



Digitized by the Internet Archive
in 2023

Annual Cumulated Index

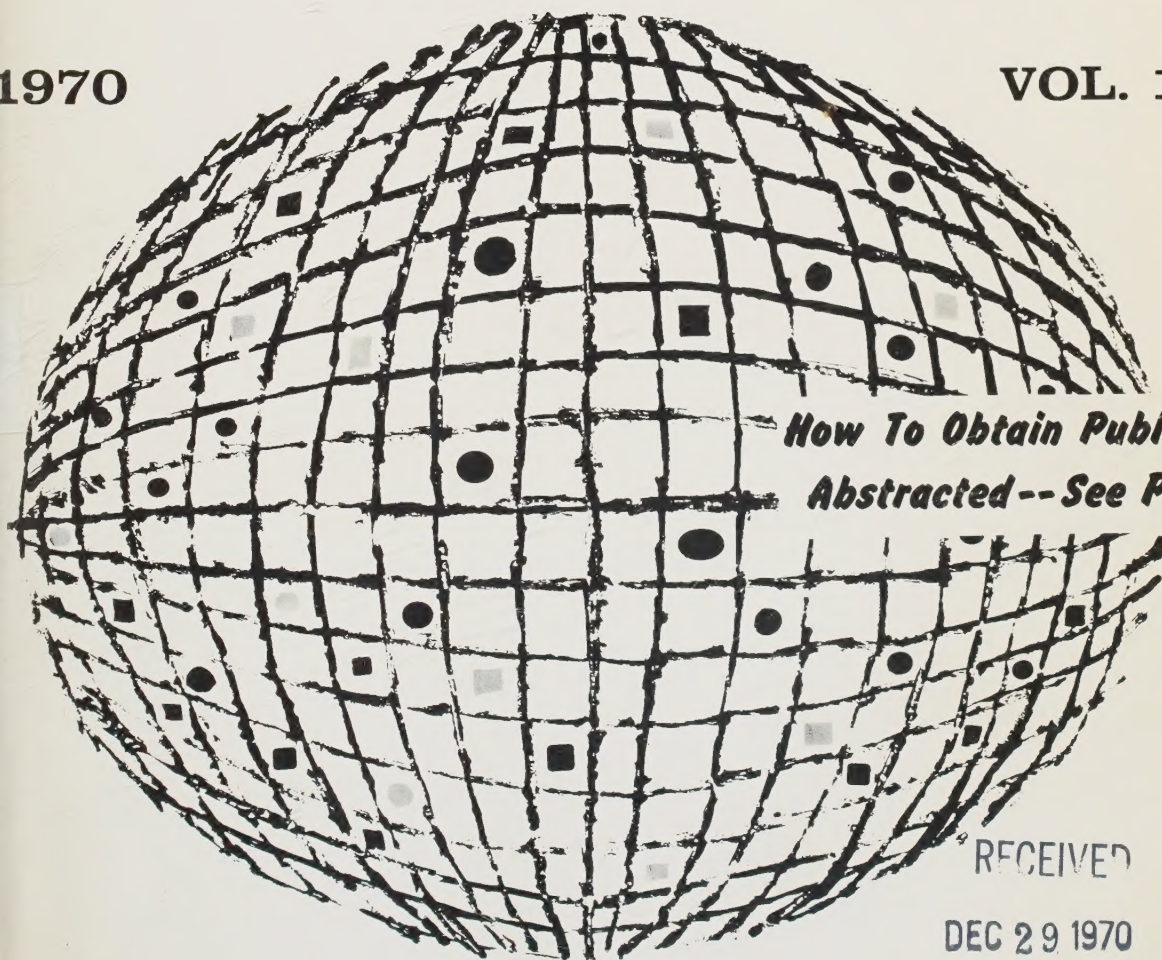
ACCESSION NOS. A70-10001 to A70-46414

INTERNATIONAL AEROSPACE ABSTRACTS

PART 2, SUBJECT INDEX, M - Z

1970

VOL. 10



*How To Obtain Publications
Abstracted -- See Page IV*

RECEIVED

DEC 29 1970

UICC SCIENCE LIBR.

PUBLISHED BY THE TECHNICAL INFORMATION SERVICE
AMERICAN INSTITUTE OF AERONAUTICS AND ASTRONAUTICS

INTERNATIONAL AEROSPACE ABSTRACTS

TL
500
I57
vol. 10
1970
Index

NK
Science

ANNUAL CUMULATED INDEX

PART 2 SUBJECT INDEX, M - Z

VOLUME 10
JANUARY - DECEMBER
1970

ACCESSION NUMBERS A70-10001 to A70-46414

INTERNATIONAL AEROSPACE ABSTRACTS is prepared and published semimonthly (except June and December, which have three issues) by the Technical Information Service, American Institute of Aeronautics and Astronautics, Inc., for the Institute and the National Aeronautics and Space Administration under Contract No. NASW-1949. Editorial and Subscription Offices: 750 Third Avenue, New York, N. Y. 10017. Copyright © 1970 by the American Institute of Aeronautics and Astronautics, Inc. (The indexes, however, may be reproduced for any bibliographic purpose.)

Telephone: 212 TN-7-8300

TWX: 212 867-7265

SUBSCRIPTION INFORMATION. Semimonthly issues: United States and Possessions, 1 year, \$75 postpaid; Foreign Countries, 1 year, \$90 postpaid. Cumulated Index Volumes: United States and Possessions, 1 year, \$30 postpaid; Foreign Countries, 1 year, \$35 postpaid. Second-class postage paid at Phillipsburg, N. J.

19 Feb 71

CONTENTS

PART 1

INTRODUCTION	iii
HOW TO OBTAIN PUBLICATIONS ABSTRACTED	iv
CROSS REFERENCES	iv
PERIODICALS SCANNED	v – xxvii
SUBJECT INDEX, A – L	A1 – A1018

PART 2

INTRODUCTION	iii
HOW TO OBTAIN PUBLICATIONS ABSTRACTED	iv
CROSS REFERENCES	iv
SUBJECT INDEX, M – Z	A1019 – 2064

PART 3

INTRODUCTION	iii
HOW TO OBTAIN PUBLICATIONS ABSTRACTED	iv
PERSONAL AUTHOR INDEX	B1 – B848
CONTRACT NUMBER INDEX	C1 – C47
MEETING PAPER & REPORT NUMBER INDEX	D1 – D30
ACCESSION NUMBER INDEX	E1 – E163

STAFF, AIAA

Administrator—Technical Information Programs, Robert R. Dexter

STAFF, TECHNICAL INFORMATION SERVICE

Director, John J. Glennon

Associate Director—Administrative, Thomas J. Meskel

Associate Director—Technical, Irene W. Bogolubsky

Abstracts Editor, Nanu Davis

Index Editor, Angelica Mihalakos

Chief Librarian, Patricia M. Marshall

INTRODUCTION

INTERNATIONAL AEROSPACE ABSTRACTS (IAA) is an abstracting and indexing service covering the world's published literature in the field of aeronautics and space science and technology. IAA is issued semimonthly, on the 1st and 15th of each month.

Coverage of Published Literature

The following types of publications are covered in IAA:

- Periodicals (including government-sponsored journals) and books.
- Meeting papers and conference proceedings issued by professional societies and academic organizations.
- Translations of journals and journal articles.

Coverage of Reports ("Unpublished" Literature)

Abstracts and indexes of report literature are issued in SCIENTIFIC AND TECHNICAL AEROSPACE REPORTS (STAR), which is published by the Scientific and Technical Information Division, National Aeronautics and Space Administration.

By special arrangement between NASA and the American Institute of Aeronautics and Astronautics, IAA is issued in coordination with the twice-monthly schedule of STAR, which appears on the 8th and 23rd of each month.

IAA and STAR both utilize identical subject categories and indexes, which are described below.

Thus the two services provide comprehensive access to the national and international unclassified report and published literature of current significance to aerospace science and technology.

Arrangement of the Semimonthly Issues

IAA is arranged in two major sections:

- (1) Abstracts Section. This section contains complete bibliographic citations with informative abstracts, arranged by appropriate subject categories to facilitate scanning. The subject categories are numbered from 01 to 34, and the scope of each category is outlined in the Table of Contents and again at the beginning of each category in the Abstracts Section. Each abstract is prefixed by the IAA accession number.
- (2) Index Section. Five indexes are contained in this section: Subject, Personal Author, Contract Number, Meeting Paper and Report Number, and Accession Number. Each index is prefaced by explanatory notes to guide the user to the desired abstract.

Cumulated Indexes

The semi-annual cumulated index is issued promptly at the end of the first six months and the annual cumulated index is issued promptly at the end of the twelve-month period.

Each cumulated index contains the following sections: A—Subject Index, B—Personal Author Index, C—Contract Number Index, D—Meeting Paper and Report Number Index, and E—Accession Number Index.

Indexing Vocabulary

The Preliminary Edition of the NASA THESAURUS (December 1967) (NASA SP-7030) is the authority for the indexing vocabulary that appears in the subject indexes to STAR and IAA. The NASA Thesaurus should be consulted for a total picture of the current indexing vocabulary and associated cross-reference structure. Copies of the NASA Thesaurus may be obtained from the National Technical Information Service or the U. S. Government Printing Office at a price of \$8.50 for the three-volume set.

how to obtain publications abstracted

Address all inquiries and requests to:

Technical Information Service
American Institute of Aeronautics
and Astronautics, Inc.
750 Third Avenue, New York, N. Y. 10017

Telephone: 212 TN-7-8300
TWX: 212 867-7265

Documents abstracted are available from the AIAA Technical Information Service as follows:

- Paper copies of accessions announced in IAA and STAR and of other documents in the TIS library are available at \$5.00 per document up to a maximum of 20 pages. The charge for each additional page is \$0.25.
- Microfiche of documents announced in IAA are available at the rate of \$1.00 per microfiche on demand. Documents available in this manner are identified by the symbol # following the accession number in the Abstracts Section and in the Meeting Paper and Report Number and the Accession Number Indexes.
- Minimum air-mail postage to foreign countries is \$1.00.
- A number of publications, because of their special characteristics, are available only for reference in the library.

PLEASE REFER TO THE ACCESSION NUMBER WHEN REQUESTING PUBLICATIONS

CROSS REFERENCES

The subject index includes two types of cross references to aid the user of the index in locating the material being sought:

1. "USE" references (U) direct the user to alternate headings under which material on the subject will be found, for example

COLUMBIUM
U NIOBIUM

2. "NARROWER TERM" references (NT) refer the user to more specific headings in the same subject area for example

LUMINESCENCE
NT ELECTROLUMINESCENCE

A Notation of Content, rather than the title of the publication, appears under each subject heading; it is listed under several subject headings which provide multiple access to the subject content of each accession. The IAA accession number is located under and to the right of the Notation of Content. It is preceded by numbers identifying the issue and page of *International Aerospace Abstracts* where the abstract is located.

To illustrate:

Issue Number	Page Number	Accession Number
01	p0196	A70-10845

M

M WINGS

U VARIABLE SWEEP WINGS

MACH CONES

Mach effect on cylinders, tracking triple point of shock interaction using 25-spark camera
[SMPT PREPRINT 103] 22 p4032 A70-43032

MACH INERTIA PRINCIPLE

Finite rotating universe model construction not possessing Goedel cosmos pathological properties, discussing relation to Mach principle
01 p0191 A70-11358

MACH NUMBER

Oblique unsteady shock wave structure propagating at large Mach numbers in plasma cylinder under steady magnetic field, showing particle velocity profile discontinuity
01 p0064 A70-10999

Hypersonic flow over blunt bodies, discussing Mach number, specific heat and blast wave limits
04 p0613 A70-14454

Flow viscosity and heat conduction effects on shock wave propagation in bent channel with weak Mach reflection
04 p0671 A70-15013

Mixture Mach number defined for collisionless plasma flow about solid body by extending cold-ion theory
04 p0729 A70-15582
[AIAA PAPER 69-78]

Nozzle exit turbulence and excess fuel combustion as low and high speed jet noise source using Lighthill theory
05 p0834 A70-16782

Gas dynamic functions using critical velocity and Laval number
06 p1033 A70-17237

Pre-set Mach number control in supersonic wind tunnel, evaluating effects of nozzle installation, stagnation temperature drop and pressure errors
06 p1028 A70-17912

Ramjet engines combustion chamber and air intake design for velocities between Mach 2 to 7
06 p1130 A70-17932

Mach disk in underexpanded exhaust plume predicted by dividing flow field into subregions
[AIAA PAPER 70-231] 06 p0974 A70-18176

Helium injection Mach number effect on supersonic jet penetration into Mach 2 air stream from flat plate determined from concentration measurements
[AIAA PAPER 70-92] 06 p0975 A70-18200

Least squares method to determine shock thickness

at arbitrary Mach number from Boltzmann equation for rigid sphere rarefied gas
06 p1051 A70-18345

Airfoil research in S-10 French wind tunnel for two dimensional flow, noting Reynolds and Mach number ranges
[ONERA-TP-766] 08 p1433 A70-21843

Aerodynamic heating of blunt bodies, investigating dependence of hypersonic limit distribution on Mach number
09 p1603 A70-22419

Blast waves in low Mach number regime with assumption of power law density profile in rear, obtaining particle velocity and pressure distributions
09 p1661 A70-23214

Flow past yawed delta wing at supersonic flight velocities, obtaining real velocity near singular surface and replacing Mach number by perturbed parameter
10 p1799 A70-24126

Closed streamline low Mach number compressible fluid flow without temperature restrictions, noting incompressible flow behavior
10 p1869 A70-24547

Regional growth functions of turbulent wakes at small Mach numbers using regression equations
11 p1976 A70-25998

Shock ionized xenon electrical conductivity measurement at high temperatures as function of Mach number, noting equilibrium effects
12 p2281 A70-27807

Gaseous injection into supersonic flow, investigating secondary Mach number and injection angle effects on flowfield in supersonic wind tunnel
[AIAA PAPER 70-552] 13 p2339 A70-29017

Inert gas ionization behind shock wave at high Mach numbers, using electrical conductivity and continuum emission measurements
13 p2388 A70-29380

Compressible fluids steady state equations invariant transformation, establishing sound speed-Mach number relation
13 p2389 A70-29458

Plasma sheath boundary as closed Mach surface, demonstrating Bohm criterion application to ion velocity component normal to sheath edge
13 p2464 A70-29465

High Mach number viscous flow past cylinder with cylindrical shock wave
13 p2391 A70-29970

Graphical plotting of critical Preston tube diameter, allowing for Mach and Reynolds numbers effects and introducing limiting line
14 p2586 A70-30871

Critical Mach numbers for transverse resistive shock waves as function of fluid/magnetic pressure ratio compared with cold plasma theory
14 p2623 A70-31036

Linearized two dimensional double vortex sheet model of inviscid compressible jet instabilities over all Mach numbers
15 p2722 A70-32375

Temperature and Mach number distributions measurements on supersonic turbulent boundary layers for reanalyzing heat transport
[AIAA PAPER 70-744] 17 p3066 A70-34499

Mach disk structure in free low density expanding supersonic jet from static pressure probe measurements
17 p3068 A70-34696

Pressure distribution measurements on wedges in compressible flow at Mach 0.5-2.2, discussing wedge angle, Mach number and boundary layer thickness effects
17 p3013 A70-35923

Axial flow compressor cascades, predicting total pressure losses for inlet relative Mach number greater than unity
[ASME PAPER 70-GT-57] 18 p3209 A70-36872

Helium injection Mach number effect on supersonic jet penetration into Mach 2 air stream from flat plate determined from concentration measurements
20 p3558 A70-39690

Mach number effect on sound propagation in tuning acoustically lined rectangular duct with uniform flow
20 p3673 A70-39709

Heat fluxes from shock-heated gas to shock tube wall and wedge surface as function of Mach number, using platinum resistance thermometers
20 p3613 A70-40343

Pressure distribution on thin nonlifting airfoils in steady two dimensional flow with freestream Mach number at or near unity
23 p4134 A70-44583

MACH-ZEHNDER INTERFEROMETERS

CW laser light sources for Mach-Zehnder interferometer, obtaining results for carbon dioxide injected through porous bottom wall into air flow
03 p0484 A70-13397

Atmospherically induced phase fluctuations for various path lengths using near ground horizontal Mach-Zehnder, discussing turbulence effects
10 p1916 A70-24413

Stress analysis using transmitted light polariscope and Mach-Zehnder interferometer for frozen-stress slice
12 p2325 A70-27620

Gas laser iterative alignment of Mach-Zehnder interferometer for monochromatic and white light fringes 19 p3424 A70-37880

Mach-Zehnder interferometer for holographic investigation of inhomogeneities in transparent media, discussing photointerpretation error reduction 20 p3633 A70-39749

Optical image hologram production, investigating gas flows around body by means of Mach-Zehnder interferometer 20 p3633 A70-39761

Mach-Zehnder interferometer for plasma diagnostics measurements, discussing optical interference method, fringe shift determination and dispersion equations 21 p3856 A70-41150

Two dimensional turbine cascade air flow, examining boundary layer regime, thickness, velocity and pressure coefficient at any point by Mach-Zehnder interferometer 22 p4026 A70-42344

MACHINE LEARNING

U LEARNING MACHINES

MACHINE LIFE

U SERVICE LIFE

MACHINE ORIENTED LANGUAGES

NT ALGOL

NT FORTRAN

SPIRAL system for free-flowing text information storage and retrieval in machine readable library 02 p0264 A70-12129

Problem oriented computer programming language and translator for solving partial differential equations 11 p2013 A70-25367

Automatic search for data in hydrology and meteorology, describing information search language development 14 p2602 A70-30141

Cost effectiveness of higher order language /HOL/ for airborne computers 16 p3003 A70-33428

Space programming language SPL/J6 replacing machine language programming in flight software capable of expressing complex vector mathematics and decision control 16 p2868 A70-33429

Common high order programming language and program debugging in aerospace software 16 p2868 A70-33430

Aerospace program oriented language /APOL/ requirements for flight programs, discussing cost, design and applicability 16 p2868 A70-33431

Aerospace compiler design for software cost reduction without affecting reliability, describing input language 16 p2868 A70-33432

Computer language related to ALGOL 60 for handling nonnumerical problems of mechanics 18 p3283 A70-36367

Digital computer input language with multiple access for engineering calculations 19 p3385 A70-38577

Soviet book on computer design and construction covering man machine interfaces, internal languages, interpretation systems, memory distribution, solution processes, etc 19 p3385 A70-38794

Interactive man computer systems evaluation considering speech communication, SKETCHPAD and graphics capabilities, FORTRAN and programming languages and future manned space missions [ALAA PAPER 70-1292] 24 p4317 A70-45928

MACHINE RECOGNITION

U ARTIFICIAL INTELLIGENCE

MACHINE STORAGE

U COMPUTER STORAGE DEVICES

MACHINE TOOLS

NT GRINDING MACHINES

NT MILLING MACHINES

Elastoplastic strains in machine element surface layers under static friction force using polarization-optical techniques 04 p0696 A70-14410

Lasers for optical inspection of components and calibration of machine tools 05 p0860 A70-16823

Machine tools used in production of Hawker Siddeley Buccaneer low level strike and reconnaissance aircraft 09 p1691 A70-22608

Rotary Ultrasonic Machining with diamond tools for hard and brittle materials compared to ultrasonic impact grinding method 09 p1692 A70-22797

Complex variable technique for electrochemical machining of insulated and uninsulated straight sided tool, using minimal computer time 10 p1894 A70-24416

Current density distribution during electroerosive machining, discussing current diagram construction and tool profile 11 p2060 A70-25935

Complex organization-processing system of experimental production, noting work specialization in machine shops 11 p2060 A70-25936

Vibration amplitudes and frequencies contactless measurement by sensor with photodiode for machining tool elements during metal working operations 12 p2235 A70-27683

Thermocompensated wire loop microtensometers for machine part stress concentration measurements, including parameter selection nomograms 13 p2409 A70-29519

Gas tungsten arc hot wire welding operational characteristics and applications 14 p2590 A70-30929

Hydraulic and pneumatic controls construction and use in machine tools 19 p3359 A70-38725

Programmable all-stored-logic numerical control system based on minicomputer, affording economy and adaptability in production tool applications 22 p3993 A70-42319

Drilling machinability of wrought Al alloys, relating tool force to hardness, feeding and cutting speed 24 p4349 A70-46195

W, Ta and Mo components economical fabrication by plasma spraying for rocket nozzles, susceptors and crucibles 24 p4350 A70-46355

MACHINE TRANSLATION

Character recognition methods applied to reading machines transforming printed material into forms acceptable to blind 13 p2360 A70-29809

MACHINERY

Rotary machine for classifying reinforcing fibers and whiskers with respect to length 05 p0855 A70-16583

Roller machine adjustment parameters determination by analytical relations allowing for intermediary zone 07 p1292 A70-18837

Filament wound bodies of revolution manufacture with consideration for linear and nonlinear winding, analyzing mechanically and electronically controlled machines 07 p1295 A70-19765

Soviet collection of articles on machine dynamics covering various rotor vibrations, machine/operator system, etc 08 p1501 A70-20693

Fatigue limits distribution functions of full-scale machine parts estimated by rupture similarity criterion, discussing stress concentration and scale factor effects 09 p1776 A70-22616

Machine parts fatigue strength calculated from failure probability parameter during unsteady loading 09 p1776 A70-22622

Machine parts lifetime dispersion determined by fatigue limits distribution during cyclic loading 09 p1776 A70-22623

Fluid mechanics and fluid machinery - Conference, Budapest, September 1969 11 p1973 A70-25776

Telemetric systems for moving machine elements tests, discussing seven channel PFM and FM/FM systems 11 p2056 A70-26451

Statistical data for optimum fatigue reliability design for dynamic and rotary machinery, considering static strength, cycle-to-failure and stress-to-failure distributions 21 p3833 A70-41004

Conduction liquid metal MHD machine channels design with baffles installed to decrease shunting effect of end zones, calculating segments by circuit theory methods 21 p3760 A70-42233

Differential equations of motion for machine assembly, using Appel equations 23 p4200 A70-44319

MACHINING

NT CHEMICAL MACHINING

NT ELECTROCHEMICAL MACHINING

NT HOT MACHINING

NT MILLING [MACHINING]

NT SPARK MACHINING

NT ULTRASONIC MACHINING

Machined surface evaluation of fabricated components by electron microscopy to identify defects 01 p0097 A70-10012

Precision machining and repair of radioactive Plum Brook Reactor core fuel grid 01 p0140 A70-10322

Algorithms for automatic control of machine elements fabrication 02 p0308 A70-12227

Manganese and sulfur content effects on martensitic stainless steels machinability, describing effects on mechanical properties, cold formability and corrosion resistance 03 p0507 A70-13135

Sputter machining thickness reduction methods for VHF resonant piezoelectric transducers 03 p0496 A70-14207

Laser characteristics relevant to microwelding and micromachining, discussing heat conduction based models limitations 05 p0857 A70-15999

Mechanical fastening, adhesive bonding and machining methods for laminated fiberglass reinforced plastic materials 05 p0856 A70-16618

Lasers industrial application to distance and flow rate measurement, automated machining and tunneling, inspection, die hole punching, welding, etc 06 p1078 A70-18431

Electron beam gun for drilling and perforation modified to include micromachining and welding 08 p1502 A70-20821

Solid state and gas lasers industrial applications in machining and nonmachining areas, discussing limiting factors 09 p1692 A70-22706

Aerospace materials machining processes guidelines to minimize structural failures caused by lack of surface integrity 12 p2239 A70-26988

Boron fibrous composite panels machining methods including drilling, routing, band sawing and reaming [ASTME PAPER MR-69-730] 12 p2240 A70-27077

Cutting speed, feed parameters and tool tip curvature effects on machined surface roughness of turned fiberglass reinforced epoxy laminates 14 p2590 A70-30873

Al-B composites forming and machining, discussing tooling, methods and filament orientation [ASM PAPER W70-5.2] 15 p2744 A70-32334

Laser and electron beam removal of material in manufacturing technology 19 p3447 A70-38451

Low stiffness optical parts bulk vibration machining 22 p4045 A70-42512

Metal matrix composite structures tooling and fabrication processes, considering forming, joining, welding, machining joining, etc [SAE PAPER 700752] 24 p4348 A70-45873

MACLAURIN SERIES

Jacobi ellipsoid quasi-static evolution by gravitational radiation, discussing direction of increasing angular velocity toward nonradiating state at bifurcation point with Maclaurin sequence 20 p3702 A70-39018

MACROCLIMATE

U CLIMATE

MACROMOLECULES

U MOLECULES

MACROSCOPIC EQUATIONS

Nonequilibrium interaction of radiative and vibrational rate processes in IR-active diatomic gas using macroscopic equations 08 p1549 A70-21574

Book on plasma dynamics covering charged particle orbit theory, macroscopic equations, hydromagnetics, hot and cold plasma waves, kinetic theory and plasma radiation 11 p2087 A70-25500

Approximate dispersion relation for MHD waves from macroscopic plasma equations including particles collision terms 16 p2859 A70-32941

Macroscopic equations of motion established by Maxwell transport equations for relativistic perfect gas 22 p4011 A70-42716

MACULAR VISION

U VISION

MAGMA

Oceanic volcanic rocks, discussing dispersed element characteristics to describe origin of magma types 15 p2731 A70-32100

Fugacities of HCl and HF compared with abundance in volcanic fumarolic emanations, indicating magma undersaturation 20 p3619 A70-39321

Compositional zoning in pyroxenes from grained Apollo 11 microgabbros, implying supercooled magma origin 21 p3899 A70-41532

Petrology, crystallization and magma origin of lunar clinopyroxene, ilmenite-rich dolerite and microgabbro from Apollo 11 samples 21 p3900 A70-41536

MAGNESIUM

NT MAGNESIUM ISOTOPES

Pressure effects on burning rate of magnesium mixtures with solid oxygen containing organic compounds, determining charge density effect on mass velocity 01 p0218 A70-11021

Stress-strain effect on dislocation densities of cylindrical Mg single crystals deformed by torsion basal slip compared to tension test 01 p0122 A70-11236

Mg vapor and oxygen surface reactions in MgO deposits, using atomic absorption spectrophotometry 02 p0250 A70-12006

- Rocket-borne spectroheliograph for taking X ray and monochromatic pictures of sun in Mg II line
03 p0570 A70-13594
- Magnesium solubility in titanium from X ray analysis of Mg distribution in diffusion zones at high temperature and pressures
09 p1703 A70-22567
- Singly ionized Mg resonance lines electron impact broadening quantum mechanical calculation
09 p1732 A70-22827
- Mg ion metabolism in neuromuscular excitability maintenance, discussing quantity requirements, detection and electromyographic recording
12 p2172 A70-28045
- Preignition and combustion kinetics in airstream of Mg and Al suspensions in aviation kerosene and gasoline
14 p2664 A70-30395
- Chemical and electrochemical corrosion resisting primers for Mg surface coatings in machine parts
14 p2598 A70-31293
- Magnesium pulse arc welding, describing procedure, techniques testing and advantages
17 p3100 A70-34635
- Solar chromosphere resonance lines, observing H and K line profiles of Mg ions
17 p3161 A70-34893
- Fabry-Perot interferometry of solar Mg II resonance lines
17 p3162 A70-34897
- Lithium-like line spectra in Mg, Al and Si observed with grazing incidence spectrometer and low inductance microfarad spark source
17 p3138 A70-35720
- Combustion of decomposition products of Mg based pyrotechnic fuel in supersonic flow, obtaining heating device characteristics
20 p3736 A70-39266
- Mg high temperature creep mechanism in high and low stress regions, using isothermal tensile creep tests
23 p4204 A70-43885
- MgH molecular lines Zeeman splitting in sunspot spectra confirmed by photoelectric observations
24 p4400 A70-45308
- Mg addition effects on impact strength and micro structure of Al-Si-Cu alloys, using Charpy test and metallographic methods
24 p4363 A70-46196
- MAGNESIUM ALLOYS**
Galvanic cell using liquid Mg chloride or Mg chloride-Ca chloride mixtures as electrolyte used to determine activities in Mg-Al liquid alloys
03 p0507 A70-13138
- Ni addition effects on Mg-Nd and Mg-Nd-Mn alloys structure and heat resistance
04 p0706 A70-15189
- Electron momentum distributions from Compton profiles of Li-Mg polycrystalline samples, exhibiting discontinuity at free electron value of Fermi momentum
05 p0892 A70-16471
- Light Mg-Li alloys physical and mechanical properties, production and treatment
[DFVLR-SONDDR-18]
07 p1306 A70-19234
- Soviet papers on casting of aluminum, magnesium and titanium alloys
08 p1504 A70-21126
- Al-Mg alloys mechanical properties and corrosion resistance during aging, noting Zr and Mo additives effects
08 p1517 A70-21129
- Al-Mg oxidation resistance and kinetics, studying Zr, Ce and Be additives effects on oxide films mechanical properties
08 p1517 A70-21130
- Carbon-bearing materials for modification of Mg-Al-Zn-Mn alloys filtration processes
08 p1505 A70-21132
- Stress concentration effect on fatigue strength of Al- and Mg-base structural alloy specimens of different sizes analyzed statistically
09 p1703 A70-22617
- Fatigue limit and rupture stress distribution patterns of Al- and Mg-base structural alloys using accelerated Prot and Enomoto methods
09 p1703 A70-22621
- Soviet monograph on intermetallic compounds with Laves phases, covering crystallographic and thermodynamic characteristics of Mg-Zn, Mg-Cu and Mg-Ni systems
12 p2252 A70-26885
- Binary and ternary Mg alloys ductile fracture mechanism, studying coherent/noncoherent particles effects
12 p2256 A70-27612
- Particles shape and phase composition in combustion products of dispersed Al-Mg alloy powders by electron diffraction and X ray analysis
14 p2664 A70-30396
- Al-Mg alloy sheets work hardened plastic properties, tensile strength and elongation
14 p2597 A70-30962
- Work hardening and tempering effects on Al-Mg alloy stress corrosion and mechanical properties
14 p2597 A70-30963
- Al-Zn-Mg weldable alloy composition, mechanical properties, heat treatment, aging effects, etc
14 p2597 A70-30964
- Al-Zn-Mg alloys aging kinetics and rupture mechanism, discussing stress corrosion, welded structures stability, activation energy, etc
14 p2597 A70-30965
- Al-Mg-Zn alloy composition, mechanical properties and structure for various heat treatments, discussing welded structures stability, stress relief, corrosion resistance and tensile strength
14 p2597 A70-30966
- Al-Mg alloys creep characteristics dependence on Ag, Si and Zn additions during aging heat treatments, establishing activation energy and stress exponents
16 p2930 A70-33086
- Al-Mg alloys recrystallization, investigating heating rate and annealing time effects on sheet grain size
19 p3450 A70-37372
- Cooling rate effect on Al-Mg equilibrium state during heat treatment after annealing
20 p3644 A70-38959
- Stressed cast Mg-Nd-Zr alloys structural transformations kinetics over temperature range by electron microscopy
20 p3646 A70-39046
- Mg-Al alloy beta phase precipitation, using metallography, hardness tests and electron microscopy
20 p3652 A70-40447
- Magnesium Al and Ti alloys electron beam welding for aerospace industry, discussing material requirements, weld quality and optimum conditions
22 p4042 A70-42338
- Light rare earth metals improving Mg alloys, Al alloys, Cu alloys and superalloys
22 p4057 A70-43575
- Al and liquid Al-Mg alloys oxidation at high temperatures, noting Mg content effect
24 p4361 A70-46174
- Al-Zn-Mg alloy prolonged aging behavior, examining Gp and intermediate zones, equilibrium phases, maximum strength and serrated stress strain curve
24 p4362 A70-46189
- Grain growth abnormality in Al-Mg ingots with small amounts of Mn and Cr during secondary recrystallization
24 p4363 A70-46197
- Alloying elements effects on corrosion resistance of Mg ingot in NaCl aqueous solution
24 p4363 A70-46198
- MAGNESIUM CELLS**
Refuelable Mg-air battery anode, electrolyte and packaging materials selection from standpoint of cell voltage, metal consumption and sludge formation
02 p0253 A70-12721
- MAGNESIUM COMPOUNDS**
NT CHLOROPHYLLS
NT ENSTATITE
NT FORSTERITE
NT MAGNESIUM FLUORIDES
NT MAGNESIUM OXIDES
NT MAGNESIUM PERCHLORATES
NT MAGNESIUM TITANATES
Crystal-chemical and geophysical implications concerning earth mantle phase transitions from beta magnesium silicate crystal structure
11 p1994 A70-25333
- MAGNESIUM FLUORIDES**
Magnon energy theory for temperature dependence of ferrous and magnesium fluorides antiferromagnetic-resonance frequency, sublattice magnetization and magnetic specific heat
09 p1739 A70-22324
- MAGNESIUM ISOTOPES**
Production rates determination for Na 24 and Mg 28 isotopes in Ar exposed to cosmic rays
03 p0561 A70-14092
- Elastic and inelastic scattering of proton beams from magnesium and silicon isotopes, using optical model
04 p0723 A70-15637
- Dating method for stone meteorites feldspar phase based on time interval between sun nebula Al 26 production and decay into Mg 26
06 p1150 A70-18479
- Magnesium hydride absorption lines in sunspot spectrograms indicating heavy Mg enhancement in sun relative to earth
08 p1571 A70-20904
- Arcturus atmosphere Mg abundances from rotational lines noting terrestrial proportions
14 p2637 A70-30540
- MAGNESIUM OXIDES**
Mg vapor and oxygen surface reactions in MgO deposits, using atomic absorption spectrophotometry
02 p0250 A70-12006
- Light scattering from thermally stable magnesium oxide particles in premixed turbulent flames used for measuring mean and fluctuating temperature values
02 p0398 A70-12039
- Defect F centers formation in MgO, discussing optical absorption bands, oscillator strengths, luminescence band, impurity centers, etc
[ALAA PAPER 70-828]
16 p2940 A70-33938
- Transparent ceramic armor fabrication using dense polycrystalline magnesia
19 p3437 A70-38422
- Solid phase stabilization of zirconium dioxide by combined addition of yttrium and magnesium oxides
19 p3455 A70-38732
- Apollo 11 magnesium-rich opaque oxide almalcolite mineral from Tranquility Base noting relation to pseudobrookite series
21 p3895 A70-41503
- Impurity dependent critical resolved shear stress of magnesium oxide single crystals, using compression testing
21 p3862 A70-41910
- MAGNESIUM PERCHLORATES**
Ammonium and magnesium perchlorate mixture thermal stability study with differential scanning calorimetry, noting exothermic decomposition of AP
20 p3688 A70-40272
- MAGNESIUM TITANATES**
Excitation, reemission and absorption spectra of Cr activated powdery Mg titanate prepared, using MgO and Ti dioxide with LiCl as flux
02 p0350 A70-11848
- MAGNESYN (TRADEMARK)**
U SERVOMOTORS
- MAGNET COILS**
NT FIELD COILS
Cryogenically cooled superconducting electromagnets design, construction and properties for research in plasma and solid state physics, considering coil systems
01 p0143 A70-10970
- Magnetic scalar potential of circular loop represented by toroidal coordinate system, solving boundary value problems determining fields of coils and toroidal magnetic conductors
18 p3215 A70-36295
- MAGNETIC ABSORPTION**
U ELECTROMAGNETIC ABSORPTION
- MAGNETIC ANOMALIES**
NT GEOMAGNETIC HOLLOW
Gravity and vertical magnetic anomalies interpretation to infer magnetization direction
09 p1729 A70-23601
- Gravitational and magnetic anomaly interpretation by regression analysis including geological field discrimination, inverse gravimetry and magnetometry, etc
12 p2223 A70-27348
- Proton magnetometer measurements from satellite Cosmos 49, observing residual and broad magnetic anomalies
18 p3248 A70-36770
- Cylindrical body with gravitational and magnetic anomalies, selecting point coordinates for body parameters
19 p3407 A70-37298
- Atmospheric Coulomb interaction influence on longitude dependence of electron intensity in anomaly region
19 p3491 A70-37305
- Spherical harmonic analysis of geomagnetic field strength for global magnetic anomaly charts
19 p3408 A70-37317
- Autocorrelation functions of anomalous gravitational and magnetic fields for ocean lines, relating Mohorovičić boundary and Cune isotherm
19 p3408 A70-37318
- Gravity and magnetic geophysical prospecting methods, discussing data acquisition, reduction and analysis in terms of underground geologic anomalies
22 p4018 A70-43086
- Geomagnetic axial dipole deviation from true north associated with earth core asymmetric motion, discussing geomagnetic reversal
22 p4020 A70-43231
- VLF signal phase and amplitude changes associated with PCA events and South Atlantic Geomagnetic Anomaly
22 p4023 A70-43292
- F region equatorial anomaly formation, investigating vertical EM drift effect
23 p4187 A70-43857
- MAGNETIC CIRCUITS**
Magnetic components design, manufacturing and handling for use in space communication satellites, noting design group role in parts construction and quality control
02 p0267 A70-12057
- Time optimal control synthesis for electromechanical devices, considering acoustical vibrations elimination in magnetically controlled contacts
08 p1472 A70-21001
- Free-running parallel inverters limitations by critical characteristics of networks, transformers and switching elements
11 p1983 A70-26628
- Electric machines magnetic circuit and motor shape, evaluating current, flux, resistance and reluctance
19 p3357 A70-37362
- MAGNETIC COILS**
NT FIELD COILS

- Computer graphics method for determining total magnetic field magnitude for various coil configurations and spacing, indicating optimum field uniformity near Helmholtz spacing
02 p0271 A70-12745
- Plasma conductivity measuring device using phenomenon of change of coil induction in electromagnetic field
09 p1737 A70-23380
- Diode coil suppression effect on two coil magnetic latching relays, showing operating time increment due to transformer action
13 p2378 A70-29348
- Magnetoplasma interaction with axially slotted delay line, examining coil behavior physical mechanisms by cold plasma model
22 p4079 A70-42365
- Superconducting magnet system design, operation and module tests, noting large and small coil systems performance data relationship
23 p4218 A70-44354
- Force-reduced superconducting toroidal magnet coils built with Cu plated Nb-Zr wire, investigating current enhancement characteristics
23 p4230 A70-44356
- Metals flaw detection, using electronic balancing type eddy current detecting coil
24 p4336 A70-45701
- MAGNETIC CONTROL**
- Magnetic torquers consisting of permanent magnets or coils for attitude stabilization of earth satellites in geomagnetic field
[IEEE PAPER 27.1] 05 p0924 A70-17000
- Aeros satellite active magnetic position control system of axis and spin noting design and operation
[DGLR-69-056] 07 p1393 A70-19148
- Time optimal control synthesis for electromechanical devices, considering acoustical vibrations elimination in magnetically controlled contacts
08 p1472 A70-21001
- Satellite stabilization one-axis control system using earth magnetic torquer
13 p2500 A70-28405
- Spinning sun oriented satellite using magnetic coil around spin axis for attitude control, detailing design
13 p2502 A70-28439
- Magnetically constrained steady state plasma production by hot cathode DC arc discharge in He
13 p2465 A70-29819
- Japanese scientific satellite magnetic attitude and spin rate control system design and computer simulation
18 p3332 A70-36065
- Square cross section waveguide with cutoff frequency, calculating density wave propagation in helical electron beam trajectories directed by magnetic field
20 p3584 A70-39256
- Magnetic compensation for attitude control of gravity gradient stabilized satellite using environmental torques and moment gyro damping
[ALAA PAPER 70-993] 20 p3668 A70-39537
- Magnetic three degree of freedom attitude control system for axisymmetric spinning spacecraft, using Kalman filter
[ALAA PAPER 70-974] 20 p3668 A70-39555
- Magnetic pressure fast opening gas puff valve for hydrogen bursts in conical theta pinch plasma source
21 p3833 A70-41472
- Optimal control of magnetic torque for bias momentum removal from attitude controller, discussing applications to Skylab
23 p4258 A70-44503
- Celestial sphere scanning by spinning symmetric satellite with open loop magnetic control of precession
23 p4216 A70-44524
- Supersonic convective electric arcs with magnetic stabilization in sulfur hexafluoride, examining aerodynamic drag and plasma column slanting
23 p4227 A70-44554
- Magnetically stabilized satellites passive roll control, discussing resonance solutions by variational approach
23 p4262 A70-44690
- MAGNETIC CORES**
- MTRAC program for transient analysis of circuits with square loop magnetic cores based on linearization of nonlinear circuit elements and Kirchhoff current law
05 p0825 A70-16999
- Lamellar magnetic core stacking pressure influence on core magnetic characteristics in variable magnetic field, noting effects on magnetic permeability
07 p1246 A70-19537
- Composite materials in Co or Fe matrix for solid rotor core materials applications at high temperature and stress, discussing magnetic properties
08 p1524 A70-21908
- Numerical analysis of magnetic frequency divider operation
09 p1649 A70-23338
- Geomagnetic micropulsations recording by transistorized saturated core magnetometers noting sensitivity
13 p2416 A70-30055

- Satellite electronics production, discussing dielectric film capacitor, solar probe magnetic oxide memory core and thin film assemblies
17 p3053 A70-35268
- MAGNETIC DIFFUSION**
- Solar wind effects on galactic cosmic rays isotropic diffusion and density distribution in interplanetary space in presence of azimuthal asymmetry
07 p1366 A70-19429
- Solar wind effects on galactic cosmic rays isotropic diffusion and density distribution in interplanetary space in presence of azimuthal asymmetry
18 p3309 A70-36903
- MAGNETIC DIPOLES**
- Geomagnetic potential optimal representation in frame of reference of eccentric inclined dipole using conversion formulas to determine harmonic coefficients
01 p0081 A70-11230
- Dipole magnetosphere model with cylindrical or spherical forbidden band for studying plasma motion in quasi-hydrodynamic approximation
01 p0082 A70-11521
- Magnetosphere boundary configuration calculated with allowance for geomagnetic dipole inclination to geographic axis and nondipole section of geomagnetic field
01 p0082 A70-11522
- Boundary conditions for equilibrium diamagnetic plasma in magnetic dipole having constant and isotropic pressure in system
01 p0153 A70-11631
- Standing bow shock in plasma flow into dipole magnetic field, measuring particle density, electron temperature, magnetic field flux and oscillations
03 p0530 A70-13158
- Converging series solutions for conducting circular disk in radiation field of vertical and horizontal magnetic dipoles to determine reemitted field
03 p0448 A70-13432
- Plane model of magnetosphere shape and structure, considering rarefied plasma flow past two dimensional magnetic dipole with dynamic and static boundary pressure, using conformal mapping
04 p0675 A70-14435
- Circularly polarized synchrotron radiation from distribution of electrically charged particle in magnetic dipole calculated for estimating Jupiter magnetic field
04 p0746 A70-14511
- Geomagnetic field secular variations relation to variations of magnetic field of optimum dipoles, noting earth core role
05 p0842 A70-16747
- Geomagnetic center position determined by coordinate system referred to dipole approximating geomagnetic field
06 p1057 A70-17844
- Gaussian approximation of parameters of arbitrarily oriented magnetic dipole representing geomagnetic field
07 p1266 A70-19441
- Pulsar model assuming magnetic dipole radiation by spinning neutron star interacting with nearby plasma
09 p1756 A70-22517
- Radiation field of electric and magnetic dipole in double layer medium, solving Sommerfeld integrals
09 p1650 A70-23550
- Charged particle motion in steady and perturbed dipole fields using laboratory earth magnetosphere plasma model
11 p2104 A70-25546
- MHD disturbances in semiinfinite electrically conducting fluid, introducing magnetic dipole to act as source of disturbance
12 p2277 A70-27156
- Plane model of magnetosphere shape and structure, considering rarefied plasma flow past two dimensional magnetic dipole with dynamic and static boundary pressure, using conformal mapping
13 p2392 A70-28460
- Earth dipole field disk dynamo model, studying connection between polarity intervals and precession effects
14 p2638 A70-30619
- Magnetosphere topology in presence of time independent ring current symmetrical with respect to earth dipole field axis
14 p2578 A70-31242
- Plasma velocity and moment equations in magnetic dipole field as function of variations along coordinate directions
16 p2956 A70-32934
- Electric and magnetic dipole VLF radiation patterns in lossy two component magnetoplasma
16 p2860 A70-32944
- Pulsar observations based on magnetic dipole model, discussing turnoff time, emission characteristics, birth rate and scale height
17 p3153 A70-34531
- Infinitesimal electric and magnetic dipoles embedded in lossy media, investigating earth effect on electromagnetic field
17 p3045 A70-35075
- Spin stabilized satellite reorientation, using magnetic dipole interaction with geomagnetic field
17 p3179 A70-35287

- High latitude magnetosphere structure, using two dipole model
18 p3312 A70-36168
- Near earth motion equations for electrically charged dust particles in gravitating dipole magnetic fields, using zero-relative-velocity surfaces and energy integral
18 p3315 A70-36606
- Gaussian approximation of parameters of arbitrarily oriented magnetic dipole representing geomagnetic field
18 p3249 A70-36915
- Magnetic bubbles in miniaturized electronic circuits, discussing fabrication and uses in communication and computers
19 p3484 A70-37574
- Geomagnetic field configuration and magnetic drift envelopes of particles with various pitch angles at equator calculated from two-dipole model of magnetosphere
20 p3619 A70-39299
- Monopole trajectory in magnetic dipole field by numerical integration on computer and Liouville theorem, using resolved Stormer cone to investigate motion
20 p3672 A70-39301
- Charged particle motion in steady and perturbed dipole fields using laboratory earth magnetosphere plasma model
21 p3882 A70-41296
- Earth magnetic dipole represented by Rikitake two-disk MHD dynamo system
22 p4013 A70-42633
- Geomagnetic axial dipole deviation from true north associated with earth core asymmetric motion, discussing geomagnetic reversal
22 p4020 A70-43231
- Geomagnetic field behavior prediction based on extrapolation of magnetic data collected by observatories and dipole model approximation
23 p4189 A70-44068
- MAGNETIC DISPERSION**
- Numerical analysis of cyclotron amplification of geomagnetic micropulsations in magnetosphere based on dispersion relation for three component cold plasma beam system
05 p0838 A70-16284
- Radiative transfer and magnetic dispersion for three dimensional wave propagation in radiation magnetodynamics
24 p4387 A70-46148
- MAGNETIC DISTURBANCES**
- NT MAGNETIC STORMS**
- Polar magnetic disturbances during IQSY characterized by SP field superposed on Sq field generated by ionospheric dynamo
01 p0075 A70-10599
- Microbarographic oscillations associated with geomagnetic activity during observation of infrasonic waves on geomagnetically disturbed days
01 p0081 A70-11298
- Magnetospheric ring current model from ground stations data to interpret observed magnetic field disturbances
01 p0082 A70-11515
- Hourly N/h profiles of F region calculated from nomograms by normal integral method during magnetic disturbance, measuring region temperature
01 p0083 A70-11548
- Polar geomagnetic disturbances global current systems representation by prototypes of equivalent current systems
01 p0084 A70-11557
- Earth magnetosphere low energy plasmas measurements via McIlwain magnetic shell parameter, showing dependence on geomagnetic disturbances
03 p0557 A70-13284
- Explorer observations of large temporal variations of midlatitude outer zone energetic electron intensities interpreted as redistribution during geomagnetic disturbances
03 p0560 A70-13989
- Magnetospheric magnetic field disturbance due to abrupt solar wind parameters change, using Explorer 26 data
04 p0738 A70-14444
- Earth magnetosphere electric fields associated with magnetic disturbances, using satellite observations
04 p0676 A70-14459
- Prediction accuracies of atmospheric models investigated for medium altitude satellites during disturbed geomagnetic conditions, discussing solar flux and geomagnetic indices as input data
[AAS PAPER 69-617] 04 p0677 A70-14647
- Magnetic disturbances and corpuscular intrusions in auroral zone, discussing daytime and nighttime magnetic activity of electron fluxes
04 p0684 A70-15752
- Magnetic disturbance associated with E layer east-west electric current calculated in terms of ionization production and loss
05 p0838 A70-16282
- Fourier spectra of Pi 1 pulsations during magnetic field sudden disturbances derived from amplitude analysis
05 p0840 A70-16641

IQSY 27-day recurrence sequence for 1964 solar and terrestrial activity, considering geomagnetic, auroral and ionospheric disturbances correlation with phase
05 p0841 A70-16646
Tangential solar wind discontinuity observed by Vela 2A satellite, producing ground magnetic disturbances conjunctively with magnetospheric, ground and ionospheric currents
05 p0903 A70-16727
Radio waves propagation along polar auroras region, obtaining ionospheric parameters for magnetic disturbances based on penetration probability
05 p0842 A70-16744
Polar auroral region displacement ascribed to distant magnetic field disturbances, proposing calculation method
05 p0842 A70-16745
Sporadic electron flux contribution to high latitude geomagnetic disturbances at outer radiation belt boundary estimated from Elektron 1 and 2 observations
05 p0843 A70-16765
Magnetic activity in Antarctica during IQSY, plotting space-time characteristics of perturbations
07 p1268 A70-19462
Magnetospheric plasmapause-high latitude electron density through relations using satellite topside ionograms, noting local time and magnetic disturbance effects
07 p1270 A70-20074
Earth ionosphere and magnetosphere electrodynamical state as function of neutral gas small scale motions, considering magnetic disturbances and ionospheric discontinuities
07 p1276 A70-20426
Statistical correlation between polar magnetic disturbances and magnetospheric energetic electron flux increase from IMP-1 satellite observations
08 p1491 A70-21714
Magnetic spikes in polar cap region due to poleward shift of narrow westward electric current filament
08 p1491 A70-21716
Solar activity analysis emphasizing sunspots, magnetic disturbances and bursts data
09 p1752 A70-22199
Excessive absorption in night E layer with and without geomagnetic disturbances for almost complete solar cycle, discussing winter increases /anomalies/
09 p1669 A70-23170
International quiet and disturbed magnetic days classification and significance
10 p1873 A70-23833
Magnetic disturbances caused by magnetosphere-solar wind filamentary inhomogeneity interaction observed by Pioneer 6
10 p1931 A70-24320
F region magnetic disturbances due to low energy solar plasma penetration during proton bursts
11 p2104 A70-25535
Exospheric density from Echo 2 orbit, observing 27 day variations associated with sun rotation and correlation with geomagnetic disturbances
11 p2046 A70-26566
Magnetospheric magnetic field disturbance due to abrupt solar wind parameters change, using Explorer 26 data
13 p2475 A70-28469
Model current system for magnetospheric substorm accounting for distribution of geomagnetic disturbance field vectors on earth surface and auroral electrons and protons
13 p2481 A70-30062
Polar cap elementary magnetic disturbance relationship to auroral electrojet
14 p2570 A70-30215
Morphology of thermal and energetic particles in inner magnetosphere during geomagnetic disturbances and solar cycles
14 p2630 A70-30358
Magnetic disturbances and corpuscular intrusions in auroral zone, discussing daytime and nighttime magnetic activity of electron fluxes
14 p2576 A70-30836
Atmospheric density near 180 km /1968-1969/ from orbit of satellite 1967-31A /ATS 2/, noting weak dependence on solar activity and correlations to geomagnetic disturbances
15 p2724 A70-31680
Geomagnetic dipole field disturbances by trapped particles, calculating self consistent equilibrium configuration for ring current dipole moments
15 p2727 A70-31905
Electrostatic turbulence in bow shock magnetic structures observed byOGO 5, explaining turbulence as ion acoustic or Buneman mode due to two stream instability
18 p3311 A70-36006
Magnetic activity in Antarctica during IQSY, plotting space-time characteristics of perturbations
18 p3250 A70-36936
Lower E region electron concentration variations relationship with geomagnetic field disturbances
18 p3255 A70-37037
Solar wind fluxes observed onboard Venera 2 and 6 compared with earth electromagnetic field pulsations and short period disturbances
19 p3494 A70-37479
LF geomagnetic micropulsations recordings by two component induction magnetometer, relating diurnal frequency and occurrence variations to local K-index changes
19 p3412 A70-37995
HF geomagnetic micropulsations recordings by two component induction magnetometer, relating diurnal frequency and occurrence variations to local K-index
19 p3412 A70-37996
Cosmic noise absorption diurnal variations at auroral zone conjugate areas during geomagnetically disturbed periods
19 p3414 A70-38379
Geomagnetic field pulsations prior to polar magnetic disturbance onset, discussing solar wind role
19 p3416 A70-38588
Geomagnetic perturbation indices indicating different solar corpuscular streams and heliogeophysical properties
20 p3618 A70-39182
Plasmapause motion in equatorial plane under sudden dawn-dusk field with constant solar wind-magnetosphere interaction
20 p3620 A70-39341
Sideband frequency disturbances at analog data magnetic storage using frequency modulation
20 p3586 A70-39706
Sporadic E layer ionization correlated with geomagnetic disturbances in northern auroral and polar regions
21 p3812 A70-40592
F 2 region critical frequency cross correlation coefficients for magnetically conjugate stations, considering magnetic disturbances effects
21 p3816 A70-41069
Low energy solar protons penetration, examining geomagnetic cutoff latitude during magnetically disturbed period
21 p3881 A70-41077
Transverse magnetic disturbances in auroral oval, examining movement, intensity, particle fluxes and field magnitude
21 p3817 A70-41090
F region magnetic disturbances due to low energy solar plasma penetration during proton bursts
21 p3882 A70-41285
Worldwide geomagnetic fluctuations during disturbed conditions computed from spectrum analysis, considering long period oscillation caused by solar wind structure changes
22 p4019 A70-43114
Total electron content and equivalent slab thickness statistical data during magnetic disturbances from AT-3 satellite VHF transmission observations
22 p4020 A70-43162
Solar wind intensity and direction correlated with intensity of earth surface magnetic disturbances and geomagnetic pi-2 type pulsations
22 p4022 A70-43284
Dynamo role in magnetospheric disturbances and ionospheric inhomogeneities, allowing for charged particle concentration height dependence
23 p4237 A70-44059
Ionospheric HF Doppler frequency dispersion at low latitudes under various geomagnetic disturbance conditions
24 p4314 A70-46129
Polar cap elementary magnetic disturbance relationship to auroral electrojet
24 p4331 A70-46290
MAGNETIC DOMAINS
Tokamak-type magnetic configurations application to thermonuclear reactor, discussing equilibrium and stability parameters minimum values, operating pattern and heating method
02 p0349 A70-12756
Ferromagnetic domain wall-dislocations magnetoelastic interaction in Fe and Ni computed as function of relative separation, discussing effects on magnetic properties
09 p1705 A70-22811
Stable colloidal dispersions of subdomain magnetite particles correlated for magnetic properties in terms of size distribution and volumetric concentration by superparamagnetic theory
12 p2284 A70-27241
Magnetic bubbles in miniaturized electronic circuits, discussing fabrication and uses in communication and computers
19 p3484 A70-37574
Magnetic surface loading of Gunn oscillators domain state for use as logic gates, pulse function generator, etc
19 p3387 A70-37819
MAGNETIC EFFECTS
NT MAGNETIC RIGIDITY
Hypothetical magnetic configurations in presence of Coriolis forces from convective cell hydromagnetic activity in solar plasma, considering dynamos with increasing magnetic field
01 p0173 A70-10133
Solar structural periodicities in quiescent prominences and filaments, considering plasma instability and supporting magnetic field characteristics
01 p0176 A70-10248
Angular momentum conservations for solar gas confined by closed field lines or outflowing along open magnetic field lines
01 p0176 A70-10251
Geomagnetic field influence on extensive air shower radio emission, discussing frequency dependency and signal polarization
01 p0069 A70-10281
Bremsstrahlung radiation in intense magnetic fields rejected for pulsar radiation mechanism
01 p0169 A70-10344
Constant magnetic fields effects on blood coagulatory processes, describing microcalorimetric determination
01 p0015 A70-10372
Magnetic field effects on point Coulomb impurity charge static shielding by quantum electron plasma
01 p0151 A70-10449
MHD wave propagation through plasma in magnetic field of current filament, developing Hamilton-Jacobi equation by geometrical optics
01 p0151 A70-10466
Entrainment of electrically conducting liquid by moving wall in long duct with rectangular cross section and magnetic induction field
01 p0151 A70-10656
Anomalous temperature-time cooling data for surface material of Tycho, Copernicus and Aristarchus craters, suggesting relation to magnetic phase transitions during lunar nights
01 p0183 A70-10825
MHD wave propagation in electrically conducting fluid contained in finite length circular cylinder subject to axial magnetic field and nonelectromagnetic forces
01 p0152 A70-10944
MHD boundary layers in transverse magnetic field with low Reynolds number, investigating suppression of separation with emphasis on behavior near rear stagnation point
01 p0152 A70-11095
Exospheric temperature variations by Thompson scatter technique, considering solar and geomagnetic activity effects
01 p0078 A70-11209
Critical current density enhancement in Ta-rich Zr alloys in magnetic fields at low temperature after aging
01 p0122 A70-11238
Satellite attitude control, discussing passive, active and hybrid stabilization methods including spin, gravity gradient and magnetic stabilization
01 p0197 A70-11264
Radio waves scattering in ionosphere, analyzing dependence on latitude, altitude, azimuth and polarization angle, considering anisotropy due to geomagnetic field
01 p0046 A70-11452
Coupling coefficients for integral charged component of cosmic rays determined from measuring azimuthal geomagnetic effect on rays observed in crossed telescopes
01 p0172 A70-11545
Magnetically balanced arcs in supersonic external flows, indicating central core with differential Lorentz forces analogous to Grashof number in free convection phenomena
02 p0347 A70-12233
Steady axially symmetric MHD flow of inviscid incompressible fluid of small conductivity in strong magnetic field past fixed axisymmetric bodies
02 p0347 A70-12234
Critical magnetic fields, frequencies and spatial structure of ion-acoustic instability of HF induction discharge plasmas in hydrogen, Ar, He and Hg vapor
02 p0348 A70-12261
Geostrophic baroclinic flow with zonal magnetic field in beta plane channel, analyzing instability, phase velocities, Alfvén-Rossby waves and Eady problem
02 p0291 A70-12284
Magnetic flux trapping experiment with Al conductor, showing decay time constant connection with sunspot theory
02 p0299 A70-12393
Geomagnetic activity effect on ionospheric electron content from statistical analysis of data obtained during three year period
02 p0293 A70-12576
LF electromagnetic waves interaction propagating in stream-magnetized cold plasma, discussing waves temporal growth and instability
02 p0262 A70-12603
Transition probabilities computed for spectral lines due to magnetic quadrupole radiation, discussing deexcitation of excited atoms in solar corona
02 p0359 A70-12706
Variable magnetic field effect on stability of Langmuir waves propagating in plasma in constant magnetic field
03 p0530 A70-13064

Geomagnetic field influence on satellite motion for various angles between field vector and satellite angular velocity vector

03 p0563 A70-13180

Transverse magnetic field effects on electrode heat fluxes in heavy-current discharge, discussing anodic space thermal ionization

03 p0531 A70-13205

Magnetic cosmological nonuniformity hypothesis leading to galaxies and clusters isolation

03 p0564 A70-13224

Geomagnetic perturbation coincidences observed at conjugate Polar Cap observatories, suggesting magnetospheric tail field lines convergence with plasma neutral layer

03 p0565 A70-13232

Plasma stability in uniform magnetic and HF electric fields, observing magnetoacoustic wave generation at electron cyclotron frequency greater than HF field frequency

03 p0532 A70-13523

Sealed-off He-Cd laser construction, describing life test, noise, Cd transport characteristics and transverse magnetic field effect

03 p0501 A70-13582

MGD finite flow regions surrounded by nonconducting gas, considering wave behavior at boundary of conducting region and magnetic field influence

03 p0533 A70-13803

Interplanetary field influence on auroral radio absorption, considering sector structure of solar wind

03 p0476 A70-13915

Solar flare cosmic rays confinement to definite solar magnetic field sectors using Laplace transformation

03 p0560 A70-13977

Sidereal cosmic ray diurnal variations from underground muon telescopes in Northern and Southern Hemispheres, proposing model producing variations at earth vicinity

03 p0560 A70-13978

Cs plasma research, discussing Q-machines, plasma confinement, magnetic field experiments, LF and HF wave propagation, etc

03 p0533 A70-14015

MHD boundary layer separation near rear stagnation point with magnetic field normal to wall solved by series expansion, calculating skin friction by numerical quadratures

03 p0469 A70-14182

Radial velocity profiles measured in plasma jet thrusters with thermal and self magnetic acceleration, discussing disturbances due to discharge current-magnetic field interactions

03 p0553 A70-14374

Electric discharges in low pressure Ar in external magnetic fields, studying change in transport coefficients and drift due to MHD forces

04 p0724 A70-14529

Conducting fluid laminar flow between parallel planes in traveling magnetic field, integrating Maxwell and Navier-Stokes equations

04 p0726 A70-14542

Transverse magnetic fields effects on velocity perturbations and vortices behind circular cylinder in electrolyte flow at various Reynolds and Stewart numbers

04 p0726 A70-14543

Interstellar gas instability, discussing thermal, magnetic and cosmic ray effects

04 p0753 A70-15072

Polarization effects of helium-neon laser emission at 3.39 micron wavelength investigated in longitudinal and transverse magnetic fields

04 p0702 A70-15227

Solar wind as one dimensional flow analogous to Laval nozzle flow, discussing rotation and magnetic field effect on model with heat conduction

04 p0754 A70-15352

Magnetohypersonic boundary layer interactions, discussing boundary layer thickness relationship to Hartmann and Reynolds numbers

04 p0729 A70-15564

Dynamic I-V characteristics of hot cathode megawatt level nitrogen propellant pulsed MPD arc plasma source for various axial magnetic fields

04 p0729 A70-15642

Prescribed circulations within conducting spheres effect on initially prescribed magnetic fields, discussing magnetic field structure in uniformly rotating stars

04 p0758 A70-15694

Poleoidal magnetic field influence on compressible fluid convection in spherical shells, using variational method to obtain stability criteria

04 p0758 A70-15695

Scattering cone of hydromagnetic waves propagating along magnetic lines in magnetized plasma with oscillating electric dipole

04 p0683 A70-15738

Magnetic declination effect on F 2 layer behavior determined from critical frequencies at two magnetically conjugate points

04 p0683 A70-15742

Thermal conductivity and hysteresis measured in cylindrical In foil under magnetic fields at temperatures below 1 K

05 p0891 A70-15792

Magnetic activity effect on ionospheric drift speeds variation with latitude, observing correlation with electron density

05 p0837 A70-15922

Electrical conductivity calculation for plasma in spatially inhomogeneous magnetic field using small-gyroradius approximation to kinetic equation

05 p0889 A70-16491

Polarization transfer equations for electromagnetic waves propagating in inhomogeneous magnetized plasma solved analytically for homogeneous magnetized plasma

05 p0890 A70-16570

Magnetic damping of homogeneous cylindrical satellite rotation about transverse axis

05 p0924 A70-16751

Flares and fast processes interrelation with active region stationary filaments, filament field magnetic envelope explosion stimulation of surges, plasma stream ascents, etc

05 p0904 A70-16910

Relativistic plasma waves in uniform ambient magnetic field analyzed for growth rate to investigate plasma instabilities of streaming cosmic rays

05 p0904 A70-16931

Kinematic characteristics of annular-blank elements extruded by pulsed magnetic fields, noting proportionality to energy stored in capacitor bank

05 p0857 A70-17018

Electron bremsstrahlung in intense magnetic fields calculated for emission rate and absorption coefficient in large quantum number limits

06 p1104 A70-17182

Synchrotron radiation rate from deexcitation of electrons in magnetic orbits of low quantum numbers, stressing electrons radiation in intense magnetic fields

06 p1108 A70-17183

Laser signal modulation at RF by subjecting emitting atoms of Xe-He laser amplifier to simultaneous DC and RF magnetic fields

06 p1079 A70-17191

Cholesteryl chloride-cholesteryl myristate /CM/ mixture liquid crystal molecular and helical axes orientation from dielectric constant change measurements in magnetic fields

06 p1126 A70-17326

Load capacity of rotating field MHD hydrostatic thrust bearing increased by rotating axial magnetic field

06 p1076 A70-17527

Ionospheric storms north-south asymmetry, discussing effects of horizontal and vertical movements of ionization controlled by asymmetric geomagnetic field

06 p1055 A70-17594

Conducting cylindrical shell in constant magnetic field analyzed for magnetoelastic disturbances using Laplace transform

06 p1056 A70-17607

Dynamic I-V characteristics of megawatt pulsed MPD-ARC plasma thruster under various axial magnetic fields given for Ar and hydrogen propellants [ALAA PAPER 70-164]

06 p1131 A70-18092

Magnetic activity effect on magnetospheric plasmopause position, measuring ion concentrations as function of local time fromOGO 5 observations

06 p1058 A70-18530

Hall current effects on anisotropic plasma magnetogravitational instability under uniform magnetic field, considering electron inertia role and plasma perturbations

07 p1348 A70-19228

Height scale of loss coefficient in F 2 region under geomagnetic perturbation at midnight based on electron number profiles, estimating thermosphere temperature

07 p1265 A70-19433

Nonlinear characteristics of electromagnetic actuating mechanism induced by magnetic field of coil

07 p1281 A70-19529

Lamellar magnetic core stacking pressure influence on core magnetic characteristics in variable magnetic field, noting effects on magnetic permeability

07 p1246 A70-19537

Plasmatron generated rarefied helium plasma parameters in external magnetic field using hot-wire anemometer Langmuir probe

07 p1349 A70-19653

Electrical conductivity of collisionless magnetoplasma in weakly turbulent magnetic field, using quasi-linear approach for diffusion equation for distribution function describing test particles

07 p1352 A70-19987

Electromagnetic wave scattering from charged particle in hot electron plasma in magnetic field, considering relativistic corrections for scattered radiation spectra

07 p1352 A70-19992

Unsteady MHD flow at forward stagnation point analyzed for magnetic field effect on transient

phenomena, using difference-differential numerical method

07 p1354 A70-20235

Electrical conductivity of fully ionized plasma in strong magnetic field computed as application of method for plasma transport coefficients

07 p1354 A70-20246

Steady pressure driven flow of conducting fluid through insulating circular pipe in transverse magnetic field

08 p1549 A70-20502

Magnetic field effects on ruby absorption in R-line region

08 p1555 A70-20543

Cosmic ray intensity increase due to meteor showers magnetic field trapping effect

08 p1560 A70-20568

Near zero magnetic fields effect on biological systems studied to determine terrestrial magnetic field absence effect on astronauts

08 p1449 A70-20724

Hypothetical magnetic configurations in presence of Coriolis forces from convective cell hydromagnetic activity in solar plasma, considering dynamos with increasing magnetic field

08 p1576 A70-21409

Plasma sheath in quadrupole and hexapole geometries, investigating magnetic field variation, particle density and electrostatic potential in transition layer

08 p1552 A70-21530

Plasma containment by spherical multipole magnetic trap, discussing injection and trapping of gun-produced plasma

08 p1553 A70-21609

Geomagnetic perturbation coincidences observed at conjugate Polar Cap observatories, suggesting magnetospheric tail field lines convergence with plasma neutral layer

08 p1580 A70-21665

Magnetic display devices covering magneto-optical displays, magnetic-electrostatic technique combinations and ferromagnetography

08 p1499 A70-21685

Chapman-Vestine and Birkeland-Alfvén electric current systems equivalence in ground geomagnetic effect explained for polar magnetic storms

08 p1491 A70-21719

Neutron beta decay in strong quantizing magnetic field using Dirac wave function for electron, noting lifetime dependence on field strength

08 p1549 A70-21744

Thin metal plate surface impedance during excitation by HF electromagnetism field as function of magnetic field, calculating line shapes

08 p1557 A70-21754

Magnetic field and conducting walls effect on laminar steady MHD Couette flow of electrically conducting incompressible viscous rarefied gas in slip regime

08 p1553 A70-21764

Magnetothermal oscillations in pressure-annealed pyrolytic graphite, relating period with angle between magnetic field and crystal c axis

08 p1557 A70-21839

Low pressure plasma stability in cylindrical crimped magnetic field, considering convective perturbations and particle velocity distribution

08 p1555 A70-21981

Anodic electric layer in self sustaining discharge in transverse magnetic field with neutral gas burnout, studying neutral atom ionization probability

09 p1734 A70-22110

Feedback stabilization of surface instabilities of highly conducting plasma, discussing application to linear pinch with uniform axial static magnetic field

09 p1734 A70-22272

Synchrotron emission of relativistic particle in magnetic field with radiative reaction force comparable to Lorentz force, emphasizing pulsar cosmic ray electron acceleration

09 p1731 A70-22273

Strong magnetic field effects on squirrel monkeys electrical and mechanical cardiac functions determined from vectorcardiogram and aortic blood flow characteristics

09 p1617 A70-22524

Magnetic field and gas thermal conductivity effects in analysis of solar wind as one dimensional, steady and spherically symmetric flow

09 p1745 A70-22687

Evanothm alloy resistance wire for applications in magnetic field, illustrating percentage change at 4.2 K

09 p1679 A70-22998

Laboratory simulations of geomagnetic field suppression, studying biological effects on human, mice, plants and microorganisms

09 p1626 A70-23113

Fast neutral particles produced in electron-ion oscillation discharge as function of gas pressure and magnetic field

09 p1736 A70-23190

- Magnetic field effect on free convection in laminar boundary layer formed by laminar flow of viscous conducting fluid along vertical wall
09 p1737 A70-23308
- Geomagnetic field orientation effects on VLF nighttime propagation, checking computer program predictions
09 p1639 A70-23664
- Small loop impedance in magnetoplasma determined for magnetic field normal and parallel to loop plane
09 p1738 A70-23671
- Asymptotic behavior in cold plasma model of magnetopause, describing boundary layer between plasma stream and vacuum magnetic field
10 p1921 A70-23835
- Magnetic funneling model proposed for accretion of matter onto neutron star to study X ray production during motion through interstellar cloud
10 p1931 A70-23902
- MF signals sky wave propagation, studying roles of geomagnetic dip and propagation direction at various latitudes
10 p1832 A70-23997
- Magnetic disturbances caused by magnetosphere-solar wind filamentary inhomogeneity interaction observed by Pioneer 6
10 p1931 A70-24320
- Plasma instability in RF discharge in Ar in magnetic field
10 p1840 A70-24540
- MHD boundary layer on rotating body in viscous incompressible conducting fluid, studying magnetic field effects on time-to-separation
10 p1924 A70-24572
- MHD exact solutions class, observing conducting flow intensification by magnetic field application
10 p1924 A70-24573
- Navier-Stokes-Maxwell equations solutions for conducting fluid flow in azimuthal magnetic field, noting jet acceleration near symmetry axis
10 p1924 A70-24574
- MHD flow turbulence suppression at small magnetic Reynolds numbers, considering MHD interaction parameter role
10 p1924 A70-24575
- Longitudinal electrical conductivity of relativistic gas in intense magnetic field
10 p1924 A70-24634
- He-Ne laser amplifier in axial magnetic field, measuring Faraday rotation and gain for various input signal intensity values
10 p1901 A70-24945
- Slow HF waves propagation under magnetic field effect in plasma waveguide surrounded by dielectrics or metal
10 p1843 A70-25106
- Hydromagnetic flute and surface wave instabilities of current-carrying plasma filament in strong longitudinal field, showing radial density stabilization
10 p1926 A70-25117
- Rapid expansion of thin walled aluminum alloy cylinders under pulsed magnetic field pressure using high speed streak camera oscillography
10 p1964 A70-25120
- Surface wave reflection during propagation along transversely magnetized ferrite plate on metal backing, using perturbation theory to find cylindrical wave field
10 p1844 A70-25163
- Extraterrestrial electrical and magnetic fields effect on meteorological observations, noting relationship between atmospheric pressure distribution and ionospheric developments
10 p1913 A70-25269
- Magnetic field effect on burst emissions in plasma frequency range, observing radiation band widening and modes transmission in terms of Appleton-Hartree theory
10 p1949 A70-25273
- HF energy nonresonance dissipation in polycrystalline yttrium-garnet ferrites subjected to constant magnetizing field
11 p2097 A70-25384
- Solid body acceleration by ideally conducting gas in constant gravity field under magnetic field, considering rarefaction, reflected waves, motion equation, wall pressure, etc
11 p2082 A70-25389
- Linear theory of cyclotron resonance maser with TEM standing wave field, considering coherent emission for nonrelativistic electrons oscillating in magnetic field
11 p2061 A70-25392
- Ionospheric magnetic activity effects on cosmic radio noise absorption diurnal and seasonal variations in auroral zone, noting K index and lowest reflection frequency roles
11 p2043 A70-25536
- Auroral pulsations photometric observation data, noting magnetic activity effects
11 p2043 A70-25540
- Magneto-photoelasticity equations derived for photoelastic model in magnetic field, developing algorithm for optical phenomena for arbitrary stress distribution
11 p2131 A70-25588
- Energy balance of self sustaining thermonuclear reaction with nonuniform magnetic field in wall-contained dense plasma, allowing for radiation losses
11 p2088 A70-25709
- Hydrodynamic equations for ions and electrons of ionized collisional plasma in inhomogeneous magnetic field based on Boltzmann kinetic equations
11 p2088 A70-25710
- Vibration generators based on magnetic field electrodynamic effect, giving design, schematic diagram and exploitation properties
11 p2032 A70-26441
- Poloidal magnetic field effects on main sequence stars core convection
11 p2117 A70-26654
- Turbulence in incompressible electrically conducting fluid with uniform applied magnetic field, discussing nonlinear energy transfer mechanisms and magnetic effects
11 p2096 A70-26771
- Barium ionic cloud formation under action of sunlight and expansion in terrestrial magnetic field using plasma model
12 p2214 A70-26892
- Energetic electron layer near magnetopause attributed to geomagnetic activity from satellite observations of fluxes
12 p2292 A70-27180
- Inhomogeneous interatomic magnetic field effects on spectral line widening and shifts of emitting atoms in low temperature plasma
12 p2278 A70-27318
- Electroacoustic conversion in low resistivity GaAs crystal surface layer, applying external magnetic field to tune converter in wide frequency range
12 p2287 A70-27483
- Maser amplifier with nonoriented Fe-doped rutile powder as active material, observing broad absorption bands under magnetic field
12 p2249 A70-27649
- Broadband traveling wave masers bandwidth increased by staggering direct current magnetic field along active structure length
12 p2249 A70-27690
- Electromagnetic wave penetration in plasma under uniform DC magnetic field, considering wave propagational direction and electric field
12 p2279 A70-27781
- Density gradient drift waves stabilization in collisionless plasma by stellator type windings, observing oscillations amplitude reduction in shear magnetic field
12 p2280 A70-27785
- Coulomb interaction effect on diffusion of plasma produced by contact ionization in magnetic field, obtaining density profiles by iterative procedure
12 p2280 A70-27789
- Linearized dispersion relation for plane wave propagation in uniform unbounded cold plasma permeated by DC magnetic field, considering two stream instability
12 p2281 A70-27881
- Externally pressurized bearing with electrically-conducting gas lubricant under axial magnetic field, considering load capacity
12 p2244 A70-28018
- Carbon dioxide laser electrical discharge stabilization against transverse gas flow by cross magnetic field
12 p2250 A70-28099
- Computerized numerical integration of nonlinear partial differential equations describing blast wave in ionosphere with finite electric conductivity under uniform magnetic field
12 p2227 A70-28212
- Magnetic field effect on frequency spectrum of vertically propagating magnetoacoustic waves and reflection conditions in inhomogeneous isothermal atmosphere
12 p2227 A70-28226
- Penumbra and geomagnetic threshold effects on ionospheric electron production by primary cosmic rays
12 p2296 A70-28366
- Finite amplitude stability of plasma column in weakly ionized gases and in semiconductor plasmas in longitudinal magnetic field
13 p2458 A70-28566
- Cs atomic spectral line broadening under simultaneous electric and magnetic fields, observing Zeeman and Stark splitting
13 p2460 A70-28711
- Proton cosmic ray flare development and spatial structure, discussing magnetic field annihilation process for particle energy and photon ejection
13 p2476 A70-29046
- Midlatitude chorus frequency spectrum changes in relation to previous local magnetic conditions
13 p2365 A70-29187
- Visual aurora properties attributed to magnetic storm following solar flare, using multiple channel photometer measurements
13 p2478 A70-29231
- Ferromagnetic cubic sulfide of Fe easy axis by electron diffraction pattern, aligning sulfide particles along magnetic field
13 p2472 A70-29712
- Thermal boundary layer separation in conducting fluids by rotating magnetized blunt body
13 p2469 A70-30008
- Constant and alternating magnetic field characteristics effects on magnetometric measurements in space near to and far from earth
13 p2401 A70-30052
- Topside ionospheric plasma scale height, showing influence of magnetic activity level
14 p2569 A70-30207
- Geomagnetic short period oscillations occurrence frequency during IQSY, discussing dependence on magnetic activity and time of day
14 p2572 A70-30242
- Quartz floating component design, discussing magnetic sensitivity temperature dependence and microseismic noise rejection properties
14 p2582 A70-30245
- Magnetoaerodynamic boundary layer of incompressible conducting fluid over right circular cylinder under magnetic field, showing flow separation
14 p2621 A70-30550
- Vlasov interaction of magnetically coupled E layer with dissipative structures including injection, trapping and drag effects
14 p2623 A70-30698
- Scattering cone of hydromagnetic waves propagating along magnetic lines in magnetized plasma with oscillating electric dipole
14 p2575 A70-30822
- Magnetic declination effect on F 2 layer behavior determined from critical frequencies at two magnetically conjugate points
14 p2575 A70-30826
- M31 continuum radio emission produced by magnetic field aligned along arms, discussing field turbulence effects
14 p2642 A70-30891
- Thermal radiative transfer and magnetic field effects on hydromagnetic stability of hot electrically conducting fluid
14 p2623 A70-30996
- Electron distribution for transport coefficients in Lorentzian plasma under magnetic field, determining electrical conductivity, thermal diffusion and viscosity
14 p2623 A70-31033
- Low density collisionless plasma sheath in planar and cylindrical geometry under weak magnetic field, considering ion-electron pair generation
14 p2624 A70-31040
- Parametric oscillation instabilities in plasma under magnetic field perpendicular to circularly polarized or hybrid electric field
14 p2624 A70-31042
- Twelve year periodicities of Jupiter decametric radiation, noting correlation with Jupiter magnetic field rotation period
14 p2648 A70-31085
- Collisionless plasma confinement using spatially uniform time varying magnetic field
14 p2624 A70-31100
- Cosmic rays geomagnetic bending and effective angles of approach for various ground stations
14 p2633 A70-31313
- Nonstationary MHD Couette flow of viscous incompressible fluid between two parallel walls caused by instantaneous fluctuations of applied transverse magnetic field
15 p2777 A70-31479
- MHD turbulence suppression by magnetic field in tubes, using conduction anemometers
15 p2778 A70-31480
- Semiconductor laser emission at band-band transitions with free carriers participation under quantizing magnetic field, using kinetic equations
15 p2749 A70-31627
- Magnetospheric protons and electron energy spectra time and magnetic activity dependence during solar maximum
15 p2792 A70-31671
- Report to COSPAR on Hungarian space research including satellite observations, upper atmosphere, geomagnetic effect, geodesy, cosmic rays, etc
15 p2830 A70-31713
- Northern Hemisphere radar aurora latitude variation, considering magnetic activity effects
15 p2697 A70-31770
- Uniform electric and magnetic fields effects on flow of conducting compressible fluid in channel, using multiple scales method
15 p2779 A70-31914
- Conducting incompressible fluid laminar flow between rotating disks in transverse magnetic field with source at center
15 p2779 A70-31915

Book on nonthermal processes in galactic and extragalactic radio sources covering plasma behavior in magnetic field, energy redistribution in spectrum by electron scattering, etc

15 p2799 A70-31999

Magnetic field effect on critical flutter speed and frequency of elastic plate in ionized gas flow, deriving dispersion equation

15 p2818 A70-32173

LF oscillatory convection characteristics in polytropic atmosphere in strong magnetic field based on sunspot theory

15 p2802 A70-32487

Magnetic hysteresis dynamic model for digital simulation of stabilized satellite attitude motions

15 p2812 A70-32509

Sunspot electric current evaluation from analyzing transverse component of magnetic field, discussing difficulties and errors in data reduction

15 p2804 A70-32615

Cosmic ray intensity increase due to meteor showers magnetic field trapping effect

15 p2795 A70-32723

Two dimensional hydromagnetic turbulence model for maintained seed field amplification, noting applications to star formation, stellar convection and gas cloud motions

15 p2781 A70-32813

Transverse magnetic field effect on CW argon laser operation with linearly polarized radiation

15 p2754 A70-32866

Plasma helix equilibrium and stability in transverse magnetic field, considering oscillation damping by ohmic heating

15 p2781 A70-32910

High strength magnetic fields effect on early embryonic development of frogs, relating growth abnormalities and paramagnetic ferritin motions

16 p2848 A70-33099

Venus retrograde axial period contradiction between radar echoes and violet-UV photographic and interferometric spectroscopic methods explained by theory using strong magnetic dipole

16 p2973 A70-33116

Magnetic dislocations effect on domain structure of postcritical Permalloy films subjected to alternating magnetic field

16 p2930 A70-33206

Unsteady hydromagnetic flow of viscous electrically conducting incompressible fluid due to rotating disk under perpendicular magnetic field

16 p2958 A70-33297

Acoustic and magnetic surface waves technologies for radar signal processing

16 p2874 A70-33390

Magnetic phase diagram of hydrated cesium-copper carbide at 1.625 Neel temperature in external magnetic fields, giving equation for spin flop field temperature dependence

16 p2961 A70-33688

Heterogeneous conducting fluid stability between fixed rigid cylinders with radiant gravitational force and magnetic field

16 p2894 A70-33784

Drift velocity for bound electron orbital motion in static axisymmetric magnetic field

16 p2959 A70-34187

Transverse magnetic field effects on Ar cross flow arc temperature distribution, cross section shape and profile, discussing forced convection effects

17 p3138 A70-34477

Reflected shock waves generation by shock produced plasma flow interaction with strong magnetic fields, determining electron density and ionization relaxation times

17 p3139 A70-34490

Magnetic field effects on Compton scattering and radiative opacity, considering longitudinal and transverse propagation with circular polarization

17 p3154 A70-34538

Transverse magnetic field influence on Gunn effect characteristics of n-type GaAs

17 p3142 A70-34622

Magnetic fields effect on probe measurements in weakly ionized Ar plasma flow at atmospheric pressure

17 p3139 A70-34693

Electrical conductivity of partially ionized gas in magnetic field by Frost mixture rules extension

17 p3141 A70-34985

Magnetic perturbation effects on magnetoactive plasma, considering Boltzmann transport equation, plasma-electromagnetic interactions, heating, cooling, etc

17 p3142 A70-35592

Solar prominences thermal and dynamical stability in terms of optically thin plasma supported by magnetic field against gravity

17 p3174 A70-35867

Coronal magnetic bottle at ten solar radii from Faraday rotation measurements of occulted spacecraft radio source

17 p3174 A70-35871

Gas laser frequency stabilization using nonlinear effects of magnetic Lamb dip

17 p3109 A70-35911

Plasmon decay by neutrinos emission in strong magnetic field, examining parallel and perpendicular propagation

18 p3305 A70-35936

Plane nonconducting elastic plate with one side impinged upon by supersonic conducting gas flow, determining magnetic field effect on flutter vibrations

18 p3336 A70-36135

Dilatometric investigation of Fe alloys phase transformations, determining magnetic field effects and Curie temperatures

18 p3276 A70-36206

Nonlinear theory for surface waves propagating in bounded magnetoactive plasma

18 p3295 A70-36412

Magnetohydrodynamic flow of electrically conducting viscous incompressible fluid past nonconducting semiofinite flat plate under transverse magnetic field

18 p3295 A70-36431

External magnetic field effect on cavitation zone behind circular cylinder, proving existence of electric charges

18 p3242 A70-36645

MHD slider bearing load carrying capacity in tangential magnetic field, observing optimum profile in step form with riser location and step height ratio

18 p3295 A70-36672

Lunar magnetic monopole charge effects on nearby magnetic field configuration

18 p3316 A70-36898

Height scale of loss coefficient in F 2 region under geomagnetic perturbation at midnight based on electron number profiles, estimating thermosphere temperature

18 p3249 A70-36907

Local spiral arm H 2 regions distribution in Cygnus direction, discussing symmetry due to magnetic field

18 p3329 A70-37180

Galactic spiral structure, discussing gravitational theory, pattern origin, radio and optical structure and magnetic field effects

18 p3332 A70-37201

Quartz astatic galvanometer resistant to geomagnetic field variations, vibrations or microseismic noise

19 p3421 A70-37337

Excitation transfer by spontaneous emission in atomic gas, investigating static magnetic field effect on radioactive cascade

19 p3443 A70-37363

Electromagnetic propagation in flat waveguide with local gyrotropic filling and transverse magnetization, using Galerkin method

19 p3470 A70-37430

Ar arc discharge magnetically induced retrograde rotation dynamics, using high speed photography

19 p3475 A70-37533

Magnetic field and permeability effects on drag in steady axisymmetric MHD flow of incompressible fluid around full and hollow spheres

19 p3477 A70-37577

Current and resistance in Hg filled space between two circular electrodes under strong magnetic field, using boundary layer techniques

19 p3477 A70-37578

Guiding center theory for relativistic plasma embedded in strong magnetic field, discussing connection with pulsar emission dynamics

19 p3479 A70-37596

Single crystal ferrite thin film microwave parameters measurement, examining susceptibility in weak magnetic fields and ferromagnetic resonance

19 p3485 A70-37628

Lifetimes and fine structure of differentially metastable autoionizing states of negative He ion in axial magnetic field, using time of flight techniques

19 p3473 A70-37746

Rubidium-85 maser, discussing continuous oscillation in low magnetic field

19 p3446 A70-37769

Magnetic coupling in solid dielectric cylinder under axial magnetic and perpendicular electric fields, noting memory and magnetostrictive effects

19 p3471 A70-37785

Magnetic surface loading of Gunn oscillators domain state for use as logic gates, pulse function generator, etc

19 p3387 A70-37819

Magnetoelastic ferromagnet linear theory, considering spin-elastic microwaves propagation in ferrimagnetic crystal subjected to pulsed magnetic fields

19 p3487 A70-37947

Geomagnetic activity effect on potential gradient and air-earth conduction current density

19 p3413 A70-38000

Conical plasma gun with Z pinching restrained by axial magnetic field, describing operating characteristics

19 p3480 A70-38018

Magnetic perturbations effect neutralization for satellite attitude stabilization by real time simulation of satellite angular motion in magnetic field

19 p3399 A70-38286

Magnetic field effect on hydromagnetic Goertler instability in boundary layer flow of conducting fluid over concave wall

19 p3481 A70-38352

VLF radiation observation at conjugate points, discussing hisses, choruses and geomagnetic effects

19 p3416 A70-38587

Slow wave propagation in plasma moving along external magnetic field, generalizing refractive index formula

19 p3417 A70-38592

Transverse magnetic field effect on emission spectrum of He-Ne laser, using scanning interferometer

19 p3448 A70-38735

Two dimensional MHD couette flow in slip regime, considering constant suction on stationary plate to determine transverse magnetic effects

20 p3677 A70-39047

Neutrino production by synchrotron process /magnetic bremsstrahlung/ in relativistic electron gas under intense magnetic field

20 p3695 A70-39050

Rarefied plasma flute oscillation stabilization in magnetic field, using controlled electron beams

20 p3677 A70-39173

Cosmic ray 27 day variations during solar activity minimum, noting unipolar magnetic regions role

20 p3696 A70-39280

Cosmic ray neutron semidiurnal variations days and night components with respect to geomagnetic and solar activity

20 p3697 A70-39288

Seasonally biased electron density enhancements in nighttime response of topside ionosphere to magnetic storms

20 p3621 A70-39342

Magnetically focused two and four stage cascade picture amplifiers for astronomy and nuclear physics applications

20 p3630 A70-39426

Interactive hybrid simulation of TRIAD satellite motions, describing attitude control system with magnetic hysteresis damping

20 p3714 A70-39536

Current distribution and interband recombination emission in bipolar semiconductor crystal under pinch effect produced by external magnetic field

20 p3677 A70-39590

Cold electron plasma nonlinear oscillations in magnetic field, using mathematical model

20 p3678 A70-39591

Charged particle interaction with fluctuation fields in nonequilibrium magnetoactive plasma

20 p3678 A70-39596

Collisionless plasmas fluid dynamical equations in presence of strong magnetic field, discussing Larmor and electron plasma frequencies

20 p3678 A70-39609

MHD nonsteady Beltrami flow between two infinite parallel walls with transverse magnetic field, calculating velocity, skin friction and induced magnetic field

20 p3678 A70-39610

Electrically conducting gas flow past slender body of arbitrary cross section in presence of crossed magnetic field by MHD Stokes approximation

20 p3558 A70-39613

Cold nonuniform plasma slab model for afterglow echoes at upper hybrid resonance in uniform magnetic field

20 p3679 A70-39664

Auroral physics, discussing visibility, relations to geomagnetism and sunspots spectrum, morphology, optical emissions and particles in magnetosphere

20 p3623 A70-39929

Viscous conducting fluid slow motion past sphere in presence of toroidal magnetic field, calculating Stokes flow perturbations

20 p3682 A70-40113

Nonlinear resonance conditions for plasma three-wave interactions, considering wave propagation modes and constant magnetic field

20 p3682 A70-40137

Plane parallel viscous conducting fluid flows stability in transverse magnetic field, considering small perturbation spectrum, Hartmann and Reynolds numbers

20 p3684 A70-40397

Scintillation LF observations with synchronous satellite radio signals at low latitude station, noting magnetic activity effects on night and day scintillations

20 p3590 A70-40488

Low pressure Hg vapor arc with remote wall, investigating magnetic self striction by ambipolar diffusion in fields

20 p3685 A70-40503

Slightly rarefied and electrically conducting gas, calculating effects of applied magnetic field on steady laminar low speed plane Couette flow

20 p3685 A70-40504

Hydromagnetic flute and surface waves instabilities of current-carrying plasma filament in strong longitudinal field, showing radial density stabilization

20 p3685 A70-40510

Rapid expansion of thin walled aluminum alloy cylinders under pulsed magnetic field pressure using high speed streak camera oscillography
20 p3735 A70-40513

Nonrelativistic electron bremsstrahlung in dense plasma with strong magnetic field
21 p3855 A70-40721

Earth magnetic field effects on midlatitude F 2 layer deviative absorption
21 p3812 A70-40727

Magnetic damper motions in rapidly spinning satellite
21 p3927 A70-40833

Artificial earth satellite orbit perigee motion, calculating perturbation effect due to gravitational and magnetic fields on orientation and rotation
21 p3884 A70-40843

Solar flaring on 25 April 1968, examining radio H alpha and X ray emission, magnetic field configuration and temperatures
21 p3879 A70-40959

Wall heat transfer for partially ionized argon laminar flow within square channel conducting walls with and without transverse magnetic field
21 p3856 A70-41032

Liquid metal heat pipes in magnetic fields of controlled fusion reactors, considering geometry, compound wick structure and vapor flow
21 p3946 A70-41046

Cylindrical plasma inhomogeneities including meteor trains diffusion in presence of magnetic field, observing dependence on angle theta
21 p3886 A70-41060

Ionospheric magnetic activity effects on cosmic radio noise absorption diurnal and seasonal variations in auroral zone, noting K index and lowest reflection frequency roles
21 p3819 A70-41286

Auroral pulsations photometric observation data, noting magnetic activity effects
21 p3819 A70-41290

Axissymmetric jet plasma flow in magnetic nozzle, measuring electric potential, electron temperature and ion density and velocity
21 p3856 A70-41380

Plasma and neutral gas collisionless interactions in magnetic field based on Alfvén critical velocity hypothesis, discussing electron energy distribution
21 p3857 A70-41383

Transport coefficients of inhomogeneous magnetized bounded and unbounded plasmas based on quasi-linear approximation
21 p3857 A70-41385

Plasma turbulence statistical theory in magnetic field based on averaging operators, deriving nonlinear dispersion relation
21 p3857 A70-41386

Turbulent plasma heating by adiabatic magnetic compression with longitudinal ring current
21 p3857 A70-41387

High power pulsed relativistic annular electron beam production and focusing by injection gun using magnetic field control
21 p3827 A70-41461

Electrical and thermal characteristics of DC magnetic annular arc operating continuously at atmospheric pressure
21 p3805 A70-41758

Rotating cold plasma wave propagation modes including Coriolis effect in absence and presence of external magnetic field
21 p3860 A70-41924

Dynamic potentials equations of guided electromagnetic wave propagating in laterally bounded plasma along magnetic field axis
21 p3860 A70-42005

Inhomogeneous interatomic magnetic field effects on spectral line widening and shifts of emitting atoms in low temperature plasma
21 p3860 A70-42059

Liquid metal turbulent jet flow dependence on longitudinal magnetic field, measuring mean velocity profiles at various cross sections
21 p3861 A70-42230

Laminar-turbulent transition in magnetic field using Plexiglas model, observing inlet conditions effect on MHD flow stability
21 p3861 A70-42234

Superimposed external DC magnetic field effect on electrodeless HF plasma density, discussing electron cyclotron waves resonance excitation and plasma electron energy gain
22 p4079 A70-42364

Statistical theory of electron-positron-photon vacuum in external magnetic field, noting magnetic activation effect at low temperatures
22 p4076 A70-43000

Biological action of constant magnetic fields, discussing axons electrical properties, biomolecules spatial orientation, electrolytes and liquids
22 p3978 A70-43138

Homogeneous helium plasma column LF wave propagation in uniform magnetic field
22 p4082 A70-43216

Magnetoplasma density modulation from LF and amplitude magnetic perturbations, using collisionless Boltzmann transport equation
22 p4082 A70-43255

Soft solar X rays cyclic variation from satellite observation, noting relation to sunspot group magnetic field complexity
22 p4096 A70-43301

MHD instability due to strong magnetic field induced scattering of plasma oscillations, using one sided Q device
23 p4223 A70-43949

Electron loss by resonant interaction with whistlers in nonuniform magnetic field, taking Fokker-Planck equation as distribution function
23 p4237 A70-44052

Gravity waves produced in liquid electric conductor by piston subjected to sinusoidal pulsation, calculating magnetic field effect on amplitude and phase velocity
23 p4225 A70-44208

Electron distribution function in homogeneous ionized plasma under oscillating electric fields and steady magnetic fields, solving Boltzmann transport equation
23 p4226 A70-44248

Kinetic transport theory for mixed dilute gases consisting of linear rotating diamagnetic molecules in external homogeneous magnetic field
23 p4223 A70-44927

Low beta surface ionized rotating streaming plasma column, determining low magnetic field effects on density and stability
23 p4229 A70-44988

Optical permittivity and dielectric permeability of electron gas in magnetic field, considering application to ferromagnetic materials
23 p4221 A70-45051

He-Ne laser with absorbing cell in magnetic field, investigating nonlinear effect in frequency dependence of output power
23 p4203 A70-45070

Homogeneous magnetic fields effects on growth rate of *Saccharomyces cerevisiae* and *Micrococcus denitrificans*
24 p4306 A70-45102

Thermal fluctuations effect on Josephson tunnel contact binding energy and external magnetic field dependence
24 p4388 A70-45203

Chromospheric heating in magnetic field above supergranular cell boundaries, using geometric optics method for energy transport by hydromagnetic shock waves
24 p4400 A70-45304

Giant cell regular structures in solar atmosphere, using magnetic synoptic charts of solar activity
24 p4400 A70-45305

Nonspherical wave excitation in solar atmosphere in presence of toroidal magnetic field
24 p4400 A70-45312

Magnetostriuctive Ni-Mn-Co ferrites and Al-Fe alloys, measuring magnetic field effect on piezomagnetic coefficients at room temperature
24 p4389 A70-45400

Strong magnetic fields effect on field emission currents in Bi, Zn, Ta and W
24 p4379 A70-45621

Differentially rotating stellar interiors nonaxisymmetric perturbation stability in toroidal and poloidal magnetic fields
24 p4413 A70-46165

Topside ionospheric plasma scale height, showing influence of magnetic activity level
24 p4330 A70-46282

Geomagnetic short period oscillations occurrence frequency during IQSY, discussing dependence on magnetic activity and time of day
24 p4332 A70-46317

MAGNETIC EQUATOR

Rarefied plasma motion in geomagnetic dipole equatorial plane near magnetosphere symmetry axis deriving approximate solution to quasi-hydrodynamic equations
04 p0681 A70-15717

Satellite observations of equatorial erosion and defocusing of VLF waves propagating at low magnetic latitudes
06 p1058 A70-18532

Numerical modeling of electron and molecular ion continuity equations describing conditions in lower F region near magnetic equator using analog computer
07 p1265 A70-19434

Vertically moving disturbance discovered in ionospheric soundings close to magnetic equator, noting correlation with electrodynamic lift
07 p1269 A70-19631

Lower ionosphere electric fields and currents vertical profiles above geomagnetic equator under quiet geomagnetic conditions from rocket data
07 p1277 A70-20453

Magnetic equator ELF noise examined with OGO 3 magnetometer, indicating unique signals in plasmasphere
08 p1488 A70-21380

Critical sunspot dependence of F 2 region noon bite-out phenomenon at various equatorial latitudes, observing magnetic dip
08 p1492 A70-21837

Low energy protons omnidirectional intensity contours in outer radiation zone at magnetic equator
09 p1747 A70-23491

Seasonal variation of spread F near magnetic equator, showing relationship with solar cycle at different geographic locations
10 p1881 A70-24818

Cosmic ray intensity fluctuations at geomagnetic equator using power spectrum analysis on mu meson records, discussing solar photosphere and interplanetary magnetic field
12 p2291 A70-27176

Lunar tide in ionospheric D region absorption near magnetic equator, noting annual variation relationship to sunspots
14 p2574 A70-30747

Rarefied plasma motion in geomagnetic dipole equatorial plane near magnetosphere symmetry axis by deriving approximate solution to quasi-hydrodynamic equations
14 p2575 A70-30801

D region rocket sounding at geomagnetic equator, measuring electron density, collision frequency, current, temperature, etc
15 p2724 A70-31668

Electric fields in lower ionosphere during solar activity minimum above magnetic equator, using vertical profiles of ionospheric current magnetic fields and electron concentration
18 p3246 A70-36098

Numerical modeling of electron and molecular ion continuity equations describing conditions in lower F region near magnetic equator using analog computer
18 p3249 A70-36908

Upper limit to primary deuteron flux and path length in space, using emulsion stack exposed near geomagnetic equator during minimum solar activity
22 p4093 A70-42673

Nighttime equatorial E region small scale irregularities detected by rocket-borne Langmuir and plasma noise probes, discussing generation mechanism
22 p4018 A70-43108

Electromagnetic variational soundings of ocean floor earth crust upper mantle near magnetic equator
23 p4189 A70-44066

MAGNETIC FIELD COILS

U FIELD COILS

MAGNETIC FIELD INTENSITY

U MAGNETIC FLUX

MAGNETIC FIELDS

NT GEOMAGNETISM

NT INTERPLANETARY MAGNETIC FIELDS

NT INTERSTELLAR MAGNETIC FIELDS

NT LUNAR MAGNETIC FIELDS

NT MAGNETOSTATIC FIELDS

NT NONUNIFORM MAGNETIC FIELDS

NT PALEOMAGNETISM

NT PLANETARY MAGNETIC FIELDS

NT SOLAR MAGNETIC FIELD

NT STELLAR MAGNETIC FIELDS

NT TRAPPED MAGNETIC FIELDS

Two layer truncated harmonic model of Rossby wave dynamo for solar cycle, accounting for maintenance and reversal of magnetic fields
01 p0174 A70-10238

Oblique unsteady shock wave structure propagating at large Mach numbers in plasma cylinder under steady magnetic field, showing particle velocity profile discontinuity
01 p0064 A70-10999

Hall generator DC brushless motor operation and applications, obtaining motor action by rotor and stator magnetic fields interaction
02 p0228 A70-12053

Interstellar space flight ramjet physical model, describing magnetic field funnel, radiation effects, relativistic effects, etc
02 p0379 A70-12782

Optical echoes using model of spins precessing in magnetic field, presenting time dependent theory of perturbation
02 p0341 A70-12830

Atomic and electron densities measurements in shock wave interactions with magnetic fields, using interferometric and spectroscopic method
03 p0529 A70-12876

Coaxial ion beams moving in opposite directions in LF magnetic field noting sliding instability development
03 p0530 A70-13061

Star rotation and meridional circulation hydrodynamic theory, considering magnetic fields and internal friction
03 p0564 A70-13228

Cyclotron resonance maser (CRM) monotron with inclined electron flux and magnetic field, considering design for performance optimization
03 p0499 A70-13455

Ionizing shock wave propagation into magnetic field from Ar gas flow characteristics in electromagnetic shock tube

03 p0532 A70-13548

Magnetic field self induction in static fluid-submerged intersecting jet system, calculating required magnetic Reynolds numbers

04 p0726 A70-14541

Charge separation effects in boundary layer between cold streaming plasma and perpendicular magnetic field with relativistic electrons

04 p0727 A70-14997

Directional pattern of waveguide radiators using Kirchhoff boundary values of electric, magnetic or electric and magnetic fields, discussing aperture reflection coefficient

04 p0653 A70-15397

Coaxial electrodes with electric and magnetic fields to study instability in MPD arcs [ALAA PAPER 69-230]

04 p0737 A70-15542

Temperature measurements in magnetic beach of steady state deuterium plasma, confirming ion-cyclotron waves thermalization

05 p0884 A70-16167

Boltzmann-type kinetic equation for homogeneous electron plasma in uniform magnetic field, describing relaxation to thermal equilibrium by convergent collision integral

05 p0888 A70-16329

Two dimensional propagation of transverse waves in plasma with embedded curl-free magnetic field, discussing cosmic ray acceleration and magnetic neutral sheet formation

05 p0888 A70-16437

Small amplitude waves and collisionless shock waves within first order Chew-Goldberger-Low equations framework, presenting modes for propagation along applied magnetic field

05 p0889 A70-16534

Surface nucleation critical field for pure superconductors at temperatures outside Landau-Ginzburg region

06 p1125 A70-17218

Monograph on MHD waves covering theories for weak discontinuities, wave propagation in inhomogeneous media and behavior in magnetic fields

06 p1114 A70-17275

Numerical solution of nonlinear Vlasov equation for collisionless plasma problems, discussing initial value problems, external electric fields, magnetic fields, etc

06 p1108 A70-17419

Steady free convection over point and horizontal line heat sources in vertical magnetic field

06 p1120 A70-17519

Relativistic electron low beta plasma oscillations in external magnetic field using covariant dispersion relations

06 p1120 A70-17542

Band extremum loops depth in CdS in electric and magnetic fields determined from calculating linear and nonlinear conductivity

06 p1126 A70-17819

Kinetic theory of plasma waves in magnetic field, covering small amplitude waves in infinite homogeneous plasma, limiting cases, etc

06 p1121 A70-17902

Cathode emission from hollow cathode controlled by variable magnetic field to ensure proper I-V characteristics for efficient ion generation in thrusters

06 p1131 A70-18032

Electric and magnetic fields of waterpouts measured by instrumented U.S. Navy aircraft

06 p1101 A70-18582

He-Cd laser output improved by transverse magnetic field application

06 p1084 A70-18619

Hall voltage and electric conductivity measurements in alternating magnetic field and current by narrow band amplifier with synchronous detector

07 p1279 A70-18944

Magnetic field filtration into time-variable and constant parts, using signal to noise analogies

07 p1266 A70-19440

Electric and magnetic field perturbation at great distances behind body moving in collisionless magnetized plasma estimated from Fourier transform

07 p1385 A70-19447

High electrical conductivity effects on alignment between magnetic field and flow velocity vector in two dimensional plasma flow

07 p1349 A70-19568

Kaufman thruster performance dependence on transmission of ion extraction optics and magnetic field shape [ALAA PAPER 69-257]

07 p1365 A70-19705

Finite amplitude disturbance propagating across magnetic field within infinite plasma, solving Vlasov equation and ordering moment equations hierarchy

07 p1352 A70-19989

Plasma sheath transition structure surrounding cylindrical probe in weak axial magnetic field on basis of moment equations

07 p1353 A70-20230

Intense quasi-steady He plasma discharge stability in magnetic field measured by Langmuir and optical techniques

07 p1354 A70-20321

Rotating shaft vibrations on assembly designed to balance rotor in magnetic field, eliminating bearings effect on shaft to determine internal friction

08 p1584 A70-20697

Effective depths of formation of absorption lines in solar atmosphere used for magnetic field recording

08 p1570 A70-20842

Rarefied plasma flow past bodies, considering determination of aerodynamic coefficients, charged states, electric and magnetic fields and plasma parameters

08 p1432 A70-21087

Slot transmission line applicability to miniature ferrite phase shifter design exploiting elliptically polarized H field existence

08 p1475 A70-21283

Radio sources model brightness distribution and internal magnetic fields deduced from long baseline interferometer observation data

08 p1577 A70-21491

Electromagnetic wave instability propagating across static magnetic field in presence of thermal anisotropy, considering interplanetary plasma and plasma devices stability

08 p1553 A70-21610

Model for magnetic field-line reconnection in conducting incompressible fluid, determining maximum reconnection rate entirely by null point conditions

08 p1553 A70-21615

Star rotation and meridional circulation hydrodynamic theory, considering magnetic fields and internal friction

08 p1580 A70-21661

Tensor analysis of four photon interaction in rarefied plasma in magnetic field, determining cubic current of plasma wave self action

08 p1554 A70-21805

Transverse particle and energy fluxes in toroidal magnetic traps magnetic fields with ionized plasmas, discussing particle diffusion coefficient and thermal conductivity

08 p1554 A70-21807

Plane shock wave stability propagating in external magnetic field determined by temperature dependence of medium electrical conductivity

09 p1658 A70-22168

Scattering matrix for resonance lines with arbitrary level splitting in magnetic field

09 p1753 A70-22452

Broadband remote sensing magnetometer for measuring fast-rising pulsed magnetic fields

09 p1676 A70-22716

One dimensional flow field behind ionizing detonation wave in magnetic field using Chapman-Jouguet hypothesis, accounting for Alfvén speed

09 p1660 A70-22722

Photoemission analyzer with finite emitter in spherically symmetric retarding field with magnetic field present, analyzing energy resolution

09 p1679 A70-22988

Magnetophotoelastic model applied to plates bending stress analysis, deriving polarized light propagation equations

09 p1728 A70-23447

Earth magnetosphere and magnetosheath magnetic field measurements by Mariner 5

09 p1670 A70-23487

Cylindrical magnetrons steady state characteristics with thick and infinitely thin cathodes for full space charge and inclined magnetic field

09 p1651 A70-23641

Small loop impedance in magnetoplasma determined for magnetic field normal and parallel to loop plane

09 p1738 A70-23671

Unsteady MHD flow in circular pipe with nonconductive walls under transverse magnetic field

10 p1921 A70-23959

Alfvén flow of dissipative conducting incompressible fluids in presence of thin airfoil in magnetic field, considering flow turbulence calculation

10 p1922 A70-24143

Plasma magnetic field measurement by scattered light, analyzing electron spectrum modulation with gyration frequency

10 p1916 A70-24401

Spectrometer design for Helios solar probe using semiconductor detectors to identify particles separated by magnetic field

10 p1888 A70-24487

Directional particle flux dependence on probe orientation with respect to external magnetic field, determining pitch angle distribution from count rates

10 p1932 A70-24497

Shift in nuclear magnetic resonance, investigating transferred hyperfine coupling near Neel temperature for magnetic and nonmagnetic systems

10 p1928 A70-24827

Microfluctuations frequency and wavelength of electromagnetic, electric and magnetic field distributions in plasma shock wave front found consistent with ion-acoustic origin hypothesis

10 p1925 A70-25031

Helium ions diffusion perpendicular to magnetic field in He gas, measuring coefficients as function of field strength and for various gas pressures

10 p1925 A70-25108

Plasma column dynamic stability breakdown in quadrupole HF magnetic field in terms of violating stability criterion for long wave deformation

10 p1926 A70-25109

Superconducting ellipsoid of revolution in alternating magnetic field, computing disturbed field components using boundary value problem

10 p1917 A70-25201

Pressure anisotropies contribution to solar wind corotation, discussing angular momentum and magnetic field

10 p1935 A70-25285

Hall effect influence on HF traveling magnetic field penetration into solid cylinder plasma device compared to magnetically contained plasma

11 p2088 A70-25712

Parametric effect maser developed by maintaining self oscillations in static amplitude modulated magnetic field, noting application as magnetometer

11 p2063 A70-25947

Background pressure and magnetic field shape effect on MPD thruster performance, testing radiation cooled thrusters

11 p2102 A70-26122

Cylindrical shock wave two dimensional propagation in conducting plasma in magnetic field, assuming isentropic flow along streamline

11 p2091 A70-26174

Homogeneous turbulent velocity effect on magnetic field distribution in electrically conducting fluid with no external source, observing dynamo action

11 p2091 A70-26545

Spherical harmonic coefficients of eccentric dipole potential and coinciding magnetic and mass center, noting geophysical prospecting applicability

11 p2047 A70-26571

Inviscid incompressible conducting fluid flow past body in aligned magnetic field at low magnetic Reynolds number, discussing small perturbations evolution

11 p2041 A70-26623

Plasma turbulent diffusion across constant magnetic field, noting magnetic, kinetic energy and relaxation times ratio effects

11 p2094 A70-26755

Magnetic field equation for gyroscopic and anisotropic turbulence, observing large scale magnetic field generation

12 p2210 A70-27546

Two dimensional MHD turbulence under strong magnetic field in Zeta device, measuring density, temperature, electric/magnetic fluctuations and various statistical characteristics

13 p2457 A70-28553

Turbulence spectrum due to density fluctuations in plasma with strong magnetic field, using hydrodynamic theory and Poisson equations

13 p2457 A70-28559

LF electrostatic waves oblique to magnetic field in plasma, evaluating dispersion relation near ion cyclotron frequency

13 p2363 A70-28641

Eddy currents magnetic field structure over surface defects in conducting objects, noting NDT applications

13 p2404 A70-28661

Plane incompressible conducting fluid laminar jets analysis in magnetic field, using boundary layer equations for zero electric field

13 p2461 A70-28964

Stationary ring vortices in unbounded conducting fluid, investigating self excitation of magnetic field by vortices

13 p2461 A70-28965

Electric field in rectangular MHD channel with ideally conducting electrodes in uniform magnetic field, considering conditions for maximum channel effectiveness

13 p2461 A70-28966

Euler potentials for magnetic fields field-line structure representation, discussing cross products of gradients of scalars in plasma physics

13 p2451 A70-29123

Magnetopause model, discussing equilibrium layer between magnetic field and cold plasma field-free stream

13 p2396 A70-29181

Vector magnetic field and energetic particle flux profiles, indicating geomagnetically aligned currents associated with visible auroral arc

13 p2397 A70-29197

Parametric excitation of potential oscillations in plasma near cyclotron frequency subjected to UHF electric and constant magnetic fields

13 p2463 A70-29281

Radio wave transmission through magnetized plasma layer as function of electron concentration and collision frequency, using coaxial accelerator

13 p2366 A70-29377

Boltzmann equation in circular magnetic field solved by Fourier series and Legendre polynomials, correcting distribution function due to Fourier harmonics

13 p2464 A70-29485

Gas parameters determination near singular point of slow magnetosonic wave propagating in conducting medium in uniform magnetic field

13 p2464 A70-29507

Magnetic field simulator for investigating magnetic properties of satellites designed for magnetometric experiments

13 p2385 A70-29556

Alouette plasma resonance stimulated perpendicularly to magnetic field by planar dipole charge sheet and permeable grids

13 p2467 A70-29907

RF admittance and electric field of plane grid capacitor in hot collision free magnetoplasma in parallel magnetic field dominated by Bernstein modes

13 p2467 A70-29910

Lithium vapor fueled applied field MPD arc jet performance using open end heat pipe vaporizer and hollow cathode

[ALAA PAPER 69-241]

13 p2475 A70-29959

Rotating plasma disturbances onset in MPD arc, determining magnetic field dependence on mass flow, background pressure and propellant

[ALAA PAPER 69-232]

13 p2475 A70-29961

Weak magnetic fields in geo- and space physics - Conference, Paris, May 1969

13 p2413 A70-30026

Superconducting lead shell shielding properties in small ambient magnetic fields

13 p2454 A70-30030

Hydromagnetic fluid model of solar wind for interpreting discontinuities in plasma and magnetic field, interaction with atmosphere, heating mechanism and chemical composition

13 p2481 A70-30067

Satellite plasma diagnostics for electric and magnetic fields and fine structure of collisionless shocks in solar wind plasma flows and interplanetary shocks

13 p2481 A70-30069

Magnetospheric particles, fields, electromagnetic waves and data on collisionless bow shock structure

13 p2484 A70-30098

Two dimensional unsteady flow of weakly conducting fluid in perpendicular magnetic field using Green function

14 p2621 A70-30180

Magnetospheric tail neutral layer magnetic field distribution, comparing satellite data with theory

14 p2570 A70-30222

Coupled temperature and electric potential distribution in finite rotational symmetric hydrogen arc column in axial magnetic field

14 p2621 A70-30656

Langmuir probe characteristics and field response in low pressure nonstationary plasma diagnostics in weak magnetic field

14 p2623 A70-30785

Oscillations and stability of rotating masses for axisymmetric equilibrium configurations with toroidal magnetic field based on virial equations

14 p2642 A70-30886

Hall, polarization and Pedersen charged particle drift velocities in static magnetic and time dependent electric field

14 p2624 A70-31046

Superconducting resistive critical field H_c of bcc region of Ti-Nb-V ternary system

15 p2782 A70-31754

Conducting incompressible fluid flow past sphere, examining effect on magnetic field for small magnetic Reynolds number

15 p2778 A70-31913

Bounded hot plasmas with/without steady magnetic field, discussing ion-electron resonances

15 p2779 A70-31997

Radial distributions and escape of charged particles across magnetic field in hot cathode Penning discharge plasma with LF oscillations

15 p2780 A70-32191

Superconducting magnetic flux detector magnetic susceptibilities or field measurements

15 p2740 A70-32431

VLF radiation resistance of short filamentary electric dipole at arbitrary angle to magnetic field in cold uniform plasma, using full wave theory

16 p2859 A70-32935

Near cathode magnetic field effect on instability in linear Hall current accelerators, using geometry of field extending from anode to cathode region

[ALAA PAPER 69-381]

16 p2959 A70-33870

German monograph on temperature distribution and motion of free burning arcs in transversal magnetic fields and gas flows, covering aerodynamic model concept

16 p2959 A70-34077

Magnetic field lines reconnection in steady incompressible hydromagnetic two dimensional flow, formulating governing equations with cylindrical polar coordinates

17 p3140 A70-34926

Supersonic conductive gas recombination fronts for arbitrarily oriented magnetic field, allowing for dissipative coefficients

18 p3294 A70-36255

Equilibrium form shapes of fluid free surface in vessel under gravitational and magnetic field with tension

18 p3240 A70-36269

Magnetic scalar potential of circular loop represented by toroidal coordinate system, solving boundary value problems determining fields of coils and toroidal magnetic conductors

18 p3215 A70-36295

Two component warm plasma wave propagation along magnetic field, considering full pressure tensor equation with momentum and pressure relaxation mechanisms

18 p3294 A70-36405

Spatially periodic dynamos, analyzing homogeneous conducting fluid motions and magnetic field forms

18 p3291 A70-36407

Degenerate relativistic electrons in intense magnetic field, computing transverse electrical conductivity

18 p3296 A70-36896

Magnetic field filtration into time-variable and constant parts, using signal to noise analogies

18 p3249 A70-36914

Electric and magnetic field perturbation at great distances behind body moving in collisionless magnetized plasma estimated from Fourier transform

18 p3316 A70-36921

Synchrotron model limitation for nonthermal spectra, demonstrating restriction to small pitch angles and strong fields

18 p3318 A70-37024

Plasma tearing instabilities involving topological changes in magnetosphere field configuration

19 p3411 A70-37491

Syrovatkii mechanism of high energy particle production near neutral line of magnetic field, noting solar flares occurrence conditions

19 p3478 A70-37581

Rubidium-85 maser, discussing continuous oscillation in low magnetic field

19 p3446 A70-37769

Gravitationally induced /Machian/ magnetic field by rotating mass-shell with centrally located stationary charged sphere, using linearized relativity theory

19 p3471 A70-37815

High magnetic fields applications, emphasizing metal forming and superconducting rings levitation

19 p3471 A70-37948

Crab Nebula electromagnetic spectrum models, considering uniform magnetic field over whole volume and strong fields in small regions

19 p3505 A70-38114

Pc-1 pulsation production by Cerenkov emission of proton beam oscillating along magnetic field line

19 p3417 A70-38590

Gas discharge in longitudinal magnetic field, investigating instability of diffusion dominated positive column

20 p3677 A70-39112

Particulate matter interaction with ionized gas in external magnetic field and nonequilibrium state, examining free electron density

20 p3677 A70-39324

Electrostatic ion waves in uniform magnetic field, calculating phase and group velocities as function of propagation angle for comparison with dispersion measurements

20 p3678 A70-39659

Solar internal rotation, examining oblateness, velocity and magnetic fields, wind structure and Li and Be abundances

20 p3707 A70-39936

Electron bombardment Hg thruster with divergent magnetic fields, investigating performance dependence on configuration and propellant utilizations

[ALAA PAPER 70-1092]

20 p3692 A70-40243

Synoptic charts of polar magnetic fields plotted in polar coordinate system for consecutive solar rotations

20 p3711 A70-40408

Electric and magnetic field components of step function excited electric dipole immersed in dissipative homogeneous medium with specified conductivity and dielectric constant

20 p3589 A70-40464

Thermal plasma model along magnetic field lines outside plasmasphere with sharp density gradient in equatorial plane, using OGO-4 ion composition measurements

21 p3815 A70-41057

Deuterium plasma three dimensional flow in coaxial accelerators, examining magnetic structure of filaments /field lines bundles/

21 p3856 A70-41321

Plasma heating by ionizing shock waves reflected by transverse magnetic field barrier, discussing discontinuity resolution

21 p3857 A70-41381

Shock waves and solitons structure propagating oblique to magnetic field in warm plasma based on two-fluid equations

21 p3857 A70-41382

Plasma source design using stellarator type magnetic field, eliminating electron beam and electrode produced impurities

21 p3858 A70-41713

Magnetotail magnetic field perturbations associated with polar magnetic substorms, using IMP-A and B satellite observations

21 p3882 A70-41720

Harmonic generation and small signal mixing in thin magnetic films subjected to static and time varying fields, generating output voltage expressions

21 p3864 A70-42012

Turbulent flow velocity profile in constant transverse magnetic field, determining resistance coefficient

21 p3861 A70-42235

Homogeneous plasma in uniform magnetic field, deriving theory for instabilities and LF wave propagation modes

22 p4079 A70-42370

Gas discharge positive column finite length effect on wave dispersion and instability, indicating critical magnetic field

22 p4079 A70-42374

Arc welding, discussing use of magnetic fields for improving quality

22 p4042 A70-42375

Unsteady hydromagnetic boundary layer flow past semiinfinite flat plate under steady magnetic field and small free stream perturbation

22 p4080 A70-42631

Compressional sound waves electromagnetic generation in metals in static magnetic fields, examining acoustic amplitude variations

22 p4074 A70-42968

Pulsed multipole magnetic field shaping short plasma blobs

22 p4083 A70-43389

Ultrasound inductive absorption coefficient of metals in quantized magnetic field

22 p4075 A70-43474

Helicon /magnetoacoustic waves/ effect on plasma instabilities, examining HF field amplitudes and magnetic fields

22 p4084 A70-43475

High speed aerospace homopolar alternator, calculating end zone three dimensional magnetic flux distribution and leakage reactance

22 p3999 A70-43585

Concentrated pulsed electromagnetic fields penetration into conductor, assuming magnetic field along metal surface

22 p4041 A70-43621

Auroral electrojet, arcs, electric and magnetic fields relationship investigated by rocket-borne magnetometers and photometers

23 p4184 A70-43835

Electrically conducting fluid hydromagnetic spin-up between infinite flat insulating plates in uniform magnetic field normal to boundaries

23 p4223 A70-43972

FSRO satellites missions and payloads, emphasizing studies of earth magnetic and electric field environment and of polar region particle measurements

23 p4191 A70-44663

Cubic monocrystalline semiconductor under critical magnetic field, using correlation function method

23 p4231 A70-44926

Electric field radial distribution measured for stationary hydrogen arc with axial magnetic field

23 p4227 A70-44933

Electron runaway suppression in fully ionized Lorentz plasma by crossed magnetic and electric fields

24 p4382 A70-45105

Ion acoustic wave propagation in collisionless gravity-supported plasma in static magnetic field calculated from linearized Vlasov equation

24 p4382 A70-45109

Quasi-ambipolar diffusion in arc discharges in magnetic field, calculating ions and electrons density distributions between anode and cathode sheaths

24 p4384 A70-45148

Porous media MHD equations for general case, considering magnetized sphere surrounded by homogeneous envelope

24 p4384 A70-45367

Magnetic field measurement by laser light scattering intensity fine structure determination in plasma

24 p4353 A70-45567

Magnetized conducting sphere steady rotation in viscous conducting liquid, solving for fluid velocity and induced magnetic field

24 p4386 A70-45609

Plasma jet motion stability in axial magnetic field of stellarator divertor and solenoid

24 p4386 A70-45660

- Full and half journal bearings in axial magnetic field, discussing hydromagnetic noncyclic squeeze fluid films 24 p4349 A70-45995
- Conducting sphere MHD rotation in viscous conducting fluid under uniform magnetic field 24 p4387 A70-46028
- Magnetospheric tail neutral layer magnetic field distribution, comparing satellite data with theory 24 p4331 A70-46297
- ### MAGNETIC FILMS
- LF creep characteristics in Block-wall Permalloy films, using high resolution Bitter pattern technique [IEEE PAPER 5.7] 05 p0893 A70-16996
- Mn-Bi films Curie point switching with laser, measuring magnetization dependence via magneto-optic effect [IEEE PAPER 9.3] 05 p0893 A70-16997
- Epitaxial magnetic oxide films grown by chemical vapor deposition 11 p2099 A70-26626
- Magnetic surface loading of Gunn oscillators domain state for use as logic gates, pulse function generator, etc 19 p3387 A70-37819
- Magneto-optic rotation and hysteresis recording instrument for thin magnetic films as function of temperature and wavelength, using Faraday effect 21 p3826 A70-41452
- Computer storage technology, discussing magnetic films, semiconductor cells, content addressable and read-only memories, etc 21 p3795 A70-41693
- Harmonic generation and small signal mixing in thin magnetic films subjected to static and time varying fields, generating output voltage expressions 21 p3864 A70-42012
- Orthogonal susceptibility of uniaxial thin nonmagnetorestrictive Permalloy films 22 p4086 A70-43011
- ### MAGNETIC FLUX
- Ruby green U/V absorption band magnetic circular dichroism calculations in linear approximation, considering spin-orbital interaction constant and magnetic field strength 01 p0156 A70-10188
- Flowmeter errors caused by nuclear magnetic relaxation decreased with increasing magnetic field strength of NMR sensor 01 p0091 A70-10981
- Electron transverse and perpendicular drift velocities calculated at moderate and strong magnetic fields for hydrogen, using Maxwellian energy distribution and equivalent pressure concept 02 p0348 A70-12654
- Computer graphics method for determining total magnetic field magnitude for various coil configurations and spacing, indicating optimum field uniformity near Helmholtz spacing 02 p0271 A70-12745
- Longitudinal magnetic field effect on output power and emission polarization of CW Ar laser employing Brewster windows 03 p0500 A70-13529
- Solar magnetic discontinuity fluxes analyzed by studying 27-day cosmic ray and geomagnetic activity variations using linear filtration method 05 p0900 A70-15969
- Human susceptibility to weak fluctuations in geomagnetic field intensity, showing frequency range 05 p0809 A70-16861
- RF probe impedance variations with magnetic field strength in hot plasma for electron gyrofrequencies less than plasma frequency explained by model 06 p1117 A70-17371
- Photospheric magnetic flux quantization away from sunspots, studying nonsunspot field strength distribution 06 p1142 A70-17992
- Proton concentrations, magnetic field strength and temperatures distribution in interplanetary plasma flows as function of latitudinal distance from center of active region 07 p1391 A70-20420
- Near zero magnetic fields effect on biological systems studied to determine terrestrial magnetic field absence effect on astronauts 08 p1449 A70-20724
- Solar magnetic field strength determination from various absorption lines, considering Rowland intensity, line lower level excitation potential, optical depth, etc 08 p1569 A70-20836
- Neutron beta decay in strong quantizing magnetic field using Dirac wave function for electron, noting lifetime dependence on field strength 08 p1549 A70-21744
- Superconductor tubes experiment, observing flux jump initiation and propagation characteristics 09 p1738 A70-22293
- Penumbral magnetic field strength on basis of photoelectric spectra of undisturbed photosphere 09 p1757 A70-22730
- Laboratory simulations of geomagnetic field suppression, studying biological effects on human, mice, plants and microorganisms 09 p1626 A70-23113
- Solar corona magnetic field estimated from type II bursts correlated with photospheric, chromospheric and geophysical phenomenon 10 p1934 A70-25275
- Archeomagnetic measurements showing westward drift of geomagnetic intensity and correlation of magnetic earth moment with radiocarbon production 11 p2044 A70-25599
- Bremsstrahlung radiation in intense magnetic field proposed as emission mechanism from pulsars, discussing absorption coefficient 11 p2104 A70-25697
- Plasma stabilizing effect of shear and magnetic flux minimum in asymmetric conductors and currents in helical stellarator winding 11 p2088 A70-25711
- Photon nature, considering light-magnetic flux similarities 11 p2084 A70-26027
- Ni-Fe thin films flux reversal with transverse bias field from dynamic magnetization configuration photographs 12 p2284 A70-27242
- Solar plasma and energy and radiation fading during microwave bursts due to synchrotron radiation losses, determining magnetic field strength 12 p2294 A70-27593
- Superposed converter magnetic field intensity normal component distribution as function of polar coordinate 13 p2348 A70-28659
- Wire loop inductive probe with compensation spur as precision sensor for magnetic field intensity in EM fields 13 p2376 A70-28817
- Magnetospheric discrete VLF emission magnetic field intensity calculation by extending Helliwell theory to include electron density model and variable frequency waves 13 p2483 A70-30087
- Interplanetary magnetic field flux relationship to Kp index of magnetic activity 14 p2570 A70-30221
- Implantable EM blood flowmeter errors due to nonsymmetrical blood flow velocity distribution and nonuniform magnetic flux density 14 p2542 A70-30797
- Measurable VLF electromagnetic fluxes from Cerenkov effect in ionosphere produced by artificial electron beams 14 p2579 A70-31249
- Earth satellite motion about center of mass, examining effects of random variations in atmospheric density, geomagnetic intensity and solar radiation 15 p2809 A70-31650
- Superconducting magnetic flux detector magnetic susceptibilities or field measurements 15 p2740 A70-32431
- Magnetic monopole flux limits in primary cosmic radiation derived from muon-poor shower data and inverse Compton scattering 16 p2972 A70-33050
- Magnetic phase diagram of hydrated cesium-copper carbide at 1.625 Neel temperature in external magnetic fields, giving equation for spin flop field temperature dependence 16 p2961 A70-33688
- MHD flow velocity and magnetic flux profiles in rectangular ducts for secondary boundary layer 16 p2959 A70-34239
- Magnetic flux measurements in quiescent solar filaments and adjacent photosphere using magnetograph observations 17 p3157 A70-34837
- Semiannual oscillation and fine structure of earth magnetic field horizontal intensity during March and September 19 p3413 A70-38004
- Magnetic field lower limit in Crab Nebula from cosmic gamma ray studies using optical reflector to detect atmospheric Cerenkov radiation 21 p3875 A70-40684
- Transverse magnetic disturbances in auroral oval, examining movement, intensity, particle fluxes and field magnitude 21 p3817 A70-41090
- Energy release during flux jump in Nb-Ti single core wires and multifilament composite superconductors 21 p3863 A70-42011
- Optically pumped magnetometers for low intensity magnetic fields measurement, reviewing atomic hyperfine levels splitting, magnetic resonance, Zeeman sublevels, etc 22 p4026 A70-42575
- High speed aerospace homopolar alternator, calculating end zone three dimensional magnetic flux distribution and leakage reactance 22 p3999 A70-43585
- Magnetic vector potential of circular ring with current in Taylor series expansion for electromagnetic axisymmetric systems 23 p4189 A70-44069
- Air spark gap to switch stored charge in LC circuit, using auxiliary triggering circuit to clamp magnetic flux 23 p4177 A70-44471
- Magnetic flux dependent interference beats in spontaneous emission of gas discharge of He-Ne laser, estimating Hertzian coherence duration 23 p4202 A70-45052
- Primeval cosmic magnetic fields origin, discussing galactic fields and limits on present intergalactic field 24 p4403 A70-45396
- Stable ellipsoidal plasma configurations in alternating electrode annular system, considering longitudinal magnetic field strength, electrode voltage and gas discharge chamber pressure 24 p3485 A70-45456
- Interplanetary magnetic field flux relationship to Kp index of magnetic activity 24 p4331 A70-46296
- ### MAGNETIC FORMING
- Magnetomotive loading of cantilevers, beams and frames, studying dynamic loading of structures 19 p3541 A70-38045
- Stainless steel sheet-to-plate tee joint resistance welded by Magnetic Force Upset Welding process, testing performance 21 p3832 A70-40792
- ### MAGNETIC INDUCTION
- Spherical conducting body effect on induction coil impedance and EMF in nondestructive testing using eddy current probes 02 p0300 A70-12478
- Electromagnetic wave propagation in homogeneous plasma waveguide satisfying Appleton-Hartree approximation without collisions in presence of longitudinal magnetic induction 02 p0349 A70-12724
- Magnetic field self induction in static fluid-submerged intersecting jet system, calculating required magnetic Reynolds numbers 04 p0726 A70-14541
- Magnetized resonantly sustained HF plasma column wave properties, obtaining above-critical density as function of static magnetic induction 04 p0728 A70-14999
- Unipolar induction to calculate moon interior electric field profiles, noting magnetic back pressure as limb shock wave and interaction with solar wind 07 p1377 A70-18970
- Inductance distribution in magnetic systems of different configuration and air gaps 07 p1282 A70-19530
- MHD flow in rectangular duct with arbitrary conductivity via modified Fourier method, obtaining magnetic induction and current for various Hartmann numbers [ASME PAPER 69-WA/APM-17] 08 p1551 A70-21308
- Magnetic moment associated with Landau levels in magnetic induction in electron gas and magnetic fields of white dwarfs and neutron stars 09 p1752 A70-22306
- Algorithm for inversion of geomagnetic induction problem, determining earth radial conductivity distribution 09 p1669 A70-23305
- Plasma conductivity measuring device using phenomenon of change of coil induction in electromagnetic field 09 p1737 A70-23380
- Linearized steady plane axisymmetric flows of inviscid finitely conducting incompressible fluid past insulator under magnetic induction with zero components 13 p2464 A70-29541
- Contactless electromagnetic level sensor for liquid metal using eddy currents 14 p2587 A70-31011
- Thermal electrodeless plasmas generation at audio frequencies with closed magnetic circuit model [AIAA PAPER 70-776] 17 p1319 A70-34478
- Electromagnetic induction in plate with two dimensional conductivity distribution for case of E polarization, representing field by Green functions 19 p3408 A70-37314
- Induction flowmeters operation, emphasizing various factors effects on induced voltage 19 p3426 A70-37936
- Energy distribution of ions transversal to magnetic field in argon plasma source with oscillating electrons, showing dependence on induction and discharge current 19 p3482 A70-38956
- Superradiation signal stationary pulse excitation, describing quantum statistical theory of condensed media and gases, forced induction, signals and echoes 20 p3642 A70-39756
- Multiphase relaxation oscillator with inductive coupling and common base resistor in feedback loop, determining circuit parameters effect on pulse length 20 p3598 A70-39791

- One wavelength MHD induction generator, discussing field pressure gradients, fluid velocities, excitation and electrical output power
20 p3566 A70-40015
- Apollo 11 rocks natural remanence and induced magnetism by triaxial magnetic gradiometer at Lunar Receiving Laboratory
21 p3914 A70-41650
- Relative pressure and excitation induction transverse distribution relationship for MHD machine model, assessing dimensionless criteria effect on pressure peaks position
21 p3760 A70-42232
- EM induction in flat plates with two dimensional conductivity distribution, describing approximation method
23 p4217 A70-44054
- MAGNETIC INDUCTION PROBES**
U MAGNETIC PROBES
- MAGNETIC MATERIALS**
NT FERRIMAGNETIC MATERIALS
NT FERROMAGNETIC FILMS
NT FERROMAGNETIC MATERIALS
NT MAGNETITE
NT PERMALLOYS [TRADEMARK]
- Co role in magnetic materials, discussing high magnetic moments in iron combinations, orbital angular momentum, quantum mechanics explanations, etc
07 p1306 A70-19074
- Superconductive materials and magnet design, discussing stabilization methods
11 p2097 A70-25613
- Magnetism and magnetic materials - Conference, Philadelphia, November 1969
12 p2283 A70-27238
- Ni-Mo-Fe magnetic alloy for EM pulse shielding, verifying saturated regions diffusion theory
12 p2201 A70-28128
- Microwave properties of infinite lossless rectangular waveguide semiinfinitely filled with magnetic material operating in specific modes
17 p3050 A70-34585
- Magnetic and nonmagnetic metals flaw detection, using orthogonal eddy current probe to reduce permeability and conductivity variations effects
24 p4344 A70-45700
- Fluorescent penetrants vs magnetic powder test for individual and continuous material inspection, discussing sensitivity and surface finish influence
24 p4338 A70-45741
- MAGNETIC MEASUREMENT**
Solar corona magnetic field determination from photospheric magnetic field line-of-sight component observations, describing various mathematical methods
01 p0176 A70-10250
- Solar magnetic field investigated with parallel beam from coelostat mounting falling on magnetograph slit of solar telescope, noting field polarity change periodicity
01 p0177 A70-10347
- Steel objects microstructure and hardness tested by continuous magnetic technique, describing experimental apparatus model
02 p0300 A70-12479
- Absorption line identification in sunspot spectra by calculating Zeeman patterns, using Zeeman splitting for magnetic field measurement
03 p0574 A70-13934
- Interplanetary magnetic field measurements from Mariner and OGO satellites at various paths, regions and intervals, finding dominant polarity effect dependent on sun latitude
03 p0575 A70-13980
- Magnetic fields neutral lines length as indicator of solar flare productivity
03 p0561 A70-14001
- Superconducting magnetic system in magnetic analyzer of positrons and electrons in primary cosmic radiation tested on board Cosmos 213
04 p0685 A70-14443
- High altitude observatory solar magnetograph installation modifications including computer control, improved Zeeman effect observation instrument, etc
04 p0691 A70-15037
- Magnetic vector directions over sunspot near central meridian passage measured, showing axisymmetric arrangement
04 p0758 A70-15697
- Miniature fluxgate magnetometer for sounding rocket measurements of two orthogonal components of external magnetic field, predicting performance by linear mathematical model
05 p0851 A70-16690
- Magnetosensitive quartz element with suspended magnet and two mirrors for recording magnetic variations
05 p0851 A70-16770
- Geomagnetic field total vector modulus secular variations from airborne measurements
07 p1278 A70-20461
- Longitudinal magnetic field measurement along H-alpha line of solar prominence
08 p1560 A70-20838
- Magnetic field measurements in geomagnetic tail from Explorers 33 and 35 indicating depressed field region centered on neutral sheet
08 p1488 A70-21379
- Mapping of normal distribution of geomagnetic elements in Bulgaria
08 p1490 A70-21433
- Broadband remote sensing magnetometer for measuring fast-rising pulsed magnetic fields
09 p1676 A70-22716
- Earth magnetosphere and magnetosheath magnetic field measurements by Mariner 5
09 p1670 A70-23487
- Solar magnetic field measurement emphasizing circular and total polarization characteristics
10 p1939 A70-24275
- Plasma magnetic field measurement by scattered light, analyzing electron spectrum modulation with gyration frequency
10 p1916 A70-24401
- Solar flare relation to local magnetic field in active regions, discussing sunspot and weak field measures
12 p2297 A70-26986
- Spectral line width and shift measured by spectrograph crossed with Fabry-Perot interferometer in pressure chamber, measuring magnetic field in sodium
12 p2238 A70-28178
- Superconducting magnetic system in magnetic analyzer of positrons and electrons in primary cosmic radiation tested on board Cosmos 213
13 p2403 A70-28468
- Wire loop inductive probe with compensation spur as precision sensor for magnetic field intensity in EM fields
13 p2376 A70-28817
- Photosphere model and magnetic field gradient effects on line contours and magnetographic calibration curves, using nonlinear source function
13 p2496 A70-29845
- Reliability and environmental testing of residual magnetic field measurements of satellite HEOS-A1 electronic equipment, using Rb vapor magnetometers
13 p2380 A70-30031
- Magnetic moment measurement of satellite in near earth orbit, using data transmitted by rectangular magnetic sensors
13 p2454 A70-30032
- Parametric resonances at zero field crossing levels of optically pumped atoms on alkali vapors, noting applications to weak magnetic measurements
13 p2456 A70-30034
- Thin ferromagnetic film sensitive elements for detection of weak magnetic fields
13 p2415 A70-30041
- Pioneer 6-9 low magnetism spacecraft for interplanetary magnetic field observation
13 p2507 A70-30046
- Stability requirements for precision magnetic field measurements on ground and in space, discussing magnetic balances and fluxgate magnetometers for geomagnetic variations and spacecraft attitude
13 p2415 A70-30050
- Magnetic field measurement of VLF wave propagating in whistler mode in magnetosphere by satellite FR-1
13 p2401 A70-30054
- Geomagnetic noise constraints on weak field measurements in upper magnetosphere
13 p2401 A70-30056
- Geomagnetic tail structure and shape from Explorer 33 and 35 and Pioneer 8 observation data, examining field lines divergence with distance from earth
13 p2402 A70-30075
- Geomagnetic field distortion in high beta magnetospheric regions from OGO observations for quiet and slightly disturbed conditions
13 p2402 A70-30076
- Geomagnetic field distant fluctuations during substorm from ATS 1 magnetometer data on abrupt recoveries of H component
13 p2482 A70-30077
- Free nuclear precession sensor with rotating sample for performing measurements in nonuniform magnetic field
14 p2582 A70-30218
- Errors magnitude in quartz variometer readings resulting from variations of geomagnetic field perpendicular component
14 p2582 A70-30244
- Magnetic fields of DA dwarfs observed with photoelectric polarimeter, noting no fields observable
17 p3154 A70-34537
- Magnetic methods of flaw detection, discussing theory and application to welded butt joints
18 p3263 A70-36521
- Interplanetary magnetic field measurements by Pioneer 8 during 25 February 1969 solar activity, discussing geomagnetic storms, cosmic rays, shock fronts and ionospheric disturbances
19 p3513 A70-37501
- Permalloy tapes uncertainty in magnetization process, discussing Barkhausen discontinuities measurement method
20 p3673 A70-40058
- Helios solar probe magnetic field measurements, discussing magnetometer systems, interplanetary magnetic field implications, shock waves, magnetic storms, etc
21 p3923 A70-42172
- Dual satellite magnetic field and plasma measurements of earth bow thick pulsation shock by Vela 3A and Explorer 33
22 p4013 A70-42470
- Magnetism in austenitic stainless steels, discussing Mossbauer measurements of temperature dependence of hyperfine field and single line width
22 p4055 A70-43012
- Global geomagnetic field fluctuations of internal and external origins, analyzing HF spectrum based on monthly mean plots
23 p4187 A70-43861
- Quartz Z-variometer for autonomous variation stations, describing construction and operation
23 p4194 A70-44089
- Beryllium orbital diamagnetic susceptibility calculated by pseudopotential method compared to experimental data
23 p4208 A70-44886
- Magnetostrictive Ni-Mn-Co ferrites and Al-Fe alloys, measuring magnetic field effect on piezomagnetic coefficients at room temperature
24 p389 A70-45400
- Magnetic field measurement by laser light scattering intensity fine structure determination in plasma
24 p4353 A70-45567
- Remanence and saturation methods for magnetic-particle flaw detection
24 p4346 A70-45726
- Defect detection by measurement of magnetic field leakage around flaw
24 p4346 A70-45727
- Free nuclear precession sensor with rotating sample for performing measurements in nonuniform magnetic field
24 p4339 A70-46293
- Errors magnitude in quartz variometer readings resulting from variations of geomagnetic field perpendicular component
24 p4339 A70-46319
- MAGNETIC MEMORIES**
U MAGNETIC STORAGE
- MAGNETIC METALS**
U MAGNETIC MATERIALS
U METALS
- MAGNETIC MIRRORS**
Plasma accumulation between mixed field accelerator and pulsed magnetic mirror, noting duration and stability
02 p0346 A70-12104
- Time resolved cavity perturbation technique to measure high plasma density in magnetic mirror compression experiment, obtaining total electron number
02 p0347 A70-12236
- Accumulated plasma density and lifetime measurement of trapped ions between accelerator and periodic magnetic mirror, showing limitation by collisions and charge exchange
03 p0532 A70-13683
- Soviet collection of papers on magnetic traps covering chamber walls effect on plasma heating, plasma in mirror trap and self sustained fusions
07 p1350 A70-19844
- Plasma properties produced in mirror magnetic trap by electron beam determined during transition from hot electron dense plasma into cold electron low density plasma
07 p1350 A70-19846
- Electromagnetic instability measurements in electron cyclotron resonance plasma produced in magnetic mirror field
10 p1921 A70-23963
- Electron diffusion in trap with magnetic mirrors under pulsed field perturbations, determining coefficients by numerical integration of drift equation
10 p1931 A70-24311
- Magnetic mirror confined plasmas, solving Fokker-Planck equation
18 p3296 A70-36795
- Ion heating during plasma instability due to interaction with electron beam in mirror magnetic trap
20 p3678 A70-39598
- Superconductive magnets with different windings and modular construction for magnetic mirror apparatus, discussing performance tests
23 p4218 A70-44355
- Plasma confinement in min-B configuration of linear multiple with mirrors, attaining additional stabilization via linear rods carrying unidirectional current
24 p4386 A70-45612
- MAGNETIC MOMENTS**
Transient magnetic resonance technique for non-destructive testing of elements with nuclei having magnetic moment, considering cereal grains, propellants, metal powder and plastics
01 p0097 A70-10014
- Disordered ferromagnetic binary alloys of transition metals magnetic moment distributions based on thermal neutron scattering experiments
05 p0893 A70-16950

Co role in magnetic materials, discussing high magnetic moments in iron combinations, orbital angular momentum, quantum mechanics explanations, etc
07 p1306 A70-19074

Magnetic moment associated with Landau levels in magnetic induction in electron gas and magnetic fields of white dwarfs and neutron stars
09 p1752 A70-22306

Archaeomagnetic measurements showing westward drift of geomagnetic intensity and correlation of magnetic earth moment with radiocarbon production
11 p2044 A70-25599

Magnetic moment measurement of satellite in near earth orbit, using data transmitted by rectangular magnetic sensors
13 p2454 A70-30032

Magnetic moment fluctuations of arbitrary solid body by fluctuation-dissipation theorem for thermal equilibrium
13 p2454 A70-30033

Isomer shift, Mossbauer recoil free fraction and nuclear quadrupole splitting for Fe57 in iron fluoride measured for lattice dynamics, fine and hyperfine structure
14 p2626 A70-30484

Ion magnetic moments in crystallographically nonequivalent lattice regions in ferrites
19 p3484 A70-37622

Optimal control of magnetic torque for bias momentum removal from attitude controller, discussing applications to Skylab
23 p4258 A70-44503

MAGNETIC PERMEABILITY

Premature saturation in strongly magnetic systems explained by model with nonuniform magnon modes, applying time dependent Green functions
02 p0338 A70-11886

Temperature dependence of magnetic susceptibility in liquid and solid states of binary Al-Mn alloys with additions of Cr, V and Ti
02 p0316 A70-12300

Magnetic susceptibility of synthetic australite and philippinite-like tektites measured in 77-560 K range, discussing origin
05 p0916 A70-16836

Normal and bottle-green microtektite glass measured for magnetic susceptibility, magnetization and Curie constants
05 p0916 A70-16839

Lamellar magnetic core stacking pressure influence on core magnetic characteristics in variable magnetic field, noting effects on magnetic permeability
07 p1246 A70-19537

Electromagnetic wave scattering from atmospheric ellipsoidal plasma formations, using arbitrary permittivity and magnetic permeability tensors
13 p2366 A70-29376

Superconducting magnetic flux detector magnetic susceptibilities or field measurements
15 p2740 A70-32431

Anisotropic temperature plasma susceptibility calculation based on velocity moment equations and circular polarized coordinates, compared to Vlasov equation solution
17 p3140 A70-34929

Thermal variation of diamagnetism and susceptibility of rhombohedral graphite
21 p3845 A70-42268

Orthogonal susceptibility of uniaxial thin nonmagnetorestrictive Permalloy films
22 p4086 A70-43011

Valent state of chromium doped barium titanate from EPR spectra and magnetic susceptibility measurements
22 p4086 A70-43133

Beryllium orbital diamagnetic susceptibility calculated by pseudopotential method compared to experimental data
23 p4208 A70-44886

Superconductive memory type chalcogenide tellurium germanium arsenide, measuring AC magnetic susceptibility and DC electrical resistivity
23 p4231 A70-44892

Ferromagnetic cylindrical specimens eddy current density distribution under influence of field strength dependent permeability corresponding to Rayleigh law
24 p4344 A70-45695

Metallic rods and tubes permeability and resistivity nondestructive measurement by AC apparatus with self balancing sensing coil, using computer program for data reduction
24 p4345 A70-45704

MAGNETIC PISTONS

Forbush decreases of cosmic rays calculated assuming semitransparent magnetic piston action with free particle exchange
07 p1372 A70-20340

Current diffusion from magnetic piston into postshock gas upstream observed in electromagnetic shock tube
09 p1736 A70-23185

MAGNETIC POLES

Polooidal magnetic field influence on compressible fluid convection in spherical shells, using variational method to obtain stability criteria
04 p0758 A70-15695

Variational and Z-expansion calculations for magnetic quadrupole transitions decay rates of He sequence
05 p0920 A70-16942

Relativistic magnetic monopoles detection in corpuscular primary cosmic rays, describing equipment and results
07 p1371 A70-20333

Altitude asymmetry of instantaneous auroral oval plotted for geomagnetic pole and earth surface
07 p1277 A70-20456

Synoptic charts of polar magnetic fields plotted in polar coordinate system for consecutive solar rotations
20 p3711 A70-40408

Magnetic monopoles electromagnetic search in Apollo 11 rock samples
21 p3912 A70-41639

Paleomagnetic reversal in 1350 year increments, measuring declination of deep sea sediment cores
21 p3820 A70-41885

MAGNETIC PROBES

Ferroprobe coercimeter with attached electromagnets for nondestructive hardness testing, describing components and mounting
02 p0301 A70-12489

Magnetovariational sounding procedure for determining vertical distribution of earth mean electrical conductivity using geomagnetic field spatial derivatives for spherical earth
05 p0843 A70-16767

Wire loop inductive probe with compensation spur as precision sensor for magnetic field intensity in EM fields
13 p2376 A70-28817

Magnetic induction sensors sensitivity for magnetotelluric surveying in geophysics
13 p2415 A70-30048

Magnetic probes effectiveness study of electron heating behind shock wave front in plasma, measuring electron temperature
18 p3294 A70-36149

Current distribution of accelerating electrodes of coaxial injector, using differential magnetic probe
22 p3965 A70-42805

Finite thickness metal plate eddy current response to pulsed field from aperture probe
24 p4344 A70-45696

Eddy current magnetic probe with frequency scanning for signal-noise discrimination in nondestructive testing of tubes
24 p4336 A70-45698

Magnetic and nonmagnetic metals flaw detection, using orthogonal eddy current probe to reduce permeability and conductivity variations effects
24 p4344 A70-45700

MAGNETIC PROPERTIES

NT ANTIFERROMAGNETISM

NT CURIE TEMPERATURE

NT DIAMAGNETISM

NT FERRIMAGNETISM

NT FERROMAGNETISM

NT GEOMAGNETISM

NT GYROFREQUENCY

NT GYROMAGNETISM

NT MAGNETIC EFFECTS

NT MAGNETIC INDUCTION

NT MAGNETIC MOMENTS

NT MAGNETIC PERMEABILITY

NT MAGNETIC RELAXATION

NT MAGNETIC RIGIDITY

NT MAGNETIC SUSPENSION

NT MAGNETOACOUSTICS

NT MAGNETOACTIVITY

NT MAGNETORESISTIVITY

NT MAGNETOSTRICTION

NT PALEOMAGNETISM

NT PARAMAGNETISM

NT POLARIZATION CHARACTERISTICS

NT REMANENCE

NT SPIN-LATTICE RELAXATION

NT THERMOMAGNETIC EFFECTS

Thickness measurement of nonmagnetic coatings on magnetic substrates taking into account surface roughness effect
02 p0302 A70-12672

Magnetic boundary layer equations applied to flow past stationary circular cylinder and sphere, showing graphical variation of slip velocity with angle
03 p0471 A70-14334

Magnetics - IEEE Conference, Amsterdam, April 1969
05 p0893 A70-16995

Ti additions influence on steel work hardening, specific weight, magnetic properties and structure
08 p1515 A70-20924

Magnetic spherules extracted from manganese nodules classified by X ray diffraction and electron

microprobe data, suggesting volcanic, stony and iron meteoritic origins
08 p1578 A70-21560

Composite materials in Co or Fe matrix for solid rotor core materials applications at high temperature and stress, discussing magnetic properties
08 p1524 A70-21908

Ferromagnetic domain wall-dislocations magnetoelastic interaction in Fe and Ni computed as function of relative separation, discussing effects on magnetic properties
09 p1705 A70-22811

Magnetism and magnetic materials - Conference, Philadelphia, November 1969
12 p2283 A70-27238

Magnesium arsenide phosphide crystal and magnetic structure using X ray and neutron diffraction
12 p2283 A70-27240

Stable colloidal dispersions of subdomain magnetite particles correlated for magnetic properties in terms of size distribution and volumetric concentration by superparamagnetic theory
12 p2284 A70-27241

Isostructural crystals of Dy compounds investigated for magnetic behavior using high resolution photoelectric optical spectroscopy
12 p2261 A70-27243

Quenched MnBi thin films measured for magnetic, magneto-optical and optical properties, noting Faraday rotation
12 p2284 A70-27246

Ni-Fe alloy sheets magnetic shielding effectiveness correlated with DC magnetic properties at various frequencies
12 p2201 A70-28127

Magnetic field simulator for investigating magnetic properties of satellites designed for magnetometric experiments
13 p2385 A70-29556

Lamellae stresses and magnetostrictive effects on magnetic properties of titanomagnetite and ilmenohematite series minerals
15 p2728 A70-31993

MAGFET devices for integrated circuits, calculating magnetic sensitivity as function of channel aspect ratio and Hall electrode position
15 p2710 A70-32572

French monograph on microwave ferrite devices, discussing paramagnetism, ferromagnetism, ferrimagnetism, gyromagnetic resonance and nonreciprocal effects, isolators, attenuators, phase shifters, etc
16 p2873 A70-33267

Spinel lithium ferrite magnetic and crystallographic properties, considering effects of Li and oxygen losses, sintering temperature and cooling rate
16 p2961 A70-33272

Magnetometric, dilatometric, pyrometric and X ray studies of phase transformations in Fe-Ni alloys, considering magnetic characteristics and formation of superstructures
18 p3276 A70-36207

Mechanical stresses effect on Vicalloy rotor packets magnetic properties
19 p3357 A70-37265

Microstructure effects on magnetic properties of polycrystalline MnZn ferrites with high permeability
19 p3484 A70-37565

Crystal dislocations and microstructure effects on magnetic properties of polycrystalline MnZn ferrites with high permeability, noting eddy currents role
19 p3484 A70-37566

Iron phosphate semiconducting glasses, determining electrical and magnetic properties dependence on thermal treatment
19 p3487 A70-37861

Azur satellite magnetic parameters simulation, noting spacecraft structure effect
19 p3400 A70-38295

Magnetoionic component of entire N/z profile on incomplete ionospheric traces, including invisible part of ionogram
19 p3419 A70-38957

Apollo 11 lunar rock pyroxenes, examining band structure and magnetic ordering by high voltage electron microscopy and electron diffraction
21 p3898 A70-41523

Apollo 11 lunar rock and dust samples thermomagnetic properties, Curie points, magnetization and demagnetization characteristics
21 p3915 A70-41661

Magnetic properties of Apollo 11 lunar breccia samples, determining natural remanent magnetization and susceptibility via paleomagnetism instruments and methods
21 p3916 A70-41668

Lunar rocks magnetic properties and natural remanent magnetization, examining pyroxene paramagnetism, ferrosilite and ilmenite antiferromagnetism and native iron ferromagnetism
21 p3917 A70-41671

Apollo 11 lunar rock and fines magnetic properties, associating remanent magnetization with lunar magnetic field
21 p3917 A70-41675

Apollo 11 lunar breccia and fines magnetic properties, examining remanence, composition, oxidation, volcanic activity and stoichiometry
21 p3918 A70-41680

Apollo 11 lunar fines glass spherules magnetic properties, considering soft and hard ferromagnetic components
21 p3918 A70-41681

Antiferro-, ferri- and ferromagnetic semiconductors properties, discussing narrow band electron correlation, electrostatic and magnetic polarons formation, etc
21 p3864 A70-42254

Magnetic and structural characteristics of ternary intermetallic systems with lanthanides, considering Ln substitution by other rare earth elements
22 p4085 A70-42481

Lanthanide zinc intermetallic compounds magnetic characteristics in 4-300 K range, observing Curie-Weiss behavior
22 p4085 A70-42482

Magnetic desaturation of inertia flywheels of satellite in equatorial or slightly inclined orbit, discussing satellite stabilization
22 p4110 A70-42488

Perovskite type oxide lanthanum manganate magnetic properties, explaining ferromagnetism by spin Hamiltonian formalism
24 p4389 A70-45601

Magnetic properties of lanthanum calcium manganate, making stoichiometric specimens by controlling oxygen partial pressure
24 p4390 A70-45602

MAGNETIC RECORDING
Recording technique for measuring short period variations of radio signal reflections altitudes from ionosphere applicable to fast ionospheric processes
07 p1277 A70-20454

Hydromagnetic emissions recordings at two Australian stations indicating simultaneous occurrence
10 p1875 A70-24441

Solar radio bursts dynamic spectra by magnetic tape recording of digital signal, obtaining frequency and time profiles and intensity layers
10 p1934 A70-25276

Solar image spectrum magnetic recording for computer, using photomultipliers with coding devices
18 p3256 A70-36107

Magnetic tape recorder for panoramic vertical ionospheric sounding data acquisition in digital form
18 p3261 A70-37041

Instrumentation magnetic recorders in aerospace industry in relation to new components and techniques development, investigating airborne recorder as flight test tool
19 p3429 A70-38516

Airborne magnetic recording flight test instrumentation of Anglo-French Jaguar aircraft
19 p3431 A70-38535

Emmanuel magnetic recording system used with airborne digital computers for aircraft in-flight tests
19 p3432 A70-38547

Magnetic recording in airborne systems, discussing printed motor-optical tachometer design for transport accuracy and ferrite spin-alloy heads
21 p3829 A70-41921

High speed three-frame electronic camera with storage tube, slow scanning and magnetic recording [SMPT PREPRINT 55]
22 p4033 A70-43038

MAGNETIC RELAXATION
NT SPIN-LATTICE RELAXATION
Flowmeter errors caused by nuclear magnetic relaxation decreased with increasing magnetic field strength of NMR sensor
01 p0091 A70-10981

MAGNETIC RESONANCE
NT ELECTRON PARAMAGNETIC RESONANCE
NT FERROMAGNETIC RESONANCE
NT NUCLEAR MAGNETIC RESONANCE
NT PARAMAGNETIC RESONANCE
NT PROTON MAGNETIC RESONANCE
NT PROTON RESONANCE
Ultra low frequency waves features in magnetosphere, considering geomagnetic pulsations, magnetic data from Explorer 33 and bounce resonance
12 p2223 A70-27573

Optically pumped He 4 magnetometers, investigating magnetic resonance signal dependence on orientation for nonresonance technique construction
13 p2414 A70-30036

Spin-spin correlation in Heisenberg magnet linear chain at infinite temperature, discussing non-monotonic frequency dependence
14 p2619 A70-30486

Apollo 11 rock and fines magnetic resonance, examining line shapes, temperature dependences and electron spin
21 p3917 A70-41670

Antiferromagnetic resonance measurement in manganese difluoride as function of microwave frequency, sample size and shape
21 p3850 A70-41908

MAGNETIC RIGIDITY

Geomagnetic latitude survey by neutron multiplicity monitor covering threshold rigidity ranges at various elevations, relating data to primary cosmic ray rigidity spectrum
04 p0741 A70-15125

Polar cap absorption midday recovery phenomenon analysis in northern and southern polar auroral regions showing increase in ionizing flux rigidity
04 p0682 A70-15729

Local time dependence of geomagnetic cut-offs for solar protons in 0.52-4.0 Mev range from satellite observations
06 p1136 A70-18529

Solar flare cosmic ray rigidity spectrum determination based on ratio of relative enhancements, assuming isotropical arrival of particles at earth
09 p1744 A70-22489

Polar cap absorption midday recovery phenomenon analysis in northern and southern polar auroral regions showing increase in ionizing flux rigidity
14 p2575 A70-30813

Secular variations calculation in cosmic ray cutoff rigidities by trajectory tracing process with geomagnetic field models
18 p3306 A70-36023

High energy charged particle observations on OSO 3 at various rigidities
19 p3505 A70-38117

Primary cosmic ray He nuclei rigidity measurement with magnetic spectrograph
19 p3505 A70-38119

Cosmic ray neutron component differential and integral barometric coefficients, showing dependence on geomagnetic cutoff rigidity and atmospheric depth
20 p3697 A70-39290

Cosmic rays cutoff rigidity variations during magnetic storms, investigating flux increase due to current flow along parallel lines on magnetic shell surface
20 p3698 A70-39300

Low energy solar protons penetration, examining geomagnetic cutoff latitude during magnetically disturbed period
21 p3881 A70-41077

Geomagnetic axial dipole deviation from true north associated with earth core asymmetric motion, discussing geomagnetic reversal
22 p4020 A70-43231

Threshold rigidity decrease during 23-24 March 1969 magnetic storm, analyzing neutron multiplicity spectrum
23 p4186 A70-43846

MAGNETIC SHIELDING
Ni-Fe alloy sheets magnetic shielding effectiveness correlated with DC magnetic properties at various frequencies
12 p2201 A70-28127

Superconducting lead shell shielding properties in small ambient magnetic fields
13 p2454 A70-30030

Spacecraft magnetic radiation shield optimization based on thickness criterion and system mass consideration
22 p3979 A70-43390

MAGNETIC SIGNALS
Superradiation signal stationary pulse excitation, describing quantum statistical theory of condensed media and gases, forced induction, signals and echoes
20 p3642 A70-39756

MAGNETIC SIGNATURES
Magnetograms by Venera 4 and Mariner 5 compared to determine interplanetary magnetic field nature in Venus proximity
04 p0744 A70-14438

Vertical incidence /VI/ F layer ionograms, magnetograms and signal amplitude data obtained during annular eclipse of 23 November 1965
09 p1671 A70-23494

Magnetospheric substorms magnetograms taken at various stations, showing preceding ring storm particles deflection into magnetic tail
10 p1876 A70-24496

Magnetograms by Venera 4 and Mariner 5 compared to determine interplanetary magnetic field nature in Venus proximity
13 p2485 A70-28463

Chromospheric photoelectric magnetograms with high resolution H alpha pictures for deriving magnetic field directly from filtergrams
17 p3096 A70-35864

MAGNETIC SPECTROSCOPY
Zeeman interaction for super 8S term in ESR Hamiltonian determined, using trivalent Gd magnetic spectrum at eightfold coordinated cubic sites of thoria
02 p0340 A70-12718

Sea level testing of magnetic spectrograph and calorimeter apparatus for studying cosmic ray spectra at different atmospheric depths
08 p1560 A70-20474

Primary cosmic ray He nuclei rigidity measurement with magnetic spectrograph
19 p3505 A70-38119

MAGNETIC STARS

Electric fields in rotating magnetic relativistic neutron stars, analyzing static fields in corotating frame and pulsar emission
02 p0379 A70-12726

Anisotropic plasma turbulence produced by two stream instability onset near light cylinder of rotating magnetic star for pulsar model
14 p2640 A70-30788

Coherent radio emission mechanisms of white dwarfs and neutron stars as magnetic pulsar models, discussing polarization
15 p2804 A70-32698

Stellar evolution covering formation, structure and time-varying properties of single spherical, nonspherical, magnetic and binary stars
19 p3531 A70-38950

Rotating magnetic star thermal behavior, discussing central nuclear burning stability, homologous changes, cooling, degeneracy and helium flash
22 p4100 A70-42855

Surface field model of rotating magnetic stars involving uniformity and Eddington-Sweet circulation suppression
23 p4251 A70-44826

Rotating magnetic star dynamic evolution, discussing magnetic and rotation axes inclinations for oblique rotator model
23 p4252 A70-44827

Heavy elements diffusive separation as explanation of metallic and magnetic A stars abundance anomalies at outer convective envelope bases
24 p4410 A70-45775

White dwarf stars continuum circular polarization as function of time and wavelength, emphasizing magnetic star search
24 p4410 A70-45776

MAGNETIC STORAGE
Multichannel ionization calorimeter data readout into electronic computer using short circuit coil magnetic storage
05 p0816 A70-15947

Sideband frequency disturbances at analog data magnetic storage using frequency modulation
20 p3586 A70-39706

Magnetic holography, considering Faraday and polar Kerr effect reconstructions and potential as computer storage
22 p3994 A70-43608

MAGNETIC STORMS
Two station simultaneous observations of auroral infrasonic wave substorms morphologies
01 p0071 A70-10411

Ionospheric auroral oval, proton aurora and midlatitude trough relationship to magnetospheric structure, trapping outer boundary, storm time belt and plasmopause
01 p0073 A70-10586

Magnetic lines of force penetration into magnetosphere accompanied by plasma insertion generating ring current responsible for main phase of magnetic storm
01 p0083 A70-11543

Midlatitude ionospheric disturbances accompanied by auroral type radio absorption observed by radio astronomy and probes during 26 May 1967 storm
01 p0084 A70-11555

Harmonic analysis of magnetic storms initial phases having steep leading edges and distinct steady portions, showing homogeneity in first approximation
01 p0084 A70-11558

Seasonal effect on F region midlatitude slab thickness diurnal variations during magnetic disturbances using monitoring VHF signals from geostationary satellites
02 p0290 A70-12160

Equatorial magnetosphere particle and field data from 18 April 1965 geomagnetic storm reanalyzed in context of drift mirror instability theory
03 p0560 A70-13976

Forbush decrease recorded on 26-27 January 1968 showing large anisotropies in cosmic ray flux after SC magnetic storm
03 p0560 A70-13979

Relationship between 6300 A monochromatic auroral arc and visible aurora during magnetic storm, determining directional speeds
03 p0478 A70-14000

Solar flare duration effect on propagation and modification of forward-reverse shock pair between sun and 1 AU, using equations of motion for spherically symmetric flow
04 p0740 A70-15104

Magnetic storms frequency and levels coincidence with solar activity variations
04 p0682 A70-15734

Cosmic ray intensity decreases in relation to geomagnetic and F 2 region disturbances characterized by Forbush decreases from vertical sounding data
05 p0898 A70-15940

Time dependent variation of first and second harmonics amplitudes of diurnal cosmic ray variations during SC magnetic storms
05 p0898 A70-15942

F 2 layer electron density changes during geomagnetic storms linked to DS current and electromagnetic disturbances

05 p0838 A70-16280

Topside ionosphere ionization compared during magnetic storms with steep onset, smooth variation and sudden commencement

05 p0838 A70-16283

Ionospheric effect sudden commencement parameters of magnetic storm related to distance from origin in polar regions

05 p0841 A70-16737

Oscillations intervals with diminishing period during magnetic storms, noting relationship to midlatitude disturbances in F region

05 p0842 A70-16746

Magnetic storm /14 September 1966/ observation by Explorer 33 in geomagnetic tail and by polar stations, studying relation in magnetosphere and on earth

05 p0843 A70-16764

Solar asymmetries associated with sun motion toward apex related to formation of N-S asymmetries of geomagnetic storms

06 p1144 A70-18011

Three dimensional model current system with magnetospheric and ionospheric sections connected by currents flowing along geomagnetic field lines proposed for polar magnetic substorms

06 p1059 A70-18535

Temporal behavior of energetic particle precipitation during auroral substorm, discussing electron energy spectra and pitch angle distributions

06 p1059 A70-18536

Geomagnetic tail natural oscillations, studying magnetospheric substorms role

07 p1268 A70-19499

Ionospheric radio wave /auroral/ absorption during substorm investigated for longitudinal and latitudinal variations by multistation riometer measurements, inferring electron precipitation characteristics

07 p1269 A70-20030

Magnetic storms effect on cosmic ray neutron component diurnal variation, determining amplitudes and phases of harmonics by harmonic analysis

07 p1372 A70-20341

Geomagnetic storms data compilation /1957-1964/, showing solar activity effect on solar corpuscular stream velocity

07 p1373 A70-20436

Magnetic field variation rates characteristics during magnetic storms investigated for longitudinal dependence and influence of equatorial electric current

07 p1276 A70-20437

Gokhberg magnetovariational sounding method for single location analysis of magnetic storms early phases, comparing ground station network observations

07 p1277 A70-20440

Low energy proton distributions in interplanetary medium, correlating intensities with main-phase geomagnetic storm development

08 p1562 A70-21376

Hydromagnetic emissions in high latitudes relationship to storm sudden commencements

08 p1491 A70-21715

Chapman-Vestine and Birkeland-Alfven electric current systems equivalence in ground geomagnetic effect explained for polar magnetic storms

08 p1491 A70-21719

Extraterrestrial ring current proton intensities asymmetric increases in outer radiation belt during magnetic storms

09 p1747 A70-23490

Neutral and ionized atmosphere parameter variations and circulation during magnetic storms observed at various heights

10 p1873 A70-24310

Two phase process for electron precipitation during polar substorm observed from balloon measurements of X rays produced by precipitated electrons in atmosphere

10 p1932 A70-24490

Magnetospheric substorms magnetograms taken at various stations, showing preceding ring storm particles deflection into magnetic tail

10 p1876 A70-24496

Aurorae and magnetic storms theory, considering ion production, motions and interactions

11 p2044 A70-25621

Geomagnetic damped type pulsations associated with storms interpreted as interaction between hydromagnetic oscillations and magnetospheric motions caused by solar wind

11 p2047 A70-26567

Corpuscular radiation intensity measurements in upper atmosphere at midlatitudes by meteorological probe during geomagnetic storm, noting radio wave absorption

11 p2106 A70-26797

Quasi-sinusoidal fluctuations of magnetic field during geomagnetic storms measured by ATS 1 in synchronous equatorial orbit

12 p2223 A70-27192

Adiabatic drawing of quasi-captured charged particles by geomagnetic trap field during phase recovery period of magnetic storm

12 p2295 A70-28258

Delayed ionization effects in midlatitude nighttime ionosphere after geomagnetic storms, noting time lag vertical distribution

12 p2277 A70-28365

Simultaneous magnetic, photometric and backscatter radio measurement of auroral and ionospheric echoes during geomagnetic storm, confirming electrojet theory

13 p2392 A70-28575

Plasmapause and polar wind, considering density discontinuity due to outer magnetosphere heating during magnetic storms

13 p2491 A70-29059

Visual aurora properties attributed to magnetic storm following solar flare, using multiple channel photometer measurements

13 p2478 A70-29231

Auroral electron precipitation and ground based magnetic field pulsations correlation for magnetic storms inception

13 p2401 A70-30053

Magnetotail plasma sheet temporal variations during substorms and plasma pressure as related to dynamic pressure of solar wind from Vela satellites observation

13 p2480 A70-30061

Trapped and polar proton and electron flux observations during 9 June 1968 magnetic storm

13 p2482 A70-30072

Geomagnetic field distant fluctuations during substorm from ATS 1 magnetometer data on abrupt recoveries of H component

13 p2482 A70-30077

Van Allen radiation belts energetic electrons injection and distribution due to magnetic storms, using satellite-borne spectrometers

13 p2483 A70-30090

High energy proton flux variations in inner belt during solar cycle and magnetic storm, using satellite and balloon measurements

13 p2483 A70-30091

Polar storm simultaneous onset and development, using observational data for geomagnetic field and aurorae

14 p2570 A70-30214

Geomagnetic storm intensity nonuniform relationship to 27 day and 11 year cycles

14 p2571 A70-30240

Aurora band theory based on three dimensional current system during magnetic substorms, discussing field aligned sheet current instability

14 p2573 A70-30671

Magnetic storms frequency and levels coincidence with solar activity variations

14 p2575 A70-30818

Nightglow OI lambda 6300 line width measurements during magnetic storm, discussing temperatures and intensity variations

14 p2579 A70-31250

Upper atmospheric short lived disturbances connected with geomagnetic storms characterized by determining equivalent duration (D) value

15 p2723 A70-31651

Polar substorm activity associated with magnetopause position variation, using Imp 2 satellite observations

15 p2728 A70-31911

Terrestrial magnetosphere dynamics in magnetospheric disturbances, analyzing solar wind-geomagnetic field interaction and storm development

15 p2729 A70-32080

Equatorial atmospheric density during geomagnetic storm and quiet days by satellite observation

15 p2811 A70-32284

Magnetosphere survey, including solar wind flow theory, observational techniques, radiation belt theory, magnetic storms, etc

15 p2732 A70-32544

Geomagnetic tail natural oscillations, studying magnetospheric substorms role

15 p2732 A70-32744

Pi 2 pulsation power spectra change with magnetospheric substorm development, relating pulsations and electron precipitation

17 p3080 A70-35641

F2 region disturbance development during magnetic storm, discussing layer height increases

17 p3080 A70-35772

Magnetic storms development via initial asymmetric inflation of evening magnetosphere, using Explorer 26 and ground observatory data

18 p3311 A70-36008

Magnetospheric plasmapause duskside bulge dynamic behavior during substorms, using whistler data

18 p3312 A70-36013

Large amplitude irregular magnetic fluctuations during expansion phase of magnetic substorms, using ATS 1 observations

18 p3312 A70-36025

Auroral protons and resonant concept of substorm, eliminating discrepancy between hydrogen emission spectroscopic and direct measurements

18 p3307 A70-36177

Electron concentration disturbances in outer ionosphere and F 2 maximum on daylight side during magnetic storm

19 p3408 A70-37307

Geomagnetic storms at ATS 1 in 1967, discussing storm-time disturbance field and associated pulsations

19 p3410 A70-37488

Interplanetary plasma observations by Vela satellites in solar wind and plasma sheet of magnetotail during magnetic storm

19 p3410 A70-37490

Polar cap absorption correlation with solar protons flux into magnetosphere, discussing diurnal and spatial variations and magnetic storm effects

19 p3411 A70-37492

Auroral substorm temporal relationship to particle kinetic energy increases within trapping region, observing geomagnetic field distortions at higher latitudes during disturbed epochs

19 p3411 A70-37494

Van Allen electrons acceleration and precipitation during magnetospheric substorms in relation to auroral processes, discussing energy and pitch angle diffusion processes

19 p3411 A70-37495

Polar electrojet and VHF auroral radio wave backscattering correlation, discussing geomagnetic disturbances effect

19 p3376 A70-37498

Traveling horizontal ionospheric waves relationship to magnetic storm onset, showing ionization displacement occurrence

19 p3413 A70-38029

Earth EM field short period pulsations distribution within magnetic storms

19 p3416 A70-38585

Auroral photographic and visual observations, discussing satellite results and substorm development

19 p3417 A70-38730

Cosmic rays cutoff rigidity variations during magnetic storms, investigating flux increase due to current flow along parallel lines on magnetic shell surface

20 p3698 A70-39300

Geomagnetic fluctuations relationship to magnetospheric ring current and plasmapause during magnetic storm

20 p3619 A70-39328

Whistler VLF radio observations of sudden magnetic impulses in plasmasphere during storms, using ground based magnetometers

20 p3620 A70-39330

Seasonally biased electron density enhancements in nighttime response of topside ionosphere to magnetic storms

20 p3621 A70-39342

Soviet book on geomagnetic storms 27-day recurrence as function of intensity and onset characteristics, establishing forecasting indices

20 p3623 A70-39897

Ionospheric electron density response to geomagnetic storms at midlatitudes, noting diurnal variations detected by ATS 3 VHF signals

20 p3623 A70-40479

High latitude F region irregularity structure during magnetic storm from multistation scintillation observations of ATS 3 transmission

20 p3624 A70-40490

Electron precipitation at geomagnetic storm sudden commencement in auroral zone from X ray balloon observations

21 p3814 A70-40937

Midlatitude F region electron and ion temperatures during magnetic storms, examining Thomson scattering, density and time dependence

21 p3817 A70-41094

F region heating by magnetic storms, discussing electron temperature, ring current conduction and red arcs

21 p3817 A70-41095

Magnetotail magnetic field perturbations associated with polar magnetic substorms, using IMP-A and B satellite observations

21 p3882 A70-41720

Substorm aspects of magnetic pulsations, discussing classification, micropulsations, generation and propagation effects

22 p4019 A70-43145

F region electron density measurement during magnetic storm by incoherent scatter technique

22 p4019 A70-43157

Magnetospheric and magnetic storms correlated to solar wind energy penetration, noting roles of energetic plasma and magnetospheric low energy plasma convection

22 p4022 A70-43287

Magnetosphere storm diagnostics from geomagnetic, auroral and airglow parameters, discussing calibration via satellite observations

22 p4022 A70-43289

Solar and geomagnetic events for maximum solar activity year 1968, correlating magnetic storms
22 p4022 A70-43290

Lower ionosphere ionization anomalies, discussing sunrise seasonal change effects in VLF-LF propagation, winter radio wave absorption and geomagnetic storm after-effects
22 p4024 A70-43311

Outer zone electrons radial diffusion coefficients and lifetimes determined as functions of magnetic shell parameter, based on satellite measurement following geomagnetic storm
23 p4236 A70-43831

Threshold rigidity decrease during 23-24 March 1969 magnetic storm, analyzing neutron multiplicity spectrum
23 p4186 A70-43846

Electron precipitation latitude extent and drift rate magnetospheric substorms from ESSA riometer data
23 p4186 A70-43850

Magnetospheric substorms model modification for growth phase inclusion prior to explosive expansion phase
23 p4186 A70-43853

Solar wind electric field relation to ground magnetic disturbances during magnetic storm from Explorer 28 and ground data
23 p4188 A70-44062

Solar flare effects in ionosphere observed at Lindau, collating with heavy geomagnetic storm
23 p4237 A70-44876

Polar storm simultaneous onset and development, using observational data for geomagnetic field and aurorae
24 p4331 A70-46289

Geomagnetic storm intensity nonuniform relationship to 27 day and 11 year cycles
24 p4332 A70-46315

MAGNETIC SURVEYS

Earth satellites magnetic survey contributions to World Magnetic Survey project (WMS/), discussing international reference standards and magnetic mapping
01 p0075 A70-10595

Secular variations distribution on earth surface, plotting isopore charts from mean annual values of magnetic elements /1960-1965/
01 p0083 A70-11540

Earth magnetic field transition recorded in basaltic lavas in southeastern Oregon
07 p1276 A70-20351

Geomagnetic variations dominant polarization direction seasonal dependence based on magnetotelluric field observations, discussing micropulsations and LF cases
11 p2044 A70-25557

Magnetic induction sensors sensitivity for magnetotelluric surveying in geophysics
13 p2415 A70-30048

Energetic particles measurements in geomagnetic tail by Explorer 33/35 for determining gross magnetic topology of distant tail and electric fields
13 p2481 A70-30070

Geomagnetic variations dominant polarization direction seasonal dependence based on magnetotelluric field observations, discussing micropulsations and LF cases
21 p3820 A70-41307

Geomagnetic field behavior prediction based on extrapolation of magnetic data collected by observatories and dipole model approximation
23 p4189 A70-44068

MAGNETIC SUSCEPTIBILITY

U MAGNETIC PERMEABILITY

MAGNETIC SUSPENSION

Liquid metal MHD, discussing conduction/induction MHD devices, measurement gages and devices for suspending liquid metal by magnetic force
04 p0724 A70-14527

Magnetic suspension and guidance of high speed vehicles realized via magnetic field interaction of vehicle-mounted superconducting magnets with eddy currents
08 p1543 A70-20576

Rotating shaft vibrations on assembly designed to balance rotor in magnetic field, eliminating bearings effect on shaft to determine internal friction
08 p1584 A70-20697

Electromagnetically suspended bearing equivalent to elastic vinculum with limit on linear displacement, relating weight, power consumption, maximum force, etc
09 p1690 A70-22421

Electromagnetic single-coil suspension for cryogenic gyroscope with superconducting sphere rotor, calculating suspension force characteristics
12 p2234 A70-27565

Materials and noncontacting design for 50,000 hour lifetime electromechanical components, noting magnetically suspended motor
17 p3100 A70-34754

MAGNETIC SWITCHING

Mn-Bi films Curie point switching with laser, measuring magnetization dependence via magneto-optic effect
[IEEE PAPER 9.3]
05 p0893 A70-16997

MAGNETIC TAPE RECORDERS

U MAGNETIC RECORDING

U TAPE RECORDERS

MAGNETIC TAPES

Linear superposition /LSP/ of isolated pulses in tape recording, discussing validity for multibit waveform synthesis
11 p2057 A70-26627

Flight loads data extraction and analysis from damaged magnetic tapes after aircraft crash
17 p3094 A70-35518

Digital computer magnetic tape recording system for flight tests of Jaguar aircraft, discussing data treatment
19 p3384 A70-38537

Magnetic tape instrumentation system installed aboard Hawker Siddeley Harrier for flight development, discussing digital format recording system
19 p3384 A70-38549

Signal modulation by pulse ratio variation in magnetic tape channel, discussing SNR characteristics
20 p3586 A70-39707

Pulse ratio modulation analysis based on information theory, emphasizing magnetic tape channel capacity optimal utilization in signal transmission
20 p3586 A70-39708

Permalloy tapes uncertainty in magnetization process, discussing Barkhausen discontinuities measurement method
20 p3673 A70-40058

MAGNETIC TRAPS

U PLASMA CONTROL

MAGNETIC VARIATIONS

NT GEOMAGNETIC MICROPULSATIONS

NT GEOMAGNETIC PULSATIONS

NT NOCTURNAL VARIATIONS

Lunar diurnal variation parameters at Irkutsk determined from IGY data concerning geometric field components
01 p0083 A70-11538

Secular variations distribution on earth surface, plotting isopore charts from mean annual values of magnetic elements /1960-1965/
01 p0083 A70-11540

Multipole analysis for earth magnetic field allowing secular variation to be illustrated by time trends in multipole parameters
02 p0288 A70-11742

Cosmic ray flux modulation in earth atmosphere produced by solar wind and geomagnetic variations, considering effects on atmospheric carbon 14 variations
04 p0680 A70-15114

Interplanetary magnetic field fluctuations stimulated by lunar wake, using Explorer 35 satellite measurements
04 p0753 A70-15122

Variational analysis of low latitude magnetic sounding data to determine structural differences between various earth mantle regions, noting additional observations required
04 p0682 A70-15735

Evening time latitudinal distribution of polar magnetic field perturbations compared with nighttime distribution, indicating evening electrojets
04 p0684 A70-15751

Magnetic field fluctuations of interplanetary plasma, considering anisotropic temperature instabilities
05 p0915 A70-16750

Magnetsensitive quartz element with suspended magnet and two mirrors for recording magnetic variations
05 p0851 A70-16770

Human susceptibility to weak fluctuations in geomagnetic field intensity, showing frequency range
05 p0809 A70-16861

Geomagnetic field variations represented by optimal electric current loops or dipoles, noting advantages over spherical polynomials
07 p1266 A70-19442

Radar measurements of magnetic dip in E region compared with surface values and spherical harmonic models for dip angles
07 p1271 A70-20163

Magnetic field variation rates characteristics during magnetic storms investigated for longitudinal dependence and influence of equatorial electric current
07 p1276 A70-20437

Geomagnetic field total vector modulus secular variations from airborne measurements
07 p1278 A70-20461

Vertical gradient of total geomagnetic field using curves based on continuous records of magnetic variations
10 p1876 A70-24589

Geomagnetic variations dominant polarization direction seasonal dependence based on magnetotelluric field observations, discussing micropulsations and LF cases
11 p2044 A70-25557

Semiannual variation of geomagnetic activity related to incident solar wind, considering Mariner 2 measurements
13 p2475 A70-28573

Geomagnetic tail structure and magnetic field fluctuations from IMP 3 satellite measurements, showing enhancement during/after SSC and sudden impulses /SI/
13 p2396 A70-29182

Sunspot electric current density accounting for magnetic field abrupt reversal
13 p2496 A70-29848

Magnetic moment fluctuations of arbitrary solid body by fluctuation-dissipation theorem for thermal equilibrium
13 p2454 A70-30033

Digital recording of geomagnetic field variations, using IBM or international telex code for radio transmission
13 p2415 A70-30043

Stability requirements for precision magnetic field measurements on ground and in space, discussing magnetic balances and fluxgate magnetometers for geomagnetic variations and spacecraft attitude
13 p2415 A70-30050

Horizontal geomagnetic force variations, considering ionospheric wind effects on ions in transition layer
13 p2402 A70-30057

Plasmapause position and density profile from ion concentration measurements byOGO-5, determining reaction to magnetic variations
13 p2482 A70-30074

Geomagnetic field distortion in high beta magnetospheric regions fromOGO observations for quiet and slightly disturbed conditions
13 p2402 A70-30076

Geomagnetic field distant fluctuations during substorm from ATS 1 magnetometer data on abrupt recoveries of H component
13 p2482 A70-30077

Magnetic fluctuations observed by ground observatories, suggesting large amplitude waves as field line resonances driven by magnetopause motion
13 p2402 A70-30078

Interplanetary magnetic field flux relationship to Kp index of magnetic activity
14 p2570 A70-30221

Geomagnetic short period oscillations occurrence frequency during IQSY, discussing dependence on magnetic activity and time of day
14 p2572 A70-30242

Errors magnitude in quartz variometer readings resulting from variations of geomagnetic field perpendicular component
14 p2582 A70-30244

Variational analysis of low latitude magnetic sounding data to determine structural differences between various earth mantle regions, noting additional observations required
14 p2575 A70-30819

Evening time latitudinal distribution of polar magnetic field perturbations compared with nighttime distribution, indicating evening electrojets
14 p2576 A70-30835

M31 continuum radio emission produced by magnetic field aligned along arms, discussing field turbulence effects
14 p2642 A70-30891

Magnetic activity intensity comparison in Northern and Southern hemispheres, noting correlation with solstices and equinoxes
14 p2580 A70-31260

Polar ionospheric electron/ion density measurements by ESRO 1 satellite, observing dependence on Kp index
15 p2724 A70-31669

Geomagnetic conjugacy variations observed via riometry in Northern and Southern Hemispheres
16 p2897 A70-33792

Magnetic perturbation effects on magnetosheath plasma, considering Boltzmann transport equation, plasma-electromagnetic interactions, heating, cooling, etc
17 p3142 A70-35592

Large amplitude irregular magnetic fluctuations during expansion phase of magnetic substorms, using ATS 1 observations
18 p3312 A70-36025

Geomagnetic latitudinal variations in Sq/H/ and Sq/Z/ in equatorial region, using electric simulation
18 p3246 A70-36099

Geomagnetic field variations represented by optimal electric current loops or dipoles, noting advantages over spherical polynomials
18 p3249 A70-36916

Geomagnetic activity relation to large scale variations in interplanetary magnetic field and solar wind deformation velocity, using satellite and space probe observations
19 p3491 A70-37304

Geomagnetic field variations recording by two variometers, correcting for variation components effects by instruments orientation
19 p3420 A70-37335

Quartz magnetic variometer allowing simultaneous recording of magnetic field variations and suspension axis inclination changes
19 p3420 A70-37336

- Magnetic field variations and structures in interplanetary space relationship to sun, discussing photospheric field lines random walk transport
19 p3494 A70-37480
- Magnetic and electric field changes across earth bow shock and magnetosheath, discussing Pioneer 8 and OGO-5 data
19 p3494 A70-37483
- Semiannual oscillation and fine structure of earth magnetic field horizontal intensity during March and September
19 p3413 A70-38004
- H sub 500 field features during natural synoptic seasons in Northern Hemisphere, including circulation characteristics
20 p3663 A70-39271
- Geomagnetic variations dominant polarization direction seasonal dependence based on magnetotelluric field observations, discussing micropulsations and LF cases
21 p3820 A70-41307
- Spherical harmonic analysis of declination and secular geomagnetic variation
21 p3820 A70-41884
- Magnetoplasma density modulation from LF and amplitude magnetic perturbations, using collisionless Boltzmann transport equation
22 p4082 A70-43255
- Geomagnetic daily variations analysis in terms of universal time components, considering solar wind-magnetosphere interactions, auroral zone effects, etc.
22 p4021 A70-43278
- Interplanetary magnetic field directional variation effect on polar caps geomagnetic field, discussing polarity reversals
22 p4022 A70-43285
- Geomagnetic variations origin from satellite space probe data, correlating DP 1 activities to interplanetary magnetic field variations
22 p4022 A70-43286
- Electromagnetic variational soundings of ocean floor earth crust upper mantle near magnetic equator
23 p4189 A70-44066
- High latitude geomagnetic secular variations determination by running 12-month means method, recommending data acquisition free of external sources effect
23 p4190 A70-44087
- Auroral electrojet return current spatial extent from model ionospheric current distribution and geomagnetic variations
23 p4192 A70-44922
- Geomagnetic activity dependence on angle between earth-sun and hourly averaged vectors of interplanetary magnetic field
24 p4405 A70-45523
- Interplanetary magnetic field flux relationship to Kp index of magnetic activity
24 p4331 A70-46296
- Geomagnetic short period oscillations occurrence frequency during IQSY, discussing dependence on magnetic activity and time of day
24 p4332 A70-46317
- Errors magnitude in quartz variometer readings resulting from variations of geomagnetic field perpendicular component
24 p4339 A70-46319
- MAGNETICALLY TRAPPED PARTICLES**
NT ARTIFICIAL RADIATION BELTS
NT INNER RADIATION BELT
NT OUTER RADIATION BELT
NT PROTON BELTS
NT RADIATION BELTS
- Energy spectrum time dependence of solar cosmic ray event of 28 January 1967 measured in Northern Hemisphere, discussing particle diffusion and magnetic trap
05 p0902 A70-16459
- Corpuscular radiation distribution function with trapped particles maximum density fixed in equatorial plane and reflection points vicinity of magnetic force line
06 p1135 A70-17894
- Transverse particle and energy fluxes in toroidal magnetic traps magnetic fields with ionized plasmas, discussing particle diffusion coefficient and thermal conductivity
08 p1554 A70-21807
- Proton injection into radiation belt, comparing solar neutron decay (SND) and cosmic ray albedo neutron decay (CRAND) as proton sources
09 p1746 A70-23489
- Gyrosynchrotron emission from nonthermal electrons trapped in magnetic dipole field to interpret center-to-limb spectrum and polarization variations of microwave impulsive bursts
12 p2294 A70-27709
- Adiabatic drawing of quasi-captured charged particles by geomagnetic trap field during phase recovery period of magnetic storm
12 p2295 A70-28258
- Energy spectrum and equatorial pitch angle distribution of charged particles trapped in magnetosphere resulting from inward diffusion due to third adiabatic invariant violation
13 p2476 A70-28942
- Satellite observation of alpha particles trapped geomagnetically in radiation belts, including Injun 5 results
13 p2484 A70-30092
- Book on geomagnetic micropulsations covering dynamic processes of magnetically trapped particles and micropulsations usability in remote sensing of magnetosphere
14 p2581 A70-31325
- Plasma containment in adiabatic magnetic traps, discussing particles, Coulomb collisions, instabilities, cyclotron resonance masers, Van Allen belts, etc.
16 p2958 A70-33232
- LF oscillations of bounded low pressure plasma under magnetic field in discharge chamber, determining spatial distribution by Langmuir sliding probes
16 p2958 A70-33254
- Auroral substorm temporal relationship to particle kinetic energy increases within trapping region, observing geomagnetic field distortions at higher latitudes during disturbed epochs
19 p3411 A70-37494
- LF oscillations of bounded low pressure plasma under magnetic field in discharge chamber, determining spatial distribution by Langmuir sliding probes
23 p4226 A70-44283
- MAGNETITE**
Metal-semiconductor transition in magnetite described on band model with electrons breaking symmetry by ordering in self induced Coulomb potential
12 p2283 A70-27239
- Stable colloidal dispersions of subdomain magnetite particles correlated for magnetic properties in terms of size distribution and volumetric concentration by superparamagnetic theory
12 p2284 A70-27241
- Lamellae stresses and magnetostrictive effects on magnetic properties of titanomagnetite and ilmenohematite series minerals
15 p2728 A70-31993
- Magnetite and ferrite spinels Hall effect, magnetoresistance and electrical conductivity over wide temperature range
19 p3485 A70-37627
- MAGNETIZATION**
Surface interactions in incompressible dynamics and stability of ferrofluid with nonlinear magnetization properties
04 p0665 A70-14451
- Generalized Watson sums evaluation without series expansions or extensive computer summations, calculating magnetization of anisotropic Heisenberg ferromagnet for cubic, bcc and fcc lattices
04 p0730 A70-14689
- Normal and bottle-green microtektite glass measured for magnetic susceptibility, magnetization and Curie constants
05 p0916 A70-16839
- Mn-Bi films Curie point switching with laser, measuring magnetization dependence via magneto-optic effect
05 p0893 A70-16997
- Forward angle microwave scattering by plasma covered magnetized metallic sphere, calculating radial electron density distribution
06 p1008 A70-17576
- Magnon energy theory for temperature dependence of ferrous and magnesium fluorides antiferromagnetic resonance frequency, sublattice magnetization and magnetic specific heat
09 p1739 A70-22324
- Gravity and vertical magnetic anomalies interpretation to infer magnetization direction
09 p1729 A70-23601
- Nonlinear spin wave theory for anisotropic antiferromagnetism, solving sublattice magnetization by thermodynamic Green function for temperature dependence
11 p2097 A70-25617
- Narrow Curie point switching transfer in Mn-Bi films by controlling magnetization direction within preselected areas
11 p2098 A70-26069
- Ni-Fe thin films flux reversal with transverse bias field from dynamic magnetization configuration photographs
12 p2284 A70-27242
- Ferrites as harmonic generators, discussing physical reasons for generation of double frequency magnetization
14 p2549 A70-30439
- Uniform bulk magnetization concept in superparamagnets related to physical statistics of magnetic first order phase transitions
15 p2785 A70-32400
- Microwave properties of uniformly magnetized slabs filling cross section of rectangular lossless waveguide operating in specific modes
17 p3050 A70-34584
- Magnetization oscillation in single crystal yttrium-iron garnet under fluctuating SHF magnetic field
19 p3484 A70-37625
- Micromagnetic theory of ferromagnets based on vector magnetization as continuous function of position, discussing free energy
19 p3471 A70-37953
- Permalloy tapes uncertainty in magnetization process, discussing Barkhausen discontinuities measurement method
20 p3673 A70-40058
- Lunar rocks magnetic properties and natural remanent magnetization, examining pyroxene paramagnetism, ferrosilite and ilmenite antiferromagnetism and native iron ferromagnetism
21 p3917 A70-41671
- MAGNETO-OPTICS**
Faraday modulator for polarized laser radiation, eliminating analyzer by oblique magneto-optical active element, converting angular modulation into amplitude modulation
05 p0858 A70-16251
- Mn-Bi films Curie point switching with laser, measuring magnetization dependence via magneto-optic effect
05 p0893 A70-16997
- Free current carriers activity in indirect magneto-optical junctions in quantized magnetic field
06 p1126 A70-17817
- Magnetic display devices covering magneto-optical displays, magnetic-electrostatic technique combinations and ferromagnetography
08 p1499 A70-21685
- Coulomb interaction during optical transitions between Landau subbands of Ge semiconductor valence and conduction bands in magnetic field, observing diamagnetic excitons
10 p1928 A70-25029
- Magneto-optical birefringence anisotropy and light propagation in terbium ferrite garnet in presence of Faraday and Cotton-Mouton effects
11 p2097 A70-25377
- Quenched MnBi thin films measured for magnetic, magneto-optical and optical properties, noting Faraday rotation
12 p2284 A70-27246
- Magneto-optics of semiconductors, taking into account intraband and interband effects with Faraday and Voigt field configurations
18 p3297 A70-35951
- Magneto-optic rotation and hysteresis recording instrument for thin magnetic films as function of temperature and wavelength, using Faraday effect
21 p3826 A70-41452
- MAGNETOACOUSTIC WAVES**
Plasma stability in uniform magnetic and HF electric fields, observing magnetoacoustic wave generation at electron cyclotron frequency greater than HF field frequency
03 p0532 A70-13523
- Thermal radiation effects on plane magnetoacoustic waves in semiinfinite expanse of radiating gas of perfect electrical conductivity
05 p0890 A70-16822
- Fast magnetoacoustic wave propagation in cylindrical plasma column with constant current density, using geometric optics
10 p1923 A70-24229
- Alfven and cylindrical magnetoacoustic waves in homogeneous unbounded conducting plasma in nonhomogeneous magnetic field, applying Weinberg method to propagation analysis
11 p2089 A70-25850
- Frequency spectrum determination of hydrodynamic instability excited in fast large amplitude magnetosonic wave
12 p2278 A70-27542
- Hall MHD generator with supersonic flow instability to magnetoacoustic waves propagating antiparallel to steady electric current in dense weakly ionized gas
12 p2281 A70-27805
- Magnetic field effect on frequency spectrum of vertically propagating magnetoacoustic waves and reflection conditions in inhomogeneous isothermal atmosphere
12 p2227 A70-28226
- Elastohydrodynamic monochromatic wave coupling in liquid filled container as model for Alfven and magnetoacoustic waves transmission in plasma
14 p2625 A70-31356
- Plasma waves with anisotropic pressure, discussing magnetoacoustic waves integral curves
15 p2777 A70-31476
- VHF radiation from plasma during electron beam interaction with fast magnetoacoustic wave stimulated by external spatially periodic currents
15 p2780 A70-32118
- Alfven magnetoacoustic waves interaction, deriving kinetic equation for distribution function and relaxation time
20 p3678 A70-39597
- Umbral flash as magnetoacoustic wave, examining Ca II K line variations formation during adiabatic compression
21 p3885 A70-40958
- Earth magnetosphere LF wave annular trap, examining high energy particle interaction with magnetosonic waves
22 p4013 A70-42300

Magnetoacoustic waves in MHD channels, investigating excitation, damping and effects on mean current density and Hall field strength 22 p4081 A70-42822

Helicon /magnetoacoustic waves/ effect on plasma instabilities, examining HF field amplitudes and magnetic fields 22 p4084 A70-43475

MAGNETOACOUSTICS

Ion-acoustic instability effect on HF EM field penetration into plasma taking into account nonlinear Ohm law 11 p2089 A70-25715

MAGNETOACTIVITY

NT MAGNETORESISTIVITY

Fourier and perturbation methods applied to radiation from uniformly moving charge in inhomogeneous magnetoactive medium, deriving expressions for radiation spectrum and energy losses 03 p0531 A70-13285

Electromagnetic finite amplitude wave beams self action in magnetoactive plasma, noting nonlinear characteristics 03 p0448 A70-13411

Thermal radiative transfer in nonuniform anisotropic magnetoactive plasma, correcting term of Zheleznyakov equation 09 p1734 A70-22514

Hydrodynamic equations to obtain transformation coefficient for HF weakly damped waves in magnetoactive plasma, applying to solar corona 13 p2463 A70-29227

Magnetomotive tools and power systems for maintenance, repair and assembly in space weightless environment 19 p3436 A70-37949

Permittivity tensor of weakly turbulent magnetoactive cold electron plasma, calculating nonlinear currents 20 p3677 A70-39296

MAGNETOELASTIC VIBRATIONS

U MAGNETOELASTIC WAVES

MAGNETOELASTIC WAVES

NT MAGNETOACOUSTIC WAVES

Magnetoelastic surface wave propagation properties in ferrites at UHF wavelengths, using numerical calculations for gallium-YIG 03 p0540 A70-13700

Solid state microwave acoustic variable delay devices for radar, fuses, repeaters, altimeters, etc, emphasizing magnetoelastic wave method 06 p1018 A70-17356

Microwave variable delay devices, discussing solid state microwave acoustic interactions 06 p1019 A70-17483

Magnetoelastic ferromagnet linear theory, considering spin-electric microwaves propagation in ferrimagnetic crystal subjected to pulsed magnetic fields 19 p3487 A70-37947

MAGNETOELASTICITY

U MAGNETOSTRICTION

MAGNETOELECTRIC MEDIA

Rectangular coaxial waveguide with internal conductor contained between inhomogeneous magneto-dielectric bars, deriving computer algorithm for natural mode fields 09 p1638 A70-23645

Magnetolectric electromotive force in media of ions and neutral molecules, using Boltzmann transport equation 21 p3855 A70-40909

MAGNETOGASDYNAMICS

U MAGNETOHYDRODYNAMICS

MAGNETOGRAMS

U MAGNETIC SIGNATURES

MAGNETOGRAPHS

U MAGNETOMETERS

U RECORDING INSTRUMENTS

MAGNETOHYDRODYNAMIC ACCELERATION

U PLASMA ACCELERATION

MAGNETOHYDRODYNAMIC FLOW

Entrainment of electrically conducting liquid by moving wall in long duct with rectangular cross section and magnetic induction field 01 p0151 A70-10656

Three dimensional instability of perturbed conducting fluid laminar boundary layer flow on concave walls in transverse magnetic field, analyzing various Hartmann numbers 01 p0152 A70-10934

Power output, Joule dissociation and generator efficiency determined for rectangular MHD channel, considering transverse and longitudinal edge effects 01 p0152 A70-10992

MHD boundary layers in transverse magnetic field with low Reynolds number, investigating suppression of separation with emphasis on behavior near rear stagnation point 01 p0152 A70-11095

MHD entrance region compressible flow characteristics, determining velocity pressure and temperature distributions, friction and heat transfer coefficients, etc 01 p0067 A70-11136

Incompressible viscous fluid flow in contact with infinite plate and rotating in perpendicular magnetic field, obtaining flow characteristics by Laplace transform 01 p0067 A70-11138

Interplanetary plasma flow simulation around earth magnetosphere and planets not considering initial conditions influence 01 p0172 A70-11488

Dipole magnetosphere model with cylindrical or spherical forbidden band for studying plasma motion in quasi-hydrodynamic approximation 01 p0082 A70-11521

Planetary atmospheres dynamics, discussing rotational and MHD effects, energy sources, etc 02 p0366 A70-11806

Mesothermal flow of collisionless plasma around conducting cylinder, calculating densities, velocities, temperatures and electrical potential [ONERA-TP-769] 02 p0346 A70-12102

Inertia effects on pressure distribution, load capacity and frictional torque in MHD hydrostatic thrust bearing lubrication flow 02 p0307 A70-12162

Steady axially symmetric MHD flow of inviscid incompressible fluid of small conductivity in strong magnetic field past fixed axisymmetric bodies 02 p0347 A70-12234

Cylindrical axial plasma flow fields velocity radial dependence measurement by double-wedge spectroscopy using Abel unfolding of Doppler shifts 02 p0349 A70-12657

Plasma velocity, electron temperature and density and ion density determined by two mutually perpendicular probes 03 p0529 A70-12940

Standing bow shock in plasma flow into dipole magnetic field, measuring particle density, electron temperature, magnetic field flux and oscillations 03 p0530 A70-13158

Nuclear fusion reactions by focused Q switched Nd doped laser beam on deuterium target, discussing neutrons from flowing plasma, electron temperature and counter experiments 03 p0501 A70-13684

Graphite sphere mass erosion in low temperature hypersonic air plasma shock flow, determining breakdown temperature and mass entrainment rates 03 p0517 A70-13741

MGD finite flow regions surrounded by nonconducting gas, considering wave behavior at boundary of conducting region and magnetic field influence 03 p0533 A70-13803

Carrying capacity and moment of friction calculated for cylindrical MHD bearing for small magnitude of radial clearance 03 p0497 A70-13877

Equilibrium model of laminar arc constrictor plasma generator, correlating heat transfer, wall shear stress, friction factor and development length 03 p0533 A70-13952

MHD laminar flow between parallel porous disks for large suction Reynolds number, solving equations of motion with singular perturbation technique 03 p0469 A70-14181

MHD boundary layer separation near rear stagnation point with magnetic field normal to wall solved by series expansion, calculating skin friction by numerical quadratures 03 p0469 A70-14182

Hall current effect on steady boundary layer flow of incompressible viscous electrically conducting fluid past semiinfinite flat plate in transverse magnetic field 03 p0469 A70-14183

Martin method for reducing determination of steady plane MHD flow to Bernoulli and direct functions satisfying quasi-linear partial differential equations 03 p0533 A70-14200

Unsteady MHD flow of viscous incompressible electrically conducting fluid through rectangular duct under transverse magnetic field 03 p0471 A70-14333

Heat transfer in steady state flow of electrically conducting incompressible viscous fluid in annular channel between coaxial circular cylinders under magnetic field 03 p0608 A70-14335

Faraday type open circuit MPD generator model obtained with allowance for temperature and pressure losses and gas transport properties dependence on static parameters 04 p0725 A70-14530

MHD flow velocity and current density distributions in annular duct with radial magnetic field 04 p0725 A70-14531

Electron temperature and particle density measurements in annular MHD duct, demonstrating Hall effect existence 04 p0725 A70-14532

Striated plasma flow in MHD duct of conducting rings using Ar with K vapor detected by high speed camera 04 p0725 A70-14533

Plasma unsteady one dimensional flow behind shock wave front in shock tube MGD channel, deriving differential gas dynamics equations 04 p0726 A70-14540

Conducting fluid laminar flow between parallel planes in traveling magnetic field, integrating Maxwell and Navier-Stokes equations 04 p0726 A70-14542

Transverse magnetic fields effects on velocity perturbations and vortices behind circular cylinder in electrolyte flow at various Reynolds and Stewart numbers 04 p0726 A70-14543

Conducting fluid as MHD lubricant for cylindrical bearings, deriving equations for ideally conducting shaft and bearing and arbitrary Reynolds numbers 04 p0697 A70-14544

Incompressible electrically conducting fluid flow along rectangular duct under transverse magnetic field, noting equivalency of Hunt solutions and thin wall restriction 04 p0726 A70-14614

MHD Stokes flow for magnetized bodies of revolution, rotating with steady motion in viscous conducting fluid at rest at infinity 04 p0726 A70-14615

Finite difference theory applied to numerical analysis of laminar equilibrium MHD flow in circular tube [ASME PAPER 69-WA/HT-55] 04 p0727 A70-14794

Heat transfer in partially ionized argon plasma flowing in water cooled circular tube as function of temperature, Reynolds number and tube entrance diameters [ASME PAPER 69-WA/HT-54] 04 p0780 A70-14795

Heat transfer rates to stagnation point of hemisphere in supersonic high enthalpy low density nitrogen plasma flow [ASME PAPER 69-WA/HT-49] 04 p0614 A70-14799

Inertia effects due to circumferential and radial velocity in MHD hydrostatic thrust bearing in axial magnetic field [ASME PAPER 69-LUB-F] 04 p0698 A70-14871

Aligned electric current effect on drag of sphere with arbitrary conductivity moving in current carrying fluid 04 p0671 A70-14993

Static pressure distributions and velocity profiles for Hg flow through circular pipes in transverse magnetic field, studying laminar and turbulent flows 04 p0728 A70-15001

Hydromagnetic flow of viscous incompressible electrically conducting fluid near accelerated infinite porous flat plate with variable suction or injection 04 p0672 A70-15095

Steady, ambipolar, low and high speed plasma transport equations developed for terrestrial ionosphere, discussing boundary conditions for supersonic and subsonic flows 04 p0679 A70-15112

Rarefied ionospheric plasma flow around rockets and satellites, studying electric field effect on ion motion by kinetic equation and similarity law 04 p0680 A70-15188

Mixture Mach number defined for collisionless plasma flow about solid body by extending cold-ion theory [AIAA PAPER 69-78] 04 p0729 A70-15582

Suction influence on skin friction fluctuations of MHD flow along infinite flat wall using Navier-Stokes equations 05 p0886 A70-15787

Heat transfer in MHD Couette flow influenced by wall electrical conductances with suction 05 p0886 A70-15823

Steady MHD shear layer velocity profiles using hot film anemometry 05 p0887 A70-15924

Entrance length and pressure drop in MHD parallel plate channel flow using one parameter Pohlhausen method 05 p0887 A70-15978

Spin-up of electrically conducting fluid between infinite flat plates under axial magnetic field, considering Ekman-Hartmann boundary layer on single plate 05 p0832 A70-16017

Mercury plasma flow rate change effect on electron temperature and density in thermoelectric converter determined by spectroscopy 05 p0887 A70-16028

Incompressible boundary layer flow of conducting fluid on solid two dimensional and axisymmetric bodies under transverse magnetic field approximated by momentum method 06 p1031 A70-17199

Multiple electrode probe characteristics in rarefied plasma flow created by ion source, noting electrode potential role 06 p1064 A70-17886

Velocity, magnetic field and drag equations for steady incompressible viscous conducting fluid flow around spherical hollow shell 06 p1122 A70-17917

Single and double cylindrical Langmuir probe responses in highly expanded low density flowing Ar plasma [ALAA PAPER 70-85] 06 p1066 A70-18207

Interplanetary plasma flow past earth and planets simulation using kinetic equations 06 p1147 A70-18292

Collisionless ions trajectories in plasma flowing about cylindrical probe calculated to determine probe ion current, ion density distribution in field and potential distribution 06 p1122 A70-18294

Numerical analysis of rarefied plasma flow interaction with charged conducting bodies of various forms and dimensions 06 p1123 A70-18298

Current collected by cylindrical Langmuir probe immersed in rarefied collisionless plasma streaming with high velocity 06 p1124 A70-18307

Earth magnetosphere physics, considering solar plasma flow, ring currents, charged particles during magnetic storms, solar wind energy transfer, etc 06 p1060 A70-18552

Steady spherical plasma flow from sun analyzed by equations of solar corona hydrodynamic model 07 p1378 A70-19033

MHD free convection of electrically conducting fluid in strong cross field using perturbation technique, considering liquid metals and ionized gases 07 p1348 A70-19208

High electrical conductivity effects on alignment between magnetic field and flow velocity vector in two dimensional plasma flow 07 p1349 A70-19568

Molybdenum single crystals orientation effect on thermal resistance to argon plasma flow 07 p1309 A70-19614

Monograph on research by Japanese Institute of Plasma Physics covering theta pinch, plasma heating, flow, diagnostics, etc 07 p1350 A70-19843

Freezing-mixing model for predicting plasma jet flow reactor yield development from analyses of thermochemical equilibrium, chemical reaction freezing and turbulent mixing 07 p1351 A70-19893

Electrical conductivity variations effects in subsonic Hartmann plasma flow under transverse magnetic field in channel with cooled walls 07 p1352 A70-19986

Unsteady MHD flow at forward stagnation point analyzed for magnetic field effect on transient phenomena, using difference-differential numerical method 07 p1354 A70-20235

Incompressible conducting fluid MHD flow at infinite plane wall forward stagnation point, considering suction or injection effects 07 p1354 A70-20237

Plasma flow structure near frontal point in earth magnetosphere, using quasi-hydrodynamic two dimensional model to obtain power series solution 07 p1391 A70-20419

Proton concentrations, magnetic field strength and temperatures distribution in interplanetary plasma flows as function of latitudinal distance from center of active region 07 p1391 A70-20420

Steady pressure driven flow of conducting fluid through insulating circular pipe in transverse magnetic field 08 p1549 A70-20502

Electron density calculation for collisionless plasma flow around conducting cylindrical body, accounting for surface absorption and mean electron velocity [ONERA-TP-792] 08 p1550 A70-20595

Rarefied plasma flow past bodies, considering determination of aerodynamic coefficients, charged states, electric and magnetic fields and plasma parameters 08 p1432 A70-21087

MHD flow in rectangular duct with arbitrary conductivity via modified Fourier method, obtaining magnetic induction and current for various Hartmann numbers [ASME PAPER 69-WA/APM-17] 08 p1551 A70-21308

Thermal sheaths effect on cooled probes for stationary and flowing plasmas measurements at high pressure 08 p1497 A70-21528

Single fluid theory for plasma laminar flow in field-free region of circular tube, obtaining friction factor and Nusselt number correlations 08 p1552 A70-21585

Magnetic field and conducting walls effect on laminar steady MHD Couette flow of electrically conducting incompressible viscous rarefied gas in slip regime 08 p1553 A70-21764

Heat transfer in MHD channel flow of viscous incompressible rarefied gas with slip flow and temperature jump boundary conditions 08 p1554 A70-21769

Tensor conductivity, magnetic field and electric field effect on heat transfer in MHD channel flow, solving for temperature and Nusselt number 08 p1554 A70-21773

MHD flow between two parallel plates, noting pressure gradient and skin friction coefficient 08 p1554 A70-21774

Turbulent MHD channel flow velocity profiles and hydraulic resistance relations for various Reynolds numbers, using two layer model 09 p1658 A70-22175

Two dimensional radial flow of inviscid infinitely conducting compressible fluid under influence of magnetic field 09 p1735 A70-22757

Thermal properties associated with temperature gradients in He-K plasma, studying mass motions initiated by cold wall contact 09 p1735 A70-22844

Hall effect on MGD flow past axisymmetric body by studying incompressible inviscid flow past body of revolution at zero incidence 09 p1661 A70-23074

Magnetic field effect on free convection in laminar boundary layer formed by laminar flow of viscous conducting fluid along vertical wall 09 p1737 A70-23308

Argon plasma interaction with RF electromagnetic field using MGD model, noting plasma-field coupling and plasma temperature exhibition of skin effect 09 p1737 A70-23433

Boundary layer of MGD flow past axisymmetric insulator body analyzed to determine torque due to Hall effect 09 p1663 A70-23579

Sandwich plates stability in conducting compressible fluid flow under magnetic field 09 p1785 A70-23621

Asymptotic behavior in cold plasma model of magnetopause, describing boundary layer between plasma stream and vacuum magnetic field 10 p1921 A70-23835

Unsteady MHD flow in circular pipe with nonconductive walls under transverse magnetic field 10 p1921 A70-23959

Two dimensional MHD flow past solid body at large Reynolds numbers, treating boundary layer transition 10 p1922 A70-24011

Unsteady MHD flows of viscous, incompressible and electrically conducting fluid, proving boundary value problem solutions existence and uniqueness 10 p1922 A70-24095

Asymptotic method for aeromagnetic flutter of plane MGD nozzle, discussing conditions of MGD nozzle stability 10 p1800 A70-24129

Alfven flow of dissipative conducting incompressible fluids in presence of thin airfoil in magnetic field, considering flow turbulence calculation 10 p1922 A70-24143

MGD model of plasma with dissipation due to finite electrical conductivity described by differential equations 10 p1922 A70-24144

MHD boundary layer flow equations solution by initial value method to eliminate iteration process 10 p1924 A70-24563

MHD boundary layer on rotating body in viscous incompressible conducting fluid, studying magnetic field effects on time-to-separation 10 p1924 A70-24572

MHD exact solutions class, observing conducting flow intensification by magnetic field application 10 p1924 A70-24573

Navier-Stokes-Maxwell equations solutions for conducting fluid flow in azimuthal magnetic field, noting jet acceleration near symmetry axis 10 p1924 A70-24574

Rotating plasma in nonuniform magnetic field analyzed for interchange instability based on MHD fluid and charged particle treatments 10 p1924 A70-24800

Book on engineering aspects of MHD power generation, discussing working gas ionization and electrical conductivity, incompressible conducting fluid motion in magnetic field, etc 11 p1982 A70-25525

Inviscid incompressible conducting fluid flow past body in aligned magnetic field at low magnetic Reynolds number, discussing small perturbations evolution 11 p2041 A70-26623

Turbulent flowing plasma, analyzing wavenumber frequency dependent spectral function and space-time correlation function 11 p2096 A70-26768

Plasmopause form in equatorial plane in presence of magnetospheric tail subsonic potential convective flow 11 p2047 A70-26796

Velocity fluctuations measurements in conducting fluids flowing through tubes 12 p2230 A70-27091

Two dimensional viscous incompressible conducting fluid flow between parallel porous walls in magnetic field, studying skin friction fluctuations 12 p2209 A70-27157

Electromagnetic effects on separation of turbulent MHD boundary layers allowing for heat transfer 12 p2278 A70-27324

Lunar limb shock wave observed by Explorer 35 satellite defined with respect to solar wind flow direction, discussing formation mechanism 12 p302 A70-27594

Flow stability of electrically conducting inviscid fluid in coaxial cylindrical annular space under influence of axial magnetic field 12 p2210 A70-27799

Turbulence energy balance equations for conducting fluid flow in longitudinal magnetic field with Joule dissipation 12 p2282 A70-28227

Current density distributions in Ar-K plasma streams through channel with segmented electrode array, measuring electron temperatures 13 p2461 A70-28732

MHD boundary layer flow past yawed flat plate in presence of pressure gradient, determining skin friction expansion terms 13 p2461 A70-28804

Electric field in rectangular MHD channel with ideally conducting electrodes in uniform magnetic field, considering conditions for maximum channel effectiveness 13 p2461 A70-28966

Laminar MHD boundary layer equations at nonconducting surface, determining flow core parameters influence on boundary characteristics 13 p2462 A70-28967

Plane electromagnetic wave interaction with compressible plasma fluid moving with uniform velocity in vacuum, calculating reflection and transmission coefficients 13 p2462 A70-29101

Collisionless electrostatic shock generation conditions, simulating homogeneous counterstreaming plasmas by computer 13 p2462 A70-29110

Magnetopause model, discussing equilibrium layer between magnetic field and cold plasma field-free stream 13 p2396 A70-29181

Wind tunnel interference for inviscid compressible conducting fluid on slender body of revolution, discussing disturbance potential 13 p2464 A70-29449

Linearized steady plane axisymmetric flows of inviscid finitely conducting incompressible fluid past insulator under magnetic induction with zero components 13 p2464 A70-29541

Incompressible, viscous and electrically conducting fluid flow due to rotating disk in uniform magnetic field, discussing hydromagnetic interaction effect on velocity and friction 13 p2465 A70-29544

MHD pressure head variations in Hg flow in square channel with conducting and insulating walls under transverse magnetic field 13 p2465 A70-29838

Steady laminar heat transfer in open circuit aligned field MHD flow past flat plate, using parametric differentiation 14 p2664 A70-30272

Solar wind interaction with earth, moon, planets and comets, using hypersonic fluid analog involving shock wave interactions 14 p2631 A70-30360

Nonsteady coupled MHD Couette flow, presenting solution by Fourier series expansion method 14 p2621 A70-30549

Magnetoaerodynamic boundary layer of incompressible conducting fluid over right circular cylinder under magnetic field, showing flow separation 14 p2621 A70-30550

Streaming thermal plasma chemistry, reviewing diagnostic techniques and product oriented research 14 p2545 A70-30905

Velocity difference across viscous tail in MHD flow, demonstrating exponential decay 14 p2623 A70-30992

Nonstationary MHD Couette flow of viscous incompressible fluid between two parallel walls caused by instantaneous fluctuations of applied transverse magnetic field 15 p2777 A70-31479

Conducting incompressible fluid flow past sphere, examining effect on magnetic field for small magnetic Reynolds number 15 p2778 A70-31913

Uniform electric and magnetic fields effects on flow of conducting compressible fluid in channel, using multiple scales method 15 p2779 A70-31914

Conducting incompressible fluid laminar flow between rotating disks in transverse magnetic field with source at center 15 p2779 A70-31915

Hydromagnetic viscous flow of incompressible conducting fluid due to electric current radial divergence from point source

15 p2780 A70-32426

Baecklund transformations applications to hodograph equations for steady two dimensional nondissipative MGD flows with aligned velocity and magnetic fields

15 p2781 A70-32453

MHD experiments showing effects of local water supply electrical conductivity from measurements of voltage distribution, pressure gradients and extracted power

16 p2957 A70-32998

Unsteady hydromagnetic flow of viscous electrically conducting incompressible fluid due to rotating disk under perpendicular magnetic field

16 p2958 A70-33297

Baecklund type matrix transformations application to hodograph equations system for aligned nondissipative MGD flows

16 p2958 A70-33747

Supersonic plasma flows charge density levels and spatial and temporal variation, discussing theory and use of electrostatic probes

16 p2912 A70-33862

MHD flow velocity and magnetic flux profiles in rectangular ducts for secondary boundary layer

16 p2959 A70-34239

Transverse magnetic field effects on Ar cross flow arc temperature distribution, cross section shape and profile, discussing forced convection effects [AIAA PAPER 70-777]

17 p1338 A70-34477

Reflected shock waves generation by shock produced plasma flow interaction with strong magnetic fields, determining electron density and ionization relaxation times [AIAA PAPER 70-761]

17 p1339 A70-34490

Hypersonic flow of shock heated plasma past axisymmetric blunt body and onboard magnetic source, using numerical method

17 p3008 A70-34491

Steady two dimensional MHD boundary layer flow with uniform suction or injection past semiinfinite flat plate in cross fields

17 p3067 A70-34618

Magnetic fields effect on probe measurements in weakly ionized Ar plasma flow at atmospheric pressure

17 p1339 A70-34693

Magnetic field lines reconnection in steady incompressible hydromagnetic two dimensional flow, formulating governing equations with cylindrical polar coordinates

17 p1340 A70-34926

Current sheet structure of hydromagnetic boundary layer formed by mixing two conducting fluid streams containing oppositely directed magnetic fields

17 p1340 A70-34930

Collisionless plasma theory modification to include effects of finite Larmor radius of ion and electron on perturbation flow mixing

17 p1341 A70-34935

Continuum plasma dynamics with electromagnetic forces of same order of magnitude as gas dynamic forces, discussing various flow problems

17 p1341 A70-35040

Turbulent gas flows shear turbulence structure at various Reynolds numbers in nonconducting channels with and without heat transfer under transverse magnetic field

17 p1341 A70-35245

Supersonic electrically conducting gas flow in flat channel with dielectric walls in inhomogeneous magnetic field

17 p1341 A70-35334

Nonlinear electrostatic vibrations in colliding antiparallel flows of rarefied plasma

17 p1341 A70-35335

Low temperature plasma flow velocity measurements using transit-time technique and high speed filming

17 p1341 A70-35345

Energy transfer processes of electron gas for pipe flow of weakly ionized nonequilibrium plasmas, noting electron temperature decrease exponentially along tube axis

17 p1342 A70-35438

MHD and thermal boundary layer, considering difference scheme for conducting medium flow past body in crossed electric and magnetic fields

18 p3293 A70-36116

Plane nonconducting elastic plate with one side impinged upon by supersonic conducting gas flow, determining magnetic field effect on flutter vibrations

18 p3336 A70-36135

Magnetohydrodynamic flow of electrically conducting viscous incompressible fluid past nonconducting semiinfinite flat plate under transverse magnetic field

18 p3293 A70-36431

Supersonic flow of rarefied plasma around plane bodies, allowing for electric field effect on ion motion

19 p3351 A70-37302

Magnetic field and permeability effects on drag in steady axisymmetric MHD flow of incompressible fluid around full and hollow spheres

19 p3477 A70-37577

Liquid with small electrical conductivity and kinematic viscosity in intense transverse magnetic field, examining plane and three dimensional duct flow

19 p3478 A70-37589

Electrically conducting perfect compressible fluid flow in semiinfinite channel under electromagnetic field, using multiple scales method

19 p3479 A70-37595

Thin airfoil theory in magnetoaerodynamics, considering steady two dimensional flow of compressible perfectly conducting inviscid fluid in presence of uniform magnetic field

19 p3351 A70-37597

Conducting gas channel and jet flow in electric and magnetic fields, using linearizing equations of motion under assumption of small magnetic Reynolds number

19 p3479 A70-37598

Compressible fluids flow with conductivity tensor in presence of thin wing under orthogonal fields, reducing integral equation to Fredholm equation

19 p3351 A70-37599

Ionization relaxation behind reflected luminous shock front in argon plasma flow interaction with magnetic fields, using spectroscopic and streak interferometric observations

19 p3479 A70-37814

Heat transfer in plasma flow incident normally on cylinder, examining laminar boundary layers in presence of turbulence

19 p3552 A70-38187

Coulombian drag on body from hybrid calculus of collisionless plasma flow around cylinder [ONERA-TP-819]

19 p3481 A70-38382

Viscous incompressible electrically conducting fluid steady flow between parallel coaxial rotating disks with transverse magnetic field

19 p3481 A70-38446

Slow wave propagation in plasma moving along external magnetic field, generalizing refractive index formula

19 p3417 A70-38592

Hydromagnetic flow past infinite impulsive motion plate, determining velocity and temperature fields distribution

19 p3482 A70-38934

Two dimensional MHD couette flow in slip regime, considering constant suction on stationary plate to determine transverse magnetic effects

20 p3677 A70-39047

MHD flow in channel of arbitrary cross section, deriving velocity and electric potential distribution by variational principle

20 p3677 A70-39360

MHD nonsteady Beltrami flow between two infinite parallel walls with transverse magnetic field, calculating velocity, skin friction and induced magnetic field

20 p3678 A70-39610

Electrically conducting gas flow past slender body of arbitrary cross section in presence of crossed magnetic field by MHD Stokes approximation

20 p3558 A70-39613

Spectral lines self rotation effects on plasma temperature and density measurement in MHD duct boundary layer

20 p3678 A70-39632

Plasma accelerator compressible turbulent boundary layers numerical calculation taking into account MHD effects, electron thermal nonequilibrium and finite rate ionization

20 p3682 A70-40017

Viscous conducting fluid slow motion past sphere in presence of toroidal magnetic field, calculating Stokes flow perturbations

20 p3682 A70-40113

Compressible plasma axisymmetric channel flow under electromagnetic forces and ohmic heating, noting velocity profiles and current density

20 p3683 A70-40239

Gas core nuclear rocket engine light and heavy species centrifugal separation by MHD-driven rotating flow, discussing fluid dynamic simulation results

20 p3671 A70-40256

Local variables in boundary layer of high temperature ionized gas flowing in magnetic field, using X ray absorption

20 p3613 A70-40344

Steady plane conducting gas flow across magnetic field in channel, calculating flow rate effect on current density distribution

20 p3684 A70-40386

Plane parallel viscous conducting fluid flows stability in transverse magnetic field, considering small perturbation spectrum, Hartmann and Reynolds numbers

20 p3684 A70-40397

Solar wind flow behind shock fronts from Mariner 5 and Explorer 34 spacecraft

20 p3701 A70-40422

Slightly rarefied and electrically conducting gas, calculating effects of applied magnetic field on steady laminar low speed plane Couette flow

20 p3685 A70-40504

Elastoviscous incompressible electrically conducting oscillating free stream flow along infinite porous plate with suction in transverse magnetic field

20 p3685 A70-40508

Electron temperature measurements in flowing high density plasma by cooled Langmuir probe, considering probe temperature variations effects in boundary layer

21 p3854 A70-40557

Viscous magnetofluidynamic one dimensional annular flow, reducing three dimensional field equation to coupled linear partial differential equations

21 p3855 A70-40889

Incompressible MHD flow in entrance region of channel with electrically conducting walls, calculating interacted laminar heat transfer by integral method

21 p3856 A70-41038

Two dimensional compressible laminar MHD boundary layer flow across flat plate with heat transfer, considering continuity, momentum and energy equations

21 p3856 A70-41039

Ionospheric conductivity effects on plasma convective flow in determining magnetospheric electric fields distribution

21 p3816 A70-41084

Rarefied ionospheric plasma flow around rockets and satellites, studying electric field effect on ion motion by kinetic equation and similarity law

21 p3819 A70-41169

Deuterium plasma three dimensional flow in coaxial accelerators, examining magnetic structure of filaments/field lines bundles/

21 p3856 A70-41321

Axisymmetric jet plasma flow in magnetic nozzle, measuring electric potential, electron temperature and ion density and velocity

21 p3856 A70-41380

Aerodynamic parameters of ionized Ar supersonic steady one dimensional nonviscous flow in thermodynamic equilibrium and subjected to Laplace accelerating forces

21 p3858 A70-41444

Two dimensional unsteady viscous incompressible MHD flow past infinite flat plate with uniform suction, considering Hartmann and Reynolds numbers

21 p3858 A70-41450

Electromagnetic effects on separation of turbulent MHD boundary layers allowing for heat transfer

21 p3860 A70-42065

Turbulent incompressible conducting fluid jets velocity and temperature characteristics in presence of longitudinal and transverse magnetic fields

21 p3860 A70-42226

One dimensional supersonic flow of ideal conducting gas in linear channel under transverse magnetic field

21 p3861 A70-42228

Thermoanemometric velocity measurements in nonstationary MHD Hg flows by insulated Pt sensors

21 p3831 A70-42229

Liquid metal turbulent jet flow dependence on longitudinal magnetic field, measuring mean velocity profiles at various cross sections

21 p3861 A70-42230

Heat and mass transfer in plane inductionless and dissipationless incompressible MHD boundary layer with longitudinal pressure gradient

21 p3861 A70-42231

High power plasma flow generation at variable pressure and rates, describing device characteristics and performance

22 p4079 A70-42367

Reverse hydromagnetic shock in solar wind as discontinuity of plasma density, proton temperature and magnetic field density, using spacecraft data

22 p4093 A70-42474

Unsteady hydromagnetic boundary layer flow past semiinfinite flat plate under steady magnetic field and small free stream perturbation

22 p4080 A70-42631

Conducting fluid supersonic flow past slender body of revolution in circular wind tunnel under inclined magnetic field, investigating MHD interference problem

22 p3958 A70-42669

MHD channel flow of suspension for prescribed wall heat flux and temperature, determining flow and heat transfer characteristics

22 p4080 A70-42670

Magnetoacoustic waves in MHD channels, investigating excitation, damping and effects on mean current density and Hall field strength

22 p4081 A70-42822

Ionization waves excitation and damping in MHD channels, investigating effects on electric conductivity, Hall parameter and electron temperature

22 p4081 A70-42823

Planar resonance probe in free molecular arc heated flowing plasma, examining shift nature in measured frequency position of minimum drawn current

22 p4081 A70-43013

Hydromagnetic theory of solar wind flow past earth extended to nonmagnetic planets Venus and Mars

22 p4095 A70-43106

- Nonequilibrium ionization during plasma flow into magnetic field, examining electrons selective heating 22 p4083 A70-43384
- MHD flow universal stability, investigating nonlinear system by energy methods 23 p4223 A70-43967
- Electrically conducting fluid hydromagnetic spin-up between infinite flat insulating plates in uniform magnetic field normal to boundaries 23 p4223 A70-43972
- Magnetic fields and electrically conducting fluids interaction with emphasis on magnetodynamics equations, investigating rectilinear flows in pipes and nozzles, shock waves, etc 23 p4223 A70-44098
- MHD incompressible viscous flow in nonconducting circular tube, determining pressure, flow rate and magnetic field level by continuum theory concepts 23 p4224 A70-44161
- MHD laminar isothermal flow in closed cylindrical tube in rotating magnetic field, determining azimuthal velocity distribution 23 p4224 A70-44162
- Gravity waves produced in liquid electric conductor by piston subjected to sinusoidal pulsation, calculating magnetic field effect on amplitude and phase velocity 23 p4225 A70-44208
- MHD equations for one dimensional plane steady flow, considering conservative difference schemes for approximation 23 p4226 A70-44307
- Conducting viscoelastic fluid flow near harmonically oscillating nonconducting flat plate under uniform transverse magnetic field, considering stress-strain rate relationship 23 p4226 A70-44375
- MHD nonstationary three dimensional problems, describing difference method 23 p4227 A70-44738
- Compressible plasma flow in axisymmetric channels under EM body forces and Joule heating 23 p4228 A70-44934
- Upstream gas photoionization caused precursor ionization effects on MHD switch-on shock structure 24 p4382 A70-45106
- Viscous conducting liquid forced vortex motion, considering radial velocity distribution and rotation effect on free surface shape 24 p4383 A70-45140
- Oscillating viscous conducting fluid laminar flow between parallel nonconducting infinite porous flat plates under suction in transverse magnetic field 24 p4383 A70-45146
- Perturbation of steady MHD Stokes flow past hollow sphere assuming small Hartmann and Reynolds numbers 24 p4384 A70-45262
- Magnetized conducting sphere steady rotation in viscous conducting liquid, solving for fluid velocity and induced magnetic field 24 p4386 A70-45609
- Conducting sphere MHD rotation in viscous conducting fluid under uniform magnetic field 24 p4387 A70-46028
- MAGNETOHYDRODYNAMIC GENERATORS**
- Power output, Joule dissociation and generator efficiency determined for rectangular MHD channel, considering transverse and longitudinal edge effects 01 p0152 A70-10992
- MHD high temperature heating equipment, describing power generation and conversion and magnetic field-working fluid interactions 02 p0348 A70-12418
- Liquid metal MHD, discussing conduction/induction MHD devices, measurement gages and devices for suspending liquid metal by magnetic force 04 p0724 A70-14527
- Faraday type open circuit MPD generator model obtained with allowance for temperature and pressure losses and gas transport properties dependence on static parameters 04 p0725 A70-14530
- MHD generators physical phenomena, discussing thermal efficiency, inlet parameters, operating principles, etc 04 p0625 A70-14716
- MHD generators developments, considering open and closed cycle systems and commercial power networks applications [ASME PAPER 69-WA/PWR-12] 04 p0625 A70-14754
- MHD generator cathode current-sheath voltage characteristics for thermionic arc spot emission mode, noting role of cathode temperature [ASME PAPER 69-WA/HT-51] 04 p0625 A70-14797
- Mechanical electromagnet model of MHD dynamo achieving direct conversion of mechanical to magnetic field energy 06 p1121 A70-17803
- Critical Hall parameter indicating instability in alkali-seeded noble gases in nonequilibrium MHD generators [AIAA PAPER 70-40] 06 p1122 A70-18107
- Electronic-vibrational coupling in nonequilibrium MHD generator with molecular gas to suppress electrode layer shorting and recombination in supersonic nozzles [AIAA PAPER 70-41] 06 p0988 A70-18222
- Electrical effects of boundary layers on insulator wall of MHD generator, considering equilibrium and nonequilibrium ionization generators performance 07 p1196 A70-19321
- Doppler shift measurements of axial and rotational velocities in MPD arc, using references from iron arc [AIAA PAPER 69-110] 07 p1364 A70-19324
- MHD generators optimum load selection by method of stepwise approach, noting agreement with pressure and density distributions to yield maximum power 10 p1923 A70-24156
- Optimal MHD generator with constant channel area, assuming small Reynolds numbers and ideal inviscid gas with arbitrary electrical conductivity 10 p1807 A70-24570
- MHD generator with generator channel consisting of two coaxial cylinders with smooth annular space, discussing internal impedance sensitivity 10 p1807 A70-24855
- Nonequilibrium plasma MHD generator critical pressures determination, applying electron energy balance equation and relation between plasma conductivity and Hall parameters 10 p1809 A70-25142
- Book on engineering aspects of MHD power generation, discussing working gas ionization and electrical conductivity, incompressible conducting fluid motion in magnetic field, etc 11 p1982 A70-25525
- NASA-Lewis closed loop MHD low temperature power generator, describing systems performances during subsonic tests 11 p1982 A70-25614
- Conducting fluid incompressible flow in entrance of MHD channel by momentum integral method, permitting edge stress existence at boundary layer free stream interface [AIAA PAPER 69-724] 11 p2035 A70-25977
- Remote controlled diaphragm exploding device associated with shock tube for MHD generator 11 p2090 A70-26170
- Insulator wall temperature effect on supersonic two temperature MHD generator channel flow at open and short circuit conditions 12 p2163 A70-27067
- Hall MHD generator with supersonic flow instability to magnetoacoustic waves propagating antiparallel to steady electric current in dense weakly ionized gas 12 p2281 A70-27805
- Mechanical electromagnet model of MHD dynamo achieving direct conversion of mechanical to magnetic field energy 13 p2460 A70-28654
- Asynchronous liquid metal MHD generator parameters, assuming constant vertical distribution of working fluid velocity 13 p2349 A70-28968
- Ohmic dissipation in MHD plasma acceleration, demonstrating interaction with electric field and magnetic induction 14 p2621 A70-30296
- MHD induction generator efficiency, investigating winding slot finite spacing and width effects 14 p2533 A70-30531
- Closed loop MHD test facility ARGAS I, describing engineering performance and test measurements 14 p2533 A70-30532
- Open cycle MHD generator operation, comparing below stoichiometric air-fuel ratios to excess air level 14 p2533 A70-30534
- MHD power generation, investigating replenishment of zirconia electrodes from plasma in open flame and duct configurations 14 p2534 A70-30535
- Faraday type MHD generators, investigating gas velocity and temperature profiles effect on electrical performance by equivalent circuits simulation 14 p2534 A70-30537
- High temperature energy systems with plasma reactors and inductive MPD converters, discussing spacecraft propulsion and ground based pollution-free power generation 15 p2791 A70-32278
- MHD power sources for onboard military aircraft electrical application 16 p2964 A70-33474
- MHD electric power generators characterized by high power level and duration for future application in space 16 p2844 A70-33711
- Nonuniform one dimensional flow of slightly ionized gas in infinitely segmented MHD generator with imperfect walls 19 p3478 A70-37588
- Liquid metal MHD conservation cycles, discussing evolution and status of power generation at various temperatures 20 p3563 A70-39325
- Plasma inhomogeneities effects on MHD generators I-V characteristics, energy conversion efficiency and optimum duct geometry 20 p3564 A70-39636
- Boundary layer separation in MHD generators, discussing differences between insulating and electrode wall boundary layers 20 p3680 A70-39985
- Liquid metal MHD power conversion system with Cs and Li as working fluids, describing hydraulic, electrical and high temperature tests results 20 p3680 A70-39986
- MHD induction generator efficiency reduction due to finite winding slots spacing and width 20 p3565 A70-39987
- MHD induction generator design, considering electrical and friction loss measurement and control 20 p3565 A70-39988
- Preionization in Cs seeded Ar nonequilibrium plasma for MHD generators, examining discharge characteristics, recombination reactions, etc 20 p3680 A70-39991
- Large scale nonequilibrium linear MHD generator performance with rare gases under strong EM-gas dynamic interactions 20 p3681 A70-39993
- Insulator wall temperature effect on supersonic nonequilibrium MHD generator channel under open and short circuit conditions 20 p3681 A70-39994
- Large MHD generator channel aerodynamics, discussing pressure distributions to stall and stagnation pressure loss 20 p3612 A70-40002
- Combustion driven Hall configuration MHD generator, discussing boundary layer analysis, gas density nonuniformity and electrode drop 20 p3566 A70-40003
- Performance comparison of diagonal conducting wall MHD generator and Hall generator of equal dimensions, investigating wall temperature effect 20 p3566 A70-40004
- Electrode size effects on combustion driven MHD generator performance, examining voltage losses, gas boundary layer temperature and surface conditions 20 p3566 A70-40005
- Projected nuclear MHD system conditions, examining electrical measurements in K vapor with diode at atmosphere pressure and high temperatures 20 p3681 A70-40006
- NASA Lewis closed loop MHD generator subsonic tests, discussing ducts, purge and Cs injection systems, electrode coating, etc 20 p3566 A70-40011
- Noble gas mixture large shock tunnel driven linear MHD generator, examining electron density, operating characteristics and electrical properties 20 p3682 A70-40012
- Conducting wall MHD generator channel current distribution, examining computer program for anode and cathode currents 20 p3566 A70-40013
- Liquid-gas separator design with reduced friction loss for MHD generators using two phase convergent-divergent nozzles 20 p3612 A70-40014
- One wavelength MHD induction generator, discussing field pressure gradients, fluid velocities, excitation and electrical output power 20 p3566 A70-40015
- Unmanned nuclear electric propelled spacecraft using reactor with liquid metal MHD power conversion system 20 p3566 A70-40016
- Continuous electrode MHD generator ionization instabilities, measuring current distribution and transverse electric field 20 p3567 A70-40018
- Effective dissociation potential measurement for alkali compound seed in MHD generator working fluid 20 p3682 A70-40159
- MHD generators nonequilibrium ionization improvement by blowing low work function particles into cold working gas to obtain required conductivity 21 p3855 A70-40794
- Electron and ion transport in cesium plasma for thermionic and MHD energy converters 21 p3859 A70-41912
- Optimal load circuits number for maximum power extraction from Hall MHD generator with nonuniform gas flow along channel 23 p4143 A70-44900
- NERVA reactor technology applied to closed Brayton cycle MHD power system [AIAA PAPER 70-1225] 24 p4377 A70-45956
- MAGNETOHYDRODYNAMIC STABILITY**
- Nonpotential waves propagating at slow phase velocity in inhomogeneous plasma, determining flute instability oscillation frequency 01 p0149 A70-10163
- Langmuir oscillations excited by electron beam in plasma during instability development investigated for temporal and spatial structure, using visualization 01 p0150 A70-10174

Particle distribution and plasma nonequilibrium field evolution with turbulence generation by microwave field, considering plasma kinetic instability 01 p0150 A70-10212

Solar structural periodicities in quiescent prominences and filaments, considering plasma instability and supporting magnetic field characteristics 01 p0176 A70-10248

Electrothermal instability and critical Hall parameter growth rates in closed cycle linear plasma generators with variable electron mobility, discussing perturbation effects 01 p0151 A70-10655

Electron trapping effect on ion-wave instability in plasma, deriving expression for saturation energy spectrum 01 p0152 A70-11361

One dimensional nonlinear model of anisotropic plasma instability with respect to Alfvén waves growth, noting applicability to solar wind processes 01 p0153 A70-11597

Ionization instability in low temperature magnetized plasma, analyzing electron concentration perturbation caused by Joule heating during electron-ion collisions 01 p0153 A70-11598

Boundary conditions for equilibrium diamagnetic plasma in magnetic dipole having constant and isotropic pressure in system 01 p0153 A70-11631

Plasma accumulation between mixed field accelerator and pulsed magnetic mirror, noting duration and stability 02 p0346 A70-12104

Unstable electron plasma initial value problem solved by numerically integrating Vlasov equation in one dimension 02 p0347 A70-12235

Warm Maxwellian plasma stabilization of velocity-space instabilities, evaluating densities and temperatures for stabilizing resonant loss-cone modes 02 p0347 A70-12237

Recombination instabilities in plasmas and gases undergoing density changes through volumetric processes, solving linearized and nonlinear cases by simplified fluid mechanics equations 02 p0348 A70-12238

Transverse Kelvin-Helmholtz instability in rotating thermally ionized alkali metal plasmas (Q machines), analyzing LF drift wave edge oscillation using dispersion equation 02 p0348 A70-12239

Critical magnetic fields, frequencies and spatial structure of ion-acoustic instability of HF induction discharge plasmas in hydrogen, Ar, He and Hg vapor 02 p0348 A70-12261

Saturation of linear or nonlinearly /explosively/ unstable HF electrostatic flute modes in mirror confined plasma 03 p0529 A70-13005

Coaxial ion beams moving in opposite directions in LF magnetic field noting sliding instability development 03 p0530 A70-13061

Variable magnetic field effect on stability of Langmuir waves propagating in plasma in constant magnetic field 03 p0530 A70-13064

Rotary equilibrium of plasma ellipsoid in external HF fields in constant magnetic field, calculating revolution frequency and effective energy potential 03 p0530 A70-13085

Van der Pol equation for finite amplitude ion-acoustic waves in unstable plasma propagating across weak magnetic field 03 p0531 A70-13404

Plasma stability in uniform magnetic and HF electric fields, observing magnetoacoustic wave generation at electron cyclotron frequency greater than HF field frequency 03 p0532 A70-13523

Electrostatic instability criterion for plasma with distribution function having discontinuities and sharp bend at minima 03 p0532 A70-13526

Thermochemical relaxation influence on shock heated plasma gases via heat transfer experiments on ionized Ar, molecular nitrogen and carbon dioxide 03 p0536 A70-14366

Plasma instabilities of Ce filled auxiliary discharge thermionic energy converter compared with Langmuir theory 03 p0415 A70-14367

Whistler mode instability due to anisotropic charged particle velocity distribution, establishing general onset conditions for variable density cold plasma containing hot electrons 03 p0537 A70-14378

Heat transfer to insulator wall of linear MGD accelerator attached to shock tube, comparing measurements with Hartmann boundary layer analysis [ASME PAPER 69-WA/HT-53] 04 p0781 A70-14796

High density nonlinear and linear growth rates of flute modes instabilities in cold plasma coexisting with low density of energetic electrons 04 p0728 A70-14998

Coaxial electrodes with electric and magnetic fields to study instability in MPD arcs 04 p0737 A70-15542

Stability and shape of magnetically balanced atmospheric cross-flow arcs in Ar noting balanced modes 04 p0729 A70-15549

Unsteady state and transit time analysis of geoeffective interplanetary plasma flux observed near earth causing magnetospheric storm of 17-19 April 1965 04 p0683 A70-15736

Steady state plasma generation in metallic waveguide without dielectric container by cold cathode discharge in He 05 p0819 A70-15803

Neutral sheet instabilities in magnetotail from collisionless plasma instabilities from shear magnetic field 05 p0887 A70-15911

Gravitational instability of finitely conducting incompressible fluid layer of finite thickness surrounded by nonconducting medium 05 p0915 A70-16696

Equatorial jet stream excitation of longitudinal waves, analyzing plasma beam instability and spectrum of short wave inhomogeneities by quasi-hydrodynamic equations 05 p0842 A70-16759

Electron ejections from nuclei of radio galaxies and quasars on basis of plasma stability, discussing role of relativistic electrons and resulting unstable pinch 05 p0917 A70-16901

Relativistic plasma waves in uniform ambient magnetic field analyzed for growth rate to investigate plasma instabilities of streaming cosmic rays 05 p0904 A70-16931

Plasma wave theory and experiments, emphasizing stable Maxwellian plasmas and transverse and longitudinal wave modes in zero and nonzero magnetic fields 06 p1116 A70-17366

Plasma waves and instabilities, detailing linearized Vlasov-Maxwell equations solution appropriate to Landau problem 06 p1118 A70-17378

Nonuniform plasma analyzed for parameters inhomogeneity effect on VLF propagation mode and instability 06 p1119 A70-17381

Anisotropic plasma instability in nonlinear stage, studying turbulent relaxation of ion distribution by quasi-linear theory 06 p1119 A70-17501

HF drift instabilities of plasma with nonuniform magnetic field, studying anomalous ion heating and resistance in Zeta installations 06 p1119 A70-17502

Heat transfer in dense high temperature plasma due to drift waves instability at trapped electrons 06 p1121 A70-17802

Remote feedback suppression method for plasma collisional drift instability using modulated microwave irradiation, describing linear heating mechanism theory 06 p1122 A70-18014

Critical Hall parameter indicating instability in alkali-seeded noble gases in nonequilibrium MHD generators 06 p1122 A70-18107

Homogeneous monoenergetic cylindrical electron beam interaction with homogeneous cold plasma, investigating system stability 06 p1125 A70-18615

Weak discontinuities propagation in quasi-linear systems for MGD, obtaining transport equations 07 p1347 A70-18676

Bogoliubov approach generalized and applied to unstable and inhomogeneous plasmas 07 p1347 A70-19108

LF ion-acoustic waves in ionosphere, considering electric and magnetic field variations, instability, etc 07 p1347 A70-19187

Hall current effects on anisotropic plasma magnetogravitational instability under uniform magnetic field, considering electron inertia role and plasma perturbations 07 p1348 A70-19228

Circumsolar plasma structural inhomogeneity origin 07 p1384 A70-19418

Quasi-linear feedback effect of enhanced ion-wave fluctuations on average electron distribution in current-carrying plasma 07 p1338 A70-19822

Ion resonance instability in nonneutral plasmas, considering ions addition to low density electron cloud with low kinetic energy 07 p1352 A70-19991

Electron clouds injection and containment by magnetic field in toroidal vacuum chamber, studying causes of cloud instability 07 p1353 A70-19994

Hydromagnetic self gravitating galactic slab embedded in halo, deriving stability criteria using models of magnetic field 07 p1390 A70-20293

Cyclotron frequency harmonics emission of PIG discharges linked to nonthermal electron plasma instability 07 p1354 A70-20316

Collective interactions and low density plasma instability in high current gas discharge showing influence on neutral gas breakdown in interelectrode space 07 p1354 A70-20317

Plasma ion-cyclotron oscillations resonance excitation in crossed electric and magnetic fields, describing instability development 07 p1354 A70-20319

Intense quasi-steady He plasma discharge stability in magnetic field measured by Langmuir and optical techniques 07 p1354 A70-20321

Diffusion coefficient of charged particles in HF stabilization of current-convective instability measured in Ge semiconductor electron hole plasma 07 p1355 A70-20365

Solar wind velocity cycles from fluid MHD viewpoint, applying Kelvin theorem on circulation stability in closed fluid system 07 p1373 A70-20441

Finite amplitude effects on MHD thermal convection in rotating layer of conducting fluid, discussing subcritical instability 08 p1563 A70-20472

Plasma-electron beam system LF dispersion characteristics noting ion instability 08 p1549 A70-20505

Inhomogeneities in interplanetary plasma formation due to instability of electron flows moving along interplanetary magnetic field lines of force 08 p1570 A70-20845

Plasma instabilities in solar wind for frequencies near proton gyrofrequency, driving instabilities by electron and proton thermal anisotropies 08 p1561 A70-21261

Plasma monochromatic wave propagation equilibrium state instability mechanisms, discussing stimulated scattering by thermal plasma particles and particle capture in wave potential well 08 p1551 A70-21422

Flute instabilities of cold magnetoactive plasma with radially dependent density and strong azimuthal particle streams, discussing nonzero perpendicular temperature effects on oscillations 08 p1552 A70-21504

Optical parametric backward-wave instabilities in unbounded medium with stopband dispersion using Fourier-Laplace integral 08 p1552 A70-21595

Electromagnetic wave instability propagating across static magnetic field in presence of thermal anisotropy, considering interplanetary plasma and plasma devices stability 08 p1553 A70-21610

Convective-current instability in finite length plasma column, analyzing spectrum of unstable harmonics 08 p1554 A70-21802

Langmuir HF turbulence effect on anisotropic plasma oscillation spectra, determining instability conditions 08 p1554 A70-21809

Axisymmetric instabilities by Z-pinch and reverse axial current discharges in plasmas of arbitrary conductivity 08 p1554 A70-21810

Turbulent diffusion and ion heating in plasmas in presence of current instability 08 p1554 A70-21813

Radial self focusing of low density electron beam by interaction with plasma in presence of beam plasma instability 08 p1554 A70-21818

Nonlinear wave scattering at plasma particles and weak plasma inhomogeneity effects on plasma current instability 08 p1554 A70-21819

Low pressure plasma stability in cylindrical crimped magnetic field, considering convective perturbations and particle velocity distribution 08 p1555 A70-21981

Trapped particle vibrations stability during quasi-neutral plasma disturbance due to centrifugal drift in stellarator electric field 08 p1555 A70-21982

Feedback stabilization of surface instabilities of highly conducting plasma, discussing application to linear pinch with uniform axial static magnetic field 09 p1734 A70-22272

Ion-acoustic wave oscillations of weak collision plasma in strong electromagnetic field, discussing instability 09 p1736 A70-23198

Plasma charge transfer in unstable beam plasma in magnetic fields system allowing for electron discharge pump operation 09 p1737 A70-23334

Beam plasma system instability, studying anomalous diffusion toward vessel walls as function of generated oscillations

09 p1737 A70-23335

Electromagnetic instability measurements in electron cyclotron resonance plasma produced in magnetic mirror field

10 p1921 A70-23963

Two-stream and cross-stream effects on nonlinear wave stability with shock in collisionless plasma

10 p1921 A70-23967

Electron-ion beam plasma system, using one dimensional quasi-linear equations for describing electron heating and stabilization

10 p1923 A70-24403

Drift dissipative instability of weakly ionized plasma, considering ion motion along magnetic lines in dispersion equation

10 p1923 A70-24407

Plasma instability in RF discharge in Ar in magnetic field

10 p1840 A70-24540

Rotating plasma in nonuniform magnetic field analyzed for interchange instability based on MHD fluid and charged particle treatments

10 p1924 A70-24800

Nonpotential waves propagating at slow phase velocity in inhomogeneous plasma, determining flute instability oscillation frequency

10 p1925 A70-25011

Langmuir oscillations excited by electron beam in plasma during instability development, investigating temporal and spatial structure using visualization

10 p1925 A70-25019

Plasma column dynamic stability breakdown in quadrupole HF magnetic field in terms of violating stability criterion for long wave deformation

10 p1926 A70-25109

Hydromagnetic flute and surface wave instabilities of current-carrying plasma filament in strong longitudinal field, showing radial density stabilization

10 p1926 A70-25117

Excitation of plasma ion-cyclotron oscillations by ion beam passing through neutral gas along magnetic field, noting radial stabilization

10 p1926 A70-25118

Two fluid hydrodynamic model of heat conductivity and viscosity effects on drift laminar flow stability of dense inhomogeneous plasma

10 p1926 A70-25125

Guiding center plasma theory, obtaining stability criteria from charged particle motion equations considerations

10 p1926 A70-25250

Statistical analysis of aurora backscatter VHF measurements, discussing related stream plasma instability theory and diurnal variation

10 p1885 A70-25263

Ultrarelativistic electrons cone instability in Van Allen radiation belts, discussing distribution function, relativistic effects and electron lifetimes

11 p2104 A70-25529

Unsteady plasma oscillation stabilization by envelope controller with spatial and temporal dispersion

11 p2087 A70-25604

Plasma stabilizing effect of shear and magnetic flux minimum in asymmetric conductors and currents in helical stellarator winding

11 p2088 A70-25711

Ion-acoustic instability effect on HF EM field penetration into plasma taking into account nonlinear Ohm law

11 p2089 A70-25715

Surface waves stability in cold bounded plasma against background of steady state electron oscillations, using nonlinear approximation

11 p2089 A70-25716

Linear theory of density gradient drift waves in stable collision dominated plasma using external excitation method

11 p2090 A70-26019

Stability of realistic inhomogeneous plasmas with sheaths, examining electron beam-stable Maxwellian plasma interaction

11 p2090 A70-26021

Trans-Alfvenic ionizing shock waves stability in absorption of rotational Alfven disturbances

11 p2090 A70-26023

Modulation coupling between electron and ion resonances in magnetoactive plasmas, discussing probeless feedback stabilization scheme

11 p2091 A70-26403

Plasma turbulence theory application to experimental phenomena using two stream instability example

11 p2096 A70-26769

Diluted plasma microinstabilities allowing for Langmuir waves propagation without magnetic field and Landau effects

12 p2277 A70-27057

Ionization instability of finite bounded plasma, investigating electrothermal waves in large disturbance domain by numerical simulation

12 p2163 A70-27065

MHD disturbances in semiinfinite electrically conducting fluid, introducing magnetic dipole to act as source of disturbance

12 p2277 A70-27156

Drift instability of Alfven waves at electron plasma sheet edge as source of auroral micropulsation instability

12 p2222 A70-27184

Stability of MHD dissipative circular flow of viscous electrically conducting fluid between concentric stationary cylinders impressed with axial magnetic and radial electric fields

12 p2277 A70-27195

Trumpet-type plane waves instability thresholds in plasma drifted by electric field, including calculation of thermodynamic equilibrium

12 p2184 A70-27236

Plasma equilibrium in stellarator type magnetic trap /vintatron/ with magnetic configuration created by strong longitudinal field

12 p2277 A70-27313

Hot-electron cold-ion plasma with anisotropic electron velocity distribution function, discussing stability under finite pressure and unstable oscillation forms

12 p2277 A70-27314

Frequency spectrum determination of hydrodynamic instability excited in fast large amplitude magnetosonic wave

12 p2278 A70-27542

Collisional drift-wave turbulence in Li Q-machine plasma far unstable regime, discussing power spectra variations of density fluctuations

12 p2280 A70-27784

Density gradient drift waves stabilization in collisionless plasma by stellarator type windings, observing oscillations amplitude reduction in shear magnetic field

12 p2280 A70-27785

Drift wave instabilities nonlinearities, discussing plasma growth rate and saturation coefficients, damping rate as function of amplitude and lower mode modification

12 p2280 A70-27786

Feedback stabilization and mode coupling of ionization waves in positive column discharges, noting dynamic stabilization of unstable bounded plasma systems

12 p2280 A70-27787

Hall MHD generator with supersonic flow instability to magnetoacoustic waves propagating antiparallel to steady electric current in dense weakly ionized gas

12 p2281 A70-27805

Impurities and electrothermal instabilities effect on conductivity of two temperature nonequilibrium plasma

12 p2281 A70-27846

Linearized dispersion relation for plane wave propagation in uniform unbounded cold plasma permeated by DC magnetic field, considering two stream instability

12 p2281 A70-27881

Nonequilibrium solid state electronic plasma instabilities due to interactions with strong electric and magnetic fields

12 p2289 A70-28363

Parametric and Raman instabilities predicted by linear theory for plasma in electromagnetic field

13 p2458 A70-28563

Finite amplitude stability of plasma column in weakly ionized gases and in semiconductor plasmas in longitudinal magnetic field

13 p2458 A70-28566

Magnetoplasmas nonlinear dielectric response function and parametric instabilities, discussing homogeneous pumping waves

13 p2459 A70-28568

Electron beam interaction with plasma in absence of magnetic field, discussing microwave radiation emission and incoherent scattering and instability spatial growth

13 p2459 A70-28569

Electron beam interaction with Maxwellian plasma, investigating temperature effects on instabilities

13 p2460 A70-28639

Propagation characteristics of instabilities represented by multidimensional Fourier integrals

13 p2454 A70-28640

Heat transfer in dense high temperature plasma due to drift waves instability at trapped electrons

13 p2460 A70-28653

Gas discharge gap preionization by thin preheated tungsten wire ignition without explosion, resulting in plasma turbulence prevention and radiation density increase

13 p2462 A70-28986

Plasma instability in TEM wave field, considering nonpotential HF oscillations buildup with frequency near external wave frequency

13 p2463 A70-29283

Drift instability and ion heating by high amplitude magnetosonic wave in plasma waveguide in constant magnetic field

13 p2463 A70-29381

Rotating plasma disturbances onset in MPD arc, determining magnetic field dependence on mass flow, background pressure and propellant

[AIAA PAPER 69-232] 13 p2475 A70-29961

Reverse flow in plasma generated in conical electromagnetic shock tube and reflected from downstream bulkhead, noting stabilization effects

13 p2469 A70-29974

HF electrostatic waves generation by electrons in magnetosphere

13 p2482 A70-30083

Hydromagnetic wave velocity and space anisotropy instabilities in magnetosphere, using dispersion relation

13 p2483 A70-30086

Two dimensional unsteady flow of weakly conducting fluid in perpendicular magnetic field using Green function

14 p2621 A70-30180

Charged particle acceleration in outer space plasma, deriving ion-acoustic instability equations

14 p2630 A70-30220

Wall stabilized arc source for spectroscopic measurements of isothermal plasma at various pressures

14 p2584 A70-30505

Convective or absolute electrostatic instability in weakly inhomogeneous hot magnetoplasma, determining density and frequency for onset

14 p2622 A70-30695

Computer models simulating plasma motion applied to sheet pinch stability, investigating relativistic and nonrelativistic regimes

14 p2623 A70-30696

Anisotropic plasma turbulence produced by two stream instability onset near light cylinder of rotating magnetic star for pulsar model

14 p2640 A70-30788

Unsteady state and transit time analysis of geoeffective interplanetary plasma flux near earth causing magnetospheric storm of 17-19 April 1965

14 p2575 A70-30820

Thermal radiative transfer and magnetic field effects on hydromagnetic stability of hot electrically conducting fluid

14 p2623 A70-30996

Sideband instability and trapped particle charge density response of large periodic Bernstein-Greene-Kruskal waves in collisionless plasma

14 p2623 A70-31039

Parametric oscillation instabilities in plasma under magnetic field perpendicular to circularly polarized or hybrid electric field

14 p2624 A70-31042

Ordinary mode electromagnetic wave propagation instability in high beta plasma, determining lower bound on growth rate

14 p2624 A70-31048

Compressible plasma gravitational instability taking into account Hall effect

14 p2624 A70-31225

Weak discontinuities propagation in quasi-linear systems for MGD, obtaining transport equations

15 p2777 A70-31470

Ellipsoidal plasmod equilibrium in external HF field, calculating rotation rate and potential energy

15 p2779 A70-32113

Dissipating instability in plasma by variational method, using relation between energy balance of wave and medium

15 p2779 A70-32115

Inhomogeneous ion beam plasma LF instability, showing oscillations amplitude maxima in radial density gradient regions

15 p2780 A70-32193

Partially ionized plasma stability with allowance for ionization and recombination processes, discussing ion-acoustic oscillations

15 p2781 A70-32823

Collisionless shock waves model in solar wind plasma, discussing instability and energy dissipation

15 p2795 A70-32825

Plasma helix equilibrium and stability in transverse magnetic field, considering oscillation damping by ohmic heating

15 p2781 A70-32910

Beam current instability and plasma heating by electron beam generated in linear discharge, discussing electron beam-cold plasma interactions

16 p2957 A70-33191

Plasma containment in adiabatic magnetic traps, discussing particles, Coulomb collisions, instabilities, cyclotron resonance masers, Van Allen belts, etc

16 p2958 A70-33232

Resonant interaction and instability produced by nonlinear coupling of modulated wave and LF mode, stimulating self focusing of plasma waves

16 p2958 A70-33285

Heterogeneous conducting fluid stability between fixed rigid cylinders with radiant gravitational force and magnetic field

16 p2894 A70-33784

Near cathode magnetic field effect on instability in linear Hall current accelerators, using geometry of field extending from anode to cathode region

[AIAA PAPER 69-381] 16 p2959 A70-33870

Electrothermal instability in nonequilibrium plasma interpreted in terms of generalized instability in gas discharge

17 p3139 A70-34550

Correlation functions of weak quasi-steady plasma turbulence determined by plasmon interactions, using computerized integral equation

17 p3139 A70-34643

Warm homogeneous magnetoplasma longitudinal cyclotron harmonic wave propagation perpendicular to static magnetic field, noting instabilities

17 p3140 A70-34927

Ring current belt stability against LF electrostatic perturbations, including effects of finite electric field along magnetic lines of force

18 p3306 A70-36009

Regular and stochastic oscillations in plasma beam discharge produced by beam instability from observing time dependent variations in spectral line luminescence intensities

18 p3294 A70-36147

Nonlinear interactions of plasma waves with positive and negative energies producing explosive instability

18 p3295 A70-36420

Electron beam interaction with ionized K plasma, considering Langmuir waves instability, turbulence and electron heating

18 p3295 A70-36614

Plasma tearing instabilities involving topological changes in magnetosphere field configuration

19 p3411 A70-37491

Finite electron beam plasma system, investigating relationship between linear fluctuations temporal growth and resulting stationary oscillations spatial growth

19 p3475 A70-37540

Inhomogeneous plasma ellipsoid equilibrium in external HF field, assuming parabolic density distribution

19 p3479 A70-37739

MHD instability of homogeneous inviscid plasma with finite electrical conductivity and anisotropic pressure, obtaining dispersion equation for model

20 p3677 A70-39048

Gas discharge in longitudinal magnetic field, investigating instability of diffusion dominated positive column

20 p3677 A70-39112

Rarefied plasma flute oscillation stabilization in magnetic field, using controlled electron beams

20 p3677 A70-39173

Steady electric field effect on dense plasma cyclotron instability

20 p3678 A70-39595

Ion heating during plasma instability due to interaction with electron beam in mirror magnetic trap

20 p3678 A70-39598

Nonuniform finite amplitude plasma waves non-linear decay and instability, discussing initial damping /or growth/ effect

20 p3678 A70-39660

Ionization stability in low temperature magnetized plasma, using physical plasma model and numerical solution

20 p3679 A70-39983

Continuous electrode MHD generator ionization instabilities, measuring current distribution and transverse electric field

20 p3567 A70-40018

Nonequilibrium plasma stability, conductivity and Hall parameter influenced by current flow parallel to magnetic field, discussing Ar-Cs and He-Cs plasma data

20 p3682 A70-40019

Potential fluctuations in intersecting plasma jet streams attributed to ion-electron instability, using external probe

20 p3682 A70-40136

Dense plasma jet kinetic instabilities and heating in strong magnetic field

20 p3682 A70-40138

Plasma nonequilibrium state formation and light absorptivity variation under high power laser pulsed radiation

20 p3684 A70-40387

Hydromagnetic flute and surface waves instabilities of current-carrying plasma filament in strong longitudinal field, showing radial density stabilization

20 p3685 A70-40510

Excitation of plasma ion-cyclotron oscillations by ion beam passing through neutral gas along magnetic field, noting radial stabilization

20 p3685 A70-40511

Two fluid hydrodynamic model of heat conductivity and viscosity effects on drift laminar flow stability of dense inhomogeneous plasma

20 p3685 A70-40518

HF electromagnetic field effect on nonhomogeneous collisionless magnetized plasma stability, deriving dispersion equation for drift cyclotron oscillations

21 p3854 A70-40622

Anomalous electromagnetic wave absorption in collisionless plasma attributed to instability excitation causing ion density fluctuations

21 p3855 A70-40754

Ultrarelativistic electrons cone instability in Van Allen radiation belts, discussing distribution function, relativistic effects and electron lifetimes

21 p3882 A70-41279

Viscous fluid cylinders electromagnetodynamic stability, discussing viscous forces effects

21 p3858 A70-41699

Laminar-turbulent transition in magnetic field using Plexiglas model, observing inlet conditions effect on MHD flow stability

21 p3861 A70-42234

Collisionless plasma shock wave instability, discussing resonance and energy dissipation through ion Landau damping

22 p4077 A70-42292

Homogeneous plasma in uniform magnetic field, deriving theory for instabilities and LF wave propagation modes

22 p4079 A70-42370

LF self excited oscillations in inhomogeneous afterglow magnetoplasma measured by Langmuir probe, noting dissipative drift instabilities

22 p4079 A70-42372

Gas discharge positive column finite length effect on wave dispersion and instability, indicating critical magnetic field

22 p4079 A70-42374

Plasma inhomogeneity and drift effects on synchrotron radiation from relativistic charged particles in magnetoplasma

22 p4082 A70-43254

Potassium plasma-electron beam interaction, studying LF instability due to electron and ion heating

22 p4083 A70-43385

Monograph on MHD, covering fluid layer stability under adverse temperature gradient, geomagnetic field origin, vector relations, etc

22 p4084 A70-43448

Current oscillations produced in finite-length electron hole semiconductors by strong electric and magnetic fields, discussing HF stabilization

22 p4084 A70-43469

Helicon /magnetoacoustic waves/ effect on plasma instabilities, examining HF field amplitudes and magnetic fields

22 p4084 A70-43475

Solar wind instability from TEM waves propagating parallel to magnetic field in electron-proton plasma

23 p4235 A70-43826

Geomagnetic tail and plasma sheet hydromagnetic oscillations, deriving dispersion equations and stability conditions

23 p4184 A70-43829

MHD instability due to strong magnetic field induced scattering of plasma oscillations, using one sided Q device

23 p4223 A70-43949

Interplanetary plasma electron density inhomogeneities formation explained by instability due to electron stream curvilinearity obtained from spacecraft data

23 p4240 A70-44070

Plasmas kinetic theory, considering crossing from instability to stability, waves decay by collisional damping and emission by bremsstrahlung

23 p4224 A70-44178

Plasma macroscopic and microscopic instabilities derivation from MHD and Vlasov equations

23 p4224 A70-44180

Plasma physics computational problems concerning controlled thermonuclear reactions, considering instability and equilibrium numerical calculations

23 p4224 A70-44181

Critical Hall parameter for linear development of MHD electrothermal instability in bounded nonequilibrium plasma

23 p4227 A70-44555

Low beta surface ionized rotating streaming plasma column, determining low magnetic field effects on density and stability

23 p4229 A70-44988

Collisionless plasma, calculating effects of energy dissipation due to weak firehose instability on steady planar flow, based on quasi-linear fluid equations

24 p4382 A70-45110

Inertia effect on low density plasma losses in toroidal MHD equilibrium in model stellarator field

24 p4383 A70-45115

Uniform HF electric field effect on ion-acoustic oscillation instability in nonisothermal magnetized current-carrying plasma

24 p4383 A70-45118

LF drift-dissipative instabilities of HF skin layer in nonuniform plasma

24 p4383 A70-45119

Acoustic plasma wave excitation by transverse electromagnetic wave beam, calculating LF instabilities and energy losses

24 p4384 A70-45149

Velocity-space homogeneous plasma instabilities due to self interaction of single species

24 p4384 A70-45253

Electrical conductivity in inhomogeneous photosphere and sunspots, suggesting sunspot plasma instabilities

24 p4400 A70-45311

MAGNETOHYDRODYNAMIC WAVES

MHD stability of tangential discontinuities in solar wind flow

24 p4396 A70-45325

Discontinuity in solar wind energy and angular distribution from 2 January 1970 ESRO satellite HEOS-1 observation

24 p4396 A70-45326

Plasma-electron beam interaction instability transition from absolute to convective in hydrogen tube system at various pressures, considering electron collision effects

24 p4385 A70-45452

Plasma heated by cyclotron resonance using waveguide method, considering properties, confinement conditions and instabilities

24 p4385 A70-45453

Stable ellipsoidal plasma configurations in alternating electrode annular system, considering longitudinal magnetic field strength, electrode voltage and gas discharge chamber pressure

24 p4385 A70-45456

Theta pinch He plasma stability using cusp coils added to mirror coil ends

24 p4386 A70-45611

Plasma confinement in min-B configuration of linear multiple with mirrors, attaining additional stabilization via linear rods carrying unidirectional current

24 p4386 A70-45612

LF instability in plasma produced by electron cyclotron resonance in nonuniform magnetic and electromagnetic fields

24 p4386 A70-45613

Plasma jet motion stability in axial magnetic field of stellarator diverter and solenoid

24 p4386 A70-45660

Large amplitude high phase velocity oscillations anomalous damping in electron-ion plasma resulting from MHD instability

24 p4387 A70-46091

Ionized matter stability in intense radiation field opposed to gravitation, explaining quasar properties

24 p4398 A70-46162

Charged particle acceleration in outer space plasma, deriving ion-acoustic instability equations

24 p4399 A70-46295

MAGNETOHYDRODYNAMIC TURBULENCE

NT PLASMA TURBULENCE

MHD flow turbulence suppression at small magnetic Reynolds numbers, considering MHD interaction parameter role

10 p1924 A70-24575

Two dimensional MHD turbulence under strong magnetic field in Zeta device, measuring density, temperature, electric/magnetic fluctuations and various statistical characteristics

13 p2457 A70-28553

Mathematical background for strong turbulence analysis in liquids and MHD

13 p2457 A70-28554

MHD turbulence suppression by magnetic field in tubes, using conduction anemometers

15 p2778 A70-31480

Two dimensional hydromagnetic turbulence model for maintained seed field amplification, noting applications to star formation, stellar convection and gas cloud motions

15 p2781 A70-32813

Steady state frequency spectra for Alfvén waves and MHD turbulence in collisionless plasma with non-linear interaction by particle scattering

24 p4383 A70-45114

MAGNETOHYDRODYNAMIC WAVES

NT ELECTROSTATIC WAVES

NT PLASMA WAVES

MHD model for microwave solar circular polarization bursts interpretation, suggesting Alfvén wave disturbances in solar atmosphere

01 p0168 A70-10254

MHD wave propagation through plasma in magnetic field of current filament, developing Hamilton-Jacobi equation by geometrical optics

01 p0151 A70-10466

MHD wave propagation in electrically conducting fluid contained in finite length circular cylinder subject to axial magnetic field and nonelectromagnetic forces

01 p0152 A70-10944

Geomagnetic field directed hydromagnetic waves propagation in lower ionosphere noting inhomogeneous conductivity, Hall effect and lines of forces role

01 p0083 A70-11546

Plasma concentration diagnostics in magnetosphere based on hydromagnetic whistlers/pearls/ dispersion

01 p0084 A70-11554

Pc 1 range geomagnetic pulsation sweepers /MHD waves/ event in evening sector, considering delay time between sweepers appearance and polar magnetic substorms onset

02 p0290 A70-12121

Geostrophic baroclinic flow with zonal magnetic field in beta plane channel, analyzing instability, phase velocities, Alfvén-Rossby waves and Eady problem

02 p0291 A70-12284

Dispersion relation governing hydromagnetic gravity waves propagation in rotating nonisotropic medium, discussing effects of constant entropy gradient

04 p0745 A70-14473

Magnetized resonantly sustained HF plasma column wave properties, obtaining above-critical density as function of static magnetic induction

04 p0728 A70-14999

Transient plane disturbance of stream angular to applied magnetic field, discussing relationship to airfoil and Alfvén waves

04 p0615 A70-15093

Geomagnetic field lines inclination effect on hydromagnetic waves propagation in lower ionosphere, using atmospheric model in plane form with integral conductivity tensor

04 p0683 A70-15737

Monograph on MHD waves covering theories for weak discontinuities, wave propagation in inhomogeneous media and behavior in magnetic fields

06 p1114 A70-17275

Self similar flow patterns arising during cylindrical shock and detonation waves propagation in gas at rest, considering MGD shock waves

06 p1119 A70-17516

Wave focusing along static magnetic field from radiating VLF source immersed in cold magnetoplasma

06 p1120 A70-17577

MHD equations including energy dissipation terms applied to irreversible processes occurring in fast hydromagnetic shock waves in solar chromosphere

06 p1143 A70-17999

Redistribution of geomagnetically trapped 55 Mev protons by Starfish nuclear explosion, discussing hydromagnetic wave interactions and multiple reflections from magnetic field inhomogeneity

06 p1137 A70-18531

Weak discontinuities propagation in quasi-linear systems for MGD, obtaining transport equations

07 p1347 A70-18678

Outer ionosphere magnetoionic and MHD waves, combining electromagnetic and plasma kinetic theory with reference to satellite observations

07 p1264 A70-19188

Hydromagnetic ionizing shock wave structure in electromagnetic fields, using model composed of strong adiabatic shock to translational equilibrium followed by ionization ionization

07 p1351 A70-19985

Ionospheric absorption of hydromagnetic waves propagated normal to magnetic field, comparing daytime to nighttime absorption

[AFCR-70-0133] 07 p1270 A70-20031

Hydromagnetic wave interaction with magnetopause and bow shock, considering solar wind turbulence and magnetopause tail stability

07 p1270 A70-20070

Alfvén wave structure mechanism of geomagnetic micropulsation type in cometary tails, assuming Kelvin-Helmholtz instability at comet plasma-solar wind interface

08 p1565 A70-20567

Hydromagnetic emissions in high latitudes relationship to storm sudden commencements

08 p1491 A70-21715

Alfvén shear waves collisionless damping from finite Larmor radius coupling to ion acoustic mode, observing longitudinal electric field existence

10 p1921 A70-23966

Hydromagnetic emissions recordings at two Australian stations indicating simultaneous occurrence

10 p1875 A70-24441

Group velocity and propagation of hydromagnetic waves in ionospheric duct, comparing calculations and measured values

10 p1875 A70-24442

Ionosphere effect on toroidal magnetodynamic waves in idealized representation, analyzing oscillations correlation between adjacent magnetospheric shells

10 p1875 A70-24444

Dynamic equations for amplitudes of interacting MHD waves bounded plasma, discussing three-plasmon interactions

11 p2088 A70-25708

Alfvén and cylindrical magnetoacoustic waves in homogeneous unbounded conducting plasma in nonhomogeneous magnetic field, applying Weinberg method to propagation analysis

11 p2089 A70-25850

Evolutionary hydromagnetic shock perturbation by incident small amplitude hydromagnetic wave calculated for diverging wave amplitudes and directions

11 p2036 A70-26017

Trans-Alfvénic ionizing shock waves stability in absorption of rotational Alfvén disturbances

11 p2090 A70-26023

Drift instability of Alfvén waves at electron plasma sheet edge as source of auroral micropulsation instability

12 p2222 A70-27184

Alfvén waves wavelengths dependence on inhomogeneous magnetic field geometry in stationary plasma, using conformal transformations

13 p2462 A70-28984

LF MHD waves propagation model through earth magnetic tail, considering analogy with hydromagnetic plasma wave duct

13 p2398 A70-29210

Compressible fluids Alfvén flow with Hall effect presence of thin foils, reducing problem to Fourier integral equation

13 p2442 A70-29484

HF instabilities effect on magnetospheric drift waves, considering Alfvén mode in auroral plasma

13 p2482 A70-30084

Earth hydromagnetic dynamo spectrum fluctuation related to secular geomagnetic field variations, using unsteady kinematic models

14 p2568 A70-30202

One dimensional Alfvén fluctuation spectrum of magnetosphere in toroidal, crimping and twisting modes, using numerical integration

14 p2569 A70-30203

Bow shock associated hydromagnetic waves generation in upstream interplanetary medium, constructing model in terms of ion cyclotron resonance

14 p2631 A70-30359

Geomagnetic field lines inclination effect on hydrodynamic waves propagation in lower ionosphere, using atmospheric model in plane form with integral conductivity tensor

14 p2575 A70-30821

Elastohydrodynamic monochromatic wave coupling in liquid filled container as model for Alfvén and magnetoacoustic waves transmission in plasma

14 p2625 A70-31356

Geomagnetic pulsations and hydromagnetic wave propagation in magnetosphere, using geometric optics approximation

15 p2722 A70-31452

Weak discontinuities propagation in quasi-linear systems for MGD, obtaining transport equations

15 p2777 A70-31470

Alfvén wave structure mechanism of geomagnetic micropulsation type in cometary tails, assuming Kelvin-Helmholtz instability at comet plasma-solar wind interface

15 p2805 A70-32722

Approximate dispersion relation for MHD waves from macroscopic plasma equations including particle collision terms

16 p2859 A70-32941

Hydromagnetic shock waves structure, investigating resistive, viscous and thermal conduction dissipation effects on discontinuities

17 p3140 A70-34928

Hydromagnetic wave propagation compared in magnetospheres of plane and cylindrical geometries

18 p3311 A70-36011

Polarization splitting of EW and NS Alfvén oscillations in axisymmetric magnetosphere

19 p3409 A70-37319

Existence theorem for piecewise-continuous solutions of waves and shocks in relativistic MHD, using Riemann manifold

19 p3477 A70-37579

Thermodynamics and velocity of MHD shock waves in perfect conducting fluid, using compressibility conditions and relativistic Hugoniot equation

19 p3477 A70-37580

Relativistic effects for MHD Riemann waves in electrically conducting fluid

19 p3478 A70-37583

Ricci curvature tensor perturbations of space-time on Alfvén wave fronts

19 p3472 A70-38935

Cosmic ray electron and proton interaction, discussing hydromagnetic waves, synchrotron radiation, magnetic field effects and wave propagation

20 p3695 A70-39012

Alfvén magnetoacoustic waves interaction, deriving kinetic equation for distribution function and relaxation time

20 p3678 A70-39597

Perturbation method for nonlinear wave propagation in inhomogeneous media, considering sound propagation in ducts and hydromagnetic waves across nonuniform magnetic field

20 p3672 A70-39611

Alfvén waves amplification propagating along sinusoidally perturbed magnetic field in argon plasma, noting parametric excitation

21 p3855 A70-40947

Magnetosheath turbulence generation by hydromagnetic waves amplification carried by solar wind through earth bowshock, computing refracted and incident energy fluxes ratio

21 p3815 A70-41059

Inner magnetosheath large amplitude hydromagnetic waves, discussing power spectrum, earth bow shock and solar wind

21 p3816 A70-41083

Radioheliograph observations of solar outbursts involving MHD waves propagation along curved paths in corona at 80 MHz

21 p3891 A70-41178

Jump relations for shocks in anisotropic collisionless magnetized plasma

21 p3856 A70-41267

Alfvén waves synchrotron emission in incompressible medium, investigating generation by rotating DC current carrying circuit

21 p3861 A70-42227

Slow and fast ionization waves in inert gas or molecular gas plasma columns, describing striation formation in neon discharge by hydrodynamic equations

22 p4079 A70-42371

Large scale magnetic field and spiral shock pattern of Galaxy, using density-wave theory

22 p4103 A70-42981

Substorm aspects of magnetic pulsations, discussing classification, micropulsations, generation and propagation effects

22 p4019 A70-43145

Magnetosphere Alfvén velocity profile relation to ELF chorus and hiss, indicating unstable wave generation by cyclotron resonance

23 p4186 A70-43851

Cyclotron instability of high energy protons in magnetosphere with refraction of growing Alfvén waves

23 p4237 A70-44073

Steady state frequency spectra for Alfvén waves and MHD turbulence in collisionless plasma with nonlinear interaction by particle scattering

24 p4383 A70-45114

Chromospheric heating in magnetic field above supergranular cell boundaries, using geometric optics method for energy transport by hydromagnetic shock waves

24 p4400 A70-45304

Earth hydromagnetic dynamo spectrum fluctuation related to secular geomagnetic field variations, using unsteady kinematic models

24 p4330 A70-46277

One dimensional Alfvén fluctuation spectrum of magnetosphere in toroidal crimping and twisting modes, using numerical integration

24 p4330 A70-46278

MAGNETOHYDRODYNAMICS

Hypothetical magnetic configurations in presence of Coriolis forces from convective cell hydromagnetic activity in solar plasma, considering dynamos with increasing magnetic field

01 p0173 A70-10133

Spatial characteristics of magnetosheath magnetic field observed simultaneously by Explorer satellites, showing zero order agreement with prediction of MGD theory

01 p0071 A70-10410

Inertia effect of electrically conducting lubricant on load capacity of hydromagnetic inclined slider bearing under magnetic field

01 p0104 A70-11389

Pulsed MHD accelerator for MHD wind tunnel application, discussing accelerator gas source, magnetic field and operation

[AIAA PAPER 68-370] 03 p0462 A70-12907

Thin airfoil magnetoaerodynamics problem revised solution to avoid divergent integrals expressing kernels of integral equations

03 p0405 A70-12933

Hydrostatic thrust bearing with electrically conducting gas lubricant under axial current induced MGD pinch

03 p0497 A70-13780

Hydromagnetic forces effects on tidal period hydrodynamic waves, explaining ionospheric tidal motion behavior

03 p0478 A70-13995

Hydromagnetic normal ionizing shock wave properties in H and D mixtures and pure gases in SUPPER 2 shock wave tube

03 p0536 A70-14365

Applied MHD and high temperature gas dynamics - Conference, Prague, May 1968

04 p0724 A70-14526

Calculus of variations used for determining optimum one dimensional MHD slider bearing with bounded control variables

[ASME PAPER 69-WA/LUB-2] 04 p0698 A70-14771

Equations governing electrofluid dynamic energy conversion processes and indicating differences between EFD and magneto fluid dynamic processes presented for mechanical engineering problems

[ASME PAPER 69-WA/ENER-9] 04 p0627 A70-14899

Hydromagnetodynamic equations of two dimensional unsteady geostrophic wind field in turbulent ionosphere

04 p0680 A70-15254

Magnetohypersonic boundary layer interactions, discussing boundary layer thickness relationship to Hartmann and Reynolds numbers

04 p0729 A70-15564

Neutral H study of binary galaxies showing departures from circular symmetry, suggesting model involving hydromagnetic interaction 04 p0759 A70-15709

Magnetized solar wind steady state inviscid single fluid model developed using MHD, including heat equation with thermal conduction 05 p0902 A70-16445

Ohms law of electromagnetohydrodynamics derived on basis of Lorentz hydrodynamic plasma model, considering plasma conductivity 05 p0890 A70-16852

Load capacity of rotating field MHD hydrostatic thrust bearing increased by rotating axial magnetic field 06 p1076 A70-17527

Hypothetical magnetic configurations in presence of Coriolis forces from convective cell hydromagnetic activity in solar plasma, considering dynamos with increasing magnetic field 08 p1576 A70-21409

Artificial satellites MHD drag, noting altitude and temperature effects 10 p1921 A70-23834

Conducting gas unsteady efflux from plane tube into vacuum, determining time dependent position of expanding rarefaction wave fronts 10 p1924 A70-24569

Electrode erosion or entrainment in MPD arcs due to excess current density, considering inner cathode and outer ring anode with axial magnetic field 10 p1925 A70-25040

Magnetopause representation by mixing region of plasma streams with different velocities and magnetic fields, assuming hydromagnetic viscosity caused by wave-particle interactions 11 p2114 A70-26563

Working body properties effects on one component liquid-metal MHD system efficiency with vapor condensation cycle 12 p2164 A70-27329

Bounds in magnetofluidynamics for angular velocity of rotating fluid mass in relative equilibrium noting generalization of Poincare theorem 13 p2463 A70-29153

Hydromagnetic coupling between neutral and ionized atmosphere perturbations, noting role of gravity waves 13 p2397 A70-29191

Earth core flow velocity field to construct kinematic model of hydromagnetic dynamo, discussing magnetic field development 13 p2398 A70-29209

Axisymmetric bodies slow rotation or rotary oscillation in hydrodynamics and MHD using boundary value problems solutions 14 p2527 A70-30276

Solar wind interaction with moon, constructing mathematical model based on MHD equations and Explorer 35 data 14 p2630 A70-30356

Critical Mach numbers for transverse resistive shock waves as function of fluid/magnetic pressure ratio compared with cold plasma theory 14 p2623 A70-31036

MHD slider bearing load carrying capacity in tangential magnetic field, observing optimum profile in step form with riser location and step height ratio 18 p3263 A70-36672

Magnetohydrodynamic calculations, discussing various models, difference methods, codes, boundary conditions, etc 18 p3296 A70-36794

Galactic spiral arm helical magnetic fields related to interstellar gas flow, using magnetohydrodynamic models 18 p3331 A70-37200

Earth magnetic field, discussing origin, field absence on planets and moon and MHD theory 19 p3410 A70-37399

Classical and relativistic MHD - Conference, Lille, France, June 1969 19 p3476 A70-37576

Relativistic and nonrelativistic fluid dynamic equations, deriving limiting procedure leading to fluid magnetodynamic Lundquist equations 19 p3478 A70-37590

Variational principle application to relativistic MHD, deriving Einstein field equations, Maxwell equations and equations of motion for self gravitating charged fluid 19 p3478 A70-37591

Boundary value problems in MHD, considering viscous and nonviscous fluids 19 p3479 A70-37592

Calculus of variations used for determining optimum one dimensional MHD slider bearing with bounded control variables [ASME PAPER 69-WA/LUB-2] 19 p3436 A70-37620

Artificial ion clouds motion in magnetosphere, using MHD model 19 p3414 A70-38378

Suction velocity effects on Rayleigh problem in MHD of flat nonmagnetic nonconducting plate, solving for velocity distribution and skin friction 19 p3481 A70-38448

Solar magnetic field origin and behavior, discussing hydromagnetic dynamos, cyclonic convection and generation times 20 p3706 A70-39927

Magnetohydrodynamics - MIT Conference, Cambridge, Mass., March 1969 20 p3679 A70-39982

Magnetohydrodynamics - JPL Conference, Padasena, March 1970 20 p3565 A70-40001

MHD measurements of gas flow velocity and boundary layer in oxyhydrogen explosions in detonation tube 21 p3942 A70-40876

Spread electron beam excitation of magnetoactive plasma waves in quasi-linear relaxation 21 p3855 A70-40948

Working body properties effects on one component liquid-metal MHD system efficiency with vapor condensation cycle 21 p3760 A70-42070

Relative pressure and excitation induction transverse distribution relationship for MHD machine model, assessing dimensionless criteria effect on pressure peaks position 21 p3760 A70-42232

Conduction liquid metal MHD machine channels design with baffles installed to decrease shunting effect of end zones, calculating segments by circuit theory methods 21 p3760 A70-42233

Earth magnetic dipole represented by Rikitake two-disk MHD dynamo system 22 p4013 A70-42633

Plasma physics and MHD in astrophysics of sun and stars, discussing stellar magnetism origin and evolution, solar and stellar atmospheres, pulsars, etc 23 p4256 A70-45042

Porous media MHD equations for general case, considering magnetized sphere surrounded by homogeneous envelope 24 p4384 A70-45367

Pre-Maxwellian electromagnetic equations application to MHD, investigating existence theorems generalization from system at rest to system with motion 24 p4386 A70-45593

Relativistic gas bulk motion nonrelativistic equations, demonstrating spatially random fluctuations damp suprathermal hydromagnetic perpendicular propagation mode to interstellar magnetic field 24 p4397 A70-45761

MPD experiments in inductive hydrodynamic shock tube with round cross section and radial magnetic field 24 p0000 A70-45798

Full and half journal bearings in axial magnetic field, discussing hydromagnetic noncyclic squeeze fluid films 24 p4349 A70-45995

Radiative transfer and magnetic dispersion for three dimensional wave propagation in radiation magnetogasdynamics 24 p4387 A70-46148

MAGNETOIONIC PLASMA
U PLASMAS (PHYSICS)
MAGNETOIONICS

Magnetoionic mode coupling in satellite transmissions through ionosphere near transverse region, showing diurnal variations and error of electron content 02 p0259 A70-12563

Magnetoionic mode coupling in satellite transmissions through ionosphere near transverse region, using electron concentration profiles for night and daytime estimates 04 p0650 A70-15131

Outer ionosphere magnetoionic and MHD waves, combining electromagnetic and plasma kinetic theory with reference to satellite observations 07 p1264 A70-19188

Radio wave reflection from ionosphere, discussing suppression of magnetoionic component with fluctuating elliptical polarization 11 p2003 A70-25534

D region electron density profiles, using magnetoionic differential-phase partial-reflection technique 21 p3818 A70-41100

Radio wave reflection from ionosphere, discussing suppression of magnetoionic component with fluctuating elliptical polarization 21 p3786 A70-41284

Zi and Ze smallness effect on complex refractive index of ionosphere for VLF propagation 23 p4164 A70-44373

MAGNETOMETERS
NT VARIOMETERS

Airborne aeromagnetic gradiometer theory and design, using superconducting thin film tunneling junctions 01 p0085 A70-10289

Solar magnetic field investigated with parallel beam from coelostat mounting falling on magnetograph slit of solar telescope, noting field polarity change periodicity 01 p0177 A70-10347

Elastic couplings applied as sliding contact-free continuous junction between permanently rotating and fixed parts in rotating coil magnetometer 02 p0298 A70-12214

High altitude observatory solar magnetograph installation modifications including computer control, improved Zeeman effect observation instrument, etc 04 p0691 A70-15037

Miniature fluxgate magnetometer for sounding rocket measurements of two orthogonal components of external magnetic field, predicting performance by linear mathematical model 05 p0851 A70-16690

Deep freezing of nuclear precession magnetometer elements for improving instrument characteristics accuracy 05 p0851 A70-16769

Multichannel magnetograph display for pattern recognition of solar feature morphology compared with spectroheliograms 06 p1142 A70-17993

Lunar surface magnetometer data interpretation by analysis of moon motion relative to interplanetary magnetic field spatial irregularities, using lunar electrical conductivity models 07 p1378 A70-18974

Error estimation of gondola encased tugged undersea magnetometer as function of turbulence parameters 07 p1281 A70-19466

Quartz magnetometer design to measure horizontal component of geomagnetic field, observing stability of H/zero/ constant 07 p1281 A70-19467

Broadband remote sensing magnetometer for measuring fast-rising pulsed magnetic fields 09 p1676 A70-22716

Solar magnetograph modified to simplify calibration, using polarimeter with special exit slit geometry 11 p2057 A70-26650

Moving object angles of rotation averaging during single measurement of geomagnetic field vector components by quantum magnetometer 12 p2234 A70-27566

Superconducting magnetometers and cryogenic refrigeration techniques, discussing liquid helium refill systems, Joule-Thompson expansion, etc 13 p2414 A70-30027

Superconducting analog and digital magnetometers, discussing instrument principles and operational limitations 13 p2414 A70-30028

Magnetometers based on flux entry into superconducting rings, discussing sensitivity and noise sources 13 p2414 A70-30029

Crossing level resonances of magnetometer in optically pumped Rb87 atoms applied to weak field measurement 13 p2454 A70-30035

Optically pumped He 4 magnetometers, investigating magnetic resonance signal dependence on orientation for nonresonance technique construction 13 p2414 A70-30036

Magnetometer design based on Hg isotopes optical pumping, discussing sensitivity improvement 13 p2414 A70-30037

Servo type Cs vapor magnetometer performance including sensitivity, orientation effect, dynamic characteristics and operational temperature range 13 p2414 A70-30038

High sensitivity magnetometers based on magnetic nuclear resonance with electronic pumping 13 p2414 A70-30039

Nuclear magnetic resonance magnetometers performance using dynamic polarization by electronic pumping 13 p2414 A70-30040

Magnetometer for geomagnetic field declination measurement, eliminating thermal drift by light modulation method 13 p2415 A70-30042

Fluxgate and Ru vapor magnetometers for space measurements over wide field intensities, reducing electronic phase shift and experiment weight 13 p2415 A70-30045

Low and high apogee satellite and rocket magnetometers for space measurements, discussing self oriented fluxgate, proton, quantum cesium and three component types 13 p2415 A70-30047

High sensitivity conditions for rapid electronic spin resonance magnetometer 13 p2415 A70-30049

Stability requirements for precision magnetic field measurements on ground and in space, discussing magnetic balances and fluxgate magnetometers for geomagnetic variations and spacecraft attitude 13 p2415 A70-30050

MAGNETOMETRY

Constant and alternating magnetic field characteristics effects on magnetometric measurements in space near to and far from earth

13 p2401 A70-30052

Geomagnetic micropulsations recording by transistorized saturated core magnetometers noting sensitivity

13 p2416 A70-30055

Superconducting magnetic flux detector magnetic susceptibilities or field measurements

15 p2740 A70-32431

Nonmagnetic explosive actuated indexing device permitting precise 180 deg rotation of magnetometer sensor on Pioneer 6 spacecraft

16 p2914 A70-34124

Nonmagnetic lightweight oscillating actuator for multiple indexing of spacecraft magnetometer

16 p2845 A70-34128

ALSEP magnetometer mission and environmental requirements and mechanical design

16 p2914 A70-34152

Active RC bandpass filter for space fluxgate magnetometer, using state variable synthesis

17 p3054 A70-35526

Fabry-Perot interferometer series as tunable optical narrow passband filter with high spectral and angular resolution, discussing performance in solar magnetograph

17 p3097 A70-35872

Error estimation of gondola encased tugged undersea magnetometer as function of turbulence parameters

18 p3260 A70-36940

Quartz magnetometer design to measure horizontal component of geomagnetic field, observing stability of H/zero/constant

18 p3260 A70-36941

LF geomagnetic micropulsations recordings by two component induction magnetometer, relating diurnal frequency and occurrence variations to local K-index changes

19 p3412 A70-37995

Lunar surface local magnetic field measurement, describing Apollo 12 magnetometer

20 p3709 A70-40087

Low noise FET amplifier for satellite magnetometer, measuring interplanetary fields

21 p3799 A70-41923

Helios solar probe magnetic field measurements, discussing magnetometer systems, interplanetary magnetic field implications, shock waves, magnetic storms, etc

21 p3923 A70-42172

Optically pumped magnetometers for low intensity magnetic fields measurement, reviewing atomic hyperfine levels splitting, magnetic resonance, Zeeman sublevels, etc

22 p4026 A70-42575

Solar activity research, discussing optical facilities, photoelectric magnetographs, magnetic field measurement, solar cycles and flares, etc

23 p4256 A70-45034

Vertical supergranular motions in solar atmosphere from multichannel magnetograph observations

24 p4400 A70-45306

MAGNETOMETRY

U MAGNETIC MEASUREMENT

MAGNETOPOUSE

Magnetopause shape determination model allowing for solar wind direction obliquely toward geomagnetic dipole axis

03 p0560 A70-13984

Plane magnetopause models assuming ionospheric electrons ability to short circuit electric fields, constructing distribution functions by Vlasov theory

05 p0840 A70-16568

Hydromagnetic wave interaction with magnetopause and bow shock, considering solar wind turbulence and magnetopause tail stability

07 p1270 A70-20070

Asymptotic behavior in cold plasma model of magnetopause, describing boundary layer between plasma stream and vacuum magnetic field

10 p1921 A70-23835

Magnetopause boundary between shocked streaming solar plasma and geomagnetic tail observed at lunar orbit by magnetometer on Explorer 35

10 p1941 A70-24436

Magnetopause representation by mixing region of plasma streams with different velocities and magnetic fields, assuming hydromagnetic viscosity caused by wave-particle interactions

11 p2114 A70-26563

Magnetopause model, discussing equilibrium layer between magnetic field and cold plasma field-free stream

13 p2396 A70-29181

Magnetic fluctuations observed by ground observatories, suggesting large amplitude waves as field line resonances driven by magnetopause motion

13 p2402 A70-30078

Electrostatic discharge at magnetopause by idealized circuit analog, discussing transmission lines and terminal impedances

14 p2579 A70-31247

Polar substorm activity associated with magnetopause position variation, using Imp 2 satellite observations

15 p2728 A70-31911

Plasma properties across bow shock and in magnetosheath as function of supersonic solar wind

19 p3494 A70-37481

Solar energetic charged particles interaction with earth bow shock and magnetopause

19 p3494 A70-37482

Earth surface magnetic field variations due to magnetopause current system

24 p4329 A70-45355

MAGNETOPLASMAS

U PLASMAS [PHYSICS]

MAGNETORESISTANCE

U MAGNETORESISTIVITY

Magnetoresistance effects in impurity conduction mode of n-type GaAs crystals below 6 K, giving electron concentration

07 p1356 A70-19796

Parallel and perpendicular negative magnetoresistance measurements as function of magnetic field in p-type GaAs at 77 K

13 p2471 A70-29374

Magnetite and ferrite spinels Hall effect, magnetoresistance and electrical conductivity over wide temperature range

19 p3485 A70-37627

Carbon resistors negative magnetoresistance measurement near absolute zero temperature by helium cryostat, noting anisotropy

20 p3687 A70-40168

Magnetoresistance nonlinearity and Hall effect in graphite in magnetic field, observing temperature dependence below 4.2 K

21 p3862 A70-40945

MAGNETOSONIC RESONANCE

Drift instability and ion heating by high amplitude magnetosonic wave in plasma waveguide in constant magnetic field

13 p2463 A70-29381

Gas parameters determination near singular point of slow magnetosonic wave propagating in conducting medium in uniform magnetic field

13 p2464 A70-29507

Magnetosonic resonance excitation in waveguide winding wrapped around plasma cylinder

22 p4082 A70-43380

MAGNETOSPHERE

NT GEOMAGNETIC TAIL

NT MAGNETOPOUSE

Solar wind-induced drag resulting from collisionless plasma shock on sunward-side of large magnetic comet, using similarity with earth magnetosphere

01 p0168 A70-10258

Spatial characteristics of magnetosheath magnetic field observed simultaneously by Explorer satellites, showing zero order agreement with prediction of MGD theory

01 p0071 A70-10410

Geomagnetic micropulsations relation to magnetospheric boundary location on sun-earth line, noting influence of solar wind pressure variations

01 p0071 A70-10412

Ionospheric auroral oval, proton aurora and midlatitude trough relationship to magnetospheric structure, trapping outer boundary, storm time belt and plasmopause

01 p0073 A70-10586

Physical processes responsible for conjugate point phenomena involving particles and waves in magnetosphere and IQSY observations

01 p0075 A70-10598

Cerenkov radiation from electrons in magnetosphere and ionosphere, analyzing radiated power relationship with frequencies and latitudes

01 p0080 A70-11226

Normal and anomalous Doppler shifted cyclotron power radiated by energetic electrons spiralling along geomagnetic line considered as VLF source from magnetosphere

01 p0080 A70-11227

Interplanetary plasma flow simulation around earth magnetosphere and planets not considering initial conditions influence

01 p0172 A70-11488

Magnetospheric ring current model from ground stations data to interpret observed magnetic field disturbances

01 p0082 A70-11515

Mariner 2 measurements of geomagnetic field and interplanetary plasma parameters, analyzing interaction between interplanetary medium and magnetosphere during decreased solar activity

01 p0192 A70-11520

Dipole magnetosphere model with cylindrical or spherical forbidden band for studying plasma motion in quasi-hydrodynamic approximation

01 p0082 A70-11521

Magnetosphere boundary configuration calculated with allowance for geomagnetic dipole inclination to geographic axis and nondipole section of geomagnetic field

01 p0082 A70-11522

Magnetic lines of force penetration into magnetosphere accompanied by plasma insertion generating ring current responsible for main phase of magnetic storm

01 p0083 A70-11543

Plasma concentration diagnostics in magnetosphere based on hydromagnetic whistlers/pearls/dispersion

01 p0084 A70-11554

Earth daily rotation effects on magnetosphere electric currents, discussing Pederson currents in dynamo region and E region ionization

02 p0293 A70-12775

Geomagnetic perturbation coincidences observed at conjugate Polar Cap observatories, suggesting magnetospheric tail field lines convergence with plasma neutral layer

03 p0565 A70-13232

Earth magnetosphere low energy plasmas measurements via McIlwain magnetic shell parameter, showing dependence on geomagnetic disturbances

03 p0557 A70-13284

Ground observations synoptic distribution importance in studying magnetosphere, emphasizing polar caps

03 p0475 A70-13849

Magnetosphere dynamic morphology model, including qualitative phenomena

03 p0475 A70-13850

Plane model of magnetosphere shape and structure, considering rarefied plasma flow past two dimensional magnetic dipole with dynamic and static boundary pressure, using conformal mapping

04 p0675 A70-14435

Magnetospheric magnetic field disturbance due to abrupt solar wind parameters change, using Explorer 26 data

04 p0738 A70-14444

Earth magnetosphere electric fields associated with magnetic disturbances, using satellite observations

04 p0676 A70-14459

Magnetospheric observations of whistler mode emissions byOGO 1 satellite over VLF and LF ranges

04 p0649 A70-15117

Rarefied plasma motion in geomagnetic dipole equatorial plane near magnetosphere symmetry axis deriving approximate solution to quasi-hydrodynamic equations

04 p0681 A70-15717

Inhomogeneous fast electron clouds stability and perturbation dynamics captured in magnetosphere geomagnetic field described by hydrodynamic equations

04 p0743 A70-15721

Neutral sheet instabilities in magnetotail from collisionless plasma instabilities from shear magnetic field

05 p0887 A70-15911

Numerical analysis of cyclotron amplification of geomagnetic micropulsations in magnetosphere based on dispersion relation for three component cold plasma beam system

05 p0838 A70-16284

Stably trapped magnetospheric plasma distribution determined from P12 micropulsations and auroral electrojet index AE

05 p0839 A70-16285

Earth bow shock and magnetopause oscillatory motions with respect to positions assumed under quiet solar wind conditions, discussing satellite observations

05 p0840 A70-16586

Low energy charged particle motion parallel with magnetic force lines analyzed in magnetosphere model with constant electric field

05 p0903 A70-16726

Pc 2-4 geomagnetic pulsations abrupt disappearance on global scale ascribed to magnetosphere boundary stabilization, noting interplanetary magnetic field role

05 p0843 A70-16766

Magnetospheric VLF emissions properties at frequencies below electron gyrofrequency

06 p1117 A70-17374

VLF and ULF whistler modes propagating along geomagnetic field-line paths in magnetosphere, studying cyclotron resonance amplification

06 p1118 A70-17379

Dynamic behavior of earth magnetosphere, discussing geophysical micropulsations, geomagnetic field diagnostics, cold plasma density, etc

06 p1139 A70-17535

Large scale artificial plasma cloud experiments for magnetosphere, solar wind and cometary physics, discussing Ba ion and ice clouds released by satellites [AJAA PAPER 70-33]

06 p1145 A70-18183

Whistler amplification in magnetosphere for electron interaction with background plasma to produce wave growth, discussing stability of various anisotropic velocity distributions

06 p1059 A70-18533

Three dimensional model current system with magnetospheric and ionospheric sections connected by currents flowing along geomagnetic field lines proposed for polar magnetic substorms

06 p1059 A70-18535

Plasmopause observations by ion spectrometer aboardOGO-5 vehicle for early orbits, obtaining O,

He and H ion concentration profiles for geomagnetic parameter

06 p1059 A70-18546

Earth magnetosphere physics, considering solar plasma flow, ring currents, charged particles during magnetic storms, solar wind energy transfer, etc

06 p1060 A70-18552

Magnetosphere and interplanetary space diagnostics by micropulsations analysis, discussing geomagnetic cavity boundary, cold plasma density, energetic particles, etc

07 p1264 A70-19191

Cerenkov generation of VLF waves in inner magnetosphere at low latitudes

07 p1265 A70-19281

Solar proton flares radiometric measurement on-board Molniya 1 satellite, detecting intensities in outer regions of magnetosphere

07 p1366 A70-19428

Electron diffusion in magnetosphere, describing experimental model

07 p1367 A70-19494

Lunar periodicity detected from radio aurora data as possible cause of lunar interaction with magnetosphere

07 p1389 A70-20164

Plasma flow structure near frontal point in earth magnetosphere, using quasi-hydrodynamic two dimensional model to obtain power series solution

07 p1391 A70-20419

Earth ionosphere and magnetosphere electrodynamic state as function of neutral gas small scale motions, considering magnetic disturbances and ionospheric discontinuities

07 p1276 A70-20426

Plasma concentration in nondipole magnetosphere model from Pc 5 pulsations periods for high geomagnetic latitudes, noting solar winds effect

07 p1277 A70-20443

Faculae and flocculi intensity relationship to orientation of magnetic fields in solar photosphere and magnetosphere

08 p1560 A70-20837

Space research in terms of earth environment in space, discussing near-earth spacecraft role in solar, magnetospheric and ionospheric studies

08 p1488 A70-21344

Magnetic equator ELF noise examined with OGO 3 magnetometer, indicating unique signals in plasmasphere

08 p1488 A70-21380

Plasma temperatures in magnetosphere, investigating ion energy balance, electron heating and agreement with rocket measurements

08 p1489 A70-21381

Magnetosphere model for quasi-circular precipitation zones of energetic particles based on geomagnetic activity distribution patterns

08 p1489 A70-21385

Geomagnetic perturbation coincidences observed at conjugate Polar Cap observatories, suggesting magnetospheric tail field lines convergence with plasma neutral layer

08 p1580 A70-21665

Energy distribution of solar wind alpha particles in magnetosheath observed by Heos A satellite

09 p1744 A70-22305

Earth magnetosphere and magnetosheath magnetic field measurements by Mariner 5

09 p1670 A70-23487

Magnetic disturbances caused by magnetosphere-solar wind filamentary inhomogeneity interaction observed by Pioneer 6

10 p1931 A70-24320

Plasmaspheric columnar electron content determination up to plasmapause by ATS-3 beacon transmitter and combining differential Doppler frequency and Faraday rotation angle methods

10 p1874 A70-24430

Ionosphere effect on toroidal magnetodynamic waves in idealized representation, analyzing oscillations correlation between adjacent magnetospheric shells

10 p1875 A70-24444

Geomagnetic pulsations /pc 4/ characteristics from analyzing magnetosphere model yielding plasma densities consistent with experimental data

10 p1875 A70-24483

Magnetospheric substorms magnetograms taken at various stations, showing preceding ring storm particles deflection into magnetic tail

10 p1876 A70-24496

Magnetosphere large-scale motions dependence on earth magnetic axis inclination against rotational axis

10 p1885 A70-25279

Charged particle motion in steady and perturbed dipole fields using laboratory earth magnetosphere plasma model

11 p2104 A70-25546

Plasma density and velocity required for simulating solar wind flow over magnetosphere /bow shock/ in plasma wind tunnel

11 p2032 A70-26372

Geomagnetic damped type pulsations associated with storms interpreted as interaction between hydromagnetic oscillations and magnetospheric motions caused by solar wind

11 p2047 A70-26567

Monograph on ambipolar diffusion and motion in stability of satellite produced artificial barium ion clouds in ionosphere and magnetosphere

11 p2048 A70-26825

Interplanetary and magnetospheric plasma structures experiments and theory

12 p2298 A70-27060

Energetic electron layer near magnetopause attributed to geomagnetic activity from satellite observations of fluxes

12 p2292 A70-27180

Ultra low frequency waves features in magnetosphere, considering geomagnetic pulsations, magnetic data from Explorer 33 and bounce resonance

12 p2223 A70-27573

Very low frequency radio noise in ionosphere, magnetosphere and solar wind, using multiple receivers to measure mathematical relations between direction magnitude and polarization characteristics

12 p2184 A70-27574

Ionospheric lowest regions and magnetosphere probing based on atmospheric observations, detecting disturbed conditions

12 p2224 A70-27734

Soft electron fluxes spatial distribution and temporal variations in magnetosphere based on Elektron 2 charged particle trap data

12 p2295 A70-28259

Plasmasphere ion concentration measurements on-board Elektron 2 and 4 satellites, observing dependence on geomagnetic activity

12 p2295 A70-28260

Plane model of magnetosphere shape and structure, considering rarefied plasma flow past two dimensional magnetic dipole with dynamic and static boundary pressure, using conformal mapping

13 p2392 A70-28460

Magnetospheric magnetic field disturbance due to abrupt solar wind parameters change, using Explorer 26 data

13 p2475 A70-28469

Cosmic rays emission by dipole magnetosphere, applying model to neutron star particle belts

13 p2476 A70-28893

Energy spectrum and equatorial pitch angle distribution of charged particles trapped in magnetosphere resulting from inward diffusion due to third adiabatic invariant violation

13 p2476 A70-28942

Plasmapause and polar wind, considering density discontinuity due to outer magnetosphere heating during magnetic storms

13 p2491 A70-29059

Magnetosheath plasma measurements by Pioneer 6 during outbound passage in dusk meridian, comparing results with various predictions

13 p2396 A70-29180

Plasmapause irregular structure and position indicated by measured distributions of hydrogen and helium thermal positive ions in duskside magnetosphere

13 p2397 A70-29185

Radio sounding of Van Allen inner belt from Antarctica, comparing American and Soviet deductions about magnetosphere structure

13 p2399 A70-29273

Perpendicular propagation of VLF waves from wave/particle interaction in vicinity of lower hybrid resonance frequency in magnetosphere

13 p2468 A70-29934

Solar wind effect on structure of magnetic field in magnetosphere and interplanetary space, noting interaction with moon

13 p2498 A70-30051

Magnetic field measurement of VLF wave propagating in whistler mode in magnetosphere by satellite FR-1

13 p2401 A70-30054

Particles and fields in magnetosphere - Conference, Santa Barbara, August 1969

13 p2479 A70-30058

Solar cosmic rays entry into magnetosphere, showing entrance on smoothly connected field lines

13 p2480 A70-30059

Model current system for magnetospheric substorm accounting for distribution of geomagnetic disturbance field vectors on earth surface and auroral electrons and protons

13 p2481 A70-30062

Magnetospheric convection models and effects on charged particle populations

13 p2402 A70-30064

Plasmapause position and density profile from ion concentration measurements by OGO-5, determining reaction to magnetic variations

13 p2482 A70-30074

Geomagnetic field distortion in high beta magnetospheric regions from OGO observations for quiet and slightly disturbed conditions

13 p2402 A70-30076

HF electrostatic waves generation by electrons in magnetosphere

13 p2482 A70-30083

Plasma wave particle interactions in outer magnetosphere, magnetosheath and solar wind, noting role of AC electric fields

13 p2483 A70-30085

Hydromagnetic wave velocity and space anisotropy instabilities in magnetosphere, using dispersion relation

13 p2483 A70-30086

Low energy charged particle distribution within earth magnetosphere and environs, suggesting solar origin for storm time ring current protons

13 p2483 A70-30089

Trapped alpha particle and proton spectra from satellite measurements, considering magnetosphere injection

13 p2484 A70-30093

Magnetospheric particles, fields, electromagnetic waves and data on collisionless bow shock structure

13 p2484 A70-30098

One dimensional Alfvén fluctuation spectrum of magnetosphere in toroidal, crimping and twisting modes, using numerical integration

14 p2569 A70-30203

Magnetosphere boundary altitude dependence on longitude, considering role of electric current density along geomagnetic lines of force

14 p2570 A70-30217

Magnetospheric tail neutral layer magnetic field distribution, comparing satellite data with theory

14 p2570 A70-30222

Morphology of thermal and energetic particles in inner magnetosphere during geomagnetic disturbances and solar cycles

14 p2630 A70-30358

Mathematical model for interaction of solar wind with geomagnetic field, predicting magnetosphere shape

14 p2574 A70-30736

Rarefied plasma motion in geomagnetic dipole equatorial plane near magnetosphere symmetry axis by deriving approximate solution to quasi-hydrodynamic equations

14 p2575 A70-30801

Inhomogeneous fast electron clouds stability and perturbation dynamics captured in magnetosphere geomagnetic field described by hydrodynamic equations

14 p2632 A70-30805

Magnetosphere topology in presence of time independent ring current symmetrical with respect to earth dipole field axis

14 p2578 A70-31242

Magnetospheric dynamic processes leading to energetic and thermal auroras in middle latitudes

14 p2581 A70-31267

Book on geomagnetic micropulsations covering dynamic processes of magnetically trapped particles and micropulsations usability in remote sensing of magnetosphere

14 p2581 A70-31325

Geomagnetic pulsations and hydromagnetic wave propagation in magnetosphere, using geometric optics approximation

15 p2722 A70-31452

VLF wave propagation direction observation by satellite after passage through magnetosphere at low and mid latitudes

15 p2697 A70-31659

Report to COSPAR on Japanese space research including satellite, rocket and balloon observations of ionosphere, magnetosphere, interplanetary space, moon, planets, cosmic rays, etc

15 p2830 A70-31720

Longitudinal electric field effect on trapped particle motion in asymmetrical magnetosphere, considering electron precipitation

15 p2728 A70-31990

Terrestrial magnetosphere dynamics in magnetospheric disturbances, analyzing solar wind-geomagnetic field interaction and storm development

15 p2729 A70-32080

Magnetosphere survey, including solar wind flow theory, observational techniques, radiation belt theory, magnetic storms, etc

15 p2732 A70-32544

Electron diffusion in magnetosphere, describing experimental model

15 p2795 A70-32739

Longitudinal and transverse electric field effects in magnetospheric electron precipitation, discussing trapped particle drift

16 p2972 A70-34188

Solstitial solar quiet currents along magnetic lines of force in magnetosphere, discussing ionospheric wind asymmetry effects

17 p3077 A70-34949

Pi 2 pulsation power spectra change with magnetospheric substorm development, relating pulsations and electron precipitation

17 p3080 A70-35641

Solar protons penetration into magnetosphere and magnetotail

18 p3306 A70-36004

Magnetic storms development via initial asymmetric inflation of evening magnetosphere, using Explorer 26 and ground observatory data

18 p3311 A70-36008

Hydromagnetic wave propagation compared in magnetospheres of plane and cylindrical geometries

18 p3311 A70-36011

Magnetospheric plasmapause duskside bulge dynamic behavior during substorms, using whistler data

18 p3312 A70-36013

Magnetospheric electric field configuration from trapped particle flux asymmetries, using Explorer 14 electron data

18 p3306 A70-36024

High latitude magnetosphere structure, using two dipole model

18 p3312 A70-36168

Solar proton flares radiometric measurement on-board Molniya 1 satellite, detecting intensities in outer regions of magnetosphere

18 p3309 A70-36902

Magnetosphere dynamics relationship with inhomogeneous electron density formation in F region, discussing scattering diurnal variations and intensity in magnetically conjugate points

18 p3255 A70-37035

Magnetospheric plasma concentration from geomagnetic pulsations periods

19 p3409 A70-37320

Nondipole geomagnetic field effect on magnetosphere boundary, presenting graphs for distance dependence on polar angle

19 p3409 A70-37321

Temporal and spectral changes in solar protons and alpha particles access to synchronous altitude in magnetosphere

19 p3494 A70-37485

Low energy solar protons temporal and spatial variations in magnetosphere by data comparison from polar orbiting satellite and Explorers 33 and 34

19 p3494 A70-37486

Trapped particle population changes associated with solar events, discussing solar wind discontinuity effects on magnetosphere

19 p3495 A70-37487

High latitudes magnetospheric electric field structure, using electrostatic probes and artificial clouds

19 p3410 A70-37489

Plasma tearing instabilities involving topological changes in magnetosphere field configuration

19 p3411 A70-37491

Polar cap absorption correlation with solar protons flux into magnetosphere, discussing diurnal and spatial variations and magnetic storm effects

19 p3411 A70-37492

Van Allen electrons acceleration and precipitation during magnetospheric substorms in relation to auroral processes, discussing energy and pitch angle diffusion processes

19 p3411 A70-37495

Artificial ion clouds motion in magnetosphere, using MHD model

19 p3414 A70-38378

Geomagnetic field configuration and magnetic drift envelopes of particles with various pitch angles at equator calculated from two-dipole model of magnetosphere

20 p3619 A70-39299

Plasmapause motion in equatorial plane under sudden dawn-dusk field with constant solar wind-magnetosphere interaction

20 p3620 A70-39341

Inner magnetosphere magnetic field mapping, deriving Pogo model

20 p3621 A70-39349

Solar wind static and dynamic pressures on earth magnetosphere, using geomagnetic parameters

21 p3878 A70-40845

Magnetosheath turbulence generation by hydromagnetic waves amplification carried by solar wind through earth bowshock, computing refracted and incident energy fluxes ratio

21 p3815 A70-41059

Steady state magnetic and electric fields in magnetosheath by linear superposition of field vectors, using axisymmetric velocity function from gas dynamics

21 p3815 A70-41063

Inner magnetosheath large amplitude hydromagnetic waves, discussing power spectrum, earth bow shock and solar wind

21 p3816 A70-41083

Ionsospheric conductivity effects on plasma convective flow in determining magnetospheric electric fields distribution

21 p3816 A70-41084

Auroral arcs formation model based on dynamic magnetosphere-ionsosphere interaction

21 p3817 A70-41089

Charged particle motion in steady and perturbed dipole fields using laboratory earth magnetosphere plasma model

21 p3882 A70-41296

Earth magnetosphere LF wave annular trap, examining high energy particle interaction with magnetosonic waves

22 p4013 A70-42300

Solar-magnetospheric neutral sheet reconnection and noise in geomagnetic tail from Explorer 33 Ames magnetometer

22 p4013 A70-42471

Large scale electric fields in ionosphere, magnetosphere and interplanetary space, considering further needs for theoretical and observational investigations

22 p4099 A70-42782

Collisionless magnetospheric plasma turbulent conductivities for weak and strong electric fields parallel to magnetic field

22 p4016 A70-42787

Magnetospheric tail magnetic field and particle motion calculation, assuming constant radius cylinder with current sheet bisecting center

22 p4019 A70-43111

Pulsar emission mechanisms, discussing possible magnetospheric physics role and optical pulse generation

22 p4105 A70-43217

Plasma-TEM wave nonlinear interactions in magnetosphere, discussing atmospheric occurrence

22 p4021 A70-43276

Magnetosphere radio propagation from ground based measurements for HF, ULF and VLF

22 p4021 A70-43280

Magnetospheric thermal plasma studies via ground based whistler method, identifying radial and longitudinal irregularities in electron density, bulk motion and plasmapause position and displacements

22 p4021 A70-43281

Micropulsations as diagnostic tool for magnetospheric research, explaining ULF and VLF results variances

22 p4021 A70-43282

Magnetospheric plasma parameters from ground observation data of Pc-1 type micropulsations, assuming radiation belt plasma cyclotron instability

22 p4022 A70-43283

Magnetospheric and magnetic storms correlated to solar wind energy penetration, noting roles of energetic plasma and magnetospheric low energy plasma convection

22 p4022 A70-43287

Magnetosphere storm diagnostics from geomagnetic, auroral and airglow parameters, discussing calibration via satellite observations

22 p4022 A70-43289

Geostationary satellites for magnetosphere and ionosphere sounding, discussing specific observational capabilities

22 p4024 A70-43397

Virial theorem for magnetospheric dynamics, discussing boundary and ring currents and densities and geomagnetic sudden impulses and commencement

23 p4184 A70-43830

Electron densities between inner edge plasma sheet and plasmasphere as function of geocentric radial distance from OGO-3 electrostatic measurements

23 p4236 A70-43834

ELF emissions dependence on plasmapause location in magnetosphere indicated from OV-3 observations

23 p4186 A70-43847

Electron precipitation latitude extent and drift rate magnetospheric substorms from ESSA riometer data

23 p4186 A70-43850

Magnetosphere Alfvén velocity profile relation to ELF chorus and hiss, indicating unstable wave generation by cyclotron resonance

23 p4186 A70-43851

Magnetospheric substorms model modification for growth phase inclusion prior to explosive expansion phase

23 p4186 A70-43853

Nonlinear frequency shift for electronic and ionic cyclotron modes in magnetospheric whistler and hydrodynamic propagation, using Vlasov equation

23 p4187 A70-43880

Geomagnetic perturbation effects on conduction along field lines and short period fluctuations associated with plasma turbulence in magnetosphere

23 p4189 A70-44065

Magnetic field and electron flux observations near magnetopause via magnetometer and triaxial electron spectrometer on OGO-E

24 p4328 A70-45350

Diurnal variations of photoelectron heat fluxes and energy production by thermal coupling between upper F2 region and magnetosphere

24 p4328 A70-45354

One dimensional Alfvén fluctuation spectrum of magnetosphere in toroidal crimping and twisting modes, using numerical integration

24 p4330 A70-46278

Magnetosphere boundary altitude dependence on longitude, considering role of electric current density along geomagnetic lines of force

24 p4331 A70-46292

Magnetospheric tail neutral layer magnetic field distribution, comparing satellite data with theory

24 p4331 A70-46297

MAGNETOSPHERIC ELECTRON DENSITY

Spacecraft surface secondary electron emission effects on electron trap measurements in magnetosphere and solar wind, noting agreement with positive ion densities

03 p0561 A70-13994

Whistlers role in ionospheric temperature, magnetospheric electron density and ionospheric composition determination

07 p1347 A70-19189

Magnetospheric plasmapause-high latitude electron density trough relations using satellite topside ionograms, noting local time and magnetic disturbance effects

07 p1270 A70-20074

Statistical correlation between polar magnetic disturbances and magnetospheric energetic electron flux increase from IMP-1 satellite observations

08 p1491 A70-21714

Magnetospheric discrete VLF emission magnetic field intensity calculation by extending Helliwell theory to include electron density model and variable frequency waves

13 p2483 A70-30087

Magnetospheric charged particle distributions in plasma sheet, pseudo- and stable-trapping regions by satellite observation

13 p2483 A70-30088

Magnetospheric protons and electron energy spectra time and magnetic activity dependence during solar maximum

15 p2792 A70-31671

Electron density large scale structure in plasmasphere identified from whistlers recorded at Antarctica near sunspot minimum

18 p3311 A70-36012

Magnetospheric thermal plasma electron density measurement during solar flare by OGO-5 satellite

19 p3411 A70-37513

Ionized magnetospheric tubes electron content, determining ionization interchange between F region and protonosphere by whistler observations

20 p3584 A70-39332

Ionosphere and magnetosphere total electron content from beacon method of measuring difference-differential-doppler (DDD) and Faraday effects via synchronous satellite signal frequencies

20 p3590 A70-40484

MAGNETOSPHERIC INSTABILITY

Regular/irregular micropulsations variations during solar cycle, noting possible magnetospheric contraction and solar wind velocity influence

01 p0075 A70-10600

Short irregular geomagnetic pulsations repetitive characteristics relationship with magnetospheric cavity dimensions

01 p0081 A70-11229

Real configuration effect of magnetic field in moderately perturbed magnetosphere on whistlers dynamic spectra, stressing geomagnetic perturbation detection

01 p0082 A70-11486

Tropospheric circulation transformation from meridional to zonal forms due to macrostructure activity of solar wind, considering magnetosphere perturbations

03 p0559 A70-13757

Equatorial magnetosphere particle and field data from 18 April 1965 geomagnetic storm reanalyzed in context of drift mirror instability theory

03 p0560 A70-13976

Ionogram conjugate echoes observed at Singapore longitudes by Alouette 2 topside sounder, attributing sequential occurrence to field-aligned irregularities in magnetosphere

03 p0477 A70-13986

Chapman-Ferraro two dimensional problem with neutral sheet, investigating magnetospheric flows and time dependence

04 p0679 A70-15109

Unsteady state and transit time analysis of geoeffective interplanetary plasma flux observed near earth causing magnetospheric storm of 17-19 April 1965

04 p0683 A70-15736

Geomagnetic tail natural oscillations, studying magnetospheric substorms role

07 p1268 A70-19499

Hydromagnetic wave interaction with magnetopause and bow shock, considering solar wind turbulence and magnetopause tail stability

07 p1270 A70-20070

Broadband and highpass LF noise in distant magnetosphere detected by VLF/LF experiment on OGO 1 satellite

12 p2222 A70-27183

Finite Larmor radius interchange and LF drift oscillations due to magnetospheric temperature and density gradient stresses in trapped plasma

13 p2401 A70-29936

HF instabilities effect on magnetospheric drift waves, considering Alfvén mode in auroral plasma

13 p2482 A70-30084

- Aurora band theory based on three dimensional current system during magnetic substorms, discussing field aligned sheet current instability
14 p2573 A70-30671
- Unsteady state and transit time analysis of geoeffective interplanetary plasma flux near earth causing magnetospheric storm of 17-19 April 1965
14 p2575 A70-30820
- Polar substorm activity associated with magnetopause position variation, using Imp 2 satellite observations
15 p2728 A70-31911
- Geomagnetic tail natural oscillations, studying magnetospheric substorms role
15 p2732 A70-32744
- Electric field strength in earth ionosphere and magnetosphere during irregular motion of fast ions and electrons
19 p3407 A70-37303
- Polarization splitting of EW and NS Alfvén oscillations in axisymmetric magnetosphere
19 p3409 A70-37319
- LF electrostatic instability of Van Allen belt in outer trapping zone causing electric field in plasmopause
22 p4099 A70-42786
- Substorm aspects of magnetic pulsations, discussing classification, micropulsations, generation and propagation effects
22 p4019 A70-43145
- Geomagnetic daily variations analysis in terms of universal time components, considering solar wind-magnetosphere interactions, auroral zone effects, etc
22 p4021 A70-43278
- Dynamo region electrostatic fields effects on magnetospheric drift, taking electrical conductivities and solar and lunar tidal modes into account
23 p4185 A70-43836
- Solar wind flux correlation with earth EM field pulsations, noting flare-generated shock front effects on magnetosphere
23 p4236 A70-44051
- Dynamo role in magnetospheric disturbances and ionospheric inhomogeneities, allowing for charged particle concentration height dependence
23 p4237 A70-44059
- Cyclotron instability of high energy protons in magnetosphere with refraction of growing Alfvén waves
23 p4237 A70-44073
- MAGNETOSPHERIC ION DENSITY**
NT MAGNETOSPHERIC PROTON DENSITY
Magnetic activity effect on magnetospheric plasmopause position, measuring ion concentrations as function of local time fromOGO 5 observations
06 p1058 A70-18530
- Magnetospheric plasma density effects on impedance of VLF electric field spacecraft antenna
13 p2397 A70-29186
- Plasmasphere bulge region morphology from hydrogen ion concentration measurement by mass spectrometer onOGO 5 satellite
18 p3312 A70-36014
- Simultaneous hydrogen ion composition measurements by upper ionospheric polar orbitingOGO 4 and eccentric orbiting magnetosphericOGO 3 at midlatitude
19 p3520 A70-38377
- Short period Pc-1 pulsations frequency spectra relationship to magnetospheric He ion concentration
19 p3417 A70-38591
- Geomagnetic fluctuations relationship to magnetospheric ring current and plasmopause during magnetic storm
20 p3619 A70-39328
- Ring current protons turbulent diffusion in magnetospheric plasmopause, considering ion cyclotron wave lifetime and geomagnetic storms
21 p3881 A70-41085
- Ionospheric electron trough and magnetospheric plasmopause movements from satellite observations, showing statistical correlation with geomagnetic field
23 p4186 A70-43854
- MAGNETOSPHERIC PROTON DENSITY**
Low energy protons penetration into magnetosphere between forbidden regions, using model of constant electric field with charge exchange as loss mechanism
13 p2477 A70-29183
- Magnetospheric charged particle distributions in plasma sheet, pseudo- and stable-trapping regions by satellite observation
13 p2483 A70-30088
- Low energy protons in outer trapping region, discussing time variations and source and transport mechanisms
13 p2484 A70-30095
- Magnetospheric protons and electron energy spectra time and magnetic activity dependence during solar maximum
15 p2792 A70-31671
- MAGNETOSTATIC FIELDS**
Nonresonant electromagnetism absorption in high density plasma used for RF heating in magnetostatic field
09 p1735 A70-22923
- Gyrotron efficiency increment at fundamental gyroresonance by applying magnetostatic field variable along length of interaction space
12 p2233 A70-27535
- MAGNETOSTATICS**
Electromagnetic to magnetostatic wave conversion loss reduction at L band by coiled transducer
16 p2913 A70-34038
- MAGNETOSTRICTION**
Semistatic acceleration sensor, using ferrite rod magnetostriction effects to convert acceleration stress to microwave resonant frequency shift
03 p0495 A70-14191
- Conducting cylindrical shell in constant magnetic field analyzed for magnetoelastic disturbances using Laplace transform
06 p1056 A70-17607
- Magnetoelastic spin Hamiltonians applied to magnetostriction of Yb in YIG
06 p1128 A70-18642
- Oscillatory transverse and longitudinal magnetostriction in single crystal Bi, obtaining deformation potentials
08 p1557 A70-21838
- Acoustic noise control on Boeing aircraft electromagnetic components, noting iron-core magnetostriction demanding transformer redesign
09 p1647 A70-22764
- Ferromagnetic domain wall-dislocations magnetoelastic interaction in Fe and Ni computed as function of relative separation, discussing effects on magnetic properties
09 p1705 A70-22811
- Co-Fe core ability to adjust roll spacing in model rolling mill determined from magnetostrictive properties
10 p1905 A70-25175
- Oscillations of longitudinal magnetostriction in silver and copper single crystals at low temperature
11 p2098 A70-25619
- Normal and unconstrained vacuum-deposited Permalloy films composition dependence of magnetization-induced uniaxial anisotropy, noting agreement with magnetostrictive constraint theory
12 p2284 A70-27244
- Ni and Ni alloys elastic properties relationship with ferromagnetic and magnetostriction effects, determining modulus of elasticity for wide temperatures and heat treatment
13 p2432 A70-28760
- Stress, strain, temperature, electric and magnetic field distributions resulting from magneto-thermoelastic interactions in infinite elastic solid subjected to transient heat source
14 p2661 A70-31229
- Magnetoelastic sensors for small force measurement, describing instrument error reduction
15 p2733 A70-31577
- Lamellae stresses and magnetostrictive effects on magnetic properties of titanomagnetite and ilmenohematite series minerals
15 p2728 A70-31993
- Magnetostrictive measurements of torque from high speed rotating shafts
17 p3093 A70-35501
- One dimensional magnetostrictive bar electromagnetically forced vibration, using Lagrange equations and normal mode analysis
19 p3472 A70-37959
- Uniaxial magnetic anisotropy in electrodeposited Permalloy films in terms of magnetostrictive mechanism
20 p3687 A70-40160
- Magnetostrictive Ni-Mn-Co ferrites and Al-Fe alloys, measuring magnetic field effect on piezomagnetic coefficients at room temperature
24 p4389 A70-45400
- MAGNETOTELLURIC PROFILING**
U GEOMAGNETISM
U MAGNETIC SURVEYS
MAGNETOVARIographs
U VARIOMETERS
MAGNETRONS
Book on negative ions and magnetron covering electron affinities determination, gases adsorption, rate processes, stability problems, etc
03 p0526 A70-12901
- Lightweight Ka band magnetron for radar system use in missile fusing and airborne applications, discussing fixed frequency operation, anode and cathode, etc
04 p0655 A70-14622
- Magnetron electron beam amplifier large signal operation analysis using model with thin beam to calculate space charge
05 p0823 A70-16884
- Electron trajectories in M-type backward wave tube, TWT and magnetron, giving output power expressions
05 p0823 A70-16885
- Magnetron amplifiers with ferrite circulators for synchronizing natural frequency, obtaining I-V characteristics and gain vs bandwidth curves
05 p0823 A70-16886
- Cylindrical magnetrons steady state characteristics with thick and infinitely thin cathodes for full space charge and inclined magnetic field
09 p1651 A70-23641
- Magnetron-type electron gun structure with high design permeance for TWT applications
09 p1651 A70-23642
- Resonator system frequency spectrum in coaxial inverted magnetron with stepped interaction space
09 p1651 A70-23643
- Magnetron diode current fluctuations in interelectrode space, considering cathode emission current amplification by various modes
10 p1853 A70-25164
- Spurious output from C band radar magnetrons, discussing measurement procedures and noise reduction by waffle-iron waveguide filters
12 p2201 A70-28141
- Tunable and fixed frequency high power magnetrons parallel operation to achieve stable output
13 p2379 A70-29667
- Coaxial, inside-out and rising-sun magnetrons for millimeter waves generation under pulsed conditions, discussing tunability, frequency stability and weight
14 p2555 A70-30429
- Transverse kinetic energy of electrons at outlet of magnetron-injection gun as function of cathode inclination and magnetic induction
15 p2707 A70-31504
- Ionization measurements by OV-3-6 satellite cold cathode ionization gage of Redhead inverted magnetron type in near circular polar orbit
15 p2723 A70-31660
- Hot cathode magnetron ionization gauge design, discussing performance and sensitivity
19 p3421 A70-37467
- Slot type oscillations electrodynamic suppression in coaxial magnetrons resonator systems, calculating long wave oscillation frequencies
19 p3387 A70-37738
- Magnetron type backward wave tube with negatively charged slow wave structure, analyzing electron beam wave interaction for starting conditions
20 p3596 A70-39251
- MAGNETS**
NT CRYOGENIC MAGNETS
NT ELECTROMAGNETS
NT HIGH FIELD MAGNETS
NT SUPERCONDUCTING MAGNETS
Optimal coercive force selection of residual inductance and energy of magnets for generators with star shaped rotors
01 p0008 A70-10192
- Iris coupled YIG tuned filters for 12-4 GHz region, including high field magnets from vanadium permendur
12 p2202 A70-28165
- Brushless DC motor consisting of permanent magnet rotor, wound stator and optical rotor position sensing
16 p2843 A70-33000
- MAGNIFICATION**
Zoom effect in magnification of reconstructed image in incoherent holography achieved by varying fringe scale via rotation of interferometer components
07 p1288 A70-20099
- Electronic zoom for low light level TV sensor employing electrostatic image intensifier coupled optically to SEC camera tube
16 p2903 A70-33128
- Autofocus for variable magnification systems, discussing conjugate concepts and linkage and cam methods for enlargers and projectors
16 p2907 A70-33182
- MAGNIFIERS**
U MAGNIFICATION
MAGNITUDE
Quasar sky distribution as function of apparent magnitude for identification with galaxies of origin
09 p1759 A70-22909
- Delta Scuti stars, determining consistent absolute magnitudes by Stromgren intermediate band colors and Crawford photoelectric H beta indices
17 p3171 A70-35443
- Supernovae frequency in Sb and Sc spiral galaxies, considering luminosity class, absolute magnitude and mass of parent galaxy
24 p4413 A70-46164
- MAGNONS**
Premature saturation in strongly magnetic systems explained by model with nonuniform magnon modes, applying time dependent Green functions
02 p0338 A70-11886
- Magnon energy theory for temperature dependence of ferrous and magnesium fluorides antiferromagnetic-resonance frequency, sublattice magnetization and magnetic specific heat
09 p1739 A70-22324
- Nonlinear spin wave theory for anisotropic antiferromagnetism, solving sublattice magnetization by thermodynamic Green function for temperature dependence
11 p2097 A70-25617

MAGNUS EFFECT

- Temperature dependence of short wavelength magnon energies correlated with heat capacity
14 p2619 A70-30487
- Bilinear scalar spin Hamiltonian inadequacy to describe electron exchange in systems containing orbitally degenerate ions, considering cobalt magnon spectra
15 p2777 A70-32399
- Antiferromagnetic and ferrimagnetic resonance frequencies, determining temperature dependence by spin wave theory
24 p4388 A70-45132
- Spin waves amplification in ferromagnetic conductor crystals, taking into account arbitrary external electric field and propagation vector orientations and space charge
24 p4392 A70-46363
- MAGNUS EFFECT**
Magnus effects on Apache sounding rocket at supersonic speeds, discussing spinning model and static tests
[AIAA PAPER 70-207] 06 p1157 A70-18103
- Aircraft development for subsonic and transonic flight dependent on methods using blowing and boundary layer control and Coanda and Magnus effect
09 p1610 A70-22220
- Freely spinning finned stabilizer static wind tunnel tests on free fall research store, determining Magnus effect, body flow interference and static stability
[AIAA PAPER 70-559] 13 p2340 A70-29024
- MAIN SEQUENCE STARS**
M dwarf stars spectroscopic, spectral and photometric parallaxes calibration based on trigonometric measurements
01 p0188 A70-11333
- M dwarf stars model atmosphere construction taking into account molecular opacities in cool stellar atmospheres
01 p0190 A70-11348
- S Doradus spectroscopic behavior study during minimum and maximum phases suggesting ejected-shell mechanism and premain sequence star classification
04 p0759 A70-15712
- Bolometric albedo of main sequence stars with deep convective envelopes in close binary systems derived as function of photometric proximity using entropy invariance
05 p0914 A70-16694
- Stellar mass loss in gravitational contraction and variation of rotation law during transition to main sequence
05 p0917 A70-16909
- Neutrino emission, mass loss and giant branch termination in young clusters with giants originating from intermediate mass main sequence stars
06 p1138 A70-17277
- Metal-poor stars evolution during hydrogen and helium burning from main sequence to giant branch, estimating relative cluster ages
09 p1755 A70-22507
- G and K stars classification /spectral type and luminosity class/ by narrow band photometry
10 p1937 A70-23945
- Polaroid magnetic field effects on main sequence stars core convection
11 p2117 A70-26654
- Vibrationally unstable high mass main sequence star, reinvestigating destruction by radial oscillations
12 p2302 A70-27587
- Neutrino astronomy for processes in stellar interiors, emphasizing thermonuclear reactions in sun and main sequence stars
13 p2490 A70-28947
- Globular cluster stars, discussing cosmological importance, stellar development models, main sequence stars, red giant models, He content, age computation, etc
17 p3171 A70-35447
- Helium abundance in unevolved main sequence eclipsing binaries by comparing to homogeneous models in mass luminosity plane
18 p3318 A70-37023
- Galactic spiral structure relation to local stellar distribution, discussing OB associations, galactic cluster, WR stars, cepheids, and common stars in sun neighborhood
18 p3329 A70-37176
- Main sequence stars faint end IR observations for luminosities and temperatures
20 p3702 A70-39014
- Main sequence II stars rapid uniform rotation effect on structure
22 p4101 A70-42859
- Polytropic premain-sequence evolutionary tracks and main sequence models of solar composition low mass stars
22 p4104 A70-42993
- UBVr colors of A0-K0 main sequence stars, deriving B-V relation to effective temperature
23 p4246 A70-44757
- Single normal main sequence stars rotational velocities compared with giant, supergiant, Be, A and metallic line stars and Population II objects
23 p4248 A70-44802

- Stellar rotation effect on internal structures, discussing angular momentum steady state distribution for main sequence stars
23 p4249 A70-44803
- Rotational velocities for main sequence stars from spectral type A5 to F9, supporting solid body rotation hypothesis
23 p4249 A70-44806
- Be stars rotation, considering emission properties and evolutionary state of main sequence
23 p4249 A70-44807
- Stellar rotation angular momentum loss in premain sequence convective phase, discussing polytropic structure, formation time and velocity changes
23 p4249 A70-44809
- Stellar rotation effects on atmospheres of early type main sequence stars, using models for surface gravity and temperature variations
23 p4249 A70-44810
- Upper main sequence and close early type binaries evolution by fission of rapidly rotating protostars
23 p4250 A70-44815
- Algol type semidetached eclipsing binaries main sequence components rotational velocities, determining deviations from synchronism
23 p4251 A70-44818
- Spectral line width distributions in main sequence stars, emphasizing B2 to A2 range rotational velocities with Maxwellian distribution
23 p4251 A70-44821
- Be star rotation dynamics phenomenon, discussing time variations on main sequence scale
23 p4252 A70-44828
- Solar rotation, discussing oblateness, solar wind torque, main sequence stars rotating core, gravitational quadrupole moments and Li and Be depletion
23 p4252 A70-44829
- Main sequence and giant stars atmospheric structure models, noting metal deficiency effects
24 p4413 A70-46159
- G8, IV subdwarf 31 Aql spectrum at 4000-6600 Å, discussing Ba II 4554 Å, G and CN bands and spectral lines
24 p4414 A70-46329

MAINTAINABILITY

- Cost model based on initial and support costs for studying availability variations effect on system total cost and maintainability and reliability interrelationship
02 p0401 A70-11674
- Automatic support systems for advanced maintainability - IEEE Conference, St. Louis, November 1969
08 p1468 A70-20651
- Avionics maintainability concepts, discussing built-in test equipment, test connectors, automatic test equipment, fault detection and fault isolation
08 p1470 A70-20664
- Apportionment optimization of reliability and maintainability by Lagrange multipliers and dynamic programming, discussing maintainability cost model and computerized simulation
09 p1792 A70-22211
- Harrier maintainability for reliability with minimum down-time and man hours, discussing servicing, turnaround, role change, inspection and engine changes
10 p1806 A70-24850
- Maintainable electronic equipment requirements for long duration manned space missions
10 p1852 A70-24895
- Three spool turbofan engine design regarding maintainability, noting on-condition module removal and overhaul
[SAE PAPER 700204] 11 p2101 A70-25877
- Systems effectiveness equated to function of performance, availability, reliability, maintainability, quality control and manufacturing, emphasizing optimization
14 p2592 A70-31112
- Project acquisition based on consideration of logistic effects /ABLE/ for tool measuring logistic consequences of reliability and maintainability
15 p2832 A70-32634
- Computer system maintainability demonstration test in accordance with MIL-STD-471, discussing techniques for failure indication and repair crew qualifications and training
15 p2706 A70-32657
- System maintainability stochastic modeling using probability density functions
15 p2748 A70-32670
- Electronic equipment maintainability in military environment, discussing myths for hardware and human performance conditions
16 p2852 A70-33664
- Field maintenance interface between human engineering and maintainability, discussing air defense system malfunction and troubleshooting deficiencies
16 p2852 A70-33665
- Maintainability assessment techniques, discussing models in terms of utility, application, validity and human engineering data
16 p2853 A70-33667
- Systems subject to failure and repair cycles, describing performance and reliability by stochastic processes in terms of excess time
17 p3099 A70-34580

- Reliability and maintainability - Conference, Detroit, July 1970, Volume 9, Assurance technology spinoffs
19 p3440 A70-38815
- Gaseous radioactive penetrant inspections for early low cycle fatigue in aircraft engine materials, discussing impact on maintainability
19 p3441 A70-38828
- TSCP700 aircraft auxiliary power unit design, fuel consumption and maintainability
[SAE PAPER 700815] 24 p4395 A70-45902
- MAINTENANCE**
NT AIRCRAFT MAINTENANCE
NT SPACE MAINTENANCE
Computerized generation of cost optimal decision logic for malfunction analysis
08 p1470 A70-20659
- Integrated man machine shipboard maintenance systems design, describing computerized model based on information flow network
08 p1465 A70-20665
- Maintenance trends for transport aircraft jet engine, considering engine and component pooling, inspection accessibility, monitoring, etc
[SAE PAPER 700316] 12 p2290 A70-27455
- Automatic engine maintenance recording system on air transport aircraft noting data reduction
[SAE PAPER 700317] 12 p2335 A70-27456
- Telecommunication satellite system operation reliability taking into account maintenance and economics, discussing spacecraft acceptance and performance tests
12 p2313 A70-27470
- On-line optimization of maintenance and verification schedules for complex system safety insurance
12 p2444 A70-28013
- Computerized Monte Carlo prediction of maintenance time distribution of complex system, concerning man hours, elapsed time and schedule meeting
13 p2524 A70-29566
- Reliability relation to mean time between failures /MTBF/ relation for long life repairable equipment with limited life components
13 p2421 A70-29567
- Multistation automatic test equipment assembly management or maintenance organization, using digital computer control
13 p2385 A70-29691
- Configuration management of software concerning automatic test systems in large maintenance depot
13 p2422 A70-29692
- Failure prediction testing and elements replacement at field maintenance level for increasing equipment reliability
13 p2423 A70-29697
- Coding procedure for Air Force maintenance technicians to record and describe equipment malfunctions compared to experimental codes
16 p2853 A70-33666
- Aircraft, helicopters and rockets aviation systems design and components service life problems, emphasizing maintenance intervals
17 p3100 A70-34686
- Management program for digital data systems maintenance and repair
17 p3200 A70-35487
- Book on optimization and probability in systems engineering covering mathematical models for reliability, repair, availability, Markov techniques and queueing
19 p3553 A70-37928
- Preventive maintenance of stationary automatic mass spectrometers
19 p3432 A70-38584
- Hazard functions, renewal and peril rates for reliability models of nonrepairable parts, sockets and repairable systems
19 p3442 A70-38839
- Reliability of redundant repairable systems with preventive maintenance, determining mean time between failures
20 p3638 A70-40181
- Optimum calibration intervals determination for obtaining instrument maintenance quality level at low cost
20 p3634 A70-40452
- Versatile Avionic Shop Test maintenance system supporting avionic equipment aboard aircraft carriers
21 p3804 A70-40772
- MAJORITY CARRIERS**
HF admittance and noise in forward-biased majority carrier Ge-Si n-n heterojunctions and Schottky barrier
03 p0539 A70-13159
- Thermoelectric power and Hall effect quantum resonances in graphite for locating majority carrier electron and hole Fermi Surfaces in Brillouin zone
24 p4389 A70-45597
- MALES**
Orthostatic tilt tolerances in young men and women noting heart rates and blood pressure
09 p1627 A70-23454
- MALFUNCTIONS**
Optimal selection of subsystems, minimizing mathematical expectation of output losses considering malfunctions
03 p0460 A70-13429

Automatic control algorithms for subsystem malfunction identification in multisubsystem plants, analyzing conditions for diagnostic tests existence
04 p0661 A70-14554

Automatic Malfunction Analysis /AMA/ digital computer software system supporting checkout and testing, defining normal system status by computer simulation
[AIAA PAPER 70-383] 10 p1861 A70-24922

Pulmonary functions disturbances producing hypoxia, discussing alveolar hypoventilation, arteriovenous admixing, blood distribution and oxygen diffusion disturbances
10 p1821 A70-25078

Coding procedure for Air Force maintenance technicians to record and describe equipment malfunctions compared to experimental codes
16 p2853 A70-33666

Test selecting and sequencing for adaptive checkout processes, determining malfunctions
20 p3659 A70-40106

MALKUS THEORY

Variational principle for turbulent shear flow between parallel plates, taking into account isothermal flow and Malkus theory
17 p3073 A70-35595

MAMMALS

NT CATS
NT CATTLE
NT CHIMPANZEES
NT DOGS
NT GOATS
NT GROUND SQUIRRELS
NT GUINEA PIGS
NT HAMSTERS
NT HUMAN BEINGS
NT MICE
NT MONKEYS
NT PRIMATES
NT RABBITS
NT RATS
NT RODENTS
NT SHEEP
NT SWINE
NT TURTLES

Brown fat thermoregulatory function and physiological control in mammals, discussing heat production and biochemical stimulation
02 p0230 A70-11683

Histochemical detection of L-glulonolactone-phenazine methosulfate oxidoreductase activity in mammals with emphasis on vitamin C synthesis in primates
04 p0647 A70-15753

Broad spectrum light sources effects on mammalian endocrine apparatus development and function determined in rats
09 p1617 A70-22335

Gamma radiation effects on higher mammals nerve activity after chronic total body exposure
09 p1619 A70-22790

Mammalian pineal organ control experiments involving light and sympathetic nerve stimulation
10 p1812 A70-24396

Mammalian ultricular macula design, considering microelectrode data and information from light and electron microscopy, behavioral experiments and computer simulation
11 p1988 A70-26231

Neurological differences in spinal projections of animals subjected to cordotomies compared with human material, using selective silver impregnation technique
13 p2350 A70-28998

Mammalian cells after X ray irradiation, showing two forms of DNA repair process
21 p3765 A70-42024

02 p0244 A70-12136

Man machine systems - IEEE/ERS Conference, Cambridge, England, September 1969, Volume 3, Decision making and mental work load
02 p0244 A70-12137

Human decision making via man-computer interaction, noting skill role in nonoptimal performance handling of simultaneous factors
02 p0245 A70-12140

Supervisor sampling frequency maximizing given value or payoff function, discussing applications to controlling vehicle, information system or institutions
02 p0307 A70-12141

Information storage and retrieval system development and operation for diversified crew/equipment task data, using general purpose digital computer
02 p0265 A70-12143

Man machine system consisting of manned station controlling distant spacecraft via wideband radio link
02 p0229 A70-12145

Adaptive man machine systems, display design - IEEE/ERS Conference, Cambridge, England September 1969, Volume 4
02 p0245 A70-12147

Adaptive man machine system for automated training of pilot dynamic control skills /decision and motion/, describing synthesis procedure
02 p0246 A70-12148

Multidimensional data efficient decomposition for communication interface between man machine system, considering decision making and pattern recognition on digital computers with orthogonal transformations
02 p0265 A70-12149

Man machine digital display low cost system for displaying black and white image data with gray levels, color image data and dot patterns
02 p0265 A70-12152

Remote sensing system for earth resources surveys temporal information employing human interpreter and machine for spatial and spectral data processings
03 p0491 A70-13668

Man machine interface in VTOL aircraft control and stabilization systems adaptation during manually controlled hovering flight
03 p0414 A70-14094

Cockpit display system to reduce aircraft pilot workload and aid judgment making during critical operations
[ASME PAPER 69-WA/BHF-12] 04 p0642 A70-14854

Tactile control in man machine systems using feed-forward loops to provide rate information, noting unmanned aircraft and machine-tool applications
[ASME PAPER 69-WA/BHF-14] 04 p0642 A70-14855

Man-machine systems design emphasizing impedance matching exemplified by visual approach landing
[ASME PAPER 69-WA/GT-15] 04 p0642 A70-14856

Human controller decision in air traffic control, discussing manpower, on-line computer use and maximized systems
[ASME PAPER 69-WA/AV-1] 04 p0643 A70-14903

Time constant of man machine system as adaptive variable in training devices derived from combined vehicle properties and human control characteristics
05 p0805 A70-16005

Computer-aided design using third generation computers and interactive graphic systems applied to transonic aerodynamics problems
05 p0816 A70-16122

Command control systems characterized as problem solving information processing systems, discussing information requirements specification prior to man-display design
05 p0806 A70-16177

MAN

U HUMAN BEINGS

MAN MACHINE SYSTEMS

Man-computer graphic systems utilization for wing/body aerodynamic design and analysis concept for subsonic vehicles
[AIAA PAPER 69-1130] 01 p0002 A70-10610

Tradeoff criteria between man machine and automated space systems applied to lunar and cosmic ray explorations
[AIAA PAPER 69-1045] 01 p0034 A70-10644

Psychological aspects of unreliability sources in man machine systems for selection and training criteria of photooptical instruments users
01 p0036 A70-10821

Automatic landing systems mission and design, discussing pilot-system task coordination, equipment characteristics and reliability, etc
01 p0138 A70-11257

Aircraft pilot-autopilot task division during automatic landing, analyzing man machine interaction in aircraft approach guidance
01 p0139 A70-11258

Electronic displays role in pilot-traffic interaction, considering flight safety, cost effectiveness, onboard data input, etc
01 p0039 A70-11260

Digital computer display techniques relationship with man in modern environment, considering human engineering and educational problems and future impact on intellectual qualities
01 p0221 A70-11281

System analysis and synthesis processes applied to educational requirements identification and programs implementation, emphasizing use of functional model with man machine interface
01 p0221 A70-11283

Dynamic structural analysis using computer graphics display, emphasizing applicability to man machine interaction at key decision making points
02 p0386 A70-11943

Man machine systems - IEEE/ERS Conference, Cambridge, England, September 1969, Volume 1, Man-computer interaction
02 p0264 A70-12126

Man machine systems - IEEE/ERS Conference, Cambridge, England, September 1969, Volume 2, Transport systems and vehicle control
02 p0334 A70-12130

Helicopter avionic systems man machine capability estimation based on pilot workload, applying results to design evolution
02 p0244 A70-12136

Man machine systems - IEEE/ERS Conference, Cambridge, England, September 1969, Volume 3, Decision making and mental work load
02 p0244 A70-12137

Human decision making via man-computer interaction, noting skill role in nonoptimal performance handling of simultaneous factors
02 p0245 A70-12140

Supervisor sampling frequency maximizing given value or payoff function, discussing applications to controlling vehicle, information system or institutions
02 p0307 A70-12141

Information storage and retrieval system development and operation for diversified crew/equipment task data, using general purpose digital computer
02 p0265 A70-12143

Man machine system consisting of manned station controlling distant spacecraft via wideband radio link
02 p0229 A70-12145

Adaptive man machine systems, display design - IEEE/ERS Conference, Cambridge, England September 1969, Volume 4
02 p0245 A70-12147

Adaptive man machine system for automated training of pilot dynamic control skills /decision and motion/, describing synthesis procedure
02 p0246 A70-12148

Multidimensional data efficient decomposition for communication interface between man machine system, considering decision making and pattern recognition on digital computers with orthogonal transformations
02 p0265 A70-12149

Man machine digital display low cost system for displaying black and white image data with gray levels, color image data and dot patterns
02 p0265 A70-12152

Remote sensing system for earth resources surveys temporal information employing human interpreter and machine for spatial and spectral data processings
03 p0491 A70-13668

Man machine interface in VTOL aircraft control and stabilization systems adaptation during manually controlled hovering flight
03 p0414 A70-14094

Cockpit display system to reduce aircraft pilot workload and aid judgment making during critical operations
[ASME PAPER 69-WA/BHF-12] 04 p0642 A70-14854

Tactile control in man machine systems using feed-forward loops to provide rate information, noting unmanned aircraft and machine-tool applications
[ASME PAPER 69-WA/BHF-14] 04 p0642 A70-14855

Man-machine systems design emphasizing impedance matching exemplified by visual approach landing
[ASME PAPER 69-WA/GT-15] 04 p0642 A70-14856

Human controller decision in air traffic control, discussing manpower, on-line computer use and maximized systems
[ASME PAPER 69-WA/AV-1] 04 p0643 A70-14903

Time constant of man machine system as adaptive variable in training devices derived from combined vehicle properties and human control characteristics
05 p0805 A70-16005

Computer-aided design using third generation computers and interactive graphic systems applied to transonic aerodynamics problems
05 p0816 A70-16122

Command control systems characterized as problem solving information processing systems, discussing information requirements specification prior to man-display design
05 p0806 A70-16177

Human controller in psychology and control engineering, discussing linear and nonlinear modeling of human behavior
05 p0807 A70-16487

Information display devices, discussing interactive graphic consoles, reusable film, magneto-optics, broadband laser, etc
05 p0851 A70-16725

VTOL aircraft control and stability with emphasis on flight characteristics and man machine interaction
05 p0809 A70-17089

Airborne computer system program for anti-submarine warfare enhancing human element in man machine system
06 p1185 A70-17974

On-line computer programs allowing for man machine interactions in linear circuits design
06 p1015 A70-18417

Concorde simulator for determining aircraft control responses and integrating pilot function into problem
07 p1249 A70-19743

Man-computer interactions in experiment design analysis, discussing applications to computer simulation
08 p1464 A70-20606

Integrated man machine shipboard maintenance systems design, describing computerized model based on information flow network
08 p1465 A70-20665

Human operator dynamic properties working to maintain given process parameters, obtaining differential equations for closed machine operator system
08 p1449 A70-20696

Control display requirements for manned spacecraft, integrating human operator with vehicle control system and determining man machine relations in stabilization, control and guidance
08 p1498 A70-21678

Human factors data standardization in NASA Apollo Applications Program for computer data processing
09 p1623 A70-22295

SIMCON digital simulation control system optimizing man machine interaction, noting capability to generate solutions with minimum computer memory
10 p1860 A70-24654

Computer aided on-line test generation for prelaunch checkout, describing interpretive test language for rapid man machine information transfer
[AIAA PAPER 70-384] 10 p1846 A70-24921

State space models of remote manipulation problem applied to human supervised or autonomous computer manipulators
10 p1828 A70-25230

Human controllers nonlinear time domain mathematical model for analyzing compensatory tracking task data
11 p1992 A70-26396

Computers graphical display devices for rapid designer-computer communication
12 p2191 A70-27013

Applied psychology role regarding human factors in man machine systems, considering boredom, skills application, age and experience, etc
12 p1716 A70-27035

Human performance as controller evaluated in man machine control system, considering pursuit or compensatory tracking tasks
12 p1717 A70-27039

Pursuit tracking during disturbance signal as function of human performance in man machine system
12 p2266 A70-27198

Apollo man-machine control design, discussing communication, integration, lunar landing, attitude control, CMC and LGC programs
13 p2357 A70-28379

Man machine function distribution optimization in spacecraft closed-loop automatic control system
13 p2380 A70-28381

Man machine eye-integration coupling in tracking task applied to helicopters, ocean-going craft and propeller aircraft
13 p2357 A70-28386

Longitudinal short-period flying qualities as closed-loop pilot-airplane system, noting acceptance values
[AIAA PAPER 70-569] 13 p2346 A70-29034

Man machine interface between operator and automatic testing equipment based on ergonomic design cost
13 p2360 A70-29687

Mathematical models for human adaptive and optimizing characteristics in manual control systems regarding behavior phase
13 p2360 A70-29780

Flight control and human role in avionics system, discussing stabilization, autopilot and ILS systems
13 p2450 A70-29997

Human temporal motor response models relating reaction, movement and manipulation time to stimulus, movement and manipulation information
14 p2540 A70-30248

Real time sonic information input/output computer system for acoustic signals and speech synthesis, concerning man machine communication
14 p2553 A70-30425

Electronic systems automatic design problems including man machine communication and data organization

14 p2554 A70-30663

Integrated circuits design by combined automatic and manual system

14 p2554 A70-30670

Workmen as environmental variables in design, introducing Human Factors Report during spacecraft components manufacture and testing

15 p2693 A70-32636

Personnel subsystem reliability through empirical approach, determining relations of man-hardware-procedure systems

15 p2804 A70-32665

Dynamic systems control and guidance by man in light of anthropotechnics, treating approaches to man machine systems optimization

16 p2850 A70-33263

Field maintenance interface between human engineering and maintainability, discussing air defense system malfunction and troubleshooting deficiencies

16 p2852 A70-33665

Interactive computer graphics in six degree of freedom control, lunar roving vehicle navigation, orbital elements calculations, drop test simulation, etc

16 p2869 A70-33726

Concorde aircraft man machine simulation and handling using fixed cabin, variable stability and ground based simulators

[AIAA PAPER 70-923]

17 p3064 A70-35834

Commercial aircraft flight deck systems controls and time sharing displays, emphasizing crew management

[AIAA PAPER 70-938]

17 p3021 A70-35847

Computer users functions to determine preparation level for effective dialog with computer, discussing teaching stages

18 p3223 A70-36077

Human operator and computer interrelations, noting sources of error

18 p3223 A70-36079

Adaptation to extreme stimulation in machine-organism system

18 p3224 A70-36529

Soviet book on man in aircraft control system covering engineering psychology, complex flight problems, human factors and instrument panels

19 p3367 A70-37236

Display/control technology for high performance input/output between man and machine, describing man-in-loop simulation

19 p3369 A70-37875

Soviet book on computer design and construction covering man machine interfaces, internal languages, interpretation systems, memory distribution, solution processes, etc

19 p3385 A70-38794

TV display simulation of instrument and visual aircraft landing approaches, investigating color, collimation and resolution effects on pilot evaluations

20 p3578 A70-39172

Aerospace digital computer and avionics systems man machine relationship optimization, considering human information and control response requirements

21 p3794 A70-41688

Computerized aerospace systems man machine interface mechanization for performance optimization, emphasizing integrated approach to avionic displays

21 p3795 A70-41689

Graphical link between operator and digital computer using CRT display and light-pen input system during automatic electronic circuit design

23 p4150 A70-43952

Electronic equipment automated testing objectives and requirements, considering man machine interaction, system controls, on-line reporting, and software/hardware availability

23 p4174 A70-44541

Integrated regenerative life support manned tests for space laboratory design and development

23 p4154 A70-44632

Manned spacecraft onboard data management systems, discussing information transfer, processing, control, display and man machine interface

23 p4167 A70-44647

Interactive man computer systems evaluation considering speech communication, SKETCHPAD and graphics capabilities, FORTRAN and programming languages and future manned space missions

[AIAA PAPER 70-1292]

24 p4317 A70-45928

Pilot interface with area navigation system, describing control and display unit for navigation situation, flight plan and system status

[AIAA PAPER 70-1335]

24 p4373 A70-45933

Computer optimization program for solid state components and integrated circuits design with conversational system for man machine dialogues

24 p4317 A70-46321

MAN OPERATED PROPULSION SYSTEMS

Man powered aircraft /MPA/ designs, considering bird flight aerodynamic characteristics

14 p2531 A70-30859

Extravehicular activity maneuvering devices, describing design and performance of Gemini project unit

21 p3929 A70-41075

MANAGEMENT

NT CONFIGURATION MANAGEMENT

NT CONTRACT MANAGEMENT

NT FINANCIAL MANAGEMENT

NT INDUSTRIAL MANAGEMENT

NT PERSONNEL MANAGEMENT

NT WATER MANAGEMENT

Management systems growth in relation to computer applications development, noting second industrial revolution

10 p1971 A70-24661

Criticism of public administration aspect of Edwards Report, noting parliamentary and constitutional difficulties in some proposals

11 p2153 A70-25857

MANAGEMENT INFORMATION SYSTEMS

Cost reduction and products reliability and quality maintenance by combining accurate cost reporting system with proper quality level control

14 p2669 A70-31108

ELDO project planning and progress monitoring system for management provided by Central Planning and Progress Monitoring Service

21 p3956 A70-41497

MANAGEMENT PLANNING

NT PRODUCTION PLANNING

Soviet book on operational maintenance of flight vehicles /civilian/, emphasizing maintenance under various climatic conditions

01 p0004 A70-10502

Mission simulation mathematical modeling technology developed for optimization of experiment program management and operational planning for manned space station missions

[AIAA PAPER 69-1065]

01 p0181 A70-10634

Operational planning system for Strategic Air Command for data accessing, generating, displaying and editing using computer complex

01 p0048 A70-11282

Book on technological forecasting covering philosophical basis, Federal Government activity, R and D management resource allocation, correlation and regression analysis, etc

01 p0221 A70-11307

Integrated materiel management for systems or product costs reduction applied to high cost spares management

02 p0401 A70-11671

Spares management of large aircraft contract in relationship to total integrated logistics support systems management

02 p0401 A70-11672

Operations research in fleet planning, discussing forecasting, frequency planning, operation simulation, traffic and revenue forecasting, etc

02 p0401 A70-11745

Technology transfer techniques within business firm, including specific examples used by successful companies

02 p0403 A70-12635

Optimum balance between program and functional organizations to promote technology transfer

02 p0403 A70-12637

Technology transfer experience in terms of aerospace company policies and technical management mechanics

02 p0389 A70-12638

Surveyor project as basis for technology transfer management exemplified by planning and organization problems

02 p0403 A70-12639

Computerized airline fleet planning methods for aircraft economics and airline operations

[SAE PAPER 690415]

03 p0609 A70-12898

European application satellite systems operation by administrative organizations dealing with communications, earth resources determination and industry participation

03 p0609 A70-13839

AMPROD /Automated Mission Profile Design/ generating schedules for long duration missions with real cost and time savings

03 p0581 A70-14023

Managerial practices of problem identification, discussing research study in operating division of large corporation

03 p0610 A70-14051

Management role in air traffic controllers stress reduction, considering human factors affecting ATC system capacity

03 p0439 A70-14316

Computer display graphic technique for business decision making, noting electronic aids

05 p0959 A70-16451

DOD systems acquisition management tools and policies, emphasizing role of development concept paper and outside personnel dialogue in DOD decision making

05 p0959 A70-16460

Cost/schedule planning and control system /C/SPCS/ providing early exposure of inadequacies in work execution and initial planning

05 p0959 A70-16461

Systems engineering management process for satisfying MIL-STD-499 requirements, detailing functional analysis, tradeoffs and resulting design analysis data

05 p0959 A70-16462

Integrated USAF acquisition management systems approach engaging top management abilities available in government and industry

05 p0959 A70-16463

R and D laboratories quality and performance evaluation techniques, describing Apstein- modified Pelz technique

06 p1185 A70-17603

Aerospace scientific and engineering work force movement between geographical areas and resource location

07 p1426 A70-18799

Decision trees application to research projects selection, cost stages, probable return on investment and control device

07 p1427 A70-19001

Team hiring of research scientists by industrial and academic organizations, discussing causes and influence on R and D organizations management and design

07 p1427 A70-19002

Isochronal maintenance inspection management of Military Airlift Command /MAC/, noting C-141 utilization rate

07 p1428 A70-19673

Ground and onboard electronics systems for space shuttle vehicles, discussing role in equipment reliability and maintainability, life cycle costs, management control, etc

[AIAA PAPER 70-261]

07 p1398 A70-20391

Automatic test equipment programming for cost reduction by eliminating duplicated effort between manufacturers of test equipment and unit to be tested

08 p1464 A70-20658

Coupling relations in product and systems development linking ideas to finished products

08 p1601 A70-20824

Machinery for management of Sea Dart missile development using managerial concepts of planning, organizing, commanding, coordinating and controlling

08 p1601 A70-21036

Management planning for French-British Martel /Missile Antiradar et Television/ project, emphasizing tasks of government agencies and contractors

08 p1601 A70-21038

International aircraft engine industry management in Europe, discussing cooperation, corporations, U.S. competition and structural changes

09 p1792 A70-22339

Government environment challenges to government sponsored big technology management illustrated by space nuclear engine research program

09 p1792 A70-22494

Quality planning for Japanese solid propellant sounding rocket motor production, discussing documentation, design, development and process controls, inspection and tests, etc

09 p1691 A70-22570

User information traffic forecasting method for operational Earth Resource Satellite System, discussing user expectations

[AIAA PAPER 70-293]

09 p1793 A70-22890

Federal contract research centers objectives, characteristics, crucial issues and future

09 p1793 A70-22971

Technology transfer or coupling from corporate viewpoint, discussing organizational responses to literature mushrooming, time compression of technological advance, etc

09 p1794 A70-23411

Technological forecasting for management planning, discussing structuring, prediction techniques, personnel selection, quantification, etc

09 p1794 A70-23413

Technological forecasting for R and D planning including project selection and resource allocation decision making

09 p1794 A70-23416

Technology or Research Quantitative Utility Evaluation /TORQUE/ system genesis and operation, with implications affecting R and D

09 p1795 A70-23418

Management planning for global atmospheric research program /GARP/ applied to climatology and weather forecasting

09 p1795 A70-23545

Models survey for evaluation and selection of research projects, discussing reasons for long range company

10 p1970 A70-24070

Integral systems management, discussing application and organizational prerequisites

10 p1970 A70-24595

Aerial photography applications to timber management programs of forest industries

10 p1879 A70-24746

- Integrated planning and testing for systems reliability improvement
[AIAA PAPER 70-391] 10 p1896 A70-24914
Apollo Lunar Module Test Program Management, discussing test requirements optimization, control, planning, etc.
[AIAA PAPER 70-368] 10 p1952 A70-24932
Personnel and organizational policies for university research management 12 p2336 A70-27750
Management science concepts tested for feasibility in large organization top management positions using questionnaire technique 13 p2524 A70-28825
Project cost estimate growth pressures on decision making by U.S. Air Force System Program Office director 14 p2667 A70-30521
Government defense contract warranties in terms of consumer interests protection and economics 14 p2667 A70-30522
Incentive earnings and payments in CPIF /cost plus incentive fee/ contracts, considering legal principles 14 p2668 A70-30523
Price estimate elements interrelationship using three dimensional matrix for computerized cost data extraction 14 p2668 A70-30524
Contractor all risk incentive contract /CARIC/, discussing innovative features and negotiation elements 14 p2668 A70-30525
Military aviation economics in UK emphasizing aircraft industry and government cooperation in meeting RAF requirements 14 p2668 A70-30938
Corrective Action systems for identification, control and resolution of manufacturing, engineering and vendor problems 14 p2669 A70-31102
Apollo project overview and quality-cost effectiveness assurance requirements for future space programs 14 p2654 A70-31103
Quality control role in configuration management, considering quality assurance organization of aircraft manufacturer 14 p2669 A70-31104
Quality control variables optimization for maximum net revenue, using computerized simulation 14 p2592 A70-31105
Quality evaluation surveys performance by contractors 14 p2669 A70-31106
Project authority relationship concerning manager authority and influence in five organization models 15 p2828 A70-31571
Decision making role in management contribution towards success of research and development based on statistical decision theory 15 p2828 A70-31573
Forecasting necessity and limitations in management decision making process 15 p2829 A70-31574
SST system safety program, discussing federal office structure, planning and control, design support, integration and evaluation, requirement analysis and failure recurrence control 15 p2675 A70-32214
Management role in flight operations safety, stressing need for confidence and discipline 15 p2831 A70-32218
Reliability program planning and organization as part of integrated Development Risk Management System, considering task identification, assignment and accomplishment 15 p2747 A70-32628
Effective R and D management working principles, discussing changing goals, policy and technology changes, environment, adequate reporting, etc. 16 p3004 A70-33663
Technological forecasting as management concept in decision making process 17 p3199 A70-34679
Management program for digital data systems maintenance and repair 17 p3200 A70-35487
Successful application development and implementation of data processing system, noting sequence, magnitude, manpower and time required 17 p3200 A70-35507
Airline maintenance department assurance of air service regularity, stressing management role 17 p3065 A70-35855
Management information systems based on Apollo program experience, considering improvements in data accuracy, display, feedback, etc. 19 p3553 A70-37862
Multi-aircraft flight test program time compression by management techniques, discussing program length and costs 19 p3355 A70-38530
Value engineering for British aerospace industry management planning 19 p3555 A70-38619
- Cost and time optimization for complex aircraft development projects via network planning 20 p3740 A70-39644
Optimal R and D planning from estimated efficiency of research projects or national programs 20 p3740 A70-39646
Predictive model for potential variance from planned schedule of R and D tasks to minimize risk in management 21 p3955 A70-41172
Military program cost effectiveness and control, considering resources and products 21 p3955 A70-41173
R and D programs engineering talent assignment case histories 21 p3955 A70-41174
Inlet data for engine stability analyses, developing technical management procedure patterns for pretest test and posttest results [AIAA PAPER 70-1214] 21 p3745 A70-41320
U.S. and Soviet space program administration and management 21 p3956 A70-41893
Lunar launch vehicles quality control and reliability, describing management procedures for test facilities, preproduction and purchased materials quality 22 p4126 A70-42384
Air cargo management problems, discussing economics, ground handling, Jumbo jets, terminal facilities, mechanization, document handling, information flow, data systems, etc. 22 p4006 A70-43269
Technology relevance to organizational structure, discussing planning models based on problem solving and performance 23 p4284 A70-43995
Space shuttle economic risk analysis, using computer program as design and management tool 23 p4261 A70-44674
International earth orbital space laboratory program, discussing objectives, management, stations, shuttles, tugs, tracking, communication, data distribution network, etc. 23 p4262 A70-44687
International Space Research Organization /ISRO/ for space operations, considering political, economic, technical and scientific requirements 23 p4286 A70-44688
Aktion X program for production efficiency, mobilizing personnel in weak points monitoring 24 p4430 A70-45624
Cost/design performance management system, noting cost reduction and avoidance needs during design definition 24 p4430 A70-45866
[SAE PAPER 700772] Financing methods for airport redevelopment and expansion, discussing economic and political framework of operations 24 p4430 A70-45920
[AIAA PAPER 70-1267] MANDELSTAM REPRESENTATION
Stimulated Mandelstam-Brillouin scattering and fracture of molten quartz and silicate glasses produced by laser giant pulse 11 p2061 A70-25380
Stimulated Mandelstam-Brillouin and entropy backscattering of light pulses, determining intensity and spectral distribution allowing for fluctuations in medium 12 p2248 A70-27550
- MANDRELS
Mandrel adhesion and cure shrinkage impact on structural integrity of solid propellant grain 09 p1742 A70-23263
- MANEUVERABILITY
Electrical signaling civil aircraft systems, discussing design and integrated maneuver demand controls 02 p0224 A70-11835
VTOL transport aircraft stability and maneuverability compared with conventional aircraft 02 p0228 A70-12759
Tactical fighter requirements and designs, considering operational environment and weapon characteristics with emphasis on turning performance [AIAA PAPER 70-516] 13 p2346 A70-29035
AH-1G Hueycobra helicopter stability, control, performance, vibration and structural loads characteristics during controlled steady state maneuvers 17 p3014 A70-34716
Maneuver load alleviation /MLA/ configurations for wing bending load relief on transport aircraft, showing improved payload and span performance [AIAA PAPER 70-877] 17 p3016 A70-34813
Single and coaxial dual rotor helicopter piloting characteristics during turning flight, discussing operational problems in snow 22 p3962 A70-43530
Lifting reentry flight test vehicle aerodynamic configuration development, emphasizing lateral stability and maneuverability [ICAS PAPER 70-02] 23 p4257 A70-44118
Maneuver demand control using electric signalling feedback technique in Avro 707C and Hunter Mk 12 aircraft 24 p4374 A70-46203
- MANEUVERABLE SATELLITES
U MANEUVERABLE SPACECRAFT
U SATELLITES
MANEUVERABLE SPACECRAFT
NT APOLLO SPACECRAFT
NT FERRY SPACECRAFT
NT LIFTING REENTRY VEHICLES
NT RENDEZVOUS SPACECRAFT
Thermal protection systems /TPS/ design criteria for maneuverable reentry spacecraft, comparing weight and cost for various alloy systems 02 p0392 A70-11940
Optimal control program using multiple maxima method for maneuvering spacecraft in earth atmosphere with aim of changing orbital plane 07 p1331 A70-19483
Optimal control program using multiple maxima method for maneuvering spacecraft in earth atmosphere with aim of changing orbital plane 15 p2813 A70-32728
Space shuttle atmospheric maneuvers, examining booster and orbiter entry, flyback and abort [AAS PAPER 70-047] 17 p1375 A70-34787
- MANEUVERS
NT EARTH ORBITAL RENDEZVOUS
NT LUNAR ORBITAL RENDEZVOUS
NT ORBITAL RENDEZVOUS
NT SPACECRAFT DOCKING
NT SPACECRAFT MANEUVERS
Loading conditions measured during aerobatic maneuvers in flight test to determine structural design requirements for aerobatic-type aircraft [SAE PAPER 700222] 11 p1980 A70-25894
Helicopter rotor blade differential pressure and structural load characteristics in transient and steady state maneuvers 17 p3016 A70-34739
- MANGANESE
NT MANGANESE ISOTOPES
Manganese and sulfur content effects on martensitic stainless steels machinability, describing effects on mechanical properties, cold formability and corrosion resistance 03 p0507 A70-13135
Pelagic sediment natural spherules identification based on formation process and manganese nodules abundance 13 p2400 A70-29859
Manganese deficiency effect on chlorophyll fluorescence in algae adapted to hydrogen, determining electron transport mechanism 16 p2848 A70-33291
Mn and Ti effects on hardening of Fe-Ni-Mn-Ti and Fe-Ni-Mn maraging martensitic steels 17 p3125 A70-35145
- MANGANESE ALLOYS
NT MANGANIN [TRADEMARK]
Temperature dependence of magnetic susceptibility in liquid and solid states of binary Al-Mn alloys with additions of Cr, V and Ti 02 p0316 A70-12300
Fe-Cr-Mn-Ni system studied to obtain high Mn austenite and establish boundaries in quaternary system 03 p0509 A70-13278
Ternary Al-Mn alloys precipitation hardening with Cr, V and Ti, investigating ferro and ferrimagnetic phases 07 p1307 A70-19390
Phase diagram of rapidly crystallized Al-Cu-Mn alloys, observing ternary solid solutions formation during high cooling rate of melt 09 p1709 A70-23786
Quenched MnBi thin films measured for magnetic, magneto-optical and optical properties, noting Faraday rotation 12 p2284 A70-27246
Internal friction in hydrogenated Ti-Mn alloys, observing relaxation peak formation under stress induced hydrogen diffusion in beta phase 16 p2930 A70-33082
Physical properties and structure of Cr-Ni austenitic stainless steels with high Mn and N content as function of temperature 17 p3125 A70-35143
Ti-Mo and Ti-Mn alloys omega transition phase, describing shape and crystallographic characteristics 24 p4361 A70-46178
- MANGANESE COMPOUNDS
NT MANGANESE PHOSPHIDES
NT PERMANGANATES
Phase equilibria in Mn-S, Mn-Se and MnS-MnSe systems by X ray diffraction after preparation by annealing 02 p0249 A70-11652
Iodine concentrations, temperature gradients and transport ampules etching effects on mass transport rate and crystal growth of MnS-MnSe-iodine system 16 p2960 A70-33088
Knudsen effusion measurements of stoichiometric MnTe sublimation at high temperature and low pressure 21 p3773 A70-41273

MANGANESE IONS

- Antiferromagnetic resonance measurement in manganese difluoride as function of microwave frequency, sample size and shape 21 p3850 A70-41908
- Magnetic properties of lanthanum calcium manganate, making stoichiometric specimens by controlling oxygen partial pressure 24 p4390 A70-45602
- ### MANGANESE IONS
- Electron paramagnetic resonance of Mn ions in single crystal and powder forsterite, testing heat treatment and proton irradiation effect on ordering 16 p2960 A70-33008
- Calcium ion role in myocardial cell electrical and mechanical trace processes under normal content and manganese blocking 18 p3221 A70-36640
- Neel temperature of thermally stable garnet orthoerites of YFeAlMn composition 19 p3484 A70-37623

MANGANESE ISOTOPES

- Half life of Mn53 calculated from measured activity in sample from Fe meteorite and isotopic ratio Mn53/Mn55 07 p1337 A70-19226
- Radioactive Mn 54 with high specific activity for short distance gamma radiography 13 p2404 A70-28658
- Apollo 11 lunar dust examination by neutron activation analysis, determining spallogenic manganese 53 21 p3908 A70-41579

MANGANESE PHOSPHIDES

- Magnesium arsenide phosphide crystal and magnetic structure using X ray and neutron diffraction 12 p2283 A70-27240

MANGANESE 53

U MANGANESE ISOTOPES

MANGANESE 54

U MANGANESE ISOTOPES

MANGANESE 56

U MANGANESE ISOTOPES

MANGANIN [TRADEMARK]

- Manganin piezoresistive shock gauge constant current supply using inductor and termination technique eliminating shunting 02 p0303 A70-12737
- Manganin in wire and thin foil geometries, measuring shock piezoresistance coefficient as function of deformation 20 p3687 A70-40166

MANIFOLDS

- Optimum manifold and injector hole area of pulsed exhaust systems of two cycle engine with turbosupercharger 22 p4091 A70-42809

MANIFOLDS [MATHEMATICS]

- Optimal control problem solution involving functional minimization along differential vector equation trajectories, considering manifold type constraints on phase coordinates 07 p1244 A70-18747
- Invariant set existence inside submanifold convex to flow established from vector field properties on submanifold boundary 07 p1324 A70-19198
- Chaplygin theorem proof for partial differential equation, using piecewise smooth manifold with unilateral conductivity 08 p1534 A70-21008
- Lagrangian nonenergetic and unconstrained systems introduced in describing Birkhoff classical dynamics, considering space of motions states as connected analytic manifold 10 p1909 A70-24190
- Integral manifolds of third order autonomous differential equations with unstable equilibrium point, investigating forward and negative asymptotic problems 12 p2261 A70-27375
- Kerr-Schild space-time manifolds with electromagnetic field, solving Einstein equations 13 p2451 A70-29166
- Grassmann manifold projective transformations into itself, considering matrix theorems 14 p2601 A70-31423

MANIPULATION

U MANIPULATORS

MANIPULATORS

- Computer controlled remote manipulator development, operation, components and applications, describing system programs consisting of executive control programs and subroutines 08 p1465 A70-20817
- State space models of remote manipulation problem applied to human supervised or autonomous computer manipulators 10 p1828 A70-25230
- Control device for micromanipulator with pacing motor during electrophysiological studies involving microelectrodes implantation into tissue 12 p2179 A70-28317
- Ground controlled remote manipulator spacecraft system through wideband radio link for satellite maintenance and repair 15 p2810 A70-31780

MANNED AERODYNAMIC REUSABLE SPACESHIP U MARS [MANNED REUSABLE SPACECRAFT]

MANNED ORBITAL LABORATORIES NT MANNED ORBITAL RESEARCH LABORATORIES

- High altitude scale model experiment to evaluate rocket plume impingement effects on Manned Orbital Workshop pressures, heating rates, forces and moments 03 p0579 A70-13646
- Manned and unmanned orbital space facilities pointing and stability requirements, noting application to stellar and solar astronomy, earth observations, etc 16 p2979 A70-34068
- Orbital international laboratory and space sciences - Conference, Cloudcroft, New Mexico, September 1969 22 p4107 A70-43626
- Manned orbital laboratories, discussing need for international cooperation 22 p4128 A70-43634
- Manned orbiting laboratory microclimate including atmosphere composition, temperature, humidity and weightlessness effects, radiation and noise protection, etc 22 p3980 A70-43636
- Alpine 11,500 ft air atmosphere for manned orbiting laboratory, noting reduced risk of dysbarism during space suit operations 22 p3980 A70-43645
- Blood-brain and blood-cerebrospinal fluid barriers alterations under various physical environments in manned orbital laboratory 22 p3973 A70-43647
- Integrated regenerative life support manned tests for space laboratory design and development 23 p4154 A70-44632
- Space technology applications to earth survey, discussing use of automatic satellites and manned space laboratories for meteorological, geophysical and related purposes 23 p4191 A70-44634
- Orbital space station utilization planning as international laboratory, discussing industry role, experiment program goals, etc 23 p4260 A70-44650
- ### MANNED ORBITAL RESEARCH LABORATORIES
- Manned lunar orbital research operations capability, systems and scientific objectives [AAS PAPER 70-022] 17 p3156 A70-34800
- Orbital biotechnology laboratory requirements concerning man systems integration, life support and protective systems 22 p3980 A70-43644
- ### MANNED ORBITAL SPACE STATIONS
- ### U ORBITAL SPACE STATIONS
- ### MANNED ORBITAL TELESCOPES
- Wide field stellar astronomical ESRO project, reviewing application of earth orbiting spin stabilized satellites and OAO 09 p1767 A70-23435
- ### MANNED ORBITAL TELESCOPES
- ### NT APOLLO TELESCOPE MOUNT
- ### MANNED REENTRY
- Earth and planetary entry vehicle designs for manned and unmanned space missions, noting thermal protection, environmental control requirements and communication systems [AIAA PAPER 68-1080] 01 p0195 A70-10826
- ### MANNED SPACE FLIGHT
- NT APOLLO 7 FLIGHT
- NT APOLLO 8 FLIGHT
- NT APOLLO 9 FLIGHT
- NT APOLLO 10 FLIGHT
- NT APOLLO 11 FLIGHT
- NT GEMINI FLIGHTS
- NT GEMINI 4 FLIGHT
- NT GEMINI 6 FLIGHT
- NT GEMINI 11 FLIGHT
- NT GEMINI 12 FLIGHT
- NT MANNED REENTRY
- Medico-engineering experiment in partially closed ecological system for long term manned space missions 01 p0032 A70-10363
- Soviet book on survival in space covering astronauts training, behavior, impressions, performance, etc, with historical considerations 01 p0033 A70-10493
- Systems design experience derived from Mercury, Gemini and Apollo projects, discussing thermal protection, launch propulsion, life support, etc [AIAA PAPER 69-1077] 01 p0193 A70-10604
- Underwater saturation habitats application as behavioral workshops for mission planning and human engineering of manned space flight, discussing Project Tektite [AIAA PAPER 69-1120] 01 p0034 A70-10611
- Manned vehicles rendezvous missions in space and hydrospace, proposing functional structure involving concurrent ship control, navigation, perception, communication and prehension [AIAA PAPER 69-1102] 01 p0034 A70-10615

- Mission simulation mathematical modeling technology developed for optimization of experiment program management and operational planning for manned space station missions [AIAA PAPER 69-1065] 01 p0181 A70-10634
- Langley integrated life support system design, discussing manned test results including system engineering, atmospheric and water chemical analyses and microbial measurements 01 p0038 A70-10973
- Manned space station system design requirements, discussing logistics interaction and station autonomy [AIAA PAPER 69-1063] 02 p0382 A70-12528
- Radiation level recordings during Soyuz manned orbital flights indicating safety standards maintenance 03 p0580 A70-13704
- Respiratory and cardiac activities, body weight variations, blood and urine electrolytic composition of astronauts during Soyuz orbital flights from medical tests 03 p0423 A70-13709
- Pharmacology for long term manned space 04 p0629 A70-14566
- Circadian rhythms characteristics in humans, animals and plants, noting possible effects of rhythm disturbances on astronauts 04 p0629 A70-14567
- Sweet potatoes productivity and nutritive value as carbohydrates source in manned space flights 04 p0641 A70-14572
- Space flight emergencies causes and consequences, underlying life threats and crew survival times, considering equipment failures, personnel errors, etc 04 p0761 A70-14926
- Parametric performance and cost comparison of separate and integral vehicle concepts for manned space activity using payload criterion 04 p0763 A70-15420
- Regenerative life support system development for multiman crews on extended space missions, considering maintainability, reliability and automation [SAE PAPER 690637] 05 p0804 A70-15845
- Command and control functions of DOD Manager for Manned Space Flight Support Operations in spacecraft recovery 05 p0827 A70-16180
- Display/control system and key technical decisions at Manned Space Mission Control Center, discussing command consoles 05 p0829 A70-16194
- Soviet book on piloted flights in near space with lunar landing, discussing flight mechanics of orbital aircraft, launching into space, maneuvering, etc 05 p0923 A70-16554
- Manned space flight requirements connected with cabin atmosphere, food/water supplies and waste disposal and environmental conditioning 05 p0807 A70-16632
- Spacecraft design for manned interplanetary missions, considering structural materials and weights, cryogenic insulation, meteoroid protection, landing gear, etc 05 p0924 A70-16720
- Electric propulsion system and initial gross weights estimation for manned Mars missions 05 p0924 A70-17093
- Dosimetry data and personal radiation sensors from Apollo and Gemini flights, noting spacecraft geometry shielding effects 06 p1134 A70-17268
- Soviet manned space flight radiation dosimetry evaluation, comparing U.S. and Soviet techniques for astronaut protection 06 p0990 A70-17271
- Systems engineering aspects of Apollo Telescope Mount spacecraft, considering design and manned space flight role 06 p1061 A70-17312
- Short duration manned Mars and Venus exploration mission planning with chemical propulsion and Saturn 5 boosters [AIAA PAPER 70-59] 06 p1147 A70-18238
- Artificial effects on atmosphere and near-earth space caused by human activity, discussing occurrence altitude, means of action and consequences 07 p1262 A70-18778
- Spacecraft incorporated emergency rescue systems, discussing design of nonseparable crew escape compartment and separable capsule 07 p1218 A70-19010
- Physiological and hygienic data on oxygen partial pressure in space cabin atmosphere analyzed for manned space flights 07 p1220 A70-19502
- Automatic control of continuous medical monitoring in manned space flight 07 p1220 A70-19512
- Astronauts visual performance during space flight, studying reduction of visual disturbances from various physiological flight factors 08 p1444 A70-20741
- Premission planning and operational radiation dose limits for manned lunar and low earth orbit missions 08 p1454 A70-21940

National Space Program relevance to human society, discussing solar system exploration, applications in meteorology, communication, etc
09 p1792 A70-22041

Manned Mars mission planning, discussing technologies and costs for planetary landing
09 p1757 A70-22676

Earth resources program function of early orbital manned space station in remote sensing
09 p1687 A70-23760

Interstellar flights, discussing human limitations, star systems with habitable planets and possible galactic communities
10 p1943 A70-24759

Maintainable electronic equipment requirements for long duration manned space missions
10 p1852 A70-24895

Radiation level recordings during Soyuz manned orbital flights indicating safety standards maintenance
11 p2121 A70-25504

Respiratory and cardiac activities, body weight variations, blood and urine electrolytic composition of astronauts during Soyuz orbital flights from medical tests
11 p1985 A70-25509

Asteroid vs planet for manned landing site, considering Martian moons mission
11 p2108 A70-25660

Physiological and hygienic data on oxygen partial pressure in space cabin atmosphere analyzed for manned space flights
11 p1991 A70-26101

Automatic control of continuous medical monitoring in manned space flight
11 p1991 A70-26111

Manned space flight role in earth orbital space astronomy, examining long range program
12 p2297 A70-26997

Manned laboratories in space - Conference, New York, October 1968
12 p2313 A70-27741

Manned Mars flyby/orbiter mission, discussing cost, scientific returns, technology advances, popular support, etc
12 p2304 A70-27749

Earth orbital parameters estimation in manned flight by manual space navigation sensors and computer
13 p2446 A70-28406

Spaceborne information processing for manned missions, describing layered system with fault tolerance and onboard checkout
13 p2372 A70-28415

Permissible radiation exposure levels during prolonged space flights based on clinical data
13 p2351 A70-29336

Stomatologic diseases during prolonged space flights simulation, discussing gingivitis, stomatitis, dental caries, parodontitis and odontogenous inflammations
13 p2352 A70-29338

Ground support real time operating system 360 for manned spaceflight, discussing system features and performance
13 p2375 A70-29937

Extraterrestrial resources for space flight maintenance and human life support in space and on extraterrestrial bodies
14 p2634 A70-30199

Weather forecasting for manned space flights, emphasizing Apollo flights and operational decisions due to forecasts
14 p2606 A70-30557

Infection resistance during extended space flights, discussing microfloral exchange, defense mechanisms, waste, etc
15 p2688 A70-31677

Lunar exploration by manned and unmanned space flights, discussing seismology, composition, surface features, etc
15 p2798 A70-31678

Astronomical observations, discussing advantages of human operators on interplanetary spacecraft or Mars
15 p2810 A70-31853

Radiation planning nomogram to display radiobiological effects of dose, onset time and shielding factors for manned space vehicles
15 p2690 A70-31894

Soyuz-9 manned space mission, outlining craft occupants personal background and statements
15 p2813 A70-32792

Spacecrew candidates leisure time preferences, discussing off-duty concepts for long space missions
16 p2853 A70-33709

Manned planetary flight systems engineering, discussing feasibility, objectives, propulsion, trans-planet injection via geospace shuttle station, energy requirements for various synodic modes
17 p3155 A70-34778

Multi-orbit injection earth departure technique for optimal thrust-weight ratio in manned interplanetary missions using NERVA engine
17 p3175 A70-34780

[AAS PAPER 70-039]

Future manned planetary missions with reusable nuclear shuttles, comparing operating modes in terms of propellant requirement, costs, complexity, etc
17 p3155 A70-34781

Manned planetary spacecraft and space stations as ecological systems, considering common features
17 p3176 A70-34799

Expandable and modular structures technology for manned and unmanned space missions, discussing expandable air lock experiment
17 p3177 A70-35230

Systems design experience derived from Mercury Gemini and Apollo projects, discussing thermal protection, launch propulsion, life support, etc
17 p3180 A70-35644

Medicobiological approach to living conditions for sustained residence and human activity during prolonged space flights, describing sealed chamber experiment
19 p3367 A70-37525

Microwave feeding system for heating and cooking prepackaged meals during extended space missions
19 p3368 A70-37747

Manned space station design, discussing durations of scientific experiments and crew operation
19 p3532 A70-37752

Space maintenance tools necessity on long duration manned space missions 1972-1980
19 p3442 A70-38836

Manned Mars lander launch-to- rendezvous analysis, using subsequent Venus swingby for mission velocity requirement reduction
19 p3530 A70-38887

Astronaut weight loss relation to flight duration during manned space missions
20 p3574 A70-40125

Medical support for long space missions based on space crews morbidity prediction, discussing onboard equipment and astronaut training
20 p3575 A70-40194

Environmental control-life support systems /ECLSS/ waste methane gas utilization in low thrust resistojet for manned space applications
20 p3568 A70-40214

Shock tube facility with high explosive driver for reentry flow conditions simulation of manned planetary flights
21 p3804 A70-40849

Gravitational experiments in manned spaceflight employing Eotvos balance in orbit and direct force technique
21 p3929 A70-41002

Book on decision making in U.S. manned lunar landing commitment covering space policy, technical planning, national interests, Apollo experience, etc
22 p4126 A70-42314

Combined space and nuclear radiation effects in manned space flight
22 p3978 A70-43184

Manned space program goals, discussing orbiting observatories, lunar bases, biological and earth resources satellites
22 p4128 A70-43627

Decompression sickness prevention in space flight, discussing suit and capsule pressure, extravehicular activity and alleviation of conditions
22 p3980 A70-43640

Biological compatibility problem in long duration space operation crew change, discussing human metabolic processes and difference effects
22 p3980 A70-43641

Space station program information management system involving data acquisition and extended manned flight operation with minimum ground support (IBM-70-U60-0015)
23 p4164 A70-44637

Manned space flight programs management, discussing organizational aspects of projects including Apollo, space shuttle and space station
23 p4286 A70-44696

Manned space flight regenerative life support systems requirements, considering weight, volume, power, cost effectiveness and integration problems
23 p4156 A70-45023

Free-flying modules interface and operation in conjunction with space station for orbital research into manned space program
24 p4417 A70-45950

[AIAA PAPER 70-1300]

MANNED SPACECRAFT

NT APOLLO SPACECRAFT

NT FERRY SPACECRAFT

NT GEMINI SPACECRAFT

NT LUNAR MODULE

NT MANNED ORBITAL LABORATORIES

NT MANNED ORBITAL RESEARCH LABORATORIES

NT MARS [MANNED SPACECRAFT]

NT MERCURY SPACECRAFT

NT ORBITAL SPACE STATIONS

NT ORBITAL WORKSHOPS

NT SOYUZ SPACECRAFT

NT SPACE SHUTTLES

NT SPACE STATIONS

Manned reusable space transportation system technology requirements and vehicle types
[AIAA PAPER 69-1116] 01 p0194 A70-10613

Manned space station power systems design and selection problems, discussing requirements based on impacts on space station design and operations
[AIAA PAPER 69-1081] 01 p0008 A70-10625

Tradeoff criteria between man machine and automated space systems applied to lunar and cosmic ray explorations
[AIAA PAPER 69-1045] 01 p0034 A70-10644

Minimum fuel consumption criteria applied to design of manned spacecraft attitude control system, using reaction jets for lateral and directional controls
01 p0196 A70-10950

Man machine system consisting of manned station controlling distant spacecraft via wideband radio link
02 p0229 A70-12145

Artificial gravitation parameters for manned compartments of spacecraft, analyzing permissible angular velocity and rotation radius regarding vestibular-vegetative disorders
04 p0760 A70-14446

Nuclear propulsion requirements for manned landing mission to Mars assuming Saturn 5-based operation
07 p1375 A70-18874

Unmanned and manned interorbital shuttle systems for satellite placement and repair and planetary spacecraft insertion, emphasizing cost analysis
[AIAA PAPER 70-267] 07 p1398 A70-20396

Control display requirements for manned spacecraft, integrating human operator with vehicle control system and determining man machine relations in stabilization, control and guidance
08 p1498 A70-21678

Manned and unmanned earth resources observation satellite program, noting international cooperation
10 p1971 A70-24636

Manned and unmanned earth observation satellite programs technology gains, discussing atmospheric temperature, pressure, winds, clouds and moisture
10 p1876 A70-24637

Nuclear pulse propulsion system for manned missions to outer planets of solar system, discussing energy and travel time requirements
11 p2082 A70-26059

Manned space stations size, crew, orbit, lifetime, resupply requirements, etc
12 p2313 A70-27742

Artificial gravitation parameters for manned compartments of spacecraft, analyzing permissible angular velocity and rotation radius regarding vestibular-vegetative disorders
13 p2503 A70-28471

Statistical error analysis of autonomous manned spacecraft navigation in long duration eccentric Mars orbits
[AIAA PAPER 69-880] 15 p2773 A70-32503

Space based reusable manned/unmanned tug, discussing potential missions, system requirements and auxiliary hydrogen oxygen propulsion system
[AIAA PAPER 70-719] 16 p2964 A70-33533

Onboard automatic checkout systems for manned space vehicles, investigating data management development costs for thorough tradeoff studies
16 p2889 A70-33803

Unmanned and manned interorbital shuttle systems for satellites placement and repair and planetary spacecraft insertion, emphasizing cost analysis
[AIAA PAPER 70-267] 17 p3172 A70-35650

Earth resources data from man operated airborne/spaceborne sensors and data handling systems, examining Apollo Applications Program
20 p3616 A70-39056

Human mass exchange parameters permissible errors for manned space vehicles life support systems design
20 p3581 A70-40200

Flame resistant nonmetallic materials for manned spacecraft and aircraft interiors, considering fibers, polymers, paper and composites
22 p4058 A70-42295

Planetary probes, orbiting space stations and manned spacecraft in interplanetary flights, discussing Mariner, Gemini and Apollo reentry and Venus landing
22 p4109 A70-42313

Decompression hazards in manned orbiting systems, considering consciousness time, survival, pathological response, water vapor and denitrogenation effects and recompression rates
22 p3973 A70-43638

Rapid decompression due to pressure loss in space vehicle or suit, discussing fulminating hypoxia, mechanical trauma and ebullism
22 p3973 A70-43639

Man-rated chamber facilities at Manned Spacecraft Center /MSC/, discussing safety requirements and criteria, environmental test chamber design and test results
23 p4152 A70-44458

- Manned spacecraft nonmetallic construction materials selection criteria, testing and configuration control, considering flammability hazard 23 p4152 A70-44462
- Manned spacecraft onboard data management systems, discussing information transfer, processing, control, display and man machine interface 23 p4167 A70-44647
- Automated and manned spacecraft design, discussing mission objectives and present and potential applications 23 p4264 A70-45003
- Manned spacecraft abort guidance and control problems, discussing various modes and emergency conditions 24 p4374 A70-46210
- MANNED SPACEFLIGHT
NT APOLLO FLIGHTS
MANOMETERS**
- Differential equations of motion of manometers in log instrument systems with allowance for viscous liquid in sensor and pulse line 12 p2234 A70-27567
- Multiple tube manometer with selector switch for measuring flow channel wall pressures 23 p4194 A70-44000
- MANPOWER
NT SCIENTISTS**
- Great Britain air transport industry manpower recruitment and training, technology changes effects and costs 02 p0402 A70-12307
- ATC procedures based on system error and aircraft accident probabilities, traffic flow and navigation control and controller manpower 11 p2078 A70-25721
- Manpowered aircraft, considering possibility as future flying sport vehicles [AIAA PAPER 70-879] 17 p3016 A70-34809
- Air cargo terminal operations analysis, discussing manpower cost reduction 20 p3607 A70-40127
- MANTLE [EARTH STRUCTURE]
U EARTH MANTLE
MANUAL CONTROL**
- Task interference model for interference among two or more continuous manual control tasks, suggesting metric for pilot mental workload 02 p0244 A70-12139
- Supervisor sampling frequency maximizing given value or payoff function, discussing applications to controlling vehicle, information system or institutions 02 p0307 A70-12141
- Speed and accuracy of foot operation of controls tested by circular targets in rows within reach of right foot 02 p0245 A70-12144
- Man machine interface in VTOL aircraft control and stabilization systems adaptation during manually controlled hovering flight 03 p0414 A70-14094
- Tactile control in man machine systems using feed-forward loops to provide rate information, noting un-manned aircraft and machine-tool applications [ASME PAPER 69-WA/BHF-14] 04 p0642 A70-14855
- Horizontal transverse vibration effects on manual tracking performance, relating tracking errors to frequency rather than acceleration 04 p0643 A70-14981
- Human controller in psychology and control engineering, discussing linear and nonlinear modeling of human behavior 05 p0807 A70-16487
- Biological model describing spacecraft operator sensorimotor activity in response to various spacecraft control stimuli, outlining computer algorithm 05 p0810 A70-17118
- Manual onboard orbit determination assuming electronic equipment failure, discussing geometric in-plane orbital parameters and safe orbit check [AIAA PAPER 70-159] 06 p1144 A70-18033
- Decision algorithms simulating human controller adaptive behavior in controlling VTOL aircraft in hover following stability augmentation system failure 07 p1216 A70-18860
- Simulator servo drive system dynamic requirements for single-axis manual control task using pilot models and computer [AIAA PAPER 70-355] 10 p1858 A70-24208
- Remote signal measurement and analysis in hazardous environment by command terminal utilizing manual or computerized control 12 p2201 A70-28134
- Manual spacecraft rendezvous system based on handheld instruments and manual computations, considering error analysis and simulation 13 p2357 A70-28392
- Manual control systems for spacecraft stabilization involved in rendezvous, midcourse correction, landing, etc 13 p2357 A70-28394

- Hypokinesia effects on working capacity of sub-jects performing manual aircraft control assignments during bed rest 13 p2352 A70-29340
- Relative cost benefits estimation of manual and automatic test systems for avionics in maintenance organization, proposing integrated maintenance and ATC data system 13 p2525 A70-29679
- Radio and electronic equipments production testing by automatic equipment combined with semiautomatic manual controller 13 p2379 A70-29680
- Mathematical models for human adaptive and optimizing characteristics in manual control systems regarding behavior phase 13 p2360 A70-29780
- Motion cue requirements in one and two axis closed loop compensatory control tracking tasks, discussing error rates 14 p2540 A70-30247
- Optimal manual control model of human compensatory tracking response 14 p2543 A70-31408
- Model for pilots optimal manual control of hovering VTOL aircraft longitudinal position 14 p2543 A70-31409
- Laser ranging and tracking system consisting of mirror tracking pedestal, instrumentation bay and control van featuring manual/automatic tracking capability 16 p2862 A70-33164
- Display-control relationships in visual display information processing, considering spatial incompatibility effects on reaction time 16 p2852 A70-33661
- Feedback delay effects on eye-hand synchronism in stimulus tracking and steering using self generated body movements 16 p2852 A70-33662
- Head up display /HUD/ flight tests, examining effects decreasing quality of manually handled instrument approach, discussing space myopia and disorientation 16 p2912 A70-33819
- Mechanical and acoustic vibrations signals analyzer, noting automatic or manual operation 17 p3054 A70-35417
- Manual attitude control for Lunar Module employing directional stability, coordinated turn and attitude command 20 p3716 A70-39683
- Longitudinal vibration effects on human reaction time and motor performance involving toggle switch and manual knob control in different working positions 22 p3977 A70-42871
- Pilot hand-held and leg-mounted controllers for precision tracking from aircraft under buffeting tested in static and dynamic motion simulator 24 p4308 A70-45513
- MANUFACTURING**
- Magnetic components design, manufacturing and handling for use in space communication satellites, noting design group role in parts construction and quality control 02 p0267 A70-12057
- Carbon materials manufacture, properties and applications in space technology, discussing carbon fibers, textiles, graphite, pyrolytic carbon, composites and vitreous carbon 03 p0516 A70-13618
- Soviet aerospace manufacturing technologies development, considering forging, extrusion, metal working and joining, etc [SAE PAPER 69-0701] 05 p0853 A70-15826
- Process specifications to control manufacturing operations, describing contents, purposes and preparation, emphasizing three levels of control 06 p1184 A70-17601
- Processing methods for manufacturing composite solid propellants, describing oxidizer, binder and fuel preparation, propellant mixing and chamber insulation and lining and instrumental analysis 07 p1361 A70-19912
- Hazards in manufacturing solid propellants evaluated to design tests and suggest process conditions 07 p1361 A70-19915
- Solid propellant technology, discussing manufacturing processes, sample testing, inspection, etc 08 p1557 A70-20690
- Composite and double base solid rocket propellants manufactured by French factory for ballistic missiles, discussing plant installations 11 p2030 A70-25520
- Manufacturing error rate and inspection efficiency relevance to hardware product reliability 12 p2244 A70-28014
- Titanium alloys powder metallurgy, considering manufacturing methods and physical, chemical and mechanical properties 13 p2435 A70-29214
- Barium fluoride film hygrometer elements for radiosondes, discussing manufacturing and testing methods 13 p2408 A70-29470

- Corrective Action systems for identification, control and resolution of manufacturing, engineering and vendor problems 14 p2669 A70-31102
- Solid state diffusion bonding applied to rocket engine injectors manufacture [AIAA PAPER 70-639] 16 p2968 A70-33597
- Space manufacturing in weightless environment, discussing unique processes, potential materials, product groups, planned experiments for Skylab Orbital Workshop mission, etc 16 p2888 A70-33716
- Orbital zero and low g environment utilization for space manufacturing processes and related operational and tooling requirements 16 p2919 A70-33718
- Systems design and instrumentation for chemical/biochemical space manufacturing at zero g, developing scaling laws for transition to larger production units 16 p2919 A70-33719
- Candidate products for manufacturing on space station, emphasizing liquid solid transformations, bubbles and droplets, polymerization, and cost effectiveness [AAS PAPER 70-036] 17 p3041 A70-34791
- Holographic projection for electronic microcircuit manufacture 17 p3088 A70-35028
- Polyimide prepreps reinforced with glass, carbon and graphite, describing processing characteristics, properties and applications 17 p3127 A70-35419
- Conical expansion nozzles manufacturing errors effect on flow expansion considered for large Mach numbers 17 p3011 A70-35662
- Soviet book on aircraft electrical and radio systems manufacturing, assembling and testing methods, considering effectiveness and standardization 19 p3357 A70-37405
- Space processing under zero gravity conditions, discussing crystal growth, metal glass and ceramic melting and casting and biological product centrifugation and electrophoresis 19 p3436 A70-37926
- Adhesive bonded aircraft structures, discussing methods and requirements for establishment and control of manufacturing procedures 19 p3438 A70-38594
- Translation gap between R and D and production occurring at design transmission to manufacturing 21 p3955 A70-40913
- Parabolic solar furnace for chemical manufacture of impurity sensitive materials in orbiting spacecraft 21 p3804 A70-41001
- Skylab Orbital Workshop fabrication experiments under space environment conditions, discussing weightlessness and vacuum effects on various manufacturing techniques 22 p4046 A70-43075
- Aircraft engine manufacturing technology, discussing metal cutting and forming, bonding, electrochemical machining and electron beam welding 24 p4341 A70-45298
- Computer-aided production engineering involving numerically controlled machines for Rolls-Royce aircraft engines manufacture 24 p4341 A70-45299
- MANY BODY PROBLEM**
- PostNewtonian equations of Brans-Dicke scalar-tensor theory for n gravitating point masses, using obtained equations of motion for radar tracking 02 p0337 A70-11777
- Singularities arising during collisions in restricted n-body problem elimination, discussing Jacobi integral and finite-mass body configuration 04 p0714 A70-15354
- State transition matrix computation method with efficient algorithm for orbit prediction in n-body gravitational field 06 p1095 A70-18497
- Thermoelasticity equations derived for regular systems of M bodies in dynamic and thermal interaction using nonlocal continuous model 07 p1407 A70-19381
- Laser-induced electron emission from metals and insulators in form of evaporated films and single crystals, discussing many-photon photoelectric effects and thermionic emission 08 p1556 A70-21509
- Molecular hydrogen parallel and perpendicular dynamic polarizabilities calculated for frequency dependence, using many body perturbation theory 09 p1731 A70-22780
- BBGKY hierarchy state functional formalism in nonequilibrium statistical mechanics for many particle system using Fourier transformation 11 p2087 A70-26548
- Bipolar moment integral in celestial mechanics formed by product of particle kinetic moments for n body problem order reduction 13 p2494 A70-29399

- Quantum-electrodynamical renormalization for electron charge in metal environment, using solid state many-body techniques 14 p2619 A70-30476
- Stable equilibrium positions for satellite consisting of many rigid bodies in circular orbit about center of gravity, using numerical method 18 p3332 A70-35963
- Many body gravitational problem, computing evolution of two groups by numerical integration with two different computers 19 p3523 A70-38692
- N body numerical integrator using virtual mass technique for computing trajectories with speed and accuracy suitable for spacecraft onboard computer applications [AIAA PAPER 70-1057] 19 p3528 A70-38872
- Coherent behavior associated with thermodynamic description projected from dynamical behavior of many body system, using relation between asymptotic operators 22 p4062 A70-42547
- Satellites with many flexibly coupled rigid bodies, calculating libration upper bounds for predicting perturbation and stability 23 p4262 A70-44682
- MANY PARTICLE THEORY**
U MANY BODY PROBLEM
MAPPING
 NT CADASTRAL MAPPING
 NT SOIL MAPPING
- Mappings of linear vector spaces induced by transformation matrix applied to linear dynamical systems 01 p0132 A70-11125
- Orbital charts development for space navigation, discussing cartography and orbital navigation 01 p0138 A70-11251
- Airborne cartographic azimuthal instrument with reflecting prism type optomechanical assembly and trihedral pyramid groscope for stabilization 01 p0093 A70-11269
- Dynamical systems with two degrees of freedom reduced to numerical investigation of quadratic area-preserving mapping 02 p0289 A70-11993
- Geodetic air mapping and surveying system, describing cartographic camera and system operation 03 p0489 A70-13655
- Artificial satellites for geodetic, topographic and cartographic purposes, outlining photographic and distance measuring equipment 03 p0475 A70-13831
- Land use mapping of southwestern U.S. using photographs from Apollo and Gemini missions [AAS PAPER 69-576] 04 p0676 A70-14640
- Line scanning IR imagery system for thermal mapping of fire, water and soil conditions 05 p0836 A70-15770
- Cartographic radiation patterns far field characteristics of aperture antenna arrays obtained by optical simulation method 05 p0820 A70-16254
- Variational methods in semigeodesic projections of analytic surfaces on plane surface, determining projections impossible by classical cartography 05 p0839 A70-16368
- Optical wave front reconstruction principles applied to sonic and seismic wave holography for mapping earth subsurface structure 05 p0850 A70-16685
- Nonlinear equation solution based on local mapping relations and global implicit function theorems for Banach space problems 06 p1092 A70-17224
- Solar magnetic field spectroheliographic mapping, discussing detection levels, resolution, applications, etc 06 p1148 A70-18454
- Holography history and applications to interferometry, contour mapping and three dimensional photography 07 p1279 A70-18900
- Automated techniques for topographic mapping, considering scales used 07 p1281 A70-19371
- Mapping of normal distribution of geomagnetic elements in Bulgaria 08 p1490 A70-21433
- Digital computer processing of airborne multispectral data, discussing automatic recognition and mapping of terrain distribution, Earth Resources Technology Satellite data channel efficiency, etc [AIAA PAPER 70-309] 09 p1668 A70-22878
- Satellite high resolution IR imagery for arctic sea ice mapping, describing sensor design and day and nighttime operation in film-strip format [AIAA PAPER 70-301] 09 p1669 A70-22884
- Mapping electric field components perpendicular to magnetic field line in ionosphere at equatorial plane, discussing discrepancy with convection patterns 10 p1875 A70-24437
- Satellite photographs for geological mapping and research assessed against interpretation of field data and conventional aerial photographs 10 p1876 A70-24640
- Photogrammetric map compilation from orbital satellite photographs, with fictitious and ground coordinates generated by electronic computer, discussing error sources 10 p1890 A70-24728
- MUSAT program and AN/USQ-28 SHIRAN controlled aerial photographs photogrammetric evaluation by U.S. Army Topographic Command, indicating bias in nadir positions 10 p1890 A70-24730
- Remote sensing techniques for water resources evaluation and hydrobiological features mapping with multiband scanner imagery 10 p1879 A70-24742
- Aerial super wide angle photography for mapping, discussing cost reduction, accuracy requirements and photographic techniques 10 p1891 A70-24756
- Universal Automatic Map Compilation Equipment /UNAMACE/ for terrain altitudes determination on uniform and dense grid in stereo model to obtain orthophotographic projection 11 p2051 A70-26042
- Mars imaging mission and astrodynamic interaction, discussing arrival geometry and orbit size effects [AIAA PAPER 69-127] 11 p2112 A70-26130
- Hydrobiological features mapping in Everglades by multispectral scanning and analog data processing 12 p2220 A70-26934
- Preprocessing data transformations for multispectral recognition mapping, reducing difficulties due to variations in environmental, observational and sensor conditions 12 p2220 A70-26935
- Airborne geological mapping by IR emission spectroscopy, describing instrumentation, materials discrimination capability, data processing, etc 12 p2330 A70-26957
- Radiophase and induced pulse transient /input/ remote sensor systems for geological mapping, describing data acquisition and reduction techniques 12 p2221 A70-26961
- Mathematical cartography, discussing uses of electronic computers in network design 13 p2395 A70-28925
- Bifurcation and stability analysis of point mappings with polynomial succession function, using parametric diagrams 13 p2383 A70-29751
- Spatial filters for ratio W/H measurement in aerial mapping 14 p2581 A70-30144
- Essa 7, Surveyor 7 and Mariner 4 space TV systems geometric distortions analysis and potentials in analytic photogrammetry and topographical mapping 14 p2586 A70-30982
- Photographic and multisensor imagery augmented by field survey for mapping vegetation boundaries and density differences within and between plant communities 17 p3079 A70-35616
- Multispectral remote sensing for detection and mapping of ecological objects and energy budget parameters measurement 17 p3079 A70-35622
- Numerical ionospheric world mapping of plasma frequency, considering height, latitude, longitude and local mean time variations 19 p3380 A70-38403
- Geological and cartographical data acquisition and processing, considering aircraft and satellite-borne photography of earth surface 20 p3616 A70-39061
- Inner magnetosphere magnetic field mapping, deriving Pogo model 20 p3621 A70-39349
- Isopotential surface maps for body surface potential relation to ECG and Frank vectorcardiogram during QRS stages in children 20 p3571 A70-39368
- Aerial cameras for topographic mapping, emphasizing geometrical image accuracy, optical picture quality and shutter performance 21 p3826 A70-41268
- Digital computer processing of airborne multispectral data, discussing automatic recognition and mapping of terrain distribution, Earth Resources Technology Satellite data, channel efficiency, etc [AIAA PAPER 70-309] 21 p3829 A70-41851
- Mapping from satellite-collected earth surface images, emphasizing optical/mechanical scanner images 22 p4037 A70-43089
- ERTS line scanning system for cartographic data of water, snow, vegetation and cultural areas 22 p4037 A70-43090
- Holo-diagrams for predicting fringe patterns in hologram interferometry caused by translation motion and rotation 22 p4040 A70-43610
- Rotating gravity gradiometer for simulated terrain mapping with subsurface density fluctuations 22 p4007 A70-43668
- Optimal timing for aerial photographic mapping of landscape types including tundra, forest, steppe, meadow, desert and mountain areas 24 p4328 A70-45196
- Optical properties of terrain for optimal time charting of aerial mapping, considering seasonal variations and atmospheric transmittance 24 p4333 A70-45199
- Field control method for aerial photograph planar tying-in, applying to cartographic reference point coordinate determination in triangulation 24 p4334 A70-45499
- Gravity measurements and adjustments of First Order Gravity Network /FOGN/ in Iran 24 p4332 A70-46409
- MAPS**
 NT ASTRONOMICAL MAPS
 NT LUNAR MAPS
 NT METEOROLOGICAL CHARTS
 NT RADAR MAPS
 NT RELIEF MAPS
- Moving map displays applications in marine and air navigation, discussing human factors and impact on ATC 01 p0139 A70-11284
- Soviet book on theory and practice of maps application in aviation, covering coordinates for objects positions determination on ground error estimation, etc 13 p2448 A70-28725
- Optimum image scale and longitudinal overlap in continuous orthophoto map production regarding sheet dimensions, instrumental ranges, flight path tolerances and ground relief 13 p2407 A70-29165
- Surface temperature color contour maps of objects undergoing aerodynamic testing, utilizing electro-optical and computer techniques 16 p2905 A70-33169
- MARAGING STEELS**
 Dimensional stability of nickel maraging steel at ambient temperature measured for applications as gage block materials 01 p0120 A70-10742
- Age hardening characteristics of maraging martensite stainless steels containing Mo and Co subjected to subzero treatment 01 p0125 A70-11641
- Calorimetric analysis and hardness test to investigate low temperature aging behavior of maraging stainless steels 01 p0125 A70-11642
- Forming techniques to overcome pressing behavior of maraging steels, noting tendency to thin during stretching and reluctance to stretch 03 p0497 A70-13620
- Maraging steels microstructure and ductility influence on stress corrosion resistance in magnesium chloride salt chamber 04 p0711 A70-15681
- Structures formed during aging of martensite in maraging steels by X ray and chemical analyses using electrolytic isolation of phases 05 p0865 A70-16871
- Maraging steels mechanical properties, studying changes in lattice constant and electric resistance to determine Al strengthening effect nature 05 p0865 A70-16872
- Maraging steel mechanical properties as function of aging temperature and time 05 p0865 A70-16873
- Maraging steel mechanical properties with Mn, Mo and Co additions in heat treated condition 05 p0865 A70-16874
- Ni maraging steel sheets tensile strength and elongation anisotropy, studying effects of directional cold work, aging and annealing 07 p1306 A70-19072
- Intermetallic precipitates development and mechanical properties of maraging steel as function of composition, tempering time and temperature using electron microscopy 07 p1310 A70-19748
- Maraging steels stress corrosion sensitivity in marine environment tested in humid atmosphere, salt fog, natural seawater and salt solutions 07 p1310 A70-19749
- Martensitic transformations during quenching and tempering of maraging steels 08 p1520 A70-21495
- Precipitation in Fe-Ni-Co maraging alloys produced by austenite plates formation from martensite, discussing effects of Ti addition 08 p1524 A70-21955
- Thermal treatment function of austenitic grain size and mechanical properties of 18 pct Ni maraging steels 09 p1704 A70-22803
- Duplex aging treatment effect on Ni-Co-Mo-Ti maraging steels mechanical properties 10 p1905 A70-25171
- Moisture effect on fatigue crack propagation and fracture path through microstructure of 300-grade maraging steel 13 p2432 A70-28607

MARIA

- Heat treatment induced shape distortions measurements in maraging steel bars, plates and sheets, noting dependence on number of anneals and product form 14 p2595 A70-30544
- Residual stresses near weld in spherical rocket motor casing constructed from maraging steel sheet, discussing moire measurement and reduction treatments 15 p2744 A70-31926
- Heat treatment effect on maraging steel fracture toughness and subcritical crack growth loaded at slow strain rate in laboratory air 15 p2760 A70-32377
- Maraging nickel steel martensitic transformation temperature reduction after interruption by nonisothermal or isothermal tempering below 460 C 16 p2932 A70-33850
- Structural hardening of nickel maraging steels related to Portevin-Le Chatelier effect in necking zone of stress-strain curves 17 p3124 A70-35141
- Impact transition behavior and strength-toughness relation of high purity Ni maraging steels, noting intergranular fracture at grain boundaries 18 p3273 A70-36043
- Maraging steels heat treatment, measuring hardness as function of temperature for various heating rates 19 p3452 A70-37807
- Microstructure and phase distribution in maraging steels subjected to austenization and subsequent aging in reversible transformation temperature range 20 p3645 A70-39038
- Heating conditions effect on microstructure, hardness, transformation temperatures and dimensional anisotropy of maraging steel 20 p3649 A70-39941
- Stainless maraging steel bolts tensile, shear and fatigue strengths and stress corrosion resistance at room and high temperatures 20 p3650 A70-39964
- High strength high Ni maraging steels crystal structure, alloying elements effects on mechanical properties, applications, etc 22 p4055 A70-43121
- Maraging steels hardening mechanisms, discussing dislocations density and distribution and Ni, Mo and Co additives effects 23 p4208 A70-44919
- Austenitic formation by rapid heating of Ni maraging steel, noting microstructural characteristics relationship to martensite before phase transformation 24 p4356 A70-45144
- Maraging steel grain size and externally applied shear stress effects on morphology of martensite formation 24 p4357 A70-45231
- MARIA**
- NT LUNAR MARIA**
- MARINE BIOLOGY**
- Remote sensing from aircraft and satellites of chlorophyll concentrations for monitoring of biological productivity of sea 12 p2217 A70-26915
- Tektite I marine laboratory underwater mission in marine biology and geology 17 p3168 A70-35306
- Remote sensing of plankton and matter in sea by determining spectral changes in scattered light measured with radiometer 17 p3079 A70-35619
- Shallow water bottom biota, sediments and morphology determination by aerial and satellite photography 17 p3079 A70-35620
- Holography application to marine ecological studies, using laser beam reduction techniques for image recording and reconstruction of large areas and volumes 21 p3823 A70-40821
- Earth-moon system age and origin from tidal evolution equations, considering growth line counts on living and fossil marine invertebrates 21 p3921 A70-41971
- MARINE NAVIGATION**
- U SURFACE NAVIGATION**
- MARINE TECHNOLOGY**
- Remote sensors application to direct and indirect fish detection in fishery research, using aerial and Gemini photography 07 p1262 A70-18957
- Maritime and aeronautics technology - Conference, Paris, May 1969 07 p1192 A70-19126
- Blind flight and helicopter navigation during prolonged maritime survival operations 07 p1193 A70-19132
- Maraging steels stress corrosion sensitivity in marine environment tested in humid atmosphere, salt fog, natural seawater and salt solutions 07 p1310 A70-19749
- Seadrome advantages and structural design concepts, describing floating runways, breakwaters, noise reduction, building costs, etc 09 p1655 A70-22243

MARINER SPACE PROBES

- NT MARINER 5 SPACE PROBE**
- MARINER PROGRAM**
- NT MARINER-MERCURY 1973**
- Mariner Mars 1971 scientific experiments, describing onboard equipment, mission objectives, etc 16 p2983 A70-34026
- Mariner 1969 test and operations program evaluated by ground tests and flight results, giving flight acceptable spacecraft recommendations 19 p3533 A70-38819
- Mission planning for 1973 Mariner Venus/Mercury flyby, discussing trajectory and navigation aspects [AIAA PAPER 70-1049] 19 p3528 A70-38864
- Geodetic parameters estimated from satellite dynamic and geometric solutions and Mariner 4 and 5 missions 24 p4312 A70-45545
- MARINER SPACE PROBES**
- NT MARINER 2 SPACE PROBE**
- NT MARINER 4 SPACE PROBE**
- NT MARINER-MERCURY 1973**
- Mars atmosphere refractivity, carbon dioxide condensation, temperature and surface pressure from Mariners 6 and 7 radio occultation measurements 05 p0908 A70-16301
- Meteorological observations of Mars polar regions, surface activity and atmosphere with astronomical telescopes during Mariner 6 and 7 flyby 09 p1754 A70-22500
- Navigation data from Mariner Mars 1969 TV pictures, estimating spacecraft trajectory to planetary center 14 p2614 A70-30468
- Mariner 7, 8 and 9 lunar photographs, discussing evidence for internally heated moon 16 p2973 A70-33112
- Soviet monograph on Venus atmosphere and Mars research covering Venera, Mariner and ground observations 18 p3332 A70-37230
- Mariners 6 and 7 orbits determination by weighted least squares estimation based on common surface features in overlapping TV pictures [AIAA PAPER 70-1066] 19 p3529 A70-38879
- MARINER SPACECRAFT**
- Structural design experience in developing large area Be solar array for Mars flyby mission, describing configurations, requirements, material and manufacturing 02 p0228 A70-11935
- Lightweight double walled meteoroid shield for Mariner Mars 1971, considering Teflon impregnated glass fabric outer sheet and multilayer thermal insulation [AIAA PAPER 69-377] 07 p1394 A70-19712
- Statistical energy concepts application to Mariner Mars 1969 spacecraft, estimating coupling of damping factors to analyze structural vibration [SAE PAPER 700171] 11 p2128 A70-25374
- Mariner-type spacecraft telemetry system optimization, considering channel capacity 11 p2008 A70-26239
- Mariner Mars 1969 navigation, guidance and control systems design, mechanization and flight testing 13 p2446 A70-28393
- Mariner spacecraft electro-optically controlled star sensors design and performance, discussing star simulation and stray light test techniques 15 p2736 A70-32033
- Mariner attitude control system limit cycle operation during cruise, noting variation from ideal case to single side operation [AIAA PAPER 69-844] 15 p2812 A70-32507
- Rocket engine prototype for Mariner Mars 71 spacecraft, describing performance test results and response, thermal and throttling characteristics [AIAA PAPER 70-716] 16 p2966 A70-33545
- TV experiment for Mariner Mars 1971 Project, providing fixed and variable feature imaging data 16 p2978 A70-34027
- IR Michelson interferometer for Mariner Mars 1971 mission, investigating atmospheric and surface temperatures and atmospheric water vapor content 16 p2978 A70-34029
- Scanning UV spectrometer for Mariner Mars 1971 orbital mission, investigating atmospheric composition for biological activity 16 p2978 A70-34030
- Space molecular sink simulator facility [Molsink] for extreme high vacuum outer space environment simulation, discussing Mariner Mars 1969 spacecraft components tests 16 p2889 A70-34167
- Mariner Mars 1971 gimbal actuator design and life test for autopilot system using hypergolic bipropellant rocket engine 17 p3022 A70-34758
- Nonlinear structural analysis of Mariner spacecraft solar panel, using damper test characteristics 17 p3022 A70-34769
- Mariner Mars 1971 mission design, discussing objectives, orbit selection, guidance, navigation and sequence analysis [AIAA PAPER 70-1048] 19 p3527 A70-38863

- Mariner spacecraft roll control star sensors and trackers design and flight performance 20 p3665 A70-39239
- Mariner-type spacecraft launch in 1971 to orbit Mars, discussing onboard experiments and instrument 20 p3716 A70-39797
- Mariner 1969 communication system modified for thermoelectric outer planet spacecraft [TOPS], noting X band addition to S band and associated problems 21 p3791 A70-41797
- Electronic parts testing for long duration Mariner spacecraft missions 21 p3799 A70-41798
- MARINER 2 SPACE PROBE**
- Semiannual variation of geomagnetic activity related to incident solar wind, considering Mariner 2 measurements 13 p2475 A70-28573
- MARINER 4 SPACE PROBE**
- Mars craters and crater-like objects catalog from Mariner 4 photographs, statistically analyzing diameter-frequency relations 01 p0179 A70-10523
- Mariner 4 guidance and control system performance from mission nominal end to final termination time 04 p0765 A70-15664
- Mariner 4 scan platform structure and actuator design, development and performance 16 p2845 A70-34106
- Mariner 4 spacecraft structural dampers construction and performance 16 p2922 A70-34120
- MARINER 5 SPACE PROBE**
- Earth magnetosphere and magnetosheath magnetic field measurements by Mariner 5 09 p1670 A70-23487
- Galactic UV emission attributed to solar radiation scattered by hydrogen atoms, using Mariner 5 measurements 17 p3163 A70-34902
- MARINER 6 SPACE PROBE**
- TV instruments for Mariners 6 and 7 providing analog and digital data, comparing resolutions and accuracies to earth based telescopes and Mariner 4 photographs 09 p1682 A70-23506
- Mariner 6 spectra establishing Fox-Duffendack-Barker bands and ionized carbon dioxide UV doublet bands as important components of Martian dayglow 10 p1938 A70-24073
- Mariner 6 and 7 navigational accuracies prior to time of planetary encounter 21 p3888 A70-41129
- Lyman alpha sky background measurements by Mariner 6 UV spectrometer 22 p4094 A70-42932
- MARINER 7 SPACE PROBE**
- TV instruments for Mariners 6 and 7 providing analog and digital data, comparing resolutions and accuracies to earth based telescopes and Mariner 4 photographs 09 p1682 A70-23506
- Mariner 7 preencounter anomaly in radio tracking data and trajectory investigated by computerized simulation [AIAA PAPER 70-1065] 19 p3534 A70-38878
- Mariner 6 and 7 navigational accuracies prior to time of planetary encounter 21 p3888 A70-41129
- MARINER-MERCURY 1973**
- Preflight error statistics of earth based Doppler tracking for Mariner navigation concerning Mars 1971 and Venus-Mercury 1973 missions [AIAA PAPER 70-1077] 20 p3670 A70-40023
- MARK 3 REENTRY BODY**
- LSI Mark 3 airborne Omega system with computerized signal processing for navigation parameters, discussing system features and flight test results 09 p1719 A70-22190
- MARKERS**
- Optimal colors for target and rescue markers, discussing influence on signal detection, response and identification 06 p1002 A70-17713
- Silica marker motion in sintering of loose spherical copper powder aggregates 20 p3647 A70-39109
- MARKETING**
- Worldwide door-to-door cargo shipping by airline, considering marketing systems approach 07 p1426 A70-18875
- Aircraft interior design styling and material selection, discussing industrial design department function and organization, styling as marketing tool, etc [SAE PAPER 700233] 11 p1980 A70-25902
- Cessna CITATION aircraft design, considering engineering, marketing and corporate cooperation [SAE PAPER 700241] 11 p1981 A70-25910
- Aircraft manufacturing market research including cost compatibility with resources and capabilities 14 p2668 A70-30937
- Corrective Action systems for identification, control and resolution of manufacturing, engineering and vendor problems 14 p2669 A70-31102

Material data file and retrieval system for designers in automotive, equipment and appliance industries, discussing applications to other FRP markets
16 p2935 A70-33352

Export market research for military aircraft
19 p3555 A70-38618

Project economic evaluation, discussing value analysis from market research recommendations
19 p3555 A70-38620

European airbuses designs, considering commercial market and financial problems
19 p3357 A70-38952

Glass drainline development and marketing, describing technology transfer role
20 p3740 A70-39100

MARKING

NT ISOTOPIC LABELING

Cross hatching on various body surfaces due to periodic surface pressure fluctuations, discussing in boundary layer
[AIAA PAPER 69-11] 09 p1662 A70-23223

MARKOV CHAINS

Communication channel average binary error and stationary Markov chain state probabilities relationship, using mathematical model and HF ionospheric FSK error sequence measurement
08 p1458 A70-20793

Viterbi decoding error probability for convolutional codes using finite Markov chain modeling
08 p1458 A70-20794

Transition matrix of Markov chain with finite states from noisy measurements of state, discussing algorithms convergence rates and computations
12 p2261 A70-27421

Limiting distributions of sums of random variables coupled in homogeneous Markov chain with finite number of states
12 p2261 A70-27551

Optimal control of systems with time transitions described by finite state stationary Markov chain, noting resetting control
13 p2382 A70-29065

Transition probabilities for Markov chain describing bond breaking and molecular energy transfer in vibrational relaxation and dissociation
16 p2953 A70-33009

Convolutional code decoder modeled as autonomous stochastic sequential machine, considering finite Markov chain theory for error probability
17 p3049 A70-34854

Limiting theorems for sums of random variables limited in Markovian chain, applying probabilistic and analytical methods
19 p3456 A70-37235

Weather regimes in statistical meteorology constructed in stochastic models representing randomly transformed Markov chain
24 p4371 A70-46035

MARKOV PROCESSES

NT MARKOV CHAINS

Tracking systems synthesis and performance analysis based on continuous Markov processes theory, particularly Fokker-Planck equation
01 p0043 A70-10776

Atomic variables elimination technique applied to Markovian laser master equation, resulting in integrodifferential equations for field statistical operator
01 p0112 A70-10884

Self excited oscillators zero crossing times distribution for Markov process formulated as boundary value problem involving Kolmogoroff backward equation
01 p0143 A70-10891

Optimal control synthesis in Markov and determinate systems using solution reduced from second order nonlinear partial differential equation
02 p0272 A70-12411

Public health services problems analyzed by statistical simulation method, using Markov process
04 p0644 A70-15356

Optimum compression ratio defined for Markov sources for compression algorithm efficiency and data compression schemes
06 p1013 A70-18624

Decision rules for incomplete a priori data, deriving informational risk estimates for Markov processes and optimal control problems
09 p1653 A70-22144

Reliability engineering for complex systems of multiple repairable parts based on analysis involving signal flow graphs and Markov renewal processes
09 p1691 A70-22574

Spherically symmetric galaxies dynamic evolution analysis, emphasizing irregular motions description using fluctuating gravitational field hypothesis to construct Markov process
09 p1758 A70-22747

Soviet book on control and search for defects in complex systems, presenting statistical optimization methods, programmings for assumed Markov processes, etc
09 p1693 A70-23540

Markov renewal processes sums convergence to multidimensional Poisson process, discussing convergence conditions
12 p2260 A70-26884

State estimation in linear discrete time systems operating in Markov dependent switching environments, using Bayes theorem for filtering
13 p2381 A70-29062

Turbulent diffusion random model of foreign substance, investigating latent parameters existence
13 p2387 A70-29211

Nonlinear optimal filtration and adaptive quasi-coherent reception of Markov signals on white noise background
13 p2369 A70-29731

Molecular Markov processes application to vibrational relaxation and dissociation, small system kinetics, nucleation and droplet growth, thermalization kinetics and diffusion processes
14 p2619 A70-30615

Phase locked automatic frequency control system, estimating duration of stabilization by theory Markov processes
18 p3228 A70-36625

Limiting distribution of additive nonnegative continuous functional of homogeneous Markovian process with conditional transfer function
23 p4212 A70-44346

MARROW

Marrow granulocyte reserve restoration in dogs exposed to chronic gamma radiation, discussing leukocyte reaction to pyrogenic agent
13 p2351 A70-29326

MARS [MANNED REUSABLE SPACECRAFT]

Reusable nuclear shuttles /RNS/ for interorbital and escape missions, discussing alternate stage configurations, radiation shielding, subsystem options, etc
[AIAA PAPER 70-678] 16 p2950 A70-33579

MARS [PLANET]

Atlas of near IR spectra of Venus, Mars, Jupiter and Saturn obtained by Fourier spectroscopy, discussing observational procedures, data recording and processing
01 p0173 A70-10078

Internal structure models of Mercury, Mars and Venus based on radar measurements of radius and mass, discussing two and three zone models
[JPL-TR-32-1439] 01 p0176 A70-10315

IR spectrometer on Mariner 7 Mars flyby recording sharp absorption near 3 microns at Martian southern polar cap
01 p0182 A70-10823

Entry and terminal deceleration systems for unmanned Martian landers, discussing parachute landing and lifting entry vehicles
[AIAA PAPER 68-1147] 01 p0195 A70-10828

Communications of lunar and planetary laboratory, Volume 6, covering Venus atmosphere and photography, Jupiter IR spectrum and Mars multicolor photometry
02 p0377 A70-12553

Mars multicolor filter photometry showing variation in whole-disk reflectivity
02 p0378 A70-12560

Martian hypothetical organisms biological model, describing nonchlorophyllous photosynthesis, epithelial hydrochrome pigments, scale insect morphology, etc
03 p0422 A70-13702

Data transmission from automatic space stations on Mars and Venus, considering relaying via artificial planet satellite or direct transmission to ground station
04 p0648 A70-14931

Orbit determination simultaneous optimal strategy and useful information set selection, discussing Mars transfer trajectory
04 p0750 A70-14940

Automated mars surface sample return /AMSSR/ mission, discussing Saturn 5 chemical and nuclear approach
[AIAA PAPER 69-1066] 04 p0764 A70-15626

Electronic packaging and cabling on Capsule System Advanced Development Lander for Mars rough landing
06 p1016 A70-17335

Short duration manned Mars and Venus exploration mission planning with chemical propulsion and Saturn 5 boosters
[AIAA PAPER 70-59] 06 p1147 A70-18238

Mariners 6 and 7 range and Doppler tracking data for studying Martian mass and earth-moon mass ratio
06 p1151 A70-18486

Qualitative analysis and comparison of hypothesis versions of Martian point flare observed by Maeda, considering solar ray reflection from ice cloud or vertical surface object
07 p1385 A70-19420

Fluid controlled solid rocket motors design for Mars mission with acceleration level as parameter, discussing mission specifications, system design and component considerations
[AIAA PAPER 69-446] 07 p1365 A70-19707

Mars planet smoothing factor determined from phase curve of integrated brightness distribution on disk
08 p1564 A70-20557

Manned Mars mission planning, discussing technologies and costs for planetary landing
09 p1757 A70-22676

Microorganisms survivability in soils near spacecraft assembly areas during simulated Martian freeze-thaw cycles
09 p1619 A70-22768

Mars biological activity suggested from metabolic energy cycle based on oxidation of carbon monoxide
[NGL-07-004-043] 09 p1765 A70-23798

Martian hypothetical organisms biological model, describing nonchlorophyllous photosynthesis, epithelial hydrochrome pigments, scale insect morphology, etc
11 p1985 A70-25502

Asteroid vs planet for manned landing site, considering Martian moons mission
11 p2108 A70-25660

Mars landing analysis and simulation for unmanned lander prototype, discussing digital simulation by Monte Carlo techniques and physical tests
11 p2032 A70-26291

Manned Mars flyby/orbiter mission, discussing cost, scientific returns, technology advances, popular support, etc
12 p2304 A70-27749

Mars and Venus radio temperature measurements by 210 ft telescope, obtaining effective brightness
12 p2309 A70-27896

Phobos image analysis on Mariner 7 frame 7F91, discussing surface darkness, limb profile and geometric albedo
13 p2492 A70-29266

Earth/moon mass ratio and Mars mass and ephemeris from Mariners range and Doppler tracking data, noting relativistic time delay measurement possibility
15 p2798 A70-31652

Astronomical observations, discussing advantages of human operators on interplanetary spacecraft or Mars
15 p2810 A70-31853

Statistical error analysis of autonomous manned spacecraft navigation in long duration eccentric Mars orbits
[AIAA PAPER 69-880] 15 p2773 A70-32503

Mars planet smoothing factor determined from phase curve of integrated brightness distribution
15 p2805 A70-32712

Mars visual observations with colored glass filters during opposition, noting southern polar cap shape irregularity and Martian atmospheric transmittance
16 p2974 A70-33658

Near equilibrium shock layers nonequilibrium radiant emission calculation, noting application to Mars entry conditions
[AIAA PAPER 70-773] 17 p3007 A70-34481

Planetary surface smoothness factor by disk brightness, Mars red light and phase curves methods, indicating superiority of visual observation
18 p3315 A70-36602

Soviet monograph on Venus atmosphere and Mars research covering Venera, Mariner and ground observations
18 p3332 A70-37230

Uranus and Mars satellite relative measures, tabulating observations
19 p3516 A70-37932

Martian photographic map during 1967 opposition in red and near IR range
19 p3516 A70-37935

Hydromagnetic theory of solar wind flow past earth extended to nonmagnetic planets Venus and Mars
22 p4095 A70-43106

Extraterrestrial life development and evolution in solar system, describing Mars suitability
22 p3975 A70-43692

International photographic planetary patrol network, discussing filmstrips of Mars and Jupiter using blue, green and red filters
23 p4242 A70-44262

MARS ATMOSPHERE

Carbon dioxide refractivity measured under simulated Martian conditions and standard temperature and pressure, comparing results with radio occultation methods
01 p0186 A70-11085

Polymers development for ablative heat shields, aeroshell structures, antennas, insulators, electronic packaging, etc, to meet Mars and Venus atmospheric entry requirements
02 p0382 A70-12525

Molecular hydrogen destruction by reaction with carbon dioxide ion in Martian ionosphere, discussing conversion into atomic hydrogen
03 p0575 A70-13997

Mars and Venus ionospheres from Mariner profiles, discussing radiative equilibrium thermal calculations and F1 layer hypothesis
04 p0753 A70-15069

Dynamic model for Martian ionosphere modification by solar wind, assuming negligible Mars magnetic moment and neutral atmosphere
04 p0753 A70-15103

Two level model for planetary atmospheres adapted to simulate atmospheric circulation and climate of Mars

04 p0756 A70-15515

Mars atmosphere refractivity, carbon dioxide condensation, temperature and surface pressure from Mariners 6 and 7 radio occultation measurements

05 p0908 A70-16301

High resolution photometry near planetary limb yielding scale height and optical depth applied to Mariner 4 Mars observations

05 p0909 A70-16387

Earth, Venus and Mars atmospheric structure, discussing gases escape, temperature, density, IR radiation and solar radiation absorption

05 p0914 A70-16628

Mayeda flare observed on Mars 4 June 1937/, suggesting oriented reflection of solar rays from ice crystals cloud or Martian surface feature

05 p0918 A70-16916

Mariner 6 and 7 missions IR spectrometric records showing evidence of solid carbon dioxide in Martian upper atmosphere

06 p1137 A70-17194

Atmospheric pressure, optical thickness and Young particle size distribution of Mars atmosphere determined from polarization observations

07 p1385 A70-19421

Vertical temperature profile diurnal variations of Mars atmosphere using models, noting aerosol influence

07 p1385 A70-19422

Mariner 4 and 5 and Venera 4 data used for comparing terrestrial planets ionospheres

07 p1386 A70-19488

Ice crystal density in Martian atmosphere from brightness of Martian parhelic halo

08 p1564 A70-20547

Meteorological observations of Mars polar regions, surface activity and atmosphere with astronomical telescopes during Mariner 6 and 7 flyby

09 p1754 A70-22500

Wind and atmospheric temperature variations on Mars, Venus and Mercury interpreted from observational data in terms of earth atmospheric processes

09 p1762 A70-23127

Mars primitive atmosphere analyzed from statistics of craters quantity as function of diameter, using Mariner 6 and 7 probe photographs

09 p1763 A70-23318

Carbon dioxide photochemistry of Mars atmosphere, noting complications due to hydrogen compounds

09 p1763 A70-23483

Mariner 6 spectra establishing Fox-Duffendack-Barker bands and ionized carbon dioxide UV doublet bands as important components of Martian dayglow

10 p1938 A70-24073

Similarity and dimensionality theory applied to large scale motions in atmospheric circulation of Mars and Venus

10 p1939 A70-24269

Blue haze hypothesis of Martian atmosphere using Mariner 6 and 7 blue filter photographs, reviewing topographic observations

10 p1943 A70-24841

Mars upper atmosphere semiempirical model, reducing density uncertainties by allowing for solar cyclic variations

11 p2111 A70-26031

Martian atmospheric models for lander and simulator design, obtaining effective sky temperatures, surface pressures and temperatures, atmospheric compositions, etc

11 p2112 A70-26141

On-line parameter updating for relationship between Martian atmospheric density and height above surface during spacecraft descent based on least squares approach

11 p2113 A70-26318

Halo rings at hexagonal ice crystals in Martian atmosphere, analyzing via bright formations with respect to planetary phase angles

13 p2493 A70-29397

Martian terrain features and atmospheric activity observation by Mariner 6 and 7

13 p2494 A70-29526

Martian atmosphere modeling for obtaining Viking lander spacecraft design margins by Monte Carlo method

14 p2637 A70-30564

Quartz crystal particulate sensor instrument for terrestrial and Mars atmospheres

14 p2585 A70-30575

Spacecraft measurements revealing hot dense Venusian and cold thin Martian carbon dioxide atmospheres

14 p2646 A70-31066

Mariner 6 radio signals frequency changes analysis during occultation measurement for determining Mars surface pressure and temperature

14 p2646 A70-31071

Mars upper atmosphere refractivity, free electron number density and plasma temperature altitude

profiles from Mariner 1969 radio occultation measurements

14 p2646 A70-31072

Mars surface, environment and electrical, thermal and mechanical properties

14 p2647 A70-31080

Water vapor abundance in Mars atmosphere from high resolution spectroscopy

14 p2649 A70-31211

Mars carbon dioxide abundance and surface pressure from growth curve based on high resolution spectra

14 p2650 A70-31218

Ice crystal density in Martian atmosphere from brightness of Martian parhelic halo

15 p2796 A70-31456

Mariner 6/7 S band radio occultation probe of Mars atmosphere concerning surface pressure, temperature and existence of ionosphere

15 p2798 A70-31681

Terrestrial planetary ionospheres, discussing charged particle density distribution of Mars daytime ionosphere and Venus day and dark sides

15 p2799 A70-31748

Martian brightness increase at 1 deg phase angle, explaining by transparent cubic crystals presence in clouds

15 p2803 A70-32499

Mariner 4 and 5 and Venera 4 data used for comparing terrestrial planets ionospheres

15 p2805 A70-32733

Spectral line formation in Mars and Venus atmospheres, discussing Lorentz and Doppler broadening

16 p2976 A70-33793

IR Michelson interferometer for Mariner Mars 1971 mission, investigating atmospheric and surface temperatures and atmospheric water vapor content

16 p2978 A70-34029

Scanning UV spectrometer for Mariner Mars 1971 orbital mission, investigating atmospheric composition for biological activity

16 p2978 A70-34030

S band occultation experiment for Mariner Mars 1971 orbiters, measuring atmospheric density and ionospheric electron density profiles

16 p2978 A70-34032

Martian blue clearing during 1967 apparition photographic observational patrol tabulated and summarized

16 p2979 A70-34035

Model calculations of Martian upper atmosphere expanding above mesopause, taking into account effects of molecular and eddy diffusion and chemical reactions

17 p3172 A70-35643

Mars UV reflectivity, examining spectrum, absorption features, planet albedo and ozone content by rocket-borne instruments and atmospheric models

18 p3317 A70-37011

Terrestrial atmospheric tidal theory applicability to Venus and Mars, considering dependence on parameters variation among planets

19 p3519 A70-38253

Mars lower atmosphere vertical temperature distributions from Mariner 6 and 7 radio occultation data, using improved trajectory estimates

21 p3884 A70-40908

Forced convection heat transfer from flat plate and cylinder in cross flow to simulated Mars atmosphere

21 p3945 A70-41026

Carbon dioxide-atomic oxygen reaction rate constant to investigate Martian ionosphere, discussing reactions involving oxygen, nitrogen molecular ions and NO

21 p3886 A70-41067

Pressure dependence and efficiency of carbon trioxide formation in Mars and Venus atmospheres

21 p3887 A70-41107

Venusian and Martian upper atmosphere chemistry, emphasizing ionization height distribution

22 p4106 A70-43312

Mars atmospheric nitrogen abundance relative to carbon from spacecraft UV spectrometer data

23 p4238 A70-43805

Martian brightness increase at 1 deg phase angle, explaining by transparent cubic crystals presence in clouds

23 p4240 A70-43920

MARS ENVIRONMENT

NT MARS ATMOSPHERE

Martian surface features and environment, discussing winds, particle sizes, moisture content, craters, etc

03 p0563 A70-12986

Chemical heat source combined with metals ignition properties considered for spacecraft heating during Mars nighttime landing

04 p0628 A70-15426

Physical and life supporting properties of hypothetical Martian biosphere, considering organism adaptation theories

05 p0803 A70-17109

Insulation materials selection for Martian soft lander to meet mission environmental conditions based on tests

[AIAA PAPER 70-11] 06 p1182 A70-18224

Microorganisms survivability in agar subjected to simulated Martian freeze-thaw cycles, discussing soil samples collection and composition

09 p1618 A70-22767

Subsystem weight trade-offs for design optimization of out-of-orbit Mars soft lander, using atmosphere and surface environmental Monte Carlo model

11 p1214 A70-26215

Cryobiological data for life mechanisms on planets in solar system emphasizing Mars

14 p2536 A70-30344

Mars surface, environment and electrical, thermal and mechanical properties

14 p2647 A70-31080

Mars geology, discussing polar caps phenomena, diurnal variations, orbital eccentricity, seasonal meteorology, volcanism, erosion, etc

15 p2800 A70-32059

Thermal conductivity of particulate basalt as function of density in simulated lunar and Martian environments, noting temperature and pressure effects

18 p3316 A70-36772

MARS EXCURSION MODULE

Nuclear propulsion requirements for manned landing mission to Mars assuming Saturn 5-based operation

07 p1375 A70-18874

Radar signal quick indication and extrapolation for terminal guidance control of Mars soft lander, reducing radar lock on loss sensitivity and engine spurious noise throttling

11 p2080 A70-26210

Martian multispectral imaging from lander emphasizing spectral bands and gray levels number for discrimination of surface constituents

12 p2229 A70-26928

MARS LANDING

Retrorocket jet size and structure for scientific instruments soft Mars landing, estimating off-optimum supersonic jet interaction with quiescent atmosphere

17 p3011 A70-35660

Manned Mars lander launch-to-rendezvous analysis, using subsequent Venus swingby for mission velocity requirement reduction

[AIAA PAPER 70-1075] 19 p3530 A70-38887

Spacecraft trajectory initial conditions expressions as parameters dependent functions, applying results to Mars lander mission

[AIAA PAPER 70-1016] 20 p3666 A70-39517

Hydrogen, N, O, Kr methane and carbon dioxide gas chromatographic examination, discussing life detection device for Mars landing

22 p3983 A70-43094

MARS PROBES

NT MARINER 4 SPACE PROBE

NT MARINER 6 SPACE PROBE

NT MARINER 7 SPACE PROBE

NT VIKING MARS PROGRAM

High gain antenna for 1973 Mars Soft Lander data transmission using sensors and digital computer to achieve autonomous precision pointing to earth

[AAS PAPER 69-578] 04 p0716 A70-14653

Statistical orbit and position determination for Mars orbiters and landers based on Viking 1973 mission requirements, discussing tracking problems

[AIAA PAPER 70-160] 06 p1158 A70-18177

Insulation materials selection for Martian soft lander to meet mission environmental conditions based on tests

[AIAA PAPER 70-11] 06 p1182 A70-18224

Visual imaging systems for Mars orbiter compared for performance and interactions with mission and spacecraft design

07 p1280 A70-19230

Ablation, transmission transparency and embrittlement of heat shield materials for Voyager tested under simulated Mars entry conditions

07 p1395 A70-19885

Mars imaging mission and astrodynamical interaction, discussing arrival geometry and orbit size effects

[AIAA PAPER 69-127] 11 p2112 A70-26130

Unmanned Mars roving vehicle navigation subsystem feasibility study covering inertial and gyrocompass-odometer systems

11 p2080 A70-26211

Satellite navigation method for locating Mars landmark or target point for exploration by roving vehicle located as center of coordinate system

11 p2080 A70-26213

Mariner Mars 1969 navigation, guidance and control systems design, mechanization and flight testing

13 p2446 A70-28393

Radio command guidance system for Mars probe ascent from surface to rendezvous with flyby vehicle on escape trajectory

13 p2447 A70-28421

Mariner, explorer, high Data Orbiters, Viking and Rover landers as required systems for unmanned Mars exploration, examining ballistic and lifting entry

[AAS PAPER 70-030] 17 p3156 A70-34805

Terminal guidance for Mars softlander utilizing Doppler and range radar for steering and propulsive control

17 p3133 A70-35286

Mars and Venus orbiter spacecraft electric propulsion system, discussing Hg electron bombardment ion engine

21 p3868 A70-41786

Statistical orbit and position determination for Mars orbiters and landers based on Viking 1973 mission requirements, discussing tracking problems

21 p3931 A70-41861

MARS SPACECRAFT

U MARINER SPACECRAFT

MARS SURFACE

Mars craters and crater-like objects catalog from Mariner 4 photographs, statistically analyzing diameter-frequency relations

01 p0179 A70-10523

Martian carbon dioxide band observations using multislit spectrophotometer, indicating surface height variations near Syrtis Major

01 p0182 A70-10723

Mars surface features, describing diagonal and meridian-latitude grid systems, continental blocks and continental drift

01 p0183 A70-10869

Martian dark area extending from Tritonius Sinus to Casius southern tip, comparing observations and charts

02 p0370 A70-12086

Martian topographic contours determined from detected carbon dioxide abundances indicating large scale differences from previous data

02 p0373 A70-12390

Martian surface features and environment, discussing winds, particle sizes, moisture content, craters, etc

03 p0563 A70-12986

Martian orbital photographic missions objectives and sensors realizable capabilities, discussing relationships between orbital parameters and imaging systems constraints

03 p0490 A70-13663

Mars surface reddish color due to carbon suboxide suggested based on spectral reflectivity measurements and matching in laboratory

04 p0743 A70-14423

Visual interpretation of moon and Mars surface photographs taken from satellites, analyzing craters and bumps

04 p0686 A70-14626

Mars atmosphere refractivity, carbon dioxide condensation, temperature and surface pressure from Mariners 6 and 7 radio occultation measurements

05 p0908 A70-16301

Martian topographical radar ranging data correlated with surface features, discussing deserts, canals and maria topography

05 p0909 A70-16388

Martian surface temperature distributions based on IR scans of disk compared with predictions of thermal properties

05 p0909 A70-16389

Mayedda flare observed on Mars 4 June 1937, suggesting oriented reflection of solar rays from ice crystals cloud or Martian surface feature

05 p0918 A70-16916

Optical parameters of Martian surface and temperature, discussing brightness distribution along diameter in red spectral region, based on photoelectric cross sections

05 p0918 A70-16917

Martian polar cap spectra interpreted with laboratory measurements of water-carbon dioxide frost spectral reflectance

07 p1388 A70-19946

Martian surface radar observation results, discussing data processing method, backscattering behavior evaluation, relief and composition model, etc

08 p1456 A70-20643

Critique of blue haze negative hypothesis in preliminary Mariner 6 data report

08 p1578 A70-21556

Carbon dioxide adsorption and desorption in Martian bright areas, discussing assumptions relative to temperature, pressure and dust adsorption

08 p1579 A70-21566

Meteorological observations of Mars polar regions, surface activity and atmosphere with astronomical telescopes during Mariner 6 and 7 flyby

09 p1754 A70-22500

Frequency-size distribution of Martian and lunar craters and oases, suggesting common mode of origin

09 p1765 A70-23810

Martian soil surface anomalies observed from polarimetric analysis of light diffused by Hellas region

10 p1943 A70-24708

Blue haze hypothesis of Martian atmosphere using Mariner 6 and 7 blue filter photographs, reviewing topographic observations

10 p1943 A70-24841

Differential thermal analysis-effluent gas analysis (DTA-EGA) experiment for lightweight Martian landed capsule

11 p2050 A70-25802

Mars surface, discussing craters, slump terraces, dry chutes, crater pair abundance, ballistic megacratering theory, etc

11 p2109 A70-25838

Multispectral imaging from lander for Martian surface constituents discrimination

11 p2051 A70-26000

Routing algorithm for computer controlled unmanned autonomous roving vehicle on Martian surface

11 p2081 A70-26317

Multichannel IR spectrophotometer to obtain albedo curves of Martian surface

12 p2229 A70-26927

Martian multispectral imaging from lander emphasizing spectral bands and gray levels number for discrimination of surface constituents

12 p2229 A70-26928

Mars border-disk brightness comparison noting atmospheric transparency effects

12 p2311 A70-28303

Martian terrain features and atmospheric activity observation by Mariner 6 and 7

13 p2494 A70-29526

Surface navigation for unmanned Martian surface roving vehicle

14 p2615 A70-30469

Mars surface, environment and electrical, thermal and mechanical properties

14 p2647 A70-31080

Mars surface topography and roughness from radar measurements

14 p2648 A70-31081

Mars radar results during 1969 opposition, presenting elevation and radar brightness as function of longitude

14 p2648 A70-31082

Mars surface material properties from radio emission observations, considering daily temperature variations distribution

14 p2648 A70-31083

Liquid water occurrence on Mars surface, considering ice melting, evaporative cooling, atmospheric moisture content, etc

14 p2651 A70-31298

Electromagnetic absorption of Martian matter based on vertical temperature variations in planet surface layer

15 p2802 A70-32491

Martian soil thermal conditions at south pole, considering polar cap annual variations and carbon dioxide sublimation

15 p2802 A70-32492

Mars photography from flybys and orbiters, communicating planetary scene information to eye-brain receiver of earth based interpreters

16 p2912 A70-33976

Organic compounds detection and identification on Mars surface for living systems existence or evolution

16 p2857 A70-33977

Mars evolution observation by gamma ray spectrometer in Martian orbit, transmitting information to earth as pulse height distribution

16 p2912 A70-33978

IR radiometer for Mariner Mars 1971 project providing surface brightness temperatures

16 p2913 A70-34028

IR Michelson interferometer for Mariner Mars 1971 mission, investigating atmospheric and surface temperatures and atmospheric water vapor content

16 p2978 A70-34029

Mars 1969 planetary surface drawing and photograph evaluation, noting dark spot east of Nodus Lacoontis

17 p3154 A70-34677

Mariner 6 and 7 TV camera pictures of Mars during approach and encounter, discussing IR spectroscopy, celestial mechanics experiment and Martian terrain

17 p3158 A70-34875

Mars surface smoothness from photometric and space probe data for atmospheric optical thickness and surface barometric pressure

19 p3512 A70-37300

Hydrogen flame ionization detector (HYFID) for life-derived organic matter in Martian/Lunar soil

19 p3426 A70-37896

Mariner-type spacecraft launch in 1971 to orbit Mars, discussing onboard experiments and instrument

20 p3716 A70-39797

Electromagnetic absorption of Martian matter based on vertical temperature variations in planet surface layer

23 p4240 A70-43913

Martian soil thermal conditions, considering polar cap annual variations and carbon dioxide sublimation

23 p4240 A70-43914

Mars topography from Mariner 6 and 7 IR spectra, discussing geographical resolution, surface carbon dioxide pressure, depressions, ridges and valleys

24 p4399 A70-45128

MARS 69 PROJECT

Optical approach navigation experiment on 1969 Mariner mission to Mars demonstrating accuracy potential of spacecraft-based measurement

[AIAA PAPER 70-70] 06 p1103 A70-18152

Navigation data from Mariner Mars 1969 TV pictures, estimating spacecraft trajectory to planetary center

14 p2614 A70-30468

MARS 71 PROJECT

Rocket engine prototype for Mariner Mars 71 spacecraft, describing performance test results and response, thermal and throttling characteristics

[AIAA PAPER 70-716] 16 p2966 A70-33545

Mariner Mars 1971 scientific experiments, describing onboard equipment, mission objectives, etc

16 p2983 A70-34026

TV experiment for Mariner Mars 1971 Project, providing fixed and variable feature imaging data

16 p2978 A70-34027

IR radiometer for Mariner Mars 1971 project providing surface brightness temperatures

16 p2913 A70-34028

Celestial mechanics experiment for Mariner Mars 1971 to test general relativity theory and improve Martian ephemeris

16 p2978 A70-34031

S band occultation experiment for Mariner Mars 1971 orbiters, measuring atmospheric density and ionospheric electron density profiles

16 p2978 A70-34032

Mariner Mars 1971 gimbal actuator design and life test for autopilot system using hypergolic bipropellant rocket engine

17 p3022 A70-34758

Mars 1971 and 1975 missions, discussing Mariner 8 and 9 and Viking lander objectives

18 p3334 A70-37224

Mariner Mars 1971 mission design, discussing objectives, orbit selection, guidance, navigation and sequence analysis

19 p3527 A70-38863

Mariner-type spacecraft launch in 1971 to orbit Mars, discussing onboard experiments and instrument

20 p3716 A70-39797

Preflight error statistics of earth based Doppler tracking for Mariner navigation concerning Mars 1971 and Venus-Mercury 1973 missions

20 p3670 A70-40023

MARTENSITE

Martensite start depressed temperatures vs pressure for steels, discussing hardness effects and microstructure

01 p0120 A70-10740

Martensite structure, discussing intensity anomalies in X ray diffraction pattern of intermetallic Ni-Nb

01 p0121 A70-10900

Ferrite and martensite precipitation hardening in Fe-Ni-Mo alloy, studying dislocation structure and aging kinetics

01 p0123 A70-11243

Martensite transformation with fcc lattice in Ti alloys containing 5.9 percent Fe as function of cooling rate, using X ray analysis

01 p0124 A70-11590

Structures formed during aging of martensite in maraging steels by X ray and chemical analyses using electrolytic isolation of phases

05 p0865 A70-16871

Martensitic transformations during quenching and tempering of maraging steels

08 p1520 A70-21495

Austenitic stainless steel hydrogen damage noting role of martensite plastic deformation

08 p1525 A70-21965

Work strengthening and microstructure of Co-Ni base alloys containing Cr and Mo, discussing deformation induced martensitic transformation

09 p1705 A70-22806

Ferritic and martensitic Fe-Ni alloys lattice parameter determined by standard X-ray techniques

12 p2256 A70-27613

Hydrogen embrittlement of martensitic Fe-Ni alloys as function of temperature via slow strain rate tensile tests

15 p2755 A70-31559

Austenite strength effect on austenite-martensite transformation in alloy steels, measuring resistance to plastic deformation

15 p2760 A70-32376

Austenitic stainless steel martensitic transformations, using transmission electron microscopy in conjunction with X ray and magnetization methods

15 p2761 A70-32379

Martensite-to-austenite reverse transformation in Fe-Ni-Co alloys, using dilatometry and coercive force measurements

15 p2761 A70-32386

Phase transformations in beta isomorphous Ti alloys, discussing effects on omega and alpha phases during quenching and aging and on martensite under stress

15 p2763 A70-32807

Maraging nickel steel martensitic transformation temperature reduction after interruption by nonisothermal or isothermal tempering below 460 C
16 p2932 A70-33850

Martensitic transformation in Ti and Ti alloys, discussing shear systems influence
17 p3118 A70-34404

Twinned hexagonal martensites crystallography in Ti alloys, discussing alpha-beta and beta-fcc transformations
17 p3118 A70-34405

Ti alloys M sub s and beta sub s points thermodynamics, considering initiation of bcc-oph martensitic transformation
17 p3193 A70-34407

Martensite transformations and cellular phase separation in Ti-Cu alloys, using electron microscopy
17 p3119 A70-34412

Martensitic transformation effects on mechanical properties of beta quenched Ti binary alloys
17 p3119 A70-34414

Mn and Ti effects on hardening of Fe-Ni-Mn-Ti and Fe-Ni-Mn maraging martensitic steels
17 p3125 A70-35145

Martensitic phase change effects in TiNi on ultrasound waves propagation in transition region, using pulse echo measurements
17 p3126 A70-35603

Precipitation hardening Co-Cu-Mo stainless steels, determining martensitic structures free from delta ferrite and residual austenite
18 p3262 A70-35965

Two phase stainless steels with microduplex structures, taking into account martensite and ferrite effects on mechanical properties
18 p3272 A70-36038

Fe-Ni alloy alpha-gamma phase transformation after heating, noting deformation planes and directions in martensite
18 p3275 A70-36204

Dynamic and static stress effects on martensite formation temperature in Fe-Ni-C alloys
19 p3451 A70-37569

Fe-Ni-C alloys austenite dispersion matrix effects on martensite structural characteristics
20 p3649 A70-39705

Zr-Nb alloys mechanical strength increase due to beta phase martensitic decomposition
21 p3840 A70-41897

Fracture behavior and tempered martensite embrittlement relationship in steel, using V- notched and fatigue precracked Charpy specimens
22 p4054 A70-42736

Orthorhombic martensite tempering behavior in Ti alloys, observing distinct stages for binary and ternary alloys
22 p4054 A70-42742

Austenitic formation by rapid heating of Ni maraging steel, noting microstructural characteristics relationship to martensite before phase transformation
24 p4356 A70-45144

Maraging steel grain size and externally applied shear stress effects on morphology of martensite formation
24 p4357 A70-45231

Crystallography of martensite transformation on /225/ type planes of austenite in Fe-Mn-Cr-C alloy
24 p4358 A70-45237

Martensite plate substructure in Fe-Mn-Cr-C alloy, using transmission electron microscopy and diffraction study
24 p4358 A70-45238

MARTENSITIC STAINLESS STEELS

Structure and mechanical properties of martensite and bainite in Fe-Ni-Co-C steels, discussing isothermal aging to obtain tough twinned martensite steels
01 p0119 A70-10733

Martensitic steel /AFC 77/ austenite grain size refinement process, noting effects on yield strength, toughness, stress corrosion resistance and fatigue crack growth rate
01 p0120 A70-10739

Age hardening characteristics of maraging martensite stainless steels containing Mo and Co subjected to subzero treatment
01 p0125 A70-11641

Calorimetric analysis and hardness test to investigate low temperature aging behavior of maraging stainless steels
01 p0125 A70-11642

Embrittlement in martensitic and semiaustenitic precipitation hardening stainless steels upon exposure to high temperatures to determine causation and controlling means
03 p0506 A70-13132

Manganese and sulfur content effects on martensitic stainless steels machinability, describing effects on mechanical properties, cold formability and corrosion resistance
03 p0507 A70-13135

Stress corrosion of martensitic and austenitic steels, discussing hydrogen embrittlement, mechanical strains, etc
04 p0710 A70-15676

Martensitic stainless steels structure related to energy dissipation capability, obtaining damping mechanism as magnetomechanical hysteresis
08 p1515 A70-20979

Martensitic stainless steels corrosion damage in jet engine compressors noting effects of temperature, surface condition, time and chloride presence
12 p2252 A70-26963

High strength martensitic stainless steel stress corrosion resistance and fatigue crack growth rate, considering austenite content, strain aging and tempering temperatures
24 p4359 A70-45245

Fe-Ni-Co martensitic alloys isothermal age hardening, comparing bcc phase energy parameters of binary systems
24 p4362 A70-46182

Fe-Ni-Mn ternary martensitic alloy, discussing metastable miscibility gap island existence in bcc phase
24 p4363 A70-46193

MARTIN MILITARY AIRCRAFT

U MILITARY AIRCRAFT

MASCONS

Lunar mascon origin theories, discussing mass transfer by excess pressure generation due to rapid cooling crust and densification by water outgassing
02 p0379 A70-12779

Nonexistence of large mascons at Mare Marginis and Mare Orientale deduced from residual acceleration analysis of Lunar Orbiter Doppler tracking data
04 p0743 A70-14424

Creep behavior of mascons to infer lunar temperatures at depth compared with electrical conductivity data and heat conduction equation
05 p0906 A70-15892

Gravity anomalies of moon mapped by time differentiation of Doppler-tracked satellite velocities, noting isostatic equilibrium
05 p0915 A70-16827

Lunar maria hypothetical simultaneous formation by impact, discussing significance of mascons
06 p1138 A70-17279

Apollo lunar orbit irregularities attributed to mascons beneath lunar surface, using short arc perturbation method
06 p1145 A70-18068

[AIAA PAPER 70-163]

Lunar mascons formation by isostatic and volcanic processes, using normal density lunar crust and mantle model
06 p1150 A70-18476

Lunar mascon effects on Apollo type spacecraft orbits calculated for minimizing orbital instabilities
07 p1387 A70-19715

Satellite impact interpretation of lunar maria surface distribution, discussing lava origins and mascon distribution
09 p1752 A70-22310

Mascons in lunar maria depressions observed by Lunar Orbiter 5 on basis of two layer model of crust
12 p2299 A70-27281

Lunar near surface gravity estimation by mass density model for agreement between Doppler tracking data from Lunar Orbiter and trajectory predictions
14 p2645 A70-31064

Lunar mascons origin explanation in terms of primordial atmosphere and hydrosphere
14 p2646 A70-31065

Pulsar gravitational waves detection by lunar mascons, discussing resonant standing vibrations
16 p2980 A70-34306

Mascon effects on close lunar orbit, using short arc perturbation technique
18 p3314 A70-36518

Lunar mascon detection in Sinus Aestuum neighborhood by Apollo 8 tracking data analysis
21 p3886 A70-41058

Lunar sea, mascon and interior composition, discussing crystallization of Apollo 11 Tranquility samples and synthetic analogs at high pressure
21 p3901 A70-41542

MASER OUTPUTS

Output characteristics of cyclotron maser with resonator field due to plane waves interference along static magnetic field, deriving tensor equations
05 p0858 A70-16260

Ammonia maser transient spiking effects under periodic oscillation condition modulation, noting frequency sweep width role
07 p1299 A70-19685

Electron paramagnetic resonance absorption curve influence on power transfer characteristics and maximum passband of multicavity maser
09 p1695 A70-22278

Broadband traveling wave masers bandwidth increased by staggering direct current magnetic field along active structure length
12 p2249 A70-27690

Multilevel maser oscillators undamped output pulsations, investigating effect of coupling between signal frequency energy storage and circuit properties at pump frequency
13 p2430 A70-29704

Rubidium-85 maser, discussing continuous oscillation in low magnetic field
19 p3446 A70-37769

Magnetic field-independent optically pumped Rb 85 maser oscillator power output
22 p4049 A70-42334

Semiconductor microwave generator design for maser simulator using transistorized amplifier, varactor frequency multiplier and diode multiplier
23 p4171 A70-43878

MASER RESONATORS

U MASERS

MASERS

NT GAS MASERS

NT TRAVELING WAVE MASERS

X band electron paramagnetic resonance spectrometer with ruby maser preamplifier, correcting misinterpretation and noise figure analysis
01 p0114 A70-11196

Cyclotron resonance maser /CRM/ monoton with inclined electron flux and magnetic field, considering design for performance optimization
03 p0499 A70-13455

Population inversion coefficient as function of optimal impurity concentrations and efficiency of ruby quantum paramagnetic amplifier in 3 cm range
03 p0499 A70-13457

Transient processes in ruby quantum paramagnetic amplifier during pumping, showing technique for saturation prevention and relaxation effects on population inversion
03 p0456 A70-13460

Atomic clock reproducibility short and long term stability, weight and power consumption characteristics, noting Rb gas cell for collision avoidance systems
04 p0688 A70-14724

Maser-like stimulated OH emission regions observed in interstellar rarefied gas
06 p1148 A70-18391

Maser coherent amplification possibility in comet atmospheres at various frequencies assuming thermodynamic nonequilibrium and nonBoltzmann populations
07 p1378 A70-19034

Multiple maser-magnet units packaging in single cryostat for maximum tunability
08 p1513 A70-21599

Double resonator ruby maser dynamic and static characteristics for centimeter band improved by pumping frequency modulation
09 p1695 A70-22188

Maser amplification in Chirp radar signals pulse paramagnetic compressors using electron spin echoes
09 p1637 A70-23321

Natural frequency of paramagnetic amplifier retuned by coupling Cr ions doped silver coated ruby resonator to passive resonator
10 p1901 A70-25138

Linear theory of cyclotron resonance maser with TEM standing wave field, considering coherent emission for nonrelativistic electrons oscillating in magnetic field
11 p2061 A70-25392

Parametric effect maser developed by maintaining self oscillations in static amplitude modulated magnetic field, noting application as magnetometer
11 p2063 A70-25947

Anomalous LF noise in receiving devices with traveling wave quantum paramagnetic amplifier
11 p2020 A70-26817

Maser amplifier with nonoriented Fe-doped rutile powder as active material, observing broad absorption bands under magnetic field
12 p2249 A70-27649

Equivalent radioelectric plan of ammoniac maser marginal type oscillator
18 p3265 A70-35946

Doubly pumped ruby maser operating in conjunction with superconducting magnet
18 p3265 A70-35953

Double resonator ruby maser for observing transitions of interstellar hydroxyl, noting incorporation in modulation radiometer of astronomical telescope
21 p3835 A70-40641

Anomalous LF noise in receiving devices with traveling wave quantum paramagnetic amplifier
24 p4351 A70-45189

Polarized maser emission from interstellar hydroxyl and water related to nonlinear weak magnetoplasma
24 p4381 A70-45258

MASKING

Target-field luminance or duration effect on target susceptibility to masking demonstrated in visual backward masking study
01 p0039 A70-11163

Contralateral remote masking /CRM/ increase of LF tone burst produced by middle ear muscle contractions
04 p0632 A70-15082

Lateralization and detection of signals under antiphase noise masking measured at various SNR levels
06 p1106 A70-17597

Visual backward masking facilitation dependence on target duration as opposed to interstimulus interval or target-onset/mask-onset interval durations
07 p1221 A70-19850

Permanent memory faults effects on sequential machines finite-state behavior, considering masking role in synthesis of fault-tolerant sequential networks
11 p2072 A70-26220

Narrow band FM noise suggested for masking studies application, discussing noise properties
11 p2011 A70-26496

Audio signals frequency and time resolution, discussing discretizing action of masking effect for higher information rate of spectrally encoded messages
13 p2450 A70-28647

MASS

NT OXYGEN MASKS

MASS

NT CRITICAL MASS

NT ELECTRON MASS

NT PARTICLE MASS

NT PLANETARY MASS

NT STELLAR MASS

Meteorite falls statistics correlations for fragmentation relationships with mass, time of fall and class
05 p0912 A70-16447

Galaxy mass loss on billion year time scale, discussing possibility on basis of bound stellar orbits
06 p1139 A70-17472

Photometric masses of bodies producing bright meteors, considering emission efficiency dependence on velocity, mass and composition
08 p1573 A70-20948

Optimum control law for minimizing mass point maximum deviation under given disturbance obtained by graph analytic method
09 p1727 A70-22534

Translational spectral bands of compressed rare gas binary mixtures, considering mass and temperature effects
12 p2275 A70-27172

Inertial and gravitational mass equivalence related to observation of anomalous K-meson decay
12 p2272 A70-27391

Galactic masses and mass-luminescence ratios from motions data
15 p2801 A70-32480

Photometric masses of bodies producing bright meteors, considering emission efficiency dependence on velocity, mass and composition
15 p2806 A70-32760

Parametric representation of brachistochrones of mass point in centrosymmetrical gravitational field
18 p3283 A70-36387

Galactic masses and mass-luminescence ratios from motions data
23 p4240 A70-43905

Supernovae frequency in Sb and Sc spiral galaxies, considering luminosity class, absolute magnitude and mass of parent galaxy
24 p4413 A70-46164

MASS BALANCE

Gravitational experiments in manned spaceflight employing Eotvos balance in orbit and direct force technique
21 p3929 A70-41002

Attitude control of artificial gravity mass-unbalanced axisymmetric orbital space stations
23 p4258 A70-44502

MASS DISTRIBUTION

Semiautomatic mass condensation transformation for reducing structural vibration calculations, including computer program and mode shape plotting
01 p0200 A70-10868

Nonlinear vibrations in mechanical systems of elastic components having equivalent circuits represented by finite number of discrete masses interconnected by weightless infinite rod
01 p0143 A70-11027

Symmetrical body rotational motion with asymmetrical mass distribution about center of mass, determining minimum initial value of angular velocity
01 p0192 A70-11482

Leonid meteoroids mass distribution law exponent evaluation based on unstable meteoric radio echo durations integral distribution
03 p0574 A70-13884

Galactic mass loss by gravitational radiation, discussing galactic expansion and nucleus mass
04 p0752 A70-15068

Mass density estimated in solar vicinity for distribution among celestial bodies
05 p0914 A70-16647

Lunar structure and evolution based on satellite measurements of mass distribution, radius moments of inertia, gravity anomalies and topographic irregularities
05 p0920 A70-16945

Meteor fragmentation in flares, determining fragments mass, time and special parameters for plotting flare brightness curves
06 p1140 A70-17734

Mass variation laws in light of Tsiolkovskii hypothesis, considering particle separation rates and thermal energy losses for actual jet engines
07 p1363 A70-19088

Mechanical vibration of beams analyzed by partial differential equations of beam vibration involving mass concentration and flexibility
07 p1411 A70-19786

Rotating rotor with mass distributed along shaft analyzed for nonlinear flexural and torsional vibrations, determining dynamic instability ranges
08 p1584 A70-20694

Boundary conditions effect on natural vibration frequencies of unloaded components and components loaded with concentrated masses, obtaining frequency equations
08 p1584 A70-20698

Matter distribution and motion in conformally flat gravitational fields, analyzing Friedmann solution to Einstein equations
08 p1544 A70-20991

Mechanical system undergoing internal mass redistribution, showing energy dissipation during motion
08 p1545 A70-21203

Motion equations and decay of rotating equal mass triple systems for random configuration integrated numerically on computer
09 p1751 A70-22160

Moon gravity field model derived from long-arc analysis of Lunar Orbiters tracking data, considering lunar mass distribution role
09 p1752 A70-22309

Angular motion of deformable earth satellite as solid-elastic system with distributed masses, applying automatic control transfer function
10 p1914 A70-24308

Iterative numerical method for determining optimal mass distribution in complex frameworks, maintaining dynamic response level
10 p1960 A70-25053

Spherical harmonic coefficients of eccentric dipole potential and coinciding magnetic and mass center, noting geophysical prospecting applicability
11 p2047 A70-26571

Diffuse matter distribution in northern region of Milky Way, examining relation with O-BO stars distribution
11 p2116 A70-26588

Mass distribution of Sikhote Alin meteorite fragmentation, noting similarity to terrestrial rocks
13 p2490 A70-28916

Motion stability of variable mass solid body with ideal liquid filled cavities about stationary point using Liapunov theorem
13 p2452 A70-29310

Rotating spherical galaxy evolution, using equations of motion for mass points representing mass distribution
13 p2492 A70-29385

Lunar near surface gravity estimation by mass density model for agreement between Doppler tracking data from Lunar Orbiter and trajectory predictions
14 p2465 A70-31064

Andromeda Galaxy M31 hydrodynamic model based on given mass distribution, determining kinematic functions
15 p2808 A70-32884

Dynamic flexible artificial earth satellites with mass distribution, considering control systems design principles
17 p3180 A70-35294

Mass distribution role in stability theory of rods under nonconservative buckling load
18 p3335 A70-35961

Mathematical model of asteroidal evolution and meteoritic mass distributions under collisional fragmentation using power law
18 p3312 A70-36213

Late-type barred spiral galaxies structure and dynamics with asymmetric mass distribution, using model consisting of small prolate spheroid displaced from disk center
18 p3331 A70-37194

Meteor luminous efficiency and luminosity factor for mass determinations
19 p3515 A70-37661

Antimatter distribution in universe, investigating mass lower limit
19 p3518 A70-38025

Multiplane balancing method for minimizing weight required for spacecraft stability [SAWE PAPER 848]
20 p3595 A70-40362

Variable mass body rotational motion stability in central Newtonian field with gyroscope on symmetry axis
21 p3849 A70-40616

Aircraft, rocket or other rigid or flexible structure, computing inertial constants based on measurements of generalized masses of natural modes
21 p3935 A70-41408

Sweepback thin cantilever wing transonic flutter characteristics, investigating concentrated mass spanwise location effects
22 p4112 A70-42274

Matter and heat balance of cosmic grains surrounded by plasma and neutral gas under radiation
22 p4097 A70-42473

Gravitational collapse for astrophysical matter distributions, discussing differential geometry, relativity, Schwarzschild metric, static equilibrium and spacetime geometries
22 p4098 A70-42579

Lunar geomorphic features and mass wasting relation, discussing landslides, rockfalls, debris slides, slump and creep play
22 p4102 A70-42972

Cosmic rays galactic propagation and confinement, discussing matter and star distributions, magnetic fields, positron flux and energy spectrum, etc
22 p4096 A70-43396

Gravitational acoustic wave emission in isothermal stellar atmosphere with mass sources
23 p4242 A70-44267

Lunar mass and gravitational fields determined from lunar satellite dynamics
24 p4407 A70-45533

Nonlinear distributed sources induced diffusion, calculating relationship between source intensity and maximum temperature or mass concentration field
24 p4380 A70-46034

MASS FILTERS

U FLUID FILTERS

MASS FLOW

Velocity and density profiles obtained from mass diffusivity time measurements in axisymmetric turbulent air pipe flow over specific Reynolds number range
02 p0295 A70-11853

Coupled diffusion of heat and vorticity in gaseous vortex caused by radial mass convection and temperature dependence of gas properties
02 p0400 A70-12858

Pressure changes associated with surface friction and geostrophic drag coefficient related, discussing mass inflow and outflow
05 p0837 A70-16151

Base mass injection effects of various gases on slender body supersonic near wake stability, diffusion and cooling
06 p0970 A70-18075

Slip flow of nitrogen gas through long circular tubes, measuring mass flow, pressure drop and cross sectional velocity profiles
06 p1051 A70-18368

Steady and unsteady flow through Napier turboblower axial flow turbine for full and partial admission, estimating mass flow and power output
07 p1189 A70-20294

Viscoelastic fluid steady flow in porous walled channel, examining mass flow solution continuity
08 p1485 A70-21639

Thermal properties associated with temperature gradients in He-K plasma, studying mass motions initiated by cold wall contact
09 p1735 A70-22844

Onset, mass motion and flash phase in 2b solar flares observed in filtergrams spanning H alpha line
11 p2105 A70-25748

Temperature distribution in opposed jet diffusion flames, discussing mass fluxes and fuel and oxygen concentrations effect
11 p2151 A70-26385

Apparent mass measurements of supersonic jet in incalculable flow regimes, determining dependence on Mach number at nozzle and on distance from exit
13 p3877 A70-28859

Residence times distribution in confined round swirling jet, considering mass conservation of hypothetical tracer substance in combustion efficiency prediction
13 p3522 A70-29609

Linear power scaling-mass flow relationship in multi-Joule pulsed carbon dioxide-nitrogen-helium laser, noting thermal effects role
15 p2751 A70-31977

Trail formation due to tidal effect in interacting galaxies during close approaches, considering mass flow hydrodynamics
15 p2801 A70-32481

Mass flow ion drift anemometer applicable to aircraft speed measurement including VISTOL
19 p3425 A70-37885

Materials jet-like ejection from metal surfaces under high density laser radiation action, investigating erosion and plasma spectrum
19 p3448 A70-38734

Trail formation due to tidal effect in interacting galaxies during close approaches, considering mass flow hydrodynamics
23 p4240 A70-43906

Friction-originated ageostrophic mass flux in ground friction layer at nonaccelerated geotropic boundary layer flow
24 p4370 A70-45133

MASS FLOW FACTORS

Material flow acceleration in jet propulsion systems, discussing acceleration by gravitational field, thermodynamic nozzle expansion, electrostatic forces and Lorentz force
04 p0671 A70-15090

Injection induced swirl effect on thrust and mass flow through nozzle in spinning rocket, discussing internal and exhaust flow measurements and visualization 09 p1606 A70-23247

MASS FLOW RATE

Electromagnetic procedures and camera-spectrometer system for studying detonation processes, measuring mass flow rates and explosives spectra 01 p0909 A70-10887

Free molecular mass flow rate through vacuum seal separating two rarefied gas environments, using coupled integral equations formulated on kinetic theory [ASME PAPER 69-WA/FE-18] 04 p0625 A70-14779

Mass flow rate calculation of methane and natural gas mixtures through critical flow nozzles [ASME PAPER 69-WA/FM-4] 04 p0667 A70-14839

Linear momentum mass flowmeter, discussing operation, damping torque-mass flow rate relationship, operation and advantages 06 p1067 A70-18427

Burning rates of monopropellant droplet evaluated by variable property models, discussing dimensionless mass flow rate 07 p1358 A70-18914

OB supergiants atmospheric expansion indicated by medium-dispersion spectra, noting mass loss rate increase with luminosity and effective temperature 11 p2117 A70-26657

High secondary/primary mass ratio multinozzle jet pump/ejector/operation feasibility [AIAA PAPER 70-579] 13 p2342 A70-29890

Oscillatory flow in turbulent boundary layer modeled by eddy viscosity distribution, deriving mass transport velocity induced by progressive and standing waves 20 p3608 A70-39358

Time-of-flight mass flow rate and thrust stand data comparison for two 100 micropound colloid thrusters [AIAA PAPER 70-114] 20 p3691 A70-40229

Colloid annular thruster performance, using low mass flow rate data and space charge formulas [AIAA PAPER 70-1113] 20 p3692 A70-40230

Colloid engine propellant mass flow distribution, determining beam current and specific charge effects on thrust, efficiency and specific impulse [AIAA PAPER 70-1109] 20 p3692 A70-40234

Tube heat transfer augmentation by helical vane inserts, noting Reynolds number and mass flow rate effects 21 p3949 A70-41318

Mass flow rate correlation for nonsteady convective heat transfer in thin walled tubes with turbulent air flow 21 p3953 A70-42087

MASS RATIOS

NT PAYLOAD MASS RATIO

NT PROPELLANT MASS RATIO

Autonomous two degrees of freedom Hamiltonian system triangular libration points found stable for all mass ratios in circular restricted three body problem 01 p0192 A70-11575

Mariners 6 and 7 range and Doppler tracking data for studying Martian mass and earth-moon mass ratio 06 p1151 A70-18486

Mass to luminosity relations in RF region derived from data for nearest galaxies 07 p1383 A70-19404

High secondary/primary mass ratio multinozzle jet pump/ejector/operation feasibility [AIAA PAPER 70-579] 13 p2342 A70-29890

Earth/moon mass ratio and Mars mass and ephemeris from Mariners range and Doppler tracking data, noting relativistic time delay measurement possibility 15 p2798 A70-31652

Solar system Eotvos experiments for measuring gravitational to inertial mass ratio of celestial bodies 16 p2978 A70-34033

Carbon isotopes abundance in primary cosmic radiation by nuclear emulsion stack exposure in high altitude balloon flight 17 p3151 A70-34914

MASS SPECTRA

Computer program to decide structure for aliphatic ketone from low resolution mass spectrum using DENDRAL algorithm 05 p0810 A70-16048

D region positive ion composition measurements by rocket-borne quadrupole mass spectrometer, discussing downleg and upleg data 06 p1137 A70-18537

Seasonal variation of F 1 region ion composition measured by rocket-borne mass spectrometer, noting altitude dependence of electron and ion temperatures 06 p1059 A70-18540

Infinite-dimensional relativistic wave equations for mass spin dependence 07 p1333 A70-18959

Evidence against electron impact induced alkyl shifts in mass spectra of alpha-hydroxy-ketones, showing thermal rearrangements 13 p2363 A70-29803

Microscopic particle mass spectra in six dimensional scalar, spinor and vector fields, noting 22 p4025 A70-42312

cosmological implications and eight dimensional theory 14 p2616 A70-30342

Wolf-Rayet associated nebulae, presenting radio observations and mass determinations 16 p2980 A70-34193

MASS SPECTROMETERS

Respiratory mass spectrometer design specifications, considering sampling and vacuum systems 01 p0041 A70-11649

Ionic collision processes in nitrogen and oxygen mixtures in mass spectrometer ion source 04 p0646 A70-14700

Mass spectrometer design and calibration for ionic composition measurements on ionosphere sounding satellite, noting effects of satellite velocity and altitude 06 p1065 A70-17908

Computerized mass spectrometer for monitoring atmosphere in astronauts suits and cabin [AIAA PAPER 69-1016] 07 p1249 A70-19730

Gaseous pyrolysis products detection and identification during eruption from polymeric surfaces subjected to flash heating by time of flight mass spectrometer 07 p1319 A70-19887

Omegatron mass spectrometer for rocket measurements of molecular nitrogen density and temperature in middle thermosphere 07 p1289 A70-20308

Monopole mass spectrometer mass range extension by voltage method, discussing sensitivity and mass scan time 08 p1497 A70-21537

Upper atmosphere research by U.S.S.R. mass spectrometers onboard French rocket probes, discussing design, payloads and equipment tests 09 p1766 A70-22658

Blood carbon dioxide and oxygen content determined by respiration mass spectrometer using carrier gas 09 p1629 A70-23584

Differential thermal analyzer coupled to mass spectrometer for kinetics of reactions giving volatile products at high temperature, considering ablative materials 14 p2664 A70-30292

E region ion composition from rocket-borne mass spectrometer data 15 p2725 A70-31689

Atmospheric density and temperature measurements by satellite- and rocket-borne pressure gages and mass spectrometers, considering error sources 15 p2731 A70-32092

Mass spectrometric analysis of lunar rocks for rare gases of solar wind, determining relative abundance, isotopic composition, rock age, exposure time, etc 18 p3320 A70-37083

Photofragment spectrometer, describing vacuum chamber, molecular beam and light sources, mass spectrometer detector, data acquisition and display system, etc 18 p3261 A70-37094

Mass spectrometer modified for use with X-Y recorder for accurate and reproducible ionization efficiency curves 18 p3262 A70-37099

Residual gases partial pressure measurement in vacuum chamber by mass spectrometer with electromagnetic scanner and electron multiplier, detecting electron current 19 p3421 A70-37466

Preventive maintenance of stationary automatic mass spectrometers 19 p3432 A70-38584

Voltage programmed RF oscillator (VPO) for spaceborne quadrupole mass spectrometer, describing transistorized circuitry 20 p3630 A70-39487

Positive ionospheric ion species concentration measurements using magnetic deflection mass spectrometer on Explorer 31 satellite 21 p3815 A70-40999

Spacecraft sheath structure, potential and velocity effects on ion current measurements by traps and mass spectrometers 21 p3816 A70-41087

Pulsed ruby laser mass spectrometry technique for flash pyrolysis of ammonium perchlorate-catalyst mixtures [AIAA PAPER 68-149] 21 p3781 A70-41729

Quadrupole mass spectrometer design for lower thermosphere neutral composition measurement, discussing atmospheric physics, installation on rockets, etc 21 p3830 A70-41990

Mass spectrometer and high voltage converter powering electrostatic plasma and wind analyzer for cosmic space studies on Sputnik 3 and Heos A satellites 22 p4025 A70-42312

Ultrahigh vacuum calibration system for vacuum gages and mass spectrometers based on pressure attenuation and molecular beam techniques 22 p4029 A70-42620

Metal vapor flow measurement by quadrupolar mass spectrometer for control of thin film depositions by evaporation 23 p4198 A70-44872

MASS SPECTROMETRY

U MASS SPECTROSCOPY

MASS SPECTROSCOPY

Secondary halo in spark source mass spectrography, determining corrections 02 p0298 A70-12211

Gas chromatography and mass spectroscopy study of fatty acids and hydroxy acids in 5000 year sediment from English Lake District 02 p0252 A70-12507

Gas chromatography and mass spectroscopy applied to porphyrin microanalysis, studying homologous porphyrin series in ancient sediments and oils 02 p0252 A70-12516

Rocket-borne cryogenic sampler for stratospheric composition measurement by mass spectrometer analysis for computing radiation balance in stratosphere [AAS PAPER 69-569] 04 p0687 A70-14661

Mass spectrometric determination of proton affinities of simple molecules determined from proton transfer and ion-molecule reactions 05 p0885 A70-17081

High resolution mass spectrography using AgBr photographic plates as ion detectors for organic chemical problems 07 p1224 A70-18894

Mass spectra of 1,2-cyclohexanediol and deuterium labeled analogs data recorded and mechanistic rationalizations of degradation processes given 07 p1225 A70-20200

Mass spectrometric sequence determination of oligopeptides via acetylacetyl derivatives, giving reliable results with small peptides 09 p1630 A70-22976

Cyclohexene oxide mass spectral fragmentation by means of deuterium labeled analogs 09 p1630 A70-23397

Aliphatic ethers low resolution mass spectra interpretation using computer program heuristic DENDRAL 09 p1631 A70-23400

Isomeric 1-phenylheptenes mass spectra, investigating electron impact induced rearrangements of double bond 09 p1631 A70-23401

Mass spectroscopy for solar system exploration, discussing ion sources, mass analyzers and ion detectors meeting mission requirements 10 p1942 A70-24612

Lunar rocks types determination by mass spectroscopy, describing results of terrestrial rocks tests 11 p2119 A70-26799

Mass spectrometric analysis of lunar material from soil vaporization products ion component by electron beam 11 p2119 A70-26800

Neutral molecule-solid surface interactions mass spectrometric techniques for measuring molecular flux and mean thermal energy after interaction 12 p2181 A70-27257

Omegatron for total and partial pressure measurement or mass spectrometer applications 12 p2231 A70-27262

Electron impact promoted phenyl migration of trans phenyltolalene, considering mass spectroscopy and stereochemistry 14 p2544 A70-30189

Ion-polar molecule collision time history plots and computer movies, calculating capture cross sections for mass spectroscopy 18 p3292 A70-36561

Upper atmospheric ions kinetic temperatures based on chromatic broadening of mass spectral lines 18 p3252 A70-36985

Optimal separation height of instrument container in atmospheric gas composition mass spectrometric studies 18 p3260 A70-36996

Exhaled alveolar air data acquisition using mass spectrometer and multichannel analyzer 19 p3367 A70-37356

Ion collision effect in quadrupole mass spectrometer, describing ion energy, total pressure in system and other parameters 19 p3421 A70-37411

Ultrahigh vacuum pressure measurement by improved residual gas analysis mass spectroscopy with magnetic section 19 p3396 A70-37465

Sealed-off carbon dioxide laser discharge deposits analyzed by mass spectroscopy 19 p3445 A70-37670

Evolved gas analysis by mass spectroscopy (EGA-MS), discussing filament heating system and data processing 19 p3374 A70-38495

Carbonaceous chondrites noble gases measurement by mass spectroscopy, discussing compositional trends and origins 20 p3703 A70-39323

- Simultaneous mass spectrometric differential thermal analysis of low pressure decompositions of nitrate salts of monomethylhydrazine and methylamine
20 p3688 A70-40475
- Apollo 11 lunar fines organic compounds detection and identification by mass spectrometry
21 p3780 A70-41632
- Mass spectroscopy analysis of neutral and ionic population of plasma in carbon dioxide laser gas mixture, discussing collision processes
21 p3838 A70-42006
- MASS TRANSFER**
- Hydrodynamics, mass and energy transfer equations for moderately dense gases multicomponent mixtures, using Bogoliubov theory
01 p1146 A70-10129
- Heat and mass transfer in Couette flow of partially ionized symmetric diatomic gas for chemical equilibrium and chemically frozen flow cases
01 p0060 A70-10290
- Laminar boundary layer analysis of heat and mass transfer in dispersed two phase flow over heated surface
01 p0214 A70-10293
- Soviet monograph on transfer processes theory in statistical mechanical systems based on probabilistic approach to random particle walk
01 p0215 A70-10650
- Mass loss rate of evaporating liquid droplet with vapor reacting with oxygen of atmosphere in combustion front
[DFVLR-SONDDR-16]
01 p0216 A70-10932
- Mass transfer analysis for axisymmetric turbulent flow in circular tube, deriving turbulent velocity profile from two part model, based on von Karman similarity hypothesis
01 p0064 A70-11092
- Nonaxisymmetric mass transfer in turbulent flow in plain circular tube, considering diametral line and discontinuous ring sources
01 p0065 A70-11093
- Aerodynamics, heat and mass transfer in vapor condensation from humid air on flat plate in longitudinal flow in asymmetrically cooled slot
01 p0004 A70-11178
- White dwarfs formation in close binary systems ascribed to mass exchange between components, describing evolutionary followup of primary from main sequence by model
01 p0189 A70-11343
- Volumetric reaction rates and mass transport coefficients as function of position for ducted two dimensional turbulent hydrogen-air diffusion flame
02 p0398 A70-12036
- Stratospheric air intrusion into troposphere calculated for speed and frequency of occurrence, considering mass and energy transfer
02 p0329 A70-12690
- Lunar mascon origin theories, discussing mass transfer by excess pressure generation due to rapid cooling crust and densification by water outgassing
02 p0379 A70-12779
- Soviet bibliography on heat and mass transfer covering thermodynamics, heat conduction, convection and radiation, phase and chemical transitions, aerodynamics, geophysics, etc
03 p0605 A70-13392
- Tropopause role in stratospheric-tropospheric exchange processes for radioactive debris transport
03 p0476 A70-13908
- Ideal fluid motion characteristics near variable volume spheres with radial mass transfer through surfaces
04 p0672 A70-15198
- Equations and techniques to analyze transient heat and mass transfer characteristics of packed adsorption beds for spacecraft life support systems
04 p0786 A70-15316
- Mass transfer and viscous interaction combined effects on axisymmetric hypersonic flow of perfect gas over slender bodies
[AIAA PAPER 68-717]
04 p0675 A70-15576
- Heat and mass transfer in reacting laminar boundary layer over porous cylinder with propane injection in wind tunnel experiments
05 p0956 A70-16289
- Soviet bibliography on heat and mass transfer covering thermodynamics, heat conduction, convective and radiant heat transfer, phase and chemical transformations, combustion, etc
05 p0957 A70-16297
- Galactic expansion due to mass energy loss by gravitational radiation
05 p0913 A70-16557
- Collection of papers on heat and mass transfer theories, measurements and applications
06 p1174 A70-17676
- Turbulent boundary layers and wall jets development investigated for effect of mass injection through porous smooth and rough surfaces
06 p1034 A70-17679
- Convective heat and mass transfer augmentation techniques including surface and displaced promoters, vortex flows, etc
06 p1174 A70-17681
- Collection of papers on heat and mass transfer, Volume 2, covering free convection, forced fluid flow, nozzle flow, boundary value problems, etc
06 p1174 A70-17682
- Heat and mass transfer in passive transpiration cooling system with two moving boundaries, observing porosities and radius of curvature effects
06 p1176 A70-17692
- Heat and mass transfer across laminar boundary layer around stagnation line of cylinder in crossflow affected by free stream turbulence intensity
06 p1176 A70-17693
- Particle ejection moments from tail of comet Ikeya-Seki determined from photographs having visible terminal synchroes
06 p1140 A70-17732
- Energy and mass transfer during elastic and inelastic molecular collisions in reacting gas mixtures, using Enskog and variational methods in solving Boltzmann equations
06 p1110 A70-17760
- Pyrolysis effect on infinite slab subjected to front heat flux, attributing increased porosity to mass loss
[WSCI PAPER 69-27]
06 p1178 A70-17978
- Hypersonic aerodynamic measurements on cone, investigating effects of oscillatory mass addition on stability
[AIAA PAPER 70-217]
06 p0974 A70-18171
- Monte Carlo analysis of free and near free molecular flow through circular tubes for mass, momentum and energy transfer
06 p1051 A70-18367
- Mass loss rates for short period comets from non-gravitational terms in equations of motion, paying particular attention to secular variations
06 p1151 A70-18490
- Integral method for time development of viscous, heat and mass conducting layer over leading edge of volatile drop instantaneously immersed in gas stream
07 p1358 A70-18916
- Fcc metals surface changes following adhesion using low energy electron diffraction (LEED), relating intersurface metal transfer to applied adhesive force
07 p1305 A70-18920
- Downstream distribution of trace element injected into boundary layer of flat plate or cone with self similar mass transfer
[SAMSO-TR-69-56]
07 p1256 A70-19313
- Electronic analog model for simulating convective mass transport in system with stationary and dynamic phases
07 p1423 A70-19740
- Stefan problem involving mass transport and phase transformations, presenting solution algorithm
08 p1596 A70-20852
- Hydrodynamics, mass and energy transfer equations for moderately dense gases multicomponent mixtures using Bogoliubov theory
08 p1548 A70-21405
- Interhemispheric mass exchange as function of eddy transfer and meridional circulation
08 p1539 A70-21922
- Heat and mass transfer coefficients in binary laminar boundary layer convection obtained with integral equations and Karman-Pohlhausen method
09 p1787 A70-22264
- Heat and mass transfer in binary turbulent boundary layer during natural convection on vertical surface, allowing for diffusional heat conduction
09 p1787 A70-22267
- Drag on sharp cones in hypersonic flow, studying effects of intense transverse mass injection through porous walls
09 p1603 A70-22441
- Turbulent heat and mass transfer from wall to plane-parallel fluid flow at large Reynolds and Peclet numbers, developing universal law
09 p1789 A70-23169
- Laminar boundary layer separation noting effect of mass slot suction
09 p1662 A70-23236
- Turbulent pipe flow with wall suction, calculating friction factor, pressure gradient, heat and mass transfer coefficients, velocity and temperature profiles
[ASME PAPER 69-HT-4]
09 p1790 A70-23558
- Heat and mass transfer during liquid surface evaporation in vacuum, calculating temperature field on basis of heat balance level
09 p1791 A70-23717
- Naphthalene rotating disk with confronting stationary disk, investigating heat and mass transfer dependence on shroud dimensions, measuring flow types
11 p2060 A70-26410
- Flat plate normal to two dimensional impinging air jet, investigating heat/mass/transfer structure using naphthalene method
11 p1977 A70-26411
- Laminar boundary layer equations solved for heat and energy transfer in binary gas mixture, investigating forced and free convection
11 p2151 A70-26558
- Simultaneous heat and mass transfer coefficients in laminar free convection boundary layers on horizontal cylinders or vertical axisymmetric bodies
11 p2151 A70-26559
- Compressibility transformation theory extended for turbulent boundary layer, involving mass transfer with/without chemical reactions
[AIAA PAPER 69-161]
12 p2211 A70-27825
- Similar laminar boundary layer solutions exhibiting separation, pressure gradient and mass transfer
12 p2211 A70-27828
- Mass transfer in close binary stars and in highly variable stars
12 p2306 A70-27858
- Bubble dynamics in subcooled nucleate boiling, deriving mathematical model based on evaporation-condensation mass transfer mechanism
12 p2333 A70-28113
- Unsteady heat or mass transfer to translating fluid sphere thermal boundary layer, determining analytical solution method accuracy
12 p2333 A70-28116
- Graphite mass removal rates under ohmic heating in reacting gas turbulent flows
13 p2519 A70-28579
- Surface erosion of sublimating graphite and naphthalene due to inequilibrium mass transfer in gas flows
13 p2437 A70-28580
- Mass transfer in electrochemically accelerated plasma, discussing recombination, ambipolar diffusion, electrode sputtering, charge exchange, electron capture and resistance forces effect on acceleration
13 p2461 A70-28862
- Laminar near wake flow field of two dimensional adiabatic circular cylinder with surface mass transfer
[AIAA PAPER 69-67]
13 p2343 A70-29951
- Reynolds momentum and mass transport at velocity half radius of coaxial jet compared to eddy viscosity models
14 p2564 A70-30260
- Two dimensional incompressible turbulent boundary layer with mass addition and heat transfer, calculating temperature and velocity profiles by marching integration
14 p2564 A70-30261
- Three dimensional boundary layer along semi-infinite swept stagnation line, assessing counteracting effects of cross flow and mass transfer
14 p2565 A70-30278
- Sonic boom minimization methods involving mass or energy addition
14 p2531 A70-30868
- Sound propagation in atmospheric fog, considering mass, momentum and energy transfer mechanisms between particles and gas
15 p2769 A70-31443
- Monograph on momentum, heat and mass transfer rates to vertical continuous cylinder moving through quiet fluid in forced and free convection
15 p2825 A70-31694
- Thermal boundary layer and heat and mass transfer at porous horizontal heated surface in presence of free convection, considering blowing and suction effects
15 p2827 A70-32133
- Distributed-lumped parameter model for impeded mass transfer and blood-gas maldistribution effects in human respiratory system
15 p2694 A70-32844
- Iodine concentrations, temperature gradients and transport ampules etching effects on mass transport rate and crystal growth of MnS-MnSe-iodine system
16 p2960 A70-33088
- Mechanical erosion concomitant with thermochemical erosion in mass and energy transfer at interface of boundary layer and ablating nylon-silica-phenol material
[AIAA PAPER 70-824]
16 p2941 A70-33942
- Iron, Ni, Cr and Co corrosion and mass transfer in high temperature Na, examining properties of stainless steels and cobalt base alloys
16 p2933 A70-34209
- Comet Alcock flareup on 27-29 May 1969, noting visible rays in coma, dust grains expulsion from nucleus, tail structure, etc
16 p2980 A70-34304
- Frequency spectra of gravitational waves radiated from celestial phenomena, suggesting mass exchange in binary containing neutron star
17 p3067 A70-34619
- Heat and mass transfer in flowing fluid, deriving conservation and constitutive equations, with application to boundary layer flow of gases
17 p3069 A70-35033
- Transient heat and mass transfer in adiabatic regenerator, solving mathematical model in terms of Green functions
17 p3197 A70-35542
- Explicit differences scheme for heat and mass transfer differential equations
18 p3345 A70-36114
- Meteorite masses evaporation during flare, showing discrepancies for luminosity factors
18 p3315 A70-36604
- Burning rate theory applied to heat and mass transfer rates of monopropellant droplets in heat-up and steady burning at wet bulb temperature
18 p3348 A70-36696

DC plasma generator with Ar stabilized arc, investigating heat and mass transfer in jet discharge channel
19 p3481 A70-38189

Phase formation and mass transport during iodine-refined Ti reaction with nitrogen at various elevated temperatures
19 p3452 A70-38364

Turbulent heat and mass transfer from wall to plane-parallel fluid flow at large Reynolds and Peclet numbers, developing universal law
19 p3552 A70-38392

Turbulent jet system with previously unmixed chemically active gases, calculating heat and mass transfers during diffusion combustion
20 p3737 A70-39813

Human mass exchange parameters permissible errors for manned space vehicles life support systems design
20 p3581 A70-40200

Flat plate boundary layer flow with surface blowing and suction /mass transfer/, investigating stability by numerical techniques
20 p3615 A70-40507

Turbulent boundary layers calculation with and without mass addition based on eddy viscosity concept, including accelerating flows
21 p3807 A70-41029

Accelerated self similar compressible laminar boundary layer flows with and without mass transfer, obtaining numerical solutions
21 p3807 A70-41031

Reentry vehicle with multicomponent gas mixture injection, calculating heat and mass transfer correlations for stagnation point flow
21 p3945 A70-41033

Thermal protection system based on radiation cooling for high altitude cruising hypersonic flight, achieving zero net mass transfer
21 p3950 A70-41745

Upstream mass injection effects on downstream heat transfer of supersonic reacting boundary layer
21 p3952 A70-42079

Turbulent heat/mass transfer from solid boundary with shear stress dependent on wall distance for various Schmidt or Prandtl numbers
21 p3953 A70-42088

Combined effects of flow unsteadiness and surface mass transfer on displacement thickness of boundary layer, using flat plate geometry
21 p3811 A70-42092

Heat and mass transfer in plane inductionless and dissipationless incompressible MHD boundary layer with longitudinal pressure gradient
21 p3861 A70-42231

Mass transfer effects on plasma electrodynamic acceleration, discussing plasma recombination and diffusion
22 p4083 A70-43386

Two phase liquid one dimensional motion in variable cross section tube, deriving mass transfer, motion and phase interaction differential equations
22 p4012 A70-43721

Mass transfer and velocity gradient fluctuations at wall in two dimensional or rotational flow for large Schmidt numbers
23 p4181 A70-44210

Heat and mass transfer for liquid film evaporation during two phase two component flow in vertical steel tube under adiabatic and nonadiabatic conditions
23 p4276 A70-44215

Mass transfer between sphere and liquid flow at small Reynolds numbers
23 p4276 A70-44219

Three dimensional laminar boundary layer separation at infinite swept stagnation line with high mass injection rates
23 p4182 A70-44568

Close binary star components axial rotation, considering synchronism, angular velocity and mass exchange
23 p4250 A70-44814

Biological life support systems mass exchange processes analysis based on mathematical models, predicting artificial ecological systems stability
23 p4149 A70-45029

German monograph on radioactive gases and decomposition products mass transport in turbulent atmospheric boundary layer, noting Boussinesq approximation and Reynolds decomposition
24 p4324 A70-45094

High speed radiographic observation of electric arc movement and metal transfer during submerged arc welding
24 p4322 A70-45724

MASSAGING

Bioelectrically controlled system for indirect heart massage, noting dynamic simulation of system on digital computers using block oriented programming languages
01 p0047 A70-10261

MATCHING

Physical identity and name sameness matchings efficiency noting role of interpolated activity
07 p1203 A70-18942

Matching operations for difference and differential equations describing discrete control systems dynamics having cyclic interruption of data quantization frequency
08 p1480 A70-20999

Helicopter engine rotor matching for tip propulsion efficiency, comparing with conventional shaft drive propulsion
18 p3215 A70-36842

MATERIAL ABSORPTION

Carbon dioxide absorption from gas streams by weak base ion exchange resins
18 p3226 A70-36767

MATERIAL BALANCE

NT WATER BALANCE

MATERIAL REMOVAL (MACHINING)

U MACHINING

MATERIALS EROSION

U EROSION

MATERIALS HANDLING

NT GROUND HANDLING

NT PROPELLANT TRANSFER

NT REMOTE HANDLING

Worldwide door-to-door cargo shipping by airline, considering marketing systems approach
07 p1426 A70-18875

Air-land demountable cargo containers specifications, establishing dimensional, structural and environmental requirements
07 p1249 A70-19599

Onboard cargo loader to make aircraft independent of specialized ground equipment
10 p1862 A70-25330

Two-point suspension system with longitudinally displaced cargo hooks for handling helicopter loads, discussing wind tunnel and flight tests
17 p3014 A70-34714

Static charge reducer for aircraft fuels handling safety, discussing performance factors
18 p3263 A70-36808

Lead alloys as shielding materials in nuclear systems, discussing physical, chemical and metallurgical properties, fabrication and applications
19 p3469 A70-37833

Surface damage of GaAs crystals by mechanical handling and polishing with hard abrasive lapping materials
20 p3686 A70-39119

Hydrogen slush characteristics, discussing advantages of liquid-solid mixture over liquid hydrogen, production methods, aging effects, transfer and pumping losses, storage, instrumentation, etc
23 p4232 A70-45075

MATERIALS RECOVERY

NT WATER RECLAMATION

Constant stress creep and recovery behavior experiments of polycarbonate under combined tension and torsion stresses in weakly nonlinear range
01 p0130 A70-11083

Creep and recovery of polyvinyl chloride reinforced by oriented cotton fibers, considering roles of fiber density and stress magnitude
03 p0516 A70-13499

Annealing properties of radiation damage in lithium-diffused silicon, formulating kinetic equation to describe processes associated with recovery and instability
20 p3687 A70-40165

Gas bubbles effect on recovery and recrystallization in W sheet deposited from tungsten fluoride vapor
24 p4358 A70-45243

MATERIALS SCIENCE

Discrete models formulated for thermomechanical behavior of materials with memory, obtaining equations of motion and heat conduction for finite elements of nonlinear continua
01 p0208 A70-11183

Optical studies of deformational structures of minerals from meteorite craters and cryptoexplosion structures
02 p0292 A70-12510

Gear materials evaluation program for space environment application with unlubricated or solid film lubricated operation mode
[ASLE PREPRINT 69-LC-6] 02 p0309 A70-12539

Papers on engineering materials covering refractory creep resistant materials, fiber reinforcement, ceramics, polymers, alloys, etc
02 p0318 A70-12709

Polymers application as engineering materials, discussing properties, physical states, etc
02 p0322 A70-12716

Servo systems for analog automatic reduction of time dependent photomechanical model materials fringe data in stress analysis
03 p0482 A70-12967

Soviet collection of papers on metal science and corrosion problems covering welding, heat treatment, Cr-Mn steel, Ti alloys, etc
03 p0509 A70-13276

Nonlinear solid applied mechanics, emphasizing nonlinear constitutive equations and related subjects, cyclic loading effect on solid materials, etc
03 p0610 A70-14230

Specific heat, electrical resistivity and thermal conductivity changes in materials properties at cryogenic temperatures, noting parasitic phenomena, mechanical and dielectric properties
03 p0525 A70-14269

Materials science experimental and diagnostic phases in mechanisms of metal erosion by impacting dust particles
[ASME PAPER 69-WA/MET-8] 04 p0704 A70-14760

Metals, plastics and ceramic materials under erosion by irregular quartz particles, using vacuum whirling arm
[ASME PAPER 69-WA/MET-6] 04 p0704 A70-14762

Materials in spatial motion criteria of stress power positiveness
05 p0929 A70-16069

Cryogenics applications to solid state physics and materials research tabulated for experimental methods and objectives
05 p0892 A70-16398

Material inhomogeneity during high temperature fatigue tests taking into account probability density of random failure coordinate distribution
07 p1401 A70-18839

Carbon fabrics and filaments, resin carbonizing and carbon-carbon composites, discussing processing parameters, initial carbonizing resin binder and reinforcement effects on laminate properties
07 p1316 A70-18932

Filamentary composite materials for commercial aircraft and engine construction noting boron, graphite and glass reinforcement
07 p1316 A70-18950

Materials selection and simulated service testing to preclude failure, considering roles of design, fabrication and maintenance
07 p1248 A70-19235

High temperature techniques, measurement and data methodology noting refractory materials
07 p1312 A70-19877

Servo systems for analog automatic reduction of time dependent photomechanical model materials fringe data in stress analysis
07 p1286 A70-20040

Strength and plasticity criteria for anisotropic reinforced materials model taking into account material structure, components properties and behavior
09 p1768 A70-22119

Book on solid materials under stress covering mechanical testing, metals and polymers structure, ceramic crystals and creep and composite materials properties
09 p1708 A70-23476

Gear materials evaluation program for space environment application with unlubricated or solid film lubricated operation mode
10 p1893 A70-23837

Materials and processing technology roles in NASA programs involving manned space stations, service spacecraft and unmanned space exploration
10 p1902 A70-23855

Book on tensor calculus in materials science covering thermodynamic equilibrium, gaseous and solid phase heat engines, solids crystalline structure, etc
12 p2282 A70-26866

Structures, structural mechanics and materials - AIAA-ASME Conference, Denver, April 1970
12 p2317 A70-27126

Acoustooptics materials selection guidelines, estimating lead molybdate figure of merit on basis of chemical composition and density
13 p2469 A70-28796

Book on high temperature, transition and hydrated ceramics covering nomenclature, natural occurrence, mechanical, thermal, sonic, electrical, magnetic and chemical properties
13 p2436 A70-29781

Elastoplastic material mechanical theory, considering constitutive equations with plastic deformations and decompositions of total velocity-strain /stretching/
14 p2661 A70-31281

Materials durability in presence of stress concentration under biharmonic loading
15 p2813 A70-31527

Materials research - Conference, Tokyo, September 1969
17 p3123 A70-34651

Materials and noncontacting design for 50,000 hour lifetime electromechanical components, noting magnetically suspended motor
17 p3100 A70-34754

Polyimide prepreps reinforced with glass, carbon and graphite, describing processing characteristics, properties and applications
17 p3127 A70-35419

Materials deformational flow theory, relating dislocation motions in solids to fluid viscosity concept
17 p3190 A70-35452

Homogeneity criteria for semiconductor materials, considering variation coefficient, goodness factor and overshoot density
18 p3298 A70-36468

Book on materials for structural and mechanical functions covering electrical engineering properties, ferrous and nonferrous metals and alloys, fabrication methods, environmental protection, etc
19 p3453 A70-38622

Soviet book on fiber reinforced composites covering strength, rheologic and elastic properties, thermal conductivity, diffusion processes, etc
19 p3456 A70-38795

Hot gas pipe thermoelastic reduction factors, determining elastic support, material and dimensions
20 p3720 A70-39624

High strength and stress corrosion resistant materials, considering Ti, Ni, Al alloys, metal-matrix composites and polymers
20 p3655 A70-39666

Photographic materials resolving power for lines and points
20 p3633 A70-39750

Materials viscous failure at various temperatures and stresses, discussing damage accumulation
20 p3725 A70-39870

Materials technology - Conference, Mexico City, August 1970
20 p3649 A70-39939

Be production, development, potential uses and properties [ASM PAPER G8-102]
20 p3650 A70-39970

Mechanics of composite materials - Conference, Philadelphia, May 1967
20 p3728 A70-40026

Composite material engineering problems, discussing tensile, compressive and shear strengths, design approaches, unidirectional properties and substance characterizations
20 p3651 A70-40027

Parabolic solar furnace for chemical manufacture of impurity sensitive materials in orbiting spacecraft
21 p3804 A70-41001

Aircraft flight propulsion systems performance improvement via materials technology for gas turbine engine components
22 p4057 A70-43573

French book on strength of materials covering potential energy theory, cutoff and matrix methods, computer calculations, etc
22 p4119 A70-43623

Papers on thermoplastics covering types, properties and applications
22 p4060 A70-43624

Materials problems in space and spacecraft environments, discussing particle density, composition and UV radiation, spacecraft structure, payloads, vibration, etc
23 p4209 A70-44328

Fibrous, cellulosic, elastomeric and plastic materials with improved flame resistant properties for space applications
23 p4152 A70-44461

Temperature dependent materials heat flow analysis using perturbation method for nonlinear boundary value problems
23 p4282 A70-44589

Fibrous composites thermomechanical properties derivation by theoretical analysis from basic constituents characteristics, presenting comparisons with experimental results
24 p4366 A70-45170

Materials design and development for engineering applications, discussing relationships and importance of strength, stiffness, weight, toughness and work of fracture
24 p4419 A70-45174

Plasticized high polymers mechanical and optical properties, studying birefringence phenomena interrelation with applied external stresses
24 p4424 A70-45590

Nondestructive testing - Conference, Hanover, June 1970, Materials properties determination, Stress measurements
24 p4347 A70-45728

MATERIALS TESTS

Nondestructive evaluation of components and materials in aerospace, weapons systems and nuclear applications - Conference, San Antonio, April 1969
01 p0095 A70-10001

Contact thermographic materials application to nondestructive materials testing based on heat capacity, costs, removal time, equipment, personnel skill and training, etc
01 p0097 A70-10007

Electronic materials nondestructive evaluation techniques, describing analytic tests for chemical, structural, electrical and optical characteristics determination
01 p0085 A70-10023

Release adiabats and recentered Hugoniot curves determination by shock reverberation techniques for compressible nonlinear materials, presenting results for epoxy resin and porous tuff
01 p0198 A70-10106

Fibrous filter materials filtering capability, comparing extruded and drawn metallic filters
01 p0007 A70-10159

Defects development in cermet materials sealing elements in high O content gas flows of turboprop and turbojet engines
01 p0161 A70-10160

Laser processing applied to optical nondestructive materials tests for surface flaws
01 p0086 A70-10416

Ultrasonic methods for materials evaluation, discussing goniometry, measuring techniques and acoustic wave propagation in various materials
01 p0104 A70-10878

Diffraction loss measurement in solid state laser to determine laser material contribution to total cavity loss
01 p0113 A70-10919

Steels tested to evaluate proposed incremental strain theories predicting loads on thin walled cylinders subjected to nonproportionate loading, discussing stress-strain diagram
01 p0202 A70-11057

Constant stress creep and recovery behavior experiments of polycarbonate under combined tension and torsion stresses in weakly nonlinear range
01 p0130 A70-11083

Microwave propagation in materials and measurement methods for inspection based on reflecting surface movement and scattering method for porosity detection
01 p0094 A70-11395

Machine element materials damping properties, determining energy dissipation during steady resonant vibrations
01 p0211 A70-11423

PKR portable xeroradiographic defectoscope for nondestructive testing of steel and Al alloys
02 p3001 A70-12486

Nb-Mo alloys in various proportions prepared by vacuum casting, showing embrittlement under hydrogen atmosphere
02 p0318 A70-12671

Test fixture for determining mechanical properties of metals and steels at moderate strain rates, detailing design and instrumentation
03 p0462 A70-12883

Apparatus for short term thermal vacuum mechanical testing of materials
03 p0463 A70-13253

Air plasma pulsed discharge jets erosive effects on metals, semiconductors and dielectrics, noting role of thermal effect
03 p0532 A70-13742

Nonflammable material development program for Apollo spacecraft, noting requirements imposed by high oxygen environments, toxic offgassing and temperature range
03 p0436 A70-14055

Structural materials mechanical properties tests during neutron bombardment, discussing atomic reactors optimal parameters calculation
04 p0775 A70-15259

Compression test for ductile materials based on Saint Venant principle of plasticity to reduce friction effects on deformation by lubricant pressurization
04 p0776 A70-15373

Stress corrosion testing method to separate corrosion and stress effects applied to Al and Ti alloys
04 p0708 A70-15374

Variable strain bending form design for determining environmental craze resistance of polymers
04 p0713 A70-15375

Reinforced plastics destructive and nondestructive testing including standard methods, equipment and procedures applicable to materials and parts
05 p0874 A70-16621

Composite materials properties test methods, discussing nondestructive method for shear or rigidity modulus of square plates
05 p0874 A70-16622

Testing equipment and methods for metallic materials selection for low temperature applications, characterizing plasticity by yield strength, tensile strength, elongation, etc
05 p0864 A70-16805

Heat resistant materials damping properties at high temperatures under distributed stresses measured in thin walled tubular specimens with vibrogram
05 p0952 A70-17049

Scale dependence and optimal sample dimensions for strength tests of brittle refractory materials
05 p0955 A70-17064

Test facilities for studying materials thermophysical properties and stress relaxation, including dynamic hardness measurement and torsion tests up to 2500 K
05 p0830 A70-17074

Recrystallization behavior of Al alloy containing Mg and Si subjected to maximum aging before cold working
06 p01085 A70-17418

Thermal and dynamic considerations of materials choice for satellite mounted telescope mirrors noting Be and silica properties
06 p1064 A70-17781

Insulation materials selection for Martian soft lander to meet mission environmental conditions based on tests
06 p1182 A70-18224

Laboratory Electronic Servo Controller for structural fatigue tests, aircraft material tests, model position and velocity control in wind tunnels
06 p0989 A70-18606

Fe-Cr-Ni alloys for use in high temperature oxidizing environments
07 p1305 A70-18966

Materials selection and simulated service testing to preclude failure, considering roles of design, fabrication and maintenance
07 p1248 A70-19235

Fiberglass reinforced materials characteristics under stress evaluated by ring test in form of split disk or hydraulic tests
07 p1410 A70-19758

Radiative heating rates and gas environments effects on ablative material performance from tests at arc image facility
07 p1319 A70-19888

Laboratory and field tests to evaluate liquid rocket propellant properties for tactical mission
07 p1362 A70-19918

Stress wave propagation in particulate loaded carbonaceous materials induced by homogeneous laser beam
07 p1302 A70-20097

Static and dynamic low temperature crack toughness behavior of steels, determining strain rate effect
08 p1518 A70-21317

High speed testing - Conference, Boston, March 1969, Volume 7, Rheology of solids
08 p1526 A70-21326

Composite materials testing and design - ASTM Conference, New Orleans, February 1969
08 p1528 A70-21876

Composite materials shear strength test problems with high modulus fibers
08 p1529 A70-21877

Inplane shear stress-strain response determined for unidirectional composites, using uniaxial test method for laminated plates
08 p1530 A70-21884

Mechanical testing of metal matrix high modulus B-Al filament composites, using unidirectional and multidirectional reinforcement
08 p1523 A70-21894

Yttrium iron garnet sintering and grain growth rates dependence on yttrium/iron ratio [ACS PAPER 16-BE-68F]
09 p1740 A70-22982

Composite window permitting visual or photographic observation and IR irradiation of test materials in ultrahigh vacuum system
09 p1698 A70-22994

Materials static tested for compatibility with pure and moisture contaminated chlorine pentafluoride at 160 F and ambient temperatures
09 p1742 A70-23250

Oxygen index flammability test for polymeric materials, showing general applicability in quality control and research
09 p1710 A70-23346

Fibrillated asbestos dispersed in thermoplastic ionomer lattices, precipitated, dried and compression molded into bars, testing for flexural modulus, flexural stress and Vicat softening temperature
10 p1906 A70-24024

Solid electrolyte high temperature fuel cells electrode materials, investigating various metal oxides
10 p1830 A70-24461

Aviation and space industry metallic and nonmetallic materials testing, discussing corrosion and ultimate fatigue due to impurities
10 p1861 A70-24664

Flammability resistance and smoke emission characteristics of aircraft interior fire retardant materials under ambient and increased temperature and zero ventilation conditions [AIAA PAPER 70-400]
10 p1908 A70-24905

Hollow cylindrical sample scale effect on accuracy of testing heat resistance of brittle materials
10 p1965 A70-25301

Stability conditions in metal specimens tension tests, considering fcc and bcc metals strain hardening, rate and gradients and temperature dependence
10 p1966 A70-25326

Stress peak distribution effects on fatigue life of test specimen excited to bending by Gaussian random vibrations
11 p2137 A70-26093

Lifting entry vehicle thermal protection system /TPS/ material performance, analyzing metallic radiator and passive transpiration systems and rigid insulation
11 p2150 A70-26368

Materials absorption coefficients determination at high temperatures based on spectrophotometric analysis of emission from samples of different thicknesses
12 p2331 A70-27305

Fracture toughness and cyclic crack propagation of surface cracked high strength aircraft structure steels 12 p2254 A70-27467

Materials life estimation under irregular load sequences, discussing computational and graphical method, applications and test and computer equipment 13 p2513 A70-29162

Transfer molding of electronic modules, discussing materials for evaluating selection and processing guidelines 13 p2421 A70-29255

Quasi-stationary analysis of thermophysical characteristics of materials, considering cylinder and plate samples under unsteady heating 15 p2826 A70-32105

Materials testing machine for tension, compression and flexure at constant strain rate and for fatigue 16 p2900 A70-33067

Ceramic material ranking, using thermal stress crack initiation method 16 p2934 A70-33274

Epoxy laminating resin evaluation for tooling industry, considering diluent, fillers, thixotropy, hardeners and physical property testing 16 p2936 A70-33360

Glass fiber reinforced resin structures evaluation by plastographic analysis using visual, macrographic, stereomicroscopic, and scanning electron microscope methods 16 p2908 A70-33361

Materials test fixture design and fabrication for vacuum testing and evaluation of slip rings and brushes, discussing dry film lubrication 16 p2920 A70-33812

Satellite-borne test instrument for determining mirror materials degradation due to long solar exposure 16 p2921 A70-34109

Materials technology for reuse capability of space shuttle, discussing normal and stress corrosion, hydrogen embrittlement and flammability 16 p2987 A70-34228

Strain rate effect on cyclic behavior of materials with hardening and softening characteristics 17 p3187 A70-34988

Fatigue life prediction under irregular stress conditions, considering material characteristics determination by standard tests 17 p3187 A70-34990

Shock wave response of metals and nonmetals under high strain rates 17 p3188 A70-35223

Temperature changes minimization techniques in specimens during microplasticity tests, describing gage assembly for plastic strain measurement 18 p3272 A70-36030

Polymers dynamic properties in hyperelastic and vitreous states as function of temperature, using torsion pendulum method 18 p3263 A70-36469

Dry friction and wear tests of various materials in vacuum at low temperatures 18 p3263 A70-36471

Dynamic hysteresis loop measurement of energy dissipation in materials, showing deformation effects on accuracy 19 p3535 A70-37346

Energy dissipation in material under complex vibrations, noting role of summary shear stress 19 p3535 A70-37347

Apparatus for short term thermal vacuum mechanical testing of materials 19 p3401 A70-38471

Jet engine roller bearings retainer candidate cage materials and coatings evaluation on test rig simulating engine conditions [ASLE PREPRINT 70AM 2D-1] 19 p3439 A70-38805

Molybdenum disulfide abrasiveness on test rings coated with bonded solid lubricant [ASLE PREPRINT 70AM 5A-1] 19 p3439 A70-38811

Carbon/carbon composites constituent characteristics effects on thermal and mechanical properties, using polarized light and scanning electron microscopy 20 p3653 A70-39204

Composite materials physical properties measurement and defect locations detection by NDT techniques 20 p3636 A70-39210

Unidirectional and multidirectional carbon/carbon composites quality and performance evaluation by NDT methods, including X ray radiography, ultrasonic test, pulse echo mapping, etc 20 p3654 A70-39211

Papers on design and materials, discussing alloys for aircraft structures, stress-rupture life of Ni base alloy, single crystal structures, etc 20 p3648 A70-39412

Composite structural materials for thermal protection in reentry vehicles applications, evaluating fused quartz yarns, silicone rubber and phenolic resins 20 p3656 A70-40031

Al alloys and stainless steels tensile properties and application in lightweight cryogenic propellant tank structures, discussing Ti alloys and reinforced composite materials tests 20 p3651 A70-40123

Integrating cavity spectroscopy for measuring absorption coefficient of material 21 p3822 A70-40817

High temperature aromatic polyester Ekonol, discussing fabrication, properties and potential applications 21 p3842 A70-41136

Turbocompressor disk materials selection by low cycle fatigue tests, discussing stop and start repetition and cracks in stress concentration zones 21 p3867 A70-41261

Aerial retrieval webbing performance characteristics, discussing structure, type of material, finishing and strength levels 21 p3843 A70-41832

Ultrasonic spectroscopy in nondestructive materials tests, discussing electronic equipment design, FM, pulse and pulsed FM methods 22 p4027 A70-42583

Scorched aluminum powder /SAP/ materials, discussing fabrication, physical and mechanical properties, applications in aircraft structural components, etc 22 p4055 A70-43084

Materials for glass-metal compressed joints, tabulating stress and thermal expansion coefficients 22 p3999 A70-43447

Manned spacecraft nonmetallic construction materials selection criteria, testing and configuration control, considering flammability hazard 23 p4152 A70-44462

Saturn Orbital Workshop experiment for testing chemically rigidized expandable materials and structures for space applications, discussing resin impregnated glass fiber cloth 23 p4264 A70-45012

Nondestructive testing - Conference, Hanover, June 1970, Electric and magnetic methods 24 p4343 A70-45693

Nondestructive defectoscopic diagnostics, applying cybernetics to materials testing 24 p4344 A70-45694

Gamma ray nondestructive tests for materials defects, discussing cinematic, geometric and radiological factors effects on detection 24 p4337 A70-45711

Oscillating pendulum equipment for nondestructive material tests, determining longitudinal and transverse elastic moduli of specimen 24 p4338 A70-45738

Potentiometer application to nondestructive tests of materials, operation principles, methodology and advantages 24 p4338 A70-45739

Fluorescent penetrants vs magnetic powder test for individual and continuous material inspection, discussing sensitivity and surface finish influence 24 p4338 A70-45741

Metal and nonmetal thermal nondestructive tests based on surface temperature distribution produced by heat treatment 24 p4348 A70-45744

Fast neutrons for radiogenic nondestructive material testing, describing defectoscope performance, sensitivity and cost efficiency 24 p4377 A70-45851

Instantaneous corrosion rate measurement, comparing coupon, resistance and polarization methods 24 p4365 A70-46390

MATHEMATICAL ANALYSIS

U APPLICATIONS OF MATHEMATICS

MATHEMATICAL LOGIC

NT ALGORITHMS

NT BOOLEAN FUNCTIONS

NT EQUIVALENCE

NT FORMULAS [MATHEMATICS]

NT LATTICES [MATHEMATICS]

NT SET THEORY

NT THRESHOLD LOGIC

Majority logic decodability of product of two majority logic decodable cyclic codes 17 p3049 A70-34853

Polynomial and logic theories of dynamic systems, explaining linear and nonlinear elements of automatic control systems 19 p3392 A70-37447

MATHEMATICAL MODELS

NT DIGITAL SIMULATION

NT THOMAS-FERMI MODEL

Mathematical model coefficients determination for planar diffused transistor, obtaining admittance parameters 01 p0048 A70-10050

Hydrogen type exciton model applied to analysis of intermediate exciton state role in two quantum absorption in semiconductors 01 p0153 A70-10068

Mathematical model of spherically symmetric quiescent droplet undergoing quasi-steady vaporization near thermodynamic critical point 01 p0213 A70-10291

Mathematical model for vestibular nystagmus adaptation to subjective sensation of rotation, noting time constants 01 p0032 A70-10362

Mathematical models for perception and skilled action in man or machine, noting sensorimotor theory 01 p0034 A70-10498

Mission simulation mathematical modeling technology developed for optimization of experiment program management and operational planning for manned space station missions [AIAA PAPER 69-1065] 01 p0181 A70-10634

Mission model construction for power limited systems, discussing flight concepts, propulsion mixes and electric propulsion 01 p0183 A70-10848

Mathematical model for studying three dimensional whirling shaft stability as function of angular to critical velocity ratio, using Liapunov method for equations of motion 01 p0143 A70-10889

Binocular brightness mixing and autocorrelation function, discussing mathematical model, computer simulation and test results 01 p0025 A70-11053

Discrete models formulated for thermomechanical behavior of materials with memory, obtaining equations of motion and heat conduction for finite elements of nonlinear continua 01 p0208 A70-11183

Book on mathematical methods of reliability theory covering probability theory, statistics, Laplace transformation, set theory, testing, quality control, mass production, sampling, etc 01 p0133 A70-11308

Nervous stress effect on coronary thrombosis, deriving mathematical theory based on biophysical and biochemical approaches 01 p0028 A70-11369

Left ventricle confocal prolate spheroid model taking into account physiologic variations of thickness 01 p0040 A70-11373

Availability model for system with exponential reliability function and constant repair time, determining start-up costs, cost-optimal mean up and down time, etc 01 p0221 A70-11382

Dynamic characteristics of model of spacecraft-astromat-tether system during approach, deriving kinetic potential 01 p0192 A70-11587

Cost model based on initial and support costs for studying availability variations effect on system total cost and maintainability and reliability interrelationship 02 p0401 A70-11674

Electron loss in heavy body collisions from free scattering model and Born approximation 02 p0342 A70-11879

Premature saturation in strongly magnetic systems explained by model with nonuniform magnon modes, applying time dependent Green functions 02 p0338 A70-11886

Mathematical model for local postbuckling strength of flat truss core sandwich panels loaded in compression, considering application to Ti structures 02 p0386 A70-11948

Mathematical models construction for predicting and measuring air traffic controller workload, using synthetic and analytic methods 02 p0332 A70-11972

Three dimensional linear combustion instability in liquid propellant rocket motors using concentrated combustion model, presenting mathematical analysis as boundary value problem 02 p0353 A70-12011

Mechanical properties of human skull specified for construction of physical and mathematical models 02 p0243 A70-12097

Mathematical model formulated in terms of feedback controller for simulation of horizontal eye movement for positioning upon objects of interest 02 p0243 A70-12098

Computer simulation of automated air traffic control concepts, formulating and implementing generalized model of automated transition/terminal area systems 02 p0335 A70-12133

Automatic flight control systems with aerodynamic characteristic and control parameters deviation from nominal values, discussing mathematical model describing aerodynamic characteristics behavior 02 p0381 A70-12408

Mathematical elastodynamic model for parametric dynamic study of forced response solution of motion equations during head trauma 02 p0238 A70-12548

Analytical scoring model design for effective evaluation of competing research and development projects 02 p0402 A70-12634

- Incremental profit and total airline profit model programs for air cargo systems
[SAE PAPER 690413] 03 p0411 A70-12899
- Mathematical model for burning rates of solid propellant rocket motors during pressure transients, coupling conservation equations with mass balance equation
03 p0543 A70-12912
- Mathematical model for ejection fraction of human left ventricle incorporated with fiber orientation and ventricular geometry, showing consistent results with biplane angiocardigraphic films
03 p0433 A70-12975
- Decision model for R and D project selection
03 p0609 A70-12991
- Laminate approximation model of randomly oriented fibrous composites estimating stiffness and thermal and expansional strains
03 p0587 A70-13126
- Negative resistance mechanism model with larger electron accumulation in conduction band than free holes
03 p0539 A70-13212
- Terrain computerized mathematical model for determining unobstructed line of sight between observer and target
03 p0455 A70-14172
- Two loop control system model of human lens accommodative system derived on basis of muscle mechanics, optics and experiments
03 p0439 A70-14275
- Deformability calculation of two phase composite solid materials through laminated structural models
03 p0602 A70-14337
- Mathematical model for computer simulation of homogeneous neuron nets with recurrent inhibition control, considering activated and inactivated states
04 p0640 A70-14553
- Mathematical model based on equivalent electrical circuit for transient radiation analysis by computer (TRAC) family of circuit analysis programs, simulating semiconductor devices
04 p0657 A70-14737
- Turbine flowmeter theoretical model
[ASME PAPER 69-WA/FM-2] 04 p0689 A70-14841
- Mathematical model building for temporal human motor responses /reaction, movement, manipulation/ by response surface technology and statistical experimental design
[ASME PAPER 69-WA/BHF-5] 04 p0642 A70-14851
- Theoretical model of fan/compressor noise blade passing frequency generation and transmission, noting duct length and configuration in engine operation
04 p0734 A70-14886
- Electron scattering by molecules, demonstrating formal equivalence of fixed nucleus and free rotator scattering models
04 p0722 A70-14949
- Conducting fluid steady convection due to combined effects of thermal gradient and DC electric field predicted by analytical model
04 p0785 A70-14989
- Resonant compression waves in geomagnetic tail estimated for frequency and spatial distribution by single layered two dimensional model
04 p0680 A70-15127
- Geometrical model for characterizing instrument landing system (ILS)/ null reference glide path utilizing CW measuring system
04 p0716 A70-15330
- Solar powered communications spacecraft weight, electrical power and communication capacity models for optimizing size and launch vehicle fractionation
04 p0763 A70-15347
- Lifting rotor blades flapping response to atmospheric turbulence, discussing time averaging and perturbation schemes
[AIAA PAPER 69-206] 04 p0624 A70-15378
- Automated modeling and structure optimization of linear dynamic systems and circuits, using hybrid computer techniques and time-domain test data
04 p0654 A70-15452
- Flowfield and chemical kinetics model to calculate nitrogen dioxide chemiluminescence wake emission
[AIAA PAPER 68-702] 04 p0620 A70-15535
- Exchange perturbation theories applied to delta function model of molecular hydrogen ion, discussing EL-HAV second order energy at large internuclear separations
05 p0884 A70-15878
- Numerical integration of linearized two level forecast model to analyze behavior of accumulated error
05 p0878 A70-16153
- Burgers one dimensional model equation for homogeneous turbulence treated by Fourier transform in space and time, using Bogoliubov expansion method
05 p0833 A70-16331
- Hartree model to study superfluid He film bound to uniform substrate
05 p0883 A70-16469
- Miniature fluxgate magnetometer for sounding rocket measurements of two orthogonal components of external magnetic field, predicting performance by linear mathematical model
05 p0851 A70-16690
- Ball lightning mechanism proposal based on mathematical model for electric discharge current in parabolic plasma shell forming vortex-type storm front
05 p0879 A70-17021
- Mathematical model for investigating satellite thermal behavior in space based on space simulation in vacuum chamber with walls maintained at liquid nitrogen temperature
05 p0924 A70-17022
- Mathematical model of optimal partially closed life support system consisting of man, recycling unit, storage unit and waste disposal outlet
05 p0809 A70-17110
- Mathematical models for describing visual perception of distance to ground during VTOL landing and takeoff
05 p0810 A70-17119
- Hazards model for probabilistic prediction of casualties by exploding solid propellant rockets, deriving casualty expectation equation
[AIAA PAPER 69-461] 06 p1154 A70-17169
- Properties of unstable confocal resonator used with carbon dioxide-nitrogen-helium laser, using geometric models and measurements
06 p1079 A70-17188
- Kolmogoroff constant determined by Heisenberg turbulence formula and model for transfer of turbulent energy between different wave numbers
06 p1034 A70-17467
- Mathematical models for progressing waves diffracted by smooth surfaces
06 p1105 A70-17533
- Mathematical models describing interactions between rarefied gas atoms and solid surfaces
06 p1036 A70-17759
- Hyperstability conditions of model reference adaptive control systems, noting applications
06 p1026 A70-17966
- Mathematical model for testing theory of solar differential rotation maintenance by two dimensional turbulence
06 p1144 A70-18009
- Experimental data to define idealized thruster discharge model power efficiency limits, computing probabilities for excitation, ionization, propellant escape and wall interception of ions
[AIAA PAPER 70-177] 06 p1131 A70-18034
- Ammonium perchlorate deflagrations, determining intrinsic stability of one dimensional burning configuration based on flame structure modeling
[AIAA PAPER 70-123] 06 p1128 A70-18044
- Flow model for steady asymmetric vortex system shed from slender body of revolution in coning motion
[AIAA PAPER 70-52] 06 p0971 A70-18118
- Combustion characteristics of blended droplets composed of monopropellant and diluent, using theoretical model to predict life histories
[AIAA PAPER 70-7] 06 p1180 A70-18141
- Gas dynamic effects of reaction center in explosive gas mixture analyzed by model and numerical computation
[AIAA PAPER 70-147] 06 p1181 A70-18144
- Modified Maxwellian models for particle reflection in free molecular flow, correlating model parameters with gas-surface properties
06 p1110 A70-18259
- Model for impact behavior of elastic body at elastic half space, measuring gas molecule impulse exchange at metal surfaces
06 p1171 A70-18260
- Three dimensional model for high energy scattering of inert gas atoms from solid surfaces, calculating trapping, accommodation and flux and velocity distributions
06 p1110 A70-18261
- Statistical model based on kinetic and probability theories to determine drag coefficient of orbiting satellites
06 p1159 A70-18289
- Solar wind interaction with moon derived for model and compared with satellite data
06 p1147 A70-18291
- Moment methods for calculating modeled diffusion gas mixture shock waves using Monte Carlo method, discussing distribution function and flow pattern
06 p1050 A70-18336
- Molecular beam continuum model to determine structure of shock waves in diatomic gases, comparing calculated profiles with measurements in nitrogen
06 p1050 A70-18338
- Kinetic model equation for shock structures in rotationally relaxing gas with internal degrees of freedom
06 p1050 A70-18340
- Monograph on models of failure covering mathematical system reliability determination and relationship to physical nature of failures
06 p1171 A70-18394
- Black box modeling of linear integrated circuits for computer analysis in frequency domain
06 p1026 A70-18416
- Stochastic model of information handling centers as typified by document storage and retrieval derived for integral equation to determine expected primary store size
06 p1016 A70-18450
- Boundary value problems and Cauchy problem considered for mathematical model of turbulent motion in liquid or gas
07 p1252 A70-18671
- Dynamic response of gas lubricated radial sliding bearing from transfer function derived from pH linearized mathematical model of gas lubrication
07 p1290 A70-18739
- Multivariate linear model and robust estimators of parameters based on rank tests
07 p1323 A70-19027
- Mathematical models of vertical antennas of finite length and height, discussing signal strength and LUF determinations
07 p1240 A70-19167
- Optical activity theory based on Kirkwood independent group model using scattering matrix
07 p1334 A70-19264
- Thermoelasticity equations derived for regular systems of M bodies in dynamic and thermal interaction using nonlocal continuous model
07 p1407 A70-19381
- Mathematical model for oxygen tension changes in dogs brain tissues under hypoxia during altitude simulation
07 p1208 A70-19505
- Real plasma isotherms using three component /atoms, electrons, positive ions/ model in search for supercooled dense plasma
07 p1349 A70-19651
- Mathematical models for photogrammetric disposition in aerial photography
07 p1284 A70-19780
- Disturbances of air flow originating from small scale mountains using numerical model
07 p1330 A70-19799
- High attenuation quantum communication channel capacity based on mathematical model
07 p1335 A70-19864
- Freezing-mixing model for predicting plasma jet flow reactor yield development from analyses of thermochemical equilibrium, chemical reaction freezing and turbulent mixing
07 p1351 A70-19893
- Mathematical model for calculating radiative heat transfer from turbulent diffusing buoyant flame and predicting liquid fuel burning rate
07 p1425 A70-20008
- Automatic control system identification with respect to optimality criteria, mathematical models, computing techniques and input signals
07 p1247 A70-20029
- Wall boundary condition model modification applied to molecular beam-solid surface scattering, noting qualitative agreement with observed distributions
07 p1342 A70-20118
- Ground wave electric field intensity prediction model in EMC applications, discussing soil conditions and polarization effects
07 p1336 A70-20217
- Finite element models for nonlinear problems analysis in coupled thermoelasticity dynamical theory, deriving heat conduction equations from energy balance considerations
07 p1417 A70-20363
- FM spectral density model with applications to radio transmitter bandwidth estimation and interference analysis
08 p1456 A70-20473
- Mathematical model of extensive air showers, calculating lateral distribution of photoelectric component at all altitudes
08 p1560 A70-20598
- Stochastic programming models for flight scheduling within airlift system accounting for cargo uncertainties, using convex programming, linear programming codes, etc
08 p1600 A70-20605
- Radio waveguides with random inhomogeneities, studying mathematical models by orthogonalization method
08 p1457 A70-20723
- Human color vision simulation by mathematical and electronic analogs for photoelectric color measurement and eye resolution
08 p1450 A70-20727
- Deductive model of vision statics formulated for Grassman laws without using operation of color composition
08 p1450 A70-20729
- Alternative equipment maintenance procedures costs by combined discrete event and continuous system simulation, discussing additional model applications
08 p1466 A70-20927
- Model characteristics selection for dynamic system behavior simulation, studying characteristics variability extent without changing trajectory behavior dependence on parameter space
08 p1544 A70-20953

Pulse neurons random homogeneous networks macroscopic description, considering operation modes in terms of input frequencies and output pulse sequences 08 p1451 A70-21000

Vertical plane and axis symmetrical numerical models for cumulus convection of moist atmosphere, discussing initial conditions 08 p1536 A70-21025

Multistage axial compressor performance described by mathematical model based on maximum probability principle 08 p1558 A70-21190

Prandtl-Kolmogoroff model of turbulence with inclusion of second order terms for stress and velocity gradient not to vanish coincidently 08 p1484 A70-21458

Civil air transportation in India, using mathematical models to estimate optimal development and efficiency of future air traffic potential 08 p1601 A70-21544

Model for magnetic field-line reconnection in conducting incompressible fluid, determining maximum reconnection rate entirely by null point conditions 08 p1553 A70-21615

Auroral zone electrojet return current spatial distribution using idealized models for stationary state 08 p1491 A70-21718

Mathematical model for finite-density non-homogeneous Newtonian cosmologies, approximating solutions using coupled Vlasov-Poisson equations 08 p1581 A70-21740

Deuterium Lyman alpha line profiles generated from microwave powered lamp for experimental testing of two layer model characterizing emission line profiles 09 p1730 A70-22066

Optimal control mathematical modeling for dynamic systems under statistically indeterminate disturbances based on game theory and pattern recognition 09 p1653 A70-22141

Vibration theory damping using mathematical model emphasizing controlling response under steady state resonance and random excitation 09 p1769 A70-22238

Pulsar mathematical model accounting for pulse width, polarization and spectrum of emitted radiation 09 p1753 A70-22383

Damage model for materials failure prediction under cyclic loading developed for strain controlled cycle with hold time 09 p1774 A70-22588

Inner-shell ionizations by proton impact calculated for cross section using impulse approximation model, comparing results with Born approximations 09 p1732 A70-22781

Error analysis of position finding techniques using analytical model composed of equations describing position error differential relationships 09 p1724 A70-23045

Incompressible homogeneous fluid model in non-relativistic generalized gravitation theory using analytical solution 09 p1762 A70-23118

Mathematical model with straight wake airfoil to determine aerodynamic forces on oscillating rotor blades in hovering flight 09 p1605 A70-23222

Polynomial force model supplementing reduced gravity model in determining accuracy of near equatorial, near synchronous and near circular satellite orbits 09 p1762 A70-23256

Pressure oscillations in LOX pump inducer of J-2 machine, using semianalytical first order model with retarded time mechanism 09 p1693 A70-23257

Shock wave structure nonequilibrium kinetic model using Boltzmann and Navier-Stokes equations 09 p1662 A70-23306

Eddy penetration model for heat transfer from trailing face of cylinder in transverse flow 09 p1791 A70-23566

Discrete dynamic models construction using Gaussian quadrature formula with Jacobian weight, noting Raleigh function role 09 p1785 A70-23597

Equivalent oscillatory model defined from asymptotes of frequency response amplitude and cut-off frequency amplitude value of plane rigid airfoil in incompressible potential flow 10 p1953 A70-23841

Supersonic leading edge problem solved by ellipsoidal model using discrete ordinate method compared with BGK model solution 10 p1797 A70-23957

MGD model of plasma with dissipation due to finite electrical conductivity described by differential equations 10 p1922 A70-24144

Balancing method for correcting mathematical model discrepancy with gas turbine based on test data 10 p1930 A70-24289

Mathematical model for determining optimal control of spacecraft reentry into atmosphere 10 p1940 A70-24318

Error propagation in flowmeter calibration on model using empirical model-transmission equation 10 p1888 A70-24391

Control synthesis method using optimization technique to design controllers making closed loop system behave as ideal system or model 10 p1855 A70-24450

Pituitary hormone ACTH stimulatory effect on steroid hormone cortisol secretion by canine adrenal cortex, constructing seventh order state variable model 10 p1819 A70-24868

Hardware and system testing mathematical model assuming stochastic design and manufacturing defects detection and nondetection probability equations analogous to reliability function 10 p1896 A70-24915

Polynomial model of uniform target motion for smoothing and extrapolating coordinates and parameters using independent radar range and velocity readings 10 p1843 A70-25136

Educational satellite TV for developing countries, giving model relating economic development to education and applied technology 11 p2152 A70-25429

Turbulence model with level and scale functions for flows including homogeneous turbulence, logarithmic boundary layer, duct center flow, linear shear layer and viscous sublayer 11 p2035 A70-25685

Mathematical model for oxygen tension changes in dogs brain tissues under hypoxia during altitude simulation 11 p1987 A70-26104

Radiant heat transfer predictions between isothermal plates based on diffuse plus specular directional property model 11 p2149 A70-26157

Regression analysis of linear statistical model experiments with stationary Gaussian error of slowly varying spectral density 11 p2073 A70-26249

Ground testing apparatus with three degrees of freedom for artificial satellites attitude control systems, establishing mathematical model by digital and analog techniques 11 p2031 A70-26290

Human controllers nonlinear time domain mathematical model for analyzing compensatory tracking task data 11 p1992 A70-26396

Asymptotic model for stationary radiative stationary transitions using Newman-Penrose spin coefficient approach to gravitational radiation for Riemann spacetime 11 p2084 A70-26547

Discrete models for boundary value problems analysis in first strain-gradient elasticity theory, using extended finite element method 11 p2142 A70-26637

Turbulent reacting wakes properties prediction models validity, discussing Lagrangian formulations and eddy diffusivity and mixing models 11 p1978 A70-26772

Linville bipolar transistor model for computer-aided design programs 11 p2021 A70-26830

Mathematical model for rats nonlinear time-varying glucocorticoid secretion control mechanism, obtaining time dependent characteristics of hypothalamic-hypophyseal complex 12 p2174 A70-26893

Spectral discrimination technique for crops remote sensing, comparing statistical irradiance model with airborne multispectral scanner data 12 p2219 A70-26931

Mathematical model of microwave probe for reentry plasma, using variational method to calculate reflection coefficient 12 p2230 A70-26983

Lunar Orbiter spacecraft vibration responses based on mathematical models, comparing results with experiment 12 p2315 A70-27098

Limited frequency range analytical model for predicting mass and stiffness changes effect on natural frequencies and normal modes 12 p2317 A70-27121

Lumped linear model parameters determined from dynamic test data on mode shapes and frequencies for approximating distributed elastic structure 12 p2317 A70-27122

Composite reinforced materials similarity criteria to relate static and dynamic fields of various physical parameters, outlining mathematical simulation 12 p2259 A70-27526

Polymer shells lasting stability mathematical simulation, discussing similarity criteria of nonlinearly and hereditarily elastic materials 12 p2259 A70-27528

Euler-Bernoulli and Timoshenko beam impact models compared for case of finite beam resting on spring supports 12 p2327 A70-27843

Radiation transfer models for diffuse reflection of quanta from turbulent medium applied to electromagnetic wave propagation in turbulent atmosphere 12 p2306 A70-27855

Mathematical model for flow within external target type thrust reverser, assuming inviscid incompressible two dimensional flow [AIAA PAPER 69-3] 12 p2291 A70-28085

Bubble dynamics in subcooled nucleate boiling, deriving mathematical model based on evaporation-condensation mass transfer mechanism 12 p2333 A70-28113

Mathematical models for radar transmitters emission spectra envelopes calculation, considering effects of pulse width, rise and fall times, corner smoothing and frequency modulation 12 p2189 A70-28136

Shock wave formation and propagation analyzed by hydrodynamic model of two directional traffic flow based on continuity equations and velocity-density empirical relations 12 p2212 A70-28196

Elssasser and statistical band models in single parameter functions representing mean absorption in given spectral range 12 p2191 A70-28295

Rotating shaft model with slight curvature for estimating maximum bending moment through Fourier series analysis 13 p2416 A70-28372

Space information systems effectiveness evaluation based on generalized homomorphous model 13 p2372 A70-28377

Crosstalk effects on data transmission in multiplex TV systems for aerospace communications analyzed by signal and noise models 13 p2363 A70-28384

Admissible controls synthesis for closed loop system [satellite] stability 13 p2500 A70-28410

Hard sphere model for reactive molecular collisions based on energy and momentum of reactants and products 13 p2361 A70-28497

Configurations stress stability liquid propellant rocket nozzle analysis by BOSOR 3 digital program, describing mathematical model construction 13 p2508 A70-28509

Mathematical background for strong turbulence analysis in liquids and MHD 13 p2457 A70-28554

Mathematical models reproducing nonlinear mode interactions in CW bounded plasma devices 13 p2458 A70-28567

Sheath structure of plasma diode using kinetic theory model of plasma-sheath transition 13 p2376 A70-28642

Detonation model, discussing combustion gases from solid explosives detonation 13 p2520 A70-28803

Mathematical model for describing flow in Hele-Shaw cell, predicting attached viscous shear layers in lifting body wake 13 p2338 A70-28818

Automatic control systems for scientific experiments, considering algorithms, mathematical models and system designs 13 p2524 A70-28887

Radar cross section sea clutter model based on slightly rough surface superposition on swell structure 13 p2366 A70-29215

High temperature dislocation model based on dislocation dynamics, rate theory and varying back stress ratio 13 p2436 A70-29563

Cost effective spares provisioning models for airline operations, minimizing availability-cost ratio for line replaceable unit and total fleet 13 p2525 A70-29571

Tubular gas turbine combustors design by analytical model, summarizing theories of combustor analysis, turbulent flame speed, microvolume burning and stirred reactors [WSCIPAPER 70-2] 13 p2474 A70-29613

Mathematical models for human adaptive and optimizing characteristics in manual control systems regarding behavior phase 13 p2360 A70-29780

Fatigue damage accumulation deterministic models for predicting longevity 14 p2656 A70-30300

Solar wind interaction with moon, constructing mathematical model based on MHD equations and Explorer 35 data 14 p2630 A70-30356

Chromium lattice vibrational properties based on fourth-nearest-neighbor tensor force model, obtaining agreement with inelastic neutron diffraction data and elastic constants 14 p2626 A70-30480

Band and localized models for electrical conduction of metal oxides, discussing Mott and semiconductor to metal transitions 14 p2627 A70-30498

- Chemically reacting ideal substance model, describing thermodynamic properties and application to energy conversion processes 14 p2533 A70-30529
- Book on automation of mathematical description of controlled plants covering signal generation, information acquisition, statistical disturbance, self adaptive systems, etc 14 p2560 A70-30629
- Soviet collection of papers on automation theory and biological systems simulation covering game theory and mathematical models 14 p2542 A70-30630
- SCAMP 4 program for electronic circuits statistical analysis in frequency domain, obtaining mathematical models and transfer functions 14 p2561 A70-30667
- Mathematical model for interaction of solar wind with geomagnetic field, predicting magnetosphere shape 14 p2574 A70-30736
- Deterministic model for cost effectiveness of avionics support programs based on subsystems support ability, test philosophy and test equipment design and manufacture [AIAA PAPER 69-305] 14 p2563 A70-30857
- Book on space flight simulation systems examining real time and real performance requirements, mathematical models and various simulation programs 14 p2563 A70-30955
- Lunar near surface gravity estimation by mass density model for agreement between Doppler tracking data from Lunar Orbiter and trajectory predictions 14 p2645 A70-31064
- Availability assurance using computerized spare allocation model for optimal selection of sufficient spares to achieve required protection against system failures 14 p2592 A70-31114
- Stress-strain relationships model for nonlinear restrained cylinders, using compression tests and finite element method 14 p2660 A70-31135
- Synchronous satellite orbits determination using mathematical model for simulating gravitational perturbations induced by terrestrial globe and foreign bodies 14 p2651 A70-31279
- Aircraft design optimization by multisearch programs, considering mathematical model role 14 p2532 A70-31400
- Kinetic gas theory mathematical models, analyzing system of N particles in cube 14 p2601 A70-31422
- Boundary value problems and Cauchy problem considered for mathematical model of turbulent motion in liquid or gas 15 p2718 A70-31463
- Model for hydraulic resistance reduction for turbulent fluid flows by injecting suspended impurities 15 p2719 A70-31489
- Numerical model of diurnal variations of minor neutral constituents in mesosphere and lower atmosphere including molecular and eddy diffusion 15 p2727 A70-31909
- Stochastic medium mathematical model for loose medium motion in potential field of forces 15 p2821 A70-32342
- Kelvin wave propagation numerical model, showing influence of mean zonal wind vertical and horizontal shear in lower stratosphere 15 p2771 A70-32370
- Spacecraft thermal mathematical model adjustment to fit measured temperatures, using iteration method 15 p2812 A70-32513
- Nonlinear time-invariant lumped parameter dynamic systems, determining mathematical model by piecewise continuous power series expansions 15 p2768 A70-32576
- System maintainability stochastic modeling using probability density functions 15 p2748 A70-32670
- Mathematical reliability model for quasi-redundant electronic system with two failure modes for each component 15 p2769 A70-32827
- Mathematical-physical parametric model of satellite geodetic laser range accuracy, false alarm and count probabilities, correlating with retroreflector signal strength 16 p2863 A70-33166
- One dimensional controlled plants structure identification with mathematical model composed of aperiodic nonlinear and delay components connected in series 16 p2883 A70-33235
- Iterative weighted nonlinear least squares parameter estimation for human respiratory control system by transfer function modeling, comparing results with visual curve fitting 16 p2851 A70-33322
- Optimal fixed-form pilot model computer program for VTOL longitudinal control hover task evaluation 16 p2851 A70-33341
- Linear systems approximate minimum energy controller, suggesting algorithm for mathematical model evaluation 16 p2886 A70-33344
- Discrete stochastic optimal control model of human operator for single loop compensatory/pursuit tracking situation, considering application to manual control system design 16 p2852 A70-33463
- Angle modulated carrier acquisition and demodulation, developing baseband model for behavior of output signal from phase lock loop 16 p2864 A70-33481
- External burning fuels environmental temperature requirements from nonlinear droplet ignition model, emphasizing droplet size importance [AIAA PAPER 70-607] 16 p2997 A70-33604
- Numerical simulation of large scale atmospheric motions, considering pressure distribution, vorticity, kinetic energy, etc 16 p2946 A70-33625
- Resonant electron scattering processes in atoms and molecules, discussing mechanistic models and use in interpretation of experiments 16 p2955 A70-33798
- Liquid rocket propellant engine exhaust plume flow field, discussing mathematical models for combustion chamber, throat region and nozzle [AIAA PAPER 70-844] 16 p3001 A70-33927
- Model relating spectral reflectance to thermal control materials properties and environment induced changes 16 p2940 A70-33934
- Monte Carlo model of V groove surface roughness effects on directional reflections in plane of incidence, employing energy localization circle [AIAA PAPER 70-820] 16 p3002 A70-33944
- Mathematical model of heat flux absorbed by heated part in radiant heating reflector systems, considering shape, spectral, directional and polarizing effects [AIAA PAPER 70-818] 16 p3002 A70-33945
- German monograph on temperature distribution and motion of free burning arcs in transversal magnetic fields and gas flows, covering aerodynamic model concept 16 p2959 A70-34077
- Nonlinear wave equations model for human torso under impulsive stress, obtaining asymptotic solution 16 p2854 A70-34247
- Nonlinear mechanical lumped dynamic systems trajectory analysis in terms of P and G sets 16 p2944 A70-34285
- Mechanical vibrations models and analysis techniques, emphasizing problem of weak couplings in discrete systems 16 p2996 A70-34290
- Annoyance assessment for sonic boom series exposure near airport 16 p2843 A70-34325
- Analytical model for jet interaction induced separation of supersonic turbulent boundary layers, conducting flat plate tests at Mach 4 [AIAA PAPER 70-765] 17 p3007 A70-34486
- Probstein-Gold model for ablated materials crosshatching patterns, using interaction between inelastic deformable surface and supersonic turbulent boundary layer [AIAA PAPER 70-768] 17 p3009 A70-34504
- Frequency analysis of cylindrically curved panel with clamped and elastic boundaries, using mathematical and panel models 17 p3181 A70-34524
- Large complex system with standby components, approximating reliability by simple model substitution 17 p3099 A70-34582
- Direction finder for point source signals, discussing mathematical model for random noise in space, S/N performance and equipment design 17 p3042 A70-34586
- Stratified-rotating fluids mathematical analogy, examining flow constraints, parameters and variables 17 p3068 A70-34664
- Weather prediction models, describing equation systems, roles of friction and heating, meteorological data analysis, fronts, convection, etc 17 p3132 A70-34668
- Horizontal gravity gradient components in outer space from Stokes function expansion, using sphere as model 17 p3154 A70-34682
- Model diffusion equation for inhomogeneous incompressible turbulent flow, applying to free turbulent flows 17 p3069 A70-34825
- Gaussian source model of image, deriving rate distortion function under mean square error criterion 17 p3049 A70-34857
- Vibrating structure mathematical model for predicting radiated noise level 17 p3187 A70-35169
- Bipolar transistor behavior identification and characterization in static regime, discussing measurement methods for parameters of IBIS model 17 p3054 A70-35414
- Transient heat and mass transfer in adiabatic regenerator, solving mathematical model in terms of Green functions 17 p3197 A70-35542
- Closed compartment fire mathematical model to analyze combustion parameter effects, atmosphere pressure and temperature during fire 17 p3198 A70-35646
- Mathematical model for short term adaptation effects in human semicircular canal response to rotation, discussing nystagmus 18 p3216 A70-35940
- Ideal fluid contained in half space with circular or strip-like aperture, formulating mathematical model to determine sloshing frequencies 18 p3238 A70-36057
- Left ventricle pumping function self regulation mathematical model, obtaining transfer function 18 p3217 A70-36080
- Astatic gyroscope subjected to steady random translational vibration, optimizing parameters by mathematical model 18 p3257 A70-36136
- Mathematical model of asteroidal evolution and meteoritic mass distributions under collisional fragmentation using power law 18 p3312 A70-36213
- Dynamic numerical weather forecasting based on balanced model consisting of closed system of equations 18 p3284 A70-36232
- Mathematical model of three dimensional separated flows with applications to small aspect ratio delta wing and flat plate 18 p3207 A70-36438
- Mathematical simulation of human thermoregulatory system, considering automatic control theory 18 p3224 A70-36530
- Autoignition, ignition and surface temperatures of M-2 double base propellant at low pressure, correcting thermocouple measurements by theoretical model 18 p3299 A70-36697
- Fuel cell cavities, analyzing fluid motion purge dynamics based on anisotropic porous media model 18 p3216 A70-36766
- Magnetohydrodynamic calculations, discussing various models, difference methods, codes, boundary conditions, etc 18 p3296 A70-36794
- Book on crack problems in classical theory of elasticity, emphasizing mathematical aspects 19 p3534 A70-37234
- Optimal control for one dimensional compressible gas flow, combustion and heat exchange, described by first order partial differential hyperbolic equations 19 p3402 A70-37240
- Asymptotic high energy behavior of Feynman integrals in scalar field theory models for elastic scattering 19 p3457 A70-37549
- CdTe nonlinear electro-optical susceptibility predicted by mathematical model using two coupled anharmonic oscillators 19 p3485 A70-37668
- Mathematical representation of heart muscle mechanical properties, examining tensile stress in parallel and series elements 19 p3368 A70-37809
- Thermoelastic composite materials, deriving crystal lattice type model of equations for predicting dynamic or thermomechanical behavior 19 p3540 A70-37958
- Blast loaded cylindrical shell collapse hinge dynamic instability prediction by mathematical model 19 p3545 A70-38334
- Lumped parameter model for multidimensional solid mechanics problems with inelasticity, discussing stress wave interaction in cylindrical cavity 19 p3458 A70-38357
- System with N independently failing subsystems minimum cost solution mathematical model based on opportunistic preventive replacement policy 19 p3437 A70-38400
- Pop-in fractures analyzed by semiquantitative model, establishing relationship between pop-in length, stress intensity factor and crack-front plastic deformation 19 p3549 A70-38626
- Operational analysis and real time computer simulation models in ATC development 19 p3468 A70-38637
- Multidimensional decision models for optimal control, using piecewise constant functions 19 p3394 A70-38679
- Rarefied gas viscoseals performance prediction by theoretical model, comparing results with experiment [ASLE PREPRINT 70AM SC-3] 19 p3439 A70-38806
- Weather occultation satellite orbit determination by radio wave measurements between master and slave satellites, formulating mathematical model [AIAA PAPER 70-1067] 19 p3529 A70-38880
- Oscillatory flow in turbulent boundary layer modeled by eddy viscosity distribution, deriving mass

transport velocity induced by progressive and standing waves 20 p3608 A70-39358

V/STOL aircraft automatic flight control, guidance and navigation by onboard computer, discussing mathematical model and simulation results [ALAA PAPER 70-1035] 20 p3665 A70-39502

Category II longitudinal approach system model taking into account inputs, gusts, ILS beam noise, man machine interaction, etc [ALAA PAPER 70-1034] 20 p3665 A70-39503

Fluidic inertial platform feasibility model for air to surface missile line-of-sight guidance, noting cost, reliability and environmental advantages [ALAA PAPER 70-1009] 20 p3667 A70-39523

Highly constrained optimal control problems, using nonlinear programming in mathematical model for trajectory optimization 20 p3600 A70-39565

Self adaptive system with standard model, using direct loop amplification factor as controlled parameter 20 p3603 A70-39832

Computer calculations automation in mathematical models construction by statistical methods, discussing programs for distributed parameter systems, stochastic approximation, etc 20 p3592 A70-39903

Stochastic approximation iterative algorithms for multivariable plants mathematical models, including steepest descent method 20 p3593 A70-39910

Generator for modeling random processes with given statistical parameters 20 p3593 A70-39915

Variable wing sweep aircraft angular motion mathematical model, analyzing inertial moments influence on control dynamics 20 p3562 A70-40182

Lunar based astronomical research program logistics model taking into account scientific mission, launch vehicle capacities, supply and support requirements, etc 20 p3710 A70-40336

Predictive model for potential variance from planned schedule of R and D tasks to minimize risk in management 21 p3955 A70-41172

Subjective probability estimation for R and D decision making, using analytical models incorporating risk and uncertainty 21 p3955 A70-41175

Regulated spacecraft solar array mathematical model for high voltage power supply regulator analysis 21 p3757 A70-41208

Mathematical model for projectile penetration into metallic targets, calculating velocity after perforation 21 p3939 A70-41968

Ablative response predictions analytical tools, discussing boundary layer edge conditions definition, atmospheric entry, rocket propulsion, etc 21 p3952 A70-42055

Computerized evaluation of Krook kinetic relaxation equation approximating Boltzmann nonlinear integral equation for rarefied gas motion 21 p3851 A70-42201

Relative pressure and excitation induction transverse distribution relationship for MHD machine model, assessing dimensionless criteria effect on pressure peaks position 21 p3760 A70-42232

Internal gravity waves mathematical model for atmosphere with arbitrary distributions of temperature, molecular weight, viscosity and conductivity, deriving wave propagation into thermosphere 21 p3821 A70-42257

Spoiler theory based on mathematical model, using two dimensional potential theory in conjunction with experimental data on wake phenomena 22 p3957 A70-42273

Fluidic amplifier with axisymmetric jets, deriving approximate mathematical model for static no-load operation [ASME PAPER 70-FLCS-4] 22 p3964 A70-42427

Viscoelastic liquids state equations, surveying various fluid models 22 p4009 A70-42541

Two dimensional incompressible flow, calculating strong suction effects on laminar boundary layer separation by linear model 22 p4010 A70-42630

Lagrange formulation for deriving energy conserving numerical approximations for Vlasov plasmas 22 p4080 A70-42750

Mathematical model of heart beat control during muscular activity in aging individuals, reflecting neutral and hormonal control circuits 22 p3969 A70-42901

Mathematical model avoiding repetitive tests costs for Nerva nuclear rocket engine 22 p4070 A70-43179

Shock wave formation and propagation analyzed by hydrodynamic model of two directional traffic flow

based on continuity equations and velocity-density empirical relations 22 p4012 A70-43321

Collision integral model for multicomponent mixture, investigating partially ionized plasma longitudinal vibrations 22 p4083 A70-43382

Discrete decision variable models formulated as linear integer programs, deriving shrinking boundary algorithm for optimization 22 p3994 A70-43497

Sequential experiments design and model discrimination, comparing Chernoff and Box-Hill approaches 22 p4064 A70-43527

Vortex induced vibration problems, deriving mathematical model for periodic lift on circular cylinder 22 p3960 A70-43546

LF passband ideal filter instantaneous pulse response, using delta function model 22 p4005 A70-43555

STOL system traffic analysis simulation model for interurban transportation system as tool for flight hardware evaluation 22 p4007 A70-43731

Gunn effect, comparing intervalley scattering model to diffusion model for dynamic domain equilibrium 23 p4229 A70-43794

Scale invariance models correlation with cosmic ray data, comparing neutrino- and antineutrino- nucleon scattering 23 p4210 A70-43800

Computerized mathematical modeling of transistors statistical and dynamic characteristics as functions of structural parameters 23 p4171 A70-43954

Mathematical models derivation for systems of interconnected elastic segments, using variational method and energy summation via difference equations 23 p4266 A70-44019

Geomagnetic field behavior prediction based on extrapolation of magnetic data collected by observatories and dipole model approximation 23 p4189 A70-44068

Wind tunnel wall interference effects for V/STOL aircraft with lift jets, using modified theoretical model for complex jet arrangements [ICAS PAPER 70-54] 23 p4139 A70-44150

Functions of two variables, using digital method for curve family modeling 23 p4166 A70-44350

Closed cell polyurethane foam for cryogenic insulation, determining thermal conductivity and net heat flow by analytical model and test 23 p4280 A70-44367

Electromagnetic ground wave propagation, deriving exact solution from two dimensional cylindrical earth model with any number of homogeneous sections 23 p4164 A70-44405

Gyro drift rate mathematical modeling based on stationary and nonstationary time series analysis techniques with random process reduction to white noise residuals [ALAA PAPER 69-838] 23 p4197 A70-44557

ESRO 1 satellites attitude reconstruction, describing torque determination from known altitude 23 p4259 A70-44614

Antenna radiation pattern modeling by power optimization under constraints 23 p4175 A70-44800

Mathematical model simulating human respiratory physiopathology, based on hypothetical stable autooscillations dependence on ventilation/ pulmonary exchange system 23 p4155 A70-44859

Biological life support systems mass exchange processes analysis based on mathematical models, predicting artificial ecological systems stability 23 p4149 A70-45029

Gravitational field fine structure representation near earth surface as sum of global model in spherical harmonics and local model in harmonic B functions 24 p4328 A70-45287

Mathematical modeling of atmospheric gusts in stratosphere, mountain wave and thunderstorm conditions relevant to aircraft design 24 p4371 A70-45420

Mathematical model for plasma expansion resulting from short energy pulse absorption 24 p4387 A70-45799

Simplex lattice mathematical models of solidus volume for quaternary Nb-W-Ti-Zr system 24 p4361 A70-45833

Short haul transportation needs in multimodal transportation systems planning, discussing modeling in Northeast Corridor Project [ALAA PAPER 70-1265] 24 p4431 A70-45925

Air traffic flow digital computer simulation model including departure, enroute and arrival phases for collision avoidance, weather effects and control constraints [ALAA PAPER 70-1316] 24 p4373 A70-45945

Weather regimes in statistical meteorology constructed in stochastic models representing randomly transformed Markov chain 24 p4371 A70-46035

Aircraft maintenance cost statistical analysis recursive regression model for aircraft failure and manhour cost data 24 p4292 A70-46125

Mode locked laser pulses picosecond structure predicted from theoretical model of Gaussian random radiation field with temporal envelope modulation 24 p4355 A70-46263

MATHEMATICAL STATISTICS U STATISTICAL ANALYSIS

MATHEMATICAL TABLES
Beginning of table calculations using difference methods for numerical integration of ordinary differential equations 13 p2440 A70-28960

MATHEMATICS

Philosophical problems arising in contemporary and modern mathematics, discussing metaphysics and psychology 07 p1327 A70-19787

Lectures on forms in many variables covering Chevalley-Waring and Lang-Nagata theorems for finite and function fields, discrete valuation rings, etc 13 p2441 A70-29454

MATHIEU EQUATION U MATHIEU FUNCTION MATHIEU FUNCTION

Mathieu equation with nonlinear terms for damping and restoring forces, investigating first order instability region 18 p3337 A70-36224

Boundedness theorem for nonlinear Mathieu equation describing motion of parametrically excited system 24 p4380 A70-46042

MATRICES

Fiber-matrix interface mechanics in composites, considering shear strength, stress distribution, fiber strength effects, etc 01 p0127 A70-10479

MATRICES (CIRCUITS)

Electroluminescent matrix displays, discussing limitations in control element 05 p0827 A70-16186

N-port resistive networks synthesis from terminal conductance matrices with two-tree port structures 06 p1023 A70-17426

Resolution, contrast and gray scale performance of CRT displays compared to dot matrix displays 08 p1500 A70-21763

Integrated image sensor matrix array derived from equivalent circuit to minimize sneak path effects 10 p1854 A70-23879

Electro-optical light modulators representation by two port matrices, deriving amplitude modulation methods 13 p2427 A70-28924

Microwave circular array with electronic beam rotation of patterns by applying linear phase tapers to Butler matrix feed 16 p2874 A70-33393

Four dimensional matrix type CRT decoder characterized by large storage capacity and high resolution 18 p3256 A70-36105

Matrix condenser for tuning hybrid thin film self excited quartz oscillator with common base transistor configuration, discussing electrical properties and fabrication 20 p3597 A70-39257

Admittance matrix of microwave networks, referring to coaxial line-waveguide coupling through 3 kMc adapter 21 p3802 A70-42250

Reprogrammable read-mostly memory /RMM/ using integrated circuit array of amorphous and crystalline semiconductor devices, discussing design and applications 22 p3996 A70-42772

One dimensional cellular logic arrays fault circumvention by bypass switching out defective cells in cascade 22 p4004 A70-43073

Optical read-write mass memory based on holographic storage and light addressable matrix array, discussing significance to computer design and usage 22 p3994 A70-43606

MATRICES [MATHEMATICS]

NT ADJOINTS

NT CANONICAL FORMS

NT EIGENVALUES

NT EIGENVECTORS

NT JORDAN FORM

Mappings of linear vector spaces induced by transformation matrix applied to linear dynamical systems 01 p0132 A70-11125

Square root filters algorithms based on covariance and invariance matrices extended to include process noise effects 01 p0144 A70-11193

- Algorithm for algebraic matrix Riccati equation, using Fletcher-Powell reformulation of Davidson function minimization 02 p0324 A70-12604
- Homogeneous waveguide solutions by finite element method using matrix operator and function minimization to assure rapid convergence to eigenvalue 03 p0457 A70-13936
- Complete solution of fifth order Runge-Kutta equations in condensed matrix form, considering coefficients of linear dependence 04 p0714 A70-15047
- Plan hybrid element generalized to arbitrary quadrilateral form, considering hybrids having constant and linear stress distributions 04 p0779 A70-15614
- Optimally ordered triangular factorization for solving symmetrical systems of linear matrix equations 05 p0876 A70-16573
- Computational algorithm for fast Hadamard matrix transform of order 12 via factorization 06 p1093 A70-17314
- Matrix Computer equisolution matrices for non-linear algebraic and integrodifferential equation systems solution 06 p1014 A70-17427
- Liapunov functions generation by matrix transformation of state-space system vector applicable to linear and nonlinear systems 06 p1023 A70-17544
- Frontal solution program for symmetric positive definite equations met in finite element applications 06 p1014 A70-17936
- Nonnegative matrices characterization by diagonal products to imply properties of stochastic matrices 06 p1094 A70-17950
- Boundary conditions and iterative procedures for plasma sheath problems, using matrix equation to represent differenced Poisson equation 06 p1123 A70-18295
- Rayleigh phase matrix solutions and albedo values for imperfect Rayleigh scattering in semiinfinite planetary atmosphere 06 p1149 A70-18460
- Capacity calculation of N identical discrete memoryless nonsingular channels cascade, discussing dependence on eigenvalues and eigenvectors of subchannel transition matrices 06 p1013 A70-18628
- Space vehicle digital control system attitude computations using quaternion matrix algebra to simplify control equations [AIAA PAPER 68-825] 07 p1393 A70-19302
- Matrix graph concept to unify signal-flow, flow- and N-graph technique approaches to representation and evaluation of matrices and linear algebraic equations 07 p1238 A70-19676
- Time-variable constrained control matrix optimization using Pontryagin principle applied to minimal time transfer, payoff and rotation maximization 07 p1247 A70-20024
- Time dependent matrix elements for multistate impact-parameter calculations for atom-atom inelastic cross sections 07 p1346 A70-20242
- Separable potential with hard core effects, treating short range repulsion in nucleon-nucleon interaction, generating T matrix for existing data 09 p1725 A70-22042
- Eigenvalues and eigenvectors evaluation for real symmetric matrices by iterating simultaneously with trial vectors 09 p1641 A70-22283
- Matrix multidimensional singular linear integral equation applied to electromagnetic radiation transfer through stratified atmosphere 09 p1711 A70-22349
- Numerical algorithms for solving Liapunov matrix equation in nonlinear stability analysis and optimal systems design 09 p1641 A70-22959
- ALGOL modified Gaussian algorithm for geodetic calculations, combining matrices for storage place economy 11 p2013 A70-25797
- Time-invariant linear dynamical systems transfer equivalence leading to algorithm for minimal realizations of transfer function matrices 11 p2072 A70-26161
- Invariance conditions and state transition matrix of linear systems 11 p2074 A70-26400
- Finite element bending stress analysis of thin rectangular and skew plates, discussing computational procedure generating stiffness matrices 11 p2143 A70-26641
- Transfer matrix spectrum for lattice gas models with finite interaction, constructing stochastic operator as stochastic matrices limit 12 p2272 A70-27343
- Transition matrix of Markov chain with finite states from noisy measurements of state, discussing algorithms convergence rates and computations 12 p2261 A70-27421
- Closed product form and simplified algorithm for efficient operation of generalized Kronecker matrices, considering role in spectral analysis 12 p2193 A70-28029
- Terminal constraints affecting matrices comprising linear impulsive guidance law for earth approach, discussing Mars mission 13 p2447 A70-28516
- Relationship between fundamental matrices of solutions to boundary value problems of parabolic and elliptical systems with Bessel functions 13 p2441 A70-29314
- Boundedness of solutions and higher derivatives for degenerate matrices, showing dependence on characteristic numbers and linear groups 13 p2443 A70-29744
- Price estimate elements interrelationship using three dimensional matrix for computerized cost data extraction 14 p2668 A70-30524
- Grassmann manifold projective transformations into itself, considering matrix theorems 14 p2601 A70-31423
- Axisymmetrical boundary value problem solution by net point method via transformation into self adjoint second order elliptic equation, obtaining positively determinate matrix 15 p2767 A70-31588
- Floquet-Liapunov theorem matrix representation derivation, improving accuracy of Liapunov classical representation 15 p2774 A70-31643
- Polarized light scattering angle relationship with Mueller matrix elements for polydisperse systems of irregular randomly oriented particles 15 p2775 A70-32040
- Multidimensional linear stationary systems controllability and observability with given transfer matrix 15 p2716 A70-32345
- Liapunov functions direct generation by state space system vector matrix transformation 15 p2768 A70-32555
- Combinational logic cells cellular arrays synthesis, considering truth table and transition matrix 15 p2712 A70-32606
- Adaptive Kalman filtering with unknown process and measurement noise covariance matrices 16 p2880 A70-32983
- Laser beam anticorrelation after attenuation by two photon amplifier, deriving density matrix in time dependent perturbation theory 16 p2928 A70-33283
- Linear multivariable feedback control systems design method based on transfer matrix, testing decoupling desirability 16 p2884 A70-33318
- Systems consisting of redundant and different modules, deriving vector and matrix expressions for effectiveness 17 p3099 A70-34581
- Lifting rotor blade motions stability computation using Floquet transition matrix 17 p3009 A70-34726
- Liapunov functions synthesis for aperiodic linear systems by inspecting traces of state matrix and products 17 p3129 A70-34955
- Matricial group representation theory for constructing elastic vibration equations of symmetric flexible mobile controlled members 17 p3180 A70-35293
- Parameter analysis of dynamical systems by matrix approach, using n-dimensional parameter space 17 p3130 A70-35300
- Hurwitz matrix of real Hurwitzian polynomial, discussing relation between eigenvalues and zeros locations 18 p3279 A70-36062
- Eigenvalues of transfer matrix and vibrations generation for passive mechanical systems with n degrees of freedom based on Laplace transformation 18 p3337 A70-36225
- Communication modulation systems unified description by conversion and indication matrices 18 p3229 A70-36942
- Nontrivial eigenvalues of stochastic matrices 19 p3456 A70-37414
- Feedback regulator synthesis for linear time invariant dynamic system with quadratic performance index, using computer algorithm for algebraic Riccati matrix equation 19 p3395 A70-38937
- Covariance matrices estimates for trajectory parameter tracking of thrust-maneuvering spacecraft [AIAA PAPER 70-1017] 20 p3666 A70-39516
- Kalman filter sizing for air-launched tactical missile via covariance sensitivity matrix [AIAA PAPER 70-954] 20 p3601 A70-39574
- Automatic digital device for evaluating matrix determinants 20 p3591 A70-39788
- Linear multivariable feedback control system, deriving conditions for existence of triangular decoupling transfer function matrices 20 p3605 A70-40118
- Rational polynomial matrices inversion by automatic computational procedures, considering Gaussian elimination and Faddeev algorithm 22 p0462 A70-42926
- Matrix transformations and minimization of computation algorithms for arbitrary linear equations systems, using direct methods 22 p0463 A70-43479
- Digital computer constructed with diodes and transistors logic for evaluating matrix determinants and minors 23 p4166 A70-43955
- Sufficient condition for bounded solution of matrix Riccati differential equation 23 p4212 A70-44896
- Large element method for stiffness matrix order reduction in two-dimensional continua problems 23 p4275 A70-44940
- Electromagnetic scattering by homogeneous gyrotropic cylinder, discussing matrix equations formulation and solution by reciprocity theorem 23 p4165 A70-44959
- Heat conduction problems numerical solution, using hypermatrices 24 p4428 A70-45127
- Matrix-vector computer program for three dimensional perspective projection and shell analysis in FORTRAN IV 24 p4419 A70-45155
- Successive iterative solution for large matrix equations reduced from Fredholm integral equations of second kind 24 p4369 A70-45164
- Approximate N-representability of density matrix by set of spin geminals 24 p4378 A70-45259
- Real matrix stability determination by right half plane eigenvalues, using symmetric solution of Liapunov equation 24 p4370 A70-46098

MATRIX ALGEBRA

U MATRICES [MATHEMATICS]

MATRIX ANALYSIS

U MATRICES [MATHEMATICS]

MATRIX METHODS

- Matrix method applied to achromatic linear phase plates design for polychromatic Ar lasers half wave phase shift 01 p0113 A70-10988
- Transfer matrix method analysis of dynamic behavior of beam structures applied to single rows of aircraft panels 01 p0209 A70-11200
- Finite element bending stiffness matrices for deflections analysis of pretwisted cantilever plate subjected to static loads 02 p0384 A70-11858
- Stiffness matrix derivation for curved beam emphasizing uncoupled normal to plane loads 03 p0584 A70-12949
- Stress-strain state of perforated shallow shells with arbitrary curvature using Green matrices 03 p0591 A70-13416
- Nonlinearity sources in elastic structures under large displacements, developing general matrix formulation 04 p0768 A70-14748
- Pressure vessel deformation and stress analysis by matrix displacement method, considering solids and membrane shells under axisymmetric and asymmetric loading [ASME PAPER 69-WA/PVP-3] 04 p0768 A70-14790
- Matrix analysis of steady state temperature field and heat flux through multilayer, plane, cylindrical or spherical partitions with internal heat sources 04 p0785 A70-14924
- Axisymmetric structures under load and temperature distribution analyzed by matrix displacement method [DGLR-69-62] 04 p0774 A70-15167
- Coefficient matrix-structural method for obtaining transfer function of linear automatic control systems 04 p0662 A70-15277
- Fundamental matrix asymptotic forms obtained for supersonic and subsonic three dimensional steady flows past body in uniform stream of viscous thermally conducting fluid 04 p0673 A70-15320
- Stiffness and mass matrices of free-free vibration structure reduced to eliminate zero frequencies 04 p0778 A70-15553
- Matrix algorithm from parallel element method derived for reducing computer time required in structural modification analysis 04 p0779 A70-15589
- Plan hybrid element generalized to arbitrary quadrilateral form, considering hybrids having constant and linear stress distributions 04 p0779 A70-15614
- Computational procedures for matrix analysis of stability and vibration of thin flat rectangular plates in longitudinal compression 05 p0927 A70-16010

Solar system resonant structure probability analyzed by matrix methods 05 p0910 A70-16397

Convergence of eigenvalues and eigenvectors in torsional vibration problems of continuous systems via improved matrix displacement analysis using points of freedom in segments 05 p0939 A70-16502

Monograph on computation of density functions of parameters in stochastic systems, giving algorithms involving only matrix computations of fixed dimensionality 06 p1093 A70-17730

Matrix method for calculating aerodynamic loads, shearing forces, bending moments, torques, etc, in hinged main rotor helicopter blades during hover and vertical flight 06 p1167 A70-17914

Green function of region near circle approximation by matrix method, considering Laplace differential equation solution, conjugate harmonic function and conformal transformation 07 p1253 A70-18924

Ideal fluid planar potential flow, approximating stream function and velocity potential by matrix method 07 p1253 A70-18925

Soviet book on matrix methods in relay and sampled data control theory described by linear differential and finite difference equations 07 p1244 A70-19069

Green matrices construction for joint shells by method of arbitrary constants variation, considering strained state symmetrical with joint lines 07 p1413 A70-20144

Automatic system of kinematic analysis (ASKA), based on matrix displacement finite element method, applied to structural strains calculations 07 p1417 A70-20362

Matrix method for converting time variable stress vector into strain vector allowing for linear creep and aging 08 p1583 A70-20531

Prismatic thin walled shells with box type cross section under torsion using Vlasov variational method in conjunction with transfer matrices 08 p1589 A70-21248

Matrix method for maximizing radar antenna directive gain and simultaneously placing nulls in far field radiation patterns 08 p1477 A70-21758

Matrix decomposition and full release methods for substructure analysis 09 p1770 A70-22258

Artifices to allow computing time reduction in recursive data elaboration for high order differential system 09 p1720 A70-22647

Forced vibrations of cylindrically curved multispan shell structures, using transfer matrix methods 10 p1962 A70-25062

Complex redundant structures matrix analysis by substructure approach, obtaining elastic properties of system by subdivision and synthesis [SAE PAPER 700217] 11 p2134 A70-25889

Finite element matrix structural analysis by direct stiffness method and use of computers, considering thin wall box beams [SAE PAPER 700218] 11 p2134 A70-25890

Finite element method using shallow shell stiffness matrix extended to cylindrical shell solution 11 p2138 A70-26159

Vector-matrix differential equation for second order sensitivity coefficients applied to trajectory optimization, modeling and compensation and guidance and control 11 p2029 A70-26324

Finite element solution procedures for inextensible beams elastica problem, using galerkin method for element stiffness matrices 11 p2143 A70-26640

Nonuniform beam element stiffness matrices for dynamic and elastic instability analysis, determining frequencies, mode shapes and critical loads 11 p2143 A70-26643

Vibrating thin beam cross sectional displacement-force equations coefficients included in coefficient matrix, considering shear deformation and rotary inertia effects on vibration modes 12 p2324 A70-27397

Shear deformation of sandwich plate cross sections with hinged opposite edges, constructing transfer matrix for state variables 13 p2508 A70-28483

Derivation procedure for dynamic flexibility matrix including material damping for triangular plate in bending, twisting and shear 13 p2509 A70-28540

Elastoplastic thermal stress analysis using finite element matrix method exemplified by cylindrical bar induction quenching 13 p2513 A70-28992

Stiffness matrices of three dimensional finite elements, considering tetrahedron, hexahedron and nodal configurations 14 p2659 A70-31127

Thin shells stiffness matrix and shear by finite curved triangular elements based on discrete Kirchhoff hypothesis 14 p2659 A70-31129

Matrix analysis of discretized dynamical system with constraints, considering case of damped oscillators 15 p2774 A70-31697

Stress-strain vector for straight bar of constant or stepwise cross section, using initial parameter matrix method 15 p2822 A70-32363

Shells of revolution nonlinear finite element analysis by matrix displacement method, including higher order strain energy terms 16 p2991 A70-33885

Twisted uniform beam element flexibility and stiffness matrices, using continuous bending theory 16 p2894 A70-33887

Nonlinear dynamic systems described by matrix equation, formulating asymptotically stable conditions, discussing motion equations of two degree of freedom system 16 p2995 A70-34281

Elastic and equilibrium matrices for semimonocoque membrane /plane stress/ elements using skin and reinforcing member transformations 17 p3185 A70-34921

Structure of flexural members, analyzing torsional and lateral stability by finite element method and matrix formulation 18 p3339 A70-36494

Matrix filtering method for stability solutions of shells and plates by finite difference method 18 p3341 A70-36580

Automatic matrix method for vibration modes of large structures with multiple degrees of freedom 18 p3342 A70-36684

Stiffness matrix correction for curved element deficient in rigid body motion 18 p3342 A70-36687

Covariance matrix of mean square response in structural systems under white noise 19 p3536 A70-37702

Finite element stiffness matrix technique for composite structures, discussing airplane component design program 20 p3730 A70-40040

Spacecraft principal inertial axis orientation estimation, comparing tangent 2 theta method with eigenvalue solution [SAWE PAPER 847] 20 p3660 A70-40361

Natural flexural vibration frequencies of bars with periodic thickness variations, comparing Hamilton principle, matrix approach and experimental investigations 20 p3735 A70-40536

Skew panels supersonic flutter and vibration calculated by matrix displacement method 21 p3933 A70-40586

Free vibration optimization analysis by reducing stiffness and mass matrices 21 p3933 A70-40587

Structural stability analysis by matrix decomposition and iteration, extending to structures with nearly equal critical loads 21 p3934 A70-40888

French book on strength of materials covering potential energy theory, cutoff and matrix methods, computer calculations, etc 22 p4119 A70-43623

Structural eigenvalue problems solved by sparsely populated matrices for structural vibrations and critical buckling, using finite element method 23 p4271 A70-44708

Finite beam element in bending, deriving shear deflection terms in stiffness matrix based on stress assumption 23 p4274 A70-44909

Feed voltages and directional gain maximization for loaded long thin-wire antennas with multiple excitations, using matrix methods 23 p4176 A70-44972

Dynamic structural stability analysis, describing integral equation matrix technique 24 p4419 A70-45156

German monograph on deformations and tensile stresses calculation in axisymmetric bodies via finite element method involving matrix displacement method 24 p4420 A70-45225

MATRIX STRESS CALCULATION U MATRIX METHODS MATRIX THEORY

Trench algorithm for Toeplitz matrix inversion, presenting proof for nonHermitian matrices case 01 p0131 A70-10456

Book on theory of matrices covering linear spaces, matrices algebra, linear algebraic equations, varia-

tional method, position vectors, perturbation theory, eigenvalues, etc 01 p0133 A70-11323

Noniterative algorithm for generalized inverse of arbitrary rectangular matrix computation 02 p0387 A70-11996

Element relations of phase transformation matrix for scattering, relating radiation field vector to scattered field vector 02 p0339 A70-12283

Matrix elements of nonadiabatic perturbation emphasized in semiempirical theory for evaluating polyatomic molecules radiationless rate constants in terms of electronic-vibrational state 04 p0722 A70-14699

Matrix elements systematic calculation method in terms of inelastic transition densities to evaluate nuclear properties 04 p0723 A70-15634

Optimally ordered triangular factorization for solving symmetrical systems of linear matrix equations 05 p0876 A70-16573

State transition matrix computation method with efficient algorithm for orbit prediction in n-body gravitational field 06 p1095 A70-18497

Regular matrix inverse computation by method of forbidden zero element removal 09 p1711 A70-22275

Matrix theory of elastic locking structures, programming for analysis under given loads and dislocations 09 p1771 A70-22396

Algorithm for transfer matrix Heaviside expansion, using Krylov and Vandermonde transformations for multiple eigenvalue case 10 p1910 A70-24705

Piecewise linear elastoplastic matrix structural theory with interacting yield planes, discussing kinematic and isotropic hardening 14 p2656 A70-30475

Sufficient conditions for convergence of infinite determinant 15 p2766 A70-31448

Generalized spectral analysis method implementing orthogonal transformations through Kronecker product representation and matrix factorization 15 p2767 A70-32099

Baecklund type matrix transformations application to hodograph equations system for aligned nondissipative MGD flows 16 p2958 A70-33747

Complex matrix eigenvalues bound derivation by constructing integral equation with degenerate kernel 17 p1311 A70-35934

Parametric functions of integral matrices representing linear differential system via continuous coefficients 18 p3279 A70-36156

Pivot search at Gaussian algorithm, investigating Hilbert matrix approach 18 p3283 A70-36364

Neighboring normal matrix pairs eigenvalues determination 19 p3459 A70-38685

Existence theorem for finite integral matrix extended to infinite matrices, prescribing upper and lower bounds for row and column deficiencies 20 p3657 A70-39445

Soviet book on matrix theory application to problem solutions in structural mechanics covering computer techniques, internal forces, initial parameter method, displacements, etc 20 p3719 A70-39600

Script-F radiative interchange matrix for enclosures with arbitrary surface emission and reflection characteristics 21 p3944 A70-41020

Nesbet algorithm modified for iterative evaluation of eigenvalues and corresponding eigenvectors for large matrices 22 p4062 A70-42749

Rational polynomial matrices inversion by automatic computational procedures, considering Gaussian elimination and Faddeev algorithm 22 p4062 A70-42926

Parallelism of two regression lines, suggesting distribution free signed rank test 22 p4064 A70-43526

Successive iterative solution for large matrix equations reduced from Fredholm integral equations of second kind 24 p4369 A70-45164

Approximate N-representability of density matrix by set of spin geminals 24 p4378 A70-45259

Real matrix stability determination by right half plane eigenvalues, using symmetric solution of Liapunov equation 24 p4370 A70-46098

MATTER (PHYSICS)

Final state of matter resulting from star contraction, white dwarfs development and neutron stars problem, explaining hydrostatic equilibrium 02 p0370 A70-12085

Equation of state for neutron, proton and electron gas mixture associated with cold matter above white dwarf densities and below nuclear density
05 p0905 A70-15756

Observational extragalactic dependences obtained within framework of Friedmann universe model with matter and neutrino background
07 p1383 A70-19407

Matter distribution and motion in conformally flat gravitational fields, analyzing Friedmann solution to Einstein equations
08 p1544 A70-20991

Equation of state for cold matter at neutron star densities, deriving equilibrium equations for nuclear interactions among hadrons
09 p1764 A70-23606

Neutron star models based on equation of state for cold degenerate matter, taking into account nuclear forces and clustering
09 p1764 A70-23607

Cosmic background radiation interactions with matter, discussing molecular excitation and black body radiation interpretation
12 p2291 A70-27054

Pulsars properties and physical nature, considering state of matter not reproducible in terrestrial laboratories
12 p2297 A70-27056

State equations of matter at high density and zero temperature, considering neutron stars relationship to supernova explosions and collapse
12 p2298 A70-27059

Cosmological constant role in closed universes with matter and radiation
13 p2490 A70-28936

Theory of matter from low energy data, discussing particle and charge classification, relativistic quantum dynamics, charge dynamics and superstrong reactions
14 p2620 A70-30783

Neutron core star models based on realistic nuclear matter calculations and hyperons equation of state
17 p3157 A70-34844

Antimatter distribution in universe, investigating mass lower limit
19 p3518 A70-38025

Antimatter detection and interaction with matter on moon, discussing radiation from electron-positron annihilation processes
19 p3521 A70-38482

Equation of state of nuclear neutron matter as function of density
19 p3524 A70-38695

Einstein-Maxwell fields in presence of matter and pressure, expressing existence conditions in terms of eigenvalues and eigenvectors of Ricci tensor
22 p4074 A70-43206

Universe cold matter structure and distribution from far IR data
22 p4096 A70-43395

MATURING U GROWTH MAXIMA

Maxima increases without limit in damped linear oscillator response to random wideband excitation interpreted by heuristic explanation
11 p2085 A70-26694

Consistent dependence of best rational Chebyshev Lp approximator on given function
23 p4210 A70-44025

MAXIMUM LIKELIHOOD ESTIMATES

Digital radar receiver based on pseudo Bayes likelihood ratio algorithms
21 p3789 A70-41353

Brittle fracture stress statistics for Weibull distribution function parameter determination, comparing linearizing, least squares curve fitting and maximum likelihood techniques
22 p4117 A70-43414

Satellite orbital element values and perturbation parameters from incomplete element system, using maximum likelihood principle
24 p4406 A70-45529

MAXIMUM PRINCIPLE

Interior estimates for second order elliptic differential or finite difference equations, applying maximum principle
01 p0131 A70-10375

Time optimal control of system variable with bounded controlling input and arbitrary disturbances, deriving necessary conditions using maximum principle [ASME PAPER 69-WA/AUT-7]
04 p0661 A70-14827

Optimization of control of oscillatory process with deviating argument in maximum principle form, reducing solution to boundary value problem
08 p1544 A70-20954

Memory systems described by integrodifferential equations with distributed time lag, obtaining optimality condition in form of maximum principle
08 p1480 A70-21177

Maximum principle optimality for nonlinear two group parameter control applicable to plants described by integrodifferential and delay equations
10 p1911 A70-25184

Maximum principle condition of optimal control of monodimensional system described by nonlinear hyperbolic equations with time delay
11 p2021 A70-25340

Maximum principle least squares (MPLS)/nonlinear filter scheme simplified, using digital simulation for stability and tracking performance
11 p2028 A70-26315

Optimal control for processes with parameters and state variable inequality constraints using gradient projection method and maximum principle
12 p2205 A70-28337

Optimal control problems solution by maximum principle, describing variational formulation simplification
12 p2205 A70-28339

Optimal control problems constraints and necessary conditions, deriving maximum principle
14 p2600 A70-31202

Optimal startup control of jacketed tubular reactor with first order reversible exothermic reaction, presenting distributed maximum principle for diffusional parameter system
16 p2885 A70-33330

Noisy stochastic pattern recognition system, determining optimal measurement sequence by discrete Pontryagin maximum principle
18 p3234 A70-36337

Optimum one dimensional journal bearing for maximum load with minimum film thickness, using Pontryagin principle [ASME PAPER 69-LUB-9]
19 p3435 A70-37614

Sufficient condition for optimal control with continuous nonlinearities, using Pontryagin maximum principle
19 p3394 A70-38717

Discrete parameter stochastic optimization problems necessary conditions, deriving maximum principle
20 p3659 A70-40107

Maximum principle for discrete systems of recurrence equations, applying Pontryagin principle
22 p4073 A70-42696

Schedule theory problem with redundancy and technological constraints reduced to optimal control problem by penalty function, making maximum principle applicable
23 p4177 A70-44304

MAXIMUM USABLE FREQUENCY

F 2 layer effects on ionospheric short wave scattering lines for operating frequencies above MUF
14 p2547 A70-30231

Short wave propagation above F2 maximum usable frequency, observing field intensity and SNR seasonal and diurnal variations
18 p3226 A70-36092

Short wave ionospheric scatter propagation, observing interference and crowding in 16-23 MHz and relationship to F 2 layer maximum usable frequency
18 p3227 A70-36093

Short radio wave propagation over single jump lines in F sub zero F 2 gradient presence, examining maximum usable frequency increase
23 p4162 A70-44076

F 2 layer effects on ionospheric short wave scattering lines for operating frequencies above MUF
24 p4316 A70-46306

MAXWELL BODIES

Spatial and temporal relaxation problems approximate solution in kinetic theory, making calculations for Maxwellian molecules and hard spheres
06 p1047 A70-18318

First collision Monte Carlo method for calculating aerodynamic drag on hard sphere and Maxwell molecular models in near-free molecular flow
06 p0983 A70-18379

Critical stresses and stability of thin Maxwell plates under random temperature fields
18 p3337 A70-36368

MAXWELL EQUATION

Inertial gravitational fields described by Maxwell equations, showing potentials defining four vector velocity field of test particles
01 p0141 A70-10140

Nonlinear modification of Maxwell equations, discussing conformal invariance and nonsingular solutions to neutral and charged states with zero mass
02 p0339 A70-12067

Electromagnetic pulse scattering in time varying inhomogeneous medium, applying finite difference method to Maxwell equations
02 p0261 A70-12588

Plasma waves and instabilities, detailing linearized Vlasov-Maxwell equations solution appropriate to Landau problem
06 p1118 A70-17378

Lagrangian invariance transformation application to steady state solution for Einstein-Maxwell equations interpreted as external field of charged isolated rotating source
06 p1106 A70-17747

Stationary solutions of Einstein-Maxwell equations constructed from Einstein-Maxwell or vacuum fields
06 p1106 A70-17748

Einstein-Maxwell equations solutions relation to Robinson and Robinson metrics compared with Reissner-Nordstrom solution relation to Schwarzschild
07 p1333 A70-18961

Surface oscillations of plasma in external HF field derived from hydrodynamics and Maxwell equations
07 p1355 A70-20367

Characteristic equations for differential symmetry operators in homogeneous and nonhomogeneous Maxwell equations
08 p1544 A70-20990

Pulse propagating in unstable plasma, determining characteristics by asymptotic expansion applied to Vlasov-Maxwell equations
09 p1734 A70-22684

Navier-Stokes-Maxwell equations solutions for conducting fluid flow in azimuthal magnetic field, noting jet acceleration near symmetry axis
10 p1924 A70-24574

Book on electromagnetic fields and waves covering electrostatic and magnetic fields, relativity, vectors, Maxwell equations and propagation
12 p2273 A70-28150

Yagi antenna field theory derived from Maxwell equations by solving in cylindrical coordinates and satisfying boundary conditions
13 p2364 A70-28898

Inductive flow measurement history, considering Maxwell, material and Poisson equations
15 p2735 A70-31823

Rough surface radiative properties, determining electromagnetic wave scattering by Maxwell equation solution [AIAA PAPER 70-862]
17 p3135 A70-34508

Maxwell equations and equations of massive-vector-meson fields in spatially homogeneous Bianchi cosmologies, obtaining formula for homogeneous EM field
17 p3156 A70-34827

Maxwell equations derivation, describing assumptions needed
17 p3136 A70-35198

Variational principle application to relativistic MHD, deriving Einstein field equations, Maxwell equations and equations of motion for self gravitating charged fluid
19 p3478 A70-37591

Maxwell equations for hybrid modes of shielded ring line with axial and coaxial region at cut-off and near cut-off conductivity
21 p3793 A70-42269

Quasi-Maxwellian equations of inertial-gravitational fields
22 p4075 A70-43223

EM wave effects on radio receiver, using Maxwell equations without taking photons into account
23 p4221 A70-44798

Pre-Maxwellian electromagnetic equations application to MHD, investigating existence theorems generalization from system at rest to system with motion
24 p4386 A70-45593

MAXWELL FLUIDS

Maxwellian fluid oscillating flow in thin walled elastic circular tube as function of tube dimensions, elastic properties, oscillation frequency, etc
21 p3810 A70-41963

MAXWELL-BOLTZMANN DENSITY FUNCTION

Quasi-linear ion oscillation theory for Maxwellian plasma, considering electron and ion distribution perturbations and energy transfer
02 p0346 A70-12105

Warm Maxwellian plasma stabilization of velocity-space instabilities, evaluating densities and temperatures for stabilizing resonant loss-cone modes
02 p0347 A70-12237

Formation of Maxwell and non-Maxwellian energy distribution in gases, noting reduction of time reversible to time irreversible equations
03 p0606 A70-13861

Distribution functions for solving moment equations of Maxwell-Boltzmann equation used in studying heat conduction through rarefied gases within concentric cylinders and spheres [ASME PAPER 69-WA/HT-17]
04 p0783 A70-14817

Maxwellian distribution perturbation in chemically reacting gas mixtures with lower inelastic collision frequency than elastic
06 p1110 A70-17761

Solar wind temperature, using distribution function for solar wind ions in anisotropic Maxwell distribution form
06 p1135 A70-17895

Modified Maxwellian models for particle reflection in free molecular flow, correlating model parameters with gas-surface properties
06 p1110 A70-18259

Plane Couette flow and heat transfer problem numerical solution, using Krook kinetic equation and Maxwell boundary condition
06 p1048 A70-18326

Chemical reaction rates corresponding to initial molecules fixed internal energy levels determinable

for multitemperature Maxwell-Boltzmann distribution as function of reagent temperatures
07 p1224 A70-18769

Globular cluster relaxation time using nonMaxwellian velocity distribution and polytropic spatial distribution
22 p4109 A70-43744

Spectral line width distributions in main sequence stars, emphasizing B2 to A2 range rotational velocities with Maxwellian distribution
23 p4251 A70-44821

MAXWELLIAN DISTRIBUTION [DENSITY]

U MAXWELL-BOLTZMANN DENSITY FUNCTION

MAYER PROBLEM

Optimal trajectory and control approximate solution by asymptotic expansion, considering Mayer variational problem solution
16 p2943 A70-33897

Optimal low thrust transfer between coplanar circular orbits, examining thrust direction and steering as Mayer problem
22 p4097 A70-42489

MAZE LEARNING

Restricted problem solving tasks /perceptual maze test/ formulated as multistage decision making, discussing use of dynamic programming and algorithms
02 p0246 A70-12321

MCDONNELL AIRCRAFT

NT C-9 AIRCRAFT

NT F-4 AIRCRAFT

MCDONNELL MILITARY AIRCRAFT

U MILITARY AIRCRAFT

MCLAURIN SERIES

U MACLAURIN SERIES

MEAN

Arithmetic mean, least squares method and standard deviation concepts in random error analysis of measurement data
11 p2117 A70-26674

Algorithm for fast digital computer recursive estimation of mean of random variable
22 p3993 A70-43074

MEAN FREE PATH

Enskog method for Boltzmann equation, analyzing asymptotic nature of integral kinetic equation for molecular mean free paths and Laplace probabilities
01 p0068 A70-11568

Flame positive ion concentration measurements with Langmuir probes with mean free path smaller than probe diameter
02 p0397 A70-12019

Cosmic ray particles inelastic nuclear interactions mean free path in iron measured in Wilson chamber and ionization calorimeter
03 p0554 A70-13030

Molecular mean free path influence on gas lubricated thrust bearings performance, discussing slip flow effect and load capacity
05 p0854 A70-15909

Asymptotic behavior /for small mean free path/ of rarefied gas steady flow over smooth solid boundary
06 p1048 A70-18328

Hyperthermal leading edge analyzed by examining adjacent relevant mean free paths for collisions, establishing basis for formal expansion of Boltzmann equation
06 p0979 A70-18347

Polarization of laser medium consisting of colliding two level molecules with velocity dependent mean free time
08 p1512 A70-20992

Stationary gas flows continuous to rarefied transition analysis based on mean free path anisotropy
15 p2721 A70-32139

Collision dominated plasma column radial structure including ambipolar diffusion region obtained from constant mean free time and path approximate formulas
16 p2959 A70-34311

Rarefied gas flow over plane wall, considering boundary layer thickness of order of mean free path
21 p3809 A70-41715

MEASURANDS

U MEASUREMENT

U PROPERTIES

MEASURE AND INTEGRATION

NT FUNCTIONAL INTEGRATION

NT INTEGRAL CALCULUS

NT NUMERICAL INTEGRATION

NT RUNGE-KUTTA METHOD

NT STIELTJES INTEGRAL

NT WEIGHTING FUNCTIONS

Algebraic properties of indefinite Riemann in integral useful in computer programming, emphasizing invariant algebras
04 p0654 A70-14683

Gaussian quadrature integration technique developed for collocation approach for integral equation of steady subsonic lifting surface theory [AIAA PAPER 70-191]
06 p0970 A70-18097

News function relation with far fields of sources obtained in linear approximation for axisymmetric case in integrating Einstein field equation
08 p1543 A70-20721

Integration of Saint Venant equations of deformation continuity for region occupied by elastic medium
08 p1587 A70-21166

Equations of motion integration for solid body in potential forces field induced by elastic springs
09 p1728 A70-23386

Analytic function integration optimal rate, discussing weighting function
10 p1909 A70-24509

Integrating sphere theory with wall mounted specular sample in reflectance and transmittance measurements
18 p3284 A70-36776

Products integration of unit vector components over all solid angles
24 p4370 A70-46029

Differential equations with integrable coefficients, proposing asymptotic integration for second order system
24 p4370 A70-46031

MEASURE THEORY

U MEASURE AND INTEGRATION

MEASUREMENT

Expected values optimal measurement, given auxiliary conditions between measured value number and quantization
02 p0299 A70-12400

Mean square error for measurement series with unknown error distribution law, specifying necessary number of terms
19 p3390 A70-38583

Monograph on estimation and optimal control with quantized measurements covering linear, nonlinear and time varying systems
20 p3658 A70-40024

Fluctuating data transmission, using measurement channel with digital logarithmic conversion
20 p3635 A70-40534

Wall thickness measurement by supersonic testing method based on resonance
24 p4336 A70-45681

MEASURING

U MEASUREMENT

MEASURING APPARATUS

U MEASURING INSTRUMENTS

MEASURING INSTRUMENTS

NT ACCELEROMETERS

NT ACTINOMETERS

NT ALTIMETERS

NT ANALYZERS

NT ANEMOMETERS

NT APPROACH INDICATORS

NT ATOMIC CLOCKS

NT ATTITUDE INDICATORS

NT BATHYTHERMOGRAPHS

NT BOLOMETERS

NT CALORIMETERS

NT CAPACITIVE FUEL GAGES

NT CATHETEROMETERS

NT CERENKOV COUNTERS

NT CHRONOMETERS

NT CINETHEODOLITES

NT CLOCKS

NT CLOUD HEIGHT INDICATORS

NT COMPARATORS

NT COUNTERS

NT DEFORMETERS

NT DENSITOMETERS

NT DICKE RADIOMETERS

NT DIFFRACTOMETERS

NT DISTANCE MEASURING EQUIPMENT

NT DOSIMETERS

NT DYNAMOMETERS

NT ELECTROMETERS

NT ELECTRON COUNTERS

NT ELECTRON PROBES

NT ELECTROPHOTOMETERS

NT ELECTROSTATIC PROBES

NT ELLIPSOMETERS

NT ENGINE ANALYZERS

NT ENGINE MONITORING INSTRUMENTS

NT ERGOMETERS

NT EXTENSOMETERS

NT FABRY-PEROT INTERFEROMETERS

NT FABRY-PEROT SPECTROMETERS

NT FIELD INTENSITY METERS

NT FLAME PROBES

NT FLIGHT LOAD RECORDERS

NT FLIGHT RECORDERS

NT FLOW DIRECTION INDICATORS

NT FLOWMETERS

NT FUEL GAGES

NT GALVANOMETERS

NT GEIGER COUNTERS

NT GEODIMETERS

NT GONIOMETERS

NT GRAVIMETERS

NT GRAVITY GRADIOMETERS

NT GYRO HORIZONS

NT GYROCOMPASSES

NT HELIOMETERS

NT HODOSCOPES

NT HOT-WIRE ANEMOMETERS

NT HOT-WIRE FLOWMETERS

NT HYDROMETERS

NT HYGROMETERS

NT HYPSONOMETERS

NT IMPEDANCE PROBES

NT INDICATING INSTRUMENTS

NT INFRARED DETECTORS

NT INFRARED INSTRUMENTS

NT INFRARED SCANNERS

NT INFRARED SPECTROMETERS

NT INFRARED SPECTROPHOTOMETERS

NT INTERFEROMETERS

NT ION PROBES

NT ION TRAPS [INSTRUMENTATION]

NT IONIZATION GAGES

NT IONOSONDES

NT KNUDSEN GAGES

NT LASER ALTIMETERS

NT LASER RANGE FINDERS

NT LIGHT SCATTERING METERS

NT LUNAR SEISMOGRAPHS

NT MACH-ZEHNDER INTERFEROMETERS

NT MAGNETIC PROBES

NT MAGNETOMETERS

NT MANOMETERS

NT METEOROLOGICAL INSTRUMENTS

NT MICHELSON INTERFEROMETERS

NT MICROBALANCES

NT MICROMETERS

NT MICROWAVE INTERFEROMETERS

NT MICROWAVE PLASMA PROBES

NT MICROWAVE PROBES

NT MICROWAVE RADIOMETERS

NT MICROWAVE SENSORS

NT MOISTURE METERS

NT MONOCHROMATORS

NT NEPHELOMETERS

NT NEUTRON COUNTERS

NT NEUTRON SPECTROMETERS

NT NOISE METERS

NT OHMMETERS

NT OMEGA NAVIGATION SYSTEM

NT OPTICAL MEASURING INSTRUMENTS

NT OPTICAL PYROMETERS

NT OPTICAL RANGE FINDERS

NT OPTICAL SCANNERS

NT OSCILLOGRAPHS

NT OXYGEN ANALYZERS

NT PARTICLE TELESCOPES

NT PENETROMETERS

NT PHASE SWITCHING INTERFEROMETERS

NT PHOTOMETERS

NT PIEZOELECTRIC GAGES

NT PLAN POSITION INDICATORS

NT PLASMA PROBES

NT PNEUMATIC PROBES

NT POLARIMETERS

NT POLARISCOPES

NT POSITION INDICATORS

NT POTENTIOMETERS [INSTRUMENTS]

NT PRESSURE GAGES

NT PROFILOMETERS

NT PROPORTIONAL COUNTERS

NT PSYCHROMETERS

NT PYRANOMETERS

NT PYROHELIOMETERS

NT PYROMETERS

NT QUANTUM COUNTERS

NT RADIATION COUNTERS

NT RADIATION DETECTORS

NT RADIATION MEASURING INSTRUMENTS

NT RADIATION PYROMETERS

NT RADIO ALTIMETERS

NT RADIO DIRECTION FINDERS

NT RADIO FREQUENCY IMPEDANCE

NT PROBES

NT RADIO INTERFEROMETERS

NT RADIOMETERS

NT RADIOSONDES

NT RANGE FINDERS

NT RAWINSONDES

NT REFLECTOMETERS

NT REFRACTOMETERS

NT RESISTANCE THERMOMETERS

NT RESONANCE PROBES

NT RHEOMETERS

NT RIOMETERS

NT SCINTILLATION COUNTERS

NT SEISMOGRAPHS

NT SEXTANTS

NT SHOCK MEASURING INSTRUMENTS

NT SIGNAL ANALYZERS

NT SILICON RADIATION DETECTORS

NT SOLAR SPECTROMETERS

NT SONDES

NT SONIC ANEMOMETERS

NT SPACECRAFT POSITION INDICATORS

NT SPARK CHAMBERS

NT SPECTROPHOTOMETERS

NT SPECTROPHOTOMETERS

NT SPEED INDICATORS

NT STRAIN GAGE ACCELEROMETERS

NT STRAIN GAGES

NT TACHOMETERS

NT TELLUROMETERS
 NT TEMPERATURE MEASURING INSTRUMENTS
 NT TEMPERATURE PROBES
 NT TENSOMETERS
 NT THEODOLITES
 NT THERMOMETERS
 NT THRESHOLD DETECTORS [DOSIMETERS]
 NT TIME MEASURING INSTRUMENTS
 NT TIMING DEVICES
 NT TORQUEMETERS
 NT TRANSITS
 NT TRANSMISSOMETERS
 NT TURBULENCE METERS
 NT ULTRAVIOLET SPECTROMETERS
 NT ULTRAVIOLET SPECTROPHOTOMETERS
 NT VACUUM GAGES
 NT VARIOMETERS
 NT VIBRATION METERS
 NT VISCOMETERS
 NT VOLTMETERS
 NT WATTMETERS
 NT WEATHER DATA RECORDERS
 NT WEIGHT INDICATORS
 NT WIND VANES

Motion equations for vibratory two degrees of freedom spring mass system subjected to rotation, discussing use for small rates of turn measurement

Apparatus for continuous creep measurement at high temperature for fine wire and thin tubular samples with small cross sectional areas

Continuous measurement and automatic recording of metals electrical resistance during fatigue testing in vacuum at elevated temperatures

Hardness measuring instrument by dynamic method at high temperatures in vacuum, using magnetic or nonmagnetic indenter balls

Handbook of transducers for electronic measuring systems covering operating principles, design features, etc

Rumanian book on shock tubes covering facility construction, gas flow, electronic measuring equipment, etc

Electronic gauging machine for multipoint measurement at preselected points around turbine blade airfoil produced by electrochemical machining

Phase detector with two value output and pulsed input for measurement and control circuits, noting construction with semiconductor elements

Flow direction and velocity measurement in three dimensional boundary layer, discussing instrument and restrictions

Sensing device to measure radial stress induced at solid propellant grain-to-case bond interfaces during wide temperature variations, detailing instrumentation and operation

Ponderomotive meter for laser energy and power measurement, discussing mechanical design and elimination of radiometric and convection disturbances

Elastic sensor for measuring linear displacements using fine crossed filaments and torsion principle

Surveyor TV camera conversion from qualitative viewing device into quantitative measuring instrument by calibration coupled with data processing program [JPL-TR-32-1374]

RF hazard measuring system for complete guided weapons electromagnetic compatibility tests with instrumented inert device replacing live igniter

Instrumentation concepts for electromagnetic compatibility measurements on electroexplosive devices, considering thin film thermocouple, electrical diode detector and microstrip transmission line techniques

Josephson effect in superconductors emphasizing Josephson junction electrical properties and applications to devices and measuring techniques

Monitoring and recording of physiological parameters, discussing heart, muscle, brain potentials, blood pressure, respiration measurements and instrumentation

Multiple optical properties measurement instrumentation for cellular specimens to classify biological cells, analyzing and displaying data by on-line computer

Radiation fluxmeters involving black plates and sensor disk respectively for use in space simulation chambers

Calibrating rods design for vibrating components stress measurement gauges

Level differences measured at 300 Hz to 200 MHz frequency range, discussing methods and measuring circuits and components

Torsion balance for measuring gravitational constant based on Langevin resonance method

Loading effects in measurements involving electrical and nonelectrical systems used in determining gas pressure and fluid flow

Acoustic fluidic amplifiers, considering receiver, transmitter and operating mode

Dynamic force measurement methods, considering reaction force and operational compensation

Aerodynamic subsonic and supersonic wind tunnels parameter measurement methods including static and total pressure, current direction, velocity, density, etc

Metal and alloys hardness measuring devices at high temperatures in ultrahigh vacuum based on use of synthetic sapphire pyramidal indenter

Instrumentation and measurement - IEEE Conference, Ottawa, May 1969

Frequency measurement in millimeter and submillimeter ranges, using high quality Fabry-Perot resonator

Plasma conductivity measuring device using phenomenon of change of coil induction in electromagnetic field

Digital wavemeter description using interferometer with parallel plates and automatic frequency readout for submillimeter band

Electron beam fluorescence probes for rarefied gas flow, describing local density and temperature measurement methods

Dynamic force measurement, evaluating hybrid system with reaction force summation and operational compensation subsystems

Solar flare videometer for measuring flare area and peak and integrated intensity in real time

Quadratic error of semiautomatic measuring apparatus for photographic plates, noting operator contribution

Measurement of dynamic mechanical quantities - Conference, Warsaw, May-June 1968

Device for measuring turbine blades natural frequencies by converting vibrations to electric current at same frequency

Connecting wires length effect on sensitivity and current-voltage characteristics of sensors for dynamic values measurement, deriving integral electrical parameters

Multichannel measurement system for inductive transducers, describing system components and capabilities

Sensor selection and telemetry measurement of physical parameters

Noise effects during mechanical parameters measurement by electronic devices, noting noise from resistors, potentiometers, power lines and wiper-type distributors

Dynamic measurements of aerospace mechanical quantities covering tensometry, vibration, torque, angular velocity, pressure, telemetry and data processing

Metals thermal properties simultaneous determination at high temperatures, describing measuring equipment operation and circuitry

Standard method for aircraft engine exhaust smoke measurement for air pollution control [SAE PAPER 700250]

Dynamic errors of electric measurement devices during three dimensional polyharmonic vibrations of foundation

Test and measuring equipment control systems analysis, discussing metrology and calibration requirements in overall quality assurance problem

Electrodynamic transducer electrical and mechanical parameters measurement, comparing various techniques

Haring x type vibration insulation table for impact sensitive measuring instruments

Large diffraction gratings by interferometrically controlled commercial measuring machine

Automatic narrow band meter for continuous readout of frequency characteristics of radiation detectors

Free nuclear precession sensor with rotating sample for performing measurements in nonuniform magnetic field

Inter-Range Instrumentation Group /IRIG/ document regarding meteorological data reliability, defining measuring process accuracy and errors

Meteorological parameters measuring instruments optimal design, presenting formalized procedure flow chart and examples

Quartz crystal particulate sensor instrument for terrestrial and Mars atmospheres

Memory systems in measurement and control equipment, describing applications to linearizing, compression and data refresh operations

Contactless electromagnetic level sensor for liquid metal using eddy currents

Magnetoelastic sensors for small force measurement, describing instrument error reduction

Laser velocimeter application to laminar-turbulent flow transition at glass tube centerline

Measuring instrument for total cross section of proton elastic scattering during sigma R reactions

Force-balance principle application to pressure and skin friction measuring instruments, discussing construction, operation and performance

Measurement transducers transforming measured quantity into forms suitable for comparison with standards in metrological sciences

High speed photoelectric measurements of lunar occultation using computer and nuclear physics instrumentation

Natural convection heat transfer from vertical cylinder outer surface to liquids, discussing apparatus design and measurements

Weak ion concentration in stratosphere and mesosphere measured using accumulated capacity amplifier

Atmospheric humidity measuring equipment and procedures for high altitudes, considering hygrometers, mass spectrometers, sondes, absorption spectra, etc

Adiabatic microwave power meter design using sodium thiosulfate phase transformations

Piezoelectric force and moment measurement by quartz multicomponent devices

Phase meter for measuring angular coordinates of reflecting meteor trails

Optical properties of system measuring atmospheric transmittance by recording light backscattered from atmospheric layers

Sensing device to measure radial stress induced at solid propellant grain-to-case bond interfaces during wide temperature variations, detailing instrumentation and operation

Fluorine-compatible apparatus for measuring temperature PVT properties of gaseous and liquid fluorine

Instruments for platforms stability determination, considering azimuth, tilt rotation and translational motion

Precise sensing systems and instruments calibration with respect to inertial frame of reference for geokinetics

Measuring and test equipment economic approach to quality levels and accuracy ratios, deriving cost tradeoffs in optimum inspection fidelity

Test measurement instruments - Conference, Houston, October 1969

Oscilloscope design involving optimum bandwidth and input sensitivity, reference measurement and second time base

- Wind tunnel response tests of cup, vane and propeller wind sensors, determining wind direction and speed parameters, damped and natural frequencies, etc 22 p4030 A70-42914
- Fluidic amplifiers in measurement technology including turbulence, pulse, Coanda, induction, vortex, arc and focusing amplifiers 23 p4142 A70-44246
- Automated high precision electrical resistance measuring system using digital computer control 24 p4334 A70-45384
- Cryogenic fluid multipoint level sensing detector circuit using carbon resistors 24 p4339 A70-46200
- Free nuclear precession sensor with rotating sample for performing measurements in nonuniform magnetic field 24 p4339 A70-46293
- Thrustmeter for direct output reading from jet engines based on stream and total port pressures 24 p4340 A70-46328
- MECHANICAL DEVICES**
- Dynamic vibration absorbers (DVA) efficiency in limiting excessive vibrations in mechanical systems by transferring motion to auxiliary system 04 p0699 A70-15306
- Sliding tube assembly for diverting carrier gas from flow pattern of Verneuil apparatus for flame fusion crystal growth 05 p0829 A70-16849
- Mechanical electromagnet model of MHD dynamo achieving direct conversion of mechanical to magnetic field energy 06 p1121 A70-17803
- Mechanical latching crossbar switches for space division electronic switching, discussing structure, performance, reliability, etc 06 p1023 A70-18413
- Mechanical system undergoing internal mass redistribution, showing energy dissipation during motion 08 p1545 A70-21203
- Hydromechanics and thermodynamics in mechanical radial face seal design 11 p2059 A70-25792
- Passive coupling of spatial six-element mechanical mixer with rotary pairs as function of element axial position and dimensions 11 p1983 A70-25933
- Mechanical electromagnet model of MHD dynamo achieving direct conversion of mechanical to magnetic field energy 13 p2460 A70-28654
- Stability loss of dynamic two dimensional mechanical elastic system with single degree of freedom under trajectory bifurcation 15 p2775 A70-32474
- Life and confidence tests of miniature self contained flexure pivots in critical mechanisms [ASME PAPER 70-DE-76] 16 p2918 A70-33522
- Collection of papers on aerospace mechanisms, Part A, covering scanning, separation, thermal and stabilization devices, booms, cameras, etc 16 p2983 A70-34101
- Nimbus weather satellites mechanical devices and subsystems, including solar array drive, fluid thermal control sensors, horizon scanners and hydraulic dampers 16 p2921 A70-34105
- Closed tubular extendible boom (Multiple Applications Storable Tube) design, fabrication and applications, including stress factors and materials 16 p2846 A70-34142
- Lunar Orbiter photo subsystem mechanisms, discussing film transport, vacuum and mechanical clamps, focal plane shutter, processor-dryer and optical mechanical scan 16 p2914 A70-34146
- Surveyor TV mechanisms, discussing camera, mirror, zoom lens, filter wheel, focal plane shutter and lubrication 16 p2914 A70-34147
- Surveyor camera double acting rotary solenoid actuated focal plane shutter utilizing two blades in parallelogram linkage 16 p2914 A70-34148
- Gemini/Agenda docking mechanism design and function, describing latch and rigidizing devices 16 p2986 A70-34151
- Collection of papers on aerospace mechanisms, Part B, Bearings and suspensions 16 p2922 A70-34154
- Rolamite low friction suspension system, describing components, force generation and applications 16 p2923 A70-34165
- Torsion, filar, flexure and coil type mechanical suspensions for space applications, considering instability due to temperature changes and magnetic, electric and force fields 16 p2924 A70-34169
- Flexural pivots for space structures, describing design, fabrication and applications 16 p2924 A70-34170

- Nonlinear mechanical systems transient motion analysis based on phase trajectories 16 p2944 A70-34283
- Nonlinear mechanical lumped dynamic systems trajectory analysis in terms of P and G sets 16 p2944 A70-34285
- Mechanical system random excitation, evaluating parameters to satisfy conditions for statistical characteristics of steady state output processes 16 p2953 A70-34296
- Mechanical system with n material points, deriving control algorithms for realizing constrained programmed motion 16 p2953 A70-34297
- High reliability release mechanism with mechanical redundancy on SERT 2 satellite 17 p3174 A70-34759
- Spacecraft separation mechanisms selection, design and use, discussing multiple device point and linear systems 17 p3175 A70-34767
- Eigenvalues of transfer matrix and vibrations generation for passive mechanical systems with n degrees of freedom based on Laplace transformation 18 p3337 A70-36225
- Mechanical systems spontaneous oscillation due to different critical velocities with and without arbitrarily small damping 18 p3338 A70-36430
- Rotating mechanical components reliability under complex fatigue, presenting design data 19 p3442 A70-38845
- Helicopter mechanical power transmission design, describing gearing, shaft bending, bearings, lubrication, weight factors, etc [SAWE PAPER 844] 20 p3563 A70-40367
- Mechanical passive cone angle amplifier for spinning sounding rockets for IR sky scanning, solving equations of motion for system 21 p3931 A70-41905
- Electro-thermal-mechanical switches based on shape-memory effect in Ti-Ni alloys 22 p3965 A70-43330
- Spacecraft fluid mechanical system design, considering environments, materials, lubrication, zero gravity and inflight maintenance [SAE PAPER 700781] 24 p4295 A70-45862
- MECHANICAL DRIVES**
- NT HELICOPTER PROPELLER DRIVE
- NT PROPELLER DRIVE
- Gear ratios series determination for planetary reduction gear having positive and negative difference between number of gear teeth 05 p0856 A70-17007
- Optimal traction drive system design for lunar roving vehicle, considering weight, energy consumption, operational flexibility, power supply, motor and power train [SAE PAPER 700023] 11 p2030 A70-25375
- X band mechanically despun antenna system with RF and motor drive assembly developed for earth coverage communications satellite [ALAA PAPER 70-422] 11 p2001 A70-25481
- Dynamic synthesis of hinged four-element mechanism with respect to driven link position, transmission relations and allowance for transmission angle 11 p1983 A70-25934
- Mechanical systems vibrations comprising tension couplings compensating misalignment between non-coaxial shafts 11 p2060 A70-26348
- Swinging gear drive, breather cartridge and hypocycloid timer mechanisms for reliable aerospace applications 16 p2921 A70-34104
- Gearhead DC/AC electric motors with wet/dry lubricants, discussing selection criteria for spacecraft boom deployment 16 p2846 A70-34139
- Brushless despin mechanical drive and control system design and performance for orientation of high gain communications antenna from spin stabilized satellite 16 p2986 A70-34161
- Discrete mechanical models of single speed gearings in torsional vibrations without teeth deformation and damping resistance 16 p2995 A70-34288
- Composite tail rotor driveshaft for next generation helicopter, discussing materials, fabrication and tests [AHS PREPRINT 451] 17 p3100 A70-34703
- Rotary relay for solar array space power transfer using clutch of low moment of inertia capable of recycling once each orbit 17 p3101 A70-34765
- Standard units and assembling of electrical driving mechanism for telescope, using audio reference oscillator, electronic power amplifier and synchronous motor 18 p3259 A70-36609
- Helicopter cost reduction by transmission overhaul frequency reduction, discussing savings with on-condition maintenance 19 p3441 A70-38824

- Rotor drive systems for rotary wing aircraft, indicating mechanical hub drive advantages over reaction blade drive 21 p3755 A70-41850
- Differential equations of motion for machine assembly, using Appel equations 23 p4200 A70-44319
- Direct drive turbine engine control components and airframe accessories, noting weight and frontal area reduction [SAE PAPER 700821] 24 p4394 A70-45896
- MECHANICAL ENGINEERING**
- Optical and mechanical techniques for space experiment structures and metals satisfying space requirements 03 p0492 A70-13848
- Equations governing electrofluid dynamic energy conversion processes and indicating differences between EFD and magnetofluid dynamic processes presented for mechanical engineering problems [ASME PAPER 69-WA/ENER-9] 04 p0627 A70-14899
- Overcut phenomenon in early stage of cutting developed as theory for tip interference in internal gears 05 p0854 A70-15885
- Mechanical engineering and mechanics-Conference, Haifa, June-July 1969 05 p0939 A70-16508
- Book on statistical methods in structural mechanics covering design, fracture, stability, random loads, damage accumulation, reliability, etc 07 p1411 A70-19849
- Book on dynamics of mechanisms with elastic connections and impact systems covering differential and finite difference equations, equations of motion, friction effects, etc 08 p1502 A70-20753
- Stress concentration effect, surface states and similarity conditions in fatigue ruptures in machine construction, considering statistical analysis 09 p1776 A70-22615
- Book on mechanical seals design covering temperature and pressure effects, leakage and wear problems, etc 12 p2238 A70-26851
- Hydraulic system pumps ratings, classification and selection 13 p2419 A70-29219
- Jet thrust reversers mechanical design limits, objectives and materials 14 p2628 A70-30500
- Cage trim control valve designs, outlining properties, advantages and limitations 14 p2534 A70-30682
- Aerospace mechanisms design attitudes effects on cost and success of space mission 16 p2985 A70-34102
- Aerospace mechanism design from test laboratory viewpoint, balancing technical, cost and schedule factors with mission objective 16 p2921 A70-34103
- High strain fatigue machine with axial loading and servocontrol for short endurance testing 17 p3063 A70-35586
- Mechanical Engineering - Conference, Haifa, July 1970 21 p3809 A70-41951
- Tension-torsion machine developed from aircraft carrier catapult principle, producing radial loading paths 22 p4117 A70-43453
- MECHANICAL IMPEDANCE**
- Bolted joints inspection using mechanical impedance algorithm method involving bolt head mechanical shock pulse response in adjacent structure 01 p0098 A70-10017
- Vibration mode response and impact time sensitivity of mechanical impedance of human skull, relating head injury factors 15 p2682 A70-31934
- MECHANICAL MEASUREMENT**
- NT DISPLACEMENT MEASUREMENT
- NT DRAG MEASUREMENT
- NT FLOW MEASUREMENT
- NT FRICTION MEASUREMENT
- NT PRESSURE MEASUREMENTS
- NT STRESS MEASUREMENT
- NT THRUST MEASUREMENT
- NT VELOCITY MEASUREMENT
- NT VIBRATION MEASUREMENT
- NT WIND MEASUREMENT
- NT WIND VELOCITY MEASUREMENT
- NT X RAY STRESS MEASUREMENT
- Metal and alloys micro and macro stress-strain behavior data correlated for linear differential transformers, strain gages, longitudinal resonance waves and X ray diffraction 01 p0092 A70-11248
- Twin wave interferometer and strain gage mechanism for press-fit measurements of contact deformation on metallic and polymer samples 03 p0484 A70-13426

Electroexplosive devices output energy measurement through metal deformation by lead block and projectile penetration methods

03 p0548 A70-14121

Tangential cutting force measurements during Ti grinding by microtols, noting properties of W, aluminum boride and zirconium carbide

04 p0697 A70-14466

Dynamic measurements of aerospace mechanical quantities covering tensometry, vibration, torque, angular velocity, pressure, telemetry and data processing

11 p2057 A70-26750

Dynamic hysteresis loop measurement of energy dissipation in materials, showing deformation effects on accuracy

19 p3535 A70-37346

Linear elastic structure with few degrees of freedom, discussing parameters experimental determination

21 p3935 A70-41409

Free vibrating reed apparatus for polymer low temperature internal friction and Young modulus measurements, discussing polystyrene properties

21 p3827 A70-41464

Rumanian book on methods, equipment and facilities for aeromechanical measurements covering fluid flow, wind and shock tunnels, flow measurements, etc

23 p4199 A70-45000

MECHANICAL OSCILLATORS

NT GYROSCOPIC PENDULUMS

NT PENDULUMS

Optical data display involving laser light deflection by vibrating mirrors actuated by mechanical resonators

01 p0108 A70-10355

Pressure and temperature sensitivity tests of fluoric oscillator for timer application, testing fluid relaxation oscillators using R-C-R feedback loops

[ASME PAPER 69-WA/FLCS-9]

04 p0626 A70-14844

Soviet book on vibrations of complex oscillatory systems with mechanical, pneumatic and electromagnetic couplings

10 p1959 A70-24650

Self-synchronization of forced frictional mechanical vibrators assuming simple harmonic combination

11 p2139 A70-26417

Simple harmonic scotch yoke mechanical oscillator for strain gauge accelerometer calibration in VLF range

16 p2900 A70-32995

Mechanical-stereomechanical analogy of two index Lagrange equations of second kind

17 p3130 A70-35192

Elastoplastic oscillator dynamic behavior with one degree of freedom compared with bilinear hysteretical model results, investigating mechanical scheme with continuous skeleton intrinsic curve

19 p3432 A70-38665

MECHANICAL PROPERTIES

NT ABRASION RESISTANCE

NT AEROELASTICITY

NT AEROTHERMOELASTICITY

NT ANELASTICITY

NT BRITTLENESS

NT BULK MODULUS

NT COMPRESSIBILITY

NT COMPRESSIVE STRENGTH

NT CREEP PROPERTIES

NT CREEP RUPTURE STRENGTH

NT CREEP STRENGTH

NT DIMENSIONAL STABILITY

NT DUCTILITY

NT ELASTIC PROPERTIES

NT ELASTOPLASTICITY

NT ELECTROSTRICTION

NT FATIGUE LIFE

NT FIBER STRENGTH

NT FLEXIBILITY

NT FRACTURE STRENGTH

NT HARDNESS

NT HIGH STRENGTH

NT HYDROELASTICITY

NT IMPACT STRENGTH

NT KNOOP HARDNESS

NT MAGNETOSTRICTION

NT MICROHARDNESS

NT MODULUS OF ELASTICITY

NT NOTCH SENSITIVITY

NT NOTCH STRENGTH

NT PHOTOELASTICITY

NT PHOTOPLASTICITY

NT PHOTOVISCOELASTICITY

NT PIEZOELECTRICITY

NT PLASTIC PROPERTIES

NT POISSON RATIO

NT PROPORTIONAL LIMIT

NT RESILIENCE

NT ROCKWELL HARDNESS

NT SHEAR CREEP

NT SHEAR PROPERTIES

NT SHEAR STRENGTH

NT SHELL STABILITY

NT STEADY STATE CREEP

NT STIFFNESS

NT STRESS CYCLES

NT STRESS RATIO

NT STRESS RELAXATION

NT STRUCTURAL STABILITY

NT TENSILE CREEP

NT TENSILE PROPERTIES

NT TENSILE STRENGTH

NT THERMAL RESISTANCE

NT THERMOELASTICITY

NT THERMOPLASTICITY

NT THERMOVISCOELASTICITY

NT TOUGHNESS

NT VISCOELASTICITY

NT VISCOPLASTICITY

NT WELD STRENGTH

NT YIELD POINT

NT YIELD STRENGTH

Combined aging and plastic deformation treatment effects on breaking point, yield stress, elongation and contraction of austenitic Fe-Ni-Ti alloy

01 p0115 A70-10064

Chemistry variations effects on mechanical properties, phase stability and microstructure of alloy Unitemp 718 /Ni-Fe-Cr alloy/ via microscopy and X ray analysis

01 p0116 A70-10092

Heat resistant alloys for gas turbine blades observed for long term heating effects on changes of hardness, tensile, impact and stress-rupture properties and microstructure

01 p0116 A70-10149

Rolled bimetallic Ni-Mo mechanical properties produced by powder metallurgy methods

01 p0116 A70-10157

Projector with paraboloid mirror solar radiation condensing lens for studying heat resistant materials mechanical properties at high temperatures

01 p0055 A70-10179

Textolites and ferromagnetodielectric wedges mechanical strengths compared for use in open grooves of compound winding

01 p0008 A70-10195

Thermomechanical processing of high strength low alloy steels to evaluate effects of composition, coiling temperature and cooling rate on mechanical properties and microstructures

01 p0118 A70-10726

Structure and mechanical properties of martensite and bainite in Fe-Ni-Co-C steels, discussing isothermal aging to obtain tough twinned martensite steels

01 p0119 A70-10733

Martensitic steel /AFC 77/ austenite grain size refinement process, noting effects on yield strength, toughness, stress corrosion resistance and fatigue crack growth rate

01 p0120 A70-10739

Digital computer for data recording in stress-strain curves and data points for mechanical tests

01 p0058 A70-11062

FeCo V plastic deformation and fracture, noting temperature and grain size effects on yield and flow stresses, ductile to brittle transition, etc

01 p0123 A70-11244

Impeller elastic and elastoplastic strength of centrifugal supercharger with curved disks and radial blades, using variational method

01 p0211 A70-11417

Dynamic loads calculation on teeth of cylindrical straight tooth gears under engaged and disengaged conditions, performing strength analysis

01 p0105 A70-11421

Al double crystals mechanical properties improvement after shock loading, studying surface and dislocation structures and active slip planes number

01 p0124 A70-11449

Beryllium properties and processing including magnesianothermal reduction, power purity, oxygen content, grain size and temperature effects on mechanical properties

01 p0124 A70-11618

Mechanical properties of carbon fiber reinforced Al, Cu and Ni, noting rope and wire applications

02 p0384 A70-11676

Mechanical properties of asbestos as reinforcing material for fiber filled thermoplastics compared with glass fiber

02 p0320 A70-11677

Fortified thermoplastic compounds for increased flame retardancy, environmental resistance and toughness

02 p0320 A70-11865

B and C fiber unidirectionally reinforced plastic composites, discussing mechanical properties, fabrication and testing

02 p0321 A70-12082

Mechanical properties of human skull specified for construction of physical and mathematical models

02 p0243 A70-12097

Mechanical strength and breakdown metallography of plate shaped structural steel and Al alloy specimen under various HF elastic vibrations

02 p0318 A70-12398

Reinforced epoxy resin performance prediction from correlation between unfilled resin and laminates mechanical properties

02 p0322 A70-12606

Co-base hardfacing alloys mechanical properties and applications, discussing mechanical and chemical wear processes in cast and wrought types

02 p0319 A70-12712

Fiber reinforced composites fabrication, properties and industrial applications, discussing modulus of elasticity and tensile strength equations, bonding and temperature applicability

02 p0322 A70-12713

Technical ceramic products physical properties compared with metals, discussing manufacturing methods and industrial and engineering applications

02 p0322 A70-12714

Chromium refractory alloys, discussing production difficulties, mechanical properties, engineering applications, etc

02 p0320 A70-12760

Test fixture for determining mechanical properties of metals and steels at moderate strain rates, detailing design and instrumentation

03 p0462 A70-12883

Mechanical properties of ordered Ni-Cr alloys, establishing hardening effect of annealing

03 p0505 A70-13105

Mechanical properties of Al composites reinforced with alpha-silicon carbide sintered whiskers, discussing voids, fiber breakage and orientation effects

03 p0506 A70-13113

Shear moduli and lattice parameters effect on screw dislocation equilibrium in bimetallic medium of soft and hard phases

03 p0587 A70-13117

Serrated plastic flow in stable austenitic steels based on Fe/Ni, showing strength dependence on C and/or Cr presence

03 p0506 A70-13134

Mechanical responses and residual defect structures in brass and stainless steel following explosive shock loading and cold reduction by rolling

03 p0507 A70-13139

Gray hypersthene Ramsdorf chondrite with thermal and mechanical alterations, discussing shock heating, metal plus troilite melt redistribution, collision and rapid cooling effects

03 p0563 A70-13147

Turbine disk strength calculations, obtaining matrix expressions and optimum algorithm for arbitrary disk shapes

03 p0588 A70-13242

Mechanical properties, optimum deformation and rupture of W wire reinforced Ni and Ti metal composites obtained by hot rolling in vacuum

03 p0508 A70-13245

Apparatus for short term thermal vacuum mechanical testing of materials

03 p0463 A70-13253

Case hardened steels structure and properties, intermetallic phases, hardness variation with depth and hardening techniques by Be and B

03 p0510 A70-13351

Polycrystalline Co strength and plastic properties tested at various temperatures and strain rates

03 p0510 A70-13352

Titanium aluminide-Mo system hardness, electrical conductivity and density as function of chemical composition, presenting creep test results

03 p0510 A70-13353

Steel crystal lattice fine structure and mechanical properties during annealing using X rays as function of temperature

03 p0511 A70-13422

Electron bombardment effects on epoxy based textolites mechanical properties, studying structural changes spectroscopically

03 p0516 A70-13735

Beta III Ti alloy cold formability, mechanical properties and heat treatment noting use for fasteners, sheet metal parts, honeycomb sandwich sections and metal matrix composites

03 p0512 A70-13776

Heat treatment effects on mechanical properties of Ti-Fe and Ti-Fe-Al alloys

03 p0512 A70-13855

Quenching temperature and deformation conditions for Ti alloy bars optimal mechanical properties emphasizing effect of primary structure

03 p0497 A70-13856

Polyethylene and polypropylene mechanical behavior under tensile and compressive loads and subject to hydrostatic pressure, obtaining tensile nominal stress-strain curves for various pressures

03 p0517 A70-14201

Electrical and mechanical instability of jets, threads and sheets of viscous fluid, noting role of deceleration

03 p0471 A70-14253

Specific heat, electrical resistivity and thermal conductivity changes in materials properties at cryogenic temperatures, noting parasitic phenomena, mechanical and dielectric properties

03 p0525 A70-14269

Thin elastic laminar shells nonlinear physical theory assuming Love-Kirchhoff hypothesis validity, rigidly connected layers and nonlinear mechanical behavior

04 p0765 A70-14419

Kamchatka regions volcanic deposits structural and mechanical characteristics compared with lunar soil characteristics

04 p0744 A70-14440

Mechanical behavior of anesthetized dog abdominal vena cava from pressure wave transmission characteristics, discussing chemical and electrical stimuli

04 p0630 A70-14630

Apparatus and techniques for investigating spacecraft materials mechanical and thermal properties, using vacuum effect to simulate space environment [ASME PAPER 69-WA/PID-22]

04 p0663 A70-14752

Structural aluminum alloy developed for Concorde Mach 2.2 flight, discussing cold mechanical properties, zero creep and fatigue resistance

04 p0706 A70-15041

Surveyor 7 highland landing soil mechanical properties and rock diameter similar to previous sites

04 p0752 A70-15063

Structural materials mechanical properties tests during neutron bombardment, discussing atomic reactors optimal parameters calculation

04 p0775 A70-15259

Gas turbine rotating disks failure analysis, studying strength as function of material properties, thermal stresses and hole dimensions

04 p0775 A70-15260

High temperature effects on mechanical properties of recrystallized Ta relating strength, hardness and yield point

04 p0707 A70-15267

Commercial Ni-Co gas tungsten arc filler metal with mechanical properties stable following stress relief

04 p0710 A70-15653

Shell directional antennas operational behavior at 2 and 4 GHz and mechanical properties

04 p0660 A70-15661

Polycrystalline metals strength factors in aircraft and aerospace construction as relation between rupture time and embrittled grain boundary at high temperatures

04 p0779 A70-15671

High temperature properties mechanisms in aluminum coated vacuum cast nickel base superalloys

04 p0711 A70-15705

Mechanical properties of eutectic superalloys compared with commercial superalloys, noting thermal stability applicability to gas turbine engines [SAE PAPER 690689]

05 p0861 A70-15827

Low melt viscosity prepolymers of diallyl phthalate and isophthalate in mold encapsulation showing dimensional, electrical and mechanical stabilities under adverse environments

05 p0869 A70-16035

Gas turbine blade material properties change effect on thermal fatigue strength after long term heating

05 p0864 A70-16700

Mechanical properties of cast light alloys at low temperatures, showing satisfactory plasticity and insensitivity to stress raisers

05 p0864 A70-16868

Stress concentration effect on mechanical properties of Ti-Ta alloys at low temperatures, showing insensitivity to notch and suitability for cryogenics

05 p0864 A70-16869

Maraging steels mechanical properties, studying changes in lattice constant and electric resistance to determine Al strengthening effect nature

05 p0865 A70-16872

Maraging steel mechanical properties as function of aging temperature and time

05 p0865 A70-16873

Maraging steel mechanical properties with Mn, Mo and Co additions in heat treated condition

05 p0865 A70-16874

Mechanical properties of nickel steels with carbon after suitable heat treatment found similar to high strength nickel steels properties without carbon

05 p0865 A70-16875

Strength and plasticity of Mo and Nb sheet in oxidizing medium at high temperatures and pressure range

05 p0865 A70-17029

Gas dynamic stand for testing turbine disks strength under mechanical and cyclic thermal loads, analyzing breakdown data for various disk geometry

05 p0953 A70-17052

Scale dependence and optimal sample dimensions for strength tests of brittle refractory materials

05 p0955 A70-17064

Metals mechanical properties with inorganic heat resistant coatings between 1900-2300 K in oxidizing medium, describing facility based on solar furnace

05 p0875 A70-17069

Red blood cell mechanical fragility independence from cell age in rats

06 p0989 A70-17221

Collection of papers on strength at small number of load cycles, problems of mechanical fatigue

06 p1160 A70-17382

Soviet monograph on nickel and Ni vacuum melted alloys, studying physicochemical, operational characteristics and gas content

06 p1085 A70-17411

Thin gas turbine disk strength under axisymmetric flexural vibrations, noting agreement of calculated and experimental rotor rpm danger zone

06 p1166 A70-17654

Mo-nitrogen interaction, studying nitriding influence at various temperatures on Mo alloys properties

06 p1089 A70-17741

Mechanical behavior of cylinders with alternating layers of reinforcing and matrix materials derived from governing equations, including equations of motion

[AIAA PAPER 70-134]

06 p1169 A70-18051

Gibeon meteorite iron strength and ductility tests, discussing fragmentation and relation to parental planet structure

06 p1150 A70-18478

Mechanical property factors influencing selection of sintered uncorked refractory metals and alloys for structural applications

[AIME PAPER F-69-4]

07 p1290 A70-18810

Oxidation, hot corrosion resistance and mechanical properties of aluminide coated superalloys, discussing failure analysis instruments and methods

07 p1305 A70-18969

Solution treating temperature and microstructure effects on hot rolled Ni base alloy properties

07 p1306 A70-18995

Heat transfer effects during solidification on mechanical properties of Al alloy castings compared with sand castings

[ASM PAPER W9-7.2]

07 p1293 A70-18998

Cobalt effects on Ni-W alloys mechanical and metallurgical properties including thermal stability, fabrication response, weldability and impact resistance

07 p1306 A70-19070

Light Mg-Li alloys physical and mechanical properties, production and treatment

[DFVLR-SONDDR-18]

07 p1306 A70-19234

Oxygen content influence on Nb-Mo alloy mechanical properties at ambient temperature in air and hydrogen

07 p1307 A70-19374

Interrelation of precipitation state, mechanical properties and electrical conductivity of wrought aluminum age hardened alloy under varied heat treatment conditions

07 p1294 A70-19389

Oriented single crystals properties obtained from Mo powder subjected to compacting, annealing in hydrogen and electron beam zone melting

07 p1308 A70-19610

Size effect on structure and mechanical properties of thin wire made of Mo single crystals deformed in recrystallized state

07 p1308 A70-19611

Structure and mechanical properties of Mo single crystals grown from gas phase using metallographic and X ray analysis

07 p1308 A70-19612

Intermetallic precipitates development and mechanical properties of maraging steel as function of composition, tempering time and temperature using electron microscopy

07 p1310 A70-19748

Selenium additions effect on structural steels transverse mechanical properties, emphasizing plasticity, shock resistance and machinability

07 p1310 A70-19750

Fiberglass reinforced materials characteristics under stress evaluated by ring test in form of split disk or hydraulic tests

07 p1410 A70-19758

Boron and carbon fiber reinforced composites mechanical properties compared with fiberglass reinforced composites

07 p1318 A70-19770

Single crystal carbides as high temperature structural materials, noting titanium carbide properties and strength-to-density ratio of B-doped crystals

07 p1312 A70-19883

Solid propellant mechanical properties tests, failure and physical deterioration /aging/

07 p1361 A70-19913

Geometrical-mechanical properties in terms of interlaminar shear stress of composite cantilever beams under end load

07 p1412 A70-19965

Glass fiber reinforced polyether composites long time strength under plane stress

07 p1321 A70-20187

Soviet book on mechanical properties of heat resistant steels and alloys at room and elevated temperatures

06 p1515 A70-20691

Glass filament reinforced plastics characteristics, considering filament protection during manufacture

08 p1526 A70-20717

Static loading effect at high temperatures in argon and liquid lithium on mechanical properties stability of steel

08 p1515 A70-20920

Steel strength under prolonged preliminary loading at elevated temperatures

08 p1515 A70-20934

Steel structure and mechanical properties under preliminary loading at elevated temperature and liquid Li at various exposure times

08 p1515 A70-20935

Mo mechanical properties dependence on surface defects and Ti films

08 p1515 A70-20937

Rare earth elements effects on microstructures and mechanical properties of cast Al, Al-Si and Al-Si-Mg alloys

08 p1516 A70-21127

Al-Mg alloys mechanical properties and corrosion resistance during aging, noting Zr and Mo additives effects

08 p1517 A70-21129

Al-Mg oxidation resistance and kinetics, studying Zr, Ce and Be additives effects on oxide films mechanical properties

08 p1517 A70-21130

Graphite molds compaction pressure effect on Ti castings nonporosity and surface layers carburization

08 p1506 A70-21143

Nickel boronizing in high temperature vacuum, studying mechanical properties and layer thickness time dependence

08 p1517 A70-21148

Mo sheet longitudinal and transverse mechanical properties and microstructure after annealing

08 p1517 A70-21199

Ti-based alloys with Al and Mo investigated for chemical composition and heat treatment effects on mechanical properties

08 p1518 A70-21200

Strain rate effects on mechanical properties of solids under dynamic loading

08 p1590 A70-21328

Dynamic mechanical properties of filled polymers as function of filler concentration, particle agglomeration and ratio of particle to polymer modulus

08 p1527 A70-21335

Nonmetallic inclusions effect on steels cyclic strength dependence on inclusion composition and metallic matrix properties derived from fatigue tests

08 p1590 A70-21413

Ultrasonic vibration effect on strength and plastic properties of metals undergoing torsion tests

08 p1520 A70-21499

Terminal mechanical characteristics of metals after ambient-temperature high energy rate forming compared with low rate processes

08 p1520 A70-21554

Turbine disk strength calculations, obtaining matrix expressions and optimum algorithm for arbitrary disk shapes

08 p1580 A70-21657

Mechanical properties and fracture behavior of chemically bonded glass matrix-metal composites

08 p1521 A70-21699

Wrought aluminum based high strength alloys structure and mechanical properties

08 p1522 A70-21708

Engineering use of filament reinforced metal matrix composites dependent on fabrication cost reduction, consistent properties and form flexibility

08 p1509 A70-21851

Cobalt modified Ti-6Al-4V plate and billet, testing effects on heat treatment response, microstructure, tensile and fatigue properties, fracture toughness, etc

08 p1523 A70-21852

Al alloy matrix composites with beta-SiC whiskers reinforcement, evaluating tensile and fatigue properties

08 p1523 A70-21856

Tension, compression and in-plane shear tests to obtain boron epoxy composite materials mechanical properties to design FB-111 wing box extension

08 p1529 A70-21879

Uniaxial and multiaxial stiffness and property characterization of anisotropic composite materials formed as thin walled cylinders

08 p1529 A70-21880

Mechanical properties characterization of unidirectional high modulus carbon fiber reinforced epoxy matrix composite

08 p1530 A70-21883

Mechanical testing of metal matrix high modulus B-Al filament composites, using unidirectional and multidirectional reinforcement

08 p1523 A70-21894

Graphite fiber/resin matrix composites for airframe structures, studying tensile, compressive and in-plane shear strengths

08 p1532 A70-21901

Fiberglass-epoxy laminates mechanical behavior under biaxial loading, describing test equipment and procedures

08 p1532 A70-21904

- Fractography of Al-B metal matrix composites to study micromechanical behavior, using scanning electron microscopy 08 p1524 A70-21913
- Metastable austenitic steel mechanical properties after thermomechanical treatment with deformation, discussing stress-strain curves to exhibit yield point 08 p1525 A70-21963
- Co-based alloy mechanical properties and physical parameters at high temperatures, discussing oxidation and hot corrosion resistance 09 p1700 A70-22025
- Strength and plasticity criteria for anisotropic reinforced materials model taking into account material structure, components properties and behavior 09 p1768 A70-22119
- Solid propellants mechanical properties under uniaxial tension 09 p1741 A70-22423
- Soviet collection of papers on mechanical fatigue from statistical standpoint 09 p1775 A70-22614
- Mechanical and physical properties of Nb-Ti binary annealed alloys as function of compound NbTi using microscopic and X ray phase analysis 09 p1704 A70-22755
- Thermal cyclic loads effects on heat resistant materials strength during strain hardening, considering role of time factors in durability 09 p1779 A70-23104
- Cellular structure and grain size effects on mechanical properties of strained and recrystallized chromium 10 p1902 A70-23862
- Ultrasonic vibrations effects on microstructure and mechanical properties of polycrystalline titanium during phase recrystallization 10 p1903 A70-23863
- Tantalum mechanical properties dependence during deformation on temperature and strain rate irregularities, discussing serrated yielding 10 p1904 A70-24386
- Duplex aging treatment effect on Ni-Co-Mo-Ti maraging steels mechanical properties 10 p1905 A70-25171
- Binary Ni-Cr alloys tensile mechanical properties at 25 C after water quenching and heat treatments 10 p1905 A70-25172
- Monograph on adhesive materials covering selection criteria tables, mechanical properties, specifications, surface preparation and joint strength 10 p1908 A70-25225
- Multicomponent Ti alloys mechanical properties for use in cryogenics describing alloying advantages with tantalum 10 p1906 A70-25295
- Shells equilibrium with large plastic deformations, discussing stability under uniaxial/biaxial tension and physical models for material mechanical properties 11 p2130 A70-25569
- Glass epoxy cross ply laminates with brittle or ductile epoxy matrices tensile tested, comparing mechanical performance 11 p2068 A70-25686
- Copper alloy composite reinforced by unidirectional solidification of pseudobinary eutectic Cu-ZrCuSi, discussing mechanical properties and electrical conductivity 11 p2066 A70-25775
- Silicon carbide whiskers properties and applications compared with other reinforcing fibers 11 p2070 A70-26340
- Measurement of dynamic mechanical quantities - Conference, Warsaw, May-June 1968 11 p2052 A70-26426
- Mechanical parameters measurement by radio telemetry during aircraft and motor vehicles tests, noting onboard recording methods 11 p2056 A70-26452
- Noise effects during mechanical parameters measurement by electronic devices, noting noise from resistors, potentiometers, power lines and wiper-type distributors 11 p2056 A70-26454
- Metals low cycle fatigue resistance, discussing repeated plastic straining effect on mechanical properties 11 p2141 A70-26609
- Earth mechanical properties and composition compared with moon and other terrestrial planets 11 p2047 A70-26616
- Mechanical properties in solids under dynamic incremental shear loading, discussing wave propagation tests on steel, Cu and Al 11 p2143 A70-26669
- Physicomechanical properties of tuff rock based on similarity to lunar surface rock, determining natural density, porosity and compression strength 11 p2119 A70-26798
- Structural materials chemical and metallurgical factors controlling mechanical properties, machinability and finished part producibility [ASTME PAPER MR-69-731] 12 p2240 A70-26992
- Wide goods fabrication of boron composites, discussing mechanical properties and cost effectiveness [ASTME PAPER EM-69-142] 12 p2240 A70-27078
- Strength conditions for orthotropic Hooke law materials with complex elasticity, giving elastic potential boundary values in tensor form 12 p2325 A70-27560
- Transpiration-cooled systems design with porous materials, considering mechanical and flow control/permeability/properties requirements 12 p2256 A70-27822
- Aluminum-boron composite material applications to structural components of F-106 aircraft, noting weight saving and mechanical properties [AIAA PAPER 68-975] 12 p2257 A70-28082
- Annealed compressed ground synthetic mica and silver dust composite materials, analyzing physicomechanical properties 12 p2260 A70-28319
- Fiber diameter effects on metal matrix composites strength from proposed model 12 p2329 A70-28370
- Kamchatka regions volcanic deposits structural and mechanical characteristics compared with lunar soil characteristics 13 p2485 A70-28465
- Glass fiber reinforced resin structures and equipment quality and physical/mechanical conditions determined by plastographic analysis 13 p2404 A70-28665
- Nonlinear theory describing mechanical behavior of prestressed laminated composites subjected to large deformations 13 p2511 A70-28738
- Collection of papers on nickel and nickel alloys covering thermal and mechanical properties during annealing and precipitation hardening behavior 13 p2432 A70-28758
- Deformation, mechanical properties and processes during recrystallization annealing of nickel and alloys single crystals 13 p2433 A70-28761
- Ni alloys hardening by solid solution precipitation and insoluble particles dispersion, emphasizing heat resistant alloys and mechanical properties 13 p2433 A70-28762
- Diffuse coatings effect on strength characteristics and corrosion resistance of steels, analyzing structure, thickness and purity of surface layers 13 p2433 A70-28888
- Electrodynamical transducer electrical and mechanical parameters measurement, comparing various techniques 13 p2406 A70-28991
- Structural Al-Zn-Mg alloys strain hardening effect on mechanical and corrosion properties, noting relationship between stress corrosion cracking and shear cracks 13 p2434 A70-29155
- Versamid cured epoxies time-dependent mechanical properties, determining loading mode, strain level and reinforcing agent effects on time-temperature shift factors 13 p2438 A70-29205
- Planar reinforced plastic resins strength and stiffness, considering mechanics of film, flake and ribbon reinforcements 13 p2438 A70-29206
- Titanium alloys powder metallurgy, considering manufacturing methods and physical, chemical and mechanical properties 13 p2435 A70-29214
- Materials selection for vibration or shock control based on cost, resonance frequency, strength, weight, etc 13 p2513 A70-29218
- Borsic-aluminum composite materials fabrication, properties and applications to aircraft parts 13 p2420 A70-29246
- Skin and tissue mechanical characteristics response to vibratory stimulation, considering effects on physiological and psychophysical tactile sensitivity measurements 13 p2354 A70-29598
- Stainless steel fiber reinforced Sn-Pb eutectic alloy composite mechanical properties, noting tensile strength and rupture behavior 13 p2436 A70-29625
- S glass fibers strength characteristics at quasi-static strain rates, considering temperature effects on elastic modulus 13 p2439 A70-29707
- Fatigue life and long term strength of polycarbonate components in pneumatic pulsating pressure equipment described by power and exponential equations 13 p2440 A70-29784
- Tensile tests on wings and wing components of plastic engine-driven aircraft, discussing design, configurations and mechanical properties 14 p2656 A70-30250
- Soviet monograph on V and V alloys covering phase diagrams, mechanical, chemical and physical properties, compounds and chemical composition 14 p2595 A70-30627
- Mission sequential environment effects on Dacron parachute material mechanical properties [AIAA PAPER 69-1018] 14 p2563 A70-30770
- Airframe critical part structural reliability on basis of ultimate static strength test data and extreme gust spectrum and maneuver loads 14 p2658 A70-30852
- Hydride segregation in Ti alloy weldments made with unalloyed Ti filler metal, determining effect on mechanical properties 14 p2591 A70-30932
- Al heat treatable alloys for welded structures, considering stress corrosion resistance, aging effects, brittle and delayed rupture resistance, etc 14 p2596 A70-30961
- Work hardening and tempering effects on Al-Mg alloy stress corrosion and mechanical properties 14 p2597 A70-30963
- Al-Zn-Mg weldable alloy composition, mechanical properties, heat treatment, aging effects, etc 14 p2597 A70-30964
- Al-Mg-Zn alloy composition, mechanical properties and structure for various heat treatments, discussing welded structures stability, stress relief, corrosion resistance and tensile strength 14 p2597 A70-30966
- Al alloy welded sheets strength and plasticity under biaxial tension, examining excess elastic energy effects on strain kinetics and rupture 14 p2597 A70-30967
- Al weldable alloys for cryogenic applications, considering plasticity, brittleness and tensile and yield strengths at low temperatures 14 p2597 A70-30968
- Lunar surface mechanical properties from Surveyor spacecraft interactions with soil /exclusive of surface sampler/ 14 p2644 A70-31055
- Piezoelectric annular disk transducer mechanical response to step voltage input with prescribed temperature field 14 p2588 A70-31228
- Book on high modulus fibers and composites providing data for preparation, microstructure, structure and properties 14 p2598 A70-31315
- Pyroceramics transient strength measurements on cylindrical and prismatic samples under static bending 15 p2764 A70-31545
- Hot rolling and warm working effects on microstructure and mechanical properties of Ni-Cu-Cb steel, noting optimum austenite plus ferrite phase field 15 p2756 A70-31566
- Filament orientation and fabrication variables effect on Ag matrix-W fiber composite mechanical properties 15 p2756 A70-31569
- Carbon reinforcing fibers, discussing mechanical properties, production, cost reduction, etc 15 p2765 A70-32246
- Superalloys commercial development, investigating strength, heat resistance and weldability of Fe- and Ni-based alloys [ASM PAPER W70-9-4] 15 p2760 A70-32335
- Thermal-mechanically treated stainless steels structure and properties, discussing stress relief aging effects 15 p2761 A70-32380
- Room temperature mechanical properties and structure of age hardened Ti-Cu alloys 15 p2761 A70-32384
- Statistical theory of material strength applied to composite materials reinforced with whiskers and noncontinuous fibers 15 p2763 A70-32833
- Book on engineering properties of thermoplastics covering strength characteristics, plastic components design, etc 15 p2766 A70-32843
- Isotropic composite materials with anisotropic components, determining microconstants for heat conduction, elasticity and thermoelasticity problems 15 p2766 A70-32896
- Anisotropic glass fiber reinforced plastics strength and deformability under cyclic axial loads 15 p2766 A70-32897
- Boron effects in austenitic stainless steels, considering chromium carbide formation, high temperature strength, ductility, etc 16 p2916 A70-33079
- Mechanically heterogeneous and optically homogeneous solid/liquid mixed laser with active centers contained in Ne bathed in liquid 16 p2926 A70-33109
- Ti-Mo cermet alloys properties and production technology, testing corrosion resistance 16 p2931 A70-33220
- Book on refractory metal properties covering nuclear reactor use, atomic, electronic and crystal structures, thermal and electrical characteristics irradiation effects, nuclear properties, etc 16 p2931 A70-33268
- Chemical structure and room temperature tensile, flexural and compressive properties of metaphen-

ylene diamine cured castings for graphite fiber reinforced epoxy resin matrices

16 p2936 A70-33358

Mechanical properties of composite materials reinforced with ribbon fibers consisting of stainless steel and polyethylene ionomer resins

16 p2988 A70-33366

Mechanical properties prediction analysis of boron filament wound reinforced composite structures verified by structural tests

16 p2937 A70-33370

Chemical and moisture resistance, electrical and mechanical properties of engineering thermosetting plastics made of HYSTL resins

16 p2938 A70-33380

Large capacity sealed nickel cadmium battery for spacecraft, describing mechanical and electrical characteristics

16 p2844 A70-33473

Beta transition mechanism dynamic mechanical properties in bisphenol-A based epoxy resins prepared with different curatives

16 p2856 A70-33500

Laminated multioriented filamentary composites strength and fracture characteristics under longitudinal tension and compression

[ASME PAPER 70-DE-31]

16 p2989 A70-33502

Fatigue life estimation from fracture mechanics data, discussing flaw geometry and propagation, mechanical properties, damage accumulation, etc

16 p2989 A70-33601

[AIAA PAPER 70-601]

16 p2989 A70-33601

Titanium electron beam welding in aerospace industry, discussing alloy properties and strength behavior

16 p2919 A70-33683

Grain boundary sliding model subjected to shear strain, discussing effect on mechanical properties

16 p2932 A70-33789

Thermal and mechanical properties of materials for spacecraft booms design

16 p2986 A70-34138

Dislocation diffusion effects on strength of whiskers and fine grained polycrystals

16 p2934 A70-34327

Chemical and structural microinhomogeneity, diffusion and mechanical properties of Ti alloys in connection with phase transformation characteristics

17 p3112 A70-34354

Electroslag melted titanium wrought shapes mechanical properties, comparing with double vacuum arc melted material properties

17 p3112 A70-34356

Interstitial impurities effect on mechanical properties of Ti alloys, discussing interaction between solutes and dislocations

17 p3116 A70-34390

Unalloyed alpha titanium mechanical properties, emphasizing grain size and interstitial content effects on strain hardening and deformation dynamics

17 p3116 A70-34391

Martensitic transformation effects on mechanical properties of beta quenched Ti binary alloys

17 p3119 A70-34414

Solution heat treatment temperature effects on strength and age hardening of Ti alloys

17 p3120 A70-34419

Shock deformation effects on strengthening and microstructure of Ti and Ti-Mo alloys

17 p3120 A70-34420

Thermal exposure effect on room temperature mechanical properties of Ti alloys, noting diffusion bonding, hot forming and heat treatment

17 p3120 A70-34422

High temperature heating and cooling effects on mechanical properties and structure of Ti welds, using notched bar impact specimens

17 p3098 A70-34423

Forged alpha/beta Ti alloys, investigating relationship between mechanical properties and microstructures produced by heating

17 p3120 A70-34427

Ultrahigh strength alpha-beta titanium alloys, examining carbon and oxygen effects on mechanical properties

17 p3121 A70-34429

High strength Ti alloys depth hardenability, discussing mechanical properties and use in aircraft components

17 p3121 A70-34434

Heat treatment effect on strength and ductility of Ti-Al-V-Sn alloy by optical and electron microscopy and X ray diffraction

17 p3122 A70-34437

Heat treatment and composition effect on mechanical properties of alpha Ti-base alloy, discussing creep resistance, tensile strength, etc

17 p3122 A70-34439

Ti alloys use in Olympus 593 engine for Concorde SST, discussing weight saving, mechanical properties and manipulation characteristics

17 p3146 A70-34449

Cold working effects on Zircaloy tubes mechanical properties and hydride orientation, discussing tubes use in nuclear power stations

17 p3123 A70-34645

Temperature and strain rate effects on polycrystalline Al strength

17 p3124 A70-34655

Composite materials in aerospace vehicle design, discussing mechanical behavior, applications and characteristics

17 p3127 A70-34674

Physical properties and structure of Cr-Ni austenitic stainless steels with high Mn and N content as function of temperature

17 p3125 A70-35143

Corrosion and mechanical properties of Cr-Ni-Mn-N austenitic stainless steels

17 p3125 A70-35144

Temperature and constant compressive loading effects on mechanical characteristics of fiberglass reinforced plastics

17 p3127 A70-35341

Collection of papers on physics of strength and plasticity, covering flow mechanisms, stress fields, alloy hardening, crack structure and initiation, rock ductility, etc

17 p3190 A70-35451

Temperature dependence of materials with protective coatings, emphasizing mechanical properties of Mo with various diffusive coatings

17 p3126 A70-35716

Composite compression tubes for VTOL aircraft components, describing weight parameters and mechanical properties

[AIAA PAPER 70-898]

17 p3193 A70-35809

Ti-Al binary and Ti-Al-X ternary alloys grain boundary precipitation kinetics and correlation with mechanical properties

18 p3272 A70-36035

Two phase stainless steels with microduplex structures, taking into account martensite and ferrite effects on mechanical properties

18 p3272 A70-36038

Ti-Al alloys room temperature mechanical properties after age hardening

18 p3274 A70-36055

Mechanical properties of binary Ti-Ni and ternary Ti-Mo-Ni alloys

18 p3275 A70-36122

Fine grained Be structure and mechanical properties under tensile deformation at temperatures from 20 to 1000 C

18 p3276 A70-36311

Thickness determination of external elastic plates in freely supported three layer structures of uniform strength under perpendicular loads

18 p3343 A70-36717

Al alloy matrix-boron fiber-stainless steel wire composites fabrication into various shapes with desired mechanical properties for aerospace structural components applications

18 p3263 A70-36837

Porosity effects on mechanical properties of Al alloy gas tungsten arc welds, noting strength loss proportional to cross sectional area loss

18 p3265 A70-37205

Normalization of mechanical properties of aircraft engine components, increasing weight efficiency and reliability

19 p3490 A70-37254

Ti and C effects on Fe-Cr-Ni alloys mechanical properties

19 p3449 A70-37271

Heat resistance of cast, forged and annealed Ti-Cu alloys, discussing forged alloys mechanical properties as function of chemical composition and temperature

19 p3449 A70-37273

Dispersion hardened Co strength and plasticity temperature dependence, determining Ti and Nb carbides additives effects

19 p3450 A70-37350

Tungsten fiber reinforced copper based composite material, investigating moulding and sintering conditions effect on mechanical properties

19 p3450 A70-37454

Ti alloys low temperature strength and plasticity, noting twinning and additives effects

19 p3450 A70-37457

Friction reducing oxide layer effects on Ti alloys low temperature plastic and mechanical properties

19 p3450 A70-37458

Electron radiation damage and stage 3 annealing effects on polycrystalline Mo properties

19 p3451 A70-37570

Mathematical representation of heart muscle mechanical properties, examining tensile stress in parallel and series elements

19 p3368 A70-37809

Graphite-polyimide composites development for high temperature environments, discussing mechanical properties

19 p3455 A70-38425

Turbine disk strength calculations, obtaining matrix expressions and optimum algorithm for arbitrary disk shapes

19 p3548 A70-38460

Mechanical properties, optimum deformation and rupture of W wire reinforced Ni and Ti metal composites obtained by hot rolling in vacuum

19 p3453 A70-38463

Apparatus for short term thermal vacuum mechanical testing of materials

19 p3401 A70-38471

Book on materials for structural and mechanical functions covering electrical engineering properties, ferrous and nonferrous metals and alloys, fabrication methods, environmental protection, etc

19 p3453 A70-38622

Pt resistance thermometers for low temperature measurements, discussing structural and mechanical characteristics

19 p3432 A70-38704

W-Mo-Nb-Ta system structure and properties at room and high temperature by microstructural analysis and hardness measurements, discussing Mo addition effects

19 p3453 A70-38713

Heat treatment and alloying element influence on phase and structure transformations in Ti alloys, investigating mechanical properties and creep resistance

20 p3645 A70-39039

Ti alloys fine structure, mechanical properties and alloying elements diffusion mobility during heat treatment, observing chemical and structural inhomogeneities

20 p3645 A70-39040

Nb-Ta and Nb-Mo alloys single crystal solid solution strengthening as function of composition, temperature and strain rate

20 p3646 A70-39105

One-component rigid epoxy foam system suitable for lightweight electronic potting, determining mechanical, electrical and thermal properties

20 p3652 A70-39167

High temperature acoustic waves, examining solid and fluid properties, weld integrity nondestructive material tests and nondisruptive process measurement

20 p3628 A70-39170

Carbon/carbon composites constituent characteristics effects on thermal and mechanical properties, using polarized light and scanning electron microscopy

20 p3653 A70-39204

Carbon/carbon composites thermal and mechanical properties measurements by NDT including image transducer, IR scanning and ultrasonic methods

20 p3636 A70-39213

Alloys for aircraft structures design, considering materials strength, corrosion resistance, producibility and cost

20 p3648 A70-39414

Stainless maraging steel bolts tensile, shear and fatigue strengths and stress corrosion resistance at room and high temperatures

20 p3650 A70-39964

Ti alloy bolts mechanical properties improvement by beta heat treatment

20 p3650 A70-39965

Beta III Ti alloy for aircraft fasteners, describing microstructure and mechanical properties

20 p3650 A70-39966

Composites potential structural performance, determining mechanical properties for fiber and matrix materials and unidirectional and isotropic composites in cylinders and box beams

20 p3651 A70-40042

Wire reinforced solid rocket propellant grains mechanical properties and failure modes

20 p3689 A70-40050

Unidirectional fiber reinforced composites strength, obtaining limit load bounds from plasticity analysis

20 p3731 A70-40051

Glass reinforced plastics /GRP/ mechanical properties degradation by water, discussing effects of temperature, pressure, environment, etc

20 p3656 A70-40056

Ti mechanical properties dependence on grain boundary size and hydride precipitation characteristics, considering transcrystalline and intercrystalline fracture

20 p3652 A70-40179

Mechanical behavior of cylinders with alternating layers of reinforcing and matrix materials derived from governing equations, including equations of motion

20 p3732 A70-40267

Elastomechanical system reciprocity relation principles using differential equations for bar with forces in two places

20 p3735 A70-40537

Multilayer three dimensionally woven fiberglass-reinforced materials, measuring strength and deformation under tension, compression, bending, torsion and shear tests

21 p3841 A70-40646

Unidirectional fiberglass-reinforced plastic, investigating binder content and porosity effects on strength

21 p3841 A70-40647

Mechanical behavior differential equation representation in presence of finite deformations using state variables

21 p3937 A70-41434

Zr-Nb alloys mechanical strength increase due to beta phase martensitic decomposition

21 p3840 A70-41897

Hot pressed zirconia-zirconia ceramic fiber reinforced ceramic matrix composites, discussing mechanical properties and failure modes

22 p4057 A70-42285

Solid rocket fuels mechanical properties, using high speed pneumatic test machine and impact tensile tester

22 p4088 A70-42342

Repair weld procedures effects on annealed Ti-Al-V weldments mechanical properties, examining defects in inert gas shielded arc welded joints

[ASME PAPER 70-MET-1] 22 p4043 A70-42425

Scorched aluminum powder /SAP/ materials, discussing fabrication, physical and mechanical properties, applications in aircraft structural components, etc

22 p4055 A70-43084

High strength high Ni maraging steels crystal structure, alloying elements effects on mechanical properties, applications, etc

22 p4055 A70-43121

Vacuum-melted and deformed Mo alloys tests, showing long term strength decrease under cyclic heating

22 p4055 A70-43123

Recrystallized and overrecrystallized Al alloys, investigating factors controlling anisotropy of mechanical properties

22 p4056 A70-43126

Al-Be-Mg alloys under solution treatment, noting aging and prolonged heating effects on mechanical properties from solid solution decomposition diagram

22 p4056 A70-43127

Polycrystalline aluminas under thermal shock, investigating strength decrease and subcritical crack formation

22 p4059 A70-43413

French book on strength of materials covering potential energy theory, cutoff and matrix methods, computer calculations, etc

22 p4119 A70-43623

Laminated composites time dependent static strength and reliability under uniaxial tension

22 p4119 A70-43678

Solidified polyglycol maleinate resin optical and mechanical properties under tensile stress creep, using hereditary photoelasticity

22 p4121 A70-43723

Mechanical properties and internal stress fields in composite materials reinforced by glass fibrous filler under transverse shear

22 p4061 A70-43724

Specific strength of unidirectional fiber reinforced metal matrix composites, using volume ratio-transfer coefficient diagrams

23 p4209 A70-43939

Statistical analysis of durability data of heat resistant alloys for gas turbine engines, using long term strength tests of melts in mass production

23 p4204 A70-43940

Fiberglass reinforced plastic strength and deformation properties under creep and stress relaxation, investigating temperature effects and load duration

23 p4209 A70-43980

German monograph on glass fiber reinforcement effect on soft thermoplastics strength, adhesion and slip properties

24 p4366 A70-45088

Fibrous composites use in compressor blades, discussing materials characteristics requirements relative to environmental and stress conditions in aircraft operational service

24 p4392 A70-45169

Fibrous composites design for mechanical properties improvement, discussing interfacial properties conflicting requirements as to interlaminar shear, transverse tensile strength, high work of fracture values, etc

24 p4419 A70-45172

Polymers strength and stiffness properties, considering different molecular chain alignments as related to elastic modulus

24 p4366 A70-45173

Materials design and development for engineering applications, discussing relationships and importance of strength, stiffness, weight, toughness and work of fracture

24 p4419 A70-45174

Superalloys dispersion strengthening and age hardening by mechanical alloying

24 p4341 A70-45246

Unimodal and bimodal distribution of fiber composite properties at different stress levels using quantitative metallography

24 p4359 A70-45250

Steel and duralumin strips with circular holes tested under axial tension, determining relationship between strength weakening and ultimate stress

24 p4420 A70-45272

Polyvinyl chloride /Novodur/ mechanical properties application to structural model testing

24 p4367 A70-45445

Caprolon B mechanical properties, comparing properties to other polyamide resins for use in machine parts fabrication

24 p4367 A70-45503

Alpha phase Ti strengthening, investigating interaction between dislocations and interstitial solute atoms

24 p4360 A70-45516

Plasticized high polymers mechanical and optical properties, studying birefringence phenomena interrelation with applied external stresses

24 p4424 A70-45590

MECHANICAL RESONANCE U RESONANT VIBRATION MECHANICAL SHOCK

Bolted joints inspection using mechanical impedance algorithm method involving bolt head mechanical shock pulse response in adjacent structure

01 p0098 A70-10017

Mechanical shock accelerometer calibration by light frequency Doppler shift measurement using laser interferometer and single sideband carrier insertion circuit

08 p1493 A70-20602

Simple high level shock machine producing trapezoidal and terminal peak sawtooth pulses with Al honeycomb impact material

19 p3396 A70-37832

Optical FM system with laser interferometer and sideband carrier circuit for measuring mechanical shock by Doppler shift

23 p4193 A70-43964

Shock and bump testing for dynamic mechanical environments effects encountered by vehicle equipment and components

23 p4195 A70-44331

Resonant fixtures utilization attaining high amplitude in shock synthesis testing, discussing test specifications

24 p4322 A70-45886

[SAE PAPER 700848] MECHANICAL TWINNING

Fast brittle crack slowing by mechanical twins in transformer steel and by slip bands in LiF and NaCl crystals

15 p2755 A70-31526

Twinning lamella formation in Nb single crystals, examining slip and shear roles in surface tilt formation

15 p2761 A70-32382

MECHANICS (PHYSICS)

Developments in mechanics - Conference, Ames, Iowa, August 1969

01 p0203 A70-11126

Holographic interferometry applications in experimental mechanics, illustrating nondestructive testing by flaw detection in bonded honeycomb

03 p0481 A70-12959

Applied mechanics - Conference, Stanford, August 1968

03 p0596 A70-14226

Nonlinear solid applied mechanics, emphasizing nonlinear constitutive equations and related subjects, cyclic loading effect on solid materials, etc

03 p0610 A70-14230

Theoretical and applied mechanics - Conference, Coimbatore, India, December 1966

03 p0601 A70-14326

Mechanical engineering and mechanics-Conference, Haifa, June-July 1969

05 p0939 A70-16508

Apollo 8 mission, spacecraft and booster details, calculating earth-moon flight parameters based on laws of mechanics

07 p1375 A70-18776

Soviet collection of papers on control mechanics and processes, computational mathematics

09 p1772 A70-22532

Applied mechanics - Conference, Bucharest, June 1969

10 p1802 A70-24776

Applied mechanics - Conference, Bucharest, June 1969

10 p1870 A70-24794

Mechanics of solid structures including shells and beams, considering three dimensional behavior laws in plasticity and creep

14 p2656 A70-30294

Mechanics - Conference, Bucharest, June 1969

16 p2893 A70-33740

Applied mathematics and mechanics - Conference, Aachen, Germany, April 1969

18 p3280 A70-36351

Computer language related to ALGOL 60 for handling nonnumerical problems of mechanics

18 p3283 A70-36367

Theoretical and applied mechanics - Conference, Tulane University, February-March 1968

19 p3543 A70-38326

Theoretical and applied mechanics - Conference, Haifa, July 1970

21 p3938 A70-41958

Applied mechanics - Conference, Bucharest, June 1969

22 p4113 A70-42601

Applied mechanics - Conference, Bucharest, June 1969

22 p4009 A70-42605

Applied mechanics - Conference, Bucharest, June 1969

22 p4113 A70-42610

Applied mechanics - Conference, Bucharest, June 1969

24 p4423 A70-45576

Applied mechanics - Conference, Bucharest, June 1969

24 p4423 A70-45586

MECHANISM

Book on dynamics of mechanisms with elastic connections and impact systems covering differential and finite difference equations, equations of motion, friction effects, etc

08 p1502 A70-20753

Equations of motion of holonomic and non-holonomic mechanical systems obtained by displacement operators

08 p1546 A70-21627

MECHANIZATION

Mechanized Algebraic Operations software package for manipulation on computer Poisson series, noting application to celestial and nonlinear mechanics and astrodynamics

10 p1845 A70-24179

Strapdown inertial system mechanization and modularized instrument packaging with self contained failure isolation, temperature control and redundant components

22 p4066 A70-42315

[AIAA PAPER 70-1027] Inertial navigation system application to air transportation, discussing system mechanization and compatibility with ATC requirements

22 p4066 A70-42654

MEDIA

NT ANISOTROPIC FLUIDS
NT ANISOTROPIC MEDIA
NT ELASTIC MEDIA
NT INTERGLACTIC MEDIA
NT INTERPLANETARY DUST
NT INTERPLANETARY GAS
NT INTERPLANETARY MEDIUM
NT METEOROID DUST CLOUDS
NT ZODIACAL DUST

Book on antennas and waves covering EM radiation, configurations, insulation, dissipative media, coupling, transmission lines, etc

12 p2194 A70-27095

Stochastic medium mathematical model for loose medium motion in potential field of forces

15 p2821 A70-32342

MEDICAL ELECTRONICS

Rocky Mountain Bioengineering - Conference, Laramie, Wyoming, May 1969

02 p0242 A70-12093

Monitoring and recording of physiological parameters, discussing heart, muscle, brain potentials, blood pressure, respiration measurements and instrumentation

03 p0439 A70-14267

Arrhythmia monitor for cardiac distress prediction, using small hybrid computer for detection of abnormal rhythm and ECG complex comparison

07 p1221 A70-19604

Electronic measurement of bronchial flow resistance in pulmonary function to determine impediment in inhaled and exhaled air passage

08 p1449 A70-20676

Electromagnetic flowmeter for cardiac output changes in unanesthetized rats, discussing construction, form and associated electronic equipment of implanted probe

09 p1627 A70-23267

ECG telemetry system within small irregular metal chamber

11 p1992 A70-26514

Dry electrodes application to ECG monitoring under primitive field conditions, noting materials storage and transportation advantages

11 p1993 A70-26524

Electromagnetic blood flow determination by catheter in external magnetic field, discussing intravascular EM flow sensor capable of percutaneous introduction into vascular system

11 p1993 A70-26663

Medical electronics and biological engineering - Conference, Nancy, France, June-July 1969

14 p2540 A70-30376

Cycloergometer with powder type electromagnetic brake for respiratory and circulatory measurements and functional rehabilitation

14 p2541 A70-30379

Bioradiotelemetry of human cardiac activity during professional activities, using ultrasonic searchless Doppler cardiography

17 p3038 A70-35365

- Cardiovascular stress testing using posterior bipolar lead for radiotelemetry monitoring
20 p3578 A70-39199
- Medical monitoring system onboard Soyuz spacecraft, describing equipment design, data acquisition and analysis, telemetric recordings, etc
20 p3581 A70-40193
- Reverse curvature silicon transistor linearizer for hot-wire and thin-film constant temperature anemometers for aorta blood flow velocity measurements
21 p3827 A70-41458
- High fidelity microelectrode recording of phase zero cardiac transmembrane action potentials, utilizing memory oscilloscope
21 p3772 A70-42163
- Real time contourographic electrocardiographic display determining heart rate from CRT face on beat-by-beat basis
23 p4150 A70-44377
- Electronic simulation of indicator-dilution curves for comparative evaluation of cardiac output computers
24 p4309 A70-46120

MEDICAL EQUIPMENT

- NT ARTIFICIAL EARS**
NT CARDIOTACHOMETERS
NT PROSTHETIC DEVICES
NT SURGICAL INSTRUMENTS
- Inexpensive schlieren system for medical ultrasonic research, discussing equipment and application to short wave transducer beam patterns used in ophthalmology
02 p0300 A70-12472
- Medical kit utility for colds, sore throats, scrapes, cuts and bruises
07 p1219 A70-19021
- Biomedical instrumentation evaluation procedure to minimize redesigns and delays and to bridge communication gap between medical and engineering fields
08 p1450 A70-20791
- Medical laser systems applications, design criteria, general functions, etc
08 p1450 A70-20819
- Laser safety programs in biomedical applications, discussing installations, techniques, hazards and protection
08 p1451 A70-21048
- Medical thermograph with modified image-pickup device characteristics and additional thermal analysis equipment
10 p1828 A70-25307
- Preflight medical examination of flying personnel, describing portable device for recording systolic/diastolic pressure, body temperature and pulse rates
13 p2357 A70-29296
- Portable battery operated system for rapid measurements of blood plasma electrolytes during aeromedical evacuation
20 p3579 A70-39433
- Multiple choice rotation chair for clinical experimental research and pilot vestibular tests
20 p3580 A70-39438
- Air transportation of respiratory failure patients, considering medical equipment adaptation for aircraft use
20 p3580 A70-39440
- Lasers biomedical applications based on thermal and ionization effects on biological targets, considering eye surgery, tumor treatment, etc
24 p4308 A70-45568
- Lasers for surgical applications, cancerous tissue treatment, ophthalmology and comparison with RF diathermy
24 p4308 A70-45569

MEDICAL PERSONNEL

- NT FLIGHT SURGEONS**
NT PHYSICIANS
- MEDICAL PHENOMENA**
NT PHENOMENOLOGY
- Medical wastage of professional aviators in military and civil aviation, discussing reasons for preventing flying license revalidation
13 p2359 A70-29440

MEDICAL SCIENCE

- NT EPIDEMIOLOGY**
NT HISTOLOGY
NT IMMUNOLOGY
NT NEUROLOGY
NT NEUROPSYCHIATRY
NT OTOTOLOGY
NT PHENOMENOLOGY
NT PSYCHIATRY
NT RADIATION MEDICINE
NT RADIOBIOLOGY
NT RADIOLOGY
NT SYMPTOMOLOGY
NT TOOTH DISEASES
- Biochemical, electron microscopy and experimental medicine data indicating pathogenetic mechanism responsible for arteriosclerosis
03 p0431 A70-14278
- Imagery in medicine - Conference, Ann Arbor, May 1969
04 p0640 A70-14556

- Real image holography of complex organism or body organs as teaching aid and research tool in medicine and biology
04 p0685 A70-14558

- Computer processing role in film scanning and digitizing for enhancing X ray and radioisotope scanner images in medical radiographs, discussing image noise reduction
04 p0654 A70-14562

- Computer program for evaluating measured lung function values by comparison with accepted norms, using matrices containing regression coefficients
04 p0644 A70-15360

- Empirical formulas derived for intuitive estimates of blood coagulability in patients to facilitate medication dosage prescription
07 p1210 A70-19558

- Pattern recognition systems design and applications in medical and photographic data classification
13 p2374 A70-29580

- Hyperthyroidism diagnosis by pattern recognition, using computerized class featuring information compression
22 p3977 A70-43732

MEDICAL SERVICES

- Ground and ditching emergency evacuation tests of C-9A aeromedical aircraft under worst possible simulated crash conditions
01 p0035 A70-10716
- Helicopters for injured or sick persons transportation as compared with ambulance use based on West Germany experience
03 p0436 A70-13822
- Public health services problems analyzed by statistical simulation method, using Markov process
04 p0644 A70-15356
- Physician-monitored central control facility communicating with remote site facilities staffed by paramedical personnel for public health care, based on aerospace experience
04 p0644 A70-15357
- Problems experienced in using computers for medical diagnosis and treatment processes, discussing Bayes formula application
04 p0644 A70-15358
- Computer aided medical diagnosis
04 p0644 A70-15359
- Victim examination, human factors and forensic problems in flight accident investigations
05 p0807 A70-16497
- Air crash rescue operations by helicopter ambulances of U.S. Army Medical Department, discussing postcrash fire suppression and injured personnel removal, emergency treatment and evacuation
06 p1002 A70-17714
- Automatic control of continuous medical monitoring in manned space flight
07 p1220 A70-19512
- Helicopter utilization in emergency transportation of civilian patients, discussing questionnaire results from medical and police agencies
08 p1454 A70-21937
- Aeromedical Evacuation System in overall treatment process for seriously ill patient
09 p1628 A70-23467
- Automatic control of continuous medical monitoring in manned space flight
11 p1991 A70-26111
- Patients emergency transportation by helicopter, discussing vehicle types and onboard medical treatment
14 p2540 A70-30191
- Survival training program preparing physicians as advisors regarding survival equipment and medicine
23 p4152 A70-44463

MEDITERRANEAN SEA

- Highly localized clear air turbulence at aircraft flight level over Mediterranean, noting simultaneous temperature rise
19 p3463 A70-38948
- Synoptic surface and upper air analysis and APT mosaics of meridional circulation over Mediterranean by remote satellite images
21 p3846 A70-41399

MEDIUM SCALE INTEGRATION

- Integrated logic circuits, considering switching properties and medium and large scale integration
13 p2372 A70-29116

MEETINGS

- U CONFERENCES**
MEISSNER EFFECT
U DIAMAGNETISM
U SUPERCONDUCTIVITY
MELLIN TRANSFORMS
- Laplace and Mellin transforms inversion in one dimensional cascade theory problems, using numerical methods for primary electron and photon spectra
20 p3675 A70-39305

MELTING

- NT ARC MELTING**
NT FUSION [MELTING]
NT VACUUM MELTING
- Transient one dimensional heat transfer analysis demonstrating infiltrant melting effect on self heat-re-

- tarding porous metal composite during surface melt layer formation
04 p0709 A70-15414

- Melting ablation for two dimensional and axisymmetric blunt bodies with body force, predicting gas-liquid interface temperature for free stream conditions
06 p1176 A70-17690

- Melting zone evolution in thermal history of earth, investigating upper mantle heat transfer effect on layer motion due to radioactive decay
06 p1056 A70-17804

- Al alloys melting in flame furnaces, studying oxidation and various sources of metal losses
08 p1505 A70-21131

- Projectile penetration of Al alloys, noting melting during intense shear band formation
08 p1522 A70-21710

- Extended chain polymer crystals temporary superheating before final melting, discussing hexagonal selenium crystals data
11 p2069 A70-25803

- Temperature, stresses and deformations in melting plates of elastic perfectly plastic material, using penetration depth concept with heat balance approach
11 p2138 A70-26134

- Polyethylene extended chain crystals melting process via electron microscopy and differential thermal analysis
12 p2258 A70-26896

- Liquid water occurrence on Mars surface, considering ice melting, evaporative cooling, atmospheric moisture content, etc
14 p2651 A70-31298

- Materials preparation processes and improvements in space weightless environment, considering metals and ceramics melting, solidification, electromagnetic process control, etc
16 p2919 A70-33717

- Ni-S melts thermodynamic properties in 700-1100 C range by continuous thermal balance method, calculating S vapor pressure
18 p3271 A70-36029

- Slab melting under hot spots, obtaining starting solutions
18 p3346 A70-36491

- Plastic deformation of melted Al-Mg single crystals, using dynamic tensile testing
19 p3450 A70-37374

- Deformable bodies rupture condition formulation by melting analogy, comparing results to experimental data
20 p3733 A70-40394

- Vapor capillary /melt/ depth in electron beam welding, considering electron energy, radiative dissipation, etc
21 p3833 A70-41124

- Lunar crystalline rock melting at atmospheric pressure under partial oxygen pressure, suggesting crystallization temperature
21 p3895 A70-41508

- Finite difference numerical integration method for melting and freezing problems extended to free convection in liquid and unequal densities for phases
21 p3953 A70-42093

- Dynamic melt properties of polymer blends, using orthogonal rheometer measurements
22 p4058 A70-43076

- Pulsed spray welding electrode melting rates for Al alloy, mild steel and stainless steel electrodes over range of pulse current levels
22 p4046 A70-43147

- One-phase Stefan problem of heat conduction with melting, proving existence and uniqueness theorems for solid and free boundary temperature determination
24 p4429 A70-46036

MELTING POINTS

- Extended chain crystals of hexagonal Se temporary superheating before final melting, presenting melting equation
01 p0126 A70-10222
- Ti-Al-Co alloys melting points and cast structures, discussing reactions with melt
01 p0125 A70-11644
- Alloying elements preventing hot cracking in weld metal by converting iron sulfides into higher melting point sulfides
07 p1293 A70-18979
- Jupiter conductive molten metallic hydrogen core of moderate temperature suggested from solids melting point temperature dependence on pressure
07 p1390 A70-20238
- Pressure effects on melting temperature curves of solids, considering Van der Waals solids, metals and ionic compounds
09 p1665 A70-22056
- Melting diagram for five element Mo-W-Nb-Ta-V system constructed by optimal projections from known composition-property relations for corresponding ternary systems with common components
09 p1702 A70-22561
- Helium melting pressure curve to calibrate cerium magnesium nitrate or NMR low temperature thermometers
09 p1728 A70-22999

Phase equilibria and maximum melting compositions determinations for compound semiconductors by differential thermal analysis compared with vapor and high pressure techniques 11 p2098 A70-25812

Linear aliphatic polyesters melting point, fusion heat and entropy correlations to molecular parameters 22 p3982 A70-42502

Subsolidus state multicomponent eutectics systems temperature range based on number and melting points ratios of individual components 24 p4367 A70-45476

MEM [EXCURSION MODULE]
U MARS EXCURSION MODULE
MEMBRANE ANALOGY
U MEMBRANE STRUCTURES
U STRUCTURAL ANALYSIS
MEMBRANE STRUCTURES
NT SKIN [STRUCTURAL MEMBER]
 Wave front discontinuities during pressure wave propagation in membranes and elastic shells by asymptotic procedure using Laplace transform 03 p0589 A70-13331

Eigenfunctions of oscillating infinite perforated membranes for various boundary conditions at holes 03 p0591 A70-13415

Tension field theory describing buckling of membranes or thin plates with boundaries subjected to excessive planar displacements 03 p0599 A70-14246

Pressure vessel deformation and stress analysis by matrix displacement method, considering solids and membrane shells under axisymmetric and asymmetric loading [ASME PAPER 69-WA/PVP-3] 04 p0768 A70-14790

Laplace transform of axial stress resultant in impacting semiinfinite elastic cylindrical membrane as exponential function involving wave propagation speed, applying continued fractions [ASME PAPER 69-APM-K] 04 p0769 A70-14859

Stereophotogrammetric measurement for dynamic deformation of circular membrane subjected to underwater detonation 05 p0927 A70-16009

Membrane stress concentration near circular cutouts in uniaxially stressed sheets reduced by predeforming immediate surroundings of hole 05 p0940 A70-16515

Membrane reinforced thin walled cylindrical shells stability as asymmetric contact problem in shell and plate theory 05 p0947 A70-17011

Unsteady interaction of compressible fluid and flat circular deforming elastic membrane analyzed by coupled computer program method [AIAA PAPER 70-75] 06 p1039 A70-18082

Elastic membranes deformation compressed by restraints using discrete dynamic programming 07 p1400 A70-18680

Membrane deformations in second order rotating surfaces with positive Gaussian curvature investigated for external couple loaded spherical shells 10 p1958 A70-24515

Thin soap membranes shape determined by photogrammetric method, using stereo camera and fluorescent light 10 p1891 A70-24735

Circular membrane creep under one-sided hydrostatic pressure, using governing equations for finite deformation 10 p1959 A70-24828

Self opening em-operated secondary and ternary mylar diaphragms for expansion tubes and tunnels 11 p2031 A70-25982

Membrane theory for thin single layer orthotropic cylindrical shells experiencing harmonic axisymmetric motion 11 p2136 A70-26084

Tension rays and load transfer from compact member via wrinkled membrane determined by variation technique using maximum strain energy 12 p2322 A70-27225

Pressurized orthotropic cylindrical membrane shells free and forced vibration, considering dynamic response dependence on internal pressure 12 p2326 A70-27815

Active and passive ion transport mechanisms in excitable animal cell maintaining constant membrane polarization 13 p2352 A70-29351

Wave front discontinuities during pressure wave propagation in membranes and elastic shells by asymptotic procedure using Laplace transform 14 p2657 A70-30710

Circular cylindrical membrane axially symmetric deformations, determining axial and circumferential stresses 14 p2657 A70-30844

Eigenvalues of membranes and plates, comparing asymptotic and numerical values 14 p2600 A70-31223

Elastic membranes deformation compressed by restraints using discrete dynamic programming 15 p2813 A70-31472

Zero moment /membrane/ theory for anisotropic thin walled shells, deriving expressions for stress-strain states and displacements under torsion 15 p2824 A70-32894

Optical membranes design, discussing properties of materials and mountings 16 p2904 A70-33148

Membrane stresses on nonspherical domes with axisymmetric loads 16 p2990 A70-33743

Vibrations of shells, plates and membranes carrying dynamic systems at discrete points on surface, obtaining eigenfunction and eigenvalue equations 16 p2993 A70-34090

Elastic and equilibrium matrices for semimonocoque membrane /plane stress/ elements using skin and reinforcing member transformations 17 p3185 A70-34921

Vibrating diaphragm gas pressure measuring system based on membrane damping, applying to prototype atmospheric entry probes 17 p3095 A70-35524

Double curved shell membrane stress calculation under arbitrary load, using stress functions 18 p3338 A70-36373

Nonhomogeneous Helmholtz vibration equation for sectorial-annular membranes and plates under arbitrary load, using Fourier method 19 p3535 A70-37343

Membrane attachment for pressure transducer with help of holographic interferometry, describing optical system 19 p3427 A70-38453

Singular integral equation formulation for torsion from membrane analogy, obtaining boundary value problem solution by computer program 20 p3718 A70-39000

Elastic membrane axisymmetric deformations, reducing nonlinear equations system to quadratures 20 p3718 A70-39230

Turtle bladder walls osmotic properties, discussing transmembrane water flow transient acceleration by sodium transport inhibition 21 p3762 A70-41223

Turtle bladders isolated mucosal and serosal fractions histological and physiological properties, discussing ion transport and oxygen consumption 21 p3762 A70-41224

Membrane theory of shells, reducing equilibrium equations to single second order partial differential equation through transformation in terms of stress function derivatives 21 p3939 A70-42031

Thin shell structural analysis by doubly curved arbitrary quadrilateral finite element, using Kirchhoff theory and cubic polynomial for membrane displacements 23 p4272 A70-44711

Rectangular cable networks covered by or embedded in membrane matrix, calculating vibration response under load by Galerkin method 24 p4421 A70-45279

MEMBRANE THEORY

U MEMBRANE STRUCTURES
U STRUCTURAL ANALYSIS
MEMBRANES
NT CHOROID MEMBRANES
NT ION EXCHANGE MEMBRANE ELECTROLYTES
NT MEMBRANE STRUCTURES
NT PLEURAE
NT SKIN [STRUCTURAL MEMBER]
 Lower bounds of Stekloff and free membrane eigenvalues for sloshing of incompressible inviscid fluid, subject to gravity in rigid tank with free surface 02 p0278 A70-11999

Gamma radiation effects on membrane permeability of isolated nuclei from white rats thymus in sucrose-calcium buffer 04 p0629 A70-14460

Hyperbaric oxygenation effects on cellular membrane permeability, analyzing rat plasma behavior of transaminases GOT and GPT and K and Na cations electrolytes 05 p0802 A70-16493

Liquids particulate contamination sizing and counting by membrane filtration, specifying procedures and apparatus used 07 p1195 A70-18804

Blasius flow stability on deformable surface of membrane using Orr-Sommerfeld equation to calculate amplitude of function for perturbation flow 09 p1658 A70-22182

Lobster giant axon membrane steady state current fluctuations measured under voltage-clamp conditions, considering current potassium component 11 p1987 A70-26006

Countercurrent sandwich type dialyzer for small animals, noting membrane support function and applicability to human use 13 p2360 A70-29950

Electronic simulation of neuron membrane demonstrating nervous impulses generation and propagation behavior 14 p2542 A70-30387

Physical principles of biological membranes - Conference, University of Miami, December 1968 16 p2847 A70-33026

Water structure role in membrane systems, considering phase transitions and thermal anomalies in surface properties 16 p2847 A70-33027

Molecular structural relationship between cellular membranes and photoreceptors in plants and animals 16 p2847 A70-33028

Membrane-like properties of synthetic proteoid microparticle systems, considering catalytic activities, size and ultrastructure 16 p2847 A70-33029

Tympanic membrane and rectal temperatures compared over wide range of ambient environments as indicators of deep body temperature 17 p3029 A70-35332

Thermodynamic effects and transport phenomena in discontinuous system of gas filled containers connected by membrane, deriving entropy production and diffusion flux in membrane 17 p3197 A70-35531

Limit surface behavior equations for structural membrane elements in terms of number, orientation and limit load of constituent fibers by limit theorems 21 p3934 A70-40778

Fluorescent probes inserted into biological membranes for molecular structural and dynamic facets 24 p4304 A70-46231

MEMORY

Neurons tracing activity and cellular memory mechanisms in cortical projection region of cutaneous analyzer of immobilized rats following electric acoustic stimuli 01 p0030 A70-11468

Long term memory effects in visual perception of apparent movement, discussing experience prior to tests 02 p0239 A70-12622

Image memory in Papio hamadryas monkeys reacting to visual and flavor food stimuli 04 p0632 A70-15219

Retroactive interference stimuli effects on pitch discrimination in short term recognition memory task 07 p1215 A70-20046

Hypoxia effect on retrograde amnesia /recent memory loss/ in albino rats subjected to shock and decompression treatments 08 p1441 A70-20477

Verbal information recall latencies as function of time interval from initial memory storage and retrieval repetitions 10 p1818 A70-24718

Short-time memory test based on model involving continuous information storage and reproduction [DFVLR-SONDDR-30] 12 p1715 A70-27027

Memory mechanisms of brain, discussing molecular physiology, information storage in living systems 12 p1668 A70-27278

Dynamic interaction between stored and active memory images in apes and monkeys with conditioned alimentary motor reflexes stimulated by visual signals 12 p1713 A70-28352

He-Ne laser memory, discussing induced oscillation excitation with radiation fed back to resonator by moving reflecting mirror 13 p2429 A70-29572

Three phase code transformation task for human subjects, determining memory aid role in problem solving phase from factor analysis 13 p2361 A70-30019

Altitude hypoxia adaptation effects on brain protein and RNA synthesis in rats, noting increase in memory resistance to environmental stress effects 17 p3030 A70-35359

Psychophysiological tests involving programmed memory device evaluating human memorization process and sensorimotor reactions to light signals 17 p3040 A70-35676

Human memory information structure, discussing pattern recognition, simultaneous attention, problem solving and logic 19 p3363 A70-38322

Alcohol effects on human short term memory, discussing pathological intoxication from flying safety viewpoint 24 p4307 A70-45345

Neurophysiology of membrane and synaptic mechanisms of prolonged trace changes in neuron activity concerning memory and cellular learning analogs 24 p4305 A70-46393

MEMORY STORAGE UNITS

U COMPUTER STORAGE DEVICES

MENISCI

Meniscus curvature correlation to viscosity contrast in capillary during fluid displacement 13 p2390 A70-29633

MENTAL HEALTH

Cardiovascular system, neuromuscular activity and mental fitness of subjects performing physical and mental assignments with prescribed work-rest schedule during confinement 03 p0425 A70-13895

Fatigue and aircraft environment effects on physical and mental state of airline flight attendants during prolonged cruises
15 p2692 A70-32211

MENTAL PERFORMANCE

Digital computer display techniques relationship with man in modern environment, considering human engineering and educational problems and future impact on intellectual qualities
01 p0221 A70-11281

Man machine systems - IEEE/ERS Conference, Cambridge, England, September 1969, Volume 3, Decision making and mental work load
02 p0244 A70-12137

Task interference model for interference among two or more continuous manual control tasks, suggesting metric for pilot mental work load
02 p0244 A70-12139

Task loading of human operator in terms of central capacity sharing model, discussing model implications for mental workload measurements
02 p0245 A70-12142

Experienced and naive subject evaluation of probabilistic data, data source determination and prediction of subsequent data in complex decision task
02 p0247 A70-12379

Recall and recognition memory in concept identification, discussing presentation time /PT/
03 p0424 A70-13767

Relative slant judgments elicited by paired comparison methods from subjects viewing computer generated slides representing rotated regular dot patterns
03 p0435 A70-13769

Cortical cells fatigue and performance in subjects doing mental work, using motion picture signal perception method
04 p0639 A70-15509

Survival psychology for civil aviation, discussing irrational behavior after forced landings resulting from exhaustion of mental resources and inappropriate activity
07 p1204 A70-19018

Aircraft pilots psychic and flight stress admissible degree not resulting in hazardous consequences, suggesting measures to increase resistance
09 p1625 A70-23006

Environmental thermal stress effect on human performance under high mental and low physical workload
10 p1812 A70-24505

Psychic functions stability during prolonged hypodynamia, discussing memory, attention span, sensometer reactions, time estimating, etc
10 p1816 A70-24685

Short-time memory test based on model involving continuous information storage and reproduction [DFVLR-SONDDR-30]
12 p2175 A70-27027

Pilot training applicant test profiles, discussing difference between intelligent and intellectual candidates
12 p2176 A70-27028

Mental blocking/incidental long reaction times/ during continuous serial performance using perceptual-selection and response theories
12 p2178 A70-27045

Flying qualities application to automobiles, discussing work load with respect to controllability and pilot behavior
13 p2347 A70-29142

Acceleration effects on mental working capacity of fighter pilots, discussing attention shift and stability, operational memory, sensorimotor reactions
13 p2351 A70-29337

Three phase code transformation task for human subjects, determining memory aid role in problem solving phase from factor analysis
13 p2361 A70-30019

Rheoencephalographic recording of healthy persons during rest and mental tension in expectation of stimulus
18 p3222 A70-37219

Decreased mental and physical performance of human beings due to T-oral and placebo vaccine reactions
19 p3359 A70-37389

Soviet monograph on secondary signaling system role in development of speech, thought, conditioned and unconditioned reflexes, human will and hypnosis, noting salivary gland function
19 p3359 A70-37407

Psychological tests for ability to learn association between event and occurrence probability
19 p3363 A70-38319

Mental performance changes due to extended exposure of man to sensory deprivation environment, discussing prevention and treatment methods
21 p3770 A70-41479

Human mental stress evaluation through chemical analysis of 17-hydrocorticosteroid level in parotid fluid
24 p4308 A70-45509

MENTAL STRESS

U STRESS [PSYCHOLOGY]

MERCAPTAN

U THIOLS

MERCAPTO COMPOUNDS

U THIOLS

MERCURY [METAL]

NT MERCURY VAPOR

Static pressure distributions and velocity profiles for Hg flow through circular pipes in transverse magnetic field, studying laminar and turbulent flows
04 p0728 A70-15001

Co and Fe base alloys corrosion in Hg tested in reflux capsules and forced flow loops
04 p0710 A70-15631

External convective heat transfer coefficients from quartz-coated cylindrical hot film anemometer probes in mercury
08 p1599 A70-21582

MHD pressure head variations in Hg flow in square channel with conducting and insulating walls under transverse magnetic field
13 p2465 A70-29838

Magnetometer design based on Hg isotopes optical pumping, discussing sensitivity improvement
13 p2414 A70-30037

Spilled Hg removal from metal surfaces, describing brush technique based on capillary action
15 p2748 A70-32775

Mercury cadmium telluride photodetectors, analyzing gain, signal current and radiation limits
16 p2905 A70-33153

Liquid mercury /LM/ cathode thruster characteristics, power conditioning and control requirements [AIAA PAPER 70-646]
16 p2965 A70-33536

Submillipound mercury electron bombardment ion thruster efficiency, noting cathode pole piece, baffle position and geometry influence on ion chamber performance
16 p2969 A70-33612

Convective diffusion and liquid velocity in Co and Fe based alloys corrosion in Hg at high temperature, using reflux capsules and forced flow loops
16 p2933 A70-34207

Dynamic behavior of eccentric annular mercury nutation damper, using variational principle of least viscous frictional power loss
17 p3023 A70-34770

Ce atom collision with excited Hg atom, measuring ionization cross section
18 p3292 A70-36154

Current and resistance in Hg filled space between two circular electrodes under strong magnetic field, using boundary layer techniques
19 p3477 A70-37578

Single crystalline mercury elastic constants calculated from propagation velocity measurements of polarized sound waves
19 p3486 A70-37770

Critical components effect on small Hg electron bombardment thruster performance, considering glass coated accelerator grids, hollow cathodes and plasma bridge neutralizers
20 p3692 A70-40238

Parameters influence on mercury hollow cathode neutralizers for Kaufman ion thruster [AIAA PAPER 70-1090]
20 p3693 A70-40245

Transient and steady state free convection heat transfer with mercury in vertical rectangular channel, measuring temperature distributions
21 p3941 A70-40773

Low specific impulse hollow cathode mercury thruster for deep space electric propulsion, using SERT 2 configuration [AIAA PAPER 70-1099]
21 p3866 A70-40893

Space compatible flight prototype ion engine power conditioning system design for Hg thruster using oxide cathode
21 p3867 A70-41006

Mercury as stainless steel heat pipe working fluid, determining wetting characteristics and heat transfer capability
21 p3947 A70-41051

Liquid metal /mercury/ cathode thruster system for operation at reduced beam voltages, discussing design and performance [AIAA PAPER 70-1103]
21 p3868 A70-41788

Thermoanemometric velocity measurements in non-stationary MHD Hg flows by insulated Pt sensors
21 p3831 A70-42229

Spectroscopic features of mercury laser associated with electron energy levels and spontaneous emission line structure, giving excitation and disruption mechanisms
23 p4202 A70-45054

MERCURY [PLANET]

Internal structure models of Mercury, Mars and Venus based on radar measurements of radius and mass, discussing two and three zone models [JPL-TR-32-1439]
01 p0176 A70-10315

Mercury atmospheric models for preliminary environmental criteria to be used in spacecraft design and engineering tradeoff studies [AIAA PAPER 69-54]
01 p0183 A70-10838

Planetary information obtained from radar installations, discussing distance and orbit measurements, rotation periods, planetary surfaces, emphasizing Mercury and Venus
01 p0185 A70-11046

Mercury flyby mission feasibility study for ESRO considering payload, picture transmitting TV system, orbits, etc [DGLR-69-12]
04 p0754 A70-15157

Mercury shape estimated with isostatic form of equilibrium controlled by situation near perihelion passage at 3-2 resonance spin rate, discussing solidification thermal effects
05 p0908 A70-16332

Radiative heat transfer in lunar and Mercurian surfaces, discussing radiative heat transfer in powders
08 p1579 A70-21569

Wind and atmospheric temperature variations on Mars, Venus and Mercury interpreted from observational data in terms of earth atmospheric processes
09 p1762 A70-23127

Mercury flyby mission feasibility study for ESRO considering payload, picture transmitting TV system, orbits, etc
09 p1763 A70-23426

Solar charge effects on Mercury perihelion motion, relativistic light deflection and gravitational red shift, using Reissner-Nordstrom solution
11 p2107 A70-25395

Mercury surface features from spectrograms of depolarized radar echoes
12 p2298 A70-27268

Thermal tidal friction and gravitation effects on Mercury libration after solidification, noting equilibrium with orbital and rotational periods locked in 3/2 resonant state
14 p2638 A70-30701

Mercury rotational angular velocity fluctuation in terms of orbital mean motion at different orbit positions
14 p2639 A70-30708

Venus and Mercury radio and radar studies concerning brightness temperature, surface reflectivity and planetary motion
14 p2647 A70-31074

Mercury disk temperature at 3.75 cm wavelength, showing variation with phase angle and hemographic longitude
14 p2647 A70-31075

Mercury mm wave observations, examining longitude dependence of disk average brightness temperature and epilith thermal parameters range
14 p2647 A70-31076

Venus and Mercury surface height variations near equators, using radar time delay and Doppler observations
14 p2647 A70-31077

Unmanned flyby missions to Mercury in 1973-1990, discussing scientific objectives and payloads [AAS PAPER 70-027]
17 p3155 A70-34798

Mercury disk temperature from microwave spectrum analysis, proposing subsurface greenhouse effect
17 p3157 A70-34838

Planet Mercury transit on photographs, noting role as test for terrestrial time systems
18 p3314 A70-36515

Mercury drawings from refractor observations during 1964-1967
18 p3315 A70-36611

Mercury transit across sun on 9 May 1970, discussing observation, equipment and photographs
18 p3319 A70-37050

Mercury photometric measurement, examining surface brightness for photometric function
18 p3319 A70-37052

Planet Mercury knowledge summary, discussing orbit, diameter, mass, density, rotation, surface features, atmosphere, polarization, albedo and color
19 p3515 A70-37930

Mission planning for 1973 Mariner Venus/Mercury flyby, discussing trajectory and navigation aspects [AIAA PAPER 70-1049]
19 p3528 A70-38864

MERCURY ARCS

Langmuir probe position-dependent ion flow effects on plasma density measurement in low pressure mercury discharge
17 p3083 A70-34995

Electron bombardment Hg thruster with divergent magnetic fields, investigating performance dependence on configuration and propellant utilizations [AIAA PAPER 70-1092]
20 p3692 A70-40243

Mercury electron bombardment thruster, measuring effect of geometry and magnetic field inside pole piece region on discharge losses and propulsion efficiency [AIAA PAPER 70-1088]
20 p3693 A70-40247

Low pressure Hg vapor arc with remote wall, investigating magnetic self striction by ambipolar diffusion in fields
20 p3685 A70-40503

MERCURY COMPOUNDS

NT MERCURY TELLURIDES

Geochemistry of venus volatile elements identifying cloud forming species as Hg compounds
14 p2650 A70-31217

MERCURY LAMPS

Mercury arc injection lamp as radiation source for testing sunlight biological effects
10 p1888 A70-24388

- Optical parametric noise from barium sodium niobate crystal pumped at 4358 Å by compact source mercury lamp 22 p4074 A70-43022
- MERCURY PROJECT**
Radiation data from manned orbital Mercury missions, correlating measurements from various additional sensors with main nuclear emulsion sensors 06 p1134 A70-17267
- MERCURY SPACECRAFT**
Astronauts celestial training, using Mercury capsule simulator and Zeiss planetarium projector for flight simulation 08 p1481 A70-21275
Power conditioning and control system prototype for Mercury spacecraft ion thruster, describing supply subsystems, circuit design, component selection and reliability [AIAA PAPER 70-649] 16 p2970 A70-33615
Space shuttle electronics requirements, considering systems in Mercury and Gemini spacecraft and Apollo lunar and command service modules 23 p4259 A70-44612
- MERCURY TELLURIDES**
Mercury cadmium telluride alloy as photoconductive IR detector material noting properties, composition and temperature dependence of energy gap 03 p0543 A70-14196
- MERCURY VAPOR**
Mercury plasma flow rate change effect on electron temperature and density in thermoelectric converter determined by spectroscopy 05 p0887 A70-16028
Secondary frequency standard obtained for Hg laser operating at microwave frequencies 05 p0859 A70-16271
Heavy negative charges formation in ionized Hg vapor by electron capture, basing demonstration on magnetic field effects on free electrons or charged droplets 08 p1550 A70-20594
Hollow cathode mercury electron bombardment thruster design, emphasizing low specific impulse operation and discharge chamber improvements 13 p2473 A70-28505
Small-orifice hollow cathode discharge properties in electron bombardment ion thrusters, using vaporized mercury propellant [AIAA PAPER 70-1087] 20 p3693 A70-40248
Microwave characteristics in plasma of short discharges in low pressure cesium and mercury vapors, noting spectral and spatial distribution of microwave power and intensities 22 p4083 A70-43392
Hg vapor thermal conductivity at various temperatures, using fine wire frequency response and kinetic theory 23 p4281 A70-44428
- MERIDIANS**
U LATITUDE
U LONGITUDE
- MERIDIONAL FLOW**
Star rotation and meridional circulation hydrodynamic theory, considering magnetic fields and internal friction 03 p0564 A70-13228
Linearized steady state hydrodynamic equations describing solar wind meridional motions used for studying zonal pressure perturbations 03 p0558 A70-13599
Tropospheric circulation transformation from meridional to zonal forms due to macrostructure activity of solar wind, considering magnetosphere perturbations 03 p0559 A70-13757
Spatial variations in zonal and meridional components of stratospheric and mesospheric winds traced over horizontal distances by Arcas ROBIN rockets 07 p1274 A70-20275
Star rotation and meridional circulation hydrodynamic theory, considering magnetic fields and internal friction 08 p1580 A70-21661
Interhemispheric mass exchange as function of eddy transfer and meridional circulation 08 p1539 A70-21922
Seasonal variation of vertical profiles of atmospheric radioactivity concentration between stratosphere and troposphere due to meridional zonal wind distribution caused by eddy diffusion 08 p1539 A70-21923
Swirling and meridional flow induced by steady rotation of gravitating sphere in compressible monatomic gas, considering compressibility effects and surface layer [ASTME PAPER MR-69-714] 11 p1978 A70-26690
Auroral absorption bays meridional motion, observing absorption onset systematic lag at various ground stations 14 p2570 A70-30216
Annual variations of monthly mean meridional circulation, discussing observations, zonal asymmetries, accuracy and transports of angular momentum and energy 16 p2945 A70-33249
Meridional circulation velocities in Roche envelope of uniformly rotating star, using nonlocal equation for radiative heat transfer 17 p3171 A70-35560
Meridional transport of angular momentum in various wavenumber-frequency domains, discussing linear and nonlinear contributions 19 p3462 A70-38258
Meridional mean eddy transport of enthalpy in Southern Hemisphere during IGY, comparing results with Northern Hemisphere 20 p3661 A70-39143
Differential rotation at solar surface caused by anisotropic turbulent viscosity in hydrogen convection zone, solving via Navier-Stokes equation 20 p3711 A70-40404
Synoptic surface and upper air analysis and APT mosaics of meridional circulation over Mediterranean by remote satellite images 21 p3846 A70-41399
Auroral absorption bays meridional motion, observing absorption onset systematic lag at various ground stations 24 p4331 A70-46291
- MEROMORPHIC FUNCTIONS**
NT ELLIPTIC FUNCTIONS
NT RATIONAL FUNCTIONS
Linear structures response to pressure fields of deterministic excitation with input function spectra as meromorphic functions of wave number and frequency 01 p0208 A70-11191
- MESH**
Heat transfer coefficients for mesh simulating porous parachute cloth, measuring Nusselt number as function of sonic Reynolds number 01 p0004 A70-10292
Bird deflection grill device for turboprop engine inlet ducts, noting effects on inlet flow characteristics, engine performance, etc 01 p0165 A70-10688
- MESON RESONANCES**
Interacting meson systems effective masses with/without secondary proton measured, detecting heavy boson resonances and fireballs, considering proton nuclear interactions 03 p0472 A70-13031
- MESON-NUCLEON INTERACTIONS**
Thermodynamic potential of meson-nucleon plasma, showing variation of Landau equation of state in hydrodynamic theory of multiple particle production 03 p0527 A70-13052
- MESONS**
NT MESON RESONANCES
Cosmic rays meson component recording by proportional counters designed for use in large telescopes 05 p0846 A70-15939
Intensity variations of cosmic ray neutrons and mesons analyzed to isolate lunar day period 07 p1368 A70-20033
Automatic system for processing data from underground meson telescopes 07 p1238 A70-20347
Interplanetary cosmic ray positrons energy spectral component with origin different from interstellar mesons decay 19 p3502 A70-38098
Automatic cosmic ray station for recording nucleon and meson components 20 p3629 A70-39314
- MESOPAUSE**
Rocket-borne sampler for collecting noctilucent cloud particles in mesopause, describing collection and analysis methods and protection against tropospheric contamination 07 p1273 A70-20266
Noctilucent clouds in mesopause over North America, discussing ground stations network, intensity variations, structure and time distribution 07 p1273 A70-20267
Nonlinear diurnal tide and gravity wave interactions at meteor heights below mesopause 14 p2579 A70-31251
- MESOSPHERE**
Upper atmosphere-lower atmosphere interactions, middle atmospheric physics and dynamics and mesospheric seasonal and large scale zonal and meridional behavior 01 p0073 A70-10581
Wind oscillations in stratosphere, lower mesosphere and meteor heights noting periodicities 01 p0074 A70-10591
Satellite and rocket probe measurements of water vapor in mesosphere 01 p0082 A70-11510
Global satellite VLF propagation system for investigating mesospheric ionization 03 p0475 A70-13827
- Clear air turbulence and mesoscale structure subsynoptic air motion experiments for numerical weather prediction 04 p0714 A70-14394
Altitude variation of mesospheric daytime sky brightness from earth based measurements of twilight sky brightness, noting inconsistency in calculations based on standard atmospheres 06 p1053 A70-17207
Photochemical calculations on mesospheric ozone for oxygen only, oxygen-hydrogen and oxygen-hydrogen-nitrogen atmospheres 07 p1273 A70-20268
Vertical eddy diffusion effect on chemical composition of mesosphere and lower thermosphere using photochemical model containing oxygen and hydrogen 07 p1274 A70-20269
Stratospheric and mesospheric circulation during winter, investigating wind fluctuations using meteorological rocket observations 07 p1274 A70-20274
Spatial variations in zonal and meridional components of stratospheric and mesospheric winds traced over horizontal distances by Arcas ROBIN rockets 07 p1274 A70-20275
Thermal structure transition of mesosphere at high altitudes from persistent summertime to dynamic wintertime case 08 p1539 A70-21649
Stratosphere-mesosphere coupling phenomena during sudden stratospheric warmings, considering ozone and ionospheric drift measurements 10 p1913 A70-24948
Mesospheric daytime/nighttime ozone abundance vertical profile diurnal variations 14 p2568 A70-30130
Upper stratosphere-mesosphere monthly-mean charts from reentry heating and atmospheric model based on hydrodynamics 14 p2608 A70-30590
Statistical mesosphere temperature, density and wind profiles models based on rocket soundings 14 p2608 A70-30593
Strong wind and vertical wind shear in upper stratosphere and mesosphere 14 p2608 A70-30594
Stratospheric and mesospheric ozone diurnal variation by rocket-borne ozonesonde in January 1968 14 p2577 A70-31170
Mesospheric levels wind oscillations in Spanish range of Arenosillo measured by meteorological rockets during February 1970 15 p2723 A70-31653
Vertical temperature profiles and global circulation patterns in stratosphere and mesosphere, discussing Northern Hemispheric seasonal, latitudinal and longitudinal variations 15 p2724 A70-31665
Upper stratosphere and mesosphere structure and circulation in Southern Hemisphere, using meteorological rockets and radiosonde data 15 p2724 A70-31683
Numerical model of diurnal variations of minor neutral constituents in mesosphere and lower atmosphere including molecular and eddy diffusion 15 p2727 A70-31909
Lidar probing of stratosphere and mesosphere using automatic data acquisition system 16 p2862 A70-33016
Weak ion concentration in stratosphere and mesosphere measured using accumulated capacity amplifier 18 p3257 A70-36179
Charged particle balance equations for stratosphere and mesosphere, noting particle composition investigation and formation and annihilation processes 19 p3491 A70-37311
Thermosphere, stratosphere and mesosphere reactions involving water, hydrogen, methane, ozone, nitric oxide and nitrogen peroxide 22 p4023 A70-43298
Noctilucent clouds blue color and rocket sounding results explained by ozone model of mesospheric clouds formation 23 p4188 A70-44048
- MESSAGES**
Message switching techniques in digital telecommunication networks, discussing automatic routing, operational and control facilities, etc 02 p0256 A70-11973
- METABOLIC WASTES**
NT FECES
NT HUMAN WASTES
NT URINE
Barometric pressure reduction effect on gaseous and volatile metabolic products elimination in men wearing oxygen-supplied rubberized suits 17 p3038 A70-33363
Heme catabolism in untreated rats and in animals treated with phenobarbital or porphyrogenic drug, comparing bilirubin and Co production 20 p3583 A70-40450
Vapor biowaste electric spacecraft propulsion system, discussing recovery cycles and subsystem

tradeoffs, specific impulse, chamber heating, power input and reaction products 21 p3866 A70-40869

Biological compatibility problem in long duration space operation crew change, discussing human metabolic processes and difference effects 22 p3980 A70-43641

METABOLISM

NT ADRENAL METABOLISM
NT CALCIUM METABOLISM
NT CARBOHYDRATE METABOLISM
NT CATABOLISM
NT ELECTROLYTE METABOLISM
NT ENZYME ACTIVITY
NT FERMENTATION
NT HORMONE METABOLISMS
NT HYPOGLYCEMIA
NT LIPID METABOLISM
NT OXYGEN METABOLISM
NT PROTEIN METABOLISM

Metabolism and biological activity of urea, citrulline, arginosuccinic acid in organism ornithine cycle, discussing role in brain and liver 01 p0019 A70-10513

Assimilation and metabolism of C atoms of pyruvate and acetate by strict autotrophs *Thiobacillus* cell, using radioactive substrates 01 p0021 A70-10788

Rats decreased muscular work and denervation effects on alpha-aminoisobutyric acid uptake by skeletal muscle 02 p0232 A70-11712

Prolonged dehydrated food diet effect on metabolism of humans, noting complete adaptation after three or four months 04 p0630 A70-14577

Hyperbaric oxygenation effects on metabolism, comparing protective agents for rats exposed to 5 absolute oxygen pressures 04 p0631 A70-14681

Myocardial metabolism in ischemic heart disease using arterial and coronary sinus catheterization 04 p0636 A70-15469

Temperature variations in organs of man and animals performing physical work as physiological base of metabolic processes and for daily activity timetable development 04 p0638 A70-15502

Human exhaled air contaminants analysis role in disease diagnosis, metabolism study and spacecraft cabin atmosphere changes 07 p1220 A70-19514

Human metabolic study showing effect of yeast RNA and allopurinol on serum and urinary uric acid formation 08 p1454 A70-20679

Thymidine tracer distribution in bone marrow chromosomes of rats and mice treated with radioprotectors, noting cell metabolic activity reduction by sulfhydryl-type radioprotectors 09 p1619 A70-22818

Brain cerebral tissues electrical impedance measurement by electrodes and bridge circuit, discussing chemical and metabolic properties 09 p1620 A70-22897

Metabolic and heart rates determined in experienced and inexperienced pilots during Hiller 12-E and 12-EL helicopters flight through standard maneuvers 09 p1627 A70-23455

Organic substrates effects on *Hydrogenomonas eutropha* autotrophic and heterotrophic metabolism 10 p1817 A70-24700

Physiology of hibernation and hypothermia, noting potential use for metabolic need reduction during long interplanetary flight 10 p1943 A70-24757

Human exhaled air contaminants analysis role in disease diagnosis, metabolism study and spacecraft cabin atmosphere changes 11 p1991 A70-26113

Metabolism in left ventricular myocardium of rabbits after asphyxiations and during postasphyxial recovery 12 p2168 A70-27624

Canoe paddlers physical training effect on cardiac output and local blood flow and metabolism at and during exercise and recovery 12 p2169 A70-27653

Mg ion metabolism in neuromuscular excitability maintenance, discussing quantity requirements, detection and electromyographic recording 12 p2172 A70-28045

Energy consumption in male subjects during walking and running in erect and supine position under simulated gravity 13 p2351 A70-29335

Epinephrine uptake and metabolic disposition in rat brain, determining pathways and turnover of endogenous brain hormone and enzymatic synthesis 14 p2536 A70-30348

Biological satellite experiment, considering long term weightlessness effects on metabolism and biological rhythms of medical leech 16 p2854 A70-33993

Plasma free fatty acids and glucose relative role in contribution to metabolic state and energy production in partially hepatectomized rats 16 p2850 A70-34319

Ergonomic and medicomilitary aspects of human adaptation to cold environments, discussing metabolic and physical protective reactions, clothing and personnel selection 16 p2850 A70-34346

Human water-salt metabolism following exposure to transverse accelerations, discussing diuresis and Cl-K excretion 17 p3038 A70-35364

Adaptive recession of gas metabolism in rats during multiple high temperature exposures 18 p3220 A70-36545

Low ambient temperature exposure effect on hamster intestinal absorption capacity, using glucose test compound 19 p3360 A70-37772

Tyrosine content and utilization in mouse liver, showing daily rhythm in composite metabolism rate 20 p3568 A70-38976

Atmospheric composition cyclic changes effects on human basal metabolism under hypokinesia 20 p3576 A70-40197

Lateral and angular acceleration effects on blood and urine contents in specific metabolic indices of healthy young men 22 p3971 A70-43136

Water and salt metabolism changes during prolonged hypokinesia of rabbits, noting blood plasma dilution, hematocrit number and hemoglobin concentration reduction, etc 23 p4146 A70-44656

Biological life support system based on mutual equilibration of human metabolism and technically controlled algae culture, discussing experimental evaluation 23 p4156 A70-45026

Vascular smooth muscle contraction regulation, discussing contractile protein, energy metabolism, excitation-contraction coupling, spontaneous rhythmicity, response to stimulants, etc 24 p4299 A70-45807

METAGALAXY

U UNIVERSE

METAL AIR BATTERIES

Refuelable Mg-air battery anode, electrolyte and packaging materials selection from standpoint of cell voltage, metal consumption and sludge formation 02 p0253 A70-12721

Mechanically rechargeable zinc-air battery, discussing electrical performance, advantages and military applications 12 p2167 A70-27928

Third electrode use in charging secondary zinc air battery, presenting performance data and operation problems 14 p2533 A70-30527

METAL ALLOYS

U ALLOYS

METAL BONDING

NT METAL-METAL BONDING
Metal fabrication shop environment contamination effect on bond strength of various adhesive system tested by humidity and salt spraying exposures 02 p0310 A70-12664

Modified explosive bonding process for welding wire reinforced Al composite materials 03 p0497 A70-13120

Bond quality and strength of high temperature adhesive films for titanium 04 p0699 A70-15158

Inertia bonded and electron beam welded joints of Waspaloy compared for suitability in aircraft gas turbine engines 04 p0700 A70-15655

Joint design for braze bonding and joining of Al-B composites using Borsic tape backed with alloy brazing foil 07 p1293 A70-18994

Collection of papers on metal bonding including technology, principles, testing, behavior calculations and applications 08 p1502 A70-20877

Metal surface adhesion to materials, examining structure and energy with allowance for environmental effect 08 p1503 A70-20878

Organic adhesives preparation and application to metal surface for bonding, examining time, pressure and temperature effects on curing 08 p1503 A70-20881

Adhesive metal bonding, considering methods for application of pressure and heat 08 p1503 A70-20882

Ceramic adhesives with glassy matrix for metal bonding, describing chemical reactions in interface, adhesive processing and application 08 p1526 A70-20883

Metal adhesive joints nondestructive tests involving acoustic and supersonic, X ray and heat flow characteristics methods 08 p1503 A70-20885

Bonds strength involving metallic, organic and ceramic adhesives at various temperatures, considering metallic additives effect 08 p1504 A70-20891

Composite materials application to structural members, considering bond or adhesive shear strength 08 p1594 A70-21855

Adhesive bonding of aircraft components, describing autoclave environmental control for curing adhesives, parts prefritting, core fitting and quality control 09 p1690 A70-22022

Titanium and titanium alloys bonding, discussing pretreatment, adhesives and assessment of temperature, environment and nuclear radiations 09 p1704 A70-22750

Adhesive bonding for structural efficiency, lower weight, reduced production costs and improved appearance in general aviation industry [SAE PAPER 700221] 11 p2134 A70-25893

Collection of papers on diffusion processes in metals covering welded joints layers, radiation effects, radioactivity, nickel grain growth 11 p2067 A70-26593

Ultrasonic Al wire bonding for microelectronic applications, discussing tensile strength dependence on machine parameters and aging 15 p2747 A70-32647

Solid state diffusion bonding applied to rocket engine injectors manufacture [AIAA PAPER 70-639] 16 p2968 A70-33597

Ti explosive bonding and forming, examining peel and shear strengths on Ti clad steel plate 17 p3098 A70-34446

Metal bonding at low temperatures, studying atmosphere and metal plating effects 18 p3265 A70-37203

Nondestructive testing of diffusion bonded metals for quality assurance 19 p3437 A70-38423

Adhesive bonded aircraft structures, discussing methods and requirements for establishment and control of manufacturing procedures 19 p3438 A70-38594

Explosive metal bonding in electronics, noting explosive strength and initial surface angle effects on bond physical and chemical properties 19 p3438 A70-38752

Book on adhesives for metals covering cleanliness, surface treatment, joint designs, sealants, etc 20 p3652 A70-39194

Optimum conditions and methods for vacuum diffusion welding of heat resistant alloys, removing thermodynamically stable surface oxide films by gaseous reaction products 20 p3636 A70-39197

Synthetic resin adhesives for aircraft components fabrication 20 p3657 A70-40532

Ultrahigh vacuum metal bonding by twist compression technique, reporting adhesion and friction coefficients for atomically ordered Pt-Co alloy 21 p3833 A70-41465

Welding electron beams metal penetration dependence on ionization phenomena, discussing model based on self focusing 22 p4043 A70-42379

Nondestructive testing of adhesively bonded metal assemblies 22 p4047 A70-43523

Holographic nondestructive testing of laminate structures, honeycomb-sandwich panels and rubber-to-metal bonds 24 p4338 A70-45755

Airframe skin panels adhesive bonding in wide-bodied jet transports, emphasizing fuselage fatigue and corrosion resistance [SAE PAPER 700863] 24 p4349 A70-45875

METAL CARBIDES

U CARBIDES

METAL COATINGS

NT ALUMINUM COATINGS
NT GOLD COATINGS
NT NICKEL COATINGS
NT ZINC COATINGS

Aluminum oxide whiskers/metal matrix composites, discussing metallic coatings effects on filament wetting, bonding and surface protection 01 p0117 A70-10480

Bridging joints resistance effect on thermoelement efficiency, describing W and Co coatings deposition on GeTe based thermoelectric alloys 01 p0159 A70-10757

Molten bridging alloy deposition on p and n type thermoelectric materials, utilizing diffusion process brief duration during contact 01 p0009 A70-10758

Vacuum deposition of Cr-Al film on Ni-Mo alloys, describing operating pressure, temperature and film thickness 01 p0124 A70-11617

Mo coated with Ni-base Nimonic and Co-base heat resistant alloys, for working degree effect on creep rupture strength 01 p0126 A70-11646

Co-base hardfacing alloys mechanical properties and applications, discussing mechanical and chemical wear processes in cast and wrought types
02 p0319 A70-12712

Cr diffusion coating influence on fatigue life of Fe and steel, discussing residual stress measurement technique
02 p0320 A70-12848

Ceramic, cermet and metallic high temperature coatings development and applications, discussing time and cost saving procedures
[SAE PAPER 690478] 03 p0515 A70-13267

Diffusion layer and protective oxide composition changed to increase chrome plated Mo heat resistance
06 p1089 A70-17742

Temperature and pressure effects as function of time in spectral and total normal emittance of metal coated refractory metals
[ALAA PAPER 70-68] 06 p1092 A70-18136

High chromium stainless steels nitriding and carburizing processes stabilized by nickel galvanic coating, enhancing nitrogen or carbon diffusion into steel
07 p1291 A70-18832

Compatibility of single metal coated carbon fibers, discussing structural recrystallization in contact with Ni or Co matrix by dissociation/ diffusion/precipitation mechanism
07 p1315 A70-20048

AlN deposition rate from gaseous phase on Mo substrate as function of temperature
07 p1357 A70-20311

Performance characteristics of low density epoxy-water emulsion corrosion resistant coating for nonferrous alloys
08 p1526 A70-20648

Nondestructive tests for diffusion-formed refractory alloy coatings used as oxidation protection for hypervelocity spacecraft and reusable systems
09 p1692 A70-22679

Sputtering method used for applying metallizing layer to ceramics in producing ceramic to metal seals
10 p1895 A70-24555

Axial flow compressor clearance control coatings at blade tip paths for efficiency
[SAE PAPER 700330] 12 p2291 A70-27462

Corrosion resistance of molybdenum coatings on steel and Pb-Bi eutectic alloy obtained by vacuum contact fusion method
12 p2258 A70-28320

Residual gas effects on critical load and brittleness of pure and molybdenum-coated niobium bars after annealing in vacuum
12 p2258 A70-28324

Heat energy transport mechanism in metallic plasma deposited coating, investigating role of elastic crystal lattice vibrations, electrons, molecules, etc
13 p2419 A70-28858

Diamond burnishing effects on wear and contact endurance of chromium coatings, investigating surface hardening and residual stresses
13 p2419 A70-28868

Structure and chemical composition of high Cr diffusion coating on Cr-Ni austenitic steels
15 p2756 A70-31634

Wear and fatigue of Ti-Mo-Al-Sn-Si /Hylite 50/ alloy with resistant Mo or Cr coatings
17 p3099 A70-34447

Fractography of fatigue and delayed fracture of hydrogenated, unplated and Cd-plated ultrahigh strength steel
17 p3124 A70-34654

Two-component metal coatings on Ni alloys for gaseous corrosion resistance increase, comparing microstructure and properties
17 p3125 A70-35393

Metallic surfaces vacuum electric spark alloying, investigating pressure effects on coating layer thickness and area
20 p3636 A70-39195

Optical multilayer metal coatings vacuum deposition by cathode sputtering, using automatic apparatus
22 p4045 A70-42510

Thermochemical method for directional crystallization of wear-resistant alloy coatings on machine parts
23 p4205 A70-44043

CW GaAs semiconductor laser fabrication by liquid epitaxy, noting Ag plating role in output power
24 p4352 A70-45468

Diffusive carbon redistribution in Mo during interaction with Ni and Cr protective coatings
24 p4364 A70-46334

High temperature coatings of high melting point alloys on graphite, determining optimum fabrication conditions
24 p4368 A70-46339

Surface alloying of alloy with three elements /Al, Si and Cr or Zr/, investigating coating stability in weight, microstructure and microhardness
24 p4364 A70-46340

Heat resistant alloys with metal coatings applied by diffusion in vacuum, investigating structure and fatigue strength at high temperatures
24 p4364 A70-46342

METAL COMBUSTION

Combustion time of Al powder, considering concentration, injection into gas flow, oxidizer composition and agglomeration
01 p0161 A70-11015

Mg vapor and oxygen surface reactions in MgO deposits, using atomic absorption spectrophotometry
02 p0250 A70-12006

BeO whiskers formation on burning Be droplets surface using scanning electron microscopy, noting temperature effects
02 p0318 A70-12641

Metal particle and wire combustion using static and flow methods, obtaining experimental results for Al, Be, Mg and B
[ONERA-TP-735] 03 p0543 A70-13633

Combustion of stationary particle of metal with boiling point lower than ignition temperature in gaseous oxidizing medium
07 p1419 A70-18753

Chemical composition effects on Zr-Ti, Zr-Si, Ni-Al and Ni-Ti alloy aerosols combustion temperature
07 p1419 A70-18755

Metal particle size relation to combustion time using statistical method applied to polydisperse Mg powder
07 p1419 A70-18756

Metal particles additives behavior in solid rocket propellant combustion, using scanning electron microscope
07 p1359 A70-19585

Two body collisions reaction mechanisms with small heats of reaction for Be and Al gaseous oxidation, noting low free energy properties of polymerization
10 p1928 A70-24089

Oxide transport and water vapor effects on flash-heated beryllium droplet combustion
10 p1969 A70-25042

Electron affinity and compound formation in hydrogen/nitrogen/oxygen flames containing potassium and boron using mass spectrometry
10 p1832 A70-25150

Chemical high energy rocket propellants, discussing metal combustion, hybrid and tribrid engines, combustion chambers, etc
11 p2100 A70-26282

Al and B particles combustion in methane-oxygen system, considering reaction zone models, energy release rate, particle kinetics, instabilities, etc
11 p2149 A70-26284

Preignition and combustion kinetics in airstream of Mg and Al suspensions in aviation kerosene and gasoline
14 p2664 A70-30395

Particles shape and phase composition in combustion products of dispersed Al-Mg alloy powders by electron diffraction and X ray analysis
14 p2664 A70-30396

Al and Be single particles combustion in various oxidizers, using pulsed Nd-glass laser and Xe flash heating device and scanning electron microscope
14 p2628 A70-30949

Aluminum spherical particles nonautonomous and autonomous combustion in O with N or Ar initiated by HF induction heating
17 p3145 A70-35042

Aluminum particle combustibility in deflagration zone of ammonium perchlorate pellets, measuring combustion rate and pyrolytic behavior
17 p3145 A70-35208

METAL COMPOUNDS
Isostructural crystals of Dy compounds investigated for magnetic behavior using high resolution photoelectric optical spectroscopy
12 p2261 A70-27243

METAL CORROSION
U CORROSION
METAL CRYSTALS
X ray topography of postannealing substructure of neutron irradiated W and Mo single crystals, indicating increase in disorientation
01 p0115 A70-10065

Al double crystals mechanical properties improvement after shock loading, studying surface and dislocation structures and active slip planes number
01 p0124 A70-11449

Recrystallization diagrams of commercially pure Mo and Mo alloyed with Fe, Co or Fe plus Ni, noting additions effect on recrystallized grain size
01 p0124 A70-11616

Constitutive equations and thermally activated dislocation processes in metals, noting temperature and strain rate relationship
02 p0316 A70-11737

Polycrystalline Ni steady state creep characteristics measurement emphasizing temperature dependence of creep rate
03 p0504 A70-13022

High temperature heat treatment effects on Mo, W, Ta and Re crystal surface order and faceting observed by electron diffraction, noting contamination role
03 p0538 A70-13097

Low energy electron diffraction structures due to Re crystal surface interaction with CO and molecular oxygen at high temperatures
03 p0440 A70-13098

Nonuniformity of dislocation structure and stress distribution in deformation of Cr samples longitudinal sections subjected to upsetting
03 p0511 A70-13488

Vacancies influence on macrodefect nucleus formation in single metal crystals under uniaxial strain explaining Griffith crack initiation
05 p0861 A70-15784

Creep in single crystal and polycrystalline Nb between 1300-1900 C under stresses, showing stress independent activation energy
05 p0862 A70-16202

Specific heat and thermal EMF increase due to radiation damage in lattice of fast neutron bombarded Cu, Mo and W specimens
05 p0863 A70-16292

Structures formed during aging of martensite in maraging steels by X ray and chemical analyses using electrolytic isolation of phases
05 p0865 A70-16871

Structural changes in polycrystalline Al subjected to HF fatigue, using transmission electron microscopy
06 p1084 A70-17127

V and Cr single crystals microhardness anisotropy and causes, noting similarity with W, Nb and silicon ferrite
06 p1088 A70-17613

Radioactive sodium and potassium diffusion in single crystal and polycrystalline Mo and Nb at various temperatures, calculating activation energies and coefficients
06 p1089 A70-17745

Inert gases scattering from Ni /111/ plane as function of beam temperature and angle of incidence compared to Au and Ag
06 p1110 A70-18263

High energy Ar atomic beams scattering from single crystal face of W measured for distribution pattern
06 p1112 A70-18270

Niobium single crystals annealed in ultrahigh vacuum, studying stress-strain behavior, secondary slip geometry and slip line morphology
06 p1090 A70-18493

Electrolyte purity effect on initiation times and growth rate of Zn dendrites in alkaline zincate solution, discussing dendrite initiation retardation
07 p1356 A70-19387

Molybdenum rolling-deformed single crystals recovery and recrystallization using diffraction electron spectroscopy
07 p1307 A70-19550

Soviet collection of articles on single crystals of rare and high melting point metals
07 p1307 A70-19606

Carbides content determination in Mo single crystals by metallographic method, establishing relation between brittle-ductile transition temperature and carbon content
07 p1308 A70-19607

Vanadium single crystals substructure on different planes to growth direction using X ray diffraction
07 p1308 A70-19608

Structure and mechanical properties of Mo single crystals grown from gas phase using metallographic and X ray analysis
07 p1308 A70-19612

Dislocation velocity-stress exponent for Nb single crystals calculated from strain rate sensitivity measurements of effective flow stress
07 p1314 A70-20011

Gruneisen parameter for metal and semiconductor single crystals obtained from measuring one dimensional thermoelastic response during exposure to pulsed electron beam
07 p1357 A70-20020

Thermal accommodation coefficients of Ar atomic beams scattered from nominal plane of Ag crystal measured by time of flight techniques
07 p1343 A70-20125

Yield stress and work hardening properties of tension-deformed vanadium single crystals as function of purity
08 p1522 A70-21750

Subboundary migration in Mo, W and W-Re alloy single crystals subjected to cyclic heating, using metallographic technique involving electrolytic polishing and special etching
09 p1701 A70-22297

Rhenium single crystals basal plane surface properties using LEED and Auger electron spectroscopy, describing gas adsorption studies
09 p1739 A70-22526

Metallic solutions formation dependence on alloying elements electron structure assumed by atoms in solvent lattice
09 p1702 A70-22560

Growth kinetics of gamma prime precipitate in Ni-Ti alloy noting Ti content variation as function of aging
09 p1706 A70-22812

Nb-W single crystal low temperature thermally activated deformation, observing slope change in temperature dependence curves of flow stress and strain rate sensitivity

09 p1708 A70-23572

Optical properties of beta prime phase CoAl, CoGa and NiGa as functions of composition and photon energy

10 p1919 A70-23986

Oxygen sticking coefficients and desorption kinetics on tungsten crystal by step desorption/ reflection technique, postulating formation and decomposition of surface oxide phases

10 p1832 A70-25147

Stability conditions in metal specimens tension tests, considering fcc and bcc metals strain hardening, rate and gradients and temperature dependence

10 p1966 A70-25326

Composition and monoclinic parameters of chromium sulfide mineral breznaita in metal matrix and silicate inclusions of Tucson meteorite using electron microprobe

11 p2110 A70-26004

Anomalous grain growth kinetics and recrystallization in electron beam annealed nickel determined by microstructural and radiographic study, noting annealing time dependence

11 p2068 A70-26596

Plastic properties of materials to elastic limit of pure metal and ionic solid crystals

12 p2283 A70-27055

Polycrystalline W-Re alloy creep tests in tension, investigating dislocation substructure formation as function of stress, temperature and strain

12 p2255 A70-27606

Contaminated Ni crystal /100/ surface photoelectric yield as function of temperature, considering effects of Ar ion bombardment and annealing

12 p2288 A70-27680

Sintering processes using boundary porosity in welded Nb bicrystal for model of final stages

13 p2434 A70-29081

Irreversible yield stress component of aluminum, Armpco iron and tantalum with fcc lattice, showing temperature dependence

13 p2436 A70-29500

Plastic deformation of Mo-Re single crystals produced by electron beam zone refining, investigating lattice frictional stress, activation volume temperature variation, etc

13 p2436 A70-29562

Cr-Ni cold worked austenitic steel dislocation structure in tensile tests at different strains

14 p2596 A70-30874

Single crystal W and W alloys dislocation structures as function of strain, temperature and dilute alloys addition, using electron microscopy

15 p2756 A70-31563

Torsional vibrations amplitude effect on polycrystalline Al stress-strain curve during uniaxial tensile test

15 p2758 A70-32125

Work hardening properties of Ni single crystals of various orientations during intermittent and continuous plastic deformation

15 p2762 A70-32394

Electron energy losses at interface of helium inclusions in aluminum irradiated by radioactive lithium

15 p2785 A70-32764

Lattice planes and interplanar spacings of small vapor deposited gold crystals, using transmission electron microscopy

16 p2961 A70-33644

Unalloyed polycrystalline Ti fatigue tests, observing cyclic stress effect on twinning

17 p3116 A70-34393

Al single crystals hardening under low temperature reactor irradiation, emphasizing yield phenomenon associated with Luders bands

17 p3123 A70-34647

Plastic deformation of melted Al-Mg single crystals, using dynamic tensile testing

19 p3450 A70-37374

Superlattice stacking faults in plastically deformed nickel aluminate /gamma prime phase/ due to interaction of antiphase boundary /APB/ type dislocation pairs

19 p3451 A70-37704

Argon hydrostatic pressure effect on self diffusion coefficients and activation energy of Al and Be single crystals

20 p3644 A70-38961

Bcc metals and alloys stress relaxation, internal stress and work hardening, discussing temperature dependence and dislocation motion

20 p3647 A70-39108

Slip band formation dislocation-diffusion mechanism for single crystal and polycrystalline metals, considering stress intensity and load cycles effects

21 p3936 A70-41416

Elemental composition and structure of metallic iron particles in lunar fines compared to meteorites, using neutron activation technique

21 p3774 A70-41556

Directional dependence of elastic shear stiffness on cubic axes for Si, Cu and Mo, making polar plots of shear stiffness coefficients

21 p3850 A70-41909

Electron tunneling through p-type GaAs point contacts on Pb single crystals at liquid He temperatures

21 p3864 A70-42017

Copper and Al polycrystalline single crystal substructure changes, examining high temperature, unsteady and diffusion creep

22 p4056 A70-43342

Polycrystalline aluminas under thermal shock, investigating strength decrease and subcritical crack formation

22 p4059 A70-43413

METAL CUTTING

Electrical discharge machining using electrical spark eroding action for machining tough metals in burr-free intricate configurations, including narrow slots and blind holes

03 p0497 A70-13564

Tangential cutting force measurements during Ti grinding by microtools, noting properties of W, aluminum boride and zirconium carbide

04 p0697 A70-14466

Overcut phenomenon in early stage of cutting developed as theory for tip interference in internal gears

05 p0854 A70-15885

Metal cutting by gas jet lasers, discussing single and multimode lasers, carbon dioxide lasers, power and power density requirements, etc

08 p1501 A70-20470

Machine tools used in production of Hawker Siddeley Buccaneer low level strike and reconnaissance aircraft

09 p1691 A70-22608

METAL DRAWING

Cold reduction effects on press formability of pure Al sheet with allowance for tensile properties and crystallographic orientation

06 p1075 A70-17145

Strain rate effects in cold metal working processes involving rolling and drawing

08 p1590 A70-21327

METAL FATIGUE

Cyclic loading test apparatus for studying ferromagnetic metals structural changes due to fatigue

01 p0116 A70-10076

Fatigue crack propagation in metals exhibiting initial crystallographic shear mode followed by noncrystallographic tensile mode

01 p0198 A70-10101

Corrosion induced fatigue damage suppression in jet engine compressor steel components, describing various surface treatment effects

01 p0165 A70-10699

Fatigue crack growth rate for high strength steels from crack length during cyclic loading and striation spacings after fracture

01 p0119 A70-10732

Aluminum alloys fatigue properties tested at ultrasonic frequencies

01 p0120 A70-10879

TD-Ni low cycle fatigue properties at high temperature, discussing grain morphology, thoria particles role and oxidation resistant coating effect

01 p0123 A70-11245

Metal fatigue in Al alloys subjected to stress cycles, determining macrocracks propagation stages

01 p0212 A70-11607

Chromium-nickel steel fatigue strength under repeated thermal cycles, showing dependence on long term fatigue buildup and single cycle fatigue damage effects

02 p0383 A70-11653

Machine parts fatigue strength under thermal cycles, studying nonlinear dependence of energy dissipation per unit volume on cycles number

02 p0383 A70-11654

Stress rupture strength dependence on specimen geometry /scale effect/ from analyzing metals failure under prolonged loads

02 p0383 A70-11655

Stress concentrations and load cycle asymmetry effect on materials stress and breakdown behavior under various load cycles

02 p0383 A70-11656

Ti alloys creep and fatigue breakdown under cyclic tensile loads at room temperature

02 p0315 A70-11660

Brazed plate-fin superalloy panels suitable for hydrogen-cooled structures, discussing fabrication techniques, performance tests and pressure containment and fatigue characteristics

02 p0306 A70-11930

F-8 wing service life extension design techniques, emphasizing fatigue design curves and procedures

02 p0386 A70-11939

Out-of-phase or nonsynchronous biaxial straining effects on low cycle fatigue observed on Al specimen by cycling tension-compression and cyclic torsion

03 p0481 A70-12955

Metals fatigue strength prediction by hysteresis loop method, presenting results for irreversible energy dissipation rules during cyclic loading

03 p0587 A70-13240

Short term creep and stress-relaxation curves analytic extrapolation for metals and alloys with lifetimes exceeding test duration

03 p0588 A70-13246

Durability of refractory tubes of small thickness under creep with account of scale factor and unsteady conditions, tabulating experimental and theoretical values

03 p0508 A70-13247

Al alloy and structural steel fatigue strength under superelastic cyclic axial stresses, describing observed plastic deformation patterns

03 p0509 A70-13271

Creep rupture and fatigue strength in solid body mechanics, considering triaxial stress state and simplified creep rupture theory variant

03 p0599 A70-14249

Dynamic equilibrium prediction for creep and fatigue of various metals under various loading conditions, using time-temperature and cyclic stress-strain parameters

[ASME PAPER 69-WA/MET-9] 04 p0704 A70-14759

Structural metals hysteresis properties under cyclic plastic loading at room temperature, considering cycle dependent creep and stress relaxation

[ASME PAPER 69-WA/MET-4] 04 p0705 A70-14763

Stress-strain spatial distribution in notched plate fatigue specimen of mild steel determined by finite element method, noting cyclic strain softening effect

[ASME PAPER 69-MET-C] 04 p0770 A70-14876

Dimensional analysis for describing steel surface microcracks growth under uniaxial fatigue loading, using stress-intensity factor and crack extension concepts of fracture mechanics

[ASME PAPER 69-MET-G] 04 p0770 A70-14879

Axial compression effect on low cycle fatigue of thin walled metal tubes in torsion

[ASME PAPER 69-MET-H] 04 p0705 A70-14880

Metals and alloys creep under tension and compression at elevated temperatures, considering plastic deformation equation applicability

04 p0707 A70-15265

Surface work hardening and stress concentrations effects on fatigue strength of alloy under asymmetric tension and compression load cycles at high temperatures

04 p0707 A70-15270

Polycrystalline metals strength factors in aircraft and aerospace construction as relation between rupture time and embrittled grain boundary at high temperatures

04 p0779 A70-15671

Hydrogen embrittlement as delayed rupture origin in high strength steels

04 p0711 A70-15682

X ray metallography methods applied to high temperature protective coating development, refractory alloys strengthening and metal fatigue studies

04 p0711 A70-15706

Book on basic metal fatigue covering microstructure, crystal structure, plastic deformation, dislocations and point defects

05 p0929 A70-16070

Test apparatus for investigating crystal defects influence on simultaneous measurement of metals thermal and electric conductivity under plastic deformation at cryogenic temperature

05 p0829 A70-16399

Al alloys crack growth effects due to gaseous environment and fatigue frequencies, suggesting role of gas adsorption

05 p0938 A70-16478

Overstress cycles sensitivity for welded specimens on basis of French fatigue damage line and Wohler S-N line

05 p0941 A70-16520

Cryogenic temperature effect on short life torsional fatigue properties of Ni-Cr-Mo steel, discussing cyclic strain range effects

05 p0864 A70-16807

Deformation and failure of refractory metals at high temperatures under constant and variable thermal loads concerning turbomachine components

05 p0865 A70-17027

Plastic deformation of refractory alloys during stress relaxation tests under vibrations, showing enhanced stability

05 p0866 A70-17033

Low cycle fatigue of alloy and steel materials under bending and cyclic heating, relating strains and number of cycles to failure

05 p0866 A70-17036

Thermocyclic creep and rupture strength of Nb, Ta and Mo refractory alloys under temperature and load variations, showing failure dependence on cycle parameters

05 p0867 A70-17043

Nickel-based alloys small cycle thermal and mechanical fatigue limit during tensile stresses and operational temperatures, analyzing fatigue curves

05 p0867 A70-17046

Fatigue life tests for heat resistant gas turbine blade alloys under power and thermal loads simulating aircraft flight 05 p0953 A70-17051

Heating influence on circular bending fatigue strength of refractory steel and alloys, using radiative and HF inductive heating 05 p0868 A70-17059

Fatigue strength of T-shaped blade roots of steam turbine regulating stages subjected to combined static tension and cyclic bending 05 p0954 A70-17060

Structural changes in polycrystalline Al subjected to HF fatigue, using transmission electron microscopy 06 p1084 A70-17127

X rays of surface residual stresses produced during fatigue process of annealed low carbon steel and copper 06 p1084 A70-17128

Plastic flow theory applied to cyclic deformation of metals under complex cyclic loads 06 p1162 A70-17385

Copper specimens stress-strain diagrams under cyclic loads of various amplitudes, noting three stage process plastic deformation 06 p1162 A70-17386

Cyclic creep curves plotted from expansion diagrams for steel, copper and brass under small numbers of cyclic compression tension loads 06 p1162 A70-17388

Stress kinetics and breakdown time of hardening Al alloys and steels under cyclic loads, noting dependence on plastic deformation 06 p1162 A70-17391

Time to crack formation determined in cylindrical and flat Al and steel specimens having various surface properties under cyclic loads 06 p1084 A70-17392

Steel elements failure during nonstationary thermal fatigue with varying strain and temperature, discussing linear damage accumulation theory 06 p1163 A70-17397

Temperature cycle duration effects on heat resistant alloys thermal fatigue resistance, noting stress relaxation occurrence 06 p1085 A70-17398

Steels crack propagation direction dependence on load magnitude in low cycle fatigue, noting groove width effects on resistance to static loading 06 p1163 A70-17401

Low cycle fatigue life of various structural steels and alloys, studying stress cycle number relations 06 p1085 A70-17402

Surface work hardening effects on steels resistance to low cycle fatigue with stress concentration, applying results to aircraft parts 06 p1085 A70-17403

Normalized steel low cycle fatigue strength under bending and torsional rotation, testing linear damage accumulation theory 06 p1163 A70-17404

Ti alloy tensile strength under cyclic loads at room and high temperatures, noting plastic deformation and damage accumulation effects 06 p1085 A70-17406

Fatigue at high temperatures - ASTM Conference, San Francisco, June 1968 06 p1086 A70-17451

Adverse effects of temperature and strain rate on low cycle fatigue resistance of austenitic stainless steels at elevated temperatures compared with tension tests 06 p1086 A70-17452

Refractory Nb alloy low cycle fatigue characteristics in vacuum at high temperatures, describing testing machine 06 p1086 A70-17453

High purity Ni fatigue in reversed bending as function of oxygen pressure and temperature 06 p1086 A70-17454

Creep-low cycle fatigue interactions in Udimet alloy at elevated temperatures, investigating cumulative damage 06 p1086 A70-17455

Elevated isothermal and low cycle thermal fatigue of Hastelloy X, investigating test temperature, cycle frequency and stress temperature effects 06 p1087 A70-17457

Microstructure effects on smooth and notched fatigue and room temperature tensile properties of Ti-Al-V alloy using heat treatment combinations 06 p1087 A70-17458

Energy dissipation patterns of metal fatigue failure during static and cyclic loading applied to untreated and heat treated steel samples 06 p1166 A70-17651

Mean cyclic stress effect on stress concentration and fatigue strength of smooth and notched steel specimens at normal and high temperatures with superimposed bending 06 p1088 A70-17653

Energy dissipation during torsional and flexural vibrations of steel and duralumin specimens subjected to plastic deformation, accounting for discrepancies due to methodical errors 06 p1166 A70-17658

Plastic zone around propagating fatigue crack in Cu single crystals, using transmission electron microscopy and X ray topography 06 p1171 A70-18494

Steels fatigue strength under biaxial tension, considering complex stress-strain state 07 p1304 A70-18823

Alloying elements preventing hot cracking in weld metal by converting iron sulfides into higher melting point sulfides 07 p1293 A70-18979

Reverse-bend and tension-tension fatigue properties of high strength Cr-Mn-N stainless steel sheet in notched and unnotched conditions 07 p1305 A70-18993

Microbiological corrosion effects on aluminum alloy fatigue properties inducing further microbiological corrosion compared to chemical corrosion effects 07 p1310 A70-19735

Stability criterion applied to asymmetric rigid cyclic strains and plastic cyclic strains, considering failure of metals 07 p1315 A70-20182

Duraluminum sheets fatigue life and corrosion fatigue strength decrease with corrosion damage area increase 08 p1515 A70-20921

Electronic recording of cyclic strain diagrams of metals in wide loading frequency range using dynamic hysteresis method 08 p1585 A70-20987

Static and dynamic low temperature crack toughness behavior of steels, determining strain rate effect 08 p1518 A70-21317

Stress corrosion-fatigue crack propagation in high strength structural steels, relating growth rates to crack tip stress intensity factor 08 p1519 A70-21452

Al alloys fatigue cracks propagation rate using electron microfractography 09 p1701 A70-22223

Metal fatigue by proliferation, diffusion and vanishing of lattice dislocations under varying loadings described by nonlinear inhomogeneous parabolic differential equations 09 p1770 A70-22253

Multiaxial thermal fatigue cracking in carbon steels predicted by elastoplastic stress-strain analysis using finite element method 09 p1773 A70-22578

Strain rate and hold time effects on steels low cycle fatigue behavior, graphing various correlations among stress amplitude, time to fracture, etc 09 p1774 A70-22589

Stress concentration effect on fatigue strength of Al- and Mg-base structural alloy specimens of different sizes analyzed statistically 09 p1703 A70-22617

Fatigue strength tests of alloy during static and programmed loading at high temperatures from statistical standpoint 09 p1703 A70-22620

High temperature fatigue crack growth in metal, suggesting condensation of vacancies at crack front after each loading cycle 09 p1776 A70-22644

Fatigue crack probability distributions under oscillatory stationary random loading, basing analysis on crack propagation model 09 p1776 A70-22683

Al alloys fatigue properties dependence on surface oxide cracking in moist and dry air, investigating oxidation and kerosene processing 09 p1707 A70-23206

Lattice defects in Al-Zn alloy due to fatigue investigated for mechanism and effect on aging kinetics by resistivity measurement 09 p1707 A70-23326

Dislocations maximal concentration during metal fatigue 10 p1955 A70-24081

Energy dissipation-fatigue strength relationships during vibrations for prestrained metals and alloys 10 p1956 A70-24244

Ti-Al-Zr-W-Si alloy fracture surface concentric markings number related to loading cycles after crack formation 10 p1904 A70-24837

Design mean stress and ground-air cycles minimum stress effect on fatigue behavior of titanium alloy in supersonic transport operating environment 11 p2128 A70-25370

[SAE PAPER 700033] VTOL aircraft metal fatigue examination by photoelasticity emphasizing stress reduction 11 p2132 A70-25622

High fatigue life resulting from titanium spot welding realized by preweld and postweld treatment 11 p2059 A70-25662

Fatigue properties of electron beam welded precipitation hardening stainless steels 11 p2059 A70-25664

Stress ratio effects on Al alloy during crack propagation and fatigue, introducing notch stress and strain approximations 11 p2066 A70-26089

METAL FATIGUE

Fatigue life tests of Al alloy under narrow and broad band random loads based on number of peaks to failure 11 p2066 A70-26095

Fatigue crack propagation in high strength steels during fatigue cycling in dry and wet environment containing NaCl 11 p2067 A70-26100

Metals low cycle fatigue resistance, discussing repeated plastic straining effect on mechanical properties 11 p2141 A70-26609

Uniaxial low cycle thermal fatigue test procedure for ductile metals, describing strain measuring system allowing direct recording of load vs mechanical deformation 11 p2034 A70-26615

Electrochemical machining effects on surface integrity and fatigue properties of steel, Ti and Al alloys [ASTME PAPER MR-69-110] 12 p241 A70-27081

Fretting and fretting fatigue in metal-metal contacts, showing friction as important parameter 12 p2253 A70-27110

Fatigue crack initiation and propagation in steel using surface plastic replication method, determining propagation rate by stress intensity 12 p3321 A70-27207

Kinetic theory for fatigue crack propagation using cyclic stress-strain relation in connection with strain hardening characteristics 12 p3322 A70-27208

Annealed stainless steel low cycle fatigue data analysis leading to method of characteristic slopes approach for correlating plastic strain range to fracture time 12 p2255 A70-27604

Fatigue crack propagation dependence on environment and load frequency in Al alloys, correlating data by stress-intensity factor 13 p2431 A70-28603

Fatigue crack growth dependence on load profile, temperature, test frequency and environment and stress in high strength Al and Ti alloys and steels 13 p2431 A70-28604

Creep properties of torsion-tension metal members subjected to nonproportionate loading at high temperatures 14 p2656 A70-30637

Erosion damage of porous sintered Fe in water or oil in test device with disk rotating near sample surface, noting relationship to metal fatigue 14 p2592 A70-31272

Al-Mg alloy nonpropagating fatigue cracks at roots of sharp notches, discussing cyclic strain hardening 14 p2598 A70-31299

Fracture mechanics and stress analyses comparison for fatigue cracked steel cantilever beam stress corrosion specimens 15 p2755 A70-31473

Plain strain fracture toughness index measurement, discussing application to metal fatigue and stress corrosion 15 p2757 A70-31927

Metallic materials damage accumulation and structural failures due to fatigue, considering surface changes, crack initiation and dislocation pattern 15 p2757 A70-31928

High temperature metal fatigue crack growth monitoring by ultrasonic detection [SESA PAPER 1622] 15 p2744 A70-32321

Pure iron and low carbon steel macroscopic stress measurements, determining correlation between residual stress, fatigue damage and fatigue life 15 p2759 A70-32322

Surface layer dislocations concentration role in metal fatigue, using variable diffusion coefficient 15 p2822 A70-32352

Metal fatigue cracks, reviewing propagation theories and structure life prediction equations 15 p2822 A70-32358

Glass bead blast induced residual stress and surface cold work effects on Ni base superalloy fatigue crack initiation and propagation 15 p2761 A70-32381

Dislocation distribution in Ta foil following yield point fatigue testing, using thin film electron microscopy 15 p2761 A70-32385

Environmental fatigue crack propagation in Al alloys at low cyclic stress intensity levels 15 p2762 A70-32390

Crack initiation and propagation in rolling contact fatigue, emphasizing electrochemical effects in ball bearing failure [ASME PAPER 70-DE-46] 16 p2931 A70-33509

Hysteresis loop behavior under tension-compression cycle fatigue related to Meyer strain hardness values of cyclically strained metals 16 p2934 A70-34334

Alpha Ti and alpha Ti-hydrogen alloys fatigue behavior, emphasizing twin formation influence and hydrogen effects 17 p3116 A70-34394

METAL FILMS

Ti-Al-Cr-Fe tensile, fatigue and creep properties at various temperatures, considering industrial applications

17 p3121 A70-34428

Weldability, tensile and fatigue properties of Ti sheet alloys, discussing TIG welds

17 p3121 A70-34431

Fatigue properties of solution treated and age hardened hot rolled Ti alloy bars, discussing sprayed tungsten carbide coatings effects on bearing properties

17 p3121 A70-34432

Fatigue characteristics of Ti alloy forgings for rotary wing vehicles, discussing effects of welding, annealing, reduction, surface finish and shot peening

17 p3122 A70-34441

Low cycle fatigue and short term tensile behavior correlation for irradiated and unirradiated stainless steels

17 p3123 A70-34627

Residual stress concentration at fatigue crack tip, using oscillating crystal X ray microbeam diffraction photographic method

17 p3183 A70-34652

Fractography of fatigue and delayed fracture of hydrogenated, unplated and Cd-plated ultrahigh strength steel

17 p3124 A70-34654

Steel and cast iron early stage fatigue failure, using photoelastic coatings

17 p3192 A70-35741

Stainless steel load-strain characteristics and cumulative damage in cyclic fatigue life

18 p3273 A70-36048

Ti alloy prior plastic deformation effect on fatigue strength under bending, tension, torsion and rolling

18 p3275 A70-36141

Chromium-nickel steel fatigue strength under repeated thermal cycles, showing dependence on long term fatigue buildup and single cycle fatigue damage effects

19 p3547 A70-38426

Machine parts fatigue strength under thermal cycles, studying nonlinear dependence of energy dissipation per unit volume on cycles number

19 p3547 A70-38427

Stress rupture strength dependence on specimen geometry /scale effect/ from analyzing metals failure under prolonged loads

19 p3547 A70-38428

Stress concentrations and load cycle asymmetry effect on materials stress and breakdown behavior under various load cycles

19 p3547 A70-38429

Ti alloys creep and fatigue breakdown under cyclic tensile loads at room temperature

19 p3452 A70-38434

Metal fatigue strength prediction by hysteresis loop method, presenting results for irreversible energy dissipation rules during cyclic loading

19 p3548 A70-38458

Short term creep and stress-relaxation curves analytic extrapolation for metals and alloys with lifetimes exceeding test duration

19 p3548 A70-38464

Durability of refractory tubes of small thickness under creep with account of scale factor and unsteady conditions, tabulating experimental and theoretical values

19 p3453 A70-38465

Gaseous radioactive penetrant inspections for early low cycle fatigue in aircraft engine materials, discussing impact on maintainability

19 p3441 A70-38828

Aluminum alloys subjected to random loading, comparing fatigue life with predictions based on linear accumulation of damage hypothesis

20 p3647 A70-39157

Low cycle metal fatigue under stress concentration, examining complex loading, cyclic strain, stress-strain state and plastic deformation

20 p3727 A70-39885

Steady state and transient fatigue behavior of stainless steel wire-Al alloy composite subjected to push-pull and pull-release frequency tests

20 p3649 A70-39946

Stainless maraging steel bolts tensile, shear and fatigue strengths and stress corrosion resistance at room and high temperatures

20 p3650 A70-39964

Notched polycrystalline Al-Mg alloy dislocation structure near propagating fatigue crack at various stress levels

21 p3839 A70-40925

Nondestructive ultrasonic measurements of crack depth in high strength steel plate weldments, studying low cycle fatigue

21 p3834 A70-41943

Stress concentration effect on perforated Al alloy panel fatigue, using theory for material critical thickness near notch

21 p3938 A70-41955

Book on fatigue crack propagation in pure Al covering tension and compression tests, single and

polycrystalline materials, elastic stress, notched and smooth specimens, etc

22 p4057 A70-43740

Fatigue limits of Ti alloy by Wohler and Locati loading methods

23 p4204 A70-43933

Crack propagation resistance-cyclic fracture strength relation for Mn-Cr-V steels, considering thermomechanical working effects

23 p4204 A70-43935

Fatigue of turbine blade stainless steels and nickel alloys as function of temperature, stress and surface layers

[ICAS PAPER 70-38]

23 p4205 A70-44135

Papers on plane strain fracture toughness testing covering metallic materials, steels and aluminum alloys

23 p4205 A70-44189

Fracture toughness testing of metallic materials including fatigue cracking, thickness limitations and crack detection

23 p4206 A70-44190

Plane strain fracture toughness testing of high strength Al alloys and steels, using fatigue cracked bend specimens

23 p4206 A70-44191

Crack and thickness effects on fracture toughness tests of high strength steel in precracked sheet and bend specimens

23 p4206 A70-44193

Specimen size and mechanical factors in plane strain fracture toughness testing of metallic materials

23 p4206 A70-44195

Bcc metals, measuring correlation between residual stress level and fatigue damage by X ray diffraction analysis

23 p4207 A70-44422

German monograph on notched structural steels fatigue properties and crack propagation under tensile-compressive alternating loads

24 p4356 A70-45086

High strength martensitic stainless steel stress corrosion resistance and fatigue crack growth rate, considering austenite content, strain aging and tempering temperatures

24 p4359 A70-45245

Cyclic loaded high purity Al samples, noting substructure around fatigue cracks

24 p4362 A70-46185

METAL FILMS

Low speed Ga lubricated sliding electrical contacts of Be in vacuum, discussing Ga film role in friction and contact resistance

01 p0099 A70-10325

Metal film graded filter fabrication for schlieren photographic system with laser light source and framing camera, using vacuum evaporation

01 p0113 A70-10921

Titanium thin films prepared in ultrahigh vacuum to determine low temperature/pressure oxidation kinetics, using electron microscopy and X ray diffraction

02 p0317 A70-12316

Frequency spectrum, Q factor and single mode selectivity of two mirror laser resonator with absorbing thin metallic films, showing agreement for Ag and Ni

03 p0500 A70-13459

Semitransparent Pt film reflectance in vacuum UV evaporated on glass, quartz, Al, Au and Cr on glass compared with opaque films

04 p0731 A70-15023

Hall voltage measurements on Ta thin films using square wave generator current, discussing parasitic effects and suppression possibilities

05 p0863 A70-16366

LF creep characteristics in Block-wall Permalloy films, using high resolution Bitter pattern technique

[IEEE PAPER 5.7]

05 p0893 A70-16996

Mn-Bi films Curie point switching with laser, measuring magnetization dependence via magneto-optic effect

[IEEE PAPER 9.3]

05 p0893 A70-16997

Calorimetric measurements determining total hemispheric emittance of thin gold films as function of temperature, demonstrating film thickness effect

[AIAA PAPER 70-63]

06 p1180 A70-18140

Crystal structure imperfections and elastic anisotropy of crystallites in condensed Ni films by X ray analysis

07 p1309 A70-19636

Low temperature oxide film effect on porous titanium carbide impregnation by liquid steel

07 p1311 A70-19805

Chromium films obtained on tungsten by sputtering, studying structure and work function at various temperatures

08 p1516 A70-21123

Strain gage for measuring strain waves amplitude on surface of fused quartz to study electromagnetic waves interaction in Permalloy films

09 p1681 A70-23349

Epitaxy of Ag deposited on Ni, observing irreversible crystallographic order transition from metastable nominal orientation by LEED

10 p1927 A70-24076

Electron energy loss spectrum in Ti measured by bombarding thin films vacuum deposited on NaCl crystal with electrons of intermediate energy

11 p2065 A70-25376

Thermal conductivity of thin metallic films and wires at cryogenic temperatures, discussing electron transport properties

11 p2083 A70-25752

Frenkel pairs and interstitial hydrogen atoms observed in thin silver films after proton bombardment

12 p2253 A70-27209

Thin films of vanadium niobium and tantalum obtained by vacuum thermal decomposition of metal iodides

12 p2253 A70-27210

Quenched MnBi thin films measured for magnetic, magneto-optical and optical properties, noting Faraday rotation

12 p2284 A70-27246

Au, Ag and Al films evaporation in ultrahigh vacuum on LiF and MgO surfaces, showing insignificant role of lattice misfit for epitaxy

12 p2285 A70-27260

Bi polycrystalline film grown by vacuum deposition on amorphous substrates investigated for electron microscope beam effects

12 p2285 A70-27261

Tantalum RF sputtered superconducting films structure and properties at various substrate temperatures, observing bcc, fcc and amorphous phases by electron microscopy

12 p2288 A70-27876

Microwave transmission through thin film screens with apertures placed in transverse plane of X band rectangular guides

12 p2202 A70-28164

Threshold light flux densities for thin Al film breakdown by laser radiation

13 p2428 A70-29383

Attenuation length of vacuum UV photoexcited electrons in evaporated metal films, observing lack of dependence on photon energy

13 p2472 A70-29711

Ta thin film integrated circuit technology including resistor and capacitor elements, conductors, cross-overs, etc

14 p2625 A70-30284

Evaporated Au-Ni-Cr alloy resistor films physical and electrical characteristics, noting dependence on composition

14 p2625 A70-30285

Au films nucleation and growth on single crystal graphite substrates in ultrahigh vacuum, using transmission electron microscopy for examination

14 p2627 A70-30499

Thin film sandwich Ag/Ni/Cu, demonstrating multiple electron diffraction

14 p2627 A70-30724

Constant temperature hot split film anemometer sensors based on velocity and heat flux distribution about probe, measuring flow rates

15 p2734 A70-31691

Au-Pd films boundary structure during diffusion annealing, noting polymerized oil vapor effect originating from vacuum pump

15 p2758 A70-32121

Thermoelectric power measurement of thin Au films, relating results to transport parameters and internal stresses

15 p2785 A70-32582

Scattering cross sections for monoenergetic Ar beams on epitaxial Ag films

16 p2956 A70-34013

Oxidation dependence on physical nature of Ti surfaces obtained by thin film techniques under ultrahigh vacuum conditions

17 p3098 A70-34364

Growth mechanism and crystal structure of Ge films deposited from molecular beam onto GaAs, Si and Ge substrates

18 p3297 A70-36415

Fe and Al impurities in bis-ethylbenzene chromium /BEC/ and in chromium films obtained by thermally induced decomposition of metal organic compound

18 p3297 A70-36463

X ray fluorescence determination of thickness and composition of Permalloy films deposited on wire surface

18 p3258 A70-36466

Adherent Ta films deposition onto Teflon disks by sputtering

18 p3264 A70-37098

Dielectric properties of thin barium titanate films from microwave resonance frequencies and resonance reflection coefficient

19 p3482 A70-37255

Substrate and thickness dependence of electrical and superconductivity properties of rhenium and molybdenum films prepared by electron beam evaporation

19 p3485 A70-37684

- Cesium films structure and work function on W /011/ face, discussing order-disorder transition
19 p3487 A70-37817
- Cooled antimony-cesium film photoelectric effect for weak luminous flux, examining electronic camera reciprocity
19 p3427 A70-38175
- Thin metal film electrical conduction current noise characteristics
19 p3487 A70-38196
- Deformation effects on metallic and semiconductor thin films conductivity
19 p3488 A70-38199
- Epitaxial GaAs films growth from solid solutions of InAs-GaAs system deposited on GaAs substrates, noting electron mobility and temperature effect
20 p3686 A70-39629
- Hydrogen emanation and distribution in metals and alloys by Nd hydrogen metal detection method
20 p3651 A70-40071
- Temperature dependent anomalous optical absorption of thin yttrium films under static ultrahigh vacuum
21 p3862 A70-40816
- Numerical solution for multilayer insulation system comprised of infinite parallel metallic films separated by optically thin dielectrics
21 p3947 A70-41054
- Nb-Zr thin films superconducting properties dependence on deposition temperature and rate and substrate material
22 p4085 A70-42623
- Thin film granular aluminum superconductors as sensitive thermometers
22 p4031 A70-43009
- Optical transmission and reflection gratings formed by standing light waves evaporation of thin metallic films in ruby laser cavity
23 p4200 A70-43817
- Crystal growth in polycrystalline Au, Ag and Au-Ag thin films annealing, observing by electron microscopy and electron diffraction
24 p4391 A70-45672
- IC metallization systems in semiconductor devices fabrication and packaging, assessing metals alternate to Al for electromigration difficulties avoidance
24 p4319 A70-46075
- Thin epitaxial Ag films on mica, measuring electrical resistivity strain dependence
24 p4391 A70-46266
- Metal layer and absorbed oxygen quantities in reactive oxidation deposition of aluminum
24 p4365 A70-46354
- ## METAL FINISHING
- ### NT ELECTROPOLISHING
- ### NT SHOT PEENING
- Nickel boronizing in high temperature vacuum, studying mechanical properties and layer thickness time dependence
08 p1517 A70-21148
- ## METAL FOILS
- DC electrical conduction in In and In-Pb alloy foils sandwich structures, discussing size effect and Pb diffusion rate
03 p0540 A70-13624
- Elastoplastic zone and instability of precracked thin sheets under uniaxial loading applied to rectangular center-notched steel foils
03 p0598 A70-14239
- Al foil exposed to solar wind on moon during Apollo 11 mission examined for helium particles, finding lunar solar wind albedo
05 p0900 A70-16093
- Swiss Solar Wind Composition Experiment, analyzing trapped particles characteristics of Apollo 11 and 12 lunar exposed aluminum foil
11 p2105 A70-25950
- Foil decarbonization process monitored by mass spectrometry of secondary carbon ion emission
12 p2254 A70-27311
- Energetic ion production by giant pulse lasers measured on Al and Au foil targets
15 p2777 A70-32333
- Dislocation distribution in Ta foil following yield point fatigue testing, using thin film electron microscopy
15 p2761 A70-32385
- Concorde engine bay thermal insulation combining stainless steel foil and polytetrafluorethylene film, considering noise level, engine fire conditions and molten Ti globules penetration
18 p3346 A70-36345
- Nonsteady combustion analysis, using method of flame front penetration through fine metal layer in solid propellant
18 p3300 A70-36704
- Fluid inertia and compressibility effects considered in equations for foil over lubricating film
19 p3435 A70-37615
- Gold foil surface thermal contact resistance, investigating temperature and pressure effects and elastic and plastic deformation of surface structure
21 p3953 A70-42166
- Thin Al foil subjected to cyclic bending stresses, investigating substructures and strain regions around fatigue crack
24 p4362 A70-46186
- ## METAL FORGING
- ### U FORGING
- ## METAL FORMING
- ### U FORMING TECHNIQUES
- ### U METAL WORKING
- ## METAL FUELS
- Chemical heat source combined with metals ignition properties considered for spacecraft heating during Mars nighttime landing
04 p0628 A70-15426
- Metallic fuels preparation by electric spark discharge process
17 p3145 A70-35214
- ## METAL GRINDING
- WC-Co alloys noting polishing and grinding effects on residual stress and crack resistance
03 p0508 A70-13145
- Tangential cutting force measurements during Ti grinding by microtools, noting properties of W, aluminum boride and zirconium carbide
04 p0697 A70-14466
- Roller bearings convex conical surfaces grinding using centerless grinder
08 p1506 A70-21192
- Material thickness tolerances control for weight minimization of aerospace vehicles by abrasive metal grinding, improving surface quality
20 p3638 A70-40358
- ## METAL HALIDES
- ### NT ALUMINUM CHLORIDES
- ### NT BARIUM FLUORIDES
- ### NT BERYLLIUM FLUORIDES
- ### NT CADMIUM FLUORIDES
- ### NT CALCIUM FLUORIDES
- ### NT COPPER CHLORIDES
- ### NT IRON CHLORIDES
- ### NT LITHIUM CHLORIDES
- ### NT LITHIUM FLUORIDES
- ### NT MAGNESIUM FLUORIDES
- ### NT POTASSIUM CHLORIDES
- ### NT SILVER HALIDES
- ### NT SILVER IODIDES
- ### NT SODIUM CHLORIDES
- ### NT SODIUM IODIDES
- ### NT STRONTIUM FLUORIDES
- ### NT TITANIUM CHLORIDES
- Polyamides /nylons/ stress cracking by metal halides and halide-like salts, investigating effects of nylon temperature, moisture content, concentration, etc
10 p1907 A70-24224
- Polyamide and secondary amide mode compounds stress cracking by metal halides using IR and nuclear magnetic resonance techniques
10 p1907 A70-24299
- Nylon 6 polyamide tensile stress cracking by metal thiocyanates in aqueous and nonaqueous solutions, comparing results with cracking by metal halides
10 p1907 A70-24300
- High temperature molecules matrix isolation in saturated vapor over refractory solids, discussing optical spectroscopy of VO, metal oxide and halide molecules
14 p2545 A70-30903
- ## METAL HARDENING
- ### U HARDENING [MATERIALS]
- ## METAL HYDRIDES
- ### NT LITHIUM HYDRIDES
- Nb-NbH solid solutions thermodynamic properties at various temperatures described by formulas
02 p0320 A70-12819
- Binary transition metal hydrides consisting of single metal and single hydrogen isotope, discussing preparation and kinetic, thermodynamic and structural properties
05 p0863 A70-16523
- Ignition of single particles of light metal hydrides, considering combustion stages and heat transfer
06 p1179 A70-17984
- Serrated yielding in hydrogenated nickel alloys, noting hydride stability role in Portevin-Le Chatelier effect
08 p1522 A70-21706
- MgH molecular lines Zeeman splitting in sunspot spectra confirmed by photoelectric observations
24 p4400 A70-45308
- ## METAL INSULATOR SEMICONDUCTORS
- ### U MIS [SEMICONDUCTORS]
- ## METAL IONS
- ### NT MANGANESE IONS
- Reduced Nd ion absorption in matrices of fluorides, fluoride mixtures or oxygen-containing compounds with various ion concentrations, analyzing optical centers statistical properties
01 p0107 A70-10210
- Positive Na and K ion effects on mitochondrial respiratory control, O uptake and adenosine triphosphate activity in rat liver
01 p0026 A70-11063
- Test program preceding first German satellite experiment using HEOS satellite for Ba ion cloud injection into deep space
02 p0380 A70-12081
- Amplification cross section of 1.06 micron transition of trivalent Nd ion in alkaline silicate glass host material, based on three level energy level diagram
02 p0312 A70-12111
- Slow waves and spikes in intestinal muscle of cat noting dependence on intracellular iontophoresis of Na
03 p0416 A70-13014
- Electron-phonon interaction model of temperature dependence of luminescence produced by multiphonon nonradiative transitions in Cr ions of ruby crystal, deriving transition probability
03 p0538 A70-13058
- Rocket-borne spectroheliograph for taking X ray and monochromatic pictures of sun in Mg II line
03 p0370 A70-13594
- He-Ne-Cd II laser operation modes for optimum pressure fill, obtaining red to blue outputs by varying current and/or temperature
04 p0702 A70-15366
- Nickel IV forbidden lines suggested from spectrum study of slow nova RR Telescopii
05 p0905 A70-15758
- Excitation of ground configuration of Fe XIII for density and temperature range in solar corona, using proton collisions, electron collision strengths, etc
05 p0902 A70-16434
- Hyperbaric oxygenation effects on cellular membrane permeability, analyzing rat plasma behavior of transaminases GOT and GPT and K and Na cations electrolytes
05 p0802 A70-16493
- Ca II 7323 forbidden line in solar Fraunhofer spectrum, estimating center-limb variation of equivalent width of transition
06 p1143 A70-17994
- Gadolinium ions in zinc tungstate single crystals, studying low symmetry effects on EPR spectrum
08 p1556 A70-21120
- Iron ions EPR lines widening in corundum crystals due to lattice defects, estimating mosaic blocks disorientation parameter and point defects density
08 p1556 A70-21122
- Excitation energy transfer processes in oxide glasses containing trivalent Tb ions in combination with other rare earth activators
09 p1738 A70-22137
- Excitation equilibrium relative populations calculations for Fe, Ni and Ca ions under solar coronal conditions
09 p1757 A70-22735
- Singly ionized Mg resonance lines electron impact broadening quantum mechanical calculation
09 p1732 A70-22827
- Energy levels predicted for various electron orbital configurations in Fe V by Slater parameters
10 p1944 A70-24953
- Natural frequency of paramagnetic amplifier retuned by coupling Cr ions doped silver coated ruby resonator to passive resonator
10 p1901 A70-25138
- Radiative lifetime for atomic transitions in UV multiplets of zinc and cadmium atoms and ions measured using phase shift method
11 p2086 A70-25363
- Electron and proton excitation of forbidden transition lines in Ca XV ground configuration determined for coronal densities and temperature
11 p2109 A70-25742
- Barium ionic cloud formation under action of sunlight and expansion in terrestrial magnetic field using plasma model
12 p2214 A70-26892
- Violet K2 emission in H and K line cores of solar calcium ions using atmospheric model in state of motion
12 p2303 A70-27701
- Lead ion effects on single crystal zinc dissolution and electrodeposition in alkaline solutions investigated microscopically
13 p2361 A70-28928
- Solar Ca II H and K lines formation, discussing double reversal, limb darkening, plage and spot lines and anomalous line ratios
13 p2494 A70-29481
- Ionized iron lines observations under coronal conditions, giving halfwidths and kinetic temperatures for forbidden lines Fe X-Fe XV
14 p2651 A70-31377
- Ferrous and ferric ions properties in corundum from observing acoustic paramagnetic resonance
15 p2784 A70-32397
- Binuclear scalar spin Hamiltonian inadequacy to describe electron exchange in systems containing orbitally degenerate ions, considering cobalt magnon spectra
15 p2777 A70-32399
- Fine structure in Ca II K line core, determining reduced high dispersion spectra at solar disk center
15 p2804 A70-32618

METAL JOINTS

Resonance and satellite lines of highly ionized iron in solar spectra, discussing spectrum features during chromospheric flares

17 p3154 A70-34541

Solar chromosphere resonance lines, observing H and K line profiles of Mg ions

17 p3161 A70-34893

Fabry-Perot interferometry of solar Mg II resonance lines

17 p3162 A70-34897

Fe II line behavior in plages near solar limb

17 p3174 A70-35866

He-Cd laser discharge, determining population densities and lifetimes for levels of Cd ion excited by He metastables

17 p3108 A70-35903

Intermediary complexes between Na-K ion stimulated ATPase/adenosine triphosphate/ and microsomal proteins of turtle bladder epithelial cells

18 p3225 A70-36233

Electron beam interaction with ionized K plasma, considering Langmuir waves instability, turbulence and electron heating

18 p3295 A70-36614

Power conditioning system for Hg ion thruster on SERT 2 spacecraft, considering performance, design, control circuits and arcing

20 p3568 A70-40216

Solar photospheric spectrum Ni II forbidden lines analysis, determining abundance of Ni for comparison with coronal and meteoritic data

20 p3711 A70-40405

Sco X-1 X ray emission data from rocket-borne measurement, indicating Fe K-emission from high ionization states

21 p3873 A70-40667

Sn and tetraethylammonium ions effects on Zn electrodeposition on Zn single crystals in aqueous KOH, using scanning electron microscopy

21 p3772 A70-40726

Molecular orbital energy level diagram for metal ion X ray emission and absorption spectra interpretation from titanium and vanadium compounds

21 p3853 A70-41901

Solar chromosphere elements abundances methods, suggesting Fe differences origin in Fe I and Fe II inconsistencies

21 p3925 A70-42194

Rb and Cs ions implanted Si analyzed by Hall effect and sheet resistivity measurements and channeling techniques

22 p4087 A70-43143

Ionization and loss processes for meteoric elements in lower ionosphere, suggesting hydrates formation role in alkali metal ions depletion

22 p4106 A70-43305

Metal phthalocyanin catalyzed oxidation by oxygen of vanadium and iron couples in externally regenerated redox fuel cell cathode

22 p3966 A70-43536

Meteoric metallic ions above F 2 peak, discussing current density and transport mechanisms

23 p4239 A70-43841

CA II chromospheric emission lines for deriving Mn in stellar luminosity, discussing calibration

23 p4242 A70-44293

Multiply ionized Fe valence and inner shell transitions from spectrum analysis, noting similarities to solar flares

24 p4401 A70-45315

Ion-ion potential for sodium vapor for second virial coefficient as function of temperature at 1200-1700 K

24 p4381 A70-45649

ESR intensities and line widths at X and Q bands of Cr and Fe molecular ions in water/glycerol mixtures

24 p4310 A70-46045

Chromium ions isothermal annealing kinetics in X ray irradiated ruby crystals, using EPR method

24 p4382 A70-46253

METAL JOINTS

NT SPOTLED JOINTS

NT SPOT WELDS

NT WELDED JOINTS

Diffusion welding of dissimilar metals with or without intermediate layers, assessing joint strength factors

03 p0498 A70-14071

Stress rupture strength of turbine blades fir tree type root joints under prolonged loads at high temperatures, studying disk teeth shearing

05 p0953 A70-17055

Turbine blades root joints endurance limit concerning tensile stress determination at stress raiser contour for elastoplastic deformation and creep

05 p0954 A70-17062

Joint design for braze bonding and joining of Al-B composites using Borsic tape backed with alloy brazing foil

07 p1293 A70-18994

Metal adhesive joints peeling and stripping strength determinations, describing static and dynamic tests

08 p1503 A70-20884

Metal adhesive joints nondestructive tests involving acoustic and supersonic, X ray and heat flow characteristics methods

08 p1503 A70-20885

Metal adhesive joints strength under tensile and torsional stresses, considering effects of dimensions, metal type and surface finishing

08 p1504 A70-20886

Metal adhesive joints behavior under prolonged static stresses, showing time dependence of tensile strength

08 p1504 A70-20887

Adhesive bonds strength in metal joints under stress cycling, examining effects of temperature and cycles frequency

08 p1504 A70-20888

Metal adhesive joints under cyclic stresses, studying stress distribution and fracture occurrence by high speed cameras

08 p1504 A70-20889

Metal adhesive joints permanence under various environmental conditions, considering surface properties effect

08 p1504 A70-20890

Shear stress distribution in metal adhesive joints, discussing methods for calculating

08 p1504 A70-20892

Metal adhesive joints strength and suitable dimensions determination, presenting parameter relations for design

08 p1584 A70-20893

Adhesive joints design, considering layer type, pipe connections and honeycomb structures for application in aircraft and automotive industries

08 p1585 A70-20894

Low cost programming system for gas tungsten arc welding process for Ti taper and stepped joint designs

08 p1507 A70-21484

Stainless steel wire-reinforced Al alloy diffusion bonded scarf joints, considering aluminum oxide coating and bonding times effects

08 p1509 A70-21906

Numerically controlled gas tungsten arc welding, discussing tape programming, fixture design and fabrication for various welded metal joint configurations

11 p2058 A70-25661

Book on metal joining techniques covering various welding and brazing processes

11 p2061 A70-26599

Polymer-metal adhesive joints rupture characteristics, considering polymer in solid or structurally fluid/elastic/ state during tests

12 p2244 A70-28341

Organic adhesives for bonding continuous surface and core-to-face joints, discussing strength, environmental resistance, producibility and reproducibility

13 p2419 A70-29118

In-place gas tungsten arc fusion welding for joining small diameter precipitation hardenable aluminum tubing

14 p2590 A70-30930

Low pressure diffusion welding for joining Ti-6Al-4V alloy in Ar atmosphere under compressive loading, evaluating performance

14 p2591 A70-30933

Transverse contraction during butt welding of plates of steel and Ti and Al alloys, showing dependence on joint thickness

16 p2916 A70-33053

Refractory alloys Li corrosion resistance, examining effects of oxygen contamination during welding

16 p2924 A70-34205

Precision electron beam welding for metal joints, discussing equipment and quality control factors

19 p3436 A70-38072

Microjoining in electronics industry, discussing technologies and nondestructive testing

19 p3437 A70-38424

Stainless steel sheet-to-plate tee joint resistance welded by Magnetic Force Upset Welding process, testing performance

21 p3832 A70-40792

Materials for glass-metal compressed joints, tabulating stress and thermal expansion coefficients

22 p3999 A70-43447

METAL MATRIX COMPOSITES

Aluminum oxide whiskers/metal matrix composites, discussing metallic coatings effects on filament wetting, bonding and surface protection

01 p0117 A70-10480

Tensile tests of heat treated silicon carbide coated B filament reinforced metals, discussing fiber strength and interfacial stability

01 p0117 A70-10483

Fiber breakage during powder metallurgy fabrication of compact Al-B composites as function of density

01 p0104 A70-10741

Tensile strength of flat specimens of Ni reinforced by W wire gauze

02 p0315 A70-11661

Mechanical properties of carbon fiber reinforced Al, Cu and Ni, noting rope and wire applications

02 p0384 A70-11676

Al-B composite missile adapter design for aerospace structures

02 p0306 A70-11951

Reversed bending fatigue tests on stainless steel fibermetal with porous structure to investigate effects of density, thickness, wire diameter, screen stiffening, etc

03 p0481 A70-12957

Mechanical properties of Al composites reinforced with alpha-silicon carbide sintered whiskers, discussing voids, fiber breakage and orientation effects

03 p0506 A70-13113

Modified explosive bonding process for welding wire reinforced Al composite materials

03 p0497 A70-13120

Al-Ni intermetallic whisker-reinforced Al microstructure and mechanical properties, studying effects of cold rolling

03 p0508 A70-13142

Mechanical properties, optimum deformation and rupture of W wire reinforced Ni and Ti metal composites obtained by hot rolling in vacuum

03 p0508 A70-13245

Composite materials possible applications, considering metal matrices reinforced by high strength metallic or nonmetallic fibers

03 p0512 A70-13857

Al and Sn composites reinforced by E glass and silicon dioxide glass fibers compared for tensile strength, noting difference due to resistivity

03 p0514 A70-14314

Titanium carbide based cermets with steel matrices, studying heat treatment effects on hardness

04 p0696 A70-14462

Electrical resistivity, contact resistance and weldability of cast Cu and Ag contact materials reinforced unidirectionally by W wire compared to powder composition

04 p0711 A70-14465

Transient one dimensional heat transfer analysis demonstrating infiltrant melting effect on self heat-retarding porous metal composite during surface melt layer formation

04 p0709 A70-15414

Ni dispersion-strengthened composites from ultrafine comminuted powders, describing forming techniques and test results

04 p0709 A70-15629

Ceramic fibers formation by particles mechanical deformation by extrusion in W matrix, describing grain structure of various extruded metal oxides

04 p0699 A70-15643

Continuous metal fiber composites tensile strength and ductility in terms of plastic instability

05 p0946 A70-16924

Joint design for braze bonding and joining of Al-B composites using Borsic tape backed with alloy brazing foil

07 p1293 A70-18994

Sapphire whisker-Al composites fabrication methods using air elutriation techniques and semiautomatic methods for fiber alignment, discussing elastic modulus, tensile strength, etc

07 p1314 A70-19956

Fiber reinforcement of metals, considering strength of boron, alumina, graphite, silicon carbide and silica glass fibers

08 p1514 A70-20471

Nickel alloy based metal fiber reinforced composites long-time structural stability at high temperatures

08 p1517 A70-21150

Aluminum-base reinforced material synthesis by liquid impregnation, investigating transition layer dependence on holding time and fiber/matrix microhardness

08 p1520 A70-21500

Axial constant load creep and strength rupture measurements of B-coated and silicon carbide-coated B filament reinforced Al alloys

08 p1521 A70-21702

Engineering use of filament reinforced metal matrix composites dependent on fabrication cost reduction, consistent properties and form flexibility

08 p1509 A70-21851

Al alloy matrix composites with beta-SiC whiskers reinforcement, evaluating tensile and fatigue properties

08 p1523 A70-21856

Transverse and shear strengths of Al-B composite materials used in F-111 aircraft components, investigating cold work, thermal treatments and steel wire addition effects

08 p1509 A70-21857

Compression test data of Al-B composites used for predicting structural element failure

08 p1523 A70-21886

Fatigue testing and thermal mechanical treatment effects on uni- and biaxial Al alloy-B composites tensile strength at room and elevated temperatures

08 p1523 A70-21893

Mechanical testing of metal matrix high modulus B-Al filament composites, using unidirectional and multidirectional reinforcement 08 p1523 A70-21894

Tensile, fatigue, creep and stress-rupture behavior of unidirectional, unidirectional off-axis and cross-ply composites of B filaments in Al alloy matrix 08 p1531 A70-21896

Stainless steel wire-reinforced Al alloy diffusion bonded scarf joints, considering aluminum oxide coating and bonding times effects 08 p1509 A70-21906

Tungsten alloy fiber reinforced Ni-base superalloy composites evaluated for high temperature turbojet engine applications, considering stress-rupture strength, oxidation and impact resistance 08 p1523 A70-21907

Composite materials in Co or Fe matrix for solid rotor core materials applications at high temperature and stress, discussing magnetic properties 08 p1524 A70-21908

Fractography of Al-B metal matrix composites to study micromechanical behavior, using scanning electron microscopy 08 p1524 A70-21913

Microstrain characteristics of continuously reinforced W-Cu composites as function of volume fraction of fibers and prestrain, discussing dislocation friction stress 08 p1524 A70-21917

Cold rolling characteristics of unidirectionally reinforced Al-B fiber composites, measuring hardness and tensile properties 08 p1524 A70-21957

Al-B composites mechanical properties, using heat treatments and transverse steel wires to increase matrix shear and transverse tensile strengths 09 p1701 A70-22551

Metal matrix fiber reinforced materials bonding, discussing brazing and fusion and diffusion welding [ASM PAPER W9-23.2] 09 p1690 A70-22557

Tungsten fiber reinforced aluminum composites tensile strength aspect ratio using foil metallurgy technique 09 p1703 A70-22627

Fiber-reinforced composite alloys prepared by controlled dissociation of Au-Ni and Al-Zn solid solutions 10 p1902 A70-23814

Filament-reinforced metallic composites corrosion control by specificity of environment and galvanic interactions between components 10 p1904 A70-24651

Copper alloy composite reinforced by unidirectional solidification of pseudobinary eutectic Cu-ZrCuSi, discussing mechanical properties and electrical conductivity 11 p2066 A70-25775

Metal matrix composites forming processes, describing liquid-metal infiltration, vapor deposition, electroforming, mechanical compaction and unidirectional solidification 11 p2060 A70-26343

Fiber reinforced Al alloys fabrication by thin sheet metallurgy techniques 12 p2252 A70-26887

Fiber diameter effects on metal matrix composites strength from proposed model 12 p2329 A70-28370

Ductile fracture in Al matrix composite reinforced with unidirectional stainless steel fibers described by critical crack tip displacement and fracture strain criteria 13 p2512 A70-28917

Borsic-aluminum composite materials fabrication, properties and applications to aircraft parts 13 p2420 A70-29246

Aluminum-boron composites for aircraft adapter fabrication 13 p2435 A70-29247

Filament reinforced metal matrix composites fabrication and engineering uses 14 p2590 A70-30542

Fe-Al and Fe-Si alloys strengthening by pyrolytic graphite fibers 14 p2595 A70-30543

Metallic base fiber and particulate composites, emphasizing silicon carbide, sapphire, boron and graphite filaments 14 p2597 A70-31168

Eutectic NiAl-Cr structure and high temperature tensile strength as function of solidification rate 15 p2755 A70-31560

Uniaxial yielding correlation with substructure in Al-stainless steel metal matrix composites, using compressive loading test 15 p2756 A70-31565

Filament orientation and fabrication variables effect on Ag matrix-W fiber composite mechanical properties 15 p2756 A70-31569

Beryllium fibers and Al matrix interactions at high temperatures and various durations, investigating diffusion by X ray diffraction, electron microscope and microprobe analysis 15 p2757 A70-31812

Al-B composites forming and machining, discussing tooling, methods and filament orientation [ASM PAPER W70-5.2] 15 p2744 A70-32334

Metal fiber multiple necking effect on uniaxial metal matrix composites ductility and plastic deformation behavior for brass-W model system 15 p2761 A70-32378

Work to fracture measurements on brittle fiber ductile-matrix metal composites, using Charpy test 15 p2763 A70-32832

Lamellar and fibrous Be-reinforced epoxy resin and metal matrix composites, describing preparation and properties 16 p2939 A70-33693

Metal matrix composite resistance spot welding, discussing value of nondestructive tests 17 p3100 A70-34636

Metal matrix alloys with base of Co, Fe or Ni reinforced by transition metal carbide fibers, discussing deformation tests at various temperatures 17 p3124 A70-35142

Deformation behavior of continuous W and B fibers reinforced Al alloy matrix composites, monitoring stress-strain characteristics by X ray diffraction 18 p3272 A70-36036

Rolled fine grained aluminum-alumina particles composites, determining creep strength dependence on temperature and tensile stress axis orientation 18 p3274 A70-36051

Fiber-metal matrix composites for gas turbine blades, discussing stress rupture strength, modulus of elasticity, fabrication, etc [ASME PAPER 70-GT-133] 18 p3302 A70-36827

Al alloy matrix-boron fiber-stainless steel wire composites fabrication into various shapes with desired mechanical properties for aerospace structural components applications 18 p3263 A70-36837

Tungsten fiber reinforced copper based composite material, investigating moulding and sintering conditions effect on mechanical properties 19 p3450 A70-37454

Longitudinal and transverse tensile strengths of Al sheet reinforced with continuous oriented steel wire of various cross sectional shapes 19 p3541 A70-38047

Tensile strength of flat specimens of Ni reinforced by W wire gauze 19 p3452 A70-38435

Mechanical properties, optimum deformation and rupture of W wire reinforced Ni and Ti metal composites obtained by hot rolling in vacuum 19 p3453 A70-38463

Duplex eutectic with Ni-Be fibers embedded in Ni-Cr solid solution matrix, discussing solidification conditions, optimum composition, heat treatment, mechanical properties and oxidation 20 p3647 A70-39107

High strength and stress corrosion resistant materials, considering Ti, Ni, Al alloys, metal-matrix composites and polymers 20 p3655 A70-39666

Ti-Be composite materials production by coextrusion of powders, investigating microstructure by microprobe analysis and X ray diffraction 20 p3649 A70-39945

Steady state and transient fatigue behavior of stainless steel wire-Al alloy composite subjected to push-pull and pull-release frequency tests 20 p3649 A70-39946

Tungsten wire reinforced copper matrix composite, determining fibers pull-out contribution to fracture work 20 p3651 A70-40047

Dynamic elastic moduli of model two phase continuous composites, using polymer and metallic foams 22 p4059 A70-43077

Composites made by unidirectional solidification of eutectics with transition metal carbide fibers embedded in metal matrix, discussing tensile tests [ONERA-TP-853] 22 p4057 A70-43457

Graphite fiber oxidation prevention in metal matrix composites, examining various thermodynamic parameters 22 p4126 A70-43676

Thin metal matrix composite rods elastic properties, examining Al-W system by Young and shear modulus measurements 22 p4061 A70-43687

Specific strength of unidirectional fiber reinforced metal matrix composites, using volume ratio-transfer coefficient diagrams 23 p4209 A70-43939

Phase equilibria, hardness and electroresistivity of Ti-Al-V alloys at solid compound section for reinforced metal composites 24 p4361 A70-45831

Metal matrix composite structures tooling and fabrication processes, considering forming, joining, welding, machining joining, etc [SAE PAPER 700752] 24 p4348 A70-45873

METAL OXIDE SEMICONDUCTORS

Digital adaptive-element building blocks in monolithic Si structures for MOS large scale integra-

METAL OXIDE SEMICONDUCTORS

tion, considering serial/parallel multiplier and shift register chips 01 p0047 A70-10458

Metal-nitride-oxide semiconductor (M/NOS) FET load devices by changing from enhancement to depletion through polarizing voltage 01 p0051 A70-10785

Junction gate and MOS field effect transistors thermal noise calculations, using circuit analysis based on equivalent circuits 02 p0258 A70-12424

MOS structure electrical characteristics dependence on silicon/silicon dioxide interfacial energy and electric charges, considering fabrication difficulties 02 p0350 A70-12541

MOSFET uses in spacecraft electronic subsystems, describing digital control unit and typical logic circuitry 03 p0456 A70-13534

Complementary symmetry MOS/CMOS integrated circuit transient response to electron irradiation 04 p0657 A70-14733

Chromium doping effect on ionizing radiation damage in MOS field effect transistors 04 p0658 A70-14744

MOS devices radiation testing for estimating anticipated threshold voltage shift at various dose levels, including gate bias intermittent application during irradiation 04 p0658 A70-14745

Bipolar n-p-n transistors fabrication to increase driving capabilities of complementary MOS transistors while retaining low power dissipation 05 p0621 A70-16419

Radiation environments effect on logic circuitry constructed of MOS and bipolar transistors, discussing permanent and transient effects 07 p1242 A70-20149

Switching and memory phenomena in semiconductor glasses, thin films and variable threshold metal-oxide-nitride-semiconductor MNOS transistor 08 p1556 A70-21304

MOS transistor amplifier circuits, analyzing circuit parameters for common-source, common-drain and common-gate configurations 09 p1643 A70-22126

MOS structures and transistors emission-current degradation mechanism at heterojunction under ionizing radiation 12 p2194 A70-27165

MOS-FET HF noise quantities computed in terms of substrate doping, angular frequency and gain-bandwidth product 12 p2196 A70-27672

Computer-aided MOS/LSI four phase logic circuit design, discussing software, design cycles and testing 13 p2380 A70-28375

Hysteresis in MOS transistors attributed to trapped charge carriers on oxide near silicon oxide interface 14 p2555 A70-30338

MOSFET integrated circuits radiation resistance measurements under electron irradiation, determining changes in threshold voltage, transconductance and on-resistance for applications in spacecraft 14 p2559 A70-31372

MAGFET devices for integrated circuits, calculating magnetic sensitivity as function of channel aspect ratio and Hall electrode position 15 p2710 A70-32572

Junction and MOSFET transistors thermal noise characteristics at cryogenic temperatures 15 p2710 A70-32585

Ion implantation doping for MOS devices, discussing improved HF performance, integrated circuitry and threshold voltage selection 16 p2872 A70-33054

High speed MOS circuitry design with application to digital equipment, noting low power and high packaging density 16 p2887 A70-33456

Portable MOS memory module with optical loading and electrical readout, using hybrid array of complementary silicon on sapphire chips 16 p2868 A70-33457

MOS transistor associative memory cell design utilizing LSI technology 16 p2869 A70-33464

MOS structure, measuring ionizing radiation effects on interface barrier energies by internal photoemission techniques 17 p3144 A70-35901

MOS devices, investigating laser radiation effects on electrical behavior 18 p3266 A70-36237

MOS structures deep depletion capacitance/voltage characteristics by ramp response method 19 p3389 A70-37972

Large scale array (LSA) MOS devices failure rate prediction model, determining reliability 19 p3391 A70-38847

Epitaxially grown Si contact for area reduction of MOS transistor circuits 20 p3596 A70-39099

METAL OXIDES

Complementary metal oxide semiconductor and bipolar transistors fabrication on same integrated circuit chip by C-squared technology 20 p3598 A70-40130

High voltage MOST silicon integrated circuits, using dielectric isolation and field plate techniques 21 p3798 A70-41214

Metal nitride oxide silicon /MNOS/ integrated circuit transistor, reviewing characteristics, operation mechanisms and applications 21 p3800 A70-42113

Silicon MOSTs LF noise model, discussing noise and gate voltages and trapping efficiency of surface states 22 p3996 A70-42916

MOS field effect transistor, measuring electrons and holes thermal emission rates and activation energies at gold centers in Si 22 p3997 A70-43016

MOS transistor trigger circuit design parameters statistical calculation and optimization by Monte Carlo method using computer 23 p4171 A70-43957

Miniature avalanche MOS diode, investigating capacitance voltage characteristics of deep depletion regime 23 p4172 A70-44007

P- and n-channel MOS transistor instability during superbreakdown voltage application to drain electrode 24 p4319 A70-45811

LSI 4-bit complementary speed /COS/ MOS parallel processor array 24 p4317 A70-46215

METAL OXIDES

NT ALUMINUM OXIDES
NT BARIUM OXIDES
NT BERYLLIUM OXIDES
NT BISMUTH OXIDES
NT CALCIUM OXIDES
NT CHROMITES
NT CHROMIUM OXIDES
NT COBALT OXIDES
NT COPPER OXIDES
NT HAFNIUM OXIDES
NT HEMATITE
NT ILMENITE
NT IRON OXIDES
NT LANTHANUM OXIDES
NT MAGNESIUM OXIDES
NT MAGNETITE
NT MOLYBDENUM OXIDES
NT NICKEL OXIDES
NT NIOBIUM OXIDES
NT POTASSIUM OXIDES
NT RUTILE
NT SAPPHIRE
NT SCANDIUM OXIDES
NT TANTALUM OXIDES
NT THORIUM OXIDES
NT TIN OXIDES
NT TITANIUM OXIDES
NT TUNGSTEN OXIDES
NT URANIUM OXIDES
NT YTTRIUM OXIDES
NT ZINC OXIDES
NT ZIRCONIUM OXIDES

Refractory metal-oxygen systems phases and phase relations 02 p0318 A70-12640

Initial oxide film on Cr-Ni steel at high temperatures observed by electron microscope, noting Ni role 04 p0708 A70-15311

Ceramic fibers formation by particles mechanical deformation by extrusion in W matrix, describing grain structure of various extruded metal oxides 04 p0699 A70-15643

Metal oxides additions effect on Ti glass crystallization, studying small and large ion radii 05 p0871 A70-16593

Density, refractivity, thermal expansion coefficient, softening point and soaking stability for glass containing barium, lead, boron, bismuth and titanium oxides 05 p0871 A70-16594

Crystallization and dielectric properties of glass containing barium, lead, titanium and boron oxides, noting frequency and temperature dependence 05 p0871 A70-16595

Oxidation behavior of metals concerning oxide plasticity role in connection with oxide film macro- and microstresses 07 p1305 A70-18968

Refractory oxides synthesized using metal alkoxide thermal decomposition, comparing thermophysical properties with conventional ceramics 07 p1320 A70-19891

Al-Mg oxidation resistance and kinetics, studying Zr, Ce and Be additives effects on oxide films mechanical properties 08 p1517 A70-21130

Al alloys melting in flame furnaces, studying oxidation and various sources of metal losses 08 p1505 A70-21131

Free radicals role in high temperature surface reactions of solid metal oxide particles interacting with unburned flame gases 09 p1629 A70-22320

High temperature fuel cell electrolytes, analyzing electrical conductivity of ternary systems of zirconium, cesium or tantalum and yttrium oxides in fluorite phase 10 p1830 A70-24460

Solid electrolyte high temperature fuel cells electrode materials, investigating various metal oxides 10 p1830 A70-24461

ETA oxides compositions in Hf-Ni-O, Ta-Ni-O and W-Ni-O systems determined by studying 1000 C isothermal sections with X ray diffraction 12 p2255 A70-27607

Low temperature oxidation of metals, discussing logarithmic kinetics of slow growth of oxides 12 p2257 A70-28006

Low resistance small area contacts on semiconductor metal oxides 12 p2288 A70-28057

Band and localized models for electrical conduction of metal oxides, discussing Mott and semiconductor to metal transitions 14 p2627 A70-30498

High temperature molecules matrix isolation in saturated vapor over refractory solids, discussing optical spectroscopy of VO, metal oxide and halide molecules 14 p2545 A70-30903

Failure mode and mechanism in dielectrically isolated IC attributed to metal bridging under planar oxide 15 p2713 A70-32648

Metal oxides thermal control coatings, investigating mechanisms of interaction between constituents by luminescent technique [AIAA PAPER 70-832] 16 p2940 A70-33936

Friction reducing oxide layer effects on Ti alloys low temperature plastic and mechanical properties 19 p3450 A70-37458

Oxide dispersed Cu alloys preparation by surface oxidation of powders, considering structural stability and stress rupture properties 20 p3646 A70-39103

Nonweldable internal flaws detection containing oxides in steel slabs by neutron activation analysis 24 p4376 A70-45750

Thermodynamic equilibrium analysis of metal oxidation and thermal dissociation of oxides in vacuum, noting decreased affinity by evaporation 24 p4361 A70-45835

Stainless steel oxide films structures and chemical compositions, examining oxidation time, polishing conditions, vapor humidity and temperature effects 24 p4362 A70-46191

METAL PARTICLES

NT METAL POWDER

NT POWDERED ALUMINUM

Metal particle and wire combustion using static and flow methods, obtaining experimental results for Al, Be, Mg and B [ONERA-TP-735] 03 p0543 A70-13633

Combustion of stationary particle of metal with boiling point lower than ignition temperature in gaseous oxidizing medium 07 p1419 A70-18753

Metal particle size relation to combustion time using statistical method applied to polydisperse Mg powder 07 p1419 A70-18756

Metal particles additives behavior in solid rocket propellant combustion, using scanning electron microscope 07 p1359 A70-19585

Particle fracture in oxide dispersed stainless steels during plastic deformation at room temperature 09 p1706 A70-22813

Liquid metallic particles fragmentation in two phase flow injected into vacuum, noting atomization enhancement by sodium nitrate 13 p2391 A70-29994

Integral model for combustion of metal particle laden jet mixing with subsonic secondary stream in duct, considering air breathing engine design [AIAA PAPER 70-736] 16 p2964 A70-33490

Aluminum spherical particles nonautonomous and autonomous combustion in O with N or Ar initiated by HF induction heating 17 p3145 A70-35042

Aluminum particle combustibility in deflagration zone of ammonium perchlorate pellets, measuring combustion rate and pyrolytic behavior 17 p3145 A70-35208

Rocket exhaust micro and mm waves attenuation attributed to low ionization potential metal particles in propellants 17 p3196 A70-35215

Kingfisher meteorite metal particles microstructures, discussing phase transformation during reheating by shock 18 p3310 A70-35970

Al particles fusion during combustion of stoichiometric mixtures of ammonium and potassium perchlorate and polyformaldehyde 18 p3299 A70-36246

Particulate matter interaction with ionized gas in external magnetic field and nonequilibrium state, examining free electron density 20 p3677 A70-39324

Thermal radiation spectrum power of small spherical tin and lead particles 20 p3737 A70-39745

Lunar breccia and fine sample metal particles, using optical and scanning electron microscopy and electron probe microanalysis 21 p3899 A70-41529

Metallic Fe grains in Apollo 12 igneous rocks, discussing Ni and Co abundances 21 p3920 A70-41881

Titanium diboride particles contact surface increase during sintering in vacuum as function of temperature 23 p4205 A70-44042

METAL PLATES

Mechanical strength and breakdown metallography of plate shaped structural steel and Al alloy specimen under various HF elastic vibrations 02 p0318 A70-12398

Electromagnetic energy transmission factors for metal-dielectric-metal system, calculating net energy flux, noting effects of metal spacing, time, temperature level, etc [ASME PAPER 69-WA/HT-8] 04 p0784 A70-14822

Radiative heat flux between two parallel copper disks at cryogenic temperature, showing dependence on emitter temperature and spacing [ASME PAPER 69-WA/HT-7] 04 p0784 A70-14823

Crack propagation rate in aluminum alloy plates under cyclic tensile and transverse shear loadings, noting sliding mode increasing effect [ASME PAPER 69-MET-1] 04 p0705 A70-14881

Thermal resistance of multiconduct heat conducting stainless steel plate stacks with different interface purities in vacuum 05 p0957 A70-16293

Thin metal plate surface impedance during excitation by HF electromagnetic field as function of magnetic field, calculating line shapes 08 p1557 A70-21754

Thermal decomposition of ammonium perchlorate and polymethylmethacrylate mixture thin layer between Ti plates in vacuum 09 p1741 A70-22109

Nonuniform stress distribution along side fillet welds and in welded plates of lap joint, discussing tangential stresses and plate width 11 p2058 A70-25598

Two plate meteoroid shields effectiveness determined by analyzing debris cloud ejected behind front plate after hypervelocity impact [AIAA PAPER 69-380] 11 p2138 A70-26132

Metal plates vibration under viscoelastic damping layers using electromagnetic transducer and impact excitation 11 p2145 A70-26702

Strain measurement over large steel plate surface ground to reasonable flatness and in welded joints by applying moire method 11 p2061 A70-26836

Heat conduction for thermally insulated bilayer metal wall for time-variable heat transfer and ambient temperature, using Green function 12 p2330 A70-27292

Dislocation structure during fretting corrosion in steel plates, analyzing via electron microscopy 12 p2258 A70-28318

Cover plates unsteady motion during explosive welding of metals, discussing edge damage 13 p2416 A70-28484

Quality control technique for predicting exfoliation and stress corrosion resistance of Al alloy sheet and plate 13 p2435 A70-29175

Sliding rigid conical indenter friction experiments over work hardenable metal flats in high adhesion conditions, observing forces, stresses and deformation modes 13 p2421 A70-29548

Convective heat transfer in Cu spherical shell and plate in supersonic rarefied gas flow at zero angle of attack from wind tunnel experiments 15 p2824 A70-31497

Charpy impact test evaluation on hot rolled metal plates for low temperature welded structures 15 p2819 A70-32235

Stress concentration around oblique circular cylindrical apertures in steel plates [SESA PAPER 1533] 15 p2820 A70-32306

Biaxial stress effect on fatigue crack propagation in Al alloy plate under reversed bending 15 p2821 A70-32324

Alternating stress required for edge crack propagation in metal plates under tensile loading cycles 15 p2762 A70-32464

Admittance measurements of rectangular or circular waveguide fed aperture antennas illuminating displaced metal plate 16 p2872 A70-32963

Transverse contraction during butt welding of plates of steel and Ti and Al alloys, showing dependence on joint thickness 16 p2916 A70-33053

Powder combustion on metal plate, investigating unburned layer thickness dependence on initial temperature 17 p3198 A70-35738

Pyrex spheres accelerated to 15 km/sec by plasma rail gun to study hypervelocity impact in twin stainless steel and Al targets [AIAA PAPER 69-378] 18 p3342 A70-36685
Welded Al plates high temperature bend tests, describing materials and procedures 18 p3278 A70-37115

High strength Al alloys plate and welds, comparing tear notch tests at cryogenic and room temperatures 23 p4206 A70-44352

Powdered flat steel plates cooling by air blown through pores, determining internal heat exchange coefficients 23 p4283 A70-44731

Finite thickness metal plate eddy current response to pulsed field from aperture probe 24 p4344 A70-45696

Defect effects on welds fatigue properties in low carbon steel plates estimated, using radiograms 24 p4347 A70-45733

Clamped parallelogram metal plate thermal deformation under single surface radiant heating 24 p4426 A70-46009

METAL POLISHING

NT ELECTROPOLISHING

WC-Co alloys noting polishing and grinding effects on residual stress and crack resistance 03 p0508 A70-13145

Band polishing machines slave mechanisms and programmed controllers, describing helicopter longerons finishing process 07 p1291 A70-18829

Gas turbine engine blades grinding and polishing procedures, considering fatigue life increase and physical properties stabilization 07 p1292 A70-18833

Mechanical and electrochemical polishing effect on turbine blade alloy fatigue strength, discussing surface strain hardening as function of temperature in mechanical polishing 07 p1304 A70-18838

Ti alloy band polished surfaces properties, obtaining required residual stresses by process control 08 p1507 A70-21198

Diamond burnishing effects on wear and contact endurance of chromium coatings, investigating surface hardening and residual stresses 13 p2419 A70-28868

Stainless steel oxide films structures and chemical compositions, examining oxidation time, polishing conditions, vapor humidity and temperature effects 24 p4362 A70-46191

METAL POWDER

NT POWDERED ALUMINUM

Rhenium powder sintering activated by palladium additions producing low porosity 01 p0117 A70-10158

Relieving microstrains in Ni powders by cold compaction at room temperature using X ray analysis, discussing polygonization process 01 p0117 A70-10161

Critical diameter and detonation parameters of nitromethane and tetranitromethane as function of powder content 01 p0217 A70-11004

Niobium powder hot pressing compaction in terms of porous body volume viscous flow, determining viscosity shift time dependence 04 p0696 A70-14461

Ni dispersion-strengthened composites from ultrafine comminuted powders, describing forming techniques and test results 04 p0709 A70-15629

Fillers effect on thermal conductivity in porous cermet elements, investigating powdered Ti plates with air replaced by Hg, benzene, ethanol, ether and water vapor 05 p0957 A70-16291

Residual free energy effects on ferrites density and structure after sintering, using powders obtained by thermal decomposition of solid solutions of salts 07 p1355 A70-18703

Chemical composition effects on Zr-Ti, Zr-Si, Ni-Al and Ni-Ti alloy aerosols combustion temperature 07 p1419 A70-18755

Oriented single crystals properties obtained from Mo powder subjected to compacting, annealing in hydrogen and electron beam zone melting 07 p1308 A70-19610

Reduction temperature effects on molybdenum powders sinterability noting dispersion role 08 p1517 A70-21145

Contact compaction methods of metal powders involving vibration, shock, detonation and hydrodynamic pressure 09 p1706 A70-23122

Propellant extinction near powder-metal contact to steady nonsteady combustion mechanism 09 p1742 A70-23228

High intensity ultrasonics for changing solids properties, discussing effects on metal powder sintering, yield strength, fatigue life, crystallization rate, etc 09 p1728 A70-23348

Powder base superalloy with superplastic behavior, ascribing mechanism to migration of second phase gamma prime particles 12 p2252 A70-26889

Porous Ti powder sintering process activation energy determination, noting influence of oxides solution in surface layer of Ti particles 12 p2254 A70-27283

Annealed compressed ground synthetic mica and silver dust composite materials, analyzing physicochemical properties 12 p2260 A70-28319

Metal powder mixtures homogenization time calculation, using Fick equation and matrix model 13 p2433 A70-28845

Powder metal parts induction sintering, comparing performance with conventional method 13 p2420 A70-29249

Tri- and bipropellants in spacecraft propulsion, discussing liquid and powder metals, hybrids, frozen tripropellants, etc 15 p2789 A70-32253

Mo powder compacting by hot pressing, determining activation energy 16 p2931 A70-33222

Carburizing spherical powders of Nb, Mo and W to obtain carbides, noting agreement between theoretical and experimental data 17 p3125 A70-35410

Powdered metallic additions effect on combustion rates of ammonium perchlorate with bitumen and polymethyl methacrylate and potassium perchlorate with bitumen mixtures 18 p3299 A70-36247

Combustion rates and self ignition vs pressure and activity in ammonium perchlorate mixtures with Al and Mg powders compressed to maximum densities 18 p3299 A70-36249

Metal powder rolling process as compaction with plastic particle deformation, deriving pressure distribution on rollers 19 p3434 A70-37451

Iron cyanide surface additives effect on photodamage to ZnO powder, using ESR method 19 p3372 A70-37543

Plasticity and strain hardening in sintered metals, considering pressure at pores and elastoplastic limit under small plastic deformation 20 p3644 A70-38962

Silica marker motion in sintering of loose spherical copper powder aggregates 20 p3647 A70-39109

Titanium powder compacts exothermic solid phase reaction ignition by focused laser pulse, obtaining temperature profile from mathematical model based on energy transport 20 p3639 A70-40473

Photoelastic stress measurement of metal powder particles during sintering, using two dimensional models 21 p3935 A70-41410

Carburization and grain size of tungsten carbide powder from W powder as function of temperature, using optical and electron micrographs 21 p3839 A70-41412

Thermal decomposition of fine-dispersion iron sulfate powders under continuous heating during ferrites manufacture 23 p4205 A70-44041

Self flammability temperature of binary alloy Al-Si powders in aerosol state as function of chemical and phase compositions 23 p4205 A70-44046

Powdered flat steel plates cooling by air blown through pores, determining internal heat exchange coefficients 23 p4283 A70-44731

Sintered material density-sound velocity relation, deriving ultrasonic wave propagation time dependence 24 p4360 A70-45731

METAL PROPELLANTS

Atmospheric contamination due to Be solid propellant exhaust products, discussing pollution levels, governmental restrictions on testing, etc [AIAA PAPER 70-117] 06 p0997 A70-18085

Solid propellant rocket engines design, considering nonlinear longitudinal combustion instability encountered in aluminized propellants 08 p1558 A70-20623

Hybrid rocket engine with solid oxidizer based on ammonium perchlorate and Al, studying performance with FORTRAN 5 program 15 p2787 A70-32273

Metallized solid propellant, calculating condensed phase distribution heterogeneity effect on performance 18 p3300 A70-37207

METAL SHEETS

Annealing effects on cold rolled titanium sheets, noting changes in Young modulus and characteristics of recrystallized titanium 01 p0124 A70-11620

Photogrammetric deformation measurement of thin steel sheets during static bending tests 02 p0302 A70-12653

Inductive eddy current strain gage for repeated strains measurement in magnetic and nonmagnetic sheets offering direct readout and remote recording 03 p0485 A70-13475

Rolling, picking and annealing influence on composition of steel sheet surface 03 p0497 A70-13775

Residual stress distribution in butt joints during welding of sheet Nb measured by extensometer, noting annealing temperature effect on stress relieving 03 p0513 A70-14072

Sound attenuation rate of rectangular flat steel plates contact and branch point relation to velocity difference and absorption length 03 p0526 A70-14353

Divergences in tension textures and values of anisotropy coefficients ascribed to imperfections in cubic texture of aluminum sheet deformed by straining 05 p0927 A70-15995

Young modulus anisotropy and recrystallization texture during annealing in cold rolled TI sheets using Fourier analysis 05 p0862 A70-16200

Stress rupture strength and relaxation and time to failure of AMG-6M sheet under creep using energy dissipation method 05 p0952 A70-17034

Cold reduction effects on press formability of pure Al sheet with allowance for tensile properties and crystallographic orientation 06 p1075 A70-17145

Cold reduction and annealing temperature effects on Al sheet ductility noting roles of hardness, crystallographic orientation and microscopic structure 06 p1075 A70-17146

Harris method for determining inverse pole figures as description of sheet metal texture 06 p1088 A70-17611

Brazing time and temperature effect on depth of Ag based brazing alloys penetration into thin Ti-Al-V sheet substantiated by microprobe analysis 06 p1078 A70-18513

Ti alloy welded sheets bending fatigue test facility, discussing test stand calibration and optimal welding 07 p1291 A70-18824

Vibration damping by sandwich structure consisting of viscoelastic layer between two high Youngs modulus metal sheets 07 p1401 A70-18845

Ni maraging steel sheets tensile strength and elongation anisotropy, studying effects of directional cold work, aging and annealing 07 p1306 A70-19072

High temperature creep rupture tests of arc cast and powder metallurgy wrought unalloyed W sheets 07 p1313 A70-19884

Mo sheet longitudinal and transverse mechanical properties and microstructure after annealing 08 p1517 A70-21199

Cubic texture components preferred orientation shares into rolling texture during cold rolling of aluminum sheets determined quantitatively 09 p1690 A70-22255

Limit and shakedown loads in creep range investigated on sheet rolled aluminum at room temperature for structural design applications 09 p1775 A70-22591

Thickness effects on elongation of sheet type Al alloys, tabulating tensile test results 10 p1887 A70-24043

Elastoplastic compressible sheet metals reinforced by isotropic work hardening under action of bending moments, analyzing stresses and strains 10 p1955 A70-24056

Fiber reinforced Al alloys fabrication by thin sheet metallurgy techniques 12 p2252 A70-26887

Aluminum sheets anomalous plastic behavior under balanced biaxial and uniaxial tensions 12 p2324 A70-27398

Quality control technique for predicting exfoliation and stress corrosion resistance of Al alloy sheet and plate 13 p2435 A70-29175

Al-Mg alloy sheets work hardened plastic properties, tensile strength and elongation 14 p2597 A70-30962

Al alloy welded sheets strength and plasticity under biaxial tension, examining excess elastic energy effects on strain kinetics and rupture 14 p2597 A70-30967

Bend formability and fracture toughness tests on Be ingot and cross-rolled powdered sheet and brake grade block materials [ASM PAPER W70-15.3] 15 p2760 A70-32337

METAL SHELLS

Lateral pressure bulging of superplastic alloy sheet, considering flat circular sheet and bulging into V grooves

16 p2916 A70-32918

Pressure forming Ti sheet alloy blanks in superplastic condition under controlled temperature and strain rate

17 p3117 A70-34402

Ti-Cu alloy sheet material age hardening, considering cold and warm work effects at various stages in aging cycle

17 p3121 A70-34430

Weldability, tensile and fatigue properties of Ti sheet alloys, discussing TIG welds

17 p3121 A70-34431

Strain gage measurements of elastic properties of Ti sheet alloys, computing polycrystalline properties from single crystal values

17 p3121 A70-34433

Ti hot forming, discussing sheet use as aircraft structural material

17 p3098 A70-34444

Forming Ti-Al-V sheet metal in heat treated conditions, showing mechanical properties improvement over mill annealed parts

17 p3098 A70-34445

Ti sheet welded construction for transport aircraft fuselages, assuming use of electron beam and plasma arc equipment

17 p3198 A70-34452

Crack initiation in wrought polycrystalline Be sheet, investigating three point loaded bend fractures of powder and ingot samples by optical and electron microscopy

17 p3122 A70-34551

Electron beam welding for thin steel, nonferrous metals and reactive metals sheets

19 p3436 A70-38073

Electron beam welding for thin copper, carbon and Cr-Ni steel sheets in precision mechanical and optical devices

19 p3436 A70-38075

Fatigue crack growth tests on Al alloy sheets under variable amplitude loading

21 p3831 A70-40749

Polyvinyl chloride sheet steel manufacture, properties and welding methods

22 p4045 A70-42479

Strained state of Ti and steel sheets during unsymmetric rolling, constructing deformed metal particles displacements rates field based on ideal fluid motion equations

22 p4045 A70-42814

Low alloy Mo sheet recovery and aging characteristics studied by X ray scattering

22 p4055 A70-43124

Temperature measurement on thin steel shield subjected to hydrogen peroxide motor exhaust heating at cryogenic temperatures in space

23 p4280 A70-44389

Metal and alloy sheets, investigating deformation and failure under biaxial stretching tensile tests

24 p4358 A70-45240

Al alloy sheets with multicolor protective coatings, measuring surface temperature under solar radiation

24 p4428 A70-45434

Metal sheets thickness measurement and monitoring by through-transmission eddy current nondestructive testing, using phase locked amplifier

24 p4344 A70-45699

METAL SHELLS

Axial compressive forces influence on steel and Al cylindrical shell stability under external pressure

03 p0593 A70-13472

Thin walled metal cylinders residual deformation microstructures under internal impulsive loading

07 p1285 A70-19969

Toroidal metallic shells stability under static loads, determining snap-through pressures in pressure chamber with nitrogen working gas

08 p1588 A70-21195

Rapid expansion of thin walled aluminum alloy cylinders under pulsed magnetic field pressure using high speed streak camera oscillography

10 p1964 A70-25120

Metallic cylindrical shells design reinforced with elastic glass fiber rings, considering elastoplastic deformation

12 p2324 A70-27530

Convective heat transfer in Cu spherical shell and plate in supersonic rarefied gas flow at zero angle of attack from wind tunnel experiments

15 p2824 A70-31497

Internal pressure deformation of thin cylindrical shells of materials with nonlinear stress-strain relations, considering Al alloy shell and axial strain

15 p2816 A70-32009

Metallic shell with passive thermal protection coating, solving boundary value problem for high temperature heating with simplified mathematical model

20 p3739 A70-40296

Rapid expansion of thin walled aluminum alloy cylinders under pulsed magnetic field pressure using high speed streak camera oscillography

20 p3735 A70-40513

METAL SPINNING NT HYDROSPINNING METAL SPRAYING

W, Ta and Mo components economical fabrication by plasma spraying for rocket nozzles, susceptors and crucibles

24 p4350 A70-46355

METAL STRIPS

Elastoplastic stress concentrations calculations in notched strips and shafts under tension, bending and torsion, using approximate method

01 p0211 A70-11425

Al alloy strips weakened by holes, analyzing limiting tensile load-carrying capacity

02 p0384 A70-11741

Coplanar waveguide consisting of thin metallic film strip on dielectric slab with ground electrodes adjacent and parallel to strip for nonreciprocal gyromagnetic device applications

08 p1475 A70-21281

Interdigitated microstrip quadrature couplers suited for monolithic or hybrid thin film microwave integrated circuitry

08 p1476 A70-21291

Radiation pattern of conducting strip excited by linear slot parallel to strip edges, deriving asymptotic solution

16 p2863 A70-33239

Minimal interference thin metal support system for dynamic stability tests of high fineness ratio wind tunnel-models

17 p3063 A70-35657

[AIAA PAPER 69-350] Plane TM wave scattering by systems of two parallel conducting elliptical cylinders, metal tapes and combinations

19 p3374 A70-37278

Scattering structures of two parallel elliptical cylinders, tapes or combinations, deriving surface current density distribution under plane TM wave excitation

19 p3375 A70-37279

Dry and water-saturated sintered fiber metal wick thermal conductivity, obtaining semicompil correlations for solid and fluid phases and void fraction

21 p3945 A70-41041

METAL SURFACES

Metal surface microscopic defects detection and display using diffused radioactive Kr-85 gaseous penetrant for anodized flaws, bearing porosity and turbine blade cracks

01 p0096 A70-10006

Oleic acid concentration effects on electron work function during surface-active agent deposition on Fe, Ni, Cu, Al and steel surfaces

01 p0099 A70-10074

Temperature effect on work function minimum of cesiated W surfaces

01 p0154 A70-10108

Surface roughness effects on dry friction between two metals, considering conical asperities and friction coefficients

01 p0102 A70-10394

[ASME PAPER 69-LUB-10] Friction and surface damage between clean metal hemispheres and flats at low sliding speeds and 25 K room temperature range

01 p0105 A70-11393

Fracture surface topography variation with specimen thickness, studying fatigue crack propagation in Al

02 p0317 A70-12317

Cu, W and oxidized W adhesion to Ni surface, examining before and after adhesion contact with low energy electron diffraction

02 p0318 A70-12535

[ASLE PREPRINT 69-LC-13] Twin wave interferometer and strain gauge mechanism for press-fit measurements of contact deformation on metallic and polymer samples

03 p0484 A70-13426

Solid lubricant films adhesion to metallic surfaces measured using pivot-twist technique

03 p0485 A70-13485

Radiative transfer between two infinite parallel metallic surfaces separated by nonconducting thick film ideal dielectric based on electromagnetic wave theory

04 p0784 A70-14824

[ASME PAPER 69-WA/HT-6] Dimensional analysis for describing steel surface microcracks growth under uniaxial fatigue loading, using stress-intensity factor and crack extension concepts of fracture mechanics

04 p0770 A70-14879

[ASME PAPER 69-MET-G] Reflectance of clean and fluoride coated aluminum surfaces in vacuum UV

05 p0883 A70-16590

Harris method for determining inverse pole figures as description of sheet metal texture

06 p1088 A70-17611

Thermal isolation characteristics of interstitial materials in vacuum environment, inserting materials between contacting metal surfaces at various pressures and temperatures

06 p1181 A70-18143

[AIAA PAPER 70-13] Accommodation coefficients ratio of He 4 to He 3 measured on W and K clean surfaces

06 p1183 A70-18257

Electromagnetic torsion balance measurement of forces exerted on clean Au surfaces by monoenergetic, steady state Ar and Kr beams, calculating thermal accommodation coefficients

06 p1066 A70-18257

Nitrogen molecule-tungsten surface interactions, computing trajectories and accommodation coefficients for various temperatures by equations of motion

06 p1110 A70-18261

Lift and drag forces measured on metal surface inclined to Ar ion stream above and below earth-satellite speeds in free molecular flow

06 p1111 A70-18269

Angular distributions of fast scattered particles resulting from noble gases collision with metal surfaces

06 p1112 A70-18271

Rare gas scattering from Ag surfaces calculated up to earth satellite energy values

06 p1112 A70-18279

Rough metal surfaces thermal constriction resistance for total heat flow through microcontacts

07 p1418 A70-18641

Fcc metals surface changes following adhesion using low energy electron diffraction (LEED), relating intersurface metal transfer to applied adhesive force

07 p1305 A70-18921

Metallic adhesion produced by surfaces compression, discussing asperities plastic deformation and macrodeformation caused by contact area growth

07 p1292 A70-18939

Contact resistance measurements used in contaminant removal and metallic adhesion on iron surfaces

07 p1293 A70-18944

Discharge circuit parameters and heat physical constants of electrode material effects on electrical erosion of metals

07 p1294 A70-19351

Specific radiant heat flow and spectral blackness degree of tungsten with different surface finish

07 p1309 A70-19666

Corrosion cracking mechanism for notched metal surface in aqueous environment under tensile stress discussing electron distribution and H ion concentration

07 p1310 A70-19739

Sand erosion of metals and plastics, discussing effects of impact conditions and impacting particles and target surface properties

07 p1314 A70-20004

Angular and energy distributions of hyperthermal K atoms scattered and ionized by W surface measured as function of beam particle energy

07 p1342 A70-20115

Electron elastic scattering from surface plane of Au and W fcc lattices using quantum mechanics

07 p1343 A70-20120

Metal surface adhesion to materials, examining structure and energy with allowance for environmental effect

08 p1503 A70-20878

Mo mechanical properties dependence on surface defects and Ti films

08 p1515 A70-20937

Metal erosion under liquid drop impingement attack, investigating damage from microplastic deformation to surface material removal using wheel and jet apparatus

08 p1519 A70-21354

Solid Mo, Ni, Ta and W surface energies determined by multiphase equilibration technique

08 p1522 A70-21749

Metals yield locus in strain hardening range in sigma-tau plane determined using slip theory, considering Bauschinger effects

09 p1771 A70-22395

Molecular vibration spectra from inelastic interaction between electrons and absorbed molecules at metal-vacuum interface

09 p1732 A70-22904

Silicon oxide films coated satellite aluminum surfaces solar absorptivity and thermal emissivity, noting suitability as temperature control coatings

09 p1613 A70-23514

Laser beam interaction with metals on basis of energy balance measurements, obtaining time dependent radiation reflectance

10 p1898 A70-23982

Intensity vs voltage curves for LEED beams from clean Ni surface, calculating Bragg spectrum with energy diagram method

10 p1927 A70-24077

Synthetic molybdenum disulfide crystal properties compared to natural crystals, discussing friction coefficient, adherence to metal surfaces, etc

10 p1907 A70-24787

Surface wave reflection during propagation along transversely magnetized ferrite plate on metal backing, using perturbation theory to find cylindrical wave field

10 p1844 A70-25163

Metal surfaces contact with cones and pyramids asperities, analyzing surface roughness effects on dry friction

11 p2060 A70-26412

DC air flow plasmatron arc chamber operation with metal surfaces used for charge stabilization, obtaining I-V characteristics and gas flow parameters in quasi-limiting region

11 p1984 A70-26738

Fretting and fretting fatigue in metal-metal contacts, showing friction as important parameter

12 p2253 A70-27110

Friction and wear of Ni sliding on Ni, Cu on Cu and Au on Au tested in vacuum at room temperature with constant load

12 p2242 A70-27229

Oxygen adsorption on W(110) surface determined for coverage as function of exposure by Auger electron spectroscopy

12 p2180 A70-27253

Nusselt numbers of nonstationary and stationary heat transfer between metal spheres and liquid flow, showing bulk heat and geometry dependence

12 p2330 A70-27288

Heat resistance of machined stainless steel and molybdenum contact pairs in vacuum, discussing compressive loads and surface defects effects

12 p2243 A70-27290

Low temperature oxidation of metals, discussing logarithmic kinetics of slow growth of oxides

12 p2257 A70-28006

Polyurethane and metal surface layers deformation related during sliding friction in presence of liquid media, noting friction coefficient- deformation relation

12 p2244 A70-28284

Pulsed plasma jet radiant heat flux effect on celophane film coated, polished and etched metals, noting erosion destruction

12 p2282 A70-28287

Metal surfaces friction and wear processes dynamic equilibrium noting loading conditions effects

13 p2423 A70-29766

Titanium effect on iron and steels nitriding at high temperature, obtaining high surface hardness

13 p2423 A70-29773

Nondestructive noncontacting microwave depth measurement of thin slits and cracks in metal surfaces

14 p2584 A70-30507

Cobalt surface X ray analysis after spark erosion treatment, revealing phase with high temperature stability

14 p2596 A70-30840

Chemical and electrochemical corrosion resisting primers for Mg surface coatings in machine parts

14 p2598 A70-31293

Wear intensity of abrasives during fine grinding of Armco Fe, Ti and Ti alloys, comparing friction and chemical composition effects

15 p2743 A70-31640

Spilled Hg removal from metal surfaces, describing brush technique based on capillary action

15 p2748 A70-32775

Metal property effects on deformation and strain energy distribution during hypervelocity projectile cratering

15 p2824 A70-32790

Intensity and velocity distributions of thermal energy argon atoms scattered from silver (111) face, using time of flight methods

16 p2953 A70-33007

Upstream wear of small metal orifices under large pressure drops in phosphate ester hydraulic fluids due to current driven electrochemical corrosion

16 p2919 A70-33629

Thermal constriction resistance between contacting metallic paraboloids applied to instrument bearings

16 p2998 A70-33902

Kirchhoff law validity for freely radiating metallic surfaces, using emissometer to measure hemispherical emittance

16 p2999 A70-33903

Contacting metal surfaces thermal conductance prediction in vacuum, formulating dimensionless parameters in terms of properties, surface measurements and load/temperature conditions of contact

16 p2932 A70-33919

Surface interaction between Al single crystals in ultrahigh vacuum, investigating galling, distortion and adhesion

16 p2924 A70-34168

Diffuse-specular models for radiant heat interchange prediction for isothermal-adiabatic surface enclosure tested for steel and gold

16 p3003 A70-34197

Anodic breakdown characteristics of Ti alloys as function of metal surface condition

17 p3113 A70-34366

Metal-silicate rock friction in ultrahigh vacuum of near environment

17 p3101 A70-34760

Metal surface ionization measurements for upper atmosphere and interplanetary space energetic neutral hydrogen analyzer design

17 p3138 A70-35309

Collection of papers on protective coatings on metals

17 p3101 A70-35390

Collection of papers on protective coatings on metals, Volume 2

17 p3102 A70-35403

Electron impact desorption kinetics of ions and neutrals from polycrystalline W surfaces, using cylindrical magnetic spectrometer

18 p3225 A70-36321

Metal surface through and part through cracks, investigating dimensions and material properties effects on fracture stresses

18 p3278 A70-36565

Low energy ion beam system for studying electron ejection from controlled metal surfaces, describing vacuum, ion source, lens and mass spectrometer components

18 p3261 A70-37086

Fcc metals surface self diffusion temperature dependence, using model based on complex defects contribution to diffusion flux at high temperatures

19 p3483 A70-37545

Critique of paper on electron diffraction study of Ce adsorption on W surface, discussing electron work function changes and data discrepancies

19 p3473 A70-37548

Materials jet-like ejection from metal surfaces under high density laser radiation action, investigating erosion and plasma spectrum

19 p3448 A70-38734

Metallic surfaces vacuum electric spark alloying, investigating pressure effects on coating layer thickness and area

20 p3636 A70-39195

Gadolinium surface work function from contact potential difference against platinum

20 p3687 A70-39996

Metal surfaces friction and wear processes dynamic equilibrium noting loading conditions effects

20 p3638 A70-40099

Heat resistance of machined stainless steel and molybdenum contact pairs in vacuum, discussing compressive loads and surface defects effects

20 p3638 A70-40340

Surface films effect on thermal contact conductance of aluminum surfaces contacting in high vacuum environment

21 p3944 A70-41024

Pt and Ag surface effects on LOX nucleate boiling heat transfer, considering embedded abrasives relationship to hysteresis

21 p3947 A70-41056

Hydrogen adsorption and coadsorption with oxygen on W single crystal surface measured by mass spectroscopy and low energy electron diffraction method

21 p3862 A70-41887

Tungsten adatoms migration and binding energies on W surfaces, taking relaxation effects into account

21 p3862 A70-41888

Ruby giant pulse laser produced plasmas from aluminum and copper surfaces, measuring electron and ion energies by time of flight and retarding potential techniques

21 p3860 A70-41925

Angular distribution of thick target bremsstrahlung produced by electron bombardment of Be, Sn and Au surfaces

21 p3854 A70-42020

Molybdenum trisilicide-tantalum trisilicide and molybdenum trisilicide-tungsten trisilicide interdiffusion for molybdenum disilicide protective coating on Ta and W surfaces

21 p3840 A70-42056

Room temperature oxygen adsorption on tungsten surfaces

22 p4087 A70-43235

Concentrated pulsed electromagnetic fields penetration into conductor, assuming magnetic field along metal surface

22 p4041 A70-43621

Damage data comparison for vibratory cavitation and liquid impact on aluminum alloy, stainless steels and pure nickel

23 p4203 A70-43870

Precious metals, measuring tension, grinding and polishing induced surface plastic deformation effects on electron work function and exoemission

23 p4204 A70-43927

Thermal radiation emissivity predictions for metal surfaces at cryogenic temperatures, comparing anomalous skin effect and Drude single electron theories

23 p4218 A70-44388

Spectral bidirectional reflectance measurements of rough metallic surfaces for reflected energy spatial distribution determination in radiative heat transfer problems

23 p4281 A70-44446

Heat resistant surface diffusion alloying of Ni alloys with Cr, Ti and Si saturation

24 p4361 A70-45834

Electrochemical corrosion of metals, discussing passivity and passivating techniques, inhibitors and resistant alloys

24 p4361 A70-46142

Thermal constriction resistance due to nonuniform metal surface conditions, considering macroscopic contact resistance for nonuniform interface pressure distribution

24 p4429 A70-46177

Spark erosion or plasma jet treatment effects on Co surface structure, describing allotropic delta phase

24 p4364 A70-46221

Diffusing element deposition on metal surface during saturation from gas phase based on calculation of equilibrium composition of reaction mixture

24 p4364 A70-46333

Diffusive carbon redistribution in Mo during interaction with Ni and Cr protective coatings

24 p4364 A70-46334

METAL VAPORS

NT MERCURY VAPOR

NT SODIUM VAPOR

Thermodynamic and transport properties of Na, K, Rb and Cs vapors to 3000 K, for use in liquid metal coolant and power systems

01 p0214 A70-10299

Helium-cadmium laser operation, using DC cathodoresis to maintain spatially uniform optimal Cd vapor concentration

01 p0110 A70-10562

Mg vapor and oxygen surface reactions in MgO deposits, using atomic absorption spectrophotometry

02 p0250 A70-12006

Sonic waves induced by shock of laser produced brass and graphite vapor in air at atmospheric pressure using high speed shadowgraphs

05 p0857 A70-15802

Electron work function variation of W in Ba-Cs-Sr vapor combinations determined using thermionic diode

05 p0891 A70-15974

Refluxing capsule tests of refractory metal alloy-boiling alkali metals corrosion compatibility, noting role of capsule geometry

06 p1087 A70-17510

Surface shielding from reentry radiation by injecting metal vapors into oxygen bearing boundary layer, calculating particle size distributions, optical depths and attenuation factors

06 p1041 A70-18163

[ALAA PAPER 70-156] He-Cd laser output improved by transverse magnetic field application

06 p1084 A70-18619

Effusion steady state pressures time dependence of carbon monoxide and calcium vapors generated during calcium oxide-graphite interaction

11 p1995 A70-26602

Parametric resonances at zero field crossing levels of optically pumped atoms on alkali vapors, noting applications to weak magnetic measurements

13 p2456 A70-30034

Microwave harmonic generation by nonlinear plasma-metal junctions noting calcium, gallium, molybdenum, gold, copper and platinum cathodes

14 p2549 A70-30438

Optimum alkali metal vapor humidity for turbine equipment estimated from energy output

14 p2535 A70-31008

Humidity measurement for alkali metal vapor in turbines by electric calorimeter with two heaters

14 p2587 A70-31009

He-Cd laser with cathaphoretic transport and diffusion return path, noting condenser critical temperature for radiation noise reduction

15 p2751 A70-31987

CW Cd vapor laser oscillation achieved with slotted hollow cathode discharge containing He carrier gas at pressures of several Torr

15 p2751 A70-31988

Initial stages of Ti vapor deposition on Mo, using secondary ion-ion emission and mass spectral analysis

15 p2757 A70-32120

Alkali metal vapors diffusion coefficients in inert gases, determining atomic interaction parameters

19 p3473 A70-38190

Binary Nb vapor systems mutual diffusion coefficients concentration and temperature dependences, discussing interatomic bonds and melting point of alloys

19 p3454 A70-38715

Metal vapors electrical conductivity and density measurement at high temperatures and supercritical pressures

20 p3648 A70-39637

Projected nuclear MHD system conditions, examining electrical measurements in K vapor with diode at atmosphere pressure and high temperatures

20 p3681 A70-40006

Low voltage slotted hollow cathode laser tube design with transverse discharge operation and uniform axial distribution of laser media, including metal vapors

21 p3834 A70-40571

Temperature, metal vapor density and energy balance in Ar shielded welding arc with Fe electrodes

22 p4043 A70-42381

Metal vapor flow measurement by quadriplanar mass spectrometer for control of thin film depositions by evaporation

23 p4198 A70-44872

METAL WHISKER REINFORCEMENT

METAL WHISKER REINFORCEMENT

U WHISKER COMPOSITES

METAL WORKING

- NT BULGING
- NT CLADDING
- NT EXPLOSIVE FORMING
- NT FORGING
- NT HYDROFORMING
- NT HYDROSPINNING
- NT MAGNETIC FORMING
- NT METAL DRAWING
- NT SIZING [SHAPING]

Mo coated with Ni-base Nimonic and Co-base heat resistant alloys, for working degree effect on creep rupture strength

01 p0126 A70-11646

Forming techniques to overcome pressing behavior of maraging steels, noting tendency to thin during stretching and reluctance to stretch

03 p0497 A70-13620

Al extrusions, discussing tooling, controls, indirect extrusion, drawn tubing and painted extrusions

03 p0512 A70-13777

Electrochemical machining based on reverse plating useful in gas turbine industry

04 p0699 A70-15398

Solution treating temperature and microstructure effects on hot rolled Ni base alloy properties

07 p1306 A70-18995

Laser systems application to automatic or semiautomatic materials processing in metal working and microelectronics, including hole drilling, silicon wafers scribing, etc

08 p1502 A70-20820

Earing during rolling of high purity aluminum on broad hot-strip mill, investigating thickness, temperature and composition relationship

09 p1692 A70-22641

Vacuum rolling of high strength hard-workable dispersion-hardened Nb base alloys excluding recrystallization

09 p1692 A70-22756

High power CW carbon dioxide laser design and operation for use as heat source in metal fusing, welding and cutting

10 p1897 A70-23816

Cost effectiveness in Ti forming, discussing materials, tooling and fabrication cost ratios

10 p1970 A70-23852

Creep forming application in producing aircraft parts from metal sheets, plates and extrusions, discussing blank forming and drawing

10 p1893 A70-23854

Metal working technology of Ti and alloys for structural parts fabrication for Concorde aircraft, describing laser cutting, electron beam welding, explosive forming, etc

10 p1895 A70-24594

Nickel base alloy as die material for creep forming titanium

11 p2060 A70-26424

Flash, gas-pressure and electron-beam welding of airframe steels

[ASTME PAPER MR-69-712] 12 p2239 A70-26987

Aerospace materials machining processes guidelines to minimize structural failures caused by lack of surface integrity

[ASTME PAPER MR-69-730] 12 p2239 A70-26988

Electrochemical machining of metals with complex shapes, discussing performance capabilities and cost efficiency

[ASTME PAPER MR-69-711] 12 p2239 A70-26989

Electric discharge machining technology, discussing quality control factors

12 p2239 A70-26990

Structural materials chemical and metallurgical factors controlling mechanical properties, machinability and finished part producibility

[ASTME PAPER MR-69-731] 12 p2240 A70-26992

Short time tensile properties of thermomechanically treated astrolloy showing improvement due to refined gamma precipitate and grain boundary carbides

12 p2256 A70-27610

Metals and metal alloys ductility development, discussing plastic flow problem in metal working

12 p2327 A70-28144

Engineering development role in metal forming industry expansion, discussing metals ductility or plasticity increase for extending processes

12 p2244 A70-28146

Die surface composition effects on lubricant efficiency in metal working judged by friction coefficient and surface damage

13 p2418 A70-28830

Cold worked metal, estimating lattice imperfections mol fractions based on reversible cell thermodynamics

15 p2676 A70-31564

Bend formability and fracture toughness tests on Be ingot and cross-rolled powdered sheet and brake grade block materials

[ASM PAPER W70-15.3] 15 p2760 A70-32337

Metallic superplasticity and superplastic alloys in simple tension, forming tubes and sheets of superplastic Sn-Pb eutectic alloy by pressure forming techniques

16 p2916 A70-32916

Ti-Al-Nb system creep strength, oxidation resistance, density, forging and rolling

17 p3120 A70-34426

Metastable ageable beta Ti-Mo-V-Fe-Al alloy, discussing plate, sheet and forgings producibility, metallurgical characteristics and structural properties

17 p3121 A70-34435

Metal powder rolling process as compaction with plastic particle deformation, deriving pressure distribution on rollers

19 p3434 A70-37451

High magnetic fields applications, emphasizing metal forming and superconducting rings levitation

19 p3471 A70-37948

Long structural shape production for titanium and super alloys, discussing rolling, extrusion, drawing, frictionless forming and filler techniques

19 p3437 A70-38420

Drilling rates improvement for Ti by adding ultrasonic vibration to conventional process

19 p3437 A70-38421

Cold form rolling of various metal-shape combinations to close tolerance net shapes without machining

20 p3637 A70-39940

Cold metal working techniques, describing electromagnetic, explosive, ultrasonic, high velocity hammering, stretch forming, deep drawing and superalloy shaping

20 p3639 A70-40445

Thermal processes during electron beam metal working, deriving relations for temperature field

21 p3833 A70-41123

Succession of passes in rolling and hot shaping of thin walled angle steel

22 p4045 A70-42813

Metal deforming machines permissible impact velocities determination

22 p4046 A70-42815

Metal matrix composite structures tooling and fabrication processes, considering forming, joining, welding, machining joining, etc

[SAE PAPER 700752] 24 p4348 A70-45873

METAL-GAS SYSTEMS

Dissolved gases and carbon effect on transition temperature from plastic to brittle state of high melting metals including niobium and vanadium

01 p0124 A70-11615

PdH system electrical resistivity, studying hydrogen concentration role

12 p2282 A70-26900

Dissociation energy of gaseous TiN molecule at high temperature

15 p2695 A70-32748

Yield strength of Nb-O single crystal solid solutions as function of temperature

15 p2763 A70-32808

Refractory metals penetration by liquid alkali metals along grain boundaries and crystallographic planes, considering threshold oxygen concentration

16 p2932 A70-34203

Physical properties and structure of Cr-Ni austenitic stainless steels with high Mn and N content as function of temperature

17 p3125 A70-35143

Corrosion and mechanical properties of Cr-Ni-Mn-N austenitic stainless steels

17 p3125 A70-35144

Yield stress in electron beam-refined Nb-N solid solution at room temperature and specific strain rate range

19 p3454 A70-38813

Niobium suboxide formation in Nb-O system from supersaturated solution of oxygen in niobium after annealing

20 p3648 A70-39630

Hydrogenated Ni elastic limit discontinuity, discussing Portevin-Le Chatelier effect

23 p4208 A70-44921

METAL-METAL BONDING

Ta-V-Cb and Ta-V-Ti alloys used as brazing fillers for refractory metals bonding, noting wetting and flow characteristics, shear strength, remelt temperatures, etc

02 p0319 A70-12753

Diffusion welding of dissimilar metals with or without intermediate layers, assessing joint strength factors

03 p0498 A70-14071

Al weld metal compositions and hydrogen content effects on weld porosity, locating hydrogen in weld by radioactive tracers

08 p1507 A70-21485

Nondestructive test procedures development and implementation for bond strength of honeycomb sandwich and metal-metal adhesive bonded structures of F-5 and T-38 aircraft

09 p1692 A70-22798

Adhesive bond stress of aircraft structural joints between metal plates of variable cross section designed for shear

10 p1957 A70-24296

Joining small components made of difficult to weld materials by percussive welding consisting of stationary and moving electrode actuated by pretensioned spring

10 p1894 A70-24298

Metal contact welding principles, materials geometries and machines

10 p1897 A70-25311

Mechanism and kinetics of intermetallic layers for mation and growth in welded joints of unlike metals

11 p2067 A70-26594

Solid state welding processes for space, nuclear and deep submergence technologies, discussing diffusor bonding of Al and stainless steels

13 p2419 A70-29117

Organic adhesives for bonding continuous surface and core-to-face joints, discussing strength, environmental resistance, producibility and reproducibility

13 p2419 A70-29118

Explosive bonding applications, safety, detonation velocity, cost and handling

13 p2419 A70-29119

Weld transition joints from explosive bonded Al-steel and Al-Cu composite plates, discussing mechanical and electrical properties

17 p3102 A70-35551

Tungsten adatoms migration and binding energies on W surfaces, taking relaxation effects into account

21 p3862 A70-41888

Hydrostatic and anisotropic piezoresistance in organometallic crystals, noting iridium and platinum complexes with maximum metal-metal interaction

22 p4086 A70-43021

METAL-WATER REACTIONS

Metal corrosion product dissolution in reactor cooling deionized water, investigating Cu, W and Cd using chemical analyses

10 p1904 A70-24398

METALLIC PLASMAS

NT CESIUM PLASMA

Transverse Kelvin-Helmholtz instability in rotating thermally ionized alkali metal plasmas /Q machines/, analyzing LF drift wave edge oscillation using dispersion equation

02 p0348 A70-12239

Heavy negative charges formation in ionized Hg vapor by electron capture, basing demonstration on magnetic field effects on free electrons or charged droplets

08 p1550 A70-20594

Ionized potassium plasma three body recombination coefficient measurements showing inverse temperature dependence

09 p1735 A70-22778

Variational model of collisional-radiative recombination of atomic ions in hydrogen and alkali plasmas

09 p1735 A70-22828

Thermal properties associated with temperature gradients in He-K plasma, studying mass motions initiated by cold wall contact

09 p1735 A70-22844

Laser-produced Al plasmas linear and nonlinear behavior, using framing camera and energy absorption measurements to study outermost ion energy increase and luminous front expansion

09 p1736 A70-23187

Nonlinear parametric excitation of stable resonant drift waves by mode-mode coupling in potassium plasma of Q device

11 p2090 A70-26020

Tuned laser radiation to diagnose and enhance local conditions in alkali metal plasma

12 p2281 A70-27793

Heat energy transport mechanism in metallic plasma deposited coating, investigating role of elastic crystal lattice vibrations, electrons, molecules, etc

13 p2419 A70-28858

He-Ne laser radiation absorption in dense Li plasma, calculating absorptivity for bremsstrahlung and photoionization

13 p2465 A70-29710

Potassium plasma-electron beam interaction, studying LF instability due to electron and ion heating

22 p4083 A70-43385

Plasma formation from transition metal target under monopulse laser radiation, noting absorbed surface density energy role in onset

24 p4385 A70-45463

METALLIZING

Wear resistance of Ti alloys chromosilicified by thermal diffusion in vacuum

01 p0115 A70-10072

Dielectric overcoatings effect on Al interconnections electromigration in IC metallization, noting longer interconnections between failures

01 p0153 A70-10083

Open circuit development in microcircuits metallization and processing to eliminate nonuniformity, voids and microcracks

02 p0316 A70-12056

Beam-lead substrate package for six stage TTL shift register, discussing metallization systems for interconnections and beams

02 p0271 A70-12846

Alloying elements effects on vanadium alloys case hardening by boronizing

07 p1303 A70-18742

Chromized molybdenum thermal stability under cyclic induction heating and subsequent air cooling

07 p1304 A70-18743

Diffraction gratings produced by holographic techniques and vacuum metallization to provide high performance

07 p1279 A70-19049

Sputtering method used for applying metallizing layer to ceramics in producing ceramic to metal seals

10 p1895 A70-24555

Thermal coated extendable boom for space applications, describing construction and vacuum metallizing technique

12 p2242 A70-27266

Plasma torch for increasing material fusion temperatures in metallization methods

12 p2244 A70-28072

Inconel 713 alloy, investigating chromaluminization treatment effect on fatigue strength at 700 C

18 p3278 A70-37211

Fluxless paste for thermomigration calorizing stainless and heat resistant steels and alloys

19 p3434 A70-37459

Titanizing Armco iron and carbon steels, examining diffusion layer structure and phase composition

19 p3451 A70-37460

Metallization systems materials for IC, discussing environmental stability, metals electromigration, electrochemical corrosion tests, etc

23 p4173 A70-44533

IC metallization systems in semiconductor devices fabrication and packaging, assessing metals alternate to Al for electromigration difficulties avoidance

24 p4319 A70-46075

METALLOGRAPHY

X ray metallography methods applied to high temperature protective coating development, refractory alloys strengthening and metal fatigue studies

04 p0711 A70-15706

Metallographic observations on slow crack growth in Be monocrystals suggesting explanation for transition regions

16 p2933 A70-34275

Metallographic preparation of materials for microstructural studies, discussing deformation- free sampling, metal polishing, microphotography and quantitative microscopy

21 p3825 A70-40895

Pulsed eddy currents in metals nondestructive testing, discussing masked probes, reflection systems, correlation and filtering methods, etc

22 p4028 A70-42593

Metallurgical interaction phenomena in welding zone of heat treated Inconel 600, using hot ductility testing and metallographic methods

22 p4046 A70-43150

Martensite plate substructure in Fe-Mn-Cr-C alloy, using transmission electron microscopy and diffraction study

24 p4358 A70-45238

METALLOIDS

NT BORON

NT BORON ISOTOPES

NT SILICON ISOTOPES

Simultaneous titration of gases, metalloids and metals in steels and refractory alloys by far UV vacuum spectrometry

[ONERA-TP-765] 08 p1455 A70-21842

Solid state plasmas waves and oscillations in metals, semimetals and semiconductors, noting applications for microwave devices

19 p3479 A70-37944

METALLORGANIC COMPOUNDS

U ORGANOMETALLIC COMPOUNDS

METALLURGY

Beryllium properties and processing including magnesium thermal reduction, power purity, oxygen content, grain size and temperature effects on mechanical properties

01 p0124 A70-11618

Cobalt effects on Ni-W alloys mechanical and metallurgical properties including thermal stability, fabrication response, weldability and impact resistance

07 p1306 A70-19070

Strength, corrosion resistance and fabricating qualities future improvements in metals and alloys, discussing chemical composition approach, dispersion hardening, superplasticity, etc

08 p1518 A70-21267

Apollo command and service modules from metallurgical viewpoint

09 p1766 A70-22792

Structural materials chemical and metallurgical factors controlling mechanical properties, machinability and finished part producibility

[ASTME PAPER MR-69-731] 12 p2240 A70-26992

Superplasticity in physical metallurgy, comparing with metal deformation modes

12 p2257 A70-28145

Physical metallurgy, discussing metals, intermetallic compounds and polymorphic metals properties, single crystals production, etc

12 p2257 A70-28272

Pure metals structure effect on friction and lubrication under steady slip in ultrahigh vacuum at low temperatures

19 p3438 A70-38729

Be production, development, potential uses and properties

[ASM PAPER GG8-102] 20 p3650 A70-39970

Metallurgical changes induced by planar shock wave propagation through metals and alloys, describing shock-hardened metals macro and substructure

20 p3652 A70-40142

Band structure contributions to elastic shear constants of hexagonal close packed metals, using optimized model potential

21 p3839 A70-40600

Metallurgical interaction phenomena in welding zone of heat treated Inconel 600, using hot ductility testing and metallographic methods

22 p4046 A70-43150

Nondestructive tests and controls in metallurgy and nuclear technology - Conference, Saclay, France, June 1968

22 p4040 A70-43617

Annealing response of explosively shock loaded Ni, thoria-Ni, Chromel-A, Inconel 600 and thoria-Chrome, noting activation temperature inverse relation with stacking fault free energy

23 p4204 A70-43883

METALS

NT ACTINIDE SERIES

NT ALKALI METALS

NT ALUMINUM

NT ALUMINUM COATINGS

NT ALUMINUM ISOTOPES

NT ALUMINUM 26

NT ALUMINUM 27

NT BARIUM

NT BERYLLIUM

NT BERYLLIUM 9

NT BERYLLIUM 10

NT BISMUTH

NT CALCIUM

NT CALCIUM ISOTOPES

NT CERIUM

NT CESIUM

NT CESIUM VAPOR

NT CHROMIUM

NT CHROMIUM ISOTOPES

NT COBALT

NT COBALT ISOTOPES

NT DYSPROSIUM

NT EUROPIUM

NT GADOLINIUM

NT GALLIUM

NT GOLD

NT GOLD COATINGS

NT HAFNIUM

NT HOLMIUM

NT INDIUM

NT IRIIDIUM

NT IRON

NT IRON ISOTOPES

NT IRON 57

NT LANTHANUM

NT LEAD [METAL]

NT LEAD ISOTOPES

NT LIQUID METALS

NT LIQUID POTASSIUM

NT LIQUID SODIUM

NT LITHIUM

NT LITHIUM ISOTOPES

NT MAGNESIUM

NT MAGNESIUM ISOTOPES

NT MANGANESE

NT MANGANESE ISOTOPES

NT MERCURY [METAL]

NT MERCURY VAPOR

NT METAL COATINGS

NT METAL CRYSTALS

NT METAL FILMS

NT METAL FOILS

NT METAL MATRIX COMPOSITES

NT METAL POWDER

NT METAL VAPORS

NT MOLYBDENUM

NT NEODYMIUM

NT NICKEL

NT NICKEL COATINGS

NT NICKEL ISOTOPES

NT NIOBIUM

NT NOBLE METALS

NT PALLADIUM

NT PLATINUM

NT PLUTONIUM ISOTOPES

NT POTASSIUM

NT POWDERED ALUMINUM

NT PRASEODYMIUM

NT RARE EARTH ELEMENTS

NT REFRACTORY METALS

NT RHENIUM

NT RHENIUM ISOTOPES

NT RHODIUM

NT RUBIDIUM

NT RUBIDIUM ISOTOPES

NT RUBIDIUM 86

NT RUTHENIUM

NT SILVER

NT SINTERED ALUMINUM POWDER

NT SODIUM

NT SODIUM ISOTOPES

NT SODIUM VAPOR

NT SODIUM 22

NT SODIUM 24

NT STRONTIUM

NT STRONTIUM ISOTOPES

NT TANTALUM

NT TERBIUM

NT THALLIUM

NT THORIUM

NT THORIUM ISOTOPES

NT TIN

NT TITANIUM

NT TRANSITION METALS

NT TUNGSTEN

NT ULTRAPURE METALS

NT URANIUM

NT URANIUM ISOTOPES

NT URANIUM 233

NT URANIUM 238

NT VANADIUM

NT YTTERBIUM

NT YTTRIUM

NT ZINC COATINGS

NT ZINC ISOTOPES

NT ZIRCONIUM

Liquid oxygen and water cavitation effects on lead, copper, nickel, iron and zinc

01 p0115 A70-10071

Antarctic twilight observation by photoelectric scanning spectrometer in search for metallic emission lines in upper atmosphere

01 p0081 A70-11231

Metal and alloys micro and macro stress-strain behavior data correlated for linear differential transformers, strain gages, longitudinal resonance waves and X ray diffraction

01 p0092 A70-11248

Acoustic emission analysis for material evaluation and polymorphic phase transformations characterization for metals and alloys, discussing electronic instrumentation and experimental techniques

02 p0276 A70-12551

Soviet collection of papers on metal science and corrosion problems covering welding, heat treatment, Cr-Mn steel, Ti alloys, etc

03 p0509 A70-13276

Optical and mechanical techniques for space experiment structures and metals satisfying space requirements

03 p0492 A70-13848

Materials science experimental and diagnostic phases in mechanisms of metal erosion by impacting dust particles

[ASME PAPER 69-WA/MET-8] 04 p0704 A70-14760

Extrusion forces required for metals and alloys determined by mathematical equations correlating extrusion pressures with process variables, discussing lubrication systems effectiveness

[ASME PAPER 69-WA/LUB-6] 04 p0697 A70-14767

Torsion tests on cylindrical plastic metals, considering shear stresses calculation as function of torsion angle and changes determination as function of increasing cold work

05 p0927 A70-15996

Micromechanisms of fracture in metals and polymers before plastic deformation onset, discussing macroscopic polymer properties from microstructure and molecular structure

05 p0937 A70-16365

Testing equipment and methods for metallic materials selection for low temperature applications, characterizing plasticity by yield strength, tensile strength, elongation, etc

05 p0864 A70-16805

Metal content effects on evolution tracks of five solar mass stars with different chemical composition, discussing Magellanic Clouds composition

05 p0919 A70-16936

Globular clusters in M31, discussing metallicity and heavy element enrichment in Andromeda

06 p1138 A70-17306

Impurities effect on grain boundaries composition and brittle fracture of metals

06 p1087 A70-17608

Time dependent relaxation model for heat flux in metals from quantum mechanical form of Boltzmann transport equation, yielding damped wave equation for temperature

06 p1090 A70-18612

Oxidation behavior of metals concerning oxide plasticity role in connection with oxide film macro- and microstresses

07 p1305 A70-18968

Ultrasonic vibration effect on strength and plastic properties of metals undergoing torsion tests

08 p1520 A70-21499

Metals thermal conductivity at high temperatures determined by direct electrical heating method, considering specimen geometry effects on radiation losses

08 p1497 A70-21526

Terminal mechanical characteristics of metals after ambient-temperature high energy rate forming compared with low rate processes

08 p1520 A70-21554

Metal-poor stars evolution during hydrogen and helium burning from main sequence to giant branch, estimating relative cluster ages

09 p1755 A70-22507

Phase diagrams of metal systems - U.S.S.R. Conference, Moscow, June 1967

09 p1702 A70-22559

Metal and alloys hardness measuring devices at high temperatures in ultrahigh vacuum based on use of synthetic sapphire pyramidal indenter

09 p1675 A70-22566

Metals and plastics tensile strain rate sensitivity tested by drop weight tests, obtaining dynamic and static stress-strain curves

09 p1704 A70-22725

Atoms diffusion mobility enhancement in metal systems during irradiation suggested due to change in electrons energy states

09 p1707 A70-23192

Metallic materials homogeneous and nonhomogeneous corrosion kinetics based on superposition principle of independent partial electrode reactions

09 p1707 A70-23422

Metal probes friction coefficient and impact temperature during impingement onto rotating chromium steel disk related to speed under various atmospheres

09 p1708 A70-23425

Enstatite chondrites and achondrites electron microprobe analysis for Si, P and Ni in metal grains and associated schreibersite and perryite

10 p1935 A70-23849

Amplitude dependence of Young modulus defect in metals during large stress HF oscillations

10 p1956 A70-24247

Thermomagnetic transport coefficients in anisotropic metals based on theory for galvanometric properties, producing closed form expression for conductivity tensor

11 p2097 A70-25618

Thermal conductivity coefficient of metals and alloys above 1000 C by longitudinal heat flow method

11 p2065 A70-25761

Thermal conductivity of metals and alloys, separating electronic and lattice contributions

11 p2098 A70-25762

Star 15 Vulpeculae metal lines analyzed by growth curve differential method

11 p2113 A70-26464

Zeeman effect on solar flares metallic lines splitting

11 p2106 A70-26592

Diffusion processes rate changes in metals and alloys resulting from radioactive emission, noting role in stress rupture strength mechanisms

11 p2068 A70-26595

Olivine and metal compositions of pallastic meteorites by electron microprobe measurements, obtaining cooling rates

12 p2296 A70-26895

Thermal metal fatigue testing, including resistance to cyclic temperature variation, operating conditions simulation and stress-strain determination

12 p2322 A70-27218

Metals thermal properties simultaneous determination at high temperatures, describing measuring equipment operation and circuitry

12 p2206 A70-27219

Metals purity, gas content and porosity effects on nature and size of material zone affected by laser beam treatment

12 p2250 A70-28219

Physical metallurgy, discussing metals, intermetallic compounds and polymorphic metals properties, single crystals production, etc

12 p2257 A70-28272

Polycrystalline lanthanides and metals resistance to deformation under compression and tension at different temperatures and strain rates

12 p2257 A70-28273

Metallic state basic parameters determined by electron transfer technique, discussing ion charges, electron and hole concentrations current scattering cross sections, etc

13 p2433 A70-28886

Metallic materials under cyclic stress conditions, investigating creep rate dependence on cycling frequency and impurities during static-to-dynamic transition

13 p2513 A70-28993

Ammonium ions elimination from atmospheric moisture condensates by treatment with metal-exchange resins, discussing volume sorption capacity

13 p2362 A70-29339

Geoactive ionizing radiation emitted by solar flares having metallic spectral lines of various brightness intensities

14 p2630 A70-30219

Concentrations model of metallic atoms and ions in upper atmosphere with deposition from meteors, using diffusion equation

14 p2580 A70-31262

Metal to hydrogen ratio for sun, Hyades and F-G stars based on photoelectric measurements of weak metal lines

14 p2652 A70-31388

Impact testing of metals - ASTM Conference, Atlantic City, June 1969

15 p2758 A70-32232

Metals and hard materials sliding wear due to granular abrasives in heated vacuum chamber

17 p3100 A70-34646

Finite element formulation for large strain and displacement problems with emphasis on elastic-plastic behavior in metals

17 p3184 A70-34905

Soft metal and dilute alloy dynamic yielding, describing high dislocation mobility effects on mechanical properties

17 p3191 A70-35459

Onsager reciprocal relations experimental validity in irreversible processes application to metals, electrokinetics, isothermal diffusion, heat conduction, chemical reactions, etc

17 p3197 A70-35538

Cryogenic attachment for cooling and tilting metal samples in electron microscope

18 p3259 A70-36474

Extrusion forces required for metals and alloys determined by mathematical equations correlating extrusion pressures with process variables, discussing lubrication systems effectiveness

[ASME PAPER 69-WA/LUB-6] 19 p3435 A70-37604

Solid state plasmas waves and oscillations in metals, semimetals and semiconductors, noting applications for microwave devices

19 p3479 A70-37944

Continuum bodies strain subjected to shearing stresses in incremental form based on slip theory of metals plasticity

19 p3549 A70-38668

Am and Ap stars metallic absorption lines, determining photometrical indices correction

19 p3523 A70-38689

Ceramic whisker and continuous filaments reinforced metals, discussing processing, properties, matrices selection of reinforced composites, etc

20 p3650 A70-39948

Metals purity, gas content and porosity effects on nature and size of material zone affected by laser beam treatment

20 p3643 A70-40094

Globular cluster color-magnitude diagram parameters, examining giant branch and metal content

21 p3889 A70-41153

Metal cracking and fracture mechanics under creep conditions at elevated temperatures, discussing notch rupture testing

21 p3937 A70-41437

Abundance ratios of metallic line star 15 UMa, using absorption spectrophotometric observations

21 p3926 A70-42270

Impurities concentration estimate in metals by low temperature residual resistivity, investigating contact and contactless measurements

22 p4052 A70-42573

Compressional sound waves electromagnetic generation in metals in static magnetic fields, examining acoustic amplitude variations

22 p4074 A70-42968

Ultrasound inductive absorption coefficient of metals in quantized magnetic field

22 p4075 A70-43474

Photometric search for metal deficient stars, using objective prism plates and four color Stromgren technique

22 p4109 A70-43736

Neutron activation determined concentrations of Ni, Ga, Ge and Ir in iron meteorites with silicate inclusions

24 p4401 A70-45376

Angle beam ultrasonic testing of metals, considering beam and depth scanning characteristics and wave reflectability of various flaws

24 p4343 A70-45687

Magnetic and nonmagnetic metals flaw detection, using orthogonal eddy current probe to reduce permeability and conductivity variations effects

24 p4344 A70-45700

Metals flaw detection, using electronic balancing type eddy current detecting coil

24 p4336 A70-45701

Metallic rods and tubes permeability and resistivity nondestructive measurement by AC apparatus with self balancing sensing coil, using computer program for data reduction

24 p4345 A70-45704

Nondestructive thermal and thermochemical treatment penetration depth measurement in metal, examining magnetic test and ultrasonic techniques

24 p4346 A70-45721

Stress-strain curves of polycrystalline metals and composites using single crystal elastoplastic model

24 p4425 A70-45779

Geoactive ionizing radiation emitted by solar flares having metallic spectral lines of various brightness intensities

24 p4398 A70-46294

METAMORPHISM [GEOLOGY]

Age and initial strontium for Guarena chondrite, determining differential evolution of Rb/Sr systems involving simple metamorphism of closed systems or multistage processes

03 p0576 A70-14088

Shock and thermal metamorphism of olivine trachybasalt by nuclear explosion at Nevada test site

05 p0843 A70-16946

Static and shock kink bands in biotite deformed by metamorphism, meteorite impact, nuclear explosion and laboratory experiments

09 p1665 A70-22053

Apollo 11 lunar crystalline rock samples petrology, discussing shock and other metamorphic effects on mineral structure

21 p3897 A70-41516

Apollo 11 lunar soil and breccia shock metamorphism, examining plastic deformation structures in plagioclase, pyroxene and olivine

21 p3897 A70-41520

Shock metamorphism, grain size and mineralogy of lunar surface regolith materials

21 p3901 A70-41543

METASTABILITY

U METASTABLE STATE

METASTABLE ATOMS

Ionization and metastable excitation in low energy collisions of ground state argon atoms formed by charge transfer

14 p2618 A70-30121

Nitrogen deactivation by ground state atomic oxygen resulting in metastable oxygen atom as auroral green line source

17 p3080 A70-35770

METASTABLE STATE

Stellar systems evolutionary stages, considering gravitational instability in rotating expanding gas, relaxation, viscosity, transition to metastable state and drift effect on geometry

02 p0376 A70-12445

Quantitative separation of metastable and cubic chromium carbides in alloyed Cr steels utilizing hydrogen peroxide

03 p0504 A70-12981

Lattice misfit influence on metastable omega phase morphology and stability in Ti transition metal alloys

03 p0508 A70-13146

Metastable diatomic N beam scattering from Teflon and Cu surfaces measured for velocity and angular distributions

06 p1112 A70-18273

Metastable tau-phase in Fe-Ni-B melt solidifying into boride, noting lattice constant and solubility

07 p1307 A70-19393

Metastable austenitic steel mechanical properties after thermomechanical treatment with deformation, discussing stress-strain curves to exhibit yield point

08 p1525 A70-21963

Metastable level populated by dissociative recombination mechanism, estimating efficiencies of various processes

09 p1745 A70-23438

Ternary metastable phase diagram for W-Ti-B system at room temperature

10 p1905 A70-25226

Metastable time-of-flight technique for measuring free molecular flow velocity distribution

12 p2231 A70-27255

Metastable He ion two photon decay, observing photon coincidence angular correlation in spectral distribution

13 p2456 A70-29811

Ionization and metastable excitation in low energy collisions of ground state argon atoms formed by charge transfer

14 p2618 A70-30121

Metastability effects on plastically deformed Al, showing superplastic flow

15 p2764 A70-32902

Metastable beta phase decomposition in Ti alloy during mechanochemical treatment and aging, determining correspondence to alpha phase segregations via electron microscopy

16 p2931 A70-33207

Phase diagrams of high strength metastable Ti beta alloys, showing minimum quantity of alloying elements for solid solution retention

17 p3119 A70-34418

Metastable ageable beta Ti-Mo-V-Fe-Al alloy, discussing plate, sheet and forgings producibility, metallurgical characteristics and structural properties

17 p3121 A70-34435

Signal to noise ratios for metastable and ion detection of excited neutral molecules in beam

18 p3262 A70-37096

Lifetimes and fine structure of differentially metastable autoionizing states of negative He ion in axial magnetic field, using time of flight techniques

19 p3473 A70-37746

Beta Ti-V-Cr-Al phase transformations below 500 C, discussing metastable phase, bcc formation and thermodynamics

20 p3646 A70-39106

Metastable excitation levels in np/4f configuration for population inversion, discussing free electron collisions, forbidden line intensity and flow density pressure 20 p3642 A70-39751

Metastable beta Ti alloy as-quenched microstructure stability with respect to thin foils transformation during electrolytic polishing and bulk specimens during cold rolling 21 p3841 A70-42150

Upper atmosphere ionization balance, examining metastable species in E and F regions 22 p4106 A70-43306

Nonequilibrium solidification and metastable stable phase transformation during heating of Al-Mo and Al-Cr alloys 24 p4360 A70-45829

Fe-Ni-Mn ternary martensitic alloy, discussing metastable miscibility gap island existence in bcc phase 24 p4363 A70-46193

METAZOA

U ANIMALS

METEOR BURSTS

U METEOROID SHOWERS

METEOR HAZARDS

U METEOROID HAZARDS

METEOR TRAILS

Ionized meteor trails initial radii statistical characteristics determined for two models 01 p0192 A70-11537

Atmospheric density in meteor region and atmospheric wind conditions determined from meteor trail drifting and artificial noctilucent clouds 03 p0563 A70-13178

Human eye image accumulation effect and meteor brightness estimation dependence on angular velocity based on visual and telescopic observations 03 p0569 A70-13358

Meteor trail drift characteristics from telescopic observations, determining velocity and diffusion coefficient 05 p0920 A70-16975

Wind velocity measurements by coherent radar pulse method of meteor trail observations 06 p1141 A70-17739

Faint meteor ablation processes, presenting evidence of solid consistency prior atmospheric entry, vaporization, wake blending and trails 06 p1151 A70-18481

Polarization- and space-diversity reception techniques for radio links based on diffraction from ionized meteor trails 07 p1378 A70-18990

Meteorite fireball track projected on earth surface determined from nearly overhead observations 07 p1387 A70-19629

Derived winds, wind shears and densities accuracies obtained by radar meteor trail technique 07 p1237 A70-20281

Meteors spectral intensity variations along flight path noting color dependence on brightness 08 p1572 A70-20946

Atmospheric particle interaction layer in front of meteor body, discussing ionization, diffusion, excitation, recombination, heat generation and luminosity 09 p1761 A70-23059

Meteor ionized trails initial expansion and diffusion resulting in dissociation and ionization of air molecules through collision, using electromagnetic wave scattering 09 p1762 A70-23177

Meteor trail angular dimensions determined by frequency scanning method involving minimum points on reflected signal characteristics 11 p2107 A70-25556

Human eye image accumulation effect and meteor brightness estimation dependence on angular velocity based on visual and telescopic observations 11 p2118 A70-26723

Auroral green line decay of atomic oxygen measured photometrically from multiple exposure spectra of meteor wakes 12 p2304 A70-27713

Small meteor streams trajectories and radiants from epsilon-Lyrids, alpha-Coronids and phi-Draconids observations by amateur astronomers 12 p2311 A70-28307

High altitude meteor winds, investigating atmospheric tides and short term wind oscillations, wind shears and drift nature 14 p2601 A70-30122

Altitude distribution of radar-signal-reflecting points and ionization in meteor trails 14 p2635 A70-30308

Meteor trail radiant, velocity and altitude measurement by obliquely incident radio waves 14 p2635 A70-30309

Transverse structural function of velocity field of turbulent motion in upper atmosphere, using meteor speed radio observations 14 p2635 A70-30312

Forward and backscattering meteor radio echo intensity variations during decay under molecular and turbulent diffusion, recombination and trapping 14 p2635 A70-30313

Phase angle gauge measurement of meteor shower radiants, using radar observations of signal scattering in meteor trails 14 p2582 A70-30314

Meteoroid radio reflections time variation based on observations at two frequencies, analyzing angular dimensions in reflecting regions 14 p2635 A70-30315

Radio wave scattering and echo intensity at inhomogeneous underdense meteor trail allowing for electron density, trail formation time and diffusion coefficient 14 p2636 A70-30316

Ionized meteor trail radio signal reflections, observing duration and echo quantity random deviations and activity coefficient at specified times 14 p2636 A70-30318

Meteor radio path activity coefficient, reflections density distribution, characteristic heights and mean durations, noting meteor velocity effects 14 p2636 A70-30319

High stability oscillators frequency check, using meteor trails and combined least squares and moving averages methods 14 p2583 A70-30320

Frequency synchronization of far spaced high stability oscillators with aid of meteor trails, discussing signal retratranslation and duplex methods 14 p2636 A70-30321

Vaporization of small meteor particles with identical surface temperature, considering radar communication based on reflection from ionized trails 14 p2636 A70-30323

Meteor radio reflections time-amplitude characteristics, discussing dependence on mirror point position in trail, wavelength, diffusion factor and initial radius 14 p2636 A70-30324

Radio echoes duration distribution from supercondensed meteoric trail emphasizing effects of recombination, adherence and turbulent diffusion 14 p2636 A70-30325

Radio wave reflection from ionized meteor trails, calculating propagation parameters by computer algorithm based on cylindrical approximation method 14 p2636 A70-30327

Wind velocity determination by radar tracking of meteor trails, investigating errors 14 p2572 A70-30328

Correlation characteristics of turbulent motions in atmospheric meteor region, discussing diversity and single point reception methods 14 p2572 A70-30329

Errors estimation in wind velocity values by radio echo observations in meteor trails of different densities 14 p2572 A70-30330

Radio observations of dense briefly visible Leonid meteor shower with fixed pencil beam antenna in coping with wave scattering in trails 15 p2796 A70-31511

Meteor radiant, drag and altitude via CW radar observation of meteor trails 15 p2800 A70-32150

Meteors spectral intensity variations along flight path noting color dependence on brightness 15 p2806 A70-32758

Fireball of 25 April 1969 crossing England, Wales, Irish Sea and northern Ireland, recovering meteorites in northern Ireland 16 p2973 A70-33117

Meteor deceleration rates in atmosphere, using base line radar measurements 18 p3313 A70-36294

Atmospheric density from radar observations of meteor trails drift, using wind velocity semidiurnal components amplitudes 18 p3253 A70-36994

Meteor radar echoes of parallel and perpendicular polarization from ionized transient trails with linear electron densities 18 p3317 A70-36995

Na D lines emission cross sections measurement from ionic and neutral gases collisions at simulated meteor conditions 18 p3318 A70-37014

Delay time between beams reflected from different parts of meteor trail, using phase invariant and frequency scanning methods 19 p3512 A70-37313

Radar tracking of meteors with slow drift velocity, improving accuracy via echo frequency multiplication 19 p3514 A70-37644

Upper atmosphere wind, density, temperature and pressure from Soviet meteor data 19 p3412 A70-37651

Meteor velocity determination by CW radar for constant phase angle, describing reflected signal processing 19 p3514 A70-37655

Meteoroid flux density from radar measurements, noting detectability dependence on initial ionized trail radius 19 p3515 A70-37660

Atmospheric turbulence scale and dissipation from 80 to 120 km, using photographic observations of Leonid meteor trails 19 p3515 A70-37663

Electron photodetachment rate from meteor radar echo duration during night and daytime observations 19 p3515 A70-37664

Optimal reception points for radar ranging measurement of angular coordinates of meteor trails, using central transmitter 19 p3515 A70-37665

Phase meter for measuring angular coordinates of reflecting meteor trails 19 p3526 A70-38777

Spectral energy distribution of meteor trail in Leonid meteor shower from photographic analysis 19 p3526 A70-38779

Spectral energy distribution curves and color indices of specific meteor trails observed on 12 August 1959 and 25 July 1963 19 p3526 A70-38780

Wind motions from meteor trails observation during IQSY, tabulating amplitudes and phases of constant, diurnal, semidiurnal and 8-hr components 19 p3526 A70-38788

Meteor trails angular coordinates, using phase difference in pairs of spaced antennas with unequal base lengths 19 p3433 A70-38789

Characteristic dimensions of large and small scale atmospheric turbulence by meteor trails photographic observations, determining energy dissipation 19 p3526 A70-38790

Meteor trail angular dimensions determined by frequency scanning method involving minimum points on reflected signal characteristics 21 p3892 A70-41306

Ionization and loss processes for meteoric elements in lower ionosphere, suggesting hydrates formation role in alkali metal ions depletion 22 p4106 A70-43305

Air current in upper atmosphere meteor zone above equator, noting diurnal and semidiurnal harmonics in wind velocity components 23 p4188 A70-44049

Meteor trails isotropic diffusion in presence of moving point source of ionization with variable intensity, calculating plasma density on and near trajectory 23 p4240 A70-44084

Upper atmosphere tidal pressure and wind variations from meteor trail drift data 23 p4215 A70-44266

METEOR 1 ROCKET VEHICLE

Meteorological rocket system Meteor 1 firing procedure 07 p1395 A70-20254

METEORITE COLLISIONS

Worldwide data inventory of rock features associated with meteorite impact structures, including photomicrographs of petrographic features 01 p0069 A70-10223

Meteoroid collision hazards of space travel, discussing meteor flux, mass and impact measurements 02 p0360 A70-11668

Meteoroid impacts as sources of seismic energy on moon, using projectile impact coupling to seismic waves in vacuum chamber experiment 04 p0751 A70-15056

Meteoroid impact mass loss and formation of planets, investigating projectile-ejecta ratio and dependence on escape speeds 05 p0910 A70-16393

Canadian Shield ridges and meteorite impact scars, discussing state of earth crust during meteoritic bombardment of earth and moon 08 p1563 A70-20500

Tungusk meteorite atmospheric shock waves obtained from simulation experiments based on forest damage 08 p1572 A70-20944

Meteorites explosive fragmentation under aerodynamic loads simulated by steel balls shot into increasing-density target, discussing parameters 08 p1572 A70-20947

Tungusk meteorite atmospheric shock waves obtained from simulation experiments based on forest damage 15 p2806 A70-32756

Meteorites explosive fragmentation under aerodynamic loads simulated by steel balls shot into increasing-density target, discussing parameters 15 p2806 A70-32759

Vredfort Ring origin, discussing paleomagnetic evidence to choose between meteorite impact or terrestrial cause 16 p2899 A70-34050

Mathematical model of asteroidal evolution and meteoritic mass distributions under collisional fragmentation using power law 18 p3312 A70-36213

Structural configurations effect on momentum imparted to spacecraft by hypervelocity meteoroid impact 21 p3938 A70-41879

Preferred disorder and shock histories of chemical group 4A meteorites from metallographic and X ray diffraction, discussing preterrestrial shock loading 21 p3920 A70-41940

Electron pulse generator for imaging of glass microspheres simulating meteorite flight and impact in evacuated vessel [SMPT PREPRINT 96] 22 p4036 A70-43059

METEORITE COMPRESSION TESTS

U COMPRESSION TESTS
U MECHANICAL PROPERTIES
U METEORITES

METEORITE CRATERS

Worldwide data inventory of rock features associated with meteorite impact structures, including photomicrographs of petrographic features 01 p0069 A70-10223

Meteor explosion theory of origin of lunar craters and round maria, suggesting endogenic origin 01 p0193 A70-11592

Optical studies of deformational structures of minerals from meteorite craters and cryptoexplosion structures 02 p0292 A70-12510

Hypervelocity impact craters formed in low and variable strength laboratory materials to provide insight into formation mechanics and resultant structures of meteorite craters 03 p0603 A70-14349

Volcanic and meteoritic processes compared as lunar cratering agency, tabulating terrestrial lopolith and cryptoexplosion structures 05 p0913 A70-16553

Tungusk meteorite as comet nucleus, discussing comet structure, composition and behavior analysis 08 p1572 A70-20943

Lunar crater meteoritic origin argument based on comparison with earth crater structure 09 p1751 A70-22195

Microscopic meteoritic spherules in soil surrounding terrestrial impact craters 09 p1758 A70-22745

Meteor explosion theory of origin of lunar craters and round maria, suggesting endogenic origin 09 p1763 A70-23436

Nonlunar origin of tektites indicated from molten glass dispersion generated by terrestrial crater-forming meteorite impact 12 p2302 A70-27584

Meteorite craters on U.S.S.R. territory, discussing impact, explosive and complex craters 12 p2311 A70-28308

Long term effects model evaluation of meteoritic impact against lunar surface compared with analyses of Lunar Orbiter photographs 14 p2645 A70-31062

Tungusk meteorite as comet nucleus, discussing comet structure, composition and behavior analysis 15 p2806 A70-32755

Lake covered ancient meteorite impact crater in Canada, noting eroded rim and microscopic shock criteria 15 p2732 A70-32849

Tenoumer crater meteorite impact origin from shock metamorphic features analysis 20 p3619 A70-39216

Shock metamorphism in lunar microbreccias and loose regolith materials, assuming crater formation by meteorite impacts 21 p3902 A70-41551

METEORITES

NT ACHONDRITES
NT AUSTRALITES
NT CARBONACEOUS METEORITES
NT CHONDRITES
NT IRON METEORITES
NT KAPOETA ACHONDRITE
NT NORTON COUNTY ACHONDRITE
NT ODESSA METEORITE
NT ORGUELL METEORITE
NT STONY METEORITES
NT TEKTITES
NT TUNGUSK METEORITE

Twilight and nightglow measurements with stratospheric balloons, discussing use for upper atmosphere exploration, meteoric influence and French network 01 p0079 A70-11217

Meteorites fossil tracks due to cosmic radiation heavy nuclei 02 p0361 A70-11748

Lunar surface samples characteristics correlation with terrestrial igneous rocks /basalts/ and eucrite meteorites based on alpha scattering analysis 07 p1380 A70-19203

Meteor ablation, investigating removal rate of molten film and droplet evaporation 09 p1754 A70-22476

Solar corpuscular streams effect on meteoric particles behavior in circular orbit around sun, determining lifetime on basis of mass loss due to pulverization 09 p1763 A70-23382

Radioactive dating of meteorites based on high temperature release of iodine-correlated Xe129 and Xe128 10 p1949 A70-25328

Serra de Mage meteorite impact history from charge particle track analysis, noting feldspar content 13 p2497 A70-29854

Astronomical, geometrical and physical selectivity factors of forward scattering radar observation concerning meteor weight 14 p2635 A70-30310

Saint-Severin meteorite thermoluminescence from mineralogical fractions separated by density 15 p2800 A70-32025

Fireball of 25 April 1969 crossing England, Wales, Irish Sea and northern Ireland, recovering meteorites in northern Ireland 16 p2973 A70-33117

Meteorites and celestial products legal status with respect to rights of property 17 p3173 A70-35793

Photometric reduction of meteor luminosity to photovisual /international/ system 19 p3515 A70-37662

Chondritic meteorite thermal histories based on K-Ar dating using Ar 39/40 method 21 p3921 A70-41974

Schenectady meteorite recovery, discussing mass, size, physical characteristics, cosmic ray track, crystalline structure and age 23 p4241 A70-44258

Meteors and meteorites research, noting fireball photointerpretation, simulated meteors, theoretical equations, etc 23 p4256 A70-45039

METEORITIC COMPOSITION

Ca-rich basalt achondrites cosmogenic isotopes characteristics, discussing lunar or cosmic origin 01 p0174 A70-10136

Petrological, X ray and chemical analyses of Muzaffarpur Ni-rich ataxite, showing kamacite, taenite and minor schreibersite composition 01 p0177 A70-10328

Chondrite-normalized lanthanide pattern of silicate inclusion of Woodbine iron meteorite, showing differences from mesosiderite phase and chondrite 01 p0177 A70-10340

Nitrogen abundances measured in enstatite chondrites by inert carrier gas fusion extraction technique, noting agglomeration of chondrules 01 p0179 A70-10475

Neutron activation analysis for U and Th in various tektites, discussing evolution and extraterrestrial origin 03 p0576 A70-14090

Isotopic composition of meteoritic Ti determined in Ivigtut galea, Plainview chondrite, Canyon Diablo troilite and Canyon Diablo metal 03 p0576 A70-14091

Isotopic composition and contents of xenon and krypton in Pesyanoe meteorite suggesting presence of solar type gas component 04 p0754 A70-15274

Allende carbonaceous chondrite radionuclide composition and concentration determined by nondestructive gamma ray spectrometry 04 p0754 A70-15275

Bronzite, hypersthene and amphibole chondrites examined by X ray diffraction for inert gas retention ages relationship to shock and reheating 05 p0912 A70-16448

Chemical compositional evidence of Needles /California/ iron meteorite, suggesting distinct fall nature 05 p0912 A70-16465

X ray diffraction analysis for composition and structure of meteorites found in Kansas, classifying as hypersthene and bronzite chondrites 05 p0912 A70-16466

I-Xe dating of Abee enstatite chondrite by combined neutron activation and mass spectrometric analysis 05 p0915 A70-16829

Microtektites chemical analysis data providing appraisal of strewn field boundaries, implying lunar origin 05 p0916 A70-16837

Ni-Cr content and variability in Ivory Coast tektites using atomic absorption and X ray emission techniques 05 p0916 A70-16837

Correlation between O isotope ratios and composition of tektites investigated for origin of tektites 05 p0917 A70-16840

Electron microprobe determinations of Si concentrations in metal of iron meteorites, showing weak evidence for Si presence in earth core 05 p0921 A70-17094

Cliftonite occurrence, internal structure, orientation within kamacite and implications on origin of diamonds in meteorites 05 p0921 A70-17095

Tektite field studies in China concerning stratigraphic occurrence and chemistry 06 p1148 A70-18393

Australasian microtektite compositional trends compared with critical plots enabling distinction between rocks formed by igneous sedimentary and vapor fractionation processes 06 p1150 A70-18477

Rb 87-Sr 87 age determination of carbonaceous chondrites, showing agreement among petrological classification types 06 p1150 A70-18480

Faint meteor ablation processes, presenting evidence of solid consistency prior to atmospheric entry, vaporization, wake blending and trails 06 p1151 A70-18481

Pueblo de Allemande chondrite unextractable carbon content using meteorite pyrolysis, obtaining aromatic hydrocarbons 07 p1380 A70-19204

Half life of Mn53 calculated from measured activity in sample from Fe meteorite and isotopic ratio Mn53/Mn55 07 p1337 A70-19226

Iron troilite meteorites lead isotopic, Pb and U concentrations, considering fractionation and terrestrial contamination effects 07 p1388 A70-20035

Bismuth concentrations in various carbonaceous and equilibrated chondrites determination by neutron activation technique 07 p1388 A70-20036

Carbonaceous chondrites primordial He and Ne isotopes variations 07 p1388 A70-20037

Satellite recording of electron-positron annihilation gamma emission on Cosmos 135 artificial earth satellite relating to meteors antimatter nature 07 p1371 A70-20334

Ti demonstrated as predominantly chalcophilic in highly reduced enstatite chondrites and achondrites 07 p1391 A70-20352

Uranium abundance in hypersthene chondrites determined by homogenized fission track analysis, comparing age estimation with iron meteorite event occurrence 07 p1391 A70-20354

Carbonaceous material genesis in Tieschitz meteorite from electron microprobe analysis, discussing chondrule formation process residue likelihood 08 p1578 A70-21561

Allende meteorite showing presence of Ca-Al-rich glasses associated with other crystalline phases 08 p1579 A70-21562

Microscopic meteoritic spherules in soil surrounding terrestrial impact craters 09 p1758 A70-22745

Rare gases abundance patterns on earth and in chondrites, proposing chemical adsorption mechanism at planetesimal stage during accretion 09 p1764 A70-23610

Carbonaceous meteorites analyzed for soluble organic compounds, carbonate and residual carbon, showing endogenous nature 10 p1935 A70-23812

Angra dos Reis stone meteorite containing cosmogenic and fissionogenic xenon 10 p1935 A70-23850

Ureilite structures and relationship to carbonaceous chondrites, considering chemical composition, diamond content, age, size, etc 10 p1941 A70-24552

Chondrites elements fractionation in solar nebula starting from carbonaceous material 10 p1949 A70-25329

Composition and monoclinic parameters of chromium sulfide mineral breznaitite in metal matrix and silicate inclusions of Tucson meteorite using electron microprobe 11 p2110 A70-26004

Olivine and metal compositions of pallastite meteorites by electron microprobe measurements, obtaining cooling rates 12 p2296 A70-26895

Iron-nickel alloy phase and diffusion relationships, composition gradients and hardness variations involving long time metallic meteorite anneals 12 p2252 A70-26964

Neutron capture effects in Gd from Norton County meteorite by isotopic composition analysis 12 p2300 A70-27524

Ar 37 and Ar 39 isotopes in recently fallen iron-ataxite and stony meteorites, discussing relevance to cosmic ray variations in space 12 p2309 A70-27950

Seymour coarse octahedrite, compositional and mineralogical relationships 13 p2487 A70-28695

Microchondrules from chondritic meteorites, investigating morphology, composition and structure 13 p2487 A70-28696

Iron meteorites electrolytic corrosion using potentiostatic technique, noting roles of Ni content and crystal structure 13 p2432 A70-28697

Holbrook chondrite specimen, discussing effects of weathering, leaching and trace elements enrichment over period of time before recovery 13 p2487 A70-28698

Pu/U ratio in St. Severin meteorite at time of Xe retention beginning 13 p2488 A70-28723

Majorite garnet in veinlet of Coorara meteorite suggesting transformation from pyroxene 13 p2492 A70-29267

Total nitrogen content determination in silicate samples of rocks, synthetic silicate standards, NBS steels and meteorites using inert carrier-gas extraction-gas chromatography 13 p2362 A70-29497

Serra de Mage meteorite impact history from charge particle track analysis, noting feldspar content 13 p2497 A70-29854

He, Ne, Ar and Xe in plagioclase concentrate separated from Serra de Mage meteorite feldspar 13 p2497 A70-29855

Weekeroo Station iron meteorite silicate inclusions chemical composition compared to chondrites 13 p2497 A70-29858

C13/C12 component composition from carbonaceous chondrites and terrestrial samples, showing similar fractional patterns but isotope variations 13 p2497 A70-29860

Gold and iridium distribution in stony meteorites, discussing metal silicate fractionation process during chondrite formation 13 p2497 A70-29862

Lunar, meteoritic and terrestrial silicate rock chemical individuality based on atomic ratios 15 p2799 A70-31896

Enstatite chondrites K, Rb and Sr concentrations, measuring ages from Sr87/Sr86 ratios 16 p2974 A70-33649

Chromatographic analysis of organic matter in Pueblito de Allende meteorite 17 p3173 A70-35754

Chondritic and achondritic meteorites Zr and Hf abundances, distributions and ratios, using thermal and neutron activation analyses 18 p3310 A70-35968

Kingfisher meteorite metal particles microstructures, discussing phase transformation during reheating by shock 18 p3310 A70-35970

Fireballs atmospheric debris collection by high altitude filtration, describing analysis results 18 p3311 A70-35971

Lunar tidal force influence on meteoritic material fission before impact, calculating internal to explain topographical features 18 p3319 A70-37051

Sodium line in meteor spectrum, determining electron temperature and number of atoms as velocity and height function 19 p3514 A70-37600

Allende Type III carbonaceous chondrite, examining rare earth and other elemental abundances 19 p3519 A70-38028

Galactic cosmic rays temporal and spatial variations in solar system, discussing nuclear active particles and spallation products depth distribution in meteorites 19 p3509 A70-38143

Thermal release profiles and retention coefficients of injected argon ions for silicates and iron simulating meteoritic materials 19 p3474 A70-38601

Chondrites and terrestrial rocks trace elements by neutron activation analysis, discussing radiochemical separation and computer analysis of gamma ray spectra 20 p3582 A70-38980

Silicate inclusions in iron meteorites analyzed by microprobe and classified according to phase assemblages, compositions and textures 20 p3701 A70-38981

Stony meteorites radionuclides gamma emission measurement, determining specific activity ratios 20 p3703 A70-39322

Carbonaceous chondrites noble gases measurement by mass spectroscopy, discussing compositional trends and origins 20 p3703 A70-39323

Chromite, zircon and quartz crystals in Muong Nong type tektites by X ray diffraction, discussing possible impact origin 20 p3709 A70-40088

Dosso stony meteorite gamma emitters radioactivity by nondestructive spectroscopy, obtaining quantitative analysis by least squares method 21 p3893 A70-41446

Mineralogy and petrology of lunar rock samples indicating meteoritic increments 21 p3900 A70-41539

Mineral chemistry of Apollo 11 igneous rocks, soil and breccia samples, comparing with meteorites 21 p3773 A70-41545

Elemental composition and structure of metallic iron particles in lunar fines compared to meteorites, using neutron activation technique 21 p3774 A70-41556

Allende meteorite age determination, probing K, U and rare gases in whole rock and chondrule samples 21 p3920 A70-41939

Preferred disorder and shock histories of chemical group 4A meteorites from metallographic and X ray diffraction, discussing preterrestrial shock loading 21 p3920 A70-41940

Chondrites Tl content by neutron activation analysis 21 p3921 A70-41941

Nitrogen content of Odessa and Canyon Diablo iron meteorites from thermal neutron activation, Kjeldahl distillation and alkali fusion methods 21 p3921 A70-41942

Lake Toba, Sumatra as possible tektite source region based on surrounding welded tuffs composition 21 p3923 A70-41996

Schenectady meteorite recovery, discussing mass, size, physical characteristics, cosmic ray track, crystalline structure and age 23 p4241 A70-44258

Fe meteorites with high Ge content, tabulating concentrations of Ni, Ga, Ge and Ir 23 p4241 A70-44259

Neutron activation determined concentrations of Ni, Ga, Ge and Ir in iron meteorites with silicate inclusions 24 p4401 A70-45376

Abiotic synthesis of meteoritic aliphatic hydrocarbons produced by open flow Fischer-Tropsch processes for hydrogen and Co interactions 24 p4402 A70-45377

Carbonaceous chondrites isomeric alkanes identification by mass spectrometry and gas chromatography 24 p4402 A70-45378

Iron meteorites graphite-troilite nodules isomeric alkane composition, using gas chromatography and mass spectrometry 24 p4402 A70-45379

Kapoeta howardite Xe abundance and isotopic composition for indications of extinct Pu 244 and I 129 decay 24 p4402 A70-45380

Terrestrial and chondrites vanadium isotopic ratios indicating irradiation histories difference 24 p4402 A70-45381

V and Cu emission spectrographic analyses in chondrite types, noting distribution patterns between groups based on meteorite chemical fractionation mechanisms 24 p4411 A70-45789

Murchison and Lost City chondrites element abundance analysis by thermal neutron activation and wet chemical techniques, noting low oxygen content 24 p4411 A70-45790

Borgo San Donino chondrite petrology and mineralogical and chemical composition, considering texture and recrystallization features 24 p4411 A70-45791

Orgueil C 1 carbonaceous meteorite mineral content, describing pyrrhotite identification by electron microprobe 24 p4411 A70-45792

Chemical composition and degree of thermodynamic equilibrium reflected in ferromagnesian silicates of chondrites 24 p4411 A70-45793

Sequential instrumental activation analysis for trace elements in rocks and stony meteorites, comparing with silicate method 24 p4310 A70-46407

METEORITIC DAMAGE

Optical properties changes of various transmitting materials under simulated micrometeoroid environment, using silicon carbide particles accelerated in shock tube 03 p0523 A70-13027

Hypervelocity impact craters formed in low and variable strength laboratory materials to provide insight into formation mechanics and resultant structures of meteorite craters 03 p0603 A70-14349

Meteorite falls statistics correlations for fragmentation relationships with mass, time of fall and class 05 p0912 A70-16447

Meteoroid hazard to spacecraft, discussing penetration and protection information reliability obtained from terrestrial and satellite observations 05 p0914 A70-16631

Tektite damage caused by micrometeoroid impact, projectile firing at glass spheres and survival time estimation 05 p0916 A70-16834

Tungusk meteorite atmospheric shock waves obtained from simulation experiments based on forest damage 08 p1572 A70-20944

Meteoroidal bombardment effects on material loss or gain in Saturn rings 11 p2113 A70-26471

Micrometeorites impact on lunar surface, using optical reflecting and stereoscan electron microscopes to investigate craters on Apollo 11 samples 13 p2485 A70-28474

Tungusk meteorite atmospheric shock waves obtained from simulation experiments based on forest damage 15 p2806 A70-32756

Lunar dimple craters formation by meteoritic erosion of concentric impact craters 15 p2807 A70-32850

Natural thermoluminescence of limestone within/near Charlevoix meteorite impact structure, discussing impact effects on quartz-rich rocks 18 p3314 A70-36499

Power loss due to cumulative meteoroid impacts on solar cells during extended planetary missions, investigating hypervelocity particle impacts into glass [ALAA PAPER 70-1139] 20 p3567 A70-40210

Meteor impact probability on spacecraft from statistical evidence from Pegasus, Explorer and Gemini spacecraft, discussing damage prevention methods 22 p4097 A70-42524

METEORITIC DIAMONDS

Cliftonite occurrence, internal structure, orientation within kamacite and implications on origin of diamonds in meteorites 05 p0921 A70-17095

METEORIC DUST

U MICROMETEORIODS

METEORITIC IONIZATION

U ATMOSPHERIC IONIZATION

U METEOR TRAILS

METEORITIC MICROSTRUCTURES

Naturally and artificially shocked iron meteorites, analyzing microstructure and alterations induced by pressure wave and high temperatures 02 p0377 A70-12506

Metallographic examination of impact induced deformation textures of Campo del Cielo iron meteorite, analyzing phase homogeneity, microstructures and shock intensity 02 p0377 A70-12511

Widmanstatten structure in iron meteorites relationship to cooling rate and meteoritic origin 04 p0751 A70-15039

Chemical compositional evidence of Needles/California/ iron meteorite, suggesting distinct fall nature 05 p0912 A70-16465

X-ray line broadening analysis for lattice damage in kamacite phase of Fe meteorites, evaluating particle size and elastic strain 05 p0915 A70-16828

Glassy drops identity and moldavites sculpturing origin in Pannonian sediments in southern Moravia 05 p0916 A70-16838

Normal and bottle-green microtektite glass measured for magnetic susceptibility, magnetization and Curie constants 05 p0916 A70-16839

Gibeon meteorite iron strength and ductility tests, discussing fragmentation and relation to parental planet structure 06 p1150 A70-18478

Shock wave compression of single olivine crystals and specimens from chondritic meteorites, observing planar deformation microstructures 07 p1391 A70-20353

Ureilite structures and relationship to carbonaceous chondrites, considering chemical composition, diamond content, age, size, etc 10 p1941 A70-24552

Iron-nickel alloy phase and diffusion relationships, composition gradients and hardness variations involving long time metallic meteorite anneals 12 p2252 A70-26964

Microchondrules from chondritic meteorites, investigating morphology, composition and structure 13 p2487 A70-28696

Compressive yield strength of iron meteorites, discussing flow stress, microstructure, grain size, plastic deformation, slip lines, etc 18 p3314 A70-36498

Cosmic ray track sources in meteoritic minerals, considering heavy primaries, secondary spallation and fission products 19 p3508 A70-38142

Borgo San Donino chondrite petrology and mineralogical and chemical composition, considering texture and recrystallization features 24 p4411 A70-45791

METEOROID CONCENTRATION

Correlation between atmospheric meteor entry and gamma and neutron radiation intensity verifying micrometeor antimatter hypothesis 03 p0454 A70-13528

Meteor particles spatial density and energy characteristics on space vehicles, using luminescent sensors coupled with photomultiplier 04 p0744 A70-14445

Meteor rate data tabulated from controlled parameter radar survey of Southern Hemisphere activity, noting diurnal and annual variations 05 p0907 A70-16001

Meteoroid hazard data comparison from terrestrial and satellite measurements supporting Whipple theory of low density meteoroid

05 p0917 A70-16900

Sporadic meteoroid particles in ionospheric spatial density determined from kinetic energy measurements

10 p1940 A70-24322

Meteor particles spatial density and energy characteristics on space vehicles, using luminescent sensors coupled with photomultiplier

13 p2485 A70-28470

Orionid and eta Aquarid meteor showers structure and association with comet Halley

13 p2491 A70-29044

Geminid and Quadrantid meteor shower densities observed on wave-channel-antenna radar

14 p2635 A70-30305

Time-amplitude characteristics and abundance in Leonid meteor shower from azimuthal radar observations

14 p2635 A70-30306

Earth and moon meteor fall probabilities calculation using hyperbolic encounters method and lunar near and far sides crater densities difference interpretation

15 p2798 A70-31658

Meteoroids origin and distribution, examining collisional and radiative processes effects

16 p2974 A70-33650

Meteoric masses evaporation during flare, showing discrepancies for luminosity factors

18 p3315 A70-36604

Meteor luminous efficiency and luminosity factor for mass determinations

19 p3515 A70-37661

METEOROID CRATERS

U METEORITE CRATERS

METEOROID DUST CLOUDS

NT ZODIACAL DUST

Micrometeoroid experiments on OGO 2 and OGO 4 satellites, measuring velocity, masses and particle orbits in earth dust cloud

01 p0086 A70-10444

Interstellar spherical dust particles from meteoritic silicates and dirty ice, calculating optical properties and scattering functions

21 p3889 A70-41147

Ephemerides for lunar-orbiting observation of dust clouds in earth-moon system libration points L4 and L5 by observer orbiting over lunar equator

22 p4097 A70-42308

METEOROID HAZARDS

Meteoroid collision hazards of space travel, discussing meteor flux, mass and impact measurements

02 p0360 A70-11668

Meteoroid hazard to spacecraft, discussing penetration and protection information reliability obtained from terrestrial and satellite observations

05 p0914 A70-16631

Meteoroid hazard data comparison from terrestrial and satellite measurements supporting Whipple theory of low density meteoroid

05 p0917 A70-16900

Meteoroid impacts on Gemini spacecraft windows, calculating flux-mass relation

19 p3520 A70-38376

Meteor impact probability on spacecraft from statistical evidence from Pegasus, Explorer and Gemini spacecraft, discussing damage prevention methods

22 p4097 A70-42524

METEOROID PROTECTION

Optimal steady state thermal design for fin-tube single and double surface space radiators, including meteoroid protection and pumping power weight penalties

01 p0215 A70-10829

Penetration criterion for double walled structures subject to hypervelocity meteoroid impact providing choice of protective material properties

03 p0584 A70-12921

Space suit meteoroid protection for extravehicular activity, discussing Gemini and lunar surface EVA suits and bumper concept

04 p0645 A70-15402

Hypervelocity projectile size and density effect on ballistic limit of dual sheet spacecraft meteoroid protection structures, considering penetration of low and high density particles

04 p0776 A70-15422

Meteoroid hazard to spacecraft, discussing penetration and protection information reliability obtained from terrestrial and satellite observations

05 p0914 A70-16631

Lightweight double walled meteoroid shield for Mariner Mars 1971, considering Teflon impregnated glass fabric outer sheet and multilayer thermal insulation

07 p1394 A70-19712

Two plate meteoroid shields effectiveness determined by analyzing debris cloud ejected behind front plate after hypervelocity impact

11 p2138 A70-26132

Penetration mechanics of multisheet structures based on discrete particle modeling of impact debris

13 p2509 A70-28521

Spacecraft meteoroid protective shield thickness sensitivity relationship to luminous efficiency

15 p2813 A70-32518

Hypervelocity impact computerized calculations, considering material response, laminated meteor bumpers, hollowed projectiles and thick target cratering

15 p2823 A70-32787

Space vehicles with shielding for protection against meteor impacts, discussing tubular radiator design for heat removal

23 p4284 A70-45008

METEOROID SHOWERS

NT GEMINID METEORIDS

NT LEONID METEORIDS

NT ORIONID METEORIDS

NT PERSEID METEORIDS

NT QUADRANTID METEORIDS

Size and spatial distribution of meteoritic showers, establishing fragment distribution pattern relationship to sorting factor

05 p0912 A70-16464

Cosmic ray intensity increase due to meteor showers magnetic field trapping effect

08 p1560 A70-20568

Minor meteor showers radiants determined close to ecliptic plane from systematic visual observations during November, December and January 1961-67

08 p1577 A70-21532

Australite fall age determination from in situ radioactive carbon and standard geological dating methods

09 p1750 A70-22055

Meteor stream 11 Canis Minorids detected and associated with Comet Mellish 1917, discussing true radiant and orbit

11 p2108 A70-25699

Small meteor streams trajectories and radiants from epsilon-Lyrids, alpha-Coronids and phi-Draconids observations by amateur astronomers

12 p2311 A70-28307

Orionid and eta Aquarid meteor showers structure and association with comet Halley

13 p2491 A70-29044

Diurnal and seasonal variations of parameter s of meteor showers on celestial sphere, using radio echo amplitude distribution from radar observations

14 p2635 A70-30307

Three-reception-point radar system for radiant and speed measurement of individual meteors in stream, using forward scattering

14 p2582 A70-30311

Phase angle gauge measurement of meteor shower radiants, using radar observations of signal scattering in meteor trails

14 p2582 A70-30314

Extraterrestrial magnetic spherules concentration in relation to meteor shower activity and rainfall probability

14 p2640 A70-30740

Radar meteor shower rate observation compared with direct cosmic dust measurements on satellites

15 p2798 A70-31682

Cosmic ray intensity increase due to meteor showers magnetic field trapping effect

15 p2795 A70-32723

Shooting star shower and solar eclipse frequencies correlation with long term climatic changes

17 p3168 A70-35310

Meteoroid flux density from radar measurements, noting detectability dependence on initial ionized trail radius

19 p3515 A70-37660

Scorpionid shower radiants measurement, discussing position, activity, physical properties and genetic relation with comet 1770 1

19 p3526 A70-38791

Cosmic ray intensity variation during maximum meteor showers periods detected on earth, noting relationship to solar activity

20 p3697 A70-39294

Radiant dispersion, position, areas and orbital axis in meteor showers by double-station photographic observations, noting Apollo group detection

21 p3884 A70-40875

METEORIDS

NT GEMINID METEORIDS

NT LEONID METEORIDS

NT METEOROID DUST CLOUDS

NT MICROMETEORIDS

NT ORIONID METEORIDS

NT PERSEID METEORIDS

NT QUADRANTID METEORIDS

NT RADIO METEORS

NT ZODIACAL DUST

Atmospheric density on basis of photographic observations of meteors, comparing vertical profile with CIRA profile

01 p0084 A70-11556

Cometary and asteroidal meteors discriminated by orbital elements in region of Jovian comet family adjoining asteroidal belt

02 p0373 A70-12371

Meteor flakes nature and statistics obtained from meteors characterized by irregular brightness curve

03 p0574 A70-13883

Frequency distribution of apparent visual magnitudes of meteors observed from November 1960 to January 1967

04 p0750 A70-14707

Meteoroids average velocity relative to spacecraft determined using sporadic meteors orbital elements data in interplanetary space

04 p0757 A70-15550

Antarctic twilight Na emission abundance and concentration in lower E region, discussing meteor ablation models

05 p0836 A70-15819

Meteor fragments motion and vaporization based on photographs

06 p1140 A70-17733

Meteor fragmentation in flares, determining fragments mass, time and special parameters for plotting flare brightness curves

06 p1140 A70-17734

Meteor motions at cosmic velocities in real atmosphere studies to determine cause of sudden flares

06 p1140 A70-17735

Atmospheric tides influence on meteors characteristics from processing observation data

06 p1140 A70-17736

Meteors orbital elements distribution in solar system from radio observation data

06 p1141 A70-17737

Meteoroids structure, composition and fragmentation, summarizing existing evidence for photographic and radio meteors and meteor luminous and ionizing efficiency

06 p1153 A70-18551

Turbulent air flow velocities determined in meteor zone of atmosphere

07 p1386 A70-19461

Meteoroids atmospheric drag and heat transfer coefficients, considering weak shielding by repelled and vaporized molecules

08 p1572 A70-20945

Photometric masses of bodies producing bright meteors, considering emission efficiency dependence on velocity, mass and composition

08 p1573 A70-20948

Meteor abundance determination by visual observation, calculating sighting probabilities for various magnitudes

08 p1573 A70-20949

Meteor flare photographs statistical analysis, noting duration and weight distribution dependence on meteor velocity

08 p1574 A70-21214

E layer atmospheric circulation model for meteor zone, noting solar thermal radiation role

08 p1575 A70-21215

Meteor astronomical parameters measurement by pulsed and CW radio methods, considering effects of wind, meteor trails, phase angle, etc

09 p1638 A70-23627

Orbital elements of small high velocity meteors, using oblique radio sounding

12 p2311 A70-28306

Bright sporadic fireballs and faint photographic meteors orbits, discussing clustering in diagram of geocentric velocity vs inclination

13 p2490 A70-29040

Meteors hyperbolicity based on statistical considerations and radiant distribution, discussing orbits perturbation and observation from earth

13 p2490 A70-29041

Radar and optical meteor observations comparison, discussing luminosity function and angular velocity

13 p2490 A70-29042

Meteors position angles determination during telescopic observations, discussing error due to angle reversion

13 p2491 A70-29043

Meteor particle orbits, comparing inclined radar reflections with photographic and straight radar observations

14 p2636 A70-30322

Meteor observation station design and operation, describing calibration difficulties and reflecting points coordinates determination

14 p2583 A70-30331

Concentrations model of metallic atoms and ions in upper atmosphere with deposition from meteors, using diffusion equation

14 p2580 A70-31262

Meteor radiant, drag and altitude via CW radar observation of meteor trails

15 p2800 A70-32150

Meteoroids atmospheric drag and heat transfer coefficients, considering weak shielding by repelled and vaporized molecules

15 p2806 A70-32757

Photometric masses of bodies producing bright meteors, considering emission efficiency dependence on velocity, mass and composition

15 p2806 A70-32760

Meteor abundance determination by visual observation, calculating sighting probabilities for various magnitudes

15 p2806 A70-32761

Meteor orbit parameters and incident particle flux measurements by radio methods, eliminating backscatter radar sensitivity limitations

15 p2807 A70-32814

Nomograms for meteor geocentric velocity and trajectory with correction for zenith attraction and radiant

18 p3315 A70-36605

Turbulent air flow velocities determined in meteor zone of atmosphere

18 p3316 A70-36935

Spectrosensitometer for standardizing meteor spectrograms

19 p3514 A70-37643

Observed meteor brightness curve shortening with respect to theoretical curves

19 p3514 A70-37645

Meteor activity during IQSY by radar observations at 7.6 m wavelength

19 p3514 A70-37654

Fine structure of solar radiation-induced electrostatic fields on dielectric surface of comets and meteoroids

19 p3514 A70-37656

Orbital elements of photographic meteors brighter than first magnitude, tabulating dates, solar longitudes, corrected radiants, velocities, major axis, etc.

19 p3526 A70-38787

Cylindrical plasma inhomogeneities including meteor trains diffusion in presence of magnetic field, observing dependence on angle theta

21 p3886 A70-41060

Ionized gas density monitor as meteoroid detector, describing operation in ionization chamber, proportional counter and glow tube modes

23 p4197 A70-44513

Meteors and meteorites research, noting fireball photointerpretation, simulated meteors, theoretical equations, etc.

23 p4256 A70-45039

Fireball end point height as indication of meteoroid existence likelihood

24 p4411 A70-45787

METEOROLOGICAL BALLOONS

NT ROBIN BALLOONS

GHOST/Global Horizontal Sounding Technique/balloon for meteorological observation over Southern Hemisphere emphasizing technique to overcome icing in clouds

04 p0622 A70-14550

Pulse radar altimeter for measuring meteorological balloon altitude, using superregenerative RF stage

05 p0845 A70-15805

Flexible nickel cadmium secondary battery as nocturnal power supply for meteorological balloons transceiver and measuring instruments

08 p1440 A70-20711

Telemetry data processing of Eole scientific weather forecasting program, discussing mathematical model simulating atmospheric circulation in Southern Hemisphere

09 p1674 A70-22200

Kalman filtering applied to moving balloon position and velocity estimates related to upper atmosphere wind measurements by balloon-satellite experiment

11 p2025 A70-26206

Si solar cell configurations for balloons and satellites, discussing critical design constraints for weather balloon power systems

14 p2670 A70-31139

Solar cell power supplies for weather balloon and satellite systems

14 p2535 A70-31146

GHOST free floating balloon system for global atmospheric circulation data acquisition in World Weather Watch

14 p2610 A70-31153

French EOLE tracking satellite-balloon network for global atmospheric data, describing satellite and electronic instrument package

14 p2611 A70-31154

Constant altitude helium filled zero pressure polyethylene balloon for stratospheric meteorological data and atmospheric tides studies

17 p3075 A70-34607

METEOROLOGICAL CHARTS

Italian fog distribution charts compiled by Italian Air Force and Istituto Centrale di Statistica compared and criticized

02 p0328 A70-12397

Ground stations and low orbiting satellite system for automatic collection of meteorological data over Italy

03 p0581 A70-13832

Global cloud cover and earth atmosphere heat budget measured from weather satellites, discussing Tiros pictures, radiation charts and albedo

03 p0479 A70-14348

Seasonal and monthly mean charts forecasting method based on variation of annual difference in atmospheric circulation

04 p0715 A70-15294

Synoptic changes associated with midwinter 1967-1968 major stratospheric warming, including pressure and wind distributions and temperature maps

07 p1275 A70-20277

Prognostic maps of geopotential and wind in middle troposphere derived from hydrodynamic equations

07 p1330 A70-20307

Lebedev nomogram determination of climatic parameters dependability, considering underlying theory and temperature sums

09 p1718 A70-23171

Analog methods of weather forecasting involving map matching, discussing weather modification

14 p2610 A70-31141

Meteorological rocket probing, noting 100 and 170 km range probes in U.S.S.R., thermobaric maps and aerological stations for high altitude aviation

15 p2771 A70-32108

Weather situation persistency, using 500 mb contour chart catalog

16 p2945 A70-32950

Climatological maps of earth mean annual radiation balance compared with satellite data

18 p3286 A70-36966

Meteorological fields objective representation by numerical analysis, discussing statistical parameters and analytic errors checking

21 p3847 A70-41400

Midwinter warming period upper stratospheric vertical motion fields, obtaining 2-mb charts

21 p3847 A70-42123

METEOROLOGICAL FLIGHT

Lower atmosphere turbulence under convective conditions, comparing Doppler radar and instrumented aircraft wind speed fluctuation measurements

09 p1716 A70-22367

Meteorological Nimbus 3 satellite and aircraft observations of thermal radiation for vertical atmospheric temperature profile measurement

11 p2075 A70-25921

Project HARP gun-launched projectiles as vertical sounding probes for upper atmospheric meteorological and geophysical measurements, discussing payloads development for high acceleration

11 p2122 A70-26047

Statistical analysis of atmospheric wind and temperature variables relationships to high altitude clear air turbulence observed by U-2 flights

12 p2264 A70-28092

Rain sampling by Varsity aircraft, determining reliability of droplet sampling instruments above aircraft top surface

19 p3463 A70-38947

METEOROLOGICAL INSTRUMENTS

NT CLOUD HEIGHT INDICATORS

NT RADIOSONDES

NT RAWINSONDES

NT WEATHER DATA RECORDERS

NT WIND VANES

Aerodynamic roughness length estimation and site roughness increase due to micrometeorological equipment

03 p0483 A70-13166

Meteorological satellite TV cameras development, discussing image sensors and tabulating characteristics

03 p0491 A70-13665

Meteorological spaceborne IR instruments associated with NASA satellites, discussing various Tiros and Nimbus instruments

03 p0491 A70-13666

IR equipment on Tiros and Nimbus 1 and 2 satellites, describing vertical atmospheric sounding

03 p0492 A70-13833

Response characteristics of height-based and time-based wind reduction techniques for meteorological rocketsondes

05 p0879 A70-17101

Acoustic piezoceramic anemometer for steady state measurements of wind turbulence on meteorological tower

07 p1285 A70-19835

Soviet collection of papers on apparatus for meteorological measurements covering error analysis, reliability engineering, use of computers, etc.

08 p1494 A70-20771

Vacuum tube signal frequency converters for meteorological telemetry measurements including blocking oscillators, multivibrator and fantastron

09 p1718 A70-23332

Atmospheric modulation transfer function measuring instrument based on Lindberg principle, discussing optical and mechanical design features and applications

09 p1688 A70-23769

Atmospheric particles photographed in situ by cameras using microsecond flash lamps, discussing required mechanical motion compensation at aircraft speed

10 p1886 A70-23930

METEOROLOGICAL PARAMETERS

Hot-film anemometers for measuring storm turbulence in presence of heavy rain

10 p1887 A70-23940

IR sensor for detecting clear air turbulence, discussing design, installation, supporting equipment and inflight test results

12 p2229 A70-26946

Wind distribution by wind frequency counter controlled by electrical direction indicator, discussing design, operation and accuracy

13 p2445 A70-29469

Viking Mars mission meteorological instruments for measurements of water vapor content, wind speed/direction, temperature and pressure

14 p2584 A70-30553

Inter-Range Instrumentation Group/IRIG/ document regarding meteorological data reliability, defining measuring process accuracy and errors

14 p2606 A70-30567

Meteorological parameters measuring instruments optimal design, presenting formalized procedure flow chart and examples

14 p2607 A70-30568

Mesoscale stratospheric turbulence recording using even activated memory recorder

14 p2573 A70-30578

Wind velocity fluctuation randomization signal probability density measurement, using statistical sampler

18 p3238 A70-36067

Lunar surface radiative balance and thermal environment measurement by portable meteorological station, considering lunar environment peculiarities for instruments design

19 p3514 A70-37631

Acoustic piezoceramic anemometer for steady state measurements of wind turbulence on meteorological tower

20 p3634 A70-40342

Meteorological TV imaging systems development in last decade, including low and synchronous altitude camera, sensors, orthicons, etc.

23 p4193 A70-43963

Aerosol impact traps for ground and airborne water vapor condensation studies

23 p4195 A70-44272

Meteorological NEXAIR/Next Generation Upper Air System/ for atmospheric data from balloon-borne instrument packages

24 p4372 A70-46049

METEOROLOGICAL PARAMETERS

Hydrothermodynamic equations used in forecasting meteorological components solved by assuming equations of motion quasi-linear and reducing to ordinary differential equations

05 p0878 A70-16195

Meteorological parameters influence on diurnal variations of radionuclide activity and resulting global air pollution

05 p0903 A70-16662

Meteorological conditions effects on SST aircraft flight safety and economics, emphasizing stratospheric information for forecasting

06 p1095 A70-17193

Meteorological data from radiosonde and radar wind observations during Indian Ocean expedition of research vessel Meteor

07 p1329 A70-19350

Soviet book on meteorological conditions analysis and prediction for aviation covering fog, storms, showers, stratospheric turbulence studies, etc.

08 p1535 A70-20772

Spectra of meteorological variables - Conference, Stockholm, June 1969

09 p1713 A70-22351

Atmospheric variables/velocity, temperature, energy, etc/ spectra in lowest few hundred meters

09 p1714 A70-22352

Tropospheric refractive index homogeneity from beam-swinging experiments, noting relationship to meteorological parameters and height

09 p1715 A70-22363

Polydisperse dielectric system distribution parameters determined from hard monochromatic polarized radiation scatter by artificial aerosols

10 p1916 A70-24500

Book on statistical processing of geophysical and meteorological data covering independent and autocorrelated data, random processes, check tests, stochastic functions, filtering, etc.

11 p2046 A70-26425

Spatial-temporal distribution of meteorological elements allowing for effects of underlying surface

12 p2263 A70-27511

CAT parameters sensitivity to horizontal wind and temperature distribution

13 p2444 A70-28587

Atmospheric turbulence and irregularities, examining classical exchange coefficient and statistical theories

13 p2445 A70-28788

Shape and location error separation in deterministic predictions of meteorological scalar fields, considering air pressure system forecasting

13 p2445 A70-28995

Weather forecasting for SST operations, discussing wind, temperature, turbulence, clouds, etc
13 p2445 A70-29494

Diurnal and seasonal variations of parameter s of meteor showers on celestial sphere, using radio echo amplitude distribution from radar observations
14 p2635 A70-30307

UHF propagation measurement over sea for varying surface refractivity and meteorological conditions, noting diurnal variations
14 p2549 A70-30513

Meteorological problems associated with accurate weather prediction affecting launch, trajectory and recovery of ballooning systems
14 p2606 A70-30555

Atmospheric elements and properties pertinent to design and operations of Space Shuttle
14 p2606 A70-30556

Inter-Range Instrumentation Group (IRIG) document regarding meteorological data reliability, defining measuring process accuracy and errors
14 p2606 A70-30567

Statistical mesosphere temperature, density and wind profiles models based on rocket soundings
14 p2608 A70-30593

CAT and small scale atmospheric motions in relation to supersonic transport and space shuttle design and operation
14 p2609 A70-30602

Meteorological effects on air and noise pollution at U.S. airports
14 p2530 A70-30610

Meteorological problems associated with proposed tests for aircraft noise certification, discussing airport near-surface environments
14 p2610 A70-30612

Toxic fuel test site selection, evaluating meteorological factors in Gypsum Canyon, California
14 p2563 A70-30613

Solar eclipse of March 1970 observation by sounding rockets, discussing ionospheric and meteorological measurements
14 p2586 A70-30800

Auroral orientation curves evaluation, testing parameters by numerical integration and revised geomagnetic coordinate system
14 p2576 A70-30918

Passive optical crossed beam detection systems monitoring meteorological parameters in rocket or aircraft environments, noting real time display
15 p2736 A70-32032

Soviet book on statistical analysis of meteorological elements based on expanding natural orthogonal functions covering horizontal, vertical and time distributions including applications
15 p2772 A70-32842

Sonic boom variation with aircraft geometry, volume, weight, weather and environment conditions, noting effects on structures and people
16 p2840 A70-32947

Annual variations of monthly mean meridional circulation, discussing observations, zonal asymmetries, accuracy and transports of angular momentum and energy
16 p2945 A70-33249

Lidar technique for remote detection and mapping of atmosphere based on weather radar and optical scattering concepts
20 p3660 A70-39079

Surface haze and vertical aerosol attenuation for various meteorological ranges within 1.2-15 km, tabulating for UV, visible and IR wavelengths
20 p3661 A70-39082

Radar angels activity seasonal variation and height distribution statistical relationship to meteorological parameters
20 p3661 A70-39169

Forecasting air temperature over North Atlantic, analyzing atmospheric parameters informativeness
20 p3663 A70-39274

Global meteorological parameters measurement by satellites, discussing IR instruments
20 p3664 A70-39711

Millimeter wave propagation measurements by ATS-5 satellite, observing attenuation dependence on meteorological parameters for communication data link performance prediction
20 p3589 A70-40311

Clear lower atmosphere meteorological parameters remote sensing for weather forecasting, comparing optical, radio and acoustic radar techniques
21 p3785 A70-40802

Optimal flight route selection with respect to meteorological prediction errors, using decision under risk and Monte Carlo method
22 p4067 A70-42656

Thunderstorm frequencies related to lunar phase and declination for ground stations in eastern and central U.S.
22 p4018 A70-42909

METEOROLOGICAL PROBES

U SONDES

METEOROLOGICAL RADAR

Lidar technique using pulsed lasers as energy sources for operational type meteorological data col-

lection including cloud height, visibility, thermal stratification, etc
01 p0042 A70-10081

Forward sounding sensors /weather radar/ development for aiding human eye in detecting flight hazards /storms and CAT/
02 p0297 A70-11989

Wind field-Doppler velocity field generalized correlation, describing horizontal velocity component measurement by single pulse Doppler radar technique
02 p0326 A70-12287

Lidar technique capabilities and limitations in meteorological applications, emphasizing data storage and display instrumentation
03 p0450 A70-13673

Airborne and ground based radar data on thunderstorm echoes compared within framework of storm reflectivity model and radar theory
06 p1010 A70-18246

Ground based radar surveillance for SST to avoid convective clouds and thunderstorm activity during transonic acceleration phase ensuring minimum demands on maneuverability
09 p1610 A70-22242

Atmospheric small scale turbulence observation by Doppler radar, noting role of tracers radial velocity spectrum
09 p1716 A70-22364

Lidar techniques for meteorology, discussing atmospheric density measurement, cloud structure and screening effect, pollutant tracking, etc
09 p1635 A70-23066

Pulsed Doppler radar technique for monitoring and diagnosing severe storms, obtaining wind velocity and direction within cloud
10 p1844 A70-25242

Meteorological radar station reception equipment for increased radio telemetry channel reliability in complex radio sounding of atmosphere
11 p2075 A70-25920

Radar signature analysis of convective precipitation, hailstorms, tornadoes, lightning, hurricanes and clear air echoes
11 p2076 A70-26039

Lidar ground-based sensing of atmospheric density, temperature, moisture content, discussing scattering theory and technique
12 p2183 A70-26945

Radar meteorology, discussing convection in lower atmosphere and clear air turbulence observations
13 p2443 A70-28475

Civil aircraft weather radar for ground collision hazard warning
13 p2447 A70-28548

Heavy squalls observations by satellite TV and radar, considering wave disturbances at cold front
13 p2444 A70-28585

Weather radar signal processing and data recording at National Severe Storms Laboratory (NSSL), providing reduction in echo variations due to relative motion of precipitation elements
13 p2363 A70-28774

Radar meteorology in electromagnetic communications to provide storm systems data, noting clear air radar echoes
13 p2445 A70-28791

Antenna design for single engine light general aviation aircraft weather radar, reviewing attenuation and terrain return problems
16 p2864 A70-33471

Meteorological laser radar, discussing basis and techniques determining atmospheric radiation attenuation constant
17 p3045 A70-35106

Soviet collection of papers on radar meteorology
18 p3287 A70-36998

Lidar technique for remote detection and mapping of atmosphere based on weather radar and optical scattering concepts
20 p3660 A70-39079

Internal gravity wave shape at temperature inversion in lower atmosphere from high resolution vertically pointing FM/CW radar sounding
23 p4162 A70-44038

METEOROLOGICAL ROCKETS

U SOUNDING ROCKETS

METEOROLOGICAL SATELLITES

- NT AEROS SATELLITE
- NT ELEKTRON 2 SATELLITE
- NT ELEKTRON 4 SATELLITE
- NT ESSA SATELLITES
- NT ESSA 9 SATELLITE
- NT EXPLORER 17 SATELLITE
- NT EXPLORER 19 SATELLITE
- NT NIMBUS SATELLITES
- NT NIMBUS 2 SATELLITE
- NT NIMBUS 3 SATELLITE
- NT NIMBUS 4 SATELLITE
- NT SAN MARCO SATELLITE
- NT SAN MARCO 2 SATELLITE
- NT TIROS SATELLITES

Weather satellites performance emphasizing designs for geostationary altitude and hydrological, oceanographic and earth science applications
[ALAA PAPER 69-1082]
01 p0135 A70-10648

Automatic picture transmission (APT) ground station design for reception of weather satellite cloud cover photographs, discussing SNR
01 p0059 A70-11451

Small read-out stations for automatic picture reception from meteorological satellites, detailing design
02 p0382 A70-12648

Meteorological satellite TV cameras development, discussing image sensors and tabulating characteristics
03 p0491 A70-13665

Ground stations and low orbiting satellite system for automatic collection of meteorological data over Italy
03 p0581 A70-13832

IR equipment on Tiros and Nimbus 1 and 2 satellites, describing vertical atmospheric sounding
03 p0492 A70-13833

Earth climatic control by reflecting satellites producing artificial solar irradiation
03 p0581 A70-13835

Atmospheric circulation in tropics using weather satellite data
06 p1095 A70-17220

Earth resources and meteorological data collection from in situ sensors via satellite, discussing system considerations
06 p1006 A70-17343

Satellite observed characteristics of severe local storms in central and eastern U.S., noting potential use for storm forecasting
06 p1102 A70-18584

Incipient tropical storm location and synoptic weather pattern analysis from environmental satellite system data utilization
07 p1329 A70-19196

Meteorological satellites motion parameters long term prediction, using final analytic relationships with allowance for zonal harmonics of gravitational field
07 p1329 A70-19650

Manned and unmanned earth observation satellite programs technology gains, discussing atmospheric temperature, pressure, winds, clouds and moisture
10 p1876 A70-24637

Numerical weather forecasting for several weeks based on global meteorological satellite network observation
10 p1913 A70-25241

Meteorological research potential of manned orbiting spacecraft, discussing electromagnetic sensing instrumentation development, specialized observing programs, etc
12 p2225 A70-27744

Meteorological satellites role in weather forecasting, discussing cloud photography and solar radiation and earth albedo measurements
12 p2265 A70-28269

Low altitude operational meteorological and navigation spacecraft, discussing need for orbit adjustment by dynamic control
13 p2500 A70-28404

Meteorological data acquisition by navigational aids, satellites and surface based indirect sensors for computer forecasting
13 p2405 A70-28773

Satellite based random Doppler environmental measurement technique for Global Atmospheric Research Program (GARP), receiving signals from balloons, buoys and land stations
13 p2407 A70-29176

Meteorological satellites TV pictures processing for hydrological information, emphasizing snow photographs interpretation
14 p2601 A70-30138

Algorithm for Fredholm integral equation in inverse problems of satellite meteorology
14 p2603 A70-30405

Soviet book on legal aspects of artificial satellites for meteorology and radio communication purposes
14 p2668 A70-30632

TIROS weather satellite TV system providing observations to ground stations via ESSA satellites
14 p2654 A70-31148

French EOLE tracking satellite-balloon network for global atmospheric data, describing satellite and electronic instrument package
14 p2611 A70-31154

Lidar for cloud height measurements from ground and meteorological satellites
14 p2611 A70-31155

Temperature profiles and wind velocities during convective cloud banks formation from meteorological satellite data
15 p2770 A70-32065

Tiros satellites window radiation applied to day and night surface temperature measurements on land and sea
17 p3081 A70-35932

Application satellites, discussing uses in communications, meteorology, earth survey and navigation
18 p3333 A70-36348

Soviet papers on atmospheric radiation processes and satellite meteorology
18 p3285 A70-36962

Meteorological satellites, discussing observation continuity, orbital characteristics onboard memory capacity and sensing methods

Weather occultation satellite orbit determination by radio wave measurements between master and slave satellites, formulating mathematical model [AIAA PAPER 70-1067]

Visible and IR imagery by meteorological satellites measuring surface temperature, atmospheric circulation and state parameters, storm development and tracking, cloud motions, etc

Atmospheric global observation for long term weather forecasts, obtaining cloud photographs and radiation data from satellites

Aeolus A satellite for position fixing and automatic meteorological signal transmission in link with balloons for tropospheric observation

Global thunderstorm activity location found by measuring differences between time of arrival of electromagnetic energy at three satellites

Large scale axisymmetric atmospheric vortex wind velocity determination, using statistical cloud data from meteorological satellites

European space applications program, discussing communication and meteorological satellites

ITOS-1 second generation meteorological satellite launched with Delta N booster, providing direct APT global readout and AVCS TV data recording for playback

Space technology applications to earth survey, discussing use of automatic satellites and manned space laboratories for meteorological, geophysical and related purposes

METEOROLOGICAL SERVICES

Lidar technique using pulsed lasers as energy sources for operational type meteorological data collection including cloud height, visibility, thermal stratification, etc

Global meteorological sounding network requirements, restraints and sensors, considering gun launched meteorological probe role

Reflected solar energy measurements by ATS satellites applied to meteorological research, emphasizing high areal resolution and dynamic range of cameras

Meteorological data provision for supersonic civil transport operations, considering various flight phases

Meteorological data processing computer center of German Weather Service, discussing equipment, data system, forecasting techniques and prediction control

ESSA system operation, describing applications of satellite meteorological data

Weather data communication, discussing transmission of radar, polar satellite and ATS satellite data to processing center and forecasts dissemination to public media

Electrostatic methods considered for using earth electric field in smog dispersion in polluted areas and for airport fog clearing

Severe storm research importance to aircraft design and operating efficiencies improvement by identifying meteorological alternatives for operations in and near adverse environments

Economic and social benefits from weather forecasting developments, noting expenditures on satellites and high speed computers

TIROS Operation Satellite /TOS/ system for daily observation of meteorological phenomena analyzed for problems of general data gathering satellite system

Tower influence of wind speed and direction measurements, comparing 150 meter meteorological tower and scale wind tunnel model

Airborne pyrotechnic cloud seeding system development, testing and application, comparing rainfall from test and control clouds

Nonlinear utility functions effects on assessor probability forecasts, discussing psychological factors

Flight test programs site selection method using computer program analysis of magnetic tape weather records

Combined statistical synoptic methods for mesometeorological forecasts

Automated Weather Network and Environmental Survey Satellite /ESSA 9/ global weather sensing systems

Digital river and rainfall data automatic transmission from remote hydrologic platforms via ATS-1, studying system economic and technological feasibility

Meteorological satellites role in weather forecasting, discussing cloud photography and solar radiation and earth albedo measurements

Apollo 9 scientific multispectral photography mission, discussing meteorological support aspect of real time planning

International cooperation in global meteorological network, outlining World Weather Watch

TIROS weather satellite TV system providing observations to ground stations via ESSA satellites

TIROS Operation Satellite /TOS/ system for daily observation of meteorological phenomena, analyzing problems of general data gathering satellite system

METEOROLOGICAL STATIONS

U WEATHER STATIONS

METEOROLOGY

NT AEROLOGY

NT HYDROMETEOROLOGY

NT LONG RANGE WEATHER FORECASTING

NT MICROMETEOROLOGY

NT NUCLEAR METEOROLOGY

NT NUMERICAL WEATHER FORECASTING

NT POLAR METEOROLOGY

NT RADIO METEOROLOGY

NT STATISTICAL WEATHER FORECASTING

NT SYNOPTIC METEOROLOGY

NT TROPICAL METEOROLOGY

NT WEATHER FORECASTING

Incomplete historical data to infer state of atmosphere based on global circulation model, noting tradeoff of temperature for wind and time for space

Atmospheric effects on passive microwave sensing in EHF region under all-weather conditions on global scale using satellites

Thermometric convection coefficients used in automatic meteorological data correction program

Thunderstorms and thunderstorm phenomena - ASM Conference, Chicago, April 1969

Barometric and atmospheric temperature corrections of cosmic ray neutron component intensity fluctuations obtained statistically from monitor recording

Nonlinear computational stability of partial difference approximations to meteorological equations

Precondensation visibility dependence on aerosol particle swelling due to increasing humidity

Orbiting satellite-borne instruments for scientific observation of earthquakes, volcanic eruptions, atmospheric phenomenon, cyclones, floods and soil erosion

Earth atmosphere circulation mechanisms, discussing zonal and meridional components and eddy motions

Atmospheric stability sensing by millimeter wave radiometry, discussing thermal radiation emitted and absorbed by oxygen molecules

Meteorological situations and fields quantitative classification and regional grouping by statistical main components application

Solar radiation absorption by atmospheric ozone observations by ground stations for meteorological data

Automatic search for data in hydrology and meteorology, describing information search language development

Atmospheric optical thickness in visual spectrum region relationship to meteorological characteristics, plotting vertical profiles of humidity and aerosol attenuation coefficient

Aerospace meteorology - AMS-AIAA Conference, Las Vegas, May 1970

Vertical mesoscale contribution to vertical wind shear profiles, using radar/Jimsphere measurements

Combined statistical synoptic methods for mesometeorological forecasts

Automated Weather Network and Environmental Survey Satellite /ESSA 9/ global weather sensing systems

Digital river and rainfall data automatic transmission from remote hydrologic platforms via ATS-1, studying system economic and technological feasibility

Meteorological satellites role in weather forecasting, discussing cloud photography and solar radiation and earth albedo measurements

Apollo 9 scientific multispectral photography mission, discussing meteorological support aspect of real time planning

International cooperation in global meteorological network, outlining World Weather Watch

Soviet collection of articles on satellite meteorology covering atmospheric cellular convection, cloud cover, wind field analysis, etc

Cloud distribution and optimal satellite picture foreshortening for global meteorological analysis of atmosphere, using Zond 7 photograph

Meteorological problems associated with space shuttle design and operations, permitting tradeoff analysis on environment effects

German monograph on atmospheric turbulence by Rn 220 as tracer, relating concentration to various meteorological parameters

Ionospheric E region winds correlations to lower atmosphere meteorological phenomena

Barometric and atmospheric temperature corrections of cosmic ray neutron component intensity fluctuations obtained statistically from monitor recording

Passive microwave sensors based on brightness temperature vs frequency model for various atmospheric conditions, presenting vegetation pictures

Atmospheric effects on passive microwave sensing in EHF region under all-weather conditions on global scale using satellites

Statistical-dynamical atmosphere model for global circulation simulation, taking into account meteorological variables of velocity, temperature, pressure and eddy statistics

Weather regimes in statistical meteorology constructed in stochastic models representing randomly transformed Markov chain

METEORS

U METEOROIDS

METERS

U MEASURING INSTRUMENTS

METHACRYLATE RESINS

U ACRYLIC RESINS

METHANE

Electric field effects on flame structure and propagation rate in methane-air mixture

Pressure and line width estimate from high resolution image tube spectra of Jupiter at 11,000 A

Rotational temperatures and methane abundances in Jovian atmosphere calculated for various Lorentz half widths

Methane photochemistry in Jupiter atmosphere, investigating acetylene, ethylene and ethane photolysis

Chemiluminescence in alkali metals and halogenated methanes diffusion flames, studying diatomic Cs spectral bands

Premixed methane-oxygen-nitrogen combustion in conical reactor fed by choked sonic flow jet, analyzing reaction products chromatographically

Chlorine dioxide-methane mixture flame stabilized in low pressure burner, determining emission spectra, burning velocity, activation energy, etc

Premixed perchloric acid-methane two flame structure, measuring burning velocities, spectra, temperatures and burned gas compositions

Ammonia/chlorine dioxide and ammonia/chlorine dioxide/methane flames burner stabilization and burst velocities

Liquefied natural gas or liquefied methane as burning propulsion system for SST, examining storage volume, fuel-tank insulation and implosion danger

He-Ne multimode laser radiation peak as function of pressure in methane-containing absorption cell installed in resonator

Burning velocity of methane-air flames inhibited by methyl bromide, using schlieren cone-nozzle burner method involving unburnt gas velocity measurement

Mass flow rate calculation of methane and natural gas mixtures through critical flow nozzles

Methane fuel systems for high Mach number supersonic transport aircraft on basis of minimum weight

Methane abundance in Jovian atmosphere deduced from line equivalent widths, obtaining line intensity for J manifolds

Combined statistical synoptic methods for mesometeorological forecasts

Automated Weather Network and Environmental Survey Satellite /ESSA 9/ global weather sensing systems

Digital river and rainfall data automatic transmission from remote hydrologic platforms via ATS-1, studying system economic and technological feasibility

Meteorological satellites role in weather forecasting, discussing cloud photography and solar radiation and earth albedo measurements

Apollo 9 scientific multispectral photography mission, discussing meteorological support aspect of real time planning

International cooperation in global meteorological network, outlining World Weather Watch

TIROS weather satellite TV system providing observations to ground stations via ESSA satellites

TIROS Operation Satellite /TOS/ system for daily observation of meteorological phenomena, analyzing problems of general data gathering satellite system

METEOROLOGICAL STATIONS

- Viscosity, thermal conductivity, specific heat and Prandtl number of hydrogen, methane and hydrogen-methane mixtures calculated for variation with temperature neglecting dissociation effects
06 p1177 A70-17700
- Fire extinguisher compounds/bromochloromethane and bromotrifluoromethane/pyrolysis products inhalation toxicities for rats
07 p1219 A70-19223
- Effective pressure and rotation line intensity in Uranus upper atmosphere obtained from methane band spectrograms, calculating maximum temperature at subsolar point
07 p1385 A70-19423
- Premixed flames of methane with chlorine dioxide and perchloric acid, comparing properties with methane-oxygen flames, suggesting unified reaction mechanism
07 p1425 A70-20007
- Absorption strengths of j-manifolds in R branch of Jupiter atmosphere methane band, discussing fine structure blending
10 p1919 A70-24473
- Gas mixture composition effect on bacteria growth oxidizing methane and propane, establishing proportional biomass concentration to hydrogen and oxygen in mixture
11 p1991 A70-25938
- Al and B particles combustion in methane-oxygen system, considering reaction zone models, energy release rate, particle kinetics, instabilities, etc
11 p2149 A70-26284
- Balloon-borne device for analyzing atmospheric carbon dioxide, moisture and methane, using cyclic analysis by gas chromatography
11 p2052 A70-26371
- Methane oxidation behind reflected shock waves between 1350-1900 K, measuring pressure, chemiluminescence and 3067 Å absorption of OH radical
11 p2150 A70-26380
- Methanol proton transfer reaction rate energy dependence
12 p2180 A70-26863
- Methane and ethane released from Apollo 11 lunar samples by crushing or acid treatment, suggesting carbides hydrolysis as main source
12 p2304 A70-27719
- Methane and ethane hydrate number measurement, alleviating liquid water occlusion and evaluating pressure effect
13 p2362 A70-29212
- Transport cross sections for isotopic methane and mixtures, considering inelastic and thermal diffusion effects
14 p2665 A70-30652
- Methane and propane flames in rotating air flow fields generated by cylindrical rotating wire mesh screen, discussing flame lengths and blowoff velocities
14 p2666 A70-31090
- Methane-air inverted flames blowoff at thin stabilization plates of twin slit inverted flame burner, determining critical values of Karlovitz flame stretch factor
14 p2666 A70-31092
- Burning velocities for methane-air mixtures with water cooled porous metal flat flame burner, discussing surrounding ambient atmospheres effects
14 p2666 A70-31093
- Hydrogen abundance in Jupiter atmosphere quadrupole line used in comparing jupiter and solar atmosphere C/H ratios
14 p2650 A70-31221
- Thermodynamic stability of methane clathrate hydrate, building up ice grains halo within comets inner coma
14 p2650 A70-31243
- Molecular hydrogen, methane, water vapor and tritium concentrations near stratosphere from air samples collected on Aerobee flight with liquid hydrogen cooled cryocondenser
15 p2728 A70-31995
- FLOX methane propellant rocket engines, describing operating conditions, injectors, thrust chambers fabrication and cooling, engine cycles, turbomachinery, etc
[AIAA PAPER 70-718] 16 p2965 A70-33540
- Photoreaction produced N-cyclohexyldiphenylketenimine from cyclohexyl isocyanide and diphenyldiazomethane
17 p3042 A70-34820
- Spectrophotometry of methane and ammonia absorption bands indicating decrease toward Jupiter disk edge
18 p3323 A70-37140
- Photoelectron spectra of methane, silane, germane, methyl fluoride, difluoromethane and trifluoromethane, describing electron spectrometer with double focusing electrostatic plates
19 p3374 A70-38269
- Environmental control-life support systems /ECLSS/ waste methane gas utilization in low thrust resistojet for manned space applications
[AIAA PAPER 70-1131] 20 p3568 A70-40214
- Methane IR filter for monochromatizing He-Ne laser
21 p3823 A70-40823
- Methane and hydrogen consumption rates during slow reactions in mixtures of molecular hydrogen, oxygen and nitrogen
21 p3772 A70-40879
- Hypersonic sound speeds measured in methane at moderate pressures by spontaneous Brillouin light scattering experiments
21 p3830 A70-41938
- Dichlorodifluoromethane ionization and attachment coefficients for wide pressure range
22 p4076 A70-42373
- METHIONINE**
Chlorella seaweed hybrid strains containing larger amounts of amino acids than original parent species
04 p0630 A70-14573
- L-dihydroxyphenylalanine intraperitoneal injection effect on S-adenosylmethionine concentration in rat brain
21 p3764 A70-41269
- METHOD OF CHARACTERISTICS**
Characteristic equations developed for two-spatial dimensional elastic wave propagating in linear elastic, isotropic and homogeneous medium
01 p0208 A70-11185
- Method of characteristic calculation of field amplitude of electromagnetic waves propagating in inhomogeneous nonlinear medium applicable for computer
03 p0448 A70-13461
- Annular nozzle shapes established via method of straight line characteristics, noting flow patterns at various regions
03 p0409 A70-13872
- Unsteady problems of gas dynamics solved by method of characteristics, Godunov method, difference methods, etc
04 p0670 A70-14958
- Method of integral relations, finite differences and method of characteristics applied to numerical solution of steady state problems of gas dynamics
04 p0670 A70-14961
- Flow distribution for short isentropic supersonic inlet diffusers, using method of characteristics and Oswatitch and Connors procedures
06 p0963 A70-17234
- Numerical method of characteristics for unsteady radiation gas dynamics, discussing surface pressures and heat transfer rates
07 p1256 A70-19314
- Three dimensional gas flow calculated by direct method of characteristics
08 p1431 A70-20860
- Survey of papers on computer calculation of two and three dimensional gas flows, emphasizing method of characteristics and finite difference techniques
09 p1603 A70-22265
- Riemann invariants, discussing method of characteristics in physical and hodograph space applications and multidimensional hyperbolic systems
10 p1865 A70-24103
- Three dimensional supersonic gas flow solution by numerical method of characteristics, discussing direct and inverse tetrahedral and semicharacteristic schemes
10 p1798 A70-24117
- Three dimensional hypersonic steady flow around blunt and pointed cones at nonzero angles of attack calculated by method of characteristics
[AIAA PAPER 69-187] 11 p1975 A70-25969
- Annealed stainless steel low cycle fatigue data analysis leading to method of characteristic slopes approach for correlating plastic strain range to fracture time
12 p2255 A70-27604
- Monge equation in small perturbation method of characteristics applied to propagation phenomena in three dimensional supersonic gas flow
13 p2386 A70-28490
- Numerical method of characteristics for three dimensional supersonic nozzle flow field calculations
13 p2338 A70-28512
- Second order hyperbolic partial differential equations solution by characteristic grid and continuous characteristic methods
15 p2768 A70-32818
- Second order hyperbolic partial differential equations analog solution based on method of characteristics, showing advantage over digital computer solution
15 p2768 A70-32819
- Parameter identification in distributed systems by method of characteristics, discussing noisy measurements and limited available transducers
16 p2942 A70-33338
- Elastic wave with discontinuities propagation, calculating decay velocities and stresses at leading wave front by theory of characteristics
17 p3189 A70-35436
- Method of characteristics for nonequilibrium flow fields analysis, reviewing theory, numerical methods and examples
17 p3071 A70-35470
- Method of characteristics for two dimensional steady supersonic gas flows with foreign particles in plane and axisymmetric nozzles
18 p3210 A70-37228
- Perfect and dissociating gas nonstationary supersonic flow around sharp profile of finite thickness analyzed by linearization and method of characteristics
19 p3351 A70-37242
- Laminar boundary layer multidimensional universal equations solution for incompressible liquid using method of characteristics
20 p3611 A70-39804
- METHODOLOGY**
Methodologies inadequacies for studying information processing rate in visual perception
07 p1203 A70-18943
- Prolonged hypodynamia effect on human organism, describing organizational and methodological principles for conducting investigations
10 p1813 A70-24667
- Rumanian book on methods, equipment and facilities for aeromechanical measurements covering fluid flow, wind and shock tunnels, flow measurements, etc
23 p4199 A70-45000
- METHODS**
U METHODOLOGY
U PROCEDURES
METHYL ALCOHOLS
Flame structure of liquid methanol burning spheres, discussing temperature and composition profiles
03 p0544 A70-13924
- Photoelimination of N from fused-ring triazoles in methanol
05 p0810 A70-16046
- Ti-6Al-4V dissolution in HCl-methanol, investigating corrosion rate
13 p2433 A70-28779
- METHYL CHLORIDE**
Modulation of carbon dioxide laser with Stark cell internal to cavity, using methyl chloride electrooptical gas
18 p3270 A70-36748
- METHYL COMPOUNDS**
Carbon dioxide lasers passive Q switching by gaseous methyl fluoride and phosphorus pentafluoride, presenting absorption coefficients
01 p0110 A70-10561
- Crossed molecular beam study of reactive asymmetry of oriented methyl iodide molecules reacting with Rb, accounting for observations with hard sphere model
07 p1225 A70-20051
- Corrosion shapes from iodine action on metals in methylic medium, discussing morphology dependence on purity, surface state and reaction products diffusion velocity
08 p1518 A70-21241
- Lil thermodynamic properties in dimethyl sulfoxide determined by emf method, discussing ionic solution energies
10 p1831 A70-25041
- Methyl fluoride calculated for ion-molecule reaction rate constants from ion cyclotron resonance spectra
12 p2180 A70-26862
- Methyl methacrylate and other vinyl monomers polymerization activation by low sulfur dioxide concentrations, noting inert solvents effect
14 p2544 A70-30246
- Methyl-nitroazobenzene-sulphenyl cyanide unit cell dimensions and space group by single crystal oscillation, rotation and Weissenberg X ray diffraction photographs
14 p2581 A70-31300
- 3-O-methyl-mannose neutral sugar identification as constituent of fungal polysaccharide
20 p3572 A70-39625
- Simultaneous mass spectrometric differential thermal analysis of low pressure decompositions of nitrate salts of monomethylhydrazine and methylamine
20 p3688 A70-40475
- Combustion products of 280-400 °C oxidation of ethyl acetate, methyl propionate and i-propyl acetate
21 p3864 A70-40882
- METHYLATION**
Methylating agents and nitrosoguanidine actions on polynucleotides, including ribonucleic acid
03 p0440 A70-13550
- METHYLENE**
Ketene and diazomethane flash photolytic measurement of reaction rates of singlet-triplet methylene deactivation
15 p2694 A70-31729
- METHYLHYDRAZINE**
Nomograms for correlation of dose to methemoglobinemia or plasma monomethylhydrazine /MMH/ concentration observed on dogs, considering human skin contact evaluation
06 p0992 A70-17298
- Behavioral changes due to repeated low doses of rocket fuel monomethylhydrazine
21 p3771 A70-41485
- Monomethylhydrazine /MMH/ missile propellant toxicity, describing symptoms and effects on blood and intellectual capacity
24 p4306 A70-45125

METRIC SPACE

- Hypothesis concerning initial spectrum of metric perturbations in Friedman model, discussing long wavelength gravitational waves energy
 - 07 p1383 A70-19406
- Vacuum metrics with null geodesic expanding shear-free congruences using holomorphic solution
 - 07 p1334 A70-19600
- Gravitational forces accompanying radiation bursts of metric outside collapsing supernova core
 - 12 p2300 A70-27393
- Four dimensional Einstein space metric of signature 2 with N type Weyl tensor and nonintegrable rays
 - 13 p2453 A70-29636
- Gravitational force and potential within static metric spaces
 - 17 p3136 A70-35597
- Stress energy tensor equal time commutation, observing metric dependence inability to satisfy relations for linearized gravitational fields
 - 19 p3536 A70-37550

METROLOGY

- Laser methods for industrial length measurements
 - 11 p2061 A70-25355
- Bonded resistance strain gages technical characteristics noting need for uniform standards
 - 11 p2053 A70-26427
- Resistance strain gages/tensometers/ for force and moment measurement in aerodynamic research, giving design and structural recommendations
 - 11 p2054 A70-26431
- Unbalanced Wheatstone bridge network operation for resistance strain gage measurements, determining dynamic transients variable extremes
 - 11 p2054 A70-26434
- Brush current collectors for strain measurements in rotating machine parts, discussing acceptance testing
 - 11 p1983 A70-26438
- Stability requirements for precision magnetic field measurements on ground and in space, discussing magnetic balances and fluxgate magnetometers for geomagnetic variations and spacecraft attitude
 - 13 p2415 A70-30050
- Nonisothermal measurement in semiconductors in presence of thermoelectric, thermomagnetic and galvanomagnetic effects
 - 16 p2960 A70-32920
- Measurement methods for forces, pressure and heat flow in hotshot hypersonic wind tunnels
 - 17 p3057 A70-34773
- He-Ne laser emission wavelength long and short term stability for metrological applications
 - 17 p3104 A70-35087
- Canadian laser stabilization program involving metrology and absolute standard replacing international meter
 - 17 p3105 A70-35089
- Measurement transducers transforming measured quantity into forms suitable for comparison with standards in metrological sciences
 - 17 p3090 A70-35432
- Piezoelectric sensors for multicomponent force and moment measurement
 - 20 p3635 A70-40533
- Rumanian book on methods, equipment and facilities for aeromechanical measurements covering fluid flow, wind and shock tunnels, flow measurements, etc
 - 23 p4199 A70-45000

MEXICO

- Geographically smoothed geomagnetic cut-offs for eliminating discontinuity in neutron monitor latitude variation in Mexico City vicinity
 - 01 p0167 A70-10229
- Solar eclipse of 7 March 1970 in Mexico, discussing characteristics, research program, equipment and photographs
 - 18 p3318 A70-37046

MICA

- NT BIOTITE
- NT MUSCOVITE
 - Thermal stability of turbine sealant mica-ceramic materials containing boron nitride
 - 04 p0712 A70-14467
 - Annealed compressed ground synthetic mica and silver dust composite materials, analyzing physicochemical properties
 - 12 p2260 A70-28319

MICE

- Lung lipid embolization effect in decompression sickness on obese mice, showing no relationship to dysbaric syndrome
 - 01 p0015 A70-10361
- Postnatal increase of immunologic competence to sheep RBC antigen in germ free and conventionally reared mice
 - 01 p0000 A70-11310
- Gnotobiotic mice with orally inoculated microorganisms observed for quantitation and fate of bacteria in intestinal tract
 - 01 p0027 A70-11312
- Protein metabolism of mice exposed to compression of air-oxygen mixture containing 27 percent oxygen, showing relationship to food intake
 - 01 p0028 A70-11363

- Altitude changes effect on brown fat content and metabolism in deer mice, noting oxygen consumption and heat production limitation by hypoxia
 - 02 p0242 A70-12865
- Radiation protective action of aminoalkylthiols, aminoalkyl disulfides, isothiuron, thiazolidine, etc, in mouse tissues, erythrocytes and yeast cells exposed to X ray doses
 - 03 p0419 A70-13307
- Radiation protective action of cystamin, cysteamine and aminoethyl in mice, noting equal decreases in redox potential
 - 03 p0419 A70-13310
- Temporary mitotic activity depression with decrease in aberrant mitoses observed in mice intestinal epithelium cells after exposure to 50 Mev proton doses
 - 03 p0423 A70-13708
- White mice hypoxia tolerance enhancement after intraabdominal administration of dilute hydrochloric and lactic acids
 - 03 p0424 A70-13718
- Antihypoxic preparations protective effect on white mice and rats subjected to gravitational accelerations
 - 03 p0425 A70-13890
- Oxygen consumption and rectal temperature in male mice confined in nitrogen and helium diluted hyperoxic atmosphere at specific temperature and humidity ranges
 - 03 p0425 A70-13891
- Corneal epithelium chromosome rearrangements in gamma irradiated white adult mice, noting radiation dosage and duration
 - 03 p0426 A70-13903
- Space cabin atmosphere effects on primary and secondary immunological responses in mice relative to spleen weight and antibody titers following antigenic stimulation
 - 03 p0437 A70-14062
- Spacecraft cabin atmosphere effects on mice primary and secondary immunological responses relative to spleen histochemical and biochemical changes in enzyme activity
 - 03 p0437 A70-14063
- Mice and hamster infection resistance following short term acceleration stress, eliminating low hydrocortisone level as protective agent
 - 03 p0428 A70-14067
- Hypokinesia effects on transversostriated muscle fibers of mice, noting changes in myofibrillar apparatus, mitochondria and sarcoplasm
 - 04 p0629 A70-14569
- Vascular resistance and constriction and muscle mass related in pulmonary arteries of mice subjected to alveolar hypoxia
 - 04 p0630 A70-14679
- Mice irradiation reactions determination from various metabolism indices including blood sugar level, leucocytes number, proteolytic processes rates, etc
 - 07 p1198 A70-18714
- Amysyl effects on conditioned passive avoidance reflexes development and reinforcement in white mice under electric shock
 - 07 p1198 A70-18717
- Resistance to decompression sickness increased and mortality rate decreased in mice after adaptation to hypoxia at normal barometric pressure
 - 07 p1206 A70-19469
- Minute volume changes under acoustic excitation of mice for measuring respiratory process without strain on organs
 - 07 p1214 A70-19824
- Atmospheric carbon dioxide and oxygen concentrations effects on white mice low temperature tolerance
 - 09 p1614 A70-22082
- Mild temperature and dehydration effects on toxicity of caffeine and dextroamphetamine in mice
 - 09 p1616 A70-22329
- Laser irradiation effects on mice skin and internal organs, observing inflammatory symptoms, hair follicles destruction and epithelial atrophy
 - 09 p1624 A70-22816
- Temporary mitotic activity depression with decrease in aberrant mitoses in mice intestinal epithelium cells after exposure to 50 Mev proton doses
 - 11 p1985 A70-25508
- White mice hypoxia tolerance enhancement after intraabdominal administration of dilute hydrochloric and lactic acids
 - 11 p1985 A70-25518
- Free radical content changes in mice organs under hyperoxia and hypoxia
 - 11 p1986 A70-25941
- Thermostability and survival rates of white mice in ambient medium with temperature variations
 - 13 p2351 A70-29330
- Compression effects in air-oxygen mixture on male mice, observing no adversity on mortality, growth and nitrogen content
 - 13 p2353 A70-29436
- Atmospheric carbon dioxide and oxygen concentrations effects on white mice low temperature tolerance
 - 15 p2685 A70-32678

- Hematology of sea level and high altitude native Sonoran deer mice, correlating hemoglobin electrophoretic patterns with oxygen affinity
 - 15 p2686 A70-32835
- Tyrosine content and utilization in mouse liver, showing daily rhythm in composite metabolism rate
 - 20 p3568 A70-38976
- Sodium pentobarbital effect on oxygen poisoned mice, observing respiratory depression coupled with lung failure
 - 21 p3764 A70-41480
- Temperature effect on radiation tolerance of mice exposed to low dose rate gamma radiation, noting mortality delay in low temperature environment
 - 23 p4148 A70-44789
- Mice intestinal epithelium, investigating high energy protons irradiation effect on cells
 - 23 p4149 A70-45028

MICHELSON INTERFEROMETERS

- Michelson interferometer with movable mirror using laser beam to measure linear by counting fringes number, discussing design features
 - 01 p0085 A70-10032
- Length measuring systems based on Michelson type interferometers, laser sources, fringe counting electronics, ambient air compensation, fringe-inch conversion and digital display
 - 01 p0108 A70-10418
- Double beam Michelson interferometer for middle IR with moving mirrors operating in constant velocity mode, applying method to atmospheric emission spectra
 - 01 p0091 A70-10909
- Interferential picture visibility in turbulent atmosphere measured at large path differences with Michelson-Twyman-Green interferometer using He-Ne laser radiation source
 - 03 p0498 A70-12869
- Laser interferometer for earth strain study, measuring Michelson arm length changes by counting fringes in interference pattern
 - 05 p0861 A70-16843
- Roof prism reversing-front Michelson interferometer for phase correlation measurements in turbulent atmosphere
 - 09 p1684 A70-23535
- Michelson interferometer usable in space for stellar spectroscopy, noting compactness achieved through mirror area reduction
 - 10 p1887 A70-24032
- Modified laser Michelson interferometer for probing highly transient plasmas occurring behind incident shock waves in shock tubes
 - 11 p2052 A70-26369
- Optical resonator longitudinal modes selection, comparing Michelson interferometer, internal slanted Fabry-Perot interferometer and absorbing film methods
 - 12 p2251 A70-28290
- Convergence corrections for absorption coefficient measurements by far IR Michelson interferometer
 - 14 p2586 A70-30988
- IR Michelson interferometer for Mariner Mars 1971 mission, investigating atmospheric and surface temperatures and atmospheric water vapor content
 - 16 p2978 A70-34029
- Nimbus 3 satellite-borne Michelson interferometer IR spectrometer for spectrum measurement, obtaining temperature, water vapor and ozone vertical distribution
 - 18 p3257 A70-36175
- Michelson IR interferometer spectrometer /IRIS/ design calibration and performance onboard Nimbus 3 satellite, demonstrating data reduction and inflight calibration
 - 20 p3626 A70-39078
- Stellar IR spectra for types A0 to M7, using Mertz type Michelson interferometer as Fourier transform spectrometer
 - 21 p3922 A70-41980
- Venus spectrum from high resolution Michelson interferometers with Fourier transform and digital computation, discussing Venus atmospheric models
 - 22 p4099 A70-42721
- Earth and atmosphere thermal emission spectra via Nimbus 4 Michelson interferometer, obtaining atmospheric temperature, humidity and ozone profiles
 - 23 p4192 A70-44866
- Millimeter wave solar radiation atmospheric absorption examined at sea level with Michelson interferometer
 - 24 p4398 A70-45785
- Thermal emission spectra of earth and atmosphere from IR Michelson interferometer onboard Nimbus 3 satellite
 - 24 p4330 A70-45977

MICROANALYSIS

- Microprobe analyzer for light elements using electronic optics probe, sample visualization devices and equipment for X photon detection and measurement [ONERA-TP-774]
 - 02 p0275 A70-12210
- Gas chromatography and mass spectrometry applied to porphyrin microanalysis, studying
 - 02 p0275 A70-12210

homologous porphyrin series in ancient sediments and oils

02 p0252 A70-12516

Electron microscope-thin film microprobe techniques in biomaterial studies of chemical segregation, species diffusion and small particle analysis

13 p2411 A70-29808

Diffusion layer microprobe analysis during chromaluminization of Inconel turbine blade

14 p2395 A70-30293

Cu-Ni diffusion couples voids and edges effect on concentration gradients measurement by electron probe microanalysis

22 p4054 A70-42740

MICROBALANCES

Uncoated quartz twin crystal microbalance for monitoring water vapor content of respiratory gases

19 p3368 A70-37844

MICROBE

U MICROORGANISMS

MICROBEAMS

Backreflection X ray microbeam camera with arrangement for positioning preselected area to study grain boundary during creep by Laue method

03 p0492 A70-13759

MICROBIOLOGY

NT BACTERIOLOGY

Germ-free biology experimental and clinical aspects - Conference, Buffalo, June 1968

01 p0027 A70-11309

Microbiological evaluation of modified vacuum probe surface sampler for handling and fallout contamination compared with swab-rinse technique

05 p0807 A70-16574

Microbiological corrosion effects on aluminum alloy fatigue properties inducing further microbiological corrosion compared to chemical corrosion effects

07 p1310 A70-19735

Carbon dioxide fixation in hydrogenomonas eutropha determined from titrating liquid culture with carbon dioxide, showing dependence on oxygen content in gas mixture

11 p1991 A70-25940

Field test for microbiological contamination of jet fuel, discussing phosphates detection

18 p3299 A70-36344

Microbial existence limits in hot springs at varying temperature and pH characteristics

22 p3970 A70-42956

Viruses response to environmental exposure emphasizing temperature, humidity, light and extraterrestrial conditions

23 p4146 A70-44398

MICROCALORIMETERS

U CALORIMETERS

MICROCIRCUITS

U MICROELECTRONICS

MICROCLIMATOLOGY

Hypodynamic effects on human external respiratory function and cardiovascular state under various microclimatic conditions

23 p4149 A70-45078

MICROCRACKS

Dimensional analysis for describing steel surface microcracks growth under uniaxial fatigue loading, using stress-intensity factor and crack extension concepts of fracture mechanics [ASME PAPER 69-MET-G]

04 p0770 A70-14879

Microfissuring of Ni base alloy weldments as function of grain size produced by solution treatment

07 p1306 A70-18996

Fracture processes in homogeneous anisotropic fiber composite materials, describing microcrack initiation, growth and unstable propagation at critical stress level

08 p1532 A70-21912

Electrical and photographic methods for measuring microcracking in fiber reinforced plastics

08 p1501 A70-21916

Precipitation hardened nickel-base alloy microcracking during gas tungsten arc and electron beam welding, studying heat affected zone hardness, phases and grain size

10 p1897 A70-25311

Laser output energy decreased by microscopical fractures masking effect in neodymium glass laser rod during monopulse operation

12 p2250 A70-28152

Ceramics microcrack propagation control through small slab with simultaneous microscopic observation of path and force changes, considering grain boundaries effects

15 p2741 A70-32434

Three dimensional stress fracture criterion for initial microcracking derived by generalizing Griffith flaw theory

19 p3540 A70-37955

Polymethyl methacrylate rupture during omnidirectional compression under laser radiation, showing pressure effect on microdefects and cracks

21 p3841 A70-40644

Polymethyl methacrylate glasses microcracks removal by dry friction

21 p3841 A70-40645

MICROELECTRONICS

NT LARGE SCALE INTEGRATION

Flip chip and beam lead methods for microcircuit assembling, discussing heat removal using heat spreader and temperature cycling effects on tensile strength

01 p0050 A70-10330

Microelectronics equipment high density packaging and heat dissipation, discussing full utilization of high speed

02 p0271 A70-12847

Design, performance and manufacturing information on various microcircuit bridges in conjunction with production of squibs, detonators and pressure cartridges

03 p0547 A70-14112

Ionizing radiation response of integrated microcircuits with different circuit functions and manufactured by different methods

04 p0658 A70-14741

Packaging and placement algorithms for modules in automated design of microelectronic equipment

04 p0659 A70-15193

Diode transistor microelectronic logic circuit reliability, efficiency and optimization using digital computer

04 p0659 A70-15210

Digital microcircuits for one kva three phase DC-AC inverter control to generate sinusoidal 400 Hz output using HF bridge chopper techniques

04 p0628 A70-15340

Concorde microelectronic power plant control system, noting overfueling prevention by throttle actuator during startup and speed governor function

05 p0896 A70-16003

Microelectronic L-band phase-lock loop receiver for data transmission between earth stations and satellites

06 p1017 A70-17338

Complex integrated avionics computer system design for navigation, guidance and control of rotary wing aircraft, emphasizing microelectronic modular assembly

06 p1014 A70-17353

Components and microelectronics - Conference, San Francisco, August 1969, Volume 13, Part 5

06 p1018 A70-17355

Large scale integration /LSI/ in electronics, discussing high density microelectronic, memory and logic circuits, fabrication and computer aided design

08 p1468 A70-20468

Microstrip integrated circuit technology in development of microwave components, discussing fabrication, design, performance and applications

08 p1471 A70-20787

Laser systems application to automatic or semiautomatic materials processing in metal working and microelectronics, including hole drilling, silicon wafers scribing, etc

08 p1502 A70-20820

Microstrip oscillator circuit design for operating with high power/efficiency avalanche diodes, describing low pass filter tuning section role

08 p1475 A70-21278

Diagnostic-control tests for automatic homogeneous microelectronic structures, considering element coupling

09 p1643 A70-22142

Integrated circuit film and hybrid technologies in microelectronics, discussing role of monolithic Si arrays

09 p1645 A70-22632

Sectorial and circular strip resonators natural oscillation modes and freely propagating waves of uniformly bent stripline

09 p1651 A70-23644

Coupled microstrip transmission lines characteristics from parameters evaluation, considering various geometries, inductive and coupling coefficients, dielectric constant and impedance

12 p2190 A70-28167

Quasi-TEM analysis justification for limit cases of guided waves on microstrip transmission lines with dielectric constant approaching free space

12 p2190 A70-28168

Resin systems for encapsulation of microelectronic packages, using thermal expansion dilatometer and gravimetric and differential analyses

13 p2439 A70-29258

Microstripline and balanced stripline, discussing parameters affecting maximum attainable Q in microwave integrated circuits

14 p2561 A70-30921

Microstrip circuit design, obtaining dimensions by computer programs incorporating subroutine sets

14 p2561 A70-30922

Airborne equipment microelectronics technology application to interrogators, transponders and UHF/VHF transceivers

14 p2558 A70-31294

Ultrasonic Al wire bonding for microelectronic applications, discussing tensile strength dependence on machine parameters and aging

15 p2747 A70-32647

Thermal design of hybrid microelectronics modules, considering resistance, assembly, joining, encapsulation and final packaging

16 p2879 A70-33957

Manufacturing and technology of hybrid microelectronics packaging in Black Arrow X-3 satellite equipment

16 p2879 A70-33959

Holographic projection for electronic microcircuit manufacture

17 p3088 A70-35028

Microelectronics in space environment, discussing circuit reliability, radiation effects, etc

17 p3053 A70-35269

Transmit only solid state radar module built with microstrip techniques for phased array systems operating at L and S dual bands

17 p3056 A70-35899

Multichip hybrid microcircuits design and construction, emphasizing reliability and cost reduction

18 p3232 A70-36759

Microelectronic systems radiation resistance, examining logic IC gates for reactor neutron irradiation

18 p3233 A70-36783

Electronically modified stroboscope as light source for multiflash photography of transient events, noting mechanical switches elimination

18 p3262 A70-37095

Thin films physics for microelectronic applications

19 p3389 A70-38194

Microjoining in electronics industry, discussing technologies and nondestructive testing

19 p3437 A70-38424

Integrated microcircuits reliability prediction models based on failure mode and mechanism knowledge

19 p3391 A70-38846

Microcircuit packaging /primarily hermetic/ and assembly techniques, considering cost reduction

20 p3597 A70-39443

Microelectronic packages encapsulation by resin systems with emphasis on thermal expansion, discussing effects of curing temperature, reactive diluents, etc

20 p3655 A70-39444

Aerospace microelectronic digital computer design, discussing optimal packaging by use of integrated circuits

21 p3795 A70-41694

High fidelity microelectrode recording of phase zero cardiac transmembrane action potentials, utilizing memory oscilloscope

21 p3772 A70-42163

Microelectronic phase lock microwave receiver packaging, discussing subassemblies interconnection minimization, shielding, RF interference, low loss and testing problems

23 p4164 A70-44536

Cumulative reference list of published books on microelectronics and reliability

24 p4322 A70-46014

High density packaging of micrologic flatpacks using high interconnection method for two-sided use of double-sided card in space flight applications

24 p4320 A70-46248

MICROFIBERS

Internal friction and shear modulus of thin glass fibers of sodium silicate, aluminosodium silicate and nonalkaline aluminoborosilicate

22 p4059 A70-43135

MICROFILMS

Threefold reduction of aerial negatives facilitating microfilming without impairing accuracy and clearness of image details

07 p1278 A70-18692

MICROGRAPHY

U PHOTOMICROGRAPHY

MICROHARDNESS

InAs-GaAs solid solutions microhardness and brittleness, studying chemical composition effects

04 p0730 A70-14464

V and Cr single crystals microhardness anisotropy and causes, noting similarity with W, Nb and silicon ferrite

06 p1088 A70-17613

Microhardness measurements of carbides, borides and nitrides in wide temperature range, considering indentation load selection

06 p1089 A70-17661

Isothermal section determination in Mo-Cr-B at 1000 C using X ray, metallographic analyses and microhardness measurements

06 p1090 A70-17847

Microhardness of transition metals carbides measured after hot compression, suggesting dependence on statistical weight of C atoms with stable sp³ configurations

08 p1516 A70-21116

Microhardness method for property changes in structural materials during sequential cyclic loading, discussing material identification, statistical fatigue theory, fine structure effects, etc

09 p1701 A70-22299

Temperature and hydrogen concentration effect on microhardness of polycrystalline beta-vanadium hydride, obtaining photomicrographs of indentations 10 p1906 A70-25227

Decomposition of supersaturated solid solutions in granulated Al alloys with Mn, Cr, Zr, Ti, V and Mo, studying microhardness and electrical resistivity 12 p2258 A70-28274

Depth measurement of gas-saturated surface layer in Ti alloys, using microhardness method 18 p3277 A70-36472

Silicon-containing pyrocarbon, relating microhardness to microstructure 18 p3279 A70-37220

MICROINDENTATION
U MICROHARDNESS
MICROINSTRUMENTATION
Thermocompensated wire loop microtensensors for machine part stress concentration measurements, including parameter selection nomograms 13 p2409 A70-29519

MICROMANOMETERS
U MANOMETERS
MICROMETEORITES
U MICROMETEORITIDS
MICROMETEORITIDS
NT METEORITID DUST CLOUDS
NT ZODIACAL DUST
Micrometeoroid experiments on OGO 2 and OGO 4 satellites, measuring velocity, masses and particle orbits in earth dust cloud 01 p0086 A70-10444

Optical properties changes of various transmitting materials under simulated micrometeoroid environment, using silicon carbide particles accelerated in shock tube 03 p0523 A70-13027

Correlation between atmospheric meteor entry and gamma and neutron radiation intensity verifying micrometeor antimatter hypothesis 03 p0454 A70-13528

Micrometeorite detection involving impact stress wave monitoring by strain gages embedded in viscoelastic plastic 03 p0487 A70-13573

Piezoelectric sensing diaphragm for detection of micrometeorites in space, noting vibration mode and effect of small beads contact time on calibration errors 04 p0695 A70-15567

Tektite damage caused by micrometeoroid impact, projectile firing at glass spheres and survival time estimation 05 p0916 A70-16834

High velocity microparticle simulation techniques for studying properties, dynamics and origin of micrometeoroids, considering accelerators and impact results [ALAA PAPER 70-30] 06 p1029 A70-18131

Micrometeor flux in near-earth space measured by satellite-borne low noise acoustic detectors 07 p1386 A70-19493

Micrometeorites impact on lunar surface, using optical reflecting and stereoscan electron microscopes to investigate craters on Apollo 11 samples 13 p2485 A70-28474

Vaporization of small meteor particles with identical surface temperature, considering radio communication based on reflection from ionized trails 14 p2636 A70-30323

Micrometeor flux in near-earth space measured by satellite-borne low noise acoustic detectors 15 p2805 A70-32738

Black Arrow X3 spacecraft design and experiments, including silicon cells performance electronic assemblies and micrometeoroid fluxes 17 p3178 A70-35256

British X 3 satellite for investigating thermal control surface finishes stability, ultrathin solar cells, electronic systems reliability and micrometeoroid flux measurement 18 p3333 A70-36511

Meteoritic dust collection in upper atmosphere by sounding rocket, discussing efficiency of sampling configurations for inertial impact 18 p3316 A70-36768

Ionization and loss processes for meteoric elements in lower ionosphere, suggesting hydrates formation role in alkali metal ions depletion 22 p4106 A70-43305

Meteoritic metallic ions above F 2 peak, discussing current density and transport mechanisms 23 p4239 A70-43841

MICROMETEOROLOGY
Periodic cellular convection in troposphere with allowance for anisotropic turbulent mixing, showing cyclone association and intervals 01 p0135 A70-10206

Aerodynamic roughness length estimation and site roughness increase due to micrometeorological equipment 03 p0483 A70-13166

Toxicity and downwind diffusion of Be rocket exhaust product measurements, using ADOBE experi-

ment and AFRPL micromet meteorological data system 14 p2628 A70-30611

MICROMETEORS
U MICROMETEORITIDS
MICROMETERS
Differential screw gauge for determining micrometer screw periodic errors and error components in level triers, using Rydberg method 04 p0693 A70-15488

Photoelectric multislit micrometer for astronomical purposes, presenting stochastic variables mean error difference formula for arbitrary power spectrum 06 p1071 A70-18458

Positional contact micrometer used to eliminate stars apparent oblique motion in astronomical universal instruments 09 p1681 A70-23342

Ring micrometer radius determination and application to right ascension changes in determining positions of comets, planets and planetary moons 11 p2057 A70-26675

Heart dimension measurement by miniature implantable ultrasonic sonomicrometer, describing system design and operation 12 p2174 A70-26897

MICROMINIATURIZATION
NT LARGE SCALE INTEGRATION
Ferrite-type phase shifter production by microstrip technique and integrated microwave system use in Gunn element Doppler radar 01 p0052 A70-11290

Book on thin film transistors microelectronics covering semiconductor physics, fabrication, analysis, applications and comparison with MOS transistors 01 p0052 A70-11329

Electron image projection tube for fabricating integrated circuits of micron size transistors 03 p0458 A70-14027

Guided elastic waves propagation on layered media, considering elastic wave circuitry design for true microminiaturization 06 p1018 A70-17476

Ultraminiature pressure transducers for use in wind tunnel models 17 p3093 A70-35492

Multipurpose microminiature multichannel biomedical telemetry system, discussing design 19 p3368 A70-37856

Epitaxially grown Si contact for area reduction of MOS transistor circuits 20 p3596 A70-39099

Compact low cost Controller/Programmer/ Evaluator for varied automatic tests, using microminiature components 21 p3803 A70-40768

MICROMINIATURIZED ELECTRONIC DEVICES
Miniaturized components in microstrips on low loss dielectric or magnetic substrates, noting suitability for microwave systems integration 01 p0052 A70-11313

Open circuit development in microcircuits metallization and processing to eliminate nonuniformity, voids and microcracks 02 p0316 A70-12056

Nd laser drilling and welding tool for microminiature electronic device fabrication 14 p2594 A70-30639

Ultraminiature piezoelectric semiconductor pressure transducers for wind tunnel models 17 p3093 A70-35491

Microminiature solid state LSI imaging system design, construction and performance characteristics 24 p4320 A70-46216

MICROMOTORS
Micromotor torsion moment-speed characteristic curve obtained by automatic recording apparatus 09 p1672 A70-22026

Optimality criterion selection for asynchronous microelectric motor design by computer 24 p4293 A70-45470

MICROMORGANISMS
NT AEROBES
NT AMOEBAS
NT AZOTOBACTER
NT BACILLUS
NT BACTERIA
NT BACTERIOPHAGES
NT CLOSTRIDIUM BOTULINUM
NT ESCHERICHIA
NT HYDROGENOMONAS
NT NITROBACTER
NT PROTOZOA
NT PSEUDOMONAS
NT SPORES
NT VIRUSES
Gnotobiotic mice with orally inoculated microorganisms observed for quantitation and fate of bacteria in intestinal tract 01 p0027 A70-11312

Mathematical planning of experiments applied to biological mineralization of human wastes, using continuous microorganism cultivation 03 p0435 A70-13715

Vacuum probe as effective device for sampling surface contamination of airborne microorganisms 05 p0808 A70-16704

Microbiological assay procedures for spacecraft sterilization and tabulation of microorganisms found on Surveyor 7 05 p0808 A70-16705

Microbial contamination levels and types detected on Apollo 9 spacecraft and related effects of various test and assembly environments 05 p0809 A70-16711

Micrococcus radiodurans and Sarcina flava radiation resistance from proton irradiation tests in carbonaceous chondrite Migei 08 p1441 A70-20550

Unicellular algae protein diet effects on animal and human enteric microflora composition 09 p1615 A70-22087

Microorganisms survivability in agar subjected to simulated Martian freeze-thaw cycles, discussing soil samples collection and composition 09 p1618 A70-22767

Microorganisms survivability in soils near spacecraft assembly areas during simulated Martian freeze-thaw cycles 09 p1619 A70-22768

Mathematical planning of experiments applied to biological mineralization of human wastes, using continuous microorganism cultivation 11 p1990 A70-25515

Microbial release from solid spacecraft materials after hard landings, testing survival during decontamination or terminal sterilization 15 p2688 A70-31664

Microbial flora in human subjects confined to long term Teklite I underwater habitat 15 p2681 A70-31879

Unicellular algae protein diet effects on animal and human enteric microflora composition 15 p2685 A70-32683

Microbial contamination levels on Apollo 6 spacecraft, discussing intramural environments for assembly and testing 16 p2849 A70-33995

Thermal stability of glycolytic enzymes from thermophilic clostridia 17 p3042 A70-33327

Circadian rhythms in single cell animals, examining cell division, temperature and light effects 19 p3365 A70-38410

Microorganisms metabolic activity effects on rocks and minerals, observing solubilization and altered IR absorption in Si-oxygen vibration region during penicillium simplicissimum growth 21 p3761 A70-40712

Lunar soil sample preparation and monitoring for viable microorganisms presence 22 p3978 A70-42973

Reaction kinetics of microbial sterilization in ultrahigh vacuum and in outer space 23 p4148 A70-44841

MICROPARTICLES
High velocity microparticle simulation techniques for studying properties, dynamics and origin of micrometeoroids, considering accelerators and impact results [ALAA PAPER 70-30] 06 p1029 A70-18131

Microparticle collection experiments during 1966 Orionid and Leonid meteor showers accomplished by Luster and ALARR /air launched-air recovered rocket/ instruments 08 p1575 A70-21393

Refractory oxide submillimeter spherical particle preparation by focused emission from carbon dioxide laser 09 p1697 A70-22984

Filamentary crystal growth associated with hypervelocity microparticles impact upon Cu foil 13 p2513 A70-29264

Microscopic particle mass spectra in six dimensional scalar, spinor and vector fields, noting cosmological implications and eight dimensional theory 14 p2616 A70-30342

Membrane-like properties of synthetic proteinoid microparticulate systems, considering catalytic activities, size and ultrastructure 16 p2847 A70-33029

Extinction parameters of submicron carbon, tungsten and Si particles in hydrogen measured at various temperatures, discussing scattering amplitude functions and Monte Carlo calculations [ALAA PAPER 70-838] 16 p3001 A70-33933

Microprobe analysis of glassy spherules from Apollo 11 lunar regolith, discussing zoning, composition and hypervelocity impact formation 21 p3903 A70-41558

MICROPHONES
First order pressure gradient microphone design based on electrostatic principle, using foil electrets to discriminate against airborne and solid-borne noises 05 p0821 A70-16402

Electret microphones application for pressure fluctuations measurements on thin aerodynamic profiles 03 p0435 A70-13715

noting operation, vibration insensitivity, robustness and cost

06 p1071 A70-18473

Microphone output level in airstream relation to sound pressure and pressure fluctuations caused by turbulent flow

07 p1334 A70-19372

Thermal porous bronze screened microphones for noise measurements in medium under large heat flow

14 p2555 A70-30298

Probe connected to microphone membrane chamber by transmission tube for fluctuating pressure measurement at discrete point in air flow

20 p3635 A70-40509

MICROPHOTOMETERS

U PHOTOMETERS

MICROPLASMAS

P-n junction and microplasmas voltage temperature coefficients during avalanche breakdown

03 p0541 A70-13729

Gas discharge avalanche breakdown in Si semiconductors, analyzing microplasmas, ionization coefficients, p-n junction voltage, electron and light emissions

04 p0731 A70-15494

Laser microplasma formation in focus of two laser beams impinging on crystalline lithium hydride targets

12 p2246 A70-27355

Microplasma and burst noise measurements on discrete silicon planar transistors indicating origin at emitter-base junction

22 p3998 A70-43331

MICROPROGRAMMING

Fourth generation systems architecture in microprogramming in terms of control logic, describing inner computer as subroutine processor for controlling interstation communication

08 p1465 A70-20816

Aerospace system design, considering use of microprogram-controlled digital computers

21 p3795 A70-41690

MICROPULSATIONS

NT GEOMAGNETIC MICROPULSATIONS

Small scale motions in solar photosphere and chromosphere using solar spectrograms

09 p1757 A70-22729

Forward and backward enhancement of auditory system sensitivity as function of short acoustic stimuli

11 p2084 A70-26495

Picosecond pulses in Q switched neodymium glass and ruby lasers, describing pulse measurement with fluorescence

17 p3108 A70-35623

Micropulsations as diagnostic tool for magnetospheric research, explaining ULF and VLF results variances

22 p4021 A70-43282

Magnetospheric plasma parameters from ground observation data of Pc-1 type micropulsations, assuming radiation belt plasma cyclotron instability

22 p4022 A70-43283

Secondary emission detector using linear signal to measure nonrepetitive microsecond ion bursts

23 p4197 A70-44475

MICROROCKET ENGINES

Simulator for testing colloid microthruster, discussing spacecraft interfaces and time of flight thrust data

[AIAA PAPER 69-314] 01 p0058 A70-10834

Pulsed plasma and ion microthrusters providing satellite attitude and position control

05 p0896 A70-16119

Ammonia micropropulsion for geostationary satellites stabilization, discussing principle and working mode of thrusters

09 p1743 A70-22660

Ammonia micropropulsion operation modes and performance for stabilizing synchronous communication satellite, noting advantages over chemical and ion propulsions

11 p2122 A70-25817

Suboptimal satellite attitude control using ionic microthrusters operating by large modulated amplitude impulses caused by electrostatic deflection of beam

13 p2501 A70-28426

Pulsed plasma microthruster propulsion system for synchronous orbit LES 6 satellite

[AIAA PAPER 69-298] 13 p2473 A70-28504

Hollow cathode mercury electron bombardment thruster design, emphasizing low specific impulse operation and discharge chamber improvements

13 p2473 A70-28505

Waste hydrogen utilization in microthrusters for spacecraft attitude control involving mass expulsion of cold gas

[AIAA PAPER 70-613] 16 p2969 A70-33609

Spacecraft attitude control microthrusters utilizing catalytically reactive gas mixtures during pulse mode and steady state operation

[AIAA PAPER 70-614] 16 p2969 A70-33611

Submillipound mercury electron bombardment ion thruster efficiency, noting cathode pole piece, baffle

position and geometry influence on ion chamber performance

[AIAA PAPER 70-616] 16 p2969 A70-33612

Low, medium and high specific impulse microthrusters development in France, using cold gases, subliming solids, hydrazine, ammonia and cesium ions

[AIAA PAPER 70-617] 16 p2969 A70-33613

One millipound cesium ion thruster for synchronous ATS-F satellite, describing power conditioning and control logic subsystems

[AIAA PAPER 70-1149] 20 p3690 A70-40205

Time-of-flight mass flow rate and thrust stand data comparison for two 100 micropound colloid thrusters

[AIAA PAPER 70-1114] 20 p3691 A70-40229

Micropound extended range thrust stand (MERTS) for testing electric thrusters for spacecraft auxiliary propulsion, providing three thrust measurement ranges and data telemetry system

[AIAA PAPER 70-1111] 20 p3607 A70-40232

Colloid microthruster system life test, discussing design and steady state performance

[AIAA PAPER 70-1110] 20 p3692 A70-40233

Critical components effect on small Hg electron bombardment thruster performance, considering glass coated accelerator grids, hollow cathodes and plasma bridge neutralizers

[AIAA PAPER 70-1100] 20 p3692 A70-40238

Composite accelerator electrodes on Cs bombardment microthrusters, testing various designs and electrode coatings

[AIAA PAPER 70-1089] 20 p3693 A70-40246

MICROSCALES

U MICROBALANCES

MICROSCOPES

NT ELECTRON MICROSCOPES

NT ION MICROSCOPES

NT OPTICAL MICROSCOPES

IR microscope and digitally programmed mirror system for printed circuit inspection, allowing two dimensional scanning and magnetic tape reference

01 p0054 A70-10024

Particulate contamination in compliance with military standard cleanliness level, using zoom microscope, charts and tables

12 p2174 A70-27010

Microscopic data importance in recognizing IC semiconductor failure characteristic traits, revealing current direction, voltage magnitude, microsurface temperature excursion and approximate transient duration

15 p2693 A70-32664

MICROSCOPY

Scanned laser microscope producing shadowgraph displays of IR transmittance variations attributed to defects in polished Si and GaAs semiconductor wafers

01 p0105 A70-10025

Holography, discussing light propagation, basic principles, skew reference wave, diffused illumination interferometry, character recognition, microscopy, high density information storage, etc

19 p3427 A70-38449

MICROSEISMS

Quartz floating component design, discussing magnetic sensitivity temperature dependence and microseismic noise rejection properties

14 p2582 A70-30245

MICROSTRUCTURE

NT METEORITIC MICROSTRUCTURES

NT WIDMANSTATTEN STRUCTURE

X ray topography of postannealing substructure of neutron irradiated W and Mo single crystals, indicating increase in disorientation

01 p0115 A70-10065

Chemistry variations effects on mechanical properties, phase stability and microstructure of alloy Unitemp 718 /Ni-Fe-Cr alloy/ via microscopy and X ray analysis

01 p0116 A70-10092

Heat resistant alloys for gas turbine blades observed for long term heating effects on changes of hardness, tensile, impact and stress-rupture properties and microstructure

01 p0116 A70-10149

Relieving microstrains in Ni powders by cold compaction at room temperature using X ray analysis, discussing polygonization process

01 p0117 A70-10161

Microstructural interfacial stability and property retention after elevated temperature exposure of eutectic composites, discussing coarsening rate relationship to interfacial area and energy

01 p0117 A70-10485

Magnetic bay microstructures occurrences at low latitude not restricted to day or night hemisphere

01 p0076 A70-10668

Thermomechanical processing of high strength low alloy steels to evaluate effects of composition, coiling temperature and cooling rate on mechanical properties and microstructures

01 p0118 A70-10726

Metal and alloys micro and macro stress-strain behavior data correlated for linear differential trans-

formers, strain gages, longitudinal resonance waves and X ray diffraction

01 p0092 A70-11248

Ni-based superalloys microstructure, describing composition, formation and characteristics of various phases

01 p0124 A70-11448

Quenched Ti-Mn alloy omega transition phase microstructure characteristics by transmission electron microscopy using thin foils

01 p0125 A70-11639

Ti-Al-Co alloys melting points and cast structures, discussing reactions with melt

01 p0125 A70-11644

Al solidification in direct chilling molds effect on as-cast structure, analyzing heat removal, casting rate and application of water to outgoing ingot

02 p0316 A70-12298

Ingot and powder metallurgy polycrystalline Be flow and fracture behavior and microstructure pressure dependence at room temperature

02 p0317 A70-12318

Steel objects microstructure and hardness tested by continuous magnetic technique, describing experimental apparatus model

02 p0300 A70-12479

Structure and segregation effects in Type 304L stainless steel weldments using transmission electron microscopy, optical microscopy and electron microprobe, comparing weld types

02 p0319 A70-12754

Microstructure and impact strength of welds of Cr-Mn steel containing nitrogen, observing grain growth dependence on nitrogen content

03 p0509 A70-13277

Grain size, forging parameter and microstructure effect on stress-rupture properties of wrought Ni-base alloy

03 p0511 A70-13567

Maraging steels microstructure and ductility influence on stress corrosion resistance in magnesium chloride salt chamber

04 p0711 A70-15681

Stroboscope lighting system for microstructural examination of fatigue test sample failure

05 p0845 A70-15882

Thermodynamics of elastic continuum with microstructure, modifying second law to include microtemperatures

05 p0930 A70-16083

Constitutive equations for isotropic elastic and thermoelastic materials with microstructure derived using free energy function, giving uniqueness theorems

05 p0932 A70-16136

Binary Al-Y system thermal and microstructural analyses at room temperature and 200 C, obtaining partial diagram and mechanical properties

05 p0864 A70-16546

Thermal conductivity and aperiodic temperature distribution in microstructure of composite materials reinforced with solid and hollow fibers

05 p0958 A70-16952

Microstructure effects on smooth and notched fatigue and room temperature tensile properties of Ti-Al-V alloy using heat treatment combinations

06 p1087 A70-17458

Graphite microstructure effect on ablation performance, discussing grain size, porosity and degree of graphitization

[AIAA PAPER 70-155] 06 p1092 A70-18147

Boundary value problems in nonlocal elasticity, considering two one dimensional media coupling with microstructure by Green function analog

07 p1399 A70-18665

Steels microstructural plastic deformation under pulsed laser irradiation

07 p1303 A70-18712

Solution treating temperature and microstructure effects on hot rolled Ni base alloy properties

07 p1306 A70-18995

Thin walled metal cylinders residual deformation microstructures under internal impulsive loading

07 p1285 A70-19969

Thin sheet and laminate bullet hole deformation zone microstructure observation by electron microscopy, considering terminal ballistics approach

07 p1413 A70-20049

Ce-Ni-Si system X ray and microstructural analysis, constructing phase diagram for Ce contents of 0-33.3 wt percent

08 p1555 A70-21115

PbTe-based Sn, Se and Ge alloys lattice constant, thermal EMF and resistance, fusibility and microstructure

08 p1555 A70-21117

Rare earth elements effects on microstructures and mechanical properties of cast Al, Al-Si and Al-Si-Mg alloys

08 p1516 A70-21127

Pyrolytic C-TiC alloys obtained by precipitation from gaseous phase, discussing microstructural properties anisotropy

08 p1517 A70-21146

- Mo sheet longitudinal and transverse mechanical properties and microstructure after annealing
08 p1517 A70-21199
- High temperature thermomechanical treatment effects on stainless steels and Ti alloys microheterogeneity, noting corrosion resistance improvement
08 p1519 A70-21444
- Silicon carbide whiskers end structure using field emission patterns
08 p1528 A70-21551
- Waspaloy gamma prime solvus temperature relationships as function of solution treatment and precipitation strengthening additives, discussing microstructure and tensile properties
08 p1520 A70-21555
- Wrought aluminum based high strength alloys structure and mechanical properties
08 p1522 A70-21708
- Nondestructive testing and inspection by acoustic emission from stressed materials, discussing microstructure effect and crack initiation detection
08 p1508 A70-21747
- Cobalt modified Ti-6Al-4V plate and billet, testing effects on heat treatment response, microstructure, tensile and fatigue properties, fracture toughness, etc.
08 p1523 A70-21852
- Microstructure of wrought arc-cast polycrystalline W sheet after high temperature creep deformation at various stress levels
08 p1525 A70-21962
- Subboundary migration in Mo, W and W-Re alloy single crystals subjected to cyclic heating, using metallographic technique involving electrolytic polishing and special etching
09 p1701 A70-22297
- Transverse and longitudinal resistive critical fields of Nb wires, discussing superconductivity in dislocation cell walls created by drawing or swaging
09 p1704 A70-22802
- Internal stresses and substructures dependence on thermomechanical histories of stainless steel during creep, noting subgrain orientation
09 p1705 A70-22805
- Work strengthening and microstructure of Co-Ni base alloys containing Cr and Mo, discussing deformation induced martensitic transformation
09 p1705 A70-22806
- Yttrium iron garnet sintering and grain growth rates dependence on yttrium/iron ratio
[ACS PAPER 16-BE-68F] 09 p1740 A70-22982
- Mo single crystals dislocation substructure strain dependence after creep using etch pitting techniques
09 p1708 A70-23544
- Ultrasonic vibrations effects on microstructure and mechanical properties of polycrystalline titanium during phase recrystallization
10 p1903 A70-23863
- Microstructure and ductility of air- and vacuum-melted heats of corrosion resistant steels, investigating tensile and yield strengths for all grain directions
10 p1905 A70-25170
- Aluminum alloys hot cracking during welding, ascribing failure to combination of strain and susceptible microstructure
10 p1897 A70-25313
- Fe-Mo-C and Fe-Ti-C alloys microstructure and hardness after rapid cooling from melt, considering phase dispersion and particle size, spacing and shape
11 p2065 A70-25774
- Anomalous grain growth kinetics and recrystallization in electron beam annealed nickel determined by microstructural and radiographic study, noting annealing time dependence
11 p2068 A70-26596
- High modulus graphite fiber structure using electron beam
11 p2071 A70-26845
- Ti alloys tensile properties correlated with microstructure for multiple heat treatment cycle variations for high strength and adequate ductility
12 p2252 A70-27107
- Low carbon Ni steels isothermal transformation characteristics, observing equiaxed ferrite and Widmanstätten and bainitic structures at various temperatures
12 p2256 A70-27615
- Uniqueness theorem in Mindlin theory of elastic materials with microstructure
13 p2508 A70-28488
- Moisture effect on fatigue crack propagation and fracture path through microstructure of 300-grade maraging steel
13 p2432 A70-28607
- Linear theory of homogeneous and anisotropic elastic media with microstructure, establishing reciprocity and variational theorems
13 p2512 A70-28951
- Junction and contact regions in electronic devices using X ray microanalysis and electron probe
14 p2590 A70-30355
- Austenization temperature, cooling rate and tempering conditions effect on steel castings structure, strength and impact properties
14 p2596 A70-30875
- Book on high modulus fibers and composites providing data for preparation, microstructure, structure and properties
14 p2598 A70-31315
- Hot rolling and warm working effects on microstructure and mechanical properties of Ni-Cu-Cb steel, noting optimum austenite plus ferrite phase field
15 p2756 A70-31566
- Boundary value problem in linear elastodynamics, investigating Ignaczak type theorems for microstructure effects in transient heat conduction problems
15 p2822 A70-32343
- High temperature scaling of Ni, investigating role of oxide microstructure and growth stresses
15 p2762 A70-32388
- Fracture of failed tensile impact and compression test pieces of hardened SAE 52100 steel, using scanning electron microscope
15 p2745 A70-32443
- Thorium phosphide anti-type microstructure of La-Rh system by X ray diffraction, discussing bcc structure, lattice constants, etc.
15 p2695 A70-32549
- Composition and heat treatment effects on Fe-Ni alloys structure, using micrographic, autoradiographic and potentiokinetic methods
16 p2916 A70-33080
- Microstructure and reaction kinetics of flat premixed fuel-rich hydrogen-oxygen-nitrogen flame at atmospheric pressure
16 p2998 A70-33900
- Aqueous stress corrosion dependence on microstructural features of Ti alloys, using optical and electron microscopy and X ray diffraction
17 p3113 A70-34370
- Shock deformation effects on strengthening and microstructure of Ti and Ti-Mo alloys
17 p3120 A70-34420
- High temperature heating and cooling effects on mechanical properties and structure of Ti welds, using notched bar impact specimens
17 p3098 A70-34423
- Forged alpha/beta Ti alloys, investigating relationship between mechanical properties and microstructures produced by heating
17 p3120 A70-34427
- Cobalt addition to Ti-Al-V alloys, examining yield strength, heat treatment, ductility and microstructure
18 p3271 A70-35964
- Binary Co-Cr alloy open circuit potential and microstructure, examining effects of composition, heat treatment, allotropic transformation and precipitation
18 p3271 A70-35966
- Kingfisher meteorite metal particles microstructures, discussing phase transformation during reheating by shock
18 p3310 A70-35970
- Microstructural changes of Ni-Cr lamellar eutectic alloy during creep deformation at 625 and 760 C
18 p3272 A70-36034
- Two phase stainless steels with microduplex structures, taking into account martensite and ferrite effects on mechanical properties
18 p3272 A70-36038
- Silicon-containing pyrocarbon, relating microhardness to microstructure
18 p3279 A70-37220
- Titanizing Armco iron and carbon steels, examining diffusion layer structure and phase composition
19 p3451 A70-37460
- Microstructure effects on magnetic properties of polycrystalline MnZn ferrites with high permeability
19 p3484 A70-37565
- Crystal dislocations and microstructure effects on magnetic properties of polycrystalline MnZn ferrites with high permeability, noting eddy currents role
19 p3484 A70-37566
- Linear micromorphic material constants determination from constituent properties based on microelasticity theory
19 p3538 A70-37795
- Stress differential equations of micropolar elasticity, considering mass forces and moments of inertia
19 p3459 A70-38672
- W-Mo-Nb-Ta system structure and properties at room and high temperature by microstructural analysis and hardness measurements, discussing Mo addition effects
19 p3453 A70-38713
- Soviet papers on heat resistant alloys and steels structure by electron microscopes
20 p3644 A70-39036
- Ni-Cr heat resistant alloys structural transformation kinetics under aging, creep and operational conditions, discussing solid solution decomposition, hardening phases coagulation and dissolution, etc.
20 p3645 A70-39037
- Microstructure and phase distribution in maraging steels subjected to austenization and subsequent aging in reversible transformation temperature range
20 p3645 A70-39038
- Heat treatment and alloying element influence on phase and structure transformations in Ti alloys, investigating mechanical properties and creep resistance
20 p3645 A70-39039
- Ti alloys fine structure, mechanical properties and alloying elements diffusion mobility during heat treatment, observing chemical and structural inhomogeneities
20 p3645 A70-39040
- Two phase Ti alloy subjected to quenching and annealing studied by diffraction electron microscope, discussing needles complex fine structure
20 p3645 A70-39043
- Al-Zn-Mg alloys structural transformations by diffraction electron microscopy, investigating grain boundary and dislocation structure as function of heat treatment and chemical composition
20 p3646 A70-39044
- Duraluminum dislocation structure dependence on deformation temperature by electron microscopy, discussing subgrain boundaries
20 p3646 A70-39045
- Stressed cast Mg-Nd-Zr alloys structural transformations kinetics over temperature range by electron microscopy
20 p3646 A70-39046
- Graphite filament composite structure shear strength decrease with modulus increase, examining fiber microstructure effect on interlaminar properties by short beam shear test
20 p3654 A70-39206
- Carbons and graphites ablation tests for predicting performance under reentry conditions, considering microstructure effects
20 p3735 A70-39214
- Variational principles in linear quasi-static theory of inhomogeneous and isotropic viscoelastic solids with microstructure
20 p3718 A70-39229
- Microstructure and composition of hafnium dioxide stabilized with Ca, Y and Mg oxides using metallographic, X ray and microprobe
20 p3654 A70-39242
- Fe-Ni-C alloys austenite dispersion matrix effects on martensite structural characteristics
20 p3649 A70-39705
- Heating conditions effect on microstructure, hardness, transformation temperatures and dimensional anisotropy of maraging steel
20 p3649 A70-39941
- Beta III Ti alloy for aircraft fasteners, describing microstructure and mechanical properties
20 p3650 A70-39966
- Metallographic preparation of materials for microstructural studies, discussing deformation-free sampling, metal polishing, microphotography and quantitative microscopy
21 p3825 A70-40895
- Carburization and grain size of tungsten carbide powder from W powder as function of temperature, using optical and electron micrographs
21 p3839 A70-41412
- Sommerfeld type radiation conditions for linear homogeneous isotropic elastic materials with microstructure, discussing field equations, displacement and rotation vector and scalar conditions
21 p3936 A70-41417
- Creep and stability of microstructural Al elements under varying temperatures, noting grain boundary migration
21 p3839 A70-41429
- Apollo 11 lunar rock and fines shock induced and melting microstructural mineral damage, discussing meteorite bombardment, phases without melting and microbreccia
21 p3902 A70-41550
- Apollo 11 lunar dust and breccia micromorphology and surface characteristics implying weathering processes
21 p3910 A70-41622
- Metastable beta Ti alloy as-quenched microstructure stability with respect to thin foils transformation during electrolytic polishing and bulk specimens during cold rolling
21 p3841 A70-42150
- Recrystallization kinetics and microstructure of low carbon Ti stabilized steel cold rolled and annealed in 800-1750 F range
22 p4053 A70-42730
- Hot work effect on properties and microstructure of wrought Waspaloy, observing temperature decrease effect on fracture ductility
22 p4054 A70-42739
- Recrystallized and nitrided Mo alloy microstructure under plastic deformation by tension at high temperatures
22 p4038 A70-43122
- Mo microstructure changes at high temperatures, noting polygonization, grain migration and crack propagation during failure
22 p4055 A70-43125
- Sound velocity in isotropic nonlinearly elastic continuum with microstructure, showing dispersion coincident with Cosserat constant
22 p4120 A70-43713
- Columnar grain and Ni alloy single crystal gas turbine engine components resistant to high temperatures produced by precision casting, using directional solidification
23 p4207 A70-44857

Austenitic formation by rapid heating of Ni maraging steel, noting microstructural characteristics relationship to martensite before phase transformation

24 p4356 A70-45144

Martensite plate substructure in Fe-Mn-Cr-C alloy, using transmission electron microscopy and diffraction study

24 p4358 A70-45238

Eutectic NiAl-Cr alloys, investigating quaternary additions effect on rod-plate transition to faceted microstructure

24 p4359 A70-45244

Cyclic loaded high purity Al samples, noting substructure around fatigue cracks

24 p4362 A70-46185

Thin Al foil subjected to cyclic bending stresses, investigating substructures and strain regions around fatigue crack

24 p4362 A70-46186

Mg addition effects on impact strength and micro structure of Al-Si-Cu alloys, using Charpy test and metallographic methods

24 p4363 A70-46196

Spark erosion or plasma jet treatment effects on Co surface structure, describing allotrope delta phase

24 p4364 A70-46221

Aluminized Armco iron and steel diffusion layers phase composition and microstructure

24 p4350 A70-46337

MICROTHRUST

Satellite spin stabilization by Cs contact ion microthrusters with beam deflection, investigating performance obtained by optimal and suboptimal laws

13 p2506 A70-29143

Microthrusters for geostationary satellites attitude and position control

15 p2791 A70-32279

Spinning satellites stationkeeping at synchronous altitude, using solid propellant pulsed plasma microthrusters

[AIAA PAPER 70-1148]

20 p3690 A70-40206

Orbital mechanics of transfer orbits under small horizontal thrust, reducing second order differential equation to linear inhomogeneous equation

23 p4245 A70-44691

MICROTOPOGRAPHY

U TERRAIN

MICROVISION LANDING AID

Electronic attitude director indicator /EADI/ for supersonic transport, employing CRT display, head down TV and microvision sensors

19 p3463 A70-37911

MICROWAVE AMPLIFIERS

Microwave generation and amplification using Gunn effect semiconductor devices

01 p0160 A70-11289

Microwave transistor amplifier design and specifications, discussing applications and economy in design, production and use

06 p1018 A70-17358

Multistage microwave transistor amplifiers design for 4 GHz band, describing poor input/output impedance matching solution

08 p1475 A70-21279

TWT amplifiers for 4-8 GHz frequency range exhibiting decreased weight and volume and increased efficiency

08 p1477 A70-21370

Broadbanding method for microwave reflection type amplifiers using additional resonators

09 p1645 A70-22604

Low noise nonreciprocal microwave parametric amplifier with up-and-down converter and idlers in cascade

09 p1647 A70-22850

Silicon diodes pulse operated in avalanche resonance pumped modes for producing stable microwave amplification

10 p1847 A70-23889

Solid state multistage high power avalanche amplifier at X band

10 p1847 A70-23890

Spacecraft S band power amplifier TWT electrical, environmental and life tests under saturated conditions

[AIAA PAPER 70-506]

11 p2016 A70-25468

Microwave amplifiers based on interaction between piezoelectric acoustic waves and collinearly drifting carriers, analyzing gain, frequency response, etc

11 p2018 A70-26164

High dynamic range low noise parametric microwave amplifier performance measurement for radar receivers

12 p2183 A70-27166

Wideband microwave transistor IF amplifier for mm wave communication system

14 p2555 A70-30283

Millimeter and submillimeter wave receivers, describing detectors, mixers, low noise amplifiers and radiometers

14 p2549 A70-30448

Computerized design of transistorized UHF wideband amplifier, using successive approximations for optimum circuit automatic selection

14 p2556 A70-30668

Microwave parametric amplifiers with nonideal circulators, deriving gain via scattering matrix theory and signal flow graphs

16 p2874 A70-33389

Millimeter wave amplification by pumped n-type gallium arsenide oscillating in limited space charge accumulation mode

16 p2875 A70-33399

Silicon avalanche transit time diodes as CW microwave generators and amplifiers

16 p2876 A70-33404

Wideband microwave IC tunnel diode amplifier /TDA/ for artificial satellites, discussing noise, size and weight reduction

17 p3053 A70-35277

SHF traveling wave tube amplifier design and characteristics

17 p3054 A70-35413

S band CW power amplifier and varactor doubler module for airborne phased arrays

18 p3231 A70-36674

Hybrid integrated microwave power amplifiers, using high-Q thin film lumped passive elements

18 p3232 A70-36760

Optimum junction area for maximum microwave output power of silicon IMPATT diodes for X band operation

23 p4167 A70-43775

Design tolerances and compensating networks for microwave transistor amplifier, using synthesis search and trial calculation by computer

23 p4168 A70-43780

Minimum noise microwave parametric amplifiers incorporating varactor diodes with frequency dependent apparent loss resistance

23 p4169 A70-43786

Ferromagnetic microwave amplifiers operation, describing longitudinal pumping amplifier using YIG

23 p4170 A70-43825

Computerized design of broadband microwave amplifiers with complex terminations, using transfer scattering parameters for analysis and optimization

24 p4316 A70-45211

MICROWAVE ANTENNAS

Compact range techniques using collimator for radar reflectivity and microwave antenna gain and pattern measurements

02 p0269 A70-12586

Numerical solutions to determinantal equation for predicting properties of periodically modulated dielectrically filled frequency scanning waveguide as microwave antenna

03 p0457 A70-13696

Analytic solutions for focal plane electric field components in parabolic reflector antennas

03 p0457 A70-13697

Shell directional antennas operational behavior at 2 and 4 GHz and mechanical properties

04 p0660 A70-15661

Variational principle used in microwave breakdown predictions for rectangular aperture antenna

05 p0824 A70-16988

High gain paraboloidal reflector antenna with horn feed for satellite and terrestrial microwave links

06 p1022 A70-18022

Bounds on near electric field outside rectangular slot in conducting ground plane applied to microwave breakdown limitation

09 p1646 A70-22696

Stripline elements centimeter wavelength emission level determination by comparison with reference antenna radiation patterns

09 p1652 A70-23650

Phased array radar system synthesis, discussing small aperture systems, effects of solid state technology and role of data processing

10 p1842 A70-24877

Integrated circuit microwave phased array radar antenna systems for multiple frequency bands and multifunction operations to save cost and space

10 p1851 A70-24878

Microwave waveguide insertion-loss calibrations, comparing cavity Q and direct measurement methods

10 p1854 A70-25315

Microwave axicon with dielectric cone at aperture of focused antenna to reduce far-field radiation pattern beamwidth

14 p2549 A70-30512

Anechoic chambers and test equipment for microwave antenna pattern measurements, discussing electromagnetic shielding and construction

14 p2557 A70-31180

Steerable microwave circular array to provide 360 deg electronic beam steering with computerized adaptive amplitude and phase control

16 p2874 A70-33392

Microwave circular array with electronic beam rotation of patterns by applying linear phase tapers to Butler matrix feed

16 p2874 A70-33393

Steerable C band waveguide arrays design for forming monopulse cluster of sum and difference beams

16 p2875 A70-33395

Compact integrated microwave antenna of composite structure involving slotted waveguide planar array capable of operating in three frequency bands

16 p2876 A70-33406

Thin window for circularly polarizing antennas, measuring circularity and VSWR performance on S and X band test sections

16 p2877 A70-33410

X band airborne antenna phased array, describing phase shifter, radiation pattern, associated computer, etc

16 p2864 A70-33454

X band aircraft antennas selection and design for defense communications satellite systems, emphasizing steerable phased array

16 p2865 A70-33712

Microwave antenna with aperture in infinite conducting plane, analyzing radiation patterns, scattering and diffraction

17 p3043 A70-35053

Microwave receiving antenna, discussing directivity, cross section, power gain, equivalent circuit, etc

17 p3044 A70-35054

Geometrical optics laws, principles and procedures applied to microwave antennas design and analysis

17 p3044 A70-35067

Impedance measurements on microwave tripole antenna for circular polarization, including expressions for radiation pattern

19 p3388 A70-37868

U.S. nationwide satellite network for multichannel community antenna TV /CATV/ operated at 12 GHz band

19 p3382 A70-38891

Lens with radial symmetry for mm wave scanning antenna

20 p3598 A70-40307

Millimeter wave reflector antennas, considering various system designs, performance, pointing capabilities, limitations and applications

20 p3599 A70-40309

Uniformly and nonuniformly spaced microwave antenna arrays, investigating directivity function and gain characteristics dependence on spacing

20 p3599 A70-40313

T, Y and ring microwave antenna array configurations for radio astronomy, comparing baseline distributions

20 p3599 A70-40317

Short cylindrical microwave antenna radiation directivity enhancement by optimum double impedance loading

20 p3599 A70-40318

Microwave antenna near field patterns analysis by spherical harmonic expansion, discussing validity conditions and convergence

21 p3796 A70-40556

Low cost microwave receiver and antenna for instructional satellite TV broadcasting in developing nations

21 p3789 A70-41355

Multiple beam earth station torus microwave antenna for satellite communication with nonplanar field of view over geostationary arc

21 p3798 A70-41357

Parabolic reflector microwave antenna flared horn primary feeds design for maximum aperture efficiency based on electric field matching

21 p3800 A70-41946

Microwave antenna array irregularity location from hologram by optical signal processing, using far field spatial filter

21 p3792 A70-42048

Near field vector evaluation of Fresnel zone field for microwave reflector antennas

23 p4161 A70-43771

Low cost microwave antenna-receiver for satellite FM TV signal reception at SHF and conversion for standard sets

23 p4164 A70-44645

Airborne radiometer slim multibeam millimetric antenna, describing design, construction and performance

24 p4316 A70-46320

MICROWAVE ATTENUATION

Attenuation vs pathlength for given fading probability of microwaves by intense rain, evaluating dual parallel path diversity

05 p0815 A70-16575

Microwave absorption by rotational transition of interstellar formaldehyde in direction of Sgr B2, Sgr A and W51

08 p1570 A70-20896

Microwaves scattering and attenuation in precipitations from raindrop size distribution curves analysis

08 p1462 A70-21096

Low pass filter structure of focusing reflectors designed for quasi-optical system, noting energy absorption

08 p1476 A70-21287

Microwave signal fading in Venus atmosphere due to turbulence, discussing atmospheric dielectric permittivity variance

09 p1764 A70-23484

Microwave power absorption in plasma investigated by transmission cavity excited in TE mode, determining electron density and collision frequency
11 p2089 A70-25841

EHF microwave absorption in compressed carbon dioxide, measuring dielectric loss as function of gas density
12 p2273 A70-27571

Anisotropic superconducting energy gap of pure Zn from microwave absorption measurements
16 p2961 A70-33776

Anisotropic energy gap model in superconducting Zn to describe microwave absorption measurements
16 p2961 A70-33777

Cosmic microwaves anomalous absorption by interstellar IR-pumped formaldehyde in dust clouds shock heated layer
17 p3154 A70-34535

External DC electric field effect on microwave absorption in plasma
23 p4226 A70-44372

MICROWAVE CIRCUITS

Microwave circuit for increasing Gunn oscillators injection locking capabilities and reducing FM resulting from bias-voltage fluctuations
01 p0050 A70-10783

Ferrite-type phase shifter production by microstrip technique and integrated microwave system use in Gunn element Doppler radar
01 p0052 A70-11290

Rise time relationship with signal bandwidth for class of TEM mode microwave delay line filters
02 p0257 A70-12185

Microwave circuits automatic analysis and design using digital computer in batch mode, describing analysis-optimization program
03 p0457 A70-13562

Dielectric loaded waveguide with symmetric microstrip line, evaluating transverse wave number by finite difference method
03 p0458 A70-14035

Self excited microwave mixer and transmitting oscillator using Gunn diode applied to short distance Doppler radar
05 p0822 A70-16678

Solid state microwave acoustic variable delay devices for radar, fuses, repeaters, altimeters, etc, emphasizing magnetoelastic wave method
06 p1018 A70-17356

Microwave transistors frequency and power characteristics and tradeoffs in relation to thermal and packaging design
06 p1023 A70-18390

Microwave mixer design to increase dynamic range applied to communications and video systems
07 p1243 A70-20216

Microstrip integrated circuit technology in development of microwave components, discussing fabrication, design, performance and applications
08 p1471 A70-20787

Wideband tunable CW Gunn effect oscillator design, discussing microwave circuit effects on performance
08 p1471 A70-20788

Controllable microwave phase shift varactor diode circuit parameters design optimization using digital computer for transmittance matrix coefficients calculation
08 p1474 A70-21230

Interference emission filtering in high power microwave transmitters, discussing spurious emissions removal or rejection by transmission line filters
08 p1474 A70-21257

Hybrid microwave integrated circuits technology and design, discussing distributed and lumped-element structures and component properties
09 p1644 A70-22225

Natural frequencies and electromagnetism field distributions in rectilinear and cylindrical dielectric resonators used in microwave circuits
09 p1644 A70-22280

Quasi-optical waveguide component (attenuator) in S-band measured for performance noting diffraction as limiting factor
09 p1647 A70-22711

Nonlinear phase distortion measurement in microwave limiters under dynamic conditions using two tone test signal
09 p1647 A70-22714

Microwave sources power stabilization, control and noise reduction using feedback techniques
09 p1649 A70-23275

Avalanche diodes and associated microwave circuits power generation in terms of IMPATT, TRAPATT, parametric, space-charge feedback and thermal modes
10 p1847 A70-23887

Hybrid microwave integrated circuits application to phased array and Data Relay Satellite System space transponder
10 p1851 A70-24879

Integrated microwave systems development taking into account cost effectiveness and anticipating kilowatt and megawatt systems
10 p1851 A70-24880

Microwave devices including gridded tubes, magnetrons, traveling wave tubes, amplifiers, solid state devices for radar and communication applications
10 p1851 A70-24885

Microwave acoustic delay lines design and fabrication for UHF to X band frequency ranges
11 p2005 A70-26163

Surface acoustic wave delay lines using interdigital transducers based on piezoelectrics with applications in VHF and UHF signal processing
11 p2005 A70-26165

Microwave surface acoustic delay lines properties, advantages, electron beam fabrication, optical probing for propagation loss measurement, etc
11 p2005 A70-26166

Computerized design of microwave circuits with S matrix
11 p2019 A70-26714

Double diffused epitaxial silicon bipolar microwave transistor design, fabrication and performance evaluation, including scattering parameters vs frequency for common-emitter amplifier
13 p2379 A70-29592

Microwave backward tunnel diodes in InAs, predicting reliability and sensitivity improvements over other materials
13 p2379 A70-29593

Microwave integrated circuit lumped element approach, showing performance as function of geometry and frequency
14 p2561 A70-30920

Microstripline and balanced stripline, discussing parameters affecting maximum attainable Q in microwave integrated circuits
14 p2561 A70-30921

GaAs-Ge heterojunction transistors with microwave planar geometry, calculating performance for comparison with Ge homojunction transistor
14 p2556 A70-30925

Computer aided design for microwave branch line couplers dimensions practical for integrated circuit microstrip fabrication
15 p2711 A70-32602

Microwave IC methods applied to solid state signal sources design, using varactor tuned transistor oscillators, resistive isolation pads, amplifiers and frequency multipliers
16 p2872 A70-33069

X band acoustic delay lines using thin film piezoelectric transducers
16 p2874 A70-33391

High Q reactance network realization for integrated microwave systems employing evanescent mode waveguide components
16 p2875 A70-33402

Wideband varactor multipliers with flat output as microwave sources in radar systems
16 p2877 A70-33412

Microwave devices with harmonized electron beam constructed from klystrons, TWT, backward wave tubes, magnetrons
18 p3231 A70-36414

Avalanche transit time diode and transferred electron oscillators in microwave systems, discussing design, performance and applications
18 p3232 A70-36675

Extrinsic photoconductive detectors, comparing performance for microwave and DC bias based on gain bandwidth product and SNR analysis
18 p3232 A70-36746

Microwave conductivity of thick film screen-printed microstrip circuits, measuring closed resonators SHF Q factors
19 p3388 A70-37964

Microwave L-band correlator using YIG delay lines varied by electronically changing magnetic bias
20 p3597 A70-39468

Microwave waveguide mount characterization of varactor diodes, using transmission resonance and Dolph-Chebyshev taper
21 p3797 A70-40759

Admittance matrix of microwave networks, referring to coaxial line-waveguide coupling through 3 kMc adapter
21 p3802 A70-42250

RLC networks and microwave components design by applying optimization technique
22 p3997 A70-43175

Stripline and microstrip junction circulators analysis for microwave integrated circuits, based on clockwise and counterclockwise rotation modes
23 p4169 A70-43787

Information processing methods in microwave measurement using digital computers, emphasizing active and passive transducers
23 p4193 A70-43795

Superheterodyne EPR spectrometer microwave bridge using single X band klystron
23 p4170 A70-43798

Semiconductor microwave generator design for maser simulator using transistorized amplifier, varactor frequency multiplier and diode multiplier
23 p4171 A70-43878

Microwave p-n diode RLC equivalent circuit parameters experimental determination
23 p4171 A70-43956

Phased array radar for missile defense, discussing development trends toward adaptive system logic control and microwave digital circuitry for signal processing
23 p4172 A70-44012

Solid state IF or baseband switching elements design for high capacity multichannel microwave systems
23 p4172 A70-44014

Phased array radar systems microwave circuit modules packaging techniques, discussing interconnections, assembly, hermetic sealing and leak testing
23 p4173 A70-44535

Ferrite junction microwave circulator bibliography /1956-1969/ covering stripline and waveguide versions theory, designs, constructions and applications
24 p4318 A70-45210

Wideband TEM quarter wave microwave coupler with continuously variable coupling range, employing even and odd mode characteristic impedance levels change
24 p4318 A70-45215

Thin film microwave acoustic transducers, calculating top electrode thickness effect on frequencies of infinite conversion loss
24 p4333 A70-45218

Packaged microwave junction diodes in reduced-height waveguide, discussing parasitics and equivalent circuit parameters measurement technique
24 p4318 A70-45220

Variable microwave attenuator using p-i-n diodes and three-port hybrids built in stripline technique
24 p4318 A70-45222

MICROWAVE COUPLING

Impedance and field distribution of bifurcated and stepped waveguide junctions with inserted diaphragm calculated by transformed singular integral equation
05 p0820 A70-16385

Interdigitated microstrip quadrature couplers suited for monolithic or hybrid thin film microwave integrated circuitry
08 p1476 A70-21291

Computer aided design for microwave branch line couplers dimensions practical for integrated circuit microstrip fabrication
15 p2711 A70-32602

Equivalent circuits and general formulas for small hole coupling of resonant cavities and waveguides
15 p2714 A70-32817

MICROWAVE EQUIPMENT

NT GYRATORS
NT MICROWAVE ANTENNAS
NT MICROWAVE FILTERS
NT MICROWAVE INTERFEROMETERS
NT MICROWAVE PLASMA PROBES
NT MICROWAVE PROBES
NT MICROWAVE RADIOMETERS
NT MICROWAVE TUBES

Microwave ILS for difficult sites or conditions, detailing capabilities and operation principles
01 p0136 A70-10301

GaAs - Conference, Dallas, October 1968
01 p0157 A70-10515

Miniaturized components in microstrips on low loss dielectric or magnetic substrates, noting suitability for microwave systems integration
01 p0052 A70-11313

GaAs microwave diode Gunn oscillator subharmonically injection phase locked at low frequency ratios
03 p0459 A70-14041

Millimeter wave fields systems application to radar guidance, radiometry, communications, radio astronomy and satellite experiments
04 p0647 A70-14621

Quasi-optical design methods applied to mm microwave resonators characterized by high Q and low spectral densities
04 p0655 A70-14623

Low loss low sidelobe N-wave microwave optical power divider for single plane electronically steerable Ku band phased array antenna
04 p0655 A70-14624

Microwave Si transistors with overlay and interdigital geometries and integrated circuit design considerations for power amplifiers, power oscillators and frequency multipliers
05 p0819 A70-16149

Microwave and IR distance measuring devices design and operational principles, discussing main circuits and reading displays
05 p0851 A70-16799

Microwave applications in measuring and heating functions, describing battery operated radar for vibration and rotation measurements
05 p0816 A70-16824

Microelectronic L-band phase-lock loop receiver for data transmission between earth stations and satellites
06 p1017 A70-17338

Bulk GaAs devices and avalanche /IMPATT and TRAPATT/ diodes compared as microwave sources
06 p1018 A70-17357

Microwave acoustic transducer and delay line properties determination from mathematical analysis
06 p1062 A70-17481

Soviet book on microwave devices employing semiconductor diodes design and synthesis covering electric field effects, optimality criteria, tabular data, etc

06 p1019 A70-17536

Lumped element microwave Y circulator, describing device performance and ALGOL program for potentials calculation

07 p1241 A70-19751

Negative differential conductivity effects in Gunn domain GaAs semiconductors, discussing physical properties and microwave applications

08 p1556 A70-21303

Inorganic ceramic materials in design and fabrication of microwave antennas, filters and stable resonators, discussing density and dielectric constant variability by ceramics foaming

09 p1689 A70-22007

Automatic phase correction for modulated subcarrier microwave systems used for control of industrial processes

09 p1632 A70-22281

High sensitivity photomultiplier TWT microwave photodetector with internal louvered secondary electron multiplier and spiral HF getter

09 p1645 A70-22413

French microwave semiconductor technology in terms of basic research, technology studies, reliability and integrated circuits

09 p1739 A70-22602

Comparator for measuring relative phase difference between identical frequency signals within microwave octave band

09 p1647 A70-22715

Signal converter for centimeter band-DC voltage transformation, noting applications to microwave power measurement by digital computers

09 p1650 A70-23629

Waveguide windows for energy outlet in microwave devices analyzed by plane /Brillouin/ modes, discussing dielectric element reflection coefficient

09 p1651 A70-23646

Coaxial energy outlets satisfying vacuum maintenance requirements of dielectric waveguide windows in dismountable prototype microwave devices

09 p1652 A70-23647

Direct domestic reception of TV signals from satellites, discussing microwave components, economics and reliability

10 p1840 A70-24448

Microwave devices excess AM and FM noise levels measurement by carrier suppression methods

10 p1841 A70-24579

Avalanche diodes microwave properties in utilization circuit, discussing negative conductance, nonlinear impedance and intrinsic noise current

10 p1850 A70-24623

Collection of papers on microwave technology covering integrated circuits, amplifiers, radar, etc

10 p1851 A70-24876

Microwave equipment reliability achievement emphasizing tests and analyses on RF amplifiers, duplexers, antennas, etc

10 p1851 A70-24882

Millimeter wave transmission, discussing atmospheric effects, system components and applications in terrestrial communication networks, synchronous satellites, etc

10 p1842 A70-24883

Microwave devices including gridded tubes, magnetrons, traveling wave tubes, amplifiers, solid state devices for radar and communication applications

10 p1851 A70-24885

Rocket- and projectile-borne microwave miniature solid state transmitters, discussing transistor oscillator-multiplier, hybrid integrated circuits, bulk effect devices, etc

10 p1852 A70-24887

Complex microwave solid state subsystems designs for specialized systems

10 p1852 A70-24889

Microwave device test system design, considering measurement ranges and parameters, calibration, repeatability, accuracy, maintainability, etc

10 p1852 A70-24890

Microwave phase shifter with rectangular ferrimagnetic toroid in waveguide longitudinal center, discussing impedance matching, phased array applications, etc

10 p1852 A70-24891

Microwave converter system for ETV satellite reception, discussing characteristics and costs for mass production

11 p2017 A70-25493

Thermal imaging device adaptable to IR, microwave or ultrasound radiation, projecting image on heat sensitive surface

11 p2050 A70-25643

SAFEGUARD ballistic missile defense radars, discussing terminal defense concept, data processing system and microwave components

11 p2005 A70-26162

V/STOL aircraft ground guidance systems using microwave instruments for approach and landing

12 p2266 A70-27458

Microwave scanning beam landing system providing aircraft radio approach guidance

12 p2269 A70-27918

Microwave avalanche diode emission frequency dependence on charge transfer across drift region, considering varactor diode output, negative resistance and noise factor

14 p2555 A70-30354

Megavolt prebunched electron beam systems for electronic sources in millimeter and submillimeter region, describing microwave accelerators and bunchers

14 p2555 A70-30431

Binary varactor diode microwave device, displaying two capacitance values in reverse bias operation for application in phased array systems and frequency control

14 p2556 A70-30919

GaAs slices efficiency as transferred electron devices, correlating impurity profiles with microwave performance

15 p2708 A70-31957

IMPATT microwave diodes small signal characterization by equivalent circuit using iterative computer procedure

15 p2708 A70-31971

Microwave power transistors design and packaging

15 p2711 A70-32589

Solid state UHF and microwave device testing by computer automated network analyzers, measuring scatter parameters

15 p2742 A70-32590

French monograph on microwave ferrite devices, discussing paramagnetism, ferromagnetism, ferrimagnetism, gyromagnetic resonance and nonreciprocal effects, isolators, attenuators, phase shifters, etc

16 p2873 A70-33267

GaAs microwave devices including diffused varactor, Schottky barrier and Gunn diode, discussing single crystals preparation and epitaxial growth layers

16 p2873 A70-33293

Integrated X band superheterodyne receiver design using planar transmission lines as components

16 p2874 A70-33388

Microwave power transistors, considering figure of merit, performance and packaging

19 p3386 A70-37691

Microwave transistors parameters measurement by scattering /S/ parameter method for characterizing noise, gain and dynamic range, reading input and output impedances from Smith chart

19 p3386 A70-37692

Microwave feeding system for heating and cooking prepackaged meals during extended space missions

19 p3368 A70-37747

Breakdown electric field strength in S band microwave cavity for dry air, water vapor and mixture

19 p3423 A70-37757

Reliability figure of merit variations for predicted microwave radio system outages, using computer method

20 p3583 A70-38987

Centimeter wave transmitting and receiving equipment for studying nanosecond pulse propagation

20 p3632 A70-39627

Microwave apparatus for resonant frequency change and loaded resonator Q measurement during DC discharge afterglow electron removal studies

20 p3679 A70-39715

Microwave transistors for power generation and amplification, discussing packaging and pellet design

20 p3599 A70-40324

Cyclotron wave rectifier with Cuccia coupler for converting microwave power into DC or LF AC

21 p3756 A70-40730

High speed photodetectors for microwave demodulation of light, discussing electrical properties, equivalent circuits and noise factors

21 p3799 A70-41420

Microwave parameters for Gunn devices with low electric field, obtaining data on characteristics and operating mode

21 p3863 A70-41989

Distance measurements by microwave tellurometers, discussing accuracy factors

22 p4039 A70-43426

Integrated 7 GHz small signal microwave balanced mixer, using microstrip transmission lines

23 p4168 A70-43777

Microwave communication - Conference, Budapest, April 1970, Volume 5, Microwave electronics, system measurements

23 p4170 A70-43793

Microelectronic phase lock microwave receiver packaging, discussing subassemblies interconnection minimization, shielding, RF interference, low loss and testing problems

23 p4164 A70-44536

MICROWAVE FILTERS

Transistors used as UHF high-Q inductance active filters, utilizing internal phase shift and energy storage characteristics

03 p0458 A70-14033

Half wave stepped digital elliptic filter design showing improvements over microwave TEM line narrow band bandpass filter

08 p1476 A70-21284

Circuit development for realizing narrow bandwidth elliptic function filters at microwave frequencies

08 p1476 A70-21285

Optimal construction of microwave filters with TWT and ferrite direct gain receivers

09 p1648 A70-23166

Capacity bounds in microwave filters computed for periodic cylindrical rods between parallel ground planes using variational principles

10 p1850 A70-24834

Microwave IC-compatible resonators for communication systems filters, comparing microstrips, disks, waveguide cavities and dielectric-loaded cavities

10 p1852 A70-24892

Microwave band-stop filters based on ladder network low pass prototypes, comparing performance with bandpass type

14 p2557 A70-31179

Microwave channelizing filters input ports interconnection techniques for signals sorting into contiguous frequency bands

14 p2558 A70-31319

Microwave filters developments, performance, production and costs

14 p2559 A70-31374

Circular and nearly rectangular irises for resonant cavities in transmission line for microwave band stop filters, discussing design based on merit factor

21 p3792 A70-41992

Signal controlled microwave modulator as filter or attenuator, using rectangular waveguide and varactor diode switching

22 p3995 A70-42718

Transmission factors of microwave filters with prescribed attenuation and group delay

22 p3997 A70-43173

MICROWAVE FREQUENCIES

NT C BAND

NT EXTREMELY HIGH FREQUENCIES

NT SUPERHIGH FREQUENCIES

Microwave holography, discussing zone plate lens design, coherent side-looking radar, large antennas, three dimensional radar display applications

01 p0086 A70-10415

Airborne instrument landing systems and ground facilities analysis and specifications, examining future use of microwave frequencies

02 p0333 A70-11982

Spectral and lasing characteristics of microwave frequency modulated He-Ne laser operating at 0.63 micron wavelength

05 p0858 A70-16257

Secondary frequency standard obtained for Hg laser operating at microwave frequencies

05 p0859 A70-16271

Microwave frequency radar terrain echoes simulation concerning variation of echo delay, Doppler shift, random fine structure and time variation

06 p1008 A70-17482

Microwave variable delay devices, discussing solid state microwave acoustic interactions

06 p1019 A70-17483

Plane light wave diffraction incident upon isotropic dielectric layer traversed by acoustic microwave using guided microwave theory

06 p1105 A70-17484

Microwave irradiation effects on rabbit eye lenses, noting injury dependence on frequency

08 p1452 A70-21273

Schottky barrier diodes microwave power rectification efficiency, developing diode losses theory based on back capacitance, series and front resistance and knee voltage

08 p1474 A70-21274

Microwave conductivity and limiting frequency in Gunn effect GaAs using drifted Maxwellian

09 p1739 A70-22849

Microwave radiation thermal and nonthermal biological effects, considering exposure limits

10 p1824 A70-24061

Microwave phase shift measurement errors caused by reflections from interference systems elements

10 p1853 A70-25130

Complex dielectric constant of alpha-AgI measured in microwave region and far IR, noting sample positioning

16 p2960 A70-33225

Microwave scintillations at sunrise indicating solar point sources at sunspot cycle peak and terrain configuration influence on ionospheric disturbances

20 p3591 A70-40493

Constant emf in bulk Ge and Si N-type semiconductors under multifrequency microwave electric field

21 p3861 A70-40636

Antiferromagnetic resonance measurement in manganese difluoride as function of microwave frequency, sample size and shape

21 p3850 A70-41908

- Microwave communication - Conference, Budapest, April 1970, Volume 1, Communication system theory 23 p4158 A70-43751
- Mossbauer spectrum of submolecular changes of oxyhemoglobin in animal blood exposed to microwave irradiation 23 p4144 A70-43788
- Cascaded varactor frequency multiplier design for microwave range 23 p4170 A70-43877
- Microwave frequency light modulators waveguides, examining optimal cross sections to increase modulator efficiency 23 p4196 A70-44409
- MICROWAVE IMAGERY**
- Microwave holography with artificial reference wave and receiver multiplier, improving linear resolution in image 13 p2408 A70-29407
- Bicylindrical microwave lenses, discussing collimating, virtual line source and point fed scanning lenses design 16 p2876 A70-33405
- Microwave holography coherent radar with improved focusing, applying to side-looking, bistatic, passive and pulse compression radars 23 p4161 A70-43874
- MICROWAVE INTERFEROMETERS**
- Plasma electron density errors in measurement by microwave interferometers, noting effects of inaccurate phase shift determination 09 p1738 A70-23634
- Fabry-Perot microwave interferometer, examining resonant system electrodynamic properties by matrix method 19 p3422 A70-37722
- Polar microwave interferometer using single null path bridge and klystron repeller voltage modulation 22 p4048 A70-42323
- Light source spatial coherence measurement, verifying laser heterodyne interferometer theory 24 p4354 A70-45665
- Confocal microwave Fabry-Perot interferometer resonator diffraction loss and field configuration measurements, noting agreement with theory 24 p4381 A70-46242
- MICROWAVE OSCILLATORS**
- Elliptically polarized microwave oscillations conversion to linearly polarized oscillations with polarization plane in original orientation 04 p0655 A70-14608
- Microwave low power electron tube oscillators and solid state technology 05 p0823 A70-16882
- Frequency response linearity for self excited microwave oscillators with complimentary cavity derived, proposing parameters selection for widening voltage tunable frequency range 05 p0824 A70-16891
- Tuning range slope steepness as criterion for evaluating microwave resonators tuning range 05 p0824 A70-16893
- Discharge current effect on shape and position of resonance curves for electron concentrations during microwave oscillation conversion in magnetoactive plasma 08 p1551 A70-20866
- P-n junction avalanche and bulk Gunn effect microwave oscillators, analyzing IMPATT and TRAPATT modes 09 p1644 A70-22224
- Microwave Gunn oscillators loaded Q factors determined on basis of frequency changes resulting from constant-depth probe movement along output line 09 p1645 A70-22601
- Tunable L band high power anomalous mode avalanche diode oscillator with coaxial circuit 10 p1847 A70-23888
- Low power microwave IMPATT oscillator as parametric amplifier pumping sources for use in radar and communication systems 10 p1847 A70-23891
- Resistive parametric mixing in GaAs oscillators at microwave frequencies resulting in negative mobility at signal frequency 10 p1849 A70-24231
- Avalanche diodes in presence of microwave instabilities related to field emission and charge transfer across depleted zone, discussing positive and negative resistance 10 p1850 A70-24621
- Silicon L-band avalanche diodes as high power pulsed microwave sources, discussing fabrication, circuit requirements, radar applications, etc 10 p1852 A70-24893
- Epitaxial or bulk GaAs for Gunn diodes in high power microwave oscillators 11 p2021 A70-26828
- Read-diode microwave oscillators performance degradation due to space charge and series resistance, discussing RF power optimization 12 p2194 A70-27167
- Coupled microwave oscillators interaction, discussing klystron operation regenerative and non-monotonic frequency pulling modes 12 p2196 A70-27847
- Tapered Gunn effect microwave oscillators frequency tuning by resistive quenching of high field domain 12 p2199 A70-27986
- X band Gunn oscillators for binary FSK regenerator operation employing signal injection triggering 12 p2199 A70-28015
- High speed linear phase and amplitude modulation of X band Gunn oscillators 12 p2199 A70-28016
- Shielded-cathode mode Gunn oscillators to eliminate constraints on operating frequency 12 p2200 A70-28056
- HF quenched-domain mode /Q mode/ Gunn effect oscillator in single frequency operation using signal analysis, obtaining instantaneous I-V transfer characteristics 12 p2202 A70-28162
- Electronic tuning range of solid state microwave oscillators, deriving equations in terms of tuning device Q factor and available power output 13 p2376 A70-28802
- High power L-band avalanche diode oscillators fabrication and performance 13 p2376 A70-28977
- High power L- and S-band transferred-electron oscillators from epitaxial GaAs 13 p2377 A70-28978
- Microwave oscillator providing transition to stable emission at harmonics with power levels comparable to fundamental frequency, considering gallium arsenide oscillation mode 13 p2471 A70-29413
- Multilevel maser oscillators undamped output pulsations, investigating effect of coupling between signal frequency energy storage and circuit properties at pump frequency 13 p2430 A70-29704
- Nonlinear effects in microwave resonators containing thin superconducting films and low values of microwave power 15 p2782 A70-31525
- Incident microwave signal in Tonks-Dattner resonance coupled to discrete LF modes in plasma column 15 p2778 A70-31756
- SHF pulsed Gunn effect GaAs oscillators for nsec pulse length radar applications 16 p2875 A70-33397
- Gunn oscillator external negative differential /END/ conductance broadband measurement noting effect of cavity control 16 p2875 A70-33398
- Millimeter wave amplification by pumped n-type gallium arsenide oscillating in limited space charge accumulation mode 16 p2875 A70-33399
- Microwave oscillator by transposing principle of spin oscillator at low frequencies in nuclear magnetic resonance in X band 16 p2877 A70-33413
- K-band high power Si avalanche diode oscillators, discussing decrease in pulse peak power output on basis of quenched plasma effect 16 p2880 A70-34260
- Phase control of locked negative resistance /Gunn/ oscillator under operational conditions, noting coupled varactor diode use 17 p3055 A70-35630
- Microwave oscillator performance of InP three level transferred electron devices 17 p3048 A70-35874
- Bulk negative resistance microwave oscillators efficiency calculation by graphical method 17 p3056 A70-35876
- Avalanche transit time diode and transferred electron oscillators in microwave systems, discussing design, performance and applications 18 p3232 A70-36675
- Fundamental microwave oscillator subharmonic phase locking for stable power, comparing with varactor frequency multipliers 19 p3386 A70-37689
- Small signal oscillation and growth for microwave loaded avalanche diodes with drift and ionization allowance 19 p3389 A70-37968
- IMPATT diode microwave oscillator with modulated bias current, discussing amplitude and frequency modulation sensitivity, thermal effects and load parameters 19 p3390 A70-38363
- Crystal controlled digital frequency setting for microwave oscillators in mobile FM radio links with remote handling 20 p3596 A70-39162
- Injection locked bilateral microwave oscillators, deriving criterion for preventing reverse locking 20 p3597 A70-39470
- Unmodulated microwave oscillations power stabilizer with semiconductor attenuator 21 p3796 A70-40635
- Avalanche diode microwave oscillators, considering Impatt and Trapatt oscillation modes 21 p3798 A70-41336
- Microwave frequency marginal oscillator for electron spin resonance spectrometer, using Gunn diode in sample cavity 21 p3827 A70-41460
- Microwave output power and impedance for InP and GaAs bulk negative resistance oscillators, using velocity/field characteristics 21 p3800 A70-42049
- Tunable high efficiency high peak power UHF avalanche diode oscillator 21 p3800 A70-42117
- CW silicon SHF TRAPATT diode oscillator, discussing double sided design and fabrication 21 p3800 A70-42118
- Tunnel diode microwave oscillator design, discussing fixed frequency or varactor tuned operation, power instabilities and load variations 22 p3997 A70-43129
- Radiosonde receiver and transmitter system optimization, obtaining increased microwave power by appropriate oscillator operating modes 22 p4038 A70-43379
- Gunn microwave oscillators I-V characteristics in quenched and retarded modes, using piecewise linear approximation 23 p4168 A70-43778
- P-n junction dependent FM noise spectrum of UHF transistor power oscillator at transit frequency 23 p4161 A70-43789
- High Q frequency stabilized cavity controlled microwave oscillator using Super Invar resonator 23 p4169 A70-43792
- S band tunable free running high Q triode oscillator phase and frequency instability measurement based on delay lines applications 23 p4170 A70-43796
- Klystron microwave signal generator power stabilization using compact low consumption integrated circuits 23 p4170 A70-43797
- High stability phase locked Gunn microwave oscillator with internal crystal reference, discussing applications as signal generator, low noise Doppler radar sources, etc 23 p4172 A70-44013
- Microwave oscillator design using Y-parameters from measured scattering parameter data at desired frequencies, applying negative resistance circuit theory 24 p4320 A70-46235
- MICROWAVE PHOTOGRAPHY**
- Acoustic /microwave/ holography for large masses by crossed linear array of microphones, discussing computer simulation of virtual holograms and image reconstruction 21 p3822 A70-40715
- MICROWAVE PLASMA PROBES**
- Electromagnetic wave reflection on thin plasma layer with Epstein electron density profile, noting use in microwave diagnostics 03 p0529 A70-13016
- Microwave nonlinear effects including mixing, harmonic generation and current rectification observed in plasma sheath surrounding Langmuir probe using PIG discharge 05 p0852 A70-16992
- Power absorption by microwave generated plasmas noting pressure effects 14 p2622 A70-30675
- Microwave probe for measuring electron density profile in supersonic arc jet plasma 15 p2741 A70-32433
- Microwave diagnostic method for amplitude variations of electron density and collision frequency in weakly ionized plasma 17 p3140 A70-34871
- Microwave diagnostics of electron density, temperature and light emission in self excited moving striations in hydrogen plasma 19 p3475 A70-37553
- Microwave diagnostics of plasma temperature and conductivity in streaming nitrogen arc with skin effect under atmospheric pressure 19 p3476 A70-37554
- MICROWAVE PROBES**
- NT MICROWAVE PLASMA PROBES**
- Microwave propagation in materials and measurement methods for inspection based on reflecting surface movement and scattering method for porosity detection 01 p0094 A70-11395
- Quadruple microwave probe applied to phase and attenuation variations measurements of HF wave propagating through dielectric media 02 p0345 A70-11898
- Atmospheric effects on passive microwave sensing in EHF region under all-weather conditions on global scale using satellites [ALAA PAPER 70-198] 06 p1010 A70-18099

Mathematical model of microwave probe for reentry plasma, using variational method to calculate reflection coefficient

12 p2230 A70-26983

Nondestructive noncontacting microwave depth measurement of thin slits and cracks in metal surfaces

14 p2584 A70-30507

Atmospheric effects on passive microwave sensing in EHF region under all-weather conditions on global scale using satellites

20 p3586 A70-39703

Microwave propagation, instrumentation and use in nondestructive testing, discussing components, methods and wave propagation equations

22 p4029 A70-42594

Nonmetallic nonconductive composite materials physical properties by swept microwave frequency nondestructive testing

24 p4345 A70-45705

MICROWAVE RADIATION

U MICROWAVES

MICROWAVE RADIOMETERS

Self calibrating radiometer for in-flight measurement of earth surface thermal microwave radiation

07 p1282 A70-19616

Atmospheric temperature measurement by microwave radiometry, considering instrument design for measurements at various barometric levels

08 p1495 A70-21041

Microwave radiometric techniques for continuous all-weather remote sensing of sea conditions from satellites, discussing foam and surface ripple effects [ALAA PAPER 70-318]

09 p1677 A70-22869

Atmospheric temperature and pressure profiles remote measurement using airborne microwave radiometer

11 p2056 A70-26502

Microwave radiometer as passive satellite sensor for observing ocean surface properties

12 p2228 A70-26902

Microwave radiometric temperature measurements generating curves relating sea state and surface temperature

12 p2215 A70-26903

Microwave radiometry assumptions relating to absorptivity, emissivity and reflectivity data for earth resources remote sensing applications

12 p2230 A70-26959

Millimeter and submillimeter wave receivers, describing detectors, mixers, low noise amplifiers and radiometers

14 p2549 A70-30448

Microwave radiometric receiver, analyzing video detector saturation effects on linearity

16 p2880 A70-34075

SHF radioheliograph with T shaped dish antenna array, noting high resolution and special applications

17 p3061 A70-35397

Shock layer microwave radiation measurements during reentry flight of spherical nose cone, determining effective plasma temperature

[ALAA PAPER 69-183]

18 p3208 A70-36694

Heterodyne millimeter wave radiometric system for observing atmospheric attenuation due to water vapor, discussing design, development and initial measurements

20 p3588 A70-40308

SHF-EHF region uses, discussing microwave radiometry and applications to radio astronomy and meteorology

21 p3799 A70-41421

Microwave radiometry and applications as material composition and temperature sensors for aircraft navigation, landing aids, pollution surveillance, meteorology and oceanology

23 p4198 A70-44648

Microwave radiometric airborne measurement of salinity of Mississippi River outflow, using P3A aircraft

24 p4330 A70-45979

MICROWAVE RESONANCE

Microwave spectral resonator and reentrant cavity as diagnostic tools to obtain discrete point data along plasma column compared with cylindrical cavity

04 p0696 A70-15650

Wobblator measurement of Q factor of microwave resonator cavities using double modulated klystron signal

05 p0822 A70-16528

Pulsed radio signals time delay due to molecular microwave resonance in earth atmosphere and interstellar medium

08 p1461 A70-20915

Dielectric properties of thin barium titanate films from microwave resonance frequencies and resonance reflection coefficient

19 p3482 A70-37255

Fabry-Perot microwave interferometer, examining resonant system electrodynamic properties by matrix method

19 p3422 A70-37722

IR microwave double resonance signals in systems of ammonia with nitrogen isotopes, using nitrous oxide laser

21 p3836 A70-41707

Resonant frequencies of microwave dielectric resonator in magnetic wall waveguide

23 p4169 A70-43784

MICROWAVE SCATTERING

Microwave propagation in materials and measurement methods for inspection based on reflecting surface movement and scattering method for porosity detection

01 p0094 A70-11395

Microwave dispersion caused by atmospheric gases at water vapor line, using microwave spectrometer based on dispersion detection in refraction spectrum

02 p0260 A70-12571

Reduced multiport equivalent scattering parameters derivation by matrix method, determining load reflection coefficients effect on signal attenuation and phase shift

03 p0458 A70-14038

Elliptically polarized microwave scattering at electrically conducting rough surface, considering probability distribution of profile angles and random reflection coefficients

04 p0650 A70-15286

Forward angle microwave scattering by plasma covered magnetized metallic sphere, calculating radial electron density distribution

06 p1008 A70-17576

Moving plasma column scattering of obliquely incident microwaves, assuming arbitrary polarization for incident plane wave

06 p1124 A70-18608

Microwave scattering from plasma column of low pressure discharge in Hg under free space conditions

06 p1125 A70-18609

Scalar radiative transport equation solved iteratively for microwaves backscattering from turbulent plasma, deriving model for direct and cross polarized cross section

07 p1353 A70-19993

Soviet collection of articles on physics of clouds modifications covering precipitations microstructure remote measurements, microwave scattering, etc

08 p1536 A70-21094

Microwaves scattering and attenuation in precipitations from raindrop size distribution curves analysis

08 p1462 A70-21096

Radar model of shower and hail clouds as two phase system of independently scattering spherical particles, stressing radar properties dependence on particle properties

08 p1536 A70-21097

Obstacle extinction cross section determination at microwave frequencies from Q factor of open resonator

09 p1637 A70-23307

Solid dielectrics permittivity measurement using beam deflection phenomenon in multislot waveguide antenna

09 p1652 A70-23656

Stratospheric water vapor measurement by submillimeter wave sounding, considering signal fluctuations due to scattering by high cirrus clouds

11 p2077 A70-26619

Microwave scattering by turbulent plasma electron density fluctuations

11 p2096 A70-26765

Double diffused epitaxial silicon bipolar microwave transistor design, fabrication and performance evaluation, including scattering parameters vs frequency for common-emitter amplifier

13 p2379 A70-29592

MICROWAVE SENSORS

Pulsed microwave spectrum analyzer using holography and Fourier spectroscopy compared with frequency methods

09 p1675 A70-22485

Waveguide gas discharge indicator of transmitted microwave power, investigating sensitivity, discharge conditions, filler gas and pressure effects

11 p2020 A70-26807

Passive microwave sensors based on brightness temperature vs frequency model for various atmospheric conditions, presenting vegetation pictures

20 p3626 A70-39054

Waveguide gas discharge indicator of transmitted microwave power, investigating sensitivity, discharge conditions, filler gas and pressure effects

24 p4317 A70-45179

MICROWAVE SPECTRA

Atmospheric models of deep atmosphere thermal emission and ionosphere free-free emission used for studying Saturn microwave spectrum

01 p0180 A70-10533

Solar microwave burst of 30 March 1969 associated with behind-limb proton flare, studying burst spectrum

[AFCRL 70-0141]

02 p0358 A70-12200

Doppler radar spectrum mean and variance derived for reflectivity gradients combined with linear wind shear velocity gradient

02 p0328 A70-12508

Microwave spectra of type 4 bursts at cm and dm waves compared to related PCA

02 p0359 A70-12774

Critical review of paper on molecular oxygen microwave spectrum analysis

09 p1732 A70-22829

Sagittarius sources A and B2 O18H absorption lines measured at microwave frequencies, determining oxygen isotopes abundance ratios

10 p1936 A70-23907

Passive remote sensing in microwave spectra for oceanographic applications including sea state, pollution and sea ice properties

12 p2216 A70-26905

Microwave solar bursts intensity and polarization measurements at 17 GHz, discussing chromospheric flares and X ray emission

12 p2293 A70-27592

Microwave lines due to hydroxyl radical in interstellar medium, discussing emission from excited OH states

13 p2484 A70-28371

Jupiter microwave spectrum from polarimetric observations and previous data

14 p2648 A70-31088

Hot universe model for demonstrating distortions in Rayleigh-Jeans region of microwave relic radiation spectrum by primeval plasma heating before recombination epoch

14 p2632 A70-31287

Mercury disk temperature from microwave spectrum analysis, proposing subsurface greenhouse effect

17 p3157 A70-34838

Planetary nebula K3-50 microwave observations, determining composite source radio spectrum

18 p3313 A70-36326

Variable radio source linear polarization at 8 GHz, examining degree, position angle and flux density

18 p3317 A70-37001

Radio sources with opaque microwave spectra near galactic equator

19 p3522 A70-38603

Solar eclipse microwave spectral observations for coronal condensation sources characteristics of solar radio emission slowly varying component, discussing ionospheric recombination coefficients

19 p3531 A70-38910

Cloud structure, atmospheric water vapor and liquid water contents from passive ground based microwave spectrum measurements

21 p3846 A70-40906

Microwave transitions for molecules in comets and interstellar space

21 p3887 A70-41110

Heavy atom skeletal molecular structure of asymmetric close-2,3-dicarbahexaborane from microwave rotational spectra

21 p3773 A70-41392

Laboratory measurement and low noise search in W3/OH for microwave emission lines in excited rotational level of interstellar OH

21 p3922 A70-41977

Atomic hydrogen 21 cm line intensity distribution in Carina arm of Milky Way galaxy

22 p4100 A70-42851

Venus atmospheric parameters from microwave spectrum, discussing brightness temperature, carbon dioxide content, opacity, water vapor, dust and models

23 p4241 A70-44256

Solar flare microwave spectra from coherent plasma emission mechanism

24 p4396 A70-45390

Delphini and Serpente Novae radio emission in microwave spectra, noting consistency with thermal radiation of expanding ionized gas envelopes

24 p4410 A70-45771

MICROWAVE SWITCHING

Three way power divider/summer fabricated symmetrically in stripline by resistive network transformation

05 p0821 A70-16386

Silicon window with double carrier injection to achieve high power broadband microwave switching, obtaining power increase over p-n diodes

10 p1847 A70-23892

Power ferrite modulator and switch for SHF band based on Faraday rotation principle

12 p2199 A70-28000

Signal controlled microwave modulator as filter or attenuator, using rectangular waveguide and varactor diode switching

22 p3995 A70-42718

MICROWAVE TRANSMISSION

Minimum microwave path clearance establishing procedures, considering relation to inverse beam bending in microwave propagation

02 p0253 A70-11746

Troposphere microwave transmission factor determined from dispersion and attenuation caused by water vapor isolated molecular resonance

02 p0261 A70-12593

Microwave transmission through afterglow of RF excited electrodeless He discharge approximating low collision frequency plasma slab of uniform electron density in magnetic field

03 p0530 A70-13152

- Rectennas design, construction and power output
04 p0660 A70-15649
- Errors arising in torsion-type ponderomotive watt-
meter connected in homogeneous microwave trans-
mission line with mismatched oscillator at input and
mismatched load at output
06 p1024 A70-17861
- Passive microwave observation from space of sea
surface degraded by atmosphere
[AIAA PAPER 70-197]
06 p1010 A70-18087
- Microwave radio refraction analysis for controlling
interference between radio relay antenna and geosta-
tionary satellites
07 p1235 A70-19363
- Step recovery frequency shift keyed retimer using
Gunn effect FSK pulse regenerator for microwave
communication
07 p1237 A70-20285
- Microwave propagation along earth-air path, study-
ing tropospheric layer role
08 p1461 A70-20968
- Polar gas phase dielectric under conditions of power
saturation interacting with microwave radiation field
in waveguide
09 p1728 A70-22908
- Microwave lines dispersion equations for ferrite
cylinder and spiral and circular waveguides
11 p2012 A70-26803
- Microwave signals covariance and spectra calcula-
tion for amplitude and phase fluctuations propagated
over line-of-sight path through turbulent atmosphere
12 p2189 A70-27963
- Microwave transmission through thin film screens
with apertures placed in transverse plane of X band
rectangular guides
12 p2202 A70-28164
- Microwave field component distribution in plasma
waveguide covered by metallic sheath in magnetic
field, using counterbalanced antenna probes for field
measurements
13 p2463 A70-29378
- Book on microwave propagation physics covering
unbounded homogeneous medium, terrain effects,
uniform refractivity gradient, nonstandard refractiv-
ity, fading, etc
14 p2551 A70-30953
- Counterrotating antenna onboard Italian satellite in
synchronous equatorial orbit for microwave propaga-
tion experiment
15 p2709 A70-32287
- Microwave propagation refractive index over India,
showing influence of humidity and vapor pressure
15 p2701 A70-32470
- Microwave transmission techniques with packaging
designs for radiation energy losses control, discussing
functions of components
15 p2714 A70-32750
- Radar ducting effects on propagation at microwave
frequencies, recording signal strength as function of
transmitter to receiver range
16 p2858 A70-32927
- Troposphere effects on microwave and optical
signals, correlating refractive index and dispersion
variabilities
16 p2862 A70-33020
- Electromagnetic wave scattering at ellipsoidal
bodies in microwave rectangular and circular
waveguides
17 p3046 A70-35346
- Nonlinear effects of harmonic generation and mix-
ing in lithium niobate microwave acoustic surface
wave delay lines measured using laser light deflection
19 p3485 A70-37698
- Worldwide multichannel air communications
system in 10 GHz to IR range by Quasi Laser Link
modulation and satellites
19 p3378 A70-37855
- SHF and EHF waves simultaneous propagation
over slant line-of-sight overwater path, comparing
phase variations and fading for signal coherence
20 p3588 A70-40301
- Millimeter waves atmospheric attenuation vs
frequency and altitude due to oxygen absorption, tu-
bulating for graphical and seasonal model atmospheres
20 p3588 A70-40302
- Millimeter and decimeter waves atmospheric
absorption as function of pressure, temperature and
water vapor density
20 p3588 A70-40303
- Rainfall effects on EM wave propagation at cen-
timeter and millimeter wavelengths
20 p3588 A70-40310
- Millimeter wave propagation measurements by
ATS-5 satellite, observing attenuation dependence on
meteorological parameters for communication data
link performance prediction
20 p3589 A70-40311
- Microwave propagation in circular waveguide con-
taining inhomogeneous gas discharge plasma
21 p3785 A70-40630
- Wideband millimeter wave communications experi-
ments for satellite applications, considering ATS-5,
radiometry and future lunar base
21 p3787 A70-41337
- Millimeter wave radio systems for relieving crowd-
ing at lower frequencies, discussing technology, at-
mosphere effects and applications
22 p3990 A70-43418
- Microwave transmission over elevated line-of-sight
path, measuring phase front distortion between pairs
of paths
22 p3991 A70-43580
- Microwave communication - Conference, Bu-
dapest, April 1970, Volume 3, Electromagnetic theory
23 p4160 A70-43764
- Multiplicative noise reduction during transmission
of analog signals over tropospheric microwave relay
links
23 p4162 A70-44090
- Directional microwave transmitter for 300 frequen-
cy division multiplexed telephone channels, discussing
transmission quality, reliability, design and operation
23 p4172 A70-44298
- Microwave lines dispersion equations for ferrite
cylinder and spiral and circular waveguides
24 p4317 A70-45178
- Microwave propagation in hollow conducting ellipti-
cal pipe waveguide, calculating successive modes cut-
off wavelengths by numerical analysis
24 p4318 A70-45212
- Microwave propagation in circular waveguide with
axially magnetized gas or solid state plasma /Faraday
configuration/, calculating twist modes
24 p4318 A70-45213
- Circular waveguide with axially magnetized plasma,
investigating twist mode propagation in InSb at 70
GHz
24 p4311 A70-45214
- Microwave propagation in waveguides, investigat-
ing trapped and slightly leaky modes in multilayered or
multiwave regions by ray-optical techniques
24 p4311 A70-45216
- Microwave transmission systems, determining elec-
tric potential functions in inhomogeneous dielectrics
by Earnshaw theorem and finite difference computa-
tion
24 p4318 A70-45217
- Microwave waveguide rotary joint using symmet-
rical excitation for mode conversion to obviate filters
24 p4318 A70-45221
- Microwave transmission in partially dielectric filled
circular waveguide, deriving cutoff wavelength and
phase velocity vs frequency
24 p4315 A70-46260
- MICROWAVE TUBES**
- Microwave devices including gridded tubes, mag-
netrons, traveling wave tubes, amplifiers, solid state
devices for radar and communication applications
10 p1851 A70-24885
- Microwave pencil triodes and cavities of miniature
design for Air Traffic Control Beacon Systems
10 p1852 A70-24886
- MICROWAVES**
- NT DECIMETER WAVES
- NT MILLIMETER WAVES
- Vertical atmospheric vapor distribution from mea-
suring microwave radiation of earth/atmosphere
system at several wavelengths
01 p0135 A70-10202
- Optical reconstruction of microwave holograms
recorded by liquid crystal detectors, emphasizing de-
pendence on IR heat bias provided by incandescent
bulb
01 p0086 A70-10421
- Microwave holography using probe scanning,
analyzing causes of distortion and effects on image
reconstruction
02 p0302 A70-12618
- Natural modes and multiple beam interference in
open resonators, taking into account centimeter wave
experiments and computations
02 p0340 A70-12829
- Book on microwave theory and applications cover-
ing transmission line theory, microwave measure-
ment, signal sources and analysis, network analysis,
etc
03 p0455 A70-13001
- Thin superconducting films nonlinear microwave
properties including impedance-amplitude relation, su-
perconducting current threshold decrease, mode
production, frequency mixing, etc
03 p0539 A70-13409
- Coherent microwave generation mechanism in indium
antimonide at high electric fields, formulating thin
plasma layer double stream interaction theory
03 p0534 A70-14214
- Solar microwave and soft X ray radiation emission
correlation to determine flare peak temperature and
solid angle
04 p0741 A70-15126
- Hologram constructed with microwaves with image
reconstruction at optical wavelengths using laser
05 p0849 A70-16659
- Heat stress due to microwave radiation, establishing
reduction factor for radiation protection guide number
under adverse thermal environments
06 p0998 A70-17202
- Whole body microwave irradiation effect on
chromosomes and protein synthesis in Chinese ham-
sters
06 p0998 A70-17203
- Peripheral blood and structural changes in
hemopoietic organs of rabbits and mice exposed to
microwave radiation
07 p1216 A70-18730
- Radar coherent linear FM microwave generation
with 14 microsecond pulse length and 1000 MHz band-
width, discussing phase error and coherency
07 p1236 A70-20064
- Solar microwave bursts with double structure,
discussing single frequency observations and flare
patrols, time variations of flux density and brightness
08 p1561 A70-21259
- Anomalous microwave recombination line at 11 cm
detected in NGC 2024, Orion A, and IC 1795,
discussing peak antenna temperature
08 p1576 A70-21399
- Microwave radiation exposure control program for
biological hazards, particularly to eye lens
09 p1623 A70-22221
- Microwave in-cavity modulation of helium-neon
laser, obtaining frequency dependence of modulation
depth
09 p1696 A70-22628
- Materials permittivity measurement at millimeter
and submillimeter wavelengths based on phase shift or
sample optical thickness
09 p1684 A70-23648
- Amplitude modulation of microwave signals
propagated through periodically varying plasma
09 p1639 A70-23673
- SID observed as VLF phase anomalies correlated
with solar microwave radio bursts
10 p1933 A70-24816
- Microwave illuminated aperture near radiation field
mapped and processed for microwave hologram suita-
ble for optical imaging for far field pattern simulation
11 p2051 A70-26025
- Pulsed and CW microwave discharge plasmatrons
design calculation, providing electrodeless plasma in
metallic chamber and nonequilibrium plasma
11 p1984 A70-26741
- Microwave radiation from electron beam generated
turbulent magnetoplasma measured, indicating
enhancement near electron cyclotron harmonic
frequencies
11 p2095 A70-26760
- Microwave conductance tensor in crystals with non-
parabolic carrier energy dissipation under crossed
constant electric and magnetic fields
12 p2288 A70-28326
- Microwave radiation effects on radar operators
myocardium functions
12 p2180 A70-28358
- Electron beam interaction with plasma in absence of
magnetic field, discussing microwave radiation emis-
sion and incoherent scattering and instability spatial
growth
13 p2459 A70-28569
- Hybrid ring microwave power divider /rat race/ for
equal or unequal power splitting
13 p2377 A70-29061
- Electron density and transverse electron tempera-
ture of magnetoactive plasma generated in circular
waveguide by microwave signal with variable polariza-
tion
13 p2462 A70-29128
- Cosmic microwave radiation origin based on dis-
crete source models
13 p2479 A70-29787
- Microwave harmonic generation by nonlinear
plasma-metal junctions noting calcium, gallium,
molybdenum, gold, copper and platinum cathodes
14 p2549 A70-30438
- Mercury disk temperature at 3.75 cm wavelength,
showing variation with phase angle and hermographic
longitude
14 p2647 A70-31075
- Microwaves in integrated military avionics systems,
discussing CNI, ECM, component reliability, etc
14 p2551 A70-31177
- X ray bursts rise and fall observed by spectrometer
onboard OSO-4
15 p2792 A70-31670
- Glass tube surrounded nonuniform plasma column
interaction with TM microwave field of cylindrical
cavity for electron density measurements
15 p2780 A70-32347
- Plasma electron density measurement for
microwave-excited pulsed discharges based on skin
effect
15 p2780 A70-32367
- X ray and microwave emissions relationship to
sources on sun, discussing development and structure
of sunspot groups
15 p2794 A70-32486
- Earth/atmosphere system outgoing microwave
radiation calculations, surveying aircraft/ satellite
measurements at various wavelengths
16 p2896 A70-33217

Microwaves - IEE Conference, London, September 1969

High power microwave pulse generation in SHF region, discussing use of boat-grown and epitaxial GaAs diodes

Optical images from microwave far field (Fourier transform/ holograms, noting carrier fringe dependence

Microwave properties of uniformly magnetized slabs filling cross section of rectangular lossless waveguide operating in specific modes

Microwave properties of infinite lossless rectangular waveguide semi-infinite filled with magnetic material operating in specific modes

Bird dispersal measure at airports, using behavioral and electrophysiological effects of high power microwave radiation

Commercial and industrial microwave hazards exposure criteria and survey techniques used in state and local governments

Galactic radio radiation observations at 610 MHz, using corner reflector antenna

Sea water temperature and salinity effects on smooth ocean surface radiation in centimeter range

Single crystal ferrite thin film microwave parameters measurement, examining susceptibility in weak magnetic fields and ferromagnetic resonance

Adiabatic microwave power meter design using sodium thiosulfate phase transformations

Magnetoelastic ferromagnet linear theory, considering spin-elastic microwaves propagation in ferrimagnetic crystal subjected to pulsed magnetic fields

Radio sources flux density and variability at microwave wavelengths

Microwave hologram recording for surface displacement, with laser beam illumination for optical reconstruction of image

Microwave emission from GaAs due to EM wave amplification within biased sample

Microwave radiation effects on maintenance personnel, investigating respiratory reaction, attention concentration, blood content of K, Ca, Na and proteins, etc

Correlated microwave bursts between adjacent active regions associated with solar flares

Crab Nebula electromagnetic spectrum deviation from power law in microwave region, investigating origin from Compton scattering of high energy electrons

Solar X-ray bursts correlation with H alpha flares and microwave bursts observed by Explorer 34 experiment

Acoustoelectric domain spectra in n-GaAs by microwave emission, comparing results with parametric conversions theory

VLF wave generation due to nonlinear interaction of two microwaves with plasma slab under high DC field

Electron beam interaction with external harmonic microwave field in planar diode gap, calculating electric field current and voltage distribution functions

Nonflaring solar X-ray and microwave radiation flux correlation from satellite data

Microwave characteristics in plasma of short discharges in low pressure cesium and mercury vapors, noting spectral and spatial distribution of microwave power and intensities

Microwave communication - Conference, Budapest, April 1970, Volume 4, Microwave theory and techniques

Safety standards and biological effects of microwave radiation, investigating cataractogenesis and heart rate in rabbits

X ray and microwave emissions relationship to sources on sun, discussing development and structure of sunspot groups

Earth/atmosphere system outgoing microwave radiation calculations, surveying aircraft/ satellite measurements at various wavelengths

Circular polarization time evolution during solar microwave impulsive bursts

Microwave emission from Maxwellian magnetoplasma in uniform magnetic field

Nondestructive examination for plastics, discussing transmission, microwave and ultrasonic tests

MICROWEIGHING

U WEIGHT MEASUREMENT

MICTURITION

U URINATION

MIDAS SATELLITES

NT MIDAS 4 SATELLITE

MIDAS 4 SATELLITE

Midas 4 satellite osculating orbital elements determined on basis of optical tracking data

MIDCOURSE GUIDANCE

Interplanetary midcourse velocity correction schedules optimization, discussing timing equations modifications, mission simulation and role of earth based radar

Optimal maneuver decision strategy for space vehicle midcourse trajectory corrections

Computational limitations of midcourse correction velocity for lunar impact trajectories, considering impact miss magnitude correction

Linearized theory for minimum fuel guidance in neighborhood of minimum fuel space trajectory, unrestricted thrust magnitude and allowances for midcourse impulses

Minimum fuel control for discrete time Gaussian processes, applying results to spacecraft midcourse guidance for earth-Mars mission

Manual control systems for spacecraft stabilization involved in rendezvous, midcourse correction, landing, etc

Onboard moon-to-earth trajectory approach guidance with or without midcourse guidance using optical angular measurements

Restricted three body interplanetary guidance scheme using midcourse fixed time of arrival velocity correction

MIDCOURSE TRAJECTORIES

Optimal maneuver decision strategy for space vehicle midcourse trajectory corrections

MIDDLE EAR

Contralateral remote masking /CRM/ increase of LF tone burst produced by middle ear muscle contractions

Tympanic membrane and rectal temperatures compared over wide range of ambient environments as indicators of deep body temperature

MIDLATITUDE ATMOSPHERE

Ionsospheric F layer in equatorial, mid and high latitude regions for various major phenomena including anomalies, neutral air winds, photoelectrons, etc

Ionsosphere total electron content diurnal and seasonal variations at midlatitudes, based on data analysis from Explorer 22 in polar orbit

Rocket sounding data on ionospheric currents at mid and low latitudes noting absence in D and above E region

Midlatitude ionospheric disturbances accompanied by auroral type radio absorption observed by radio astronomy and probes during 26 May 1967 storm

Explorer observations of large temporal variations of midlatitude outer zone energetic electron intensities interpreted as redistribution during geomagnetic disturbances

Balloon-borne experiments with directional scintillators to measure low energy gamma radiation spectrum in midlatitude atmosphere for photons origin and gamma albedos investigation

Diurnal fluctuations of quiet F 2 region intensity at midlatitude based on vertical probe observations during solar activity minimum

Oscillations intervals with diminishing period during magnetic storms, noting relationship to midlatitude disturbances in F region

Midlatitude F 2 perturbations from vertical sounding stations data during solar activity minimum, discussing F 2 region critical frequency variation

Midlatitude upper atmosphere soft electron energy flux nighttime measurements by sounding rocket

Winter midlatitude electron density trough from length fluctuation of Faraday signal fading period of satellite Explorer 22, noting characteristic seasonal variation

Small dispersion whistlers characteristics and propagation at midlatitudes based on observation at Tohokata, Japan

Simultaneous Thomson scatter measurements for middle and low latitudes, comparing electron density and temperature and exospheric and global temperature distributions

Midlatitude sporadic E layer critical frequencies dependence on solar activity using vertical ionospheric sounding data, observing ionization correlation

Tropical and midlatitude stratospheric dust by twilight photometry, considering possible causes of anomalous turbidity levels

Midlatitude upper atmospheric low energy proton intensity obtained from meteorological rocket data

Solar activity effects on midlatitude upper atmosphere corpuscular radiation intensity via rocket sounding

Delayed ionization effects in midlatitude nighttime ionosphere after geomagnetic storms, noting time lag vertical distribution

Midlatitude chorus frequency spectrum changes in relation to previous local magnetic conditions

Geomagnetic field influence on annual F 2 layer longitudinal ionization at midlatitudes, relating solar activity level

Diurnal fluctuations of quiet F 2 region intensity at midlatitude based on vertical probe observations during solar activity minimum

Midlatitude upper atmosphere soft electron energy flux nighttime measurements by sounding rocket

Winter anomaly of radio wave absorption in midlatitude lower ionosphere in terms of meteorological influences and particle influx enhancements

Midlatitude F 2 perturbations from vertical sounding stations data during solar activity minimum, discussing F 2 region critical frequency variation

Atmospheric ozone longitudinal variation in lower middle latitudes of Southern Hemisphere

Simultaneous hydrogen ion composition measurements by upper ionospheric polar orbiting OGO 4 and eccentric orbiting magnetospheric OGO 3 at midlatitude

Midlatitude atmospheric neutron density height dependence during minimum solar activity

Atmospheric dynamic effect on cosmic ray intensity, showing extremum and seasonal variation at midlatitudes

Earth magnetic field effects on midlatitude F 2 layer derivative absorption

Midlatitude stratosphere and lower ionosphere density model, discussing vertical, diurnal and seasonal variations effects on spacecraft trajectories

Midlatitude F 2 layer electron density structure using theoretical model, accounting for atmospheric physical and chemical processes

Midlatitude F region electron and ion temperatures during magnetic storms, examining Thomson scattering, density and time dependence

Photoelectron production and escape flux at midlatitudes, using spectrometric measurements from ISIS-1 satellite

F region night airglow in equatorial and midlatitudes, discussing red and blue emission origins

F 2 layer nighttime ionization at mid-latitudes, investigating conjugate point effects on observation point

Geomagnetic field influence on annual F 2 layer longitudinal ionization at midlatitudes, relating solar activity level 24 p4331 A70-46300

MIDLATITUDES

U TEMPERATE REGIONS

MIE SCATTERING

NT RAYLEIGH SCATTERING

Holograms of light scattered by clouds of water droplets to determine drop size, noting agreement with Mie theory 02 p0296 A70-11890

Mie scattering and polarization functions of atmospheric aerosols determined on basis of logarithmic Gaussian distributions 05 p0879 A70-16664

Field theory of moving dislocations in Cosserat continuum considered incomplete regarding constitutive equations, basing analysis on Mie-developed mathematical analogy to electrodynamics 07 p1334 A70-19564

Circumterrestrial dust component in Doppler shifted zodiacal light, considering Mie theory 11 p2045 A70-25698

Scattered radiation from plane parallel Mie atmosphere containing spherical particles by Fourier transform method 16 p2952 A70-33983

MIE THEORY

U MIE SCATTERING

MIL AIRCRAFT

Mil-10 Soviet giant helicopter cargo and altitude record, VTOL and STOL capability and weight design 03 p0414 A70-14286

MILITARY AIR FACILITIES

Air breathing engine testing at propulsion Wind Tunnel Facility at Arnold Engineering Development Center 11 p2031 A70-25852

MILITARY AIRCRAFT

Blended wing-body design concept for F-15 air superiority fighter, providing fixed wing planform for maneuverability at transonic speed 04 p0622 A70-14395

Protection methods for increasing ground fire survivability of military aircraft hydraulic systems classified by cost, system and component design criteria 05 p0797 A70-15777

Emergency auxiliary hydraulic and electric power for commercial and military aircraft control, proposing self contained monofueled turbine system [SAE PAPER 690658] 05 p0797 A70-15838

Design safety requirement and philosophy differences distinguishing commercial from military aircraft programs 05 p0792 A70-15855

V/STOL and fixed wing tactical transport aircraft survivability while supporting forward area logistics bases, noting V/STOL advantage [SAE PAPER 690705] 05 p0792 A70-15857

British military and civilian aircraft and flying between World War I and II, discussing weapons systems and accidents 05 p0794 A70-16113

Integrated USAF acquisition management systems approach engaging top management abilities available in government and industry 05 p0959 A70-16463

Swedish VIGGEN program for aircraft weapons system development emphasizing management methods 05 p0960 A70-16717

Lift fan V/STOL tactical aircraft performance capabilities determination, using digital computer program 07 p1191 A70-18975

Isochronal maintenance inspection management of Military Airlift Command/MAC/, noting C-141 utilization rate 07 p1428 A70-19673

Remote control turboprop drone aircraft for long unmanned electronic intelligence or tactical communications relay missions 08 p1435 A70-20625

V/STOL transport aircraft design in Germany, analyzing demands in military and civil sectors 08 p1435 A70-20639

Lead-acid and vented nickel cadmium batteries compared in redesign of military aircraft battery for cells reduction, low current density, etc 08 p1440 A70-20712

Integrated display for crowded tactical aircraft cockpits, presenting multisensor information for weapons and fire control systems 08 p1500 A70-21760

Fiat G-222 aircraft featuring high wing twin engine retractable landing gear for military cargo transport 10 p1805 A70-24381

Large scale project grading into stepwise decision stages exemplified by aircraft weapon system development program 10 p1971 A70-24596

Military specification revision of Flying Qualities of Piloted Airplanes evaluated by flight test including

Flight Path Stability and Roll Rate Oscillation techniques [AIAA PAPER 70-372] 10 p1806 A70-24930

Gas turbine engine technology for military and commercial aircraft, discussing operations economy, design matching to missions and fabrication methods 11 p2101 A70-25873

Aircraft turbofan and turbojet engines military-commercial interrelationships [SAE PAPER 700268] 12 p2290 A70-27436

VORTAC system providing navigation service to civil and military air traffic on worldwide basis 12 p2269 A70-27919

Rigid wing subsonic and supersonic civil and military aircraft utilizing aerodynamic lift at takeoff and landing 13 p2344 A70-28543

European Panavia 100/200 two engine variable wing military aircraft, noting prototype design, use and production sharing 13 p2347 A70-29051

USAF undergraduate pilot trainees responses in prototype spatial orientation trainer 13 p2359 A70-29439

Avionics on military combat-reconnaissance aircraft, discussing automatic systems testing and cost effectiveness model 13 p2380 A70-29698

Airborne pulse Doppler radar for tactical aircraft velocity vector measurement, improving navigation system performance 16 p2840 A70-33448

Emergency auxiliary electric and/or hydraulic power for commercial and military aircraft using self contained monofueled gas turbine system 16 p2964 A70-33472

MHD power sources for onboard military aircraft electrical application 16 p2964 A70-33474

Emergency auxiliary hydraulic and electric power for commercial and military aircraft control, proposing self contained monofueled turbine system [AIAA PAPER 70-651] 16 p2970 A70-33616

Equipment and subsystems application to flight management avionics in military and commercial aircraft, noting role of ground-air information transfer 16 p2878 A70-33724

Tactical aircraft performance, discussing electro-optical devices, weaponry, communication and navigational networks, information displays and real time remotely manned control systems 17 p3013 A70-34672

Military aircraft avionics central digital computers, discussing memory capacity, computational speed requirements, cost and tradeoffs 17 p3049 A70-34673

Avionics problems in future Army aviation, discussing communications, navigation, instrumentation, automatic flight control, electronic countermeasures, fire control, etc 17 p3051 A70-34725

Variable sweep high thrust-weight ratio multirole combat aircraft/MRCA/, discussing British-French cooperation, development programs and requirements 17 p3017 A70-34916

Airborne data acquisition and flight recorder systems, comparing civil and military aircraft requirements 17 p3094 A70-35515

USAF aviation accidents diagnostic patterns of injury and death, noting increase in fire and/or associated complications 17 p3039 A70-35574

System engineering process for survival enhancement of military aircraft to meet stringent requirements of general nuclear war [AIAA PAPER 70-893] 17 p3019 A70-35810

Air to air armament selection effect on aircraft configuration [AIAA PAPER 70-939] 17 p3021 A70-35848

RAF aircraft damage due to bird strikes in U.K., discussing preventive measures at airfields 18 p3211 A70-35978

German Air Force aircraft bird strikes statistics 18 p3211 A70-35979

Military airlift command bird hazard minimization near airfields by environmental control, including uses of scare devices, chemicals, trapping, etc 18 p3212 A70-35988

YF-12A interceptor aircraft development and testing, discussing titanium alloys application, aerodynamics and thermodynamics, escape systems for high speed and altitude tests 18 p3213 A70-36451

Military aircraft engines performance increase and cost reduction [SAE PAPER 700272] 18 p3302 A70-36817

Military and commercial transports turbofan propulsion systems impact on future aircraft design and development [SAE PAPER 700267] 18 p3214 A70-36820

High angle of attack aerodynamic characteristics of swept wing navy aircraft designs improved via leading edge modifications [AIAA PAPER 70-904] 19 p3355 A70-37392

USAF operations integration into ATC system 19 p3465 A70-38229

Military Airlift Command jet aircraft computerized area navigation system operational procedures 19 p3465 A70-38232

Export market research for military aircraft 19 p3555 A70-38618

Comparative demand forecasting for military helicopter spare parts, stressing exponential smoothing model 20 p3740 A70-39643

Military and commercial aircraft maintenance costs reduction, discussing labor/material ratio, spare parts use, diagnostic systems, etc 21 p3749 A70-40750

Integrated communication, navigation and identification for worldwide needs of military aircraft 21 p3786 A70-41132

High temperature liquid metal cooled nuclear reactor for military aircraft with long flight endurance and range 22 p4071 A70-43188

Fluidics in naval avionics, discussing CH-46A helicopter stability augmentation and approach power compensator for carrier-based aircraft 24 p4293 A70-45428

Nondestructive testing technology impact on military aircraft maintenance, discussing training, applications and advantages 24 p4342 A70-45678

Fluidically augmented artificial feel system for fighter and attack aircraft control, discussing improved handling qualities [SAE PAPER 700785] 24 p4294 A70-45859

MILITARY AVIATION

Operational planning system for Strategic Air Command for data accessing, generating, displaying and editing using computer complex 01 p0048 A70-11282

Aviation environment master plan concerning public relations problems confronted by USAF bases with adjoining communities 05 p0960 A70-16634

Combat and noncombat ejection/extraction fatalities and major injuries to USAF crewmen 07 p1192 A70-19023

Psychological measures in RAF operational aircrew to obtain details for comparison of flying anxiety casualties from same population 07 p1214 A70-19941

SOAR/Simulation of Airlift Resources/ model for stochastic productivity variations of strategic airlift systems 08 p1466 A70-20930

Pilots anxiety in military milieu using interviews and questionnaires noting effect on proficiency 12 p2179 A70-27051

Medical wastage of professional aviators in military and civil aviation, discussing reasons for preventing flying license revalidation 13 p2359 A70-29440

Economic factors in aviation - RAS Conference, London, May 1970 14 p2668 A70-30935

Military aviation economics in UK emphasizing aircraft industry and government cooperation in meeting RAF requirements 14 p2668 A70-30938

International cooperation in military aviation emphasizing cost effectiveness in R and D, production and export prospects 14 p2669 A70-30939

Predicting retention rate of naval pilots and flight officers beyond initial obligated duty tour based on training performance 15 p2690 A70-31888

Asymptotic myocardial infarction in USAF flyers detected by annual electrocardiograms 15 p2690 A70-31889

Motion sickness among USAF flying personnel, examining organic and psychiatric factors 15 p2690 A70-31890

Combat and noncombat ejection/extraction fatalities and major injuries to USAF crewmen 17 p3039 A70-35576

Aeroatelectosis and pneumothorax in fighter pilot postflight chest pains, noting decompression role 17 p3041 A70-35920

Training simulation improving ejection decision making in naval aviation 23 p4178 A70-44467

Army aviation requirements in high intensity conflicts, discussing transportation, communications, intelligence acquisition, organization and suitable aircraft types 23 p4142 A70-44855

MILITARY HELICOPTERS

NT CH-3 HELICOPTER

NT CH-46 HELICOPTER

NT CH-47 HELICOPTER

NT CH-54 HELICOPTER

NT OH-6 HELICOPTER

NT SA-330 HELICOPTER

T-63 gas turbine engine air induction system protection for OH-58A light observation helicopter against

- debris with minimum power loss and intake air distortion 01 p0164 A70-10681
- Helicopter advantages in airlift operation over conventional fixed-wing aircraft in Vietnam war 05 p0795 A70-16718
- Air crash rescue operations by helicopter ambulances of U.S. Army Medical Department, discussing postcrash fire suppression and injured personnel removal, emergency treatment and evacuation 06 p1002 A70-17714
- Forward looking airborne radar (FLAR) moving target indicator for military helicopter mounting 08 p1462 A70-21358
- AH-1G helicopters combat flight loads from on-board oscillograph data recording, defining performance in terms of critical variables 17 p3013 A70-34706
- UH-1C, AH-1G and UH-1H helicopters combat operational flight profiles, considering airspeed, altitude, rotor speed, load factor, etc 17 p3014 A70-34717
- Attack helicopter fire control system with day and night detection, recognition and kill capabilities, discussing system components, operation and reliability 17 p3043 A70-34732
- Flight loads spectrum data for army CH-47A, UB-1B and CH-54A helicopters components compared with fatigue life spectra 18 p3210 A70-35955
- U.S. Army rotary wing mishap experience for product assurance and accident prevention 19 p3356 A70-38825
- U.S. Army UH-1/AH-1 helicopter maintainability and reliability field program, including statistical data 19 p3356 A70-38827
- Armor airframed helicopter for aerial armored reconnaissance vehicle, noting design, fabrication and weight 23 p4137 A70-44095
- SA-341 Gazelle French military helicopter configuration, performance, flight characteristics, technological particulars and design 23 p4142 A70-44854
- Military helicopter test program application to commercial VTOL operations, discussing military-civil design and development relationships [AIAA PAPER 70-1242] 24 p4292 A70-46327
- MILITARY SATELLITES**
- NT VELA SATELLITES**
- MILITARY SPACECRAFT**
- NT MIDAS 4 SATELLITE**
- Low noise tunable parametric amplifier for tactical satellite communications, discussing characteristics and varactor diode mount 08 p1471 A70-20806
- Communications and attitude control on Phase 2 satellite for Defense Satellite Communication System [AIAA PAPER 70-493] 11 p1998 A70-25427
- Temperature control of USAF tactical communications satellite (TACSAT) by passive techniques [AIAA PAPER 70-461] 11 p2120 A70-25441
- Lunar spaceports for military uses from legal viewpoint, considering Space Treaty 12 p2336 A70-27774
- TDMA applicability to military satellites, describing synchronization process 12 p2187 A70-27916
- Tactical communications satellite (TACSAT) design, emphasizing communications repeater characteristics 16 p2983 A70-34051
- Book on law relating to activities of man in space covering liability, space communication, international organization, military implications, etc 19 p3553 A70-37676
- MILITARY TECHNOLOGY**
- Military inertial navigation technology applied to civil air transport aircraft 01 p0137 A70-10311
- Humanoid unmanned reconnaissance and assault vehicle maneuvers, describing cover-seeking and obstacle-avoidance functions from physiological and engineering viewpoint 01 p0033 A70-10495
- Military aeronautical R and D contributions to civil aviation since 1905, discussing jet engine and supersonic aircraft introduction, air traffic control, etc [AIAA PAPER 69-1114] 01 p0005 A70-10614
- National air traffic control system modernization based on Department of Defense military experience to achieve safe and efficient air space utilization [AIAA PAPER 69-1113] 01 p0137 A70-10616
- Particle removal efficiency of engine inlet separator-filter devices evaluated at Naval inlet test facility for simulated engine airflows, scavenging conditions, etc 01 p0163 A70-10679
- Real-world physical simulators application to tactical and strategical optical hardware 01 p0089 A70-10819
- IR systems in military intelligence and space research including aerospace and planetary investigations, discussing IR detection and IR and earth radiation 01 p0144 A70-11255
- Automatic IR control and tracking systems for aviation, space flights and military use, discussing sensor elements 01 p0139 A70-11262
- CL-84 tilt wing V/STOL program to develop best configuration for ground support operations 01 p0007 A70-11317
- Integrated materiel management for systems or product costs reduction applied to high cost spares management 02 p0401 A70-11671
- Cost effectiveness analysis applicable to DOD military system selection and acquisition, using model to study airborne electronics subsystem 02 p0401 A70-11673
- Structural qualification testing of experimental tactical communication satellite (TAC COM SAT) 02 p0274 A70-11936
- High temperature coatings in industrial, military and space applications, noting use in metal melting and working, furnace protection, propulsion systems, rocket engines, etc 04 p0709 A70-15630
- Electronic search and rescue system developed for West German Air Force, consisting of personal transceiver and automatic distress signal transmitter unit, etc 05 p0793 A70-15904
- Command and control display operational requirements within Allied Command Europe (ACE), information flow, decision making and evaluation 05 p0959 A70-16178
- Aircraft life support systems and equipment evaluated in Vietnam combat environment, discussing combat ejection conditions, injuries cause and severity, fatalities, etc 05 p0806 A70-16298
- Computer controlled radar guided tactical missile system using digital techniques in performing target detection, acquisition, tracking and illumination 05 p0814 A70-16328
- Systems engineering management process for satisfying MIL-STD-499 requirements, detailing functional analysis, tradeoffs and resulting design analysis data 05 p0959 A70-16462
- Future U.S. aerospace power in terms of military technology and defense policies and attitudes 05 p0960 A70-16633
- Army aviation personnel ear protection, evaluating APH-5 and SPH-4 helmets 06 p1002 A70-17703
- Life support and survival gear design, testing, manufacture, supply and maintenance for combat ejections over rugged enemy terrain, discussing pilot injuries 06 p1002 A70-17706
- RAPIDJET escape, recovery and survival system providing rapid escape for large aircrew complement by manual bailout system utilizing semiautomatic escape slide 06 p0986 A70-17719
- Material Acquisition Division of Naval Air Systems Command, discussing engineering and testing functions in providing air weapons systems to operating forces 06 p1185 A70-17973
- Thickening of fluids with tetrafluoroethylene polymer to provide physically and chemically stable grease type lubricants for military applications 07 p1292 A70-18863
- Pilot Airborne Recovery Device (PAR/D) using hot air ballute, noting capability to ascend or descend by flow control valve controlling butane burner 07 p1192 A70-19019
- Flying ejection seat providing capability for leaving hostile area before vertical descent by parachute, using Princeton Sailing and bypass fanjet 07 p1192 A70-19020
- Plastic semiconductor devices encapsulation materials and fabrication techniques, considering device performance in various environments and military applications 08 p1468 A70-20626
- Molten carbonate fuel cells power source for military applications, considering catalytic recycle reformer 08 p1439 A70-20703
- Nickel zinc secondary battery low cost and high performance in military applications, discussing maintenance and rapid recharge requirements 08 p1440 A70-20710
- Book on navigation and communication satellites for military uses, considering design, operation, computers role, etc 08 p1582 A70-21298
- Navy Navigation Satellite System program development and present status, discussing satellite design and system accuracy-geodesy connection 09 p1723 A70-23039
- R and D resources allocation model based on correlated Navy technological forecast (NTF) and exploratory development goals (EDG) 09 p1794 A70-23412
- Resource allocation model with cost-effectiveness relationship for Army long range R and D 09 p1795 A70-23417
- Communications and attitude control on Phase 2 satellite for Defense Satellite Communication System [AIAA PAPER 70-493] 11 p1998 A70-25427
- Digital techniques application to military communication satellite systems, discussing 40 Mbps quadruphase modem, convolutional encoders, TDMA, etc [AIAA PAPER 70-495] 11 p2002 A70-25488
- Trends in military communication satellite repeaters, noting influence by increased payload size, weight and complexity 11 p2009 A70-26258
- SHF tactical satellite communications ground terminals, discussing system concepts, relationship to satellites and design problems 11 p2031 A70-26259
- Integral relay operations effectiveness based on random spatial distribution of aircraft under control of Army flight operations center 11 p2080 A70-26265
- Nuclear environments determination methodology for ground military equipment hardening, considering personnel and equipment responses to detonation in atmosphere 12 p2271 A70-27097
- Rotating combustion engine design offering low life cycle costs for military applications [SAE PAPER 700273] 12 p2290 A70-27438
- TDMA applicability to military satellites, describing synchronization process 12 p2187 A70-27916
- Self organization and adaptive routing communication system for military network, describing routing algorithm and entropy organization measure based on stochastic switching matrices 12 p2187 A70-27934
- Hazardous X ray bremsstrahlung from military radio electronic equipment, discussing radiation protection and operating safety standards 12 p2180 A70-28360
- Space-surface path loss due to atmospheric gases, rain and clouds, considering military ground site location for space communication 14 p2608 A70-30596
- Microwaves in integrated military avionics systems, discussing CNI, ECM, component reliability, etc 14 p2551 A70-31177
- Parts standardization in military electronics industry for cost reduction and reliability, discussing design transform from software to hardware 15 p2831 A70-32632
- Reliability factors in design and development staging systems (DDSS) for military and space exploration programs 15 p2747 A70-32639
- Reliability test facilities for military shipboard electronic equipment, subjecting equipment to combined thermal shock and vibration cycles 16 p2888 A70-33125
- Low light level TV (LLLTV) tube, camera and sensor development for military and space applications 16 p2903 A70-33129
- Phased arrays, discussing ground based, shipboard and airborne research programs for military 16 p2863 A70-33264
- In-flight thrust reverser for tactical/attack aircraft, discussing system influence on airplane stability and control [AIAA PAPER 70-699] 16 p2841 A70-33561
- Electronic equipment maintainability in military environment, discussing myths for hardware and human performance conditions 16 p2852 A70-33664
- Coding procedure for Air Force maintenance technicians to record and describe equipment malfunctions compared to experimental codes 16 p2853 A70-33666
- Air superiority fighter design philosophy, including tradeoffs between armament, detection capability, thrust, speed and load factor [AIAA PAPER 70-930] 17 p3021 A70-35840
- Cost effectiveness methodology for space program, industry, military sector, etc 19 p3554 A70-38402
- Military electronic equipment reliability limitations in terms of mean time to failure, considering quality control of components 19 p3390 A70-38596
- RAMMIT (reliability and maintainability management improvement techniques) for processing maintenance data relevant to Army aircraft operations and support 19 p3441 A70-38826
- Laser beam for military weapons applications, investigating energy levels and beam guidance 20 p3641 A70-39421

Electronic equipment test capability, programming methods and operation-modes of General Purpose Automatic Test System, describing updating by USN 21 p3803 A70-40769

General Purpose Automatic Test System using building block concept for avionic systems evaluation at military depot level 21 p3803 A70-40771

Disposable load drop effect on aircraft range, using Breguet equations for graphic determination of bombing range 21 p3750 A70-40868

Military program cost effectiveness and control, considering resources and products 21 p3955 A70-41173

Military sealed thin sintered plate Ni-Cd rechargeable batteries, comparing performance with other systems 22 p3966 A70-43538

Plastic encapsulated IC for military environments, discussing cooker, corrosion and thermal shock tests 23 p4173 A70-44534

Army aviation requirements in high intensity conflicts, discussing transportation, communications, intelligence acquisition, organization and suitable aircraft types 23 p4142 A70-44855

MILITARY VEHICLES

Computer program (TACTICS) for simulating three vehicles simultaneous motion in space, considering interceptor-target guidance and intercept trajectories 07 p1239 A70-20414

Ground effect machine, discussing tactical transport support role 16 p2843 A70-34265

MILK

Transport ratio for I-131 air to milk concentrations, determining mean value and statistical variation from Project Rover data 19 p3361 A70-38012

MILKY WAY GALAXY

Radial velocities determined from prism spectrograms for O and B stars in Milky Way field in Scorpius 02 p0369 A70-12062

Symmetric cosmologies within gamma ray measurement context showing antimatter limits in Milky Way and metagalaxy 02 p0371 A70-12196

Ionized matter complex at galactic periphery deduced from neutral hydrogen line and continuous spectrum observations 03 p0564 A70-13222

Galactic bending dynamics, discussing omega and zeta motions coupling of neutral hydrogen in outer region 03 p0570 A70-13553

BV photometry of Population I Cepheids in Magellanic Clouds, Galaxy and M31 03 p0578 A70-14287

Radio telescopic observations at 408 and 5000 MHz in galactic plane, describing two sources 04 p0746 A70-14514

Neutral atomic hydrogen in Virgo A cluster and between Galaxy and Virgo A, using emission and absorption measurements 04 p0758 A70-15707

NonJeans gravitational instability of stars and interstellar gas in Galaxy due to wave interaction with stars having velocity near wave phase velocity 05 p0917 A70-16906

Density wave theory and Schmidt model applied to Milky Way spiral structure, considering systematic motion of interstellar neutral hydrogen 05 p0918 A70-16928

H I gas and H II regions kinematics, comparing radial velocities near galactic center 06 p1149 A70-18459

Milky way and interstellar clouds brightness fluctuations statistical analysis by surface photometry, studying dust distribution, cloud absorption and dimensions, star distribution, etc 06 p1149 A70-18463

Flux densities and positions for Southern Milky Way sources at 1410 MHz, determining spectral indices 07 p1387 A70-19682

Earth observations of collapsing star neutrinos and neutrino oscillations in Milky Way galaxy 07 p1371 A70-20331

Ionized matter complex at galactic periphery deduced from neutral hydrogen line and continuous spectrum observations 08 p1580 A70-21655

Far IR radiation at galactic center suggested as thermal emission by dust particles 09 p1744 A70-22502

Galactic halo origin and evolution postulated from chemical evolution assuming stellar evolution details 09 p1758 A70-22742

Planetary faint nebulae containing northern Milky Way portion in direction of galactic anticenter observed with spectral Schmidt camera, noting stellar appearance 09 p1761 A70-23051

Galactic sources H109 alpha line and continuum surveys, showing thermal continuum spectrum for sources with radio recombination lines 10 p1936 A70-23903

Galactic radio sources examined for hydroxyl lines associated with H II regions, making observations in absorption and emission 10 p1936 A70-23904

Formaldehyde absorption profile in direction of Milky Way center observed using lunar occultation 10 p1936 A70-23905

Milky Way expansion, explaining Weber gravitation signals by collisions between neutron and normal star 10 p1943 A70-24698

Radial velocities of superegiant distant stars in southern Milky Way regions of I Sco Association 11 p2113 A70-26465

Diffuse matter distribution in northern region of Milky Way, examining relation with O-BO stars distribution 11 p2116 A70-26588

Pulsar research, discussing possibilities in probing galactic medium 12 p2301 A70-27577

Milky Way large scale structure from radio recombination line surveys 12 p2301 A70-27580

Diffuse galactic radiation and absorbing clouds luminescence illuminated by integral stellar radiation in Milky Way 12 p2307 A70-27866

Cosmic rays intensity frequency spectrum near earth, indicating relativistic electron energy spectra similarity in interstellar space and galactic particles existence 13 p2478 A70-29388

High energy cosmic ray muons, investigating arrival from both low and high galactic latitudes 13 p2478 A70-29482

Density wave theory and spiral gravitational field effects in migrating stars orbits and origins in Milky Way spiral arm, using Schmidt model 13 p2495 A70-29801

Near Galactic plane condensations of spectral A stars in HD catalog, investigating by Monte Carlo method and Poisson formula 15 p2797 A70-31616

Galactic structure of Milky Way towards Taurus based on two dimensional classification and three color photography of star group 15 p2797 A70-31621

Milky Way galaxy continuous background radio emission observed at various longitude intervals 18 p3322 A70-37130

Milky Way spiral structure - Conference, Basel, August-September 1969 18 p3324 A70-37151

Milky Way and other galaxies spiral arms configuration, comparing to Andromeda 18 p3326 A70-37154

Spiral galaxies pattern statistics, examining morphological type of Milky Way galaxy 18 p3326 A70-37155

Neutral H spiral structure in Milky Way galaxy, discussing map derivation, pattern interpretation, arm characteristics and kinematics 18 p3327 A70-37161

H 2 region and neutral gas spiral structure and radial distribution, using optical observations and radio continuum surveys 18 p3327 A70-37162

Milky Way galaxy spiral structure analysis, using neutral H Hat Creek survey with southern observations 18 p3327 A70-37164

Continuum source counts in galactic plane 18 p3327 A70-37165

Neutral H concentrations far from galactic plane associated with spiral arms 18 p3327 A70-37166

Milky way galactic plane corrugation, discussing maximum hydrogen brightness temperature oscillating in sinusoidal pattern 18 p3328 A70-37167

Neutral hydrogen distribution in galactic region surveyed with radiotelescope 18 p3328 A70-37169

Radial velocities of neutral hydrogen in anticenter region of Galaxy 18 p3328 A70-37170

H I local spiral arm drift curves from radio telescope operation 18 p3328 A70-37171

Galactic spiral structure relation to local stellar distribution, discussing OB associations, galactic cluster, WR stars, cepheids, and common stars in sun neighborhood 18 p3329 A70-37176

Local spiral arm H 2 regions distribution in Cygnus direction, discussing symmetry due to magnetic field 18 p3329 A70-37180

Milky Way appearance and galactic spiral structure, using models with variable and different absorption values of arms 18 p3329 A70-37181

Integrated Milky Way spectrum, examining composition and galactic structure in solar neighborhood 18 p3329 A70-37182

Interstellar dust spatial distribution, indicating galactic spiral structure 18 p3329 A70-37183

Large scale spiral galaxy structure interpretation, examining density wave theory, Milky Way System and spiral form origin 18 p3331 A70-37196

Young star velocity ellipse vertex deviation, discussing formation at right angles to galactic center direction 18 p3331 A70-37199

Galactic spiral arm helical magnetic fields related to interstellar gas flow, using magnetohydrodynamic models 18 p3331 A70-37200

Cosmic rays - Conference, Budapest, August-September 1969, Volume 1, Origin and galactic phenomena, covering supernovae, ray spectra, pulsar gamma rays, etc 19 p3497 A70-38076

Cosmic rays propagation and production in Milky Way galaxy, using equilibrium model 19 p3510 A70-38157

Expansion motions in inner Galaxy, discussing lower velocity absorption features, mass estimation method and model 19 p3522 A70-38602

Radio sources with opaque microwave spectra near galactic equator 19 p3522 A70-38603

H II region radial velocity comparison to galactic spiral structure, using optical and radio investigations 19 p3524 A70-38698

Cepheids in Galaxy spherical component, determining periodic variations by distribution function technique 19 p3525 A70-38768

Pulsars discovery at low galactic latitudes, investigating dispersion, pulse shape and period 21 p3923 A70-41995

Atomic hydrogen 21 cm line intensity distribution in Carina arm of Milky Way galaxy 22 p4100 A70-42851

OB star distribution statistical analysis in Southern Milky Way, discussing concentrations, relations and systematic deviations 22 p4100 A70-42854

H alpha emission objects in Southern Milky Way, discussing positions, photometric data and relation to galactic structure 22 p4101 A70-42865

Alpha hydrogen recombination lines 156, 166, 167 and 168 from galactic center, using radio telescope 22 p4103 A70-42980

Large scale magnetic field and spiral shock pattern of Galaxy, using density-wave theory 22 p4103 A70-42981

Galactic plane continuum surveys at 8000 MHz, presenting radio contour map and sources list 22 p4109 A70-43747

Radio astronomy research covering solar radio emission, Milky Way radiation, molecular radio line spectra, etc 23 p4256 A70-45041

German monograph on Milky Way spiral structure, describing elliptic orbit model 24 p4399 A70-45100

Discrete source interpretation of isotropic component of diffuse gamma radiation in Milky Way galaxy 24 p4398 A70-46166

MILLIMETER WAVES

Millimeter background discrete source model, deriving required source density from small scale anisotropy upper limit 01 p0173 A70-10041

Astronomical studies at millimeter wavelengths, describing radio meter and Fabry-Perot interferometer design for submillimeter range 01 p0185 A70-10975

Variable atmospheric attenuation of 5 mm wavelength band, considering oxygen absorption spectrum and attenuation for reference atmosphere 02 p0260 A70-12570

Radio telescope efficiency improved at 8 mm wavelength by quantum paramagnetic amplifier and multimirror antenna system 03 p0455 A70-13083

Millimeter wave fields systems application to radar guidance, radiometry, communications, radio astronomy and satellite experiments 04 p0647 A70-14621

Quasi-optical design methods applied to mm microwave resonators characterized by high Q and low spectral densities 04 p0655 A70-14623

MM wave outbursts of 1 and 2 November 1968, discussing wavelength dependence of flux density 05 p0912 A70-16441

Radio astronomical observations in millimeter wavelength region, discussing sun, moon, planets, galactic and extragalactic sources, etc 06 p1139 A70-17417

Solar bursts of enhanced intensity at millimeter wavelengths suggested for limb brightening mechanism

06 p1153 A70-18545

Plastic symmetrical trough waveguides with metalized surfaces for hybrid millimeter-wave integrated circuit systems, discussing ferrite resonant isolator

07 p1243 A70-20151

Millimeter wave CW Gunn oscillators construction by packaging free from spurious resonance, using sapphire ring and Au cap

08 p1468 A70-20482

Millimeter guided wave communication systems information transmission capacity increase, using quaternary and higher order modulation techniques

08 p1462 A70-21506

Permittivity of thin films in millimeter and submillimeter wavelengths measured by diffraction grating method

08 p1464 A70-21985

Frequency measurement in millimeter and submillimeter ranges, using high quality Fabry-Perot resonator

09 p1680 A70-23141

Klystrons operation at millimeter band, using efficiently bunching drift fields for steady power output at critical wavelength

09 p1651 A70-23636

Millimeter band direct-transit klystrons oscillation and amplification at improved output power obtained by electron bunching in nonuniform drift fields

09 p1651 A70-23637

Adaptive multiple access satellite communication system at millimeter wavelengths in time- and frequency-division modes, compensating rainfall attenuation

10 p1838 A70-24358

Multiple access technique for millimeter wave satellite communications, noting weight and size of on-board equipment

10 p1838 A70-24359

Solar mapping using millimeter wave radio telescope, comparing results with H alpha photographs and magnetograms

10 p1945 A70-24963

Solar flares period, core and physical nature of areas by measurements at millimeter wavelengths, discussing radio source center

10 p1934 A70-25277

Beam switching Cassegrain antenna for millimeter wave radio astronomical measurements, describing RF and electronic systems

11 p2019 A70-26374

Atmospheric stability sensing by millimeter wave radiometry, discussing thermal radiation emitted and absorbed by oxygen molecules

12 p2263 A70-26955

Solar radio emission maps at 8.6 mm using parabolic antenna and TV camera for optical control

12 p2293 A70-27591

Electromagnetic radiation attenuation in rain at cm and mm wavelengths, determining rainfall rates and drop size distribution

13 p2364 A70-28783

Millimeter wave probing for vertical distribution of atmospheric water vapor, comparing ground, balloon and satellite observation techniques

13 p2394 A70-28785

Millimeter and submillimeter radio waves propagation, outlining molecular and aerosol attenuation in real atmosphere together with transmitters and receivers

13 p2366 A70-29401

Atmospheric optical thickness from radio telescopic measurements of wave absorption at millimeter wavelengths, showing dependence on lower atmospheric moisture content

14 p2546 A70-30127

Book on millimeter and submillimeter waves covering generation, transmission, components and detection

14 p2548 A70-30426

Millimeter and submillimeter waves applications, discussing klystron oscillators for spectral purity and coherence

14 p2548 A70-30427

Coaxial, inside-out and rising-sun magnetrons for millimeter waves generation under pulsed conditions, discussing tunability, frequency stability and weight

14 p2555 A70-30429

HF backward wave oscillators with emphasis on limiting factors in millimeter waves generation, discussing ohmic and circuit imperfection losses

14 p2555 A70-30430

Megavolt prebunched electron beam systems for electronic sources in millimeter and submillimeter region, describing microwave accelerators and bunchers

14 p2555 A70-30431

Millimeter and submillimeter waves generation as difference frequencies of mixed laser beams

14 p2593 A70-30434

Millimeter waves generation by tunnel, Gunn and avalanche diodes, tabulating frequency, efficiency and power data

14 p2548 A70-30435

Nonlinear resistance and reactance type harmonic generator diodes performance with output in millimeter wave decade

14 p2548 A70-30436

Harmonic generation in gas discharge by frequency multipliers, assessing multipliers capabilities for millimeter wavelength operation

14 p2549 A70-30437

Circular low loss waveguides for millimeter waves, discussing construction, geometry, surface texture, etc

14 p2556 A70-30442

Surface wave transmission lines used at millimeter wavelengths

14 p2549 A70-30443

Millimeter waveguide components, discussing impedance measuring equipment, matched loads, variable short circuits and attenuators, power measurement equipment, etc

14 p2556 A70-30446

Millimeter and submillimeter wave receivers, describing detectors, mixers, low noise amplifiers and radiometers

14 p2549 A70-30448

Millimeter wave applications, considering waveguide and plasma communications, ground surveillance radars, vibration analysis equipment, decoders, etc

14 p2549 A70-30449

Quasi-optical filters with bandpass and pseudohigh pass structures for millimeter wave and far IR frequencies

14 p2558 A70-31318

TWT noise level minimization in 8 mm band with circular spiral slow wave structure and five electrode gun

15 p2707 A70-31519

Instrument for visualization of EM field in open resonators in mm range

16 p2908 A70-33213

Millimeter wave amplification by pumped n-type gallium arsenide oscillating in limited space charge accumulation mode

16 p2875 A70-33399

High speed millimetric horn antenna with small azimuth and elevation beamwidths for airfield radar

16 p2876 A70-33407

Millimeter wave radar for high resolution aircraft landing aid, describing experiments to obtain backscatter data from airborne platform

17 p3133 A70-34721

Lunar millimeter wavelength thermal radiation measurement noting surface roughness effect on polarization

17 p3171 A70-35559

Hour-angle and declination center-to-limb profiles of quiet sun 3.3mm brightness temperature distribution

17 p3174 A70-35868

High altitude humidity from millimeter-band water vapor lines, using EHF atmospheric spectral transparency calculation

19 p3461 A70-37633

Millimeter waves atmospheric attenuation vs frequency and altitude due to oxygen absorption, tabulating for graphical and seasonal model atmospheres

20 p3588 A70-40302

Millimeter and decimeter waves atmospheric absorption as function of pressure, temperature and water vapor density

20 p3588 A70-40303

Millimeter wave observation of sun, deriving empirical relationships between atmospheric attenuation, emission and water vapor

20 p3623 A70-40304

Millimeter wave and optical astronomical refraction differential measurements, showing dependence on atmospheric water vapor

20 p3588 A70-40305

Atmospheric turbulence and wind velocity remote probing by millimeter waves, comparing results with conventional anemometer measurement

20 p3665 A70-40306

Lens with radial symmetry for mm wave scanning antenna

20 p3598 A70-40307

Heterodyne millimeter wave radiometric system for observing atmospheric attenuation due to water vapor, discussing design, development and initial measurements

20 p3588 A70-40308

Millimeter wave reflector antennas, considering various system designs, performance, pointing capabilities, limitations and applications

20 p3599 A70-40309

Rainfall effects on EM wave propagation at centimeter and millimeter wavelengths

20 p3588 A70-40310

Millimeter wave propagation measurements by ATS-5 satellite, observing attenuation dependence on meteorological parameters for communication data link performance prediction

20 p3589 A70-40311

Solar active regions at millimeter wavelengths, discussing brightness temperature, background radiation, electron density, optical thickness, polarization and chromospheric magnetic fields

21 p3886 A70-40960

Millimeter wave space-to-space and space-to-ground satellite communication links frequency allocation problems

21 p3787 A70-41335

Wideband millimeter wave communications experiments for satellite applications, considering ATS-5, radiometry and future lunar base

21 p3787 A70-41337

Millimeter wave high gain Cassegrain antenna for wide bandwidth data link between communications satellites, obtaining accurate parabolic contours

21 p3799 A70-41359

Millimeter wave radio systems for relieving crowding at lower frequencies, discussing technology, atmosphere effects and applications

22 p3990 A70-43418

Millimeter band electromagnetic scattering from weakly doped GaAs, calculating reflection coefficient and phase angle

23 p4229 A70-43926

Uranus and Neptune millimeter wave observations, showing brightness temperatures in excess of black body equilibrium temperatures derived from solar heating

24 p4403 A70-45398

Millimeter wave solar radiation atmospheric absorption examined at sea level with Michelson interferometer

24 p4398 A70-45785

Mm wavelength radiometer for recording solar activity and radiation attenuation in atmosphere as function of time

24 p4315 A70-46236

MILLING [MACHINING]

Apparatus for studying vibrations via contactless HF resonant transducers during milling

09 p1691 A70-22625

Rotary Ultrasonic Machining with diamond tools for hard and brittle materials compared to ultrasonic impact grinding method

09 p1692 A70-22797

Laser applications of metal machining and micromachining, discussing drilling, cutting, milling, welding, dynamic balancing, automation, etc

12 p2241 A70-27082

Surface alterations by machining processes for gas turbine engine materials, emphasizing effects of milling on Ti and grinding on high strength steels

18 p3264 A70-36888

MILLING [MIXING]

U COMPOUNDING

MILLING MACHINES

Spark erosion milling machines adaptable to piece and mass production

15 p2744 A70-31899

Digitally controlled milling machine for complex aerodynamic profiles and prismatic blades

22 p4046 A70-43117

MILNE METHOD

Milne problem for anisotropic atmospheric scattering, determining radiation transmission at particular angle with arbitrary scattering indicatrices and particle albedo

15 p2801 A70-32477

Thick plane fog layers reflection and transmission properties, using emerging light angular distribution for Milne problem

18 p3284 A70-35944

Milne problem for anisotropic atmospheric scattering, determining radiation transmission at particular angle with arbitrary scattering indicatrices and particle albedo

23 p4239 A70-43902

MINER RULE

U PALMGREN-MINER RULE

MINERAL DEPOSITS

Gravity and magnetic geophysical prospecting methods, discussing data acquisition, reduction and analysis in terms of underground geologic anomalies

22 p4018 A70-43086

MINERAL OILS

Potentiometric analysis for determining acidity and alkalinity in dark mineral oils with additives

05 p0810 A70-15898

Distilled water and mineral oils heated to 50-80 C studied for effect on residual stresses in fiberglass reinforced plastics

08 p1526 A70-20925

MINERALOGY

Differential thermal analysis capabilities in mineralogy for determining present/past planetary environmental parameters having significance for biological experiment

11 p1994 A70-25811

Synthetic pyroxenoid stability and crystallography, noting pyroxenoid structure similar to yellow lunar mineral from Mare Tranquillitatis

12 p2226 A70-28022

Seymour coarse octahedrite, compositional and mineralogical relationships 13 p2487 A70-28695

Early Precambrian chert porosity and permeability, investigating hydrocarbon content origin 13 p2400 A70-29863

Apollo 11 lunar rocks mineralogy and petrology, noting anorthosite in powder and breccia 18 p3320 A70-37081

Lunar surface spectral reflectivity measured with ground based telescopes for remote mineralogical analysis 20 p3709 A70-39977

Apollo 11 lunar science - NASA Conference, Houston, January 1970, Volume 1, Mineralogy and petrology 21 p3893 A70-41501

Titanian and aluminian chromites and chromian ulvöspinel in Apollo 11 fines, microbreccias and basaltic type igneous rocks 21 p3895 A70-41505

Apollo 11 lunar rock and fines chemistry, mineralogy and petrology, discussing composition, igneous rocks, microbreccias, glasses and pyroxene relations 21 p3895 A70-41507

Mineralogy and chemistry of Apollo 11 lunar soil samples, using three-channel electron microprobe analyzer 21 p3896 A70-41509

Apollo 11 lunar rocks, breccias, dust and chip mineralogy and petrology, examining composition, texture, grain size and morphologies 21 p3896 A70-41511

Apollo 11 lunar igneous rocks mineralogical, chemical and petrological features by optical and electron microscopy and X ray spectrometry 21 p3896 A70-41512

Petrology, mineralogy and deformation of Apollo 11 rock samples using microscopic, X ray and electron microprobe methods 21 p3897 A70-41517

Tranquility Base lunar soil origin, establishing component nature, size distribution, density, mineralogy, constructional or destructional history 21 p3897 A70-41519

Apollo 11 lunar rock mineralogy, examining petrographic and chemical features by light microscopy, electron microprobe microanalysis and detector system 21 p3898 A70-41525

Bulk chemical compositions, mineral and glass analyses, X ray data and physical properties of Apollo 11 lunar fines and rocks 21 p3898 A70-41526

Plagioclases, pyroxenes and olivines in lunar soils and rocks, using X ray diffraction and Mossbauer effect 21 p3899 A70-41528

Lunar breccia and fine sample metal particles, using optical and scanning electron microscopy and electron probe microanalysis 21 p3899 A70-41529

Type 1 carbonaceous chondrites contribution to lunar soil, comparing mineralogical and trace element evidence 21 p3899 A70-41533

Apollo 11 lunar samples mineralogical and compositional studies concerning lunar origin hypothesis 21 p3899 A70-41534

Apollo 11 lunar igneous rocks minerals and glassy phases characteristics, using electron probe microanalysis 21 p3900 A70-41538

Mineralogy and petrology of lunar rock samples indicating meteoritic increments 21 p3900 A70-41539

Lunar rocks petrography, mineralogy and petrogenesis from Apollo 11 samples 21 p3902 A70-41554

Apollo 11 lunar igneous rock mineralogy and petrology, emphasizing ferrobasalt minerals microanalysis electron probe 21 p3903 A70-41557

Lunar rocks mineralogy and visible and near IR reflectivity, discussing depression in telescopic curve 21 p3912 A70-41637

Hydrous Cu-Ca silicate mineral /kinoite/ from Arizona occurring as single crystals and veinlets 24 p4329 A70-45459

MINERALS

NT ALUMINUM SILICATES

NT ASBESTOS

NT BIOTITE

NT CALCIUM SILICATES

NT CHROMITES

NT ENSTATITE

NT FELDSPARS

NT FORSTERITE

NT GARNETS

NT HEMATITE

NT ILMENITE

NT KAMACITE

NT KAOLINITE

NT MAGNETITE

NT MICA

NT MUSCOVITE

NT OBSIDIAN GLASS

NT OLIVINE

NT PEROVSKITES

NT PYROXENES

NT SCHREIBERSITE

NT SILICATES

NT SODIUM SILICATES

NT SPINEL

NT TROILITE

NT YTTRIUM-ALUMINUM GARNET

NT YTTRIUM-IRON GARNET

Optical studies of deformational structures of minerals from meteorite craters and cryptoexplosion structures 02 p0292 A70-12510

Existence probability of useful mineral resources on moon, considering physical features and geological formations 03 p0563 A70-13170

Composition and monoclinic parameters of chromium sulfide mineral breznaitite in metal matrix and silicate inclusions of Tucson meteorite using electron microprobe 11 p2110 A70-26004

Reinforced plastics adhesion to hydrophilic mineral surfaces by using silane coupling agents 16 p2937 A70-33374

Minerals radiative thermal conductivity at high temperatures from IR measurement of absorption coefficient and refractive index 16 p2897 A70-33648

Cosmic ray track sources in meteoritic minerals, considering heavy primaries, secondary spallation and fission products 19 p3508 A70-38142

Microorganisms metabolic activity effects on rocks and minerals, observing solubilization and altered IR absorption in Si-oxygen vibration region during penicillium simplicissimum growth 21 p3761 A70-40712

Apollo 11 mafic crystalline rocks and mineral assemblages, discussing collection, classification and sample environments 21 p3894 A70-41502

Apollo 11 magnesium-rich opaque oxide armalcolite mineral from Tranquility Base noting relation to pseudobrookite series 21 p3895 A70-41503

Trace elements in Apollo 11 lunar glass clinopyroxene, plagioclase and ilmenite, using ion microprobe mass analyzer 21 p3896 A70-41510

Petrologic analyses of minerals and glass spherules in Apollo 11 lunar rocks, indicating little fractionation and shallow-level differentiation 21 p3897 A70-41521

Apollo 11 lunar rock fluorapatite and trace minerals, examining pressure and oxidizing conditions of formation, grain and crystallization 21 p3898 A70-41527

Apollo 11 lunar rocks and minerals oxygen 18-oxygen 16 ratios 21 p3777 A70-41609

X ray powder and chemical data on monoclinic secondary mineral guildite from mine fire at Jerome site 24 p4330 A70-46274

MINES [EXCAVATIONS]

X ray powder and chemical data on monoclinic secondary mineral guildite from mine fire at Jerome site 24 p4330 A70-46274

MINIATURE ELECTRONIC EQUIPMENT

Miniature piezoresistive pressure transducers for catheter and external physiological measurements in small animals 07 p1220 A70-19297

Standing wave ratio frequency dependence in miniature stripline power dividers and ring structure hybrid junction 09 p1652 A70-23653

Miniature wireless strain and temperature radio telemetry transmitters for measurements in areas inaccessible to direct wire connections 15 p2738 A70-32301

Solid state dipole antenna array miniaturization by etching microstrip components on alumina substrate having high dielectric constant 16 p2876 A70-33409

Subminiature solid state piezoresistive accelerometer using diffused four arm Wheatstone bridge sensor 17 p3094 A70-35522

Magnetic bubbles in miniaturized electronic circuits, discussing fabrication and uses in communication and computers 19 p3484 A70-37574

Miniature pressure transducers using piezoelectric or semiconductor elements 20 p3628 A70-39226

MINIATURIZATION

NT MICROMINIATURIZATION

NT SUBMINIATURIZATION

MINIMUM DRAG

Printed circuit board connector selection techniques based on miniaturization reliability, cost and compatibility with intended application 02 p0268 A70-12473

Microwave pencil triodes and cavities of miniature design for Air Traffic Control Beacon Systems 10 p1852 A70-24886

Miniature electromechanical gallium antimonide tunnel diode transducer theory fabrication and performance 12 p2236 A70-28055

Life and confidence tests of miniature self contained flexure pivots in critical mechanisms [ASME PAPER 70-DE-76] 16 p2918 A70-33522

Ultraminiature pressure transducer for airplane model and inlet/engine subsystem in wind tunnel tests, considering design, calibration, environments, etc 19 p3430 A70-38523

Miniaturized programmer-comparator MINI-BACE /Basic Automatic Checkout Equipment/, discussing design, mechanization, etc 21 p3803 A70-40767

Helicopter rotors fatigue testing using small scale models of full scale components [ICAS PAPER 70-34] 23 p4267 A70-44131

Miniaturized VHF transmitter with bonded circular printed circuits for withstanding high shock loads, discussing design, production, packaging and testing 23 p4164 A70-44537

MINIMA

Final state vector norm minimizing in linear optimal control, using successive approximation and quadratic programming 10 p1856 A70-25188

Minimum principles for rate solution in elastoplastic work hardening materials with regular yield surface 13 p2513 A70-29152

MINIMAX TECHNIQUE

Necessary and sufficient conditions for constrained extrema without use of Lagrange multipliers 07 p1325 A70-19335

Discrete process max-min problem, using dynamic programming to obtain upper and lower bounds 08 p1533 A70-20604

Optimum control law for minimizing mass point maximum deviation under given disturbance obtained by graph analytic method 09 p1727 A70-22534

Sufficiency conditions and Lagrange multipliers in maxima and minima theory with results restricted to ordinary extremal points, considering constrained optimization 11 p2073 A70-26232

Minimax one step and recursive nonlinear predictors for linear discrete time-invariant first order plant driven by unknown bounded forcing function 12 p2204 A70-28069

Soviet book on numerical methods of Chebyshev approximation covering minimax problems, computer methods, linear programming, etc 19 p3456 A70-37232

Unilateral and minimax control with functional restrictions, including pursuit and evasion games 23 p4177 A70-44906

Relaxed minimax control with functional restrictions by Uryson integral financial equation 23 p4213 A70-44907

Algorithm for Chebyshev solution of n plus 1 inconsistent linear equations in n unknowns, using minimax technique 24 p4370 A70-46241

MINIMIZATION

U OPTIMIZATION

MINIMUM DRAG

Surface shape determination for thin delta wing with variable geometry to minimize drag for given open and closed configurations and cruising supersonic speeds 01 p0002 A70-10547

Minimum drag hypersonic delta wing, analyzing shape for given planform, lift, pitching moment and volume using correction for pressure coefficient 01 p0002 A70-10557

Slender bodies optimum aerodynamic shape for supersonic velocities, discussing minimum wave drag and total drag two step analysis using calculus of variations 03 p0408 A70-13801

Two dimensional and axisymmetric bodies shapes providing minimum wave drag to supersonic flow of perfect gas, considering bodies around which flow causes bound shock waves 03 p0409 A70-13863

Streamlining design for high altitude hypersonic flight vehicles based on drag minimization at flight condition 07 p1189 A70-19717

Numerical solutions of variational problems concerning symmetrical wings with minimum drag and optimal aerodynamic efficiency in hypersonic flow 09 p1603 A70-22433

Generatrix shape determined for body of revolution moving at supersonic speed with minimum wave drag 09 p1603 A70-22434

Optimal deformation and minimum wave drag for wings with supersonic leading and straight trailing edge, solving variational problem by Ritz method
09 p1604 A70-22444

Shape of minimum drag slender body of revolution in Newtonian flow for given volume, length and maximum cross section determined by stochastic optimality principle
10 p1802 A70-24278

Minimum drag thin symmetrical cruciform wing fitted with central ridge, reducing problem to linear algebraic finite system of equations
10 p1803 A70-24784

Planar wing with end plates in ground effect, calculating minimum induced drag by approximation theory
21 p3743 A70-40919

Optimum thickness ratio and minimum drag of slender bodies in hypersonic viscous flow as function of altitude
23 p4134 A70-44571

MINKOWSKI SPACE

Pseudoisotropic surfaces in Minkowski space-time with proof of existence, formulating congruencies of normal fiber
13 p2452 A70-29634

MINORITY CARRIERS

Hole mobility in n-type InSb semiconductors determined from solving kinetic equation for minority carriers allowing for scatterings
01 p0155 A70-10185

Resistivity, temperature and injection level dependence of minority carrier lifetime in neutron irradiated p- and n-type Si
04 p0730 A70-14729

Minority current carriers diffusion in heterojunctions and p-n junctions in AlAs-GaAs, using X ray microanalyzer performing electron beam scanning
06 p1126 A70-7816

Minority carriers lifetime following CdS and ZnTe spontaneous luminescence relaxation after electron beam excitation
07 p1302 A70-20318

Volt-ampere characteristics of metal-semiconductor contacts for Schottky barrier diodes, investigating suppression of minority carriers and frequency response
09 p1741 A70-23352

Transient analysis of transistor under large input signal accounting for minority carrier life and base collector capacity
10 p1849 A70-24383

MIS varactors applications as nonlinear reactances, discussing charge-voltage characteristics and minority carriers effect
12 p2196 A70-27685

Minority carrier diffusion lengths on sides of copper sulfide-cadmium sulfide heterojunctions measured by light microprobes
13 p2471 A70-29709

Spectral distribution of GaAs photoconductivity, allowing for coordinate dependence of minority carrier lifetime in surface space charge region
15 p2782 A70-31626

Alloy junction transistors with emitter larger than collector, analyzing minority carrier distribution in base region and effect on current amplification
15 p2714 A70-32703

Conducting state propagation in p-n-p structure involving minority carrier diffusion between regions
23 p4232 A70-45068

Electron recombination effect on current transmission through insulator-semiconductor junction with large diffusion length of minority carriers
24 p4390 A70-45634

MINUTEMAN ICBM

Minuteman 3 Reentry System real time laboratory aging and surveillance test program to evaluate long-term storage effects on equipment behavior
[AIAA PAPER 70-395] 10 p1952 A70-24910

MINUTEMAN MISSILES

U MINUTEMAN ICBM

MIRRORS

NT CELESTROSCOPES

NT MAGNETIC MIRRORS

NT PARABOLOID MIRRORS

NT ROTATING MIRRORS

Optical data display involving laser light deflection by vibrating mirrors actuated by mechanical resonators
01 p0108 A70-10355

Absorber positioning inaccuracy influence in concentrating solar unit mirror on unit energy parameters, discussing defocusing
01 p0010 A70-10763

High reflectivity mirror construction for H Lyman alpha line using vacuum deposited Al layer coated by magnesium fluoride
02 p0299 A70-12367

Autostereoscopic display using vibrating varifocal mirrors, including laboratory computer generated real time image and movie projection systems
02 p0302 A70-12631

Multimirror illumination system for radio telescope antenna with reduced noise temperature, narrow
07 p1293 A70-19119

radiation pattern and optimal specular cross section, noting sensitivity
03 p0455 A70-13082

Complex profile aspherical mirrors used in He-Ne gas laser to obtain single mode emission
03 p0500 A70-13465

UHF self modulation in GaAs laser coupled to external cavity, focusing convergent beam on external mirror
04 p0701 A70-14718

Thermal and dynamic considerations of materials choice for satellite mounted telescope mirrors noting Be and silica properties
06 p1064 A70-17781

Mirror material for satellite-borne telescopes, considering Be and CER-VIT or ULE silica thermal and mechanical properties
07 p1279 A70-19000

Spatial and energy characteristics of laser with nonuniform transmittance across resonator mirrors, analyzing transverse modes interaction
08 p1514 A70-21816

Astronomical high power telescopes construction, discussing rough casting, forming, precision polishing, Foucaultage principle for spherical mirrors, thermal effects, etc
09 p1674 A70-22218

Lightweight mirror blanks of titanium silicate for OAO-4 providing thermal and dimensional stability
09 p1678 A70-22952

Interference proof characteristics and shielding capability of mirror antennas improved by peripheral sheet metal or wire screens, reducing rear lobe level
09 p1648 A70-23151

Optical resonators formed by spherical mirrors, deriving mode density-output power relationship by ray analysis
09 p1729 A70-23521

Mirror-grating system optical properties emphasizing coma-type aberration elimination
09 p1729 A70-23528

Antenna array circular polarization adjustment using reflections from horn radiator and mirror
09 p1650 A70-23633

Temperature insensitive telescope with metallic mirror at Milan-Merate Observatory
10 p1889 A70-24584

Mirror adjustment effect on transverse structure, time dependence and spatial coherence of pulsed UV molecular nitrogen laser emission
11 p2062 A70-25394

Selective optical coatings of alternate Ni and silicon dioxide layers, describing optical and spectral characteristics of black mirror
12 p2272 A70-27307

Gallium arsenide laser with external mirror excited by electron beam, measuring radiation patterns
12 p2247 A70-27482

Modal expansion method applied to thin deformable primary mirror surface control for orbiting astronomical observatory
13 p2403 A70-28427

Thermal control coatings, windows and mirrors for 1973 Mars Viking Lander vehicles under simulated Martian surface conditions
[AIAA PAPER 69-1023] 13 p2384 A70-28530

Gas laser radiation focusing with spherical mirrors, calculating field distribution and beam path
13 p2424 A70-28592

Two mirror astigmatic resonator mode fields and stability determined by writing Fredholm equation suitable to geometrical optics approximation
13 p2424 A70-28596

Fabry-Perot resonator mirrors with local reflecting inhomogeneities within perimeter of single crystal wafer for application in optically coupled semiconductor lasers
13 p2427 A70-28884

Reflecting surface nonplane parallelism effects on Fabry-Perot interferometers superposition bands contrast and multiplied length measurement accuracy
13 p2408 A70-29366

Fabry resonator X band model with step or slope rimmed mirrors, noting periodical trend of power losses
14 p2558 A70-31320

Shemakha observatory telescope main mirror spherical aberration, coma, astigmatism and light concentration, describing support system and adjustment and control mechanisms
15 p2738 A70-32203

Mirror damage problem with mode locked ruby laser system solved by rough stack mirror fabricated from microscope coverslips
15 p2753 A70-32546

Beryllium mirrors optical performance, describing causes and effects of anisotropy and dimensional instability
16 p2904 A70-33146

Reflecting X ray telescopes with glancing incidence mirror, discussing design, manufacture and testing
16 p2904 A70-33150

IR reflectometer system using Fourier transform spectrometer and ellipsoidal mirror, describing design, construction and performance
16 p2905 A70-33171

Automatic active optic control of alignment and figure of primary mirror of spacecraft-borne telescope with response time stability
16 p2907 A70-33189

Low threshold electron beam pumped CdS lasers with improved Al coated Fabry-Perot mirrors in end-pumped configuration
16 p2928 A70-33642

Laser beam photography by multiple reflections from partially reflecting mirrors
16 p2913 A70-33985

Scanning mirror system for Apollo telescope mount UV spectroheliometer, describing design, fabrication and testing
17 p3083 A70-34764

Primary mirror development problems for large orbiting telescopes
17 p3083 A70-34873

Spaceborne lightweight mirror blanks made from ceramics fabricated from glass crystallization
18 p3263 A70-36559

Cardioid condenser as radiometer mirror objective in low temperature radiometry, describing optical characteristics
19 p3420 A70-37261

Optical Schmidt system shortening with spherical, ellipsoidal and flattened spherical mirrors
19 p3433 A70-38767

Power diffraction losses at mirrors of asymmetric confocal laser interferometers with output coupling apertures
20 p3628 A70-39130

Mirror deformation effect on laser emission angular distribution, estimating output parameters by geometric optics
20 p3642 A70-39741

Thermally induced mirror deformations and wavefront distortions under radially nonuniform heating
21 p3942 A70-40806

Q switched free running mode-locked lasers with cavity mirror consisting of thin glass plates suitable for high power use
21 p3836 A70-40807

Surface contamination and degradation effect on reflectance of evaporated vacuum UV mirrors and temperature control coatings under simulated space environments
21 p3842 A70-40815

Optical devices contaminated mirror surfaces restoration with atomic oxygen from RF plasma by noncontaminating nondestructive oxidation of polymer film
22 p4029 A70-42622

Spheroidal three mirror telescopes distortion involving dioptrics combination
23 p4194 A70-44213

MIS (SEMICONDUCTORS)

MIS varactors applications as nonlinear reactances, discussing charge-voltage characteristics and minority carriers effect
12 p2196 A70-27685

Broadband frequency multipliers optimum efficiency solutions, realizing linear charge-voltage characteristics with MIS varactors
14 p2557 A70-31159

MIS structures with silicon nitride film deposited by RF glow discharge, observing doping increase in epitaxial substrate
17 p3055 A70-35873

Surface density, charge and field effect mobilities for electrons and holes on MIS insulator-semiconductor structure on narrow bandgap HgCdTe
22 p4086 A70-43018

MIS model applied to memory transistor with thin insulator consisting of silicon nitride on silicon dioxide
23 p4172 A70-44197

Tunneling electron and local mode phonon interaction in MIS n-type semiconductors
23 p4231 A70-44916

MISALIGNMENT

Misalignment and eccentricity effect on face seal, discussing leakage dependence on phase angle
[ASLE FICFS PREPRINT 15A] 02 p0308 A70-12171

Fabry-Perot resonator misalignment effect on TEM wave transmission coefficient in gas laser
03 p0492 A70-13749

Mode patterns and losses for laser resonator with identical tilted spherical rectangular reflectors in stable and unstable configurations
04 p0701 A70-15021

Shaft misalignment effect on accuracy of precision digital shaft angle encoders, using test fixture and optical methods
05 p0844 A70-15769

Hydrostatic journal bearing calculation for case of shaft misalignment, deriving linear inhomogeneous equations with symmetrical matrix for pressure
07 p1293 A70-19119

- Electron bombardment ion engine thrust variations, considering effects of electrode misalignment and ion current changes 12 p2291 A70-27808
- Continuous elastic turboshaft flexible journal bearings, analyzing radial misalignment effects on operation [ASME PAPER 70-DE-71] 16 p2918 A70-33521
- Gyro misalignment and encoder quantization effects for strapdown attitude error sources 22 p4040 A70-43588
- Tracking elevation/azimuth errors due to frame misalignment, presenting least squares procedure for determining true bias and misalignment angle and axis 23 p4215 A70-44518
- MISIBILITY**
U SOLUBILITY
- MISFIRES**
U FIRING [IGNITING]
- MISMATCH**
U IMPEDANCE MATCHING
- MISORIENTATION**
U MISALIGNMENT
- MISS DISTANCE**
Missile miss distance evaluation model with emphasis on statistical nature, noting application to systems analysis 01 p0193 A70-10118
- MISSILE ANTENNAS**
Quartz-polyimide for missile radome exhibiting low dielectric constant and thin wall for use over broader frequency range 13 p2417 A70-28664
- MISSILE COMPONENTS**
NT MISSILE ANTENNAS
Al-B composite missile adapter design for aerospace structures 02 p0306 A70-11951
- Reduced ambient pressure effects on hot wire sensitivity of initiating materials of electroexplosive devices used in missiles 03 p0549 A70-14139
- Thermal control through fusible materials for missile S band transmitter package, using computer analysis 18 p3231 A70-36349
- Vacuum brazed stainless steel hot gas actuators for guided weapons 18 p3265 A70-37202
- Fluidic applications in missile components production, discussing various types of fluidic control and logic in relation to functional requirements [ASME PAPER 70-FLCS-11] 22 p3963 A70-42416
- MISSILE CONFIGURATIONS**
Asymmetric missile nonlinear angular motion, describing quasi-linear relations for frequencies, damping rates and swerving motion amplitude [AIAA PAPER 70-534] 13 p2506 A70-29002
- Pitch damping derivatives computation for missile configurations undergoing small amplitude oscillations at subsonic speeds, using static aerodynamic data [AIAA PAPER 70-537] 13 p2339 A70-29004
- Bistable fluidic thrusters and circular sonic control jets interaction with airstream surrounding tactical missile configuration, investigating effect on amplification factors 13 p2391 A70-29887
- Static longitudinal aerodynamic characteristics predictions for missile configurations at various angles of attack, using digital computer [AIAA PAPER 70-581] 20 p3558 A70-39548
- Otomat surface to surface missile with turbojet engine for extended range subsonic cruise and two solid propellant rocket engines for launch 22 p4110 A70-43211
- MISSILE CONSTRUCTION**
U MISSILE STRUCTURES
- MISSILE CONTROL**
Antitank guided missiles guidance and control systems using optical tracking 01 p0139 A70-11261
- Fluid oscillators for sensing and missile control, discussing performance, design, frequency variation and applications [ASME PAPER 69-WA/FLCS-8] 04 p0626 A70-14845
- Supersonic missile drag reduction through wake heating assuming conical shaped missile tail and flow nonseparation [DFVLR-SONDDR-36] 04 p0616 A70-15165
- Fluidic sun sensor design and breadboard test for spacecraft and missile attitude control systems 04 p0716 A70-15415
- Computer controlled radar guided tactical missile system using digital techniques in performing target detection, acquisition, tracking and illumination 05 p0814 A70-16328
- Policies and controller design for pursuing vehicle developed in terms of pursuit-evasion differential games 06 p1025 A70-17955
- Dynamic instability of finned missiles occurring as angle of attack undamping and caused by differential lift from windward and leeward fins [AIAA PAPER 70-206] 06 p1158 A70-18178
- Range safety philosophy and practice concerning malfunctioning missile and space vehicle launch and flight [AIAA PAPER 70-249] 07 p1250 A70-20369
- IR technology in aircraft, satellite and rocket electronics, discussing photography, scanners, search and pursuit devices, guided rockets, pilot warning devices, etc 08 p1494 A70-20687
- Linear high order aircraft and missile control systems design using Horowitz frequency response method 09 p1654 A70-22835
- Air to air missile guidance to moving target via optimal feedback strategies 11 p2080 A70-26244
- Quasi-optimum proportional navigation for attack situations with large missile and target maneuvers, showing advantage over linearized optimization 11 p2081 A70-26316
- Fighter-missile launch and control using direct radar information for guidance to reduce computation time and computer storage space 11 p2015 A70-26332
- Airborne computer design for short range attack missile /SRAM/ to perform aircraft navigation and missile fire control 12 p2192 A70-27800
- Maximum thrust and drag reduction for supersonic missiles by base burning, showing dependence on chemical reaction and Mach number 12 p2158 A70-28208
- Nonlinear rolling motion of four-finned missile, investigating function of angle of attack and cubic damping 13 p2503 A70-28531
- Missile roll rate from yawing motion frequencies determined by epicyclic theory [AIAA PAPER 70-536] 13 p2506 A70-29075
- Electromagnetic interference /EMI/ effects on TALOS missile guidance receiver by expanding computer simulation test results 14 p2655 A70-31345
- Terminal kinematic variables prediction for missile homing, discussing line of sight angle, rate and acceleration 15 p2773 A70-32525
- Ballistic missile instrument orientation optimization based on CEP criterion, considering acceleration induced errors 16 p2947 A70-33317
- Cross product steering for space vehicles and ballistic missiles guidance during powered vacuum flight, pointing thrust acceleration vector to null velocity at termination 16 p2947 A70-33440
- Fluidic attitude control for boost phase of tactical surface to surface missile 16 p2844 A70-33447
- Missile homing on moving target, assuming closing velocity vector angular rate proportional to line of sight 16 p2949 A70-34054
- Tactical missiles electromechanical control actuator with reduced size and weight, describing mathematical model for analog simulation 16 p2845 A70-34111
- Stability analysis parameter plane technique for tactical missile control system design, correlating variable parameters with characteristic equation roots location 19 p3532 A70-37853
- Fluidic inertial platform feasibility model for air to surface missile line-of-sight guidance, noting cost, reliability and environmental advantages [AIAA PAPER 70-1009] 20 p3667 A70-39523
- Fluidic gyro compatible with PDM missile guidance system, discussing spherical gas bearing design [AIAA PAPER 70-1008] 20 p3631 A70-39524
- Cruciform-finned missiles dynamic stability investigation by nonlinear differential equations of motion, considering roll lock-in, resonance instability and catastrophic yaw [AIAA PAPER 70-969] 20 p3715 A70-39560
- Low cost gimballed inertial guidance platform providing medium accuracy in missile environment [AIAA PAPER 70-1026] 20 p3669 A70-39721
- UpSTAGE interceptor missile flight control system, discussing command logic to capitalize on lifting body advantages to enhance roll maneuver 21 p3927 A70-40782
- ACRA supersonic antitank missile with IR laser beam guidance system 22 p4110 A70-43212
- High performance military aircraft missile command and control signal data processor microelectronics packaging, using integrated and printed circuit modules 23 p4174 A70-44542
- Single stage warm gas directed jet valve for missile attitude control, noting servovalve and auxiliary power unit control applications [SAE PAPER 700778] 24 p4295 A70-45864
- Onboard digital information processing, discussing applications to tactical missile guidance and manned vehicles [AIAA PAPER 70-1230] 24 p4317 A70-45976
- Cleanliness levels for missile guidance package as function of component design complexity 24 p4349 A70-46250
- MISSILE DEFENSE**
U S. Safeguard plan suitability as hardpoint missile defense system, discussing technical controversy over Sentinel components 04 p0760 A70-14502
- ABM perimeter acquisition radar effectiveness, discussing time limitation and burden on Missile Site Radar/Sprint combination 04 p0647 A70-14503
- Radar system for Safeguard ballistic missile system, detailing perimeter acquisition and data processing system 09 p1638 A70-23421
- Weapon Systems Level testing methods and machines application to missiles, manned space flight vehicles and Safeguard System [AIAA PAPER 70-380] 10 p1862 A70-24923
- Phased array radar for missile defense, discussing development trends toward adaptive system logic control and microwave digital circuitry for signal processing 23 p4172 A70-44012
- MISSILE DEFENSE SYSTEMS**
U MISSILE SYSTEMS
- MISSILE DESIGN**
Performance characteristics of RDX-metal sheath systems, using high speed motion picture photography for missile design applications 03 p0550 A70-14141
- Design and qualification test criteria for components derived by enveloping peaks of shock response spectra in ground tests of missile stages explosive separation [SAE PAPER 690616] 05 p0922 A70-15849
- Soviet book on guided ballistic missiles design and construction employing liquid and solid propellant engines with emphasis on aerodynamic heating 06 p1155 A70-17410
- Computer program /SAFETE/ for evaluating missile launch risk on near real time basis [AIAA PAPER 70-248] 07 p1250 A70-20370
- Machinery for management of Sea Dart missile development using managerial concepts of planning, organizing, commanding, coordinating and controlling 08 p1601 A70-21036
- Missile radome design optimization, considering compromise between conflicting aerodynamic, thermal and structural aspects 11 p2134 A70-25862
- Wind profiles derivation for environmental influence upon missile systems design, limiting bulky input into computer programs 14 p2608 A70-30586
- Hypervelocity impact damage on complex targets, considering spacecraft and missile design 15 p2824 A70-32791
- Stability analysis parameter plane technique for tactical missile control system design, correlating variable parameters with characteristic equation roots location 19 p3532 A70-37853
- Slender axisymmetric power-law missile bodies with minimum ballistic factor, using Newton-Busemann centrifugal theory with skin friction 21 p3746 A70-41756
- MISSILE DETECTION**
NT RADAR DETECTION
- MISSILE ENGINE CASES**
U ROCKET ENGINE CASES
- MISSILE GUIDANCE**
U MISSILE CONTROL
- MISSILE LAUNCHERS**
Hydraulic drive mechanism for moving missile tower between launch pad and storage site 02 p0276 A70-12862
- Missile and rail launching structure combined dynamic response determined by discrete element dynamic analysis 12 p2312 A70-27116
- Elastomeric liner material for missile launch system design, developing bowed-knotted strut for compression-deflection characteristics 13 p2513 A70-29256
- Missile tube liner design with cast polyurethane elastomers, discussing effect of polymer composition and processing on physical properties 13 p2439 A70-29257
- MISSILE RANGES**
Missile miss distance evaluation model with emphasis on statistical nature, noting application to systems analysis 01 p0193 A70-10118
- Enhanced real time operational impact and casualty analysis /ERIOCA/ for range safety, discussing computer-driven CRT display and missile flight parameters selection [AIAA PAPER 70-247] 07 p1251 A70-20371

- Missile and space vehicle range safety policies and practices using past statistical performance data and cost consideration
[AIAA PAPER 70-246] 07 p1251 A70-20372
- British national and Commonwealth collaborative sounding rocket programs, discussing organization, scope and range facilities
13 p2523 A70-28685
- ESRange-high altitude sounding rocket range for European space research, discussing location, safety, equipment, instrumentation, staff and programs
13 p2523 A70-28690
- Shipborne day/night star tracker assisting Missile Guidance System monitoring in Atlantic and Pacific Missile Ranges
16 p2905 A70-33156
- Enhanced real time operational impact and casualty analysis for range safety, discussing computer-driven CRT display and missile flight parameters selection
[AIAA PAPER 70-247] 23 p4178 A70-44517
- British National and Commonwealth collaborative sound rocket programs, discussing organization, scope and range facilities
24 p4431 A70-46124
- MISSILE ROLL CONTROL**
U LATERAL CONTROL
U MISSILE CONTROL
MISSILE SIMULATION [MATH MODELS]
U MATHEMATICAL MODELS
U MISSILES
MISSILE SIMULATORS [TRAINING]
U MISSILES
U TRAINING SIMULATORS
MISSILE STABILIZATION
U MISSILE CONTROL
U STABILIZATION
MISSILE STAGING
U MISSILES
U STAGE SEPARATION
MISSILE STORAGE
Electroexplosively powered release valve for high pressure N stored in hermetically sealed container of missile, discussing design and performance tests
03 p0546 A70-14106
- MISSILE STRUCTURES**
Airframes dynamic response during simulated launchings of externally carried missile measured in laboratory, describing dynamic load simulation and structural analysis
06 p1159 A70-18439
- Al alloys flash welding for rings used in Poseidon program
06 p1078 A70-18502
- Al alloys missile splice rings fabrication, discussing extrusion, draw forming, flash butt welding and stretch sizing
18 p3264 A70-37112
- High intensity noise testing of missile and spacecraft structures, simulating acoustically induced vibrations due to aerodynamic turbulence
19 p3531 A70-37697
- MISSILE SYSTEMS**
NT GROUND OPERATIONAL SUPPORT SYSTEM
Poseidon missile optimized and automated computer aided electronic packaging design, considering partitioning, placement, internal and external cable, etc
10 p1853 A70-25210
- Rocket and supersonic aircraft weapon systems, discussing missile delivery and interception
13 p2507 A70-30000
- Wind profiles derivation for environmental influence upon missile systems design, limiting bulky input into computer programs
14 p2608 A70-30586
- Missile systems accuracy determination, analyzing pertinent errors statistical properties
[AIAA PAPER 70-1007] 20 p3657 A70-39525
- MISSILE TEST LABORATORIES**
U LABORATORIES
U MISSILE TESTS
MISSILE TEST RANGES
U MISSILE RANGES
MISSILE TESTS
Computer applications in French missile testing center, describing real and delayed time equipment and computations
01 p0057 A70-10798
- Optimal data filtering techniques and hardware for centrifuge testing of missile inertial platforms
[AIAA PAPER 70-405] 10 p1861 A70-24901
- Minuteman 3 Reentry System real time laboratory aging and surveillance test program to evaluate long-term storage effects on equipment behavior
[AIAA PAPER 70-395] 10 p1952 A70-24910
- Weapon Systems Level testing methods and machines application to missiles, manned space flight vehicles and Safeguard System
[AIAA PAPER 70-380] 10 p1862 A70-24923
- Seismic analysis of lunar module impact and missile-earth impact, comparing recorded signal parameters
11 p2118 A70-26748

- Missile aerodynamic characteristics investigation in subsonic low turbulence wind tunnel with three degrees of freedom angular motions
[AIAA PAPER 70-578] 13 p2342 A70-29891
- Army missile command /AMICOM/ plasma jet wind tunnel automatic control system design
16 p2888 A70-33303
- Ground environmental simulation test for captive carrying cycling of air launched missiles
17 p3060 A70-35182
- S band telemetry antenna with electronic tracking and polarity diversity for remote location missile testing
19 p3388 A70-37901
- Missiles aerodynamic coefficients parameter sensitivity from test data, using least squares analysis
23 p4133 A70-44525
- MISSILE TRACKING**
Antitank guided missiles guidance and control systems using optical tracking
01 p0139 A70-11261
- Laser range finding by mobile missile station compared with geodesic satellite telemetry by ground station
02 p0312 A70-12212
- Missile tracer mixture performance control facility noting chamber for pressure measurement during operation
03 p0544 A70-13758
- Missile impact location visual identification by marker system using pyrotechnic aboard to produce dense white smoke detectable to unaided eye, including flight test
03 p0582 A70-14104
- Tracking of goal seeking attack vehicles, discussing error improvement and destination estimating by tracking station observer
11 p2080 A70-26243
- Shipborne day/night star tracker assisting Missile Guidance System monitoring in Atlantic and Pacific Missile Ranges
16 p2905 A70-33156
- MISSILE TRAJECTORIES**
Kalman-Bucy filtering for nonlinear system consisting of missile in flight, discussing state variables values selected by estimator
11 p2025 A70-26221
- Controlled missile reentry trajectory through dense atmosphere, describing digital computer solution of differential equations of motion
12 p2314 A70-27768
- Missile impact and trajectory for water entry with zero angle of attack, including deceleration measuring instrumentation
[AIAA PAPER 70-531] 13 p2387 A70-29039
- Digital computer six degree of freedom wind tunnel separation simulator for air launched missile trajectory analysis
17 p3063 A70-35509
- Air to air missile launch range maximization for plane trajectories and nonmaneuvering targets, discussing optimal fuel burning rate
[AIAA PAPER 70-980] 20 p3668 A70-39549
- Spinning missile gravity induced angular motion for various trajectory portions, considering quasi-steady state assumption validity
[AIAA PAPER 70-968] 20 p3715 A70-39561
- Aerodynamic forces on flexible launch vehicles and missiles in supersonic flight based on first order method, solving boundary value problem for surface velocities
21 p3746 A70-41853
- MISSILE VIBRATION**
Saturn 5 launch vehicle design, role in exploration and anomalous structural vibration and oscillation
[AIAA PAPER 69-1094] 01 p0194 A70-10620
- Dynamical characteristics of variable-mass flexible spinning rocket with internal flow, investigating rigid body motion, elastic displacements and vibrations
09 p1767 A70-23252
- Missile oscillations in plane during pitching moment hysteresis, discussing test coefficients suitability for predicting motion
09 p1606 A70-23258
- Structural incompressible liquid element for discrete linear idealization of missile and propellant vibration analysis
16 p2991 A70-33852
- Ground vibration testing for aircraft and missile flutter prevention
[ONERA-TP-816] 18 p3339 A70-36508
- Discrete element idealization of missile and liquid propellant for vibration analysis, deriving sloshing theory
[SAE PAPER 700847] 24 p4326 A70-45885
- MISSILE WINGS**
U LOW ASPECT RATIO WINGS
MISSILES
NT AIR TO AIR MISSILES
NT AIR TO SURFACE MISSILES
NT ANTIAIRCRAFT MISSILES
NT ANTIMISSILE MISSILES
NT ANTITANK MISSILES
NT BALLISTIC MISSILES
NT CRUISE MISSILES

- NT HAWK MISSILE
NT MINUTEMAN ICBM
NT RAMJET MISSILES
NT SURFACE TO AIR MISSILES
NT SURFACE TO SURFACE MISSILES
NT TALOS MISSILE
RF hazard measuring system for complete guided weapons electromagnetic compatibility tests with instrumented inert device replacing live igniter
03 p0495 A70-14132
- Soviet SS-9 ICBM role in international debates over antiballistic missile, multiple independently targeted reentry vehicles, superhard silos and offensive forces
04 p0760 A70-14501
- Structural reliability of missile and aircraft solid propellant engines, estimating effect of loads variance, geometrical dimensions and mechanical strength
10 p1930 A70-24294
- MISSILRY**
U MISSILES
MISSION PLANNING
Solar and nuclear electric propelled spacecraft applications to planetary and interplanetary missions, considering asteroid survey, out-of- ecliptic, Mercury orbiter, comet rendezvous, etc
[AIAA PAPER 69-1108] 01 p0181 A70-10619
- Mission simulation mathematical modeling technology developed for optimization of experiment program management and operational planning for manned space station missions
[AIAA PAPER 69-1065] 01 p0181 A70-10634
- Mission model construction for power limited systems, discussing flight concepts, propulsion mixes and electric propulsion
01 p0183 A70-10848
- Solar photoelectric power ion propelled probe of asteroid region, describing design and mission planning
[AIAA PAPER 69-1105] 02 p0382 A70-12529
- Martian orbital photographic missions objectives and sensors realizable capabilities, discussing relationships between orbital parameters and imaging systems constraints
03 p0490 A70-13663
- Mission design, spacecraft characteristics, communications and experimental approaches for Viking 1973 Mars Project
03 p0576 A70-14020
- AMPROD /Automated Mission Profile Design/ generating schedules for long duration missions with real cost and time savings
03 p0581 A70-14023
- Apollo spacecraft pyrotechnics on lunar landing mission, considering standard initiator, modular cartridges, noninterchangeability of special purpose devices, postmanufacture indexing and data system
03 p0582 A70-14102
- Interplanetary trajectory selection, discussing transfer orbits, energy considerations, launch window computation, hyperbolic encounters and capture maneuvers
03 p0577 A70-14149
- Experiment selection in orbital program planning based on broad system synthesis, discussing identification and grouping of objectives, critical issues and experimental equipment requirements
[AAS PAPER 69-580] 04 p0749 A70-14652
- Automated parameter search techniques applied to low thrust mission design, stressing trajectories and mission optimization
[AIAA PAPER 69-261] 04 p0736 A70-15404
- Automated mars surface sample return /AMSSR/ mission, discussing Saturn 5 chemical and nuclear approach
[AIAA PAPER 69-1066] 04 p0764 A70-15626
- Manned space stations development, objectives, supply, storage and waste disposal, launching and artificial gravity
05 p0923 A70-16042
- Space programs and future missions assessment based on technical feasibility, considering effects of economic and social factors
06 p1185 A70-17644
- Return to earth abort capability for Apollo missions for various mission phases
[AIAA PAPER 70-94] 06 p1156 A70-18035
- Reentry targeting philosophy for Apollo missions emphasizing premission planning activities and real time targeting decisions, discussing Apollo 10 post-flight results
[AIAA PAPER 70-28] 06 p1158 A70-18149
- Apollo 11 lunar landing mission planning, control and evaluation of launch window and translunar, lunar parking orbit and transearth trajectories
[AIAA PAPER 70-24] 06 p1158 A70-18168
- Viking Mars orbiter/lander mission planning, studying sun, earth and star occultations sensitive mission characteristics
[AIAA PAPER 70-62] 06 p1146 A70-18193
- Apollo 11 premission planning, real time situation and postflight analysis for lunar descent and ascent phases, providing navigation correction capability for Apollo 12
[AIAA PAPER 70-25] 06 p1159 A70-18227

- Outer solar system exploration, discussing swingby and junction missions, Jovian satellite grand tours, mission energy requirements, etc
[AIAA PAPER 70-58] 06 p1147 A70-18229
- Analytic Trajectory Optimization Model to develop computational techniques for low thrust mission analysis
[AIAA PAPER 70-96] 06 p1159 A70-18230
- Short duration manned Mars and Venus exploration mission planning with chemical propulsion and Saturn 5 boosters
[AIAA PAPER 70-59] 06 p1147 A70-18238
- Space probe investigation of comets, discussing feasibility, instrumentation, mission planning, etc
06 p1153 A70-18550
- Nuclear propulsion requirements for manned landing mission to Mars assuming Saturn 5-based operation
07 p1375 A70-18874
- SERT 2 thruster system performance over expected mission parameters, noting operational lifetime excess over mission requirements
[AIAA PAPER 69-235] 07 p1364 A70-19702
- Fluid controlled solid rocket motors design for Mars mission with acceleration level as parameter, discussing mission specifications, system design and component considerations
[AIAA PAPER 69-446] 07 p1365 A70-19707
- Air breathing engines for long range Mach 4 transport, discussing airplane mission profile- engine configuration interface
[AGARDGRAPH-120] 08 p1560 A70-21934
- Premission planning and operational radiation dose limits for manned lunar and low earth orbit missions
08 p1454 A70-21940
- Manned Mars mission planning, discussing technologies and costs for planetary landing
09 p1757 A70-22676
- Manned Spacecraft Center spacecraft development, mission design and planning, flight crew operations for Apollo, discussing spacecraft design principles
09 p1767 A70-23703
- Apollo crew procedures, simulation and flight planning, discussing navigation, guidance and control procedures
09 p1657 A70-23706
- Apollo Program flight control operations personnel premission planning and training, discussing presolution of launch problems and emergencies
09 p1768 A70-23707
- Spacecraft mission planning for trajectory control after establishing mission objectives, trajectory plan and crew timeline for Apollo flights
09 p1725 A70-23709
- Apollo mission planning process, discussing flight schedule evolution from panels, meetings and working groups
09 p1768 A70-23710
- Operational planning for earth resources surveys using spacecraft
09 p1672 A70-23762
- Mass spectroscopy for solar system exploration, discussing ion sources, mass analyzers and ion detectors meeting mission requirements
10 p1942 A70-24612
- Franco-German telecommunication satellite Symphonie mission objectives and system design
[AIAA PAPER 70-406] 11 p1996 A70-25401
- Titan 3 launch vehicles capabilities communication satellites deployment modes, presenting cost and availability data for preliminary mission planning
[AIAA PAPER 70-482] 11 p2121 A70-25451
- Launch vehicle selection, utilization and mission planning and analysis in Comsat programs, discussing INTELSAT I-IV
[AIAA PAPER 70-484] 11 p2002 A70-25489
- Planetology and space mission planning - Conference, New York, October 1967
11 p2110 A70-26026
- Signature theory application to space mission planning and archeological project
11 p2051 A70-26034
- Interstellar exploration mission profiles, considering technical constraints, propulsion modes, environmental hazards, spacecraft communications and control, etc
11 p2112 A70-26065
- Spacecraft propulsion systems selection for particular exploration missions including planets, comets and interstellar space
11 p2112 A70-26066
- Low thrust mission simulation dependence on hardware definition, discussing power plant characteristics, jet velocity and thruster efficiency
13 p2486 A70-28517
- Planetary trajectory handbooks for mission and system analysis covering opportunities for Mercury, outer planets and Mars, contour charts, etc
13 p2486 A70-28525
- Navigation for planetary orbiter and lander missions, considering orbit insertion, trim corrections and capsule descent for poor planetary gravity field model
13 p2448 A70-28706
- Weather forecasting for manned space flights, emphasizing Apollo flights and operational decisions due to forecasts
14 p2606 A70-30557
- Cloud size clear area spacing statistics development for satellite mission and simulation analyses
14 p2609 A70-30598
- Apollo 9 scientific multispectral photography mission, discussing meteorological support aspect of real time planning
14 p2610 A70-30614
- Radiation planning nomogram to display radiobiological effects of dose, onset time and shielding factors for manned space vehicles
15 p2690 A70-31894
- Lunar exploration program based on U.S. antarctic research experience, considering man role, environment, logistics, transportation, economics, etc
15 p2800 A70-32058
- American-German solar probe HELIOS mission parameters for interplanetary and close proximity solar research, discussing spacecraft building and launching
15 p2801 A70-32281
- Space program planning for scientific and application earth satellites, stressing image sensors development
15 p2812 A70-32289
- Mission analysis in system evolution, determining subtasks sequence to accomplish performance goals
15 p2804 A70-32627
- Space based reusable manned/unmanned tug, discussing potential missions, system requirements and auxiliary hydrogen oxygen propulsion system
[AIAA PAPER 70-719] 16 p2964 A70-33533
- NERVA flight engine operating characteristics and reliability requirements for missions, noting conditioning, startup shutdown, reactor cooldown, fuel consumption, etc
[AIAA PAPER 70-676] 16 p2951 A70-33951
- Space station experiments, payloads and activity planning
16 p2983 A70-34067
- Aerospace mechanism design from test laboratory viewpoint, balancing technical, cost and schedule factors with mission objective
16 p2921 A70-34103
- Unmanned flyby missions to Mercury in 1973-1990, discussing scientific objectives and payloads
[AAS PAPER 70-027] 17 p3155 A70-34798
- Subsystem selection integration and technology for space base and planetary mission module /PMM/ of space station program
[AAS PAPER 70-021] 17 p3023 A70-34801
- NASA ten year space station operational concepts, discussing mission planning, crew scheduling and management
[AAS PAPER 70-031] 17 p3176 A70-34804
- M-4 SS launch vehicle capabilities and development schedule for low energy interplanetary missions
17 p3168 A70-35253
- OGOs design evolution with respect to scientific mission requirements
17 p3180 A70-35303
- German monograph on heavy space probes for solar system investigation covering systems analysis, mission success, flight programs, Saturn 5 launch vehicle, etc
17 p3168 A70-35378
- System analysis to determine orbital parameters influence on mission scientific objectives under engineering constraints, using value function
[AIAA PAPER 68-1052] 17 p3172 A70-35648
- Commercial air transport mission payload and range capability analysis, noting on-line flight planning computers
[AIAA PAPER 70-899] 17 p3204 A70-35815
- Comet de Arrest 1976 opportunity mission analysis, considering flyby and rendezvous trajectories and guidance problems
[AIAA PAPER 70-1073] 19 p3513 A70-37426
- Future space missions for observing solar events, magnetospheric problems, cosmic rays and low energy plasma, considering use of multiple satellites
19 p3513 A70-37523
- Mission success model for unmanned space exploration, combining expected data return with computer technique
19 p3527 A70-38838
- Mariner Mars 1971 mission design, discussing objectives, orbit selection, guidance, navigation and sequence analysis
[AIAA PAPER 70-1048] 19 p3527 A70-38863
- Mission planning for 1973 Mariner Venus/Mercury flyby, discussing trajectory and navigation aspects
[AIAA PAPER 70-1049] 19 p3528 A70-38864
- Pioneer-F Jupiter flyby mission planning, considering use of optimum broken plane trajectories to increase launch opportunity and/or payload capability
[AIAA PAPER 70-1050] 19 p3528 A70-38865
- Jupiter swingbys and multiplanet Jupiter swingby trajectory modes for outer planet missions, comparing in terms of passage conditions
[AIAA PAPER 70-1071] 19 p3530 A70-38884
- Future spacecraft mission for short period comets rendezvous, considering trajectory requirements and launch vehicle payload capabilities
[AIAA PAPER 70-1072] 19 p3530 A70-38885
- Manned Mars lander launch-to-rendezvous analysis, using subsequent Venus swingby for mission velocity requirement reduction
[AIAA PAPER 70-1075] 19 p3530 A70-38887
- Spacecraft trajectory initial conditions expressions as parameters dependent functions, applying results to Mars lander mission
[AIAA PAPER 70-1016] 20 p3666 A70-39517
- SERT 2 for testing ion thruster reliability and operational characteristics, discussing design and mission objectives
[AIAA PAPER 70-1124] 20 p3716 A70-40221
- Solar system unmanned exploration decision making, discussing resource utilization, sequence optimization, etc
20 p3710 A70-40335
- Life support systems oxygen generation mode selection based on mission parameters, including duration, crew size, resupply, vehicle leakage, etc
21 p3768 A70-40991
- Waste management for large space stations, discussing removal, venting, utilization, processing techniques, etc
21 p3769 A70-40996
- Mission analysis and trajectory simulation /MATS/ program, discussing computer controls, modular design, integration evaluation
[AIAA PAPER 69-939] 21 p3920 A70-41872
- Apollo lunar surface experiment package-SNAP 27 program, discussing mission profile, design and performance characteristics
22 p4071 A70-43194
- Space shuttle mission and economics, discussing cost effectiveness, capabilities, satellite transportation payloads and traffic forecasts
22 p4127 A70-43505
- Space station mission and configuration concepts, discussing experimental/operational capability, crew assignments, accommodation and module sizing
22 p4111 A70-43517
- Manned space program goals, discussing orbiting observatories, lunar bases, biological and earth resources satellites
22 p4128 A70-43627
- Space station requirements and design, discussing space shuttles, operational personnel, long term effects, logistical systems, functions, etc
23 p4259 A70-44606
- Solar-electric ion propulsion mission analysis and spacecraft designs, discussing thruster, power conditioning, propellant storage and feed, etc
23 p4234 A70-44631
- Apollo spacecraft program evolution, discussing Apollo 13 accident, command and service module modifications, oxygen tank design, mission objectives, etc
23 p4245 A70-44640
- Orbital space station utilization planning as international laboratory, discussing industry role, experiment program goals, etc
23 p4260 A70-44650
- Helios solar probe for automated spacecraft exploration of interplanetary space near sun, considering design, mission planning and U.S.-German cooperation
23 p4245 A70-44689
- Automated and manned spacecraft design, discussing mission objectives and present and potential applications
23 p4264 A70-45003
- Jupiter Orbiting Vehicle for Exploration system for gathering Jupiter atmosphere, magnetic, radiation, gravitation, temperature, topography and interplanetary data
23 p4264 A70-45010
- Space vehicle for interstellar flight, discussing propulsion concepts, mission implications and international cooperation
23 p4254 A70-45011
- Manned earth orbital space astronomy instruments, facilities and research objectives
24 p4415 A70-45825
- Orbital space station program, discussing common module design, support, space shuttles and objectives
[SAE PAPER 700755] 24 p4415 A70-45852
- Automated mission requirements for outer planets, discussing flyby spacecraft, orbiters, atmospheric entry and grand tour missions
[AIAA PAPER 70-1246] 24 p4411 A70-45919
- Skylab mission in 1972, describing orbital workshop configuration and three man crew integration for operational experiments
[AIAA PAPER 70-1328] 24 p4417 A70-45939
- Planetary exploration for solar system origin and evolution, identifying outer planet mission scientific values
[AIAA PAPER 70-1244] 24 p4411 A70-45962
- Long life spacecraft design and reliability based on marine practices and advanced system technology project, considering grand tour outer planets mission
[AIAA PAPER 70-1247] 24 p4412 A70-45964

MITOCHONDRIA

Book on lunar rocks covering pre-Apollo lunar scientific knowledge, Apollo and future lunar mission planning, lunar mineralogy, petrology and geochemistry, etc

24 p4412 A70-46025

MITOCHONDRIA

Gamma-aminobutyric acid effect on oxidative phosphorylation of rabbit and rat brain mitochondria, noting dependence on ionic concentration, temperature and amount of additions

01 p0019 A70-10509

Positive Na and K ion effects on mitochondrial respiratory control, O uptake and adenosine triphosphate activity in rat liver

01 p0026 A70-11063

Enzyme beta-hydroxybutyrate dehydrogenase concentration in mitochondria from bovine and sheep liver

03 p0430 A70-14198

Critical oxygen supply of cerebral mitochondria and intercapillary oxygen transport

10 p1821 A70-25080

Electronmicroscopical structure of laser irradiated Garding-Passy melanoma cell organelles, noting mitochondria damage

18 p3224 A70-36636

Senescent *Drosophila melanogaster* flight muscle electron microscopic examination showing mitochondria in stages of degeneration

20 p3574 A70-40075

Oxidative phosphorylation and oxygen intake during circulatory hypoxia in mitochondria of liver and brain in rats subjected to acute ischemia

23 p4145 A70-44315

Oxidative phosphorylation and oxygen consumption during hypoxia in mitochondria preparations and tissue homogenates from white rat liver

23 p4146 A70-44316

Monovalent cations active transport model in mitochondria, noting membrane potential as driving force and ion pump omission

24 p4304 A70-46230

MITOSIS

Temporary mitotic activity depression with decrease in aberrant mitoses observed in mice intestinal epithelium cells after exposure to 50 Mev proton doses

03 p0423 A70-13708

Chronic gamma irradiation effects on bone marrow mitotic activity and chromosome aberrations in dogs

09 p1614 A70-22083

Temporary mitotic activity depression with decrease in aberrant mitoses in mice intestinal epithelium cells after exposure to 50 Mev proton doses

11 p1985 A70-25508

Chronic gamma irradiation effects on bone marrow mitotic activity and chromosome aberrations in dogs

15 p2685 A70-32679

Mitotic activity and aberrant mitoses frequency in mice corneal and duodenal epithelium cells under fast fission neutron irradiation

17 p3026 A70-35319

MIXED CRYSTALS

Optical phonons in mixed sodium potassium tantalate crystals as function of temperature and composition, using IR and Raman spectra

03 p0542 A70-14002

MIXED FLOW

U MULTIPHASE FLOW

MIXERS

Germanium, silicon and gallium arsenide point contact and Schottky barrier diodes as submillimetric wavelength detectors and mixers

11 p2017 A70-25736

Passive coupling of spatial six-element mechanical mixer with rotary pairs as function of element axial position and dimensions

11 p1983 A70-25933

MIXING

NT COLLOIDING
NT COMPOUNDING
NT DISSOLVING
NT HOMOGENIZING
NT LAMINAR MIXING
NT SIGNAL MIXING
NT SUSPENDING [MIXING]
NT TURBULENT MIXING

Multiphase two dimensional mixing and combustion of flow fields suspended in gaseous medium for propulsion systems problems, obtaining governing equations

[AIAA PAPER 70-145] 06 p1181 A70-18175

MIXING CIRCUITS

Nonlinear distortion in switching transistor mixer predicted by modifying analysis used for diode modulator and mixer circuitry

02 p0268 A70-12423

Schottky barrier diodes design for wideband radiometer mixers to obtain optimum noise performance and broadband operation by DC bias application

03 p0457 A70-13968

Self excited microwave mixer and transmitting oscillator using Gunn diode applied to short distance Doppler radar

05 p0822 A70-16678

Microwave mixer design to increase dynamic range applied to communications and video systems

07 p1243 A70-20216

Cross modulation due to nonlinearity and linear cross modulation due to local oscillator pulling in FET FM receiver, discussing mixer operating points

08 p1460 A70-20818

Diode mixer analysis for arbitrary I-V characteristics and commensurate levels of converted signals, using modulation characteristics method

20 p3588 A70-40147

Low noise GaAs Schottky barrier beam lead mixer and chip style diodes, discussing fabrication and performance

22 p3998 A70-43333

Integrated 7 GHz small signal microwave balanced mixer, using microstrip transmission lines

23 p4168 A70-43777

MIXING LENGTH FLOW THEORY

Mixing length relationship in Prandtl theory for turbulent channel and pipe flow, deriving universal velocity distribution law

02 p0277 A70-11911

Compression wave mechanism of supersonic combustion controlled by mixing, discussing multiple injector design, thermal compression and geometry effect

02 p0399 A70-12041

Extended mixing length method for computing turbulent shear stress distribution required in calculating two dimensional incompressible turbulent boundary layer

02 p0282 A70-12333

Mixing length theory improvement to calculate turbulent boundary layers based on velocity profiles

02 p0284 A70-12342

Dissimilar coaxial axisymmetric jets confined laminar mixing obtained from numerical solution of boundary layer equations, considering binary, isothermal and nonreacting system

04 p0621 A70-15579

Prandtl mixing length and effective Schmidt number distributions from wall jet and wake data to predict film cooling

06 p1035 A70-17688

Isoenergetic mixing and reattachment processes of two dimensional supersonic turbulent separated flow, modeling mixing process by constant pressure theory [AIAA PAPER 70-108]

06 p1037 A70-18039

Elastic coatings effect on turbulent friction using turbulence flow theory based on mixing length concept

08 p1483 A70-21227

Solid particles or liquid drops admixture effect on propagation of inhomogeneous turbulent gas jet, using Prandtl mixing length theory to estimate pulsation velocities

12 p2213 A70-28218

Collisionless plasmas strong turbulence in terms of mixing length and Hamilton-Jacobi theories

13 p2458 A70-28562

Turbulent boundary layer characteristics on simple shapes in hypersonic flow, using mixing length theory and eddy exchange coefficient

14 p2564 A70-30262

Turbulent boundary layer instability on rotating cylinder in axial stream, correlating mixing length to Richardson number

15 p2722 A70-32372

Turbulent kinetic energy equation for determining turbulent flow fields applied to free mixing problem of constant density streams

16 p2894 A70-33856

Solid particles or liquid drops admixture effect on propagation of inhomogeneous turbulent gas jet, using Prandtl mixing length theory to estimate pulsation velocities

20 p3612 A70-40091

Compressible hypersonic turbulent boundary layers solution by finite difference method, relating mixing length to velocity profile shape factor

20 p3684 A70-40269

Turbulent near wake of symmetrical airfoil, determining universal constant in mixing length formula for inner wake

20 p3559 A70-40276

Upstream disturbances propagation during hypersonic flow boundary layer interaction

21 p3748 A70-42205

Turbulent boundary layer velocity profiles and shear stress distributions computation based on mixing length approach

23 p4182 A70-44574

MIXTURES

NT ADMIXTURES
NT AEROSOLS
NT AQUEOUS SOLUTIONS
NT BINARY FLUIDS
NT BINARY MIXTURES
NT COLLOIDAL PROPELLANTS
NT COLLOIDS
NT DETONABLE GAS MIXTURES
NT DISPERSIONS
NT EMULSIONS
NT EUTECTIC ALLOYS
NT EUTECTICS

NT FOG

NT GAS MIXTURES

NT LIQUID-GAS MIXTURES

NT METAL MATRIX COMPOSITES

NT NUCLEAR EMULSIONS

NT PHOTOGRAPHIC EMULSIONS

NT PLASTISOLS

NT SMOKE

NT SOLID SOLUTIONS

NT SOLUTIONS

Digital control valve for high speed aerospace blending, considering propellant and cryogenics applications

06 p0989 A70-18602

Vapor-liquid equilibria predictions for multicomponent cryogenic mixtures, applying to correlation selection in critical and low temperature regions

14 p2616 A70-31015

Dynamic melt properties of polymer blends, using orthogonal rheometer measurements

22 p4058 A70-43076

MOBILE LOUNGES

Mobile lounges and airport productivity concepts for optimal handling of passengers at airport terminal [AIAA PAPER 70-918]

17 p3064 A70-35830

MOBILITY

NT ELECTRON MOBILITY

NT HOLE MOBILITY

NT IONIC MOBILITY

Dopant effect on dislocation mobility in elastically loaded silicon crystal using internal friction and modulus defect measurements

11 p2099 A70-26394

Soft metal and dilute alloy dynamic yielding, describing high dislocation mobility effects on mechanical properties

17 p3191 A70-35459

Mechanical structure dynamic response to vibration environment, using mobility method analysis

23 p4269 A70-44334

MODAL RESPONSE

Finite element method for calculating natural frequencies and mode shapes of pretwisted cantilever plates assembly of flat triangular elements

02 p0384 A70-11859

Natural mode shapes of longitudinal oscillations and resonant frequencies of thin rods of constant curvature and rings with slit, noting use for crack determination

03 p0588 A70-13283

Optical waves in round metallic and dielectric waveguides calculated using geometrical optics and model analysis for anisotropic wall impedance model

04 p0652 A70-15396

Avalanche diodes and associated microwave circuits power generation in terms of IMPATT, TRAPATT, parametric, space-charge feedback and thermal modes

10 p1847 A70-23887

Natural frequencies and mode shapes of vibrating shells and shell combinations determined using variational finite difference method in conjunction with Hamilton principle

10 p1961 A70-25056

Modal expansion method applied to thin deformable primary mirror surface control for orbiting astronomical observatory

13 p2403 A70-28427

Transmission line modal analysis for nonlinear polarizability in optical and quasi-optical waveguides

21 p3784 A70-40564

MODE OF VIBRATION

U VIBRATION MODE

MODE SHAPES

U MODAL RESPONSE

MODE TRANSFORMERS

Signal processing by differential data and common mode amplifiers and active filters, emphasizing low level transducers

19 p3431 A70-38529

MODELS

NT AIRCRAFT MODELS
NT ASTRONOMICAL MODELS
NT ATMOSPHERIC MODELS
NT DIGITAL SIMULATION
NT DYNAMIC MODELS
NT ENVIRONMENT MODELS
NT GUTENBERG ZONE
NT LIGHTHILL GAS MODEL
NT MATHEMATICAL MODELS
NT REFERENCE ATMOSPHERES
NT SCALE MODELS
NT SPACECRAFT MODELS
NT THOMAS-FERMI MODEL
NT WIND TUNNEL MODELS

Vaporization interaction liquid rocket performance model, discussing performance loss evaluation and test data

01 p0160 A70-10832

Reliability model for analyzing operational phase test programs developed from R and D phase models, processing data according to test scope [AIAA PAPER 70-389]

10 p1896 A70-24916

Star tracker linear and nonlinear model selection influence on satellite attitude stability

10 p1953 A70-25231

Photoplastic method for modeling of plane elastoplastic problems, comparing results with photoelastic coating method to estimate transition errors from model to prototype 10 p1965 A70-25320

MODERATION [ENERGY ABSORPTION]
 NT NEUTRON THERMALIZATION
 NT THERMALIZATION [ENERGY ABSORPTION]

Modes
 NT COUPLED MODES
 NT LASER MODES
 NT PROPAGATION MODES
 NT UNCOUPLED MODES
 NT VIBRATION MODE

GaAs relaxation and hybrid modes properties and formation conditions 11 p2099 A70-26827

MODIFIERS
 U ADDITIVES

MODULATION
 NT AMPLITUDE MODULATION
 NT DELTA MODULATION
 NT FEEDBACK FREQUENCY MODULATION
 NT FM/PM [MODULATION]
 NT FREQUENCY MODULATION
 NT FREQUENCY SHIFT KEYING
 NT INTERMODULATION
 NT IONOSPHERIC CROSS MODULATION
 NT LIGHT MODULATION
 NT PHASE MODULATION
 NT PHASE SHIFT KEYING
 NT PULSE AMPLITUDE MODULATION
 NT PULSE CODE MODULATION
 NT PULSE DURATION MODULATION
 NT PULSE FREQUENCY MODULATION
 NT PULSE FREQUENCY MODULATION TELEMETRY
 NT PULSE MODULATION
 NT PULSE POSITION MODULATION
 NT PULSE TIME MODULATION
 NT TRAVELING WAVE MODULATION
 NT ULTRASONIC LIGHT MODULATION

Laser and quasi-laser systems modulation for wide spectrum communications, discussing global potentials and application as low cost satellite links 08 p1459 A70-20802

He-Ne laser emission modulation by varying discharge current, studying gas pressure effect and role of ballast resistor 09 p1695 A70-22411

Inertialess nonlinear quadrupole output of oscillations modulated by normal noise, analyzing correlation functions 09 p1637 A70-23159

Review of 1969 London International Conference on Digital Satellite Communication session covering modulation, synchronization and coding [AIAA PAPER 70-464] 11 p1997 A70-25409

Multiplicative modulation noise of helium-neon traveling wave laser amplifier at micron wavelength 11 p2020 A70-26816

Spectral analysis of LF pulses from defects obtained by modulation method of monitoring using eddy currents with superposed converter 13 p2404 A70-28660

Optical absorption due to imperfections in CdS by sensitive differential technique using laser excitation 13 p2430 A70-29708

Soviet monograph on modulation of cosmic rays in interplanetary space, covering anisotropic diffusion approximation, diffusion equation, Forbush effects energy spectrum, etc 16 p2971 A70-32911

Resonant interaction and instability produced by nonlinear coupling of modulated wave and LF mode, stimulating self focusing of plasma waves 16 p2958 A70-33285

Pulsars PSR 1451-68, 1749-28 and 2045-16, discussing modulation effects associated with second periodicity 18 p3314 A70-36334

Communication modulation systems unified description by conversion and indication matrices 18 p3229 A70-36942

Residual solar modulation of relativistic cosmic ray nuclei in galaxy over eleven years, observing magnitude at solar activity minima 18 p3309 A70-37009

Monochromatic radiation from laser modulated electron beams 19 p3444 A70-37572

Analog communication optimal nonlinear modulation scheme design for large SNR through transformation into inner product functions 20 p3587 A70-39973

Diode mixer analysis for arbitrary I-V characteristics and commensurate levels of converted signals, using modulation characteristics method 20 p3588 A70-40147

Outer space galactic cosmic rays energy spectrum and modulation region boundary determination, using meteorite observations 23 p4236 A70-44050

Multiplicative modulation noise of helium-neon traveling wave laser amplifier at micron wavelength 24 p4317 A70-45188

MODULATORS
 Palladium alloy transmodulator for gas chromatograph, demonstrating sensitivity gain for thermal conductivity and ionization cross section detectors 03 p0442 A70-14325

Modem selection for satellite communications system, considering bandwidth and power constraints, propagation characteristics, point-to-multipoint operation, etc 08 p1459 A70-20807

Iterative solution for balanced diode modulator performance, obtaining output spectrum using Fourier transformation 10 p1849 A70-24232

Communication satellite PSK modulator-demodulator /modem/ implementation requirements and design for optimal performance 10 p1835 A70-24336

Modulation-demodulation system for multiple access tactical satellite communication 12 p2187 A70-27915

Power ferrite modulator and switch for SHF band based on Faraday rotation principle 12 p2199 A70-28000

Laser acoustooptic quartz modulators inserted inside He-Ne and argon cavities for internal power extraction 13 p2430 A70-29705

Elongation characteristics of modulation type charged particle traps and analyzers, discussing ions and electrons trapping 18 p3307 A70-36171

He-Cd pulsed laser mode locking at 4416 and 3250 A using intracavity acoustic loss modulator 18 p3266 A70-36314

Si controlled thyristors applied to pulse modulators in ionospheric stations 18 p3233 A70-37043

Radar transmitters modulating circuits protection with microsec rapidly by power elimination, discussing electronic switches 21 p3792 A70-41987

Signal controlled microwave modulator as filter or attenuator, using rectangular waveguide and varactor diode switching 22 p3995 A70-42718

Soviet book on modulation-type frequency converters based on electromagnetic and semiconductor elements covering modulators static and dynamic characteristics, optimal operating conditions, etc 24 p4319 A70-45626

Output signal/quantization noise ratio, dynamic range and transmission error effects for syllabically companded delta-sigma modulator systems 24 p4320 A70-46152

MODULES
 NT COMMAND MODULES
 NT COMMAND SERVICE MODULES
 NT ELECTRONIC MODULES
 NT LANDING MODULES
 NT LUNAR LANDING MODULES
 NT LUNAR MODULE
 NT MARS EXCURSION MODULE
 NT SERVICE MODULES
 NT SPACECRAFT MODULES

Water electrolysis module long term operation in providing oxygen for life support systems 05 p0804 A70-15843

F-111 crew escape module, describing main parachute and pyrotechnics severance improvements, parachute deployment and inflation, etc [AIAA PAPER 70-1210] 21 p3751 A70-41807

MODULUS OF ELASTICITY
 Annealing effects on cold rolled titanium sheets, noting changes in Young modulus and characteristics of recrystallized titanium 01 p0124 A70-11620

High strength high modulus carbon fibers for use in structural reinforced plastics, describing carbonizing and pyrolysis processes 02 p0320 A70-11856

Unidirectional composite materials properties, discussing stiffer filaments effect on Young modulus and shear coupling constant relating shear strain to longitudinal strain 03 p0587 A70-13128

Carbon effect on high temperature elasticity modulus and long term hardness of Nb, indicating diffusion enhancement and counteractive Zr addition 03 p0509 A70-13252

Complex Young modulus of plastics during flexural vibration, discussing deformation of viscoelastic bodies and test results of various plastics [ONERA-TP-715] 03 p0487 A70-13645

Elasticity theory of orthotropic materials applied to steady rotation of long cylindrical tubes of filament reinforced plastics 03 p0602 A70-14331

Energy balance relations for elastic material with different elastic moduli in two regions of deformation space 05 p0925 A70-15824

Torsion testing apparatus for refractory materials at 2400 C, measuring applied torsion moment, twisting angle and second order modulus of elasticity 05 p0825 A70-15881

Young modulus anisotropy and recrystallization texture during annealing in cold rolled Ti sheets using Fourier analysis 05 p0862 A70-16200

Structure and interstitial impurities effects on Nb modulus of elasticity at normal and high temperatures, noting rolling 05 p0866 A70-17040

Materials stress rupture strength and elastic constants at liquid hydrogen temperature, describing method and facility 05 p0955 A70-17076

Deformation pattern, interstitial impurities and alloying elements effects on temperature dependence of elasticity modulus of Nb and alloys 06 p1088 A70-17659

Dynamic elastic modulus of graphites and composites measured as function of temperature using thin rod resonance method 06 p1070 A70-18447

Saint Venant principle in cantilever sandwich beams under two statically equivalent load systems, considering Young moduli effects 07 p1406 A70-19328

Isotropic elastic body occupying half plane assuming elasticity coefficients of certain class 07 p1407 A70-19376

Vibrating composite beam test method for determining complex dynamic modulus of viscoelastic materials over broad frequency and temperature ranges 07 p1320 A70-19955

Complex modulus measurement for rigid linear viscoelastic materials over audio frequency spectrum by harmonic end displacement ratio method 07 p1413 A70-20044

Elastoplastic bending of inhomogeneous rectangular plates with modulus of elasticity and yield stress varying over plate thickness 08 p1583 A70-20530

Modulus of elasticity of fiber glass reinforced plastic under transverse bending as function of length-to-height ratio in laminates 08 p1526 A70-20532

Fiberglass reinforced plastics creep behavior under axial compression, studying time dependence of elasticity modulus and Poisson coefficient 08 p1526 A70-21174

Microphotometric spectral reflectivity correlation to static Young moduli of carbon and graphite yarn filaments as optical testing method 08 p1497 A70-21350

Variable modular elasticity theory demonstrated for anisotropic body subjected to plane stressed state, deriving expression for potential energy of deformation 09 p1769 A70-22152

Stress distribution in shells of revolution with variable elastic moduli, considering material rigidity and strain state 09 p1781 A70-23286

Amplitude dependence of Young modulus defect in metals during large stress HF oscillations 10 p1956 A70-24247

Dynamic shear modulus and depth of dominant layer of vibrating elastic medium, assuming foundation as isotropic stratum on rigid bed 10 p1957 A70-24481

Processing temperature effects on breaking strength-modulus relation for carbonized acrylic fibers 10 p1907 A70-24533

Resonant frequencies and Young/shear moduli of unidirectional graphite epoxy composite beams under high modes of vibration 11 p2136 A70-26082

Length effect on modulus determination test for thin laminated tube under combined loading using shell theory 11 p2136 A70-26086

Elastic moduli of fiber reinforced composites calculated, deriving reinforcement factor in Halpin-Tsai equation from volume fraction 11 p2070 A70-26087

Dopant effect on dislocation mobility in elastically loaded silicon crystal using internal friction and modulus defect measurements 11 p2099 A70-26394

Anisotropic fiber reinforced composites elastic moduli determined by analytical matrix method 11 p2141 A70-26488

High modulus graphite fiber structure using electron beam 11 p2071 A70-26845

Elastic moduli and damping coefficients for glass- and boron-epoxy beams determined from resonant frequencies and bandwidths during lateral forced vibrations 12 p2253 A70-27120

Complex moduli of isotropic viscoelastic composites from elastic moduli 13 p2511 A70-28735

Ni and Ni alloys elastic properties relationship with ferromagnetic and magnetostriction effects, determining modulus of elasticity for wide temperatures and heat treatment

13 p2432 A70-28760

Laminated composite materials dynamic elastic properties, outlining resonant frequency effect on apparent Young modulus

13 p2515 A70-29467

High temperature elastic moduli of slender polycrystalline aluminum rods with elastic waves generated by Q switched laser energy

14 p2595 A70-30638

Book on high modulus fibers and composites providing data for preparation, microstructure, structure and properties

14 p2598 A70-31315

Fiber reinforced viscoelastic composites complex elastic moduli derivation

15 p2816 A70-32003

High temperature elastic moduli in polycrystalline Al rods from propagation velocity of elastic waves generated by Q switched laser

[SESA PAPER 1641]

15 p2759 A70-32304

Activation energy for creep at intermediate temperatures, allowing for elastic modulus change

16 p2991 A70-33790

Beta-Ti and Ti-Cr single crystals elastic moduli, determining λ ratio temperature dependence

17 p3115 A70-34380

Longitudinal shear modulus of unidirectional fibrous composite, involving series solution of Laplace equation

17 p3183 A70-34564

Plastic materials Poisson ratio and Young modulus measurements by triaxial compression method

17 p3089 A70-35048

Graphite fibers made from polyacrylonitrile yarn examining density-Young modulus relationship

17 p3127 A70-35149

Viscoelastic materials cut growth, discussing strain, fracture and modulus of elasticity dependence on temperature variations

17 p3146 A70-35220

German monograph on stress and displacement in plane elastic circular rings, disk strips and wedges, considering single load distributions

17 p3189 A70-35370

Graphite modulus of elasticity as function of temperature, considering effects of moisture content in pores

18 p3278 A70-36470

Nonlinear elasticity law for elastic moduli of plastics

18 p3344 A70-36947

Hydrostatic pressure derivatives of adiabatic elastic moduli of single crystal zirconium, noting high temperature Gruneisen-thermal expansion deviation

19 p3486 A70-37763

Carbon effect on high temperature elasticity modulus and long term hardness of Nb, indicating diffusion enhancement and counteractive Zr addition

19 p3453 A70-38470

Graphite filament composite structure shear strength decrease with modulus increase, examining fiber microstructure effect on interlaminar properties by short beam shear test

20 p3654 A70-39206

Thermal stress and changes in modulus of elasticity and expansion coefficient effects on dynamical properties of turbine disks at high temperatures

20 p3721 A70-39783

Composite material dynamic properties, discussing modulus and damping during constant strain rate, viscoelasticity, fracture strength and high loading tests

20 p3731 A70-40048

Nonhomogeneous elastic cylinder under internal pressure with modulus in terms of Fermi-Dirac distribution function series, discussing fibers rigidity and modulus change

20 p3731 A70-40052

High strength and modulus continuous graphite fibers from pitch, describing production process from asphalt and specifications

21 p3842 A70-40732

Thermomechanical theory for elastic material with different moduli in tension and compression, noting heteroresistance

21 p3937 A70-41428

Free vibrating reed apparatus for polymer low temperature internal friction and Young modulus measurements, discussing polystyrene properties

21 p3827 A70-41464

Novozhilov complex transformation method extended to Timoshenko theory of elastic shells constructed with allowance for transverse shear deformation

21 p3941 A70-42237

Compatibility equations in superelastic domain for permanent deformation hypotheses

22 p4114 A70-42611

Dynamic elastic moduli of model two phase continuous composites, using polymer and metallic foams

22 p4059 A70-43077

Ultrasonic wave velocity measurements for flaw detection and modulus of elasticity of carbon-carbon composites

22 p4047 A70-43519

Numerical solution of first boundary value problem of elasticity theory involving biharmonic stress function relating to rim loads

23 p4275 A70-44942

High modulus carbon fibers production and properties describing polymer chains intermolecular structuring by pyrolysis and strength increase by fibers stretching at 2700 C

24 p4366 A70-45166

Oscillating pendulum equipment for nondestructive material tests, determining longitudinal and transverse elastic moduli of specimen

24 p4338 A70-45738

MOHR CIRCLES

U FRACTURE MECHANICS

MOIRE EFFECTS

Epitaxial PbSe films formation mechanism-defect structure relation using moire rotation method, discussing elastic strains, dislocations, boundary formation, etc

01 p0155 A70-10182

Optical spatial amplitude filtering techniques application to moire fringe patterns processing

01 p0058 A70-11060

Strain distribution measurement in plastically deformed region around crack tip in metals using moire grid and optical interference

03 p0513 A70-14019

Basic equations governing optical properties of telecentric lens systems for moire analysis, discussing suitability for stress analysis

07 p1248 A70-19238

Lens effects applied to measurement of stresses on plane transparent models in photoelastic analyses, visualizing stresses from moire fringes

07 p1409 A70-19746

Green and Cauchy deformation tensors determined from moire fringe pitch and angle measurements, deriving equations by specimen and master grid geometries indicial representation

[ASME PAPER 69-APMW-21]

08 p1591 A70-21462

Tensile and compressive strain measurements close to weld deposits, using moire fringe technique and mismatch grating

10 p1890 A70-24591

Deformed grating frequency multiplication by filtering in Fourier plane of lens, forming moire pattern in image plane by mechanical interference

10 p1890 A70-24592

Grid shadow moire method to measure displacement contours of large plates, discussing sensitivity changes

11 p2131 A70-25589

Profile plane state of stress in wedge with and without external notch using combined photoelastic analysis and moire method

11 p2131 A70-25591

Optical filtering applied to moire method for measuring small structural strains

11 p2131 A70-25595

Moire-holographic technique for deformed plane spatial displacements determination, describing diffraction patterns generation and stress analysis

11 p2140 A70-26487

Moire theory applied to direct strain measurement methods based on light diffraction

11 p2058 A70-26835

Strain measurement over large steel plate surface ground to reasonable flatness and in welded joints by applying moire method

11 p2061 A70-26836

Surface contours generation by Moire patterns

12 p2235 A70-27753

Hologram interferometry using moire method to determine bending moments of object surface

13 p2409 A70-29474

Holographic interferometry for moire strain analysis, discussing theory and applications

16 p2904 A70-33149

Book on elasticity theory covering end effects, Saint Venant principle, edge and screw dislocations, moire method, thermoelasticity, cavity and inclusion effects, Muskhelishvili methods, etc

17 p3183 A70-34603

Normally loaded thin plate displacements, bending moments and stresses determined by hologram interferometry and indirect moire and superposition of grilles

17 p3085 A70-35011

Combined lens-hologram system for strain measurements by moire technique

17 p3087 A70-35024

Shadow moire method for comparing diffusely reflecting component against holographically recorded master shape, noting turbine blade measurement

17 p3088 A70-35025

Bent plates strain analysis using in-plane moire method for small and large deflections

19 p3535 A70-37383

Welded joint strain measurement by grating etching and moire fringe technique

19 p3428 A70-38513

Strain analysis by moire technique, using triangular and square root of 2 gratings

19 p3432 A70-38720

Light intensity distributions within successive slits imaged by transmission gratings, using theory for spatial moire fringe blurring

23 p4217 A70-43819

Moire technique application to fracture toughness tests on Zr alloys, measuring crack opening displacements and plastic flow beneath notch

23 p4208 A70-44914

MOISTURE

Moisture absorptivity and hydrolytic stability effects on operational parameters of gas turbine engine lubricants

06 p1075 A70-17222

Moisture effect on fatigue crack propagation and fracture path through microstructure of 300-grade maraging steel

13 p2432 A70-28607

Moisture induced failure of glass-resin composites at interface, discussing water adsorption, crack propagation, wet strength and nonsilicate reinforcements

16 p2937 A70-33373

Aqueous stress corrosion dependence on microstructural features of Ti alloys, using optical and electron microscopy and X ray diffraction

17 p3113 A70-34370

MOISTURE CONTENT

NT ATMOSPHERIC MOISTURE

Venusian atmosphere water content determined by airborne interferometer

02 p0377 A70-12554

He-Ne laser emission attenuation coefficient relation to water content of artificial fogs for 0.63, 1.15 and 3.39 microns

06 p1079 A70-17209

Atmospheric integral moisture content determination from thermal radio emission measurements by Cosmos 243 satellite

07 p1329 A70-19649

Balloon-borne device for analyzing atmospheric carbon dioxide, moisture and methane, using cyclic analysis by gas chromatography

11 p2052 A70-26371

Atmospheric hemispheric general circulation model numerical time integration with moist processes and uniform earth surface

12 p2262 A70-26882

Atmospheric optical thickness from radio telescopic measurements of wave absorption at millimeter wavelengths, showing dependence on lower atmospheric moisture content

14 p2546 A70-30127

Atmospheric moisture balance solution for altitude dependent vertical velocity and turbulence coefficient, considering cloud water content and boundaries height calculation

14 p2601 A70-30137

Visual reflectance of wet soils, attributing darkening to internal reflection of radiation in water layer enveloping soil particles

14 p2577 A70-31236

Visible polarization signature for remote sensing of soil surface moisture, noting invariance to partial shadowing in plowed or rough soils

15 p2724 A70-31667

Radar and DC pulse signatures of multiple reflection from dry, damp and wet earth for vertical and horizontal polarization

16 p2861 A70-32977

Graphite modulus of elasticity as function of temperature, considering effects of moisture content in pores

18 p3278 A70-36470

Water separation index modified (WSIM) test for jet fuel surface active materials in relation to filter/separator performance

[SAE PAPER 700279]

18 p3300 A70-36815

Atmospheric moisture content vertical profile from terrestrial radiation measurements, using statistical regularization procedure

19 p3460 A70-37418

Uncoated quartz twin crystal microbalance for monitoring water vapor content of respiratory gases

19 p3368 A70-37844

Optical hydrometer measuring water vapor content in vertical atmosphere column, using interference filters and thermoelectric sensitive element

20 p3625 A70-39027

Cloud structure, atmospheric water vapor and liquid water contents from passive ground based microwave spectrum measurements

21 p3846 A70-40906

Apollo 11 lunar material water content and H and C isotope abundance, examining changes in deuterium and O by solar winds

21 p3774 A70-41570

Initial water content on moon implied from hypothetical falling temperature lunar accretion as original earth satellite
22 p4102 A70-42954

MOISTURE DETECTORS
U MOISTURE METERS
MOISTURE METERS
NT HYGROMETERS
NT PSYCHROMETERS
Moisture detector for evaluating trapped water effects in thermal insulation, describing equipment and test procedure
10 p1891 A70-24829

MOL [ORBITAL LABORATORIES]
U MANNED ORBITAL LABORATORIES
MOLABS
U LUNAR MOBILE LABORATORIES
MOLDAVITE
Glassy drops identity and moldavites sculpturing origin in Pannonian sediments in southern Moravia
05 p0916 A70-16838

MOLDING MATERIALS
Bag molding process for molding laminates of reinforced preimpregnated material containing thermosetting resin
05 p0856 A70-16612
Matched die molding technology working principles, mat materials, mold taper, preforms, etc
05 p0856 A70-16613
Preimpregnated materials processing, discussing molding, resin-reinforcement, unidirectional materials, ablative applications, mechanical data and air-frame uses
05 p0874 A70-16614
Optimum composition of sand-bentonite materials for aluminum alloy casting in molds compacted by high pressure
08 p1506 A70-21137
Nickel base alloy as die material for creep forming titanium
11 p2060 A70-26424
Molding procedure to orient filaments relative to loads for optimizing structural component/compressor blades/ of filament reinforced composite
13 p2417 A70-28663
Thermal stresses and curing in electronic modules transfer molding, discussing various design test models
13 p2420 A70-29252
Transfer molding process in fabrication of electronic modules components, emphasizing criticality and unfavorable characteristics
13 p2420 A70-29253
Internal stresses in transfer molding of electronic modules by photoelastic technique, discussing component failure
13 p2420 A70-29254
Transfer molding of electronic modules, discussing materials for evaluating selection and processing guidelines
13 p2421 A70-29255
Anisotropic composite materials comprised of B and graphite fibers in polymer matrix, discussing precision molding technologies
[ASME PAPER 70-GT-126] 18 p3264 A70-36852

MOLDS
Al solidification in direct chilling molds effect on as-cast structure, analyzing heat removal, casting rate and application of water to outgoing ingot
02 p0316 A70-12298
Matched die molding technology working principles, mat materials, mold taper, preforms, etc
05 p0856 A70-16613
Mold canting effects on nonporosity of Al alloys flat castings noting decreased metal losses
08 p1517 A70-21134
Graphite shell molds for Al castings mass production
08 p1505 A70-21135
Thermal interaction between casting and mold at beginning of cooling using mathematical model for temperature field
08 p1506 A70-21139
Heat exchange during solidification of castings in molds, studying thermal properties effect for achieving constant mold surface temperature
08 p1506 A70-21141
Solidification thermal conditions during Ti casting by melting out patterns in graphite molds, investigating heat accumulation coefficients in molds
08 p1506 A70-21142
High service temperature glass reinforced premix compound on Glastic grade electrical laminate, discussing optimum molding and applications
16 p2936 A70-33356
Matched-die compression molding of complex shape structures from composite materials
[SAE PAPER 700751] 24 p4348 A70-45874

MOLECULAR ABSORPTION
Jupiter Red Spot continuous spectrum intensity distribution and methane/ammonia absorption between 3300-6500 A
02 p0374 A70-12427

Troposphere microwave transmission factor determined from dispersion and attenuation caused by water vapor isolated molecular resonance
02 p0261 A70-12593
Molecular vibration spectra from inelastic interaction between electrons and absorbed molecules at metal-vacuum interface
09 p1732 A70-22904
Air polluting sulfur dioxide and nitrogen dioxide remote sensing based on radiation molecular absorption using long line correlation spectrometer
20 p3633 A70-39793

MOLECULAR BEAMS
Particle velocity distributions in low density supersonic jets measured by molecular beam sampling technique and multidisk velocity analyzer
02 p0276 A70-11849
Differential elastic scattering cross section of Ar nozzle beam in nitrogen considered with rainbow effect in determining intermolecular potential well depth
02 p0344 A70-12722
Molecular beam laser short term frequency instability found dependent on laser and measuring device noise
03 p0455 A70-13091
Nitrous oxide molecular beam reflection and dissociation on tungsten surface at high temperatures from angular distribution measurements
06 p1004 A70-17493
Molecule spatial and velocity distributions of supersonic molecular beams, measuring scattering cross sections of He and Ar on noncondensable gases
06 p1043 A70-18252
Intensity measurements of molecular beams skimmed from nearly inviscid nitrogen and Ar free jets, interpreting beam attenuation in terms of collisional models
06 p1043 A70-18254
Cold molecular beam of helium impinging on LiF or Si crystals investigated for gas-surface interactions, using time of flight method
06 p1043 A70-18255
Nitrogen molecule-tungsten surface interactions, computing trajectories and accommodation coefficients for various temperatures by equations of motion
06 p1110 A70-18262
Velocity distributions of incident and reflected Ar beams, determining partial energy accommodation coefficients for reflection from copper and carbon dioxide deposited surfaces
06 p1111 A70-18264
Time of flight spectroscopic measurements in arc heated supersonic molecular beam using algebraic relations, sensing modulated beam by Orbitron type detector
06 p1111 A70-18266
Molecular He and Ar nozzle-type beams scattering from room temperature LiF crystal surfaces, measuring particles flux and speed distributions
06 p1111 A70-18267
Momentum transfer from neutral nitrogen molecules to solid surfaces measured for various incident beam molecule energies
06 p1112 A70-18272
Metastable diatomic N beam scattering from Teflon and Cu surfaces measured for velocity and angular distributions
06 p1112 A70-18273
Ar beam scattering and UV radiation from glass target surface with adsorbed gas layer
06 p1112 A70-18274
Supersonic molecular free jets using electron diffraction technique, discussing vibrational and condensation states
06 p1044 A70-18301
Molecular beam continuum model to determine structure of shock waves in diatomic gases, comparing calculated profiles with measurements in nitrogen
06 p1050 A70-18338
Crossed molecular beam study of reactive asymmetry of oriented methyl iodide molecules reacting with Rb, accounting for observations with hard sphere model
07 p1225 A70-20051
High and medium energy molecular beams - Conference, Cannes, July 1969
07 p1339 A70-20101
Atomic and molecular beams produced by nozzle beams aerodynamic acceleration, discussing condensation effects, internal energy, scattering cross sections, etc
07 p1341 A70-20102
Skimmer interaction influences on nozzle beam production explaining intensity maxima, proposing model assuming normal shock across skimmer mouth
07 p1341 A70-20103
Supersonic molecular beam source operation, discussing dominant degradation factors and nozzle beam generation intensities and energies improvement
07 p1341 A70-20104
Binary mixture molecular beam apparatus combining aerodynamic acceleration and arc heating techniques, discussing particle energy and density
07 p1341 A70-20106

Single junction vacuum thermocouple measuring thermal beam effect with reference to velocity distribution perturbation in molecular beam scattering
07 p1341 A70-20107
Time of flight resolution of fast excited atoms from thermal molecular beam
07 p1341 A70-20108
Low and moderate energy gas molecule-solid surface interactions using molecular beams
07 p1328 A70-20116
Wall boundary condition model modification applied to molecular beam-solid surface scattering, noting qualitative agreement with observed distributions
07 p1342 A70-20118
Molecular beam interactions with solid crystalline surface with fcc lattice elementary cell, investigating intensity distribution of scattered particles
07 p1342 A70-20119
Solid surface roughness influence on reflection of thermal energy molecular jets, showing shock determined by incidence angle
07 p1343 A70-20121
Reflected molecular beam intensity distribution interpreted in terms of disturbances in boundary layer between gas and solid
07 p1343 A70-20122
Crystalline structure effect on molecular beam reflection from rough polycrystalline Au surfaces
07 p1343 A70-20123
Gas molecules scattering by solid surface for monoenergetic and Maxwellian beams, discussing model with different values for magnitude and velocity direction
07 p1343 A70-20124
Satellite-borne experiments of neutral molecular beam-solid surface interactions, describing Molsink chamber, densitometer, sphere and paddlewheel satellites
07 p1344 A70-20128
Helium high energy molecular beams for insulating body heating and thermal constants determination
07 p1344 A70-20129
Molecular beam approximation introduced in Boltzmann equation to investigate high speed rarefied flows
07 p1261 A70-20130
Molecular beam research at low, intermediate and high energies, discussing inelastic processes, intermolecular potentials, etc
07 p1344 A70-20131
Nitrogen molecules pulsed high energy beams transit time measurement by gated time of flight procedure and by multichannel analyzer
07 p1345 A70-20136
Energy dependence of elastic total collision cross section of identical He molecules, using velocity selected primary beams at low target temperature
07 p1545 A70-20137
Hydrogen triatomic molecules existence, stability and ionization in molecular beams
07 p1345 A70-20139
Rotational temperature of molecular beam by electron excited fluorescence method, discussing signal level, background light and scattering effects
07 p1345 A70-20140
Supersonic gas jets applicability as vacuum locks for molecular fluxes at thermal velocity in magnetic trap
07 p1549 A70-20509
Molecular beams and particle adsorbing surfaces interactions in state of relaxation, determining reflection parameters as function of gas characteristics
08 p1547 A70-21078
Molecular beams and particle adsorbing surfaces interaction with allowance for deposited atoms relaxation, determining reflected flux
08 p1547 A70-21079
Molecular beam and pure surface interactions on background of external forces field
08 p1547 A70-21080
Shock heated molecular beams of argon, oxygen and mixtures with helium, measuring particle velocities and gas dissociation
09 p1733 A70-23180
Deuterium atom reaction with hydrogen molecule yielding HD and H using modulated crossed beams, plotting angular distributions and reaction velocities
10 p1920 A70-25148
Nozzle source design for high intensity thermal energy molecular beam with small dispersion in velocity suitable for scattering experiments
11 p2086 A70-25973
High temperature gaseous molecular beams impingement on Cu surfaces at cryogenic temperatures measured for condensation rates
12 p2271 A70-27265
Molecular beam carbon dioxide laser Q switching by ethylene as saturating filter, reducing pulse duration by varying ethylene pressure and active mixture composition
12 p2248 A70-27509
Glorified shadows in molecular beam scattering, considering undulation spacing, bound states number and extrema amplitudes in terms of optical analogies
13 p2454 A70-28624

Molecular beams formation from high pressures, discussing detection, diagnosis and applications in high temperature chemistry

14 p2545 A70-30904

Scattering cross sections for monoenergetic Ar beams on epitaxial Ag films

16 p2956 A70-34013

Signal to noise ratios for metastable and ion detection of excited neutral molecules in beam

18 p3262 A70-37096

Capture coefficients and reflected flux measurements for gaseous nitrogen molecular beams impinging on solid nitrogen cryodeposit surface

20 p3675 A70-39390

Cesium beam velocity attenuation by He, Kr and Xe, determining scattering cross sections from gas pressure and density measurements

20 p3675 A70-39618

Monoenergetic nitrogen free molecule beam impingement on solid surface, calculating satellite drag coefficients from momentum transfer measurements

21 p3745 A70-41743

Solid surface interaction between surface with normal molecular beam, generalizing model by energy parameter simulating dissipative forces

23 p4223 A70-44994

MOLECULAR BONDS

U CHEMICAL BONDS

MOLECULAR CHAINS

Polymeric materials properties, discussing tensile stress disadvantage and compensation by reinforcement and polymer chain directional alignment

02 p0321 A70-12305

Polyethylene extended chain crystals melting process via electron microscopy and differential thermal analysis

12 p2258 A70-26896

Polymers as cryogenic adhesives, evaluating role of chain structure below glass transition temperature

21 p3783 A70-42142

Human hemoglobin chain, noting zeta chain synthesis during embryonic development

24 p4297 A70-45406

MOLECULAR COLLISIONS

Multistate impact parameter treatment of hydrogen-helium excitation collisions, considering distortion, back- and rotational-coupling and virtual transition sequence

01 p0147 A70-10285

Rotational excitation and scattering of diatomic molecules by structureless atoms, comparing approximation methods

01 p0147 A70-10470

Nitrogen and helium collisional effect on rotational relaxation rate of carbon dioxide upper laser level, noting thermalization

01 p0110 A70-10567

Vibrational energy exchange between colliding diatomic molecules modulated by harmonic oscillators with insignificant frequency difference

01 p0147 A70-11035

Molecular reaction rates and ion/electron vertical profile and concentrations in equatorial ionosphere, applying computer simulation to numerical solution of continuity equations

01 p0083 A70-11549

Hydrodynamic equations and Grad transport coefficients for nonequilibrium rarefied monatomic gases developed for molecular collisions

01 p0068 A70-11567

Enskog method for Boltzmann equation, analyzing asymptotic nature of integral kinetic equation for molecular mean free paths and Laplace probabilities

01 p0068 A70-11568

Oscillations and decomposition of diatomic gas molecules at high temperatures during atom-molecule collisions, deriving kinetic equations for energy level changes

01 p0148 A70-11630

Oxygen molecules dissociation by molecular and atomic collisions in shock tube from measuring molecular O concentration behind shock wave front

01 p0149 A70-11632

Vibrational energy exchange between molecules during collision behind normal shock front as function of wave velocity

03 p0468 A70-13873

Electron scattering by molecules, demonstrating formal equivalence of fixed nucleus and free rotor scattering models

04 p0722 A70-14949

Diatomic oxygen-nitrogen collisions in mixtures with CO, determining vibration-vibration energy exchange probabilities

04 p0723 A70-15562

Vibration effects on ion-molecule collision lifetimes and multiple reflections

04 p0723 A70-15638

Vibrational energy transfer in oriented nonlinear collisions between diatomic molecule and atom, considering molecular vibration excitation

05 p0885 A70-17080

Slow electron attachment to O molecules forming stable O-ions, discussing formation rate constant

06 p1109 A70-17488

Approximate solution to Boltzmann gas kinetics equation, using moment relations of collision integral and reverse collision operator

06 p1036 A70-17758

Energy and mass transfer during elastic and inelastic molecular collisions in reacting gas mixtures, using Enskog and variational methods in solving Boltzmann equations

06 p1110 A70-17760

Model for impact behavior of elastic body at elastic half space, measuring gas molecule impulse exchange at metal surfaces

06 p1171 A70-18260

Collision cross sections direct measurement for determining macroscopic reaction rates in inelastic molecular collision processes in gas dynamics

06 p1113 A70-18276

Evaporation rate from spherical drop into vacuum influenced by molecular collisions occurring in gas cloud formed by emitted particles

06 p1113 A70-18283

Knudsen iteration for predicting cooled blunt body near free molecular drag in hypersonic stream, using BGK model for collisions

06 p0979 A70-18313

Monte Carlo method for modeling gas flow by simulated molecules concurrently followed through collisions and boundary interactions in simulated physical space within computer

06 p1113 A70-18314

Hyperthermal leading edge analyzed by examining adjacent relevant mean free paths for collisions, establishing basis for formal expansion of Boltzmann equation

06 p0979 A70-18347

Angular distribution of nonreactively scattered molecules in reactive collision, analyzing relation to reaction probability using gray sphere optical model

07 p1225 A70-18903

Molecular beam interactions with solid crystalline surface with fcc lattice elementary cell, investigating intensity distribution of scattered particles

07 p1342 A70-20119

Ion production cross sections determined for alkali atoms and bromine molecules collisions, noting charge transfer

07 p1345 A70-20138

Polarization of laser medium consisting of colliding two level molecules with velocity dependent mean free time

08 p1512 A70-20992

Scattering equations and cross sections for rotational excitation in collisions of rigid diatomic molecules interacting through soft potential

09 p1732 A70-22901

Binary collision-induced rotational far IR spectrum of tetrahedral molecular gas, using induced absorption theory

09 p1732 A70-22905

Meteor ionized trails initial expansion and diffusion resulting in dissociation and ionization of air molecules through collision, using electromagnetic wave scattering

09 p1762 A70-23177

Fast electrons spatial distribution for multiple scattering in nitrogen and argon, noting target thickness and incident energy

09 p1735 A70-23179

Vibrational energy exchange between colliding diatomic molecules modulated by harmonic oscillators with insignificant frequency difference

10 p1920 A70-25004

Molecular reflection effects on aerodynamic characteristics of rarefied gas flow past plate

11 p1973 A70-25386

Hard sphere model for reactive molecular collisions based on energy and momentum of reactants and products

13 p2361 A70-28497

Flame ionization, extra-equilibrium excitation and electronic temperature resulting from electron collisions with gas molecules

14 p2666 A70-31096

Atomic oxygen 1D excitation state obtained by metastable He atoms collision with ground state oxygen molecules in O-He discharge

14 p2579 A70-31248

Fragment ion products velocity vector distribution for dissociative collisions of molecular ions with He

16 p2953 A70-33005

Photodissociation and fluorescence cross sections for hydrogen by Lyman-alpha photons emission from collisional quenching

16 p2953 A70-33006

Total cross sections for production of free electrons in collisions of low energy negative atomic oxygen ions with molecular nitrogen

18 p3292 A70-36188

Ion-polar molecule collision time history plots and computer movies, calculating capture cross sections for mass spectrometry

18 p3292 A70-36561

Atomic H electron transition induced by H atom collisional-excitation rates at various thermal energies, explaining anomalous recombination lines in H I regions

18 p3253 A70-37021

Ion-molecule pair relative motion in capture collisions, using computer-made movies

19 p3474 A70-38796

Molecular and noble gas rotational collision numbers from thermal transpiration measurements

20 p3738 A70-39995

Dynamical theorems to control number of collisions for sequences in generalized Boltzmann equation, discussing binary collisions involving three molecules

21 p3852 A70-40946

Rotational transition probabilities of molecular collisions, using time dependent perturbation theory along linear trajectories

21 p3853 A70-41390

Numerical molecular rotational transition probabilities and cross sections in HCN-HCN and ICN-ICN collisions, using perturbation theory and multipole potentials

21 p3853 A70-41391

Vibrationally adiabatic model for reaction dynamics of atomic and molecular hydrogen systems, using zero point energy path

21 p3773 A70-41397

Turbomolecular pumps efficiency calculation by Maxwell transport equation, assuming gas molecules perfect specular reflection from blade surface

22 p4009 A70-42607

Enskog theory extended to three particle collisions for gas transport properties

23 p4222 A70-44427

Electronic energy collisional transfer between atomic and molecular hydrogen, measuring excited molecule vibrational distribution

24 p4381 A70-45650

MOLECULAR DIFFUSION

Chromoluminescing process protecting alloys for gas turbines against oxidation at high temperatures by diffusion mechanism

04 p0711 A70-15683

Dissolved macromolecules effect on flow resistance due to turbulent friction in nonNewtonian liquids, considering physical parameters and hydrodynamic conditions

08 p1483 A70-21228

Diatomic gases, describing rotational distribution function evolution by diffusion equation approximation, discussing apparent relaxation times

08 p1548 A70-21521

Critique of paper on diffusion in Si isotopes and excess vacancies generation by motions of diffusion induced dislocations

08 p1553 A70-21696

Global atmospheric models computations based on treating molecular and eddy diffusion as dynamic processes

14 p2606 A70-30561

Nitrogen and nitric oxide production and diffusion, examining photochemistry and transport at high altitudes

20 p3620 A70-39339

MOLECULAR DISSOCIATION

U DISSOCIATION

MOLECULAR ELECTRONICS

NT LARGE SCALE INTEGRATION

Matrix elements of nonadiabatic perturbation emphasized in semiempirical theory for evaluating polyatomic molecules radiationless rate constants in terms of electronic-vibrational state

04 p0722 A70-14699

MOLECULAR ENERGY LEVELS

NT INTERMOLECULAR FORCES

Oscillations and decomposition of diatomic gas molecules at high temperatures during atom-molecule collisions, deriving kinetic equations for energy level changes

01 p0148 A70-11630

Quadrupole moment matrix elements in adiabatic approximation for transition bands of hydrogen, HD and deuterium molecules in ground electronic state

02 p0342 A70-11822

Intramolecular triplet-triplet energy transfer between nonconjugated molecular chromophores held together by rigid molecular frame at known separation distance and mutual orientation

02 p0251 A70-12277

Morse eigenfunctions for variational calculation of diatomic molecules vibrational-rotational energy level analysis, showing better convergence than harmonic oscillator basis

02 p0344 A70-12519

Dissociative recombination coefficients temperature dependence in molecular neon and argon ions measured under equal gas, ion and electron temperature

04 p0722 A70-14668

Excited oxygen molecules concentration in upper atmosphere calculated, considering deactivation during interactions in various energy states

04 p0684 A70-15750

Nitrogen ionization rate increase by admixing neutral molecules of electronically excited nitrogen, noting nitrogen decay controlled by spontaneous radiation and wall collisions

05 p0884 A70-15918

Radiative lifetimes of transitions to ground state for CS, SO and diatomic sulfur, showing relationship to absolute transition probabilities in terms of physicochemical applications

05 p0885 A70-16456

Chemical reaction rates corresponding to initial molecules fixed internal energy levels determinable for multitemperature Maxwell-Boltzmann distribution as function of reagent temperatures

07 p1224 A70-18769

Extrema behavior in nonlinear absorption of organic compounds under high power laser radiation interpreted by triple absorption molecular energy level models

07 p1302 A70-20100

Coupled Schrodinger equations for diatomic molecules internal motion solved using best adiabatic approximation to obtain energy correction to Born-Oppenheimer method

08 p1548 A70-21522

Compound state resonance energies and widths in elastic scattering of diatomic molecule at energies below rotational excitation threshold

08 p1548 A70-21523

Lyman-Birge-Hopfield nitrogen bands high resolution emission spectrum, giving energy values of particular states together with corresponding rotational constants and band origins

09 p1730 A70-22067

Quasi-bound levels determination method for molecular hydrogen ground state

10 p1919 A70-24395

API state lifetime of CO measured using molecular level crossing spectroscopy

10 p1920 A70-24629

Transitions in interstellar OH observed at National Radio Astronomy Observatory

10 p1948 A70-25000

Pulsed CO₂ laser calculating upper level lifetime of carbon dioxide molecule with allowance for gas heating at relaxation

12 p2251 A70-28296

Microwave lines due to hydroxyl radical in interstellar medium, discussing emission from excited OH states

13 p2484 A70-28371

Dissociation energy and long range interatomic potential of diatomic molecules from vibrational spacings of higher levels

13 p2454 A70-28495

Energy resonances between laser levels of carbon dioxide and diatomic and triatomic molecular impurity species, discussing population inversion due to superelastic collisions

13 p2425 A70-28622

IR spectroscopy, determining relative populations of carbon dioxide vibrational energy levels by comparing emission intensities

13 p2455 A70-29131

Carbon dioxide molecular vibrational energy levels above carbon monoxide-oxygen premixed flame, discussing vibration modes leading to population inversion and relaxation time variance

13 p2455 A70-29132

Excited oxygen molecules concentration in upper atmosphere calculated, considering deactivation during interactions in various energy states

14 p2576 A70-30834

Molecular nitrogen excitation under electron bombardment at auroral and airglow impact levels, using computerized Monte Carlo method

14 p2620 A70-31269

NaI molecular and ionic electronic states, discussing valence formulation, Hartree-Fock calculations, wave functions, excited state potential, etc

15 p2776 A70-31728

Acrolein photoisomerization in lower excited states, determining fluorescence and phosphorescence quantum yields

15 p2694 A70-31730

Three level molecular coherence effects in stimulated Raman scattering, considering molecular relaxation and field inhomogeneity

15 p2752 A70-32350

Perfect nonrelativistic bounded gas thermodynamics and surface tension, assuming single particle energy level density dependence on external potential

23 p4284 A70-44928

MOLECULAR FLOW

NT SLIP FLOW

NT TRANSITION FLOW

Output power and gain saturation characteristics for high speed flowing gas molecular lasers, discussing electrically excited fluid mixing carbon dioxide laser

01 p0107 A70-10103

Molecular velocity distribution function measured in normal He shock wave in low density wind tunnel by electron beam fluorescence technique

02 p0299 A70-12229

Molecular mean free path influence on gas lubricated thrust bearings performance, discussing slip flow effect and load capacity

05 p0854 A70-15909

Unsteady nonlinear molecular flow problems concerning plane Couette flow, heat transfer between parallel plates and density discontinuity propagation solved by Monte Carlo method

06 p1113 A70-18321

Thermal molecular flow kinetic theory, discussing anisotropic distribution function, thermal transpiration, thermal conduction, entropy production, etc

06 p1113 A70-18369

Simple molecules viscosity as function of temperature and density using empirical equation

09 p1731 A70-22292

Macroscopic properties of thermal molecular flow between coaxial cylinders and concentric spheres, using transpiration theory in Knudsen gas

09 p1788 A70-22906

Molecular, viscomolecular and laminar gas flows in tubes and porous bodies at low pressures

10 p1869 A70-24287

Rarefied gas mixtures efflux from opening at various pressures, calculating component discharge coefficients for molecular flow conditions

15 p2721 A70-32137

Time correlation functions approach to calculation of properties of nonequilibrium ensembles in fluid molecular motions

17 p3197 A70-35535

Low density gas jet from short circular cylindrical tube, calculating molecular flux radial density variation

22 p4076 A70-43430

Molecular jet velocity distribution, investigating adiabatic focalization conditions

24 p4351 A70-45370

Narrow capillary supermolecular flow density relation to vapor molecule specular reflection, considering Knudsen flow conditions

24 p4381 A70-45491

MOLECULAR GASES

NT DIATOMIC GASES

NT POLAR GASES

NT POLYATOMIC GASES

Mathematical model for saturable absorbers consisting of molecular gases for use in IR applied to carbon dioxide laser radiation absorption by sulfur hexafluoride

01 p0109 A70-10429

Total cross section for electron impact excitation and ionization in He, CO, nitrogen, oxygen, carbon dioxide, ethylene and benzene, emphasizing threshold values

01 p0147 A70-10489

Atomic O, H and D and molecular oxygen, deuterium and sulfur hexafluoride effects on nitrogen vibrational population distribution in nitrogen afterglow

01 p0148 A70-11356

Compact 4 micron radiation band from high temperature air and gases measured on arc jet and shock tube, noting molecular O and N source

02 p0392 A70-11901

Rotational compound state resonances in subthreshold atom-diatom scattering determined for lowest state molecular hydrogen and deuterium model systems scattered by Xe

03 p0526 A70-13006

Hydrogen molecule formation relation to galaxy formation, discussing cosmic plasma neutralization role

03 p0577 A70-14152

Electronic-vibrational coupling in nonequilibrium MHD generator with molecular gas to suppress electrode layer shorting and recombination in supersonic nozzles

[AIAA PAPER 70-41]

06 p0988 A70-18222

Thermomolecular pressure corrections in tubes and at orifices for errors in gaseous pressure measurements by temperature gradients

06 p1113 A70-18371

IR spectra excited by fast electrons in nitrogen, oxygen, carbon monoxide, carbon dioxide, nitrogen oxide, methane, ammonia and water molecules

07 p1337 A70-19045

Molecular oxygen concentration determined by absorption spectroscopy of solar hydrogen Lyman alpha line

08 p1490 A70-21390

Molecular hydrogen parallel and perpendicular dynamic polarizabilities calculated for frequency dependence, using many body perturbation theory

09 p1731 A70-22780

Fast argon beam scattering by gas molecules measured to study atomic and molecular two body systems involving nitrogen and oxygen atoms

09 p1732 A70-22902

Binary collision-induced rotational far IR spectrum of tetrahedral molecular gas, using induced absorption theory

09 p1732 A70-22905

Transient stimulated rotational and vibrational Raman scattering in gases using mode locked ruby laser

09 p1700 A70-23568

Emission and absorption by nonhomogeneous gases with vibration-rotation bands determined by scaling approximation

10 p1968 A70-24474

Acetone formation mechanisms during neopentane oxidation when added to slowly reacting molecular hydrogen and oxygen

11 p1995 A70-26379

Predissociation of excited molecules in molecular hydrogen and deuterium by electric field as linear function of field strength

13 p2362 A70-29479

Molecular gases ionization and dissociation by low energy atoms, using mass spectroscopy on secondary ionic products of collisions

14 p2619 A70-30723

Rotational transition of interstellar formaldehyde in absorption in direction of galactic and extragalactic objects

14 p2641 A70-30878

Flame ionization, extra-equilibrium excitation and electronic temperature resulting from electron collisions with gas molecules

14 p2666 A70-31096

Nitrogen dioxide continuum in green-white afterglow of molecular oxygen and nitrogen, using spectrometry and photometry

14 p2579 A70-31254

Molecular oxygen emissions in airglow, inverting calculation to determine ozone distribution from observed altitude profiles

14 p2580 A70-31265

Vibration-rotation band absorbance for nonisothermal gaseous radiation in terms of parameters describing isothermal gas

15 p2825 A70-31816

Dissociation energy of gaseous TiN molecule at high temperature

15 p2695 A70-32748

Gaseous diatomic molecules quantum mechanical treatment, calculating Hamiltonian matrix elements for interpretation of electron resonance spectra

16 p2955 A70-33799

Ionic and molecular gas lasers, discussing pumping, transitions, emission, discharge tube dimensions, cooling, pressures, optical elements and applications

19 p3449 A70-38751

Positive ion and electron production in H atom collisions with atomic and molecular gases, deriving ionization cross sections

20 p3675 A70-39605

Book on molecular and aerosol backscatter measurement from stratosphere by means of ground based laser beams

20 p3623 A70-39925

Venusian atmosphere carbon dioxide, water, molecular oxygen and nitrogen contents from Venera 5 and 6 data

21 p3883 A70-40837

Slow and fast ionization waves in inert gas or molecular gas plasma columns, describing striation formation in neon discharge by hydrodynamic equations

22 p4079 A70-42371

Carbon dioxide laser vibrational temperature measurement, determining ground state vibration level populations in various molecular gases

22 p4051 A70-43391

Atomic or molecular gases excited state lifetime measurements, using time to amplitude conversion and multichannel analyzer

23 p4198 A70-44946

MOLECULAR INTERACTIONS

NT MOLECULAR COLLISIONS

Mass spectrometric determination of proton affinities of simple molecules determined from proton transfer and ion-molecule reactions

05 p0885 A70-17081

Kinetic analysis of ion-molecule reactions in Ar-N₂ mixtures with H₂, deuterium and HD using ion ejection mode of ion-cyclotron-resonance spectroscopy

06 p1108 A70-17332

Molecular dipole moments-electric field interaction induction of cholesteric liquid crystal transition to nematic phase

07 p1225 A70-20053

Low and moderate energy gas molecule-solid surface interactions using molecular beams

07 p1328 A70-20116

Gas molecules scattering by solid surface for monoenergetic and Maxwellian beams, discussing model with different values for magnitude and velocity direction

07 p1343 A70-20124

Molecular beams and particle adsorbing surfaces interactions in state of relaxation, determining reflection parameters as function of gas characteristics

08 p1547 A70-21078

Molecular beams and particle adsorbing surfaces interaction with allowance for deposited atoms relaxation, determining reflected flux

08 p1547 A70-21079

Molecular beam and pure surface interactions on background of external forces field

08 p1547 A70-21080

Chemical high pressure laser action produced by stimulated phototransition of electrons at contact moment between pair of reacting nonexcited gas molecules

08 p1513 A70-21412

Elementary processes cross sections in charged states changes during proton-hydrogen molecule interactions

08 p1549 A70-21817

F region ion-molecule reaction rate constants laboratory measurements, observing reactions energy dependence

10 p1872 A70-23825

Transfer coefficients calculation for equations of motion of medium, presenting mathematical experiment requiring molecular interactions only

10 p1919 A70-24157

Molecular densities and population inversion pulse shape in working gas in mixture with thermally excited auxiliary gas

10 p1920 A70-25112

Methyl fluoride calculated for ion-molecule reaction rate constants from ion cyclotron resonance spectra

12 p2180 A70-26862

Neutral molecule-solid surface interactions mass spectrometric techniques for measuring molecular flux and mean thermal energy after interaction

12 p2181 A70-27257

Heat conductivity of Xe-He binary gas mixtures, allowing for molecular transfer and polarity effects

15 p2827 A70-32107

Molecular velocity influence of optically active medium in gas dynamic quantum amplifier on monochromatic radiation transport, using corpuscular light model

15 p2721 A70-32356

Molecular interactions, surface pressures and potentials of mixed monolayers of stearic acid and stearyl alcohol with inorganic substructures

15 p2695 A70-32547

Ion-molecule reactions produced in phosphine by ion cyclotron resonance

16 p2855 A70-33061

Ethyl nitrate positive and negative ion-molecule chemistry investigated by ion cyclotron single/double resonance techniques

16 p2855 A70-33090

Thermal energy negative ion-molecule reactions in photoionized NO-water vapor mixtures, determining rate constants by stationary afterglow system

16 p2954 A70-33280

Thermal product distributions and energy dependencies of ion-molecule reactions in allene and propyne, using ion cyclotron resonance

16 p2856 A70-33651

Hydrogen ion-molecule reactions analysis by flowing afterglow technique, noting application to proton affinity measurement

16 p2857 A70-34005

Inelastic energy losses in oxygen ion beams collisions with neutral molecules, determining vibrational transition probabilities

16 p2955 A70-34011

Ethylene and ethylene-acetylene mixtures ion-molecule reaction product distributions calculation using quasi-equilibrium theory of unimolecular reactions

16 p2858 A70-34012

Ion-molecule reactions investigation by resonance principle, discussing ion paths in crossed fields

17 p3081 A70-34574

Liquid Fe-Cr-C, Fe-P-C and Fe-Cr-P systems, evaluating interaction coefficients

18 p3272 A70-36032

Atmospheric ions interaction with rocket exhaust gas water molecules, using sounding rocket mass spectrometric data

18 p3293 A70-36982

Book on thermal radiative properties of air, Volume 2, covering reaction rates, photons and charged particles interactions with air molecules, secondary air excitation, etc

19 p3552 A70-38010

Fluid intermolecular potential and virial calculation, noting relationships to Boyle and Joule-Thompson inversion temperatures

20 p3671 A70-38988

Hydrogen negative ion thermal energy reactions with oxygen, nitric oxide, carbon monoxide and nitrous oxide, determining rate constants

20 p3583 A70-39616

Ion-molecule reactions in mixtures of hydrogen sulfide with ethylene and acetylene from deuterium labeling studies via ion cyclotron resonance spectroscopy

21 p3773 A70-41200

Ion cyclotron resonance spectroscopy for detecting trapped gaseous ions in analyzer cell, observing ion-molecule reactions

23 p4196 A70-44390

Beam laser operational efficiency relation to molecule /atom/ interaction in focusing system, explaining lasing power drop at large flow rates

24 p4351 A70-45457

MOLECULAR IONS

Collision induced dissociations of 2000 ev diatomic O, N, CO and NO positive molecular ions as function of reactant ion internal energy

01 p0148 A70-11354

Dissociative recombination coefficients temperature dependence in molecular neon and argon ions measured under equal gas, ion and electron temperature

04 p0722 A70-14668

Temperature dependence of reaction rate for dissociative recombination in vibrationally excited gases, using electronic threshold law for diatomic ions

04 p0722 A70-14669

Ionic collision processes in nitrogen and oxygen mixtures in mass spectrometer ion source

04 p0646 A70-14700

NO ion dissociative recombination rate coefficient determined in high temperature air plasma from electron temperature and number density measurements

04 p0675 A70-15583

Exchange perturbation theories applied to delta function model of molecular hydrogen ion, discussing EL-HAV second order energy at large internuclear separations

05 p0884 A70-15878

Absolute values of emission cross sections for vibrational Meinel bands of molecular nitrogen ions excited by electron impact

05 p0901 A70-16279

Electron temperature dependence of molecular neon ions recombination with electrons using microwave afterglow/mass spectrometer, obtaining recombination coefficient

05 p0885 A70-16468

Stationary nitric oxide afterglow, studying molecular ionic species by time resolved mass spectrometry

06 p1114 A70-18635

Numerical modeling of electron and molecular ion continuity equations describing conditions in lower F region near magnetic equator using analog computer

07 p1265 A70-19434

Molecular ion concentrations, using flap probe collector trap on Cosmos 5 satellite at 200-300 km

07 p1276 A70-20421

Uranyl ion luminescence and absorption cross section in silicate glass excited by high power light beam, considering Q switching action of ion

08 p1510 A70-20516

Dialkyl ketone ion in double McLafferty rearrangement, applying ion cyclotron resonance to structural study

08 p1454 A70-20525

Molecular cesium ion production by arc discharge in inhomogeneous cesium plasma, describing probable reaction mechanism

08 p1551 A70-20849

Electron, oxygen and NO molecular ions concentrations for E region from computer calculations of diurnal model compared to observations

08 p1490 A70-21391

Nitrogen oxide ions mobility in air calculated at high plasma temperatures

12 p2776 A70-27845

Molecular oxygen positive ion density in upper ionosphere as function of photoionization, ambipolar diffusion velocity and altitude effect

13 p2399 A70-29233

Charge, hydrogen atom and ion transfer in collisions involving deuterium-labeled methanol- acetaldehyde system and molecular ions

14 p2543 A70-30110

Electron impact excitation cross sections of oxygen ion first negative bands, considering relationship to oxygen ionization cross section

14 p2620 A70-31363

Rare gas diatomic ions reactions with molecules and rare gas atoms, measuring rate coefficients and product channels by flowing afterglow technique

15 p2776 A70-31726

Rare gas diatomic and hydride ions reactions with hydrogen, determining rate coefficients and product channels by flowing afterglow technique

15 p2776 A70-31727

NaLi molecular and ionic electronic states, discussing valence formulation, Hartree-Fock calculations, wave functions, excited state potential, etc

15 p2776 A70-31728

Fragment ion products velocity vector distribution for dissociative collisions of molecular ions with He

16 p2953 A70-33005

Effective cross sections for molecular hydrogen and hydrogen positive ion formation in collisions between He, Ne and Ar ions or atoms

16 p2954 A70-33193

NO and oxygen ions vibrational excitation due to inelastic scattering from He, calculating scattering angle variation

16 p2955 A70-34010

Diatomic nitrogen ions branch overlapping, discussing rotational line structure in first negative system vibrational bands

16 p2956 A70-34254

Nighttime E region molecular ion production rate estimation, taking into account windshear effect

18 p3245 A70-36022

Comet Morehouse CO ions lifetime and density from photometric analysis

18 p3313 A70-36324

Numerical modeling of electron and molecular ion continuity equations describing conditions in lower F region near magnetic equator using analog computer

18 p3249 A70-36908

Signal to noise ratios for metastable and ion detection of excited neutral molecules in beam

18 p3262 A70-37096

Indeterminacy interval reduction for ionospheric reaction rate constants by imposing supplementary condition on NO/oxygen molecular ion concentrations ratio

19 p3408 A70-37309

Nitrogen dioxide and molecular oxygen ions densities in lower ionosphere as function of solar corpuscular radiation

19 p3409 A70-37325

Ammonium molecules dissociation and ionization in comet atmospheres due to solar corpuscular and photon radiation

19 p3514 A70-37642

Collision induced dissociation of nitric oxide and molecular oxygen ions at low kinetic energies, noting internal ionic excitation effects

21 p3773 A70-41398

F I region positive nitric oxide and oxygen ions concentrations ratio and conversion rates from rocket data and theoretical formulas

23 p4189 A70-44075

Autoionization theory application to partial solar photoionization cross sections for production rates of vibrationally excited positive molecular oxygen ions

23 p4222 A70-44785

ESR intensities and line widths at X and Q bands of Cr and Fe molecular ions in water/glycerol mixtures

24 p4310 A70-46045

MOLECULAR ORBITALS

Plasma pi-electrons effects in annulene molecules, obtaining dispersion relation for plasma oscillations by Hueckel theory

14 p2621 A70-30116

Molecular orbital wave functions for water molecule, using minimum set of Slater orbitals

14 p2544 A70-30119

Papers on chemical physics covering photoelectron angular distribution, molecular orbital theories, electron impact spectrometry, resonant electron scattering, etc

16 p2857 A70-33796

Molecular orbital energy level diagram for metal ion X ray emission and absorption spectra interpretation from titanium and vanadium compounds

21 p3853 A70-41901

MOLECULAR OSCILLATIONS

Vibrational energy exchange between colliding diatomic molecules modulated by harmonic oscillators with insignificant frequency difference

01 p0147 A70-11035

Transient molecular vibration excitation by picosecond laser pulses found dependent on shape of Stokes pulses in Raman scattering study

04 p0702 A70-15298

Vibrational energy transfer in oriented nonlinear collisions between diatomic molecule and atom, considering molecular vibration excitation

05 p0885 A70-17080

Molecular vibration energy distributions of polyatomic molecules, formulating energy criterion valid for nth order general case

08 p1511 A70-20597

Pulsed radio signals time delay due to molecular microwave resonance in earth atmosphere and interstellar medium

08 p1461 A70-20915

Thermospheric molecular nitrogen vibrational temperature, studying various chemical reactions and collisions as energy sources

10 p1872 A70-23827

Diatomic molecules vibrational levels distribution near dissociation limit determined using WKB approximation

10 p1919 A70-24041

Vibrational energy exchange between colliding diatomic molecules modulated by harmonic oscillators with insignificant frequency difference

10 p1920 A70-25004

Fermi triplet resonance between fundamental molecular vibrations possible in presence of harmonic or composite tone of same symmetry

12 p2275 A70-27502

Electron beam measurement of rotational and high vibrational temperature in molecular nitrogen

13 p2412 A70-29980

Resonance excitation of oscillations in diatomic molecules by slow electrons, calculating scattering on spherical potential well

20 p3642 A70-39753

Oscillator strengths for aluminum oxide molecular electronic sigma band system from intensity measurements in cyanogen-oxygen flame system

20 p3676 A70-40474

Vibrational relaxation measurements of specific carbon dioxide vibrational-rotational states from tunable carbon dioxide laser beam absorption

23 p4221 A70-44011

Carbon dioxide molecular vibration excitation by Q switched carbon dioxide laser, obtaining accommodation and diffusion coefficients by relaxation measurements

24 p4351 A70-45369

Two point hydrodynamic equation for molecular fluctuations divergent growth in classical shear flow via B-B-G-K-Y procedure and double series moment expansion

24 p4382 A70-46254

MOLECULAR OSCILLATORS

IR light beam modulation in Gunn oscillator near fundamental edge of GaAs, investigating mechanism

03 p0539 A70-13160

SiH molecular absorption lines in solar disk spectrum, determining maximum equivalent widths and oscillator strength

06 p1143 A70-17996

Ionization energies and oscillator strengths for Fe XVI, Co XVII and Ni XVIII by frozen core approximation, noting applications to solar corona

06 p1150 A70-18465

MOLECULAR PHYSICS

Interstellar molecular radio frequency lines significance to galactic physics, noting abundance relation to constituent atoms indicating dust catalytic formation

19 p3521 A70-38496

MOLECULAR PUMPS

Aerospace coldness and vacuum simulation, discussing uses of cryogenic, titanium sublimation, ion and molecular pumps

19 p3396 A70-37462

Turbomolecular pumps with uniformly distributed small plane blades, calculating rotor efficiency

22 p3964 A70-42604

Turbomolecular pumps efficiency calculation by Maxwell transport equation, assuming gas molecules perfect specular reflection from blade surface

22 p4009 A70-42607

MOLECULAR RELAXATION

Vibrational relaxation and optimum population inversion of carbon dioxide molecules under unsteady conditions during pulsed electron excitation, discussing laser output increase

03 p0528 A70-13408

Carbon dioxide supersonic flows, describing numerical integration procedure for chemical and vibrational relaxation

03 p0440 A70-13743

Vibrational relaxation and continuous spectrum transition during dissociation of diatomic low temperature plasma

04 p0721 A70-14539

Numerical analysis of near equilibrium flow regions in chemically relaxing gas mixtures past blunt bodies at supersonic speeds

04 p0666 A70-14603

Matrix elements of nonadiabatic perturbation emphasized in semiempirical theory for evaluating polyatomic molecules radiationless rate constants in terms of electronic-vibrational state

04 p0722 A70-14699

High temperature thermal transport and ionization relaxation in Ar from measurements by thin film surface thermometer in high pressure shock tube end wall

04 p0787 A70-15607

Kinetic Boltzmann equations for spatially uniform two component gas mixture solved with allowance for relaxation processes, assuming differing temperatures

06 p1109 A70-17754

Kinetic relaxation and Boltzmann equations for studying shock waves propagating in gas composed of rigid ideally elastic spherical molecules without internal degrees of freedom

06 p1036 A70-17756

Iteration for Boltzmann equation solution for relaxation of gas having solid molecules with time variable and velocity dependent distribution function

06 p1109 A70-17757

Translational relaxation in low density axisymmetric hypersonic free gas jet, describing transition from isentropic to free molecular flow

06 p1043 A70-18277

Spatial and temporal relaxation problems approximate solution in kinetic theory, making calculations for Maxwellian molecules and hard spheres

06 p1047 A70-18318

Kinetic theory study of shock wave structure in rotationally relaxing diatomic gases

06 p1050 A70-18339

Kinetic model equation for shock structures in rotationally relaxing gas with internal degrees of freedom

06 p1050 A70-18340

Sound waves dispersion and attenuation produced in gas flow by relaxation effects of solid particles presence

07 p1258 A70-19567

Coupled vibrational relaxation in mixtures of diatomic gases, showing energy pumping phenomenon between species

07 p1338 A70-19627

Carbon dioxide laser emission spectrum, considering working mixture emission power and rotational relaxation characteristics

08 p1511 A70-20539

Oscillatory relaxation of binary system of heat conducting viscous gases composed of nonspherical molecules

08 p1547 A70-21085

Diatomic gases, describing rotational distribution function evolution by diffusion equation approximation, discussing apparent relaxation times

08 p1548 A70-21521

Rotational-translational energy transfer in collisions between homonuclear diatomic molecules and rotational relaxation time in diatomic gases

10 p1918 A70-23956

Vibrational and dissociation relaxation effects on plane shock wave structure and supersonic flow around blunt bodies

10 p1801 A70-24150

Liquid crystal of cholesteryl chloride and myristate measured for complex dielectric constant, noting role of molecular rotation modes in dipole relaxation

12 p2180 A70-26859

Weak plane waves propagation in binary mixtures of diatomic gases subject to vibrational relaxation, solving piston problem in acoustic approximation

12 p2209 A70-27151

Vibrational relaxation time and transition probability in bromine collisions with He, Ne, Ar, Xe atoms determined by shock wave method

12 p2275 A70-27353

Coupled relaxation dependence on translational and vibrational temperature and number of modes in polyatomic gases, noting molecular dissociation

12 p2276 A70-27797

Piston formed weak steady shock wave propagation in relaxing gases, investigating via characteristics method

12 p2212 A70-28206

Vibrational relaxation effect on supersonic flow past nose section of blunted body

12 p2159 A70-28231

Vibrational dissociation relaxation effects on chemical reactions, molecular energy and thermal quanta in air flow behind direct shock wave

12 p2213 A70-28232

Pulsed CO2 laser calculating upper level lifetime of carbon dioxide molecule with allowance for gas heating at relaxation

12 p2251 A70-28296

Strontium chloride lanthanum ion system with dynamic Jahn-Teller effect, indicating isotropic EPM spectrum resulting from averaging by relaxation

13 p2470 A70-29109

Hydrogen impurities anelastic relaxation effect on internal friction alpha peak in cold worked tantalum and niobium

13 p2435 A70-29350

Molecular Markov processes application to vibrational relaxation and dissociation, small system kinetics, nucleation and droplet growth, thermalization kinetics and diffusion processes

14 p2619 A70-30615

Three level molecular coherence effects in stimulated Raman scattering, considering molecular relaxation and field inhomogeneity

15 p2752 A70-32350

Transition probabilities for Markov chain describing bond breaking and molecular energy transfer in vibrational relaxation and dissociation

16 p2953 A70-33009

Chemical energy conversion in lasers, discussing vibrational inversions in diatomic and multiatomic molecules and chain reactions

16 p2927 A70-33233

Nonequilibrium vibrational energy and relaxation equation for carbon dioxide-nitrogen molecular gas mixtures in supersonic free jet exhausting into vacuum [AIAA PAPER 70-867]

16 p2895 A70-33910

Vibrational nonequilibrium nozzle flow problems, obtaining similar solutions for various initial conditions and nozzle geometries

17 p3065 A70-34459

Vibrational relaxation and energy transfer processes in gas dynamic flows, discussing cross sections, atom-molecule interactions, molecular rotation, kinetic equations, etc

17 p3068 A70-34670

Shock tube flow of dissociating oxygen with chemical relaxation using Lax method

17 p3070 A70-35243

Relaxation gas dynamics with chemical reactions, emphasizing differences and similarities with classical gas dynamics behavior

17 p3071 A70-35467

Nonequilibrium nozzle flows involving molecular vibrational energy relaxation and composition changes from gas phase chemical reactions respectively

17 p3071 A70-35469

Nonequilibrium gas states evolution in detached wave front of hypersonic blunt body, comparing vibrational relaxation in free flight and wind tunnel flow

18 p3335 A70-35962

Relaxation peaks associated with interaction clusters of Zr and N dissolved in Nb

18 p3274 A70-36056

Reacting gas relaxation with particle sink removing products from system calculating relaxation processes during equilibrium state approach

18 p3292 A70-36291

Relaxation time for nitrogen molecule vibration temperature in ionosphere due to thermal electron collisions

19 p3409 A70-37324

HD molecule nuclear relaxation time in liquid state as function of temperature, discussing various mechanisms

19 p3473 A70-37367

Laminar boundary layer equations on plate with arbitrary catalytic properties in diatomic gas flow undergoing vibrational dissociative relaxation

20 p3611 A70-39802

Weak steady shock waves formation in relaxing binary gas mixture, discussing vibrational specific heat temperature dependence

20 p3614 A70-40350

Rotational relaxation of diatomic molecular excited electronic state at high temperatures, discussing nonequilibrium region behind shock wave front in nitrogen

21 p3854 A70-42060

Diluent molecules effect on polymers relaxation behavior at cryogenic temperatures from internal friction measurements, noting loss peaks shift

21 p3844 A70-42138

Ultrasonic absorption in gaseous molecular relaxation processes, considering error due to neglecting thermal conductivity effect on frequency dependence

22 p4073 A70-42649

Hot air temperature decay, discussing relaxation process of lightning channel behavior

22 p4016 A70-42781

Relaxation gas dynamics, discussing vorticity and drag generation by relaxation, linearized theory and shock waves structure

23 p4178 A70-43889

CO vibrational relaxation measurements in shock tube expansion wave generated in argon heat bath

23 p4180 A70-44009

Vibrational relaxation measurements of specific carbon dioxide vibrational-rotational states from tunable carbon dioxide laser beam absorption

23 p4221 A70-44011

MOLECULAR ROTATION

Rotational excitation and scattering of diatomic molecules by structureless atoms, comparing approximation methods

01 p0147 A70-10470

Nitrogen and helium collisional effect on rotational relaxation rate of carbon dioxide upper laser level, noting thermalization

01 p0110 A70-10567

Rotational temperature of molecular nitrogen Vegard-Kaplan bands determined from auroral spectra, including variations in vibrational levels populations

01 p0076 A70-10873

Carbon dioxide laser with incorporated grating for measuring line strength to width ratio for various rotational lines

01 p0112 A70-10916

Rotational temperatures and methane abundances in Jovian atmosphere calculated for various Lorentz half widths

02 p0366 A70-11809

Quadrupole moment matrix elements in adiabatic approximation for transition bands of hydrogen, HD and deuterium molecules in ground electronic state

02 p0342 A70-11822

Rotation-vibration matrix elements of quadrupole moments and absorption coefficients of ground electronic states of hydrogen, HD and deuterium

02 p0342 A70-11823

Molecular rotations and kinetics from spectral features of molecular Raman spectra, using light scattering spectroscopy

02 p0343 A70-12077

Atmospheric oxygen A band individual rotational lines intensities and half widths measurements

02 p0344 A70-12656

Rotational compound state resonances in subthreshold atom-diatom scattering determined from lowest state molecular hydrogen and deuterium model systems scattered by Xe

03 p0526 A70-13006

Self broadened semihalf widths measurement in pure rotational spectrum of carbon monoxide compared with vibration-rotation calculation

05 p0886 A70-17086

Density effects on rotational temperature measurements in nitrogen by electron beam excitation, discussing emission intensity distribution
06 p1067 A70-18306

Hydrogen fluoride fundamental vibration rotation band spectral line shift and broadening due to carbon dioxide
07 p1337 A70-19365

Diatomic Br molecular vibration-rotation coupling effects on energy transfer during Br-Br collisions, determining probability distributions
07 p1339 A70-20054

Molecular N rotational temperature effect on rare gases scattering cross section
07 p1344 A70-20134

Rotational temperature of molecular beam by electron excited fluorescence method, discussing signal level, background light and scattering effects
07 p1345 A70-20140

Carbon dioxide laser emission spectrum, considering working mixture emission power and rotational relaxation characteristics
08 p1511 A70-20539

Diatomic gases, describing rotational distribution function evolution by diffusion equation approximation, discussing apparent relaxation times
08 p1548 A70-21521

Helical twisting power of steroidal solutes in cholesteric mesophases, discussing nematic temperature shift dependence on ester chain
08 p1455 A70-21524

Relative rotational lines intensities of carbon dioxide, considering sigma-sigma transitions for abundant isotopes
08 p1549 A70-21575

Lyman-Birge-Hopfield nitrogen bands high resolution emission spectrum, giving energy values of particular states together with corresponding rotational constants and band origins
09 p1730 A70-22067

Perturbation rotational levels in triplet states of CO emission spectra attributed to resonance fluorescence process involving optically forbidden transitions
09 p1731 A70-22282

Scattering equations and cross sections for rotational excitation in collisions of rigid diatomic molecules interacting through soft potential
09 p1732 A70-22901

Binary collision-induced rotational far IR spectrum of tetrahedral molecular gas, using induced absorption theory
09 p1732 A70-22905

Liquid crystal of cholesteryl chloride and myristate measured for complex dielectric constant, noting role of molecular rotation modes in dipole relaxation
12 p2180 A70-26859

Book on rotational structure of diatomic molecules spectra covering multiplets, intensity distributions and perturbations
12 p2274 A70-27094

CO vibration-rotation bands, calculating high resolution and temperature steradiance and spectral absorption coefficient
12 p2275 A70-27171

Rotational, vibrational and equilibrium molecular constants for Phillips system of diatomic carbon
12 p2275 A70-27174

Electron beam measurement of rotational and high vibrational temperature in molecular nitrogen
13 p2412 A70-29980

HF and DF continuous chemical lasers vibrational and rotational spectra, comparing lines and relative intensities
14 p2593 A70-30274

Rotational transition of interstellar formaldehyde in absorption in direction of galactic and extragalactic objects
14 p2641 A70-30878

Vibration-rotation band absorbance for nonisothermal gaseous radiation in terms of parameters describing isothermal gas
15 p2825 A70-31816

Vibrational energies, rotational constants and internuclear potential of ground state molecular iodine, using reanalyzed spectroscopic data
16 p2954 A70-33056

Night airglow hydroxyl rotational brightness temperature determined from emission spectra
19 p3412 A70-37777

Polar gas rotational relaxation time calculation, comparing volume viscosity and energy equation definitions
19 p3473 A70-38266

Diatomic molecules inelastic collision cross sections for specific rotational transitions, discussing S matrix energy requirements for statistical analysis
19 p3474 A70-38268

Formaldehyde rotational transition hyperfine components measured by molecular beam maser
20 p3702 A70-39008

Hydrogen molecules rotational excitation cross sections by electron impact in adiabatic excitation, discussing polarization and distortion effects
20 p3675 A70-39606

Molecular and noble gas rotational collision numbers from thermal transpiration measurements
20 p3738 A70-39995

Carbon dioxide and CO IR vibration-rotation spectral absorption coefficients, noting harmonic oscillator approximation
21 p3851 A70-40589

Electron collision frequency profile for energy loss rate in ionospheric G factor for air, considering rotational excitations of molecular oxygen and nitrogen
21 p3812 A70-40618

Rotational transition probabilities of molecular collisions, using time dependent perturbation theory along linear trajectories
21 p3853 A70-41390

Numerical molecular rotational transition probabilities and cross sections in HCN-HCN and ICN-ICN collisions, using perturbation theory and multipole potentials
21 p3853 A70-41391

Heavy atom skeletal molecular structure of asymmetric close-2,3-dicarbahexaborane from microwave rotational spectra
21 p3773 A70-41392

Laboratory measurement and low noise search in W3/OH for microwave emission lines in excited rotational level of interstellar OH
21 p3922 A70-41977

Rotational relaxation of diatomic molecular excited electronic state at high temperatures, discussing nonequilibrium region behind shock wave front in nitrogen
21 p3854 A70-42060

Liquid crystals orientational ordering molecular field theory examined by cluster variation method, predicting first order transition
22 p4085 A70-42485

Hydrogen chloride self broadened fundamental vibration rotation band intensity variation with pressure investigated by absorption spectroscopy analysis
22 p3983 A70-42945

Strong coupled rotational excitation problem in atom-diatom molecule scattering system, discussing transition probability matrices statistical analysis
23 p4212 A70-44600

Kinetic transport theory for mixed dilute gases consisting of linear rotating diamagnetic molecules in external homogeneous magnetic field
23 p4223 A70-44927

Rotational quantum numbers from iodine molecule resonance fluorescence measurements during laser excitation using Fabry-Perot interferometer
23 p4202 A70-44938

Narrow resonances in saturated absorption at molecular vibrational-rotational transitions in carbon dioxide laser
23 p4202 A70-45059

Rate equation study of multiwavelength far IR laser oscillations in water vapor, taking into account molecular rotation-vibration interaction
24 p4354 A70-45812

MOLECULAR SIEVES

U ABSORBENTS

MOLECULAR SPECTRA

NT ELECTRONIC SPECTRA

NT RAMAN SPECTRA

NT VIBRATIONAL SPECTRA

Carbon dioxide laser with incorporated grating for measuring line strength to width ratio for various rotational lines
01 p0112 A70-10916

Dispersed fluorescence spectra from vacuum UV photon impact on COS, noting absence of emission from higher vibrational levels
01 p0148 A70-11353

CH and CD molecules UV absorption spectra, using flash photolysis of diazomethane
02 p0341 A70-11795

Methane and ammonia absorption bands and possible structure of Jupiter and Saturn cloud layers by spectrophotometric observations
02 p0366 A70-11807

NH bands in stellar spectra by visual inspection of spectrograms, noting abundance of N in normal and strong CN stars
02 p0379 A70-12708

G values of hyperfine components of OH radical molecular vibrational-rotational levels determined using optical RF double resonance
02 p0345 A70-12822

IR spectra of M stars and alpha Tau obtained with Michelson interferometer, observing molecular features and water vapor absorption
04 p0747 A70-14548

Low resolution spectra of IR stars NML Tau, CIT 3, 6 and 13 considered inadequate for molecular band identification
04 p0748 A70-14591

Laser action observation on IR bands of first positive system of molecular nitrogen using pulsed excitation
04 p0704 A70-15625

Molecular fluorescence emission rate factors for strong bands of nitric oxide gamma systems, noting day airglow temperature dependence
05 p0886 A70-17085

Particle, momentum and energy flux spatial distributions of molecules scattered in collisions of low energy Ar atoms with mica and Ag surfaces
06 p1111 A70-18268

Excitation emission of diatomic nitrogen molecule for first negative band broadening, considering high energy primary beam with secondary electrons
06 p1124 A70-18305

Methylamine crystals lattice vibrations IR spectra recordings, making spectral band assignments according to translational and librational motions
07 p1356 A70-18958

Rotating and oscillating spectra in diatomic molecule excited by slow and fast electrons, discussing Boltzmann distribution of excited molecules
07 p1337 A70-19044

Pressure-narrowing theory applied to calculating equivalent widths of lines in quadrupole rotation-vibration spectrum of molecular hydrogen
07 p1338 A70-19366

Rotational temperature of molecular beam by electron excited fluorescence method, discussing signal level, background light and scattering effects
07 p1345 A70-20140

Perturbation rotational levels in triplet states of CO emission spectra attributed to resonance fluorescence process involving optically forbidden transitions
09 p1731 A70-22282

CH, CD and CH ion excited states decay rates determined from phase shift and frequency data, discussing implications for astrophysics
09 p1731 A70-22513

Critical review of paper on molecular oxygen microwave spectrum analysis
09 p1732 A70-22829

Photoelectric measurements of dust and CN/C2 molecular emission in atmosphere of Comet Ikeya-Seki
09 p1761 A70-23058

Emission and absorption by nonhomogeneous gases with vibration-rotation bands determined by scaling approximation
10 p1968 A70-24474

Interstellar atomic and molecular hydrogen abundance and physical state using rocket observations of Lyman alpha absorption line and ground based observations
10 p1941 A70-24551

Molecular line identification in sunspot spectrum of CN, diatomic carbon, TiO, MgH, CaH, NiH and water vapor
12 p2302 A70-27590

Electron impact excitation cross section of /O, first negative band of nitrogen ion from threshold to 3 keV, using photon counting techniques
12 p2276 A70-27880

Spectrographic measurements of Jovian Red Spot and Southern Tropical Zone molecular absorption bands related to cloud cover density and depth
12 p2311 A70-28305

CH molecule line formation mechanism for 4300 A transition in solar photosphere, noting collisions with hydrogen atoms
12 p2311 A70-28309

Stark cell with high electric fields for studying inactive IR spectrum of homonuclear diatomic gas molecules
13 p2450 A70-28499

Formation mechanism of molecular CN violet bands in solar photosphere
13 p2493 A70-29393

Atmospheric molecular oxygen photometric absorption spectral bands, calculating growth curves
14 p2572 A70-30403

High temperature molecules matrix isolation in saturated vapor over refractory solids, discussing optical spectroscopy of VO, metal oxide and halide molecules
14 p2545 A70-30903

Nitrogen dioxide continuum in green-white afterglow of molecular oxygen and nitrogen, using spectrometry and photometry
14 p2579 A70-31254

Vapor phase fluorescence spectra from benzene and deuterated benzene at zero point vibrational level
15 p2694 A70-31731

Hydrogen molecules rotational excitation cross sections by electron impact in adiabatic excitation, discussing polarization and distortion effects
20 p3675 A70-39606

Method of moments for determining wave functions used in calculating molecular properties
20 p3675 A70-39997

Oscillator strengths for aluminum oxide molecular electronic sigma band system from intensity measurements in cyanogen-oxygen flame system
20 p3676 A70-40474

Microwave transitions for molecules in comets and interstellar space
21 p3887 A70-41110

Absorption diffuse band systems of diatomic argon molecule in vacuum UV region

21 p3853 A70-41395

Steepest descent method for determining lowest ground state eigenvectors for molecular wave configurations

22 p4062 A70-42747

MgH molecular lines Zeeman splitting in sunspot spectra confirmed by photoelectric observations

24 p4400 A70-45308

MOLECULAR SPECTROSCOPY

NT RAMAN SPECTROSCOPY

Spectroscopic calibration of laser lines at simultaneous carbon dioxide and nitrous oxide transitions in gas flow, showing abnormal line intensity

03 p0501 A70-13685

API state lifetime of CO measured using molecular level crossing spectroscopy

10 p1920 A70-24629

Molecular I ground state dissociation energy value, proposing spectroscopic reassignment

12 p2180 A70-26861

IR spectroscopy, determining relative populations of carbon dioxide vibrational energy levels by comparing emission intensities

13 p2455 A70-29131

Atomic physics of lasers and active materials, noting multiplet spectra of atoms, molecular spectroscopy, energy level population distribution and amplification

[AIAA PAPER 69-63]

18 p3316 A70-36700

Saturated absorption spectroscopy of various molecules using emission spectra of carbon dioxide and nitrous oxide lasers

22 p4050 A70-43239

MOLECULAR STRUCTURE

Electric field effects on dielectric properties and molecular arrangements of cholesteric liquid crystals with temperature dependent helical pitch

01 p0160 A70-11352

Intramolecular triplet-triplet energy transfer between nonconjugated molecular chromophores held together by rigid molecular frame at known separation distance and mutual orientation

02 p0251 A70-12277

Biophysics research, discussing supramolecular biological structures, synthesis of proteins, nucleic acids and genetic codes, biological membranes, coding in nervous system, etc

03 p0420 A70-13491

Peroxides, superoxides and ozonides applications in industrial chemistry, semiconductors and rocket motor fuels, discussing chemical structure and properties and nomenclature

05 p0810 A70-15768

Computer program to decide structure for aliphatic ketone from low resolution mass spectrum using DENDRAL algorithm

05 p0810 A70-16048

Cytosine-thymine transitions from cytosine-5-H3 decay in bacteriophage S13 DNA, discussing coding change efficiency

05 p0803 A70-16948

Kinetic relaxation and Boltzmann equations for studying shock waves propagating in gas composed of rigid ideally elastic spherical molecules without internal degrees of freedom

06 p1036 A70-17756

Dialkyl ketone ion in double McLafferty rearrangement, applying ion cyclotron resonance to structural study

08 p1454 A70-20525

Amino acid sequence of Chromatium ferredoxin molecule compared with other ferredoxins concerning structural, functional and evolutionary relationships

13 p2361 A70-28921

Structural and functional properties of phosphates in biochemical reactions, discussing linkages

14 p2544 A70-30346

Water structure role in membrane systems, considering phase transitions and thermal anomalies in surface properties

16 p2847 A70-33027

Molecular structural relationship between cellular membranes and photoreceptors in plants and animals

16 p2847 A70-33028

Organic molecules topology, discussing Hamilton circuits, DENDROL applications, etc

16 p2855 A70-33298

Vibrational spectra and structure of oxalyl chloride in crystalline and fluid states, discussing molecular and space group symmetry

16 p2857 A70-34006

IR Raman and vibrational spectra and structure of gaseous and liquid 1-pyrazoline

16 p2857 A70-34007

IR and Raman spectra of gaseous and liquid germylcyclopentane, determining torsional barriers and skeletal ring atom symmetry

16 p2858 A70-34008

Heavy atom skeletal molecular structure of asymmetric close-2,3-dicarbahexaborane from microwave rotational spectra

21 p3773 A70-41392

Combustion rate as function of oxidizer molecular refractivity in perchlorates and nitrates of aliphatic and aromatic mono- and polyamines explosives

21 p3783 A70-42241

Atomic and molecular spin in cosmic medium

22 p4107 A70-43460

High modulus carbon fibers production and properties describing polymer chains intermolecular structuring by pyrolysis and strength increase by fibers stretching at 2700 C

24 p4366 A70-45166

Polymers strength and stiffness properties, considering different molecular chain alignments as related to elastic modulus

24 p4366 A70-45173

Fluorescent probes inserted into biological membranes for molecular structural and dynamic facets

24 p4304 A70-46231

MOLECULAR THEORY

Absorption and luminescence in complex molecules and semiconductors, describing particle distribution and Fermi quasi-levels dependence on temperature and excitation intensity

08 p1555 A70-20510

Molecular-statistical theory of second-harmonic light generation by isotropic bodies immersed in external AC or DC electric field

10 p1916 A70-24379

Resonant electron scattering processes in atoms and molecules, discussing mechanistic models and use in interpretation of experiments

16 p2955 A70-33798

Liquid crystals orientational ordering molecular field theory examined by cluster variation method, predicting first order transition

22 p4085 A70-42485

MOLECULAR TRAJECTORIES

Molecular size dependent steric effects in translation-vibration energy transfer by velocity dispersions in cyclopropane-inert mixtures

21 p3780 A70-41706

MOLECULAR WEIGHT

NT LOW MOLECULAR WEIGHTS

Critical impurity concentrations of He-Ne laser quenching determined with mass spectrometer, giving impurities molecular weight and ionization potential for input powers

01 p0110 A70-10491

Laminar isothermal entrance flows in circular cross section ducts with uniform mass injection at wall from boundary layer equations, discussing molecular weight effects

02 p0288 A70-12859

Polysiloxanes morphology crystallized isothermally from melt using electron microscopy, noting fracture ease increment with molecular weight decrease

03 p0517 A70-14203

Unsaponifiable, molecular weight acids, alcohols and esters effect on rheological properties of lithium lubricants based on synthetic fatty acids

06 p1076 A70-17800

Two temperature gasdynamics for binary gas mixtures of differing molecular weight components, analyzing ultrasound and shock wave propagation

08 p1486 A70-21808

Injectant stagnation temperature and molecular weight variation effect on flow field generated from secondary gas injection into supersonic stream

09 p1733 A70-23217

[AIAA PAPER 69-1]

Injectant stagnation temperature and molecular weight effects in jet interaction flowfield

11 p2036 A70-25989

Fluidic oscillator molecular weight of flowing mono- and polyatomic gases, discussing frequency dependence on pressure drop and temperature

17 p3081 A70-34515

Mean molecular mass determination method for upper atmosphere based on Nicolet equation for scale height, using satellite orbit and spin decay data

17 p3138 A70-35773

ELF and VLF propagation for perturbed ionosphere models, discussing effects of ion collision frequencies and molecular weights

20 p3585 A70-39454

T4 phage proteins radioisotopic examination, determining quantitative analysis and molecular weight by autoradiography

20 p3583 A70-40325

Poly/perfluoroalkylene oxides/ preparation and curing, considering molecular weight and thermal stability

21 p3783 A70-42145

Propellant binder prepolymers functionality distribution, examining solute concentration, solvent type and temperature effects on number average molecular weight measurements

21 p3865 A70-42146

MOLECULES

NT DIATOMIC MOLECULES

NT MONATOMIC MOLECULES

NT POLYATOMIC MOLECULES

NT TRIATOMIC MOLECULES

Source power molecule lifetime, acceleration and particle velocity in region near comet nucleus determined from brightness

07 p1378 A70-19036

K and M star molecular constituent density calculations using model atmospheres and observations

20 p3702 A70-39015

Photoelimination reactions of macromolecules, emphasizing intermediate pathways heuristic description via energy level diagrams

23 p4157 A70-44391

MOLIERE FORMULA

U COSMIC RAY SHOWERS

U SECONDARY COSMIC RAYS

U SPATIAL DISTRIBUTION

MOLLUSKS

Aplysias periodic spontaneous gill movements controlled by central neuron activity in abdominal ganglion

04 p0629 A70-14425

MOLNIYA SATELLITES

Molniya 1 communication satellite attitude control involving automatic solar panel and antenna orientation, using powered gyroscopic stabilizers

13 p2499 A70-28387

Soviet communication satellites orbit and design characteristics, operational uses and ground stations, discussing Molniya 1 series transmitting television, multichannel radio, telephone and telegraphy

18 p3230 A70-37225

SECAM video and audio color TV transmission over Molniya satellite relay path

23 p4162 A70-44091

MOLTEN SALT ELECTROLYTES

Molten carbonate fuel cells power source for military applications, considering catalytic recycle reformer

08 p1439 A70-20703

Fuel cells phase equilibria between carbonate melt and Li, Na and K solid aluminate electrolytes, analyzing thermal and electrical conductances

10 p1830 A70-24458

Molten lithium sodium carbonate electrolyte decomposition and evaporation at high temperatures in various atmospheres, noting water and carbon dioxide additives effects

12 p2166 A70-27763

MOLYBDATES

NT LEAD MOLYBDATES

MOLYBDENUM

X ray topography of postannealing substructure of neutron irradiated W and Mo single crystals, indicating increase in disorientation

01 p0115 A70-10065

Disk-shaped Mo and Nb specimens solar radiation reflection and absorption characteristics observed for temperature effect

01 p0117 A70-10176

Polycrystalline Mo ductility at low pressures in tension at ambient temperature, discussing H type embrittlement mechanism

01 p0121 A70-11234

Recrystallization diagrams of commercially pure Mo and Mo alloyed with Fe, Co or Fe plus Ni, noting additions effect on recrystallized grain size

01 p0124 A70-11616

Mo coated with Ni-base Nimonic and Co-base heat resistant alloys, for working degree effect on creep rupture strength

01 p0126 A70-11646

Molybdenum cylinders strength and plasticity under various compression and cyclic tensile loads

02 p0315 A70-11662

Temperature effects on tensile deformation mechanism of Mo single crystals, investigating stress-strain characteristics and slip geometry

02 p0316 A70-11699

Thermionic emission characteristics of W and Mo subjected to focused CW carbon dioxide laser radiation, discussing direct energy conversion

02 p0312 A70-12068

Titanium aluminide-Mo system hardness, electrical conductivity and density as function of chemical composition, presenting creep test results

03 p0510 A70-13353

Brittle fracture in neutron irradiated and nonirradiated Mo specimens tested in tension and compression at low temperature

03 p0513 A70-14013

Mo/Mo cylindrical thermionic converter steady state performance, measuring efficiency and power density at various low emitter and collector temperatures

04 p0627 A70-14947

Ductile-brittle transition temperature relation with grain size in polycrystalline Mo as function of annealing temperature

05 p0862 A70-15907

Binary system Mo-C determined in temperature range 1250-2270 C, using microscopic and thermal analyses and microhardness testing

05 p0862 A70-16198

Strength and plasticity of Mo and Nb sheet in oxidizing medium at high temperatures and pressure range

05 p0865 A70-17029

Chromized molybdenum thermal stability under cyclic induction heating and subsequent air cooling

07 p1304 A70-18743

Molybdenum rolling-deformed single crystals recovery and recrystallization using diffraction electron spectroscopy

07 p1307 A70-19550

Carbides content determination in Mo single crystals by metallographic method, establishing relation between brittle-ductile transition temperature and carbon content

07 p1308 A70-19607

Cylindrical Mo single crystals during cyclic heating, studying characteristic dislocation changes at various stages of thermal fatigue

07 p1308 A70-19609

Oriented single crystals properties obtained from Mo powder subjected to compacting, annealing in hydrogen and electron beam zone melting

07 p1308 A70-19610

Size effect on structure and mechanical properties of thin wire made of Mo single crystals deformed in recrystallized state

07 p1308 A70-19611

Structure and mechanical properties of Mo single crystals grown from gas phase using metallographic and X ray analysis

07 p1308 A70-19612

Rolling texture and recrystallization of Mo single crystals and deformation effect on texture formation using X ray transmission technique

07 p1309 A70-19613

Molybdenum single crystals orientation effect on thermal resistance to argon plasma flow

07 p1309 A70-19614

Interstitial atoms effect on dislocation relaxation and aging of Mo and Nb single crystals

07 p1309 A70-19638

Tracks shape associated with dislocation motion during etching of Mo single crystals

07 p1309 A70-19639

Fatigue crack growth in polycrystalline Mo at room temperature under cyclic loads observed along grain boundaries

07 p1314 A70-20013

AIN deposition rate from gaseous phase on Mo substrate as function of temperature

07 p1357 A70-20311

Low energy ions incidence angle effects on secondary electron emission from molybdenum cylinders in low pressure plasma, noting role of Langmuir sheath around target

07 p1355 A70-20356

Mo effect on structure and properties of Ni-Al-Nb system alloys in gamma and gamma prime solid solutions range, discussing high temperature strength

08 p1514 A70-20549

Mo mechanical properties dependence on surface defects and Ti films

08 p1515 A70-20937

Reduction temperature effects on molybdenum powders sinterability noting dispersion role

08 p1517 A70-21145

Combined solubility of group IVA metals and carbon in solid state molybdenum at various temperatures

09 p1704 A70-22754

Thermochemical predictions for high temperature oxidation of Mo and W, discussing oxide films or scales, reactant gases flow rate, etc

09 p1630 A70-22943

Molybdenum heat capacity, electrical resistivity and thermal radiation measurements at high temperatures with millisecond resolution

09 p1706 A70-22955

D-pattern changes of helium ions irradiated polycrystalline Mo and Ni specimens, observing line splitting

09 p1707 A70-23197

Mo single crystals creep behavior temperature and stress dependences using X ray analysis

09 p1708 A70-23543

Mo single crystals dislocation substructure strain dependence after creep using etch pitting techniques

09 p1708 A70-23544

Oxygen solubility in liquid Mo in presence of volatile oxides, determining equilibrium constant of dissolution reaction

09 p1709 A70-23784

High temperature creep of prestrained molybdenum single crystals as function of physical treatment and crystal orientation

10 p1902 A70-23860

Chemisorption on Mo single crystal surfaces observed by LEED techniques, discussing bcc planes and adsorbed gases

12 p2181 A70-27256

Foil decarbonization process monitored by mass spectrometry of secondary carbon ion emission

12 p2254 A70-27311

Polycrystalline molybdenum desorption of adsorbed hydrogen, oxygen and water by electron impact

12 p2182 A70-27679

Interstitial solid solutions stability in cast molybdenum subjected to heat treatment

12 p2257 A70-28225

Corrosion resistance of molybdenum coatings on steel and Pb-Bi eutectic alloy obtained by vacuum contact fusion method

12 p2258 A70-28320

Pure Mo recrystallization deformed by cold rolling using transmission electron microscopy

14 p2597 A70-31284

Initial stages of Ti vapor deposition on Mo, using secondary ion-ion emission and mass spectral analysis

15 p2757 A70-32120

Stress relaxation of Mo under plastic deformation controlled by diffusion of interstitial atoms and dislocations, determining activation energy

15 p2758 A70-32124

Flow stress and dislocation density dependence on temperature in polycrystalline molybdenum

16 p2930 A70-33085

Mo powder compacting by hot pressing, determining activation energy

16 p2931 A70-33222

Constant grain size cast Mo ductile-brittle transition temperature dependence on annealing temperature using tensile test

16 p2933 A70-34274

Siliconizing of Mo in medium with silicon chloride, comparing reaction probabilities for various heating methods

17 p3102 A70-35392

Diffusion during high temperature exposure of protective coatings on Mo, noting compact layers and carbide forming elements effect on thermal stability

17 p3125 A70-35404

Baron thermal diffusion effects on plastic of pure Mo subjected to recrystallization

17 p3102 A70-35408

Temperature dependence of materials with protective coatings, emphasizing mechanical properties of Mo with various diffusive coatings

17 p3126 A70-35716

Electron radiation damage and stage 3 annealing effects on polycrystalline Mo properties

19 p3451 A70-37570

Substrate and thickness dependence of electrical and superconductivity properties of rhenium and molybdenum films prepared by electron beam evaporation

19 p3485 A70-37684

Nitrogen diffusion coefficient in Mo and W using degassing method

19 p3452 A70-37828

Molybdenum cylinders strength and plasticity under various compression and cyclic tensile loads

19 p3453 A70-38436

Mo-Si system phase diagram by X ray, microstructural and thermal differential analyses, identifying eutectic, peritectic and eutectoid equilibria

20 p3649 A70-39773

Mo microstructure changes at high temperatures, noting polygonization, grain migration and crack propagation during failure

22 p4055 A70-43125

Mo single crystals tensile properties at different orientations, noting asymmetric slip in plastic behavior

22 p4056 A70-43155

Slip, fracture and rupture in sintered and cast ductile and brittle polycrystalline Mo under tension, using optical and electron microscopy

23 p4204 A70-43884

Convective diffusion limited oxidation of Mo, measuring kinetics up to 2000 K by rotating disk method

24 p4358 A70-45233

Aluminum oxide growth rate in molybdenum cermet after high temperature annealing

24 p4359 A70-45478

Diffusive carbon redistribution in Mo during interaction with Ni and Cr protective coatings

24 p4364 A70-46334

MOLYBDENUM ALLOYS

NT RENE 41

Roller bimetallic Ni-Mo mechanical properties produced by powder metallurgy methods

01 p0116 A70-10157

Recrystallization diagrams of commercially pure Mo and Mo alloyed with Fe, Co or Fe plus Ni, noting additions effect on recrystallized grain size

01 p0124 A70-11616

Nb-Mo alloys in various proportions prepared by vacuum casting, showing embrittlement under hydrogen atmosphere

02 p0318 A70-12671

Complexonometric analysis of alloys containing Mo without component separation, treating molybdenum aluminides, zirconium boride-molybdenum silicide, molybdenum carbide in Ti, etc

03 p0504 A70-12980

Mo separation from W during chemical analysis of W in binary Mo-W alloys, using organic reagents for precipitation and extraction

03 p0504 A70-12982

Phase alteration quenching effects in Ni-Mo alloys, discussing high temperature alpha region, isothermal annealing below peritectoid temperature and metastable nickel molybdenide phase

03 p0508 A70-13143

Nb-Mo alloy interstitial oxygen concentration determined by measuring internal friction /Snoek/ peak

03 p0512 A70-13763

Extension characteristics of delta and sigma related phases in Mo-Ni ternary systems and evaluation of unit cell dimension variations on alloying

04 p0704 A70-14392

Oxidation behavior of TiC base alloys containing Mo

04 p0708 A70-15312

Book on optimization by variational methods covering use of differential equations, Pontryagin minimum principle, optimal and feedback control, dynamic programming, etc

06 p1093 A70-17650

Mo-nitrogen interaction, studying nitriding influence at various temperatures on Mo alloys properties

06 p1089 A70-17741

Diffusion layer and protective oxide composition changed to increase chrome plated Mo heat resistance

06 p1089 A70-17742

Annealing atmosphere effect on permeability of Mo Permalloy

07 p1304 A70-18814

Oxygen content influence on Nb-Mo alloy mechanical properties at ambient temperature in air and hydrogen

07 p1307 A70-19374

Mo sheet longitudinal and transverse mechanical properties and microstructure after annealing

08 p1517 A70-21199

Cr-Mo steel strength and structural stability during tubular stress-rupture testing with high pressure hydrogen, discussing welding effect on strengths

08 p1519 A70-21455

Ni-Mo surface alloys investigated by low energy electron diffraction, using tabulated symmetry and extinction properties of space groups and phase diagrams

08 p1557 A70-21603

Dynamic strain aging effect on Mo-Ti-C alloy creep, relating carbides precipitation during plastic deformation to mobile dislocations density

08 p1524 A70-21954

Cleavage fracture of Ta-Mo bcc alloys, investigating short range ordering and size effects by X ray diffraction

09 p1708 A70-23573

Hot shortness of molybdenum alloys under tensile testing due to molybdenum carbide precipitation on grain boundaries

11 p2066 A70-25914

Heat resistance and elastic properties of binary Ti-Mo alloys as function of phase structure and chemical composition

11 p2066 A70-25915

Carbide-strengthened Mo alloys dynamic strain aging processes

12 p2255 A70-27605

Plastic deformation of Mo-Re single crystals produced by electron beam zone refining, investigating lattice frictional stress, activation volume temperature variation, etc

13 p2436 A70-29562

Nitrogen solubility in Nb-Mo solid solutions, determining relationship between N partial pressure, temperature and concentration

14 p2598 A70-31285

Beta phase decomposition kinetics and strain hardening inhibitions in Ti-base Mo alloys, using metallographic, dilatometric and X ray analyses

15 p2764 A70-32855

Ti-Mo cermet alloys properties and production technology, testing corrosion resistance

16 p2931 A70-33220

Working fluid /Ar/ purity and stability effects on fatigue life and creep of Nb and Mo alloys using gas analysis, microstructure and microhardness data

17 p3126 A70-35715

Mechanical properties of binary Ti-Ni and ternary Ti-Mo-Ni alloys

18 p3275 A70-36122

Cross sectional phase diagram of Nb-Ti-Mo-V, discussing continuous crystallization and composition dependent hardness and resistance

18 p3275 A70-36125

Mo alloying additions effects on carbide phases in Nb-C alloys

20 p3646 A70-39104

Nb-Ta and Nb-Mo alloys single crystal solid solution strengthening as function of composition, temperature and strain rate

20 p3646 A70-39105

Sintered boron-alloyed Mo electron beam welding behavior examined by texture-revealing color etching method

21 p3833 A70-41411

Ni-Nb-Mo, Ni-Nb and Ni-Mo alloys phase equilibrium

21 p3840 A70-41898

Recrystallized and nitrided Mo alloy microstructure under plastic deformation by tension at high temperatures

22 p4038 A70-43122

Vacuum-melted and deformed Mo alloys tests, showing long term strength decrease under cyclic heating 22 p4055 A70-43123

Low alloy Mo sheet recovery and aging characteristics studied by X ray scattering 22 p4055 A70-43124

Mo alloys strengthening by hydrostatic extrusion, combining dynamic strain aging with low temperature strain hardening 24 p4341 A70-45251

Phase regions and lattice parameters of isothermal section of Mo-Zr-Cr system at 1100 C from microstructural and X ray analyses 24 p4361 A70-45832

Ti-Mo and Ti-Mn alloys omega transition phase, describing shape and crystallographic characteristics 24 p4361 A70-46178

MOLYBDENUM CARBIDES

Carbides content determination in Mo single crystals by metallographic method, establishing relation between brittle-ductile transition temperature and carbon content 07 p1308 A70-19607

Phase equilibria, crystallization and solidus surface in transition conode triangle of ternary system Mo-Ti-C at high temperatures 07 p1310 A70-19804

Phase transformations of molybdenum carbide under elevated temperature in vacuum, using X ray and differential thermographic analysis 13 p2433 A70-28852

Carburizing spherical powders of Nb, Mo and W to obtain carbides, noting agreement between theoretical and experimental data 17 p3125 A70-35410

Molybdenum carbization in methane-based plasma glow discharge, considering possible pyrocarbon layer formation and temperature effects 19 p3434 A70-37456

MOLYBDENUM COMPOUNDS

NT LEAD MOLYBDATES
NT MOLYBDENUM DISULFIDES
NT MOLYBDENUM OXIDES

Synthetic molybdenum diselenide oxidation kinetics between 375-530 C, determining isothermally reaction rate constants in dry air [ASLE PREPRINT 69-LC-8] 02 p0321 A70-12537

German monograph on sintered molybdenum silicide recrystallization following high temperature heating in oxidizing atmosphere 24 p4367 A70-45575

Molybdenum disilicate and aluminum oxide coating sealing heat resistance tests 24 p4364 A70-46341

MOLYBDENUM DISULFIDES

Molybdenum disulfide surface and bulk properties, comparing endurance of fractions and grades with synthetic chalcogenides at same layer thickness in dry atmospheres [ASLE PREPRINT 69-LC-7] 02 p0322 A70-12538

Molybdenum disulfide solid film lubricant with increased wear life developed from in situ conversion of electrodeposited molybdenum trioxide 06 p1091 A70-17339

Burnishing load and time effect on deposition, endurance limit of lubrication and wear-in characteristics of molybdenum disulfide powder films 08 p1508 A70-21516

Service life and friction coefficient of molybdenum disulfide-silicon lubricating coating as function of load, sliding rate and vacuum level 11 p2060 A70-25943

Transformations on surfaces of molybdenum disulfide-stem system during friction in air, noting Mo oxides formation and friction coefficient increase 13 p2421 A70-29427

Molybdenum disulfide and phenol formaldehyde resin lubricants for hydroextrusion of steel 15 p2743 A70-31639

Molybdenum disulfide abrasiveness on test rings coated with bonded solid lubricant [ASLE PREPRINT 70AM 5A-1] 19 p3439 A70-38811

MOLYBDENUM OXIDES

Transformations on surfaces of molybdenum disulfide-stem system during friction in air, noting Mo oxides formation and friction coefficient increase 13 p2421 A70-29427

MOLYBDENUM SULFIDES

NT MOLYBDENUM DISULFIDES
Synthetic molybdenum disulfide crystal properties compared to natural crystals, discussing friction coefficient, adherence to metal surfaces, etc 10 p1907 A70-24787

Molybdenum disulfide dry film lubricant wear life as film sintering process dependent on binder, additive or atmosphere chemical effects 11 p2058 A70-25571

MOMENT DISTRIBUTION

Moment methods for calculating modeled diffusion gas mixture shock waves using Monte Carlo method, discussing distribution function and flow pattern 06 p1050 A70-18336

Differential equations of motion for body with stationary point, allowing for Kovalevskaja conditions and assuming nonzero gyrostatic moment 09 p1726 A70-22149

Zero moments surface in problem of two immovable centers, taking into account cosmic dust accumulation before binary apex moving forward with periastron of bright component 18 p3324 A70-37147

Mathematical theory of constitutive relations connecting surface tractions and moments with motion of single body in continuum 20 p3672 A70-39495

Method of moments for determining wave functions used in calculating molecular properties 20 p3675 A70-39997

MOMENTS

NT BENDING MOMENTS
NT DIPOLE MOMENTS
NT DISTRIBUTION MOMENTS
NT ELECTRIC MOMENTS
NT LOADING MOMENTS
NT MAGNETIC MOMENTS
NT MEAN
NT MOMENTS OF INERTIA
NT PITCHING MOMENTS
NT ROLLING MOMENTS
NT STABILITY DERIVATIVES
NT STANDARD DEVIATION
NT TORQUE
NT VARIANCE [STATISTICS]
NT YAWING MOMENTS

Dynamic behavior and moments of oscillatory systems under steady perturbations using linear differential equations 12 p2261 A70-27555

Bipolar moment integral in celestial mechanics formed by product of particle kinetic moments for n body problem order reduction 13 p2494 A70-29399

Delayed moment of force relativistic definition within reference of inertia, discussing lever bent at right angles 13 p2452 A70-29635

Piezoelectric force and moment measurement by quartz multicomponent devices 19 p3426 A70-37937

Piezoelectric sensors for multicomponent force and moment measurement 20 p3635 A70-40533

Non-Chebyshevian moments induced by system of linearly independent functions expanding to semi-infinite programs 23 p4211 A70-44243

Algorithm for moment problems in Chebyshev system with applications to numerical integration, series summation and function approximation 23 p4211 A70-44244

MOMENTS OF INERTIA

Inertia forces effect in turbulent and laminar, self acting and infinitely long film bearings, considering compressible and incompressible lubricants [ASME PAPER 69-LUB-2] 01 p10103 A70-10400

Inertia cross coupling during aircraft design stage allowing later flight testing, discussing analysis complexity and sensitivity to aerodynamic data change 01 p0007 A70-11315

Sinusoidal test for measuring knee moment increase required to flex and extend for various conditions of knee angle, angular velocity and steady knee moment 02 p0238 A70-12546

Eddington equation for white dwarf pulsation solved by treating eigenfunctions as differential moment of inertia functions 04 p0751 A70-15050

Human body turning /orienting/ in unsupported /weightless/ position by own muscular forces, determining inertia moments of body and parts relative to various axes 07 p1207 A70-19495

Perturbed gyroscopic system consisting of disk hinged by rigid weightless rod, investigating stability condition at axial and equatorial inertia moments 08 p1496 A70-21210

Ionosphere sounding satellite attitude variation dependence on transverse moments of inertia 10 p1949 A70-23918

Uniform beams flexural vibration natural frequencies approximate calculation showing effect of shear flexibility and rotatory inertia 10 p1959 A70-24562

Inplane and rotary inertia effects on free vibration frequencies of circular cylindrical shells eccentrically stiffened by orthogonal set of stringers and/or rings 11 p2135 A70-25993

Free elastic rotating beam with tip masses and inertia, developing solutions for flexible modes and natural frequencies of H-type configuration 12 p2273 A70-27820

Circular orbit gravitationally stabilized satellite oscillation damping by changes of moments of inertia 13 p2501 A70-28420

Effective moment of inertia in quantum mechanical three body problem, applying specific decoupling to wave functions 13 p2452 A70-29478

Human body turning /orienting/ in unsupported /weightless/ position by own muscular forces, determining inertia moments of body and parts relative to various axes 15 p2685 A70-32740

Optimal orientation of axisymmetric spin stabilized rigid bodies as function of moments of inertia ratios, using single jet for alignment [DFVLR-SONDDR-50] 16 p2976 A70-33773

Inertia forces effect in turbulent and laminar, self acting and infinitely long film bearings, considering compressible and incompressible lubricants [ASME PAPER 69-LUB-2] 19 p3435 A70-37613

Stress differential equations of micropolar elasticity, considering mass forces and moments of inertia 19 p3459 A70-38672

Variable wing sweep aircraft angular motion mathematical model, analyzing inertial moments influence on control dynamics 20 p3562 A70-40182

Shape factors for weight prediction and design optimization of structural members requiring given area moment of inertia [SAWE PAPER 828] 20 p3732 A70-40354

Optimal moments of inertia of rigid satellite in circular orbit by generalization of Beletskij concept, discussing libration boundaries 23 p4261 A70-44677

MOMENTUM

NT ANGULAR MOMENTUM

Turbulent boundary layers behavior prediction by strip integral momentum equation method, considering velocity profiles and shear stresses 02 p0282 A70-12332

Momentum integral method for turbulent boundary layers based on equilibrium profiles family, considering weighting function specification techniques 02 p0284 A70-12345

Spatial distribution function calculation for muons in extensive air shower model and secondary particles mean transverse momentum estimation 03 p0556 A70-13039

Atmospheric momentum and heat flux height variations in surface boundary layer, stressing instrument performance and measurement techniques 09 p1715 A70-22359

Laminar boundary layer in adverse pressure gradient calculated for momentum thickness from approximate equation, analyzing error 09 p1660 A70-22832

Vertical momentum flux correction for planetary scale gravity waves in equatorial lower stratosphere 13 p2445 A70-29623

Electron momentum distribution function of p-type semiconductor with arbitrary band structure under electric and magnetic fields 17 p3144 A70-35704

Subcritical and supercritical boundary layer problems, reviewing various momentum integral solution methods 18 p3242 A70-36705

Liquid fuel jet engine thrust aftereffect momentum, investigating switching off transient process 19 p3490 A70-37249

Insular system energy and momentum definition in external gravitational field, using dynamic equations and Einstein theory 19 p3513 A70-37412

Jet momentum for flow separation control of air past circular cylindrical surface 24 p4288 A70-46011

MOMENTUM ENERGY

U KINETIC ENERGY

MOMENTUM PRECESSION

U PRECESSION

MOMENTUM THEORY

Equations of hydrodynamics governing perfect fluid in second postNewtonian approximation to general relativity, deriving energy momentum tensor equation 02 p0337 A70-11776

Integral method for turbulent shear flow based on momentum and moment-of-momentum equations and Cole velocity profile family, determining shear stress integral 02 p0282 A70-12329

Modified Granville moment of momentum method used with integral equations in integral moment method for turbulent boundary layer flow, considering pressure gradient influence 02 p0282 A70-12334

Momentum integral method using auxiliary equation for two and three dimensional flow problems 02 p0284 A70-12344

Mean flow velocity distribution calculated from momentum deficit superposed behind single cylinders in finite array of arbitrarily spaced parallel cylinders [ASME PAPER 69-WA/FE-11] 04 p0614 A70-14781

Na abundance in terrestrial upper atmosphere, solving steady state continuity and momentum equations for Na atoms and ions 05 p0840 A70-16475

MOMENTUM TRANSFER

Suddenly started laminar flow in circular tube entrance region, obtaining integral momentum equation for boundary layer thickness, entrance length, velocity profile, etc

06 p1034 A70-17528

Momentum considerations in thunderstorm dissipation by disrupting organized cloud base updraft structure

06 p1100 A70-18570

Turbulent flow downstream from abrupt widening of circular jet, using flow and momentum equations

10 p1870 A70-24782

Momentum theory of small elastic-plastic deformations, proving minimum potential energy, simple loading and elastic unloading theorems

11 p2128 A70-25387

Energy and canonical momentum relationship in relativistic mechanics, discussing particle production and annihilation

13 p2453 A70-29721

Maximum impact accelerations of spherical and conical bodies landing on water, using momentum theorem

15 p2722 A70-32524

Fermi momentum upper limit for universe neutrinos in cosmic ray propagation, determining maximum proton energy

20 p3700 A70-39592

Momentum source interaction with viscous uniform stream, constructing perturbation solutions from nonlinear equations

24 p4327 A70-46040

MOMENTUM TRANSFER

Two phase flow in cylindrical channel, formulating maximum momentum flow variational principle for laminated adiabatic vapor- and gas-liquid flows

01 p0213 A70-10216

Wet vapor flow with/without inert diluent, assuming momentum and heat transfer between phases according to Stokes law and Nusselt number of unity

01 p0061 A70-10332

Prediction systems for turbulent boundary layers, noting momentum integral equation use in all integral methods

02 p0281 A70-12327

Method of weighted residuals /MWR/ for nonlinear partial differential equations applied to incompressible two dimensional turbulent boundary layer momentum and continuity equations

02 p0281 A70-12328

Heat and momentum transfer efficiency of thermal convection, calculating eddy coefficients for vertical transfer

05 p0831 A70-15876

Laminar sublayer resistance to momentum and heat transfer, noting effects of Prandtl number and surface roughness using mathematical model and experiments

06 p1034 A70-17680

Momentum transfer from neutral nitrogen molecules to solid surfaces measured for various incident beam molecule energies

06 p1112 A70-18272

Monte Carlo analysis of free and near free molecular flow through circular tubes for mass, momentum and energy transfer

06 p1051 A70-18367

Tropospheric and stratospheric turbulent horizontal heat and momentum transfer spectral density profiles calculations from radio launchings data

07 p1269 A70-19646

Correlation functions for resistance to heat and momentum transfer in viscous sublayer at rough walls defined for varied geometry flows [ASME PAPER 69-HT-2]

08 p1486 A70-21833

Heat, moisture and momentum fluxes measurement in atmospheric boundary layer, discussing instrumental accuracy necessary for various measuring techniques

09 p1717 A70-22379

Momentum transport bounds in turbulent shear flow using variational methods

11 p2039 A70-26535

Reynolds momentum and mass transport at velocity half radius of coaxial jet compared to eddy viscosity models

14 p2564 A70-30260

Sound propagation in atmospheric fog, considering mass, momentum and energy transfer mechanisms between particles and gas

15 p2769 A70-31443

Monograph on momentum, heat and mass transfer rates to vertical continuous cylinder moving through quiet fluid in forced and free convection

15 p2825 A70-31694

Optimal desaturation of angular momentum exchange controllers in spacecraft attitude control systems, using natural environmental torques

16 p2947 A70-33345

Gas-particle mixture cascade flow over turbine blades, considering momentum/heat transfer and particle trajectories

16 p2835 A70-33569

Stellar mass loss, considering radiation field momentum transfer or coronal heating as mechanisms

17 p3157 A70-34841

Energy and momentum exchange between gases in elastic collisions at different temperatures and velocities

19 p3551 A70-37538

Periodic thermal forcing role in Venus atmosphere dynamics, investigating momentum transport to support mean shear for channel flow

19 p3519 A70-38251

Meridional transport of angular momentum in various wavenumber-frequency domains, discussing linear and nonlinear contributions

19 p3462 A70-38258

Intercomponent momentum and energy exchange in weakly ionized gases, examining kinetic theory of subsonic and supersonic transport processes

19 p3482 A70-38945

Thin radiating shock layer about axisymmetric blunt bodies, investigating energy-momentum transport coupling

21 p3950 A70-41746

Structural configurations effect on momentum imparted to spacecraft by hypervelocity meteoroid impact

21 p3938 A70-41879

Energy deposition in solar corona associated with momentum transfer from heating wave in transition region, discussing wave pressures

21 p3925 A70-42190

Plasma sheath boundary in anisotropic plasma taking into account ionization rate, momentum transferring collisions and finite ion temperature

22 p4077 A70-42291

MONATOMIC GASES

Atomic O, H and D and molecular oxygen, deuterium and sulfur hexafluoride effects on nitrogen vibrational population distribution in nitrogen afterglow

01 p0148 A70-11356

Hydrodynamic equations and Grad transport coefficients for nonequilibrium rarefied monatomic gases developed for molecular collisions

01 p0068 A70-11567

Shock wave structure determination in simple monatomic gas, using statistical counting and successive approximation algorithm

01 p0068 A70-11601

D-2 experiments measuring atomic oxygen emission from terrestrial atmosphere and polarization rate and emission intensity from geocoronal hydrogen

03 p0559 A70-13828

Hydrogen molecule formation relation to galaxy formation, discussing cosmic plasma neutralization role

03 p0577 A70-14152

Monatomic gas steady expansion into cylindrical vacuum, considering Maxwell molecules with cylindrical symmetry

04 p0674 A70-15557

Time dependent expansions into vacuum of monatomic gases with spherical symmetry, obtaining moments expressions for Maxwellian molecules

05 p0831 A70-16015

Particle, momentum and energy flux spatial distributions of molecules scattered in collisions of low energy Ar atoms with mica and Ag surfaces

06 p1111 A70-18268

Monatomic gas flow past moderate curvature body, obtaining approximate solutions to Boltzmann equation under form of matched asymptotic expansions

06 p0979 A70-18316

Boltzmann equation fourth moment numerically solved to study distribution function characteristics during monatomic gases spherical expansions into vacuum

06 p1048 A70-18320

Normal shock wave structure in binary gas mixtures of chemically inert monatomic molecules, using kinetic theory moment method

06 p1051 A70-18343

Monatomic gas rarefaction wave structure in unsteady one dimensional flow from high to low pressure zones, describing numerical solution technique

09 p1604 A70-22449

Fast argon beam scattering by gas molecules measured to study atomic and molecular two body systems involving nitrogen and oxygen atoms

09 p1732 A70-22902

Coupled Boltzmann and rate equations for free electron distribution function and level populations in monatomic partially ionized gas including nonelastic collisions

10 p1918 A70-23958

Thermal conductivity of monatomic binary gas mixtures at moderately low temperatures and pressures, considering various Ar-He mixtures

11 p2147 A70-25755

Swirling and meridional flow induced by steady rotation of gravitating sphere in compressible monatomic gas, considering compressibility effects and surface layer

[ASTME PAPER MR-69-714]

11 p1978 A70-26690

Ionization kinetics of Ar, Xe and Hg monatomic gas behind shock wave front at high temperatures

12 p2210 A70-27319

Ionization and metastable excitation in low energy collisions of ground state argon atoms formed by charge transfer

14 p2618 A70-30121

Strong shock waves profiles in monatomic perfect gases by Monte Carlo simulation, obtaining maximum density slope thicknesses

14 p2567 A70-31031

Continuum radiative flux from nonisothermal stagnation shock layer of nongray atomic gases, employing ionization edges and bound free spectral forms [AIAA PAPER 70-837]

16 p3001 A70-33932

Axisymmetric detached shock preceding blunt body immersed in hypersonic monatomic gas flow, considering radiative ionization in cold precursor by differential approximation

16 p2839 A70-34252

Collisionless monatomic gas flow density and velocity distribution on axis of diffusely reflecting circular cone at zero attack angle with free stream

16 p2839 A70-34273

Fluidic oscillator molecular weight of flowing monatomic and polyatomic gases, discussing frequency dependence on pressure drop and temperature

17 p3081 A70-34515

Light gas atoms adsorption on solid surfaces, calculating wave function, energy, mobility, sticking coefficient, etc

18 p3225 A70-36186

Monatomic inert gas molecules interaction with continuous elastic solid of alkaline and nonalkaline metals, calculating energy exchange

19 p3373 A70-37816

Atomic hydrogen population distribution in far UV of comets

19 p3526 A70-38782

Plasma and neutral gas collisionless interactions in magnetic field based on Alfvén critical velocity hypothesis, discussing electron energy distribution

21 p3857 A70-41383

Axisymmetric detached shock before blunt body in hypersonic monatomic gas flow, obtaining radiative ionization patterns in cold precursor

21 p3950 A70-41731

Ionization kinetics of Ar, Xe and Hg monatomic gas behind shock wave front at high temperatures

21 p3854 A70-42061

Gravitating sphere high speed rotation in monatomic gas, discussing viscous and thermal boundary layers, velocity fields, temperature effects and fluid motion

23 p4131 A70-43944

Atomic or molecular gases excited state lifetime measurements, using time to amplitude conversion and multichannel analyzer

23 p4198 A70-44946

MONATOMIC MOLECULES

Thermal diffusion of isotropic, nonisotropic and multicomponent mixtures with monatomic and polyatomic molecules, considering kinetic theory and experimental results

17 p3197 A70-35537

MONAURAL SIGNALS

Monaural detection and filtering of sinusoidal signals in noise, using amplitude model

17 p3033 A70-35610

MONGE-AMPERE EQUATION

Sonic surface and Cauchy problem of Monge-Ampère equations in plane unsteady transonic channel flow solved by hodographic analysis

12 p2156 A70-27299

Monge equation in small perturbation method of characteristics applied to propagation phenomena in three dimensional supersonic gas flow

13 p2386 A70-28490

MONITORS

Monitoring behavior in three source visual task, studying selective attention by response observation method

03 p0435 A70-13770

Monitoring and recording of physiological parameters, discussing heart, muscle, brain potentials, blood pressure, respiration measurements and instrumentation

03 p0439 A70-14267

Physician-monitored central control facility communicating with remote site facilities staffed by paramedical personnel for public health care, based on aerospace experience

04 p0644 A70-15357

Monitor for linearizing nonlinear characteristics of thermistors used for temperature sensors in Apollo Telescop Mount, optimizing circuit values with FORTRAN IV computer program

05 p0851 A70-16692

Contamination control of spacecraft for planetary exploration missions emphasizing monitoring equipment and cleaning procedures

05 p0808 A70-16702

Weld quality monitor for production testing of welding strength in electronic circuitry

05 p0856 A70-16722

Frequency monitor design, analyzing relationships between time constants, gain, etc, emphasizing white noise filtration

07 p1227 A70-18991

- Divided attention utility for monitoring information processing during encoding, retention and recall of words
07 p1224 A70-20047
- TV system for satellite antenna boom position monitoring, describing camera system and programming, imaging techniques, position calibration, etc
10 p1891 A70-24898
- Spectral analysis of LF pulses from defects obtained by modulation method of monitoring using eddy currents with superposed converter
13 p2404 A70-28660
- Tiros solar proton monitor program, describing detector design, operational data processing and early warning network
17 p3180 A70-35304
- Remote sonic monitoring system for Saturn V noise measurement and recording
17 p3094 A70-35521
- High altitude neutron supermonitor investigation of cosmic ray microvariations
18 p3307 A70-36104
- Automatic sound monitoring system for measuring aircraft noise in airport vicinity
19 p3397 A70-37908
- Computer controlled aircraft noise monitoring system at Stuttgart airport
19 p3397 A70-37909
- SUREFIRE /system for utilization of remote equipment for failure investigation and reliability evaluation/ monitoring reliability in closed loop failure reporting and corrective action system
19 p3555 A70-38834
- Inertial platform with integral dynamic self test and fault monitoring scheme, describing design and operation
[AIAA PAPER 70-1013] 20 p3667 A70-39520
- Self calibrating TRIM gyromonitor inertial platform with gyroflex gyro, describing operation and performance
[AIAA PAPER 70-1012] 20 p3667 A70-39521
- Medical monitoring system onboard Soyuz spacecraft, describing equipment design, data acquisition and analysis, telemetric recordings, etc
20 p3581 A70-40193
- Communications satellite carrier instrumentation, using computer controlled frequency shift radiometer for power monitoring
21 p3826 A70-41345
- Multichannel monitor for repetitive short scan Auger electron spectroscopy for surface composition changes, using low energy electron diffraction
21 p3827 A70-41467
- Supervisor /monitor/ sampling frequency maximizing payoff function, using Bayesian preposterior information analysis
22 p4127 A70-43498
- Aircraft onboard radar system with landing monitor perspective display of runway operating independently of ground based electronic equipment
[AIAA PAPER 70-1336] 24 p4373 A70-45932
- MONKEYS**
- Photoperiod variation effects on ambulatory primate Cebus albifrons deep body temperature /DBT/, locomotor activity /LMA/ phase relationships and DBT waveform
01 p0011 A70-10035
- Male macaque monkey physiological deterioration in Biosatellite 3, noting falling brain temperature, lowered central venous pressure, fluid loss, blood redistribution into visceral pools, etc
01 p0022 A70-10822
- Renal hemodynamics and clearances alterations in owl monkey, using hemorrhagic shock procedure
02 p0234 A70-11732
- Visual half field central integration and monocular performance in split-brain monkeys after transection of chiasm, anterior commissure and corpus callosum
03 p0421 A70-13625
- Image memory in Papio hamadryas monkeys reacting to visual and flavor food stimuli
04 p0632 A70-15219
- Amphetamine effects on observing and monitoring performance in squirrel monkeys, investigating lever and key responses using food reinforcements
05 p0806 A70-16128
- Pre-space flight tests effects on Macaca nemestrina monkeys spermatogenesis, considering immobilization and exposure time effects
06 p0991 A70-17287
- Macaque monkey stereoscopic vision, obtaining behavioral evidence by random dot stereoscopic patterns and finding cells sensitive to binocular depth in cortex
07 p1205 A70-19276
- Macaque monkey stereoscopic vision demonstrated behaviorally by combining random dot patterns with standard operant conditioning
07 p1205 A70-19277
- Delayed trace reaction under stable and unstable pauses in apes and monkeys, noting independence of conditioned reflex
08 p1446 A70-21446
- Phase correlation of conditioned and electrophysiological postirradiation disturbances in central nervous system of monkeys
08 p1446 A70-21447
- Rhesus monkey active bone marrow distribution and volume studied by radioactive tracing techniques
09 p1616 A70-22301
- Urinary calcium phosphate and carbonate precipitates reduction by protein and carbohydrate diet change to casein and sucrose in Macaca nemestrina
09 p1621 A70-23456
- Macaca nemestrina total body water measurement by dilution technique
20 p3577 A70-40333
- Balloon-borne monkeys possible brain damage due to cosmic rays, discussing thindown tracks and acute vasculitis
21 p3764 A70-41476
- Rhesus monkeys PC02 tolerance in low pressure environments, observing hypothermia and heart and respiratory rates depression
21 p3765 A70-41486
- Biosatellite 3 experiment with male macaca nemestrina monkey, discussing cardiac rate, vascular data, water balance, weight loss and brain temperature
22 p3973 A70-43646
- MONOCHROMATIC RADIATION**
- Human eye integration of short monochromatic light flashes at TV frame frequencies
02 p0238 A70-12463
- Numerically stable solutions existence for one dimensional monochromatic radiative transfer, using linear algebra including vector and matrix norms, convergence, etc
02 p0340 A70-12643
- Electromagnetic field structure and interaction inside and outside of spherical shell of arbitrary linear media excited by monochromatic plane wave
03 p0443 A70-13151
- Relationship between 6300 A monochromatic auroral arc and visible aurora during magnetic storm, determining directional speeds
03 p0478 A70-14000
- Brightness distributions and widths determined from monochromatic radiation intensity at earth during lunar occultation of RF source
05 p0920 A70-16941
- Liquid fuel combustion luminous flame monochromatic radiation distribution, considering soot particle clouds effective emission thickness
06 p1172 A70-17142
- Monochromatic radiation emissivity temperature dependence of monocarbides of Ti, Nb and alloys in homogeneity region
08 p1516 A70-20994
- Plasma monochromatic wave propagation equilibrium state instability mechanisms, discussing stimulated scattering by thermal plasma particles and particle capture in wave potential well
08 p1551 A70-21422
- Fluorel spectral reflectance, transmittance and absorbance under monochromatic irradiation, considering thermal analysis and surface finish
09 p1710 A70-22794
- Structural detail in transparent object through holographic measurement of scattered monochromatic light, noting similarity to crystal structure reconstruction in X ray diffraction experiments
11 p2048 A70-25360
- Monochromatic light propagation in medium with large scale Markov nonuniformities of dielectric constant using parabolic equation approximation
12 p2272 A70-27359
- Mutual coherence functions for quasi-monochromatic illumination measured by image holography
12 p2237 A70-28124
- Quasi-monochromatic radiation field polarization representation and transformation of state, including instrumental effects
13 p2451 A70-28829
- Planar absorbing and emitting layer exposed to monochromatic collimated radiation, analyzing line or band shape effect on radiative transfer
13 p2451 A70-29135
- Electronic heterodyne astronomical spectroscopy, using lasers for absolute monochromatic flux and polarization measurements on star-like objects
13 p2408 A70-29473
- Elastohydrodynamic monochromatic wave coupling in liquid filled container as model for Alfvén and magnetoacoustic waves transmission in plasma
14 p2625 A70-31356
- Normally incident plane monochromatic electromagnetic wave reflection and scattering from expanding dielectric slab, using invariant imbedding concept
15 p2695 A70-31438
- Molecular velocity influence of optically active medium in gas dynamic quantum amplifier on monochromatic radiation transport, using corpuscular light model
15 p2721 A70-32356
- Solar prominences monochromatic images in He I D3 and He II 4686 lines allowing for contamination in 4686 images
15 p2803 A70-32614
- Monochromatic electromagnetic wave diffraction on moving ideally conducting half plane, deriving parameters and spectral composition after diffraction
16 p2863 A70-33216
- Spectrophotometric and visual observations of twilight glow from Soyuz 5, comparing vertical monochromatic brightness profiles with calculations for Elterman aerosol model
16 p2896 A70-33218
- Monochromatic radiation angular distribution surface reflectance measurement using photographic reflectometer
[AIAA PAPER 70-859] 16 p2912 A70-33904
- Optically excited homogeneous bulk semiconductor lasers, examining quantum mechanical rate equations and monochromatic light field pump source
18 p3270 A70-36741
- Monochromatic radiation from laser modulated electron beams
19 p3444 A70-37572
- Plane monochromatic EM wave diffraction by rectangular metal bar tapered grating, examining amplitude and polarization parameters
19 p3377 A70-37721
- Frequency shifted diffraction of monochromatic Gaussian light beam by reflection off ultrasonic surface wave
21 p3850 A70-41907
- Monochromatic acoustic wave interaction with turbulent jet fluctuating vorticity field, using Fourier analysis to extend spectral relations
[ASME PAPER 70-FLCS-6] 22 p4008 A70-42426
- Monochromatic radiant flux angular distribution reflected from water and carbon dioxide cryodeposits, discussing incidence, deposit thickness and wavelengths
[ASME PAPER 70-HT-34] 22 p4122 A70-42433
- Monochromatic light propagation in medium with large scale Markov nonuniformities of dielectric constant using parabolic equation approximation
22 p4075 A70-43600
- Unsteady radiating nongray gas diffuse boundary conditions, emphasizing monochromatic radiation slip and one dimensional radiant flux
23 p4282 A70-44593
- Quantum noise in narrow-band ring laser, noting mode amplification of weak monochromatic signals
23 p4202 A70-45056
- Spectrophotometric and visual observations of twilight glow from Soyuz 5, comparing vertical monochromatic brightness profiles with calculations for Elterman aerosol model
24 p4328 A70-45193
- Monochrome radiography for contrast strengthening to increase color images detectability by human eye
24 p4337 A70-45708
- MONOCHROMATIZATION**
- Methane IR filter for monochromatizing He-Ne laser
21 p3823 A70-40823
- MONOCHROMATORS**
- Emission flame spectrometer based on double diffraction monochromator, describing design features and operating characteristics
08 p1493 A70-20545
- Vacuum-UV monochromators polarization and effective transmittance measurements, comparing characteristics of parallel and pyramidal biotite polarizers
08 p1546 A70-21791
- Airborne monochromator and photoelectric filter radiometer for solar spectral irradiance measurements, estimating instrument errors
09 p1683 A70-23515
- Solar radiation energy distribution simulated using vacuum monochromator, discussing Ar-Kr-Xe-methane mixture
10 p1931 A70-24317
- Solar horizontal telescope performance improvement by adding birefringent monochromator and diffraction grating
11 p2057 A70-26590
- Monochromators dispersion and resolution increased by multiple passage of light through singly dispersive element, comparing optical schemes
12 p2237 A70-28160
- Monochromator design for UV and visible wavenumbers linear output, noting application to absorption coefficient measurement
24 p4336 A70-45669
- MONOCOQUE CYLINDERS**
- U CYLINDRICAL SHELLS**
- U MONOCOQUE STRUCTURES**
- MONOCOQUE STRUCTURES**
- Elastic and equilibrium matrices for semimonocoque membrane /plane stress/ elements using skin and reinforcing member transformations
17 p3185 A70-34921

MONOCULAR VISION

Superior recognition of right visual field of left eye with monocular viewing of letters as interaction of visual acuity and right superiority

02 p0239 A70-12623

Visual half field central integration and monocular performance in split-brain monkeys after transection of chiasm, anterior commissure and corpus callosum

03 p0421 A70-13625

Human eye contribution to visual evoked responses under different color stimuli during all possible monocular and binocular combinations

05 p0801 A70-16382

Binocular fusion and rivalry effects on cortically evoked human potential, obtaining pattern characteristic responses to monocular stimulation

07 p1215 A70-20214

Monocular and interocular threshold luminance changes during flicker stimulation, noting interflash duration effects

08 p1453 A70-21792

Choice reaction time task involving right or left hand button pressing in monocular and binocular visual response to directional commands by colored lights

11 p1990 A70-25830

Visually evoked responses in man to different light stimuli intensities, noting marked increase in binocular over monocular visual response

22 p3972 A70-43408

MONOLITHIC CIRCUITS

U INTEGRATED CIRCUITS

MONOMERS

Polymer optical properties in terms of interaction matrix coupling monomers, applying to polypeptide alpha helix, beta sheets and polyproline helices

14 p2544 A70-30118

Methyl methacrylate and other vinyl monomers polymerization activation by low sulfur dioxide concentrations, noting inert solvents effect

14 p2544 A70-30246

Physicochemical properties of monomer and associated aluminosilicates, determining heats of combustion

22 p4124 A70-42677

MONOMOLECULAR FILMS

Molecular interactions, surface pressures and potentials of mixed monolayers of stearic acid and stearyl alcohol with inorganic subolutions

15 p2695 A70-32547

MONOPLANES

NT A-7 AIRCRAFT
NT AVRO 707 AIRCRAFT
NT B-52 AIRCRAFT
NT BAC 111 AIRCRAFT
NT BOEING 707 AIRCRAFT
NT BOEING 737 AIRCRAFT
NT BUCCANEER AIRCRAFT
NT C-47 AIRCRAFT
NT C-135 AIRCRAFT
NT C-141 AIRCRAFT
NT DC 8 AIRCRAFT
NT DH 121 AIRCRAFT
NT DH 125 AIRCRAFT
NT DO-31 AIRCRAFT
NT F-4 AIRCRAFT
NT F-5 AIRCRAFT
NT F-8 AIRCRAFT
NT F-28 TRANSPORT AIRCRAFT
NT F-104 AIRCRAFT
NT F-106 AIRCRAFT
NT G-91 AIRCRAFT
NT G-222 AIRCRAFT
NT HFB-320 AIRCRAFT
NT OV-10 AIRCRAFT
NT T-33 AIRCRAFT
NT TU-134 AIRCRAFT
NT XV-4 AIRCRAFT
NT XV-5 AIRCRAFT

MBB Bo-209 Monsun travel, commuter and acrobatics aircraft, discussing configurations, specifications, structure and handling characteristics

19 p3355 A70-37388

MONOPOLE ANTENNAS

Input impedance of monopole antenna in rectangular waveguide assuming sinusoidal current distribution, noting accuracy limitation to specific monopole lengths

03 p0457 A70-13698

Impedance and radiation pattern of quarter wave monopole and half wave dipole antennas in isotropic plasma, considering plasma density role

06 p1117 A70-17372

Induced electromotive force method for determining impedance changes of monopole on base of large cone

06 p1019 A70-17558

Radiation patterns from finite conducting cone excited by quarter wave monopole protruding from center of base computed on digital computer

06 p1020 A70-17559

Quasi-near zone electric field intensity and current distribution of monopole antenna on finite conductive earth

09 p1645 A70-22691

Dipole and monopole antenna radiation patterns, considering effects of soil conductivity and elevation above ground

12 p2129 A70-27979

Mutual and self admittances for array with two monopoles, solving integral equations for current distributions

16 p2860 A70-32957

Rod antenna radiation representation by instantaneous pictures of electric field lines, considering wave detachment mechanism

17 p3050 A70-34575

Complex impedance measurements for monopole antenna for electron densities in/out of OGO satellite wake in upper ionosphere

17 p3080 A70-35771

Dielectric filled tubular monopole antenna driven by coaxial line with TEM mode, calculating current distribution from integral equation

23 p4175 A70-44953

Broadside-endfire array of cylindrical dipoles and monopoles driven by interconnecting transmission lines, calculating admittance and field patterns

23 p4176 A70-44955

Two monopole antennas on perfectly conducting sphere, calculating radiation pattern by numerical technique

23 p4165 A70-44968

MONOPOLES

Hot universe model for determining magnitude constraints on Dirac monopole annihilation cross section and mass in cosmic rays

07 p1371 A70-20330

Relativistic magnetic monopoles detection in corpuscular primary cosmic rays, describing equipment and results

07 p1371 A70-20333

Monopole mass spectrometer mass range extension by voltage method, discussing sensitivity and mass scan time

08 p1497 A70-21537

Magnetic monopole flux limits in primary cosmic radiation derived from muon-poor shower data and inverse Compton scattering

16 p2972 A70-33050

Lunar magnetic monopole charge effects on nearby magnetic field configuration

18 p3316 A70-36898

Monopole trajectory in magnetic dipole field by numerical integration on computer and Liouville theorem, using resolved Stormer cone to investigate motion

20 p3672 A70-39301

Magnetic monopoles electromagnetism search in Apollo 11 rock samples

21 p3912 A70-41639

MONOPROPELLANTS

NT AEROZINE

Hydrazine monopropellant performance and characteristics, describing various catalysts and propulsion systems

02 p0352 A70-12265

Combustion characteristics of blended droplets composed of monopropellant and diluent, using theoretical model to predict life histories

06 p1180 A70-18141

Burning rates of monopropellant droplet evaluated by variable property models, discussing dimensionless mass flow rate

07 p1358 A70-18914

Quasi-steady adiabatic vaporization and exothermic decomposition of monopropellant spherical droplet in inert and reactive environments

07 p1359 A70-19580

Pilot chamber initiated thermal decomposition reactor concept for monopropellant thruster, discussing thrust levels and throttling ratios

13 p2473 A70-28507

First pulse vacuum startup measurements of monopropellant hydrazine thrust reactors with spontaneous catalyst, simulating spacecraft control dynamics

14 p2628 A70-30753

Monopropellant rocket combustion one dimensional theory with uniform velocity and size droplets injection, obtaining chamber length

14 p2629 A70-30773

Monopropellant hydrazine RCS rocket engine module, discussing operating conditions, development, thermal control and valve internal leakage

16 p2965 A70-33544

Small rocket engines tailoff impulse and tailoff repeatability, comparing monopropellant hydrazine and storable bipropellant engines impulse data

16 p2967 A70-33576

Chemical rocket propellant research covering composite liquid monopropellants, lateral thrust in solid propellant rockets, ELDO third stage, friction losses, etc

17 p3148 A70-35211

Burning rate theory applied to heat and mass transfer rates of monopropellant droplets in heat-up and steady burning at wet bulb temperature

18 p3348 A70-36696

MONOPULSE ANTENNAS

Transportable telemetry acquisition system (TTAS) as mobile tracker featuring pseudomonopulse method

01 p0045 A70-11120

Phased array monopulse autotracking, radio interferometer and Doppler frequency methods for radio tracking systems for artificial satellite orbits

15 p2697 A70-31836

Search radar antennas for monopulse direction finding with radiation pattern for sum and difference operation

15 p2704 A70-32674

Steerable C band waveguide arrays design for forming monopulse cluster of sum and difference beams

16 p2875 A70-33395

Dual mode log periodic spiral DF antenna system, using monopulse to provide azimuth and bearing elevation data

16 p2863 A70-33450

Parabolic antenna properties generated by dual band circularly polarized focused two channel monopulse feed system, discussing tracking data from helicopter, Apollo 8 and Cassiopeia A

20 p3589 A70-40323

Monopulse tracking antenna beam broadening by feed displacement defocusing in parabolic reflector

23 p4165 A70-44956

Phase and tracking errors due to mutual scattering in phase monopulse phase-scanned antenna

24 p4315 A70-46135

Dual channel circularly polarized feed of monopulse tracking antenna system, noting axial ratio and gain and open loop mode autotracking

24 p4321 A70-46259

MONOPULSE RADAR

Antenna far field noise effect on monopulse type and conical scanning radar angle meters performance

05 p0813 A70-16256

Monopulse radar signal detection efficiency with fully polarized reception taking into account target with fluctuating polarization

05 p0813 A70-16270

Three channel traveling wave maser with cryogenic superconducting magnet for C-band monopulse radar system, describing construction and electrical characteristics

10 p1900 A70-24894

Celestial radio source angle tracking techniques using monopulse antenna receiving system applied to angle tracking radar

22 p3991 A70-43582

Monopulse radar excited by Gaussian signal and thermal noise in multiple targets, calculating angle error output probability density function for predicting tracking performance

22 p3992 A70-43593

MONOSACCHARIDES

Temperature, solvent, catalyst and formaldehyde concentration effects on monosaccharide synthesis from formaldehyde condensation

13 p2362 A70-29327

MONOSCOPES

Pseudo three dimensional effect on monoscopic radar imagery for topographic relief differentiation, using offset superposition of transparencies

22 p4031 A70-42965

MONOSTABLE MULTIVIBRATORS

Pulse duration approximation in tunnel diode monostable multivibrator during low duty cycle operation

08 p1472 A70-20867

MONOTONE FUNCTIONS

Bounded region satisfying regularity necessary to Korn inequalities and Sobolev immersion theories, discussing plasticity theory operator monotony in Minty-Browder sense

02 p0387 A70-12109

Relaxation functions of one dimensional viscoelastic linear and nonlinear materials having monotone decreasing time properties

11 p2141 A70-26556

Monotonic difference schemes for parabolic differential equations with nonlinear boundary conditions, discussing convergence and stability

18 p3282 A70-36361

Linear algebraic system stability and monotony, investigating plane structures by finite element method

23 p4213 A70-44996

Stochastic boundary value problem involving differential equation with random forcing function, proving monotone property of solution covariance variation

24 p4426 A70-46039

MONOTONY

Performance in monotonous work situations, discussing various factors affecting efficiency

18 p3224 A70-36317

MONTE CARLO METHOD

Monte Carlo methods for calculating simple and multiple integrals and random variables characteristics, noting applications to Europa 2 booster

03 p0454 A70-13535

Nonlinear boltzmann equation for heat transfer in rarefied gases between parallel plates at different temperatures using Monte Carlo method
[ASME PAPER 69-WA/HT-23] 04 p0782 A70-14811

Fast neutron transport characteristics of helical ducts using Monte Carlo code FASTER, computing neutron fluxes and attenuation 05 p0884 A70-16163

Monte Carlo radiative transfer techniques applied to develop height dependent spicule model, computing contrast curves of model against chromospheric background 05 p0911 A70-16431

Monte Carlo calculations of nonequilibrium radiative transport, including weighting and biasing techniques 05 p0958 A70-17084

Chain pooling tests for two level factorial replication-free experiments using Monte Carlo methods 06 p1093 A70-17305

Probability distributions and error estimates for Monte Carlo solutions of radiation heat transfer problems, considering wavelength and direction of emitted photon bundles 06 p1175 A70-17683

Monte Carlo method for modeling gas flow by simulated molecules concurrently followed through collisions and boundary interactions in simulated physical space within computer 06 p1113 A70-18314

Monte Carlo method applied to Boltzmann collision integral in solving heat transfer between plates at different temperatures in elastic spheres gas 06 p1183 A70-18324

Monte Carlo simulation for shock wave formation by specularly reflecting piston, discussing reflection from specularly reflecting wall 06 p1049 A70-18334

Monte Carlo method applied to solving nonlinear Boltzmann equation for plane shock waves in elastic sphere gases 06 p1050 A70-18335

Moment methods for calculating modeled diffusion gas mixture shock waves using Monte Carlo method, discussing distribution function and flow pattern 06 p1050 A70-18336

Model sampling or Monte Carlo applied to normal shock, giving temperature and density profiles for Mach 10 shock 06 p1050 A70-18337

Monte Carlo analysis of free and near free molecular flow through circular tubes for mass, momentum and energy transfer 06 p1051 A70-18367

First collision Monte Carlo method for calculating aerodynamic drag on hard sphere and Maxwell molecular models in near-free molecular flow 06 p0983 A70-18379

Book on some methods of solving boundary value problems of mathematical physics covering linear operators, boundary conditions, perturbation and Monte Carlo methods 07 p1326 A70-19696

Electromagnetic component of extensive air showers to three dimensional Monte Carlo simulations of hadronic component using electromagnetic cascade theory 07 p1368 A70-19967

Reliability estimations precision evaluated by Monte Carlo simulation, analyzing causes of data inaccuracy 09 p1689 A70-22019

Thermally emitted photons of atmospheric molecules and aerosols and planetary surface followed by Monte Carlo method, using anisotropic single scattering functions 09 p1719 A70-23524

Ionospheric photoelectrons resulting from solar UV radiation interaction with atmospheric gases, obtaining escape fluxes using Monte Carlo method 09 p1747 A70-23667

Monte Carlo method research development covering techniques for variance reduction, linear equations solutions and use of various random sequences 10 p1910 A70-24844

Earth interior structure models using geophysical data in Monte Carlo inversion procedure 11 p2042 A70-25332

Flow near leading edge of sharp insulated and cooled flat plates, using Monte Carlo direct molecular simulation 11 p1975 A70-25968

Computerized Monte Carlo prediction of maintenance time distribution of complex system, concerning man hours, elapsed time and schedule meeting 13 p2524 A70-29566

Martian atmosphere modeling for obtaining Viking lander spacecraft design margins by Monte Carlo method 14 p2637 A70-30564

Monte Carlo model of V groove surface roughness effects on directional reflections in plane of incidence, employing energy localization circle [AIAA PAPER 70-820] 16 p3002 A70-33944

Pulsars spatial distribution, comparing actual distribution to Monte Carlo computations 17 p3173 A70-35755

Nonlinear stochastic discrete time processes prediction and filtering by Monte Carlo techniques 18 p3234 A70-36338

Luminous intensity profile of optically thick Sr artificial clouds in upper atmosphere, using Monte Carlo calculations 19 p3415 A70-38388

TSF-SNAP reactor neutron radiation leakage, comparing Monte Carlo calculations with experimental and analytical determinations 20 p3671 A70-39156

Three dimensional Monte Carlo simulation of extensive air shower processes, comparing with hadrons and electrons energy spectra 20 p3699 A70-39442

Prior distributions computer aided selection for generating Monte Carlo confidence bounds on system reliability 20 p3658 A70-39641

Design component size index as function of various system demands, using Monte Carlo method 21 p3846 A70-41870

Radiation shielding calculations using multidimensional Monte Carlo computer programs 23 p4217 A70-43809

Radiation shielding calculations, discussing Monte Carlo concepts for point fluxes with random sampling of source distributions 23 p4217 A70-43810

MOS transistor trigger circuit design parameters statistical calculation and optimization by Monte Carlo method using computer 23 p4171 A70-43957

Multidimensional integral Monte Carlo evaluation applying regression analysis to linear unbiased estimators 24 p4370 A70-46100

MOON

Low energy proton flux in neighborhood of Moon measured by Luna 12 satellite indicating magnetized plasma region effect on burst 01 p0172 A70-11493

Kinetics of solar wind interaction with moon and planetary bodies using perturbation scheme to obtain ion density distribution on antisolal side [AIAA PAPER 70-61] 06 p1136 A70-18192

Solar wind flow different interactions with earth, Venus and moon 06 p1136 A70-18284

Solar wind interaction with moon derived for model and compared with satellite data 06 p1147 A70-18291

Lunar science - NASA Conference, Houston, January 1970, covering moon rock composition, magnetic, electrical and physical properties, etc 08 p1565 A70-20587

Moon perigees and apogees for years 1-3000, tabulating parameters for calculations 08 p1568 A70-20635

Radiative heat transfer in lunar and Mercurian surfaces, discussing radiative heat transfer in powders 08 p1579 A70-21569

Computer program for generating tables to calculate lunar libration at any epoch 09 p1752 A70-22313

Textured gray-scale imagery by computer simulating lunar display 09 p1642 A70-23771

Seismology as tool for investigation of planets, discussing earth rigidity, tides and long period oscillations 11 p2111 A70-26040

Earth mechanical properties and composition compared with moon and other terrestrial planets 11 p2047 A70-26616

Computer techniques for determining physical libration of moon in longitude 13 p2488 A70-28765

Heliometric lunar libration series joined to obtain uniform equation 13 p2490 A70-28949

Solar wind interaction with moon, constructing mathematical model based on MHD equations and Explorer 35 data 14 p2630 A70-30356

Delaunay reduced Hamiltonian verification in lunar ephemeris theory based on Lie transforms 16 p2978 A70-33972

Moon origin, surface, exploration, Apollo 11 landing, subsidence/uplift crater formation and Transient Lunar Phenomena 20 p3701 A70-38977

Lunar ephemeris computerized analytical solution, considering literal expansions generation 20 p3705 A70-39479

MOON ILLUSION

Moon illusion on basis of perceived size relativity, discussing dependence on objective characteristics of visual field 09 p1752 A70-22248

MOON-EARTH TRAJECTORIES

Reentry trajectories from lunar surface and orbit obtained by computer with allowance for initial data spread 01 p0191 A70-11476

Earth-moon-earth flight characteristics, discussing spacecraft trajectory, velocity and corrections for close distance placement and return for soft landing 03 p0569 A70-13483

Apollo translunar and transearth orbit determination and navigation using ground and onboard systems [AIAA PAPER 70-27] 06 p1103 A70-18124

Hybrid patched conic technique as iterative procedure for generating translunar and transearth trajectories emphasizing computing time saving 06 p1152 A70-18495

Hybrid patched conic iterative technique for accurate moon-earth /transearth/ trajectory generation 09 p1760 A70-22929

Onboard moon-to-earth trajectory approach guidance with or without midcourse guidance using optical angular measurements 14 p2615 A70-30470

French photographic observations of Apollo 12 translunar trajectory 15 p2697 A70-31676

MOONMOBILES

U LUNAR SURFACE VEHICLES

MOORING

Automatic rendezvous and mooring-coupling of spin stabilized satellites, discussing configuration, guidance and dynamics model 13 p2499 A70-28397

MOORINGS

U MOORING

MOPS (PROPULSION SYSTEMS)

U MAN OPERATED PROPULSION SYSTEMS

MOREHOUSE COMET

Comet Morehouse /190811/ tail rays waviness interpreted in terms of fluctuations in solar wind direction 11 p2117 A70-26649

Comet Morehouse CO ions lifetime and density from photometric analysis 18 p3313 A70-36324

MORL

U MANNED ORBITAL RESEARCH LABORATORIES

MORPHINE

Pineal C14-indoles synthesis in rats noting no direct effect of morphine 11 p1988 A70-26299

MORPHOLOGY

NT GEOMORPHOLOGY

NT ISOMORPHISM

NT LUNG MORPHOLOGY

NT POLYMORPHISM

Noctilucent clouds morphological and kinematic characteristics based on photographs 03 p0476 A70-13885

Temperature and morphological changes of animals adipose tissue under various nutrition conditions, based on measurements by thermocouples implanted in fat deposits 04 p0640 A70-15514

Isomorphous beta type Ti-Mo alloy omega phase transformations and morphology by electron microscopy, relating hardness to aging 10 p1902 A70-23817

Microdissection morphology of vestibular apparatus sensory regions in guinea pig, rabbit, cat, squirrel, monkey and man 10 p1811 A70-24200

Coma cluster of galaxies morphological and statistical characteristics, determining major and minor axes 10 p1948 A70-25194

Centrifuging acceleration tolerance of various animals, relating physiological and morphological effects 12 p2174 A70-28361

Omega phase morphology in Ti alloy by electron microscope techniques, noting cubic structure 17 p3118 A70-34410

Spiral galaxies pattern statistics, examining morphological type of Milky Way galaxy 18 p3326 A70-37155

Lunar sinuous rilles morphological and distributional observations and implications on theories of origin concerning surface water erosion 19 p3521 A70-38442

Al-Be eutectic alloys structure, using laue X ray method and electron microscopy in studying fibrous morphology due to unidirectional solidification 24 p4356 A70-45143

MORPHOTROPISM

U ISOMORPHISM

MORSE POTENTIAL

Morse eigenfunctions for variational calculation of diatomic molecules vibrational-rotational energy level analysis, showing better convergence than harmonic oscillator basis 02 p0344 A70-12519

MORTALITY

Diurnal and seasonal variations of mortality due to cardiac and circulatory failure using model representing daylight regulation of human organism
05 p0802 A70-16663

Fatal ejections in USN, suggesting initiation delay as prime causal factor
07 p1191 A70-19006

Resistance to decompression sickness increased and mortality rate decreased in mice after adaptation to hypoxia at normal barometric pressure
07 p1206 A70-19469

Temperature effect on radiation tolerance of mice exposed to low dose rate gamma radiation, noting mortality delay in low temperature environment
23 p4148 A70-44789

MOS [SEMICONDUCTORS]

U METAL OXIDE SEMICONDUCTORS

MOSAICS

Pulse-biased phototransistor imaging mosaics behavior measurement showing significant photovoltaic mode at high light levels
10 p1846 A70-23880

MOSS [SPACE STATIONS]

U ORBITAL SPACE STATIONS

MOSSBAUER EFFECT

Mossbauer temperature dependent isomer shift, proposing electron density change at resonant nucleus site by lattice phonons
14 p2626 A70-30483

Isomer shift, Mossbauer recoil free fraction and nuclear quadrupole splitting for Fe57 in iron fluoride measured for lattice dynamics, fine and hyperfine structure
14 p2626 A70-30484

Fe 57 contaminant in Ni, studying Mossbauer effect as function of temperature
15 p2784 A70-32023

Low temperature anharmonicity in thorium dioxide with Co 57 impurities, using Mossbauer effect of Fe 57
21 p3862 A70-40975

High transmission Mylar window He cryostat for Mossbauer measurements
21 p3828 A70-41470

Mossbauer spectra of Apollo 11 lunar fines and microbreccia, showing iron oxidation, site symmetry and magnetic state
21 p3915 A70-41657

Mossbauer effect spectrometry application to Apollo 11 lunar rocks composition, using nuclear gamma resonance measurements for nuclide Fe 57
21 p3916 A70-41662

Apollo 11 lunar dust, breccia and igneous rocks, using Mossbauer spectroscopy and petrographic techniques
21 p3916 A70-41664

Temperature distribution measurement inside solid samples by Mossbauer effect, considering application to turbine blades
21 p3830 A70-42165

Magnetism in austenitic stainless steels, discussing Mossbauer measurements of temperature dependence of hyperfine field and single line width
22 p4055 A70-43012

Mossbauer spectrum of submolecular changes of oxyhemoglobin in animal blood exposed to microwave irradiation
23 p4144 A70-43788

Mossbauer effect analysis of Fe impurity atoms in n- and p-type semiconductor compounds with wide and narrow forbidden gaps
24 p4388 A70-45204

Fe-Cr and Fe-Cr-V system miscibility gap, using differential thermal analysis and Mossbauer effect measurements
24 p4362 A70-46190

Al substituted YIG crystal chemistry by cation distribution determination as function of Al concentration using Mossbauer spectroscopy
24 p4392 A70-46364

MOT [ORBITAL TELESCOPES]

U MANNED ORBITAL TELESCOPES

MOTHS

Circadian oscillations and photoperiodic time measurement in *Pectinophora gossypiella*
18 p3221 A70-36893

MOTILITY

U LOCOMOTION

MOTION

NT SPACECRAFT MOTION

Airborne simulator program for evaluation of motion and visual cue effects on pilot performance in roll, using compensatory tracking tasks
[AIAA PAPER 70-351] 10 p1857 A70-24202

Flight simulation data on motion cues effects in controlling compensatory tracking tasks
[AIAA PAPER 70-352] 10 p1859 A70-24211

Ground based moving-base aircraft flight simulator using computer program to establish motion requirements
[AIAA PAPER 70-348] 10 p1859 A70-24213

Size effects on velocity threshold for real movement during narrow stimulus object length increase
11 p1989 A70-26662

Motion cue requirements in one and two axis closed loop compensatory control tracking tasks, discussing error rates
14 p2540 A70-30247

Sphere slow motion in viscous fluid with solid particle suspension, considering Stokes flow pattern small relaxation time perturbation
16 p2896 A70-34272

MOTION AFTEREFFECTS

Motion coordination capacity of persons subjected to 40 days bed rest using dynamographic technique, discussing nature of slackening
03 p0425 A70-13896

Human motion coordination under acceleration followed by weightlessness during jet flights along Keplerian orbits, discussing initial disturbance and subsequent subsiding
03 p0425 A70-13897

Aerodynamic velocity field induced by plate in motion correlated with ideal gas flow at specific Reynolds number, discussing wake formation
03 p0410 A70-14270

MOTION EQUATIONS

U EQUATIONS OF MOTION

MOTION PERCEPTION

U SPACE PERCEPTION

MOTION PICTURES

Computer evaluation of photographic imagery of left ventricle volume obtained by cineangiography, including densitometric measurements
03 p0434 A70-13678

Variable anamorphic motion picture system to produce visual display for use with flight simulator [ASME PAPER 69-WA/BHF-8] 04 p0642 A70-14852

Solar photographs taken with motion picture cameras in integral light
05 p0920 A70-16974

Holographic 3D movie of front-lighted opaque objects, recording diffuse reflection with CW laser and high resolution film
09 p1684 A70-23533

Motion picture holography using continuously pumped ruby laser illumination system in repetitive Q switched mode
09 p1689 A70-23782

Heterogeneous combustion observation by motion picture holography, considering light source requirements and hologram separation at higher sampling rates
[WSCIP PAPER 70-10] 13 p2409 A70-29610

Cloud cover stationary pictures by spin-scan camera in synchronous orbit over Pacific converted into motion pictures showing cloud pattern changes and storm development
14 p2587 A70-31150

Galactic 21 cm line emission motion picture film, discussing contour maps on neutral hydrogen distribution
18 p3327 A70-37163

High speed pin registered intermittent camera, discussing film transport, magazines operating speed, motor drive and boresighting provisions
[SMPT PREPRINT 78] 22 p4036 A70-43066

High speed holographic methods for supersonic phase objects movement and replacement of conventional optical processes in shock tubes, firing tunnels, etc
[SMPT PREPRINT 77] 22 p4037 A70-43067

High speed X ray flash motion picture installation for ballistic photography
[SMPT PREPRINT 76] 22 p4037 A70-43068

Highspeed raster motion picture cameras with high aperture ratios
24 p4335 A70-45651

Motion picture B and W photographic materials characteristic curves, describing geometry by three-component set
24 p4335 A70-45653

Motion picture B and W photographic materials characteristic curves, describing geometry by three-component set
24 p4335 A70-45653

Motion picture B and W photographic materials characteristic curves, describing geometry by three-component set
24 p4335 A70-45653

Motion picture B and W photographic materials characteristic curves, describing geometry by three-component set
24 p4335 A70-45653

Motion picture B and W photographic materials characteristic curves, describing geometry by three-component set
24 p4335 A70-45653

Motion picture B and W photographic materials characteristic curves, describing geometry by three-component set
24 p4335 A70-45653

Motion picture B and W photographic materials characteristic curves, describing geometry by three-component set
24 p4335 A70-45653

Motion picture B and W photographic materials characteristic curves, describing geometry by three-component set
24 p4335 A70-45653

Motion picture B and W photographic materials characteristic curves, describing geometry by three-component set
24 p4335 A70-45653

Motion picture B and W photographic materials characteristic curves, describing geometry by three-component set
24 p4335 A70-45653

Motion picture B and W photographic materials characteristic curves, describing geometry by three-component set
24 p4335 A70-45653

Motion picture B and W photographic materials characteristic curves, describing geometry by three-component set
24 p4335 A70-45653

Motion picture B and W photographic materials characteristic curves, describing geometry by three-component set
24 p4335 A70-45653

Motion picture B and W photographic materials characteristic curves, describing geometry by three-component set
24 p4335 A70-45653

Motion picture B and W photographic materials characteristic curves, describing geometry by three-component set
24 p4335 A70-45653

Motion picture B and W photographic materials characteristic curves, describing geometry by three-component set
24 p4335 A70-45653

Motion picture B and W photographic materials characteristic curves, describing geometry by three-component set
24 p4335 A70-45653

Motion picture B and W photographic materials characteristic curves, describing geometry by three-component set
24 p4335 A70-45653

Motion picture B and W photographic materials characteristic curves, describing geometry by three-component set
24 p4335 A70-45653

Motion picture B and W photographic materials characteristic curves, describing geometry by three-component set
24 p4335 A70-45653

Motion picture B and W photographic materials characteristic curves, describing geometry by three-component set
24 p4335 A70-45653

Motion picture B and W photographic materials characteristic curves, describing geometry by three-component set
24 p4335 A70-45653

Motion picture B and W photographic materials characteristic curves, describing geometry by three-component set
24 p4335 A70-45653

Motion picture B and W photographic materials characteristic curves, describing geometry by three-component set
24 p4335 A70-45653

Motion picture B and W photographic materials characteristic curves, describing geometry by three-component set
24 p4335 A70-45653

Motion picture B and W photographic materials characteristic curves, describing geometry by three-component set
24 p4335 A70-45653

Motion picture B and W photographic materials characteristic curves, describing geometry by three-component set
24 p4335 A70-45653

Motion picture B and W photographic materials characteristic curves, describing geometry by three-component set
24 p4335 A70-45653

Motion picture B and W photographic materials characteristic curves, describing geometry by three-component set
24 p4335 A70-45653

Motion picture B and W photographic materials characteristic curves, describing geometry by three-component set
24 p4335 A70-45653

Motion picture B and W photographic materials characteristic curves, describing geometry by three-component set
24 p4335 A70-45653

Motion picture B and W photographic materials characteristic curves, describing geometry by three-component set
24 p4335 A70-45653

Motion picture B and W photographic materials characteristic curves, describing geometry by three-component set
24 p4335 A70-45653

Motion picture B and W photographic materials characteristic curves, describing geometry by three-component set
24 p4335 A70-45653

Motion sickness among USAF flying personnel, examining organic and psychiatric factors
15 p2690 A70-31890

Airsickness frequency, pathogenesis and prevention, discussing cadet selection
17 p3037 A70-35129

Hypoglycemia role in air sickness, aggravating effects of hypoxia and acceleration
17 p3040 A70-35914

Soviet book on peripheral vestibular apparatus and higher nervous system roles in motion sickness covering Coriolis acceleration tests, pilot training and selection, drugs, etc
19 p3359 A70-37406

Reflex vestibular disturbances and motion sickness prevention in artificial gravity of rotating space base, by incremental adaptation tests and drugs
23 p4154 A70-44625

Sea sickness symptoms in relation to reduced minute blood volumes in human after Coriolis acceleration
23 p4149 A70-45079

Head movement role in motion sickness as function of angular velocity, discussing prediction of human tolerance in space station
24 p4297 A70-45341

Head movement role in motion sickness as function of angular velocity, discussing prediction of human tolerance in space station
24 p4297 A70-45341

Head movement role in motion sickness as function of angular velocity, discussing prediction of human tolerance in space station
24 p4297 A70-45341

Head movement role in motion sickness as function of angular velocity, discussing prediction of human tolerance in space station
24 p4297 A70-45341

Head movement role in motion sickness as function of angular velocity, discussing prediction of human tolerance in space station
24 p4297 A70-45341

Head movement role in motion sickness as function of angular velocity, discussing prediction of human tolerance in space station
24 p4297 A70-45341

Head movement role in motion sickness as function of angular velocity, discussing prediction of human tolerance in space station
24 p4297 A70-45341

Head movement role in motion sickness as function of angular velocity, discussing prediction of human tolerance in space station
24 p4297 A70-45341

Head movement role in motion sickness as function of angular velocity, discussing prediction of human tolerance in space station
24 p4297 A70-45341

Head movement role in motion sickness as function of angular velocity, discussing prediction of human tolerance in space station
24 p4297 A70-45341

Head movement role in motion sickness as function of angular velocity, discussing prediction of human tolerance in space station
24 p4297 A70-45341

Head movement role in motion sickness as function of angular velocity, discussing prediction of human tolerance in space station
24 p4297 A70-45341

Head movement role in motion sickness as function of angular velocity, discussing prediction of human tolerance in space station
24 p4297 A70-45341

Head movement role in motion sickness as function of angular velocity, discussing prediction of human tolerance in space station
24 p4297 A70-45341

Head movement role in motion sickness as function of angular velocity, discussing prediction of human tolerance in space station
24 p4297 A70-45341

Head movement role in motion sickness as function of angular velocity, discussing prediction of human tolerance in space station
24 p4297 A70-45341

Head movement role in motion sickness as function of angular velocity, discussing prediction of human tolerance in space station
24 p4297 A70-45341

Head movement role in motion sickness as function of angular velocity, discussing prediction of human tolerance in space station
24 p4297 A70-45341

Head movement role in motion sickness as function of angular velocity, discussing prediction of human tolerance in space station
24 p4297 A70-45341

Head movement role in motion sickness as function of angular velocity, discussing prediction of human tolerance in space station
24 p4297 A70-45341

Head movement role in motion sickness as function of angular velocity, discussing prediction of human tolerance in space station
24 p4297 A70-45341

Head movement role in motion sickness as function of angular velocity, discussing prediction of human tolerance in space station
24 p4297 A70-45341

Head movement role in motion sickness as function of angular velocity, discussing prediction of human tolerance in space station
24 p4297 A70-45341

Head movement role in motion sickness as function of angular velocity, discussing prediction of human tolerance in space station
24 p4297 A70-45341

Head movement role in motion sickness as function of angular velocity, discussing prediction of human tolerance in space station
24 p4297 A70-45341

Head movement role in motion sickness as function of angular velocity, discussing prediction of human tolerance in space station
24 p4297 A70-45341

Head movement role in motion sickness as function of angular velocity, discussing prediction of human tolerance in space station
24 p4297 A70-45341

Head movement role in motion sickness as function of angular velocity, discussing prediction of human tolerance in space station
24 p4297 A70-45341

Head movement role in motion sickness as function of angular velocity, discussing prediction of human tolerance in space station
24 p4297 A70-45341

Head movement role in motion sickness as function of angular velocity, discussing prediction of human tolerance in space station
24 p4297 A70-45341

Head movement role in motion sickness as function of angular velocity, discussing prediction of human tolerance in space station
24 p4297 A70-45341

Head movement role in motion sickness as function of angular velocity, discussing prediction of human tolerance in space station
24 p4297 A70-45341

Head movement role in motion sickness as function of angular velocity, discussing prediction of human tolerance in space station
24 p4297 A70-45341

Head movement role in motion sickness as function of angular velocity, discussing prediction of human tolerance in space station
24 p4297 A70-45341

Head movement role in motion sickness as function of angular velocity, discussing prediction of human tolerance in space station
24 p4297 A70-45341

Head movement role in motion sickness as function of angular velocity, discussing prediction of human tolerance in space station
24 p4297 A70-45341

Head movement role in motion sickness as function of angular velocity, discussing prediction of human tolerance in space station
24 p4297 A70-45341

Head movement role in motion sickness as function of angular velocity, discussing prediction of human tolerance in space station
24 p4297 A70-45341

Head movement role in motion sickness as function of angular velocity, discussing prediction of human tolerance in space station
24 p4297 A70-45341

Head movement role in motion sickness as function of angular velocity, discussing prediction of human tolerance in space station
24 p4297 A70-45341

Head movement role in motion sickness as function of angular velocity, discussing prediction of human tolerance in space station
24 p4297 A70-45341

Head movement role in motion sickness as function of angular velocity, discussing prediction of human tolerance in space station
24 p4297 A70-45341

Head movement role in motion sickness as function of angular velocity, discussing prediction of human tolerance in space station
24 p4297 A70-45341

Head movement role in motion sickness as function of angular velocity, discussing prediction of human tolerance in space station
24 p4297 A70-45341

Head movement role in motion sickness as function of angular velocity, discussing prediction of human tolerance in space station
24 p4297 A70-45341

Head movement role in motion sickness as function of angular velocity, discussing prediction of human tolerance in space station
24 p4297 A70-45341

Head movement role in motion sickness as function of angular velocity, discussing prediction of human tolerance in space station
24 p4297 A70-45341

Head movement role in motion sickness as function of angular velocity, discussing prediction of human tolerance in space station
24 p4297 A70-45341

Head movement role in motion sickness as function of angular velocity, discussing prediction of human tolerance in space station
24 p4297 A70-45341

Head movement role in motion sickness as function of angular velocity, discussing prediction of human tolerance in space station
24 p4297 A70-45341

Head movement role in motion sickness as function of angular velocity, discussing prediction of human tolerance in space station
24 p4297 A70-45341

Head movement role in motion sickness as function of angular velocity, discussing prediction of human tolerance in space station
24 p4297 A70-45341

Head movement role in motion sickness as function of angular velocity, discussing prediction of human tolerance in space station
24 p4297 A70-45341

Head movement role in motion sickness as function of angular velocity, discussing prediction of human tolerance in space station
24 p4297 A70-45341

Head movement role in motion sickness as function of angular velocity, discussing prediction of human tolerance in space station
24 p4297 A70-45341

Head movement role in motion sickness as function of angular velocity, discussing prediction of human tolerance in space station
24 p4297 A70-45341

Head movement role in motion sickness as function of angular velocity, discussing prediction of human tolerance in space station
24 p4297 A70-45341

Head movement role in motion sickness as function of angular velocity, discussing prediction of human tolerance in space station
24 p4297 A70-45341

Head movement role in motion sickness as function of angular velocity, discussing prediction of human tolerance in space station
24 p4297 A70-45341

Head movement role in motion sickness as function of angular velocity, discussing prediction of human tolerance in space station
24 p4297 A70-45341

Head movement role in motion sickness as function of angular velocity, discussing prediction of human tolerance in space station
24 p4297 A70-45341

Head movement role in motion sickness as function of angular velocity, discussing prediction of human tolerance in space station
24 p4297 A70-45341

Head movement role in motion sickness as function of angular velocity, discussing prediction of human tolerance in space station
24 p4297 A70-45341

Head movement role in motion sickness as function of angular velocity, discussing prediction of human tolerance in space station
24 p4297 A70-45341

Head movement role in motion sickness as function of angular velocity, discussing prediction of human tolerance in space station
24 p4297 A70-45341

Head movement role in motion sickness as function of angular velocity, discussing prediction of human tolerance in space station
24 p4297 A70-45341

Head movement role in motion sickness as function of angular velocity, discussing prediction of human tolerance in space station
24 p4297 A70-45341

Head movement role in motion sickness as function of angular velocity, discussing prediction of human tolerance in space station
24 p4297 A70-45341

Head movement role in motion sickness as function of angular velocity, discussing prediction of human tolerance in space station
24 p4297 A70-45341

Head movement role in motion sickness as function of angular velocity, discussing prediction of human tolerance in space station
24 p4297 A70-45341

Head movement role in motion sickness as function of angular velocity, discussing prediction of human tolerance in space station
24 p4297 A70-45341

Head movement role in motion sickness as function of angular velocity, discussing prediction of human tolerance in space station
24 p4297 A70-45341

Head movement role in motion sickness as function of angular velocity, discussing prediction of human tolerance in space station
24 p4297 A70-45341

Head movement role in motion sickness as function of angular velocity, discussing prediction of human tolerance in space station
24 p4297 A70-45341

Head movement role in motion sickness as function of angular velocity, discussing prediction of human tolerance in space station
24 p4297 A70-45341

- Spatial amplification criteria for hyperbolic wave equations extended to include parabolic equations, discussing convective and absolute instabilities
03 p0519 A70-13522
- Motion stability and time dependent deflections of thin flexible cylinder with zero bending rigidity in viscous stream
03 p0595 A70-13783
- Generalized Keplerian orbits for large cylindrical satellites noting orbit stability
03 p0578 A70-14252
- Time history of spin and forward motion accuracy of rocket launched from smoothbore, using analytical model and motion coupling through dynamic friction coefficient
03 p0582 A70-14311
- Heaving and pitching motion analysis of wave action-induced pressure gradients in captured air bubble /CAB/ ship bubble chamber, discussing fan system design
[ASME PAPER 69-WA/AV-6] 04 p0622 A70-14902
- Unsteady flows effects on aircraft longitudinal motion, flight stability and control, discussing horizontal and vertical effects of rough air
04 p0623 A70-15172
- Bottom topography effect on jets stability in baroclinic fluid, discussing two layer model
04 p0715 A70-15518
- Single degree of freedom nutation damper motion instability on dual spin stabilized spacecraft ascribed to parametric excitation by transverse angular rates
04 p0764 A70-15585
- Proportional controlled pneumatic servomechanisms analysis extended to include motion along stroke, considering position effect on stability
05 p0797 A70-15891
- Gravitational radiation damping effect on motion of two bodies, evaluating field components in approximation by Einstein-Infeld-Hoffman method
05 p0882 A70-16308
- Motion stability of ideally plastic medium flow in conical matrix, studying surface and velocity distribution for minimum plastic deformation energy
05 p0945 A70-16854
- Hydrodynamic coefficients of algebraic equations for boundary value problems in disturbed motion of body with rib-reinforced liquid filled cavity
05 p0836 A70-16956
- Steady three dimensional motions using classical differential geometry, considering Navier-Stokes and helical flows
05 p0884 A70-17100
- Helicopter dynamics structural model extended to LF longitudinal motions by including stabilizing feedback loop representing forward velocity influence on main rotor
06 p0987 A70-17910
- Dynamic instability of motion of rigid and elastic bodies with liquid filled cavities associated with practical problems of rocket technology
06 p1107 A70-18415
- Optimal guaranteeing control for single switching representable in form of two different successive stages in time, ensuring invariance with respect to motion perturbations
07 p1332 A70-18664
- Routh theorem and Chetaev method for construction of Liapunov function to investigate steady state motions, obtaining stability conditions
07 p1332 A70-18677
- Partial stabilization of given quantities on steady motions of nonlinear control systems with initial perturbations based on observation theory
07 p1333 A70-18686
- Nonlinear differential equations solution behavior near zero point of phase space examined in material system perturbed motion
07 p1333 A70-18772
- Anisotropically elastic rotor vibrations stability analysis allowing for damper mass and internal/external friction, determining regions of steady and unsteady motions
07 p1403 A70-19059
- Lagrange rotational motion stability of heavy symmetrical body attached at point to platform moving forward using Liapunov theorem
07 p1334 A70-19641
- Meteorological satellites motion parameters long term prediction, using final analytic relationships with allowance for zonal harmonics of gravitational field
07 p1329 A70-19650
- Stability criteria for systems of nonlinear stochastic differential equations on finite time interval, considering stable motion of physical processes
08 p1533 A70-20488
- Dynamic discrete systems unsteady motions stability, formulating theorem for finite characteristic numbers existence
08 p1543 A70-20493
- Soviet book on motion of guided rockets in space covering aerodynamic and structural aspects, stabilized and disturbed rocket motion, etc
08 p1582 A70-20756
- Elastic body with incompressible fluid filled cavities, studying motion and stability by deriving motion equations starting from principle of least action
08 p1544 A70-20951
- Fluid motion convective stability between vertical parallel planes with longitudinal temperature gradient, solving boundary value problem for amplitudes of normal perturbations
08 p1482 A70-20952
- Steady motions and stability of gravitating gyrostat and spheroid, considering dynamically asymmetrical and symmetrical conditions
08 p1544 A70-20965
- Stability in whole of motion determined by system of nonlinear third order differential equations, using Liapunov functions
08 p1545 A70-21003
- Stability of continuously differentiable functions representing approximate solution to system of differential equations of perturbed motion
08 p1545 A70-21167
- Minimization of motion deviation from prescribed motion as differential game of converging motions using equations of motion
08 p1546 A70-21626
- Steady state motion of sinusoidally excited primary system with impact damper solved analytically by piecewise linear technique
08 p1546 A70-21858
- Stable equilibrium of rotor in pressurized gas bearing, considering perturbed rotor motion equation together with Reynolds equations for pressures in lubricant layer
09 p1690 A70-22544
- Error analysis in calculating periodic limiting state of rotor motion
09 p1727 A70-22624
- Spherically symmetric galaxies dynamic evolution analysis, emphasizing irregular motions description using fluctuating gravitational field hypothesis to construct Markov process
09 p1758 A70-22747
- Stability characteristics of near periodic orbits using variational equations, with results applied to phase space and stability problems
09 p1760 A70-22917
- Motions stability about triangular points in elliptic restricted problem of three bodies, using perturbation scheme
09 p1728 A70-23205
- Missile oscillations in plane during pitching moment hysteresis, discussing test coefficients suitability for predicting motion
09 p1606 A70-23258
- Sphere motion in laminar flow, postulating absolute velocity as resultant of entrainment and fall velocities and stable position in tube with ascending flow
09 p1663 A70-23309
- Elongated rotating configuration evolution by gravitational radiation and secular instability using homogeneous figures of Maclaurin and Jacobi
10 p1916 A70-24404
- Small plane perturbations stability losses in uniform rectilinear motion of nonrigid deformable rocket, using slender bodies pressure theory
10 p1950 A70-24528
- Orbital stability of geostationary vehicle at arbitrary latitude, considering nonlinear equations and deducing stability conditions by Liapunov method
10 p1950 A70-24783
- Polynomial model of uniform target motion for smoothing and extrapolating coordinates and parameters using independent radar range and velocity readings
10 p1843 A70-25136
- Linearized equations of motion solved for stability of dual spin satellite with two dampers, comparing to Floquet analysis
[AIAA PAPER 70-431] 11 p2120 A70-25440
- Structural synthesis of automatic control systems for body motion along trajectory, using inverse method and nonlinear coordinate transformations
11 p2077 A70-25611
- Stability conditions of rotational motions of symmetrical solid body on vibrating base in potential force field
11 p2098 A70-25916
- Nonconservative problems motion stability analysis based on restricted admissible displacements, establishing two variational principles
11 p2138 A70-26172
- Motion stability of rapidly spinning satellite, discussing elastic booms effect
11 p2128 A70-26784
- Monograph on ambipolar diffusion and motion instability of satellite produced artificial barium ion clouds in ionosphere and magnetosphere
11 p2048 A70-26825
- Clamped beams steady state free and forced response and stability for large amplitude motion, discussing multimode analytical and numerical technique
12 p2327 A70-27821
- Satellite stationary motions stabilization using rotors with axes fixed inside spacecraft
13 p2499 A70-28389
- Cover plates unsteady motion during explosive welding of metals, discussing edge damage
13 p2416 A70-28484
- Stability of single periodic symmetrical solutions of plane circular restricted three body problem, using digital computer for numerical integration of equations of motion
13 p2490 A70-28950
- Numerical solution of satellite rotational damping by onboard motors using Euler equations, local variations and finite control time
13 p2505 A70-28963
- Motion stability of variable mass solid body with ideal liquid filled cavities about stationary point using Liapunov theorem
13 p2452 A70-29310
- Free and forced motion characteristics in absolutely stable nonstationary nonlinear system analysis by variational approach
13 p2453 A70-29716
- Material system equations of motion, determining programmed motion variable mass systems stability
13 p2453 A70-29717
- Third order dynamic relay control system, determining periodic motion and motion stability
13 p2507 A70-29719
- Satellite orientation control and stabilization by gyro with statically and dynamically balanced rotors, showing steady motions and stability region augmentation
13 p2507 A70-29769
- Steady motions stability of gyrostat satellite in central Newtonian gravitational field
14 p2653 A70-30718
- Vibration stability of particle in plane restrained by two nonidentical springs with initial stress using Floquet theory and perturbations
14 p2657 A70-30843
- Routh theorem and Chetaev method for construction of Liapunov function to investigate steady state motions, obtaining stability conditions
15 p2774 A70-31469
- Motion and small vibration frequency stability of correctable gyroscope with correction moment at arbitrary angle with mismatch plane
15 p2738 A70-32154
- Motion and stability characteristics of dual spin satellite system with pendulous type nutation dampers, noting mass unbalance effect
[AIAA PAPER 69-857] 15 p2812 A70-32508
- Asymptotic motion stability bound for non-holonomic nonlinear electrodynamic systems, using energy metric algorithm for Liapunov functions generation
15 p2768 A70-32556
- Perturbation complex potential and aerodynamic forces determined for rectilinear profile motion under free surface, using linear theory
16 p2837 A70-33848
- Lifting rotor blade motions stability computation using Floquet transition matrix
17 p3009 A70-34726
- Circular orbit stability in stationary axisymmetric space-times dependence on angular momentum per unit mass increases outward from symmetry axis
18 p3317 A70-37004
- Motion stability in periodic cubic force field, using nonlinear differential equation integration with time periodic square wave function and Jacobian table
18 p3284 A70-37065
- Dynamic systems stability in sense of Poisson, relating motions commutative and stable families
19 p3472 A70-38936
- Elastic body with incompressible fluid filled cavities, studying motion and stability by deriving motion equations starting from principle of least action
20 p3672 A70-39376
- Fluid motion convective stability between vertical parallel planes with longitudinal temperature gradient, solving boundary value problem for amplitudes of normal perturbations
20 p3608 A70-39377
- Steady motions and stability of gravitating gyrostat and spheroid, considering dynamically asymmetrical and symmetrical conditions
20 p3672 A70-39387
- Asymmetric boundary layer transition effects on slender reentry vehicle motion by changing static stability characteristics
[AIAA PAPER 70-987] 20 p3557 A70-39542
- Harmonic forced transverse vibrations effects on rectangular plates with cross braces, deriving motion stability equations
20 p3725 A70-39867
- Satellite steady state motion and relative equilibrium position optimal stabilization by additional forces application
21 p3849 A70-40606
- Elastic deformable satellite motion stability in central Newtonian force field
21 p3927 A70-40827

Automatically controlled motion of object with finite degrees of freedom under parametric periodic disturbances
22 p4005 A70-43561

MOTIVATION

Motivation changes in rabbits exposed to increasing hypoxia in pressure chamber altitude simulation
07 p1208 A70-19506

Numerical payoff influence on reaction time to second stimulus in subjects receiving successive signals at short intervals
10 p1818 A70-24715

Motivation changes in rabbits exposed to increasing hypoxia in pressure chamber altitude simulation
11 p1987 A70-26105

Stochastic automata as learning system models in random environments with penalty-nonpenalty expectations, demonstrating convergence
13 p2374 A70-29587

Hypothalamic motivation, presenting data supporting less anatomical specificity
13 p2355 A70-29794

Eating, drinking and gnawing motivation interchangeability under hypothalamic stimulation, noting role of neural substrate activation
13 p2356 A70-29814

MOTOR SYSTEMS (BIOLOGY)

U EFFERENT NERVOUS SYSTEMS

MOTORS

NT ELECTRIC MOTORS

NT MICROMOTORS

NT SERVOMOTORS

NT SYNCHRONOUS MOTORS

NT TORQUE MOTORS

Multiplying digital device for measuring motor speed, torque and power, discussing optional applications and design
02 p0297 A70-12076

Positive displacement low pressure air motors for Boeing 747 fan thrust reverser pneumatic actuators and controls
03 p0550 A70-12881

Hydraulic synchronizers for motors and actuators speed equalization, describing operation and technical specifications
21 p3756 A70-40800

MOUNTAIN INHABITANTS

Blood plasma and red cell volumes simultaneous measurement in native group living at high altitude
15 p2684 A70-32537

Lung diffusing capacity for CO in Caucasians native to 3100 m noting membrane diffusing capacity, lung capillary volume and age effects
17 p3031 A70-35427

Hemodynamic changes in Andean native after two years at sea level, measuring intravascular pressures, cardiac output, heart rate and stroke index
20 p3571 A70-39427

MOUNTAINS

High temperature effects on evolution of Venus upper lithosphere, considering magnetic differentiation, isostatic adjustments, surface relief, mountain building time and distance scales, etc
02 p0371 A70-12207

Disturbances of air flow originating from small scale mountains using numerical model
07 p1330 A70-19799

Air flow disturbances over mountains in terms of turbulent boundary layer separation dissolution
07 p1330 A70-19800

Lee wave flow disturbances due to mountains by midtroposphere balloon and aircraft observation, noting flow features nonstationarity
12 p2262 A70-26883

Mountain climbing and prolonged stays at high altitudes effects on blood composition
13 p2352 A70-29355

Lunar rotary motion predetermination for spacecraft landing in mountainous region
15 p2773 A70-32266

MOUNTING

Turbine rotor and stator blades twist inaccuracies in assembly due to shroud induced stresses and blade root mountings clearances
07 p1291 A70-18827

Square Van Atta reflector with/without conducting plate used for mounting antenna half wave dipoles, considering scattering cross sections
09 p1646 A70-22695

Disk elements perpendicular mounting by rotation on vibrating shaft, obtaining orientation by centrifugal force
15 p2733 A70-31580

Mechanical design and mounting technique of Apollo 11 fused silica laser ranging retroreflector array at Tranquility Base
17 p3082 A70-34763

Accelerometer installation resonant frequency, discussing mounting methods, structure material, geometry and total mass
17 p3089 A70-35174

Flush mounted lightweight antennas for rockets, discussing construction radiation patterns, input impedance, etc
17 p3053 A70-35273

MOUNTS

U SUPPORTS

MOUTH

Silicon strain gage transducer for measurement of pressure between tongue and teeth, developing two types of temperature compensated strain gages
02 p0242 A70-12054

Stomatologic diseases during prolonged space flights simulation, discussing gingivitis, stomatitis, dental caries, parodontitis and odontogenous inflammations
13 p2352 A70-29338

Antidiuresis associated with oral cavity stimulation during food ingestion by rats
13 p2355 A70-29813

MOVEMENT

U MOTION

MOVING TARGET INDICATORS

Moving targets automatic identification by radar signals digital processing, describing radar echoes properties, moving window detector system and circuits design
01 p0137 A70-10358

ATC surveillance radar for high density traffic, discussing optimum electronic scanning rates, 3D radar and MTI
02 p0330 A70-11958

Target velocity effects on resolution of synthetic aperture side-looking radar
02 p0268 A70-12582

Visual prediction accuracy in estimating point coincidence of two moving targets as function of viewing opportunity and length of period
03 p0428 A70-14084

Forward looking airborne radar (FLAR) moving target indicator for military helicopter mounting
08 p1462 A70-21358

Target velocity and approach angle effects on accuracy of moving targets intersection estimation tested on human subjects
09 p1628 A70-23578

Two frequency moving target indicator system overcoming clutter motion relative to radar
11 p2004 A70-25737

Pilot midair collision warning instrument based on optical radar MTI, discussing target cross section enhancement by passive retroreflector
12 p2234 A70-27646

Subclutter visibility (SCV), resolution and interclutter of MTI or Doppler search radars in land, sea and weather clutter
12 p2188 A70-27940

Digital range tracking, Doppler filtration and moving target selection in multichannel automatic surveillance radars
13 p2380 A70-29735

MTBF

Failure rate and MTBF in reliability engineering, clarifying ambiguous terminology
20 p3638 A70-40061

Reliability of redundant repairable systems with preventive maintenance, determining mean time between failures
20 p3638 A70-40181

MTI RADAR

U MOVING TARGET INDICATORS

MUBIS (SCANNERS)

U MULTIPLE BEAM INTERVAL SCANNERS

MUCOUS

Pesinogens A, C and D from stomach mucosae of smooth dogfish separated by chromatography on DEAE cellulose
11 p1987 A70-26007

MUFFLERS

Noise damping model for complex configuration mufflers operating under conditions prevailing in diffuse acoustic field
08 p1545 A70-21009

Acoustic and gas dynamic characteristics of jet noise muffler using adapters at outlet section of exhaust nozzle
12 p2160 A70-27295

MULTICHANNEL COMMUNICATION

Temporal position of pulse signals measured by multichannel storage devices, discussing interference immunity and required storage time
03 p0448 A70-13435

Broad beam Tracking Data Relay Satellite (TDRS) for manned and automated spacecraft using VHF bands
06 p1006 A70-17345

PCM time division satellite multiple access communication system to increase time slot utility, considering individual earth station control and common signaling circuit features
06 p1011 A70-18409

Acquisition system design and experimental results for time division multiple access satellite communication system
06 p1011 A70-18410

Multiple access channel control system operating in variable destination multiple access mode for application in PCM-TDMA satellite communication system
06 p1011 A70-18412

Multichannel sequential detection of stationary signal, deriving analytical expressions for probabilities of erroneous solutions and mean duration of tests
07 p1227 A70-18762

Multichannel correlator for turbulent signal processing in real time scale using natural delay
07 p1284 A70-19832

Injection lasers for multichannel optical communication using composite cavities to improve spectral output
09 p1698 A70-23359

TDMA system burst synchronizer with periodic channel slots reallocation feature
10 p1835 A70-24331

Multichannel PCM/TDMA INTELSAT network with time preassignment and time assignment speech interpolation features for field test
10 p1835 A70-24332

Three channel traveling wave maser with cryogenic superconducting magnet for C-band monopulse radar system, describing construction and electrical characteristics
10 p1900 A70-24894

Geostationary satellite communication bandwidth increase by reusing same frequency band in multiple independent earthward beams, discussing modulation and interference noise allocation effects
11 p1996 A70-25405

Multiple-access and demand-assignment techniques, discussing compatibility of PCM-FDMA/SPADE/, PCM-TDMA, ATIC and INTELSAT 4 systems
11 p1997 A70-25415

Multiple channel communication satellite interchannel interference including preamplifier intermodulation, direct interference, multipath amplification, crosstalk and multiplexer reflections considered for capacity maximization
11 p2002 A70-25483

Symphonic satellite telecommunication network for multiple access telephone, telegraph, data transmission, radio and TV dissemination
11 p2005 A70-26008

Multiple access to communication satellite by limiting repeater, considering model of n signals plus band limited white Gaussian noise in zero memory device
11 p2008 A70-26229

Controlled digital data relay satellite system to provide multiple access between central station and user terminals, noting computer time sharing operation
11 p2008 A70-26230

Passive and active satellite systems for point-to-point communication network with multiple access capacity, comparing technical and economic competitiveness
11 p2011 A70-26335

Nonlinear phase shift equation derived from TWT single carrier performance, predicting multicarrier performance of communications satellites
12 p2195 A70-27248

Frequency-time coded multichannel communication system error probability bounds to investigate frequency selective fading effect on performance
12 p2184 A70-27416

Modulation-demodulation system for multiple access tactical satellite communication
12 p2187 A70-27915

Multiple user satellite system for air navigation and traffic control, presenting comparative error analyses for position determination by spherical and hyperbolic ranging
12 p2270 A70-27925

Statistical output characteristics of harmonic cosine and sinusoidal inertialess phase periodic converters in two channel system with frequency multiplication
13 p2370 A70-29741

Demand assigned domestic satellite communications system with capability of single hierarchy switching and serving terrestrial common carriers and direct users
14 p2552 A70-31351

Compact integrated microwave antenna of composite structure involving slotted waveguide planar array capable of operating in three frequency bands
16 p2876 A70-33406

Multiple access discrete address system for satellite networks
16 p2865 A70-33729

Multichannel sequential detection of stationary signal, deriving analytical expressions for probabilities of erroneous solutions and mean duration of tests
18 p3229 A70-37106

Worldwide multichannel air communications system in 10 GHz to IR range by Quasi Laser Link modulation and satellites
19 p3378 A70-37855

Multipurpose microminiature multichannel biomedical telemetry system, discussing design
19 p3368 A70-37856

U.S. nationwide satellite network for multichannel community antenna TV (CATV) operated at 12 GHz band
19 p3382 A70-38891

Multichannel iterative servosystems operators for useful signals reproduction 20 p3603 A70-39836

Frequency division multiple access satellite communication system, calculating bandwidth variations effects on intermodulation distortion 21 p3787 A70-41328

Multicarrier FM communication system, calculating adjacent channel interference due to impulse noise 21 p3789 A70-41343

Multiple channel VHF testing on ATS 1 and 3, describing transponder intermodulation and compression corrections 21 p3791 A70-41366

Multiple access communication satellite systems providing reliable speech communication for low density use in remote areas [JPL-TR-32-1501] 21 p3791 A70-41368

Wideband detection of frequency uncertain M-ary frequency shift-keyed [MFSK] transmission in Gaussian noise, deriving symbol error rate for limiting SNR cases 21 p3792 A70-42177

Multichannel correlation filter devices for processing periodic fluctuating signals in noise background 22 p3987 A70-42557

Solid state IF or baseband switching elements design for high capacity multichannel microwave systems 23 p4172 A70-44014

MULTICHANNEL RECEIVERS
U MULTICHANNEL COMMUNICATION RECEIVERS

MULTICHANNEL TRANSMITTERS
U MULTICHANNEL COMMUNICATION TRANSMITTERS

MULTILAYER INSULATION
Multilayer insulation blankets with slits normal to energy transfer direction for thermal control of spacecraft and cryogenic tankage [AIAA PAPER 70-15] 06 p1156 A70-18076

Effective thermal conductivity parallel to laminations of multilayer insulation as function of temperature, layer density and length [AIAA PAPER 70-846] 16 p2999 A70-33913

Radiation and conduction of open joint multilayer insulation systems, analyzing dependence on contact area by numerical methods [AIAA PAPER 70-848] 16 p2939 A70-33915

Cryogenic multilayer insulation (MLI), comparing radiation magnitudes, gas conduction and contact solid conduction to calorimeter and tank data [AIAA PAPER 70-850] 16 p2939 A70-33917

Multilayer insulation thermal scale modeling, discussing surface control techniques 21 p3951 A70-41865

Guarded electrical cylindrical calorimeter measuring multilayer insulation thermal conductivity, discussing construction, test and error 23 p4195 A70-44366

Gas pressure differential across multilayer insulation blanket during rapid evacuation predicted, using one dimensional flow theory [AIAA PAPER 69-608] 23 p4282 A70-44522

MULTILAYER STRUCTURES
U LAMINATES

MULTILOOP SYSTEMS
U CASCADE CONTROL

MULTIMODE RESONATORS
Multimode excitation of large aperture horn antennas to produce electronic deflections of directional pattern 01 p0046 A70-11454

Sectorial and circular strip resonators natural oscillation modes and freely propagating waves of uniformly bent stripline 09 p1651 A70-23644

Free carriers mobility and concentration in microwave semiconductors measurable by two mode resonator over temperature ranges and magnetic fluxes 13 p2470 A70-28881

Mode intensity fluctuations in unlocked multiple mode He-Ne laser related to LF noise 21 p3837 A70-41918

Multifrequency autooscillatory systems, comparing reflex klystron with He-Ne laser 22 p3995 A70-42404

MULTIPATH TRANSMISSION
Multipath spectral and statistical characteristics in VHF satellite-aircraft link, discussing geometric considerations and reflection from Gaussian surfaces 02 p0259 A70-12565

Channel constraints on multiple access systems obtained from airborne propagation tests via satellites, studying disparities in received signal strength 02 p0260 A70-12569

Azimuth information transmission by PCM signals with equal repetition and scanning frequencies, investigating antenna characteristics 02 p0270 A70-12619

Recognition problem in multipositional symmetrical channel solved by special separation of observational

space with preference to signal arriving at reception point 03 p0446 A70-13197

Intrinsic noise of passive waveguide multipoint with losses, obtaining mean values and wave correlation functions using scattering matrix 04 p0655 A70-14402

HF oblique ionospheric soundings over long temperate latitude path, discussing measured angles of elevation and multipath time dispersion 05 p0847 A70-15998

Shielded multiconductor transmission line capacitance calculated by integral equations with Green function kernel 05 p0820 A70-16383

Field strength determination at reception point for long range short wave paths, taking into account multiple ray paths and antenna radiation patterns 07 p1237 A70-20435

Intermodulation noise performance of FM FDM trunk radio systems in two path fading situations, calculating noise/power ratio and baseband enhancements 09 p1632 A70-22237

Sensitivity of nondiffuse double exposure holographic interferometry with transparent medium increased via multiple beam passage through medium placed in optical cavity 09 p1682 A70-23360

Nonresonant multipath carbon dioxide laser amplifier small signal gain of 39 dB utilizing White optical reflector design 09 p1699 A70-23365

Amplifier properties and oscillator mode structure of multipath carbon dioxide laser 09 p1699 A70-23538

VHF satellite transponders for ranging and position fixing, studying ionospheric and multipath effects [AIAA PAPER 70-489] 11 p1999 A70-25433

System configuration requirements and detectability performance characteristics analysis for optimizing array reception of multipath 11 p2018 A70-26264

Multipath tolerant ranging and data acquisition for air-ground-air links in ATC based on mathematical scattering theory 12 p2268 A70-27642

Ladder networks total transmittance and voltage transfer ratio and impedance or admittance, investigating signal flow graph open paths and Fibonacci sequence 15 p2715 A70-32344

Group delay times criterion of multibeam propagation of ionospheric radio echoes for communications systems 19 p3375 A70-37332

Satellite communications performance improvement by use of multipath signal for channel models including noncoherent FSK 21 p3787 A70-41329

Microwave transmission over elevated line-of-sight path, measuring phase front distortion between pairs of paths 22 p3991 A70-43580

Multibeam communication channel identification from output signal autocorrelation function analysis 23 p4159 A70-43761

MULTIPHASE FLOW
NT TWO PHASE FLOW

Multiphase fluid continuum model and hydrothermodynamic equations under phase transformations, including dimensionless and similarity parameters 07 p1254 A70-19085

Viscid-inviscid equations solution, describing flows with coupled mixing, combustion and lateral pressure gradients [AIAA PAPER 69-166] 15 p2718 A70-32516

Nonequilibrium combustion products and condensables containing reactive multiphase rocket nozzle flows and exhaust plumes characterization using generalized kinetics streamtube program (MGKS) [AIAA PAPER 70-845] 16 p3001 A70-33928

MULTIPLE BEAM INTERVAL SCANNERS
Multiple beam earth station torus microwave antenna for satellite communication with nonplanar field of view over geostationary arc 21 p3798 A70-41357

MULTIPLE DEGREES OF FREEDOM
U DEGREES OF FREEDOM

MULTIPLETS
U FINE STRUCTURE

MULTIPLEX TRANSMISSION
U MULTIPLEXING

MULTIPLEXERS
U MULTIPLEXING

MULTIPLEXING
NT FREQUENCY DIVISION MULTIPLEXING
NT TIME DIVISION MULTIPLEXING

Communications subsystem configuration for orbital manned space station, describing data rates and processing, multiplexing and associated modulation methods [AIAA PAPER 69-1079] 01 p0043 A70-10627

Bandwidth reduction for interlacing two voice and three additional teletype subchannels in standard phone frequency range for use in VHF/UHF satellite link 03 p0450 A70-13623

Group delay characteristics curvature in radio relay systems, analyzing crosstalk in picture- sound and beamed multiplex signal transmission by nonlinear distortion method 05 p0815 A70-16774

Binary cyclic coding schemes for multiplex spectrometry in terms of linear least mean square unbiased estimate 06 p1013 A70-17217

Coding and signal selection for data relay satellite interrogation channel serving many low- powered unattended user terminals 06 p1006 A70-17347

Hologram spatial bandwidth reduction by space-time multiplexing 09 p1673 A70-22074

Gigahertz rate circuits requirements for high speed digital data communication from component and system viewpoint, emphasizing coding and multiplexing techniques 09 p1633 A70-22605

Channel separation in RF transponder for communication satellite achieved with RF multiplexers consisting of microwave filters and combiners with superior electrical performance [AIAA PAPER 70-509] 11 p2016 A70-25457

Large capacity long distance transmission by circular waveguides, describing artery frequency modulation and equipment for multiplexed telephone messages transmission 12 p2194 A70-27233

Multiplexer-interface system for digital nuclear and position control data transfer from high altitude balloons to earth monitoring instruments 12 p2233 A70-27407

Crosstalk effects on data transmission in multiplex TV systems for aerospace communications analyzed by signal and noise models 13 p2363 A70-28384

Wave front multiplexing on spatially distinct area of single piece hologram 15 p2738 A70-32054

Frame synchronization in biorthogonal coded multiplex communication system, describing PCM, pattern insertion and double encoding methods 17 p3045 A70-35266

Service multiplex for communications network via satellite, discussing reliability 18 p3229 A70-36667

Solid state multiplexed electrical power distribution system for future generation military and commercial airplanes [SAE PAPER 700301] 18 p3216 A70-36803

Aircraft electrical system multiplexing, discussing design features and advantages over conventional hard wired systems [SAE PAPER 700303] 18 p3216 A70-36811

Aircraft digital interior communication systems, combining multiplexing techniques with solid state integrated circuits technology and systems integration [SAE PAPER 700302] 18 p3216 A70-36813

Dispersive spectrometer multiplexing light in entrance and exit slit positions compared with Michelson interferometric spectrometers 21 p3823 A70-40848

FM transmission of multiplex telephone signals by communication satellites, deriving impulse noise due to adjacent channel interference 21 p3787 A70-41330

Multiple beam antenna system for regional communications satellite directing high radiated power toward specific earth areas 21 p3790 A70-41358

Boeing 747 aircraft passenger entertainment and service system controls electronics design and wire installation improvement by multiplexing techniques 23 p4174 A70-44543

Boeing 747 airliner passenger entertainment and service electronics multiplexing system, discussing cable and connectors selection and design 23 p4174 A70-44544

MULTIPLICATION
Multiplication theorem for Sbrauts characteristic functions of quasi-Hermitian operators, including open systems coupling 05 p0877 A70-16880

Trachtenberg rapid calculation methods for multiplication, describing triangular or double product method and general algebraic theory 07 p1327 A70-19785

Algorithm for Fast Two Dimensional Fourier Transform requiring logarithm additions and multiplication 11 p2073 A70-26250

Walsh functions electrical generation with small orthogonality error based on multiplication theory, presenting circuit diagram for 32 channel analyzer 13 p2364 A70-28900

Nondiverging filter with single additional multiplication by fixed scalar s at each observation time, proposing algorithm 16 p2887 A70-33872

MULTIPLIER PHOTOTUBES

U PHOTOMULTIPLIER TUBES

MULTIPLIERS

Feedback time sharing analog electronic multiplier for two quantities, noting linearity, accuracy and stability of measurements 02 p0268 A70-12422

Multiplier and gradient methods in computing variational and optimal control problems 07 p1325 A70-19267

Parallel multiplier design with carry-save scheme and constructed from series integrated circuits, discussing speed, complexity and cost 08 p1467 A70-21784

Theorem for highest statically admissible multiplier for plates and shells, noting association with stress field satisfying yield equality at all cross sections 08 p1595 A70-21977

Flexible channel multiplier for particle counting with electron conductive polymer composition, discussing secondary electron emission, gain distribution and degradation 17 p3054 A70-35279

Strain multiplier for fatigue sensor in moderate amplitude cyclic strain applications 20 p3628 A70-39159

Analog three dimensional electrical signal multiplier circuit based on Hall effect, considering division and square root extraction 24 p4319 A70-45484

MULTIPOLAR FIELDS

Multipole analysis for earth magnetic field allowing secular variation to be illustrated by time trends in multipole parameters 02 p0288 A70-11742

Plasma containment by spherical multipole magnetic trap, discussing injection and trapping of gun-produced plasma 08 p1553 A70-21609

Multipole analysis applied to 1965 International Geomagnetic Reference Field, separating secular variation field into drifting and nondrifting components 09 p1666 A70-22065

Multipolarized radar imagery for detecting high return linear cultural features in geographic areas including channel markers, bridges, railroad and power-line networks, etc 12 p2228 A70-26911

Pulsed multipole magnetic field shaping short plasma blobs 22 p4083 A70-43389

Earth quadrupole moment indirect effect on satellite gyroscope precession 23 p4217 A70-43799

MULTIPOLES

Multipole coupling circuits for wideband radio amplifiers 08 p1474 A70-21225

Asymptotic stability of multivariable autonomous control systems using Liapunov vector function method 11 p2083 A70-25606

Asymptotic stabilization of multivariable dynamic systems, using subsystem decomposition and Liapunov second method 11 p2023 A70-25607

Acoustic field scattering from multipole point sources by solid spherical surface 22 p4010 A70-42693

MULTIPROGRAMMING

IBM System/360 Operating System submodel simulator for multiprogramming, discussing language and structure 02 p0266 A70-12281

Airborne multiprocessor building blocks, discussing central processor, input/output controller and interface, memory unit and power supply 16 p2869 A70-33465

MULTIROPELLANTS

U ROCKET PROPELLANTS

MULTISPECTRAL BAND SCANNERS

Multispectral scanner technology for earth resources exploration from space 03 p0492 A70-13671

Multispectral scanner for Earth Resources Technology Satellite, discussing agriculture applications and advantages over return beam vidicon 03 p0493 A70-13957

Earth resources program data management system, discussing mission control, processing and distribution of data from satellite vidicon cameras and multispectral line sensors [AIAA PAPER 70-321] 09 p1792 A70-22854

Wheat fields recognition, mapping and acreage measurement by multispectral scanning with real time analog data processing, considering seasonal and observation altitude effects 12 p2219 A70-26930

Spectral discrimination technique for crops remote sensing, comparing statistical irradiance model with airborne multispectral scanner data 12 p2219 A70-26931

Collapse prone land detected by multispectral scanning and photography with analog data processing 12 p2220 A70-26933

Hydrobiological features mapping in Everglades by multispectral scanning and analog data processing 12 p2220 A70-26934

Preprocessing data transformations for multispectral recognition mapping, reducing difficulties due to variations in environmental, observational and sensor conditions 12 p2220 A70-26935

ERTS multispectral scanner with optimal sensitivity and resolution for agricultural scenes signature analysis 12 p2229 A70-26941

Airborne multispectral sensing, describing multichannel scanners, pattern recognition techniques and equipment, etc 17 p3083 A70-34874

Multispectral UV sky mapping and heavenly body intensity measurement onboard OAO 2 satellite 17 p3179 A70-35264

Remote multispectral sensing of environmental and vegetative gradients in Yellowstone National Park by intercomparison of thermal IR and visible band imagery 17 p3079 A70-35617

Earth resources satellite orbits and imaging sensors, discussing multispectral spin scanner design 20 p3626 A70-39053

Multispectral IR scanner system for earth resources survey programs 22 p4037 A70-43087

MULTISPECTRAL PHOTOGRAPHY

NT INFRARED PHOTOGRAPHY

NT RADAR PHOTOGRAPHY

Photographic and IR multiband spectral discrimination for rock and soil mapping from orbiting ERTS satellites [AIAA PAPER 70-303] 09 p1668 A70-22882

Multispectral imaging from lander for Martian surface constituents discrimination 11 p2051 A70-26000

Martian multispectral imaging from lander emphasizing spectral bands and gray levels number for discrimination of surface constituents 12 p2229 A70-26928

Engineering soils mapping by multispectral techniques, describing image interpretation by visual means, densitometric measurements and automatic spectral response classification 12 p2220 A70-26932

Collapse prone land detected by multispectral scanning and photography with analog data processing 12 p2220 A70-26933

Remote sensing techniques for earth resources inventory, describing image enhancement role in multiband space photography 12 p2220 A70-26936

Multispectral color aerial photography, describing instrumentation, oceanographic and agricultural applications, atmospheric effects on images, etc 12 p2220 A70-26937

Apollo 9 scientific multispectral photography mission, discussing meteorological support aspect of real time planning 14 p2610 A70-30614

Remote sensing experiment demonstrating utility of multispectral color aerial photography for detection of differences among vegetative species 17 p3095 A70-35615

Multispectral remote sensing for detection and mapping of ecological objects and energy budget parameters measurement 17 p3079 A70-35622

Multispectral photography in earth resources research, noting three return beam vidicons for technology satellites 20 p3628 A70-39128

Multispectral hydrometeorological environment monitoring in Earth Resources Survey Program 23 p4191 A70-44664

MULTISTAGE COMPRESSORS

U TURBOCOMPRESSORS

MULTISTAGE ROCKET VEHICLES

NT ANTARES ROCKET VEHICLE

NT ATLAS CENTAUR LAUNCH VEHICLE

NT ATLAS LAUNCH VEHICLES

NT BERNICE ROCKET VEHICLE

NT BLACK KNIGHT ROCKET VEHICLE

NT DIAMANT LAUNCH VEHICLE

NT ELDO LAUNCH VEHICLE

NT JAVELIN ROCKET VEHICLE

NT SATURN LAUNCH VEHICLES

NT SATURN IB LAUNCH VEHICLES

NT SATURN 5 LAUNCH VEHICLES

NT SCOUT LAUNCH VEHICLE

NT SKYLARK ROCKET VEHICLE

NT THOR DELTA LAUNCH VEHICLE

NT THOR LAUNCH VEHICLES

NT TITAN LAUNCH VEHICLES

NT TITAN 3 LAUNCH VEHICLE

Optimum angle of attack control for multistage rocket as function of phase coordinates and time by solving functional equation with finite difference method 02 p0381 A70-12407

Shooting method for real time optimization of multiple burn rocket flights, presenting analysis, algorithm and test results 04 p0761 A70-14932

Multistage rocket optimum ascent regime obtained by height function of engine gas outlet velocity 06 p1155 A70-17585

Launch vehicle first stage cost reduction, considering weight factors, mass production, recoverability, etc 11 p2126 A70-26285

Two stage rocket booster-ram rocket launcher combination compared to single and two stage rockets 11 p2126 A70-26287

Cost optimal carrier rocket system for European satellite TV, communication, navigation and earth survey networks 13 p2502 A70-28448

Spin-stabilized rockets stage separation dynamics, considering guide shoe-guide rail lateral motion constraint system 13 p2503 A70-28508

Delta launch vehicle for scientific and application satellites, describing three stage liquid and solid propulsion systems 15 p2810 A70-31783

Europa 3 configurations for launching payloads into geostationary orbit using various rocket stage combinations 15 p2789 A70-32254

Two stage reusable space shuttle consisting of booster and orbiter 15 p2789 A70-32255

Multistage rocket weight optimization for payload and velocity at burnout, considering specific impulse, drag, etc 15 p2813 A70-32519

Modular launch vehicle system for European commercial satellites using Eldo-A/I Astris and French rocket stages 16 p2987 A70-34342

Black Arrow launch vehicle for inexpensive and reliable payload injection into low polar orbits 17 p3178 A70-35255

Europa 2 booster perigee stage engine design, discussing total and propellant masses, spin stabilization, materials, etc 23 p4234 A70-44672

MULTIVARIATE STATISTICAL ANALYSIS

NT BIVARIATE ANALYSIS

NT CORRELATION

NT COVARIANCE

NT DISCRETE FUNCTIONS

NT ORTHOGONALITY

NT REGRESSION ANALYSIS

Multivariate analysis - Conference, Dayton, June 1968 07 p1323 A70-19026

Multivariate linear model and robust estimators of parameters based on rank tests 07 p1323 A70-19027

Multidimensional stochastic approximation theorems useful for infinite-dimensional Hilbert space or Banach space 07 p1324 A70-19029

Multidimensional Kiefer-Wolfowitz stochastic approximation algorithm modified to locate regression function minimum 07 p1247 A70-20028

Ballistocardiograms hypertensive observations multivariate analysis, discussing factors for various groups discrimination 21 p3763 A70-41230

Pattern recognition system design, discussing criteria and algorithm for grouping multivariate data without supervision 24 p4316 A70-45103

MULTIVIBRATORS

NT FLIP-FLOPS

NT MONOSTABLE MULTIVIBRATORS

Pneumatic fluidic oscillator consisting of bistable multivibrator, analyzing feedback loop operation based on electropneumatic analog system 02 p0229 A70-12673

Transistor bistable multivibrator design by graphic analytic method, considering effects of loading and supply voltages, temperature and component values on circuit performance 10 p1848 A70-23995

Interference free and frequency stable transistorized multivibrator circuits using High Level Logic /HLL/ units 14 p2561 A70-31163

Multivibrator designs incorporating distributed R-C-NR thin film structures 24 p4321 A70-46395

Multivibrators with improved stability and frequency-division capacity, using distributed R-C-NR structures 24 p4321 A70-46396

MUONS

Cosmic ray latitude survey in western U.S. and Hawaii in summer 1966 using neutron and muon monitors 01 p0167 A70-10228

High energy nuclear interactions defined by computerized determination of sea level lateral distribution of muons from primary cosmic ray air showers 01 p0171 A70-10667

Angular distribution of muon poor extensive air showers flatter than normal showers, discussing initiation by passive particles produced by cosmic ray-atmospheric nuclei 02 p0357 A70-12079

Inelastic muon-nucleon scattering implications on cosmic rays, studying equation validity for absorption cross section 02 p0359 A70-12702

Cosmic ray muon source implied from hadrons X pairs produced in primary cosmic ray collisions 02 p0360 A70-12845

High energy muon production and interaction, analyzing ionization burst spectra 03 p0555 A70-13037

Spatial distribution function calculation for muons in extensive air shower model and secondary particles mean transverse momentum estimation 03 p0556 A70-13039

Scintillation counters hodoscopic system for studying spatial distribution of muon and muon- number fluctuations in extensive air showers 03 p0482 A70-13042

Density spectrum exponent of penetrating muon component of extensive air showers determined for hodoscopic assembly of Geiger-Muller counters with lead absorber 03 p0556 A70-13043

Sidereal cosmic ray diurnal variations from underground muon telescopes in Northern and Southern Hemispheres, proposing model producing variations at earth vicinity 03 p0560 A70-13978

Muonic and hadronic component arrival time distribution in EAS measured under rock compared to Monte Carlo computation 03 p0562 A70-14187

Isothermal atmospheric temperature effects on extensive air shower characteristics and muon numbers computed at various temperature and observation levels 05 p0898 A70-15945

Angular distribution and production probability of secondary shower particles produced by high energy cosmic ray muons using scintillation counter facility 05 p0899 A70-15957

Muon-electron ratio measurements in extensive air showers, showing anomaly due to chemical composition change of primary cosmic radiation 05 p0901 A70-16274

Neutron formation multiplicity during capture of cosmic ray muons by Zn and Sb nuclei, noting agreement with one-third law 08 p1560 A70-20718

Extensive air shower simulation for determining inelasticity effect on electrons, hadrons and muons variation at sea level 08 p1563 A70-21674

K-mesons role in high energy cosmic ray muons angular distribution and nuclear interaction 09 p1748 A70-23731

Cosmic ray muons continuous recordings, describing design and performance of plastic scintillators with photomultipliers 10 p1889 A70-24489

Muon energy measurements using pair production, bremsstrahlung cross sections, burst sampling and Monte Carlo calculations 10 p1920 A70-24857

Sidereal time variations in cosmic ray intensity observed by inclined muon telescopes 10 p1933 A70-24858

Cosmic ray intensity fluctuations at geomagnetic equator using power spectrum analysis on mu meson records, discussing solar photosphere and interplanetary magnetic field 12 p2291 A70-27176

Muon intensity meter for cosmic ray muon flux underground using scintillation telescope consisting of two coincidence counters 12 p2295 A70-28176

Low momentum muon intensity dependence on geomagnetic latitude 13 p2476 A70-28919

Cosmic ray muon energy spectra at large zenith angles measured by optical spark chamber magnetic spectrometer 13 p2476 A70-28933

Cosmic ray muons energy spectra and zenith angle distributions by analyzing tracks recorded in high field heavy liquid bubble chamber 13 p2476 A70-28934

Cosmic ray vertical muon flux measurements at sea level using spectrometer 13 p2477 A70-29124

High energy cosmic ray muons, investigating arrival from both low and high galactic latitudes 13 p2478 A70-29482

Statistical accuracy of standard muon azimuthal semicubic telescope for solar cosmic rays, discussing rms error 18 p3256 A70-36103

Azimuthal muon telescope installation at cosmic ray station, noting photorecorder circuitry 18 p3256 A70-36108

Cosmic ray muon intensity deep underground vs depth measured with liquid scintillation detector hodoscope 18 p3308 A70-36897

High energy primary cosmic ray muons arrival directions examined for anisotropies underground 19 p3508 A70-38141

Sidereal daily variation in cosmic ray muon intensity at 60 mwe depth, indicating extragalactic origin 19 p3509 A70-38149

Sidereal cosmic ray diurnal variations using underground mu-meson telescopes in Northern and Southern Hemispheres 19 p3510 A70-38150

Muon deficient showers intensity distribution as function of sidereal time, obtaining anisotropy upper limit by statistical analysis and Monte Carlo method 19 p3511 A70-38483

Muonic atoms nuclear excitation in Zn 66 and 68 20 p3674 A70-39221

Primary cosmic rays spectrographic measurement, using hard muon component intensity variations data 20 p3629 A70-39320

Secondary cosmic ray muon inelasticity in high energy neutrino interactions for deep mine experiments, using lepton current 21 p3845 A70-41139

Cosmic ray signal anisotropy around 0900 h sidereal time and 30-60 degree declination, investigating muon events in liquid scintillator 21 p3882 A70-41994

Anomalous angular distribution and inelastic cross section of muon-nucleon interaction for penetrating underground cosmic ray particles 22 p4095 A70-43232

MUSCLES

NT MYOCARDIUM

Somatic motor unit spikes human biceps during posture holding, obtaining Markov chain and random variable behavior patterns 03 p0416 A70-13011

Plethysmographic investigation of myogenic load influencing sportsmen central nervous systems state, tabulating short and long distance running results 03 p0420 A70-13403

Pathologic findings of left ventricular papillary muscle related to electrocardiogram, discussing papillary muscle dysfunction syndrome 03 p0426 A70-13942

Hypokinesia effects on transversostriated muscle fibers of mice, noting changes in myofibrillar apparatus, mitochondria and sarcoplasm 04 p0629 A70-14569

Human skin temperature variations in supramuscular areas under physical activity and rest 04 p0638 A70-15505

Synchronous variations in skin and muscle temperatures of musculus gastrocnemius and flexor carpi in human subjects performing intermittent physical exercises 04 p0639 A70-15506

Muscle temperature variations and respiratory activity of athletes under various exercise regimens, outlining optimal weight lifting training programs 04 p0639 A70-15507

Skin-muscle temperatures ratio variations in dogs during periods of activity and rest 04 p0639 A70-15508

Orthostatic tolerance in humans increased by lower limb muscles electrostimulation, correlating subjective feelings with heart and pulse rate measurements 09 p1615 A70-22089

Vibration effects on receptors in frog toe muscles at various frequencies 12 p2179 A70-28344

Oxygen and carbon dioxide effects on airway smooth muscle following pulmonary vascular occlusion in dogs 13 p2356 A70-29943

Electrophysiological characteristics of rabbit eye muscles tonic fibers, measuring postsynaptic and membrane rest potentials 15 p2679 A70-31604

Portal vein smooth muscles electrical properties, using double saccharose bridge method 15 p2679 A70-31605

Orthostatic tolerance in humans increased by lower limb muscles electrostimulation, correlating subjective feelings with heart and pulse rate measurements 15 p2685 A70-32685

Skeletal muscle proteins fractional composition in white rats during hypokinesia, noting water content changes 17 p3030 A70-35356

Bone and muscle tissue morphological changes in caged and immobilized rodents and in myasthenic humans 17 p3030 A70-35357

Analog computer for continuous recording of oxygen consumption of muscular area in canine foot via blood flow rate and oxygen saturation 19 p3367 A70-37354

Senescent *Drosophila melanogaster* flight muscle electron microscopic examination showing mitochondria in stages of degeneration 20 p3574 A70-40075

MUSCOVITE

Neutrinos line patterns in Muscovite mica, refuting Russel assumption by analysis of multiple Coulomb scattering of charged particles and track comparison 03 p0556 A70-13047

MUSCULAR FATIGUE

Heart rate augmentation during constant performance in excess of endurance limit, considering muscle fatigue 03 p0431 A70-14292

Activity and rest alternation effect on fatigue and rehabilitation behavior of trained athletes, discussing muscle performance characteristics 04 p0639 A70-15510

Intraocular tension due to muscular fatigue in overheated albino rats, determining Na and K content in eye tissue 14 p2535 A70-30159

Signal processing methods application to myoelectric studies of muscular fatigue, employing surface electrodes 23 p4151 A70-44378

MUSCULAR FUNCTION

Rats decreased muscular work and denervation effects on alpha-aminoisobutyric acid uptake by skeletal muscle 02 p0232 A70-11712

Frog sartorius muscle heat production and work effect measured under isotonic and isometric conditions, using gradient layer calorimetry 02 p0232 A70-11715

Polarographic method for determining cat papillary muscle oxygen consumption used to investigate Fenn effect involving afterloaded and isometric contractions 02 p0234 A70-11726

Spinal cord and skin temperature effects on tension-extension diagrams in cats red and pale muscles 02 p0236 A70-12092

Sensory and muscular factors interaction in space perception via empirical test of summative hypothesis derived from sensory tonic field theory 02 p0239 A70-12626

Slow waves and spikes in intestinal muscle of cat noting dependence on intracellular iontophoresis of Na 03 p0416 A70-13014

Two loop control system model of human lens accommodative system derived on basis of muscle mechanics, optics and experiments 03 p0439 A70-14275

Lactate accumulation and anaerobic work threshold in subjects exercised on bicycle ergometer, considering muscle contraction effect on oxygen supply 03 p0431 A70-14293

Contralateral remote masking /CRM/ increase of LF tone burst produced by middle ear muscle contractions 04 p0632 A70-15082

Human unloading reflex, using experimental setup unloading muscle without tension increase 06 p1000 A70-17450

Oxygen tension change effects on rats smooth vascular muscles electrical and contractile properties 07 p1198 A70-18715

Surface and underwater swimming tests for statistical correlation to linear maximum accelerations effects 07 p1201 A70-18788

Acceleration and weightlessness effects on efficiency, reliability and capacity in pilots and astronauts muscular system 07 p1202 A70-18797

Human body turning /orienting/ in unsupported /weightless/ position by own muscular forces, determining inertia moments of body and parts relative to various axes 07 p1207 A70-19495

Veloergometric assembly using two bicycles for simultaneously measuring muscular motor activity of persons in competition 07 p1221 A70-19525

Electromyograms cross correlation analysis to study time relationships between motor unit discharges of human musculus biceps and triceps brachii during physical work 07 p1213 A70-19791

Human esophagus physiology, studying sphincter function from data on healthy and afflicted subjects 07 p1214 A70-19793

Step tracking in normal human subjects, studying muscle system around ankle joint 10 p1824 A70-23898

Initial period of muscular energy expenditure in athletes performing exercises on veloergometer, considering oxygen consumption

12 p2172 A70-28313

Human forearm motion control mechanism, examining mechanogram, instantaneous velocity, acceleration and biopotentials of biceps and triceps brachii

12 p2173 A70-28314

Myocardium potential working capacity in relation to diastola duration of ventricles

13 p2355 A70-29767

Heart rate elicitation and blood pressure increase, considering parasympathetic and sympathetic nervous outflows adjustments of initial cardiovascular response to muscular contraction

15 p2684 A70-32535

Human body turning /orienting/ in unsupported /weightless/ position by own muscular forces, determining inertia moments of body and parts relative to various axes

15 p2685 A70-32740

Muscular behavior analog simulation model from generalization of laws governing viscoelastic behavior of polymeric materials

15 p2693 A70-32820

Cardiac structure-functional relations, discussing muscle strand continuum, basal fibrous skeleton, epicardial, endocardial and myocardial layers

15 p2685 A70-32834

Human power output dependence on muscle mechanical properties and kinematics of input motion, describing ergometer

16 p2853 A70-33669

Human muscular function in conditioned and unconditioned thermoregulatory reflex changes of gaseous metabolism during repeated cooling

18 p3218 A70-36528

Thermoregulation of hedgehogs during muscular activity in cold environment, recording electrical activity, oxygen consumption and body temperature during work-rest cycles

18 p3219 A70-36542

Diaphragmatic muscle reactions and pneumogram changes in rats immediately after air passage obstruction

19 p3360 A70-37804

Myocardial contractile function in rats under acute overstrain, evaluating role of preliminary training to altitude hypoxia

19 p3360 A70-37805

Muscle function mechanics across knee joint in walking, relating tension to length, velocity and energy absorption

19 p3368 A70-37810

Perfusion peristaltic pump for determining smooth muscle reaction in vascular bed, discussing applications to physiological and pharmacological investigations

19 p3372 A70-38958

Skeletal muscle force generation stochastic model based on motor unit, discussing Poisson distribution and dynamic force response

21 p3769 A70-41199

Elastic bounce of body resulting from falling to ground with calf muscles in sustained contraction and without knee bending

21 p3765 A70-42151

Muscular group response to sinusoidal and trapezoidal force applied to forearm, discussing frequency dependent limb oscillations and neuromuscular effects

21 p3767 A70-42161

Motor activity and aging - Conference, Kiev, April 1968

22 p3967 A70-42893

Muscular activity in regulation of organism functions during aging, considering hypokinesia effects

22 p3968 A70-42894

Muscular activity influence on energetic processes and functions in aging organism, relating oxygen consumption to aerobic metabolism

22 p3968 A70-42895

Adaptation of cardiovascular system in aging and old individuals under muscular activity

22 p3968 A70-42896

Aged conditioned changes in muscular working capacity, relating developments in functionally labile nerve centers

22 p3969 A70-42898

Body oxygen control under muscular activity in aging individuals

22 p3969 A70-42899

Mathematical model of heart beat control during muscular activity in aging individuals, reflecting neural and hormonal control circuits

22 p3969 A70-42901

Physical training effects on blood circulation, respiratory and muscular functions in aging persons

22 p3970 A70-42905

Contractive function of myocardium in middle and advanced age individuals under high physical loads during prolonged periods

22 p3970 A70-42907

Vascular smooth muscle contraction regulation, discussing contractile protein, energy metabolism, ex-

citation-contraction coupling, spontaneous rhythmicity, response to stimulants, etc

24 p4299 A70-45807

Sympathetic-adrenal system activity of trained organism during muscular work and emotional excitation

24 p4300 A70-45841

Esophageal swallowing pattern of longitudinal and circular muscular layer contraction, using intraluminal pressure recordings

24 p4300 A70-45844

MUSCULAR STRENGTH

Muscle force and electromyogram behavior with alteration in blood flow and composition in anesthetized cats

02 p0231 A70-11708

Veloergometric assembly using two bicycles for simultaneously measuring muscular motor activity of persons in competition

07 p1221 A70-19525

Human muscular strength capacity relationship to maximal or submaximal dynamic work performance

16 p2853 A70-33668

Training effect on strength per unit cross sectional area of arm muscle, using ultrasonic measurement

17 p3024 A70-34592

Hand held device for finger /thumb/ strength measurements

24 p4309 A70-46121

MUSCULAR TONUS

NT HYPOTONIA

Polymethylene-bis-lepidine dibromides effect on blood pressure and peripheral vessel tonus in dogs, analyzing depressor reaction as function of binding chain

04 p0632 A70-15204

Blood pressure variations resulting in permanent irreversible hypertonia in air force pilots subjected to repeated stress situations and emotional irritations

09 p1626 A70-23011

Transmural stimulation elicited phasic and tonic contractile responses in circular and longitudinal axes of small intestine under nerve-blocking drugs

09 p1622 A70-23547

Physiological mechanisms of cold adaptation in terms of individual, type and population categories, examining thermoregulatory muscular reflex

18 p3218 A70-36527

Cerebrum electrical activity and myogenic tonus relation in subjects performing tasks in response to visual and acoustic stimuli

18 p3221 A70-37216

Muscular mechanics of intact heart contraction, discussing effects of altered fiber length, afterload and inotropic state

20 p3571 A70-39363

Fatigue effects on relationship between oxygen consumption, electromyographic activity and isometric contraction in human leg muscles

21 p3766 A70-42159

MUSCULOSKELETAL SYSTEM

NT BONES

NT CARTILAGE

NT CEREBRUM

NT CONNECTIVE TISSUE

NT CONSTRUCTORS

NT CRANIUM

NT FEMUR

NT FLEXORS

NT JOINTS [ANATOMY]

NT KNEE [ANATOMY]

NT MARROW

NT SCIATIC REGION

NT SKULL

NT ULNA

NT VERTEBRAE

NT VERTEBRAL COLUMN

Skeletal status evaluation in space flight, describing instrumentation for bone mineral measurement and acoustic velocity method for bone elasticity

01 p0032 A70-10369

Cr 51 osteotropic properties for osseous system studies, discussing binding to bones, experiments on rats and rabbits, applications for human osseous system diagnosis, etc

01 p0029 A70-11403

Alpha-aminoisobutyric acid accumulation by soleus and plantaris muscles of rat in vivo during work induced growth, showing amino acid transport variation with work level

02 p0232 A70-11711

Rats decreased muscular work and denervation effects on alpha-aminoisobutyric acid uptake by skeletal muscle

02 p0232 A70-11712

Local contractures in K depolarized amphibian skeletal muscle fibers by intracellular injection or by microperfusion, discussing intracellular Ca ion concentration

02 p0234 A70-11728

Oxygen consumption, lactic acid production and mechanical performance of anesthetized dog gastrocnemius muscle with increased blood flow

02 p0235 A70-12090

Reactive forces and torques of musculoskeletal system during lifting and carrying materials, using computerized biomechanical models

02 p0247 A70-12549

Purification and properties of diphosphopyridine nucleotide-linked glycerol 3-phosphate dehydrogenases from chicken breast muscle and liver

03 p0442 A70-14047

Human nerve and muscle system changes under prolonged hypodynamia

10 p1815 A70-24681

Tissue oxygen partial pressure measurement in resting skeletal gracilis muscle of cat, using microelectrode

11 p1989 A70-26664

Repeated local spine cooling effect on gas exchange and electrical activity of white rats skeletal muscles

18 p3219 A70-36541

Respiratory activity of internal organs and skeletal muscles in rats exposed to long term heat and cold

18 p3220 A70-36546

Respiratory gas metabolism, tissue respiration and enzyme distribution in white rats skeletal muscles following long term cold acclimatization

18 p3220 A70-36548

White rats adaptation to multiple high temperature exposures, examining oxygen tension in skeletal muscles

18 p3220 A70-36549

Macroscopic architectural changes of cancellous and cortical bone in Rhesus monkey following long term immobilization and chemical removal of calcium

20 p3569 A70-38983

Plasma tocopherol concentrations and vitamin E deficiency in dogs, noting pathologic changes in smooth muscle, central nervous system, skeletal muscle and retina

20 p3569 A70-38991

Visceral blood flow during exercise in sled dogs, testing hypothetical compensatory decrease as cardiovascular reserve for skeletal muscle by biotelemetry

20 p3571 A70-39366

Ulnar resonant frequency reproducibility as objective measure of skeletal status, discussing forearm and hand positioning effect

20 p3579 A70-39432

Skeletal muscles static tension influence on dog respiratory center functional properties, showing increased frequency volume and sensitivity under stimulation

20 p3574 A70-40174

Skeletal muscle force generation stochastic model based on motor unit, discussing Poisson distribution and dynamic force response

21 p3769 A70-41199

Linear lumped parameter mechanical model of muscle spindle in postural control

22 p3979 A70-43496

Calcium metabolic balance reports discrepancies with radiologic indications of astronaut bone loss

23 p4148 A70-44838

Hypogravic skeletal atrophy model, considering bone maintenance as feedback control system

24 p4296 A70-45328

MUTATIONS

Chromosome of temperature-sensitive mutant of bacillus subtilis 168, observing multiforked replication at normal temperature and transfer of DNA

09 p1615 A70-22206

X ray effects on central nervous system noting mutations in rats, guinea pigs, chickens, dogs and rabbits

09 p1620 A70-22821

Spaceflight effects on dry crepis capillaris seeds in five day orbit, showing chromosome rearrangements and increased mutagenic sensitivity

10 p1811 A70-24323

MYELIN

Time course of end bulb material formation in vitro in rodent myelinated nerve fibers, confirming elastic capillary concept

02 p0233 A70-11725

MYLAR [TRADEMARK]

High transmission Mylar window He cryostat for Mossbauer measurements

21 p3828 A70-41470

MYOCARDIUM

P wave changes in serial ECG in patients with acute myocardial infarction

01 p0013 A70-10272

Serologic evidence of immune mechanisms, including heart muscle antibodies in patients with idiopathic cardiomyopathy, showing no autoimmune disease in majority

01 p0014 A70-10276

Atrial and ventricular gallops incidence during acute myocardial infarction by serial auscultation and phonocardiograms

01 p0014 A70-10277

Patients with/without coronary heart disease inhaled various gas mixtures to induce arterial hypoxemia and hyperoxia, noting O availability for myocardial metabolism

01 p0016 A70-10440

Myocardial infarct and other psychosomatic disturbances n Conference, Wiesbaden, West Germany, August 1967, Part 3
01 p0023 A70-10864

External environmental factors, life habits and personality structure effects on development of coronary artery disease, discussing psychosomatic aspects of myocardial infarction
01 p0023 A70-10866

Organic and psychological risk factors in myocardial infarction, presenting characteristic case history graphically
01 p0024 A70-10867

Physiological significance of myocardial fibers curvature in left ventricle wall determined by numerical solutions based on mathematical description
01 p0039 A70-11368

Left ventricular muscle time varying elastic properties, using dynamic model and Fourier series representations
01 p0040 A70-11371

Adrenal function in patients with acute myocardial infarction correlated with prognosis
01 p0029 A70-11405

Hyperbaric oxygenation /OHP/ effect on left ventricular function evaluated by measurement on anesthetized dogs of myocardial contractility
02 p0230 A70-11701

Cardiac relaxation mechanics from isolated preparation of cat papillary muscle, noting inotropic influences role
02 p0231 A70-11709

Heart rate change effect on myocardial oxygen consumption and nutritional circulation with constant coronary blood flow suggesting oxygen extraction independence of capillary surface
02 p0235 A70-11991

Frequency and postextrasystolic potentiations in guinea pig isolated auricles and dog heart in vitro and in situ, noting myocardial diagnostic use
02 p0235 A70-12088

Arterial counterpulsation effect on mechanics of left ventricular contraction and myocardial oxygen consumption in normal and abnormal animals
03 p0416 A70-13009

Myocardial changes in rabbits after general chronic ionizing irradiation attributed to lower cardiac activity, hypotrophy and dystrophy
03 p0425 A70-13888

External work and energy expenditure relations of heart, including myocardial oxygen consumption
03 p0426 A70-13940

Production mechanism of abnormal Q waves in obstructive cardiomyopathy
03 p0427 A70-13943

Acute myocardial infarction - Conference, Phoenix, March 1969
04 p0633 A70-15455

Pathological manifestations of acute myocardial ischemia without acute myocardial necrosis and myocardial infarction, discussing subjects with chronic occlusive coronary atherosclerosis
04 p0634 A70-15456

Primary and secondary pathological changes in small coronary arteries and role in acute myocardial infarction development, discussing coronary arteries distribution
04 p0635 A70-15457

Platelet function in coronary artery disease and myocardial infarction, considering thrombosis, atherosclerosis, emboli in microcirculation, etc
04 p0635 A70-15458

Clinicopathological studies of coronary artery occlusion and acute myocardial infarction, discussing coronary thrombosis
04 p0635 A70-15459

Psychosocial factors in myocardial infarction and sudden death, considering possible causes of fatal cardiac arrhythmia
04 p0635 A70-15462

Myocardial infarction therapeutic prevention possibilities on basis of epidemiologic and dietary studies involving hypercholesterolemia and hyperlipemia in coronary disease
04 p0635 A70-15463

Plasma lipids and lipoprotein changes following myocardial infarction, discussing rise and normal return times of free fatty acids, cholesterol and beta lipoproteins
04 p0636 A70-15464

Heparin role in anticoagulant therapy for myocardial infarction based on proved application to other venous thrombotic diseases, noting hemorrhagic complications controllability
04 p0636 A70-15465

Exercise relation to acute myocardial infarction, coronary thrombosis, stenosis and obstruction, discussing prevention value of physical reconditioning in heart patients
04 p0636 A70-15466

Familial aggregation for coronary artery disease and familial similarities in coronary anatomy, considering possible genetic analysis of myocardial infarction
04 p0636 A70-15467

Myocardial blood flow in patients with acute myocardial infarction determined from measuring effective capillary flow /ECF/ by direct counting of rubidium 86 uptake
04 p0636 A70-15468

Myocardial metabolism in ischemic heart disease using arterial and coronary sinus catheterization
04 p0636 A70-15469

Ventricular performance as function of infarcting myocardium, discussing dynamic characteristics
04 p0637 A70-15470

Acute myocardial infarction clinical features, discussing gallop rhythm, ventricular arrhythmias, ventricular tachycardia, bradycardia, etc
04 p0637 A70-15471

Sudden and early death in acute myocardial infarction, discussing prophylactic measures
04 p0637 A70-15472

Glucagon infusion effect on human coronary circulation, relating changes in cardiac dynamics to myocardial oxygen consumption and blood flow
05 p0800 A70-16101

Myocardial scarring sites localized in human subjects by HF ECG components
05 p0800 A70-16104

Acute myocardial ischemic injury and infarction in dogs related to changes in man using oxygraph tracings
06 p0997 A70-18405

Biochemical disturbances during early myocardial ischemia, examining coronary sinus lactate and K levels using electrocardiographic correlation
06 p0997 A70-18406

Ventricular ectopic beats and bradyarrhythmia associated with myocardial infarction, discussing enhanced automaticity, reentry activity, drugs and heart pacing
06 p0998 A70-18407

Bradycardic rhythms in acute myocardial infarction, investigating pathophysiologic, hemodynamic and electrophysiologic aspects and ECG interpretation
06 p0998 A70-18408

Perfusion pressure effect on myocardial oxygen consumption and coronary flow in stable nonworking rat heart
07 p1202 A70-18865

ECG changes attributed to reduction of blood supply to myocardium during orthostatic tests after prolonged hypokinesia
07 p1209 A70-19513

Left ventricular function myocardial infarction induced acute depression and subsequent recovery in intact conscious dogs
07 p1211 A70-19615

Physiological responses during exercise recorded in patients with healed myocardial infarction, considering work tolerance
07 p1212 A70-19693

Myocardium, endocardium and/or epicardium disease characteristics, discussing primary and secondary cardiomyopathy groups
09 p1616 A70-22277

Postinfectious noncoronary affections of myocardium in flight personnel, discussing clinical record, atherosclerotic differentiation and ECG variation
09 p1617 A70-22474

Cardiac muscle intercellular junctions ultrastructural appearance, considering macula adherens, fascia adherens and nexus junctional specializations
09 p1620 A70-23061

Idiopathic myocardial disease patients investigated for serological anomalies and markers of immunopathology
09 p1621 A70-23301

Wolff-Parkinson-White syndrome simulation of myocardial infarction, indicating false positive tests for exercise electrocardiograms
09 p1622 A70-23468

Hyperbaric oxygen effect on heart muscle contractions in mammals, considering cells enzymatic activity and substrate utilization
09 p1623 A70-23586

Body vibration effects in cats on myocardial ECG recordings, discussing electrodes implantation and tracings
10 p1810 A70-24007

Prolonged hypodynamia effect on heart size and myocardium function obtained from human chest X ray studies
10 p1814 A70-24673

Electrocardiac activity, myocardium and hemodynamic disorders in subjects after prolonged hypodynamia with or without physical exercises and during orthostatic test
10 p1817 A70-24692

Aerobic metabolism of heart muscle cells and oxygen utilization of coronary artery blood
10 p1821 A70-25081

ECG changes attributed to reduction of blood supply to myocardium during orthostatic tests after prolonged hypokinesia
11 p1988 A70-26112

Myocardial individual fibers length calculation based on ellipsoidal model of left ventricle and fibers helicoidal course, noting distension nonuniform effect
12 p2174 A70-27020

Metabolism in left ventricular myocardium of rabbits after asphyxiations and during postasphyxial recovery
12 p2168 A70-27624

Rats myocardial contractility depression by free fatty acids during hypoxia or anoxia, noting mechanical performance improvement by glucose
12 p2170 A70-27898

Microwave radiation effects on radar operators myocardium functions
12 p2180 A70-28358

Myocardium potential working capacity in relation to diastola duration of ventricles
13 p2355 A70-29767

Asymptomatic myocardial infarction in USAF flyers detected by annual electrocardiograms
15 p2690 A70-31889

Cardiac structure-functional relations, discussing muscle strand continuum, basal fibrous skeleton, epicardial, endocardial and myocardial layers
15 p2685 A70-32834

Contractile mechanics of cat papillary muscle during hypoxia and reoxygenation recovery
15 p2686 A70-32836

Autonomic drugs induced contractures of cardiac muscle of frogs, relating inotropic action with Ca influx during low membrane potential
15 p2686 A70-32837

Primary myocardial disease, describing hemodynamic and angiocardigraphic observation of left ventricular volume and wall changes
16 p2848 A70-33110

Coxsackie B virus as cause of myopericarditis in adults
17 p3025 A70-34860

Focal myocarditis associated with aircraft accidents, discussing difficulties in diagnosis and assessment
17 p3033 A70-35571

Calcium ion role in myocardial cell electrical and mechanical trace processes under normal content and manganese blocking
18 p3221 A70-36640

Myocardial contractile function in rats under acute overstrain, evaluating role of preliminary training to altitude hypoxia
19 p3360 A70-37805

Mathematical representation of heart muscle mechanical properties, examining tensile stress in parallel and series elements
19 p3368 A70-37809

Intracellular myocardium potentials under vagus inhibition by electrometric DC amplifiers with positive and negative feedback
19 p3370 A70-38213

Electrocardiogram vs vectorcardiogram for myocardial infarction diagnosis
19 p3371 A70-38362

Hemodynamic effect of lidocaine given by infusion and bolus injections in myocardial infarction, examining cardiac output, heart rate, systolic left ventricular and aortic pressures
19 p3366 A70-38575

Antigens immunological response during myocardial infarction
20 p3570 A70-39151

Mechanical analysis involving clamping apparatus for cardiac muscle contractile response
20 p3570 A70-39362

Muscular mechanics of intact heart contraction, discussing effects of altered fiber length, afterload and inotropic state
20 p3571 A70-39363

Determinants of human ventricular dimensions and myocardial free velocity relations during maximum and submaximum exercise levels
20 p3571 A70-39365

Myocardial Na and K content of rats exposed to high altitude, preparing isolated right ventricular strip
20 p3577 A70-40541

Myocardial blood flow response to cardioacceleration by right atrial pacing in normal subjects, using coincidence counting
21 p3760 A70-40576

Postexercise electrocardiogram detection of latent coronary heart disease in flyers prior to myocardial infarction
21 p3771 A70-41494

Serum enzymes lactate dehydrogenase, creatine phosphokinase and isoenzymes in conditioned male after marathon run, noting little myocardium damage
21 p3766 A70-42158

Contractive function of myocardium in middle and advanced age individuals under high physical loads during prolonged periods
22 p3970 A70-42907

Myocardium bioelectric activity electrocardiogram simulator, describing block diagram and operation
22 p3979 A70-43553

Indirect serial determination of left ventricular systolic ejection time changes in human patients with acute transmural and nontransmural myocardial infarctions
23 p4144 A70-43946

Hypercapnia effect on oxygen tension in ischemic myocardium in dogs using polarographic method
24 p4300 A70-45843

MYOELECTRIC POTENTIALS

Calcium ion role in myocardial cell electrical and mechanical trace processes under normal content and manganese blocking
18 p3221 A70-36640

MYOELECTRICITY

NT MYOELECTRIC POTENTIALS

Myocardium bioelectric activity electrocardiogram simulator, describing block diagram and operation
22 p3979 A70-43553

Signal processing methods application to myoelectric studies of muscular fatigue, employing surface electrodes
23 p4151 A70-44378

MYOPIA

Hypoxia effects on aviators visual accommodation, convergence and stereoacuity, noting myopia increase with altitude
20 p3569 A70-38996

N

N ELECTRONS

Tunable adjustable solid state bandwidth filter using N path system for low pass to bandpass filter transformation
02 p0270 A70-12666

N-N JUNCTIONS

HF admittance and noise in forward-biased majority carrier Ge-Si n-n heterojunctions and Schottky barrier
03 p0539 A70-13159

N-P JUNCTIONS

U P-N JUNCTIONS

Bipolar n-p-n transistors fabrication to increase driving capabilities of complementary MOS transistors while retaining low power dissipation
05 p0821 A70-16419

Hybrid ion implanted diffused emitter n-p-n transistor two dimensional doping profiles, considering emitter oxide window edge shape effect
22 p3997 A70-42924

N-TYPE SEMICONDUCTORS

Current carrier mobility in n-InSb calculated by Schwinger variational method over temperature range
01 p0154 A70-10098

Natural absorption band absorption coefficient frequency and temperature dependences in doped n-InSb
01 p0154 A70-10100

Hole mobility in n-type InSb semiconductors determined from solving kinetic equation for minority carriers allowing for scatterings
01 p0155 A70-10185

Plasma injection occurrence as function of temperature in n-InSb subjected to low electric field strengths and fitted with Ohmic contacts
01 p0159 A70-11176

Free carrier light absorption in n-type GaAs, InAs and Ge semiconductors with mechanically polished surfaces as function of thickness and crystal structure
03 p0538 A70-13057

N-GaAs pulsed Gunn effect oscillators for decimeter band, discussing synchronization by external sinusoidal current
03 p0499 A70-13204

GaAs n-type single crystals thermoreflectance spectra at various energies
03 p0541 A70-13721

Carrier concentration profiles and surface resistance of Ohmic contacts to solution epitaxial n-type GaAs wafers measured by Schottky barrier capacitance
03 p0543 A70-14213

Resistivity, temperature and injection level dependence of minority carrier lifetime in neutron irradiated p- and n-type Si
04 p0730 A70-14729

N-type layer formation with ion implanted nitrogen or Sb in p-type alpha-SiC, evaluating electrical characteristics, discussing junction devices formed
04 p0732 A70-15685

Doped n-type Ga-As electrophysical parameters determinable from IR reflection spectra
05 p0892 A70-16540

Field emission mechanism of hot electrons from semiconductors, discussing experiments with n-Si of high resistivity
06 p1126 A70-17749

Magnetoresistance effects in impurity conduction mode of n-type GaAs crystals below 6 K, giving electron concentration
07 p1356 A70-19796

Ohmic contacts to n- and p-type semiconductors obtained by ruby laser, noting linear current-voltage characteristics
07 p1299 A70-19797

N-type InAs single crystals optical properties with various carrier concentrations at 1-6 mu wavelengths and 300-78 K temperatures, studying absorption spectra
08 p1555 A70-20512

Gunn diode parallel combinations fabricated for X band with n-type GaAs crystals, discussing output power at CW operation
08 p1477 A70-21296

Al n-type Si Schottky barrier diode characteristics, discussing I-V, barrier height, temperature dependence, photoemission, LF noise, etc
09 p1644 A70-22210

Absorption spectra of n-type GaAs before and after proton irradiation, discussing dependence on wavelength
09 p1739 A70-22753

Frequency dependent negative resistance of n-type semiconductor doped at acceptor level near valence band top
10 p1927 A70-24273

Helicon wave dispersion in cold multicomponent plasma of n-type Si and Ge semiconductors in linear hydrodynamic approximation
10 p1928 A70-24832

Helical propagation in multivalley semiconductors of n-Ge type, obtaining polarization anisotropy
10 p1928 A70-24842

Thin n-type Ge film electrical conductivity effect on ferromagnetic barium titanate single crystals as function of magnitude and sign of polarizing field
11 p2097 A70-25383

GaAs-Au surface barrier n-type photodiode structure, electrical parameters and response characteristics
12 p2194 A70-26969

Electric field heating effect on edge photoluminescence of n-type GaAs, noting increase in electron energy
12 p2286 A70-27368

Cu doped GaAs n- to p-type transition after fast reactor neutron irradiation, measuring Hall effect and photoconductivity to determine Cu electrical activation
12 p2287 A70-27490

Thin plates finite length effects on thermal conductivity measurement by impulse method, verifying results with n-type silicon samples
12 p2332 A70-28047

Electric field distribution in rectangular waveguide loaded with magnetized n-InSb at room temperature obtained by solving boundary value problem by variational method
12 p2202 A70-28163

N-type GaAs carrier mobility and concentrations increased slow cooling after heat treatment
12 p2289 A70-28343

N-type Te-doped gallium antimonide conversion to p-type by electron irradiation, noting thermal conductivity variations
13 p2470 A70-29167

Metal-Ge n-type semiconductor tunnel junctions, discussing Sb and As doped units and conductance and barrier heights air cleavage effects
14 p2626 A70-30482

Bulk n-type InP single crystal transferred-electron oscillators, investigating current instabilities
14 p2556 A70-30686

Acceptor level formation kinetics from measuring Hall constant as function of temperature after diffusion of copper into n-type GaAs
15 p2782 A70-31633

Millimeter wave amplification by pumped n-type gallium arsenide oscillating in limited space charge accumulation mode
16 p2875 A70-33399

Transverse magnetic field influence on Gunn effect characteristics of n-type GaAs
17 p3142 A70-34622

Submillimeter lasers radiation measurement with n-InSb detectors at liquid He temperature
17 p3107 A70-35109

Wideband UHF amplification in bulk n-type GaAs during domain generation, comparing cut-off and Gunn frequency
17 p3143 A70-35684

Shallow acceptor level in Au-doped n-type GaAs, using photoconductivity temperature dependence
17 p3143 A70-35702

Photoconductivity relaxation kinetics of low resistivity n- and p-type GaAs, showing nonradiative recombination
17 p3143 A70-35703

Absorption coefficient of n-type indium arsenide single crystals with varying electron and doping concentrations, investigating spectral dependence
17 p3144 A70-35705

Electrical properties of n-type GaAs epitaxial films grown by gas transport method
17 p3144 A70-35706

Visible light-emitting p-n junctions formed in AlAs via Zn diffusion into single crystal n-type vapor grown AlAs layers
18 p3297 A70-36316

Electrical conductivity, Hall constant and differential thermal emf n-type GaAs-CdS solid solutions
18 p3298 A70-36596

Energy zone bending near surface of n-type semiconductor, discussing surface plasma level
18 p3298 A70-36619

Constant emf in bulk Ge and Si n-type semiconductors under multifrequency microwave electric field
21 p3861 A70-40636

Acoustoelectric domain spectra in n-GaAs by microwave emission, comparing results with parametric conversions theory
21 p3863 A70-42002

Fermi energy and bandtail parameters in heavily doped and degenerate n-type GaAs, calculating conduction band density of states by screened Coulomb potential
21 p3864 A70-42018

Holographic recording on n-type Si single crystal surface by photoanodic engraving
22 p4026 A70-42332

N-type GaAs samples doped with Ag, Se and Te respectively, measuring absorption coefficients spectral dependences at room temperature
23 p4229 A70-43928

N type GaAs doped with Si, conductivity anisotropy observed from measurement and explanation in terms of electron distribution
23 p4231 A70-44890

Tunneling electron and local mode phonon interaction in MIS n-type semiconductors
23 p4231 A70-44916

Mossbauer effect analysis of Fe impurity atoms in n- and p-type semiconductor compounds with wide and narrow forbidden gaps
24 p4388 A70-45204

Czochralski thermal probe for current carrier concentration in strip shaped area of n-type GaAs single crystals active growth
24 p4389 A70-45481

P- and n-channel MOS transistor instability during superbreakdown voltage application to drain electrode
24 p4319 A70-45811

N-156 AIRCRAFT

U F-5 AIRCRAFT

NA-300 AIRCRAFT

U OV-10 AIRCRAFT

NACELLES

Airframe flow field effects on propulsion system performance in transonic flight, studying case of underwing aft mounted turbojet engine nacelles
01 p0004 A70-10321

Boeing 747 nacelle development programs involving outdoor and ground test rigs, flying test bed, flight tests, etc
03 p0550 A70-12894

[SAE PAPER 690389] Pressure distribution about finite axisymmetric nacelle determined using Douglas Neumann program for cowl surfaces and inlet external surface
07 p1190 A70-20412

Thrust follower force stability in pod mounted jet engine and nacelle whirl using multiple degrees of freedom model
10 p1930 A70-25070

DC-10 aircraft wing engine calibration, isolated- and wing-nacelle testings using air-driven engine simulator [AIAA PAPER 70-590]
13 p2342 A70-29881

Powered nacelles simulating exhaust flow for propulsion and airframe problems in subsonic flow [AIAA PAPER 70-636]
16 p2888 A70-33594

NASA acoustically treated nacelle program reducing noise under commercial transport flight path near airports
22 p4089 A70-42529

Aerodynamic problems due to mixed subsonic and supersonic/ transonic flows on swept wings, nacelle lips and helicopter rotor blades [ICAS PAPER 70-14]
23 p4132 A70-44125

L-1011 aircraft optimum minimum noise pod design, describing technology, restraints and system requirements [SAE PAPER 700805]
24 p4393 A70-45877

NAMING

NT NORMS

NAPHTHALENE

Naphthalene rotating disk with confronting stationary disk, investigating heat and mass transfer dependence on shroud dimensions, measuring flow types
11 p2060 A70-26410

Surface erosion of sublimating graphite and naphthalene due to inequilibrium mass transfer in gas flows
13 p2437 A70-28580

NARCOTICS

NT MORPHINE

NASA PROGRAMS

NT APOLLO APPLICATIONS PROGRAM

NT APOLLO PROJECT

NT CENTAUR PROJECT

NT EARTH RESOURCES PROGRAM

NT GEMINI PROJECT

NT MARINER PROGRAM
 NT MARS 69 PROJECT
 NT MARS 71 PROJECT
 NT MERCURY PROJECT
 NT ROVER PROJECT
 NT SKYLAB PROGRAM
 NT SURVEYOR PROJECT
 NT SYNCHRONOUS COMMUNICATIONS
 SATELLITE PROJ
 NT TEKITE PROJECT
 NT TIROS PROJECT
 NT VIKING MARS PROGRAM
 NASA Technology Utilization Program extending space exploration and upper atmosphere R and D to X ray pictures, safer highways, TV cameras, etc
 01 p0220 A70-10282
 Space rescue techniques and equipment in NASA recovery programs, considering low earth orbit and water landing
 01 p0035 A70-10717
 Apollo spacecraft contamination control program, considering NASA role in management, contractor controls, criteria establishment and enforcement, etc
 01 p0220 A70-11076
 Meteorological spaceborne IR instruments associated with NASA satellites, discussing various Tiros and Nimbus instruments
 03 p0491 A70-13666
 NASA Source Evaluation Board process for major contractor selection, discussing procurement practices and management techniques
 03 p0610 A70-13962
 NASA research studies supporting tracked air cushion vehicle /TACV/ program illustrating aerospace technology application to ground transportation
 [AAS PAPER 69-565] 04 p0622 A70-14639
 Helium properties and utilization in NASA projects, discussing pressurization of fuel tanks cooling of superconducting magnets
 04 p0720 A70-15633
 NASA aerospace system safety program implementation and supporting organization with emphasis on background, concepts, constraints, methods and results
 [SAE PAPER 690710] 05 p0792 A70-15856
 Sterile access system using pilot assembly sterilizer system /PASS/ for NASA Planetary Quarantine Program
 05 p0808 A70-16708
 U.S. space research and technology applications in aviation, astronomy, weather information, intercontinental communication and space shuttle design
 05 p0921 A70-17091
 NASA solar particle alert network /SPAN/ operated by Manned Spacecraft Center giving 24 hr coverage of solar activity at optical and radio frequencies
 06 p1029 A70-18013
 Space flight candidate selection and physical training, comparing American and Soviet training programs for efficiency and physical requirements
 07 p1216 A70-18792
 Azur satellite program, describing NASA-German cooperative effort
 [DGLR-69-052] 07 p1391 A70-18815
 NASA three meter orbital telescope discussing configuration, optical geometry, launching, power supply, etc
 07 p1280 A70-19150
 Midwestern political economy and federal R and D funds distribution, surveying bidding practices and NASA contracts for five year period
 07 p1428 A70-19733
 Small Astronomy Satellite /SAS/ program providing Explorer class Scott launched satellite capability for astronomical observations
 08 p1581 A70-20608
 National Space Program relevance to human society, discussing solar system exploration, applications in meteorology, communication, etc
 09 p1792 A70-22041
 NASA earth-orbit shuttle /EOS/ for achieving routine arrival, conventional landing after orbital flight and reentry
 09 p1766 A70-22677
 Earth Resources Satellite Information Systems, discussing NASA Space Application Program relation to national goals, federal spending, cost effectiveness analysis, information sales, etc
 [AIAA PAPER 70-333] 09 p1793 A70-22860
 NASA Geodetic Satellite Program applications to long range navigation, spacecraft orbit prediction, navigation experiments calibration, etc
 09 p1724 A70-23048
 NASA future space programs, discussing space shuttle and station, nuclear propulsion, manned Mars landing, unmanned Venus-Mercury probes, etc
 09 p1762 A70-23065
 Photo-optical processes and optical measuring techniques in research programs at Ames Research Center for aerodynamics, life sciences and space sciences
 09 p1657 A70-23501

NASA operation of Convair 990 jet transport as airborne scientific research platform for optical observations
 09 p1682 A70-23504
 Optical equipment development at Jet Propulsion Laboratory, discussing flight TV systems and associated digital image processing laboratory, planetary spectroscopy, spacecraft guidance, etc
 09 p1657 A70-23505
 Optical research at NASA Electronics Research Center applied to air pollution measurement, pulse formation, pilot warning systems, star field mapper, etc
 09 p1657 A70-23513
 Marshall Space Flight Center optical research programs technology base for launch vehicle development support, discussing Apollo Telescope Mount
 09 p1657 A70-23518
 Lewis Research Center applications of optics to research in flight propulsion and space power generation, discussing gas density visualization, radiative heat transfer, etc
 09 p1657 A70-23522
 Materials and processing technology roles in NASA programs involving manned space stations, service spacecraft and unmanned space exploration
 10 p1902 A70-23855
 Environmental engineering at NASA MSC, surveying Lunar Receiving Laboratory, microbe incinerator, radon adsorption, Apollo Post-Landing Environmental Test Tank and vacuum chamber
 10 p1860 A70-24411
 Automatic Malfunction Analysis /AMA/ digital computer software system supporting checkout and testing, defining normal system status by computer simulation
 [AIAA PAPER 70-383] 10 p1861 A70-24922
 Space shuttle program, considering vehicle configurations mission capabilities and cost estimates with emphasis on ground and flight tests
 [AIAA PAPER 70-739] 10 p1953 A70-25074
 NASA-Lewis closed loop MHD low temperature power generator, describing systems performances during subsonic tests
 11 p1982 A70-25614
 Low cycle fatigue testing facility and methods used at NASA Lewis Research Center
 11 p2033 A70-26610
 Aerospace environment models development by NASA for engineering use in Space Vehicle Design Criteria program
 14 p2637 A70-30554
 Tropical storms and hurricanes critical winds forecasting accuracy by NASA Manned Spacecraft Center
 14 p2606 A70-30558
 European information retrieval network for interlocking NASA master file on space literature using computer terminals
 14 p2670 A70-31174
 Report to COSPAR on U.S. space science program, discussing NASA projects, stellar and solar astronomy, lunar and planetary research, cosmic particles, upper atmosphere, etc
 15 p2831 A70-31724
 Ten year NASA manned space station in low earth orbit, grouping experiments in functional program elements /FPE/
 [AAS PAPER 70-033] 17 p3156 A70-34802
 NASA ten year space station operational concepts, discussing mission planning, crew scheduling and management
 [AAS PAPER 70-031] 17 p3176 A70-34804
 NASA program for international cooperation in space involving developing and advanced nations, discussing television instruction for India, resource surveys, etc
 18 p3349 A70-36514
 Soviet and American lunar exploration by probes, manned surveillance flights and lunar landings, discussing NASA program
 18 p3238 A70-37079
 Integrated environmental control/life support resistojet systems, surveying NASA programs
 [AIAA PAPER 70-1130] 20 p3690 A70-40215
 NASA automatic checkout systems for Saturn 5 stages and instrument units
 21 p3803 A70-40770
 U.S. and Soviet space program administration and management
 21 p3956 A70-41893
 U.S. and European space program costs and resources with particular reference to telecommunication satellites
 22 p4126 A70-43247
 European participation in U.S. space projects, discussing economics, space shuttles and tugs and earth orbital space station
 22 p4126 A70-43407
 European-U.S. cooperation in shuttle and space station program, noting experience in unmanned systems
 22 p4127 A70-43508
 European cooperation possibilities in future NASA space programs
 22 p4127 A70-43510

European participation in small space shuttle development, discussing design, test vehicle program and European applications
 22 p4111 A70-43511
 Orbital laboratories and international cooperation, discussing national and foreign viewpoints
 22 p4128 A70-43631
 Space station development and missions, discussing general design philosophy, successive project lineage and applications programs
 22 p4108 A70-43653
 International space program cooperation, discussing NASA projects, Apollo 11 flight and European and Soviet programs
 22 p4129 A70-43655
 NASA research in turbojet aircraft propulsion noting inlet, compressor, combustor, turbine and nozzle component technology
 [ICAS PAPER 70-46] 23 p4233 A70-44144
 NASA design objectives for space transportation, discussing space shuttle, airlines-aerospace industry cooperation, computerization, etc
 23 p4257 A70-44173
 European space policy decisions regarding continuation of existing programs and participation in U.S. post-Apollo programs
 23 p4285 A70-44325
 NASA safety related research programs based on technology transfer involving information summarizing, indexing and storage from global aerospace research and development
 23 p4285 A70-44457
 NASA information fall-out, discussing Technology Utilization Program providing aerospace related data to civilian economy
 23 p4285 A70-44500
 Commercial transport aircraft fatigue loading data from NASA VGH /airspeed-acceleration-altitude/ program, discussing instrumentation, sample sizes, etc
 23 p4270 A70-44548
 NACA/NASA rotary wing aircraft research covering autogyro and helicopter development, noting flight safety
 23 p4142 A70-44851
 NACA/NASA rotating wing aircraft research history 1915-1970, Part 2, autogyro flight test experiences, rotor blade dynamics research, interest in helicopters, etc
 23 p4142 A70-44852
 NACA/NASA rotary wing aircraft research history 1915-1970, Part 3, covering rotor and helicopter theory, related flight and wind tunnel testing, etc
 23 p4142 A70-44853
 NACA/NASA rotating wing aircraft research history 1915-1970, Part 3, covering rotor dynamics and flying qualities, hovering tests, rotor flow, loads, etc
 23 p4142 A70-44856
 Systems and design requirements for NASA Manned Space Station, discussing projected experiment program for applications and science
 [AIAA PAPER 70-1298] 24 p4417 A70-45952
 Integrated electronics for NASA space shuttle program, discussing costs, configurations and technologies application
 [AIAA PAPER 70-1252] 24 p4418 A70-45966
 International participation in U.S. post-Apollo program involving reusable space transportation system and multipurpose space station
 24 p4431 A70-46123
NATIONAL AIRSPACE UTILIZATION SYSTEM
 General aviation requirements for national aviation system of 1970s including use of airspace and airports under all conditions
 [SAE PAPER 700296] 12 p2335 A70-27446
 Short range VOR/DME area navigation techniques in U.S. National Airspace System
 16 p2948 A70-33470
 Time-frequency national airspace system, using distributed sensors and closed loop control to meet safety and traffic handling requirements
 16 p2948 A70-33478
 National airspace system /NAS/, describing en route stage A automated air traffic control
 18 p3289 A70-36399
 National Airspace System air traffic control automation program for en route and terminal facilities
 19 p3464 A70-37914
 Area navigation system charting, discussing effect on flight information publications
 19 p3465 A70-38231
 Airline area navigation in national airspace system, emphasizing moving map display for navigation charting
 19 p3465 A70-38233
 ATC and general aviation growth, considering airport capacity, radars, navigation, National Airspace System, etc
 19 p3467 A70-38631
 ATC integration of SST, discussing en route and terminal projects of national airspace system, modular automation, instrument flight rules, etc
 19 p3467 A70-38633
 Air traffic control, future national airspace system improvements in view of air transportation growth, computerized automation technology, etc
 [AIAA PAPER 70-1263] 24 p4374 A70-45969

NATURAL FREQUENCIES

U RESONANT FREQUENCIES

NATURAL SATELLITES

- NT MOON
NT PHOBOS
Io and Europa mass and density anomalies, indicating asteroid capture by Jupiter as comet origin theory
01 p0182 A70-10671
Jupiter mass determined from observations of Jupiter fourth satellite right ascension and declination differences
02 p0370 A70-12087
Undiscovered satellites of solar system major planets, predicting Jupiter satellites
03 p0569 A70-13360
Jovian decametric radiation periodicities analysis refuting evidence of Bigg for new Jovian satellites
06 p1138 A70-17280
Eccentric and inclined motions of satellite of spherical planet in planet centered coordinate system, applying formulas to Jupiter motion
07 p1374 A70-18693
Photometric profiles of Jupiter shadows cast by large natural satellites used as upper atmosphere probes
08 p1579 A70-21571
Saturn globe, rings and satellites observations /1968-1969/
09 p1751 A70-22198
Bode law development from dynamical relaxation suggested from comparison of Jupiter, Saturn and Uranus inner satellite systems with planetary system
09 p1765 A70-23796
Jupiter decametric emission modulation by planetary rotation and Io position, suggesting role of magnetic tail diurnal swings
10 p1940 A70-24434
Motion of negligible mass body near large mass body affected by larger third body applied to Phoebe-Saturn-sun system
10 p1945 A70-24960
Observational data for distributions of physical and optical companions to spiral galactic systems and number of satellites as function of central galaxy size
10 p1948 A70-25247
Asteroid vs planet for manned landing site, considering Martian moons mission
11 p2108 A70-25660
Undiscovered satellites of solar system major planets, predicting Jupiter satellites
11 p2118 A70-26725
Light pressure induced secular effect contributing to planetary satellites and lunar orbits evolution calculated by numerical integration
11 p2118 A70-26777
Fuel savings by Jupiter moon gravity assisted transfer trajectories from earth, considering initial energy, mass ratio, approach angle, timing and aiming errors
14 p2640 A70-30761
Perturbative effects of Jupiter moons on spacecraft flyby and postencounter heliocentric trajectories, noting precision targeting
[AIAA PAPER 70-932]
18 p3316 A70-36680
Jupiter decametric radio emission modulation by Io simulated by DC circuit model
18 p3321 A70-37120
Uranus and Mars satellite relative measures, tabulating observations
19 p3516 A70-37932
Galilean satellites touring by Jupiter spacecraft, discussing orbit calculation and encounter geometry
[AIAA PAPER 70-1070]
19 p3530 A70-38883
Navigation instrument geometrical calibration by natural satellites and reference stars during interplanetary flight
[AIAA PAPER 70-1023]
20 p3669 A70-39586
Spacecraft-based navigation instruments for outer planet missions using celestial directions to outer planet natural satellites
[AIAA PAPER 69-902]
20 p3669 A70-39681
Initial water content on moon implied from hypothetical falling temperature lunar accretion as original earth satellite
22 p4102 A70-42954
Minor planets, comets and natural satellites positions and motions, discussing orbit and ephemerides calculation, Icarus asteroid, etc
23 p4256 A70-45038
Albedo and thermal emission of Jovian satellites I-IV at 3 to 12 micron wavelengths
24 p4413 A70-46171

NAVIER-STOKES EQUATION

- Navier-Stokes equation generalized solutions to initial boundary value problems, considering uniqueness theorem and smoothness
01 p0132 A70-11068
Navier-Stokes hypersonic weak interaction theory for viscous heat conducting compressible fluid flow past slender axisymmetric body
01 p0003 A70-11097
Navier-Stokes equations for compressible gas, generalizing viscous channel flow of heat conducting gas to slip flow of rarefied gas
01 p0068 A70-11579

Turbulent fluid flow analysis described by Navier-Stokes equations, introducing asymmetric tensors for anisotropic cases
01 p0068 A70-11605

Navier-Stokes difference equations numerically integrated by computer for viscous fluid flow along parallel flat plate at low Reynolds number
02 p0277 A70-11909

Computer application to Navier-Stokes equations numerical integration for incompressible viscous fluid deflected flow with large Reynolds number
02 p0287 A70-12376

Interstellar media under action of supernova or nova, solving Navier-Stokes equations of hydrogen plasma for motion during shock wave formation
03 p0564 A70-13221

Viscous incompressible laminar two dimensional flows using Navier-Stokes equations, emphasizing near wake and flow around leading edge
[ONERA-TP-757]
03 p0467 A70-13640

Viscous supersonic flow near wall with large local curvature, using asymptotic solutions to Navier-Stokes equations
03 p0468 A70-13867

Navier-Stokes boundary value problem describing viscous incompressible fluid flow between coaxial fixed and rotating cylinders, emphasizing stability analysis
03 p0470 A70-14242

Asymptotic form of axisymmetric solution with Dirichlet integral for Navier-Stokes equations applied to flow past bodies of revolution with smooth surfaces
03 p0471 A70-14303

Incompressible two dimensional time dependent Navier-Stokes equations for oscillating body with rectangular boundaries
[AIAA PAPER 69-185]
04 p0779 A70-15616

Non-Newtonian fluids in continuum mechanics, classical Navier-Stokes theory limitations and theory of incompressible fluids for viscometric flows
06 p1037 A70-17926

Navier-Stokes equations numerical integration in Eulerian coordinates, applying results to compressible and incompressible fluids steady flow
[AIAA PAPER 70-2]
06 p1040 A70-18113

Finite difference solution of time dependent Navier-Stokes equations for two and three dimensional laminar incompressible flow, discussing results for flat plates
[AIAA PAPER 70-46]
06 p1041 A70-18170

Transition regime gas flows using Navier-Stokes equations and boundary conditions set, considering heat transfer, torque and drag in spherical geometry
06 p1049 A70-18331

Finite difference analysis of partial differential equations derived from Navier-Stokes equations in hypersonic leading edge problem in merged gas flow-layer regime
06 p0980 A70-18349

Trailing edge region of flat plate in laminar incompressible flow examined for high Reynolds numbers limit using Navier-Stokes reduced equations
07 p1255 A70-19213

Navier-Stokes equations solved for unsteady incompressible three dimensional stagnation point flow, noting reduction to two dimensional and axisymmetric cases
07 p1188 A70-19343

Book on mathematical theory of viscous incompressible flow covering stationary and nonstationary boundary value problems for linearized and nonlinear Navier-Stokes equations
07 p1258 A70-19697

Oscillations of highly viscous incompressible fluid in partially filled cavity of body moving about fixed point, solving Navier-Stokes equations by asymptotic method
08 p1485 A70-21632

Navier-Stokes equations exact solutions for two dimensional steady flow of compressible viscous heat conducting perfect gas
08 p1485 A70-21638

Interstellar media under action of supernova or nova, solving Navier-Stokes equations of hydrogen plasma for motion during shock wave formation
08 p1580 A70-21654

Cauchy problem solution for linearized Navier-Stokes equations of incompressible rotating viscous fluid, discussing velocity and angular momentum effect on asymptotic behavior
09 p1659 A70-22326

Navier-Stokes equation for plane unsteady axisymmetric rotation of viscous fluid in steady radial flow from source or sink
09 p1660 A70-22437

Navier-Stokes equation approximation for non-homogeneous case obtained by relating Burgers equation to Riccati equation through similarity transformation
09 p1711 A70-22613

Navier-Stokes equations for laminar near wake of blunt based body, obtaining numerical solutions for adiabatic and constant wall temperatures
09 p1605 A70-23176

Shock wave structure nonequilibrium kinetic model using Boltzmann and Navier-Stokes equations
09 p1662 A70-23306

Laminar viscous flow past semiinfinite flat plate parallel to uniform stream, solving Navier-Stokes equation to determine local skin friction coefficient
09 p1663 A70-23581

Nonlinear stability problem posed by Navier-Stokes equations in case of laminar flows stability using semigroups theory
[ONERA-TP-755]
10 p1863 A70-24094

One dimensional Navier-Stokes equations solution for viscous heat conducting gas flow involving spherical sink for finite pressure at infinity
10 p1865 A70-24104

Finite difference methods stability for time dependent Navier-Stokes equations coupled to energy equation with quadratic terms in velocity gradients
10 p1866 A70-24106

Cascade theory of turbulence, applying cascade decomposition resulting from Navier-Stokes application to hydrodynamic turbulence to Riemann equation for atmospheric and plasma turbulence
10 p1868 A70-24167

Navier-Stokes solution to laminar flow past semiinfinite flat plate valid for any Reynolds number, discussing skin friction, displacement thickness, etc
10 p1869 A70-24415

Navier-Stokes-Maxwell equations solutions for conducting fluid flow in azimuthal magnetic field, noting jet acceleration near symmetry axis
10 p1924 A70-24574

Nonlinear disturbance decay in unbounded viscous fluid calculated by iterative solution of Navier-Stokes equations
10 p1871 A70-24854

Stability analysis using energy method applied to Navier-Stokes equations for unsteady viscous flow
11 p2042 A70-26849

Boundary value problem for Navier-Stokes equations to obtain stationary flows as limits of nonstationary solutions
14 p2600 A70-31347

Navier-Stokes equations derivation for multicomponent gas with internal nonrotary degrees of freedom, using moment equations
15 p2672 A70-31649

Series expansions convergence of solutions to boundary value problem for Navier-Stokes equations, introducing small parameter in boundary conditions
16 p2890 A70-33243

Exact and normal solutions of Boltzmann equation linearized around total equilibrium, yielding Navier-Stokes and Burnett transport coefficients
17 p3128 A70-34628

Turbulence theory from Liouville equation for Navier-Stokes velocity field distribution
17 p3073 A70-35629

Fluid turbulence unified heuristic model, defining determinate solutions for Navier-Stokes equations numerical integration at high Reynolds numbers
17 p3074 A70-35884

Multistage solution algorithm for solving Navier-Stokes equations stationary problem, considering plane motion of incompressible fluid
18 p3239 A70-36216

Similarity equations for rotating flow near disk, using Navier-Stokes equations for case of complicated boundary conditions
18 p3239 A70-36223

Boundary value problem for Navier-Stokes equations of viscous incompressible fluid flow, discussing convergence of iterative solution
18 p3241 A70-36290

Nonlinearized exact solution of Navier-Stokes equations for fluid motion between two coaxial circular disks rotating at equal velocity
18 p3241 A70-36381

Unsteady laminar incompressible fluid flow in parallel plate channels and circular tubes, solving Navier-Stokes equations for prescribed discharge
19 p3405 A70-38347

Round laminar jet with swirl, reducing Navier-Stokes equations to ordinary differential equations by similarity transformations
19 p3405 A70-38349

Compressible and incompressible Stokesian fluids motion described by finite element analog of Navier-Stokes equation
20 p3607 A70-38999

Unsteady flow in rectangular cavity with moving wall, using iterative solution of Navier-Stokes equations
21 p3807 A70-41317

Navier-stokes equations solutions in two way flows of Newtonian fluids with constant kinematic viscosity
21 p3810 A70-41961

Thermoelasticity theory concerning Navier-Stokes-Fourier type fluid universal motion characterization in absence of body forces and external heat supply
22 p4010 A70-42637

Navier-Stokes equations for discrete flows of viscous fluids, using grid cell representation
23 p4181 A70-44220

Channel vs deflection flow in boundary layer theory, considering Navier-Stokes equations 23 p4183 A70-44736

Incompressible laminar swirling jet flow, obtaining similarity solution for Navier-Stokes equations 23 p4184 A70-44982

Viscous heat conducting compressible fluid flow past slender axisymmetric body, presenting Navier-Stokes hypersonic strong interaction theory 24 p4289 A70-46020

Nonlinear parabolic initial value problems, including Navier-Stokes equations 24 p4370 A70-46414

NAVIGATION

NT AIR NAVIGATION

NT ALL-WEATHER AIR NAVIGATION

NT ASTRONAVIGATION

NT CELESTIAL NAVIGATION

NT DEAD RECKONING

NT DECCA NAVIGATION

NT DIGITAL NAVIGATION

NT DOPPLER NAVIGATION

NT GIMBALLLESS INERTIAL NAVIGATION

NT HYBRID NAVIGATION SYSTEMS

NT HYPERBOLIC NAVIGATION

NT INERTIAL NAVIGATION

NT INTERPLANETARY NAVIGATION

NT LORAN

NT LORAN C

NT LORAN D

NT OMEGA NAVIGATION SYSTEM

NT RADAR NAVIGATION

NT RADIO NAVIGATION

NT SPACE NAVIGATION

NT SURFACE NAVIGATION

NT TACAN

NT VHF OMNIRANGE NAVIGATION

Proportional navigation law three dimensional vectorial equation analyzed in kinematic conditions, discussing perturbation effects on linearized trajectory 09 p1720 A70-22420

Parameter estimates effectiveness from independent discrete and continuous navigation measurements of circular orbital plane 10 p1914 A70-24303

Quasi-optimum proportional navigation for attack situations with large missile and target maneuvers, showing advantage over linearized optimization 11 p2081 A70-26316

Nonlinear phase locked loops compared with linear loops in communication and navigation, considering interference vulnerability 12 p2187 A70-27909

Discrete approximation of differential game of navigation, considering control of object transfer to given set by finite time 15 p2775 A70-32472

Soviet book on complex signals in ranging, navigation and communications, discussing correlation and ambiguity functions and bandwidth effect 20 p3587 A70-39723

Position finding and navigation in space, air and sea - Conference, Hamburg, October 1969, Volume 1 21 p3847 A70-41126

Gravity error propagation in dynamic gravimetry associated with navigation and gradient measurement errors, emphasizing standard error limits in navigation data 22 p4068 A70-43660

Position finding and navigation in space, air and sea - Conference, Hamburg, October 1969, Volume 2 23 p4162 A70-44227

NAVIGATION AIDS

NT AIRPORT BEACONS

NT BEACONS

NT GYROCOMPASSES

NT LASER ALTIMETERS

NT NAVIGATION INSTRUMENTS

NT OMNIDIRECTIONAL RADIO RANGES

NT RADAR BEACONS

NT RADIO BEACONS

NT RADIO DIRECTION FINDERS

Airborne DME minimum operational characteristics for air traffic control navigation and communication systems including equipment specifications, environmental conditions, accuracy and range 01 p0138 A70-11050 [DO-141]

Computerized navigation system for controlling aircraft movement on airports under zero visibility conditions 02 p0274 A70-1978

Aircraft navigation systems performance, discussing navigation aid integration by digital management computer coupling navigation sensors to display and control devices 02 p0334 A70-11984

Airborne computer civil navigation system designed for output coordination from navigation sensors 02 p0334 A70-11986

Navigation system with twin gyro platform and Doppler sensor, discussing performance and cost advantage over inertial systems 02 p0334 A70-11987

Nonlinear gyroscopic navigation system intrinsic error derived as function of linear operator 03 p0522 A70-13373

Apollo program navigation processing using Kalman optimal linear computer, emphasizing position vector and error matrix and command and lunar landing extrapolation module navigation 03 p0522 A70-13604

Optimum estimation equations as simple averaging extension, considering application to Kalman filtering in integrated space navigation system 03 p0522 A70-13608

V/STOL Flight Profile Indicator display system development to present pilot situation information in vertical plane [SAE PAPER 690694] 05 p0792 A70-15861

Polar diagrams control for distributed radiating systems, generating localizer planes for high flying aircraft navigation aids 05 p0812 A70-16150

Onboard computer requirements for inertial navigation of spinning and maneuvering vehicle, determining design parameters [AIAA PAPER 68-839] 06 p1013 A70-17161

Commercial navigation systems for long range subsonic transports, discussing accuracy, avionics hardware and crew responsibility optimization 06 p1102 A70-17638

Optimal timing of measurements to minimize dispersion of navigational observation parameters by least squares method applied to Keplerian orbit elements 06 p1103 A70-17878

Solid state VHF omnirange navigation system operation, principle, equipment, applications, advantages, etc 07 p1241 A70-19622

Navigational techniques - NATO/AGARD Conference, Milan, September 1967 09 p1721 A70-23026

Long range navigational aids requirements for airlines, discussing self contained navigation systems capabilities 09 p1722 A70-23028

Hybrid long range en route navigation system extended to short range role meeting ATC and terrain problems 09 p1722 A70-23032

Doppler VOR offering increased course accuracy and allowing precise area coverage in conjunction with DME ground station 09 p1723 A70-23036

Sequential collation of range /SECOR/ satellite tracking system using electronic phase comparison for measuring ground station-satellite distance 09 p1724 A70-23047

NASA Geodetic Satellite Program applications to long range navigation, spacecraft orbit prediction, navigation experiments calibration, etc 09 p1724 A70-23048

French geodetic satellites Diademe I and II experiments in navigation, noting laser and Doppler devices 09 p1725 A70-23049

Harrier navigation/attack system to provide successful single pass attack for close support and strike roles, noting target finding optimization 10 p1914 A70-24847

Inertial navigation systems, describing platform servos, computer, measurement devices, etc 10 p1914 A70-24861

North-finding gyroscope applicability for directional gyros and stabilized platforms 10 p1891 A70-24865

Area navigation system advantages for pilots, flight control systems and improved accuracy through rejection of VOR course scalloping [SAE PAPER 700214] 11 p2079 A70-25885

Soviet book on air navigation covering position determination methods, wind measurement, equipment design and use, etc 12 p2266 A70-26875

Area navigation for reducing cockpit navigation workload, permitting aircraft operations on desired course and enhancing pilot response to ATC instructions [SAE PAPER 700283] 12 p2266 A70-27426

Airborne computer design for short range attack missile /SRAM/ to perform aircraft navigation and missile fire control 12 p2192 A70-27800

Course deviation indicator /CDI/ display applicability to tracking Omega lines of position, providing reduction in weight, volume, cost and complexity 12 p2269 A70-27920

Spacecraft based data processing stages to perform navigation during outer planet missions 13 p2448 A70-28704

Soviet book on theory and practice of maps application in aviation, covering coordinates for objects positions determination on ground error estimation, etc 13 p2448 A70-28725

Meteorological data acquisition by navigational aids, satellites and surface based indirect sensors for computer forecasting 13 p2405 A70-28773

Pictorial display area navigation system for air traffic control in terms of cockpit utilization, interface with ground navigation aids, parallel multiple routes, etc [AIAA PAPER 69-798] 13 p2449 A70-29171

Low cost VHF and UHF navigation aids IFR procedures for low density airports [SAE PAPER 700230] 13 p2385 A70-29607

Gyroscopic navigation systems errors as function of sensor errors in terms of arbitrary operators requiring optimization 15 p2773 A70-32155

Airborne pulse Doppler radar for tactical aircraft velocity vector measurement, improving navigation system performance 16 p2840 A70-33448

Fifty percent coverage problem /Circular Error Probable/ of general bivariate Gaussian distribution from viewpoint of navigation systems error analysis 16 p2948 A70-33451

Blinking warning lights for air navigation, signaling of obstacles and glider onboard marker lights 16 p2889 A70-34302

Air traffic control, discussing precision instrument landing, approach lighting, collision avoidance, navigation aids, etc 17 p3133 A70-35185

Navigation aids evolution and trends, noting ground stations, Intelsat 3 and navigation satellites 17 p3048 A70-35879

STOL navigation systems, evaluating Vector Analog Computer, Decca Omnitrac IIB and inertial system 18 p3289 A70-36513

SATRAM, multiple trajectory landing system for aircraft position indication within large airspace 18 p3289 A70-36948

Area navigation system charting, discussing effect on flight information publications 19 p3465 A70-38231

Pictorial display methods for pilot error reduction in area navigation via guidance control and capability beyond visual field 19 p3465 A70-38234

Eurocontrol evaluation of navigational aid systems air traffic control, examining HARCO and VORDAC systems 19 p3468 A70-38641

Aircraft navigation light visibility, discussing visual threshold, source intensity, atmospheric transmissivity, color, background luminance, etc 20 p3564 A70-39719

Apollo program navigation processing using Kalman optimal linear computer, emphasizing position vector and error matrix and command and lunar landing extrapolation module navigation 21 p3848 A70-41127

Integrated air navigation by least square adjustment, analyzing Doppler navigation errors 22 p4067 A70-42655

Kalman filters for data mixing in optimally aided inertial navigation systems 22 p4067 A70-42661

Automatic ship navigation system using Transit satellites and onboard digital computer for routine tasks of dead reckoning 22 p4068 A70-42666

NAVIGATION INSTRUMENTS

NT GYROCOMPASSES

Two axis spherical gage bearing gyro for accurate measurements of space vehicle position and attitude rates while maintaining compatibility with exotic environments 01 p0086 A70-10308

Inertial navigation systems, discussing role as flight control sensor with advent of all digital interface automatic flight control systems and cost and reliability 02 p0334 A70-11988

Lateral separations using navigation error analysis, showing values for aircraft with or without Discreurs and inertial control under North Atlantic conditions 02 p0336 A70-12607

Readjustment of aircraft navigation systems based on inertial platforms, discussing errors, corrections and damping stressing single platform 02 p0336 A70-12608

Self contained and ground referenced radio systems combination for tactical air navigation, including Loran D and hybrid Loran /HYLO/ 04 p0716 A70-14628

Tacan navigation system developments for accuracy and reliability improvements, data transmission, tie-in with airborne computers, etc 07 p1331 A70-19621

Solid state VHF omnirange navigation system operation, principle, equipment, applications, advantages, etc 07 p1241 A70-19622

Apollo space vehicles guidance and navigation using data obtained onboard, discussing inertial platforms, accelerometers and trajectory calculations 08 p1541 A70-21023

Sector Tactical Air Navigation System to supply on-board information on bearings, slant range and elevation and computer input signals
09 p1720 A70-22491

Doppler radar aircraft navigation system with gyroscopic reference platform and computer, showing error propagation dependence on velocity and latitude
13 p2449 A70-29621

Operational and environmental factors constraining onboard navigation system design for outer planet flyby missions
14 p2614 A70-30467

Apollo navigation methods and data analysis covering inertial guidance with gyro-stabilized platforms, acceleration sensors, sextants and telescopes, ergodicity, filtering, etc
15 p2772 A70-31549

Tactical aircraft performance, discussing electro-optical devices, weaponry, communication and navigational networks, information displays and real time remotely manned control systems
17 p3013 A70-34672

Loran C principles, ground station operation and navigation equipment
17 p3135 A70-35881

Manned lunar roving vehicle (MLRV) navigation scheme based on dead reckoning concept, discussing instruments effectiveness for vehicle velocity and orientation measurements
19 p3396 A70-37849

Military Airlift Command jet aircraft computerized area navigation system operational procedures
19 p3465 A70-38232

Airborne navigation systems operational aspects in ATC, discussing sensors, digital computer, cockpit displays, etc
19 p3468 A70-38640

Navigation errors and time delays in prediction techniques for air traffic control
19 p3468 A70-38642

Navigation instrument geometrical calibration by natural satellites and reference stars during interplanetary flight
[AIAA PAPER 70-1023] 20 p3669 A70-39586

Spacecraft-based navigation instruments for outer planet missions using celestial directions to outer planet natural satellites
[AIAA PAPER 69-902] 20 p3669 A70-39681

Aircraft navigation control system by digital computer combined with inertial platform, considering emergency backup, slow drift and system malfunctions
24 p4374 A70-46092

NAVIGATION SATELLITES
NT EXPLORER 22 SATELLITE
NT TRANSIT SATELLITES

Aeronautical satellites for monitoring positions of many commercial aircraft simultaneously crossing North Atlantic, discussing navigational error correction and atmospheres
01 p0178 A70-10454

Continuous and pulsed parameter stabilization for circular orbits of navigation and communication satellites under perturbing effects of oblateness and atmospheric drag
02 p0374 A70-12402

Earth space signal propagation characteristics obtained by satellite-borne radio interferometer provide phase information in addition to amplitude for improving navigation accuracy
02 p0260 A70-12567

Airplane navigation based on VHF ranging between aircraft and geostationary satellite, examining errors by unknown propagation characteristics of signal in ionosphere
02 p0262 A70-12594

Aeronautical satellite system for civil flight safety, discussing operational, technical and economic aspects
03 p0522 A70-13610

Navy navigation satellite passes predicted by equations for rise and set times, elevation and azimuth in plane circular polar orbit about spherical earth
04 p0764 A70-15431

Aeronautical satellites application to supersonic air transportation economy, discussing navigational information relay between aircraft and control center
07 p1191 A70-18988

Book on navigation and communication satellites for military uses, considering design, operation, computers role, etc
08 p1582 A70-21298

Satellite potential for long range air traffic control, discussing airline navigation requirements and ATC requirements for position determination
09 p1722 A70-23027

Navy Navigation Satellite System program development and present status, discussing satellite design and system accuracy-geodesy connection
09 p1723 A70-23039

Aeronautical satellite system for North Atlantic air traffic position monitoring, discussing simultaneous position display
09 p1723 A70-23040

SPOT navigation satellite system for near instantaneous fixes or continuous tracks providing height, velocity and automatic guidance and control signals
09 p1723 A70-23041

Navigation satellite system with 10-meter accuracy, continuous coverage, rapid position determination, simultaneous service and interference immunity achieved by synchronous satellites
09 p1723 A70-23042

VHF aerosat antenna design and system interactions, analyzing impact of spacecraft dynamics, control system, power supply and propulsion
[AIAA PAPER 70-486] 11 p2120 A70-25439

Navigation-traffic control satellite system application to transoceanic traffic surveillance
[AIAA PAPER 70-487] 11 p2000 A70-25462

Satellite Integrated Communications, Navigation and Identification System for implementing worldwide command-control system and equipment and signal integration
[AIAA PAPER 70-503] 11 p2000 A70-25466

Navigation satellite communication experimental design emphasizing mobile, ship or aircraft station technical characteristics
[AIAA PAPER 70-407] 11 p2001 A70-25469

Air traffic control surveillance and data system using synchronous satellites in inclined elliptical orbits for communications and aircraft position determination
12 p2268 A70-27644

North Atlantic air traffic control system using aeronautical satellites, discussing flight levels, surveillance and positioning, terminals, etc
12 p2268 A70-27645

Low altitude satellite system for aircraft navigation, considering cost factors, military applications, traffic control capabilities, etc
12 p2270 A70-27922

Midaltitude satellite system for continuous three dimensional navigation, considering elevation angles, constellations and orbits
12 p2270 A70-27923

Navigation systems using 24-hour orbit satellites, discussing system concept options for U.S., Western Hemisphere and global coverage
12 p2270 A70-27924

Hard wired modular multipurpose global navigation system using cluster noncoplanar synchronous satellites
13 p2446 A70-28385

Low altitude operational meteorological and navigation spacecraft, discussing need for orbit adjustment by dynamic control
13 p2500 A70-28404

Navigation satellite systems, analyzing error sources in signal processing and propagation developing computer programs
13 p2447 A70-28429

Aircraft and ship navigation using precision time measurement signals transmitted between vehicles and earth satellites
13 p2448 A70-28748

Synchronous navigation satellite system for ships and aircraft applicable to earth orbital and lunar operations
14 p2614 A70-30463

Satellite communication/navigation/surveillance systems for domestic and transoceanic ATC
16 p2949 A70-33479

Aircraft/ship navigation system using three synchronous satellites positioned over equator for Pacific applications
17 p3134 A70-35302

Navigation aids evolution and trends, noting ground stations, Intelsat 3 and navigation satellites
17 p3048 A70-35879

Ground and cockpit initiated collision avoidance commands system based on satellites surveillance of aircraft position and velocity data
19 p3466 A70-38242

Telecommunication, ATC and navigation satellite systems, examining economic bases for aeronautical and maritime space systems
20 p3740 A70-39407

Optimum altitudes for passive ranging satellite navigation systems, using electronic clocks in satellite and navigator receiver
21 p3883 A70-40724

Sea and air navigation in U.S. with satellites, considering cost estimates
21 p3848 A70-41130

Aeronautical satellite system for civil flight safety, discussing operational, technical and economic aspects
21 p3848 A70-41131

Global digital navigation and traffic control system via satellites, discussing position determination, surveillance and communication requirements
21 p3848 A70-41133

Diocures project for ATC over Atlantic Ocean, describing distance measurement by simultaneous use of two geostationary satellites
21 p3848 A70-41258

Air navigation Diocures project satellites, discussing spin or three axis stabilization, system replenishment strategies and subsystem reliability
21 p3929 A70-41259

Air traffic safety problems, discussing satellite radiobeacons applications to aerial navigation
22 p4066 A70-42652

Position experiments for navigation satellite system parameters determination, using satellite ATS-3 distance measurements
22 p4066 A70-42653

Radio navigation system using multiple satellite beacons (NAVSTAR) for large area air and sea coverage
22 p4067 A70-42662

Position fixing by distance measuring to geostationary satellites, discussing ATS-3 and ship experiment accuracy and orbit interference
23 p4215 A70-44232

Worldwide common satellite network for sea and air navigation, discussing cost estimate and economics
23 p4216 A70-44608

Satellite technology applications to ATC, including communications, navigation, surveillance over water and data acquisition
[AIAA PAPER 70-1301] 24 p4373 A70-45922

Satellite based navigation/air traffic control information systems for short range STOL air carrier aircraft
[AIAA PAPER 70-1338] 24 p4373 A70-45930

Position experiments for navigation satellite parameters system using ATS-3 distance measurements
24 p4374 A70-46201

NAVIGATORS
Soviet book on air navigation covering civil navigator training, geographic concepts, navigation means, flight and meteorological conditions, instrument errors, etc
06 p1103 A70-17642

NAVY
Material Acquisition Division of Naval Air Systems Command, discussing engineering and testing functions in providing air weapons systems to operating forces
06 p1185 A70-17973

Oxygen equipment design for USN patrol and attack aircraft, considering masks, regulators, helmets and hoses
07 p1191 A70-19005

Fatal ejections in USN, suggesting initiation delay as prime causal factor
07 p1191 A70-19006

Fire resistant protective flight clothing program for USN aircrewmembers, presenting accident case histories
07 p1218 A70-19013

Navy Navigation Satellite System program development and present status, discussing satellite design and system accuracy-geodesy connection
09 p1723 A70-23039

Predicting retention rate of naval pilots and flight officers beyond initial obligated duty tour based on training performance
15 p2690 A70-31888

NEAR INFRARED RADIATION
Atlas of near IR spectra of Venus, Mars, Jupiter and Saturn obtained by Fourier spectroscopy, discussing observational procedures, data recording and processing
01 p0173 A70-10078

Jupiter and Saturn near IR spectra for relative abundances of atmospheric constituents and distribution with altitude, noting rough solar composition
01 p0179 A70-10526

Near IR reflection spectra of artificial cumulus clouds with progressive droplet sizes
01 p0076 A70-10911

Angular distribution measurements of visible and near IR radiation reflected from carbon dioxide cryodeposits formed on liquid nitrogen cooled surface in vacuum
[AIAA PAPER 69-63] 04 p0720 A70-15538

Dispersive resonator for near IR frequency control of neodymium-silicate glass laser
08 p1512 A70-20850

Noncontact thermometer designed around YIG modulator to demonstrate usefulness of optical component in near IR systems
09 p1676 A70-22788

High resolution Fourier interference near IR spectrometer for aircraft, balloon and spacecraft remote sensing applications
09 p1683 A70-23508

Water depth determination by remote measurement of near IR reflectance of underwater plants, discussing effects of water path length changes
10 p1878 A70-24741

Near IR radiation diurnal variations in corn canopy accounted for by Duntley equations for unidirectionally incident light propagation through diffusing medium
11 p2082 A70-25364

Terrestrial clouds near IR light scattering compared to reflectivity of water and ice particles, discussing Mie and multiple scattering 11 p2045 A70-25649

Star HBV 475 emission spectra in near IR due to H, He I, OI and Ca II, confirming symbiotic character 13 p2495 A70-29641

Reflectivity measurement in near IR using black bodies near room temperature for light sources 14 p2588 A70-31210

Lasers and GaAs diode emitters near IR radiation intensity distributions, using IR films and IR display phosphors 15 p2753 A70-32607

Broadband image pick-up tube with high near IR sensitivity, comparing performance with other vidicons 16 p2907 A70-33186

Near IR electronic emission spectrum of positive column in flowing oxygen electric discharge, noting vibrational temperature 16 p2955 A70-33981

Airborne illumination using argon vortex-stabilized arc lamp, noting applicability in near IR spectral range 17 p3023 A70-35152

Semiconductor luminescence and photodetector diodes near IR region transmission, describing frequency response measurements 22 p4087 A70-43445

NEAR ULTRAVIOLET RADIATION

Nimbus 3 satellite observations of near UV solar flux intensity and variability, describing instrumentation and measurement of radiation producing molecular oxygen photodissociation 02 p0291 A70-12295

Stratospheric balloon measurement of near UV from early type stars, discussing gondola, observation method, telescope and photographic recordings analysis 04 p0750 A70-14704

Stellar observations in near UV by camera having two color photometric slides, discussing atmospheric models 13 p2498 A70-30013

Spectral classification of relatively bright stars in near UV based on moderate and low dispersion spectra including F, G and K stars 15 p2797 A70-31614

Spectral classification and continuous spectrum photometry of weak late stars in visual and near UV regions, noting anomalous C star in CH Cyg 15 p2797 A70-31615

NEBULAE

NT CASSIOPEIA A

NT CRAB NEBULA

NT PLANETARY NEBULAE

Stellar emission line spectra from comet-like nebulae, discussing stellar position instability and shell movements 01 p0174 A70-10198

Nebular variables and flare stars in Orion aggregate 03 p0567 A70-13319

H alpha line for emission nebulae analyzed by Fabry-Perot etalon, noting Doppler profile 05 p0917 A70-16907

Nonstellar 5 micron source in Orion nebula, noting intensity nonvariance and energy distribution calculation of temperature 08 p1575 A70-21375

Internal radial velocities of diffuse emission nebulae in H II region, using photographic Fabry-Perot interferometer 08 p1581 A70-21952

Bright rims in North America Nebula, measuring electron temperature to derive profile characteristics 10 p1944 A70-24956

Orion Nebula region search, giving characteristics and locations of flare type variable stars 10 p1949 A70-25249

Stars of galactic nebulae - Conference, Biurakan, Armenian SSR, September 1968 12 p2304 A70-27851

Comet-like nebulae, describing brightness and spectral characteristics of variable stars in nebulae 12 p2307 A70-27863

Stellar and nebular magnetic fields formation, considering role of high temperature plasma random charge and current fluctuations 12 p2307 A70-27864

Merope /IC 349/ nebula, noting luminescence and continuous spectrum fine structure 12 p2307 A70-27867

Forbidden Ne iv lines intensity in high excitation gaseous nebulae based on upper level-j populations 12 p2277 A70-28215

Galactic continuum surveys at 8000 MHz by radio telescope, noting North American nebula and Cyg X region 13 p2491 A70-29096

Gaseous nebulae electron densities based on interpretation of forbidden CI III lines using collisional strengths and transition probabilities 15 p2798 A70-31746

Cygnus loop nebula H alpha line halfwidths and radial velocities 15 p2802 A70-32482

Orion Nebula photographed at H alpha line with half angstrom filter 15 p2807 A70-32805

Wolf-Rayet associated nebulae, presenting radio observations and mass determinations 16 p2980 A70-34193

Luminous nebulae near Sco X-1 indicating H beta emission 17 p3156 A70-34829

Lyman alpha radiation from gaseous hydrogen nebula model, taking into account absorption by dust and interstellar neutral hydrogen 17 p3163 A70-34904

Orion nebula core radio recombination line intensities, showing variations in mean electron temperatures and physical conditions 18 p3313 A70-36329

Nebula K3-50 IR radiation source observation, noting energy distribution resembling NGC 7027 and W51-IRS2 20 p3701 A70-39003

Carina nebula NGC 3372 continuum map at 5 GHz compared to optical photographs, discussing H alpha lines 21 p3887 A70-41109

Reflection nebulae dust density, noting lower limit dependence on absolute magnitude of illuminating star 21 p3889 A70-41149

Preferential galactic orientation based on inclination statistics of predominantly elliptical clustered nebula 22 p4099 A70-42627

Orion nebula H alpha/forbidden N II ratio measurement using wide field multislit spectrograph 22 p4101 A70-42857

B-V and U-B colors and B and V polarization calculation in single scattering for slab model reflection nebulae with dielectric or graphite grains 22 p4103 A70-42984

Electron impact induced transitions in ions with configurations 3p/q responsible for forbidden lines in gaseous nebulae 22 p4105 A70-43234

Solar nebula rings and planet formation by sedimentation of solid particles in mechanical equilibrium, including Jupiter and Saturn protoplanets 23 p4239 A70-43867

H II region dust grains thermal emission, examining effect on diffuse nebulae 24 p4413 A70-46158

NEEDLE BEARINGS

Load rating methods for cage-type and full complement needle bearings dynamic capacity [ASLE PREPRINT 70AM 3D-2] 19 p3438 A70-38802

NEEL TEMPERATURE

Shift in nuclear paramagnetic resonance frequency of ligand nuclei in ferromagnets above Neel temperature 10 p1928 A70-24826

Shift in nuclear magnetic resonance, investigating transferred hyperfine coupling near Neel temperature for magnetic and nonmagnetic systems 10 p1928 A70-24827

Magnetic phase diagram of hydrated cesium-copper carbide at 1.625 Neel temperature in external magnetic fields, giving equation for spin flop field temperature dependence 16 p2961 A70-33688

Neel temperature of thermally stable garnet orthoferrites of YFeAlMn composition 19 p3484 A70-37623

NEGATIVE CONDUCTANCE

Negative resistance mechanism model with larger electron accumulation in conduction band than free holes 03 p0539 A70-13212

GaAs nonlinear I-V characteristics and negative differential conductivity associated with electron heating by electric field 03 p0540 A70-13720

Semiconductor electronic devices applications in microelectronics, optical/dielectric electronics and photography and electron-acoustical phenomena and negative differential conductivity 05 p0822 A70-16863

Semiinsulating GaAs doped with Cr, discussing negative resistance segment in current-voltage curves of S diodes 07 p1242 A70-19798

Negative differential conductivity effects in Gunn domain GaAs semiconductors, discussing physical properties and microwave applications 08 p1556 A70-21303

Parallel and perpendicular negative magnetoresistance measurements as function of magnetic field in p-type GaAs at 77 K 13 p2471 A70-29374

He-Ne laser focused beam effect on negative Si diodes base I-V characteristics 13 p2378 A70-29517

Microwave avalanche diode emission frequency dependence on charge transfer across drift region, considering varactor diode output, negative resistance and noise factor 14 p2555 A70-30354

Gunn oscillator external negative differential /END/ conductance broadband measurement noting effect of cavity control 16 p2875 A70-33398

Frequency dependence of Gunn oscillator maximum negative conductance 23 p4172 A70-44198

NEGATIVE FEEDBACK

NT SENSORY FEEDBACK

Differential equations of optimal degenerate problem reduced to autonomous form with multiple control, noting D-stationarity application for optimal motions 01 p0053 A70-11022

Respiratory center functional organization established as automatism with negative feedback, based on experimental data of dogs and cats artificial respiration and hypocapnic apnea 03 p0417 A70-13069

Response characteristics of negative feedback galvanometer amplifier with inductive source impedance for geomagnetic micropulsation detection 07 p1242 A70-19998

Transient response analysis of nanosecond pulsed transistor amplifier having common-emitter configuration with negative feedback 08 p1474 A70-21229

Ruby laser spatial and temporal characteristics improvement with bleachable dye filter, using local negative feedback 15 p2754 A70-32865

Voltage-to-frequency transducers with negative feedback, analyzing errors and conversion transconductance 20 p3601 A70-39789

NEGATIVE RESISTANCE CIRCUITS

Rotator and symmetrizer negative resistance circuits application in electronic function generator 05 p0824 A70-15991

Instability of semiconductor circuit with nonlinear current-voltage characteristics, showing potential negative differential conductivity effect 07 p1240 A70-19274

Terminal negative resistance of X band Gunn diodes, discussing frequency conditions for modulation and parametric amplification 16 p2877 A70-33417

Microwave oscillator design using Y-parameters from measured scattering parameter data at desired frequencies, applying negative resistance circuit theory 24 p4320 A70-46235

Multivibrator designs incorporating distributed R-C-NR thin film structures 24 p4321 A70-46395

Multivibrators with improved stability and frequency-division capacity, using distributed R-C-NR structures 24 p4321 A70-46396

NEGATIVE RESISTANCE DEVICES

Negative resistance light emitting lateral GaAs diode, analyzing oscillation frequency, I-V characteristics, temperature and magnetic effects 01 p0050 A70-10565

Frequency dependent negative resistance of n-type semiconductor doped at acceptor level near valence band top 10 p1927 A70-24273

Negative resistance and cut-off voltage of doped Si p-i-n diodes subject to deep acceptor levels 10 p1849 A70-24274

Avalanche diodes microwave properties in utilization circuit, discussing negative conductance, nonlinear impedance and intrinsic noise current 10 p1850 A70-24623

Phase control of locked negative resistance /Gunn/ oscillator under operational conditions, noting coupled varactor diode use 17 p3055 A70-35630

Bulk negative resistance microwave oscillators efficiency calculation by graphical method 17 p3056 A70-35876

Negative resistance and conductivity segments in I-V curves of diode structures, taking into account injection junction imperfections 18 p3231 A70-36413

Carbon resistors negative magnetoresistance measurement near absolute zero temperature by helium cryostat, noting anisotropy 20 p3687 A70-40168

Wave instabilities in avalanche diode bulk semiconductors with negative field dependent drift velocity and carrier temperature, noting validity for gas plasma 21 p3863 A70-41915

Microwave output power and impedance for InP and GaAs bulk negative resistance oscillators, using velocity/field characteristics 21 p3800 A70-42049

NEGATRONS

Thermally induced oscillations and negative resistance in seminsulating oxygen-doped GaAs double injection devices via heating beyond critical temperature

22 p4084 A70-42326

Current-controlled negative resistance and conductivity memory state in Si-doped single crystal YIG wafers

22 p4085 A70-42331

Current twisting in double injection ohmic contact long p-n diodes with S-shaped current-voltage curve, showing unstable density at negative resistance segment

23 p4176 A70-45061

High cutoff negative resistance silicon carbide diodes, noting temperature independent current-voltage curve

23 p4176 A70-45067

NEGATRONS

Cosmic ray positrons and negatrons differential energy spectra and solar modulation, using balloon-borne magnetic spectrometer

19 p3503 A70-38100

Energy spectrum of primary cosmic ray electrons /negatron and positron/ in interstellar region observed near 1965 solar minimum

19 p3503 A70-38101

Cosmic ray positrons and negatrons differential intensities near north geomagnetic pole from balloon flight measurements, noting solar modulation effects

19 p3503 A70-38102

NEODYMIUM

Reduced Nd ion absorption in matrices of fluorides, fluoride mixtures or oxygen-containing compounds with various ion concentrations, analyzing optical centers statistical properties

01 p0107 A70-10210

Oscillation and doubling of 0.946 micron line in Nd ion doped YAG, calculating optimum nonlinear coupling to internal Q switched laser

01 p0113 A70-11169

Amplification cross section of 1.06 micron transition of trivalent Nd ion in alkaline silicate glass host material, based on three level energy level diagram

02 p0312 A70-12111

Laser gain investigated for amplifications of short emission pulses in neodymium glass, discussing line broadening nonuniform mechanism

04 p0702 A70-15226

Nd glass laser emission spectral width reproducibility as function of flash intervals and pump energy

07 p1297 A70-18869

Neodymium-yttrium fluoride crystal laser free and Q switched operating characteristics

08 p1511 A70-20523

Neodymium laser frequency doubling based on nonlinear functional relation between polarization and electric vector in matter

08 p1512 A70-20677

Holographic recording of Q switched neodymium laser beam achieved through lens testing on reconstructed beam

09 p1697 A70-22845

Neodymium/YAG laser emission characteristics, studying spectral selection at various excitation energy levels and output-pumping power relationship

10 p1899 A70-24261

Neodymium spectral line widths in various glasses, studying role of inhomogeneous broadening

10 p1900 A70-24266

Thermo-optical constant of laser neodymium glasses measured with interferometer

13 p2430 A70-29761

Temporal structure and spectral evolution of Nd laser emission with self locking axial modes, noting gain saturation effects

13 p2430 A70-29776

Lasing characteristics of Nd glass, measuring efficiency, pump threshold energy and absorption under test conditions instability

13 p2431 A70-29873

Optical resonator thermal deformations during pumping of circular cylindrical interferometer rods in illuminators, measuring thermo-optical constants of neodymium glass

15 p2754 A70-32863

Crystal and glass lasers activated by Nd ions, examining stimulated emission temperature dependence by high temperature spectroscopy

17 p3106 A70-35105

Energy levels and spectral broadening of neodymium ions in laser glass from fluorescence and absorption spectra

19 p3445 A70-37760

Giant pulse neodymium glass laser emission spectrum structure, showing cavity geometry effect on fine structure

20 p3641 A70-39450

YAG-Nd laser volume limits condition for high power fundamental mode operation

21 p3836 A70-40808

Laser characteristics of Nd doped lithium germanate and silicate glasses, discussing spectroscopic properties

21 p3838 A70-42010

Giant pulses by actively and passively Q-switched inorganic neodymium-liquid lasers with varying modulation due to mode coupling

23 p4202 A70-44937

NEODYMIUM ALLOYS

Phase diagram of Nd-Rh system determined by powder X ray diffraction, metallography and differential thermal analysis methods

08 p1522 A70-21711

NEODYMIUM COMPOUNDS

Inorganic liquid lasers, discussing Nd salts solution preparation and handling methods

23 p4201 A70-44929

NEON

NT NEON ISOTOPES

Electron temperature dependence of molecular neon ions recombination with electrons using microwave afterglow/mass spectrometer, obtaining recombination coefficient

05 p0885 A70-16468

Neutral Ne emission line in visible solar spectrum during bright events in inner corona, noting 1958 outburst of RS Oph

05 p0920 A70-16944

Inelastic scattering of He ions by Ne as function of angle, initial energy and energy loss using collision spectroscopy

07 p1346 A70-20243

Line strength and radiative lifetimes for Ne II determined from spontaneous emission data obtained from CW neon laser discharge

09 p1730 A70-22070

Acoustic perturbations in stationary weakly ionized pulsed neon plasma

11 p2096 A70-26842

Forbidden Ne iv lines intensity in high excitation gaseous nebulae based on upper level-j populations

12 p2277 A70-28215

Stepwise ionization effect on electron distribution, transport and balance coefficients in low voltage low pressure neon plasma

19 p3476 A70-37555

Transition probabilities of visible and near-IR neon lines, using gas-driven shock tube spectroscopy

20 p3674 A70-39134

Gaseous neon plasma positive column electrons density and drift velocities measurements by Langmuir probe technique

20 p3683 A70-40163

Methane IR filter for monochromatizing He-Ne laser

21 p3823 A70-40823

Optimum tube diameter for maximum radiation output of single and multimode He-Ne lasers

21 p3836 A70-40916

He-Ne gas laser, construction, operation and characteristic mode patterns

22 p4049 A70-42959

NEON ISOTOPES

Elastic and inelastic scattering of proton beam from Ne 20 measured for cross sections to interpret polarization data

04 p0723 A70-15636

Carbonaceous chondrites primordial He and Ne isotopes variations

07 p1388 A70-20037

Induced nuclear processes role in radiogenic Ne-21 production in earth atmosphere

12 p2227 A70-28367

Coupled channel calculation of inelastic proton scattering from Ne 20 using Hartree-Fock wave functions

17 p3137 A70-34517

NEON 19

U NEON ISOTOPES

NEOPENTANE

Initial pyrolysis kinetics of neopentane, showing decomposition rate tendency to equal formation rate at high temperature

01 p0215 A70-10706

Acetone formation mechanisms during neopentane oxidation when added to slowly reacting molecular hydrogen and oxygen

11 p1995 A70-26379

NEOPLASMS

NT CANCER

NEOPRENES

U CHLOROPRENE RESINS

NEPHELOMETERS

Prototype cloud physics laser nephelometer design and performance, determining droplet concentration and size from scattered light pulse count and amplitudes

20 p3626 A70-39081

NEPTUNE (PLANET)

Rotation, diameter, mass, atmosphere and constitution of planet Neptune, with emphasis on visual observations

05 p0913 A70-16552

Meridian circle observations before and after occultation of ZC 2232 by Neptune on 7 April 1968, correcting ephemeris for star and Neptune

06 p1151 A70-18489

Neptune and Pluto oblateness inferred from analogous similarities of mass, diameter and mean density with Uranus and Mars planets

09 p1750 A70-22096

Gravitational disturbance by exterior planets, considering Brown transformation of longitudinal perturbation problem in relation to planet Neptune discovery

11 p2117 A70-26658

Neptune data from photoelectric observations of 7 April 1968 occultation of BD-17 deg 4388, determining hydrogen dominance and molecular density

14 p2642 A70-30890

Neptune position errors by meridian observations compared with photoelectric observation of stellar occultation

19 p3518 A70-38008

Neptune orbit residual, discussing recently discarded Lalande prediscovers

21 p3922 A70-41986

Travel time for trips to Neptune, calculating earth gravitational field escape hyperbola and waiting time before return

23 p4245 A70-44653

Uranus and Neptune millimeter wave observations, showing brightness temperatures in excess of black body equilibrium temperatures derived from solar heating

24 p4403 A70-45398

NERVA [ENGINE]

U NUCLEAR ENGINE FOR ROCKET VEHICLES

NERVES

Simulated responses of depressed and hyperpolarized single-modulated nerve fibers, using Frankenhaeuser-Huxley equations

02 p0231 A70-11706

Time course of end bulb material formation in vitro in rodent myelinated nerve fibers, confirming elastic capillary concept

02 p0233 A70-11725

Electrical polarization effects on discharges in individual auditory nerve fibers following current application to cochlear partition

17 p3033 A70-35609

Continuous functions transformation by artificial neuron networks, investigating electrophysiological data for nerve tissues excitability

18 p3223 A70-36081

Vagus nerve blockage effect on arterial carbon dioxide tension and breathing regulation in dogs

24 p4303 A70-46112

NERVOUS SYSTEM

NT AFFERENT NERVOUS SYSTEMS

NT AUTONOMIC NERVOUS SYSTEM

NT AXONS

NT BRAIN

NT BRAIN STEM

NT CENTRAL NERVOUS SYSTEM

NT CEREBELLUM

NT CEREBRAL CORTEX

NT CEREBRUM

NT DIENCEPHALON

NT EFFERENT NERVOUS SYSTEMS

NT GANGLIA

NT HIPPOCAMPUS

NT MYELIN

NT NERVES

NT NEURONS

NT PERIPHERAL NERVOUS SYSTEM

NT SPINAL CORD

NT SPINE

NT SYMPATHETIC NERVOUS SYSTEM

NT SYNAPSES

NT THALAMUS

Posture and motion control for functional organizations of nervous systems, emphasizing reflexes and relation between suprasegmental structures and controlling organs

01 p0017 A70-10499

Electrochemical mechanisms of nervous tension generation and expansion based on neural impulse expansion theory, noting ion transport

01 p0020 A70-10518

Corticovisceral interrelations concept, summarizing contributions in form of diagram showing interactions between cortical and nervous activity of organs

01 p0029 A70-11463

Vasomotor activity of neurons located in spinal cord lateral crescent in curarized decerebrated and intact cats

01 p0030 A70-11471

Phasic phrenic nerve electrical activity relation to systemic blood pressure oscillations produced in paralyzed dogs by ventilation arrest or hemorrhage

03 p0416 A70-13010

Degenerate retinal fibers in duck photoreceptor path connecting to supraoptical hypothalamic region detected following optic nerve dissection

03 p0427 A70-13955

Nervous system influence on erythema radiation reactions from soft X ray irradiation, discussing blood supply effect

06 p0993 A70-17430

Vasomotor center neuron responses to vertical rocking movement stimulus of vestibular apparatus in cats

06 p0995 A70-17805

Hypothermia effect at various temperatures and durations on nervous activity and vegetative functions of rats, discussing pulse and respiratory rates
07 p1197 A70-18696

Ciliary nerve stimulation and lens motion data to identify open-loop plant dynamics of lens accommodation
07 p1216 A70-18858

Gamma radiation effects on higher mammals nerve activity after chronic total body exposure
09 p1619 A70-22790

Soviet book on nervous stress and cardiac activity covering hypothalamus and cardiovascular reactions and cardiac component of complex conditioned reflexes and emotional reactions
10 p1809 A70-23873

Human nerve and muscle system changes under prolonged hypodynamia
10 p1815 A70-24681

Hypodynamia aftereffects on nervous system, investigating organic microsymptoms, asthenia, vegetative-vascular instability and skin muscle akinetic hypotrophy
10 p1825 A70-24691

Pattern recognition with time interval modulation information coding (TIMIC), considering channel capacity of switching device, similarity with nervous system, etc
11 p2010 A70-26267

Short duration high workload effects in pilot rr interval and finger tremor during Boeing 747 aircraft let-down, approach and landing
11 p1993 A70-26521

Hippocampus nerve cells protein fractions synthesis in rats, noting relation to learning process during transfer of handedness
12 p2172 A70-28217

Nervous system response fluctuation measurement during perceptual and learning tasks in terms of signal to noise ratio of electrical and tactile stimuli
13 p2354 A70-29595

Speech signals reflection in nervous system, constructing functional perception model for signals conversion into phonetic patterns
15 p2687 A70-32870

Soviet book on peripheral vestibular apparatus and higher nervous system roles in motion sickness covering Coriolis acceleration tests, pilot training and selection, drugs, etc
19 p3359 A70-37406

Oxidative enzymes histochemistry in nervous system, liver and kidney of rats in immediate and remote periods after 24-hr artificial hypobiosis
21 p3764 A70-41478

Aged conditioned changes in muscular working capacity, relating developments in functionally labile nerve centers
22 p3969 A70-42898

Sinus and diaphragmatic nerves impulse activity during hypoxia compared with normal respiration in cats
23 p4145 A70-44312

NETHERLANDS

Fighter pilot selection and training in Royal Netherlands Air Force
12 p2176 A70-27029

Report to COSPAR on Netherlands space research /1969/ including solar and stellar X radiation and UV spectrophotometry, cosmic ray measurements, satellite geodesy, etc
15 p2830 A70-31719

NETS

NT NEURAL NETS

NETWORK ANALYSIS

NT CRITICAL PATH METHOD

Trigger scaling circuits with pulsed and blanking feedback analysis for minimizing number of couplings
01 p0047 A70-10984

Time sharing computer systems to perform circuit design and analysis, discussing effectiveness in terms of immediate access, accuracy and cost
02 p0265 A70-12187

Pneumatic fluidic oscillator consisting of bistable multivibrator, analyzing feedback loop operation based on electropneumatic analog system
02 p0229 A70-12673

Book on microwave theory and applications covering transmission line theory, microwave measurement, signal sources and analysis, network analysis, etc
03 p0455 A70-13001

Optimal selection of centralized communication network of combined radial and linear structures minimizing disconnected peripheral points
03 p0446 A70-13238

Microwave circuits automatic analysis and design using digital computer in batch mode, describing analysis-optimization program
03 p0457 A70-13562

Analytic solutions for focal plane electric field components in parabolic reflector antennas
03 p0457 A70-13697

Resistance, capacitance and inductance in passive hydraulic circuits considered in analogy with electric circuits to determine dynamic characteristics
03 p0415 A70-13931

Device modeling for computer aided design and analysis of integrated circuits, discussing list of desirable properties and applications to transistor design
03 p0454 A70-14026

Reduced multiport equivalent scattering parameters derivation by matrix method, determining load reflection coefficients effect on signal attenuation and phase shift
03 p0458 A70-14038

Tunnel diode studied for oscillations initiation resulting in hysteresis involving supply voltage and load conductance variations
03 p0459 A70-14284

Silicon bipolar transistors primary photocurrent calculation using manufacturers data
04 p0657 A70-14736

Mathematical model based on equivalent electrical circuit for transient radiation analysis by computer /TRAC/ family of circuit analysis programs, simulating semiconductor devices
04 p0657 A70-14737

Digital computers for calculating coefficients of electronic circuit functions polynomials, developing algorithm
04 p0659 A70-15205

Bifurcation frequency and nonlinear distortions determined in nonlinear semiconductor circuit with series-opposed connections of p-n junctions operating in forced oscillation mode
04 p0659 A70-15206

Amplitude and phase frequency characteristics relations established by analyzing forced resonant oscillations in nonlinear circuit operating at power source frequency
04 p0662 A70-15207

Nonlinear networks computer analysis by recursive decomposition, discussing network graphs construction rules
04 p0662 A70-15451

Sensitivity functions of nonlinear circuits obtained by calculation of dependent linear model responses, topologically equivalent to original circuit
05 p0824 A70-16125

Fluidics background, operational principles, constituent elements, system assemblies and applications, discussing integrated and multiple function circuits, cost and reliability advantages, etc
05 p0798 A70-16146

Ferroelectric control circuits controlling electroluminescent cells in matrix, pointer, bargraph, alphanumeric and other displays
05 p0827 A70-16187

VHF field effect transistors thermal noise characteristics and effects of feedback and parasitic impedance
05 p0814 A70-16420

MTRAC program for transient analysis of circuits with square loop magnetic cores based on linearization of nonlinear circuit elements and Kirchhoff current law
05 p0825 A70-16999

Waveform-shaping transfer function rational polynomial approximation method with application to network problem in PCM communications
06 p1007 A70-17459

Linear circuit output waveform calculation without first resolving transfer functions on complex frequency plane, applied to current switching circuit analysis
06 p1018 A70-17460

Microwave acoustic transducer and delay line properties determination from mathematical analysis
06 p1062 A70-17481

Klystron amplifier output circuit large signal frequency response, showing dependence on distance between cavities
06 p1021 A70-17672

Oscillator discharge properties of capacitance power storage circuit used for pumping pulse lasers
06 p1081 A70-17668

Black box modeling of linear integrated circuits for computer analysis in frequency domain
06 p1026 A70-18416

Network analysis for systems application program /NASAP/ computer-aided circuit design program for network analysis, discussing application in education
06 p1015 A70-18418

Computer aided network design course using FORTRAN 4 emphasizing modeling of semiconductor devices
06 p1015 A70-18419

Signal flow graph, obtaining numeric and symbolic expressions for network function in terms of component parameters and sensitivity coefficients
06 p1026 A70-18420

NASAP program FORTRAN subroutine LOOPS for loop detection in circuit analysis, discussing automatic instrumentation process for computation time reduction
06 p1015 A70-18421

Hybrid NASAP program module for direct design of linear dynamic circuits using simple optimization without sophisticated computer programming
06 p1015 A70-18422

Computerized FORTRAN equations simulation of linear and nonlinear circuits for symbolic analysis and transient response
06 p1026 A70-18424

Self adaptive servosystems operating with incomplete input signal information, proposing schemes for parameter adjustment by employing differential circuit containing frequency filters
07 p1239 A70-18734

Frequency monitor design, analyzing relationships between time constants, gain, etc, emphasizing white noise filtration
07 p1227 A70-18991

Rectangular waveguides broad wall longitudinal slot equivalent networks, noting series/parallel function dependence on slot length
07 p1240 A70-19221

Energy transfer from pulse network to mass associated with propagating current sheet in linear pinch discharge, discussing pulsed plasma accelerator efficiency
07 p1348 A70-19323

Fourth order polynomial RC-RL decomposition conditions
07 p1326 A70-19686

Linear control circuits transfer function analysis, revising Nyquist criterion
07 p1328 A70-20212

Frequency characteristics optimization of symmetrical octupole bridge networks based on relationships between electrical parameters functions and impedance matrices eigenvalues
08 p1468 A70-20572

Impedance behavior of inductive posts with small capacitive gap in waveguide
08 p1468 A70-20644

Circuit analysis of pulse integrator and square-law receiver used as optimal filter during incoherent radio pulse reception on background fluctuating noise
08 p1461 A70-20865

Electronic equipment complexity estimation based on information-recognition characteristics and ease of utilization
08 p1474 A70-21222

Transient response analysis of nanosecond pulsed transistor amplifier having common-emitter configuration with negative feedback
08 p1474 A70-21229

TRAPATT oscillator circuit characteristics determined from measurements and equivalent circuit calculations
08 p1475 A70-21277

Photolithographically produced thin film lumped element circulator, assuring physical and electrical symmetry by interweaving junction conductors
08 p1476 A70-21293

Circuit allowing direct combining of power from several avalanche diodes, discussing CW power output, single and multiple diode oscillators, etc
08 p1477 A70-21295

Reticular formation of central nervous system in vertebrates described as behavior controlling circuit of interconnected modules, proposing hybrid computer method for operational scheme
08 p1447 A70-21461

Algorithm for evaluating nth order partial derivatives of network functions and corresponding sensitivity functions
08 p1467 A70-21643

MOS transistor amplifier circuits, analyzing circuit parameters for common-source, common-drain and common-gate configurations
09 p1643 A70-22126

LC circuit with time dependent resistance containing wire explosion physics, solving differential equation of discharge circuit
09 p1726 A70-22492

Distributed RC notch filter normalized constants for dominant and nondominant transmission zero
09 p1654 A70-23025

Optimal decomposition of nth order filter into cascaded second order sections
09 p1650 A70-23367

Pulse-shaping transistor circuit analysis, considering circuit elements roles and temperature, pulse duration and leading and trailing edges durations effects
09 p1650 A70-23628

Integrated image sensor matrix array derived from equivalent circuit to minimize sneak path effects
10 p1854 A70-23879

Component tolerances effect on transfer function of networks, calculating sum variance for two terminal networks
10 p1833 A70-24223

Iterative solution for balanced diode modulator performance, obtaining output spectrum using Fourier transformation
10 p1849 A70-24232

DICAP system to analyze digital sequential switching circuits, studying simulation technique range and limitations of applicability
10 p1845 A70-24236

PCM-TDMA satellite communication systems operation modes and applicability, considering efficient circuit utility, equipment cost and control complexity
10 p1837 A70-24352

Traffic simulation in telephone network via communication satellite with presassigned and demand assigned circuits
10 p1838 A70-24356

Integrated circuits involving long-strip heat source surrounded by multiple layers, expressing temperature distribution by Fourier transformation obtained integrals
10 p1850 A70-24620

Computer-aided circuit design by imbedding singular elements to transform network synthesis into analysis problem
10 p1855 A70-24762

Coupled systems stability and oscillatory behavior analysis using Liapunov theory
10 p1855 A70-24763

Error propagation in rectangular grid leveling networks assuming fixed height of center of mass
11 p2045 A70-25798

Test pattern generation algorithm and program for failure detection in asynchronous sequential logic circuits, using combinational method
11 p2024 A70-26205

Optimal directed circuit and cycle elimination in weighted diagraphs by edge reversal orientation
11 p2072 A70-26219

Topological symbolic analysis of circuits defined by topological constraints, utilizing digital computers
11 p2029 A70-26330

Circuitry for phase modulated synchrotronized electronic oscillators for measuring minor reactance changes during remote sensing
11 p2052 A70-26373

Analog fluidic elements/operational amplifiers/with beam deflector proportional amplifiers incorporated into close coupled circuit
12 p2164 A70-27072

Computer programmed automatic circuit analyzers, discussing unit adaptation, wire data processing and analyzer programming [SME PAPER MS-70-727]
12 p2241 A70-27084

Amplitude stabilization transient processes at output of four terminal network with arbitrary phase and amplitude characteristics by representing pulse transfer function in series
12 p2184 A70-27537

Distributed-lumped-active network to produce transfer function with pair of high Q zero real part sensitivity poles
12 p2196 A70-27652

Sinusoidal signal harmonics measurement to determine nonlinear resistance junction I-V equation, discussing applications to circuit analysis
12 p2204 A70-28132

Diode coil suppression effect on two coil magnetic latching relays, showing operating time increment due to transformer action
13 p2378 A70-29348

Similarity theory in design of isofunctional electric converters, relating input-output criteria
14 p2533 A70-30374

SCAMP 1 DC statistical circuit analysis program for linear and nonlinear circuits, describing program structure
14 p2560 A70-30664

SCAMP 2 program for statistical analysis of electronic circuit sensitivity to variations in parameters and DC input values
14 p2560 A70-30665

SCAMP 3 program for calculation of electronic circuit DC performances statistical distribution as function of component parameters variation
14 p2560 A70-30666

SCAMP 4 program for electronic circuits statistical analysis in frequency domain, obtaining mathematical models and transfer functions
14 p2561 A70-30667

IMPATT microwave diodes small signal characterization by equivalent circuit using iterative computer procedure
15 p2708 A70-31971

Ladder networks total transmittance and voltage transfer ratio and impedance or admittance, investigating signal flow graph open paths and Fibonacci sequence
15 p2715 A70-32344

Feedback in electrical networks, discussing transient processes within cybernetics framework
15 p2716 A70-32362

Solid state UHF and microwave device testing by computer automated network analyzers, measuring scatter parameters
15 p2742 A70-32590

Large signal junction FET model involving piecewise linear approximation for ECAP circuit analysis program
15 p2711 A70-32596

Circuits and systems - Conference, Pacific Grove, California, December 1969
16 p2881 A70-33031

Optimal linear filter analysis from singular optimal control viewpoint, considering white and correlated measurement noise
16 p2885 A70-33320

Fluid amplifiers equivalent circuit with stagnation pressure source in series with orifice and load, discussing applications to small signal circuit analysis
16 p2844 A70-33446

High speed MOS circuitry design with application to digital equipment, noting low power and high packaging density
16 p2887 A70-33456

Nonlinear circuits with linear gain relations, examining input-output relations of two ports for analysis, synthesis and design
18 p3230 A70-36000

Phase plane method for Hill equation in problems involving EM wave expansion in elliptical waveguides or single circuit parametric systems analysis
18 p3227 A70-36424

Inverse Laplace transform of network function with allowance for initial differential equation solution, determining circuit temporal characteristics
19 p3456 A70-37269

Network function sensitivity to parameter variations, describing indirect calculation method
19 p3394 A70-37966

Frequency multipliers with charge storage diode, analyzing turn-off transient effect on performance by charge control model
19 p3391 A70-38748

Second order automatic phase control system with proportionately integrating filter, calculating transient response by harmonic linearization method
20 p3584 A70-39253

Soviet book on radio transmitting equipment, covering vacuum tube and transistorized devices, amplifier stages, AM transmitters, oscillator circuits, etc
20 p3597 A70-39599

Real time network support simulation allowing network configuration for nominal or perturbed trajectory for Saturn vehicles, applicable to any flight azimuth [AIAA PAPER 69-936]
20 p3591 A70-39684

Multiphase relaxation oscillator with inductive coupling and common base resistor in feedback loop, determining circuit parameters effect on pulse length
20 p3598 A70-39791

Ga-as Gunn diodes small signal admittance in dipole oscillation mode, analyzing RC model
20 p3598 A70-40062

Ideal limiter with polyharmonic signal input, calculating output spectral composition by Fourier series expansion
20 p3587 A70-40143

Diode mixer analysis for arbitrary I-V characteristics and commensurate levels of converted signals, using modulation characteristics method
20 p3588 A70-40147

Satellite networks queueing analysis, examining graph-theoretic model based on stochastic inputs and time delay factors
20 p3589 A70-40338

DC transistorized Nor logic gates design based on graphic analytic method permitting influence of circuit parameters variations for reliability improvement
21 p3793 A70-40765

Book on pulse and switching circuits covering remote control, TV, computers, radar, telemetry and automation devices
21 p3798 A70-41324

Frequency multipliers with charge controlled junction diode model, predicting operational behavior
22 p3998 A70-43421

Transistor circuit analysis at high frequencies and large signals, considering collector current, inertia and conductance conditioned by diffusion and recombination
23 p4161 A70-43779

Stripline and microstrip junction circulators analysis for microwave integrated circuits, based on clockwise and counterclockwise rotation modes
23 p4169 A70-43787

Electroacoustic circuits transient behavior, examining loudspeaker effectiveness
24 p4321 A70-45374

Modified time-domain reflectometer method for waveguide system evaluation, detecting and displaying radar echoes as function of time
24 p4315 A70-46234

Failure analysis methods for connectors and interconnections, discussing visual inspection, X ray vidicon analysis, electrical evaluation, etc
24 p4320 A70-46249

NETWORK SYNTHESIS

Flip chip and beam lead methods for microcircuit assembling, discussing heat removal using heat

spreader and temperature cycling effects on tensile strength

01 p0050 A70-10330

Digital adaptive-element building blocks in monolithic Si structures for MOS large scale integration, considering serial/parallel multiplier and shift register chips
01 p0047 A70-10458

Wide range pulse height discriminator with milliwatt power drain for use in nuclear experiments on scientific satellites
01 p0088 A70-10749

Microwave circuit for increasing Gunn oscillators injection locking capabilities and reducing FM resulting from bias-voltage fluctuations
01 p0050 A70-10783

Miniaturized components in microstrips on low loss dielectric or magnetic substrates, noting suitability for microwave systems integration
01 p0052 A70-11313

Message switching techniques in digital telecommunication networks, discussing automatic routing, operational and control facilities, etc
02 p0256 A70-11973

Functionally integrated superheterodyne receivers design by applying microwave IC technology, providing weight reduction, interconnecting cables elimination and circuit interface problems minimization
02 p0267 A70-12055

Time sharing computer systems to perform circuit design and analysis, discussing effectiveness in terms of immediate access, accuracy and cost
02 p0265 A70-12187

Multistop time-to-pulse-height conversion unit to extend capability of pulse height analyzer for multichannel time analysis with narrow channel widths
02 p0271 A70-12749

Design methods for self steerable antenna arrays in unidirectional and two directional radio links
03 p0456 A70-13196

Unstable problems stabilization in antenna synthesis from Fredholm equations solution, using least squares method and Chebyshev polynomials
03 p0456 A70-13452

Microwave circuits automatic analysis and design using digital computer in batch mode, describing analysis-optimization program
03 p0457 A70-13562

Optimal synthesis and design of distributed parameter system for waveguides using gradient technique with devised algorithm to overcome convergence problem
03 p0449 A70-13563

Wideband parametric and tunnel diode amplifiers synthesizing method for obtaining maximum flat amplitude frequency response
03 p0457 A70-13727

Variable RF signals in pulsed radar, examining circuits design for required functions
03 p0452 A70-14281

Quasi-optical design methods applied to mm microwave resonators characterized by high Q and low spectral densities
04 p0655 A70-14623

Radiation hardening of electronic systems for nuclear weapons using shielding, circuit design techniques and hardened components
04 p0657 A70-14738

Circuit parameter equations for effective circuit synthesis taking into account ratios between coefficients of polynomials in numerator and denominator
04 p0659 A70-15208

Microwave Si transistors with overlay and interdigital geometries and integrated circuit design considerations for power amplifiers, power oscillators and frequency multipliers
05 p0819 A70-16149

Transistorized wideband amplifiers synthesis by combining dynamic parameters method with poles and zeros method
05 p0819 A70-16249

Adjustable pulse delay circuit design utilizing slow switching action of storage diodes emphasizing thermal stability
05 p0820 A70-16343

Transistor circuit design with junction compensation techniques to reduce transient gamma radiation effects
05 p0821 A70-16418

Broadband two way switch obtained by p-n diodes deposited on alumina substrate
05 p0821 A70-16526

Transversal filters with continuously tapped delay lines, emphasizing synthesis of low pass filter and phase shifter
05 p0822 A70-16652

N-port resistive networks synthesis from terminal conductance matrices with two-tree port structures
06 p1023 A70-17426

Guided elastic waves propagation on layered media, considering elastic wave circuitry design for true microminiaturization
06 p1018 A70-17476

- Surface acoustic wave components for performing transduction, amplification and coupling functions, considering compatible component configurations
06 p1018 A70-17477
- Soviet book on microwave devices employing semiconductor diodes design and synthesis covering electric field effects, optimality criteria, tabular data, etc
06 p1019 A70-17536
- Complex control follow-up systems in transient modes, suggesting synthesis for transfer function of control signal coupling
06 p1023 A70-17775
- Circular antenna arrays synthesis, minimizing peak sidelobe level by dynamic programming
06 p1022 A70-18021
- On-line computer programs allowing for man machine interactions in linear circuits design
06 p1015 A70-18417
- Computer aided network design course using FORTRAN 4 emphasizing modeling of semiconductor devices
06 p1015 A70-18419
- Size reduction and low noise temperature in receiving antennas obtained by transistor integration and resonance frequency modulation
07 p1241 A70-19353
- AC to DC converter design for transforming average AC values into DC voltage
08 p1438 A70-20601
- Galvanoplasty process for parts for UHF circuits, discussing cost, safety and quality
08 p1468 A70-20611
- Monolithic, thick film, thin film and multichip integrated circuit techniques applied to communication equipment design
08 p1471 A70-20785
- Equivalent transformations method for minimizing electronic equipment sensitivity to circuit components value variations during operation
08 p1474 A70-21221
- Microstrip oscillator circuit design for operating with high power/efficiency avalanche diodes, describing low pass filter tuning section role
08 p1475 A70-21278
- Five resonator broadband frequency doubler design using charge storage diodes
08 p1475 A70-21280
- Half wave stepped digital elliptic filter design showing improvements over microwave TEM line narrow band bandpass filter
08 p1476 A70-21284
- Circuit development for realizing narrow bandwidth elliptic function filters at microwave frequencies
08 p1476 A70-21285
- Commensurate transmission line circuits design approximating periodic frequency characteristics on digital computer
08 p1476 A70-21286
- Low pass filter structure of focusing reflectors designed for quasi-optical system, noting energy absorption
08 p1476 A70-21287
- UHF and VHF stacked ferrite loaded junction circulators construction, improving cost to power performance
08 p1476 A70-21292
- Parallel multiplier design with carry-save scheme and constructed from series integrated circuits, discussing speed, complexity and cost
08 p1467 A70-21784
- Adaptive equalizer consisting of canonical link structure with minimum number of delay elements applied to fast data transmission
09 p1640 A70-22039
- Nonlinear circuits reducing nonlinear distortions in amplifiers, discussing wideband nonlinear distortion compensating circuits
09 p1643 A70-22131
- Hybrid microwave integrated circuits technology and design, discussing distributed and lumped-element structures and component properties
09 p1644 A70-22225
- Current distribution determination necessary for given directional characteristic of antennas in nonlinear synthesis problem
09 p1644 A70-22403
- Linear antenna array synthesis by variational calculus, minimizing sidelobe level for fixed input powers and field strengths
09 p1644 A70-22404
- Antenna arrays phase synthesis method based on properties of fast fluctuating phase distribution
09 p1645 A70-22414
- One dimensional discrete time nonlinear filters synthesis using Bayes theorem and digital techniques
09 p1654 A70-22934
- Photoemission energy distribution curves measuring circuit using AC retarding potential method, offering improved noise performance
09 p1679 A70-22996
- Optimal construction of microwave filters with TWT and ferrite direct gain receivers
09 p1648 A70-23166
- Roundoff noise output-dynamic range interaction in digital filters, discussing filter synthesis with transpose configurations concept
09 p1649 A70-23366
- Reactance filters for matching circuits design with optimum transforming performance
09 p1650 A70-23404
- Curvilinear horn antennas synthesis having smoothly changing cross sections, studying methods for solving Fourier integral equation
09 p1652 A70-23660
- Transistor bistable multivibrator design by graphic analytic method, considering effects of loading and supply voltages, temperature and component values on circuit performance
10 p1848 A70-23995
- Directional broadband couplers with lumped elements obtained by insertion of LC networks between sum and difference ports of equal hybrids
10 p1848 A70-24221
- Demand assignment signaling and switching subsystems /DASSS/ design for communication satellite, examining voice channels modulation
10 p1837 A70-24348
- Integrated TDMA switching/transmission system implementation into existing network
10 p1837 A70-24354
- Computer-aided class C amplifier design, discussing algorithm and computer program
10 p1849 A70-24447
- Control synthesis method using optimization technique to design controllers making closed loop system behave as ideal system or model
10 p1855 A70-24450
- Computer-aided circuit design by imbedding singular elements to transform network synthesis into analysis problem
10 p1855 A70-24762
- Phased array radar system synthesis, discussing small aperture systems, effects of solid state technology and role of data processing
10 p1842 A70-24877
- Integrated circuit microwave phased array radar antenna systems for multiple frequency bands and multifunction operations to save cost and space
10 p1851 A70-24878
- Book on integrated electronic systems covering integrated circuit design, device and material properties, quality control, applications, etc
10 p1853 A70-25049
- Single bit latching reciprocal ferrite phase shifter design, operation and performance, noting linear phase response and low phase nonreciprocity
10 p1853 A70-25243
- Thyratron based fast pulse generator circuits noting applications
11 p2017 A70-25570
- Low sensitivity optimal controls synthesis for gyro stabilizer stabilization circuit using variable structure systems theory
11 p2048 A70-25580
- Circuit for analog computing system to determine function extremum of many variables in presence of constraints
11 p2023 A70-25927
- Time correlation telemetering systems design, describing structural scheme
11 p2004 A70-25929
- Microwave acoustic delay lines design and fabrication for UHF to X band frequency ranges
11 p2005 A70-26163
- Constrained complex optimization method for synthesizing distributed-lumped-active networks
11 p2024 A70-26204
- Permanent memory faults effects on sequential machines finite-state behavior, considering masking role in synthesis of fault-tolerant sequential networks
11 p2072 A70-26220
- Computerized design of microwave circuits with S matrix
11 p2019 A70-26714
- Broadband 2 GHz transhorizon radio relay system design and performance for transmission on four channel pairs
11 p2034 A70-26820
- T2L logic circuits design and coherent noise immunity
11 p2021 A70-26833
- Distributed-lumped-active network to produce transfer function with pair of high Q zero real part sensitivity poles
12 p2196 A70-27652
- Computer aided electronic circuit design, describing calculations, graph and table generation, data storage, etc
12 p2192 A70-27769
- Photodetector-electronic circuit matching channels for optical communication system, using minimum risk design criterion
12 p2237 A70-28153
- Computer-aided MOS/LSI four phase logic circuit design, discussing software, design cycles and testing
13 p2380 A70-28375
- Gauss-Newton nonlinear programming algorithm applications to optimization of optimal control law parameters and closed loop control system synthesis
13 p2381 A70-28435
- MELVIN compact inexpensive multipurpose automatic test system, utilizing MSI single printed circuits to work optimally with computer
13 p2374 A70-29683
- Redundant threshold logic elements synthesis based on von Neumann multiplexing principle for automatic error correction
13 p2376 A70-29940
- Similarity theory in design of isofunctional electric converters, relating input-output criteria
14 p2533 A70-30374
- State-space synthesis of multiport passive reciprocal networks with minimum number of resistors, using Gauss factorization procedure
14 p2556 A70-30516
- Linear control systems identification and synthesis from data containing modulus and phase information as frequency functions
14 p2559 A70-30520
- Integrated circuits design by combined automatic and manual system
14 p2554 A70-30670
- Root locus of active distributed RC circuit for synthesis of magnitude response of parabolic filters
14 p2562 A70-31323
- Axisymmetric multibeam annular antenna array with interacting radiating elements synthesized by partial radiation patterns
15 p2707 A70-31513
- Transistorized amplifiers synthesis with multiloop feedback
15 p2707 A70-31518
- Lossless pulse-shaping active line for unipolar transmission, considering construction by loading two terminal Esaki diode to coaxial cable
15 p2697 A70-31827
- Synthesis of vertically polarized omnidirectional pattern with cascade dipole antennas on conducting cylinder
15 p2697 A70-31832
- Low pass filter synthesis with transfer function having frequency response boost in pass band
15 p2708 A70-31833
- Cascade synthesis of multistage logical network with multiple outputs capable of realizing arbitrary logical function from algebraic viewpoint
15 p2715 A70-31840
- Multiple wiring algorithm for automatic pattern design for AI interconnections and printed wiring in integrated circuits
15 p2715 A70-31842
- Microwave power transistors design and packaging
15 p2711 A70-32589
- Topology and component values in computerized design of distributed lumped active networks
15 p2711 A70-32595
- Combinational logic cells cellular arrays synthesis, considering truth table and transition matrix
15 p2712 A70-32606
- Circuit design characteristics and reliability relationship in electronic power supplies for performance requirements
15 p2712 A70-32644
- Practical electronic components criteria accommodating reliability engineer and circuit designer
15 p2832 A70-32653
- Real time variable range digital filter design in suitable form for LSI realization, satisfying reduced deadband requirement for input interface element
16 p2882 A70-33040
- Control strategy for linear system performance based on synthesis of optimal closed loop controller with both sensitivity and state feedback
16 p2882 A70-33042
- Microwave IC methods applied to solid state signal sources design, using varactor tuned transistor oscillators, resistive isolation pads, amplifiers and frequency multipliers
16 p2872 A70-33069
- Suboptimal nonlinear feedback control synthesis for linear time-invariant system with convex cost functional
16 p2886 A70-33334
- High Q reactance network realization for integrated microwave systems employing evanescent mode waveguide components
16 p2875 A70-33402
- High speed MOS circuitry design with application to digital equipment, noting low power and high packaging density
16 p2887 A70-33456
- MOS transistor associative memory cell design utilizing LSI technology
16 p2869 A70-33464
- Nonlinear lumped system synthesis by inverse delta method
16 p2943 A70-34278
- Kinetic synthesis for multivariable system by asymptotic equivalence method
16 p2944 A70-34279

Multibandswitch AC Wheatstone bridge design with large circuit factor

17 p3051 A70-34616

Book on design of resonant piezoelectric devices covering linear piezoelectric materials, Green function, variational methods for dimensional motions and modes, etc

17 p3143 A70-35188

Adaptive system synthesized to compensate stochastic feedback or external disturbance, obtaining quasi-optimal compensation algorithms

17 p3056 A70-35368

Observation space transforming for synthesis of automatic optimization systems with memory tracking randomly walking extremum

18 p3234 A70-36073

Multichannel time marker network synthesis device for physiological data assembly, transformation and processing, generating pulses

18 p3223 A70-36083

Electronic circuits design by discrete equivalent transformations for selecting components parameters within given limits

18 p3231 A70-36239

Microwave devices with harmonized electron beam constructed from klystrons, TWT, backward wave tubes, magnetrons

18 p3231 A70-36414

Funnel shaped vector radiation pattern realized by synthesizing axisymmetric distribution of elliptically polarized currents on body of revolution

19 p3392 A70-37277

Low pass linear phase active feedback circuit synthesis using distributed RC networks to realize flat magnitude response

19 p3392 A70-37707

Automatic control systems synthesis based on root locus trajectories theory

19 p3392 A70-37808

Digital filter synthesis, discussing transfer function determination based on prescriptions for frequency or time response properties

19 p3391 A70-38746

Pulse shaper circuits with tunnel diodes and transistors, describing recovery time decrease

20 p3596 A70-38972

Optimal synthesis of linear active RC filters with controlled source, using feedforward and feedback weighted signals

20 p3596 A70-39163

Two dynamic systems synthesis achieving limited influence on each other by coordinates invariance criteria method involving determinant

20 p3604 A70-39841

Low noise requirements of DC current sources used in circuit design

21 p3797 A70-40854

Power IC fabrication methods covering monolithic chip, monobrid chips and IC driver with external power transistors

21 p3797 A70-41212

High power IC technical limits involving packaging, bonding wires, interconnect metal, power transistors

21 p3797 A70-41213

Coherent receiver as hybrid carrier tracking loop consisting of standard phase locked and modified Costas loop

21 p3802 A70-41351

Fluid logic sequential circuits with optional input signals, describing synthesis procedure

[ASME PAPER 70-FLCS-19] 22 p3963 A70-42408

Fluid logic circuits with combined feedback input signals, describing synthesis procedure

[ASME PAPER 70-FLCS-18] 22 p3963 A70-42409

RLC networks and microwave components design by applying optimization technique

22 p3997 A70-43175

Stripline bandstop filter design method, discussing response shape and resonator number determination, reactance calculation, etc

22 p3999 A70-43488

Gyrostabilizer design based on composite optimal controls with respect to different regional criteria

22 p4040 A70-43559

Algorithm for communication network synthesis from limited elements selection, considering fixed reliability requirements

23 p4160 A70-43763

Design tolerances and compensating networks for microwave transistor amplifier, using synthesis search and trial calculation by computer

23 p4168 A70-43780

Optimal design of electronic circuits, using mathematical methods for solving nonlinear multivariable function extremum

23 p4171 A70-43951

Graphical link between operator and digital computer using CRT display and light-pen input system during automatic electronic circuit design

23 p4150 A70-43952

Digital computer algorithm for automatic electronic circuit design using design engineer experience

23 p4171 A70-43953

Radio electronic circuits precision, deriving relationship between frequency response and component variations solvable by linear programming

23 p4171 A70-43958

Transistorized LF RC filter circuit design for desired frequency response characteristics

23 p4171 A70-43962

Computerized algorithm facilitating automatic synthesis of time invariant linear compensation for highly complex multiloop control systems

[AIAA PAPER 69-941] 23 p4177 A70-44561

General Optimization Software Package for Electrical network and system design, noting application to engineering problems and education

23 p4177 A70-44750

Sequential logic circuit synthesis using truth table, minimizing by Quine-McCluskey method

23 p4167 A70-44861

Microwave oscillator design using Y-parameters from measured scattering parameter data at desired frequencies, applying negative resistance circuit theory

24 p4320 A70-46235

NETWORKS

Soviet monograph on gas dynamics one dimensional problems in variable networks, discussing difference schemes, boundary conditions and discontinuities

19 p3407 A70-38930

NEUMANN PROBLEM

Shells with holes using Neumann method, obtaining Fredholm alternative for singular integral equations

03 p0589 A70-13347

Neumann problem reformulation for regions having boundaries with limited rotation

07 p1325 A70-19538

Scalar plane wave LF scattering by prolate spheroid of revolution, obtaining iterative solution for Neumann problem

11 p2085 A70-26622

Shells with holes using Neumann method, obtaining Fredholm alternative for singular integral equations

14 p2657 A70-30721

Saint Venant principle treating Neumann problem with nonthin two dimensional domain

15 p2767 A70-31855

NEURAL NETS

Neural information processing taking into account differences between living brain and artificial processor

09 p1617 A70-22496

Hypothalamic electric stimulation intensity effects on elicited behavior, considering possible neural circuit threshold reduction

13 p2355 A70-29807

Eating, drinking and gnawing motivation interchangeability under hypothalamic stimulation, noting role of neural substrate activation

13 p2356 A70-29814

Neural pulse frequency modulation system stability, using feedback control model

17 p3056 A70-35553

Brightness contrast by human observer binocular matching, discussing neural networks models

19 p3366 A70-38924

NEUROLOGY

Cortex functional interrelationships with hypothalamus and formatio reticularis, studying role of corticofugal effects in anesthetized cats

01 p0012 A70-10051

Electrochemical mechanisms of nervous tension generation and expansion based on neural impulse expansion theory, noting ion transport

01 p0020 A70-10518

Neuroregulatory agents instrumentation based on compounds brain level, enzymatic formation and radio labeling

14 p2536 A70-30347

Otoneurology - Conference, Basel, 1969

14 p2538 A70-30908

Auditory perception by neuroelectrical tests based on logic coincidence among several detectors, discussing bullfrog inner ear

21 p3765 A70-41991

NEUROMUSCULAR TRANSMISSION

Respiratory muscles neuromotor units activity as function of volley from electric discharge features study on dogs and cats

03 p0417 A70-13068

Mg ion metabolism in neuromuscular excitability maintenance, discussing quantity requirements, detection and electromyographic recording

12 p2172 A70-28045

Excitation conduction velocity maximum along motor fibers of peripheral nerves as function of age in healthy subjects

15 p2679 A70-31602

Muscular group response to sinusoidal and trapezoidal force applied to forearm, discussing frequency dependent limb oscillations and neuromuscular effects

21 p3767 A70-42161

Sympathetic transmission model, discussing transmitter liberation capacity under various stresses by mobilization of stores, acceleration of synthesis, etc

24 p4299 A70-45804

NEURON TRANSMISSION

U BIOELECTRICITY

NEURONS

Corticofugal effects of various cortical regions on neuron activity in hypothalamus posterior lateral sections in cats

01 p0012 A70-10053

Microelectrophysiological study of cerebellar neuron responses to stimulation of vestibular apparatus by vertical rocking performed on anesthetized adult cats

01 p0012 A70-10124

Neurons and perineuronal glial cells quantitative relations in visual cortex from anesthetized dogs

01 p0025 A70-11030

Temporary interneuron connections mechanisms during conditioned reflexes development

01 p0025 A70-11040

Human and cat visual neuron properties, discussing encoding orientation and dimensions of retinal images

01 p0028 A70-11360

Neurons tracing activity and cellular memory mechanisms in cortical projection region of cutaneous analyzer of immobilized rats following electric acoustic stimuli

01 p0030 A70-11468

Rabbits and cats cortical neurons responses to light and acoustic signals, using microelectrodes inserted at different depths into cortex

01 p0030 A70-11469

Neuron activity in somatosensory cortex region of guinea pigs and rats with intracortical connections severed by circular incision

01 p0030 A70-11470

Vasomotor activity of neurons located in spinal cord lateral crescent in curarized decerebrated and intact cats

01 p0030 A70-11471

Direct links existence between rabbit temporal cortex neurons and neurons in each division of hippocampus, discussing topographic arrangement and axons quantity

03 p0417 A70-13071

Tegmental nucleus neurons of cats cerebellum, considering responses to acceleration changes and natural stimulation of vestibular apparatus

03 p0421 A70-13510

Early and late response component of associative cortical area in cerebral hemispheres of cats connected with mono and polysensory neuron activity

03 p0421 A70-13688

Origin and functional designation of associative evoked potentials in orbital cortex of cats, showing phases connected with neuron activity and excitation

03 p0422 A70-13689

Aplysia periodic spontaneous gill movements controlled by central neuron activity in abdominal ganglion

04 p0629 A70-14425

Mathematical model for computer simulation of homogeneous neuron nets with recurrent inhibition control, considering activated and inactivated states

04 p0640 A70-14553

High altitude environmental effects on adrenal glands and hypothalamic neurosecretion in rats

04 p0629 A70-14568

Small amplitude discharges and neuron activity in dorsal hippocampus of cats recorded simultaneously with pyramid cell activity

04 p0632 A70-15221

Nonspecific influences on rabbits neurons reaction to nonvisual stimuli in central visual pathway using microelectrodes implantation in visual cortex

05 p0802 A70-16624

Vasomotor center neuron responses to vertical rocking movement stimulus of vestibular apparatus in cats

06 p0995 A70-17805

Connection character of rubrospinal tract fibers with various neuron groups of spinal cord on basis of electrophysiological and morphological investigations

07 p1206 A70-19468

Respiratory neurons pulsating activity in medulla oblongata of anesthetized cats during imposed rhythm

07 p1213 A70-19774

Respiratory neurons activity in respiratory center of medulla oblongata during suspension and forced recovery of respiratory motions

07 p1213 A70-19775

Guinea pigs visual analyzer during stimulations by diffuse light, nonspecific thalamic nuclei and microelectrodes polarization, determining A- neuron activity

07 p1213 A70-19788

Midbrain reticular neurons activity in cats during response to individual and coincident cortical and hypothalamic stimulations

07 p1213 A70-19789

Pulse neurons random homogeneous networks macroscopic description, considering operation modes in terms of input frequencies and output pulse sequences

08 p1451 A70-21000

- Neuron processing of retinal activity in estimating distances and sizes of objects in field of vision
12 p2172 A70-28312
- Neuron activity of cortical motor and visual regions and corpus geniculatum laterale in cats during diffuse thalamic electrostimulation combined with light signals
12 p2173 A70-28355
- Electronic simulation of neuron membrane demonstrating nervous impulses generation and propagation behavior
14 p2542 A70-30387
- Pulse activity records to investigate neuron functioning dynamics based on construction of frequency graph
15 p2679 A70-31601
- Lemniscus neurons in switching nucleus of thalamus, showing switching cells with direct cortical projections into somatosensory cortical zones
16 p2848 A70-33262
- Arterial blood carbon dioxide tension effects on rhythmic volley activity of respiratory medulla oblongata neurons in cats
17 p3030 A70-35354
- Continuous functions transformation by artificial neuron networks, investigating electrophysiological data for nerve tissues excitability
18 p3223 A70-36081
- Posterior ventral thalamic nucleus neuron reactions converging lemniscus and spinothalamic signals in cats
18 p3221 A70-36639
- Extracellular spontaneous sequences of action potentials of thalamic neurons during asphyxia in rats under artificial respiration
19 p3361 A70-38306
- Acetylcholinesterase and simple esterases distribution in squirrel monkey brain, examining activity in neuropil and postrema area neurons
20 p3569 A70-38993
- Rat neuron impulsive reactions and frequency response differences to varying sound signals, discussing time constant, signal intensity and frequencies
20 p3574 A70-40172
- Spatial summation of retinal neurons receptive field centers excitation from single optic tract fibers action potential in light-adapted cats
22 p3971 A70-43403
- Bioelectric activity changes in rats lumbar neurons, membrane and postsynaptic potential and discharge frequency during and after asphyxiation
22 p3971 A70-43404
- Time analysis of pulsed activity of neurons, using amplitude analyzer with programmable control unit
22 p3972 A70-43551
- Visual system recording neuron pulse potential spatial and temporal responses to sinusoidal stimuli
23 p4144 A70-43922
- Peripheral stimulations of various modalities effect on neurons impulse activity in hippocamp dorsal area of rabbits, noting excitation and latent periods
23 p4145 A70-44311
- Forebrain participation in motor response suppression reaction during stimulation of caudate nucleus in rats and cats, noting brain damage effects
24 p4299 A70-45836
- Neurophysiology of membrane and synaptic mechanisms of prolonged trace changes in neuron activity concerning memory and cellular learning analogs
24 p4305 A70-46393
- NEUROPHYSIOLOGY**
- Neurophysiological vertical and horizontal visual coordinates localization in man
06 p0998 A70-18484
- Corneal stroma transparency analysis based on refractive index and lattice theories
09 p1618 A70-22675
- Vestibular analyzer and otolithic apparatus disturbances and normalization under prolonged hypodynamia, noting pathological effects of repeated caloric testing
10 p1816 A70-24686
- Neurophysiological mechanism of motor activity during simple reaction time situation performance
10 p1818 A70-24724
- Psychovegetative and neurovegetative stress syndroms in flying personnel removed prematurely from active service as result of psychophysiological complementary diagnostics [DFVLR-SONDDR-31]
12 p2177 A70-27041
- Motor reactions and neural negative induction duration in male and female human subjects of different ages
12 p2174 A70-28356
- Neurological differences in spinal projections of animals subjected to cordotomies compared with human material, using selective silver impregnation technique
13 p2350 A70-28998
- Electrode placement ancillary technique for obtaining stereotaxic atlas of infant rat hypothalamus
13 p2350 A70-29322
- Electronic simulation of neuron membrane demonstrating nervous impulses generation and propagation behavior
14 p2542 A70-30387
- Neurophysiological framework for binocular single vision and depth discrimination, concerning construction of horopter for cat
14 p2539 A70-31348
- Enhanced evoked potentials sited by auditory stimuli in complex task, considering EEG and neurophysiological basis of selective attention
19 p3363 A70-38318
- Prolonged transverse acceleration effects on rats kidney and posterior hypophysis neurosecretions
20 p3575 A70-40188
- Peripheral stimulations of various modalities effect on neurons impulse activity in hippocamp dorsal area of rabbits, noting excitation and latent periods
23 p4145 A70-44311
- Neurogenically maintained blood pressure component, discussing autonomic nervous system activity in hypertension and normotension, sympatholytic agents effectiveness in hypertensive treatment, etc
24 p4299 A70-45805
- NEUROPSYCHIATRY**
- Soviet book on higher cortical functions of man and disorders due to local brain injuries, describing methods for neuropsychological studies of motor functions
01 p0017 A70-10503
- NEUROSCIENCE**
- U NEUROLOGY**
- NEUROSES**
- Psychic state changes during prolonged bed rest, discussing effects of physical exercise and medicine
10 p1816 A70-24684
- Student pilot case diagnosis of hysterical neurosis with syncopal and epileptiform symptoms
21 p3771 A70-41493
- NEUROTIC DEPRESSION**
- Neurotic syndromes in aviation medicine, discussing acute reactions, anxiety, depressions, structured syndromes and psychosomatic disorders
21 p3771 A70-41490
- NEUTRAL BEAMS**
- NT MOLECULAR BEAMS**
- NT NEUTRON BEAMS**
- NEUTRAL PARTICLES**
- NT FAST NEUTRONS**
- NT NEUTRONS**
- NT PHOTONEUTRONS**
- NT THERMAL NEUTRONS**
- Ionospheric ion and neutral constituents composition from D region to magnetopause, noting ion-chemical reaction rates
01 p0074 A70-10588
- Charged particles motion in isotropic weakly ionized plasma acoustic wave associated with difference in electrons and ions entrainment by neutral particles
03 p0530 A70-13087
- Electron density and temperature in ionized gas created by thermal collisions between neutral particles, analyzing chemical ionization and inelastic collisions influence [ONERA-TP-752]
03 p0532 A70-13631
- Neutral particle flux measurements in plasma wind tunnel using BeCu detector, discussing role in collisionless flow dissipation processes
04 p0727 A70-14994
- Axial neutral gas pressure gradient calculated in cylindrical positive column of DC discharge due to driving volume force
04 p0671 A70-15003
- Chapman-Ferraro two dimensional problem with neutral sheet, investigating magnetospheric flows and time dependence
04 p0679 A70-15109
- Ion-neutral coupling in plasma acceleration revealed by velocity disparities determined spectroscopically [ALAA PAPER 70-166]
06 p1133 A70-18219
- Electron density, excited state density and neutral particle temperature in Ar and Ne nonequilibrium laminar plasma jets
08 p1550 A70-20596
- Fast neutral particles produced in electron-ion oscillation discharge as function of gas pressure and magnetic field
09 p1736 A70-23190
- Boltzmann equations for distribution functions of gas, analyzing neutral or ionized components by linearization method
11 p2090 A70-25946
- Upper atmospheric ion and neutral composition from rocketborne mass spectrometry, allowing for rocket velocity and analyzers orientation with respect to velocity vector
14 p2568 A70-30140
- Neutral particle temperature, pressure and velocity measurements in argon plasma jet, using refraction index
14 p2625 A70-31350
- Scalar-tensor theory in canonical form, discussing neutral particle and electron self energy problem
15 p2773 A70-31439
- Ionospheric spacecraft flight conditions simulation in vacuum chamber, discussing low energy ion sources
15 p2717 A70-31814
- Neutral particle and electron density measurements by Explorer 32 proving thermospheric gravity waves association with wave-like structure in F region electron density
15 p2727 A70-31907
- Rocket and satellite data on upper atmospheric neutral/charged particles, short wave solar radiation, temperature and photochemical reactions
15 p2730 A70-32089
- Metal surface ionization measurements for upper atmosphere and interplanetary space energetic neutral hydrogen analyzer design
17 p3138 A70-35309
- Upper atmosphere neutral component temperature measurement from thermal spread of charged particles beam
18 p3247 A70-36182
- Elastic energy transfer cross sections calculation of H-H scattering to estimate neutralized solar wind particles thermalization
18 p3309 A70-36951
- Upper atmospheric neutral components temperature determination by rocket-borne mass spectrometers
18 p3252 A70-36983
- Upper atmospheric layers neutral composition by rocket-borne mass spectrometers, indicating gravitational separation of argon from molecular nitrogen
18 p3252 A70-36984
- Magnetolectric electromotive force in media of ions and neutral molecules, using Boltzmann transport equation
21 p3855 A70-40909
- Plasma and neutral gas collisionless interactions in magnetic field based on Alfvén critical velocity hypothesis, discussing electron energy distribution
21 p3857 A70-41383
- Quadrupole mass spectrometer design for lower thermosphere neutral composition measurement, discussing atmospheric physics, installation on rockets, etc
21 p3830 A70-41990
- NEUTRALIZERS**
- Wire dischargers at helicopter propeller blade tips reducing electrostatic RF interference, substituting stainless steel wire tufts for nichrome wire
05 p0848 A70-16320
- Parameters influence on mercury hollow cathode neutralizers for Kaufman ion thruster [ALAA PAPER 70-1090]
20 p3693 A70-40245
- NEUTRINOS**
- High luminosity white dwarfs possible evolution from planetary nebulae, discussing plasma neutrino processes
01 p0189 A70-11342
- Neutrino in nonquantum and quantum gravitation theories, neutrino sea, etc, discussing classical neutrino dynamics
02 p0341 A70-11669
- Neutrinos line patterns in Muscovite mica, refuting Russel assumption by analysis of multiple Coulomb scattering of charged particles and track comparison
03 p0556 A70-13047
- Solar structure models for neutrino flux prediction compared with solar structure, suggesting modification in solar and stellar evolution calculations
05 p0906 A70-15895
- Solar neutrino spectroscopy using various radiochemical detectors for Be 7, N 13, O 15 and B 8 neutrino fluxes, noting Li 7 suitability for determining CNO cycle
05 p0898 A70-15949
- Assessing background magnitude caused by earth natural radiation sources during underground detection of solar neutrinos by radiochemical methods
05 p0899 A70-15950
- Solar interior temperature measurement by Cl, Ga and Li isotopic detectors of solar neutrinos, discussing effectiveness and upper temperature bound
05 p0899 A70-15951
- Time variation of gravitational constant on structure of central solar region and neutrino luminosity
05 p0899 A70-15952
- Solar neutrino detectors calibration with artificial neutrino sources produced by reactors, electron and proton accelerators
05 p0846 A70-15953
- Deuteron splitting by solar neutrinos for neutrino detection, describing deuterium scintillation detector characteristics
05 p0899 A70-15954
- Gallium trichloride and aqueous solution of lithium chloride as solar neutrino detectors
05 p0899 A70-15956
- Neutrinos production by primary cosmic rays in rarefied and dense media, calculating spectra
05 p0899 A70-15963
- Solar neutrinos detection from recording high-energy electrons in reactions, using Li 7, Be 9 and B 11 as detectors
05 p0899 A70-15964

Experimental determination of solar neutrino activity from interaction cross section between neutrinos and target nuclei

05 p0900 A70-15965

Experimental observations of neutrino in collapsing stars in Galaxy, showing detector capability of recording positrons or electrons from antineutrino-neutrino flux induced reactions

05 p0900 A70-15966

Nonequilibrium processes and initial conditions in early universe, discussing neutrino viscosity efficiency at removing shear anisotropy and Misner model

05 p0907 A70-16002

Solar core opacity influence on revised photospheric iron abundances, discussing neutrino flux prediction doubling in solar models

05 p0905 A70-16985

Neutrino emission, mass loss and giant branch termination in young clusters with giants originating from intermediate mass main sequence stars

06 p1138 A70-17277

Observational extragalactic densities obtained within framework of Friedman universe model with matter and neutrino background

07 p1383 A70-19407

Lepton charge and neutrino astrophysics, discussing oscillations role in solar neutrino detection difficulties

07 p1371 A70-20329

Earth observations of collapsing star neutrinos and neutrino oscillations in Milky Way galaxy

07 p1371 A70-20331

Relativistic gravitational stellar collapse calculations for stars exceeding neutron star limit, discussing results in terms of supernovae or neutrinos

09 p1749 A70-21991

Supernovae hydrodynamics, discussing early light curves energy requirements and shock wave dynamics in terms of neutrino diffusion

09 p1749 A70-21992

Neutrinos kinetic theory for anisotropic cosmological models

09 p1753 A70-22453

Electron-neutrino weak interaction and beat decay coupling constants found nearly equal, describing astrophysical tests based on white dwarf stars luminosity intervals

09 p1733 A70-23451

Neutrino emission effect on collapse of supermassive stars, estimating energy radiated, discussing envelope explosion

10 p1938 A70-24022

Universe neutrino energy density estimation based on photon-neutrino weak interaction coupling theory

10 p1920 A70-24567

Stellar plasma neutrino pair emission, comparing photon neutrino coupling with current current coupling theory and white dwarf evolution

12 p2297 A70-26976

Solar neutrino flux measurement based on neutrino capture by large chlorine mass and subsequent Ar 37 decay in low noise environment

12 p2293 A70-27389

Cosmic neutrinos detection, using inverse beta decay and elastic scattering by electrons to overcome solar neutrino problem

12 p2293 A70-27390

Dissipation mechanism and period rate increase in neutron star pulsar model with neutrino emission for damping

12 p2312 A70-28368

Neutrino astronomy for processes in stellar interiors, emphasizing thermonuclear reactions in sun and main sequence stars

13 p2490 A70-28947

Thermonuclear reactions in interior of sun, discussing models for He isotope concentration and flow to interpret solar neutrino generation

13 p2494 A70-29573

Low energy neutrino cosmic background, discussing energy density, black body radiation, beta decay, scattering process and origin

13 p2479 A70-30001

Nucleosynthesis in supernova models based on neutrino energy transport

17 p3153 A70-34529

Solar neutrino fluxes, calculating capture rates and primordial helium abundance

17 p3151 A70-34847

Plasmon decay by neutrinos emission in strong magnetic field, examining parallel and perpendicular propagation

18 p3305 A70-35936

Electron correlations and solar neutrino counts, correcting frequency independent Thomson cross section

18 p3308 A70-36485

Critique of metagalactic origin of high energy cosmic rays, reviewing neutrino hypothesis

19 p3500 A70-38082

Energy spectrum distortion of ultrahigh energy cosmic rays due to interactions with photons and neutrinos in universe

19 p3510 A70-38155

Solar neutrinos flux upper limit determination, describing detection equipment and procedures

19 p3511 A70-38486

Neutrino production by synchrotron process /magnetic bremsstrahlung/ in relativistic electron gas under intense magnetic field

20 p3695 A70-39050

Solar B8-Be8 decay neutrinos energy spectrum and absorption cross sections calculation

20 p3698 A70-39307

Inverse beta decay thermonuclear reactions induced by neutrinos proposed for neutrino detection from solar interior

20 p3704 A70-39471

Fermi momentum upper limit for universe neutrinos in cosmic ray propagation, determining maximum proton energy

20 p3700 A70-39592

Cosmic ray superhigh energy electrons and neutrinos propagation in degenerate neutrino gas universe, considering gas density in cosmological models

20 p3700 A70-39593

Secondary cosmic ray muon inelasticity in high energy neutrino interactions for deep mine experiments, using lepton current

21 p3845 A70-41139

High energy neutrinos generated by cosmic ray interactions with earth atmosphere, discussing detection, plotted energy spectrum and underground muons

22 p4093 A70-42310

Scale invariance models correlation with cosmic ray data, comparing neutrino- and antineutrino- nucleon scattering

23 p4210 A70-43800

Neutrino processes in lepton era as primordial fireball relic, discussing coupling constant for muon-electron neutrinos interactions

23 p4253 A70-44849

Red supergiants location in H-R diagram, discussing significance of mass loss, rotational mixing and neutrino emission as stellar model mechanisms

24 p4403 A70-45393

NEUTRON ACTIVATION ANALYSIS

Stony meteorite trace elements groups neutron activation analysis with computer reduction of Ge/Li spectra

02 p0249 A70-11680

Neutron activation analysis for U and Th in various tectites, discussing evolution and extraterrestrial origin

03 p0576 A70-14090

Bismuth concentrations in various carbonaceous and equilibrated chondrites determination by neutron activation technique

07 p1388 A70-20036

High energy neutron activation method for remote extraterrestrial in situ rock surface constituents analysis

10 p1932 A70-24614

Chondrites and terrestrial rocks trace elements by neutron activation analysis, discussing radiochemical separation and computer analysis of gamma ray spectra

20 p3582 A70-38980

Apollo 11 lunar dust examination by neutron activation analysis, determining spallogenic manganese 53

21 p3908 A70-41579

Neutron activation analysis for Re and Os in Apollo 11 volcanic rocks, discussing possible meteorite contamination of secondary rocks and fines

21 p3775 A70-41589

Apollo 11 lunar rocks and soil chemical elements analysis by neutron activation scheme

21 p3777 A70-41612

Apollo 11 fines and rocks major and trace elements data obtained by combined instrumental and neutron activation analysis

21 p3910 A70-41615

Chondrites Ti content by neutron activation analysis

21 p3921 A70-41941

Neutron activation determined concentrations of Ni, Ga, Ge and Ir in iron meteorites with silicate inclusions

24 p4401 A70-45376

Nonweldable internal flaws detection containing oxides in steel slabs by neutron activation analysis

24 p4376 A70-45750

Murchison and Lost City chondrites element abundance analysis by thermal neutron activation and wet chemical techniques, noting low oxygen content

24 p4411 A70-45790

Radiochemical neutron activation analysis of In, Cd, Y and rare earth elements in rocks

24 p4310 A70-46375

NEUTRON BEAMS

Neutron radiography for visual nondestructive failure analysis and production inspection of ordnance components compared with X ray radiography

03 p0494 A70-14122

Neutron radiography in cold, resonance or epithermal, and fast neutron energy ranges, discussing converter materials for direct exposure or transfer method

22 p4028 A70-42590

Image contrast enhancement on neutron radiograph by energy tailored beams

24 p4376 A70-45748

NEUTRON COUNTERS

NT NEUTRON SPECTROMETERS

Cosmic ray latitude survey in western U.S. and Hawaii in summer 1966 using neutron and muon monitors

01 p0167 A70-10228

Geographically smoothed geomagnetic cut-offs for eliminating discontinuity in neutron monitor latitude variation in Mexico City vicinity

01 p0167 A70-10229

Cosmic ray neutron monitors data comparison for various stations using one factor model, considering atmospheric effects and cut-off rigidities

01 p0087 A70-10460

Geomagnetic latitude survey by neutron multiplicity monitor covering threshold rigidity ranges at various elevations, relating data to primary cosmic ray rigidity spectrum

04 p0741 A70-15125

High energy neutron counter designed for recording slow neutrons produced in lead detector

05 p0845 A70-15935

Diurnal cosmic ray intensity variations first and second harmonics amplitudes during sudden phase variations diagrammed from neutron monitor data during IGY

05 p0898 A70-15936

Neutron monitor calibration method to eliminate natural cosmic ray background, decreasing errors due to ray intensity variation

05 p0846 A70-15938

High energy solar flare data from neutron monitor stations supplemented by low energy data from interplanetary space probes Pioneer 6 and 7

05 p0902 A70-16443

Satellite mounted device for detecting and recording 20-110 Mev solar neutrons

10 p1889 A70-24488

Neutron monitor air pressure attenuation coefficient dependent on neutron energy being recorded

10 p1889 A70-24491

Multiplicity recorder for cosmic rays neutron component studies, reducing star redistribution errors by coincidence effect compensation

11 p2103 A70-25527

First harmonic of diurnal variation in pressure corrected cosmic ray neutron monitor rate, discussing amplitude variation with height and observed time dependence

12 p2291 A70-27177

Statistical analysis of cosmic radiation neutron component monitor error, taking into account generation multiplicity

18 p3307 A70-36097

High altitude neutron supermonitor investigation of cosmic ray microvariations

18 p3307 A70-36104

Neutron monitor NM-64 design and operation, using Setun digital computer for around clock processing

20 p3629 A70-39310

Diurnal anisotropy variations of cosmic ray intensity, taking into account neutron monitors data

20 p3699 A70-39346

Barometric coefficient altitude dependence of cosmic ray neutron monitor for vertical flux

20 p3699 A70-39347

Multiplicity recorder for cosmic rays neutron component studies, reducing star redistribution errors by coincidence effect compensation

21 p3882 A70-41277

Fast neutron radiography, considering sources and transfer and scintillator-film detectors

24 p4376 A70-45749

NEUTRON DECAY

Neutron beta decay in strong quantizing magnetic field using Dirac wave function for electron, noting lifetime dependence on field strength

08 p1549 A70-21744

Proton injection into radiation belt, comparing solar neutron decay /SND/ and cosmic ray albedo neutron decay /CRAND/ as proton sources

09 p1746 A70-23489

Proton distribution in radiation belt inner zone from radial diffusion addition to cosmic ray produced albedo-neutron decay and atmospheric collision loss

17 p3150 A70-34644

NEUTRON DETECTORS

U NEUTRON COUNTERS

NEUTRON DIFFRACTION

Long range order formation in Ni-Cr alloys analyzed by direct neutron diffraction, considering disorder-order transition temperature and chemical composition

01 p0124 A70-11600

Order-disorder transition temperatures for Ni-Cr alloys determined by neutron diffraction, discussing homogeneous ordering of atoms

09 p1707 A70-23196

Chromium lattice vibrational properties based on fourth-nearest-neighbor tensor force model, obtaining

agreement with inelastic neutron diffraction data and elastic constants 14 p2626 A70-30480

Neutron diffraction of ordered atomic oxygen structures in titanium suboxides, noting compositional dependence of physical properties 22 p4053 A70-42735

NEUTRON DISTRIBUTION

Cosmic ray neutrons energy spectrum and angular distribution at sea level based on measurement results 03 p0556 A70-13046

Geomagnetic latitude survey by neutron multiplicity monitor covering threshold rigidity ranges at various elevations, relating data to primary cosmic ray rigidity spectrum 04 p0741 A70-15125

Neutron and proton distributions rms radii in nuclei by optical model analysis of low energy pion-nucleus interactions 07 p1337 A70-19360

NEUTRON EMISSION

Time dependent telegrapher equation solution for studying transient neutron waves propagation 01 p0130 A70-10086

Focused deuterium plasma discharge neutrons and X rays energy spectra, flux and time resolved collimation measurement with nuclear emulsions and scintillation detectors 02 p0348 A70-12241

Nuclear fusion reactions by focused Q switched Nd doped laser beam on deuterium target, discussing neutrons from flowing plasma, electron temperature and counter experiments 03 p0501 A70-13684

Lunar neutron flux due to cosmic radiation interaction with lunar surface layer, determining angular distribution and energy spectrum 04 p0738 A70-14442

Gamma radiation integral fluxes and production rate evaluation from ground and neutron production in Plexiglas and Fe to calculate optimum recoil electron threshold 05 p0899 A70-15955

Solar cosmic ray flare /28 January 1967/ observed by neutron monitors, determining emission and particle spectrum at atmosphere boundary 05 p0903 A70-16752

Neutron flux due to cosmic radiation interaction with lunar surface layer, determining angular distribution and energy spectrum 13 p2475 A70-28467

TSF-SNAP reactor neutron radiation leakage, comparing Monte Carlo calculations with experimental and analytical determinations 20 p3671 A70-39156

NEUTRON FLUX

U FLUX (RATE)

NEUTRON FLUX DENSITY

Correlation between atmospheric meteor entry and gamma and neutron radiation intensity verifying micrometeor antimatter hypothesis 03 p0454 A70-13528

Large amplitude wave trains in cosmic ray neutron intensity compared with diurnal variations, determining interplanetary space directional distribution from monitor data 03 p0559 A70-13912

Forbush effect on intensity of neutron component of cosmic rays during quiet sun period 05 p0897 A70-15795

Fast neutron transport characteristics of helical ducts using Monte Carlo code FASTER, computing neutron fluxes and attenuation 05 p0884 A70-16163

Neutron flux measurements on Cosmos 53, equipment and calculation of secondary neutrons due to bombardment of satellite components 05 p0905 A70-17112

High energy neutrons searched for during solar flares by balloon flights, giving upper limits for gamma ray and neutron fluxes 06 p1136 A70-18008

Barometric and atmospheric temperature corrections of cosmic ray neutron component intensity fluctuations obtained statistically from monitor recording 07 p1366 A70-19430

Cosmic rays effect on atmospheric temperature and wind, discussing planetary distribution of neutron component of radiation intensity 07 p1373 A70-20346

Altitude dependence of low latitude cosmic ray diurnal variations from cosmic ray neutron data 13 p2479 A70-29792

High altitude neutron supermonitor investigation of cosmic ray microvariations 18 p3307 A70-36104

Barometric and atmospheric temperature corrections of cosmic ray neutron component intensity fluctuations obtained statistically from monitor recording 18 p3309 A70-36904

Neutron flux measurement in nuclear reactors based on logarithmic techniques and digital approach, discussing temperature effects compensation 19 p3427 A70-37939

Midlatitude atmospheric neutron density height dependence during minimum solar activity 20 p3697 A70-39285

Cosmic ray neutron semidiurnal variations day and night components with respect to geomagnetic and solar activity 20 p3698 A70-39298

Earth atmosphere cosmic ray neutron albedo from balloon measurement of flux vertical distribution 20 p3698 A70-39298

Cosmic ray albedo neutron flux latitude and altitude dependence, using OGO-6 polar orbiting satellite 20 p3698 A70-39326

Barometric coefficient altitude dependence of cosmic ray neutron monitor for vertical flux 20 p3699 A70-39347

Atmospheric neutron flux increase during solar proton event, measuring flux and energy spectrum of particles by balloon sounding 21 p3881 A70-41076

High energy solar neutron flux via balloon measurement of flux difference from solar direction and from symmetrical direction about zenith 23 p4236 A70-43881

Solar neutron flux density relation to solar flare of 28 September 1968, using high altitude balloon-borne neutron detector 23 p4238 A70-44925

NEUTRON IRRADIATION

X ray topography of postannealing substructure of neutron irradiated W and Mo single crystals, indicating increase in disorientation 01 p0115 A70-10065

High temperature ductility improvement in stainless steels containing He, analyzing lattice damage and interphase cavities after fast neutron irradiation 01 p0123 A70-11246

Silicon solar cells I-V characteristics, spectral response and diffusion length measured after neutron irradiation 03 p0537 A70-13025

DNA penetration into normal and fast neutron irradiated yeast cells, using immunofluorescent microscopy 03 p0417 A70-13072

Neutron bombardment effect on ordering and disordering state of alloys phase diagrams, noting temperature dependence 03 p0506 A70-13107

Superconducting properties of polycrystalline disordered cold worked Nb-Ti-V alloys showing unexpected sensitivity to fast neutron irradiation 03 p0508 A70-13144

Brittle fracture in neutron irradiated and nonirradiated Mo specimens tested in tension and compression at low temperature 03 p0513 A70-14013

Neutron induced defect clusters in high field space charge region of Si p-n junctions, noting rate of volume damage dependence on electric field strength 04 p0730 A70-14728

Resistivity, temperature and injection level dependence of minority carrier lifetime in neutron irradiated p- and n-type Si 04 p0730 A70-14729

Neutron irradiation effect on space charge limited current of electrons in high purity silicon, noting SCLC sensitivity in detecting traps and changes 04 p0731 A70-14730

Structural materials mechanical properties tests during neutron bombardment, discussing atomic reactors optimal parameters calculation 04 p0775 A70-15259

Specific heat and thermal EMF increase due to radiation damage in lattice of fast neutron bombarded Cu, Mo and W specimens 05 p0863 A70-16292

Neutron irradiation and annealing effects on lattice constants of titanium and chromium carbides analyzed for X ray diffractions 07 p1303 A70-18702

Antiradiation chemical substances for modifying radiation damage in peas during seed irradiation with fast neutrons 07 p1208 A70-19510

Neutron irradiation damage in W, observing consistency of activation energy for self diffusion with vacancy mechanism 07 p1314 A70-20012

Gamma-neutron irradiation effect on miniature pig, observing incapacitation with severe convulsions and performance decrement 09 p1622 A70-23461

Thermal conductivity of neutron irradiated copper at low temperature noting lattice defects 11 p2148 A70-25757

Antiradiation chemical substances for modifying radiation damage in peas during seed irradiation with fast neutrons 11 p1988 A70-26109

Cu doped GaAs n- to p-type transition after fast reactor neutron irradiation, measuring Hall effect and photoconductivity to determine Cu electrical activation 12 p2287 A70-27490

Combined neutron and gamma ray irradiation effects on piezoresistive accelerometers 13 p2405 A70-28814

Electromotive force appearance in fissionable material semiconductor during thermal neutrons irradiation 13 p2469 A70-28879

Neutron irradiation effect on n-channel GaAs junction FET performance, considering transconductance, drain current, pinch-off voltage and cut-off frequency 13 p2376 A70-28932

Dimensional measurements of nuclear fuel cylindrical specimens by scanning neutron radiographic negative with microdensitometer, taking into account specimen geometry and neutron cross section 15 p2735 A70-31769

Void formation and creep during fast neutron irradiation of austenitic stainless steel based on thermodynamic approach, calculating nucleation and growth rates 17 p3123 A70-34626

Neutron irradiation effects on stress corrosion susceptibility of Al alloy 17 p3124 A70-34822

Microelectronic systems radiation resistance, examining logic IC gates for reactor neutron irradiation 18 p3233 A70-36783

Neutron irradiation effect on unijunction transistors and SCRs, developing damage prediction technique 19 p3388 A70-37848

Flexible shallow shell with plastic inhomogeneity due to yield point-fast neutron flux relation, examining stability under uniform load 20 p3734 A70-40437

Neutron irradiation effect on elevated temperature fracture of various fcc alloys 22 p4054 A70-42957

NEUTRON SCATTERING

Lunar and planetary surface chemical composition analysis using neutron inelastic scattering as optimum for unmanned missions 10 p1942 A70-24613

Polarized Co59 target using He3-He4 dilution refrigerator, analyzing fast neutron scattering 14 p2584 A70-30508

Initial value transport of monoenergetic neutrons migrating in slab with infinite reflectors for isotropic scattering as function of material properties 21 p3854 A70-41999

Neutron-electron collision damping and displacing of space echo in plasmas, indicating use for density measurement 22 p4082 A70-43244

Transverse and longitudinal current correlations in fluids from modeled kinetic equations, noting inelastic neutron scattering from liquids 24 p4378 A70-45261

NEUTRON SOURCES

Nondestructive testing of Apollo CSM /Command and Service Module/ spacecraft ordnance explosive devices by indirect and direct neutron radiography 03 p0494 A70-14123

Neutron formation multiplicity during capture of cosmic ray muons by Zn and Sb nuclei, noting agreement with one-third law 08 p1560 A70-20718

High speed shock wave propagation in deuterium gas, observing neutron production 21 p3806 A70-40744

Reactor, isotropic and accelerator neutron sources for thermal neutron radiography 24 p4375 A70-45746

Equipment, sources and safety in neutron radiography for industrial quality control 24 p4376 A70-45747

Scintillator-film neutron radiography converter combinations efficiency gain for small sources by cooling 24 p4376 A70-45751

NEUTRON SPECTRA

Fast neutron spectrum produced by galactic cosmic ray protons in atmosphere, presenting Monte Carlo transport calculation results 04 p0742 A70-15130

Solar cosmic rays diffusion enclosure in interplanetary space magnetic boundary suggested from balloon, satellite and ground observations of solar flare neutron component 05 p0904 A70-16753

Threshold rigidity decrease during 23-24 March 1969 magnetic storm, analyzing neutron multiplicity spectrum 23 p4186 A70-43846

NEUTRON SPECTROMETERS

Liquid scintillator neutron spectrometer using pulse shape discrimination and two parameter analyzer 18 p3290 A70-36563

NEUTRON STARS

Final state of matter resulting from star contraction, white dwarfs development and neutron stars problem, explaining hydrostatic equilibrium

02 p0370 A70-12085

Neutron star atmospheric composition as function of time, including effects of diffusion, cooling and nucleosynthesis

02 p0378 A70-12698

Hyperon and resonance particle effects on neutron star vibration, discussing vibrational energy storage and atmospheric electromagnetic generation

02 p0379 A70-12699

Electric fields in rotating magnetic relativistic neutron stars, analyzing static fields in corotating frame and pulsar emission

02 p0379 A70-12726

Neutron star X synchrotron radiation from gas accretion producing strong magnetic field with high electron temperature

03 p0557 A70-13220

Rotational properties of neutron star models for Crab Nebula energy source, using expressions for angular momentum and rotational kinetic energy

03 p0571 A70-13817

Pulsars observed properties and interpretation based on oblique rotator model for neutron stars

03 p0577 A70-14099

Superfluid states of matter in interior of neutron stars, discussing strong interaction forces role

03 p0578 A70-14219

Neutron star electrical conductivity, discussing stellar flux and magnetic field decay times

03 p0578 A70-14220

Pulsars pulse duration and shape as key to neutron stars linkage with supernova explosions

04 p0750 A70-14749

Neutron star vulcanism and seismicity, discussing neutron star volcano size and shape possibilities

04 p0753 A70-15070

Hydrostatic equilibrium solutions of internal structure of neutron stars using Brueckner equation

06 p1139 A70-17541

Angular velocities and equilibrium of rotating neutron stars compared with white dwarfs

07 p1376 A70-18911

Landau Orbital Ferromagnetism in electron gas as magnetic field source for neutron stars

07 p1380 A70-19279

Neutron stars equation of state derived, suggesting three body forces inclusion at high densities

07 p1388 A70-19924

Pulsar magnetorelativistic model assuming neutron star with magnetic field

08 p1563 A70-20478

Neutron star X synchrotron radiation from gas accretion producing strong magnetic field with high electron temperature

08 p1563 A70-21653

Supernovae and remnants - Conference, New York, November 1967

09 p1748 A70-21987

Supernovae and remnants, data concerning radio brightness distribution of Tycho supernova remnant and Cassiopeia and Crab Nebula origin

09 p1748 A70-21989

Supernovae remnants evolution, properties and galactic distribution, discussing criteria for catalog listing and remnants as X ray sources

09 p1749 A70-21990

Relativistic gravitational stellar collapse calculations for stars exceeding neutron star limit, discussing results in terms of supernovae or neutrinos

09 p1749 A70-21991

Neutron stars properties, using static cold stellar model to examine relation between central density and mass, and cool hyperonic matter composition

09 p1749 A70-21995

Gravitational radiation detection from pulsating neutron star, considering asymmetries in gravitational collapse of massive stars as origin

09 p1749 A70-21996

Supernovae remnants X ray emission associated with explosion process generating relativistic particles, indicating Crab Nebula as X ray object

09 p1749 A70-21998

Crab Nebula continuing energetic activity study indicating origin in nebula center and association with supernova remnant

09 p1750 A70-22000

Magnetic moment associated with Landau levels in magnetic induction in electron gas and magnetic fields of white dwarfs and neutron stars

09 p1752 A70-22306

Pulsar model assuming magnetic dipole radiation by spinning neutron star interacting with nearby plasma

09 p1756 A70-22517

Pulsars period distribution not related to decay of magnetic field in rotating neutron star

09 p1756 A70-22518

Pulsars as tiny superdense neutron stars with spin to explain galactic cosmic rays and radiation from supernova remnants

09 p1756 A70-22631

Equation of state for cold matter at neutron star densities, deriving equilibrium equations for nuclear interactions among hadrons

09 p1764 A70-23606

Neutron star models based on equation of state for cold degenerate matter, taking into account nuclear forces and clustering

09 p1764 A70-23607

Magnetic funneling model proposed for accretion of matter onto neutron star to study X ray production during motion through interstellar cloud

10 p1931 A70-23902

Pulsars in supernova remnants emitting X rays

10 p1933 A70-24627

Longitudinal electrical conductivity of relativistic gas in intense magnetic field

10 p1924 A70-24634

Milky Way expansion, explaining Weber gravitation signals by collisions between neutron and normal star

10 p1943 A70-24698

State equations of matter at high density and zero temperature, considering neutron stars relationship to supernova explosions and collapse

12 p2298 A70-27059

Pulsar properties association with neutron star rotation energy, discussing alternate pulsar theories

12 p2301 A70-27579

Pulsar theory of rotating and precessing neutron stars, rejecting relevance of forced precession to behavior

12 p2308 A70-27884

Dwarf and neutron stars as pulsar energy sources, considering Crab Nebula X ray emission and gravitational collapse

12 p2310 A70-27990

Dissipation mechanism and period rate increase in neutron star pulsar model with neutrino emission for damping

12 p2312 A70-28368

Crab pulsar /neutron star NP 0532/ possible spherical asymmetry indicated by pulse arrival time anomalies

13 p2486 A70-28618

Cosmic rays emission by dipole magnetosphere, applying model to neutron star particle belts

13 p2476 A70-28893

Superfluidity and superconductivity under cosmic conditions, discussing Bose-Einstein condensation, neutron stars, white dwarfs, etc

15 p2795 A70-31454

Pulsar formation mechanism, showing core collapse to neutron star state

15 p2806 A70-32773

Neutron stars gamma and radio emission in gas accretion state, determining surface gravitational potential

15 p2808 A70-32883

Hot small mass neutron stars cooling time and internal characteristics, discussing evolution based on H-R diagram

15 p2808 A70-32886

Frequency spectra of gravitational waves radiated from celestial phenomena, suggesting mass exchange in binary containing neutron star

17 p3067 A70-34619

Neutron core star models based on realistic nuclear matter calculations and hyperons equation of state

17 p3157 A70-34844

Pulsars theories review, discussing geometrical model picturing pulsar as rotating neutron star with high magnetic field

17 p3164 A70-35117

Superheavy nuclei origin in primary cosmic rays, proposing neutron stars /pulsars/ as sources

18 p3308 A70-36403

Pulsars pulsation mechanism, using neutron star model with oblique rotation axis

18 p3319 A70-37048

Electrical and thermal conductivities in white dwarf stars cores and neutron stars outer layers, calculating electron-photon collisions transition probability

20 p3702 A70-39016

Collapsing or neutronizing stars detection by recording neutrino and antineutrino flux, calculating antineutrino-deuteron interaction cross section and positron energy and angular distribution

20 p3698 A70-39302

Equilibrium theory of white dwarfs, neutron and hyperon stars, deriving equations for nonrotating objects composed of degenerate cold electron or neutron gas

20 p3704 A70-39472

Neutron stars, discussing equations of state and stellar interiors, models, atmosphere, cooling, vibration, rotation and magnetic fields

20 p3706 A70-39932

Neutron star superfluid turbulent state, applying dynamic model to conditions in pulsars

20 p3713 A70-40429

Proper motion evidence for existence of X ray stars associated with Sco X-1 and Cen X-2, indicating formation by neutron stars

21 p3873 A70-40673

Rotating neutron stars, pulsars and cosmic X ray sources relationship, discussing stellar model with mass loss in presence of magnetic field

21 p3874 A70-40678

Pulsar research review, discussing characteristics, neutron star theory and galactic origin

21 p3886 A70-41072

Pulsars and neutron stars origin and properties, discussing superdense star angular velocity, blackholes, supernovae remnants, rotation, etc

21 p3923 A70-42171

Neutron star crust conductivity, obtaining electrical conductivity formula for outer kilometer

24 p4403 A70-45394

Neutron star or defunct pulsar accretion of interstellar matter, discussing effects on total luminosity and radiation spectrum

24 p4403 A70-45397

Pulsar distributions without magnetic decay, concerning age dependence of surface field and radio luminosity of neutron stars

24 p4413 A70-46138

NEUTRON THERMALIZATION

Nuclear rocket engine core thermal and neutronic transient and steady state dynamics digital simulation, showing advantages over lump model analysis

[ASME PAPER 69-WA/NE-3] 04 p0717 A70-14757

NEUTRON TRANSMUTATION

U NUCLEAR REACTIONS

NEUTRONS

NT FAST NEUTRONS

NT PHOTONEUTRONS

NT THERMAL NEUTRONS

Cosmic rays neutron component solar-diurnal variations as function of solar activity using magnetically quiet data

05 p0898 A70-15941

Intensity variations of cosmic ray neutrons and mesons analyzed to isolate lunar day period

07 p1368 A70-20033

Magnetic storms effect on cosmic ray neutron component diurnal variation, determining amplitudes and phases of harmonics by harmonic analysis

07 p1372 A70-20341

Diurnal variations of cosmic ray neutrons following solar proton flares, proposing anisotropic diffusion model for phase and amplitude

07 p1372 A70-20342

Boundary value problems in one speed transport theory, applying Green function technique to neutrons with spherical symmetry

08 p1542 A70-21253

Neutron capture effects in Gd from Norton County meteorite by isotopic composition analysis

12 p2300 A70-27524

Cosmic ray neutron component differential and integral barometric coefficients, showing dependence on geomagnetic cutoff rigidity and atmospheric depth

20 p3697 A70-39290

Cosmic ray beta neutron component barometric coefficients planetary distribution during IQSY, establishing latitude dependence for mountain and sea level equations

20 p3697 A70-39292

Extremely high temperature deuterium examination, using coaxial plasma accelerators to determine neutron production and vorticity

23 p4227 A70-44452

X ray and neutron propagation in multilayer film composite, discussing boundary conditions in interferential systems

24 p4380 A70-46095

NEW MEXICO

New Mexico Bandera lava tube systems, noting similarities with lunar surface sinuous rilles

23 p4254 A70-44884

NEWTON SECOND LAW

Energy derivation for mechanics and thermodynamics with generalization to systems of more than two dynamic variables, considering transformations and Newton and Kepler laws

12 p2164 A70-27070

NEWTON THEORY

Human rectal temperature cooling rate during refrigeration in mortuary, applying Newton law

01 p0017 A70-10471

Kharlamova solution for solid body motion in Newtonian force field represented as rolling, without slipping, of mobile hodograph of angular velocity vector

01 p0145 A70-11431

Translational-rotational motion of long dumbbell in Newtonian central force field, analyzing plane center of mass trajectory with perpendicular kinetic moment vector

04 p0744 A70-14427

Stellar configurations of cold static neutral plasma consisting of nuclei and degenerate electron gas, calculating integral parameters by Newton gravitation theory

07 p1376 A70-18912

Mass point motion in celestial mechanics, investigating two and three body problems without equal counteraction assumption

08 p1565 A70-20562

- Mathematical model for finite-density non-homogeneous Newtonian cosmologies, approximating solutions using coupled Vlasov- Poisson equations
08 p1581 A70-21740
- Particle escape from Newtonian gravitational system of positive energy
10 p1938 A70-24183
- Different gravitational force fields effecting optimal rocket trajectories and queried validity of Newtonian law
10 p1943 A70-24820
- Kantorovich theorem application as weak Newton method used in boundary value problems containing Euler-Lagrange equation for variational problems and ordinary differential equations
12 p2260 A70-27002
- Translational-rotational motion of long dumbbell in Newtonian central force field, analyzing plane center of mass trajectory with perpendicular kinetic moment vector
13 p2485 A70-28452
- Mass point motion in celestial mechanics, investigating two and three body problems without equal counteraction assumption
15 p2805 A70-32717
- Newtonian gravity law in light of relativistic theories, considering deviations of quasars and red shift deviations from Newton theory
16 p2976 A70-33722
- Newtonian hypersonic aerodynamic theory for arbitrary bodies, discussing computational difficulty for shadowed areas
21 p3747 A70-41866
- Newton and Einstein gravitation theories applied to light velocity in gravitational field
24 p4379 A70-45487
- Earth-moon laser distance measurements, examining relationship between Newtonian and relativistic field coordinates
24 p4413 A70-46160
- NEWTON-BUSEMANN LAW**
Slender axisymmetric power-law missile bodies with minimum ballistic factor, using Newton-Busemann centrifugal theory with skin friction
21 p3746 A70-41756
- NEWTON-RAPHSON METHOD**
Differential equations in two point boundary value problems solved by combining Newton-Raphson iterative method with parameter variation extrapolation
12 p2260 A70-27003
- Inverse boundary value problems involving elliptic equations solved by Newton method and discrete invariant imbedding
13 p2440 A70-28650
- Newton-Raphson method analog accelerating convergence of multidimensional stochastic approximation algorithm to local minimum for attitude controller design
13 p2382 A70-29069
- Quasi-linearization /generalized Newton-Raphson process/ in orbit determination, comparing with differential correction method
17 p3168 A70-35235
- Normalized multidimensional Newton-Raphson method eliminating initial guess, using two-transformation technique
19 p3457 A70-37822
- Newton regularized method for nonlinear boundary value problems in combination with conjugate gradients
22 p4064 A70-43480
- NEWTONIAN FLUIDS**
Film-vapor interface shape for thin liquid lubricating film, analyzing two dimensional Newtonian flow including gravity, inertia and surface tension effects [ASME PAPER 69-LUB-3]
01 p0103 A70-10399
- Newtonian liquid lubricated spiral groove bearing load capacity and power loss dependence on viscosity variations with temperature
02 p0309 A70-12533
- Critical thermal regimes in Couette flow, investigating temperature and velocity profiles of nonisothermal steady state Newtonian flow between two parallel plates
03 p0466 A70-13388
- Laminar steady radial flow of simple fluid of short memory between two parallel disks, demonstrating relation to Newtonian fluid
06 p1037 A70-17915
- Shape of minimum drag slender body of revolution in Newtonian flow for given volume, length and maximum cross section determined by stochastic optimality principle
10 p1802 A70-24278
- Newtonian fluid laminar throughflow between coaxial corotating cones, applying solution for flow between disks
11 p2038 A70-26491
- Newtonian fluid laminar boundary layer flow over flat plate with nonNewtonian fluid injection
12 p2209 A70-27212
- Wave propagation through Newtonian fluid in compressible thick walled viscoelastic tube, considering blood flow in arteries
15 p2691 A70-31938
- Post-Newtonian equations of hydrodynamics and radiation reaction in general relativity
17 p3156 A70-34828
- Unsteady state Newtonian liquid diffusion in laminar flow in circular tube, using mathematical model
17 p3072 A70-35544
- Film-vapor interface shape for thin liquid lubricating film, analyzing two dimensional Newtonian flow including gravity, inertia and surface tension effects [ASME PAPER 69-LUB-3]
19 p3435 A70-37610
- NonNewtonian boundary layer flow having arbitrary potential velocities from methods for Newtonian fluids
19 p3407 A70-38932
- Navier-stokes equations solutions in two way flows of Newtonian fluids with constant kinematic viscosity
21 p3810 A70-41961
- Incompressible Newtonian fluid laminar radial flow between parallel stationary disks, obtaining integral solution for Navier-Stokes equation
22 p4007 A70-42302
- Newtonian fluid turbulent flow development characteristics in inlet region of smooth concentric annulus from momentum integral equations
22 p3957 A70-42304
- Newtonian hydrodynamic analogies for homogeneous anisotropic models in general relativity
22 p4075 A70-43472
- Incompressible Newtonian fluid flow between closely spaced corotating disks, showing radial pressure distribution similar to laminar flow
24 p4324 A70-45293
- Constitutive equations in fluid dynamics, discussing Newtonian, Oldroyd and Walter, Reiner-Rivlin, Rivlin-Ericksen, Noll, Bingham and oriented fluids
24 p4327 A70-46149
- Inertia effects and suspension rheology for incompressible Newtonian fluid shear flow around neutrally buoyant rigid sphere
24 p4327 A70-46243
- NICHROME [TRADEMARK]**
Strengthening mechanisms in dispersion hardened Nichrome /TDNiC/ analyzed in 70-2000 F range, discussing solid solution, dislocation substructure and grain refinement
08 p1525 A70-21961
- NICKEL**
NT NICKEL ISOTOPES
Coherent precipitates effect on explosive shock hardening of pure nickel and Inconel alloy sandwich assemblies determined from simultaneous shock loading at specific pressures
01 p0116 A70-10107
- Crack propagation mode in laminated steel-Ni composites, analyzing softer layer effect using impact tests and C replica fractographs
01 p0120 A70-10743
- Tensile strength of flat specimens of Ni reinforced by W wire gauze
02 p0315 A70-11661
- Impurity diffusion in Ni using diffusion theory, considering activation energies for Mo and W
02 p0317 A70-12396
- Hydrogen, oxygen and nitrogen effects on gas shielded arc weld porosity of Ni, comparing MIG and TIG processes
02 p0310 A70-12543
- Polycrystalline Ni steady state creep characteristics measurement emphasizing temperature dependence of creep rate
03 p0504 A70-13022
- Mechanical properties, optimum deformation and rupture of W wire reinforced Ni and Ti metal composites obtained by hot rolling in vacuum
03 p0508 A70-13245
- Ni dispersion-strengthened composites from ultrafine comminuted powders, describing forming techniques and test results
04 p0709 A70-15629
- Nickel IV forbidden lines suggested from spectrum study of slow nova RR Telescopii
05 p0905 A70-15758
- High purity Ni fatigue in reversed bending as function of oxygen pressure and temperature
06 p1086 A70-17454
- Ni effect on nitrogen activity in Fe-Ni-N austenite between 600-1200 C using Strohlein analysis
06 p1088 A70-17612
- Inert gases scattering from Ni /111/ plane as function of beam temperature and angle of incidence compared to Au and Ag
06 p1110 A70-18263
- Ionization energies and oscillator strengths for Fe XVI, Co XVII and Ni XVIII by frozen core approximation, noting applications to solar corona
06 p1150 A70-18465
- Heat transfer in Ni wires in laminar air flow from wind tunnel investigation
07 p1420 A70-19064
- Crystal structure imperfections and elastic anisotropy of crystallites in condensed Ni films by X ray analysis
07 p1309 A70-19636
- Nickel boronizing in high temperature vacuum, studying mechanical properties and layer thickness time dependence
08 p1517 A70-21148
- Weld porosity in TIG welding of technical Ni in ternary mixtures of Ar with H, O and N
08 p1518 A70-21345
- Hydrogenated Ni activation energy difference for lower and higher critical temperatures due to hydride dislocations binding energy
08 p1522 A70-21705
- Ni L alpha X ray emission line shape and position as function of bombarding electron energy, observing differential self absorption in anode
09 p1731 A70-22777
- D-pattern changes of helium ions irradiated polycrystalline Mo and Ni specimens, observing line splitting
09 p1707 A70-23197
- Epitaxy of Ag deposited on Ni, observing irreversible crystallographic order transition from metastable nominal orientation by LEED
10 p1927 A70-24076
- Intensity vs voltage curves for LEED beams from clean Ni surface, calculating Bragg spectrum with energy diagram method
10 p1927 A70-24077
- Raney alloy catalyst activity and stability in fuel cell anodes, noting properties of ternary phases of nickel, aluminum and iron, molybdenum or titanium
10 p1831 A70-24466
- Raney catalyst preparation and continuous operation in molecular hydrogen and oxygen electrodes noting improved voltage, manipulation and energy yield
10 p1831 A70-24467
- Electrochemically optimal structure for Raney alloy catalysts based on molecular hydrogen polarization temperature, noting beta and gamma phases and particle size influence
10 p1831 A70-24468
- Heat transfer in Ni wires in laminar air flow from wind tunnel investigation
10 p1970 A70-25215
- Fatigue life of Ni vibrated in reversed bending at 300 C in oxygen and in water vapor at various pressures
11 p2067 A70-26098
- Anomalous grain growth kinetics and recrystallization in electron beam annealed nickel determined by microstructural and radiographic study, noting annealing time dependence
11 p2068 A70-26596
- Selective optical coatings of alternate Ni and silicon dioxide layers, describing optical and spectral characteristics of black mirror
12 p2272 A70-27307
- Stress-strain state effects on Cu and Ni tubular samples plasticity and strength using polarization-optical technique
12 p2323 A70-27341
- Contaminated Ni crystal /100/ surface photoelectric yield as function of temperature, considering effects of Ar ion bombardment and annealing
12 p2288 A70-27680
- Collection of papers on nickel and nickel alloys covering thermal and mechanical properties during annealing and precipitation hardening behavior
13 p2432 A70-28758
- Ni and Ni alloys thermal properties, discussing expansion and conductivity, melting and boiling points, vapor pressure, specific heat, entropy, etc
13 p2432 A70-28759
- Ni and Ni alloys elastic properties relationship with ferromagnetic and magnetostriction effects, determining modulus of elasticity for wide temperatures and heat treatment
13 p2432 A70-28760
- Deformation, mechanical properties and processes during recrystallization annealing of nickel and alloys single crystals
13 p2433 A70-28761
- Zirconium additions effect on Ni internal friction behavior and relaxation spectrum
13 p2435 A70-29498
- Ferromagnetic Ni band structure and Fermi surface including spin-orbit and exchange interactions obtained by Mueller interpolation scheme
14 p2626 A70-30479
- Ionization equilibria and ionization and recombination rates for Fe and Ni ions, discussing dielectronic recombination
14 p2631 A70-30727
- Fe 57 contaminant in Ni, studying Mossbauer effect as function of temperature
15 p2784 A70-32023
- Work hardening properties of Ni single crystals of various orientations during intermittent and continuous plastic deformation
15 p2762 A70-32394
- Ni-S melts thermodynamic properties in 700-1100 C range by continuous thermal balance method, calculating S vapor pressure
18 p3271 A70-36029
- Gas bubbles thermal rejection and formation in Ni electrodeposit during annealing over 200-1000 C range
18 p3272 A70-36039

Lunar anorthosites Ni-Fe grains from Mare Tranquillitatis, discussing contamination by meteoritic metal, magnetic fractionation and fractional crystallization
19 p3519 A70-38032

Tensile strength of flat specimens of Ni reinforced by W wire gauze
19 p3452 A70-38435

Mechanical properties, optimum deformation and rupture of W wire reinforced Ni and Ti metal composites obtained by hot rolling in vacuum
19 p3453 A70-38463

Solar photospheric spectrum Ni II forbidden lines analysis, determining abundance of Ni for comparison with coronal and meteoritic data
20 p3711 A70-40405

Pure Ni plastic flow threshold measurement under combined ultrasonic and static loadings, noting annealing
22 p4053 A70-42644

Nickel surface layer fine structure changes in super-sonic air flows at various temperatures and times
22 p4056 A70-43341

Fe meteorites with high Ge content, tabulating concentrations of Ni, Ga, Ge and Ir
23 p4241 A70-44259

Oxygen pressure effects on Ni oxidation kinetics at high temperatures
23 p4208 A70-44920

Hydrogenated Ni elastic limit discontinuity, discussing Portevin-Le Chatelier effect
23 p4208 A70-44921

Cu and Ni doped n-p and p-n silicon solar cells, examining radiation damage and isochronal annealing properties
24 p4294 A70-45810

Pure Ni recrystallization, noting stacking faults and parallel sided and thin annealed twins formation during boundary migration
24 p4363 A70-46192

Ni/sulfuric acid AC voltage polarization curves for anodic dissolution region
24 p4364 A70-46220

Hydrogen effect on deformation and fracture of polycrystalline nickel
24 p4365 A70-46372

NICKEL ALLOYS
NT HASTELLOY [TRADEMARK]
NT INCONEL [TRADEMARK]
NT KAMACITE
NT NICHROME [TRADEMARK]
NT RENE 41
NT UDIMET ALLOYS
NT WASPALLOY

Chemistry variations effects on mechanical properties, phase stability and microstructure of alloy Unitemp 718 /Ni-Fe-Cr alloy/ via microscopy and X ray analysis
01 p0116 A70-10092

Rolled bimetallic Ni-Mo mechanical properties produced by powder metallurgy methods
01 p0116 A70-10157

Creep deformation modes of Ni-base austenitic superrefractory alloy as function of test temperature
01 p0118 A70-10704

Transmission electron microscope study of deformation mode during rapid tensile testing of Ni-base superalloy, discussing twinning and stacking fault modes
01 p0118 A70-10705

Tungsten effect on phase transformations and carbide reactions to attain equilibrium at 850 C in Ni-base superalloys
01 p0118 A70-10727

Hot corrosion reactions in Ni, Co and NiAl-base alloys exposed to salt-sulfur containing simulated gas turbine combustion atmospheres
01 p0118 A70-10728

Precipitation in Ni-base superalloy analysis with dark field electron microscopy and electron and X ray diffraction
01 p0119 A70-10730

Intrinsic/extrinsic stacking fault pairs observed during creep of single crystals of gamma prime precipitation hardened Ni-base alloy, developing viscous slip model
01 p0119 A70-10731

Offset yield strengths of TD-Ni and Al-aluminum oxide SAP type two phase alloys in tension and compression
01 p0119 A70-10736

Martensite structure, discussing intensity anomalies in X ray diffraction pattern of intermetallic Ni-Nb
01 p0121 A70-10900

Phase changes in Ni/Ti alloys with equiatomic composition, resolving discrepancy on non-Martensitic eutectoidal decomposition of B2 structure and intermediate precipitate
01 p0121 A70-11232

Vapor pressures of cobalt over pure cobalt and over Ni-Co alloys determined as function of temperature by isotope exchange method
01 p0121 A70-11233

High temperature internal friction measurements on miniature torsional pendulum specimens from TD

nickel bar, showing damping differences due to microstructural anisotropy
01 p0122 A70-11237

TD-Ni low cycle fatigue properties at high temperature, discussing grain morphology, theta particles role and oxidation resistant coating effect
01 p0123 A70-11245

Semicoherent interface dislocations in directionally solidified Ni-Al-Cr eutectic, discussing lattice mismatch
01 p0123 A70-11247

Ni-based superalloys microstructure, describing composition, formation and characteristics of various phases
01 p0124 A70-11448

Long range order formation in Ni-Cr alloys analyzed by direct neutron diffraction, considering disorder-order transition temperature and chemical composition
01 p0124 A70-11600

Vacuum deposition of Cr-Al film on Ni-Mo alloys, describing operating pressure, temperature and film thickness
01 p0124 A70-11617

Size distribution of Ni-Si particles precipitated from Si solid solution in Ni measured as function of concentration, aging time and temperature
02 p0317 A70-12320

Potential lubricants in friction and cup forming tests of stainless steel, Ti- and Ni-base alloys, considering boron nitride, graphitic materials and Mo oxides
02 p0309 A70-12540

Heat and creep resistant Ni- and Fe-base alloys application in gas turbines, superheaters, steam pipes, chemical and petrochemical plants and heat treatment equipment
02 p0319 A70-12711

Strain hardening on single crystals of aging Ni-based alloys with ordered separated phase
03 p0505 A70-13104

Mechanical properties of ordered Ni-Cr alloys, establishing hardening effect of annealing
03 p0505 A70-13105

Microdeformation resistance in Ni alloys with ordered phase diagrams related to strain level, analyzing Bauschinger effect
03 p0505 A70-13106

Phase alteration quenching effects in Ni-Mo alloys, discussing high temperature alpha region, isothermal annealing below peritectoid temperature and metastable nickel molybdenide phase
03 p0508 A70-13143

Grain size, forging parameter and microstructure effect on stress-rupture properties of wrought Ni-base alloy
03 p0511 A70-13567

Ni-Nb intermetallic compound precipitation effect on various phase formations in strained samples of Alloy 718 /wrought Ni base alloy/
03 p0511 A70-13568

Al and Ti single additions effects on recrystallization of Ni-Cr alloys, noting phase transformation and hardness variations
03 p0513 A70-14300

Ni-Cr alloy oxidation resistance dependence on small amount of Al at high temperatures, noting role of protective oxide layer
03 p0514 A70-14315

Extension characteristics of delta and sigma related phases in Mo-Ni ternary systems and evaluation of unit cell dimension variations on alloying
04 p0704 A70-14392

Prealloyed powders of Ni base alloys, made by inert gas atomization for improved strength and ductility
04 p0706 A70-14951

Nickel base alloy, WAZ-20 with improved strength in 2000-2200 F range for application to gas turbine engine stator vanes
04 p0706 A70-15097

Ni addition effects on Mg-Nd and Mg-Nd-Mn alloys structure and heat resistance
04 p0706 A70-15189

Fatigue tests results parametric representation for nickel base alloys tested at various temperatures and times to failure
04 p0707 A70-15264

Ni-V alloys precipitation behavior with 15.4/16.5 wt percent V content, observing tetragonal equilibrium theta phase precipitation
04 p0708 A70-15368

High temperature properties mechanisms in aluminum coated vacuum cast nickel base superalloys
04 p0711 A70-15705

Thin film transmission electron microscopy study of precipitation in Fe-Ni-Cr-Mo alloy with added Be and specific thermoelastic properties
05 p0862 A70-16022

Alloy EI 602 ingots low ductility during forging ascribed to nonferrous metal atoms, decreasing iron diffusion and forming brittle nitride and carbide compounds
05 p0863 A70-16545

Refractory Ni alloys defects accumulation under creep and cyclic temperature variations assessed by relative lifetime additive method
05 p0866 A70-17032

Nickel-based alloys small cycle thermal and mechanical fatigue limit during tensile stresses and operational temperatures, analyzing fatigue curves
05 p0867 A70-17046

Heat resistant steel and nickel alloys stress rupture strength at operating temperatures, discussing endurance diagrams under cyclic bending loads
05 p0868 A70-17047

Soviet monograph on nickel and Ni vacuum melted alloys, studying physicomechanical, operational characteristics and gas content
06 p1085 A70-17411

Ni-Cr alloys oxidation dependence on temperature and Cr concentration
06 p1087 A70-17609

Ni-Cr alloys effects of grain size and surface deformation on oxidation properties at high temperature
06 p1088 A70-17610

Ni-Fe alloys texture formation, studying strong deoxidizers role in secondary recrystallization
06 p1088 A70-17614

Aluminosilicate coatings for increased Ni-Cr alloys heat resistance due to silicon properties
06 p1089 A70-17743

Isothermal sections in Ti-Ni-B, Mo-Ni-B and W-Ni-B at 800 C determined by X ray analysis
06 p1090 A70-17846

Roll diffusion bonding applicability to Ti, Ni and Fe alloys, discussing fabrication temperatures and tooling [AIME PAPER F-69-3]
07 p1290 A70-18813

Ni influence in high temperature oxidation of austenitic Fe-Cr-Ni alloys investigated thermogravimetrically, metallographically and by electron probe microanalysis
07 p1305 A70-18965

Solution treating temperature and microstructure effects on hot rolled Ni base alloy properties
07 p1306 A70-18995

Microfissuring of Ni base alloy weldments as function of grain size produced by solution temperature
07 p1306 A70-18996

Cobalt effects on Ni-W alloys mechanical and metallurgical properties including thermal stability, fabrication response, weldability and impact resistance
07 p1306 A70-19070

Phase equilibrium and homogeneity regions of solid solutions system Ni-Nb-O at elevated temperature
07 p1315 A70-20313

Ce-Ni-Si system X ray and microstructural analysis, constructing phase diagram for Ce contents of 0-33.3 wt percent
08 p1555 A70-21115

Nickel alloy based metal fiber reinforced composites long-time structural stability at high temperatures
08 p1517 A70-21150

Quadratic precipitate transformation into orthorhombic phase with conservation of maximal atomic density planes in Ni-Cr-Nb and Ni-Cr-Ta alloys during prolonged reheating
08 p1518 A70-21240

Matrix stiffened nickel-chromium welding products featuring high tensile strength at room and elevated temperatures and high impact strength at cryogenic temperatures
08 p1508 A70-21488

Iron base and nickel base alloys susceptibilities to internal hydrogen and hydrogen environment embrittlements, studying crack initiation inside and at metal surface
08 p1520 A70-21515

Ni-Mo surface alloys investigated by low energy electron diffraction, using tabulated symmetry and extinction properties of space groups and phase diagrams
08 p1557 A70-21603

Gamma-gamma prime mismatch effects on stress rupture of Ni and Fe-Ni based alloys with Al and Ti hardeners
08 p1521 A70-21701

Serrated yielding in hydrogenated nickel alloys, noting hydride stability role in Portevin-Le Chatelier effect
08 p1522 A70-21706

Tungsten alloy fiber reinforced Ni-base superalloy composites evaluated for high temperature turbojet engine applications, considering stress-rupture strength, oxidation and impact resistance
08 p1523 A70-21907

Yield strength of cold worked MP Co-Ni alloys during aging at elevated temperatures, noting behavior in overaged condition
08 p1525 A70-21960

Sigma and mu phase formations in Ni heat resistant alloys x ray analysis using phase isolation by anodic dissolution
09 p1700 A70-22079

Powder metallurgy all-inert processing method for producing nickel base superalloys forgings, discussing

- microstructure, reproducibility, mechanical properties, etc
09 p1701 A70-22553
- Time, temperature and composition dependent regularities in Ni-Al and Ni-Nb alloys oxidation processes, discussing Oxygen ion migration and Ni ion diffusion
09 p1704 A70-22752
- Work strengthening and microstructure of Co-Ni base alloys containing Cr and Mo, discussing deformation induced martensitic transformation
09 p1705 A70-22806
- Ordered Ni₈Ta phase in nickel-rich binary alloy using electron microscopy and diffraction analysis
09 p1705 A70-22808
- Creep deformation in single crystals of gamma prime precipitation hardened nickel base alloys at intermediate temperatures
09 p1705 A70-22809
- Growth kinetics of gamma prime precipitate in Ni-Ti alloy noting Ti content variation as function of aging
09 p1706 A70-22812
- Ni-Cr superalloys hot corrosion, studying sulfidation-oxidation in various synthetic controlled gas mixtures
09 p1706 A70-22944
- Electrical resistivity of TiNi and TiCo compounds and alloys measured at various temperatures after quenching or annealing
09 p1707 A70-23194
- Gamma prime phase structure ordering effect on critical shear stresses of aging Ni-Al alloys and mimonin
09 p1707 A70-23195
- Order-disorder transition temperatures for Ni-Cr alloys determined by neutron diffraction, discussing homogeneous ordering of atoms
09 p1707 A70-23196
- Ni alloys with Ir and Rh using X ray diffraction and microscopy, exhibiting continuous solid solutions
09 p1708 A70-23423
- Adiabatic elastic stiffness of single crystals of Ni-Co alloys, determining bulk modulus dependence on chemical composition
10 p1904 A70-24699
- Ni-Cr alloys hardened by complex alloying with Ti-Al or Ti-Zr-C additions, improving strength at elevated temperatures in oxidizing atmosphere
10 p1904 A70-24836
- Binary Ni-Cr alloys tensile mechanical properties at 25 C after water quenching and heat treatments
10 p1905 A70-25172
- Stacking faults developed in double hexagonal closed-packed phase of Ni-Ti alloy in cold worked and annealed conditions, using X ray line broadening
10 p1906 A70-25228
- Precipitation hardened nickel-base alloy microcracking during gas tungsten arc and electron beam welding, studying heat affected zone hardness, phases and grain size
10 p1897 A70-25311
- Nickel base alloy as die material for creep forming titanium
11 p2060 A70-26424
- Iron-nickel alloy phase and diffusion relationships, composition gradients and hardness variations involving long time metallic meteorite anneals
12 p2252 A70-26964
- Ni-Nb-O system state diagram by reduction equilibria and X ray analysis, discussing oxidation resistance based on metal surface protective layers makeup
12 p2253 A70-27158
- Resistivity anomalies of nickel-chromium alloy with Al additions subjected to deformation and heating, studying K-state
12 p2254 A70-27496
- Dispersion strengthened Ni-Cr alloys elastic and plastic properties at room temperature, studying preferred crystallographic orientation effect
12 p2255 A70-27609
- Short time tensile properties of thermomechanically treated astrolloy showing improvement due to refined gamma precipitate and grain boundary carbides
12 p2256 A70-27610
- Ferritic and martensitic Fe-Ni alloys lattice parameter determined by standard X-ray techniques
12 p2256 A70-27613
- Superplastic nickel superalloys fabrication by controlled densification during direct extrusion
12 p2257 A70-28020
- Ni-Fe alloy sheets magnetic shielding effectiveness correlated with DC magnetic properties at various frequencies
12 p2201 A70-28127
- Ni-Mo-Fe magnetic alloy for EM pulse shielding, verifying saturated regions diffusion theory
12 p2201 A70-28128
- Collection of papers on nickel and nickel alloys covering thermal and mechanical properties during annealing and precipitation hardening behavior
13 p2432 A70-28758
- Ni and Ni alloys thermal properties, discussing expansion and conductivity, melting and boiling points, vapor pressure, specific heat, entropy, etc
13 p2432 A70-28759
- Ni and Ni alloys elastic properties relationship with ferromagnetic and magnetostriction effects, determining modulus of elasticity for wide temperatures and heat treatment
13 p2432 A70-28760
- Deformation, mechanical properties and processes during recrystallization annealing of nickel and alloys single crystals
13 p2433 A70-28761
- Ni alloys hardening by solid solution precipitation and insoluble particles dispersion, emphasizing heat resistant alloys and mechanical properties
13 p2433 A70-28762
- Phase transformations in TiNi with equiatomic composition, using internal friction, electrical resistivity and dilatometry
13 p2435 A70-29499
- Ni-Fe base superalloy notch and rupture properties as function of thermal and chemical changes, using electron microscopy
13 p2437 A70-29829
- Short term creep of Ni in vacuum, stationary air and high speed air flow at various temperatures and loads
14 p1594 A70-30167
- Fine grained structure effect on steels and Ni alloys short term heat resistance at high temperatures
14 p1594 A70-30168
- Growth kinetics of strengthening phase during aging of Ni-Cr-W-Mo-Al-Ti alloys, considering gamma prime particles at different Al/Ti ratios
14 p1594 A70-30169
- Metallic thermoelectric materials, measuring electrical resistivities and Seebeck coefficients of binary Ni alloys
14 p2533 A70-30530
- Carrier distillation DC arc emission spectrography, determining lead, bismuth and tin traces in nickel base alloys after conversion to oxides
14 p2546 A70-30957
- Hydrogen embrittlement of martensitic Fe-Ni alloys as function of temperature via slow strain rate tensile tests
15 p2755 A70-31559
- Portevin-Le Chatelier effect in carburized nickel and Ni-Co alloys, discussing carbide stability and carbon diffusion roles
15 p2756 A70-31562
- High temperature oxidation of Ni-Cr alloys and stainless steels in molten salt, observing grain boundary corrosion with electron probe
15 p2757 A70-31875
- Superalloys commercial development, investigating strength, heat resistance and weldability of Fe- and Ni-based alloys
15 p2760 A70-32335
- Glass bead blast induced residual stress and surface cold work effects on Ni base superalloy fatigue crack initiation and propagation
15 p2761 A70-32381
- Cellular precipitation in laminar eutectic and cast Ni-Cr alloys
15 p2761 A70-32383
- Fe-Ni-P phase diagrams for high temperatures, providing phase equilibria data for Widmanstatten pattern in iron meteorites
15 p2762 A70-32391
- Composition and heat treatment effects on Fe-Ni alloys structure, using micrographic, autoradiographic and potentiokinetic methods
16 p2916 A70-33080
- Quench hardening and Ni content relationship in Ti-Ni intermetallic compounds, investigating heat treatment effect on mechanical properties
16 p2930 A70-33084
- Physical properties and structure of Cr-Ni austenitic stainless steels with high Mn and N content as function of temperature
17 p3125 A70-35143
- Two-component metal coatings on Ni alloys for gaseous corrosion resistance increase, comparing microstructure and properties
17 p3125 A70-35393
- Ni alloys with protective coatings for gas turbine blades, testing corrosion resistance in diesel fuel combustion products with intermittent salt water sprays
17 p3125 A70-35394
- Martensitic phase change effects in TiNi on ultrasound waves propagation in transition region, using pulse echo measurements
17 p3126 A70-35603
- Microstructural changes of Ni-Cr lamellar eutectic alloy during creep deformation at 625 and 760 C
18 p3272 A70-36034
- Sodium sulfate induced accelerated oxidation of Ni and superalloys, investigating thermodynamics and reaction mechanism
18 p3272 A70-36037
- Cr-Ni system activities and phase boundaries determined by solid electrolyte technique
18 p3273 A70-36040
- Ni-Al-Nb superalloy, determining temperature effect on phase relationships in Ni-rich portion of phase diagram
18 p3273 A70-36041
- Mechanical properties of binary Ti-Ni and ternary Ti-Mo-Ni alloys
18 p3275 A70-36122
- Magnetometric, dilatometric, pyrometric and X ray studies of phase transformations in Fe-Ni alloys, considering magnetic characteristics and formation of superstructures
18 p3276 A70-36207
- Fe diffusion in equiatomic Ni-Co alloy, using thin radioactive deposit method with tagged element Fe 59
18 p3277 A70-36440
- Papers on cracking during postweld heat treatment of Ni alloys covering Rene 41 mechanical properties and resistance to strain age cracking
18 p3277 A70-36522
- Oxygen role in crack initiation and growth in Ni alloys postwelding heat treatment
18 p3277 A70-36525
- Ni superalloys for gas turbine engines, discussing chemical composition, microstructure, strength, solidification, etc
18 p3278 A70-36831
- Superlattice stacking faults in plastically deformed nickel aluminate /gamma prime phase/ due to interaction of antiphase boundary /APB/ type dislocation pairs
19 p3451 A70-37704
- High vacuum effects on creep properties of single crystal low carbon nickel base superalloy
19 p3451 A70-37705
- Plastic deformation in Ni-Cr-Nb alloy precipitation hardened at different long terms of high temperature
19 p3451 A70-37706
- Dispersion strengthened Ni-Cr alloys creep properties, investigating temperature, applied stress and thorium dioxide particles effects
20 p3644 A70-38984
- Ni-Cr heat resistant alloys structural transformation kinetics under aging, creep and operational conditions, discussing solid solution decomposition, hardening phases coagulation and dissolution, etc
20 p3645 A70-39037
- Solidification and composition model of macroscopic freckles in nickel base superalloys single crystals
20 p3646 A70-39101
- Duplex eutectic with Ni-Be fibers embedded in Ni-Cr solid solution matrix, discussing solidification conditions, optimum composition, heat treatment, mechanical properties and oxidation
20 p3647 A70-39107
- Hot corrosive environment effect on stress rupture and fatigue strength of Ni heat resistant alloy used in gas turbine rotating blade
20 p3647 A70-39241
- High temperature Ni base superalloy stress-rupture life dependence on casting variables and section size
20 p3648 A70-39413
- Creep resistant Ni-base superalloys ductility and thermal shock resistance improvement by precision casting technique, producing columnar grain and single crystal structures
20 p3648 A70-39415
- Ni base alloys sulfidation kinetics, examining roles of sodium/sulfur compounds-substrate interactions in accelerated oxidation
20 p3651 A70-40072
- Solid state butt and lap joint welding of TD-nickel bar, evaluating performance by stress rupture and shear tests
21 p3832 A70-40790
- Ni-Nb-Mo, Ni-Nb and Ni-Mo alloys phase equilibrium
21 p3840 A70-41898
- Ni-Cu-C solid solutions, measuring temperature dependence of graphite solubility by vapor transport method
21 p3841 A70-42149
- Stacking faults in gamma prime precipitation hardened high temperature Ni base alloys, relating fault energy to strength
22 p4053 A70-42728
- Grain boundary damping characteristics of Cu-Ni alloys solid solutions, discussing height, temperature and activation energy of solute peak
22 p4053 A70-42729
- Ni base superalloy for gas turbines, describing heat treatment for precipitation hardening
22 p4055 A70-43099
- Electro-thermal-mechanical switches based on shape-memory effect in Ti-Ni alloys
22 p3965 A70-43330
- Fatigue of turbine blade stainless steels and nickel alloys as function of temperature, stress and surface layers
23 p4205 A70-44135
- ICAS PAPER 70-38]
23 p4207 A70-44423
- Ni base superalloys gamma prime phase long range order parameter measured by X ray diffraction
23 p4207 A70-44423
- Columnar grain and Ni alloy single crystal gas turbine engine components resistant to high temperatures

NICKEL CADMIUM BATTERIES

produced by precision casting, using directional solidification 23 p4207 A70-44857

Ni-Fe-Cr-Nb alloy, investigating precipitation hardening of Ni3Nb phases by transmission electron microscopy 24 p4357 A70-45226

Fe-Ni alloy plastic flow behavior during reversible austenite-martensite transformation under constant load 24 p4357 A70-45228

Eutectic NiAl-Cr alloys, investigating quaternary additions effect on rod-plate transition to faceted microstructure 24 p4359 A70-45244

Prestraining effect on cellular precipitation in Ni-Cr lamellar eutectic during creep testing 24 p4359 A70-45247

Stress dependent creep rate in nickel based superalloy single crystals 24 p4359 A70-45289

Ni-Nb-W and Ni-W alloys phase equilibrium, obtaining diagrams from analysis of liquid and solid phases separated electromagnetically before tempering 24 p4359 A70-45372

Notch sensitivity dependence on plastic strain in Al alloy, heat resistant steels and Ni alloys under tensile tests at room temperature 24 p4360 A70-45827

High purity Cr-Ni heat resisting steels, investigating phase transformations with microhardness measurements magnetic analysis, X ray diffraction and microstructure examination 24 p4362 A70-46181

Fe-Ni-Co martensitic alloys isothermal age hardening, comparing bcc phase energy parameters of binary systems 24 p4362 A70-46182

NICKEL CADMIUM BATTERIES

Sealed Ni-Cd aerospace battery design, discussing recombination of gases produced during prolonged overcharging at low temperature, separator material, plate balance, etc 05 p0798 A70-16096

Nickel-cadmium batteries rapid deterioration due to destructive demand pulse charging methods 08 p1439 A70-20706

Flexible nickel cadmium secondary battery as nocturnal power supply for meteorological balloons transceiver and measuring instruments 08 p1440 A70-20711

Lead-acid and vented nickel cadmium batteries compared in redesign of military aircraft battery for cells reduction, low current density, etc 08 p1440 A70-20712

Nickel cadmium battery for aircraft jet engine starting, discussing selection for optimum service life and reliability under maintenance and environmental conditions [SAE PAPER 700211] 11 p1980 A70-25883

Generator regulator for Ni-Cd batteries capable of sensing temperature, reducing charge rate and limiting output to increase batteries life [SAE PAPER 700212] 11 p1983 A70-25884

Nickel cadmium battery construction capabilities and limitations from design engineer and aircraft operator viewpoint [SAE PAPER 700227] 11 p1983 A70-25898

Large capacity sealed nickel cadmium battery for spacecraft, describing mechanical and electrical characteristics 16 p2844 A70-33473

Ni-Co aerospace batteries thermal and mechanical design for orbiting space vehicles 21 p3757 A70-41012

Ni-Cd cell plates screening and selection by weight for reliability and uniformity improvement 21 p3760 A70-42147

Sealed Ni-Cd cells, investigating carbonate effect on performance 22 p3965 A70-43535

Military sealed thin sintered plate Ni-Cd rechargeable batteries, comparing performance with other systems 22 p3966 A70-43538

NICKEL COATINGS

Residual stress of electroless nickel deposits on beryllium from bow deformation measurements, noting role of phosphorus content 19 p3451 A70-37708

NICKEL COMPOUNDS

NT NICKEL OXIDES

NT SCHREIBERSITE

Quantitative method developed for photometric determination of B in nickel or titanium borides, using magnezon I reagent in alkaline solutions at various pH 03 p0504 A70-12983

Nickel chromite structural changes, thermal conductivity and dilatation during tetragonal-cubic transition, noting phonon-lattice effect 13 p2437 A70-28855

Weak itinerant ferromagnetism theory for Ni-Ga and Ni-Al intermetallics, allowing for molecular field parameter magnetization dependence 22 p4087 A70-43197

Electrochemical properties of sintered and film nickel hydroxide electrodes 22 p3966 A70-43542

NICKEL ISOTOPES

Pionic transition in Ni isotopes to measure nuclear interaction effects, observing level shift and broadening 05 p0885 A70-16682

NICKEL OXIDES

High temperature scaling of Ni, investigating role of oxide microstructure and growth stresses 15 p2762 A70-32388

NICKEL PLATE

Cu, W and oxidized W adhesion to Ni surface, examining before and after adhesion contact with low energy electron diffraction [ASLE PREPRINT 69-LC-13] 02 p0318 A70-12535

NICKEL STEELS

Dimensional stability of nickel maraging steel at ambient temperature measured for applications as gage block materials 01 p0120 A70-10742

Chromium-nickel steel fatigue strength under repeated thermal cycles, showing dependence on long term fatigue buildup and single cycle fatigue damage effects 02 p0383 A70-11653

Fe-Cr-Mn-Ni system studied to obtain high Mn austenite and establish boundaries in quaternary system 03 p0509 A70-13278

Niobium addition effect on alpha-gamma transformation temperature during continuous cooling of low carbon Ni-Cu steel 04 p0706 A70-15134

Initial oxide film on Cr-Ni steel at high temperatures observed by electron microscope, noting Ni role 04 p0708 A70-15311

Mechanical properties of nickel steels with carbon after suitable heat treatment found similar to high strength nickel steels properties without carbon 05 p0865 A70-16875

Energy dissipation in heat resistant Ni steels under cyclic tension and compression at room temperature 08 p1516 A70-20981

Ultrahigh strength Ni steels fracture toughness analysis, studying effects of chemical composition, yield strength, air melting, vacuum melting, etc 09 p1701 A70-22552

Thermal treatment function of austenitic grain size and mechanical properties of 18 pct Ni maraging steels 09 p1704 A70-22803

Phenomenological properties of stress relief embrittlement in nickel steel, noting toughness recovery via retempering 11 p2059 A70-25665

Low carbon Ni steels isothermal transformation characteristics, observing equiaxed ferrite and Widmanstätten and bainitic structures at various temperatures 12 p2256 A70-27615

Charpy V notch and dynamic tear tests compared for fracture toughness characterization of Ni-Cr-Mo-V steel 14 p2596 A70-30931

Hot rolling and warm working effects on microstructure and mechanical properties of Ni-Cu-Cb steel, noting optimum austenite plus ferrite phase field 15 p2756 A70-31566

Structure and chemical composition of high Cr diffusion coating on Cr-Ni austenitic steels 15 p2756 A70-31634

Preprecipitation and reversion stages in Ni-Co-Mo steel, observing dislocation nucleated phase growth initiation by aging 16 p2929 A70-33047

Structural hardening of nickel maraging steels related to Portevin-Le Chatelier effect in necking zone of stress-strain curves 17 p3124 A70-35141

Impact transition behavior and strength-toughness relation of high purity Ni maraging steels, noting intergranular fracture at grain boundaries 18 p3273 A70-36043

Chromium-nickel steel fatigue strength under repeated thermal cycles, showing dependence on long term fatigue buildup and single cycle fatigue damage effects 19 p3547 A70-38426

High strength high Ni maraging steels crystal structure, alloying elements effects on mechanical properties, applications, etc 22 p4055 A70-43121

NICKEL ZINC BATTERIES

Nickel zinc secondary battery low cost and high performance in military applications, discussing maintenance and rapid recharge requirements 08 p1440 A70-20710

Ni-Zn high energy secondary battery cycle life and discharge capability 22 p3966 A70-43540

NICOTINAMIDE

Nicotinamide adenine dinucleotide (NAD)/deamination and role of nicotinamide hypoxanthine dinucleotide (deamino-NAD) in forming ammonia from amino acids in rats/rabbits brain and liver tissue 01 p0018 A70-10505

Nicotinamide adenine dinucleotide phosphate (NADP)/specific isocitrate dehydrogenase (ICDH)/inactivation from obligate halophile at low NaCl levels 15 p2685 A70-32671

NIGHT

Positive ion concentration profiles in lower nighttime midlatitude ionosphere calculated from corpuscular radiation measurements and ion recombination constants 04 p0738 A70-14436

Nighttime radio wave absorption in ionosphere during moderate solar activity based on echo observations 06 p1056 A70-17840

Nighttime recombination model of O ion plasma in upper ionosphere, showing temporal behavior and variation of electron concentration 07 p1265 A70-19432

Geomagnetic field orientation effects on VLF nighttime propagation, checking computer program predictions 09 p1639 A70-23664

Positive ion concentration profiles in lower nighttime midlatitude ionosphere calculated from corpuscular radiation measurements and ion recombination constants 13 p2475 A70-28461

Electro-optical sensor night time capabilities with laser illuminator, determining current per unit area from photocathode 16 p2907 A70-33183

Nighttime recombination model of O ion plasma in upper ionosphere, showing temporal behavior and variation of electron concentration 18 p3249 A70-36906

Intermode coupling processes in nighttime D and E regions, using thin film optical method for propagation phenomena at LF and VLF 19 p3413 A70-38003

Aircraft nighttime and daytime accident rate comparison, considering darkness, flight phase, etc 21 p3751 A70-41489

NIGHT AIRGLOW

U AIRGLOW

U NIGHT SKY

NIGHT E LAYER

U E REGION

U NIGHT SKY

NIGHT F LAYER

U F REGION

U NIGHT SKY

NIGHT SKY

Far IR night sky emission above 120 km over millimeter range, using rocket-borne telescope 01 p0069 A70-10040

Nighttime F layer thickness relations to atmospheric temperature 01 p0078 A70-11211

Quasi-trapped particle currents having discontinuities on daytime and nighttime side of earth 01 p0171 A70-11487

Pc 1 range geomagnetic pulsation sweepers (MHD waves)/event in evening sector, considering delay time between sweepers appearance and polar magnetic storms onset 02 p0290 A70-12121

Night airglow emission intensities during IQSY concerning Na, OH and H alpha lines compared with intensities during IGY 02 p0292 A70-12433

Stellar X ray effect on nighttime lower ionosphere wave reflection suggested from VLF propagation data 03 p0562 A70-14224

Excitation of H-alpha and H-beta lines in night sky, calculating solar L radiations variation with altitude 04 p0679 A70-15075

Evening time latitudinal distribution of polar magnetic field perturbations compared with nighttime distribution, indicating evening electrojets 04 p0684 A70-15751

Compact and fully automatic fixed photometer for zenith measurements of night airglow intensities, calibrating sky observation through filter by constant intensity light source 05 p0845 A70-15821

Night airglow variations observed during Cosmos satellite orbits, determining atmospheric albedo wavelength dependence for solid and medium cloudiness and clear skies 05 p0841 A70-16728

D region electron density distribution during night and presunrise period, using full wave integration method for propagation parameters for waves reflected from electron density model 06 p1054 A70-17587

Ray tracing techniques applied to night sky wave medium frequency propagation, modifying program for absorption and polarization coupling losses 07 p1230 A70-19164

Ionospheric reflection coefficients from vertical and oblique incidence pulse amplitude data, discussing night conditions effect on Ottawa pulse transmissions 07 p1232 A70-19176

Nighttime ionospheric F region velocity component and recombination coefficient computer calculation 07 p1277 A70-20449

Spectral intensity distribution of night airglow noting visual spectra distribution difference from G2 stars 07 p1277 A70-20457

Excessive absorption in night E layer with and without geomagnetic disturbances for almost complete solar cycle, discussing winter increases/anomalies/ 09 p1669 A70-23170

Astronomic observation balloon Thisbe, discussing telescope, stabilization, basket control, data processing and objectives including zodiacal light and night sky brightness measurements 10 p1804 A70-23915

Nighttime concentration profiles of O, NO and molecular oxygen ions in ionosphere calculated from daytime values 10 p1874 A70-24428

Night time upper atmosphere light phenomena and Tungusk meteorite observed on 30 June 1908 10 p1876 A70-24499

Field-aligned plasma velocity dependence on plasma diffusion and wind velocity illustrated with model of night F 2 layer 10 p1881 A70-24814

Nocturnal E layer electron density profile dependence on solar activity 10 p1885 A70-25265

Nocturnal F layer electron density profile and temperature dependence on solar activity 10 p1885 A70-25266

Night sky X ray sources at low galactic latitudes, describing rocket survey experiment 12 p2292 A70-27386

Topside ionosphere nighttime structure over Japan deduced from Alouette 2 satellite plasma frequency measurements 12 p2226 A70-28063

Terrestrial ELF waves F layer nighttime reflections, discussing effects of electron density, geomagnetic field radial component and absorption by ions 13 p2365 A70-29190

Earth-ionosphere waveguide electric field strength calculation based on nighttime ionospheric models, comparing results to measurements 14 p2574 A70-30748

Lower ionospheric drift motions observed from VHF radio signal, relating to three paths near auroral zone during dark hours 14 p2574 A70-30749

Evening time latitudinal distribution of polar magnetic field perturbations compared with nighttime distribution, indicating evening electrojets 14 p2576 A70-30835

Night airglow space and time variations from jet aircraft observations, measuring conjugate enhancements 14 p2580 A70-31266

Night sky atmospheric continuum, zodiacal light and OI line observations with photoelectric color telescope 14 p2581 A70-31268

Hydrogen UV geocorona photoionizing effect on nighttime E region electron density in low and midlatitudes, comparing with ionosonde data 14 p2581 A70-31270

Night sky visible brightness at minus 19 degrees declination from July 1965-June 1966 in Tsumeb, South West Africa 14 p2581 A70-31390

Earth-ionosphere cavity resonances diurnal variations by considering different propagation characteristics at day and night hemispheres 15 p2728 A70-31910

Night sky brightness in UV and visible region by photoelectric photometers on Cosmos 51 and 213 satellites 17 p3163 A70-34901

Night F 2 layer underside morphology for magnetically quiet period at sunspot minimum 17 p3076 A70-34937

Nighttime E region structure variations observed by Wallops Island rocket flights, obtaining electron density profiles by Langmuir probe during ascent 17 p3076 A70-34941

Nighttime E region molecular ion production rate estimation, taking into account windshear effect 18 p3245 A70-36022

Submillimeter wavelength night sky radiation background, observing effects on various cosmic ray phenomena 18 p3308 A70-36330

Night airglow hydroxyl rotational brightness temperature determined from emission spectra 19 p3412 A70-37777

Night airglow oxygen red lines predawn enhancement calculations, confirming role of photoelectrons from magnetic conjugate ionospheric

Seasonally biased electron density enhancements in nighttime response of topside ionosphere to magnetic storms 20 p3621 A70-39342

Nighttime lightning activity observations by orbiting solar satellite OSO-B, determining thunderstorms positions by optical radiation detection 20 p3623 A70-39978

Anomalous nighttime ionospheric total electron content increases seasonal and solar cycle dependences attributed to ionization sources due to electrodynamic drifts 21 p3815 A70-41061

F 2 layer nighttime ionization at mid-latitudes, investigating conjugate point effects on observation point 23 p4188 A70-44055

E region ion composition nighttime variations, examining nitrogen monoxide and O ion nonequilibrium concentrations by ionic-molecular reactions 23 p4189 A70-44074

NIGHT VISION

RF holographic vision through rain, fog or darkness, discussing cholesterol ester-coated Mylar sheets and pyroelectric hot plates detectors and antenna sensory matrix 02 p0305 A70-12843

Landing performance of BLEU static cockpit simulator compared with flight data for night conditions in clear and limited visibility 10 p1859 A70-24215

Night vision systems with integrated pulse gated viewing and laser ranging, analyzing transmitter and viewer 12 p2236 A70-27902

Oxygen effect on night vision tested in men at 5,000 ft above sea level, obtaining threshold curves of dark adaptation 13 p2359 A70-29443

Imaging type electro-optical detection systems design for passive night surveillance, building camera system and testing in helicopters and fixed wing aircraft 16 p2903 A70-33127

Illumination level and contrast loss distribution in atmosphere to evaluate passive night vision equipment with image intensifier tubes 16 p2907 A70-33184

Aircraft pilot and nonpilot night vision adaptation comparison, using Goldmann-Weekers adaptometer 17 p3038 A70-35138

Scotopic responses conditions, using stimulus alternation method to elicit electroretinogram 17 p3034 A70-35897

NIGHTGLOW

Oxygen collisional quenching rate in F region determined by comparing nightglow intensities with intensities calculated from electron density profiles 01 p0070 A70-10403

Twilight and nightglow measurements with stratospheric balloons, discussing use for upper atmosphere exploration, meteoric influence and French network 01 p0079 A70-11217

Predawn enhancement of emission rate of 6300 A forbidden O I line in nightglow spectrum, discussing onset time 07 p1275 A70-20286

Excitation and layers heights for 5577 A and O2 bands of atmospheric and Herzberg systems in night airglow estimated, suggesting Chapman reaction for emission 08 p1492 A70-21755

Summertime midnight airglow enhancement of 6300 A line by sensitive continuum compensating photometer, suggesting F 2 region electron density increase for emission 12 p2225 A70-27895

F region nightglow emissions rocket data, discussing rate coefficient for oxygen atoms quenching by molecular nitrogen 13 p2398 A70-29200

Nightglow OI lambda 6300 line width measurements during magnetic storm, discussing temperatures and intensity variations 14 p2579 A70-31250

Tropical UV nightglow, considering oxygen ion-ion neutralization reaction as primary source 18 p3244 A70-36015

Lyman alpha geocoronal emission rate as function of altitude at midnight during solar minimum, solving radiative transfer equations 20 p3619 A70-39329

Tropical UV nightglow measurement by Ogo-4 spectrometer, considering ionospheric recombination excitation mechanism 20 p3620 A70-39338

UV oxygen nightglow observation by OGO-4, examining ion-ion neutralization and radiative recombination production mechanisms 20 p3621 A70-39344

Nightglow Na D line excitation rate in winter and summer 21 p3814 A70-40934

Auroral UV night airglow radiation distribution over latitude range, using scanning spectrometer onboard Convair 990 aircraft 21 p3818 A70-41106

Nighttime equatorial E region small scale irregularities detected by rocket-borne Langmuir and plasma noise probes, discussing generation mechanism 22 p4018 A70-43108

Nightglow Na-D lines excitation, attributing emission to Chapman mechanism 22 p4023 A70-43294

F region night airglow in equatorial and midlatitudes, discussing red and blue emission origins 23 p4185 A70-43839

NIMBOSTRATUS CLOUDS

Refractive index complex part effect on polarization and radiance of reflected and transmitted light for continental haze and nimbostratus cloud models 21 p3847 A70-41724

NIMBUS CLOUDS

U NIMBOSTRATUS CLOUDS

NIMBUS SATELLITES

NT NIMBUS 2 SATELLITE

NT NIMBUS 3 SATELLITE

NT NIMBUS 4 SATELLITE

TIROS, Nimbus, ESSA and ATS weather satellites configurations, onboard equipment and cloud photographs 09 p1765 A70-22227

Nimbus high resolution IR radiometer (HRIR) data processed by color display enhancement system, demonstrating meteorological, oceanographic and geomorphological applications 11 p2049 A70-25636

Nimbus weather satellite as laboratory for sensors collecting data for global weather system, describing launching, attitude control systems and cameras 14 p2654 A70-31149

Solid lubricated contacts performance in Nimbus and OAO spacecraft, discussing slip ring assembly and noise problems in Ag-graphite brushes 16 p2920 A70-33810

Nimbus weather satellites mechanical devices and subsystems, including solar array drive, fluid thermal control sensors, horizon scanners and hydraulic dampers 16 p2921 A70-34105

Tracking and data relay satellite system performance by ATS and Nimbus spacecraft for range and range rate tracking and command and data transmission [ALAA PAPER 70-1306] 24 p4374 A70-45949

NIMBUS 2 SATELLITE

Ocean currents and sea surface temperature remote sensing by Nimbus 2 High Resolution IR Radiometer 24 p4332 A70-46400

NIMBUS 3 SATELLITE

Nimbus 3 satellite carrying IR spectrometer to measure spectral radiances and retrieve atmospheric temperature profiles 04 p0675 A70-14393

SNAP 19 radioisotope fueled thermoelectric power supply orbital performance on Nimbus 3, ascribing power output decrease to decreasing generator output currents [ALAA PAPER 70-480] 11 p2120 A70-25435

Meteorological Nimbus 3 satellite and aircraft observations of thermal radiation for vertical atmospheric temperature profile measurement 11 p2075 A70-25921

Michelson IR interferometer spectrometer /IRIS/ design calibration and performance onboard Nimbus 3 satellite, demonstrating data reduction and inflight calibration 20 p3626 A70-39078

Temperature and height data for synoptic stratospheric evaluation, using Nimbus 3 satellite IR spectrometer 22 p4064 A70-42618

Thermal emission spectra of earth and atmosphere from IR Michelson interferometer onboard Nimbus 3 satellite 24 p4330 A70-45977

NIMBUS 4 SATELLITE

Atmospheric temperature profiles using Nimbus 4 selective chopper radiometer 23 p4192 A70-44865

Earth and atmosphere thermal emission spectra via Nimbus 4 Michelson interferometer, obtaining atmospheric temperature, humidity and ozone profiles 23 p4192 A70-44866

NIMONIC ALLOYS

Nimonic Ni-Cr based alloys fracture characteristics used to determine temperature and time effects on equicohesive points positions 01 p0116 A70-10073

Gamma prime phase structure ordering effect on critical shear stresses of aging Ni-Al alloys and nimonic 09 p1707 A70-23195

Massive eutectic and fine gamma phases precipitation in cast nimonic 100 alloy at 900 C aging 16 p2930 A70-33083

NIMPHE [ENGINE]

Wrought Nimonic alloy, measuring stress redistribution due to creep under variable load and temperature

23 p4274 A70-44911

NIMPHE [ENGINE]

U HYDRAZINE ENGINES

NIOBATES

Nonlinear optical properties of lithium niobate single crystals, considering optically induced index inhomogeneity and second harmonic generation

01 p0157 A70-10422

Birefringences and phase retardations in lithium niobate crystals for light propagation directions near optical axis, considering electro-optic modulation

02 p0313 A70-12451

Alkali-alkaline earth niobates phase equilibrium study revealing tetragonal tungsten bronze-type solid solutions existence range

09 p1740 A70-22983

Intense light effect on refractive index of potassium niobate crystals

09 p1698 A70-23317

Optical parametric noise from barium sodium niobate crystal pumped at 4358 Å by compact source mercury lamp

22 p4074 A70-34022

Far field diffraction spreading of surface acoustic waves on cut Li-niobate in two directions

23 p4230 A70-44199

NIOBUM

Disk-shaped Mo and Nb specimens solar radiation reflection and absorption characteristics observed for temperature effect

01 p0117 A70-10176

Ti, Zr and Nb characteristics, processing procedures and applications in corrosive environments, nuclear reactors and aerospace structures

02 p0319 A70-12710

Carbon effect on high temperature elasticity modulus and long term hardness of Nb, indicating diffusion enhancement and counteractive Zr addition

03 p0509 A70-13252

Residual stress distribution in butt joints during welding of sheet Nb measured by extensometer, noting annealing temperature effect on stress relieving

03 p0513 A70-14072

Niobium powder hot pressing compaction in terms of porous body volume viscous flow, determining viscosity shift time dependence

04 p0696 A70-14461

Niobium addition effect on alpha-gamma transformation temperature during continuous cooling of low carbon Ni-Cu steel

04 p0706 A70-15134

Creep in single crystal and polycrystalline Nb between 1300-1900 C under stresses, showing stress independent activation energy

05 p0862 A70-16202

Recrystallization annealing third stage of cold worked polycrystalline niobium by measuring electrical resistance at liquid nitrogen temperature

05 p0863 A70-16204

Strength and plasticity of Mo and Nb sheet in oxidizing medium at high temperatures and pressure range

05 p0865 A70-17029

Structure and interstitial impurities effects on Nb modulus of elasticity at normal and high temperatures, noting rolling

05 p0866 A70-17040

Niobium single crystals annealed in ultrahigh vacuum, studying stress-strain behavior, secondary slip geometry and slip line morphology

06 p1090 A70-18493

Oxide transformation during oxidation of Nb in terms of O diffusion

07 p1305 A70-18967

Interstitial atoms effect on dislocation relaxation and aging of Mo and Nb single crystals

07 p1309 A70-19638

Dislocation velocity-stress exponent for Nb single crystals calculated from strain rate sensitivity measurements of effective flow stress

07 p1314 A70-20011

Transverse and longitudinal resistive critical fields of Nb wires, discussing superconductivity in dislocation cell walls created by drawing or swaging

09 p1704 A70-22802

Tensile strain rate and oxygen concentration effects on peaks of niobium hardening zones involving interstitial atoms

12 p2252 A70-27001

Residual gas effects on critical load and brittleness of pure and molybdenum-coated niobium bars after annealing in vacuum

12 p2258 A70-28324

Sintering processes using boundary porosity in welded Nb bicrystal for model of final stages

13 p2434 A70-29081

Hydrogen impurities anelastic relaxation effect on internal friction alpha peak in cold worked tantalum and niobium

13 p2435 A70-29350

Upper critical field dependence on s- and p-wave scattering of Frenkel effects in electron irradiated niobium

13 p2471 A70-29535

Nb single crystal faces electron work functions and comparison of thermionic emission patterns with Ba-Nb system

14 p2625 A70-30162

Twinned lamella formation in Nb single crystals, examining slip and shear roles in surface tilt formation

15 p2761 A70-32382

Carbon effect on high temperature elasticity modulus and long term hardness of Nb, indicating diffusion enhancement and counteractive Zr addition

19 p3453 A70-38470

Nb effects on steel susceptibility to brittle fracture at various temperatures, discussing impact strength and nucleation energy of crack formation

19 p3453 A70-38709

Alumina effects on Nb creep activation energy at elevated temperatures, noting independence from chemical composition and creep stresses

19 p3453 A70-38710

Niobium yield stress at room temperature for various nitrogen and oxygen concentrations

19 p3454 A70-38814

Nb single and polycrystalline thermal properties at high temperatures

20 p3648 A70-39639

Orientation and applied stress effects on pure Nb-6W bcc single crystals yield stress, discussing thermal activation strengthening and crystal dislocations

22 p4052 A70-42318

Thermal decomposition of freeze dried Ta and mixed lithium-niobium oxalate, using surface area and electron micrographs

24 p4363 A70-46212

NIOBUM ALLOYS

Tensile tests of polycrystalline Nb-H alloys at low temperatures, noting cooling rate effect on ductility in terms of microstructure

01 p0122 A70-11240

Nb-Mo alloys in various proportions prepared by vacuum casting, showing embrittlement under hydrogen atmosphere

02 p0318 A70-12671

Nb-NbH solid solutions thermodynamic properties at various temperatures described by formulas

02 p0320 A70-12819

Superconducting properties of polycrystalline disordered cold worked Nb-Ti-V alloys showing unexpected sensitivity to fast neutron irradiation

03 p0508 A70-13144

Nb binary and tertiary alloys density changes found proportional to alloying element content

03 p0511 A70-13489

Niobium ditelluride single crystals production with purity dependent on initial materials, discussing X ray structural and chemical analysis and electrical properties

03 p0542 A70-13753

Nb-Mo alloy interstitial oxygen concentration determined by measuring internal friction /Snoek/ peak

03 p0512 A70-13763

Stress rupture tests with Nb-based alloys in 1273-1673 K temperature range

05 p0952 A70-17039

Refractory Nb alloy low cycle fatigue characteristics in vacuum at high temperatures, describing testing machine

06 p1086 A70-17453

Book on optimization by variational methods covering use of differential equations, Pontryagin minimum principle, optimal and feedback control, dynamic programming, etc

06 p1093 A70-17650

Deformation pattern, interstitial impurities and alloying elements effects on temperature dependence of elasticity modulus of Nb and alloys

06 p1088 A70-17659

Structure, phase composition and heat resistance of diffusion layers obtained by surface alloying of Nb alloy with Cr, Ti and Si

06 p1089 A70-17744

High melting point oxides effects on niobium alloys recrystallization temperature and grain growth

07 p1303 A70-18741

Oxygen content influence on Nb-Mo alloy mechanical properties at ambient temperature in air and hydrogen

07 p1307 A70-19374

Silicide-coated columbium alloys reuse capabilities under flight conditions, considering coating local damage and emittance

[AIAA PAPER 70-279]

07 p1315 A70-20388

Interstitial sinks effect on structure and creep behavior of dispersion-strengthened Nb base alloy

08 p1521 A70-21703

Recrystallization in austenite phases of vanadium and columbium HSLA steel alloys determined in high temperature deformation tests

08 p1521 A70-21704

Vacuum rolling of high strength hard-workable dispersion-hardened Nb base alloys excluding recrystallization

09 p1692 A70-22756

Phase equilibrium diagram and heat resistance of Ti-Al-Nb alloys along radial section by thermal and microstructural analysis

09 p1709 A70-23789

Nb and Nb alloys activation in polarized light by etching technique, observing grain contrast improvement

10 p1906 A70-25229

Ni-Nb-O system state diagram by reduction equilibria and X ray analysis, discussing oxidation resistance based on metal surface protective layers makeup

12 p2253 A70-27158

Superconducting thin films of beta-tungsten structure Nb-Al-Ge compound, discussing high purity sputtering preparation techniques and properties in magnetic fields

12 p2285 A70-27259

Nitrogen solubility in Nb-Mo solid solutions, determining relationship between N partial pressure, temperature and concentration

14 p2598 A70-31285

Yield strength of Nb-O single crystal solid solutions as function of temperature

15 p2763 A70-32808

Optical properties of electropolished cubic Nb-Ti alloys at cryogenic and room temperatures in visible and near IR spectral range

16 p2930 A70-33205

Working fluid /Ar/ purity and stability effects on fatigue life and creep of Nb and Mo alloys using gas analysis, microstructure and microhardness data

17 p3126 A70-35715

Omega transformation in Hf-Nb alloys, investigating aging at various temperatures

18 p3273 A70-36044

Cross sectional phase diagram of Nb-Ti-Mo-V, discussing continuous crystallization and composition dependent hardness and resistance

18 p3275 A70-36125

Nb-based Ti-Zr alloy surface phase recrystallization characteristics, using field emission microscope

18 p3276 A70-36309

Superconducting Nb-Ti-Zr alloy, investigating structure and decomposition at high temperatures by X ray and electron microscopy

18 p3276 A70-36310

Nb-Sn superconductors multiphase structure with three intermetallic phase, constructing diagram based on phase stability and composition

18 p3299 A70-37221

Age hardening of Nb-Hf-C alloys investigated by metallography and X ray diffraction, discussing tests in various temperature ranges

19 p3452 A70-37826

Oxygen solubility in Nb-Hf alloys at elevated temperatures, using isothermal sections for Nb-rich part

19 p3453 A70-38708

Ti-Nb-Zr alloys strength and plasticity at various temperatures, noting compositional effects on tensile and yield strength

19 p3453 A70-38712

Binary Nb vapor systems mutual diffusion coefficients concentration and temperature dependences, discussing interatomic bonds and melting point of alloys

19 p3454 A70-38715

Yield stress in electron beam-refined Nb-N solid solution at room temperature and specific strain rate range

19 p3454 A70-38813

Mo alloying additions effects on carbide phases in Nb-C alloys

20 p3646 A70-39104

Nb-Ta and Nb-Mo alloys single crystal solid solution strengthening as function of composition, temperature and strain rate

20 p3646 A70-39105

Ni-Nb-Mo, Ni-Nb and Ni-Mo alloys phase equilibrium

21 p3840 A70-41898

Nb-Zr thin films superconducting properties dependence on deposition temperature and rate and substrate material

22 p4085 A70-42623

Nb-Zr alloy and yttria corrosion by high velocity Li flow, discussing material removal depth

22 p4055 A70-43100

Solid solutions properties in Nb-oxygen system, examining atomic bond nature by elastic modulus measurement

22 p4056 A70-43345

Nb-Ru equiatomic alloys reversible phase transformations, using electrical resistivity, hot stage optical metallography, X ray diffraction and magnetic susceptibility measurements

23 p4208 A70-44858

Zr-Nb alloys athermal omega transformation studied by transmission electron microscopy

24 p4358 A70-45234

Heat treatment effects on dispersion strengthening of Ni alloys, showing enhanced long term creep strength at 1100 C

24 p4360 A70-45828
Simplex lattice mathematical models of solidus volume for quaternary Nb-W-Ti-Zr system
24 p4361 A70-45833
Heat resistant surface diffusion alloying of Ni alloys with Cr, Ti and Si saturation

24 p4361 A70-45834
Anions and cations diffusion during oxidation of Ni-V-Ti alloys, using chemical and electron microprobe analyses

24 p4364 A70-46335
NIOBUM CARBIDES
Parameters effect on radius of dispersion during plasma and detonation spray coating process of niobium and zirconium carbides

06 p1076 A70-17849
Monochromatic radiation emissivity temperature dependence of monocarbides of Ti, Nb and alloys in homogeneity region
08 p1516 A70-20994
Congruent vaporization rates of niobium monocarbide phase at high temperatures in vacuum, using method of least squares

12 p2254 A70-27320
WC as densification aid for NbC-C composites, examining fabrication temperature, mechanical properties, solid solution composition, etc
15 p2757 A70-31797

Niobium carbides formation in Nb containing steels during gamma-alpha transformation, establishing relationship between brittleness and carbide distribution characteristics

15 p2758 A70-32123
Carburizing spherical powders of Nb, Mo and W to obtain carbides, noting agreement between theoretical and experimental data

17 p3125 A70-35410
NIOBUM COMPOUNDS
NT NIOBATES
NT NIOBIUM CARBIDES
NT NIOBIUM OXIDES
Nb metal-like compounds energy band structures using X ray fluorescence technique

04 p0707 A70-15213
Mechanical and physical properties of Nb-Ti binary annealed alloys as function of compound NbTi using microscopical and X ray phase analysis

09 p1704 A70-22755
HF electrodeless plasma discharge synthesis of niobium and vanadium intermetallic compounds

11 p2061 A70-26746
Niobium oxychloride conversion to niobium pentachloride by vapor phase chlorination with phosgene, examining reaction kinetics

18 p3272 A70-36031
Superconductivity and crystalline structure of laminar solid solutions of niobium-selenide-niobium-telluride single crystals

22 p4088 A70-43464
Niobium nitride precipitation associated with stacking faults in Cr-Ni-Nb austenitic stainless steels, using electron microscopy

24 p4365 A70-46369
NIOBUM OXIDES
Oxide transformation during oxidation of Nb in terms of O diffusion

07 p1305 A70-18967
Stoichiometric compositions of niobium dioxide to pentoxide range, investigating X ray characteristics and thermal stability

07 p1315 A70-20312
Phase equilibrium and homogeneity regions of solid solutions system Ni-Nb-O at elevated temperature

07 p1315 A70-20313
Niobium suboxide formation in Nb-O system from supersaturated solution of oxygen in niobium after annealing

20 p3648 A70-39630
NITRATES
NT AMMONIUM NITRATES
NT CELLULOSE NITRATE
NT HYDRAZINE NITRATE
NT ORGANIC NITRATES
NT SILVER NITRATES

Ethyl nitrate positive and negative ion-molecule chemistry investigated by ion cyclotron single/ double resonance techniques

16 p2855 A70-33090
NITRATION
Nitrification reactions in soil with constant ammonium solution entry rate and nitrifying organisms, considering ion concentrations as functions of time and distance

02 p0252 A70-12518
High temperature kinetics of pyrolytic silicon carbide oxidation and nitridation in dissociated gases

13 p2361 A70-29077
NITRIC ACID
Passive film on stainless steels in boiling nitric medium studied by recording constant potential on sample subjected to polarizations

09 p1700 A70-22010

Ignition delay-reducing catalyst for furfuryl alcohol-red fuming nitric acid hypergolic bipropellant

13 p2473 A70-29992
NITRIC OXIDE
NO ion dissociative recombination rate coefficient determined in high temperature air plasma from electron temperature and number density measurements

04 p0675 A70-15583
Molecular fluorescence emission rate factors for strong bands of nitric oxide gamma systems, noting day airglow temperature dependence

05 p0886 A70-17085
Jet aircraft air pollutant production and dispersion of nitric oxide and soot, discussing mixing process [AIAA PAPER 70-115]

06 p1131 A70-18070
Nitric oxide free jet expansion, studying molecular cluster formation, inhibition and chemiluminescence

06 p1044 A70-18281
Stationary nitric oxide afterglow, studying molecular ionic species by time resolved mass spectrometry

06 p1114 A70-18635
Production rate constants for hydrated positive ions in photoionized nitric oxide-water afterglows

07 p1346 A70-20245
Gas turbine engines contribution to air pollution, using model combustor to study burned gas composition, emphasizing nitric oxide concentration

08 p1559 A70-21481
Ar and nitric oxide free jets dimmer and cluster abundance dependence on nozzle diameter and reservoir temperature and pressure

09 p1733 A70-22907
Chemiluminescence from NO adiabatically expanded against supersonic H atoms stream in inert carrier

10 p1831 A70-24566
Nitric oxide gas IR radiation properties at high temperatures, determining spectral mean fine structure and total band absorbance correlations

16 p3003 A70-34253
NO in earth atmosphere, describing theory of formation for explaining observed density distribution

18 p3245 A70-36019
Nitric oxide and atomic nitrogen in mesosphere and stratosphere, discussing photochemical equilibrium

19 p3415 A70-38389
Nitrogen and nitric oxide production and diffusion, examining photochemistry and transport at high altitudes

20 p3620 A70-39339
Collision induced dissociation of nitric oxide and molecular oxygen ions at low kinetic energies, noting internal ionic excitation effects

21 p3773 A70-41398
F I region positive nitric oxide and oxygen ions concentrations ratio and conversion rates from rocket data and theoretical formulas

23 p4189 A70-44075

NITRIDES
NT ALUMINUM NITRIDES
NT BERYLLIUM NITRIDES
NT BORON NITRIDES
NT SILICON NITRIDES
NT TITANIUM NITRIDES

Vapor deposited GaN single crystals tested for electrical and optical properties, determining band gap energy, electron concentration, etc

04 p0732 A70-15688
Superconducting properties of Nb-Ti-N thin films prepared by reactive sputtering process, obtaining transition temperature maximums

04 p0732 A70-15689
Strontium nitride hydrolysis, investigating hydrazine presence among products

23 p4158 A70-44598
Vanadium subnitride crystal structure with ordered array of nitrogen atoms in V sublattice

24 p4360 A70-45519
Niobium nitride precipitation associated with stacking faults in Cr-Ni-Nb austenitic stainless steels, using electron microscopy

24 p4365 A70-46369

NITRIDING
Internal nitriding kinetics of W-base alloys containing Hf, investigating morphology of resulting Hf nitride dispersion

02 p0317 A70-12319
Mo-nitrogen interaction, studying nitriding influence at various temperatures on Mo alloys properties

06 p1089 A70-17741
Chromium stainless steels nitrided cases formation and phase composition, studying temperature effects

07 p1304 A70-18744
High chromium stainless steels nitriding and carburizing processes stabilized by nickel galvanic coating, enhancing nitrogen or carbon diffusion into steel

07 p1291 A70-18832
Austenitic Fe-Cr-Ni-Ti alloys at high temperature to determine activation energy for nitrogen diffusion, noting oxygen role

08 p1522 A70-21707
Internal nitridation temperature effect on dispersion hardening of austenitic stainless Fe-Cr-Ni-Ti steels,

investigating interparticle spacing and layer thickness effects

09 p1705 A70-22810
Tensile strength of nitrided boron-aluminum alloy composite modules, noting effect of Ti cladding on panel surfaces

11 p2066 A70-26085
Titanium effect on iron and steels nitriding at high temperature, obtaining high surface hardness

13 p2423 A70-29773
Phase formation and mass transport during iodine-refined Ti reaction with nitrogen at various elevated temperatures

19 p3452 A70-38364

NITRILES
Replicating molecules on primordial earth, suggesting chemical evolution on Jupiter via demonstrable alpha-aminonitriles synthesis

14 p2536 A70-30364
Lattice resolution of layer planes in polyacrylonitrile based carbon fibers ground and dispersed by ultrasonic irradiation

14 p2598 A70-30793

NITRITES
Ferroelectric sodium nitrite single crystals LF linear electro-optical coefficients as function of temperature

01 p0154 A70-10104

NITRO COMPOUNDS
NT NITROBENZENES
NT NITROMETHANE
NT TRINITROTOLUENE

Agents for deoxygenation of nitro and nitroso groups

17 p3042 A70-35329
Microgram 2-nitro-1-butyl pyridinium sulfate /NBPS/ inhibition of growth of *Bacillus subtilis* by blocking thymidylate synthetase

23 p4158 A70-44998

NITROBACTER
Nitrification reactions in soil with constant ammonium solution entry rate and nitrifying organisms, considering ion concentrations as functions of time and distance

02 p0252 A70-12518

NITROBENZENES
NT TRINITROTOLUENE
Isolation and structural characterization of adduct formed from propionaldehyde, sym-trinitrobenzene and triethylamine

02 p0251 A70-12275
Red bicyclic condensation product from reaction of acetone with sym-trinitrobenzene and diethylamine

02 p0251 A70-12278
Turbulent charge diffusion during unipolar injection in nitrobenzene between plane-parallel electrodes, discussing liquid motion at high voltages

22 p4080 A70-42719

NITROCELLULOSE
U CELLULOSE NITRATE
NITROGEN
NT LIQUID NITROGEN
NT NITROGEN ATOMS
NT NITROGEN IONS
NT NITROGEN ISOTOPES

Primary cosmic ray nitrogen nuclei intensity and spectrum measured by balloons and Pioneer 8 space probe, obtaining abundance difference from solar atmosphere

01 p0169 A70-10319
Nitrogen abundances measured in enstatite chondrites by inert carrier gas fusion extraction technique, noting agglomeration of chondrules

01 p0179 A70-10475
Sulfur compound effects on carbon monoxide-nitrogen laser emission stability, obtaining continuous operation independently of tube quality

01 p0111 A70-10660
Rotational temperature of molecular nitrogen Vegard-Kaplan bands determined from auroral spectra, including variations in vibrational levels populations

01 p0076 A70-10873
Biochemical characteristics, nitrogenase activity and nitrogen fixation in heterocysts of blue green algae

01 p0024 A70-10894
Atomic O, H and D and molecular oxygen, deuterium and sulfur hexafluoride effects on nitrogen vibrational population distribution in nitrogen afterglow

01 p0148 A70-11356
Physiological equivalents of air with rare gases and H substitutes for nitrogen in inhaled gas mixtures providing normal oxygen intake

02 p0249 A70-12798
Microstructure and impact strength of welds of Cr-Mn steel containing nitrogen, observing grain growth dependence on nitrogen content

03 p0509 A70-13277
Electron spectrometer for nitrogen energy loss spectrum in 12-14 eV region, detailing relative intensities of transition bands

03 p0528 A70-13577
Static breakdown voltage of air and nitrogen measured under uniform field conditions for specific gas number densities, comparing results with Paschen law

03 p0528 A70-14086

Ionization spatial growth similarity with Paschen law in air and nitrogen for specific electric field/gas number density values, discussing ionization coefficients

03 p0528 A70-14087

Laser action observation on IR bands of first positive system of molecular nitrogen using pulsed excitation

04 p0704 A70-15625

Nitrogen ionization rate increase by admixing neutral molecules of electronically excited nitrogen, noting nitrogen decay controlled by spontaneous radiation and wall collisions

05 p0884 A70-15918

Intramolecular formation of azo-linkage accompanying N elimination from bis-azide

05 p0810 A70-16052

Absolute values of emission cross sections for vibrational Meinel bands of molecular nitrogen ions excited by electron impact

05 p0901 A70-16279

Electrically discharged O effect on N first positive band emission in surface catalyzed excitation

06 p1109 A70-17489

Nonequilibrium excitation in recombining N plasma nozzle flows

[AIAA PAPER 70-44]

06 p1122 A70-18061

Momentum transfer from neutral nitrogen molecules to solid surfaces measured for various incident beam molecule energies

06 p1112 A70-18272

Metastable diatomic N beam scattering from Teflon and Cu surfaces measured for velocity and angular distributions

06 p1112 A70-18273

Excitation emission of diatomic nitrogen molecule for first negative band broadening, considering high energy primary beam with secondary electrons

06 p1124 A70-18305

Density effects on rotational temperature measurements in nitrogen by electron beam excitation, discussing emission intensity distribution

06 p1067 A70-18306

Slip flow of nitrogen gas through long circular tubes, measuring mass flow, pressure drop and cross sectional velocity profiles

06 p1051 A70-18368

Fat embolism and decompression sickness similarities, studying lipid stability changes resulting from liver tissue injury by nitrogen bubbles

07 p1222 A70-19936

Photodissociation of diatomic O and N molecules in far UV

07 p1338 A70-20052

Nitrogen IR emission spectra from atomic and molecular excited electronic states transitions, studying DC discharges at various pressures

07 p1339 A70-20092

Molecular N rotational temperature effect on rare gases scattering cross section

07 p1344 A70-20134

Nitrogen molecules pulsed high energy beams transit time measurement by gated time of flight procedure and by multichannel analyzer

07 p1345 A70-20136

Omegatron mass spectrometer for rocket measurements of molecular nitrogen density and temperature in middle thermosphere

07 p1289 A70-20308

Nitrogen molecule photoabsorption and photoionization cross sections determination, discussing ionization probability variations and radiationless transitions

07 p1347 A70-20358

Inert gases and nitrogen determined at high temperature, discussing revision of existing functions representing intermolecular energy

08 p1598 A70-21525

Ionization of rare gases /H and N/ by nitrogen ions, determining cross sections of formation of slow ions and electrons

08 p1549 A70-21801

Lyman-Birge-Hopfield nitrogen bands high resolution emission spectrum, giving energy values of particular states together with corresponding rotational constants and band origins

09 p1730 A70-22067

Fixed low pressures of nitrogen generated by chemical dissociation in system at equilibrium at constant temperature, applying results to vacuum measurement device calibration

09 p1630 A70-22954

Fast electrons spatial distribution for multiple scattering in nitrogen and argon, noting target thickness and incident energy

09 p1735 A70-23179

Acoustic velocity in rarefied argon and nitrogen using Brillouin scatter and Burnett equations

09 p1698 A70-23314

Thermospheric molecular nitrogen vibrational temperature, studying various chemical reactions and collisions as energy sources

10 p1872 A70-23827

High energy oxygen positive-ion reaction with molecular nitrogen, presenting semiempirical model with assumed crossing of potential energy surfaces

10 p1920 A70-25146

Nitrogen content effect on proportional limit and work hardening rate of austenitic stainless steel at 302 F

10 p1905 A70-25169

Thermal conductivity of nitrogen in 350-1500 K range using hot-wire diffusion columns

11 p2147 A70-25756

Threshold photoionization cross sections for homonuclear diatomic N molecules calculated from Slater orbitals and Coulomb waves

11 p2086 A70-25833

Electrical conductivity of impact-ionized nitrogen across magnetic field, deriving electron collision frequency

11 p2091 A70-26461

Nitrogen transport properties to 26,000 degrees K, measuring current-field intensity properties and radial temperature distributions in molecular nitrogen cascade

11 p2151 A70-26841

Spectral absorption characteristics for C atom radiative processes in carbon dioxide-nitrogen mixtures at high temperatures corresponding to Venusian atmosphere

12 p2275 A70-27317

Nitrogen respiratory elimination by human lung, analyzing expired air by mass spectrometry and volume displacement in closed systems

13 p2351 A70-29325

Compression effects in air-oxygen mixture on male mice, observing no adversity on mortality, growth and nitrogen content

13 p2353 A70-29436

Total nitrogen content determination in silicate samples of rocks, synthetic silicate standards, NBS steels and meteorites using inert carrier-gas extraction-gas chromatography

13 p2362 A70-29497

Electron beam measurement of rotational and high vibrational temperature in molecular nitrogen

13 p2412 A70-29980

Low pressure nitrogen and air spectra excitation by low energy proton bombardment, using spectroscopic, photometric and microphotometric analyses

14 p2619 A70-30653

V-N and V-O solid solutions magnetic, electrical, crystallographic and mechanical properties as function of gas concentration

14 p2596 A70-30842

Molecular nitrogen excitation under electron bombardment at auroral and airglow impact levels, using computerized Monte Carlo method

14 p2620 A70-31269

Nitrogen solubility in Nb-Mo solid solutions, determining relationship between N partial pressure, temperature and concentration

14 p2598 A70-31285

Pressurization system for nitrogen generation based on hydrazine catalytic decomposition, describing metal membrane configuration, fuel additives, etc [AIAA PAPER 70-682]

16 p2962 A70-33583

Diatomic nitrogen ions branch overlapping, discussing rotational line structure in first negative system vibrational bands

16 p2956 A70-34254

Cr-Ni stainless steels room temperature yield and tensile strengths improvement by nitrogen addition

17 p3122 A70-34553

NTWO Fortran IV family of subroutines for thermodynamic and transport properties of nitrogen

17 p3195 A70-34746

Aniline and o-anisidine production by photoelimination of nitrogen from fused ring triazoles

17 p3042 A70-34821

High temperature plasmas of mixtures of nitrogen with rare gases, calculating equilibrium thermodynamic properties

17 p3195 A70-34932

Nitrogen deactivation by ground state atomic oxygen resulting in metastable oxygen atom as auroral green line source

17 p3080 A70-35770

Nitrogen solubility calculation in transition metals liquid binary systems, using quasi-chemical model

18 p3273 A70-36045

Total cross sections for production of free electrons in collisions of low energy negative atomic oxygen ions with molecular nitrogen

18 p3292 A70-36188

Compressibility factors and virial coefficients for He-N mixture, He and nitrogen at low temperatures and high pressures

18 p3290 A70-36250

Physiosorption isotherms for nitrogen on stainless steel at various temperatures and very low pressures

18 p3226 A70-36322

Interstellar hot low density intercloud medium in H I region, estimating diffuse emission in forbidden lines O I at 6300 A and N I at 5200 A

18 p3310 A70-37020

Relaxation time for nitrogen molecule vibration temperature in ionosphere due to thermal electron collisions

19 p3409 A70-37324

Nitrogen diffusion coefficient in Mo and W using degassing method

19 p3452 A70-37828

Niobium yield stress at room temperature for various nitrogen and oxygen concentrations

19 p3454 A70-38814

Nitrogen and nitric oxide production and diffusion, examining photochemistry and transport at high altitudes

20 p3620 A70-39339

Capture coefficients and reflected flux measurements for gaseous nitrogen molecular beams impinging on solid nitrogen cryodeposit surface

20 p3675 A70-39390

Emission cross sections of nitrogen in vacuum UV by electron impact

20 p3675 A70-39617

Nitrogen viscosity coefficient at high pressure, describing viscosimeter operation and kinetic theory calculations

20 p3738 A70-40140

Oxygen-nitrogen generation for long manned space flight based on liquid center dual matrix electrolysis cell

21 p3768 A70-40992

Nitrogen photoelectron excitation in dayglow, examining 3371 A band intensity, energy spectrum and flux in ionosphere

21 p3882 A70-41093

Carbon and nitrogen abundances in Apollo 11 rocks, basaltic achondrites and terrestrial basalts, using meteorite analytical techniques

21 p3776 A70-41592

Carbon monoxide-nitrogen laser mechanism vibrational populations, discussing operational characteristics and walls condition and nature

21 p3837 A70-41716

Carbon monoxide-nitrogen laser luminescent phenomena by electronic spectroscopy

21 p3837 A70-41717

Carbon monoxide-nitrogen system vibrational distribution of populations and kinetics in fundamental and harmonic regions, investigating vibroluminescence

21 p3837 A70-41718

Carbon dioxide-He-nitrogen gas mixture pulsed discharge system afterglow gain measurements up to one atmosphere, using CW laser

21 p3837 A70-41719

Helium and nitrogen role in carbon dioxide laser excitation, discussing optimum gas mixture

21 p3837 A70-41919

Nitrogen content of Odessa and Canyon Diablo iron meteorites from thermal neutron activation, Kjeldahl distillation and alkali fusion methods

21 p3921 A70-41942

Spectral absorption characteristics for c atom radiative processes in carbon dioxide-nitrogen mixtures at high temperatures corresponding to Venusian atmosphere

21 p3854 A70-42058

Mars atmospheric nitrogen abundance relative to carbon from spacecraft UV spectrometer data

23 p4238 A70-43805

Auroral spectrophotometer measurements from 1968 NASA airborne expedition, discussing oxygen and nitrogen spectral lines

23 p4186 A70-43855

Auroral molecular nitrogen bands tentative identification based on rocket-borne spectrometer results

23 p4186 A70-43856

Three body recombination and dissociation rate coefficients of nitrogen in Ar atoms heat bath, using modified phase-space theory

23 p4221 A70-44008

Cryogenic fluids nitrogen, argon and carbon monoxide nucleate boiling from atmospheric to near critical pressure

23 p4279 A70-44359

Saturated nitrogen vapors condensing coefficients measurement by cryostat, comparing results with theoretical prediction

23 p4218 A70-44364

Molecular oxygen ions 1Ng band and molecular nitrogen 1Pg band relative intensities in normal and type B auroras

23 p4191 A70-44408

Nitrogen deficient algae nitrification, showing cellular N compounds oxidized to nitrate and nitrite followed by nitrate reductase

24 p4297 A70-45407

Nitrogen abundance of subgiant nu Indi from observed and computed stellar spectra of CN violet bands

24 p4404 A70-45411

Energy loss spectra and collision cross sections for positive ion impact on molecular nitrogen, noting Lyman-Birge-Hopfield system excitation

24 p4381 A70-45599

TROGEN ATOMS

- N atom recombination rate coefficient in static system pressure dependent at low pressure
01 p0147 A70-10450
- Kinetics of attack of SiC in monoatomic mixtures of N and O generated by microwave discharge dissociation
07 p1421 A70-19332
- Vacuum UV atomic nitrogen and oxygen lines contribution to energy transfer in high density plasma, noting f values and Stark half widths
09 p1730 A70-22229
- Electron density reduction in plasma surrounding reentry vehicle due to N atom removal by water droplets injection
09 p1737 A70-23237
- Upper atmospheric atomic nitrogen reaction with carbon tetrachloride, estimating radiation intensity and brightness of artificial luminescent cloud
18 p3252 A70-36989
- Emission spectral distribution of atomic nitrogen reaction with carbon tetrachloride for artificial luminescent clouds
18 p3293 A70-36990
- Nitric oxide and atomic nitrogen in mesosphere and stratosphere, discussing photochemical equilibrium
19 p3415 A70-38389
- Ionization rates in auroras detected by atomic oxygen and nitrogen lines
22 p4024 A70-43308
- Vanadium subnitride crystal structure with ordered array of nitrogen atoms in V sublattice
24 p4360 A70-45519

TROGEN COMPOUNDS

- ALUMINUM NITRIDES
- AMIDES
- AMMONIA
- AMMONIUM NITRATES
- ATROPINE
- AZIDES [INORGANIC]
- AZIDES [ORGANIC]
- AZO COMPOUNDS
- BERYLLIUM NITRIDES
- BORON NITRIDES
- CAFFEINE
- CELLULOSE NITRATE
- CYANO COMPOUNDS
- FOLIC ACID
- HYDRAZINE NITRATE
- HYDROGEN CYANIDES
- IMIDES
- IMINES
- ISOCYANATES
- LIQUID AMMONIA
- MORPHINE
- NICOTINAMIDE
- NITRATES
- NITRIC ACID
- NITRIC OXIDE
- NITRIDES
- NITRITES
- NITRO COMPOUNDS
- NITROBENZENES
- NITROGEN DIOXIDE
- NITROGEN OXIDES
- NITROGEN TETROXIDE
- NITROMETHANE
- NITROSO COMPOUNDS
- NITROSYL CHLORIDES
- NITROUS OXIDES
- ORGANIC NITRATES
- POLYIMIDES
- RDX
- SILICON NITRIDES
- SILVER NITRATES
- THYMIN
- TITANIUM NITRIDES
- TRINITROTOLUENE
- TRYPTOPHAN
- UREAS
- URIC ACID
- XANTHINES
- Ionic polymers, investigating cyclic and linear compounds and reaction products from tetramethyldiaminoalkanes and dibromoalkanes using NMR, IR and mass spectroscopy
06 p1004 A70-17511

- Nitrogenous compounds from Colorado Green River Formation oil shale using high resolution mass spectrometry
11 p2047 A70-26620

- Ketene and diazomethane flash photolytic measurement of reaction rates of singlet-triplet methylene deactivation
15 p2694 A70-31729

- Product distribution of organic nitrogen compounds plasma sources computed by assuming high temperature limited thermodynamic equilibrium
18 p3226 A70-36764

TROGEN DIOXIDE

- Flowfield and chemical kinetics model to calculate nitrogen dioxide chemiluminescence wake emission [AIAA PAPER 68-702]
04 p0620 A70-15535

- Nitrogen dioxide presence in solar atmosphere from balloon-borne spectrometer observations, presenting graph of sunset solar spectrum
08 p1575 A70-21262

- Kinetics of homogeneous nitrogen dioxide-carbon monoxide atom transfer reaction in single pulse shock tube, carrying out product analysis by vapor phase chromatography
08 p1455 A70-21263

- Nitrogen dioxide continuum in green-white afterglow of molecular oxygen and nitrogen, using spectrometry and photometry
14 p2579 A70-31254

- Heat transfer coefficient of chemically reacting gas mixture as function of Lewis-Semenov number, discussing nitrogen dioxide decomposition
19 p3550 A70-37251

- Thermal decomposition of nitrogen tetroxide and nitrogen dioxide induced by shock waves, examining temperature effects
19 p3373 A70-38265

- Nitrogen dioxide continuous visible emission under thermal and recombination excitation, examining spectral characteristics
19 p3374 A70-38267

- Air polluting sulfur dioxide and nitrogen dioxide remote sensing based on radiation molecular absorption using long line correlation spectrometer
20 p3633 A70-39793

NITROGEN IONS

- Lifetimes of upper levels of N II and N III UV multiplets determined from radiative deexcitation of excited ions
03 p0527 A70-13074

- Ionization of rare gases /H and N/ by nitrogen ions, determining cross sections of formation of slow ions and electrons
08 p1549 A70-21801

- Stark broadening of singly ionized nitrogen lines measured in dense high temperature plasma behind reflected shock wave in T tube
09 p1731 A70-22776

- N and O ions electron impact ionization rates calculated from approximate cross sections
12 p2275 A70-27173

- Electron impact excitation cross section of /O,0/ first negative band of nitrogen ion from threshold to 3 keV, using photon counting techniques
12 p2276 A70-27880

- Nitrogen and air bombardment by relativistic electrons, determining absolute fluorescence intensity of nitrogen molecular ion first negative band
16 p2954 A70-33279

- Orion nebula H alpha/forbidden N II ratio measurement using wide field multislit spectrograph
22 p4101 A70-42857

NITROGEN ISOTOPES

- IR spectra of N isotopes adsorbed on nickel-on-Aerosil catalysts, investigating effects of intermolecular interaction and isotopic substitution
03 p0440 A70-13099

- Carbon dioxide-nitrogen and nitrous oxide-nitrogen laser systems, substituting diatomic N 15 for N 14 to investigate radiation intensity
15 p2750 A70-31761

- Carbon-nitrogen-oxygen isotope bi-cycle function in solar evolution, noting first cycle role in solar energy release and neutrino production
20 p3698 A70-39306

- Apollo 11 lunar matter rare gas, H and N concentrations and isotopic abundances, discussing solar wind, gas diffusion loss from silicates and spallation component
21 p3908 A70-41583

- IR microwave double resonance signals in systems of ammonia with nitrogen isotopes, using nitrous oxide laser
21 p3836 A70-41707

NITROGEN OXIDES

- NITRIC OXIDE
- NITROGEN DIOXIDE
- NITROGEN TETROXIDE
- NITROUS OXIDES

- Ozone formation in presence of nitrogen oxides and hydrocarbons during long wave UV irradiation, noting energy yield
09 p1629 A70-22328

- Nitrogen oxide ions mobility in air calculated at high plasma temperatures
12 p2276 A70-27845

- NO and nitrogen dioxide influence on ozone concentration and production rate in stratosphere
14 p2568 A70-30125

- Air pollution by turbojets and gas turbines, discussing control of carbon particles and nitrogen oxides
16 p2963 A70-32922

- Reactive stream separation high speed color photography for impinging streams of nitrogen tetroxide and hydrazine [AIAA PAPER 70-608]
16 p2998 A70-33605

NITROGEN PLASMA

- Heat transfer rates to stagnation point of hemisphere in supersonic high enthalpy low density nitrogen plasma flow [ASME PAPER 69-WA/HT-49]
04 p0614 A70-14799

- Continuum radiation of nitrogen plasma at atmospheric pressure at high temperatures
10 p1923 A70-24472

- Interference holograms of low temperature nitrogen plasma jet using fundamental and second harmonic ruby laser emissions
13 p2464 A70-29384

- Electric field intensity and extension of space charge sheath for ion extraction from nitrogen plasma
14 p2652 A70-30661

- Oxygen, nitrogen and argon plasma total radiation measurement at various wavelengths and temperatures
17 p3139 A70-34547

- Microwave diagnostics of plasma temperature and conductivity in streaming nitrogen arc with skin effect under atmospheric pressure
19 p3476 A70-37554

- Equilibrium compositions of helium-nitrogen, argon-nitrogen and xenon-nitrogen plasmas at atmospheric pressure between 5000 and 35,000 K
19 p3552 A70-37831

- Collisionless nitrogen plasma drift velocity measurement by ion acoustic wave method
21 p3859 A70-41760

- Spatial energy loss and ionization deposition distributions of fluorescent radiation emission induced by electron beam in nitrogen gas
21 p3853 A70-41913

- Nitrogen transport coefficients as function of high temperature in stationary plasma produced in cascade arc chamber
22 p4082 A70-43373

- Nitrogen plasma viscosity measurements as function of velocity and axial static pressure gradient
23 p4226 A70-44439

NITROGEN TETROXIDE

- Liquid nitrogen tetroxide enthalpy measured by indirect heating techniques, obtaining data at supercritical temperatures
06 p1005 A70-18560

- Caloric data determining saturated vapor pressure of nitrogen tetroxide and heat of sublimation for sublimation curve
07 p1358 A70-19206

- Enthalpy of nitrogen tetroxide in liquid phase using direct heating of test substance in calorimeter
07 p1358 A70-19207

- Optimum penetration and separation mixing of unlike doublet injector element with hypergolic hydrazine and nitrogen tetroxide propellants [JPL-TR-32-1487]
11 p2099 A70-25995

- Combustion stability effects of additives on hydrazine/nitrogen tetroxide propellant combination by measuring droplet burning rates
11 p2100 A70-26283

- Nitrogen tetroxide thermodynamic properties calculation from pressure-volume-temperature equation of state in gas and liquid phases
12 p2332 A70-27975

- Stress corrosion cracking of Ti and Ti-Al-V alloy in liquid dinitrogen tetroxide
15 p2755 A70-31475

- Odor threshold levels for unsymmetrical dimethylhydrazine /UDMH/ and nitrogen tetroxides
18 p3224 A70-36227

- Thermal decomposition of nitrogen tetroxide and nitrogen dioxide induced by shock waves, examining temperature effects
19 p3373 A70-38265

NITROMETHANE

- Critical diameter and detonation parameters of nitromethane and tetranitromethane as function of powder content
01 p0217 A70-11004

NITROSO COMPOUNDS

- Methylating agents and nitrosoguanidine actions on polynucleotides, including ribonucleic acid
03 p0440 A70-13550

- Agents for deoxygenation of nitro and nitroso groups
17 p3042 A70-35329

- Gaseous and liquid fluorine exposure effects on nitroso rubbers at ambient and cryogenic temperatures, using impact tests and IR spectroscopy
21 p3844 A70-42140

NITROSYL CHLORIDES

- Nitrosyl chloride reagent effects on phenylalanine peptides
12 p2181 A70-27471

NITROUS OXIDES

- Dissociative attachment of low energy electrons in nitrous oxide as function of gas temperature
03 p0441 A70-14006

- Potential energy surface shapes for lowest states of temporary negative ions of nitrous oxide and carbon dioxide
03 p0441 A70-14008

Nitrous oxide molecular beam reflection and dissociation on tungsten surface at high temperatures from angular distribution measurements

06 p1004 A70-17493

Tunable nitrous oxide laser cavity losses and absorption by carbon dioxide determined spectroscopically

11 p2061 A70-25361

Cyanogen-nitrous oxide flame temperature determination for different concentrations of mixture in flat stainless steel diffusion flame burner

11 p2101 A70-26386

Nitrous oxide chemisorption by rhodium filament at low pressures at various temperatures, determining sticking probability

12 p2181 A70-27678

Nitrous oxide and carbon dioxide laser Q switching by ammonia Stark effect

13 p2431 A70-29835

Thermal energy negative ion-molecule reactions in photoionized NO-water vapor mixtures, determining rate constants by stationary afterglow system

16 p2954 A70-33280

Q switching of nitrous oxide laser with Freon 12 and sulfurhexafluoride absorbers, comparing wavelengths with carbon dioxide laser outputs

21 p3834 A70-40567

NO molecule gamma system in emission spectra of polar auroras in far UV by monochromator aboard Skylark rocket

21 p3821 A70-42261

NOBLE GASES

U RARE GASES

NOBLE METALS

NT GOLD

NT RUTHENIUM

NT SILVER

Noble metals band structure effects on shielding cloud around impurity and alloys electronic properties in weak scattering limit

09 p1740 A70-22953

Superconductivity in noble metal rich hexagonal close packed phases and fcc solid solutions ascribed to Fermi surface-Brillouin zone interaction

15 p2785 A70-32398

Precious metals, measuring tension, grinding and polishing induced surface plastic deformation effects on electron work function and exoemission

23 p4204 A70-43927

NOCTILUCES

U LUMINESCENCE

NOCTILUCENT CLOUDS

Noctiluculent cloud observation stations and international cooperation in exchanging climatological data concerning annual variations, height distribution and latitude dependence

01 p0072 A70-10579

Atmospheric density in meteor region and atmospheric wind conditions determined from meteor trail drifting and artificial noctiluculent clouds

03 p0563 A70-13178

Noctiluculent clouds morphological and kinematic characteristics based on photographs

03 p0476 A70-13885

Nacreous and noctiluculent cloud physics, discussing earth-impacting meteor dust accumulation and mesopause water vapor

07 p1273 A70-20265

Rocket-borne sampler for collecting noctiluculent cloud particles in mesopause, describing collection and analysis methods and protection against tropospheric contamination

07 p1273 A70-20266

Noctiluculent clouds in mesopause over North America, discussing ground stations network, intensity variations, structure and time distribution

07 p1273 A70-20267

Lower thermosphere dust particle layers correlated with polarization anomaly twilight fluctuations and noctiluculent clouds frequency distribution

10 p1944 A70-24949

Auroras and noctiluculent clouds simultaneous occurrence in middle latitudes, discussing mesopause temperature variations and mesosphere heating

20 p3621 A70-39402

Noctiluculent cloud kinematics, examining wave structure and lengths, velocities and general motion

20 p3622 A70-39403

Noctiluculent clouds blue color and rocket sounding results explained by ozone model of mesospheric clouds formation

23 p4188 A70-44048

NOCTURNAL VARIATIONS

Cosmic radio absorption nightly variations, considering ionospheric structure and composition and various scattering mechanisms

07 p1367 A70-19456

Nighttime D region ionization irregularities deduced from vertically incident VLF radio wave

09 p1671 A70-23663

Sodium night airglow analyzed by Chapman mechanism, considering nocturnal intensity seasonal behavior and location in upper atmosphere

10 p1873 A70-23829

Cosmic radio absorption nightly variations, considering ionospheric structure and composition and various scattering mechanisms

18 p3309 A70-36930

Total ionospheric electron content nocturnal and latitudinal variations in winter at midlatitudes

20 p3624 A70-40480

Scintillation LF observations with synchronous satellite radio signals at low latitude station, noting magnetic activity effects on night and day scintillations

20 p3590 A70-40488

Sodium D lines airglow nocturnal and seasonal variations in upper atmosphere

22 p4023 A70-43295

NODES [STANDING WAVES]

Clamped skew plates influence coefficients, natural vibration frequencies and nodal patterns measurement, comparing to Galerkin method results

16 p2988 A70-33124

Mechanical models of single speed gears for torsional vibrations, taking into account nodes of first free vibration mode

16 p2995 A70-34289

Nodal patterns on thin elastic circular plate vibrating in flexure, considering natural and compounded modes

19 p3543 A70-38245

Lunar theory literal solution for average node and perigee movements compared with Delaunay results, using Lie transforms for Hamiltonian function

24 p4399 A70-45141

NOISE [SOUND]

NT AERODYNAMIC NOISE

NT AIRCRAFT NOISE

NT ENGINE NOISE

NT JET AIRCRAFT NOISE

NT ROCKET ENGINE NOISE

NT SONIC BOOMS

NT THERMAL NOISE

Intermittent vs continuous noise effects on signal detection measures during audio visual checking task performance

01 p0039 A70-11167

Noise generation in turbulent premixed flames, turbulent diffusion flames and liquid-spray combustion of hydrocarbon fuels, using optical method

02 p0399 A70-12040

Pulsed noise biological effects on human organism, showing stimulation of auditory duct and baric and mechanical reception system causing neural functional shift

03 p0433 A70-13476

Near noise fields of choked axisymmetric air jet, discussing sound pressure levels surrounding jet

05 p0834 A70-16783

Ionic noise during plasma turbulent heating in toroidal facility, discussing oscillation spectrum

07 p1349 A70-19552

Human complex responses to noise, considering individual variations, social and psychological factors, adaptation, etc

09 p1617 A70-22392

Acoustic noise control on Boeing aircraft electromagnetic components, noting iron-core magnetostatic demanding transformer redesign

09 p1647 A70-22764

Noise-flutter interrelation in flight vehicle flexible plate and shell configurations immersed in fluid flow

11 p2132 A70-25726

Ionic noise during plasma turbulent heating in toroidal facility, discussing oscillation spectrum

15 p2777 A70-31459

Noise effects on arousal level in auditory vigilance from EEG parameters

19 p3364 A70-38325

NOISE ATTENUATION

U NOISE REDUCTION

NOISE ELIMINATION

U NOISE REDUCTION

NOISE HAZARDS

U HAZARDS

U NOISE [SOUND]

NOISE INJURIES

Audiograms for aviators unexposed and exposed to high intensity LF noise of maritime patrol aircraft indicating no permanent effects

01 p0032 A70-10365

Guinea pig cochlear hair cell damage after exposure to impulse noise

02 p0236 A70-12322

Ship engineers cardiovascular system functional changes during HF internal combustion engine noise, investigating EKG recordings and arterial pressure

20 p3582 A70-40292

NOISE INTENSITY

Signal discrimination from sequence of interference and noise by determining parameter value probability density using random process

01 p0044 A70-11024

He-Ne laser using K-activated alumina cold cathode and coaxial construction, discussing output, low noise applications, construction and testing

03 p0501 A70-13583

Schottky barrier diodes design for wideband radiometer mixers to obtain optimum noise performance and broadband operation by DC bias application

03 p0457 A70-1396

Plume-induced X band radar attenuation, AM and PM noise measured in aluminized solid propellant motor firings

04 p0736 A70-1540

Aircraft noise suppression, discussing community aspects of jet and fan noise and physical mechanism of jet noise

05 p0795 A70-1677

Acoustic intensity determined from time, length and velocity scales in mixing region of jet from nozzle with turbulent boundary layers

05 p0834 A70-1677

Subsonic circular jet noise radiation intensity and directional distribution, based on effects of refraction and Lighthill quadrupole model for aerodynamic noise

05 p0834 A70-1678

Antenna noise temperature of large aperture reflectors from feed system RF characteristics, discussing spillover and blockage factors

06 p1008 A70-1750

Acoustic power output from supersonic jets, considering aerodynamic and acoustic characteristics for supersonic exhaust velocities

06 p1132 A70-18115

Acoustic characteristics of high subsonic model cold jet using imaging technique and measurements of energy flux of flow, calculating energy flux from flow-field measurements

06 p1040 A70-18125

Perceived aircraft noise level based on objective acoustic measurements related to subjective response, tabulating noys as function of sound pressure

07 p1190 A70-18803

Signal strength of sky waves and noise levels near LUF, suggesting importance of changing mode structure

07 p1229 A70-19158

HF radio noise environment, discussing local storm effects, noise power estimation, noise measurement methods, etc

07 p1231 A70-19172

HF ion-acoustic noise /whistlers/ during turbulent heating of plasma, using matched magnetic probe

07 p1348 A70-19551

Acoustic turbulence generated noise intensity and spectrum using statistical thermodynamics

07 p1194 A70-19618

Temporary and permanent threshold shifts in hearing of guinea pigs exposed to intense rocket booster engine noise

07 p1214 A70-19931

Random synchronization errors in PN and PSK systems reduce input signal power and introduce additional self noise

07 p1236 A70-20069

Roundoff noise output-dynamic range interaction in digital filters, discussing filter synthesis with transpose configurations concept

09 p1649 A70-23366

Pure-tone air conduction audiogram for diagnosis of patients exposed to intense noise indicating conductive or sensorineural origin of loss

09 p1621 A70-23457

Microwave devices excess AM and FM noise levels measurement by carrier suppression methods

10 p1841 A70-24579

Optimal stochastic control investigated for linear systems with driving noise intensity proportional to control input

10 p1856 A70-25234

Aerial and ground UHF noise measurement in Phoenix area, correlating air and ground data

11 p2001 A70-25480

Takeoff noise minimization by prescribing optimum takeoff trajectories, considering aircraft parameters influencing noise intensity at takeoff

11 p1979 A70-25814

THEMIS source encoding systems research program to investigate inherent quantizing noise and degradation of analog to digital conversion

11 p2014 A70-26255

Commercial aircraft peak cockpit noise level during cruise and high speed descent, discussing damage risk criteria and interplot speech interference

11 p1991 A70-26275

Pro- and anticoagulants dynamics in rats blood during early phases of prolonged sound effect

12 p2168 A70-27347

STOL aircraft noise level certification based on aircraft type, landing and takeoff paths and airports

12 p2161 A70-27459

Aircraft noise reduction effects on airport capacity and community exposure levels

12 p2207 A70-27628

MOS-FET HF noise quantities computed in terms of substrate doping, angular frequency and gain-bandwidth product

12 p2196 A70-27672

High intensity noise effects on auditory thresholds, blood pressure and time response to light stimuli, showing permissible levels during space flights
13 p2358 A70-29334

Noise level influence on optimal recognition of non-stationary random processes in white noise
13 p2369 A70-29729

HF ion-acoustic noise /whistlers/ during turbulent heating of plasma, using matched magnetic probe
15 p2777 A70-31458

Noise effect on modulation transfer function of visual channel by threshold measurements
15 p2698 A70-32013

Intensity correlations in optical parametric noise and second harmonic generation measured by two photon delayed coincidence counting
15 p2753 A70-32603

Helicopter rotors noise intensity prediction for high tip Mach number, including compressibility and thickness effects
17 p3015 A70-34729

Vibrating structure mathematical model for predicting radiated noise level
17 p3187 A70-35169

High intensity noise enveloping space vehicle as distributed excitation, examining correlation effects on structural response
17 p3059 A70-35170

High intensity noise testing of missile and spacecraft structures, simulating acoustically induced vibrations due to aerodynamic turbulence
19 p3531 A70-37697

Temporal and spectra combination effects on aircraft sound judged noisiness, using human subjects in anechoic chamber
20 p3580 A70-39712

Frequency synchronization channel pulse fluctuations effect on noise stability of binary signal reception
20 p3587 A70-40145

Aircraft noise reduction, discussing generation sources in propulsion system, noise levels and subjective responses
23 p4140 A70-44395

Intense white pulsed jet engine noise effects on cochlea biocurrents in cats
23 p4157 A70-45076

NOISE MEASUREMENT

U ACOUSTIC MEASUREMENTS

NOISE METERS

Remote sonic monitoring system for Saturn V noise measurement and recording
17 p3094 A70-35521

Sound measurement, discussing impulse level meters, noise exposure index, sound level recorder and classification, frequency analysis and filters
17 p3097 A70-35925

NOISE PROPAGATION

Discrete noise generation and propagation due to fan engine rotor forcing excitation and interaction with downstream stator
05 p0896 A70-16791

Far field directionality and acoustic power of noise radiated by axial flow fans and compressors using fluctuating forces model
08 p1547 A70-21860

Ground reflection effect on plane uniform sound source distribution applicable to compressor and fan noise under far field conditions
09 p1726 A70-22240

Collection of papers on aerodynamic noise covering noise generation, solid boundaries effect, strength distribution, jet noise, perturbation theory, etc
17 p3071 A70-35448

Buzz-saw noise of transonic compressor due to rotating pressure field at supersonic blade tip speeds [ASME PAPER 70-GT-54]
18 p3303 A70-36838

Triboelectric noise in mechanically flexed low level signal cables for piezoelectric transducers with high gain amplifiers
21 p3825 A70-40866

Microplasma and burst noise measurements on discrete silicon planar transistors indicating origin at emitter-base junction
22 p3998 A70-43331

Jet engine noise propagation near porous surface, predicting anomalous LF dip from direct and reflected waves interference with phase delay
24 p3395 A70-46068

Axial flow compressor fan discrete tone noise radiation directivity pattern measurement and theoretical explanation for cut-off effect, power and harmonics
24 p4380 A70-46069

NOISE REDUCTION

Noise reduction for V/STOL aircraft operation by introducing quiet propellers, discussing variable camber propellers, propeller aerodynamics, etc [AIAA PAPER 69-1038]
01 p0005 A70-10646

Jet engine noise sources and design of noise suppressors used during airport runway engine tests
02 p0275 A70-12222

Touring aircraft, discussing vibration and noise reduction, instrumentation, STOL aircraft, etc
02 p0227 A70-12663

Multimirror illumination system for radio telescope antenna with reduced noise temperature, narrow radiation pattern and optimal specular cross section, noting sensitivity
03 p0455 A70-13082

Phase lock loop circuit for spacecraft communication noise filtration, describing linear study of first-four-order loops
03 p0448 A70-13537

Fan rotors aerodynamic noise tonal annoyance reduction by blade unequal circumferential spacing, noting sound-pressure wave shape determination [ASME PAPER 69-WA/FE-23]
04 p0614 A70-14776

Turbine noise significance in civil aircraft noise problem
04 p0734 A70-14884

Optimum low speed ducted fan design for minimum noise generation
04 p0734 A70-14891

Ar laser as suitable source for LF heterodyne anemometer experiments through noise spectrum suppression under optimum conditions
04 p0702 A70-15569

Noise suppressor research for jet engine components, describing test equipment and facilities for models work
05 p0825 A70-15808

Rotor noise reduction in helicopter design for increased blade loadings and higher tip speed [SAE PAPER 690684]
05 p0792 A70-15865

Airport noise silencers for aircraft engines, discussing design, operation and damping efficiency
05 p0829 A70-16353

First order pressure gradient microphone design based on electrostatic principle, using foil electrets to discriminate against airborne and solid-borne noises
05 p0821 A70-16402

Aircraft noise suppression, discussing community aspects of jet and fan noise and physical mechanisms of jet noise
05 p0795 A70-16777

Engineering methods developed for controlling boundary layer, jet and compressor noise, discussing theoretical formulations usefulness
05 p0896 A70-16778

Propeller noise research for achieving noise reductions in future propeller design
05 p0796 A70-16793

Aircraft configurations designed for eliminating sonic boom due to lift
05 p0791 A70-16798

Jet noise theory application in noise prediction and reduction at source for subsonic and supersonic jets
06 p1038 A70-18066

Interacting coaxial supersonic jet flows noise reduction based on noise distribution characteristics measurement in anechoic chamber [AIAA PAPER 70-236]
06 p1040 A70-18112

Magnetic, electrostatic and RF fields noise reduced for strain gage data acquisition
06 p1069 A70-18435

Aircraft noise reduction certifications program by tripartite draft plan
07 p1426 A70-18876

Frequency monitor design, analyzing relationships between time constants, gain, etc, emphasizing white noise filtration
07 p1227 A70-18991

V/STOL intercity airliner potential and development noting benefits of noise reduction, ground space economy, etc
08 p1434 A70-20619

Threshold extension techniques using impulse noise detection and elimination implemented at phase lock loop demodulator output
08 p1460 A70-20811

Noise damping model for complex configuration mufflers operating under conditions prevailing in diffuse acoustic field
08 p1545 A70-21009

SHF avalanche transit time oscillator with FM noise reduction by injection phase locking
08 p1462 A70-21594

Mean flow and turbulent velocity over noise-producing regions of subsonic jet nozzle with and without delta wings
09 p1610 A70-22239

Jet aircraft engine noise control, discussing noise sources and built-in acoustic absorbers
09 p1743 A70-22759

Acoustic noise control on Boeing aircraft electromagnetic components, noting iron-core magnetostatic demanding transformer redesign
09 p1647 A70-22764

Microwave sources power stabilization, control and noise reduction using feedback techniques
09 p1649 A70-23275

Takeoff noise minimization by prescribing optimum takeoff trajectories, considering aircraft parameters influencing noise intensity at takeoff
11 p1979 A70-25814

Fourier and Hadamard transformation codings for multidimensional data channel noise immunity and bandwidth reduction
11 p2011 A70-26329

Pilot helmets, discussing sound attenuation, noise protection and speech intelligibility
12 p2177 A70-27040

Proportional fluid amplifiers noise and instability sources related to geometry and power jet flow, considering noise reduction methods
12 p2164 A70-27071

Aircraft noise reduction effects on airport capacity and community exposure levels
12 p2207 A70-27628

Transportation vehicle noise control measures and acceptability, discussing physical and operational source modifications using aircraft noise examples
12 p2336 A70-27849

Binary-valued digital pictures noise cleaning by propagation processes
12 p2188 A70-27937

Noise reduction design of Enstrom F-28A helicopter, noting operation at lower tip speeds and blade loading
12 p2162 A70-28096

Spurious output from C band radar magnetrons, discussing measurement procedures and noise reduction by waffle-iron waveguide filters
12 p2201 A70-28141

Noise characteristics and measurement, discussing aircraft noise generation and reduction
13 p2473 A70-28443

VTOL and STOL design and operation, discussing noise and vibration reduction
13 p2344 A70-28544

Jet engines for civil and military aircraft, discussing turbine designs and noise reduction
13 p2474 A70-28546

Noise rejection during synchronous quasi-coherent radio signal reception with binary narrow band linear filter used for voltage shaping
13 p2369 A70-29737

Quartz floating component design, discussing magnetic sensitivity temperature dependence and microseismic noise rejection properties
14 p2582 A70-30245

Climatology of safe threshold Mach number and airplane ground speed for boomless supersonic cruise, considering San Francisco-New York route
14 p2530 A70-30606

Noise of large commercial V/STOL aircraft and effect on design and operation, predicting acoustic signatures
14 p2531 A70-30854

Sonic boom minimization methods involving mass or energy addition
14 p2531 A70-30868

Commercial jet aircraft engine noise evaluation, discussing noise reduction and effects on airport neighbors
14 p2630 A70-31335

TWT noise level minimization in 8 mm band with circular spiral slow wave structure and five electrode gun
15 p2707 A70-31519

Combined radio and physical navigation systems, considering noise rejection and corrections of position and speed
15 p2772 A70-31623

He-Cd laser with cathaphoretic transport and diffusion return path, noting condenser critical temperature for radiation noise reduction
15 p2751 A70-31987

Aircraft fan and turbine noise reduction, discussing blade wake interaction, jet mixing and duct acoustic linings
16 p2963 A70-32946

Solid state spectrum centered receiver for eliminating externally generated pulse type interference between radar sets
16 p2862 A70-33066

Phase modulated holography for inherent noise reduction using thicker recording media, increasing signal beamwidth or beam ratio
16 p2904 A70-33137

Curved porous wall channels for noise suppression in power plants, ventilation systems, etc
18 p3216 A70-36302

Optimal incoherent signal reception in discrete information transmission systems with fluctuation and concentration noise, including Rayleigh fading
18 p3228 A70-36600

Sound transmission and suppression in turbomachinery fans and compressor ducts, using three dimensional wave equation [ASME PAPER 70-GT-58]
18 p3304 A70-36873

Noise rejection characteristics of ionospheric radiosondes via phase-code modulated signals, noting nonoptimal filter role in power loss
18 p3229 A70-37042

Ferrite reactive modulation amplifier design, using yttrium garnet for noise reduction
19 p3386 A70-37629

RF communication signal to noise improvement by time variant tracking filter with high Q superconductive resonant cavity
19 p3391 A70-38892

- FM demodulation threshold extension by correlation detection implemented in impulse noise cancellation system 19 p3382 A70-38893
- Traveling wave antenna arrays with resistance elements for coupling, measuring noise elimination capabilities 20 p3598 A70-40146
- Objective and subjective laser speckle noises in holography, discussing causes and methods of elimination 21 p3835 A70-40716
- Electro-optical modulation lock-in techniques for minimizing statistical fluctuations and eliminating internal noise in sampling of light signals 21 p3827 A70-41462
- Information transmission techniques by discrete amplitudes and increments, comparing effectiveness for noise rejection 22 p3986 A70-42495
- NASA acoustically treated nacelle program reducing noise under commercial transport flight path near airports 22 p4089 A70-42529
- Structural and environmental design criteria for acoustical duct-lining materials in turbofan noise suppression 22 p4089 A70-42531
- Duct lining parameters effects on engine inlet and fan discharge noise reduction during fan jet landing 22 p4090 A70-42532
- Test rig vehicle design for noise research on single stage high bypass ratio fans for quieter turbofan power plants [ALAA PAPER 69-492] 22 p4090 A70-42708
- Turbojet engines noise-suppressing nozzles flow rate and thrust characteristics calculation 22 p4092 A70-43371
- VHF omnidirectional range (VOR) receiver, considering noise reduction problem and active filter importance to signal improvement and system accuracy 22 p3992 A70-43586
- Coherent radar backscatter, calculating autocorrelation and power spectrum of spuri noise from periodic random phase injections for filter design to eliminate noise 22 p3992 A70-43591
- Picture transmitting systems noise rejection enhancement via redundancy, discussing video coding and decoding and signal filtration 23 p4159 A70-43760
- Phased locked AFC circuit, calculating internal harmonic noise reduction by proportionately integrating filter 23 p4161 A70-43960
- Multiplicative noise reduction during transmission of analog signals over tropospheric microwave relay links 23 p4162 A70-44090
- Jet aircraft noise reduction devices directed at turbulence fluctuation noise sources, noting effects on flight characteristics [ICAS PAPER 70-21] 23 p4233 A70-44112
- Aircraft noise reduction, discussing generation sources in propulsion system, noise levels and subjective responses 23 p4140 A70-44395
- Noise reduction regulations effects on subsonic transport design and configuration [SAE PAPER 700806] 24 p4290 A70-45876
- L-1011 aircraft optimum minimum noise pod design, describing technology, restraints and system requirements [SAE PAPER 700805] 24 p4393 A70-45877
- Noise suppression for high-bypass ratio CF6 turbofan engine in DC-10 airplane, considering effect on engine design [SAE PAPER 700804] 24 p4393 A70-45878
- STOL aircraft augmentor wing concept, examining noise suppression, flight research vehicle program and application to turbofan production aircraft [SAE PAPER 700812] 24 p4290 A70-45903
- Boeing 2707 SST design for low community noise, discussing engine-airframe matching effect [SAE PAPER 700808] 24 p4290 A70-45906
- Noise reduction design for subsonic transport turbofan engines [SAE PAPER 700807] 24 p4395 A70-45907
- SST sonic boom noise level reduction by thermal simulation of long body aircraft, considering thermal spike or keel [AIAA PAPER 70-1323] 24 p4291 A70-45942
- ### NOISE SPECTRA
- Absorbed RF plasma wave noise spectrum in region of anomalous dispersion, noting peak in far IR region 01 p0150 A70-10286
- Noise power spectrum characteristics for He-Ne laser as function of discharge characteristics, measuring effect of cold vs hot cathodes 01 p0111 A70-10745
- Correlation between sunspot number index and solar radio noise index relative to ionospheric propagation, noting computer analysis program and hysteresis effect 02 p0289 A70-12107
- Noise source model of Si planar diffused bipolar IC transistors in operational amplifiers, noting base-emitter junction burst noise 02 p0257 A70-12192
- Rate distortion function for class of sources, proving positive and negative sides of Shannon encoding theorem for noisy channels 02 p0266 A70-12611
- Sealed-off He-Cd laser construction, describing life test, noise, Cd transport characteristics and transverse magnetic field effect 03 p0501 A70-13582
- Discrete frequency noise generation from axial flow compressor blade row, using experiments in small scale Freon loop [ASME PAPER 69-WA/FE-22] 04 p0733 A70-14777
- Discrete frequency noise generation associated with wakes due to fluid flow over turbomachine blades, supporting spokes, flat plates, etc [ASME PAPER 69-WA/GT-13] 04 p0733 A70-14883
- Residential structures vibration response to aircraft flyover noise, discussing noise transmission, rattle phenomenon, spectra, etc [ASME PAPER 69-WA/GT-8] 04 p0770 A70-14887
- Discrete components in noise spectrum of heated and unheated supersonic air jets, using axisymmetric and conical nozzles 04 p0618 A70-15247
- Sound levels and frequency spectra of noises measured in AN-24 and IL-18 turboprop aircraft cockpits 05 p0796 A70-16925
- Two port isotropic antenna excited by independent noise sources for uniform power radiation in all directions and polarizations 06 p1021 A70-17574
- Noise field from ground testing of nuclear rocket engines operated at various reactor power levels 06 p1133 A70-18234
- Acoustic turbulence generated noise intensity and spectrum using statistical thermodynamics 07 p1194 A70-19618
- Spectral amplitude distribution of lightning spherics predicted over VLF-SHF range using theoretical analysis of lightning streamers 07 p1272 A70-20215
- Noise mean duration in surface communications links due to communications satellites interference, discussing irradiation emission and termination 08 p1456 A70-20570
- Noise variance extreme value estimator for biorthogonally block coded high rate telemetry system for Mariner missions 08 p1459 A70-20799
- Optimal satellite communication system design concerning station spectrum and interference limits 08 p1459 A70-20805
- Noise and gain formulas for wideband distributed-gain amplifiers using quadrupole elements and transmission line configurations 08 p1472 A70-20863
- Noise effects on joint operation of signal follow-up system with search device using semi-Markov random technique 08 p1461 A70-20864
- Effective noise temperature of planar aperture antennas in lossy inhomogeneous plasma slabs calculated by computer 09 p1646 A70-22704
- Quantizing noise measured for single integration delta modulation coders using unequal positive and negative integrator step sizes 09 p1638 A70-23368
- Broad band power amplification with Gunn effect diodes, describing frequency response and saturation characteristics and FM/AM noise spectrum measurements for reflection amplifier in X band 10 p1847 A70-23886
- Observation noise model for human controller remnant 10 p1823 A70-23893
- Human operator remnant data normalization noting observation noise spectral characteristics for compensatory tracking 10 p1824 A70-23899
- GaAs light amplifier p-n junction gain and output noise determination for wide photon energy ranges, studying input noise levels effects on sensitivity 10 p1928 A70-25167
- Differential Pulse Code Modulation (DPCM) system with quantizer separating slope overload and granular noise, using Fokker-Planck-Kolmogorov equation 10 p1844 A70-25204
- Nomograms simplifying noise and natural loop bandwidths calculation for phase locked loop receiver, determining limiter suppression factor 10 p1844 A70-25244
- Narrow band FM noise suggested for masking studies application, discussing noise properties 11 p2011 A70-26496
- Thermal plasma devices with discrete modes, describing periodic pulling and transition to continuous noise spectrum characteristic of turbulence 11 p2094 A70-26754
- Anomalous LF noise in receiving devices with traveling wave quantum paramagnetic amplifier 11 p2020 A70-26817
- Broadband and highpass LF noise in distant magnetosphere detected by VLF/LF experiment on OGO 1 satellite 12 p2222 A70-27183
- Liquid He temperature fluctuation effects on cryogenic superconducting bolometer noise spectrum, deriving transfer functions 12 p2237 A70-28156
- In-flight shock cell noise generation by static jets, discussing frequency prediction formula 13 p2347 A70-29078
- Noise rejection and spurious reception probability in optimal channel for continuous sequenced signal with undetermined arrival and overlapping spectra 15 p2696 A70-31509
- Frequency locked noise effect on beat frequency measurement of angular velocity with ring laser, comparing gyroscope and phase methods 15 p2749 A70-31551
- Noise sources and identification in low noise RF amplifiers via noise temperature or factors 15 p2708 A70-31952
- Radiometer employing frequency domain coding of noise-like signal spectrum, comparing with Dicke system 16 p2871 A70-32926
- Recording instrumental noise resolution of standard algorithm for cosmic ray stations 18 p3307 A70-36100
- High field noise emission from indium antimonide, suggesting electron-hole plasma as source 19 p3486 A70-37767
- Flow noise mechanisms, considering discharge, propeller, ventilator, jet engine, boundary layer, water pipe and supersonic aircraft sources 19 p3406 A70-38474
- Discrete components formation in noise spectra of axial turbocompressor intake, considering relationship between blades and rotor disk 19 p3353 A70-38652
- Rod surface roughness effect on eddying sound frequency and intensity and on aerodynamic resistance 19 p3353 A70-38654
- Supersonic air jet noise spectrum analysis at various pressures 19 p3354 A70-38659
- Supersonic jets noise spectra, using linear equations of moving medium acoustics 19 p3354 A70-38660
- Discrete components of noise frequency spectrum of free supersonic jet 19 p3354 A70-38661
- Noise spectra of two dimensional jet flowing from nozzle ejector, using dispersion equation 19 p3354 A70-38662
- Sound level vs duration evaluated for noise exposure using different exchange rates [ASA PAPER FF2] 20 p3578 A70-39125
- Noise field from ground testing of nuclear rocket engines operated at various reactor power levels 20 p3689 A70-39688
- Temporal and spectra combination effects on aircraft sound judged noisiness, using human subjects in anechoic chamber 20 p3580 A70-39712
- Photographic emulsions and photosensitive materials for holography, measuring noise spectral power density at high spatial frequencies by scattered light method 21 p3822 A70-40812
- Superconducting Sn bolometer under isothermal and nonisothermal conditions, measuring noise spectra dependence on displacement current and resistance 22 p4026 A70-42397
- Acoustic lining technology and materials for turbofan engine ducts, considering environmental factors and noise spectra 22 p4089 A70-42530
- Global thunderstorm activity experiment by Ariel 3 satellite, investigating lightning discharge number and noise power 22 p4015 A70-42778
- Silicon MOSTs LF noise model, discussing noise and gate voltages and trapping efficiency of surface states 22 p3996 A70-42916
- P-n junction dependent FM noise spectrum of UHF transistor power oscillator at transit frequency 23 p4161 A70-43789
- Aircraft noise sources, examining compressors with dynamic pressure devices and jets with turbulence investigations [ICAS PAPER 70-22] 23 p4232 A70-44111
- Anomalous LF noise in receiving devices with traveling wave quantum paramagnetic amplifier 24 p4351 A70-45189
- ### NOISE STORMS
- Metric type I and decametric type III bursts relationship, suggesting common generation by high energy electron outward streams from photosphere or low chromosphere 06 p1150 A70-18466

- Jupiter decametric noise storm commencement time defining constant planetary rotation period
08 p1580 A70-21572
- Two dimensional structure of 20 May 1966 noise storm from solar eclipse data obtained at ground stations
13 p2493 A70-29390
- Circularly polarized emission from types I and 4 bursts and noise storms, considering mode coupling in warm plasma, gyroradiation and Cerenkov radiation
13 p2479 A70-29851
- Type I solar radio burst chains during noise storms, determining lifetime, bandwidth, frequency drift and fine structure
13 p2479 A70-30002
- NOISE SUPPRESSORS**
U NOISE REDUCTION
- NOISE THRESHOLD**
Threshold extension techniques using impulse noise detection and elimination implemented at phase lock loop demodulator output
08 p1460 A70-20811
- Multichannel performance measurement of threshold extension FM demodulators using click suppression techniques
08 p1460 A70-20812
- FM noise threshold reduction achieved through narrow bandwidth of self synchronized N-path filter tracking incoming FM carrier
10 p1833 A70-24233
- Noise threshold performance of suboptimum PPM telemetry receivers using slicer for detector
11 p2010 A70-26273
- Automatic threshold regulation for radar applications, using feedback control device based on noise peak probabilities
11 p2012 A70-26717
- FM threshold extension for system performance improvement, comparing impulse noise elimination, correlation detection and delta modulation signal processing techniques implemented at demodulator output
21 p3787 A70-41334
- Threshold output characteristic of FM signals, generalizing Gaussian baseband modulation solution to obtain autocorrelation function of output signal plus FM discriminator noise
24 p4313 A70-46063
- NOISE TOLERANCE**
Residential structures vibration response to aircraft flyover noise, discussing noise transmission, rattle phenomenon, spectra, etc
[ASME PAPER 69-WA/GT-8] 04 p0770 A70-14887
- Noise effects on tracking performance, electroencephalography /EEG/ and galvanic skin resistance /GSR/
04 p0643 A70-14977
- T2L logic circuits design and coherent noise immunity
11 p2021 A70-26833
- Geomagnetic noise constraints on weak field measurements in upper magnetosphere
13 p2401 A70-30056
- Jet engine noise technology evaluation, noting effects on airport neighbor
16 p2971 A70-34262
- Annoyance assessment for sonic boom series exposure near airport
16 p2843 A70-34325
- Ear protection for persons exposed to various jet aircraft noise environments
24 p4306 A70-45121
- NOMINAL VALUES**
U APPROXIMATION
- NOMOGRAMS**
U NOMOGRAPHS
- NOMOGRAPHS**
Solid bodies unsteady thermal conductivity in presence of quasi-steady heat transfer under combined radiant and thermal fluxes, presenting thermodynamic nomograms
01 p0213 A70-10215
- Transistor behavior prediction at threshold of large signal conditions, using nomograms to evaluate maximum drive levels before distortion onset
03 p0452 A70-13966
- Nomographical solution of electroexplosive device firing time equation permitting firing data prediction from blueprint data
03 p0548 A70-14117
- Nomograms for spectral transparency of atmosphere at 2.8-5.6 microns
06 p1053 A70-17208
- Nomograms for ultrasonic shadow defectoscope acoustic channel parameters calculation
06 p1065 A70-17921
- Specifications nomographs for earth resources IR radiometers, considering ground resolution, aperture diameters, detector arrays, etc
[AIAA PAPER 70-317] 09 p1677 A70-22870
- Lebedev nomogram determination of climatic parameters dependability, considering underlying theory and temperature sums
09 p1718 A70-23171
- Nomogram selecting dimensions of steel or Al alloy cantilever beams for transducer design using strain gages
10 p1890 A70-24593
- Nomograms simplifying noise and natural loop bandwidths calculation for phase locked loop receiver, determining limiter suppression factor
10 p1844 A70-25244
- Nomograms for thermoelastic stress in plate determined as function of dimensions and heat transfer
10 p1965 A70-25300
- Nomographic Richardson-Dushman equation solutions for thermionic electron emission devices, giving current density for various work functions and electrode temperatures
12 p2271 A70-26894
- Nomogram construction for graphical solution of two body problem using radius-vector and velocity components applied to solar system
12 p2311 A70-28310
- Nomogram for true and apparent radiometric temperatures of remote graybodies in presence of atmosphere
14 p2577 A70-31231
- Radiation planning nomogram to display radiobiological effects of dose, onset time and shielding factors for manned space vehicles
15 p2690 A70-31894
- Nomograms for meteor geocentric velocity and trajectory with correction for zenith attraction and radiant
18 p3315 A70-36605
- Traveling wave antenna array single lobe design using mode charts to reduce errors
19 p3376 A70-37688
- Safety factor estimation by nomographic techniques for eye protection against direct viewing of laser beam
21 p3768 A70-40761
- Effective pressure ratio nomographs for mechanical energy conversion and heat transfer of closed regenerative Stirling engines, using isothermal theory
22 p4091 A70-42757
- Gas turbine design by nomograms with minimal preliminary calculations
22 p3960 A70-43368
- Tunnel diode amplifier design, using gain-bandwidth nomograph
22 p3999 A70-43487
- Corrected geomagnetic midnight local time calculations, using nomogram
23 p4187 A70-43862
- NONADIABATIC CONDITIONS**
U ADIABATIC CONDITIONS
- NONADIABATIC THEORY**
Length calculation method for nonadiabatic imaginary tip extension of heat exchanger fins, predicting heat conduction rate
01 p0215 A70-10842
- Thermal imbalance effect on stellar pulsational stability using linear quasi-adiabatic pulsation theory
10 p1946 A70-24980
- NONAXISYMMETRY**
U ASYMMETRY
- NONCONDUCTORS**
U ELECTRICAL INSULATION
- NONCONSERVATIVE FORCES**
Thermomechanical coupling effect on stability of elastic continuous systems subjected to nonconservative forces, reducing flutter load by thermal damping
08 p1589 A70-21245
- Nonconservative problems motion stability analysis based on restricted admissible displacements, establishing two variational principles
11 p2138 A70-26172
- Linear dynamic systems under nonconservative and harmonic forces, examining stability conditions
16 p2952 A70-33896
- Mass distribution role in stability theory of rods under nonconservative buckling load
18 p3335 A70-35961
- Group variational procedure for first integrals of nonconservative dynamical systems
19 p3458 A70-38060
- Mechanical destabilizing model of nonlinear damping in nonconservative systems with follower forces, using Liapunov method
19 p3542 A70-38065
- Continuous one dimensional nonconservative elastic systems under complex forces, examining stability theory
19 p3546 A70-38341
- Elastic bodies stability criteria, investigating loss under nonconservative forces influence
20 p3722 A70-39785
- Undamped elastic cantilever column with concentrated masses, considering transition from stability to divergence under nonconservative forces
24 p4421 A70-45286
- NONDESTRUCTIVE TESTS**
NT PRELAUNCH TESTS
- NT STATIC FIRING**
Nondestructive evaluation of components and materials in aerospace, weapons systems and nuclear applications - Conference, San Antonio, April 1969
01 p0095 A70-10001
- Inspection penetrant systems reliability and performance predictability for nondestructive flaw detection
01 p0096 A70-10005
- Metal surface microscopic defects detection and display using diffused radioactive Kr-85 gaseous penetrant for anodized flaws, bearing porosity and turbine blade cracks
01 p0096 A70-10006
- Contact thermographic materials application to nondestructive materials testing based on heat capacity, costs, removal time, equipment, personnel skill and training, etc
01 p0097 A70-10007
- Eddy current inspection method for detecting fatigue cracks location and depth in fastener holes
01 p0097 A70-10008
- S/N fatigue life gage for nondestructive evaluation of cumulative damage, discussing calibration and two step, block and random tests
01 p0053 A70-10009
- Nondestructive testing and fatigue life analysis of cyclically loaded mechanism, determining dynamic responses to velocity shocks by computer techniques
01 p0053 A70-10010
- Transient magnetic resonance technique for nondestructive testing of elements with nuclei having magnetic moment, considering cereal grains, propellants, metal powder and plastics
01 p0097 A70-10014
- Acoustic emission to monitor metal structures, pipes, pressure vessels and graphite shapes to detect structural deterioration before failure, emphasizing nuclear reactor pressure systems
01 p0054 A70-10015
- Ultrasonics inspection applied to reentry vehicle heat shields and composite materials, verifying anomalies by microscopic area examination
01 p0097 A70-10016
- Bolted joints inspection using mechanical impedance algorithm method involving bolt head mechanical shock pulse response in adjacent structure
01 p0098 A70-10017
- Cessna single engine aircraft tubular and flat steel landing gear springs, describing quality control through nondestructive testing
01 p0098 A70-10018
- Lamb wave techniques using guided ultrasonic waves for solid cylindrical objects nondestructive testing
01 p0098 A70-10019
- Nondestructive X ray stress measurement equipment for large specimen, using diffractometer focusing
01 p0085 A70-10022
- Electronic materials nondestructive evaluation techniques, describing analytic tests for chemical, structural, electrical and optical characteristics determination
01 p0085 A70-10023
- Nondestructive testing for Apollo Command and Service Module, describing requirements added to quality control scope
01 p0098 A70-10026
- NDT used in airline and aircraft maintenance emphasizing practicability, reliability and costs
01 p0098 A70-10027
- NDT peculiar to airline maintenance, emphasizing inspection of complex parts hidden within assembly
01 p0099 A70-10028
- Laser processing applied to optical nondestructive materials tests for surface flaws
01 p0086 A70-10416
- Ultrasonic imaging system for flaw detection, analyzing welds
01 p0104 A70-10881
- Ultrasonic holography in nondestructive testing, discussing metal block with simulated defects
01 p0089 A70-10882
- Aircraft nondestructive testing, discussing radiography requirements, ultrasonic bond testing technique, etc
01 p0104 A70-11319
- Nondestructive inspection program for DC 10 aircraft maintenance
02 p0308 A70-12273
- Sandwich structures nondestructive testing by holographic interferometry, discussing system operation, specimen stressing, acoustic vibration, etc
02 p0309 A70-12274
- Spherical conducting body effect on induction coil impedance and EMF in nondestructive testing using eddy current probes
02 p0300 A70-12478
- Steel objects microstructure and hardness tested by continuous magnetic technique, describing experimental apparatus model
02 p0300 A70-12479
- Ultrasonic tracking type transducers for testing ribbed and smooth walled pipes using shadow and two probe echo methods
02 p0300 A70-12480
- Piezoprobe parameters calculation for controlling angular welded connections of boiler assembly elements
02 p0300 A70-12481

Electrodynamic contactless method for ultrasonic nondestructive testing of materials based on natural frequencies shift with and without defects
02 p0301 A70-12483

PKR portable xeroradiographic defectoscope for nondestructive testing of steel and Al alloys
02 p0301 A70-12486

Programming device for positioning samples under X ray beam in testing welded seams and parts
02 p0301 A70-12488

Ferroprobe coercimeter with attached electromagnets for nondestructive hardness testing, describing components and mounting
02 p0301 A70-12489

Sheath-enclosed steel cable inspection using induction coil transducer in conical sleeve
02 p0301 A70-12490

Acoustic emission analysis for material evaluation and polymorphic phase transformations characterization for metals and alloys, discussing electronic instrumentation and experimental techniques
02 p0276 A70-12551

Lamb waves behavior applied to defect evaluation in nondestructive tests of solid elongated cylindrical objects
02 p0276 A70-12552

Holographic interferometry applications in experimental mechanics, illustrating nondestructive testing by flaw detection in bonded honeycomb
03 p0481 A70-12959

Honeycomb structure fracture initiation flaw detection method using liquid crystal determination of stress concentration sites, noting absence of external heat source
03 p0515 A70-13121

Neutron radiography for visual nondestructive failure analysis and production inspection of ordnance components compared with X ray radiography
03 p0494 A70-14122

Nondestructive testing of Apollo CSM/Command and Service Module/ spacecraft ordnance explosive devices by indirect and direct neutron radiography
03 p0494 A70-14123

Nondestructive test procedures for maintaining and determining serviceability of penetrant inspection materials during use
05 p0844 A70-15780

Reinforced plastics destructive and nondestructive testing including standard methods, equipment and procedures applicable to materials and parts
05 p0874 A70-16621

Composite materials properties test methods, discussing nondestructive method for shear or rigidity modulus of square plates
05 p0874 A70-16622

Correlations between 100 percent inspection by automatic equipment and quality control acceptance sampling in vacuum tube industry
06 p1077 A70-17986

Acoustic impedance method for nondestructive testing exploiting phase defect of signal from piezoelectric transducer
06 p1074 A70-18629

Metal adhesive joints nondestructive tests involving acoustic and superasonic, X ray and heat flow characteristics methods
08 p1503 A70-20885

Nondestructive process control analyzer for spot welds in aircraft structural components, monitoring expansion, current and spotweld properties
08 p1507 A70-21486

Liquid oxygen usage inspection penetrant systems combining nonreactivity with flaw detection sensitivity
08 p1508 A70-21745

Nondestructive betatron radiographic testing techniques for Ti billets, evaluating various lead screen, film and geometry combinations
08 p1508 A70-21746

Nondestructive testing and inspection by acoustic emission from stressed materials, discussing microstructure effect and crack initiation detection
08 p1508 A70-21747

Nondestructive testing of small metal tubing, discussing eddy current, ultrasonic and electromagnetic inspection and dye penetrants
08 p1509 A70-21748

Thermomechanical tests effectiveness and determination of stress level defining boundary between destructive and nondestructive testing
09 p1689 A70-22004

Destructive and nondestructive tests optimum procedure for quality control based on information theory, decision statistics and cost optimization
09 p1691 A70-22573

Nondestructive tests for diffusion-formed refractory alloy coatings used as oxidation protection for hypervelocity spacecraft and reusable systems
09 p1692 A70-22679

Nondestructive test procedures development and implementation for bond strength of honeycomb sandwich and metal-metal adhesive bonded structures of F-5 and T-38 aircraft
09 p1692 A70-22798

Reliability testing of waveguide ferrite devices based on quantitative technique using circular charts with filled in endurance test results
09 p1652 A70-23661

Silicon high resistivity surface barrier detectors fabrication for nondestructive tests, discussing long term sensitivity and calibration
10 p1893 A70-24169

Ultrasonic traveling waves for nondestructive testing, discussing scattering and velocity anisotropy in polycrystalline metals, propagation in glass, epoxy resins shear moduli, etc
10 p1894 A70-24171

Thermal transducer for rapid nondestructive testing, discussing imaging of specimen bond defects and thermal property differences
10 p1894 A70-24173

Acoustic emission monitoring methods to detect crack formation and growth in ceramics
10 p1894 A70-24174

Acoustic impact technique /AIT/ for aerospace structures nondestructive testing, describing theory, instrumentation and applications
10 p1894 A70-24175

X ray laminography for nondestructive testing based on synchronous rotation of source, sample and image forming planes
10 p1895 A70-24577

Cost and deadline planning for system development, suggesting theoretical methods tests regarding applicability
10 p1971 A70-24597

C-5A airframe composite materials fabrication, tooling, processing, quality assurance and nondestructive test methods
11 p2058 A70-25572

Heat flow comparator for nondestructive testing of resin-impregnated fiber glass, detecting nonuniformities leading to thermal properties variation
11 p2059 A70-25764

NDT methods for fiberglass, graphite and boron fiber composites for aircraft structures
12 p2243 A70-27465

Eddy currents magnetic field structure over surface defects in conducting objects, noting NDT applications
13 p2404 A70-28661

NDT techniques in manufacturing of Apollo command and service modules
13 p2420 A70-29243

High speed thermal transducer for imaging bond defects and thermal property differences within test specimens during nondestructive tests
13 p2420 A70-29244

Radio Influence Voltage /RIV/ nondestructive test method for detecting voids in neoprene-steel structures or other elastomers bonded to metal
13 p2420 A70-29245

Nondestructive noncontacting microwave depth measurement of thin slits and cracks in metal surfaces
14 p2584 A70-30507

Nondestructive bond inspection by interferometric holography of ultrasonically excited plates
14 p2588 A70-31166

Nondestructive screen test efficiency, determining potential failures of electric components by Bayes theorem
15 p2748 A70-32659

Collection of papers on nondestructive testing covering automatic profile recording, holography, radiography, leak detection, etc
15 p2742 A70-32776

Holography for nondestructive testing, describing theory, equipment and applications
15 p2742 A70-32779

Leak detection techniques, describing back pressurizing and calibrating methods
15 p2743 A70-32781

NDT for structural corrosion evaluation, including ultrasonics, X rays, penetrating liquids and induced currents
16 p2929 A70-32924

Electrical, electronic, electromechanical, pneumatic and hydraulic subsystems failure pattern determination, discussing sensing techniques in signature analysis
16 p2917 A70-33505

[ASME PAPER 70-DE-34] Metal matrix composite resistance spot welding, discussing value of nondestructive tests
17 p3100 A70-34636

Fiberglass reinforced plastics fatigue properties, describing electric model and nondestructive testing
17 p3183 A70-34658

Fatigue and surface crack detection using holographic techniques
17 p3086 A70-35015

IR NDT bond inspection system for helicopter rotor blade honeycomb box assemblies, using closed circuit slow scan video system to detect bondline voids
17 p3101 A70-35184

Magnetic methods of flaw detection, discussing theory and application to welded butt joints
18 p3263 A70-36521

Pulsed laser holographic nondestructive testing optimization technique, monitoring honeycomb panel surface temperature during thermal stressing
18 p3259 A70-36754

Acoustical holography forming optical wavefield analog for nondestructive testing, medical diagnosis, underwater and seismic imaging
19 p3425 A70-37887

Nondestructive testing of diffusion bonded metals for quality assurance
19 p3437 A70-38423

Microjoining in electronics industry, discussing technologies and nondestructive testing
19 p3437 A70-38424

Gaseous radioactive penetrant inspections for early low cycle fatigue in aircraft engine materials, discussing impact on maintainability
19 p3441 A70-38828

Holographic ultrasonic imager using liquid surface detector for real time imaging of test objects moving through viewfield, discussing nondestructive test applications
19 p3433 A70-38829

Condition Monitored Maintenance program for turbine engines eliminating total overhauls at specified time, using NDT
19 p3441 A70-38830

Semiconductor silicon power diodes nondestructive quality control, discussing optimal sampling procedures
20 p3595 A70-38969

Composite materials physical properties measurement and defect locations detection by NDT techniques
20 p3636 A70-39210

Unidirectional and multidirectional carbon/carbon composites quality and performance evaluation by NDT methods, including X ray radiography, ultrasonic test, pulse echo mapping, etc
20 p3654 A70-39211

Laser holography for nondestructive testing of C composite structures, reducing fringe patterns to radial deformation and surface strain for cylinders and cones
20 p3718 A70-39212

Carbon/carbon composites thermal and mechanical properties measurements by NDT including image transducer, IR scanning and ultrasonic methods
20 p3636 A70-39213

Surface adsorbed and absorbed radioactive Kr 85 gas for displaying surface microdefects in materials
20 p3638 A70-39950

Optical thermal testing by IR radiation, reviewing thermistor bolometer, various detectors, radiometric microscopes, NDT equipment, etc
21 p3831 A70-40747

Nondestructive ultrasonic measurements of crack depth in high strength steel plate weldments, studying low cycle fatigue
21 p3834 A70-41943

Carbon fiber reinforced polymer /CFRP/ failure mechanism, discussing nondestructive testing, destructive and cyclic loads
22 p4058 A70-42476

Papers on research techniques in nondestructive testing covering acoustic emission, ultrasonic spectroscopy, imaging systems angle reflectivity and holography, optical methods, etc
22 p4026 A70-42581

Acoustic emissions method for monitoring structural stability of solid materials assemblies via crack formation and movement detection
22 p4027 A70-42582

Ultrasonic spectroscopy in nondestructive materials tests, discussing electronic equipment design, FM, pulse and pulsed FM methods
22 p4027 A70-42583

Ultrasonic imaging systems of nondestructive testing, discussing photographic and chemical systems, thermal, optical and mechanical methods and electronic systems
22 p4027 A70-42584

Ultrasonic Rayleigh critical angle reflectivity of liquid-solid interface energy, detecting near-surface properties changes
22 p4027 A70-42585

Ultrasonic holography for nondestructive testing, discussing reference beams and analogies to optical and electronic methods
22 p4028 A70-42586

Laser application to nondestructive testing via holography and hologram interferometry
22 p4028 A70-42587

Data handling and processing methods for non-destructive test data translation and interpretation, using scanning test model
22 p3993 A70-42588

Communication network approach to submillimeter wave applications in nondestructive testing, deriving transport equations for EM wave propagation
22 p4028 A70-42591

Multiparameter eddy current test methods, describing test coil output signal amplification, demodulation and recombination
22 p4028 A70-42592

Pulsed eddy currents in metals nondestructive testing, discussing masked probes, reflection systems, correlation and filtering methods, etc

22 p4028 A70-42593

Microwave propagation, instrumentation and use in nondestructive testing, discussing components, methods and wave propagation equations

22 p4029 A70-42594

IR radiation, transmission and detection in non-destructive testing, discussing atmospheric transmission, thermal and photon-type detectors, etc

22 p4029 A70-42595

Aircraft engine diagnostics and defectoscopy, considering radioactive isotopes testing for component wear and performance

22 p4046 A70-43083

Nondestructive testing by ultrasonic acousto-optical imaging in opaque objects

22 p4047 A70-43518

Ultrasonic wave velocity measurements for flow detection and modulus of elasticity of carbon-carbon composites

22 p4047 A70-43519

Modulation transfer function applied to optimal holographic nondestructive testing systems, using edge gradient analysis

22 p4039 A70-43520

Nondestructive measurement of elastic and plastic deformation in soldered joints and printed circuit boards by holographic interferometry

22 p4047 A70-43521

Nondestructive testing of adhesively bonded metal assemblies

22 p4047 A70-43523

Nondestructive tests for flaw detection during various aircraft production and operation phases

22 p4047 A70-43531

Nondestructive tests and controls in metallurgy and nuclear technology - Conference, Saclay, France, June 1968

22 p4040 A70-43617

Acoustic and scanned holography for nondestructive testing, showing defects in metal samples

22 p4041 A70-43620

Fatigue crack growth detection by acoustic emission techniques

23 p4194 A70-44214

Photochromic paint nondestructive testing for survival equipment, detecting bond defects and sandwich water

23 p4197 A70-44490

Thermal IR nondestructive testing of adhesively bonded boron composite/Al honeycomb structures, discussing surface, cross section and instrumentation sensitivity effects

24 p4341 A70-45570

Ultrasonic delta technique inspection method for flaw detection in weldments or wrought materials

24 p4335 A70-45572

Reflector materials flow size and orientation using ultrasonic spectral frequency analysis

24 p4335 A70-45573

X ray attenuation factor calculation as function of radiation energy and test material nature and thickness for nondestructive defectoscopy

24 p4341 A70-45581

Nondestructive testing - Conference, Hanover, June 1970, General problems

24 p4342 A70-45676

Nondestructive testing for aircraft maintenance, considering economics

24 p4342 A70-45677

Nondestructive testing technology impact on military aircraft maintenance, discussing training, applications and advantages

24 p4342 A70-45678

Nondestructive testing technology, emphasizing component designer role in facilitating inspection of surface defects

24 p4342 A70-45679

Nondestructive testing - Conference, Hanover, June 1970, Ultrasound, Part I, Instruments, methods and defect evaluation

24 p4342 A70-45680

Nondestructive testing - Conference, Hanover, June 1970, Electric and magnetic methods

24 p4343 A70-45693

Nondestructive defectoscopic diagnostics, applying cybernetics to materials testing

24 p4344 A70-45694

Finite thickness metal plate eddy current response to pulsed field from aperture probe

24 p4344 A70-45696

Eddy current nondestructive tests for surface defects detection, determining optimum test parameters based on calculation

24 p4344 A70-45697

Eddy current magnetic probe with frequency scanning for signal-noise discrimination in nondestructive testing of tubes

24 p4336 A70-45698

Metal sheets thickness measurement and monitoring by through-transmission eddy current nondestructive testing, using phase locked amplifier

24 p4344 A70-45699

Encasing and welded pipes flaws detection with high resolution by nondestructive testing, using eddy current method

24 p4345 A70-45702

Nondestructive tests of work-hardening Al alloy structural deterioration due to overheating, using eddy current conductivity techniques

24 p4345 A70-45703

Metallic rods and tubes permeability and resistivity nondestructive measurement by AC apparatus with self balancing sensing coil, using computer program for data reduction

24 p4345 A70-45704

Nonmetallic nonconductive composite materials physical properties by swept microwave frequency nondestructive testing

24 p4345 A70-45705

Nondestructive testing - Conference, Hanover, June 1970, Radiography

24 p4345 A70-45706

Radiography for nondestructive tests, considering image quality specification and choice of geometric progression for determining visibility

24 p4337 A70-45709

Gamma ray nondestructive tests for materials defects, discussing cinematic, geometric and radiological factors effects on detection

24 p4337 A70-45711

Industrial radiography for nondestructive control of products quality, discussing exposure time determination method

24 p4337 A70-45712

Nondestructive testing - Conference, Hanover, June 1970, Material properties determination

24 p4345 A70-45717

NDT for aircraft service life extension, discussing fatigue tests and crack detection

24 p4346 A70-45719

Nondestructive examination for plastics, discussing transmission, microwave and ultrasonic tests

24 p4346 A70-45720

Nondestructive thermal and thermochemical treatment penetration depth measurement in metal, examining magnetic test and ultrasonic techniques

24 p4346 A70-45721

Radiography and stray flux methods in nondestructive testing - Conference, Hanover, June 1970

24 p4346 A70-45722

Automatic TV radioscopic X ray control for mass NDT of refractories and grinding wheels

24 p4368 A70-45723

Remanence and saturation methods for magnetic-particle flaw detection

24 p4346 A70-45726

Defect detection by measurement of magnetic field leakage around flaw

24 p4346 A70-45727

Nondestructive testing - Conference, Hanover, June 1970, Materials properties determination, Stress measurements

24 p4347 A70-45728

Residual stress measurement using programmed horizontal X ray diffractometer

24 p4425 A70-45729

Nondestructive inspection methods for welded structures affected by stress corrosion

24 p4347 A70-45730

Nondestructive testing - conference, Hanover, June 1970, Material properties determination, covering electric, magnetic, liquid penetrant and thermal methods

24 p4347 A70-45735

Nondestructive tests for performance levels, discussing signature analysis as methodology

24 p4338 A70-45736

Oscillating pendulum equipment for nondestructive material tests, determining longitudinal and transverse elastic moduli of specimen

24 p4338 A70-45738

Potentiometer application to nondestructive tests of materials, operation principles, methodology and advantages

24 p4338 A70-45739

DC potentiometer for nondestructive tests of structural components, obtaining crack detection, depths and angles and wall thicknesses

24 p4338 A70-45740

Inspection penetrant development for flaw detection, considering entrapment efficiency and dimensional sensitivity

24 p4348 A70-45743

Metal and nonmetal thermal nondestructive tests based on surface temperature distribution produced by heat treatment

24 p4348 A70-45744

Nondestructive testing - Conference, Hanover, June 1970, Neutron radiography and holography

24 p4375 A70-45745

Nonweldable internal flaws detection containing oxides in steel slabs by neutron activation analysis

24 p4376 A70-45750

Holographic interferometry for NDT inspection of adhesive bonded honeycomb sandwich aerospace structures

24 p4338 A70-45754

Holographic nondestructive testing of laminate structures, honeycomb-sandwich panels and rubber-to-metal bonds

24 p4338 A70-45755

Radiative flaw detection problems, calculating gamma radiation scattering

24 p4348 A70-45848

Liquid compensators for gamma ray flow detection of complex metal product configurations, considering radiation source energy spectrum and specimen density

24 p4348 A70-45849

Betatron monoenergetic electron beams in radiometric, spectrometric and radiographic testing of composite materials

24 p4339 A70-45850

Fast neutrons for radiogenic defectoscopy performance, sensitivity and cost efficiency

24 p4377 A70-45851

NONEQUILIBRIUM CONDITIONS

Nonequilibrium and equilibrium schemes studies of nuclear symmetry energy of finite nuclei, discussing binding energy of nuclei with neutron excess

01 p0148 A70-11106

Nonequilibrium initial condition combustion effects on propellant performance for hydrazine/ chlorine pentafluoride and hydrogen/fluorine with equilibrium, kinetic and frozen nozzle flow

04 p0732 A70-15423

Ballistic range measurements of vibrational nonequilibrium effects on leading edge shock wave shape for cone-cylinders fired through chlorine atmosphere at supersonic speeds

04 p0621 A70-15601

Nonequilibrium processes and initial conditions in early universe, discussing neutrino viscosity efficiency at removing shear anisotropy and Misner model

05 p0907 A70-16002

Nonequilibrium models describing two phase critical discharge of initially saturated or subcooled liquid through sharp edged and smooth inlet geometries

05 p0956 A70-16162

Monte Carlo calculations of nonequilibrium radiative transport, including weighting and biasing techniques

05 p0958 A70-17084

Witham radiative acoustics, analyzing nonequilibrium waves propagating in nongray radiating and absorbing gas

06 p1173 A70-17514

Nonequilibrium processes behind shock wave in shock tube supersonic air and nitrogen flow, using photoelectrical shadow method

06 p1053 A70-18562

BBGKY hierarchy state functional formalism in nonequilibrium statistical mechanics for many particle system using Fourier transformation

11 p2087 A70-26548

Nonequilibrium self gravitating medium unified thermodynamics theory based on propagators, describing spatial and temporal fluctuations and coupling for galactic formation

12 p2310 A70-27978

Collision coefficients of reaction and inverse reaction for nonequilibrium processes with variable distribution functions and cross sections

13 p2461 A70-28920

Plane electromagnetic waves propagation in isotropic medium in electromagnetic nonequilibrium conditions

15 p2790 A70-32275

Rotational relaxation of diatomic molecular excited electronic state at high temperatures, discussing nonequilibrium region behind shock wave front in nitrogen

21 p3854 A70-42060

NONEQUILIBRIUM DRAG

U FRICTION DRAG

NONEQUILIBRIUM FLOW

Nonequilibrium flows covering small disturbance theories, steady one dimensional flow, gas particle flow relaxation and expansion flow gas dynamics

01 p0062 A70-10802

Linear small disturbance theories applied to two component gas mixture with fluid motion accompanied by nonequilibrium effects, discussing linear convection and reaction processes

01 p0062 A70-10803

Nonequilibrium effect of expanding water vapor condensation on supersonic nozzle flows with or without inert carrier gas

01 p0063 A70-10806

Integral theory for two dimensional incompressible turbulent boundary layer in nonequilibrium flows, describing velocity profile in momentum and energy equations

02 p0283 A70-12335

Dissipation integral method for turbulent boundary layer problem based on nonequilibrium flow, analyzing inner and outer regions

02 p0283 A70-12338

Nonequilibrium two phase forced convection flow, describing pressure, temperature and void fraction measurement techniques

02 p0305 A70-12838

Supersonic nonequilibrium two phase flow in Laval nozzle from numerical solution of quasi-linear hyperbolic equations

04 p0617 A70-15229

Classical Couette flow for emitting and conducting gas media, discussing velocity distribution and temperature effects at LTE and non-LTE

04 p0787 A70-15675

Radiating gas flows during hypersonic planetary reentry, discussing atmospheric composition, shock layer characteristics, nonequilibrium flows, etc

06 p0985 A70-18558

Frozen flow effect in hypersonic wind tunnel nozzle on parameters of nonequilibrium incident flow past wedge

09 p1604 A70-22446

Time dependent analysis for quasi one dimensional, vibrational and chemical nonequilibrium nozzle flows approaching steady state solution by finite difference technique

11 p1976 A70-25974

Population inversions in rapidly expanded flows of nonequilibrium gases, discussing kinetic processes in cooled mixtures of shock heated nitrogen and carbon dioxide

11 p2041 A70-26572

Pressure distribution over lateral surface of truncated cones in nonequilibrium flow, analyzing physicochemical transformations effect

12 p2159 A70-28246

Pseudo one dimensional dissociational nonequilibrium nozzle flows, obtaining equilibrium and nonequilibrium solution through similar transformation of governing equations

14 p2527 A70-30264

Linearized gas mixture nonequilibrium flow fields, analyzing consequences of multiplicity of principal relaxation frequencies

14 p2566 A70-30474

Supersonic nonequilibrium gas mixture flow past segmental bodies nose areas to simulate Venusian atmosphere, determining temperature, pressure and concentration distributions

15 p2796 A70-31483

Maximum thrust nozzles design for rotational or nonequilibrium simple dissociating gas flows, including boundary layer effects

[ALAA PAPER 70-707]

16 p2891 A70-33567

Experimental and numerical nonequilibrium shock layer around cones in hypersonic pure oxygen flows with simultaneous rotational, vibrational and dissociation relaxation

[ALAA PAPER 69-136]

16 p2894 A70-33858

Inviscid air nonequilibrium shock layer properties correlation based on plenum entropy, predicting composition of downstream converging-diverging nozzle expanding air flow

[ALAA PAPER 70-866]

16 p2838 A70-33909

Vibrational nonequilibrium nozzle flow problems, obtaining similar solutions for various initial conditions and nozzle geometries

[ALAA PAPER 70-804]

17 p3065 A70-34459

Collection of papers on nonequilibrium flows, Part 2, covering relaxation gas dynamics, nozzle flow, method of characteristics, etc

17 p3071 A70-35466

Weak nonlinear one dimensional wave propagation in nonequilibrium flow, using governing system characteristics for reference coordinates

17 p3071 A70-35468

Nonequilibrium nozzle flows involving molecular vibrational energy relaxation and composition changes from gas phase chemical reactions respectively

17 p3071 A70-35469

Method of characteristics for nonequilibrium flow fields analysis, reviewing theory, numerical methods and examples

17 p3071 A70-35470

Isotropic fluid systems in nonequilibrium, investigating thermodynamic characteristics of transport phenomena

17 p3072 A70-35529

Nonequilibrium fluid system with two subsystems in local equilibrium, investigating thermodynamic properties including entropy creation

17 p3196 A70-35530

Time correlation functions approach to calculation of properties of nonequilibrium ensembles in fluid molecular motions

17 p3197 A70-35535

Dilute gas transport expressions experimental substantiation, emphasizing nonequilibrium thermodynamics as macroscopic theory rather than empirical postulate

17 p3072 A70-35536

Nonequilibrium gas states evolution in detached wave front of hypersonic blunt body, comparing vibrational relaxation in free flight and wind tunnel flow

18 p3335 A70-35962

Nonequilibrium ionized hypersonic flow over blunt body at low Reynolds number, using thin shock layer assumption in analysis

18 p3208 A70-36689

Multicomponent chemically unstable nonequilibrium gas flow past body, taking into account boundary layer behavior

19 p3373 A70-38182

Solid body nonelastic deformation in terms of thermodynamic principles of nonequilibrium processes

20 p3718 A70-39246

Nonequilibrium processes and body geometry as stagnation point conditions in blunt body inviscid flow

20 p3557 A70-39355

Convergent-divergent nonequilibrium nozzle flow numerical solution by time dependent technique, investigating rapid vibrational nonequilibrium super-sonic expansion of gas mixture with population inversion

20 p3609 A70-39655

Compressible hypersonic turbulent boundary layers solution by finite difference method, relating mixing length to velocity profile shape factor

20 p3684 A70-40269

Nonequilibrium flow adjacent to cooling tube wall confining cascade arc plasma electrical discharge

21 p3805 A70-41763

Equations for unsteady frozen nonequilibrium flow of dissociating and relaxing gas, using Lighthill ideal dissociating diatomic gas for thermochemical model

22 p4124 A70-42754

Computerized nonequilibrium thermochemical gas dynamic solutions for nozzle, shock tube and stream tube flow with arbitrary species and kinetic reactions numbers

22 p3982 A70-42762

Dissociative nonequilibrium hypersonic flow of low density gas mixtures over flat plate in free stream, noting catalytic wall effect on flow field

23 p4135 A70-44604

Non-LTE radiative gas flow conservation equations

24 p4325 A70-45610

NONEQUILIBRIUM IONIZATION

Disturbances effect in Langmuir layer at cathode on ionization rate in arc discharge, estimating ion density and width of nonequilibrium ionization region

01 p0150 A70-10171

Gas dynamics theory with nonequilibrium radiative and collisional ionization applied to strong normal shock wave structure

05 p0831 A70-15870

Disturbances effect in Langmuir layer at cathode on ionization rate in arc discharge, estimating ion density and width of nonequilibrium ionization region

10 p1925 A70-25017

Small parameter structure and propagation velocity of ionization front in gas, applying nonequilibrium plasma model and electron equation

10 p1926 A70-25191

Gas mixture plasma ionized and heated by discharge and ejected into vacuum, considering nonequilibrium ionization calculation with gap between electron and heavy particle temperatures

11 p2092 A70-26732

Nonequilibrium air ionization in hypersonic viscous shock layers in flow about axisymmetric blunt bodies

17 p3008 A70-34501

Low voltage arc nonequilibrium ionization rate, taking into account atom-electron collisions

20 p3684 A70-40389

MHD generators nonequilibrium ionization improvement by blowing low work function particles into cold working gas to obtain required conductivity

21 p3855 A70-40794

Nonequilibrium ionization during plasma flow into magnetic field, examining electrons selective heating

22 p4083 A70-43384

Normal shock waves structured by nonequilibrium radiative and electron-atom collisional ionization, using generalized radiation model

24 p4324 A70-45290

Carbon ionization equilibrium in dense interstellar clouds, discussing grains and neutral atoms attenuation effects

24 p4402 A70-45387

NONEQUILIBRIUM PLASMAS

Particle distribution and plasma nonequilibrium field evolution with turbulence generation by microwave field, considering plasma kinetic instability

01 p0150 A70-10212

Nonequilibrium potassium seeded Ar plasma electrical conductivity at atmospheric pressure, noting current density role

02 p0347 A70-12232

Plasma optical transparency criterion, estimating nonequilibrium plasma layer optical density limit

03 p0531 A70-13255

Nonequilibrium cesium plasma of low voltage arc discharge, measuring electron temperature and distribution function and diffuse-series excited level populations

03 p0532 A70-13740

Photon absorption and emissivity of nonequilibrium cylindrical plasma in Doppler broadened lines and hemisphere approximation

04 p0724 A70-14411

Electron heat transfer to spherical body in nonequilibrium quiescent plasma by asymptotic solution

[ASME PAPER 69-WA/HT-56] 04 p0727 A70-14793

Nonequilibrium Cs plasma electron density, temperature and sustaining field using theoretical analysis and probe measurements

05 p0887 A70-16108

Visible light emission from nonequilibrium Cs plasma measured for spectral intensity distribution, suggesting excitation mechanism in terms of collision-radiation model

05 p0887 A70-16109

Thermal conductivity and diffusion-thermal coefficients analysis for nonequilibrium and highly ionized plasmas based on particle velocities

06 p1120 A70-17698

Nonequilibrium excitation in recombining N plasma nozzle flows

[ALAA PAPER 70-44]

06 p1122 A70-18061

Critical Hall parameter indicating instability in alkali-seeded noble gases in nonequilibrium MHD generators

[ALAA PAPER 70-40]

06 p1122 A70-18107

Electron energy equation for nonequilibrium plasmas, assuming large electron diffusion velocity and current density and enhanceable electron temperature

06 p1123 A70-18299

Electron density, excited state density and neutral particle temperature in Ar and Ne nonequilibrium laminar plasma jets

08 p1550 A70-20596

Scalar potential nonlinear fluctuations in quasi-stationary plasma, deriving expressions for potential spectral function and Langmuir and ion-acoustic fluctuations spectral densities

08 p1550 A70-20844

Correlation functions of fluctuations in electrical characteristics of nonequilibrium electron gas during scattering, determining spectral densities and populations by kinetic equation Green function

08 p1554 A70-21806

Nonequilibrium plasma MHD generator critical pressures determination, applying electron energy balance equation and relation between plasma conductivity and Hall parameters

10 p1809 A70-25142

Small parameter structure and propagation velocity of ionization front in gas, applying nonequilibrium plasma model and electron equation

10 p1926 A70-25191

Unsteady plasma oscillation stabilization by envelope controller with spatial and temporal dispersion

11 p2087 A70-25604

Pulsed and CW microwave discharge plasmotrons design calculation, providing electrodeless plasma in metallic chamber and nonequilibrium plasma

11 p1984 A70-26741

Impurities and electrothermal instabilities effect on conductivity of two temperature nonequilibrium plasma

12 p2281 A70-27846

Nonequilibrium solid state electronic plasma instabilities due to interactions with strong electric and magnetic fields

12 p2289 A70-28363

Langmuir probe characteristics and field response in low pressure nonstationary plasma diagnostics in weak magnetic field

14 p2623 A70-30785

Energy bands shape effect on fluctuations in nonequilibrium low resistance semiconductor plasma

15 p2784 A70-32192

Electrothermal instability in nonequilibrium plasma interpreted in terms of generalized instability in gas discharge

17 p3139 A70-34550

Energy transfer processes of electron gas for pipe flow of weakly ionized nonequilibrium plasmas, noting electron temperature decrease exponentially along tube axis

17 p3142 A70-35438

Nonequilibrium plasma from pulsed discharge in crossed electric and magnetic fields

17 p3142 A70-35727

Relaxation properties of nonequilibrium electronic solid state plasma during nonlinear interaction with external fields, using kinetic equation

18 p3297 A70-36423

Inhomogeneous nonequilibrium plasma stratification in magnetic field, investigating electrical conductivity

19 p3481 A70-38191

Charged particle interaction with fluctuation fields in nonequilibrium magnetoactive plasma

20 p3678 A70-39596

Electrothermal mode wave propagation in nonequilibrium partially ionized gas, using model with finite ionization

20 p3680 A70-39984

Preionization in Cs seeded Ar nonequilibrium plasma for MHD generators, examining discharge characteristics, recombination reactions, etc

20 p3680 A70-39991

Large scale nonequilibrium linear MHD generator performance with rare gases under strong EM-gas dynamic interactions 20 p3681 A70-39993

Insulator wall temperature effect on supersonic nonequilibrium MHD generator channel under open and short circuit conditions 20 p3681 A70-39994

Nonequilibrium plasma stability, conductivity and Hall parameter influenced by current flow parallel to magnetic field, discussing Ar-Cs and He-Cs plasma data 20 p3682 A70-40019

Charge separated and quasi-neutral solutions of electron heat transfer to spherical body in quiescent nonequilibrium plasma, noting diagnostic applications 21 p3860 A70-42080

Critical Hall parameter for linear development of MHD electrothermal instability in bounded nonequilibrium plasma 23 p4227 A70-44555

NONEQUILIBRIUM RADIATION

Nonequilibrium zone radiation intensity profiles behind strong shock waves in air determined for specific wavelengths and shock velocities 03 p0535 A70-14364

Gas dynamics theory with nonequilibrium radiative and collisional ionization applied to strong normal shock wave structure 05 p0831 A70-15870

Cepheids nonequilibrium continuous emission at maximum brightness, considering phase shift between radiation intensity and stellar contraction 15 p2802 A70-32483

Nonequilibrium radiation from stagnation region of high velocity spherical gas cap traveling through air 22 p4124 A70-42758

Cepheids nonequilibrium continuous emission at maximum brightness, considering phase shift between radiation intensity and stellar contraction 23 p4240 A70-43907

NONEUCLIDIAN GEOMETRY

U DIFFERENTIAL GEOMETRY

NONFLAMMABLE MATERIALS

Tetrabromophthalic anhydride /TBPA/ in polyester and epoxy resins, studying fire retardant capabilities by comparative combustion tests 05 p0811 A70-16584

Nonflammable coatings for polycarbonate to meet NASA safety standards, discussing alkali silicate and arc plasma deposition of glass and ceramic oxide [WSCI PAPER 69-34] 06 p1092 A70-17977

Hyperbaric environment combustion, discussing burning rate data and fire resistance scale 14 p2665 A70-30626

Flame resistant nonmetallic materials for manned spacecraft and aircraft interiors, considering fibers, polymers, paper and composites 22 p4058 A70-42295

Nonflammable fibrous textile materials for injury and personnel loss prevention in fires by aircraft accidents 23 p4153 A70-44481

Fireproof nonmetallic materials for spacecraft and aircraft, discussing functional utility, durability and aesthetic requirements relative to environmental conditions 23 p4210 A70-44610

NONGRAY ATMOSPHERES

Nongray and constant radiative flux model atmosphere for K dwarf stars with 4000 K effective temperature and 4.5 log surface gravity 01 p0191 A70-11350

Radiative transfer in nongray gas between parallel walls, solving heat flux and temperature distribution 02 p0392 A70-11907

Convective nongray stellar atmospheres construction for stellar stability studies, accounting for convective flow nonlocality and nongray radiative transfer 04 p0745 A70-14472

Witham radiative acoustics, analyzing nonequilibrium waves propagating in nongray radiating and absorbing gas 06 p1173 A70-17514

Radiatively driven plane acoustic wave in nongray radiating and absorbing gas assuming local molecular equilibrium 06 p1173 A70-17515

Radiative transport in nongray cylindrical medium using total band absorbance 09 p1790 A70-23553

Nongray surfaces radiative interchange calculation, considering surface radiative properties 09 p1790 A70-23561

Band or line shape effect on radiative transfer in nongray medium between parallel walls, discussing temperature distribution and radiative flux 13 p2521 A70-29136

Continuum radiative flux from nonisothermal stagnation shock layer of nongray atomic gases, employing ionization edges and bound free spectral forms [AIAA PAPER 70-837] 16 p3001 A70-33932

Nongray radiant heat transfer corrections to thermal conductivity measurements for water vapor at atmospheric pressure 16 p3003 A70-34200

Unsteady radiating nongray gas diffuse boundary conditions, emphasizing monochromatic radiation slip and one dimensional radiant flux 23 p4282 A70-44593

NONHOMOGENEITY

U INHOMOGENEITY

NONISENTROPICITY

Perturbation theory of supersonic steady anisentropic flow with radiative heat transfer using hyperbolic characteristic coordinates 12 p2334 A70-28203

Plane shock wave decay by interaction with simple wave, solving nonisentropic equations of gas dynamics 23 p4179 A70-43969

NONISOTHERMAL PROCESSES

U ISOTHERMAL PROCESSES

NONISOTROPIC PLATES

U ANISOTROPIC PLATES

NONISOTROPY

U ANISOTROPY

NONLIFTING VEHICLES

U BALLISTIC VEHICLES

NONLINEAR EQUATIONS

NT CUBIC EQUATIONS

NT DUFFING DIFFERENTIAL EQUATION

NT MONGE-AMPERE EQUATION

NT QUADRATIC EQUATIONS

Nonlinear electrodynamic equations solutions for electromagnetic media with one dimensional unsteady electromagnetic field based on wave functions determined from boundary conditions 01 p0149 A70-10165

Atmospheric dynamics nonlinear equations reduction to spectral form using generalized spherical functions series 01 p0135 A70-10203

Asymptotic and approximate wave construction for system of first order quasi-linear partial differential equations 01 p0131 A70-10800

Nonlinear stress-strain equations for incompressible hyperelastic media developed for undeformed and deformed continuum states 01 p0201 A70-10892

Nonlinear equations solvability for elastic cylindrical shells found existing for arbitrary load and clamping conditions 01 p0212 A70-11572

Algorithm for solving Dirichlet problem of nonlinear elliptical differential equations representing atmospheric dynamics balance equation 01 p0134 A70-11609

Nonlinear waves in parallel shear flows, discussing laminar flow breakdown due to free stream disturbances 02 p0277 A70-11876

Quasi-linear stress-strain deviators relations in viscoelastic theory, indicating kernels and functions determinable from creep relaxation loading and deformation tests 02 p0390 A70-12804

Stability criteria for first approximation solutions of nonlinear ordinary differential equations of motion 03 p0524 A70-13431

Averaging over finite and infinite intervals derived for nonlinear integrodifferential equations with varying variables 03 p0594 A70-13507

Nonlinear differential equations for determining radiation density of three level pulsed gas laser as function of power losses, active medium parameters and time 03 p0502 A70-13745

Wave propagation in inhomogeneous media, reducing quasi-linear hyperbolic partial differential equations to single nonlinear equation integratable by method of characteristics 03 p0525 A70-14184

Nonlinear solid applied mechanics, emphasizing nonlinear constitutive equations and related subjects, cyclic loading effect on solid materials, etc 03 p0610 A70-14230

Nonlinear stochastic differential equations formulated during random loading processes generation, designing testing devices with stable performance parameters 03 p0598 A70-14236

Plasma turbulence theory formulated using averaging operators, obtaining nonlinear dispersion relation for turbulent diffusion coefficients 03 p0537 A70-14377

Initial value method for solution of nonlinear two point boundary value problems in fluid mechanics, considering Blasius equation and unsteady gas flow [ASME PAPER 69-WA/FE-8] 04 p0667 A70-14782

Numerical analysis of nonlinear boundary value problems for ordinary differential equations, considering patch bases and monotone methods 04 p0714 A70-15046

Nonlinear equations for TWT derived allowing for electron beam defocusing and slow wave structure deposition current 05 p0823 A70-16887

Existence and uniqueness, stability and asymptotic stability of nonlinear operator differential equation 05 p0878 A70-17098

Existence and stability problems of nonlinear operator differential equations containing linear operator with domain and range contained in real Hilbert space 05 p0878 A70-17099

Nonlinear equation solution based on local mapping relations and global implicit function theorems for Banach space problems 06 p1092 A70-17224

Numerical solution of nonlinear hyperbolic systems of differential equations using methods of differences, applying results to invariant cross section gas flow 06 p0964 A70-17236

Soviet monograph on branching theory of nonlinear equations, covering solutions with analytical operators dependent on numerical or functional parameters 06 p1093 A70-17412

Matric Computer equisolution matrices for nonlinear algebraic and integrodifferential equation systems solution 06 p1014 A70-17427

Nonlinear differential equations variational formulation, giving practical applications 06 p1093 A70-17635

Discrete ordinate technique for nonlinear Boltzmann equation tuned for computing collision integrals to instantaneous nature of distribution function 06 p1047 A70-18319

Monte Carlo method applied to solving nonlinear Boltzmann equation for plane shock waves in elastic sphere gases 06 p1050 A70-18335

Asymptotic behavior of approximate solutions of nonlinear differential equations 07 p1322 A70-18891

Nonlinear spinning shallow spherical shell equations solved for equilibrium stress and displacement distributions, discussing inertia loading 07 p1406 A70-19342

Isotropic plate stress-strain state weakened by doubly periodic curvilinear holes using nonlinear theory 07 p1408 A70-19544

Short term weather forecast hydrodynamic equations reduced to solving nonlinear differential equations by introducing dependent variables 07 p1329 A70-19647

Asymptotically periodic solution of nonlinear differential equations, discussing digital or analog computer utilization 07 p1326 A70-19782

Ritz method applied to second order nonlinear differential-difference equations subjected to sinusoidal driving functions, studying stability criteria and resonance properties 07 p1327 A70-20023

Parameters identification in nonlinear boundary value problems by successive approximations technique, using Lagrange multipliers and Newton-Raphson method 07 p1327 A70-20025

Nonlinear integral equations for inhomogeneous atmospheres derived from radiative transfer equations global form, noting relations to Ueno and Chandrasekhar equations 07 p1336 A70-20059

Temperature renormalization for improving velocity distribution function representation in solving nonlinear Vlasov equation, transforming Hermite polynomials 07 p1328 A70-20201

Nonlinear computational stability of partial difference approximations to meteorological equations 08 p1534 A70-21024

Nonlinear transport equations linearization by hodograph and inversion techniques 08 p1597 A70-21125

Nonlinear equations for large fluid oscillations in axisymmetric rotating cavities with radial partitions 09 p1660 A70-22438

Vortex and potential motions interactions in relativistic hydrodynamics, noting effects of gravitation equations nonlinearity 09 p1754 A70-22461

Nonlinear stability theory for applying perturbed equations to dynamical system based on Liapunov stability theorem 09 p1727 A70-22612

Nonlinear differential equations approximate periodic solutions generation by finding equivalent system in sense of minimum mean square difference 09 p1712 A70-22666

Nonlinear partial differential inequalities treated by comparison function μ associated with continuity and growth conditions 10 p1908 A70-23836

Analytic systems theory using Volterra calculus of functionals applied to nonlinear differential equations 10 p1908 A70-23845

Numerical method for linear differential equations extended to nonlinear ordinary differential equations, liquidating residuals by setting integrals equal to zero 10 p1909 A70-24419

Nonlinear operational equation iteration solution error estimation, discussing Banach space nonlinear operator equation

10 p1909 A70-24508

Existence theorem for periodic solutions of nonlinear differential equations with deviating arguments

10 p1910 A70-24605

Orbital stability of geostationary vehicle at arbitrary latitude, considering nonlinear equations and deducing stability conditions by Liapunov method

10 p1950 A70-24783

Nonlinear electrodynamic equations solutions for electromagnetic media with one dimensional unsteady electromagnetic field based on wave functions determined from boundary conditions

10 p1925 A70-25013

Equilibrium properties of nearly normal turbulence assuming near-Gaussian nonlinear model equations and real turbulence

11 p2039 A70-26533

Nonlinear thin shell theory equations reduced to equations in unknowns with boundary conditions

11 p2143 A70-26653

Nonlinear equations systems iterative solution convergence by extending classical algorithm with optimization process

11 p2074 A70-26850

Nonlinear integral equations of radiation transfer of stellar and planetary atmospheres

12 p2305 A70-27852

Nonlinear Vlasov equation treatment by Fourier-Hermite expansion techniques for plasma problems

13 p2457 A70-28556

Averaging over finite and infinite intervals derived for nonlinear integrodifferential equations with varying variables

13 p2440 A70-28656

Nonlinear differential equations systems, deriving periodic solutions existence conditions

13 p2440 A70-29049

Finite difference methods for approximating first order nonlinear hyperbolic differential equations, considering convergence

13 p2441 A70-29098

Nonlinear integrodifferential equations of radiative transfer solved by invariant imbedding approach, discussing Rayleigh phase matrix

13 p2451 A70-29130

Nonlinear equations boundary value problem solution by Galerkin method in integrodifferential equations form, determining Lipschitz conditions constant and proving existence and uniqueness

13 p2442 A70-29513

Nonlinear branching point problems in fluid mechanics using perturbation technique

14 p2565 A70-30471

Canonical representation for nonlinear differential equations periodic solutions

14 p2658 A70-30846

Monograph on nonlinear oscillation equations resonance solutions and solution stability, considering Green matrix, differential equations reduction to integrodifferential equations, etc

14 p2618 A70-31417

Nonlinear higher order canonical time lag equations initial and boundary value problems solutions by approximate iterative two way integration

15 p2767 A70-32171

Nonlinear differential equations for smoothing density function and smoothed expectation of arbitrary function of state

16 p2941 A70-33057

Nonlinear elasticity equations in displacements by Green and Hencky deformation tensors, discussing stress-strain of body with spherical cavity

16 p2988 A70-33251

Parameter identification algorithm for nonlinear equations describing VTOL aircraft longitudinal response

16 p2942 A70-33327

Particular solutions for nonlinear two point boundary differential equations with initial and final conditions

16 p2942 A70-33692

Nonlinear partial differential equations initial value problems asymptotic solution using two time method

16 p2943 A70-34245

Nonlinear wave equations model for human torso under impulsive stress, obtaining asymptotic solution

16 p2854 A70-34247

Existence and uniqueness theorem for boundary value problem solutions to nonlinear canonical ordinary differential equations

17 p3131 A70-35339

Power series solutions to linear and nonlinear differential equations in region of asymptotic stability

18 p3279 A70-36155

Mathieu equation with nonlinear terms for damping and restoring forces, investigating first order instability region

18 p3337 A70-36224

Nonlinear second order differential equations with periodic coefficients and solutions, examining stability by phase and amplitude plots by marginal range diagrams

18 p3282 A70-36356

Nonlinear approximation under auxiliary conditions in normed space involving minimum solution

18 p3282 A70-36363

Nonlinearized exact solution of Navier-Stokes equations for fluid motion between two coaxial circular disks rotating at equal velocity

18 p3241 A70-36381

Nonlinear two point boundary value problem, examining quadrature error effects in approximate numerical solutions by variational techniques

19 p3458 A70-37979

Nonlinear integral equations formal solution method, noting relationship to Fredholm solutions of linear integral equations

19 p3458 A70-38063

Numerical integration of finite difference analogs of nonlinear partial differential equations, investigating data smoothing, filtering and boundary effects on computational instability

19 p3459 A70-38417

Planetary scale unsteady atmospheric motions nonlinear problem, considering two level solenoidal model

20 p3662 A70-39177

Elastic membrane axisymmetric deformations, reducing nonlinear equations system to quadratures

20 p3718 A70-39230

Nonlinear differential equations solutions in power series with indefinite coefficients, determining type of singular points

20 p3658 A70-39766

Iterative solutions for systems of nonlinear equations and discretization of elliptic differential equations

21 p3845 A70-40736

Numerical procedure for second order nonlinear differential equations, discussing temperature distribution in semiinfinite solid homogeneous medium

21 p3950 A70-41449

Quasi-linear higher order differential equations, examining periodic solutions existence and stability

22 p4062 A70-42698

Numerical solution of nonlinear master equation for diatomic molecule dissociation and recombination from uncoupled differential equations

22 p4062 A70-42746

Wave front arbitrary curvature, examining integration of weak discontinuities growth equation in quasi-linear hyperbolic system

22 p4062 A70-42953

Nonlinear differential equations system under small perturbation, considering uniqueness for autonomous unperturbed system

22 p4062 A70-42969

Polynomial approximation process for scalar nonlinear equation solution, applying to Cauchy problem

22 p4064 A70-43482

Nonlinear elasticity equations in displacements by Green and Hencky deformation tensors, discussing stress-strain of body with spherical cavity

23 p4268 A70-44287

Computer program for nonlinear differential equations related to nonlinear boundary value problems based on Newtonian iteration process difference analog of linearization method

23 p4212 A70-44338

Nonlinear free boundary value problems involving region bounded by curvilinear ring consisting of smooth curves, reducing problem to nonlinear equations in Banach space

23 p4212 A70-44342

Nonlinear properties of first order differential equations for axisymmetric velocity vector fields of ideal incompressible fluid, using nonlinear singular integral equation

23 p4181 A70-44343

Nonlinear equations of motion approximate solution, determining ordnance weapons aerodynamic stability coefficients from angle of attack

23 p4133 A70-44515

German monograph on Hamilton principle and Hermetian polynomials for solving linear and nonlinear differential equations via computer method

24 p4369 A70-45091

Fifth-order pseudo-Runge-Kutta methods for numerical solution of ordinary differential equations, determining optimal parameters

24 p4369 A70-45163

Eigenvalue problem in elasticity theory, treating nonlinear equations solutions multiplicity by topological methods

24 p4420 A70-45273

Virtual work equations steady state subharmonic solutions by Newton-Raphson method, developing generalized iterative procedure for nonlinear differential equations

24 p4423 A70-45577

Nonlinear second order differential equation periodic solutions, describing water column oscillation in U-tube

24 p4369 A70-46021

Perturbation effects on nonlinear first order wave equations discontinuous solutions decay, discussing boundary value problem for stress wave propagation in rod with viscous damping

24 p4426 A70-46026

Boundedness theorem for nonlinear Mathieu equation describing motion of parametrically excited system

24 p4380 A70-46042

NONLINEAR FEEDBACK

Optimal servocontrol via nonquadratic performance index and linear plant dynamics obtainable as nonlinear function of error between controllable states and input vector

02 p0273 A70-12732

Popov criterion generalization for asymptotic stability of nonlinear feedback systems

14 p2658 A70-30849

Distributed sampled-data control systems with memoryless nonlinear feedback element, deriving frequency domain stability criterion

16 p2884 A70-33308

Suboptimal nonlinear feedback control synthesis for linear time-invariant system with convex cost functional

16 p2886 A70-33334

NONLINEAR FILTERS

Generalized approach for optimal corrector in mean squared sense for predictor-corrector filter structure, illustrating signal modes with nonlinear and linear dynamics

03 p0520 A70-14170

Optimal nonlinear filtering for nonlinear dynamic system subjected to additive white Gaussian noise with corrupted observations, using successive linearization scheme

03 p0461 A70-14340

Stochastic differential equations for approximate continuous nonlinear minimal variance filtering, discussing existence and uniqueness conditions

07 p1245 A70-19092

Matched filter rectangular pulse compression nonlinear FM waveform design with low time sidelobes and zero mismatch loss due to spectral weighting

07 p1242 A70-20065

PSK demodulation by optimal carrier and bit synchronization methods based on nonlinear filter theory, relating error probability to signal to noise ratios

08 p1458 A70-20795

Quasi-linear estimator algorithms to achieve both optimal nonlinear filtration and signal interpolation resulting in significant gain of estimate accuracy

09 p1633 A70-22408

Optimal inertialess nonlinear filters synthesis with various optimality criteria for signal distributions differing from normal

09 p1654 A70-22543

One dimensional discrete time nonlinear filters synthesis using Bayes theorem and digital techniques

09 p1654 A70-22934

Maximum principle least squares (MPLS) nonlinear filter scheme simplified, using digital simulation for stability and tracking performance

11 p2028 A70-26315

Markov nonlinear optimal filtration theory exact equations replaced by finite system of approximate differential equations

11 p2012 A70-26805

Nonlinear filtering methods for attitude computation in strapdown inertial navigation system

13 p2382 A70-29067

Book on stochastic processes and filtering theory covering probability theory, Markov processes, linear and nonlinear filters, etc

13 p2442 A70-29575

Nonlinear optimal filtration and adaptive quasi-coherent reception of Markov signals on white noise background

13 p2369 A70-29731

Dynamic nonlinear estimation, deriving general algorithms for filtering, smoothing and prediction for continuous and discrete systems

14 p2562 A70-31366

Homomorphic filters, discussing nonlinear filters for generalized linear system

15 p2710 A70-32580

Stochastic linearization approximation to solve nonlinear dynamical systems filtering problems in Markovian framework

17 p3056 A70-34953

Continuous time nonlinear filter for space vehicle attitude determination, using estimation theory

17 p3130 A70-35291

Nonlinear stochastic discrete time processes prediction and filtering by Monte Carlo techniques

18 p3234 A70-36338

Optimal nonlinear filtration for continuous automatic data transmission with radio signal under white, narrow band and Markov noise

22 p4004 A70-42891

Nonlinear filtering for linear parabolic distributed parameter systems with white noise, considering stochastic boundary value problem

23 p4177 A70-44905

Laser operation instability with nonlinear filter, deriving electrons differential velocity distribution functions on inhomogeneous emitter

24 p4352 A70-45469

NONLINEAR PROGRAMMING

Dual type method solving discrete optimal control problems with linear plants, convex cost and constraint taking into account dynamic structure

03 p0461 A70-14274

Unconstrained minimization techniques efficiency in mathematical nonlinear programming, discussing gradient and variable metric types

06 p1094 A70-17968

Second order necessary conditions of optimality with straightforward application to nonlinear programming of optimal control problems

07 p1322 A70-18850

Numerical solution of optimal control with dimensionality not exceeding phase space, using nonlinear programming and traveling wave method

10 p1911 A70-25185

Gauss-Newton nonlinear programming algorithm applications to optimization of optimal control law parameters and closed loop control system synthesis

13 p2381 A70-28435

Penalty function algorithm for linear/nonlinear programming optimization problems subject to equality/inequality constraints, discussing feasibility determination capability

13 p2373 A70-29462

Nonlinear digital programming techniques for air-plane stability augmentation systems design

16 p2840 A70-33343

Buckling problem numerical analysis by nonlinear programming and minimum energy formulation

18 p3339 A70-36495

Minimum weight design for structures with stability constraint by nonlinear programming

18 p3344 A70-37068

Highly constrained optimal control problems, using nonlinear programming in mathematical model for trajectory optimization

20 p3600 A70-39565

Nonlinear programming for minimizing inertial guidance systems costs via optimal subsystem selection

20 p3740 A70-39645

Book on theory of optimal control and mathematical programming covering linear, nonlinear, quadratic programmings, etc

21 p3845 A70-40891

Real functions and sets representation theorems derivation and application to nonlinear programming, using Bellman quasi-linearization technique

24 p4370 A70-46099

NONLINEAR SYSTEMS

Nonlinear closed-loop automatic control systems steady state characteristics calculation by graphic method

01 p0052 A70-10194

Book on nonlinear stress waves propagation in elastic solids covering adiabatic shocks, isentropic plane waves, Lagrange equation, spherical waves, heat conduction effect, etc

01 p0202 A70-10966

Algebraic criteria for absolute stability and equilibrium position in nonlinear continuous automatic control systems, using complex gain amplifier substitution

01 p0053 A70-11041

Nonlinear system under random excitation, discussing analytic solution method and statistical properties

01 p0206 A70-11149

Wave propagation in nonlinear viscoplastic medium, deriving first order system of coupled equations in stress and particle velocity components

01 p0207 A70-11154

Stressed state of isotropic nonlinear multiply connected media with large deformations, using nonlinear elasticity theory

01 p0212 A70-11446

Second order dynamic systems stability, analyzing nonlinear and self excited oscillations by using two differential equations

01 p0146 A70-11604

Popov type nonlinear control systems from synthesis viewpoint, using state variable feedback results to insure absolute stability

02 p0271 A70-12194

Harmonic vibration testing of aircraft structural nonlinearities caused by dry friction, describing pitch control system

02 p0387 A70-12215

Automatic control nonlinear systems with random inputs, determining phase coordinates probability densities

02 p0272 A70-12414

Soviet book on oscillations of quasi-linear time lag systems, emphasizing asymptotic methods in nonlinear oscillation theory

02 p0340 A70-12826

Frozen stress techniques for photoelastic analysis of orthotropic plate on nonlinear foundation, providing results to compare with future finite element analysis

03 p0480 A70-12952

Nonlinear gyroscopic navigation system intrinsic error derived as function of linear operator

03 p0522 A70-13373

Method of characteristic calculation of field amplitude of electromagnetic waves propagating in inhomogeneous nonlinear medium applicable for computer

03 p0448 A70-13461

Nonlinear feedback control system analysis and synthesis by parametric plane method, investigating frequency response by describing functions

03 p0460 A70-13970

Generation-recombination noise theory extension to nonlinear devices applied to double injection diode in various operation modes

03 p0458 A70-14028

Closed loop nonlinear optimal control systems sensitivity to small parameter variations noting influence of feedback

03 p0461 A70-14171

Linear system theory in abstract algebraic framework applied to nonlinear machines in automata theory, discussing Ho algorithm, convolution and Kalman module theory

03 p0520 A70-14273

Optimal nonlinear filtering for nonlinear dynamic system subjected to additive white Gaussian noise with corrupted observations, using successive linearization scheme

03 p0461 A70-14340

Nonlinear control systems with linear controls appearance defined for controllability concepts and sufficient conditions to reduce to lower dimensional problem

04 p0660 A70-14524

Optimal control of multidimensional distributed parameters plants described by linear or nonlinear partial differential equations, considering boundary conditions

04 p0660 A70-14551

Modified harmonic balance method applied to critical values determination of nonlinear automatic control system parameters

04 p0661 A70-14555

Recursive nonlinear system state estimation for arbitrary path magnetic navigation tested on simplified model by Monte Carlo simulation, considering derived error expression

04 p0715 A70-14627

Light pulses propagation in nonlinear laser medium, obtaining equations of motion for density matrix

04 p0700 A70-14687

Transient heat conduction solution by finite element methods application to nonlinear boundary condition problems

[ASME PAPER 69-WA/HT-36] 04 p0781 A70-14804

Coupled nonlinear systems with two degrees of freedom using transformation techniques

04 p0714 A70-15084

Bifurcation frequency and nonlinear distortions determined in nonlinear semiconductor circuit with series-opposed connections of p-n junctions operating in forced oscillation mode

04 p0659 A70-15206

Amplitude and phase frequency characteristics relations established by analyzing forced resonant oscillations in nonlinear circuit operating at power source frequency

04 p0662 A70-15207

Nonlinear systems periodic oscillations with resonance from differential equations solutions

04 p0720 A70-15258

Nonlinear networks computer analysis by recursive decomposition, discussing network graphs construction rules

04 p0662 A70-15451

Book on theory of nonlinear control systems covering nonlinear oscillations, Liapunov stability, control systems stability and theory, differential equations, etc

04 p0663 A70-15500

Barium titanate ceramics with nonlinear electrical conduction, noting I-V relationship dependence on temperature, impurities and electrodes

05 p0891 A70-15990

Heated isotropic shallow shells results extended to solving nonlinear problem in bending theory of orthotropic shallow shells clamped, heated and under pressure

05 p0927 A70-15993

Hybrid computer simulation of small nonlinearities effects in human arterial system, using perturbation techniques

05 p0805 A70-16045

Sensitivity functions of nonlinear circuits obtained by calculation of dependent linear model responses, topologically equivalent to original circuit

05 p0824 A70-16125

Averaging analysis of oscillations attenuation of relaxing one dimensional linear viscoelastic systems under external force at resonance applied to nonlinear multidimensional systems

05 p0933 A70-16208

Mathematical problem of stability of nonlinear automatic control systems solved using linear criteria

05 p0825 A70-16866

Inertial parameters and functions of dissipative and restoring forces in quasi-linear oscillatory system determined from free motion characteristics

05 p0884 A70-16951

N-port resistive networks synthesis from terminal conductance matrices with two-tree port structures

06 p1023 A70-17426

Time optimal control of nonlinear systems with distributed parameters, proposing approximate algorithm

06 p1024 A70-17814

Suboptimal control to minimize quadratic cost functional for nonlinear systems, using Taylor series representation for feedback gain matrix

06 p1025 A70-17961

Signal stabilization and performance of nonlinear sampled data systems, suggesting oscillations injection at input

06 p1026 A70-17970

Nonlinear control systems stability with stochastic coefficients, applying Liapunov function

06 p1026 A70-17971

Nonlinear feedback control systems frequency domain stability criterion obtained using gain-phase plot

06 p1026 A70-17972

Iterative solution of nonlinear optimal control delineated for sufficient conditions for convergence

06 p1027 A70-18507

Nonlinear system theory for optimal linearization in holography, discussing generalized method for photographic emulsion and first order amplitude transmittance

06 p1072 A70-18521

Partial stabilization of given quantities on steady motions of nonlinear control systems with initial perturbations based on observation theory

07 p1333 A70-18686

Approximate linearization of nonlinear automatic control systems with two frequency forced oscillations

07 p1243 A70-18687

Absolute stability ranges of forced motions and damping in nonlinear systems determined by Sturm theorem

07 p1243 A70-18688

Periodic motions and dynamic stability of nonlinear distributed sampled data system of closed loop of pulsed element governed by heat conduction equation

07 p1226 A70-18749

Electromagnetic waves phase modulation index during propagation in nonlinear media found dependent on mismatch between interacting waves group velocities, relaxation time and losses

07 p1227 A70-18763

Control system composed of linear and nonlinear components and distributed parameters, deriving stability criterion for simple critical case

07 p1246 A70-19539

Steady oscillations under random forces of nonlinear system described by stochastic partial differential difference equations with distributed parameters and delayed argument

08 p1542 A70-20486

Stability criteria for systems of nonlinear stochastic differential equations on finite time interval, considering stable motion of physical processes

08 p1533 A70-20488

Nonlinear quasi-harmonic systems forced vibrations using one degree of freedom system as example

08 p1543 A70-20700

Book on solution of nonlinear systems covering stability theory, differential equations analysis, analog and digital simulation, etc

08 p1533 A70-20755

Periodic and almost periodic solutions to vibrations of quasi-linear nonautonomous systems in presence of resonance, determining principal amplitudes

08 p1544 A70-20966

Conditionally optimal control coefficients for nonlinear plant obtained from weighting functions derivatives of conjugate linear model for plant

08 p1479 A70-20995

Stability in whole of motion determined by system of nonlinear third order differential equations, using Liapunov functions

08 p1545 A70-21003

Spectral densities of phase coordinates of nonlinear automatic systems in steady states at random disturbances determined by statistic linearization

08 p1480 A70-21016

Pairs existence of symmetrical equilibrium forms in nonlinear shallow shell under load applicable to nonshallow shells equilibrium

08 p1591 A70-21416

Nonlinear system oscillations analysis based on small parameter method and difference equations, including resonant case and stability criterion for periodic solutions

08 p1546 A70-21629

Nonlinearity of human eye movement control system in two dimensional tracking tasks, explaining visual axis lags as time delays dependent on target motion

08 p1447 A70-21724

Nonlinear circuits reducing nonlinear distortions in amplifiers, discussing wideband nonlinear distortion compensating circuits

09 p1643 A70-22131

Combination resonance in two degree of freedom dissipative nonlinear system using small parameter and Ritz-Galerkin methods

09 p1727 A70-22667

Nonlinear periodic oscillations problem solved by solving nonlinear operator equations, discussing iterative methods based on equations linearization

09 p1728 A70-22668

Statistical linearization technique for nonlinear control systems with feedback and zero memory under random input excitation evaluated for output signal characteristics

09 p1654 A70-22960

Inertialess nonlinear quadrupole output of oscillations modulated by normal noise, analyzing correlation functions

09 p1637 A70-23159

Vibration decrement of nonlinear elastic system from resonance peak width of displacement amplitude curve of perturbing force

09 p1782 A70-23295

Soviet monograph on accelerated convergence method in nonlinear mechanics, discussing quasi-periodic differential equations solutions, smoothing techniques, etc

09 p1729 A70-23726

Nonlinear many degrees of freedom systems steady state forced vibrations analysis, expressing response in nonlinear normal coordinates

10 p1954 A70-24010

Hodograph or Riemann invariants method generalization for nonelliptic systems, discussing three dimensional potential supersonic flows

10 p1863 A70-24087

Electrohydraulic fast response servosystem design and operation, describing nonlinear model based on component limitations

10 p1807 A70-24578

One dimensional wave processes in distributed nonlinear systems, surveying mathematical methods

10 p1843 A70-25151

Maximum principle optimality for nonlinear two group parameter control applicable to plants described by integrodifferential and delay equations

10 p1911 A70-25184

Slowly varying parameters as engineering problem in nonlinear lumped systems

10 p1856 A70-25239

Nonlinear system with piecewise linear spring characteristic response to stochastic excitation of white noise type process, discussing technical stability

10 p1918 A70-25323

Necessary and sufficient conditions for absolute stability of nonstationary nonlinear system, showing equivalency to asymptotic instability in small position equilibrium piecewise linear systems

11 p2021 A70-25337

Stability of multiconnected nonlinear controlled systems with nonsingle equilibrium position, representing lumped parameter system with characteristic equation having complex roots

11 p2021 A70-25338

Maximum principle condition of optimal control of monodimensional system described by nonlinear hyperbolic equations with time delay

11 p2021 A70-25340

Correlation functions of nonlinear auto-oscillatory system under nonstationary conditions determined by statistic linearization

11 p2022 A70-25341

Control theory, Volume 1, covering linear, nonlinear, stochastic, optimal, adaptive and learning systems, sensitivity analysis, etc

11 p2023 A70-25771

Coupled nonlinear systems analysis based on reducing coupled differential equations to equivalent uncoupled equations amenable to existing techniques

11 p2072 A70-25956

Sequential filter equations for nonlinear system dynamics and observational model with linear estimator, comparing difference between white and colored noise filter results

11 p2024 A70-26126

Kalman-Bucy filtering for nonlinear system consisting of missile in flight, discussing state variables values selected by estimator

11 p2025 A70-26221

Nonlinear control systems on-off oscillations with instants of commutation determined by simultaneous equations, noting feedback control

11 p2027 A70-26254

Suboptimal nonlinear state estimation from noise corrupted measurements in ballistic trajectory, using simplified extended Kalman filter

11 p2028 A70-26303

Time optimal control for nonlinear second order system containing positive parameter and measurable control function

11 p2028 A70-26308

Optimum damping and stiffness in nonlinear single degree of freedom systems, discussing protection from ground and velocity shock during landing impact

11 p2145 A70-26695

Nonlinear time-varying multivariable adaptive control system design using signal synthesis technique

12 p2203 A70-27415

IR image conversion into visible using nonlinear KDP crystal

12 p2248 A70-27543

Nonlinear phase locked loops compared with linear loops in communication and navigation, considering interference vulnerability

12 p2187 A70-27909

Statistical analysis of control system with nonlinear zero-memory element evaluated for error using Fokker-Planck equation

12 p2204 A70-27985

Nonlinear discrete time sampled systems optimal control by dynamic programming, with application to stochastic systems

12 p2204 A70-28068

Nonlinear rotating systems optimal control problems approximation by modified Krylov-Bogoliubov averaging technique

12 p2273 A70-28192

Quasi-linear autonomous systems of second order equations, considering periodic solutions asymptotic stability

12 p2273 A70-28193

Quasi-linear elastic gyroscopic systems with distributed and lumped parameters, studying periodic solutions stability

12 p2238 A70-28194

Output signal spectrum analysis for nonlinear active element in presence of distorted modulating voltage

12 p2191 A70-28342

Soviet book on theory of oscillations of linear and nonlinear time lag systems

13 p2450 A70-28699

Nonlinear servo system stability criteria based on plus or minus controlled data theory

13 p2381 A70-28939

Random-input describing function as linear approximation to instantaneous nonlinearity in terms of minimum mean-squared error

13 p2382 A70-29070

Nonlinear control systems optimization applied to asymmetrical spacecraft

13 p2382 A70-29071

Multistep formulations of optimized Lax-Wendroff method for nonlinear hyperbolic systems in space variables

13 p2440 A70-29086

Computer modeling of nonlinear phase automatic frequency control systems under noise and oscillating disturbance

13 p2383 A70-29303

Free and forced motion characteristics in absolutely stable nonstationary nonlinear system analysis by variational approach

13 p2453 A70-29716

Multiple period oscillations in nonlinear systems, using nonautonomous differential equations and Hammerstein operator

13 p2443 A70-29745

Unsteady nonlinear aerodynamic loads measurements in wind tunnel, using linearized mathematical analog

[AIAA PAPER 70-573]

13 p2343 A70-29896

Controllability test for second order differential systems, noting applicability to linear first order time dependent systems

13 p2443 A70-29972

Statistical linearization synthesis of nonlinear self adjusting systems with frequency filters and input signal under white noise

14 p2559 A70-30156

Nonlinear sampled data system transportation lag effect on limit cycle nature

14 p2560 A70-30623

Limit cycle and stability analysis of multivariable nonlinear systems using function decomposition

14 p2560 A70-30624

First harmonic precision improvement of dual input describing function, applying to self oscillation of nonlinear systems

14 p2560 A70-30625

SCAMP I DC statistical circuit analysis program for linear and nonlinear circuits, describing program structure

14 p2560 A70-30664

Off-axis nonlinear holograms, defining spurious distortion and SNR

14 p2588 A70-31206

Dynamic nonlinear estimation, deriving general algorithms for filtering, smoothing and prediction for continuous and discrete systems

14 p2562 A70-31366

Stochastic terminal optimal control for nonlinear dynamical systems with state independent noise

14 p2600 A70-31420

Nonlinear effects in microwave resonators containing thin superconducting films and low values of microwave power

15 p2782 A70-31525

Computer control of nonlinear systems with varying performance specifications, using Popov stability and nonlinear programming

15 p2715 A70-31973

Nonlinear systems absolute stability by graphic methods, noting use of Nichol chart and analog computer

15 p2715 A70-31974

Stochastic linearized state estimator for nonlinear dynamic systems with Markovian noise, using digital simulation

15 p2715 A70-31975

Soviet book on mathematical theory of linear and nonlinear control systems covering differential and difference equations, calculus variations, etc

15 p2715 A70-32200

Nonlinear feedback control systems forced asymptotic stability, using linear transformation of circle criterion

15 p2716 A70-32554

Asymptotic motion stability bound for non-holonomic nonlinear electrodynamic systems, using energy metric algorithm for Liapunov functions generation

15 p2768 A70-32556

Nonlinear time-invariant lumped parameter dynamic systems, determining mathematical model by piecewise continuous power series expansions

15 p2768 A70-32576

Augmented state variable method of nonlinear discrete system identification with noise corrupted input observations

15 p2704 A70-32592

Parameter plane method of stability analysis applied to spacecraft attitude control system with two nonlinearities related by nonlinear differential equation

16 p2881 A70-33032

Nonlinear systems stabilization with linear system estimator output state to provide feedback for asymptotic stability of overall system

16 p2881 A70-33033

Nonlinear discrete systems absolute stability exponential property proved by modified frequency condition, applying analog transformation to Szego-Kalman equations

16 p2882 A70-33044

One dimensional controlled plants structure identification with mathematical model composed of aperiodic nonlinear and delay components connected in series

16 p2883 A70-33235

Oscillatory and wave processes in nonlinear distributed systems by asymptotic method analogous to Bogoliubov concentrated systems

16 p2951 A70-33252

State estimation for nonlinear discrete time systems with quantized measurements, obtaining recursive algorithm through boundary value problem linearization

16 p2867 A70-33305

Popov and circle criteria for stability of nonlinear feedback control systems, using parameter plane representation

16 p2884 A70-33314

Controllability of nonlinear dynamic feedback systems based on Liapunov-like stability approach and optimal control theory

16 p2885 A70-33321

Optimal control in nonlinear systems, discussing conditions for analytical solutions for Hamilton-Jacobi equations

16 p2886 A70-33335

Recurrence scheme for parameter estimation by quasi-linear equations of motion method and Kalman filtering for nonlinear dynamical systems

16 p2887 A70-33349

Geometrically nonlinear theory for sandwich type plates symmetrically built of three elastically and thermally anisotropic layers, considering nonuniform temperature field

16 p2990 A70-33744

Solutions behavior of nonlinear system of linear Volterra integral equations, discussing applicability of standard fixed point theorems

16 p2943 A70-34000

Potential stability theory for linear and nonlinear systems trajectory

16 p2943 A70-34042

Linear, nonlinear and random vibrations - Conference, Poznan, Poland, April 1968

16 p2994 A70-34276

Nonlinear lumped system synthesis by inverse delta method

16 p2943 A70-34278

Nonlinear dynamic systems described by matrix equation, formulating asymptotically stable conditions, discussing motion equations of two degree of freedom system

16 p2995 A70-34281

Nonlinear mechanical systems transient motion analysis based on phase trajectories

16 p2944 A70-34283

- Linear and nonlinear systems natural frequency and stability determination, using theorems for degenerate systems 16 p2944 A70-34284
- Nonlinear mechanical lumped dynamic systems trajectory analysis in terms of P and G sets 16 p2944 A70-34285
- Nonlinear systems excitation by two harmonic forces, analyzing vibration by linearization of differential equation of motion 16 p2995 A70-34286
- Arterial wall nonlinear distensibility effects on blood flow velocity profiles, considering various mathematical and physical artery models 17 p3035 A70-34468
- Automatic stabilization and control of computerized nonlinear processes, proposing algorithm for stability criteria 17 p3049 A70-34640
- Continuous time nonlinear feedback control systems, using modified gradient procedure for parameters adaptation 17 p3056 A70-34952
- Stochastic linearization approximation to solve nonlinear dynamical systems filtering problems in Markovian framework 17 p3056 A70-34953
- Imperfect solid deformation, presenting formalism for elastic theory nonlinear aspects of continuous distributions of dislocations and point defects 17 p3190 A70-35456
- Perturbation method for finite elastodynamic deformation of nonlinear systems 17 p3191 A70-35590
- Third order accuracy for nonlinear hyperbolic system of partial differential equations extended to equations with independent variables 17 p3131 A70-35891
- Nonlinear circuits with linear gain relations, examining input-output relations of two ports for analysis, synthesis and design 18 p3230 A70-36000
- Optimum spectral control of nonlinear plant, using Newton iteration and linear programming 18 p3234 A70-36075
- Frequency filters in nonlinear self adaptive system design for noncorrelated input and noise signals 18 p3234 A70-36119
- Stability conditions for control system third-order differential equations with double nonlinearity, using Liapunov function 18 p3280 A70-36157
- Nonlinear stochastic discrete time processes prediction and filtering by Monte Carlo techniques 18 p3234 A70-36338
- Asymptotic, averaging and Ritz methods for steady state periodic vibrations of nonlinear systems with many degrees of freedom 18 p3338 A70-36437
- Computerized Pontryagin stability analysis of nonlinear multiple delay systems 18 p3235 A70-36477
- Discrete automatic control theories, including linear, nonlinear, feedback, optimal and adaptive systems and bibliographies 18 p3235 A70-36626
- Creep bending of rectangular plates with stress-strain and strain displacement nonlinearities 18 p3343 A70-36703
- Electromagnetic waves phase modulation index during propagation in nonlinear media found dependent on mismatch between interacting waves group velocities, relaxation time and losses 18 p3229 A70-37107
- Spiral structure gravitational theory, discussing separation between linear and nonlinear effects 18 p3330 A70-37189
- Tightly wound spiral nonlinear density waves in pressureless self gravitating disk with external gravitational field, examining solid body and differential rotation 18 p3331 A70-37192
- Soviet book on vibrations in flight vehicle engines covering linear and nonlinear systems, computer methods, etc 18 p3305 A70-37229
- Soviet book on statistical calculation methods for linear and nonlinear automatic aircraft control systems design, using correlation theory of stochastic processes 19 p3463 A70-37403
- Traveling wave tube with two mixed different velocity electron beams, analyzing nonlinear operation by integro-differential equations 19 p3387 A70-37742
- Modified differential equation for stability of oscillating nonlinear system 19 p3458 A70-37823
- Stress relaxation interpretation at wave fronts in one dimensional media by nonlinear viscoelastic models, giving constitutive equations 19 p3542 A70-38057
- Periodic solutions of nonlinear second order differential systems containing symmetries, noting Marlin criteria 19 p3458 A70-38064
- Mechanical destabilizing model of nonlinear damping in nonconservative systems with follower forces, using Liapunov method 19 p3542 A70-38065
- Multivariable nonlinear systems absolute stability criteria, emphasizing nonzero entry functions 19 p3394 A70-38171
- Undamped forced two degree of freedom system with one linear and one nonlinear spring, analyzing subharmonic vibrations by Ritz averaging method 19 p3544 A70-38329
- Sufficient condition for optimal control with continuous nonlinearities, using Pontryagin maximum principle 19 p3394 A70-38717
- Oscillations of nearly nonlinear systems with conditions for main amplitude equations 19 p3472 A70-38726
- Optimal control time for second order nonlinear system with motion subject to specified conditions, determining switching line points 19 p3460 A70-38939
- Nonlinear LC circuit with p-n junction capacitance, examining relaxation vibrations during automatic biasing 20 p3596 A70-38970
- Two dimensional detonations structure by nonlinear theory for systems with hydrodynamically unstable steady state solutions, imposing periodic boundary conditions 20 p3609 A70-39658
- Perturbation theory for nonlinear systems of differential equations 20 p3658 A70-40104
- Nonlinear closed loop systems frequency response determination by graphical method 20 p3605 A70-40122
- Nonlinear dynamic systems phase coordinate variations statistical characteristics, describing data reduction method 20 p3674 A70-40183
- Quasi-linearization relationship with Kalman filtering for nonlinear systems parameter estimation in process noise absence 21 p3845 A70-41749
- Nonlinear coupling in systems with two degrees of freedom, deriving transformation laws for uncoupling 21 p3940 A70-42054
- Hollow spheres and hemispheres nonlinear axisymmetric deformation, using shell theory reduced to two point boundary value problem for differential equations 22 p4112 A70-42288
- Periodic motions of arbitrarily long periods for idealized nonlinear spring-mass systems with two or more degrees of freedom 22 p4073 A70-42699
- Soviet papers on harmonic linearization method in design of nonlinear automatic control systems 22 p3999 A70-42826
- Harmonic linearization method for nonlinear automatic control systems, describing theoretical fundamentals 22 p4000 A70-42827
- Harmonic linearization of nonlinear hysteretic elements in automatic control systems 22 p4000 A70-42828
- Harmonic linearization method for periodic regimes in nonlinear control systems based on periodic solution sensitivity to higher harmonics and small parameters 22 p4000 A70-42829
- Amplitude and phase frequency characteristics of open and closed multiloop nonlinear automatic control systems by graphical methods 22 p4000 A70-42830
- Nonlinear automatic control systems transient response by frequency response curves of amplitude and phase characteristics 22 p4001 A70-42831
- Harmonic linearization equations for frequency and amplitude of self oscillations in nonlinear automatic control systems 22 p4001 A70-42832
- Harmonic linearization method for periodic regimes in discrete nonlinear automatic control systems performing signal quantization with respect to level or time 22 p4001 A70-42833
- Asymptotic method for nonlinear automatic control systems involving differential equations in Cauchy form with nonlinearities 22 p4001 A70-42834
- Harmonic linearization for nonsearching self adaptive automatic control systems described by nonlinear differential equations 22 p4001 A70-42835
- Harmonic linearization method for nonlinear automatic control systems with finite automata, discussing self oscillating modes of operation 22 p4001 A70-42836
- Periodic solutions to complex nonlinear automatic control systems with initial deviations, considering system stability and self oscillation conditions 22 p4002 A70-42839
- Harmonic linearization method application to automatic phase control system with periodic nonlinearities 22 p4002 A70-42840
- Harmonic linearization method for automatic control systems having hydraulic or pneumatic actuating device with two nonlinear elements 22 p4002 A70-42841
- Soviet papers on statistical methods in nonlinear automatic control systems design 22 p4002 A70-42881
- Statistical methods for nonlinear automatic control systems, including Monte Carlo method, equivalent perturbations, linearization and analytical techniques 22 p4002 A70-42882
- Signal accuracy prediction in nonlinear steady or unsteady continuous and discrete automatic control systems in random noise, using statistical linearization 22 p4003 A70-42883
- Dynamic characteristics of autooscillatory nonlinear self adaptive systems under random noise, using statistical and harmonic linearization 22 p4003 A70-42884
- Output probability of nonlinear systems from coupling moments for input random parameters, using equivalent perturbations method 22 p4003 A70-42885
- Interpolation method for nonlinear automatic control systems accuracy, discussing numerical integration optimal step and node number selection 22 p4003 A70-42886
- Quantitative reduction of statistical nodes for nonlinear automatic control system with random noise, using minimal approximating polynomials 22 p4003 A70-42887
- Output coordinates probability distribution density of nonlinear automatic control systems at fixed time, using multiple integrals 22 p4003 A70-42888
- Statistically optimal nonlinear automatic control systems synthesis in presence of random perturbations, using gradient or steepest descent methods 22 p4003 A70-42889
- Digital statistical modeling of nonlinear automatic control systems including accuracy analysis, generation of random perturbations and parameter optimization 22 p4004 A70-42892
- Conjunctors and traditors circuit realizations, discussing resistive and dynamic nonlinear networks 22 p3996 A70-42919
- Nonlinear rotating systems optimal control problems approximation by modified Krylov-Bogoliubov averaging technique 22 p4004 A70-43317
- Quasi-linear autonomous systems of second order equations, considering periodic solutions asymptotic stability 22 p4075 A70-43318
- Quasi-linear elastic gyroscopic systems with distributed and lumped parameters, studying periodic solutions stability 22 p4038 A70-43319
- Nonlinear heat transport in structural elements due to radiative transfer, analyzing temperature field dynamics 22 p4125 A70-43360
- Nonlinear control systems described by linear equations, discussing quasi and local controllability as functions of time and stationary state 22 p4063 A70-43427
- Criterion for global asymptotic stability of system with power-law nonlinearity, reducing to Nyquist criterion for linear system cases 22 p4063 A70-43428
- Stochastic optimal control for nonlinear dynamical systems under noisy observations, designing suboptimal state estimates and feedback controls 22 p4063 A70-43429
- Newton regularized method for nonlinear boundary value problems in combination with conjugate gradients 22 p4064 A70-43480
- Free motion of second order nonlinear automatic control device with vibration damping 22 p4075 A70-43554
- Nonlinear automatic optimal control for discrete system with delay 22 p4005 A70-43563
- Flexural vibrations of clamped circular plate with nonlinear elasticity for small strains and displacements, using variational principle 22 p4120 A70-43719
- MHD flow universal stability, investigating nonlinear system by energy methods 23 p4223 A70-43967
- Hamilton-Jacobi theorem for nonlinear dynamic system moving with holonomic Cetaev constraints, investigating necessary and sufficient conditions 23 p4210 A70-44024
- Krylov-Bogoliubov virtual work principal, investigating nonlinear vibrations, extending to heteronomous vibrations 23 p4266 A70-44028

NONLINEARITY

- Nonlinear differential equation systems overall stability, using qualitative methods 23 p4211 A70-44092
- Nonlinear elasticity theory, deriving geometrical relations applicable to small deformation tensor components 23 p4267 A70-44167
- Fluidic networks nonlinear component AC and DC behavior, discussing Bernoulli equation, nonlinear resistances, transmission lines and various flows 23 p4142 A70-44296
- Single-frequency oscillations mode in nonlinear catenary systems, considering factors promoting stabilization and uniformity 23 p4218 A70-44344
- Spectral and real time computation for acoustic absorbers with nonlinear material characteristics 23 p4219 A70-44393
- Nonlinear material and geometric behavior of shell structures studied by Eulerian and Lagrangian approaches 23 p4273 A70-44718
- Nonlinear shell analysis by finite difference energy method, using BOSOR3 and STAGS computer programs 23 p4273 A70-44723
- Pendulum dynamic stability under parametric excitation, presenting transient and steady state solutions by linear and nonlinear theory applications 24 p4379 A70-45587
- Nonlinear systems subharmonic oscillations under polyharmonic disturbance and viscous damping 24 p4427 A70-46378

NONLINEARITY

- Nonlinearity sources in elastic structures under large displacements, developing general matrix formulation 04 p0768 A70-14748
- Perturbation technique for numerically sensitive nonlinear two point boundary value problems 04 p0713 A70-15045
- Transmission channel nonlinearity effect on signal detector performance for signal received by synthesized antenna indicating SNR change 04 p0659 A70-15287
- Sonic boom theory of geometric acoustics with nonlinear effects modification, emphasizing horizontally stratified atmospheric propagation, discussing failure near caustic 05 p0796 A70-16794
- Light beam intensity variations during propagation in nonlinear medium taking into account combination scattering, solving equations by difference method 08 p1461 A70-20858
- Automatic control system stability with restricted nonlinearity, investigating lumped and distributed parameter systems and unique and nonunique equilibrium positions 08 p1479 A70-20996
- Weakly nonlinear dispersive cold plasma waves propagation by two time scale expansion, taking into account amplitude dispersion and coupling 08 p1553 A70-21613
- Second harmonic generation and frequency conversion efficiencies for laser beam shaping in nonlinear medium 08 p1514 A70-21984
- Photographic emulsion nonlinear response effect on image quality, discussing holography for multiple exposures 09 p1676 A70-22718
- Nonlinear effects related to plane electromagnetic wave propagation in weakly ionized plasma 09 p1735 A70-22842
- Spectral criteria for approximating tunnel diode nonlinear characteristics obtained by minimizing deviations of moduli of harmonic amplitudes 09 p1649 A70-23340
- Hamilton modified principal applied to nonlinear control problems including time delay, servosystem with ideal relay and liquid level control 09 p1614 A70-23693
- Nonlinear wave interactions in quiescent plasma column with external disturbance creating broadened frequency spectrum and weakly turbulent plasma 10 p1922 A70-24146
- LF ion-acoustic wave nonlinear interaction with HF Langmuir waves in nonisothermal plasma, establishing criteria for ion plasma turbulence 10 p1925 A70-25103
- Electromagnetic waves propagation in nonlinear medium, investigating polarized plane wave incident on vacuum-plasma interface in magnetic field 10 p1844 A70-25156
- Recording nonlinearities effect on image reconstruction from hologram of diffuse object 11 p2050 A70-25641
- Book on quasi-linearization and nonlinear fluid and orbital mechanics covering ablating wall, electrostatic probe, laminar boundary stability, pipe flow and optimum bang-bang transfer 11 p2072 A70-26225

Asymptotics of linear diffusion processes altered by weak nonlinear effects, discussing deterministic and statistical initial value problems 11 p2074 A70-26686

Electron beam-plasma interaction nonlinear development in time and space using computer simulation 11 p2095 A70-26758

Nonlinear optical effects in solids, gases and liquids with light from laser sources, discussing self focusing and absorption of light, transclucidity, harmonics, etc 12 p2245 A70-27277

Drift wave instabilities nonlinearities, discussing plasma growth rate and saturation coefficients, damping rate as function of amplitude and lower mode modification 12 p2280 A70-27786

Liapunov functions construction through conversion of differential equation with polynomial nonlinearities into auxiliary exact differential equation using algorithm 12 p2262 A70-28070

Nonlinear effects of oscillatory disturbances produced by viscous excitations in rotating fluid inside of cylindrical tank 13 p2386 A70-28819

Asymmetric missile nonlinear angular motion, describing quasi-linear relations for frequencies, damping rates and swerving motion amplitude [AIAA PAPER 70-534] 13 p2506 A70-29002

Finned configurations with nonlinear aerodynamic properties, obtaining solutions for angular motion at and near resonance [AIAA PAPER 70-535] 13 p2506 A70-29026

Random-input describing function as linear approximation to instantaneous nonlinearity in terms of minimum mean-squared error 13 p2382 A70-29070

Output correlation function of nonlinearity: filter system and phase modulated oscillations influence on system 13 p2366 A70-29411

Finite element method applications to structural analysis problems involving geometric and material nonlinearities 14 p2660 A70-31134

Human postural motor control systems nonlinearities, describing physiological experiments and mathematical models 15 p2693 A70-32568

Waves nonlinear propagation in fluids due to convection, reviewing various solution methods 17 p3068 A70-34666

Stress concentration near holes in plate in plane problem of thermoelasticity, taking into account physical and geometrical nonlinearities 18 p3336 A70-36133

Nonlinear elasticity law for elastic moduli of plastics 18 p3344 A70-36947

CdTe nonlinear electro-optical susceptibility predicted by mathematical model using two coupled anharmonic oscillators 19 p3485 A70-37668

Physically nonlinear elastic solid three dimensional and generalized plane strain problem, discussing application to composite materials 19 p3538 A70-37798

Boundary value problem solution in nonlinear viscoelasticity by constitutive equations 19 p3544 A70-38330

Elastic body steady forced oscillations under monoharmonic excitation, investigating hereditary nonlinearity effects on systems dynamic characteristics 20 p3733 A70-40395

Nonlinear heaving motion of plenum-chamber air cushion vehicles induced by sinusoidal ground irregularity 22 p3961 A70-42280

Image holography nonlinearities analysis, using photographic film characteristics for phase deviation enhancement 22 p4031 A70-42951

Nonlinear shell theory formulated in Lagrangian stress and moment resultants, deriving equilibrium equations 22 p4118 A70-43545

Wheel force and roll moment nonlinearities effect on light STOL aircraft handling qualities during approach [ICAS PAPER 70-55] 23 p4139 A70-44151

NONNEWTONIAN FLOW

Incompressible slow viscous nonNewtonian flow with free surface solved by finite element method, showing computerized results for squeezed fluid between two plates 01 p0066 A70-11131

NonNewtonian boundary layer flow having arbitrary potential velocities from methods for Newtonian fluids 19 p3407 A70-38932

NonNewtonian fluids flow and heat transfer characteristics past flat plate, determining velocity and temperature distributions 21 p3806 A70-40900

NONNEWTONIAN FLUIDS

Non-Newtonian fluids in continuum mechanics, classical Navier-Stokes theory limitations and theory of incompressible fluids for viscometric flows 06 p1037 A70-17926

Dissolved macromolecules effect on flow resistance due to turbulent friction in nonNewtonian liquids, considering physical parameters and hydrodynamic conditions 08 p1483 A70-21228

Sliding bearings with nonNewtonian lubricants, noting pressure gradient change effect caused by speed fluctuation and material constants 10 p1893 A70-24015

Newtonian fluid laminar boundary layer flow over flat plate with nonNewtonian fluid injection 12 p2209 A70-27212

Dimensionless heat transfer and resistance coefficients during stabilized nonNewtonian fluid flow in circular pipe 20 p3613 A70-40176

Integral transforms applied to convective heat transfer during nonNewtonian fluid flow with power rheology in pipes and channels 20 p3613 A70-40177

Flow past streamlined obstacles under nonNewtonian fluid injection into hydrodynamic laminar and turbulent boundary layer 21 p3812 A70-42266

NonNewtonian fluids variational problems, discussing generalized solutions existence and uniqueness 23 p4179 A70-43987

Ladyzhenskaja-type fluids linear flow stability criteria for two dimensional case 23 p4218 A70-44238

NonNewtonian fluids injection into boundary layer, comparing flow and pressure effects with water injection 24 p4324 A70-45364

Colloidal alumina nonNewtonian suspension in propylene glycol, examining thixotropic behavior at various structural levels 24 p4310 A70-45625

Constitutive equations in fluid dynamics, discussing Newtonian, Oldroyd and Walter, Reiner-Rivlin, Rivlin-Ericksen, Noll, Bingham and oriented fluids 24 p4327 A70-46149

NONOHMIC EFFECT

Hazards due to nonohmic materials responsible for electrostatic failures in missile and space programs and ground equipment 01 p0141 A70-10088

NONPARAMETRIC STATISTICS

Nonparametric statistical pattern recognition conditions of finite probability distribution mixtures in non-supervised adaptive detection 03 p0454 A70-14078

Nonparametric rank tests detection performance for signals in Gaussian noise, considering radar application 14 p2551 A70-31119

Nonparametric reliability application to numerical data involving failure distribution, using mathematical model 15 p2748 A70-32669

Light signals detection on noise background, comparing algorithms based on nonparametric statistics 22 p3989 A70-42569

NONREFLECTION

U ENERGY ABSORPTION

NONRELATIVISTIC MECHANICS

Incompressible homogeneous fluid model in non-relativistic generalized gravitation theory using analytical solution 09 p1762 A70-23118

Relativistic and nonrelativistic fluid dynamic equations, deriving limiting procedure leading to fluid magnetodynamic Lundquist equations 19 p3478 A70-37590

Nonrelativistic electron bremsstrahlung in dense plasma with strong magnetic field 21 p3855 A70-40721

Relativistic and nonrelativistic generalizations of classical approach in quantum mechanics applied to equations of motion in electromagnetic field 24 p4378 A70-45275

Relativistic gas bulk motion nonrelativistic equations, demonstrating spatially random fluctuations damp suprathermal hydromagnetic perpendicular propagation mode to interstellar magnetic field 24 p4397 A70-45761

NONRESONANCE

Optically pumped He 4 magnetometers, investigating magnetic resonance signal dependence on orientation for nonresonance technique construction 13 p2414 A70-30036

NONRIGIDITY

U FLEXIBILITY

NONSTABILIZED OSCILLATION

Energy analysis of unstable gravitational oscillations in galaxies, using two component model for normal spiral galaxies

03 p0570 A70-13532

NONUNIFORM FLOW

Turbine blade tip clearance effect on aerodynamic characteristics in nonuniform flow

07 p1187 A70-18980

Real gas behavior effect on shock tube temperature and pressure flow nonuniformity for range of Mach numbers

07 p1257 A70-19337

Supersonic wind tunnel flow discontinuities effect on oscillatory pressures

07 p1257 A70-19338

Stepwise averaged parameters of nonuniform three dimensional flow through turbine blade cascade determined from conservation conditions

09 p1606 A70-23611

Shock wave initiated two dimensional time dependent ducted flows in nonuniform regions using fluid-in-cell method, discussing density, pressure and energy distributions

09 p1665 A70-23740

Implantable EM blood flowmeter errors due to nonsymmetrical blood flow velocity distribution and nonuniform magnetic flux density

14 p2542 A70-30797

Viscometric Poiseuille or Couette flow kinematics, considering nonuniform shear rate

14 p2567 A70-31282

Flow nonuniformity effects on heat exchangers efficiency

15 p2827 A70-32140

Kinetic energy correction factor for nonuniform flow at Vena Contracta, using experimental data and modified Bernoulli equation

[ASME PAPER 70-FE-34] 16 p2892 A70-33639

Nonuniform external flow near blunt body stagnation point in diverging hypersonic thin shock layer

18 p3206 A70-36267

Nonuniform one dimensional flow of slightly ionized gas in infinitely segmented MHD generator with imperfect walls

19 p3478 A70-37588

Book on nonuniform gas theory covering viscosity, thermal conduction, diffusion, Maxwell-Boltzmann equations, density, quantum theory, transport phenomena, mixtures, electric fields, etc

20 p3673 A70-40135

Turbulent boundary layers produced by nonuniform shock tube flow, considering effects on chemical kinetic measurements

21 p3807 A70-41315

Nonuniform free stream supersonic flow past aerodynamic decelerators, calculating inviscid flow fields by method of characteristics

[AIAA PAPER 70-1176] 21 p3746 A70-41837

Centrifugal compressor losses as function of suction chamber exit nonuniform flow field delivered to impeller

21 p3747 A70-41954

Nonuniform radiation heat transfer between two coaxial cylinders, obtaining temperature distribution by Fourier series expansion

21 p3952 A70-42082

Nonuniform flow parameters for maximum thrust in nozzle, discussing specific impulse determination

22 p3960 A70-43366

Optimal load circuits number for maximum power extraction from Hall MHD generator with nonuniform gas flow along channel

23 p4143 A70-44900

NONUNIFORM MAGNETIC FIELDS

Contactless asynchronous flowmeter for measuring liquid metal coolant small flow rates, describing design and characteristics

03 p0483 A70-13211

Nutational NMR nonuniform magnetic field stabilizer for beta spectrometer, structural details and circuit schematics

03 p0485 A70-13467

Resonance frequency shift in motional field-averaging system due to nonuniformities in static magnetic or electric field may cause unexpected systematic errors

04 p0721 A70-14665

Whistler mode wave propagation in collisionless Vlasov plasma along nonuniform magnetic field

05 p0889 A70-16533

HF drift instabilities of plasma with nonuniform magnetic field, studying anomalous ion heating and resistance in Zeta installations

06 p1119 A70-17502

Plasma ion cyclotron resonance acceleration in nonuniform magnetic field by RF field

07 p1353 A70-20229

Diamagnetic plasma in nonuniform magnetic fields, determining equilibrium plasma configurations in and near neutral point for low and high pressure

09 p1734 A70-22478

Rotating plasma in nonuniform magnetic field analyzed for interchange instability based on MHD fluid and charged particle treatments

10 p1924 A70-24800

Alfven waves wavelengths dependence on inhomogeneous magnetic field geometry in stationary plasma, using conformal transformations

13 p2462 A70-28984

Free nuclear precession sensor with rotating sample for performing measurements in nonuniform magnetic field

14 p2582 A70-30218

Natural convection problem solution along nonuniformly heated vertical plate with variable transverse magnetic field

20 p3735 A70-39144

LF electrostatic ion cyclotron wave energy resonant power absorption in plasma in axially nonuniform magnetic field

24 p4386 A70-45608

Free nuclear precession sensor with rotating sample for performing measurements in nonuniform magnetic field

24 p4339 A70-46293

NONUNIFORM PLASMAS

Nonpotential waves propagating at slow phase velocity in inhomogeneous plasma, determining flute instability oscillation frequency

01 p0149 A70-10163

Thermal emission of inhomogeneous plasma sphere having dielectric constant as function of radius

01 p0149 A70-10164

Quasar 3C 273 scintillation intensity, considering role of interplanetary plasma inhomogeneities

01 p0174 A70-10199

Quasi-linear relaxation of electron beam in plasma with concentration nonuniformities, noting electron velocity role

01 p0150 A70-10213

Inhomogeneous plasma containing weak electron beam using Vlasov equation, noting wave-wave coupling effect

02 p0345 A70-11882

Permittivity tensor calculations of weakly inhomogeneous plasma with monoenergetic component, using distribution function of particles produced by thermonuclear reactions

03 p0529 A70-13055

Interplanetary plasma inhomogeneity size, shape and spatial orientation and drift velocity and direction determined from radio telescope data

03 p0565 A70-13231

Dispersive compression of plane frequency modulated waves in inhomogeneous plasma based on generalizing geometric optics approximation to unsteady quasi-harmonic processes

03 p0447 A70-13287

Nonlinear drift wave buildup in inhomogeneous plasma faster than in linear approximation

03 p0531 A70-13509

Electrical conductivity calculation for plasma in spatially inhomogeneous magnetic field using small-gyroradius approximation to kinetic equation

05 p0889 A70-16491

Polarization transfer equations for electromagnetic waves propagating in inhomogeneous magnetized plasma solved analytically for homogeneous magnetized plasma

05 p0890 A70-16570

Monograph on MHD waves covering theories for weak discontinuities, wave propagation in inhomogeneous media and behavior in magnetic fields

06 p1114 A70-17275

Ionospheric resonances observed by swept frequency Alouette topside sounders, discussing plasma nonlinearity

06 p1115 A70-17362

Plasma resonances, considering unbounded and bounded uniform and nonuniform plasmas and nonlinear effects

06 p1116 A70-17365

Transmission and emission of radiation from dense inhomogeneous finite laboratory plasma column in magnetic field with interpretation by cold plasma theory

06 p1116 A70-17367

Nonuniform plasma analyzed for parameters inhomogeneity effect on VLF propagation mode and instability

06 p1119 A70-17381

Linear transformation of waves in nonuniform magnetoactive plasma by solving wave equation with/without allowance for spatial dispersion

06 p1119 A70-17498

Variational ray path calculation method for HF electromagnetic wave in anisotropic inhomogeneous lossless ionospheric plasma

06 p1055 A70-17592

Symmetrical H mode wave propagation in inhomogeneous plasma filled circular waveguide solved by hypergeometric functions, noting use for microwave diagnostics and computer programs verification

06 p1009 A70-17825

Inhomogeneous plasma cylinder skin effect, surface impedance, radiation transport and mean noise temperature

07 p1347 A70-19107

Bogoliubov approach generalized and applied to unstable and inhomogeneous plasmas

07 p1347 A70-19108

Waves and differential equations for electromagnetic field in nonuniform magnetized plasma described for all orders in electron and ion temperature

07 p1350 A70-19823

Inhomogeneities in interplanetary plasma formation due to instability of electron flows moving along interplanetary magnetic field lines of force

08 p1570 A70-20845

Longwave and shortwave mode transformation in resonant layer of inhomogeneous plasma

08 p1550 A70-20847

Molecular cesium ion production by arc discharge in inhomogeneous cesium plasma, describing probable reaction mechanism

08 p1551 A70-20849

Interplanetary plasma inhomogeneity size, shape and spatial orientation and drift velocity and direction determined from radio telescope data

08 p1580 A70-21664

Nonlinear wave scattering at plasma particles and weak plasma inhomogeneity effects on plasma current instability

08 p1554 A70-21819

Thermal radiative transfer in nonuniform anisotropic magnetoactive plasma, correcting term of Zheleznyakov equation

09 p1734 A70-22514

Effective noise temperature of planar aperture antennas in lossy inhomogeneous plasma slabs calculated by computer

09 p1646 A70-22704

Nonpotential waves propagating at slow phase velocity in inhomogeneous plasma, determining flute instability oscillation frequency

10 p1925 A70-25011

Thermal emission of inhomogeneous plasma sphere having dielectric constant as function of radius

10 p1925 A70-25012

Two fluid hydrodynamic model of heat conductivity and viscosity effects on drift laminar flow stability of dense inhomogeneous plasma

10 p1926 A70-25125

Radiation fields of sources in plane stratified plasma medium calculated for amplitude transformation coefficient

10 p1843 A70-25155

Stability of realistic inhomogeneous plasmas with sheaths, examining electron beam-stable Maxwellian plasma interaction

11 p2090 A70-26021

Electrostatic wave propagation and growth rate in electron beam-inhomogeneous plasma confined by magnetic field

11 p2091 A70-26460

Plasma resonance excitation by small pulsed dipole in weakly inhomogeneous plasma determined using WKB solutions and stationary phase approximations

12 p2777 A70-27188

Electrostatic wave modes in inhomogeneous adiabatic plasma, discussing waves with gamma-fold ion and electron drift velocity

12 p2280 A70-27783

Tonks-Dattner resonances in plasma columns, considering viscosity effect on radial oscillations in nonuniform plasmas

12 p2281 A70-27792

Inhomogeneous one dimensional plasma in electrostatic normal modes, considering interactions of waves and particles

13 p2460 A70-28638

Laser radiation interaction with hot nonuniform plasma, determining thermal and electromagnetic forces for various temperatures and densities

13 p2460 A70-28643

Electromagnetic waves extraordinary mode scattering by small diameter nonuniform plasma column in magnetic field

13 p2460 A70-28644

Nonlinear drift wave buildup in inhomogeneous plasma faster than in linear approximation

13 p2460 A70-28652

Cross coupling relations in Boltzmann equations solution for inhomogeneous plasmas, using spherical harmonics expansion and Laguerre-Sonine polynomial

13 p2464 A70-29539

Cylindrical antenna admittance during immersion in ionospheric plasma, noting influence of ion sheath and plasma anisotropy

13 p2371 A70-29922

Whistler mode wave packets propagation in hot inhomogeneous collisionless plasma immersed in nonuniform ambient magnetic field

13 p2468 A70-29931

Convective or absolute electrostatic instability in weakly inhomogeneous hot magnetoplasma, determining density and frequency for onset

14 p2622 A70-30695

Anisotropic plasma turbulence produced by two stream instability onset near light cylinder of rotating magnetic star for pulsar model

14 p2640 A70-30788

Em wave reflection and transmission at boundary between free space and semiinfinite anisotropic plasma 15 p2778 A70-31830

Particle acceleration by electrostatic waves propagation in inhomogeneous plasma in terms of phase velocity, magnetic field and wave amplitude 15 p2778 A70-31912

Inhomogeneous ion beam plasma LF instability, showing oscillations amplitude maxima in radial density gradient regions 15 p2780 A70-32193

Glass tube surrounded nonuniform plasma column interaction with TM microwave field of cylindrical cavity for electron density measurements 15 p2780 A70-32347

Born approximation limit for plane wave multiple scattering by inhomogeneous electron density distribution in plasma 16 p2957 A70-32981

Tonks-Dattner resonances in warm inhomogeneous plasma column, examining kinetic theory for waveform shapes and resonance location 19 p3475 A70-37534

Inhomogeneous plasma ellipsoid equilibrium in external HF field, assuming parabolic density distribution 19 p3479 A70-37739

Inhomogeneous nonequilibrium plasma stratification in magnetic field, investigating electrical conductivity 19 p3481 A70-38191

Nonuniform electron plasma trapped in one dimensional potential well, determining linear oscillations by normal mode approach 19 p3482 A70-38944

Electromagnetic waves scattering from dense turbulent plasma, calculating radar cross sections of inhomogeneous plasma for peak electron densities 20 p3586 A70-39459

Nonuniform finite amplitude plasma waves nonlinear decay and instability, discussing initial damping/or growth/ effect 20 p3678 A70-39660

Two fluid hydrodynamic model of heat conductivity and viscosity effects on drift laminar flow stability of dense inhomogeneous plasma 20 p3685 A70-40518

HF electromagnetic field effect on nonhomogeneous collisionless magnetized plasma stability, deriving dispersion equation for drift cyclotron oscillations 21 p3854 A70-40622

Microwave propagation in circular waveguide containing inhomogeneous gas discharge plasma 21 p3785 A70-40630

Cylindrical plasma inhomogeneities including meteor trains diffusion in presence of magnetic field, observing dependence on angle theta 21 p3886 A70-41060

Transport coefficients of inhomogeneous magnetized bounded and unbounded plasmas based on quasi-linear approximation 21 p3857 A70-41385

Electromagnetic wave propagation through cold slowly varying plasma layers in absence of external magnetic field 21 p3860 A70-42000

LF self excited oscillations in inhomogeneous afterglow magnetoplasma measured by Langmuir probe, noting dissipative drift instabilities 22 p4079 A70-42372

Plasma inhomogeneity and drift effects on synchrotron radiation from relativistic charged particles in magnetoplasma 22 p4082 A70-43254

EM wave second harmonic generation by plasma wave, discussing decay processes in inhomogeneous plasma layer 22 p4083 A70-43381

Interplanetary plasma electron density inhomogeneities formation explained by instability due to electron stream curvilinearity obtained from spacecraft data 23 p4240 A70-44070

LF drift-dissipative instabilities of HF skin layer in nonuniform plasma 24 p4383 A70-45119

NONUNIFORMITY

Power and location prediction at critical heat flux onset under nonuniform axial heating conditions, using local approach method 01 p0219 A70-11303

Monochromatic light propagation in medium with large scale Markov nonuniformities of dielectric constant using parabolic equation approximation 12 p2272 A70-27359

TV photograph image instability of stars, developing discontinuity and variability criteria as elementary approximate method for comparing nonuniformities 16 p2979 A70-34177

Monochromatic light propagation in medium with large scale Markov nonuniformities of dielectric constant using parabolic equation approximation 22 p4075 A70-43600

NONVISCIOUS FLOW

U TURBULENT FLOW

NOON

Critical sunspot dependence of F 2 region noon bite-out phenomenon at various equatorial latitudes, observing magnetic dip 08 p1492 A70-21837

NORADRENALINE

Sleep-wakefulness cycle regulation role of serotonin, noradrenalin and acetylcholine in CNS of animals 15 p2680 A70-31745

Intact femoral artery pressure-diameter relationship in man, discussing noradrenaline infusions effects 18 p3222 A70-37222

Human elbow induced forearm and hand vessels tachyphylaxis to angiotensin, noradrenaline and acetylcholine compared to vascular response of vasopressin 21 p3761 A70-40577

NOREPINEPHRINE

Rats sympathoadrenomedullary response to increased oxygen tensions, measuring catecholamines, norepinephrine and epinephrine in adrenal gland, hypothalamus, serum and urine 01 p0024 A70-10979

Ambient temperature effects on rats excretion of epinephrine, norepinephrine and major metabolites 02 p0232 A70-11714

Blood flow changes in portal vein and hepatic artery of anesthetized cats following intraportal and intrahepatic arterial administration of isoproterenol, epinephrine and norepinephrine 02 p0232 A70-11718

Oxygen tension and pressure effects on hyperbaric oxygenation induced depletion of brain norepinephrine and 5-hydroxytryptamine in mice 02 p0235 A70-11992

Brain norepinephrine synthesis rate in gonadectomized and control rats treated with alpha-methyl paratyrosine 03 p0416 A70-12987

Norepinephrine release associated with vasoconstrictor response during selective activation of arterial and venous sympathetic nerves in dog hindpaw 03 p0416 A70-13012

Norepinephrine-induced depolarization effects on brown fat thermogenesis in cold-acclimated rats determined from in vivo measurement of intracellular potentials 05 p0799 A70-16020

Time course of changes in rat brain norepinephrine levels after olfactory bulb lesions, discussing automatic and biological mechanisms 08 p1448 A70-21841

Norepinephrine synthesis inhibition effect on arousal triggering and maintenance in hibernating golden hamsters, examining sympathetic activity 23 p4148 A70-44874

NORMAL DENSITY FUNCTIONS

Mie scattering and polarization functions of atmospheric aerosols determined on basis of logarithmic Gaussian distributions 05 p0879 A70-16664

Convolution formulas for Cauchy and standard normal random variable distributions derived from geometry of circular symmetric distribution on plane 07 p1323 A70-18946

Distributional results pertaining to complex Wishart processes and time varying spectral estimators on null hypothesis of stationary Gaussian time series 07 p1323 A70-19028

Complex Gaussian processes with complex density functions, computing covariances and marginal distributions 10 p1915 A70-24057

Regression analysis of linear statistical model experiments with stationary Gaussian error of slowly varying spectral density 11 p2073 A70-26249

Fifty percent coverage problem /Circular Error Probable/ of general bivariate Gaussian distribution from viewpoint of navigation systems error analysis 16 p2948 A70-33451

Gaussian source model of image, deriving rate distortion function under mean square error criterion 17 p3049 A70-34857

Gaussian gravity field structure, calculating gravity correlation function using differential equation from density correlation function 20 p3617 A70-39075

NORMAL DISTRIBUTIONS

U NORMAL DENSITY FUNCTIONS

NORMAL FORCE DISTRIBUTION

U FORCE DISTRIBUTION

NORMAL SHOCK WAVES

Normal shock waves in frozen, partly frozen and equilibrium flow in gas-solid particle mixtures 01 p0065 A70-11100

Molecular velocity distribution function measured in normal He shock wave in low density wind tunnel by electron beam fluorescence technique 02 p0299 A70-12229

Vibrational energy exchange between molecules during collision behind normal shock front as function of wave velocity 03 p0468 A70-13873

Numerical integration of differential equations governing one dimensional flow of reactive gas, discussing flows of converging-diverging nozzle and normal shock waves 04 p0671 A70-14992

Flow fields construction for normal shock waves with nonequilibrium chemical reactions reflected from shock tube end wall [AIAA PAPER 68-732] 04 p0674 A70-15537

Gas dynamics theory with nonequilibrium radiative and collisional ionization applied to strong normal shock wave structure 05 p0831 A70-15870

Numerical results for perturbed downstream flow field resulting from entropy wave interaction with normal shock and oblique shock generated by wedge flow 05 p0835 A70-16788

Model sampling or Monte Carlo applied to normal shock, giving temperature and density profiles for Mach 10 shock 06 p1050 A70-18337

Normal hypersonic shock wave structure in diatomic gas, measuring density by electron beam fluorescence technique 06 p1050 A70-18341

Normal shock waves produced in argon and helium flow by holder with variable downstream porosity, measuring DC moments, component velocities and density 06 p1051 A70-18342

Normal shock wave structure in binary gas mixtures of chemically inert monatomic molecules, using kinetic theory moment method 06 p1051 A70-18343

Single component two phase pipe flow choking and shock phenomena, including flashing flow vibratory effects 13 p2386 A70-28846

Gas-liquid two phase flow dynamics, explaining behavior under normal and oblique shocks 16 p2893 A70-33684

Normal shock structure in thermally perfect gas, using perturbation methods 17 p3070 A70-35244

Plane normal shock front diffraction along free interface between half planes of homogeneous fluids at rest, using method of characteristics and Whitham technique 17 p3074 A70-35886

Normal shock waves structured by nonequilibrium radiative and electron-atom collisional ionization, using generalized radiation model 24 p4324 A70-45290

NORMALITY

Seminormality and upper semicontinuity of variable sets in optimal control 22 p4061 A70-42461

NORMALIZING [STATISTICS]

Quantum-electrodynamics renormalization for electron charge in metal environment, using solid state many-body techniques 14 p2619 A70-30476

Normalization of mechanical properties of aircraft engine components, increasing weight efficiency and reliability 19 p3490 A70-37254

NORMS

International norms establishment for direct TV broadcast by satellites 17 p3201 A70-35780

NORTH AMERICA

Cosmic ray latitude survey in North America in summer using neutron and muon monitors operating near sea level and on mountains 01 p0167 A70-10226

Noctilucent clouds in mesopause over North America, discussing ground stations network, intensity variations, structure and time distribution 07 p2173 A70-20267

GEOS 1 satellite short arc optical observations over North American network to improve survey coordinates of tracking stations 24 p4312 A70-45542

NORTH AMERICAN AIRCRAFT

NT B-70 AIRCRAFT

NT OV-10 AIRCRAFT

NT X-15 AIRCRAFT

NORTH AMERICAN MILITARY AIRCRAFT

U MILITARY AIRCRAFT

NORTH CAROLINA

North Carolina continental shelf discolored water origin, movement and dissipation from Apollo 9 photograph interpretation 24 p4329 A70-45361

NORTHERN HEMISPHERE

NT ARCTIC REGIONS

Lowell Observatory Northern Hemisphere proper motion survey, analyzing preliminary data for low luminosity stars 01 p0187 A70-11332

Soviet book on nonperiodic processes in Northern Hemisphere stratosphere, discussing seasonal temperature fields, geopotential and circulation formation 07 p1261 A70-18733

Horizontal ionospheric drift over Northern Hemisphere during low solar activity, studying spatiotemporal distribution patterns of drift parameters

07 p1266 A70-19438

Atmospheric ground pressure seasonal changes after corpuscular flux arrival shown for Northern Hemisphere

08 p1487 A70-20554

Interhemispheric mass exchange as function of eddy transfer and meridional circulation

08 p1539 A70-21922

Hydrogen ion flux detected along earth magnetic force lines in Northern Hemisphere midlatitudes, determining flux magnitude

10 p1874 A70-24321

Long term ionospheric absorption measurements in Northern Hemisphere from IGY through IQSY, discussing annual and diurnal variations correlation with solar activity

12 p2226 A70-28060

F 2 layer ionization asymmetry for Northern and Southern Hemispheres during solstice periods due to electron density variations and aerodynamic conditions

14 p2569 A70-30206

Northern Hemisphere temperature atlas for SST cruise altitudes, estimating probabilities of enroute temperatures and risk increase

14 p2609 A70-30609

Magnetic activity intensity comparison in Northern and Southern hemispheres, noting correlation with solstices and equinoxes

14 p2580 A70-31260

Exospheric density at opposite hemispheres, showing variations from winter helium bulge

15 p2724 A70-31679

Northern Hemisphere radar aurora latitude variation, considering magnetic activity effects

15 p2697 A70-31770

Atmospheric ground pressure seasonal changes after corpuscular flux arrival shown for Northern Hemisphere

15 p2732 A70-32709

Horizontal ionospheric drift over Northern Hemisphere during low solar activity, studying spatiotemporal distribution patterns of drift parameters

18 p3249 A70-36912

Global scale atmospheric circulation processes numerical simulation leading to long range weather forecasts for Northern Hemisphere

19 p3462 A70-38753

Atmospheric zonal kinetic energy balance for Northern Hemisphere, assuming frictional destruction due to stresses across horizontal surfaces

20 p3661 A70-39145

Geopotential fields forecasting on isobaric surfaces over Northern Hemisphere by linear four level nonadiabatic model, discussing eddy transport and heat flux equations

20 p3662 A70-39179

Atmospheric circulation indices in Northern Hemisphere on isobaric surfaces, comparing mean diurnal, monthly and climatic values

20 p3662 A70-39180

Solar activity effects on Northern Hemisphere atmospheric temperature, mapping gradients for 11 year solar cycle

20 p3662 A70-39188

Air circulation spring restructuring in Northern Hemisphere upper stratosphere, investigating summer stratospheric anticyclone evolution

22 p4066 A70-43378

F 2 layer ionization asymmetry for Northern and Southern Hemispheres during solstice periods due to electron density variations and aerodynamic conditions

24 p4330 A70-46281

NORTHROP AIRCRAFT

NT F-5 AIRCRAFT

NORTHROP MILITARY AIRCRAFT

U MILITARY AIRCRAFT

NORTON COUNTY ACHONDRITE

Neutron capture effects in Gd from Norton County meteorite by isotopic composition analysis

12 p2300 A70-27524

NOSE [ANATOMY]

Human nostril airflow resistance during supported sitting and lateral recumbency and crutch pressure, discussing ipsilateral nasal congestion mechanisms

08 p1448 A70-21874

NOSE CAPS

U NOSE CONES

NOSE CONES

NT ABLATIVE NOSE CONES

NT ROCKET NOSE CONES

Shock wave shapes in hypersonic flow past blunt conical nosed circular cylinders, using analogy with Savic perturbed hypersonic blast wave theory

02 p0277 A70-11862

Scaling laws for nose bluntness effects on hypersonic aerodynamics of bodies of revolution

04 p0620 A70-15530

Porous matrix flow, surface liquid layer and hot gaseous boundary layer interactions at nose tip of reentry vehicle

06 p1037 A70-18028

Nose cone modifications for Meteor-1 meteorological sounding rocket used for wind velocity measurements

09 p1767 A70-23406

Photo-optical instrumentation for temperature estimates of nose cone in simulated reentries, using rocket monorail sleds and artificial rainfields for rain erosion effects

09 p1688 A70-23778

Transonic static and dynamic stability of large angle spherically blunted high-drag cones

[AIAA PAPER 70-564] 13 p2341 A70-29029

Cone boundary layer transition location and Reynolds number as function of nose bluntness combined effect with Ar, air and He mass injection

[AIAA PAPER 69-706] 13 p2343 A70-29954

Blunt nose effects on drag of flared conical body in supersonic flow, considering pressure loss through shock layer during atmospheric near orbital entry at high altitudes, using finite rate chemistry

16 p2837 A70-33865

Atmospheric reentry nosetip shape changes supersonic flow, considering rough surface effects on heat transfer

[AIAA PAPER 70-827] 17 p3196 A70-35193

Shock layer microwave radiation measurements during reentry flight of spherical nose cone, determining effective plasma temperature

18 p3208 A70-36694

NOSE INLETS

Pressure distribution about finite axisymmetric nacelle determined using Douglas Neumann program for cowl surfaces and inlet external surface

07 p1190 A70-20412

NOSE WHEELS

Steerable landing gear system consisting of freely castoring corotating wheel nose gear, tiltable axle and main gear skids for lifting body spacecraft

[AIAA PAPER 69-790] 13 p2344 A70-28514

Boeing 737 aircraft nose gear gravel deflector and engine vortex dissipator

[AIAA PAPER 70-912] 17 p3020 A70-35824

Large wheel and tire imperfection effects on nosegear parametric shimmy instability, using Mathieu equation

18 p3213 A70-36455

NOSES [FOREBODIES]

NT ABLATIVE NOSE CONES

NT NOSE CONES

NT ROCKET NOSE CONES

Vibrational relaxation effect on supersonic flow past nose section of blunted body

12 p2159 A70-28231

Viscous gas hypersonic flow past blunt nosed bodies based on Navier-Stokes equation

15 p2671 A70-31481

Supersonic nonequilibrium gas mixture flow past segmental bodies nose areas to simulate Venusian atmosphere, determining temperature, pressure and concentration distributions

15 p2796 A70-31483

Heat transfer and pressure drag of axisymmetric body in hypersonic flow, obtaining minimum energy nose and leading edge shapes by Pontryagin principle

[AIAA PAPER 70-825] 16 p3001 A70-33940

NOSTOC

Amino acid composition of protein in blue green algae *Stratonostoc Linckia*

14 p2540 A70-30158

NOTATION

U CODING

NOTCH SENSITIVITY

Stress distribution in vicinity of arbitrarily shaped slender notches as function of notch symmetry using photoelastic analysis

07 p1404 A70-19240

Ni-Fe base superalloy notch and rupture properties as function of thermal and chemical changes, using electron microscopy

13 p2437 A70-29829

Transient overloads effect on long term fatigue strength of notches and smooth steel samples, emphasizing heat treatment effect on notch sensitivity at high temperatures

15 p2814 A70-31546

Drop-weight tear test evaluation taking into account operator, test machine, specimen thickness, notch type and strength level effects

15 p2759 A70-32241

Glass fiber reinforced cross ply and quasi-isotropic plastics, considering notches effect on fatigue behavior for comparison with metals

19 p3455 A70-37951

Notch sensitivity dependence on plastic strain in Al alloy, heat resistant steels and Ni alloys under tensile tests at room temperature

24 p4360 A70-45827

NOTCH STRENGTH

Elastoplastic stress concentrations calculations in notched strips and shafts under tension, bending and torsion, using approximate method

01 p0211 A70-11425

Notch-bend strength of titanium, aluminum and copper base alloys, noting geometrical size effect

[ASME PAPER 69-MET-D] 04 p0705 A70-14878

Notched cylindrical shells of nonuniform thickness using two dimensional photoelastic models mounted on elastic foundations

07 p1249 A70-19239

Hypercritical crack growth resistance and notch toughness of aluminum alloys derived from fracture tests

11 p2064 A70-25331

Thin cut plate quasi-brittle breakdown under tensile stress, considering elastoplastic equilibrium under Tresca-St. Venant yield conditions

12 p2329 A70-28325

Strength and thickness effects on energy absorption criteria for transition temperatures in Charpy V-notch impact tests

15 p2819 A70-32234

Axial stress at notch root of shafts under axially symmetric loading, utilizing integrated birefringent patterns in transmitted light at room temperature

[SESA PAPER 1970] 15 p2821 A70-32315

Viscoelastic materials cut growth, discussing strain, fracture and modulus of elasticity dependence on temperature variations

17 p3146 A70-35220

Notch stress intensity factor representation as boundary traction weighted average, deriving weight functions from stress field boundary displacements

23 p4266 A70-44021

Brittle fracture of welded notched steels with different stress concentrations, using subzero tensile tests

24 p4347 A70-45732

NOTCH TESTS

NT CHARPY IMPACT TEST

Ultrasonic detection system for crack initiation and propagation in notched low cycle axial fatigue testing using surface and longitudinal waves

01 p0096 A70-10004

Stressed state of circular notched plane in tension under creep conditions

01 p0210 A70-11410

Elastoplastic zone and instability of precracked thin sheets under uniaxial loading applied to rectangular center-notched steel foils

03 p0598 A70-14239

Thermal stress concentration produced by cracks, notches and fillets in plates free from external loads measured photoelastically

03 p0600 A70-14310

Stress-strain spatial distribution in notched plate fatigue specimen of mild steel determined by finite element method, noting cyclic strain softening effect

[ASME PAPER 69-MET-C] 04 p0770 A70-14876

Hammer forces and specimen bending moment-time responses and fracture resistance during notched beam impact test

05 p0938 A70-16479

Analog to Burger model applied to rotating disk creep problem solution and stress-strain state of plane sample with hyperbolic groove

05 p0952 A70-17038

Corrosion cracking mechanism for notched metal surface in aqueous environment under tensile stress, discussing electron distribution and H ion concentration

07 p1310 A70-19737

Stress and strain spatial distribution in notched steel plate under cyclic loading determined by finite element method

08 p1590 A70-21315

Profile plane state of stress in wedge with and without external notch using combined photoelastic analysis and moire method

11 p2131 A70-25591

Mechanical notches and saltwater corrosion effects on flexural fatigue behavior of high strength structural alloys, investigating yield strength to density ratio

11 p2066 A70-26097

Spherically cut space elastic properties, determining normal and tangential stresses for uniform axisymmetric edge loading

12 p2328 A70-28200

Contour notch position effects on stress concentration in taper section of dumbbell shafts, using photoelastic shaft models and cyclic tests

13 p2517 A70-29750

Charpy V notch and dynamic tear tests compared for fracture toughness characterization of Ni-Cr-Mo-V steel

14 p2596 A70-30931

Structural components strength calculation with design required functional notches, noting stress limit for ductile materials under static loads

15 p2815 A70-31874

Microscopic residual stress in crystals at fatigue crack tip in notched specimen in terms of flow stress and dislocation density

17 p3183 A70-34653

Stress concentration in notched flat samples under plane plastic deformation

18 p3340 A70-36570

Critical loads for notched square Al alloy rods under tension 18 p3343 A70-36718

Notched sheet failure prediction based on Dugdale crack model, including work hardening and finite width effects, strain fracture criterion and yield failure mechanism 19 p3548 A70-38624

Elastoplastic deformation in strip with symmetrical semicircular notches simulating stress strain-state on celluloid models by polarization-optical method 20 p3720 A70-39735

Low cycle notch fatigue tests on Inconel and low alloy steel, giving fatigue strength reduction factors for design 22 p4055 A70-43103

Spherically cut space elastic properties, determining normal and tangential stresses for uniform axisymmetric edge loading 22 p4117 A70-43324

High strength Al alloys plate and welds, comparing tear notch tests at cryogenic and room temperatures 23 p4206 A70-44352

Moire technique application to fracture toughness tests on Zr alloys, measuring crack opening displacements and plastic flow beneath notch 23 p4208 A70-44914

German monograph on notched structural steels fatigue properties and crack propagation under tensile-compressive alternating loads 24 p4356 A70-45086

NOTCHED METALS

U NOTCH TESTS

NOTCHED STEEL

U NOTCH TESTS

U STEELS

NOTCHES

Plastic strains at sharp notch roots in Perspex plates using interference patterns formed by gas laser monochromatic light beam for fracture initiation 11 p2131 A70-25594

Stress concentration factors determined for U-shaped and semielliptical edge notches in semiinfinite sheet under uniaxial tension parallel to edge 13 p2509 A70-28535

Al-Mg alloy nonpropagating fatigue cracks at roots of sharp notches, discussing cyclic strain hardening 14 p2598 A70-31299

Stresses in plate containing circular hole with notch under uniaxial tension, determining parametric coefficients by Fourier transforms 14 p2661 A70-31326

Half plane with stress-free surface deformed by protrusions or notches, deriving edge force or screw dislocation by linear elastic analysis 21 p3939 A70-42028

NOVAE

NT HERCULES NOVA

Nova Delphini 1967 emission line spectrum at 8400-9600 Å, using diffraction spectrograph attached to astronomical telescope 01 p0182 A70-10675

Binary system Nova WZ Sge model with nonequilibrium secondary component contribution to total light explaining W UMa type light curve 03 p0568 A70-13324

Nickel IV forbidden lines suggested from spectrum study of slow nova RR Telescopii 05 p0905 A70-15758

SS Cygni outburst origin in G type star indicated from radial velocity variations of hydrogen absorption lines during rising light 05 p0915 A70-16695

Nova Delphini 1967 brightness visual evaluations by amateurs, discussing effect of personal factors and instruments on accuracy 08 p1568 A70-20634

Stellar formation and explosions in compact gas clouds to explain quasar phenomenon, discussing temporary star concept 08 p1578 A70-21548

Celestial sources energy spectrum and absolute flux by rocket flights, attributing short lived outbursts to shock wave from nova expanding into circumstellar medium 11 p2113 A70-26297

Pulsars nature based on hypothesis for main energy of novae and supernovae bursts equaling gravitational energy of collapse 11 p2117 A70-26708

Nova Delphini brightness variations, observing absorption lines shift toward violet 12 p2306 A70-27860

Nova Ser 1970 and Aql 1970 luminous IR emission, discussing stellar brightness, grain formation and optical decay 20 p3701 A70-39004

Nova Vulpeculae 1968 Number 1 medium dispersion spectra, using radial velocity line identification and line profile reductions 21 p3889 A70-41152

Nova HR Delphini 1967 UVB photoelectric photometry, examining absolute magnitude, distance, response curves and spectra 21 p3889 A70-41154

Delphini and Serpentis Novae radio emission in microwave spectra, noting consistency with thermal radiation of expanding ionized gas envelopes 24 p4410 A70-45771

Novae and supernovae envelope properties, observing optical polarization and magnetic field for Crab Nebula 24 p4413 A70-46169

NOXIOUS MATERIALS

U CONTAMINANTS

NOZZLE COEFFICIENT

U NOZZLE FLOW

NOZZLE DESIGN

Nozzle throat ablative materials for controlled high regression rates in tactical rocket motors, primarily nylon reinforced thermosetting resins [AIAA PAPER 69-423] 04 p0713 A70-15428

Heat transfer to hydrogen calculated with reference to design of cooled rocket nozzles and combustion chambers 06 p1174 A70-17677

Analytical method for design of supersonic flow and maximum thrust nozzles for chemically reacting gases, noting surface geometry 06 p0971 A70-18108

Free piston compression with sonic flow outlet for determining orifice size by matching with bounce parameters 07 p1249 A70-19334

Approximation for axisymmetric hodograph equation for nozzle calculation 07 p1188 A70-19347

Mean flow and turbulent velocity over noise-producing regions of subsonic jet nozzle with and without delta wings 09 p1610 A70-22239

Harrier engine nozzle actuation system role in short ground takeoff run facility, discussing pneumatic system, air motor servo unit and pilot control 09 p1610 A70-22606

Three dimensional supersonic nozzle geometry optimization using Lagrange multipliers and iteration for solving variational problem 10 p1798 A70-24115

Nozzle source design for high intensity thermal energy molecular beam with small dispersion in velocity suitable for scattering experiments 11 p2086 A70-25973

Monograph on relaxation processes at high temperatures for thrust nozzle calculation and optimization covering real gas effects, reaction kinetics, heat transfer, etc 11 p2103 A70-26475

Monograph on nozzle design effect on starting process initiated by plane shock wave in reflected shock tunnel 15 p2672 A70-31692

Auxiliary inlet ejector and plug nozzle flight performance, describing design variation effects for high supersonic speeds [AIAA PAPER 70-701] 16 p2841 A70-33563

Maximum thrust nozzles design for rotational or nonequilibrium simple dissociating gas flows, including boundary layer effects [AIAA PAPER 70-707] 16 p2891 A70-33567

Close-spaced nozzles twin jet configuration, achieving low nozzle and total afterbody drag [AIAA PAPER 70-934] 17 p3149 A70-35844

Supersonic air intake unsteady buzz phenomenon, examining shear layer under cowling and boundary layer detachment at shock wave base for design improvement 21 p3744 A70-41262

Concorde downstream thrust reversal nozzle, noting weight saving by use of welded stainless steel honeycomb construction 22 p4092 A70-43213

Axisymmetrical nozzle aerodynamic shape design for conical to axially uniform flow conversion, using method of characteristics 23 p4136 A70-44991

NOZZLE EFFICIENCY

F-106B aircraft in-flight study of airframes installation effects on propulsion system performance at transonic speeds 08 p1437 A70-21732

Aerodynamic performance of axisymmetric body traveling at transonic Mach numbers for predicting installed nozzle flow fields and efficiency [AIAA PAPER 70-700] 16 p2835 A70-33562

NOZZLE EXPANSION

U GAS EXPANSION

U NOZZLE FLOW

NOZZLE FLOW

Nonequilibrium effect of expanding water vapor condensation on supersonic nozzle flows with or without inert carrier gas 01 p0063 A70-10806

Mach numbers, electron density and temperature in partially ionized frozen equilibrium flows of Ar in hypersonic nozzle 01 p0063 A70-10994

Air flow density measurements with interferometer in supersonic square Laval nozzle, showing flow core motion and wave structure 01 p0064 A70-11000

Heat transfer in turbulent boundary layer of airflow injected on smooth plate from nozzle in subsonic stepwise heated wind tunnel 01 p0216 A70-11001

Compressible swirling inviscid nozzle flows approximate solution showing changed choking at throat, axial velocity distributions and reversing in subsonic region 01 p0003 A70-11128

Supersaturated vapor condensation in supersonic nozzles, obtaining flow and droplet growth equations for local equilibrium condition 02 p0279 A70-12049

Swirling flow equations in converging nozzles, comparing analytical and experimental data 03 p0405 A70-12929

Laminar-turbulent transition in free axisymmetric viscous incompressible jet from shaped nozzle and long cylindrical tube 03 p0466 A70-13396

Turbulence in hypersonic nozzle due to two phase flow of ideal gas and solid spherical particles, discussing thermal and dynamic differences 03 p0407 A70-13494

Flow parameters of two interacting submerged turbulent jets from rectangular nozzles, determining total pressure profiles of coincident flow 03 p0466 A70-13504

Difference method for calculating one dimensional nozzle flow and expansion with allowance for relaxation, friction and heat losses, discussing fluorine-hydrogen mixture application 03 p0408 A70-13804

Chaplygin equation solution for wedge flows applied to Rethy flows, evaluating drag coefficient and approximate hodograph equations for subsonic and transonic regimes 04 p0614 A70-14613

Mass flow rate calculation of methane and natural gas mixtures through critical flow nozzles [ASME PAPER 69-WA/FM-4] 04 p0667 A70-14839

Supersonic nonequilibrium two phase flow in Laval nozzle from numerical solution of quasi-linear hyperbolic equations 04 p0617 A70-15229

Supersonic jet flow from diverging nozzle into space with given pressure or into supersonic slipstream, noting barrel shock formation inside jet 04 p0617 A70-15235

Mixed nozzle flows solution complex boundary value problem reducible to Cauchy problem for hyperbolic system with three dependent variables by applying flow stabilization method 04 p0617 A70-15236

Solar wind as one dimensional flow analogous to Laval nozzle flow, discussing rotation and magnetic field effect on model with heat conduction 04 p0754 A70-15352

Nonequilibrium initial condition combustion effects on propellant performance for hydrazine/ chlorine pentafluoride and hydrogen/fluorine with equilibrium, kinetic and frozen nozzle flow [AIAA PAPER 69-469] 04 p0732 A70-15423

One dimensional steady adiabatic source nonequilibrium flow of thermally and calorically perfect gas in conical nozzle, considering exit divergence and nonuniform flow effects 04 p0619 A70-15427

Approximate solution for far downstream flow of condensation in hypersonic wind tunnels and nozzles for colloidal thrusters and EHD generators 04 p0621 A70-15600

Inert, oxidizing or reducing fluids wall injection into combustion gas boundary layer of variable composition noting effects on wall temperature 05 p0956 A70-15919

Acoustic intensity determined from time, length and velocity scales in mixing region of jet from nozzle with turbulent boundary layers 05 p0834 A70-16779

Acoustic radiation from underexpanded supersonic main jet flow from nozzle impinged upon by annular jet 05 p0835 A70-16784

Liquid flow through cylindrical slot of constant and variable thickness, calculating flow variations 06 p1034 A70-17630

Nonequilibrium excitation in recombining N plasma nozzle flows [AIAA PAPER 70-44] 06 p1122 A70-18061

Viscous core of incompressible swirling flow through nozzle using momentum-integral equations [AIAA PAPER 70-51] 06 p1038 A70-18079

Exhaust plume from underexpanded sonic and supersonic nozzles including boundary mixing analyzed by approximate model to predict Mach disk location [AIAA PAPER 70-229] 06 p0972 A70-18135

Particle density of jet plumes exhausting in vacuum calculated for He, Ar and N 06 p1052 A70-18388

Dense gas effects in free piston hypersonic wind tunnel, discussing Longshot facility, free piston cycle, reservoir conditions decay and hypersonic nozzle flow [AIAA PAPER 69-169] 07 p1249 A70-19310

- Skimmer interaction influences on nozzle beam production explaining intensity maxima, proposing model assuming normal shock across skimmer mouth
07 p1341 A70-20103
- Local heat transfer coefficients for unsteady conditions in tube determined by gradient method, noting use in reacting flow and jet nozzle protection
08 p1598 A70-21189
- Shallow water waves simulation method for studying aerodynamic noise of free jet emitted from nozzle with variable wall roughness
08 p1485 A70-21608
- Mean flow and turbulent velocity over noise-producing regions of subsonic jet nozzle with and without delta wings
09 p1610 A70-22239
- Aerodynamic characteristics of plane straight walled diffusers initial and stabilized flow segments, assuming incompressible fluid and turbulent boundary layer
09 p1659 A70-22430
- Axisymmetric nozzles flow regimes with subsonic ejection velocities analyzed by stabilization method, noting role of pressure in nozzle exit section
09 p1660 A70-22440
- Book on fundamental aspects of solid propellant rockets covering nozzle flow, solid propellants performance, ignition, combustion instability, etc [AGARDGRAPH-116]
09 p1743 A70-22635
- Relaxation time influence on mass output calculation errors for gases in small diameter sonic nozzles
09 p1604 A70-22841
- Injectant stagnation temperature and molecular weight variation effect on flow field generated from secondary gas injection into supersonic stream [AIAA PAPER 69-1]
09 p1733 A70-23217
- Dissociative-recombination rate coefficient measured for dissociative recombination reaction in inviscid nozzle flow of reflected shock tunnel, using high temperature and pressure nitrogen
09 p1737 A70-23225
- Injection induced swirl effect on thrust and mass flow through nozzle in spinning rocket, discussing internal and exhaust flow measurements and visualization
09 p1606 A70-23247
- Undried atmospheric air humidity effect on pressure and water vapor supercooling in supersonic wind tunnel nozzles
09 p1606 A70-23613
- Gas flow from nozzle into duct with enlarged cross section investigated for flow pattern and boundary conditions, noting oscillation behavior
10 p1799 A70-24123
- Asymptotic method for aeromagnetic flutter of plane MGD nozzle, discussing conditions of MGD nozzle stability
10 p1800 A70-24129
- External supersonic potential flow effects on turbojet engine ring and needle nozzle performance, considering gas overexpansion operation
10 p1930 A70-24286
- Compressible flow equations of motion applied to incompressible fluid flow through nozzle with eddies and springs
10 p1871 A70-24796
- Time dependent analysis for quasi one dimensional, vibrational and chemical nonequilibrium nozzle flows approaching steady state solution by finite difference technique
11 p1976 A70-25974
- One dimensional compound compressible nozzle flow solution dependence on initial conditions and nozzle geometry, discussing applications to bypass turbojets and solid propellant motors
11 p1976 A70-26137
- Cavity pressure and velocities distributions of interfering two dimensional dual jets from parallel slot nozzles
11 p2037 A70-26419
- Rarefied gas stream density measurements with electron beam fluorescence experiment, determining pressures and densities behind plane shock wave and in supersonic nozzles
11 p2087 A70-26743
- Ducted propellers design with flow accelerating and retarding nozzle analyzed by impulse theory
12 p2155 A70-26876
- Oxygen cation electron dissociative recombination rate coefficient measurement during expanding oxygen flow in nozzle
12 p2276 A70-27802
- Convergent-divergent nozzle operation at low pressure ratios causing separation of internal flow, discussing stability and flow field
12 p2157 A70-28084
- Free flow field from underexpanded rocket motor nozzle and impingement effects of pressure and heat transfer to flat plate [AIAA PAPER 69-568]
13 p2473 A70-28510
- Numerical method of characteristics for three dimensional supersonic nozzle flow field calculations
13 p2338 A70-28512
- Apparent mass measurements of supersonic jet in incalculable flow regimes, determining dependence on Mach number at nozzle and on distance from exit
13 p2387 A70-28859
- Inviscid thermally nonconducting gas unsteady and steady motions in Laval nozzle of known geometry, obtaining solutions for subsonic, transonic and supersonic regions
13 p2391 A70-29756
- Carbon dioxide jet plumes condensation on model nozzle in vacuum chamber, noting particle size and growth rate
13 p2523 A70-29983
- Liquid metallic particles fragmentation in two phase flow injected into vacuum, noting atomization enhancement by sodium nitrate
13 p2391 A70-29994
- Pseudo one dimensional dissociational nonequilibrium nozzle flows, obtaining equilibrium and nonequilibrium solution through similar transformation of governing equations
14 p2527 A70-30264
- Flow disturbances and side forces in supersonic rocket nozzle due to gaseous secondary injection analyzed by semiempirical models
14 p2629 A70-30756
- Superradiant pulsed 5401 A neon laser for interferograms of gas flow through nozzles in shock tunnel
15 p2750 A70-31763
- Gas-particle efflux from nozzle at critical velocities, noting particle size and concentration effects on inlet pressure
15 p2721 A70-32136
- Steady state one dimensional nozzle flow of reacting inviscid gas mixtures, giving numerical solution procedure for hydrogen-oxygen reactions
15 p2694 A70-32269
- Stationary hydrodynamic equations of gas channel and nozzle flow with inlet tangential discontinuities
16 p2833 A70-33247
- Exhaust nozzle model tests at high subsonic Mach numbers, investigating differences in nozzle drag in contrast to engine conditions
16 p2967 A70-33573
- Flow and diffusion phenomena in rarefied gas mixtures associated with separation nozzle process, using molecular pressure probe and mass spectrometer
16 p2893 A70-33699
- Operation modes of nozzles with emerging pointed and central bodies, discussing external flow effects on internal performance
16 p2970 A70-33760
- Thin wire Langmuir probe measurements of electron temperature and density in transition and free molecular nozzle flow of short duration reflected shock tunnel
16 p2912 A70-33864
- Inviscid air nonequilibrium shock layer properties correlation based on plenum entropy, predicting composition of downstream converging-diverging nozzle expanding air flow [AIAA PAPER 70-866]
16 p2838 A70-33909
- ATS-C satellite rocket exhaust plume convective heating measurements of VHF whip antennas, discussing nozzle flow and heating rate [AIAA PAPER 70-843]
16 p3000 A70-33926
- Nonequilibrium combustion products and condensables containing reactive multiphase rocket nozzle flows and exhaust plumes characterization using generalized kinetics streamtube program [MGKS/ [AIAA PAPER 70-845]
16 p3001 A70-33928
- Boundary layer formation on walls of conical pressure nozzle during vortex flow
16 p2896 A70-34299
- Rocket chambers combustion products isentropic expansion effects within nozzle on dissociation degree, assuming shifting and frozen equilibria
16 p2963 A70-34341
- Low Reynolds number flow inside Delaval nozzle, examining gas density and rotational temperatures by electron beam techniques
17 p3065 A70-34454
- Vibrational nonequilibrium nozzle flow problems, obtaining similar solutions for various initial conditions and nozzle geometries [AIAA PAPER 70-804]
17 p3065 A70-34459
- Convergent-divergent nozzle flow under influence of friction drag, determining heat transfer rate as function of nozzle geometry
17 p3194 A70-34694
- Optimum nozzle geometry for minimum heat transfer to convergent-divergent nozzle wall from high enthalpy flow
17 p3196 A70-35238
- Nonequilibrium nozzle flows involving molecular vibrational energy relaxation and composition changes from gas phase chemical reactions respectively
17 p3071 A70-35469
- Conical expansion nozzles manufacturing errors effect on flow expansion considered for large Mach numbers
17 p3011 A70-35662
- Real gas effects in blowdown analysis of leakage through choked nozzle in air flask
17 p3073 A70-35670
- Steam-water jet discharge heat transfer features, examining critical region parameters from nozzle into submerged space with large counterpressure
18 p3345 A70-36117
- Compressible flow of two component two phase mixtures through convergent nozzles and orifices, determining initially or annular dispersed flow patterns
18 p3239 A70-36231
- Gas particle mixtures nozzle flow at high loading ratios
18 p3208 A70-36693
- Method of characteristics for two dimensional steady supersonic gas flows with foreign particles in plane and axisymmetric nozzles
18 p3210 A70-37228
- Noise spectra of two dimensional jet flowing from nozzle ejector, using dispersion equation
19 p3354 A70-38662
- Rocket attitude stabilization using exhaust gas flow spinning plug nozzle as gyroscopic mass [AIAA PAPER 70-67]
20 p3715 A70-39562
- Convergent-divergent nonequilibrium nozzle flow numerical solution by time dependent technique, investigating rapid vibrational nonequilibrium supersonic expansion of gas mixture with population inversion
20 p3609 A70-39655
- Ion concentrations in premixed propane-air two dimensional laminar nozzle burner flames with seeding, discussing dependence on temperature and equivalence ratio
21 p3772 A70-40880
- Perfect gas irrotational isentropic nozzle flow by solving partial differential equations set
21 p3744 A70-41240
- Axisymmetric jet plasma flow in magnetic nozzle, measuring electric potential, electron temperature and ion density and velocity
21 p3856 A70-41380
- Heat transfer and friction effects on flow parameters in nozzle with independent cooling
21 p3951 A70-41769
- Viscous gas flow through Laval nozzle, calculating velocity coefficient and pressure recovery in contracting and expanding parts
21 p3746 A70-41774
- Inviscid thermally nonconducting gas unsteady and steady motions in Laval nozzle of known geometry, obtaining solutions for subsonic, transonic and supersonic regions
21 p3811 A70-42074
- Two layer gas flows in supersonic axisymmetric nozzles, using method of characteristics
21 p3748 A70-42210
- Acoustic waves generation from decay region of pulsating supersonic jet expelled from nozzle
21 p3748 A70-42211
- Stagnation temperature of two phase nozzle gas jet containing solid particles on particle density and velocity
21 p3748 A70-42220
- LF acoustic disturbances effect on root portion of turbulent jet from conical nozzle
21 p3954 A70-42223
- Equilibrium sonic velocity in reacting gas mixture in nozzle flow for unlimited species and independent chemical reactions
22 p4074 A70-42753
- Nonequilibrium gasdynamic and thermodynamic properties of chemically reacting gas mixtures in high expansion subsonic and supersonic nozzles for selected rocket propellants
22 p3982 A70-42761
- Computerized nonequilibrium thermochemical gas dynamic solutions for nozzle, shock tube and stream tube flow with arbitrary species and kinetic reactions numbers
22 p3982 A70-42762
- Cavitation characteristics of jet nozzles, formulating relationship between pressure differential and fluid flow rate
22 p3965 A70-43369
- Wave drag due to swirling flow through convergent-divergent nozzle, deriving approximate solution for specified nozzle shape at various swirl ratios
23 p4179 A70-43971

NOZZLE GEOMETRY

- Monograph on aircraft aerodynamic nozzle asymmetry effects for pressure drag reduction in critical conditions
03 p0465 A70-13003
- Annular nozzle shapes established via method of straight line characteristics, noting flow patterns at various regions
03 p0409 A70-13872
- Ablative throat nozzle performance, plotting change in thrust, exit pressure and Mach number as function of ablated to initial area ratio
03 p0410 A70-14336
- Discrete components in noise spectrum of heated and unheated supersonic air jets, using axisymmetric and conical nozzles
04 p0618 A70-15247

Exit geometry effects on peripheral jet device lift, considering operating height, curtain thickness, base extension, etc

04 p0619 A70-15388

Free plane turbulent jet virtual origin using tests determining influence of upstream conditions and nozzle shape

04 p0674 A70-15554

Air inlet and exhaust nozzle form and location effect in afterburning turbofan engines, discussing stalling, afterburner blowouts and thrust losses prevention

05 p0895 A70-15807

Aerobell extendible nozzle rocket engine design and performance, cold flow and simulated hot flow test results

[AIAA PAPER 69-4] 06 p1129 A70-17168

Vortex refrigerators characteristics, examining configurations with cylindrical and conical hot ends with and without diffuser

06 p0988 A70-17855

Liquid propellant rocket nozzle configurations maximum stress and stability limits using computer program for composite ring-stiffened shells of revolution

[AIAA PAPER 70-138] 06 p1014 A70-18053

Circular nozzle contraction and Reynolds number effects on turbulent pulsation damping, measuring longitudinal and transverse components

07 p1259 A70-19830

Supersonic molecular beam source operation, discussing dominant degradation factors and nozzle beam generation intensities and energies improvement

07 p1341 A70-20104

Condensation start dependence on air humidity at inlet and nozzle geometry applied to supersonic wind tunnel using undried atmospheric air

09 p1606 A70-23614

Three dimensional supersonic nozzle geometry optimization using Lagrange multipliers and iteration for solving variational problem

10 p1798 A70-24115

Nozzle fuel and air system geometrical parameters to determine mean diameter of fuel droplets, dispersion angle and spectrum and flame jet shape

10 p1930 A70-24295

Interior ballistics for wide temperature throttling of solid propellant rockets by variable-throat-area nozzle, noting composition effect screening

11 p2103 A70-26154

Base pressure effects on cone angle of fixed length conical nozzle yielding maximum thrust

11 p1977 A70-26156

Rao optimization method for thrust nozzles at given length, analyzing control surface flow field conditions

12 p2158 A70-28202

Supersonic jet spoilers flow fields with various nozzle shapes to determine secondary jets penetration depth and mixing in wake

13 p2338 A70-28480

Configurations stress stability liquid propellant rocket nozzle analysis by BOSOR 3 digital program, describing mathematical model construction

13 p2508 A70-28509

Turbulent base flowfields in multinozzle configurations, considering adiabatic flow and determining base pressure distribution from reverse jet impingement

[AIAA PAPER 69-570] 13 p2538 A70-28511

Forward inclined two dimensional circular arc slot nozzle jet flaps at hypersonic speeds, considering amplification and interaction processes

13 p2340 A70-29018

Auxiliary inlet ejector and plug nozzle flight performance, describing design variation effects for high supersonic speeds

[AIAA PAPER 70-701] 16 p2841 A70-33563

Operation modes of nozzles with emerging pointed and central bodies, discussing external flow effects on internal performance

16 p2970 A70-33760

Convergent-divergent nozzle flow under influence of friction drag, determining heat transfer rate as function of nozzle geometry

17 p3194 A70-34694

Optimum nozzle geometry for minimum heat transfer to convergent-divergent nozzle wall from high enthalpy flow

17 p3196 A70-35238

Constant chamber pressure thrust throttling of expansion-deflection rocket nozzle, calculating wall static pressure and thrust by characteristic method, discussing performance

[AIAA PAPER 69-435] 17 p3149 A70-35655

Nozzle geometry effects on turbine gas ejector characteristics

21 p3867 A70-41765

Plasma arc welding torches nozzle dimensions and shape dependence on thermal and electrical characteristics, optimizing energy output

22 p4042 A70-42378

Starting shock and contact surface measurement reflection nozzle, using HF spark camera and interference techniques

[SMPT PREPRINT 89] 22 p3959 A70-43064

Radial flow microturbines deflection and wave losses in circular nozzle ring oblique exit section

22 p3965 A70-43359

Nonuniform flow parameters for maximum thrust in nozzle, discussing specific impulse determination

22 p3960 A70-43366

Variable geometry radial inflow turbine performance estimation based on one dimensional flow theory

22 p3960 A70-43738

Two stream ejector type propelling nozzles for supersonic aircraft, investigating various configuration effects over range of secondary/primary air flow ratios

[ICAS PAPER 70-48] 23 p4133 A70-44145

Contoured nozzle shock tunnel condensation point, determining flow supercooling over specified pressure range

23 p4182 A70-44588

Radial inflow turbine optimum design geometry, calculating nozzle and rotor geometrical parameters efficiency

24 p4395 A70-46012

NOZZLE INSERTS

Low cost fabrication for solid rocket nozzles using carbon or graphite reinforcements in throat inserts

[SAE PAPER 700796] 24 p4349 A70-45897

NOZZLE THRUST COEFFICIENTS

Installed thrust vector for scarfed attitude control nozzles flush mounted with spacecraft cylindrical surface, predicting pressure distributions for internal thrust

06 p1154 A70-17167

Transonic flow in convergent and convergent-divergent conical nozzles with nonuniform inlet predicted by time dependent flow equations, discussing discharge and thrust coefficients

[AIAA PAPER 70-635] 16 p2834 A70-33548

Turbofan engine gross thrust dependence on nozzle pressure ratio and simulated flight Mach number, considering altitude chamber test data

[AIAA PAPER 70-612] 16 p2969 A70-33608

NOZZLE WALLS

Graphite rocket engine nozzles chemical erosion at various temperatures, comparing reaction and diffusion rates

03 p0516 A70-13619

Boundary layer formation on walls of conical pressure nozzle during vortex flow

16 p2896 A70-34299

Nozzle wall hypersonic turbulent boundary layers at free stream Mach number using pitot, hot wire, and wall fluctuation and static pressure measurements

[AIAA PAPER 70-746] 17 p3065 A70-34497

Real gas transonic flow transition through critical velocity in Laval nozzle, examining reasons for increment of viscosity and heat conduction effects

18 p3239 A70-36217

Jet flow reattachment to walls of various shapes, measuring undeveloped velocity profiles at nozzle exit

[ASME PAPER 70-FLCS-2] 22 p4008 A70-42429

NOZZLES

NT ANNULAR NOZZLES

NT CONICAL NOZZLES

NT CONVERGENT NOZZLES

NT CONVERGENT-DIVERGENT NOZZLES

NT DIVERGENT NOZZLES

NT DUAL THRUST NOZZLES

NT EXHAUST NOZZLES

NT HYPERSONIC NOZZLES

NT INLET NOZZLES

NT PLUG NOZZLES

NT ROCKET NOZZLES

NT SONIC NOZZLES

NT SUPERSONIC NOZZLES

NT TRANSONIC NOZZLES

NT TURBINE EXHAUST NOZZLES

NT WIND TUNNEL NOZZLES

NRX REACTORS

NERVA nuclear rocket reactors, considering NRX and XE technology tests

22 p4069 A70-43178

NRX-A REACTOR

U NRX REACTORS

U NUCLEAR ENGINE FOR ROCKET VEHICLES

NUCLEAR AUXILIARY POWER UNITS

NT SNAP

NT SNAP 8

NT SNAP 19

NT SNAP 27

NT SPACE POWER UNIT REACTORS

Guidebook on application of space nuclear power systems covering radioisotope and reactor systems, static and dynamic systems, power system suppliers and users, etc

01 p0140 A70-10942

Weights, sizes and costs of nuclear and nonnuclear spacecraft power systems with reference to mission duration

11 p2082 A70-26260

NUCLEAR BINDING ENERGY

Symmetry energy of infinite nuclear matter calculated for cases of constant density and minimum saturation energy by density variation, considering finite compressibility effects

01 p0148 A70-11105

Nonequilibrium and equilibrium schemes studies of nuclear symmetry energy of finite nuclei, discussing binding energy of nuclei with neutron excess

01 p0148 A70-11106

Thermal fluctuations effect on Josephson tunnel contact binding energy and external magnetic field dependence

24 p4388 A70-45203

NUCLEAR CAPTURE

NT ELECTRON CAPTURE

NUCLEAR CHEMISTRY

Reagent translational energy effect on dynamics of ionic and atomic reactions, using nuclear recoil and chemical accelerator methods

11 p1995 A70-26005

NUCLEAR ELECTRIC POWER GENERATION

NT NUCLEAR AUXILIARY POWER UNITS

NT NUCLEAR ENERGY

NT NUCLEAR POWER PLANTS

NT NUCLEAR POWER REACTORS

NT SNAP

NT SNAP 8

NT SNAP 19

NT SNAP 27

NT SPACE POWER UNIT REACTORS

Rankine cycle technology concerning high temperature, refractory alloy and liquid metal experience, showing applicability to nuclear Brayton and thermionic power systems

02 p0229 A70-12513

Nuclear converter with porous metal adsorption reservoir working with or without liquid cesium

10 p1915 A70-25039

Rankine 10 MWe nuclear electric space power system design, discussing reactor power, fuel, coolant, structural material, control system, shield, etc

11 p2082 A70-26123

Brayton, Hg, organic-Rankine and potassium-Rankine dynamic space power systems for use with nuclear energy sources

13 p2450 A70-29492

Spacecraft electric power supplied by isotope nuclear sources, discussing heat sources, energy converters and heat rejection systems

14 p2616 A70-31147

Nuclear space power three stage potassium turbine erosion testing in stainless steel loop with various contamination levels

21 p3756 A70-41005

Aerospace nuclear applications - Conference, Huntsville, Alabama, April 1970

22 p4069 A70-43177

Brayton, Hg, organic-Rankine and potassium-Rankine dynamic space power systems for use with nuclear energy sources

22 p4071 A70-43189

Space nuclear power system design and operation related to safety, discussing SNAP flights

22 p4071 A70-43192

NUCLEAR ELECTRIC PROPULSION

Performance boundaries of space propulsion systems containing nuclear electric stages

[AIAA PAPER 69-249] 01 p0196 A70-10839

Unmanned nuclear electric propelled spacecraft using reactor with liquid metal MHD power conversion system

20 p3566 A70-40016

NUCLEAR EMULSIONS

Cosmic ray electron spectrum above 200 Gev based on pure nuclear emulsion stack using horizontal sandwich assembly

06 p1135 A70-17473

Primary cosmic ray electron flux above 30 GeV, using nuclear emulsion plate chamber

19 p3504 A70-38110

Carbon isotopic composition in primary cosmic radiation by nuclear emulsions exposure in balloon flights

19 p3507 A70-38129

Upper limit to primary deuteron flux and path length in space, using emulsion stack exposed near geomagnetic equator during minimum solar activity

22 p4093 A70-42673

Electronographic camera for ultrahigh speed photography, using nuclear emulsion as recording medium

[SMPT PREPRINT 54] 22 p4033 A70-43039

Cosmic ray jet studies, evaluating nuclear emulsion technique

22 p4096 A70-43399

NUCLEAR ENERGY

Solar, nuclear, chemical and thermal energy sources for short and long duration exploration on moon

14 p2634 A70-30195

NUCLEAR ENERGY LABORATORIES

U LABORATORIES

U NUCLEAR RESEARCH

NUCLEAR ENGINE FOR ROCKET VEHICLES

- Air backflow in nuclear exhaust system duct for ground testing of NERVA engines, noting overpressure effect
[AIAA PAPER 69-325] 06 p1027 A70-17174
- NERVA nuclear rocket engine design for Saturn 5 third stage, comparing nuclear and chemical engines performance
12 p2270 A70-26871
- Nerva nuclear subsystem diagnostics and control instrumentation, discussing transducers
[AIAA PAPER 70-659] 16 p2949 A70-33551
- NERVA rocket engine program reliability, design, performance and managerial approaches
[AIAA PAPER 70-711] 16 p2950 A70-33568
- Vapor fraction dependence on liquid hydrogen propellant outflow during NERVA operation under stored gas or autogenous pressurization, using computer simulation
[AIAA PAPER 70-677] 16 p2950 A70-33578
- NERVA engine chamber pressure control, investigating replacement of TPCV with fluidic vortex valve
[AIAA PAPER 70-658] 16 p2970 A70-33620
- NERVA XE-Prime test series, discussing computer simulation, full power and high specific impulse operation and startup under varying initial conditions
[AIAA PAPER 70-709] 16 p2951 A70-33950
- NERVA flight engine operating characteristics and reliability requirements for missions, noting conditioning, startup shutdown, reactor cooldown, fuel consumption, etc
[AIAA PAPER 70-676] 16 p2951 A70-33951
- Multiorbit injection earth departure technique for optimal thrust-weight ratio in manned interplanetary missions using NERVA engine
[AAS PAPER 70-039] 17 p3175 A70-34780
- NERVA engine operational cycle and performance, discussing startup, thrust buildup and shutdown
17 p3135 A70-35653
- Post Apollo space research, discussing Saturn Workshop/Skylab, Nerva nuclear rocket engine and international cooperation
21 p3956 A70-41496
- NERVA nuclear rocket reactors, considering NRX and XE technology tests
22 p4069 A70-43178
- Mathematical model avoiding repetitive tests costs for Nerva nuclear rocket engine
22 p4070 A70-43179
- NERVA nuclear rocket engine design technology program, discussing probabilistic techniques for reliability engineering
[SAE PAPER 700801] 24 p4377 A70-45910
- NERVA reactor technology applied to closed Brayton cycle MHD power system
[AIAA PAPER 70-1225] 24 p4377 A70-45956
- ## NUCLEAR EXPLOSION EFFECT
- Shock and thermal metamorphism of olivine trachybasalt by nuclear explosion at Nevada test site
05 p0843 A70-16946
- Redistribution of geomagnetically trapped 55 Mev protons by Starfish nuclear explosion, discussing hydromagnetic wave interactions and multiple reflections from magnetic field inhomogeneity
06 p1137 A70-18531
- Nuclear environments determination methodology for ground military equipment hardening, considering personnel and equipment responses to detonation in atmosphere
12 p2271 A70-27097
- Electromagnetic pulse generator for simulation of EMP associated with nuclear explosions, describing electronic equipment vulnerability testing
12 p2208 A70-28135
- Artificial aurora generated by Starfish in northern conjugate region and afterglow spectra
14 p2578 A70-31245
- Solar constant measurements by high altitude balloon sounding, noting anomalous turbidity in upper atmospheric layers due to nuclear explosions and volcanic eruptions
20 p3703 A70-39375
- Quasi-periodic ionospheric oscillations associated with nuclear explosions, thunderstorms and quiet conditions
21 p3814 A70-40938
- Artificial injection of trapped electrons into geomagnetic field by low altitude nuclear explosions, examining electron flux and energy
21 p3816 A70-41086
- ## NUCLEAR EXPLOSIONS
- ### NT THERMONUCLEAR EXPLOSIONS
- Backscattering from rough surface of nuclear fireball measured by two way directive radar antenna on reentry vehicle
09 p1634 A70-22703
- Silicon monolithic integrated circuits technology for radiation environment near nuclear detonation
09 p1647 A70-23076
- Hydrodynamic energy flow down horizontal tunnel from nuclear explosive detonated underground, recording shock front luminosity and time of arrival
10 p1857 A70-23985

- Fireball role in N-N interactions at primary cosmic ray energies, using fireball model to explain particle production
13 p2476 A70-28913
- ## NUCLEAR FISSION
- Tektites age from fission track method, discussing elimination technique for strain caused spurious tracks
13 p2488 A70-28721
- Fission track uranium distribution studies of Apollo 11 lunar volcanic rocks, using Lexan plastic print method
21 p3900 A70-41537
- ## NUCLEAR FORCES
- ### U NUCLEAR BINDING ENERGY
- ### NUCLEAR FUEL ELEMENTS
- Thermal mapping vacuum chamber tests of nuclear fuel capsules for lunar surface experiments, using remote IR radiometric microscope
15 p2718 A70-32800
- Thermionic reactor program for electric propulsion, considering internally fueled flashlight concept
[AIAA PAPER 70-1108] 20 p3568 A70-40235
- ## NUCLEAR FUELS
- Precision machining and repair of radioactive Plum Brook Reactor core fuel grid
01 p0140 A70-10322
- Dimensional measurements of nuclear fuel cylindrical specimens by scanning neutron radiographic negative with microdensitometer, taking into account specimen geometry and neutron cross section
15 p2735 A70-31769
- Ground test reactor design based on colloid fueled reactor concept
[AIAA PAPER 70-688] 16 p2950 A70-33587
- Turbulent coaxial flow analysis predicting fuel volume fraction in gas core nuclear rocket reactor cavity, using free-jet computer code and eddy viscosity equation
18 p3290 A70-36560
- Optimum fuel utilization for Plum Brook Reactor, using criticality data for effects of neutron leakage and burnup uniformity in core point model
20 p3671 A70-39110
- Aeromechanical characteristics of colloidal fuel core nuclear reactor in relation to cavity geometry and propellant gas injection
[AIAA PAPER 70-1222] 24 p4377 A70-45958
- ## NUCLEAR FUSION
- ### NT CONTROLLED FUSION
- Three mode galactic age model for nucleosynthesis of solar radioisotopic material produced by r-processes
01 p0182 A70-10720
- Steady state deuterium-tritium fusion reactor approximate parameters prediction possibility based on interim assumptions of plasma confinement, model, etc
02 p0349 A70-12755
- Nuclear fusion reactions by focused Q switched Nd doped laser beam on deuterium target, discussing neutrons from flowing plasma, electron temperature and counter experiments
03 p0501 A70-13684
- Fusion reactions generation by high power laser beams focused on solid deuterium target
05 p0857 A70-15992
- He to carbon fusion reaction rate enhancement in dense matter by inelastic scattering processes, discussing C 12 deexcitation to ground state
05 p0885 A70-16934
- Soviet collection of papers on magnetic traps covering chamber walls effect on plasma heating, plasma in mirror trap and self sustained fusions
07 p1350 A70-19844
- Emission containment and working temperature reduction possibility in thermonuclear reactor by increasing plasma densities and introducing large atomic number contaminants
07 p1350 A70-19847
- Self sustained fusion reaction in dense deuterium-tritium plasma, considering large atomic number contaminants optimal concentration calculations
07 p1351 A70-19848
- Iron peak nuclei synthesis by charged particles under supernova mechanism conditions predicted by hydrodynamic conditions
09 p1749 A70-21994
- Preplanetary matter irradiation by solar particles, noting isotopic abundances for evidence of nucleosynthesis induced by proton and alpha bombardment
13 p2486 A70-28619
- Galactic cosmic ray actions on interstellar medium for origin of Li, Be and boron in stellar atmospheres and solar system
14 p2640 A70-30786
- O-Of stellar evolution yielding Wolf-Rayet type, considering spectral evidence and H-He interaction
15 p2800 A70-32202
- Galactic composition differences, considering stellar and galactic nucleosynthesis
16 p2976 A70-33791
- Nucleosynthesis in supernova models based on neutrino energy transport
17 p3153 A70-34529

- Laser applications in thermonuclear fusion, analyzing plasma acceleration under laser pulse action
18 p3265 A70-36110
- Heavy cosmic ray abundance attributed to thermal nucleosynthesis during silicon burning at high temperature and density
19 p3507 A70-38132
- Nuclear fusion realization by focusing from intense beam neodymium glass laser
19 p3447 A70-38167
- Laser beam and matter interaction models for positive energy balance in nuclear fusion, obtaining Lawson criterion
19 p3447 A70-38168
- Explosive nucleosynthesis as heavy nuclei source for stars
20 p3712 A70-40426
- Nuclear fusion reactor spacecraft propulsion system using ion rocket with charged deuterium nuclei fuel, emphasizing nuclear plasma confinement problem
21 p3867 A70-41498
- Stellar surface and solar system light element abundances, explaining formation by energetic proton flux nucleosynthetic effect
24 p4398 A70-46163
- Atmospheric composition of cool stars in relation to nucleosynthesis and galactic evolution
24 p4414 A70-46227
- ## NUCLEAR GYROSCOPES
- Unconventional gyros, discussing nuclear magnetic resonance, induction, cryogenic, electrostatic and laser technology
03 p0481 A70-12960
- Quantum gyroscopic theory for instrument design
16 p2927 A70-33229
- ## NUCLEAR INTERACTIONS
- ### NT ELECTRON CAPTURE
- ### NT SPIN-ORBIT INTERACTIONS
- Angular distribution of muon poor extensive air showers flatter than normal showers, discussing initiation by passive particles produced by cosmic ray atmospheric nuclei
02 p0357 A70-12079
- Cosmic ray nuclear interactions under paraffin and lead, using counter controlled multilayer cloud chamber
03 p0553 A70-12877
- Cosmic ray particles inelastic nuclear interactions mean free path in iron measured in Wilson chamber and ionization calorimeter
03 p0554 A70-13030
- Interacting meson systems effective masses with/without secondary proton measured, detecting heavy boson resonances and fireballs, considering proton nuclear interactions
03 p0472 A70-13031
- Pion and nucleon interactions with atomic nuclei at 200 Gev using Wilson chamber and ionization calorimeter, determining pion collisions characteristics
03 p0555 A70-13034
- High energy muon production and interaction, analyzing ionization burst spectra
03 p0555 A70-13037
- Light-gathering amplitude and intrinsic resolution of large-area flat scintillation detectors used for cosmic rays-nuclear interaction experiments at high energies
03 p0484 A70-13466
- Pionic transition in Ni isotopes to measure nuclear interaction effects, observing level shift and broadening
05 p0885 A70-16682
- Neutron and proton distributions rms radii in nuclei by optical model analysis of low energy pion-nucleus interactions
07 p1337 A70-19360
- Neutron formation multiplicity during capture of cosmic ray muons by Zn and Sb nuclei, noting agreement with one-third law
08 p1560 A70-20718
- Cross sections measured for symmetric p, 2p/ reactions on deuterium and He, discussing nonsymmetric p, 2p/ events in He
08 p1548 A70-21233
- Equation of state for cold matter at neutron star densities, deriving equilibrium equations for nuclear interactions among hadrons
09 p1764 A70-23606
- Neutron star models based on equation of state for cold degenerate matter, taking into account nuclear forces and clustering
09 p1764 A70-23607
- Cosmic radiation low energy positrons flux estimation compared with calculation from solar modulation models
10 p1932 A70-24537
- Rare earth energy band structure effect on RKKY magnetic interaction between atomic spins
13 p2472 A70-29799
- Th 232 and U 238 pionic X ray energies and widths, suggesting anomalous effect for interaction between high-Z nuclei and pion
15 p2776 A70-31738

Electrons lateral distribution in large air showers determining inelasticity of high energy nuclear interactions

18 p3305 A70-35947
Nuclear-electromagnetic cascades longitudinal development in glass, Fe and W absorbers, presenting Monte Carlo simulation

18 p3293 A70-36895
Galactic cosmic rays lifetime based on nuclei and matter interactions, discussing ionization losses effect

20 p3695 A70-38965
Muonic atoms nuclear excitation in Zn 66 and 68

20 p3674 A70-39221

NUCLEAR ISOBARS

Pion production characteristics during high energy nucleons interactions from data on production in upper atmosphere by gamma-quanta families /isobaric production/

03 p0555 A70-13032

NUCLEAR MAGNETIC RESONANCE

NT PROTON MAGNETIC RESONANCE

NT PROTON RESONANCE

Transient magnetic resonance technique for non-destructive testing of elements with nuclei having magnetic moment, considering cereal grains, propellants, metal powder and plastics

01 p0097 A70-10014

Sq data acquisition and analysis, noting automatic standard observatories using nuclear magnetometers and ionospheric current information from instrumented rockets

01 p0075 A70-10597

Flowmeter errors caused by nuclear magnetic relaxation decreased with increasing magnetic field strength of NMR sensor

01 p0091 A70-10981

Nutational NMR nonuniform magnetic field stabilizer for beta spectrometer, structural details and circuit schematic

03 p0485 A70-13467

Te nuclear magnetic resonance in amorphous semiconducting sample cycled between conducting and nonconducting states

08 p1557 A70-21697

Spin-lattice NMR and EPR relaxation time measurements, using train signals and free induction decays

09 p1679 A70-22995

Helium melting pressure curve to calibrate cerium magnesium nitrate or NMR low temperature thermometers

09 p1728 A70-22999

Shift in nuclear paramagnetic resonance frequency of ligand nuclei in ferromagnets above Neel temperature

10 p1928 A70-24826

Shift in nuclear magnetic resonance, investigating transferred hyperfine coupling near Neel temperature for magnetic and nonmagnetic systems

10 p1928 A70-24827

Precise sweep calibrations and simultaneous spectrum recording for high resolution nuclear magnetic resonance spectroscopy

11 p2052 A70-26375

High sensitivity magnetometers based on magnetic nuclear resonance with electronic pumping

13 p2414 A70-30039

Nuclear magnetic resonance magnetometers performance using dynamic polarization by electronic pumping

13 p2414 A70-30040

Microwave oscillator by transposing principle of spin oscillator at low frequencies in nuclear magnetic resonance in X band

16 p2877 A70-33413

Frequency locking and control of autodyne oscillating NMR detector for signal averaging

21 p3827 A70-41454

Drift reducing NMR stabilization of Hall regulated electromagnet, applying error signal to bias coil

21 p3827 A70-41456

NMR spin-spin coupling constants between vinyl protons in cyclopentadiene, 1,3-cyclohexadiene and 1,3-cyclooctadiene from spectrum analysis

21 p3780 A70-41704

Chondritic meteorites electron and nuclear magnetic resonance spectra at various frequencies

23 p4239 A70-43897

Al-27 NMR saturation effects on ruby electron cross relaxation and inversion

23 p4230 A70-43932

NUCLEAR METEOROLOGY

Induced nuclear processes role in radiogenic Ne-21 production in earth atmosphere

12 p2227 A70-28367

NUCLEAR PARTICLES

NT ALPHA PARTICLES

NT ANTINEUTRINOS

NT ANTIPARTICLES

NT BETA PARTICLES

NT BOSONS

NT HYPERONS

NT MESON RESONANCES

NT MESONS

NT NUCLEONS

NT PHOTONS

NT PIONS

NT POSITRONS

Cosmic ray protons, He nuclei and electrons solar modulation by betatron deceleration mechanism during interplanetary space passage

02 p0357 A70-12123

Fossil nuclear particle tracks in extraterrestrial matter using high voltage electron microscope and chemical etching

19 p3519 A70-38031

Rigidity spectra of primary cosmic ray nuclei groups from satellite-borne Cerenkov spectrometer

19 p3508 A70-38135

Nuclear particle tracks in Apollo 11 samples due to galactic cosmic rays and solar flares relationship to dynamic surface processes

21 p3914 A70-41648

NUCLEAR PHYSICS

NT BOHR THEORY

NT FIELD THEORY (PHYSICS)

NT PLASMA PHYSICS

NT QUANTUM THEORY

Symmetry energy of infinite nuclear matter calculated for cases of constant density and minimum saturation energy by density variation, considering finite compressibility effects

01 p0148 A70-11105

Instrumentation system for nuclear experiments on scientific satellites allowing highest priority event selection during telemetry sequence and periodic change of priority order

03 p0453 A70-13024

Matrix elements systematic calculation method in terms of inelastic transition densities to evaluate nuclear properties

04 p0723 A70-15634

Book on nuclear and astrophysical aspects of cosmic rays covering kinematics in collisions and decays, cascade theory, high energy interactions, origin, etc

07 p1368 A70-19666

Nuclear science and nuclear power systems engineering - IEEE Conference, San Francisco, October 1969

12 p2232 A70-27401

Cryogenics and nuclear physics, discussing particle beam handling magnets, superconducting accelerators, detectors, moderators, low temperature irradiation facilities, etc

14 p2616 A70-31014

NUCLEAR POWER

U NUCLEAR ENERGY

U NUCLEAR POWER GENERATION

U NUCLEAR ELECTRIC POWER GENERATION

U NUCLEAR POWER PLANTS

Aircraft impact against nuclear containment vessel and associated structures for dangers in vessel-nuclear power station collisions

11 p2144 A70-26683

Nuclear science and nuclear power systems engineering - IEEE Conference, San Francisco, October 1969

12 p2232 A70-27401

Cold working effects on Zircaloy tubes mechanical properties and hydride orientation, discussing tubes use in nuclear power stations

17 p3123 A70-34645

NUCLEAR POWER REACTORS

NT SNAP 8

NT SPACE POWER UNIT REACTORS

Nuclear power systems for manned orbiting space stations, noting Brayton aggregate and NASA objectives

13 p2450 A70-29493

Ground test reactor design based on colloid fueled reactor concept

[AIAA PAPER 70-688]

16 p2950 A70-33587

Nuclear power systems for manned orbiting space stations, noting Brayton aggregate and NASA objectives

22 p4071 A70-43193

NERVA Technology Reactor design integrated with Brayton cycle space power conversion systems, considering space bases and shielding analysis

[AIAA PAPER 70-1226]

24 p4377 A70-45955

NUCLEAR PROPELLED AIRCRAFT

Nuclear propulsion systems types, discussing relative capabilities and future roles in aerospace applications

11 p2082 A70-26055

Heat pipes in nuclear aircraft propulsion system, describing core, heat exchangers, and reactor to jet engine heat transport system

[AIAA PAPER 70-662]

16 p2950 A70-33623

High temperature liquid metal cooled nuclear reactor for military aircraft with long flight endurance and range

22 p4071 A70-43188

NUCLEAR PROPULSION

NT NUCLEAR ELECTRIC PROPULSION

Shield mass optimization of low thrust nuclear powered space vehicle for occupant shielding against reactor radiation

03 p0523 A70-13575

Ar plasma interaction with concentric cool hydrogen sheath for simulation study for gaseous core nuclear space propulsion system

03 p0536 A70-14375

Nuclear and electric propulsion systems performance, considering applications in future European space activities

05 p0897 A70-16898

Rankine cycle two loop Li boiling Ka facility for nuclear turbopump simulation, studying alkali metal corrosion for operation with and without hot traps

[AIME PAPER F-69-1]

07 p3104 A70-18809

Nuclear propulsion requirements for manned landing mission to Mars assuming Saturn 5-based operation

07 p1375 A70-18874

Book on spaceflight propulsion covering jet thrust, energy release, chemical, nuclear and electric propulsion, transportable and environmental systems

09 p1742 A70-22202

NASA future space programs, discussing space shuttle and station, nuclear propulsion, manned Mars landing, unmanned Venus-Mercury probes, etc

09 p1762 A70-23065

Algorithm for propellant flow rate increase of nuclear rocket in minimum time without exceeding maximum allowable stress in reactor core

10 p1914 A70-24870

Technological feasibility, economical and operational compatibility of subsonic aircraft nuclear propulsion /ANP/ compared with conventional propulsion systems

11 p2081 A70-26050

Interstellar transport vehicles design around thermodynamic propulsion plants, discussing weight, mission velocity, acceleration time and fuel costs

11 p2123 A70-26054

Nuclear propulsion systems types, discussing relative capabilities and future roles in aerospace applications

11 p2082 A70-26055

Nuclear pulse propulsion system for manned missions to outer planets of solar system, discussing energy and travel time requirements

11 p2082 A70-26059

Lunar and planetary exploration costs and technology, discussing role of nuclear propelled passenger vehicles

11 p2082 A70-26061

Rankine 10 MWe nuclear electric space power system design, discussing reactor power, fuel, coolant, structural material, control system, shield, etc

11 p2082 A70-26123

Optimal control of nuclear propulsion and energetic plants of space vehicle, considering thermionic generator

13 p2450 A70-28436

High temperature energy systems with plasma reactors and inductive MPD converters, discussing spacecraft propulsion and ground based pollution-free power generation

15 p2791 A70-32278

Reusable ferry spacecraft program, discussing space shuttles, cost reduction and nuclear propulsion for deep space missions

15 p2791 A70-32300

Fluid mechanics and engine dynamics and start-up experiments simulating thermal environment in nuclear light bulb engine

16 p2949 A70-33552

Nuclear orbital launch stages for interplanetary departure, comparing parallel and tandem spacecraft configurations

[AIAA PAPER 70-680]

16 p2950 A70-33580

Metal corrosion effects in Rankine cycle lithium-boiling potassium test loop simulating working fluids of spacecraft nuclear turbopump propulsion system

16 p2933 A70-34204

Reusable nuclear shuttle /RNS/ for space program providing low cost transportation beyond earth orbit

[AIAA PAPER 70-679]

17 p3174 A70-34512

Future manned planetary missions with reusable nuclear shuttles, comparing operating modes in terms of propellant requirement, costs, complexity, etc

[AAS PAPER 70-040]

17 p3155 A70-34781

Low thrust high impulse nuclear and electric space propulsion systems, discussing performance capabilities for space missions

18 p3290 A70-36566

Nuclear fusion reactor spacecraft propulsion system using ion rocket with charged deuterium nuclei fuel, emphasizing nuclear plasma confinement problem

21 p3867 A70-41498

Aerospace nuclear applications - Conference, Huntsville, Alabama, April 1970

22 p4069 A70-43177

Plasma accelerators for nuclear EM propulsion, considering power supply requirements and differences between plasma and ion engines

22 p4070 A70-43186

Nuclear electric space propulsion, emphasizing systems uncertainties and cost aspects

22 p4070 A70-43187

NUCLEAR RADIATION

NT BETA PARTICLES
NT FAST NEUTRONS
NT GAMMA RAY BEAMS
NT NEUTRON BEAMS
NT PHOTONEUTRONS
NT SPALLATION
NT THERMAL NEUTRONS

Radioactive nuclei alpha radiation investigation methods, discussing nuclear emulsions, scintillation spectrometry, ionization chambers, semiconductor counters and magnetic spectrographs

03 p0485 A70-13479
Nuclear environmental testing techniques, discussing radiation effects, measurements, instrumentation hardening, simulation source selection, dosimetry, noise sources and noise reduction, etc

03 p0523 A70-13540
Shield mass optimization of low thrust nuclear powered space vehicle for occupant shielding against reactor radiation

03 p0523 A70-13575
Nuclear and space radiation effects - IEEE Conference, Pennsylvania State University, July 1969

04 p0656 A70-14726
Gaging system utilizing nuclear radiation to obtain mass measurement of fuel quantity

05 p0880 A70-15832
[SAE PAPER 690673]
Elastic stress-strain states in spherical reservoir and thick walled tube during nuclear radiation induced phase transformations

10 p1894 A70-24513
Electropneumatic actuation systems for rocket engines in extreme environment applications involving high nuclear radiation levels and high and cryogenic temperatures

14 p2535 A70-31343
Calcium tungstate crystals, investigating electron paramagnetic resonance centers produced by neutrons and gamma rays to obtain information on lattice vacancies, defects, etc

16 p2961 A70-33963
Al single crystals hardening under low temperature reactor irradiation, emphasizing yield phenomenon associated with Luders bands

17 p3123 A70-34647
Nuclear irradiation effect on embrittlement of Ti and Ti alloys at cryogenic temperature, determining radiation damage threshold as function of tensile properties changes

18 p3278 A70-36567
Lead alloys as shielding materials in nuclear systems, discussing physical, chemical and metallurgical properties, fabrication and applications

19 p3469 A70-37833
Combined space and nuclear radiation effects in manned space flight

22 p3978 A70-43184

NUCLEAR REACTIONS

NT ALPHA DECAY
NT ANNIHILATION REACTIONS
NT CONTROLLED FUSION
NT ELECTRON CAPTURE
NT ELECTRON SCATTERING
NT HIGH ENERGY INTERACTIONS
NT NEUTRON EMISSION
NT NEUTRON SCATTERING
NT NUCLEAR FISSION
NT NUCLEAR FUSION
NT NUCLEAR INTERACTIONS
NT NUCLEAR SCATTERING
NT PROTON SCATTERING
NT PROTON-PROTON REACTIONS
NT RADIOACTIVE DECAY
NT RESONANCE SCATTERING
NT SPALLATION
NT SPIN-ORBIT INTERACTIONS
NT THERMONUCLEAR REACTIONS

Cross sections of fragments emitted in spallation reactions of carbon and nitrogen nuclei emulsion with alpha particles

09 p1733 A70-23549
Cepheid type variable stars nuclear reaction and opacity pulsation excitation mechanisms

10 p1940 A70-24409
Induced nuclear processes role in radiogenic Ne-21 production in earth atmosphere

12 p2227 A70-28367
Wave properties of nuclear optical model for barrier penetration by charged particles, considering square well reflection, absorption and resonance

14 p2619 A70-30491
Nuclear reactions and elementary particle reactions in Friedman universe with positive lepton abundance and degenerate electrons, discussing prestellar helium synthesis

14 p2620 A70-30877
Electron capture involving iron nuclei in contracting iron stars treated as endothermic nuclear reaction

22 p4104 A70-42992
Solid core nuclear reactor engine variables, considering specific impulse, engine weight, operating life and engine thrust

22 p4070 A70-43181

Radiography using photo-nuclear reaction emulsion to improve picture contrast by eliminating scattered photons in sample

24 p4337 A70-45716

NUCLEAR REACTOR CONTROL

Forced cooling water flow temporary loss accident at Plum Brook Reactor, discussing inspection and corrective action

01 p0140 A70-10323
Material evaluation and selection for compact nuclear reactor control bearings operating at high temperature in vacuum
[ASME PAPER 69-WA/LUB-11]

04 p0697 A70-14765
Bearings for nuclear reactor control components in space environment, discussing sliding friction, compatibility and prototype assemblies tests

16 p2923 A70-34162
SNAP reactor control system mechanisms development for operation in space environment

16 p2951 A70-34163

NUCLEAR REACTOR MATERIALS

U REACTOR MATERIALS

NUCLEAR REACTORS

NT GAS COOLED REACTORS
NT GASEOUS FISSION REACTORS
NT HEAVY WATER REACTORS
NT HIGH TEMPERATURE NUCLEAR REACTORS

NT LIQUID COOLED REACTORS

NT NUCLEAR POWER REACTORS

NT PLUM BROOK REACTOR

NT SNAP 8

NT SPACE POWER UNIT REACTORS

NT THERMAL REACTORS

Steady state deuterium-tritium fusion reactor approximate parameters prediction possibility based on inter assumptions of plasma confinement, model, etc

02 p0349 A70-12755
Nuclear reactor surface temperatures probability calculations allowing for some uncertainties and MTR type test reactor application

03 p0523 A70-12997
Thermionic diode development for nuclear reactor systems

04 p0717 A70-14900
[ASME PAPER 69-WA/ENER-5]
Structural materials mechanical properties tests during neutron bombardment, discussing atomic reactors optimal parameters calculation

04 p0775 A70-15259
Emission containment and working temperature reduction possibility in thermonuclear reactor by increasing plasma densities and introducing large atomic number contaminants

07 p1350 A70-19847
Hydrogen, oxygen and carbon dioxide in off-gas stream from nuclear reactor experiment using on-line gas chromatography

11 p1994 A70-25615
Controllable thermonuclear reactor with free- floating HF discharge plasma in deuterium

12 p2271 A70-27351
Thermionic diode development for nuclear reactor systems

15 p2773 A70-31959
[ASME PAPER 69-WA/ENER-5]
Nuclear rocket engine testing, monitoring reactor and facility performance with real time digital computer

17 p3135 A70-35212
Turbulent coaxial flow analysis predicting fuel volume fraction in gas core nuclear rocket reactor cavity, using free-jet computer code and eddy viscosity equation

18 p3290 A70-36560
Open cycle gas core nuclear rocket reactor, evaluating critical mass for U isotopes

18 p3290 A70-36564
Neutron flux measurement in nuclear reactors based on logarithmic techniques and digital approach, discussing temperature effects compensation

19 p3427 A70-37939
Unmanned nuclear electric propelled spacecraft using reactor with liquid metal MHD power conversion system

20 p3566 A70-40016
Liquid metal heat pipes in magnetic fields of controlled fusion reactors, considering geometry, compound wick structure and vapor flow

21 p3946 A70-41046
Nuclear light bulb and coaxial flow gaseous core nuclear rocket reactors based on energy transfer via thermal radiation

22 p4070 A70-43182
Controllable thermonuclear reactor with free- floating HF discharge plasma in deuterium

22 p4084 A70-43595
Aeromechanical characteristics of colloidal fuel core nuclear reactor in relation to cavity geometry and propellant gas injection

24 p4377 A70-45958
[AIAA PAPER 70-1222]

NUCLEAR RESEARCH

Nondestructive tests and controls in metallurgy and nuclear technology - Conference, Saclay, France, June 1968

22 p4040 A70-43617

NUCLEAR RESEARCH AND TEST REACTORS

NT HIGH TEMPERATURE NUCLEAR REACTORS

NT NRX REACTORS

NT PLUM BROOK REACTOR

NUCLEAR ROCKET ENGINES

Nuclear light bulb engine critical fuel mass and design changes effects

01 p0140 A70-10835
[AIAA PAPER 68-571]
Optimal control for thermionic nuclear reactor space power plant utilizing state variable feedback with limited input simplifying computation

03 p0461 A70-14342
Nuclear rocket engine core thermal and neutronic transient and steady state dynamics digital simulation, showing advantages over lump model analysis

04 p0717 A70-14757
[ASME PAPER 69-WA/NE-3]
Gas core nuclear reactors feasibility based on gas core hydrodynamics, heat transfer and neutronics development, noting spacecraft weight and trip time reduction potential

04 p0717 A70-15639
Flow characteristics of curved porous wall gas core reactors for nuclear rocket engines, visualizing simulated fuel flow with air-smoke combination

06 p1104 A70-17509
Noise field from ground testing of nuclear rocket engines operated at various reactor power levels

06 p1133 A70-18234
Constant flux gas core nuclear rocket acoustic instabilities, presenting idealized physical model with gas dynamic field perturbed by wave phenomena

09 p1725 A70-23227
Reusable earth-moon and deep space return transportation, assuming extraterrestrial nuclear rocket propellant source

14 p2653 A70-30766
Nuclear solid core rocket engine performance for interplanetary orbital launch of spacecraft by multi-orbit injection

14 p2616 A70-30767
[AIAA PAPER 69-535]
Nuclear light bulb reactor and coaxial flow reactor for gas core nuclear rocket engines

16 p2949 A70-33532
[AIAA PAPER 70-708]
Engine weight estimation for showing effect on thrust, specific impulse and uranium loss rate for open cycle gas fueled nuclear rocket engine

16 p2949 A70-33553
[AIAA PAPER 70-690]
Gas-core nuclear rocket engine simulation by induction coupled plasma torch, determining gas flow patterns

16 p2950 A70-33555
[AIAA PAPER 70-691]
Reusable nuclear shuttles (RNS) for interorbital and escape missions, discussing alternate stage configurations, radiation shielding, subsystem options, etc

16 p2950 A70-33579
[AIAA PAPER 70-678]
Nuclear rocket nozzle cooling passages, discussing heat transfer and friction correlations for single-phase hydrogen turbulent flow

16 p2950 A70-33622
[AIAA PAPER 70-661]
Nuclear rocket engine testing, monitoring reactor and facility performance with real time digital computer

17 p3135 A70-35212
Turbulent coaxial flow analysis predicting fuel volume fraction in gas core nuclear rocket reactor cavity, using free-jet computer code and eddy viscosity equation

18 p3290 A70-36560
Crew radiation dosage from fission fragments in plume from gas core nuclear rocket

18 p3224 A70-36562
Open cycle gas core nuclear rocket reactor, evaluating critical mass for U isotopes

18 p3290 A70-36564
Environmental surveillance associated with ground tests of nuclear rocket engine prototypes, determining statistical nature of radioactive effluent

19 p3470 A70-38013
Nuclear rocket engine fluidic chamber pressure control, discussing design concepts for static and dynamic subsystems

20 p3688 A70-39585
[AIAA PAPER 70-1010]
Noise field from ground testing of nuclear rocket engines operated at various reactor power levels

20 p3689 A70-39688
Thermionic reactor program for electric propulsion, considering internally fueled flashlight concept

20 p3568 A70-40235
[AIAA PAPER 70-1108]
Gas core nuclear rocket engine light and heavy species centrifugal separation by MHD-driven rotating flow, discussing fluid dynamic simulation results

20 p3671 A70-40256
Thermionic reactor electric propulsion for unmanned outer planets exploration, discussing spacecraft design, launch vehicle, weight factors, etc

20 p3717 A70-40524
[AIAA PAPER 70-1122]

Nuclear rockets for interorbit transportation, discussing reuse economics, propulsion system performance, etc 21 p3886 A70-40987

Nuclear rocket engines design and performance, discussing fission reactors, radiation leakage and shielding, heat transfer, etc 21 p3870 A70-42044

Nuclear rocket applications in Nuclear Flight Propulsion Module (NFPM) and Reusable Nuclear Shuttle (RNS) 22 p4070 A70-43180

Solid core nuclear reactor engine variables, considering specific impulse, engine weight, operating life and engine thrust 22 p4070 A70-43181

Nuclear light bulb and coaxial flow gaseous core nuclear rocket reactors based on energy transfer via thermal radiation 22 p4070 A70-43182

Operational safety of nuclear rockets in orbit-to-orbit transportation in regard to radiation doses from plume and reactor, including malfunction condition 22 p4070 A70-43183

Thermionic reactors for spacecraft auxiliary power and electric propulsion, discussing in-core conversion system and diodes 22 p4071 A70-43191

NERVA nuclear rocket engine design technology program, discussing probabilistic techniques for reliability engineering [SAE PAPER 700801] 24 p4377 A70-45910

NUCLEAR SCATTERING

NT NEUTRON SCATTERING

NT RESONANCE SCATTERING

Electron scattering from diatomic molecular systems including coupling of partial waves in fixed-nuclei approximation 06 p1114 A70-18633

Anomalous angular distribution and inelastic cross section of muon-nucleon interaction for penetrating underground cosmic ray particles 22 p4095 A70-43232

NUCLEAR SHIELDING

U RADIATION SHIELDING

NUCLEAR SPIN

Deep freezing of nuclear precession magnetometer elements for improving instrument characteristics accuracy 05 p0851 A70-16769

Rare earth energy band structure effect on RKKY magnetic interaction between atomic spins 13 p2472 A70-29799

Free nuclear precession sensor with rotating sample for performing measurements in nonuniform magnetic field 14 p2582 A70-30218

Free nuclear precession sensor with rotating sample for performing measurements in nonuniform magnetic field 24 p4339 A70-46293

NUCLEAR STRUCTURE

Neutron and proton distributions rms radii in nuclei by optical model analysis of low energy pion-nucleus interactions 07 p1337 A70-19360

Inverted coexistence possibility of spherical and deformed states in Si 28 and S 32 nuclei 17 p3137 A70-34518

Primary cosmic rays nuclear transitions, determining fragmentation parameters 20 p3696 A70-39284

NUCLEAR SUBMARINES

U SUBMARINES

NUCLEAR WARFARE

System engineering process for survival enhancement of military aircraft to meet stringent requirements of general nuclear war [AIAA PAPER 70-893] 17 p3019 A70-35810

NUCLEAR WEAPONS

Radiation hardening of electronic systems for nuclear weapons using shielding, circuit design techniques and hardened components 04 p0657 A70-14738

UN treaty based on U.S.-U.S.S.R.-UK agreement banning nuclear arms in space and establishing international law covering space exploration 07 p1428 A70-19106

NUCLEAR-ELECTRIC MOMENTS

U ELECTRIC MOMENTS

NUCLEATE BOILING

NT LEIDENFROST PHENOMENON

Organic liquid nucleate pool boiling experiments determining stresses, surface tension, viscosity and gravitation relationships to bubble shape and microlayer formation 01 p0218 A70-11180

Microlayers evaporation contribution to vapor bubbles growth rate from heated wall in liquid near saturation temperature during nucleate pool boiling 01 p0218 A70-11181

Heat transfer during nucleate boiling, discussing transfer from heated surface to superheated liquid layer and exchange on gas-liquid interface 06 p1176 A70-17695

Initial vapor bubble growth on horizontal heated wall during saturated nucleate boiling using combined streak and high speed frame photography 08 p1542 A70-21584

Reduced gravity effect on nucleate boiling using drop tower method with high speed motion pictures and telemetry 10 p1969 A70-25096

Bubble dynamics in subcooled nucleate boiling, deriving mathematical model based on evaporation-condensation mass transfer mechanism 12 p2333 A70-28113

Nucleate pool boiling, calculating sinusoidal and square wave pressure variations effect on heat flux for comparison with measurements 14 p2616 A70-30254

Pt and Ag surface effects on LOX nucleate boiling heat transfer, considering embedded abrasives relationship to hysteresis 21 p3947 A70-41056

Nucleation role in boiling and cavitation - ASME Conference, Detroit, May 1970 21 p3948 A70-41201

Site activation in saturated nucleate boiling tests involving various fluids boiled on transparent oxide coated glass surface, correlating site density data with surface temperature 21 p3948 A70-41202

Heated surface orientation and reduced gravity effects on Freon 113 nucleate 21 p3948 A70-41204

Nucleation phenomena associated with boiling heat transfer in pure liquids at solid heating surfaces 21 p3948 A70-41205

Surface tension role in microliquid layer formation on solid surface with growing bubble in nucleate boiling, using optical method 21 p3953 A70-42089

Cryogenic fluids nitrogen, argon and carbon monoxide nucleate boiling from atmospheric to near critical pressure 23 p4279 A70-44359

NUCLEATION

NT CLOUD SEEDING

Ice nucleating properties of dust particles above 80 km compared with soil and AgI particles 01 p0081 A70-11296

Water vapor condensation by homogeneous nucleation measured for cluster number using laser light scattering compared with theory in condensing supersonic flow 02 p0279 A70-12048

Surface nucleation critical field for pure superconductors at temperatures outside Landau-Ginzburg region 06 p1125 A70-17218

Liquid nucleation in vapor condensation on wettable, unwettable, smooth, rough and cavitating surfaces, showing positive effect of roughness elements 06 p1177 A70-17838

Efferent and afferent fibers presence in optic nerves determined by unilateral and bilateral enucleation of dogs and cats 07 p1207 A70-19476

Vapor-liquid-solid nucleation mechanism of alpha-aluminum oxide filamentary single crystal growth, suggesting combination with suboxide condensation and disproportionation mechanism 07 p1313 A70-19890

Atmospheric condensation nuclei activity with rough surface with decreasing spherical hollows 09 p1718 A70-23172

Nucleation and heteroepitaxial GaAs film growth on sapphire using electrical measurements, reflection diffraction and electron microscopy 11 p2098 A70-26393

Tribonucleation emphasizing viscosity-velocity product in gas nuclei formation and cavitation 12 p2170 A70-27661

Molecular Markov processes application to vibrational relaxation and dissociation, small system kinetics, nucleation and droplet growth, thermalization kinetics and diffusion processes 14 p2619 A70-30615

Spall nucleating mechanism for Al, noting microcracks in embedded particles 16 p2991 A70-33894

Kinetic theory of fatigue crack propagation, discussing stochastic nucleation process and power exponent relation 16 p2992 A70-33968

Titanium hydride deformation assisted nucleation in alpha-beta titanium alloy, showing low strain rate embrittlement and stress corrosion crack propagation in aqueous environments 17 p3116 A70-34395

Fatigue crack propagation in solids in terms of nucleation theory, explaining temperature dependence of fatigue strength and size effect 17 p3191 A70-35464

Nucleation processes associated with thermal decomposition sites formation in ammonium perchlorate single crystals, using optical and electron microscopy 20 p3582 A70-39494

Water vapor homogeneous nucleation in simulated spacecraft debris clouds 22 p4110 A70-43115

NUCLEI

Dust growth, density distribution and collisions in interior of cometary head atmosphere, considering gravitational attraction to nucleus 07 p1379 A70-19039

Comet nuclei internal structure from photometric measurements, discussing gas emanation and free surface ice evaporation 19 p3514 A70-37640

NUCLEI [NUCLEAR PHYSICS]

NT ALPHA PARTICLES

NT DEUTERONS

NT EVEN-EVEN NUCLEI

NT HEAVY NUCLEI

NT TRITONS

Energy dependence of intensity ratio of Li, Be and B on C, N, O and F nuclei /L/M ratio in primary cosmic rays, analyzing data discrepancy 01 p0169 A70-10316

Nucleons and high energy pions inelastic interactions with complex nuclei involving external diffraction production of pions 03 p0526 A70-13029

Basis functions with harmonic oscillator radial dependence in Hartree-Fock calculations for light deformed nuclei 04 p0723 A70-15635

Experimental determination of solar neutrino activity from interaction cross section between neutrinos and target nuclei 05 p0900 A70-15965

Effective potential of electron screening of Coulomb nuclei field leading to thermonuclear reaction rate increase using self consistent field method 07 p1346 A70-20206

High energy electrons elastic scattering from 2s-1d shell nuclei based on Dirac equation solution in Glauber approximation 09 p1730 A70-22043

Cosmic ray particle abundance in upper atmosphere during minimum solar activity estimated by nuclear photographic emulsions on balloon flight 10 p1932 A70-24438

Electrostatic shielding of nuclei Coulomb field during thermonuclear reactions in degenerate gases of arbitrary densities 11 p2087 A70-26578

Nucleon spectra, particle multiplicities and radiochemical cross sections following stopped-pion absorptions by complex nuclei, comparing calculated and experimental data 14 p2618 A70-30341

Inverted coexistence possibility of spherical and deformed states in Si 28 and S 32 nuclei 17 p3137 A70-34518

Neutron core star models based on realistic nuclear matter calculations and hyperons equation of state 17 p3157 A70-34844

Warm fog clearing effectiveness by seeding with hygroscopic nuclei as function of fog droplet and seedling nuclei distribution 17 p3132 A70-35928

Superheavy nuclei origin in primary cosmic rays, proposing neutron stars/pulsars/ as sources 18 p3308 A70-36403

Residual solar modulation of relativistic cosmic ray nuclei in galaxy over eleven years, observing magnitude at solar activity minima 18 p3309 A70-37009

Primary cosmic ray He nuclei rigidity measurement with magnetic spectrograph 19 p3505 A70-38119

Galactic cosmic ray energy spectra of light and medium nuclei from IMP-4 satellite measurements, investigating L/M ratio 19 p3506 A70-38124

Cosmic ray nuclei charge composition of elements Ne to Ni, using emulsion stacks exposure in balloon flights 19 p3506 A70-38126

Cosmic ray nuclei chemical composition and energy spectra in 3-30 Z range by balloon flight and Pioneer 8 space probe, noting propagation models 19 p3507 A70-38131

Relativistic cosmic rays nuclei abundances from Gemini 11 flight 19 p3509 A70-38144

Cosmic ray nuclei transformation and propagation in interstellar space, considering diffusion equation, cross sections, solar modulation, etc 19 p3509 A70-38145

Geomagnetically trapped energetic nuclei Z greater than or equal to 3 in earth outer radiation zone, measuring intensity ratio to alpha particles 20 p3698 A70-39327

Relativistic cosmic ray LH nuclei abundance via Cerenkov scintillator telescope on polar orbiting OV1-10 satellite 24 p4397 A70-45522

NUCLEIC ACIDS

NT RIBONUCLEIC ACIDS

Biophysics research, discussing supramolecular biological structures, synthesis of proteins, nucleic acids and genetic codes, biological membranes, coding in nervous system, etc
03 p0420 A70-13491

Nucleic acid and protein synthesis dynamics in rat brain and heart during adaptation to high altitude hypoxia
07 p1209 A70-19518

Nucleic acids constituents reactions with singlet oxygen, determining oxidation mechanism in photodynamic processes
21 p3781 A70-42025

NUCLEON-NUCLEON INTERACTIONS
Pion production characteristics during high energy nucleons interactions from data on production in upper atmosphere by gamma-quanta families /isobaric production/
03 p0555 A70-13032

Charged particles distribution according to multiplicity during pion-nucleon and nucleon-nucleon interactions at high energies
03 p0555 A70-13033

Separable potential with hard core effects, treating short range repulsion in nucleon-nucleon interaction, generating I matrix for existing data
09 p1725 A70-22042

Pion and nucleon interactions, tabulating average multiplicity and inelasticity values for various primary cosmic ray energy levels
09 p1745 A70-22775

NUCLEONICS
Gaging system utilizing nuclear radiation to obtain mass measurement of fuel quantity [SAE PAPER 690673]
05 p0880 A70-15832

NUCLEONS
Cosmic rays nucleon component measurements interpretation in terms of geomagnetic field model
01 p0169 A70-10354

Inelastic muon-nucleon scattering implications on cosmic rays, studying equation validity for absorption cross section
02 p0359 A70-12702

Pion and nucleon interactions with atomic nuclei at 200 Gev using Wilson chamber and ionization calorimeter, determining pion collisions characteristics
03 p0555 A70-13034

Extensive air shower characteristics for inelasticity coefficient, nucleon-pion interaction cross sections and secondary particles, noting parameter interchangeability
05 p0898 A70-15946

Neutron and proton distributions rms radii in nuclei by optical model analysis of low energy pion-nucleus interactions
07 p1337 A70-19360

Nucleons split-up into quarks disregarded as energy source for quasars
08 p1547 A70-20583

Cosmic ray diurnal anisotropy, demonstrating two-solar-cycle variations for nucleonic component
09 p1746 A70-23478

Nucleon spectra, particle multiplicities and radiochemical cross sections following stopped-pion absorptions by complex nuclei, comparing calculated and experimental data
14 p2618 A70-30341

Three dimensional nucleon-pion cascade equations solution for cosmic ray extensive air showers by pion-links method
17 p3150 A70-34597

Solar cosmic rays emission spectrum for 23 February 1956 flare, taking into account nucleon diffusion coefficient dependence on particle rigidity and distance to sun
20 p3697 A70-39287

Automatic cosmic ray station for recording nucleon and meson components
20 p3629 A70-39314

Scale invariance models correlation with cosmic ray data, comparing neutrino- and antineutrino- nucleon scattering
23 p4210 A70-43800

NUCLEOSIDES
NT ADENOSINE DIPHOSPHATE [ADP]
NT ADENOSINE TRIPHOSPHATE [ATP]
NT ADENOSINES
Uridine phosphorylation by heating with inorganic orthophosphates achieved via nucleoside reactions
23 p4158 A70-44837

NUCLEOSYNTHESIS
U NUCLEAR FUSION

NUCLEOTIDES
NT ADENOSINE DIPHOSPHATE [ADP]
NT ADENOSINE TRIPHOSPHATE [ATP]
NT ADENOSINES
NT PYRIDINE NUCLEOTIDES
Nicotinamide adenine dinucleotide /NAD/ deamination and role of nicotinamide hypoxanthine dinucleotide /deamino-NAD/ in forming ammonia from amino acids in rats/rabbits brain and liver tissue
01 p0018 A70-10505

Thyroidin influence on RNA content and nucleotide composition in hypothalamus, cortex and phenolic fractions of cerebral hemispheres resulting in accelerated protein biosynthesis
01 p0019 A70-10511

Methylating agents and nitrosoguanidine actions on polynucleotides, including ribonucleic acid
03 p0440 A70-13550

Acid soluble nucleotides content in normal and gamma irradiated rat spleens, presenting table
06 p0995 A70-17799

Partial nucleotide sequences for fragments isolated from ribonuclease digests of tobacco mosaic virus RNA, suggesting genetic duplication possibility
13 p2363 A70-29798

Nicotinamide adenine dinucleotide phosphate /NADP/ specific isocitrate dehydrogenase /ICDH/ inactivation from obligate halophile at low NaCl levels
15 p2685 A70-32671

NUCLIDES
NT ALUMINUM ISOTOPES
NT ALUMINUM 26
NT ALUMINUM 27
NT ARGON ISOTOPES
NT BERYLLIUM 9
NT BERYLLIUM 10
NT BORON ISOTOPES
NT CALCIUM ISOTOPES
NT CARBON ISOTOPES
NT CARBON 12
NT CARBON 13
NT CARBON 14
NT CESIUM VAPOR
NT CHROMIUM ISOTOPES
NT COBALT ISOTOPES
NT DEUTERIUM
NT HELIUM ISOTOPES
NT HYDROGEN ISOTOPES
NT IODINE ISOTOPES
NT IODINE 131
NT IRON ISOTOPES
NT IRON 57
NT ISOTOPES
NT KRYPTON ISOTOPES
NT KRYPTON 85
NT LEAD ISOTOPES
NT LITHIUM ISOTOPES
NT MANGANESE ISOTOPES
NT NEON ISOTOPES
NT NICKEL ISOTOPES
NT NITROGEN ISOTOPES
NT OXYGEN ISOTOPES
NT OXYGEN 18
NT PLUTONIUM ISOTOPES
NT RADIOACTIVE ISOTOPES
NT RUBIDIUM ISOTOPES
NT RUBIDIUM 86
NT SODIUM ISOTOPES
NT SODIUM 22
NT SODIUM 24
NT STRONTIUM ISOTOPES
NT TELLURIUM
NT TELLURIUM ISOTOPES
NT THORIUM ISOTOPES
NT TRITIUM
NT URANIUM ISOTOPES
NT URANIUM 233
NT URANIUM 238
NT XENON ISOTOPES
NT XENON 129
NT XENON 133
NT ZINC ISOTOPES

NULL HYPOTHESIS
Distributional results pertaining to complex Wishart processes and time varying spectral estimators on null hypothesis of stationary Gaussian time series
07 p1323 A70-19028

NULL REFERENCE GLIDE PATH
U GLIDE PATHS

NULL ZONES
Matrix method for maximizing radar antenna directive gain and simultaneously placing nulls in far field radiation patterns
08 p1477 A70-21758

Pulsars null pulse spacing significance, determining fluctuation power spectrum
23 p4238 A70-43814

NUMBER THEORY
NT ADDITION THEOREM
NT ARITHMETIC
NT DIVIDING [MATHEMATICS]
NT EXPONENTS
NT INTEGERS
NT MULTIPLICATION
NT SUBTRACTION
Negative radix conversion results applied to logical design of serial converter
09 p1642 A70-22967

NUMBERS
Readability of segmented numerals under critical accuracy and limited exposure time, comparing with conventional displays
24 p4308 A70-45514

NUMERICAL ANALYSIS
NT APPROXIMATION

NT BORN APPROXIMATION
NT BORN-OPPENHEIMER APPROXIMATION
NT CHEBYSHEV APPROXIMATION
NT DIFFERENCE EQUATIONS
NT EDDINGTON APPROXIMATION
NT ERROR ANALYSIS
NT FINITE DIFFERENCE THEORY
NT HARTREE APPROXIMATION
NT INTERPOLATION
NT ITERATION
NT ITERATIVE SOLUTION
NT LEAST SQUARES METHOD
NT MILNE METHOD
NT MONTE CARLO METHOD
NT NEWTON-RAPHSON METHOD
NT NOMOGRAPHS
NT NUMERICAL INTEGRATION
NT OSEEN APPROXIMATION
NT RAYLEIGH-RITZ METHOD
NT RELAXATION METHOD [MATHEMATICS]
NT RITZ AVERAGING METHOD
NT RUNGE-KUTTA METHOD
NT SCHWARTZ METHOD
NT SOMMERFELD APPROXIMATION
NT TRUNCATION ERRORS

Burning program for sounding rocket to reach maximum altitude with given initial and propellant masses, discussing numerical parameter optimization technique
01 p0161 A70-10150

Textbook on applied numerical methods covering interpolation, approximation, integration, matrices, etc, with emphasis on digital computer algorithms
01 p0132 A70-11306

Book on numerical solution of partial differential equations, discussing methods for physical and chemical problems on digital computer
01 p0134 A70-11326

Physiological significance of myocardial fibers curvature in left ventricle wall determined by numerical solutions based on mathematical description
01 p0039 A70-11368

Dynamical systems with two degrees of freedom reduced to numerical investigation of quadratic area-preserving mapping
02 p0289 A70-11993

Numerically stable solutions existence for one dimensional monochromatic radiative transfer, using linear algebra including vector and matrix norms, convergence, etc
02 p0340 A70-12643

Numerical method for attacking-lifting problems of general three dimensional wing executing arbitrary motion in potential flow [AIAA PAPER 69-23]
03 p0405 A70-12930

Centrally clamped spinning circular disk free transverse vibration analysis within accuracy of numerical computations
03 p0584 A70-12931

Alternating direction implicit difference schemes for solving Laplace and biharmonic elliptic equations
03 p0518 A70-13026

Axisymmetric and three dimensional gas flow around blunt bodies using numerical methods, discussing finite difference algorithms for gas dynamic equations
03 p0410 A70-14251

Shell theory resolving equations transformation to second order partial differential equations suited for solution by numerical algorithms of network method
04 p0767 A70-14495

Computer programs for numerical analysis of shell structures, considering series expansion, numerical integration, finite differences and finite elements
04 p0768 A70-14787

Numerical methods of solving problems in mechanics of continuous media - Conference, Kiev, Ukrainian SSR, June-July 1966
04 p0669 A70-14956

Small parameter method applied to numerical solution of conformal mapping and viscous fluid motion problems
04 p0719 A70-14960

Perturbation technique for numerically sensitive nonlinear two point boundary value problems
04 p0713 A70-15045

Numerical analysis of nonlinear boundary value problems for ordinary differential equations, considering patch bases and monotone methods
04 p0714 A70-15046

Numerical method for calculating gust effect on wing of complex planform at subsonic speeds by converting continuous to discrete processes
04 p0618 A70-15242

Numerical solution of transient heat conduction with radiating surface, imposing Runge-Kutta type integration on surface
04 p0787 A70-15613

Numerical solution for differential equations describing nonlinear beam-plasma interactions based on dispersion relation analysis
05 p0886 A70-15799

Numerical analysis of cyclotron amplification of geomagnetic micropulsations in magnetosphere based

on dispersion relation for three component cold plasma beam system

05 p0838 A70-16284

Book on digital computer methods in engineering covering numerical and programming methods, algebraic and differential equations solutions, time-frequency domain analysis, etc

05 p0877 A70-16771

Stratified cloud transport and evolution, solving kinetic equations by numerical method

06 p1053 A70-17210

Numerical solution of nonlinear hyperbolic systems of differential equations using methods of differences, applying results to invariant cross section gas flow

06 p0964 A70-17236

Soviet collection of papers on numerical methods in rarefied gas theory

06 p1035 A70-17751

Numerical methods for solving Boltzmann gas kinetics equation, assessing various methods effectiveness

06 p1036 A70-17752

Numerical solution of control optimization problems by systematic search in initial costate space, using Newton-Raphson method

06 p1025 A70-17964

Seeding effects on isolated cumulus clouds, using numerical model of microphysics and dynamics factors, measuring rainfall amounts and duration

06 p1098 A70-18243

Numerical analysis of rarefied plasma flow interaction with charged conducting bodies of various forms and dimensions

06 p1123 A70-18298

Optimal control problem converted Cauchy problem for obtaining numerical solutions through invariant imbedding

06 p1027 A70-18508

Numerical methods for computing solutions in optimal control of variable lift reentry spacecraft, applying digital computer techniques

07 p1245 A70-19093

Numerical method of characteristics for unsteady radiation gas dynamics, discussing surface pressures and heat transfer rates

[AIAA PAPER 68-163]

07 p1256 A70-19314

Numerical analysis of low-g fluid flow and heating problems encountered with liquid propellant storage and supply

[AIAA PAPER 69-567]

07 p1394 A70-19719

Numerical calculation and applied mathematics - Conference, Tours, France, July 1965

07 p1326 A70-19781

Point matching technique for plane elastic problems extended to axisymmetrically loaded elastic body of revolution, developing general computer program

07 p1416 A70-20303

Numerical procedure for determining horizontal wind from geopotential height in barotropic model, discussing solutions for resultant simultaneous equations

08 p1540 A70-21968

Stellar evolution computations numerical instability due to coupling between hydrostatic equilibrium and thermal processes

09 p1755 A70-22508

Numerical algorithms for solving Liapunov matrix equation in nonlinear stability analysis and optimal systems design

09 p1641 A70-22959

Two dimensional numerical analysis of current saturation mechanism for junction field effect transistors with small and large length-to-width ratio values

09 p1740 A70-23110

Lebedev nomogram determination of climatic parameters dependability, considering underlying theory and temperature sums

09 p1718 A70-23171

Numerical analysis of magnetic frequency divider operation

09 p1649 A70-23338

Numerical methods of viscous liquid dynamics, considering unsteady flow in simply and multiply connected regions

10 p1866 A70-24110

Continuous media mechanics by applying fractional steps method to numerical solutions, outlining theoretical basis for computer algorithms

10 p1866 A70-24114

Three dimensional supersonic gas flow solution by numerical method of characteristics, discussing direct and inverse tetrahedral and semicharacteristic schemes

10 p1798 A70-24117

Hydrodynamic lubrication theory two dimensional problem, comparing numerical methods for elliptical nonlinear differential equations

10 p1893 A70-24164

Numerical method for linear differential equations extended to nonlinear ordinary differential equations, liquidating residuals by setting integrals equal to zero

10 p1909 A70-24419

Quasi-linearization extension to numerical solution of multipoint boundary value problems for ordinary

differential equations arising from state constrained optimal control problems

10 p1909 A70-24421

Monograph on numerical treatment method for harmonically oscillating wings covering pressure distributions, logarithmic singularity, etc

11 p1219 A70-25497

Stiffened cylindrical shells under internal pressure numerically analyzed based on C-5A fuselage material parameters

[AIAA PAPER 68-29]

11 p2135 A70-25961

Numerical techniques and solutions for compressible and incompressible laminar separated flows using time dependent finite difference equations

[AIAA PAPER 68-741]

11 p2035 A70-25972

Bidirectional reflectance of three dimensional surfaces described by diffuse triangular subareas network for spacecraft thermal design, giving numerical technique

11 p2084 A70-26354

Multidata and collocation methods compared for numerical Laplace transform inversion

11 p2074 A70-26639

Numerical solution for steady supersonic inviscid flow around smooth conical bodies by solving elliptic partial differential equations for conical flow

12 p2155 A70-27202

Aerodynamic coefficients from observed motion of body in flight, eliminating need for closed form solutions by employing numerical solutions to equations of motion

[AIAA PAPER 69-134]

12 p2156 A70-27824

Numerical quadratures application to integral equations for radiative heat transfer computations, discussing validity for parallel and adjoint plates

12 p2332 A70-27840

Numerical solution of satellite rotational damping by onboard motors using Euler equations, local variations and finite control time

13 p2505 A70-28963

Aircraft turbulence penetration performance numerical rating, applying concept to large subsonic jet transports

[AIAA PAPER 70-543]

13 p2347 A70-29074

Dilute gas transport properties calculation, investigating numerical techniques to minimize computation time to prescribed accuracy

13 p2441 A70-29089

Algorithms based on Newton formula for polynomial interpolation and numerical differentiation

13 p2441 A70-29100

First order node to node satellite orbital elements perturbations due to arbitrary zonal geopotential harmonic, determining computation methods and time

14 p2638 A70-30703

Eigenvalues of membranes and plates, comparing asymptotic and numerical values

14 p2600 A70-31223

Numerical solution to Laplace equation in spherical coordinates with axial symmetry, using Dirichlet method to obtain difference equations

15 p2767 A70-31751

Attitude dynamics of slowly spinning axisymmetric satellites under influence of gravity gradient torques, using analytical and numerical techniques

15 p2809 A70-31778

Automatic numerical analysis of velocity information from Doppler effect ultrasonic blood flow meter

15 p2691 A70-31920

Vector displacement numerical calculations for rectangular parallelepipeds of infinite and finite lengths

15 p2767 A70-32018

Nonparametric reliability application to numerical data involving failure distribution, using mathematical model

15 p2748 A70-32669

Second order hyperbolic partial differential equations solution by characteristic grid and continuous characteristic methods

15 p2768 A70-32818

Reference stress evaluated by numerical analysis techniques, discussing rectangular beam in pure bending

16 p2987 A70-32921

Variance reduction technique for hybrid computer generated random walk solutions of partial differential equations, comparing to analytical solution

16 p2942 A70-33731

Continuous space discrete time /CSDT/ method using initial value formulation for partial differential equations, discussing applications to one dimensional problem

16 p2943 A70-33736

Hypervelocity impact of spheres on thin targets using numerical solutions utilizing STEEP code two dimensional technique based on hydrodynamic elastoplastic model

16 p2991 A70-33853

Radiation and conduction of open joint multilayer insulation systems, analyzing dependence on contact area by numerical methods

[AIAA PAPER 70-848]

16 p2939 A70-33915

Fluid mechanics phenomena numerical modeling, considering present methods three dimensional problems, turbulence treatment, etc

17 p3068 A70-34663

Numerical solutions for velocity and concentration profiles to nonsimilar isothermal diffusion laminar boundary layer equations for uniform injection of foreign gas

17 p3069 A70-34824

Method of characteristics for nonequilibrium flow fields analysis, reviewing theory, numerical methods and examples

17 p3071 A70-35470

Multistage solution algorithm for solving Navier-Stokes equations stationary problem, considering plane motion of incompressible fluid

18 p3239 A70-36216

Unsteady two dimensional gas flow calculation axisymmetric shock tube of variable cross section, using numerical method

18 p3240 A70-36275

Hypotheses concerning optimal methods of solving mathematical physics problems, choosing algorithms employable in digital computers

18 p3291 A70-36284

Numerical differentiation of analytic functions involving Cauchy formula and error estimation

18 p3282 A70-36362

Buckling problem numerical analysis by nonlinear programming and minimum energy formulation

18 p3339 A70-36495

Two dimensional turbulent film cooling, predicting initial region temperature distribution by solving finite difference form of thermal energy equation

18 p3346 A70-36497

Vlasov high temperature plasmas numerical analysis, using Hamilton variational principle

18 p3296 A70-36793

Laminar incompressible flow in arbitrary cross sectioned entrance region of ducts by numerical technique after transformation to boundary value problem

[ASME PAPER 70-GT-91]

18 p3243 A70-36878

Numerical ionospheric world mapping of plasma frequency, considering height, latitude, longitude and local mean time variations

19 p3380 A70-38403

Nonlinear acoustic absorbers behavior analysis, discussing spectral and temporal computation methods

20 p3672 A70-39237

Plane electromagnetic scattering from perfectly conducting bodies, comparing exact numerical solution with experiment

20 p3585 A70-39394

Nonstationary random processes prediction by numerical method

20 p3673 A70-39762

Plasma accelerator compressible turbulent boundary layers numerical calculation taking into account MHD effects, electron thermal nonequilibrium and finite rate ionization

20 p3682 A70-40017

Numerical solution for multilayer insulation system comprised of infinite parallel metallic films separated by optically thin dielectrics

21 p3947 A70-41054

Cantilever bending under gradual contact with cylindrical supporting surface compared with solution by elasticity theory

21 p3934 A70-41251

Bond stresses between fiber and matrix of fiber reinforced composite materials determined by numerical method based on superposition

21 p3934 A70-41252

Meteorological fields objective representation by numerical analysis, discussing statistical parameters and analytic errors checking

21 p3847 A70-41400

Atmospheric scattering governed by Rayleigh phase function with absorption, calculating radiative transfer by numerical solution of Chandrasekhar integral equations

22 p4072 A70-42340

Optimal design of electronic circuits, using mathematical methods for solving nonlinear multivariable function extremum

23 p4171 A70-43951

Plasma physics computational problems concerning controlled thermonuclear reactions, considering instability and equilibrium numerical calculations

23 p4224 A70-44181

Elastic continua structural optimization analysis decisions for maximizing calculation accuracy, insuring efficient complex numerical analyses

23 p4271 A70-44706

Numerical methods for mixed boundary value problem of axisymmetric shells of revolution, using truncated series expansion and finite difference expressions

23 p4272 A70-44712

Numerical solution of first boundary value problem of elasticity theory involving biharmonic stress function relating to rim loads

23 p4275 A70-44942

Statistical interpolation for numerical analysis of middle troposphere AT potential based on geopotential and wind observations
24 p4371 A70-45135

Numerical solutions of three dimensional static elasticity, using physical analogies
24 p4419 A70-45195

Numerical analysis of fuel combustion in supersonic stationary flows of hydrogen air mixture past bodies by two-component reaction kinetics model
[ICAS PAPER 70-52] 24 p4428 A70-45500

NUMERICAL CONTROL

Book on numerical control covering principles, electromechanical system using digital logic circuits, binary numbers and arithmetic, etc
10 p1854 A70-24023

Numerically controlled gas tungsten arc welding, discussing tape programming, fixture design and fabrication for various welded metal joint configurations
11 p2058 A70-25661

Economical inspection of numerical-control produced parts through critical dimensions determination and dimension measurement reduction
[SME PAPER IQ-70-710] 12 p2241 A70-27086

Numerically controlled N/C machines reliability program based on organized failure reporting and analysis system for cost effectiveness and downtime reduction
15 p2747 A70-32635

Asymmetric closed and cylindrical shells variable surface machining for desired wall thickness profile by chemical milling with digital computer numerical control
20 p3637 A70-39942

Programmable all-stored-logic numerical control system based on minicomputer, affording economy and adaptability in production tool applications
22 p3993 A70-42319

Digitally controlled milling machine for complex aerodynamic profiles and prismatic blades
22 p4046 A70-43117

Computerized air cargo clearing, discussing London Airport Cargo Electronic-data-processing Scheme
22 p4007 A70-43272

Computer-aided production engineering involving numerically controlled machines for Rolls-Royce aircraft engines manufacture
24 p4341 A70-45299

NUMERICAL INTEGRATION

NT RUNGE-KUTTA METHOD

Integration time reduction for equations of motion of vehicle center of mass during parabolic reentry, using Runge principle
01 p0134 A70-11483

Navier-Stokes difference equations numerically integrated by computer for viscous fluid flow along parallel flat plate at low Reynolds number
02 p0277 A70-11909

Unstable electron plasma initial value problem solved by numerically integrating Vlasov equation in one dimension
02 p0347 A70-12235

Second order ordinary differential equations solution extended to higher order or partial differential equations using numerical integration
02 p0324 A70-12280

Computer application to Navier-Stokes equations numerical integration for incompressible viscous fluid deflected flow with large Reynolds number
02 p0287 A70-12376

Numerical integration methods in electromagnetic theory, discussing scattering and radiation from thin wire structures
02 p0262 A70-12600

Carbon dioxide supersonic flows, describing numerical integration procedure for chemical and vibrational relaxation
03 p0440 A70-13743

Optimum numerical integration with application to real time digital simulation of continuous systems, deriving three step methods
03 p0455 A70-14173

Elliptic system of twelfth order equations describing elastic equilibrium of plate with kinematic functions analyzed by integration procedure
03 p0600 A70-14306

Numerical integration of differential equations governing one dimensional flow of reactive gas, discussing flows of converging-diverging nozzle and normal shock waves
04 p0671 A70-14992

Boundary layer along flat plate at zero incidence with homogeneous suction using momentum and kinetic energy integral equations through boundary layer velocity profile
04 p0615 A70-15052

Thin elastic shallow shell static problem solved using numerical integration of differential equation
04 p0778 A70-15558

Numerical integration of linearized two level forecast model to analyze behavior of accumulated error
05 p0878 A70-16153

Electron flux-atmosphere interaction solved by numerical integration on computer, discussing auroral ionosphere
05 p0842 A70-16755

Numerical integration of equations of motion of three dimensional laminar compressible boundary layers
[DVL-915] 06 p1033 A70-17229

Equations of motion for hypersonic friction layers integrated using quadrature procedures
[DVL-913] 06 p1033 A70-17230

Optimal quadrature formulae for numerical integration of 2 pi-periodic functions involving integrand derivative values at knots
06 p1093 A70-17582

Boltzmann equation direct numerical integration using successive iterations algorithm
06 p1036 A70-17755

Numerical method for field problems analysis using algorithm based on generalized Betti-Maxwell theorem
06 p1094 A70-17942

Navier-Stokes equations numerical integration in Eulerian coordinates, applying results to compressible and incompressible fluids steady flow
[AIAA PAPER 70-2] 06 p1040 A70-18113

Plane elastic-relaxing plastic shock wave yielding of Fe numerically integrated by two step stable difference scheme without pseudoviscosity
06 p1172 A70-18618

Integration by orthogonalizations of envelopes of revolution loaded asymmetrically, introducing boundary conditions and structure discontinuities
07 p1404 A70-19128

Penetrative thermal convection stability for statically unstable layer surmounted by statically stable layer from numerical integration of linearized equations of motion and heat conduction
07 p1269 A70-19947

Digital differential analyzers improved speed and accuracy by extended resolution on Euler integration for differential equations solution programming
08 p1467 A70-21756

Negative radix conversion results applied to logical design of serial converter
09 p1642 A70-22967

Numerical integration method for function and solution of differential equation, considering equations governing two dimensional motion of particle in air stream
10 p1910 A70-25099

One-step numerical integration of linear differential equations based on Labotto quadrature, including higher order applications and stability analysis
11 p2071 A70-25840

Spin stabilized satellite attitude and orbital maneuvers computation, considering required accuracy and computer time in numerical integration procedures
11 p2125 A70-26278

Coefficients for finite difference methods of numerical integration of products of Fourier and ordinary polynomials
11 p2074 A70-26848

Atmospheric hemispheric general circulation model numerical time integration with moist processes and uniform earth surface
12 p2262 A70-26882

Algorithm for integrating ordinary differential equations system determined for stability condition by trial-and-error procedure programmed on computer
12 p2262 A70-28030

Computerized numerical integration of nonlinear partial differential equations describing blast wave in ionosphere with finite electric conductivity under uniform magnetic field
12 p2227 A70-28212

Stability of single periodic symmetrical solutions of plane circular restricted three body problem, using digital computer for numerical integration of equations of motion
13 p2490 A70-28950

Beginning of table calculations using difference methods for numerical integration of ordinary differential equations
13 p2440 A70-28960

Numerical integration or quadrature technique for evaluating Fourier integrals in theory of infinite cylindrical antenna
13 p2440 A70-29088

Numerical integration of differential equations with widely separated eigenvalues, outlining solution stability and accuracy problems
13 p2441 A70-29213

Tesseral and sectorial harmonics effect on satellite perturbations using numerical integration
13 p2494 A70-29531

Differential equations stiff systems numerical solution by linear one step integration methods
14 p2599 A70-30645

Planetary motion zero-rank effects numerical integration, using Hill secular perturbation method and trace of dyadics
14 p2639 A70-30704

Thermoelasticity of incompressible solids, integrating linearized equations using Helmholtz solution
14 p2660 A70-31224

Hypersonic internal flow investigation by differential equation numerical integration, determining shock shape and surface pressure
16 p2838 A70-33881

Algebraic aspects of generalized Riemann invariants method of integration of quasi-linear partial differential equations
16 p2944 A70-34329

Differential equations numerical integration by one step method of high order accuracy
16 p2945 A70-34333

Fluid turbulence unified heuristic model, defining determinate solutions for Navier-Stokes equations numerical integration at high Reynolds numbers
17 p3074 A70-35884

Numerical quadrature of singular functional equations, tabulating integral functions, Cauchy principle values and integral transformations for optimal error function
18 p3280 A70-36219

Spherical gas lubricated sliding bearing with forced injection, determining pressure distribution by numerical integration
18 p3262 A70-36273

Linear differential equation integration method, using Eulerian technique for error reduction
18 p3282 A70-36358

Tropical circulation structure and energetics from numerical time integration of global atmospheric model with realistic orography
19 p3462 A70-38257

Numerical integration of finite difference analogs of nonlinear partial differential equations, investigating data smoothing, filtering and boundary effects on computational instability
19 p3459 A70-38417

Many body gravitational problem, computing evolution of two groups by numerical integration with two different computers
19 p3523 A70-38692

N body numerical integrator using virtual mass technique for computing trajectories with speed and accuracy suitable for spacecraft onboard computer applications
[AIAA PAPER 70-1057] 19 p3528 A70-38872

Linear homogeneous differential equations nonautonomous systems integration techniques, deriving finite forms of solutions
19 p3460 A70-38938

Aircraft and rocket guidance systems navigation error analysis, discussing numerical integration techniques and computer program
[AIAA PAPER 70-1004] 20 p3667 A70-39527

Finite difference numerical integration method for melting and freezing problems extended to free convection in liquid and unequal densities for phases
21 p3953 A70-42093

Interpolation method for nonlinear automatic control systems accuracy, discussing numerical integration optimal step and node number selection
22 p4003 A70-42886

Cloud droplet growth rapid computation using number density mean value for integrating stochastic coalescence equation into differential equation
22 p4064 A70-42910

Digital differential analyzers one step integration method with iteration procedure truncation to single step
22 p3996 A70-42921

Numerical integration of Orr-Sommerfeld equation for flat plate Blasius boundary layer transition
23 p4179 A70-43973

Shell analysis based on discretization into one, two and three dimensional configurations, comparing finite difference, numerical integration and finite element methods
23 p4272 A70-44715

Numerical integration of equations of motion from finite element analysis in structural mechanics, using computer program
24 p4420 A70-45278

Rapid satellite orbit prediction program by numerical integration including oblateness squared and radiation pressure effects over long time spans
24 p4406 A70-45528

Multidimensional integral Monte Carlo evaluation applying regression analysis to linear unbiased estimators
24 p4370 A70-46100

NUMERICAL WEATHER FORECASTING

Finite difference schemes compared for numerical weather prediction by application to shallow water equations on hemisphere, noting mesh spacing
01 p0135 A70-11064

Numerical forecasting scheme for hurricane and typhoon trajectories applied to 1967 Atlantic storm data
03 p0520 A70-13162

Weather prediction technique based on hydrodynamical equations, outlining atmospheric circulation models
[AAS PAPER 69-619] 04 p0714 A70-14646

Localized numerical weather forecasts via interpolation from primitive equation model outputs, analyzing winter season results in terms of snow prediction

06 p1098 A70-18241

Global atmospheric research program data requirements analysis based on two level numerical model

08 p1539 A70-21650

Global real data numerical forecasting with two layer NCAR /National Center for Atmospheric Research/ general circulation model, testing different data initialization schemes

09 p1713 A70-22303

Numerical weather forecasting for several weeks based on global meteorological satellite network observation

10 p1913 A70-25241

Shape and location error separation in deterministic predictions of meteorological scalar fields, considering air pressure system forecasting

13 p2445 A70-28995

Extratropical planetary high altitude frontal zones statistical analysis and position forecasting by eigenfunction expansion

13 p2445 A70-29673

Numerical weather prediction requirements for global satellite observing systems using atmospheric models

14 p2610 A70-31152

Dynamic numerical weather forecasting based on balanced model consisting of closed system of equations

18 p3284 A70-36232

Numerical scheme for weather forecasting, considering interaction mechanism between cyclonic and ultralong waves and climate

18 p3285 A70-36646

Simulation studies for first GARP global experiment, discussing data redundancy, measured and derived data, sampling, etc

18 p3285 A70-36785

Orography and friction effects on numerical forecast of atmospheric pressure variation

24 p4370 A70-45112

NUSSELT NUMBER

Forced convection of hot wire in hypersonic flow, determining Nusselt-Reynolds number relationship for hot-wire anemometers

02 p0223 A70-12101

Thermal entrance region effect on Nusselt number determination in asymmetrically heated rectangular duct with uniform heat flux

07 p1425 A70-20223

Thermal boundary layer thickness and Nusselt number approximations for heat transfer in laminar flow along flat plate with power law heat flux distribution

08 p1599 A70-21583

Single fluid theory for plasma laminar flow in field-free region of circular tube, obtaining friction factor and Nusselt number correlations

08 p1552 A70-21585

Heat transfer coefficient to gas in tube under unsteady heat flow conditions, studying Nusselt number dependence on Reynolds and Prandtl numbers

09 p1787 A70-22173

Local Nusselt numbers beyond abrupt circular channel expansion tested for Reynolds numbers with air as working fluid

09 p1790 A70-23554

Nusselt numbers of nonstationary and stationary heat transfer between metal spheres and liquid flow, showing bulk heat and geometry dependence

12 p2330 A70-27288

Laminar flow heat transfer in annuli, discussing correlation of local Nusselt numbers

17 p3197 A70-35545

NUTATION

Rotational motion of self excited symmetric gyroscopes applied to attitude control and nutation damping of space vehicles

01 p0143 A70-10929

Inertial damper optimum parameter selection for achieving maximum nutation damping factor for gyroscopic stabilizer

01 p0091 A70-10985

Nutational NMR nonuniform magnetic field stabilizer for beta spectrometer, structural details and circuit schematic

03 p0485 A70-13467

Single degree of freedom nutation damper motion instability on dual spin stabilized spacecraft ascribed to parametric excitation by transverse angular rates

04 p0764 A70-15585

Liquid filled dampers for nutation damping of spacecraft with momentum wheel for attitude stabilization

06 p1154 A70-17163

Cross coupled rotational motions of free solid body carrying nutation-damping pendulums

07 p1335 A70-19808

Heavy solid body motion about stationary point at small nutation angle, estimating region of series convergence representing periodic solutions to motion equations

07 p1336 A70-20298

Earth free diurnal nutation parameters determination from latitude observations, establishing amplitude and phase time-independent variations

08 p1488 A70-21154

Nutation damping in gyrostabilization for multispin satellites in terms of energy momentum and damping torque arguments

11 p2119 A70-25357

TACSAT 1 communication satellite design, dual-spin stabilization principles and dynamic characteristics, noting nutation behavior

[AIAA PAPER 70-455]

11 p2120 A70-25447

Spin axis motion of n-body coaxially mounted cluster of differentially spinning bodies, considering combined precession and nutation

11 p2123 A70-26128

Fluid sphere gyro satellite nutation sensor

11 p2057 A70-26504

Dual spin satellite stability with four mass nutation damper

12 p2314 A70-27842

Nutation damper for dual-spin spacecraft, considering various two degree of freedom systems with two natural frequencies

14 p2655 A70-31367

Motion and stability characteristics of dual spin satellite system with pendulous type nutation dampers, noting mass unbalance effect

[AIAA PAPER 69-857]

15 p2812 A70-32508

Ball in tube nutation damper for spinning satellite, describing design, testing and fabrication techniques for achieving low friction level

16 p2985 A70-34136

Precession-nutation dependence on earth structure based on oscillations theory of ellipsoid with rotating fluid contained in rigid envelope

16 p2980 A70-34316

Dynamic behavior of eccentric annular mercury nutation damper, using variational principle of least viscous frictional power loss

17 p3023 A70-34770

Critique of Ruderman theory of Crab pulsar LF wobble as long wavelength oscillation of superfluid vortex lattice

19 p3522 A70-38604

Torque free spinning satellite with flexible appendages, investigating design parameters effects on nutational stability

[AIAA PAPER 70-1046]

19 p3534 A70-38861

Nutational stability and closed loop position control of dual spin spacecraft with despun platform

[AIAA PAPER 70-975]

20 p3715 A70-39554

Variable parameter nutation damper SAS-A dual spin satellite, discussing design and expected in-flight performance by digital simulation

[AIAA PAPER 70-972]

20 p3669 A70-39557

Dual spin bodies stability, controlling nutation by passive damper fitted to despun platform

22 p4110 A70-42486

Correctable gyroscope stability estimation by energy method taking into account nutation and precession motions

22 p4039 A70-43556

Rigid body rotation about fixed point under oscillatory precession and nutation due to noncentral attractive force, showing errors in Euler equations

23 p4247 A70-44792

NUTATIONAL OSCILLATION

U NUTATION

Heart rate change effect on myocardial oxygen consumption and nutritional circulation with constant coronary blood flow suggesting oxygen extraction independence of capillary surface

02 p0235 A70-11991

Dehydrated food effects on human functional state, noting published literature on food composition, preparation, caloric and nutritional values, digestibility, etc

03 p0435 A70-13703

Nutrition and atherosclerosis - Conference, Bad Ragaz, Switzerland, October 1968

03 p0430 A70-14276

Statistical data to demonstrate atherosclerotic diseases affected by cholesterol and saturated fatty acids in foods

03 p0430 A70-14277

Interactions between nutrition, blood coagulation and atherosclerosis by Duguid theory, emphasizing fibrinolysis, thrombosis and alimentary lipids

03 p0431 A70-14280

Chlorella seaweed hybrid strains containing larger amounts of amino acids than original parent species

04 p0630 A70-14573

Temperature and morphological changes of animals adipose tissue under various nutrition conditions, based on measurements by thermocouples implanted in fat deposits

04 p0640 A70-15514

Nutritive value of mycelium of *Cantharellus cibarius* mushroom on rats compared with eggs and fresh and sour milk

05 p0809 A70-17111

Dehydrated food effects on human functional state, noting food composition, preparation, caloric and nutritional values, digestibility, etc

11 p1989 A70-25503

Space diets with pure nutrition for balanced nutrition obtained through biological and physicochemical synthesis

23 p4157 A70-45027

NUTRITIONAL REQUIREMENTS

NT CALORIC REQUIREMENTS

Human capacity to discriminate between poorly and well balanced diets and liability to select amino acid imbalanced mixtures for deficient nutrient

01 p0028 A70-11314

Hypokinesia and nutrition deficiency effect on blood coagulation, noting combination with accelerations may lead to hypocoagulation

04 p0630 A70-14578

Aircraft crews in-flight medically controlled feeding, discussing physiological and nutritive value of foods

06 p1001 A70-17669

Atrophic changes in tortoises during roundtrip to moon on Zond 5 ascribed to hunger and space flight factors

07 p1207 A70-19496

Space diets tests for mean DAR of proteins, carbohydrates, fats and water, considering body weight and required energy expenditure

09 p1623 A70-22088

Fasting and postprandial serum amino acid patterns of human males fed protein-free or protein-sufficient diets

09 p1621 A70-23399

Prolonged hypodynamia effect on human nutritional habits and protein metabolism, noting decrease in energy requirement and body weight

10 p1814 A70-24675

Space diets tests for mean DAR of proteins, carbohydrates, fats and water, considering body weight and required energy expenditure

15 p2693 A70-32684

Atrophic changes in tortoises during roundtrip to moon on Zond 5 ascribed to hunger and space flight factors

15 p2685 A70-32741

Dietary amino acids combination allowing maximum growth in rat

16 p2850 A70-34320

NUTS [FASTENERS]

Resilience coefficient of intermediate elements of threaded connection related to transverse and axial nut dimensions by least squares method

05 p0856 A70-17012

Nut and bolt locking, describing cotter pins, lock washers, elastic washers, prestressing, nut with lock nut and self locking nuts

06 p1075 A70-17436

NYLON [TRADEMARK]

Nylon 6 polyamide tensile stress cracking by metal thiocyanates in aqueous and nonaqueous solutions, comparing results with cracking by metal halides

10 p1907 A70-24300

Hypersonic wind tunnel testing of Plexiglas and nylon hemispheres instrumented with strain gages and thermocouples, comparing with calculated strain, temperature and ablation

13 p2520 A70-28727

Packable near weightless nylon cloth wings without rigid members for improved aeronautical efficiency in cargo delivery, powered flight and rocket and spacecraft recovery

[AIAA PAPER 70-880]

17 p3017 A70-34815

Phenolic nylon thermal decomposition, considering surface reradiation and physical parameters effects

17 p3196 A70-35242

Longitudinal tension impact tests on nylon tape and Apollo pilot parachute riser construction, determining wave propagation effects

[AIAA PAPER 70-1182]

21 p3843 A70-41831

NYLON RESINS

U POLYAMIDE RESINS

NYQUIST FREQUENCIES

Linear control circuits transfer function analysis, revising Nyquist criterion

07 p1328 A70-20212

Prelaunch dynamic response test parameter selection for control systems for space complexes with form of Nyquist locus

13 p2381 A70-28423

NYSTAGMUS

Astronaut vestibular fitness determined from threshold labyrinthine tests on isolated horizontal and vertical semicircular canals

03 p0437 A70-14059

Quantitative characteristics of central compensatory process, investigating nystagmus responses in guinea pigs subjected to bilateral labyrinthectomy

06 p0995 A70-17806

Postcaloric nystagmus clinical evaluation by analog computer measuring fast-phase eye displacement in Vestibular Function laboratory

08 p1448 A70-21942

Alcoholic beverages effect on positional nystagmus and Coriolis acceleration 11 p1993 A70-26520

Anatomical and physiological correlations between mathematical model components for vestibular nystagmus mechanisms 13 p2351 A70-29331

Gravity effect on positional alcohol nystagmus in man and rabbits, observing threshold value in weightless state 13 p2359 A70-29442

Vestibular nystagmic and electrical responses facilitation, inhibition and habituation, noting modulation by subcortical and cortical systems 14 p2538 A70-30909

Vestibular nystagmus evocation by conditioned reflexes technique after pure tone stimulation 14 p2538 A70-30910

Arousal effects on vestibular nystagmus in man, discussing forced alertness in mental arithmetics form 14 p2538 A70-30911

Ocular fixation index and vestibular stimulation by caloric tests, discussing central processes for nystagmic rhythm regulation 14 p2538 A70-30912

Pattern center hypothesis for habituation to centrifugal and linear accelerations in man, investigating aftereffects by nystagmography 14 p2538 A70-30913

Electronystagmographical responses comparison with electroencephalographic record during prolonged torsion swing vestibular tests under cortical and subcortical factors influence 14 p2539 A70-30917

Hearing loss thresholds and spontaneous and caloric nystagmus correlationship in test pilots 15 p2690 A70-31893

Vestibular stimulation by square wave acceleration, evaluating Ewald laws for nystagmus behavior 17 p3037 A70-35127

Nystagmic response to directional inert shift of endolymph in semicircular canals in frontal plane head subject rotation 18 p3220 A70-36635

Vestibular thermal stimulation method using distilled water injected into ear, discussing nystagmus appearance and duration 19 p3367 A70-37355

O

O RING SEALS

Ring seal elements structural parameters influence on fluid leakage at various shaft speeds and fluid pressures 07 p1294 A70-19123

O STARS

Radial velocities determined from prism spectrograms for O and B stars in Milky Way field in Scorpius 02 p0369 A70-12062

Catalog of faint Ob stars between Carina and Centaurus 02 p0370 A70-12075

Anomalous fast OB stars separation method based on spatial kinematic characteristics measurements, noting accuracy 03 p0565 A70-13230

Color difference method for interstellar extinction laws applied to O stars study 06 p1140 A70-17641

O star red shift considering gravitation interpretation effects on stellar masses 07 p1391 A70-20465

O and B type stars neutral He lines, studying UV line blanketing effects on predicted departures from LTE 08 p1571 A70-20912

Von Zeipel 1128 O star spectrum analysis, discussing mass, He/H ratio, metal abundances, etc 08 p1571 A70-20913

Anomalous fast OB stars separation method based on spatial kinematic characteristics measurements, noting accuracy 08 p1580 A70-21663

O-Of stellar evolution yielding Wolf-Rayet type, considering spectral evidence and H-He interaction 15 p2800 A70-32202

Luminosity criteria in O stars via narrow band photoelectric photometry suggesting VI Cygni proximity 15 p2807 A70-32804

Lyman alpha absorption by interstellar neutral hydrogen observed in O and B stars UV spectra 17 p3162 A70-34898

Observational evidence concerning validity of Saha and Boltzmann laws in O, B and A stellar atmospheres 17 p3170 A70-35387

O type stellar clusters hydrogen line observation revealing associated gas clouds 18 p3328 A70-37172

Carina spiral feature progress report covering O and B star distribution, optical and radio H 2 and H 1 sources and cosmic dust 18 p3330 A70-37185

O and B stars velocity dispersion, considering Oort terms and average residual radial velocity 18 p3330 A70-37188

O-B5 stars mean ages estimation by hyperbolic approximation based on distribution in stellar associations 19 p3524 A70-38762

OB star distribution statistical analysis in Southern Milky Way, discussing concentrations, relations and systematic deviations 22 p4100 A70-42854

Stellar ring 274 reality confirmed by photometric measurements of OB member stars, determining variable shell star P Cygni location 22 p4101 A70-42868

Of stars mean spectrophotometric gradients and Balmer jump data with corrections for interstellar absorption 24 p4409 A70-45632

OA O

NT OAO 2
NT OAO 3
NT OSO
NT OSO-B
NT OSO-1
UV photometry of stars and galaxies from OAO-2, discussing instruments and observational results 02 p0378 A70-12580

UV photometry from OAO, observing planets, gaseous nebulae, X ray source, quasars, Crab Nebula, extragalactic nebulae, etc 02 p0303 A70-12705

OAO thermal subsystem design to provide temperature control for experiments and spacecraft electronic devices 04 p0765 A70-15668

Monograph on OAO design, experiments, testing, mission operations and history 07 p1393 A70-19100

Lightweight mirror blanks of titanium silicate for OAO-4 providing thermal and dimensional stability 09 p1678 A70-22952

Modal expansion method applied to thin deformable primary mirror surface control for orbiting astronomical observatory 13 p2403 A70-28427

Celelescope TV photometer system operation on-board OAO by mathematical simulation 16 p2906 A70-33174

Solid lubricated contacts performance in Nimbus and OAO spacecraft, discussing slip ring assembly and noise problems in Ag-graphite brushes 16 p2920 A70-33810

Interstellar Lyman alpha observations with OAO, providing upper limit to neutral hydrogen column density 17 p3162 A70-34899

Multispectral UV sky mapping and heavenly body intensity measurement onboard OAO 2 satellite 17 p3179 A70-35264

Lunar based vs orbiting astronomical observatories, discussing limitations imposed by geocorona 22 p4108 A70-43630

OA O

UV photometry from OAO-2, describing Wisconsin instrumentation and equipment 20 p3624 A70-39009

Orbiting Astronomical Observatory II systems performance 21 p3928 A70-40980

OAO 2 for UV telescope sky mapping and spectrophotometric measurements of celestial bodies 23 p4261 A70-44666

OAO 2 satellite Telescope astronomical TV system, describing various developmental problems for future guidelines 24 p4415 A70-45824

OA O

Heat pipes in OAO 3 spacecraft for minimizing structural temperature gradients and validating thermal control approach 21 p3946 A70-41045

OA O

U OAO

OBLATE SPHEROIDS

Oblate earth gravitational field effect on ballistic missile trajectories, including body range determination and quadratures expressed by elementary functions 01 p0178 A70-10423

Earth oblateness effects on lunar and interplanetary trajectories, using algorithm based on orbital elements variations [AIAA PAPER 70-97] 06 p1146 A70-18203

Body surface curvature effect on surrounding laminar flow field, investigating oblate spheroids of various thicknesses 07 p1259 A70-19977

Solar oblateness and gravitational quadrupole moment related under assumption of magnetic and

OBSERVATION AIRCRAFT

velocity fields absence in surface layers, including rotation effects 08 p1570 A70-20902

Neptune and Pluto oblateness inferred from analogous similarities of mass, diameter and mean density with Uranus and Mars planets 09 p1750 A70-22096

Space probe trajectory near second order integration under influence of solar oblateness and gravitation 14 p2635 A70-30288

EM wave scattering and diffraction by acoustically soft and hard oblate spheroids 15 p2701 A70-32413

Prolate and oblate wave functions for EM radiation from spheroidal antenna in surrounding inhomogeneous medium 17 p3044 A70-35063

Plane wave incident on oblate spheroid or disk, deriving LF field scattering 18 p3335 A70-35974

Earth ellipticity in past, using hydrostatic equations based on density distribution and angular velocity to obtain oblateness 21 p3820 A70-41973

Solar rotation, discussing oblateness, solar wind torque, main sequence stars rotating core, gravitational quadrupole moments and Li and Be depletion 23 p4252 A70-44829

Nonspherical stars thermal stability, considering solar rotational models and oblateness problem 23 p4252 A70-44833

Solar oblateness calculation based on Stockly differential rotation law application to polytropes 23 p4253 A70-44835

OBLIQUE SHOCK WAVES

Oblique unsteady shock wave structure propagating at large Mach numbers in plasma cylinder under steady magnetic field, showing particle velocity profile discontinuity 01 p0064 A70-10999

Rocket nozzle originated oblique shock waves effect on near-field plume impingement flows, heat transfer and pressure distribution 04 p0737 A70-15421

Numerical results for perturbed downstream flow field resulting from entropy wave interaction with normal shock and oblique shock generated by wedge flow 05 p0835 A70-16788

Supersonic oblique shock wave reflection on turbulent boundary layer, considering layer separation and pressure effects 07 p1255 A70-19210

Oblique blast wave interaction with small bend along plane wall analyzed for diffraction using conformal transformation and complex variable techniques 10 p1869 A70-24524

Evolutionary hydromagnetic shock perturbation by incident small amplitude hydromagnetic wave calculated for diverging wave amplitudes and directions 11 p2036 A70-26017

Oblique shock initiated by 7 July 1966 proton flare in solar wind observed by satellite magnetometers outside magnetosphere 11 p2105 A70-26562

Gas-liquid two phase flow dynamics, explaining behavior under normal and oblique shocks 16 p2893 A70-33684

Shock waves and solitons structure propagating oblique to magnetic field in warm plasma based on two-fluid equations 21 p3857 A70-41382

OBSCURATION

U OCCULTATION

OBSCURATION

NT SATELLITE OBSERVATION

NT VISUAL OBSERVATION

Least squares adjustment of observation equations for hybrid systems solved by regarding constraints as observations with zero variances 02 p0289 A70-11798

Optimal control of continuous and discrete observations described by linear differential and recurrent algebraic equations in presence of random perturbations 03 p0447 A70-13341

Optimal control of continuous and discrete observations described by linear differential and recurrent algebraic equations in presence of random perturbations 14 p2561 A70-30717

Linear stationary systems observability with stochastic inputs for linearly independent row vectors, determining state vector components mean values 15 p2716 A70-32346

Linear systems simultaneous optimal stochastic control and observation strategies, assuming quadratic observation cost 16 p2886 A70-33346

Duality of optimal control and observation problems in cases of bounded coordinates and continuously acting perturbations respectively 21 p3801 A70-40605

OBSERVATION AIRCRAFT

NT CL-84 AIRCRAFT

NT G-91 AIRCRAFT

NT OH-6 HELICOPTER

- NT OV-10 AIRCRAFT
 NT RECONNAISSANCE AIRCRAFT
 T-63 gas turbine engine air induction system protection for OH-58A light observation helicopter against debris with minimum power loss and intake air distortion 01 p0164 A70-10681
 NASA operation of Convair 990 jet transport as airborne scientific research platform for optical observations 09 p1682 A70-23504

OBSERVATORIES

- NT ASTRONOMICAL OBSERVATORIES
 NT GEOPHYSICAL OBSERVATORIES
 NT LUNAR OBSERVATORIES
 NT OAO
 NT OGO
 NT OGO-A
 NT OGO-B
 NT OGO-D
 NT OGO-E
 NT OGO-F
 NT OSO
 NT OSO-B
 NT OSO-I

OBSIDIAN

- NT MOLDAVITE
 OBSIDIAN GLASS
 Rhyolitic obsidian glass devitrification rate in water and alkali solutions, noting increase in Na or K rich solutions 11 p2070 A70-26003

OBSTACLES

U BARRIERS

OBSTRUCTING

U BLOCKING

OCCIPITAL LOBES

- Electrical recording of retinal and occipital potentials in response to stimulation of human visual system used at levels from receptor to striate cortex 07 p1220 A70-19364
 Sensory deprivation induced EEG changes, discussing duration effect on poststimulation occipital alpha frequency 13 p2350 A70-29242
 Occipital migraine in flying personnel, discussing diagnosis and flight status disposition 24 p4297 A70-45344

OCCLUSION

- Acute coronary occlusion effects on adjacent unoccluded artery resistance, discussing responsible mechanisms in ischemic heart 04 p0637 A70-15473
 Occlusion training during hypodynamia with inflatable thigh cuffs to prevent unfavorable effects on cardiovascular system 10 p1816 A70-24689
 Methane and ethane hydrate number measurement, alleviating liquid water occlusion and evaluating pressure effect 13 p2362 A70-29212
 Steady flow of incompressible fluid through converging-diverging tube, considering implications in occlusive vascular disease 15 p2691 A70-31936
 Water and blood flow characteristics in converging-diverging plastic tube, considering implications in occlusive vascular disease 15 p2691 A70-31937

OCCULTATION

NT LUNAR OCCULTATION

NT SOLAR ECLIPSES

NT STELLAR OCCULTATION

- Venus atmosphere ionization distribution, temperature and pressure profiles determined from amplitudes and differential Doppler of radio signals to Mariner 5 during occultation 01 p0186 A70-11084
 Wilson effect in sunspot structure as penumbra foreshortening and disappearance or penumbra occultation by photosphere, analyzing intensity profiles on disk passage photographs 06 p1143 A70-18001
 Mariner 6/7 S band radio occultation probe of Mars atmosphere concerning surface pressure, temperature and existence of ionosphere 15 p2798 A70-31681
 S band occultation experiment for Mariner Mars 1971 orbiters, measuring atmospheric density and ionospheric electron density profiles 16 p2978 A70-34032
 Weather occultation satellite orbit determination by radio wave measurements between master and slave satellites, formulating mathematical model [AIAA PAPER 70-1067] 19 p3529 A70-38880
 Mars lower atmosphere vertical temperature distributions from Mariner 6 and 7 radio occultation data, using improved trajectory estimates 21 p3884 A70-40908
 Taurus A 21 cm radiation anomalous frequency decrease during occultation by sun attributed to particle streams propagating in solar corona 21 p3886 A70-41064

OCCUPATION

- Occupational and age composition of working population of U.S.S.R., comparing cardiovascular and respiratory systems 22 p3969 A70-42904

OCEAN BOTTOM

- Continental migration role in lunar maria formation, suggesting similarity with geological formation of earth ocean floor 09 p1765 A70-23797
 Oceanic ridge volcanic rocks alkali metal, alkaline earth, rare earth, nickel and major element content, observing partial melting 10 p1877 A70-24648
 Water depth determination by various remote sensing techniques, discussing bottom reflection, wave analysis, thermal anomalies and laser ranging by time difference 12 p2217 A70-26916
 Shallow water bottom biota, sediments and morphology determination by aerial and satellite photography 17 p3079 A70-35620
 Amino acid racemization as enantiomers in core sediment samples 21 p3781 A70-41896
 Electromagnetic variational soundings of ocean floor earth crust upper mantle near magnetic equator 23 p4189 A70-44066
 Ocean floor-spreading tectonic effects, considering Arabian Shield separation from African continent 24 p4332 A70-46408

OCEAN CURRENTS

- Circulation model of joint ocean-atmosphere system constructed with ocean and atmospheric models, discussing heat transfer by ocean currents 04 p0680 A70-15297
 Inertial Navigation System /INS/, geodetic reference and optimal data smoothing for estimating vertical deflection and ocean currents 22 p4069 A70-43665
 Ocean currents and sea surface temperature remote sensing by Nimbus 2 High Resolution IR Radiometer 24 p4332 A70-46400

OCEAN SURFACE

- Interaction between turbulent air flow and water surface based on Fourier analysis of finite intervals of field 11 p2042 A70-26775
 Microwave radiometer as passive satellite sensor for observing ocean surface properties 12 p2228 A70-26902
 Microwave radiometric temperature measurements generating curves relating sea state and surface temperature 12 p2215 A70-26903
 Sea and sea ice remote sensing by four-frequency radar /4FR/ system in EC-121 aircraft 12 p2215 A70-26904
 Sea roughness effect on bandwidth of radar backscatter, analyzing Doppler signals of eight millimeter aircraft navigation system 12 p2228 A70-26906
 Microwaves reflection, absorption and thermal emission at smooth air-water interface, tabulating calculated coefficients 12 p2183 A70-27169
 Laser profilometer for airborne ocean wave profile measurement 12 p2249 A70-28003
 Radar cross section sea clutter model based on slightly rough surface superposition on swell structure 13 p2366 A70-29215
 Motion equation derivation for incompressible fluid flow in baroclinic ocean, allowing for horizontal macroturbulent exchange 14 p2601 A70-30136
 Sun glitter on sea surface from space photographs, considering wind and sea conditions effect on shape and brightness of patterns 14 p2572 A70-30345
 UHF propagation measurement over sea for varying surface refractivity and meteorological conditions, noting diurnal variations 14 p2549 A70-30513
 Sea surface temperature and atmospheric moisture determination from satellite measurements of atmospheric thermal radio emission on quiet and cloudy windy days 15 p2770 A70-32069
 Anomalous dark areas in sunglint patterns from ATS photographs, considering water temperature effect on ocean surface conditions 16 p2897 A70-33725
 Sea water temperature and salinity effects on smooth ocean surface radiation in centimeter range 18 p3250 A70-36968
 Atmospheric layer attenuation of thermal radiation from water surface by airborne radiation thermometer measurements 18 p3260 A70-36969
 Autocorrelation functions of anomalous gravitational and magnetic fields for ocean lines, relating Mohorovičić boundary and Curie isotherm 19 p3408 A70-37318

- Forecasting air temperature over North Atlantic, analyzing atmospheric parameters informativeness 20 p3663 A70-39274
 Ocean swell wavelength and propagation direction measurements, using Fourier optical analysis of Apollo 7 space photography 22 p4029 A70-42766
 Sea surface temperature relationship with ocean currents, using bathythermograph data 22 p4014 A70-42768
 Ocean roughness determination from satellite photographs sunglint patterns, indicating surface wind speeds 22 p4014 A70-42770
 Airborne optical scanning gyro for measuring sea surface radiation emission 22 p4039 A70-43558
 Ocean wave spectra from bistatic radar scatter data, using time delay Doppler-frequency map 23 p4184 A70-43802
 Ocean currents and sea surface temperature remote sensing by Nimbus 2 High Resolution IR Radiometer 24 p4332 A70-46400
- OCEANOGRAPHY
 NT MARINE BIOLOGY
 Reworking of deep-sea sediments as indicated by vertical dispersion of Australasian and Ivory Coast microtektite horizons, implying years of deposition 01 p0178 A70-10474
 UHF radio telemetry system using pulse signal to measure and transmit sea waves amplitude and frequencies data to shore-based recorder 03 p0453 A70-14352
 Earth environmental satellite data for oceanography and hydrology, discussing sea surface temperature mapping, low level wind conditions, snow and ice mapping, etc 04 p0676 A70-14635
 Bottom topography effect on jets stability in baroclinic fluid, discussing two layer model 04 p0715 A70-15518
 Remote sensors for measurement and mapping of ocean color variations, discussing Widerange Image Spectrophotometer and Water Color Spectrometer 06 p1073 A70-18592
 Spatial resolution and repetition intervals for optimum utilization of space-derived remotely sensed data of ocean surface features 06 p1060 A70-18593
 Aerospace technology contributions to oceanography, discussing lightweight structures, electronics, automatic systems and submarine laboratory application 07 p1263 A70-19135
 Range positioning system as automatic indicator in oceanography, aboard land vehicles and aircraft 08 p1541 A70-21360
 Abstracts with references to literature sources on oceanography from space and aircraft 09 p1665 A70-22014
 Turbulence and internal waves in stably stratified atmosphere and ocean, proposing velocity and temperature spectral behavior model 09 p1716 A70-22370
 Internal waves breaking on sloping surface in two fluid system, studying interfacial shear instability by capacitance probe on-line computer system 09 p1717 A70-22371
 Microwave radiometric techniques for continuous all-weather remote sensing of sea conditions from satellites, discussing foam and surface ripple effects [AIAA PAPER 70-318] 09 p1677 A70-22869
 Satellite remote sensors for oceanographic applications, estimating resolution requirements for temperature, spatial interval, roughness patterns, wind speeds, etc 09 p1668 A70-22880
 Microwave radiometer as passive satellite sensor for observing ocean surface properties 12 p2228 A70-26902
 Passive remote sensing in microwave spectra for oceanographic applications including sea state, pollution and sea ice properties 12 p2216 A70-26905
 Aerial oceanographic photographic image enhancement by including blue spectral region, presenting Apollo 9 space photographs 12 p2217 A70-26917
 Oceanographic potential of spacecraft, discussing synoptic scanning, International Decade of Ocean Exploration, etc 12 p2225 A70-27746
 Spacecraft tracking methods applied to solid earth and ocean physics 15 p2809 A70-31685
 Oceanic volcanic rocks, discussing dispersed element characteristics to describe origin of magma types 15 p2731 A70-32100
 Oceanographic phenomena inference from satellite cloud photographs, developing seasonal cloud climatology for Peru Current area 16 p2897 A70-33713
 Fluidic technology applications to space and oceanography, discussing control, monitoring, sequencing and signal processing 16 p2845 A70-33714

- Aerial IR surveys of surface temperature patterns of Hudson Bay during ice free seasons
17 p3079 A70-35621
- Criticism of theory for cosmogenic tritium produced oceanic He 3 excess
21 p3920 A70-41883
- Earth orbital experiments synthesis in space programs methodology, discussing examples in astronomy, biology and oceanography research
22 p4097 A70-42500
- Ocean swell wavelength and propagation direction measurements, using Fourier optical analysis of Apollo 7 space photography
22 p4029 A70-42766
- Space and astronomic methods applied to solid earth and ocean physics
22 p4025 A70-43669
- North Carolina continental shelf discolored water origin, movement and dissipation from Apollo 9 photograph interpretation
24 p4329 A70-45361
- ## OCEANS
- ### NT ATLANTIC OCEAN
- ### NT INDIAN OCEAN
- ### NT PACIFIC OCEAN
- Earth surface hydrology effect incorporated into atmospheric circulation mathematical model for climate, considering ocean as atmospheric moisture reservoir
04 p0680 A70-15296
- Earth rotational velocity irregularities and horizontal motions of continental blocks at expense of oceanic hemisphere, noting seasonal distance changes
04 p0681 A70-15477
- Sea surface sunglint pattern irregularities in earth orbiting satellite photographs, observing dark patches
05 p0838 A70-16152
- Ocean surface roughness time variation effect on incident laser beam, analyzing motion picture data by computer program
05 p0860 A70-16687
- Wave surface elevation and velocity fluctuations in ocean upper layer under wind waves, discussing correlation coefficients between vertical and horizontal velocity components
06 p1097 A70-17792
- Backscattered sun and skylight spectra from sea obtained from low flying aircraft as measure of chlorophyll concentration
09 p1666 A70-22250
- Oceanic wind and wave predictions by satellite radar radiometer using single receiver to determine wind velocity
09 p1668 A70-22877
- [AIAA PAPER 70-310] Survival on sea following air accident, based on medical and technical considerations, emphasizing life jackets
09 p1625 A70-23008
- Wastes dispersion discharged into sea analyzed by aerial photography, measuring diffusion
10 p1879 A70-24749
- ## OCTAHEDRAL RESEARCH SATELLITES
- ### U ENVIRONMENTAL RESEARCH SATELLITES
- ## OCTAHEDRITE
- ## U MINERALS
- ## OCTAHEDRONS
- Octahedral solid-solid phase transitions by differential thermal analyzer and scanning calorimeter module, discussing entropy change causes
21 p3784 A70-42264
- ## OCULAR CIRCULATION
- Binocular fundus refectometry and plethysmography in rabbits and man after dye injection and in patients with carotid occlusion
24 p4310 A70-46345
- ## OCULOGRAPHIC ILLUSIONS
- Illusory visual signals experienced by pilots ascribed to aerodynamic forces interference with normal functional relationships between sensory systems
09 p1627 A70-23131
- Pilot disorientation in dark night takeoff accident type, presenting illusory angular displacement of vertical, flight paths and sequential accelerations
13 p2359 A70-29441
- ## OCULOMOTOR NERVES
- Neurons and perineuronal glial cells quantitative relations in visual cortex from anesthetized dogs
01 p0025 A70-11030
- Eye movements during two dimensional tracking tasks, showing oculomotor system transfer characteristics function of target motion spectral content
03 p0427 A70-13948
- Human saccadic system properties, discussing eye movements and correction saccades with and without visual fixation points
03 p0427 A70-13949
- Efference role in eye tracking of moving targets, discussing oculomotor system role
03 p0439 A70-14345
- Non-specific influences on rabbits neurons reaction to nonvisual stimuli in central visual pathway using microelectrodes implantation in visual cortex
05 p0802 A70-16624
- Efferent and afferent fibers presence in optic nerves determined by unilateral and bilateral enucleation of dogs and cats
07 p1207 A70-19476
- Nonlinearity of human eye movement control system in two dimensional tracking tasks, explaining visual axis lags as time delays dependent on target motion
08 p1447 A70-21724
- Prolonged hypodynamia effects on visual analyzer, investigating functional weakening, fundus oculi appearance change and restoration after normal activity resumption
10 p1816 A70-24687
- Anatomical and physiological correlations between mathematical model components for vestibular nystagmus mechanisms
13 p2351 A70-29331
- ## ODESSA METEORITE
- Nitrogen content of Odessa and Canyon Diablo iron meteorites from thermal neutron activation, Kjeldahl distillation and alkali fusion methods
21 p3921 A70-41942
- ## ODORS
- Odor threshold levels for unsymmetrical dimethylhydrazine/UDMH/ and nitrogen tetroxides
18 p3224 A70-36227
- ## OFF-ON CONTROL
- Picosecond on-off light gate based on Kerr cell design, using optical pulses to induce birefringence in liquids
01 p0111 A70-10571
- Monolithic zero crossing AC trigger IC for thyristor power control systems operating in on-off mode
08 p1478 A70-20786
- Nonlinear control systems on-off oscillations with instants of commutation determined by simultaneous equations, noting feedback control
11 p2027 A70-26254
- Laser field transient properties in switching-on processes, discussing Q switching, detuning switch-off and pump power switch-on
11 p2064 A70-26843
- Performance cost functions for reaction-jet controlled spacecraft during on-off-on limit cycle
13 p2382 A70-29072
- Book on differential dynamic programming covering algorithms for continuous time control, bang-bang, discrete time and stochastic systems
14 p2560 A70-30631
- Initial condition sensitivity functions in bang-bang and optimal control, considering discontinuous functions, perturbation equations, iteration algorithms terminal states, cost functions, etc
16 p2885 A70-33325
- Bang-bang control of electrohydraulic servomechanisms, approximating optimal control by quasi-optimal controls
16 p2887 A70-33685
- Start-stop dynamics as cost effective method for computerized testing of digital modules and subassemblies, providing static and dynamic capability
17 p3062 A70-35504
- Performance cost functions of on-off limit cycle controllers for reaction jet controlled system
17 p3056 A70-35552
- Steady state off-on attitude control strategy for minimizing propellant consumption and thrust ignitions of satellite in presence of environmental disturbance torques
17 p3180 A70-35556
- Bang-Bang principle and vector functions at extreme points, considering Lebesgue measure and Liapunov theorem
23 p4176 A70-44237
- ## OGEE WINGS
- ## U VARIABLE SWEEP WINGS
- ## OGIVES
- Inviscid transonic approximation theory, calculating mixed flow field around nonlifting slender ogive body, accounting for shock wave generation, strength and location
06 p0972 A70-18132
- [AIAA PAPER 70-189] Pointed ogival body of revolution in supersonic flow field, investigating local pressure distributed by variational methods
23 p4136 A70-44992
- ## OGO
- ### NT OGO-A
- ### NT OGO-B
- ### NT OGO-D
- ### NT OGO-E
- ### NT OGO-F
- OGO spacecraft structures, thermal control systems, attitude control, weight and power supplies
15 p2810 A70-31782
- OGOs design evolution with respect to scientific mission requirements
17 p3180 A70-35303
- Complex impedance measurements for monopole antenna for electron densities in/out of OGO satellite wake in upper ionosphere
17 p3080 A70-35771
- OGO 5 observations of quasi-trapped electromagnetic waves in solar wind at 70 kHz
18 p3306 A70-36005
- Electron intensity long term variations above 500 MeV by OGO-5 satellite-borne cosmic ray electron detector, supporting diffusion-convection theory of solar modulation
19 p3497 A70-37522
- Extraterrestrial gamma radiation from Cygnus region of galactic disk, using OGO-5 observations
19 p3501 A70-38087
- Electron densities between inner edge plasma sheet and plasmasphere as function of geocentric radial distance from OGO-3 electrostatic measurements
23 p4236 A70-43834
- ## OGO-A
- Magnetospheric observations of whistler mode emissions by OGO 1 satellite over VLF and LF ranges
04 p0649 A70-15117
- Electron density profiles along OGO 1 orbit portions calculated by measuring harmonic radio beacon transmissions differential Doppler frequencies and Faraday polarization rotation angle
04 p0741 A70-15118
- ## OGO-B
- Micrometeoroid experiments on OGO 2 and OGO 4 satellites, measuring velocity, masses and particle orbits in earth dust cloud
01 p0086 A70-10444
- ## OGO-D
- Micrometeoroid experiments on OGO 2 and OGO 4 satellites, measuring velocity, masses and particle orbits in earth dust cloud
01 p0086 A70-10444
- GEOS A and OGO-4 satellite orbits and trajectory analysis using Definitive Orbit Determination System, discussing tracking stations error rate
24 p4407 A70-45536
- ## OGO-E
- OGO 5 satellite scientific observations, payloads, parameters and objectives
15 p2812 A70-32364
- Cosmic ray electron and positron differential energy spectra during solar quiet times from OGO-5 satellite observations in interplanetary space
19 p3502 A70-38096
- Interstellar cosmic ray electron spectrum flattening below 3 GeV from OGO-5 observations
19 p3504 A70-38106
- ## OGO-F
- Ionospheric electric fields variations in ELF-VLF, confirming OV-1 satellite measurements with OGO 6 data
13 p2403 A70-30082
- ## OH-6 HELICOPTER
- Inertial particle separator-type turbine engine air cleaner for OH-6A light observation helicopter, describing evolution
01 p0164 A70-10682
- ## OHMIC DISSIPATION
- Joule dissipation model for sunspot magnetic field, discussing field fine structure and lifetime
02 p0373 A70-12374
- Heat transmission by current carriers to cryogenic region, ascribing heat flux to Joule effect in conductor
05 p0881 A70-16025
- Heating rate of radio electronic equipment with variable power shown dependent on initial dissipated power
10 p1853 A70-25134
- Gravity wave attenuation in F region investigated for role of ohmic losses
10 p1885 A70-25264
- Ionosphere dynamo region thermal input by Joule heating and solar radiation and coupling to various thermotidal modes, observing semi-diurnal and semi-monthly effects
11 p2047 A70-26569
- Turbulence energy balance equations for conducting fluid flow in longitudinal magnetic field with Joule dissipation
12 p2282 A70-28227
- Infrasonic waves generated by pulsating aurora, using Joule heating and Lorentz force coupling
13 p2399 A70-29236
- Flat plate and cylinder with periodic Joulian heating from time dependent heat source, analyzing transient temperature distribution
14 p2664 A70-30269
- Ohmic dissipation in MHD plasma acceleration, demonstrating interaction with electric field and magnetic induction
14 p2621 A70-30296
- Compressible plasma flow in axisymmetric channels under EM body forces and Joule heating
23 p4228 A70-44934
- ## OHMMETERS
- Portable megaohmmeter for measuring insulation resistance of strain gauge ceramic installations
05 p0848 A70-16378
- ## OHMS LAW
- Ohms law of electromagnetohydrodynamics derived on basis of Lorentz hydrodynamic plasma model, considering plasma conductivity
05 p0890 A70-16852

Ion-acoustic instability effect on HF EM field penetration into plasma taking into account nonlinear Ohm law

11 p2089 A70-25715

Electron-neutral interaction parameters for Ohm law coefficients in multicomponent nonisothermal plasmas tabulated as function of electron temperature

22 p4081 A70-43015

OIL ADDITIVES

Potentiometric analysis for determining acidity and alkalinity in dark mineral oils with additives

05 p0810 A70-15898

Liquid and solid lubricants, discussing properties, temperature ranges, costs, environmental effects and outlook

07 p1316 A70-18953

OILS

NT CRUDE OIL

NT LUBRICATING OILS

NT MINERAL OILS

Purity requirements for oil in hydraulic systems of modern aircraft, discussing filtering devices and Swedish Air Force and SAAB specifications

01 p0130 A70-11359

Diffusivities of argon, krypton and xenon determined in olive oil by curve-fitting analysis of sorption curves

03 p0429 A70-14159

Vibration damping of oil hydraulic system using bladder type accumulator composed of rubber, measuring frequency response of shock absorber

06 p0988 A70-17140

Free incompressible oil jet interaction with mobile plate, discussing plate configuration, oil feed pressure and nozzle diameter, applications to electrohydraulic converter design, etc

09 p1613 A70-22825

Oil pollution remote sensing by aircraft, utilizing 9-14 micron IR mapper, 19.35 GHz microwave radiometer, aerial cameras and multiband video system

10 p1878 A70-24740

Pressure loss in tubulature of oil-hydraulic drive mechanism, allowing for viscosity changes associated with oil temperature and pressure increases

10 p1809 A70-25209

Proportional and flip-flop elements in hydraulic circuits using oils, noting cavitation effect on switching stability in digital elements

14 p2534 A70-30677

U.S. Coast Guard air delivered antipollution transfer system for oil, discussing deployment method, trajectory analysis, rigging techniques and full scale testing [AIAA PAPER 70-1205]

21 p3752 A70-41813

OLEFINS

U ALKENES

OLEIC ACID

Oleic acid concentration effects on electron work function during surface-active agent deposition on Fe, Ni, Cu, Al and steel surfaces

01 p0099 A70-10074

OLFACTORY PERCEPTION

Cortical induction phases estimated by retinal mobility index concerning activity of acoustic, olfactory and cutaneous analysors

08 p1443 A70-20735

Odor threshold levels for unsymmetrical dimethylhydrazine (UDMH) and nitrogen tetroxides

18 p3224 A70-36227

OLIVINE

Abundance levels of K, Rb, Sr and Ba in pyroxenes, olivines and garnets of ultramafic rocks for upper mantle composition

03 p0472 A70-13149

Shock and thermal metamorphism of olivine trachybasalt by nuclear explosion at Nevada test site

05 p0843 A70-16946

Shock wave compression of single olivine crystals and specimens from chondritic meteorites, observing planar deformation microstructures

07 p1391 A70-20353

Olivine and metal compositions of pallassitic meteorites by electron microprobe measurements, obtaining cooling rates

12 p2296 A70-26895

Plagioclases, pyroxenes and olivines in lunar soils and rocks, using X ray diffraction and Mossbauer effect

21 p3899 A70-41528

Apollo 11 lunar rock lavas and breccias, examining opaque minerals and olivine by reflection microscopy, electron probe and optical absorption measurements

21 p3899 A70-41530

OMEGA NAVIGATION SYSTEM

Mark III airborne Omega system designed as receiver-computer to demonstrate real time operation, discussing flight test results

01 p0136 A70-10302

Omega position location experiment applied to ship navigation, air traffic control and moving vehicle surveillance, noting daytime and night fixing accuracy

01 p0136 A70-10307

Satellite navigation efficiency compared with inertial and Omega navigation techniques

01 p0139 A70-11263

Omega position location equipment /OPLE/ experiment data analysis, obtaining quantitative measure of statistical performance of system

02 p0336 A70-12180

User problems in navigation methods, discussing Omega method, Navy Navigation Satellite System and VLF methods

03 p0522 A70-13603

VLF radio wave propagation variations occurring in earth-ionosphere waveguide contributing to errors in OMEGA position lines used to obtain worldwide navigational fixes

03 p0523 A70-13614

OMEGA frequencies propagation characteristics measured to estimate navigation errors from multiple waveguide propagation modes close to transmitter, comparing day and night errors

07 p1330 A70-19222

Earth-ionosphere waveguide propagation variations effects on Omega navigation system position errors

08 p1541 A70-21564

LSI Mark 3 airborne Omega system with computerized signal processing for navigation parameters, discussing system features and flight test results

09 p1719 A70-22190

Omega Position Location Experiment with synchronous satellite /ATS-3/ as radio relay for merchant shipping, air traffic control and moving vehicle location and communication

09 p1720 A70-22193

Omega Position Location Equipment /OPLE/ system, testing operational feasibility of centralized global meteorological data collection system

09 p1722 A70-23030

Signal format for eight station Omega network, considering integrating /DR/ receiver and concept combining time multiplex and frequency multiplex signals

09 p1722 A70-23031

Loran-C and Omega radio navigation systems, discussing hostile environment operation and hardware processing

11 p2081 A70-26507

Course deviation indicator /CDI/ display applicability to tracking Omega lines of position, providing reduction in weight, volume, cost and complexity

12 p2269 A70-27920

Decca, Loran C/D and Omega LF and VLF hyperbolic navigation systems

23 p4215 A70-43865

General aviation aircraft influences on federal airways systems, considering area and Omega navigation examples [AIAA PAPER 70-1314]

24 p4373 A70-45929

OMEGATONS

Omegatron for total and partial pressure measurement or mass spectrometer applications

12 p2231 A70-27262

OMICRON CETI STAR

Omicron Ceti [Mira/ spectrophotometry before, during and after 1969 maximum, noting TiO bandwidth variations

23 p4242 A70-44294

OMNIDIRECTIONAL ANTENNAS

NT MONOPOLE ANTENNAS

S-band omnidirectional antenna patterns measurement procedure and results for Apollo spacecraft configurations, tabulating measure gains

06 p1019 A70-17507

Design features and experimental results of E-fed cavity type suppressed omnidirectional antenna for VHF operation

06 p1022 A70-18020

Stacked, vertically polarized collinear arrays of independently fed omnidirectional antennas for flight testing Doppler radar aircraft warning system

12 p2199 A70-27968

Synthesis of vertically polarized omnidirectional pattern with cascade dipole antennas on conducting cylinder

15 p2697 A70-31832

OMNIDIRECTIONAL RADIO RANGES

VHF omnidirectional range /VOR/ receiver, considering noise reduction problem and active filter importance to signal improvement and system accuracy

22 p3992 A70-43586

Aircraft Doppler VHF omnidirectional range /DVOR/ performance test, noting improvement over VOR system

24 p4375 A70-46240

OMNIRANGE NAVIGATION

U VHF OMNIRANGE NAVIGATION

ON-LINE PROGRAMMING

On-line electronic integration of aortic flow during systole to provide beat by beat readout of stroke volume

01 p0038 A70-11044

Hardware-software integrated time sharing computer system for testing transmission control units and associated terminals on line

02 p0275 A70-12189

Computer program for on-line analysis of exercise ECG considered for improved diagnosis of ischemic heart disease

05 p0805 A70-16105

Display Oriented Computer Usage System /DOCUS/, discussing on-line display console management in multiaccess environment, display oriented language, compiler, etc

05 p0817 A70-16181

BR-90 visual analysis control as flexible and versatile display for command and control, discussing on-line data processing, maintenance, etc

05 p0827 A70-16182

Flight plans monitoring in real time with on-line computer for optimal route, fuel consumption and speed

05 p0817 A70-16362

On-line system transmitting experimental data from optical spectrometer to central computing facility for magnetic tape recording

05 p0818 A70-16846

On-line computer programs allowing for man machine interactions in linear circuits design

06 p1015 A70-18417

Computer-generated shaded flicker-free on-line digital video display, allowing superimposed vector graphics with light-pen interaction

09 p1640 A70-22033

Computer aided on-line test generation for prelaunch checkout, describing interpretive test language for rapid man machine information transfer [AIAA PAPER 70-384]

10 p1846 A70-24921

Space vehicle velocity-attitude optimal control for on-line trajectory control schemes

11 p2025 A70-26216

Spacecraft launch computerized simulator, discussing operational characteristics applicable to on-line real time process control

11 p2013 A70-26217

Space vehicle on-line tracking with impulsive thrust maneuver by sequential estimation scheme, reducing radius measurement error

11 p2008 A70-26237

On-line parameter updating for relationship between Martian atmospheric density and height above surface during spacecraft descent based on least squares approach

11 p2113 A70-26318

Computerized on-line industrial inspection involving automatic machine sequential control and product geometry error correction, discussing hardware and software requirements [SME PAPER IQ-70-712]

12 p2241 A70-27088

Suboptimal control of discrete input system with bounded state and control variables, developing algorithm for on-line computation

12 p2203 A70-27409

On-line reduction of nystagmic data during vestibular bithermal caloric testing by analog technique

15 p2685 A70-32570

On-line computer aided design of fixed point digital filters simulating direct, cascade and parallel bit representations

15 p2711 A70-32598

Filters design by on-line graphic interface computerized synthesis utilizing three screen CRT display

16 p2867 A70-33041

On-line optical data processing using CRT with electro-optic target crystal

16 p2903 A70-33132

Direct access on-line information retrieval system combining computer assisted instruction and bibliographic retrieval, using thesaurus for literature indexing

17 p3048 A70-34600

On-line final V/STOL Wind Tunnel Data Encoding and Evaluation System /WINDEE/ for complex powered models, using computer monitoring

17 p3049 A70-35494

On-line display of pulsed rocket engine performance data using hybrid computer

17 p3063 A70-35512

Computer driven on-line CRT graphics displays for data acquisition and reduction

17 p3063 A70-35513

Solid state display for on-line information retrieval using light emitting crystals, integrated circuits and hybrid packaging

17 p3063 A70-35514

Commercial air transport mission payload and range capability analysis, noting on-line flight planning computers [AIAA PAPER 70-899]

17 p3204 A70-35815

Data management methodology for test facilities, considering on-line analog/digital computers

19 p3383 A70-37922

Pulsar single pulse search at Jodrell Bank by on-line computer

21 p3923 A70-42102

ONBOARD EQUIPMENT

NT AIRBORNE EQUIPMENT

NT AIRBORNE/SPACEBORNE COMPUTERS

NT SPACECRAFT ELECTRONIC EQUIPMENT

Onboard radar self contained all-weather landing and taxiing /SALT/ system, discussing concept, requirements and results [AIAA PAPER 69-1053]

01 p0138 A70-10641

Si solar cells for powering artificial satellites onboard equipment, discussing fabrication and substitute materials

01 p0011 A70-11253

Radiation dosimetry and shielding onboard Cosmos 110 artificial satellite, noting earth belt proton radiation

01 p0198 A70-11518

Digital onboard telecommunications and tracking equipment based on Dioscures two satellite system for L band operation

03 p0442 A70-12990

Digital telemetry systems for geophysical satellites, describing onboard and ground systems design criteria and experimental results

03 p0451 A70-13837

Cockpit information transfer between pilot and flight control information displays improved by onboard data processing system

03 p0436 A70-14021

Optical approach navigation experiment on 1969 Mariner mission to Mars demonstrating accuracy potential of spacecraft-based measurement

[AIAA PAPER 70-70]

06 p1103 A70-18152

Baseline length and orientation of closely co-orbiting satellites estimated by combined onboard sensor and ground tracking data

[AIAA PAPER 70-39]

06 p1146 A70-18186

Onboard and ground checkout systems for space station and space shuttle operations

[AIAA PAPER 70-245]

07 p1251 A70-20373

MADAR onboard maintenance system designed for C-5 aircraft monitoring line replaceable units in electrical, avionics, environmental, mechanical and propulsion systems

[AIAA PAPER 70-243]

07 p1195 A70-20375

Onboard automatic test equipment design, evaluating failure detection and reporting ability

08 p1470 A70-20667

Engine performance monitoring system (EPMS) for aircraft jet onboard operation analysis and failure detection

08 p1558 A70-20668

Built-in test equipment for automatic flight control systems, discussing testing programs and fail safe hybrid circuitry

08 p1471 A70-20670

Liquid helium cryostat for onboard satellite storing designed with allowance for overloads and vibrations during powered flight

08 p1440 A70-21220

Grand tour space probe optics for observation of objects on planet, considering atmospheric refraction indices effect

09 p1700 A70-23768

Multiple access technique for millimeter wave satellite communications, noting weight and size of onboard equipment

10 p1838 A70-24359

Onboard cargo loader to make aircraft independent of specialized ground equipment

10 p1862 A70-25330

Open magnetic electron multipliers (MEM) with continuous dynode and field strips for satellite-borne detection systems, emphasizing extreme UV detectors

11 p2049 A70-25628

Digital closed-loop inflight calibration system for spaceborne particle spectrometers, utilizing cesium iodide crystal and programmable photomultiplier dynode supply

12 p2232 A70-27405

Intercoms 2 equipment for measurement of positive ion concentration, electron temperature and energy distribution, electron concentration between satellite and ground reception points, etc

12 p2207 A70-27500

Checkout systems for shuttle and orbiting space stations, discussing shift from ground to onboard operation

12 p2208 A70-27691

Space navigation for Apollo 11 mission, emphasizing ground and onboard systems, interfaces with guidance and use in phases of lunar landing

13 p2447 A70-28547

Onboard navigational requirements for future planetary missions, discussing major subsystems

13 p2448 A70-28701

Spacecraft based data processing stages to perform navigation during outer planet missions

13 p2448 A70-28704

Spaceborne logarithmic variable prescaling counters for automatic compression of particle measurement data, discussing statistical error

13 p2406 A70-28931

Projectiles yawing and rolling over long flight paths, describing onboard solar aspect sensor and telemetry link to ground stations

13 p2406 A70-29005

Onboard automatic checkout systems for manned space vehicles, investigating data management development costs for thorough tradeoff studies

16 p2889 A70-33803

Nimbus weather satellites mechanical devices and subsystems, including solar array drive, fluid thermal

control sensors, horizon scanners and hydraulic dampers

16 p2921 A70-34105

Scan platform servomechanical actuator for Mariner Mars 1969 spacecraft, emphasizing gear arrangement and train dynamics

16 p2845 A70-34108

Spacecraft hydraulic timers design and qualifications testing, discussing oil selection and temperature dependence

16 p2914 A70-34112

Aircraft onboard maintenance recording system, discussing design and effectiveness

17 p3094 A70-35516

Engine vibration monitoring system for Boeing 747 aircraft, including piezoelectric transducer, transmission assembly and differential charge converter

19 p3426 A70-37898

Logic, arithmetic, control and instruction capacities of dedicated onboard telemetry preprocessor

19 p3383 A70-37904

Satellite electrometer for weak DC currents due to charged particle flux

19 p3428 A70-38485

Free air temperature by onboard satellite IR spectrometer (SIRS), measuring earth spectral radiance in carbon dioxide 15 micrometer band

20 p3660 A70-39077

Michelson IR interferometer spectrometer (IRIS)/design calibration and performance onboard Nimbus 3 satellite, demonstrating data reduction and inflight calibration

20 p3626 A70-39078

ATC by scanning beam ILS and onboard control systems, increasing airport capacity and terminal area safety

[AIAA PAPER 70-1033]

Onboard velocity sensors for VOR/DME navigation systems positional accuracy improvement, describing optimal and suboptimal data filtering

[AIAA PAPER 70-1024]

Medical monitoring system onboard Soyuz spacecraft, describing equipment design, data acquisition and analysis, telemetric recordings, etc

20 p3581 A70-40193

Medical support for long space missions based on space crews morbidity prediction, discussing onboard equipment and astronaut training

20 p3575 A70-40194

X ray astronomy instruments on sounding rockets, balloons and satellites, investigating sources distribution on celestial sphere

21 p3821 A70-40652

Baseline length and orientation of closely coorbiting satellites estimated by combined onboard sensor and ground tracking data

[AIAA PAPER 70-39]

Spacecraft radioisotope thermoelectric generator interference in onboard instrument operation, using analytical models to determine necessary shielding

24 p4375 A70-45175

C5 Malfunction Detection Analysis and Recording (MADAR) subsystem for onboard fault isolation including engines

[SAE PAPER 700820]

Aircraft onboard radar system with landing monitor perspective display of runway operating independently of ground based electronic equipment

[AIAA PAPER 70-1336]

Space shuttle onboard cost effective data management system, discussing checkout, fault isolation, redundant element switching and crew interaction

[AIAA PAPER 70-1293]

Onboard digital information processing, discussing applications to tactical missile guidance and manned vehicles

[AIAA PAPER 70-1230]

ONBOARD NAVIGATION
U NAVIGATION
ONE DIMENSIONAL FLOW

Steady one dimensional flow in gas filled cylindrical tube, studying shock induced compression wave generated by sudden piston acceleration

01 p0062 A70-10804

Relaxation in gas-particle flow, analyzing thermodynamic properties, interactions, single particles and one dimensional flow equations

01 p0062 A70-10805

Plasma unsteady one dimensional flow behind shock wave front in shock tube MGD channel, deriving differential gas dynamics equations

04 p0726 A70-14540

Numerical integration of differential equations governing one dimensional flow of reactive gas, discussing flows of converging-diverging nozzle and normal shock waves

04 p0671 A70-14992

One dimensional unsteady gas flows formation theories extended to include viscosity, heat conductivity, diffusion and chemical reactions effects

04 p0672 A70-15230

Solar wind as one dimensional flow analogous to Laval nozzle flow, discussing rotation and magnetic field effect on model with heat conduction

04 p0754 A70-15352

One dimensional steady adiabatic source nonisentropic flow of thermally and calorically perfect gas in conical nozzle, considering exit divergence and nonuniform flow effects

04 p0619 A70-15427

One dimensional unsteady heat conduction with variable boundary conditions solved by difference-differential method using rectangular and cylindrical coordinates

05 p0957 A70-16295

Burgers one dimensional model equation for homogeneous turbulence treated by Fourier transform in space and time, using Bogoliubov expansion method

05 p0833 A70-16331

Unbranched chain reaction in hydrogen bromide for studying laminar one dimensional flame propagation, determining temperature dependence, velocity and concentrations at fixed time

06 p1177 A70-17797

Interference between body and porous walls of water tunnels by one dimensional solution for usable length of tunnel

07 p1248 A70-19078

One dimensional steady neutral shock wave structure, using expanding Boltzmann equation distribution function in terms of Hermite polynomials

07 p1260 A70-19984

Numerical solutions of one dimensional expanding flow of dissociating gas initially in frozen state for variations in recombination rate

08 p1484 A70-21531

Plane one dimensional motion of shock wave with moving inner boundary investigated for given shock wave front position and gas mass and energy

09 p1659 A70-22432

Monatomic gas rarefaction wave structure in unsteady one dimensional flow from high to low pressure zones, describing numerical solution technique

09 p1604 A70-22449

Magnetic field and gas thermal conductivity effects in analysis of solar wind as one dimensional, steady and spherically symmetric flow

09 p1745 A70-22687

Finite plates impact flow field analysis from isentropic one dimensional flow equations solution through hodograph transformation

09 p1776 A70-22721

One dimensional flow field behind ionizing detonation wave in magnetic field using Chapman-Jouguet hypothesis, accounting for Alfvén speed

09 p1660 A70-22722

Steady and unsteady viscous incompressible one dimensional flows parameters in deformable cylindrical tube determined, solving continuity and motion equations by Galerkin method

09 p1664 A70-23715

Quasi-one dimensional motion of perfect compressible fluid through pipe, considering one dimensional schemes in aerodynamics

10 p1865 A70-24102

One dimensional Navier-Stokes equations solution for viscous heat conducting gas flow involving spherical sink for finite pressure at infinity

10 p1865 A70-24104

One dimensional fluid flows with shock waves described by constructing discontinuous solution for gas dynamic equations, using successive approximation

10 p1866 A70-24113

Radiating shock wave reflection from rigid wall studied for velocity and structural changes, assuming unsteady and one dimensional flow

10 p1867 A70-24140

Partial differential equation describing one dimensional heat transmission problems solved by eigenvalues for initial and boundary conditions

10 p1969 A70-25098

One dimensional compressible constant entropy flows stability, noting unstable regions with fluid particles undergoing compression

11 p2034 A70-25679

Time dependent analysis for quasi one dimensional, vibrational and chemical nonequilibrium nozzle flows approaching steady state solution by finite difference technique

11 p1976 A70-25974

One dimensional compound compressible nozzle flow solution dependence on initial conditions and nozzle geometry, discussing applications to bypass turbojets and solid propellant motors

11 p1976 A70-26137

One dimensional compressible flow with heat addition in nonconstant area duct extended for friction addition, discussing critical thermal shocking

11 p2041 A70-26651

One dimensional perfect gas motion under spatial pressure distribution, investigating self similar solutions

12 p2212 A70-28189

One dimensional steady state flows and discontinuities in radiation gas dynamics, neglecting radiation pressure, viscosity and heat conduction

13 p2387 A70-28937

Contraction coefficients for compressible discharge through axisymmetric sharp edged orifice, obtaining approximate analytical expression based on one dimensional theory

13 p2389 A70-29549

Unsteady one dimensional motion of reacting gas mixtures in presence of supercompressed detonation waves, discussing transformation into Chapman-Jouguet wave

13 p2522 A70-29772

One dimensional Alfvén fluctuation spectrum of magnetosphere in toroidal, crimping and twisting modes, using numerical integration

14 p2569 A70-30203

Pseudo one dimensional dissociational nonequilibrium nozzle flows, obtaining equilibrium and nonequilibrium solution through similar transformation of governing equations

14 p2527 A70-30264

Gas flow calculations application to gas turbines simulations, considering engine dynamics, one dimensional flow and program structure

14 p2629 A70-30990

Monograph on steady shock waves in one dimensional frictionless gas flows with thermodynamic relaxation, using continuum mechanics

16 p2891 A70-33294

Weak nonlinear one dimensional wave propagation in nonequilibrium flow, using governing system characteristics for reference coordinates

17 p3071 A70-35468

Viscous heat-conducting one dimensional piston driven gas flow, assuming sharp shock discontinuity

17 p3075 A70-35890

One dimensional steady gas flow, deriving algorithm for iterative solution of Boltzmann kinetic equation by statistical approach

18 p3241 A70-36285

Axisymmetric one dimensional compressible flow theory applications to compressible fluids ducted flow [ASME PAPER 70-GT-82]

18 p3243 A70-36882

Optimal control for one dimensional compressible gas flow, combustion and heat exchange, described by first order partial differential hyperbolic equations

19 p3402 A70-37240

Nonuniform one dimensional flow of slightly ionized gas in infinitely segmented MHD generator with imperfect walls

19 p3478 A70-37588

One dimensional channel flow theory for ram wings, deriving lift and drag laws for comparison with wind tunnel and free flight tests results

20 p3558 A70-39558

Perturbation method for nonlinear acoustic wave propagation in steady one dimensional flow through variable cross section duct

20 p3673 A70-39612

Alfvén critical velocity concept in MPD arcs analysis, obtaining exhaust velocity relationship from one dimensional flow model

20 p3683 A70-40240

One dimensional unsteady equilibrium flow stability of relaxing two phase medium consisting of perfect gas and incompressible liquid

20 p3613 A70-40295

Viscous magnetofluid dynamic one dimensional annular flow, reducing three dimensional field equation to coupled linear partial differential equations

21 p3855 A70-40889

Aerodynamic parameters of ionized Ar supersonic steady one dimensional nonviscous flow in thermodynamic equilibrium and subjected to Laplace accelerating forces

21 p3858 A70-41444

One dimensional supersonic flow of ideal conducting gas in linear channel under transverse magnetic field

21 p3861 A70-42228

One dimensional perfect gas motion under spatial pressure distribution, investigating self similar solutions

22 p4012 A70-43314

Two phase liquid one dimensional motion in variable cross section tube, deriving mass transfer, motion and phase interaction differential equations

22 p4012 A70-43721

MHD equations for one dimensional plane steady flow, considering conservative difference schemes for approximation

23 p4226 A70-44307

Gas pressure differential across multilayer insulation blanket during rapid evacuation predicted, using one dimensional flow theory

23 p4282 A70-44522

One dimensional collisionless electron-proton plasma, obtaining exact electrostatic shock solution to Vlasov and Poisson equations

24 p4382 A70-45107

One-dimensional propagation of elastic spherical waves in inhomogeneous unbounded medium under normal stress on cavity surface

24 p4424 A70-45631

One dimensional gas pressure as function of activity, using Poisson-type partition function for perturbation calculation of thermodynamic limit

24 p4430 A70-46269

One dimensional Alfvén fluctuation spectrum of magnetosphere in toroidal crimping and twisting modes, using numerical integration

24 p4330 A70-46278

ONISOTROPY

U ANISOTROPY

ONSAGER RELATIONSHIP

Book on rational thermodynamics covering homogeneous processes, internal dissipation, Coleman theorem, wave propagation in dissipative materials, diffusion, chemical reactions, Onsager relationship, etc

03 p0525 A70-14042

Onsager reciprocal relations experimental validity in irreversible processes application to metals, electrokinetics, isothermal diffusion, heat conduction, chemical reactions, etc

17 p3197 A70-35538

OPACITY

M dwarf stars model atmosphere construction taking into account molecular opacities in cool stellar atmospheres

01 p0190 A70-11348

Collective interactions effect on electron scattering opacity in stellar interiors, using Debye-Hückel radial distribution function and neglecting collisions

02 p0364 A70-11789

Sodium-titanium-boron-silicate glass opacity and fusibility increase during partial substitution of K for Na, noting phase composition changes

05 p0871 A70-16598

Opacity-probability distributions for CO, computing theoretical spectra of line absorption coefficient, discussing effects of temperature and/or turbulent velocity

05 p0919 A70-16938

Solar core opacity influence on revised photospheric iron abundances, discussing neutrino flux prediction doubling in solar models

05 p0905 A70-16985

Electrical conductivity and conductive opacity for relativistic electron gas in presence of ions taking into account ion-ion interaction

09 p1727 A70-22509

Free-free opacity of stellar interiors by ion correlations applied to red giant degenerate cores

09 p1755 A70-22510

Cepheid type variable stars nuclear reaction and opacity pulsation excitation mechanisms

10 p1940 A70-24409

Triatomic hydrogen ion role in solar photosphere opacity implied from limb darkening and specific intensity data

11 p2104 A70-25739

Thermal diffusivity of opaque materials by phase shift method, using modulated radiation beam from carbon arc to heat material

11 p2068 A70-25767

Rossland stellar opacity calculation allowing for photon absorption in spectral lines using non-relativistic dipole approximation

13 p2495 A70-29752

Venus atmosphere opacity law determination as function of wavelength, comparing interferometric and integrated brightness temperatures with model calculations for various atmospheric compositions

14 p2646 A70-31069

Massive homogeneous star pulsation stability, determining maximum mass by opacity formula

17 p3154 A70-34533

Magnetic field effects on Compton scattering and radiative opacity, considering longitudinal and transverse propagation with circular polarization

17 p3154 A70-34538

UV solar opacity observations, comparing solar model predictions

17 p3160 A70-34884

Plasma opacity measurements using CW He-Ne and Ar lasers as light sources

17 p3106 A70-35107

Continuous UV opacity effects on visual spectrum observations and predictions for solar photosphere

17 p3169 A70-35385

Solar core opacity, investigating individual heavy elements influence and effect of changes in abundances

18 p3317 A70-37005

Backscattering of collimated light beam emitted by pulsed point source into opaque medium

19 p3461 A70-37421

Smoke chamber measurements of opacity developed in polymer pyrolysis or combustion, including Materials Smoke Obscurity Index/MSOI

20 p3736 A70-39404

Plate illumination relation to opacity in photometry and spectrophotometry, using digital techniques

20 p3630 A70-39475

Opaque minerals in Apollo 11 lunar igneous and fragmental rocks, using reflecting microscope and electron microprobe

21 p3896 A70-41513

Quantitative optical and electron probe studies of opaque phases in Apollo 11 lunar rocks

21 p3902 A70-41552

Rossland stellar opacity calculation allowing for photon absorption in spectral lines using non-relativistic dipole approximation

21 p3923 A70-42072

Cool star atmospheric structure, discussing models with and without graphite particle inclusion opacity

24 p4410 A70-45765

OPENINGS

NT APERTURES

NT IRISES [MECHANICAL APERTURES]

NT PORTS [OPENINGS]

NT SLITS

Buckling of elastic cylinders with rectangular cut-outs and reinforcements under axial or lateral loading, using modified Newton method

[ALAA PAPER 69-92] 09 p1780 A70-23208

Natural vibration analysis of uniform cylindrical and cantilever rectangular tubes with cutouts

10 p1961 A70-25057

Coupled integral equations for cutouts in shallow shells

17 p3186 A70-34970

German monograph on stress concentration around doubly symmetrical cut-out in cylindrical shells subjected to symmetrical load, using elliptical cut-out theory

24 p4418 A70-45092

Cylindrical shells with unreinforced openings, determining limit pressures and deformation patterns

24 p4419 A70-45158

OPERATING SYSTEMS [COMPUTERS]

Computer simulation of automated ATC systems, discussing operational gaming and mathematical models

02 p0274 A70-11968

IBM System/360 Operating System submodel simulator for multiprogramming, discussing language and structure

02 p0266 A70-12281

Ground support real time operating system 360 for manned spaceflight, discussing system features and performance

13 p2375 A70-29937

OPERATING TEMPERATURE

Mass action law-polynomial optimization analogy, illustrating optimal temperature determination in chemical reactors in series

01 p0143 A70-10925

Thermal discomfort by changing operational temperature of human subjects environment found to follow power law

01 p0041 A70-11647

Solar cell array fabrication methods extending operating temperature by pulsed spot welding techniques and deletion of adhesives

02 p0228 A70-12080

Correlation function procedure applied to quartz clock rate analysis, noting operating temperature control

04 p0693 A70-15487

Workpiece temperature during asymmetrical plane polishing by wheel face, deriving temperature distribution formulas for maximum heat source intensity

07 p1291 A70-18828

Emission containment and working temperature reduction possibility in thermonuclear reactor by increasing plasma densities and introducing large atomic number contaminants

07 p1350 A70-19847

Creep and stability of perforated and unperforated turbine disks under operating conditions

09 p1779 A70-23097

Long time static strength, durability and thermal stability relations determined for heat resistant alloys at operational temperatures

10 p1903 A70-24238

Fuel cells with alkaline electrolyte consuming H and O and operating near ambient temperature, discussing electrodes composition and performance

12 p2163 A70-26993

Medium temperature hydrogen fuel cells design, operational characteristics and performance

12 p2163 A70-26996

Natural gas-air fuel cell battery with sulfuric acid electrolyte for low temperature operation

12 p2166 A70-27766

Superconducting bolometer operating temperature stabilization

13 p2412 A70-29868

Commercial aircraft brake temperatures under HF landing conditions, using energy input and heat transfer computer programs

14 p2532 A70-31341

Posterior electrode structural modification for reducing silicon photovoltaic cells absorptivity and operating temperature

19 p3358 A70-38492

Cryogenic pipelines cooldown to operating temperature, calculating cryogen flow rate limits due to thermal stresses in steel and Al alloys

23 p4280 A70-44368

OPERATIONAL CALCULUS

Operational calculus for semisimple complex Lie group 07 p1321 A70-18658

OPERATIONAL HAZARDS

Hazards due to nonohmic materials responsible for electrostatic failures in missile and space programs and ground equipment 01 p0141 A70-10088

Atmosphere classification according to fire hazard based on heat capacity per mole of oxygen, noting exponential growth rate 03 p0607 A70-14054

Detonator insensitive to highest level of electrostatic voltage on human body for precise synchronization 03 p0547 A70-14111

Preventive measures against fire and blast hazards in high oxygen concentration chambers 08 p1599 A70-21795

Solid rocket motors potential hazards explosive reactions and temperature and blast effects 14 p2629 A70-30782

Approximating hazard rate function parameters estimation from failure data, using computer program 14 p2592 A70-31113

Evolution and current status of Apollo crew safety, discussing hazard aspects, program approach and measures and activities incorporated in project [AAS PAPER 70-051] 17 p3176 A70-34790

Operational requirements for NASA space shuttle Survival and Flight Equipment, discussing protection during launch and ascent 23 p4258 A70-44484

OPERATIONAL PROBLEMS

Soviet book on operational maintenance of flight vehicles /civilian/, emphasizing maintenance under various climatic conditions 01 p0004 A70-10502

Three dimensional navigation and guidance system for transport aircraft to alleviate operational problems, noting application to STOL aircraft 02 p0334 A70-11983

Nonlinear operational equation iteration solution error estimation, discussing Banach space nonlinear operator equation 10 p1909 A70-24508

Report on 1969 London International Conference on digital satellite communication session on operational requirements covering circuit operation modes, demand-assignment control, etc [AIAA PAPER 70-466] 11 p1997 A70-25412

Low cycle fatigue problems, environmental influence of operational differences on component life, life limits and controls for safe operation of jet engines [SAE PAPER 700207] 11 p2102 A70-25879

Supply phase voltage loss detection failure by voltage sensors in industry 13 p2378 A70-29349

Accident prevention in laser operation emphasizing eye protection 13 p2361 A70-30018

Noise of large commercial V/STOL aircraft and effect on design and operation, predicting acoustic signatures 14 p2531 A70-30854

Solar furnaces in space for treatment of high purity products in space vacuum, discussing design and operational problems 15 p2717 A70-31802

Mirror damage problem with mode locked ruby laser system solved by rough stack mirror fabricated from microscope coverslips 15 p2753 A70-32546

Stable operating range of supersonic mixed compression inlet increase by air flow removal via throat bleed system 16 p2967 A70-33585

Gas turbine engine compressor rotor roller bearing operation conditions analysis by computer calculation of thermal regime 21 p3834 A70-41777

High voltage solar array operational problems in earth orbit environment, discussing conducting surfaces, power loss, plasma effects, leakage, etc 22 p3967 A70-43544

Geometry and ionosphere effects on radio beacon operation for distress signal monitoring at sea, comparing night performance to daytime 23 p4163 A70-44229

Cactus high sensitivity accelerometer flight tests, discussing operation and experimental conditions [ONERA-TP-875] 23 p4198 A70-44660

Space Station long term operations and logistics concerning inventory, configuration and cargo management [SAE PAPER 700757] 24 p4416 A70-45871

STOL aircraft operational constraints, considering economics, short haul market characteristics, community acceptance, speed, propulsion system, takeoff/landing performance and maneuverability [AIAA PAPER 70-1283] 24 p4374 A70-45972

OPERATIONS RESEARCH

NT CRITICAL PATH METHOD

NT DYNAMIC PROGRAMMING

NT GAME THEORY

NT LINEAR PROGRAMMING

NT MINIMAX TECHNIQUE

NT NONLINEAR PROGRAMMING

NT SADDLE POINTS [GAME THEORY]

N binomial events approximations to high probabilities of overall success for reliability situations and mission accomplishment, including operations research implications 01 p0134 A70-11475

Operations research in fleet planning, discussing forecasting, frequency planning, operation simulation, traffic and revenue forecasting, etc 02 p0401 A70-11745

Managerial practices of problem identification, discussing research study in operating division of large corporation 03 p0610 A70-14051

Experiment selection in orbital program planning based on broad system synthesis, discussing identification and grouping of objectives, critical issues and experimental equipment requirements [AAS PAPER 69-580] 04 p0749 A70-14652

Deterministic and stochastic simulation models for obtaining optimal solution in operations research by trial and error 08 p1464 A70-20579

Reliability model for analyzing operational phase test programs developed from R and D phase models, processing data according to test scope [AIAA PAPER 70-389] 10 p1896 A70-24916

System effectiveness apportionment for constraints existing on accountable factors using Lagrange multiple method 14 p2669 A70-31111

Operational analysis and real time computer simulation models in ATC development 19 p3468 A70-38637

OPERATOR PERFORMANCE

Task loading of human operator in terms of central capacity sharing model, discussing model implications for mental workload measurements 02 p0245 A70-12142

Vigilance of human monitors detecting additions and deletions of relevant and irrelevant signals presented on computer matrix display 02 p0246 A70-12377

Automatic inspection data collecting and processing by human operator using display devices and computerized mathematical reduction for real time evaluation 02 p0266 A70-12469

Psychological factors in training and education of pilots and astronauts for optimal matching between human operator and vehicle control system 05 p0809 A70-16967

Human operator dynamic properties working to maintain given process parameters, obtaining differential equations for closed machine operator system 08 p1449 A70-20696

Airborne sidescan radar for fix-point navigation at low flight altitudes involving computerized sensing evaluated for operator performance 08 p1541 A70-21563

Drug-alcohol and hypoxia effects on multiple task operator performance tested at altitude and pressure chamber treatments 08 p1448 A70-21939

Observation noise model for human controller remnant 10 p1823 A70-23893

Pilot model based on Kalman filtering and optimal control, investigating evaluation for time stationary conditions and sine-wave tracking 10 p1823 A70-23894

Human operator transinformation sensitivity to display gain and forcing function bandwidth in rate control tracking task 10 p1823 A70-23896

Human operator remnant data normalization noting observation noise spectral characteristics for compensatory tracking 10 p1824 A70-23899

Modified fast Fourier transform for hybrid computer program data processing of human operator describing functions 10 p1824 A70-23900

Hypokinesia effects on working capacity of subjects performing manual aircraft control assignments during bed rest 13 p2352 A70-29340

Mathematical models for human adaptive and optimizing characteristics in manual control systems regarding behavior phase 13 p2360 A70-29780

Human operator ocular tracking and decay time stimulation response measurements using information, statistical, point process and random analysis 14 p2537 A70-30388

CRT symbol generators design for high speed computer data display as function of electro-optical and human operator constraints 16 p2850 A70-33133

OPERATORS [MATHEMATICS]

Feedback analysis of learning and performance in hand-yoked, steering and stimulus tracking control of breath-produced visual target 16 p2852 A70-33660

Human operator and computer interrelations, noting sources of error 18 p3223 A70-36079

Radar consoles with various display components under different illumination levels to determine optimal operator performance, discussing push-button design recommendations 20 p3580 A70-39713

OPERATORS [MATHEMATICS]

Five dimensional rotations and representation of isomorphic spinor groups by boson operators calculus, expanding Gelfand states in Weyl patterns 01 p0147 A70-10521

Atomic variables elimination technique applied to Markovian laser master equation, resulting in integrodifferential equations for field statistical operator 01 p0112 A70-10884

Bounded region satisfying regularity necessary to Korn inequalities and Sobolev immersion theories, discussing plasticity theory operator monotony in Minty-Browder sense 02 p0387 A70-12109

Variational principles in dynamic viscoplasticity theory, based on operator approach combined with time independent variations in elasticity theory 02 p0391 A70-12818

Nonlinear gyroscopic navigation system intrinsic error derived as function of linear operator 03 p0522 A70-13373

Asymptotic behavior at infinity of mixed boundary value problem analyzed for Sobolev equation involving operator 03 p0518 A70-13433

Homogeneous waveguide solutions by finite element method using matrix operator and function minimization to assure rapid convergence to eigenvalue 03 p0457 A70-13936

Generalized transform theory for causal operators developed, using Gelfand theory for commutative Banach algebras 03 p0520 A70-14167

Plasma turbulence theory formulated using averaging operators, obtaining nonlinear dispersion relation for turbulent diffusion coefficients 03 p0537 A70-14377

Chaplygin equation algebraic classification with respect to ring admitted by equation, extending results to include lambda function tolerating second order symmetry operators 04 p0613 A70-14412

Euler-Lagrange linear operators in variational embedding with one dependent function 05 p0881 A70-16058

Stationarization problems involving nonlocal and null class Euler-Lagrange operators, considering vector spaces of function spaces 05 p0881 A70-16059

Nonlocal variational mechanics with one field variable, developing algorithm for Euler-Lagrange operator calculation 05 p0882 A70-16137

Nonlocal Euler-Lagrange operator nature and characteristics, discussing operation of class of all Lagrangian functions 05 p0882 A70-16138

Compressible fluid flow satisfying perfect gas equation in presence of thin foil, developing operators characterizing incompressible and compressible flows without Hall effect 05 p0790 A70-16158

Self adjoint boundary value problems with interior point boundary conditions using differential operator in Hilbert space 05 p0876 A70-16423

Green operator structure and eigenvalue approximation of boundary value problems regarding vibrations and buckling of clamped plates using orthogonal invariants 05 p0876 A70-16563

Dirichlet problem of biharmonic operator in boundary region containing infinite number of pieces 05 p0877 A70-16878

Multiplication theorem for Shtraus characteristic functions of quasi-Hermitian operators, including open systems coupling 05 p0877 A70-16880

Boundary value problems in closed spaces with fine grained Liapunov boundary described by second order elliptic differential operators 05 p0877 A70-16881

Fourier series localization conditions for fundamental system of Beltrami operator functions in arbitrary n-dimensional space 05 p0877 A70-16972

Existence and uniqueness, stability and asymptotic stability of nonlinear operator differential equation 05 p0878 A70-17098

Existence and stability problems of nonlinear operator differential equations containing linear operator with domain and range contained in real Hilbert space
05 p0878 A70-17099

Observation operators and cosmology, constructing equations for cosmological aggregates governed by Einstein field equations
06 p1105 A70-17529

Discrete spectrum of fourth order differential operator estimating number of eigenvalues in bounded interval of real line
06 p1094 A70-17740

Existence results for Cauchy problem for linear variable coefficient hyperbolic operators with multiple characteristics
06 p1094 A70-17898

Hilbert transform as operator in function space defined on harmonic analysis groups, noting application to noise stability, modulation and signal detection
07 p1235 A70-19644

Perturbations classes for self adjoint operator limit spectrum preservation
07 p1327 A70-19807

Self adjoint operator generated by differential expression and pseudodifferential boundary conditions, using Berezanskii procedure for operator eigenfunction expansion
07 p1327 A70-19809

Infinite order differential operator in S type spaces for Cauchy problem solution uniqueness
08 p1533 A70-20722

Characteristic equations for differential symmetry operators in homogeneous and nonhomogeneous Maxwell equations
08 p1544 A70-20990

Half space elasticity problems solved by operator method
08 p1586 A70-21013

Boundary value problem for linear elliptic differential operator degenerating on region boundary
08 p1534 A70-21119

Clock corrections smoothing by linear transformation operator, calculating operator transfer function and averaged errors deviations
08 p1574 A70-21155

Optical coherence theory functional formalism developed in radiation field probability functional terms, noting role of P representation of density operator
08 p1545 A70-21254

Volterra operators extension, considering structure of complete operators and invariant subspaces
09 p1711 A70-22146

Asymptotic distribution of operator eigenvalues for self adjoint elliptic boundary value problem in unbounded region using Green function
09 p1711 A70-22148

Nonlinear periodic oscillations problem solved by solving nonlinear operator equations, discussing iterative methods based on equations linearization
09 p1728 A70-22668

Nonlinear partial differential operators eigenvalue solution using modified Newton iteration method, noting advantages over perturbation method
11 p2074 A70-26423

Transfer matrix spectrum for lattice gas models with finite interaction, constructing stochastic operator as stochastic matrices limit
12 p2272 A70-27343

Operator representing anisotropic element in gas laser resonator, considering phase crystalline and rotating plates
13 p2424 A70-28593

Operator originated by Schroedinger equation having inhomogeneous boundary conditions on portion of boundary of Hilbert spaces orthogonal sum, defining region of self conjugation
13 p2442 A70-29514

Extremum conditions for optimal control with operator constraints using gradient algorithms
14 p2559 A70-30181

Operator form added to equations of state of continuous media in case of small and large deformations
14 p2656 A70-30473

Multichannel scattering variational bounds reformulation without using projection operators, calculating resonance-energy relations
14 p2619 A70-30490

Control system teaching based on preferred response data, discussing operator determination from purpose control function
15 p2716 A70-32449

Elliptic boundary value problems involving pseudodifferential operators on bounded manifold, examining solutions analyticity
16 p2941 A70-33269

Linear partial differential equations solvability, deriving necessary conditions for pseudo differential operator
19 p3457 A70-37677

Singularities of solutions of partial differential equations, discussing smallest convex set in manifold with differential operator
19 p3457 A70-37680

Sufficient conditions for local solvability of linear partial differential equations with operator on complex functions
19 p3457 A70-37682

Helmholtz equation initial value problem solution by integral operators
19 p3459 A70-38680

Perturbation calculation for linear ordinary differential operators, considering equivalence to eigenvalue problems
19 p3459 A70-38681

Simultaneous approximation of function and product with given operator, applying to boundary value problems of partial differential equations
19 p3459 A70-38682

Coordinate sequences for regions with complex geometries and various boundary conditions, using linear operators
19 p3460 A70-38940

Kinetic equations derivation for correlation functions and time dependent distribution functions of irreversible processes, using projection operators
20 p3672 A70-39588

Multichannel iterative servosystems operators for useful signals reproduction
20 p3603 A70-39836

Structures of linear field theories concerning constitutive equations and operators dual relationship
21 p3851 A70-42098

Dubovitskii and Milyutin formalism applied to optimization problems involving equality and operator constraints via mathematical programming in normed linear space
22 p4061 A70-42462

Coherent behavior associated with thermodynamic description projected from dynamical behavior of many body system, using relation between asymptotic operators
22 p4062 A70-42547

Whole operator with infinite defective numbers for Sturm-Liouville differential equation, describing spectral functions
23 p4210 A70-43977

Shooting method for computing eigenvalues of Hermitian differential operators
23 p4210 A70-44020

Approximate bounds for differential eigenvalues of self adjoint linear operators in Hilbert space
23 p4211 A70-44245

Integration operators for transient structural response in qualification tests for internal components of dynamically loaded structures
23 p4273 A70-44719

Cauchy problem for singular parabolic equation, establishing existence, uniqueness and representation theorem by integral operator techniques in conjunction with function-theoretic methods
23 p4212 A70-44895

Linear operator convex closed set, considering range-domain or output-input implications
24 p4369 A70-46023

OPERATORS [PERSONNEL]

NT AIRCRAFT PILOTS
NT PILOTS [PERSONNEL]
NT TEST PILOTS
Discrete stochastic optimal control model of human operator for single loop compensatory/pursuit tracking
16 p2851 A70-33340

OPHTHALMOLOGY

NT EYE EXAMINATIONS
Occupational and medicative hazards in ophthalmology - Conference, Amsterdam, June 1968
01 p0022 A70-10855
Space or atmospheric flight caused or aggravated ophthalmic lesions, noting retinal and conjunctival hemorrhages from barometric pressure fall and rapid acceleration and deceleration
01 p0022 A70-10858
Cine recording ophthalmoscope with TV monitoring for retinal photography during centrifugation
06 p1061 A70-17286
Ophthalmological treatment of severe thermomechanical eye injuries investigated on radiant-energy burned rabbit eyelids
09 p1617 A70-22473
Lasers for surgical applications, cancerous tissue treatment, ophthalmology and comparison with RF diathermy
24 p4308 A70-45569
Binocular fundus reflectometry and plethysmography in rabbits and man after dye injection and in patients with carotid occlusion
24 p4310 A70-46345

OPTICAL ABSORPTION

U ELECTROMAGNETIC ABSORPTION

U LIGHT TRANSMISSION

OPTICAL AMPLIFIERS

U LIGHT AMPLIFIERS

OPTICAL COMMUNICATION

Error probability, signal to noise ratio and average signal level for coherent heterodyne and photon limited laser communication systems, using Poisson distributions
02 p0255 A70-11914

Laser transmitter and optical superheterodyne receiver performance tests at 6328 Å, demonstrating aperture size effect and noncoherent operation superiority
03 p0450 A70-13675

Laser communication system for outer space, beam guiding and fiber optical guiding systems
04 p0649 A70-15038

Light signals frequency converters and amplifiers applied to detection problems
05 p0813 A70-16264

Information transmission capability of hologram without distortion, considering confocal resonator reconstructible transparencies for bounded hologram
05 p0848 A70-16265

Maximum likelihood receiver /MLR/ to detect pulsed signal propagated through turbulent medium, assuming optical propagation over long path in atmosphere
07 p1227 A70-19146

Laser and quasi-laser systems modulation for wide spectrum communications, discussing global potentials and application as low cost satellite links
08 p1459 A70-20802

Modal excitation and scattering in retinal receptors of human and insect visual systems investigated with dielectric rod uniform wave and irregularities
08 p1452 A70-21289

Narrow width pulse-position modulated optical communication system design, determining performance in terms of error probability and information rates
08 p1463 A70-21778

Injection lasers for multichannel optical communication using composite cavities to improve spectral output
09 p1698 A70-23359

Optical transmission technology for aerospace launch operations investigated on ground communication systems projects involving use of gallium arsenide lasers and diodes
09 p1640 A70-23776

Portable optical communcator for voice transmission combining pulse position modulation and low power gallium arsenide diode
10 p1840 A70-24530

Laser systems for deep space communications, considering high data rates, laser types, systems operation, earth atmosphere effects, hardware reliability, etc
11 p2005 A70-26036

Photodetector-electronic circuit matching channels for optical communication system, using minimum risk design criterion
12 p2237 A70-28153

Analog information transmission device using He-Ne laser radiation, discussing optical telemetric channel transfer characteristics for pulsed nanosecond analog signals
12 p2250 A70-28184

Injection lasers as logic elements in optical communication systems with time division multiplexing, examining optimal switching and pulse duration reduction
13 p2428 A70-29406

Lunar communications systems considering use of satellites, metallic particle belts, rockets, lasers and particle beams
14 p2634 A70-30196

Optical and quasi-optical transmission of EM wave beams of type in directional antennas Fresnel region, examining free space and waveguide modes
14 p2549 A70-30445

Satellite laser communication system using dual scan acquisition technique
14 p2552 A70-31197

Temporal dependence of photoelectron multiplier output waveform and focusing under photocathode alternating modulation, noting thresholds for optical reception
15 p2696 A70-31505

FM optical signals detection, using Fabry-Perot interferometer with air gap between mirrors
15 p2733 A70-31523

Atmospheric turbulence effects on optical communication systems in geosciences
16 p2900 A70-33019

Troposphere effects on microwave and optical signals, correlating refractive index and dispersion variabilities
16 p2862 A70-33020

Injection laser communication link for high data rate transmission, discussing design and construction of transmitter and receiver
16 p2862 A70-33139

Drosograph high brilliance display device for rapid line-pattern projections and optical signal processing
16 p2906 A70-33179

Deep space optical communications link, fabricating operational prototype of flight hardware for spaceborne terminal
16 p2863 A70-33190

HE sub 11 mode launching in optical communication system, considering fiber tapering effect on excitation efficiency
16 p2875 A70-33400

Optical spacecraft communication system, discussing size, weight, power, etc 16 p2864 A70-33484

GaAs injection lasers for optical communication, synthesizing high bit rate data link between synchronous relay satellites 16 p2865 A70-33710

Blinking warning lights for air navigation, signaling of obstacles and glider onboard marker lights 16 p2889 A70-34302

Fiber optics in functional electronic circuits, considering multichannel optical communication 18 p3290 A70-36235

Worldwide multichannel air communications system in 10 GHz to IR range by Quasi Laser Link modulation and satellites 19 p3378 A70-37855

Optical communications in space, considering multiple access low earth orbit-to-synchronous and synchronous-to-synchronous links 19 p3379 A70-37878

Information optical transmission parameters with electroluminescent GaAs diode as radiation source, calculating energy received over various distances 19 p3389 A70-38069

Light focusing glass fiber with variable refractive index using ion exchange process, discussing applications to laser communications and data processing 20 p3671 A70-39129

Planar thin film optical waveguides for integrated circuits, utilizing information carrying potential of laser light in optical communication 20 p3598 A70-40129

Deep space microwave and optical communications, describing grand tour requirements 21 p3784 A70-40546

Amplitude modulated optical band signal detection, comparing optimal direct photodetection and superheterodyne receivers sensitivities 21 p3785 A70-40633

Space-to-ground link wideband digital laser communications system design and performance tests 21 p3787 A70-41331

Carbon dioxide laser systems for various space communication links between ground, satellites and Mars probe 21 p3787 A70-41338

Optical communications system for transmission and detection of PCM word pattern at gigahertz rates, discussing optical and electrical modulation 21 p3788 A70-41339

Wideband high speed PCM/AM optical communication system using mode locked He-Ne laser, noting simultaneous signal transmission and bit rate 21 p3789 A70-41354

Optical communication in turbulent media, investigating error rate for binary single path fading channels by photocount detection 21 p3837 A70-41935

Optical communication waveguides with diffused boundaries, calculating modal propagation fields by perturbation theory 21 p3792 A70-42045

Atmospheric communication channel modeling for laser wavelengths, considering point, area, heterodyne and direct detection receivers, nonplanar and infinite plane wave propagations, etc 21 p3793 A70-42179

Optimal heterodyne receiver for laser signals element-by-element wavefront detection 22 p3987 A70-42558

Fluctuating light pulses detection and arrival time estimation for heterodyne reception 22 p3987 A70-42560

Light signals detection on noise background, comparing algorithms based on nonparametric statistics 22 p3989 A70-42569

Frequency modulated gas laser communication system, discussing Raman-Nath effect, Doppler shifting phase grating, monochromatic light, pseudostanding wave, optical heterodyne detector, etc 22 p3989 A70-42966

Ultrasonic light modulation using single crystal lithium niobate transducers in laser communication and information processing systems 22 p3992 A70-43734

Signal arrival time variance in optical communication system with high lag photodetectors, examining input, detection and amplification noise 23 p4196 A70-44410

OPTICAL CORRECTION PROCEDURE

Microscope objective effect on accuracy of optical systems modulation-transfer function based on corrected high speed lens measurements 07 p1334 A70-19147

Sunspot minimum intensity dependence on area, including correction for blurring or image motion, scattered light and line absorption 13 p2496 A70-29846

Foreground presence for computer generated and painted three dimensional photographic displays using fly eye lenslets 16 p2906 A70-33177

Automatic active optic control of alignment and figure of primary mirror of spacecraft-borne telescope with response time stability 16 p2907 A70-33189

OPTICAL COUPLING

Small signal opto-electronic wideband transformer with coupling element ensuring fast response and low sensibility to parasitic magnetic fields 03 p0459 A70-14266

Injection laser amplifier with emitting and amplifying diodes coupled by planar polyharmonic beam waveguide 04 p0702 A70-15292

Cylindrical confocal laser resonator with circular coupling aperture in center of mirror calculated for diffraction losses by numerical iteration 06 p1079 A70-17187

GaAs diode amplifiers and switching devices behavior, describing optical coupling between two GaAs lasers 07 p1241 A70-19399

Semiconductor laser signals coupling into thin optical platelet waveguides 07 p1301 A70-20019

Fabry-Perot resonator mirrors with local reflecting inhomogeneities within perimeter of single crystal wafer for application in optically coupled semiconductor lasers 13 p2427 A70-28884

Radiation coherent enhancement of single frequency emission fields in Q modulated coupled ruby lasers 14 p2593 A70-30152

Whisker diode coupling to polarized IR laser beam by orientation based on antenna theory 17 p3048 A70-35902

Radiation divergence from gas laser resonator with coupling aperture 20 p3642 A70-39752

Radiation coherent enhancement of single frequency emission fields in Q modulated coupled ruby lasers 21 p3839 A70-42076

Prism film device coupling laser beam into thin film dielectric light guides, discussing operational theory 22 p4030 A70-42947

Prism film device for high efficiency laser beam coupling into light guiding thin film, deriving operation theory by plane wave analysis 22 p4030 A70-42948

Helicons and transverse optical phonons coupling in degenerate polar semiconductors investigated from electromagnetic linear response theory and field method 24 p4390 A70-45603

OPTICAL DATA PROCESSING

On-line system transmitting experimental data from optical spectrometer to central computing facility for magnetic tape recording 05 p0818 A70-16846

Optical data processing systems with spatial filters for two dimensional signals detection, using film nonlinearities to record Fourier transform hologram 07 p1287 A70-20094

Optical information processing in noncoherent light, considering applicability to simulating antenna radiation patterns using field distribution in aperture obtained by Fourier transformation 08 p1494 A70-20971

Hologram data efficiency improvement by spatial offset removal, analyzing plane and spherical reference waves and plane and solid objects 08 p1500 A70-21787

Automatic photographic data processing system with transient reproducer to obtain digital format for computer analysis 09 p1673 A70-22030

Optical signal processing using circular array and spatial frequency filtering to yield azimuthal distribution of sources 09 p1678 A70-22969

Optical processing of signals from circular aerial arrays involving use of spatial filter 09 p1678 A70-22970

Compound semiopaque thin films quality control for thickness uniformity by observing fringe patterns generated by optical data processing techniques 09 p1687 A70-23765

Image processing for motion blur removal, discussing methods for measuring degradation and filter design for image restoration 09 p1688 A70-23773

Optical image processor using Fourier transform corrective function for image restoration 09 p1688 A70-23774

Computer texture analysis for two dimensional scenery pictures involving periodicity invariance under Fourier transform 11 p2014 A70-26251

Two dimensional remote sensing displays based on diffraction patterns generated by coherent light, discussing optical processing of photographs, drawings, maps, etc 12 p2229 A70-26944

Optical processing for measuring frequency spectrum of PM wave induced by turbulent medium in laser beam 12 p2249 A70-27756

Binary-valued digital pictures noise cleaning by propagation processes 12 p2188 A70-27937

Book on synthetic aperture radar imaging systems theory and design covering SNR, optical data processing, phase and motion errors, ambiguity function, etc 13 p2368 A70-29603

Sufficient statistics for optimal correlation function in classifying optical images in pattern recognition, using permissible transformations 14 p2553 A70-30421

Computerized control for beam scanning and optical data processing concerning symbols, letters and photographic images 14 p2553 A70-30424

Photoemission optical analysis from thin films with uniaxial anisotropy, discussing reflectance, transmittance and divergence of Poynting vector 15 p2774 A70-32012

Onboard IR receiver and ground photorecorder for Meteor satellite cloud tracking, using computer processed data 15 p2738 A70-32112

Data compression techniques, considering two dimensional image coding problem 15 p2705 A70-32558

Image processing and picture enhancement by computer, using fast binary log-antilog conversion 15 p2768 A70-32567

Radiograph images digital processing by linear and nonlinear position invariant techniques, obtaining contrast enhancement 15 p2706 A70-32569

Lunar color differentiation by computer image processing compared to earth based photoelectric photometry [JPL-TR-32-1472] 16 p2900 A70-33097

On-line optical data processing using CRT with electro-optic target crystal 16 p2903 A70-33132

Optical spatial phase modulator array using membrane light modulator for coherent optical processing and character recognition 16 p2904 A70-33147

Drosograph high brilliance display device for rapid line-pattern projections and optical signal processing 16 p2906 A70-33179

Coherent optical computer system driven by membrane light modulator (MLM), describing electro-optical properties and operating characteristics 16 p2871 A70-34055

Image distortion in reconstructions from phase only holograms, noting savings in collection and processing of acoustic holographic data 16 p2915 A70-34324

Human lung internal surface area automated measurement by computerized image processing techniques, grading emphysema 17 p3035 A70-34578

Light focusing glass fiber with variable refractive index using ion exchange process, discussing applications to laser communications and data processing 20 p3671 A70-39129

Automatic measurement of drainage networks for lengths and areas by copper plate etching or flying spot scanner on transparencies or radar images 20 p3633 A70-39794

Image detection in pattern recognition through bipolar correlation, discussing reference generating algorithms and digital simulation results 20 p3633 A70-39972

Digital optical storage for information system components 21 p3823 A70-40852

Two dimensional data array contour tracing algorithm for reduction of image coding bits number 21 p3786 A70-41327

Microwave antenna array irregularity location from hologram by optical signal processing, using far field spatial filter 21 p3792 A70-42048

Ultrashort time perceiving electron-optical conversion methods, discussing image quality and brightness, quantum yield and time resolution 22 p4038 A70-43424

Ultrasonic light modulation using single crystal lithium niobate transducers in laser communication and information processing systems 22 p3992 A70-43734

Line-by-line and two dimensional image processing performance, considering transmission rates and distortion 23 p4160 A70-43762

Integrated data processor-operation controller for stellar TV photometer systems in spaceborne observatory, considering limited channel transmission capacity 23 p4167 A70-44649

Electronic data handling and CRT display of ATS satellite cloud pictures 24 p4371 A70-46048

Seeding particles motion recording in fluid flow by holographic velocimetry, using optical matched spatial filtering to determine particle location 24 p4340 A70-46350

OPTICAL DENSITY

Energy distributions of emitted electrons from Si, GaP and ZnS semiconductors, determining relative core levels and Si valence band states optical density 03 p0537 A70-12879

Optical density measurements in high speed confined air vortex, discussing light deflection mapping of vortex density field at off axis positions [AIAA PAPER 68-694] 03 p0480 A70-12906

Plasma optical transparency criterion, estimating nonequilibrium plasma layer optical density limit 03 p0531 A70-13255

Stellar light absorption in optically dense cometary atmospheres 06 p1141 A70-17738

Optical density vs illumination amount characteristic curve determined for photometric calibration of astronomical photographs of celestial bodies 07 p1279 A70-19046

Polychromatic nonlinear light scattering in plane parallel layer solved by self consistent optical depths method 09 p1762 A70-23117

Aerial IR film optical density related to preharvest crop yield indicators in micro experiments with remote sensors 12 p2217 A70-26918

Quantitative analytic composite photography, performing image density point-to-point subtraction of two negatives 13 p2406 A70-28905

Photoemission from evaporated gold films, measuring quantum yield, photoelectric energy distribution curves and optical density states 14 p2626 A70-30481

Earth atmosphere transmission coefficients determination by relation between transparency and daytime sky brightness, noting limits of applicability 16 p2899 A70-34180

Atmospheric optical properties stability determination for various optical densities, assuming horizontally homogeneous medium with properties constant during observation 16 p2899 A70-34181

Atmosphere spectral transparency and stability spectrophotometric studies based on measuring solar aureole brightness 16 p2899 A70-34183

Optical density of valence and conduction states by UV photoelectric spectroscopy, outlining experimental techniques and inelastic scattering effects 19 p3471 A70-37711

Photographic images formation mechanism, examining streaks resolving power and total densities 20 p3632 A70-39747

OPTICAL EMISSION

U LIGHT EMISSION

OPTICAL EMISSION SPECTROSCOPY

Strontium fluoride crystals containing trivalent neodymium cations investigated for laser action and radiation characteristics by spectroscopy 10 p1899 A70-24253

Picosecond pulse frequency sweep measurement using time resolved spectroscopy 17 p3108 A70-35904

Gas lasers intensity expression derived by theory of double resonance spectroscopy, comparing results with He-Ne laser experimental data 19 p3445 A70-37672

Thin optically pumped pulsed CdSe platelet lasers, detecting mode jumping and tuning effects by time-resolved spectroscopy 22 p4049 A70-42946

Simultaneous X ray and optical observations of Scorpius XR-1, comparing rocket data from various flights 22 p4094 A70-42987

OPTICAL EQUIPMENT

NT ASTRONOMICAL TELESCOPES

NT BAKER-NUNN CAMERA

NT BALLISTIC CAMERAS

NT CAMERAS

NT CATHETOMETERS

NT CELESCOPES

NT CINETHODOLITES

NT COLLIMATORS

NT DIFFRACTOMETERS

NT ELECTROPHOTOMETERS

NT ELLIPSOMETERS

NT FRAMING CAMERAS

NT GEODIMETERS

NT HELIOMETERS

NT HIGH SPEED CAMERAS

NT IMAGE CONVERTERS

NT IMAGE TUBES

NT INFRARED SPECTROMETERS

NT INFRARED SPECTROPHOTOMETERS

NT LALLEMAND CAMERAS

NT LIGHT SCATTERING METERS

NT MULTISPECTRAL BAND SCANNERS

NT NEPHELOMETERS

NT OPTICAL GYROSCOPES

NT OPTICAL MEASURING INSTRUMENTS

NT OPTICAL MICROSCOPES

NT OPTICAL PYROMETERS

NT OPTICAL RADAR

NT OPTICAL RANGE FINDERS

NT OPTICAL SCANNERS

NT PANORAMIC CAMERAS

NT PHOTOMETERS

NT POLARIMETERS

NT POLARISCOPE

NT PRISMATIC BARS

NT PRISMS

NT PYROHELIOMETERS

NT REFLECTOMETERS

NT REFRACTOMETERS

NT SCHMIDT CAMERAS

NT SEXTANTS

NT SPECTROPHOTOMETERS

NT SPECTROSCOPIC TELESCOPES

NT STROBOSCOPES

NT TELEVISION CAMERAS

NT THEODOLITES

NT TRANSITS

NT TRANSMISSOMETERS

NT ULTRAVIOLET SPECTROMETERS

NT ULTRAVIOLET SPECTROPHOTOMETERS

NT WIDE ANGLE LENSES

NT X RAY TELESCOPES

Interferometer for compressing linearly FM light pulses and analyzing spectra of picosecond pulses 01 p0111 A70-10670

Photooptical techniques in simulators - Conference, South Fallsburg, N.Y., April 1969 01 p0057 A70-10807

Motion perception sensitivity measurement in various portions of retina for operation accuracy of photooptical systems of simulation 01 p0036 A70-10820

Psychological aspects of unreliability sources in man machine systems for selection and training criteria of photooptical instruments users 01 p0036 A70-10821

Airborne cartographic azimuthal instrument with reflecting prism type optomechanical assembly and trihedral pyramid gyroscope for stabilization 01 p0093 A70-11269

Optical and radioastronomical observations of 1966 solar eclipse, discussing data and instruments 01 p0191 A70-11472

Low loss low sidelobe N-way microwave optical power divider for single plane electronically steerable Ku band phased array antenna 04 p0655 A70-14624

Optical facilities of Apollo 11 mission and NASA Manned Spacecraft Center noting Fاذow telescopes, lunar cartography, photometric surface analysis, etc 04 p0687 A70-14690

Apollo lunar mission optics concerning liftoff alignment theodolites, spacecraft atmosphere electro-optical sensor, helmet optical coating and laser experiment 04 p0688 A70-14693

Emission modulation in multifunctional injection laser-photodiode system used as optical memory, pulse generator, multivibrator and trigger 05 p0859 A70-16268

Visual simulation in Lunar Module Mission simulator provided by computer controlled infinity optics system 06 p1031 A70-18603

NASA three meter orbital telescope discussing configuration, optical geometry, launching, power supply, etc 07 p1280 A70-19150

Optical polygon calibration by interferometric method using He-Ne laser light source 07 p1287 A70-19227

Anamorphic optics to focus luminous wakes of hypervelocity projectiles onto focal plane of slitless spectrograph in free flight ballistic range launching 07 p1287 A70-20082

Axicon systems for spectroscopy of light emitted by foil-excited accelerator beams, discussing scattering contribution to spectral line widths 07 p1287 A70-20083

Detector for focus assessment of laser on target, scanning image by fiber optics 07 p1302 A70-20089

Low pass filter structure of focusing reflectors designed for quasi-optical system, noting energy absorption 08 p1476 A70-21287

Acousto-optic receiver and spectrum analyzer for electromagnetic signals in VHF-UHF range 08 p1463 A70-21780

Photo-optical instrumentation applications and theory - Conference, San Francisco, August 1969 09 p1672 A70-22029

Solar eclipse coronal polarization and intensity measurements, discussing equipment, calibration, photometric reduction and results 09 p1757 A70-22736

Stereo photographs conjugate image area matching, comparing automatic optical and electronic correlation techniques 09 p1680 A70-23067

Optical devices for enhancement of semitransparent photocathode quantum efficiency applied to TV camera tubes, image intensifiers and other imaging detectors 09 p1682 A70-23502

Optical equipment development at Jet Propulsion Laboratory, discussing flight TV systems and associated digital image processing laboratory, planetary spectroscopy, spacecraft guidance, etc 09 p1657 A70-23505

Marshall Space Flight Center optical research programs technology base for launch vehicle development support, discussing Apollo Telescope Mount 09 p1657 A70-23518

Lewis Research Center applications of optics to research in flight propulsion and space power generation, discussing gas density visualization, radiative heat transfer, etc 09 p1657 A70-23522

Photo-optical instrumentation - Conference, San Francisco, August 1969 09 p1684 A70-23751

Grand tour space probe optics for observation of objects on planet, considering atmospheric refraction indices effect 09 p1700 A70-23768

Holographic optical memory feasibility for digital data storage using Ar ion laser, acousto-optic beam deflector system, hologram storage plane and photodetector array 09 p1642 A70-23780

Laser Doppler velocimeter optics, noting minimal heterodyne alignment needs and stress and vibration stability 10 p1889 A70-24556

Orthophoto Attachment for A8 autograph to produce black and white and color aerial photographs on negative film 10 p1891 A70-24739

Holographic optical memory systems operational principles and potential advantages, discussing feasibility of 100 million bit memory capacity and one microsecond random access time 10 p1892 A70-25245

Transfer functions application to optical system specification, design and evaluation, calculating diffraction limited MTF 11 p2082 A70-25354

Spacecraft window cleaning with methyl alcohol and low pressure nitrogen providing filming control for Apollo optical experiments 11 p2051 A70-26143

Optical IR system as low cost pilot warning indicator providing audible and visual collision warnings to general aviation aircraft 12 p2234 A70-27647

Aperture field modal decomposition of optical system in terms of integral equation eigenfunctions during detection and estimation of incoherent objects 12 p2273 A70-28121

Ocular focus stimulator with provision for optical distance change between object and observer without brightness and visual angle variation 12 p2237 A70-28125

Soviet optical instrument industry development trend (1971-1975), considering spectral, test, measuring, reading and microscopic equipment 13 p2412 A70-29864

Quasi-optical power transmission in overmoded waveguides in interferometers, millimeter wave spectrometers, polarizers, etc 14 p2556 A70-30447

Astronomical telescope system design and construction, considering optical configurations, components, mounting, atmospheric limitations, etc 15 p2736 A70-31950

Passive optical crossed beam detection systems monitoring meteorological parameters in rocket or aircraft environments, noting real time display 15 p2736 A70-32032

Air cell optical phase shifter for holography based on refractive index variation with air pressure 15 p2741 A70-32439

Optical membranes design, discussing properties of materials and mountings 16 p2904 A70-33148

Holography techniques, discussing fringe pattern formation, various systems advantages and optical elements 17 p3084 A70-35002

Optical system of absorption tubes for planetary atmosphere spectra simulation 18 p3314 A70-36408

Contaminated optical surface investigation technique in near UV, visible and near IR range, investigating property changes of systems in transmission and reflection 18 p3292 A70-36786

Holographic interferometry applications in stress analysis of photoelastic resins, describing holographic interferometry assembly 18 p3262 A70-37209

Coherent light communication system quasi-optical lens line output field examination, using laser assembly to study parasitic, radiative and overall power losses 19 p3443 A70-37288

Inlet optics modification in Raman laser spectrometer, discussing high pressure gas storage and support plate enlargement 19 p3443 A70-37361

Membrane attachment for pressure transducer with help of holographic interferometry, describing optical system 19 p3427 A70-38453

Coherent light beam characteristics with Gaussian radial intensity variation during propagation along optical system axis, determining radius from diffraction theory 20 p3639 A70-39086

Encircled energy calculation in optical systems with central obstruction, observing focus error, spherical aberration and central stop effects on image contrast 20 p3627 A70-39088

Optical aperture tapering for attenuating sidelobe impairing LF signals detection 20 p3639 A70-39089

OPL astrolabe catalog corrections, discussing Danton prototype, color-magnitude effect, time and latitude values 21 p3887 A70-41111

Optical pulsar search instrument in radio pulsar fields, showing performance on NP 0532 21 p3826 A70-41156

Light modulator design based on Fabry-Perot interferometer controlled by electro-optical effect 22 p4026 A70-42507

Optical multilayer metal coatings vacuum deposition by cathode sputtering, using automatic apparatus 22 p4045 A70-42510

Low stiffness optical parts bulk vibration machining 22 p4045 A70-42512

Optical devices contaminated mirror surfaces restoration with atomic oxygen from RF plasma by noncontaminating nondestructive oxidation of polymer film 22 p4029 A70-42622

Prism film device coupling laser beam into thin film dielectric light guides, discussing operational theory 22 p4030 A70-42947

Prism film device for high efficiency laser beam coupling into light guiding thin film, deriving operation theory by plane wave analysis 22 p4030 A70-42948

Optical waveguides and resonators propagation modes detection and discrimination techniques evaluated for circular cylinder dielectrics/optical fibers 22 p4030 A70-42949

Low pressure supersonic wake measurement by differential interferometer in double pass polarized light [SMPT PREPRINT 95] 22 p4036 A70-43060

Two-component optical system for laser radiation collimation, calculating tolerances for fabrication and assembly 22 p4051 A70-43560

Optical read-write mass memory based on holographic storage and light addressable matrix array, discussing significance to computer design and usage 22 p3994 A70-43606

Optical system for read-write holographic memory capable of high storage density 22 p3994 A70-43607

Reflection echelon and Fabry-Perot interferometer with surface imperfections, comparing spectral resolution limit with Rayleigh limit 22 p4040 A70-43612

High dispersion stellar spectroscopy with echelle grating, discussing instrument design, operation and performance 22 p4040 A70-43613

Apollo TV cameras, detailing general characteristics, principal features, optical systems and operational requirements 23 p4195 A70-44382

OPTICAL FILTERS

NT INFRARED FILTERS

NT ULTRAVIOLET FILTERS

Semiconductors as optical limiters for Q switched lasers, reporting temperature values for nonlinear absorption coefficients of Si, CdSe, CdTe and GaAs 01 p0158 A70-10563

Metal film graded filter fabrication for schlieren photographic system with laser light source and framing camera, using vacuum evaporation 01 p0113 A70-10921

Optical spatial amplitude filtering techniques application to moire fringe patterns processing 01 p0058 A70-11060

Interference filter for photography of comet heads, tabulating filter characteristics 02 p0303 A70-12707

Collection of papers on optics covering dielectric multilayer filter synthesis, photographic image, light interaction with free electrons, laser radiation, optical echoes, etc 02 p0340 A70-12828

Longitudinal and transverse mode locking in laser with passive filter, discussing giant pulse development and duration 03 p0502 A70-13746

Laser pulse power effect on edge absorption of glass filter used for Q switching applications 07 p1299 A70-19855

Image processing for motion blur removal, discussing methods for measuring degradation and filter design for image restoration 09 p1688 A70-23773

Color schlieren photography with complete spectrum displayed in single photograph, discussing filter matrix 10 p1857 A70-23913

IR light dispersion filters of compressed mixed powdered crystals, discussing optimal preparation procedures, passbands temperature dependence and stability 10 p1915 A70-24256

Deformed grating frequency multiplication by filtering in Fourier plane of lens, forming moire pattern in image plane by mechanical interference 10 p1890 A70-24592

Blue haze hypothesis of Martian atmosphere using Mariner 6 and 7 blue filter photographs, reviewing topographic observations 10 p1943 A70-24841

Optical filtering applied to moire method for measuring small structural strains 11 p2131 A70-25595

Evaporated multilayer optical bandpass filters in solar radiation technology, discussing design and construction 13 p2411 A70-29665

Quasi-optical filters with bandpass and pseudohigh pass structures for millimeter wave and far IR frequencies 14 p2558 A70-31318

Bleachable dye filters selection for periodic undamped output power oscillations in laser 15 p2753 A70-32859

Ruby laser spatial and temporal characteristics improvement with bleachable dye filter, using local negative feedback 15 p2754 A70-32865

Book on holography covering principles, applications, spatial and temporal coherence, interference and diffraction theory and optical filtering 16 p2908 A70-33266

Optical filtering applied to aerial photointerpretation of oceanographic, archeologic and town planning data 17 p3081 A70-34620

Fabry-Perot interferometer series as tunable optical narrow passband filter with high spectral and angular resolution, discussing performance in solar magnetograph 17 p3097 A70-35872

Bandlimiting in coherent optical matched filtering for pattern recognition, eliminating confusion between cross correlations and autocorrelations 19 p3446 A70-37889

Thin films optical constants and thickness measurements and UV bandpass interference filters design 19 p3488 A70-38204

Self oscillatory operation of laser with bleachable light filters, solving power balance equations by computer algorithm 20 p3641 A70-39738

Sun photographs with violet interference filter, determining photospheric magnetic fields position by cospatial network 20 p3634 A70-40410

Corrective light filter performance evaluation by spectral transmittance normalization 22 p4072 A70-42503

Interference-polarization light filter, calculating phase shifter errors effects on transmittance by Poincare sphere method 22 p4072 A70-42505

Color filter schlieren photography for visualization of wind tunnel shock and pressures, liquid mixing and convection currents 22 p4036 A70-43065

Single mode ruby and Nd glass lasers axial mode selection by dye filters, noting radiation spectra and spatial coherence 24 p4352 A70-45462

Partially space coherent diffraction by slit aperture with apodizing filter, calculating tolerance and apodization coefficients for correlation interval numbers 24 p4354 A70-45814

OPTICAL GENERATORS

U LASERS

OPTICAL GYROSCOPES

Unconventional gyros, discussing nuclear magnetic resonance, induction, cryogenic, electrostatic and laser technology 03 p0481 A70-12960

Laser gyro status for major obstacles impeding exploitation, comparing biasing methods 04 p0704 A70-15659

Airborne optical scanning gyro for measuring sea surface radiation emission 22 p4039 A70-43558

OPTICAL HETERODYNYING

He-Ne laser heterodyne system evaluating dispersive effect in He-Ne laser, measuring dispersion as function of cavity loss, excitation level, etc 01 p0107 A70-10102

Chirped pulses observation by heterodyning single frequency Q switched carbon dioxide laser with stable CW local oscillator and beat signal display on oscilloscope 01 p0109 A70-10433

Error probability, signal to noise ratio and average signal level for coherent heterodyne and photon limited laser communication systems, using Poisson distributions 02 p0255 A70-11914

Signal to noise ratio for optical heterodyne with inhomogeneous partially coherent signal and local oscillator fields, using phase-quadrature description 02 p0255 A70-11915

Ar laser as suitable source for LF heterodyne anemometry experiments through noise spectrum suppression under optimum conditions 04 p0702 A70-15569

Optical heterodyne quantum detector response, calculating signal to noise ratios 06 p1008 A70-17524

Optical and electronic mixing in avalanche photodiode during variable amplitude signal demodulation in optical heterodyne receiver, considering conversion losses 07 p1243 A70-20282

Signal properties and measurement accuracy of noncontacting optical heterodyne velocity sensing method used in differential Doppler velocity measurements 09 p1678 A70-22926

Optical heterodyning of Doppler shifted signal with minimal instrumental spectral broadening and high SNR, applying to turbulence structure measurement by CW laser 11 p2062 A70-25630

Electronic heterodyne astronomical spectroscopy, using lasers for absolute monochromatic flux and polarization measurements on star-like objects 13 p2408 A70-29473

Laser Doppler heterodyning system for velocity measurements without directional ambiguity, employing incident beams of different frequencies through rotating diffraction grating or Bragg cell application 15 p2751 A70-31986

Optical heterodyne interferometer for stellar diameter measurements 16 p2925 A70-33025

Far field antenna patterns synthesis and steering for optical heterodyne receivers 16 p2866 A70-34261

Magnetized plasma electron density measurement by laser self heterodyne 17 p3141 A70-34996

IR heterodyne signal statistics, discussing receiver characteristics and design 17 p3105 A70-35096

Cryogenically cooled photoconductive IR radiation detectors, determining wideband optical heterodyne performance 20 p3627 A70-39085

Laser heterodyne system for nonsinusoidal vibration measurements, describing calibration and use 22 p4049 A70-42526

Optimal heterodyne receiver for laser signals element-by-element wavefront detection 22 p3987 A70-42558

Fluctuating light pulses detection and arrival time estimation for heterodyne reception 22 p3987 A70-42560

Light source spatial coherence measurement, verifying laser heterodyne interferometer theory 24 p4354 A70-45665

OPTICAL ILLUSION

Horizontal-vertical illusion and foreshortening of receding horizontal lines during visual observations 02 p0249 A70-12839

Human oculogyral illusion thresholds determined on Ames Man-Carrying Rotation Device to establish stimulus duration effect on angular acceleration thresholds 03 p0424 A70-13765

Illusions of rotation perception with oscillating trapezoid and oscillation perception with rotating trapezoid, correlating magnitudes 05 p0807 A70-16673

Perceptual selection and integration of sensory data conveyed to brain, explaining various optical illusions 10 p1827 A70-24766

Oculogyral illusion provoked by angular accelerations during flying stationary and spiral turns in jet aircraft, considering semicircular canals stimulation 11 p1992 A70-26512

- Visual effects in astronauts and pilots, discussing optical illusions and distance estimation errors due to accelerations, runway factors, lack of oxygen, etc
18 p3225 A70-36777
- OPTICAL IMAGES**
U IMAGES
OPTICAL MASER MODULATION
U LIGHT MODULATION
OPTICAL MASERS
U LASERS
OPTICAL MEASUREMENT
NT ASTRONOMICAL PHOTOMETRY
NT COLORIMETRY
NT ELECTROPHOTOMETRY
NT OPTOMETRY
NT PHOTOMETRY
NT POLARIMETRY
NT SPECTROPHOTOMETRY
NT STELLAR SPECTROPHOTOMETRY
NT TELEPHOTOMETRY
NT ULTRAVIOLET PHOTOMETRY
NT VISUAL PHOTOMETRY
- Optical measurements of mirrors reflectance and solar radiation transmittance to solve problems specific to solar energy engineering by standard optical equipment
01 p0010 A70-10765
- Pritchard photometer analyzed for in-focus and out-of-focus operation using radial weighting function
01 p0091 A70-10918
- Photochronographic measurements of high speed rotor vibrations, showing precision and nutation components
01 p0093 A70-11268
- CRT resolution measurements by double slit method, relating light spot response to slit width
01 p0093 A70-11278
- Optical scintillation measurements applied to turbulence diagnostics, inferring spatial spectrum of turbulent scatterers, using Monte Carlo numerical procedure
02 p0296 A70-11892
- Chemical kinetics in reaction zone of shock heated hydrogen-carbon monoxide-oxygen mixtures, measuring density field behind normal shock wave by optical interferometry
02 p0250 A70-12022
- CuCl single crystal refractive index measurement at room temperature using V-block refractometer
02 p0350 A70-12453
- Optical studies of deformational structures of minerals from meteorite craters and cryptoexplosion structures
02 p0292 A70-12510
- Photoelectronic measurement of distance from laser beam axis to reference plane, discussing applications to surveying, vibration measurements and atmospheric investigations
02 p0314 A70-12785
- Stress-optic law for orthotropic composites photoelastic stress analysis, investigating use of transparent filament-resin composites
03 p0481 A70-12956
- Lunar limb ellipsoid orientation and parameters based on Greenwich meridional measurements of visible lunar diameters, noting use for observation reduction for various librations
03 p0569 A70-13356
- Third harmonic generation detection for strongly absorbing media in reflection with neodymium-glass mode-locked laser, measuring nonlinear susceptibilities of semiconductors and metals
03 p0501 A70-13649
- Airborne optics control subsystem /AOCs/ in optical measurement program for radiation originating in reentry events in project PRESS /Pacific range electromagnetic signature study/
03 p0489 A70-13652
- Optical telescope spectrograph to obtain radiometric and spectrographic data on vehicles reentering atmosphere, discussing performance criteria and tests
03 p0489 A70-13653
- Strain distribution measurement in plastically deformed region around crack tip in metals using moire grid and optical interference
03 p0513 A70-14019
- Measurement method for second and third order photon intensity correlation functions, using optical field produced by gas laser operating near oscillation threshold
04 p0700 A70-14686
- Surface roughness measurements by coherent optics and interferometry, including theory and experimental verification
04 p0689 A70-15015
- Solid carbon dioxide measured for complex index of refraction at IR wavelengths
04 p0719 A70-15036
- Multiple optical properties measurement instrumentation for cellular specimens to classify biological cells, analyzing and displaying data by on-line computer
04 p0644 A70-15361

- Polarimeter for atmospheric radiation with three optical channels enabling precision measurement of polarization
04 p0695 A70-15573
- Temporal behavior of NP 0532 in radio and optical bands compared for second derivative of period
05 p0906 A70-15893
- Length shifts measurement with single 2-mode laser by observing beat frequency, obtaining frequency shift proportional to length shifts
05 p0859 A70-16356
- Optical crossbeam technique for remote sensing of wind speeds, relating light fluctuations to convective wind velocity by space-time correlation methods
05 p0850 A70-16688
- Optical surface degradation during measurements with high power laser, considering atmospheric dust and cleaning solvents
05 p0861 A70-16848
- Displacement measurement using single reflecting phase grating
06 p1060 A70-17148
- Displacement measurement to fractions of micron using laser interferometer
06 p1060 A70-17149
- Properties of unstable confocal resonator used with carbon dioxide-nitrogen-helium laser, using geometric models and measurements
06 p1079 A70-17188
- Optical approach navigation experiment on 1969 Mariner mission to Mars demonstrating accuracy potential of spacecraft-based measurement
[AIAA PAPER 70-70] 06 p1103 A70-18152
- Earth axis position and displacements measured by earth-moon laser telemetry
06 p1058 A70-18452
- Remote sensing of winds and atmospheric turbulence by cross correlation of passive optical signals, discussing results for power spectrum of fluctuations and winds
06 p1072 A70-18553
- Multiple beam interferometer coherence analyzer for temporal and spatial study of laser beams, emphasizing application to pulsed lasers, holography and nonlinear optics
07 p1297 A70-19145
- Wave numbers, intensity and half width of lines of vibration-rotation relative to carbon monoxide transition, noting band center displacement dependence on pressure
07 p1338 A70-19380
- Specular reflectivity measurement method for optical thin film coating in 10.6 micron IR region using carbon dioxide laser source
07 p1302 A70-20084
- Holographic system to obtain time-bandwidth product improvement in spectral analysis without sacrificing multichannel processing capability
07 p1288 A70-20098
- Quasi-optical beam splitter, using grid diffraction of plane wave at dielectric cylinder, suitable for millimeter and submillimeter wavelengths and thread measuring
08 p1496 A70-21219
- Microphotometric spectral reflectivity correlation to static Young moduli of carbon and graphite yarn filaments as optical testing method
08 p1497 A70-21350
- Quantum mechanical form of Cramer-Rao inequality used to determined error lower bound for radiating object parameter observed by quantum-limited optical system
09 p1694 A70-22072
- Polarization-optical studies of large deformations in nonlinear theory of elasticity and plasticity, considering procedures based on photoelastic coatings and transparent models
09 p1768 A70-22120
- Small-scale local flow velocity measurements with laser using differential Doppler method
09 p1694 A70-22125
- Plasma discharge absorption coefficients measurement using Q switched ruby laser
09 p1694 A70-22139
- Earth satellite orbit determined by small separated optical observations at two stations
09 p1751 A70-22162
- Real time hologram-interferometry application to optical aspheric surfaces testing explained by geometrical optics
09 p1676 A70-22717
- Compact unequal-path radial shearing laser interferometer designed for small angular aperture wave front testing
09 p1696 A70-22719
- Coherent optical beam propagation measurement of fine scale turbulent atmosphere structure, inferring microscale size and permittivity spectra
09 p1635 A70-22963
- Photo-optical processes and optical measuring techniques in research programs at Ames Research Center for aerodynamics, life sciences and space sciences
09 p1657 A70-23501

- NASA operation of Convair 990 jet transport as airborne scientific research platform for optical observations
09 p1682 A70-23504
- Optical tools in aeronautical and space research at Langley Research Center, discussing schlieren photography of aeronautical and space models in wind tunnels
09 p1657 A70-23510
- Optical research at NASA Electronics Research Center applied to air pollution measurement, pulse formation, pilot warning systems, star field mapper, etc
09 p1657 A70-23513
- Roof prism reversing-front Michelson interferometer for phase correlation measurements in turbulent atmosphere
09 p1684 A70-23535
- Atmospheric water vapor profiles remote measurements using Raman component of high powered Q switched laser backscatter
10 p1886 A70-23938
- Microwave surface acoustic delay lines properties, advantages, electron beam fabrication, optical probing for propagation loss measurement, etc
11 p2005 A70-26166
- Divergence measurement of beam emitted by ruby laser in relaxation mode as function of cavity length and excitation voltage
11 p2063 A70-26462
- Lunar limb ellipsoid orientation and parameters based on Greenwich meridional measurements of visible lunar diameters, noting use for observation reduction for various librations
11 p2118 A70-26721
- Electron concentration measurement range expansion in plasma by laser interferometer with optical signal phase modulation
12 p2278 A70-27328
- Stress concentrations and optimum shape minimum-weight reinforcement of circular holes in plates determined by polarization-optical technique
13 p2512 A70-28864
- Radar and optical meteor observations comparison, discussing luminosity function and angular velocity
13 p2490 A70-29042
- Vertical tropospheric turbidity distribution determination from intensity measurements of inclined searchlight beams
13 p2445 A70-29471
- Interferometric measurement of spatial correlation function of optical radiation fields propagating through turbulent atmosphere
13 p2454 A70-29825
- Spatial filters for ratio W/H measure in aerial mapping
14 p2581 A70-30144
- Air cell optical phase shifter for holography based on refractive index variation with air pressure
15 p2741 A70-32439
- Erroneous height correlation coefficients in physical optics formulation of rough surface scatter
16 p2859 A70-32938
- Spatial vectors determination by two laser measurements and one optical observation of artificial satellite
16 p2926 A70-33118
- Optical system and light source imperfection effects interference image contrast lowering in laser interferometer for length measurements
16 p2928 A70-33292
- Materials real time strain measurements by optical correlation techniques, noting sensitivity
16 p2913 A70-33980
- Optical system measurement of density and rotational temperature in gaseous plume simulating auxiliary propulsion and oxygen hydrogen burner of S-4B
16 p2913 A70-34023
- Jovian planets polar and equatorial diameters and lateral dimensions of Saturn rings by optical measurements
16 p2979 A70-34034
- Luminous emissions related to Apollo 12 mission observed in Belgium, discussing flight chronology, gas ejection, stage separation, etc
16 p2981 A70-34318
- Holodiagram for making and evaluating holograms for large objects dimension, deformation and vibration measurement
17 p3084 A70-35004
- Holographic interferometry measurements, including low frequency quartz vibration and relaxation effects in materials following strain or impacts
17 p3085 A70-35005
- Standards for measuring pulsed laser energy, CW laser power and HCN laser frequency
17 p3105 A70-35097
- Optical rectification /polarization/ and measurement of Q switched laser energy and time parameters, using crystals and parallel plate capacitor
17 p3105 A70-35098
- Plasma opacity measurements using CW He-Ne and Ar lasers as light sources
17 p3106 A70-35107

Clear air turbulence /CAT/ remote sensing feasibility by optical signal covariance measurement, taking into account refractive index fluctuations

17 p3132 A70-35723
Picosecond light pulse measurement by two beam overlap technique using nonlinear photoelectric effect

17 p3097 A70-35912
Optical observation of laminar convective flow caused by combined action of concentration and temperature fields

18 p3346 A70-36276
Optical observation of structure, composition, thermal spectra and aerosol layers of giant planet atmospheres

18 p3315 A70-36601
Integrating sphere theory with wall mounted specular sample in reflectance and transmittance measurements

18 p3284 A70-36776
Silicon elastic constant measurement by Debye-Sears effect, using He-Ne laser source

18 p3298 A70-36952
Atmospheric particle distribution spectrum by optical methods, estimating aerosol concentration from scattering coefficient

18 p3251 A70-36980
Daylight sky brightness at different wavelengths by airborne photometer, investigating statistical characteristics

19 p3460 A70-37419
Atmospheric scattering indicatrices from daytime sky brightness balloon measurements in presence of cloud cover

19 p3460 A70-37420
Atmospheric aerosols optical and microphysical measurements comparison, evaluating sample collection equipment, errors, etc

19 p3421 A70-37637
Transparent spherical rotor spin axis orientation by measuring Fresnel drag effect of optical beam inside ring laser cavity

19 p3445 A70-37669
Two photon absorption-fluorescence measurement of laser pulse width, using three level model of absorber

19 p3422 A70-37671
Laser aided frequency and amplitude analysis of vacuum test chamber vibration during alignment of orbiting UV spectroheliograph

19 p3396 A70-37877
High accuracy length measurement by fringe counting using laser interferometer

19 p3447 A70-38050
Thin films optical properties and measurements

19 p3487 A70-38197
Thin films optical constants and thickness measurements and UV bandpass interference filters design

19 p3488 A70-38204
Strain analysis by moire technique, using triangular and square root of 2 gratings

19 p3432 A70-38720
Earth continental drift and polar wandering measurements by laser ranging to two synchronous satellites

19 p3529 A70-38882
Pulse light amplification by stimulated thermal Rayleigh scattering measured as function of time, absorption coefficient and interaction length

20 p3640 A70-39114
Smoke chamber measurements of opacity developed in polymer pyrolysis or combustion, including Materials Smoke Obscurity Index /MSOI/

20 p3736 A70-39404
Small angle of rotation measurement of coherent radiation polarization plane, discussing technique for increasing sensitivity and accuracy

20 p3643 A70-39759
Extrasolar X ray source optical observations, discussing identification method and individual characteristics

20 p3700 A70-39930
He/Ne laser amplifier and oscillator threshold bandwidth measurement by double laser device

20 p3643 A70-40126
Optical reflection measurement at grazing incidence from shock front at Mach 1.94 in air at atmospheric pressure

20 p3674 A70-40167
Millimeter wave and optical astronomical refraction differential measurements, showing dependence on atmospheric water vapor

20 p3588 A70-40305
Turbulence characteristics determination by measuring light beam arrival angle fluctuation using photoelectric recording shadow devices

20 p3634 A70-40401
Optical photometric observations of nonsolar gamma and X ray sources WX Cen, NGC 5189 and GX3 plus 1

21 p3873 A70-40669
Optical thermal testing by IR radiation, reviewing thermistor bolometer, various detectors, radiometric microscopes, NDT equipment, etc

21 p3831 A70-40747

Bubble frequencies random distribution during boiling of pure liquids and binary liquid mixtures by optical measurement

21 p3941 A70-40775
Clear lower atmosphere meteorological parameters remote sensing for weather forecasting, comparing optical, radio and acoustic radar techniques

21 p3785 A70-40802
Fuel nozzle sprays mean droplet diameter based on computerized analysis of small angle forward scattered light profile

21 p3806 A70-40805
Photographic emulsions and photosensitive materials for holography, measuring noise spectral power density at high spatial frequencies by scattered light method

21 p3822 A70-40812
Integrating cavity spectroscopy for measuring absorption coefficient of material

21 p3822 A70-40817
F region radar and optical temperature measurements, discussing Doppler and backscatter ion temperature

21 p3818 A70-41103
Heat transfer measurements based on optical methods with temperature dependence of refractive index making temperature field visible

21 p3826 A70-41373
Quantitative optical and electron probe studies of opaque phases in Apollo 11 lunar rocks

21 p3902 A70-41552
Catalog 4C radio sources optical identification, determining distribution, coordinates and radio luminosity

21 p3922 A70-41978
Accurate tuning methods for laser mode locking device, using diffracted light measurement and photodiode with LF spectrum analyzer

21 p3838 A70-42047
Electron concentration measurement range expansion in plasma by laser interferometer with optical signal phase modulation

21 p3860 A70-42069
Optical solar observatory for investigation of solar activity and impact on earth environment, discussing site selection and equipment

22 p4005 A70-42349
Plasma diagnostics by two-beam optical interferometry and holographic techniques, discussing plasma parameter spatial distribution recording insensitivity to radiation and variable- sensitivity interferometry

22 p4079 A70-42382
Crab pulsar observations with refractor and on-line data acquisition, indicating optical pulse arrival times at variance with previously assumed 77 day periodic wobble

22 p4097 A70-42464
Three dimensional hologram diffractive efficiency measurement by spectrographic attachment

22 p4026 A70-42508
Optical glasses photoelastic constants measurement, tabulating results

22 p4072 A70-42509
Large collimator objectives lenses focal lengths measurement in vibrations and temperature gradients

22 p4073 A70-42511
Fiber optic components quality control by image transmission intensity distribution measurement

22 p4045 A70-42513
Single and crossed light beam techniques for optical measurement of fluid turbulence with refractive index fluctuations

22 p4011 A70-42694
Crab Nebula pulsar NP 0532 optical timing, measuring frequency, arrival times and pulse interval

22 p4102 A70-42936
Optical waveguides and resonators propagation modes detection and discrimination techniques evaluated for circular cylinder dielectrics /optical fibers/

22 p4030 A70-42949
High purity surface-free GaAs epitaxial layer carrier lifetime measurement by optical transmission and excitation technique

22 p4086 A70-43017
Ruby laser mode excitation, spatial coherence and free emission kinetics investigated by high speed camera scanning

22 p4051 A70-43461
Material transfer image recording using focused laser beam, discussing experimental setup and test results

22 p4040 A70-43605
Optical FM system with laser interferometer and sideband carrier circuit for measuring mechanical shock by Doppler shift

23 p4193 A70-43964
Laser applications in length measurement and holography, describing principles and techniques, modulated laser beams and pulse transit time

23 p4201 A70-43998
Microwave propagation in waveguides, investigating trapped and slightly leaky modes in multilayered or multiwave regions by ray-optical techniques

24 p4311 A70-45216

Laser sensors as alignment instrument for control and measurement of five degrees of freedom

24 p4351 A70-45383
Laser measurements in semidynamic space geodesy on D1-D satellite using Mediterranean stations

24 p4352 A70-45541
GEOS 1 satellite short arc optical observations over North American network to improve survey coordinates of tracking stations

24 p4312 A70-45542
Electro-optical light speed measurements with interference comparator using He-Ne lasers with light modulators

24 p4353 A70-45562
Mode locked neodymium-glass pulsed laser stimulated picosecond time resolved light emission observation by cross beam technique

24 p4354 A70-45647
D2A satellite optical experiments, examining atmospheric atomic H and solar and extraterrestrial 1216 A emission

24 p4339 A70-46094
Phosphorus and selenium oxychloride based liquid laser transmission loss measurement

24 p4355 A70-46265
Laser Doppler shift theory and applications to vibration and flow velocity field measurements

24 p4340 A70-46351

OPTICAL MEASURING INSTRUMENTS

NT CATHETOMETERS
NT CINETHOODOLITES
NT DIFFRACTOMETERS
NT ELECTROPHOTOMETERS
NT ELLIPSOMETERS
NT GEODIMETERS
NT INFRARED SPECTROMETERS
NT INFRARED SPECTROPHOTOMETERS
NT LIGHT SCATTERING METERS
NT NEPHELOMETERS
NT OPTICAL PYROMETERS
NT OPTICAL RANGE FINDERS
NT OPTICAL SCANNERS
NT PHOTOMETERS
NT POLARIMETERS
NT REFLECTOMETERS
NT REFRACTOMETERS
NT SEXTANTS
NT SPECTROPHOTOMETERS
NT THEODOLITES
NT TRANSITS
NT TRANSMISSOMETERS
NT ULTRAVIOLET SPECTROMETERS
NT ULTRAVIOLET SPECTROPHOTOMETERS

Real-world physical simulators application to tactical and strategical optical hardware

01 p0089 A70-10819
Turbulence intensity, light intensity fluctuations and frequency optical measurement in diffusion flames of city gas with air, deriving turbulence spectral functions

02 p0398 A70-12038
Gas pressure differences and diffusion rates recording using He-Ne laser interferometer, discussing aerodynamic applications and avionic instrumentation problems

02 p0299 A70-12272
Photo-optical instrumentation - Conference, Washington, D.C., August 1968, Volume 1

03 p0487 A70-13651
Laser velocimeter measurements on drag reducing polyacrylamide solution compared to water

03 p0502 A70-13821
Holographic method for measuring optical instruments transfer function, using laser light source and beams interference

03 p0493 A70-13946
Precision and accuracy evaluation of convergence angles for measuring vertical and horizontal components of space position applicable to geodesy and flight measurement

04 p0676 A70-14634
[AAS PAPER 69-605]
Prismatic astrolabe errors, analyzing focal plane displacement due to temperature, micrometer motor adjustment, instrument and personal errors

04 p0693 A70-15485
Cine recording ophthalmoscope with TV monitoring for retinal photography during centrifugation

06 p1061 A70-17286
Cosmic rays induced Cerenkov light pulses effect on stellar intensity interferometer from measuring correlated pulses

08 p1497 A70-21492
Signal properties and measurement accuracy of noncontacting optical heterodyne velocity sensing method used in differential Doppler velocity measurements

09 p1678 A70-22926
Optical signal processing using circular array and spatial frequency filtering to yield azimuthal distribution of sources

09 p1678 A70-22969
Single and clad glass fibers radii and refractive indices measurements on basis of laser light scattering

09 p1699 A70-23444

Mirror-grating system optical properties emphasizing coma-type aberration elimination

09 p1729 A70-23528

Aluminized epoxy integrating hemiellipsoidal reflector, discussing fabrication, focusing properties and selection of detector size

09 p1683 A70-23530

Instrument localizing-resolving powers relationship as function of luminous source coherence

10 p1898 A70-23911

Vacuum chamber for adjusting and calibrating spaceborne optical instruments used in studying UV radiations

10 p1860 A70-24479

Plate coordinate measurements obtained with Zeiss precision monocomparator at satellite observation station

10 p1889 A70-24501

Laser methods for industrial length measurements

11 p2061 A70-25355

Visible light sensors application in LES control system for circular near equatorial orbits

[AIAA PAPER 70-477] 11 p2107 A70-25432

Length shifts measurement with two mode laser, noting frequency shift proportionality to mirror displacement

11 p2062 A70-25632

Instrument for measuring and recording strains and birefringence in glasses and crystal under compressive, tensile or bending loads at low/high temperatures and in vacuum

12 p2237 A70-28161

Laser beam photography utilization in engineering for optical pointers, interferometers and holographic visualization of surface strain and vibration

13 p2406 A70-28914

Statistical estimation of resolvability of incoherently radiating object sampled at aperture field of observing optical instrument, using Cramer-Rao inequality

13 p2453 A70-29823

Atmospheric absorption, scattering and turbulence effect on visible and IR radiation propagation, discussing optical systems performance

14 p2583 A70-30399

Balloon-borne optical dew point hygrometer and radiosonde measurements of atmospheric range refractive index

14 p2585 A70-30573

Satellite attitude control via optical-inertial stabilization, using Bucy-Kalman linear statistical filtering

15 p2811 A70-32265

Servocontrolled laser strainmeter based on Michelson-Morley interferometer, determining dynamic characteristics dependence on feedback loop filter type

16 p2925 A70-33022

Optical heterodyne interferometer for stellar diameter measurements

16 p2925 A70-33025

Laser anemometer for fluid flow measurements, noting sample size restraint, frequency response and velocity range

16 p2926 A70-33141

Laser Doppler-shift velocimeter with self aligning optics, discussing performance parameters

16 p2926 A70-33143

Gas laser components optical properties determination, describing measuring apparatus and techniques

17 p3106 A70-35104

He-Ne CW laser emission line width measurement, describing apparatus and technique

17 p3106 A70-35108

Humidity measurement and calibration systems, considering automatic optical dew point hygrometry

17 p3089 A70-35172

Instrumental measurement of projection center coordinates for aerial triangulation with independent models

18 p3248 A70-36780

Photofragment spectrometer, describing vacuum chamber, molecular beam and light sources, mass spectrometer detector, data acquisition and display system, etc

18 p3261 A70-37094

Balloon-borne spectrophotometer with diffraction grating for upper atmospheric solar radiation attenuation measurement

19 p3422 A70-37639

Optimum laser beam deflection for instrument design, considering tandem, rotary mirror and analog methods

19 p3446 A70-37879

Optical hydrometer measuring water vapor content in vertical atmosphere column, using interference filters and thermoelectric sensitive element

20 p3625 A70-39027

Optical interferometry device for large amplitude vibration measurement

20 p3630 A70-39488

Agricultural crop identification, using optical Stokes parameters such as wavelength, geometry, and bidirectional photometric and polarization factors

22 p4014 A70-42769

Projectile velocity measurement, using laser and Fabry-Perot interferometer for Doppler shift determination

[SMPT PREPRINT 29] 22 p4034 A70-43046

Laser application to deformation and vibration analysis, discussing optical alignment, contactless measurement and holographic interferometry

23 p4201 A70-44335

Solar activity research, discussing optical facilities, photoelectric magnetographs, magnetic field measurement, solar cycles and flares, etc

23 p4256 A70-45034

OPTICAL METHODS

U OPTICS

OPTICAL MICROSCOPES

Microscope objective effect on accuracy of optical systems modulation-transfer function based on corrected high speed lens measurements

07 p1334 A70-19147

OPTICAL MODULATION

U LIGHT MODULATION

OPTICAL PATHS

Optical paths inequality of nonuniform power opposing waves in ring lasers

01 p0107 A70-10209

Holographic interferometry for determining optical path variations resulting from photographic plate emulsion thickness and refractive index changes during development

01 p0087 A70-10666

Interferential picture visibility in turbulent atmosphere measured at large path differences with Michelson-Twyman-Green interferometer using He-Ne laser radiation source

03 p0498 A70-12869

Light signals amplification efficiency, considering double-pass regenerative amplifier

04 p0702 A70-15225

Maximum likelihood receiver (MLR) to detect pulsed signal propagated through turbulent medium, assuming optical propagation over long path in atmosphere

07 p1227 A70-19146

Radiation focusing properties of gravitational bodies associated with curving light trajectories analyzed by geometrical and waveguide optics approximations

07 p1384 A70-19411

Laser beam trajectory equation in scanning ultrasonic cell for nonzero incidence angle, relating input and output beam divergence

07 p1300 A70-19865

Total optical field in inhomogeneous medium, questioning uniqueness of division into direct and reversed wave propagation

08 p1546 A70-21785

Atmospheric ray paths calculations applied to determination of optical air mass and twilight ray paths in earth atmosphere

10 p1873 A70-23830

Diffuse light transmission from point sources over horizontal paths in lower atmosphere, discussing effect of range

10 p1912 A70-24424

Composite cylindrical laser rods end region stress and optical pathlength change with thermal expansion or contraction between core and cladding

13 p2429 A70-29703

Aircraft clear line of sight probability data for various altitudes and view angles

14 p2608 A70-30595

Interferograms of window wave front deformations to measure angular deviations to line of sight

15 p2737 A70-32038

GaAs lasers with light propagation along curved junctions, discussing threshold current density variation with radius of curvature

18 p3269 A70-36738

Transmission line modal analysis for nonlinear polarizability in optical and quasi-optical waveguides

21 p3784 A70-40564

Numerical model of light diffraction on plane shock waves at optical phase jump region for shadow and schlieren techniques

[SMPT PREPRINT 97] 22 p4035 A70-43058

OPTICAL POLARIZATION

Icarus surface reflectivity estimated from reflected light polarization, combining estimate with inferred absolute magnitude to obtain radius

01 p0180 A70-10537

Stress concentration in optically active fiberglass reinforced plastics during static loading determined by optical polarization method

02 p0390 A70-12812

Optical rotatory power measurement for compensated cholesteric liquid crystal helical structure to observe thermally induced inversion and electric field perturbations

03 p0542 A70-14003

Polarimeter for atmospheric radiation with three optical channels enabling precision measurement of polarization

04 p0695 A70-15573

Holographic method for reconstructing polarization of light emitted by photoelastic model, obtaining isochromatic and isoclinic fringe patterns

06 p1063 A70-17643

Optical activity theory based on Kirkwood independent group model using scattering matrix

07 p1334 A70-19264

Thermal stress freezing during optical polarization study of perforated disk three dimensional thermoelasticity

09 p1780 A70-23105

Lower thermosphere dust particle layers correlated with polarization anomaly twilight fluctuations and noctilucent clouds frequency distribution

10 p1944 A70-24949

Holographic method for reconstructing polarization of light emitted by photoelastic model, obtaining isochromatic and isoclinic fringe patterns

13 p2405 A70-28726

He-Ne laser beam transmission through atmosphere, investigating intensity, spot size, polarization and power spectrum fluctuations

13 p2427 A70-29103

Optical polarization, discussing radiation intensity and state measurement by two beam interferometer

15 p2736 A70-32035

Optically active organic compounds origin on primordial earth, emphasizing role of asymmetric catalyst

17 p3024 A70-34700

Optically active alpha-amino acids synthesis from esters of alpha-keto acids by hydrogenolytic asymmetric transamination

17 p3041 A70-34749

Optical rectification/polarization/ and measurement of Q switched laser energy and time parameters, using crystals and parallel plate capacitor

17 p3105 A70-35098

Polarization optical determination of plane stress plastic region, using celluloid model

18 p3343 A70-36723

Carbon dioxide laser producing nearly 100 percent amplitude modulation of output by intracavity polarization modulation technique

18 p3270 A70-36747

Zodiacal light observations at elongation angles from sun, examining surface brightness, color index and polarization degree by balloon-borne instruments

18 p3318 A70-37012

Amino acid racemization as enantiomers in core sediment samples

21 p3781 A70-41896

Optical activity of nonenantiomorphous biaxial crystals with mirror planes, investigating polarization plane rotation

21 p3850 A70-41934

Interference-polarization light filter, calculating phase shifter errors effects on transmittance by Poincaré sphere method

22 p4072 A70-42505

Crab Nebula pulsar optical polarization compared with surrounding nebula and radio polarization

22 p4105 A70-43227

Holographic exposure and reconstruction processes, considering illumination beam polarization effects on image brightness

22 p4040 A70-43616

Novae and supernovae envelope properties, observing optical polarization and magnetic field for Crab Nebula

24 p4413 A70-46169

Optical solar polarization broadband measurement interpretation with depolarization factor due to elastic collisions or additional source

24 p4414 A70-46172

OPTICAL PROPERTIES

K factor analysis of target visibility, considering target size contrast, background luminance, glare, atmospheric scattering and optical sight parameters

01 p0142 A70-10420

Nonlinear optical properties of lithium niobate single crystals, considering optically induced index inhomogeneity and second harmonic generation

01 p0157 A70-10422

Flow velocity pulsations effect on frequency spectrum of flow optical fluctuations, discussing methods for separating turbulence characteristics

01 p0092 A70-10996

Venus atmosphere optical properties on basis of Venera 4 data, proposing models for measured rotational temperature and subcloud atmosphere radiative equilibrium

01 p0192 A70-11507

Diamond-like glassy semiconductor compound of cadmium germanium arsenide, determining optical lattice vibrations from IR reflection spectra

01 p0160 A70-11599

Diffuse isotropic light interaction with compact corn leaf, using transparent plate model with rough plane-parallel surfaces

02 p0338 A70-11893

Collection of papers on optical properties of planetary atmospheres

02 p0374 A70-12426

Intermediate air layer optical properties explained by assuming presence of small and large size aerosol particles

02 p0328 A70-12436

Aerosol induced light scattering optical properties in atmospheric boundary layer measured with three photometer setup with He-Ne laser

02 p0328 A70-12437

Two band Drude model validity for analysis of IR optical properties of transition metals obtained from experimental dielectric constant data

02 p0339 A70-12452

Optical properties changes of various transmitting materials under simulated micrometeoroid environment, using silicon carbide particles accelerated in shock tube

03 p0523 A70-13027

Displacement interferograms and schlieren pictures of optical inhomogeneities in transparent media obtainable from single exposure hologram, using non-monochromatic and laser light for reconstruction

03 p0483 A70-13258

Optical variations of quasars and other radio bright sources using photographic photometry, emphasizing highly optically violently variable (OVV) quasars properties

03 p0568 A70-13328

Quasi-optical propagation in frequency wave range above 100 MHz as user problem in VOR, ILS, navigation satellite and CAT detection and warning systems

03 p0523 A70-13613

Optical inhomogeneity of GaAs associated with current carrier distribution analyzed quantitatively using magnetooptical Faraday effect and transmittance method

03 p0541 A70-13726

Optical phonons in mixed sodium potassium tantalate crystals as function of temperature and composition, using IR and Raman spectra

03 p0542 A70-14002

Planetary nebulae with concordant and discordant radio and optical fluxes, discussing possible causes of discordances

04 p0747 A70-14516

Optical systems for coude focus spectroscopic telescopes, discussing advantages over Newtonian and Cassegrain foci

04 p0685 A70-14522

Optimum planetary image intensity at Tv camera cathodes, exemplifying with Saturn orthicon image

04 p0688 A70-14694

External optical phonon modes in ammonium and deuteroammonium halides phase transitions as function of temperature, using IR and Raman spectra

04 p0646 A70-14695

Surface coating optical and thermal properties investigated in preparation for HELIOS solar probe [DGLR-69-46]

04 p0762 A70-15163

Multiple optical properties measurement instrumentation for cellular specimens to classify biological cells, analyzing and displaying data by on-line computer

04 p0644 A70-15361

Optical, electrical and structural properties of transition metal dichalcogenides

05 p0890 A70-15755

Light collecting properties of polystyrene scintillator designed for counting particles of electron-photon showers generated by high energy cosmic ray particles

05 p0846 A70-15944

Elliptically shaped lenses to eliminate reflection losses by positioning obliquely in optical line

05 p0812 A70-16244

Photostability of Nd-activated glass elements as function of dopant concentration and laser mode operation

05 p0858 A70-16266

Diffuse far UV radiation analysis in connection with stars and dust grains distribution and grains optical properties

05 p0903 A70-16571

Beam transformation laws and matrices for Gaussian beams, discussing propagation, reflection and refraction in geometrical optics

05 p0883 A70-16773

Optical parameters of Martian surface and temperature, discussing brightness distribution along diameter in red spectral region, based on photoelectric cross sections

05 p0918 A70-16917

Yttrium-iron garnet optical properties at various wavelengths and temperatures, noting absorptivity decrease in IR region

06 p1126 A70-17767

Optical parameters effect on directional emittance near edge of two dimensional ceramic coating, using Monte Carlo techniques [AIAA PAPER 70-67]

06 p1106 A70-18138

Optical properties of Gabor holograms with pure reference beam, discussing image reconstruction using He-Ne laser

06 p1072 A70-18565

Basic equations governing optical properties of telecentric lens systems for moire analysis, discussing suitability for stress analysis

07 p1248 A70-19238

Solar installations optical properties selectivity increase by light-collecting surfaces mechanical treatment, describing plate grinding with abrasive powders

07 p1196 A70-19625

Elastic and optical properties anisotropy in fiberglass reinforced epoxy plates using photoelastic method

07 p1416 A70-20295

N-type InAs single crystals optical properties with various carrier concentrations at 1-6 μ m wavelengths and 300-78 K temperatures, studying absorption spectra

08 p1555 A70-20512

Optical suitability to pilot visual requirements in head-up displays, discussing telecentric viewed system permitting binocular disparity tests

08 p1449 A70-20675

Astronomical telescope performance at transfer process from object to image using optical transfer function and brightness standards

08 p1493 A70-20685

Optical parametric backward-wave instabilities in unbounded medium with stopband dispersion using Fourier-Laplace integral

08 p1552 A70-21595

Coherent light beams scanning and propagation direction control by acoustooptical method for laser applications

09 p1695 A70-22315

F-104 jet windshield components research concerning plate glass optical deviation problems to meet quality standards

09 p1691 A70-22571

Quasi-optical waveguide component (attenuator) in S-band measured for performance noting diffraction as limiting factor

09 p1647 A70-22711

Room temperature cholesteric liquid crystals retention of information on past electric field excitation by changes in optical transmission properties

09 p1740 A70-22924

Electrical narrowband noise model for laser speckle pattern, obtaining image intensity statistical properties

09 p1638 A70-23370

Mirror-grating system optical properties emphasizing coma-type aberration elimination

09 p1729 A70-23528

Optical properties of beta prime phase CoAl, CoGa and NiGa as functions of composition and photon energy

10 p1919 A70-23986

CW Nd-doped YAG laser rods, measuring thermal and optical properties before and during pumping with W lamps

10 p1900 A70-24942

Electrical analogs for optical systems based on linear system concepts and communication theory analysis

10 p1854 A70-25246

Macrodon elastic-plastic strain model, studying stress-strain relationship and optico-mechanical properties

11 p2128 A70-25385

Magneto-photoelasticity equations derived for photoelastic model in magnetic field, developing algorithm for optical phenomena for arbitrary stress distribution

11 p2131 A70-25588

Optical and radio homologues of solar flares, studying correlation from astronomical telescope pictures

11 p2105 A70-25747

Resonant oscillations of passive Fabry-Perot resonator in optically anisotropic medium, using parabolic equations for wave vector amplitudes polarized components

11 p2063 A70-25869

Piezo-rotatory coefficients R_{11} and R_{12} of isotropic non-enantiomorphic optically active crystals from fourth rank axial tensor, discussing stress effects

11 p2098 A70-26298

Quenched MnBi thin films measured for magnetic, magneto-optical and optical properties, noting Faraday rotation

12 p2284 A70-27246

Selective optical coatings of alternate Ni and silicon dioxide layers, describing optical and spectral characteristics of black mirror

12 p2272 A70-27307

Waveguide optical properties effect on injection GaAs laser threshold lasing and field distribution in near/far zones for various parameters of active region

12 p2246 A70-27365

Quasar optical properties, red shift and models

12 p2299 A70-27379

Field cotton leaves reflectance and transmittance measurement, predicting linear dimension related to cellular structure

12 p2273 A70-28122

Temperature dependence of electrical conductivity and optical properties of strontium titanate semiconductor single crystals doped with Ce and Nb

12 p2288 A70-28328

Nonoriented cadmium silicon arsenide single crystals optical properties, determining spectral distribution of IR absorptivity for various photon energies

13 p2470 A70-28883

Reflecting surface nonplane parallelism effects on Fabry-Perot interferometers superposition bands contrast and multiplied length measurement accuracy

13 p2408 A70-29366

Stimulated emission cut-off characteristics of laser based on crystals with Nd ions under UV irradiation

13 p2429 A70-29505

Thermooptical constant of laser neodymium glasses measured with interferometer

13 p2430 A70-29761

Polymer optical properties in terms of interaction matrix coupling monomers, applying to polypeptide alpha helix, beta sheets and polyproline helices

14 p2544 A70-30118

Continuous operation He-Ne lasers, discussing excitation, structural and optical design, mode selection and performance specifications

14 p2593 A70-30353

Atmospheric optical aerosol model based on vertical attenuation profile, particle concentration and size distribution and air conductivity

14 p2603 A70-30410

Wave properties of nuclear optical model for barrier penetration by charged particles, considering square well reflection, absorption and resonance

14 p2619 A70-30491

Lunar surface optical properties differences for lunar and planetary nature and evolution determination

14 p2645 A70-31063

Photoemission optical analysis from thin films with uniaxial anisotropy, discussing reflectance, transmittance and divergence of Poynting vector

15 p2774 A70-32012

Goddard Space Flight Center optical studies, noting UV and soft X ray regions, lasers and holography, vision, photography and testing

15 p2775 A70-32026

Glancing incidence extreme UV telescopes optical design in solar physics applications, employing surfaces of revolution

15 p2736 A70-32029

Shemakha observatory telescope main mirror spherical aberration, coma, astigmatism and light concentration, describing support system and adjustment and control mechanisms

15 p2738 A70-32203

Elastic and optical properties of polyurethane rubber under large deformation using natural stress concept derived from stress-strain linear relationship [SESA PAPER 1608]

15 p2821 A70-32319

Atmospheric optical properties at various altitudes, using lunar disk photometric observations at different wavelengths during eclipse

15 p2801 A70-32476

Composition dependence of optical energy gap and diffuse reflectance in MnSe-CdSe solid solutions

16 p2960 A70-33094

Mechanically heterogeneous and optically homogeneous solid/liquid mixed laser with active centers contained in Ne bathed in liquid

16 p2926 A70-33109

Beryllium mirrors optical performance, describing causes and effects of anisotropy and dimensional instability

16 p2904 A70-33146

Optical properties of electropolished cubic Nb-Ti alloys at cryogenic and room temperatures in visible and near IR spectral range

16 p2930 A70-33205

Tropospheric inhomogeneities properties and wind conditions in relation to lunar limb image deformations

16 p2979 A70-34178

Atmospheric optical properties stability determination for various optical densities, assuming horizontally homogeneous medium with properties constant during observation

16 p2899 A70-34181

Earth atmosphere transmission coefficient and optical stability based on solar aureole observation

16 p2899 A70-34186

Electronic narrow sweep antenna array active element number reduction, discussing optical considerations

16 p2866 A70-34266

Glass laser materials characteristics, discussing refractive index thermal coefficient, stress optical coefficients, spontaneous emission, etc

17 p3105 A70-35091

Gas laser components optical properties determination, describing measuring apparatus and techniques

17 p3106 A70-35104

InAs p-n junction laser electrical and optical characteristics during spontaneous and stimulated radiative recombination

18 p3269 A70-36739

Upper atmospheric dust composition and optical properties by crepuscular technique, using photometric measurements in 5200 Å region

18 p3251 A70-36978

Spiral structure definition in external galaxies, discussing optical form types, Messier 33 outer and inner parts and differences in arms

18 p3326 A70-37153

Galactic spiral structure, discussing gravitational theory, pattern origin, radio and optical structure and magnetic field effects

18 p3332 A70-37201

Cardioid condenser as radiometer mirror objective in low temperature radiometry, describing optical characteristics

19 p3420 A70-37261

Nd glass laser ultrashort light impulse optical rectification, presenting lower harmonics angular dependence

19 p3443 A70-37287

Trichroic IR absorption lines of triglycine selenate, computing optical and dielectric constants from transmission and reflection data

19 p3470 A70-37366

Soviet reference book on highly refractory elements and compounds covering crystalline, chemical, thermodynamic, thermophysical, electrical, optical and nuclear properties

19 p3451 A70-37470

Thin films optical properties and measurements

19 p3487 A70-38197

Antireflection titanium dioxide thin films for aerospace silicon solar cells

19 p3358 A70-38201

Thin films optical constants and thickness measurements and UV bandpass interference filters design

19 p3488 A70-38204

Optical system mtf measurement by photographic technique for comparing telescopic sight with simulator, discussing performance

19 p3428 A70-38511

Light characteristics and geometry of photoelectric photometer system measuring light attenuated by atmosphere, discussing error sources

20 p3625 A70-39030

Optical properties of system measuring atmospheric transmittance by recording light backscattered from atmospheric layers

20 p3660 A70-39033

Ronchi test interferometer for optical quality checking of laser crystals

20 p3627 A70-39094

Organic liquid scintillators with high transparency, describing optical and chemical properties

20 p3629 A70-39319

Solar flare parameters, statistical relationships and energy estimates from optical characteristics

20 p3699 A70-39465

Holographic recording in transparent bodies with optical characteristics changeable under intensive light

20 p3633 A70-39999

Temperature dependent anomalous optical absorption of thin yttrium films under static ultrahigh vacuum

21 p3862 A70-40816

Optical properties of off-axis multibeam resonators with spherical mirrors, discussing application to He-Ne lasers

21 p3836 A70-40914

Interstellar spherical dust particles from meteoritic silicates and dirty ice, calculating optical properties and scattering functions

21 p3889 A70-41147

Extended extragalactic bright radio sources with complex structure, comparing radio to optical field

21 p3892 A70-41189

Apollo 11 lunar fines, rocks and breccias luminescence, electron paramagnetic resonance and optical properties, discussing reflection spectra, heating effects and dipole resonance

21 p3914 A70-41654

Apollo 11 lunar powder optical and HF electrical properties, discussing reflectivity, polarization, absorption, differential mass spectrum and albedo

21 p3915 A70-41655

Apollo 11 lunar fines, investigating solar radiation effects on optical properties by standing and heating

21 p3915 A70-41660

Optical properties of amorphous polymers, considering one state calculations for flexible polypeptides in solution and disordered regions of films or proteins

21 p3780 A70-41702

Electro-optic device using ferroelectric bismuth titanate, discussing electrical and optical properties and matrix addressed display

21 p3830 A70-42114

Optical devices contaminated mirror surfaces restoration with atomic oxygen from RF plasma by noncontaminating nondestructive oxidation of polymer film

22 p4029 A70-42622

Liquid crystals as solid state organic material with physical properties of liquid, discussing electro-optical properties and applications

22 p4085 A70-42724

X ray sources identification with optical counter-parts, noting lack of radio and pulsar type emissions

22 p4094 A70-42929

Sources of variability in laboratory carbon arc weathering of light stabilized polyester resin

22 p4059 A70-43080

Solidified polyglycol maleinate resin optical and mechanical properties under tensile stress creep, using hereditary photoelasticity

22 p4121 A70-43723

Optical point characteristics of static spherically symmetric space-times of de Sitter universe, Einstein universe and exterior Schwarzschild field

23 p4239 A70-43821

Atmospheric optical properties at various altitudes, using lunar disk photometric observation at different wavelengths during eclipse

23 p4239 A70-43901

Holographic primary and conjugate images properties, considering applications in moving scenes recording and multiple images storage and retrieval

23 p4193 A70-43924

YIG single crystals piezo-optical effect and magnetic double refraction, describing stress measurement technique

23 p4230 A70-43931

Upper atmosphere optical properties sounding by twilight observation and successive brightness approximation

23 p4187 A70-44047

Spheroidal three mirror telescopes distortion involving dioptrics combination

23 p4194 A70-44213

EUV reflectance data for optical constants obtained in digital form directly on punched cards by data acquisition system

23 p4197 A70-44470

Optical permittivity and dielectric permeability of electron gas in magnetic field, considering application to ferromagnetic materials

23 p4221 A70-45051

Short and long term stabilized optical frequency standard of gas laser, using two absorption cells

23 p4202 A70-45057

Optical properties of terrain for optimal time charting of aerial mapping, considering seasonal variations and atmospheric transmittance

24 p4333 A70-45199

OPTICAL PUMPING

Spectral efficiency of coaxial flash lamp pumping gas laser, noting dependence on geometrical and physical parameters of source and active body

01 p0106 A70-10061

Combination absorption effect on Raman scattering and Stokes component gain in presence of pumping in antiStokes region, giving relation for radiation conversion

01 p0107 A70-10141

CW laser perturbation by coupled optical transition at strong pumping with incoherent and coherent perturbing radiation, considering disappearance of laser effect

01 p0108 A70-10231

Superradiant traveling wave laser emission observed with polymethine cyanine dyes pumped by mode locked ruby laser for picosecond duration pulse generation

01 p0110 A70-10564

Frequency control of ruby laser pumped lithium niobate singly resonant parametric oscillator by radiation injection of CW Nd-YAG laser

01 p0110 A70-10566

Raman effect liquid laser power as function of cavity length, using Q switched ruby laser beam focused by cylindrical lens for optical pump

01 p0111 A70-10674

Solar energy concentrator with truncated conical mirror and toroidal lens to illuminate cylindrical thermoelectric generators or radiation pumped lasers

01 p0010 A70-10760

Polarization level dependence of dye lasers emission on angles between direction of forced radiation and pumping laser resonator axis

01 p0113 A70-11037

Laser transitions to valence band or acceptor in low loss uniformly pumped crystal structure p-type GaAs at 77 K

01 p0113 A70-11168

Optical parametric oscillator pumped by continuously repetitively Q switched Nd:YAG laser output

01 p0113 A70-11171

CW visible ring cavity parametric oscillator, discussing pump depletion, conversion efficiency and improved stability resulting from optical isolation

01 p0052 A70-11173

High output neodymium glass laser with small emission divergence angle using four lamp pumping system

01 p0114 A70-11267

Soviet book on methods in laser design, Volume 2, covering pumping radiation in active rods, unsteady modes, ruby and Nd glass lasers

02 p0310 A70-11691

Light induced modulation of optical absorption of CdS crystals by chopped laser excitation, noting use for fast recombination center detection

02 p0310 A70-11846

Ballistic compressor performance as high intensity pulsed light source, discussing Xe gas heating and laser pumping

02 p0311 A70-11921

Kr, Xe and W-iodine lamps efficiencies for pumping Nd-doped YAG compared for use in high continuous power lasers

02 p0311 A70-11922

Book on ruby laser output power calculation as function of pumping efficiency, considering energy density distribution, absorption, induced emission and excited Cr ions

02 p0314 A70-12692

Resonant energy transfer of trivalent Yb into trivalent Eb for optical pumping improvement for fluorophosphate glass lasing

02 p0314 A70-12725

High intensity short pulse flash lamps using quartz envelopes and wire electrodes for pumping high energy organic dye lasers

02 p0314 A70-12741

Steady state inversion coefficient for active substance in quantum paramagnetic amplifier with push-pull pumping determined by nonstationary methods

03 p0455 A70-13088

Transverse mode controlled hydrogen Stokes laser oscillator optically pumped by pulsed ruby laser

03 p0498 A70-13153

Flash lamp-pumped organic dye scintillator lasers using coaxial Xe-filled lamp, tabulating blue-violet organic liquid lasers characteristics

03 p0499 A70-13161

Transient processes in ruby quantum paramagnetic amplifier during pumping, showing technique for saturation prevention and relaxation effects on population inversion

03 p0456 A70-13460

Pumping energy distribution over cross section of active ruby laser elements in relation to smoothly polished, roughly polished and dull lateral cylindrical surfaces

04 p0700 A70-14607

Optical effects in parallel glass fibers irradiated by He-Ne laser beam, studying resonance tunneling and periodic power repumping between fibers

04 p0702 A70-15215

Flashlamp pumped coumarin dye laser mode locked by intracavity loss modulation operating in blue region

04 p0703 A70-15622

Aminocoumarin derivatives and 2-hydroxyquinoline compounds for flash pumped organic lasers

04 p0703 A70-15624

Continuous wave chemical laser operation in carbon dioxide pumped by vibrational energy released from DF and HF molecular formation

04 p0704 A70-15686

Power output of gas laser pumped by laser contained in single resonator

05 p0858 A70-16259

Frequency shift in Rb-87 atomic frequency standards dependence on filter temperature interpreted for optical pumping radiation improvement

05 p0859 A70-16269

Parametric coupling between space-time harmonics of electromagnetic wave propagating in dielectrics modulated by pump wave

05 p0815 A70-16660

Pumping techniques, design and properties of pulsed and CW lasers based on Nd-glass, ruby, barium fluoride and calcium tungstate crystals

05 p0860 A70-16821

Flash lamp pumped tunable organic dye laser, using capacitor bank for reliable operation

05 p0861 A70-16845

Oscillatory discharge properties of capacitance power storage circuit used for pumping pulse lasers

06 p1081 A70-17768

Pumping light distribution in rectangular laser rods showing corner maxima and overall nonhomogeneity

07 p1300 A70-19871

Electro-optical shutter for optical pumping experiments using Kerr cell controlled by high voltage modulator

07 p1286 A70-19972

Dye laser stimulation by pumping with pulsed nitrogen laser line to obtain entire visible spectrum

07 p1301 A70-20016

Raman effect in liquid nitrogen resonator with light from Q modulated Nd laser pumped into resonator at small angle to axis

07 p1303 A70-20366

Optical pumping energy effects on lasing pulse duration during pulse excitation of alcohol solutions of rhodamine 6G

08 p1511 A70-20522

Neodymium glass laser stimulated by pinch discharge radiation in He and Kr, increasing power, energy and pulse repetition frequency by improved pumping energy coupling

08 p1512 A70-21213

Alkali seeded plasma electron density and temperature enhancement by laser resonance pumping

08 p1552 A70-21576

Double resonator ruby maser dynamic and static characteristics for centimeter band improved by pumping frequency modulation 09 p1695 A70-22188

Book on lasers, light amplifiers and oscillators covering optical resonators, optical pumping, pulsed lasers, etc 09 p1700 A70-23541

Laser pumped optical parametric oscillators (OPO), considering phase matching, threshold power, transient response, etc 10 p1898 A70-23999

Neodymium/YAG laser emission characteristics, studying spectral selection at various excitation energy levels and output-pumping power relationship 10 p1899 A70-24261

CW Nd-doped YAG laser rods, measuring thermal and optical properties before and during pumping with W lamps 10 p1900 A70-24942

He-Ne optical laser CW operation under DC excitation, considering output power, discharge current, total pressure, mixture ratio, etc 11 p2062 A70-25827

Giant Stokes radiation pulse generation during stimulated combination scattering, emphasizing pulses traveling counter to pumping wave 12 p2250 A70-28288

Dye laser small signal gain via pumping by UV nitrogen laser 13 p2426 A70-28811

Ruby laser output calculated as function of pumping power, taking into account pumping energy density spatial distribution and laser level depopulation 13 p2427 A70-28985

Solid state laser optical pumping energy density calculations for case of circular cylindrical image of pumping lamp formed in rod 13 p2429 A70-29476

Operation characteristics of flash, arc, incandescent and explosion type laser pump lamps 13 p2431 A70-29874

Parametric resonances at zero field crossing levels of optically pumped atoms on alkali vapors, noting applications to weak magnetic measurements 13 p2456 A70-30034

Crossing level resonances of magnetometer in optically pumped Rb87 atoms applied to weak field measurement 13 p2454 A70-30035

Optically pumped He 4 magnetometers, investigating magnetic resonance signal dependence on orientation for nonresonance technique construction 13 p2414 A70-30036

Magnetometer design based on Hg isotopes optical pumping, discussing sensitivity improvement 13 p2414 A70-30037

Optically pumped Rb laser theory, taking into account superfine and Zeeman structure of atoms 15 p2749 A70-31521

Luminescent line broadening effect on axial mode selectivity in pulsed neodymium lasers with Fabry-Perot resonator at above-threshold pumping power 15 p2749 A70-31554

CW nonspiking single mode ruby laser operation by end pumping ruby with CW argon ion laser output 15 p2751 A70-31981

Optically pumped cadmium phosphide laser, obtaining IR coherent oscillation from Q switched Nd doped YAG laser excitation 15 p2751 A70-31985

Optical resonator thermal deformations during pumping of circular cylindrical interferometer rods in illuminators, measuring thermo-optical constants of neodymium glass 15 p2754 A70-32863

Gas dynamic molecular laser with electrons in ground state, using incoherent optical pumping from stationary shock wave 16 p2927 A70-33255

Lasing action and reduced output without beam distortion from misaligned carbon dioxide lasers by DC-Tesla coil pumping 16 p2929 A70-33986

Light propagation-shift relationships in optically pumped atomic vapors, discussing susceptibilities, birefringence, conversion efficiencies, coupling, etc 17 p3103 A70-35000

Doubly pumped ruby maser operating in conjunction with superconducting magnet 18 p3265 A70-35953

Electron energy effect on output power and beam divergence of electron beam pumped GaAs lasers 18 p3269 A70-36740

Optically excited homogeneous bulk semiconductor lasers, examining quantum mechanical rate equations and monochromatic light field pump source 18 p3270 A70-36741

Power, energy and efficiency of emission from dye solutions pumped by incoherent light pulses, allowing for particle accumulation at metastable level 19 p3448 A70-38738

Nonactive absorption by silicate neodymium glasses at emission wavelength as function of pumping flash rate 19 p3448 A70-38739

Pulsed laser emission at IR transitions of xenon and neon under electron beam pumping 19 p3449 A70-38743

Solid state laser glass filters for absorbing UV light emitted by pumping tubes 20 p3641 A70-39739

Smooth periodic wavelength retuning in organic dye laser, using neodymium glass laser with YAG for pumping 20 p3642 A70-39742

Normal mode pulsed ruby laser system with Xe flash lamp pumping, trigger circuit and transistorized power supply 20 p3643 A70-40355

Flash lamp pumped organic dye laser intensity for dye solutions in contact with different argon-oxygen compositions, noting effect of oxygen partial pressure 21 p3834 A70-40569

Continuous wave laser action in chlorine, Ar and He gas mixtures, observing energy transfer between Ar and chlorine by pumping action 21 p3834 A70-40570

Carbon dioxide laser pulse shape, duration and power dependence on repetition rate during continuous pumping 21 p3835 A70-40634

IR microwave double resonance signals in systems of ammonia with nitrogen isotopes, using nitrous oxide laser 21 p3836 A70-41707

Magnetic field-independent optically pumped Rb 85 maser oscillator power output 22 p4049 A70-42334

Solid state laser optical pumping systems design and evaluation 22 p4049 A70-42514

Optically pumped magnetometers for low intensity magnetic fields measurement, reviewing atomic hyperfine levels splitting, magnetic resonance, Zeeman sublevels, etc 22 p4026 A70-42575

Thin optically pumped pulsed CdSe platelet lasers, detecting mode jumping and tuning effects by time-resolved spectroscopy 22 p4049 A70-42946

Optical parametric noise from barium sodium niobate crystal pumped at 4358 Å by compact source mercury lamp 22 p4074 A70-43022

Rhodamine 6G triplet lifetime under continuous pumping by Ar laser 22 p4050 A70-43225

Gas dynamic molecular laser with electrons in ground state, using incoherent optical pumping from stationary shock wave 23 p4201 A70-44284

Two-bulb switchable pulsed spectral lamp with Cs and Xe for optical pumping studies 23 p4197 A70-44478

Amplification factor time dependence of dye lasing under rectangular pumping pulse, noting threshold conditions and burnout time relation to material parameters and resonator 24 p4352 A70-45473

Nitrogen laser pumped exciplex 4-Methylumbelliferone and rhodamine 6G dye laser amplifier, measuring single pass power gain vs wavelength 24 p4355 A70-46088

Spectral anomalies due to inhomogeneous optical pumping in masked ruby laser, using mathematical model 24 p4355 A70-46264

OPTICAL PYROMETERS

Photographic pyrometry for surface temperature measurements on ablation models, discussing technique accuracy and limitations 04 p0694 A70-15536

Optically dense high temperature flame pyrometric diagnostics based on modified Kirchhoff formula 10 p1967 A70-24251

OPTICAL RADAR

Lidar technique using pulsed lasers as energy sources for operational type meteorological data collection including cloud height, visibility, thermal stratification, etc 01 p0042 A70-10081

Cirrus clouds signature analysis, discussing light scattering pertinent to lidar equation 01 p0076 A70-10913

Atmospheric density profiles based on laser radar return from ruby laser detected by photomultiplier 01 p0079 A70-11220

CW laser ranging systems power and signal to power ratio characteristics, finding possible advantages over pulsed systems 01 p0114 A70-11321

Lidar technique capabilities and limitations in meteorological applications, emphasizing data storage and display instrumentation 03 p0450 A70-13673

Carbon dioxide laser radar system for studying radar techniques application to IR, discussing automatic tracking capability provision 03 p0450 A70-13676

Lidar and IR radiometer mobile laboratory for atmospheric optics research, including construction details and support equipment 03 p0463 A70-13677

Raman backscatter of frequency doubled ruby laser beam by water vapor in atmosphere observed by optical radar, calculating water vapor mixing ratio profile 04 p0677 A70-14950

Depolarization factor measurements of clear atmospheric air by lidar techniques and laser light scattering 06 p1083 A70-18244

Short coherent laser radar detection of backscattered signal in measuring Doppler shift due to atmospheric temperature 07 p1297 A70-19368

Airport runway and slant visual ranges determination using single scanning lidar/laser radar/ 09 p1696 A70-22490

Lidar techniques for meteorology, discussing atmospheric density measurement, cloud structure and screening effect, pollutant tracking, etc 09 p1635 A70-23066

Lidar ground-based sensing of atmospheric density, temperature, moisture content, discussing scattering theory and technique 12 p2183 A70-26945

Pilot midair collision warning instrument based on optical radar MTI, discussing target cross section enhancement by passive retroreflector 12 p2234 A70-27646

Upper atmosphere probing based on light scattering from laser radar beam by atmospheric constituents 12 p2185 A70-27740

Upper atmospheric composition by nitrogen molecules radiative transition analysis, using laser resonance backscattering effect 12 p2227 A70-28267

Laser tracking system for space guidance, describing equipment and operations 13 p2447 A70-28529

Laser radar systems for atmospheric structure, conditions and processes, discussing clouds delineation, thermal stratification and smoke diffusion and transport 13 p2425 A70-28787

Threshold sensitivity of pulsed optical radar with discrete signal storage, considering different operating modes 13 p2370 A70-29871

Laser radar measurements for atmospheric scattering properties, observing aerosol content, atmospheric density and composition 14 p2550 A70-30746

Lidar for cloud height measurements from ground and meteorological satellites 14 p2611 A70-31155

Bistatic lidar/laser radar/ detection of atmospheric aerosol size distribution, using angular scattering measurements of polarization parameters 15 p2704 A70-32609

Atmospheric structure studies using lidar method to detect particulate content in clear air 16 p2862 A70-33014

Tropospheric turbidity detection and measurements by lidar, considering performance limitations and thickness resolution vs range curve 16 p2862 A70-33015

Lidar probing of stratosphere and mesosphere using automatic data acquisition system 16 p2862 A70-33016

Semiremote laser Raman spectroscopy application in pipes, reactors, hot cells, jet and rocket engines and air pollution studies, discussing LIDAR model for chemical analysis 16 p2926 A70-33161

Meteorological laser radar, discussing basis and techniques determining atmospheric radiation attenuation constant 17 p3045 A70-35106

Laser radar tracking systems, calculating atmospheric turbulence effects on angular errors 19 p3379 A70-37857

Atmospheric free Na atoms layer measurement during twilight and throughout night by laser radar 19 p3413 A70-37999

Lidar technique for remote detection and mapping of atmosphere based on weather radar and optical scattering concepts 20 p3660 A70-39079

Raman spectroscopy with lidar for remote mapping of air pollutants and concentrations 20 p3627 A70-39126

Pulsed laser lidar measurements of atmospheric turbidity, diffusion, pollution, visibility and cloud physics 20 p3584 A70-39127

Spectroscopic detection of sulfur dioxide and carbon dioxide molecules and concentrations in polluted atmosphere by laser-Raman radar technique 20 p3640 A70-39389

Book on molecular and aerosol backscatter measurement from stratosphere by means of ground based laser beams

20 p3623 A70-39925

Spurious photomultiplier response to short intense overexposure of atmospheric return using optical radar

21 p3828 A70-41474

Target velocity estimation by lidar, examining range measurements with time response and cross correlation technique

22 p3988 A70-42567

Pulsed laser radar tracking and ranging system for monitoring and directing TV camera at astronaut position on lunar surface

22 p3992 A70-43604

Optical laser radar for upper atmospheric density and aerosol concentration measurements

24 p4353 A70-45561

OPTICAL RANGE FINDERS

NT LASER RANGE FINDERS

Automatic aiming system for laser range finders using directional information carried by light beam transmission

[ONERA-TP-761] 03 p0450 A70-13637
Apollo 11 lunar laser reflector for earth-moon distance measurement

10 p1898 A70-23847

Phase modulated optical range finder with RF coaxial delay line

13 p2412 A70-29872

Modulation method for phase detection in electro-optical light modulator of optical range finder

16 p2914 A70-34213

Earth continental drift and polar wandering measurements by laser ranging to two synchronous satellites

[AIAA PAPER 70-1069] 19 p3529 A70-38882

Pulsed laser radar tracking and ranging system for monitoring and directing TV camera at astronaut position on lunar surface

22 p3992 A70-43604

OPTICAL REFLECTION

Disk-shaped Mo and Nb specimens solar radiation reflection and absorption characteristics observed for temperature effect

01 p0117 A70-10176

French laser reflectors for lunar telemetry functioning with ruby laser, discussing applications to lunar orbital parameters, continental drift, gravity constant secular variations, etc

04 p0700 A70-14609

Carbon dioxide laser resonator design and operation, discussing performance with dish reflector made of leucosapphire

05 p0859 A70-16272

Single crystal Ge surface etching characteristics using laser beam reflection pattern

05 p0860 A70-16656

Doppler shift of laser beam reflected from shock wave measuring velocity through optical mixing

05 p0852 A70-16993

Reflected light directional diagram effects on scintillating surface luminescence yield, considering scattering function gradient

12 p2231 A70-27310

Visual reflectance of wet soils, attributing darkening to internal reflection of radiation in water layer enveloping soil particles

14 p2577 A70-31236

Planetary atmospheric light diffuse reflection and transmission, applying anisotropic scattering theory

15 p2802 A70-32493

Attenuation, refraction and multiple reflection effects on light reflection from shock front at near grazing incidence

16 p2953 A70-34271

Spontaneous megawatt pulsing in ruby laser with output beam reflected back into cavity

17 p3108 A70-35909

First luminous lunar echoes obtained by laser telemetry of Pic Du Midi observatory

18 p3310 A70-35948

Contaminated optical surface investigation technique in near UV, visible and near IR range, investigating property changes of systems in transmission and reflection

18 p3292 A70-36786

Narrow band IR photometry of star alpha Orion, testing hypothetical correlation of emission peak with starlight-reflecting silicate dust

22 p4105 A70-43229

Planetary atmospheric light diffuse reflection and transmission, applying anisotropic scattering theory

23 p4240 A70-43915

Delta function approximation in diffuse transmission and reflection of light for phase function with sharp forward peak, using scattering compensation

23 p4214 A70-44034

Laser light pulse reflection by atmospheric boundary layer calculated on computer by Monte Carlo method, comparing results with full scale measurement

23 p4166 A70-45072

Light reflectance from optically inhomogeneous medium due to space charge near semiconductor surface

24 p4390 A70-45661

Interference fringes on gas laser beam reflected by total reflection prism

24 p4356 A70-46272

Binocular fundus reflectometry and plethysmography in rabbits and man after dye injection and in patients with carotid occlusion

24 p4310 A70-46345

OPTICAL RESONANCE

Difference frequency generation by resonant three photon process during optical mixing in ruby laser medium with simultaneous emission of optical transitions

01 p0108 A70-10350

Maximum power transfer theorem, discussing rotation symmetry with respect to optic axis and confocal optical resonators

02 p0339 A70-12454

G values of hyperfine components of OH radical molecular vibrational-rotational levels determined using optical RF double resonance

02 p0345 A70-12822

Optical resonator reaction to coupled laser frequency, attributing differences between theory and experiment to errors in mirror reflection efficiency measurement

05 p0859 A70-16354

Frequency reaction of optical resonator to coupled laser in mismatch case, measuring laser and resonator axes displacements

05 p0859 A70-16355

Tunable optical parametric oscillators including Gaussian beams amplification, threshold, tuning techniques, spectral output, etc

05 p0822 A70-16651

Properties of unstable confocal resonator used with carbon dioxide-nitrogen-helium laser, using geometric models and measurements

06 p1079 A70-17188

Polarization of interacting atoms resonance fluorescence and coherence transfer due to excitation exchange, considering electrostatic dipole-dipole and electromagnetic radiative interactions

08 p1548 A70-21341

Lyman alpha wing resonance broadening opacity effects on solar spectrum in 1500 A to 8000 A range

17 p3169 A70-35383

Resonant modes of GaAs junction laser beams with Hermite-Gaussian rectangular symmetry, using stripe geometry with lens-slit combination

18 p3268 A70-36732

Gas lasers intensity expression derived by theory of double resonance spectroscopy, comparing results with He-Ne laser experimental data

19 p3445 A70-37672

Periodic resonant reflector with thin air intervals for YAG-Nd pulsed laser for retinal safety

19 p3445 A70-37673

Gaseous media absorption coefficient and refractive index in field of two nonmonochromatic radiation streams quasi-resonant with combining atoms and molecules transitions

19 p3448 A70-38740

Short light pulse coherent absorption in homogeneously broadened resonant medium, discussing influence of input pulse area and atomic coherence on propagation properties

21 p3784 A70-40565

Narrow resonances in saturated absorption at molecular vibrational-rotational transitions in carbon dioxide laser

23 p4202 A70-45059

OPTICAL RESONATORS

U LASERS

OPTICAL SCANNERS

NT MULTISPECTRAL BAND SCANNERS

Flying spot scanner design and performance to generate images for visual flight simulation

01 p0089 A70-10816

Flying spot scanners evaluation as image processing devices, discussing scan patterns effect on video signal

01 p0089 A70-10817

Planetary film system /PFS/ camera-processor-scanner for scientific spaceborne applications, detailing design and performance

03 p0490 A70-13664

Repetitive scanner for wave velocity measurements in annular two phase gas or liquid flow using pivoted mirror

06 p1062 A70-17618

Optical system with orthogonal standing waves in liquid used for two dimensional scanning of laser beam in ultrasonic field

07 p1296 A70-18765

Rapid scanning high resolution photoelectric spectrometer for sunspot spectra study

07 p1289 A70-20291

Coherent light beams scanning and propagation direction control by acoustooptical method for laser applications

09 p1695 A70-22315

Multiband high resolution spaceborne imagery telemetry with optical mechanical scanners from earth orbiting satellites in earth resource applications

[AIAA PAPER 70-314] 09 p1677 A70-22873

Real time wide angle multicolor scanned laser display for visual flight simulators, utilizing flying-spot camera and rotating optical polygons

[AIAA PAPER 70-361] 10 p1857 A70-24203

Scanning Fabry-Perot interferometer for plasma diagnostics, determining kinetic temperatures

12 p2231 A70-27215

Computerized control for beam scanning and optical data processing concerning symbols, letters and photographic images

14 p2553 A70-30424

Satellite laser communication system using dual scan acquisition technique

14 p2552 A70-31197

Linked and fiber optic components, describing applications as punched card and tape reading, geometrical converters and sensing and scanning probes

16 p2904 A70-33145

Optical scanners efficiency criterion based on geometrical factors including boundary losses overlap, holes, field of view, etc

16 p2904 A70-33151

Scanning celestial attitude determination system /SCADS/, providing triaxial information for earth stabilized satellites

16 p2946 A70-33159

Nd-YAG Q switched laser using feedback loss control to increase switching speed for digital scanning

18 p3270 A70-36744

Optical system with orthogonal standing waves in liquid used for two dimensional scanning of laser beam in ultrasonic field

18 p3271 A70-37109

High speed three-frame electronic camera with storage tube, slow scanning and magnetic recording [SMPTTE PREPRINT 55]

22 p4033 A70-43038

Airborne optical scanning gyro for measuring sea surface radiation emission

22 p4039 A70-43558

OPTICAL SENSORS

U OPTICAL MEASURING INSTRUMENTS

OPTICAL SIGNALS

U OPTICAL COMMUNICATION

OPTICAL SPECTRUM

U LIGHT [VISIBLE RADIATION]

U SPECTRA

OPTICAL THICKNESS

Velocity distribution and optical depth of line formation in solar atmosphere using blue and red wing filtergram and numerical experiment

01 p0175 A70-10241

Jovian polar zones enhanced optical transparency causes, discussing thin clouds and difference in molecular optical depth between north and south poles

01 p0180 A70-10531

Albedo variations for single scattering in atmosphere of arbitrary optical thickness by linearizing transfer equations with perturbation technique

02 p0338 A70-11790

Radiation effects on postshock gas state, noting shock wave optical thinness dependence on radiative cooling and photon flight time

02 p0277 A70-11867

High resolution photometry near planetary limb yielding scale height and optical depth applied to Mariner 4 Mars observations

05 p0909 A70-16387

Unusual IR object IRC plus 10216 interpreted as galactic source surrounded by optically thick dust shells, noting resemblance to black body energy distribution

05 p0920 A70-16976

Laser radiation attenuation coefficient in artificial fog related to water droplet concentration, suggesting single scattering for given optical thickness

07 p1296 A70-18725

Step profile decay of initial perturbations of radiating gas as function of optical depth and Boltzmann number

07 p1255 A70-19212

Atmospheric pressure, optical thickness and Young particle size distribution of Mars atmosphere determined from polarization observations

07 p1385 A70-19421

Relaxation time calculation for ground and excited states of H atoms and H-like ions in optically thin and thick plasmas, considering electron density role

07 p1353 A70-20058

Diffuse radiation intensity determination in finite optical thickness atmosphere illuminated by parallel light beams

07 p1389 A70-20204

Spectral line intensities in hydrogen plasma, calculating relative intensities and Balmer line width for various electron temperatures and optical thicknesses in H alpha line

07 p1389 A70-20205

Optical hardness effect on dispersed particles spectrum determination accuracy by spectral transmittance

07 p1330 A70-20309

Radiant energy transport in plane semiinfinite atmosphere with scattering indicatrix and quantum survival probability as arbitrary functions of optical depth 08 p1564 A70-20548

Resonance radiation transport in optically thick layer, obtaining conservative light scattering solution 09 p1753 A70-22451

Solar IR Fraunhofer line damping constants empirical values and variation with optical depth, noting discrepancy with theoretical constants 09 p1757 A70-22726

Materials permittivity measurement at millimeter and submillimeter wavelengths based on phase shift or sample optical thickness 09 p1684 A70-23648

Resonance radiation transport in optically thick plane gas layer with two-level atoms 12 p2305 A70-27853

Atmospheric optical thickness from radio telescopic measurements of wave absorption at millimeter wavelengths, showing dependence on lower atmospheric moisture content 14 p2546 A70-30127

Atmospheric optical thickness in visual spectrum region relationship to meteorological characteristics, plotting vertical profiles of humidity and aerosol attenuation coefficient 14 p2603 A70-30407

Radiation effects on heat transfer in turbulent channel flow for small optical depths and optically thin limit 14 p2665 A70-30548

Radiant energy transport in plane semiinfinite atmosphere with scattering indicatrix and quantum survival probability as arbitrary functions of optical depth 15 p2796 A70-31457

Mars surface smoothness from photometric and space probe data for atmospheric optical thickness and surface barometric pressure 19 p3512 A70-37300

Luminous intensity profile of optically thick Sr artificial clouds in upper atmosphere, using Monte Carlo calculations 19 p3415 A70-38388

Ionization degree in moving stellar envelopes with large optical thickness 19 p3525 A70-38763

Resonance radiation transport in optically thick media, investigating complete frequency redistribution mathematical assumption 20 p3671 A70-39021

Optically thin plasma population and ionization equilibrium, taking into account heavy particle collisions 22 p4082 A70-43219

Atomic levels occupation numbers and ionization degree for optically thin hydrogen plasma with self consistent electron velocity distribution 23 p4227 A70-44932

OPTICAL TRACKING

Simulation technique to evaluate TV contrast trackers standard scan performance using video tape recording 01 p0058 A70-10812

Voluntary control over velocity of smooth pursuits, discussing saccadic and saccade free modes and switching during tracking 01 p0026 A70-11056

Antitank guided missiles guidance and control systems using optical tracking 01 p0139 A70-11261

Satellite orbital elements optical determination accuracy by differential corrections, presenting computations for data distributed along small arc 02 p0254 A70-11754

Automatic four axle satellite tracking camera design and operational principle, examining lens aberration 02 p0294 A70-11771

Laser position finding of satellites fitted with corner reflectors, discussing atmospheric attenuation and applications to global triangulation and gravitational field measurements 02 p0256 A70-12083

Laser range finding by mobile missile station compared with geodesic satellite telemetry by ground station 02 p0312 A70-12212

Earth satellites optical observations accuracy for geodetic purposes based on errors in station position determinations 03 p0445 A70-13183

Satellite optical tracking data in space geodesy, determining stations position from minimum number of stations and observations with time errors 03 p0446 A70-13195

Ruby laser experiment in illuminating satellites equipped with retroreflectors to determine satellite position in space from range and photographic data 03 p0450 A70-13674

Eye movements during two dimensional tracking tasks, showing oculomotor system transfer characteristics function of target motion spectral content 03 p0427 A70-13948

Visual prediction accuracy in estimating point coincidence of two moving targets as function of viewing opportunity and length of period 03 p0428 A70-14084

Missile impact location visual identification by marker system using pyrotechnic aboard to produce dense white smoke detectable to unaided eye, including flight test 03 p0582 A70-14104

Effence role in eye tracking of moving targets, discussing oculomotor system role 03 p0439 A70-14345

Monograph on probability of aircraft detection by ground visual observation using mathematical model based on Poisson process, considering laws of ocular physiology 05 p0794 A70-16558

Triaxial universal astronomic instrument for tracking artificial satellite path with eyepiece cross-wire, considering instrument errors 05 p0851 A70-16698

Optimal control of elevation and azimuth of automatic tracking device carrying pulse laser and receiving telescope [ONERA-TP-785] 06 p1011 A70-18469

Visual tracking of horizontally moving object, noting acuity dependence on target angular velocity and observation time 08 p1444 A70-20745

Target velocity and approach angle effects on accuracy of moving targets intersection estimation tested on human subjects 09 p1628 A70-23578

Pilot model based on Kalman filtering and optimal control, investigating evaluation for time stationary conditions and sine-wave tracking 10 p1823 A70-23894

Human operator transinformation sensitivity to display gain and forcing function bandwidth in rate control tracking task 10 p1823 A70-23896

IR electro-optical tracker Oculometer using human eye motions for pointing and tracking 11 p1989 A70-25352

Optimal linear estimation and control theory application to high precision optical spacecraft tracking systems design 11 p2028 A70-26302

Man machine eye-integration coupling in tracking task applied to helicopters, ocean-going craft and propeller aircraft 13 p2357 A70-28386

Laser tracking system for space guidance, describing equipment and operations [AIAA PAPER 69-870] 13 p2447 A70-28529

Human operator ocular tracking and decay time stimulation response measurements using information, statistical, point process and random analysis 14 p2537 A70-30388

Aircraft clear line of sight probability data for various altitudes and view angles 14 p2608 A70-30595

Sequential event tracking dependence on stimulus rate and simultaneously displayed information categories 14 p2538 A70-30900

Feedback analysis of learning and performance in hand-yoked, steering and stimulus tracking control of breath-produced visual target 16 p2852 A70-33660

Feedback delay effects on eye-hand synchronism in stimulus tracking and steering using self generated body movements 16 p2852 A70-33662

Receiver for artificial satellite transmission and optical tracking time signals, using crossed dipole directional antenna 16 p2867 A70-34303

ILS glide slope calibration using optically projected digital codes as reference 19 p3464 A70-37912

Visual target tracking with active head rotation, indicating independent eye response due to vestibulo-ocular reflex 22 p3979 A70-43492

Pulsed laser radar tracking and ranging system for monitoring and directing TV camera at astronaut position on lunar surface 22 p3992 A70-43604

Visual acuity during ocular tracking movements as function of field illumination density 23 p4147 A70-44777

Retinal image tracking movement effect on discriminatory perceptibility of orifice orientations of Landolt ring 23 p4147 A70-44778

Stroboscopic stereophenomenon, investigating depth shift of oscillating target motion binocularly viewed for interocular luminance differences 23 p4147 A70-44781

Human tracking performance as function of information precision in electrocutaneous display 24 p4308 A70-45508

Pilot hand-held and leg-mounted controllers for precision tracking from aircraft under buffeting tested in static and dynamic motion simulator 24 p4308 A70-45513

Human compensatory two dimensional visual display tracking performance with superimposed apparent vertical vibration, studying frequency dependent eye pursuit movements 24 p4309 A70-46078

OPTICAL TRANSITION

CW laser perturbation by coupled optical transition at strong pumping with incoherent and coherent perturbing radiation, considering disappearance of laser effect 01 p1018 A70-10231

Difference frequency generation by resonant three photon process during optical mixing in ruby laser medium with simultaneous emission of optical transitions 01 p1018 A70-10350

Solution crystallization method to obtain gallium indium phosphide semiconductor alloys, discussing optical absorption thresholds and transitions 01 p10158 A70-10661

Excitation cross sections for bound-bound transitions in optical levels in hydrogenlike atoms induced by fast charged particles 09 p1730 A70-22230

Coulomb interaction during optical transitions between Landau subbands of Ge semiconductor valence and conduction bands in magnetic field, observing diamagnetic excitons 10 p1928 A70-25029

Upper atmospheric composition by nitrogen molecules radiative transition analysis, using laser resonance backscattering effect 12 p2227 A70-28267

Two-photon transitions effect on two-frequency generation threshold in media with line broadening, considering laser radiation effect on amplification in second channel 12 p2251 A70-28289

Optical transformation of field ion micrographs providing orthographic, gnomonic projections and perspective images of hemispheric metal surface 14 p2584 A70-30506

Gold impurity photovoltaic effect in silicon, determining optical cross section for transition 14 p2627 A70-30528

Optical charge transfer transitions in N-alkyl iodide salts, examining transient absorptions due to flash photolysis 18 p3226 A70-36765

Lasing transitions time delay in carbon monoxide laser under pulsed electrical excitation, attributing inversion to anharmonic decoupling 22 p4048 A70-42330

Carbon dioxide amplification coefficient measurement for lines in laser transition range, determining rotational temperature and upslon levels populations 23 p4201 A70-44204

OPTICS

Geometrical optics method for obtaining radar cross section of perfectly conducting sphere with inhomogeneous dielectric coating 02 p0262 A70-12599

Acoustooptical processing for amplification of weak radar echoes, describing design and operation of modulators, correlators, filters, etc 02 p0266 A70-12630

Collection of papers on optics covering dielectric multilayer filter synthesis, photographic image, light interaction with free electrons, laser radiation, optical echoes, etc 02 p0340 A70-12828

Optical and mechanical techniques for space experiment structures and metals satisfying space requirements 03 p0492 A70-13848

Kirchhoff wave scattering geometric optics theory accuracy, using multifrequency acoustic wave backscatter data obtained from rough surfaces 05 p0814 A70-16401

Modulation transfer function [MTF] of eye-visual system as spatial frequency filter 07 p1216 A70-18870

Optical coherence theory functional formalism developed in radiation field probability functional terms, noting role of P representation of density operator 08 p1545 A70-21254

Optical research at NASA Electronics Research Center applied to air pollution measurement, pulse formation, pilot warning systems, star field mapper, etc 09 p1657 A70-23513

Light storage by Venus machine using refractive properties of gas and involving fluid mechanical optics 11 p2114 A70-26575

Nonlinear optical effects in solids, gases and liquids with light from laser sources, discussing self focusing and absorption of light, translucidity, harmonics, etc 12 p2245 A70-27277

Acoustooptics materials selection guidelines, estimating lead molybdate figure of merit on basis of chemical composition and density

13 p2469 A70-28796

Goddard Space Flight Center optical studies, noting UV and soft X ray regions, lasers and holography, vision, photography and testing

15 p2775 A70-32026

Soviet collection of papers on atmospheric optics covering transmittance, sky brightness, dust component, etc

16 p2899 A70-34176

Geometrical optics laws, principles and procedures applied to microwave antennas design and analysis

17 p3044 A70-35067

Astrophotograph optical center coordinates and camera focal length calculations

18 p3260 A70-36992

Interference wave functions for diffraction on cylinder and sphere, including noninterfering waves of geometric optics

19 p3380 A70-38398

Soviet papers on actinometry, atmospheric optics and ozonometry

20 p3624 A70-39026

Diffraction theory relationship to ray optics for coherent light propagation through lens systems

21 p3829 A70-41929

Self focusing in nonlinear optics, discussing physical processes of wave propagation in dielectrics

22 p4074 A70-43207

OPTIMAL CONTROL

NT TIME OPTIMAL CONTROL

Optimization of distributed parameter control systems described by linear integro-partial differential parabolic equation with delayed argument, using dynamic programming

01 p0131 A70-10548

Dynamic programming for optimizing distributed parameter control systems described by parabolic linear integrodifferential equation with delayed argument

01 p0131 A70-10556

Aircraft optimal spin recovery by aileron, elevator and rudder control calculated using Pontryagin principle to minimize altitude loss

01 p0006 A70-10924

Differential equations of optimal degenerate problem reduced to autonomous form with multiple control, noting D-stationarity application for optimal motions

01 p0053 A70-11022

Optimal control problems concerning vector determination and trajectory of point motion toward target in n-dimensional phase space

01 p0053 A70-11028

Algorithm for L-shaped linear programs in optimal control problems and stochastic programming, outlining cutting hyperplane

01 p0047 A70-11069

Optimal structural design including service requirements on strength, buckling and natural frequency stated as optimal control problem

01 p0207 A70-11158

Optimal control algorithm for spacecraft descent in atmosphere based on nominal trajectory and acceleration measurements

01 p0197 A70-11499

Optimum thrust control of satellite along given trajectory to rendezvous at zero velocity with orbited satellite

01 p0197 A70-11500

Optimal motion control of spacecraft refueling during flight by liquefying atmospheric gas along prescribed trajectory under constant thrust

01 p0197 A70-11502

Observation process optimization in system described by linear differential equations of motion reducible to optimal control problem

01 p0047 A70-11574

Optimal control synthesis in flight dynamics, solving Hamilton-Jacobi-Bellman equation by finite difference technique

02 p0336 A70-12403

Optimum angle of attack control for multistage rocket as function of phase coordinates and time by solving functional equation with finite difference method

02 p0381 A70-12407

Optimal control of aircraft angle of attack based on minimum terminal velocity during passive flight in spherical nonrotating earth atmosphere

02 p0227 A70-12409

Optimal control synthesis in Markov and determinate systems using solution reduced from second order nonlinear partial differential equation

02 p0272 A70-12411

Optimal linear controller synthesis with allowance for continuous perturbations effect, describing weighting factors selection

02 p0272 A70-12413

Analytical design of optimum linear multivariable control systems with randomly sampled stationary

random signals, evaluating matrix complex convolution integral using Laplace transforms

02 p0272 A70-12610

Optimal servocontrol via nonquadratic performance index and linear plant dynamics obtainable as nonlinear function of error between controllable states and input vector

02 p0273 A70-12732

Optimal strategies for controlled plant guidance into convex space assuming linear differential equations of motion

03 p0459 A70-13339

Control problem of linear system with phase coordinate constraints, discussing solution properties, boundary conditions and function minimization procedure

03 p0460 A70-13340

Optimal control of continuous and discrete observations described by linear differential and recurrent algebraic equations in presence of random perturbations

03 p0447 A70-13341

Optimal selection of subsystems, minimizing mathematical expectation of output losses considering malfunctions

03 p0460 A70-13429

Apollo program navigation processing using Kalman optimal linear computer, emphasizing position vector and error matrix and command and lunar landing extrapolation module navigation

03 p0522 A70-13604

Automatic aiming system for laser range finders using directional information carried by light beam transmission

[ONERA-TP-761]

03 p0450 A70-13637

Two point boundary value problem arising from Pontryagin maximum principle application in optimal control, describing solution based on combined existing methods

03 p0460 A70-13699

Optimum automatic system for controlling helicopter formation flight, stressing transient response Q factor and transmission ratios

03 p0413 A70-13859

Existence theorems for optimal control problems with multiple integrals

03 p0460 A70-14075

Closed loop nonlinear optimal control systems sensitivity to small parameter variations noting influence of feedback

03 p0461 A70-14171

Dual type method solving discrete optimal control problems with linear plants, convex cost and constraint taking into account dynamic structure

03 p0461 A70-14274

Optimal control for thermionic nuclear reactor space power plant utilizing state variable feedback with limited input simplifying computation

03 p0461 A70-14342

Optimal strategies for observation system subject to recognition using data transmission along symmetrical channel

04 p0647 A70-14401

Optimal space vehicle reentry control ensuring minimum scattering of landing points based on accelerometer and free pitch-angle gyroscope data

04 p0760 A70-14431

Optimum power and operation mode of space vehicle engine with control error allowance as function of mass and velocity

04 p0760 A70-14433

Optimal control of multidimensional distributed parameters plants described by linear or nonlinear partial differential equations, considering boundary conditions

04 p0660 A70-14551

Graphical solution of optimum trajectories for third order systems depending on single control function, including maximum error and switching time

[ASME PAPER 69-WA/AUT-6]

04 p0661 A70-14828

Pontryagin principle applied to minimum structural weight design problem in optimal control theory with state and control inequality constraints

[ASME PAPER 69-WA/AUT-1]

04 p0769 A70-14832

Optimal control of thrust limited minimum-propellant rocket-powered vehicle using expansion about optimal trajectory

04 p0750 A70-14928

Axial misalignment control of gimbal pivots and rotors in gyroscopes

04 p0692 A70-15282

Soviet monograph on optimal space flight trajectory control, covering vehicle CG trajectory and synthesis of automatic stabilization system using variational calculus

04 p0764 A70-15493

Optimal lift control of hypersonic lifting body during planetary entry, assuming exponential variation of atmospheric density

04 p0620 A70-15532

Analytic guidance and control for minimum fuel expenditure and optimal guidance corrections for low thrust vehicle in Martian orbit

[AIAA PAPER 68-862]

04 p0716 A70-15544

Terminal states and time specifications influence on optimum control systems, using Pontryagin principle for boundary value problems application

05 p0824 A70-15877

Optimization of control forces in rocket nozzle produced by multipoint secondary gaseous injection

05 p0923 A70-15887

Optimal stabilization of spinning body motion about dynamic symmetry axis by controllable gyroscope

05 p0923 A70-16222

Weighting function of optimal correctable gyroscope servosystem in random narrow band noise

05 p0880 A70-16222

Real time computer control system queueing model to optimize preemptible and nonpreemptible job priority assignment

05 p0817 A70-16414

Suboptimal stabilization of axially symmetric satellite angular velocity, using ionic propulsion system as control torque

06 p1155 A70-17554

Identification experiments and computational algorithms allowing synthesis of adaptive optimization process for real dynamic plants

06 p1023 A70-17634

Optimality conditions determined for control involving trajectory with singular component equations of motion

06 p1024 A70-17813

Closed form variational synthesis of optimally fast acting stabilization systems for rigid single axis gyroscopic platforms using integrating nonanalytic equations

06 p1103 A70-17860

Slack variable to transform optimal control problem with scalar inequality constraint on state variables into unconstrained problem

06 p1024 A70-17952

Optimal control generated by Kalman filter and least mean-squared predictor for linear systems with time delay

06 p1025 A70-17959

Suboptimal control to minimize quadratic cost functional for nonlinear systems, using Taylor series representation for feedback gain matrix

06 p1025 A70-17961

M measurement optimal feedback control algorithm for stochastic discrete time systems, considering nonlinear plant, constrained controls, nonquadratic cost and simulations

06 p1025 A70-17962

Numerical solution of control optimization problems by systematic search in initial costate space, using Newton-Raphson method

06 p1025 A70-17964

Control system employing adaptive modeler to estimate state, dynamics and future trajectory of unknown plant through performance index minimization

06 p1025 A70-17965

Separation theorem for nonlinear measurements, discrete-time linear systems and quadratic cost to achieve stochastic control without dynamic programming

06 p1026 A70-17967

Linear optimal stochastic control systems described by covariance matrix correlating errors and estimates of state variables, analyzing instability under parameter variations

[AIAA PAPER 70-36]

06 p1095 A70-18054

Optimum filter for aircraft inertial navigator and radio position fix data mixing using mathematical model of error propagation

[AIAA PAPER 70-35]

06 p1103 A70-18184

Optimal control of elevation and azimuth of automatic tracking device carrying pulse laser and receiving telescope

[ONERA-TP-785]

06 p1011 A70-18469

Growth conditions used in existence theorem for calculus of variations in optimal control problems

06 p1027 A70-18506

Iterative solution of nonlinear optimal control delineated for sufficient conditions for convergence

06 p1027 A70-18507

Optimal control problem converted Cauchy problem for obtaining numerical solutions through invariant imbedding

06 p1027 A70-18508

Optimal guaranteeing control for single switching representable in form of two different successive stages in time, ensuring invariance with respect to motion perturbations

07 p1332 A70-18664

Constraint optimization on phase coordinates and controls noting extension to functional spaces

07 p1330 A70-18683

Optimal nonparametric amplitude and phase methods for synthesizing signal detection systems invariant to noise distribution and noise-signal combination

07 p1226 A70-18684

Optimal control problem solution involving functional minimization along differential vector equation trajectories, considering manifold type constraints on phase coordinates

07 p1244 A70-18747

- Optimal control for distributed parameter systems described by biharmonic linear partial differential equation using dynamic programming
07 p1244 A70-18843
- Second order necessary conditions of optimality with straightforward application to nonlinear programming of optimal control problems
07 p1322 A70-18850
- Stochastic automata for parameter self optimization with multimodal performance criteria
07 p1244 A70-18861
- Suboptimal computational algorithm for terminal control of random linear dynamical system, noting increasing optimality with random variations degeneration to deterministic quantities
07 p1324 A70-19091
- Numerical methods for computing solutions in optimal control of variable lift reentry spacecraft, applying digital computer techniques
07 p1245 A70-19093
- Optimal control of dynamical systems with transport lag determined using differential-integral equations
07 p1245 A70-19094
- Optimal control of linear distributed parameter systems using functional analysis
07 p1245 A70-19096
- Multiplier and gradient methods in computing variational and optimal control problems
07 p1325 A70-19267
- Optimum systems synthesis in computation of programmed movements including dynamical programming methods, control under uncertainty and division problem
07 p1325 A70-19270
- Primal and dual algorithms for discrete optimal control incorporating antijamming procedures
07 p1245 A70-19271
- Optimal control program using multiple maxima method for maneuvering spacecraft in earth atmosphere with aim of changing orbital plane
07 p1331 A70-19483
- Efficiency of terminal state control systems defined, relating efficiency, random parameters and reliability
07 p1246 A70-19528
- Book on optimal control and guidance theory covering state and transition equations and canonical forms of linear systems, systems stability, servo loops, etc
07 p1246 A70-19668
- Suboptimal attitude control system for Nimbus satellite using motor-driven inertia wheels as control torque source for three dimensional control
07 p1331 A70-20027
- Multidimensional Kiefer-Wolfowitz stochastic approximation algorithm modified to locate regression function minimum
07 p1247 A70-20028
- Quasi-optimum design of aircraft landing control system, performing worst case simulation for jet transport
07 p1195 A70-20405
- Optimal spare parts inventory determined for stochastically failing components using mathematical model
08 p1501 A70-20603
- Optimal control systems design involving time delays as functions of time and system state, considering stability constraints
08 p1478 A70-20779
- Optimal feedback control synthesis for linear system with time delay through error criterion minimization
08 p1478 A70-20780
- Phase space variations method proved not applicable to optimal control problems
08 p1479 A70-20856
- Linear differential controller equations for optimal automatic control system with disturbances
08 p1479 A70-20870
- Optimization of control of oscillatory process with deviating argument in maximum principle form, reducing solution to boundary value problem
08 p1544 A70-20954
- Conditionally optimal control coefficients for nonlinear plant obtained from weighting functions derivatives of conjugate linear model for plant
08 p1479 A70-20995
- Optimal control synthesis for flight vehicle in vertical plane involving digital and analog computers
08 p1479 A70-20997
- Optimal linear control system with multiple controls, determining stability margins with respect to phase, amplitude, oscillation index and cut-off frequency
08 p1480 A70-21015
- Variational problem of determining optimal heat transfer from gas flow to porous plate boundary layer
08 p1597 A70-21176
- Memory systems described by integrodifferential equations with distributed time lag, obtaining optimality condition in form of maximum principle
08 p1480 A70-21177
- Optimal control conditions for elastic aircraft motion with delayed wing downwash determined by hyperbolic partial differential equations with delay
08 p1480 A70-21178
- Optimal synthesis of linear steady multidimensional systems with common output ensuring minimum rms error in reproducing control action
08 p1480 A70-21497
- Existence theorem for linear stochastic systems optimal control described by differential equation with random coefficients, providing rms stabilization
08 p1480 A70-21637
- Random perturbation procedure for control variable functions optimization using hybrid computer method for analog solutions and digital storage
08 p1467 A70-21783
- Optimal control mathematical modeling for dynamic systems under statistically indeterminate disturbances based on game theory and pattern recognition
09 p1653 A70-22141
- Decision rules for incomplete a priori data, deriving informational risk estimates for Markov processes and optimal control problems
09 p1653 A70-22144
- Optimality condition for singular control problems derived using differential dynamic programming to obtain expression for change in cost produced by control variation
09 p1653 A70-22345
- One dimensional Poisson production process under costly surveillance, considering maximum attainable income rate approximation
09 p1653 A70-22347
- Optimal amplitude modulated radio signal reception on white and narrow band background noise, using nonlinear filtration and phase locked control
09 p1633 A70-22416
- Optimum control law for minimizing mass point maximum deviation under given disturbance obtained by graph analytic method
09 p1727 A70-22534
- Optimum control for shock absorber of elastic body solved by graph analytic method
09 p1727 A70-22535
- Fourth order differential equation system with complex conjugate eigenvalues, deriving optimal control for fuel minimum
09 p1759 A70-22831
- Control system design for maximum weapon delivery missions effectiveness, discussing analysis and simulation methods
09 p1611 A70-23022
- Soviet book on aircraft control systems design covering optimal functional or function parameters, circuits controlling pitch, roll, yaw motions, human operator systems, etc
09 p1725 A70-23472
- Soviet book on new methods of variational calculus in aerospace vehicle flight dynamics covering controlled processes optimization theory analysis
09 p1767 A70-23473
- Soviet book on control and search for defects in complex systems, presenting statistical optimization methods, programmings for assumed Markov processes, etc
09 p1693 A70-23540
- Optimal control of distributed parameter systems, discussing necessary and sufficient optimality conditions based on functional analysis with emphasis on thermal processes
09 p1654 A70-23542
- Optimizing control system design using fluidic digital circuitry and FM type transducers
09 p1614 A70-23690
- Optimum coding of information for symmetric channel described by code word transformation probability
09 p1639 A70-23694
- Pilot model based on Kalman filtering and optimal control, investigating evaluation for time stationary conditions and sine-wave tracking
10 p1823 A70-23894
- Degenerate variational problem of optimum gliding along zero proximity line, determining number of control switchings and deviation during perturbed motion
10 p1854 A70-24277
- Optimization of controlled systems with allowance for failures of parallel connected elements dependent on control inputs and phase coordinates
10 p1854 A70-24279
- Mathematical model for determining optimal control of spacecraft reentry into atmosphere
10 p1940 A70-24318
- Quasi-linearization extension to numerical solution of multipoint boundary value problems for ordinary differential equations arising from state constrained optimal control problems
10 p1909 A70-24421
- Control synthesis method using optimization technique to design controllers making closed loop system behave as ideal system or model
10 p1855 A70-24450
- Discrete calculus of variations for optimal control involving use of discrete time sequence and functionals
10 p1910 A70-24702
- Linear control systems design with restricted number of feedbacks based on optimization criteria concerning responses to initial disturbance
10 p1855 A70-24703
- Stochastic predictor model for process control, discussing multivariable search techniques and effect of forcing function and noise
10 p1856 A70-24872
- Maximum principle optimality for nonlinear two group parameter control applicable to plants described by integrodifferential and delay equations
10 p1911 A70-25184
- Numerical solution of optimal control with dimensionality not exceeding phase space, using nonlinear programming and traveling wave method
10 p1911 A70-25185
- Final state vector norm minimizing in linear optimal control, using successive approximation and quadratic programming
10 p1856 A70-25188
- Optimal stochastic control investigated for linear systems with driving noise intensity proportional to control input
10 p1856 A70-25234
- Large angle suboptimal attitude control of rigid spinning spacecraft
10 p1856 A70-25236
- Fuel suboptimal attitude control of spin stabilized axisymmetric spacecraft
10 p1953 A70-25237
- Maximum principle condition of optimal control of monodimensional system described by nonlinear hyperbolic equations with time delay
11 p2021 A70-25340
- Low sensitivity optimal controls synthesis for gyrostatizer stabilization circuit using variable structure systems theory
11 p2048 A70-25580
- Soviet papers on complex control systems covering hierarchical structures, accuracy and stability analysis, optimal and self adjusting control, etc
11 p2022 A70-25601
- Optimal two level air traffic control avoiding conflict on runway and in flight and minimizing landing time deviations
11 p2077 A70-25603
- Control theory, Volume 1, covering linear, nonlinear, stochastic, optimal, adaptive and learning systems, sensitivity analysis, etc
11 p2023 A70-25771
- Space vehicle velocity-attitude optimal control for on-line trajectory control schemes
11 p2025 A70-26216
- Spacecraft stochastic optimal control, discussing design of least upper bound fuel optimal system with measurement uncertainty
11 p2025 A70-26222
- Algorithm for infinite dimensional optimal control problems associated with maximum deviation cost functionals distributed systems
11 p2073 A70-26234
- Linear systems optimal control problems with sensitivity considerations for restriction to linear feedback of output variables
11 p2026 A70-26235
- Air to air missile guidance to moving target via optimal feedback strategies
11 p2080 A70-26244
- Optimal fixed digital control for handling wide range plant parameters uncertainty involving random disturbances and measurement errors
11 p2026 A70-26248
- Optimal linear estimation and control theory application to high precision optical spacecraft tracking systems design
11 p2028 A70-26302
- Suboptimal nonlinear state estimation from noise corrupted measurements in ballistic trajectory, using simplified extended Kalman filter
11 p2028 A70-26303
- Quasi-optimum proportional navigation for attack situations with large missile and target maneuvers, showing advantage over linearized optimization
11 p2081 A70-26316
- Fuel-optimal retrothrust control in state dependent retarding force fields, taking into consideration synthesis for vertical trajectory system configuration
11 p2126 A70-26321
- Optimum transmitter strategy and receiver gain for linear feedback communication in nonstationary additive noise
11 p2011 A70-26328
- Rendezvous problems formulated as optimal control problems in combined state space, considering decomposition in optimality criteria and solution existence
11 p2127 A70-26331
- Environmental control of confined spaces and life support systems by Pontryagin maximum principle of optimal control theory, discussing cabins, heat exchanger, etc
11 p1991 A70-26363
- Markov nonlinear optimal filtration theory exact equations replaced by finite system of approximate differential equations
11 p2012 A70-26805

Suboptimal control of discrete input system with bounded state and control variables, developing algorithm for on-line computation 12 p2203 A70-27409

Computational methods for multiinput linear control systems applied to designing lateral and longitudinal autopilots for jet transports subject to gust loads 12 p2203 A70-27417

Optimal and suboptimal aircraft lateral directional stability augmentation applying optimal control and model-following techniques 12 p2162 A70-27812

Nonlinear rotating systems optimal control problems approximation by modified Krylov-Bogoliubov averaging technique 12 p2273 A70-28192

Optimization for control processes with first and higher order constraints on phase coordinates 12 p2205 A70-28195

Spacecraft optimal impulsive braking by onboard engine to ensure maximum angle of atmospheric reentry 12 p2310 A70-28253

Optimal control for processes with parameters and state variable inequality constraints using gradient projection method and maximum principle 12 p2205 A70-28337

Optimal control problems solution by maximum principle, describing variational formulation simplification 12 p2205 A70-28339

Man machine function distribution optimization in spacecraft closed-loop automatic control system 13 p2380 A70-28381

Stochastic optimal trajectory control for spacecraft reentry at supercircular velocity, deriving computer algorithm 13 p2499 A70-28382

Spacecraft rendezvous control at minimal propellant consumption, deriving algorithm 13 p2499 A70-28400

Self contained optimal control synthesis for spacecraft entering atmosphere at first cosmic speed, considering landing spots dispersion component decrease 13 p2500 A70-28407

Spacecraft orientation control system optimization by plotting controlled motion kinematic models 13 p2501 A70-28417

Suboptimal satellite attitude control using ionic microthrusters operating by large modulated amplitude impulses caused by electrostatic deflection of beam 13 p2501 A70-28426

Stochastic processes optimal control theory application to launcher attitude control under wind disturbance 13 p2501 A70-28428

Gauss-Newton nonlinear programming algorithm applications to optimization of optimal control law parameters and closed loop control system synthesis 13 p2381 A70-28435

Optimal control of nuclear propulsion and energetic plants of space vehicle, considering thermionic generator 13 p2450 A70-28436

Optimum filtering techniques for radio guidance of third stage of Europa 1 booster compared for effectiveness 13 p2381 A70-28437

Optimal space vehicle reentry control ensuring minimum scattering points based on accelerometer and free pitch-angle gyroscope data 13 p2503 A70-28456

Optimum power and operation mode of space vehicle engine with control error allowance as function of mass and velocity 13 p2503 A70-28458

Numerical solution of satellite rotational damping by onboard motors using Euler equations, local variations and finite control time 13 p2505 A70-28963

Optimal constant output feedback gains for linear multivariable systems, noting control vector as time invariant function of output vector 13 p2382 A70-29064

Optimal control of systems with time transitions described by finite state stationary Markov chain, noting resetting control 13 p2382 A70-29065

Optimal singular controls made nonsingular for decreasing epsilon values by adding integral quadratic functional of control to cost functional 13 p2382 A70-29066

Nonlinear control systems optimization applied to asymmetrical spacecraft 13 p2382 A70-29071

Training algorithms in designing multilevel quasi-optimal controllers for dynamic processes, using pattern recognition methods 13 p2383 A70-29581

Adaptive optimization methods involving minimization of unknown function, determining new input location via sequential search 13 p2383 A70-29583

Optimal policy for linearly distributed parameter control system, describing sufficient conditions 13 p2384 A70-29899

Terminal guidance by dynamic programming to obtain optimal feedback control law in nominal trajectory neighborhood for minimum energy consumption 13 p2449 A70-29963

Extremum conditions for optimal control with operator constraints using gradient algorithms 14 p2559 A70-30181

Optimal spatial discretization and brightness quantization of graphical symbols for pattern recognition, considering illumination and reflection coefficient 14 p2553 A70-30423

Optimal control of continuous and discrete observations described by linear differential and recurrent algebraic equations in presence of random perturbations 14 p2561 A70-30717

Sequential gradient restoration algorithm for optimal control requiring state, control and parameter to satisfy vector differential equation, initial and final conditions 14 p2561 A70-31099

Availability assurance using computerized spare allocation model for optimal selection of sufficient spares to achieve required protection against system failures 14 p2592 A70-31114

Time lag system performance index bounds determination and optimal feedback controller design based on min-max criteria 14 p2561 A70-31185

Optimum adaptive reception for binary sequences, using posteriori probability density function computing device synthesized from correlator, instantaneous nonlinearity and multiplier 14 p2552 A70-31188

Dynamical optimal control for infinite dimensional linear systems, examining Balakrishnan solution technique 14 p2562 A70-31201

Optimal control problems constraints and necessary conditions, deriving maximum principle 14 p2600 A70-31202

Pontryagin principle for thin vibrating plates under mixed boundary conditions, examining optimal control 14 p2660 A70-31205

Penalty functions for state-space constraints elimination in continuous optimal control problems 14 p2562 A70-31353

Aircraft optimal roll stabilization control system design using performance index with weighting matrix 14 p2532 A70-31395

Optimal manual control model of human compensatory tracking response 14 p2543 A70-31408

Model for pilots optimal manual control of hovering VTOL aircraft longitudinal position 14 p2543 A70-31409

Optimal control theory for system model dependence on state and control variables history 14 p2562 A70-31410

Dynamical systems optimal control approximation without solving differential equations, considering linear systems with quadratic cost functional 14 p2562 A70-31411

Robot motion optimal control in partially unknown environment, using dynamic programming and heuristic methods 14 p2543 A70-31413

Stochastic terminal optimal control for nonlinear dynamical systems with state independent noise 14 p2600 A70-31420

Synergetic plane change maneuver optimal control, combining aerodynamic and propulsive flight phases for efficiency 15 p2715 A70-31784

Optimal control theory of asymptotically stable closed systems synthesis regarding product requirements 15 p2716 A70-32473

Optimal control theory applied to oligopoly, considering economic problems and Nash equilibrium solutions 15 p2831 A70-32552

Optimal control stochastic problem with initial conditions treated as random variables, using matrix minimum principle 15 p2716 A70-32563

Sequential and combined gradient restoration algorithms for functional minimization in control theory 15 p2716 A70-32574

Real time computer algorithm for achieving optimal position of tracking antenna with nonlinear control system 15 p2703 A70-32575

Optimal control program using multiple maxima method for maneuvering spacecraft in earth atmosphere with aim of changing orbital plane 15 p2813 A70-32728

Pursuit-evasion differential games involving two linear dynamic systems with state and control dependent thermal noise 16 p2881 A70-32985

Classical and modern approaches to tracking problem, discussing optimal control in frequency domain and time domain terms 16 p2882 A70-3303

Control strategy for linear system performance based on synthesis of optimal closed loop controller with both sensitivity and state feedback 16 p2882 A70-3304

Regularization techniques for optimal control problems in polynomial algorithms of data handling b groups 16 p2867 A70-3323

Optimal adaptive digital autopilot design for reentry vehicle flight path control 16 p2946 A70-3330

Minimum energy feedback control for electrically driven vehicles by dynamic programming 16 p2884 A70-3331

Optimal interceptor-target allocation and guidance for linear interception and rendezvous using real time and storage computer 16 p2947 A70-3331

Desensitized linear servo model following feedback control systems design using specific optimal control concepts 16 p2884 A70-3331

Optimal control surface location for flexible aircraft determined by matrix minimum principle and calculus of variations 16 p2840 A70-3331

Optimal linear filter analysis from singular optimal control viewpoint, considering white and correlated measurement noise 16 p2885 A70-33320

Controllability of nonlinear dynamic feedback systems based on Liapunov-like stability approach and optimal control theory 16 p2885 A70-33321

Output feedback control systems design, considering closed loop system sensitivity to plant parameters based on linear optimal control problem 16 p2885 A70-33324

Initial condition sensitivity functions in bang-bang and optimal control, considering discontinuous functions, perturbation equations, iteration algorithms terminal states, cost functions, etc 16 p2885 A70-33325

Optimal startup control of jacketed tubular reactor with first order reversible exothermic reaction, presenting distributed maximum principle for diffusional parameter system 16 p2885 A70-33330

Jacobi conditions for singular optimization problems by transforming singular accessory minimum problem into nonclassical nonsingular form, considering optimal control theory applicability 16 p2885 A70-33331

Constrained and constant coefficient optimal controls compared in optimizing performance criteria of vibrating beams 16 p2886 A70-33332

Suboptimal nonlinear feedback control synthesis for linear time-invariant system with convex cost functional 16 p2886 A70-33334

Optimal control in nonlinear systems, discussing conditions for analytical solutions for Hamilton-Jacobi equations 16 p2886 A70-33335

Distributed parameter feedback systems with quadratic cost criteria, obtaining optimal controls characterization 16 p2886 A70-33339

Discrete stochastic optimal control model of human operator for single loop compensatory/pursuit tracking 16 p2851 A70-33340

Optimal fixed-form pilot model computer program for VTOL longitudinal control hover task evaluation 16 p2851 A70-33341

Linear systems approximate minimum energy controller, suggesting algorithm for mathematical model evaluation 16 p2886 A70-33344

Linear systems simultaneous optimal stochastic control and observation strategies, assuming quadratic observation cost 16 p2886 A70-33346

Optimal distributed feedback surface temperature control of inertial grade floated rate integrating gyroscope, minimizing instrument degradation 16 p2908 A70-33347

Neighboring optimum feedback control scheme for aerospace vehicles to handle small disturbances from nominal trajectory with unspecified final time 16 p2887 A70-33438

Optimal open loop controller and suboptimal feedback law to minimize terminal error of entry vehicle 16 p2947 A70-33439

Optimal control solution for dynamic entry vehicle along planar trajectory, using hybrid computer simulation 16 p2981 A70-33443

- Discrete stochastic optimal control model of human operator for single loop compensatory/pursuit tracking situation, considering application to manual control system design 16 p2852 A70-33463
- Bang-bang control of electrohydraulic servomechanisms, approximating optimal control by quasi-optimal controls 16 p2887 A70-33685
- Optimal trajectory and control approximate solution by asymptotic expansion, considering Mayer variational problem solution 16 p2943 A70-33897
- Book on random processes, communications and radar covering optimum filtering, detection, information theory, ergodic theory, probability and integration axioms, parameter estimation, coding, etc 17 p3043 A70-34602
- Servosystems with random input signals, obtaining optimal transfer function by variational calculus 17 p3056 A70-34617
- Aircraft optimal operating procedure development by integral-variational performance analysis methods, discussing flight paths, fuel consumption, mission requirements, etc 17 p3016 A70-34812
- [AIAA PAPER 70-876] Optimal control problems solution using Cartesian product of space of right-hand sides of differential equations with Euclidean n space 17 p3129 A70-34868
- Optimal filter problem related to tracking, discussing mathematical formulation and reduction to variational problem 17 p3056 A70-34869
- Optimal control problems solution using epsilon technique to avoid solving dynamical equations 17 p3129 A70-34870
- Optimal control problem solution methods, comparing Euler-Lagrange equations, Pontryagin principle, dynamic programming and invariant imbedding 17 p3057 A70-35589
- Existence and uniqueness of optimal control for one dimensional linear system with distributed control parameter using input-output integral with quadratic functional 17 p3057 A70-35627
- Satellite optimal guidance, discussing gyroscope application for stabilization and orientation control 17 p3181 A70-35691
- STOL takeoff trajectory optimization for heavily loaded helicopter, using optimal control theory 17 p3021 A70-35841
- Stochastic processes with linear dynamics and quadratic control cost, considering application to aircraft landing approach path optimization 18 p3279 A70-35973
- Observation space transforming for synthesis of automatic optimization systems with memory tracking randomly walking extremum 18 p3234 A70-36073
- Optimum spectral control of nonlinear plant, using Newton iteration and linear programming 18 p3234 A70-36073
- Optimal orientation control of axisymmetric rotating space vehicle, using cyclic sliding mode theory 18 p3332 A70-36162
- Noisy stochastic pattern recognition system, determining optimal measurement sequence by discrete Pontryagin maximum principle 18 p3234 A70-36337
- Necessary and sufficient conditions for optimal control law existence for model following system, discussing applications to aircraft control 18 p3235 A70-36443
- Tangential descent direction determination for optimum control problems based on problem of moments 18 p3235 A70-36574
- Discrete automatic control theories, including linear, nonlinear, feedback, optimal and adaptive systems and bibliographies 18 p3235 A70-36626
- Optimal control for one dimensional compressible gas flow, combustion and heat exchange, described by first order partial differential hyperbolic equations 19 p3402 A70-37240
- Two stage turbine engine parts adjustment optimization in terms of fuel consumption or thrust control by linear programming techniques 19 p3489 A70-37241
- Merlons amplitude optimal value for open loop part characteristics in control systems design, obtaining global extremum of stipulation numbers 19 p3392 A70-37448
- Linear stochastic continuous feedback system with white noise and control input, investigating combined problem of filtering and optimal control 19 p3393 A70-37850
- Linear time varying systems optimal control through decoupling of boundary value problems 19 p3393 A70-37866
- Optimum stabilized variable frequency multiple input phase locked oscillator in mutually synchronized systems 19 p3389 A70-37969
- Geometrical interpretation of controlled evolution of optimal systems with mixed state constraints, using Pontryagin and variational methods 19 p3542 A70-38056
- Boron and boron carbide coatings formation on graphite by vapor deposition, determining optimum parameters for reaction control 19 p3455 A70-38250
- Control error effect on performance index in Pontryagin principle calculation of optimum control 19 p3394 A70-38501
- Multidimensional decision models for optimal control, using piecewise constant functions 19 p3394 A70-38679
- Optimal control systems sensitivity analysis, discussing trajectory tracking 19 p3394 A70-38716
- Sufficient condition for optimal control with continuous nonlinearities, using Pontryagin maximum principle 19 p3394 A70-38717
- Optimal control of processes with lags, including linear analytical regulator problem 19 p3395 A70-38718
- Control moment gyro /CMG/ for spacecraft attitude control, determining optimal gimbal angle rate for desired torque 19 p3433 A70-38857
- [AIAA PAPER 70-1042] Launch vehicle injection error sensitivity minimization by trajectory shaping using excess booster capability 19 p3534 A70-38889
- [AIAA PAPER 70-1078] Spacecraft fuel optimal controls for out-of-plane motion about translunar libration point based on phase plane methods 19 p3530 A70-38890
- [AIAA PAPER 70-1079] Book on optimal control covering optimization, estimation, dynamic and linear control systems, programming, probability and random processes, environmental influence, etc 20 p3600 A70-39124
- Optimal control of distributed parameter systems via functional analysis 20 p3600 A70-39136
- Thor launch vehicles steering filters design using automated method of optimizing large order linear stochastic systems control 20 p3600 A70-39543
- [AIAA PAPER 70-986] Satellite-based air traffic control system for North Atlantic, applying stochastic optimal control theory 20 p3669 A70-39563
- [AIAA PAPER 70-966] Saturn 5 suboptimal continuous guidance design, eliminating discontinuous control encountered in SA-502 flight 20 p3600 A70-39564
- [AIAA PAPER 70-965] Highly constrained optimal control problems, using nonlinear programming in mathematical model for trajectory optimization 20 p3600 A70-39565
- [AIAA PAPER 70-964] Sensitivity optimization for linear optimal control systems design, describing aircraft lateral-directional control case study 20 p3600 A70-39567
- [AIAA PAPER 70-962] Nonlinear adaptive reaction jet attitude control for long life space vehicles, providing optimal performance over bias acceleration disturbances 20 p3716 A70-39680
- [AIAA PAPER 69-945] Optimal control problems with moving ends in presence of phase constraints, deriving difference approximation stability condition 20 p3601 A70-39730
- Dynamic plants optimal control, deriving algorithm for determining a posteriori probability density of generalized state vector 20 p3604 A70-39907
- German monograph on satellite orbit synergetic plane change maneuver optimal control by entry into denser atmosphere 20 p3705 A70-39924
- Monograph on estimation and optimal control with quantized measurements covering linear, nonlinear and time varying systems 20 p3658 A70-40024
- Linear feedback control system with quadratic penalty function, deriving lower bound on optimal performance for suboptimality evaluation 20 p3604 A70-40116
- Jacobi-type conditions for singular optimization problems obtained by transformation to nonsingular form adaptable to linear quadratic optimal control theory 20 p3659 A70-40262
- Duality of optimal control and observation problems in cases of bounded coordinates and continuously acting perturbations respectively 21 p3801 A70-40605
- Satellite steady state motion and relative equilibrium position optimal stabilization by additional forces application 21 p3849 A70-40606
- Optimal terminal control stochastic synthesis for linear systems by Bellman second order nonlinear partial differential equation 21 p3801 A70-40607
- Optimal and conventional good control systems relationships, considering open and closed loop characteristics, cost functions, etc 21 p3926 A70-40781
- Conventional closed loop controller design treated as particular formulation of optimal control problem through gain and integration derivations 21 p3927 A70-40783
- Computer algorithm for optimal linear impulse corrections to satellite orbit under inequality type constraints 21 p3801 A70-40828
- Optimal control of composite spacecraft propulsion system incorporating high thrust-weight ratio chemical engine and low thrust ion engine 21 p3865 A70-40831
- Book on theory of optimal control and mathematical programming covering linear, nonlinear, quadratic programmings, etc 21 p3845 A70-40891
- Optimal control problem for plant including dynamics and input constraints parameters treated by calculus of variations and Pontryagin maximum principle 21 p3801 A70-40899
- Apollo program navigation processing using Kalman optimal linear computer, emphasizing position vector and error matrix and command and lunar landing extrapolation module navigation 21 p3848 A70-41127
- Inequality constrained optimal control problems by function space method, using integral equation representation of second variation 21 p3802 A70-41266
- Control processes and optimization problems solutions by stochastic differential equations, discussing dynamic models and programming, linear filtering and optimal feedback 21 p3802 A70-41275
- Control space properties of pareto-optimal and cooperative solutions for static continuous and differential games involving vector cost criteria 22 p4061 A70-42460
- Seminormality and upper semicontinuity of variable sets in optimal control 22 p4061 A70-42461
- Optimal control of coordinate space cells inspection order during search for unknown number of objects 22 p3999 A70-42552
- Maximum principle for discrete systems of recurrence equations, applying Pontryagin principle 22 p4073 A70-42696
- Oscilloscope design involving optimum bandwidth and input sensitivity, reference measurement and second time base 22 p3996 A70-42820
- Statistically optimal nonlinear automatic control systems synthesis in presence of random perturbations, using gradient or steepest descent methods 22 p4003 A70-42889
- Optimal self adaptive control systems with incomplete input information, ensuring minimum error dispersion 22 p4004 A70-42890
- Optimal nonlinear filtration for continuous automatic data transmission with radio signal under white, narrow band and Markov noise 22 p4004 A70-42891
- Nonlinear rotating systems optimal control problems approximation by modified Krylov-Bogoliubov averaging technique 22 p4004 A70-43317
- Optimization for control processes with first and higher order constraints on phase coordinates 22 p4004 A70-43320
- Stochastic processes control optimization, selecting elastic aircraft stabilizer planform 22 p4004 A70-43352
- Two stage gas turbine engine optimal tuning for RPM, thrust, fuel rate and gas temperature, describing automated bench tests 22 p4092 A70-43361
- Stochastic optimal control for nonlinear dynamical systems under noisy observations, designing suboptimal state estimates and feedback controls 22 p4063 A70-43429
- Suboptimum extraction of pattern features from continuous measurements, assuming different Gaussian random classes 22 p3991 A70-43493
- Modulation transfer function applied to optimal holographic nondestructive testing systems, using edge gradient analysis 22 p4039 A70-43520
- Gyrostabilizer design based on composite optimal controls with respect to different regional criteria 22 p4040 A70-43559
- Optimal transducers distribution for estimating random field values in presence of additive noise 22 p4005 A70-43562
- Linear control plant identification by solving integral equation obtained from input and output signals 22 p4005 A70-43565

Stochastic control optimization, examining self organizing approach for performance adaptive controller with asymptotic optimal properties 22 p4005 A70-43733

Discrete systems with and without time lags, deriving necessary conditions for singular optimal control 23 p4176 A70-44301

Linear programming problems in optimal control numerical analysis, discussing iterative solution 23 p4177 A70-44303

Schedule theory problem with redundancy and technological constraints reduced to optimal control problem by penalty function, making maximum principle applicable 23 p4177 A70-44304

Optimal control of magnetic torque for bias momentum removal from attitude controller, discussing applications to Skylab 23 p4258 A70-44503

Optimal adaptive digital autopilot design and operation, discussing linear differential equations of motion, algorithms, etc 23 p4215 A70-44504

Unilateral and minimax control with functional restrictions, including pursuit and evasion games 23 p4177 A70-44906

Relaxed minimax control with functional restrictions by Uryson integral financial equation 23 p4213 A70-44907

Singular and nonsingular optimal control problems, deriving sufficient conditions for nonnegativity of second variation 23 p4213 A70-44908

Optimal asymptotic stability laws of control systems with unstable plant, using piecewise coordinate functions 24 p4321 A70-45494

Closed loop synthesis algorithm and comparison to sensitivity of open loop system, noting applicability to optimal control 24 p4322 A70-46013

Optimum finite memory model for sequential minimum-mean-square-error estimation of random variable in added noise 24 p4317 A70-46052

Optimum pulse radar signal-receiver design, considering implementation errors for maximum target detectability in clutter 24 p4313 A70-46055

Algebraic structure convolutional codes using minimal encoders with feedback-free delay-free inverses 24 p4313 A70-46058

Optimal noiseless linear information feedback estimation for additive white Gaussian noise channels, applicable to digital transmission 24 p4313 A70-46064

Suboptimum sequential algorithm for recovery decoding errors in convolutional codes, using Hamming distance criterion 24 p4314 A70-46066

Optimal temperature control for confined spaces and life support systems, using mathematical models of environmental control systems 24 p4295 A70-46373

OPTIMIZATION

NT FLIGHT OPTIMIZATION

NT OPTIMAL CONTROL

NT TIME OPTIMAL CONTROL

NT TRAJECTORY OPTIMIZATION

Optimum R and D organization in aircraft engine production illustrated on turbofan engine 01 p0161 A70-10080

Optimal damping of flexibly mounted rotor by providing system with additional degrees of freedom and applying damping to additional masses 01 p0199 A70-10121

Optimal coercive force selection of residual inductance and energy of magnets for generators with star shaped rotors 01 p0008 A70-10192

Four dimensional optimal interpolation for maximum wind velocity components, calculating spatiotemporal correlation functions 01 p0135 A70-10205

STOL aircraft configurations optimization including cost effectiveness, considering propulsive lift systems [AIAA PAPER 69-1131] 01 p0162 A70-10609

High temperature solar energy converter cavity absorbers geometry, considering absorption parameters of radiation reflected by concentrator 01 p0010 A70-10761

Optimal steady state thermal design for fin-tube single and double surface space radiators, including meteoroid protection and pumping power weight penalties 01 p0215 A70-10829

Functional optimization within partial differential equation solutions class by choosing optimum boundary values 01 p0131 A70-10922

Mass action law-polynomial optimization analogy, illustrating optimal temperature determination in chemical reactors in series 01 p0143 A70-10925

Minimum fuel consumption criteria applied to design of manned spacecraft attitude control system, using reaction jets for lateral and directional controls 01 p0196 A70-10950

Trigger scaling circuits with pulsed and blanking feedback analysis for minimizing number of couplings 01 p0047 A70-10984

Inertial damper optimum parameter selection for achieving maximum nutation damping factor for gyroscopic stabilizer 01 p0091 A70-10985

Accelerated memory gradient method for minimization of functions with unconstrained variables, investigating generalization of Fletcher-Reeves algorithm 01 p0132 A70-11194

Runge-Kutta method with position dependent optimal parameter alpha for initial value problem solution to minimize total error 01 p0134 A70-11364

Redundant components optimal quantity determination for maximizing reliability of series system subject to multiple resource restrictions 01 p0104 A70-11383

Optimal moments for trajectory parameters measurements determined by linear analysis to minimize error for initial conditions 01 p0094 A70-11478

Optimal dynamic design of system consisting of elastic cantilever rod with two concentrated masses subjected to harmonic vibrations under force at free end 02 p0384 A70-11739

Minimum microwave path clearance establishing procedures, considering relation to inverse beam bending in microwave propagation 02 p0253 A70-11746

Airborne secondary surveillance radar transponders performance and system optimization for automatic altitude reporting, separation standards maintenance and automatic plot extraction 02 p0267 A70-11990

ALGOL Dynamic Display System for debugging and optimizing computer source language program, providing real time portrayal of static and dynamic block structure, etc 02 p0264 A70-12128

Wing design optimization for steady and unsteady supersonic flow through computerized simulation and study of leading and trailing edge shape 02 p0223 A70-12208

Expected values optimal measurement, given auxiliary conditions between measured value number and quantization 02 p0299 A70-12400

Optimal fuel consumption for climbing, cruising and landing flight conditions for medium range subsonic, high supersonic and hypersonic aircraft 02 p0227 A70-12404

Optimization potential selection in control system design by analytical method 02 p0272 A70-12412

Optimum balance between program and functional organizations to promote technology transfer 02 p0403 A70-12637

Optimal lift-drag ratio of cascades dependence on optimal pitch of cascades calculated for axial flow turbomachinery 02 p0356 A70-12750

Signal waveform algorithmic construction with optimal autocovariance properties, using isosum integer partitions, applied to clustered multipath distribution measurement 02 p0263 A70-12773

Optimal redundancy for maximizing systems reliability of mixed series and parallel network consisting of N modules including I module with specified reliability cost function 03 p0585 A70-12995

Pulse signals optimal filtration in superregenerative receiver and resulting SNR effect 03 p0456 A70-13203

Optimal selection of centralized communication network of combined radial and linear structures minimizing disconnected peripheral points 03 p0446 A70-13238

Optimal nonlinear correcting of vertical gyro obtainable with correction containing nonlinear elements with variable linearized coefficients 03 p0483 A70-13363

Optimal stabilization of free solid body equilibrium state with gyroscope, using solution of three flywheel system stabilization 03 p0484 A70-13364

Optimal radar resolution of objects during detection and measurements, giving diagrams of resolution characteristics vs echo signals parameters 03 p0448 A70-13453

Microwave circuits automatic analysis and design using digital computer in batch mode, describing analysis-optimization program 03 p0457 A70-13562

Optimal synthesis and design of distributed parameter system for waveguides using gradient technique

with devised algorithm to overcome convergence problem

03 p0449 A70-13563

Shield mass optimization of low thrust nuclear powered space vehicle for occupant shielding against reactor radiation 03 p0523 A70-13575

Optimum estimation equations as simple averaging extension, considering application to Kalman filtering in integrated space navigation system 03 p0522 A70-13608

Wide strut analysis for determining weight minimizing cross sectional dimensions of panels having unflanged integral stiffeners 03 p0596 A70-14145

Generalized approach for optimal corrector in mean squared sense for predictor-corrector filter structure, illustrating signal modes with nonlinear and linear dynamics 03 p0520 A70-14170

Optimum numerical integration with application to real time digital simulation of continuous systems, deriving three step methods 03 p0455 A70-14173

Aircraft structural weight optimization for given fundamental vibration frequency obtained by aeroelastic constraints 03 p0598 A70-14231

Optimization problems computing methods - Conference, San Remo, Italy, September 1968 03 p0461 A70-14338

Optimal nonlinear filtering for nonlinear dynamic system subjected to additive white Gaussian noise with corrupted observations, using successive linearization scheme 03 p0461 A70-14340

Optimum planetary image intensity at Tv camera cathodes, exemplifying with Saturn orbicon image 04 p0688 A70-14694

Algorithm for optimal decoding of convolutional codes confirmed using error probability upper bound 04 p0654 A70-15067

Integral-criterion optimization of transient processes in mechanical systems synthesis with favorable dynamic and damping characteristics 04 p0720 A70-15218

Radar signals optimal synthesis characterized by ambiguity surfaces minimized over predetermined regions of ambiguity plane, noting weighted error criterion role 04 p0651 A70-15328

Wiener-Hopf equation development and Kalman filter derivation using Leibnitz equation for differentiating integral 04 p0660 A70-15338

Solar powered communications spacecraft weight, electrical power and communication capacity models for optimizing size and launch vehicle fractionation 04 p0763 A70-15347

Energy state approximation for supersonic aircraft performance optimization with extension to maximum range problems, noting comparison with complex dynamic models 04 p0623 A70-15376

Analog computer schemes for solving dynamic plants identification reducible to optimizing parametric problem of many variables function 04 p0654 A70-15435

Automated modeling and structure optimization of linear dynamic systems and circuits, using hybrid computer techniques and time-domain test data 04 p0654 A70-15452

Differential equations for minimum variance linear filter separating signals from additive correlated noise, using discrete time optimum formulas [AIAA PAPER 69-73] 04 p0663 A70-15586

Optimized compressor blades, examining Le Foll boundary layers theory possibilities as design method 04 p0621 A70-15667

Fighter aircraft design combining optimal qualities with economy 05 p0793 A70-15902

Radar signals synthesis using steepest descent for minimizing Hermitian form 05 p0812 A70-16247

Shape optimization of elastic rod compressed by force directed toward point on undeformed rod axis, deriving optimal bending line 05 p0937 A70-16373

Algorithm for constrained optimization problems providing rapid convergence 05 p0877 A70-16714

Optimal strategy for searching for object hidden in box involving use of optimal return function 05 p0877 A70-16715

Assignment problem for finite set elements pairing, discussing probabilistic formulations and applications to satellite communications problems 05 p0815 A70-16716

Optimal electron bunching in two cavity klystron by varying parameters and nonlinear one dimensional approximation 05 p0823 A70-16888

Mathematical model of optimal partially closed life support system consisting of man, recycling unit, storage unit and waste disposal outlet
05 p0809 A70-17110

Computer optimization of spacecraft optical coatings for temperature control, using finite element analysis and matrix inversion
[AIAA PAPER 69-979] 06 p1172 A70-17180

Optimum signals for phase locked or delay locked loops determined as function of signal to noise ratio
06 p1023 A70-17523

Optimal quadrature formulae for numerical integration of 2 pi-periodic functions involving integrand derivative values at knots
06 p1093 A70-17582

Book on optimization by variational methods covering use of differential equations, Pontryagin minimum principle, optimal and feedback control, dynamic programming, etc
06 p1093 A70-17650

Unconstrained minimization techniques efficiency in mathematical nonlinear programming, discussing gradient and variable metric types
06 p1094 A70-17968

Hybrid NASAP program module for direct design of linear dynamic circuits using simple optimization without sophisticated computer programming
06 p1015 A70-18422

Nonlinear system theory for optimal linearization in holography, discussing generalized method for photographic emulsion and first order amplitude transmittance
06 p1072 A70-18521

Direction finding characteristics of nonlinear antenna, including current determination and optimal angle for sidelobe level
06 p1023 A70-18561

Optimum compression ratio defined for Markov sources for compression algorithm efficiency and data compression schemes
06 p1013 A70-18624

Clutter symmetry as indication of matching optimum signal filter pair, comparing mismatched and matched systems
06 p1013 A70-18626

Optimal signal detection with random phase on Gaussian noise background, estimating error probabilities
07 p1226 A70-18685

Optimal scale selection for aerial surveys by analyzing aerial photography data
07 p1278 A70-18690

Optimal receiver synthesis for signal detection on background noise resulting from nonlinear filtration of Gaussian noise
07 p1226 A70-18760

Energy optimal osculating elliptical transfer orbit from low eccentricity orbit constructed for prolonged circling in equatorial plane of axisymmetric planet
07 p1374 A70-18774

Paraboloidal- and spherical-reflector antennas efficiency optimization obtained from optimum combination of amplitude and phase of hybrid modes propagating in guide
07 p1240 A70-19220

Computing methods in optimization problems - Conference, San Remo, September 1968, Volume 2
07 p1324 A70-19266

Necessary and sufficient conditions for constrained extrema without use of Lagrange multipliers
07 p1325 A70-19335

Sequential gradient-restoration algorithm for minimization of function subject to constraint
07 p1325 A70-19355

Minimum weight design of elastic sandwich beams with deflection constraints using n-dimensional space of discretized bending stiffness
07 p1407 A70-19358

Sufficient conditions of optimality for strategic couple in theory of quantitative differential games
07 p1245 A70-19379

Optimal localized heat treatment of welded products, analyzing temperature fields and stresses during heating and cooling of ferromagnetic materials
07 p1294 A70-19477

Integrated switching circuits design optimization by ALGOL program, analyzing circuits transient behavior
07 p1242 A70-19752

Self sustained fusion reaction in dense deuterium-tritium plasma, considering large atomic number contaminants optimal concentration calculations
07 p1351 A70-19848

Automatic control system identification with respect to optimality criteria, mathematical models, computing techniques and input signals
07 p1247 A70-20029

Optimal distance between satellite communication system ground stations for surface network cost equivalent, analyzing economic efficiency for various cases
08 p1456 A70-20569

Discrete analog filters circuits for optimal noncoherent processing of phase manipulated signals
08 p1456 A70-20571

Frequency characteristics optimization of symmetrical octupole bridge networks based on relationships between electrical parameters functions and impedance matrices eigenvalues
08 p1468 A70-20572

Discrete process max-min problem, using dynamic programming to obtain upper and lower bounds
08 p1533 A70-20604

Parallel wire antenna arrays analysis and design, emphasizing directive power gain maximization and sidelobe reduction
08 p1471 A70-20789

Gain-to-noise temperature ratio (G/T) optimization by dish antenna shaping for nonuniform aperture field distribution
08 p1471 A70-20790

PSK demodulation by optimal carrier and bit synchronization methods based on nonlinear filter theory, relating error probability to signal to noise ratios
08 p1458 A70-20795

Frequency locked loop optimization, showing advantages in frequency shift keying detection and FM signal demodulation
08 p1460 A70-20808

Optimal linear antenna synthesis, determining current distribution resulting in specified radiation pattern for superdirective antennas
08 p1472 A70-20972

Controllable microwave phase shift varactor diode circuit parameters design optimization using digital computer for transmittance matrix coefficients calculation
08 p1474 A70-21230

Optimal inextensional buckling of uniformly loaded simply supported arches with large opening angle
08 p1589 A70-21310

Minimization of motion deviation from prescribed motion as differential game of converging motions using equations of motion
08 p1546 A70-21626

Tunnel diode parametric phase locked oscillators as memory elements, considering optimum subharmonic pumping frequencies determination
08 p1477 A70-21642

Matrix method for maximizing radar antenna directive gain and simultaneously placing nulls in far field radiation patterns
08 p1477 A70-21758

Conjugate direction procedures for function minimization compared for convergence, recommending modified conjugate gradient procedure
08 p1535 A70-21875

Electronic equipment optimal design variant selection method, based on relative characteristics of feasible versions, widening weighting coefficients determination basis
09 p1643 A70-22129

Apportionment optimization of reliability and maintainability by Lagrange multipliers and dynamic programming, discussing maintainability cost model and computerized simulation
09 p1792 A70-22211

Optimizing shape of elastic bar compressed by polar force obtained by determining functional extremum representing volume of bar at constant critical force
09 p1769 A70-22252

Minimum weight design for two dimensional bodies with given load system determined by variational method
09 p1771 A70-22400

Quasi-linear estimator algorithms to achieve both optimal nonlinear filtration and signal interpolation resulting in significant gain of estimate accuracy
09 p1633 A70-22408

Optimal adjusting of laser with instantaneously increasing Q without pumping and relaxation effects during pulse, using nonlinear differential equation
09 p1695 A70-22412

Optimal deformation and minimum wave drag for wings with supersonic leading and straight trailing edge, solving variational problem by Ritz method
09 p1604 A70-22444

Shock absorbing forces for absorber with one degree of freedom optimized for given acceleration during periodic disturbances by variational method
09 p1727 A70-22537

Nonlinear complexing problem in measuring random signal, proposing optimal data processing algorithm with minimum error variance criterion
09 p1654 A70-22542

Optimal inertialess nonlinear filters synthesis with various optimality criteria for signal distributions differing from normal
09 p1654 A70-22543

Thermo-elastic analysis and optimum start-up in power plant, discussing transfer function for thermally loaded bodies with restricted boundary temperature
09 p1774 A70-22584

Liapunov stability conditions for critical point of ordinary differential equation, determining optimal criterion
09 p1727 A70-22664

Weight function minimization of multiweb box beam in pure bending
09 p1777 A70-22769

Fault finding strategy optimization in systems with single defective element
09 p1693 A70-22974

Temperature fields in cylindrical shell under axisymmetric heating, ensuring optimal stressed state
09 p1778 A70-23081

Combined gyromotors optimal starting and operating conditions, considering size and weight characteristics
09 p1680 A70-23146

Optimal construction of microwave filters with TWT and ferrite direct gain receivers
09 p1648 A70-23166

Prestressing in minimum weight design of statically indeterminate structures
09 p1781 A70-23231

Electric propulsion design, considering effects of weight, impedance matching, beam voltage regulation and operating point variations in formulating system mass and reliability
09 p1743 A70-23248

Payload optimization factors for orbital storage of liquid hydrogen, considering payload cost of agitation, tank pressure, pressurant weight, etc
[AIAA PAPER 69-1007] 09 p1767 A70-23262

Wedges calculated for lift-drag ratios at hypersonic speeds to find optimum surface geometry
09 p1606 A70-23282

Parameter optimization of V and rhombic antennas with sloped wires, determining radiation angle from radiation pattern
09 p1649 A70-23336

Optimal decomposition of nth order filter into cascaded second order sections
09 p1650 A70-23367

Reactance filters for matching circuits design with optimum transforming performance
09 p1650 A70-23404

Single-pass multimode carbon dioxide laser amplifier power gain optimization
10 p1897 A70-23815

Optimization in epiphydrostatics and epiphydrodynamics, discussing liquid in rectangular tank, electro-magneto-epiphydrodynamics and thermal instability
10 p1866 A70-24108

Three dimensional supersonic nozzle geometry optimization using Lagrange multipliers and iteration for solving variational problem
10 p1798 A70-24115

MHD generators optimum load selection by method of stepwise approach, noting agreement with pressure and density distributions to yield maximum power
10 p1923 A70-24156

Digital satellite communication system using multiphase modulation optimized for phase positions number to maximize transmission capacity
10 p1835 A70-24334

Communication satellite PSK modulator-demodulator /mode/ implementation requirements and design for optimal performance
10 p1835 A70-24336

Analytic function integration optimal rate, discussing weighting function
10 p1909 A70-24509

Optimal trusses design, considering minimal volume /weight/ and elastoplastic stability in compressed and stretched bars
10 p1958 A70-24514

Optimal MHD generator with constant channel area, assuming small Reynolds numbers and ideal inviscid gas with arbitrary electrical conductivity
10 p1807 A70-24570

SIMCON digital simulation control system optimizing man machine interaction, noting capability to generate solutions with minimum computer memory
10 p1860 A70-24654

Dynamic programming successive approximations optimization technique involving system state variables reduction with convergence proofs
10 p1845 A70-24871

Optimal data filtering techniques and hardware for centrifuge testing of missile inertial platforms
[AIAA PAPER 70-405] 10 p1861 A70-24901

Avionics test station optimum design by computerized simulation involving iteration of computer run, analysis and model change
[AIAA PAPER 70-398] 10 p1861 A70-24907

Time-optimal testing sequence for system failure detection, considering maintenance and reliability data
10 p1896 A70-25048

Iterative numerical method for determining optimal mass distribution in complex frameworks, maintaining dynamic response level
10 p1960 A70-25053

Airborne side-looking radar antenna optimum directional characteristics analysis from viewpoint of maximum surveillance range
10 p1843 A70-25139

Generalized control theory, discussing optimization and table classifying control theory fields
10 p1856 A70-25238

Optimal efficiency of axial turbomachines limit loading of blade root and hydrodynamic criteria
11 p1975 A70-25791

Missile radome design optimization, considering compromise between conflicting aerodynamic, thermal and structural aspects

11 p2134 A70-25862

Ram wing tube ground transportation vehicle, analyzing optimum lift-drag ratio and induced power requirements

11 p1975 A70-25966

Constrained complex optimization method for synthesizing distributed-lumped-active networks

11 p2024 A70-26204

Optimal pulse compression time-invariant filter for signal reception with sidelobe constraints under white noise in radar and communications systems

11 p2025 A70-26218

Sufficiency conditions and Lagrange multipliers in maxima and minima theory with results restricted to ordinary extremal points, considering constrained optimization

11 p2073 A70-26232

Mariner-type spacecraft telemetry system optimization, considering channel capacity

11 p2008 A70-26239

Optimal strategies for game with nature and two-automata zero sum game under finite memory constraints

11 p2073 A70-26241

Optimum symbol sequence interleavers realization taking into account storage capacity and encoding delay

11 p2014 A70-26246

Satellite communication systems optimal utilization achievable through supervisory control system

11 p2009 A70-26261

System configuration requirements and detectability performance characteristics analysis for optimizing array reception of multipath

11 p2018 A70-26264

Computerized tradeoff analysis for planetary landing vehicle entry capsule and lander design optimization, emphasizing weight allocation for Mars 1973 missions

11 p2126 A70-26320

Flat-top airfoil determined for lower surface shape to maximize lift drag ratio at hypersonic speeds using calculus of variations

11 p1977 A70-26397

Optimal phase-manipulated signals synthesis from autocorrelation function using algorithm

11 p2012 A70-26804

Nonlinear equations systems iterative solution convergence by extending classical algorithm with optimization process

11 p2074 A70-26850

Optimum binary digital detector of radar targets, using confidence ratio as criterion of target presence

12 p2182 A70-26890

PAM-FM modulation system optimal receiver derivation, assessing threshold performance assuming uniformly distributed modulating signal

12 p2183 A70-27155

Dynamic systems absolute stability, optimality and passivity algebraic criterion in terms of real even polynomial coefficients

12 p2261 A70-27412

Composite resonator for semiconductor laser to increase single mode power generation, determining optimal length of passive part

12 p2247 A70-27484

Optimal linear band limited time invariant data transmission systems, discussing pulse interference tolerance based on eye parameters as quality criteria

12 p2185 A70-27688

Optimum distribution over circular aperture in ground plane for best mean square approximation to specified radiation pattern

12 p2197 A70-27952

Redundancy optimization based on partial failure modes effect on system reliability to reduce cost

12 p2243 A70-28010

On-line optimization of maintenance and verification schedules for complex system safety insurance

12 p2244 A70-28013

Rao optimization method for flow nozzles at given length, analyzing control surface flow field conditions

12 p2158 A70-28202

He-Ne laser optimal mixture component ratio for generating IR radiation at two wavelengths

12 p2251 A70-28293

Molding procedure to orient filaments relative to loads for optimizing structural component (compressor blades) of filament reinforced composite

13 p2417 A70-28663

Inertial hybrid navigation system optimization, discussing performance curves and numerical filters synthesis and error elimination

13 p2448 A70-28747

Noise stability of optimal binary detection receiver of rectangular-pulse and discrete pseudorandom signals under nonideal synchronization

13 p2364 A70-28869

Elastoplastic continuum under specified rates of body forces, surface tractions and displacements, formulating minimum principle for solving boundary value problem

13 p2513 A70-29154

Differential equations of controller providing optimum transient response for plant with indeterminate parameters, allowing for nonadditive random noise

13 p2382 A70-29278

Multilens quasi-optical transmission lines construction by determining lens profile for optimal conversion of source field into specified field at receiver end

13 p2366 A70-29403

Light transmission losses in optical resonators partially filled with inhomogeneous dielectric, specifying optimal geometrical parameters

13 p2378 A70-29404

Penalty function algorithm for linear/nonlinear programming optimization problems subject to equality/inequality constraints, discussing feasibility determination capability

13 p2373 A70-29462

Minimum weight structural member size and configuration simultaneous optimization using computer program

13 p2516 A70-29550

Stochastic analog approximation method minimizing criterion functions and for recovering functions from noisy measurements of values in learning systems

13 p2442 A70-29585

Centrifugal pump design optimization, assuming one dimensional throughflow of viscous fluid as driving force

13 p2391 A70-29748

Cylinders and airfoils drag tests and simulation in two dimensional sheared flow, considering shapes optimization

[AIAA PAPER 70-576]

13 p2342 A70-29893

Amplitude-frequency characteristics selection for minimum phase channel allowing for intersymbol interference and smooth noise during data transmission, calculating mean error probability

14 p2547 A70-30150

Parameters optimization of nonlinear electric servo actuator on basis of statistical criteria

14 p2559 A70-30157

State-space synthesis of multiport passive reciprocal networks with minimum number of resistors, using Gauss factorization procedure

14 p2556 A70-30516

Meteorological parameters measuring instruments optimal design, presenting formalized procedure flow chart and examples

14 p2607 A70-30568

Size and cost of Al mirror IR photometric telescopes optimized for scientific information acquisition

14 p2586 A70-30896

Optimum diffusion welding temperature for Ti-6Al-4V alloy determined from tensile and creep tests

14 p2591 A70-30934

Civil aircraft design optimization, considering operating and seat mile costs, speed, wing and fuselage, engine location, etc

14 p2531 A70-30941

Optimum alkali metal vapor humidity for turbine equipment estimated from energy output

14 p2535 A70-31008

Quality control variables optimization for maximum net revenue, using computerized simulation

14 p2592 A70-31105

Optimum interleavers realization procedure for reordering contiguous symbols sequence to satisfy minimum distance requirement for improving communication system performance

14 p2554 A70-31121

Rank order statistics for optimum detection of binary pulsed signals in white noise and DC drift

14 p2551 A70-31122

Analytical solutions to optimum orbit modifications including atmospheric maneuver

14 p2649 A70-31171

High speed dynamic systems synthesis with optimal damping of elastic vibrations, using gradient method

14 p2617 A70-31354

S band transmitters frequency deviations optimization enabling designer to determine optimum value within constraints of associated receiving equipment

14 p2559 A70-31373

Aircraft design optimization by multisearch programs, considering mathematical model role

14 p2532 A70-31400

Optimal search algorithm for stationary object hidden in one of N regions with a priori probability

15 p2767 A70-31843

Optimal design for composite material structure, considering internal and external reinforcement

15 p2816 A70-32005

Gyroscopic navigation systems errors as function of sensor errors in terms of arbitrary operators requiring optimization

15 p2773 A70-32155

Optimal questionnaires characteristics and design algorithms

15 p2705 A70-32450

Multistage rocket weight optimization for payload and velocity at burnout, considering specific impulse, drag, etc

15 p2813 A70-32519

Phase locked loop damping characteristics optimization based on input rms error rate minimization and transient error integral square value limitation

15 p2704 A70-32604

Human element in system development to achieve optimum tradeoffs among reliability, cost and other system criteria

15 p2693 A70-32629

Optimum reliability programs, suggesting simulation to provide cost effectiveness basis for systems design configurations evaluation as alternative to demonstration testing

15 p2831 A70-32631

Computerized optimal redundancy analysis, considering cost, size, weight, volume, etc

15 p2712 A70-32642

Multihorn array antenna performance improvement by shaping beam for optimum earth coverage from stabilized synchronous satellites

16 p2860 A70-32952

Airborne electro-optical imaging sensor subsystems performance optimization, comparing mathematical and graphical methods for providing maximum SNR

16 p2906 A70-33172

Discrete signals optimal reception by lowering synchronization requirements for communications or radar purposes

16 p2863 A70-33242

Dynamic systems control and guidance by man in light of anthropotechnics, treating approaches to man machine systems optimization

16 p2850 A70-33263

Ballistic missile instrument orientation optimization based on CEP criterion, considering acceleration induced errors

16 p2947 A70-33317

Aircraft stability augmentation systems design by parameter optimization techniques and feedback selection

16 p2840 A70-33342

Dynamic structures design optimization subject to shock spectrum, describing conversational type computer program

[ASME PAPER 70-DE-28]

16 p2989 A70-33501

Fixed and variable sweep wing structure computerized design optimization

[ASME PAPER 70-DE-41]

16 p2869 A70-33506

Reliability-cost model to determine optimum failure rate for minimization of systems total life cycle cost

[ASME PAPER 70-DE-43]

16 p3004 A70-33507

Maximum thrust nozzles design for rotational or nonequilibrium simple dissociating gas flows, including boundary layer effects

[AIAA PAPER 70-707]

16 p2891 A70-33567

Lunar flying vehicle propulsion system optimization, discussing weight, performance, engine life, reliability, etc

[AIAA PAPER 70-605]

16 p2969 A70-33602

Optimal design of structures with constraints on strength and natural frequency, developing steepest descent boundary value method

16 p2991 A70-33854

Antenna reflectors of evolution and double curvature optimization by iteration method

16 p2866 A70-34267

Linear system under ergodic random processes, determining optimal dynamic characteristics by approximation of spectral density by Laguerre series

16 p2944 A70-34280

Optimization - Conference, Toronto, June 1968

17 p3181 A70-34542

Mathematical techniques for optimal design of single purpose structures under dynamic deflection

17 p3182 A70-34544

VTOL aircraft power plants optimization for future helicopter missions without restrictions of limited off-shelf inventory

17 p3147 A70-34708

V/STOL 5000 hp engine design optimization, considering component arrangements, rotor design, blade cooling method and fuel control

17 p3147 A70-34709

Spatial filter properties of antennas, discussing system performance optimization and incoherent source transfer functions

17 p3045 A70-35077

Optimal receiving systems for satellite broadcasting, considering costs, power requirements, service area, etc

17 p3046 A70-35272

Digital self optimizing distortionless filter for hybrid navigation system

17 p3054 A70-35281

Single gap klystron output resonator optimization, showing maximum electronic efficiency during bunched beam excitation

17 p3055 A70-35681

Optimal filters design predicting electronic systems parameters, preventing equipment failure due to wear and aging

17 p3055 A70-35744

- Receiving antenna for ionospheric scatter lines, calculating input power versus height and energy flux density spreading for position optimization
18 p3230 A70-36094
- Astatic gyroscope subjected to steady random translational vibration, optimizing parameters by mathematical model
18 p3257 A70-36136
- Constraint optimization in state coordinates by variable structure system flexibility, using mathematical model
18 p3281 A70-36353
- Nonlinear approximation under auxiliary conditions in normed space involving minimum solution
18 p3282 A70-36363
- Turbofan engine performance optimization by closed form solution of operating cycle parameter functions
[ASME PAPER 70-GT-65] 18 p3303 A70-36840
- Boundary layer optimization for high turning axial flow compressor blades, using flow theory and conformal mapping
[ASME PAPER 70-GT-88] 18 p3209 A70-36879
- Optimal receiver synthesis for signal detection on background noise resulting from nonlinear filtration of Gaussian noise
18 p3229 A70-37104
- Discrete signals synthesis optimal with respect to given criterion, determining ambiguity function extremum
19 p3374 A70-37270
- Optimization model for evaluating information management systems for handling control functions of long duration space station missions
19 p3532 A70-37851
- Book on optimization and probability in systems engineering covering mathematical models for reliability, repair, availability, Markov techniques and queueing
19 p3553 A70-37928
- Quadratically convergent algorithms for function minimization, discussing unified method and applications to quadratic and nonquadratic functions
19 p3458 A70-38302
- Minimum weight design of sandwich beams with elementwise constant cross section for prescribed compliances under alternative loads
19 p3543 A70-38303
- Slender hypersonic airfoil shape optimization for maximum lift to drag ratio for given profile area, chord and free stream conditions
19 p3352 A70-38304
- Optimum attention allocation, discussing distraction resistance and multiple task performance
19 p3362 A70-38316
- Optimum reliability level in terms of economic benefits and external constraints
19 p3554 A70-38595
- Optimum fuel utilization for Plum Brook Reactor, using criticality data for effects of neutron leakage and burnup uniformity in core point model
20 p3671 A70-39110
- Uncertainty principle in optimum communication theory, discussing existence and value of minimum product of pulse duration in terms of calculus of variations and differential equations
20 p3584 A70-39161
- Cost and time optimization for complex aircraft development projects via network planning
20 p3740 A70-39644
- Soviet book on flight vehicle optimal design algorithms, covering mathematical theory of variational method, multistage spacecraft, etc
20 p3716 A70-39898
- Analog communication optimal nonlinear modulation scheme design for large SNR through transformation into inner product functions
20 p3587 A70-39973
- Cylindrical or tapered composite shell structures optimal design with closed circular or elliptical cross section under combined bending and torsional loads
20 p3730 A70-40043
- Structural synthesis concept in optimal design of composite material structural systems, considering failure modes of rectangular fiber composite plate
20 p3731 A70-40044
- Discrete parameter stochastic optimization problems necessary conditions, deriving maximum principle
20 p3659 A70-40107
- Aircraft engine design combining turbojet and ramjet features to ensure optimum performance
20 p3690 A70-40148
- RF ion source for electrostatic spacecraft propulsion, discussing RIT-10 performance optimization and development
[AIAA PAPER 70-1102] 20 p3692 A70-40236
- Minimum bias criteria for selecting data fitting curves, allowing for unknown true equation in improving data predictability
20 p3659 A70-40261
- Shape factors for weight prediction and design optimization of structural members requiring given area moment of inertia
[SAWE PAPER 828] 20 p3732 A70-40354
- Structural weight design optimization by computer aided geometrical programming technique
[SAWE PAPER 822] 20 p3733 A70-40357
- Fuselage frames minimum weight analysis by automatic iterative method
[SAWE PAPER 826] 20 p3733 A70-40370
- Mathematical techniques for optimal design of single purpose structures under dynamic deflection
20 p3733 A70-40381
- Elastic beams optimal design for multipurpose loading, considering compliance and minimum cross section constraints
20 p3733 A70-40382
- Optimum calibration intervals determination for obtaining instrument maintenance quality level at low cost
20 p3634 A70-40452
- Free vibration optimization analysis by reducing stiffness and mass matrices
21 p3933 A70-40587
- Lifting reentry vehicle two dimensional motion optimization with inequality constraints explicitly containing control by perturbation method
21 p3845 A70-41265
- Transfer function optimization for linear follow-up frequency filter with controlled resonance, analyzing noise band performance
22 p3985 A70-42402
- Dubovitskii and Milyutin formalism applied to optimization problems involving equality and operator constraints via mathematical programming in normed linear space
22 p4061 A70-42462
- Optimal weight design of axisymmetric rotating elastic disks for specific edge radial displacement
22 p4112 A70-42463
- Optimal binary and ternary signal system synthesis by information divergence procedure for communication channels with colored Gaussian noise
22 p3985 A70-42491
- Optimum pressure distribution and airfoil profiles for maximum lift without separation in incompressible flow determined by second order theory
[AIAA PAPER 69-739] 22 p3959 A70-42704
- RLC networks and microwave components design by applying optimization technique
22 p3997 A70-43175
- Spacecraft magnetic radiation shield optimization based on thickness criterion and system mass consideration
22 p3979 A70-43390
- Matrix transformations and minimization of computation algorithms for arbitrary linear equations systems, using direct methods
22 p4063 A70-43479
- Discrete decision variable models formulated as linear integer programs, deriving shrinking boundary algorithm for optimization
22 p3994 A70-43497
- Air transport system technical and operational functions optimization
22 p3962 A70-43532
- MOS transistor trigger circuit design parameters statistical calculation and optimization by Monte Carlo method using computer
23 p4171 A70-43957
- Signal shape optimization by minimizing dispersion in temporal position estimates for radio pulse in presence of additive white noise
23 p4161 A70-43961
- Linear phased arrays computer aided design, discussing search algorithms in multivariable optimization program
23 p4172 A70-44015
- Minimum weight structural design within given stress limits due to different loads or natural frequency vibrations, using finite element method for structural analysis
23 p4268 A70-44226
- Optimal algorithm for searching extremum of single variable unimodal function satisfying Lipschitz condition based on maximum possible error criteria
23 p4177 A70-44305
- Microwave frequency light modulators waveguides, examining optimal cross sections to increase modulator efficiency
23 p4196 A70-44409
- Structural optimization of designs with requirements including restrictions on structure dynamic response and characteristics
23 p4270 A70-44562
- Optimal design of minimum weight bar and beam structures under static loads, comparing computer time with nonlinear programming methods
23 p4271 A70-44702
- Gradient minimization and higher order discrete elements application to shell buckling and vibration eigenproblems, using 48 degree of freedom Bogner cylindrical panel element
23 p4271 A70-44705
- Elastic continua structural optimization analysis decisions for maximizing calculation accuracy, insuring efficient complex numerical analyses
23 p4271 A70-44706
- General Optimization Software Package for Electrical network and system design, noting application to engineering problems and education
23 p4177 A70-44750
- Optimum input pulse signal synthesis for transmission through lossless homogeneous isotropic plasma, using matched filter theory
23 p4228 A70-44962
- Parameter optimization of gravity gradient stabilized satellite in circular orbit, considering minimum transition time and eccentricity oscillation
23 p4264 A70-45014
- Boron and boron-carbide coatings formation by vapor deposition, determining optimum thermodynamic parameters from experiment
24 p3466 A70-45241
- Optimality criterion selection for asynchronous microelectric motor design by computer
24 p4293 A70-45470
- Combinatorial optimization problems design on permutation set, considering applicability of variants successive analysis method
24 p4321 A70-45472
- Planning criteria for optimum metropolitan airport system considering operational, physical, social and economic factors
[AIAA PAPER 70-1266] 24 p4430 A70-45921
- Computer optimization program for solid state components and integrated circuits design with conversational system for man machine dialogues
24 p3417 A70-46321
- Satellite launch vehicle guidance equations for programmed optimization applied to Eldo inertial guidance system
24 p4375 A70-46359
- OPTIMUM CONTROL**
U OPTIMAL CONTROL
- OPTIMUM THRUST PROGRAMMING**
U THRUST PROGRAMMING
- OPTOMETRY**
Servocontrolled IR optometer providing electrical signal proportional to refractive power of human eye
12 p2237 A70-28123
- OR-GATES**
U GATES [CIRCUITS]
- ORBIS**
NT ORBIS CAL SATELLITE
- ORBIS CAL SATELLITE**
Ionospheric ducting of satellite beacon signals observed on Orbis Cal satellite experiment
20 p3591 A70-40495
- ORBIT CALCULATION**
Solar motion effects on planetary orbits, discussing preferred coordinate systems of scalar theory of gravitation
01 p0186 A70-11104
- Orbital charts development for space navigation, discussing cartography and orbital navigation
01 p0138 A70-11251
- Satellite orbital elements optical determination accuracy by differential corrections, presenting computations for data distributed along small arc
02 p0254 A70-11754
- Secular and short period perturbations calculation of satellite orbital elements under action of solar radiation pressure
02 p0362 A70-11763
- Orbital period determination for satellite from single station visual observations, assuming known orbit inclination, ascending node length and node precession
02 p0254 A70-11765
- Cosmos 44 quasi-draconic period analytical and graphical determination, comparing moments of meridian intersection with INTEROBS observations
02 p0363 A70-11767
- Satellite 1965-11-4/Cosmos 54 rocket/braking, rotation periods and revolution from INTEROBS and SPIN observations, comparing K-index and solar activity parameters
02 p0363 A70-11768
- Lunar gravitational field determination from analysis of Lunar Orbiter spacecraft tracking data
03 p0562 A70-12915
- Midast 4 satellite osculating orbital elements determined on basis of optical tracking data
03 p0443 A70-13177
- Orbits computation from double lined spectra of eclipsing binaries 31 Men and 9 Cha, emphasizing systemic velocity and mass ratio derivation method
03 p0565 A70-13268
- Earth satellite orbit parameters determination from angle measurements using computer program and least squares estimation technique
03 p0573 A70-13843
- Geocentric orbital elements of lunar particles expelled into space by meteorite impact, using spheres of influence method
03 p0574 A70-13880
- Generalized Keplerian orbits for large cylindrical satellites noting orbit stability
03 p0578 A70-14252

Orbit determination program for launching and stationkeeping of 24 hr geostationary satellites, using azimuth and elevation of single autotrack antenna
03 p0578 A70-14339

Singularity-free universal orbit calculation satisfying two position vectors and time interval
04 p0750 A70-14930

Orbit determination simultaneous optimal strategy and useful information set selection, discussing Mars transfer trajectory
04 p0750 A70-14940

Navy navigation satellite passes predicted by equations for rise and set times, elevation and azimuth in plane circular polar orbit about spheroidal earth
04 p0764 A70-15431

Hybrid system for allocating domestic synchronous communication satellites in concentric circles within inclined elliptical synchronous orbits
05 p0906 A70-15801

Ionospheric air density profiles revision based on satellite orbits analysis
05 p0839 A70-16287

Error analysis of resonant orbits for geodesy, discussing high order geopotential coefficient recovery by resonance and gravity model errors
05 p0909 A70-16341

Satellites and space probes orbital parameters calculation, considering circular and elliptical trajectories and rendezvous maneuver example
06 p1140 A70-17583

Second order secular perturbations formulas of distant earth satellite motion valid for nearly circular orbits with small inclination to ecliptic plane
06 p1141 A70-17823

Manual onboard orbit determination assuming electronic equipment failure, discussing geometric in-plane orbital parameters and safe orbit check
[AIAA PAPER 70-159] 06 p1144 A70-18033

Apollo translunar and transearth orbit determination and navigation using ground and onboard systems
[AIAA PAPER 70-27] 06 p1103 A70-18124

Statistical orbit and position determination for Mars orbiters and landers based on Viking 1973 mission requirements, discussing tracking problems
[AIAA PAPER 70-160] 06 p1158 A70-18177

Translunar Apollo orbit analysis from elementary equations relating to elliptical and hyperbolic orbits in inverse square force field
06 p1148 A70-18397

State transition matrix computation method with efficient algorithm for orbit prediction in n-body gravitational field
06 p1095 A70-18497

Satellite orbit using analytic partial derivatives of perturbed motion based on state transition matrices
07 p1381 A70-19301

Maximum probability estimates for satellite orbital plane, reducing computational labor by eliminating use of maximum likelihood principle in differential formulation
07 p1386 A70-19486

Satellite circular orbital plane rotation by jet thrust, minimizing fuel for fixed time
07 p1393 A70-19497

Computer scheduling model and timeline plot for Apollo Telescope Module /ATM/ experiments using orbital trajectory simulation
07 p1394 A70-19572

Moon perigees and apogees for years 1-3000, tabulating parameters for calculations
08 p1568 A70-20635

Orbit analysis of hypothetical comets formed by Jupiter surface eruptions using Lagrange origin hypothesis
08 p1573 A70-21012

Earth satellite orbit determined by small separated optical observations at two stations
09 p1751 A70-22162

Spherical coordinate intermediaries for calculating satellite orbits
09 p1760 A70-22914

Periodic orbits in highly perturbed dynamical systems, studying characteristic curves of various families in galactic-type potential
09 p1760 A70-22916

Orbit determination from two position vectors and periaips radius, introducing polar equation for conic to obtain solution
09 p1760 A70-22932

Satellite orbital characteristics selection techniques, tools and methods for mission objectives and constraints
[AAS PAPER 68-136] 09 p1761 A70-22937

Center of mass small displacement effects on satellite orbits by solving variational equations for scalar potential function employing matrix formalism
09 p1761 A70-22938

Polynomial force model supplementing reduced gravity model in determining accuracy of near equatorial, near synchronous and near circular satellite orbits
09 p1762 A70-23256

Short arc method and spatial fitting of orbit in satellite triangulation, establishing sequential order between methods
09 p1670 A70-23440

Satellite orbit prediction formulas for Vinti dynamic model with three coordinates expressed in terms of independent variable
10 p1939 A70-24188

Geopotential resonance effects on low altitude satellites orbit determination, analyzing GEOS 2 orbit variations to determine even-degree coefficients
10 p1939 A70-24189

Parameter estimates effectiveness from independent discrete and continuous navigation measurements of circular orbital plane
10 p1914 A70-24303

Minimal characteristic velocity of single impulse transfer between coplanar elliptical orbits with allowance for thrust action finite time
10 p1940 A70-24304

Satellite orbit prediction using computer program based on first order secular node-to-node drag perturbations
10 p1943 A70-24822

Short period hypothetical orbits distribution formed by flaring on Jovian satellites
11 p2109 A70-25925

Mars imaging mission and astrodynamic interaction, discussing arrival geometry and orbit size effects
[AIAA PAPER 69-127] 11 p2112 A70-26130

Spin stabilized satellite attitude and orbital maneuvers computation, considering required accuracy and computer time in numerical integration procedures
11 p2125 A70-26278

Comet-asteroid evolutionary relationship based on Hidalgo orbital analysis
11 p2114 A70-26472

Light pressure induced secular effect contributing to planetary satellites and lunar orbits evolution calculated by numerical integration
11 p2118 A70-26777

Errors in determining controlled satellite rotation periods, proposing scheme for corrected trajectory calculation of small eccentricity orbits
11 p2118 A70-26779

Satellite motion initial phase vector estimation for calculating satellite motion from selection of complete or increasing volume of measurements
11 p2118 A70-26781

Vinti potential with spheroidal coordinates for equations of motion in earth satellite orbit computation
13 p2486 A70-28503

First order node to node satellite orbital elements perturbations due to arbitrary zonal geopotential harmonic, determining computation methods and time
14 p2638 A70-30703

Synchronous satellite orbits determination using mathematical model for simulating gravitational perturbations induced by terrestrial globe and foreign bodies
14 p2651 A70-31279

Orbit calculation based on first integrals of two body problem in spherical coordinates
15 p2797 A70-31620

Restricted three body problem taken for intermediate orbit in constructing analytical trigonometric motion theory for resonance asteroids, calculating perturbations by Bogoliubov method
15 p2803 A70-32498

Matrizant of two body problem or integrable dynamic system for applications to computing perturbations and differential correction of orbits with observations
15 p2768 A70-32611

Maximum probability estimates for satellite orbital plane, reducing computational labor by eliminating use of maximum likelihood principle in differential formulation
15 p2805 A70-32731

Satellite circular orbital plane rotation by jet thrust, minimizing fuel for fixed time
15 p2813 A70-32742

Satellite equations of motion in noninertial instantaneous astronomical system, taking into account perturbation equations terms
17 p3155 A70-34684

Quasi-linearization /generalized Newton-Raphson process/ in orbit determination, comparing with differential correction method
17 p3168 A70-35235

Scientific satellites orbit determination and improvement procedures for tracking system based on Doppler frequency and angular measurements
17 p3046 A70-35280

Interplanetary probes trajectory optimization for minimum energy expenditures, neglecting solar and terrestrial perturbations within earth sphere of influence
17 p3168 A70-35366

Echo 2 satellite orbital elements from optical observations covering last passages over Milan before orbital decay
17 p3172 A70-35628

System analysis to determine orbital parameters influence on mission scientific objectives under engineering constraints, using value function
[AIAA PAPER 68-1052] 17 p3172 A70-35648

Parking orbit optimal orientation for minimal impulsive maneuvers total velocity increment in three dimensional capture-escape mission
[AIAA PAPER 69-918] 17 p3172 A70-35649

Intermediate orbit calculation, allowing for spacecraft large gravitational perturbation during motion near planetary sphere of influence
18 p3312 A70-36166

Satellite path geometry along Keplerian elliptical orbit, taking earth flattening into consideration
18 p3312 A70-36167

Intermediate elliptical orbits for planetary satellites with small inclination to equatorial plane
18 p3312 A70-36174

Artificial satellite orbital motion numerical integration, computing spherical harmonic terms for earth gravitational potential
18 p3334 A70-37063

Plane galactic orbits near spiral field particle resonance, calculating numerically for ring orbits librating near maxima at Lagrangian points
18 p3331 A70-37193

Optimal three dimensional impulsive orbit transfer at cuspidal point of primer locus in terms of three parameters to facilitate computation and tabulation
[AIAA PAPER 70-1037] 19 p3527 A70-38852

Manned space station orbit selection, considering ground truth sites, sensors, film resolution, ground swaths, etc
[AIAA PAPER 70-1063] 19 p3529 A70-38877

Mariners 6 and 7 orbits determination by weighted least squares estimation based on common surface features in overlapping TV pictures
[AIAA PAPER 70-1066] 19 p3529 A70-38879

Weather occultation satellite orbit determination by radio wave measurements between master and slave satellites, formulating mathematical model
[AIAA PAPER 70-1067] 19 p3529 A70-38880

Orbit determination accuracy in synchronous satellite tracking analysis, using weighted least squares method
[AIAA PAPER 70-1068] 19 p3529 A70-38881

Galilean satellites touring by Jupiter spacecraft, discussing orbit calculation and encounter geometry
[AIAA PAPER 70-1070] 19 p3530 A70-38883

Visual binary stars orbits computation catalog from data obtained in 1939-1969 period
19 p3530 A70-38895

Computer algorithm for optimal linear impulse corrections to satellite orbit under inequality type constraints
21 p3801 A70-40828

Statistical orbit and position determination for Mars orbiters and landers based on Viking 1973 mission requirements, discussing tracking problems
[AIAA PAPER 70-160] 21 p3931 A70-41861

Solar eclipse calculation and prediction, discussing relationship between possible forms and earth-moon orbital configurations
21 p3924 A70-42173

Restricted three body problem taken for intermediate orbit in constructing analytical trigonometric motion theory for resonance asteroids, calculating perturbations by Bogoliubov method
23 p4240 A70-43919

Interplanetary periodic orbits and flyby dates for multiple earth-Venus swingby missions, describing various iterative solutions for trajectory
[AIAA PAPER 69-931] 23 p4243 A70-44508

Practical stability of highly eccentric orbits quasi-normal to ecliptic, discussing lunar effects on orbital lifetime
23 p4243 A70-44510

Doppler effect simplification to classical Laplacian orbit determination, deriving equations in perturbed gravity field for initial point determination
23 p4246 A70-44697

Minor planets, comets and natural satellites positions and motions, discussing orbit and ephemerides calculation, Icarus asteroid, etc
23 p4256 A70-45038

Orbital elements from secular acceleration in motion assumption, proving Comet Harrington identity with Comet Wolf
23 p4257 A70-45045

Rapid satellite orbit prediction program by numerical integration including oblateness squared and radiation pressure effects over long time spans
24 p4406 A70-45528

Satellite orbital element values and perturbation parameters from incomplete element system, using maximum likelihood principle
24 p4406 A70-45529

Satellite orbital elements calculation using ellipsoidal harmonics for geopotential representation
24 p4406 A70-45531

Solar and terrestrial perturbations on lunar satellite calculated by Brown theory
24 p4407 A70-45534

- GEOS A and OGO-4 satellite orbits and trajectory analysis using Definitive Orbit Determination System, discussing tracking stations error role 24 p4407 A70-45536
- Error analysis of satellite orbits obtained by synchronous satellites range and range rate measurements 24 p4407 A70-45539
- Satellite motion deviations from reference orbit by generalized Fourier analysis, discussing earth gravitational field parameters determination and errors 24 p4408 A70-45546
- ORBIT DECAY**
- Artificial satellite around Venus, investigating orbital lifetime based on atmospheric drag effect on periaapsis height 14 p2637 A70-30563
- Echo 2 satellite orbital elements from optical observations covering last passages over Milan before orbital decay 17 p3172 A70-35628
- ORBIT EQUATIONS**
- U ORBITAL MECHANICS**
- ORBIT PERTURBATION**
- NT SATELLITE PERTURBATION**
- Continuous and pulsed parameter stabilization for circular orbits of navigation and communication satellites under perturbing effects of oblateness and atmospheric drag 02 p0374 A70-12402
- Midast 4 satellite osculating orbital elements determined on basis of optical tracking data 03 p0443 A70-13177
- Beta Lyr spectral and brightness characteristics long period variations related to orbital motion perturbations 03 p0564 A70-13229
- U Geminorum type variables properties, orbital period changes in close binaries and origin of outbursts 03 p0567 A70-13322
- Gyrostabil motion stabilization with respect to unperturbed circular orbit vector radius, considering gravitational, aerodynamic, perturbation moments action and zero dry friction moment 03 p0484 A70-13370
- Osculating transfers between two prescribed trajectories without considering optimization problem, obtaining in-space launching point of artificial cosmic bodies 03 p0575 A70-13972
- Earth figure parameters from satellite orbit dynamics, including potential on geoidal surface and scale factor for lengths 05 p0840 A70-16638
- Apollo lunar orbit irregularities attributed to mascons beneath lunar surface, using short arc perturbation method [AIAA PAPER 70-163] 06 p1145 A70-18068
- Three body problem involving sun and perturbing and perturbed planets, examining perturbed motion equations of Brouwer and Encke methods 07 p1374 A70-18773
- Lunar mascon effects on Apollo type spacecraft orbits calculated for minimizing orbital instabilities 07 p1387 A70-19715
- Beta Lyr spectral and brightness characteristics long period variations related to orbital motion perturbations 08 p1580 A70-21662
- Major planets secular perturbations represented in trigonometric form using canonical transformations 09 p1751 A70-22176
- Climate variations and earth orbital elements secular perturbations, noting solar radiation and celestial mechanics roles 09 p1666 A70-22177
- Nongravitational effects, systematic residuals and close Jupiter approach problems in motions of comets 09 p1759 A70-22913
- Periodic orbits in highly perturbed dynamical systems, studying characteristic curves of various families in galactic-type potential 09 p1760 A70-22916
- Motions stability about triangular points in elliptic restricted problem of three bodies, using perturbation scheme 09 p1728 A70-23205
- Variations after one revolution in semimajor axis, period and eccentricity computed for orbit using variable drag coefficient involving satellite and air thermal speeds 10 p1951 A70-24824
- Dynamic orbital mixing in self gravitating spherical stellar system using water bag model 10 p1945 A70-24965
- Orbital perturbations earth satellite due to zonal and tesseral earth gravitational harmonics and external body fields 12 p2302 A70-27671
- Variational equations from Herrick variation of parameters method for Icarus encounter with earth 13 p2488 A70-28823
- Long period comets energy change due to planetary perturbations tabulated, obtaining orbital major axes before and after passage 13 p2489 A70-28906
- Meteors hyperbolicity based on statistical considerations and radiant distribution, discussing orbits perturbation and observation from earth 13 p2490 A70-29041
- Planetary motion zero-rank effects numerical integration, using Hill secular perturbation method and trace of dyadics 14 p2639 A70-30704
- Planetary orbit after central star supernova explosion, discussing effect on pulsar period 14 p2640 A70-30787
- Restricted three body problem taken for intermediate orbit in constructing analytical trigonometric motion theory for resonance asteroids, calculating perturbations by Bogoliubov method 15 p2803 A70-32498
- Matrizant of two body problem or integrable dynamic system for applications to computing perturbations and differential correction of orbits with observations 15 p2768 A70-32611
- Artificial planetary satellites long term orbital evolution under strong perturbations, considering solar and lunar gravitational effects [AAS PAPER 70-038] 17 p3155 A70-34779
- Intermediate orbit calculation, allowing for spacecraft large gravitational perturbation during motion near planetary sphere of influence 18 p3312 A70-36166
- Satellite path geometry along Keplerian elliptical orbit, taking earth flattening into consideration 18 p3312 A70-36167
- Solar quadrupole moment effect on secular perturbations of planetary orbital elements 18 p3313 A70-36325
- Mascon effects on close lunar orbit, using short arc perturbation technique 18 p3314 A70-36518
- Perturbative effects of Jupiter moons on spacecraft flyby and postencounter heliocentric trajectories, noting precision targeting [AIAA PAPER 69-932] 18 p3316 A70-36680
- Stellar velocity field in M 51 from image tube spectra 18 p3327 A70-37158
- Planetary orbiter parameters long term variations under central body oblateness, solar and atmospheric drag perturbations [AIAA PAPER 70-1055] 19 p3528 A70-38870
- Drag-free satellite design and propulsion requirements, noting orbit perturbation mechanisms [AIAA PAPER 70-1145] 20 p3717 A70-40523
- Oscillation stability of stars moving along axis of symmetry in galaxy, discussing first order orbit perturbations in general resonance case 21 p3884 A70-40873
- Perturbation of body motion in vicinity of smallest primary according to Huang model of restricted four body problem, discussing near lunar satellite application 21 p3884 A70-40874
- Restricted three body problem taken for intermediate orbit in constructing analytical trigonometric motion theory for resonance asteroids, calculating perturbations by Bogoliubov method 23 p4240 A70-43919
- Jupiter perturbations on short period comets during close approaches, discussing orbital distribution 23 p4241 A70-44252
- Orbital eccentricity effects on solutions of eclipsing binary light curves, comparing circular orbits solutions 23 p4242 A70-44290
- Practical stability of highly eccentric orbits quasi-normal to ecliptic, discussing lunar effects on orbital lifetime 23 p4243 A70-44510
- Moderately elliptic reference orbit perturbed motion, applying linearized perturbation equations for circular orbit 23 p4244 A70-44590
- Eclipsing binary stars minima variations related to orbit perturbations and rotational angular momentum of component interiors 23 p4251 A70-44819
- Satellite orbital element values and perturbation parameters from incomplete element system, using maximum likelihood principle 24 p4406 A70-45529
- Resonant satellites geodesy, determining orbit perturbation and gravity constant via mean Kepler elements high speed analysis 24 p4408 A70-45540
- Echo 1 and PAGEOS 1 orbital elements variations, determining perturbing effects of earth albedo radiation pressure 24 p4409 A70-45558
- ORBITAL ASSEMBLY**
- Environmental control of Apollo applications program orbital assembly, analyzing thermal and life support systems [SAE PAPER 690622] 05 p0922 A70-15847
- Automatically controlled rendezvous and docking for orbital assembly of spacecraft, deriving motion equations for mass centers 07 p1393 A70-19481
- Automatically controlled rendezvous and docking for orbital assembly of spacecraft, deriving motion equations for mass centers 15 p2813 A70-32726
- ORBITAL ELEMENTS**
- Algorithm for solving autonomous artificial satellite orbital elements, using successive approximations 01 p0139 A70-11503
- Satellite orbital elements optical determination accuracy by differential corrections, presenting computations for data distributed along small arc 02 p0254 A70-11754
- Satellite tracking at several stations at synchronized time to obtain satellite positions, station coordinates and to improve orbital elements accuracy 02 p0254 A70-11760
- Period changes of satellite 1963 53 A due to accelerations from atmospheric drag and solar radiation pressure 02 p0362 A70-11764
- Orbital period determination for satellite from single station visual observations, assuming known orbit inclination, ascending node length and node precession 02 p0254 A70-11765
- Cometary and asteroidal meteors discriminated by orbital elements in region of Jovian comet family adjoining asteroidal belt 02 p0373 A70-12371
- Midast 4 satellite osculating orbital elements determined on basis of optical tracking data 03 p0443 A70-13177
- Nonperiodic changes in radiation connected with orbital period in eclipsing conventional binaries observed in R Canis Majoris 03 p0568 A70-13326
- Earth satellite orbit parameters determination from angle measurements using computer program and least squares estimation technique 03 p0573 A70-13843
- Geocentric orbital elements of lunar particles expelled into space by meteorite impact, using spheres of influence method 03 p0574 A70-13880
- Differential correction procedures, using residuals to obtain celestial body orbital elements by linear programming 04 p0751 A70-14943
- Color photoelectric study of eclipsing binary RY Gemini for determining orbital elements and structure 04 p0754 A70-15217
- Satellites and space probes orbital parameters calculation, considering circular and elliptical trajectories and rendezvous maneuver example 06 p1140 A70-17583
- Meteors orbital elements distribution in solar system from radio observation data 06 p1141 A70-17737
- Balloon satellite orbital time and eccentricity correlated, investigating earth shadow and solar radiation effects 06 p1142 A70-17892
- Asteroid families and jet streams, searching for regularities and resonances in mean family elements 06 p1151 A70-18491
- Maximum probability estimates for satellite orbital plane, reducing computational labor by eliminating use of maximum likelihood principle in differential formulation 07 p1386 A70-19486
- Satellite orbital characteristics selection techniques, tools and methods for mission objectives and constraints [AAS PAPER 68-136] 09 p1761 A70-22937
- Optimal trajectory measurement program for orbit parameter determination, assuming random errors and nondegenerate weighting matrix of normal equations 10 p1940 A70-24302
- Pages 1 satellite characteristics, design, structure and orbital elements 10 p1941 A70-24585
- Orbital stability of geostationary vehicle at arbitrary latitude, considering nonlinear equations and deducing stability conditions by Liapunov method 10 p1950 A70-24783
- Satellite motion initial phase vector estimation for calculating satellite motion from selection of complete or increasing volume of measurements 11 p2118 A70-26781
- Orbital elements of small high velocity meteors, using oblique radio sounding 12 p2311 A70-28306
- Earth orbital parameters estimation in manned flight by manual space navigation sensors and computer 13 p2446 A70-28406
- Navigation for lunar parking orbit with time varying osculating orbital elements, using Apollo 11 Doppler tracking data 14 p2613 A70-30457
- Churimov-Gerasimenko 1969h comet photographs and preliminary orbital characteristics 15 p2800 A70-32146

Maximum probability estimates for satellite orbital plane, reducing computational labor by eliminating use of maximum likelihood principle in differential formulation

15 p2805 A70-32731

Meteor orbit parameters and incident particle flux measurements by radio methods, eliminating backscatter radar sensitivity limitations

15 p2807 A70-32814

Secular variations in osculating orbital elements of particle in Saturn ring gravitational field, considering motion in both external and internal space

16 p2973 A70-33226

Periodic comet Slaughter-Burnham improved ephemeris for 1970-71, based on 1958-59 and 1969 orbital elements

17 p3158 A70-34863

System analysis to determine orbital parameters influence on mission scientific objectives under engineering constraints, using value function

[AIAA PAPER 68-1052] 17 p3172 A70-35648

Solar quadrupole moment effect on secular perturbations of planetary orbital elements

18 p3313 A70-36325

Leonid meteoroids orbital elements mean values from photographic observations

19 p3526 A70-38776

Orbital elements of photographic meteors brighter than first magnitude, tabulating dates, solar longitudes, corrected radiants, velocities, major axis, etc

19 p3526 A70-38787

Planetary orbiter parameters long term variations under central body oblateness, solar and atmospheric drag perturbations

[AIAA PAPER 70-1055] 19 p3528 A70-38870

Orbital and physical parameters of calibration satellites launched into right circular cylinder and right circular cone

19 p3382 A70-38894

Binary stars dynamical parallaxes, masses, absolute magnitudes and provisional orbits, fitting deduced masses into empirical visual mass-luminosity relations

19 p3531 A70-38896

SERT 2 measurements for spacecraft and ion beam potential as function of thruster and orbital parameters, using hot wire emissive probes

[AIAA PAPER 70-1127] 20 p3691 A70-40218

Radiant dispersion, position, areas and orbital axis in meteor showers by double-station photographic observations, noting Apollo group detection

21 p3884 A70-40875

Comet Bennett basic characteristics, discussing orbits, periods and observational summaries of other comets

21 p3890 A70-41164

Terrestrial satellites ground tracks by FORTRAN IV computer program, investigating orbital parameters effects

21 p3892 A70-41325

Neptune orbit residual, discussing recently discarded Lalande prediscovery

21 p3922 A70-41986

Orbital elements from secular acceleration in motion assumption, proving Comet Harrington identity with Comet Wolf

23 p4257 A70-45045

Satellite orbital element values and perturbation parameters from incomplete element system, using maximum likelihood principle

24 p4406 A70-45529

Satellite orbital elements determination by differential correction procedure, considering observation stations distribution influence on accuracy

24 p4406 A70-45530

Satellite orbital elements calculation using ellipsoidal harmonics for geopotential representation

24 p4406 A70-45531

Geophysical parameters from artificial earth satellite orbital elements evolution data, discussing atmospheric density and zonal harmonics

24 p4330 A70-45551

Echo 1 and PAGEOS 1 orbital elements variations, determining perturbing effects of earth albedo radiation pressure

24 p4409 A70-45558

Short period hypothetical and real comets in Jupiter sphere of influence distributed according to orbital elements

24 p4409 A70-45637

ORBITAL LAUNCHING

Osculating transfers between two prescribed trajectories without considering optimization problem, obtaining in-space launching point of artificial cosmic bodies

03 p0575 A70-13972

Optimum second stage sizes for Blue Streak first stage for maximum payload injection into various orbits, tabulating sizes and payloads

05 p0924 A70-16589

Orbit-to-orbit shuttle for launch in earth-to-orbit shuttle vehicle, discussing design requirements

[AIAA PAPER 70-268] 07 p1399 A70-20397

Nuclear solid core rocket engine performance for interplanetary orbital launch of spacecraft by multibit injection

[AIAA PAPER 69-535] 14 p2616 A70-30767

Scramjets for recoverable booster transporting payloads into earth orbits

15 p2811 A70-32258

Nuclear orbital launch stages for interplanetary departure, comparing parallel and tandem spacecraft configurations

[AIAA PAPER 70-680] 16 p2950 A70-33580

Light weight integrated spin-up launch mechanism for rocket propelled payload

16 p2845 A70-34113

Multiorbit injection earth departure technique for optimal thrust-weight ratio in manned interplanetary missions using NERVA engine

[AAS PAPER 70-039] 17 p3175 A70-34780

Black Arrow launch vehicle for inexpensive and reliable payload injection into low polar orbits

17 p3178 A70-35255

ORBITAL MECHANICS

NT KEPLER LAWS

Periodic motion of satellite with magnetic damper along circular orbit, assuming small value of damping coefficient

01 p0197 A70-11481

Optimum orbital transfer of material point subjected to reactive force with minimum mass loss, discussing Kepler motion kinematics

01 p0192 A70-11514

Conditionally periodic orbits existence in restricted problem of three bodies, using similarity transformation

02 p0369 A70-11997

Three-body gravity gradient satellite orbital plane motion analysis, studying transient damping of proposed tethered orbiting interferometer (TOI)

02 p0383 A70-12781

Optimal two impulse transfer through 180 degree range angle between Keplerian noncoplanar orbits, minimizing impulse by transfer plane optimal orientation

[AIAA PAPER 68-93] 03 p0562 A70-12914

Tidal disturbing functions developed with amplitude factor and lag angle expressed as sums of zonal spherical harmonics, discussing lunar formation and orbit evolution

03 p0576 A70-14083

Phobos motion observational results compared with Sharpless determination of secular acceleration

04 p0743 A70-14399

Satellite motion in earth gravitational field under additional forces using Stokel theorem

04 p0760 A70-14432

Stationary and periodic solutions for commensurable cases of mean motions in restricted three body problems by expanding disturbing functions

04 p0745 A70-14474

Singularity-free universal orbit calculation satisfying two position vectors and time interval

04 p0750 A70-14930

Orbit mechanical investigations for increasing Europa 2 booster rocket payload to place German-French communications satellite Symphonie into 24 hr orbit

04 p0754 A70-15153

Predictor-corrector algorithm for continuing analytically families of periodic orbits beyond collision trajectories in restricted three bodies problem

05 p0908 A70-16333

Resonance effects on satellite orbits due to tesseral harmonics in potential field

05 p0908 A70-16335

Motion near collision singularity in perturbed two body problem, applying method to boundedness proof for Sperling cluster energy

05 p0909 A70-16339

Critique of solar system resonant structure hypothesis based on planetary orbital frequencies errors

05 p0910 A70-16394

Computation methods for optimal rocket trajectories closely approaching gravitating celestial bodies, alleviating computational difficulties with regularizing techniques

[AIAA PAPER 70-95] 06 p1146 A70-18202

Plane motion of two mass points coupled by flexible inelastic thread assuming system mass center moving along circular orbit

07 p1386 A70-19484

Pulsar formation effect on orbits of preexisting planets and postformation planets effects on pulsar period and phase residuals

08 p1570 A70-20898

Periodic solutions with moderate eccentricities and high inclinations for three dimensional restricted three body problem by expanding disturbing functions by high speed computer

09 p1759 A70-22773

Periodic orbits in highly perturbed dynamical systems, studying characteristic curves of various families in galactic-type potential

09 p1760 A70-22916

Stability characteristics of near periodic orbits using variational equations, with results applied to phase space and stability problems

09 p1760 A70-22917

Triangular Lagrangian equilibrium points stability in planar restricted problem of three bodies at order two mass ratio using two variable expansion method

10 p1939 A70-24184

Periodic orbits for reduced problem of conservative Hamiltonian system with two degrees of freedom, discussing emergence from resonant equilibrium

10 p1939 A70-24187

Spacecraft and boosters for earth resources surveys, discussing design, payloads, orbits, etc

10 p1950 A70-24641

Evolution discontinuities and genealogy of long period orbit families at Lagrangian equilibrium point of restricted three body problem

10 p1945 A70-24958

Motion of negligible mass body near large mass body affected by larger third body applied to Phoebe-Saturn-sun system

10 p1945 A70-24960

Dynamic orbital mixing in self gravitating spherical stellar system using water bag model

10 p1945 A70-24965

Book on quasi-linearization and nonlinear fluid and orbital mechanics covering ablating wall, electrostatic probe, laminar boundary stability, pipe flow and optimum bang-bang transfer

11 p2072 A70-26225

Coplanar transfer orbits optimal trajectories in central Newtonian gravitational field, using Krotov sufficient criteria

12 p2310 A70-28252

Nomogram construction for graphical solution of two body problem using radius-vector and velocity components applied to solar system

12 p2311 A70-28310

Satellite motion in earth gravitational field under additional forces using Stokel theorem

13 p2503 A70-28457

Variational equations from Herrick variation of parameters method for Icarus encounter with earth

13 p2488 A70-28823

Bright sporadic fireballs and faint photographic meteors orbits, discussing clustering in diagram of geocentric velocity vs inclination

13 p2490 A70-29040

Harmonic functions defining geopotential and gravity derived from satellite orbit dynamics, applying to earth shape parameters

13 p2398 A70-29208

Lunar spring board effect to minimize impulses for given velocity at great distance of earth-moon system, discussing nonimpulsive grazing passage

14 p2635 A70-30289

Artificial satellite around Venus, investigating orbital lifetime based on atmospheric drag effect on periapsis height

14 p2637 A70-30563

Analytical solutions to optimum orbit modifications including atmospheric maneuver

14 p2649 A70-31171

Third integral of stellar dynamics, considering Contopoulos galactic system model separability

14 p2651 A70-31288

Book on celestial mechanics covering perturbation methods, two body problems, astronomical coordinates, orbital mechanics, satellite rotation, gravitational effects, etc

15 p2799 A70-31998

Jet assisted orbital spacecraft trajectories equations derivation, considering Kepler trajectories and orbital velocities

15 p2800 A70-32260

Plane motion of two mass points coupled by flexible inelastic thread assuming system mass center moving along circular orbit

15 p2805 A70-32729

Periodic solutions close to commensurabilities in three body problem, considering restricted and planar nonrestricted problems

17 p3172 A70-35561

Computation methods for optimal rocket trajectories closely approaching gravitating celestial bodies, alleviating computational difficulties with regularizing techniques

17 p3172 A70-35666

Low thrust station keeping guidance scheme for gravity gradient stabilized 24-hour satellite, solving equations of motion for near circular equatorial orbit

18 p3289 A70-36676

Minimum-fuel multiple impulse orbital fixed time rendezvous in circular orbit vicinity

18 p3289 A70-36682

Circular orbit stability in stationary axisymmetric space-times dependence on angular momentum per unit mass increases outward from symmetry axis

18 p3317 A70-37004

Iterative Hansen method of general perturbations programmed for digital computer, evaluating major and minor planetary theory

18 p3320 A70-37060

General potential function in triaxially ellipsoidal coordinates for Laplace equation, examining near earth satellites and Vinti potential

18 p3334 A70-37064

Satellite orbit theory error bounds and initialization, investigating first order von Zeipel method in axisymmetric force field

18 p3320 A70-37067

- Bestser comet 1946k-1947I orbit, showing original and future orbits as long period ellipses
19 p3515 A70-37931
- Burnham-Slaughter 1958e-1959I comet orbit, showing nearly parabolic ellipse
19 p3516 A70-37933
- Humason 1960e-1959X comet hyperbolic orbit, indicating solar system permanent membership
19 p3516 A70-37934
- Periodic collision orbits in plane elliptic three body problem of infinitesimal mass under gravitational field of two finite masses
20 p3705 A70-39603
- Global geoid sections determined by satellite orbit dynamics, using best fitting ellipses
21 p3812 A70-40591
- Titius-Bode law conclusions regarding solar system planetary distances numerical relations, considering planetary evolution
22 p4101 A70-42863
- Jupiter perturbations on short period comets during close approaches, discussing orbital distribution
23 p4241 A70-44252
- Moderately elliptic reference orbit perturbed motion, applying linearized perturbation equations for circular orbit
23 p4244 A70-44590
- Three body elliptic restricted problem triangular points, deriving second order expression for transition curves and characteristic exponents
23 p4244 A70-44595
- Restricted osculating two body orbit with time derivative of eccentric anomalies difference position as independent variable in perturbation differential equations
23 p4244 A70-44635
- Orbital mechanics of transfer orbits under small horizontal thrust, reducing second order differential equation to linear inhomogeneous equation
23 p4245 A70-44691
- Celestial mechanics covering two body problem, orbital improvement, perturbation theory and dynamics, planetary and satellite theory, lunar motion, etc
23 p4255 A70-45032
- Balloon satellite perturbations in orbital period involving air drag, lunar gravity and solar and terrestrial radiation pressures
24 p4414 A70-45358
- Resonant satellites geodesy, determining orbit perturbation and gravity constant via mean Kepler elements high speed analysis
24 p4408 A70-45540
- ORBITAL MOTION**
U ORBITS
ORBITAL RENDEZVOUS
NT EARTH ORBITAL RENDEZVOUS
NT LUNAR ORBITAL RENDEZVOUS
Optimal rendezvous between satellite and spacecraft, determining power and time optimal coplanar rendezvous in circular orbit
01 p0139 A70-11479
- Optimum thrust control of satellite along given trajectory to rendezvous at zero velocity with orbited satellite
01 p0197 A70-11500
- Medium duration optimal rendezvous between near circular noncoplanar orbits with close orbital planes, analyzing six impulse solutions
03 p0571 A70-13639
- Orbital rendezvous for inspection, rescue, etc, discussing launch bases number, warning time and alert status effect on reaction time
06 p1027 A70-17173
- Rendezvous control law for spacecraft moving in central gravitational field along trajectory representing target vehicle Keplerian orbit
08 p1582 A70-21636
- Optimal longitude rendezvous for geostationary satellite by using inertially fixed orientation thrust for performing final positioning
10 p1941 A70-24541
- Soviet book on rendezvous in orbit, flight dynamics and control of spacecraft covering trajectory synthesis, optimization and control for approach stage
10 p1950 A70-24656
- Satellite rendezvous programmed control with allowance for thrust limitation by free trajectories method, determining impulse duration, magnitude and time
12 p2314 A70-28257
- Earth-pointing satellites joined by tether, discussing reel back and drag brake orbital deployment techniques and dynamic behavior
15 p2799 A70-31776
- Automatic control of Cosmos spacecraft docking maneuvers in two successive encounter phases
23 p4264 A70-45016
- ORBITAL SIMULATORS**
U SPACE SIMULATORS
ORBITAL SPACE STATIONS
NT EOSS
NT ORBITAL WORKSHOPS
Long life subsystems design and testing for orbital space station programs, considering nuclear genera-
- tion, electromechanical equipment, positive expulsion of fluids, instrumentation, etc
[AIAA PAPER 69-1080] 01 p0103 A70-10626
- Communications subsystem configuration for orbital manned space station, describing data rates and processing, multiplexing and associated modulation methods
[AIAA PAPER 69-1079] 01 p0043 A70-10627
- Manned space station system analysis for identifying control subsystem functions/weight penalties/and system characteristics to minimize penalties
[AIAA PAPER 69-1078] 01 p0194 A70-10628
- Orbital space station operations requirements and interactions, considering experimentation, support vehicles, ground support and follow-on growth
[AIAA PAPER 69-1062] 01 p0195 A70-10636
- Reusable airbreathing launcher for manned space station ferry operations, considering nozzles, intakes, thrust, acceleration, flight plan, weight analysis, etc
02 p0381 A70-12502
- Manned space station system design requirements, discussing logistics interaction and station autonomy
[AIAA PAPER 69-1063] 02 p0382 A70-12528
- Support facilities requirements and goals for manned and unmanned solar and stellar orbital astronomy
[MDAC-WD-1258] 05 p0847 A70-16074
- NASA three meter orbital telescope discussing configuration, optical geometry, launching, power supply, etc
07 p1280 A70-19150
- Modular earth orbiting space station design, configuration and operation
08 p1568 A70-20688
- Earth resources program function of early orbital manned space station in remote sensing
09 p1687 A70-23760
- Materials and processing technology roles in NASA programs involving manned space stations, service spacecraft and unmanned space exploration
10 p1902 A70-23855
- Soyuz 6, 7 and 8 group flight as step in Soviet space program to place manned station in earth orbit
11 p2121 A70-25623
- Manned space flight role in earth orbital space astronomy, examining long range program
12 p2297 A70-26997
- Checkout systems for shuttle and orbiting space stations, discussing shift from ground to onboard operation
12 p2208 A70-27691
- Manned space stations size, crew, orbit, lifetime, resupply requirements, etc
12 p2313 A70-27742
- Meteorological research potential of manned orbiting spacecraft, discussing electromagnetic sensing instrumentation development, specialized observing programs, etc
12 p2225 A70-27744
- Lunar spaceports for military uses from legal viewpoint, considering Space Treaty
12 p2336 A70-27774
- Nuclear power systems for manned orbiting space stations, noting Brayton aggregate and NASA objectives
13 p2450 A70-29493
- Maintenance vs redundancy for manned space station economy, considering costing structure and time increase for maintenance
15 p2713 A70-32666
- Outer space exploration and utilization, analyzing 1967 UN treaty provisions from standpoint of war potential inherent in space stations existence
16 p3003 A70-33100
- Experiment space module combined with space station and serviced by shuttle for low total cost and maximum flexibility in funding and scheduling
[AAS PAPER 70-034] 17 p3175 A70-34777
- Manned planetary flight systems engineering, discussing feasibility, objectives, propulsion, transplanet injection via geospace shuttle station, energy requirements for various synodic modes
[AAS PAPER 70-037] 17 p3155 A70-34778
- Space shuttle-manned space station integration, discussing design and operation, crew rotation, station resupply, docking, etc
[AAS PAPER 70-051] 17 p3176 A70-34789
- Manned planetary spacecraft and space stations as ecological systems, considering common features
[AAS PAPER 70-023] 17 p3176 A70-34799
- Ten year NASA manned space station in low earth orbit, grouping experiments in functional program elements/FPE/
[AAS PAPER 70-033] 17 p3156 A70-34802
- NASA ten year space station operational concepts, discussing mission planning, crew scheduling and management
[AAS PAPER 70-031] 17 p3176 A70-34804
- Orbiting space stations and interplanetary flights, discussing spacecraft design, facilities, Mariner probes, etc
19 p3533 A70-38487
- Manned space station orbit selection, considering ground truth sites, sensors, film resolution, ground swaths, etc
[AIAA PAPER 70-1063] 19 p3529 A70-38877
- Skylab scientific space station, discussing crew living quarters and supplies, artificial atmosphere and manned solar observatory
20 p3713 A70-39481
- Motion and stability of rotating connected two body space station satellite system, developing Lagrangian equations of motion and optimizing damping system parameters
[AIAA PAPER 69-919] 20 p3716 A70-39678
- Parameterized design data and selection criteria of biowaste resistojet system for orbit keeping and control moment gyro desaturation of manned space station
[AIAA PAPER 70-1132] 20 p3567 A70-40213
- Planetary probes, orbiting space stations and manned spacecraft in interplanetary flights, discussing Mariner, Gemini and Apollo reentry and Venus landing
22 p4109 A70-42313
- Nuclear power systems for manned orbiting space stations, noting Brayton aggregate and NASA objectives
22 p4071 A70-43193
- Geolunar space development with transportation based on shuttle stations, discussing communication, orbits, logistics, etc
22 p4108 A70-43628
- Attitude and orbit control electric propulsion systems for long term space stations, discussing resistojets and electron bombardment and contact ionization ion thrusters
22 p4092 A70-43654
- Attitude control of artificial gravity mass-unbalanced axisymmetric orbital space stations
23 p4258 A70-44502
- Rotating cable-connected orbital space stations deployment dynamics, considering cable mass and motion equation
23 p4258 A70-44529
- Earth orbital space station electrical power systems, discussing power sources, effect on structural configuration, environmental control and launch and resupply operations
[MDAC-WD-1461] 23 p4143 A70-44605
- Free flight remote controlled teleoperator system applications in manned orbital space station/space shuttle program
23 p4260 A70-44644
- Orbital space station utilization planning as international laboratory, discussing industry role, experiment program goals, etc
23 p4260 A70-44650
- Manned earth orbital space astronomy instruments, facilities and research objectives
24 p4415 A70-45825
- Orbital space station program, discussing common module design, support, space shuttles and objectives
[SAE PAPER 700755] 24 p4415 A70-45852
- Space station design, discussing existing technology base for earth orbital operations program implementation
[SAE PAPER 700756] 24 p4416 A70-45872
- Free-flying modules interface and operation in conjunction with space station for orbital research into manned space program
[AIAA PAPER 70-1300] 24 p4417 A70-45950
- Earth-orbiting manned space station design, describing shuttle support and experimentation in attached and free-flying modules
[AIAA PAPER 70-1299] 24 p4417 A70-45951
- Systems and design requirements for NASA Manned Space Station, discussing projected experiment program for applications and science
[AIAA PAPER 70-1298] 24 p4417 A70-45952
- ORBITAL TRANSFER**
U TRANSFER ORBITS
ORBITAL VELOCITY
Growth test vehicle /GTV/ flight test program for development of hypersonic flight to orbital speeds, discussing design, costs, capabilities, etc
03 p0582 A70-14188
- Hodographic determination of required velocity changes for space vehicle transfer orbit, involving only launching point and trajectory plane
08 p1577 A70-21505
- Minor planets orbits coordinates and velocities data at osculation time
09 p1756 A70-22654
- Jet assisted orbital spacecraft trajectories equations derivation, considering Kepler trajectories and orbital velocities
15 p2800 A70-32260
- Radio meteor orbit velocity and radiant measurements by pulse diffraction technique
18 p3315 A70-36603
- Nomograms for meteor geocentric velocity and trajectory with correction for zenith attraction and radiant
18 p3315 A70-36605

- Position and velocity of geodetic drag free satellite in near circular orbit, including lunar- solar gravitational effects and zonal and tesseral harmonics [AIAA PAPER 70-1054] 19 p3528 A70-38869
- Optimal fixed-time impulsive transfer trajectories minimizing characteristic orbital velocity, determining sufficient conditions 23 p4255 A70-45015
- Interorbital optimum trajectories with specified transfer angle in inverse square gravitational field, examining minimum velocity increment 24 p4412 A70-46003
- ORBITAL WORKERS**
- Orbital zero and low g environment utilization for space manufacturing processes and related operational and tooling requirements 16 p2919 A70-33718
- ORBITAL WORKSHOPS**
- Expandable space hangar with composite wall for orbiting maintenance shelter, providing radiation and meteoroid protection for occupants 02 p0380 A70-11934
- Spent Saturn S-4B stage conversion into orbital workshop in Apollo Applications Program 11 p2122 A70-26044
- Saturn IB Orbital Workshop solar array thermal and performance analysis for various vehicle orientations and orbital conditions, emphasizing modeling and data handling 11 p2127 A70-26357
- Solar X rays observation from manned orbiting workshop of Apollo Applications Program, describing telescope/camera assembly and X ray event analyzer 11 p2057 A70-26506
- Atmospheric density variations and functional dependence of aerodynamic moment coefficient on incident angle from Saturn Workshop flight experiment 14 p2528 A70-30559
- Space manufacturing in weightless environment, discussing unique processes, potential materials, product groups, planned experiments for Skylab Orbital Workshop mission, etc 16 p2888 A70-33716
- Materials preparation processes and improvements in space weightless environment, considering metals and ceramics melting, solidification, electromagnetic process control, etc 16 p2919 A70-33717
- Candidate products for manufacturing on space station, emphasizing liquid solid transformations, bubbles and droplets, polymerization, and cost effectiveness [AAS PAPER 70-036] 17 p3041 A70-34791
- Parabolic solar furnace for chemical manufacture of impurity sensitive materials in orbiting spacecraft 21 p3804 A70-41001
- Skylab Orbital Workshop fabrication experiments under space environment conditions, discussing weightlessness and vacuum effects on various manufacturing techniques 22 p4046 A70-43075
- Orbital laboratories and international cooperation, discussing national and foreign viewpoints 22 p4128 A70-43631
- Manned orbital laboratories, discussing need for international cooperation 22 p4128 A70-43634
- International earth orbital space laboratory program, discussing objectives, management, stations, shuttles, tugs, tracking, communication, data distribution network, etc 23 p4262 A70-44687
- Saturn Orbital Workshop experiment for testing chemically rigidized expandable materials and structures for space applications, discussing resin impregnated glass fiber cloth 23 p4264 A70-45012
- Skylab mission in 1972, describing orbital workshop configuration and three man crew integration for operational experiments [AIAA PAPER 70-1328] 24 p4417 A70-45939
- ORBITALS**
- NT ELECTRON ORBITALS
- NT MOLECULAR ORBITALS
- NT SLATER ORBITALS
- ORBITER PROJECT**
- Orbiter imagery analysis program for Apollo landing site selection, using photographic interpretive techniques 03 p0571 A70-13660
- Visual imaging systems for Mars orbiter compared for performance and interactions with mission and spacecraft design 07 p1280 A70-19230
- ORBITING ASTRONOMICAL OBSERVATORY**
- U OAO
- ORBITING GEOPHYSICAL OBSERVATORY**
- U OGO
- ORBITING SATELLITES**
- U ARTIFICIAL SATELLITES
- ORBITING SOLAR OBSERVATORY**
- U OSO
- ORBITS**
- NT APOGEEES
- NT CIRCULAR ORBITS

- NT EARTH ORBITS
- NT ECCENTRIC ORBITS
- NT ELLIPTICAL ORBITS
- NT EQUATORIAL ORBITS
- NT INTERPLANETARY TRANSFER ORBITS
- NT LUNAR ORBITS
- NT PARKING ORBITS
- NT PERIGEEES
- NT PERIHELIONS
- NT PLANETARY ORBITS
- NT POLAR ORBITS
- NT SATELLITE ORBITS
- NT SOLAR ORBITS
- NT SPACECRAFT ORBITS
- NT STATIONARY ORBITS
- NT TRANSFER ORBITS
- NT TROJAN ORBITS
- NT TWENTY-FOUR HOUR ORBITS
- Faye comet motion and secular orbital evolution of short period comets 07 p1379 A70-19048

ORDER-DISORDER TRANSFORMATIONS

- Long range order formation kinetics in lithium ferite octahedral sublattice after stepwise annealing and quenching in water, using X ray analysis 03 p0537 A70-12867
- High temperature heat treatment effects on Mo, W, Ta and Re crystal surface order and faceting observed by electron diffraction, noting contamination role 03 p0538 A70-13097
- Atom ordering and effects on alloy properties - Conference, Kiev, Ukrainian SSR, 1969 03 p0505 A70-13101
- Interstitial atoms ordering effects on low and high temperature phase transformations in alloys with bcc lattice 03 p0505 A70-13102
- Two phase theory of ordered to disordered state transition in ternary alloys with fcc lattice, constructing phase diagrams 03 p0505 A70-13103
- Strain hardening on single crystals of aging Ni-based alloys with ordered separated phase 03 p0505 A70-13104
- Mechanical properties of ordered Ni-Cr alloys, establishing hardening effect of annealing 03 p0505 A70-13105
- Microdeformation resistance in Ni alloys with ordered phase diagrams related to strain level, analyzing Bauschinger effect 03 p0505 A70-13106
- Neutron bombardment effect on ordering and disordering state of alloys phase diagrams, noting temperature dependence 03 p0506 A70-13107
- Two phase transitions existence in Hubbard model of interacting electrons using one particle Green function solution 05 p0884 A70-16099
- Gamma prime phase structure ordering effect on critical shear stresses of aging Ni-Al alloys and nimonic 09 p1707 A70-23195
- Order-disorder transition temperatures for Ni-Cr alloys determined by neutron diffraction, discussing homogeneous ordering of atoms 09 p1707 A70-23196
- Cleavage fracture of Ta-Mo bcc alloys, investigating short range ordering and size effects by X ray diffraction 09 p1708 A70-23573
- Initial value problem of macroscopic disorder-order transformation in random thermal convection phase of fluid heated from below 09 p1791 A70-23679
- Minimum entropy production at microscopic level, obtaining stationary state by Pauli master equation 14 p2616 A70-30654
- Electron paramagnetic resonance of viscous nematic liquid crystal, investigating order as function of temperature 16 p2960 A70-33058
- Fe ion, Mg order-disorder in natural orthopyroxenes as function of temperature 16 p2896 A70-33087
- Kinetic simulation of atom rearrangements in order-disorder transformation for point defect movement in Ti alloys, considering vacancies and interstitials properties 17 p3115 A70-34381
- Ti alloys martensitic transformations, metastable beta-phase decomposition and alpha-phase ordering 17 p3118 A70-34403
- Cesium films structure and work function on W /011/ face, discussing order-disorder transition 19 p3487 A70-37817
- Liquid crystals orientational ordering molecular field theory examined by cluster variation method, predicting first order transition 22 p4085 A70-42485
- Neutron diffraction of ordered atomic oxygen structures in titanium suboxides, noting compositional dependence of physical properties 22 p4053 A70-42735

- Short range order and Fermi surface effects in copper-rich Cu-Al alloys single crystals from X ray scattering measurements 23 p4204 A70-43886

ORDINATES
U COORDINATES
ORDNANCE

- Ordnance circuit RF filter in backshell of standard connector, discussing design, physical- electrical specifications and tests 03 p0494 A70-14113
- Neutron radiography for visual nondestructive failure analysis and production inspection of ordnance components compared with X ray radiography 03 p0494 A70-14122
- Statistical control charts for evaluating instrumentation performance during ordnance devices testing, discussing evolution, interpretation and application 03 p0494 A70-14126
- Harrier armament system design for ordnance carriage to full combat load factors, describing Weapon Control Panel 10 p1807 A70-24848
- Ordnance flight dynamics, considering trajectory analysis and inaccuracies due to projectile wobble [AIAA PAPER 70-533] 13 p2506 A70-29001
- Agenda D vehicle self destruct charge ordnance component, discussing design, performance and tests 16 p2963 A70-34126
- Apollo ordnance systems design and reliability, stressing redundant components role 17 p3179 A70-35263
- Air to air armament selection effect on aircraft configuration [AIAA PAPER 70-939] 17 p3021 A70-35848
- Nonlinear equations of motion approximate solution, determining ordnance weapons aerodynamic stability coefficients from angle of attack [AIAA PAPER 69-135] 23 p4133 A70-44515
- OREGON**
- Earth magnetic field transition recorded in basaltic lavas in southeastern Oregon 07 p1276 A70-20351
- ORES**
- U MINERALS
- ORGANIC ALUMINUM COMPOUNDS**
- Physicochemical properties of monomer and associated aluminokalks, determining heats of combustion 22 p4124 A70-42677
- ORGANIC CHEMISTRY**
- Organic synthesis by electrical discharge in simulated Jovian atmosphere, noting appearance of orange-red cyanogen-ammonia polymer nonvolatile fraction 01 p0179 A70-10529
- Book on chemical evolution of life covering molecular paleontology, prebiotic chemistry, membrane structures, molecular evolution and structure, etc 02 p0230 A70-11685
- Carbonaceous complex use as indicators of geothermal history and high temperature organic geochemistry 17 p3042 A70-35331
- ORGANIC COMPOUNDS**
- NT ACETIC ACID
- NT ADENOSINE DIPHOSPHATE [ADP]
- NT ADENOSINE TRIPHOSPHATE [ATP]
- NT ADENOSINES
- NT AMINO ACIDS
- NT ASPARTIC ACID
- NT CHOLINE
- NT CYSTEINE
- NT FATS
- NT FATTY ACIDS
- NT FLUORINE ORGANIC COMPOUNDS
- NT FLUOROCARBONS
- NT FLUOROHYDROCARBONS
- NT FOLIC ACID
- NT GLUTAMIC ACID
- NT GLUTAMINE
- NT GLYCINE
- NT HISTIDINE
- NT LEUCINE
- NT LYSINE
- NT METHIONINE
- NT NUCLEOTIDES
- NT OLEIC ACID
- NT ORGANIC LIQUIDS
- NT ORGANIC SULFUR COMPOUNDS
- NT OXIDASE
- NT PHENYLALANINE
- NT PYRIDINE NUCLEOTIDES
- NT THYROXINE
- NT TRYPTOPHAN
- Electron mobility in single component aromatic hydrocarbons, considering crystals structures and electrical properties, energy dissipation and fluctuation, etc 01 p0158 A70-10517
- Pressure effects on burning rate of magnesium mixtures with solid oxygen containing organic compounds, determining charge density effect on mass velocity 01 p0218 A70-11021

- Apollo lunar module descent engine exhaust organic combustion products, estimating ion intensities of various species in all mass spectra 02 p0356 A70-12693
- Low molecular weight organic semiconductors photoelectron UV emission spectra, studying electron energy distribution and optical ionization, dark bulk conductivity, etc 03 p0541 A70-13728
- Activated carrier mobility confinement in organic solids 06 p1004 A70-17325
- Organic compounds synthesis by electric discharges in simulated primitive atmosphere, considering mechanism for biologically significant molecules formation 07 p1225 A70-19104
- Pueblo de Alameda chondrite unextractable carbon content using meteorite pyrolysis, obtaining aromatic hydrocarbons 07 p1380 A70-19204
- Extrema behavior in nonlinear absorption of organic compounds under high power laser radiation interpreted by triple absorption molecular energy level models 07 p1302 A70-20100
- Free radical destruction by gamma irradiation in organic solids at low temperature measured by electron spin resonance spectroscopy, noting dosage relationship 07 p1225 A70-20324
- Bonds strength involving metallic, organic and ceramic adhesives at various temperatures, considering metallic additives effect 08 p1504 A70-20891
- Thermal conductivity for organic compound gases at atmospheric pressure 08 p1597 A70-21026
- Organic compounds chemical reactions during burning in laminar diffusive flames, describing technique for pyrolysis and combustion products sampling 09 p1787 A70-22107
- Conditions for life in universe, analyzing evolutionary stages of matter to determine steps producing complex organic compounds 09 p1762 A70-23121
- Organic substrates effects on *Hydrogenomonas eutropha* autotrophic and heterotrophic metabolism 10 p1817 A70-24700
- Carbonaceous chondrites composition by gas chromatography for light hydrocarbons and carbon, discussing origin of organic matter 10 p1949 A70-25327
- Nitrogenous compounds from Colorado Green River Formation oil shale using high resolution mass spectrometry 11 p2047 A70-26620
- Organic adhesives for bonding continuous surface and core-to-face joints, discussing strength, environmental resistance, producibility and reproducibility 13 p2419 A70-29118
- Biogeocenosis applicability to artificial closed ecological systems consisting of plants creating organic matter and heterotrophic organisms 13 p2353 A70-29501
- Electron impact promoted phenyl migration of trans phenylacetalone, considering mass spectrometry and stereochemistry 14 p2544 A70-30189
- Organic solutes diffusion in stagnant blood plasma and red cell suspensions, using models from transport theory 15 p2686 A70-32847
- Organic molecules topology, discussing Hamilton circuits, DENDROL applications, etc 16 p2855 A70-33298
- Organic compounds detection and identification on Mars surface for living systems existence or evolution 16 p2857 A70-33977
- Atmospheric oxygen history, using primeval anoxic terrestrial atmosphere simulation to show organic molecule formation by abiogenic process 16 p2898 A70-33990
- Optically active organic compounds origin on primordial earth, emphasizing role of asymmetric catalyst 17 p3024 A70-34700
- Product distribution of organic nitrogen compounds plasma sources computed by assuming high temperature limited thermodynamic equilibrium 18 p3226 A70-36764
- Solid-solid phase transitions in molecular crystals of organic tetrahedral substances, using differential scanning calorimetry 19 p3373 A70-38193
- P32 labeled organic phosphate esters in water extracts of soil 20 p3615 A70-38979
- Apollo 11 lunar fines examined for organic compounds via solvent extraction, vacuum crushing, programmed heating and hydrofluoric acid etching 21 p3778 A70-41619
- Apollo 11 lunar fines carbon compounds, examining chemical state of porphyrins, fatty and amino acids, purines, pyrimidines and carbohydrates, etc 21 p3779 A70-41625
- Apollo 11 lunar samples organic compounds analysis by mass spectroscopy, gas and liquid chromatography and nuclear magnetic resonance 21 p3779 A70-41629
- Apollo 11 lunar fines organic compounds detection and identification by mass spectrometry 21 p3780 A70-41632
- Organic solvent extracts of Apollo 11 bulk fine sample examined for porphyrins using spectrofluometry 21 p3780 A70-41635
- Organic spiropolymers synthesis for thermal stability by condensation of aliphatic spirotetraamines and aromatic dianhydrides 21 p3782 A70-42128
- Carbonaceous chondrites isomeric alkanes identification by mass spectrometry and gas chromatography 24 p4402 A70-45378
- ORGANIC FLUORINE COMPOUNDS**
- U FLUORINE ORGANIC COMPOUNDS**
- ORGANIC LASERS**
- Superradiant traveling wave laser emission observed with polymethine cyanine dyes pumped by mode locked ruby laser for picosecond duration pulse generation 01 p0110 A70-10564
- Frequency locking of flashlamp pumped Rhodamine 6G dye lasers to D lines of Na vapor by Faraday rotation, noting doublet splitting 01 p0110 A70-10568
- Polarization level dependence of dye lasers emission on angles between direction of forced radiation and pumping laser resonator axis 01 p0113 A70-11037
- High intensity short pulse flash lamps using quartz envelopes and wire electrodes for pumping high energy organic dye lasers 02 p0314 A70-12741
- Threshold energy value of organic laser emission from coronene in methyl-cyclohexane-isopentane at 100 K 03 p0498 A70-12878
- Flash lamp-pumped organic dye scintillator lasers using coaxial Xe-filled lamp, tabulating blue-violet organic liquid lasers characteristics 03 p0499 A70-13161
- Flashlamp pumped coumarin dye laser mode locked by intracavity loss modulation operating in blue region 04 p0703 A70-15622
- Aminocoumarin derivatives and 2-hydroxyquinoline compounds for flash pumped organic lasers 04 p0703 A70-15624
- Flash lamp pumped tunable organic dye laser, using capacitor bank for reliable operation 05 p0861 A70-16845
- Laser emission from organic molecules under neodymium laser harmonics excitation, describing absorption and photochemical inversions effects and emission spectra characteristics 07 p1300 A70-19866
- Dye laser stimulation by pumping with pulsed nitrogen laser line to obtain entire visible spectrum 07 p1301 A70-20016
- Optical pumping energy effects on lasing pulse duration during pulse excitation of alcohol solutions of rhodamine 6G 08 p1511 A70-20522
- Retunable lasers with organic dye dispersive resonators, studying space-angular, spectral and energy emission characteristics 08 p1511 A70-20538
- Pulsed nitrogen gas laser to obtain continuously tunable dye laser action to 3550 Å with output at 3771 Å in UV 08 p1513 A70-21553
- Dye laser tuned to sodium D line used for measuring ionospheric atomic sodium 08 p1492 A70-21757
- Organic dyes investigated for amplification characteristics of Raman emission stimulated by Q switched ruby laser 09 p1694 A70-22134
- Potassium iodide and paratoluidine fluorescent quenching effect on lasing threshold in rhodamine 6G alcohol solutions 09 p1696 A70-22487
- Green light laser using sodium fluorescein pumped by xenon pulse tubes, describing output power spectral characteristics 12 p2246 A70-27316
- Dye laser small signal gain via pumping by UV nitrogen laser 13 p2426 A70-28811
- Flashlamp-excited organic liquid UV lasers 13 p2427 A70-29141
- Organic dye lasers output bandwidth and tunability extension by acidification of solution 19 p3445 A70-37675
- Smooth periodic wavelength retuning in organic dye laser, using neodymium glass laser with YAG for pumping 20 p3642 A70-39742
- Organic laser spectral and energy characteristics, discussing practical operation principles, low generation threshold and harmonic energy 20 p3642 A70-39754
- Flash lamp pumped organic dye laser intensity for dye solutions in contact with different argon-oxygen compositions, noting effect of oxygen partial pressure 21 p3834 A70-40569
- Excited state complexes laser action in coumarin dyes indicated from stimulated fluorescence time dependence 22 p4048 A70-42328
- Rhodamine 6G triplet lifetime under continuous pumping by Ar laser 22 p4050 A70-43225
- Low threshold laser action of Nd-containing chelate in host media consisting of polymethyl methacrylate and organic liquid 23 p4201 A70-44869
- Laser excited atoms quenching by iodine molecules from light pulse induced photodissociation of perfluoropropyl iodide active media 24 p4352 A70-45467
- Amplification factor time dependence of dye lasing under rectangular pumping pulse, noting threshold conditions and burnout time relation to material parameters and resonator 24 p4352 A70-45473
- Nitrogen laser pumped exciplex 4-Methylumbelliferone and rhodamine 6G dye laser amplifier, measuring single pass power gain vs wavelength 24 p4355 A70-46088
- Laser gain coefficient increased via organic compounds addition to rhodamine 6G aqueous solution 24 p4356 A70-46273
- ORGANIC LIQUIDS**
- Organic liquid nucleate pool boiling experiments determining stresses, surface tension, viscosity and gravitation relationships to bubble shape and microlayer formation 01 p0218 A70-11180
- Gas chromatography based on sampling gas-vapor phase at liquid surface for determining volatile oxygen containing compounds in biological media 04 p0646 A70-14580
- Film properties of organic liquids squeezed between two solid flats using order liquid model, discussing applications to boundary layer lubrication 08 p1508 A70-21601
- Interfacial energy and free energy estimation by quasi-continuum approximation for two component water-organic or organic-organic liquid systems 10 p1915 A70-23843
- Fluorocarbon fluid Rankine cycle system utilizing gas turbine exhaust heat for environmental control [SAE PAPER 700160] 11 p1982 A70-25371
- Reciprocating Rankine-cycle engine with organic working fluids, noting piston speed and efficiency [SAE PAPER 700162] 11 p1982 A70-25372
- Propylene carbonate applications in nonaqueous electrolyte batteries, describing impurities identification by gas-liquid chromatographic analysis 12 p2164 A70-27069
- High energy density nonaqueous battery with lithium metal anodes, cupric chloride cathodes and organic aprotic solvent electrolyte [AIAA PAPER 70-530] 13 p2349 A70-29038
- Organic liquid scintillators with high transparency, describing optical and chemical properties 20 p3629 A70-39319
- ORGANIC MATERIALS**
- High resolution mass spectroscopy using AgBr photographic plates as ion detectors for organic chemical problems 07 p1224 A70-18894
- Thermal Analysis - Conference Worcester, Mass., August 1968, Volume 1, Instrumentation, organic materials and polymers 11 p2069 A70-25801
- Chromatographic analysis of organic matter in Pueblito de Allende meteorite 17 p3173 A70-35754
- Rhodamine C chemiluminescent material for atmospheric ozone measurements, describing preparation and luminescence spectrum 19 p3373 A70-37638
- Apollo 11 lunar samples organic carbon content analysis by pyrolysis hydrogen flame ionization detection 21 p3779 A70-41624
- Lunar carbonaceous, organic and organoanionic materials analysis by mass spectroscopy, gas chromatography and various other methods 21 p3780 A70-41633
- High temperature organic resin binders and solid lubricant thermal and oxidative behavior examined by thermogravimetric analysis [ASME PAPER 70-HT-30] 22 p4058 A70-42436
- Liquid crystals as solid state organic material with physical properties of liquid, discussing electro-optical properties and applications 22 p4085 A70-42724
- ORGANIC NITRATES**
NT CELLULOSE NITRATE

ORGANIC PHOSPHORUS COMPOUNDS

Peroxyacetyl nitrate decomposition products under continued and discontinued irradiations determined by IR spectral analysis
22 p3983 A70-42944

ORGANIC PHOSPHORUS COMPOUNDS

Benzoyl cyanide deoxygenation, describing reaction kinetics and products
17 p3041 A70-34750

Carbon dioxide content of dialyzed human hemoglobin measured at specific pressure and varying pH values as function of 2,3 diphosphoglycerate
19 p3364 A70-38367

ORGANIC SEMICONDUCTORS

Organic semiconductor electrodes for electrochemical generators, discussing redox association with ion and electron conductivity in polyanilines
10 p1830 A70-24463

Thermoresistor parameters of organic semiconductor polymers with conjugated bond system, plotting temperature and EV characteristics
20 p3595 A70-38966

ORGANIC SILICON COMPOUNDS

Silicon organic binding materials properties, assessing ethyl silicate-50 perspectives in fabrication of precision castings
08 p1506 A70-21144

Gas-liquid chromatographic separation applied in derivatization chemistry of protein amino acids as N-trimethylsilyl/TMS/ esters
09 p1629 A70-22337

Lunar fines hydrochloric acid hydrolyses examination by gas-liquid chromatography indicating presence of organosiloxanes
21 p3779 A70-41627

ORGANIC SULFUR COMPOUNDS

Sulfur trichloride-Al tetrachloride complex ionic structure from Raman spectra and nuclear quadrupole resonance data
21 p3772 A70-40912

Aromatic polysulfone thermomechanical behavior by torsional braid analysis, discussing structure, synthesis, thermal stability, radiation effects, etc
21 p3783 A70-42134

ORGANISMS

Amino acid stability in pyrolyzed Pleistocene Mercenaria shells, comparing decomposition rates for aqueous solution
03 p0472 A70-13150

Radiation damage recuperation process in living organisms and justified risk dose in prolonged space flights using Blair model
03 p0423 A70-13705

Gravitational effects on organisms - Conference, Warsaw, March 1969
07 p1200 A70-18784

Radiation damage recuperation process in living organisms and justified risk dose in prolonged space flights using Blair model
11 p1985 A70-25505

Acceleration effects on human organisms, describing centrifuge, rocket sleds and catapult simulators
22 p3979 A70-43528

Living organisms physiological death as biological problem, discussing hypotheses, theories and facts
23 p4145 A70-44225

Organism reactions to gravity forces, discussing experimental zero and hyper g simulation studies with frog and nematode eggs
23 p4146 A70-44630

ORGANIZATIONS

NT TEAMS

Aerospace laboratories organization concepts, discussing dependence on product, size, location and technological trends
03 p0612 A70-14313

Earth resources data exploitation, describing potential organizational structures for data handling and various political, economic and technological problems
09 p1793 A70-22859

Integral systems management, discussing application and organizational prerequisites
10 p1970 A70-24595

European company for providing and operating European application satellite systems /EUROSAT/, discussing organization, tasks and financial structure
12 p2335 A70-27469

Quality control role in configuration management, considering quality assurance organization of aircraft manufacturer
14 p2669 A70-31104

Project authority relationship concerning manager authority and influence in five organization models
15 p2828 A70-31571

Management organization of European operational application satellite systems, concerning interurban telecommunication and air traffic control
22 p4127 A70-43502

European Space Research and Technology Center space science department, examining cosmic ray, ionospheric and surface physics divisions
24 p4323 A70-46356

ORGANIZING

Correlations between organizational factors and individual engineer performance, analyzing stability of relationships and time lags in measurement
02 p0246 A70-12378

Machinery for management of Sea Dart missile development using managerial concepts of planning, organizing, commanding, coordinating and controlling
08 p1601 A70-21036

Complex organization-processing system of experimental production, noting work specialization in machine shops
11 p2060 A70-25936

Technology relevance to organizational structure, discussing planning models based on problem solving and performance
23 p4284 A70-43995

ORGANOMETALLIC COMPOUNDS

NT CARBOXYHEMOGLOBIN

NT CHLOROPHYLLS

NT FERROCENES

NT HEMOGLOBIN

NT ORGANIC ALUMINUM COMPOUNDS

NT OXYHEMOGLOBIN

Refractory oxides synthesized using metal alkoxide thermal decomposition, comparing thermophysical properties with conventional ceramics
07 p1320 A70-19891

Fe and Al impurities in bis-ethylbenzene chromium /BEBC/ and in chromium films obtained by thermally induced decomposition of metal organic compound
18 p3297 A70-36463

ESR spectrum of gamma irradiated cycloheptatriene silver perchlorate, indicating free radicals and trapped electrons
19 p3374 A70-38272

Hydrostatic and anisotropic piezoresistance in organometallic crystals, noting iridium and platinum complexes with maximum metal-metal interaction
22 p4086 A70-43021

ORGANS

NT BLADDER

NT ESOPHAGUS

NT KIDNEYS

NT LIVER

NT LUNGS

NT OVARIES

NT PITUITARY GLAND

NT SPLEEN

NT STOMACH

NT TESTES

Corticovisceral interrelations concept, summarizing contributions in form of diagram showing interactions between cortical and nervous activity of organs
01 p0029 A70-11463

Temperature variations in organs of man and animals performing physical work as physiological base of metabolic processes and for daily activity timetable development
04 p0638 A70-15502

White rats parenchymatous organs morphological changes following convulsion-producing exposure to pure hyperbaric oxygen
07 p1207 A70-19503

Vascular and dystrophic disturbances in rat parenchymatous organs in hyperbaric pure oxygen atmospheres, observing increased tissue eosinophilia
07 p1207 A70-19504

White rats parenchymatous organs morphological changes following convulsion-producing exposure to pure hyperbaric oxygen
11 p1987 A70-26102

Intense deceleration effects on mice and rats, including internal organs damage and enzyme activity increase
17 p3025 A70-35132

Respiratory activity of internal organs and skeletal muscles in rats exposed to long term heat and cold
18 p3220 A70-36546

Gravity effects on perinatal organ growth in chicks
24 p4297 A70-45342

ORGUEIL METEORITE

Orgueil C 1 carbonaceous meteorite mineral content, describing pyrrhotite identification by electron microprobe
24 p4411 A70-45792

ORIENTATION

X ray diffraction method to determine degree of orientation of crystallites in extruded graphites
03 p0517 A70-13964

Stiffener inclination effect on pressurized cylinder instability under pure bending
04 p0769 A70-14868

Catalog systems orientation based on major and minor planets observation, discussing zero points corrections
08 p1574 A70-21152

Spacecraft orientation control system optimization by plotting controlled motion kinematic models
13 p2501 A70-28417

Disk elements perpendicular mounting by rotation on vibrating shaft, obtaining orientation by centrifugal force
15 p2733 A70-31580

Optimum fiber orientation for minimum weight boron/epoxy shear panel design
17 p3182 A70-34562

Optimum filament orientation for maximum strength in composite with combined normal and shear stresses
17 p3183 A70-34563

FK4 catalog system equinox and equator point corrections from lunar transit circle observations, discussing validity of moon for orientation
21 p3922 A70-41985

Orientation detectors in human visual cortex, suggesting mutual lateral inhibition
23 p4144 A70-43813

ORIFICE FLOW

Statistical model equations to predict discharge coefficients for concentric orifice plates as function of line size, diameter ratio and Reynolds number
04 p0667 A70-14837

Actively participating bounding surfaces effect on free molecule flow through slit or annular orifice situated in wall separating different pressure regions
04 p0668 A70-14906

Helmholtz resonator associated flow field analysis in nonlinear regime, considering external pressure, mean flow, velocity fluctuations and orifice flow
06 p1038 A70-18065

Orifice effect investigated for sharp flat plate in hypersonic rarefied flow, measuring surface pressure
06 p0982 A70-18366

Pipe orifice conductance for rarefied gas flow measured for specific Knudsen numbers and pressure ratios
06 p1052 A70-18370

Very small diameter laminar flow orifice coefficient calculation as function of Reynolds number
08 p1484 A70-21321

Turbulent jet injection from circular opening into unbounded transverse shear flow, determining velocity distribution along axis
09 p1659 A70-22427

Near-free molecular flow through orifice measured for velocity distribution dependence on Knudsen number and angular position using time-of-flight technique
10 p1918 A70-23969

Flow structure around incurved lateral jet issuing from narrow orifices, determining interaction zone geometry with main current by hot wire technique
10 p1868 A70-24165

Turbine flow meters dynamic calibration employing sinusoidally perturbed orifice flow
12 p2236 A70-28033

Contraction coefficients for compressible discharge through axisymmetric sharp edged orifice, obtaining approximate analytical expression based on one dimensional theory
13 p2389 A70-29549

Jet flow through rectangular orifices in cylindrical wall using conformal mapping for potential, velocity, volume flow rate, viscosity, etc
14 p2567 A70-31359

Hydraulic characteristics of flow through miniature slot orifices for rocket engine injectors, observing stability of effluent liquid streams
16 p2891 A70-33566

Upstream wear of small metal orifices under large pressure drops in phosphate ester hydraulic fluids due to current driven electrochemical corrosion
16 p2919 A70-33629

Kinetic energy correction factor for nonuniform flow at Vena Contracta, using experimental data and modified Bernoulli equation
16 p2892 A70-33639

Shock tube orifice effect on gas flow velocity and pressure drop, using pressure probes and Jenny friction formula
17 p3069 A70-34699

Air jets from sonic orifice, investigating three zones of isochor families by visualization and density measurement
17 p3070 A70-35046

Orifice length-to-diameter ratio effect on spray mixture uniformity from unlike impinging jets
17 p3073 A70-35671

Compressible flow of two component two phase mixtures through convergent nozzles and orifices, determining initially or annular dispersed flow patterns
18 p2329 A70-36231

Knudsen effusion in free molecular flows in supersonic jet during expansion through circular orifice, discussing power and heat transmission
18 p3346 A70-36379

Exhaust plume rarefaction from sonic orifice, considering continuum to transitional behavior for perfect gas
21 p3745 A70-41742

Supersonic air flow interaction with transverse gas jet from plate orifice
21 p3749 A70-42222

Vortices growth in vortex sheets bounding jets flowing from two dimensional slit and circular orifice observed by computer experiments
24 p4327 A70-46244

ORIFICES

At thermofluid pressure corrections in tubes and at orifices for errors in gaseous pressure measurements by temperature gradients
06 p1113 A70-18371

Orifice diameter for low Reynolds number flowmeter dependent on pipeline diameter tolerances
08 p1482 A70-20684

Liquid rocket engine injector elements design criteria, using noncircular orifice geometry to predict efficiency [AIAA PAPER 70-704]
16 p2967 A70-33565

ORIGINS

Free plane turbulent jet virtual origin using tests determining influence of upstream conditions and nozzle shape
04 p0674 A70-15554

ORION CONSTELLATION

Multicolor photometry of Orion flare stars in U, B, V and R, constructing diagrams confirming flare stars scattering about main sequence
03 p0567 A70-13317

Nebular variables and flare stars in Orion aggregate
03 p0567 A70-13319

Psi Orionis light variations, using photoelectric photometry, indicating ellipsoidal variability
03 p0570 A70-13552

Radiative excitation in planetary and Orion nebulae by solving transfer equations for Lyman line and continuum radiation, using normalized on-the-spot [NOS] approximation
04 p0758 A70-15700

Nonstellar 5 micron source in Orion nebula, noting intensity nonvariance and energy distribution calculation of temperature
08 p1575 A70-21375

Sigma Orionis E hydrogen-deficient atmosphere, using grid of constant-flux model atmospheres to determine abundances of five elements
09 p1755 A70-22504

Orion Nebula region search, giving characteristics and locations of flare type variable stars
10 p1949 A70-25249

Model for FU Orion irregular variable to determine turbulent convection characteristics in atmosphere at optical transparency level
11 p2115 A70-26580

Orion Nebula photographed at H alpha line with half angstrom filter
15 p2807 A70-32805

Orion stars far UV intensities, considering photometric data and electronographic spectra from rocket sounding
17 p3160 A70-34882

Orion nebula core radio recombination line intensities, showing variations in mean electron temperatures and physical conditions
18 p3313 A70-36329

Orion arm local structure and kinematics, discussing outward or inward motion to galactic center and component direction
18 p3329 A70-37177

BM Orionis eclipsing binary spectra, determining radial velocity curve
21 p3890 A70-41161

Orion nebula H alpha/forbidden N II ratio measurement using wide field multislit spectrograph
22 p4101 A70-42857

Narrow band IR photometry of star alpha Orion, testing hypothetical correlation of emission peak with starlight-reflecting silicate dust
22 p4105 A70-43229

Hydrogen I region anomalous alpha lines recombination in Orion B spectrum, identifying carbon emitter by measured frequency separation
24 p4410 A70-45773

ORIONID METEOROIDS

Microparticle collection experiments during 1966 Orionid and Leonid meteor showers accomplished by Luster and ALARR /air launched-air recovered rocket/instruments
08 p1575 A70-21393

Upper atmospheric ion composition during Orionid meteor shower activity by rocket-borne RF mass spectrometer
18 p3247 A70-36183

OROGRAPHY

Friction and orography influence on wave motions in real atmosphere, discussing planetary boundary layer and propagation in free atmosphere
09 p1718 A70-23331

Earth orography shape effect on cyclogenetic properties of atmosphere noting mountain height, slope, and mass thermal properties, etc
10 p1913 A70-25196

Atmospheric pressure variations as function of vertical movements caused by friction and orography, considering numerical forecasting
11 p2076 A70-26073

Nonlinear orographic waves in atmosphere, investigating influence of meteorological parameters, temperature jump, incident flow and ridge geometry on flow patterns
12 p2263 A70-27517

Computer plotting of flow patterns and orographic cloud over/in lee wave flow, including rotors, blocking and high level turbulence
12 p2264 A70-27722

Tropical circulation structure and energetics from numerical time integration of global atmospheric model with realistic orography
19 p3462 A70-38257

Nonlinear orographic waves in atmosphere, investigating influence of meteorological parameters, temperature jump, incident flow and ridge geometry on flow patterns
21 p3846 A70-41165

Wind directions in free atmosphere and on ground, discussing deflections by orographical factors in Upper Rhine plain
22 p4065 A70-43245

Orography and friction effects on numerical forecast of atmospheric pressure variation
24 p4370 A70-45112

ORRERIES

U ASTRONOMICAL MODELS

ORTHICONS

NT IMAGE ORTHICONS

ORTHO HYDROGEN

Thermal separation of ortho and para hydrogen and deuterium, discussing kinetic theory of nonspherical molecules in terms of rotational collision numbers
22 p3983 A70-43154

ORTHOGONAL FUNCTIONS

Orthogonal polynomials in three dimensional contact problems without friction, discussing construction of kernels over finite and seminfinite intervals
08 p1594 A70-21634

Book on information transmission by orthogonal functions covering mathematical foundations, direct signal transmission, carrier transmission, statistical variables, etc
09 p1636 A70-23125

Simultaneous singular integral equations approximate solution in orthogonal polynomials
10 p1909 A70-24603

Orthogonal expansion of multivalued functions for weights in threshold function realization
15 p2767 A70-31838

Generalized spectral analysis method implementing orthogonal transformations through Kronecker product representation and matrix factorization
15 p2767 A70-32099

Soviet book on statistical analysis of meteorological elements based on expanding natural orthogonal functions covering horizontal, vertical and time distributions including applications
15 p2772 A70-32842

F 2 region critical frequency diurnal variation forecasting, using series expansion of natural orthogonal components
19 p3409 A70-37327

Geomagnetic Sq variation examination, using field expansion into natural orthogonal component series
23 p4188 A70-44063

ORTHOGONALITY

Orthogonality of aircraft natural vibration modes by calculating complete matrix of generalized masses [DGLR-69-59]
04 p0774 A70-15150

Perturbation effects on elastic material deformation due to nonorthogonality of curves defining curvilinear aeolotropy, with application to circular cylindrical tube
05 p0929 A70-16065

Optical system with orthogonal standing waves in liquid used for two dimensional scanning of laser beam in ultrasonic field
07 p1296 A70-18765

Optical system with orthogonal standing waves in liquid used for two dimensional scanning of laser beam in ultrasonic field
18 p3271 A70-37109

Orthogonality of eigenmodes of aircraft vibrations based on F-104G ground measurements
23 p4274 A70-44766

ORTHOGRAPHY

Universal Automatic Map Compilation Equipment /UNAMACE/ for terrain altitudes determination on uniform and dense grid in stereo model to obtain orthophotographic projection
11 p2051 A70-26042

ORTHONORMAL FUNCTIONS

Trigonometric interpolation of polynomials by Lagrangian type orthonormal functions, noting satellite geodesy applications
10 p1909 A70-24185

Three dimensional elasticity by Ritz method, using coordinate system orthonormalized in energy metric of operator to avoid precision loss
10 p1957 A70-24511

ORTHOPHOTOGRAPHY

Optimum image scale and longitudinal overlap in continuous orthophoto map production regarding

ORTHOTROPIC CYLINDERS

sheet dimensions, instrumental ranges, flight path tolerances and ground relief
13 p2407 A70-29165

ORTHOSTATIC TOLERANCE

Ventilation function, pulse rate and blood pressure measured for adaptation to vertical upright and head-down positions
07 p1201 A70-18794

ECG changes attributed to reduction of blood supply to myocardium during orthostatic tests after prolonged hypokinesia
07 p1209 A70-19513

Statistical analysis of pulmonary ventilation and gas exchange indices during orthostatic tests before and after water immersion
07 p1209 A70-19517

Antigravitation suit effects on rheoencephalography changes during Valsalva maneuver and horizontal-passive orthostatism transition in humans
07 p1212 A70-19738

Human physiological responses to lower body negative pressure /LBNP/, studying presence or absence of change for orthostatic tolerance as function of time
07 p1222 A70-19933

Orthostatic tolerance in humans increased by lower limb muscles electrostimulation, correlating subjective feelings with heart and pulse rate measurements
09 p1615 A70-22089

Orthostatic tilt tolerances in young men and women noting heart rates and blood pressure
09 p1627 A70-23454

Amphetamine, caffeine and securinine effects on hypodynamic syndrome in subjects during orthostatic tests and transverse G-forces under prolonged hypokinesia
10 p1817 A70-24690

Electrocardiac activity, myocardium and hemodynamic disorders in subjects after prolonged hypodynamia with or without physical exercises and during orthostatic test
10 p1817 A70-24692

Cardiovascular reactions and orthostatic stability during hypodynamia determined from ECG, seismocardiograms, phonocardiograms, sphygmograms and tachy-oscillograms
10 p1817 A70-24694

ECG changes attributed to reduction of blood supply to myocardium during orthostatic tests after prolonged hypokinesia
11 p1988 A70-26112

Statistical analysis of pulmonary ventilation and gas exchange indices during orthostatic tests before and after water immersion
11 p1988 A70-26116

Incremental lower body negative pressure as assay method for human orthostatic tolerance
11 p1992 A70-26518

Physiological reactions of humans to orthostatic heat tolerance and natural acclimatization in summer and winter using tilt-table test and bicycle ergometer
12 p2169 A70-27656

Nine-alpha-fluorohydrocortisone preventing bedrest induced orthostatism, considering plasma volume decrease effects on cardiovascular performance
13 p2358 A70-29433

Position dependent variations in intrapericardial, pleural and esophageal pressures and cardiac output in thorax of dogs
13 p2356 A70-29946

Orthostatic tolerance in humans increased by lower limb muscles electrostimulation, correlating subjective feelings with heart and pulse rate measurements
15 p2685 A70-32685

Minnesota Impedance Cardiograph method evaluated by applying to cardiac output measurements in postural stress studies
17 p3031 A70-35431

Orthostatic tolerance increase in animals by application of hyperoxic and hypercapnic gas mixtures
20 p3574 A70-40185

Orthostatic stability reduction in experiments with simulated weightlessness, investigating functional compensation mechanisms
23 p4149 A70-45025

Syncope prevention in orthostatic heat test by inflating cuffs around legs and lower abdomen
24 p4306 A70-45331

ORTHOTROPIC CYLINDERS

Strain rates and stresses relations in plasticity theory for consolidatable orthotropic bodies having three elastic planes of symmetry
02 p0389 A70-12686

Axisymmetric problem analysis for cylindrically anisotropic elastic bodies with restricted orthotropy based on Love-Lekhnitsky stress function generalization
03 p0601 A70-14327

Elasticity theory of orthotropic materials applied to steady rotation of long cylindrical tubes of filament reinforced plastics
03 p0602 A70-14331

Thin orthotropic composite circular cylindrical shells buckling under axial and radial loads, satisfying

end boundary conditions for clamped and simply supported shells
[ASME PAPER 69-WA/APM-21]

04 p0771 A70-14910
Material coupling in two layered orthotropic cylindrical shell subjected to normal external pressure

04 p0778 A70-15547
Thick walled orthotropic cylinder subjected to internal pressure analyzed for stress distribution and creep rates, using constitutive equations and Norton law

07 p1416 A70-20234
End plugs bending moment and shear loads reduction during compression tests of composite orthotropic cylinders

08 p1594 A70-21889
Eccentrically stiffened orthotropic cylinders with intermittently attached stiffeners under bending and axial load, analyzing instability and buckling

13 p2518 A70-29966
Anisotropic axisymmetric elastic shell theory including transverse stress effects, with application to orthotropic cylinder

19 p3545 A70-38337
Stress distribution at hole in orthotropic cylindrical sandwich shell under internal pressure

20 p3734 A70-40440
Orthotropic fiberglass-reinforced plastic cylindrical shell with allowance for material creep, calculating stress-strain state during bending under external pressure

21 p3842 A70-40649

ORTHOTROPIC PLATES

Buckling of orthotropic sandwich plates derived for sixth order governing differential equation by variational theorem

01 p0204 A70-11139
Clamped skew plates of orthotropic material under transverse load analyzed by stationary potential energy method and compared with isotropic case

01 p0205 A70-11140
Strain rates and stresses relations in plasticity theory for consolidatable orthotropic bodies having three elastic planes of symmetry

02 p0389 A70-12686
Frozen stress techniques for photoelastic analysis of orthotropic plate on nonlinear foundation, providing results to compare with future finite element analysis

03 p0480 A70-12952
Stability analysis of orthotropically symmetric strip under uniformly distributed compressive forces applied to shorter ends, deriving critical load formula

03 p0590 A70-13402
Stress-strain relations for rigidly sealed orthotropic planes with finite number of slits

03 p0592 A70-13447
Natural oscillation frequencies lower bounds of orthotropic plates determined as coupled elastic systems

03 p0592 A70-13451
Boundary value problems for orthotropic half plane and infinite orthotropic plane with cuts, considering loads at various points

03 p0593 A70-13497
Shear testing and data reduction based on torsion analysis to obtain elastic shear constants of thin orthotropic Be sheets

04 p0664 A70-15552
Shear wave and plate velocity expressions derived for orthotropic elastic plate with shear coupling, considering propagation direction

07 p1412 A70-19961
Temperature and stress fields in orthotropic plate with partial surface insulation, examining boundary conditions

09 p1777 A70-23078
Bending of homogeneous orthotropic rectangular plate of variable thickness supported on opposite edges, obtaining solution as Fourier series

10 p1955 A70-24083
Thermal stress concentration in constant thickness orthotropic plate with rounded square hole

12 p2323 A70-27338
Glass fiber reinforced thin rectilinear orthotropic plastic plates bending using finite difference method with allowance for creep

12 p2324 A70-27531
Orthotropic plates bending with shallow and sharp fillets, determining normal stresses

12 p2325 A70-27533
Iteration procedures for boundary value problem of orthotropic rectangular plate under bending loads, discussing convergence of procedures

12 p2325 A70-27552
Shear buckling and uniaxial compression dependence on mechanical properties of clamped orthotropic plates, using Ritz method to compute bifurcation type loads

12 p2326 A70-27817
Finite element displacement method for elastoplastic bilinear strain hardening orthotropic plates and shells, comparing initial and tangent stiffness

14 p2660 A70-31136

Clamped orthotropic rectangular sandwich plates bending using approximate solution

14 p2661 A70-31429

Homogeneous orthotropic cantilevered rectangular plate with reinforcing ribs, calculating flutter in supersonic gas flow

18 p3336 A70-36140

Buckling of fiber reinforced composite orthotropic plates

18 p3343 A70-36706

Elastic bending, vibration and buckling of simply supported thick orthotropic rectangular plates and laminates

22 p4116 A70-43205

Transverse bending of orthotropic glass fiber reinforced plastic plates under uniformly distributed loads

22 p4120 A70-43720

Elastic orthotropic plates vibration analysis by finite strip method via eigenvalue matrix, obtaining natural frequencies and modal vectors by small computer

24 p4423 A70-45579

ORTHOTROPIC SHELLS

NT CYLINDRICAL SHELLS

Natural oscillation frequencies of closed circular orthotropic cylindrical shells having freely supported end faces, particularly with stringers

01 p0210 A70-11413

Strain rates and stresses relations in plasticity theory for consolidatable orthotropic bodies having three elastic planes of symmetry

02 p0389 A70-12686

Orthotropic cylindrical shell with initial deflection under long term effect of external hydrostatic pressure, solving bending problem

02 p0390 A70-12809

Elastic orthotropic fiberglass reinforced plastic shells stability under axial compression, analyzing shear modulus influence

04 p0712 A70-14490

Orthotropic axially compressed conical shell stability, evaluating lower critical load and postbuckling state

04 p0772 A70-14921

Orthotropic sandwich cylinders buckling under axial compression, presenting linear theory approximate design equations

04 p0776 A70-15381

Heated isotropic shallow shells results extended to solving nonlinear problem in bending theory of orthotropic shallow shells clamped, heated and under pressure

05 p0927 A70-15993

Geometrically linear anisotropic shell deformation under transverse shear applied to stability analysis of orthotropic shells of revolution sustaining axisymmetric stresses

05 p0933 A70-16212

Stress-strain state of circular orthotropic shells under bending, considering distributed loads applied to shell center

05 p0934 A70-16217

Stability analysis of deflected shallow thin walled elastic noncircular conical and cylindrical orthotropic shells using straight lines method

06 p1167 A70-17865

Shallow orthotropic shell of rectangular planform with edges under dynamic load, studying forced vibrations by anisotropic shell theory

07 p1403 A70-19057

Natural vibration frequencies and mode shapes for laminated orthotropic shells of revolution using finite element method

07 p1411 A70-19951

Multilayer orthotropic conical shell cyclic deformation equation obtained in hypergeometric functions

09 p1777 A70-23079

Axisymmetric free vibrations of orthotropic cylindrical shell loaded on ends by constant axial force, investigating nonlinear elasticity

09 p1785 A70-23625

Solutions existence for nonlinear partial differential equations describing orthotropic and nonlinear shallow shells under loads and temperature effects

10 p1954 A70-24019

Finite deformations of flexible inelastic orthotropic shells of revolution for generalized plastic flow and deformation theories

10 p1955 A70-24079

Truncated, structurally orthotropic and round conical shell oscillations taking into account reinforcing ribs eccentricity

10 p1964 A70-25195

Clamping edges effect on critical parameters of cylindrical orthotropic shell under axial compression using undetermined Lagrange multipliers

11 p2130 A70-25567

Transient bending and shear stresses at clamped support of orthotropic circular cylindrical shells

11 p2135 A70-25985

Stability analysis of ring-stiffened orthotropic, multilayered shells of revolution under axisymmetric torsionless loads by digital computer

12 p2320 A70-27143

Pressurized orthotropic cylindrical membrane shells free and forced vibration, considering dynamic response dependence on internal pressure

12 p2326 A70-27815

Strain induced in laminated orthotropic fiberglass plastic cylindrical shell by normal concentrated load, using equations free from rectilinear normals hypothesis

12 p2328 A70-28279

Linear compressive orthotropic stability theory for shallow-stiffened cylinders

13 p2518 A70-30022

Finite element displacement method for elastoplastic bilinear strain hardening orthotropic plates and shells, comparing initial and tangent stiffness

14 p2660 A70-31136

Composite orthotropic cylindrical shells linear thermoelastic equations solution for fixed end boundary conditions, noting heterogeneity effects on stress distribution

17 p3184 A70-34909

Long orthotropic pressurized circular cylindrical shell under radial line loads along equally spaced generators, analyzing stresses and deflections by linearization

19 p3545 A70-38338

Structurally closed orthotropic circular cylindrical reinforced shell stability, developing approximate method to obtain various boundary conditions

20 p3727 A70-39886

Orthotropic shells under arbitrary loads, deriving approximation equations

20 p3734 A70-40436

Circular cylindrical orthotropic fiberglass-reinforced shell buckling under longitudinal impact, assuming initial surface imperfections

22 p4117 A70-43347

Curved element approximation of orthotropic axisymmetric thin shells under axial loads

24 p4419 A70-45152

ORTHOTROPISM

Constitutive equations for orthotropic bilinear elastic materials in plane stress case, discussing unidirectional composites

03 p0587 A70-13127

Book on analysis of laminated composite structures covering orthotropic materials stress-strain relations, laminated composite shells, plates, beams and columns

05 p0938 A70-16467

Deformation theory for small elastic-plastic strains in orthotropic material and discretization and iterative solution techniques

11 p2144 A70-26684

Strength conditions for orthotropic Hooke law materials with complex elasticity, giving elastic potential boundary values in tensor form

12 p2325 A70-27560

Orthotropic fiberglass reinforced plastic deformation during stretching with allowance for binder breakdown in transverse layer

12 p2259 A70-28283

Nonlinear electromagnetic constitutive equations with coupling to thermal gradients for holohedral and hemihedral materials, extending analysis to orthotropic media

19 p3552 A70-37786

Yield condition and Bauschinger effect in transition conditions for isotropic and orthotropic bodies

19 p3542 A70-38061

Equations of state in quadratic viscoelasticity for orthotropic media, deriving tensors of creep and relaxation centers

22 p4119 A70-43711

Incremental complementary energy method of stress analysis of orthotropic nonlinear materials having different behavior in tension and compression [AIAA PAPER 69-119]

23 p4270 A70-44563

OSCILLATING CYLINDERS

Natural oscillation frequencies of partially liquid-filled cylindrical shells determined by resonance method

03 p0592 A70-13444

Stationary and vibrating circular cylinders for boundary layer separation point, determining vortex excited oscillation range

04 p0670 A70-14988

Periodic drag of vibrating cylinders as function of excitation amplitude and frequency, noting similarity to nonlinear oscillator subjected to forced vibration

04 p0691 A70-15148

Interaction of infinite shallow draft cylinder oscillating at free surface with train of oblique waves

04 p0618 A70-15321

Transverse oscillation periods of cylinder containing flowing fluid obtained by solving nonlinear partial differential equations describing transverse and longitudinal motion

08 p1592 A70-21480

Acoustic radiation produced in response to harmonically oscillating circular cylinder rotating in viscous fluid solved within Lighthill-Curle formalism for aerodynamically generated sound

09 p1726 A70-22391

Oscillating infinite cylinder as acoustic waves source in homogeneous viscous medium, deriving scalar and vector potentials 12 p2274 A70-28240

Unsteady aerodynamic forces on oscillating circular cylinder, using wind tunnel two dimensional dynamic model 14 p2529 A70-31050

Unsteady flow and heat transfer in viscous incompressible fluid due to infinite porous cylinder oscillations about axis with suction at surface 19 p3406 A70-38445

Two dimensional boundary layer growth with suction for oscillating circular cylinder, considering stream functions and phase angles 24 p4326 A70-46002

OSCILLATING FLOW

Inviscid surface pressures calculated on slender wedges and cones at low frequencies and large oscillation amplitudes in hypersonic flow 01 p0003 A70-10854

Pulsation frequency affecting boundary layer separation from channel wall in incompressible fluid flow calculated by equation 03 p0466 A70-13399

Incompressible viscous fluid rectilinear flow along arbitrary cross section duct under pressure gradients oscillating at large frequencies 03 p0468 A70-14147

Pulsatile flows in living animals and model arteries, discussing flow profiles, instability and wall shear 03 p0430 A70-14244

Instantaneous heat transfer from oscillating wire in free convection in still air as function of time [ASME PAPER 69-WA/HT-15] 04 p0783 A70-14819

Inviscid flow through staggered airfoil cascades in oscillatory and distorted flow simulating axial flow compressor [AIAA PAPER 70-131] 06 p0969 A70-18049

Supersonic wind tunnel flow discontinuities effect on oscillatory pressures 07 p1257 A70-19338

Oscillations of highly viscous incompressible fluid in partially filled cavity of body moving about fixed point, solving Navier-Stokes equations by asymptotic method 08 p1485 A70-21632

Natural oscillation frequencies of subsonic gas flow past plate array, solving eigenvalue problem by splicing method 09 p1603 A70-22117

Nonlinear equations for large fluid oscillations in axisymmetric rotating cavities with radial partitions 09 p1660 A70-22438

Gas flow from nozzle into duct with enlarged cross section investigated for flow pattern and boundary conditions, noting oscillation behavior 10 p1799 A70-24123

Plane Couette oscillating flow stability to small disturbances under composed unsteady velocity at high Reynolds number 10 p1868 A70-24197

Viscous incompressible flows nonlinear stability theory, considering perturbed flows tending toward stationary or flow periodic in time [ONERA-TP-802] 10 p1869 A70-24542

Time dependent analysis for quasi one dimensional, vibrational and chemical nonequilibrium nozzle flows approaching steady state solution by finite difference technique 11 p1976 A70-25974

Three dimensional periodic boundary layer flow noting successive approximations method, noting steady streaming in first order cross flow 11 p2037 A70-26296

Aerodynamic loadings on planar wings in oscillatory subsonic flow determined by collocation for performing Gaussian quadrature integration of pressure and kernel functions 12 p2155 A70-27102

Incompressible two dimensional and axisymmetric oscillating laminar boundary layer flows approximated by momentum integral equation, discussing flow along flat plate 12 p2158 A70-28205

Free convection flow and heat transfer from semi-finite horizontal flat plate with time-oscillating temperature, using successive approximations process 13 p2522 A70-29537

Oscillatory flow in porous channel with suction and injection, using Laplace transform technique 13 p2389 A70-29538

Interfacial and free surface mode instabilities of time periodic flows of viscosity and density stratified fluids at various Froude numbers 14 p2566 A70-31026

LF oscillatory convection characteristics in polytropic atmosphere in strong magnetic field based on sunspot theory 15 p2802 A70-32487

Admittance calibration of short HF through flow pneumatic lines, using hot-wire anemometer [ASME PAPER 70-FE-10] 16 p2891 A70-33628

Compression and expansion characteristics of steady supersonic flow passing along yawing slender body of rotation, linearizing differential equations 18 p3207 A70-36382

WKB method for asymptotic oscillatory solutions of nonlinear equations of relativistic fluid mechanics 19 p3403 A70-37587

Unsteady incompressible planar gas jets with stable vortex street, investigating near flow field region to establish oscillatory component 19 p3404 A70-37799

Boundary layer oscillatory flow interaction with nonuniformly rotating lamina, calculating velocity distribution and transitional frequencies 19 p3406 A70-38443

Sound field produced in uniform moving ideal fluid stream by nonuniform oscillating elastic wall 19 p3353 A70-38657

Oscillatory flow in turbulent boundary layer modeled by eddy viscosity distribution, deriving mass transport velocity induced by progressive and standing waves 20 p3608 A70-39358

Wedge angle large amplitude slow oscillations in hypersonic and supersonic flows, examining attached bow shock 20 p3559 A70-40288

Elastoviscous incompressible electrically conducting oscillating free stream flow along infinite porous plate with suction in transverse magnetic field 20 p3685 A70-40508

Resonance tube fluid dynamics, examining oscillation start and growth by wave diagram and gas-speed/sound-speed diagram 21 p3807 A70-41244

Rectangular wing with oscillating control surface, measuring induced unsteady pressure field for comparison with computations based on lifting surface theory 21 p3935 A70-41407

Maxwellian fluid oscillating flow in thin walled elastic circular tube as function of tube dimensions, elastic properties, oscillation frequency, etc 21 p3810 A70-41963

Forced harmonic vibrations of clamped circular plate in inviscid fluid, calculating radiation pressure and power distributions 22 p4073 A70-42646

Thermal boundary layer near stagnation point in three dimensional fluctuating incompressible flow, using Lighthill method 22 p4124 A70-42685

Time-mean velocity and skin friction of laminar boundary layer near two dimensional stagnation point with oscillating oncoming flow 22 p4010 A70-42686

Expiratory gas flow oscillations during forced vital capacity maneuvers in atmospheres of various composition and pressure 22 p3981 A70-43702

Thermal-acoustic oscillations in forced convection, giving time delay analog for perturbation feedback 23 p4280 A70-44369

Cryogenic fluid heat exchanger flow oscillation automatic feedback control, discussing design and simulation 23 p4280 A70-44370

Oscillatory flow measurements by directionally sensitive laser velocimeter, discussing concept, design and construction 23 p4197 A70-44473

Oscillating viscous conducting fluid laminar flow between parallel nonconducting infinite porous flat plates under suction in transverse magnetic field 24 p4383 A70-45146

OSCILLATION DAMPERS

Single degree of freedom nutation damper motion instability on dual spin stabilized spacecraft ascribed to parametric excitation by transverse angular rates 04 p0764 A70-15585

Liquid filled dampers for nutation damping of spacecraft with momentum wheel for attitude stabilization 06 p1154 A70-17163

Cross coupled rotational motions of free solid body carrying nutation-damping pendulums 07 p1335 A70-19808

Active and passive geomagnetic rate dampers for attitude control systems of geomagnetically, gravitationally or spin stabilized spacecraft 09 p1766 A70-22936

Dual spin satellite stability with four mass nutation damper 12 p2314 A70-27842

Nutation damper for dual-spin spacecraft, considering various two degree of freedom systems with two natural frequencies 14 p2655 A70-31367

Motion and stability characteristics of dual spin satellite system with pendulous type nutation dampers, noting mass unbalance effect [AIAA PAPER 69-857] 15 p2812 A70-32508

Book on passive gravity gradient libration dampers covering design, flight experience, evaluation criteria, performance monitoring, failure prevention, etc 16 p2983 A70-33954

Spacecraft gravity gradient stabilization by damping out oscillatory motions by energy dissipation, using combined eddy current and hysteresis dampers / Combination Passive Damper/ 16 p2985 A70-34133

Ball in tube nutation damper for spinning satellite, describing design, testing and fabrication techniques for achieving low friction level 16 p2985 A70-34136

Dynamic behavior of eccentric annular mercury nutation damper, using variational principle of least viscous frictional power loss 17 p3023 A70-34770

Surface oscillations energy and attenuation in damped spectral region of semibounded degenerate electron plasma 18 p3293 A70-36143

High speed and long life bearings and dampers for future jet engines, considering design factors [SAE PAPER 700318] 18 p3263 A70-36800

Gravitational effects on impact damper performance, discussing dynamic stability and kinematically viable periodic motion and resonant conditions 20 p3717 A70-38975

Variable parameter nutation damper SAS-A dual spin satellite, discussing design and expected in-flight performance by digital simulation [AIAA PAPER 70-972] 20 p3669 A70-39557

Aircraft vertical gyro with hydraulic damping device, calculating ballistic deviations limitation conditions 20 p3632 A70-39733

Magnetic damper motions in rapidly spinning satellite 21 p3927 A70-40833

Dual spin bodies stability, controlling nutation by passive damper fitted to despun platform 22 p4110 A70-42486

Electronic damped plasma oscillations eigenfrequency in presence of external electric field 22 p4082 A70-43253

Sliding mass and damper boom damping mechanisms for gravity-oriented satellites, using method of characteristic roots coalescence 22 p4110 A70-43436

Automatic control systems small oscillations suppression by nonlinear correcting elements 22 p4005 A70-43564

Large amplitude high phase velocity oscillations anomalous damping in electron-ion plasma resulting from MHD instability 24 p4387 A70-46091

OSCILLATIONS

NT ELECTRON OSCILLATIONS

NT H WAVES

NT HARMONIC OSCILLATION

NT HYDROFOIL OSCILLATIONS

NT MOLECULAR OSCILLATIONS

NT NONSTABILIZED OSCILLATION

NT PLASMA OSCILLATIONS

NT PRESSURE OSCILLATIONS

NT SELF OSCILLATION

NT STABLE OSCILLATIONS

NT TRANSIENT OSCILLATIONS

NT TRANSVERSE OSCILLATION

NT UNDAMPED OSCILLATIONS

NT WING OSCILLATIONS

Mathematical pendulum oscillations under clockwise and counterclockwise impact impulse, deriving differential equations describing trajectories 01 p0141 A70-10153

Soviet book on oscillations of quasi-linear time lag systems, emphasizing asymptotic methods in nonlinear oscillation theory 02 p0340 A70-12826

Random function theory for determining influence of system oscillation characteristics on load distribution 02 p0324 A70-12852

Liquid film stability relation to angle of attack oscillations during reentry body deceleration 03 p0406 A70-12939

Nonlinear systems periodic oscillations with resonance from differential equations solutions 04 p0720 A70-15258

Earth bow shock and magnetopause oscillatory motions with respect to positions assumed under quiet solar wind conditions, discussing satellite observations 05 p0840 A70-16586

Illusions of rotation perception with oscillating trapezoid and oscillation perception with rotating trapezoid, correlating magnitudes 05 p0807 A70-16673

Resonant oscillations of coupled physical pendulums, investigating phase trajectories by Struble method 08 p1544 A70-20964

Radiative relaxations of chromospheric oscillations generated by granule, assuming isothermal atmosphere and linearizing equations of motion 08 p1576 A70-21395

Human biological organism analysis based on physiological determination of regulating and control functions dependence on oscillatory properties 08 p1452 A70-21460

Plane double front detonation wave attenuation by pursuing rarefaction waves, analyzing oscillations, onset mechanism and stability during transition to Chapman-Jouguet mode 08 p1485 A70-21633

Oscillatory transverse and longitudinal magnetostriiction in single crystal Bi, obtaining deformation potentials 08 p1557 A70-21838

Magnetothermal oscillations in pressure-annealed pyrolytic graphite, relating period with angle between magnetic field and crystal c axis 08 p1557 A70-21839

Relaxational oscillations produced by interaction between rarefaction wave in external two dimensional supersonic flow and turbulent near wake 09 p1603 A70-22426

Nonlinear periodic oscillations problem solved by solving nonlinear operator equations, discussing iterative methods based on equations linearization 09 p1728 A70-22668

Si avalanche diodes oscillations external current waveform measurement using coaxial current monitoring assembly with negligible phase error 10 p1849 A70-24234

Hertzian differential polarimeter-clipsonometer with single detector designed for multiwave oscillations analysis 10 p1888 A70-24477

Oscillations of longitudinal magnetostriction in silver and copper single crystals at low temperature 11 p2098 A70-25619

Initial parameter conditions influence on sustained unstable oscillations of attitude control system for large space vehicle, calculating stable region by nonlinear method 11 p2124 A70-26149

Nonlinear control systems on-off oscillations with instants of commutation determined by simultaneous equations, noting feedback control 11 p2027 A70-26254

Hydraulic piston-valve-type slave mechanism oscillations with rigid feedback and inertial load at actuated shaft, using harmonic linearization method 12 p2167 A70-28340

Limit cycle oscillations in satellite attitude control system, producing control moment by pulse modulated controller 13 p2502 A70-28430

Soviet book on theory of oscillations of linear and nonlinear time lag systems 13 p2450 A70-28699

Oscillatory perturbed motion of elastic body in general relativity space time, discussing energy tensor, unitary speed vector and density 13 p2451 A70-28954

Multiple period oscillations in nonlinear systems, using nonautonomous differential equations and Hammerstein operator 13 p2443 A70-29745

GaAs junction lasers output oscillations, analyzing time dependent equations for low temperatures 14 p2593 A70-30335

Oscillations and stability of rotating masses for axisymmetric equilibrium configurations with toroidal magnetic field based on virial equations 14 p2642 A70-30886

GaAs Gunn devices oscillatory modes under various operating conditions 14 p2557 A70-31158

Monograph on nonlinear oscillation equations resonance solutions and solution stability, considering Green matrix, differential equations reduction to integrodifferential equations, etc 14 p2618 A70-31417

CW oscillation in carbon monoxide chemical laser 15 p2748 A70-31432

Semiconducting gallium arsenide LF oscillations, considering domain behavior and illumination effects 15 p2783 A70-31972

Difference schemes approximating boundary value problem for heat conductivity and oscillation equations, considering brute force method stability 16 p2951 A70-33245

Oscillatory and wave processes in nonlinear distributed systems by asymptotic method analogous to Bogoliubov concentrated systems 16 p2951 A70-33252

Pisarenko generalized equations for hysteresis loop contour applied to oscillations of one degree of freedom system 17 p3137 A70-35710

Current oscillations of GaAs Gunn diodes over wide voltage range, discussing diode behavior dependence on polarity and applied voltage 18 p3230 A70-36197

Oscillations of rigidly clamped elastic liquid filled hemispherical shell with gas bubble 18 p3242 A70-36583

Large scale galactic oscillations, discussing observational evidence and theoretical modal calculations 18 p3330 A70-37191

Algorithm for steady state oscillations in irregular waveguide structures with conducting walls 19 p3470 A70-37427

Quasi-static thickness-shear approximation of radiation of electromagnetic energy accompanying oscillation of piezoelectric crystal plates 19 p3487 A70-37945

Oscillations of nearly nonlinear systems with conditions for main amplitude equations 19 p3472 A70-38726

Resonant oscillations of coupled physical pendulums, investigating phase trajectories by Struble method 20 p3672 A70-39386

Quasi-periodic ionospheric oscillations associated with nuclear explosions, thunderstorms and quiet conditions 21 p3814 A70-40938

Vertical oscillations in solar temperature minimum suggested as acoustic-gravity waves modes dependent on height at chromosphere-corona interface 21 p3926 A70-42196

Thermally induced oscillations and negative resistance in seminsulating oxygen-doped GaAs double injection devices via heating beyond critical temperature 22 p4084 A70-42326

Striations due to mechanical oscillations in fast wire explosions, using dispersion for elastic waves in solid cylinders 22 p4074 A70-43002

Low gravity fuel sloshing in axisymmetric rigid tank, calculating oscillations by modified Galerkin method 24 p4324 A70-45292

Hough eigenfunctions of lunar diurnal and semidiurnal atmospheric oscillations using matrix and group methods 24 p4328 A70-45351

OSCILLATORS

NT AUTODYNES
NT CRYSTAL OSCILLATORS
NT GYROSCOPIC PENDULUMS
NT HARMONIC OSCILLATORS
NT MECHANICAL OSCILLATORS
NT MICROWAVE OSCILLATORS
NT MOLECULAR OSCILLATORS
NT PENDULUMS
NT RELAXATION OSCILLATORS
NT SYNCHRONIZED OSCILLATORS
NT VACUUM TUBE OSCILLATORS

Delay times elimination in pulse operated X band Gunn effect oscillators, using RF power injection 01 p0050 A70-10463

Microwave circuit for increasing Gunn oscillators injection locking capabilities and reducing FM resulting from bias-voltage fluctuations 01 p0050 A70-10783

Self excited oscillators zero crossing times distribution for Markov process formulated as boundary value problem involving Kolmogoroff backward equation 01 p0143 A70-10891

Random vibration of interconnected systems, analyzing power flow and energy levels in linear oscillator interacting with environments, using Thevenin-Norton representations 01 p0207 A70-11161

He isoelectronic sequence 3d-nf transitions, determining UV wavelengths and oscillator strengths 04 p0739 A70-14601

Equivalent circuit for acoustoelectric oscillator providing practical device analog, discussing oscillation suppression and resonant frequency changes under reactive load 04 p0656 A70-14719

Fluidic oscillator use as volume flowmeter, discussing effects of setback, aspect ratio, splitter distance and feedback location on oscillation frequency [ASME PAPER 69-WA/FM-3] 04 p0688 A70-14840

Fluid oscillators for sensing and missile control, discussing performance, design, frequency variation and applications [ASME PAPER 69-WA/FLCS-8] 04 p0626 A70-14845

Kinetic, potential and dissipative energies computed in systems of randomly excited coupled oscillators, using Liapunov stability method 05 p0821 A70-16407

Phase, frequency and amplitude fluctuations in avalanche diode oscillators, studying noise origin 05 p0823 A70-16883

Inertial parameters and functions of dissipative and restoring forces in quasi-linear oscillatory system determined from free motion characteristics 05 p0884 A70-16951

Analytical expressions for amplitude and frequency modulation characteristics of bias modulated tunnel diode oscillator on steady state mode 06 p1022 A70-17836

Equivalent scheme for tunnel diode oscillator operating mode and parameters effect on LF modulating signal phase correlations 07 p1241 A70-19287

CW high power operation of transferred-electron oscillators realized by low thermal resistance, describing fabrication 07 p1241 A70-19300

Millimeter wave CW Gunn oscillators construction by packaging free from spurious resonance, using sapphire ring and Au cap 08 p1468 A70-20482

Wideband tunable CW Gunn effect oscillator design, discussing microwave circuit effects on performance 08 p1471 A70-20788

Ti I spectrum oscillator strengths, determining formula for relative-absolute values transition 08 p1569 A70-20832

TRAPATT oscillator circuit characteristics determined from measurements and equivalent circuit calculations 08 p1475 A70-21277

Microstrip oscillator circuit design for operating with high power/efficiency avalanche diodes, describing low pass filter tuning section role 08 p1475 A70-21278

Circuit allowing direct combining of power from several avalanche diodes, discussing CW power output, single and multiple diode oscillators, etc 08 p1477 A70-21295

Oscillator strengths of Fe II lines and solar iron abundance measured by arc burning in Ar with iron chloride admixture 08 p1576 A70-21398

Monograph on normal frequency generator serving devices measuring differential Doppler effect, discussing generator design for ionospheric research satellites frequencies 09 p1645 A70-22531

Ferrimagnetically tunable transistor oscillator in common collector configuration 09 p1645 A70-22603

X band Gunn oscillators amplitude modulation by pulse signals from another Gunn diode 09 p1646 A70-22707

Fabrication effects on current instability during injection and breakdown of p-n junctions in GaAs oscillators 09 p1740 A70-23351

Amplifier properties and oscillator mode structure of multipath carbon dioxide laser 09 p1699 A70-23538

Book on lasers, light amplifiers and oscillators covering optical resonators, optical pumping, pulsed lasers, etc 09 p1700 A70-23541

Born approximation used in calculating wave functions of helium atom for determining generalized oscillator strengths in first ionized continuum of helium 10 p1919 A70-24072

Gunn oscillator current noise correlation with frequency modulation noise 10 p1848 A70-24230

Oscillator strengths relative values determined from flame atom absorption line sensitivity measurements 10 p1828 A70-24259

Signal frequency capture probability vs frequency search rates and AFC loop parameters determined in phase locked oscillator 11 p1996 A70-25349

Forced oscillations of oscillator matched to transistor as active element, obtaining stability conditions by Liapunov first method 11 p2018 A70-25945

Maxima increases without limit in damped linear oscillator response to random wideband excitation interpreted by heuristic explanation 11 p2085 A70-26694

Temperature effects on width of current-voltage characteristics of GaAs Gunn oscillators 11 p2020 A70-26819

Dynamic behavior and moments of oscillatory systems under steady perturbations using linear differential equations 12 p2261 A70-27555

Gunn oscillator voltage supply influence on domain capacity, considering frequency stability 13 p2377 A70-29302

Self excited cavity oscillators with tunnel and parametric diodes and nonequilibrium medium, noting single and multimodes, energy capabilities and frequency interactions 13 p2366 A70-29405

Oscillators frequency instability and spectral purity relations [ONERA-TP-829] 13 p2383 A70-29637

Frequency synchronization of far spaced high stability oscillators with aid of meteor trails, discussing signal retranalysis and duplex methods 14 p2636 A70-30321

HF backward wave oscillators with emphasis on limiting factors in millimeter waves generation, discussing ohmic and circuit imperfection losses 14 p2555 A70-30430

Bulk n-type InP single crystal transferred- electron oscillators, investigating current instabilities 14 p2556 A70-30686

Equivalent linearization for random vibration, considering stationary statistics of bilinear hysteretic one degree of freedom oscillator response 14 p2661 A70-31428

Matrix analysis of discretized dynamical system with constraints, considering case of damped oscillators 15 p2774 A70-31697

Voltage-frequency conversion technique using FM principle and RF oscillator beating with crystal oscillator output 15 p2705 A70-32705

Frequency instability of oscillator perturbed by internal thermal noise [ONERA-TP-838] 16 p2872 A70-33105

Univibrator analysis with glow discharge thyatrons, increasing time lag for equal R and C values 16 p2873 A70-33237

Self excited systems limiting states with traveling wave, analyzing oscillator moving along string under tension 16 p2990 A70-33781

Fluidic oscillator molecular weight of flowing mono- and polyatomic gases, discussing frequency dependence on pressure drop and temperature 17 p3081 A70-34515

Hysteresis effects during retuning of n-type GaAs Gunn oscillator with bias source and LCR circuit, showing range of domain damping by low field 17 p3055 A70-35689

Equivalent radioelectric plan of ammoniac maser marginal type oscillator 18 p3265 A70-35946

Equivalent circuit of Gunn oscillators for quenched domain mode operation, noting optimal working conditions 18 p3229 A70-36668

Giant pulses in passively Q switched laser oscillator, calculating time constant of light flux exponential increase 18 p3270 A70-36953

Random vibration first threshold crossing probability density function for linear oscillator 19 p3427 A70-38038

Axiomatic approach to homeostasis, discussing living systems as oscillators with input-output and transit variables in duration and elongation 19 p3365 A70-38411

Matrix condenser for tuning hybrid thin film self excited quartz oscillator with common base transistor configuration, discussing electrical properties and fabrication 20 p3597 A70-39257

Transistorized quartz oscillators, testing frequency and amplitude stabilities and functions of input and output capacitances, supply voltage and feedback 20 p3597 A70-39258

Voltage programmed RF oscillator (VPO) for spaceborne quadrupole mass spectrometer, describing transistorized circuitry 20 p3630 A70-39487

Signal frequency capture probability vs frequency search rates and AFC loop parameters determined in phase locked oscillator 20 p3589 A70-40461

Magnetic field-independent optically pumped Rb 85 maser oscillator power output 22 p4049 A70-42334

Parametric phenomena in oscillatory system with unlimited number of degrees of freedom, illustrating segment of long line loaded at one end 22 p3995 A70-42395

Fluidic oscillators frequency stability evaluation, noting analog circuits superiority over digital [ASME PAPER 70-FLCS-20] 22 p3963 A70-42407

Gunn diode oscillators in domain suppression mode, showing dynamic I-V curve shape relationship to donor concentration and crystal thickness 22 p3997 A70-43128

Frequency dependence of Gunn oscillator maximum negative conductance 23 p4172 A70-44198

Stable clock precision timing systems, discussing quartz crystal, rubidium, cesium and hydrogen oscillators 23 p4195 A70-44289

Temperature effects on width of current-voltage characteristics of GaAs Gunn oscillators 24 p4318 A70-45191

Jet interaction type proportional fluid amplifier as feedback oscillators, measuring frequency response 24 p4292 A70-45291

OSCILLOGRAMS

U OSCILLOGRAPHS

OSCILLOGRAPHS

Pulse characteristics of scintillator-photomultiplier-cathode ray tube channel for oscillographic recording

of nanosecond pulses from neutron, gamma or X ray sources 08 p1496 A70-21218

OSCILLOSCOPES

General purpose automatic test system (GPATS) for electronic equipment fault location, discussing software and hardware for integrating programmable oscilloscope 08 p1470 A70-20656

Optically bistable crystal applications, discussing photochromaticity, catochromatic tubes, oscilloscopes, computer storage devices and laser systems 19 p3446 A70-37860

Oscilloscope polar coordinate displays for multidimensional analog signals, noting human detection capability 21 p3823 A70-40853

Adaptive AC null detector with tuned compression amplifier used for oscilloscope display drive 21 p3828 A70-41469

Oscilloscope design involving optimum bandwidth and input sensitivity, reference measurement and second time base 22 p3996 A70-42820

OSCULATIONS

U DOUBLE CUSPS

OSCULATORY INTERPOLATION

U ORBIT CALCULATION

U ORBIT PERTURBATION

OSEEN APPROXIMATION

Hydrodynamic fields of revolution around sphere in unbounded fluid governed by Oseen equation, emphasizing streamlines and attached vortex 05 p0832 A70-16157

Plane flow of electrically conducting fluids around oscillating plate, using equations linearized by Oseen method 09 p1734 A70-22316

OSMOSIS

Food ingestion initiation, investigating role of hyposmotic solutions from observation of rats under water deprivation 13 p2353 A70-29495

Turtle bladder walls osmotic properties, discussing transmembrane water flow transient acceleration by sodium transport inhibition 21 p3762 A70-41223

OSMOTIC PRESSURE

U OSMOSIS

OSO

NT OSO-B

NT OSO-1

NT OSO-3

NT OSO-4

OSO 1-6 spacecraft design, payloads and performance for continuous solar observation, discussing instrumentation and Delta launch vehicle characteristics 14 p2638 A70-30691

Orbiting solar telescope design for solar disturbances location and monitoring in H alpha line 16 p2907 A70-33188

OSO-B

Nighttime lightning activity observations by orbiting solar satellite OSO-B, determining thunderstorms positions by optical radiation detection 20 p3623 A70-39978

OSO-1

EUV solar spectrometer in orbiting solar observatory (OSO-1), describing satellite, optics and detector, data coding, etc 15 p2736 A70-32027

OSO-3

High energy gamma ray flux enhancement towards galactic plane from OSO-3 particle telescope observations 19 p3501 A70-38089

OSO-4

X ray bursts rise and fall observed by spectrometer onboard OSO-4 15 p2792 A70-31670

OTOLITH ORGANS

Cerebello-otolith system represented by axons of Purkinje cells, studying inhibitory vestibular efferent system relation to cerebellum in frog 01 p0014 A70-10352

Vestibular sensing system role in providing information concerning vertical, linear and angular head movements to central organs 02 p0246 A70-12191

Motion sickness causes and prevention during prolonged space flights, discussing vestibular system and characteristics of visual-inertial and canal-otolith incongruities 03 p0421 A70-13542

Vestibular analyzer and otolith apparatus disturbances and normalization under prolonged hypodynamia, noting pathological effects of repeated caloric testing 10 p1816 A70-24686

Mammalian utricle macula design, considering microelectrode data and information from light and electron microscopy, behavioral experiments and computer simulation 11 p1988 A70-26231

Semicircular canals-otoliths interactions for antagonistic and synergistic information 22 p3976 A70-43704

Spatial disorientation of human subjects in centrifuge, examining otolith role in reorientation and eye sensory mechanisms 22 p3976 A70-43707

OTOLOGY

Otoneurology - Conference, Basel, 1969 14 p2538 A70-30908

OUTER PLANETS EXPLORERS

Outer solar system exploration, discussing planetary data, interplanetary environment, atmospheric models, data acquisition, etc 11 p2112 A70-26062

Thermal analysis of deployable parabolic antenna for Outer Planetary Explorer program, discussing spacecraft spin and radioisotope thermoelectric generators effect 11 p2127 A70-26359

Spacecraft based data processing stages to perform navigation during outer planet missions 13 p2448 A70-28704

Course correction requirements for ballistic grand tours and outer planet missions, considering trajectory disturbances by random nongravitational forces 13 p2448 A70-28707

Operational and environmental factors constraining onboard navigation system design for outer planet flyby missions 14 p2614 A70-30467

Thermally powered reciprocating piston pump for temperature control fluid transport on Thermoelectric Outer Planet Spacecraft (TOPS) 17 p3101 A70-34757

Jupiter swingbys and multiplanet Jupiter swingby trajectory modes for outer planet missions, comparing in terms of passage conditions 19 p3530 A70-38884

Thermionic reactor electric propulsion for unmanned outer planets exploration, discussing spacecraft design, launch vehicle, weight factors, etc [AIAA PAPER 70-1071] 20 p3717 A70-40524

RF requirements of deep space-outer planet spacecraft communications for Jupiter, Saturn, Uranus and Neptune flyby missions 21 p3791 A70-41369

TOPS /thermoelectric outer planet spacecraft/ project integrating R and D for specific space missions 21 p3920 A70-41793

Scientific motivation for outer planets exploration covering solar system clues, atmosphere comparisons with earth, radiation and planetary radii measurement, etc 21 p3920 A70-41794

Thermoelectric outer planet spacecraft (TOPS) /flight environment, systems design and Titan 3D/Centaur launch vehicle with Burner II upper stage 21 p3930 A70-41795

Thermoelectric outer planet spacecraft (TOPS) data subsystems for 12 year missions compared with Mariner subsystem 21 p3795 A70-41796

Mariner 1969 communication system modified for thermoelectric outer planet spacecraft (TOPS), noting X band addition to S band and associated problems 21 p3791 A70-41797

Trajectory correction propulsion subsystem (TCPS), attitude propulsion subsystem (APS) and pyrotechnic subsystem of thermoelectric outer planet spacecraft (TOPS) 21 p3868 A70-41800

Thermoelectric outer planets spacecraft (TOPS) /attitude control subsystem providing accurate antenna pointing and trajectory correction engine thrust vector orientation 21 p3930 A70-41801

Thermoelectric outer planet spacecraft (TOPS) /solar-independent power subsystem 21 p3760 A70-41802

Thermoelectric outer planet spacecraft (TOPS) /structural problems associated with high gain antenna and electronic equipment 21 p3930 A70-41803

Automated mission requirements for outer planets, discussing flyby spacecraft, orbiters, atmospheric entry and grand tour missions [AIAA PAPER 70-1246] 24 p4411 A70-45919

Long life spacecraft design and reliability based on marine practices and advanced system technology project, considering grand tour outer planets mission [AIAA PAPER 70-1247] 24 p4412 A70-45964

OUTER RADIATION BELT

High latitude capture region boundary for electrons in upper radiation belt determined relative to current electrojets in ionosphere from satellite observations 01 p0172 A70-11516

Explorer observations of large temporal variations of midlatitude outer zone energetic electron intensities interpreted as redistribution during geomagnetic disturbances 03 p0560 A70-13989

Solar proton latitude profiles relation to outer radiation zone electron measurements by Alouette 2 satellite

- lite charged particle detectors during quiet magnetic conditions
04 p0740 A70-15105
- Sporadic electron flux contribution to high latitude geomagnetic disturbances at outer radiation belt boundary estimated from Elektron 1 and 2 observations
05 p0843 A70-16765
- Outer radiation belt high energy electron fluxes correlated with VLF hiss ground observations
07 p1367 A70-19498
- Extraterrestrial ring current proton intensities asymmetric increases in outer radiation belt during magnetic storms
09 p1747 A70-23490
- Low energy protons omnidirectional intensity contours in outer radiation zone at magnetic equator
09 p1747 A70-23491
- Low energy protons in outer trapping region, discussing time variations and source and transport mechanisms
13 p2484 A70-30095
- Outer belt electron intensity variations related to geomagnetic activity indices, using Elektron measurements
14 p2630 A70-30201
- Outer radiation belt high energy electron fluxes correlated with VLF hiss ground observations
15 p2795 A70-32743
- Book on dynamics of geomagnetically trapped radiation, covering radiation belts control, adiabatic theory, trapped particle diffusion, etc
16 p2972 A70-34300
- Acceleration and precipitation of Van Allen outer zone energetic electrons, using correlation experiment between magnetosphere and auroral zone
18 p3306 A70-36010
- Geomagnetically trapped energetic nuclei Z greater than or equal to 3 in earth outer radiation zone, measuring intensity ratio to alpha particles
20 p3698 A70-39327
- LF electrostatic instability of Van Allen belt in outer trapping zone causing electric field in plasmapause
22 p4099 A70-42786
- Outer zone electrons radial diffusion coefficients and lifetimes determined as functions of magnetic shell parameter, based on satellite measurement following geomagnetic storm
23 p4236 A70-43831
- High altitude outer radiation zone boundary region electron energy measurement by satellite Injun 3, noting angular distribution dependence on local time, latitude, etc
23 p4236 A70-43833
- Outer belt electron intensity variations related to geomagnetic activity indices, using Elektron measurements
24 p4398 A70-46276
- OUTGASSING**
- Lunar mascon origin theories, discussing mass transfer by excess pressure generation due to rapid cooling crust and densification by water outgassing
02 p0379 A70-12779
- Air sample removal from hermetically sealed cavities during studies of toxic gas emanations from polymeric materials
07 p1221 A70-19516
- Volatile toxic products outgassed by polymer construction materials, discussing physico-chemical classification of outgassing reduction methods
09 p1709 A70-22085
- Silicone products with low outgassing characteristics for spacecraft applications, discussing fluids, compounds and elastomers
10 p1906 A70-23914
- Air sample removal from hermetically sealed cavities during studies of toxic gas emanations from polymeric materials
11 p1991 A70-26115
- Outgassing pressure variation with time near perigee in satellite-borne pressure gages, using Langmuir model of surface adsorption
13 p2408 A70-29202
- Volatile toxic products outgassed by polymer construction materials, discussing physico-chemical classification of outgassing reduction methods
15 p2766 A70-32681
- Lunar luminescence phenomena, examining gas eruptions from volcanic activity, solar radiation and color
21 p3886 A70-41070
- OUTLETS**
- Coaxial energy outlets satisfying vacuum maintenance requirements of dielectric waveguide windows in dismountable prototype microwave devices
09 p1652 A70-23647
- OUTPUT**
- NT LASER OUTPUTS**
- NT MASER OUTPUTS**
- Output autocorrelation properties of ideal limiters driven by binary deterministic signal plus stationary zero-mean Gaussian noise
06 p1013 A70-18625
- Optimal constant output feedback gains for linear multivariable systems, noting control vector as time invariant function of output vector
13 p2382 A70-29064
- OV-1 SATELLITES**
- High sensitivity particle spectrometer for onboard OV-1-18 satellite measurements of precipitating protons, electrons and alpha particles during PCA events
12 p2232 A70-27402
- Ionospheric electric fields variations in ELF-VLF, confirming OV-1 satellite measurements with OGO 6 data
13 p2403 A70-30082
- OV-3 SATELLITES**
- Ionization measurements by OV-3-6 satellite cold cathode ionization gage of Redhead inverted magnetron type in near circular polar orbit
15 p2723 A70-31660
- OV-10 AIRCRAFT**
- OV-10A forward air control and light attack aircraft design, specifications and performance [SAE PAPER 700837]
24 p4290 A70-45883
- OVARIES**
- High speed fluorescent cell sorting system for sorting mouse spleen cells from Chinese hamster ovarian tumor cells
02 p0240 A70-12695
- OVERCAST**
- U CLOUD COVER**
- OVERESTIMATION**
- U ESTIMATING**
- OVEREXPOSURE**
- U RADIATION DOSAGE**
- OVERPRESSURE**
- Sonic boom overpressures generated by aircraft level rectilinear flight at supersonic speed in temperature and wind stratified atmosphere, calculating atmospheric correction factor
05 p0794 A70-16411
- Air shock tube driven by exploding mixture of propane and oxygen investigated for shock overpressure variation with distance
10 p1863 A70-23992
- Shock impedance definition consistent with acoustic limit, considering use of impedance mismatch to reduce sonic boom overpressure
10 p1805 A70-24522
- Overpressure, rise time and wave period of sonic boom signatures at ground level from unaccelerated supersonic overflights
14 p2530 A70-30608
- Supersonic transport sonic boom theory and effect reduction, discussing Whitham rule, bow shock, overpressure, engine and aircraft design and shock wave control
16 p2843 A70-34263
- Lower bounds for sonic boom, considering negative overpressure region in configuration tailoring
18 p3241 A70-36456
- Combustion velocity in high pressure chamber, determining fire mechanism in overpressure environment
24 p4393 A70-45447
- OVERTONES**
- U HARMONICS**
- OVERVOLTAGE**
- Thermal loads on semiconductors in solid state converters during short circuit and overload
15 p2709 A70-32205
- OXALATES**
- Second and third harmonic simultaneous generation in ammonium oxalate crystals achieved by three frequency interactions
10 p1901 A70-25159
- OXAZOLE**
- Cyclization of N-allylamides to disubstituted-2-oxazolines, giving melting points, yields, picrate melting points and NMR spectra
02 p0249 A70-11681
- OXIDASE**
- Histochemical detection of L-gulonolactone-phenazine methosulfate oxidoreductase activity in mammals with emphasis on vitamin C synthesis in primates
04 p0647 A70-15753
- OXIDATION**
- NT ELECTROCHEMICAL OXIDATION**
- NT PHOTOOXIDATION**
- Mass loss rate of evaporating liquid droplet with vapor reacting with oxygen of atmosphere in combustion front [DFVLR-SONDR-16]
01 p0216 A70-10932
- Artificial hypobiosis state maintenance in animals exposed to cooling after administering lytic mixtures for suppressing oxidation
01 p0029 A70-11464
- Be oxidation in carbon dioxide at high temperatures, explaining observed kinetic discontinuity in terms of oxide morphology
01 p0124 A70-11638
- Reactor surface and propylene role during vapor phase partial oxidation of propane in continuous flow tubular reactors
02 p0250 A70-12017
- Titanium thin films prepared in ultrahigh vacuum to determine low temperature/pressure oxidation kinetics, using electron microscopy and X ray diffraction
02 p0317 A70-12316
- Co-Cr alloy oxidation behavior at high temperatures and various oxygen pressures
02 p0319 A70-12720
- Initial oxide film on Cr-Ni steel at high temperatures observed by electron microscope, noting Ni role
04 p0708 A70-15311
- Particle removal in ablation of artificial graphite linked to oxidation, using high speed motion pictures in analysis
04 p0787 A70-15610
- Chromoluminizing process protecting alloys for gas turbines against oxidation at high temperatures by diffusion mechanism
04 p0711 A70-15683
- High temperature Hf oxidation in air and oxygen using thermogravimetry, X ray diffraction and electron microscopy
05 p0863 A70-16522
- Ni-Cr alloys oxidation dependence on temperature and Cr concentration
06 p1087 A70-17609
- Thermal emittance of Cu measured in vacuum in spherical enclosure by calorimetric method to investigate oxidation effect [AIAA PAPER 70-66]
06 p1180 A70-18139
- Oxide transformation during oxidation of Nb in terms of O diffusion
07 p1305 A70-18967
- Oxidation behavior of metals concerning oxide plasticity role in connection with oxide film macro- and microstresses
07 p1305 A70-18968
- Oxidation, hot corrosion resistance and mechanical properties of aluminate coated superalloys, discussing failure analysis instruments and methods
07 p1305 A70-18969
- W oxidation kinetics as function of ribbon temperature and absorption time using flash technique with sweep pulse mass spectrometer
07 p1306 A70-19275
- Low temperature oxide film effect on porous titanium carbide impregnation by liquid steel
07 p1311 A70-19805
- Al alloys melting in flame furnaces, studying oxidation and various sources of metal losses
08 p1505 A70-21131
- Transition kinetics during linear to parabolic oxidation of Cr in water-hydrogen gas mixture measured thermogravimetrically
08 p1521 A70-21558
- LEED pattern and germanium surface conductivity during oxidation indicating electron states annihilation
09 p1738 A70-22215
- Time, temperature and composition dependent regularities in Ni-Al and Ni-Nb alloys oxidation processes, discussing Oxygen ion migration and Ni ion diffusion
09 p1704 A70-22752
- Thermochemical predictions for high temperature oxidation of Mo and W, discussing oxide films or scales, reactant gases flow rate, etc
09 p1630 A70-22943
- Dual photon emission from chemiluminescent S-O reaction, proposing two step emission mechanism
09 p1630 A70-23001
- Al alloys fatigue properties dependence on surface oxide cracking in moist and dry air, investigating oxidation and kerosene processing
09 p1707 A70-23206
- Mars biological activity suggested from metabolic energy cycle based on oxidation of carbon monoxide [NGL-07-004-043]
09 p1765 A70-23798
- Two body collisions reaction mechanisms with small heats of reaction for Be and Al gaseous oxidation, noting low free energy properties of polymerization
10 p1928 A70-24089
- Electrodes oxidation processes involving fuel cell molecules or derived adsorbed intermediates reacting with anodically generated surface oxide, considering Pt electrochemical reduction
10 p1830 A70-24465
- Electrocatalytic activity of oxides in redox reactions without adsorption, noting application to hydrogen oxidation in acid medium
10 p1831 A70-24470
- Oxide transport and water vapor effects on flash-heated beryllium droplet combustion
10 p1969 A70-25042
- Pyrolytic graphite oxidation kinetics as function of temperature, air velocity and surface area
11 p0270 A70-25809
- Gas mixture composition effect on bacteria growth oxidizing methane and propane, establishing proportional biomass concentration to hydrogen and oxygen in mixture
11 p1991 A70-25938
- Acetone formation mechanisms during neopentane oxidation when added to slowly reacting molecular hydrogen and oxygen
11 p1995 A70-26379

Methane oxidation behind reflected shock waves between 1350-1900 K, measuring pressure, chemiluminescence and 3067 Å absorption of OH radical
11 p2150 A70-26380

Powdered titanium oxycarbides, carbonitrides and oxynitrides oxidation by X ray phase analysis, determining titanium dioxide as final product
12 p2254 A70-27285

Temperature and metallic contact effects on composition and structure of solid phase deposits during reactive fuel oxidation
12 p2289 A70-27493

Solid tar deposits from hydrocarbon fuels oxidation during prolonged storage
12 p2289 A70-27494

Anaerobic and aerobic oxidation efficiency in muscular work performance before and after achieving oxygen steady state consumption
12 p2169 A70-27658

Surface oxidation effects on thermionic work functions of Be determined by visual observation and X ray diffraction patterns analysis
12 p2288 A70-28004

Alloy oxidation at high temperatures emphasizing binary and ternary alloys
12 p2257 A70-28005

Low temperature oxidation of metals, discussing logarithmic kinetics of slow growth of oxides
12 p2257 A70-28006

Vacuum annealing treatments effect on oxidation rate of Co-Cr alloy at high temperatures
12 p2257 A70-28007

Phenolic aldehydes generated from lignin in fossil woods and carbonaceous sediments by oxidative degradation
13 p2361 A70-28911

High temperature kinetics of pyrolytic silicon carbide oxidation and nitridation in dissociated gases
13 p2361 A70-29077

Molar growth yields from chemostat cultures of *Hydrogenomonas eutropha* on succinate and on fumarate, noting equivalence to ATP via oxidation
13 p2350 A70-29113

High temperature oxidation of Ni-Cr alloys and stainless steels in molten salt, observing grain boundary corrosion with electron probe
15 p2757 A70-31875

Linear regression rate of spherical solid hybrid fuel grains oxidized in reducing gas flow
15 p2786 A70-32263

Graphite oxidation on exposure to high temperature flow field based on surface coupled model [AIAA PAPER 70-823]
16 p2940 A70-33941

Oxidation dependence on physical nature of Ti surfaces obtained by thin film techniques under ultrahigh vacuum conditions
17 p3098 A70-34364

Ti alloys crack formation during oxidation under stress, considering annealing and recrystallizing effects
17 p3114 A70-34374

Oxidized alpha Ti crystals strain analysis based on X ray divergent beam, discussing hardening effects
17 p3115 A70-34387

Sodium sulfate induced accelerated oxidation of Ni and superalloys, investigating thermodynamics and reaction mechanism
18 p3272 A70-36037

Carbon monoxide oxidation by molecular oxygen in incident shock waves, accounting for chain branching in shock tubes
19 p3374 A70-38271

Oxide dispersed Cu alloys preparation by surface oxidation of powders, considering structural stability and stress rupture properties
20 p3646 A70-39103

High temperature Ni, Co and Fe alloys for gas turbines, examining sulfidation-oxidation corrosion test methods
20 p3651 A70-39971

Ni base alloys sulfidation kinetics, examining roles of sodium/sulfur compounds-substrate interactions in accelerated oxidation
20 p3651 A70-40072

Spacecraft wet oxidation for human waste processing, discussing temperature and gas pressure effects, catalyst types, pump requirements, etc
21 p3769 A70-40997

Metal phthalocyanin catalyzed oxidation by oxygen of vanadium and iron couples in externally regenerated redox fuel cell cathode
22 p3966 A70-43536

Oxygen pressure effects on Ni oxidation kinetics at high temperatures
23 p4208 A70-44920

Convective diffusion limited oxidation of Mo, measuring kinetics up to 2000 K by rotating disk method
24 p4358 A70-45233

Thermodynamic equilibrium analysis of metal oxidation and thermal dissociation of oxides in vacuum, noting decreased affinity by evaporation
24 p4361 A70-45835

Al and liquid Al-Mg alloys oxidation at high temperatures, noting Mg content effect
24 p4361 A70-46174

Anions and cations diffusion during oxidation of Ni-V-Ti alloys, using chemical and electron microprobe analyses
24 p4364 A70-46335

Metal layer and absorbed oxygen quantities in reactive oxidation deposition of aluminum
24 p4365 A70-46354

OXIDATION RESISTANCE

Annular metal specimens protection against oxidation during high temperature relaxation testing by covering specimens with Al powder thinned with alcohol
01 p0121 A70-11109

Silicide, aluminide and boride coatings transition temperature holdability, considering nitridation/oxidation protection for Cr alloys
01 p0122 A70-11241

TD-Ni low cycle fatigue properties at high temperature, discussing grain morphology, thoria particles role and oxidation resistant coating effect
01 p0123 A70-11245

Chemical composition of cermet material for radial sealing of high temperature gas turbines, ensuring structural stability and oxidation resistance
01 p0124 A70-11621

Tungsten metal oxidation retardation by W-F bonds
02 p0249 A70-11651

B-C alloys chemical composition effect on high temperature stability in pure oxygen
03 p0514 A70-12978

Oxidation resistance of mixed silicon nitride and silicon carbide refractory materials at high temperatures
03 p0514 A70-12979

Oxidation and sulfidation resistant diffusion coatings for superalloys, discussing processing methods, composition, properties and application [SAE PAPER 690479]
03 p0509 A70-13266

Free radical antioxidant reactions in lipids from blood, liver, spleen, brain and intestines of rats exposed to ionizing radiation
03 p0419 A70-13309

Ni-Cr alloy oxidation resistance dependence on small amount of Al at high temperatures, noting role of protective oxide layer
03 p0514 A70-14315

Oxidation behavior of TiC base alloys containing Mo
04 p0708 A70-15312

Polymers with high temperature oxidation resistance, discussing problems caused by aromatic heterocyclic structures and manufacturing methods
05 p0873 A70-16604

Strength and plasticity of Mo and Nb sheet in oxidizing medium at high temperatures and pressure range
05 p0865 A70-17029

Metals mechanical properties with inorganic heat resistant coatings between 1900-2300 K in oxidizing medium, describing facility based on solar furnace
05 p0875 A70-17069

Ni-Cr alloys effects of grain size and surface deformation on oxidation properties at high temperature
06 p1088 A70-17610

Ni influence in high temperature oxidation of austenitic Fe-Cr-Ni alloys investigated thermogravimetrically, metallographically and by electron probe microanalysis
07 p1305 A70-18965

Fe-Cr-Ni alloys for use in high temperature oxidizing environments
07 p1305 A70-18966

Al-Mg oxidation resistance and kinetics, studying Zr, Ce and Be additives effects on oxide films mechanical properties
08 p1517 A70-21130

Co-based alloy mechanical properties and physical parameters at high temperatures, discussing oxidation and hot corrosion resistance
09 p1700 A70-22025

Nondestructive tests for diffusion-formed refractory alloy coatings used as oxidation protection for hypervelocity spacecraft and reusable systems
09 p1692 A70-22679

Ni-Nb-O system state diagram by reduction equilibria and X ray analysis, discussing oxidation resistance based on metal surface protective layers makeup
12 p2253 A70-27158

Commercial Co base superalloys oxidation and hot corrosion resistance under controlled environments, examining role of various alloying elements [ASME PAPER D-8-21-5]
12 p2256 A70-27974

Phosphorus compounds inhibition effect on oxidation and wear of graphite lubricants
13 p2437 A70-28854

Preoxidation treatment alleviating silicide pest in protective coatings for refractory metals, discussing effectiveness against high temperature oxidation
13 p2434 A70-29082

Aliphatic diesters as high temperature lubricants, discussing viscosity range extension, oxidation inhibition and thermal stability
13 p2438 A70-29125

High temperature scaling of Ni, investigating role of oxide microstructure and growth stresses
15 p2762 A70-32388

Ta oxygen concentration effects on corrosion resistance to NaK in SNAP 8 boilers
16 p2932 A70-34202

Ti-Al-Nb system creep strength, oxidation resistance, density, forging and rolling
17 p3120 A70-34426

Oxidation and atmospheric contamination protective coatings for high temperature materials, using burner ring tests
17 p3127 A70-34519

Surface degradation by oxidation, temperature fluctuations and hot corrosion of Ni- and Co-base superalloys in gas turbine engines
22 p4057 A70-43574

Graphite fiber oxidation prevention in metal matrix composites, examining various thermodynamic parameters
22 p4126 A70-43676

German monograph on use of Ge as oxidation resistant refractory materials alloy component covering base materials, test samples processing methods and apparatus, etc
24 p4367 A70-45525

OXIDES

NT ALUMINUM OXIDES
NT ANHYDRIDES
NT BARIUM OXIDES
NT BERYLLIUM OXIDES
NT BISMUTH OXIDES
NT BORON OXIDES
NT CALCIUM OXIDES
NT CARBON DIOXIDE
NT CARBON MONOXIDE
NT CHLORINE OXIDES
NT CHROMITES
NT CHROMIUM OXIDES
NT COBALT OXIDES
NT COPPER OXIDES
NT ENSTATITE
NT HAFNIUM OXIDES
NT HEMATITE
NT HYDROGEN PEROXIDE
NT ILMENITE
NT INORGANIC PEROXIDES
NT IRON OXIDES
NT LANTHANUM OXIDES
NT MAGNESIUM OXIDES
NT MAGNETITE
NT METAL OXIDES
NT MOLYBDENUM OXIDES
NT MUSCOVITE
NT NICKEL OXIDES
NT NIOBIUM OXIDES
NT NITRIC OXIDE
NT NITROGEN DIOXIDE
NT NITROGEN OXIDES
NT NITROGEN TETROXIDE
NT NITROUS OXIDES
NT PEROXIDES
NT POTASSIUM OXIDES
NT PYROXENES
NT QUARTZ
NT RUTILE
NT SAPPHIRE
NT SCANDIUM OXIDES
NT SILICON DIOXIDE
NT SILICON OXIDES
NT SULFUR OXIDES
NT TANTALUM OXIDES
NT THORIUM OXIDES
NT TIN OXIDES
NT TITANIUM OXIDES
NT TUNGSTEN OXIDES
NT URANIUM OXIDES
NT YTTRIUM OXIDES
NT ZINC OXIDES
NT ZIRCONIUM OXIDES

Oxides and silicates universal equations of state based on experimental data including elastic properties, density, mean atomic weight relations and geophysics interpretations
02 p0294 A70-12778

Negative O, NO and nitrous oxide ions formation by electron impact on nitrous oxide as function of pressure
03 p0441 A70-14007

Mars surface reddish color due to carbon suboxide suggested based on spectral reflectivity measurements and matching in laboratory
04 p0743 A70-14423

High melting point oxides effects on niobium alloys recrystallization temperature and grain growth
07 p1303 A70-18741

Excitation energy transfer processes in oxide glasses containing trivalent Tb ions in combination with other rare earth activators
09 p1738 A70-22137

Refractory oxide submillimeter spherical particle preparation by focused emission from carbon dioxide laser
09 p1697 A70-22984

- Cyclohexene oxide mass spectral fragmentation by means of deuterium labeled analogs
09 p1630 A70-23397
- Epitaxial magnetic oxide films grown by chemical vapor deposition
11 p2099 A70-26626
- Fuel cells with solid oxide electrolyte, principles, advantages and drawbacks
12 p2163 A70-26994
- Gaseous monoxides dissociation energies and free energy functions tabulation for calculating partial pressures
14 p2545 A70-30902
- Oxide film and liquid effects on friction coefficient, surface relief and dislocation density along depth related to plastic deformation
15 p2743 A70-31638
- High temperature reaction kinetics between oxygen difluoride and CO in shock tube, discussing carbon dioxide formation
16 p2855 A70-33010
- Pressure effects on quantum yields of carbon trioxide formation in gas phase ozone photolysis with carbon dioxide
16 p2856 A70-33653
- Oxides compounds heats of formation isocomponent and primary product composition relationship in binary systems
22 p3982 A70-42679
- Perovskite type oxide lanthanum manganate magnetic properties, explaining ferromagnetism by spin Hamiltonian formalism
24 p4389 A70-45601

OXIDIZERS

- NT FLOX
NT LIQUID OXIDIZERS
NT LIQUID OXYGEN
NT ROCKET OXIDIZERS
- Hydrogen reactions with nitrogen dioxide, oxygen and mixtures of oxygen and nitric oxide in adiabatic flow reactor measured as function of temperature and pressure
02 p0250 A70-12020
- Condensed fuel mixtures and oxidizers combustion rates as function of pressure and particle size
09 p1786 A70-22104
- Oxidizer particle size and binder type effects on nonacoustic combustion instability of solid propellants [AIAA PAPER 69-175]
12 p2332 A70-27804
- Reaction rates temperature dependence for artificial carbon-graphites of various densities in oxidizing gas media
13 p2519 A70-28577
- Thermal decomposition mechanism of inorganic oxidizers, discussing reactivity of alkali and alkali earth salts
18 p3299 A70-36240
- Chemical kinetics effect on combustion rates of fuel plate in turbulent oxidizer flow, deriving conservation equations in boundary layer and diffusion equation
18 p3346 A70-36245
- Hybrid rocket engine with solid oxidizer, noting applications as apogee or perigee motor
18 p3301 A70-36655
- Anomalous substrate oxidizing specificities among red brown and green algal peroxidases and land plants
19 p3360 A70-37773
- Combustion rate as function of oxidizer molecular refractivity in perchlorates and nitrates of aliphatic and aromatic mono- and polyamines explosives
21 p3783 A70-42241

OXIMETRY

- Continuous blood oxygen analyzer standardized with atmospheric air, demonstrating on dogs during occlusion of left anterior descending coronary artery
21 p3772 A70-42162

OXYFLUORIDES

- Carbon oxyfluoride IR radiation from boundary layer formed by arc-heated air passing over Teflon surface
10 p1968 A70-24475

OXYGEN

- NT HIGH PRESSURE OXYGEN
NT LIQUID OXYGEN
NT OXYGEN ATOMS
NT OXYGEN ISOTOPES
NT OXYGEN 18
NT OZONE
NT OZONIDES
- Iron group nuclei abundance relative to oxygen determined for solar cosmic ray event of 2 September 1966
01 p0167 A70-10042
- Oxygen molecules dissociation by molecular and atomic collisions in shock tube from measuring molecular O concentration behind shock wave front
01 p0149 A70-11632
- Reaction analysis of acetylene-oxygen flames with known concentrations and temperature profiles, integrating one dimensional flame equations numerically
02 p0251 A70-12035
- Diurnal variations of intensity and height profile of diatomic O concentration from photometric rocket measurements compared with balloon data
02 p0297 A70-12066

- Nimbus 3 satellite observations of near UV solar flux intensity and variability, describing instrumentation and measurement of radiation producing molecular oxygen photodissociation
02 p0291 A70-12295
- Low energy electron diffraction structures due to Re crystal surface interaction with CO and molecular oxygen at high temperatures
03 p0440 A70-13098
- Nb-Mo alloy interstitial oxygen concentration determined by measuring internal friction (Snoek) peak
03 p0512 A70-13763
- Fire prevention problems in closed oxygen-rich environments, discussing ignition temperature and flame propagation rate
03 p0607 A70-13961
- Temperature and hemoglobin concentration effect on oxygen solubility in blood, constructing table for Bunsen solubility coefficients
03 p0428 A70-14156
- Tensile tests on alpha Ti containing oxygen and hydrogen at various temperatures and strain rates to determine deformation and fracture
04 p0706 A70-15133
- Polymorphic transformation effects on oxygen diffusion rate in alpha and beta phases of Ti, considering temperature effects and activation energy
04 p0707 A70-15211
- Threshold oxygen concentration for corrosion determined for Ta specimens subjected to low pressure contamination in NaK
04 p0709 A70-15628
- Vertical profiles of atomic and excited molecular oxygen concentration in upper atmosphere calculated from spectral band intensity, determining excitation reaction rates
04 p0682 A70-15733
- Excited oxygen molecules concentration in upper atmosphere calculated, considering deactivation during interactions in various energy states
04 p0684 A70-15750
- Pressure wave formation induced by absorption of radiation in oxygen, noting wave driving after radiation pulse decay by frozen dissociation energy
05 p0833 A70-16306
- Quasi-equilibrium treatment of heterogeneous reactions applied to evaporation rate/desorption/ computation for volatile species formed in oxygen reactions with W, Mo and graphite
06 p1004 A70-17330
- Quasi-equilibrium treatment of heterogeneous reactions applied to flash desorption data for oxygen reaction with tungsten surface, discussing species desorption dependence on adsorption temperature
06 p1004 A70-17331
- Slow electron attachment to O molecules forming stable O⁻ ions, discussing formation rate constant
06 p1109 A70-17488
- Electrically discharged O effect on N first positive band emission in surface catalyzed excitation
06 p1109 A70-17489
- Earth oxygen atmosphere age estimated from sulfur isotope composition of geological phlogopite and lazurite deposits from South Baikal region
06 p1056 A70-17798
- Absorption cross sections for single and double molecules of oxygen and in UV region noting disagreement with Beer law
06 p1114 A70-18632
- Oxygen content influence on Nb-Mo alloy mechanical properties at ambient temperature in air and hydrogen
07 p1307 A70-19374
- Photodissociation of diatomic O and N molecules in far UV
07 p1338 A70-20052
- Altitude profiles and absolute intensities of far UV emission features in aurora measured by filterwheel photometer in Aerobee rocket, determining molecular oxygen densities
08 p1489 A70-21384
- Atmospheric carbon dioxide and oxygen concentrations effects on white mice low temperature tolerance
09 p1614 A70-22082
- Critical review of paper on molecular oxygen microwave spectrum analysis
09 p1732 A70-22829
- Stainless steel corrosion rates in flowing liquid Na from mechanism based on thermodynamic partitioning of oxygen
09 p1706 A70-22942
- Oxygen pressure, volume and temperature data and derived thermodynamic properties presented in tabular form
09 p1788 A70-22956
- Oxygen index flammability test for polymeric materials, showing general applicability in quality control and research
09 p1710 A70-23346
- Blood carbon dioxide and oxygen content determined by respiration mass spectrometer using carrier gas
09 p1629 A70-23584

- Oxygen solubility in liquid Mo in presence of volatile oxides, determining equilibrium constant of dissolution reaction
09 p1709 A70-23784
- Oxygen-kerosene combustion product composition and characteristics in engine thermodynamic design allowing for intermolecular interaction forces
10 p1968 A70-24284
- Charge transfer reactions of negative ions with oxygen investigated for energy dependence, yielding evidence on oxygen electron affinity
10 p1919 A70-24402
- Oxygen reduction reaction mechanism and catalysis, considering metal electrode surfaces and substrates, hydrogen peroxide role, adsorption, metal-oxygen bonds, etc
10 p1829 A70-24452
- Oxygen electrode ring and disk currents analysis, studying oxygen reduction on platinum via peroxy intermediates
10 p1829 A70-24453
- Oxygen reduction in sulfuric acid with phthalocyanine-carbon catalysts
10 p1829 A70-24456
- Oxygen-hydrazine interactions on partially immersed metal electrodes, studying conjugated electrochemical reactions
10 p1830 A70-24457
- Specific intensity production from photolysis of ozone-oxygen mixtures at 2537 Å, investigating mechanism
10 p1831 A70-24565
- Oxygen diffusion in presence of hemoglobin taking into account chemical kinetics, showing approximate and computer solutions
10 p1819 A70-24772
- Critical oxygen supply of cerebral mitochondria and intercapillary oxygen transport
10 p1821 A70-25080
- Partial oxygen pressure in hyperaemic earlobe capillary blood under hypoxic conditions, noting correlation with age and body weight
10 p1822 A70-25088
- Light scattering, turbulent disturbances and absorption by binary oxygen complexes in atmospheric layers
10 p1843 A70-25126
- High energy oxygen positive-ion reaction with molecular nitrogen, presenting semiempirical model with assumed crossing of potential energy surfaces
10 p1920 A70-25146
- Oxygen sticking coefficients and desorption kinetics on tungsten crystal by step desorption/ reflection technique, postulating formation and decomposition of surface oxide phases
10 p1832 A70-25147
- Hydrogen, oxygen and carbon dioxide in off-gas stream from nuclear reactor experiment using on-line gas chromatography
11 p1994 A70-25615
- Fatigue life of Ni vibrated in reversed bending at 300 C in oxygen and in water vapor at various pressures
11 p2067 A70-26098
- Styrene-oxygen copolymer preparation methods, discussing burning rates for rocket solid propellants mixtures with ammonium perchlorate
11 p2100 A70-26146
- Al and B particles combustion in methane-oxygen system, considering reaction zone models, energy release rate, particle kinetics, instabilities, etc
11 p2149 A70-26284
- Ionic composition of Class I auroras based on 1965 CIRA atmospheric model atomic/molecular oxygen ratios, noting ion loss rates
11 p2046 A70-26565
- Tensile strain rate and oxygen concentration effects on peaks of niobium hardening zones involving interstitial atoms
12 p2252 A70-27001
- N and O ions electron impact ionization rates calculated from approximate cross sections
12 p2275 A70-27173
- Oxygen adsorption on W(110)/ surface determined for coverage as function of exposure by Auger electron spectroscopy
12 p2180 A70-27253
- Oxygen and hydrogen diffusion coefficients in aqueous potassium hydroxide electrolyte solutions at various temperatures and concentrations
12 p2181 A70-27575
- Oxygen interaction on rhodium filament, considering sticking probability as function of temperature
12 p2181 A70-27677
- Gold alloys electrocatalytic activity in cathodic reduction of oxygen in potassium hydroxide
12 p2182 A70-27760
- Hydrogen oxygen fuel cell investigated for oxygen transfer to Pt cathode surface
12 p2166 A70-27848
- Oxygen diffusion facilitation in vivo and nonsteady state conditions under physiological circumstances, emphasizing hemoglobin in red cells and myoglobin in muscle
12 p2171 A70-28024

- Quenching efficiency of molecular oxygen relative to nitrogen, carbon monoxide, carbon dioxide and argon, involving photolysis of gas mixtures
13 p2361 A70-28498
- Predawn forbidden OI 6300 Å airglow seasonal variations by isophoto maps, discussing photoelectron precipitation
13 p2395 A70-28944
- Postdusk and predawn seasonal variations of forbidden OI 6300 Å airglow, discussing photoelectron precipitation
13 p2395 A70-28945
- Oxygen motion velocity effect at various pressures on heatproof and heat resistant steels and alloys ignition, noting minimum ignition temperature
13 p2434 A70-29168
- Molecular oxygen positive ion density in upper ionosphere as function of photoionization, ambipolar diffusion velocity and altitude effect
13 p2399 A70-29233
- Earth atmosphere formation and oxygen-carbon dioxide balance mechanisms, including water vapor photodissociation, photosynthesis, fossil fuel burning, etc
14 p2572 A70-30350
- Atmospheric molecular oxygen photometric absorption spectral bands, calculating growth curves
14 p2572 A70-30403
- Vertical profiles of atomic and excited molecular oxygen concentration in upper atmosphere calculated from spectral band intensity, determining excitation reaction rates
14 p2575 A70-30817
- Excited oxygen molecules concentration in upper atmosphere calculated, considering deactivation during interactions in various energy states
14 p2576 A70-30834
- V-N and V-O solid solutions magnetic, electrical, crystallographic and mechanical properties as function of gas concentration
14 p2596 A70-30842
- Nonequilibrium dissociation effect on supersonic oxygen flow past inverted blunted cones at angle of attack, considering thermal fluxes and aerodynamic forces
15 p2671 A70-31496
- Oxygen interlayer diffusion effects on wear change during gliding friction of normalized steel samples
15 p2743 A70-31636
- Electron mobility, diffusion, drift velocity and attachment in oxygen, determining Townsend primary ionization coefficient
15 p2776 A70-31969
- Atmospheric carbon dioxide and oxygen concentrations effects on white mice low temperature tolerance
15 p2685 A70-32678
- Oxygen-hemoglobin reaction rate constants in red cells obtained by applying in vitro blood data to solutions of differential equations describing intracellular oxygen transport
15 p2686 A70-32846
- Diffusion coefficient of dissolved oxygen in blood proteins aqueous solutions
15 p2686 A70-32848
- Experimental and numerical nonequilibrium shock layer around cones in hypersonic pure oxygen flows with simultaneous rotational, vibrational and dissociation relaxation
[AIAA PAPER 69-136]
16 p2894 A70-33858
- Long term helium-oxygen atmosphere effects on rats and mice, investigating biochemical and metabolic changes
16 p2849 A70-33996
- Molecular oxygen role in photolytic decomposition of ozone by intermediate quantum yield method, presenting rate constants
16 p2858 A70-34009
- Inelastic energy losses in oxygen ion beams collisions with neutral molecules, determining vibrational transition probabilities
16 p2955 A70-34011
- Refractory metals penetration by liquid alkali metals along grain boundaries and crystallographic planes, considering threshold oxygen concentration
16 p2932 A70-34203
- Refractory alloys Li corrosion resistance, examining effects of oxygen contamination during welding
16 p2924 A70-34205
- Liquid metal corrosion of heat pipe refractory alloys at high temperatures, noting oxygen role
16 p2933 A70-34208
- Homogeneity of commercially pure Ti and Ti-Al-V ingots, discussing oxygen distribution uniformity over cross section
17 p3112 A70-34353
- Phase transformations and equilibrium diagram of titanium-oxygen alloys, using electron and optical metallography
17 p3119 A70-34413
- Ultrahigh strength alpha-beta titanium alloys, examining carbon and oxygen effects on mechanical properties
17 p3121 A70-34429
- Hypersonic flow of chemically reacting binary mixture of oxygen atoms and molecules past blunt body, presenting viscous shock layer equations - slip boundary conditions
[AIAA PAPER 70-805]
17 p3005 A70-34458
- Oxygen, nitrogen and argon plasma total radiation measurement at various wavelengths and temperatures
17 p3139 A70-34547
- Aluminum spherical particles nonautonomous and autonomous combustion in O with N or Ar initiated by HF induction heating
17 p3145 A70-35042
- Combustion efficiency and rate in oxygen enriched spacecraft atmosphere
17 p3177 A70-35210
- Shock tube flow of dissociating oxygen with chemical relaxation using Lax method
17 p3070 A70-35243
- Oxygen dilute solutions in liquid Fe-Ni-Co alloys, investigating thermodynamic properties by hydrogen-water vapor equilibrium
18 p3272 A70-36033
- Oxygen pressure effect on stainless steel cyclic hardening during vibration tests at resonant frequency
18 p3273 A70-36042
- Oxygen absorption coefficients at Lyman alpha line and other transmission windows, verifying dependence on pressure source line width and doublet separation
18 p3293 A70-36753
- Oxygen solubility in Nb-Hf alloys at elevated temperatures, using isothermal sections for Nb-rich part
19 p3453 A70-38708
- Flash lamp pumped organic dye laser intensity for dye solutions in contact with different argon-oxygen compositions, noting effect of oxygen partial pressure
21 p3834 A70-40569
- Turbulent mixing effect on vertical distribution of ionospheric atomic and molecular oxygen, using equations of motion and continuity
21 p3813 A70-40907
- Molecular oxygen density and vibrational distribution in lower atmosphere, observing solar UV radiation absorption by satellite OSO-4
21 p3816 A70-41066
- Hydroxyl atmospheric airglow secondary production processes, discussing vibrationally excited oxygen molecules and rapid quenching by atomic O and HO sub 2
21 p3816 A70-41068
- Collision induced dissociation of nitric oxide and molecular oxygen ions at low kinetic energies, noting internal ionic excitation effects
21 p3773 A70-41398
- Apollo 11 lunar rocks and fines oxygen, Si and Al content determination by neutron activation analysis
21 p3774 A70-41566
- Nucleic acids constituents reactions with singlet oxygen, determining oxidation mechanism in photodynamic processes
21 p3781 A70-42025
- Oxygen diffusion coefficient of alpha-Ti from oxidation of saturated and unsaturated beta phase in 932-1142 C range
22 p4053 A70-42731
- Diffusion effect on hydrogen and oxygen constituents height distributions in atmosphere and lower thermosphere, solving diffusion and continuity equations
22 p4020 A70-43160
- Room temperature oxygen adsorption on tungsten surfaces
22 p4087 A70-43235
- Solid solutions properties in Nb-oxygen system, examining atomic bond nature by elastic modulus measurement
22 p4056 A70-43345
- Interdiffusion coefficients for hydrogen-carbon dioxide and oxygen-carbon dioxide systems at low temperatures
22 p4076 A70-43393
- Hydrazine-oxygen fuel cell design and operation, discussing efficiency, electrolyte space, etc
22 p3966 A70-43541
- F1 region positive nitric oxide and oxygen ions concentrations ratio and conversion rates from rocket data and theoretical formulas
23 p4189 A70-44075
- Diurnal variation symmetry of upper atmosphere molecular oxygen concentration in terms of ozone photodissociation
23 p4190 A70-44083
- Autoionization theory application to partial solar photoionization cross sections for production rates of vibrationally excited positive molecular oxygen ions
23 p4222 A70-44785
- Blood oxygen, carbon dioxide and pN during hypothermia induced by He-oxygen mixture and cold exposure in hamsters, comparing with hibernation state
23 p4147 A70-44787
- Photosystem II and oxygen evolution kinetics
24 p4305 A70-46411
- OXYGEN AFTERGLOW**
Chemiluminescent reaction rates measurements for emission of diatomic oxygen molecules Herzberg bands in oxygen and oxygen-inert-gas afterglows
03 p0440 A70-13579
- Photoelectric intensity measurements on emission bands of oxygen Herzberg I system excited in argon-oxygen afterglow
03 p0528 A70-14350
- Hydronium ion formation mechanism for D region, obtaining experimental support from mass spectrometer observation of ion production in oxygen glow discharge
09 p1671 A70-23500
- Flowing afterglow system below 300 K for rate constants of certain gases association with helium third body, investigating oxygen cluster ions formation and reactions
10 p1920 A70-25144
- OXYGEN ANALYZERS**
Continuous blood oxygen analyzer standardized with atmospheric air, demonstrating on dogs during occlusion of left anterior descending coronary artery
21 p3772 A70-42162
- Atomic oxygen height profile measurements in upper atmosphere by sensor consisting of thin silver film on small pyrex rod permitting molecular transport
24 p4329 A70-45359
- OXYGEN ATOMS**
Atomic oxygen reaction with carbon dioxide and carbon dioxide dissociation in shock waves, using nitrous oxide decomposition for oxygen source
03 p0440 A70-13578
- Ionospheric inhomogeneities motion and vertical profile of atomic oxygen concentration associated with solar particle absorption in upper layer
04 p0681 A70-15724
- Atomic oxygen and chlorine attack on refractory materials studied for kinetics of chemical reactions of free radicals and atoms
07 p1313 A70-19903
- Reactive scattering from solid surfaces, discussing atom beam reaction of O with heated Ge and Si single crystals
07 p1342 A70-20117
- Bromine monoxide formation by atomic oxygen-bromine reaction in flash photolysis of bromine-nitrous oxide and bromine-nitrogen dioxide mixtures
08 p1455 A70-21342
- Vacuum UV atomic nitrogen and oxygen lines contribution to energy transfer in high density plasma, noting f values and Stark half widths
09 p1730 A70-22229
- Neutral atomic oxygen auroral and nebular emissions in twilight airglow, suggesting photodissociation of molecules by sunlight
10 p1873 A70-23832
- Atomic oxygen IR emission in earth atmospheric models, using reduction factor for comparison with optically thin atmosphere
10 p1875 A70-24439
- Thermal diffusion effects on F2 region ion densities, deriving diffusion coefficients for partially ionized atomic oxygen plasma
13 p2398 A70-29232
- Ionospheric inhomogeneities motion and vertical profile of atomic oxygen concentration associated with solar particle absorption in upper layer
14 p2575 A70-30808
- F1 layer formation and ion production rates related to F layer stratification, atomic oxygen, zenith angle and solar activity periods
15 p2730 A70-32086
- Nitrogen deactivation by ground state atomic oxygen resulting in metastable oxygen atom as auroral green line source
17 p3080 A70-35770
- Atomic oxygen beams interaction with various surfaces at low pressure, discussing reflection probability and recombination reactions
18 p3225 A70-36187
- Total cross sections for production of free electrons in collisions of low energy negative atomic oxygen ions with molecular nitrogen
18 p3292 A70-36188
- Positive atomic oxygen ion reactions with carbon dioxide detected using ion cyclotron and double resonance methods
18 p3225 A70-36189
- Carbon dioxide-atomic oxygen reaction rate constant to investigate Martian ionosphere, discussing reactions involving oxygen, nitrogen molecular ions and NO
21 p3886 A70-41067
- Atomic oxygen density and temperature diurnal variation determination by F region incoherent scatter measurements, using nonlinear regression analysis
21 p3817 A70-41096
- Optical devices contaminated mirror surfaces restoration with atomic oxygen from RF plasma by noncontaminating nondestructive oxidation of polymer film
24 p4029 A70-42622

Neutron diffraction of ordered atomic oxygen structures in titanium suboxides, noting compositional dependence of physical properties

22 p4053 A70-42735

Ionization rates in auroras detected by atomic oxygen and nitrogen lines

22 p4024 A70-43308

EPR method for elementary reaction kinetics of vapor phase oxygen atoms interacting with molecular hydrogen

22 p3983 A70-43349

Oxygen atom catalytic recombination and flame inhibition mechanism literature survey

23 p4157 A70-44002

Solar spectrum O I, obtaining high resolution UV line profiles from rocket-borne spectrograms

24 p4410 A70-45766

OXYGEN BREATHING

Cardiac output and coronary blood flow during steady state hypoxia, considering room air and different oxygen concentration breathings

01 p0014 A70-10360

Dynamic testing instrumentation for oxygen breathing equipment emphasizing demand regulators and masks, connecting hose, helmets and individual components

01 p0041 A70-11458

Noble gases breathing effects on free amino acid pool increase in rat brains, considering O mixtures with He, Ar and Ne

04 p0632 A70-15086

Electrocardiographic changes during positive headward acceleration of normal human subjects after oxygen breathing and propranolol administration

05 p0808 A70-16675

Vigilance time degradation, studying effects of breathing gas mixtures with varying oxygen and carbon dioxide content

06 p1000 A70-17293

Respiration behavior of men during inhalation of various gas mixtures, observing spontaneous changes in breathing rates

07 p1206 A70-19471

Vital capacity measurements made preflight and postflight on jet fighter aircrew breathing pure oxygen at various G forces

07 p1222 A70-19934

Rats acute hypoxia and altitude tolerances after prolonged exposure to hyperoxic atmospheres

08 p1446 A70-21437

Dogs breathing air or oxygen during slow and rapid decompression, measuring intraocular and cardiovascular pressure changes and retinal responses

09 p1621 A70-23460

Prolonged hyperbaric oxygen breathing effect on human physical performance at rest and during severe exercise

19 p3364 A70-38369

Human and animal tolerances to hyperbaric oxygen, discussing response variation, toxicity modification, etc

22 p3976 A70-43701

Systolic and diastolic pressure in central artery of retina in deep-sea divers during oxygen inhalation at atmospheric pressure

23 p4150 A70-45081

Oxygen breathing effects in exercise on respiration, circulation and metabolism during high altitude acclimatization

24 p4303 A70-46110

OXYGEN COMPOUNDS

Reduced Nd ion absorption in matrices of fluorides, fluoride mixtures or oxygen-containing compounds with various ion concentrations, analyzing optical centers statistical properties

01 p0107 A70-10210

Vibrational spectra and structure of oxalyl chloride in crystalline and fluid states, discussing molecular and space group symmetry

16 p2857 A70-34006

OXYGEN CONSUMPTION

Oxygen uptake increase following sodium L-lactate isomer infusion into anesthetized dogs

02 p0233 A70-11721

Polarographic method for determining cat capillary muscle oxygen consumption used to investigate Fenn effect involving afterloaded and isometric contractions

02 p0234 A70-11726

Heart rate change effect on myocardial oxygen consumption and nutritional circulation with constant coronary blood flow suggesting oxygen extraction independence of capillary surface

02 p0235 A70-11991

Endtidal oxygen and carbon dioxide partial pressures, oxygen uptake and carbon dioxide after apnea and during apneic diving

02 p0235 A70-12089

Oxygen consumption, lactic acid production and mechanical performance of anesthetized dog gastrocnemius muscle with increased blood flow

02 p0235 A70-12090

Physiological equivalents of air with rare gases and H substitutes for nitrogen in inhaled gas mixtures providing normal oxygen intake

02 p0249 A70-12798

Altitude changes effect on brown fat content and metabolism in deer mice, noting oxygen consumption and heat production limitation by hypoxia

02 p0242 A70-12865

Arterial counterpulsation effect on mechanics of left ventricular contraction and myocardial oxygen consumption in normal and abnormal animals

03 p0416 A70-13009

Oxygen consumption and rectal temperature in male mice confined in nitrogen and helium diluted hyperoxic atmosphere at specific temperature and humidity ranges

03 p0425 A70-13891

External work and energy expenditure relations of heart, including myocardial oxygen consumption

03 p0426 A70-13940

Oxygen consumption and body temperatures during acute hypoxia in man, based on low oxygen mixture breathing tests

03 p0439 A70-14291

Perfusion pressure effect on myocardial oxygen consumption and coronary flow in stable nonworking rat heart

07 p1202 A70-18865

Oxygen uptake increase phenomena in passively hyperventilated anesthetized and paralyzed dogs

07 p1205 A70-19293

Carbon dioxide effect on oxygen uptake during hyperventilation in normal man

07 p1205 A70-19294

Statistical analysis of pulmonary ventilation and gas exchange indices during orthostatic tests before and after water immersion

07 p1209 A70-19517

Physical training effects on sedentary men with stable activity pattern, recording heart rates and oxygen uptake

07 p1215 A70-20171

Oxygen uptake by brain as function of oxygen tension in rats using venous outflow method and blood gas analysis

08 p1446 A70-21436

Esophageal, rectal and quadriceps muscle temperatures, oxygen uptake, weight changes, skin conductance and skin evaporation during thermal transients caused by bicycle exercise

10 p1810 A70-24006

External respiration, hemodynamics, oxygen transport and consumption in lungs during static load tests

10 p1822 A70-25176

Statistical analysis of pulmonary ventilation and gas exchange indices during orthostatic tests before and after water immersion

11 p1988 A70-26116

Cyclic strain energy method determining oxygen consumption rate of intact working human left ventricle by closed chest measurements

12 p2167 A70-27018

Brain tissular respiration and oxygen consumption in rats during hypothermia

12 p2168 A70-27345

Anaerobic and aerobic oxidation efficiency in muscular work performance before and after achieving oxygen steady state consumption

12 p2169 A70-27658

Initial period of muscular energy expenditure in athletes performing exercises on velocometer, considering oxygen consumption

12 p2172 A70-28313

Maximum oxygen uptake correlation to age of subjects performing physical and sedentary work

13 p2350 A70-29112

Human respiratory responses to gas mixtures with different oxygen content under rarefied atmospheric conditions

13 p2353 A70-29521

Maximal oxygen intake, pulse heart rate and lactate levels variations with physical activity in middle aged man free of cardiovascular disease

13 p2356 A70-29826

Hot environment and hyperthermy effects on oxygen consumption in subjects performing muscular exercise

13 p2360 A70-29947

High oxygen pressure effect on consumption rate constant for in vivo tissues

15 p2679 A70-31608

Metabolic Rate Monitor for measuring continuous oxygen consumption during changes in work in real time

15 p2741 A70-32540

Hybrid computer simulation of steady state oxygen transport and consumption in capillary-tissue system

15 p2694 A70-32845

Heart rate variations due to influence of body position rapid changes, emphasizing oxygen consumption in crouching position

17 p3024 A70-34591

Arterial pH change effects on circulation and oxygen consumption in dogs, discussing respiratory

acidosis heart rate, cardiac output and arterial blood pressure

17 p3024 A70-34593

Oxygen uptake capacity, ventilation, heart rate and acid base values during bicycle ergometer exercise

17 p3036 A70-34594

Tissue respiration measurement with membrane-covered oxygen electrode, discussing effects of electrode deterioration and diffusion artifacts on accuracy

17 p3026 A70-35186

Body temperature-maximum oxygen intake relations in hot humid air

17 p3038 A70-35424

Oxygen uptake and cardiac output in males during submaximal and maximal treadmill and bicycle exercise

17 p3039 A70-35428

Analog computer for continuous recording of oxygen consumption of muscular area in canine foot via blood flow rate and oxygen saturation

19 p3367 A70-37354

Psychotropic drugs radioprotective effects in mice, noting oxygen consumption and body temperature decrease after X ray exposure

19 p3367 A70-37558

Coulometric microrespirometer for long term numerical recording of oxygen consumption in respiratory chamber under sterile conditions

19 p3371 A70-38372

Oxygen pressure effects on tracking control training for stable reactions, investigating muscles bioelectrical activity changes during elevated pressure breathing

20 p3581 A70-40291

Oxygen uptake at alveolar capillary membrane, investigating ventilation variability at exercise onset

20 p3577 A70-40331

Liver blood flow in dogs during increased oxygen consumption

20 p3577 A70-40448

Turtle bladders isolated mucosal and serosal fractions histological and physiological properties, discussing ion transport and oxygen consumption

21 p3762 A70-41224

Body position effect on oxygen saturation of regional pulmonary venous blood and arterial-venous shunts in intact dogs

21 p3766 A70-42153

Fatigue effects on relationship between oxygen consumption, electromyographic activity and isometric contraction in human leg muscles

21 p3766 A70-42159

Muscular activity influence on energetic processes and functions in aging organism, relating oxygen consumption to aerobic metabolism

22 p3968 A70-42895

Body oxygen control under muscular activity in aging individuals

22 p3969 A70-42899

Oxidative phosphorylation and oxygen intake during circulatory hypoxia in mitochondria of liver and brain in rats subjected to acute ischemia

23 p4145 A70-44315

Oxidative phosphorylation and oxygen consumption during hyperoxia in mitochondria preparations and tissue homogenates from white rat liver

23 p4146 A70-44316

Human cardiovascular compensatory responses to environmental cold stress, relating heart stroke to increased oxygen consumption

24 p4302 A70-46103

Oxygen transport, arterial resistance and consumption in normovolemic and hypovolemic dogs in hemorrhagic shock

24 p4302 A70-46106

OXYGEN DEFICIENCY

U HYPOXIA

OXYGEN DETECTORS

U OXYGEN ANALYZERS

OXYGEN FLUORIDES

Oxygen difluoride-diborane reaction measured for pressure-temperature relationships and gas composition dependence on time, noting possible applications as hypergolic rocket propellants

11 p1995 A70-26138

Oxygen difluoride-diborane reaction kinetics and boron fluoride formation rate [WSCI PAPER 70-11]

13 p2362 A70-29611

Oxygen difluoride/diborane propellant thrust chamber and injector technology, discussing engine duty cycles and performance

16 p2962 A70-33550

Gelled space-storable oxygen difluoride and diborane analysis, including particle preparation, yield stresses, viscosities and storability [AIAA PAPER 70-609]

16 p2962 A70-33607

OXYGEN ISOTOPES

NT OXYGEN 18

Correlation between O isotope ratios and composition of tektites investigated for origin of tektites

05 p0917 A70-16840

Bowen levels of O III radiative lifetimes and transition probabilities measurements by beam-foil spectroscopy

10 p1936 A70-23909

Carbon-nitrogen-oxygen isotope bi-cycle function in solar evolution, noting first cycle role in solar energy release and neutrino production

20 p3698 A70-39306

Apollo 11 lunar rocks oxygen isotope ratios, examining relationship to terrestrial basalts

21 p3776 A70-41596

Oxygen isotope fractionation and formation temperature of minerals from Apollo 11 rocks, including plagioclase-clinopyroxene-magnetite concordancy diagram

21 p3776 A70-41597

Apollo 11 lunar rocks and minerals oxygen 18- oxygen 16 ratios

21 p3777 A70-41609

OXYGEN MASKS

Closed circuit respiration studies on subjects at rest and work, demonstrating potassium superoxide as oxygen source in breathing apparatus

15 p2688 A70-31500

Continuous flow requirements in aircraft passenger oxygen systems using phased dilution principle, discussing breathing mask efficiencies

23 p4141 A70-44483

OXYGEN METABOLISM

Patients with/without coronary heart disease inhaled various gas mixtures to induce arterial hypoxemia and hyperoxia, noting O availability for myocardial metabolism

01 p0016 A70-10440

Positive Na and K ion effects on mitochondrial respiratory control, O uptake and adenosine triphosphate activity in rat liver

01 p0026 A70-11063

Humans and dogs breathing CO in closed system, discussing distribution on blood, body stores and oxygen metabolism

02 p0234 A70-11727

Stimulated thyroid gland temperature variations and oxygen metabolism in decorticated dogs and anesthetized rabbits and rats

04 p0639 A70-15511

Equation describing atmospheric oxygen conductance to human tissues compared with experiments, ascribing discrepancies to inhomogeneity in diffusion/perfusion relationships

06 p0993 A70-17434

Protective ability of various compounds against hyperoxia at 5, 7, 9 and 11 atmosphere of pure oxygen

08 p1441 A70-20629

Prolonged hypodynamia effect on human external respiration, arterial blood oxygenation, circulation rate and gas exchange under various physical stress conditions

10 p1814 A70-24674

Aerobic metabolism of heart muscle cells and oxygen utilization of coronary artery blood

10 p1821 A70-25081

Hypoxia diagnosis based on excess lactate determination as indicator of oxidative metabolism changes

10 p1822 A70-25084

Pure oxygen effect on amino acids uptake and metabolism of *Pseudomonas saccharophila* stationary cells

14 p2536 A70-30343

Metabolic Rate Monitor for measuring continuous oxygen consumption during changes in work in real time

15 p2741 A70-32540

Hematology of sea level and high altitude native Sonoran deer mice, correlating hemoglobin electrophoretic patterns with oxygen affinity

15 p2686 A70-32835

Sodium oxybutyrate effects on brain tissue oxidation during hypoxia in mice

15 p2686 A70-32851

OXYGEN PRODUCTION

Atmospheric water vapor photodissociation and resulting O evolution recalculated for determining O abundance in absence of biological activity

01 p0081 A70-11294

Water electrolysis module long term operation in providing oxygen for life support systems

05 p0804 A70-15843

Space stations life support systems for air purification, water reclamation and oxygen recovery

08 p1449 A70-20630

Hill reaction color sensitivity in red and blue light during chloroplast disintegration, considering oxygen evolution capacity

15 p2684 A70-32548

Atmospheric oxygen history, using primeval anoxic terrestrial atmosphere simulation to show organic molecule formation by abiogenic process

16 p2898 A70-33990

Carbon dioxide electric discharge dissociation producing oxygen molecules

17 p3138 A70-35588

Solid oxygen generator for oxygen gas production from sodium chlorate decomposition, discussing reliability, safety and maintenance

18 p3225 A70-36211

Unicellular hot spring acidophilic alga *Cyanidium cadarium* cultured in pure carbon dioxide, examining

packed cell volume, oxygen production and growth rate

20 p3572 A70-39492

Prototype electrolyzer for generating oxygen from water vapor under various atmospheric conditions, noting spacecraft cabin application

20 p3564 A70-39696

Integrated Life Support System hardware tests, discussing oxygen and water recovery, contaminant control, personal accommodations and failure detection

21 p3833 A70-40989

OXYGEN RECOMBINATION

Nighttime recombination model of O ion plasma in upper ionosphere, showing temporal behavior and variation of electron concentration

07 p1265 A70-19432

Auroral green line rocket measurements, showing roles of atomic and molecular oxygen dissociative recombinations

10 p1874 A70-24432

Recombination in hydrogen-oxygen reaction studied by monitoring IR emission from water vapor formed by shock initiated combustion

11 p1995 A70-26377

Oxygen cation electron dissociative recombination rate coefficient measurement during expanding oxygen flow in nozzle

12 p2276 A70-27802

Atomic oxygen beams interaction with various surfaces at low pressure, discussing reflection probability and recombination reactions

18 p3225 A70-36187

Nighttime recombination model of O ion plasma in upper ionosphere, showing temporal behavior and variation of electron concentration

18 p3249 A70-36906

Hydrogen-oxygen flames recombination rates measurements analysis, taking into account reverse reaction rates

20 p3583 A70-40470

Winter predawn enhancement of 6300 A airglow at higher midlatitudes, considering roles of oxygen dissociative recombination and photoelectrons production at magnetically conjugate point

22 p4019 A70-43110

Oxygen atom catalytic recombination and flame inhibition mechanism literature survey

23 p4157 A70-44002

OXYGEN REGULATORS

Commercial flight crew oxygen system using mask mounted diluter demand regulator

06 p1002 A70-17715

OXYGEN SENSORS

U OXYGEN ANALYZERS

OXYGEN SPECTRA

Oxygen collisional quenching rate in F region determined by comparing nightglow intensities with intensities calculated from electron density profiles

01 p0070 A70-10403

Predawn O I 6300 A airglow enhancement, observing time variations and suggesting mechanism

02 p0289 A70-12120

Variable atmospheric attenuation of 5 mm wavelength band, considering oxygen absorption spectrum and attenuation for reference atmosphere

02 p0260 A70-12570

Atmospheric oxygen A band individual rotational lines intensities and half widths measurements

02 p0344 A70-12656

Transition probabilities for diatomic oxygen Schumann-Runge bands determined from shock tube emission studies

02 p0344 A70-12658

Vertical profiles of atomic and excited molecular oxygen concentration in upper atmosphere calculated from spectral band intensity, determining excitation reaction rates

04 p0682 A70-15733

Vertical air density profile from satellite measurements of atmospheric oxygen radio emission at 40-70 km altitudes

06 p1056 A70-17788

Predawn enhancement of emission rate of 6300 A forbidden O I line in nightglow spectrum, discussing onset time

07 p1275 A70-20286

Molecular oxygen concentration determined by absorption spectroscopy of solar hydrogen Lyman alpha line

08 p1490 A70-21390

OI 6300 A airglow intensity decrease at dawn ascribed to scattered solar radiation

08 p1492 A70-21720

Excitation and layers heights for 5577 A and O2 bands of atmospheric and Herzberg systems in night airglow estimated, suggesting Chapman reaction for emission

08 p1492 A70-21755

Hydroxyl emission during auroras, noting absence of correlation with O I brightness fluctuations for IBC II-III aurora of 1 November 1968

09 p1671 A70-23496

IR oxygen emission transmission characteristics in atmosphere compared with ground-based observation

10 p1876 A70-24538

Seasonal changes in thermospheric composition in middle latitudes, investigating molecular oxygen density and solar activity effects

10 p1881 A70-24817

Vertical air density profile from satellite measurements of atmospheric oxygen radio emission at 40-70 km altitudes

10 p1882 A70-25020

Auroral enhancement of IR oxygen band at 1.27 micron compared with molecular nitrogen band intensity

12 p2222 A70-27185

Auroral green line decay of atomic oxygen measured photometrically from multiple exposure spectra of meteor wakes

12 p2304 A70-27713

Vertical profiles of atomic and excited molecular oxygen concentration in upper atmosphere calculated from spectral band intensity, determining excitation reaction rates

14 p2575 A70-30817

5577 A /OI/ airglow emission diurnal variations during IGY by normalization method, observing seasonal effects

14 p2578 A70-31239

Excitation and radiative transport of 1304 A triplet of atomic oxygen for dayglow and aurora

14 p2578 A70-31241

Atomic oxygen 1D excitation state obtained by metastable He atoms collision with ground state oxygen molecules in O-He discharge

14 p2579 A70-31248

Nightglow OI lambda 6300 line width measurements during magnetic storm, discussing temperatures and intensity variations

14 p2579 A70-31250

Molecular oxygen emissions in airglow, inverting calculation to determine ozone distribution from observed altitude profiles

14 p2580 A70-31265

Night sky atmospheric continuum, zodiacal light and OI line observations with photoelectric color telescope

14 p2581 A70-31268

Electron impact excitation cross sections of oxygen ion first negative bands, considering relationship to oxygen ionization cross section

14 p2620 A70-31363

Triply ionized oxygen atom spectrum between 500-8000 A, determining energy levels and ionization limit

15 p2777 A70-32428

Near IR electronic emission spectrum of positive column in flowing oxygen electric discharge, noting vibrational temperature

16 p2955 A70-33981

Telluric lines seasonal variations, discussing oxygen and water vapor photoelectric recordings in solar spectrum

16 p0000 A70-34185

Spectrophotometric airglow intensity measurements of OH, O I 6300, hydrogen H alpha and oxygen Herzberg I bands by airborne laboratory

17 p3080 A70-35769

Tropical UV nightglow, considering oxygen ion-ion neutralization reaction as primary source

18 p3244 A70-36015

Direction and time variations of O I 4368 A emission following evening twilight

18 p3245 A70-36026

Vertical distribution of upper atmospheric 7600 A oxygen glow, discussing 8645 A band and nitric oxide data

18 p3251 A70-36977

Interstellar hot low density intercloud medium in H I region, estimating diffuse emission in forbidden lines O I at 6300 A and N I at 5200 A

18 p3310 A70-37020

Night airglow oxygen red lines predawn enhancement calculations, confirming role of photoelectrons from magnetic conjugate ionospheric

19 p3414 A70-38380

Auroral enhancement of IR oxygen band, considering electric field excitation mechanisms

19 p3414 A70-38383

Evening twilight airglow oxygen IR band ground based observation by two-channel photometric technique

19 p3415 A70-38385

Pi sub u states of positive ionized diatomic oxygen by photoelectron spectrometry

19 p3474 A70-38488

UV oxygen nightglow observation by OGO-4, examining ion-ion neutralization and radiative recombination production mechanisms

20 p3621 A70-39344

Anomalous IR auroral emission observation during rocket flight, indicating unknown energy sources of oxygen excitation

20 p3621 A70-39350

Decay lifetimes and electron impact cross sections of vacuum UV O I and O II emission multiplets, using pulsed electron beam in low pressure gases
21 p3852 A70-40718

Auroral optical emission measurements, examining oxygen atmospheric and IR bands by rocket sounding
21 p3817 A70-41092

Predawn enhancement of O I 6300 Å line, considering magnetically conjugate photoelectron effects on atomic oxygen excitation
22 p4095 A70-43113

Auroral spectrophotometer measurements from 1968 NASA airborne expedition, discussing oxygen and nitrogen spectral lines
23 p4186 A70-43855

Molecular oxygen ions 1Ng band and molecular nitrogen 1Pg band relative intensities in normal and type B auroras
23 p4191 A70-44408

Doubly excited antiferrodielectrics absorption spectrum band and bound states, discussing zero approximation 0-0 transitions of alpha oxygen molecules and permeability tensor
24 p4392 A70-46362

OXYGEN SUPPLY EQUIPMENT

NT OXYGEN MASKS

Chemical and physical adsorption of gaseous oxygen contaminants to maintain purity for respiratory purposes, noting trichlorethylene and carbon tetrachloride
01 p0031 A70-10236

Dynamic testing instrumentation for oxygen breathing equipment emphasizing demand regulators and masks, connecting hose, helmets and individual components
01 p0041 A70-11458

Physiological training programs and equipment for life support in transports, discussing changes in protective helmet and quick donning harness
06 p1002 A70-17708

Fleet evaluation program of AOH-1 helmet for replacement of standard flight helmet, oxygen mask retainer kit and oxygen regulator
06 p1002 A70-17709

Commercial flight crew oxygen system using mask mounted diluter demand regulator
06 p1002 A70-17715

Physiological and environmental factors influencing oxygen breathing system design and use for passengers and aircrews of high flying aircraft
06 p1003 A70-17716

Oxygen equipment design for USN patrol and attack aircraft, considering masks, regulators, helmets and hoses
07 p1191 A70-19005

Personnel protection against accidental decompression in transport aircraft at high altitudes, recommending flight stations with capsule to achieve ground level oxygen equivalent
09 p1627 A70-23459

Supercritical pressure system heat transfer characteristics for cryogenic space oxygen storage and supply
14 p2667 A70-31342

Portable contingency transfer life support system for crewman of Apollo missions providing oxygen and cooling
20 p3580 A70-39441

NASA aircrew oxygen system, describing carbon dioxide control and oxygen generation subsystems
21 p3768 A70-40990

Life support systems oxygen generation mode selection based on mission parameters, including duration, crew size, resupply, vehicle leakage, etc
21 p3768 A70-40991

Oxygen-nitrogen generation for long manned space flight based on liquid center dual matrix electrolysis cell
21 p3768 A70-40992

OXYGEN SYSTEMS

U OXYGEN SUPPLY EQUIPMENT

OXYGEN TENSION

NT HYPOXEMIA

Rats sympathoadrenomedullary response to increased oxygen tensions, measuring catecholamines, norepinephrine and epinephrine in adrenal gland, hypothalamus, serum and urine
01 p0024 A70-10979

Hyperbaric oxygenation (OHP) effect on left ventricular function evaluated by measurement on anesthetized dogs of myocardial contractility
02 p0230 A70-11701

Oxygen tension and pressure effects on hyperbaric oxygenation induced depletion of brain norepinephrine and 5-hydroxytryptamine in mice
02 p0235 A70-11992

Oxygen and carbon dioxide partial pressures bloodless determination in mixed venous blood, using platinum electrode and IR carbon dioxide meter
02 p0236 A70-12091

Co-Cr alloy oxidation behavior at high temperatures and various oxygen pressures
02 p0319 A70-12720

Dithiols protective effect against ionizing radiation in mice, noting oxygen pressure drop role
03 p0420 A70-13311

Time varying blood flow in pulmonary capillaries affecting overall diffusing capacity and alveolar-arterial oxygen tension gradient
03 p0421 A70-13570

Increased oxygen partial pressure effects on cerebral bioelectric activity from EEG recordings on unanesthetized dogs
03 p0422 A70-13690

Hyperbaric oxygenation effects on metabolism, comparing protective agents for rats exposed to 5 absolute oxygen pressures
04 p0631 A70-14681

White single-comb Leghorn chick embryonic development at increased pressures at various hyperbaric gas mixtures for ten day periods
06 p0991 A70-17296

Oxygen tension change effects on rats smooth vascular muscles electrical and contractile properties
07 p1198 A70-18715

Physiological and hygienic data on oxygen partial pressure in space cabin atmosphere analyzed for manned space flights
07 p1220 A70-19502

Mathematical model for oxygen tension changes in dogs brain tissues under hypoxia during altitude simulation
07 p1208 A70-19505

Automatic control theory found effective in studying arterial blood saturation with oxygen during ascent to 4000 m in pressure chamber
07 p1210 A70-19523

Oxygen uptake by brain as function of oxygen tension in rats using venous outflow method and blood gas analysis
08 p1446 A70-21436

Physiological and hygienic data on oxygen partial pressure in space cabin atmosphere analyzed for manned space flights
11 p1991 A70-26101

Mathematical model for oxygen tension changes in dogs brain tissues under hypoxia during altitude simulation
11 p1987 A70-26104

Tissue oxygen partial pressure measurement in resting skeletal gracilis muscle of cat, using microelectrode
11 p1989 A70-26664

Compression effects in air-oxygen mixture on male mice, observing no adversity on mortality, growth and nitrogen content
13 p2353 A70-29436

Oxygen and carbon dioxide effects on airway smooth muscle following pulmonary vascular occlusion in dogs
13 p2356 A70-29943

Wustite partial oxygen pressure measurements using emf in zirconia solid electrolyte
16 p2961 A70-33965

White rats adaptation to multiple high temperature exposures, examining oxygen tension in skeletal muscles
18 p3220 A70-36549

Hypercapnia effect on oxygen tension in ischemic myocardium in dogs using polarographic method
24 p4300 A70-45843

Adrenocorticotrophic hormone effect on oxygen tension in rabbit kidney
24 p4301 A70-45845

OXYGEN TOXICITY

U HYPEROXIA

OXYGEN 18

Sagittarius sources A and B2 O18H absorption lines measured at microwave frequencies, determining oxygen isotopes abundance ratios
10 p1936 A70-23907

Oxygen 18 concentration in Greenland ice core correlation to solar activity index, indicating earth temperature control by solar activity
13 p2489 A70-28909

OXYGENATION

Oxygen tension and pressure effects on hyperbaric oxygenation induced depletion of brain norepinephrine and 5-hydroxytryptamine in mice
02 p0235 A70-11992

Elastic interaction energy involved in Ti solution hardening by oxygen determined using anisotropic elasticity, presenting atomistic calculations and chemical bonds breaking role
05 p0862 A70-15906

Hyperbaric oxygenation effects on cellular membrane permeability, analyzing rat plasma behavior of transaminases GOT and GPT and K and Na cations electrolytes
05 p0802 A70-16493

Hyperbaric oxygenation treatment physiology and techniques, discussing limitations of equipment
09 p1620 A70-23017

Physiology of oxygen transport in human organism and genesis of tissue hypoxia, discussing pulmonary functions, blood transport properties and tissue blood flow and diffusion
10 p1821 A70-25077

Physiology and pathophysiology of oxygen transport in human blood, discussing fluctuations in O2 capacity and affinity
10 p1821 A70-25079

Oxygen transport after cardiopulmonary resuscitation from asystole and ventricular fibrillation in dogs
10 p1822 A70-25085

Brain oxygen supply during cerebral edema, examining venous and arterial blood gases, circulation, oxygen uptake, blood volume and pressure and EEG
10 p1822 A70-25087

Long term weightlessness effects on cardiovascular system of rats using miniaturized pump oxygenator
16 p2854 A70-33999

Benzoyl cyanide deoxygenation, describing reaction kinetics and products
17 p3041 A70-34750

Rene 41 ductility reduction by environmental oxygen promoting intergranular cracking at high temperatures
18 p3277 A70-36524

Oxygen role in crack initiation and growth in Ni alloys postwelding heat treatment
18 p3277 A70-36525

Temperature dependence of anisotropic reaction kinetics of oxygen with pyrolytic graphite
19 p3373 A70-37709

Interstitial oxygen effect on properties and precipitation processes in pure V and V-Ti alloys, using electron microscope
19 p3454 A70-38812

Niobium yield stress at room temperature for various nitrogen and oxygen concentrations
19 p3454 A70-38814

Rats brain oxygenation during hyperventilation with air or oxygen-nitrogen mixture, measuring creatine phosphate concentration and lactate/pyruvate ratio
21 p3762 A70-41225

OXYHEMOGLOBIN

Oxygen diffusion in presence of hemoglobin taking into account chemical kinetics, showing approximate and computer solutions
10 p1819 A70-24772

Mossbauer spectrum of submolecular changes of oxyhemoglobin in animal blood exposed to microwave irradiation
23 p4144 A70-43788

OZONE

NT OZONIDES

Vertical ion concentration profile in troposphere and stratosphere from ozone distribution satellite measurements using aeronautical reactions
02 p0291 A70-12389

Soviet collection of papers on radiation fluxes and ozone in atmosphere covering concentration, UV radiation scattering, etc
03 p0473 A70-13293

Mean and extreme atmospheric ozone concentration calculated as function of altitude and seasons in Northern Hemisphere
03 p0474 A70-13294

Temporal autocorrelation functions of ozone content and autocorrelation from data of Soviet and U.S. stations, obtaining statistical stability
03 p0474 A70-13295

UV radiation scattering and rocking instrument error source in vertical ozone profile determination with optical ozone probes
03 p0557 A70-13296

Atmospheric absorption anomalies of UV sunlight near 50 km altitude in rocket-borne radiometer determination of ozone distribution
03 p0478 A70-14197

Statistical model of ozone absorption bands for calculating intensity, rotational line position and transmission functions of complex spectral regions
04 p0680 A70-15252

Vertical profile of angular mass distribution of atmospheric water vapor and ozone as gas proportion function
06 p1097 A70-17794

Atmospheric ozone content and mass effect on solar radiation flux measured during total solar eclipse of 22 September 1968
07 p1275 A70-20310

Atomic bond rupture rate in rubber subjected to uniaxial tensile strain in ozone environment monitored by electron paramagnetic resonance measurements
08 p1527 A70-21454

Ozone formation in presence of nitrogen oxides and hydrocarbons during long wave UV irradiation, noting energy yield
09 p1629 A70-22328

Aeronomic neutral reaction rates, describing ozone excited state photochemistry
10 p1872 A70-23824

Downward ozone transport from troposphere to atmospheric boundary layer by turbulent diffusion calculated by model, estimating annihilation rate
10 p1875 A70-24486

Specific intensity production from photolysis of ozone-oxygen mixtures at 2537 Å, investigating mechanism
10 p1831 A70-24565

Vertical profile of angular mass distribution of atmospheric water vapor and ozone as gas proportion function
10 p1913 A70-25025

Atmospheric absorption by ozone of solar radiation measured by balloon-borne spectrometer in 9-10 micron region
11 p2045 A70-25627

IR absorption in ozone band, including atmospheric inhomogeneity effects on accuracy of transmittance calculations
12 p2223 A70-27515

Lower stratosphere ozone formation, suggesting origin in cosmic rays absorption
13 p2400 A70-29472

Middle stratospheric circulation in Southern Hemisphere, associating temperature changes and ozone content with planetary wave passage in Antarctic polar vortex
14 p2568 A70-30123

NO and nitrogen dioxide influence on ozone concentration and production rate in stratosphere
14 p2568 A70-30125

Mesospheric daytime/nighttime ozone abundance vertical profile diurnal variations
14 p2568 A70-30130

Winter stratospheric circulation quasi-geostrophic model based on joint radiative-photochemical equilibrium, investigating ozone cycle and warming
16 p2945 A70-33250

Pressure effects on quantum yields of carbon trioxide formation in gas phase ozone photolysis with carbon dioxide
16 p2856 A70-33653

Molecular oxygen role in photolytic decomposition of ozone by intermediate quantum yield method, presenting rate constants
16 p2858 A70-34009

Ozone content effect on presunrise fall in LF radio waves amplitude from Radio Tashkent to Delhi, noting UV light role
17 p3077 A70-34947

Flux emissivity tables for water vapor, carbon dioxide and ozone based on wavelength dependent absorption coefficients and flux transmissivities
17 p3081 A70-35927

Ozone concentration in San Francisco Bay Area, discussing temperature inversion, air pollution, destruction rate and distribution patterns of oxidants
18 p3284 A70-35945

Mars UV reflectivity, examining spectrum, absorption features, planet albedo and ozone content by rocket-borne instruments and atmospheric models
18 p3317 A70-37011

Atmospheric ozone longitudinal variation in lower middle latitudes of Southern Hemisphere
18 p3256 A70-37117

Rhodamine C chemiluminescent material for atmospheric ozone measurements, describing preparation and luminescence spectrum
19 p3373 A70-37638

Ozone effect on stratospheric electricity based on numerical calculations of ion densities
19 p3413 A70-38005

Atmospheric ozone remote sensing by high resolution IR interferometer spectrometer /IRIS/ aboard Nimbus 3 satellite
19 p3414 A70-38262

Ozone concentration variations in upper atmosphere during solar eclipses
19 p3418 A70-38906

Anomalous seasonal variation in worldwide ozone above 40 km from Umkehr measurement, considering turbidity effects
23 p4187 A70-44037

Noctilucent clouds blue color and rocket sounding results explained by ozone model of mesospheric clouds formation
23 p4188 A70-44048

Diurnal variation symmetry of upper atmosphere molecular oxygen concentration in terms of ozone photodissociation
23 p4190 A70-44083

OZONIDES
Peroxides, superoxides and ozonides applications in industrial chemistry, semiconductors and rocket motor fuels, discussing chemical structure and properties and nomenclature
05 p0810 A70-15768

OZONOMETRY
Network ozonometer compared to ozonometers with narrow interference filters, finding fictitious day lapse in data
06 p1064 A70-17791

Arcas rocket-borne chemiluminescent ozonesonde for measuring ozone concentration after deployment above stratopause level
07 p1396 A70-20263

Photochemical calculations on mesospheric ozone for oxygen only, oxygen-hydrogen and oxygen-hydrogen-nitrogen atmospheres
07 p1273 A70-20268

Umkehr observation days selectivity effects on calculated mean ozone distributions in layers 2 and 3
08 p1492 A70-21970

Ozone measurement from satellite by direct beam and scattered light methods employing UV sunlight attenuation
10 p1890 A70-24639

Network ozonometer compared to ozonometers with narrow interference filters, finding fictitious day lapse in data
10 p1892 A70-25023

Gravity waves structure simultaneous determination from airborne ozone and temperature sensors and satellite observations data
11 p2076 A70-26072

Atmospheric ozone vertical distribution measurement based on luminescence of solid organic substances, noting chemical and optical methods
14 p2573 A70-30409

Stratospheric and mesospheric ozone diurnal variation by rocket-borne ozonesonde in January 1968
14 p2577 A70-31170

Molecular oxygen emissions in airglow, inverting calculation to determine ozone distribution from observed altitude profiles
14 p2580 A70-31265

Soviet papers on actinometry, atmospheric optics and ozonometry
20 p3624 A70-39026

Atmospheric ozone content during May 1966 solar eclipse, noting solar disk darkening effect on measurements
20 p3615 A70-39031

Aerosol correction for atmospheric ozone content measurements using direct sunlight
20 p3615 A70-39032

Ionospheric transition and ozone correction from D region sunrise auroral rocket flight
21 p3814 A70-40935

Vertical atmospheric ozone distribution according to direct solar radiation received on ground, using UV and IR observations
22 p4023 A70-43296

Ozone vertical distribution from satellite IR data, discussing Fredholm equations for radiation transfer
23 p4191 A70-44269

OZONOSPHERE
Umkehr observation days selectivity effects on calculated mean ozone distributions in layers 2 and 3
08 p1492 A70-21970

Ozonosphere heating between 20-60 km during high solar activity, determining positive heating rate gradient directions and maximum heating altitude
12 p2223 A70-27514

Solar radiation absorption by atmospheric ozone observations by ground stations for meteorological data
13 p2400 A70-29642

P

P WAVES
P wave changes in serial ECG in patients with acute myocardial infarction
01 p0013 A70-10272

Right and left atrial polarization time sequence as guide to p wave origin in heart diseased patients following electrical stimulation of atria and ventricles
01 p0015 A70-10437

P wave and P loop changes during transvenous pacing of specific locations in coronary sinus and left atrium in dogs and man
08 p1445 A70-21266

First order scattering formulae for s- and p-light reflected and transmitted by rough plane surface using perturbation theory
11 p2086 A70-26840

Upper critical field dependence on s- and p-wave scattering of Frenkel effects in electron irradiated niobium
13 p2471 A70-29535

Seismic refraction profiles of ash flow in Valley of Ten Thousand Smokes, Alaska, obtaining P wave velocities
14 p2573 A70-30493

Circadian rhythms from electrocardiogram and cardiachogram of patient with human heart transplant, noting P waves relationship between donor and recipient tissues
20 p3570 A70-39166

Apollo 11 lunar sample elastic wave velocities at high pressures, examining P and S waves, Q value and geophysical implications
21 p3916 A70-41666

P-I-N DIODES
U DIODES
U P-I-N JUNCTIONS
P-I-N JUNCTIONS
High efficiency oscillator using avalanche square wave diode, considering case of silicon p-i-n diode
05 p0819 A70-15815

Current carrier motion and diffusion capacity in p-i-n junctions with highly doped regions under large variable signal
05 p0892 A70-16197

Broadband two way switch obtained by p-i-n diodes deposited on alumina substrate
05 p0821 A70-16526

Negative resistance and cut-off voltage of doped Si p-i-n diodes subject to deep acceptor levels
10 p1849 A70-24274

Nonequilibrium charge carriers transient accumulation in p-i-n diode at superhigh injection levels
15 p2714 A70-32908

Microwave p-i-n diode RLC equivalent circuit parameters experimental determination
23 p4171 A70-43956

Variable microwave attenuator using p-i-n diodes and three-port hybrids built in stripline technique
24 p4318 A70-45222

P-N JUNCTIONS
Electrical properties of Si-doped GaAs p-n structures obtained by liquid phase epitaxy, considering charge buildup
01 p0155 A70-10132

Current-voltage characteristics of p-n junctions in cadmium telluride, discussing spectral sensitivity bands
01 p0160 A70-11596

Gradual linear p-n junctions characteristics, including diffusion voltage value and temperature coefficient, space charge zone thickness and junction capacitance
02 p0268 A70-12493

Semiconductor injection laser modes, considering inhomogeneous lasing action levels over p-n junction area
03 p0499 A70-13410

P-n junction and microplasmas voltage temperature coefficients during avalanche breakdown
03 p0541 A70-13729

P-n heterojunction diode strain sensor fabricated by vacuum evaporation onto substrate, investigating mechanical input and output impedance characteristics
03 p0495 A70-14192

Neutron induced defect clusters in high field space charge region of Si p-n junctions, noting rate of volume damage dependence on electric field strength
04 p0730 A70-14728

Bifurcation frequency and nonlinear distortions determined in nonlinear semiconductor circuit with series-opposed connections of p-n junctions operating in forced oscillation mode
04 p0659 A70-15206

Equivalent conductances and resistances vs pumping oscillation modes of p-n junction in parallel and series-connected three-frequency parametric circuits
04 p0659 A70-15209

Gas discharge avalanche breakdown in Si semiconductors, analyzing microplasmas, ionization coefficients, p-n junction voltage, electron and light emissions
04 p0731 A70-15494

P-n-n structure dynamic I-V characteristics at high injection levels mathematically determined, showing rectifying capability decrease with increasing harmonic signal frequency
05 p0892 A70-16196

Minority current carriers diffusion in heterojunctions and p-n junctions in AlAs- GaAs, using X ray microanalyzer performing electron beam scanning
06 p1126 A70-17816

P-n junction depth in semiconductors, using electron beam of scanning electron microscope
06 p1127 A70-17820

GaAs p-n junction lasers operating properties under ideal and thermal conditions
07 p1298 A70-19396

GaAs lasers fabrication, discussing p-n junctions formation, laser die mounting, low resistance electrical contacts, optical cavities, etc
07 p1298 A70-19398

Electrical properties of Si-doped GaAs p-n structures obtained by liquid phase epitaxy, considering charge buildup
08 p1556 A70-21408

P-n junction avalanche and bulk Gunn effect microwave oscillators, analyzing IMPATT and TRAPATT modes
09 p1644 A70-22224

Fabrication effects on current instability during injection and breakdown of p-n junctions in GaAs oscillators
09 p1740 A70-23351

Natural oscillation mode in symmetrically graded p-n junction using Missawa small signal equations for avalanche diode
09 p1653 A70-23804

GaAs light amplifier p-n junction gain and output noise determination for wide photon energy ranges, studying input noise levels effects on sensitivity
10 p1928 A70-25167

Ionization gage with reverse biased silicon carbide p-n junction hot electron emitter as source
12 p2231 A70-27263

Emission field and Fermi quasi-levels distribution in injection laser with n-p heterojunction, determining frequency and threshold current temperature dependence
13 p2426 A70-28876

Modulation phase distribution over emitting surface of p-n junction GaAs laser at micron wavelength
13 p2431 A70-29866

Photodetector properties influence on opton transfer functions achieving light conversion by separating photocarriers with p-n junction

14 p2555 A70-30161

Iodide concentration effects on epitaxial GaAs p-n junctions growth characteristics

14 p2625 A70-30171

Regenerative semiconductor parametric amplifier saturation in forward current mode, assuming harmonic voltages /signal, pumping and difference frequencies/ action at p-n junction

15 p2708 A70-31522

Diffused p-n junction devices impurity profile from capacitance-voltage measurements

15 p2710 A70-32562

High voltage photoelectric generator containing semiconductor plates with series- and parallel- connected p-n junctions forming solid circuit for super-high light flux concentrations

16 p2843 A70-33201

Solar cells based on homogeneous diffusion p-n junctions in epitaxial GaAs films grown on Ge single crystal substrate

16 p2843 A70-33202

Indium arsenide p-n junctions fabrication and electrical and photoelectric properties

17 p3143 A70-35120

Photosensitivity and electroluminescence spectra of GaAs-indium gallium arsenide p-n heterojunctions at room temperature

17 p3144 A70-35708

Visible light-emitting p-n junctions formed in AlAs via Zn diffusion into single crystal n-type vapor grown AlAs layers

18 p3297 A70-36316

InAs p-n junction laser electrical and optical characteristics during spontaneous and stimulated radiative recombination

18 p3269 A70-36739

P-n junction photovoltaic cell excitation by two photon absorption with low bandgap energy

19 p3446 A70-37764

Current carrier mobility under dynamic regime in p-n junctions by computerized method, emphasizing transitory phase

19 p3487 A70-38169

Photovoltaic effects in p-n junction semiconductors, discussing conduction and electro- optical mechanism in thermal equilibrium

19 p3488 A70-38476

Impurity distribution in diffused p-n junction in thin epitaxial film, calculating space charge region width and junction capacitance

20 p3685 A70-38967

Nonlinear LC circuit with p-n junction capacitance, examining relaxation vibrations during automatic biasing

20 p3596 A70-38970

Degenerate p-n diode junction capacitance calculation, taking into account quantum and temperature effects

20 p3596 A70-39117

P-n junction dependent FM noise spectrum of UHF transistor power oscillator at transit frequency

23 p4161 A70-43789

Current twisting in double injection ohmic contact long p-n diodes with S-shaped current-voltage curve, showing unstable density at negative resistance segment

23 p4176 A70-45061

P-n junction conductance at superhigh frequencies in breakdown region with simultaneous tunneling and impact ionization

23 p4232 A70-45064

GaAs injection lasers, calculating effect of active region displacement from p-n junction waveguide on wave generation

23 p4203 A70-45074

Cu and Ni doped n-p and p-n silicon solar cells, examining radiation damage and isochronal annealing properties

24 p4294 A70-45810

P-N-P JUNCTIONS

Germanium p-n-p transistor frequency oscillation dependence on emitter current, noting forced air cooling effect

09 p1741 A70-23354

UHF Si p-n-p transistors with low noise and high gain for small signal applications

14 p2557 A70-31161

P-N-P-N JUNCTIONS

Conducting state propagation in p-n-p-n structure involving minority carrier diffusion between regions

23 p4232 A70-45068

P-TYPE SEMICONDUCTORS

Edge luminescence effect in doped p-GaAs single crystals with various hole concentrations, determining band structure at liquid nitrogen and room temperature

01 p0154 A70-10097

Laser transitions to valence band or acceptor in low loss uniformly pumped crystal structure p-type GaAs at 77 K

01 p0113 A70-11168

Autoelectron and autophotoelectron emission from Fe-doped p-type GaAs cathodes in vacuum, noting I-V and emission characteristics dependence on light flux

03 p0538 A70-13067

Resistivity, temperature and injection level dependence of minority carrier lifetime in neutron irradiated p- and n-type Si

04 p0730 A70-14729

N-type layer formation with ion implanted nitrogen or Sb in p-type alpha-SiC, evaluating electrical characteristics, discussing junction devices formed

04 p0732 A70-15685

Ohmic contacts to n- and p-type semiconductors obtained by ruby laser, noting linear current- voltage characteristics

07 p1299 A70-19797

Cu doped GaAs n- to p-type transition after fast reactor neutron irradiation, measuring Hall effect and photoconductivity to determine Cu electrical activation

12 p2287 A70-27490

Active region characteristics of double injection laser employing electron-hole plasma in p-type indium antimonide

12 p2247 A70-27491

N-type Te-doped gallium antimonide conversion to p-type by electron irradiation, noting thermal conductivity variations

13 p2470 A70-29167

Parallel and perpendicular negative magnetoresistance measurements as function of magnetic field in p-type GaAs at 77 K

13 p2471 A70-29374

P-type GaAs laser diodes spontaneous emission power temperature dependence, considering radiative recombination mechanism

13 p2378 A70-29545

Photoconductivity relaxation kinetics of low resistivity n- and p-type GaAs, showing nonradiative recombination

17 p3143 A70-35703

Electron momentum distribution function of p-type semiconductor with arbitrary band structure under electric and magnetic fields

17 p3144 A70-35704

Temperature and bias voltage dependence of zero bias tunneling structure in p-type GaAs-Au Schottky junctions

21 p3863 A70-41917

Electron tunneling through p-type GaAs point contacts on Pb single crystals at liquid He temperatures

21 p3864 A70-42017

Intraband absorption in p-type GaAs associated with carrier transitions between heavy and light hole in valence band

23 p4232 A70-45066

Mossbauer effect analysis of Fe impurity atoms in n- and p-type semiconductor compounds with wide and narrow forbidden gaps

24 p4388 A70-45204

P- and n-channel MOS transistor instability during superbreakdown voltage application to drain electrode

24 p4319 A70-45811

PACIFIC ISLANDS

NT JAPAN

PACIFIC OCEAN

Pacific ocean equatorial trough zone disturbances structure, discussing organized convective downdrafts role in rapid structural decay

06 p1101 A70-18578

LOF observations of long distance transequatorial step frequency radio circuits in Pacific Area during sunspot minimum period

07 p1232 A70-19174

PACKAGES

NT APOLLO LUNAR SURFACE EXPERIMENTS PACKAGE

PACKAGING

NT ELECTRONIC PACKAGING

Refuelable Mg-air battery anode, electrolyte and packaging materials selection from standpoint of cell voltage, metal consumption and sludge formation

02 p0253 A70-12721

Equipment container with sandwich type structure for packing delicate parts

10 p1852 A70-24899

Polymers industrial applications in textiles, building materials, furniture, aviation, automobile industry and packaging

19 p3455 A70-38700

PACKING DENSITY

Conductive heat transfer coefficients of densely packed electronic subassemblies

01 p0051 A70-10990

Spacecraft electronics packaging methods, discussing mechanical engineering aspect of high density component packing in single housing

06 p1017 A70-17337

Miniwire method of packaging high density electronic equipment shown in photographs, including OAO applications

24 p4320 A70-46247

High density packaging of micrologic flatpacks using high interconnection method for two-side use of double-sided card in space flight applications

24 p4320 A70-46248

PAD

Hydrodynamically lubricated rectangular taper-land bearing pads, analyzing geometry, viscosity, load capacity, friction and operating temperature conditions

13 p2418 A70-28740

PAGEOS SATELLITE

Spatial direction Riga-Cairo determined using simultaneous photographic observations of Pageos A satellite

06 p1054 A70-17550

Pageos I satellite characteristics, design, structure and orbital elements

10 p1941 A70-24585

PAINTS

Airline aircraft finishes for protection against corrosion, air pollution, discussing paint application and polyurethane technology

03 p0497 A70-14053

Paint technology findings and recommendations for airline aircraft surface finishes emphasizing use of polyurethanes

05 p0869 A70-16106

Computer optimization of spacecraft optical coatings for temperature control, using finite element analysis and matrix inversion

06 p1172 A70-17180

Corrosion resistant paint systems for aircraft structural parts under severe environmental conditions simulated in carrier test stand

14 p2598 A70-31292

Photochromic paint nondestructive testing for survival equipment, detecting bond defects and sandwich water

23 p4197 A70-44490

PAIR PRODUCTION

Electron-positron pair formation in electromagnetic field created by coherent laser light focused into vacuum with ideal lens

08 p1513 A70-21411

Photon bremsstrahlung from relativistic hydrogen plasma determined by studying electron-positron pairing effect on plasma radiation intensity

09 p1735 A70-22986

Electron-hole pair creation in semiconductors /Zener effect and impact ionization/ defined from qualitative study of electron-phonon collisions

10 p1928 A70-24624

Low density collisionless plasma sheath in planar and cylindrical geometry under weak magnetic field, considering ion-electron pair generation

14 p2624 A70-31040

Average triton energy required to produce electron-hole pair in silicon measured, describing precision charge calibration of amplifier system

15 p2784 A70-32396

Energy loss of high energy cosmic rays traversing isotropic radiation field of arbitrary energy spectrum in pair producing collisions with ambient photons

17 p3150 A70-34598

Simultaneity in optical photon pairs parametric production, verifying quantum mechanical description of fluorescence

17 p3143 A70-35187

PAKISTAN

Report to COSPAR on space research in Pakistan, covering rocket, satellite and ground based investigations, etc

15 p2830 A70-31718

PALEOMAGNETISM

Cyclonic convective cell fluctuation and nonuniform core rotation effects on reversal of geomagnetic field, investigating fossil magnetism

04 p0676 A70-14600

Earth magnetic field transition recorded in basaltic lavas in southeastern Oregon

07 p1276 A70-20351

Archeomagnetic measurements showing westward drift of geomagnetic intensity and correlation of magnetic earth moment with radiocarbon production

11 p2044 A70-25599

Australasian and Ivory Coast deep sea microtektites fission track ages compared to deposition ages from paleomagnetic data

12 p2310 A70-28021

Vredefort Ring origin, discussing paleomagnetic evidence to choose between meteorite impact or terrestrial cause

16 p2899 A70-34050

Cretaceous rock paleomagnetism from Israel lava fields, determining original magnetization directions

19 p3413 A70-38034

Paleomagnetic reversal in 1350 year increments, measuring declination of deep sea sediment cores

21 p3820 A70-41885

PALEONTOLOGY

Amino acid stability in pyrolyzed Pleistocene Mercenaria shells, comparing decomposition rates for aqueous solution

03 p0472 A70-13150

Apollo 11 lunar dust and microbreccia micropaleontological examination, discussing biological morphology 21 p3778 A70-41620

Palaeogeophysics - Conference, University of Newcastle-upon-Tyne, England, April 1968 21 p3921 A70-41969

Biology of fossil genus Kakabekia and living species Kakabekia barghoorniana Siegel cultured from Alaskan soil samples 24 p4304 A70-46232

PALLADIUM

Rhenium powder sintering activated by palladium additions producing low porosity 01 p0117 A70-10158

Au-Pd films boundary structure during diffusion annealing, noting polymerized oil vapor effect originating from vacuum pump 15 p2758 A70-32121

PALLADIUM ALLOYS

Palladium alloy transmodulator for gas chromatograph, demonstrating sensitivity gain for thermal conductivity and ionization cross section detectors 03 p0442 A70-14325

PALLADIUM COMPOUNDS

PdH system electrical resistivity, studying hydrogen concentration role 12 p2282 A70-26900

Cellulose ion exchanger palladium catalysts preparation and applications in asymmetric hydrogenation reactions 17 p3042 A70-35125

PALMGREN-MINER RULE

Miner rule for cumulative fatigue damage, obtaining upper and lower bounds on load cycle number to failure 24 p4426 A70-46024

PAM [MODULATED]

U PULSE AMPLITUDE MODULATION

PANEL FLUTTER

Curved cylindrical panel flutter in presence of uniform compressive load, taking into account relationship between actual and ideal shape 01 p0202 A70-10946

Transfer matrix method analysis of dynamic behavior of beam structures applied to single rows of aircraft panels 01 p0209 A70-11200

Rectangular clamped panel flutter characteristics at various oncoming flow angles of attack 03 p0590 A70-13382

Rib-reinforced rectangular plate flutter in gas flow, considering shell stability, rib torsional rigidity, etc 03 p0593 A70-13498

Radiation from and panel response to supersonic turbulent boundary layer, emphasizing panel mode coupling to acoustic field 04 p0615 A70-15081

Liapunov second method extension to dynamical systems stability, illustrating wing torsional divergence and panel supersonic flutter 05 p0941 A70-16564

Aerodynamic forces for boundary layer profiles of flexible plate under transient motion in shear flow using computer programs [AIAA PAPER 70-76] 06 p0972 A70-18122

Panel flutter theory applied to aeroelastic stability of flat unloaded plates and cylindrical shells 11 p2134 A70-25951

Wind tunnel interference effect on fluttering airfoils and panels supersonic speeds, studying pressure distributions for various tunnel aspect ratios and roof conditions 12 p2155 A70-27103

Nonlinear panel flutter for random excitation and linear/nonlinear aerodynamic loading, using Rayleigh-Ritz approximation to Hamilton variational principle 12 p2316 A70-27105

Supersonic flutter solutions using finite elements, analyzing rectangular plate bending elements, square simply supported and clamped panels, low aspect ratio configurations, etc 12 p2327 A70-27823

Circular cylindrical shells with clamped ends, investigating supersonic panel flutter by two mode approach and Galerkin method 17 p3184 A70-34695

Supersonic panel flutter of circular cylindrical shells at critical dynamic pressure 17 p3188 A70-35227

Probability theory of stresses during random vibrations of flat panel in acoustic field of jet engine exhaust 18 p3301 A70-36301

Flutter design charts for isotropic panels stressed to verge of buckling for tropical values of structural damping 18 p3338 A70-36446

Infinite elastic plates traveling wave flutter in compressible flow, investigating viscous damping effects on critical flow velocity 18 p3343 A70-36701

Thin plates and thin walled cylinders aeroelastic stability in fluid flow, analyzing panel flutter 19 p3546 A70-38342

Elastic panel nonlinear free vibrations, analyzing small amplitude phenomena 20 p3672 A70-39493

Skew panels supersonic flutter and vibration calculated by matrix displacement method 21 p3933 A70-40586

Circular cylindrical shell supersonic panel flutter nonlinear analysis, using averaging and numerical integration methods 22 p4112 A70-42275

Thin circular cylindrical panels in supersonic gas current parallel to generatrices, calculating heterogeneity effect on flutter 22 p4113 A70-42603

Fluttering isotropic rectangular flat plate fatigue life estimation, taking into account stress, dynamic pressure, frequency, Mach number and plate thickness 23 p4270 A70-44577

Aeroelastic and aerothermoelastic development of winged interorbital space shuttle concerning panel flutter, stability and nonstationary lifting surface theory 23 p4273 A70-44760

ONERA calculations in aeroelasticity including lifting surface optimization, control surface vibration, pressure fields, aircraft transfer functions and panel flutter 23 p4274 A70-44762

PANELS

NT CURVED PANELS

NT RECTANGULAR PANELS

NT WING PANELS

Wide strut analysis for determining weight minimizing cross sectional dimensions of panels having unflanged integral stiffeners 03 p0596 A70-14145

Fatigue life of stiffened skin pannels under acoustic loading of wideband frequencies to achieve structural resistance optimization [DGLR-69-63] 04 p0774 A70-15140

Pseudosound field wall pressure correlation obtained to predict response characteristics of aircraft panel mounted along jet wake 05 p0835 A70-16785

Stability equations of three layer panels with allowance for rigid filler transverse deformations 07 p1415 A70-20186

Sound energy transmission and radiation into room by flexible structural panels subjected to acoustic excitation using wave equations 10 p1964 A70-25224

Core shear deformations effects on stress, deflection and buckling load calculations for sandwich panels 15 p2815 A70-31931

Optimum fiber orientation for minimum weight boron/epoxy shear panel design 17 p3182 A70-34562

Core flexibility effects on deformation of uniformly loaded clamped parallelogrammic sandwich panels using linear theory 17 p3185 A70-34920

Sandwich panels geometrically and physically nonlinear theory, obtaining equations of motion and boundary conditions consistent with strain displacement relations 19 p3547 A70-38360

PANORAMIC CAMERAS

Holocamera holographic system for wide angle panoramic view, discussing dual laser beam illumination, side and top view diagrams, etc 16 p2913 A70-33984

PANORAMIC SCANNING

Panoramic vertical sounding method of ionosphere, noting drawbacks 18 p3255 A70-37040

Celestial sphere scanning by spinning symmetric satellite with open loop magnetic control of precession 23 p4216 A70-44524

PAPERS

Photographic paper as emulsion film substitute in industrial radiography, evaluating sensitivity and image contrast 24 p4337 A70-45715

PARA HYDROGEN

Far IR spectra of liquid hydrogen at para concentrations, noting absorption coefficient variation consistent with composition 04 p0718 A70-14696

Viscosity and thermal conductivity of dilute gaseous para and normal hydrogen at various temperatures 19 p3551 A70-37710

Solid para hydrogen IR and Raman spectra frequency analysis, examining lattice vibration effects 21 p3853 A70-41721

Thermal separation of ortho and para hydrogen and deuterium, discussing kinetic theory of nonspherical molecules in terms of rotational collision numbers 22 p3983 A70-43154

Thermodynamic properties, tables and equations of state of liquid para hydrogen from liquid-gas and liquid-solid phase equilibria 23 p4220 A70-44434

PARABOLIC BODIES

PARABOLAS

Stagnation point position and entropy at surfaces of supersonic paraboloids in perfect gas 12 p2160 A70-28250

PARABOLIC ANTENNAS

Satellite mounted mm wave parabolic dish antenna for tracking communication satellite in synchronous orbit 02 p0392 A70-11933

Far field radiation pattern determination particularly suitable for large parabolic antennas, detailing measurement errors 02 p0267 A70-12399

Analytic solutions for focal plane electric field components in parabolic reflector antennas 03 p0457 A70-13697

Aerodynamic damping measured for parabolic satellite communication antenna with pronounced flexibility in azimuth drive, simulating by scaled wind tunnel models 05 p0938 A70-16455

Geometrical and electrical characteristics of two mirror parabolic antenna for tropospheric radio relay communications lines in centimeter band, analyzing radiation patterns 07 p1240 A70-19125

Rotating parabolic mirror /antenna/ ou multisupported suspension analyzed for static rigidity, determining elastic deformation under mirror weight 08 p1586 A70-21055

Rotating parabolic mirror /antenna/ cantilever suspension rigidity with emphasis on rigidity of central bushing 08 p1586 A70-21056

Statistical analysis of model parabolic mirror rigidity on multisupported suspension under symmetrically distributed load represented by mirror weight 08 p1586 A70-21057

Multisupported radially symmetrical suspension systems designs for parabolic antennas, assessing performance in terms of maximum rigidities 08 p1586 A70-21058

Parabolic antenna for automatic tracking compared for characteristics between multimode and four horn feed systems 10 p1847 A70-23920

Parabolic antenna radiation pattern synthesis under laboratory conditions with space limitations obtainable by defocused antenna method 10 p1853 A70-25132

Thermal analysis of deployable parabolic antenna for Outer Planetary Explorer program, discussing spacecraft spin and radioisotope thermoelectric generators effect 11 p2127 A70-26359

Far field radiation patterns of Cassegrain, offset paraboloid and horn reflector antennas by stationary phase approximation method 11 p2019 A70-26659

Deformed parabolic mirror antenna equivalent geometrical parameters based on known points coordinates on real profile of reflector 14 p2563 A70-30147

UHF ground communication dish antennas transmit and receive gains calibration by communication satellite repeater 16 p2872 A70-32967

Aerodynamic admittance of paraboloid dish aerial in scaled atmospheric turbulent boundary shear layer simulated in wind tunnel by vortex generators 16 p2878 A70-33766

Computation and measurement methods for parabolic antennas design with high front to back ratio 18 p3231 A70-36666

Parabolic antennas for satellite communications network and radio telescopes, investigating surface utilization coefficient 19 p3395 A70-37267

Experimental model for random phase errors caused by surface irregularities in paraboloid reflector antennas 19 p3388 A70-37927

Parabolic antenna properties generated by dual band circularly polarized focused two channel monopulse feed system, discussing tracking data from helicopter, Apollo 8 and Cassiopeia A 20 p3589 A70-40323

Optimum performance of corrugated waveguide feed horns for paraboloidal reflector antennas via radiation pattern shaping with digital computer 24 p4320 A70-46222

PARABOLIC BODIES

Hyperboloids and paraboloids in flow of Reynolds number 22-65000 and Mach number 10, discussing viscous interactions effects on pressure, drag and skin friction [AIAA PAPER 70-182] 06 p0976 A70-18240

Elastic paraboloid of revolution under axisymmetrical and nonaxisymmetrical loads, using Bessel functions of real and imaginary arguments with trigonometric functions 08 p1587 A70-21165

Singularities of boundary layer conditions on parabolic cylinder in homogeneous incompressible

viscous flow with leading edge, using Weyl integral equation 12 p2210 A70-27559

Hypersonic gas flow characteristics incident on elliptic paraboloid and triaxial ellipsoid at arbitrary angles of attack 15 p2672 A70-31647

Wave diffraction by parabolic cylinder, solving boundary value problems for two dimensional wave equations via separation of variables 15 p2700 A70-32408

Convex infinite paraboloid of revolution, describing geometry and applications to electromagnetic wave scattering and antennas 15 p2701 A70-32415

Thermal constriction resistance between contacting metallic paraboloids applied to instrument bearings [AIAA PAPER 70-857] 16 p2998 A70-33902

Paraboloid of revolution, examining mixed axisymmetric buckling problem 20 p3727 A70-39892

PARABOLIC DIFFERENTIAL EQUATIONS

Optimization of distributed parameter control systems described by linear integro-partial differential parabolic equation with delayed argument, using dynamic programming 01 p0131 A70-10548

Stochastic processes providing exposition of differential-integral calculus for Brownian motion paths, with applications to diffusion processes and related parabolic partial differential equations 01 p0133 A70-11322

Summary representations method to analyze finite difference schemes for integrating parabolic equations with constant coefficients, solving boundary value problems 03 p0518 A70-13078

Spatial amplification criteria for hyperbolic wave equations extended to include parabolic equations, discussing convective and absolute instabilities 03 p0519 A70-13522

Boundary layer on sharp flat plate in low density flow computed by continuum approach, obtaining parabolic partial differential equation system [DVL-914] 06 p1034 A70-17250

Positive time-periodic solutions to parabolic problems with Stefan-Boltzmann boundary conditions using straight lines method 07 p1333 A70-18748

Existence and uniqueness theorem for boundary value problem solution for parabolic equation in domain with singular points on boundary 07 p1322 A70-18853

First boundary value problem for quasi-elliptic and quasi-parabolic equations, discussing solvability and boundary behavior near characteristic points 07 p1322 A70-18854

Nonuniqueness of Cauchy problem for parabolic equation of order 2b with rapidly increasing coefficients at infinity 07 p1322 A70-18855

Toupin and Knowles elasticity theory applied to spatial decay estimate for parabolic heat equation used in diffusive temperature field 07 p1409 A70-19565

Cauchy-Dirichlet problem for linear inhomogeneous polycaloric /polyparabolic/ equation with constant coefficients under certain boundary conditions 08 p1597 A70-21006

Alternating direction implicit method for solving parabolic equation with variable coefficients in two space dimensions with mixed derivative 09 p1711 A70-22284

Integral relations describing laws of conservation and Sobolev theorem used in deriving a priori estimates for nonlinear parabolic equations first boundary value problem 10 p1908 A70-23924

Mixed boundary value problem for linear parabolic equations with discontinuous coefficients, proving solution existence and uniqueness by functional method 10 p1911 A70-25304

Monochromatic light propagation in medium with large scale Markov nonuniformities of dielectric constant using parabolic equation approximation 12 p2272 A70-27359

Linear and nonlinear parabolic boundary value problems with first boundary conditions solved by method of lines, estimating error 12 p2262 A70-28031

Mixed boundary value problems for pseudoparabolic partial differential equations solved in Hilbert space, demonstrating solution existence and uniqueness 14 p2599 A70-30635

Finite difference schemes for systems of elliptic and parabolic equations, using brute force algorithm 16 p2941 A70-33246

First boundary value problem solution for parabolic equation by differential invariant method 17 p1311 A70-35340

Incompressible laminar boundary layer, vortex and axisymmetric wake/jet flow parabolic equations solution by weighted residuals method, describing use of exponentials 17 p3074 A70-35883

Monotonic difference schemes for parabolic differential equations with nonlinear boundary conditions, discussing convergence and stability 18 p3282 A70-36361

Monochromatic light propagation in medium with large scale Markov nonuniformities of dielectric constant using parabolic equation approximation 22 p4075 A70-43600

Cauchy problem solution for parabolic equation with variable coefficients, using differential invariant method and Volterra integral equation 23 p4210 A70-43979

Cauchy problem for singular parabolic equation, establishing existence, uniqueness and representation theorem by integral operator techniques in conjunction with function-theoretic methods 23 p4212 A70-44895

Nonlinear parabolic initial value problems, including Navier-Stokes equations 24 p4370 A70-46414

PARABOLIC FLIGHT

Human factors research with simulated reduced gravity conditions by parabolic flight technique with aircraft [AMRL-TR-69-16] 01 p0037 A70-10962

Integration time reduction for equations of motion of vehicle center of mass during parabolic reentry, using Runge principle 01 p0134 A70-11483

Burnham-Slaughter 1958e-1959f comet orbit, showing nearly parabolic ellipse 19 p3516 A70-37933

PARABOLIC REFLECTORS

NT PARABOLOID MIRRORS

Monograph on radio telescopes covering developments from simple parabolic reflectors to computer based image forming instruments 01 p0046 A70-11250

Field pattern near paraboloid reflectors focus for low f/D ratios, considering vectorial character of electromagnetic field 02 p0268 A70-12474

Analytic solutions for focal plane electric field components in parabolic reflector antennas 03 p0457 A70-13697

Electrical and mechanical characteristics and specifications of second parabolic reflector antenna at Pleumeur-Bodou space communications center 05 p0819 A70-15982

High gain paraboloidal reflector antenna with horn feed for satellite and terrestrial microwave links 06 p1022 A70-18022

Paraboloidal- and spherical-reflector antennas efficiency optimization obtained from optimum combination of amplitude and phase of hybrid modes propagating in guide 07 p1240 A70-19220

Gain-to-noise temperature ratio /G/T/ optimization by dish antenna shaping for nonuniform aperture field distribution 08 p1471 A70-20790

Parabolic reflectors profile error compensation by means of multielement feed array with controllable phasing 09 p1644 A70-22236

Monograph on analysis of reflector antennas covering electromagnetic field equations, computer aided design, etc 13 p2367 A70-29600

Asymmetric phase error in antenna circular apertures, emphasizing beam squint resulting from distortion of paraboloidal reflector 16 p2859 A70-32942

Paraboloidal reflectors aperture fields from stereographic mapping of feed polarization pattern, illustrating electric and magnetic dipoles and Huygens sources 16 p2871 A70-32962

Paraboloidal and spherical reflectors focal region fields matching over corrugated waveguide open end propagating hybrid modes 16 p2861 A70-32966

Axially symmetric parabolic reflector with incident linearly polarized plane wave, determining Poynting vector behavior 17 p3043 A70-34615

Physical and electrical sizes in large antennas, discussing paraboloid reflectors, arrays, slot antennas, etc 17 p3053 A70-35079

Parabolic reflector microwave antenna flared horn primary feeds design for maximum aperture efficiency based on electric field matching 21 p3800 A70-41946

Monopulse tracking antenna beam broadening by feed displacement defocusing in parabolic reflector 23 p4165 A70-44956

PARABOLIC VELOCITY

U ESCAPE VELOCITY

PARABOLOID MIRRORS

Projector with paraboloid mirror solar radiation condensing lens for studying heat resistant materials mechanical properties at high temperatures 01 p0055 A70-10179

Direct solar radiation concentration by paraboloid mirrors, analyzing energy transport and distribution functions, based on statistically distributed imperfections of reflecting surfaces 01 p0010 A70-10762

Radio astronomical antenna structure synthesis based on excitation of unshaded mirror surfaces with symmetrical caustics and virtual sources outside of focal axis 07 p1239 A70-18758

Telescopic paraboloid mirrors optical distortion from surface deformation due to gravity loads 07 p1281 A70-19254

Statistical analysis of model parabolic mirror rigidity on multisupported suspension under symmetrically distributed load represented by mirror weight 08 p1586 A70-21057

Cassegrain antenna with parabolic mirror and switch designed for broadband transhorizon radio relays, using antenna scale model to determine parameters and electrical properties 11 p2020 A70-26823

Deformed parabolic mirror antenna equivalent geometrical parameters based on known points coordinates on real profile of reflector 14 p2563 A70-30147

Radio astronomical antenna structure synthesis based on excitation of unshaded mirror surfaces with symmetrical caustics and virtual sources outside of focal axis 18 p3233 A70-37102

PARABOLOIDS

U PARABOLIC BODIES

PARACHUTE DESCENT

Coordination technique for pressure, density and temperature measurements by probes during parachute reentry into planetary atmospheres, taking into account reentry dynamics 01 p0197 A70-11495

Functional state changes in organism awaiting and performing parachute jump using orthostatic test, respiration retention and Howard step test 03 p0420 A70-13477

Distance of spacecraft descending on parachute through planetary atmosphere measured from center of planetary mass using onboard instrument data 06 p1155 A70-17897

Three dimensional motion of nonrigid parachute and payload system analyzed for dynamic stability [AIAA PAPER 70-209] 06 p0987 A70-18062

Opening distance and inflation time prediction for parachutes deployed supersonically based on subsonic performance 07 p1394 A70-19725

Parachute wind sensors used in Arcas and Loki sounding rocket systems for stratospheric sounding, describing position data acquisition via radar tracking 07 p1395 A70-20259

Heart frequency profiles of persons during parachute jumps measured by electrocardiograms recorded directly and telemetrically to investigate psychical and physical stresses 09 p1626 A70-23010

Flat circular parachute stress analysis in steady vertical descent, using computer program for design change effects on shape, drag and stress 14 p2531 A70-30863

Free fall sport jumping with parachute, discussing exercises for changing positions 16 p2842 A70-34175

Buoyant Venus station balloon for deployment and inflation during parachute descent into Venus atmosphere tested with scale model balloons in wind tunnels 17 p3063 A70-35658

Significant terms in equations of motion for parachutes inflating in free air and in wind tunnel experiments [AIAA PAPER 68-924] 18 p3213 A70-36449

Aircraft-borne and descent systems performance and weight optimized for midair retrieval [AIAA PAPER 70-1201] 21 p3751 A70-41805

Optimum drogue gun firing angle of stabilization times for MEW /Minimal Envelope and Weight/ ejection seat system, considering zero and high velocities [AIAA PAPER 70-1208] 21 p3751 A70-41810

Pilot airborne recovery device /PARD/ midair rescue system, discussing buoyancy, midair pickup, seat ejection energy absorber, homing avionics and human factors [AIAA PAPER 70-1206] 21 p3752 A70-41812

U.S. Coast Guard air delivered antipollution transfer system for oil, discussing deployment method, trajectory analysis, rigging techniques and full scale testing [AIAA PAPER 70-1205] 21 p3752 A70-41813

Extraction parachute deployment for airdropping multiple loads from C-5A aircraft [AIAA PAPER 70-1203] 21 p3752 A70-41814

Parachute decelerator towline energy absorber shock attenuation characteristics, discussing drop test results
[AIAA PAPER 70-1202] 21 p3752 A70-41815

Attached inflated BALLUTE /balloon-parachute/ for stabilization and retardation of aircraft stores, high altitude descent devices and planetary entry vehicles
[AIAA PAPER 70-1200] 21 p3752 A70-41816

Ballistic trajectory, packageability, deployment and flight stability of attached ram air inflatable decelerator for high speed/low altitude store delivery
[AIAA PAPER 70-1199] 21 p3752 A70-41817

Stress distribution and shape in arbitrarily shaped gore parachute under unsteady pressure distribution during inflation and descent
[AIAA PAPER 70-1197] 21 p3752 A70-41819

Gliding parachute air cargo systems using nonproportional and proportional automatic manual control, estimating wind effects on ground track and impact computer simulation
[AIAA PAPER 70-1193] 21 p3753 A70-41823

Reefing systems for Parawings, Sailwings, Paraflyers, Paraplanes and Volplanes, discussing performance tests
[AIAA PAPER 70-1192] 21 p3753 A70-41824

All-flexible parawing as primary descent system for large spacecraft landing, discussing configuration, structural arrangement, multistage reefing and L/D performance tests
[AIAA PAPER 70-1187] 21 p3754 A70-41828

Basket weave fabrics for gliding descent decelerators with polyurethane and nylon coatings for tearing strength and pressure packing
[AIAA PAPER 70-1180] 21 p3843 A70-41833

Parachute decelerator system for 1975 Viking Mars Lander mission, discussing configuration selection, design factors, trajectory simulation, weight and mass analysis, etc
[AIAA PAPER 70-1162] 21 p3931 A70-41849

Solid cloth personnel parachutes opening forces, discussing loading conditions, flight path shock parameters, mass ratio variations and elasticity of system
[AIAA PAPER 70-1167] 23 p4137 A70-43992

Parachute trajectory and opening load prediction based on inflation process and added mass, determining drag area as function of distance
[AIAA PAPER 70-1168] 23 p4137 A70-43993

PARACHUTE FABRICS

Heat transfer coefficients for mesh simulating porous parachute cloth, measuring Nusselt number as function of sonic Reynolds number
01 p0004 A70-10292

Mission sequential environment effects on Dacron parachute material mechanical properties
[AIAA PAPER 69-1018] 14 p2563 A70-30770

Euler buckling of inflated toroidal drag bodies, including packaging and load deflection tests for Mylar, dacron-neoprene and stainless steel-silicone fabrics
[AIAA PAPER 70-1198] 21 p3938 A70-41818

Longitudinal tension impact tests on nylon tape and Apollo pilot parachute riser construction, determining wave propagation effects
[AIAA PAPER 70-1182] 21 p3843 A70-41831

Parachutes lightweight coated fabrics air permeability under axial tensile loading and load cycling at room temperatures
[AIAA PAPER 70-1178] 21 p3843 A70-41835

Stretch fabric materials for personnel high speed escape parachute systems
23 p4141 A70-44482

PARACHUTES

NT DRAG CHUTES

NT RECOVERY PARACHUTES

Parachute inflation dispersion studied by plotting dimensionless products characterizing incompressible flow process
01 p0006 A70-10849

Parachute design for decelerating upper atmosphere rocket probes at high altitudes, using high drag coefficients in Stokes flow regime
[AIAA PAPER 68-949] 04 p0624 A70-15410

Parachute altitude wind sensor /PAWS/ project for real time wind profile determination, using modified HASP I sounding rocket
14 p2585 A70-30577

Flat circular parachute stress analysis in steady vertical descent, using computer program for design change effects on shape, drag and stress
14 p2531 A70-30863

Small rocket systems research programs, discussing Apollo-Pacemaker and planetary entry parachute flight tests
17 p3177 A70-35203

Spacecraft parachute stress analysis, using finite elements with nonlinear elastic properties to obtain shape and load distribution
[AIAA PAPER 70-1195] 21 p3753 A70-41821

Drag prediction for Ballute and parachute trailing decelerators at supersonic speed and zero angle of attack, using flow field computations
[AIAA PAPER 70-1177] 21 p3746 A70-41836

Parachute canopy surfaces transient aerodynamic pressures during unsteady processes, using piston theory
[AIAA PAPER 70-1175] 21 p3754 A70-41838

Continuous surface of revolution parachute for supersonic/hypersonic speeds, performing wind tunnel tests
[AIAA PAPER 70-1173] 21 p3754 A70-41840

Reefed and unreefed disk gap band parachutes tested in supersonic and subsonic wind tunnels to determine stability and performance
[AIAA PAPER 70-1172] 21 p3754 A70-41841

Three body problem for parachute system dynamics during inflation
[AIAA PAPER 70-1170] 21 p3755 A70-41843

Tethered parachutes vibration modes, determining fundamental frequencies from canopy/lines mass ratio and materials elastic properties
[AIAA PAPER 70-1169] 21 p3755 A70-41844

Parachute flexibility as performance parameter, discussing stiffness-weight index, inflation process, squidding, etc
[AIAA PAPER 70-1166] 21 p3755 A70-41845

Parachutes for low density atmospheres, describing low and high altitude test results
[AIAA PAPER 70-1164] 21 p3755 A70-41846

Para-foil application programs and test results, discussing flight and glide performance, turn control, deployment inflation, etc
22 p3961 A70-42706

Testing laboratory for safety, survival and life support equipment concerning parachutes, aircrew protective helmets and maintenance manuals
23 p4141 A70-44488

Parachute opening load amplification due to suspension line elasticity, using two-body spring-mass model
23 p4142 A70-44531

PARACHUTING

U PARACHUTE DESCENT

PARACHUTING INJURY

Temporary or permanent visual field injury in test parachutists compared to control group
07 p1223 A70-19943

PARADOXES

Sleep biphasic paradoxical stage in cats, correlating brain structures electroencephalographic data with various somatic and vegetative signs
12 p2173 A70-28345

PARAFFINS

Cosmic ray nuclear interactions under paraffin and lead, using counter controlled multiplate cloud chamber
03 p0553 A70-12877

PARAGLIDERS

NT FLEXIBLE WINGS

NT PARAWINGS

Hi-glide personnel canopy /Para-Foil, Parawing, Sailwing, Volplane/ technology capability requirements identification from performance parameters tradeoffs
[AIAA PAPER 70-1194] 21 p3753 A70-41822

Static and dynamic longitudinal stability of semirigid parafoil gliding descent system in pitching motion
[AIAA PAPER 70-1191] 21 p3753 A70-41825

Parafoil flight performance predictions and test results based on wind tunnel data and manned free flight
[AIAA PAPER 70-1190] 21 p3754 A70-41826

Para-foil application programs and test results, discussing flight and glide performance, turn control, deployment inflation, etc
22 p3961 A70-42706

PARALLAX

Visual simulation limitations, discussing parallax error correction in display system, wraparound system, image generation, TV and motion picture film systems
01 p0036 A70-10813

M dwarf stars spectroscopic, spectral and photometric parallaxes calibration based on trigonometric measurements
01 p0188 A70-11333

HR diagram calibration based on proper motions and radial velocities, deriving absolute magnitudes and statistical parallaxes
06 p1149 A70-18456

Geodetic satellite positional problems taking into account parallax refraction
09 p1765 A70-22653

Binary stars dynamical parallaxes, masses, absolute magnitudes and provisional orbits, fitting deduced masses into empirical visual mass-luminosity relations
19 p3531 A70-38896

PARALLEL PLATES

Dipolar fluid effect on back flow between parallel plates, considering generalized Couette flow
01 p0062 A70-10545

Gas jets collision flowing from parallel wall channels, applying solution to calculating geometrical characteristics or fluid jet amplifiers
01 p0011 A70-11569

Radiative transfer in nongray gas between parallel walls, solving heat flux and temperature distribution
02 p0392 A70-1907

Navier-Stokes difference equations numerically integrated by computer for viscous fluid flow along parallel flat plate at low Reynolds number
02 p0277 A70-11909

Polarization diversity provided to parallel plate antennas in airborne radar applications by orthogonal vector processing
03 p0452 A70-13967

MHD laminar flow between parallel porous disks for large suction Reynolds number, solving equations of motion with singular perturbation technique
03 p0469 A70-14181

Conducting fluid laminar flow between parallel planes in traveling magnetic field, integrating Maxwell and Navier-Stokes equations
04 p0726 A70-15452

Radiative heat transfer through dust clouds in radiative equilibrium and isothermal conditions between parallel plates measured with heat flowmeter
[ASME PAPER 69-WA/HT-41] 04 p0781 A70-14802

Radiative heat flux between two parallel copper disks at cryogenic temperature, showing dependence on emitter temperature and spacing
[ASME PAPER 69-WA/HT-7] 04 p0784 A70-14823

Radiative transfer between two infinite parallel metallic surfaces separated by nonconducting thick film ideal dielectric based on electromagnetic wave theory
[ASME PAPER 69-WA/HT-6] 04 p0784 A70-14824

Rarefied H, He, air, carbon dioxide and water vapor flow rates between parallel optically flat glass surfaces measured, giving flow equation describing channel flow
05 p0833 A70-16525

Parallel plate TEM waveguides radiation pattern slope diffraction analysis
06 p1021 A70-17570

Laminar steady radial flow of simple fluid of U memory between two parallel disks, demonstrating relation to Newtonian fluid
06 p1037 A70-17915

Unsteady nonlinear molecular flow problems concerning plane Couette flow, heat transfer between parallel plates and density discontinuity propagation solved by Monte Carlo method
06 p1113 A70-18321

Plane Couette flow and heat transfer between parallel plates problems treated by generalizing BGK model and applying variational principle to linearized Boltzmann equation
06 p1048 A70-18323

Monte Carlo method applied to Boltzmann collision integral in solving heat transfer between plates at different temperatures in elastic spheres gas
06 p1183 A70-18324

Rarefied gas flows and heat transfer between parallel plates, concentric cylinders and spheres in presence of fractionally accommodating boundaries
06 p1049 A70-18330

Free steady convective flow stability relative to three dimensional disturbances between parallel planes reduced to equivalent plane disturbances problem
07 p1252 A70-18669

Flow velocity distribution near boundaries of model of plates of parallel faces, obtaining Laplace equation solution
07 p1258 A70-19378

Temperature gradients, viscosity and conduction measurements in air stream between parallel plates, investigating limiting value of total Prandtl number
07 p1260 A70-19999

Transient phenomena accompanying heating of fluid situated between heat conducting plane horizontal plates, using interferometry and streak photography
08 p1596 A70-20592

Fluid motion convective stability between vertical parallel plates with longitudinal temperature gradient, solving boundary value problem for amplitudes of normal perturbations
08 p1482 A70-20952

Laminar radial flow between parallel disks, estimating static wall pressure distribution perturbation caused by characteristic time
08 p1484 A70-21377

Symmetrical laminar distorted velocity profiles between flat parallel plates, analyzing decay using integral method
08 p1433 A70-21325

Forced convection heat transfer between two parallel plates analyzed numerically for effect of constant heat transfer coefficient boundary condition
08 p1598 A70-21425

MHD flow between two parallel plates, noting pressure gradient and skin friction coefficient
08 p1554 A70-21774

Open-sided shielded stripline and other parallel plate waveguide structures propagation modes
09 p1634 A70-22712

Digital wavemeter description using interferometer with parallel plates and automatic frequency readout for submillimeter band
09 p1652 A70-23658

Velocity profile and volume flow rate for rarefied gas flowing isothermal parallel plates, solving linearized Boltzmann equation by BGK model
11 p2037 A70-26168

Parallel isotropic flat plates vibration and flutter in supersonic/subsonic flow over one surface, observing plane loadings and elastic medium stiffness effects
12 p2316 A70-27104

Radiative energy transfer in hydrogen plasma having uniform heat source and bounded by parallel black plates
12 p2278 A70-27695

Numerical quadratures application to integral equations for radiative heat transfer computations, discussing validity for parallel and adjoint plates
12 p2332 A70-27840

Coupling between parallel plate waveguides excited in TE modes using integral and differential equations, noting dielectric plug loading effect
12 p2198 A70-27954

Semiinfinite parallel plate waveguide modes reflection coefficients with propagation constants near cut-off and excited at open end for microwave-optical frequency range
12 p2198 A70-27959

Free steady convective flow stability relative to three dimensional disturbances between parallel planes reduced to equivalent plane disturbances problem
15 p2718 A70-31461

Linear integral equations for radiative transfer between parallel plates, using least squares method
15 p2826 A70-31822

Finite parallel plate waveguide arrays edge effects, comparing element radiation patterns and reflection coefficients vs scan
16 p2860 A70-32953

Thermal conductivity along parallel radiation shields, proposing calculation method for energy transport
[AIAA PAPER 70-847] 16 p3000 A70-33914

Lateral heat transfer along parallel conducting and radiating plates spaced by absorbing and isotropically scattering dielectric
[AIAA PAPER 70-849] 16 p2939 A70-33916

Hydrodynamic entry length for laminar flow between parallel porous plates, using finite difference theory for flow equations
17 p3069 A70-34983

Variational principle for turbulent shear flow between parallel plates, taking into account isothermal flow and Malkus theory
17 p3073 A70-35595

Critical height phenomenon for vertical jet exhausting into horizontal parallel plates channel simulating aircraft surfaces
18 p3243 A70-36709

Fluid motion convective stability between vertical parallel planes with longitudinal temperature gradient, solving boundary value problem for amplitudes of normal perturbations
20 p3608 A70-39377

MHD nonsteady Beltrami flow between two infinite parallel walls with transverse magnetic field, calculating velocity, skin friction and induced magnetic field
20 p3678 A70-39610

Surface roughness effects on thermal radiant energy interchange between opaque interacting surfaces formulated for unequal temperature adjoint plates
21 p3944 A70-41018

Radiation heat transfer from parallel plates with grooved surfaces for direction dependent radiation properties
21 p3944 A70-41021

Interface interaction of colliding plates of different materials, reducing flow problem to differential equation via hodograph transformation
21 p3747 A70-41962

Incompressible Newtonian fluid laminar radial flow between parallel stationary disks, obtaining integral solution for Navier-Stokes equation
22 p4007 A70-42302

Plasma-air junction problem in parallel plate waveguide, obtaining discontinuity admittance expression
22 p3994 A70-42350

Ray theory of diffraction from open-ended parallel plate waveguides, using Wiener-Hopf technique
23 p4219 A70-44404

Radiation and phase-scanning properties of planar array of parallel plate waveguides, using wedge diffraction theory
23 p4166 A70-44973

PARALLELEPIPEDS

Elastic equilibrium of quasi-completely regular rectangular parallelepiped with rigidly clamped lateral faces, obtaining Lamé equations in double Fourier series
04 p0765 A70-14418

Boundary value problem in parallelepiped constructed for linear partial differential equation with constant coefficients using expansions in Riesz bases
10 p1911 A70-25305

Vector displacement numerical calculations for rectangular parallelepipeds of infinite and finite lengths
15 p2767 A70-32018

Rumanian book on spatial problems in elasticity theory covering deformation geometry, temperature effects, elastic parallelepipeds, etc
23 p4275 A70-44999

PARALLOGRAMS

Core flexibility effects on deformation of uniformly loaded clamped parallelogrammic sandwich panels using linear theory
17 p3185 A70-34920

Infinite periodic phased array over ground plane with dipole elements in parallelogram lattice, calculating driving impedance and gain loss due to mismatch
23 p4172 A70-44004

Clamped parallelogram metal plate thermal deformation under single surface radiant heating
24 p4426 A70-46009

PARALYSIS

Asymptomatic pilot with idiopathic paralysis of hemidiaphragm, discussing clinical picture and aeromedical significance
07 p1215 A70-19942

PARAMAGNETIC AMPLIFIERS

U MASERS

PARAMAGNETIC RESONANCE

Shift in nuclear paramagnetic resonance frequency of ligand nuclei in ferromagnets above Neel temperature
10 p1928 A70-24826

Ferrous and ferric ions properties in corundum from observing acoustic paramagnetic resonance
15 p2784 A70-32397

Ultrasonic and electron paramagnetic double resonance in Fe-doped corundum
22 p4074 A70-43010

PARAMAGNETISM

Uniform bulk magnetization concept in superparamagnets related to physical statistics of magnetic first order phase transitions
15 p2785 A70-32400

High strength magnetic fields effect on early embryonic development of frogs, relating growth abnormalities and paramagnetic ferritin motions
16 p2848 A70-33099

PARAMETERIZATION

Parameter introduction during boundary value problem solution for second order nonlinear ordinary differential equations
10 p1909 A70-24510

VLF radio noise statistical parameters observed as functions of azimuth, considering atmospheric distribution and parameters correlations
10 p1884 A70-25259

Complete sample estimation techniques for reparameterizations of Weibull density function to assign probabilities to components and systems lifetimes
12 p2243 A70-28012

Extrema of functions of many variables in presence of constraints from modified simplex method with variable search step
13 p2382 A70-29277

Book on aerodynamics of bodies of revolution covering hypersonic flow parameters effects, method of characteristics, slender body drag, blunt bodies, rarefied gas aerodynamics, etc
16 p2834 A70-33271

Parameter identification algorithm for nonlinear equations describing VTOL aircraft longitudinal response
16 p2942 A70-33327

Parameter analysis of dynamical systems by matrix approach, using n-dimensional parameter space
17 p3130 A70-35300

Atmospheric noise statistical parameters analysis on digital computer designed to measure short duration atmospheric radio noise
17 p3170 A70-35396

Bipolar transistor behavior identification and characterization in static regime, discussing measurement methods for parameters of IBIS model
17 p3054 A70-35414

Algebraic manipulation of empirical relationships between geophysical parameters, discussing invalid results
17 p3080 A70-35760

Parametric functions of integral matrices representing linear differential system via continuous coefficients
18 p3279 A70-36156

Turbofan engine performance optimization by closed form solution of operating cycle parameter functions
[ASME PAPER 70-GT-65] 18 p3303 A70-36840

Booster parameterized guidance algorithms investigated on basis of steering forms validity, discussing exoatmospheric ascent applications
[AIAA PAPER 70-1006] 20 p3669 A70-39584

Invariance conditions for control systems with time varying parameters
20 p3602 A70-39827

Parameter methods generalization and D decomposition, using function minimization methods
24 p4322 A70-46155

PARAMETERS

U INDEPENDENT VARIABLES

PARAMETRIC AMPLIFIERS

Frequency control of ruby laser pumped lithium niobate singly resonant parametric oscillator by radiation injection of CW Nd-YAG laser
01 p0110 A70-10566

Optical parametric oscillator pumped by continuously repetitively Q switched Nd/YAG laser output
01 p0113 A70-11171

CW visible ring cavity parametric oscillator, discussing pump depletion, conversion efficiency and improved stability resulting from optical isolation
01 p0052 A70-11173

Wideband parametric and tunnel diode amplifiers synthesizing method for obtaining maximum flat amplitude frequency response
03 p0457 A70-13727

Group delay characteristics of C band nondegenerate parametric amplifier determined by Nyquist method and compared to phase frequency derivative measurement
03 p0458 A70-14037

Low noise amplification equipment for telecommunications, considering France-Portugal link parametric amplifiers
05 p0819 A70-15983

Tunable optical parametric oscillators including Gaussian beams amplification, threshold, tuning techniques, spectral output, etc
05 p0822 A70-16651

Phase velocities of intrinsic normal waves of electron beam in three frequency parametric amplifier of space charge waves, determining optimal wave interaction conditions
05 p0823 A70-16890

Parametric interactions in three frequency TWT parametric amplifier, using power series
05 p0824 A70-16895

Increasing sensitivity of tuning fork gyroscope by parametric signal amplification
07 p1289 A70-20297

Low noise tunable parametric amplifier for tactical satellite communications, discussing characteristics and varactor diode mount
08 p1471 A70-20806

Radiometers with low noise parametric amplifiers at centimeter wavelengths for radio telescope, discussing design, performance and Venus observations
08 p1495 A70-21065

Parametric amplifier for spectral radiometer of U.S.S.R. astronomical telescope, showing improved sensitivity observations of neutral H emission
08 p1473 A70-21066

Low noise nonreciprocal microwave parametric amplifier with up-and-down converter and idlers in cascade
09 p1647 A70-22850

Low power microwave IMPATT oscillator as parametric amplifier pumping sources for use in radar and communication systems
10 p1847 A70-23891

Laser pumped optical parametric oscillators (OPO), considering phase matching, threshold power, transient response, etc
10 p1898 A70-23999

Resistive parametric mixing in GaAs oscillators at microwave frequencies resulting in negative mobility at signal frequency
10 p1849 A70-24231

Amplitude and phase constants of interacting waves in three frequency nondegenerate parametric amplifier of fast space charges using coupled wave technique
10 p1853 A70-25133

Varactor diode equivalent circuit determination for application to cooled parametric amplifiers design
11 p2017 A70-25573

Parametric effect maser developed by maintaining self oscillations in static amplitude modulated magnetic field, noting application as magnetometer
11 p2063 A70-25947

High dynamic range low noise parametric microwave amplifier performance measurement for radar receivers
12 p2183 A70-27166

Single and multistage parametric amplifiers for broadband communications, noting nonideal circular characteristics by scattering parameter and signal flow graph
12 p2197 A70-27933

Parametric amplifier as preamplifier for microwave receivers in space probes, presenting block diagrams and test results
13 p2379 A70-29559

Regenerative semiconductor parametric amplifier saturation in forward current mode, assuming harmonic voltages /signal, pumping and difference frequencies/ action at p-n junction
15 p2708 A70-31522

Microwave parametric amplifiers with nonideal circulators, deriving gain via scattering matrix theory and signal flow graphs
16 p2874 A70-33389

Terminal negative resistance of X band Gunn diodes, discussing frequency conditions for modulation and parametric amplification 16 p2877 A70-33417

Mechanical parametric amplification, improving SNR of acoustic systems in hostile environments 19 p3422 A70-37695

Flux intensity measurements of radio sources at 10.69 GHz by radome protected telescope using cryogenically cooled parametric amplifier as receiver 19 p3524 A70-38750

Parametric phenomena in oscillatory system with unlimited number of degrees of freedom, illustrating segment of long line loaded at one end 22 p3995 A70-42395

Signal and noise properties of degenerate and quasi-degenerate nonreciprocal parametric amplifiers without circulators 22 p3990 A70-43423

Minimum noise microwave parametric amplifiers incorporating varactor diodes with frequency dependent apparent loss resistance 23 p4169 A70-43786

Low noise dual receiver system for satellite communication earth station using parametric and transistor amplifiers 23 p4169 A70-43791

Ionospheric parametric amplification and frequency mixing due to polarized TEM waves nonlinear interaction with longitudinal electrostatic waves 23 p4185 A70-43838

PARAMETRIC DIODES

Self excited cavity oscillators with tunnel and parametric diodes and nonequilibrium medium, noting single and multimodes, energy capabilities and frequency interactions 13 p2366 A70-29405

PARAMETRIC FREQUENCY CONVERTERS

IR CW sum-frequency up-conversion of carbon dioxide laser radiation using phase matched prostrate as nonlinear crystal 01 p0111 A70-10786

Equivalent conductances and resistances vs pumping oscillation modes of p-n junction in parallel and series-connected three-frequency parametric circuits 04 p0659 A70-15209

High level parametric upconverter for radio link using evanescent mode waveguide 22 p3997 A70-42925

Nonreciprocal double-pumped parametric converter eliminating separate pump signals 22 p3998 A70-43252

Intermodulation distortion reduction in four frequency parametric converter by low impedance path 23 p4169 A70-43785

PARAMETRIC OSCILLATORS

U PARAMETRIC AMPLIFIERS

PARASITES

Biological satellite experiment, considering long term weightlessness effects on metabolism and biological rhythms of medical leech 16 p2854 A70-33993

Unnatural environment behavior of leeches for long term biosatellite experiment, determining temperature, humidity, oxygen pressure, carbon dioxide concentration, calcium hydroxide limits, etc 16 p2854 A70-33994

PARATHYROID GLAND

Parathyroidectomy effects on high altitude adaptation and adrenal cortex activity in rats exposed to chronic hypoxia 08 p1442 A70-20719

White Leghorn laying hens parathyroid glands fine structure from electron microscopic studies, noting electron dense membrane bound mature secretory granules in cytoplasm 09 p1619 A70-22800

PARAWINGS

Contour, pressure distribution and aerodynamic parameters calculations of slender highly cambered parawings in symmetric and asymmetric inviscid flow 03 p0408 A70-13800

Lift and drag characteristics of flexible parawings at subsonic speeds, predicting angle of attack for trailing edge flutter commencement 12 p2157 A70-28079

Parawing canopy behavior during deployment in free flight at specific altitudes and dynamic pressures [AIAA PAPER 70-1189] 21 p3751 A70-41804

AERCAB /Aircrew Escape/Rescue Capability/ Flying ejection seat, considering rotary wings, fixed wings and parawings 21 p3751 A70-41806

Finite element analysis of critical stress distribution in canopy of deployed twin keel parawing, predicting fatigue stress levels 21 p3753 A70-41820

Hi-glide personnel canopy /Para-Foil, Parawing, Sailing, Volplane/ technology capability requirements identification from performance parameters tradeoffs [AIAA PAPER 70-1194] 21 p3753 A70-41822

Reefing systems for Parawings, Sailwings, Para-Flyers, Paraplanes and Volplanes, discussing performance tests 21 p3753 A70-41824

All-flexible parawings aerodynamic performance prediction based on slender wing theory and circular arc approximations for canopy shape [AIAA PAPER 70-1188] 21 p3754 A70-41827

All-flexible parawing as primary descent system for large spacecraft landing, discussing configuration, structural arrangement, multistage reefing and L/D performance tests 21 p3754 A70-41828

Glide and landing performance of twin-keel parawings, discussing wind tunnel, radio flight and simulator tests 21 p3754 A70-41829

PARITY

Gravitational radiation scattering by Schwarzschild horizon, discussing odd parity waves of angular momentum 21 p3878 A70-40731

PARKING ORBITS

Navigation for lunar parking orbit with time varying osculating orbital elements, using Apollo 11 Doppler tracking data 14 p2613 A70-30457

Optimal explicit guidance equation using maximum principle for two stage vehicle injecting satellite into parking orbit 17 p3134 A70-35289

Parking orbit optimal orientation for minimal impulsive maneuvers total velocity increment in three dimensional capture-escape mission [AIAA PAPER 69-918] 17 p3172 A70-35649

Optimum launch trajectories for ATS-E mission with noncircular parking orbits, considering apogee motor size, perigee radius and duration constraints [AIAA PAPER 70-1051] 19 p3528 A70-38866

PAROTID GLAND

U SALIVARY GLANDS

PARTIAL DIFFERENTIAL EQUATIONS

NT BIHARMONIC EQUATIONS

Energy inequality solutions properties pertaining to mixed boundary value problem of partial differential equations, using Fourier method 01 p0130 A70-10154

Asymptotic and approximate wave construction for system of first order quasi-linear partial differential equations 01 p0131 A70-10800

Functional optimization within partial differential equation solutions class by choosing optimum boundary values 01 p0131 A70-10922

Book on function theoretic methods for partial differential equations covering complex variables, harmonic functions, envelope method for singularities, operators, etc 01 p0133 A70-11325

Book on numerical solution of partial differential equations, discussing methods for physical and chemical problems on digital computer 01 p0134 A70-11326

Second order ordinary differential equations solution extended to higher order or partial differential equations using numerical integration 02 p0324 A70-12280

Method of weighted residuals /MWR/ for nonlinear partial differential equations applied to incompressible two dimensional turbulent boundary layer momentum and continuity equations 02 p0281 A70-12328

Optimal control synthesis in Markov and determinate systems using solution reduced from second order nonlinear partial differential equation 02 p0272 A70-12411

Wave propagation in inhomogeneous media, reducing quasi-linear hyperbolic partial differential equations to single nonlinear equation integratable by method of characteristics 03 p0525 A70-14184

Boundary value problems for partial differential equations representing steady gas flow hydrodynamic problems 03 p0469 A70-14228

Shell theory resolving equations transformation to second order partial differential equations suited for solution by numerical algorithms of network method 04 p0767 A70-14495

Augmented small parameter gas film equation for squeeze film journal bearing solved in terms of radial displacement [ASME PAPER 69-WA/LUB-9] 04 p0697 A70-14766

Finite difference analysis of partial differential equations derived from Navier-Stokes equations in hypersonic leading edge problem in merged gas flow-layer regime 06 p0980 A70-18349

Kolmogoroff partial differential equations for non-Markovian stochastic processes, noting applications to reliability theory 07 p1323 A70-18938

Simultaneous partial integrodifferential equations for transverse oscillations of uniform short beams 07 p1406 A70-19306

Partial differential equations hyperbolic systems solutions by finite difference methods, considering schemes stability and viscosity from first differential approximation standpoint 07 p1326 A70-19559

Mechanical vibration of beams analyzed by partial differential equations of beam vibration involving mass concentration and flexibility 07 p1411 A70-19786

Functions describing spatial-temporal temperature distribution in hyperbolic partial differential equations for nonstationary heat exchange between fluid flow and boundary wall 07 p1423 A70-19839

Steady oscillations under random forces of nonlinear system described by stochastic partial differential difference equations with distributed parameters and delayed argument 08 p1542 A70-20486

Chaplygin theorem proof for partial differential equation, using piecewise smooth manifold with unilateral conductivity 08 p1534 A70-21008

Optimal control conditions for elastic aircraft motion with delayed wing downwash determined by hyperbolic partial differential equations with delay 08 p1480 A70-21178

Nonlinear partial differential inequalities treated by companion function mu associated with continuity and growth conditions 10 p1908 A70-23836

Partial differential equation describing one dimensional heat transmission problems solved by eigenvalues for initial and boundary conditions 10 p1969 A70-25098

Boundary value problem in parallelepiped constructed for linear partial differential equation with constant coefficients using expansions in Riesz bases 10 p1911 A70-25305

Problem oriented computer programming language and translator for solving partial differential equations 11 p2013 A70-25367

Nonlinear partial differential operators eigenvalue solution using modified Newton iteration method, noting advantages over perturbation method 11 p2074 A70-26423

Computerized numerical integration of nonlinear partial differential equations describing blast wave in ionosphere with finite electric conductivity under uniform magnetic field 12 p2227 A70-28212

Hybrid computing techniques for solving parabolic and hyperbolic partial differential equations, discussing serial method accuracy and use of parallel logic for integrator control 13 p2373 A70-29461

Shallow shell theory partial differential equations, obtaining integral representations of general solutions 13 p2517 A70-29764

Second order hyperbolic partial differential equations solution by characteristic grid and continuous characteristic methods 15 p2768 A70-32818

Second order hyperbolic partial differential equations analog solution based on method of characteristics, showing advantage over digital computer solution 15 p2768 A70-32819

Variance reduction technique for hybrid computer generated random walk solutions of partial differential equations, comparing to analytical solution 16 p2942 A70-33731

Invariant imbedding application to solution of partial differential equations by continuous-space discrete-time /CSDT/ method, discussing time dependent heat diffusion 16 p2942 A70-33735

Continuous space discrete time /CSDT/ method using initial value formulation for partial differential equations, discussing applications to one dimensional problem 16 p2943 A70-33736

German monograph on stress-strain state determination for rotors of turbomachines covering strain equations, partial differential equations, boundary conditions, etc 16 p2971 A70-34078

Nonlinear partial differential equations initial value problems asymptotic solution using two time method 16 p2943 A70-34245

Forces on two dimensional oscillating airfoil in subsonic compressible wind tunnel flow, solving partial differential equation for pressure potential by integral transform technique 16 p2839 A70-34248

Algebraic aspects of generalized Riemann invariants method of integration of quasi-linear partial differential equations 16 p2944 A70-34329

Stochastic approximation for identification of distributed parameter system solutions described by linear partial differential equations

17 p3131 A70-35557

Third order accuracy for nonlinear hyperbolic system of partial differential equations extended to equations with independent variables

17 p3131 A70-35891

Class of third order difference methods for hyperbolic equations in one and two dimensions applicable to nonlinear initial value problems

17 p3131 A70-35893

Adiabatic invariant of nonlinear periodic wave described by partial differential equations in weakly inhomogeneous medium

18 p3291 A70-36642

Book on abstract methods in partial differential equations, covering functional analysis and distributions, elliptic theory, linear and nonlinear problems, evolution equations, etc

18 p3284 A70-36782

Augmented small parameter gas film equation for squeeze film journal bearing solved in terms of radial displacement

[ASME PAPER 69-WA/LUB-9] 19 p3435 A70-37609

Linear partial differential equations solvability, deriving necessary conditions for pseudo differential operator

19 p3457 A70-37677

Initial boundary value problems for hyperbolic partial differential equations, including Cauchy problem

19 p3457 A70-37678

Singularities of solutions of partial differential equations, discussing smallest convex set in manifold with differential operator

19 p3457 A70-37680

Sufficient conditions for local solvability of linear partial differential equations with operator on complex functions

19 p3457 A70-37682

Numerical integration of finite difference analogs of nonlinear partial differential equations, investigating data smoothing, filtering and boundary effects on computational instability

19 p3459 A70-38417

Simultaneous approximation of function and product with given operator, applying to boundary value problems of partial differential equations

19 p3459 A70-38682

Dirichlet problem for elliptic linear system of partial differential equations with constant first order coefficients

20 p3657 A70-39120

Parametric boundary layer theory numerical solution in two parameter approximation, solving partial differential equation by finite difference method

20 p3611 A70-39807

Shallow shell theory partial differential equations, obtaining integral representations of general solutions

20 p3732 A70-40102

Optimal terminal control stochastic synthesis for linear systems by Bellman second order nonlinear partial differential equation

21 p3801 A70-40607

Viscous magnetofluid dynamic one dimensional annular flow, reducing three dimensional field equation to coupled linear partial differential equations

21 p3855 A70-40889

Membrane theory of shells, reducing equilibrium equations to single second order partial differential equation through transformation in terms of stress function derivatives

21 p3939 A70-42031

Ducted propeller subsonic rotational flow with free boundaries, presenting second-order partial differential equation solution without linearizing assumptions

24 p4287 A70-45269

Continuous structural systems stability under random load excitation from linear partial differential equations of motion

24 p4421 A70-45281

PARTIAL PRESSURE

NT HYPOXEMIA

NT OXYGEN TENSION

Endtidal oxygen and carbon dioxide partial pressures, oxygen uptake and carbon dioxide after apnea and during apneic diving

02 p0235 A70-12089

Partial oxygen pressure in hyperaemic carotid capillary blood under hypoxic conditions, noting correlation with age and body weight

10 p1822 A70-25088

Gaseous monoxides dissociation energies and free energy functions tabulation for calculating partial pressures

14 p2545 A70-30902

Residual gases partial pressure measurement in vacuum chamber by mass spectrometer with electromagnetic scanner and electron multiplier, detecting electron current

19 p3421 A70-37466

PARTICLE ACCELERATION

Heavy nuclei survival in cosmic rays Colgate supernova acceleration model, assuming plasma wave instability in shock wave

02 p0357 A70-11788

Multiparticle processes in acceleration energy region, comparing various models, noting role of diffraction

03 p0526 A70-13044

Electrostatic charged particle acceleration and ion thruster function in geostationary satellite station-keeping and attitude control, orbital transfer and drag compensation

[ONERA-TP-764] 04 p0735 A70-14934

Ionization losses effect on energy spectra of cosmic ray heavy nuclei with Fermi acceleration, using transfer equation

04 p0742 A70-15201

Particle acceleration during 1966-1967 radio burst of 3C 273, indicating breaking down of model of expanding source emitting synchrotron radiation

05 p0918 A70-16927

Criteria for particle motion with constant acceleration in curved space-time

06 p1104 A70-17186

Quasi-steady coaxial MPD arcs characteristics, studying Ar ion velocities, electrostatic ion acceleration mechanism and arc voltage gradient

[AIAA PAPER 70-165] 06 p1132 A70-18208

Coherent synchrotron emission in Crab Nebula associated with electron gyromotion, discussing models for high energy particle acceleration

07 p1375 A70-18848

Ion acceleration in spherical and cylindrical plasma layers formed by spherical plasmoid expansion in plasma cylinders

07 p1384 A70-19414

Electromagnetic acceleration and energy losses of charged chromospheric-coronal plasma electrons and protons in unsteady magnetic fields of sunspots

07 p1384 A70-19417

Atomic and molecular beams produced by nozzle beams aerodynamic acceleration, discussing condensation effects, internal energy, scattering cross sections, etc

07 p1341 A70-20102

Binary mixture molecular beam apparatus combining aerodynamic acceleration and arc heating techniques, discussing particle energy and density

07 p1341 A70-20106

Light ions acceleration to high energy by pulsed high intensity electron beams

08 p1553 A70-21694

Synchrotron emission of relativistic particle in magnetic field with radiative reaction force comparable to Lorentz force, emphasizing pulsar cosmic ray electron acceleration

09 p1731 A70-22273

Magnetospheric substorms magnetograms taken at various stations, showing preceding ring storm particles deflection into magnetic tail

10 p1876 A70-24496

Particle acceleration during solar plasma ejection, disregarding magnetic effects on flux

11 p2107 A70-25526

Plasma turbulence theory, discussing particles stochastic acceleration in strong electric field

11 p2094 A70-26753

Primary cosmic rays electron-positron component, considering relative roles of collision-produced and directly accelerated electrons

12 p2292 A70-27382

Stochastic particle acceleration by VLF in weakly turbulent plasma in magnetic field, considering nonlinear cyclotron damping

13 p2468 A70-29935

Charged particle acceleration in outer space plasma, deriving ion-acoustic instability equations

14 p2630 A70-30220

Particle acceleration by electrostatic waves propagation in inhomogeneous plasma in terms of phase velocity, magnetic field and wave amplitude

15 p2778 A70-31912

German monograph on artificially accelerated proton measurements for ionization calorimeter calibration and cosmic radiation energy spectrum analysis during balloon flight

17 p3081 A70-34572

Pulsars as cosmic ray sources, emphasizing time properties of acceleration mechanisms

17 p3151 A70-34913

Acceleration and precipitation of Van Allen outer zone energetic electrons, using correlation experiment between magnetosphere and auroral zone

18 p3306 A70-36010

Van Allen electrons acceleration and precipitation during magnetospheric substorms in relation to auroral processes, discussing energy and pitch angle diffusion processes

19 p3411 A70-37495

Acceleration of high energy cosmic rays by pulsar LF electromagnetic radiation

19 p3501 A70-38085

Cosmic electron spectrum formation by acceleration, considering metagalactic background X radiation

20 p3695 A70-39174

Particle acceleration phase in solar flare development, discussing H alpha maximum, hard X ray burst and bremsstrahlung

21 p3880 A70-40971

Particle acceleration during solar plasma ejection, disregarding magnetic effects on flux

21 p3892 A70-41276

Hot electrons bunch spread deceleration in collisionless plasma, discussing stationary moving jump formation similar to shock wave

22 p4077 A70-42299

Charged particle acceleration in outer space plasma, deriving ion-acoustic instability equations

24 p4399 A70-46295

PARTICLE ACCELERATOR TARGETS

Polarized Co59 target using He3-He4 dilution refrigerator, analyzing fast neutron scattering

14 p2584 A70-30508

Bremsstrahlung and photoneutrons from electron-photon cascades in thick tungsten and tantalum targets bombarded with low energy electrons

20 p3674 A70-39222

High energy alpha particle beam exposed to plastic scintillators, determining spallation cross section for C12/alpha, alpha n/C11

21 p3852 A70-41138

PARTICLE ACCELERATORS

NT BETATRONS

NT ELECTRON ACCELERATORS

NT ION ACCELERATORS

NT LINEAR ACCELERATORS

NT OMEGATRONS

NT SYNCHROCYCLOTRONS

NT SYNCHROTRONS

NT VAN DE GRAAFF ACCELERATORS

Electron and proton accelerators design characteristics, performance capabilities and specifications, emphasizing opposite-beam techniques for elementary particles interactions studies

03 p0527 A70-13045

High energy neutron accelerator as fast neutron radiography source, comparing contrasts with gamma and X radiography

05 p0844 A70-15779

High velocity microparticle simulation techniques for studying properties, dynamics and origin of micrometeoroids, considering accelerators and impact results

06 p1029 A70-18131

Axicon systems for spectroscopy of light emitted by foil-excited accelerator beams, discussing scattering contribution to spectral line widths

07 p1287 A70-20083

Electrons radial motion and beam focusing in linear accelerator allowing for perturbing forces, calculating particle trajectory

10 p1926 A70-25110

Electrodeless traveling wave accelerator for wind tunnel use, determining gas stream density for subsonic and supersonic operation

16 p2889 A70-33868

Thermal neutron radiography with small accelerators using optimized collimator and fission increased flux

24 p4376 A70-45752

PARTICLE BEAMS

NT ATOMIC BEAMS

NT ELECTRON BEAMS

NT ION BEAMS

NT MOLECULAR BEAMS

NT NEUTRON BEAMS

NT PION BEAMS

NT PROTON BEAMS

Electron and proton accelerators design characteristics, performance capabilities and specifications, emphasizing opposite-beam techniques for elementary particles interactions studies

03 p0527 A70-13045

Electromagnetic wave growth effect on wave field propagating along beam-plasma slab, showing Poynting vector component

04 p0651 A70-15293

Transverse particle and energy fluxes in toroidal magnetic traps magnetic fields with ionized plasmas, discussing particle diffusion coefficient and thermal conductivity

08 p1554 A70-21807

Fast argon beam scattering by gas molecules measured to study atomic and molecular two body systems involving nitrogen and oxygen atoms

09 p1732 A70-22902

Lunar communications systems considering use of satellites, metallic particle belts, rockets, lasers and particle beams

14 p2634 A70-30196

Cryogenics and nuclear physics, discussing particle beam handling magnets, superconducting accelerators, detectors, moderators, low temperature irradiation facilities, etc

14 p2616 A70-31014

PARTICLE CLOUDS

U CLOUDS

PARTICLE COLLISIONS

LF electromagnetic waves theory for turbulent plasma based on expansion of particle collision and turbulent pulsation integrals 01 p0150 A70-10211

Oxygen collisional quenching rate in F region determined by comparing nightglow intensities with intensities calculated from electron density profiles 01 p0070 A70-10403

Daytime ionospheric electron temperature as function of electron-neutral particle collision reaction and nonlocal heating effect 01 p0170 A70-10407

Soviet book on plasma physics covering noninteracting and colliding particle motion, elementary processes, electric discharges, kinetic equations, macrocharacteristics, plasmoids, etc 01 p0151 A70-10500

Collision induced dissociations of 2000 eV diatomic O, N, CO and NO positive molecular ions as function of reactant ion internal energy 01 p0148 A70-11354

Evolution and entropy of partially ionized collision dominated plasmas interacting with radiation based on statistical analogs of irreversible thermodynamics 02 p0346 A70-11902

Cosmic ray muon source implied from hadrons X pairs produced in primary cosmic ray collisions 02 p0360 A70-12845

Cosmic ray particles inelastic nuclear interactions mean free path in iron measured in Wilson chamber and ionization calorimeter 03 p0554 A70-13030

Interacting meson systems effective masses with/without secondary proton measured, detecting heavy boson resonances and fireballs, considering proton nuclear interactions 03 p0472 A70-13031

Pion and nucleon interactions with atomic nuclei at 200 GeV using Wilson chamber and ionization calorimeter, determining pion collisions characteristics 03 p0555 A70-13034

Multiparticle processes in acceleration energy region, comparing various models, noting role of diffraction 03 p0526 A70-13044

Angle of incidence effect on oblique impact crater formed by high speed solid spherical particles colliding with massive lead targets 03 p0592 A70-13449

Density effects on transport coefficients of gaseous mixtures, solving modified Boltzmann equation including collisional transfer and three-particle collision effects 03 p0606 A70-13576

Radar Thomson backscatter observations of ion temperature and ion-neutral collision frequency used to investigate reversible heating in E region 03 p0477 A70-13988

Singularities arising during collisions in restricted n-body problem elimination, discussing Jacobi integral and finite-mass body configuration 04 p0714 A70-15354

Single impact data considered ineffective in estimating target damage induced by micron-sized particle cloud impingement 04 p0737 A70-15425

Motion near collision singularity in perturbed two body problem, applying method to boundedness proof for Sperling cluster energy 05 p0909 A70-16339

Collisions effects on cylindrical antenna impedance near plasma frequency of isotropic nonMaxwellian plasma, allowing for collision frequency dependence on electron energy 06 p1020 A70-17567

Ion-neutral coupling in plasma acceleration revealed by velocity disparities determined spectroscopically [AIAA PAPER 70-166] 06 p1133 A70-18219

Modified Maxwellian models for particle reflection in free molecular flow, correlating model parameters with gas-surface properties 06 p1110 A70-18259

Gas stream-elastic solid surface scattering characteristics, calculating trajectories, particle flux angular distributions, velocities, transfer coefficients, etc 06 p1111 A70-18265

Particle, momentum and energy flux spatial distributions of molecules scattered in collisions of low energy Ar atoms with mica and Ag surfaces 06 p1111 A70-18268

Heavy particle impact ionization in hot gases analyzed for ionization rates relationships 06 p1113 A70-18278

Particles and surface brightness distributions in nonionized cometary tails, considering near nucleus source and particle acceleration 07 p1378 A70-19035

Stress tensor for relativistic weakly ionized plasma in HF electromagnetic field taking into account collisions 07 p1348 A70-19197

Diatomic Br molecular vibration-rotation coupling effects on energy transfer during Br-Ar collisions, determining probability distributions 07 p1339 A70-20054

Inelastic scattering of He ions by Ne as function of angle, initial energy and energy loss using collision spectroscopy 07 p1346 A70-20243

Deviating and nondeviating absorption of radiowaves in ionosphere, deriving vertical distribution of particle collisions in E layer 08 p1490 A70-21431

Heavy particle collisions impact parameter and wave equations for direct excitation and electron capture processes 08 p1548 A70-21502

Fast argon beam scattering by gas molecules measured to study atomic and molecular two body systems involving nitrogen and oxygen atoms 09 p1732 A70-22902

Electromagnetic wave propagation through weakly inhomogeneous plasma layer with frequent electron-molecule collisions, noting applicability to ionosphere 11 p2003 A70-25530

Hydrodynamic equations for ions and electrons of ionized collisional plasma in inhomogeneous magnetic field based on Boltzmann kinetic equations 11 p2088 A70-25710

Linear theory of density gradient drift waves in stable collision dominated plasma using external excitation method 11 p2090 A70-26019

Collisional drift-wave turbulence in Li Q-machine plasma far unstable regime, discussing power spectra variations of density fluctuations 12 p2280 A70-27784

Glorified shadows in molecular beam scattering, considering undulation spacing, bound states number and extrema amplitudes in terms of optical analogies 13 p2454 A70-28624

Electrical conductivity without particle-particle or wave-particle collisional noise or radiation 13 p2463 A70-29238

Radio wave transmission through magnetized plasma layer as function of electron concentration and collision frequency, using coaxial accelerator 13 p2366 A70-29377

Collision and motion effect on rocket-borne quadrupole probe transfer impedance near lower hybrid resonance in ionosphere 13 p2371 A70-29919

Plasma kinetic equation, expressing interaction term as sum of binary collisions between close and collective interactions among remote particles 14 p2625 A70-31297

Semiclassical collision theory for computing fine structure proton impact excitation rates and cross sections for positive ions, presenting excitation rate tables 14 p2652 A70-31383

Potential gradient effect on charge separation mechanism during interaction of polarized snow crystals with ice sphere 15 p2769 A70-31445

Approximate dispersion relation for MHD waves from macroscopic plasma equations including particles collision terms 16 p2859 A70-32941

Effective cross sections for molecular hydrogen and hydrogen positive ion formation in collisions between He, Ne and Ar ions or atoms 16 p2954 A70-33193

Multistate impact parameter treatment of heavy particle collisions modified to include higher state couplings for electronic wave functions 16 p2956 A70-34309

Lorentz plasma electron velocity distribution with allowance for elastic and inelastic collisions, using Legendre polynomial and spherical harmonic expansions in Boltzmann equation 16 p2945 A70-34337

Krook gas particle collision model for relaxation from nonequilibrium to equilibrium Boltzmann distribution in spatially uniform gases 17 p3068 A70-34697

Na D lines emission cross sections measurement from ionic and neutral gases collisions at simulated meteor conditions 18 p3318 A70-37014

Photon pair annihilation process in graviton pair, examining IR emission in two scalar particle collision 19 p3472 A70-38172

Collisions in one, two and three dimensional plasmas of finite sized particles and clouds, obtaining scattering cross sections and Fokker-Planck coefficients 20 p3679 A70-39663

Charged particle collisions, discussing electron impact ionization of positive ions, detachment from negative ions, ion collisions, etc 20 p3676 A70-40154

Low voltage arc nonequilibrium ionization rate, taking into account atom-electron collisions 20 p3684 A70-40389

Configuration space three body elastic scattering theory for initially free independently moving particles collisions under short range forces 21 p3852 A70-40595

Coupling constant and binary collision expansions for ion motion in plasma line broadening 21 p3855 A70-40722

Electromagnetic wave propagation through weakly inhomogeneous plasma layer with frequent electron-molecule collisions, noting applicability to ionosphere 21 p3786 A70-41280

Electron-neutral collisional damping of longitudinal electron oscillations in weakly ionized plasma, solving linearized Boltzmann-Vlasov equation 21 p3860 A70-42014

Plasma sheath boundary in anisotropic plasma taking into account ionization rate, momentum transferring collisions and finite ion temperature 22 p4077 A70-42291

Neutron-electron collision damping and displacing of space echo in plasmas, indicating use for density measurement 22 p4082 A70-43244

Ionospheric bremsstrahlung X ray flux and ionization rate, considering electron-atom and electron-ion collisions as function of altitude 22 p4095 A70-43293

Upper atmosphere photoionization by extreme UV solar radiation compared with ionization by charged particles collisions 22 p4096 A70-43302

Scale invariance models correlation with cosmic ray data, comparing neutrino- and antineutrino-nucleon scattering 23 p4210 A70-43800

Classical calculations for energy transfer to diatomic molecules with rotational and vibrational degrees of freedom in atom-diatom-molecule collisions 23 p4221 A70-44010

Enskog theory extended to three particle collisions for gas transport properties 23 p4222 A70-44427

Normal shock waves structured by nonequilibrium radiative and electron-atom collisional ionization, using generalized radiation model 24 p4324 A70-45290

Plasma concentration and heavy particle-electron collision frequency in open cylindrical cutoff resonator based on frequency shift and passband broadening data 24 p4385 A70-45455

Plane parallel collision between two solid bodies of similar shape, discussing kinetic energy losses and motion after impact 24 p4427 A70-46376

Plane parallel collision of two solid spherical bodies with mass centers coincident with geometrical centers 24 p4427 A70-46377

PARTICLE COUNTERS

U RADIATION COUNTERS

PARTICLE DECAY

U RADIOACTIVE DECAY

PARTICLE DENSITY [CONCENTRATION]

NT ELECTRON DENSITY [CONCENTRATION]

NT ELECTRON DENSITY PROFILES

NT ELECTRON DISTRIBUTION

NT ION DENSITY [CONCENTRATION]

NT IONOSPHERIC ELECTRON DENSITY

NT IONOSPHERIC ION DENSITY

NT MAGNETOSPHERIC ELECTRON DENSITY

NT MAGNETOSPHERIC ION DENSITY

NT MAGNETOSPHERIC PROTON DENSITY

NT PLASMA DENSITY

NT PROTON DENSITY [CONCENTRATION]

Particle distribution and plasma nonequilibrium field evolution with turbulence generation by microwave field, considering plasma kinetic instability 01 p0150 A70-10212

Solid hydrogen condensation on interstellar grain surfaces at extremely low temperatures related to H atoms density 01 p0183 A70-10896

Electromagnetic showers fluctuations produced by electrons and photons in heavy materials, determining moments of particle numbers and bremsstrahlung differential cross sections 01 p0171 A70-11026

Extensive air shower axis position determined using energy methods and radial distribution geometry of particle density 01 p0171 A70-11252

Charged particles distribution according to multiplicity during pion-nucleon and nucleon-nucleon interactions at high energies 03 p0555 A70-13033

Density spectrum exponent of penetrating muon component of extensive air showers determined for hodoscopic assembly of Geiger-Muller counters with lead absorber 03 p0556 A70-13043

Equatorial magnetosphere particle and field data from 18 April 1965 geomagnetic storm reanalyzed in context of drift mirror instability theory 03 p0560 A70-13976

Charged particle distribution in heterogeneous medium using dispersion model to describe quasi-charged particles interaction with internal surfaces
03 p0536 A70-14370

Electron temperature and particle density measurements in annular MHD duct, demonstrating Hall effect existence
04 p0725 A70-14532

Interplanetary dust measurements near earth compared to theories predicting dust characteristics, discussing concentration, flux, impact rate and solar radiation pressure
04 p0749 A70-14619

Charged particle concentration emitted by inhomogeneous plasma determinable from emission spectral lines broadening, suggesting error correction procedure
05 p0889 A70-16541

Electric field determination from charged particle concentration in wake of body moving in rarefied plasma, noting hydrodynamics similarity
05 p0915 A70-16754

Particle density of jet plumes exhausting in vacuum calculated for He, Ar and N
06 p1052 A70-18388

Individual extensive air showers axes localized by measurement of charged particle densities, assuming age parameter
07 p1365 A70-18777

Particles infinite systems equilibrium state by canonical ensemble theory, demonstrating existence and uniqueness of limiting distribution functions dependence on density
07 p1333 A70-18936

Optical hardness effect on dispersed particles spectrum determination accuracy by spectral transmittance
07 p1330 A70-20309

Meteor abundance determination by visual observation, calculating sighting probabilities for various magnitudes
08 p1573 A70-20949

Plasma sheath in quadrupole and hexapole geometries, investigating magnetic field variation, particle density and electrostatic potential in transition layer
08 p1552 A70-21530

Sporadic meteoroid particles in ionospheric spatial density determined from kinetic energy measurements
10 p1940 A70-24322

Polarization of solar scattered radiation measured by radio probes for aerosol particle concentration and size distribution as function of altitude
10 p1884 A70-25253

Low energy charged particle distribution within earth magnetosphere and environs, suggesting solar origin for storm time ring current protons
13 p2483 A70-30089

Meteor abundance determination by visual observation, calculating sighting probabilities for various magnitudes
15 p2806 A70-32761

Solar wind observations by Pioneer 6, considering particle density, flux and kinetic energy
16 p2972 A70-32949

Gamma phase particle distribution changes in homogeneous segregation in Co-Ti alloy attributed to elastic interaction during aging temperature changes
16 p2931 A70-33208

Positron fraction among primary cosmic ray low energy electrons, using pure emulsion stack exposed under residual atmosphere
19 p3504 A70-38109

Schlieren method application in plasma diagnostics, obtaining density change of neutral, ion and electron gases
21 p3825 A70-40950

Stagnation temperature of two phase nozzle gas jet containing solid particles on particle density and velocity
21 p3748 A70-42220

One dimensional radiation transfer equation in non-homogeneous particle field, discussing spatial variations, particle number density, temperature, size distribution and optical properties
23 p4281 A70-44445

PARTICLE DETECTORS

U RADIATION COUNTERS

PARTICLE DIFFUSION

NT ELECTRON DIFFUSION

Particle diffusion distribution function of two component ionized degenerate gas from Boltzmann transport equation, giving tables for various spin and mass ratios
01 p0151 A70-10318

Diffusion categories and propagation of radioactive elements in lower atmosphere determined with respect to measured radiation balance, temperature gradient and wind
03 p0521 A70-14290

Galactic cosmic rays scattering by solar wind magnetic field fluctuations, considering energy and momentum transfer
04 p0739 A70-14596

Energy spectrum time dependence of solar cosmic ray event of 28 January 1967 measured in Northern Hemisphere, discussing particle diffusion and magnetic trap
05 p0902 A70-16459

Minority current carriers diffusion in heterojunctions and p-n junctions in AlAs-GaAs, using X ray microanalyzer performing electron beam scanning
06 p1126 A70-17816

Kinetic theory applied to free flow in spherical geometry to study collisionless thermal escape of particles from planetary atmospheres
06 p1147 A70-18293

Mass variation laws in light of Tsiolkovskii hypothesis, considering particle separation rates and thermal energy losses for actual jet engines
07 p1363 A70-19088

Electrical conductivity of collisionless magnetoplasma in weakly turbulent magnetic field, using quasi-linear approach for diffusion equation for distribution function describing test particles
07 p1352 A70-19987

Cosmic ray microvariations relation to solar wind structure, particle scattering models, spatial distribution, time variations, etc
07 p1372 A70-20336

Diffusion coefficient of charged particles in HF stabilization of current-convective instability measured in Ge semiconductor electron hole plasma
07 p1355 A70-20365

Horizontal turbulent diffusion model of cloud, determining particles dispersion as function of time
08 p1538 A70-21111

Boltzmann systems dynamics, discussing excitation spectrum, momentum relaxation time, particle diffusion trajectory, macroscopic theory of quasi-collective processes, hydrodynamics, etc
08 p1545 A70-21421

Diffusion layer correspondence to phase diagram in terms of constituent phases and composition
09 p1702 A70-22563

Cosmic rays diffusion through interstellar plasma noting microstabilities role
10 p1931 A70-23972

Plasma turbulent diffusion across constant magnetic field, noting magnetic, kinetic energy and relaxation times ratio effects
11 p2094 A70-26755

Nonlinear effects in beam-plasma type interactions, studying particle redistribution under inhomogeneous oscillating electric field
11 p2095 A70-26759

Dispersion/peak broadening in gel chromatography measured with nonporous and porous column packings, suggesting diffusion controlled separation with linear permeation isotherm
12 p2181 A70-27474

Boron particles combustion behavior prediction by incorporating condensed phase effect into diffusion controlled model
13 p2472 A70-29612

Radial diffusion role in radiation belt dynamics from flux profiles time variations observations or equilibrium states analysis
13 p2484 A70-30094

Trapped particles radial diffusion in formation and decay of radiation belts
13 p2484 A70-30096

Trapped protons population explanation by combined pitch angle scattering and radial diffusion across L shells
13 p2484 A70-30097

Diffusion layer microprobe analysis during chromalumination of Inconel turbine blade
14 p2595 A70-30293

Cosmic ray transport in solar wind generalized with anisotropic diffusion approximation
14 p2632 A70-30887

Aerosol particle convective diffusion from gas medium into obstacle, solving Fokker-Planck equation for particle distribution
15 p2774 A70-31493

Beryllium fibers and Al matrix interactions at high temperatures and various durations, investigating diffusion by X ray diffraction, electron microscope and microprobe analysis
15 p2757 A70-31812

Stress relaxation of Mo under plastic deformation controlled by diffusion of interstitial atoms and dislocations, determining activation energy
15 p2758 A70-32124

Two phase axisymmetric jet, studying dispersion of pulverized impurity consisting of particles of various sizes
15 p2721 A70-32135

Book on dynamics of geomagnetically trapped radiation, covering radiation belts control, adiabatic theory, trapped particle diffusion, etc
16 p2972 A70-34300

Proton distribution in radiation belt inner zone from radial diffusion addition to cosmic ray produced albedo-neutron decay and atmospheric collision loss
17 p3150 A70-34644

Alloy hardening statistical theory, applying flow stress to second phase randomly dispersed particles
17 p3191 A70-35458

Electrons and ions diffusion effect on vertical distribution in F region, discussing diurnal variations at various heights
18 p3254 A70-37027

Solar protons directional and omnidirectional measurements during particle event of 25 February 1969 by Heos 1 spacecraft, indicating particle diffusion in interplanetary space
19 p3496 A70-37506

PARTICLE EMISSION

NT ELECTRON EMISSION

NT FIELD EMISSION

NT ION EMISSION

NT NEUTRON EMISSION

NT PHOTOELECTRIC EMISSION

NT SECONDARY EMISSION

Alpha particle emissivity measurement of moon by Explorer 35 spacecraft for U 238 abundance in outer crust
01 p0181 A70-10573

Gas flow proportional counter for measuring high emission rates of alpha particles, discussing design and operation
04 p0695 A70-15570

Neutrino emission, mass loss and giant branch termination in young clusters with giants originating from intermediate mass main sequence stars
06 p1138 A70-17277

Particle ejection moments from tail of comet Ikeya-Seki determined from photographs having visible terminal synchrones
06 p1140 A70-17732

Laser characteristics and applications in high temperature research including metal heating, welding, machining, surface particle emission and plasma production
07 p1301 A70-19881

Nonthermal mechanism for high energy radiation and particle emission from X-stars and pulsars
08 p1575 A70-21364

Neutrino emission effect on collapse of supermassive stars, estimating energy radiated, discussing envelope explosion
10 p1938 A70-24022

Dissipation mechanism and period rate increase in neutron star pulsar model with neutrino emission for damping
12 p2312 A70-28368

Plasma turbulence in Van Allen belts, examining weak turbulent electromagnetic wave properties, with emphasis on trapped energetic particles radiation
13 p2486 A70-28555

Comet Ikeya-Seki 1965 f tail formed by dust particles continuous ejection, using perihelion photographs
19 p3527 A70-38792

Particle ejections in solar atmosphere and chromosphere structure, discussing dark halo exhibited by H alpha line in active region
20 p3699 A70-39464

Emitting plasma probes floating potential, discussing emission rate dependence on probe temperature and surface coverage by seed
20 p3632 A70-39607

PARTICLE ENERGY

NT ELECTRON ENERGY

NT ELECTRON STATES

NT PROTON ENERGY

Electric power generators performance based on kinetic energy conversion of radioactive isotope decay products, noting space applications
01 p0140 A70-10217

Multiparticle processes in acceleration energy region, comparing various models, noting role of diffraction
03 p0526 A70-13044

Earth magnetosphere low energy plasmas measurements via McIlwain magnetic shell parameter, showing dependence on geomagnetic disturbances
03 p0557 A70-13284

Electron and positron flux steady state in interstellar space relationship to differential energy spectrum exponent in cosmic rays, discussing galactic halo and age
03 p0561 A70-14151

Spectral line widths in MPD arc jet measured to determine plasma electron density and heavy particle temperature
03 p0536 A70-14371

Satellite observation of energetic particles and magnetic fields, discussing radiation belts, magnetosphere, galactic cosmic rays, etc
04 p0740 A70-14620

Quarks discovery in cores of energetic extensive air showers, discussing results evaluation and interpretation
04 p0722 A70-15299

Bethe function for ionization losses in energy of elementary particles heavier than electron
05 p0899 A70-15961

- High energy solar flare data from neutron monitor stations supplemented by low energy data from interplanetary space probes Pioneer 6 and 7
05 p0902 A70-16443
- Cold molecular beam of helium impinging on LiF or Si crystals investigated for gas-surface interactions, using time of flight method
06 p1043 A70-18255
- Momentum transfer from neutral nitrogen molecules to solid surfaces measured for various incident beam molecule energies
06 p1112 A70-18272
- Attractive potential effects on free and bound particles distribution in dissociating gas, studying recombination reaction effects on gas kinetic structure
06 p1044 A70-18280
- Energetic particle intensity fluctuations during bright aurora, using rocket-borne measurements
06 p1060 A70-18548
- Source power molecule lifetime, acceleration and particle velocity in region near comet nucleus determined from brightness
07 p1378 A70-19036
- High and medium energy molecular beams - Conference, Cannes, July 1969
07 p1339 A70-20101
- Molecular beam research at low, intermediate and high energies, discussing inelastic processes, intermolecular potentials, etc
07 p1344 A70-20131
- Intermolecular potential of atoms and/or molecules determined from scattering cross sections of supersonic He and/or Ar atomic beams
07 p1344 A70-20132
- Scattering cross sections of K atoms on bromine molecules determined as function of particle energy using supersonic atomic beams
07 p1344 A70-20133
- Charge exchange and electron loss measurements in steam target exposed to high energy hydrogen ions beam, using equilibrium fractions method
07 p1345 A70-20142
- Highly variable component protons and alpha particles identified in low energy cosmic rays by IMP 4
07 p1369 A70-20199
- Relativistic magnetic monopoles detection in corpuscular primary cosmic rays, describing equipment and results
07 p1371 A70-20333
- Longitudinal nuclear-electromagnetic cascade in ionization spectrometer simulated by Monte Carlo method, noting energy relationship to particle sum recording
08 p1500 A70-21743
- Low pressure plasma stability in cylindrical crimped magnetic field, considering convective perturbations and particle velocity distribution
08 p1555 A70-21981
- Shock heated molecular beams of argon, oxygen and mixtures with helium, measuring particle velocities and gas dissociation
09 p1733 A70-23180
- Fast neutral particles produced in electron-ion oscillation discharge as function of gas pressure and magnetic field
09 p1736 A70-23190
- Satellite-borne spectrometer for low energy ion measurement
10 p1874 A70-24314
- Satellite mounted device for detecting and recording 20-110 Mev solar neutrons
10 p1889 A70-24488
- Neutron monitor air pressure attenuation coefficient dependent on neutron energy being recorded
10 p1889 A70-24491
- Universe neutrino energy density estimation based on photon-neutrino weak interaction coupling theory
10 p1920 A70-24567
- Muon energy measurements using pair production, bremsstrahlung cross sections, burst sampling and Monte Carlo calculations
10 p1920 A70-24857
- Highest energy primary cosmic ray particles, considering air shower characteristics and energy spectrum shape
12 p2292 A70-27381
- Cosmic ray muon energy spectra at large zenith angles measured by optical spark chamber magnetic spectrometer
13 p2476 A70-28933
- Vector magnetic field and energetic particle flux profiles, indicating geomagnetically aligned currents associated with visible auroral arc
13 p2397 A70-29197
- High energy cosmic ray muons, investigating arrival from both low and high galactic latitudes
13 p2478 A70-29482
- Low energy charged particle distribution within earth magnetosphere and environs, suggesting solar origin for storm time ring current protons
13 p2483 A70-30089
- Superhigh energy particles detection by transition radiation, measuring Lorentz factor of emitted spectra
14 p2616 A70-31003
- Neutral particle temperature, pressure and velocity measurements in argon plasma jet, using refraction index
14 p2625 A70-31350
- Average triton energy required to produce electron-hole pair in silicon measured, describing precision charge calibration of amplifier system
15 p2784 A70-32396
- Electrons, positrons and photon energy distribution inside hydrogen plasma injected with high energy electrons
15 p2781 A70-32429
- Metal surface ionization measurements for upper atmosphere and interplanetary space energetic neutral hydrogen analyzer design
17 p3138 A70-35309
- Miniature multigrid probes for measuring energy spectra of charged particles and absolute plasma densities, comparing results to microwave measurements
18 p3294 A70-36150
- Upper atmosphere neutral component temperature measurement from thermal spread of charged particles beam
18 p3247 A70-36182
- Low energy solar and galactic cosmic rays propagation in interplanetary medium observed by Zond and Venus space probes, discussing shock waves retardation
19 p3493 A70-37475
- Auroral substorm temporal relationship to particle kinetic energy increases within trapping region, observing geomagnetic field distortions at higher latitudes during disturbed epochs
19 p3411 A70-37494
- Energetic storm particle events observation, noting association with solar protons and interplanetary shock waves
19 p3496 A70-37518
- Atmospheric fluorescence observation of supernova energetic photon short pulse burst, using photomultiplier
19 p3500 A70-38079
- High energy charged particle observations on OSO 3 at various rigidities
19 p3505 A70-38117
- Charge spectrum of high and low energy heavy cosmic ray nuclei, using balloon-borne nuclear emulsions
19 p3507 A70-38130
- Primary cosmic rays above 4.5 GV, measuring charge composition from balloon flight
19 p3507 A70-38133
- High energy primary cosmic ray muons arrival directions examined for anisotropies underground
19 p3508 A70-38141
- Energetic cosmic ray particles transfer through interstellar space based on galactic disk model
19 p3511 A70-38158
- Dense plasma thermodynamic and electromagnetic properties, discussing correlation energy
19 p3480 A70-38181
- Solar wind and flare energetic particles properties and interactions, surveying interplanetary magnetic field, planetary bow shock waves, neutrons, neutrinos, etc
19 p3511 A70-38418
- Equilibrium energy spectra of cascade electrons and photons in light and heavy materials as function of total shower energy
20 p3675 A70-39304
- Geomagnetically trapped energetic nuclei Z greater than or equal to 3 in earth outer radiation zone, measuring intensity ratio to alpha particles
20 p3698 A70-39327
- Ionization spectrometer for hadron energy measurement, analyzing instrument accuracy by Monte Carlo model for nuclear-EM cascade in iron absorber
20 p3635 A70-40456
- Temporal and spatial origin of hot ions in turbulent plasma heating, using particle analysis
21 p3855 A70-40824
- Energy losses frequency distributions for fast charged particles in small pathlengths in equimolar He-carbon dioxide mixture
21 p3852 A70-40973
- Earth magnetosphere LF wave annular trap, examining high energy particle interaction with magnetosonic waves
22 p4013 A70-42300
- Galactic X ray background due to inner bremsstrahlung associated with suprathermal particles, taking into account interstellar gas self absorption and ionization rate
22 p4093 A70-42465
- Solar high energy particles penetration into ionospheric heights at equator, analyzing optical flare and solar proton data from ATS-1 and Explorer 34
23 p4235 A70-43816
- Spallation limits on low energy cosmic and nuclear gamma rays interstellar fluxes, evaluating fast particle effects on interstellar medium
24 p4397 A70-45758
- Translational temperature measurement of atoms and ions in plasma based on wavelength reduction by X ray spectroscopy
24 p4388 A70-46208
- PARTICLE FLUX
U FLUX [RATE]
PARTICLE FLUX DENSITY
NT ELECTRON FLUX DENSITY
NT NEUTRON FLUX DENSITY
NT PROTON FLUX DENSITY
- Interplanetary dust measurements near earth compared to theories predicting dust characteristics, discussing concentration, flux, impact rate and solar radiation pressure
04 p0749 A70-14619
- Neutral particle flux measurements in plasma wind tunnel using BeCu detector, discussing role in collisionless flow dissipation processes
04 p0727 A70-14994
- Solar neutrino spectroscopy using various radiochemical detectors for Be 7, N 13, O 15 and B 8 neutrino fluxes, noting Li 7 suitability for determining CNO cycle
05 p0898 A70-15949
- Solar flare alpha to proton flux ratios on 23 May 1967 observed following interplanetary disturbances, suggesting electric fields as cause of modulations
05 p0902 A70-16444
- Solar core opacity influence on revised photospheric ion abundances, discussing neutrino flux prediction doubling in solar models
05 p0905 A70-16985
- Corpuscular radiation distribution function with trapped particles maximum density fixed in equatorial plane and reflection points vicinity of magnetic force line
06 p1135 A70-17894
- Angular distributions of fast scattered particles resulting from noble gases collision with metal surfaces
06 p1112 A70-18271
- Energetic particle intensity fluctuations during bright aurora, using rocket-borne measurements
06 p1060 A70-18548
- Atmospheric X ray photons measured regularly by sounding balloons in U.S.S.R., discussing X ray photon flux relation to charged particle fluxes
07 p1367 A70-19445
- Micrometeor flux in near-earth space measured by satellite-borne low noise acoustic detectors
07 p1386 A70-19493
- Intensity variations of cosmic ray neutrons and mesons analyzed to isolate lunar day period
07 p1368 A70-20033
- Molecular beam interactions with solid crystalline surface with fcc lattice elementary cell, investigating intensity distribution of scattered particles
07 p1342 A70-20119
- Reflected molecular beam intensity distribution interpreted in terms of disturbances in boundary layer between gas and solid
07 p1343 A70-20122
- Particle flux densities in electric field near spherical body moving in rarefied plasma
07 p1355 A70-20368
- Cosmic ray air showers simulation, discussing high energy nuclear interaction and linear relation of primary particle energy to number
09 p1744 A70-22048
- Charged particle albedo latitude dependence estimated from balloon-borne Geiger telescopes
09 p1746 A70-23481
- Cosmic ray particle abundance in upper atmosphere during minimum solar activity estimated by nuclear photographic emulsions on balloon flight
10 p1932 A70-24438
- Directional particle flux dependence on probe orientation with respect to external magnetic field, determining pitch angle distribution from count rates
10 p1932 A70-24497
- Universe neutrino energy density estimation based on photon-neutrino weak interaction coupling theory
10 p1920 A70-24567
- Muon energy measurements using pair production, bremsstrahlung cross sections, burst sampling and Monte Carlo calculations
10 p1920 A70-24857
- Siderial time variations in cosmic ray intensity observed by inclined muon telescopes
10 p1933 A70-24858
- Solar neutrino flux measurement based on neutrino capture by large chlorine mass and subsequent Ar 37 decay in low noise environment
12 p2293 A70-27389
- Deposition zone on sphere and aerosol particles flux onto sphere as functions of flow Reynolds and Stokes numbers, discussing drop deformation effects
12 p2263 A70-27513
- Muon intensity meter for cosmic ray muon flux underground using scintillation telescope consisting of two coincidence counters
12 p2295 A70-28176
- Low momentum muon intensity dependence on geomagnetic latitude
13 p2476 A70-28919

Cosmic ray vertical muon flux measurements at sea level using spectrometer 13 p2477 A70-29124

Vector magnetic field and energetic particle flux profiles, indicating geomagnetically aligned currents associated with visible auroral arc 13 p2397 A70-29197

Radial diffusion role in radiation belt dynamics from flux profiles time variations observations or equilibrium states analysis 13 p2484 A70-30094

Micrometeor flux in near-earth space measured by satellite-borne low noise acoustic detectors 15 p2805 A70-32738

Meteor orbit parameters and incident particle flux measurements by radio methods, eliminating backscatter radar sensitivity limitations 15 p2807 A70-32814

Cosmic ray muon intensity deep underground vs depth measured with liquid scintillation detector hodoscope 18 p3308 A70-36897

Atmospheric X ray photons measured regularly by sounding balloons in U.S.S.R., discussing X ray photon flux relation to charged particle fluxes 18 p3309 A70-36919

Flare associated high energy photon and particle fluxes characterized by short rise times and longer lasting decays, discussing plasma emissions 19 p3493 A70-37473

Solar wind fluxes observed onboard Venera 2 and 6 compared with earth electromagnetic field pulsations and short period disturbances 19 p3494 A70-37479

Trapped particle population changes associated with solar events, discussing solar wind discontinuity effects on magnetosphere 19 p3495 A70-37487

Solar cosmic ray protons and electrons increase during 25 February-5 March 1969 observed by Venus 5 and 6 space probes, discussing interplanetary medium disturbance 19 p3495 A70-37504

Particle flux diagnostics of nonisothermal low pressure plasma, using corpuscular passive method 19 p3476 A70-37556

Cosmic ray positrons and negatrons differential intensities near north geomagnetic pole from balloon flight measurements, noting solar modulation effects 19 p3503 A70-38102

Solar neutrinos flux upper limit determination, describing detection equipment and procedures 19 p3511 A70-38486

Transverse magnetic disturbances in auroral oval, examining movement, intensity, particle fluxes and field magnitude 21 p3817 A70-41090

Upper limit to primary deuteron flux and path length in space, using emulsion stack exposed near geomagnetic equator during minimum solar activity 22 p4093 A70-42673

Low density gas jet from short circular cylindrical tube, calculating molecular flux radial density variation 22 p4076 A70-43430

PARTICLE INTENSITY

Low energy electron beam diffraction, calculating intensity as wavelength function 14 p2619 A70-30489

Primary cosmic rays spectrographic measurement, using hard muon component intensity variations data 20 p3629 A70-39320

Geomagnetically trapped energetic nuclei Z greater than or equal to 3 in earth outer radiation zone, measuring intensity ratio to alpha particles 20 p3698 A70-39327

PARTICLE INTERACTIONS

NT ELECTRON CAPTURE

NT ION ATOM INTERACTIONS

NT MOLECULAR COLLISIONS

NT MOLECULAR INTERACTIONS

NT NUCLEAR INTERACTIONS

NT SPIN-ORBIT INTERACTIONS

Gas-particle primary and pure gas secondary streams turbulent mixing, solving for various mixing zone flow field parameters 01 p0061 A70-10337

Coulomb, Gaussian and harmonic oscillator potentials for particle pairs in three body system, using S wave expansion 01 p0147 A70-10519

Relaxation in gas-particle flow, analyzing thermodynamic properties, interactions, single particles and one dimensional flow equations 01 p0062 A70-10805

Convective red dwarfs Kr 60 A and 60 B structure and stability taking into account electrostatic interactions between gas particles 01 p0188 A70-11337

Cosmic ray primaries and secondaries direct heating of thermal electrons for computation of H I regions electron densities and temperatures 02 p0363 A70-11782

Direct interaction between hydrogen atom and positive ion with one electron, using Born and two and four state impact parameter treatments 02 p0344 A70-12703

Soviet book on quantum electrodynamics covering photon mechanics, electron relativistic mechanics, electromagnetic interactions, corrections to Green functions, particle interactions, etc 02 p0345 A70-12827

Multiple particle production at high energy levels and associated peripheral interaction and statistical theories 03 p0555 A70-13035

Cosmic ray particles high energy interactions during extensive air showers, noting inelastic superhigh energy collisions 03 p0556 A70-13040

Electron and proton accelerators design characteristics, performance capabilities and specifications, emphasizing opposite-beam techniques for elementary particles interactions studies 03 p0527 A70-13045

Electron flux interaction with electromagnetic field in comb type waves via linear approximation assuming small space charge 03 p0447 A70-13291

One and two center Coulomb, hybrid and exchange integrals contributing to orbit-orbit interaction in diatomic molecules evaluated for Slater orbitals combinations 03 p0528 A70-14010

Energy spectrum of cosmic radiation primary nuclei calculated from collisions against stellar light photons and 3 K black body radiation 03 p0561 A70-14185

Charged particle distribution in heterogeneous medium using dispersion model to describe quasi-charged particles interaction with internal surfaces 03 p0536 A70-14370

Lunar neutron flux due to cosmic radiation interaction with lunar surface layer, determining angular distribution and energy spectrum 04 p0738 A70-14442

Particle removal in ablation of artificial graphite linked to oxidation, using high speed motion pictures in analysis 04 p0787 A70-15610

Elastic and inelastic scattering of proton beam from Ne 20 measured for cross sections to interpret polarization data 04 p0723 A70-15636

Extensive air shower characteristics for inelasticity coefficient, nucleon-pion interaction cross sections and secondary particles, noting parameter interchangeability 05 p0898 A70-15946

Multichannel spectrometer electronic circuitry for ionization colorimeter providing data on low energy particle interactions, emphasizing reliability and accuracy 05 p0846 A70-15948

Deuteron splitting by solar neutrinos for neutrino detection, describing deuterium scintillation detector characteristics 05 p0899 A70-15954

Extensive air showers with nuclear particle interactions using ionization colorimeters, neutron monitor, scintillation and Cerenkov radiation counters 05 p0846 A70-15958

Experimental determination of solar neutrino activity from interaction cross section between neutrinos and target nuclei 05 p0900 A70-15965

Two phase transitions existence in Hubbard model of interacting electrons using one particle Green function solution 05 p0884 A70-16099

Muon-electron ratio measurements in extensive air showers, showing anomaly due to chemical composition change of primary cosmic radiation 05 p0901 A70-16274

Attractive potential effects on free and bound particles distribution in dissociating gas, studying recombination reaction effects on gas kinetic structure 06 p1044 A70-18280

Surface-particle interaction and atmospheric parameters measurements by paddlewheel satellites, discussing angular distribution of re-emitted molecules and accommodation coefficients 06 p1067 A70-18287

Rocket rectilinear motion, comparing Meshcherskii and Gantmacher-Levin equations in light of contact interaction hypothesis 07 p1392 A70-19087

Cs jet device eliminating wall influence in nonlinear radiation-atom interaction phenomena 07 p1342 A70-20109

Angular and energy distributions of hyperthermal K atoms scattered and ionized by W surface measured as function of beam particle energy 07 p1342 A70-20115

Atomic gas particles interactions with self and solid surfaces based on rarefied gas dynamics and classical mechanics 08 p1547 A70-21077

Dominant radiation field interaction with gas flow field using matched asymptotic expansion method 08 p1598 A70-21579

Geoactive low energy particles and fresh photoelectrons interactions with upper atmosphere observed by satellite Cosmos 261 08 p1492 A70-21796

Pion and nucleon interactions, tabulating average multiplicity and inelasticity values for various primary cosmic ray energy levels 09 p1745 A70-22775

Charged particle interaction influence on photoionization cross section of negative hydrogen ion, considering initial state polarization leading to free s wave electron 09 p1732 A70-22826

Atmospheric particle interaction layer in front of meteor body, discussing ionization, diffusion, excitation, recombination, heat generation and luminosity 09 p1761 A70-23059

Electron-neutrino weak interaction and heat decay coupling constants found nearly equal, describing astrophysical tests based on white dwarf stars luminosity intervals 09 p1733 A70-23451

Space charge parameters influence on electron wave and traveling wave interactions in TWT 09 p1652 A70-23654

Ionospheric photoelectrons resulting from solar UV radiation interaction with atmospheric gases, obtaining escape fluxes using Monte Carlo method 09 p1747 A70-23667

Dissipative parameters determination for relativistic gas within kinetic theory framework based on particle interaction model, assuming constant differential effective interaction cross section 10 p1867 A70-24148

Tachyons /faster than light particles/ on basis of relativity theory, noting reaction with light speed particles and relation to quantum theory 10 p1916 A70-24385

Universe neutrino energy density estimation based on photon-neutrino weak interaction coupling theory 10 p1920 A70-24567

Warm clouds electrification calculated for electro-magnetic field growth by inductive mechanism, noting role of water drop pair interaction 10 p1913 A70-24807

Quantization of Wheeler-Feynman electrodynamics, discussing spontaneous emission and connection between quantum and classical interparticle action theories 11 p2108 A70-25700

Suspended Stokes particle-single wave interaction effect on energy dissipation and vorticity of random turbulent incompressible fluid approximated by Fourier-Stieltjes integral 12 p2213 A70-28236

Neutron flux due to cosmic radiation interaction with lunar surface layer, determining angular distribution and energy spectrum 13 p2475 A70-28467

Inhomogeneous one dimensional plasma in electrostatic normal modes, considering interactions of waves and particles 13 p2460 A70-28638

Heavy particle spectroscopy, deducing collision parameters from empirical observations 13 p2456 A70-29810

Nucleon spectra, particle multiplicities and radiochemical cross sections following stopped-pion absorptions by complex nuclei, comparing calculated and experimental data 14 p2618 A70-30341

Time dependent simultaneous solution for continuity, heat conduction and motion equations of system involving neutral, electron and ion gases 14 p2665 A70-30744

Nuclear reactions and elementary particle reactions in Friedman universe with positive lepton abundance and degenerate electrons, discussing prestellar helium synthesis 14 p2620 A70-30877

Ion line Stark broadening, considering electron-ion quadrupole excitation and electron resonant scattering 14 p2620 A70-31376

Elementary particles gravitational interactions, identifying tensor field with local gravitation 15 p2776 A70-31732

Interactions of electrons, phonons and magnons with crystalline surfaces - Conference, University of Lille, France, September 1969 15 p2785 A70-32763

Ion-molecule reactions produced in phosphine by ion cyclotron resonance 16 p2855 A70-33061

Dusty gas dynamics, examining shock wave structure, boundary layers stability, flow equations, acoustic damping, velocity and density perturbations, etc 17 p3068 A70-34671

Particle penetration of solid or liquid combustible airstreams injected into air breathing combustors 17 p3073 A70-35665

Charge source density during interaction between atmosphere and electron/proton fluxes at prescribed boundary parameters 18 p3307 A70-36178

Solar energetic charged particles interaction with earth bow shock and magnetopause 19 p3494 A70-37482

Elastic materials consisting of particles with rotary inertia, long range force and dipole interactions, deriving constitutive relations 19 p3538 A70-37794

Three level gas laser amplifier theory, considering quantum mechanical atomic system in interaction with two monochromatic EM waves 19 p3446 A70-37829

Cosmic rays deuterons abundance calculation from H and He nuclei collisions with interstellar matter 19 p3506 A70-38125

Solar wind and flare energetic particles properties and interactions, surveying interplanetary magnetic field, planetary bow shock waves, neutrons, neutrinos, etc 19 p3511 A70-38418

Deep inelastic lepton-hadron scattering cross sections universality properties based on Wilson theory 20 p3674 A70-39150

Magnetron type backward wave tube with negatively charged slow wave structure, analyzing electron beam wave interaction for starting conditions 20 p3596 A70-39251

Wave particle resonances broadening by particles random motion in turbulent electric field, determining cyclotron instabilities saturation level from vanishing nonlinear growth rate 20 p3679 A70-39661

Variational formalism in mechanics of continuous media in four dimensional event space, considering model with local particle interactions 20 p3724 A70-39855

Universe homogeneous isotropic model with thermal radiation at outset, considering nucleons and antinucleons interactions 21 p3884 A70-40910

Electron exchange coupling of Gd and Gd-Y alloy dihydrides from ESR indicating negative hydrogen ion entry 21 p3862 A70-41703

Electron-ion wave interaction due to scattering by electrons, using kinetic wave equation to describe wave-particle interaction 21 p3858 A70-41712

Monoenergetic nitrogen free molecule beam impingement on solid surface, calculating satellite drag coefficients from momentum transfer measurements 21 p3745 A70-41743

Earth magnetosphere LF wave annular trap, examining high energy particle interaction with magnetosonic waves 22 p4013 A70-42300

Statistical theory of electron-positron-photon vacuum in external magnetic field, noting magnetic activation effect at low temperatures 22 p4076 A70-43000

Electron-neutral interaction parameters for Ohm law coefficients in multicomponent nonisothermal plasmas tabulated as function of electron temperature 22 p4081 A70-43015

Scattering indicatrix of electromagnetic radiation in plasma caused by electron-ion interactions 22 p3989 A70-43141

Solar wind instability from TEM waves propagating parallel to magnetic field in electron-proton plasma 23 p4235 A70-43826

Solid particles interactions during entrainment by viscous incompressible fluid in pipe, calculating interaction force as function of radius, distance and Reynolds number 23 p4181 A70-44310

Neutrino processes in lepton era as primeval fireball relic, discussing coupling constant for muon-electron neutrinos interactions 23 p4253 A70-44849

Solid surface interaction between surface with normal molecular beam, generalizing model by energy parameter simulating dissipative forces 23 p4223 A70-44994

Velocity-space homogeneous plasma instabilities due to self interaction of single species 24 p4384 A70-45253

Hoyle-Narlikar gravitation theory, considering Bohr quantization of direct interparticle action over all pairs 24 p4403 A70-45405

Solar wind two fluid model with boundary conditions describing electron and proton behavior in expanding corona 24 p4397 A70-45770

PARTICLE MASS

NT ELECTRON MASS

Field equations in particle neighborhood for spherically symmetric metric in conformal gravitation theory, considering particle inertial mass as function of position 01 p0142 A70-10492

Optical and radio pulses from pulsars as test of light speed variation with frequency and photon mass possible existence 02 p0373 A70-12394

Charged aerosol charge/mass ratio measurement and colloidal propulsion system thrust, efficiency and exhaust velocity determinations 03 p0551 A70-12936

Scintillation spectrometer design for mass and energy spectra of elementary particles, discussing block diagram 05 p0846 A70-15962

Relativity theory and quantum mechanics relation concerning point charge velocity and motion at light speed, deriving elementary particle mass formula 06 p1106 A70-17833

Heavy particles separation at sea level from overall flux of cosmic radiation, discussing method and device recording subrelativistic particles 09 p1684 A70-23732

Electrical conductivity hypothesis based on concept of transition temperature being inversely proportional to ionic mass square root 12 p2282 A70-26880

Free carriers effective mass and relaxation time in semiconductors determined from IR spectra of light reflection 12 p2285 A70-27362

Sr 83, 85 and 87 level structure and mass defect, using stripping and pickup reactions 17 p3138 A70-34625

Primary mass effects on extensive air shower characteristics, using Monte Carlo simulation 23 p4238 A70-44930

PARTICLE MOTION

Solar radiation pressure effects on zodiacal dust particle orbital velocity, computing Doppler shift of H-beta absorption line as function of elongation 01 p0070 A70-10348

Soviet book on plasma physics covering noninteracting and colliding particle motion, elementary processes, electric discharges, kinetic equations, macrocharacteristics, plasmoids, etc 01 p0151 A70-10500

Soviet monograph on transfer processes theory in statistical mechanical systems based on probabilistic approach to random particle walk 01 p0215 A70-10650

Cosmic dust particle direction, velocity and mass from ionization and momentum measurements by dust sensor during impact on Pioneer 8 satellite 01 p0088 A70-10748

Aerosol particles Brownian motion under inertial forces in absence/presence of obstacle 01 p0143 A70-10997

Normal shock waves in frozen, partly frozen and equilibrium flow in gas-solid particle mixtures 01 p0065 A70-11100

Mass point motion in inertial reference system of special relativity, finding motion equations analogous to relative motion equations in classical mechanics 01 p0145 A70-11442

Motion equations of material point in general relativity theory found analogous to equations in classical mechanics for metric in introduced physical space 01 p0146 A70-11443

Lagrange and Hamilton equations of motion of mass point in physical space of general theory of relativity based on least action principle 01 p0146 A70-11444

Dynamics of turbulent motion of incompressible viscous fluid particles, using Lagrangian functions 01 p0068 A70-11603

Particle velocity distributions in low density supersonic jets measured by molecular beam sampling technique and multidisk velocity analyzer 02 p0276 A70-11849

Charged particle self resonant motion in field of plane electromagnetic wave, showing trapped particles existence in whistlers 02 p0256 A70-12116

Geodesic motion of massless particles inside static sphere of small volume, analyzing relativistic effect of energy accumulation and release 02 p0339 A70-12117

Cosmic ray protons, He nuclei and electrons solar modulation by betatron deceleration mechanism during interplanetary space passage 02 p0357 A70-12123

Adiabatic invariance of action integral for motion in nonregular fields, explaining charged particles motion through magnetic shock front in interplanetary space 02 p0359 A70-12788

Charged particles motion in isotropic weakly ionized plasma acoustic wave associated with difference in electrons and ions entrainment by neutral particles 03 p0530 A70-13087

Galactic bending dynamics, discussing omega and zeta motions coupling of neutral hydrogen in outer region 03 p0570 A70-13553

Air-glass particle suspensions flows in shock tubes, deriving effective drag coefficients from simultaneous particle concentration and pressure measurements [ASME PAPER 69-WA/FE-21] 04 p0667 A70-14778

Relative motion of two spheroidal homogeneous rigid bodies of isolated binary system, obtaining potential energy 05 p0880 A70-15760

Motion generated by spherical body moving along axis of uniformly rotating fluid, measuring particle velocities ahead of and behind body 05 p0789 A70-16013

Formula for energy radiated from particles system applied to electromagnetic and gravitational radiation and illustrated by charged particle motion in magnetic field 05 p0882 A70-16309

Low energy charged particle motion parallel with magnetic force lines analyzed in magnetosphere model with constant electric field 05 p0903 A70-16726

Criteria for particle motion with constant acceleration in curved space-time 06 p1104 A70-17186

Charged particles motion in field of whistler mode wave packet, discussing trajectories 06 p1118 A70-17377

Relativity theory and quantum mechanics relation concerning point charge velocity and motion at light speed, deriving elementary particle mass formula 06 p1106 A70-17833

Motion of gaseous medium with uniform deformation with respect to three dimensional Cartesian coordinates 06 p1036 A70-17854

Particle nonlinear motion near equatorial libration points in restricted three body problem [AIAA PAPER 70-98] 06 p1146 A70-18226

Solar flare protons motion in sun radial magnetic field, considering protons interaction with interplanetary field inhomogeneities 07 p1366 A70-19427

Charged particle replacement by external plasma particles in ionized inhomogeneities moving in ionosphere, considering magnetic field role 07 p1266 A70-19435

Approximate method for celestial mechanics problems, considering particle motion under gravitation from central body in cylindrical coordinate system 07 p1387 A70-19626

Material particles unrealizability of periodic motion near libration points of triaxial ellipsoid rotating steadily about polar axis 08 p1543 A70-20491

Vibration stability of two identical particles constrained to plane and restrained by three linear springs with initial stress 08 p1591 A70-21466

Solar attraction effects on zero-mass body planar motion near triangular earth-moon libration points, obtaining variational equations of motion 09 p1754 A70-22477

Book on electrodynamics of particles and plasmas covering Cerenkov and gyro radiation, point charge motion, magneto-ionic theory, Boltzmann-Vlasov equations, etc 09 p1734 A70-22637

Charged particle self oscillatory motion in plane condenser field, applying results to electrical measuring instruments theory 09 p1680 A70-23144

Charged particles velocity profile across shock determined by induction velometry, considering eddy currents effects on induced potential gradient 09 p1738 A70-23677

Velocity synchronized Fourier transform hologram camera system for recording hypervelocity particles 09 p1688 A70-23775

Newtonian gravitational system of three point masses with oscillatory motion at time approaching infinity, discussing particles mutual distance 10 p1938 A70-24182

Particle escape from Newtonian gravitational system of positive energy 10 p1938 A70-24183

Tachyons /faster than light particles/ on basis of relativity theory, noting reaction with light speed particles and relation to quantum theory 10 p1916 A70-24385

Numerical integration method for function and solution of differential equation, considering equations governing two dimensional motion of particle in air stream 10 p1910 A70-25099

Electrons radial motion and beam focusing in linear accelerator allowing for perturbing forces, calculating particle trajectory 10 p1926 A70-25110

Charged particle motion in steady and perturbed dipole fields using laboratory earth magnetosphere plasma model 11 p2104 A70-25546

Transformed distribution function of particle velocity of plasma in Debye thermodynamic equilibrium approximation based on statistical mechanics 11 p2091 A70-26459

Elastic scattering effect on photoelectron transport and escape in upper sunlit atmosphere 12 p2222 A70-27187

Solid particle motions in dusty gas in inviscid hypersonic shock layers of slender wedges and cones and stagnation regions of cylinders and spheres 12 p2156 A70-27827

Kinetic theory of gas composed of identical particles with discrete velocity distribution, using Chapman-Enskog method 12 p2213 A70-28211

Solid particles or liquid drops admixture effect on propagation of inhomogeneous turbulent gas jet, using Prandtl mixing length theory to estimate pulsation velocities 12 p2213 A70-28218

Gas temperature effects on aerodynamic drag of carbon particles burning during nonisothermal motion 13 p2520 A70-28582

Low energy solar flare electrons scatter-free propagation through interplanetary medium, considering rise, decay and travel times 13 p2477 A70-29194

Self gravitating collisionless particles instability related to anisotropic random velocity distribution function in presence of disk-galaxy type spiral wave perturbations 13 p2492 A70-29299

Vibration spectra, kinetic and dispersion equations of solid spherical particles moving in incompressible weakly viscous liquid 13 p3388 A70-29368

Trapped particle interactions with plasma waves, analyzing pitch angle scattering, oscillating electric field, transverse waves and resonance effects 13 p2468 A70-29929

Laminar flow of suspension over flat plate, analyzing particulate velocity and concentration profiles relationships to drag and lift forces 14 p2565 A70-30270

Evaporation and combustion kinetics of droplets and particles in hot air stream, observing luminous trace 14 p2664 A70-30392

Quantum mechanical Boltzmann equation for atomic gas of composite particles, considering excited level degeneracy 14 p2619 A70-30651

Vibration stability of particle in plane restrained by two nonidentical springs with initial stress using Floquet theory and perturbations 14 p2657 A70-30843

Longitudinal electric field effect on trapped particle motion in asymmetrical magnetosphere, considering electron precipitation 15 p2728 A70-31990

Alumina particles marker transport in Ag wires during early sintering as function of plastic deformation by slip 15 p2745 A70-32392

Secular variations in osculating orbital elements of particle in Saturn ring gravitational field, considering motion in both external and internal space 16 p2973 A70-33226

Drift velocity for bound electron orbital motion in static axisymmetric magnetic field 16 p2959 A70-34187

Thermophoresis of aerosol particles in nearly free molecular nonuniformly heated gas, using linearized Boltzmann equation 18 p3292 A70-36254

Parametric representation of brachistochrones of mass point in centrosymmetrical gravitational field 18 p3283 A70-36387

Near earth motion equations for electrically charged dust particles in gravitating dipole magnetic fields, using zero-relative-velocity surfaces and energy integral 18 p3315 A70-36606

Gas particle mixtures nozzle flow at high loading ratios 18 p3208 A70-36693

Solar flare protons motion in sun radial magnetic field, considering protons interaction with interplanetary field inhomogeneities 18 p3309 A70-36901

Charged particle replacement by external plasma particles in ionized inhomogeneities moving in ionosphere, considering magnetic field role 18 p3249 A70-36909

Electric field strength in earth ionosphere and magnetosphere during irregular motion of fast ions and electrons 19 p3407 A70-37303

Coordinates for diagonalizing kinetic energy of particle system relative motion, discussing potential energy surface 19 p3373 A70-37841

Heavy and super heavy nuclei steady state spectra, comparing propagation parameters of light and medium nuclei 19 p3508 A70-38140

Energetic cosmic ray particles transfer through interstellar space based on galactic disk model 19 p3511 A70-38158

Ion-molecule pair relative motion in capture collisions, using computer-made movies 19 p3474 A70-38796

Adiabatic bounce periods of particle gyrophase coherence in earth field for cyclotron echo and triggered emission analyses 20 p3621 A70-39343

Solid particles or liquid drops admixture effect on propagation of inhomogeneous turbulent gas jet, using Prandtl mixing length theory to estimate pulsation velocities 20 p3612 A70-40091

Electric propulsion research involving MPD thrusters, current sheets and neutral-ion motion coupling [AIAA PAPER 70-1086] 20 p3683 A70-40249

Fraunhofer holography for small spherical particles three dimensional position and velocity measurements 21 p3822 A70-40811

Charged particle motion in steady and perturbed dipole fields using laboratory earth magnetosphere plasma model 21 p3882 A70-41296

Initial value transport of monoenergetic neutrons migrating in slab with infinite reflectors for isotropic scattering as function of material properties 21 p3854 A70-41999

Stagnation temperature of two phase nozzle gas jet containing solid particles on particle density and velocity 21 p3748 A70-42220

Magnetospheric tail magnetic field and particle motion calculation, assuming constant radius cylinder with current sheet bisecting center 22 p4019 A70-43111

Two particles relative motion in elliptical orbits in inverse square central force field 23 p4244 A70-44576

Particle motions in magnetic field, demonstrating existence of adiabatic region in particle phase space for Van Allen belt region 23 p4238 A70-44898

Particle motion in constant density dynamic viscosity random translational velocity fluid 24 p4324 A70-45139

Transition radiation due to charged particle moving in periodically stratified cold isotropic plasma 24 p4384 A70-45254

Faster-than-light particles impossibility in causal loops using nonquantum special relativity framework, considering tachyons 24 p4378 A70-45424

Two spherical particles rotation and slow motion about axis of circular cylinder in direction perpendicular to line of centers, considering fluid flow characteristics 24 p4325 A70-45781

Seeding particles motion recording in fluid flow by holographic velocimetry, using optical matched spatial filtering to determine particle location 24 p4340 A70-46350

PARTICLE PRODUCTION

Particle-antiparticle creation in galactic nuclei, expelling particles while retaining antiparticles 02 p0371 A70-12195

Cosmic ray muon source implied from hadrons X pairs produced in primary cosmic ray collisions 02 p0360 A70-12845

Nucleons and high energy pions inelastic interactions with complex nuclei involving external diffraction production of pions 03 p0526 A70-13029

Pion production characteristics during high energy nucleon interactions from data on production in upper atmosphere by gamma-quanta families/isobaric production/ 03 p0555 A70-13032

Multiple particle production at high energy levels and associated peripheral interaction and statistical theories 03 p0555 A70-13035

High energy muon production and interaction, analyzing ionization burst spectra 03 p0555 A70-13037

Thermodynamic potential of meson-nucleon plasma, showing variation of Landau equation of state in hydrodynamic theory of multiple particle production 03 p0527 A70-13052

Permittivity tensor calculations of weakly inhomogeneous plasma with monoenergetic component, using distribution function of particles produced by thermonuclear reactions 03 p0529 A70-13055

Negative O, NO and nitrous oxide ions formation by electron impact on nitrous oxide as function of pressure 03 p0441 A70-14007

Angular distribution and production probability of secondary shower particles produced by high energy cosmic ray muons using scintillation counter facility 05 p0899 A70-15957

Neutrinos production by primary cosmic rays in rarefied and dense media, calculating spectra 05 p0899 A70-15963

Carbon particles formation and growth model for cool variable carbon star atmosphere with sinusoidal carbon star atmosphere with sinusoidal temperature variations 07 p1380 A70-19260

Carbon particles formation and growth in Mira variables atmospheres, considering extinction effects on stellar structure and appearance 07 p1380 A70-19261

Quark search in cores of air showers with four million GeV mean energy, deducing rough production rate 07 p1368 A70-19925

Electron production rate enhancement by solar cosmic rays in lower ionosphere, considering particle distribution and polar cap absorption 07 p1369 A70-20153

Electron production in lower ionosphere by solar cosmic rays, calculating rates by computer as function of nuclear charge number, energy spectrum and height 07 p1373 A70-20348

Electrodynamic plasma accelerators fast particle generation mechanism during entrainment, studying polarization field potential structure 08 p1549 A70-20506

Relativistic particles formation associated with supermassive outbursts estimated to determine relativistic electrons mechanism in Crab Nebula 08 p1564 A70-20552

Vacuum UV photons production during ground state neutral argon atomic collisions, measuring relative cross sections energy dependence 09 p1731 A70-22333

Hydronium ion formation mechanism for D region, obtaining experimental support from mass spectrometer observation of ion production in oxygen glow discharge 09 p1671 A70-23500

Cross sections of fragments emitted in spallation reactions of carbon and nitrogen nuclei emulsion with alpha particles 09 p1733 A70-23549

Cosmic gamma ray spectrum from secondary neutral pion production in p-p interactions, discussing delta isobar, fireball and nuclear interactions effects 11 p2106 A70-26707

Solar L alpha and X ray emission contribution to lower ionosphere ion production, discussing altitudinal, latitudinal and temporal variations 11 p2106 A70-26789

Cosmic rays emission by dipole magnetosphere, applying model to neutron star particle belts 13 p2476 A70-28893

Fireball role in N-N interactions at primary cosmic ray energies, using fireball model to explain particle production 13 p2476 A70-28913

Elastic scattering formation and decay of unstable particle gases, discussing density and corrections to chemical and nuclear statistical equilibrium equations 13 p2455 A70-29223

Thermonuclear reactions in interior of sun, discussing models for He isotope concentration and flow to interpret solar neutrino generation 13 p2494 A70-29573

Primary cosmic ray flux and p-carbon cross sections measurements by satellites showing heavy particle production at high energies 15 p2792 A70-31733

Relativistic particles formation associated with supermassive outbursts estimated to determine relativistic electrons mechanism in Crab Nebula 15 p2805 A70-32707

Statistical analysis of cosmic radiation neutron component monitor error, taking into account generation multiplicity 18 p3307 A70-36097

Syrovatskii mechanism of high energy particle production near neutral line of magnetic field, noting solar flares occurrence conditions 19 p3478 A70-37581

Interstellar electron and positron intensity, observing pion production spectrum from nuclear collisions at machine energies 19 p3504 A70-38111

Cosmic rays deuterons abundance calculation from H and He nuclei collisions with interstellar matter 19 p3506 A70-38125

Cosmic rays propagation and production in Milky Way galaxy, using equilibrium model 19 p3510 A70-38157

Neutrino production by synchrotron process /magnetic bremsstrahlung/ in relativistic electron gas under intense magnetic field 20 p3695 A70-39050

Electron formation by cosmic rays in atmosphere, taking into account impinging particles energy variations 20 p3697 A70-39293

High speed shock wave propagation in deuterium gas, observing neutron production
21 p3806 A70-40744

PARTICLE SIZE DISTRIBUTION

Size distribution of Ni-Si particles precipitated from Si solid solution in Ni measured as function of concentration, aging time and temperature
02 p0317 A70-12320

Aerosol size distribution from data on atmospheric spectral transmittance and solar corona brightness spectral and angular variations
02 p0292 A70-12434

Intermediate air layer optical properties explained by assuming presence of small and large size aerosol particles
02 p0328 A70-12436

Aerosols size distribution and chemical composition and carbon monoxide, nitrous oxide and sulfur dioxide concentrations measured in pure atmosphere
03 p0521 A70-14289

Hypervelocity projectile size and density effect on ballistic limit of dual sheet spacecraft meteoroid protection structures, considering penetration of low and high density particles
04 p0776 A70-15422

Size and spatial distribution of meteoritic showers, establishing fragment distribution pattern relationship to sorting factor
05 p0912 A70-16464

Vacuum probe sampler to monitor particle contamination on surfaces within clean environments
05 p0808 A70-16703

Automatic particle counters and fluid contamination problems, misconceptions relating to sampling, size measurement, calibration, etc
05 p0851 A70-16706

Cepheus light attenuation curve explained by applying polymodal particle size distribution, obtaining interstellar dust density
05 p0918 A70-16915

Metal particle size relation to combustion time using statistical method applied to polydisperse Mg powder
07 p1419 A70-18756

Liquids particulate contamination sizing and counting by membrane filtration, specifying procedures and apparatus used
07 p1195 A70-18804

Atmospheric pressure, optical thickness and Young particle size distribution of Mars atmosphere determined from polarization observations
07 p1385 A70-19421

Microwaves scattering and attenuation in precipitations from raindrop size distribution curves analysis
08 p1462 A70-21096

Vacuum probe sampler to monitor particle contamination on surfaces within clean environments
09 p1623 A70-22340

Interstellar dust, discussing effective particle size, composition, formation and effects on astronomical observations
09 p1763 A70-23374

Electro-optical technique for size distributions of cloud and precipitations particles using linear array of photodetectors
10 p1912 A70-23929

Polarization of solar scattered radiation measured by radar probes for aerosol particle concentration and size distribution as function of altitude
10 p1884 A70-25253

Particle size distributions used in analyzing snow size spectra and radar reflectivity
11 p2004 A70-25651

Stable colloidal dispersions of subdomain magnetite particles correlated for magnetic properties in terms of size distribution and volumetric concentration by superparamagnetic theory
12 p2284 A70-27241

Scattering particle distribution relation to halo formation in polydisperse clouds, using Kirchhoff approximation for halos theory construction
12 p2264 A70-27522

Leonid meteor shower radar observation data, analyzing flux rates and particle size distribution
13 p2487 A70-28694

Griffith flaws limitation effect on glass matrix-tungsten composites strength, considering dispersed phase with wide particle size distribution
13 p2437 A70-28827

Two phase convex corner flows of particle imbedded inviscid incompressible fluid using small perturbations method
14 p2565 A70-30279

Particles shape and phase composition in combustion products of dispersed Al-Mg alloy powders by electron diffraction and X ray analysis
14 p2664 A70-30396

Quartz crystal particulate sensor instrument for terrestrial and Mars atmospheres
14 p2585 A70-30575

Polarized light scattering angle relationship with Mueller matrix elements for polydisperse systems of irregular randomly oriented particles
15 p2775 A70-32040

Two phase axisymmetric jet, studying dispersion of pulverized impurity consisting of particles of various sizes
15 p2721 A70-32135

Bistatic lidar /laser radar/ detection of atmospheric aerosol size distribution, using angular scattering measurements of polarization parameters
15 p2704 A70-32609

Airborne electro-optical array system design and performance for particle size measurement
16 p2906 A70-33175

Aerodynamic drag coefficients of micron size particle clouds in compressible transonic flow, using light extinction method
16 p2894 A70-33882

Fraunhofer holography for recording small particles to determine size distribution without disturbing sample
17 p3086 A70-35016

Erosion by solid particles, discussing impacting velocity effects, natural sand quartz particle size distribution and composition, artificial industrial abrasives, etc
17 p3126 A70-35600

Hypersonic flow containing dust, investigating for cosmic dust collection and analysis, discussing conditions for collected particle size distribution correspondence to original distribution
17 p3012 A70-35921

Interstellar cloud collisions, examining gas and dust particles separation by size
18 p3313 A70-36323

Atmospheric particle distribution spectrum by optical methods, estimating aerosol concentration from scattering coefficient
18 p3251 A70-36980

Atmospheric aerosols vertical distribution from aerostat measurements, considering particle size distribution
19 p3461 A70-37636

Primary cosmic rays energy spectrum, investigating extensive air shower /EAS/ size spectrum in 2,000-1,000,000 eV range
19 p3510 A70-38154

Collisions in one, two and three dimensional plasmas of finite sized particles and clouds, obtaining scattering cross sections and Fokker-Planck coefficients
20 p3679 A70-39663

Circumstellar system crushing processes described by integrodifferential equations, deriving particle size distribution of fragments in interplanetary space
21 p3889 A70-41148

Tranquility Base lunar soil origin, establishing component nature, size distribution, density, mineralogy, constructional or destructional history
21 p3897 A70-41519

Polarization of radiation reflected and transmitted by earth atmosphere, calculating scattering matrix for aerosol size distribution model
21 p3820 A70-41725

Tank collection and spectrophotometric tests in determining aluminum oxide particle size produced by small rocket engine
21 p3867 A70-41727

Particle size, shape and absorptivity effects on inclusion damage of Nd-doped barium crown laser glass
22 p4050 A70-43007

Spectral radiation extinction at atmospheric aerosol particles, discussing particles complex refractive indices and size distributions
22 p4065 A70-43171

PARTICLE SPIN

Self excited electron-phonon-spin spontaneous oscillations generation, deriving dispersion equation
16 p2878 A70-33779

Sound velocity in isotropic nonlinear elastic Cosserat continuum with constrained particle rotation, analyzing uniaxial and hydrostatic compression
20 p3734 A70-40434

Rarita-Schwinger fields in general relativity, extending equations for Fermion motion in linearized gravitational field to higher spin particles
24 p4380 A70-45818

PARTICLE TELESCOPES

Sidereal cosmic ray diurnal variations from underground muon telescopes in Northern and Southern Hemispheres, proposing model producing variations at earth vicinity
03 p0560 A70-13978

Block diagram for eliminating counting errors and spurious coincidences in telescope used at cosmic ray stations
05 p0845 A70-15931

Azimuthal telescope with proportional counters for underground recording of hard/soft cosmic ray components
05 p0846 A70-15937

Assessing background magnitude caused by earth natural radiation sources during underground detection of solar neutrinos by radiochemical methods
05 p0899 A70-15950

PARTICLE TRAJECTORIES

Azimuthal telescope for recording cosmic rays intensity, noting statistical error for vertical and oblique incident component
05 p0846 A70-15967

Automatic system for processing data from underground meson telescopes
07 p1238 A70-20347

Particle spectrometer for Apollo measurements of trapped protons and electrons, using directional telescope composed of solid state and scintillation counters
12 p2232 A70-27404

Digital closed-loop inflight calibration system for spaceborne particle spectrometers, utilizing cesium iodide crystal and programmable photomultiplier dynode supply
12 p2232 A70-27405

Muon intensity meter for cosmic ray muon flux underground using scintillation telescope consisting of two coincidence counters
12 p2295 A70-28176

Quark search in cosmic radiation near sea level, using scintillation counter telescope
15 p2793 A70-31737

Solar spar telescope of Lockheed Solar Observatory with closed tube protection from dust and wind
16 p2911 A70-33794

Statistical accuracy of standard muon azimuthal semicubic telescope for solar cosmic rays, discussing rms error
18 p3256 A70-36103

Azimuthal muon telescope installation at cosmic ray station, noting photorecorder circuitry
18 p3256 A70-36108

Sidereal cosmic ray diurnal variations using underground mu-meson telescopes in Northern and Southern Hemispheres
19 p3510 A70-38150

Five-channel azimuthal underground cosmic ray telescope using proportional counters suitable for continuous recording
20 p3629 A70-39312

PARTICLE THEORY

Fireball detection and discovery, investigating angular distribution of secondary particles using Van Hove and Amati theory
09 p1747 A70-23729

Book on plasma dynamics covering charged particle orbit theory, macroscopic equations, hydrodynamics, hot and cold plasma waves, kinetic theory and plasma radiation
11 p2087 A70-25500

Finite size particle physics for plasma computerized simulation, considering longitudinal oscillations, scattering cross sections, diffusion coefficients, etc
18 p3296 A70-36791

PARTICLE TRACKS

U PARTICLE TRAJECTORIES

PARTICLE TRAJECTORIES

NT ELECTRON TRAJECTORIES

Particle trajectory and associated wave determined for nonclassical trajectory problem from nonprobabilistic point of view, discussing discontinuity arising from unbounded velocities
01 p0142 A70-10657

Optimal control problems concerning vector determination and trajectory of point motion toward target in n-dimensional phase space
01 p0053 A70-11028

Quasi-trapped particle currents having discontinuities on daytime and nighttime side of earth
01 p0171 A70-11487

Galaxy model formulated in cylindrical coordinate system using Fokker-Planck equation for cosmic radiation particles propagation, discussing trajectories of high energy particles
03 p0553 A70-12880

Neutrinos line patterns in Muscovite mica, refuting Russel assumption by analysis of multiple Coulomb scattering of charged particles and track comparison
03 p0556 A70-13047

Theoretical and experimental cascade curves comparison for heavy materials used for particle absorption in tracking experiments, discussing Coulomb scattering
03 p0527 A70-13051

Laser beam for measuring particles velocity in two phase air-water jets by heterodyning, describing signal properties
05 p0858 A70-16258

Linear damping of sinusoidal oscillation in plasma, solving linearized Vlasov equation by integration along particle trajectories
05 p0888 A70-16304

Charged particles motion in field of whistler mode wave packet, discussing trajectories
06 p1118 A70-17377

High energy and contemporaneous cosmic ray tracks in bubble chamber picture noting evidence of quarks
12 p2276 A70-27997

Serra de Mage meteorite impact history from charge particle track analysis, noting fieldspar content
13 p2497 A70-29854

Charged particles focusing and sorting in bispiral systems, deriving differential equations for relativistic trajectories 15 p2707 A70-31520

Gas-particle mixture cascade flow over turbine blades, considering momentum/heat transfer and particle trajectories [AIAA PAPER 70-712] 16 p2835 A70-33569

HEOS 1 low energy proton measurements in interplanetary space, discussing particle direction during solar event and anisotropy time history 19 p3495 A70-37505

Fossil nuclear particle tracks in extraterrestrial matter using high voltage electron microscope and chemical etching 19 p3519 A70-38031

Erasure fission tracks in soda-lime glass, tektite, biotite and apatite by shock loading, determining dynamic pressure and associated temperature effects 19 p3414 A70-38035

Distribution functions of cosmic ray path length, obtaining exponential type for high and low energy data 19 p3509 A70-38146

Bubble chamber photography and track image reconstruction by holography, discussing measurement apparatus, accuracy and tolerances 19 p3428 A70-38510

Square cross section waveguide with cutoff frequency, calculating density wave propagation in helical electron beam trajectories directed by magnetic field 20 p3584 A70-39256

Solar radio U burst second branch low relative intensity, contradicting previous theory for trajectories 21 p3880 A70-40966

Nuclear particle tracks in Apollo 11 samples due to galactic cosmic rays and solar flares relationship to dynamic surface processes 21 p3914 A70-41648

Rock particle tracks of primary cosmic rays, spallation recoil nuclei, nuclear fission and solar wind ions, observing time scale multiple soil orientation 21 p3914 A70-41652

Apollo 11 bulk and core tube fines and rock cosmic ray tracks, discussing material history and corpuscular radiation flux and energy spectra near moon 21 p3916 A70-41667

PARTICLES

NT AEROSOLS
NT ALPHA PARTICLES
NT ANIONS
NT ANTINEUTRINOS
NT ANTIPARTICLES
NT ARTIFICIAL RADIATION BELTS
NT BARYON RESONANCES
NT BETA PARTICLES
NT BOSONS
NT CATIONS
NT CHARGED PARTICLES
NT CONDUCTION ELECTRONS
NT CORPUSCULAR RADIATION
NT CYCLOTRON RADIATION
NT DEUTERONS
NT DROPS [LIQUIDS]
NT ELECTRON BEAMS
NT ELECTRON PRECIPITATION
NT ELECTRON RADIATION
NT ELECTRONS
NT ELEMENTARY PARTICLES
NT FAST NEUTRONS
NT FERMIONS
NT FINES
NT FLAKES
NT FOG
NT FREE ELECTRONS
NT HADRONS
NT HIGH ENERGY ELECTRONS
NT HIGH TEMPERATURE PLASMAS
NT HOT ELECTRONS
NT HYPERONS
NT INNER RADIATION BELT
NT ION CYCLOTRON RADIATION
NT LEPTONS
NT MAGNETICALLY TRAPPED PARTICLES
NT MANGANESE IONS
NT MESON RESONANCES
NT MESONS
NT METAL IONS
NT METAL PARTICLES
NT METAL POWDER
NT MICROPARTICLES
NT N ELECTRONS
NT NEGATONS
NT NEUTRAL PARTICLES
NT NEUTRINOS
NT NEUTRON BEAMS
NT NEUTRONS
NT NUCLEAR PARTICLES
NT NUCLEONS
NT OUTER RADIATION BELT
NT PHOTOELECTRONS
NT PHOTONEUTRONS
NT PHOTONS
NT PI-ELECTRONS
NT PIONS

NT POSITRONS
NT POWDER [PARTICLES]
NT POWDERED ALUMINUM
NT PRIMARY COSMIC RAYS
NT PROTON BELTS
NT PROTONS
NT RADIATION BELTS
NT RAINDROPS
NT RELATIVISTIC PARTICLES
NT SOLAR CORPUSCULAR RADIATION
NT SOLAR COSMIC RAYS
NT SOLAR PROTONS
NT SOOT
NT STELLAR WINDS
NT THERMAL NEUTRONS
NT TRAPPED PARTICLES
NT TRITONS

Transillumination holography in environmental tests, discussing camera design, particle field and applications, including flow visualization in wind tunnel tests 03 p0486 A70-13539

Particles infinite systems equilibrium state by canonical ensemble theory, demonstrating existence and uniqueness of limiting distribution functions dependence on density 07 p1333 A70-18936

Oxidizer particle size and binder type effects on nonacoustic combustion instability of solid propellants [AIAA PAPER 69-175] 12 p2332 A70-27804

Plastic deformation of two phase alloy with small nondeformable particles in ductile matrix, discussing cross slip, yield and flow stress, work hardening etc 17 p3126 A70-35460

PARTICULATE FILTERS

U FLUID FILTERS

PARTITIONS [MATHEMATICS]

Partition functions and equilibrium constants for ScO, YO and LaO computed for 1000-8000 K, assuming doublet ground electronic state 10 p1946 A70-24970

Partitioning formalism for degenerate, almost degenerate and electron exchange perturbation problems 16 p2955 A70-34001

Partitioning perturbation theory for electron exchange problems, generalizing Hirschfelder-Silbey formalism 16 p2955 A70-34003

Ordinary differential equations piecewise polynomial approximation using subpartitioning to liquidate residuals 19 p3458 A70-38356

PARTITIONS [STRUCTURES]

Matrix analysis of steady state temperature field and heat flux through multilayer, plane, cylindrical or spherical partitions with internal heat sources 04 p0785 A70-14924

PARTS

U COMPONENTS

PAS

ELDO-PAS apogee motor prequalification test to determine specifications for constructing units for qualification testing 03 p0581 A70-13854

PASCHEN SERIES

Chromospheric slitless spectrometers at 1962 eclipse, discussing Balmer-Paschen line intensities, continuum data, reduction and source error 01 p0175 A70-10244

LTE departures in late B stars from measurements of Balmer and Paschen discontinuities 05 p0919 A70-16937

PASSBANDS

U BANDPASS FILTERS

U BANDWIDTH

PASSENGER AIRCRAFT

NT BAC 111 AIRCRAFT
NT BOEING 707 AIRCRAFT
NT BOEING 727 AIRCRAFT
NT BOEING 737 AIRCRAFT
NT BOEING 747 AIRCRAFT
NT BOEING 707 AIRCRAFT
NT CH-3 HELICOPTER
NT CH-46 HELICOPTER
NT CH-47 HELICOPTER
NT CH-54 HELICOPTER
NT DC 8 AIRCRAFT
NT DH 121 AIRCRAFT
NT DH 125 AIRCRAFT
NT F-28 HELICOPTER
NT F-28 TRANSPORT AIRCRAFT
NT G-222 AIRCRAFT
NT HFB-320 AIRCRAFT
NT L-1011 AIRCRAFT
NT TU-134 AIRCRAFT

Human vibration test program for airline passenger reaction to vibration environments of large commercial aircraft 02 p0244 A70-12132

Touring aircraft, discussing vibration and noise reduction, instrumentation, STOL aircraft, etc 02 p0227 A70-12663

Forward and rearward facing passenger seats effects in postdecompression emergency descent of high speed high altitude aircraft 03 p0437 A70-14061

Airline passenger food service, discussing public health measures, low temperature and cryogenic galley cooling 05 p0804 A70-15833

DO-231 fixed wing V/STOL airliner project based on DO-31 development, construction and flight tests, considering design problems, controls, safety, performance targets, etc 05 p0793 A70-15901

L-1011 TriStar design for transcontinental airline requirements, discussing propulsion, noise suppression, configuration, passenger comfort, etc 05 p0793 A70-16098

Safety analysis of VTOL aircraft for passenger transport based on accidental failures caused by technical defects, human error, weather, sabotage, etc 05 p0794 A70-16348

Unstable spiral precursor to jet upset /Mach tucks/ in executive jet transports 06 p0987 A70-18248

Civil air transport passenger escape devices design and installation criteria [SAE-ARP-495A] 07 p1191 A70-18805

Hansa 330 fan jet design for executive and commuter market, discussing forward-swept wing concept and standardized structures and systems 07 p1194 A70-19619

Particle properties and solar flare radiation hazards for passengers in supersonic flight 08 p1435 A70-20632

Jet lift passenger aircraft considered better suited for medium stage routes than rotor/ propeller designs for VTOL transport 08 p1436 A70-21347

Lift fan propulsion for VTOL passenger aircraft, discussing design, thrust augmentation, optimum element combination, engine-wing integrations and tests [DGLR-70-007] 10 p1929 A70-24049

Low cost lightweight flight control systems for business aircraft providing equivalent performance to larger equipment [SAE PAPER 700213] 11 p2079 A70-25886

Air conditioning systems design for turboprop commuter and business aircraft [SAE PAPER 700224] 11 p1980 A70-25895

Business aircraft fuel management system using capacitance and mass flow rate measurements, displaying fuel quantity and flow rate and flight time remaining [SAE PAPER 700225] 11 p1983 A70-25896

Twin turbofan executive aircraft /Falcon/ development, describing modifications and antinoise features 12 p2162 A70-28026

Falcon 10 economical executive aircraft development involving dimensions of cabin, powerplant and range 12 p2162 A70-28027

Falcon 10 simplified airliner-type equipment for operation under Category 2 weather conditions 12 p2167 A70-28028

Passenger aircraft structures accelerated testing for safety and fatigue durability under operational conditions, describing tests planning and evaluation 15 p2673 A70-31541

Emergency evacuation on land of passengers and crew of airliners, discussing training, equipment, standardization, communication and protective fabrics 15 p2675 A70-32220

High energy chemical systems for postcrash emergency evacuation of commercial passenger aircraft, discussing exit opening via explosive methods 15 p2675 A70-32221

Passenger survival and evacuation of civil jet transport aircraft after ditching at sea 15 p2676 A70-32223

Mercury passenger aircraft development schedule, cost, delivery and features, emphasizing weight balance and convenience 15 p2676 A70-32365

Corporate aircraft operations in Europe, discussing meteorological conditions, flight planning, airport arrival and departure procedures and language differences 16 p2842 A70-33820

Reliability maintenance problems in corporate aircraft operations, discussing equipment calibration, aircraft systems analysis and repair facility selection 16 p2921 A70-33821

Aircraft utilization rate vs invested money as factor determining financial justification of corporate aircraft operations, discussing maintenance engineering 16 p2921 A70-33822

Aircraft passenger tie-down failure, comparing injury patterns in various accidents to aid reconstruction 17 p3039 A70-35572

Mobile lounges and airport productivity concepts for optimal handling of passengers at airport terminal [AIAA PAPER 70-918] 17 p3064 A70-35830

- Central passenger traffic schedule role in air traffic control, discussing computer solutions, aircraft optimal use, etc
18 p3289 A70-36397
- Soviet book on passenger aircraft aerodynamics covering motions of gases and immersed bodies, similarity laws, boundary layer theory, finite span wing, etc
18 p3208 A70-36507
- Mass air transportation, discussing aircraft characteristics, traffic growth, scheduling, passenger and cargo handling, etc
18 p3350 A70-36656
- Passenger seaplanes virtues and drawbacks, discussing bases, servicing, refueling, passenger conveyance, prospects, etc
23 p4137 A70-43887
- Continuous flow requirements in aircraft passenger oxygen systems using phased dilution principle, discussing breathing mask efficiencies
23 p4141 A70-44483
- Superjet airliners wiring connectors for power distribution, signal circuitry and self ejecting push buttons for passenger seats
23 p4174 A70-44545
- ## PASSENGERS
- Systems engineering applied to airborne, airport and community socioeconomic structure in determining air freight and passenger demand impact on airport location and configuration
[ALAA PAPER 69-1091]
01 p0055 A70-10605
- Cardiology role in aviation medicine, evaluating jumbo jet and SST flight stress effects on pilots and passengers in age factor study of arteriosclerosis
05 p0803 A70-16721
- C-5 design features for entire environment assuring human integration as crew member or troop passenger
09 p1609 A70-22021
- Commercial jet passenger emergency oxygen needs for cabin decompression studied in determining time of safe unconsciousness
11 p1992 A70-26511
- Automatic air transportation passenger handling and postflight financial and statistical data processing
12 p2335 A70-27016
- Air terminal design, describing mechanical systems for moving people, baggage and cargo
[SAE PAPER 700259]
12 p2206 A70-27431
- Aircraft characteristics effects on traffic control and community, considering passengers and freight
14 p2612 A70-30108
- Rest periods assignment on long distance air travel of passengers based on physiological stress factor
15 p2690 A70-31892
- Concorde aircraft design for emergency passenger evacuation, emphasizing overwing inflatable escape slides and kinetic heating effects
15 p2675 A70-32222
- Human survival problems of transport aircraft in various airport ground-air situations and environmental conditions
15 p2676 A70-32224
- Passenger awareness of airline industry problems, discussing safety, traffic control, convenience, etc
15 p2831 A70-32225
- Space shuttle safety program for low risk passenger transportation, combining large aircraft experience with spacecraft technology
[AAS PAPER 70-055]
17 p3176 A70-34793
- Air freight carrier liabilities in passenger transportation international regulations, noting conflicting interpretations
19 p3553 A70-37562
- Air passenger legal rights and obligations, discussing contracting states, formalities, hygiene, inoculation and deinfestation
22 p4127 A70-43500
- Passengers physiological and medical problems on subsonic and supersonic aircraft
23 p4150 A70-44223
- Space rescue operations in orbit during heavy traffic of spacecraft with large passenger loadings, noting role of space shuttles and tugs
23 p4260 A70-44619
- ## PASSIVATION
- ### U PASSIVITY
- ## PASSIVE SATELLITES
- ### NT BEACON SATELLITES
- ### NT ECHO SATELLITES
- ### NT ECHO 1 SATELLITE
- ### NT ECHO 2 SATELLITE
- ### NT EXPLORER 22 SATELLITE
- ### NT PAGEOS SATELLITE
- Airborne SHF communication system for operation with passive satellites installed in C-121 aircraft
01 p0045 A70-11122
- Passive satellite coordinates correlations to instants of observation in U.S.S.R. ground stations, reducing quasi-synchronous observations by interpolation
11 p2007 A70-26192
- Passive and active satellite systems for point-to-point communication network with multiple access capacity, comparing technical and economic competitiveness
11 p2011 A70-26335
- ## PASSIVITY
- Dynamic systems absolute stability, optimality and passivity algebraic criterion in terms of real even polynomial coefficients
12 p2261 A70-27412
- ## PASTES
- Fluxless paste for thermomdiffusion calorizing stainless and heat resistant steels and alloys
19 p3434 A70-37459
- ## PATCHING
- ## U MAINTENANCE
- ## PATENTS
- Collection of patent papers on liquid crystals applications including radiation detection, polarizing, thermal imaging, etc
08 p1556 A70-21346
- Book on solar cells U.S. patent literature, discussing Si semiconductors, panel fabrication techniques, photoemissive devices, Cd, Ga and organic compounds, etc
09 p1612 A70-22050
- ## PATHOGENESIS
- Biochemical, electron microscopy and experimental medicine data indicating pathogenetic mechanism responsible for arteriosclerosis
03 p0431 A70-14278
- Hormones excreted by adrenal cortex function in rhesus monkeys pathogenesis after irradiation by sublethal dose
09 p1620 A70-22822
- Lumbar vertebrae transverse processes fractures in air crashes, considering factors involved, incidence and pathogenesis
17 p3033 A70-35578
- Etiopathogenesis of auditory disorders in flying personnel and aircraft engineers resulting from exposure to acoustic stresses
17 p3034 A70-35677
- ## PATHOLOGICAL EFFECTS
- Catecholamines biosynthesis, distribution, combining, uptake, deposition, release and metabolism in physiological and pathological reactions of organism
01 p0019 A70-10512
- Respiratory and cardiac activities, body weight variations, blood and urine electrolytic composition of astronauts during Soyuz orbital flights from medical tests
03 p0423 A70-13709
- Pathological Q waves in various diseases in absence of myocardial infarction, discussing electrophysiological mechanism
03 p0426 A70-13941
- EKG, EEG, pneumograms and X ray pictures showed no pathological effect after prolonged confinement in sealed chamber having artificial atmosphere with variable gas composition
05 p0810 A70-17121
- Long bone necrosis in response to reduced atmospheric pressure exposure, comparing lesions with caisson disease
08 p1449 A70-21944
- Physiopathological effects of weightlessness, showing desirability of partial gravity for long voyages via spacecraft rotation
09 p1621 A70-23439
- Pure-tone air conduction audiogram for diagnosis of patients exposed to intense noise indicating conductive or sensorineural origin of loss
09 p1621 A70-23457
- Vasoactive agent effects on decompression sickness in rats, noting increased severity of bends by serotonin and platelet role
10 p1811 A70-24176
- Physiology and pathophysiology of oxygen transport in human blood, discussing fluctuations in O2 capacity and affinity
10 p1821 A70-25079
- Respiratory and cardiac activities, body weight variations, blood and urine electrolytic composition of astronauts during Soyuz orbital flights from medical tests
11 p1985 A70-25509
- Physiopathologic effects on organs of longitudinal and tangential accelerations, decelerations, vibrations and weightlessness
11 p1986 A70-25821
- Plasma tocopherol concentrations and vitamin E deficiency in dogs, noting pathologic changes in smooth muscle, central nervous system, skeletal muscle and retina
20 p3569 A70-38991
- Laser radiation effects on lens lipid content in adult Rana temporaria frogs during cataract development
22 p3978 A70-43139
- Decompression hazards in manned orbiting systems, considering consciousness time, survival, pathological response, water vapor and denitrogenation effects and recompression rates
22 p3973 A70-43638
- Passengers physiological and medical problems on subsonic and supersonic aircraft
23 p4150 A70-44223
- Heme biosynthesis defect in vitamin E-deficient rats affecting bone marrow synthesis of delta-
- aminolevulinic acid and liver formation of porphobilinogen
24 p4304 A70-46146
- ## PATHOLOGY
- ### NT HUMAN PATHOLOGY
- Stainless steel micropipettes implantation in rat amygdala to study role in gastric secretion
02 p0234 A70-11729
- Pathophysiology of congenital heart disease - Conference, University of California, Los Angeles, July 1967
20 p3570 A70-39361
- ## PATIENTS
- Aeromedical Evacuation System in overall treatment process for seriously ill patient
09 p1628 A70-23467
- Air transport of cardiac patients with aorticuloventricular blocks, noting feasibility due to portable surveillance and treatment apparatus
12 p2172 A70-28041
- Patients emergency transportation by helicopter, discussing vehicle types and onboard medical treatment
14 p2540 A70-30191
- Air transportation of respiratory failure patients, considering medical equipment adaptation for aircraft use
20 p3580 A70-39440
- Optimum bed rest time schedules for cardiovascular patients from neurological, dynamometric, electromyographic and myogenic-tonus tests
23 p4149 A70-45077
- ## PATTERN DISTRIBUTION
- ### U DISTRIBUTION [PROPERTY]
- ## PATTERN RECOGNITION
- ### NT CHARACTER RECOGNITION
- Dynamic shape recognition scheme with two dimensional image mapped by spatial integration onto one dimensional time varying function, discussing corner information preservation
01 p0033 A70-10496
- Pattern recognition concepts applied to synthesis of aircraft approach progress monitor as adjunct to pilot decision process, discussing feasibility experiments [SRCC-106]
02 p0335 A70-12138
- Multidimensional data efficient decomposition for communication interface between man machine system, considering decision making and pattern recognition on digital computers with orthogonal transformations
02 p0265 A70-12149
- Instruments and procedures for photogrammetry automation, discussing automatic pattern recognition, data correlation and computer role
02 p0302 A70-12652
- Signal orientation insensitive filter for pattern recognition
02 p0266 A70-12701
- Lines and letters identification and localization relationships to stimulus attributes in visual perception supporting hierarchical processing hypothesis
03 p0425 A70-13825
- Nonparametric statistical pattern recognition conditions of finite probability distribution mixtures in non-supervised adaptive detection
03 p0454 A70-14078
- Error correction training procedures convergence for committee solution to pattern recognition problem
05 p0817 A70-16175
- Classification analysis methods application to plant identification for case with incomplete initial statistical information
06 p1014 A70-17632
- Image recognition problem analyzed by deterministic approach yielding criteria for operation of recognition algorithm
06 p1014 A70-17633
- Multichannel magnetograph display for pattern recognition of solar feature morphology compared with spectroheliograms
06 p1142 A70-17993
- Consistent and inconsistent linear inequalities evaluating speed and efficiency of algorithm for pattern recognition problems
08 p1467 A70-21782
- Algorithms based on continuous-group pattern recognition, distinguishing human faces, speech and handwritten characters
09 p1640 A70-22143
- Invariant recognition of visual patterns in translational conversions, describing patterns by differential method
09 p1641 A70-22824
- Automatic change discrimination applications to weather prediction, land resource management and city planning, using photographic, IR and radar sensor imagery
[ALAA PAPER 70-311]
09 p1677 A70-22876
- Digital computer processing of airborne multispectral data, discussing automatic recognition and mapping of terrain distribution, Earth Resources Technology Satellite data channel efficiency, etc
[ALAA PAPER 70-309]
09 p1668 A70-22878

Star field pattern recognition methods for spacecraft attitude determination without a priori knowledge of star position-vehicle attitude relationship

09 p1725 A70-23516

Diffraction pattern sampling for automatic pattern recognition in photographic imagery

09 p1689 A70-23802

Pattern prerecognition processing for multibject pictures, describing illumination, contour and curvature computation

10 p1845 A70-24659

Airborne remote sensing automatic data processing for forest identification through pattern discrimination, utilizing power spectrum analysis

10 p1878 A70-24734

Pattern recognition model simulating human physiology based on two dimensional Fourier transform of input images

10 p1827 A70-24770

Symbols design for machine displays based on Gestalt pattern perception theory, considering symbol learning, perceptibility, detail, boundaries, etc

10 p1827 A70-24771

Radar observation of landscape regions, discussing dependence on recognition of variations in texture patterns on radar image

11 p2004 A70-25642

Computer texture analysis for two dimensional scenery pictures involving periodicity invariance under Fourier transform

11 p2014 A70-26251

Pattern recognition with time interval modulation information coding (TIMIC), considering channel capacity of switching device, similarity with nervous system, etc

11 p2010 A70-26267

Preprocessing data transformations for multispectral recognition mapping, reducing difficulties due to variations in environmental, observational and sensor conditions

12 p2220 A70-26935

Binary-valued digital pictures noise cleaning by propagation processes

12 p2188 A70-27937

Computer program for flying spot scanner pattern recognition, analyzing human chromosome contour

12 p2170 A70-27938

Descriptive pattern analysis methods, considering grammar formalism for broad application

12 p2193 A70-28102

Algorithm for feature extraction in pattern recognition, using internal and universal criterion in computerized process

12 p2193 A70-28103

Holographic identification of similar two dimensional images by linear transformation of space by spherical lens using white light correlator

12 p2238 A70-28185

Book on automatic recognition of visual patterns and mechanization of creativity, presenting computer program termed Arithmetic

13 p2373 A70-29451

Collection of papers on theory and applications of learning and pattern recognition systems covering statistics and algorithms, adaptive optimization, stochastic processes, etc

13 p2373 A70-29576

Pattern recognition involving machine extraction of characteristic features and classification based on associated values, discussing design and decision rules for optimal recognition

13 p2373 A70-29577

Statistical methods for feature selection and ordering, mode estimation and pattern classification in pattern recognition, describing sequential decision model

13 p2374 A70-29578

Error correcting algorithms for pattern classification, finding optimal approximation to unknown optimal decision function

13 p2374 A70-29579

Pattern recognition systems design and applications in medical and photographic data classification

13 p2374 A70-29580

Training algorithms in designing multilevel quasi-optimal controllers for dynamic processes, using pattern recognition methods

13 p2383 A70-29581

Stochastic reinforcement learning model synthesizing control and pattern recognition systems with learning attributes

13 p2374 A70-29584

Stochastic approximation methods applied to pattern classification, estimation and control

13 p2442 A70-29586

Soviet papers on image recognition covering sequential optimization, self learning processes, transformations statistics, spatial discretization, optical information processing, etc

14 p2552 A70-30418

Maximum convergence function in image recognition using dynamic programming and sequential optimization

14 p2553 A70-30419

Learning self learning relationship in image recognition, analyzing resolving function with minimum probability for erroneous recognition

14 p2553 A70-30420

Sufficient statistics for optimal correlation function in classifying optical images in pattern recognition, using permissible transformations

14 p2553 A70-30421

Standard pattern recognition with spatial discretization, concerning discrete cell or segment viewing

14 p2553 A70-30422

Optimal spatial discretization and brightness quantization of graphical symbols for pattern recognition, considering illumination and reflection coefficient

14 p2553 A70-30423

Computerized control for beam scanning and optical data processing concerning symbols, letters and photographic images

14 p2553 A70-30424

Airphoto interpretation, discussing descriptive, digital and photographic methods of representing recognition process results

14 p2585 A70-30642

Mathematical pattern recognition, using potential functions superposition methods for reconstructing probability density from samples

14 p2554 A70-30926

Error probability bounds for M-ary pattern recognition, proposing adaptive feature extraction criteria

15 p2703 A70-32564

Pattern recognition procedure for electronic systems data classification

15 p2706 A70-32566

Human and machine pattern discrimination correlated by statistical correlation method from pattern recognition task involving computer simulation and humans

16 p2852 A70-33461

Generalized iterative inverse algorithm for linear inequalities set involved in pattern recognition and threshold logic requiring decision functions determination

16 p2870 A70-33739

Noisy stochastic pattern recognition system, determining optimal measurement sequence by discrete Pontryagin maximum principle

18 p3234 A70-36337

Simultaneous optimal detection and parameter estimation of signals in noise, considering multiple solution, learning and image recognition

18 p3228 A70-36597

Neutral H spiral structure in Milky Way galaxy, discussing map derivation, pattern interpretation, arm characteristics and kinematics

18 p3327 A70-37161

Observation classification/image identification/for two normal sets with common covariance matrix, investigating error probability asymptotic behavior

19 p3375 A70-37283

Sample images division into teaching and checking sequences in pattern recognition problems, determining coefficients based on statistical properties of set

19 p3382 A70-37449

Bandlimiting in coherent optical matched filtering for pattern recognition, eliminating confusion between cross correlations and autocorrelations

19 p3446 A70-37889

Eye movements during visual search and meaningless pattern discrimination

19 p3361 A70-38054

Human memory information structure, discussing pattern recognition, simultaneous attention, problem solving and logic

19 p3363 A70-38322

Close range atmospheric shape classification, using image recognition theory concepts

19 p3416 A70-38572

Image detection in pattern recognition through bipolar correlation, discussing reference generating algorithms and digital simulation results

20 p3633 A70-39972

Statistical pattern recognition and threshold learning in signal detection of noisy binary pulses

21 p3794 A70-41332

Adaptive pattern recognition systems design based on notions of convergence and feedforward interconnection of two systems

21 p3794 A70-41499

Digital computer processing of airborne multispectral data, discussing automatic recognition and mapping of terrain distribution, Earth Resources Technology Satellite data, channel efficiency, etc

[AIAA PAPER 70-309]

Suboptimum extraction of pattern features from continuous measurements, assuming different Gaussian random classes

22 p3991 A70-43493

Hyperthyroidism diagnosis by pattern recognition, using computerized class featuring information compression

22 p3977 A70-43732

Automatic detection of K-complex waveforms in sleep electroencephalograms, using pattern recognition

23 p4151 A70-44379

PATTERNS

Open pattern winding technique for composite materials, laying fibers without weaving around pillars at edge of table and to stiff beam

11 p2060 A70-26344

Pattern center hypothesis for habitation to centrifugal and linear accelerations in man, investigating aftereffects by nystagmography

14 p2538 A70-30913

PATTERSON MAP

Orthorhombic form of crystalline formylmethionine transfer RNA, obtaining Patterson function from three dimensional X ray diffraction data

05 p0803 A70-16947

PAYLOAD MASS RATIO

Single stage reusable ballistic space shuttle, featuring minimum payload mass ratios and high propulsive efficiency

23 p4262 A70-44686

All-body configuration hypersonic transport aircraft performance by computer synthesis, considering sonic boom constraint, maximum payload ratio and optimal cruise speed

[AIAA PAPER 70-1224]

24 p4291 A70-45957

PAYLOADS

Airport terminal configurations payload flow-through characteristics and space allocations, discussing passenger processing, baggage systems, etc

[AIAA PAPER 69-1088]

01 p0000 A70-10622

Cost reductions achieved by space payload life extension through manned maintenance and increased transportation economies via refueling and improved space propulsion

01 p0196 A70-10844

Geostationary satellite payload-optimal injection trajectory from nonequatorial firing range, describing dog-legging maneuvers

03 p0573 A70-13845

TD-1 satellite design and scientific payload

[DGLR-69-11]

04 p0762 A70-15142

Javelin research rocket payload suspension ensuring limited vibrational accelerations, using viscoelastic materials for damping

[DGLR-69-61]

04 p0774 A70-15147

Yo-Yo system for satellite Azur to reduce payload angular velocity after separation from booster, analyzing final spin error

[DGLR-69-43]

04 p0762 A70-15152

ASTRID two axis stabilization system for rocket payloads, aligning optical axis of experiment with star

[DGLR-69-42]

04 p0762 A70-15161

Parametric performance and cost comparison of separate and integral vehicle concepts for manned space activity using payload criterion

04 p0763 A70-15420

Sounding rocket Vera 15 design with emphasis on operation safety, discussing payload capacity

04 p0765 A70-15669

Airframe production factors involving choice of materials and fabrication methods, emphasizing weight reduction to increase payload

05 p0854 A70-15925

Optimum second stage sizes for Blue Streak first stage for maximum payload injection into various orbits, tabulating sizes and payloads

05 p0924 A70-16589

Solid propellant motors relative performance as related to intermediate payload missions, considering reusable liquid strap-on stages for post-Saturn payloads

05 p0897 A70-16897

Three dimensional motion of nonrigid parachute and payload system analyzed for dynamic stability

[AIAA PAPER 70-209]

06 p0987 A70-18062

Air cargo transportation systems in 1970s, discussing market expansion, payload capacity and fleet growth, containerization, etc

07 p1250 A70-19875

Electronic timing device for light balloon payloads, describing circuit

07 p1286 A70-19975

ARCAS meteorological rocket system designed for upper atmospheric soundings to provide thermodynamic and wind data, discussing payloads

07 p1395 A70-20256

Payload optimization factors for orbital storage of liquid hydrogen, considering payload cost of agitation, tank pressure, pressurant weight, etc

[AIAA PAPER 69-1007]

09 p1767 A70-23262

TD-1 satellite design and scientific payload

09 p1767 A70-23429

Yo-Yo system for satellite Azur to reduce payload angular velocity after separation from booster, analyzing final spin error

09 p1767 A70-23430

Spacecraft and boosters for earth resources surveys, discussing design, payloads, orbits, etc

10 p1950 A70-24641

Titan 3C boost phase inertia loads on payload estimated for satellite design, using frequency and interface acceleration methods

[AIAA PAPER 70-485]

Accelerated gradient projection method applied to rocket trajectory optimization for minimizing fuel required for placing payload in circular orbits

11 p2120 A70-25446

13 p2485 A70-28395

- Gyroless attitude control system for pointing Aerobee sounding rocket payload at sun using solar sensors
13 p2501 A70-28422
- Space environment effects on spacecraft payload materials and performance, discussing atmospheric pressure, outgassing, radiation and meteoroid collision
13 p2485 A70-28434
- Mesosphere payload to measure neutral gas density, positive and negative ions concentration and mobility in D region
13 p2393 A70-28682
- Petrel payloads taking into consideration rocket stability after launch and compartment design
13 p2503 A70-28683
- Attitude control system of three axis stabilized payload for spectral survey of comet head light
13 p2505 A70-28770
- RESY parachute recovery for payloads launched by Skylark high altitude sounding rocket, noting flotation system and location aids
13 p2505 A70-28771
- OGO 5 satellite scientific observations, payloads, parameters and objectives
15 p2812 A70-32364
- Space station experiments, payloads and activity planning
16 p2983 A70-34067
- Light weight integrated spin-up launch mechanism for rocket propelled payload
16 p2845 A70-34113
- Reliable latch diaphragm release mechanism for separation of payload from spacecraft, discussing design, operation and tests
16 p2921 A70-34117
- Reliable collet release mechanism design for separation and ejection of reentry vehicle payload from booster
16 p2922 A70-34118
- Titan 3 launch vehicle for scientific space missions, discussing building blocks, performance and payloads
17 p3178 A70-35260
- Delta launch vehicle design modifications for increased payload and space research programs
17 p3179 A70-35261
- Commercial air transport mission payload and range capability analysis, noting on-line flight planning computers
17 p3204 A70-35815
- [AIAA PAPER 80-899]
Future spacecraft mission for short period comets rendezvous, considering trajectory requirements and launch vehicle payload capabilities
19 p3530 A70-38885
- [AIAA PAPER 70-1072]
Surveyor spacecraft characteristics and operation, discussing scientific payloads, landing sites, etc
20 p3716 A70-39951
- Weight growth factor in aircraft design, discussing fixed and variable weight, payload, performance, flight quality, structural criteria and life expectancy
20 p3562 A70-40363
- [SAWE PAPER 839]
Aircraft loadability design by computerized loading program using graphic plotter
20 p3562 A70-40364
- [SAWE PAPER 836]
Aircraft stretch efficiency factor as function of productivity and payload growth
20 p3563 A70-40369
- [SAWE PAPER 838]
Space shuttle with reusable launch system, discussing payload sensitivities regarding orbiter and booster weight and engine reliability
20 p3716 A70-40377
- [SAWE PAPER 849]
Optimal low thrust power plant for spacecraft payload-maneuver tradeoff
21 p3866 A70-40832
- Disposable load drop effect on aircraft range, using Breguet equations for graphic determination of bombing range
21 p3750 A70-40868
- Rocket motion and space propulsion systems, discussing exhaust velocity effect on payload
21 p3869 A70-42039
- Low disk loading rotors in high speed VTOL aircraft for economical vertical payload lift
23 p4139 A70-44153
- [ICAS PAPER 70-57]
Europa III SLV payload for geostationary equatorial orbit, describing engine thrust and propellant capacity for high energy second stage
24 p4414 A70-46357
- links, using programmable switch for improved traffic handling and frequency coordination
10 p1837 A70-24346
- Time division multiple access (TDMA) system for Symphonie communication satellite using PCM phase shift keyed RF carrier
10 p1837 A70-24353
- Real time Apollo PCM telemetry data compression and transmission using zero order predictor
14 p2550 A70-30768
- Analog data transmission over PCM telemetry link, comparing noncoherent FSK vs PSK reception performance for waveform error
14 p2552 A70-31187
- PCM telemetry transmitters, command and receiver and ground control for German research satellite Azur
16 p2890 A70-34349
- PCM command control system for high altitude ballooning operations, discussing component equipment
20 p3587 A70-40085
- SKYNET PCM telemetry and command station, discussing system design, pseudomonopulse feed, command and computer subsystems, etc
20 p3589 A70-40322
- Digital PCM telemetry link coding techniques, discussing encoding-decoding complexity, and concatenated block scheme for channel
24 p4315 A70-46258
- PDM [MODULATION]**
U PULSE DURATION MODULATION
- PEACETIME**
Peaceful uses of outer space, discussing committee reports and recommendations, direct broadcast satellites, administrative and financial implications, etc
07 p1428 A70-19688
- PEAKS**
Optimal synthesis of filters maximizing peak-sideobe ratio of arbitrary zone of mutual ambiguity function
13 p2369 A70-29734
- PECLET NUMBER**
Transverse flow convective instability spectrum in vertical channel with porous walls, noting Peclet number effects
12 p2333 A70-28199
- Two dimensional body slow motion through stratified fluid bounded by parallel vertical walls, examining flow at different Peclet numbers
21 p3744 A70-41246
- PEDALS**
Speed and accuracy of foot operation of controls tested by circular targets in rows within reach of right foot
02 p0245 A70-12144
- PEDOLOGY**
U SOIL SCIENCE
- PEELING**
Metal adhesive joints peeling and stripping strength determinations, describing static and dynamic tests
08 p1503 A70-20884
- PEENING**
NT SHOT PEENING
- PELAGIC ZONE**
Pelagic sediment natural spherules identification based on formation process and manganese nodules abundance
13 p2400 A70-29859
- PELLETS**
Steel balls impact on polyurethane foam, porous rubber and fiber materials, noting effects on both pellets and targets
09 p1769 A70-22123
- PENALTIES**
Reliability guarantee vs cost of capital, analyzing contract compliance delay and discounted penalty expenditures
13 p2525 A70-29570
- Penalty functions for state-space constraints elimination in continuous optimal control problems
14 p2562 A70-31353
- PENDULOUS GYROSCOPES**
U GYROSCOPIC PENDULUMS
- PENDULUMS**
NT GYROSCOPIC PENDULUMS
Mathematical pendulum oscillations under clockwise and counterclockwise impact impulse, deriving differential equations describing trajectories
01 p0141 A70-10153
- Lorentz invariance test using bar magnet on torsion fiber, analyzing preferred reference frame in space assuming earth velocity coupled to electron spin through specific term
02 p0341 A70-12849
- Astronomical clock pendulum oscillations isosynchronization noting effects of suspension elastic moment, fabrication, calibration errors and rotation center displacement
03 p0484 A70-13367
- N degree of freedom pendulum with suspension point vibrating vertically, determining conditions for parametric resonance occurrence
03 p0524 A70-13368
- Cross coupled rotational motions of free solid body carrying nutation-damping pendulums
07 p1335 A70-19808
- Time optimal control for rotation of solid supporting body with aid of pendulum, obtaining motion equations by algorithm
07 p1337 A70-20299
- Dynamic stability of pendulum-weight system during vertical HF small amplitude vibration of suspension point by averaging method
08 p1543 A70-20494
- Resonant oscillations of coupled physical pendulums, investigating phase trajectories by Struble method
08 p1544 A70-20964
- Spherical pendulum equations of motion solved using Hamilton-Jacobi theory
08 p1546 A70-21465
- Bifilar pendulum vibration absorber for counteracting helicopter main motor vibratory forces
10 p1805 A70-24657
- Support vibration effect on zero shift of damped vertical pendulum, using equivalent linearization with perturbation scheme
10 p1917 A70-25205
- Polymers dynamic properties in hyperelastic and vitreous states as function of temperature, using torsion pendulum method
18 p3263 A70-36469
- Soviet book on dynamic systems with cylindrical phase space covering differential equations with angular coordinates, parameter estimation, multidimensional and discontinuous systems, pendulums, etc
19 p3470 A70-37468
- Multiaxis clusters of single axis pendulous accelerometers with coincident centers of angular motion insensitivity
19 p3431 A70-38539
- Resonant oscillations of coupled physical pendulums, investigating phase trajectories by Struble method
20 p3672 A70-39386
- Inverted torsion pendulum performance improvement, describing dashpot to dampen lateral vibrations
23 p4202 A70-44950
- Pendulum dynamic stability under parametric excitation, presenting transient and steady state solutions by linear and nonlinear theory applications
24 p4379 A70-45587
- Oscillating pendulum equipment for nondestructive material tests, determining longitudinal and transverse elastic moduli of specimen
24 p4338 A70-45738
- PENETRANTS**
Inspection penetrant systems reliability and performance predictability for nondestructive flaw detection
01 p0096 A70-10005
- Nondestructive test procedures for maintaining and determining serviceability of penetrant inspection materials during use
05 p0844 A70-15780
- Liquid oxygen usage inspection penetrant systems combining nonreactivity with flaw detection sensitivity
08 p1508 A70-21745
- Nondestructive testing of small metal tubing, discussing eddy current, ultrasonic and electromagnetic inspection and dye penetrants
08 p1509 A70-21748
- Fluorescent penetrants vs magnetic powder test for individual and continuous material inspection, discussing sensitivity and surface finish influence
24 p4338 A70-45741
- Commercial fluorescent penetrants for natural and artificial cracks, considering indication characteristics
24 p4348 A70-45742
- Inspection penetrant development for flaw detection, considering entrapment efficiency and dimensional sensitivity
24 p4348 A70-45743
- PENETRATING PARTICLES**
U CORPUSCULAR RADIATION
- PENETRATION**
Penetration criterion for double walled structures subject to hypervelocity meteoroid impact providing class of protective material properties
03 p0584 A70-12921
- Penetration depth calculation of high speed non-deformable sphere into massive body, approximating force on sphere by ideal incompressible fluid cavitating flow
04 p0776 A70-15269
- Hard electron bremsstrahlung measurement during intense polar aurorae in January and February 1968, determining electron flux penetration region
04 p0682 A70-15731
- Point source intensity fluctuations dependence on penetration depth of wave propagating in statistically homogeneous and isotropic media
09 p1636 A70-23133
- Penetration mechanics of multisheet structures based on discrete particle modeling of impact debris
13 p2509 A70-28521
- Low energy protons penetration into magnetosphere between forbidden regions, using model of constant electric field with charge exchange as loss mechanism
13 p2477 A70-29183

- Hard electron bremsstrahlung measurement during intense polar aurorae in January and February 1968, determining electron flux penetration region
14 p2575 A70-30816
- Particle penetration of solid or liquid combustible additives injected into air breathing combustors airstreams
17 p3073 A70-35665
- Welding electron beams metal penetration dependence on ionization phenomena, discussing model based on self focusing
22 p4043 A70-42379
- Isothermal kinetic rates of penetration of polymer by spherical indenter, using thermomechanical analyzer
22 p4059 A70-43079
- Nondestructive thermal and thermochemical treatment penetration depth measurement in metal, examining magnetic test and ultrasonic techniques
24 p4346 A70-45721

PENETRATION BALLISTICS

U TERMINAL BALLISTICS

PENETRAMETERS

- Wire and hole type penetrometers minimum perceptible image contrast level on radiograph, considering X ray quality and films effects
24 p4337 A70-45713

PENNING DISCHARGE

- Quasi-linear mode coupling in confined hot-ion Penning discharge plasma, discussing externally imposed excitation and internally generated oscillations
05 p0888 A70-16166
- Microwave nonlinear effects including mixing, harmonic generation and current rectification observed in plasma sheath surrounding Langmuir probe using PIG discharge
05 p0852 A70-16992
- Cyclotron frequency harmonics emission of PIG discharges linked to nonthermal electron plasma instability
07 p1354 A70-20316
- Kaufman thruster with predominant radial field, noting electron mobility across ion extraction screen and advantages of uniform plasma distribution [AIAA PAPER 69-259]
11 p2102 A70-26120
- Discharge effects on LF oscillations and ion extraction in hot cathode Penning plasma
13 p2463 A70-29370
- Penning pump argon stability, noting influence of pressure and ion incidence angle on cathode surface
15 p2744 A70-31847
- Radial distributions and escape of charged particles across magnetic field in hot cathode Penning discharge plasma with LF oscillations
15 p2780 A70-32191

PENNING EFFECT

- Hg and Cd seeded Ce plasma wide-spaced diode without external light source investigated for Penning effect on diode performance
10 p1808 A70-25038

PENTACHLORIDES

U CHLORIDES

PENTANES

NT NEOPENTANE

PENTOBARBITAL SODIUM

- Sodium pentobarbital effect on oxygen poisoned mice, observing respiratory depression coupled with lung failure
21 p3764 A70-41480

PENTOLITE

- Pentolite spherical charge gaseous explosion products expansion into vacuum, using Taylor similarity solution for flow in detonation wave
15 p2774 A70-31764

PENUMBRAS

- Penumbras forms and magnetic polarity distribution relationship in sunspot groups
01 p0184 A70-10955
- Penumbras visibility of earth on lunar disk related to moon distance during lunar eclipse, discussing moon vanishing
03 p0569 A70-13361
- Hydrostatic models of sunspot penumbra and umbra, analyzing spot transparency influence on Wilson effect
03 p0571 A70-13596
- Wilson effect in sunspot structure as penumbra foreshortening and disappearance or penumbra occultation by photosphere, analyzing intensity profiles on disk passage photographs
06 p1143 A70-18001
- Penumbras during lunar eclipses analyzed photometrically, considering effects of earth upper atmosphere and lunar luminescence
07 p1377 A70-18973
- Penumbral magnetic field strength on basis of photoelectric spectra of undisturbed photosphere
09 p1757 A70-22730
- Penumbras visibility of earth on lunar disk related to moon distance during lunar eclipse, discussing moon vanishing
11 p2118 A70-26726
- Penumbras and geomagnetic threshold effects on ionospheric electron production by primary cosmic rays
12 p2296 A70-28366

- Photoelectric spectra of photosphere and sunspot umbra and penumbra ranging from 3900 to 8000 Å
20 p3712 A70-40412
- Sunspot intensity profiles near solar limb, observing center side penumbra photosphere border
21 p3885 A70-40957
- Sunspot umbras and penumbras magnetically nonsplit lines measured photographically by spot contrast discriminator
21 p3887 A70-41115
- Sunspot penumbra velocity field spatial structure by filament spectrum analysis, plotting radial velocities relative to undisturbed photosphere
24 p4400 A70-45310

PEPSIN

- Pesinogens A, C and D from stomach mucosae of smooth dogfish separated by chromatography on DEAE cellulose
11 p1987 A70-26007
- Stereospecificity and reaction rate of enzymatic hydrolysis of racemic substrate by pepsin determined by nuclear magnetic resonance spectroscopy
12 p2181 A70-27472

PEPTIDES

- Optical transmission spectra of polypeptide films showing exciton structure near 1600 Å for alpha and polyproline II helices
02 p0345 A70-12723
- Chloride and sulfhydryl activators in glucagon degradation and secretion by purified rat liver dipeptidyl aminopeptidase I/Cathepsin C/
04 p0631 A70-14682
- Peptides removal from Merrifield solid phase by transesterification with anion exchange resin
06 p1003 A70-17154
- Peptide formation by stepwise tetramer-mediated condensation of alpha-amino acid as possible prebiotic process
07 p1204 A70-19202
- Mass spectrometric sequence determination of oligopeptides via acetylacetyl derivatives, giving reliable results with small peptides
09 p1630 A70-22976
- Peptide formation during glycine reaction with linear polyphosphates and cyclic metaphosphates, considering prebiotic synthesis
09 p1630 A70-23395
- Nitrosyl chloride reagent effects on phenylalanine peptides
12 p2181 A70-27471
- Polymer optical properties in terms of interaction matrix coupling monomers, applying to polypeptide alpha helix, beta sheets and polyproline helices
14 p2544 A70-30118
- Amino acids changes distribution in specificity regions of light polypeptide chains of immunoglobulins showing correspondence with Poisson distribution
14 p2536 A70-30349
- Taro ferredoxin amino acid sequence determined from chymotryptic and thermolysin peptides sequence
14 p2544 A70-30351
- Optical properties of amorphous polymers, considering one state calculations for flexible polypeptides in solution and disordered regions of films or proteins
21 p3780 A70-41702
- Stereochemical course of sterically controlled syntheses of dipeptides, using optically active amino acids
22 p3983 A70-43095
- Lipoprotein lipase activation on emulsified triglycerides by specific glycopeptides of human serum lipoproteins
24 p4298 A70-45802

PERCEPTION

- NT AUDITORY PERCEPTION
NT CONSCIOUSNESS
NT CRITICAL FLICKER FUSION
NT KINESTHESIA
NT OLFACTORY PERCEPTION
NT PROPRIOCEPTION
NT SENSORY PERCEPTION
NT SPACE PERCEPTION
NT TACTILE DISCRIMINATION
NT TASTE
NT VERTICAL PERCEPTION
NT VIBRATION PERCEPTION
NT VISUAL DISCRIMINATION
NT VISUAL PERCEPTION
- Air traffic vibration effects on human organs and sensations, considering blood circulation, lungs, eyes and muscles
09 p1625 A70-23007

PERCEPTRONS

U SELF ORGANIZING SYSTEMS

PERCEPTUAL SPEED

U PERCEPTUAL TIME CONSTANT

PERCEPTUAL TIME CONSTANT

- Perceptual tuning in tachistoscopic identification task with alternatives provided after or before and after stimulus
11 p1986 A70-25829
- Hypoxia effects on voluntary response time to peripherally located visual stimuli
24 p4302 A70-46107

PERCHLORATES

NT AMMONIUM PERCHLORATES

NT MAGNESIUM PERCHLORATES

NT POTASSIUM PERCHLORATES

- Thermal decomposition of perchlorates evaluated by mass spectrometer, with regard to composite propellants combustion processes
17 p3145 A70-34638

- Al particles fusion during combustion of stoichiometric mixtures of ammonium and potassium perchlorate and polyformaldehyde
18 p3299 A70-36246

- Powdered metallic additions effect on combustion rates of ammonium perchlorate with bitumen and polymethyl methacrylate and potassium perchlorate with bitumen mixtures
18 p3299 A70-36247

PERCHLORIC ACID

- Premixed perchloric acid-methane two flame structure, measuring burning velocities, spectra, temperatures and burned gas compositions
02 p0352 A70-12034

- Premixed flames of methane with chlorine dioxide and perchloric acid, comparing properties with methane-oxygen flames, suggesting unified reaction mechanism
07 p1425 A70-20007

PERCUSSION

- Linearization of elastic forces in vibration system with percussion
10 p1958 A70-24516

PERFECT GAS

U IDEAL GAS

PERFLUORO COMPOUNDS

- Photodissociation of perfluoroalkyl iodides filler of pulsed laser operating cavity, discussing thermal molecular dissociation and unexcited iodine atoms formation
08 p1513 A70-21418
- Poly(perfluoroalkylene oxides) preparation and curing, considering molecular weight and thermal stability
21 p3783 A70-42145

PERFORATED PLATES

- Thin anisotropic elliptical plate elastic equilibrium weakened by hole and under concentrated loads
01 p0211 A70-11445
- Curvature and hole spacing effects on stress concentration of isotropic plate weakened by two curvilinear holes, applying small parameter method
01 p0212 A70-11447
- Elastic deformation of plates with circular holes, determining stress concentration factors for compressible and incompressible materials on digital computer
02 p0390 A70-12810
- Complex stress functions and stress intensity factors at tips of star-shaped contour hole in infinite tensile sheet, including crack forking with arbitrary angle
03 p0585 A70-12974
- Stress state of brittle alloy turbine disks with eccentric hole distributions, studying stress concentrations, hole number effects, etc
03 p0588 A70-13243
- Plane longitudinal elastic monochromatic wave diffraction on stress free circular holes in infinite plate, calculating stresses between holes
03 p0589 A70-13375
- Hole reinforcement providing stressed state beyond hole equivalent to plate stress without hole, reducing problem to annulus region mapping
03 p0590 A70-13378
- Eigenfunctions of oscillating infinite perforated membranes for various boundary conditions at holes
03 p0591 A70-13415
- Stress-strain state of perforated shallow shells with arbitrary curvature using Green matrices
03 p0591 A70-13416
- Stress-strain state of infinite isotropic perforated plate under cyclic symmetry, assuming finite strains and nonlinear material
03 p0592 A70-13445
- Equivalent rigidity of doubly periodic symmetrically perforated infinite plate strengthened by elastic ring under isotropic tension
03 p0595 A70-13754
- Stress distribution in anisotropic half plane with reinforced circular hole under external loads applied at plane infinity and ring edge
04 p0765 A70-14417
- Perforated plates bending for multiply connected regions, proving quasi-regularity and uniqueness of boundary value equations
04 p0767 A70-14481
- Statistical model equations to predict discharge coefficients for concentric orifice plates as function of line size, diameter ratio and Reynolds number [ASME PAPER 69-WA/FM-6]
04 p0667 A70-14837
- Reinforced openings effect on burst strength of ductile circular plates subjected to pressure loads
05 p0943 A70-16810
- Stress-strain state of plates weakened by reinforced hole and under tensile and bending loads, including boundary conditions
05 p0945 A70-16856

Bending problem for homogeneous transversely isotropic plate weakened by curvilinear hole
05 p0946 A70-19659

Bending stress concentrations in elastic square plate with central hole under uniform load, using finite element solutions of modified Rayleigh-Ritz method
06 p1168 A70-17940

Critical stresses for plate with circular hole and cracks assuming symmetrical load
07 p1402 A70-19054

Effect of uniformly distributed circular holes infinite double row on stress distribution in transversely bent strip, based on Kirchhoff bending theory
07 p1407 A70-19385

Stressed state of plate with reinforced circular hole under tension and bending using Airy stress functions
07 p1407 A70-19540

Isotropic plate stress-strain state weakened by doubly periodic curvilinear holes using nonlinear theory
07 p1408 A70-19544

Critical stress-strain diagrams for brittle plate possessing notch-type stress raisers under biaxial tension
07 p1408 A70-19547

Stress concentrations calculation at holes in plates and shells of positive Gaussian curvature applicable to hyperbolic shells
07 p1408 A70-19548

Boundary value problems solution for infinite elastic isotropic plane weakened by arbitrarily distributed circular holes based on using series in Taylor functions
07 p1408 A70-19549

Thin sheet and laminate bullet hole deformation zone microstructure observation by electron microscopy, considering terminal ballistics approach
07 p1413 A70-20049

Plate electromagnetic wave diffraction on conducting plate with circular hole
08 p1456 A70-20503

Limiting equilibrium of unbounded cracked elastic plate with circular hole, studying crack propagation under compression
09 p1769 A70-22121

Stressed state in region of strain raisers round holes/ in plate subjected to two axial tension associated with plastic yield
09 p1771 A70-22464

Stress concentrations and load transfer around cutouts in fiber reinforced laminates, discussing boron epoxy plates with circular holes
09 p1710 A70-22793

Creep and stability of perforated and unperforated turbine disks under operating conditions
09 p1779 A70-23097

Thermal stress freezing during optical polarization study of perforated disk three dimensional thermoelasticity
09 p1780 A70-23105

Stress concentrations in turbine disks with eccentric holes under steady creep
09 p1780 A70-23200

Stress concentration at circular hole in plate, considering material creep and aging effects
09 p1782 A70-23290

Steady harmonic oscillations of half space with circular holes, deriving algebraic equations for boundary value problems
09 p1782 A70-23296

Stress concentration in plate with hole reinforced by elastic cylinder described by equations of three dimensional elasticity theory
09 p1784 A70-23592

Stress distribution in strip with asymmetrically positioned infinite row of equal and equally spaced circular holes subjected to longitudinal tension or transverse bending
10 p1955 A70-24082

Equivalent rigidity of doubly periodic symmetrically perforated infinite plate strengthened by elastic ring under isotropic tension
10 p1960 A70-25009

Fatigue crack propagation rate in sheet alloys with holes as stress concentrators related to duration of various development phases
10 p1965 A70-25290

Pinhole expansion in anisotropic plastic disks determined by obtaining solutions for Tresca and Mises yield functions, assuming plane stressed state
11 p2138 A70-26171

Thermal stress concentration in constant thickness orthotropic plate with rounded square hole
12 p2323 A70-27338

Transmission coefficient for perforated screen related to orientation of rectangular and cross shaped narrow openings and field polarization during normal wave incidence
12 p2191 A70-28174

Steel plates with penetration of oblique circular cylindrical aperture tested for effects on stress concentration
13 p2510 A70-28728

Stress concentrations and optimum shape minimum-weight reinforcement of circular holes in plates determined by polarization-optical technique
13 p2512 A70-28864

Stress distribution in isotropic plates weakened by elliptical holes under bending based on elastic shallow shell theory and small parameter technique
13 p2514 A70-29291

Stressed state of infinite plate with circular hole induced by displacement discontinuity in form of cracks
13 p2514 A70-29292

Stress-strain state of infinite isotropic plate weakened by curvilinear slit
13 p2514 A70-29293

Elastic isotropic circular perforated plate stress-strain state, proving quasi-regularity of infinite linear algebraic equations
13 p2515 A70-29317

Isotropic plates weakened by circular holes, investigating bending by Ambartsumian plate theory
13 p2515 A70-29509

Stress concentration coefficient around hole in isotropic nonlinear plate under shear, reducing solution to integrating fourth order differential equation
13 p2516 A70-29510

Tensile test on perforated Al-filled rectangular plate of photoelastic material, obtaining stress concentration at hole by photoelastic visualization
13 p2516 A70-29628

Surface heat transfer coefficients under perforated plate of multiple square array round impinging air jets [ASME PAPER 69-GT-4]
14 p2666 A70-31025

Stresses in plate containing circular hole with notch under uniaxial tension, determining parametric coefficients by Fourier transforms
14 p2661 A70-31326

Axisymmetric nonuniform initial thickness disk under pressure and twisting along interior surface of circular hole using incremental theory of plasticity for deformation analysis
15 p2816 A70-32004

Stress analysis of polystyrene plate weakened by doubly periodic system of equal circular holes
15 p2817 A70-32166

Point heat source generation of thermal stresses in elliptical plate with circular hole, using functions of complex variable for stress field determination
15 p2818 A70-32182

Stress concentration problems for partially strengthened circular hole in plate under uniaxial tension
15 p2819 A70-32185

Stress concentration in flat rectangular and skew panels with circular holes from photoelastic verification of direct stiffness method [SESA PAPER 1633]
15 p2820 A70-32303

Stress distribution around oblique holes in uniaxially loaded plate using three dimensional photoelastic analysis [SESA PAPER 1618]
15 p2820 A70-32305

Stress concentration around oblique circular cylindrical apertures in steel plates [SESA PAPER 1533]
15 p2820 A70-32306

Thin plates with central circular holes, investigating creep behavior for biaxial edge tractions
15 p2822 A70-32359

Hydrostatic stability and damping characteristics of perforated plates and screens for passive propellant control schemes from drop tower tests [AIAA PAPER 69-531]
15 p2787 A70-32510

Elastic layer with circular cylindrical cavity under axial tension /Kirsch problem/, determining stress concentration from boundary value problem
18 p3335 A70-36130

Stress concentration near holes in plate in plane problem of thermoelasticity, taking into account physical and geometrical nonlinearities
18 p3336 A70-36133

Nonlinearly elastic plate with hole of general shape, determining stress concentration
18 p3336 A70-36139

Elastic bending of perforated inhomogeneous plane with circular holes or inclusions
18 p3340 A70-36579

Stress state of brittle alloy turbine disks with eccentric hole distributions, studying stress concentrations, hole number effects, etc
19 p3548 A70-38461

Disk equations to determine tensions around arbitrary hole or stiffening contours
20 p3720 A70-39623

Infinite elastic plate with pair of insulated unequal circular holes, calculating thermal stresses
20 p3720 A70-39672

Elastoplastic equilibrium of thin infinite plate with periodic slit system along straight line under tension, investigating localized plastic deformation domains
20 p3721 A70-39769

Cross shaped plates with circular hole, determining stress concentrations under uniaxial and biaxial tension
20 p3734 A70-40443

Perforated infinite plate finite elastic deformation under biaxial tension, using successive approximation

in connection with complex variable method of plane elasticity
21 p3932 A70-40551

Perforated cantilever beams and plates vibration damping capacity improvement by stress concentration introduction
21 p3933 A70-40729

Perforated steel strip axial tension load limit, considering various hole diameters and numbers
21 p3936 A70-41415

Stress concentration effect on perforated Al alloy panel fatigue, using theory for material critical thickness near notch
21 p3938 A70-41955

Stresses and strains concentration around elliptic hole in finite plates subjected to uniform load, using photoelasticity, moire effect and grids
22 p4114 A70-42697

Shock wave damping by perforated walls in gas channel, visualizing curved fronts with 24-spark HF camera [SMPE PREPRINT 104]
22 p4032 A70-43031

Stress concentration near holes in nonlinear viscoelastic plate, using elastic theory
23 p4266 A70-43989

Heat conduction of doubly connected square and triangular isotropic plates with hole, applying small parameter method
23 p4276 A70-44217

Steel and duralumin strips with circular holes tested under axial tension, determining relationship between strength weakening and ultimate stress
24 p4420 A70-45272

Infinite plate perforated with rounded corner square hole under uniform partial loading, examining elasticity with conformal mapping
24 p4427 A70-46367

PERFORATING
Plastic film precise perforation using carbon dioxide laser and optical tooling permitting double exposure to laser beam
03 p0497 A70-13565

PERFORATION
Subsonic boundary lift interference in wind tunnels with perforated walls, using point matching method
14 p2563 A70-30869

Perforated solid body moving in ideal incompressible fluid, deriving equations of motion in Lagrangian form
20 p3610 A70-39732

PERFORMANCE
Performance characteristics analysis of large area roll-up solar arrays based on support structure size and weight [ASME PAPER 69-WA/ENER-11]
04 p0770 A70-14898

Linear regulator optimal for exponentially time-weighted quadratic performance indices, using cost equivalence concept in infinite terminal time solution
04 p0663 A70-15604

Minimum performance standards established by Radio Technical Commission for Aeronautics for airborne radio marker receiving equipment operating on 75 MHz
13 p2364 A70-28999

Time lag system performance index bounds determination and optimal feedback controller design based on min-max criteria
14 p2561 A70-31185

PERFORMANCE CHARACTERISTICS
U PERFORMANCE
PERFORMANCE DECUREMENT
U PERFORMANCE
PERFORMANCE PREDICTION
NT PREDICTION ANALYSIS TECHNIQUES
Performance boundaries of space propulsion systems containing nuclear electric stages [AIAA PAPER 69-249]
01 p0196 A70-10839

Mathematical models construction for predicting and measuring air traffic controller workload, using synthetic and analytic methods
02 p0332 A70-11972

Prediction systems for turbulent boundary layers, noting momentum integral equation use in all integral methods
02 p0281 A70-12327

Method of weighted residuals /MWR/ applied to turbulent boundary layer equations, describing two parameter prediction technique
02 p0282 A70-12330

Evaluation of performance of prediction methods for mandatory flows
02 p0286 A70-12359

Resistance strain gauge performance prediction, investigating response during temperature change for preattachment matching
02 p0302 A70-12498

Reinforced epoxy resin performance prediction from correlation between unfilled resin and laminates mechanical properties
02 p0322 A70-12606

Steady state deuterium-tritium fusion reactor approximate parameters prediction possibility based on

interim assumptions of plasma confinement, model, etc 02 p0349 A70-12755

Turbulent and wall jets with wide varieties of geometries and boundary conditions, predicting jet-in-flow effects on entrainment rate, lift, drag, etc 02 p0288 A70-12840

Flow development in conical diffusers, delaying stall with high velocity air injection through annular slot at diffuser inlet predicted by finite difference method 02 p0224 A70-12866

Ground clutter characteristics from moving receiver in bistatic radar system, developing method for performance prediction and problem analysis 03 p0449 A70-13586

Transistor behavior prediction at threshold of large signal conditions, using nomographs to evaluate maximum drive levels before distortion onset 03 p0452 A70-13966

Computerized approximations for quantitative predictions of EED firing characteristics based on header geometry and electrical leads 03 p0548 A70-14118

Piezoelectric transducers performance in ultrasonic devices evaluated from loss and admittance measurements, using Mason equivalent circuit method 03 p0496 A70-14206

Ablative throat nozzle performance, plotting change in thrust, exit pressure and Mach number as function of ablated to initial area ratio 03 p0410 A70-14336

Ball bearing performance prediction using analytical technique based on race profilometry data, considering torque variation [ASME PAPER 69-WA/LUB-4] 04 p0698 A70-14769

Nonequilibrium initial condition combustion effects on propellant performance for hydrazine/ chlorine pentafluoride and hydrogen/fluorine with equilibrium, kinetic and frozen nozzle flow [AIAA PAPER 69-469] 04 p0732 A70-15423

Computerized thermal model simulating environment control system, crew and vehicle structure in performance prediction for Apollo lunar module [SAE PAPER 690621] 05 p0922 A70-15848

Antenna far field noise effect on monopulse type and conical scanning radar angle meters performance 05 p0813 A70-16256

Composite strength and stiffness prediction from fiber and matrix properties using computer 05 p0870 A70-16579

Miniature fluxgate magnetometer for sounding rocket measurements of two orthogonal components of external magnetic field, predicting performance by linear mathematical model 05 p0851 A70-16690

Turboblowers and compressors air tests for gas operation performance prediction 06 p1129 A70-17136

Flight performance prediction for throttling bipropellant rocket engine utilizing ablative combustion chamber throat, discussing lunar module descent engine [AIAA PAPER 69-452] 06 p1130 A70-17176

Optimal feedback controls design for linear systems relative to time-multiplied performance indices 06 p1025 A70-17960

Spherical gas bearings static characteristics and performance, discussing materials selection, optimum clearances and surface hardness 07 p1294 A70-19122

LUF /lowest useful frequency/ prediction for HF sky wave communication, emphasizing prediction methods using computers 07 p1229 A70-19156

Radio propagation characteristics and communication system performance, discussing concepts of MUF, LUF, error rate, communication system modeling, prediction techniques, etc 07 p1229 A70-19157

SERT 2 thruster system performance over expected mission parameters, noting operational lifetime excess over mission requirements [AIAA PAPER 69-235] 07 p1364 A70-19702

ICRPG liquid propellant thrust chamber performance evaluation methodology, reviewing imperfections and limitations [AIAA PAPER 69-468] 07 p1365 A70-19728

Freezing-mixing model for predicting plasma jet flow reactor yield development from analyses of thermochemical equilibrium, chemical reaction freezing and turbulent mixing 07 p1351 A70-19893

Missassignment prevention in aviation specialties, using multiple regression analyses and dichotomous pass vs fail criterion to develop prediction equations 07 p1222 A70-19929

Multichannel performance measurement of threshold extension FM demodulators using click suppression techniques 08 p1460 A70-20812

Multistage axial compressor performance described by mathematical model based on maximum probability principle 08 p1558 A70-21190

Computer program predicting thermal response of fusion welding tooling chill bars and holding fixtures, simulating moving heat source and contact 08 p1508 A70-21487

Compound state resonance energies and widths in elastic scattering of diatomic molecule at energies below rotational excitation threshold 08 p1548 A70-21523

Beam delay line for introducing variable gradients in Molonglo radio telescope, discussing circuits and performance 08 p1478 A70-21824

Reliability estimations precision evaluated by Monte Carlo simulation, analyzing causes of data inaccuracy 09 p1689 A70-22019

DASSS operational parameters and performance in SPADE satellite voice communication system 10 p1837 A70-24350

Electrode structural parameters effect on polarization characteristics of air-hydrogen cells to obtain optimum performance, reliability and service life 10 p1831 A70-24471

Linear time-varying systems transient responses prediction, using Krylov-Bogoliubov method and parameter plane analysis 10 p1855 A70-24704

High intensity shock wave propagation and generation of high enthalpy hypersonic flow studied to determine IMF-2 hypersonic shock tube performance limit 10 p1871 A70-24795

Hydrostatic oil journal bearings performance with several supply holes and incompressible lubricant, analyzing Reynolds pressure equation by numerical method 10 p1895 A70-24851

Solar activity forecasting using normalized sunspot curves deduced from 200 years of observations, discussing parameters of running 11 year cycle 10 p1949 A70-25287

Gas turbine engine performance prediction with water-methanol injection, describing analytical method [SAE PAPER 700208] 11 p2102 A70-25881

Reusable ballistic orbital-global transportation systems using rocket sled-assist-takeoff compared to SST systems in terms of effectiveness and cost 11 p2122 A70-26048

Solid rocket motor performance prediction including motor pressure, thrust and propellant parameters, discussing mathematical modeling of flow fields [AIAA PAPER 69-732] 11 p2102 A70-26117

Embossed/crinkled aluminized film multilayer insulation blankets with joints performance variation with temperature predicted by radiation heat transfer correlation 11 p2150 A70-26365

Lifting entry vehicle thermal protection system /TPS/ material performance, analyzing metallic radiator and passive transpiration systems and rigid insulator 11 p2150 A70-26368

Chemical milling characteristics, development and applications, outlining performance capabilities with Al, Ti, Fe and Mg alloys 12 p2240 A70-26991

PAM-FM modulation system optimal receiver derivation, assessing threshold performance assuming uniformly distributed modulating signal 12 p2183 A70-27155

Nonlinear phase shift equation derived from TWT single carrier performance, predicting multicarrier performance of communications satellites 12 p2195 A70-27248

Spherical reflector antenna with Gregorian correctors, calculating gain, far field radiation pattern and efficiency as functions of subreflector and feed positions 12 p2200 A70-28052

Gust response calculations compared with flight measurements for two fighter aircraft and jet transport to determine accuracy [AIAA PAPER 68-892] 12 p2162 A70-28077

Externally pressurized air journal bearing performance prediction, obtaining pressure distribution by numerical solution of Reynolds equation 13 p2418 A70-28743

Inertial hybrid navigation system optimization, discussing performance curves and numerical filters synthesis and error elimination 13 p2448 A70-28747

Pogo sticks concept for lunar exploration, showing improved performance over lunar surface or flying vehicles 13 p2505 A70-28891

Neutron irradiation effect on n-channel GaAs junction FET performance, considering transconductance, drain current, pinch-off voltage and cut-off frequency 13 p2376 A70-28932

Computer program for system reliability prediction, using probability tree approach and block probabilities 13 p2373 A70-29565

Computerized Monte Carlo prediction of maintenance time distribution of complex system, concerning man hours, elapsed time and schedule meeting 13 p2524 A70-29566

Beneficial and detrimental effects of value engineering change proposals on system reliability, relating cost improvement and performance factors 13 p2524 A70-29568

Reliability prediction techniques accuracy and optimal timing including true and project control predictions 13 p2524 A70-29569

Failure prediction testing and elements replacement at field maintenance level for increasing equipment reliability 13 p2423 A70-29697

Nuclear magnetic resonance magnetometers performance using dynamic polarization by electronic pumping 13 p2414 A70-30040

Agna propulsion system performance model for predicting propellant flow rate, mixture ratio, thrust time and specific impulse [AIAA PAPER 69-453] 14 p2629 A70-30754

GaAs-Ge heterojunction transistors with microwave planar geometry, calculating performance for comparison with Ge homojunction transistor 14 p2556 A70-30925

System effectiveness apportionment for constraints existing on accountable factors using Lagrange multiple method 14 p2669 A70-31111

Systems effectiveness equated to function of performance, availability, reliability, maintainability, quality control and manufacturing, emphasizing optimization 14 p2592 A70-31112

Wideband PCM/FM discriminator detection, predicting effects of predetection and postdetection filtering on system performance 14 p2558 A70-31192

Radial flow impellers design for maximum machine performance, using straight cascade characteristics 15 p2672 A70-31825

Field correlation theorem for deducing Cassegrain antennas performance from internal field distributions, considering two reflector diffraction problems 15 p2698 A70-31953

Cost effective reliability prediction techniques, discussing precision gyros procurement by NASA 15 p2736 A70-31964

Hybrid rocket engine with solid oxidizer based on ammonium perchlorate and Al, studying performance with FORTRAN 5 program 15 p2787 A70-32273

Constrained and constant coefficient optimal controls compared in optimizing performance criteria of vibrating beams 16 p2886 A70-33332

Rolling element bearings fatigue life prediction and extension, using elastohydrodynamic lubrication theory [ASME PAPER 70-DE-19] 16 p2917 A70-33423

Dynamic seal effectiveness prediction, considering bearing and sealing pressure distributions, friction coefficient, flow characteristics, etc [ASME PAPER 70-DE-53] 16 p2918 A70-33514

Liquid rocket engine injector elements design criteria, using noncircular orifice geometry to predict efficiency [AIAA PAPER 70-704] 16 p2967 A70-33565

Motor design parameters effects on solid propellant extinguishment predicted from mathematical combustion model 16 p2962 A70-33571

Optimal Kalman tracking filter performance estimation for manned maneuvering targets 16 p2949 A70-34057

Incoherent Manchester coded FSK system performance based on optimal signal detection theory, plotting instantaneous frequency vs time 16 p2866 A70-34074

Single stage /rigid/, two stage and stretch yo-yo despin mechanisms, discussing advantages, disadvantages and flight tests 16 p2985 A70-34114

Flow control valve without moving parts used in ATS A and D, describing design, operation and theoretical performance 16 p2846 A70-34132

Helicopter rotor blades flapwise bending moments prediction by transfer function/superposition techniques 17 p3013 A70-34704

Aircraft optimal operating procedure development by integral-variational performance analysis methods, discussing flight paths, fuel consumption, mission requirements, etc [AIAA PAPER 70-876] 17 p3016 A70-34812

Extrinsic photoconductive detectors, comparing performance for microwave and DC bias based on gain bandwidth product and SNR analysis 18 p3232 A70-36746

Axial gas turbine performance prediction method improvements based on comparison with tests [ASME PAPER 70-GT-2] 18 p3304 A70-36859

Transonic high turning low aspect ratio stator cascades flow field performance prediction, reducing secondary flows by partial slots [ASME PAPER 70-GT-63] 18 p3209 A70-36875

End wall boundary layers effect included in performance prediction method for multistage axial compressors
[ASME PAPER 70-GT-80] 18 p3210 A70-36884

Systems reliability numerical prediction
19 p3389 A70-38205

Solid state laser with transverse mode selection to increase brightness, discussing plano-concave resonator
19 p3447 A70-38508

Optical system mtf measurement by photographic technique for comparing telescopic sight with simulator, discussing performance
19 p3428 A70-38511

Contact-relay circuits failure free operation probability, taking into account coil winding breakage
19 p3390 A70-38579

Frequency multipliers with charge storage diode, analyzing turn-off transient effect on performance by charge control model
19 p3391 A70-38748

Instrument ball bearings running torque prediction at high speed under combined radial and axial loads
[ASLE PREPRINT 70AM 3D-3] 19 p3438 A70-38803

Rarefied gas viscoseals performance prediction by theoretical model, comparing results with experiment
[ASLE PREPRINT 70AM 5C-3] 19 p3439 A70-38806

Computer program for assessment and modification of mechanical component life predictions by discrete formulation of Bayes theorem
19 p3440 A70-38816

Long life reliability measurement for reentry and recovery systems, noting applicability to program monitoring, optimum resources allocation, etc
19 p3442 A70-38832

Integrated structural analysis for reliability prediction of solid propellant rocket motors
19 p3489 A70-38844

Carbons and graphites ablation tests for predicting performance under reentry conditions, considering microstructure effects
20 p3735 A70-39214

Nonlinear acoustic absorbers behavior analysis, discussing spectral and temporal computation methods
20 p3672 A70-39237

Apollo Lunar Module strapdown Abort Guidance system, correlating performance prediction with flight test results
[AIAA PAPER 70-1028] 20 p3666 A70-39509

Rocket course correction by lateral air expulsion (ram air control), deriving model for performance prediction
[AIAA PAPER 70-90] 20 p3715 A70-39559

Nonstationary random processes prediction by numerical method
20 p3673 A70-39762

Linear feedback control system with quadratic penalty function, deriving lower bound on optimal performance for suboptimality evaluation
20 p3604 A70-40116

Electrostatic plasma probe inverse process I-V properties from current voltage characteristics, improving accuracy and reliability by theory in terms of new variables
20 p3683 A70-40162

Minimum bias criteria for selecting data fitting curves, allowing for unknown true equation in improving data predictability
20 p3659 A70-40261

Third stage engine performance from mass properties data for space vehicles with side-by-side tanks
[SAWE PAPER 846] 20 p3717 A70-40378

Externally pressurized air lubricated journal bearing with multiple supply holes, predicting load carrying capacity, flow requirement and stiffness
20 p3639 A70-40505

Slender wings of low aspect ratio and sharp leading edges, predicting inviscid maximum lift
21 p3743 A70-40585

Fusion welding cooling rates, peak temperatures and heating duration relationships to distance from fusion line predicted by theory for comparison with experiment
21 p3832 A70-40791

Solar arrays for Venus-Mercury flyby, evaluating temperature and power performance
21 p3756 A70-41010

Predictive model for potential variance from planned schedule of R and D tasks to minimize risk in management
21 p3955 A70-41172

OP-EX, optimal explicit guidance algorithm for powered flight outside atmosphere
[AIAA PAPER 68-869] 21 p3848 A70-41734

All-flexible parawings aerodynamic performance prediction based on slender wing theory and circular arc approximations for canopy shape
[AIAA PAPER 70-1188] 21 p3754 A70-41827

GaAs point contact diodes quick response performance with glass-metal or metal-ceramic bases, obtaining Schottky-type rectifying barriers by half period currents
22 p3995 A70-42406

Variable geometry radial inflow turbine performance estimation based on one dimensional flow theory
22 p3960 A70-43738

Survival probability of randomly excited structures, using maximum entropy principle
23 p4270 A70-44582

Biological life support systems mass exchange processes analysis based on mathematical models, predicting artificial ecological systems stability
23 p4149 A70-45029

PERFORMANCE TESTS

Flight test experiments for H-19 helicopter to evaluate aided inertial system performance for terminal guidance
01 p0136 A70-10303

Visual fatigue symptoms, causes, relation to general fatigue and psychological aspects, discussing testing for sensory and visual fatigue
01 p0022 A70-10857

Visual attention testing, considering perception focusing on stimulus object and eyelid blinking recording, measuring eye distance to work plane
01 p0023 A70-10861

Langley integrated life support system design, discussing manned test results including system engineering, atmospheric and water chemical analyses and microbial measurements
01 p0038 A70-10973

Brazed plate-fin superalloy panels suitable for hydrogen-cooled structures, discussing fabrication techniques, performance tests and pressure containment and fatigue characteristics
02 p0306 A70-11930

Test program preceding first German satellite experiment using HEOS satellite for Ba ion cloud injection into deep space
02 p0380 A70-12081

Omega position location equipment /OPL/ experiment data analysis, obtaining quantitative measure of statistical performance of system
02 p0336 A70-12180

Single stage experimental front fan designed for aircraft engines, measuring overall and blade element performances
02 p0355 A70-12258

Sliding steel specimens anomalous friction behavior in vacuum, noting friction-time plot dependence on oxide film rupture, load, environmental pressure, etc
02 p0321 A70-12534

Optical telescope spectrograph to obtain radiometric and spectrographic data on vehicles reentering atmosphere, discussing performance criteria and tests
03 p0489 A70-13653

Laser transmitter and optical superheterodyne receiver performance tests at 6328 A, demonstrating aperture size effect and noncoherent operation superiority
03 p0450 A70-13675

Statistical control charts for evaluating instrumentation performance during ordnance devices testing, discussing evolution, interpretation and application
03 p0494 A70-14126

Performance characteristics of RDX-metal sheath systems, using high speed motion picture photography for missile design applications
03 p0550 A70-14141

Electroencephalograms recorded for chimpanzees performance to play game, selecting parameters by computer analysis to discriminate between game phases and decisions
04 p0640 A70-14387

High hub/tip ratio centrifugal compressor with pipe and vaned cascade diffusers for turbofan engines, determining impeller performance
[ASME PAPER 69-WA/FE-28] 04 p0733 A70-14774

Nonextension lines characteristic to human skin utilized to provide natural mobility and minimal ballooning in full pressure suits noting mapping, testing, construction, etc
[ASME PAPER 69-WA/AUT-22] 04 p0642 A70-14826

Tangential jet, tandem, jet flap and vortex generator blade concepts investigated for turbine blade loading efficiency
[ASME PAPER 69-WA/GT-5] 04 p0734 A70-14890

Thermionic converter with oriented W electrodes, describing test method and computerized data acquisition for performance mapping
04 p0627 A70-14945

Optical performance of image intensifier system with good resolution for exposure times down to 1 nsec
04 p0695 A70-15568

Small three stage hydraulic turbine for aerospace and commercial applications, discussing design and performance
04 p0628 A70-15640

Simulation equipment for extraterrestrial solar radiation for spacecraft components evaluation tests, describing spectral characteristics
04 p0665 A70-15663

Nondestructive test procedures for maintaining and determining serviceability of penetrant inspection materials during use
05 p0844 A70-15780

Laboratory bench technique assessing performance of explosives, using brass small arms cartridge cases as witness vessels
05 p0894 A70-16323

Axial and nonlinear bending performance compared for compression moldings laminated from random glass fiber mat
05 p0870 A70-16577

Turboblowers and compressors air tests for gas operation performance prediction
06 p1129 A70-17136

Cooper aircraft handling rating scale on basis of test pilot experience
06 p1003 A70-18018

Back-up rings and special sealing devices performance qualification testing specifications
[SAE-ARP-979] 07 p1290 A70-18802

Design concept, materials application and performance characteristics of high temperature fasteners
[AIME PAPER F-69-6] 07 p1290 A70-18811

Specification of minimum performance standards and test procedures for automatic pressure altitude digitizer equipment
[SAE-AS-855] 07 p1279 A70-18901

Advanced concept ejection seat /ACES/ system design and performance, considering gyro-controlled vernier rocket motor and electronic time delays
07 p1192 A70-19016

Veloergometric assembly using two bicycles for simultaneously measuring muscular motor activity of persons in competition
07 p1221 A70-19525

Twin spool hydrogen turbopump performance at zero net positive suction pressure /NPSF/ saturated fluid in propellant tank, including steady state and simulated transient engine tests
[AIAA PAPER 69-550] 07 p1295 A70-19709

Visual acuity performance during various vibration stresses found differentially degraded for near, intermediate and distant vision
07 p1223 A70-19939

Water tests with N 300 Naviplanes confirming flexible skirt concept regarding speeds and stability
08 p1435 A70-20622

Astronomical telescope operation at transfer process from object to image using optical transfer function and brightness standards
08 p1493 A70-20685

Nickel zinc secondary battery low cost and high performance in military applications, discussing maintenance and rapid recharge requirements
08 p1440 A70-20710

Wideband tunable CW Gunn effect oscillator design, discussing microwave circuit effects on performance
08 p1471 A70-20788

Air brake with compressed air fed bearings for testing small turbines, determining power and friction moment
08 p1481 A70-21188

UHF transistor power amplifier, discussing CW and pulse performance and power gain
08 p1477 A70-21294

Display devices luminance and luminous efficiency measurement as function of angle
08 p1500 A70-21762

Resolution, contrast and gray scale performance of CRT displays compared to dot matrix displays
08 p1500 A70-21763

Crossed field amplifiers properties and applications, comparing performance to TWT
09 p1642 A70-22008

Lossless three-port H-plane waveguide junction circulator performance evaluation using computerized design
09 p1646 A70-22710

Spacecraft conditions influencing remote imaging sensor performance, discussing altitude, temperature and moisture at sensor, air turbulence, vehicle motion, etc
[AIAA PAPER 70-291] 09 p1677 A70-22853

Circulation-controlled lifting rotor built and tested on hovering rig, analyzing performance
09 p1611 A70-23284

Qualification and testing procedures for Apollo Spacecraft Program components and systems, discussing vibration tests
09 p1693 A70-23705

Tandem axial compressor performance for various blade stagger and flap angle values of rotor row, investigating gap influence
09 p1608 A70-23736

Turbojet engines departure from equilibrium performance during thermal soak transient attributed to heat absorption in turbine and compressor metals, observing thrust loss
09 p1744 A70-23739

Compressor blade performance dependence on Reynolds number, turbulence intensity and axial velocity ratio, considering wind tunnel tests with porous side walls
09 p1609 A70-23748

Photoelectric photometer for astronomic observations, discussing design and performance
10 p1886 A70-23917

Raney catalyst preparation and continuous operation in molecular hydrogen and oxygen electrodes noting improved voltage, manipulation and energy yield 10 p1831 A70-24467

Traveling wave tube amplifier performance in numerous orbiting communication satellites, emphasizing life test data 11 p2015 A70-25406 [AIAA PAPER 70-507]

SNAP 19 radioisotope fueled thermoelectric power supply orbital performance on Nimbus 3, ascribing power output decrease to decreasing generator output currents 11 p2120 A70-25435 [AIAA PAPER 70-480]

Satellite communications subsystem performance testing from initial integration through launch under all environmental exposure 11 p2030 A70-25445 [AIAA PAPER 70-448]

Despin ball bearing assemblies performance data for TACSAT and Intelsat 4, discussing technology needed for accelerated testing, higher precision, failure detection and lubricants 11 p2058 A70-25471 [AIAA PAPER 70-459]

CW chemical laser performance using molecular hydrogen diffused into supersonic fluorine atoms streams 11 p2063 A70-26067

High speed sequential decoding machine design and performance test for deep space channels 11 p2014 A70-26245

Mars landing analysis and simulation for unmanned lander prototype, discussing digital simulation by Monte Carlo techniques and physical tests 11 p2032 A70-26291

Broadband 2 GHz transhorizon radio relay system design and performance for transmission on four channel pairs 11 p2034 A70-26820

Medium temperature hydrogen fuel cells design, operational characteristics and performance 12 p2163 A70-26996

Aircraft pilot ability tests validity, applying correction methods in decision making regarding applicant acceptance 12 p2176 A70-27031 [DFVLR-SONDDR-32]

Electromagnetic differential flowmeter design and performance, considering SNR 12 p2231 A70-27162

High dynamic range low noise parametric microwave amplifier performance measurement for radar receivers 12 p2183 A70-27166

Read-diode microwave oscillators performance degradation due to space charge and series resistance, discussing RF power optimization 12 p2194 A70-27167

Frequency-time coded multichannel communication system error probability bounds to investigate frequency selective fading effect on performance 12 p2184 A70-27416

Xenon arc lamp searchlight performance and application during Apollo 8 launch 12 p2207 A70-27662

Grating spectrometer performance in measuring earth IR radiance determined from balloon flights 12 p2235 A70-27752

Porous hydrogen electrode performance with Ni skeleton catalyst, studying effects of temperature, active layer thickness, etc 12 p2182 A70-27759

Mechanically rechargeable zinc-air battery, discussing electrical performance, advantages and military applications 12 p2167 A70-27928

Plenum-chamber air-bearing and labyrinth-seal types air cushion lifting mechanisms performance in simulated hovering flight 12 p2162 A70-27981

Minimum performance standards for airborne radio receiving and direction finding equipment covering normal and environmental test procedures 13 p2365 A70-29000

Barium fluoride film hygrometer elements for radiosondes, discussing manufacturing and testing methods 13 p2408 A70-29470

Protective coatings with Si-Zr alloys for graphite, discussing wettability, spreading kinetics and impregnation 13 p2439 A70-29503

Flight test experiments for H-19 helicopter to evaluate aided inertial system performance for terminal guidance 13 p2449 A70-29622

Automatic test equipment performance and effectiveness below customer expectations, discussing design factors 13 p2525 A70-29677

Turbojet engine testing in ground level facilities with automatic instrument reading and parameters calculation 13 p2474 A70-29688

Feedback control systems automatic testing by examining frequency response 13 p2423 A70-29696

DC-10 aircraft wing engine calibration, isolated- and wing-nacelle testings using air-driven engine simulator [AIAA PAPER 70-590] 13 p2342 A70-29881

Closed loop MHD test facility ARGAS I, describing engineering performance and test measurements 14 p2533 A70-30532

Microwave integrated circuit lumped element approach, showing performance as function of geometry and frequency 14 p2561 A70-30920

Low pressure diffusion welding for joining Ti-6Al-4V alloy in Ar atmosphere under compressive loading, evaluating performance 14 p2591 A70-30933

Soviet book on bearing capacity of turbomachine rotor elements covering testing methods, stress analysis, design factors on stability, etc 14 p2658 A70-30958

Microwave band-stop filters based on ladder network low pass prototypes, comparing performance with bandpass type 14 p2557 A70-31179

Microwave filters developments, performance, production and costs 14 p2559 A70-31374

Axial flow fans performance dependence on aspect ratio from empirical relationships, plotting various component losses and stage efficiency 14 p2529 A70-31418

Thermocouples performance during fast varying temperature measurements in solids, considering physical parameters effects on accuracy 15 p2734 A70-31646

SHF radio telescope for solar radio wave observation, describing design and performance 15 p2717 A70-31897

CW HCN laser driven phase matched traveling wave lithium niobate electro-optic light modulator performance 15 p2750 A70-31976

Centrifugal pump performance correlation parameter under cavitation conditions for handling different liquids based on bubble growth theory 15 p2720 A70-32098

Air intake distortions effect on compressor performance, discussing radial and peripheral gradients 15 p2787 A70-32248

High gain helix radiators for spacecraft phased arrays, measuring performance vs design parameters 15 p2678 A70-32600

Electronic equipment reliability performance measurements during tests correlated to performance observed under field use 15 p2712 A70-32645

Boeing 707 and 727 aircraft components on condition maintenance program based on statistical analysis and performance monitoring for replacing scheduled overhauls 15 p2748 A70-32656

Electro-optical sensor night time capabilities with laser illuminator, determining current per unit area from photocathode 16 p2907 A70-33183

Electromechanical velocity feeder redesign for functional performance in random vibration environments [ASME PAPER 70-DE-25] 16 p2917 A70-33425

Real time video data display at visual and thermal IR wavelengths, demonstrating performance improvement for target recognition 16 p2910 A70-33436

Adhesives selection based on bond performance requirements, considering joint design, stress distribution, temperature effects, etc [ASME PAPER 70-DE-69] 16 p2939 A70-33519

Throttleable thruster system for Mars soft landing, selecting catalytic decomposition engine from system weight and performance studies [AIAA PAPER 70-652] 16 p2966 A70-33549

NERVA rocket engine program reliability, design, performance and managerial approaches [AIAA PAPER 70-711] 16 p2950 A70-33568

Turbofan engine compressor system performance dependence on circumferential extent, magnitude and rate of change of inlet temperature in altitude test facility [AIAA PAPER 70-625] 16 p2968 A70-33590

Axial flow multistage turbines performance, examining profile manufacturing tolerances effects on cost 16 p2970 A70-33677

Operation modes of nozzles with emerging pointed and central bodies, discussing external flow effects on internal performance 16 p2970 A70-33760

Ablative materials performance in high radiative heat flux environments produced by CW carbon dioxide laser [AIAA PAPER 70-864] 16 p2939 A70-33907

Al radiator with thin stainless steel tube liner using liquid metal coolant tested for heat rejection system of SNAP-8 Rankine cycle power system [AIAA PAPER 70-855] 16 p3000 A70-33922

Mariner 4 scan platform structure and actuator design, development and performance 16 p2845 A70-34106

Spacecraft hydraulic timers design and qualifications testing, discussing oil selection and temperature dependence 16 p2914 A70-34112

Explosively actuated /pyromechanical/, devices for spacecraft, discussing guidelines for design, testing, application and cost efficiency 16 p2963 A70-34125

Ball in tube nutation damper for spinning satellite, describing design, testing and fabrication techniques for achieving low friction level 16 p2985 A70-34136

Lubrication system flight performance and laboratory test data for space applications, considering torque motors, slip rings, bearings and gears 16 p2923 A70-34157

Nonextension lines characteristic to human skin utilized to provide natural mobility and minimal ballooning in full pressure suits noting mapping, testing, construction, etc 17 p3036 A70-34951

Heat pipe performance tests under longitudinal harmonic vibration 17 p3193 A70-35751

Multistage electrocardiographic exercise tests for cardiovascular performance measurement 17 p3034 A70-35878

Prototype grill device for turboprop aircraft engine inlet protection against bird ingestion, discussing performance tests 18 p3212 A70-35996

Deep space spacecraft radioisotope thermoelectric generators, discussing testing and evaluating for future missions 18 p3215 A70-36229

Position sensitive planar photocells based on silicon-silicon dioxide systems, discussing photoelectromotive force generation mechanism, light intensity and load characteristics 18 p3297 A70-36236

Avalanche transit time diode and transferred electron oscillators in microwave systems, discussing design, performance and applications 18 p3232 A70-36675

High bypass ratio aircraft turbofan engines, discussing program of factory, flight and operational suitability testing [SAE PAPER 700290] 18 p3302 A70-36806

Static charge reducer for aircraft fuels handling safety, discussing performance factors [SAE PAPER 700277] 18 p3263 A70-36808

Two dimensional compressor cascades of double circular arc and wedge shape blades testing performance in transonic and supersonic wind tunnels [ASME PAPER 70-GT-7] 18 p3302 A70-36829

Supersonic cascade wind tunnel performance evaluation, using compressor blades of simple geometric shapes [ASME PAPER 70-GT-110] 18 p3238 A70-36848

Tailpipe effects on gas turbine diffuser performance with fully developed inlet conditions [ASME PAPER 70-GT-86] 18 p3210 A70-36881

Hot cathode magnetron ionization gauge design, discussing performance and sensitivity 19 p3421 A70-37467

Electronic equipment reliability improvement, based on reliability control group qualification, burn-in and diagnostic tests 19 p3554 A70-38401

ONERA accelerometer flight test of performance in zero gravity environment, using Vesta sounding rocket for simulation 19 p3431 A70-38541

Runway test vehicle for lifting rotor performance in simulated forward flight, comparing with wind tunnel tests 19 p3402 A70-38611

Jet engine roller bearings retainer candidate cage materials and coatings evaluation on test rig simulating engine conditions [ASLE PREPRINT 70AM 2D-1] 19 p3439 A70-38805

Molybdenum disulfide abrasiveness on test rings coated with bonded solid lubricant [ASLE PREPRINT 70AM 5A-1] 19 p3439 A70-38811

Cryogenically cooled photoconductive IR radiation detectors, determining wideband optical heterodyne performance 20 p3627 A70-39085

In-Au contacts for GaAs, discussing fabrication and performance tests on transverse Gunn mode oscillator 20 p3686 A70-39118

Carbon/carbon composites constituent characteristics effects on thermal and mechanical properties, using polarized light and scanning electron microscopy 20 p3653 A70-39204

Unidirectional and multidirectional carbon/carbon composites quality and performance evaluation by NDT methods, including X ray radiography, ultrasonic test, pulse echo mapping, etc 20 p3654 A70-39211

- Transistorized quartz oscillators, testing frequency and amplitude stabilities and functions of input and output capacitances, supply voltage and feedback
20 p3597 A70-39258
- Choice reaction and movement time dependence on hypoxia induced by air pressure reduction inside decompression chamber, discussing adult human performance
20 p3573 A70-39714
- Liquid metal MHD power conversion system with Cs and Li as working fluids, describing hydraulic, electrical and high temperature tests results
20 p3680 A70-39986
- Large scale nonequilibrium linear MHD generator performance with rare gases under strong EM-gas dynamic interactions
20 p3681 A70-39993
- Performance comparison of diagonal conducting wall MHD generator and Hall generator of equal dimensions, investigating wall temperature effect
20 p3566 A70-40004
- Electrode size effects on combustion driven MHD generator performance, examining voltage losses, gas boundary layer temperature and surface conditions
20 p3566 A70-40005
- NASA Lewis closed loop MHD generator subsonic tests, discussing ducts, purge and Cs injection systems, electrode coating, etc
20 p3566 A70-40011
- Filament wound composites, investigating interaction of fabrication variables and untoward environments by delineating effect of each on structural performance
20 p3731 A70-40055
- Airborne atmospheric turbulent flux measurement system with fast response wind velocity, temperature, humidity and aircraft motion sensors, discussing performance and data reduction
20 p3665 A70-40109
- Concorde aircraft flight test program for verifying design features of wing vortices, fuel transfer, longitudinal stability, etc
21 p3749 A70-40580
- Helicopter vibration measurement techniques, discussing in-service fault diagnosis
21 p3749 A70-40582
- Helicopter dynamic tests for aeroelastic and mechanical instabilities and forced vibration problems
21 p3749 A70-40583
- Tooling concepts providing gas shielding in mechanized open air arc welding of Ti, evaluating effectiveness by various mechanical tests
21 p3832 A70-40788
- Solid state butt and lap joint welding of TD-nickel bar, evaluating performance by stress rupture and shear tests
21 p3832 A70-40790
- Stainless steel sheet-to-plate tee joint resistance welded by Magnetic Force Upset Welding process, testing performance
21 p3832 A70-40792
- Integrated Life Support System hardware tests, discussing oxygen and water recovery, contaminant control, personal accommodations and failure detection
21 p3833 A70-40989
- Working fluids liquid property variations effects on cryogenic heat pipe performance
21 p3946 A70-41043
- Heat pipe performance map with ammonia as working fluid, comparing thermal transport efficiency with water pipe
21 p3947 A70-41050
- ATS-5 spacecraft L band propagation performance, describing up and downlink test methods
21 p3790 A70-41363
- Parafol flight performance predictions and test results based on wind tunnel data and manned free flight
21 p3754 A70-41826
- Reefed and unreefed disk gap band parachutes tested in supersonic and subsonic wind tunnels to determine stability and performance
21 p3754 A70-41841
- Low aspect ratio compressor blade cascade performance at blade span center, discussing pressure loss, angle of attack and staggering
22 p3957 A70-42272
- Gas lubricated foil bearing performance as support for turborotor simulator, examining heating and thermal gradient effects
22 p4044 A70-42448
- High temperature fuel cell with thin disk solid electrolyte, evaluating performance as function of electrolyte, electrode and current collector resistance ratio
22 p3964 A70-42499
- Corrective light filter performance evaluation by spectral transmittance normalization
22 p4072 A70-42503
- Three dimensional hologram diffractive efficiency measurement by spectrographic attachment
22 p4026 A70-42508
- NERVA nuclear rocket reactors, considering NRX and XE technology tests
22 p4069 A70-43178
- Sealed Ni-Cd cells, investigating carbonate effect on performance
22 p3965 A70-43555
- Military sealed thin sintered plate Ni-Cd rechargeable batteries, comparing performance with other systems
22 p3966 A70-43538
- Superconducting magnet system design, operation and module tests, noting large and small coil systems performance data relationship
23 p4218 A70-44354
- Superconductive magnets with different windings and modular construction for magnetic mirror apparatus, discussing performance tests
23 p4218 A70-44355
- Guarded electrical cylindrical calorimeter measuring multilayer insulation thermal conductivity, discussing construction, test and error
23 p4195 A70-44366
- Plastic encapsulated IC for military environments, discussing cooker, corrosion and thermal shock tests
23 p4173 A70-44534
- Space vehicle for testing electric propulsion systems in space, powering by cluster of six electrostatic ion motors regulated by automatic thrust control
23 p4259 A70-44616
- Hypersonic wind tunnel facility for hypersonic aircraft and recoverable booster systems development [DFVLR-SONDDR-19]
23 p4178 A70-44799
- Cryogenic thermocouples of various metal pairs for low temperature measurements, discussing performance tests and calibrations
24 p4378 A70-45385
- Fluidic elements operation and performance, considering wall attachment, jet interaction, turbulence, gain load, operating ranges, etc
24 p4293 A70-45430
- Spark gap triggering with Q switched laser, comparing performance with electrical method
24 p4353 A70-45560
- Nondestructive tests for performance levels, discussing signature analysis as methodology
24 p4338 A70-45736
- Orbit-to-orbit space shuttle toroidal propellant tank design, construction and testing for outflow and slosh characteristics
24 p4417 A70-45940
- [AIAA PAPER 70-1325] Carrier injection-limited Gunn diode wideband performance, deriving expression for admittance
24 p4319 A70-46081
- Aircraft Doppler VHF omnidirectional radio range /DVOR/ performance test, noting improvement over VOR system
24 p4375 A70-46240
- Apollo 11 deployed solar cells, investigating degradation of surface properties and thermal control due to lunar module ascent effects
24 p4295 A70-46262
- PERFUSION**
U DIFFUSION
PERIDOTITE
NT ENSTATITE
NT OLIVINE
NT PYROXENES
PERIGEEES
Moon perigees and apogees for years 1-3000, tabulating parameters for calculations
08 p1568 A70-20635
- Space mechanics problem of passing from perigee to radial distance in given time determined by fitting conic to radii, using iteration method
09 p1760 A70-22927
- Echo 2 satellite orbital elements from optical observations covering last passages over Milan before orbital decay
17 p3172 A70-35628
- Comet brightness curves asymmetry with respect to perigee attributed to pre- and post-heating
19 p3526 A70-38781
- Artificial earth satellite orbit perigee motion, calculating perturbation effect due to gravitational and magnetic fields on orientation and rotation
21 p3884 A70-40843
- Europa 2 booster perigee stage engine design, discussing total and propellant masses, spin stabilization, materials, etc
23 p4234 A70-44672
- Lunar theory literal solution for average node and perigee movements compared with Delaunay results, using Lie transforms for Hamiltonian function
24 p4399 A70-45141
- PERIHELIONS**
Planetary perihelion precession with velocity-dependent gravitational mass in terms of special relativity
09 p1765 A70-23800
- Comet Ikeya-Seki 1965 f tail formed by dust particles continuous ejection, using preperihelion photographs
19 p3527 A70-38792
- PERIOD EQUATIONS**
U PERIODIC FUNCTIONS
PERIODIC FUNCTIONS
NT TANGENTS
NT TRIGONOMETRIC FUNCTIONS
- Periodic motions and integral stability for systems with quasi-cyclic coordinates applied to current carrying conductor oscillations and linear case of Routh equations
01 p0212 A70-11573
- Periodic solutions for two dimensional cubic differential equation, covering one dimensional traveling wave and two dimensional types
03 p0519 A70-13581
- Cosmic ray time series periodicity using variance analysis allowing for intensity variations and meteorological factors
06 p1135 A70-17543
- Optimal quadrature formulae for numerical integration of 2 pi-periodic functions involving integrand derivative values at knots
06 p1093 A70-17582
- Positive time-periodic solutions to parabolic problems with Stefan-Boltzmann boundary conditions using straight lines method
07 p1333 A70-18748
- Periodic motions and dynamic stability of nonlinear distributed sampled data system of closed loop of pulsed element governed by heat conduction equation
07 p1226 A70-18749
- Periodic solution with nondegenerate orbit for functional differential equations taking into account small perturbation
07 p1324 A70-19199
- Asymptotically periodic solution of nonlinear differential equations, discussing digital or analog computer utilization
07 p1326 A70-19782
- Radial heat conduction in infinite hollow cylinder with circular cross section and periodic heat transfer coefficient at inner and outer cylinder surfaces
07 p1423 A70-19816
- Quasi-stable linear differential equations systems with nearly periodic coefficients, noting application to equations with zero real portions of matrix characteristic roots
08 p1533 A70-20492
- Periodic and almost periodic solutions to vibrations of quasi-linear nonautonomous systems in presence of resonance, determining principal amplitudes
08 p1544 A70-20966
- Liapunov vector functions for asymptotically stable omega-periodic solution existence in case of finite dimensional system
08 p1534 A70-21002
- Extension of Liapunov systems to time lag systems with small periodic parameter
08 p1546 A70-21628
- Nonlinear system oscillations analysis based on small parameter method and difference equations, including resonant case and stability criterion for periodic solutions
08 p1546 A70-21629
- Error analysis in calculating periodic limiting state of rotor motion
09 p1727 A70-22624
- Periodic solutions with moderate eccentricities and high inclinations for three dimensional restricted three body problem by expanding disturbing functions by high speed computer
09 p1759 A70-22773
- Stability characteristics of near periodic orbits using variational equations, with results applied to phase space and stability problems
09 p1760 A70-22917
- Existence theorem for periodic solutions of nonlinear differential equations with deviating arguments
10 p1910 A70-24605
- Periodic solution existence theorem using harmonic linearization method
11 p2023 A70-25725
- Linear periodic coefficient differential equations stability analysis by infinite determinate method, considering applications to damped mechanical systems motion and dual spin satellite
12 p2261 A70-27813
- Stability of single periodic symmetrical solutions of plane circular restricted three body problem, using digital computer for numerical integration of equations of motion
13 p2490 A70-28950
- Nonlinear differential equations systems, deriving periodic solutions existence conditions
13 p2440 A70-29049
- Statistical output characteristics of harmonic cosine and sinusoidal inertialess phase periodic converters in two channel system with frequency multiplication
13 p2370 A70-29741
- Multiple period oscillations in nonlinear systems, using nonautonomous differential equations and Hammerstein operator
13 p2443 A70-29745
- Canonical representation for nonlinear differential equations periodic solutions
14 p2658 A70-30846
- Periodic solutions close to commensurabilities in three body problem, considering restricted and planar nonrestricted problems
17 p3172 A70-35561

- Nonlinear second order differential equations with periodic coefficients and solutions, examining stability by phase and amplitude plots by marginal range diagrams 18 p3282 A70-36356
- Periodic solutions of nonlinear second order differential systems containing symmetries, noting Marlin criteria 19 p3458 A70-38064
- Quasi-linear higher order differential equations, examining periodic solutions existence and stability 22 p4062 A70-42698
- Harmonic linearization method for periodic regimes in nonlinear control systems based on periodic solution sensitivity to higher harmonics and small parameters 22 p4000 A70-42829
- Periodic solutions to complex nonlinear automatic control systems with initial deviations, considering system stability and self oscillation conditions 22 p4002 A70-42839
- Three body problem periodic solutions, considering near equilibrium conservative Hamiltonian system consisting of two harmonic oscillators with rationally related frequencies 23 p4213 A70-44897
- Periodic boundary value problems with cyclic totally positive Green functions, and spline applications in vibrating physical systems and scaling theory 23 p4213 A70-44899
- Nonlinear second order differential equation periodic solutions, describing water column oscillation in U-tube 24 p4369 A70-46021
- PERIODIC ORBITS**
U ORBITS
PERIODIC OSCILLATIONS
U OSCILLATIONS
PERIODIC PROCESSES
U CYCLES
PERIODIC VARIATIONS
NT ANNUAL VARIATIONS
NT DIURNAL VARIATIONS
NT NOCTURNAL VARIATIONS
 Periodic cellular convection in troposphere with allowance for anisotropic turbulent mixing, showing cyclone association and intervals 01 p0135 A70-10206
- Male rats locomotor activity responses to altered photoperiods during exposure to varied-light artificial days 01 p0015 A70-10367
- Stellar system DQ Herculis photometry by synchronous signal averaging, indicating sinusoidal light curve with increasing binary period 02 p0373 A70-12392
- Beta Lyr spectral and brightness characteristics long period variations related to orbital motion perturbations 03 p0564 A70-13229
- Cosmic ray variations concepts with reference to 11, 22 and 80-90 year solar cycles Wolf number variations 03 p0568 A70-13355
- Astronomical clock pendulum oscillations isosynchronization noting effects of suspension elastic moment, fabrication, calibration errors and rotation center displacement 03 p0484 A70-13367
- Dynamic spectra of quasi-periodic VLF emissions noting association with geomagnetic micropulsations 03 p0477 A70-13985
- Galactic water vapor radio sources spectral observation suggesting correlation between time variation and polarization 04 p0747 A70-14547
- Solar Lyman-alpha radiation observed by OGO 4 spacecraft showing short term fluctuations superposed with monthly variation 04 p0741 A70-15128
- Tropospheric periodic responses to chromospheric flares, analyzing stations atmospheric pressure power spectra 04 p0742 A70-15524
- Latitude-period relation existence in geomagnetic micropulsations, discussing coupling between components of geomagnetic field fluctuations 05 p0838 A70-16278
- Periodic observation errors in air temperature, relative humidity, vapor and air pressure 05 p0879 A70-16665
- Oscillations intervals with diminishing period during magnetic storms, noting relationship to midlatitude disturbances in F region 05 p0842 A70-16746
- Periodicities in solar activity variation from correlation spectral analysis, establishing monotonically decreasing component and secular variations in activity 05 p0918 A70-16913
- Ionospheric absorption at oblique incidence during IQSY, studying seasonal and diurnal variations as solar zenith angle function 06 p1009 A70-17905

- HF periodic velocity oscillations effect on axisymmetric wake diffusion flames [AIAA PAPER 70-10] 06 p1182 A70-18179
- RW Aur-type variables in Taurus, studying temporal variations from photographic and photometric observations and B, B-V diagram 07 p1376 A70-18906
- Latitudinal dependence of period and amplitude of steady Pc 3-4 pulsations observed at group of widely spaced stations 07 p1268 A70-19464
- Lunar periodicity detected from radio aurora data as possible cause of lunar interaction with magnetosphere 07 p1389 A70-20164
- Heavy solid body motion about stationary point at small nutation angle, estimating region of series convergence representing periodic solutions to motion equations 07 p1336 A70-20298
- Material particles unrealizability of periodic motion near libration points of triaxial ellipsoid rotating steadily about polar axis 08 p1543 A70-20491
- Binary star spectrum analysis establishing seasonal and season-to-season variations in He II emission band intensity and shift toward long wave region 08 p1569 A70-20827
- Beta Lyr spectral and brightness characteristics long period variations related to orbital motion perturbations 08 p1580 A70-21662
- Pulsars period distribution not related to decay of magnetic field in rotating neutron star 09 p1756 A70-22518
- Two dimensionally periodic slow wave structure, verifying Shein formulas 09 p1637 A70-23143
- Periodic intensity fluctuations in pulsars from VHF phased array measurements 09 p1764 A70-23793
- Sideral time variations in cosmic ray intensity observed by inclined muon telescopes 10 p1933 A70-24858
- Zero-point of period-luminosity-relation of Cepheids based on proper motions, radial velocities and photometric data, applying secular parallax method 10 p1945 A70-24964
- Microfluctuations frequency and wavelength of electromagnetic, electric and magnetic field distributions in plasma shock wave front found consistent with ion-acoustic origin hypothesis 10 p1925 A70-25031
- Human finger tips skin temperature periodical variations process and influencing factors using electronic analog model 10 p1823 A70-25306
- Ionospheric magnetic activity effects on cosmic radio noise absorption diurnal and seasonal variations in auroral zone, noting K index and lowest reflection frequency roles 11 p2043 A70-25536
- Three dimensional periodic boundary layer flow noting successive approximations method, noting steady streaming in first order cross flow 11 p2037 A70-26296
- Cosmic ray variations concepts with reference to 11, 22 and 80-90 year solar cycles Wolf number variations 11 p2118 A70-26720
- Climatic phenomena cyclic behavior from forecasting viewpoint, considering geomagnetic, upper atmospheric and solar activity effects 12 p2265 A70-28268
- Cosmic radiation periodic variations measurements noting second harmonic importance of daily variations 13 p2478 A70-29230
- Diurnal and seasonal variations of parameter s of meteor showers on celestial sphere, using radio echo amplitude distribution from radar observations 14 p2635 A70-30307
- Continuity equation plasma oscillation, discussing ion current waveform flowing from discharge and implications for periodic astrophysical phenomena 14 p2638 A70-30618
- Planetary orbit after central star supernova explosion, discussing effect on pulsar period 14 p2640 A70-30787
- Twelve year periodicities of Jupiter decametric radiation, noting correlation with Jupiter magnetic field rotation period 14 p2648 A70-31085
- Jupiter decimeter radiation long term variations from flux density measurements, suggesting correlation with solar activity 14 p2648 A70-31087
- Cosmic ray shortest term regular intensity variations, measuring particle dispersion as time function 14 p2633 A70-31314
- Harmonic analysis of digital data from satellite measurements of periodic phenomena with unknown periodicity 14 p2554 A70-31415

- Cyg XR-1 X ray spectrum variability by balloon-borne detectors as eclipsing properties of binary system 15 p2799 A70-31750
- Pulsars MP 0031 and CP 1919 periodic variations in pulse intensity, considering radio emission models with plasma waves 17 p3157 A70-34843
- Periodic cosmic ray variations near Southern magnetic pole related to chromospheric flares 18 p3307 A70-36102
- Pulsars PSR 1451-68, 1749-28 and 2045-16, discussing modulation effects associated with second periodicity 18 p3314 A70-36334
- Pulsars period galactic equator concentration correlation, discussing period-radio luminosity relation and spatial distribution 18 p3314 A70-36335
- Latitudinal dependence of period and amplitude of steady Pc 3-4 pulsations observed at group of widely spaced stations 18 p3250 A70-36938
- Motion stability in periodic cubic force field, using nonlinear differential equation integration with time periodic square wave function and Jacobian table 18 p3284 A70-37065
- Wolf numbers monthly fluctuations, giving histogram of fluctuation amplitude distribution 18 p3323 A70-37137
- Periodic thermal forcing role in Venus atmosphere dynamics, investigating momentum transport to support mean shear for channel flow 19 p3519 A70-38251
- Vibration signals analysis in random and periodic modes, presenting analyzers block diagrams 19 p3430 A70-38526
- Pc-1 pulsations during solar activity maximum and minimum, discussing diurnal, seasonal and cyclic variations 19 p3416 A70-38586
- Cepheids in Galaxy spherical component, determining periodic variations by distribution function technique 19 p3525 A70-38768
- Cepheids periodic variations photographic analysis 19 p3525 A70-38769
- Pulsars CP 0834, AP 1237 and CP 1919 radiation intensity periodic variations, discussing power spectra fluctuations in circulating plasma model 20 p3701 A70-39007
- Plane horizontal fluid film convective stability with free boundaries in vertical circular cylinder for periodic modulation of vertical temperature gradient or gravitational field 21 p3941 A70-40608
- Field-ion microscope image formation, determining periodic surface potential variation effects on high field tunneling 21 p3862 A70-40974
- Ionospheric magnetic activity effects on cosmic radio noise absorption diurnal and seasonal variations in auroral zone, noting K index and lowest reflection frequency roles 21 p3819 A70-41286
- Dispersion equation for impedance elements periodic structures phase velocity calculation, discussing approximate solution methods 22 p3984 A70-42392
- Crab pulsar observations with refractor and on-line data acquisition, indicating optical pulse arrival times at variance with previously assumed 77 day periodic wobble 22 p4097 A70-42464
- Periodic motions of arbitrarily long periods for idealized nonlinear spring-mass systems with two or more degrees of freedom 22 p4073 A70-42699
- Harmonic linearization method for periodic regimes in discrete nonlinear automatic control systems performing signal quantization with respect to level or time 22 p4001 A70-42833
- Ionospheric electron content measurement during solar activity cycle, noting temporal and spatial variations 22 p4020 A70-43159
- EUV solar spectral intensity distribution and cyclic variations 22 p4106 A70-43299
- Earth surface magnetic field variations due to magnetopause current system 24 p4329 A70-45355
- PERIODICITY**
U PERIODIC VARIATIONS
PERIODICITY (BIOLOGY)
U RHYTHM (BIOLOGY)
PERIPHERAL CIRCULATION
 Human thermoregulatory responses as function of peripheral thermoreceptors during imposed negative heat load in different ambient environments 01 p0024 A70-10977
- Constant-inflow and constant-pressure perfusion effect on vascular responses of dog 02 p0232 A70-11716

Polyethylene-bis-lepidine dibromides effect on blood pressure and peripheral vessel tonus in dogs, analyzing depressor reaction as function of binding chain

04 p0632 A70-15204

Peripheral arterial piezography for cardiological screening tests and checkups of flying personnel

05 p0807 A70-16495

Intracerebral, peripheral and central blood circulation relationship in humans during transverse accelerations

07 p1209 A70-19520

Intermittent forced inspirations or expirations effects on venous tone and blood flow in human skin vessels

17 p3024 A70-34595

Peripheral vasculocapillary blood circulation by plethysmography

19 p3370 A70-38212

Human peripheral blood flow rearming in cold ambient temperature, examining skin, rectal and tympanic membrane and oxygen uptake

20 p3576 A70-40327

Dynamic response of peripheral blood flow to hypothalamic temperature waveforms in baboon, using implanted thermodes

24 p4303 A70-46116

PERIPHERAL JET FLOW

Exit geometry effects on peripheral jet device lift, considering operating height, curtain thickness, base extension, etc

04 p0619 A70-15388

Secondary peripheral air injection effects on subsonic airflow through slotted tube, discussing primary flow, flow separation, static and stagnation pressures and temperature changes

11 p2036 A70-26140

Inviscid flow theory for ACV high speed peripheral jets, considering component inefficiencies, pressure losses, nozzle geometry, etc

12 p2156 A70-27211

Two dimensional peripheral turbulent jet curtain structure, determining curved and impinging jet flow field by pressure and velocity measurements

22 p3957 A70-42277

Static and dynamic spring constants of peripheral jet air cushion vehicle in heaving motion, obtaining sinusoidal input response characteristics

22 p3960 A70-42279

Peripheral jet ground effect machine model heaving motion, investigating static hover and forced and free vibration characteristics

22 p3961 A70-42281

PERIPHERAL NERVOUS SYSTEM

Nerve cell response to change in chemical constitution of surroundings used to investigate animal periphery sensory mechanisms

01 p0033 A70-10497

Functional model of signal analysis and pulse sequence conversion in nervous system at periphery of hearing

10 p1827 A70-25127

Excitation conduction velocity maximum along motor fibers of peripheral nerves as function of age in healthy subjects

15 p2679 A70-31602

Peripheral stimulations of various modalities effect on neurons impulse activity in hippocamp dorsal area of rabbits, noting excitation and latent periods

23 p4145 A70-44311

PERIPHERIES

U BOUNDARIES

PERTONEUM

Gamma-aminobutyric acid influence on 5- hydroxytryptamine in rat brain after intraperitoneal administration

01 p0019 A70-10510

PERMALLOYS [TRADEMARK]

LF creep characteristics in Block-wall Permalloy films, using high resolution Bitter pattern technique [IEEE PAPER 5.7]

05 p0893 A70-16996

Annealing atmosphere effect on permeability of Mo Permalloy

07 p1304 A70-18814

Normal and unconstrained vacuum-deposited Permalloy films composition dependence of magnetization-induced uniaxial anisotropy, noting agreement with magnetostrictive constraint theory

12 p2284 A70-27244

Permalloy evaporation rates from resistance heated W boat, revealing departure from free molecular flow

13 p2452 A70-29203

Magnetic dislocations effect on domain structure of postcritical Permalloy films subjected to alternating magnetic field

16 p2930 A70-33206

X ray fluorescence determination of thickness and composition of Permalloy films deposited on wire surface

18 p3258 A70-36466

Permalloy tapes uncertainty in magnetization process, discussing Barkhausen discontinuities measurement method

20 p3673 A70-40058

Uniaxial magnetic anisotropy in electrodeposited Permalloy films in terms of magnetostrictive mechanism

20 p3687 A70-40160

Orthogonal susceptibility of uniaxial thin nonmagnetostrictive Permalloy films

22 p4086 A70-43011

PERMANGANATES

Potassium permanganate catalytic effects on ammonium perchlorate deflagration, studying catalyst dispersion degree role

07 p1358 A70-19329

PERMEABILITY

NT DIELECTRIC PERMEABILITY

Gamma radiation effects on membrane permeability of isolated nuclei from white rats thymus in sucrose-calcium buffer

04 p0629 A70-14460

Annealing atmosphere effect on permeability of Mo Permalloy

[AIME PAPER F-69-7]

07 p1304 A70-18814

Permeability disturbances in skin capillaries of rabbits and rats following exposure to Sr90-Y90 beta radiation

09 p1619 A70-22789

Transpiration-cooled systems design with porous materials, considering mechanical and flow control /permeability/ properties requirements

12 p2256 A70-27822

Microstructure effects on magnetic properties of polycrystalline MnZn ferrites with high permeability

19 p3484 A70-37565

Crystal dislocations and microstructure effects on magnetic properties of polycrystalline MnZn ferrites with high permeability, noting eddy currents role

19 p3484 A70-37566

Magnetic field and permeability effects on drag in steady axisymmetric MHD flow of incompressible fluid around full and hollow spheres

19 p3477 A70-37577

Parachutes lightweight coated fabrics air permeability under axial tensile loading and load cycling at room temperatures

21 p3843 A70-41835

EM wave propagation in inhomogeneous media, examining permittivity and permeability

23 p4217 A70-43768

PERMEATING

Early Precambrian chert porosity and permeability, investigating hydrocarbon content origin

13 p2400 A70-29863

PERMUTATIONS

Rank permutation codes equivalence to binary code class capable of generation and detection through direct and inverse transformations respectively

20 p3594 A70-39975

Combinatorial optimization problems design on permutation set, considering applicability of variants successive analysis method

24 p4321 A70-45472

PEROVSKITES

Perovskite crystals phase transitions based on group theory, considering lattice vibration modes as instability source

24 p4389 A70-45206

Perovskite type oxide lanthanum manganate magnetic properties, explaining ferromagnetism by spin Hamiltonian formalism

24 p4389 A70-45601

PEROXIDES

NT HYDROGEN PEROXIDE

NT INORGANIC PEROXIDES

Oxygen electrode ring and disk currents analysis, studying oxygen reduction on platinum via peroxy intermediates

10 p1829 A70-24453

Self heating accompanying exothermic decomposition of gaseous diethyl peroxide in spherical vessel measured positionally by thermocouple

12 p2330 A70-27223

Thermal testing of decomposition and spontaneous ignition of diethyl peroxide before explosion

12 p2330 A70-27224

Free radical coupling of silyl peroxides in reinforced plastics, laminates and adhesives

16 p2937 A70-33377

PERSEID METEORIDS

Radar and photographic studies of meteors from Leonid and Perseid showers, presenting velocities, luminence and ionization

01 p0193 A70-11602

Perseids time distribution, based on observations during meteor showers, contradicting appearance of homogeneous Poisson process

09 p1750 A70-22099

Parameter S mean values measurement in Perseid meteor shower, discussing wind effects and accuracy

19 p3526 A70-38778

PERSONALITY

Headache and personality traits related to visual acuity and brightness sensitivity increases from sea level to high altitude

04 p0633 A70-15444

Professional personality formation and organization of aviator, discussing infancy motivation, identification with instructor during training, emotional life, etc

05 p0799 A70-15767

Pilots personality studies, considering roles of defense mechanisms, Oedipus complex, infant sexuality, Icarus complex, etc

10 p1825 A70-24660

PERSONALITY TESTS

Impression formation model extended to personality traits, noting curvilinear relationship between probability and liking ratings

05 p0803 A70-16670

Ego strength relationship to respiration in response to sound and light stimulation tested in subjects balanced for alertness-drowsiness by EEG criteria

09 p1616 A70-22331

Minnesota Multiphasic Personality Inventory scores compared with various pilot training proficiency levels, noting low correlation

12 p2176 A70-27032

Aptitude test validity taking into account selection board subjective decisions on pilot applicant acceptance

19 p3371 A70-38507

Age, grade, educational institution and attitude effects on pilot personality test performance

22 p3977 A70-42870

Jet pilots psychological survey on troubles, frustrations and personality trends by questionnaire

22 p3978 A70-42876

PERSONNEL

NT AIRCRAFT PILOTS

NT ASTRONAUTS

NT COSMONAUTS

NT FLIGHT CREWS

NT FLIGHT SURGEONS

NT FLYING PERSONNEL

NT GROUND CREWS

NT INSTRUCTORS

NT NAVIGATORS

NT OPERATORS [PERSONNEL]

NT ORBITAL WORKERS

NT PHYSICIANS

NT PILOTS [PERSONNEL]

NT SCIENTISTS

NT SPACECREWS

NT TEST PILOTS

Aerospace scientific and engineering work force movement between geographical areas and resource location

07 p1426 A70-18799

Mission Control Center and Apollo flight controller team, discussing personnel qualifications, equipment and individual evaluation

21 p3805 A70-41197

PERSONNEL DEVELOPMENT

Digital real time simulation for training and evaluating ATC controllers, discussing system hardware, software, design and implementation

02 p0274 A70-11977

Great Britain air transport industry manpower recruitment and training, technology changes effects and costs

02 p0402 A70-12307

Cooperation of NASA and DOD Quality Assurance personnel concerning Apollo 11, considering personnel training

07 p1428 A70-19674

Apollo Program flight control operations personnel premission planning and training, discussing presolution of launch problems and emergencies

09 p1768 A70-23707

Human engineering in weapon systems development, considering flying and ground personnel training plans

12 p2177 A70-27038

Personnel and organizational policies for university research management

12 p2336 A70-27750

Quality control organization for miniature resistance welding of electronic equipment, examining planning phase and personnel training program

14 p2592 A70-31107

ATC personnel training at International ATC Academy, discussing objectives and syllabus

19 p3372 A70-38650

PERSONNEL MANAGEMENT

Predicting retention rate of naval pilots and flight officers beyond initial obligated duty tour based on training performance

15 p2690 A70-31888

Systems engineering approach to comparison by emphasis for employee performance evaluation

17 p3130 A70-35298

Air traffic controller stress reduction, discussing work-rest intervals and various management and human factors

19 p3371 A70-38647

R and D programs engineering talent assignment case histories

21 p3955 A70-41174

Aktion X program for production efficiency, mobilizing personnel in weak points monitoring

24 p4430 A70-45624

PERSONNEL PROPULSION SYSTEMS

U SELF MANEUVERING UNITS

PERSONNEL SELECTION

NT PILOT SELECTION

Psychological aspects of unreliability sources in man machine systems for selection and training criteria of photooptical instruments users

01 p0036 A70-10821

Space flight candidate selection and physical training, comparing American and Soviet training programs for efficiency and physical requirements

07 p1216 A70-18792

Team hiring of research scientists by industrial and academic organizations, discussing causes and influence on R and D organizations management and design

07 p1427 A70-19002

Aircraft pilot and captain selection system on basis of STANINE/standard nine/ method of psychological assessment

10 p1825 A70-24504

Age discrimination in employment policies of air carriers, discussing legislative measures, hiring practices and retirement rules concerning stewardesses and FAA pilots

12 p2336 A70-27772

Ergonomic and medicomilitary aspects of human adaptation to cold environments, discussing metabolic and physical protective reactions, clothing and personnel selection

16 p2850 A70-34346

Wolff-Parkinson and White syndrome applicability in aeromedical appraisal for aircrew selection, noting effects of paroxysmal tachycardia

17 p3040 A70-35916

UK organization of ATC services, considering responsibilities, facilities and personnel recruitment

19 p3467 A70-38634

PERSONNEL SUBSYSTEMS

Air traffic control procedures pertaining to personnel, hardware and regulations

11 p2078 A70-25720

Personnel subsystem reliability through empirical approach, determining relations of man-hardware-procedure systems

15 p2804 A70-32665

Project managers problems of anomalies and ambiguities in complex missions operation and implementation, discussing interactions with personnel

23 p4284 A70-43996

PERSPEX (TRADEMARK)

Plastic strains at sharp notch roots in Perspex plates using interference patterns formed by gas laser monochromatic light beam for fracture initiation

11 p2131 A70-25594

PERSPIRATION

Esophageal, rectal and quadriceps muscle temperatures, oxygen uptake, weight changes, skin conductance and skin evaporation during thermal transients caused by bicycle exercise

10 p1810 A70-24006

Human sweating transient state characterized by time constant following abrupt ambient temperature rise

21 p3761 A70-41140

PERT

Installation planning of electronic data processing unit using network and PERT program features

03 p0454 A70-13969

Book on project management with critical path method and PERT, covering manual and computerized calculation of scheduling, networks, time-cost tradeoffs, etc

22 p4128 A70-43625

PERTURBATION

NT ORBIT PERTURBATION

NT SATELLITE PERTURBATION

Motion stability over finite interval of time for perturbed mechanical systems

01 p0146 A70-11560

Optimal linear controller synthesis with allowance for continuous perturbations effect, describing weighting factors selection

02 p0272 A70-12413

Perturbed motion of solid body with cylindrical cavity partially filled with viscous fluid, using Rabinovich equations

04 p0766 A70-14476

Lifting rotor blades flapping response to atmospheric turbulence, discussing time averaging and perturbation schemes

[AIAA PAPER 69-206] 04 p0624 A70-15378

Perturbation solution for fins taking into consideration interaction of conduction with radiation and convection

07 p1422 A70-19333

Electric and magnetic field perturbation at great distances behind body moving in collisionless magnetized plasma estimated from Fourier transform

07 p1385 A70-19447

Evolutionary hydromagnetic shock perturbation by incident small amplitude hydromagnetic wave calculated for diverging wave amplitudes and directions

11 p2036 A70-26017

Annular gas laser, considering external periodic perturbation effect on difference frequency of oppositely moving waves

12 p2251 A70-28291

Self gravitating collisionless particles instability related to anisotropic random velocity distribution function in presence of disk-galaxy type spiral wave perturbations

13 p2492 A70-29299

Two dimensional jet velocity profile evolution under symmetrical and antisymmetrical perturbations

14 p2567 A70-31200

Perturbed motion of body with partially filled cylindrical cavity with damping ribs, discussing vibrations boundary value problems of liquid filling

15 p2775 A70-32157

Independent integrals of perturbed motion equations of spatial gyrohorizon compass

17 p3090 A70-35344

Electric and magnetic field perturbation at great distances behind body moving in collisionless magnetized plasma estimated from Fourier transform

18 p3316 A70-36921

Plane waveguide field with complex geometric inhomogeneity, describing perturbed section by integral equations

19 p3381 A70-38567

Stratospheric perturbation sources from atmospheric circulation as function of season, geographic latitude and altitude, suggesting high energy protons in atmosphere

20 p3618 A70-39183

Magnetotail magnetic field perturbations associated with polar magnetic substorms, using IMP-A and B satellite observations

21 p3882 A70-41720

PERTURBATION THEORY

Critique of double resonance theory in gaseous lasers, including correction regarding saturation parameter for small RF perturbations and line width dependence

01 p0109 A70-10432

Rayleigh method convergence for linear development of perturbations in unsteady plane parallel flow of ideal fluid, formulating and proving theorem

01 p0064 A70-11032

Upper atmospheric thermal fluctuations study based on correlation characteristics of rapid thermal perturbations, using linear differential equations

02 p0288 A70-11761

Asymptotic method based on Landahl small perturbation theory applied to perturbation velocity potential for oscillating delta wing in transonic flow

02 p0223 A70-11775

Perturbation method developed for linearizing nonlinear singular equation for inhomogeneous stratified atmosphere H-function in theory of radiative transfer

02 p0338 A70-11791

Singular perturbation problem solution asymptotic expansions applied to linearized theory of elasticity equilibrium problem with stress couples

02 p0389 A70-12685

Optical echoes using model of spins precessing in magnetic field, presenting time dependent theory of perturbation

02 p0341 A70-12830

Multiple periodicities in beta Canis Majoris Star 16 Lacertae attributed to tidal perturbation effects on pulsation mode of structural changes

03 p0567 A70-13320

Dead zone initial disturbance of sensitive element dynamic coordinate in two rotor gyrocompass determined using method of averages

03 p0484 A70-13419

Approximate method of boundary perturbation to solve elasticity and viscoelasticity problems for non-canonical bodies of revolution applied to stress concentration at ellipsoidal cavity

03 p0591 A70-13439

Potential determination from gravity disturbances along fixed direction in analysis of residuals of Doppler tracking of Lunar Orbiter satellites for moon gravity field

03 p0577 A70-14177

Matrix elements of nonadiabatic perturbation emphasized in semiempirical theory for evaluating polyatomic molecules radiationless rate constants in terms of electronic-vibrational state

04 p0722 A70-14699

Perturbation technique for numerically sensitive nonlinear two point boundary value problems

04 p0713 A70-15045

Rate equation analysis of steady state behavior of double cavity GaAs diode laser, noting solution stability by perturbation method

04 p0703 A70-15618

Coordinates computation method using spherical harmonic expansion of geomagnetic field, discussing direct computations by perturbation method

05 p0837 A70-15820

Exchange perturbation theories applied to delta function model of molecular hydrogen ion, discussing EL-HAV second order energy at large internuclear separations

05 p0884 A70-15878

Continuum, harmonic and finite element perturbation studies of elastica to yield postbuckling path derivatives from nonlinear energy formulation

05 p0927 A70-16011

Periodic perturbations of plane Poiseuille flow, observing neutral curve relationship to disturbance amplitude

05 p0832 A70-16019

Hybrid computer simulation of small nonlinearities effects in human arterial system, using perturbation techniques

05 p0805 A70-16045

Perturbation effects on elastic material deformation due to nonorthogonality of curves defining curvilinear acotropy, with application to circular cylindrical tube

05 p0929 A70-16065

Perturbation theory based on Lie transforms, reducing Deprit equation to generate general recursion formulas

05 p0908 A70-16336

Motion near collision singularity in perturbed two body problem, applying method to boundedness proof for Spherling cluster energy

05 p0909 A70-16339

Bounded operator functionals used for deriving nonlocal interaction Hamiltonian of quantum electrodynamics corresponding to converging series for scattering matrix in perturbation theory

05 p0883 A70-16876

Bounded nonlocal operator used in deriving series of subtracting Hamiltonians representing S matrix in perturbation theory after transition to local limit

05 p0883 A70-16877

Randomly perturbed linear differential equation involving first derivative of n-vector function of real variable

05 p0878 A70-17096

Excitation coefficients for arrays with shaped beam patterns by perturbation of roots which lie off unit circle

06 p1021 A70-17572

Time dependent pressure fluctuations effect on laminar film pool boiling on vertical flat plate by perturbation method to predict heat transfer

06 p1177 A70-17696

Degenerate and nondegenerate energy states and wave functions formulated by Rayleigh-Schrodinger perturbation theory

06 p1110 A70-17764

Ammonium perchlorate deflagrations, determining intrinsic stability of one dimensional burning configuration based on flame structure modeling

[AIAA PAPER 70-123] 06 p1128 A70-18044

Three body problem involving sun and perturbing and perturbed planets, examining perturbed motion equations of Brouwer and Encke methods

07 p1374 A70-18773

Propagation in perturbed magnetically focused electron beams, noting influence of spatially varying drift velocity and damping effect

07 p1239 A70-18867

Periodic solution with nondegenerate orbit for functional differential equations taking into account small perturbation

07 p1324 A70-19199

Step profile decay of initial perturbations of radiating gas as function of optical depth and Boltzmann number

07 p1255 A70-19212

Satellite orbit using analytic partial derivatives of perturbed motion based on state transition matrices

07 p1381 A70-19301

Hypothesis concerning initial spectrum of metric perturbations in Friedman model, discussing long wavelength gravitational waves energy

07 p1383 A70-19406

Perturbations classes for self adjoint operator limit spectrum preservation

07 p1327 A70-19807

Single junction vacuum thermocouple measuring thermal beam effect with reference to velocity distribution perturbation in molecular beam scattering

07 p1341 A70-20107

Axial-vector current divergence in external gravitational field, using perturbation approach in Minkowski space

07 p1336 A70-20167

Single frequency oscillations of variable cross section rods with random perturbations using asymptotic methods of nonlinear mechanics, discussing wedge oscillations

08 p1583 A70-20487

Phase shift effect on astatic gyro axis drift and stability during periodic perturbations, describing motion by nonlinear differential equations

08 p1493 A70-20489

Stability in systems finite over given time interval under permanent perturbations bounded in mean

08 p1543 A70-20490

Soviet book on motion of guided rockets in space covering aerodynamic and structural aspects, stabilization and disturbed rocket motion, etc

08 p1582 A70-20756

- Libration limits of satellite in Keplerian circular orbit, estimating potential energy of perturbing forces 08 p1582 A70-20967
- Stability of continuously differentiable functions representing approximate solution to system of differential equations of perturbed motion 08 p1545 A70-21167
- Incompressible laminar boundary layer stability of incompressible fluid for nonparallel oncoming flow, deriving perturbed motion equation 08 p1483 A70-21179
- Quasi-geostrophic baroclinic instability in non-separable parallel flow, using perturbation theory 08 p1539 A70-21604
- Random perturbation procedure for control variable functions optimization using hybrid computer method for analog solutions and digital storage 08 p1467 A70-21783
- Stress analysis of composite materials reinforced with glass ribbons embedded in epoxy matrix by photoelastic technique, discussing perturbation effect 08 p1594 A70-21862
- Gravitational collapse models with magnetic dipole and gravitational quadrupole, treating asymmetries as small perturbations 09 p1752 A70-22274
- Perturbation rotational levels in triplet states of CO emission spectra attributed to resonance fluorescence process involving optically forbidden transitions 09 p1731 A70-22282
- Integral equation perturbation technique, discussing applications to electrostatics, hydrodynamics, MHD, heat and mass transfer, etc 09 p1711 A70-22350
- Optimum control law for minimizing mass point maximum deviation under given disturbance obtained by graph analytic method 09 p1727 A70-22534
- Nonlinear stability theory for applying perturbed equations to dynamical system based on Liapunov stability theorem 09 p1727 A70-22612
- Molecular hydrogen parallel and perpendicular dynamic polarizabilities calculated for frequency dependence, using many body perturbation theory 09 p1731 A70-22780
- Periodic solutions of restricted three body libration point perturbation due to fourth body gravitational and radiative influence using Huang model 09 p1761 A70-23053
- Amplitude and phase correlations of spherical waves propagating in turbulent atmosphere using smooth perturbation method 09 p1636 A70-23139
- Motions stability about triangular points in elliptic restricted problem of three bodies, using perturbation scheme 09 p1728 A70-23205
- Inviscid hypersonic small disturbance theory applied to flow behind concave and convex exponential shock waves, determining supporting two dimensional airfoil surfaces 09 p1605 A70-23220
- Laminar boundary layers behavior in shock tube flows behind primary moving shock wave using perturbation method 09 p1662 A70-23281
- Streamwise perturbations in flow downstream of self excited blades cascade calculated by two dimensional theory, discussing periodic circulation shedding 09 p1608 A70-23746
- Gravitational instability theory for large density perturbations growth during expansion of matter without pressure 10 p1945 A70-24961
- Radiative transfer in inhomogeneous atmospheres using simplified matrix equations in perturbation method 10 p1933 A70-24984
- Polarized radiation transfer through inhomogeneous semiinfinite atmosphere by matrix perturbation method, giving nonlinear singular integral equation 10 p1933 A70-24985
- Rayleigh method convergence for linear development of perturbations in unsteady plane parallel flow of ideal fluid, formulating and proving theorem 10 p1871 A70-25001
- Ideal fluid flow containing small spherical particles past cylinder and flat plate normal to stream using small perturbations method 11 p1976 A70-26012
- Spacecraft temperature prediction and heat conduction problems with nonlinear radiation boundary conditions by perturbation theory, applying to heat shield analysis 11 p2150 A70-26355
- Hydrogen-air reaction by singular perturbation methods for temperature and pressure values of supersonic combustion, changing reaction velocity by initial stoichiometry 11 p1995 A70-26624
- Gravitational disturbance by exterior planets, considering Brown transformation of longitudinal perturbation problem in relation to planet Neptune discovery 11 p2117 A70-26658
- Elastic postbuckling and imperfection sensitivity of discrete structural systems using perturbation approach 11 p2143 A70-26668
- Aerodynamic sound emission from compact eddy region by singular perturbation approach, discussing Lighthill and Ribner theories 11 p1977 A70-26687
- Linearized perturbation theory for quasi-static equilibrium stellar interior models, obtaining correction through bidirectional quadrature 11 p2118 A70-26709
- Wave propagation in continuous random media solved by partial differential equations with random coefficients, describing perturbation methods for obtaining solutions statistical properties 11 p2085 A70-26761
- Differential equations perturbed linear systems convergence, extending Bridgland results 12 p2260 A70-27011
- Solar wind structure as function of corotating coronal inhomogeneities determined using perturbation equations for spherical polar coordinate system 12 p2292 A70-27179
- Dynamic behavior and moments of oscillatory systems under steady perturbations using linear differential equations 12 p2261 A70-27555
- Perturbation theory of supersonic steady anisotropic flow with radiative heat transfer using hyperbolic characteristic coordinates 12 p2334 A70-28203
- Perturbation function of first order general planetary theory using Hori canonical variables, revealing mixed secular term of determining function 13 p2487 A70-28708
- Oscillatory perturbed motion of elastic body in general relativity space time, discussing energy tensor, unitary speed vector and density 13 p2451 A70-28954
- Banach space stability in presence of constantly acting perturbations bounded in mean, investigating differential operator equation 13 p2452 A70-29309
- Nonlinear branching point problems in fluid mechanics using perturbation technique 14 p2565 A70-30471
- Steady plane relativistic flow small irrotational perturbation theory determining subsonic, transonic and supersonic approximation 14 p2566 A70-30472
- Spiral structure of disk galaxies as nonaxisymmetric perturbations in density, using pressure free hydrodynamical equations 14 p2639 A70-30731
- Singular perturbation problems in theory of differential equations with almost periodic coefficients 14 p2599 A70-30847
- Flow velocity distributions in laminar boundary layer by perturbation methods 14 p2566 A70-30850
- Adiabatic relation between initial plasma density perturbations and radiation temperature fluctuations during galaxies formation, discussing relic radiation fluctuations 14 p2632 A70-31286
- Red giant model, investigating inclusion of semirelativistic partially degenerate gas characteristics by perturbationary technique 14 p2651 A70-31290
- Book on celestial mechanics covering perturbation methods, two body problems, astronomical coordinates, orbital mechanics, satellite rotation, gravitational effects, etc 15 p2799 A70-31998
- Circular free boundary problem associated with phase transformation by first order perturbation solution, discussing radial solidification and melting of fluid over cylindrical rod 16 p2941 A70-33003
- Plasma echo oscillations due to superposition of consecutive perturbations separated by intervals greater than characteristic decay time 16 p2957 A70-33198
- Equations of supersonic and hypersonic motion past circular cone by linearized method based on small perturbations with respect to nearly incompressible flow 16 p2835 A70-33746
- Partitioning formalism for degenerate, almost degenerate and electron exchange perturbation problems 16 p2955 A70-34001
- Coupled simple harmonic oscillators with almost degenerate energy levels, comparing partitioning perturbation techniques with Rayleigh-Schrodinger approach 16 p2955 A70-34002
- Partitioning perturbation theory for electron exchange problems, generalizing Hirschfelder-Silbey formalism 16 p2955 A70-34003
- German monograph on supersonic flows calculation past slender bodies of revolution using perturbation approach based on Poincare-Lighthill-Kuo method 16 p2839 A70-34082
- Longitudinal wave propagation in variable section bars, solving hyperbolic equation of motion by perturbation method 16 p2993 A70-34088
- Shear flow perturbations in inviscid incompressible stratified fluid of given density, comparing stability characteristics with jet flow 16 p2895 A70-34243
- Perturbation method to obtain analytical expressions for attenuation of plane wave sound propagation in lined ducts 17 p3136 A70-34523
- Singular perturbations of boundary value problems, investigating asymptotic solutions to finite difference equations 17 p3128 A70-34613
- Boundary conditions for electrodynamics of wave reflection from conducting bodies, using perturbation technique 17 p3128 A70-34633
- Satellite equations of motion in noninertial instantaneous astronomical system, taking into account perturbation equations terms 17 p3155 A70-34684
- Plasma waves parametric excitation by external electric field, using perturbation method of multiple scales 17 p3140 A70-34933
- Bounded ionospheric layers gradient instability, discussing perturbation growth and lifetime 17 p3076 A70-34944
- Normal shock structure in thermally perfect gas, using perturbation methods 17 p3070 A70-35244
- Perturbation method for finite elastodynamic deformation of nonlinear systems 17 p3191 A70-35590
- Magnetic perturbation effects on magnetoactive plasma, considering Boltzmann transport equation, plasma-electromagnetic interactions, heating, cooling, etc 17 p3142 A70-35592
- Couette flow stability between coaxial rotating cylinders, calculating eigenvector in first approximation small perturbation equations 17 p3073 A70-35695
- Hydrodynamic flow stability, formulating localizability properties for short wave perturbation 17 p3073 A70-35735
- Motion perturbation equations for guided space vehicles, allowing for sloshing liquid propellant viscosity effects 18 p3332 A70-36160
- Nonperturbability conditions and equations of motion of bigyroscopic vertical below escape velocity 18 p3259 A70-36592
- Schwarzschild exterior metric stability against perturbations from asymptotic behavior of Einstein field equations solution in Kruskal coordinates 18 p3291 A70-36650
- Iterative Hansen method of general perturbations programmed for digital computer, evaluating major and minor planetary theory 18 p3320 A70-37060
- Artificial satellite theory main problem for small and moderate eccentricities, using perturbation techniques based on Lie transforms for computer programming 18 p3334 A70-37062
- Differential equations for odd and even parity Regge-Wheeler perturbations on Schwarzschild metric 19 p3457 A70-37573
- Frames nonlinear elastic postbuckling behavior, using static perturbation technique 19 p3542 A70-38058
- Radio wave propagation over inhomogeneous terrains, determining perturbing effects of details on wave characteristics 19 p3381 A70-38573
- Perturbation calculation for linear ordinary differential operators, considering equivalence to eigenvalue problems 19 p3459 A70-38681
- Rotating stellar systems cooperative phenomena, estimating star-star collisions effect on perturbation rate and damping 19 p3525 A70-38772
- Second and higher order perturbation theory for two body trajectories, using recursive formulas [AIAA PAPER 70-1056] 19 p3528 A70-38871
- Ricci curvature tensor perturbations of space-time on Alfvén wave fronts 19 p3472 A70-38935
- Libration limits of satellite in Keplerian circular orbit, estimating potential energy of perturbing forces 20 p3713 A70-39388
- Perturbation method for nonlinear wave propagation in inhomogeneous media, considering sound propagation in ducts and hydromagnetic waves across nonuniform magnetic field 20 p3672 A70-39611
- Perturbation method for nonlinear acoustic wave propagation in steady one dimensional flow through variable cross section duct 20 p3673 A70-39612

Flow rate, momentum and energy perturbations during gas motions through shock wave, discussing acoustic waves impinging from supersonic region

20 p3612 A70-39815

Cylindrical gas suspension lubricating layer pressure distribution calculation by perturbation method, determining angular rigidity

20 p3637 A70-39818

Perturbation theory for nonlinear systems of differential equations

20 p3658 A70-40104

Boundary value problems in dynamic elasticity by perturbation method with displacement components

20 p3732 A70-40111

Viscous conducting fluid slow motion past sphere in presence of toroidal magnetic field, calculating Stokes flow perturbations

20 p3682 A70-40113

Perturbation method for stress-strain state of circular cylindrical shell with large curvilinear hole

20 p3734 A70-40442

Perturbed motion linear equations of body rigidly coupled to thin walled elastic shell partially filled with heavy compressible fluid

21 p3806 A70-40602

External field perturbations by local inhomogeneities in elastic medium, deriving expressions for interaction energy and forces between defects

21 p3933 A70-40604

Duality of optimal control and observation problems in cases of bounded coordinates and continuously acting perturbations respectively

21 p3801 A70-40605

Electromagnetic wave propagation in one dimensional periodic waveguide slow wave systems, deriving dispersion curves by perturbation theory

21 p3784 A70-40628

Secondary flow model for planetary boundary layer, considering flow as finite perturbation

21 p3813 A70-40904

Lifting reentry vehicle two dimensional motion optimization with inequality constraints explicitly containing control by perturbation method

21 p3845 A70-41265

Plasma wave echo, observing oscillatory behavior of perturbed distribution with different phases and amplitudes

21 p3858 A70-41389

Rotational transition probabilities of molecular collisions, using time dependent perturbation theory along linear trajectories

21 p3853 A70-41390

Numerical molecular rotational transition probabilities and cross sections in HCN-HCN and ICN-ICN collisions, using perturbation theory and multipole potentials

21 p3853 A70-41391

Bending stress at clamped support of impulsively loaded semiinfinite conical shell, obtaining formulas from perturbation theory

21 p3938 A70-41759

Quasi-conical supersonic wings with curved subsonic leading edges, discussing perturbation potential, boundary conditions, homogeneous flow and gothic and ogee planforms

21 p3747 A70-42108

Output probability of nonlinear systems from coupling moments for input random parameters, using equivalent perturbations method

22 p4003 A70-42885

Perturbation method with small parameter applied to turbulent transfer equation in lower atmosphere, solving longitudinal diffusion effect on evaporation

22 p4065 A70-42911

Nonlinear differential equations system under small perturbation, considering uniqueness for autonomous unperturbed system

22 p4062 A70-42969

Metric evolution in oscillatory mode of approach to singularity in homogeneous cosmological models in asymptotic region, showing Kasner epoch dependence on perturbation

22 p4075 A70-43478

Perturbation theories based on canonical transformations, examining von Zeipel theory and Hamiltonian functions

22 p4109 A70-43749

Book on guided EM wave theory covering mathematical methods transmission lines cavity resonators, perturbation theory, electrostatics, electric and magnetic fields, propagation, etc

23 p4172 A70-44242

Temperature dependent materials heat flow analysis using perturbation method for nonlinear boundary value problems

23 p4282 A70-44589

Moderately elliptic reference orbit perturbed motion, applying linearized perturbation equations for circular orbit

23 p4244 A70-44590

Restricted osculating two body orbit with time derivative of eccentric anomalies difference position as independent variable in perturbation differential equations

23 p4244 A70-44635

Doppler effect simplification to classical Laplacian orbit determination, deriving equations in perturbed gravity field for initial point determination

23 p4246 A70-44697

Celestial mechanics covering two body problem, orbital improvement, perturbation theory and dynamics, planetary and satellite theory, lunar motion, etc

23 p4255 A70-45032

High energy close approach trajectories within planar free fall three body problem, using perturbation theory

24 p4412 A70-45984

Perturbation effects on nonlinear first order wave equations discontinuous solutions decay, discussing boundary value problem for stress wave propagation in rod with viscous damping

24 p4426 A70-46026

Krylov and Bogoliubov perturbation method extension to difference equations based on analogy between differential and difference equations

24 p4370 A70-46027

Momentum source interaction with viscous uniform stream, constructing perturbation solutions from non-linear equations

24 p4327 A70-46040

Perfect gas statistical relations by perturbation form of state equation for atmosphere

24 p4372 A70-46071

Ionospheric wave propagation, using medium model, perturbation theory for vertical variation and computer eigenvalues of matrix system

24 p4314 A70-46132

Differentially rotating stellar interiors nonaxisymmetric perturbation stability in toroidal and poloidal magnetic fields

24 p4413 A70-46165

One dimensional gas pressure as function of activity, using Poisson-type partition function for perturbation calculation of thermodynamic limit

24 p4430 A70-46269

Linear stationary systems rms stability under parametric disturbances by white noise random processes

24 p4427 A70-46379

PERVEANCE

Magnetron-type electron gun structure with high design perveance for TWT applications

09 p1651 A70-23642

PETROGRAPHY

Worldwide data inventory of rock features associated with meteorite impact structures, including photomicrographs of petrographic features

01 p0069 A70-10223

Optical studies of deformational structures of minerals from meteorite craters and cryptoexplosion structures

02 p0292 A70-12510

Tenoumer crater meteorite impact origin from shock metamorphic features analysis

20 p3619 A70-39216

Electron microprobe and petrographic analyses of crystalline rock and separates from Apollo 11 lunar soil samples

21 p3895 A70-41506

Petrography and shock vaporization origin of Apollo 11 lunar breccias and glasses compared to terrestrial impactites and chondrites

21 p3898 A70-41524

Apollo 11 lunar rock mineralogy, examining petrographic and chemical features by light microscopy, electron microprobe microanalysis and detector system

21 p3898 A70-41525

Lunar rocks petrography, mineralogy and petrogenesis from Apollo 11 samples

21 p3902 A70-41554

Apollo 11 lunar dust, breccia and igneous rocks, using Mossbauer spectroscopy and petrographic techniques

21 p3916 A70-41664

Apollo 11 lunar crystalline rock and breccias petrography and luminescent properties, spectral analysis, color, emission bands and shock effects

21 p3918 A70-41678

PETROLEUM

U CRUDE OIL

PETROLOGY

NT PETROGRAPHY

Petrological, X ray and chemical analyses of Muz-zaffarpur Ni-rich ataxite, showing kamacite, taenite and minor schreibersite composition

01 p0177 A70-10328

Methane and ethane released from Apollo 11 lunar samples by crushing or acid treatment, suggesting carbides hydrolysis as main source

12 p2304 A70-27719

Apollo 11 lunar rocks mineralogy and petrology, noting anorthosite in powder and breccia

18 p3320 A70-37081

Chondrites and terrestrial rocks trace elements by neutron activation analysis, discussing radiochemical separation and computer analysis of gamma ray spectra

20 p3582 A70-38980

Apollo 11 lunar science - NASA Conference, Houston, January 1970, Volume 1, Mineralogy and petrology

21 p3893 A70-41501

Apollo 11 lunar rock and fines chemistry, mineralogy and petrology, discussing composition, igneous rocks, microbreccias, glasses and pyroxene relations

21 p3895 A70-41507

Apollo 11 lunar rocks, breccias, dust and chip mineralogy and petrology, examining composition, texture, grain size and morphologies

21 p3896 A70-41511

Apollo 11 lunar igneous rocks mineralogical, chemical and petrological features by optical and electron microscopy and X ray spectrometry

21 p3896 A70-41512

Apollo 11 lunar crystalline rock samples petrology, discussing shock and other metamorphic effects on mineral structure

21 p3897 A70-41516

Petrology, mineralogy and deformation of Apollo 11 rock samples using microscopic, X ray and electron microprobe methods

21 p3897 A70-41517

Petrologic analyses of minerals and glass spherules in Apollo 11 lunar rocks, indicating little fractionation and shallow-level differentiation

21 p3897 A70-41521

Petrology, crystallization and magma origin of lunar clinopyroxene, ilmenite-rich dolerite and microgabbro from Apollo 11 samples

21 p3900 A70-41536

Mineralogy and petrology of lunar rock samples indicating meteoritic increments

21 p3900 A70-41539

Apollo 11 lunar basalt petrogenesis, examining internal constitution and origin by high pressure

21 p3901 A70-41547

Lunar petrology of silicate melt inclusions from Apollo 11 rock samples, discussing heating experiments

21 p3902 A70-41548

Apollo 11 lunar igneous rock mineralogy and petrology, emphasizing ferrobasalt minerals microanalysis electron probe

21 p3903 A70-41557

Apollo 11 lunar basalt chemical composition and petrogenesis, using stable isotope dilution method

21 p3907 A70-41573

Crystalline rocks from Mare Tranquillitatis and Oceanus Procellarum, determining K-Ar ages

23 p4238 A70-43803

Terrestrial and synthetic lunar igneous rocks thermal conductivities in melting range, discussing thermal gradient

23 p4238 A70-43804

Apollo 11 ilmenite basalts petrology from regolith samples

23 p4239 A70-43898

Borgo San Donino chondrite petrology and mineralogical and chemical composition, considering texture and recrystallization features

24 p4411 A70-45791

PFM (MODULATION)

U PULSE FREQUENCY MODULATION

PM

Acidosis effects on anoxic rat heart cardiac performance and anaerobic energy generation

04 p0635 A70-15461

Potentiometric analysis for determining acidity and alkalinity in dark mineral oils with additives

05 p0810 A70-15898

PH variation effect on sea water on stress corrosion cracking behavior of Ti alloys

13 p2435 A70-29174

Corrosion and stress corrosion behavior comparison of aged Al-Zn-Mg alloy in aqueous chloride solution, discussing pH variation effect

18 p3271 A70-36028

Microbial existence limits in hot springs at varying temperature and pH characteristics

22 p3970 A70-42956

Blood oxygen, carbon dioxide and pN during hypothermia induced by He-oxygen mixture and cold exposure in hamsters, comparing with hibernation state

23 p4147 A70-44787

PH FACTOR

Acid base responses of arterial plasma of anesthetized man during acute carbon dioxide partial pressure changes, discussing anesthesia effects

01 p0020 A70-10651

H ion increased activity effect on sodium transport across short circuited turtle bladder

02 p0234 A70-11730

Blood pH effects on adrenomedullary response to hemorrhage, studying catecholamines release in anesthetized dogs

02 p0235 A70-11733

Arterial pH change effects on circulation and oxygen consumption in dogs, discussing respiratory acidosis heart rate, cardiac output and arterial blood pressure

17 p3024 A70-34593

PHARMACOLOGY

Pharmacology for long term manned space
04 p0629 A70-14566

PHARYNX

Electroencephalographic study of flying personnel utilizing nasopharyngeal electrodes to determine neurological disorders
06 p1000 A70-17302

PHASE ANGLE

U PHASE SHIFT

PHASE CHANGES

U PHASE TRANSFORMATIONS

PHASE COHERENCE

White noise and nonlinear effects in telemetry RF links, analyzing received process to phase coherent receiver
08 p1460 A70-20823

Holographic technique of coherent light field transformation with desirable phase distribution from laser light beams of arbitrary wavefront characteristics
08 p1497 A70-21410

Phase noise and cycle slip optimization of steady state digital data transition tracking loop used as bit synchronizer in phase-coherent receiver
11 p2024 A70-26202

Cardiac and respiratory cycles phase coincidence detection device, making photographic plates under physiological conditions
14 p2541 A70-30381

Alpha rhythm phase coherence during photic blocking, examining pacemaker model
19 p3368 A70-37811

Current-phase relationship in short superconducting weak links, using one dimensional model
24 p4389 A70-45224

PHASE CONTRAST

Object visualization in phase contrast using non-linear interferential holography by successive recording of intensities on photographic plate
05 p0848 A70-16273

Scattered field amplitude and phase determined from hologram light intensity distribution, noting biological applications
08 p1500 A70-21786

Comparator for measuring relative phase difference between identical frequency signals within microwave octave band
09 p1647 A70-22715

Phase meter for measuring angular coordinates of reflecting meteor trails
19 p3526 A70-38777

PHASE CONTROL

Radiation patterns containing multiple beams generated by aperture phase control
01 p0050 A70-10462

Minimum time frequency transitions in phase locked loops with phase and frequency controls using Pontryagin principle, obtaining switchless control strategies
04 p0652 A70-15339

Lateralization and detection of signals under antiphasic noise masking measured at various SNR levels
06 p1106 A70-17597

Constraint optimization on phase coordinates and controls noting extension to functional spaces
07 p1330 A70-18683

Optimal nonparametric amplitude and phase methods for synthesizing signal detection systems invariant to noise distribution and noise-signal combination
07 p1226 A70-18684

Discrete diode phase inverter for meter wavelengths providing north-south antenna control of radio telescope by diffraction method
08 p1473 A70-21064

Cross type radio telescope beam forming and steering system, describing switched delay lines and phasing circuits
08 p1477 A70-21823

Parabolic reflectors profile error compensation by means of multielement feed array with controllable phasing
09 p1644 A70-22236

Automatic phase correction for modulated subcarrier microwave systems used for control of industrial processes
09 p1632 A70-22281

TDMA system control, considering access process control and switching process control, discussing burst transmission phase control and channel selection at receiving end
10 p1839 A70-24366

Switched self balancing comparison radiometer with coupling between channels, showing measurement errors due to coupling correctable by phase switching
11 p2018 A70-26269

Atomic frequency standards for phase calibration of large aerial arrays applied to radiotelegraph
11 p2019 A70-26300

Optimal phase-manipulated signals synthesis from autocorrelation function using algorithm
11 p2012 A70-26804

Optimization for control processes with first and higher order constraints on phase coordinates
12 p2205 A70-28195

Automatic phase control of demodulating signal in one dimensional extremal system with harmonic tracking oscillations
12 p2205 A70-28338

Computer modeling of nonlinear phase automatic frequency control systems under noise and oscillating disturbance
13 p2383 A70-29303

Noise effect on single band modulation receiver using phase automatic frequency control for carrier wave at arbitrary SNR
13 p2370 A70-29739

Statistical output characteristics of harmonic cosine and sinusoidal inertialess phase periodic converters in two channel system with frequency multiplication
13 p2370 A70-29741

Transfer properties of scanning phase discriminator with intermediate storage, explaining sampling method and sample-hold-sample circuit
15 p2714 A70-32672

Phase control of locked negative resistance /Gunn/ oscillator under operational conditions, noting coupled varactor diode use
17 p3055 A70-35630

Soviet book on dynamic systems with cylindrical phase space covering differential equations with angular coordinates, parameter estimation, multidimensional and discontinuous systems, pendulums, etc
19 p3470 A70-37468

Second order automatic phase control system with proportionately integrating filter, calculating transient response by harmonic linearization method
20 p3584 A70-39253

Digital frequency and phase flip-flop comparator for slave oscillators fine control by master frequency
22 p3996 A70-42819

Harmonic linearization method application to automatic phase control system with periodic nonlinearities
22 p4002 A70-42840

Amplitude-phase characteristics of relay slave mechanisms with AC and DC motors under dynamic braking, using harmonic linearization
22 p4002 A70-42842

Optimization for control processes with first and higher order constraints on phase coordinates
22 p4004 A70-43320

Linear systems with phase coordinates bounded by given time functions, obtaining optimal control by iterative solution involving Lagrange multipliers
23 p4177 A70-44302

PHASE DEMODULATORS

Phase feedback demodulation technique to analyze telemetry performance degradation caused by voice interference in modes of Apollo communication system, providing linear detection scheme
04 p0648 A70-14660

Carrier recovery circuits synchronization for PSK demodulators used in TDMA satellite communication
10 p1835 A70-24338

PHASE DETECTORS

Phase detector with two value output and pulsed input for measurement and control circuits, noting construction with semiconductor elements
02 p0266 A70-11900

AFC by digital phase lock loop consisting of zone error detector with phase quantizing circuit and discrete frequency regulator with reversible counter
02 p0258 A70-12542

M-type transmission line with cyclotron waves to achieve phase inverter and delay line operation, showing phase sensitivity to magnetic field changes near cyclotron resonance
03 p0447 A70-13292

Linear phase detection using FM demodulation for Apollo S band communication system eliminating baseband voice interference with telemetry
04 p0648 A70-14659

Backscatter radar signal phase determination from amplitude data, measuring phase and amplitude in laboratory
05 p0815 A70-16507

Turbine blade vibration measurement by contactless discrete-phase method, discussing sensor positioning for displacement amplitudes and flutter speeds determination
09 p1681 A70-23199

Weak phase objects detection based on interferential and streak photography methods, noting fringe deformation role
10 p1916 A70-24587

LF signals phase determination during solar eclipse of 22 September 1968, noting frequency shift magnitude
14 p2547 A70-30238

Modulation method for phase detection in electro-optical light modulator of optical range finder
16 p2914 A70-34213

Pulse superposition measurements of small ultrasonic waves velocity changes using automatic recording phase sensitive detection
21 p3827 A70-41468

PHASE DIAGRAMS

LF signals phase determination during solar eclipse of 22 September 1968, noting frequency shift magnitude
24 p4316 A70-46313

PHASE DEVIATION

Earth space signal propagation characteristics obtained by satellite-borne radio interferometer provide phase information in addition to amplitude for improving navigation accuracy
02 p0260 A70-12567

Phase distortion and Faraday rotation of wideband radio waves propagating through ionosphere
03 p0449 A70-13584

Interferograms taken by phase difference amplification technique with nonlinear hologram, considering amplified image accuracy
08 p1500 A70-21788

Nonlinear phase distortion measurement in microwave limiters under dynamic conditions using two tone test signal
09 p1647 A70-22714

Roof prism reversing-front Michelson interferometer for phase correlation measurements in turbulent atmosphere
09 p1684 A70-23535

Atmospherically induced phase fluctuations for various path lengths using near ground horizontal Mach-Zehnder, discussing turbulence effects
10 p1916 A70-24413

Holographic compensation for atmospherically induced phase distortion of IR laser beam
11 p2049 A70-25638

Periodic high temperature effects on human systolic phase dynamics
12 p2174 A70-28359

Obliquely incident spherical wave amplitude and phase fluctuations, deriving formulae to compare variances behavior for refractive index fluctuation autocorrelation functions
14 p2574 A70-30750

Asymmetrical transient attenuation effects of bridge circuit phase discriminator on accuracy of phase difference measurements
15 p2707 A70-31508

Sudden phase anomaly /SPA/ in VLF radio wave propagation during Proton Flare Project, noting corresponding solar X-ray flux intensity enhancement
15 p2794 A70-32294

Polar cap disturbance of 7 June 1969 due to small proton enhancement, describing detection by transpolar VLF phase measurement
15 p2794 A70-32295

Negative sudden phase anomaly /SPA/ in VLF radio transmission, noting solar X ray flux intensity and zenith angle effects
15 p2699 A70-32297

Multiple sensor arrays phase difference estimation, assuming Gaussian signal and noise statistics
16 p2866 A70-34064

Nonlinear dynamic systems phase coordinate variations statistical characteristics, describing data reduction method
20 p3674 A70-40183

Image holography nonlinearities analysis, using photographic film characteristics for phase deviation enhancement
22 p4031 A70-42951

Lissajous figures for phase response of N-path signal filter transfer functions, using switched modulators
22 p3998 A70-43256

VLF phase disturbances, HF absorption and solar protons in 1967 PCA events, using ionization model
24 p4314 A70-46128

PHASE DIAGRAMS

Phase diagrams for binary mixtures at high pressures suggesting layered structures existence in Jupiter and Saturn atmospheres resulting from phase separations in hydrogen-helium mixture
02 p0368 A70-11819

Refractory metal-oxygen systems phases and phase relations
02 p0318 A70-12640

Two phase theory of ordered to disordered state transition in ternary alloys with fcc lattice, constructing phase diagrams
03 p0505 A70-13103

Microdeformation resistance in Ni alloys with ordered phase diagrams related to strain level, analyzing Bauschinger effect
03 p0505 A70-13106

Neutron bombardment effect on ordering and disordering state of alloys phase diagrams, noting temperature dependence
03 p0506 A70-13107

Ti-Al-V alloys after annealing investigated for equilibrium diagram at high temperatures
04 p0708 A70-15313

Ternary Ti-Al-Mo part phase diagrams constructed from Mo corner to plane titanium aluminate, including isothermal phase diagram for 600 C
05 p0864 A70-16548

Phase equilibria, crystallization and solidus surface in transition conode triangle of ternary system Mo-Ti-C at high temperatures
07 p1310 A70-19804

Carbide layer formation on Ta and Ta-W alloys, discussing Ta-C phase diagram and phases 07 p1320 A70-19892

Knudsen effusion cells high temperature uses, discussing binary alloys phase boundary determination and volume and surface diffusion studies 07 p1424 A70-19900

Phase equilibrium and homogeneity regions of solid solutions system Ni-Nb-O at elevated temperature 07 p1315 A70-20313

Ce-Ni-Si system X ray and microstructural analysis, constructing phase diagram for Ce contents of 0-33.3 wt percent 08 p1555 A70-21115

Phase diagram of dysprosium oxide-chromium oxide system constructed by microstructural analysis in 1600-2400 C range in argon atmosphere 08 p1556 A70-21118

Phase diagram of Nd-Rh system determined by powder X ray diffraction, metallography and differential thermal analysis methods 08 p1522 A70-21711

Phase diagrams of metal systems - U.S.S.R. Conference, Moscow, June 1967 09 p1702 A70-22559

Melting diagram for five element Mo-W-Nb-Ta-V system constructed by optimal projections from known composition-property relations for corresponding ternary systems with common components 09 p1702 A70-22561

Vacuum melting and heat treating equipment for high melting point metals from phase equilibria studies viewpoint 09 p1655 A70-22562

Diffusion layer correspondence to phase diagram in terms of constituent phases and composition 09 p1702 A70-22563

Binary and ternary systems phase diagrams construction by diffusion layer method and X ray analysis, studying concentration dependence of diffusion coefficient 09 p1703 A70-22564

Mechanical and physical properties of Nb-Ti binary annealed alloys as function of compound NbTi using microscopic and X ray phase analysis 09 p1704 A70-22755

Ordered Ni8Ta phase in nickel-rich binary alloy using electron microscopy and diffraction analysis 09 p1705 A70-22808

Alkali-alkaline earth niobates phase equilibrium study revealing tetragonal tungsten bronze-type solid solutions existence range 09 p1740 A70-22983

Phase diagram of rapidly crystallized Al-Cu-Mn alloys, observing ternary solid solutions formation during high cooling rate of melt 09 p1709 A70-23786

Phase diagram of Ti-Ta-Cr system, plotting isothermal and polythermal sections by microstructural and X ray analysis 09 p1709 A70-23787

Phase diagram of Ti-Ta-V system, determining solubility of sigma Ta and V in alpha and beta Ti in solid solutions 09 p1709 A70-23788

Phase equilibrium diagram and heat resistance of Ti-Al-Nb alloys along radial section by thermal and microstructural analysis 09 p1709 A70-23789

Fuel cells phase equilibria between carbonate melt and Li, Na and K solid aluminate electrolytes, analyzing thermal and electrical conductances 10 p1830 A70-24458

Electrochemically optimal structure for Raney alloy catalysts based on molecular hydrogen polarization temperature, noting beta and gamma phases and particle size influence 10 p1831 A70-24468

Enthalpy-entropy, enthalpy-pressure and composition diagrams of fluorine-hydrogen system, noting possible applications to rocket propulsion systems 10 p1929 A70-25100

Ternary metastable phase diagram for W-Ti-B system at room temperature 10 p1905 A70-25226

Ni-Nb-O system state diagram by reduction equilibria and X ray analysis, discussing oxidation resistance based on metal surface protective layers makeup 12 p2253 A70-27158

Ternary phase diagrams and quaternary excess free energy prediction using binary data, applied to Pb-Sn-Zn, Ag-Pd-Cu and Pb-Sn-Cd-Bi systems 12 p2254 A70-27475

Cu-Fe-Ti ternary system via microscopic, X ray and thermal analyses, measuring microhardness, electrical resistivity and magnetometry 13 p2433 A70-28863

Soviet monograph on V and W alloys covering phase diagrams, mechanical, chemical and physical properties, compounds and chemical composition 14 p2595 A70-30627

Binary Co-In system thermal analysis, X ray diffraction and microscopy, discussing phase diagram 14 p2595 A70-30838

Be-Al-Ti system liquidus surfaces and invariant equilibria by chemical, thermal, X ray and microscopic methods, discussing phase diagrams 14 p2595 A70-30839

High temperature solid-solid reactions and solid-liquid or condensed phase-gas equilibria, using solar furnace 14 p2545 A70-30907

Ternary phase diagram of liquid epitaxially grown gallium arsenide antimonide, considering use as high quantum efficiency long wavelength photoemitter 15 p2782 A70-31758

Fe-Ni-P phase diagrams for high temperatures, providing phase equilibria data for Widmanstätten pattern in iron meteorites 15 p2762 A70-32391

Ti-Cu-Ag phase diagrams and liquidus surface structure, using metallographic, thermal and X ray techniques 16 p2931 A70-33221

Magnetic phase diagram of hydrated cesium-copper carbide at 1.625 Neel temperature in external magnetic fields, giving equation for spin flop field temperature dependence 16 p2961 A70-33688

Titanium base binary systems phase diagrams, describing component activity and compound phases heat of formation 17 p3114 A70-34379

Ti interaction with elements of periodic systems, considering binary system phase diagrams 17 p3115 A70-34384

Phase transformations and equilibrium diagram of titanium-oxygen alloys, using electron and optical metallography 17 p3119 A70-34413

Phase diagrams of high strength metastable Ti beta alloys, showing minimum quantity of alloying elements for solid solution retention 17 p3119 A70-34418

Cr-Ni system activities and phase boundaries determined by solid electrolyte technique 18 p3273 A70-36040

Ni-Al-Nb superalloy, determining temperature effect on phase relationships in Ni-rich portion of phase diagram 18 p3273 A70-36041

Isothermal phase equilibria in Ti rich ternary Ti-Al-Fe alloys, noting eutectoidal transformation 18 p3275 A70-36123

Polythermal phase equilibrium and heat resistance of Ti-rich Ti-Zr-Al alloys, noting creep and tensile tests 18 p3275 A70-36124

Cross sectional phase diagram of Nb-Ti-Mo-V, discussing continuous crystallization and composition dependent hardness and resistance 18 p3275 A70-36125

Electron microscopic investigation of alpha-epsilon phase transformations in Co-Ni alloys above and under phase equilibrium temperature 18 p3276 A70-36205

Interferometric holograms of vibrating body via numerical analysis of oscillations amplitude and phases 18 p3258 A70-36303

Nb-Sn superconductors multiphase structure with three intermetallic phase, constructing diagram based on phase stability and composition 18 p3299 A70-37221

Phase equilibrium of Fe-rich Fe-Al alloys using single crystal X ray diffraction 19 p3452 A70-37838

Mo-Si system phase diagram by X ray, microstructural and thermal differential analyses, identifying eutectic, peritectic and eutectoid equilibria 20 p3649 A70-39773

Ni-Nb-Mo, Ni-Nb and Ni-Mo alloys phase equilibrium 21 p3840 A70-41898

Cd-Se and Cd-Te systems phase diagrams based on regular solutions theory, discussing molecular interaction energy dependence on composition 22 p4085 A70-42678

Phase relations in system Ag-Fe-S in 700-1200 C range at various vapor pressures by quenching and differential thermal analysis, observing liquid-immiscibility fields 22 p4053 A70-42732

Phase diagrams and nonvariant equilibria points of Ti-Si alloys subjected to prior annealing, determining phase transformations, decomposition and other properties as function of temperature 22 p4057 A70-43350

Thermodynamics and statistical physics of dense plasma with particle interaction energy exceeding kinetic energy, discussing three-component model phase equilibrium 23 p4229 A70-45073

Ni-Nb-W and Ni-W alloys phase equilibrium, obtaining diagrams from analysis of liquid and solid phases separated electromagnetically before tempering 24 p4359 A70-45372

Phase equilibria, hardness and electroresistivity of Ti-Al-V alloys at solid compound section for reinforced metal composites 24 p4361 A70-45831

Phase regions and lattice parameters of isothermal section of Mo-Zr-Cr system at 1100 C from microstructural and X ray analyses 24 p4361 A70-45832

Al-Zn-Mg alloy prolonged aging behavior, examining Gp and intermediate zones, equilibrium phases, maximum strength and serrated stress strain curve 24 p4362 A70-46189

Fe-Ni-Mn ternary martensitic alloy, discussing metastable miscibility gap island existence in bcc phase 24 p4363 A70-46193

PHASE ERROR

Rapid fading intensity distribution formula for analysis of aperture phase and amplitude errors influence on antenna arrays directional characteristics 03 p0456 A70-13463

Statistical characteristics of field of linear antenna with square phase characteristics, deriving formulas for presence of amplitude phase errors 05 p0820 A70-16255

Radar coherent linear FM microwave generation with 14 microsecond pulse length and 1000 MHz bandwidth, discussing phase error and coherency 07 p1236 A70-20064

Large-base radio interferometer with separate heterodyne receivers and electrical length automatic control, studying causes of phase errors 09 p1650 A70-23631

Line source antenna arrays containing random dissimilarities in waveguide cross section analyzed for phase errors to determine sidelobe deterioration 11 p2018 A70-26177

Stationary phase error variance for second order phase locked loop for low signal to noise ratios 13 p2383 A70-29590

Phase errors of hydraulic input impedance of arterial bed due to proximal or distal pressure measurements 15 p2682 A70-31940

Asymmetric phase error in antenna circular apertures, emphasizing beam squint resulting from distortion of paraboloidal reflector 16 p2859 A70-32942

Amplitude distribution selection in antenna aperture in presence of phase amplitude errors from relation between sidelobe level probabilistic and phase amplitude errors characteristics 16 p2873 A70-33241

Experimental model for random phase errors caused by surface irregularities in paraboloid reflector antennas 19 p3388 A70-37927

Synthetic aperture terrain-imaging radar systems, calculating tropospheric turbulence induced phase errors for comparison with microwave propagation experiment 22 p3991 A70-43579

Microwave transmission over elevated line-of-sight path, measuring phase front distortion between pairs of paths 22 p3991 A70-43580

Resolution limits and corresponding linear antenna apertures in presence of propagation phase errors, considering pattern angle 22 p3991 A70-43581

Phase and tracking errors due to mutual scattering in phase monopulse phase-scanned antenna 24 p4315 A70-46135

PHASE LOCK DEMODULATORS

Threshold extension techniques using impulse noise detection and elimination implemented at phase lock loop demodulator output 08 p1460 A70-20811

Delta modulation threshold extension technique for phase lock loop FM demodulator 15 p2703 A70-32559

Phase lock loop acquisition and tracking of carrier frequency modulated by single sinusoid, obtaining parameter values through mathematical model and digital simulation 15 p2703 A70-32578

Angle modulated carrier acquisition and demodulation, developing baseband model for behavior of output signal from phase lock loop 16 p2864 A70-33481

Threshold extension capabilities of phase lock loop and FM feedback demodulators, calculating output SNR for broadband systems 18 p3229 A70-36784

Recursive differential equation for moments of time-to-cycle slip in first and second order phase lock loops 21 p3802 A70-41350

Coherent receiver as hybrid carrier tracking loop consisting of standard phase locked and modified Costas loop 21 p3802 A70-41351

PHASE LOCKED SYSTEMS

AFC by digital phase lock loop consisting of zone error detector with phase quantizing circuit and discrete frequency regulator with reversible counter 02 p0258 A70-12542

Phase lock loop circuit for spacecraft communication noise filtration, describing linear study of first-order loops 03 p0448 A70-13537

GaAs microwave diode Gunn oscillator subharmonically injection phase locked at low frequency ratios 03 p0459 A70-14041

Minimum time frequency transitions in phase locked loops with phase and frequency controls using Pontryagin principle, obtaining switchless control strategies 04 p0652 A70-15339

Microelectronic L-band phase-lock loop receiver for data transmission between earth stations and satellites 06 p1017 A70-17338

Optimum signals for phase locked or delay locked loops determined as function of signal to noise ratio 06 p1023 A70-17523

Phase locked loop method for waveshaping rectangular wave frequency modulation signals in phase coherent VLF-FSK systems, reducing transient effects and adjacent channel interference 08 p1459 A70-20803

SHF avalanche transit time oscillator with FM noise reduction by injection phase locking 08 p1462 A70-21594

Tunnel diode parametric phase locked oscillators as memory elements, considering optimum subharmonic pumping frequencies determination 08 p1477 A70-21642

Laser frequency measurement and active and passive stabilization techniques, emphasizing HCN laser phase locking to frequency standard output 09 p1697 A70-22951

Atmospheric phase jitter for He-Ne locked laser measured by retroreflector for half mile round trip 09 p1699 A70-23539

Digital sampled-data loop of phase lock control containing digital zone error detector and digital frequency regulator with reversible counter as memory unit 10 p1833 A70-24085

Digital controlled phase-locked loop in burst mode operation, comparing recovery characteristics with carrier and bit-timing recovery techniques based on statistical analysis 10 p1835 A70-24333

Nomograms simplifying noise and natural loop bandwidths calculation for phase locked loop receiver, determining limiter suppression factor 10 p1844 A70-25244

Absolute frequency wideband high resolution determination, using frequency synthesizer as phase locked loop local oscillator 10 p1854 A70-25316

Signal frequency capture probability vs frequency search rates and AFC loop parameters determined in phase locked oscillator 11 p1996 A70-25349

Nonlinear phase locked loops compared with linear loops in communication and navigation, considering interference vulnerability 12 p2187 A70-27909

HCN laser 890 GHz line phase locked to multiplied standard frequency with wide bandwidth loop, narrowing line widths 13 p2426 A70-28798

HCN laser far IR line phase locked to absolute frequency standard 13 p2426 A70-28810

Carrier synchronization system for PSK signals, using direct regenerative repeater and phase locked loop/DR-PLL/ 15 p2697 A70-31826

Phase locked loop damping characteristics optimization based on input rms error rate minimization and transient error integral square value limitation 15 p2704 A70-32604

CW argon lasers simultaneous mode selection and phase locking by electro-optic KDDP crystals 15 p2753 A70-32610

Model probability distribution for hybrid phase locked loop derived by Fokker-Planck techniques, providing superior performance for all SNR 16 p2882 A70-33038

Cycle slipping rate in first order phase locked loop, extending Viterbi analysis 16 p2865 A70-34058

Gas laser phase locking due to loss modulation with double mode spacing 17 p3107 A70-35474

Internally loss modulated multimode ring gas laser, showing pulse peak intensity with detuning for phase locking 17 p3107 A70-35475

Phase locked automatic frequency control system, estimating duration of stabilization by theory Markov processes 18 p3228 A70-36625

Fundamental microwave oscillator subharmonic phase locking for stable power, comparing with varactor frequency multipliers 19 p3386 A70-37689

Optimum stabilized variable frequency multiple input phase locked oscillator in mutually synchronized systems 19 p3389 A70-37969

Injection locked bilateral microwave oscillators, deriving criterion for preventing reverse locking 20 p3597 A70-39470

Signal frequency capture probability vs frequency search rates and AFC loop parameters determined in phase locked oscillator 20 p3589 A70-40461

Digital bit synchronization phase locked loop steady state and transient performance in white Gaussian noise 21 p3802 A70-41352

Dynamic noise performance equivalence of phase locked or double superheterodyne tracking loops, using noise free external generator 21 p3793 A70-42180

Transient behavior of first order phase locked loop in presence of noise, solving Fokker-Planck equation for loop dynamics by numerical integration 21 p3802 A70-42181

Phase locked solid state laser with picosecond pulses applied to high speed cinematography [SMPTE PREPRINT 22] 22 p4034 A70-43051

Phase locked AFC circuit, calculating internal harmonic noise reduction by proportionately integrating filter 23 p4161 A70-43960

High stability phase locked Gunn microwave oscillator with internal crystal reference, discussing applications as signal generator, low noise Doppler radar sources, etc 23 p4172 A70-44013

Microelectronic phase lock microwave receiver packaging, discussing subassemblies interconnection minimization, shielding, RF interference, low loss and testing problems 23 p4164 A70-44536

Metal sheets thickness measurement and monitoring by through-transmission eddy current nondestructive testing, using phase locked amplifier 24 p4344 A70-45699

PHASE MODULATION

NT FM/PM [MODULATION]

NT PHASE SHIFT KEYING

Zero crossings of signal harmonic function with normal phase distribution, deriving relations with spectrum and modulating process parameters 03 p0447 A70-13289

Spectrum parameters analysis of signal in form of radio pulses sequence with harmonic angular modulation 03 p0448 A70-13511

PCM signal transmission testing over radio links with two level phase modulation 03 p0452 A70-14282

Half octave bandwidth traveling wave X band optical phase modulator, noting multiple interactions of optical and microwave fields in electro-optical crystal 06 p1079 A70-17192

Two cavity mode locking of He-Ne laser using electro-optic phase modulator 06 p1083 A70-17947

Electromagnetic waves phase modulation index during propagation in nonlinear media found dependent on mismatch between interacting waves group velocities, relaxation time and losses 07 p1227 A70-18763

Equivalent scheme for tunnel diode oscillator operating mode and parameters effect on LF modulating signal phase correlations 07 p1241 A70-19287

Phase and amplitude modulated signals transmission over band limited channel disturbed by additive white Gaussian noise 07 p1237 A70-20195

Millimeter guided wave communication systems information transmission capacity increase, using quaternary and higher order modulation techniques 08 p1462 A70-21506

Correlation function of oscillation modulated in amplitude, phase and frequency by random processes causing spectral density maximum shift away from carrier frequency 09 p1633 A70-22409

Pulse train transition in Nd-YAG and He-Ne lasers mode-locked by intracavity phase modulator 09 p1697 A70-22919

Digital satellite communication system using multiphase modulation optimized for phase positions number to maximize transmission capacity 10 p1835 A70-24334

Digital transmission techniques optimal utilization of assigned frequency spectrum for phase modulation of frequency carriers 10 p1839 A70-24365

Circuitry for phase modulated synchronized electronic oscillators for measuring minor reactance changes during remote sensing 11 p2052 A70-26373

Biased measurement of angular coordinates of phase modulated signals under meter input quantization 11 p2012 A70-26806

Phased array radar for automatic random search using pseudorandom sequences to generate random phase characteristics of currents together with suitable gating 12 p2183 A70-26984

Transient processes in n-stage aperiodic amplifier during instantaneous change in phase and amplitude of emf at input 12 p2195 A70-27536

Amplitude and phase fluctuations in laser with non-linear absorption due to spontaneous emission, studying lasing instability near hysteresis threshold 12 p2248 A70-27548

Optical processing for measuring frequency spectrum of PM wave induced by turbulent medium in laser beam 12 p2249 A70-27756

Phase modulated laser light beam statistical analysis, using Michelson interferometer with piezoelectric crystal driven mirror connected to Gaussian random noise generator 12 p2249 A70-27877

Radar transmitter waveforms for multifunction operation, emphasizing phase and frequency modulation for CW radars 12 p2188 A70-27939

High speed linear phase and amplitude modulation of X band Gunn oscillators 12 p2199 A70-28016

Output correlation function of nonlinearity-filter system and phase modulated oscillations influence on system 13 p2366 A70-29411

Amplitude and phase modulation of laser beams by tetragonal crystal cuts 13 p2429 A70-29533

Quasi-optimal sequential detection of phase modulated signal of varying frequency on white noise background, using Markov theory 13 p2369 A70-29732

Thermally self induced laser beam phase modulation resulting in far field aberrational rings, describing structure and profile 13 p2431 A70-29834

Modulation phase distribution over emitting surface of p-n junction GaAs laser at micron wavelength 13 p2431 A70-29866

Phase modulated optical range finder with RF coaxial delay line 13 p2412 A70-29872

Frequency conversion during multiple phase modulation of supply voltage by pulse width technique 14 p2548 A70-30372

Hard limiting bandpass limiter output signal to noise ratio in PM signal detection calculated using probability density function 14 p2552 A70-31194

Phase modulated holography for inherent noise reduction using thicker recording media, increasing signal beamwidth or beam ratio 16 p2904 A70-33137

Optical spatial phase modulator array using membrane light modulator for coherent optical processing and character recognition 16 p2904 A70-33147

Holographic stereo model, comparing stereoscopic perception of phase and amplitude to model consisting of overlapping photos 16 p2908 A70-33228

Self phase modulation of stimulated Raman light in carbon disulfide, discussing Stokes and anti-Stokes spectrum regions 18 p2366 A70-36422

Noise rejection characteristics of ionospheric radioesondes via phase-code modulated signals, noting nonoptimal filter role in power loss 18 p3229 A70-37042

Electromagnetic waves phase modulation index during propagation in nonlinear media found dependent on mismatch between interacting waves group velocities, relaxation time and losses 18 p3229 A70-37107

Cosmic ray anisotropy sidereal-diurnal effects isolation by solving simultaneous amplitude and phase modulation problem 20 p3696 A70-39282

Active filter operation, examining angle modulated signal at input by various approximation methods 22 p3997 A70-43130

Crosstalk error in binary phase modulated communications systems due to RFI and thermal noise 23 p4158 A70-43752

Power spectrum of digital signals pulse modulated with random sequences, discussing phase modulation and z transform techniques 24 p4315 A70-46151

PHASE SHIFT

Matrix method applied to achromatic linear phase plates design for polychromatic Ar lasers half wave phase shift 01 p0113 A70-10988

Phase fluctuations measurements of obliquely incident signal reflected from ionosphere performed over distance of 1300 km, showing amplitude dependence

01 p0046 A70-11533

Quadruple microwave probe applied to phase and attenuation variations measurements of HF wave propagating through dielectric media

02 p0345 A70-11898

Dispersive Doppler shift and Faraday rotation second order theory for curved earth-ionosphere geometry, calculating phase path differences

02 p0260 A70-12574

Spectral polarization characteristics phase variations used for classifying lunar surface features

03 p0565 A70-13234

O-C diagrams of RR Lyrae variables in M5, considering representation by parabolas or intersecting straight lines

03 p0567 A70-13321

Reduced multiport equivalent scattering parameters derivation by matrix method, determining load reflection coefficients effect on signal attenuation and phase shift

03 p0458 A70-14038

Holographic technique for transferring phase perturbation of subject waves onto spherical waves focusable through aperture and examinable by interferometric and schlieren methods

04 p0691 A70-15034

VLF phase disturbances and HF absorption during solar proton events of 28 August and 2 September 1966 related to proton intensities, energies and cut-off latitudes

04 p0741 A70-15124

Phase and amplitude level of plane light wave propagation in medium with randomly discontinuous refractive index, discussing wave phase dependence on dielectric constant

04 p0650 A70-15288

Lunar tides in midday critical frequency of F2 layer, determining phase reversal location

04 p0651 A70-15309

Diurnal cosmic ray intensity variations first and second harmonics amplitudes during sudden phase variations diagrammed from neutron monitor data during IGY

05 p0898 A70-15936

Electromagnetic wave phase characteristics after free space passage through statistical medium with wave disturbance producing density and ionization

05 p0815 A70-16735

Leading edge phase shift of output pulse from threshold-type pulse shaping circuit determined as function of triggering threshold

06 p1009 A70-17675

Acoustic impedance method for nondestructive testing exploiting phase defect of signal from piezoelectric transducer

06 p1074 A70-18629

Ionospheric data of local and integral electron concentration obtained by measuring phase shift of satellite emitted coherent radio waves

07 p1276 A70-20422

Phase shift effect on astatic gyro axis drift and stability during periodic perturbations, describing motion by nonlinear differential equations

08 p1493 A70-20489

Spectral polarization characteristics phase variations used for classifying lunar surface features

08 p1580 A70-21667

CH, CD and CH ion excited states decay rates determined from phase shift and frequency data, discussing implications for astrophysics

09 p1731 A70-22513

Rectangular waveguides filled with magnetized ferrite with/without dielectric, calculating phase shift and attenuation by Ritz method

09 p1645 A70-22548

Tape recorder performance characteristics relevant to signal types handled, considering phase response and envelope delay

09 p1679 A70-22975

Materials permittivity measurement at millimeter and submillimeter wavelengths based on phase shift or sample optical thickness

09 p1684 A70-23648

Prolonged hypodynamia effect on human cardiac cycle phases using poly- and kinetocardiographic data

10 p1814 A70-24672

SID observed as VLF phase anomalies correlated with solar microwave radio bursts

10 p1933 A70-24816

Microwave phase shifter with rectangular ferrimagnetic toroid in waveguide longitudinal center, discussing impedance matching, phased array applications, etc

10 p1852 A70-24891

Microwave phase shift measurement errors caused by reflections from interference systems elements

10 p1853 A70-25130

Thermal diffusivity of opaque materials by phase shift method, using modulated radiation beam from carbon arc to heat material

11 p2068 A70-25767

Quantum mechanical inverse problem of elastic scattering theory, discussing Hylleraas solution for determining potential energy function from phase shift

12 p2274 A70-26899

Remote sensing of lunar photometric function at small phase angles by Apollo 8 command service module

12 p2297 A70-26926

Phase characteristics of nonperiodic slow EM wave delay structures determined by phase shift measurements

12 p2230 A70-26967

Nonlinear phase shift equation derived from TWT single carrier performance, predicting multicarrier performance of communications satellites

12 p2195 A70-27248

Ionospheric electron content calculations based on satellite measurements of Faraday rotation and phase path length variations

12 p2294 A70-27739

Circular loop antenna with traveling wave current distribution, considering phase change effects on radiation pattern and gain

12 p2198 A70-27965

Radiation patterns of phased array scanning antenna using digital phase shifter, reducing peak sidelobe level

13 p2380 A70-29785

Phase angle gauge measurement of meteor shower radiants, using radar observations of signal scattering in meteor trails

14 p2582 A70-30314

Digital filter facilitating biological data analysis through zero or linear phase shift filtering without distorting time relationship in data

14 p2542 A70-30796

Balloon localization with transponder system, measuring payload distance by phase difference in ground transmitted and received CW signal

14 p2588 A70-31308

Phase shift ultrasonic flowmeter measuring transit time between oppositely propagating waves in blood vessels

15 p2691 A70-31921

Prolonged upper ionospheric observations from Sputnik 3, Transit 4A and Explorer 22 signals Faraday fading and phase shifts, showing electron content dependence on solar activity

15 p2731 A70-32093

Air cell optical phase shifter for holography based on refractive index variation with air pressure

15 p2741 A70-32439

Cepheids nonequilibrium continuous emission at maximum brightness, considering phase shift between radiation intensity and stellar contraction

15 p2802 A70-32483

Vector valued Gaussian random processes with Gaussian measurement noise, estimating phase and time delay parameters by maximum likelihood theory

15 p2704 A70-32593

Annular lasers energy, polarization, radiation loss and frequency characteristics dependence on phase shift due to anisotropic plate introduction

15 p2753 A70-32860

Phase stability measurements at 2695 MHz with radio link interferometer, discussing atmospheric water content effect

16 p2861 A70-32959

Optimum carrier phase delay estimation for one way ranging aircraft navigation, investigating receiver signal processing

16 p2947 A70-33449

Cycle slipping rate in first order phase locked loop, extending Viterbi analysis

16 p2865 A70-34058

Sound wave phase fluctuations from ultrasonic waves traveling through turbulent wakes of circular cylinders and plates, using multichannel pulse height analysis

16 p2839 A70-34086

Ionospheric scatter communications channel phase frequency characteristics measuring method, considering probability density function

18 p3256 A70-36091

Incompressible fluid flow past array of arbitrary profiles vibrating with arbitrary phase shift, taking into account blade displacement and vortex wake effect

18 p3206 A70-36277

Amplitude and phase fluctuations of opposing waves in ring laser with allowance for waves coupling due to backscattering

18 p3267 A70-36618

Phase delay of solid earth tide, minimizing ocean and atmosphere loading by strain seismograph measurement

18 p3255 A70-37077

Bounded electromagnetic wave propagation in randomly inhomogeneous medium, calculating correlation in amplitude and phase fluctuations

19 p3375 A70-37282

Phase shift direct and balance measurement procedures between signals over wide frequency range classified by conversion schemes

19 p3391 A70-38702

Meteor trails angular coordinates, using phase difference in pairs of spaced antennas with unequal base lengths

19 p3433 A70-38789

Mutual synchronization of oscillators at multiple frequencies, analyzing effect of tuning on frequency and phase

20 p3597 A70-39252

Transistor amplifier with back coupled emitter and parallel inductive correction, calculating optimal frequency and phase characteristics under complex load

20 p3598 A70-39790

SHF and EHF waves simultaneous propagation over slant line-of-sight overwater path, comparing phase variations and fading for signal coherence

20 p3588 A70-40301

Strip array excitation by field with large phase shift per period, deriving approximate solution from averaged boundary conditions

21 p3784 A70-40627

Electromagnetic field amplitude and phase scattering diagrams analysis for shape information capacity

21 p3785 A70-40637

Convergent numerical method for principal value integrals in dispersion relations of coupled channel scattering problem involving wave phase shifts

22 p4062 A70-42748

Amplitude and phase frequency characteristics of open and closed multiloop nonlinear automatic control systems by graphical methods

22 p4000 A70-42830

Coherent radar backscatter, calculating autocorrelation and power spectrum of spuri noise from periodic random phase injections for filter design to eliminate noise

22 p3992 A70-43591

S band tunable free running high Q triode oscillator phase and frequency instability measurement based on delay lines applications

23 p4170 A70-43796

Cepheids nonequilibrium continuous emission at maximum brightness, considering phase shift between radiation intensity and stellar contraction

23 p4240 A70-43907

Millimeter band electromagnetic scattering from weakly doped GaAs, calculating reflection coefficient and phase angle

23 p4229 A70-43926

D region LF and VLF sky waves opposite phase perturbation behavior

23 p4162 A70-44006

Varian HA-100 spectrometer eliminating phase change by compensation network in synchronous audio detector reference signals

23 p4199 A70-44949

X band horn antennas precision phase center measurement technique for high resolution system applications

23 p4176 A70-44966

Holographic interferometry of phase object by double exposure method, showing no effect of photographic emulsion compression on order of interference

24 p4334 A70-45368

PHASE SHIFT CIRCUITS

NT CIRCULATORS (PHASE SHIFT CIRCUITS)

Ferrite-type phase shifter production by microstrip technique and integrated microwave system use in Gunn element Doppler radar

01 p0052 A70-11290

Diagram compression by spatiotemporal coding of antenna array fitted with phase shifters

05 p0811 A70-15989

Transversal filters with continuously tapped delay lines, emphasizing synthesis of low pass filter and phase shifter

05 p0822 A70-16652

Radiation patterns of scanning antenna using digital phase shifters to obtain suitable phase distribution to move sidelobes into invisible region

05 p0822 A70-16676

Polarization insensitive phase shifter for phased array antennas, discussing limitations, design optimization and experimental results

06 p1019 A70-17508

Controllable microwave phase shift varactor diode circuit parameters design optimization using digital computer for transmittance matrix coefficients calculation

08 p1474 A70-21230

Slot transmission line applicability to miniature ferrite phase shifter design exploiting elliptically polarized H field existence

08 p1475 A70-21283

Phase interpolation circuits for scanning phased array antennas, using doublers and frequency multipliers

09 p1646 A70-22701

Single bit latching reciprocal ferrite phase shifter design, operation and performance, noting linear phase response and low phase nonreciprocity

10 p1853 A70-25243

C band radar antenna with pencil beam steered in plane by ferrite phase shifters 16 p2875 A70-33394

Artificial pilot phased array /APPA/ for use as multiple narrow beam communication satellite, obtaining beam steering from phase shifter setting 16 p2983 A70-34070

Low pass linear phase active feedback circuit synthesis using distributed RC networks to realize flat magnitude response 19 p3392 A70-37707

Ferrite phase shifter for array antennas, discussing design trends, production, performance characteristics and future developments 19 p3388 A70-37864

Interference-polarization light filter, calculating phase shifter errors effects on transmittance by Poincare sphere method 22 p4072 A70-42505

PHASE SHIFT KEYING

Binary decoding extension to achieve unquantized demodulation performance for nonfading phase shift keyed coherent channel with white Gaussian noise 06 p1008 A70-17525

Random synchronization errors in PN and PSK systems reduce input signal power and introduce additional self noise 07 p1236 A70-20069

PSK demodulation by optimal carrier and bit synchronization methods based on nonlinear filter theory, relating error probability to signal to noise ratios 08 p1458 A70-20795

Error probability upper and lower bounds determined for self synchronized binary PSK communications systems, presenting maximum-likelihood and Monte Carlo computer simulation 08 p1463 A70-21777

Communication satellite PSK modulator-demodulator /modem/ implementation requirements and design for optimal performance 10 p1835 A70-24336

Carrier recovery circuits synchronization for PSK demodulators used in TDMA satellite communication 10 p1835 A70-24338

PSK distortion spectra generated in satellite transponders by interactions of FDMA PSK modulated carriers, developing computer programs for multichannel FDMA PSK modulated systems 10 p1839 A70-24364

Pseudonoise phase shift keying /PN/PSK/ and frequency hopping /PN/FH/ modulation technique for low altitude satellite receiving /VHF/ transmissions [AIAA PAPER 70-496] 11 p1999 A70-25436

Power spectral density and autocorrelation functions of sinusoidal carrier amplitude modulated by split phase PCM and PSK 11 p2008 A70-26203

Performance characteristics of quadriphase PSK communication system with noisy reference signal, formulating error probability 12 p2187 A70-27907

Analog data transmission over PCM telemetry link, comparing noncoherent FSK vs PSK reception performance for waveform error 14 p2552 A70-31187

Carrier synchronization system for PSK signals, using direct regenerative repeater and phase locked loop /DR-PLL/ 15 p2697 A70-31826

Communication satellite UHF link with FSK or PSK modulation, considering coded digital transmissions 16 p2867 A70-34331

PHASE SWITCHING INTERFEROMETERS

Phase switching method application to radio telescopic observations showing increase in reliability of radio source coordinates determination 07 p1240 A70-18909

PHASE TRANSFORMATIONS

NT ARC MELTING

NT BOILING

NT EVAPORATION

NT FILM BOILING

NT FLASHING [VAPORIZING]

NT FREEZING

NT FUSION [MELTING]

NT LEIDENFROST PHENOMENON

NT LIQUEFACTION

NT MELTING

NT NUCLEATE BOILING

NT PROPELLANT EVAPORATION

NT SUBLIMATION

NT TRANSPIRATION

NT VACUUM MELTING

NT VAPORIZING

Glass formation region of chalcogenide semiconductor arsenic triselenide-antimony triselenide system and vitreous-crystalline transformation, investigating electrical and optical properties 01 p0153 A70-10085

Shock wave structure in two phase media with temperature and velocity gradients and possible phase transitions 01 p0060 A70-10147

Second phase formation in Czochralski grown Cr-doped GaAs crystals by metallography, radioactive indicators and X ray analysis 01 p0156 A70-10189

Tungsten effect on phase transformations and carbide reactions to attain equilibrium at 850 C in Ni-base superalloys 01 p0118 A70-10727

Phase changes in Ni/Ti alloys with equiatomic composition, resolving discrepancy on nonMartensitic eutectoidal decomposition of B2 structure and intermediate precipitate 01 p0121 A70-11232

Martensite transformation with fcc lattice in Ti alloys containing 5.9 percent Fe as function of cooling rate, using X ray analysis 01 p0124 A70-11590

Ti-Mn alloy quenched in brine and aged at high temperature studied for structural transformations using electron microscope 01 p0125 A70-11640

Phase equilibria in Mn-S, Mn-Se and MnS-MnSe systems by X ray diffraction after preparation by annealing 02 p0249 A70-11652

Acoustic emission analysis for material evaluation and polymorphic phase transformations characterization for metals and alloys, discussing electronic instrumentation and experimental techniques 02 p0276 A70-12551

Interstitial atoms ordering effects on low and high temperature phase transformations in alloys with bcc lattice 03 p0505 A70-13102

Two phase theory of ordered to disordered state transition in ternary alloys with fcc lattice, constructing phase diagrams 03 p0505 A70-13103

Strain hardening on single crystals of aging Ni-based alloys with ordered separated phase 03 p0505 A70-13104

Austenitic fcc Cr-Mn-N stainless steels ductile-to-brittle transition behavior noting role of deformation faulting 03 p0506 A70-13133

Phase alteration quenching effects in Ni-Mo alloys, discussing high temperature alpha region, isothermal annealing below peritectoid temperature and metastable nickel molybdenide phase 03 p0508 A70-13143

Ni-Nb intermetallic compound precipitation effect on various phase formations in strained samples of Alloy 718 /wrought Ni base alloy/ 03 p0511 A70-13568

Al and Ti single additions effects on recrystallization of Ni-Cr alloys, noting phase transformation and hardness variations 03 p0513 A70-14300

Extension characteristics of delta and sigma related phases in Mo-Ni ternary systems and evaluation of unit cell dimension variations on alloying 04 p0704 A70-14392

External optical phonon modes in ammonium and deuterammonium halides phase transitions as function of temperature, using IR and Raman spectra 04 p0646 A70-14695

Pressure-volume-temperature measurements on H, calculating fugacity coefficients 04 p0719 A70-15057

Niobium addition effect on alpha-gamma transformation temperature during continuous cooling of low carbon Ni-Cu steel 04 p0706 A70-15134

Ductile-brittle transition temperature relation with grain size in polycrystalline Mo as function of annealing temperature 05 p0862 A70-15907

Two phase transitions existence in Hubbard model of interacting electrons using one particle Green function solution 05 p0884 A70-16099

Dilatometric diagrams of phase transformations at low temperatures in Re steels, studying dilatation coefficient behavior 05 p0862 A70-16201

Sodium-titanium-boron-silicate glass opacity and fusibility increase during partial substitution of K for Na, noting phase composition changes 05 p0871 A70-16598

Structures formed during aging of martensite in maraging steels by X ray and chemical analyses using electrolytic isolation of phases 05 p0865 A70-16871

Thermal control of spacecraft via solid-liquid phase change materials [AIAA PAPER 70-12] 06 p1092 A70-18137

Internal friction and shear modulus of Co under dynamic and steady state conditions, discussing peak at alpha-epsilon transition 07 p1306 A70-19073

Multiphase fluid continuum model and hydrothermodynamic equations under phase transformations, including dimensionless and similarity parameters 07 p1254 A70-19085

Alloying elements effect on polymorphic alpha-beta transformation temperature of Ti systems, discussing heat resistance 07 p1307 A70-19555

Dynamic pearlite-austenite transformation and melt temperatures measured in laser-irradiated steel, discussing thermal response as function of heating rate 07 p1301 A70-19897

Molecular dipole moments-electric field interaction induction of cholesteric liquid crystal transition to nematic phase 07 p1225 A70-20053

Stefan problem involving mass transport and phase transformations, presenting solution algorithm 08 p1596 A70-20852

Elastic oscillations amplitude-dependent damping during phase transformations in two phase systems 08 p1556 A70-21121

Quadratic precipitate transformation into orthorhombic phase with conservation of maximal atomic density planes in Ni-Cr-Nb and Ni-Cr-Ta alloys during prolonged reheating 08 p1518 A70-21240

Irreversible phase transition analysis of atmospheric condensation-crystallization processes 08 p1538 A70-21427

Automatic cladding method for submerged arc stainless steel welding, discussing delta ferrite to sigma phase transformation for surfacing with low ferrite stainless steel 08 p1508 A70-21489

Martensitic transformations during quenching and tempering of maraging steels 08 p1520 A70-21495

Temperature dependence of microplastic yield and flow stress and transient creep responses of gamma prime phase 08 p1522 A70-21709

Temperature, transformation and strain rate effects on tensile ductility properties of stable and metastable compositions of austenitic stainless steels 08 p1524 A70-21956

Duplex Fe-Cr-Ni-Ti alloy sigma phase formation mechanism using electron microscope 08 p1525 A70-21958

Sigma and mu phase formations in Ni heat resistant alloys x ray analysis using phase isolation by anodic dissolution 09 p1700 A70-22079

Work strengthening and microstructure of Co-Ni base alloys containing Cr and Mo, discussing deformation induced martensitic transformation 09 p1705 A70-22806

Gamma prime phase structure ordering effect on critical shear stresses of aging Ni-Al alloys and nimonic 09 p1707 A70-23195

Isomorphous beta type Ti-Mo alloy omega phase transformations and morphology by electron microscopy, relating hardness to aging 10 p1902 A70-23817

Transformation kinetics of Ti alloy under isothermal conditions in solution treatment as function of temperature 10 p1903 A70-24025

Elastic stress-strain states in spherical reservoir and thick walled tube during nuclear radiation induced phase transformations 10 p1894 A70-24513

Phase equilibria and maximum melting compositions determinations for compound semiconductors by differential thermal analysis compared with vapor and high pressure techniques 11 p2098 A70-25812

Soviet monograph on intermetallic compounds with Laves phases, covering crystallographic and thermodynamic characteristics of Mg-Zn, Mg-Cu and Mg-Ni systems 12 p2252 A70-26885

Metal-semiconductor transition in magnetite described on band model with electrons breaking symmetry by ordering in self induced Coulomb potential 12 p2283 A70-27239

Low carbon Ni steels isothermal transformation characteristics, observing equiaxed ferrite and Widmanstatten and bainitic structures at various temperatures 12 p2256 A70-27615

Phase equilibria in quasi-ternary alloys by microstructural, thermographic and X ray analyses, showing continuous solid solutions formation in titanium-niobium-titanium aluminide 12 p2258 A70-28275

Phase transformations of molybdenum carbide under elevated temperature in vacuum, using X ray and differential thermographic analysis 13 p2433 A70-28852

Nickel chromite structural changes, thermal conductivity and dilatation during tetragonal-cubic transition, noting phonon-lattice effect 13 p2437 A70-28855

Nonaggressive liquid media effect on residual strains and phase transformations initiation and

PHASE TRANSFORMATIONS

development in polyurethane parts operating in lubricants, discussing wear resistance

13 p2439 A70-29431

Thick plate titanium alloy welds using filler wire to regulate chemical composition and plate phase constitution

13 p2435 A70-29456

Phase transformations in TiNi with equiatomic composition, using internal friction, electrical resistivity and dilatometry

13 p2435 A70-29499

Growth kinetics of strengthening phase during aging of Ni-Cr-W-Mo-Al-Ti alloys, considering gamma prime particles at different Al/Ti ratios

14 p1594 A70-30169

Cobalt surface X ray analysis after spark erosion treatment, revealing phase with high temperature stability

14 p2596 A70-30840

High temperature transformation of high speed steel low temper hardened in vacuum or atmosphere furnace

15 p2756 A70-31568

Niobium carbides formation in Nb containing steels during gamma-alpha transformation, establishing relationship between brittleness and carbide distribution characteristics

15 p2758 A70-32123

Austenite strength effect on austenite-martensite transformation in alloy steels, measuring resistance to plastic deformation

15 p2760 A70-32376

Austenitic stainless steel martensitic transformations, using transmission electron microscopy in conjunction with X ray and magnetization methods

15 p2761 A70-32379

Martensite-to-austenite reverse transformation in Fe-Ni-Co alloys, using dilatometry and coercive force measurements

15 p2761 A70-32386

Uniform bulk magnetization concept in superparamagnets related to physical statistics of magnetic first order phase transitions

15 p2785 A70-32400

Phase transformations in beta isomorphous Ti alloys, discussing effects on omega and alpha phases during quenching and aging and on martensite under stress

15 p2763 A70-32807

Beta phase decomposition kinetics and strain hardening inhibitions in Ti-base Mo alloys, using metallographic, dilatometric and X ray analyses

15 p2764 A70-32855

Circular free boundary problem associated with phase transformation by first order perturbation solution, discussing radial solidification and melting of fluid over cylindrical rod

16 p2941 A70-33003

Water structure role in membrane systems, considering phase transitions and thermal anomalies in surface properties

16 p2847 A70-33027

Preprecipitation and reversion stages in Ni-Co-Mo steel, observing dislocation nucleated phase growth initiation by aging

16 p2929 A70-33047

Massive eutectic and fine gamma phases precipitation in cast nimonic 100 alloy at 900 C aging

16 p2930 A70-33083

Beta transition mechanism dynamic mechanical properties in bisphenol-A based epoxy resins prepared with different curatives

16 p2856 A70-33500

Maraging nickel steel martensitic transformation temperature reduction after interruption by nonisothermal or isothermal tempering below 460 C

16 p2932 A70-33850

Constant grain size cast Mo ductile-brittle transition temperature dependence on annealing temperature using tensile test

16 p2933 A70-34274

Metallographic observations on slow crack growth in Be monocrystals suggesting explanation for transition regions

16 p2933 A70-34275

Chemical and structural microinhomogeneity, diffusion and mechanical properties of Ti alloys in connection with phase transformation characteristics

17 p3112 A70-34354

Heating effect above beta transus at intermediate and final stages of processing on Ti alloys properties

17 p3097 A70-34359

Ti-Al alloy crystallographic structure, observing hexagonality for alpha phase

17 p3114 A70-34377

Thermodynamic properties of bcc beta phase in Ti-Cu and Ti-Al systems, discussing activities determination technique

17 p3114 A70-34378

Oxidized alpha Ti crystals strain analysis based on X ray divergent beam, discussing hardening effects

17 p3115 A70-34387

Single phase alpha Ti alloy welds breaking strength, discussing delayed failure and cold cracking with various oxygen and hydrogen contents

17 p3117 A70-34399

Temperature cycling through phase transformation effects on plastic deformation of Ti and Ti-Al-V alloy under torsion and tension

17 p3117 A70-34400

Ti alloys martensitic transformations, metastable beta-phase decomposition and alpha-phase ordering

17 p3118 A70-34403

Martensitic transformation in Ti and Ti alloys, discussing shear systems influence

17 p3118 A70-34404

Twinned hexagonal martensites crystallography in Ti alloys, discussing alpha-beta and beta-fcc transformations

17 p3118 A70-34405

Cooling rate effect on beta phase transformation temperature in Ti-Nb and Ti-Al alloys

17 p3118 A70-34406

Ti alloys M sub s and beta sub s points thermodynamics, considering initiation of bcc-cph martensitic transformation

17 p3193 A70-34407

Ti binary alloys beta phase continuous cooling transformation, investigating additives effects

17 p3118 A70-34408

Metastable Ti alloys beta-omega-alpha decomposition and Ti-8Al alpha-ordered alpha transformation, using automatic measuring apparatus

17 p3118 A70-34409

Martensite transformations and cellular phase separation in Ti-Cu alloys, using electron microscopy

17 p3119 A70-34412

Phase transformations and equilibrium diagram of titanium-oxygen alloys, using electron and optical metallography

17 p3119 A70-34413

Martensitic transformation effects on mechanical properties of beta quenched Ti binary alloys

17 p3119 A70-34414

Martensitic phase change effects in TiNi on ultrasound waves propagation in transition region, using pulse echo measurements

17 p3126 A70-35603

Epitaxial beta SiC film formation on SiC by reactive evaporation or sputtering at low temperature

17 p3144 A70-35906

Cobalt binary alloys allotropic transformation and thermal expansion at various temperatures

18 p3271 A70-35967

Kingfisher meteorite metal particles microstructures, discussing phase transformation during reheating by shock

18 p3310 A70-35970

Ni-Al-Nb superalloy, determining temperature effect on phase relationships in Ni-rich portion of phase diagram

18 p3273 A70-36041

Omega transformation in Hf-Nb alloys, investigating aging at various temperatures

18 p3273 A70-36044

Transformation induced plasticity (TRIP)/high strength steels resistance to hydrogen embrittlement

18 p3273 A70-36047

Soviet papers on phase transformations of Fe, Ni, Co and Al alloys

18 p3275 A70-36201

Fe-Co alloys critical points during rapid heating, determining alpha-gamma phase transformations onset from dilatometric curves

18 p3275 A70-36203

Fe-Ni alloy alpha-gamma phase transformation after heating, noting deformation planes and directions in martensite

18 p3275 A70-36204

Electron microscopic investigation of alpha-epsilon phase transformations in Co-Ni alloys above and under phase equilibrium temperature

18 p3276 A70-36205

Dilatometric investigation of Fe alloys phase transformations, determining magnetic field effects and Curie temperatures

18 p3276 A70-36206

Magnetometric, dilatometric, pyrometric and X ray studies of phase transformations in Fe-Ni alloys, considering magnetic characteristics and formation of superstructures

18 p3276 A70-36207

Nb-based Ti-Zr alloy surface phase recrystallization characteristics, using field emission microscope

18 p3276 A70-36309

Interstellar gas thermal instability under cosmic ray heating, investigating perturbations causing transition to dense cool phase in pressure equilibrium with intercloud phase

18 p3309 A70-37003

Adiabatic microwave power meter design using sodium thiosulfate phase transformations

19 p3422 A70-37743

CdS conversion by cation exchange to single crystal CuS, examining phases structural relationship

19 p3486 A70-37766

Yield condition and Bauschinger effect in transition conditions for isotropic and orthotropic bodies

19 p3542 A70-38061

Solid-solid phase transitions in molecular crystals of organic tetrahedral substances, using differential scanning calorimetry

19 p3373 A70-38193

Ni-Cr heat resistant alloys structural transformation kinetics under aging, creep and operational conditions, discussing solid solution decomposition, hardening phases coagulation and dissolution, etc

20 p3645 A70-39037

Microstructure and phase distribution in maraging steels subjected to austenization and subsequent aging in reversible transformation temperature range

20 p3645 A70-39038

Heat treatment and alloying element influence on phase and structure transformations in Ti alloys, investigating mechanical properties and creep resistance

20 p3645 A70-39039

Beta Ti alloy decomposition study during aging by diffraction electron microscopy, forming finely dispersed coherent precipitates

20 p3645 A70-39041

Al-Zn-Mg alloys structural transformations by diffraction electron microscopy, investigating grain boundary and dislocation structure as function of heat treatment and chemical composition

20 p3646 A70-39044

Stressed cast Mg-Nd-Zr alloys structural transformations kinetics over temperature range by electron microscopy

20 p3646 A70-39046

Beta Ti-V-Cr-Al phase transformations below 500 C, discussing metastable phase, bcc formation and thermodynamics

20 p3646 A70-39106

Phonons and band structure role in metal-insulator phase transition, developing model of electron interactions with lattice vibrations

20 p3686 A70-39149

Ti binary alloys with V, Nb and Mo, determining phase boundaries by diffusion layers method and electron microscope analysis

20 p3649 A70-39727

RF spectral recombination lines from atomic level transitions, discussing populations, H lines, electron temperature, density and emission and formation

20 p3706 A70-39934

Heating conditions effect on microstructure, hardness, transformation temperatures and dimensional anisotropy of maraging steel

20 p3649 A70-39941

Mg-Al alloy beta phase precipitation, using metallography, hardness tests and electron microscopy

20 p3652 A70-40447

High temperature combined differential thermal analysis and spectrophotometric cell for phase transformation monitoring of evaporated thin film and bulk phthalocyanine

21 p3827 A70-41459

Earth upper mantle phase change instability, discussing temperature gradient, transformation influence on fluid, olivine-spinel phase flow patterns and tectonics

21 p3820 A70-41895

Zr-Nb alloys mechanical strength increase due to beta phase martensitic decomposition

21 p3840 A70-41897

Metastable beta Ti alloy as-quenched microstructure stability with respect to thin foils transformation during electrolytic polishing and bulk specimens during cold rolling

21 p3841 A70-42150

Octahedral solid-solid phase transitions by differential thermal analyzer and scanning calorimeter module, discussing entropy change causes

21 p3784 A70-42264

M phase thyristor amplifier operation, investigating state and transition equations by state variable methods

22 p3996 A70-42918

Ti phase transformation effects on thermal conductivity, electrical resistivity and spectral and total emissivities at 1100-1500 K

22 p4056 A70-43222

Phase diagrams and nonvariant equilibria points of Ti-Si alloys subjected to prior annealing, determining phase transformations, decomposition and other properties as function of temperature

22 p4057 A70-43350

Allotropic transformation points and linear thermal expansion coefficients of Co-base binary alloy terminal solutions, using dilatometric method

23 p4203 A70-43864

Nb-Ru equiatomic alloys reversible phase transformations, using electrical resistivity, hot stage optical metallography, X ray diffraction and magnetic susceptibility measurements

23 p4208 A70-44858

Austenitic formation by rapid heating of Ni maraging steel, noting microstructural characteristics relationship to martensite before phase transformation

24 p4356 A70-45144

Perovskite crystals phase transitions based on group theory, considering lattice vibration modes as instability source 24 p4389 A70-45206

Fe-Ni alloy plastic flow behavior during reversible austenite-martensite transformation under constant load 24 p4357 A70-45228

Zr-Nb alloys athermal omega transformation studied by transmission electron microscopy 24 p4358 A70-45234

Crystallography of martensite transformation on /225/ type planes of austenite in Fe-Mn-Cr-C alloy 24 p4358 A70-45237

Weak superstructure line patterns of ternary phases with TiFeSi and ordered iron phosphides by single crystal, Guinier powder and diffractometer techniques 24 p4359 A70-45249

Alpha phase Ti strengthening, investigating interaction between dislocations and interstitial solute atoms 24 p4360 A70-45516

Phase transitions in FeW doped strontium and barium oxides, using X ray diffraction and Mossbauer effect for transition temperature 24 p4390 A70-45605

Nonequilibrium solidification and metastable-stable phase transformation during heating of Al-Mo and Al-Cr alloys 24 p4360 A70-45829

Statistical characteristics of stability of single phase one component system under external force 24 p4381 A70-46144

Ti-Mo and Ti-Mn alloys omega transition phase, describing shape and crystallographic characteristics 24 p4361 A70-46178

High purity Cr-Ni heat resisting steels, investigating phase transformations with microhardness measurements magnetic analysis, X ray diffraction and microstructure examination 24 p4362 A70-46181

Spaak erosion or plasma jet treatment effects on Co surface structure, describing allotropic delta phase 24 p4364 A70-46221

Transition entropy during dissociation, investigating Trouton-Pictet rule applicability to diatomic molecules [DFVLR-SONDDYR-58] 24 p4430 A70-46412

PHASE VELOCITY

Nonpotential waves propagating at slow phase velocity in inhomogeneous plasma, determining flute instability oscillation frequency 01 p0149 A70-10163

Characteristic equation for phase velocity of surface wave propagating on helix for forbidden zone, suggesting current distribution function 05 p0815 A70-16775

Phase velocities of intrinsic normal waves of electron beam in three frequency parametric amplifier of space charge waves, determining optimal wave interaction conditions 05 p0823 A70-16890

NonJeans gravitational instability of stars and interstellar gas in Galaxy due to wave interaction with stars having velocity near wave phase velocity 05 p0917 A70-16906

Prestrain effect on waves propagation along slender low density unoriented polyethylene rod, indicating uniform phase velocity change over audio frequency range 07 p1248 A70-19237

Rayleigh and Love wave phase velocities for great circle paths from ordinary seismograms of World Wide Standard Seismographic Network /WWSSN/ stations 09 p1672 A70-23702

Nonpotential waves propagating at slow phase velocity in inhomogeneous plasma, determining flute instability oscillation frequency 10 p1925 A70-25011

Phase velocity and direction estimation of unknown signal propagating across two dimensional array in dispersive waveguide, showing dependence on SNR 11 p2018 A70-26274

Circular elastic helix phase velocities determined by internal constraints method, comparing results with other theories 11 p2085 A70-26557

Electron amplification and phase velocity of plane harmonic Rayleigh wave in gallium arsenide crystals under constant electric field 12 p2285 A70-27294

Turbulent flow phase velocity fluctuations measurement by hot-wire anemometers, obtaining cross-spectral density by Fourier analysis digital techniques 19 p3404 A70-38019

Electrostatic ion waves in uniform magnetic field, calculating phase and group velocities as function of propagation angle for comparison with dispersion measurements 20 p3678 A70-39659

Phase velocity and attenuation of shear waves in cases from sampled-CW ultrasonic crystal resonator reflection measurement 21 p3827 A70-41457

Acoustic surface waves phase velocity on lithium niobate with gold layer for propagation modes, predicting LF cut-off by substrate anisotropy 21 p3863 A70-42001

Dispersion equation for impedance elements periodic structures phase velocity calculation, discussing approximate solution methods 22 p3984 A70-42392

ELF and VLF waves in waveguide propagation mode, calculating lower ionosphere effect on attenuation and phase velocity 22 p3989 A70-42960

Interferometric investigation of rapidly varying frequency dependent phase objects, using ruby laser waves [SMPT PREPRINT 26] 22 p4034 A70-43049

Gravity waves produced in liquid electric conductor by piston subjected to sinusoidal pulsation, calculating magnetic field effect on amplitude and phase velocity 23 p4225 A70-44208

Phase and group velocity variations of LF transmission compared against crystal oscillator 23 p4163 A70-44228

Turbulent plasma without external magnetic field, observing low phase velocity ion wave mode 23 p4227 A70-44893

Microwave transmission in partially dielectric filled circular waveguide, deriving cutoff wavelength and phase velocity vs frequency 24 p4315 A70-46260

PHASE-SPACE INTEGRAL

Nonlinear differential equations solution behavior near zero point of phase space examined in material system perturbed motion 07 p1333 A70-18772

Phase space variations method proved not applicable to optimal control problems 08 p1479 A70-20856

Phase variable canonical form for time varying multivariable systems requiring less computational effort 08 p1463 A70-21645

Numerical solution of optimal control with dimensionality not exceeding phase space, using nonlinear programming and traveling wave method 10 p1911 A70-25185

Diffusion processes on multidimensional cylindrical phase space for studying stochastic processes for physical systems with angular measurements, developing model for satellite under torque 12 p2273 A70-28067

PHASED ARRAYS

Phased array antennas bandwidth and range resolution, discussing delay elements and antenna size affecting radiation patterns 01 p0042 A70-10262

Phase measuring scheme for large radio telescope array, describing constant-phase calibration signal production 02 p0269 A70-12583

Plane electromagnetic wave diffraction at periodic arrays obtained by direct summation of multiple reflection between arrays 03 p0442 A70-13095

Low loss low sidelobe N-way microwave optical power divider for single plane electronically steerable Ku band phased array antenna 04 p0655 A70-14624

Polarization insensitive phase shifter for phased array antennas, discussing limitations, design optimization and experimental results 06 p1019 A70-17508

Phased-array radars and parallel processing computers system in high target density environment, input-output, array steering and data storage and handling 07 p1236 A70-20150

Antenna arrays phase synthesis method based on properties of fast fluctuating phase distribution 09 p1645 A70-22414

Equivalent circuit for radiation admittance of infinite planar array of phased rectangular waveguide apertures 09 p1646 A70-22692

Phase interpolation circuits for scanning phased array antennas, using doublers and frequency multipliers 09 p1646 A70-22701

Periodic intensity fluctuations in pulsars from VHF phased array measurements 09 p1764 A70-23793

Phased array radar system synthesis, discussing small aperture systems, effects of solid state technology and role of data processing 10 p1842 A70-24877

Integrated circuit microwave phased array radar antenna systems for multiple frequency bands and multifunction operations to save cost and space 10 p1851 A70-24878

Hybrid microwave integrated circuits application to phased array and Data Relay Satellite System space transponder 10 p1851 A70-24879

Single bit latching reciprocal ferrite phase shifter design, operation and performance, noting linear phase response and low phase nonreciprocity 10 p1853 A70-25243

Air traffic control system using ground controlled satellite-borne phased array antenna to overcome UHF downlink path loss 11 p2077 A70-25421

[AIAA PAPER 70-497] 11 p2077 A70-25421

Spacecraft phased array antenna techniques, discussing tape helix radiators design for applications in navigation, TV broadcasting and data relay systems [AIAA PAPER 70-425] 11 p2015 A70-25452

S band communications repeater using retrodirective phased array on synchronous altitude data relay satellite /DRS/ for intersatellite and ground links [AIAA PAPER 70-424] 11 p2001 A70-25472

Phased array radar for automatic random search using pseudorandom sequences to generate random phase characteristics of currents together with suitable gating 12 p2183 A70-26984

Spacecraft high efficiency phased arrays with deployable helix radiating elements, considering gain and weight factors 12 p2197 A70-27930

Radiation patterns of phased array scanning antenna using digital phase shifter, reducing peak sidelobe level 13 p2380 A70-29785

Binary varactor diode microwave device, displaying two capacitance values in reverse bias operation for application in phased array systems and frequency control 14 p2556 A70-30919

Antenna research, discussing efficiency and design considerations in phased and strip line arrays and conical scan telemetry antennas 14 p2559 A70-31375

Phased array monopulse autotracking, radiointerferometer and Doppler frequency methods for radio tracking systems for artificial satellite orbits 15 p2697 A70-31836

High gain helix radiators for spacecraft phased arrays, measuring performance vs design parameters 15 p2678 A70-32600

Phased arrays, discussing ground based, shipboard and airborne research programs for military 16 p2863 A70-33264

Solid state phased array radar employing MIC modules in radiating elements, achieving reliability by redundancy 16 p2877 A70-33411

X band airborne antenna phased array, describing phase shifter, radiation pattern, associated computer, etc 16 p2864 A70-33454

Phased arrays universal figure of merit, including aperture efficiency, sidelobe level, scanning frequency and noise temperature 16 p2864 A70-33482

X band aircraft antennas selection and design for defense communications satellite systems, emphasizing steerable phased array 16 p2865 A70-33712

Artificial pilot phased array /APPA/ for use as multiple narrow beam communication satellite, obtaining beam steering from phase shifter setting 16 p2983 A70-34070

Gas tube isolator circuit for arcing amplifier in phased arrays, using programmed charge of capacitance bank during interpulse 16 p2879 A70-34072

Linear phased antenna arrays, calculating influence of interaction between radiating elements on radiation pattern 17 p3048 A70-35686

Transmit only solid state radar module built with microstrip techniques for phased array systems operating at L and S dual bands 17 p3056 A70-35899

S band CW power amplifier and varactor doubler module for airborne phased arrays 18 p3231 A70-36674

Directivity characteristics of planar antenna arrays with discrete identical elements and uniform phase progression 20 p3597 A70-39458

Scattering matrix for external coupling effects in dielectric covered phased array 23 p4160 A70-43766

Infinite periodic phased array over ground plane with dipole elements in parallelogram lattice, calculating driving impedance and gain loss due to mismatch 23 p4172 A70-44004

Phased array radar for missile defense, discussing development trends toward adaptive system logic control and microwave digital circuitry for signal processing 23 p4172 A70-44012

Linear phased arrays computer aided design, discussing search algorithms in multivariable optimization program 23 p4172 A70-44015

Phased array radar systems microwave circuit modules packaging techniques, discussing interconnections, assembly, hermetic sealing and leak testing 23 p4173 A70-44535

Radiation and phase-scanning properties of planar array of parallel plate waveguides, using wedge diffraction theory

23 p4166 A70-44973

PHASED LOCKED SYSTEMS

Stationary phase error variance for second order phase locked loop for low signal to noise ratios

13 p2383 A70-29590

PHASES

A priori initial phase distribution influence on optimal nonenergetic parameter estimation of rectangular narrow band radio signals on white noise background

13 p2369 A70-29730

PHENOBARBITAL

Aerzine-50 toxicity therapeutic treatment by pyridoxine and phenobarbital resulting in 100 percent survival of mice

07 p1222 A70-19926

Heme catabolism in untreated rats and in animals treated with phenobarbital or porphyrinogenic drug, comparing bilirubin and Co production

20 p3583 A70-40450

PHENOL FORMALDEHYDE

Polymer structure and cross-link density effects on thermal analysis of phenol-formaldehyde polymers pyrolysis products

11 p2069 A70-25804

Molybdenum disulfide and phenol formaldehyde resin lubricants for hydroextrusion of steel

15 p2743 A70-31639

PHENOLIC RESINS

Parietal ablation in phenolic resins using chemical kinetics

[ONERA-TP-734] 03 p0606 A70-13634

Phenolics and silicones characteristics, history, chemical composition, available forms, impregnation process, manufacture, productivity, electrical applications and temperature resistance

05 p0873 A70-16603

Phenolic nylon ablative thermal effectiveness in arc heated nitrogen, air and nitrogen-carbon dioxide streams

[AIAA PAPER 70-154] 06 p1183 A70-18233

Antifriction reinforced plastics based on polyamide fibers in epoxy phenolic resins, determining optimum ratios to obtain desired mechanical properties

09 p1710 A70-23675

Filament winding process for boron modified phenolic resin tape used in high temperature applications

12 p2242 A70-27204

Molybdenum disulfide and phenol formaldehyde resin lubricants for hydroextrusion of steel

15 p2743 A70-31639

Phenolic nylon thermal decomposition, considering surface reradiation and physical parameters effects

17 p3196 A70-35242

Phenolic nylon ablative thermal effectiveness in arc heated nitrogen, air and nitrogen-carbon dioxide streams

[AIAA PAPER 70-154] 23 p4282 A70-44520

PHENOLS

Ionol concentration variations in oncological patients blood, using liquid gas chromatography to determine removal by urine and feces

07 p1209 A70-19519

PHENOMENOLOGY

Choice prediction in partially repeatable decision situations, discussing phenomenological analysis

19 p3366 A70-38504

PHENYLALANINE

Feline hypersexuality, aggression and perceptual disorientation resulting from p-chlorophenylalanine administration

12 p2167 A70-27271

Nitrosyl chloride reagent effects on phenylalanine peptides

12 p2181 A70-27471

L-dihydroxyphenylalanine intraperitoneal injection effect on S-adenosylmethionine concentration in rat brain

21 p3764 A70-41269

PHENYLS

Electron impact promoted phenyl migration of trans phenyltolalene, considering mass spectrometry and stereochemistry

14 p2544 A70-30189

PHILOSOPHY

Philosophical problems arising in contemporary and modern mathematics, discussing metaphysics and psychology

07 p1327 A70-19787

Space orientation vs geocentrism in science and philosophy

19 p3553 A70-37397

PHOBIAS

Clinicnosographic criteria of flight phobia and differentiation from other psychopathologic syndromes, noting sociofamilial and operative factors

01 p0031 A70-10235

PHOBOS

Phobos motion observational results compared with Sharpless determination of secular acceleration

04 p0743 A70-14399

Phobos and Deimos photographic reconnaissance feasibility during 1971 orbiter and 1973 Viking missions, studying trajectory

[AIAA PAPER 70-60] 06 p1146 A70-18191

Phobos image analysis on Mariner 7 frame 7F91, discussing surface darkness, limb profile and geometric albedo

13 p2492 A70-29266

Phobos and Deimos photographic reconnaissance feasibility during 1971 Orbiter and 1973 Viking missions, studying trajectory

[AIAA PAPER 70-60] 23 p4243 A70-44507

PHONOARTERIOGRAPHY

Blood pressure indirect recording using ceramic crystal pick-up over brachial artery and under pneumatic cuff

06 p0992 A70-17299

PHONOCARDIOGRAMS

U PHONOCARDIOGRAPHY

PHONOCARDIOGRAPHY

Mitral stenosis and atrial flutter with atrial sounds heard and recorded, discussing sound generating mechanism

01 p0013 A70-10271

Atrial and ventricular gallops incidence during acute myocardial infarction by serial auscultation and phonocardiograms

01 p0014 A70-10277

Phonocardiographic and ultrasound observations of acute rejection following cardiac transplantation, considering rejection treatment at early stage

03 p0415 A70-12888

Ultrasonic Doppler method for timing mitral and aortic valves rapid movements, using filter to eliminate LF signals due to heart walls

03 p0432 A70-12891

Functional and organic systolic murmur differentiation using phonocardiography test

03 p0420 A70-13478

Phonocardiographic and mechanocardiographic features of patients with nonejection clicks and mid- or late-systolic murmurs

03 p0427 A70-13944

Hemodynamic determinants of gallop sounds in patients with aortic valve disease based on clinical, hemodynamic and angiographic observations

04 p0633 A70-15308

Ejection click of valvular pulmonic stenosis by external phonocardiograms and intracardiac pressure recordings during successive respiratory cycles

04 p0633 A70-15440

Frequency analysis of arterial sounds used in studying atherosclerosis, correlating spectra with jet flow turbulence past occlusion

06 p1003 A70-18220

On-line computer for heart rate, isovolumetric contraction time, ejection time, stroke volume and cardiac output using vibrophonocardiogram signals

07 p1224 A70-20196

Diastolic and equivocal fluttering of mitral valve in aortic insufficiency by echocardiography

09 p1615 A70-22209

X ray irradiation effects on phonocardiograms, EKGs, cardiac activity phases and Kunos-Garan mechano-electrical coefficient in dogs

13 p2350 A70-28890

Ultrasonic nonsearch Doppler cardiography for cycle phase analysis, recording single functions

20 p3581 A70-40199

Chest wall vibrations conversion measured by different transducers for simultaneous velocity, displacement, acceleration and phonocardiograms

21 p3770 A70-41236

PHONONS

Phonon-photon scattering intensity and line shape used to study laser-excited impurity centers dynamic characteristics in stimulated induction regime

03 p0499 A70-13256

Optical phonons in mixed sodium potassium tantalate crystals as function of temperature and composition, using IR and Raman spectra

03 p0542 A70-14002

Semiconductors low temperature photoconductivity fluctuations occurrence during energy relaxation probability by optical phonons

04 p0730 A70-14413

External optical phonon modes in ammonium and deuteroammonium halides phase transitions as function of temperature, using IR and Raman spectra

04 p0646 A70-14695

Phonon spectrum of mixed semiconductor crystals based on AIII-BV and AII-BVI compounds, studying frequency spectrum as function of crystal composition

07 p1300 A70-19867

Two parameter model for lattice vibrations applicable to diamond structured crystals, calculating phonon dispersion curves from dielectric screening theory

07 p1357 A70-19920

Laser light investigations of atoms, molecules and plasmas, considering Raman molecular spectroscopy,

acoustic phonons interactions and plasma diagnostics by light scattering

12 p2245 A70-27063

Self excited electron-phonon-spin spontaneous oscillations generation, deriving dispersion equation

16 p2878 A70-33779

Laser Raman spectroscopy, discussing scattering from vibrational modes in solid and from phonons above optical gap

17 p3081 A70-34599

Phonons and band structure role in metal-insulator phase transition, developing model of electron interactions with lattice vibrations

20 p3686 A70-39149

Helicons and transverse optical phonons coupling in degenerate polar semiconductors investigated from electromagnetic linear response theory and field method

24 p4390 A70-45603

PHOSGENE

Niobium oxychloride conversion to niobium pentachloride by vapor phase chlorination with phosgene, examining reaction kinetics

18 p3272 A70-36031

PHOSPHATES

NT ADENOSINE DIPHOSPHATE [ADP]

NT ADENOSINE TRIPHOSPHATE [ATP]

NT ADENOSINES

NT AMMONIUM PHOSPHATES

NT CALCIUM PHOSPHATES

NT DIPHOSPHATES

NT NUCLEOTIDES

NT POTASSIUM PHOSPHATES

NT PYRIDINE NUCLEOTIDES

Phospholipid metabolism intensity in brains of adrenalectomized and pseudo operated rats under hypoxia

01 p0012 A70-10054

Peptide formation during glycine reaction with linear polyphosphates and cyclic metaphosphates, considering prebiotic synthesis

09 p1630 A70-23395

Structural and functional properties of phosphates in biochemical reactions, discussing linkages

14 p2544 A70-30346

P32 labeled organic phosphate esters in water extracts of soil

20 p3615 A70-38979

Uridine phosphorylation by heating with inorganic orthophosphates achieved via nucleoside reactions

23 p4158 A70-44837

PHOSPHIDES

NT GALLIUM PHOSPHIDES

NT INDIUM PHOSPHIDES

NT MANGANESE PHOSPHIDES

NT SCHREIBERSITE

Optically pumped cadmium phosphide laser, obtaining IR coherent oscillation from Q switched Nd doped YAG laser excitation

15 p2751 A70-31985

Solid solutions of quasi-binary cross section CdP-CdTe and ZnP-CdTe, using X ray, thermal, microstructural and microhardness analyses

22 p4086 A70-43132

Weak superstructure line patterns of ternary phases with TiFeSi and ordered iron phosphides by single crystal, Guinier powder and diffractometer techniques

24 p4359 A70-45249

PHOSPHINES

Ion-molecule reactions produced in phosphine by ion cyclotron resonance

16 p2855 A70-33061

PHOSPHORESCENCE

Acrolein photoisomerization in lower excited states, determining fluorescence and phosphorescence quantum yields

15 p2694 A70-31730

PHOSPHORS

Transient hologram recording with fluorescein-boric acid glass organophosphor, noting effects of dye concentration, sample thickness, laser power and excited state lifetime

04 p0690 A70-15027

Projection CRT with liquid-cooled phosphor faceplate, showing linear relationship between brightness and beam current

09 p1673 A70-22034

Current-sensitive single gun color CRT with phosphor screen for display systems

12 p2195 A70-27373

Absolute quantum efficiency of phosphor calcium tungstate-lead under monochromatic far UV illumination

15 p2729 A70-32017

Visual IR laser beam display, using cathode ray tube phosphor with variable sensitivity and range control

15 p2752 A70-32441

Phosphor-output image intensifier response to single photon inputs in multichannel spectrophotometer for faint optical sources

23 p4195 A70-44291

Flickerless regeneration rates for CRT displays as function of scan order and phosphor persistence, using computer experiment 24 p4298 A70-45511

PHOSPHORUS
Fe-Ni-P phase diagrams for high temperatures, providing phase equilibria data for Widmanstätten pattern in iron meteorites 15 p2762 A70-32391
Direct gap conduction band and alloy composition monitoring InAlP, using electron microprobe cathodoluminescence and X ray emission 22 p4086 A70-43019
GaAs crystal surface Raman scattering from phosphorus impurities localized modes, using Ar ion laser line 24 p4391 A70-46255

PHOSPHORUS COMPOUNDS
NT ADENOSINE DIPHOSPHATE [ADP]
NT ADENOSINE TRIPHOSPHATE [ATP]
NT ADENOSINES
NT AMMONIUM PHOSPHATES
NT CALCIUM PHOSPHATES
NT DIPHOSPHATES
NT GALLIUM PHOSPHIDES
NT INDIUM PHOSPHIDES
NT MANGANESE PHOSPHIDES
NT NUCLEOTIDES
NT ORGANIC PHOSPHORUS COMPOUNDS
NT PHOSPHATES
NT PHOSPHIDES
NT PHOSPHINES
NT POTASSIUM PHOSPHATES
NT PYRIDINE NUCLEOTIDES
NT SCHREIBERSITE
Carbohydrate-phosphorus metabolites content in gophers brains under normal conditions during hypothermia and spontaneous warming at room temperature 01 p0012 A70-10055
Carbon dioxide lasers passive Q switching by gaseous methyl fluoride and phosphorus pentafluoride, presenting absorption coefficients 01 p0110 A70-10561
Acute hypoxia effect on mono-, di- and triphosphoinositides metabolism and content in white rats cerebral tissues, using chromatographic analysis 07 p1199 A70-18721
Electric discharge reactions in mixtures of phosphine with methane, ammonia and water, obtaining biologically significant inorganic and organic phosphorus compounds 09 p1630 A70-23396
Phosphorus compounds inhibition effect on oxidation and wear of graphite lubricants 13 p2437 A70-28854
Spatial-angular characteristics of Nd doped phosphorus oxychloride liquid lasers, discussing beam divergence effects 18 p3266 A70-36416
Solid phosphorus triamide derivatives as ignition aids in hypergolic propellant systems, testing characteristics in interaction with oxidizers 21 p3865 A70-41404

PHOSPHORYLATION
Gamma-aminobutyric acid effect on oxidative phosphorylation of rabbit and rat brain mitochondria, noting dependence on ionic concentration, temperature and amount of additions 01 p0019 A70-10509
Oxidative phosphorylation and oxygen intake during circulatory hypoxia in mitochondria of liver and brain in rats subjected to acute ischemia 23 p4145 A70-44315
Oxidative phosphorylation and oxygen consumption during hyperoxia in mitochondria preparations and tissue homogenates from white rat liver 23 p4146 A70-44316
Uridine phosphorylation by heating with inorganic orthophosphates achieved via nucleoside reactions 23 p4158 A70-44837

PHOTICS
Alpha rhythm phase coherence during photic blocking, examining pacemaker model 19 p3368 A70-37811

PHOTOABSORPTION
Cs seeding effect on bound-free UV photoabsorption of Cs-H plasma at constant electron density and energies below H ionization 02 p0343 A70-11904
Nitrogen molecule photoabsorption and photoionization cross sections determination, discussing ionization probability variations and radiationless transitions 07 p1347 A70-20358
Extreme UV spectroscopy with synchrotron radiation storage ring light sources in 40-400 Å range, including thin film photoabsorption measurements 21 p3826 A70-41451

PHOTOCATHODES
Photocathode internal light scattering effect on photomultiplier time response 05 p0845 A70-15806

Optical devices for enhancement of semitransparent photocathode quantum efficiency applied to TV camera tubes, image intensifiers and other imaging detectors 09 p1682 A70-23502
Spectral characteristics of secondary emission alloys for photocathodes in extra atmospheric radiation open-type detectors in UV range 14 p2582 A70-30166
Temporal dependence of photoelectron multiplier output waveform and focusing under photocathode alternating modulation, noting thresholds for optical reception 15 p2696 A70-31505
High efficiency semitransparent III-V semiconductor photocathodes fabrication and operation 19 p3486 A70-37756

PHOTOCELLS
U PHOTOELECTRIC CELLS
PHOTOCHEMICAL REACTIONS
NT PHOTOCROMISM
NT PHOTODECOMPOSITION
NT PHOTOLYSIS
NT PHOTOSYNTHESIS
NT RADIIOLYSIS
Aeronomy of Jovian upper atmosphere at pressures below 25 mb, discussing stratospheric heat sources, thermal emissivity, photochemistry of methane, ammonia, etc 02 p0366 A70-11804
Lower atmospheric photochemistry, discussing tropospheric, stratospheric, mesospheric and polluted atmospheric chemical and photochemical reactions 06 p1058 A70-18485
Photochemical calculations on mesospheric ozone for oxygen only, oxygen-hydrogen and oxygen-hydrogen-nitrogen atmospheres 07 p1273 A70-20268
Carbon dioxide photochemistry of Mars atmosphere, noting complications due to hydrogen compounds 09 p1763 A70-23483
Aeronomic neutral reaction rates, describing ozone excited state photochemistry 10 p1872 A70-23824
Chemical kinetic model for photoexcitation and photoionization of cold argon ahead of strong shock wave, predicting electron and excited atom concentrations [AIAA PAPER 68-666] 11 p2090 A70-25953
Sterically hindered arylidiazonium salts absorption spectra and quantum yield data interpretation, considering photochemical properties 12 p2182 A70-28300
Acrolein photoisomerization in lower excited states, determining fluorescence and phosphorescence quantum yields 15 p2694 A70-31730
Rocket and satellite data on upper atmospheric neutral/charged particles, short wave solar radiation, temperature and photochemical reactions 15 p2730 A70-32089
Photoreaction produced N-cyclohexyldiphenylketenimine from cyclohexyl isocyanide and diphenyldiazomethane 17 p3042 A70-34820
Book on ionospheric chemistry, covering chemical and photochemical reactions above 60 km and ionization processes 18 p3247 A70-36212
Nitric oxide and atomic nitrogen in mesosphere and stratosphere, discussing photochemical equilibrium 19 p3415 A70-38389
Nitrogen and nitric oxide production and diffusion, examining photochemistry and transport at high altitudes 20 p3620 A70-39339
Total reflectance of composite light diffuser with nonuniform absorption by two beam model, noting application to photochemistry 21 p3829 A70-41936
Trap filling dependence on intensity, temperature and wavelength of photoexcitation in CdS crystals subjected to electron radiation damage and annealing 21 p3864 A70-42013
Peroxyacetyl nitrate decomposition products under continued and discontinued irradiations determined by IR spectral analysis 22 p3983 A70-42944
Photoelimination reactions of macromolecules, emphasizing intermediate pathways heuristic description via energy level diagrams 23 p4157 A70-44391

PHOTOCHEMISTRY
U PHOTOCHEMICAL REACTIONS
PHOTOCROMISM
UV sensitive spiropyran films coloration mechanism and color structure stabilization, discussing film and laser applications to optical data recording and storage 01 p0086 A70-10357
Photochromic aminotriarylmethane filter solutions for flash blindness protection, noting stability against xenon flash UV exposure 04 p0690 A70-15028

Hologram storage and retrieval in photochromic SrTiO₃ crystals at ruby laser wavelengths 06 p1072 A70-18519
Photochromism of dihydroquinoline compounds and absorption spectra of color forms, noting color development upon UV light irradiation and thermal eradication 09 p1629 A70-22334
Optically bistable crystal applications, discussing photochromaticity, catochromatic tubes, oscilloscopes, computer storage devices and laser systems 19 p3446 A70-37860
Inorganic photochromic and cathodochromic recording materials, examining transition metal doped strontium titanates, rare earth doped calcium fluorides and Fe or S doped sodalite 22 p4088 A70-43601
Photochromic paint nondestructive testing for survival equipment, detecting bond defects and sandwich water 23 p4197 A70-44490

PHOTOCONDUCTIVE CELLS
Electro-optical transducers based on photoconductive cells, phototransistors and microminiature incandescent and solid state light emitters 16 p2904 A70-33144

PHOTOCONDUCTIVITY
Photoconductivity and photomagnetic effect measurements in Ge for determining nonequilibrium current carrier concentration produced by Q switched neodymium laser 01 p1017 A70-10099
Photoconductivity growth and decay curves green edge emission and integral flux in optical flare of cadmium sulfide crystals due to hole trapping process 03 p0540 A70-13503
Mercury cadmium telluride alloy as photoconductive IR detector material noting properties, composition and temperature dependence of energy gap 03 p0543 A70-14196
Semiconductors low temperature photoconductivity fluctuations occurrence during energy relaxation probability by optical phonons 04 p0730 A70-14413
Two photon photoconductivity of CdS crystals stimulated by ruby laser, showing emission self focusing during pumping 07 p1302 A70-20322
Photoconductivity detected in pigmented epithelium of eye during illumination by visible light 08 p1444 A70-20738
Ge-Cu IR detector photoconducting characteristics and application to carbon dioxide laser mode pattern measurement 10 p1898 A70-23922
Chromium doped GaAs photoconductivity spectral distribution at various temperatures, determining temperature dependence of impurity maximum 12 p2286 A70-27366
Fe and Ni doped GaAs photoconductivity at various temperatures, determining activation energy level 12 p2287 A70-27489
Self focusing of ruby laser radiation in CdS single crystal, considering effect on crystal photoconductivity 12 p2248 A70-27540
Surface field effect, contact potential and photoconductivity measurements on p- and n-type heteroepitaxial single crystal silicon films on sapphire 13 p2470 A70-29372
Photoconductive and thermal IR detectors development 13 p2410 A70-29656
Spectral distribution of GaAs photoconductivity, allowing for coordinate dependence of minority carrier lifetime in surface space charge region 15 p2782 A70-31626
Photoconductivity relaxation kinetics of low resistivity n- and p-type GaAs, showing nonradiative recombination 17 p3143 A70-35703
Photon capture cross sections for surface silicon electronic states using IR photoconductivity measurements 17 p3144 A70-35707
Extrinsic photoconductive detectors, comparing performance for microwave and DC bias based on gain bandwidth product and SNR analysis 18 p3232 A70-36746
Semiconductor solar energy converter, deriving conditions for occurrence of photoconductivity quenching 24 p4391 A70-46325

PHOTOCONDUCTORS
As₂Se₃ crystal production technology concerning substitution-type solid solution structure and photoconducting ferroelectric properties 04 p0729 A70-14409
Extrinsic photoconductor with reduced background under uniform illumination, describing frequency response as function of recombination and dielectric relaxation times and load resistances 14 p2586 A70-30989

PHOTOCURRENTS

Semiconductor image detectors in photodiode and photoconductor forms, describing construction and operation modes 15 p2714 A70-32673

Cryogenically cooled photoconductive IR radiation detectors, determining wideband optical heterodyne performance 20 p3627 A70-39085

Integrated ferroelectric photoconductor device for hologram storage, discussing improved phase readout technique for reconstruction 22 p3994 A70-43609

PHOTOCURRENTS

U ELECTRIC CURRENT
U PHOTOELECTRIC EMISSION

PHOTODECOMPOSITION

Photodecomposition of 1,4-dichlorobutane sensitized by n, pi singlet state of acetone as chemical process 04 p0646 A70-15319

Disproportionation to combination ratio of hydrazyl radicals generated in absence of hydrazine direct decomposition 14 p2544 A70-30120

Molecular oxygen role in photolytic decomposition of ozone by intermediate quantum yield method, presenting rate constants 16 p2858 A70-34009

PHOTODETACHMENT

Ion cyclotron resonance spectroscopy technique for determining electrons photodetachment energy from negative ions in gas phase 11 p1995 A70-26001

Electron photodetachment rate from meteor radar echo duration during night and daytime observations 19 p3515 A70-37664

PHOTODETECTORS

U PHOTOMETERS

PHOTODIODES

Semiconductor laser-photodiode system used as optical logic elements for electronic circuits describing storage elements, dynamic trigger and multivibrator 03 p0499 A70-13456

Silicon photodiode arrays with total active area noting element isolation 03 p0459 A70-14195

Emission modulation in multifunctional injection laser-photodiode system used as optical memory, pulse generator, multivibrator and trigger 05 p0859 A70-16268

Optical and electronic mixing in avalanche photodiode during variable amplitude signal demodulation in optical heterodyne receiver, considering conversion losses 07 p1243 A70-20282

Photosensitivity and scanning of planar Si photodiode image detector arrays, using most ring counter and shift register 10 p1846 A70-23881

GaAs-Au surface barrier n-type photodiode structure, electrical parameters and response characteristics 12 p2194 A70-26969

Vibration amplitudes and frequencies contactless measurement by sensor with photodiode for machining tool elements during metal working operations 12 p2235 A70-27683

Photovoltaic effects in diodes with generation-recombination process in space charge region 15 p2709 A70-32427

Information optical transmission parameters with electroluminescent GaAs diode as radiation source, calculating energy received over various distances 19 p3389 A70-38069

Constant false alarm rate bias technique to control avalanche photodiode laser receiver over varying operating conditions of temperature, ambient illumination, etc 20 p3641 A70-39483

Accurate tuning methods for laser mode locking device, using diffracted light measurement and photodiode with LF spectrum analyzer 21 p3838 A70-42047

Semiconductor luminescence and photodetector diodes near IR region transmission, describing frequency response measurements 22 p4087 A70-43445

PHOTODISSOCIATION

Atmospheric water vapor photodissociation and resulting O evolution recalculated for determining O abundance in absence of biological activity 01 p0081 A70-11294

Radiative-convective equilibrium model to investigate photodissociation of water in Venus atmosphere, considering greenhouse effect 04 p0757 A70-15516

Unsensitized gaseous fuel-air mixtures photochemical ignition due to molecular oxygen photodissociation by radiant energy absorption [AIAA PAPER 70-149] 06 p1183 A70-18225

Photodissociation of diatomic O and N molecules in far UV 07 p1338 A70-20052

Photodissociation of perfluoroalkyl iodides filler of pulsed laser operating cavity, discussing thermal molecular dissociation and unexcited iodine atoms formation 08 p1513 A70-21418

Photodissociation and fluorescence cross sections for hydrogen by Lyman-alpha photons emission from collisional quenching 16 p2953 A70-33006

Ammonium molecules dissociation and ionization in comet atmospheres due to solar corpuscular and photon radiation 19 p3514 A70-37642

Diurnal variation symmetry of upper atmosphere molecular oxygen concentration in terms of ozone photodissociation 23 p4190 A70-44083

Laser excited atoms quenching by iodine molecules from light pulse induced photodissociation of perfluoropropyl iodide active media 24 p4352 A70-45467

PHOTOELASTIC ANALYSIS

NT PHOTOGRAMMETRY

Dynamic stress concentration factor in strut containing symmetrically located elliptical discontinuity, using photoelastic technique with modulated ruby laser light source 02 p0388 A70-12495

Photoelastic stress analysis of shouldered shafts with keyways in shanks under direct loading and torsion, including keyway and shoulder fillet stresses 02 p0388 A70-12496

Piezoelectric transducer for photoelastic analysis of HF stress waves in thick ring subjected to transient loads 02 p0389 A70-12500

Photoelasticity extension to plane elastic problems with stress state depending on Poisson ratio, discussing multiple connected body with nonzero surface tractions on internal boundaries [SESA PAPER 1570] 03 p0583 A70-12884

Out-of-plane restraint effect on plane-stress solutions near straight boundaries, predicting deviation of two dimensional photoelastic results 03 p0584 A70-12951

Frozen stress techniques for photoelastic analysis of orthotropic plate on nonlinear foundation, providing results to compare with future finite element analysis 03 p0480 A70-12952

Stress-optic law for orthotropic composites photoelastic stress analysis, investigating use of transparent filament-resin composites 03 p0481 A70-12956

Hologram interferometry to study stresses in fixed two dimensional photoelastic models and three dimensional slice qualitative analysis [SESA PAPER 1530] 03 p0482 A70-12964

Pseudo two dimensional photoelastic test method applied to axisymmetric solid propellant rocket grains under pressure and thermal loads [SESA PAPER 1482] 03 p0482 A70-12968

Scattered light photoelastic stress analysis using doubly refracting materials and lasers 03 p0594 A70-13657

Transient thermal stresses in photoelastic models of various shapes under various steady state or transient temperature conditions, describing instrumentation and experimental methods 03 p0600 A70-14308

Thermal stress concentration produced by cracks, notches and fillets in plates free from external loads measured photoelastically 03 p0600 A70-14310

Two dimensional plane stress photoelastic models of star configurations in elastic case bonded solid propellant rocket motors under transverse body force loading 03 p0582 A70-14312

Stress analysis based on observing birefringence effects in photoelastic surface coating 04 p0689 A70-14922

Photoelastic and photorheological analysis of time-dependent variation of stress distribution in long strip compressed oppositely with elastic flat punches 05 p0928 A70-16012

Three dimensional photoelastic model for structural analysis of aircraft bulkhead to improve fatigue life 05 p0937 A70-16376

Holographic method for reconstructing polarization of light emitted by photoelastic model, obtaining isochromatic and isoclinic fringe patterns 06 p1063 A70-17643

Notched cylindrical shells of nonuniform thickness using two dimensional photoelastic models mounted on elastic foundations 07 p1249 A70-19239

Lens effects applied to measurement of stresses on plane transparent models in photoelastic analyses, visualizing stresses from moire fringes 07 p1409 A70-19746

Photoelastic stress analysis of composite structures subjected to gravitational forces using immersion analogy, considering constant acceleration stresses 07 p1413 A70-20038

Magnetophotoelastic model applied to plates bending stress analysis, deriving polarized light propagation equations 09 p1728 A70-23447

Dynamic photoelastic analysis of fracturing plastic plates, studying elastic and stress fields around propagating cracks 09 p1783 A70-23448

Profile plane state of stress in wedge with and without external notch using combined photoelastic analysis and moire method 11 p2131 A70-25591

Transient and steady state thermal stresses measured by holographic extension of photoelastic analysis 11 p2049 A70-25592

Stress distributions in thin walled pressure vessels analyzed by scattered light photoelasticity technique compared to strain gage analysis 11 p2131 A70-25593

Photoelasticity stress analysis, determining principal stress differences and orientation, using holographic interferometry to obtain sum and separation 11 p2049 A70-25596

VTOL aircraft metal fatigue examination by photoelasticity emphasizing stress reduction 11 p2132 A70-25622

Two dimensional photoelastic investigation of crack propagation in fiber-reinforced composites consisting of glass and polyester resin layers 11 p2136 A70-26078

Photoelastic analysis using fringe multiplication instrument applied to two dimensional models under load and frozen stress slices 11 p2061 A70-26834

Interferometric stress analysis in three dimensional photoelasticity, including practical measurements and analysis in terms of refractive index 12 p2326 A70-27621

Wing rib structure transient thermal stresses analysis using photothermoelastic method 12 p2327 A70-27982

Holographic method for reconstructing polarization of light emitted by photoelastic model, obtaining isochromatic and isoclinic fringe patterns 13 p2405 A70-28726

Tensile test on perforated Al-filled rectangular plate of photoelastic material, obtaining stress concentration at hole by photoelastic visualization 13 p2516 A70-29628

Photoelastic stress analysis, discussing holographic interferometry for main stresses separation and polyester resins application to birefringence pattern superposition elimination 15 p2815 A70-31809

Stress distribution around oblique holes in uniaxially loaded plate using three dimensional photoelastic analysis [SESA PAPER 1618] 15 p2820 A70-32305

Fringe interpretation in stress-holo- interferometry, emphasizing isopachic-isochromatic interaction effects in photoelastic analysis [SESA PAPER 1642] 15 p2739 A70-32309

Scattered light rosette using three polarized light beams intersecting at surface point to evaluate photoelastic stress data 15 p2739 A70-32320

Steel and cast iron early stage fatigue failure, using photoelastic coatings 17 p3192 A70-35741

Stress measurements in rotating plane disks with notched disturbed symmetry, using stroboscopic photoelasticity and numerical methods [ASME PAPER 70-GT-26] 18 p3344 A70-36867

Holographic interferometry applications in stress analysis of photoelastic resins, describing holographic interferometry assembly 18 p3262 A70-37209

Holographic registration of isochromatic and isopachous diffraction patterns of photoelastic birefringent objects, showing stress concentrations 19 p3422 A70-37649

Photographic patterns from brittle coatings, grids, photoelasticity and moire, considering variability, association with other images and esthetic value 19 p3546 A70-38343

Granular medium particles contact forces distribution measurement by absolute retardation method using photoelastic techniques 19 p3427 A70-38344

Maximum secondary principal stress axis and isotropic points determination in scattered light photoelastic analysis, considering bar in uniaxial tension and rectangular beam 19 p3546 A70-38345

Welded joint strain measurement by grating etching and moire fringe technique 19 p3428 A70-38513

Strain analysis by moire technique, using triangular and square root of 2 gratings 19 p3432 A70-38720

Three dimensional photoelastic analysis of stresses and strains in hollow circular cylinders with conical ends bonded to shell and shrunk 20 p3720 A70-39686

Strains and stresses along interfaces and near fiber ends in composite structures made of reinforced matrix, using photoelastic methods 20 p3730 A70-40035

Circular cylindrical shell stability under axial compressive load, analyzing buckling process by high speed photographic recording of photoelastic isoclinic pattern changes 20 p3735 A70-40528

Photoelastic stress measurement of metal powder particles during sintering, using two dimensional models 21 p3935 A70-41410

Clad glass fibers axial stress measurement by photoelastic techniques 22 p4060 A70-43415

Isoclinic parameter determination from intersection points of secondary isochromatics lines in photoelastic analysis, discussing polariscope theory and imperfect quarter wave plates error effect 23 p4198 A70-44910

PHOTOELASTIC MATERIALS

Out-of-plane displacement restraint at thin photoelastic plates bonded to rigid boundaries of inclusions inducing transverse stress components causing plane stress solution deviation 01 p0202 A70-11059

Servo systems for analog automatic reduction of time dependent photomechanical model materials fringe data in stress analysis 03 p0482 A70-12967

High speed photography for instability onset and subsequent buckling process in photoelastic circular cylindrical shells under axial compression 03 p0594 A70-13659

Two dimensional plane stress photoelastic models of star configurations in elastic case bonded solid propellant rocket motors under transverse body force loading 03 p0582 A70-14312

Residual strains determination in rotating disks from photoelastic coatings interference 05 p0955 A70-17063

Servo systems for analog automatic reduction of time dependent photomechanical model materials fringe data in stress analysis 07 p1286 A70-20040

Magneto-photoelasticity equations derived for photoelastic model in magnetic field, developing algorithm for optical phenomena for arbitrary stress distribution 11 p2131 A70-25588

Plane electromagnetic waves propagation in nonabsorbing photoelastic material with finite deformations, formulating theory from Eulerian and Lagrangian point of view 11 p2139 A70-26173

PHOTOELASTIC STRESS MEASUREMENT

U PHOTOELASTIC ANALYSIS

PHOTOELASTICITY

NT PHOTOVISCOELASTICITY

Holographic interferometry as stress analysis technique for crack propagation studies, discussing advantages over classic interferometric and conventional photoelastic methods 01 p0198 A70-10002

Successive small birefringences undergone by polarized light ray crossing photoelastic model represented by rotations in equatorial plane on Poincare sphere 06 p1168 A70-17918

Warped wave front viewpoint in analyzing object plane resolution, contrast and location in polariscopes 07 p1280 A70-19236

Photoplastic method for modeling of plane elastoplastic problems, comparing results with photoelastic coating method to estimate transition errors from model to prototype 10 p1965 A70-25320

Poincare sphere application to automatic polarization forms measurements and two/three dimensional photoelasticity by scattered light 11 p2142 A70-26633

Ellipsometry with Poincare sphere representation, describing application to automatic two and three dimensional photoelasticity by scattered light 17 p3086 A70-35014

Neumann and Maxwell photoelasticity laws reformulation with aid of characteristic tensor of mechanical state 17 p3187 A70-35044

Equal thickness interference fringe networks behavior in singularities region of photoelasticity 21 p3941 A70-42260

Optical glasses photoelastic constants measurement, tabulating results 22 p4072 A70-42509

PHOTOELECTRIC CELLS

Conflicting requirements for reflection reduction, thermal stabilization and radiation protection satisfied by three layer coatings on Si photocells 01 p0159 A70-10768

Coordinate-sensitive photocells with heterojunctions between wideband semiconductors, noting increased longitudinal photovoltage 03 p0541 A70-13722

Photocell uses in semiconductor integrated circuit, discussing scanned arrays applications and economics 03 p0459 A70-14265

Biplanar photocell in various holders noting intrinsic properties, emphasizing rise time characteristics 04 p0695 A70-15572

Divided photoelectric cell position sensitive detectors in laser alignment systems, obtaining independent signals for displacements in orthogonal directions 06 p1081 A70-17624

Photoelectric exposure meter for meridian circle readings photographic recording 08 p1496 A70-21159

Transverse Dember effect in elastically bent Ge single crystal illuminated by light beam, considering EMF distribution and photocell application 09 p1740 A70-23191

Photoelectric devices for object position fixation and superposition of two images 09 p1684 A70-23635

Photoelectric receiver and light beam alignment in gas laser aerial photography, considering directrix rectilinearity verification 12 p2247 A70-27476

Si photocells fabrication, reliability and energy conversion efficiency 19 p3358 A70-38479

Cadmium sulfide photocell development, noting plastic support base, film deposition and interconnection 19 p3358 A70-38480

PHOTOELECTRIC EFFECT

NT PHOTOIONIZATION

Rapid photoprocesses decay kinetics, using CW Ar ion laser beam interrupted periodically by electro-optical shutter 02 p0314 A70-12742

Rapid scanning high resolution photoelectric spectrometer for sunspot spectra study 07 p1289 A70-20291

Chemical high pressure laser action produced by stimulated phototransition of electrons at contact moment between pair of reacting nonexcited gas molecules 08 p1513 A70-21412

Laser-induced electron emission from metals and insulators in form of evaporated films and single crystals, discussing many-photon photoelectric effects and thermionic emission 08 p1556 A70-21509

Photoelectric detector sensitivity variation effect on long term instability of servomagnet variometers 14 p2588 A70-31261

Picosecond light pulse measurement by two beam overlap technique using nonlinear photoelectric effect 17 p3097 A70-35912

Cooled antimony-cesium film photoelectric effect for weak luminous flux, examining electronic camera reciprocity 19 p3427 A70-38175

Detonation front position determination in explosive by photoelectric technique 22 p4121 A70-42341

Battery operated electronic servo governed photoelectric polarimeter for airborne measurements of skylight polarization, discussing design and operation principles 23 p4199 A70-45006

Time evolution of instantaneous light intensity mean and variance for Q switched single mode laser near oscillation threshold 24 p4355 A70-46090

PHOTOELECTRIC EMISSION

Autoelectron and autophotoelectron emission from Fe-doped p-type GaAs cathodes in vacuum, noting I-V and emission characteristics dependence on light flux 03 p0538 A70-13067

Low molecular weight organic semiconductors photoelectron UV emission spectra, studying electron energy distribution and optical ionization, dark bulk conductivity, etc 03 p0541 A70-13728

Photoelectric intensity measurements on emission bands of oxygen Herzberg I system excited in argon-oxygen afterglow 03 p0528 A70-14350

Competition mechanism for free carriers in junction isolated transistor collector suggested by current dependence of photocurrent 04 p0657 A70-14732

Silicon bipolar transistors primary photocurrent calculation using manufacturers data 04 p0657 A70-14736

Inelastic scattering of electrons by surface plasma oscillation for low energy electron diffraction and photoemission, interpreting surface plasmon excitation 07 p1337 A70-19359

Two photon photoconductivity of CdS crystals stimulated by ruby laser, showing emission self focusing during pumping 07 p1302 A70-20322

Time resolved photoelectric light detection, discussing photoelectric emission probability time dependence and radiation interaction with bound charge 09 p1726 A70-22232

Photoemission analyzer with finite emitter in spherically symmetric retarding field with magnetic field present, analyzing energy resolution 09 p1679 A70-22988

Photoemission energy distribution curves measuring circuit using AC retarding potential method, offering improved noise performance 09 p1679 A70-22996

Thermal lens effect produced by photocurrent in CdS, using focused laser beam to generate photocurrent causing local heating changes of refractivity 10 p1898 A70-23980

Photographs of ferroelectric tungsten oxide crystal domains obtained with photoemission microscope, noting memory effect after electron beam sweeping 11 p2099 A70-26463

Contaminated Ni crystal 100/ surface photoelectric yield as function of temperature, considering effects of Ar ion bombardment and annealing 12 p2288 A70-27680

Photoemission from evaporated gold films, measuring quantum yield, photoelectric energy distribution curves and optical density states 14 p2626 A70-30481

Photoemission of electrons and holes from Al into aluminum oxide, giving approximate energy band diagram of Al-aluminum oxide interface 15 p2783 A70-31759

Steady state potential distributions near photoemitting plate immersed in plasma, noting overshoot effects role for sheaths around satellites in interplanetary plasma 15 p2778 A70-31906

Photoemission optical analysis from thin films with uniaxial anisotropy, discussing reflectance, transmittance and divergence of Poynting vector 15 p2774 A70-32012

Peak emission currents from tungsten under ruby laser focused radiation, describing integral emission by heat conduction theory and Richardson equation 15 p2754 A70-32875

MOS structure, measuring ionizing radiation effects on interface barrier energies by internal photoemission techniques 17 p3144 A70-35901

Photoemitting cesium antimonide thin films for IR detectors 19 p3488 A70-38202

Photocurrent multiplication in single crystal n-type epitaxial GaAs due to impact ionization of shallow donors 22 p4087 A70-43218

PHOTOELECTRIC GENERATORS

Solar photoelectric power ion propelled probe of asteroid region, describing design and mission planning [AIAA PAPER 69-1105] 02 p0382 A70-12529

Photoelectric composite multicell solar generator, deriving empirical equation for external I-V characteristic 07 p1196 A70-19623

Solar energy direct conversion into electricity, surveying photoelectric, thermoelectric and thermoelectric methods 15 p2677 A70-31598

High voltage photoelectric generator containing semiconductor plates with series- and parallel-connected p-n junctions forming solid circuit for super-high light flux concentrations 16 p2843 A70-33201

Heterogeneous solar cells based on polycrystalline cadmium sulfide and selenide, discussing preparation methods and photoelectric and electric properties 18 p3215 A70-36238

PHOTOELECTRIC MATERIALS

Ternary phase diagram of liquid epitaxially grown gallium arsenide antimonide, considering use as high quantum efficiency long wavelength photoemitter 15 p2782 A70-31758

PHOTOELECTRIC PHOTOMETRY

U ELECTROPHOTOMETERS

PHOTOELECTRICITY

Parameters defining elliptic vibration of light reflected from surface using photoelectric ellipsometer 08 p1546 A70-21673

Structural and material design of contactless photopotentiometers operating in forward and reverse modes with given output characteristics 09 p1681 A70-23357

Carrier drift due to electromagnetic impulse, deriving expressions for photo EMF generated in transverse magnetic field manifesting monopolar photomagnetic effect 13 p2452 A70-29282

- Photoelectric device for recording plant rhythmic leaf movements in space 16 p2849 A70-33998
- Indium arsenide p-n junctions fabrication and electrical and photoelectric properties 17 p3143 A70-35120
- Lunar occultation photoelectric measurements, investigating irregularities of occulted stars 17 p3171 A70-35442
- Delta Scuti stars, determining consistent absolute magnitudes by Stromgren intermediate band colors and Crawford photoelectric H beta indices 17 p3171 A70-35443
- Adsorption influence on electrical and photoelectric properties of CdSe thin films 17 p3143 A70-35674
- Prebreakdown ionization growth in gases based on initial photocurrents production from high voltage uniform field electrodes 22 p4026 A70-42353
- Time resolving X ray grating polychromator, discussing photoelectric attachment with surface barrier semiconductor detectors [SMPT PREPRINT 75] 22 p4037 A70-43069
- PHOTOELECTROMAGNETIC DETECTORS**
- U RADIATION MEASURING INSTRUMENTS**
- PHOTOELECTRONICS**
- U ELECTRONICS**
- U PHOTOELECTRICITY**
- PHOTOELECTRONICS**
- Hot photoelectrons in semiconductors assuming short lived photoexcited current carriers, deriving expressions for energy distribution function of semiconductor current carriers 01 p0153 A70-10066
- Photomultiplier tubes for counting photoelectrons from photocathode, discussing pulse height distributions, SNR, quantum counting, statistical correlation and dark current properties 01 p0090 A70-10902
- Spectral distribution of X ray atmospheric absorption used to determine high energy photoelectrons spectrum 01 p0172 A70-11494
- Absorption of EUV sunlight by Jupiter upper atmosphere, discussing photoelectron energy loss, thermal equilibrium and heating efficiencies 02 p0367 A70-11816
- Photoelectron energy spectra and partial photoionization cross sections for carbon dioxide determined with spectrometer at monochromatic incident radiation wavelengths 02 p0343 A70-11903
- Photoelectrons entry into F region detected at conjugate point during winter night by Thomson scatter observations of plasma lines appearing in signal spectrum 08 p1489 A70-21386
- Protonospheric heating by photoelectrons from conjugate ionosphere using Explorer 31 data 08 p1489 A70-21387
- Geoelectric low energy particles and fresh photoelectrons interactions with upper atmosphere observed by satellite Cosmos 261 08 p1492 A70-21796
- Auroral electrons and photoelectrons spatial, energy and angular distributions measurements using low energy electron spectrometer onboard satellite Cosmos-261 08 p1500 A70-21797
- Ionospheric photoelectrons resulting from solar UV radiation interaction with atmospheric gases, obtaining escape fluxes using Monte Carlo method 09 p1747 A70-23667
- Satellite studies geoelectric particles and photoelectrons, including interactions with earth atmosphere 10 p1874 A70-24312
- Satellite-borne spectrometer for low energy electrons measurement, describing virgin photoelectrons equilibrium energy spectrum for different latitudes and pitch angles 10 p1874 A70-24313
- Elastic scattering effect on photoelectron transport and escape in upper sunlit atmosphere 12 p2222 A70-27187
- Attenuation length of vacuum UV photoexcited electrons in evaporated metal films, observing lack of dependence on photon energy 13 p2472 A70-29711
- Temporal dependence of photoelectron multiplier output waveform and focusing under photocathode alternating modulation, noting thresholds for optical reception 15 p2696 A70-31505
- F 2 layer heating by photoelectrons reconsidered in terms of electron inelastic collisions effect on temperature 15 p2727 A70-31870
- Papers on chemical physics covering photoelectron angular distribution, molecular orbital theories, electron impact spectrometry, resonant electron scattering, etc 16 p2857 A70-33796
- Photoelectron spectra of methane, silane, germane, methyl fluoride, difluoromethane and trifluoromethane, describing electron spectrometer with double focusing electrostatic plates 19 p3374 A70-38269
- Night airglow oxygen red lines predawn enhancement calculations, confirming role of photoelectrons from magnetic conjugate ionospheric 19 p3414 A70-38380
- Pi sub u states of positive ionized diatomic oxygen by photoelectron spectrometry 19 p3474 A70-38488
- Nitrogen photoelectron excitation in dayglow, examining 3371 A band intensity, energy spectrum and flux in ionosphere 21 p3882 A70-41093
- Photoelectron production and escape flux at ISIS-1 satellite 21 p3818 A70-41102
- Winter predawn enhancement of 6300 A airglow at higher midlatitudes, considering roles of oxygen dissociative recombination and photoelectrons production at magnetically conjugate point 22 p4019 A70-43110
- Predawn enhancement of O I 6300 A line, considering magnetically conjugate photoelectrons effects on atomic oxygen excitation 22 p4095 A70-43113
- Diurnal variations of photoelectron heat fluxes and energy production by thermal coupling between upper F 2 region and magnetosphere 24 p4328 A70-45354
- Quantum detector with impinging EM field, discussing photoelectron counting distribution and signal with white noise 24 p4312 A70-46051
- PHOTOEMISSION**
- U PHOTOELECTRIC EMISSION**
- PHOTOEMISSIVITY**
- U EMISSIVITY**
- U PHOTOELECTRIC EMISSION**
- PHOTOEMITTERS**
- U PHOTOELECTRIC MATERIALS**
- PHOTOENGRAVING**
- Holographic recording on n-type Si single crystal surface by photoanodic engraving 22 p4026 A70-42332
- Monolithic precision castings using photoetched plastic and lost-wax investment techniques [ASME PAPER 70-FLCS-8] 22 p4043 A70-42419
- PHOTO GEOLOGY**
- Diffraction limited resolution criteria for geoscene imagery 02 p0297 A70-11924
- Photogeological mapping at medium to small scales, comparing satellite transparencies with aerial photographs 02 p0298 A70-12202
- Geological interpretation of aerial photographs, discussing picture quality, scale, film material and applications 05 p0840 A70-16499
- Earth resources observation satellite [EROS/ program, discussing geologic terrain and land-use planning maps [SPE PAPER 2703] 06 p1053 A70-17155
- Satellite photographs for geological mapping and research assessed against interpretation of field data and conventional aerial photographs 10 p1876 A70-24640
- Photography for geological interpretation, comparing color, color IR, and black-and-white photographs from spacecraft and aircraft 12 p2221 A70-26956
- Airborne geological mapping by IR emission spectroscopy, describing instrumentation, materials discrimination capability, data processing, etc 12 p2230 A70-26957
- Air photographs or imagery linear features, assessing sensors performance and developing interpretation criteria in photogeological research 14 p2573 A70-30641
- PHOTOGRAMMETRY**
- Instruments and procedures for photogrammetry automation, discussing automatic pattern recognition, data correlation and computer role 02 p0302 A70-12652
- Photogrammetric deformation measurement of thin steel sheets during static bending tests 02 p0302 A70-12653
- Stereoscopic device for photogrammetric points selection and marking on aerial photographs 03 p0482 A70-13109
- Automatic universal-code digital data recorder for photogrammetric measurements 03 p0483 A70-13110
- Ranger, Surveyor and Lunar Orbiter televised and reconstructed picture quality, suggesting improvements in existing photographic systems 03 p0490 A70-13656
- Satellite orbit and attitude determination and planetary gravity and astronomical constants from earth-based radio Doppler and orbital photogrammetric observations 04 p0750 A70-14938
- Cameras photogrammetric parameters determined from stellar photographs, considering distortion components, reference points, etc 05 p0852 A70-16921
- Photogrammetric processing of aerial photographs using setting values of phototriangulation by stereocomparator and electronic computer 07 p1278 A70-18691
- Visual and quantitative image definition, evaluating microdetail clarity in panchromatic, IR, color and color IR aerial photographs 07 p1281 A70-19369
- Photogrammetry - Conference, Karlsruhe, West Germany, September 1969 07 p1284 A70-19776
- Mathematical models for photogrammetric disposition in aerial photography 07 p1284 A70-19780
- Holography in terms of photogrammetry, reviewing interferometry role, wave construction and reconstruction, etc 09 p1674 A70-22260
- Errors in aerial stereo photogrammetry, deriving equation to account for lens distortion and internal orientation 09 p1682 A70-23394
- Photogrammetry - Conference, Washington, D.C., March 1970 10 p1877 A70-24726
- Photogrammetric map compilation from orbital satellite photographs, with fictitious and ground coordinates generated by electronic computer, discussing error sources 10 p1890 A70-24728
- Analytical aerial triangulation iterative solution mathematical convergence parameters tests, considering photogrammetric relations for standard conditions in variable size block 10 p1878 A70-24729
- MUSAT program and AN/USQ-28 SHIRAN controlled aerial photographs photogrammetric evaluation by U.S. Army Topographic Command, indicating bias in nadir positions 10 p1890 A70-24730
- Photogrammetric three dimensional control extension investigated by plotter and method of Independent Model Aerotriangulation 10 p1890 A70-24731
- Thin soap membranes shape determined by photogrammetric method, using stereo camera and fluorescent light 10 p1891 A70-24735
- Photogrammetry methods for experimental structural mechanics, describing Balplex 525 Plotter camera system, image measurement and displacement vector computation 10 p1827 A70-24736
- Numerical photogrammetric techniques application to cadastral surveys and mapping, discussing standard errors 10 p1880 A70-24753
- Polluted air mass concentration determined by photogrammetry, producing topographic type map with respect to vertical and oblique aerial photographs 10 p1880 A70-24755
- Extraterrestrial photogrammetry role in lunar photographs analysis, considering landing site triangulation and selection, coordinate system improvement, etc 10 p1948 A70-25046
- Volcanic terrain by high precision photogrammetry for studying planetary surface roughness traversability by three wheeled vehicle 10 p1882 A70-25047
- Vertical tilt and horizontal position of antenna rotating device in radio astronomy and radar observations using photogrammetric methods 12 p2195 A70-27478
- Essa 7, Surveyor 7 and Mariner 4 space TV systems geometric distortions analysis and potentials in analytic photogrammetry and topographical mapping 14 p2586 A70-30982
- Statistical analysis of photogrammetrically surveyed three dimensional space points sets for aerospace vehicles and projectiles position location 15 p2733 A70-31550
- Stress analysis for plate with large displacements by multicamera photogrammetry, comparing results with numerical solution by finite differences 15 p2821 A70-32313
- Partial coherence theory in holography with photogrammetry applications, reconstructing images with fringes representing constant range contours 17 p3087 A70-35023
- Computer programs for photogrammetric aerial triangulation with independent models 18 p3248 A70-36778
- Aerial terrain analysis by color and color IR photography, analyzing physical factors affecting final image 22 p4018 A70-42963
- PHOTOGRAPH INTERPRETATION**
- U PHOTOINTERPRETATION**

PHOTOGRAPHIC DEVELOPERS

Optimum developer for aerial photofilms processing, relating light sensitivity and information capacity 18 p3258 A70-36283

PHOTOGRAPHIC EMULSIONS

NT NUCLEAR EMULSIONS

Holographic interferometry for determining optical path variations resulting from photographic plate emulsion thickness and refractive index changes during development 01 p0087 A70-10666

High resolution silver halide photoemulsions by holographic resolvometry using Ne-He laser to obtain interference patterns 01 p0095 A70-11633

Spectrophotometric facility for measuring spectral characteristics of color filters, photomultipliers and photographic plates as function of temperature 02 p0301 A70-12494

Photographic emulsions used for astronomical photography in U.S., discussing hypersensitization, exposure, processing and image evaluation methods 06 p1071 A70-18516

High resolution mass spectrography using AgBr photographic plates as ion detectors for organic chemical problems 07 p1224 A70-18894

Holographic recording of information contained in evanescent wave fields in high resolution photographic emulsions 07 p1281 A70-19367

Book on holography principles and applications, discussing imaging properties, coherence, photographic emulsions, optical analog computers, etc 07 p1283 A70-19739

Photographic emulsions design for increased water depth penetration during aerial multispectral recording of light absorption and scattering in water masses 09 p1674 A70-22261

Photographic emulsion nonlinear response effect on image quality, discussing holography for multiple exposures 09 p1676 A70-22718

Primary cosmic ray particles location in photographic emulsions exposed to balloon elevations by spark chambers, noting stack alignment 09 p1679 A70-22990

High resolution holography with pulsed radiation source, testing various emulsions for sensitivity and reciprocity behavior 09 p1681 A70-23175

Crop species and soil conditions identification from space by comparison of multivase and multiemulsion photography, assigning standard signature to optical fields 10 p1879 A70-24745

Chilled emulsion photography for astronomy and spectrography, reducing long exposures with chilled plates 14 p2585 A70-30649

Heterochromatic spectrophotometry, discussing maxima and integral techniques for line measurement, photoemulsion properties and Eberhard effect 14 p2585 A70-30784

Planetary and lunar photography at French observatory, discussing Pic du Midi facilities and various photographic emulsions 17 p3082 A70-34676

Plate illumination relation to opacity in photometry and spectrophotometry, using digital techniques 20 p3630 A70-39475

Photographic materials resolving power for lines and points 20 p3633 A70-39750

Photographic emulsions and photosensitive materials for holography, measuring noise spectral power density at high spatial frequencies by scattered light method 21 p3822 A70-40812

Photographic processing methods for high efficiency low noise phase holograms on silver halide emulsions 22 p4025 A70-42286

Holographic interferometry sensitivity augmentation by use of nonlinear properties of photoemulsion 22 p4038 A70-43140

Holographic interferometry of phase object by double exposure method, showing no effect of photographic emulsion compression on order of interference 24 p4334 A70-45368

Cobb chart resolution in photographic system including independent sources of image spread and single source of granularity 24 p4334 A70-45450

Motion picture B and W photographic materials characteristic curves, describing geometry by three-component set 24 p4335 A70-45653

Optical image reconstruction from holograms, discussing photographic materials resolution, response linearity, spatial noise, etc 24 p4335 A70-45654

Exposed photographic layers blackening phenomenon energy spectrum and mean square 24 p4336 A70-45655

Industrial radiography, discussing photographic emulsion layers granular structure formation due to ionizing radiation 24 p4337 A70-45714

Photographic paper as emulsion film substitute in industrial radiography, evaluating sensitivity and image contrast 24 p4337 A70-45715

Radiography using photo-nuclear reaction emulsion to improve picture contrast by eliminating scattered photons in sample 24 p4337 A70-45716

PHOTOGRAPHIC EQUIPMENT

NT BAKER-NUNN CAMERA

NT BALLISTIC CAMERAS

NT CAMERAS

NT FRAMING CAMERAS

NT HIGH SPEED CAMERAS

NT LALLEMAND CAMERAS

NT PANORAMIC CAMERAS

NT PHOTOGRAPHIC PROCESSING EQUIPMENT

NT SCHMIDT CAMERAS

NT TELEVISION CAMERAS

Scinticamera resolving power in radioactivity measurements, discussing mathematical principle of division of radioisotope concentration in biological experiments 01 p0040 A70-11404

Stereoscopic device for photogrammetric points selection and marking on aerial photographs 03 p0482 A70-13109

Martian orbital photographic missions objectives and sensors realizable capabilities, discussing relationships between orbital parameters and imaging systems constraints 03 p0490 A70-13663

Photoobjective and camera resolution tests regarding entire frame using two dimensional azimuth mark 05 p0852 A70-16864

Photo-optical instrumentation applications and theory - Conference, San Francisco, August 1969 09 p1672 A70-22029

Earth resources data transmission, describing picture reception and reproduction equipment [AIAA PAPER 70-328] 09 p1634 A70-22856

Photo-optical instrumentation - Conference, San Francisco, August 1969 09 p1684 A70-23751

Photographic apparatus for lunar orbiters and Apollo spacecraft, describing lunar surface closeup camera for astronauts, launch photographing, etc 13 p2406 A70-28926

Lunar Orbiter photo subsystem mechanisms, discussing film transport, vacuum and mechanical clamps, focal plane shutter, processor-dryer and optical mechanical scan 16 p2914 A70-34146

Surveyor camera double acting rotary solenoid actuated focal plane shutter utilizing two blades in parallelogram linkage 16 p2914 A70-34148

Image intensifier apparatus photographing nuclear electromagnetic cascades in ionization spectrometer 18 p3261 A70-37091

Soviet book on aerial photo plotting of aerogeophysical routes and anomalies covering techniques, equipment, low altitude surveys, etc 19 p3410 A70-37408

Photographic polarimeter based on Savart and lambda/4 plates combination for linear polarization measurements of coronal and prominence emission lines during solar eclipse 20 p3627 A70-39092

Vibration transfer coefficient of aerial camera-photographic assembly system for shock absorption during surveys 24 p4333 A70-45200

Apollo and Skylab photographic systems, describing equipment and missions 24 p4333 A70-45360

Image forming performance in photographic system design, considering Cobb chart resolution as figure of merit 24 p4334 A70-45449

PHOTOGRAPHIC FILM

NT MICROFILMS

UV sensitive spiropyran films coloration mechanism and color structure stabilization, discussing film and laser applications to optical data recording and storage 01 p0086 A70-10357

Broad bandwidth electronic analysis of high resolution photographic film using flying spot CRT or rotating mirror devices 02 p0302 A70-12613

Photographic negatives analysis, storage and reconstruction using facility permitting photography conditions simulation and computer image treatment 02 p0302 A70-12614

Interferogram contrast as spatial frequency function measured for photographic materials used in holography by He-Ne laser 03 p0485 A70-13530

Dichromated gelatin holographic films preparation, sensitization, exposure and development, giving diffraction efficiencies and reconstruction SNR 04 p0691 A70-15031

Automatic measurement of frequency-contrast characteristics of photographic films using linear, photoelectric and high speed comparator devices 05 p0852 A70-16865

Previous radiation exposure effect on photographic film noting increased sensitivity at UV frequencies 06 p1065 A70-17890

Minimum altitudes for illumination levels of aerial color photographic film calculated for different landscapes 07 p1283 A70-19633

Photographic film imagery, degraded by long term artificial atmospheric turbulence, restored by spatial filters placed in Fourier transform plane 07 p1336 A70-20090

Reconstructed holographic image complex amplitude expression derived, showing effects of film optical transfer function, size and shape 08 p1500 A70-21789

Hypersensitization of IR films for use in stellar photometry, discussing laboratory and astronomical tests 09 p1673 A70-22158

Aerophoto film emulsion layer and backing deformation magnitude and direction, suggesting use of photoplates for astrophotography 09 p1673 A70-22166

Color radiography with photographic negative film exposed to X rays, obtaining same thickness latitude with improved detail sensitivity on single emulsion line 10 p1887 A70-24168

Equidensity film advantages in photointerpretation relating to remote sensing in hydrology and land use 10 p1889 A70-24502

Orthophoto Attachment for A8 autograph to produce black and white and color aerial photographs on negative film 10 p1891 A70-24739

Photographic films for astronomy and spectroscopy, discussing resolving power, light sensitivity, antihalo lacquer and emulsions 10 p1892 A70-25129

Film reduction and time keeping used at Smithsonian Astrophysical Observatory for Baker-Nunn films 11 p2007 A70-26196

Quantitative analytic composite photography, performing image density point-to-point subtraction of two negatives 13 p2406 A70-28905

Photographic enhancement by slightly offset film sandwiching 14 p2586 A70-30979

Coherent or spatially incoherent light recordings of Fourier transform holograms, investigating resolution cells film grain and signal to noise ratio 14 p2588 A70-31207

Photographic materials for holography, discussing spectral sensitivity, grain size, resolution, transfer functions, diffraction efficiency, etc 17 p3084 A70-35003

Reciprocity law between radiation intensity and exposure time for photographic films in vacuum UV spectrum region, investigating departure at various wavelengths 18 p3257 A70-36281

Optimum developer for aerial photofilms processing, relating light sensitivity and information capacity 18 p3258 A70-36283

Meteor spectrosensitometric properties of panchromatic plates and films for aerial photos, investigating parametric conditions effect on image quality 19 p3422 A70-37653

Color film /XRC/ application in Mexico during solar eclipse of 7 March 1970, showing little color and tone distortion 19 p3423 A70-37751

Efficiency, low noise and photochromic effects suppression in bleached silver halide holography with various films 20 p3627 A70-39097

Pulsating light source afterglow increasing high speed film information content, discussing streak image, tearing process and impact stress tests [SMPTE PREPRINT 66] 22 p4032 A70-43036

Degraded photographic image enhancement limitations due to film grain noise 23 p4193 A70-43820

Diazo compounds purity effect on photosensitive photographic film quality, determining color image reproduction density 24 p4334 A70-45498

Photo copying in diapositive form, using ruby laser light on IR film 24 p4352 A70-45559

X ray films sensitometric investigation in medical and industrial radiography, evaluating HVL and ISO methods for X ray quality

24 p4337 A70-45710

Photographic paper as emulsion film substitute in industrial radiography, evaluating sensitivity and image contrast

24 p4337 A70-45715

PHOTOGRAPHIC MEASUREMENT

Photochronographic measurements of high speed rotor vibrations, showing precision and nutation components

01 p0093 A70-11268

Two phase flow visualization by various photographic and optical methods, describing equipment and lighting used and types of data obtainable

02 p0305 A70-12834

Interferogram contrast as spatial frequency function measured for photographic materials used in holography by He-Ne laser

03 p0485 A70-13530

Photo-optical instrumentation - Conference, Washington, D.C., August 1968, Volume 1

03 p0487 A70-13651

Photographic pyrometry for surface temperature measurements on ablation models, discussing technique accuracy and limitations

04 p0694 A70-15536

High speed photographic study of breakdown, crack formation, thermal explosions and molecular weight of transparent plastic dielectrics under laser beam

05 p0869 A70-16210

Optimal scale selection for aerial surveys by analyzing aerial photography data

07 p1278 A70-18690

Transistorized circuit for automatic control of photographic studies of pupillary reaction transient states in rabbits subjected to light stimulus

07 p1216 A70-18731

Color and black-and-white photomicrographs and photomicrographs of Apollo 11 moon rock sample consisting of spongy gray mass of pumice-like material

07 p1288 A70-20224

Atmospheric turbulence parameters in meteor zone determined from simultaneous photographic and radar observations, determining turbulent diffusion coefficient dependence on height

08 p1563 A70-20546

Atmospheric particles photographed in situ by cameras using microsecond flash lamps, discussing required mechanical motion compensation at aircraft speed

10 p1886 A70-23930

Quadratic error of semiautomatic measuring apparatus for photographic plates, noting operator contribution

11 p2051 A70-26182

Spatial geodesy calculations based on photographs of satellites against star background, recommending ECHO type satellites

11 p2046 A70-26191

Photographic techniques for artillery projectile flight evaluation, emphasizing high speed range and drum film image synchronized cameras

13 p2407 A70-29159

Atmospheric turbulence parameters in meteor zone determined from simultaneous photographic and radar observations, determining turbulent diffusion coefficient dependence on height

15 p2796 A70-31455

Upper atmosphere turbulence spectra of passive contaminants deposited by rockets from radiometrically calibrated photographs of chemical trails

15 p2725 A70-31688

Monochromatic radiation angular distribution surface reflectance measurement using photographic reflectometer

[AIAA PAPER 70-859] Cumulative jets during shock induced collapse of air cavities in thin fluid layers, using high speed motion picture photography

17 p3074 A70-35742

Atmospheric turbulence scale and dissipation from 80 to 120 km, using photographic observations of Leonid meteor trails

19 p3515 A70-37663

Optical system mtf measurement by photographic technique for comparing telescopic sight with simulator, discussing performance

19 p3428 A70-38511

Auroral photographic and visual observations, discussing satellite results and substorm development

19 p3417 A70-38730

Comet Ikeya-Seki 1965 f tail formed by dust particles continuous ejection, using preperihelion photographs

19 p3527 A70-38792

Aircraft trajectory postflight reconstruction involving photographic starfield and landmark referenced to inertial navigator output, discussing optimal data smoothing technique

[AIAA PAPER 70-1022]

20 p3666 A70-39512

Shock wave and surface velocity measurements in exploding foil testing by streak photography with image converter camera

21 p3824 A70-40863

Photographic determination of star positions at closed block plate adjustment, considering accuracy expectancy

21 p3889 A70-41146

Low pressure supersonic wake measurement by differential interferometer in double pass polarized light [SMPT PREPRINT 95]

22 p4036 A70-43060

Supersonic wakes visualization and photographic measurement by schlieren techniques, using amplitude subtraction and He-Ne laser

22 p4036 A70-43061

CW laser beam power density distribution monitoring by self calibrating photographic dosimetry technique

24 p4307 A70-45343

Photographic measurement of droplets size, velocity and number during sprayed liquid fuel combustion, using Xe flash bulbs

24 p4429 A70-46008

Photographic representation of localization center of anomalous retinal correspondence

24 p4310 A70-46343

PHOTOGRAPHIC PROCESSING

Automatic photo-optical technique for processing of cineangiograms to find time-course history of left ventricular volume

04 p0641 A70-14559

Computer processing role in film scanning and digitizing for enhancing X ray and radioisotope scanner images in medical radiographs, discussing image noise reduction

04 p0654 A70-14562

Dichromated gelatin holographic films preparation, sensitization, exposure and development, giving diffraction efficiencies and reconstruction SNR

04 p0691 A70-15031

Photographic emulsions used for astronomical photography in U.S., discussing hypersensitization, exposure, processing and image evaluation methods

06 p1071 A70-18516

Bleach process giving high efficiency low noise holograms using potassium ferricyanide, noting drying procedure and developer

06 p1072 A70-18520

Photogrammetric processing of aerial photographs using setting values of phototriangulation by stereocomparator and electronic computer

07 p1278 A70-18691

Threefold reduction of aerial negatives facilitating microfilming without impairing accuracy and clearness of image details

07 p1278 A70-18692

Optimum image scale and longitudinal overlap in continuous orthophoto map production regarding sheet dimensions, instrumental ranges, flight path tolerances and ground relief

13 p2407 A70-29165

Pattern recognition systems design and applications in medical and photographic data classification

13 p2374 A70-29580

Herschel effect in UV solar photography in developing autotopographic photographic film for bright photospheric recording

13 p2497 A70-29853

Airphoto interpretation, discussing descriptive, digital and photographic methods of representing recognition process results

14 p2585 A70-30642

Photographic enhancement by slightly offset film sandwiching

14 p2586 A70-30979

Optimum developer for aerial photofilms processing, relating light sensitivity and information capacity

18 p3258 A70-36283

Photographic processing methods for high efficiency low noise phase holograms on silver halide emulsions

22 p4025 A70-42286

Combined hypersensitization and rapid in situ processing for time-average observation in real time hologram interferometry

22 p4025 A70-42321

Degraded photographic image enhancement limitations due to film grain noise

23 p4193 A70-43820

PHOTOGRAPHIC PROCESSING EQUIPMENT

Photogrammetric processing of aerial photographs using setting values of phototriangulation by stereocomparator and electronic computer

07 p1278 A70-18691

Stereo photographs conjugate image area matching, comparing automatic optical and electronic correlation techniques

09 p1680 A70-23067

PHOTOGRAPHIC RECORDING

Electromagnetic procedures and camera-spectrometer system for studying detonation processes, measuring mass flow rates and explosives spectra

01 p0090 A70-10887

Artillery type projectiles field photography in flight in connection with service integrity evaluation of weapon components under real environment conditions

03 p0490 A70-13658

Rotating prism method for obtaining time correlation between streak photographs and characteristic waveforms of flash X ray discharges

03 p0492 A70-13762

Performance characteristics of RDX-metal sheath systems, using high speed motion picture photography for missile design applications

03 p0550 A70-14141

Schwerd color drawings of amplitude and intensity distributions of Fraunhofer diffraction patterns, verifying accuracy with computer generated diffraction plate photographs

04 p0719 A70-15014

Simultaneous recording of near and far field diffraction patterns at several exposures for single laser pulse

04 p0701 A70-15022

Hologram recording materials properties and limitations, discussing diffraction efficiency of thick and thin amplitude and phase holograms, silver and non-silver halide noise effects, etc

04 p0690 A70-15026

Transient hologram recording with fluorescein-boric acid glass organophosphor, noting effects of dye concentration, sample thickness, laser power and excited state lifetime

04 p0690 A70-15027

Cine recording ophthalmoscope with TV monitoring for retinal photography during centrifugation

06 p1061 A70-17286

Photoelectric exposure meter for meridian circle readings photographic recording

08 p1496 A70-21159

Automatic photographic data processing system with transient reproducer to obtain digital format for computer analysis

09 p1673 A70-22030

Small contrast objects detection by photographic technique, measuring gradients, granularity noise and density variations for emulsions

09 p1673 A70-22157

Stars photographic position determination errors with NAFA-3C/25 camera, comparing films and plates

09 p1673 A70-22164

High temperature vacuum dilatometer for continuous photographic recording of expansion curves for refractory materials, determining thermal expansion coefficient

09 p1675 A70-22565

Time lapse photographic recording and scoring in-flight performance of helicopter aviator trainees during hypothetical tactical instrument mission

09 p1624 A70-22900

Control system for high speed photographic diagnostics based on rotating mirror action

09 p1679 A70-22993

Satellites equatorial topocentric coordinates determination from photographic observations

09 p1763 A70-23328

Holographic 3D movie of front-lighted opaque objects, recording diffuse reflection with CW laser and high resolution film

09 p1684 A70-23533

Meteor particle orbits, comparing inclined radio reflections with photographic and straight radar observations

14 p2636 A70-30322

Hologram superposition on photosensitive surface for multiimage successive recording, examining resolution, SNR, etc

15 p2734 A70-31596

Onboard IR receiver and ground photorecorder for Meteor satellite cloud tracking, using computer processed data

15 p2738 A70-32112

Aerospectrometric camera facilitating spectral brightness coefficients determination for object identification

16 p2908 A70-33227

Four dimensional recording using synchronous multiple pulse ruby laser holography

17 p3088 A70-35027

High speed photographic recording of bursting rotor in fragment control device

17 p3063 A70-35523

Systematic errors in rotating mirror framing cameras and film records for quantitative high speed motion analysis

17 p3095 A70-35632

Fiber optics lens for transferring specimen image to camera during vibration tests

17 p3095 A70-35633

Large photographic telescope characteristics for stellar and planetary observations, noting differential refraction influence on plate scale factors

18 p3259 A70-36608

Photographic patterns from brittle coatings, grids, photoelasticity and moiré, considering variability, association with other images and esthetic value

19 p3546 A70-38343

Holographic recording in transparent bodies with optical characteristics changeable under intensive light 20 p3633 A70-39999

Circular cylindrical shell stability under axial compressive load, analyzing buckling process by high speed photographic recording of photoelastic isoclinic pattern changes 20 p3735 A70-40528

Artificial rain erosion effects on missile and spacecraft recorded via high speed photography 20 p3635 A70-40531

Particulate boron levitated electrostatically in air and ignited by pulsed laser to avoid contamination, investigating combustion by high speed photography [SMPT PREPRINT 100] 22 p4032 A70-43034

Electronographic camera for ultrahigh speed photography, using nuclear emulsion as recording medium [SMPT PREPRINT 54] 22 p4033 A70-43039

High speed stroboscopic photography, discussing multiple flash and motion picture photography and TV operated strobe light [SMPT PREPRINT 42] 22 p4033 A70-43040

Orthogonal multistreak recording by framing camera applied to arrival of detonation wave at front surface of explosive charge [SMPT PREPRINT 32] 22 p4034 A70-43045

High speed holographic recording of transient events by single shot ruby and Nd-doped pulsed lasers, applying to shock tubes and wind tunnels [SMPT PREPRINT 3] 22 p4035 A70-43056

Material transfer image recording using focused laser beam, discussing experimental setup and test results 22 p4040 A70-43605

Computer photokymographic recording of gravitational-inertial force environment effects on cardiovascular and respiratory systems on centrifuge 22 p3976 A70-43709

Holographic primary and conjugate images properties, considering applications in moving scenes recording and multiple images storage and retrieval 23 p4193 A70-43924

Hologram superposition on photosensitive surface for multiimage successive recording, examining resolution, SNR, etc 23 p4195 A70-44280

PHOTOGRAPHIC RECORDING INSTRUMENTS

U OPTICAL MEASURING INSTRUMENTS

U PHOTOGRAPHIC RECORDING

U RECORDING INSTRUMENTS

PHOTOGRAPHIC TRACKING

Mathematical relations and procedures for automatic satellite tracking by four axis Zeiss camera, discussing motion along small circle approximation and punch tape criteria 02 p0255 A70-11770

Automatic camera theodolite at Sophia satellite tracking station, discussing instrument constants 02 p0273 A70-11774

Q switched and high energy pulse laser devices for location of satellite photographed by night against background of stars, including optimization in noise [ONERA-TP-753] 02 p0313 A70-12369

Computerized method for processing photographic earth satellite observation results, transforming coordinates by nonconformal approximation of polynomial function 05 p0814 A70-16367

Artificial earth satellites photographic observation without chronometric recording aids, determining location and time by single indicator 09 p1635 A70-23055

Satellite photograph equatorial coordinates dependence on magnitude of evaluated region, objective distortion and transformation methods 09 p1679 A70-23056

Soviet cameras for photographic observation of artificial celestial bodies, noting equatorial platform mount, mirror lenses and installations 10 p1892 A70-25128

Method of dependence involving triangulation applied to reducing photographs of earth satellites 11 p2006 A70-26185

Schmidt photographs reduction, noting film bending during exposure and mean error of satellite position 11 p2007 A70-26195

Satellites photographic positions accuracy compared with stars based on stellar coordinates, investigating causes of difference 11 p2008 A70-26198

Satellite coordinates estimation precision by comparing artificial satellite positions obtained simultaneously by photographic cameras 11 p2008 A70-26199

Photographic satellite plates reduction by astrometric method at geodetic institute at Potsdam, discussing star coordinates, astronomic refraction, etc 11 p2008 A70-26200

French photographic observations of Apollo 12 translunar trajectory 15 p2697 A70-31676

Bubble chamber photography and track image reconstruction by holography, discussing measurement apparatus, accuracy and tolerances 19 p3428 A70-38510

Artificial satellites photographic observation by camera, describing sighting system, tracking adjustments and shutter controls 19 p3433 A70-38793

PHOTOGRAPHS

NT CLOUD PHOTOGRAPHS

NT LUNAR PHOTOGRAPHS

NT MOTION PICTURES

Collection of papers on optics covering dielectric multilayer filter synthesis, photographic image, light interaction with free electrons, laser radiation, optical echoes, etc 02 p0340 A70-12878

Photographic image reconstruction of spatially incoherent illuminated object using twofold holography 09 p1675 A70-22486

Foreground presence for computer generated and painted three dimensional photographic displays using fly eye lenses 16 p2906 A70-33177

Holographic stereo model, comparing stereoscopic perception of phase and amplitude to model consisting of overlapping photos 16 p2908 A70-33228

Photographic image deblurring method, using image forming holograph and amplitude weighting transparency 22 p4042 A70-43670

PHOTOGRAPHY

NT AERIAL PHOTOGRAPHY

NT ASTRONOMICAL PHOTOGRAPHY

NT AUTORADIOGRAPHY

NT CHRONOPHOTOGRAPHY

NT CINEMATOGRAPHY

NT CLOUD PHOTOGRAPHY

NT COLOR PHOTOGRAPHY

NT ELECTRO-OPTICAL PHOTOGRAPHY

NT FRAME PHOTOGRAPHY

NT INFRARED IMAGERY

NT INFRARED PHOTOGRAPHY

NT LUNAR PHOTOGRAPHY

NT MICROWAVE PHOTOGRAPHY

NT MULTISPECTRAL PHOTOGRAPHY

NT PHOTOMICROGRAPHY

NT PHOTORECONNAISSANCE

NT RADAR PHOTOGRAPHY

NT ROCKET-BORNE PHOTOGRAPHY

NT SATELLITE-BORNE PHOTOGRAPHY

NT SCHLIENEN PHOTOGRAPHY

NT SHADOWGRAPH PHOTOGRAPHY

NT SPACEBORNE PHOTOGRAPHY

NT SPECTROHELIOGRAPHS

NT SPECTROPHOTOGRAPHY

NT STEREOPHOTOGRAPHY

NT ULTRAVIOLET PHOTOMETRY

Book on photographic action of ionizing radiations in dosimetry and medical, industrial, neutron, auto- and microradiography, emphasizing photographic materials reaction to photons and particles 02 p0337 A70-11696

Photographic relief images with arbitrary profile produced by using image relief height as spatial frequency function 02 p0300 A70-12462

Three dimensional X ray imaging technique from conventional radiograph set photoreduced and projected by special purpose imaging system 04 p0686 A70-14561

Holography history and applications to interferometry, contour mapping and three dimensional photography 07 p1279 A70-18900

High resolution multiple spark photography, discussing facility 09 p1680 A70-23070

Diffraction pattern sampling for automatic pattern recognition in photographic imagery 09 p1689 A70-23802

Transistorized differed synchronizer for delaying photoflash initiation in scientific photography 12 p2228 A70-26879

Laser beam photography utilization in engineering for optical pointers, interferometers and holographic visualization of surface strain and vibration 13 p2406 A70-28914

Laser beam photography by multiple reflections from partially reflecting mirrors 16 p2913 A70-33985

Electronically modified stroboscope as light source for multiflash photography of transient events, noting mechanical switches elimination 18 p3262 A70-37095

Magnetically focused two and four stage cascade picture amplifiers for astronomy and nuclear physics applications 20 p3630 A70-39426

Photographic images formation mechanism, examining streaks resolving power and total densities 20 p3632 A70-39747

High speed stroboscopic photography, discussing multiple flash and motion picture photography and TV operated strobe light [SMPT PREPRINT 42] 22 p4033 A70-43040

PHOTOINTERPRETATION

Satellite topocentric equatorial coordinates determination from photographic observations 02 p0363 A70-11773

Photointerpreters information extraction, studying psychological effects of image contrast and resolution on accuracy of target detection 02 p0300 A70-12459

Photographic negatives analysis, storage and reconstruction using facility permitting photography conditions simulation and computer image treatment 02 p0302 A70-12614

Stereocomparator and electronic computer used to determine aerial photographs relative orientation elements, discussing measurement error elimination 03 p0482 A70-13108

Space research photography role in studying earth and moon atmospheres and surfaces, determining spectral bands for contrast 03 p0483 A70-13168

Solar corona photographs for isophotes during solar eclipse of 22 September 1968 revealing chromospheric flare and prominences 03 p0569 A70-13362

Photometry as aid for aerial photography, discussing resolution, mapping, etc 03 p0486 A70-13554

Orbiter imagery analysis program for Apollo landing site selection, using photographic interpretive techniques 03 p0571 A70-13660

Lower E region turbulence interpretation based on high resolution photographs of artificial sodium vapor trails 03 p0476 A70-13913

Visual interpretation of moon and Mars surface photographs taken from satellites, analyzing craters and bumps 04 p0686 A70-14626

Cloud cover consequence on earth photographic space missions simulated by Monte Carlo method using worldwide statistics 04 p0676 A70-14636

Apollo 9 space photography of earth surface and use for quantitative analysis of earth resources, including supporting aircraft photography [AAS PAPER 69-572] 04 p0687 A70-14650

Plasma camera photographs of K plasma spatial distribution with electric fields and density gradients perpendicular to magnetic field, observing rotating irregularities around edge 04 p0728 A70-15005

Band shaped polar auroras widths from photographs analysis, noting wider bands for midnight hours and winter solstice 04 p0682 A70-15732

Geological contribution of satellite photography, discussing synoptic surveyability of vast areas and reduced scale maps of little known remote territories 05 p0837 A70-16073

Geological interpretation of aerial photographs, discussing picture quality, scale, film material and applications 05 p0840 A70-16499

Cartographic tying-in of Zond 3 lunar surface photographs to verify maps of moon far side 05 p0918 A70-16918

Meteor fragments motion and vaporization based on photographs 06 p1140 A70-17733

Optimal scale selection for aerial surveys by analyzing aerial photography data 07 p1278 A70-18690

Visual and quantitative image definition, evaluating microdetail clarity in panchromatic, IR, color and color IR aerial photographs 07 p1281 A70-19369

Visual perception of black-and-white photo in aerial photographic interpretation, examining processes in human brain 07 p1221 A70-19777

Aerial photographs interpretation methodology based on soil sciences taking into consideration reference level of photointerpreter 07 p1284 A70-19778

Lunar photography interpretation, discussing topographic maps obtained by spacecraft 07 p1284 A70-19779

Selenodetic investigations based on lunar photographs with background stars, converting equatorial coordinates to orbital using Cracovian formulas 08 p1564 A70-20560

Lunar Orientale region structure geological interpretation based on Lunar Orbiter 4 photographs 09 p1751 A70-22196

Remote sensing systems for vegetation analysis, discussing machine-aided photointerpretation methods for data analysis [AIAA PAPER 70-308] 09 p1678 A70-22879

Earth resources remotely sensed data analysis with emphasis on machine analysis over manual photointerpretation, discussing pattern recognition techniques, information systems, etc [AIAA PAPER 70-292] 09 p1678 A70-22891

Satellite photograph equatorial coordinates dependence on magnitude of evaluated region, objective distortion and transformation methods 09 p1679 A70-23056

Satellites equatorial topocentric coordinates determination from photographic observations 09 p1763 A70-23328

Analytical phototriangulation block equalization by two stage polygon method, discussing computer algorithm for problem solution 09 p1681 A70-23344

Photointerpretation applications to kaolin deposit detection, railway tunnel collapse analysis and highway drainage 10 p1873 A70-24075

Equidensity film advantages in photointerpretation relating to remote sensing in hydrology and land use 10 p1889 A70-24502

Satellite photographs for geological mapping and research assessed against interpretation of field data and conventional aerial photographs 10 p1876 A70-24640

Remote sensor input radiation at aperture, signals within and sensed data processing by computer techniques, noting automatic image interpretation 10 p1841 A70-24733

Intercensus population estimate by air photos, topographic maps and local and state census of population and housing 10 p1878 A70-24737

Forest inventory data collection by 70 mm photography, creating correction surface over model area of large scale pair 10 p1880 A70-24754

Polluted air mass concentration determined by photogrammetry, producing topographic type map with respect to vertical and oblique aerial photographs 10 p1880 A70-24755

Laser-light spatial-domain scanning function for deconvolution of blurred photographs using point-spread and holographic Fourier transform division filter 11 p2050 A70-25832

Classical astronomical photographic methods for reducing satellite photographs taking into account linear and nonlinear methods, analyzing random errors 11 p2006 A70-26184

Method of dependence involving triangulation applied to reducing photographs of earth satellites 11 p2006 A70-26185

Satellite observations reduction, determining continuous transformation over whole field of photograph by local transformations 11 p2007 A70-26187

Algorithms for transforming coordinates from photographic plate system to equatorial coordinates, noting applicability with unknown optical center position in plate system 11 p2007 A70-26188

Plate reduction method for Schmidt satellite camera, considering satellite position, distortion parameters, etc 11 p2007 A70-26193

Photographic plate reduction method at Polish Academy of Sciences based on sufficient reference stars, correcting x and y coordinates 11 p2007 A70-26194

Schmidt photographs reduction, noting film bending during exposure and mean error of satellite position 11 p2007 A70-26195

Film reduction and time keeping used at Smithsonian Astrophysical Observatory for Baker-Nunn films 11 p2007 A70-26196

Photographic reduction techniques at Meudon Observatory, discussing computation of standard and measured coordinates 11 p2007 A70-26197

Satellites photographic positions accuracy compared with stars based on stellar coordinates, investigating causes of difference 11 p2008 A70-26198

Photographic satellite plates reduction by astrometric method at geodetic institute at Potsdam, discussing star coordinates, astronomic refraction, etc 11 p2008 A70-26200

Solar corona photographs for isophotes during solar eclipse of 22 September 1968 revealing chromospheric flare and prominences 11 p2118 A70-26727

Residential urban environment data extraction from high and low resolution images 12 p2216 A70-26907

Gemini 12 photographs examined for urban and transportation data content 12 p2228 A70-26909

Spaceborne photography for detecting and identifying road networks, using color separation plates and photograph enlargement 12 p2216 A70-26910

Photography for geological interpretation, comparing color, color IR, and black-and-white photographs from spacecraft and aircraft 12 p2221 A70-26956

Landscape structure interpreting from aerial photos taken vertically from overflying aircraft 12 p2231 A70-27237

Aerial reconnaissance of soils, rocks, vegetation and streams, comparing color, IR color, and black-and-white photography 12 p2236 A70-27873

Automatic image interpretation and classification - Conference, Pisa-Tirrenia, Italy, August-September 1968 12 p2193 A70-28101

Automatic image interpretation and classification using two dimensional digital Fourier transforms 12 p2193 A70-28106

Methodology for machine processing for identification of individual crop types, discussing discriminant photoanalysis 12 p2227 A70-28108

Earth global photography by satellites, discussing photointerpretation 12 p2227 A70-28270

Venus photographs analysis during synoptic periods, noting inconclusive results on cloud layer and planetary surface structures 12 p2311 A70-28311

Satellite photographs interpretation for cloud types and patterns with allowance for transmission characteristics, image cut-off at corners and sun angle and glint 13 p2394 A70-28786

Quantitative analytic composite photography, performing image density point-to-point subtraction of two negatives 13 p2406 A70-28905

Photographic techniques and optical equipment in orbiter missions for lunar surface photography 13 p2407 A70-29164

Phobos image analysis on Mariner 7 frame 7F91, discussing surface darkness, limb profile and geometric albedo 13 p2492 A70-29266

Monograph on troposphere pressure, temperature and humidity and satellite TV photographs interpretation 13 p2446 A70-29786

Meteorological satellites TV pictures processing for hydrological information, emphasizing snow photographs interpretation 14 p2601 A70-30138

Sun glitter on sea surface from space photographs, considering wind and sea conditions effect on shape and brightness of patterns 14 p2572 A70-30345

Air photographs or imagery linear features, assessing sensors performance and developing interpretation criteria in photogeological research 14 p2573 A70-30641

Airphoto interpretation, discussing descriptive, digital and photographic methods of representing recognition process results 14 p2585 A70-30642

Band shaped polar auroras widths from photographs analysis, noting wider bands for midnight hours and winter solstice 14 p2575 A70-30815

Land use classification system of photointerpretation from remote sensor imagery 14 p2576 A70-30976

Soil characteristics determination from black and white, color and IR aerial photographs 14 p2577 A70-30980

Mixed hardwoods and pine area forest cover types identification by aerial photography 14 p2577 A70-30981

Lunar soil and rocks photometric and polarimetric properties from high resolution Surveyor pictures 14 p2644 A70-31054

Fringe interpretation in stress-holo- interferometry, emphasizing isopachic-isochromatic interaction effects in photoelastic analysis [SESA PAPER 1642] 15 p2739 A70-32309

Transistor densitometer used for variable star interpretation by amateur photographers 15 p2740 A70-32348

Lunar atmospheric pressure based on twilight horizon photographic data from Surveyor 7 15 p2803 A70-32500

Selenodetic investigations based on lunar photographs with background stars, converting equatorial coordinates to orbital using Cracovian formulas 15 p2805 A70-32715

Mariner 7, 8 and 9 lunar photographs, discussing evidence for internally heated moon 16 p2973 A70-33112

Optical filtering applied to aerial photointerpretation of oceanographic, archeologic and town planning data 17 p3081 A70-34620

Day and night IR imagery compared for interpreting vegetation 17 p3079 A70-35618

Gemini spacecraft photograph patterns revealing relationship between cloud formation and topography 18 p3258 A70-36298

Turbulent flows shadowgraph analysis, solving electromagnetic equations for optical response 18 p3242 A70-36692

Geometric methods for processing TV images of earth cloud cover 18 p3286 A70-36964

Lunar volcanic ridges features from interpretation of photographs by telescopes and satellites 19 p3418 A70-37992

Satellite TV cloud picture digital representation, deriving algorithms for statistical analysis of geometrical features 19 p3463 A70-38755

Mach-Zehnder interferometer for holographic investigation of inhomogeneities in transparent media, discussing photointerpretation error reduction 20 p3633 A70-39749

Orbital photography interpretation from test rockets and Apollo-Gemini spacecraft, considering environmental applications 20 p3634 A70-40321

Impact times measurement by photography, correlating projectile velocity with projectile- target distance 20 p3635 A70-40530

Natural and cultural landscape pattern classification in aerial photointerpretation using land-system concept 21 p3826 A70-41401

Internal and integral photointerpretation in aerial photography, discussing landscape information reliability increase by interdisciplinary method 21 p3826 A70-41403

Instrumental and atmospheric observational problems regarding dark mottles, fibrils and H alpha solar limb photographic interpretations 21 p3926 A70-42199

Image holography nonlinearities analysis, using photographic film characteristics for phase deviation enhancement 22 p4031 A70-42951

Horizontal passpoint error in block analytic aerotriangulations with dense perimeter ground control 22 p4031 A70-42964

Mapping from satellite-collected earth surface images, emphasizing optical/mechanical scanner images 22 p4037 A70-43089

Lunar atmospheric pressure based on twilight horizon photographic data from Surveyor 7 23 p4240 A70-43921

North Carolina continental shelf discolored water origin, movement and dissipation from Apollo 9 photograph interpretation 24 p4329 A70-45361

Flood plain boundaries delineation by panchromatic and color airphoto interpretation 24 p4329 A70-45362

PHOTOIONIZATION

Spectral distribution of X ray atmospheric absorption used to determine high energy photoelectrons spectrum 01 p0172 A70-11494

Diffuse soft X ray photoionization and heating of H I regions compared to cosmic ray heating 02 p0364 A70-11784

Photoelectron energy spectra and partial photoionization cross sections for carbon dioxide determined with spectrometer at monochromatic incident radiation wavelengths 02 p0343 A70-11903

Production rate constants for hydrated positive ions in photoionized nitric oxide-water afterglows 07 p1346 A70-20245

Nitrogen molecule photoabsorption and photoionization cross sections determination, discussing ionization probability variations and radiationless transitions 07 p1347 A70-20358

Charged particle interaction influence on photoionization cross section of negative hydrogen ion, considering initial state polarization leading to free s wave electron 09 p1732 A70-22826

Quasars photoionization of intergalactic high density hydrogen gas to interpret absorption features absence, noting gas temperature 10 p1942 A70-24628

Threshold photoionization cross sections for homonuclear diatomic N molecules calculated from Slater orbitals and Coulomb waves 11 p2086 A70-25833

Chemical kinetic model for photoexcitation and photoionization of cold argon ahead of strong shock wave, predicting electron and excited atom concentrations [AIAA PAPER 68-666] 11 p2090 A70-25953

Ruby laser beam used to trigger high voltage spark discharge in vacuum, studying auxiliary photoionization during firing delay or failure 12 p2249 A70-27999

Radial wave functions and photoionization cross sections for neutral atoms from central potential model based on Slater and Klein-Brueckner approximations 13 p2455 A70-29133

Molecular oxygen positive ion density in upper ionosphere as function of photoionization, ambipolar diffusion velocity and altitude effect 13 p2399 A70-29233

F I region ion structure diurnal variations, calculating photoionization rates 14 p2571 A70-30227

Hydrogen UV geocorona photoionizing effect on nighttime E region electron density in low and midlatitudes, comparing with ionosonde data 14 p2581 A70-31270

Thermal energy negative ion-molecule reactions in photoionized NO-water vapor mixtures, determining rate constants by stationary afterglow system 16 p2954 A70-33280

Cosmic X rays interstellar absorption, giving atomic He total photoionization cross section 18 p3308 A70-36899

F region photoionization rate vs height twin peak profile in presence of temperature maximum, taking into account ionization of atmospheric gases by quasi-monochromatic radiation 18 p3254 A70-37031

Alkali metals ionization by photons and atomic projectiles, discussing results in first Born approximation 20 p3676 A70-40153

Photoionization cross sections for atoms and ions of carbon, nitrogen, oxygen and neon as function of wavelength for H II regions and planetary nebulae 22 p4104 A70-42997

Upper atmosphere photoionization by extreme UV solar radiation compared with ionization by charged particles collisions 22 p4096 A70-43302

Bremsstrahlung X rays caused by energetic electrons precipitating into upper atmosphere, calculating photoionization rate as function of altitude 22 p4096 A70-43310

Laser induced gas breakdown, considering plasma generation and properties 23 p4225 A70-44185

Multiphoton gas ionization by coherent radiation, showing electron transitions role with gas ionization model 23 p4201 A70-44205

Autoionization theory application to partial solar photoionization cross sections for production rates of vibrationally excited positive molecular oxygen ions 23 p4222 A70-44785

Upstream gas photoionization caused precursor ionization effects on MHD switch-on shock structure 24 p4382 A70-45106

F I region ion structure diurnal variations, calculating photoionization rates 24 p4331 A70-46302

PHOTOLUMINESCENCE

NT X RAY FLUORESCENCE

Rapid photoprocesses decay kinetics, using CW Ar ion laser beam interrupted periodically by electro-optical shutter 02 p0314 A70-12742

Reflected light directional diagram effects on scintillating surface luminescence yield, considering scattering function gradient 12 p2231 A70-27310

Electric field heating effect on edge photoluminescence of n-type GaAs, noting increase in electron energy 12 p2286 A70-27368

Semiconductor luminescence and photodetector diodes near IR region transmission, describing frequency response measurements 22 p4087 A70-43445

Daytime near horizon atmospheric luminescence measurement by Cosmos 224 satellite, discussing contributions of nitrogen and aerosol and Rayleigh scatterings 23 p4188 A70-44061

Threshold characteristics of injection and electron excitation semiconductor lasers having photoluminescence properties of n-type GaAs single crystals 23 p4203 A70-45065

UV excited powdery fluorescent products, describing cryostat for photo and thermoluminescence at various temperatures 24 p4339 A70-46097

PHOTOLYSIS

NT RADIOLYSIS

Methane photochemistry in Jupiter atmosphere, investigating acetylene, ethylene and ethane photolysis 02 p0367 A70-11815

Xenon sensitized photolysis of carbon dioxide compared with direct photolysis at 1470 A resonance line 03 p0441 A70-14005

Vacuum UV flash photolysis of carbon suboxide, noting pressure dependent reaction rates of carbon atoms with various gases 04 p0645 A70-14391

Photoelimination of N from fused-ring triazoles in methanol 05 p0810 A70-16046

Dicyanostilbene formation from phenylethyne azide and isocyanate 05 p0811 A70-16054

Radicals in low pressure supersonic free jets, investigating production by flash photolysis 07 p1343 A70-20126

Bromine monoxide formation by atomic oxygen-bromine reaction in flash photolysis of bromine-nitrous oxide and bromine-nitrogen dioxide mixtures 08 p1455 A70-21342

Photolytic reactions mechanism in photochromic glass with silver halide crystals formed during glass manufacture, discussing properties and applications 08 p1499 A70-21683

Specific intensity production from photolysis of ozone-oxygen mixtures at 2537 A, investigating mechanism 10 p1831 A70-24565

Quenching efficiency of molecular oxygen relative to nitrogen, carbon monoxide, carbon dioxide and argon, involving photolysis of gas mixtures 13 p2361 A70-28498

Ketene and diazomethane flash photolytic measurement of reaction rates of singlet-triplet methylene deactivation 15 p2694 A70-31729

Direct sensitized photolysis of various dichlorobutanes yielding HCl 16 p2855 A70-33089

Pressure effects on quantum yields of carbon trioxide formation in gas phase ozone photolysis with carbon dioxide 16 p2856 A70-33653

Surface recombination centers protecting against discoloration of thermal control coatings due to chemical changes induced by photoproducts holes and electrons in oxide pigments 16 p2940 A70-33935

[AIAA PAPER 70-830] Molecular oxygen role in photolytic decomposition of ozone by intermediate quantum yield method, presenting rate constants 16 p2858 A70-34009

Oxadiazolone pyrolytic and photolytic fragmentation, noting intramolecular cyclizations and intermediate azomethine nitrene production 17 p3041 A70-34771

Photolysis of 3-phenyl-oxadiazol-5-one by UV irradiation, eliminating carbon dioxide 17 p3041 A70-34772

Aniline and o-anisidine production by photoelimination of nitrogen from fused ring triazoles 17 p3042 A70-34821

Optical charge transfer transitions in N-alkyl iodide salts, examining transient absorptions due to flash photolysis 18 p3226 A70-36765

Photolytic model of Jupiter belt excess temperatures and coloration compared to solid ammonia clouds, using IR and visual observations 19 p3513 A70-37410

PHOTOMAGNETIC EFFECTS

Photoconductivity and photomagnetic effect measurements in Ge for determining nonequilibrium current carrier concentration produced by Q switched neodymium laser 01 p0107 A70-10099

Carrier drift due to electromagnetic impulse, deriving expressions for photo emf generated in transverse magnetic field manifesting monopolar photomagnetic effect 13 p2452 A70-29282

PHOTOMECHANICS

U PHOTOGRAPHY

U PRINTING

PHOTOMETERS

NT ELECTROPHOTOMETERS

NT ULTRAVIOLET SPECTROMETERS

NT ULTRAVIOLET SPECTROPHOTOMETERS

Pritchard photometer analyzed for in-focus and out-of-focus operation using radial weighting function 01 p0091 A70-10918

In-flight radiometric calibration of low brightness OGO 4 airglow photometer 04 p0696 A70-15645

Compact and fully automatic fixed photometer for zenith measurements of night airglow intensities, calibrating sky observation through filter by constant intensity light source 05 p0845 A70-15821

Atmospheric turbidity measurements over U.S. using Volz sunphotometer 06 p1098 A70-18245

Photometric error analysis and optimum use of photomultipliers, discussing pulse-height spectra, detection and weighting systems 06 p1071 A70-18517

Analog computing spectral photometer for high temperature measurements in gas flames 07 p1285 A70-19896

Word organized photodetector array design for holographic read-only optical memories 07 p1288 A70-20148

High sensitivity photomultiplier TWT microwave photodetector with internal lowered secondary electron multiplier and spiral HF getter 09 p1645 A70-22413

Photodetector-electronic circuit matching channels for optical communication system, using minimum risk design criterion 12 p2237 A70-28153

Ballistic pulsed photometer calibration without etalon light pulse using radiation sensitivity, oscillation period and galvanometer damping 12 p2338 A70-28179

Balloon-borne photometer for collecting twilight and daytime OH intensity and rotational temperature variations data 13 p2399 A70-29240

Photodetector properties influence on optron transfer functions achieving light conversion by separating photocarriers with p-n junction 14 p2555 A70-30161

Photothermometer response to thermal shock, considering rapidly varying surface temperature measurement 16 p2901 A70-33104

Mercury cadmium telluride photodetectors, analyzing gain, signal current and radiation limits 16 p2905 A70-33153

Twilight sky brightness measurements at 5200 A for estimating upper atmospheric dust component, discussing error rates 16 p2899 A70-34184

Photodetector frequency response measurement, using beat light signals from mixed single mode He-Ne lasers 17 p3108 A70-35688

Far UV photometer for space research, isolating specific bands by combining spectral response of individual solar blind photocathodes with thin metallic films transmission qualities 17 p3096 A70-35766

Azimuthal moon telescope installation at cosmic ray station, noting photorecorder circuitry 18 p3256 A70-36108

Angular and geometric properties of actinometers, pyroheliometers and photometers, measuring direct and scattered circumsolar radiation 20 p3625 A70-39028

Amplitude modulated optical band signal detection, comparing optimal direct photodetector and superheterodyne receivers sensitivities 21 p3785 A70-40633

High speed photodetectors for microwave demodulation of light, discussing electrical properties, equivalent circuits and noise factors 21 p3799 A70-41420

Fluctuating light pulse packet detection by inertialess photodetector, deriving optimal algorithm 22 p3987 A70-42554

Semiconductor luminescence and photodetector diodes near IR region transmission, describing frequency response measurements 22 p4087 A70-43445

Signal arrival time variance in optical communication system with high lag photodetectors, examining input, detection and amplification noise 23 p4196 A70-44410

Subminiature transistor photosensor for direct measurements of capillary blood cell motion 24 p3409 A70-46119

PHOTOMETRY

NT ASTRONOMICAL PHOTOMETRY

NT ELECTROPHOTOMETRY

NT SPECTROPHOTOMETRY

NT STELLAR SPECTROPHOTOMETRY

NT TELEPHOTOMETRY

NT ULTRAVIOLET PHOTOMETRY

NT VISUAL PHOTOMETRY

Quantitative method developed for photometric determination of B in nickel or titanium borides, using magnezon I reagent in alkaline solutions at various pH 03 p0504 A70-12983

Photometry as aid for aerial photography, discussing resolution, mapping, etc 03 p0486 A70-13554

Optical facilities of Apollo 11 mission and NASA Manned Spacecraft Center noting Fzadow telescopes, lunar cartography, photometric surface analysis, etc 04 p0687 A70-14690

Prelaunch photometric calibration of Surveyor TV system for reconstruction of lunar terrain televised pictures permitting system lunar performance prediction [AIAA PAPER 68-1138] 04 p0692 A70-15405

Automatic measurement of frequency-contrast characteristics of photographic films using linear, photoelectric and high speed comparator devices 05 p0852 A70-16865

Sensitivity distribution in working field of electro-optical converter tubes, noting use for photometric research 09 p1673 A70-22159

Auroral pulsation observed by Aerobee rocket instruments and ground multichannel photometer indicating primarily temporal fluctuation 09 p1671 A70-23497

Remote sensing of lunar photometric function at small phase angles by Apollo 8 command service module

12 p2297 A70-26926

Photometric determination of Ti with diantipyryl-methane in steels containing Se

18 p3277 A70-36465

Projection of integrating photometric spheres, discussing angular dependence on wall thickness, radiation losses and aperture dimensions

18 p3260 A70-36974

PHOTOMICROGRAPHY

Electrical and photographic methods for measuring microcracking in fiber reinforced plastics

08 p1501 A70-21916

Ti-Al-Zr-W-Si alloy fracture surface concentric markings number related to loading cycles after crack formation

10 p1904 A70-24837

Impact crater cross section in fused silica, describing photomicrographic technique for distinguishing hypervelocity from low energy impacts

[ALAA PAPER 69-367] 11 p2138 A70-26133

Water drop-solid surface collision experiments to study rain impact erosion process, using gas gun projectiles, high speed photography, photomicrography and profilometry techniques

22 p4116 A70-43096

PHOTOMULTIPLIER TUBES

Photomultiplier tubes for counting photoelectrons from photocathode, discussing pulse height distributions, SNR, quantum counting, statistical correlation and dark current properties

01 p0090 A70-10902

Spectrophotometric facility for measuring spectral characteristics of color filters, photomultipliers and photographic plates as function of temperature

02 p0301 A70-12494

Photocathode internal light scattering effect on photomultiplier time response

05 p0845 A70-15806

Duration measurements for sampling function in dynamic crossed field photomultiplier

05 p0849 A70-16655

Response variation and detection efficiency of funnelled channel electron multipliers for low energy protons and Ar ions

06 p1021 A70-17623

Photometric error analysis and optimum use of photomultipliers, discussing pulse-height spectra, detection and weighting systems

06 p1071 A70-18517

Signal to noise ratios and fluctuation spectrum of photomultiplier illuminated by laser passing through laser amplifier, noting population level effect

07 p1300 A70-19869

Heavy positive ions pulse counting by spiral-type continuous channel electron multiplier, noting long pulse rise time composed of numerous after pulsing

07 p1286 A70-19970

Secondary electron emission coefficients and energy distributions to investigate interaction between positive ions and Cu/Be dynodes of electron multiplier

07 p1344 A70-20127

Pulse characteristics of scintillator-photomultiplier-cathode ray tube channel for oscillographic recording of nanosecond pulses from neutron, gamma or X ray sources

08 p1496 A70-21218

High sensitivity photomultiplier TWT microwave photodetector with internal lowered secondary electron multiplier and spiral HF getter

09 p1645 A70-22413

Preamplifier-discriminator-gate generator in printed circuit for use with photomultipliers, noting pulse sensitivity and cost

09 p1679 A70-22997

Fatigue effects of incident illumination on area sensitivity, dynode gain stability and anode output for end-on photomultipliers

09 p1683 A70-23511

Channel electron multipliers design and operation, investigating parameters influencing amplification, resolving power and response probability

10 p1888 A70-24484

Cosmic ray muons continuous recordings, describing design and performance of plastic scintillators with photomultipliers

10 p1889 A70-24489

Lead type channel electron multipliers gain degradation in ultrahigh vacuum

10 p1849 A70-24557

Open magnetic electron multipliers (MEM) with continuous dynode and field strips for satellite-borne detection systems, emphasizing extreme UV detectors

11 p2049 A70-25628

Hybrid Cockcroft Walton multidynode photomultiplier supply for space applications, using miniature components and thick film technology

12 p2233 A70-27406

Photomultipliers single electron response by measuring electron pulse height distribution

12 p2236 A70-27850

Photomultiplier tubes for liquid scintillation equipment, emphasizing detection efficiency and coincidence background

14 p2587 A70-31005

Temporal dependence of photoelectron multiplier output waveform and focusing under photocathode alternating modulation, noting thresholds for optical reception

15 p2696 A70-31505

Photomultiplier tubes high quantum efficiency attainment by optical enhancement techniques

15 p2735 A70-31767

Open type secondary electron multipliers, discussing circuitry, emission recording, component materials and performance

16 p2873 A70-33231

Residual gases partial pressure measurement in vacuum chamber by mass spectrometer with electromagnetic scanner and electron multiplier, detecting electron current

19 p3421 A70-37466

Spurious photomultiplier response to short intense overexposure of atmospheric return using optical radar

21 p3828 A70-41474

Continuous channel electron multipliers (Channeltron) gain improvement via blanking method avoid detection of unwanted particles

23 p4197 A70-44477

PHOTON ABSORPTION

U ELECTROMAGNETIC ABSORPTION

PHOTON BEAMS

NT LIGHT BEAMS

Laser radiation coherence origin explainable by mechanism consisting of many photon emission process by many atoms

05 p0883 A70-16500

Photon propulsion with constant power in exhaust beam and intragalactic travel in force free space from solving relativistic rocket equations

06 p1132 A70-18105

Photon scattering in inhomogeneous medium, deriving expressions for mean number of photons escaping or annihilated in medium

07 p1376 A70-18910

P-n junction photovoltaic cell excitation by two photon absorption with low bandgap energy

19 p3446 A70-37764

High power neodymium laser with aspherical lenses to focus photon beam for nuclear fusion experiments

19 p3447 A70-38165

CW gas laser improvement, discussing optimum efficiency and photon beam spatial distribution

21 p3836 A70-41419

Photon flow delay regarding fluctuating source field in two points, applying correlation statistics by Pearson method of moments

22 p3988 A70-42564

PHOTON DENSITY

Constricted DC Ar arc with N or O additions calibrated as vacuum UV radiation standard for photon flux measurements

02 p0343 A70-11905

Superfluorescence losses in large aperture disk laser systems using Monte Carlo method, determining maximum population inversion from enhanced photon flux density considerations

03 p0503 A70-14209

Measurement method for second and third order photon intensity correlation functions, using optical field produced by gas laser operating near oscillation threshold

04 p0700 A70-14686

Very high energy cosmic rays disintegration and energy degradation by intense blue shifted photon fields of supernovae quasars and pulsar models

04 p0742 A70-15300

Optical position estimation model based on defining photon density profile center of gravity in noise, using photon Poisson process theory

04 p0652 A70-15337

Atmospheric X ray photons measured regularly by sounding balloons in U.S.S.R., discussing X ray photon flux relation to charged particle fluxes

07 p1367 A70-19445

Radiation field photon density matrix for gas laser with ring resonator determined from double level atomic model, considering photon dispersion and wave reflection feedback

08 p1513 A70-21420

Solar XUV lines photon flux based on one dimensional model of chromosphere-corona transition region

10 p1949 A70-25271

Atmospheric X ray photons measured regularly by sounding balloons in U.S.S.R., discussing X ray photon flux relation to charged particle fluxes

18 p3309 A70-36919

Photon occurrence moments probability distribution in partially coherent light signals

22 p3988 A70-42563

PHOTON-ELECTRON INTERACTION

Dispersed fluorescence spectra from vacuum UV photon impact on COS, noting absence of emission from higher vibrational levels

01 p0148 A70-11353

Collection of papers on optics covering dielectric multilayer filter synthesis, photographic image, light interaction with free electrons, laser radiation, optical echoes, etc

02 p0340 A70-12828

Nonlinear parameter of two intersecting laser beams in interaction with free electrons plane wave external field coupling

09 p1695 A70-22213

Photon capture cross sections for surface silicon electronic states using IR photoconductivity measurements

17 p3144 A70-35707

Laser light effects on electron beams, considering absence or presence of crystalline optically transparent solid

24 p4353 A70-45564

PHOTONEUTRONS

Bremsstrahlung and photoneutrons from electron-photon cascades in thick tungsten and tantalum targets bombarded with low energy electrons

20 p3674 A70-39222

PHOTONIC PROPULSION

Photon propulsion with constant power in exhaust beam and intragalactic travel in force free space from solving relativistic rocket equations

06 p1132 A70-18105

PHOTONS

Threshold laser power density-atom density relation in cesium vapor optical breakdown, suggesting two photon ionization process

01 p0110 A70-10569

Radiation effects on postshock gas state, noting shock wave optical thinness dependence on radiative cooling and photon flight time

02 p0277 A70-11867

Optical and radio pulses from pulsars as test of light speed variation with frequency and photon mass possible existence

02 p0373 A70-12394

Soviet book on quantum electrodynamics covering photon mechanics, electron relativistic mechanics, electromagnetic interactions, corrections to Green functions, particle interactions, etc

02 p0345 A70-12827

Transparent bodies photon thermal conductivity temperature dependence

03 p0515 A70-13206

Phonon-photon scattering intensity and line shape used to study laser-excited impurity centers dynamic characteristics in stimulated induction regime

03 p0499 A70-13256

Balloon-borne experiments with directional scintillators to measure low energy gamma radiation spectrum in midlatitude atmosphere for photons origin and gamma albedos investigation

03 p0561 A70-13996

Photon number per mode for laser with nonresonant feedback for homogeneous and inhomogeneous atomic line broadening

06 p1081 A70-17746

Laser emission photons scattering by semiconductor conduction electrons allowing for electron-phonon interaction

07 p1357 A70-19857

Tensor analysis of four photon interaction in rarefied plasma in magnetic field, determining cubic current of plasma wave self action

08 p1554 A70-21805

Two photon interaction between ultrashort light pulse and medium, showing pulse propagation through medium without absorption

08 p1514 A70-21820

Photon scattering by Ar in vacuum UV measured for cross sections

09 p1730 A70-22071

Vacuum UV photons production during ground state neutral argon atomic collisions, measuring relative cross sections energy dependence

09 p1731 A70-22333

Dual photon emission from chemiluminescent SO-O reaction, proposing two step emission mechanism

09 p1630 A70-23001

Coherent photon responses production in liquids and glasses by superposing trains of giant laser pulses, achieving spatial separation of responses by combining pulse trains

10 p1900 A70-24564

GaAs light amplifier p-n junction gain and output noise determination for wide photon energy ranges, studying input noise levels effects on sensitivity

10 p1928 A70-25167

Photon nature, considering light-magnetic flux similarities

11 p2084 A70-26027

Saturation homogeneity ascribed to resonant photon capture in emission of neon laser

12 p2247 A70-27508

- Photon lifetime dependence on hole and electron concentration in GaAs from IR reflection spectra analysis 13 p2470 A70-28882
- Metastable He ion two photon decay, observing photon coincidence angular correlation in spectral distribution 13 p2456 A70-29811
- Atom excited state mean lifetime measurement, using correlated cascade photons method 14 p2620 A70-31378
- Cosmic X ray and gamma ray spectral energy distribution slope change explained by measurement process involving photon spectrum 15 p2792 A70-31431
- Time controllable continuous photon emission from plasma produced by pulsed laser vacuum spark applied to absorption spectroscopy in vacuum UV 15 p2734 A70-31757
- Continuous differential energy pulse height spectra reduction to photon upper atmospheric spectra 15 p2694 A70-31800
- Low light intensities measured using photon counting method, comparing signal to noise ratio with lock-in method 16 p2911 A70-33524
- Probabilistic model for radiative transfer of photons in inhomogeneous infinite cylindrical shell medium, noting radiation intensity relation to scattering and transmission functions 16 p2952 A70-33785
- Critique of paper on Crab Nebula pulsar pulsed gamma ray emission, considering photon flux and statistical data analysis 17 p3149 A70-34565
- Energy loss of high energy cosmic rays traversing isotropic radiation field of arbitrary energy spectrum in pair producing collisions with ambient photons 17 p3150 A70-34598
- Simultaneity in optical photon pairs parametric production, verifying quantum mechanical description of fluorescence 17 p3143 A70-35187
- Light combinatorial scattering by longitudinal photons with frequency near forbidden zone width, calculating Raman scattering cross sections 19 p3444 A70-37444
- Flare associated high energy photon and particle fluxes characterized by short rise times and longer lasting decays, discussing plasma emissions 19 p3493 A70-37473
- Atmospheric fluorescence observation of supernova energetic photon short pulse burst, using photomultiplier 19 p3500 A70-38079
- High energy galactic gamma rays photons, suggesting two-component cosmic ray source model 19 p3505 A70-38115
- Energy spectrum distortion of ultrahigh energy cosmic rays due to interactions with photons and neutrinos in universe 19 p3510 A70-38155
- Photon pair annihilation process in graviton pair, examining IR emission in two scalar particle collision 19 p3472 A70-38172
- High energy cosmic ray-photon interactions, discussing ion production, nuclear fission, proton energy loss, red shift, etc 20 p3696 A70-39283
- Gas dynamic quantum amplifier improvement, discussing power utilization, photon distribution and radiation transport 21 p3836 A70-41418
- Phosphor-output image intensifier response to single photon inputs in multichannel spectrophotometer for faint optical sources 23 p4195 A70-44291
- Scattered photon effects on cosmic diffuse X ray spectrum at balloon altitude, noting overcorrection for absorption of primary X rays 23 p4237 A70-44794
- Radiation detectors with superconducting weak links response to single photons, considering Mercereau ring interferometer 24 p4391 A70-46256
- PHOTOOXIDATION**
Electron transfer mechanism between photoact I and II from redox reactions observation with modulated polarograph 13 p2363 A70-29815
- Nucleic acids constituents reactions with singlet oxygen, determining oxidation mechanism in photodynamic processes 21 p3781 A70-42025
- PHOTOPIEZOELECTRICITY**
U PHOTOELECTRICITY
U PIEZOELECTRICITY
PHOTOPLASTICITY
Photoplastic method for modeling of plane elastoplastic problems, comparing results with photoelastic coating method to estimate transition errors from model to prototype 10 p1965 A70-25320
- Macrolon elastic-plastic strain model, studying stress-strain relationship and optico-mechanical properties 11 p2128 A70-25385
- Photoplastic material thickness change from mechanical and holographic measurements, showing correlation with isochromatics during plastic yielding 15 p2821 A70-32314
- PHOTORECEPTORS**
Degenerate retinal fibers in duck photoreceptor path connecting to suprachiasmatic hypothalamic region detected following optic nerve dissection 03 p0427 A70-13955
- Molecular structural relationship between cellular membranes and photoreceptors in plants and animals 16 p2847 A70-33028
- Human eye early receptor potential, investigating contributions of rods and cones 17 p3034 A70-35896
- Isochromic change in bleaching of rhodopsin, showing additional intermediate without detectable color change 23 p4147 A70-44776
- PHOTORECONNAISSANCE**
Royal Air Force air reconnaissance function, discussing cameras, films, processing and printing, photointerpretation, etc 03 p0495 A70-14144
- Wideband transmission of photographic reconnaissance information over long distances using Initial Defense Communication Satellite Program satellites 06 p1006 A70-17346
- PHOTOREDUCTION**
U PHOTOCHEMICAL REACTIONS
U REDUCTION (CHEMISTRY)
- PHOTORESISTIVITY**
U PHOTOCONDUCTIVITY
- PHOTORESISTORS**
U PHOTOCONDUCTORS
- PHOTOSENSITIVITY**
NT LIGHT ADAPTATION
NT PHOTOTROPISM
Light pulse demodulator using zero crossing technique to eliminate photomultiplier bandwidth and sensitivity limitations 02 p0271 A70-12744
- Coordinate-sensitive photocells with heterojunctions between wideband semiconductors, noting increased longitudinal photovoltage 03 p0541 A70-13722
- Previous radiation exposure effect on photographic film noting increased sensitivity at UV frequencies 06 p1065 A70-17890
- Human eye sensitization and dark adaptation, noting annular surrounding light addition effect on rod threshold 08 p1447 A70-21723
- Hypersensitization of IR films for use in stellar photometry, discussing laboratory and astronomical tests 09 p1673 A70-22158
- Sensitivity distribution in working field of electro-optical converter tubes, noting use for photometric research 09 p1673 A70-22159
- High resolution holography with pulsed radiation source, testing various emulsions for sensitivity and reciprocity behavior 09 p1681 A70-23175
- Photosensitivity and scanning of planar Si photodiode image detector arrays, using most ring counter and shift register 10 p1846 A70-23881
- Color radiography with photographic negative film exposed to X rays, obtaining same thickness latitude with improved detail sensitivity on single emulsion line 10 p1887 A70-24168
- Differential luminance sensitivity of human eye using signal detection theory, correlating discrimination and detection results with electrophysiological data 10 p1812 A70-24599
- Nb and Nb alloys activation in polarized light by etching technique, observing grain contrast improvement 10 p1906 A70-25229
- Optical absorption due to imperfections in CdS by sensitive differential technique using laser excitation 13 p2430 A70-29708
- Electron transfer mechanism between photoact I and II from redox reactions observation with modulated polarograph 13 p2363 A70-29815
- Protective coatings for silicon photosensitive elements to reflect incident energy at wavelengths not participating in conversion into electricity 15 p2677 A70-31599
- Disadapting photostimulation effect on light sensitivity restoration of human visual analyzer, obtaining dark adaptation curves 15 p2679 A70-31603
- B, In or Ga doped Si photosensitivity dependence on sample temperature, supply voltage and illumination intensity, determining optimal operating conditions 15 p2782 A70-31631
- Steady state evoked potentials Fourier analysis from human scalp during psychophysical procedure of heterochromatic flicker photometry, obtaining spectral sensitivity curve 15 p2682 A70-32015
- Brightness matching and sensitivity to sinusoidal flicker for various contrasts as function of surround field luminance 15 p2683 A70-32016
- Thin film solar cells photosensitivity improvement by semiconductors with graded energy gap, describing construction techniques and electrical properties 15 p2678 A70-32420
- Visual IR laser beam displayer, using cathode ray tube phosphor with variable sensitivity and range control 15 p2752 A70-32441
- Hill reaction color sensitivity in red and blue light during chloroplast disintegration, considering oxygen evolution capacity 15 p2684 A70-32548
- Broadband image pick-up tube with high near IR sensitivity, comparing performance with other vidicons 16 p2907 A70-33186
- Photographic materials for holography, discussing spectral sensitivity, grain size, resolution, transfer functions, diffraction efficiency, etc 17 p3084 A70-35003
- Photosensitivity and electroluminescence spectra of GaAs-indium gallium arsenide p-n heterojunctions at room temperature 17 p3144 A70-35708
- Visual contrast sensitivity adaptation to temporal frequencies using high modulation sinusoidal grating 17 p3034 A70-35898
- Circadian oscillations and photoperiodic time measurement in *Pectinophora gossypiella* 18 p3221 A70-36893
- Meteor spectrosensitometric properties of panchromatic plates and films for aerial photos, investigating parametric conditions effect on image quality 19 p3422 A70-37653
- Circadian rhythms in single cell animals, examining cell division, temperature and light effects 19 p3365 A70-38410
- Photoperiodism in animal organism, discussing retinal epithelium photosensitive substance accumulation and retino-hypothalamo-hypophyseal mechanism of pigmentation 19 p3365 A70-38413
- Photographic emulsions and photosensitive materials for holography, measuring noise spectral power density at high spatial frequencies by scattered light method 21 p3822 A70-40812
- Holographic photopolymer recording systems, discussing sensitivity, reconstruction, fixing, etc 21 p3829 A70-41926
- Diazo compounds purity effect on photosensitive photographic film quality, determining color image reproduction density 24 p4334 A70-45498
- X ray films sensitometric investigation in medical and industrial radiography, evaluating HVL and ISO methods for X ray quality 24 p4337 A70-45710
- Photographic paper as emulsion film substitute in industrial radiography, evaluating sensitivity and image contrast 24 p4337 A70-45715
- PHOTOSENSORS**
U PHOTOELECTRICITY
U RADIATION MEASURING INSTRUMENTS
- PHOTOSPHERE**
Photospheric Fe I abundance variation with excitation potential 01 p0175 A70-10239
- Solar corona magnetic field determination from photospheric magnetic field line-of-sight component observations, describing various mathematical methods 01 p0176 A70-10250
- Solar photosphere temperature fluctuations from model consistent with convection hypothesis agreeing with limb darkening data 03 p0570 A70-13591
- One dimensional magnetograph scans studying photospheric velocity oscillations and supergranulation, noting downward flows coincident with chromospheric network 03 p0570 A70-13593
- Solar photospheric Fe abundance determined from IR supermultiplet line spectra, considering LTE effects 04 p0749 A70-14597
- Solar radio emission intensity-solar flare index and 5303 A coronal line intensity-proton flare numbers relations 05 p0911 A70-16438

Flare radiation influence on high photospheric and low chromospheric lines in H alpha, H and K regions
05 p0902 A70-16439

Solar core opacity influence on revised photospheric iron abundances, discussing neutrino flux prediction doubling in solar models
05 p0905 A70-16985

Photospheric magnetic flux quantization away from sunspots, studying nonsunspot field strength distribution
06 p1142 A70-17992

Wilson effect in sunspot structure as penumbra foreshortening and disappearance or penumbra occultation by photosphere, analyzing intensity profiles on disk passage photographs
06 p1143 A70-18001

Turbulent velocities of convective motions in active and unperturbed photospheric faculae based on spectral observations
07 p1384 A70-19415

Faculae and flocculi intensity relationship to orientation of magnetic fields in solar photosphere and magnetosphere
08 p1560 A70-20837

Brightness distribution of spectroheliograms taken in metal lines reflecting velocity field structure in photosphere
08 p1570 A70-20839

Solar and stellar convection regions and coronas using photospheric models, taking into account molecule formation
08 p1581 A70-21953

Fe abundance in solar photosphere, evaluating various determination methods
09 p1753 A70-22382

Sunspots photospheric layers magnetic field structure, analyzing anomalous Zeeman pi-components in umbra
09 p1757 A70-22685

Homogeneous model solar photosphere in strict radiative equilibrium with depth-dependent line blanketing by neutral and ionized metals
09 p1757 A70-22728

Small scale motions in solar photosphere and chromosphere using solar spectrograms
09 p1757 A70-22729

Penumbra magnetic field strength on basis of photoelectric spectra of undisturbed photosphere
09 p1757 A70-22730

Triatomic hydrogen ion role in solar photosphere opacity implied from limb darkening and specific intensity data
11 p2104 A70-25739

Solar photospheric turbulence from observing Ti I line profiles at different center to limb distances, showing anisotropy
11 p2116 A70-26591

CH molecule line formation mechanism for 4300 A transition in solar photosphere, noting collisions with hydrogen atoms
12 p2311 A70-28309

Dark band in H alpha solar chromosphere above photospheric limb, outlining approaches to obtain spectrally pure observational results
13 p2486 A70-28627

Magnetic field spatial structure in sunspot with photospheric bridge, using photographic observations of solar spectrum lines
13 p2493 A70-29391

Formation mechanism of molecular CN violet bands in solar photosphere
13 p2493 A70-29393

Photosphere model and magnetic field gradient effects on line contours and magnetographic calibration curves, using nonlinear source function
13 p2496 A70-29845

Sudden disappearance of large quiescent prominence on solar disk with subsequent brightenings, using photospheric and gravitational model
13 p2497 A70-29850

Herschel effect in UV solar photography in developing autographic photographic film for bright photospheric recording
13 p2497 A70-29853

Polar and equatorial limb darkening related to solar rotation and thermal flow, using photospheric models
15 p2807 A70-32812

Photospheric magnetic fields by magnetograph during and one week before and after eclipse of 7 March 1970
16 p2977 A70-33844

Solar disk center to limb variation of Fraunhofer lines, comparing measurements to predictions by BCA, Elste and Holweger models
16 p2980 A70-34307

Magnetic flux measurements in quiescent solar filaments and adjacent photosphere using magnetograph observations
17 p3157 A70-34837

Continuous UV opacity effects on visual spectrum observations and predictions for solar photosphere
17 p3169 A70-35385

Solar photosphere temperature constancy in thin CO layer from equivalent spectral line width determination
18 p3322 A70-37134

Cosmic ray elements abundance at sources relative to carbon, comparing near-earth composition and solar photosphere
19 p3509 A70-38147

Solar atmospheric hydrodynamic response to stationary random forces homogeneous over horizontal planes, discussing common energy argument, various models and photospheric oscillation
19 p3523 A70-38690

Sun photographs with violet interference filter, determining photospheric magnetic fields position by cospatial network
20 p3634 A70-40410

Photospheric pore magnetic field model, investigating pore-sunspot distinctions
20 p3711 A70-40411

Photoelectric spectra of photosphere and sunspot umbra and penumbra ranging from 3900 to 8000 A
20 p3712 A70-40412

Coronal streamers structure and evolution from photographic and K-coronameter data, indicating photospheric bipolar magnetic regions as origin
20 p3712 A70-40416

Photospheric magnetic field differential rotation using synoptic charts for autocorrelation technique
21 p3885 A70-40951

Solar photosphere vertical velocities and horizontal wave propagation, discussing magnetic fields, phase coherence and behavior and oscillations
21 p3885 A70-40952

Solar photosphere absorption line weakened region, examining temperature increase effects on neutral and ionized lines
21 p3885 A70-40953

Solar coronal and photospheric iron abundances from absorption forbidden lines, discussing discrepancy with permitted lines
21 p3925 A70-42195

Photospheric metallic line profiles numerical experiment, investigating physical processes causing shape and asymmetry change
22 p4101 A70-42866

Solar photosphere negative viscosity phenomenon, examining Rossby wave on differentially rotating isothermal spherical shell of nonconducting inviscid ideal gas
22 p4109 A70-43748

Spectroscopic differential photosphere and chromosphere rotation with height in solar envelope
23 p4252 A70-44831

High resolution upper photosphere images obtained by slow raster scanning device and germanium bolometer, noting points around sunspots
24 p4400 A70-45307

Electrical conductivity in inhomogeneous photosphere and sunspots, suggesting sunspot plasma instabilities
24 p4400 A70-45311

Coherent motion effects on brightness of clouds moving above photosphere, describing H alpha Doppler brightening and Lyman alpha Doppler dimming in solar prominences
24 p4400 A70-45313

PHOTOSYNTHESIS

Photosynthesis and respiration rate in vegetables in controlled temperature, humidity, illumination levels, carbon dioxide and oxygen contents
03 p0425 A70-13892

Thermodynamics of radiation and photosynthesis, discussing Ross-Calvin maximal efficiencies, Duysens method, light and dark conditions and polarized light
03 p0428 A70-14011

UV radiation effects on pea plant chloroplasts photosynthesis at high altitudes, noting disruption of electron-transport chain reactions and cyclic phosphorylation
08 p1445 A70-21216

Biological conversion of solar energy, discussing photosynthesis and nonphotosynthesis mechanisms
15 p2688 A70-31600

Space cabin atmosphere regeneration by unicellular algae photosynthesis, discussing Chlorella cultivation procedures and additional functions in life support systems
23 p4154 A70-44655

Pigments absence in photosystem II of photosynthesis in heterocysts of blue-green algae
23 p4148 A70-44870

Photosystem II and oxygen evolution kinetics
24 p4305 A70-46411

PHOTOTHERMOTROPISM

U ANISOTROPY

U PHOTOTROPISM

U TEMPERATURE EFFECTS

PHOTOTRANSISTORS

Output and frequency limitations of functional converter using photopotentiometer with shaped resistor
09 p1682 A70-23358

Pulse-biased phototransistor imaging mosaics behavior measurement showing significant photovoltaic mode at high light levels
10 p1846 A70-23880

Electro-optical transducers based on photoconductive cells, phototransistors and microminiature incandescent and solid state light emitters
16 p2904 A70-33144

PHOTOTROPISM

Monopulse ruby laser with phototropic Q switch based on radiation density increase due to beam distribution
15 p2754 A70-32867

PHOTOTUBES

NT PHOTOMULTIPLIER TUBES

PHOTOVISCOELASTICITY

Polyurethane rubber time- and temperature- dependent visco- and photoviscoelastic coefficients using two dimensional strain and stress wave propagation photoviscoelastic analysis
03 p0599 A70-14243

PHOTOVOLTAGES

Coordinate-sensitive photocells with heterojunctions between wideband semiconductors, noting increased longitudinal photovoltage
03 p0541 A70-13722

Surface photovoltage regeneration mechanism in GaAs dependent on free carrier concentration, space charge density and minority carriers
15 p2783 A70-31951

PHOTOVOLTAIC CELLS

SNR for IR photovoltaic semiconductor cell generalized for astronomical case, noting stars approximation to black body radiators
05 p0849 A70-16645

Applied space research covering photovoltaic cells, electric propulsion, onboard data storage, vacuum lubrication and NASA-European organizations budgets
06 p1141 A70-17780

Photovoltaic InSb IR detectors design and operation, emphasizing performance in restricted field of view
16 p2926 A70-33152

Position sensitive planar photocells based on silicon-silicon dioxide systems, discussing photoelectromotive force generation mechanism, light intensity and load characteristics
18 p3297 A70-36236

P-n junction photovoltaic cell excitation by two photon absorption with low bandgap energy
19 p3446 A70-37764

Cadmium telluride photocells, discussing performance and mass production
19 p3358 A70-38481

Posterior electrode structural modification for reducing silicon photovoltaic cells absorptivity and operating temperature
19 p3358 A70-38492

Heat treatment and photovoltaic properties of copper disulfide-cadmium sulfide heterojunctions, measuring I-V characteristics, capacitance and spectral response
21 p3862 A70-41911

PHOTOVOLTAIC CONVERSION

Advanced reconnaissance electric planetary spacecraft /AREPS/ concept for repeated coverage of Mars or Venus surface, using solar photovoltaic system
01 p0196 A70-10837

Electrical power system adaptable to intermediate solar probes, discussing thermoelectric, thermionic, photovoltaic systems and battery for energy storage
04 p0625 A70-14753

PHOTOVOLTAIC EFFECT

Pulse-biased phototransistor imaging mosaics behavior measurement showing significant photovoltaic mode at high light levels
10 p1846 A70-23880

Gold impurity photovoltaic effect in silicon, determining optical cross section for transition
14 p2627 A70-30528

Photovoltaic effects in diodes with generation-recombination process in space charge region
15 p2709 A70-32427

Photovoltaic effects in p-n junction semiconductors, discussing conduction and electro-optical mechanism in thermal equilibrium
19 p3488 A70-38476

Photovoltaic effects in semiconductors, considering excess load carrier transport and I-V characteristics
19 p3488 A70-38477

PHTHALATES

Low melt viscosity prepolymers of diallyl phthalate and isophthalate in mold encapsulation showing dimensional, electrical and mechanical stabilities under adverse environments
05 p0869 A70-16035

Potassium acid phthalate crystal X ray spectrometric properties measurements, discussing parallel position rocking curves and reflection coefficients
23 p4230 A70-44420

PHTHALOCYANIN

Oxygen reduction in sulfuric acid with phthalocyanine-carbon catalysts

10 p1829 A70-24456

High temperature combined differential thermal analysis and spectrophotometric cell for phase transformation monitoring of evaporated thin film and bulk phthalocyanine

21 p3827 A70-41459

Metal phthalocyanin catalyzed oxidation by oxygen of vanadium and iron couples in externally regenerated redox fuel cell cathode

22 p3966 A70-43536

PHUGOID OSCILLATIONS

U OSCILLATIONS

U OSCILLATORS

U PITCH (INCLINATION)

PHYSICAL CHEMISTRY

Collection of Soviet papers on physicochemistry of radiation damage covering free radical processes in cellular organelles, protective action of pyridine derivatives, etc

03 p0418 A70-13301

Thermal analysis - Conference, Holy Cross College, August 1968, Volume 2, Inorganic materials and physical chemistry

11 p2070 A70-25808

Physicochemical methods of producing formaldehyde for carbohydrate synthesis in life support systems

15 p2693 A70-32676

Papers on chemical physics covering photoelectron angular distribution, molecular orbital theories, electron impact spectrometry, resonant electron scattering, etc

16 p2857 A70-33796

Physicochemical properties of monomer and associated aluminokyls, determining heats of combustion

22 p4124 A70-42677

PHYSICAL ENDURANCE

U PHYSICAL FITNESS

PHYSICAL EXAMINATIONS

Human response in Apollo flights emphasizing astronaut food, water, waste management, physical examination, preventive medicine problems, etc

02 p0239 A70-12669

SAS pilot selection system, discussing assessment variables, physiological examinations, psychological tests, recruiting procedure, etc

03 p0433 A70-13262

Human response in Apollo flights emphasizing astronaut food, water, waste management, physical examination, preventive medicine problems, etc

13 p2353 A70-29434

Wolff-Parkinson and White syndrome applicability in aeromedical appraisal for aircrew selection, noting effects of paroxysmal tachycardia

17 p3040 A70-35916

Soviet monograph on automated physiological measurements with onboard computers, covering EKG, EEG, electromyogram, respiration, muscular activity, etc

19 p3372 A70-38797

Multiple choice rotation chair for clinical experimental research and pilot vestibular tests

20 p3580 A70-39438

Astronauts medical examination, using thermal load as functional and diagnostic test

20 p3575 A70-40195

Jet pilot aging effects on physical functions based on medical examinations during six years, noting visual accommodation changes

22 p3978 A70-42878

PHYSICAL EXERCISE

Computer analysis and comparison of ST segment on Frank and bipolar lead electrocardiograms of healthy persons and cardiac patients during exercise, noting physiological responses

01 p0013 A70-10270

Apollo space cabin atmospheres, evaluating diluent N effect on decompression sickness in intermittently exercising men

01 p0032 A70-10368

Absolute ULF ballistocardiogram /BCG/ values as pulsatile fluid pumping values in cardiodynamic function before and after exercise

02 p0248 A70-12677

Motion coordination capacity of persons subjected to 40 days bed rest using dynamographic technique, discussing nature of slackening

03 p0425 A70-13896

Prolonged hypokinesia effect on human resistance to physical stress, noting prophylactic influence of physical exercises

03 p0425 A70-13898

Cardiac output and coronary blood flow changes in patients at rest and during peak exertion, stating correlation coefficients

03 p0428 A70-14065

Civil aviation personnel cardiovascular rehabilitation using single-lead electrocardiographic telemetry for monitoring and assessing cardiovascular status during supervised exercise

03 p0438 A70-14069

Airway resistance effect on ventilation and gas exchange during exercise, discussing minute volume and work of breathing response

03 p0429 A70-14157

Lactate accumulation and anaerobic work threshold in subjects exercised on bicycle ergometer, considering muscle contraction effect on oxygen supply

03 p0431 A70-14293

Exercise relation to acute myocardial infarction, coronary thrombosis, stenosis and obstruction, discussing prevention value of physical reconditioning in heart patients

04 p0636 A70-15466

Human skin temperature variations in supramuscular areas under physical activity and rest

04 p0638 A70-15505

Synchronous variations in skin and muscle temperatures of musculus gastrocnemius and flexor carpi in human subjects performing intermittent physical exercises

04 p0639 A70-15506

Muscle temperature variations and respiratory activity of athletes under various exercise regimens, outlining optimal weight lifting training programs

04 p0639 A70-15507

Skin-muscle temperatures ratio variations in dogs during periods of activity and rest

04 p0639 A70-15508

Activity and rest alternation effect on fatigue and rehabilitation behavior of trained athletes, discussing muscle performance characteristics

04 p0639 A70-15510

Physical exercise and rest regime evaluation by thermoelectric method recording skin temperature above gastrocnemius muscle

04 p0640 A70-15513

Computer program for on-line analysis of exercise ECG considered for improved diagnosis of ischemic heart disease

05 p0805 A70-16105

Standardized bicycle ergometer training effects at sea level and simulated altitudes, indicating hypoxia potentiating role

05 p0807 A70-16674

Cardiac work limiting factors during exercise under hypoxia, studying cardiac output and coronary blood flow capacities

06 p0991 A70-17282

Centripetal acceleration tolerance level correlated with circulatory system functional tests and physical exercises, discussing strength and speed endurance

07 p1201 A70-18787

Left ventricular wall motion in normal man at rest and after exercise using echocardiogram

07 p1210 A70-19573

Collection of papers on physical activity and aging, discussing physiology, biochemistry, coronary patients cardiovascular performance, electrocardiography, pathology, epidemiology, etc

07 p1211 A70-19689

Energy cost and heart rate responses to single stage nonsteady state submaximal exercise procedures used in diagnostic and functional testing

07 p1211 A70-19690

Physical training effects on factors in cardiovascular system influenced by age

07 p1212 A70-19691

Exercise habits and environmental emotional stresses role in origin and prevention of degenerative heart disease

07 p1212 A70-19692

Physiological responses during exercise recorded in patients with healed myocardial infarction, considering work tolerance

07 p1212 A70-19693

Physical activity and epidemiology of coronary heart disease

07 p1212 A70-19694

Epidemiologic investigation of physical activity and fitness effect on prevention of premature clinical coronary heart disease

07 p1212 A70-19695

Exercise influence on cardiac output and coronary blood flow during hypoxia, correlating CO and systolic pressure with blood flow changes

07 p1214 A70-19928

Human renal function, electrolyte and water metabolism during bed rest with daily leg exercise

07 p1223 A70-19937

Physical training effects on sedentary men with stable activity pattern, recording heart rates and oxygen uptake

07 p1215 A70-20171

Multistage treadmill exercise tests on healthy business executives noting S-T-segment responses

08 p1445 A70-21265

Hypercapnic atmosphere effect on human organisms found tolerable in state of rest or performing light labor

09 p1615 A70-22094

Aircraft pilots physical exercise program to maintain optimal state of fitness, discussing harmful effects caused by nervous and psychic strains

09 p1626 A70-23014

Body training type and amount effect on physiological functions and physical fitness of pilots, discussing pulse frequency

09 p1626 A70-23015

Serum lactate dehydrogenase /LDH/ isoenzyme in males before and after muscular exertion, observing change in skeletal muscle and liver fraction

10 p1809 A70-24002

Esophageal, rectal and quadriceps muscle temperatures, oxygen uptake, weight changes, skin conductance and skin evaporation during thermal transients caused by bicycle exercise

10 p1810 A70-24006

Prolonged hypodynamia effect on human blood coagulation, noting antithrombotic effect of physical exercise

10 p1815 A70-24678

Human motor functions changes following prolonged hypodynamia, including physical training and hypokinesia roles in standing and walking

10 p1815 A70-24682

Psychic state changes during prolonged bed rest, discussing effects of physical exercise and medicine

10 p1816 A70-24684

Physical exercise effects on man during prolonged bed rest, investigating muscle performance, static endurance, walking coordination and psychomotor functions

10 p1816 A70-24688

Body temperature effect on pulmonary ventilation response to exercise

10 p1819 A70-24773

Human pulmonary ventilation during exercise in high altitude and sea level acclimated subjects

10 p1819 A70-24774

Rats heart rate change during running at simulated altitude, discussing respiratory-circulatory training effect

11 p1985 A70-25671

Free fatty acids, glycerol and triglyceride levels in arterial and femoral venous blood in humans before and after physical training

12 p2169 A70-27625

Canoe paddlers physical training effect on cardiac output and local blood flow and metabolism at and during exercise and recovery

12 p2169 A70-27653

Initial period of muscular energy expenditure in athletes performing exercises on veloergometer, considering oxygen consumption

12 p2172 A70-28313

Soviet book on flight stress covering physiological bases, prediction and prevention methods, physical training, etc

13 p2357 A70-28775

Serum uric acid reduction in men during chronic physical exercise

13 p2355 A70-29802

Maximal oxygen intake, pulse heart rate and lactate levels variations with physical activity in middle aged man free of cardiovascular disease

13 p2356 A70-29826

Resting concentrations of fibrinogen, plasminogen and levels of euglobulin fibrinolytic activity, plasmin inhibitors and urokinase in blood in inactive and exercising men

13 p2356 A70-29942

Hot environment and hyperthermy effects on oxygen consumption in subjects performing muscular exercise

13 p2360 A70-29947

Inspired carbon dioxide pressure effects on human response to physical exercise, noting dyspnea and intercostal muscle pain

13 p2360 A70-29949

Swimming activity effect on dysbarism in rats in simulated free ascent from deep water

15 p2681 A70-31877

Human renal response to various exercise rates, measuring endogenous creatinine clearance, urine volume, solutes, acid, elements and protein excretion

15 p2684 A70-32534

Hypercapnic atmosphere effect on human organisms found tolerable in state of rest or performing light labor

15 p2685 A70-32690

Human power output dependence on muscle mechanical properties and kinematics of input motion, describing ergometer

16 p2853 A70-33669

Human circadian coronary circulatory rhythms during space flight weightlessness or bedrest with and without exercise

16 p2854 A70-33991

Training effect on strength per unit cross sectional area of arm muscle, using ultrasonic measurement

17 p3024 A70-34592

Oxygen uptake capacity, ventilation, heart rate and acid base values during bicycle ergometer exercise

17 p3036 A70-34594

Blood glucose and plasma immunoreactive insulin concentrations before, during and after intermittent short duration maximal exercise and glucose infusion

17 p3030 A70-35420

Oxygen uptake and cardiac output in males during submaximal and maximal treadmill and bicycle exercise 17 p3039 A70-35428

Multistage electrocardiographic exercise tests for cardiovascular performance measurement 17 p3034 A70-35878

Cutaneous liquid crystal temperature sensors for thermographic patterns of angina pectoris induced by treadmill exercise 19 p3364 A70-38361

Prolonged hyperbaric oxygen breathing effect on human physical performance at rest and during severe exercise 19 p3364 A70-38369

Human body core temperature control dependence during exercise on heat dissipation, noting sweating control 20 p3570 A70-38997

Determinants of human ventricular dimensions and myocardial free velocity relations during maximum and submaximum exercise levels 20 p3571 A70-39365

Visceral blood flow during exercise in sled dogs, testing hypothetical compensatory decrease as cardiovascular reserve for skeletal muscle by biotelemetry 20 p3571 A70-39366

Preliminary physical training for human water immersion resistance improvement 20 p3576 A70-40196

Ethanol ingestion effect on human response to submaximal and maximal exercise, measuring cardiac output and intraarterial pressure 21 p3761 A70-41135

Postexercise electrocardiogram detection of latent coronary heart disease in flyers prior to myocardial infarction 21 p3771 A70-41494

Body composition and weight changes estimation after physical exercise by prediction equations based on skinfold and girth measurements 21 p3766 A70-42155

Serum enzymes lactate dehydrogenase, creatine phosphokinase and isoenzymes in conditioned male after marathon run, noting little myocardium damage 21 p3766 A70-42158

Physical training effects on blood circulation, respiratory and muscular functions in aging persons 22 p3970 A70-42905

Hemodynamic indices of aged individuals engaging in physical exercises over long period of time 22 p3970 A70-42906

Contractive function of myocardium in middle and advanced age individuals under high physical loads during prolonged periods 22 p3970 A70-42907

Age determined hemodynamic reactions in men and women performing walking motions in lying position 22 p3970 A70-42908

Low carbon dioxide concentration breathing effects on exercise tolerance, discussing aerobic capacity decrement and hypercapnia occurrence 22 p3973 A70-43637

Decompression sickness relationship to physical exercise during simulated Apollo flight 24 p4307 A70-45336

Cardiovascular dimensions changes and heart volume in physically trained young men, comparing with response in old age 24 p4303 A70-46109

PHYSICAL FACTORS

Screen filtration pressure of human blood, establishing time, anticoagulant, red cells, platelets and leucocytes as physical determinants 07 p1210 A70-19590

Physical methods in applied climatology, analyzing meteorological effects on human body and building thermal conditions and plant biomass growth 15 p2771 A70-32111

Jet pilot aging effects on physical functions based on medical examinations during six years, noting visual accommodation changes 22 p3978 A70-42878

PHYSICAL FITNESS

Epidemiologic investigation of physical activity and fitness effect on prevention of premature clinical coronary heart disease 07 p1212 A70-19695

Body training type and amount effect on physiological functions and physical fitness of pilots, discussing pulse frequency 09 p1626 A70-23015

Antiair sickness medications effectiveness and secondary effects during low altitude transport of troops, observing sleepiness but no impairment of physical capacity 12 p2179 A70-28038

Fatigue and aircraft environment effects on physical and mental state of airline flight attendants during prolonged cruises 15 p2692 A70-32211

Statistical data on waivers granted to airline flight crew members by French Civil Aviation Medical Board based on ICAO medical standards 21 p3771 A70-41491

Heart rate-time curves before, during and after step-up exercise in relation to physical fitness 22 p3978 A70-42873

PHYSICAL OPTICS

Confocal parameters, spot sizes, waist positions and stability conditions of astigmatic Gaussian beams formed by spherical mirror laser cavity resonators 01 p0108 A70-10426

Book on coherent optics and holography covering image restoration, holographic interferometry, lensless Fourier transform holography, etc 01 p0144 A70-11074

Kerr physical optics formula usefulness for calculation of radar reflectivity of metallic bodies of revolution in terms of electric and magnetic dipoles 02 p0262 A70-12598

Optical echoes using model of spins precessing in magnetic field, presenting time dependent theory of perturbation 02 p0341 A70-12830

Laser emission intensity fluctuations influence on optical second and higher harmonic production and optical mixing arising from multimode oscillation 04 p0701 A70-14688

Optical waves in round metallic and dielectric waveguides calculated using geometrical optics and model analysis for anisotropic wall impedance model 04 p0652 A70-15396

Optical coherence and light fluctuations, determining statistical distributions of light from photoelectric counting experiments 09 p1728 A70-23372

Deformed grating frequency multiplication by filtering in Fourier plane of lens, forming moire pattern in image plane by mechanical interference 10 p1890 A70-24592

Ocular focus stimulator with provision for optical distance change between object and observer without brightness and visual angle variation 12 p2237 A70-28125

Microwave axicon with dielectric cone at aperture of focused antenna to reduce far-field radiation pattern beamwidth 14 p2549 A70-30512

PHYSICAL PROPERTIES

Technical ceramic products physical properties compared with metals, discussing manufacturing methods and industrial and engineering applications 02 p0322 A70-12714

Polymers application as engineering materials, discussing properties, physical states, etc 02 p0322 A70-12716

Field effect transistors with controlled p-n junction and metal-dielectric-semiconductor transistors investigated for radiation effects on physical and electrical properties 04 p0730 A70-14500

Cobalt alloys physical properties and heat treatment, discussing service conditions and critical problems 04 p0711 A70-15684

Aluminosilicate glass physical properties and chemical stability in water, alkaline and acidic agents, studying titanium oxides additions effect 05 p0871 A70-16596

Observed objects physical properties influence on boundary conditions of visibility perception by human eye 06 p0994 A70-17631

Gas turbine engine blades grinding and polishing procedures, considering fatigue life increase and physical properties stabilization 07 p1292 A70-18833

GaAs preparation techniques, crystal structure, electrical and physical properties, single crystal growth, impurities properties and distribution, thermal and optical properties, etc 07 p1356 A70-19397

Einstein gravitational equations general solution having physical singularity with respect to time 08 p1546 A70-21424

Oxygen pressure, volume and temperature data and derived thermodynamic properties presented in tabular form 09 p1788 A70-22956

Chimkurgan reservoir algae life and physicochemical characteristics 09 p1627 A70-23148

Rigid fire-retardant polyurethane foams obtained from phosphonopropionate polyols, discussing physical properties and shelf stability tests 10 p1907 A70-24063

Hydrodynamic analogy in restricted three body problem of celestial mechanics, discussing mass and momentum conservation and physical properties uniqueness 10 p1938 A70-24180

Ar-arc-produced dust of iron, carbon, silicon carbide and silica, investigating shapes, sizes, grouping and optical absorption to simulate interstellar grains 10 p1944 A70-24957

Sensor selection and telemetry measurement of physical parameters 11 p2011 A70-26453

Physicomechanical properties of tuff rock based on similarity to lunar surface rock, determining natural density, porosity and compression strength 11 p2119 A70-26798

Pulsars properties and physical nature, considering state of matter not reproducible in terrestrial laboratories 12 p2297 A70-27056

Composite reinforced materials similarity criteria to relate static and dynamic fields of various physical parameters, outlining mathematical simulation 12 p2259 A70-27526

High modulus carbon fibers low angle X ray diffraction correlation to physical properties 12 p2259 A70-28050

Annealed compressed ground synthetic mica and silver sput composite materials, analyzing physicochemical properties 12 p2260 A70-28319

Temperature-dependent physical properties effects on turbulent heat transfer, determining corrective factor for semiempirical equations 13 p2520 A70-28847

Visualized multicomponent systems subsolidus structures, studying physicochemical characteristics 13 p2470 A70-28885

Fiberglass reinforcement effects on injection molded thermoplastics physical properties, noting role of binder and glass content 13 p2438 A70-29204

Evaporated Au-Ni-Cr alloy resistor films physical and electrical characteristics, noting dependence on composition 14 p2625 A70-30285

Bi-Sb alloys, discussing structural data, crystal preparation, band structure, pressure, nonohmic conductivity, thermoelectric, thermomagnetic and magnetothermal effects 14 p2625 A70-30332

Soviet book on physical libration constants of moon based on visual and photographic observations of two craters by position angle method 14 p2642 A70-30959

Fluid urethane laminating resin for bonding nylon and glass fabrics, giving physical properties as function of room temperature curing time 16 p2938 A70-33381

Ti alloys beta forging effect on physical properties and tensile ductility 17 p3097 A70-34358

Ti alloys systems physical properties and structural phase stability, discussing electronic Fermi state density variation 17 p3114 A70-34376

Interstellar H I gas physical conditions, discussing ionization ratio average values and temperature conditions 18 p3328 A70-37175

Ferrite single crystals physical properties - Conference, Krasnoyarsk, U.S.S.R., June-July 1969 19 p3484 A70-37621

Ferrite single crystals physical properties - Conference, Krasnoyarsk, U.S.S.R., June-July 1969 19 p3485 A70-37626

Physical properties of comet heads, considering apparent diameters and internal magnitudes 19 p3514 A70-37641

Two dimensional electromagnetic fields in presence of cylindrical objects of arbitrary physical properties and cross sections, using scattering matrix approximation 19 p3471 A70-37778

Linear micromorphic material constants determination from constituent properties based on microelasticity theory 19 p3538 A70-37795

Space environment physical properties near earth, discussing neutral atmosphere, solar radiation, ionosphere, electric and magnetic fields and radiation belts 19 p3520 A70-38277

Electrophysical properties of refractory and rare earth metallic single crystals, discussing work function, transition temperature, resistivity and superconductivity 19 p3454 A70-38731

High temperature acoustic waves, examining solid and fluid properties, weld integrity nondestructive material tests and nondisruptive process measurement 20 p3628 A70-39170

Composite materials physical properties measurement and defect locations detection by NDT techniques 20 p3636 A70-39210

Chemical and physical factors effect on smoke evolution from polymers 20 p3736 A70-39405

Composite materials physical properties based on linearly reinforced media models and complex variable functions theory 20 p3655 A70-39860

High temperature aromatic polyester Ekonol, discussing fabrication, properties and potential applications

21 p3842 A70-41136

Apollo 11 lunar rock and soil mechanical behavior and physical characteristics, discussing color, specific gravity, density, shapes and adhesive and cohesive properties

21 p3913 A70-41646

Scorched aluminum powder (SAP) materials, discussing fabrication, physical and mechanical properties, applications in aircraft structural components, etc

22 p4055 A70-43084

PHYSICAL SCIENCES

Astronomy role in physical science and space exploration

10 p1940 A70-24373

PHYSICAL WORK

Alpha-aminobutyric acid accumulation by soleus and plantaris muscles of rat in vivo during work induced growth, showing amino acid transport variation with work level

02 p0232 A70-11711

Life support system model using heart rate to monitor man doing physical work in space suits under simulated space environment

02 p0245 A70-12146

Autocorrelation and cross correlation analysis of slow EEG potentials in rhythm of movement as cortical activity pattern of cerebral hemispheres during work

03 p0421 A70-13687

Diurnal variations of phase coupling between heart beat and respiration under resting conditions and modification by quantitatively regulated physical effort

03 p0431 A70-14294

Temperature variations in organs of man and animals performing physical work as physiological base of metabolic processes and for daily activity timetable development

04 p0638 A70-15502

Catecholine excretion, cardiovascular functions and subjective effort in healthy male subjects under various physical work loads

05 p0801 A70-16141

Alveolar ventilation difference in nasal and oral breathing in hyperventilation due to work

05 p0802 A70-16492

Blood clotting and fibrinolysis under short term physical work in healthy men measured using thrombelastograms

06 p0992 A70-17423

Pulmonary CO diffusing capacity in young men during muscular exercise

06 p0993 A70-17432

Symmetrical motor centers inequality significance in humans during interaction under conditions of successive innervations during exercise

07 p1213 A70-19790

Electromyograms cross correlation analysis to study time relationships between motor unit discharges of human musculus biceps and triceps brachii during physical work

07 p1213 A70-19791

Work and energy theorems in linear elasticity, discussing potential energy, real work, complementary energy and energy coefficients

11 p2142 A70-26625

Respiratory gas exchange, heart rate, arterial acidemia and hypocapnia responses to physical work in hyperbaric environments and hyperoxia conditions

12 p2169 A70-27655

Anaerobic and aerobic oxidation efficiency in muscular work performance before and after achieving oxygen steady state consumption

12 p2169 A70-27658

Maximum oxygen uptake correlation to age of subjects performing physical and sedentary work

13 p2350 A70-29112

Stochastic processes for physiological analysis of cardiac rhythm dynamics during work

15 p2680 A70-31609

Metabolic Rate Monitor for measuring continuous oxygen consumption during changes in work in real time

15 p2741 A70-32540

Cooling hood effect on physiological responses to work in hot environment, discussing body temperature

17 p3031 A70-35422

Glucose-free fatty acid interactions in working heart, noting increase in glucose uptake, oxidation and glycogenolysis with physiologic work increment

17 p3031 A70-35429

Decreased mental and physical performance of human beings due to T-oral and placebo vaccine reactions

19 p3359 A70-37389

Anaerobic carbohydrate metabolism in aging individuals under physical loads

22 p3969 A70-42900

Occupational and age composition of working population of U.S.S.R., comparing cardiovascular and respiratory systems

22 p3969 A70-42904

Virtual work equations steady state subharmonic solutions by Newton-Raphson method, developing generalized iterative procedure for nonlinear differential equations

24 p4423 A70-45577

Sympathetic-adrenal system activity of trained organism during muscular work and emotional excitation

24 p4300 A70-45841

PHYSICIANS

Physician-monitored central control facility communicating with remote site facilities staffed by paramedical personnel for public health care, based on aerospace experience

04 p0644 A70-15357

Survival training program preparing physicians as advisors regarding survival equipment and medicine

23 p4152 A70-44463

PHYSICS

Book on technical acoustics physics covering propagation, dissipation, reflection, field perturbation in real solids, liquids and gases, lumped constants, resonators, etc

01 p0144 A70-11328

Collection of papers on high temperature physics and chemistry covering shock tube chemistry, plasmas, exploding wires, etc

06 p1063 A70-17726

Growth points of physics - Conference, Florence, April 1969

12 p2297 A70-27053

PHYSICOCHEMISTRY

Physicochemical methods of producing formaldehyde for carbohydrate synthesis in life support systems

09 p1623 A70-22080

PHYSIOGRAPHY

U GEOMORPHOLOGY

PHYSIOLOGICAL DEFENSES

Phonocardiographic and ultrasound observations of acute rejection following cardiac transplantation, considering rejection treatment at early stage

03 p0415 A70-12888

Free radical antioxidant reactions in lipids from blood, liver, spleen, brain and intestines of rats exposed to ionizing radiation

03 p0419 A70-13309

PHYSIOLOGICAL EFFECTS

NT HEMODYNAMIC RESPONSES

NT PHYSIOLOGICAL RESPONSES

Biophysical symptoms and clinical treatment of ailments resulting from pressure drop, considering exposure to higher and lower pressure changes

[DVL-894] 01 p0011 A70-10036

Arterial pressure pulse waves mathematical analysis applied to variations in stroke volume in anesthetized dogs subjected to spine-to-breast accelerations

01 p0012 A70-10125

Sea-level pressure interval to prevent decompression sickness in humans flying in commercial aircraft after diving

01 p0032 A70-10366

Physiological significance of myocardial fibers curvature in left ventricle wall determined by numerical solutions based on mathematical description

01 p0039 A70-11368

Lactate rise diminution in anesthetized paralyzed dogs subjected to hypoxia by gas mixtures before and after beta-adrenergic blockade

02 p0233 A70-11724

Stainless steel micropipettes implantation in rat amygdala to study role in gastric secretion

02 p0234 A70-11729

Health hazards and physiological effects of atmospheric infrasonic waves, discussing sources, ear protecting devices and electrochemical detectors

02 p0247 A70-12467

Physiological equivalents of air with rare gases and H substitutes for nitrogen in inhaled gas mixtures providing normal oxygen intake

02 p0249 A70-12798

Slow waves and spikes in intestinal muscle of cat noting dependence on intracellular iontophoresis of Na

03 p0416 A70-13014

Motion coordination capacity of persons subjected to 40 days bed rest using dynamographic technique, discussing nature of slackening

03 p0425 A70-13896

Human motion coordination under acceleration followed by weightlessness during jet flights along Keplerian orbits, discussing initial disturbance and subsequent subsiding

03 p0425 A70-13897

Physiological effects on men of 10 hr exposure to nitrogen-oxygen mixture followed by pure oxygen 4 hr exposure, simulating conditions during EVA

03 p0436 A70-13899

Human alveolar-arterial oxygen differences during rest, sleep and exercise in initial hypoxia induced by simulated high altitude exposure

03 p0429 A70-14161

PHYSIOLOGICAL EFFECTS

Circadian rhythms characteristics in humans, animals and plants, noting possible effects of rhythm disturbances on astronauts

04 p0629 A70-14567

Hypokinesis effects on transversostrated muscle fibers of mice, noting changes in myofibrillar apparatus, mitochondria and sarcoplasm

04 p0629 A70-14569

Autonomic nervous system role in controlling body functions after rapid decompression, increasing tolerance to pressure gradients by physical training

04 p0630 A70-14575

Physiological and physiopathological effects of transverse accelerations on spacecraft crews, discussing cardiovascular and respiratory systems

05 p0799 A70-15763

Heat exchanges between man and environment due to incidents or accidents during aircraft operation evaluated by combined heat transfer coefficient

05 p0799 A70-15764

Radiation environment in space and effect on man, discussing particulate and high energy electromagnetic radiation components

05 p0903 A70-16630

Standardized bicycle ergometer training effects at sea level and simulated altitudes, indicating hypoxia potentiating role

05 p0807 A70-16674

Pre-space flight tests effects on Macaca nemestrina monkeys spermatogenesis, considering immobilization and exposure time effects

06 p0991 A70-17287

High temperature effects on pilots psychomotor performance and physiological function, discussing measurements taken during complex tasks

06 p0999 A70-17290

Aircraft crews in-flight medically controlled feeding, discussing physiological and nutritive value of foods

06 p1001 A70-17669

Recumbency effect on human heel bone density during bed rest using X rays

06 p0996 A70-17850

Heart rate and circulatory load as ergonomic criteria based on muscular work, environment temperature, mental stress, etc

06 p0997 A70-18017

Mice irradiation reactions determination from various metabolism indices including blood sugar level, leucocytes number, proteolytic processes rates, etc

07 p1198 A70-18714

Carbon dioxide effect on oxygen uptake during hyperventilation in normal man

07 p1205 A70-19294

Traumatic rupture of aortic arch and descending thoracic aorta resulting from abrupt linear body deceleration

07 p1206 A70-19295

Physiological and hygienic data on oxygen partial pressure in space cabin atmosphere analyzed for manned space flights

07 p1220 A70-19502

Human vertical perception with body tilt in median plane tested with luminous rod in upright to supine position with backward and lateral tilt

07 p1224 A70-20045

Visual analyzer physiology under effects of gravitation, atmospheric pressure, mechanical vibrations, etc

08 p1444 A70-20740

Acute gasoline poisoning toxicology and prophylaxis, manner of ingestion and effects on organs and systems

08 p1451 A70-20976

Microwave irradiation effects on rabbit eye lenses, noting injury dependence on frequency

[IMPI PAPER DA-4] 08 p1452 A70-21273

Human sea-level natives physiological changes during high altitude physical exercise, considering carbon dioxide arterial pressure, plasma cortisol, adrenal function indexes, etc

08 p1453 A70-21873

Optic chiasm damage effects on human depth perception implying interhemispheric link for binocular integration in central vision

09 p1618 A70-22669

Corpus callosum damage effects on human depth perception implying interhemispheric link for binocular integration in central vision

09 p1618 A70-22670

Air traffic vibration effects on human organs and sensations, considering blood circulation, lungs, eyes and muscles

09 p1625 A70-23007

Body training type and amount effect on physiological functions and physical fitness of pilots, discussing pulse frequency

09 p1626 A70-23015

Hyperbaric oxygenation treatment physiology and techniques, discussing limitations of equipment

09 p1620 A70-23017

Physiopathological effects of weightlessness, showing desirability of partial gravity for long voyages via spacecraft rotation

09 p1621 A70-23439

Serum lactate dehydrogenase /LDH/ isoenzyme in males before and after muscular exertion, observing change in skeletal muscle and liver fraction
10 p1809 A70-24002

Mineral saturation in calcaneal bone and hand finger phalanx in humans under prolonged hypodynamia by X ray analysis, observing Ca salts reduction
10 p1815 A70-24676

Prolonged hypodynamia effects on visual analysis, investigating functional weakening, fundus oculi appearance change and restoration after normal activity resumption
10 p1816 A70-24687

Hypodynamia aftereffects on nervous system, investigating organic microsymptoms, asthenia, vegetative-vascular instability and skin muscle akinetic hypotrophy
10 p1825 A70-24691

Hypodynamia effects on humans during prolonged bed rest, investigating immunological resistance, psychic disorders, myocardium changes, responses to pharmaceuticals, etc
10 p1817 A70-24696

Physiology and pathophysiology of oxygen transport in human blood, discussing fluctuations in O₂ capacity and affinity
10 p1821 A70-25079

Physiological and psychological human reactions during space flight concerning hypokinesia, space kinetosis, isolation and limited room conditions
11 p1986 A70-25707

Physiopathologic effects on organs of longitudinal and tangential accelerations, decelerations, vibrations and weightlessness
11 p1986 A70-25821

Vestibular adaptation to heat and rotary stimulation in animals and men
11 p1986 A70-25822

Inflight aircraft cockpit noise levels effect on pilot hearing sensitivity
11 p1990 A70-25875

Physiological and hygienic data on oxygen partial pressure in space cabin atmosphere analyzed for manned space flights
11 p1991 A70-26101

Oxygen diffusion facilitation in vivo and nonsteady state conditions under physiological circumstances, emphasizing hemoglobin in red cells and myoglobin in muscle
12 p2171 A70-28024

Microwave radiation effects on radar operators myocardium functions
12 p2180 A70-28358

Centrifuging acceleration tolerance of various animals, relating physiological and morphological effects
12 p2174 A70-28361

Paced respiration and selective attention effects on heart rate and finger pulse amplitude in adult females subjected to visual stimuli
13 p2350 A70-29241

Sensory deprivation induced EEG changes, discussing duration effect on postisolation occipital alpha frequency
13 p2350 A70-29242

High altitude effects on total protein content and composition in rats blood serum
13 p2352 A70-29346

Medical wastage of professional aviators in military and civil aviation, discussing reasons for preventing flying license revalidation
13 p2359 A70-29440

Gravity effect on positional alcohol nystagmus in man and rabbits, observing threshold value in weightless state
13 p2359 A70-29442

Oxygen effect on night vision tested in men at 5,000 ft above sea level, obtaining threshold curves of dark adaptation
13 p2359 A70-29443

Arousal effects on vestibular nystagmus in man, discussing forced alertness in mental arithmetics form
14 p2538 A70-30911

Swimming activity effect on dysbarism in rats in simulated free ascent from deep water
15 p2681 A70-31877

High altitude liver function and blood flow, determining bromsulphthalein transport maximum and storage capacity and galactose elimination
15 p2683 A70-32531

Long term helium-oxygen atmosphere effects on rats and mice, investigating biochemical and metabolic changes
16 p2849 A70-33996

Exercise and rest of humans under hypoxia and hyperoxia, determining blood acid-base state, ventilation and carbon dioxide partial pressure
16 p2849 A70-34256

Complex accelerations effects on vestibular apparatus from physical and mathematical viewpoint
17 p3037 A70-35128

Intense deceleration effects on mice and rats, including internal organs damage and enzyme activity increase
17 p3025 A70-35132

Repeated decelerations effects on mice and rats, noting fibrotic changes in liver
17 p3025 A70-35133

Dehydration effects on rabbits acceleration resistance
17 p3025 A70-35134

Vibration effects on vestibular components, noting applications to spacecraft artificial gravity
17 p3038 A70-35322

Prototype space foods effects on humans, determining changes in bacterial fecal flora content
17 p3032 A70-35565

Bird dispersal measure at airports, using behavioral and electrophysiological effects of high power microwave radiation
18 p3222 A70-35993

Microwave radiation effects on maintenance personnel, investigating respiratory reaction, attention concentration, blood content of K, Ca, Na and proteins, etc
20 p3581 A70-40289

Ship engineers cardiovascular system functional changes during HF internal combustion engine noise, investigating EKG recordings and arterial pressure
20 p3582 A70-40292

Cardiac glycosides and beta receptor blocking agent effect on ULF displacement ballistocardiogram in healthy young men, measuring heart rate and blood pressure
21 p3763 A70-41227

Hypoxia and hyperoxia effect on ballistocardiogram of healthy males, determining systolic and minute cardiac forces
21 p3763 A70-41231

Work load effect on ballistocardiogram by minute cardiac force /MF/ measurement, using bicycle ergometer
21 p3763 A70-41233

Activation energies of acceleration and hypoxia stress in man and rats, noting brain function survival
21 p3764 A70-41484

Behavioral changes due to repeated low doses of rocket fuel monomethylhydrazine
21 p3771 A70-41485

Chicken lymphopenia and body mass loss resulting in death from chronic restraint, developing physiologically unstressful restraint for space environmental testing
21 p3765 A70-41488

Valsalva maneuver beat-to-beat effects on systolic cardiac intervals compared with time based measurements
22 p3972 A70-43484

Space flight effects on dogs cardiac activity, brain circulation and systemic-tissue circulation interactions
22 p3972 A70-43635

Passengers physiological and medical problems on subsonic and supersonic aircraft
23 p4150 A70-44223

Gravity effects on perinatal organ growth in chicks
24 p2977 A70-45342

Desoxycorticosterone action on human kidneys and sweat glands as function of temperature tested with various DOCA and NaCl doses
24 p4301 A70-45988

Vagus nerve blockage effect on arterial carbon dioxide tension and breathing regulation in dogs
24 p4303 A70-46112

Sonic boom effects on guinea pigs Corti organ, comparing auditory damage in cochlea with hair cell damage
24 p4305 A70-46374

PHYSIOLOGICAL FACTORS

NT PHYSICAL FACTORS

Biological rhythm disturbances of astronauts during air and space travel, discussing sleeping habits, alertness under weightlessness conditions, etc
02 p0241 A70-12763

Physiological limitations of air traffic controllers, considering stress factors connected with workload
04 p0716 A70-15314

External environment changes effect on animal activity, considering reactions on molecular, physiological and behavioral levels
07 p1199 A70-18782

Astronauts visual performance during space flight, studying reduction of visual disturbances from various physiological flight factors
08 p1444 A70-20741

Human factors responsibility for aircraft accidents, discussing cooperation between air safety service and flight surgeons
09 p1626 A70-23016

Human body homeostatic mechanisms autoregulation, discussing feedback control systems for blood pressure and flow regulation, bodily movements and postural control, etc
10 p1810 A70-24038

Period length calculation method for physiological rhythms by digital computer
10 p1811 A70-24380

Soviet book on flight stress covering physiological bases, prediction and prevention methods, physical training, etc
13 p2357 A70-28775

Physiological indices criteria for human thermal stress tolerance, discussing rectal temperature, body surface condition, body temperature and local cooling effects
13 p2351 A70-29332

Perception threshold in rapidly changing circumstances, discussing stimuli signals recognition
15 p2687 A70-32872

Instrumentation safety for physiological research in hyperbaric chamber environment, taking into account pressure, isolation, atmosphere, electricity and fire
18 p3222 A70-35939

Electronic differentiator for physiological research, discussing electrical voltage derivatives reproduction, sensitivity, etc
19 p3371 A70-38219

Human vigilance paradigm and physiology, discussing relationships between vigilance, signal detection and animal discrimination
19 p3364 A70-38324

PHYSIOLOGICAL INDEXES

U PHYSIOLOGICAL TESTS

PHYSIOLOGICAL RESPONSES

NT HEMODYNAMIC RESPONSES

Photoperiod variation effects on ambulatory primate Cebus albifrons deep body temperature /DBT/, locomotor activity /LMA/ phase relationships and DBT waveform
01 p0011 A70-10035

Physiological research on humans in hypothermia resulting from confinement to life raft on open sea, analyzing thermal conditions, thermoregulation and survival
01 p0013 A70-10233

Computer analysis and comparison of ST segment on Frank and bipolar lead electrocardiograms of healthy persons and cardiac patients during exercise, noting physiological responses
01 p0013 A70-10270

Reciprocal rhythm occurring with impulses of atrial or atrioventricular /A-V/ nodal or ventricular origin, noting role of A-V nodal pathways
01 p0016 A70-10442

Catecholamines biosynthesis, distribution, combining, uptake, deposition, release and metabolism in physiological and pathological reactions of organism
01 p0019 A70-10512

Male macaque monkey physiological deterioration in Biosatellite 3, noting falling brain temperature, lowered central venous pressure, fluid loss, blood redistribution into visceral pools, etc
01 p0022 A70-10822

UV radiation effects on mucopolysaccharide compounds in tears and on cornea epithelium of albino rabbits
01 p0037 A70-10860

Rats sympathoadrenomedullary response to increased oxygen tensions, measuring catecholamines, norepinephrine and epinephrine in adrenal gland, hypothalamus, serum and urine
01 p0024 A70-10979

Target-field luminance or duration effect on target susceptibility to masking demonstrated in visual backward masking study
01 p0039 A70-11163

Line length effects on sequential blanking in visual perception demonstrated by computer-based CRT display and interpreted with information processing model
01 p0039 A70-11164

Heart rate and skin conductance measurements during attention-direction tasks involving proprioceptive stimuli position on environmental acceptance and rejection continuum
01 p0026 A70-11166

Rabbits and cats cortical neurons responses to light and acoustic signals, using microelectrodes inserted at different depths into cortex
01 p0030 A70-11469

Comfort and thermal sensations and associated physiological responses during exercise at various ambient temperatures, noting effects on sensory estimates
01 p0031 A70-11648

Hyperbaric oxygenation /OHP/ effect on left ventricular function evaluated by measurement on anesthetized dogs of myocardial contractility
02 p0230 A70-11701

Chest, abdominal wall and diaphragm displacements of rabbits during partial and whole body exposure to shock waves produced by hexotol charges
02 p0231 A70-11704

Rat water intake and urine output during chronic centrifugation at resultant inertial fields of 1.7 and 3.0 g
02 p0231 A70-11705

Simulated responses of depressed and hyperpolarized single-medullated nerve fibers, using Frankenhauser-Huxley equations
02 p0231 A70-11706

Muscle force and electromyogram behavior with alteration in blood flow and composition in anesthetized cats
02 p0231 A70-11708

Constant-inflow and constant-pressure perfusion effect on vascular responses of dog

02 p0232 A70-11716

Polycythemia and hypercapnia effects on apparent oxygenation of rat brain during acute hypoxia by changes in creatine phosphate concentration and lactate/pyruvate ratio

02 p0232 A70-11717

Blood flow changes in portal vein and hepatic artery of anesthetized cats following intraportal and intrahepatic arterial administration of isoproterenol, epinephrine and norepinephrine

02 p0232 A70-11718

H ion increased activity effect on sodium transport across short circuited turtle bladder

02 p0234 A70-11730

Starvation effect on intestinal amino acid absorption of rats, noting protein synthesis reduction

02 p0234 A70-11731

Oxygen consumption, lactic acid production and mechanical performance of anesthetized dog gastrocnemius muscle with increased blood flow

02 p0235 A70-12090

Vestibular sensing system role in providing information concerning vertical, linear and angular head movements to central organs

02 p0246 A70-12191

Accelerative and decelerative heart rate responses in human subjects given differential conditioning trials by auditory and electric shock stimuli under paced respiration

02 p0239 A70-12628

Human response in Apollo flights emphasizing astronaut food, water, waste management, physical examination, preventive medicine problems, etc

02 p0239 A70-12669

Sensor, vegetative, motor and vestibulosomatic reactions to brief weightlessness in fighter pilots and laymen, ascribing disorders absence to statokinetic stability of organism

02 p0241 A70-12799

Cross adaptations of physiological functions, discussing results for heat, altitude and cold adapted animals

02 p0242 A70-12824

Cross adaptation criteria and modifications in physiologic and biochemical processes in man and mammals, demonstrating positive cross acclimation between hypertension and hypoxia exposure

02 p0242 A70-12825

Altitude changes effect on brown fat content and metabolism in deer mice, noting oxygen consumption and heat production limitation by hypoxia

02 p0242 A70-12865

Mathematical model for ejection fraction of human left ventricle incorporated with fiber orientation and ventricular geometry, showing consistent results with biplane angiocardigraphic films

03 p0433 A70-12975

Light synchronization of deep body temperature rhythms in Macaca nemestrina, investigating efficiency

03 p0416 A70-13013

Evoked potentials arising in entorhinal cortex of rabbits in response to stimulation of somatic nerves, light and sound

03 p0417 A70-13070

Somatosensory cortex removal effect on blocking action of skin stimulation on associative response to light flash in cats

03 p0420 A70-13430

Functional state changes in organism awaiting and performing parachute jump using orthostatic test, respiration retention and Howard step test

03 p0420 A70-13477

Tegmental nucleus neurons of cats cerebellum, considering responses to acceleration changes and natural stimulation of vestibular apparatus

03 p0421 A70-13510

Early and late response component of associative cortical area in cerebral hemispheres of cats connected with mono and polysensory neuron activity

03 p0421 A70-13688

Respiratory and cardiac activities, body weight variations, blood and urine electrolytic composition of astronauts during Soyuz orbital flights from medical tests

03 p0423 A70-13709

Diurnal rhythms of physiological functions and human adaptation to shifted sleep-wakefulness schedule on healthy pilots subjected to solitary confinement

03 p0423 A70-13711

Diurnal periodicity of physiological functions of flight crews flying through several time zones found to correspond to time zone of permanent residence

03 p0425 A70-13894

Space cabin atmosphere effects on primary and secondary immunologic responses in mice relative to spleen weight and antibody titers following antigenic stimulation

03 p0437 A70-14062

Unrestrained chimpanzees cortical and subcortical electrical activity during sleep recorded by telemetry and compared with human beings and other mammals

03 p0432 A70-14347

Immobilization effects on alpha rhythm, locomotor coordination and visual alimentary motor reflexes of cats

04 p0629 A70-14570

High altitude acclimatization effects on cardiovascular system, external respiration, blood composition, optical and vestibular analyzers in human subjected to various stresses

04 p0630 A70-14576

Mathematical model building for temporal human motor responses /reaction, movement, manipulation/ by response surface technology and statistical experimental design

[ASME PAPER 69-WA/BHF-5] 04 p0642 A70-14851

Pilots hearing level based on pure tone threshold audiograms compared with personnel not exposed to job noise

04 p0631 A70-14982

Plasma free fatty acid level relationship to acute and chronic exposure to cold in rabbits, rats and humans

04 p0631 A70-14983

Physiological load of exercise at altitude evaluated by heart rate and recovery rate measurements

04 p0631 A70-14984

Temporary suppression of cortical associative responses in cats with electrocoagulated thalamic relay nuclei lesions

04 p0632 A70-15220

Collection of Soviet papers on physiological foundation of activity regimes covering human cerebral cortex, skin and muscles responses to stimuli, etc

04 p0638 A70-15501

Amphetamine effects on observing and monitoring performance in squirrel monkeys, investigating lever and key responses using food reinforcements

05 p0806 A70-16128

Rod and cone contributions to S potentials from cat retina using spectral sensitivity observation

05 p0801 A70-16379

Rod-cone interaction in cat S potentials, analyzing effect of wavelength and intensity upon dark adapted responses

05 p0801 A70-16380

Rod aftereffect relationship to percent rhodopsin bleached in S potentials from cat retina

05 p0801 A70-16381

Human eye contribution to visual evoked responses under different color stimuli during all possible monocular and binocular combinations

05 p0801 A70-16382

Nonspecific influences on rabbits neurons reaction to nonvisual stimuli in central visual pathway using microelectrodes implantation in visual cortex

05 p0802 A70-16624

Cerebellar cortex reactions to sciatic nerve stimulation in rats under transverse accelerations in centrifuge

05 p0804 A70-17116

Human heart chronotropic reactions during centrifuge acceleration tests up to tolerance limit, establishing sinus tachycardia in various degrees

05 p0804 A70-17120

Nervous system influence on erythema radiation reactions from soft X ray irradiation, discussing blood supply effect

06 p0993 A70-17430

Human unloading reflex, using experimental setup unloading muscle without tension increase

06 p1000 A70-17450

Bioelectrical reactions in anesthetized cats cortical zones in response to stimulation of contralateral sciatic nerve

07 p1199 A70-18722

Thalamic N.VPL role in distributing afferent flux in anesthetized cats cortex, using stimulating contralateral sciatic nerve

07 p1199 A70-18723

Physiological reactions of living organisms to aircraft and spacecraft acceleration, discussing physical, pharmacological and training methods to increase tolerance

07 p1200 A70-18785

Physiological effects of prolonged human motor activity restriction, discussing oxygen transport system, work capacity relationships, body fluids volume and distribution, metabolism, etc

07 p1200 A70-18786

Acceleration effects on chest organs by X ray studies noting heart shape changes, pulmonary areas, diaphragm position, etc

07 p1201 A70-18791

Ciliary nerve stimulation and lens motion data to identify open-loop plant dynamics of lens accommodation

07 p1216 A70-18858

Human visual performance, discussing effects of object size and exposure time

07 p1204 A70-19050

Atrophic changes in tortoises during roundtrip to moon on Zond 5 ascribed to hunger and space flight factors

07 p1207 A70-19496

Somato-vegetative and behavioral reactions of rabbits to electric stimulation of hypothalamus after injecting aminazine

07 p1209 A70-19521

Involvement reactions in dying and reanimated cats with nucleus reticular hypothalamicus stimulated by rectangular electric pulses

07 p1209 A70-19522

Left ventricular wall motion in normal man at rest and after exercise using echocardiogram

07 p1210 A70-19573

Physiological responses during exercise recorded in patients with healed myocardial infarction, considering work tolerance

07 p1212 A70-19693

Midbrain reticular neurons activity in cats during response to individual and coincident cortical and hypothalamic stimulations

07 p1213 A70-19789

Adaptive reactions in thyroidectomized rats blood and brain during adaptation to hypoxia compared with intact animals

07 p1214 A70-19794

Minute volume changes under acoustic excitation of mice for measuring respiratory process without strain on organs

07 p1214 A70-19824

Acceleration environment duplication difficulties, considering human physiological responses dependence on centrifuges performance characteristics and geometries

07 p1222 A70-19927

Human physiological responses to lower body negative pressure /LBNP/, studying presence or absence of change for orthostatic tolerance as function of time

07 p1222 A70-19933

Temporary or permanent visual field injury in test parachutists compared to control group

07 p1223 A70-19943

Physiology of high altitude, studying animal and man adaptation and changes in body processes due to life stresses and hypoxia

08 p1441 A70-20469

Operator analysis of electroretinograms, investigating eye reaction dependence on stimulation using amplitude-phase-frequency characteristics

08 p1450 A70-20730

Delayed trace reaction under stable and unstable pauses in apes and monkeys, noting independence of conditioned reflex

08 p1446 A70-21446

Thoracic cage, heart and extirpated lung dimensions measurement for dogs before and after explosive decompression and after ground level recompression

08 p1448 A70-21793

Acceleration training schedules performed with animals and test subjects, assessing schedules effectiveness in increasing tolerances to transverse acceleration

09 p1623 A70-22086

Hypercapnic atmosphere effect on human organisms found tolerable in state of rest or performing light labor

09 p1615 A70-22094

Flashtube photostimulators for examining human physiological response, discussing design and calibration

09 p1624 A70-22673

Hormones excreted by adrenal cortex function in rhesus monkeys pathogenesis after irradiation by sublethal dose

09 p1620 A70-22822

Physiological reactions detection, transmission and data evaluation of aircraft pilots subjected to various stress environments, using radio telemetry

09 p1626 A70-23009

Human tolerance to short duration high acceleration in centrifuge concerning peripheral or central vision trouble or syncope

09 p1626 A70-23112

Water cooled space suits automatic control based on physiological changes in astronaut during hard work

09 p1627 A70-23458

Dogs breathing air or oxygen during slow and rapid decompression, measuring intraocular and cardiovascular pressure changes and retinal responses

09 p1621 A70-23460

Startle auditory stimuli effects on motor performance and recovery characteristics from heart rate and skin conductance recordings

09 p1628 A70-23577

Blood lactate changes during prolonged exhaustive running at varied intensities and durations

10 p1809 A70-24001

Prolonged hypodynamia effects on hemodynamics using dye dilution method, noting adaptability in cardiovascular system

10 p1814 A70-24671

Prolonged hypodynamia effect on human cardiac cycle phases using poly- and kinetocardiographic data

10 p1814 A70-24672

Prolonged hypodynamia effect on heart size and myocardium function obtained from human chest X ray studies

10 p1814 A70-24673

Immunity indices in humans subjected to hypodynamia, noting infection resistance lowering

10 p1815 A70-24679

Human central nervous system changes during hypodynamia, noting unidirectional shifts in brain hemodynamics, rheographic wave propagation time reduction, etc

10 p1815 A70-24680

Human nerve and muscle system changes under prolonged hypodynamia

10 p1815 A70-24681

Psychic functions stability during prolonged hypodynamia, discussing memory, attention span, sensometer reactions, time estimating, etc

10 p1816 A70-24685

Physical exercise effects on man during prolonged bed rest, investigating muscle performance, static endurance, walking coordination and psychomotor functions

10 p1816 A70-24688

Human peripheral blood circulation during prolonged underwater activity, showing compensation for high humidity, noise levels, low water temperatures, isolation and confinement

10 p1822 A70-25178

Human cardiovascular system function during adaptation at various high altitudes using simultaneous EKG and phono-KG recordings

10 p1823 A70-25179

High altitude acclimatization effect on tissue capillarity, investigating physiological evidence in rats by tissue diffusing capacity measurement

10 p1823 A70-25220

Respiratory and cardiac activities, body weight variations, blood and urine electrolytic composition of astronauts during Soyuz orbital flights from medical tests

11 p1985 A70-25509

Diurnal rhythms of physiological functions and human adaptation to shifted sleep-wakefulness schedule on healthy pilots subjected to solitary confinement

11 p1985 A70-25511

Rats heart rate change during running at simulated altitude, discussing respiratory-circulatory training effect

11 p1985 A70-25671

Cold air inhalation effect on vital physiological functions of dogs, describing heat exchange simulator of upper respiratory tract

11 p1985 A70-25672

Free radical content changes in mice organs under hyperoxia and hypoxia

11 p1986 A70-25941

Incremental lower body negative pressure as assay method for human orthostatic tolerance

11 p1992 A70-26518

Pilots psychophysiological reactions to various aircraft types and flight maneuvers, considering recorded comments, blood pressure and heart rate

12 p2177 A70-27042

Pro- and anticoagulants dynamics in rats blood during early phases of prolonged sound effect

12 p2168 A70-27347

Metabolism in left ventricular myocardium of rabbits after asphyxiations and during postasphyxial recovery

12 p2168 A70-27624

Canoe paddlers physical training effect on cardiac output and local blood flow and metabolism at and during exercise and recovery

12 p2169 A70-27653

Cerebral circulatory reactions of smokers and non-smokers exposed to altitude, measuring vasomotor, blood flow and cardiac frequency indexes using scalp electrodes

12 p2172 A70-28042

Rats cardiac aerobic and anaerobic pathways response to hyperbaric oxygen exposure

13 p2349 A70-28833

Hypothermia and ionizing radiation effects on hamsters influenza immune response

13 p2349 A70-28834

Psychophysiological characteristics of pilot activity during various landing approaches with different instrumentation levels, studying heart and respiratory rates

13 p2358 A70-29297

Marrow granulocyte reserve restoration in dogs exposed to chronic gamma radiation, discussing leukocyte reaction to pyrogenic agent

13 p2351 A70-29326

Daily electrolyte excretion dynamics of subjects with shifted work-rest schedule, noting disagreement with Scharp results

13 p2358 A70-29343

Vegetative cardiovascular, motor and electrophysiological reactions to electrical stimulation of limbic and reticular formations in cerebrum after adrenalin and aminazine injections

13 p2352 A70-29352

Human response in Apollo flights emphasizing astronauts food, water, waste management, physical examination, preventive medicine problems, etc

13 p2353 A70-29434

Cardiac cycle and phases shortening observations from analyzing electro- and phonocardiographic data recorded during Gemini flights

13 p2359 A70-29437

Food ingestion initiation, investigating role of hypotonic solutions from observation of rats under water deprivation

13 p2353 A70-29495

Skin receptors afferent discharge characteristics during vibrotactile stimulation

13 p2354 A70-29594

Nervous system response fluctuation measurement during perceptual and learning tasks in terms of signal to noise ratio of electrical and tactile stimuli

13 p2354 A70-29595

Skin and tissue mechanical characteristics response to vibratory stimulation, considering effects on physiological and psychophysical tactile sensitivity measurements

13 p2354 A70-29598

Motion sickness in man and animals as normal response with individual susceptibility dependent on motion duration

13 p2355 A70-29793

Electronic simulation of neuronic membrane demonstrating nervous impulses generation and propagation behavior

14 p2542 A70-30387

Vestibular nystagmic and electrical responses facilitation, inhibition and habituation, noting modulation by subcortical and cortical systems

14 p2538 A70-30909

Electronystagmographical responses comparison with electroencephalographic record during prolonged torsion swing vestibular tests under cortical and subcortical factors influence

14 p2539 A70-30917

Intrinsic heart rate /IHR/ range and variability in healthy subjects measured showing age as important determinant in absence of heart disease

15 p2678 A70-31433

Infection resistance during extended space flights, discussing microfloral exchange, defense mechanisms, waste, etc

15 p2688 A70-31677

Physiological examination of healthy human beings, considering repose situation abnormal

15 p2691 A70-31923

Isolated human heart measurements for time course and instantaneous distribution of normal heart excitatory process

15 p2683 A70-32471

Human postural motor control systems nonlinearities, describing physiological experiments and mathematical models

15 p2693 A70-32568

Acceleration training schedules performed with animals and test subjects, assessing schedules effectiveness in increasing tolerances to transverse acceleration

15 p2693 A70-32682

Hypercapnic atmosphere effect on human organisms found tolerable in state of rest or performing light labor

15 p2685 A70-32690

Atrophic changes in tortoises during roundtrip to moon on Zond 5 ascribed to hunger and space flight factors

15 p2685 A70-32741

Muscular behavior analog simulation model from generalization of laws governing viscoelastic behavior of polymeric materials

15 p2693 A70-32820

Electrical potentials in response to auditory stimuli recorded in cat brains by averaging computer

15 p2685 A70-32831

Human and animal adaptation and responses to time intervals and temporal activity cycles, discussing conditioned reflexes in terms of physiological factors

15 p2687 A70-32869

Visual and auditory reactions in dogs to alimentary stimuli before and after partial removal of cerebellum, noting complete recovery within month

15 p2687 A70-32892

Cryobiotic potentialities on earth, investigating life forms physiological response to temperature, cryotolerance mechanisms, etc

16 p2848 A70-33093

Eating and digestion effects on arterial pressure and mesenteric and aortic blood flows in intact unanesthetized dogs

17 p3024 A70-34848

Physiological reactions of Soyuz 6, 7 and 8 crew during group flights, noting cardiovascular and respiratory reaction to submaximum stresses after flight

17 p3038 A70-35361

Barometric pressure reduction effect on gaseous and volatile metabolic products elimination in men wearing oxygen-supplied rubberized suits

17 p3038 A70-35363

Blood glucose and plasma immunoreactive insulin concentrations before, during and after intermittent short duration maximal exercise and glucose infusion

17 p3030 A70-35420

Sheep cardiac rate, respiration rate, hematocrit, erythrocytes per cubic mm and hemoglobin concentration responses to elevated ambient carbon dioxide

17 p3030 A70-35421

Cooling hood effect on physiological responses to work in hot environment, discussing body temperature

17 p3031 A70-35422

Mountain climbing effects on urinary excretion of vanillylmandelic and homovanillic acids, discussing circulatory system acclimatization

17 p3039 A70-35425

Ambient temperature effects on venous reactivity to hydrostatic stress, discussing posture changes and lower body negative pressure effects on index of compliance

17 p3031 A70-35426

Glucose-free fatty acid interactions in working heart, noting increase in glucose uptake, oxidation and glycogenolysis with physiologic work increment

17 p3031 A70-35429

Mathematical model for short term adaptation effects in human semicircular canal response to rotation, discussing nystagmus

18 p3216 A70-35940

Environmental heat stress indices of human subjects in bicycle ergometer experiment

18 p3224 A70-36226

Habituation and dishabituation in semiautact Aplysia preparation with central nervous system removed

18 p3217 A70-36517

Soviet papers on physiological adaptation to heat and cold covering thermoregulatory reflexes, bionics, temperature gradients, hypothalamus, gas exchange, heat generation, etc

18 p3217 A70-36526

Physiological mechanisms of cold adaptation in terms of individual, type and population categories, examining thermoregulatory muscular reflex

18 p3218 A70-36527

Varying thermoregulatory responses of different rodent species to long term heat and cold

18 p3218 A70-36534

Thermoregulation processes in oxygen consumption, blood and body temperatures and skeletal muscles in adult nutria and muskrats in air and water

18 p3218 A70-36535

Gas exchange, body temperature and electrical activity of neck and back muscles of cold-acclimated white rats subjected to various temperatures

18 p3219 A70-36540

Repeated local spine cooling effect on gas exchange and electrical activity of white rats skeletal muscles

18 p3219 A70-36541

Thermoregulation of hedgehogs during muscular activity in cold environment, recording electrical activity, oxygen consumption and body temperature during work-rest cycles

18 p3219 A70-36542

Prolonged cold adaptation effect on heat transfer during recovery period after hypothermia in white rats

18 p3220 A70-36543

Low ambient temperature exposure effect on hamster intestinal absorption capacity, using glucose test compound

19 p3360 A70-37772

Human spatio-temporal visual evoked response characteristics, showing potential graded rotation in same period as input stimulus

19 p3360 A70-37845

Human brain LF activity in visual evoked response, determining relationship to stimulation

19 p3360 A70-37846

Human response time to visual stimulus preceding or following auditory stimulus as function of interstimulus interval

19 p3362 A70-38311

Prolonged hyperbaric oxygen breathing effect on human physical performance at rest and during severe exercise

19 p3364 A70-38369

Mongrel dogs pulmonary and systemic circulatory responses to dopamine infusion

20 p3569 A70-38986

Determinants of human ventricular dimensions and myocardial free velocity relations during maximum and submaximum exercise levels

20 p3571 A70-39365

Skeletal muscles static tension influence on dog respiratory center functional properties, showing increased frequency volume and sensitivity under stimulation

20 p3574 A70-40174

Athletes ventilation and heart rate dynamic responses to supine leg exercise with sinusoidal work load

20 p3576 A70-40329

Human elbow induced forearm and hand vessels tachyphylaxis to angiotensin, noradrenaline and acetylcholine compared to vascular response of vasopresin

21 p3761 A70-40577

Visual vigilance task with standard, binary or rating procedures as response indicators based on signal detection theory, noting relationship to psychophysical procedures

21 p3761 A70-40743

Click-evoked potentials in rat auditory cortex, medial geniculate body, reticulate formation and hippocampus during natural sleep and waking

21 p3761 A70-40917

Ethanol ingestion effect on human response to submaximal and maximal exercise, measuring cardiac output and intraarterial pressure

21 p3761 A70-41135

Human sweating transient state characterized by time constant following abrupt ambient temperature rise

21 p3761 A70-41140

Rats brain oxygenation during hyperventilation with air or oxygen-nitrogen mixture, measuring creatine phosphatase concentration and lactate/pyruvate ratio

21 p3762 A70-41225

L-dihydroxyphenylalanine intraperitoneal injection effect on S-adenosylmethionine concentration in rat brain

21 p3764 A70-41269

Dehydrogenases activities in rabbit retina homogenates exposed to oxygen at high partial pressure for various time periods

21 p3765 A70-41487

Human leg blood flow distribution between deep and superficial veins during alternate treadmill work-rest periods

21 p3767 A70-42160

Muscular group response to sinusoidal and trapezoidal force applied to forearm, discussing frequency dependent limb oscillations and neuromuscular effects

21 p3767 A70-42161

Jet pilot EEG radio telemetry showing psychomotor stresses during takeoff and acceleration

22 p3978 A70-42877

Lateral and angular acceleration effects on blood and urine contents in specific metabolic indices of healthy young men

22 p3971 A70-43136

Visually evoked responses in man to different light stimuli intensities, noting marked increase in binocular over monocular visual response

22 p3972 A70-43408

Human postural control system response to mechanical torque disturbance, using second order differential equation with state dependent parameters for approximate analysis

22 p3979 A70-43494

Normal human postural control system reflex response to tendon jerk disturbance

22 p3979 A70-43495

Decompression hazards in manned orbiting systems, considering consciousness time, survival, pathological response, water vapor and denitrogenation effects and recompression rates

22 p3973 A70-43638

Biosatellite 3 experiment with male marmoset nemestrina monkey, discussing cardiac rate, vascular data, water balance, weight loss and brain temperature

22 p3973 A70-43646

Apollo program medical data contribution to knowledge of human response to space environment

22 p3980 A70-43651

Semicircular canals dynamic cross coupled responses to rotational movement, discussing mechanical model applicability

22 p3981 A70-43703

Orientation detectors in human visual cortex, suggesting mutual lateral inhibition

23 p4144 A70-43813

Human tolerance and ventilatory response to inspiratory mechanical loads

23 p4144 A70-43822

Human ventilatory response to resistance unloading during muscular exercise

23 p4144 A70-43823

Pilot influence on dynamic aircraft design, taking into account physiological state during various operational tasks

23 p4138 A70-44134

Water and salt metabolism changes during prolonged hypokinesia of rabbits, noting blood plasma dilution, hematocrit number and hemoglobin concentration reduction, etc

23 p4146 A70-44656

Mammal and human acoustic reflex for impulsive sound, investigating immunization effectiveness

24 p4297 A70-45373

PSYCHOLOGICAL TELEMETRY

U BIOTELEMETRY

PHYSIOLOGICAL TESTS

NT BODY SWAY TEST

NT CARBOXYHEMOGLOBIN TEST

NT EAR PRESSURE TEST

NT VESTIBULAR TESTS

Serologic evidence of immune mechanisms, including heart muscle antibodies in patients with idiopathic cardiomyopathy, showing no autoimmune disease in majority

01 p0014 A70-10276

Lipid and carbohydrate behavioral abnormalities in patients with angiographically documented coronary artery disease observed by glucose tolerance tests

01 p0016 A70-10441

Functional state changes in organism awaiting and performing parachute jump using orthostatic test, respiration retention and Howard step test

03 p0420 A70-13477

Respiratory and cardiac activities, body weight variations, blood and urine electrolytic composition of astronauts during Soyuz orbital flights from medical tests

03 p0423 A70-13709

White mice hypoxia tolerance enhancement after intraabdominal administration of dilute hydrochloric and lactic acids

03 p0424 A70-13718

Simplified laboratory test program yielding serviceable information for possible direct laboratory diagnosis of risk factors affecting atherosclerosis

03 p0431 A70-14279

Oxygen consumption and body temperatures during acute hypoxia in man, based on low oxygen mixture breathing tests

03 p0439 A70-14291

Efferent model to test inhibitory influence of inferotemporal cortex lesions on visual discrimination of monkeys, using paired flashes of light

04 p0629 A70-14449

QRS and ST-T areas in multiple bipolar chest leads during normal and abnormal activation in patient measured for checking ventricular gradient concept

04 p0632 A70-15307

Solar and geomagnetic effects on variations in physiological tests using alimentary reflex of dogs

04 p0639 A70-15512

Surface and underwater swimming tests for statistical correlation to linear maximum accelerations effects

07 p1201 A70-18788

Circulatory system tests during linear, intermittent and continuous accelerations on centrifuge, noting lack of statistical correlation between centrifuge tests and functional tests

07 p1201 A70-18789

Tolerance level to z axis acceleration from centrifuge techniques, noting irreducibility of intermittent stepwise increasing accelerations tests

07 p1201 A70-18790

Ventilation function, pulse rate and blood pressure measured for adaptation to vertical upright and head-down positions

07 p1201 A70-18794

Physiological pilot training program of FAA, discussing slides on Aeronautical Center and Civil Aeromedical Institute

07 p1218 A70-19012

Energy cost and heart rate responses to single stage nonsteady state submaximal exercise procedures used in diagnostic and functional testing

07 p1211 A70-19690

Electromyograms cross correlation analysis to study time relationships between motor unit discharges of human musculus biceps and triceps brachii during physical work

07 p1213 A70-19791

Syncope proneness correlation with episodes of impaired consciousness in pilots during flight using physiological tests

07 p1223 A70-19944

Multistage treadmill exercise tests on healthy business executives noting S-T-segment responses

08 p1445 A70-21265

Various phases of human isometric left ventricle contraction, comparing results with previously published data

09 p1620 A70-23111

Biological performance studies under extreme environmental stresses for gaining insight into potential of earth-type life here and in universe

09 p1623 A70-23699

Cardiovascular reactions and orthostatic stability during hypodynamia determined from ECG, seismocardiograms, phonocardiograms, sphygmograms and tachy-oscillograms

10 p1817 A70-24694

Respiratory and cardiac activities, body weight variations, blood and urine electrolytic composition of astronauts during Soyuz orbital flights from medical tests

11 p1985 A70-25509

White mice hypoxia tolerance enhancement after intraabdominal administration of dilute hydrochloric and lactic acids

11 p1985 A70-25518

Hypoxia tolerance of albino rats in He-oxygen and Ar-oxygen environments in heat-pressure chamber, discussing He-oxygen mixture cooling effect

11 p1987 A70-26103

Open circuit gas washout test of lungs under inspiration-expiration transmission symmetry, using Hilbert-Schmidt operators

12 p2175 A70-27021

Perivascular pH influence on arteriolar diameter on brain surface of anesthetized rats and cats by micropipette technique

12 p2168 A70-27623

Electrode placement ancillary technique for obtaining stereotaxic atlas of infant rat hypothalamus

13 p2350 A70-29322

Hunger, thirst and environmental stimuli roles in development and elicitation of stimulus bound eating and drinking in animals

13 p2355 A70-29806

2000 meter race for endurance testing, using heart rate radiotelemetry before, during and after

14 p2543 A70-31173

Physiological examination of healthy human beings, considering repose situation abnormal

15 p2691 A70-31923

Physiological tests of sampled data hypothesis in human motor control system

16 p2851 A70-33323

Gas exchange adaptation to heat and cold in rats with different ecological backgrounds

18 p3218 A70-36533

Soviet monograph on automated physiological measurements with onboard computers, covering EKG, EEG, electromyogram, respiration, muscular activity, etc

19 p3372 A70-38797

Circadian rhythms from electrocardiogram and cardiogram of patient with human heart transplant, noting P waves relationship between donor and recipient tissues

20 p3570 A70-39166

Orthostatic stability reduction in experiments with simulated weightlessness, investigating functional compensation mechanisms

23 p4149 A70-45025

Biological life support system based on mutual equilibration of human metabolism and technically controlled algae culture, discussing experimental evaluation

23 p4156 A70-45026

Optimum bed rest time schedules for cardiovascular patients from neurological, dynamometric, electromyographic and myogenic-tonus tests

23 p4149 A70-45077

PHYSIOLOGY

NT AUDIOLOGY

NT BODY COMPOSITION (BIOLOGY)

NT ELECTROPHYSIOLOGY

NT HEMATOPOIETIC SYSTEM

NT LAMELLA

NT NEUROPHYSIOLOGY

NT PSYCHOPHYSIOLOGY

NT RESPIRATORY PHYSIOLOGY

Physiological interpretation of blood velocity curves recorded in right heart cavities of dogs by ultrasonic directional probe, using Doppler effect

01 p0035 A70-10709

Digital computer program for physiological measurements, outlining interpolation of mathematical functions describing signals time variations

03 p0436 A70-13900

Human esophagus physiology, studying sphincter function from data on healthy and afflicted subjects

07 p2124 A70-19793

Soviet collection of papers on physiology of vision under normal and extremal conditions

08 p1442 A70-20726

Compartmented physiological system dynamics by bilinear control model, relating homeostasis to system

15 p2693 A70-32571

Soviet papers on physiological data collection and analysis methods

19 p3369 A70-38206

Living organisms physiological death as biological problem, discussing hypotheses, theories and facts

23 p4145 A70-44225

Functional systems in biology, discussing interscientific demarcation, research strategy, physiological experiment, operational architectures, etc

24 p4305 A70-46391

PI-ELECTRONS

Plasma pi-electrons effects in annulene molecules, obtaining dispersion relation for plasma oscillations by Hueckel theory

14 p2621 A70-30116

PIASECKI MILITARY AIRCRAFT

U MILITARY AIRCRAFT

PICKLING

U CHEMICAL CLEANING

PICTURES

U PHOTOGRAPHS

PIEZOELECTRIC CRYSTALS

Plane harmonic Rayleigh wave propagation in piezoelectric semiconductor GaAs crystals, using successive approximation procedure

01 p0154 A70-10131

Piezoelectric ultrasonic crystal on cardiac catheter tip measuring cardiac diameter in vitro and in excised canine hearts

01 p0038 A70-11025

Plane harmonic Rayleigh wave propagation in piezoelectric semiconductor GaAs crystals, using successive approximation procedure

08 p1556 A70-21407

SnTe of various nominal hole concentrations measured for longitudinal piezoresistance effect along different crystallographic directions

10 p1927 A70-23993

Acoustic wave amplification and generation in piezoelectric semiconductors and semimetals by superionic carrier drift currents

10 p1925 A70-25030

Piezo-rotatory coefficients $R_{11}/$ and $R_{12}/$ of isotropic non-enantiomorphic optically active crystals from fourth rank axial tensor, discussing stress effects

11 p2098 A70-26298

Elastic, piezoelectric and dielectric properties of barium titanate single crystals of laminar domain structure

12 p2288 A70-28329

Piezoelectric scattering effects on electron temperature and mobility in IIB-VIA semiconductor compounds with nonparabolic conduction band

13 p2471 A70-29373

Numerical model of piezoelectric surface wave propagation on free and metallized cubic and hexagonal crystals

19 p3486 A70-37754

Piezoelectric force and moment measurement by quartz multicomponent devices

19 p3426 A70-37937

Quasi-static thickness-shear approximation of radiation of electromagnetic energy accompanying oscillation of piezoelectric crystal plates

19 p3487 A70-37945

Ultrasonic surface waves amplification in piezoelectric crystal-Si semiconductor system, observing dependence on permittivity

19 p3488 A70-38675

Hydrostatic and anisotropic piezoresistance in organometallic crystals, noting iridium and platinum complexes with maximum metal-metal interaction

22 p4086 A70-43021

YIG single crystals piezo-optical effect and magnetic double refraction, describing stress measurement technique

23 p4230 A70-43931

Single crystal piezoelectric materials growth characteristics and wave propagation properties for surface acoustic wave applications

24 p4367 A70-45399

PIEZOELECTRIC GAGES

Piezoprobe parameters calculation for controlling angular welded connections of boiler assembly elements

02 p0300 A70-12481

Piezovibrator operation with two side acoustical loading in pulse mode

02 p0301 A70-12482

Piezoelectric sensing diaphragm for detection of micrometeorites in space, noting vibration mode and effect of small beads contact time on calibration errors

04 p0695 A70-15567

Piezoelectric accelerometer transverse sensitivity calibration using reference accelerometer comparison technique

06 p1073 A70-18599

Piezoelectric quartz and tourmaline pressure gages static calibration, evaluating errors

09 p1675 A70-22599

Piezoelectric field effect strain gage with semiconducting film for extremely small strains in electrically noisy background

15 p2739 A70-32317

Piezoelectric accelerometer reference systems calibration by function separation

17 p3089 A70-35173

PIEZOELECTRIC TRANSDUCERS

NT PIEZOELECTRIC GAGES

Piezoelectric transducer for photoelastic analysis of HF stress waves in thick ring subjected to transient loads

02 p0389 A70-12500

Piezojunction effect and applications in transducers, showing needle and mesa configurations as most promising methods

03 p0496 A70-14193

Solid state digital pressure transducer incorporating Si diaphragm with piezoresistive sensing elements for computerized supersonic and subsonic data applications

03 p0496 A70-14194

Piezoelectric transducers performance in ultrasonic devices evaluated from loss and admittance measurements, using Mason equivalent circuit method

03 p0496 A70-14206

Sputter machining thickness reduction methods for VHF resonant piezoelectric transducers

03 p0496 A70-14207

Electrical impedance, conversion loss and bandwidth for piezoelectric film or plate transducers used for generating planar volume-acoustic waves at microwave frequencies

06 p1062 A70-17480

Turbulence measurement by piezoceramic acoustic sensors, considering capacitance

07 p1284 A70-19829

Acoustic piezoceramic anemometer for steady state measurements of wind turbulence on meteorological tower

07 p1285 A70-19835

Two component piezoelectric skin friction force transducer for hypersonic flow tunnel

13 p2405 A70-28815

Piezoelectric annular disk transducer mechanical response to step voltage input with prescribed temperature field

14 p2588 A70-31228

X band acoustic delay lines using thin film piezoelectric transducers

16 p2874 A70-33391

Ultraminiature piezoelectric semiconductor pressure transducers for wind tunnel models

17 p3093 A70-35491

Interdigital Rayleigh wave transducers piezoelectric coupling coefficient from bulk constants, permitting equivalent circuit parameters prediction

17 p3055 A70-35875

Miniature pressure transducers using piezoelectric or semiconductor elements

20 p3628 A70-39226

Acoustic piezoceramic anemometer for steady state measurements of wind turbulence on meteorological tower

20 p3634 A70-40342

Piezoelectric sensors for multicomponent force and moment measurement

20 p3635 A70-40533

Triboelectric noise in mechanically flexed low level signal cables for piezoelectric transducers with high gain amplifiers

21 p3825 A70-40866

PIEZOELECTRICITY

Static deformation of radially polarized inhomogeneous rotating cylindrical shaft of barium titanate using elasticity, electric field and constitutive equations for piezoelectric materials

01 p0118 A70-10549

Piezojunction effect and applications in transducers, showing needle and mesa configurations as most promising methods

03 p0496 A70-14193

Peripheral arterial piezography for cardiological screening tests and checkups of flying personnel

05 p0807 A70-16495

Electro-optic effects in ferroelectric ceramics with electrically variable coefficients of piezoelectricity and birefringence, discussing applications

09 p1739 A70-22633

SnTe of various nominal hole concentrations measured for longitudinal piezoresistance effect along different crystallographic directions

10 p1927 A70-23993

Microwave amplifiers based on interaction between piezoelectric acoustic waves and collinearly drifting carriers, analyzing gain, frequency response, etc

11 p2018 A70-26164

Surface acoustic wave delay lines using interdigital transducers based on piezoelectrics with applications in VHF and UHF signal processing

11 p2005 A70-26165

Sound generation and detection by distributed piezoelectric sources using frequency response and equivalent circuit

11 p2085 A70-26701

Piezoelectric effects in ferroelectric ceramics using equivalent circuits and admittance matrices

12 p2283 A70-27005

Book on design of resonant piezoelectric devices covering linear piezoelectric materials, Green function, variational methods for dimensional motions and modes, etc

17 p3143 A70-35188

Two dimensional piezoelectric problems of electroelasticity, formulating general solutions in terms of stress and electric potentials using complex variables

19 p3487 A70-37946

Manganin in wire and thin foil geometries, measuring shock piezoresistance coefficient as function of deformation

20 p3687 A70-40166

Rayleigh wave scalar electric potential analysis on piezoelectric medium, using iterative techniques for Poisson equation

22 p4074 A70-42967

PIEZORESISTIVE TRANSDUCERS

NT PIEZORESISTIVE GAGES

Manganin piezoresistive shock gauge constant current supply using inductor and termination technique eliminating shunting

02 p0303 A70-12737

Miniature piezoresistive pressure transducers for catheter and external physiological measurements in small animals

07 p1220 A70-19297

Combined neutron and gamma ray irradiation effects on piezoresistive accelerometers

13 p2405 A70-28814

Subminiature solid state piezoresistive accelerometer using diffused four arm Wheatstone bridge sensor

17 p3094 A70-35522

Piezoresistive Si pressure transducer design for Digital Air Data Computers, achieving optimum resistor matching and long term stability

19 p3430 A70-38521

Sensing elements piezoresistive Si and indium antimonide film sensing elements for high sensitivity pressure transducers and accelerometers, discussing airborne telemetry applications

19 p3431 A70-38538

PIGEONS

Selective visual stimulus control by part of compound S delta in pigeons

01 p0021 A70-10796

Pigeon response to concurrent variable interval reinforcement schedules, investigating relative and changeover rates regarding key color

05 p0800 A70-16126

Chronic hypoxia effects on heart size and hematocrit ratios tested in pigeons

12 p2172 A70-28075

Fixed-ratio performance patterns of pigeon key-peck responses to fractional punishments by electric shock

22 p3971 A70-43375

PIGGYBACK SYSTEMS

Small satellites for scientific technological and operational missions, discussing piggyback launching, command, battery storage, telemetry and attitude control systems

15 p2810 A70-31781

PIGMENTS

NT CHLOROPHYLLS

Joint Chlorella-yeast cultivation on metabolites, investigating biomass accumulation and pigment synthesis

07 p1197 A70-18655

Dark adaptation correlated with in vivo visual pigments regeneration as function of bleaching during monomolecular time course

08 p1447 A70-21722

Radiation stable refractory oxides in white spacecraft thermal control coatings, discussing photocatalysis application to degradation analysis

11 p2067 A70-26364

Bidirectional reflectance and transmittance calculation for irradiated layer of monodisperse matrix suspended pigment particles

16 p2940 A70-33923

UV irradiation effects on ZnO used as pigment for spacecraft thermal control coatings

16 p2940 A70-33937

Rhodamine C chemiluminescent material for atmospheric ozone measurements, describing preparation and luminescence spectrum

19 p3373 A70-37638

Photoperiodism in animal organism, discussing retinal epithelium photosensitive substance accumulation and retino-hypothalamo-hypophyseal mechanism of pigmentation

19 p3365 A70-38413

Ruby laser radiation injury relationship to position and number of energy absorbing pigment particles in iris

20 p3579 A70-39425

Apollo 11 lunar fines porphyrin-like pigments content demonstrated by fluorescence spectrometry and analytical demetallation, suggesting rocket exhaust source

21 p3910 A70-41626

Isochromic change in bleaching of rhodopsin, showing additional intermediate without detectable color change

23 p4147 A70-44776

Pigments absence in photosystem II of photosynthesis in heterocysts of blue-green algae

23 p4148 A70-44870

PIGS [SWINE]

U SWINE

PILOT ERROR

Biphasic nature of pilot error in gliding, suggesting means of reducing aircraft accidents

03 p0433 A70-13261

Pilot visual information display systems influence on flight safety, discussing aircraft accidents and human error factors

04 p0691 A70-15143

Book on human factor in aircraft accidents covering desire to please, fatigue, diurnal rhythm, psychology, etc

06 p0987 A70-18249

Flight safety evaluation based on ICAC and German flight accident data indicating pilot role and tabulating statistical analysis

11 p1981 A70-25948

Reference systems for two dimensional visual indications as correction device for pilot guidance errors associated with rotation effects

12 p2177 A70-27036

Pilot disorientation in dark night takeoff accident type, presenting illusory angular displacement of vertical, flight paths and sequential accelerations

13 p2359 A70-29441

Corporate aircraft accident statistics, causes and prevention, noting pilot errors, mechanical failures, etc

16 p2842 A70-33814

Low cost headup displays /HUD/ for pilot error reduction during takeoff, approach and landing, discussing displayed functions vs cost tradeoffs

16 p2911 A70-33818

Pictorial display methods for pilot error reduction in area navigation via guidance control and capability beyond visual field

19 p3465 A70-38234

PILOT PERFORMANCE

Concorde aircraft flight simulator, describing piloting system refinement and pilot training

01 p0057 A70-10797

Aircraft pilot-autopilot task division during automatic landing, analyzing man machine interaction in aircraft approach guidance

01 p0139 A70-11258

Electronic displays role in pilot-aircraft interaction, considering flight safety, cost effectiveness, onboard data input, etc

01 p0039 A70-11260

Navy/pilot aircraft control performance during day and night final approach to landing on carriers for empirical performance criteria

02 p0243 A70-12131

Helicopter automatic hybrid navigation system for increased accuracy over unfamiliar terrain and above-human performance, comparing navigating pilot performance with machine

02 p0335 A70-12134

Air traffic control system for intercity and metropolitan VTOL airway reducing pilot and air traffic controller workloads

02 p0335 A70-12135

Helicopter avionic systems man machine capability estimation based on pilot workload, applying results to design evolution

02 p0244 A70-12136

Task interference model for interference among two or more continuous manual control tasks, suggesting metric for pilot mental work load

02 p0244 A70-12139

Intermittent EKG recordings during hypoxia test for detection and diagnosis of heart disorders in airmen

02 p0242 A70-12850

Biphasic nature of pilot error in gliding, suggesting means of reducing aircraft accidents

03 p0433 A70-13261

Commercial pilots susceptibility to emphysema and respiratory impairment in hypobaric environment, discussing flying disability implications

03 p0438 A70-14068

Cockpit display system to reduce aircraft pilot work load and aid judgment making during critical operations [ASME PAPER 69-WA/BHF-12]

04 p0642 A70-14854

Aircraft pilots vertigo during flight using questionnaire and interviews, emphasizing bank directional disorientation

04 p0643 A70-14979

Pilots hearing level based on pure tone threshold audiograms compared with personnel not exposed to job noise

04 p0631 A70-14982

Pilot response to stability augmentation system failures and design implications [AIAA PAPER 68-819]

04 p0624 A70-15379

Cardiology role in aviation medicine, evaluating jumbo jet and SST flight stress effects on pilots and passengers in age factor study of arteriosclerosis

05 p0803 A70-16721

High temperature effects on pilots psychomotor performance and physiological function, discussing measurements taken during complex tasks

06 p0999 A70-17290

High fidelity simulations for environmental stress evaluations, describing carbon dioxide effects on pilots simulated ground target tracking and reentry vehicle landing

06 p0999 A70-17291

Pilot emotional state during stressful situations from tape recorded vocal utterances of air to ground radio communications using spectrographic analysis

06 p1000 A70-17297

Anxiety-stress effects on pilot performance in execution of acquisition tracking task minimized by training

06 p1003 A70-18016

Cooper aircraft handling rating scale on basis of test pilot experience

06 p1003 A70-18018

Emotional stability relationship to pilot acceleration tolerance tested on centrifuge, confirming instability correlation to poor resistance

07 p1201 A70-18793

Vestibular semicircular canal excitation thresholds of experienced and candidate pilots for imposed angular accelerations

07 p1201 A70-18795

Acceleration and weightlessness effects on efficiency, reliability and capacity in pilots and astronauts muscular system

07 p1202 A70-18797

Decision algorithms simulating human controller adaptive behavior in controlling VTOL aircraft in hover following stability augmentation system failure

07 p1216 A70-18860

Pilot limitations role in USAF midair collisions, discussing information systems for collision avoidance

07 p1192 A70-19022

Ground terrain blurring during aircraft flight at low altitude and high speed, calculating theoretical blur zone

07 p1220 A70-19285

Concorde simulator for determining aircraft control responses and integrating pilot function into problem

07 p1249 A70-19743

Missassignment prevention in aviation specialties, using multiple regression analyses and dichotomous pass vs fail criterion to develop prediction equations

07 p1222 A70-19929

Vital capacity measurements made preflight and postflight on jet fighter aircrew breathing pure oxygen at various G forces

07 p1222 A70-19934

Syncope proneness correlation with episodes of impaired consciousness in pilots during flight using physiological tests

07 p1223 A70-19944

Visual aspects of collision avoidance, describing prudent mid-air maneuvers

08 p1449 A70-20481

Attack aircraft cockpit displays, discussing design requirements and pilot ability as controller

08 p1435 A70-20674

Optical suitability to pilot visual requirements in head-up displays, discussing telecentric viewed system permitting binocular disparity tests

08 p1449 A70-20675

Flight crews spatial vision, estimating absolute distance perception of pilots and navigators with emmetropic refraction

08 p1450 A70-20742

Convergence role in distance perception during aircraft landing, testing subjects with normal binocular vision, emmetropic refraction and visual acuity

08 p1450 A70-20744

Aircraft flight testing techniques modification to cover maximum performance values

08 p1437 A70-21735

Pilot and copilot task distribution schedules adopted by European civil aviation for landing approaches under poor weather conditions

08 p1542 A70-21850

Circadian rhythm of pilot efficiency and multiple time zone travel effects [DFVLR-SONDDR-29]

08 p1453 A70-21935

Time lapse photographic recording and scoring in-flight performance of helicopter aviator trainees during hypothetical tactical instrument mission

09 p1624 A70-22900

Flight stress effect on blood clotting stabilization of Starfighter aircraft pilots, observing no change in thrombocytes number

09 p1625 A70-23005

Aircraft pilots psychic and flight stress admissible degree not resulting in hazardous consequences, suggesting measures to increase resistance

09 p1625 A70-23006

Psychic stress causing factors and reactions in aircraft pilots on duty, analyzing harmful effects on organism

09 p1620 A70-23012

Body training type and amount effect on physiological functions and physical fitness of pilots, discussing pulse frequency

09 p1626 A70-23015

Metabolic and heart rates determined in experienced and inexperienced pilots during Hiller 12-E and 12-EL helicopters flight through standard maneuvers

09 p1627 A70-23455

Visual search activity decrease observed as function of time-on-task for skilled and unskilled helicopter pilots, recording eye movements and blinks

09 p1628 A70-23463

Pilot/vehicle dynamics from flight test records, discussing close-loop attitude control tasks

10 p1824 A70-23897

Airborne simulator program for evaluation of motion and visual cue effects on pilot performance in roll, using compensatory tracking tasks

10 p1857 A70-24202

Ground-based and in-flight simulation using variable stability aircraft, investigating pilot rating

10 p1858 A70-24209

Statistical methods for flying quality research concerning sailplane dynamic stability, maneuverability, sensitivity, rolling and pilot induced oscillations

10 p1805 A70-24582

Ground based simulation for hypersonic reusable lifting reentry vehicle design with pilot-in-loop, discussing six degree of freedom simulation

10 p1861 A70-24920

Pilots with high vestibular stability studied for spatial orientation, noting activity impairment due to alternating angular acceleration and optokinetic stimuli

10 p1828 A70-25180

Japanese jet aircraft pilots instrument reading and checking procedures during landing operation under contact flight rules

11 p2078 A70-25667

Pilot electroencephalograms during F-104 flights recorded by telemetering noting alpha, beta and theta activities

11 p1990 A70-25668

Aged pilots hearing acuity using speech audiometry, noting discrimination loss for HF verbal sounds

11 p1990 A70-25669

Inflight aircraft cockpit noise levels effect on pilot hearing sensitivity

11 p1990 A70-25875

Short duration high workload effects in pilot rr interval and finger tremor during Boeing 747 aircraft let-down, approach and landing

11 p1993 A70-26521

Agricultural pilots fatigue based on flight and environmental effects

11 p1993 A70-26522

Aviation psychological research - Conference, Zurich, September 1969

12 p2175 A70-27026

Minnesota Multiphasic Personality Inventory scores compared with various pilot training proficiency levels, noting low correlation

12 p2176 A70-27032

Aircraft pilot candidates reactions under simulated flight conditions tested using precision coordination analyzer /PCA II/ and instrument coordination analyzer /ICA/

12 p2176 A70-27034

Pilots psychophysiological reactions to various aircraft types and flight maneuvers, considering recorded comments, blood pressure and heart rate

12 p2177 A70-27042

Pilots anxiety in military milieu using interviews and questionnaires noting effect on proficiency

12 p2179 A70-27051

Psychological tests of pilot adaptation to accident situation using photo display assessment

12 p2179 A70-27052

Area navigation for reducing cockpit navigation workload, permitting aircraft operations on desired course and enhancing pilot response to ATC instructions

[SAE PAPER 700283]

12 p2266 A70-27426

Airborne equipment for Air Traffic Control System, improving pilot/controller cooperation

[SAE PAPER 700300]

12 p2266 A70-27448

Visual aircraft-to-aircraft detection effectiveness in collision avoidance as function of pilot performance and closing speed

12 p2267 A70-27633

Man machine eye-integration coupling in tracking task applied to helicopters, ocean-going craft and propeller aircraft

13 p2357 A70-28386

Frequency and amplitude during longitudinal control surface pumping by pilots in precise flight path handling for aircraft design

[AIAA PAPER 70-567]

13 p2346 A70-29032

Pilot-aircraft closed-loop characteristics, using pilot transfer functions for handling qualities prediction

[AIAA PAPER 70-568]

13 p2346 A70-29033

Longitudinal short-period flying qualities as closed-loop pilot-airplane system, noting acceptance values

[AIAA PAPER 70-569]

13 p2346 A70-29034

Military pilots visual estimation of point location coordinates within rectangular area

13 p2357 A70-29121

Flying qualities application to automobiles, discussing work load with respect to controllability and pilot behavior

13 p2347 A70-29142

Psychophysiological characteristics of pilot activity during various landing approaches with different instrumentation levels, studying heart and respiratory rates

13 p2358 A70-29297

Acceleration effects on mental working capacity of fighter pilots, discussing attention shift and stability, operational memory, sensorimotor reactions

13 p2351 A70-29337

Cardiac cycle and phases shortening observations from analyzing electro- and phonocardiographic data recorded during Gemini flights

13 p2359 A70-29437

Man powered aircraft /MPA/ designs, considering bird flight aerodynamic characteristics

14 p2531 A70-30859

V/STOL control systems design for aircraft stabilization and pilot workload reduction

14 p2615 A70-31278

Model for pilots optimal manual control of hovering VTOL aircraft longitudinal position

14 p2543 A70-31409

Heat stress levels in cockpit of AH-1G Hueycobra helicopter parked in sunlight with closed canopy, using sweating copper mannikin

15 p2689 A70-31881

Pitch and Coriolis illusions effects on pilot pitch angle adjustment in simulated takeoff

15 p2689 A70-31885

Pilots brake-takeoff decision at critical engine failure speed, discussing operational aspects of accelerate-stop criteria

15 p2675 A70-32219

Aircraft accident prevention via reduction of pilot attention distractions

15 p2692 A70-32226

Medical and professional disadaptation in fighter pilots, considering fatigue, digestive disorders, anxiety, absenteeism, efficiency loss and accident proneness

16 p2850 A70-34347

Aircraft pilot and nonpilot night vision adaptation comparison, using Goldmann-Weekers adaptometer

17 p3038 A70-35138

Fatal general aviation accidents examined by pathologists, determining pilot incapacity, accident sequence, aircraft design modification and crash protection performance

17 p3033 A70-35567

Safety in airline operations, discussing roles of aircraft designer and pilot

[AIAA PAPER 70-907] 17 p3019 A70-35819

Integrated flight management system for commercial aircraft pilot using computer

[AIAA PAPER 70-908] 17 p3134 A70-35820

Acrobatic pilots equilibrium behavior in vestibular training, discussing labyrinth reactions and fluid intake role

17 p3041 A70-35919

Optokinetic and vestibular effects on human operator reliability in aircraft control systems

18 p3223 A70-36184

Visual effects in astronauts and pilots, discussing optical illusions and distance estimation errors due to accelerations, runway factors, lack of oxygen, etc

18 p3225 A70-36777

Computer simulated decision hierarchical model of helicopter and VTOL pilot for multiloop closure and tracking characteristics of man-vehicle system

19 p3372 A70-38921

Comfort plane switch mounting design for helicopter collective controls, noting mock-up evaluation by test pilots

19 p3372 A70-38922

Hypoxia effects on aviators visual accommodation, convergence and stereoacuity, noting myopia increase with altitude

20 p3569 A70-38996

Bobweights effects on pilot induced oscillations, noting role in flying qualities and control system design

[AIAA PAPER 70-1002] 20 p3560 A70-39529

Pilot scanning dwell times and control workload in simulated instrument approach, using eye-point-of-regard (EPR) measurements

[AIAA PAPER 70-999] 20 p3580 A70-39532

Turbulence effects on lateral directional flying qualities, examining pilot task performance, control workload and compensatory behavior

[AIAA PAPER 70-998] 20 p3560 A70-39533

Student pilot case diagnosis of hysterical neurosis with syncopal and epileptiform symptoms

21 p3771 A70-41493

Postexercise electrocardiogram detection of latent coronary heart disease in flyers prior to myocardial infarction

21 p3771 A70-41494

Age, grade, educational institution and attitude effects on pilot personality test performance

22 p3977 A70-42870

Aircraft handling qualities specifications and definitions evolution based on test pilot rating correlation with engineering data and piloting ease evaluation with transfer functions

[ICAS PAPER 70-19] 23 p4138 A70-44114

Pilot influence on dynamic aircraft design, taking into account physiological state during various operational tasks

[ICAS PAPER 70-37] 23 p4138 A70-44134

Aircraft crew and pilot in-flight work load measurement and simulator

[ICAS PAPER 70-43] 23 p4138 A70-44141

Pilot trainees psychological screening, correlating Rorschach test parameters with subsequent training performance

24 p4306 A70-45123

Pilot heart rate during in-flight simulated ILS approaches in general aviation aircraft

24 p4306 A70-45333

Pilot navigation efficiency in low altitude terrain following flight, using synchronized TV and simulator with inertial guidance

24 p4307 A70-45506

Pilot hand-held and leg-mounted controllers for precision tracking from aircraft under buffeting tested in static and dynamic motion simulator

24 p4308 A70-45513

Biotechnological design of shirt/sleeve side-by-side crew station for shuttle vehicle, including pilot vision and landing experience from X-15 program

[AIAA PAPER 70-1327] 24 p4416 A70-45923

Pilot interface with area navigation system, describing control and display unit for navigation situation, flight plan and system status

[AIAA PAPER 70-1335] 24 p4373 A70-45933

PILOT PLANTS

Pilot model based on Kalman filtering and optimal control, investigating evaluation for time stationary conditions and sine-wave tracking

10 p1823 A70-23894

Complex organization-processing system of experimental production, noting work specialization in machine shops

11 p2060 A70-25936

PILOT SELECTION

Scientifically oriented pilot selection objectives criteria taking into account data concerning accident causes

[DVL-892] 02 p0242 A70-11684

Scandinavian Airlines system of pilot selection, considering personality traits, behavior characteristics, clinical examination, etc

03 p0433 A70-13260

SAS pilot selection system, discussing assessment variables, physiological examinations, psychological tests, recruiting procedure, etc

03 p0433 A70-13262

Missassignment prevention in aviation specialties, using multiple regression analyses and dichotomous pass vs fail criterion to develop prediction equations

07 p1222 A70-19929

Cardiovascular aging and aeromedical maintenance programs for selecting test pilots

08 p1453 A70-21739

Vestibulometric techniques for medical examination and pilot selection using Coriolis accelerations for instability prognosis

09 p1617 A70-22475

Pilot leadership qualities as criteria for selection, examining command training

11 p1993 A70-26607

Pilot training applicant test profiles, discussing difference between intelligent and intellectual candidates

12 p2176 A70-27028

Fighter pilot selection and training in Royal Netherlands Air Force

12 p2176 A70-27029

Elementary flight training study in Royal Netherlands Air Force for improving pilot selection, discussing instructor and social science roles

12 p2176 A70-27030

Aircraft pilot ability tests validity, applying correction methods in decision making regarding applicant acceptance

[DFVLR-SONDDR-32] 12 p2176 A70-27031

Ab initio pilots selection and training in Swissair, describing preselection, in-flight and final selection tests and interviews

12 p2176 A70-27033

Flying accident liability predictions reliability from pilot trainee aptitude test performance at selection, discounting accident proneness theory

12 p2178 A70-27048

Radiological studies of young adult spines for selecting aircrew personnel and collecting data to compile reference dossiers in case of accidents

12 p2171 A70-28039

Scandinavian airlines /SAS/ pilot selection system validity based on scores

15 p2689 A70-31772

French airline pilots training program at Montpellier and St-Yan, considering selection, licensing and simulators

16 p2853 A70-33675

Airsickness frequency, pathogenesis and prevention, discussing cadet selection

17 p3037 A70-35129

Medicopsychological and labyrinthine exploration of flight crew candidates aeronautical adaptation, using electronystagmographic method of swinging chair

17 p3041 A70-35918

Aptitude test validity taking into account selection board subjective decisions on pilot applicant acceptance

19 p3371 A70-38507

Airline transport pilots selection based on psychiatric and psychological testing

22 p3981 A70-43697

Pilot trainees psychological screening, correlating Rorschach test parameters with subsequent training performance

24 p4306 A70-45123

Aviation psychiatry role in pilots selection and treatment

24 p4296 A70-45124

Psychological training and selection of airline pilots for stress resistance

[DFVLR-SONDDR-53] 24 p4310 A70-46413

PILOT TRAINING

Concorde aircraft flight simulator, describing pilot training system refinement and pilot training

01 p0057 A70-10797

Adaptive man machine system for automated training of pilot dynamic control skills /decision and motion/, describing synthesis procedure

02 p0246 A70-12148

Visual spaceflight simulators for spacemen and aircraft pilot training

04 p0663 A70-14691

Visual, motion and auditory stimuli role in enhancing aircraft pilot training simulators realism, considering motion perception research

[ASME PAPER 69-WA/BHF-9] 04 p0642 A70-14853

Professional personality formation and organization of aviator, discussing infancy motivation, identification with instructor during training, emotional life, etc

05 p0799 A70-15767

Adaptive training applied to simulated pilot training system, discussing methods for variables selection, error measurement, trainee feedback, etc

05 p0805 A70-16007

Psychological factors in training and education of pilots and astronauts for optimal matching between human operator and vehicle control system

05 p0809 A70-16967

Anxiety-stress effects on pilot performance in execution of acquisition tracking task minimized by training

06 p1003 A70-18016

Crash control for reduction of operational hazards and flight accidents to survivable level, discussing pilot training for emergencies

07 p1191 A70-19008

Physiological pilot training program of FAA, discussing slides on Aeronautical Center and Civil Aeromedical Institute

07 p1218 A70-19012

Aviation medicine, discussing pilots physical fitness and training, spatial orientation, ground crew, data flow, etc

08 p1451 A70-20977

Jet pilot trainee qualification requirements, training process methods and equipment, considering German-French joint trainer aircraft program

08 p1452 A70-21348

Air transport total in-flight simulator /AT/TIFS/ equipped with six degree of freedom variable stability system for aircraft development and pilot training

08 p1437 A70-21736

Flight simulators for pilot training, discussing need for aircraft motion cues

09 p1655 A70-22296

Time lapse photographic recording and scoring in-flight performance of helicopter aviator trainees during hypothetical tactical instrument mission

09 p1624 A70-22900

Air combat simulator with attacker and evader pilots control capability, comparing simulated interceptions with flight test maneuvers

[AIAA PAPER 70-340] 09 p1656 A70-23023

Psychological fitness capacity of students in pilot training, determining unfavorable traits for flight

11 p1985 A70-25670

Civil airlines training captains heart rate response to simulator stress, base conversion and line training

11 p1992 A70-26519

Pilot leadership qualities as criteria for selection, examining command training

11 p1993 A70-26607

Pilot training applicant test profiles, discussing difference between intelligent and intellectual candidates

12 p2176 A70-27028

Fighter pilot selection and training in Royal Netherlands Air Force

12 p2176 A70-27029

Elementary flight training study in Royal Netherlands Air Force for improving pilot selection, discussing instructor and social science roles

12 p2176 A70-27030

Minnesota Multiphasic Personality Inventory scores compared with various pilot training proficiency levels, noting low correlation

12 p2176 A70-27032

Ab initio pilots selection and training in Swissair, describing preselection, in-flight and final selection tests and interviews

12 p2176 A70-27033

Aircraft pilot candidates reactions under simulated flight conditions tested using precision coordination analyzer /PCA II/ and instrument coordination analyzer /ICA/

12 p2176 A70-27034

Civilian pilot trainee stress level dependence on individual flying instructors, detecting psychophysiological variables by inflight recording

12 p2178 A70-27044

Preparatory aviation training applicants intelligence correlated with number of brothers and sisters

12 p2178 A70-27050

Airline flight crews training need, emphasizing pilot flight maneuver capabilities for emergencies

13 p2345 A70-28974

USAF undergraduate pilot trainees responses in prototype spatial orientation trainer

13 p2359 A70-29439

DC-9 aircraft pilot training including jet introduction, DC-9 conversion and route training

14 p2542 A70-30417

French airline pilots training program at Montpellier and St-Yan, considering selection, licensing and simulators

16 p2853 A70-33675

Variable stability trainer modification of F-106 to reproduce flight characteristics of aircraft for pilot training in potentially dangerous situations
16 p2842 A70-33815

Soviet book on peripheral vestibular apparatus and higher nervous system roles in motion sickness covering Coriolis acceleration tests, pilot training and selection, drugs, etc
19 p3359 A70-37406

Boeing 747 pilot transition training, discussing takeoff, landing, eyelevel, flareout taxi speeds, inertial navigation and electrical, fuel and hydraulic systems
20 p3562 A70-40083

Highlift and blown wing types slow speed STOL aircraft, comparing pilot training requirements with jet airline flying
[AIAA PAPER 70-1282] 24 p4292 A70-45971

Psychological training and selection of airline pilots for stress resistance
[DFVLR-SONDDR-53] 24 p4310 A70-46413

PILOTTED CENTRIFUGES
U HUMAN CENTRIFUGES

PILOTLESS AIRCRAFT
NT DRONE AIRCRAFT
NT TARGET DRONE AIRCRAFT

PILOTS (PERSONNEL)
NT AIRCRAFT PILOTS
NT TEST PILOTS

Human communication in pilots and in maintenance and administrative personnel, noting time factor influence
04 p0644 A70-14985

Pilots temporal lobe epilepsy case history and diagnosis
06 p1000 A70-17301

Flight doctor-pilot relationship, studying personal motivation
12 p2178 A70-27049

Age discrimination in employment policies of air carriers, discussing legislative measures, hiring practices and retirement rules concerning stewardesses and FAA pilots
12 p2336 A70-27772

Pilots EEG characteristics, noting alpha and beta rhythms prevalence
13 p2358 A70-29342

Vestibular habituation among pilots and flying staff from training and seniority standpoint
14 p2538 A70-30914

Sympathoadrenals activity in pilots during supersonic flight, investigating urinary catecholamine output
15 p2690 A70-31891

Characteristic injuries from aircraft controls inflicted in fatal accidents, showing pilot position and hand location upon impact
17 p3039 A70-35573

Pilot assessment aspects of flight simulation in terms of experiment planning, facility and results reporting and analysis
23 p4153 A70-44546

PINCH EFFECT
NT PLASMA PINCH
NT THETA PINCH

Pinch characteristics of simple band structure semiconductor and nondegenerate electron gas during bimolecular current carrier recombination, determining hole pairs spatial and recombination spectral distribution
03 p0538 A70-13062

Recombination emission of InSb semiconductor at low temperature during pinch effect with electron gas degeneration, calculating spectral distribution and effective temperature vs current
03 p0539 A70-13406

Magnetic field effect on recombination radiation intensity under pinch effect in semiconductor nondegenerate electron hole plasma with recombination time exceeding carrier lifetime
03 p0540 A70-13508

Hydrostatic thrust bearing with electrically conducting gas lubricant under axial current induced MGD pinch
03 p0497 A70-13780

Anodic precursors of convergent cylindrical shock wave of z-pinch discharges in He and Ar
07 p1261 A70-20357

Degenerate pinch in bipolar electron-hole plasma in semiconductors
13 p2472 A70-29760

Current distribution and interband recombination emission in bipolar semiconductor crystal under pinch effect produced by external magnetic field
20 p3677 A70-39590

Semiconductors with bipolar conductivity under electron-hole scattering, calculating plasma pinch effect on I-V characteristics
24 p4390 A70-45659

PINEAL GLAND
Dibutyltryl cyclic adenosine monophosphate stimulation of melatonin and serotonin synthesis from C-14 labeled tryptophan by rat pineals in organ culture
01 p0022 A70-10824

Melatonin biosynthesis, discussing regulation by light and sympathetic nerves, daily pineal rhythms, estrous rhythms and ovarian hormones
03 p0424 A70-13809

Mammalian pineal organ control experiments involving light and sympathetic nerve stimulation
10 p1812 A70-24396

Pineal C14-indoles synthesis in rats noting no direct effect of morphine
11 p1988 A70-26299

PINHOLES
Pinhole expansion in anisotropic plastic disks determined by obtaining solutions for Tresca and Mises yield functions, assuming plane stressed state
11 p2138 A70-26171

PION BEAMS
Extensive air shower characteristics for inelasticity coefficient, nucleon-pion interaction cross sections and secondary particles, noting parameter interchangeability
05 p0898 A70-15946

Neutron and proton distributions rms radii in nuclei by optical model analysis of low energy pion-nucleus interactions
07 p1337 A70-19360

Nucleon spectra, particle multiplicities and radiochemical cross sections following stopped-pion absorptions by complex nuclei, comparing calculated and experimental data
14 p2618 A70-30341

PIONEER SPACE PROBES
NT PIONEER 6 SPACE PROBE
NT PIONEER 8 SPACE PROBE
NT PIONEER 9 SPACE PROBE

High energy solar flare data from neutron monitor stations supplemented by low energy data from interplanetary space probes Pioneer 6 and 7
05 p0902 A70-16443

Pioneer 6-9 low magnetism spacecraft for interplanetary magnetic field observation
13 p2507 A70-30046

Pioneer-F Jupiter flyby mission planning, considering use of optimum broken plane trajectories to increase launch opportunity and/or payload capability
[AIAA PAPER 70-1050] 19 p3528 A70-38865

SNAP 19 radioisotope thermoelectric generator module for Viking Lander and Pioneer applications, discussing design requirements, environmental and mission constraints, life, performance and reliability characteristics, etc
22 p4071 A70-43195

PIONEER 6 SPACE PROBE
Transient Faraday rotation of S-band telemetry carrier observed during Pioneer 6 occultation by solar corona, correlating with decametric solar radio bursts
02 p0369 A70-12059

Pioneer 6 radio signal spectrograms during solar occultation, noting solar event effects on bandwidth
02 p0369 A70-12060

Magnetosheath plasma measurements by Pioneer 6 during outbound passage in dusk meridian, comparing results with various predictions
13 p2396 A70-29180

Solar wind observations by Pioneer 6, considering particle density, flux and kinetic energy
16 p2972 A70-32949

Nonmagnetic explosive actuated indexing device permitting precise 180 deg rotation of magnetometer sensor on Pioneer 6 spacecraft
16 p2914 A70-34124

PIONEER 8 SPACE PROBE
Primary cosmic ray nitrogen nuclei intensity and spectrum measured by balloons and Pioneer 8 space probe, obtaining abundance difference from solar atmosphere
01 p0169 A70-10319

Geomagnetic tail observations by Pioneer 8 probe
03 p0475 A70-13851

Geomagnetic tail observations by Pioneer 8 at 500 earth radii, analyzing time-averaged magnetic field data
03 p0575 A70-13983

Interplanetary magnetic field measurements by Pioneer 8 during 25 February 1969 solar activity, discussing geomagnetic storms, cosmic rays, shock fronts and ionospheric disturbances
19 p3513 A70-37501

Primary interplanetary electron energy spectrum, using Pioneer 8 measurements
19 p3502 A70-38094

Pioneer 8 and 9 cosmic ray detector system, discussing mechanical, electrical and data conditioning properties
23 p4195 A70-44300

PIONEER 9 SPACE PROBE
Pioneer 8 and 9 cosmic ray detector system, discussing mechanical, electrical and data conditioning properties
23 p4195 A70-44300

PIONS
Nucleons and high energy pions inelastic interactions with complex nuclei involving external diffraction production of pions
03 p0526 A70-13029

Pion production characteristics during high energy nucleons interactions from data on production in upper atmosphere by gamma-quanta families/isobaric production/
03 p0555 A70-13032

Charged particles distribution according to multiplicity during pion-nucleon and nucleon-nucleon interactions at high energies
03 p0555 A70-13033

Pion and nucleon interactions with atomic nuclei at 200 Gev using Wilson chamber and ionization calorimeter, determining pion collisions characteristics
03 p0555 A70-13034

Pionic transition in Ni isotopes to measure nuclear interaction effects, observing level shift and broadening
05 p0885 A70-16682

Pion and nucleon interactions, tabulating average multiplicity and inelasticity values for various primary cosmic ray energy levels
09 p1745 A70-22775

Cosmic gamma ray spectrum from secondary neutral pion production in p-p interactions, discussing delta isobar, fireball and nuclear interactions effects
11 p2106 A70-26707

High energy break in isotropic gamma ray spectrum predicted from critical test of cosmological pion-decay hypothesis
11 p2106 A70-26844

Th 232 and U 238 pionic X ray energies and widths, suggesting anomalous effect for interaction between high-Z nuclei and pion
15 p2776 A70-31738

Galactic gamma rays from OSO-3 observations attributed to decay of neutral pions produced by cosmic rays interaction with interstellar gas nucleons
17 p3150 A70-34567

Three dimensional nucleon-pion cascade equations solution for cosmic ray extensive air showers by pion-links method
17 p3150 A70-34597

Interstellar electron and positron intensity, observing pion production spectrum from nuclear collisions at machine energies
19 p3504 A70-38111

Background gamma ray observations attributed to decay of pi-mesons produced by extragalactic cosmic ray protons collisions, noting radiation sources age
21 p3877 A70-40703

PIPE FLOW
Heat transfer in tube flow with forced convection, internal radiation exchange, axial wall heat conduction and arbitrary wall heat generation
01 p0214 A70-10294

Steady one dimensional flow in gas filled cylindrical tube, studying shock induced compression wave generated by sudden piston acceleration
01 p0062 A70-10804

Flow stability criterion in rough pipes, deriving laminar to turbulent flow transition characteristics and drag as function of Reynolds number
01 p0064 A70-10998

Mass transfer analysis for axisymmetric turbulent flow in circular tube, deriving turbulent velocity profile from two part model, based on von Karman similarity hypothesis
01 p0064 A70-10992

Nonaxisymmetric mass transfer in turbulent flow in plain circular tube, considering diametral line and discontinuous ring sources
01 p0065 A70-11093

Mixing length relationship in Prandtl theory for turbulent channel and pipe flow, deriving universal velocity distribution law
02 p0277 A70-11911

Pressure drops in turbulent flow through circular or plane parallel section pipes, obtaining mean velocity expressions suitable for application to lubrication
02 p0277 A70-11912

Average pressure at downstream end of pipe discharging into reservoir with upstream end under pulsed flow, considering application to pneumatic control system
02 p0279 A70-12110

Axial flow reversal in swirling incompressible tube flow, discussing static pressure, velocity profiles and turbulent Navier-Stokes equation
03 p0465 A70-13017

Wall temperatures and heat transfer coefficients for solid-vapor mixtures of para hydrogen and nitrogen flowing in heated tube
03 p0604 A70-13018

Unsteady heat transfer equations for laminar fluid flow in pipe with varying wall temperature
03 p0604 A70-13207

Swirling flow through axisymmetrically deformed tube without consideration of viscosity and compressibility, noting wall flow for critical Rossby number values
03 p0468 A70-13788

Structural similarity hypothesis for fully developed turbulence in smooth circular tubes, using intensity correction procedure
04 p0665 A70-14453

Blood flow through veins and collapsible tubes simulated by physical model, downstream pressure effect and importance of collapse phenomena

04 p0641 A70-14631

Finite difference theory applied to numerical analysis of laminar equilibrium MHD flow in circular tube [ASME PAPER 69-WA/HT-55]

04 p0727 A70-14794

Heat transfer in partially ionized argon plasma flowing in water cooled circular tube as function of temperature, Reynolds number and tube entrance diameters

[ASME PAPER 69-WA/HT-54]

04 p0780 A70-14795

Heat transfer to absorbing fluid by coupled thermal radiation and laminar forced convection at pipe entry region, considering gray and nongray absorption

[ASME PAPER 69-WA/HT-16]

04 p0783 A70-14818

Laminar and turbulent flows of compressible media in rotating pipes, analyzing velocity distribution, angular velocity and Coriolis effects using Abel equation

04 p0672 A70-15159

Entrance shape effects on tube rarefied flow in transition regime, noting role of Reynolds number in shape selection

04 p0675 A70-15593

Unsteady flow equations for periodic axisymmetric laminar flow of second order fluids in circular cylindrical pipes

05 p0831 A70-15871

Closed form solutions describing nonlinear motions of incompressible fluid flowing in thin walled tube buckled by uniform external pressure

05 p0832 A70-16090

Laminar flow in circular pipe with arbitrary axial variation of wall temperature or heat flux, using integral type approximation

05 p0957 A70-16519

Free molecular flow through long circular tube rotating with constant angular velocity about axis, discussing rotation speed effect on mass flow

05 p0836 A70-16994

Steady laminar flow with frictionless central core surrounded by boundary layer in circular curved pipe, discussing friction factor and flowmeter discharge coefficient

05 p0836 A70-17107

Viscoelastic fluid flow through circular tube under time dependent pressure gradient superposed on steady Poiseuille flow

06 p1032 A70-17200

Frictional drag reducing polymer solution injection into boundary for turbulent pipe flow, discussing Reynolds number, injection rate, injection points and concentration

06 p1032 A70-17215

Suddenly started laminar flow in circular tube entrance region, obtaining integral momentum equation for boundary layer thickness, entrance length, velocity profile, etc

06 p1034 A70-17528

One dimensional compressible flow analysis for near field aerodynamics of tube-vehicles, showing drag coefficient dependence

[AIAA PAPER 70-140]

06 p1038 A70-18077

Monte Carlo analysis of free and near free molecular flow through circular tubes for mass, momentum and energy transfer

06 p1051 A70-18367

Slip flow of nitrogen gas through long circular tubes, measuring mass flow, pressure drop and cross sectional velocity profiles

06 p1051 A70-18368

Pipe orifice conductance for rarefied gas flow measured for specific Knudsen numbers and pressure ratios

06 p1052 A70-18370

Plastic lubricants motion in circular pipes, determining drag and cross sectional velocity profile of laminar flows

07 p1290 A70-18652

Gas detonation in rough walled pipe, calculating Chapman-Jouguet detonation velocity, deriving existence criterion

07 p1419 A70-18752

Approximate solution for heat transfer in incompressible fluid laminar flow in circular tube

07 p1253 A70-19060

Laminar flow forced convection heat transfer in circular pipe entrance region for constant wall temperature and constant wall heat flux

07 p1420 A70-19215

Cylindrical tubes steady axisymmetric inlet flow at lower Reynolds numbers, applying results to blood vessels entry flow

07 p1205 A70-19244

Spectral functions of airflow velocity pulsations in circular pipe at various Reynolds numbers, considering laminar, transition and turbulent regimes

07 p1259 A70-19826

Large axisymmetric disturbances generated in laminar pipe flow by sleeve oscillating at wall, measuring flow with laser-Doppler velocimeter

07 p1286 A70-19995

Damped turbulent whirling tube flow friction characteristics and heat exchange, solving equation of maximum tangential flow rate

07 p1261 A70-20464

Steady pressure driven flow of conducting fluid through insulating circular pipe in transverse magnetic field

08 p1549 A70-20502

Local heat transfer coefficients for unsteady conditions in tube determined by gradient method, noting use in reacting flow and jet nozzle protection

08 p1598 A70-21189

Unsteady flow in circular tube of constant section with time dependent discharge, determining pressure gradient and velocity distribution

08 p1484 A70-21477

Transverse oscillation periods of cylinder containing flowing fluid obtained by solving nonlinear partial differential equations describing transverse and longitudinal motion

08 p1592 A70-21480

Solid layer effect on laminar heat transfer and pressure drop in medium surrounding pipe with liquid flows below freezing point, discussing wall temperature effects

08 p1485 A70-21589

Heat transfer augmentation in tubes by surface roughness and twisted tape generated swirl flow

08 p1600 A70-21830

Gas flow in pipe with uniform wall heat flux, analyzing turbulent heat transfer using heat balance equation [ASME PAPER 69-HT-H]

08 p1486 A70-21834

Radiative transport in nongray cylindrical medium using total band absorptance

09 p1790 A70-23553

Turbulent pipe flow with wall suction, calculating friction factor, pressure gradient, heat and mass transfer coefficients, velocity and temperature profiles [ASME PAPER 69-HT-4]

09 p1790 A70-23558

Velocity distribution along cylindrical pipe in adiabatic flow with friction and known inlet parameters

09 p1607 A70-23616

Steady and unsteady viscous incompressible one dimensional flows parameters in deformable cylindrical tube determined, solving continuity and motion equations by Galerkin method

09 p1664 A70-23715

Fluid boiling heated nonuniformly in pipe, deriving formulas for unsteady temperature field by integrating energy equation

09 p1791 A70-23716

Progressive shock waves propagation, reflection and transmission through sudden changes in pipe cross sectional area, obtaining boundary conditions for quasi-steady junction flow

09 p1664 A70-23738

Unsteady MHD flow in circular pipe with nonconductive walls under transverse magnetic field

10 p1921 A70-23959

Quasi-one dimensional motion of perfect compressible fluid through pipe, considering one dimensional schemes in aerodynamics

10 p1865 A70-24102

Molecular, viscomolecular and laminar gas flows in tubes and porous bodies at low pressures

10 p1869 A70-24287

Turbulent flow nonresonant pressure pulsations effects on local convective heat transfer in tube flow

10 p1968 A70-24288

Hydraulic loss and secondary circulation of fluid flow in three dimensional bend commercial conduits, discussing relationship to velocity distribution

10 p1871 A70-25094

Approximate solution for heat transfer in incompressible fluid laminar flow in circular tube

10 p1871 A70-25211

Secondary peripheral air injection effects on subsonic airflow through slotted tube, discussing primary flow, flow separation, static and stagnation pressures and temperature changes

11 p2036 A70-26140

Sound radiation from rigid flow spoilers correlated with fluctuating forces, measuring jet-pipe drag and lift components with transducers

11 p2085 A70-26699

Velocity fluctuations measurements in conducting fluids flowing through tubes

12 p2230 A70-27091

Turbulent heat diffusion coefficients in air and water tube flow calculated from statistical characteristics, extending method to boundary layers

12 p2210 A70-27322

Tube relaminarization, predicting turbulent-to-laminar flow transition

12 p2212 A70-28118

Hydrodynamic entrance length in channels and tubes of varying cross section with arbitrary initial velocity profile [DFVLR-SONDDR-39]

12 p2212 A70-28210

Lateral motions of vertical uniform tubular cantilever conveying fluid, considering oscillatory instability at high flow velocities

13 p2511 A70-28741

Unsteady compressible pipe flows with large cross sectional variations studied by two dimensional difference method

13 p2386 A70-28806

Single component two phase pipe flow choking and shock phenomena, including flashing flow vibratory effects

13 p2386 A70-28846

Preston tube errors in pipe flow wall shear stress determination due to velocity distribution deviations

13 p2387 A70-28848

Boundary conditions and initial value lines for unsteady homentropic flow, performing straight pipe calculations

13 p2392 A70-30023

Velocity circulation in laminar motion of fluid in cylindrical tube, assuming equilibrium under dissipative forces

14 p2564 A70-30164

Incompressible turbulent fluid flow through ducts and pipes by integral boundary layer techniques, considering entrainment principles

14 p2564 A70-30258

Rarefied gas flow in slip regime through cylindrical tube assuming parabolic velocity profile

14 p2565 A70-30263

Karman vortex shedding phenomenon for flow rate measurement in channel or pipe

14 p2588 A70-31333

Natural vibrations frequency of tubular cantilever pipe with fluid flow, solving differential equation of motion by Ritz method

14 p2567 A70-31426

MHD turbulence suppression by magnetic field in tubes, using conduction anemometers

15 p2778 A70-31480

Turbulent flow theory of dilute linear polymer solutions in smooth and rough tubes based on Reynolds equation

15 p2719 A70-31491

Incompressible viscous fluid steady flow admission into bounded space from cylindrical tube, demonstrating solvability of plane and three dimensional versions

15 p2720 A70-31642

Pressure-flow relation for fluid in pipe obeying Casson equation, considering applicability to human blood

15 p2690 A70-31917

Steady flow of incompressible fluid through converging-diverging tube, considering implications in occlusive vascular disease

15 p2691 A70-31936

Water and blood flow characteristics in converging-diverging plastic tube, considering implications in occlusive vascular disease

15 p2691 A70-31937

Boundary layer equations for laminar flow, drag and heat transfer of gas in circular tube, considering parabolic and uniform entrance velocity profiles

15 p2722 A70-32692

Incompressible viscous fluid divergent turbulent flow detection in conical tube of revolution based on measuring wall pressure differences along tube generatrix

16 p2894 A70-33849

Turbulent shear flow asymptotic theory, discussing channel, pipe and two dimensional boundary layers

16 p2895 A70-34244

Mathematical model of pulsatile viscous entrance flow in thick walled elastic tube, investigating flow development effects in large arteries

17 p3035 A70-34471

Energy transfer processes of electron gas for pipe flow of weakly ionized nonequilibrium plasmas, noting electron temperature decrease exponentially along tube axis

17 p3142 A70-35438

Unsteady state Newtonian liquid diffusion in laminar flow in circular tube, using mathematical model

17 p3072 A70-35544

Unsteady convective heat transfer in pipes in presence of heat flux density and flow rate aperiodic variations

17 p3198 A70-35730

Tailpipe effects on gas turbine diffuser performance with fully developed inlet conditions [ASME PAPER 70-GT-86]

18 p3210 A70-36881

Lift forces acting on spheres in cylindrical tube laminar flow

19 p3352 A70-37647

Unsteady laminar incompressibles fluid flow in parallel plate channels and circular tubes, solving Navier-Stokes equations for prescribed discharge

19 p3405 A70-38347

Integral transforms applied to convective heat transfer during nonNewtonian fluid flow with power rheology in pipes and channels

20 p3613 A70-40177

Laminar fluid flow in pipes of rectangular cross section, determining critical Reynolds numbers and maximum instability locations

20 p3614 A70-40400

Heat transfer in cooled turbulent tube flow downstream region at high bulk-to-wall temperature ratios

21 p3945 A70-41037

Poiseuille pipe flow instability, considering asymptotic analysis for small wave number disturbances

21 p3807 A70-41241

- Resonance tube fluid dynamics, examining oscillation start and growth by wave diagram and gas-speed/sound-speed diagram 21 p3807 A70-41244
- Heat transfer and skin friction in quasi-steady axisymmetric turbulent pipe flow of incompressible fluid with variable physical properties 21 p3808 A70-41375
- Maxwellian fluid oscillating flow in thin walled elastic circular tube as function of tube dimensions, elastic properties, oscillation frequency, etc 21 p3810 A70-41963
- Vibrational response of thin walled pipes to internal turbulent water flow as function of Strouhal number 21 p3940 A70-42052
- Turbulent heat diffusion coefficients in air and water tube flow calculated from statistical characteristics, extending method to boundary layers 21 p3811 A70-42063
- Mass flow rate correlation for nonsteady convective heat transfer in thin walled tubes with turbulent air flow 21 p3953 A70-42087
- Wave number spectral correlation of temperature and longitudinal velocity fluctuations in fully developed pipe flow 21 p3811 A70-42090
- Turbulent air flow measurements through heated pipe, determining local heat flux from simultaneous velocity and temperature fluctuation 21 p3811 A70-42091
- Isothermal steady laminar flow through tube with change in wall temperature, examining velocity profile relationship to temperature profile [ASME PAPER 70-HT-C] 22 p4008 A70-42421
- Downstream heat transfer and wall friction predictions for quasi-developed strongly heated turbulent pipe flow, using mixing length model [ASME PAPER 70-HT-8] 22 p4008 A70-42439
- Cantilevered tube conveying fluid, calculating forced vibration under time dependent loading and arbitrary initial conditions 22 p4010 A70-42650
- High velocity isothermal viscous compressible steam flow in circular tubes, measuring pressure drops 22 p4011 A70-42845
- Two phase liquid one dimensional motion in variable cross section tube, deriving mass transfer, motion and phase interaction differential equations 22 p4012 A70-43721
- MHD incompressible viscous flow in nonconducting circular tube, determining pressure, flow rate and magnetic field level by continuum theory concepts 23 p4224 A70-44161
- MHD laminar isothermal flow in closed cylindrical tube in rotating magnetic field, determining azimuthal velocity distribution 23 p4224 A70-44162
- Heat and mass transfer for liquid film evaporation during two phase two component flow in vertical steel tube under adiabatic and nonadiabatic conditions 23 p4276 A70-44215
- Subsonic Ludwig/simple expansion/ tube as shock tube for aerodynamic testing, examining flow characteristics 23 p4182 A70-44578
- Transition zone heat exchange during air mixed flow in pipes with conical duct or Vitoshinski nozzle inlets 23 p4283 A70-44729
- Critical heat flux during forced pipe flow of boiling ethanol-water and acetone-water binary mixtures 23 p4283 A70-44730
- Viscous compressible gas flows in pipe initial section, calculating friction and heat transfer coefficients 23 p4135 A70-44734
- Turbulent heat exchange coefficient and Prandtl number in turbulent air flow through heated pipe with constant heat flux 23 p4183 A70-44740
- Cross correlation measurement errors for fluid pipe flow with pseudorandom sequence generated temperature fluctuations, considering transport time, impulse response and laminar flow 24 p4333 A70-45111
- Pulsatile flow in circular rigid tube with and without longitudinal vibration, obtaining momentum integral solution 24 p4325 A70-45623
- Porous tube inlet region, calculating fluid injection effect on laminar flow from integral form boundary layer equations 24 p4326 A70-45782
- Long wave approximation for peristaltic transport in circular cylindrical tube, noting inertia and wavelength effects on backward flow 24 p4309 A70-46224
- PIPES**
- Orifice diameter for low Reynolds number flowmeter dependent on pipeline diameter tolerances 08 p1482 A70-20684
- Differential equation formulation for pipeline in hydraulic automatic control system considered as lumped or distributed parameter plant 09 p1612 A70-22823
- Aviation kerosene pipeline column separation after valve closure, solving differential equations for transient pressures propagation to predict vapor cavities duration 09 p1665 A70-23744
- Pressure and velocity ratios and energy requirements dependence on flow parameters of cylindrical capsule in horizontal pipeline 09 p1665 A70-23747
- Lumped parameter pipeline and hydraulic systems stability, deriving equations of motion for closed and open cycle control systems 18 p3216 A70-36946
- Cryogenic pipelines cooldown to operating temperature, calculating cryogen flow rate limits due to thermal stresses in steel and Al flanges 23 p4280 A70-44368
- PIPES (TUBES)**
- NT GAS PIPES**
- Volterra equations for stresses, strains and displacements of viscoelastic tube with variable radius encased in shell under pressure and unsteady temperature field 02 p0384 A70-11663
- Ultrasonic tracking type transducers for testing ribbed and smooth walled pipes using shadow and two probe echo methods 02 p0300 A70-12480
- Durability of refractory tubes of small thickness under creep with account of scale factor and unsteady conditions, tabulating experimental and theoretical values 03 p0508 A70-13247
- Stress wave propagation tests in thin walled tubes under combined tension and torsion, discussing predicted and observed strain-time profiles discrepancies 03 p0599 A70-12425
- Elasticity theory of orthotropic materials applied to steady rotation of long cylindrical tubes of filament reinforced plastics 03 p0602 A70-14331
- Axial compression effect on low cycle fatigue of thin walled metal tubes in torsion [ASME PAPER 69-MET-H] 04 p0705 A70-14880
- Stress concentration in long thick cylindrical tube under diametrically opposite normal loads using elasticity theory 05 p0939 A70-16505
- Stress analysis of curved tubes capable of accounting for all end effects based on shell theory equations 05 p0944 A70-16811
- Stability of conical hydraulic poppet valve with elastic support and inlet and outlet piping 06 p1075 A70-17139
- Pipe bounding walls effect on sound waves dispersion in rarefied gas, deriving integral equations showing frequency range decrease with container size 06 p1107 A70-18315
- Precision tungsten alloy tubing manufacture and properties, discussing direct conversion of metal powder to finished tubing with high temperature structural stability 07 p1292 A70-18928
- Wall temperature variation of transpiration cooled tube surrounding plasma arc calculated from gas mass flow and wall properties 07 p1420 A70-19214
- Stress analysis of multiaxially loaded tubes of fiberglass reinforced composite wound in three directions 07 p1318 A70-19755
- Air bubble free glass fiber-plastic laminates fabricated by wet-winding method using vacuum, noting void free filament wound pipes 07 p1295 A70-19766
- Autocollimation technique for determining flexure of tube of Wanschaff vertical circle 08 p1496 A70-21158
- Nondestructive testing of small metal tubing, discussing eddy current, ultrasonic and electromagnetic inspection and dye penetrants 08 p1509 A70-21748
- Boiling heat transfer enhancement inside tubes using integral fins, discussing water film retention on walls 08 p1599 A70-21825
- Tubing materials for gas turbine engines covering fabrication, selection, etc 08 p1559 A70-21854
- Structural analysis of boron filament-epoxy composite laminate tubes for use as spacecraft long column members 08 p1595 A70-21911
- Superconductor tubes experiment, observing flux jump initiation and propagation characteristics 09 p1738 A70-22293
- Miniaturized program oriented automatic pipe/tube welding system for in-place joining of fluid systems, controlling timing functions and weld current sequence 09 p1692 A70-22795
- Circumferential wall temperature gradients in spacecraft radiator tubes as function of tube wall fins 09 p1789 A70-23261
- Transient response of fin-tube space radiators under steady state operation halting and system cooling 09 p1790 A70-23564
- Natural vibration analysis of uniform cylindrical and cantilever rectangular tubes with cutouts 10 p1961 A70-25057
- Welding techniques for Nb-stainless steel bimetal tubing for liquid metal containment, determining structural integrity and bond interface condition after thermal cycling 10 p1897 A70-25309
- Thin walled tubes plastic instability under combined internal pressure and axial load for open and closed end conditions 12 p3232 A70-27216
- Stress-strain state effects on Cu and Ni tubular samples plasticity and strength using polarization-optical technique 12 p3233 A70-27341
- In-place gas tungsten arc fusion welding for joining small diameter precipitation hardenable aluminum tubing 14 p2590 A70-30930
- Film condensation in tubes, considering liquid-vapor interface, zero gravity and electrostatic field conditions 15 p2828 A70-32541
- Dangerous plane stressed state surfaces for fiberglass reinforced plastic pipes, using fourth degree polynomial 15 p2766 A70-32852
- Storable tubular extensible member /STEM/, discussing advantages of BI-STEM for erecting unfurlable structures in space 16 p2846 A70-34141
- Cold working effects on Zircaloy tubes mechanical properties and hydride orientation, discussing tubes use in nuclear power stations 17 p3123 A70-34645
- Elastoplastic deformations during explosive extrusion of pipes of different materials with linear strain hardening law 18 p3335 A70-36132
- Flow stability of incompressible heavy viscous fluid along wall of vertical circular cylindrical pipes, relating flow parameters to stability 18 p3240 A70-36278
- Loading history effect on work of plastic deformation in Ni and Cu pipes, taking into account stress and strain deviators deviation from similarity 18 p3344 A70-36945
- Fatigue strength in pulsed tension of butt-welded tubular joints, evaluating test results statistically 19 p3433 A70-37357
- Volterra equations for stresses, strains and displacements of viscoelastic tube with variable radius encased in shell under pressure and unsteady temperature field 19 p3547 A70-38437
- Durability of refractory tubes of small thickness under creep with account of scale factor and unsteady conditions, tabulating experimental and theoretical values 19 p3453 A70-38465
- Glass drainline development and marketing, describing technology transfer role 20 p3740 A70-39100
- Hot gas pipe thermoelastic reduction factors, determining elastic support, material and dimensions 20 p3720 A70-39624
- Resonance tube fluid dynamics, examining oscillation start and growth by wave diagram and gas-speed/sound-speed diagram 21 p3807 A70-41244
- Eddy current magnetic probe with frequency scanning for signal-noise discrimination in nondestructive testing of tubes 24 p4336 A70-45698
- Encasing and welded pipes flaws detection with high resolution by nondestructive testing, using eddy current method 24 p4345 A70-45702
- Tubing, fitting and flexible line designs and testing for production aircraft hydraulic distribution systems [SAE PAPER 700789] 24 p4294 A70-45856
- Thermosetting glass reinforced plastics fabrication and use for pressure vessels, vacuum vessels and pipes 24 p4350 A70-46388
- PISTON ENGINES**
- Aircraft piston engines air cooling analysis, discussing forced cooling for high altitude aircraft and helicopters 02 p0355 A70-12224
- Stirling free piston engine operating principles, performance limitations, heat transfer problems, fluid flow, mechanical design, test results and applications [ASME PAPER 69-WA/ENER-15] 04 p0627 A70-14895
- Heat transfer data for rotary piston and conventional piston engines, studying compression energy losses due to working fluid leakage 05 p0897 A70-17002

- Selection criteria for nonturbocharged air or liquid cooled reciprocating type prime movers used in aircraft ground support equipment 07 p1248 A70-18801 [SAE-ARP-1052]
- Supersonic fluid bistable amplifier used as air motor, converting supply air flow energy into reciprocating piston motion 10 p1807 A70-24791
- Reciprocating Rankine-cycle engine with organic working fluids, noting piston speed and efficiency [SAE PAPER 700162] 11 p1982 A70-25372
- Temperature distribution in cylinders of aircraft internal combustion rotary piston engine under air cooling 23 p4234 A70-44742
- PISTON THEORY**
- Steady one dimensional flow in gas filled cylindrical tube, studying shock induced compression wave generated by sudden piston acceleration 01 p0062 A70-10804
- Piston theory application to plates and shells stability in supersonic gas flows, considering critical velocities determination for asymmetric flows and oscillations 04 p0617 A70-15196
- Flow field between infinitely massive wall and rigid piston accelerated by detonation products, comparing analytical results to finite difference numerical integration 05 p0830 A70-15782
- Monte Carlo simulation for shock wave formation by specularly reflecting piston, discussing reflection from specularly reflecting wall 06 p1049 A70-18334
- Plane exponential reactive shock waves following piston impact on gamma-law gas solved by similarity method, including Whitham conditions and shock acceleration 10 p1967 A70-24194
- Piston formed weak steady shock wave propagation in relaxing gases, investigating via characteristics method [DFVLR-SONDDR-38] 12 p2212 A70-28206
- High Reynolds number flow in moving corner, observing vortex motion at piston and cylinder wall interface by flow visualization techniques 16 p2895 A70-34240
- Viscous heat-conducting one dimensional piston driven gas flow, assuming sharp shock discontinuity 17 p3075 A70-35890
- Shock and expansion waves formation by moving piston based on kinetic theory of gases, solving Bhatnagar-Gross-Krook equation by numerical method 21 p3808 A70-41377
- Piston problem numerical solution by Boltzmann collision integral, considering shock waves and thermal disturbances evolution at gas-solid interfaces 21 p3808 A70-41378
- PISTONS**
- NT MAGNETIC PISTONS**
- Radial clearance, pressure and piston length and diameter dependence of friction force at rest in piston type hydraulic devices 14 p2534 A70-30872
- Low friction seal for axial loading piston in triaxial soil testing cells 23 p4199 A70-43873
- Pneumatic actuator rod and piston head seals, examining materials at various temperatures, pressures and speeds [SAE PAPER 700791] 24 p4294 A70-45855
- PITCH**
- Fan rotors aerodynamic noise tonal annoyance reduction by blade unequal circumferential spacing, noting sound-pressure wave shape determination [ASME PAPER 69-WA/FE-23] 04 p0614 A70-14776
- Contralateral remote masking /CRM/ increase of LF tone burst produced by middle ear muscle contractions 04 p0632 A70-15082
- Retroactive interference stimuli effects on pitch discrimination in short term recognition memory task 07 p1215 A70-20046
- Axial flow compressor fan discrete tone noise radiation directivity pattern measurement and theoretical explanation for cut-off effect, power and harmonics 24 p4380 A70-46069
- PITCH [INCLINATION]**
- Multiple skirt air cushion vehicle /ACV/ pitch and heave dynamic characteristics, describing mathematical modeling and analog computer simulation 04 p0624 A70-15389
- Vortex sheets pitch along constant aerodynamic pitched propeller blade at zero traction, discussing calculation, construction and wind tunnel testing 05 p0790 A70-16159
- Pitch angle anisotropy instabilities of electromagnetic waves in space, discussing warm plasma, solar wind and Van Allen belts 06 p1118 A70-17380
- Mold canting effects on nonporosity of Al alloys flat castings noting decreased metal losses 08 p1517 A70-21134

- Shock wavefront configurations before inclined obstacles in supersonic flow, studying inclination angle role 09 p1604 A70-22443
- Electron flux independence of pitch angle distribution /0-90 degrees/ observed from sounding rocket measurements in auroral arc 10 p1932 A70-24492
- Directional particle flux dependence on probe orientation with respect to external magnetic field, determining pitch angle distribution from count rates 10 p1932 A70-24497
- Linearly tapered zigzag antenna of constant pitch angle observed for radiation and impedance characteristics 12 p2199 A70-27988
- Pitch damping derivatives computation for missile configurations undergoing small amplitude oscillations at subsonic speeds, using static aerodynamic data [AIAA PAPER 70-537] 13 p2339 A70-29004
- Solar proton structure across polar cap and anomalous latitude cut-off explained by local pitch angle variations 15 p2792 A70-31672
- Pitch and Coriolis illusions effects on pilot pitch angle adjustment in simulated takeoff 15 p2689 A70-31885
- Synchrotron model limitation for nonthermal spectra, demonstrating restriction to small pitch angles and strong fields 18 p3318 A70-37024
- Ballistic reentry vehicle roll-pitch coupling, showing influence of nose asymmetries 21 p3930 A70-41736
- Pitch-angle distribution of electron fluxes in auroral zone as function of geomagnetic latitude 23 p4192 A70-44878
- Energy dependence of equatorial pitch angle distribution for protons trapped in radiation belt, based on adiabatic theory and observational data 23 p4192 A70-44923
- Pitch illusion in flight personnel under centripetal acceleration 24 p4306 A70-45330
- PITCH [MATERIAL]**
- High strength and modulus continuous graphite fibers from pitch, describing production process from asphalt and specifications 21 p3842 A70-40732
- PITCH ANGLES**
- U PITCH [INCLINATION]**
- PITCH ATTITUDE CONTROL**
- U LONGITUDINAL CONTROL**
- PITCHING MOMENTS**
- Minimum drag hypersonic delta wing, analyzing shape for given planform, lift, pitching moment and volume using correction for pressure coefficient 01 p0002 A70-10557
- Pitching moment coefficient changes due to ground effect in fixed wing aircraft flight test method, considering constant angle of attack approach 04 p0619 A70-15394
- Upper surface suction effect on thin plate aerodynamic characteristics, considering relations for lift and pitching moment coefficients 06 p0968 A70-17851
- Missile oscillations in plane during pitching moment hysteresis, discussing test coefficients suitability for predicting motion 09 p1606 A70-23258
- Rolling reentry body velocity as function of roll, pitch, yaw rates and angle of attack 13 p2343 A70-29991
- Bearing force and moment produced by motion of inclined plate supported by compressed air in ground effect machines with small angle of attack 20 p3557 A70-39140
- Static and dynamic longitudinal stability of semirigid parafoil gliding descent system in pitching motion [AIAA PAPER 70-1191] 21 p3753 A70-41825
- Radiation forces on flat plate in ecliptic earth orbit applicable to satellite attitude dynamics during pitching libration 22 p4125 A70-43437
- Low speed airfoil two dimensional testing in wind tunnel with slotted wall, examining lift, drag and pitching moments [ICAS PAPER 70-08] 23 p4132 A70-44119
- PITOT STATIC TUBES**
- U PITOT TUBES**
- U SPEED INDICATORS**
- PITOT TUBES**
- Pitot tube measurements of mixing zone of turbulent shear flow, discussing velocity gradient effects 01 p0066 A70-11134
- Pitot boundary layer probes with position indicators using extensometric gauges for boundary layers on wind tunnel test models [ONERA-TP-754] 03 p0487 A70-13628
- Calibration for five hole spherical pitot probe plotting data for velocity, inclination and static pressure factors 06 p1063 A70-17621

- Velocity measurements with Pitot tubes in polymer solutions /polyethylene oxide/ in water, noting viscoelastic properties effect on measured pressure value 10 p1887 A70-24093
- Preston tube errors in pipe flow wall shear stress determination due to velocity distribution deviations 13 p2387 A70-28848
- Pitot probe for high altitude atmospheric density measurements integrated with telemetry system mounted on two stage Super Loki sounding rocket 14 p2585 A70-30576
- Graphical plotting of critical Preston tube diameter, allowing for Mach and Reynolds numbers effects and introducing limiting line 14 p2586 A70-30871
- Velocity fluctuations in temperature gradient turbulent jets and in turbulent flames, using hot wire in cooled pitot tube 17 p3096 A70-35749
- PITTING**
- Zr and stainless steel pitting in acidic and near neutral chloride media, comparing controlled potential and conventional chemical corrosion tests results 09 p1706 A70-22939
- 18-8 stainless steels pitting corrosion, examining grain boundaries influence 24 p4362 A70-46184
- PITUITARY GLAND**
- Glutethimide and aminoglutethimide reversible inhibitory effect on rat pituitary adrenal system in response to stress 07 p1203 A70-18902
- Circadian variation of pituitary-adrenal steroid levels, noting light role 14 p2540 A70-31430
- Mathematical model of human pituitary gland mechanism controlling secretions of serum growth hormone in response to glucose deficiency 20 p3569 A70-38995
- Serotonin, 5-hydroxyindoleacetic acid /5-HIAA/ and monoamine oxidase in bovine pituitary organ and median eminence 21 p3761 A70-40850
- PITUITARY HORMONES**
- Thyrotropin /TSH/ effects on thyroidal iodine metabolism during hypoxia in rats 02 p0231 A70-11703
- Extraction, analysis and properties of rat prolactin isolated from pituitary glands 07 p1203 A70-18895
- Pituitary hormone ACTH stimulatory effect on steroid hormone cortisol secretion by canine adrenal cortex, constructing seventh order state variable model 10 p1819 A70-24868
- Melatonin or water deprivation effects on pituitary serotonin content in rats 17 p3034 A70-35625
- Human gluco-regulatory hormone reserve depressions following acute and chronic acceleration exposure 20 p3572 A70-39436
- PIVOTED WING AIRCRAFT**
- U TILT WING AIRCRAFT**
- PIVOTS**
- Odessa observatory meridian circle pivots wear determined during observations of eclipsing variables 08 p1574 A70-21160
- Variable sweep wing pivot joint design utilizing double shear tilted spherical journal bearings with Teflon fabric liners 12 p2318 A70-27135
- Flexural pivots applications as bearings, hinges, force sensing devices, torsion springs, sensing elements, etc [ASME PAPER 70-DE-51] 16 p2918 A70-33513
- Life and confidence tests of miniature self contained flexure pivots in critical mechanisms [ASME PAPER 70-DE-76] 16 p2918 A70-33522
- Flexural pivots for space structures, describing design, fabrication and applications 16 p2924 A70-34170
- Optimum automatic selection of redundancies, discussing weighting and pivot choice and rigid element incorporation 20 p3732 A70-40264
- Liquid lubricant unsteady motion and pressure distribution during pivot harmonic vibration in hydrodynamic bearing 23 p4200 A70-44163
- PLAGES [FACULAE]**
- U FACULAE**
- PLAN POSITION INDICATORS**
- Ultrasonic imaging system for flaw detection, analyzing welds 01 p0104 A70-10881
- Air traffic control CRT plan position indicators, considering alphanumeric symbols strokes design 19 p3469 A70-38645
- PLANAR STRUCTURES**
- Planar Gunn effect devices using various surface electrode configurations, discussing limitations by breakdown on Ga arsenide exposed surface 01 p0049 A70-10287

Steady thermoelastic state of inhomogeneous plane with circular discontinuity on perimeter, studying stress concentration at thermally insulated crack
03 p0595 A70-13738

Radiative heat transfer from longitudinal rectangular conducting fins on plane wall involving mutual irradiation, using iterative method
[ASME PAPER 69-WA/HT-22] 04 p0782 A70-14812

Steady state electrical characteristics of double diffused planar transistor calculated by iterative algorithm under arbitrary bias conditions
06 p1016 A70-17125

Axisymmetric or plane bodies temperature distribution from heat conduction analysis using computer program based on finite element method
09 p1788 A70-22581

Heat conduction analysis for plane body with boundary condition and time variable heat exchange coefficient, applying automatic control technique
10 p1966 A70-23869

Stress analysis of plane, shell and three dimensional structures using finite element method
12 p2315 A70-26886

Statistical design of density tapered planar circular and elliptical arrays for radiation patterns with good sidelobe behavior
12 p2199 A70-27987

Electromagnetic wave diffraction by heterogeneous planar dielectric structures, showing field distributions by single variable Fredholm equations
15 p2695 A70-31436

Drag optimal stern section of plane body at supersonic flow, allowing for friction forces
18 p3206 A70-36261

Transient stresses and strains in plane wedge under dynamic load, using photoelastic, high speed photographic and strain gage studies
[SMPT PREPRINT 93] 22 p4036 A70-43062

Dirichlet problem with singularities for plane with cutouts along circumference, determining analytical function
23 p4211 A70-44239

Radiation and phase-scanning properties of planar array of parallel plate waveguides, using wedge diffraction theory
23 p4166 A70-44973

PLANE WAVES

Natural oscillation modes two dimensional resonator determined in form of superimposed uniform plane waves with arbitrary coefficients of wave reflection
01 p0140 A70-10057

Plane harmonic Rayleigh wave propagation in piezoelectric semiconductor GaAs crystals, using successive approximation procedure
01 p0154 A70-10131

Plane sinusoidal wave propagation through material reinforced with parallel fibers, using integral formulation for multiple scattering in infinite slab
01 p0130 A70-11187

Electromagnetic plane wave diffraction by slit and circular apertures in nonplanar conducting screens, presenting equireadance contour maps
02 p0340 A70-12455

Self consistent field method to calculate effective dynamic characteristics of elastic media with filler for plane longitudinal wave propagation
02 p0388 A70-12485

Plane electromagnetic wave diffraction at periodic arrays obtained by direct summation of multiple reflection between arrays
03 p0442 A70-13095

Electromagnetic field structure and interaction inside and outside of spherical shell of arbitrary linear media excited by monochromatic plane wave
03 p0443 A70-13151

Dispersive compression of plane frequency modulated waves in inhomogeneous plasma based on generalizing geometric optics approximation to unsteady quasi-harmonic processes
03 p0447 A70-13287

Plane longitudinal elastic monochromatic wave diffraction on stress free circular holes in infinite plate, calculating stresses between holes
03 p0589 A70-13375

Dispersion equation and coupling impedance of two dimensionally periodic slow wave structure of cellular cylinder type with parallel perpendicular diaphragms
03 p0456 A70-13438

Plane electromagnetic wave diffraction at conducting stripline, calculating surface current density and far field scattering using edge wave and factorization methods
03 p0451 A70-13755

Integrodifferential equation solved for plane wave reflection and transmission by random medium assuming homogeneous background refractive index
04 p0649 A70-14970

Phase and amplitude level of plane light wave propagation in medium with randomly discontinuous refractive index, discussing wave phase dependence on dielectric constant
04 p0650 A70-15288

Inhomogeneity and water vapor absorption influence on frequency spectrum of amplitude fluctua-

tions of plane wave propagating in turbulent atmosphere
05 p0813 A70-16252

Output characteristics of cyclotron maser with resonator field due to plane waves interference along static magnetic field, deriving tensor equations
05 p0858 A70-16260

Thermal radiation effects on plane magnetoacoustic waves in semiinfinite expanse of radiating gas of perfect electrical conductivity
05 p0890 A70-16822

Radiatively driven plane acoustic wave in nongray radiating and absorbing gas assuming local molecular equilibrium
06 p1173 A70-17515

Backscattered field determination at edge on incidence from thin circular plates illuminated by plane waves
06 p1008 A70-17563

Scattering and depolarization of plane horizontally polarized electromagnetic wave from slightly rough lossless dielectric layer, using small perturbation theory
06 p1010 A70-18019

Monte Carlo method applied to solving nonlinear Boltzmann equation for plane shock waves in elastic sphere gases
06 p1050 A70-18335

Moving plasma column scattering of obliquely incident microwaves, assuming arbitrary polarization for incident plane wave
06 p1124 A70-18608

Plane electromagnetic wave penetration into ferromagnetic half space solved for nonlinear parabolic equations using difference method
07 p1227 A70-18992

Plane electromagnetic wave reflection from laminar anisotropic medium, analyzing piecewise-constant permittivity tensor as boundary value problem
07 p1235 A70-19448

Plane electromagnetic wave diffraction on conducting plate with circular hole
08 p1456 A70-20503

Plane electromagnetic wave scattering at apex of conical body, presenting scattered field calculations for various cone sizes and surface impedances
08 p1461 A70-20974

Plane E-polarized wave diffraction by slit in conducting screen using Fredholm integral equations of second kind
08 p1461 A70-21004

Plane electromagnetic wave scattering by perfectly conducting cylinder coated with moving dielectric or plasma sheath, using relativity theory, Lorentz transformations, etc
08 p1551 A70-21251

Plane harmonic Rayleigh wave propagation in piezoelectric semiconductor GaAs crystals, using successive approximation procedure
08 p1556 A70-21407

Multiple scattering of plane time harmonic compressional elastic wave impinged on parallel circular cylindrical inclusions in finite domain, analyzing stress field
08 p1592 A70-21469

Monochromatic plane electromagnetic wave incident from vacuum on plane boundary of plasma half space, discussing specular reflection and diffuse scattering boundary conditions
08 p1553 A70-21611

Plane double front detonation wave attenuation by pursuing rarefaction waves, analyzing oscillations, onset mechanism and stability during transition to Chapman-Jouguet mode
08 p1485 A70-21633

Nonlinear effects related to plane electromagnetic wave propagation in weakly ionized plasma
09 p1735 A70-22842

Amplitude measurement of plane light wave propagating in turbulent atmosphere, giving log amplitude dependence on dispersion of logarithm fluctuations
09 p1636 A70-23136

Plane electromagnetic wave diffraction on circular cylinder
09 p1638 A70-23339

Plane electromagnetic wave scattering by conducting circular cylinder/wire in air/vacuum, computing scattering cross sections by Wiener-Hopf method
09 p1638 A70-23347

Plane electromagnetic wave diffraction at conducting stripline, calculating surface current density and far field scattering using edge wave and factorization methods
10 p1842 A70-25002

Electromagnetic waves propagation in nonlinear medium, investigating polarized plane wave incident on vacuum-plasma interface in magnetic field
10 p1844 A70-25156

Diffraction of plane cylindrical and spherical waves in wedge-shaped regions with reflecting edge, using asymptotic expansions
10 p1911 A70-25186

Unsteady problems of finite amplitude plane and cylindrical wave propagation in dissipative spatially symmetrical media
11 p2034 A70-25399

Plane electromagnetic waves propagation in nonabsorbing photoelastic material with finite deformations, formulating theory from Eulerian and Lagrangian point of view
11 p2139 A70-26173

Plane wave disturbances introduced in turbulent channel flow by vibrating ribbons near each wall, obtaining amplitude and relative phase
11 p2039 A70-26537

Scalar plane wave LF scattering by prolate spheroid of revolution, obtaining iterative solution for Dirichlet problem
11 p2085 A70-26621

Scalar plane wave LF scattering by prolate spheroid of revolution, obtaining iterative solution for Neumann problem
11 p2085 A70-26622

Weak plane waves propagation in binary mixtures of diatomic gases subject to vibrational relaxation, solving piston problem in acoustic approximation
12 p2209 A70-27151

Plane electromagnetic wave diffraction by perfectly reflecting half plane calculated by elementary method
12 p2184 A70-27234

Trumpet-type plane waves instability thresholds in plasma drifted by electric field, including calculation of thermodynamic equilibrium
12 p2184 A70-27236

Plane periodic diffraction of elastic waves propagating in medium with infinite sequence of circular holes
12 p2325 A70-27557

Linearized dispersion relation for plane wave propagation in uniform unbounded cold plasma permeated by DC magnetic field, considering two stream instability
12 p2281 A70-27881

Plane wave three dimensional diffraction through circular aperture in infinite screen computed for normal incidence, using Babinet principle
12 p2197 A70-27951

Plane electromagnetic waves anomalous reflections from diffraction grating with periodic array of rectangular holes in dielectric layer, observing resonant character
12 p2191 A70-28175

Plane electromagnetic wave interaction with compressible plasma fluid moving with uniform velocity in vacuum, calculating reflection and transmission coefficients
13 p2462 A70-29101

Plane electromagnetic wave reflection at interface of two semiinfinite dielectric media in relative motion perpendicular to incidence plane, noting polarization change
13 p2365 A70-29102

Plane electromagnetic wave in moving conductive medium, analyzing without approximation of velocity limitation
13 p2462 A70-29104

Elastic plane wave diffraction and scattering at convex obstacle in semibounded regions, using method of images
13 p2452 A70-29289

Plane cylindrical and spherical explosion waves propagation in detonating gas mixtures with counterpressure, calculating perturbed flow parameters by numerical method of integral relations
13 p2388 A70-29308

Plane harmonic wave steady state diffraction at cylinder in elastic half space, applying method of images
13 p2366 A70-29320

Electromagnetic plane wave oblique reflection from flat surface with spatially modulated surface impedance, computing wave spectrum
13 p2367 A70-29527

LF plane wave scattering from semielliptic groove in conducting ground plane noting validity for arbitrary polarization, incidence, directions and eccentricity
13 p2453 A70-29822

Plane waves propagation in elastic layer using Cauchy theory of initial stress
14 p2658 A70-30998

Plane wave ray optical scattering by two spheres for arbitrary angle of incidence and observation, noting importance of first order interaction terms
14 p2551 A70-31157

Normally incident plane monochromatic electromagnetic wave reflection and scattering from expanding dielectric slab, using invariant imbedding concept
15 p2695 A70-31438

Monograph on nozzle design effect on starting process initiated by plane shock wave in reflected shock tunnel
15 p2672 A70-31692

Plane EM wave reflection and transmission at moving boundary, discussing frequency disparity with incident wave
15 p2697 A70-31834

Plane electromagnetic waves propagation in isotropic medium in electromagnetic nonequilibrium conditions 15 p2790 A70-32275

Wave scattering from elliptic cylinder, solving boundary value problem for two dimensional wave equation 15 p2700 A70-32404

Plane wave scattering by strip of elliptical cylinder, considering geometrical diffraction theory 15 p2700 A70-32405

Acoustic and EM scattering by hyperbolic cylinder, considering plane wave incidence and line sources 15 p2700 A70-32406

Equation of state of solids measured by shock wave techniques, considering elastic-plastic flow in plane wave geometry 15 p2824 A70-32789

Plane wave diffraction by cylinder tipped half plane, demonstrating localized behavior by geometrical theory 16 p2872 A70-32975

Born approximation limit for plane wave multiple scattering in inhomogeneous electron density distribution in plasma 16 p2957 A70-32981

Electromagnetic waves scattering in uniformly moving media, using transformation formulas for plane waves 16 p2865 A70-33690

Plane harmonic sound wave reflection and transmission in flowing medium by infinite set of arbitrary spaced and staggered flat plates 16 p2971 A70-34016

Plane acoustic wave interaction with elastic spherical shell, discussing effects of membrane, bending, rotatory inertia and shear deformation 16 p2993 A70-34087

Plane wave reflection decay rate representation by slowness diagrams 16 p2952 A70-34089

Perturbation method to obtain analytical expressions for attenuation of plane wave sound propagation in lined ducts 17 p3136 A70-34523

Axially symmetric parabolic reflector with incident linearly polarized plane wave, determining Poynting vector behavior 17 p3043 A70-34615

Plane wave incident on oblate spheroid or disk, deriving LF field scattering 18 p3335 A70-35974

Electromagnetic wave Poynting vector trajectories in absorbing inhomogeneous media, discussing reversibility and energy propagation of spherical and plane structures 18 p3293 A70-36144

Plane wave diffraction by periodic grating reduced to waveguide problem, determining asymptotic behavior of integral solution 18 p3291 A70-36286

Plane electromagnetic waves diffraction by periodic structure of infinite system of parallel strips, reducing problem to solution of linear algebraic equations 18 p3227 A70-36287

Viscoplastic solids, computing plane shock wave propagation structure from nonlinear constitutive relations 18 p3338 A70-36435

Plane electromagnetic wave reflection from laminar anisotropic medium, piecewise-constant permittivity tensor as boundary value problem 18 p3229 A70-36922

Plane TM wave scattering by systems of two parallel conducting elliptical cylinders, metal tapes and combinations 19 p3374 A70-37278

Scattering structures of two parallel elliptical cylinders, tapes or combinations, deriving surface current density distribution under plane TM wave excitation 19 p3375 A70-37279

Plane electromagnetic wave diffraction by infinite grid above finite dielectric layer, calculating field distribution 19 p3375 A70-37281

Electric field equations of plane EM wave diffraction at lattice of conducting cylinders, using Hankel function 19 p3375 A70-37289

Plane EM wave diffraction by conducting strip, using algorithm for reducing integral to linear algebraic equations 19 p3376 A70-37433

Plane electromagnetic wave diffraction by thin metal gratings, using mathematical method of elasticity theory 19 p3376 A70-37712

Plane polarized electromagnetic wave diffraction by dielectric grating, obtaining linear algebraic equations for field coefficients 19 p3376 A70-37713

Plane wave diffraction by serrated surface, examining wave transformation matrix coefficients 19 p3377 A70-37715

Plane EM wave diffraction by ribbon periodic grating, determining diffraction spectrum wave amplitudes 19 p3377 A70-37718

Plane EM wave diffraction by bounded and unbounded periodic gratings 19 p3377 A70-37719

Plane monochromatic EM wave diffraction by rectangular metal bar tapered grating, examining amplitude and polarization parameters 19 p3377 A70-37721

Ponderomotive forces of plane electromagnetic wave incident at arbitrary angle on metal grating, based on diffraction results 19 p3377 A70-37723

Plane EM wave diffraction in cylindrical plasma-electron beam system 19 p3378 A70-37740

Diffraction amplitudes in plane H-polarized electromagnetic wave incident obliquely on grating with closely spaced conducting rectangular bars, obtaining transmission coefficient 19 p3378 A70-37745

Plane waves superposed on solid during steady state isothermal creep deformation subjected to unidirectional constant initial tensile stress 19 p3537 A70-37791

Synchrotron radiation emissivity function containment in dispersion equation for plane wave propagation in magnetoactive plasma 19 p3480 A70-38017

Plane wave reflection from stratified isotropic medium using ray tracing in complex space, noting agreement with phase integral method 19 p3380 A70-38404

Pressure field behind plane shock wave interacting with curved boundary 19 p3406 A70-38447

Plane waveguide field with complex geometric inhomogeneity, describing perturbed section by integral equations 19 p3381 A70-38567

Plane VLF wave propagation in waveguide formed by earth and inhomogeneous anisotropic ionosphere, determining excitation coefficients and attenuation functions 19 p3381 A70-38568

Space-time rays relation to plane wave dispersion surfaces in radiation and diffraction problems, using ray tracing diagrams 20 p3671 A70-39220

Plane electromagnetic scattering from perfectly conducting bodies, comparing exact numerical solution with experiment 20 p3585 A70-39394

Unsteady problems of finite amplitude plane and cylindrical wave propagation in dissipative spatially symmetrical media 20 p3673 A70-40093

Metallurgical changes induced by planar shock wave propagation through metals and alloys, describing shock-hardened metals macro and substructure 20 p3652 A70-40142

Plane electromagnetic waves diffraction on thin filaments cloud/passive dipoles/, discussing field fluctuations and mean power 20 p3588 A70-40298

Plane wave diffraction by periodic array at boundary between two media, discussing asymptotic behavior of reflection and transmission coefficients 21 p3806 A70-40614

Electromagnetic wave diffraction by ideally conducting wedge of finite radius, deriving asymptotic formula for plane wave scattering 21 p3784 A70-40626

Plane stationary shock wave reflection from rigid concave wall at low Mach numbers 21 p3811 A70-42204

Plane electromagnetic waves diffraction by moving periodic metal strip grating, writing E polarized wave of unit amplitude by Lorentz transforms 22 p3984 A70-42388

Plane electromagnetic wave propagation at normal incidence in isotropic lossless plane-stratified inhomogeneous gyrational medium, calculating varying profiles from constitutive equations 22 p4073 A70-42640

Ultrasonic transducer diffraction fields in highly anisotropic crystals obtained by plane waves angular spectrum 22 p4029 A70-42643

Elastic cylindrical shell transient response to plane acoustic shock wave traveling through light fluid medium 22 p4114 A70-42647

Plane shock wave decay by interaction with simple wave, solving nonisentropic equations of gas dynamics 23 p4179 A70-43969

Conducting bodies of revolution, calculating surface currents due to axially incident plane electromagnetic wave by computer program 23 p4162 A70-44005

Plane plasma waves in homogeneous conducting fluid with magnetic field, considering oscillations of two-fluid, cold and hot plasmas 23 p4224 A70-44179

Dipolar resonant scattering of H-polarized plane waves by axially magnetized plasma column with perfectly conducting core 23 p4228 A70-44977

Plane wave diffraction by infinite strips and slitted planes, obtaining asymptotic expansions valid for HF 24 p4426 A70-46019

Two identical conducting thin cylinders illuminated by plane wave at arbitrary incidence angle, determining backscattering cross sections and induced current 24 p4314 A70-46133

PLANET EPHEMERIDES

Dichotomy of Venus in eastern and western elongations, determining time of occurrence by graphical method 03 p0574 A70-13886

Optimum planetary image intensity at TV camera cathodes, exemplifying with Saturn orthicon image 04 p0688 A70-14694

Planetary ephemerides accuracy and navigation during interplanetary missions, discussing machine readable ephemerides for outer planets 13 p2448 A70-28703

Planetary tidal force effect on solar activity cycle, showing amplitude proportionality to solar and gravity center deviation 14 p2649 A70-31199

Celestial mechanics experiment for Mariner Mars 1971 to test general relativity theory and improve Martian ephemeris 16 p2978 A70-34031

PLANET ORIGINS

U PLANETARY EVOLUTION

PLANETARIUMS

Astronauts celestial training, using Mercury capsule simulator and Zeiss planetarium projector for flight simulation 08 p1481 A70-21275

PLANETARY ATMOSPHERES

NT JUPITER ATMOSPHERE

NT MARS ATMOSPHERE

Nonlinear flow conductance and convective terms effects on planetary thermospheres heating diurnal variations, emphasizing solar EUV heating 01 p0178 A70-10413

Atmospheric models of deep atmosphere thermal emission and ionosphere free-free emission used for studying Saturn microwave spectrum 01 p0180 A70-10533

Minor circle maneuver solution to equations of motion of vehicle in spherical planet atmosphere for gliding and cruising, discussing cylindrical planet case 01 p0184 A70-10949

Plane and spherical albedos of planet surrounded by infinite optical thickness atmosphere, with application to Venusian atmosphere 01 p0193 A70-11591

Lorentz absorption line shape computations in radiation scattered by homogeneous planetary atmosphere compared with results for isotropic scattering by van de Hulst similarity relations 02 p0364 A70-11792

Jovian planets atmosphere - Conference, Tucson, April-May 1969 02 p0364 A70-11801

Hydrogen pressure-induced IR absorption spectra, noting applications to planetary atmosphere studies 02 p0341 A70-11805

Planetary atmospheres dynamics, discussing rotational and MHD effects, energy sources, etc 02 p0366 A70-11806

Mutual diffusion coefficient of hydrogen atoms and molecules in upper atmospheres of major planets calculated as function of temperature, using Chapman-Enskog theory 02 p0342 A70-11817

Polarization observations of Saturn in UV and visible regions compared with Jupiter data, noting multiple scattering 02 p0368 A70-11818

Radiative transfer in plane parallel atmospheres computed by discrete space techniques based on invariance concept for application to planetary atmospheres 02 p0338 A70-11825

Absorption spectra computation for model planetary atmosphere using Neumann series for solving semiinfinite radiative transfer equation 02 p0342 A70-11826

Rocket telescope spectrometer precision pointing achieved by servocontrolling secondary mirror, discussing use for planetary atmospheres far UV spectrum studies 02 p0296 A70-11916

Collection of papers on optical properties of planetary atmospheres 02 p0374 A70-12426

Venusian atmosphere water content determined by airborne interferometer 02 p0377 A70-12554

- Optimal lift control of hypersonic lifting body during planetary entry, assuming exponential variation of atmospheric density 04 p0620 A70-15532
- Wind speed and potential temperature vertical profile in day/night planetary atmospheres estimated by similarity theory of boundary layer parameters 06 p1141 A70-17827
- Optimal information selection for determining spacecraft trajectory, considering atmosphere, light speed and series expansion coefficients of planetary gravitational potentials 06 p1142 A70-17891
- Kinetic theory applied to free flow in spherical geometry to study collisionless thermal escape of particles from planetary atmospheres 06 p1147 A70-18293
- Rayleigh phase matrix solutions and albedo values for imperfect Rayleigh scattering in semiinfinite planetary atmosphere 06 p1149 A70-18460
- Radiating gas flows during hypersonic planetary reentry, discussing atmospheric composition, shock layer characteristics, nonequilibrium flows, etc 06 p0985 A70-18558
- Planetary atmospheric entry optimal three dimensional glide paths, considering polar curve altitude dependence, flight path changes, braking maneuvers, etc 07 p1378 A70-18985
- Effective pressure and rotation line intensity in Uranus upper atmosphere obtained from methane band spectrograms, calculating maximum temperature at subsolar point 07 p1385 A70-19423
- Integral methods of obtaining electron density profile of planetary ionospheres and interplanetary gases 07 p1388 A70-20160
- Evaporation rates from rotating planet, showing augmentation over stationary planet 07 p1390 A70-20290
- Solar radiation reflection function for plane-parallel atmosphere with isotropic phase function calculated by successive scattering method, noting application to planetary atmospheres 08 p1571 A70-20909
- Absorption lines in hazy planetary atmosphere with isotropic scattering, examining phase variations of equivalent width 08 p1571 A70-20910
- Saturn ring atmosphere absorption spectrum observation during earth passage through ring plane 09 p1754 A70-22497
- Thermal controls for spacecraft in space and planetary atmospheres, including heat inputs by solar radiation and planetary albedos 09 p1789 A70-23130
- Grand tour space probe optics for observation of objects on planet, considering atmospheric refraction indices effect 09 p1700 A70-23768
- Solar and solar system planetary atmospheres including interplanetary space filled with solar wind 10 p1942 A70-24611
- Nonlinear integral equations of radiation transfer of stellar and planetary atmospheres 12 p2305 A70-27852
- Laminar multicomponent boundary layer for large injection and heat transfer, with particular reference to vehicle entry into planetary atmosphere 12 p2159 A70-28234
- Seed germination in simulated planetary atmospheres, considering biological responses of various organisms 14 p2537 A70-30692
- Planetary atmospheres and surfaces - Conference, Woods Hole, Mass., August 1969 14 p2643 A70-31051
- Solar wind interaction with planetary ionosphere, considering flow behavior across bow MHD shock 14 p2647 A70-31073
- Angular distribution of diffusely reflected solar rays over spherical shell planetary atmosphere, determining halo brightness 14 p2632 A70-31222
- Satellite probing method for transmission absorption spectroscopy of planetary atmospheres 14 p2650 A70-31230
- Polarization role in radiation scattering by planetary atmosphere, considering luminance variation and Rayleigh scattering 14 p2651 A70-31302
- Diffusely transmitted and reflected radiation fields for planetary isotropically scattering atmosphere bounded by Lambert law reflector 14 p2617 A70-31305
- Jupiter Red Spot, explaining motion rate in terms of cellular convection in liquid hydrogen-helium layer 15 p2799 A70-31895
- Power plant using carbon dioxide planetary atmosphere as working fluid, noting weight reduction 15 p2828 A70-32262
- Planetary atmospheres parameters use in spacecraft guidance 15 p2773 A70-32267
- Planetary atmospheric light diffuse reflection and transmission, applying anisotropic scattering theory 15 p2802 A70-32493
- Planetary atmospheric entry optimal three dimensional glide paths, considering polar curve altitude dependence, flight path changes, braking maneuvers, etc [DFVLR-SONDDR-49] 16 p2982 A70-33771
- Optical system of absorption tubes for planetary atmosphere spectra simulation 18 p3314 A70-36408
- Optical observation of structure, composition, thermal spectra and aerosol layers of giant planet atmospheres 18 p3315 A70-36601
- Planetary atmospheres energy balance, considering models in terms of radiative control or large scale fluid motions 19 p3521 A70-38499
- Soviet papers on planetary atmosphere dynamics and hydrodynamic long range weather forecasting covering atmospheric motions, wind field, model, etc 20 p3661 A70-39176
- Planetary scale unsteady atmospheric motions nonlinear problem, considering two level solenoidal model 20 p3662 A70-39177
- Planetary wind field from observed pressure field by linearized balance equation, assuming solenoidal air motion 20 p3662 A70-39178
- Cloudy planetary atmospheres model, assessing nonlocal thermodynamic equilibrium role 21 p3813 A70-40903
- Reacting planetary carbon dioxide-nitrogen atmospheres high temperature equilibrium thermodynamic and transport properties 21 p3950 A70-41747
- Planetary atmospheres X ray fluorescence, calculating Mercury, Venus, earth, Mars and Jupiter emissions 22 p4105 A70-43230
- Planetary atmospheric light diffuse reflection and transmission, applying anisotropic scattering theory 23 p4240 A70-43915
- EM radiation beams higher directivity from sources in two layer plasma in planetary atmosphere 23 p4242 A70-44261
- Absorption line multiple scattering in thick planetary atmosphere, using successive scattering method for single-scattering phase function based on line profile and equivalent width 23 p4222 A70-44550
- Internal constitution of terrestrial and giant planets, planetary surfaces and atmospheres 23 p4256 A70-45036
- Ashen light origin, considering atmospheric refraction of sunlight illuminating dark side of planet 24 p4399 A70-45113
- Planetary atmosphere diffuse radiative transfer reflection and transmission, deriving reciprocity relations from integrodifferential equations 24 p4409 A70-45756
- PLANETARY BASES**
Subsystem selection integration and technology for space base and planetary mission module /PMM/ of space station program [AAS PAPER 70-021] 17 p3023 A70-34801
- PLANETARY COMPOSITION**
Spectroscopically active compounds observability in Jupiter atmosphere using solar composition adiabatic equilibrium model 01 p0180 A70-10530
- Gibeon meteorite iron strength and ductility tests, discussing fragmentation and relation to parental planet structure 06 p1150 A70-18478
- Unmanned exploration program to study magnetic fields and chemical composition of five outer planets in solar system 07 p1375 A70-18871
- Data on Jupiter chemical composition, internal structure and energy sources, discussing Jovian planets origin and role played by gas 07 p1386 A70-19487
- Solar system objects /earth, moon, planets, meteorites, etc/ chemical composition data and analysis techniques 10 p1942 A70-24609
- Lunar and planetary surface chemical composition analysis using neutron inelastic scattering as optimum for unmanned missions 10 p1942 A70-24613
- Multispectral imaging from lander for Martian surface constituents discrimination 11 p2051 A70-26000
- Earth mechanical properties and composition compared with moon and other terrestrial planets 11 p2047 A70-26616
- Martian multispectral imaging from lander emphasizing spectral bands and gray levels number for discrimination of surface constituents 12 p2229 A70-26928
- Planetary gamma and X radiation by remote sensing and passive observation for gross chemical composition 15 p2793 A70-31749
- Lunar, meteoritic and terrestrial silicate rock chemical individuality based on atomic ratios 15 p2799 A70-31896
- Electromagnetic absorption of Martian matter based on vertical temperature variations in planet surface layer 15 p2802 A70-32491
- Data on Jupiter chemical composition, internal structure and energy sources, discussing Jovian planets origin and role played by gas 15 p2805 A70-32732
- Venus deep mantle water degassing rate from atmospheric hydrogen escape data 17 p3154 A70-34610
- Planetary interior density depth relationship, using modified Emden equation 18 p3321 A70-37122
- Electromagnetic absorption of Martian matter based on vertical temperature variations in planet surface layer 23 p4240 A70-43913
- Internal constitution of terrestrial and giant planets, planetary surfaces and atmospheres 23 p4256 A70-45036
- PLANETARY ENTRY**
U ATMOSPHERIC ENTRY
PLANETARY ENVIRONMENTS
NT JUPITER ATMOSPHERE
NT MARS ATMOSPHERE
NT MARS ENVIRONMENT
NT PLANETARY ATMOSPHERES
Microorganisms survivability in soils near spacecraft assembly areas during simulated Martian freeze-thaw cycles 09 p1619 A70-22768
- Differential thermal analysis capabilities in mineralogy for determining present/past planetary environmental parameters having significance for biological experiment 11 p1994 A70-25811
- PLANETARY EVOLUTION**
Nonthermal convection permissible modes in planetary mantles, using self gravitating homogeneous non-rotating sphere containing core and overlying viscous mantle 01 p0176 A70-10317
- Planetary mass and radii determinations indicating earth-moon-Mars and Mercury-Venus systems origin from two unstable planetary body breakups 01 p0177 A70-10342
- Solar system evolution based on Darwin theory, discussing energy inputs effect on primeval atmospheric molecules 02 p0229 A70-11666
- High temperature effects on evolution of Venus upper lithosphere, considering magnetic differentiation, isostatic adjustments, surface relief, mountain building time and distance scales, etc 02 p0371 A70-12207
- Moon-earth historical relationship, comparing differences in figure and interior with terrestrial planets 03 p0562 A70-12875
- Soviet Venus probes Venera 1, 2, 3, 4 and 5 emphasizing aims, implementation means and information yields influence on theory of solar system planets origin and evolution 04 p0757 A70-15672
- Meteoroid impact mass loss and formation of planets, investigating projectile-ejecta ratio and dependence on escape speeds 05 p0910 A70-16393
- Solar orbiting planets formation theory agreement with actual planetary system proved in terms of planetary masses and distances 05 p0913 A70-16567
- Manned or unmanned missions to asteroids close to earth as intermediate stage in planets formation 06 p1139 A70-17551
- Solar system evolution theories to explain planetary orbits, angular momentum and matter distribution, satellite systems and chemical composition 07 p1376 A70-18898
- Data on Jupiter chemical composition, internal structure and energy sources, discussing Jovian planets origin and role played by gas 07 p1386 A70-19487
- Thermal convection determination in earth, Venus, Mars and moon interiors based on thermal stability analysis, obtaining viscosity depth profiles 07 p1272 A70-20203
- Compressibility effect on density explaining Mercury-Venus density near equality to earth- Mars-moon, discussing theory of rotational break-up of parent planets 08 p1563 A70-20496
- Solar system origin theory emphasizing brother star approaching nebula for instability of boundary layer 08 p1568 A70-20638
- Soviet monograph on preplanetary cloud evolution and earth and planet formation covering convection, turbulence, gravitational instability and distribution function of bodies by size 08 p1568 A70-20725

PLANETARY EXPLORATION

Small planets observation methods, classification and designation, discussing asteroid belt origin
08 p1572 A70-20939

Asteroids uniaxial rotation as evidence against origin by collisional fragmentation of larger bodies
08 p1581 A70-21951

Extinct radioactive isotopes of solar system, discussing decay during nuclear synthesis and planetary formation periods
09 p1762 A70-23126

Mars primitive atmosphere analyzed from statistics of craters quantity as function of diameter, using Mariner 6 and 7 probe photographs
09 p1763 A70-23318

Soviet book on solar activity influence on earth natural processes covering atmospheric circulation and pressure, air temperature, precipitations and hydrological changes
09 p1719 A70-23471

Gerstenkorn moon capture theory taking into account tidal evolution of earth-moon system, discussing marine organisms time rate synopsis for earth rotation retardation
10 p1943 A70-24840

Jupiter atmospheric composition, gas and dust cloud formation as clues to origin and evolution of solar system
11 p2108 A70-25654

Differential thermal analysis capabilities in mineralogy for determining present/past planetary environmental parameters having significance for biological experiment
11 p1994 A70-25811

Earth continents and ocean basins as clues to planetary evolution, considering crust composition, moon origin, continental drift, etc
11 p2111 A70-26032

Comet-asteroid evolutionary relationship based on Hidalgo orbital analysis
11 p2114 A70-26472

Preplanetary matter irradiation by solar particles, noting isotopic abundances for evidence of nucleosynthesis induced by proton and alpha bombardment
13 p2486 A70-28619

Lunar surface optical properties differences for lunar and planetary nature and evolution determination
14 p2645 A70-31063

Data on Jupiter chemical composition, internal structure and energy sources, discussing Jovian planets origin and role played by gas
15 p2805 A70-32732

Small planets observation methods, classification and designation, discussing asteroid belt origin
15 p2805 A70-32751

Planetary origin theories, discussing lunar probes and manned landings data, accretion and fission formation models, etc
16 p2973 A70-33115

Mars evolution observation by gamma ray spectrometer in Martian orbit, transmitting information to earth as pulse height distribution
16 p2912 A70-33978

Gaseous disk in equatorial plane of solar nebula, determining dimensions from accretional theory for planets formation
17 p3172 A70-35584

Asteroidal parent bodies heating by electrical induction during early solar evolution
18 p3310 A70-35938

Mathematical model of asteroidal evolution and meteoritic mass distributions under collisional fragmentation using power law
18 p3312 A70-36213

Earth-moon system age and origin from tidal evolution equations, considering growth line counts on living and fossil marine invertebrates
21 p3921 A70-41971

Earth-moon system formation theory, discussing condensation from terrestrial hot extended silicate atmosphere
22 p4098 A70-42548

Apollo 11 data for lunar formation by earth breakup, discussing moon heating phase and correlation with planetary evolution
22 p4098 A70-42549

Titius-Bode law conclusions regarding solar system planetary distances numerical relations, considering planetary evolution
22 p4101 A70-42863

Solar nebula rings and planet formation by sedimentation of solid particles in mechanical equilibrium, including Jupiter and Saturn protoplanets
23 p4239 A70-43867

Venus polywater hydrosphere, discussing vapor phase, surface temperature, evolution, observations and model data
23 p4242 A70-44260

Venus atmospheric speculations compared to Soviet and American probe findings, discussing composition, evolution cloud layer and ionosphere
23 p4253 A70-44863

Planetary exploration for solar system origin and evolution, identifying outer planet mission scientific values
[AIAA PAPER 70-1244] 24 p4411 A70-45962

PLANETARY EXPLORATION
U SPACE EXPLORATION
PLANETARY GRAVITATION
Patch-conic method accuracy and limitations in determining space trajectories as function of planetary zones of influence
04 p0750 A70-14941

Optimal information selection for determining spacecraft trajectory, considering atmosphere, light speed and series expansion coefficients of planetary gravitational potentials
06 p1142 A70-17891

Gravitational field signatures for planetary fine structure analysis, describing lunar orbiter, selenodesy experiment and gravity field and earth gravity field satellite observation
11 p2111 A70-26029

Gravitational disturbance by exterior planets, considering Brown transformation of longitudinal perturbation problem in relation to planet Neptune discovery
11 p2117 A70-26658

Terrestrial external gravitational field approximation using sphere and ellipsoid attraction, showing mass, angular velocity and size dependence
12 p2300 A70-27477

Navigation for planetary orbiter and lander missions, considering orbit insertion, trim corrections and capsule descent for poor planetary gravity field model
13 p2448 A70-28706

Intermediate orbit calculation, allowing for spacecraft large gravitational perturbation during motion near planetary sphere of influence
18 p3312 A70-36166

Pluto space probe using swingby technique with Jupiter, Saturn and Uranus gravitation fields for acceleration
21 p3886 A70-41073

PLANETARY LANDING
Entry and terminal deceleration systems for unmanned Martian landers, discussing parachute landing and lifting entry vehicles
[AIAA PAPER 68-1147] 01 p0195 A70-10828

Spacecraft horizontal maneuvers in homogeneous gravitational field to achieve soft landing on planetary surface, including optimal liftoff and orbital transfer
01 p0197 A70-11501

Dry heat resistance of bacillus subtilis var. niger spores on selected planetary lander capsule surface materials
04 p0645 A70-15442

Electronic packaging and cabling on Capsule System Advanced Development Lander for Mars rough landing
06 p1016 A70-17335

Thermal testing of planetary lander vehicle in vacuum chamber, modeling electronics modules and experiments using resistance heaters
06 p1157 A70-18128

Nuclear propulsion requirements for manned landing mission to Mars assuming Saturn 5-based operation
07 p1375 A70-18874

Sterilized solid propellant motors applicability to planetary landing capsule spin stabilization
[AIAA PAPER 69-823] 07 p1365 A70-19716

Manned Mars mission planning, discussing technologies and costs for planetary landing
09 p1757 A70-22676

Differential thermal analysis-effluent gas analysis /DTA-EGA/ experiment for lightweight Martian landed capsule
11 p2050 A70-25802

Rough-landing space capsule for omnidirectional touchdown in lunar and Martian missions, tabulating design characteristics and functional capabilities
11 p2123 A70-26053

Mars landing analysis and simulation for unmanned lander prototype, discussing digital simulation by Monte Carlo techniques and physical tests
11 p2032 A70-26291

Computerized tradeoff analysis for planetary landing vehicle entry capsule and lander design optimization, emphasizing weight allocation for Mars 1973 missions
11 p2126 A70-26320

Navigation for planetary orbiter and lander missions, considering orbit insertion, trim corrections and capsule descent for poor planetary gravity field model
13 p2448 A70-28706

Throttleable thruster system for Mars soft landing, selecting catalytic decomposition engine from system weight and performance studies
[AIAA PAPER 70-652] 16 p2966 A70-33549

Planetary probes, orbiting space stations and manned spacecraft in interplanetary flights, discussing Mariner, Gemini and Apollo reentry and Venus landing
22 p4109 A70-42313

PLANETARY LONGITUDE
U PLANET EPHEMERIDES

PLANETARY MAGNETIC FIELDS

Dynamo theory of stellar and planetary magnetic fields, discussing mathematical analysis and electronic computation of eigenvalue problems and field parameters
01 p0185 A70-10957

Particle flux and dose rates in Jupiter Van Allen belts based on assumed synchrotron radiation from trapped electrons in dipole magnetic field
[AIAA PAPER 69-18] 04 p0742 A70-15543

Unmanned exploration program to study magnetic fields and chemical composition of five outer planets in solar system
07 p1375 A70-18871

Venus exploration by space probes, discussing orbital and physical data, planetary rotation, atmosphere, surface conditions and magnetic field
18 p3319 A70-37047

Earth magnetic field, discussing origin, field absence on planets and moon and MHD theory
19 p3410 A70-37399

Magnetospheric tail magnetic field and particle motion calculation, assuming constant radius cylinder with current sheet bisecting center
22 p4019 A70-43111

PLANETARY MASS
Planetary mass and radii determinations indicating earth-moon-Mars and Mercury-Venus systems origin from two unstable planetary body breakups
01 p0177 A70-10342

Jupiter mass determined from observations of Jupiter fourth satellite right ascension and declination differences
02 p0370 A70-12087

Geogravitational constants and mass determination, discussing Cavendish constant and measurement theory and technique
03 p0473 A70-13236

Mass and radius relations for zero temperature spheres of chemical elements, using equation of state and numerical integration
04 p0749 A70-14599

Meteoroid impact mass loss and formation of planets, investigating projectile-ejecta ratio and dependence on escape speeds
05 p0910 A70-16393

Solar orbiting planets formation theory agreement with actual planetary system proved in terms of planetary masses and distances
05 p0913 A70-16567

Mariners 6 and 7 range and Doppler tracking data for studying Martian mass and earth-moon mass ratio
06 p1151 A70-18486

Soviet monograph on constant of gravitation, mass and density of earth covering torsion balance, weight experiments and nonlinear vibration techniques
08 p1487 A70-20764

Geogravitational constants and mass determination, discussing Cavendish constant and measurement theory and technique
08 p1491 A70-21669

Earth/moon mass ratio and Mars mass and ephemeris from Mariners range and Doppler tracking data, noting relativistic time delay measurement possibility
15 p2798 A70-31652

Large planets mass determination based on Kepler law and gravitational effects
18 p3318 A70-37045

Uranus and Saturn reciprocal mass determination based on astronomical observations of Saturn and Jupiter respectively
20 p3705 A70-39477

Pluto mass from Saturn, Uranus and Neptune masses
23 p4243 A70-44295

Planetary masses determined from radar measurement data and radio tracking of space probes
24 p4407 A70-45535

PLANETARY MOTION
U SOLAR ORBITS
PLANETARY NEBULAE
IR emission from planetary nebulae, W-R, Of and symbiotic stars, discussing dust hypothesis for IR excess
01 p0173 A70-10039

High luminosity white dwarfs possible evolution from planetary nebulae, discussing plasma neutrino processes
01 p0189 A70-11342

Planetary nebulae with concordant and discordant radio and optical fluxes, discussing possible causes of discordances
04 p0747 A70-14516

Carbon atom RF recombination lines evaluated for conditions in H II regions and planetary nebulae
04 p0748 A70-14587

Radiative excitation in planetary and Orion nebulae by solving transfer equations for Lyman line and continuum radiation, using normalized on-the-spot /NOS/ approximation
04 p0758 A70-15700

Planetary nebula formation mechanism based on slow mass loss due to radiation pressure on grains
08 p1575 A70-21374

- Planetary faint nebulae containing northern Milky Way portion in direction of galactic anticenter observed with spectral Schmidt camera, noting stellar appearance
09 p1761 A70-23051
- Hydrogen rich material forming planetary nebula ejected from contracted core of evolved star with 20,000 times solar luminosity
10 p1936 A70-23906
- Planetary nebula NGC 7027, discussing hydrogen recombination lines
13 p2486 A70-28629
- Planetary nebula K3-50 microwave observations, determining composite source radio spectrum
18 p3313 A70-36326
- Planetary nebula NGC 7027 radio component, determining brightness temperature from fringe amplitude
18 p3313 A70-36327
- Image tube observations of Large and Small Magellanic Clouds and southern planetary nebulae at Cerro Tololo Observatory
20 p3705 A70-39480
- Planetary nebulae radial velocities using prime focus or coude spectra
21 p3889 A70-41157
- Planetary nebula NGC 7027 IR line spectra emission, examining S IV and AR III line intensities
22 p4094 A70-42933
- Orion Nebula and 32 other planetary nebulae spectra in yellow-green obtained with electronic camera, discussing forbidden N I and II lines
22 p4103 A70-42983
- Photoionization cross sections for atoms and ions of carbon, nitrogen, oxygen and neon as function of wavelength for H II regions and planetary nebulae
22 p4104 A70-42997
- Planetary nebulae NGC 7662 and NGC 7009 axially symmetric models from density distributions, H continuum threshold optical depths and central star temperatures
24 p4409 A70-45757
- Planetary nebula NGC 3242 monochromatic photographs and isophotic contours
24 p4411 A70-45788
- PLANETARY ORBITS**
- Planetary information obtained from radar installations, discussing distance and orbit measurements, rotation periods, planetary surfaces, emphasizing Mercury and Venus
01 p0185 A70-11046
- Optimal descent maneuver from planetary orbit for fixed atmospheric reentry angle, considering minimum impulse /fuel consumption/
04 p0745 A70-14496
- Patch-conic method accuracy and limitations in determining space trajectories as function of planetary zones of influence
04 p0750 A70-14941
- Analytic guidance and control for minimum fuel expenditure and optimal guidance corrections for low thrust vehicle in Martian orbit
04 p0716 A70-15544 [AIAA PAPER 78-862]
- Interplanetary swingby trajectory correcting maneuvers for space vehicles return to earth after planet orbiting, with emphasis on singular points
06 p1142 A70-17877
- Statistical orbit and position determination for Mars orbiters and landers based on Viking 1973 mission requirements, discussing tracking problems
06 p1158 A70-18177 [AIAA PAPER 70-160]
- Energy optimal osculating elliptical transfer orbit from low eccentricity orbit constructed for prolonged circling in equatorial plane of axisymmetric planet
07 p1374 A70-18774
- Dynamical constraints on planetary fission events, calculating maximum possible excursions of planetary orbits
07 p1381 A70-19280
- Pulsar formation effect on orbits of preexisting planets and postformation planets effects on pulsar period and phase residuals
08 p1570 A70-20898
- Major planets secular perturbations represented in trigonometric form using canonical transformations
09 p1751 A70-22176
- Minor planets orbits coordinates and velocities data at osculation time
09 p1756 A70-22654
- Thermal interface between edge of planetary disk and space for providing attitude reference during orbiting of planet
13 p2403 A70-28442
- Long period comets energy change due to planetary perturbations tabulated, obtaining orbital major axes before and after passage
13 p2489 A70-28906
- Venus obliquity dynamic implications, developing equations for independent parameter set to define spin vector
13 p2489 A70-28907
- Thermal tidal friction and gravitation effects on Mercury libration after solidification, noting equilibrium with orbital and rotational periods locked in 3/2 resonant state
14 p2638 A70-30701
- Mercury rotational angular velocity fluctuation in terms of orbital mean motion at different orbit positions
14 p2639 A70-30708
- Planetary orbit after central star supernova explosion, discussing effect on pulsar period
14 p2640 A70-30787
- Intermediate elliptical orbits for planetary satellites with small inclination to equatorial plane
18 p3312 A70-36174
- Solar quadrupole moment effect on secular perturbations of planetary orbital elements
18 p3313 A70-36325
- Planet Mercury transit on photographs, noting role as test for terrestrial time systems
18 p3314 A70-36515
- Planetary orbiter parameters long term variations under central body oblateness, solar and atmospheric drag perturbations
19 p3528 A70-38870 [AIAA PAPER 70-1055]
- Statistical orbit and position determination for Mars orbiters and landers based on Viking 1973 mission requirements, discussing tracking problems
21 p3931 A70-41861 [AIAA PAPER 70-160]
- Neptune orbit residual, discussing recently discarded Lalande precovery
21 p3922 A70-41986
- Jupiter perturbations on short period comets during close approaches, discussing orbital distribution
23 p4241 A70-44252
- PLANETARY QUARANTINE**
- Collection of papers on planetary quarantine and spacecraft sterilization covering microbiology, spacecraft components, launching and environments, planetary landing, etc
03 p0433 A70-12996
- Sterile access system using pilot assembly sterilizer system /PASS/ for NASA Planetary Quarantine Program
05 p0808 A70-16708
- PLANETARY RADIATION**
- Local thermal emission from Jupiter at 5 microns discussing North Equatorial Belt and atmospheric transparency
01 p0173 A70-10043
- Internal powers and effective temperatures of Jupiter and Saturn measured by aircraft mounted telescope, noting restraints on planetary structure and atmosphere models
01 p0173 A70-10045
- Far UV spectroscopy of Jupiter by rocket-borne spectrograph
01 p0179 A70-10528
- Atmospheric models of deep atmosphere thermal emission and ionosphere free-free emission used for studying Saturn microwave spectrum
01 p0180 A70-10533
- Icarus asteroid rotation period and brightness variation values obtained from photometric observations at Cassegrain reflector focus
01 p0180 A70-10536
- Jovian decameter radiation polarization during 1966-1967 apparition compared with cyclotron model predictions
02 p0364 A70-11793
- Venus and Jupiter Aerobee rocket photoelectric UV spectra, determining geometric albedos using reflecting layer and cloud models
02 p0367 A70-11812
- Absorption spectra computation for model planetary atmosphere using Neumann series for solving semiinfinite radiative transfer equation
02 p0342 A70-11826
- Mars multicolor filter photometry showing variation in whole-disk reflectivity
02 p0378 A70-12560
- Jupiter radio telescope observations at cm wavelengths, describing radiation belt emission characteristics and planetary brightness temperature spectrum
03 p0565 A70-13233
- Daily variations of winter stratospheric zonal wind and planetary waves based on synoptic charts from balloon observation
05 p0878 A70-16148
- Mayeda flare observed on Mars 4 June 1937/, suggesting oriented reflection of solar rays from ice crystals cloud or Martian surface feature
05 p0918 A70-16916
- Circular polarization measurements of Jovian decimeter radiation by 210-ft radio telescope at Goldstone, California
05 p0921 A70-16986
- Jovian decametric radiation periodicities analysis refuting evidence of Bigg for new Jovian satellites
06 p1138 A70-17280
- Cosmic rays effect on atmospheric temperature and wind, discussing planetary distribution of neutron component of radiation intensity
07 p1373 A70-20346
- Mars planet smoothing factor determined from phase curve of integrated brightness distribution on disk
08 p1564 A70-20557
- Jupiter and Saturn IR reflection spectra observed with Michelson interferometer- spectrometer, eliminating effects of terrestrial atmospheric absorption, solar spectral lines, etc
08 p1570 A70-20895
- Modulation lanes in fine structure of dynamic spectra of Jovian L bursts possibly due to ionosphere or magnetosphere
08 p1576 A70-21394
- Fine structure morphology in dynamic spectra of Jupiter decametric radiation determined from spectral recordings
08 p1562 A70-21514
- Critique of blue haze negative hypothesis in preliminary Mariner 6 data report
08 p1578 A70-21556
- Jupiter decametric noise storm commencement time defining constant planetary rotation period
08 p1580 A70-21572
- Jupiter radio telescope observations at cm wavelengths, describing radiation belt emission characteristics and planetary brightness temperature spectrum
08 p1580 A70-21666
- Book on solar and planetary radio emission covering solar system physical characteristics, quiet Sun, thermal and nonthermal emission, etc
09 p1752 A70-22201
- Baseline measurements of Jupiter decametric radiation providing upper size limit to coherent and incoherent sources
09 p1755 A70-22512
- Saturn disk temperature obtained from centimeter wavelength, suggesting possibility of nonthermal radiation
09 p1759 A70-22912
- Thermal controls for spacecraft in space and planetary atmospheres, including heat inputs by solar radiation and planetary albedos
09 p1789 A70-23130
- Jupiter brightness temperature values and standard deviations from EHF radio telescope observations
09 p1765 A70-23809
- Jupiter decametric emission modulation by planetary rotation and Io position, suggesting role of magnetic tail diurnal swings
10 p1940 A70-24434
- Radio telescopic observations of Jupiter, Venus and radio source 3C 273 at 2 and 8 mm wavelengths, determining brightness temperatures and radiation flux densities
10 p1948 A70-25153
- Stellar and planetary IR spectra from spectrometer with rotating circular variable thickness interference filter
11 p2113 A70-26468
- Thermal interface between edge of planetary disk and space for providing attitude reference during orbiting of planet
13 p2403 A70-28442
- Jupiter decametric radio bursts observed by tape recording fringe interferometer
13 p2486 A70-28626
- Jupiter luminosity as indication of internal energy magnitude, comparing limb darkening with predicted brightness distribution
14 p2643 A70-30984
- Mercury mm wave observations, examining longitude dependence of disk average brightness temperature and epilith thermal parameters range
14 p2647 A70-31076
- Thermal radio emission from major planets at mm and cm wavelengths and at decimeter wavelengths for Jupiter and Saturn
14 p2648 A70-31084
- Twelve year periodicities of Jupiter decametric radiation, noting correlation with Jupiter magnetic field rotation period
14 p2648 A70-31085
- Lunar occultation observation of Jupiter by radio telescope, determining one dimensional strip brightness distribution
14 p2648 A70-31086
- Jupiter decimeter radiation long term variations from flux density measurements, suggesting correlation with solar activity
14 p2648 A70-31087
- Jupiter microwave spectrum from polarimetric observations and previous data
14 p2648 A70-31088
- Synchrotron model involving electron trapping in dipolar magnetic field for Jupiter decimeter radiation
14 p2649 A70-31089
- Planetary gamma and X radiation by remote sensing and passive observation for gross chemical composition
15 p2793 A70-31749
- Martian brightness increase at 1 deg phase angle, explaining by transparent cubic crystals presence in clouds
15 p2803 A70-32499
- Mars planet smoothing factor determined from phase curve of integrated brightness distribution
15 p2805 A70-32712

- Mars evolution observation by gamma ray spectrometer in Martian orbit, transmitting information to earth as pulse height distribution 16 p2912 A70-33978
- Jovian decimeter radiation, discussing electron drift velocity in dipole field, characteristic time for energy loss and radiation belt dimensions 16 p2980 A70-34192
- Jupiter decametric radio emission modulation by Io simulated by DC circuit model 18 p3321 A70-37120
- Jovian continuum radiation observation by RAE-1 during lunar occultations 19 p3512 A70-38608
- Jupiter RF spectrum in 80 to 10,000 MHz range for dipolar model, noting independent synchrotron component 21 p3891 A70-41185
- Martian brightness increase at 1 deg phase angle, explaining by transparent cubic crystals presence in clouds 23 p4240 A70-43920
- Jupiter flux density changes at 2695 MHz correlated with 10.7 cm solar activity, suggesting magnetic anomaly explanation 23 p4246 A70-44751
- Pluto albedo at various wavelengths from spectrophotometric measurements 24 p4399 A70-45129
- ### PLANETARY ROTATION
- Rotation period of Jupiter based on decametric component of radio emission, suggesting anticorrelation with sunspot number for drift observed 01 p0173 A70-10044
- Icarus asteroid rotation period and brightness variation values obtained from photometric observations at Cassegrain reflector focus 01 p0180 A70-10536
- Planetary information obtained from radar installations, discussing distance and orbit measurements, rotation periods, planetary surfaces, emphasizing Mercury and Venus 01 p0185 A70-11046
- Planetary atmospheres dynamics, discussing rotational and MHD effects, energy sources, etc 02 p0366 A70-11806
- Equations of conservation of mass, energy and momentum applied to rotation effects on convective motion in planetary interiors 05 p0905 A70-15759
- Telescopic circular polarization observations of Jupiter at 9.26 cm related to Jovicentric declination of earth 05 p0906 A70-15896
- Theory for describing rotating fluid planets external geometry in state of hydrostatic equilibrium, noting role of equipotential surfaces 06 p1153 A70-18559
- Planets rotation axes inclinations related to Titius-Bode rule of solar distances, noting estimation of unknown inclinations 07 p1386 A70-19557
- Evaporation rates from rotating planet, showing augmentation over stationary planet 07 p1390 A70-20290
- Spin angular momentum of planets based on particle accretion, discussing particles cloud condensation 08 p1576 A70-21400
- Jupiter decametric noise storm commencement time defining constant planetary rotation period 08 p1580 A70-21572
- Asteroids uniaxial rotation as evidence against origin by collisional fragmentation of larger bodies 08 p1581 A70-21951
- Optimal transfer ellipse obtained by complete rotation in gravitational field of axisymmetric planet 09 p1751 A70-22161
- Venus rotation period determination by radar observation of surface features 09 p1759 A70-22911
- Thermal tidal friction and gravitation effects on Mercury libration after solidification, noting equilibrium with orbital and rotational periods locked in 3/2 resonant state 14 p2638 A70-30701
- Mercury rotational angular velocity fluctuation in terms of orbital mean motion at different orbit positions 14 p2639 A70-30708
- Venus radar anomalous features, examining rotation period, polarized and cross polarized scattering properties and topography 14 p2647 A70-31079
- Retrograde rotation of equatorial spots of Venus cloudy exterior layer, using UV photographic and spectroscopic observations 14 p2649 A70-31215
- Venus spin-orbit resonance resulting in consistent inferior conjunction with earth, suggesting solar atmosphere tidal influence 14 p2650 A70-31216
- Venus retrograde axial period contradiction between radar echoes and violet-UV photographic and interferometric spectroscopic methods explained by theory using strong magnetic dipole 16 p2973 A70-33116
- Convective heat transport role in determining rotating planets climatic temperature zones 22 p4099 A70-42626
- ### PLANETARY SPACE FLIGHT
- #### U INTERPLANETARY FLIGHT
- #### PLANETARY SPACECRAFT
- #### U INTERPLANETARY SPACECRAFT
- #### PLANETARY SURFACES
- #### NT MARS SURFACE
- Slopes distribution over finite span on planetary surface excavated by primary impact craters, including typical lunar mare crater densities 01 p0178 A70-10443
- Moon-earth historical relationship, comparing differences in figure and interior with terrestrial planets 03 p0562 A70-12875
- Automated mars surface sample return /AMSSR/ mission, discussing Saturn 5 chemical and nuclear approach [AIAA PAPER 69-1066] 04 p0764 A70-15626
- Space temperature determination, discussing planet or satellite absorption and radiation rate dependence on surface characteristics, solar radiation, planet albedo and thermal radiation 05 p0914 A70-16629
- Planetary boundary layer thickness estimation, considering geostrophic wind speed and potential temperature average vertical gradient 07 p1377 A70-18922
- Optimal photometric data processing for planetary characteristics and surface details, considering errors due to image blurring in telescope 07 p1384 A70-19419
- Orbit analysis of hypothetic comets formed by Jupiter surface eruptions using Lagrange origin hypothesis 08 p1573 A70-21012
- Venus surface temperature calculations with non-gray radiation balance model and Mariner 5 and Venera 4 vertical temperature profile data 08 p1579 A70-21568
- Radiative heat transfer in lunar and Mercurian surfaces, discussing radiative heat transfer in powders 08 p1579 A70-21569
- Thermally emitted photons of atmospheric molecules and aerosols and planetary surface followed by Monte Carlo method, using anisotropic single scattering functions 09 p1719 A70-23524
- Venus planetary surface and atmosphere, reviewing American and Soviet probe results 10 p1943 A70-24761
- Volcanic terrain by high precision photogrammetry for studying planetary surface roughness traversability by three wheeled vehicle 10 p1882 A70-25047
- Unmanned exploration of planetary surfaces in preparation for manned landings, describing Surveyor lunar probes 11 p2112 A70-26056
- Mars imaging mission and astrodynamic interaction, discussing arrival geometry and orbit size effects [AIAA PAPER 69-127] 11 p2112 A70-26130
- Mercury surface features from spectrograms of depolarized radar echoes 12 p2298 A70-27268
- Unmanned vehicles for planet surface exploration, discussing design and control using self adjusting and logic circuits 13 p2384 A70-28418
- Cratered planetary surface distribution and covariance functions of elevations using statistical model 13 p2488 A70-28763
- Planetary atmospheres and surfaces - Conference, Woods Hole, Mass., August 1969 14 p2643 A70-31051
- Venus surface temperature poleward variation from radio interferometry measurements 14 p2646 A70-31068
- Venus atmosphere-lithosphere interactions, predicting electrically conducting cloud masses presence 14 p2646 A70-31070
- Mercury mm wave observations, examining longitude dependence of disk average brightness temperature and epilith thermal parameters range 14 p2647 A70-31076
- Venus and Mercury surface height variations near equators, using radar time delay and Doppler observations 14 p2647 A70-31077
- Venus radar mapping using fixed base line interferometer for hemispheric ambiguity resolution 14 p2647 A70-31078
- Venus radar anomalous features, examining rotation period, polarized and cross polarized scattering properties and topography 14 p2647 A70-31079
- Dual mode algorithm for routing unmanned autonomous roving vehicle around obstacles on planets, using dynamic programming and terrain information [JPL-TR-32-1484] 14 p2655 A70-31183
- Mars carbon dioxide abundance and surface pressure from growth curve based on high resolution spectra 14 p2650 A70-31218
- Venus atmosphere and surface conditions, describing temperature, accumulation of carbon dioxide and runaway greenhouse effect 15 p2806 A70-32771
- Atmospheric boundary layer model, considering air-surface interaction, heat and humidity exchange, wind, temperature and humidity profiles, etc 17 p3132 A70-34667
- Planetary surface smoothness factor by disk brightness, Mars red light and phase curves methods, indicating superiority of visual observation 18 p3315 A70-36602
- Venus exploration by space probes, discussing orbital and physical data, planetary rotation, atmosphere, surface conditions and magnetic field 18 p3319 A70-37047
- Mercury photometric measurement, examining surface brightness for photometric function 18 p3319 A70-37052
- Planetary surface inhomogeneities detection by reflected and transmitted light polarimetry, using symmetry principles 18 p3319 A70-37057
- Aeolian regime of Venus surface resulting from high surface temperature and pressure, discussing spurious radar echoes, dust and sand transport and deposition 21 p3885 A70-40929
- Thin walled spherical shell spacecraft skin heating in planetary surface proximity, considering skin temperature distribution 21 p3944 A70-41019
- Jupiter varied color surface area observations /1926-1964/ 22 p4107 A70-43594
- Internal constitution of terrestrial and giant planets, planetary surfaces and atmospheres 23 p4256 A70-45036
- Jupiter red spot darkness parameter and solar activity as clue to Jupiter-solar relationship 24 p4402 A70-45391
- Jupiter surface drawings and photographs concerning quasi-periodic oscillations of red spot 24 p4411 A70-45800
- ### PLANETARY TEMPERATURE
- Internal powers and effective temperatures of Jupiter and Saturn measured by aircraft mounted telescope, noting restraints on planetary structure and atmosphere models 01 p0173 A70-10045
- Venus upper atmosphere average rotational temperature determined from high dispersion spectroscopic observations of 7883 A carbon dioxide band 01 p0184 A70-10912
- Jupiter atmosphere temperature and density profiles determined from thermal models based on thermal structure above dense cloud level 02 p0367 A70-11814
- Optical parameters of Martian surface and temperature, discussing brightness distribution along diameter in red spectral region, based on photoelectric cross sections 05 p0918 A70-16917
- Effective pressure and rotation line intensity in Uranus upper atmosphere obtained from methane band spectrograms, calculating maximum temperature at subsolar point 07 p1385 A70-19423
- Venus surface temperature calculations with non-gray radiation balance model and Mariner 5 and Venera 4 vertical temperature profile data 08 p1579 A70-21568
- Saturn disk temperature obtained from centimeter wavelength, suggesting possibility of nonthermal radiation 09 p1759 A70-22912
- Martian atmospheric models for lander and simulator design, obtaining effective sky temperatures, surface pressures and temperatures, atmospheric compositions, etc 11 p2112 A70-26141
- Mars and Venus radio temperature measurements by 210 ft telescope, obtaining effective brightness 12 p2309 A70-27896
- Upper atmospheric temperature-gravitational potential relationship for sun, earth and several planets 13 p2495 A70-29765
- Mercury disk temperature at 3.75 cm wavelength, showing variation with phase angle and hermographic longitude 14 p2647 A70-31075
- Martian soil thermal conditions at south pole, considering polar cap annual variations and carbon dioxide sublimation 15 p2802 A70-32492
- Venus atmosphere and surface conditions, describing temperature, accumulation of carbon dioxide and runaway greenhouse effect 15 p2806 A70-32771

Mercury disk temperature from microwave spectrum analysis, proposing subsurface greenhouse effect 17 p3157 A70-34838

Photolytic model of Jupiter belt excess temperatures and coloration compared to solid ammonia clouds, using IR and visual observations 19 p3513 A70-37410

Upper atmospheric temperature-gravitational potential relationship for sun, earth and several planets 20 p3710 A70-40090

Martian soil thermal conditions, considering polar cap annual variations and carbon dioxide sublimation 23 p4240 A70-43914

Jupiter model thermal profiles, examining metallic core and molecular envelope in convective equilibrium 23 p4241 A70-44251

Venus carbon dioxide band, deriving rotational temperatures at various phase angles 23 p4241 A70-44257

PLANETOCENTRIC COORDINATES

NT GEOCENTRIC COORDINATES

Three camera method for studying upper atmosphere winds via smoke trails providing wind velocity, earth coordinate data and error indication 14 p2607 A70-30572

Earth to planet radar signal time delay in general relativity expressed in relativistic spherical polar coordinates of earth and planet 15 p2806 A70-32801

PLANETOLOGY

Nonthermal convection permissible modes in planetary mantles, using self gravitating homogeneous non-rotating sphere containing core and overlying viscous mantle 01 p0176 A70-10317

Planetary mass and radii determinations indicating earth-moon-Mars and Mercury-Venus systems origin from two unstable planetary body breakups 01 p0177 A70-10342

Giant planets structure, calculating Jupiter and Saturn densities using Russell solar mixture and internal heat from central core radioactivity 01 p0181 A70-10663

Mars surface features, describing diagonal and meridian-latitude grid systems, continental blocks and continental drift 01 p0183 A70-10869

DC dynamo models for planetary electromagnetic conditions, considering nonrotationally symmetric turbulence induction actions and critical values for field maintenance 01 p0185 A70-10956

Radar probing of solar system noting contributions to knowledge on planets 01 p0192 A70-11485

Long range solar flare forecasting noting correlation between planetary conjunctions and proton events [AAS PAPER 69-624] 04 p0740 A70-14658

Satellite orbit and attitude determination and planetary gravity and astronomical constants from earth-based radar Doppler and orbital photogrammetric observations 04 p0750 A70-14938

Mercury shape estimated with isostatic form of equilibrium controlled by situation near perihelion passage at 3-2 resonance spin rate, discussing solidification thermal effects 05 p0908 A70-16332

Soviet book on Jupiter atmosphere covering structure, chemical composition, cloud cover, temperature conditions, etc 05 p0910 A70-16412

Rotation, diameter, mass, atmosphere and constitution of planet Neptune, with emphasis on visual observations 05 p0913 A70-16552

Physical and life supporting properties of hypothetical Martian biosphere, considering organism adaptation theories 05 p0803 A70-17109

Tabulated corrections of data concerning reduction of photographs of small planets obtained at Bucharest Astronomical Observatory 06 p1139 A70-17549

Dynamical constraints on planetary fission events, calculating maximum possible excursions of planetary orbits 07 p1381 A70-19280

Planets rotation axes inclinations related to Titius-Bode rule of solar distances, noting estimation of unknown inclinations 07 p1386 A70-19557

Martian polar cap spectra interpreted with laboratory measurements of water-carbon dioxide frost spectral reflectance 07 p1388 A70-19946

Thermal convection determination in earth, Venus, Mars and moon interiors based on thermal stability analysis, obtaining viscosity depth profiles 07 p1272 A70-20203

Jupiter conductive molten metallic hydrogen core of moderate temperature suggested from solids melting point temperature dependence on pressure 07 p1390 A70-20238

Figure of gravitating inhomogeneous rotating liquid, applying results to Jupiter and Saturn model construction 08 p1564 A70-20558

Small planets observation methods, classification and designation, discussing asteroid belt origin 08 p1572 A70-20939

Catalog systems orientation based on major and minor planets observation, discussing zero points corrections 08 p1574 A70-21152

Hori canonical equations analytical solution generalization resulting from elimination of short period terms of first order planetary theory 08 p1575 A70-21239

Neptune and Pluto oblateness inferred from analogous similarities of mass, diameter and mean density with Uranus and Mars planets 09 p1750 A70-22096

Major planets secular perturbations represented in trigonometric form using canonical transformations 09 p1751 A70-22176

Rayleigh number effects on convection in planetary mantles, considering conservation equations of mass, energy and momentum 09 p1752 A70-22312

Planetary perihelion precession with velocity-dependent gravitational mass in terms of special relativity 09 p1765 A70-23800

Einstein theory applied to sample modeling of planetary orbits and light beams touching sun in solar gravitational field 10 p1939 A70-24268

Laboratory simulation for shock waves around earth, moon and Venus based on artificial solar wind and magnetic dipole interaction study 10 p1948 A70-25182

Planetary and space mission planning - Conference, New York, October 1967 11 p2110 A70-26026

Earth mechanical properties and composition compared with moon and other terrestrial planets 11 p2047 A70-26616

Ring micrometer radius determination and application to right ascension changes in determining positions of comets, planets and planetary moons 11 p2057 A70-26675

Planet Venus motion, mass, dimensions, shape, topography and atmosphere 12 p2311 A70-28301

Perturbation function of first order general planetary theory using Hori canonical variables, revealing mixed secular term of determining function 13 p2487 A70-28708

Soviet monograph on minor planets origin and physical nature, considering orbits, investigative techniques, etc 13 p2488 A70-28800

Mars geology, discussing polar caps phenomena, diurnal variations, orbital eccentricity, seasonal meteorology, volcanism, erosion, etc 15 p2800 A70-32059

Figure of gravitating inhomogeneous rotating liquid, applying results to Jupiter and Saturn model construction 15 p2805 A70-32713

Small planets observation methods, classification and designation, discussing asteroid belt origin 15 p2805 A70-32751

Planetary origin theories, discussing lunar probes and manned landings data, accretion and fission formation models, etc 16 p2973 A70-33115

Mars 1969 planetary surface drawing and photograph evaluation, noting dark spot east of Nodus Lacontis 17 p3154 A70-34677

Mercury drawings from refractor observations during 1964-1967 18 p3315 A70-36611

Lunar and planetary laboratory communications, Volume 8 covering IR astronomy, Mercury, Mars, Uranus, comets, etc 19 p3515 A70-37929

Planet Mercury knowledge summary, discussing orbit, diameter, mass, density, rotation, surface features, atmosphere, polarization, albedo and color 19 p3515 A70-37930

Einstein theory applied to sample modeling of planetary orbits and light beams touching sun in solar gravitational field 19 p3520 A70-38393

Astronomical events observed in 1970 by amateur astronomers, discussing sun and moon eclipses and planets visibility 21 p3886 A70-41074

Planetary unipolar electric generator system theoretical model based on polarization charges deposition by solar wind 22 p4100 A70-42790

Jupiter varied color surface area observations /1926-1964/ 22 p4107 A70-43594

Pluto mass from Saturn, Uranus and Neptune masses 23 p4243 A70-44295

PLANETS

NT EARTH [PLANET]

NT JUPITER [PLANET]

NT MARS [PLANET]

NT MERCURY [PLANET]

NT NEPTUNE [PLANET]

NT PLUTO [PLANET]

NT SATURN [PLANET]

NT URANUS [PLANET]

NT VENUS [PLANET]

Sun-planetary systems capture and catapult capacity for interstellar bodies under close flyby conditions 04 p0753 A70-15144

Kinetics of solar wind interaction with moon and planetary bodies using perturbation scheme to obtain ion density distribution on antisolar side [AIAA PAPER 70-61] 06 p1136 A70-18192

Barnard two planet solar system, dwarf star perturbations, orbital parameters and comparison with Solar system 10 p1943 A70-24758

Jovian planets polar and equatorial diameters and lateral dimensions of Saturn rings by optical measurements 16 p2979 A70-34034

Planetary and lunar photography at French observatory, discussing Pic du Midi facilities and various photographic emulsions 17 p3082 A70-34676

Planetary theory construction to second order of disturbing masses, applying to motions of any set of two or three planets in solar system 19 p3523 A70-38687

Extrasolar planets photometric observations by telescopic mirror system on moon far side 20 p3710 A70-40131

PLANFORMS

NT CARET WINGS

NT DELTA WINGS

NT RECTANGULAR PANELS

NT RECTANGULAR PLANFORMS

NT RECTANGULAR PLATES

NT RECTANGULAR WINGS

NT SWEPTBACK WINGS

NT TRAPEZOIDAL WINGS

NT VARIABLE SWEEP WINGS

NT WING PLANFORMS

Arbitrary planform plates with edge clamping and elastic beam spanwise support using Green function 14 p2655 A70-30182

Horizontal flight speed effects on aerodynamic characteristics of air cushion vehicles with elliptical planform 22 p3959 A70-42801

PLANIMETRY

U DIMENSIONAL MEASUREMENT

PLANKTON

Remote sensing of plankton and matter in sea by determining spectral changes in scattered light measured with radiometer 17 p3079 A70-35619

PLANNING

NT AIRPORT PLANNING

NT PRODUCTION PLANNING

Cost and deadline planning for system development, suggesting theoretical methods tests regarding applicability 10 p1971 A70-24597

PLANT ROOTS

Ca ion reversible effects of hydrochloric acid and ammonia water on betacyanin leakage from beetroot sections 19 p3365 A70-38375

PLANTS [BOTANY]

NT ALGAE

NT AUTOTROPHS

NT AZOTOBACTER

NT BACILLUS

NT BACTERIA

NT BLUE GREEN ALGAE

NT CHLORELLA

NT CLOSTRIDIUM BOTULINUM

NT ESCHERICHIA

NT EUGENIA

NT FUNGI

NT GRASSES

NT HYDROGNOMONAS

NT LEAVES

NT NITROBACTER

NT NOSTOC

NT PARASITES

NT PSEUDOMONAS

NT SACCCHAROMYCES

NT SCENEDESMUS

NT SPORES

NT TOBACCO

NT TREES [PLANTS]

NT YEAST

Gas chromatographic-mass spectrometric identification of aliphatic hydroxy acids in plants and sediments 02 p0252 A70-12521

Phytotron design and operation, discussing closed air conditioned plant growing system at Stockholm including greenhouse, light controlled rooms, darkrooms, etc

03 p0435 A70-13716

Carrot plants growing during 374 days in conveyor type aeroponic assembly, noting yield and morphological features

03 p0436 A70-13902

Unicellular algae protein diet effects on animal and human enteric microflora composition

09 p1615 A70-22087

Water depth determination by remote measurement of near IR reflectance of underwater plants, discussing effects of water path length changes

10 p1878 A70-24741

Phytotron design and operation, discussing closed air conditioned plant growing system at Stockholm including greenhouse, light controlled rooms, darkrooms, etc

11 p1990 A70-25516

Light-induced electron paramagnetic resonance signal detected in *Anacystis nidulans*

11 p1989 A70-26847

Plant leaves discrimination by multispectral reflectance indicated in transmittance measurements via remote sensing from aircraft and spacecraft

12 p2218 A70-26920

Plant cultivation in closed biological cycles by hydroponic method using keramit/alumoferrisilicate/substrate

13 p2358 A70-29328

Venus water presence from Venera 4 and Mariner 5 data suggesting polar seas and oceans saturated with hydrochloride and carbon dioxide as plant life source

14 p2637 A70-30365

Physical methods in applied climatology, analyzing meteorological effects on human body and building thermal conditions and plant biomass growth

15 p2771 A70-32111

Unicellular algae protein diet effects on animal and human enteric microflora composition

15 p2685 A70-32683

False color aerial photography with IR film for distinguishing vegetation types and assessing plant vigor based on leaf reflectance

17 p3078 A70-35613

Remote sensing experiment demonstrating utility of multispectral color aerial photography for detection of differences among vegetative species

17 p3095 A70-35615

Photographic and multisensor imagery augmented by field survey for mapping vegetation boundaries and density differences within and between plant communities

17 p3079 A70-35616

Anomalous substrate oxidizing specificities among red brown and green algal peroxidases and land plants

19 p3360 A70-37773

Cosmos 110 satellite experiments concerning radiation effects on lysogenic bacteria and plants

23 p4149 A70-45030

PLANTS [INDUSTRIES]

U INDUSTRIAL PLANTS

PLASMA ACCELERATION

Steady state spherically symmetric model for solar plasma acceleration with distance, showing essential role of viscosity

01 p0172 A70-11519

Acceleration mechanisms in pulsed plasma accelerator with rail electrodes driven by capacitor discharge

02 p0348 A70-12501

Steady, homogeneous, electromagnetic plasma acceleration fields, demonstrating electric and magnetic fields effects on dynamic behavior

03 p0529 A70-12989

Solar wind acceleration and coronal plasma heating above plage regions from spectra of solar radio echoes, computing temperature rise and energy input

04 p0470 A70-15049

Neutral gas ionization and ion recombination effect on electrodynamic plasma acceleration in coaxial and flat electrode accelerators

04 p0728 A70-15222

Plasma acceleration by induced Hall currents, discussing Hall-to-current ratio maximum at critical magnetic field

04 p0729 A70-15596

Ion-neutral coupling in plasma acceleration revealed by velocity disparities determined spectroscopically

06 p1133 A70-18219

Plasma ion cyclotron resonance acceleration in nonuniform magnetic field by RF field

07 p1353 A70-20229

Light ions acceleration to high energy by pulsed high intensity electron beams

08 p1553 A70-21694

Quasi-steady state plasma acceleration in coaxial electrode geometry during synchronized application of tailored pulses of mass flow and current

09 p1736 A70-23204

Particle acceleration during solar plasma ejection, disregarding magnetic effects on flux

11 p2107 A70-25526

Mass transfer in electrodynamic accelerated plasma, discussing recombination, ambipolar diffusion, electrode sputtering, charge exchange, electron capture and resistance forces effect on acceleration

13 p2461 A70-28862

Ohmic dissipation in MHD plasma acceleration, demonstrating interaction with electric field and magnetic induction

14 p2621 A70-30296

Solar wind velocity profile in rapid acceleration of coronal plasma from type I, III and V bursts

17 p3152 A70-35745

Laser applications in thermonuclear fusion, analyzing plasma acceleration under laser pulse action

18 p3265 A70-36110

Acceleration processes in MPD arc jet in Ar for symmetric discharge layer and rotating spoke types

20 p3680 A70-39992

Particle acceleration during solar plasma ejection, disregarding magnetic effects on flux

21 p3892 A70-41276

Stochastic kinetic theory for plasma turbulent heating by random fields, predicting acceleration effects

21 p3859 A70-41899

Mass transfer effects on plasma electrodynamic acceleration, discussing plasma recombination and diffusion

22 p4083 A70-43386

PLASMA ACCELERATORS

NT COAXIAL PLASMA ACCELERATORS

Plasma accumulation between mixed field accelerator and pulsed magnetic mirror, noting duration and stability

02 p0346 A70-12104

Acceleration mechanisms in pulsed plasma accelerator with rail electrodes driven by capacitor discharge

02 p0348 A70-12501

Pulsed MHD accelerator for MHD wind tunnel application, discussing accelerator gas source, magnetic field and operation

03 p0462 A70-12907

Heat transfer to insulator wall of linear MGD accelerator attached to shock tube, comparing measurements with Hartmann boundary layer analysis

[ASME PAPER 69-WA/HT-53] 04 p0781 A70-14796

Crossed field plasma accelerator designed as element of hypersonic wind tunnel driver

06 p1119 A70-17471

Quasi-steady coaxial MPD arcs characteristics, studying Ar ion velocities, electrostatic ion acceleration mechanism and arc voltage gradient

06 p1132 A70-18208

Repetitively pulsed quasi-steady vacuum arc magnetoplasma dynamic accelerator for propulsion, using electrolytic capacitors as power source

[AIAA PAPER 70-167] 06 p1133 A70-18228

Current sheet pattern and gas flow stabilization in pulsed plasma accelerators

[AIAA PAPER 69-112] 07 p1348 A70-19322

Energy transfer from pulse network to mass associated with propagating current sheet in linear pinch discharge, discussing pulsed plasma accelerator efficiency

[AIAA PAPER 69-113] 07 p1348 A70-19323

Electrodynamic plasma accelerators fast particle generation mechanism during entrainment, studying polarization field potential structure

08 p1549 A70-20506

Inert gas plasma jets diagnostics in accelerator by spectroscopy, determining flow velocities, excitation and gas temperatures

11 p2093 A70-26744

Energy spectrum of electrons accelerated in linear plasma betatron close to potential compared to cyclic betatron results

13 p2463 A70-29379

Hypervelocity gas, electromagnetic, explosive drive and exploding wire accelerometers and high explosive, shaped charge, plasma drag and electrostatic accelerators for projectile impact studies

15 p2718 A70-32783

Electroless traveling wave accelerator for wind tunnel use, determining gas stream density for subsonic and supersonic operation

16 p2889 A70-33868

Experimental and theoretical investigation of mass injection effect on high current MPD arc

16 p2959 A70-33869

Near cathode magnetic field effect on instability in linear Hall current accelerators, using geometry of field extending from anode to cathode region

[AIAA PAPER 69-381] 16 p2959 A70-33870

Fluid dynamics of pulsed plasma accelerators, discussing energy transfer and losses limitations

18 p3301 A70-36660

Langley 20 megawatt plasma accelerator design and operation, describing arc heater modifications, exit parameters, electrical properties, etc

20 p3606 A70-40010

Plasma accelerator compressible turbulent boundary layers numerical calculation taking into account MHD effects, electron thermal nonequilibrium and finite rate ionization

20 p3682 A70-40017

Multimegawatt quasi-steady MPD arc accelerator in millisecond pulses, noting applicability to experiments requiring long exposure times

[AIAA PAPER 70-1095] 20 p3683 A70-40241

Composite accelerator electrodes on Cs bombardment microthrusters, testing various designs and electrode coatings

[AIAA PAPER 70-1089] 20 p3693 A70-40246

Plasma accelerators for nuclear EM propulsion, considering power supply requirements and differences between plasma and ion engines

22 p4070 A70-43186

Eroding-dielectric plasma accelerators energy characteristics, discussing current distribution

22 p4083 A70-43387

Extremely high temperature deuterium examination, using coaxial plasma accelerators to determine neutron production and vorticity

23 p4227 A70-44452

PLASMA ARC SPRAYING

U ARC SPRAYING

U PLASMA SPRAYING

PLASMA ARC WELDING

Plasma beam welding of light metal and heat resistant alloys, discussing weld characteristics, beam I-V characteristics, etc

09 p1690 A70-22077

Plasma arc welding torches nozzle dimensions and shape dependence on thermal and electrical characteristics, optimizing energy output

22 p4042 A70-42378

PLASMA ARCS

U PLASMA JETS

PLASMA CHEMISTRY

Streamline thermal plasma chemistry, reviewing diagnostic techniques and product oriented research

14 p2545 A70-30905

PLASMA CLOUDS

Needle-shaped filament artificial ion cloud drift and diffusion in F1 region plasma in presence of neutral wind and uniform electric field

01 p0070 A70-10401

Thermal and dynamical evolution of gas clouds in transparent and opaque stages by comparing rates of cooling, heating, contraction and expansion

05 p0907 A70-16041

Large scale artificial plasma cloud experiments for magnetosphere, solar wind and cometary physics, discussing Ba ion and ice clouds released by satellites

[AIAA PAPER 70-33] 06 p1145 A70-18183

Atmospheric thermodynamic properties determined from radar studies of detonation waves from cesium-seeded explosive bursts in lower ionosphere

06 p1012 A70-18542

Expansion and deceleration of rocket-released artificial ion cloud in terms of snowplow expansion model and drag deceleration

07 p1271 A70-20159

Magnetic funneling model proposed for accretion of matter onto neutron star to study X ray production during motion through interstellar cloud

10 p1931 A70-23902

Monograph on ambipolar diffusion and motion instability of satellite produced artificial barium ion clouds in ionosphere and magnetosphere

11 p2048 A70-26825

Plasma experiments in space including electric fields measurement, collisionless plasma studies and artificial Ba cloud generation

12 p2214 A70-26868

Barium ionic cloud formation under action of sunlight and expansion in terrestrial magnetic field using plasma model

12 p2214 A70-26892

Electromagnetic wave scattering from atmospheric ellipsoidal plasma formations, using arbitrary permittivity and magnetic permeability tensors

13 p2366 A70-29376

Signal decoder for barium USA Germany /BUG/ project command reception system, discussing Ba ion cloud propagation and expansion along geomagnetic field

13 p2367 A70-29557

Solar radar echo characteristics, discussing coronal compressional waves and refraction by plasma clouds and moving plasma irregularities

13 p2370 A70-29852

Auroral and polar cap ionospheric electric fields and tensor conductivity elements using ion clouds data of Ba release experiment

13 p2402 A70-30080

Many body correlation and conditional probability functions of plasma shield clouds surrounding test particles

14 p2623 A70-31034

Spherical ionized cloud movement in ionosphere uniform anisotropic plasma as function of electric field applied to rocket released ion clouds

15 p2726 A70-31867

Barium ion clouds striation formation above E layer ascribed to LF gradient drift instability

15 p2727 A70-31908

Striation formation in artificial ion clouds aligned with local geomagnetic fields, considering visual indi-

cation of ionospheric electric field transferal along magnetic field

19 p3415 A70-38387

Moving type 4 solar burst on 1 March 1969 observed at 80 MHz, discussing plasma cloud associated with prominence

21 p3880 A70-40967

Solar wind free electron number density measurement by Pioneer 6 spacecraft after solar proton flare, constructing plasma cloud models

21 p3881 A70-41079

PLASMA COMPOSITION

Cs seeding effect on bound-free UV photoabsorption of Cs-H plasma at constant electron density and energies below H ionization

02 p0343 A70-11904

Stellar configurations of cold static neutral plasma consisting of nuclei and degenerate electron gas, calculating integral parameters by Newton gravitation theory

07 p1376 A70-18912

Cesium plasma composition as equilibrium mixture of ideal gases assuming chemical equilibrium attainable by specified reactions

07 p1349 A70-19660

Steady state spherically symmetrical ejection of multicomponent plasma from sun determined with hydrogen approximation, considering ion composition

07 p1391 A70-20418

Solar wind properties and helium abundance determined from satellite-borne electrostatic analyzers

09 p1746 A70-23482

Dynamics of multicomponent plasma involving charged or neutral gases with transport phenomena for case of no magnetic field

09 p1738 A70-23580

Helicon wave dispersion in cold multicomponent plasma of n-type Si and Ge semiconductors in linear hydrodynamic approximation

10 p1928 A70-24832

Stationary and nonstationary nonlinear waves propagation in multicomponent collisionless plasma, considering dispersion relations for acoustic oscillations

10 p1844 A70-25166

Gas mixture plasma ionized and heated by discharge and ejected into vacuum, considering nonequilibrium ionization calculation with gap between electron and heavy particle temperatures

11 p2092 A70-26732

Reciprocity principle for biased and two component compressible plasmas

12 p2282 A70-27971

Cesium plasma composition as equilibrium mixture of ideal gases, assuming chemical equilibrium attainable by specified reactions

15 p2781 A70-32697

Photoresonant cesium plasma ionization, discussing pumping spectra, electron gas, molecular-atomic ion ratio and dynamics

19 p3474 A70-37440

Equilibrium compositions of helium-nitrogen, argon-nitrogen and xenon-nitrogen plasmas at atmospheric pressure between 5000 and 35,000 K

19 p3552 A70-37831

Electron-neutral interaction parameters for Ohm law coefficients in multicomponent nonisothermal plasmas tabulated as function of electron temperature

22 p4081 A70-43015

Collision integral model for multicomponent mixture, investigating partially ionized plasma longitudinal vibrations

22 p4083 A70-43382

PLASMA CONDUCTIVITY

Equilibrium state of high current discharge in low conductivity plasmas, obtaining light sources at low temperatures

01 p0152 A70-10993

Nonequilibrium potassium seeded Ar plasma electrical conductivity at atmospheric pressure, noting current density role

02 p0347 A70-12232

HF electromagnetic field penetration of plasma with finite conductivity and Hall constant for containment of hot plasmas, formulating nonlinear electrodynamic problem

05 p0889 A70-16490

Electrical conductivity calculation for plasma in spatially inhomogeneous magnetic field using small-gyroradius approximation to kinetic equation

05 p0889 A70-16491

HF conductivity tensor of isotropic plasma, taking into account particle correlations describing weakly Langmuir turbulent plasma

05 p0889 A70-16532

Ohms law of electromagnetohydrodynamics derived on basis of Lorentz hydrodynamic plasma model, considering plasma conductivity

05 p0890 A70-16852

Electrical conductivity of collisionless magnetoplasma in weakly turbulent magnetic field, using quasi-linear approach for diffusion equation for distribution function describing test particles

07 p1352 A70-19987

Induced current density of fully ionized stationary plasma in externally applied HF electric field, discussing frequency range of fluctuations

07 p1352 A70-19988

Electrical conductivity of fully ionized plasma in strong magnetic field computed as application of method for plasma transport coefficients

07 p1354 A70-20246

Plasma finite DC resistivity quantum theory, considering electron-molecule collisions energy absorption, noise generation, etc

08 p1551 A70-21099

Axisymmetric instabilities by Z-pinch and reverse axial current discharges in plasmas of arbitrary conductivity

08 p1554 A70-21810

Feedback stabilization of surface instabilities of highly conducting plasma, discussing application to linear pinch with uniform axial static magnetic field

09 p1734 A70-22272

Plasma conductivity measuring device using phenomenon of change of coil induction in electromagnetic field

09 p1737 A70-23380

Small loop impedance in magnetoplasma determined for magnetic field normal and parallel to loop plane

09 p1738 A70-23671

MGD model of plasma with dissipation due to finite electrical conductivity described by differential equations

10 p1922 A70-24144

Nonequilibrium plasma MHD generator critical pressures determination, applying electron energy balance equation and relation between plasma conductivity and Hall parameters

10 p1809 A70-25142

Thermal conductivity of argon, nitrogen and air plasmas at atmospheric pressure and 6500-16500 K range, discussing electric arc source

11 p2148 A70-25760

Cylindrical shock wave two dimensional propagation in conducting plasma in magnetic field, assuming isentropic flow along streamline

11 p2091 A70-26174

Electromagnetic inductive shock tube design and wave velocity, electron temperature and plasma conductivity measurements

12 p2206 A70-27400

Impurities and electrothermal instabilities effect on conductivity of two temperature nonequilibrium plasma

12 p2281 A70-27846

RF method for recording temperature dependence of electrical conductivity of solids, liquids and multicomponent plasma mixtures

13 p2459 A70-28583

Electromagnetic shock tube demonstrations of electrode spark breakdown, strong shock behavior, plasma conductivity and hypersonic shock flow over blunt body

13 p2404 A70-28623

Electrical conductivity of partially ionized gas in magnetic field by Frost mixture rules extension

17 p3141 A70-34985

Microwave diagnostics of plasma temperature and conductivity in streaming nitrogen arc with skin effect under atmospheric pressure

19 p3476 A70-37554

Equilibrium homogeneous steady state highly ionized non-Debye plasma for investigation of electrical conductivity, viscosity, dynamic properties, etc

19 p3480 A70-38183

Inhomogeneous nonequilibrium plasma stratification in magnetic field, investigating electrical conductivity

19 p3481 A70-38191

MHD instability of homogeneous inviscid plasma with finite electrical conductivity and anisotropic pressure, obtaining dispersion equation for model

20 p3677 A70-39048

Nonequilibrium plasma stability, conductivity and Hall parameter influenced by current flow parallel to magnetic field, discussing Ar-Cs and He-Cs plasma data

20 p3682 A70-40019

Coaxial three coil probe measuring local electrical conductivity and velocity in plasma streams, discussing operations in electrolytes and axisymmetric plasma stream

20 p3684 A70-40259

Electromagnetic wave propagation in colloidal plasmas analyzed by kinetic approach, obtaining expressions for current density, DC and microwave conductivities, etc

20 p3685 A70-40502

MHD generators nonequilibrium ionization improvement by blowing low work function particles into cold working gas to obtain required conductivity

21 p3855 A70-40794

Collisionless magnetospheric plasma turbulent conductivities for weak and strong electric fields parallel to magnetic field

22 p4016 A70-42787

Geomagnetic perturbation effects on conduction along field lines and short period fluctuations associated with plasma turbulization in magnetosphere

23 p4189 A70-44065

Scaling laws for turbulent plasma anomalous conductivity dependent on electrostatic fluctuation spectrum

23 p4227 A70-44796

Semiconductors with bipolar conductivity under electron-hole scattering, calculating plasma pinch effect on I-V characteristics

24 p4390 A70-45659

PLASMA CONFINEMENT

U PLASMA CONTROL

PLASMA CONTROL

Plasma accumulation between mixed field accelerator and pulsed magnetic mirror, noting duration and stability

02 p0346 A70-12104

Magnetic flux trapping experiment with Al conductor, showing decay time constant connection with sunspot theory

02 p0299 A70-12393

Ceramic plasma containers construction by soldered seal technique for ion lasers, noting moly- manganese process

02 p0314 A70-12746

Steady state deuterium-tritium fusion reactor approximate parameters prediction possibility based on interim assumptions of plasma confinement, model, etc

02 p0349 A70-12755

Tokamak-type magnetic configurations application to thermonuclear reactor, discussing equilibrium and stability parameters minimum values, operating pattern and heating method

02 p0349 A70-12756

Saturation of linear or nonlinearly/explosively/ unstable HF electrostatic flute modes in mirror confined plasma

03 p0529 A70-13005

Cs plasma research, discussing Q-machines, plasma confinement, magnetic field experiments, LF and HF wave propagation, etc

03 p0533 A70-14015

Plasma nature, properties and applications, discussing echoes, shocks, phase mixing and hot plasma containment

05 p0887 A70-16130

Quasi-linear mode coupling in confined hot-ion Penning discharge plasma, discussing externally imposed excitation and internally generated oscillations

05 p0888 A70-16166

HF electromagnetic field penetration of plasma with finite conductivity and Hall constant for containment of hot plasmas, formulating nonlinear electrodynamic problem

05 p0889 A70-16490

Plasma resonances, considering unbounded and bounded uniform and nonuniform plasmas and nonlinear effects

06 p1116 A70-17365

Remote feedback suppression method for plasma collisional drift instability using modulated microwave irradiation, describing linear heating mechanism theory

06 p1122 A70-18014

Soviet collection of papers on magnetic traps covering chamber walls effect on plasma heating, plasma in mirror trap and self sustained fusions

07 p1350 A70-19844

Magnetic trap chamber walls adverse effect on plasma heating produced by electron beam injected at low hydrogen pressures

07 p1350 A70-19845

Electron clouds injection and containment by magnetic field in toroidal vacuum chamber, studying causes of cloud instability

07 p1353 A70-19994

Plasma density measurement by LC tank circuit with plasma contained in induction coil, deriving expressions for circuit resistance and resonant frequency

08 p1550 A70-20846

Plasma sheath in quadrupole and hexapole geometries, investigating magnetic field variation, particle density and electrostatic potential in transition layer

08 p1552 A70-21530

Plasma containment by spherical multipole magnetic trap, discussing injection and trapping of gun-produced plasma

08 p1553 A70-21609

Guiding center plasma theory, obtaining stability criteria from charged particle motion equations considerations

10 p1926 A70-25250

Unsteady plasma oscillation stabilization by envelope controller with spatial and temporal dispersion

11 p2087 A70-25604

Plasma energy confinement time as function of discharge parameters for plasma thermal insulation in Tokamak-3

11 p2088 A70-25713

Electrostatic wave propagation and growth rate in electron beam inhomogeneous plasma confined by magnetic field 11 p2091 A70-26460

Plasma equilibrium in stellarator type magnetic trap /vintatron/ with magnetic configuration created by strong longitudinal field 12 p2277 A70-27313

Feedback stabilization and mode coupling of ionization waves in positive column discharges, noting dynamic stabilization of unstable bounded plasma systems 12 p2280 A70-27787

Stable auroral red /SAR/ arc alignment-movement relationship, suggesting dominant local time control 13 p2397 A70-29193

Collisionless plasma confinement using spatially uniform time varying magnetic field 14 p2624 A70-31100

Plasma containment in adiabatic magnetic traps, discussing particles, Coulomb collisions, instabilities, cyclotron resonance masers, Van Allen belts, etc 16 p2958 A70-33232

Surface oscillations energy and attenuation in damped spectral region of semibounded degenerate electron plasma 18 p3293 A70-36143

Magnetic mirror confined plasmas, solving Fokker-Planck equation 18 p3296 A70-36795

Energy loss of fast protons in cold Li plasma confined by magnetic field, using precession around axis to develop large interaction length 19 p3474 A70-37364

Laser-produced plasmas production and containment, studying expansion in uniform magnetic field and charge quantity as power density function 19 p3444 A70-37535

Conical plasma gun with Z pinching restrained by axial magnetic field, describing operating characteristics 19 p3480 A70-38018

Nonuniform electron plasma trapped in one dimensional potential well, determining linear oscillations by normal mode approach 19 p3482 A70-38944

Pair correlations effect in equilibrium and nonequilibrium theory, taking Coulomb collisions into account for ionized plasmas confined to half space by reflecting boundary 20 p3679 A70-39662

Transport coefficients of inhomogeneous magnetized bounded and unbounded plasmas based on quasi-linear approximation 21 p3857 A70-41385

Nuclear fusion reactor spacecraft propulsion system using ion rocket with charged deuterium nuclei fuel, emphasizing nuclear plasma confinement problem 21 p3867 A70-41498

Nonequilibrium flow adjacent to cooling tube wall confining cascade arc plasma electrical discharge 21 p3805 A70-41763

Dynamic potentials equations of guided electromagnetic wave propagating in laterally bounded plasma along magnetic field axis 21 p3860 A70-42005

Plasma injection and confinement in closed quadrupole magnetic trap 22 p4083 A70-43388

High density plasmas production and containment in theta pinch device, discussing shock and Joule heating 23 p4225 A70-44186

Critical Hall parameter for linear development of MHD electrothermal instability in bounded nonequilibrium plasma 23 p4227 A70-44555

Electron runaway suppression in fully ionized Lorentz plasma by crossed magnetic and electric fields 24 p4382 A70-45105

Plasma heated by cyclotron resonance using waveguide method, considering properties, confinement conditions and instabilities 24 p4385 A70-45453

Plasma confinement in min-B configuration of linear multiple with mirrors, attaining additional stabilization via linear rods carrying unidirectional current 24 p4386 A70-45612

PLASMA CYLINDERS

Oblique unsteady shock wave structure propagating at large Mach numbers in plasma cylinder under steady magnetic field, showing particle velocity profile discontinuity 01 p0064 A70-10999

Calorimetric measurement of electron temperature in collisionless shock wave propagating in plasma column, discussing role of H beta line Stark broadening 01 p0153 A70-11589

Cylindrical axial plasma flow fields velocity radial dependence measurement by double-wedge spectroscopy using Abel unfolding of Doppler shifts 02 p0349 A70-12657

Measurement techniques for determining density and temperature distributions along radius of plasma cylinder by electron cyclotron resonance, microwave refraction and acoustic resonance 02 p0349 A70-12758

Electric potential fluctuations beyond long collisionless plasma cylinder in uniform magnetic field, noting thermal noise intensity 03 p0530 A70-13086

Electromagnetic wave propagation through stratified positive plasma column in waveguide, noting stratification travel effects on wave amplitude and phase shift 03 p0443 A70-13096

Surface wave attenuation in homogeneous plasma cylinder caused by resonance in transition layer between plasma and vacuum 03 p0447 A70-13286

Photon absorption and emissivity of nonequilibrium cylindrical plasma in Doppler broadened lines and hemisphere approximation 04 p0724 A70-14411

Magnetized resonantly sustained HF plasma column wave properties, obtaining above-critical density as function of static magnetic induction 04 p0728 A70-14999

Electrostatic oscillations in cylindrical column of laboratory plasmas excited by electromagnetic waves, investigating resonances by cold plasma theory 06 p1116 A70-17368

Inhomogeneous plasma cylinder skin effect, surface impedance, radiation transport and mean noise temperature 07 p1347 A70-19107

Ion acceleration in spherical and cylindrical plasma layers formed by spherical plasmoid expansion in plasma cylinders 07 p1384 A70-19414

Plane electromagnetic wave scattering by perfectly conducting cylinder coated with moving dielectric or plasma sheath, using relativity theory, Lorentz transformations, etc 08 p1551 A70-21251

Free plasma column discharge in HF field in high pressure deuterium atmosphere, discussing high plasma temperature inside column and reliable thermonuclear reaction achievement 08 p1551 A70-21417

Convective-current instability in finite length plasma column, analyzing spectrum of unstable harmonics 08 p1554 A70-21802

Microwave-induced ionization oscillations in resonant plasma column excited by low pressure mercury DC discharge 10 p1922 A70-23988

Nonlinear wave interactions in quiescent plasma column with external disturbance creating broadened frequency spectrum and weakly turbulent plasma 10 p1922 A70-24146

Fast magnetoacoustic wave propagation in cylindrical plasma column with constant current density, using geometric optics 10 p1923 A70-24229

Plasma column dynamic stability breakdown in quadrupole HF magnetic field in terms of violating stability criterion for long wave deformation 10 p1926 A70-25109

Hydromagnetic flute and surface wave instabilities of current-carrying plasma filament in strong longitudinal field, showing radial density stabilization 10 p1926 A70-25117

Hall effect influence on HF traveling magnetic field penetration into solid cylinder plasma device compared to magnetically contained plasma 11 p2088 A70-25712

Tonks-Dattner resonances in plasma columns, considering viscosity effect on radial oscillations in nonuniform plasmas 12 p2281 A70-27792

Finite amplitude stability of plasma column in weakly ionized gases and in semiconductor plasmas in longitudinal magnetic field 13 p2458 A70-28566

Electromagnetic waves extraordinary mode scattering by small diameter nonuniform plasma column in magnetic field 13 p2460 A70-28644

Energy loss radial dependence due to K resonance radiation for infinitely long plasma cylinder, using approximation method for integrals 13 p2461 A70-28731

Electron temperature and concentration determined from longitudinal electron cyclotron harmonic waves in finite plasma column 13 p2467 A70-29916

Coupled temperature and electric potential distribution in finite rotational symmetric hydrogen arc column in axial magnetic field 14 p2621 A70-30656

Plasma cylinder surface drive current buildup, using theta pinch two dimensional model 14 p2624 A70-31049

Incident microwave signal in Tonks-Dattner resonance coupled to discrete LF modes in plasma column 15 p2778 A70-31756

Glass tube surrounded nonuniform plasma column interaction with TM microwave field of cylindrical cavity for electron density measurements 15 p2780 A70-32347

Resonance excitation of high amplitude waves in plasma cylinder by HF azimuthal axially periodic current flowing through coil encircling plasma 16 p2957 A70-33194

Collision dominated plasma column radial structure including ambipolar diffusion region obtained from constant mean free time and path approximate formulas 16 p2959 A70-34311

Multiple narrow beam antenna system with plasma column and electromagnetic wave ring source, discussing radiation pattern and electronic scannability 18 p3294 A70-36346

Ion density and electron temperature variations as function of maximum electric field density in independently excited plasma column striations 19 p3475 A70-37552

Helium plasma ionization rate in positive column with DC discharge, considering gas pressure, electron density, electric field strength and plasma radius 19 p3476 A70-37559

Stationary DC discharge positive column in helium, determining production balance and loss of charge carriers 19 p3476 A70-37560

Plane EM wave diffraction in cylindrical plasma-electron beam system 19 p3378 A70-37740

Hydromagnetic flute and surface waves instabilities of current-carrying plasma filament in strong longitudinal field, showing radial density stabilization 20 p3685 A70-40510

Slow and fast ionization waves in inert gas or molecular gas plasma columns, describing striation formation in neon discharge by hydrodynamic equations 22 p4079 A70-42371

Gas discharge positive column finite length effect on wave dispersion and instability, indicating critical magnetic field 22 p4079 A70-42374

Ion and electron ambipolar velocity distribution near plasma sheath boundary in collisional positive column 22 p4080 A70-42542

Magnetosonic resonance excitation in waveguide winding wrapped around plasma cylinder 22 p4082 A70-43380

Supersonic convective electric arcs with magnetic stabilization in sulfur hexafluoride, examining aerodynamic drag and plasma column slanting 23 p4227 A70-44554

Dipolar resonant scattering of H-polarized plane waves by axially magnetized plasma column with perfectly conducting core 23 p4228 A70-44977

German monograph on thermal and nonthermal phenomena in quasi-stationary convectionless plasma arc column, using 13-moment approximation for Boltzmann equation 24 p4382 A70-45089

Quasi-homogeneous approximation validity for electron velocity distribution function disturbance in gas plasma column ionization waves discharge involving high currents 24 p4386 A70-45794

Plasma positive column impedance in low current noble gas discharges, using Boltzmann equation for electrons 24 p4387 A70-45796

PLASMA DECAY

Wave-wave coupling of two HF electromagnetic waves launched into warm plasma across constant confining magnetic field, using Maxwell-Vlasov equations for electrons 02 p0349 A70-12757

Maximum plasma decay rate in heterogeneous medium determined from deionization process in rarefied gases 03 p0536 A70-14369

Upper cesium levels population inversion during cesium discharge plasma decay 08 p1550 A70-20848

Electron temperature and concentration in decaying He and Ar plasmas with cesium vapor additions 11 p2092 A70-26733

Resonant and nonresonant coupling between two coherent electron plasma waves propagating in opposite directions, considering parametric decay 12 p2279 A70-27780

Plasmon decay by neutrinos emission in strong magnetic field, examining parallel and perpendicular propagation 18 p3305 A70-35936

HF oscillations excitation in decaying plasma-electron beam system, noting Coulomb collisions and nonlinear effects role

18 p3294 A70-36145

Fully ionized magnetized rotating plasma interaction with neutral gas blanket, discussing plasma decay and velocity field

19 p3481 A70-38489

PLASMA DENSITY

Plasma density and electroacoustic resonance effects on coupled cylindrical antennas self and mutual impedances measured in Hg-arc discharge

01 p0050 A70-10461

Stable geomagnetic pulsations related to plasma density shock position in magnetosheath and to magnitude of diurnal variations

01 p0082 A70-11508

Plasma electron temperature and density in Tokamak T3 toroidal discharge measured by Thomson scattering of laser light

02 p0346 A70-12199

Time resolved cavity perturbation technique to measure high plasma density in magnetic mirror compression experiment, obtaining total electron number

02 p0347 A70-12236

Recombination instabilities in plasmas and gases undergoing density changes through volumetric processes, solving linearized and nonlinear cases by simplified fluid mechanics equations

02 p0348 A70-12238

Measurement techniques for determining density and temperature distributions along radius of plasma cylinder by electron cyclotron resonance, microwave refraction and acoustic resonance

02 p0349 A70-12758

Nonisothermal plasma perturbed by supersonic body, studying plasma rarefaction and condensation cones, particle density, etc. in wake

03 p0407 A70-13413

Accumulated plasma density and lifetime measurement of trapped ions between accelerator and periodic magnetic mirror, showing limitation by collisions and charge exchange

03 p0532 A70-13683

Plasma jet temperature and density determination from intensity ratio of H beta line and continuous spectrum

04 p0725 A70-14535

Electron plasma frequency exchange corrections temperature dependence at high densities, using equation of motion for coupled particle-hole pair operators

04 p0727 A70-14714

High density nonlinear and linear growth rates of flute modes instabilities in cold plasma coexisting with low density of energetic electrons

04 p0728 A70-14998

Magnetized resonantly sustained HF plasma column wave properties, obtaining above-critical density as function of static magnetic induction

04 p0728 A70-14999

Plasma camera photographs of K plasma spatial distribution with electric fields and density gradients perpendicular to magnetic field, observing rotating irregularities around edge

04 p0728 A70-15005

Nonequilibrium Cs plasma electron density, temperature and sustaining field using theoretical analysis and probe measurements

05 p0887 A70-16108

Stably trapped magnetospheric plasma distribution determined from Pi2 micropulsations and auroral electrojet index AE

05 p0839 A70-16285

Coupling between LF oscillations and third harmonic frequency resonances of bounded plasma capacitor system, discussing density profile variation

05 p0890 A70-16654

Transmission and emission of radiation from dense inhomogeneous finite laboratory plasma column in magnetic field with interpretation by cold plasma theory

06 p1116 A70-17367

Impedance and radiation pattern of quarter wave monopole and half wave dipole antennas in isotropic plasma, considering plasma density role

06 p1117 A70-17372

Pulsed dense argon plasma arcs radiation spectra in visible and UV regions as function of current and pressure

07 p1349 A70-19652

Plasma properties produced in mirror magnetic trap by electron beam determined during transition from hot electron dense plasma into cold electron low density plasma

07 p1350 A70-19846

Emission containment and working temperature reduction possibility in thermonuclear reactor by increasing plasma densities and introducing large atomic number contaminants

07 p1350 A70-19847

Self sustained fusion reaction in dense deuterium-tritium plasma, considering large atomic number contaminants optimal concentration calculations

07 p1351 A70-19848

Relaxation time calculation for ground and excited states of H atoms and H-like ions in optically thin and thick plasmas, considering electron density role

07 p1353 A70-20058

Plasma concentration in nondipole magnetosphere model from Pc 5 pulsations periods for high geomagnetic latitudes, noting solar winds effect

07 p1277 A70-20443

Plasma density measurement by LC tank circuit with plasma contained in induction coil, deriving expressions for circuit resistance and resonant frequency

08 p1550 A70-20846

Laser interferometric technique involving use of unstable external resonator to facilitate electron density measurements in presence of transverse plasma density gradients

08 p1499 A70-21693

Laser radiation absorption in xenon plasma, noting dependence on intensity due to atoms ionization

08 p1554 A70-21803

Plasma electron density determination by number of extreme resolved line, considering broadening action by Doppler effect for Balmer, Lyman and Paschen series

09 p1734 A70-22731

Stark broadening of singly ionized nitrogen lines measured in dense high temperature plasma behind reflected shock wave in T tube

09 p1731 A70-22776

Plasma electron density errors in measurement by microwave interferometers, noting effects of inaccurate phase shift determination

09 p1738 A70-23634

Geomagnetic pulsations /pc 4/ characteristics from analyzing magnetosphere model yielding plasma densities consistent with experimental data

10 p1875 A70-24483

Stationary low pressure plasma enclosed in emitting surfaces calculated for spatial charge density distribution

10 p1923 A70-24539

Plasma cumulation, with and without shell under concentric pressure impulse using perfect gas theory, estimating critical parameters

10 p1926 A70-25322

Wind shear caused ionospheric E region irregularities investigated by horizontal plasma density gradients determination

11 p2045 A70-25652

Seeded dense plasma-electrode system behavior, studying effect of adsorption and emission from boundary surfaces

11 p2090 A70-25952

Plasma density and velocity required for simulating solar wind flow over magnetosphere (bow shock) in plasma wind tunnel

11 p2032 A70-26372

Homogeneous plasma turbulence growth limits, determining bounds on density and electromagnetic field nonlinear fluctuations in thermodynamic terms

11 p2096 A70-26767

Optimal conditions for obtaining dense low temperature cesium plasma in shock tube with heating calculated by Debye theory

12 p2278 A70-27327

Collisional drift-wave turbulence in Li Q-machine plasma far unstable regime, discussing power spectra variations of density fluctuations

12 p2280 A70-27784

Density gradient drift waves stabilization in collisionless plasma by stellarator type windings, observing oscillations amplitude reduction in shear magnetic field

12 p2280 A70-27785

Coulomb interaction effect on diffusion of plasma produced by contact ionization in magnetic field, obtaining density profiles by iterative procedure

12 p2280 A70-27789

Magnetospheric plasma density effects on impedance of VLF electric field spacecraft antenna

13 p2397 A70-29186

Solar wind turbulence, demonstrating radio source interplanetary scintillation consistent with plasma density correlation

14 p2642 A70-30888

Adiabatic relation between initial plasma density perturbations and radiation temperature fluctuations during galaxies formation, discussing relic radiation fluctuations

14 p2632 A70-31286

Ultrahigh speed camera with high optical resolution for dense plasma diagnosis

14 p2590 A70-31407

Plasma concentration measurement in coaxial accelerator, using gas laser and multiple wave interferometer in vacuum chamber

15 p2781 A70-32858

Probe measurements in Cs plasma formed by contact ionization with hot wire for density, electron temperature and space potential

16 p2958 A70-33624

Collisions effects on ion collection by Langmuir probes, determining plasma density

17 p3139 A70-34494

Langmuir probe position-dependent ion flow effects on plasma density measurement in low pressure mercury discharge

17 p3083 A70-34995

Magnetized plasma electron density measurement by laser self heterodyne

17 p3141 A70-34996

Ar plasma generation by focused Q switched ruby laser beam, measuring density and temperature by electro-optical spectroscopy

17 p3107 A70-35111

Type 2 irregularities in equatorial electrojet associated with plasma density vertical gradients

18 p3244 A70-36017

Miniature multigrid probes for measuring energy spectra of charged particles and absolute plasma densities, comparing results to microwave measurements

18 p3294 A70-36150

Magnetospheric plasma concentration from geomagnetic pulsations periods

19 p3409 A70-37320

Laser radiation and solid target interaction, calculating temperature and plasma density as function of intensity

19 p3447 A70-38166

Dense plasma thermodynamic and electromagnetic properties, discussing correlation energy

19 p3480 A70-38181

Steady electric field effect on dense plasma cyclotron instability

20 p3678 A70-39595

Spectral lines self rotation effects on plasma temperature and density measurement in MHD duct boundary layer

20 p3678 A70-39632

Gaseous neon plasma positive column electrons density and drift velocities measurements by Langmuir probe technique

20 p3683 A70-40163

Solar corona current free magnetic field distribution relationship to plasma density structure

20 p3712 A70-40415

Electron temperature measurements in flowing high density plasma by cooled Langmuir probe, considering probe temperature variations effects in boundary layer

21 p3854 A70-40557

Nonrelativistic electron bremsstrahlung in dense plasma with strong magnetic field

21 p3855 A70-40721

Extended homogeneous stationary field-free spherical plasma source, including radial density measurement with Langmuir probe in argon

21 p3805 A70-41463

Optimal conditions for obtaining dense low temperature cesium plasma in shock tube with heating calculated by Debye theory

21 p3860 A70-42068

Low density plasma in region of orbital-motion-limited /OML/ currents in presence of cylindrical Langmuir probes

22 p4078 A70-42360

Superimposed external DC magnetic field effect on electrodeless HF plasma density, discussing electron cyclotron waves resonance excitation and plasma electron energy gain

22 p4079 A70-42364

Neutron-electron collision damping and displacing of space echo in plasmas, indicating use for density measurement

22 p4082 A70-43244

Magnetoplasma density modulation from LF and amplitude magnetic perturbations, using collisionless Boltzmann transport equation

22 p4082 A70-43255

Solar X-ray data from rocket and satellites, discussing hot dense plasmas and correlation with H alpha flares, calcium plages and microwave emission

22 p4096 A70-43300

Solar wind flux correlation with earth EM field pulsations, noting flare-generated shock front effects on magnetosphere

23 p4236 A70-44051

Meteor trails isotropic diffusion in presence of moving point source of ionization with variable intensity, calculating plasma density on and near trajectory

23 p4240 A70-44084

High density plasmas production and containment in theta pinch device, discussing shock and Joule heating

23 p4225 A70-44186

Low beta surface ionized rotating streaming plasma column, determining low magnetic field effects on density and stability

23 p4229 A70-44988

Quasi-ambipolar diffusion in arc discharges in magnetic field, calculating ions and electrons density distributions between anode and cathode sheaths

24 p4384 A70-45148

Temperature, densities and electric field strength of cascaded arcs burning in He under normal pressure

24 p4384 A70-45425

Plasma concentration and heavy particle-electron collision frequency in open cylindrical cutoff resonator

tor based on frequency shift and passband broadening data 24 p4385 A70-45455

Density correlation measurements for diffusion coefficient in magnetized He plasma 24 p4386 A70-45614

PLASMA DIAGNOSTICS

Plasma concentration diagnostics in magnetosphere based on hydromagnetic whistlers/pearls/dispersion 01 p0084 A70-11554

Calorimetric measurement of electron temperature in collisionless shock wave propagating in plasma column, discussing role of H beta line Stark broadening 01 p0153 A70-11589

Plasma velocity, electron temperature and density and ion density determined by two mutually perpendicular probes 03 p0529 A70-12940

Supersonic plasma jets studied spectroscopically, determining atomic levels populations, population inversion conditions, electron temperature and concentration distributions, etc 03 p0531 A70-13254

Plasma optical transparency criterion, estimating nonequilibrium plasma layer optical density limit 03 p0531 A70-13255

Earth magnetosphere low energy plasma measurements via McIlwain magnetic shell parameter, showing dependence on geomagnetic disturbances 03 p0557 A70-13284

Nonequilibrium cesium plasma of low voltage arc discharge, measuring electron temperature and distribution function and diffuse-series excited level populations 03 p0532 A70-13740

Electron temperature of hydrogen-oxygen flame plasma obtained by floating probe method compared to spectroscopic method results 03 p0608 A70-14380

Microwave spherical resonator and reentrant cavity as diagnostic tools to obtain discrete point data along plasma column compared with cylindrical cavity 04 p0696 A70-15650

Charge carriers recombination and diffusion coefficients for confined gas discharge plasma obtained from data on radial particle distribution profile 05 p0888 A70-16330

Slide rule for calculating electron number density, Debye length and Debye sphere particles in plasma parameters determination 05 p0852 A70-16847

Diagnostic methods for field-free plasmas with medium dispersed optical-spectrographic and source monitoring equipment 06 p1063 A70-17728

Spectroscopic quantitative diagnostics of high density plasma sources encountered in aerospace applications and chemistry 06 p1063 A70-17729

Uranium plasma design and characteristics, measuring emission and absorption coefficients as function of temperature and pressure [AIAA PAPER 70-43] 06 p1122 A70-18084

Magnetosphere and interplanetary space diagnostics by micropulsations analysis, discussing geomagnetic cavity boundary, cold plasma density, energetic particles, etc 07 p1264 A70-19191

Circumsolar plasma structural inhomogeneity origin 07 p1384 A70-19418

Plasmatron generated rarefied helium plasma parameters in external magnetic field using hot-wire anemometer Langmuir probe 07 p1349 A70-19653

Plasma properties produced in mirror magnetic trap by electron beam determined during transition from hot electron dense plasma into cold electron low density plasma 07 p1350 A70-19846

Intense quasi-steady He plasma discharge stability in magnetic field measured by Langmuir and optical techniques 07 p1354 A70-20321

Solar wind structural characteristics determination from cosmic ray variations in interplanetary medium, considering interplanetary magnetic field structure and spatial orientation 07 p1372 A70-20337

Time dependent electrostatic probe theory relating measurements to internal properties of plasma, calculating free stream ion density from collected electric charge 07 p1289 A70-20466

Rarefied plasma flow past bodies, considering determination of aerodynamic coefficients, charged states, electric and magnetic fields and plasma parameters 08 p1432 A70-21087

Thermal sheaths effect on cooled probes for stationary and flowing plasmas measurements at high pressure 08 p1497 A70-21528

Pulse propagating in unstable plasma, determining characteristics by asymptotic expansion applied to Vlasov-Maxwell equations 09 p1734 A70-22684

Diagnostics of inhomogeneous plane stratified plasma with arbitrary electron concentration distribution, solving differential equation for electromagnetic wave propagation normal to plasma layers 09 p1735 A70-23160

Transient partially ionized plasmas observation by two wavelength holographic interferometry, describing electron density measurements 09 p1736 A70-23186

Laser-produced Al plasmas linear and nonlinear behavior, using framing camera and energy absorption measurements to study outermost ion energy increase and luminous front expansion 09 p1736 A70-23187

Electrostatic cylindrical probes applicability to hypersonic flow field diagnostics 11 p2086 A70-25684

Plasma transport properties at temperatures up to 15000 K, considering electrical and thermal conductivity, radiation source strength and viscosity 11 p2089 A70-25759

Microwave power absorption in plasma investigated by transmission cavity excited in TE mode, determining electron density and collision frequency 11 p2089 A70-25841

Modified laser Michelson interferometer for probing highly transient plasmas occurring behind incident shock waves in shock tubes 11 p2052 A70-26369

Inert gas plasma jets diagnostics in accelerator by spectroscopy, determining flow velocities, excitation and gas temperatures 11 p2093 A70-26744

Spectroscopic diagnostics of erosion plasma jets from cylindrical pulsed plasma generator operating in vacuum 11 p2093 A70-26745

Radar interferometry as diagnostic method for remote probing of turbulent plasma 11 p2096 A70-26766

Interplanetary and magnetospheric plasma structures experiments and theory 12 p2298 A70-27060

Laser light investigations of atoms, molecules and plasmas, considering Raman molecular spectroscopy, acoustic phonons interactions and plasma diagnostics by light scattering 12 p2245 A70-27063

Scanning Fabry-Perot interferometer for plasma diagnostics, determining kinetic temperatures 12 p2231 A70-27215

Electron concentration measurement range expansion in plasma by laser interferometer with optical signal phase modulation 12 p2278 A70-27328

Portable low cost shearing interferometer for plasma and flow analysis and instruction aid 12 p2235 A70-27754

Tuned laser radiation to diagnose and enhance local conditions in alkali metal plasma 12 p2281 A70-27793

Plasma diagnostics by high sensitivity holographic interferometry 12 p2235 A70-27794

SERT 2 mercury vapor fed hollow cathode operated in bell jar, determining volt-ampere characteristics and flow rates for plasma diagnostics [AIAA PAPER 69-258] 13 p2473 A70-28515

Nonlinear Vlasov equation treatment by Fourier-Hermite expansion techniques for plasma problems 13 p2457 A70-28556

Mass transfer in electrostatically accelerated plasma, discussing recombination, ambipolar diffusion, electrode sputtering, charge exchange, electron capture and resistance forces effect on acceleration 13 p2461 A70-28862

Rotational and vibrational temperature effects on neutral gas and electron temperature and density in high pressure discharge plasma diagnostics 13 p2462 A70-29129

Magnetosheath plasma measurements by Pioneer 6 during outbound passage in dusk meridian, comparing results with various predictions 13 p2396 A70-29180

Stark broadening of neutral helium line in plasmas for electron densities measurements accuracy, comparing to H beta determined densities 13 p2456 A70-29225

Satellite plasma diagnostics for electric and magnetic fields and fine structure of collisionless shocks in solar wind plasma flows and interplanetary shocks 13 p2481 A70-30069

Wall stabilized arc source for spectroscopic measurements of isothermal plasma at various pressures 14 p2584 A70-30505

Plasma refractive index determination by propagation method allowing simultaneous electron concentration and density measurements by reflected damped wave 14 p2622 A70-30658

Langmuir probe characteristics and field response in low pressure nonstationary plasma diagnostics in weak magnetic field 14 p2623 A70-30785

Streaming thermal plasma chemistry, reviewing diagnostic techniques and product oriented research 14 p2545 A70-30905

Ultrahigh speed camera with high optical resolution for dense plasma diagnosis 14 p2590 A70-31407

Langmuir probe comparison to electron temperature probe measurements of ionospheric electron temperature during rocket flights 15 p2734 A70-31674

RF floating double probe for plasma ionization density and electron temperature 15 p2778 A70-31755

Discharged cleaned surface effect on accuracy and reliability of electron density and temperature measurements by Langmuir probes 15 p2778 A70-31765

Concentric polarization Fabry-Perot duochromator for spectral line displacement measurements applied to ion drifts in hollow cathode plasma 15 p2737 A70-32042

Probe measurements in Cs plasma formed by contact ionization with hot wire for density, electron temperature and space potential 16 p2958 A70-33624

Electrostatic probe measurements of vortex streets growth in plasmas bounded shear flow [AIAA PAPER 70-758] 17 p1319 A70-34493

Plasma diagnostic data from onboard Langmuir probes, reflectometers, antenna VSWR and beacon and telemetry attenuation for blunt body reentry flow field [AIAA PAPER 70-756] 17 p3008 A70-34495

Microwave diagnostic method for amplitude variations of electron density and collision frequency in weakly ionized plasma 17 p3140 A70-34871

Magnetized plasma electron density measurement by laser self heterodyne 17 p3141 A70-34996

Time dependent characteristics of dense argon plasma formed by pulsed lasers, measuring shock wave front velocity with streak camera 17 p3104 A70-35083

Excited atoms transfer mechanism in helium plasma, using He-Ne laser 17 p3106 A70-35102

Plasma opacity measurements using CW He-Ne and Ar lasers as light sources 17 p3106 A70-35107

Pulsed plasmas refractive index measurement by two-wavelength He-Ne laser interferometry, estimating effects of heavy atoms and neutral gas density 17 p3107 A70-35110

Low temperature plasma flow velocity measurements using transit-time technique and high speed filming 17 p3141 A70-35345

Electron concentration distribution over plasma discharge cross section, using interferometry 17 p3142 A70-35732

Vlasov high temperature plasmas numerical analysis, using Hamilton variational principle 18 p3296 A70-36793

Electron temperature and concentration profiles behind shock front from IR emission and absorption simultaneous measurement, applying method to xenon ionization and recombination processes 19 p3402 A70-37443

Microwave diagnostics of electron density, temperature and light emission in self excited moving striations in hydrogen plasma 19 p3475 A70-37553

Stepwise ionization effect on electron distribution, transport and balance coefficients in low voltage low pressure neon plasma 19 p3476 A70-37555

Particle flux diagnostics of nonisothermal low pressure plasma, using corpuscular passive method 19 p3476 A70-37556

Equilibrium homogeneous steady state highly ionized non-Debye plasma for investigation of electrical conductivity, viscosity, dynamic properties, etc 19 p3480 A70-38183

Ionospheric movements measurement methods and data interpretation 19 p3415 A70-38415

Gas discharge in longitudinal magnetic field, investigating instability of diffusion dominated positive column 20 p3677 A70-39112

Surface contaminated Langmuir probe measurements in glow discharge plasmas, discussing errors 20 p3633 A70-40161

Electrostatic plasma probe inverse process I-V properties from current voltage characteristics, improving accuracy and reliability by theory in terms of new variables 20 p3683 A70-40162

Gaseous neon plasma positive column electrons density and drift velocities measurements by Langmuir probe technique

20 p3683 A70-40163

Collisionless cylindrical Langmuir probe response in turbulent plasma for mean and statistical properties

20 p3684 A70-40258

Shock waves formation in rarefied plasma investigated by Thomson scattering of ruby laser light

20 p3643 A70-40388

Passive corpuscular diagnostics of high temperature plasma based on charge exchange neutrals, calibrating stripping chamber

20 p3685 A70-40398

Schlieren method application in plasma diagnostics, obtaining density change of neutral, ion and electron gases

21 p3825 A70-40950

Mach-Zehnder interferometer for plasma diagnostics measurements, discussing optical interference method, fringe shift determination and dispersion equations

21 p3856 A70-41150

Book on electrical probes for plasma diagnostics covering kinetic theory, carrier distribution, current characteristics, plasma resonance, etc

21 p3829 A70-41790

Mass spectroscopy analysis of neutral and ionic population of plasma in carbon dioxide laser gas mixture, discussing collision processes

21 p3838 A70-42006

Low electron temperature plasma measurements by electrostatic planar guard ring probe with floating potential electrode, discussing electronic circuit

21 p3830 A70-42015

Electron concentration measurement range expansion in plasma by laser interferometer with optical signal phase modulation

21 p3860 A70-42069

Charge separated and quasi-neutral solutions of electron heat transfer to spherical body in quiescent nonequilibrium plasma, noting diagnostic applications

21 p3860 A70-42080

Spontaneous emission intensification at 6911 Å in potassium to evaluate plasma local conditions, using low pressure arc and Q switched ruby laser

22 p4049 A70-42359

Uranium plasma diagnostics, measuring emission and absorption coefficients as function of pressure and temperature

22 p4069 A70-42361

Stationary hydrogen RF plasma, using quadrupole mass analyzer for ion composition and extraction study

22 p4078 A70-42363

Carbon dioxide-nitrogen He discharge gas temperature measurements involving plasma refractivity determination by interferometer

22 p4049 A70-42366

Plasma diagnostics by two-beam optical interferometry and holographic techniques, discussing plasma parameter spatial distribution recording insensitivity to radiation and variable-sensitivity interferometry

22 p4079 A70-42382

Electron energy distribution in time-varying plasmas, using difference quotient circuits for Langmuir probe characteristics measurement

22 p4082 A70-43220

Magnetospheric thermal plasma studies via ground based whistler method, identifying radial and longitudinal irregularities in electron density, bulk motion and plasmaphase position and displacements

22 p4021 A70-43281

Micropulsations as diagnostic tool for magnetospheric research, explaining ULF and VLF results variances

22 p4021 A70-43282

Magnetospheric plasma parameters from ground observation data of Pc-1 type micropulsations, assuming radiation belt plasma cyclotron instability

22 p4022 A70-43283

Magnetosphere storm diagnostics from geomagnetic, auroral and airglow parameters, discussing calibration via satellite observations

22 p4022 A70-43289

Geomagnetic wake in solar wind at 500 earth radii, correlating Explorer 35 and Pioneer 8 data

23 p4184 A70-43828

Ionospheric ion temperature measurements by retarding potential analyzer onOGO-6 satellite

23 p4185 A70-43840

Plasma diagnostics based on light beam refractivity, considering laser interferometry and holographic methods

23 p4225 A70-44188

Hydrogen cluster beam discharges, determining transient plasma ion density from Stark broadening measurements of H beta line

23 p4228 A70-44939

Equatorial E region electrojet plasma irregularities, discussing electron density, drift velocity, profile structure, etc

24 p4384 A70-45150

Magnetic field measurement by laser light scattering intensity fine structure determination in plasma

24 p4353 A70-45567

Plasma jet motion stability in axial magnetic field of stellarator diverter and solenoid

24 p4386 A70-45660

Energy-mass analysis for steady state plasma by electrostatic analyzer and time of flight mass spectrometer, determining ion species temperature and density ratios

24 p4387 A70-45813

PLASMA DIFFUSION

Needle-shaped filament artificial ion cloud drift and diffusion in F1 region plasma in presence of neutral wind and uniform electric field

01 p0070 A70-10401

Charged particle distribution in heterogeneous medium using dispersion model to describe quasi-charged particles interaction with internal surfaces

03 p0536 A70-14370

Plasma turbulence theory formulated using averaging operators, obtaining nonlinear dispersion relation for turbulent diffusion coefficients

03 p0537 A70-14377

Steady, ambipolar, low and high speed plasma transport equations developed for terrestrial ionosphere, discussing boundary conditions for supersonic and subsonic flows

04 p0679 A70-15112

Plasma transport models of polar ionosphere, discussing physical processes involved and effects on electron concentration, ion composition and speeds

04 p0679 A70-15113

Periodic potential probe for diffusive flux to wall measurements in negative glow and back diffusion plasmas

06 p1074 A70-18617

Optical parametric backward-wave instabilities in unbounded medium with stopband dispersion using Fourier-Laplace integral

08 p1552 A70-21595

Turbulent diffusion and ion heating in plasmas in presence of current instability

08 p1554 A70-21813

Current diffusion from magnetic piston into postshock gas upstream observed in electromagnetic shock tube

09 p1736 A70-23185

Beam plasma system instability, studying anomalous diffusion toward vessel walls as function of generated oscillations

09 p1737 A70-23335

Comets ionized shells, studying plasma expansion in corpuscular solar wind magnetic field

10 p1940 A70-24372

Drift dissipative instability of weakly ionized plasma, considering ion motion along magnetic lines in dispersion equation

10 p1923 A70-24407

Field-aligned plasma velocity dependence on plasma diffusion and wind velocity illustrated with model of night F2 layer

10 p1881 A70-24814

Solid state plasma drift velocity effect on helicon propagation constant assuming isotropic momentum relaxation time and effective mass

10 p1928 A70-24831

Kaufman thruster with predominant radial field, noting electron mobility across ion extraction screen and advantages of uniform plasma distribution

11 p2102 A70-26120

Plasma turbulent diffusion across constant magnetic field, noting magnetic, kinetic energy and relaxation times ratio effects

11 p2094 A70-26755

Plasma turbulence spectral theory, considering cascade processes in collisional and collisionless dissipation

11 p2095 A70-26756

Diffusion coefficients measurements in velocity space from ion-ion collisions and ion wave microturbulence, supporting theoretical calculations and diffusion equations in plasma

12 p2279 A70-27777

Drift waves relation to anomalous cross field diffusion in fully ionized magnetoplasmas, introducing model predicting amplitude, correlation time, fluctuation spectrum and diffusion process

12 p2280 A70-27788

Coulomb interaction effect on diffusion of plasma produced by contact ionization in magnetic field, obtaining density profiles by iterative procedure

12 p2280 A70-27789

Frequency modulated RF pulses compression with dispersive property of lossless, isotropic and homogeneous plasma used to enhance receiver transmission resolution

12 p2282 A70-27960

Collision dominated plasma column radial structure including ambipolar diffusion region obtained from constant mean free time and path approximate formulas

16 p2959 A70-34311

Two component fully ionized plasma in HF electric field, demonstrating suppression of runaway electrons in Lorentz plasma

17 p3140 A70-34934

Plasma anomalous diffusion relation to self excited LF oscillations

19 p3480 A70-38016

MHD instability of homogeneous inviscid plasma with finite electrical conductivity and anisotropic pressure, obtaining dispersion equation for model

20 p3677 A70-39048

Gas discharge in longitudinal magnetic field, investigating instability of diffusion dominated positive column

20 p3677 A70-39112

Cylindrical plasma inhomogeneities including meteor trains diffusion in presence of magnetic field, observing dependence on angle theta

21 p3886 A70-41060

Laser torch plasma dispersion gas dynamics from motion and kinetics of ionization processes

21 p3839 A70-42238

Plasma inhomogeneity and drift effects on synchrotron radiation from relativistic charged particles in magnetoplasma

22 p4082 A70-43254

Meteor trails isotropic diffusion in presence of moving point source of ionization with variable intensity, calculating plasma density on and near trajectory

23 p4240 A70-44084

PLASMA DIODES

Hg and Cd seeded Ce plasma wide-spaced diode without external light source investigated for Penning effect on diode performance

10 p1808 A70-25038

Sheath structure of plasma diode using kinetic theory model of plasma-sheath transition

13 p2376 A70-28642

Collisionless alkali plasma diode with two electrodes emitting electrons and ions with half-Maxwellian velocities, analyzing potential distribution

14 p2622 A70-30660

PLASMA DISCHARGES

U PLASMA JETS

PLASMA DISPERSION

U PLASMA DIFFUSION

PLASMA DYNAMICS

Moving plasmas with small angular divergence without guide field produced by modified Ti-washer gun for plasma interaction studies

01 p0054 A70-10109

Magnetic field effects on point Coulomb impurity charge static shielding by quantum electron plasma

01 p0151 A70-10449

Electron distribution function for steady homogeneous plasma of arbitrary ionization degree under strong electric fields, discussing kinetic equations for elastic and nonelastic encounters

02 p0346 A70-12231

Interplanetary plasma inhomogeneity size, shape and spatial orientation and drift velocity and direction determined from radio telescope data

03 p0565 A70-13231

Electrostatic instability criterion for plasma with distribution function having discontinuities and sharp bend at minima

03 p0532 A70-13526

Ionospheric aerodynamics concerning plasma flow and stability, ion motion, radio wave scattering, etc

03 p0479 A70-14386

Discharges in Ar flow in membrane shock tube at Mach 5, discussing plasma compression, shock wave position and effect on electrode region

04 p0725 A70-14534

Rarefied plasma motion in geomagnetic dipole equatorial plane near magnetosphere symmetry axis deriving approximate solution to quasi-hydrodynamic equations

04 p0681 A70-15717

Two dimensional plasma modes involving geometry and velocity spaces, discussing Vlasov equation

05 p0890 A70-17025

Radiation from dipole in dispersive anisotropic magnetized plasmas using Fourier analysis

06 p1116 A70-17363

Interplanetary plasma flow past earth and planets simulation using kinetic equations

06 p1147 A70-18292

Electron beam generated plasma behavior, showing electron pressure local nonisotropy capability for generating supersonic-subsonic transitions

06 p1123 A70-18296

Kinetic processes in plasma subjected to randomly fluctuating electric field, obtaining chain of single particle distribution functions

07 p1349 A70-19553

Finite amplitude disturbance propagating across magnetic field within infinite plasma, solving Vlasov equation and ordering moment equations hierarchy

07 p1352 A70-19989

Expansion and deceleration of rocket-released artificial ion cloud in terms of snowplow expansion model and drag deceleration

07 p1271 A70-20159

Electrodynamic plasma accelerators fast particle generation mechanism during entrainment, studying polarization field potential structure

08 p1549 A70-20506

Spark track plasma of electrical discharge in fluid, describing energy dissipation, particle formation and density, plasma temperature, etc

08 p1551 A70-21202

Interplanetary plasma inhomogeneity size, shape and spatial orientation and drift velocity and direction determined from radio telescope data

08 p1580 A70-21664

Laser heating of plasma, motion pattern and shock wave parameters during absorption burst in solid body vapor, using numerical analysis

09 p1695 A70-22181

Dynamics of multicomponent plasma involving charged or neutral gases with transport phenomena for case of no magnetic field

09 p1738 A70-23580

Book on plasma dynamics covering charged particle orbit theory, macroscopic equations, hydromagnetics, hot and cold plasma waves, kinetic theory and plasma radiation

11 p2087 A70-25500

Plasma self Q switching in pulsed far IR lasers, discussing lens effect of plasma electrons delaying laser pulses

11 p2062 A70-25634

Magnetopause representation by mixing region of plasma streams with different velocities and magnetic fields, assuming hydromagnetic viscosity caused by wave-particle interactions

11 p2114 A70-26563

Flow dynamics effects on characteristics of high temperature plasmatron, describing plasma burner design and HF discharge plasma experiment

11 p1984 A70-26740

Rarefied plasma motion in geomagnetic dipole equatorial plane near magnetosphere symmetry axis by deriving approximate solution to quasi-hydrodynamic equations

14 p2575 A70-30801

Many body correlation and conditional probability functions of plasma shield clouds surrounding test particles

14 p2623 A70-31034

Comparative sets of higher order adiabatic motion equations for plasmas in electric and magnetic fields with slow variations

14 p2624 A70-31043

Compressible plasma gravitational instability taking into account Hall effect

14 p2624 A70-31225

Kinetic processes in plasma subjected to randomly fluctuating electric field, obtaining chain of single particle distribution functions

15 p2777 A70-31460

Distant radiation from magnetic line source in moving isotropic plasma, discussing dependence on velocity

15 p2778 A70-31835

Plasma velocity and moment equations in magnetic dipole field as function of variations along coordinate directions

16 p2956 A70-32934

Collection of papers on gas dynamics covering hypersonic flow, rarefied gas and plasma dynamics, heat and mass transfer, etc

17 p3069 A70-35031

Continuum plasma dynamics with electromagnetic forces of same order of magnitude as gas dynamic forces, discussing various flow problems

17 p3141 A70-35040

Photoresonant cesium plasma ionization, discussing pumping spectra, electron gas, molecular-atomic ion ratio and dynamics

19 p3474 A70-37440

Ar arc discharge magnetically induced retrograde rotation dynamics, using high speed photography

19 p3475 A70-37533

Gas discharge in longitudinal magnetic field, investigating instability of diffusion dominated positive column

20 p3677 A70-39112

Magnetospheric and magnetic storms correlated to solar wind energy penetration, noting roles of energetic plasma and magnetospheric low energy plasma convection

22 p4022 A70-43287

HF plasma propagation, discussing RF discharge by exciting axially symmetric mode of plasma column

22 p4084 A70-43671

Thermodynamics and statistical physics of dense plasma with particle interaction energy exceeding kinetic energy, discussing three-component model phase equilibrium

23 p4229 A70-45073

MPD experiments in inductive hydrodynamic shock tube with round cross section and radial magnetic field

24 p0000 A70-45798

Mathematical model for plasma expansion resulting from short energy pulse absorption

24 p4387 A70-45799

PLASMA ELECTRODES

Acceleration mechanisms in pulsed plasma accelerator with rail electrodes driven by capacitor discharge

02 p0348 A70-12501

Plasma acceleration by induced Hall currents, discussing Hall-to-current ratio maximum at critical magnetic field

[AIAA PAPER 69-280] 04 p0729 A70-15596

Electron temperature distribution in thermal boundary layer about probe electrodes calculated by successive approximations allowing for electron heating by arc

09 p1734 A70-22167

Quasi-steady state plasma acceleration in coaxial electrode geometry during synchronized application of tailored pulses of mass flow and current

[AIAA PAPER 69-267] 09 p1736 A70-23204

Silver cathodes and plasma-sprayed anodes for cold effective hydrogen/oxygen fuel cells with solid zirconium dioxide electrolyte, considering carbon precipitation avoidance

10 p1830 A70-24459

Radial distribution of plasma parameters for thermionic converters with electrode shielding by plane sapphire rings, showing lateral surface effect

10 p1808 A70-25124

Seeded dense plasma-electrode system behavior, studying effect of adsorption and emission from boundary surfaces

11 p2090 A70-25952

Heat exchange in linear vortex plasmatron with bilateral ejection, noting dependence on electrodes geometry and gas flow rates

11 p1984 A70-26737

Electron bombardment ion engine thrust variations, considering effects of electrode misalignment and ion current changes

12 p2291 A70-27808

Surface parameters influence on energy transfer to arc jet anode, discussing work function, accommodation coefficient and diffuse reflection coefficient of electrons

[AIAA PAPER 69-107] 12 p2281 A70-27809

Electric field in rectangular MHD channel with ideally conducting electrodes in uniform magnetic field, considering conditions for maximum channel effectiveness

13 p2461 A70-28966

Lithium vapor fueled applied field MPD arc jet performance using open end heat pipe vaporizer and hollow cathode

[AIAA PAPER 69-241] 13 p2475 A70-29959

Microwave harmonic generation by nonlinear plasma-metal junctions noting calcium, gallium, molybdenum, gold, copper and platinum cathodes

14 p2549 A70-30438

MHD power generation, investigating replenishment of zirconia electrode from plasma in open flame and duct configurations

14 p2534 A70-30535

Collisionless alkali plasma diode with two electrodes emitting electrons and ions with half-Maxwellian velocities, analyzing potential distribution

14 p2622 A70-30660

Coaxial electrode arc discharge plasma accelerators at reduced pressure under crossed fields, employing Hall effect

15 p2779 A70-32104

Laminar Cu-W electrode erosion resistivity in single chamber electric arc hydrogen plasmatrons with gas vortex stabilization

15 p2780 A70-32130

Combustion driven Hall configuration MHD generator, discussing boundary layer analysis, gas density nonuniformity and electrode drop

20 p3566 A70-40003

Electrode size effects on combustion driven MHD generator performance, examining voltage losses, gas boundary layer temperature and surface conditions

20 p3566 A70-40005

Continuous electrode MHD generator ionization instabilities, measuring current distribution and transverse electric field

20 p3567 A70-40018

Radial distribution of plasma parameters for thermionic converters with electrode shielding by plane sapphire rings, showing lateral surface effect

20 p3568 A70-40517

Plasma source design using stellarator type magnetic field, eliminating electron beam and electrode produced impurities

21 p3858 A70-41713

Arc ignition and cathode spot movement dynamics of thermionically emitting cathode surfaces in heat feedback plasma

21 p3859 A70-41903

Current distribution of accelerating electrodes of coaxial injector, using differential magnetic probe

22 p3965 A70-42805

PLASMA ENGINES

Spectral line widths in MPD arc jet measured to determine plasma electron density and heavy particle temperature

03 p0536 A70-14371

Current stream function, Hall current density, force densities and pressure distribution for typical MPD thruster

03 p0552 A70-14372

Radial velocity profiles measured in plasma jet thrusters with thermal and self magnetic acceleration, discussing disturbances due to discharge current-magnetic field interactions

03 p0553 A70-14374

Pulsed plasma and ion microthrusters providing satellite attitude and position control

05 p0896 A70-16119

Dynamic I-V characteristics of megawatt pulsed MPD-ARC plasma thruster under various axial magnetic fields given for Ar and hydrogen propellants

[AIAA PAPER 70-164] 06 p1131 A70-18092

LES-6 satellite solid Teflon pulsed plasma thruster performance, determining energy balance, thrust and circuit parameters

[AIAA PAPER 70-179] 06 p1132 A70-18206

Pulsed plasma vacuum-arc thruster system incorporating throttle and thrust vector controls for long life satellite control applications

[AIAA PAPER 70-180] 06 p1133 A70-18232

Segmented anode current and heat distribution in MPD engine measured with current shunts and calorimetric methods

[AIAA PAPER 69-244] 09 p1613 A70-23238

Three axis attitude control of earth oriented non-spinning synchronous communications satellite, using gimbal-mounted momentum wheel and pulsed plasma thrusters

[AIAA PAPER 70-456] 11 p2119 A70-25431

Background pressure and magnetic field shape effect on MPD thruster performance, testing radiation cooled thrusters

[AIAA PAPER 69-243] 11 p2102 A70-26122

Pulsed plasma microthruster propulsion system for synchronous orbit LES 6 satellite

[AIAA PAPER 69-298] 13 p2473 A70-28504

Continuously working plasma thrusters, describing operating principles of Hall current and self magnetic acceleration systems

15 p2790 A70-32277

RFI measurements at X band on LES-7 prototype pulsed plasma thruster

17 p3149 A70-35669

RF plasma thrusters for synchronous satellites, estimating weights and efficiencies of various types

20 p3689 A70-40124

Spinning satellites stationkeeping at synchronous altitude, using solid propellant pulsed plasma microthrusters

[AIAA PAPER 70-1148] 20 p3690 A70-40206

Electric propulsion research involving MPD thrusters, current sheets and neutral-ion motion coupling

[AIAA PAPER 70-1086] 20 p3683 A70-40249

Low power MPD arc thruster performance with downstream cathode, using Xe propellant

[AIAA PAPER 70-1084] 20 p3693 A70-40251

Cathode geometry effect on performance of radiation cooled MPD arc thruster in continuous mode

[AIAA PAPER 70-1083] 20 p3693 A70-40252

Electrolytic capacitor current pulse networks for quasi-steady MPD arc thrusters, determining series resistance effects on energy transfer

[AIAA PAPER 70-1082] 20 p3568 A70-40253

Quasi-steady MPD arc thruster average thrust measurements, considering time-of-flight velocity determination by ion collecting probes

[AIAA PAPER 70-1080] 20 p3694 A70-40255

Repetitively pulsed MPD propulsion systems, considering thruster performance

[AIAA PAPER 70-1093] 20 p3695 A70-40522

Pulsed plasma and low pressure detonator thrusters for long life secondary spacecraft propulsion, considering satellite stationkeeping and attitude control

[AIAA PAPER 70-1147] 21 p3868 A70-41782

High temperature acceleration of propellants in electrothermal thrusters including resistojets, arcjets, thermionic and plasma configurations

22 p4091 A70-42763

PLASMA FLOW

U MAGNETOHYDRODYNAMIC FLOW

PLASMA FLUX MEASUREMENTS

Ionization studies in collision dominated high pressure flame plasma using electrostatic probes

03 p0534 A70-14212

Unsteady state and transit time analysis of geoeffective interplanetary plasma flux observed near earth causing magnetospheric storm of 17-19 April 1965

04 p0683 A70-15736

Periodic potential probe for diffusive flux to wall measurements in negative glow and back diffusion plasmas

06 p1074 A70-18617

Unsteady state and transit time analysis of geoeffective interplanetary plasma flux near earth causing magnetospheric storm of 17-19 April 1965

14 p2575 A70-30820

Negative hydrogen ion balance in high intensity plasma source, measuring flux as function of discharge current

15 p2780 A70-32195

- Dual satellite magnetic field and plasma measurements of earth bow thick pulsation shock by Vela 3A and Explorer 33 22 p4013 A70-42470
- Plasma with oriented charged particle fluxes macroscopic parameter measurement by multigrid probes facing and reversed to drift, noting graphical data processing 24 p4385 A70-45454
- PLASMA FREQUENCIES
 - Bremsstrahlung emission from thermal plasma coexisting with relativistic electron tails, noting enhancement at electron plasma frequency harmonics 02 p0348 A70-12240
 - Saturation of linear or nonlinearly /explosively/ unstable HF electrostatic flute modes in mirror confined plasma 03 p0529 A70-13005
 - Inhomogeneous plasma oscillations in counterstreaming plasmas analyzed for electric fields and resonant frequencies from Vlasov equation 04 p0726 A70-14671
 - Electron plasma frequency exchange corrections temperature dependence at high densities, using equation of motion for coupled particle-hole pair operators 04 p0727 A70-14714
 - RF probe impedance variations with magnetic field strength in hot plasma for electron gyrofrequencies less than plasma frequency explained by model 06 p1117 A70-17371
 - Collisions effects on cylindrical antenna impedance near plasma frequency of isotropic nonMaxwellian plasma, allowing for collision frequency dependence on electron energy 06 p1020 A70-17567
 - High electron density plasma generation by ionized gaseous filament explosion, noting plasma frequency effect on spectral brightness 10 p1915 A70-23961
 - Nonlinear wave interactions in quiescent plasma column with external disturbance creating broadened frequency spectrum and weakly turbulent plasma 10 p1922 A70-24146
 - Cyclotron waves absorption study in bounded rarefied plasma having Larmor electron frequency exceeding plasma frequency 10 p1925 A70-25101
 - Narrow band radiation from longitudinal plasma waves nonlinear interactions during solar bursts, comparing flux intensities for Corona single or double shock wave frequencies 10 p1934 A70-25272
 - Magnetic field effect on burst emissions in plasma frequency range, observing radiation band widening and modes transmission in terms of Appleton-Hartree theory 10 p1949 A70-25273
 - HF and LF plasma waves interaction in three wave approximation taking into account linear damping 11 p2089 A70-25714
 - Topside ionosphere nighttime structure over Japan deduced from Alouette 2 satellite plasma frequency measurements 12 p2226 A70-28063
 - Electrostatic waves for upper ionospheric plasma model, obtaining solutions to dispersion relation at multiples of electron cyclotron frequency 13 p2400 A70-29914
 - LF oscillations of bounded low pressure plasma under magnetic field in discharge chamber, determining spatial distribution by Langmuir sliding probes 16 p2958 A70-33254
 - Numerical ionospheric world mapping of plasma frequency, considering height, latitude, longitude and local mean time variations 19 p3380 A70-38403
 - Antennas impedances in warm isotropic plasma, using hydrodynamic and kinetic /Vlasov/ equations 19 p3380 A70-38406
 - Topside plasma frequency resonance below electron cyclotron frequency, discussing ray paths and delay times 20 p3620 A70-39336
 - Positive ions energy dispersion effused from RF plasma, presenting ion extraction model for plasma sheath system and equivalent circuit 20 p3678 A70-39608
 - Collisionless plasmas fluid dynamical equations in presence of strong magnetic field, discussing Larmor and electron plasma frequencies 20 p3678 A70-39609
 - Superimposed external DC magnetic field effect on electrodeless HF plasma density, discussing electron cyclotron waves resonance excitation and plasma electron energy gain 22 p4079 A70-42364
 - Homogeneous plasma in uniform magnetic field, deriving theory for instabilities and LF wave propagation modes 22 p4079 A70-42370
 - LF oscillations of bounded low pressure plasma under magnetic field in discharge chamber, determining spatial distribution by Langmuir sliding probes 23 p4226 A70-44283
- LF drift-dissipative instabilities of HF skin layer in nonuniform plasma 24 p4383 A70-45119
- PLASMA GENERATION
 - U PLASMA GENERATORS
 - PLASMA GENERATORS
 - NT PLASMA GUNS
 - NT PLASMATRONS
 - Electrothermal instability and critical Hall parameter growth rates in closed cycle linear plasma generators with variable electron mobility, discussing perturbation effects 01 p0151 A70-10655
 - Giant pulse Q switched lasers generated plasmas, noting VUV spectral line shifts, asymmetries and existence of satellite lines 02 p0345 A70-11894
 - Local thermodynamic equilibrium conditions in superhigh pressure He plasma produced by laser action, obtaining threshold electric field relationship with gas pressure and temperature 02 p0312 A70-12078
 - Cs plasma research, discussing Q-machines, plasma confinement, magnetic field experiments, LF and HF wave propagation, etc 03 p0533 A70-14015
 - Hot cathode reflex discharges investigated to improve ion generation efficiency in space ion thrusters 03 p0536 A70-14368
 - Transpiration-cooled electric arcs for high temperature high density plasma generation, considering uncertainties in plasma transport properties and temperature distributions 04 p0729 A70-15591
 - Dynamic I-V characteristics of hot cathode megawatt level nitrogen propellant pulsed MPD arc plasma source for various axial magnetic fields 04 p0729 A70-15642
 - Steady state plasma generation in metallic waveguide without dielectric container by cold cathode discharge in He 05 p0819 A70-15803
 - Electron beam generated plasma behavior, showing electron pressure local nonisotropy capability for generating supersonic-subsonic transitions 06 p1123 A70-18296
 - Electrohydrodynamic /EHD/ technique for generating ions from liquid metals by using electrostatic forces to overcome surface tension forces for field emission of ions 06 p1125 A70-18610
 - Chemical synthesis in streaming thermal plasmas including HCN from cold methane and N plasma discharge chemistry 07 p1351 A70-19879
 - Transpiration-cooled constricted arc for plasma generation, considering transport properties, LTE assumptions and porous tube flow characteristics 07 p1351 A70-19898
 - Plasma generation and heating by controlled thermonuclear fusion reactions using pulsed lasers 09 p1734 A70-22249
 - Laser-produced Al plasmas linear and nonlinear behavior, using framing camera and energy absorption measurements to study outermost ion energy increase and luminous front expansion 09 p1736 A70-23187
 - Subnanosecond laser pulses for plasma production obtained via mode selecting uncoated flats inserted in laser cavity 09 p1699 A70-23364
 - High electron density plasma generation by ionized gaseous filament explosion, noting plasma frequency effect on spectral brightness 10 p1915 A70-23961
 - Radiative capacity measurement for plasmas produced from nonconducting materials by pulsed discharges in magnetic field 10 p1923 A70-24252
 - Plasma production by solid hydrogen-giant pulse laser interaction, studying time dependent distributions of plasma density, temperature and velocity 10 p1902 A70-25222
 - Electrode erosion during high voltage vacuum breakdown measured by neutron activation analysis and gamma ray spectrometry, noting plasma formation from electrode material 10 p1854 A70-25317
 - Soviet collection of articles on low temperature plasma generators covering electrical discharges, plasma jets, electrodes, generator applications, etc 11 p2091 A70-26728
 - Spectroscopic diagnostics of erosion plasma jets from cylindrical pulsed plasma generator operating in vacuum 11 p2093 A70-26745
 - Laser microplasma formation in focus of two laser beams impinging on crystalline lithium hydride targets 12 p2246 A70-27355
 - Far UV emission spectrum of plasma produced by laser beam impact on Al target observed as function of time, determining electron temperature 13 p2460 A70-28729
- Electron density and transverse electron temperature of magnetoactive plasma generated in circular waveguide by microwave signal with variable polarization 13 p2462 A70-29128
- Magnetically constrained steady state plasma production by hot cathode DC arc discharge in He 13 p2465 A70-29819
- Plasma ionization enhancement by laser line radiation matched to specific atomic transitions [ALAA PAPER 69-47] 13 p2468 A70-29958
- Plasma production by irradiating solid hydrogen foils with intense pulse ruby laser 14 p2622 A70-30659
- Probe measurements in Cs plasma formed by contact ionization with hot wire for density, electron temperature and space potential 16 p2958 A70-33624
- Plasma production by long wavelength lasers applied to controlled thermonuclear reactions [ALAA PAPER 70-779] 17 p3103 A70-34476
- Thermal electrodeless plasmas generation at audio frequencies with closed magnetic circuit model [ALAA PAPER 70-776] 17 p3139 A70-34478
- Nonequilibrium plasma from pulsed discharge in crossed electric and magnetic fields 17 p3142 A70-35727
- Product distribution of organic nitrogen compounds plasma sources computed by assuming high temperature limited thermodynamic equilibrium 18 p3226 A70-36764
- Laser-produced plasmas production and containment, studying expansion in uniform magnetic field and charge quantity as power density function 19 p3444 A70-37535
- Ion temperatures and incident intensities in plasmas produced by solid target irradiation with Q switched laser beam 19 p3479 A70-37765
- DC plasma generator with Ar stabilized arc, investigating heat and mass transfer in jet discharge channel 19 p3481 A70-38189
- Multidimensional control systems synthesized in accord with polyinvariance and coordinating couplings principles 20 p3604 A70-39837
- LTE verification for argon plasma generated in free burning arc by measuring atomic line transition probability at various pressures 21 p3854 A70-40588
- Extended homogeneous stationary field-free spherical plasma source, including radial density measurement with Langmuir probe in argon 21 p3805 A70-41463
- Magnetic pressure fast opening gas puff valve for hydrogen bursts in conical theta pinch plasma source 21 p3833 A70-41472
- Plasma source design using stellator type magnetic field, eliminating electron beam and electrode produced impurities 21 p3858 A70-41713
- Ruby giant pulse laser produced plasmas from aluminum and copper surfaces, measuring electron and ion energies by time of flight and retarding potential techniques 21 p3860 A70-41925
- High power plasma flow generation at variable pressure and rates, describing device characteristics and performance 22 p4079 A70-42367
- Plasma vortices during electrodynamic distortion of curved copper wire exploding in atmospheric air, using shadowgraphs 22 p4081 A70-42807
- Plasma generation by pulsed laser heating, investigating ionization effects on temperature 22 p4082 A70-43224
- Nitrogen transport coefficients as function of high temperature in stationary plasma produced in cascade arc chamber 22 p4082 A70-43373
- Laser induced gas breakdown, considering plasma generation and properties 23 p4225 A70-44185
- High density plasmas production and containment in theta pinch device, discussing shock and Joule heating 23 p4225 A70-44186
- Ion source emitter plasma column generated by electron beam injection through gas filled chamber, compensating ion space charge with fast discharge electrons 24 p4385 A70-45451
- Plasma formation from transition metal target under monopulse laser radiation, noting absorbed surface density energy role in onset 24 p4385 A70-45463
- Cs ion beam space charge and current neutralization by electron capture for partially ionized plasma formation, investigating longitudinal electrostatic wave excitation 24 p4385 A70-45465

PLASMA GUNS

Moving plasmas with small angular divergence without guide field produced by modified Ti-washer gun for plasma interaction studies

01 p0054 A70-10109

Pyrex spheres accelerated to 15 km/sec by plasma rail gun to study hypervelocity impact in twin stainless steel and Al targets

18 p3342 A70-36685

[AIAA PAPER 69-378]
Conical plasma gun with Z pinching restrained by axial magnetic field, describing operating characteristics

19 p3480 A70-38018

Axial propellant density gradients and circuit capacitance correlated with pulsed coaxial plasma gun efficiency

21 p3858 A70-41726

Air spark gap to switch stored charge in LC circuit, using auxiliary triggering circuit to clamp magnetic flux

23 p4177 A70-44471

Coaxial plasma deflagration gun for accelerating particles to high velocities at low thermal energy for plasma injection experiments

24 p4383 A70-45120

W, Ta and Mo components economical fabrication by plasma spraying for rocket nozzles, susceptors and crucibles

24 p4350 A70-46355

PLASMA HEATING

Equilibrium model of laminar arc constrictor plasma generator, correlating heat transfer, wall shear stress, friction factor and development length

03 p0533 A70-13952

Nonthermal heating mechanism in quiet solar wind, tabulating observed and predicted parameters

03 p0561 A70-13998

Thermochemical relaxation influence on shock heated plasma gases via heat transfer experiments on ionized Ar, molecular nitrogen and carbon dioxide

03 p0536 A70-14366

Kinetic theory of cracks network formation on LiF crystal surface exposed to plasma jet using high speed camera

04 p0730 A70-14458

Solar wind acceleration and coronal plasma heating above plage regions from spectra of solar radio echoes, computing temperature rise and energy input

04 p0740 A70-15049

Remote feedback suppression method for plasma collisional drift instability using modulated microwave irradiation, describing linear heating mechanism theory

06 p1122 A70-18014

HF ion-acoustic noise /whistlers/ during turbulent heating of plasma, using matched magnetic probe

07 p1348 A70-19551

Ionic noise during plasma turbulent heating in toroidal facility, discussing oscillation spectrum

07 p1349 A70-19552

Monograph on research by Japanese Institute of Plasma Physics covering theta pinch, plasma heating, flow, diagnostics, etc

07 p1350 A70-19843

Soviet collection of papers on magnetic traps covering chamber walls effect on plasma heating, plasma in mirror trap and self sustained fusions

07 p1350 A70-19844

Magnetic trap chamber walls adverse effect on plasma heating produced by electron beam injected at low hydrogen pressures

07 p1350 A70-19845

Turbulent diffusion and ion heating in plasmas in presence of current instability

08 p1554 A70-21813

Pulse indicators using thermoelectric effect of hot carriers caused by nonuniform heating of electron gas in HF field

09 p1643 A70-22127

Laser heating of plasma, motion pattern and shock wave parameters during absorption burst in solid body vapor, using numerical analysis

09 p1695 A70-22181

Plasma generation and heating by controlled thermonuclear fusion reactions using pulsed lasers

09 p1734 A70-22249

Solar wind heating, determining roles of various energy sources from Explorer 34 observations

09 p1755 A70-22511

Nonresonant electromagnetic absorption in high density plasma used for RF heating in magnetostatic field

09 p1735 A70-22923

Laser radiation conversion into kilovolt X rays using planar heated plasma, discussing electron temperature role

10 p1921 A70-23987

Deuterium plasma expansion resulting from thermal shock produced by laser impulse

10 p1923 A70-24526

Gas mixture plasma ionized and heated by discharge and ejected into vacuum, considering nonequilibrium ionization calculation with gap between electron and heavy particle temperatures

11 p2092 A70-26732

Optimal conditions for obtaining dense low temperature cesium plasma in shock tube with heating calculated by Debye theory

12 p2278 A70-27327

Plasma torch for increasing material fusion temperatures in metallization methods

12 p2244 A70-28072

Pulsed plasma jet radiant heat flux effect on celophane film coated, polished and etched metals, noting erosion destruction

12 p2282 A70-28287

Macroscopic plasma response to absorption of high intensity laser radiation in one dimensional geometry

13 p2459 A70-28636

Kinetic theory of cracks network formation on LiF crystal surface exposed to plasma jet using high speed camera

13 p2510 A70-28655

Drift instability and ion heating by high amplitude magnetosonic wave in plasma waveguide in constant magnetic field

13 p2463 A70-29381

Power absorption by microwave generated plasmas noting pressure effects

14 p2622 A70-30675

Hot universe model for demonstrating distortions in Rayleigh-Jeans region of microwave relic radiation spectrum by primeval plasma heating before recombination epoch

14 p2632 A70-31287

HF ion-acoustic noise /whistlers/ during turbulent heating of plasma, using matched magnetic probe

15 p2777 A70-31458

Ionic noise during plasma turbulent heating in toroidal facility, discussing oscillation spectrum

15 p2777 A70-31459

Ions energy spectra in plasma heated by shock wave, using passive corpuscular diagnostic technique

15 p2781 A70-32821

Beam current instability and plasma heating by electron beam generated in linear discharge, discussing electron beam-cold plasma interactions

16 p2957 A70-33191

Electron beam interaction with ionized K plasma, considering Langmuir waves instability, turbulence and electron heating

18 p3295 A70-36614

Plasma satellites near He I forbidden lines during turbulent heating

19 p3475 A70-37441

Surface layer heating of solid body by dense gas discharge plasma radiation, comparing vaporization and reversible opacity onset times in quartz

19 p3482 A70-38733

Ion heating during plasma instability due to interaction with electron beam in mirror magnetic trap

20 p3678 A70-39598

High radiation intensity neodymium glass laser, describing installation for heating plasmas to high temperatures

20 p3643 A70-39758

Dense plasma jet kinetic instabilities and heating in strong magnetic field

20 p3682 A70-40138

Nonlinear resonant heating in magneto-plasma, calculating energy absorption by ions and plasma wave amplitude

20 p3685 A70-40467

Temporal and spatial origin of hot ions in turbulent plasma heating, using particle analysis

21 p3855 A70-40824

Plasma heating by ionizing shock waves reflected by transverse magnetic field barrier, discussing discontinuity resolution

21 p3857 A70-41381

Turbulent plasma heating by adiabatic magnetic compression with longitudinal ring current

21 p3857 A70-41387

Stochastic kinetic theory for plasma turbulent heating by random fields, predicting acceleration effects

21 p3859 A70-41899

Numerical analysis of inductive electrodeless discharge of thermal Ar plasma column heated by RF axial magnetic field

21 p3859 A70-41902

Optimal conditions for obtaining dense low temperature cesium plasma in shock tube with heating calculated by Debye theory

21 p3860 A70-42068

Small high temperature rotary plasma-heated furnace for refractory material high purity processing, discussing design and operation

22 p4005 A70-42368

Planar resonance probe in free molecular arc heated flowing plasma, examining shift nature in measured frequency position of minimum drawn current

22 p4081 A70-43013

Stochastic heating of plasma in toroidal trap /stellarator/, showing discharge ignition potential dependence on microwave oscillator frequency

22 p4084 A70-43394

High density plasmas production and containment in theta pinch device, discussing shock and Joule heating

23 p4225 A70-44186

Plasma heated by cyclotron resonance using waveguide method, considering properties, confinement conditions and instabilities

24 p4385 A70-45453

PLASMA INSTABILITY
U MAGNETOHYDRODYNAMIC STABILITY
PLASMA INTERACTIONS
NT PLASMA-ELECTROMAGNETIC INTERACTION

Moving plasmas with small angular divergence without guide field produced by modified Ti-washer gun for plasma interaction studies

01 p0054 A70-10109

Geomagnetic bays produced by neutral sheet plasma earthward movement resulting from solar wind enlargement of geomagnetic tail

01 p0071 A70-10409

Solar electric spacecraft field interaction with space plasma affecting collection and interpretation of scientific data, emphasizing required system configurations and constraints

[AIAA PAPER 69-1106] 01 p0162 A70-10601

Mariner 2 measurements of geomagnetic field and interplanetary plasma parameters, analyzing interaction between interplanetary medium and magnetosphere during decreased solar activity

01 p0192 A70-11520

Magnetic lines of force penetration into magnetosphere accompanied by plasma insertion generating ring current responsible for main phase of magnetic storm

01 p0083 A70-11543

Evolution and entropy of partially ionized collision dominated plasmas interacting with radiation based on statistical analogs of irreversible thermodynamics

02 p0346 A70-11902

Coaxial ion beams moving in opposite directions in LF magnetic field noting sliding instability development

03 p0530 A70-13061

Coherent microwave generation mechanism in indium antimonide at high electric fields, formulating thin plasma layer double stream interaction theory

03 p0534 A70-14214

Ionization study of gas discharge parameters behind shock wave front produced by moving plasma pulse interaction with immovable gas discharge plasma

03 p0535 A70-14361

Ar plasma interaction with concentric cool hydrogen sheath for simulation study for gaseous core nuclear space propulsion system

03 p0536 A70-14375

Energy modes nonlinear interactions in rarefied plasmas, presenting wave energy and momentum definitions and kinetic equations for mode density in wave number space

04 p0726 A70-14701

Radiation-convection interaction in plasma free jet, using two-thermal-domain model for enthalpy distribution determination

[ASME PAPER 69-WA/HT-50] 04 p0781 A70-14798

Pulsed supersonic plasma jets induced surface ablations and cracks in polymers, using X ray and IR analysis

06 p1091 A70-17763

Remote feedback suppression method for plasma collisional drift instability using modulated microwave irradiation, describing linear heating mechanism theory

06 p1122 A70-18014

High altitude telemetry plasma attenuation for hypersonic blunt nose slender reentry bodies

[AIAA PAPER 70-220] 06 p1010 A70-18088

Solar wind flow different interactions with earth, Venus and moon

06 p1136 A70-18284

Collective interactions and low density plasma instability in high current gas discharge showing influence on neutral gas breakdown in interelectrode space

07 p1354 A70-20317

Alfven wave structure mechanism of geomagnetic micropulsation type in cometary tails, assuming Kelvin-Helmholtz instability at comet plasma-solar wind interface

08 p1565 A70-20567

Monograph on solar wind covering solar physics, space observation methods, solar system interactions, etc

09 p1745 A70-23475

Magnetic disturbances caused by magnetosphere-solar wind filamentary inhomogeneity interaction observed by Pioneer 6

10 p1931 A70-24320

Solar wind-geomagnetic field interactions, considering day and night hemispheres, satellite observations, shock and magnetopause motion, shock structure, etc

10 p1932 A70-24553

Monograph on ionosphere-satellite interactions, discussing ionosphere layers, plasma sheaths and waves, electromagnetic wave propagation, spacecraft antennas, etc

10 p1944 A70-24900

- LF ion-acoustic wave nonlinear interaction with HF Langmuir waves in nonisothermal plasma, establishing criteria for ion plasma turbulence 10 p1925 A70-25103
- F region magnetic disturbances due to low energy solar plasma penetration during proton bursts 11 p2104 A70-25535
- Dynamic equations for amplitudes of interacting MHD waves bounded plasma, discussing three-plasmon interactions 11 p2088 A70-25708
- Energy balance of self sustaining thermonuclear reaction with nonuniform magnetic field in wall-contained dense plasma, allowing for radiation losses 11 p2088 A70-25709
- Hydrodynamic equations for ions and electrons of ionized collisional plasma in inhomogeneous magnetic field based on Boltzmann kinetic equations 11 p2088 A70-25710
- HF and LF plasma waves interaction in three wave approximation taking into account linear damping 11 p2089 A70-25714
- Magnetopause representation by mixing region of plasma streams with different velocities and magnetic fields, assuming hydromagnetic viscosity caused by wave-particle interactions 11 p2114 A70-26563
- Coulomb interaction effect on diffusion of plasma produced by contact ionization in magnetic field, obtaining density profiles by iterative procedure 12 p2280 A70-27789
- Mathematical models reproducing nonlinear mode interactions in CW bounded plasma devices 13 p2458 A70-28567
- Landau damping in plasma cyclotron wave interaction by symmetrical counterstreaming double electron beam with uniform magnetic field 13 p2468 A70-29917
- Ohmic dissipation in MHD plasma acceleration, demonstrating interaction with electric field and magnetic induction 14 p2621 A70-30296
- Container wall-collision plasma sheath model for charge carrier investigation using velocity distribution [DFVLR-SONDDR-51] 14 p2622 A70-30662
- Vlasov interaction of magnetically coupled E layer with dissipative structures including injection, trapping and drag effects 14 p2623 A70-30698
- Solar wind interaction with planetary ionosphere, considering flow behavior across bow MHD shock 14 p2647 A70-31073
- Plasma kinetic equation, expressing interaction term as sum of binary collisions between close and collective interactions among remote particles 14 p2625 A70-31297
- VHF radiation from plasma during electron beam interaction with fast magnetoacoustic wave stimulated by external spatially periodic currents 15 p2780 A70-32118
- Shock wave propagation during moving pulsed plasma interaction with stationary gas discharge plasma 15 p2780 A70-32197
- Alfven wave structure mechanism of geomagnetic micropulsation type in cometary tails, assuming Kelvin-Helmholtz instability at comet plasma-solar wind interface 15 p2805 A70-32722
- Collisionless shocks structure in turbulent wave-particle interactions, obtaining ion distribution function 16 p2959 A70-33970
- Solar wind interaction with earth, moon, Venus and Mars, reviewing literature on continuum fluid model, spacecraft observations, plasma characteristics, etc 17 p3150 A70-34669
- Nonlinear electrostatic vibrations in colliding antiparallel flows of rarefied plasma 17 p3141 A70-35335
- Temporal and spatial covariation of high latitude geophysical phenomena, using unified mechanism of solar plasma stream interaction with geomagnetic field 18 p3247 A70-36404
- Solar wind and flare energetic particles properties and interactions, surveying interplanetary magnetic field, planetary bow shock waves, neutrons, neutrinos, etc 19 p3511 A70-38418
- Fully ionized magnetized rotating plasma interaction with neutral gas blanket, discussing plasma decay and velocity field 19 p3481 A70-38489
- Interactions between moving alkali-metal seeded dense plasma and metallic thermionically emitting electrode with surface properties influenced by seed particle absorption 20 p3681 A70-40007
- Auroral arcs formation model based on dynamic magnetosphere-ionosphere interaction 21 p3817 A70-41089
- F region magnetic disturbances due to low energy solar plasma penetration during proton bursts 21 p3882 A70-41285
- Magnetoplasma interaction with axially slotted delay line, examining coil behavior physical mechanisms by cold plasma model 22 p4079 A70-42365
- Electric propulsion plasma thrust beam and ambient space plasma electrostatic equilibration, considering various charged particle parameters involved in bi-plasma system interactions [AIAA PAPER 70-1142] 22 p4091 A70-42974
- Steady state frequency spectra for Alfven waves and MHD turbulence in collisionless plasma with nonlinear interaction by particle scattering 24 p4383 A70-45114
- Velocity-space homogeneous plasma instabilities due to self interaction of single species 24 p4384 A70-45253
- PLASMA JET SYNTHESIS**
- HF electrodeless plasma discharge synthesis of niobium and vanadium intermetallic compounds 11 p2061 A70-26746
- PLASMA JET WIND TUNNELS**
- Plasma arc wind tunnel gas velocity measurement with electron beam probe using closed-loop electronic controller to stabilize beam position 01 p0092 A70-11195
- Neutral particle flux measurements in plasma wind tunnel using BeCu detector, discussing role in collisionless flow dissipation processes 04 p0727 A70-14994
- Ion density profile across shock in partially ionized gas measured in plasma jet wind tunnel for comparison with Rankine-Hugoniot relation 09 p1662 A70-23235
- Army missile command /AMICOM/ plasma jet wind tunnel automatic control system design 16 p2888 A70-33303
- Steady state plasma wind tunnel for flow around ionospheric satellites, studying wakes of cylinders and spheres 16 p2837 A70-33866
- PLASMA JETS**
- Pulsed arcs in argon and helium at superhigh pressures, noting plasma ionization and temperature and charged particle density 01 p0149 A70-10168
- Negative resistance I-V characteristics of low voltage arc discharge in Cs plasma 01 p0150 A70-10172
- Magnetically balanced arcs in supersonic external flows, indicating central core with differential Lorentz forces analogous to Grashof number in free convection phenomena 02 p0347 A70-12233
- Focused deuterium plasma discharge neutrons and X rays energy spectra, flux and time resolved collimation measurement with nuclear emulsions and scintillation detectors 02 p0348 A70-12241
- Critical magnetic fields, frequencies and spatial structure of ion-acoustic instability of HF induction discharge plasmas in hydrogen, Ar, He and Hg vapor 02 p0348 A70-12261
- Millimeter and nanosecond resolution of fast neutrons in pulse dense high temperature deuterium plasma discharge with polyethylene collimators and photomultipliers 02 p0303 A70-12739
- Anomalous behavior of arc motion in high pressure cross-field plasma devices in terms of electromagnetic effects 03 p0529 A70-12938
- Laser emission action at 4880 Å in plasma discharge from injecting electron beam into Ar at different pressures 03 p0530 A70-13063
- Supersonic plasma jets studied spectroscopically, determining atomic levels populations, population inversion conditions, electron temperature and concentration distributions, etc 03 p0531 A70-13254
- Turbulent submerged plasma jet boundaries calculated theoretically and compared with experimental results from dynamic head profiles 03 p0532 A70-13515
- Air plasma pulsed discharge jets erosive effects on metals, semiconductors and dielectrics, noting role of thermal effect 03 p0532 A70-13742
- Equilibrium model of laminar arc constrictor plasma generator, correlating heat transfer, wall shear stress, friction factor and development length 03 p0533 A70-13952
- Hot cathode reflex discharges investigated to improve ion generation efficiency in space ion thrusters 03 p0536 A70-14368
- Spectral line widths in MPD arc jet measured to determine plasma electron density and heavy particle temperature 03 p0536 A70-14371
- Entrainment rate of ambient medium by MPD arc jet, discussing flow field in and around jet and pressure distribution along vacuum tank wall 03 p0553 A70-14373
- Electron efflux effectiveness from discharge plasma into vacuum, investigating various electrodes influence 04 p0724 A70-14415
- Radiation-convection interaction in plasma free jet, using two-thermal-domain model for enthalpy distribution determination [ASME PAPER 69-WA/HT-50] 04 p0781 A70-14798
- Pulsed high current arc burning in hydrogen at pressures to 400 atm, discussing stability and discharge plasma parameters 04 p0729 A70-15224
- Stability and shape of magnetically balanced atmospheric cross-flow arcs in Ar noting balanced modes 04 p0729 A70-15549
- Plasma gas jets high velocity propagation, studying radiation precursor and divergence and expansion chamber effects 04 p0675 A70-15594
- Axial and rotational velocity profiles of plasma jet from Doppler shift of spectral lines [DFVLR-SONDDR-27] 04 p0729 A70-15612
- Dynamic I-V characteristics of hot cathode megawatt level nitrogen propellant pulsed MPD arc plasma source for various axial magnetic fields 04 p0729 A70-15642
- Exploding wire discharges in high vacuum, discussing particle emission MHD instabilities, plasma temperature and electron density 05 p0890 A70-16820
- Ball lightning mechanism proposal based on mathematical model for electric discharge current in parabolic plasma shell forming vortex-type storm front 05 p0879 A70-17021
- Diagnostic methods for field-free plasmas with medium dispersed optical-spectrographic and source monitoring equipment 06 p1063 A70-17728
- Pulsed supersonic plasma jets induced surface ablations and cracks in polymers, using X ray and IR analysis 06 p1091 A70-17763
- Plasma arc tests to simulate stagnation reentry heating on spherical subized models of nuclear heat source to investigate heat shield materials ablation characteristics [AIAA PAPER 70-200] 06 p0974 A70-18172
- Quasi-steady coaxial MPD arcs characteristics, studying Ar ion velocities, electrostatic ion acceleration mechanism and arc voltage gradient [AIAA PAPER 70-165] 06 p1132 A70-18208
- Repetitively pulsed quasi-steady vacuum arc magnetoplasdynamic accelerator for propulsion, using electrolytic capacitors as power source [AIAA PAPER 70-167] 06 p1133 A70-18228
- Microwave scattering from plasma column of low pressure discharge in Hg under free space conditions 06 p1125 A70-18609
- Wall temperature variation of transpiration cooled tube surrounding plasma arc calculated from gas mass flow and wall properties 07 p1420 A70-19214
- Doppler shift measurements of axial and rotational velocities in MPD arc, using references from iron arc [AIAA PAPER 69-110] 07 p1364 A70-19324
- Pulsed dense argon plasma arcs radiation spectra in visible and UV regions as function of current and pressure 07 p1349 A70-19652
- Chemical synthesis in streaming thermal plasmas including HCN from cold methane and N plasma discharge chemistry 07 p1351 A70-19879
- Freezing-mixing model for predicting plasma jet flow reactor yield development from analyses of thermochemical equilibrium, chemical reaction freezing and turbulent mixing 07 p1351 A70-19893
- Transpiration-cooled constricted arc for plasma generation, considering transport properties, LTE assumptions and porous tube flow characteristics 07 p1351 A70-19898
- Dispersion of ion-acoustic waves in quiescent rare gas discharge plasmas, discussing model simulating ion waves generated by finite sine wave bursts 07 p1352 A70-19990
- Cyclotron frequency harmonics emission of PIG discharges linked to nonthermal electron plasma instability 07 p1354 A70-20316
- Electron density, excited state density and neutral particle temperature in Ar and Ne nonequilibrium laminar plasma jets 08 p1550 A70-20596
- Thermal and nonthermal plasmas for ion production, discussing gas pressure, voltage and discharge current effects on electron temperature 09 p1734 A70-22037
- Plasma discharge absorption coefficients measurement using Q switched ruby laser 09 p1694 A70-22139

PLASMA LAYERS

Plasma discharge studies by holographic interferometry using ruby laser pulse for light source
09 p1674 A70-22171

Doppler effect induced small spectral line shifts measured by modified duochromator in MPD arc jet
09 p1684 A70-23531

HF electromagnetic wave detector based on study of volt-ampere characteristics of luminescent plasma discharge
10 p1922 A70-24030

Plasma energy confinement time as function of discharge parameters for plasma thermal insulation in Tokamak-3
11 p2088 A70-25713

Inert gas plasma jets diagnostics in accelerator by spectroscopy, determining flow velocities, excitation and gas temperatures
11 p2093 A70-26744

Spectroscopic diagnostics of erosion plasma jets from cylindrical pulsed plasma generator operating in vacuum
11 p2093 A70-26745

Controllable thermonuclear reactor with free-float HF discharge plasma in deuterium
12 p2271 A70-27351

Pulsed plasma jet radiant heat flux effect on cellophane film coated, polished and etched metals, noting erosion destruction
12 p2282 A70-28287

SERT 2 mercury vapor fed hollow cathode operated in bell jar, determining volt-ampere characteristics and flow rates for plasma diagnostics
[AIAA PAPER 69-258] 13 p2473 A70-28515

DC plasma arc jet excitation and emission characteristics for solution analysis with economical inert gas flow rates
13 p2362 A70-29107

Interference holograms of low temperature nitrogen plasma jet using fundamental and second harmonic ruby laser emissions
13 p2464 A70-29384

Thermal induction plasma discharge characteristics, considering radiation and conduction losses
13 p2465 A70-29702

Lithium vapor fueled applied field MPD arc jet performance using open end heat pipe vaporizer and hollow cathode
[AIAA PAPER 69-241] 13 p2475 A70-29959

Neutral particle temperature, pressure and velocity measurements in argon plasma jet, using refraction index
14 p2625 A70-31350

Teflon and polymethyl methacrylate sublimation breakdown in plasma jets, using electric arc heated argon, nitrogen, air and oxygen
15 p2765 A70-32103

High energy electron temperature in beam plasma discharge pulsed laser measured by bremsstrahlung X radiation spectrum
15 p2752 A70-32194

Negative hydrogen ion balance in high intensity plasma source, measuring flux as function of discharge current
15 p2780 A70-32195

Plasma electron density measurement for microwave-excited pulsed discharges based on skin effect
15 p2780 A70-32367

Microwave probe for measuring electron density profile in supersonic arc jet plasma
15 p2741 A70-32433

Discharge chamber plasma processes in electron bombardment ion thrusters, considering factors affecting thruster performance
[AIAA PAPER 69-494] 15 p2791 A70-32501

Electron density fluctuations in transitional zone of turbulent plasma jet, using digital analysis of Langmuir probe signals
[AIAA PAPER 70-731] 16 p2958 A70-33495

Gas-core nuclear rocket engine simulation by induction coupled plasma torch, determining gas flow patterns
[AIAA PAPER 70-691] 16 p2950 A70-33555

Ni particles induced quenching measured by probes in afterglow plasma of pulsed linear discharge, determining deionization rate
16 p2958 A70-33687

Experimental and theoretical investigation of mass injection effect on high current MPD arc
[AIAA PAPER 69-266] 16 p2959 A70-33869

Transverse magnetic field effects on Ar cross flow arc temperature distribution, cross section shape and profile, discussing forced convection effects
[AIAA PAPER 70-777] 17 p3138 A70-34477

Electron concentration distribution over plasma discharge cross section, using interferometry
17 p3142 A70-35732

Thermal stability test assembly for refractory materials cylindrical specimens, using argon plasma jet
19 p3395 A70-37351

Molybdenum carbization in methane-based plasma glow discharge, considering possible pyrocarbon layer formation and temperature effects
19 p3434 A70-37456

Elementary chemical reaction kinetics effect on electrophysical parameters of low temperature plasma jets, calculating relaxation time for C fuels
19 p3481 A70-38184

Low temperature underexpanded supersonic gas plasma jets behind shock wave, analyzing rarefaction and viscosity effects on parameters distribution
19 p3352 A70-38185

DC plasma generator with Ar stabilized arc, investigating heat and mass transfer in jet discharge channel
19 p3481 A70-38189

Acceleration processes in MPD arc jet in Ar for symmetric discharge layer and rotating spoke types
20 p3680 A70-39992

Potential fluctuations in intersecting plasma jet streams attributed to ion-electron instability, using external probe
20 p3682 A70-40136

Dense plasma jet kinetic instabilities and heating in strong magnetic field
20 p3682 A70-40138

Alfven critical velocity concept in MPD arcs analysis, obtaining exhaust velocity relationship from one dimensional flow model
[AIAA PAPER 70-1096] 20 p3683 A70-40240

Multimegawatt quasi-steady MPD arc accelerator in millisecond pulses, noting applicability to experiments requiring long exposure-times
[AIAA PAPER 70-1095] 20 p3683 A70-40241

Arc luminosity in cathode region of quasi-steady MPD arc jet, using high speed photography and electric and magnetic field probes
[AIAA PAPER 70-1094] 20 p3683 A70-40242

Supersonic weakly ionized plasma jet in argon, investigating axial and radial temperature profiles by electrical probe techniques and spectroscopic and photographic methods
20 p3685 A70-40463

Axisymmetric jet plasma flow in magnetic nozzle, measuring electric potential, electron temperature and ion density and velocity
21 p3856 A70-41380

Nonequilibrium flow adjacent to cooling tube wall confining cascade arc plasma electrical discharge
21 p3805 A70-41763

Intense high ionization degree discharge plasma initiation at low gas pressures, using auxiliary discharge
22 p4078 A70-42356

Spatial stability of transferred arc anode spots during cutting with plasma jets, noting currents associated with microspots
22 p4043 A70-42380

Transpiration cooling of porous constrictor walls of high intensity electric arc in plasma
[ASME PAPER 70-HT-35] 22 p4122 A70-42432

Electric propulsion plasma thrust beam and ambient space plasma electrostatic equilibration, considering various charged particle parameters involved in bi-plasma system interactions
[AIAA PAPER 70-1142] 22 p4091 A70-42974

High speed plasma jet propagation, obtaining time of arrival measurements, brightness temperature, pressure and impact data
22 p4012 A70-43014

Controllable thermonuclear reactor with free-float HF discharge plasma in deuterium
22 p4084 A70-43595

Temperature distribution and thermal conductivity determination in Ar plasma cascade arc
23 p4226 A70-44438

Five-moments approximation calculation of magnetoplasma dynamic hydrogen arc radial pressure profile as function of ambient pressure and superimposed magnetic field
23 p4228 A70-44935

Magnetoplasma dynamic hydrogen arc radial pressure profile as function of ambient pressure and superimposed magnetic field, using thirteen-moments approximation
23 p4228 A70-44936

German monograph on thermal and nonthermal phenomena in quasi-stationary convectionless plasma arc column, using 13-moment approximation for Boltzmann equation
24 p4382 A70-45089

Temperature, densities and electric field strength of cascaded arcs burning in He under normal pressure
24 p4384 A70-45425

Plasma jet motion stability in axial magnetic field of stellarator diverter and solenoid
24 p4386 A70-45660

Spark erosion or plasma jet treatment effects on Co surface structure, describing allotropic delta phase
24 p4364 A70-46221

PLASMA LAYERS

Transmission and reflection of electromagnetic waves by bounded moving plasma layer in slow wave space
01 p0042 A70-10167

Radiation enhancement from spherical antenna by overdense plasma coating, noting use for reentry vehicle blackout prevention
02 p0262 A70-12601

Electromagnetic wave reflection on thin plasma layer with Epstein electron density profile, noting use in microwave diagnostics
03 p0529 A70-13016

Geomagnetic perturbation coincidences observed at conjugate Polar Cap observatories, suggesting magnetospheric tail field lines convergence with plasma neutral layer
03 p0565 A70-13232

Plasma optical transparency criterion, estimating nonequilibrium plasma layer optical density limit
03 p0531 A70-13255

Energy distribution function of electrons in weakly ionized plasma layer at electrode calculated, allowing for possible plasma concentration inhomogeneities
03 p0540 A70-13525

Coherent microwave generation mechanism in indium antimonide at high electric fields, formulating thin plasma layer double stream interaction theory
03 p0534 A70-14214

Rectangular-slot antenna pair self and mutual admittances in inhomogeneous plasma layer on slender conical body, calculating VSWR and isolation
06 p1020 A70-17565

Ion acceleration in spherical and cylindrical plasma layers formed by spherical plasmoid expansion in plasma cylinders
07 p1384 A70-19414

S- and p-polarized electromagnetic wave incident on semifinite laminar plasma layers, analyzing reflection and absorption characteristics
08 p1456 A70-20504

Spectrum of waves emitted from waveguide of two plane dielectric or isotropic plasma layers, solving dispersion equations numerically by computer
08 p1472 A70-20973

Geomagnetic perturbation coincidences observed at conjugate Polar Cap observatories, suggesting magnetospheric tail field lines convergence with plasma neutral layer
08 p1580 A70-21665

Anodic electric layer in self sustaining discharge in transverse magnetic field with neutral gas burnout, studying neutral atom ionization probability
09 p1734 A70-22110

Diagnostics of inhomogeneous plane stratified plasma with arbitrary electron concentration distribution, solving differential equation for electromagnetic wave propagation normal to plasma layers
09 p1735 A70-23160

Oblique E-mode electromagnetic wave in plane stratified collisionless plasma taking into account plasma temperature
09 p1639 A70-23674

Transmission and reflection of electromagnetic waves by bounded moving plasma layer in slow wave space
10 p1842 A70-25015

Vacuum arc discharge phases before total breakdown, studying high combustion voltage relation to interplasma double layer potential difference
10 p1969 A70-25115

Electromagnetic wave propagation through weakly inhomogeneous plasma layer with frequent electron-molecule collisions, noting applicability to ionosphere
11 p2003 A70-25530

Radio wave transmission through magnetized plasma layer as function of electron concentration and collision frequency, using coaxial accelerator
13 p2366 A70-29377

Magnetotail plasma sheet temporal variations during substorms and plasma pressure as related to dynamic pressure of solar wind from Vela satellites observation
13 p2480 A70-30061

Spatial distribution and directional anisotropies of tail plasma sheet energetic electrons from measurements by electrostatic analyzer and energetic particle experiments on Vela 4
13 p2482 A70-30071

Interplanetary plasma observations by Vela satellites in solar wind and plasma sheet of magnetotail during magnetic storm
19 p3410 A70-37490

Inhomogeneous nonequilibrium plasma stratification in magnetic field, investigating electrical conductivity
19 p3481 A70-38191

Electromagnetic wave propagation through weakly inhomogeneous plasma layer with frequent electron-molecule collisions, noting applicability to ionosphere
21 p3786 A70-41280

Electromagnetic wave propagation through cold slowly varying plasma layers in absence of external magnetic field
21 p3860 A70-42000

Slow and fast ionization waves in inert gas or molecular gas plasma columns, describing striation formation in neon discharge by hydrodynamic equations
22 p4079 A70-42371

Interferometric investigation of rapidly variable frequency dependent phase objects, using ruby laser waves
[SMPT PREPRINT 26] 22 p4034 A70-43049

EM radiation beams higher directivity from sources in two layer plasma in planetary atmosphere 23 p4242 A70-44261

LF drift-dissipative instabilities of HF skin layer in nonuniform plasma 24 p4383 A70-45119

PLASMA LIFETIME

Plasma accumulation between mixed field accelerator and pulsed magnetic mirror, noting duration and stability 02 p0346 A70-12104

Accumulated plasma density and lifetime measurement of trapped ions between accelerator and periodic magnetic mirror, showing limitation by collisions and charge exchange 03 p0532 A70-13683

PLASMA LOSS

F 2 field-aligned ion velocity measurement compared with theoretical results, discussing difference at sunspot minimum and daytime ion velocity-plasma loss relation 10 p1881 A70-24815

Inertia effect on low density plasma losses in toroidal MHD equilibrium in model stellarator field 24 p4383 A70-45115

PLASMA OSCILLATIONS

Nonpotential waves propagating at slow phase velocity in inhomogeneous plasma, determining flute instability oscillation frequency 01 p0149 A70-10163

Langmuir oscillations excited by electron beam in plasma during instability development investigated for temporal and spatial structure, using visualization 01 p0150 A70-10174

Quasi-linear ion oscillation theory for Maxwellian plasma, considering electron and ion distribution perturbations and energy transfer 02 p0346 A70-12105

Time resolved cavity perturbation technique to measure high plasma density in magnetic mirror compression experiment, obtaining total electron number 02 p0347 A70-12236

Transverse Kelvin-Helmholtz instability in rotating thermally ionized alkali metal plasmas /Q machines/, analyzing LF drift wave edge oscillation using dispersion equation 02 p0348 A70-12239

Satellite lines of forbidden transition in laser-produced He plasma attributed to longitudinal plasma oscillations 02 p0379 A70-12717

Spectrum function in Booker scattering formula /first order Born approximation/ for dielectric constant fluctuations in hypersonic wake plasmas 03 p0529 A70-12908

Variable magnetic field effect on stability of Langmuir waves propagating in plasma in constant magnetic field 03 p0530 A70-13064

Ion-cyclotron oscillations in plasmas, considering plasma waves and oscillation characteristics 03 p0530 A70-13065

Nonisothermal plasma perturbed by supersonic body, studying plasma rarefaction and condensation cones, particle density, etc, in wake 03 p0407 A70-13413

Temporal and statistical characteristics of HF oscillations from electron beam interaction with plasma in magnetic field 03 p0532 A70-13524

Electrostatic drift-dissipative plasma instability and nocturnal equatorial spread F irregularities, discussing amplification in collision dominated medium 03 p0477 A70-13990

Inhomogeneous plasma oscillations in counterstreaming plasmas analyzed for electric fields and resonant frequencies from Vlasov equation 04 p0726 A70-14671

Plasma camera photographs of K plasma spatial distribution with electric fields and density gradients perpendicular to magnetic field, observing rotating irregularities around edge 04 p0728 A70-15005

Quasi-linear mode coupling in confined hot-ion Penning discharge plasma, discussing externally imposed excitation and internally generated oscillations 05 p0888 A70-16166

Linear damping of sinusoidal oscillation in plasma, solving linearized Vlasov equation by integration along particle trajectories 05 p0888 A70-16304

Coupling between LF oscillations and third harmonic frequency resonances of bounded plasma capacitor system, discussing density profile variation 05 p0890 A70-16654

Plasma oscillations, resonances and wave propagation characteristics analyzed by radio pulse sounders for application to space measurements 06 p1115 A70-17360

Ionospheric observations of resonance oscillations using satellite-borne radio sounding instruments 06 p1115 A70-17361

Electrostatic oscillations in cylindrical column of laboratory plasmas excited by electromagnetic waves, investigating resonances by cold plasma theory 06 p1116 A70-17368

Relativistic electron low beta plasma oscillations in external magnetic field using covariant dispersion relations 06 p1120 A70-17542

Kinetic theory of longitudinal ion oscillations pertaining to LF plasma oscillations monitored in Ariel 1 satellite wake due to ions trapped in potential trough 06 p1120 A70-17591

Hall current effects on anisotropic plasma magnetogravitational instability under uniform magnetic field, considering electron inertia role and plasma perturbations 07 p1348 A70-19228

Inelastic scattering of electrons by surface plasma oscillation for low energy electron diffraction and photoemission, interpreting surface plasmon excitation 07 p1337 A70-19359

Ionic noise during plasma turbulent heating in toroidal facility, discussing oscillation spectrum 07 p1349 A70-19552

Induced current density of fully ionized stationary plasma in externally applied HF electric field, discussing frequency range of fluctuations 07 p1352 A70-19988

Plasma ion-cyclotron oscillations resonance excitation in crossed electric and magnetic fields, describing instability development 07 p1354 A70-20319

Plasma physics relating turbulence to cosmic rays covering oscillations, turbulent acceleration, subcosmic rays, langmuir turbulence spectra and acceleration, etc 07 p1371 A70-20332

Surface oscillations of plasma in external HF field derived from hydrodynamics and Maxwell equations 07 p1355 A70-20367

He-Ne laser plasma vibrations and radiation power during active medium discharge excitation by DC current, noting characteristic energy hysteresis 08 p1511 A70-20519

Plasma oscillations analytic second order theory verification by computerized simulation, using Fourier-Hermitian expansion of distribution function in phase space 08 p1550 A70-20636

Scalar potential nonlinear fluctuations in quasi-stationary plasma, deriving expressions for potential spectral function and Langmuir and ion-acoustic fluctuations spectral densities 08 p1550 A70-20844

Flute instabilities of cold magnetoactive plasma with radially dependent density and strong azimuthal particle streams, discussing nonzero perpendicular temperature effects on oscillations 08 p1552 A70-21504

Whistler type electromagnetic waves excitation by electron beam in plasma, noting intensity dependence on electron frequency 08 p1554 A70-21804

Low pressure plasma stability in cylindrical crimped magnetic field, considering convective perturbations and particle velocity distribution 08 p1555 A70-21981

Trapped particle vibrations stability during quasi-neutral plasma disturbance due to centrifugal drift in stellarator electric field 08 p1555 A70-21982

Ion-acoustic wave oscillations of weak collision plasma in strong electromagnetic field, discussing instability 09 p1736 A70-23198

Beam plasma system instability, studying anomalous diffusion toward vessel walls as function of generated oscillations 09 p1737 A70-23335

Microwave-induced ionization oscillations in resonant plasma column excited by low pressure mercury DC discharge 10 p1922 A70-23988

Ionosphere effect on toroidal magnetodynamic waves in idealized representation, analyzing oscillations correlation between adjacent magnetospheric shells 10 p1875 A70-24444

Nonpotential waves propagating at slow phase velocity in inhomogeneous plasma, determining flute instability oscillation frequency 10 p1925 A70-25011

Langmuir oscillations excited by electron beam in plasma during instability development, investigating temporal and spatial structure using visualization 10 p1925 A70-25019

Nonlinear interaction between plasma and HF field near cyclotron frequency, studying plasma oscillations generation in strong magnetic field 10 p1925 A70-25102

Excitation of plasma ion-cyclotron oscillations by ion beam passing through neutral gas along magnetic field, noting radial stabilization 10 p1926 A70-25118

Unsteady plasma oscillation stabilization by envelope controller with spatial and temporal dispersion 11 p2087 A70-25604

Surface waves stability in cold bounded plasma against background of steady state electron oscillations, using nonlinear approximation 11 p2089 A70-25716

Wakes of cylinder in collision-free plasma wind tunnel simulating ionospheric satellite conditions, noting decaying oscillation 11 p1976 A70-26018

Linear theory of density gradient drift waves in stable collision dominated plasma using external excitation method 11 p2090 A70-26019

Acoustic perturbations in stationary weakly ionized pulsed neon plasma 11 p2096 A70-26842

Hot-electron cold-ion plasma with anisotropic electron velocity distribution function, discussing stability under finite pressure and unstable oscillation forms 12 p2277 A70-27314

Plasma turbulence due to nonlinear wave interaction, considering second sound LF oscillations propagation and plasmons scattering at ions 12 p2278 A70-27358

Density gradient drift waves stabilization in collisionless plasma by stellarator type windings, observing oscillations amplitude reduction in shear magnetic field 12 p2280 A70-27785

Tonks-Dattner resonances in plasma columns, considering viscosity effect on radial oscillations in nonuniform plasmas 12 p2281 A70-27792

Stellar and nebular magnetic fields formation, considering role of high temperature plasma random charge and current fluctuations 12 p2307 A70-27864

Plasma properties investigation by laser beam probes, considering direct observation of oscillation mode 13 p2458 A70-28564

Nonlinear dielectric function and propagators of plasma submitted to electric field by Vlasov equation iterative solution, considering electron plasma in thermodynamic equilibrium 13 p2458 A70-28565

Mathematical models reproducing nonlinear mode interactions in CW bounded plasma devices 13 p2458 A70-28567

Parametric excitation of potential oscillations in plasma near cyclotron frequency subjected to UHF electric and constant magnetic fields 13 p2463 A70-29281

Discharge effects on LF oscillations and ion extraction in hot cathode Penning plasma 13 p2463 A70-29370

Finite Larmor radius interchange and LF drift oscillations due to magnetospheric temperature and density gradient stresses in trapped plasma 13 p2401 A70-29936

Rotating plasma disturbances onset in MPD arc, determining magnetic field dependence on mass flow, background pressure and propellant [ALAA PAPER 69-232] 13 p2475 A70-29961

Landau and Doppler-shifted cyclotron damping effects on helicon-like and plasma excitations of many-valley semiconductors 13 p2472 A70-30016

Plasma pi-electrons effects in annulene molecules, obtaining dispersion relation for plasma oscillations by Hueckel theory 14 p2621 A70-30116

Continuity equation plasma oscillation, discussing ion current waveform flowing from discharge and implications for periodic astrophysical phenomena 14 p2638 A70-30618

Parametric oscillation instabilities in plasma under magnetic field perpendicular to circularly polarized or hybrid electric field 14 p2624 A70-31042

Ionic noise during plasma turbulent heating in toroidal facility, discussing oscillation spectrum 15 p2777 A70-31459

Radial distributions and escape of charged particles across magnetic field in hot cathode Penning discharge plasma with LF oscillations 15 p2780 A70-32191

Energy bands shape effect on fluctuations in nonequilibrium low resistance semiconductor plasma 15 p2784 A70-32192

Inhomogeneous ion beam plasma LF instability, showing oscillations amplitude maxima in radial density gradient regions 15 p2780 A70-32193

Partially ionized plasma stability with allowance for ionization and recombination processes, discussing ion-acoustic oscillations 15 p2781 A70-32823

Plasma helix equilibrium and stability in transverse magnetic field, considering oscillation damping by ohmic heating 15 p2781 A70-32910

PLASMA PERTURBATION

Plasma echo oscillations due to superposition of consecutive perturbations separated by intervals greater than characteristic decay time

16 p2957 A70-33198

Ion beam scattering at turbulent plasma oscillations in glass chamber containing low pressure air

16 p2958 A70-33253

LF oscillations of bounded low pressure plasma under magnetic field in discharge chamber, determining spatial distribution by Langmuir sliding probes

16 p2958 A70-33254

Collisionless plasma theory modification to include effects of finite Larmor radius of ion and electron on perturbation flow mixing

17 p3141 A70-34935

Magnetic perturbation effects on magnetoactive plasma, considering Boltzmann transport equation, plasma-electromagnetic interactions, heating, cooling, etc

17 p3142 A70-35592

Surface oscillations energy and attenuation in damped spectral region of semibounded degenerate electron plasma

18 p3293 A70-36143

HF oscillations excitation in decaying plasma-electron beam system, noting Coulomb collisions and nonlinear effects role

18 p3294 A70-36145

Regular and stochastic oscillations in plasma beam discharge produced by beam instability from observing time dependent variations in spectral line luminescence intensities

18 p3294 A70-36147

Finite size particle physics for plasma computerized simulation, considering longitudinal oscillations, scattering cross sections, diffusion coefficients, etc

18 p3296 A70-36791

Hydrodynamic model analogy to water bag/incompressible homogeneous fluid in phase space/, investigating nonlinear collisionless plasma oscillations

19 p3474 A70-37365

Homogeneous plasma electrostatic oscillations excitation by electromagnetic waves nonlinear interaction in magnetic field, deriving expression for density perturbation

19 p3475 A70-37536

Finite electron beam plasma system, investigating relationship between linear fluctuations temporal growth and resulting stationary oscillations spatial growth

19 p3475 A70-37540

Plasma lasers, investigating striation oscillations and excess noise phenomena and generation mechanisms

19 p3446 A70-37858

Solid state plasmas waves and oscillations in metals, semiconductors, noting applications for microwave devices

19 p3479 A70-37944

Plasma anomalous diffusion relation to self excited LF oscillations

19 p3480 A70-38016

Nonuniform electron plasma trapped in one dimensional potential well, determining linear oscillations by normal mode approach

19 p3482 A70-38944

Rarefied plasma flute oscillation stabilization in magnetic field, using controlled electron beams

20 p3677 A70-39173

Cold electron plasma nonlinear oscillations in magnetic field, using mathematical model

20 p3678 A70-39591

Electromagnetic waves and oscillations excited by magnetic current ring source around infinitely long compressible plasma column, deriving radiation field distribution

20 p3685 A70-40506

Excitation of plasma ion-cyclotron oscillations by ion beam passing through neutral gas along magnetic field, noting radial stabilization

20 p3685 A70-40511

HF electromagnetic field effect on nonhomogeneous collisionless magnetized plasma stability, deriving dispersion equation for drift cyclotron oscillations

21 p3854 A70-40622

Statistical analysis of random oscillations excited in electron beam-plasma system based on signal recording data

21 p3855 A70-40631

Plasma and spiraling electron beam interactions, observing oscillations above integral multiples of electron cyclotron frequency

21 p3857 A70-41388

Plasma wave echo, observing oscillatory behavior of perturbed distribution with different phases and amplitudes

21 p3858 A70-41389

Two probe electron energy distribution measurements in gaseous discharges with random and coherent oscillations, giving xenon results at low pressures

21 p3828 A70-41471

Electron-neutral collisional damping of longitudinal electron oscillations in weakly ionized plasma, solving linearized Boltzmann-Vlasov equation

21 p3860 A70-42014

LF self excited oscillations in inhomogeneous afterglow magnetoplasma measured by Langmuir probe, noting dissipative drift instabilities

22 p4079 A70-42372

Electron beam instability in cylindrical magnetically confined plasma column, calculating quasi-static spatial growth increments

22 p4080 A70-42403

Electronic damped plasma oscillations eigenfrequency in presence of external electric field

22 p4082 A70-43253

Collision integral model for multicomponent mixture, investigating partially ionized plasma longitudinal vibrations

22 p4083 A70-43382

Potassium plasma-electron beam interaction, studying LF instability due to electron and ion heating

22 p4083 A70-43385

Electric field finite amplitude oscillations of electron hole plasma during pinch effect, considering impurities stabilizing effect

22 p4084 A70-43468

Plasma turbulence due to nonlinear wave interaction, considering second sound LF oscillations propagation and plasmons scattering at ions

22 p4084 A70-43599

Geomagnetic tail and plasma sheet hydromagnetic oscillations, deriving dispersion equations and stability conditions

23 p4184 A70-43829

MHD instability due to strong magnetic field induced scattering of plasma oscillations, using one sided Q device

23 p4223 A70-43949

Plane plasma waves in homogeneous conducting fluid with magnetic field, considering oscillations of two-fluid, cold and hot plasmas

23 p4224 A70-44179

Collisionless plasma weak turbulence theory derivation from Vlasov equations, considering interactions between oscillation modes

23 p4225 A70-44182

Homogeneous plasma in unidirectional oscillatory electric field, solving Boltzmann equation by electron distribution function expansion

23 p4225 A70-44240

Ion beam scattering at turbulent plasma oscillations in glass chamber containing low pressure air

23 p4226 A70-44282

LF oscillations of bounded low pressure plasma under magnetic field in discharge chamber, determining spatial distribution by Langmuir sliding probes

23 p4226 A70-44283

Uniform HF electric field effect on ion-acoustic oscillation instability in nonisothermal magnetized current-carrying plasma

24 p4383 A70-45118

Electron plasma oscillations excitation by ion-acoustic waves

24 p4386 A70-45607

LF instability in plasma produced by electron cyclotron resonance in nonuniform magnetic and electromagnetic fields

24 p4386 A70-45613

Resonant electrons interaction with turbulent ion-acoustic plasma oscillations consisting of superimposed three dimensional random phase wave packets

24 p4386 A70-45658

Large amplitude high phase velocity oscillations anomalous damping in electron-ion plasma resulting from MHD instability

24 p4387 A70-46091

PLASMA PERTURBATION U PLASMA OSCILLATIONS PLASMA PHYSICS

Soviet book on plasma physics covering noninteracting and colliding particle motion, elementary processes, electric discharges, kinetic equations, macrocharacteristics, plasmoids, etc

01 p0151 A70-10500

Cryogenically cooled superconducting electromagnets design, construction and properties for research in plasma and solid state physics, considering coil systems

01 p0143 A70-10970

One dimensional nonlinear model of anisotropic plasma instability with respect to Alfvén waves growth, noting applicability to solar wind processes

01 p0153 A70-11597

Collection of papers on advances in plasma physics, Volume 2, covering Cs plasma, waves in interstellar plasma and shock waves

03 p0533 A70-14014

Shock wave research in plasma physics, discussing classical gas dynamic shock wave theory, detonation waves, collisional shocks, relativistic velocity shock waves, etc

03 p0533 A70-14017

Phenomena in ionized gases - Conference, Bucharest, September 1969

03 p0534 A70-14359

Plasma nature, properties and applications, discussing echoes, shocks, phase mixing and hot plasma containment

05 p0887 A70-16130

Collection of papers on advances in plasma physics, Volume 3

06 p1121 A70-17901

Plasma dielectric tensor derived quantum mechanically, emphasizing similarity in classical and quantum mechanical methods, discussing linear wave propagation, kinetic equations, etc

06 p1121 A70-17904

Superposition of dressed particles in plasma kinetic theory proved by using generalized stochastic equation for conditional probability density for one particle

06 p1124 A70-18500

Argon ion CW lasers, discussing design, inverse population, plasma, radiative transition probabilities, pumping, frequency spectra and active medium

07 p1298 A70-19642

Real plasma isotherms using three component /atoms, electrons, positive ions/ model in search for supercooled dense plasma

07 p1349 A70-19651

Monograph on research by Japanese Institute of Plasma Physics covering theta pinch, plasma heating, flow, diagnostics, etc

07 p1350 A70-19843

Plasma physics relating turbulence to cosmic rays covering oscillations, turbulent acceleration, subcosmic rays, langmuir turbulence spectra and acceleration, etc

07 p1371 A70-20332

Vlasov equations and irreversibility in plasma physics and stellar dynamics, calculating statistical entropy and relaxation time

08 p1550 A70-20556

Solar wind ejection, analyzing regions of heat conducting fluxes and laminar patterns

08 p1561 A70-21059

Monochromatic plane electromagnetic wave incident from vacuum on plane boundary of plasma half space, discussing specular reflection and diffuse scattering boundary conditions

08 p1553 A70-21611

Collective approach to thermodynamics of N-particle electron gas including transverse radiation, calculating internal energy and pressure of modes

08 p1553 A70-21612

Model for magnetic field-line reconnection in conducting incompressible fluid, determining maximum reconnection rate entirely by null point conditions

08 p1553 A70-21615

Vacuum UV atomic nitrogen and oxygen lines contribution to energy transfer in high density plasma, noting f values and Stark half widths

09 p1730 A70-22229

Diamagnetic plasma in nonuniform magnetic fields, determining equilibrium plasma configurations in and near neutral point for low and high pressure

09 p1734 A70-22478

Book on electrodynamics of particles and plasmas covering Cerenkov and gyro radiation, point charge motion, magneto-ionic theory, Boltzmann-Vlasov equations, etc

09 p1734 A70-22637

Boltzmann collisionless transport equation for relativistic plasma solved by expanding distribution function in terms of unnormalized spherical harmonics

10 p1923 A70-24228

Waveguides consisting of three concentric regions suitable for plasma experiments, showing dispersion characteristics and cut-off frequencies

10 p1850 A70-24835

Cascade mechanism of closure associated with nonlinear wave interactions between modes in turbulent plasmas, using hydrodynamical model

11 p2087 A70-25358

Transformed distribution function of particle velocity of plasma in Debye thermodynamic equilibrium approximation based on statistical mechanics

11 p2091 A70-26459

Quiescent plasma physics - Conference, Paris, September 1969, Part 1

12 p2279 A70-27776

Physics of quiescent plasmas - Conference, Paris, September 1969, Part 2

12 p2279 A70-27782

Physics of quiescent plasmas - Conference, Paris, September 1969, Part 3

12 p2280 A70-27790

Simulated isotropic lossless plasma radiating apertures located on nonplanar models, relating results to antenna radiation patterns

12 p2282 A70-27969

Reciprocity principle for biased and two component compressible plasmas

12 p2282 A70-27971

Nonlinear effects in plasmas - Conference, Orsay, Essonne, France, September 1966

13 p2456 A70-25551

Sheath structure of plasma diode using kinetic theory model of plasma-sheath transition

13 p2376 A70-28642

- Collision coefficients of reaction and inverse reaction for nonequilibrium processes with variable distribution functions and cross sections
13 p2461 A70-28920
- Alfven waves wavelengths dependence on inhomogeneous magnetic field geometry in stationary plasma, using conformal transformations
13 p2462 A70-28984
- Book on plasma physics covering properties, particle and wave motion, instabilities, shock waves, application to light nuclei controlled fusion, etc
13 p2465 A70-29783
- Raman scattering cross sections in solid state semiconductor plasma in magnetic field from phonon fluctuations
14 p2621 A70-30485
- Electron distribution for transport coefficients in Lorentzian plasma under magnetic field, determining electrical conductivity, thermal diffusion and viscosity
14 p2623 A70-31033
- Thermal relaxation rate in one and two dimensional electron plasma models with positive background, using particle in cell simulation
14 p2624 A70-31047
- Report to COSPAR on Swedish space research /1969/ including rocket-borne auroral particle experiments, plasma physics, atmospheric, solar, cosmic radiation, etc
15 p2830 A70-31722
- Plasma reflection edge in thin film InAs semiconductors, calculating refractive index and extinction coefficient from free charge parameters
15 p2783 A70-31966
- Vlasov equations and irreversibility in plasma physics and stellar dynamics, calculating statistical entropy and relaxation time
15 p2781 A70-32711
- Lorentz plasma electron velocity distribution with allowance for elastic and inelastic collisions, using Legendre polynomial and spherical harmonic expansions in Boltzmann equation
16 p2945 A70-34337
- Electrothermal instability in nonequilibrium plasma interpreted in terms of generalized instability in gas discharge
17 p3139 A70-34550
- Laboratory experiments applicability to interplanetary plasma physics, describing simulations of solar wind interactions, magnetosphere, collisionless shock waves, etc
17 p3164 A70-35123
- Nonideal plasma thermodynamics data, discussing particle interactions, Coulomb potential, stability, etc
17 p3142 A70-35733
- Magnetic probes effectiveness study of electron heating behind shock wave front in plasma, measuring electron temperature
18 p3294 A70-36149
- Collisional contribution to finite wavelength high frequency dielectric constant of Coulomb plasma
18 p3295 A70-36439
- Collection of papers on methods in computational physics, plasma physics covering Vlasov equation, simulation, finite difference, etc
18 p3295 A70-36787
- Electrostatic sheet model for plasma, emphasizing computer solutions of various problems
18 p3295 A70-36788
- Fourier and Hermite transform methods for Vlasov equation solutions in plasma physics
18 p3296 A70-36789
- Finite size particle physics for plasma computerized simulation, considering longitudinal oscillations, scattering cross sections, diffusion coefficients, etc
18 p3296 A70-36791
- Finite difference methods for collisionless plasma models, taking into account Eulerian form of Vlasov equation in phase space
18 p3296 A70-36792
- Collisions in one, two and three dimensional plasmas of finite sized particles and clouds, obtaining scattering cross sections and Fokker-Planck coefficients
20 p3679 A70-39663
- Gas dynamics turbulence of controlled properties effect on electrical discharge across plasma stream, preventing filamentary nature
20 p3681 A70-40008
- High speed cameras for submicrosecond exposures in plasma research involving theta and zeta pinches
20 p3635 A70-40526
- Schrodinger equation for hydrogen solved for high pressure behavior of materials, applying to stellar atmospheres and laboratory plasmas
21 p3849 A70-40933
- Binary Boltzmann operator for quantum statistical second virial coefficient for real gases and plasmas in two-particle scattering problem involving Jost function
22 p4081 A70-42824
- Hot plasmas physics - Conference, Newbattle Abbey, Scotland, July-August 1968
23 p4224 A70-44176
- Plasma kinetic theory, applying Boltzmann equation, Lorentz gas model and relaxation method
23 p4224 A70-44177
- Plasma kinetic theory, considering crossing from instability to stability, waves decay by collisional damping and emission by bremsstrahlung
23 p4224 A70-44178
- Plasma macroscopic and microscopic instabilities derivation from MHD and Vlasov equations
23 p4224 A70-44180
- Plasma physics computational problems concerning controlled thermonuclear reactions, considering instability and equilibrium numerical calculations
23 p4224 A70-44181
- Plasma physics and MHD in astrophysics of sun and stars, discussing stellar magnetism origin and evolution, solar and stellar atmospheres, pulsars, etc
23 p4256 A70-45042
- PLASMA PINCH**
NT THETA PINCH
Energy transfer from pulse network to mass associated with propagating current sheet in linear pinch discharge, discussing pulsed plasma accelerator efficiency
[AIAA PAPER 69-113] 07 p1348 A70-19323
- Axisymmetric instabilities by Z-pinch and reverse axial current discharges in plasmas of arbitrary conductivity
08 p1554 A70-21810
- Feedback stabilization of surface instabilities of highly conducting plasma, discussing application to linear pinch with uniform axial static magnetic field
09 p1734 A70-22272
- Pinched plasma reversed current induction due to relativistic electron beam injection
09 p1736 A70-23183
- Computer models simulating plasma motion applied to sheet pinch stability, investigating relativistic and nonrelativistic regimes
14 p2623 A70-30696
- Gas kinetic pressure profile and mass density of propagating current sheet in argon pinch discharge, using piezoelectric transducer
14 p2624 A70-31041
- Gas pressure effects on visible and UV laser action in small argon Z-pinch plasma discharge, using streak photographs
15 p2750 A70-31968
- Pinch effect in degenerate and nondegenerate electron hole plasma in semiconductors during bimolecular bulk recombination
18 p3298 A70-36620
- Conical plasma gun with Z pinching restrained by axial magnetic field, describing operating characteristics
19 p3480 A70-38018
- Laser interferometry with unstable external resonator, determining radial electron density distributions during implosion phase of linear z-pinch discharge in argon
20 p3630 A70-39420
- High speed cameras for submicrosecond exposures in plasma research involving theta and zeta pinches
20 p3635 A70-40526
- Electric field finite amplitude oscillations of electron hole plasma during pinch effect, considering impurities stabilizing effect
22 p4084 A70-43468
- PLASMA POTENTIALS**
Probe impedance loss in cold magnetoplasma related to distribution of point charge potentials
02 p0346 A70-12124
- Thermodynamic potential of meson-nucleon plasma, showing variation of Landau equation of state in hydrodynamic theory of multiple particle production
03 p0527 A70-13052
- Plasma space potential measurement by RF characteristics of Langmuir probe
07 p1288 A70-20233
- Scalar potential nonlinear fluctuations in quasi-stationary plasma, deriving expressions for potential spectral function and Langmuir and ion-acoustic fluctuations spectral densities
08 p1550 A70-20844
- Vacuum arc discharge phases before total breakdown, studying high combustion voltage relation to interplasma double layer potential difference
10 p1969 A70-25115
- Emissive probes for measuring plasma potentials over different ion density ranges on SERT spacecraft, detailing calibration and mechanical and electronic configurations
13 p2404 A70-28519
- Collisionless alkali plasma diode with two electrodes emitting electrons and ions with half-Maxwellian velocities, analyzing potential distribution
14 p2622 A70-30660
- Spherical electrostatic probe in uniform quiescent continuum slightly ionized gas for range of bias potential and radius-Debye length ratio
16 p2912 A70-33863
- Plasma space potential measurement with heavy ion beam probe using cesium gun and electrostatic energy analyzer
16 p2960 A70-34339
- Potential calculation from given source distribution, including direct and iterative methods, error analysis, convergence, computer programs and applications in plasma physics
18 p3284 A70-36790
- Phase rate of plasma potential variations in fast ionization waves without electron distribution assumptions
21 p3856 A70-40949
- LF resonances and potential in plane nonisothermal plasma layer, considering electromagnetic field interaction and ionic collisions
24 p4383 A70-45116
- Spatial potential measurements in magnetized non-Maxwellian hydrogen plasma, using Zaitsev-Mnev method
24 p4385 A70-45464
- PLASMA POWER SOURCES**
NT PLASMA ENGINES
Kaufman thruster with predominant radial field, noting electron mobility across ion extraction screen and advantages of uniform plasma distribution
[AIAA PAPER 69-259] 11 p2102 A70-26120
- Army Missile Command 8000 kw plasma facility automatic control system design
20 p3606 A70-39689
- Plasma accelerators for nuclear EM propulsion, considering power supply requirements and differences between plasma and ion engines
22 p4070 A70-43186
- PLASMA PROBES**
NT ELECTROSTATIC PROBES
Probe impedance loss in cold magnetoplasma related to distribution of point charge potentials
02 p0346 A70-12124
- Spherical probe impedance in infinite collisional isotropic plasma investigated for ionospheric applications, selecting electron density
06 p1117 A70-17369
- RF probe admittance in ionosphere investigated for cold anisotropic and warm isotropic plasma diagnostics
06 p1117 A70-17370
- RF probe impedance variations with magnetic field strength in hot plasma for electron gyrofrequencies less than plasma frequency explained by model
06 p1117 A70-17371
- Quadrupole probe for ionospheric plasma resonances involving measurement of mutual impedance between pairs of electrodes
06 p1117 A70-17373
- Sweeping W wire probe in rotational high temperature plasmas for local heat transfer measurement
06 p1120 A70-17699
- Diagnostic methods for field-free plasmas with medium dispersed optical-spectrographic and source monitoring equipment
06 p1063 A70-17728
- Multiple electrode probe characteristics in rarefied plasma flow created by ion source, noting electrode potential role
06 p1064 A70-17886
- Periodic potential probe for diffusive flux to wall measurements in negative glow and back diffusion plasmas
06 p1074 A70-18617
- Plasma sheath transition structure surrounding cylindrical probe in weak axial magnetic field on basis of moment equations
07 p1353 A70-20230
- Thermal sheaths effect on cooled probes for stationary and flowing plasmas measurements at high pressure
08 p1497 A70-21528
- Electron temperature distribution in thermal boundary layer about probe electrodes calculated by successive approximations allowing for electron heating by arc
09 p1734 A70-22167
- Electron and proton temperature differential near earth bow shock determined from plasma probe measurements by Vela 4B satellite
09 p1670 A70-23486
- Plasma magnetic field measurement by scattered light, analyzing electron spectrum modulation with gyration frequency
10 p1916 A70-24401
- Transfer impedance measurement for HF quadrupole probe immersed in hot magnetoplasma
10 p1877 A70-24709
- Neutral-dominated plasma turbulence, discussing space-time plasma probe correlation functions for electron density fluctuations measurements
11 p2095 A70-26757
- Mathematical model of microwave probe for reentry plasma, using variational method to calculate reflection coefficient
12 p2230 A70-26983
- E region plasma parameters measurement by in situ probes, considering electron density and temperature
12 p2225 A70-27737

PLASMA PROPULSION

Emissive probes for measuring plasma potentials over different ion density ranges on SERT spacecraft, detailing calibration and mechanical and electronic configurations [AIAA PAPER 69-272] 13 p2404 A70-28519

Plasma properties investigation by laser beam probes, considering direct observation of oscillation mode 13 p2458 A70-28564

RF floating double probe for plasma ionization density and electron temperature 15 p2778 A70-31755

Magnetic fields effect on probe measurements in weakly ionized Ar plasma flow at atmospheric pressure 17 p3139 A70-34693

Continuum theory of spherical electrostatic probes as measuring devices in high density weakly ionized gases 17 p3140 A70-34931

Plasma resonance phenomena related to ionospheric plasma parameters using gyroplasma probe on Kappa 8-15 sounding rocket 17 p3077 A70-35307

Winter ionosphere electron density profile from rocket-borne gyro-plasma probe observations 17 p3078 A70-35308

Ionospheric sounding with gyro-plasma probe on Kappa 8-15 rocket, discussing electron density profiles and plasma resonance 17 p3079 A70-35638

Miniature multigrid probes for measuring energy spectra of charged particles and absolute plasma densities, comparing results to microwave measurements 18 p3294 A70-36150

Plasma properties across bow shock and in magnetosheath as function of supersonic solar wind 19 p3494 A70-37481

Emitting plasma probes floating potential, discussing emission rate dependence on probe temperature and surface coverage by seed 20 p3632 A70-39607

Coaxial three coil probe measuring local electrical conductivity and velocity in plasma streams, discussing operations in electrolytes and axisymmetric plasma stream 20 p3684 A70-40259

Maintenance voltage of RF argon thermal induction plasma at atmospheric pressure as function of ring probe 21 p3859 A70-41904

Probe technique for plasma electron temperature measurements at medium and high pressures, examining thermal boundary effects 22 p4078 A70-42362

Nonzero electron temperature effect on mutual impedance of quadrupole probe in hot isotropic plasma 22 p4080 A70-42720

Plasma with oriented charged particle fluxes macroscopic parameter measurement by multigrid probes facing and reversed to drift, noting graphical data processing 24 p4385 A70-45454

PLASMA PROPULSION

Chemical engineering problems of resistojets, pulsed plasma, ion bombardment and colloid thrusters 01 p0166 A70-10974

TV data transmitted by Iantars series automatic ionospheric laboratories released by geophysical rockets at 100-400 km, discussing plasma-ion propulsion system performance 04 p0735 A70-14936

Plasma devices for spacecraft propulsion taking into account electrothermal, electromagnetic and electrostatic systems 05 p0895 A70-15817

Repetitively pulsed quasi-steady vacuum arc magnetoplasmadynamic accelerator for propulsion, using electrolytic capacitors as power source [AIAA PAPER 70-167] 06 p1133 A70-18228

Pulsed plasma transfer systems weight analysis, studying propellant density gradients effects on coaxial plasma gun performance [AIAA PAPER 70-168] 06 p1133 A70-18231

Kaufman thruster performance dependence on transmission of ion extraction optics and magnetic field shape 07 p1365 A70-19705

RF interference emanating from satellite-borne pulse plasma thruster by measuring RF power at UHF antenna having plasma in near field 11 p2103 A70-26136

Lithium vapor fueled applied field MPD arc jet performance using open end heat pipe vaporizer and hollow cathode [AIAA PAPER 69-241] 13 p2475 A70-29959

Rotating plasma disturbances onset in MPD arc, determining magnetic field dependence on mass flow, background pressure and propellant [AIAA PAPER 69-232] 13 p2475 A70-29961

Continuously working plasma thrusters, describing operating principles of Hall current and self magnetic acceleration systems 15 p2790 A70-32277

Axial propellant density gradients and circuit capacitance correlated with pulsed coaxial plasma gun efficiency 21 p3858 A70-41726

PLASMA RADIATION

Equilibrium state of high current discharge in low conductivity plasmas, obtaining light sources at low temperatures 01 p0152 A70-10993

Bremsstrahlung emission from thermal plasma coexisting with relativistic electron tails, noting enhancement at electron plasma frequency harmonics 02 p0348 A70-12240

Focused deuterium plasma discharge neutrons and X rays energy spectra, flux and time resolved collimation measurement with nuclear emulsions and scintillation detectors 02 p0348 A70-12241

Cylindrical axial plasma flow fields velocity radial dependence measurement by double-wedge spectroscopy using Abel unfolding of Doppler shifts 02 p0349 A70-12657

Laser emission action at 4880 Å in plasma discharge from injecting electron beam into Ar at different pressures 03 p0530 A70-13063

Electron relaxation in shock heated Ar plasma estimated by measuring radiation intensity at various frequencies 03 p0535 A70-14363

Photon absorption and emissivity of nonequilibrium cylindrical plasma in Doppler broadened lines and hemisphere approximation 04 p0724 A70-14411

Phase lock technique study of 10.6 micron radiation effect in carbon dioxide laser plasmas on 2.4 micron spontaneous emissions and plasma impedance 05 p0857 A70-16071

Electron distribution function in quasi-static free moderately ionized plasma with partial radiation trapping determined from electron-electron collisions 05 p0889 A70-16452

Charged particle concentration emitted by inhomogeneous plasma determinable from emission spectral lines broadening, suggesting error correction procedure 05 p0889 A70-16541

Astrophysical plasmas radio emission interpreted as collective bremsstrahlung due to ultrarelativistic electron tails, discussing Crab Nebula, quasars and Jupiter 05 p0904 A70-16932

Transmission and emission of radiation from dense inhomogeneous finite laboratory plasma column in magnetic field with interpretation by cold plasma theory 06 p1116 A70-13767

Cerenkov radiation in infinite anisotropic electron plasma linearly polarized in magnetic field having linear electron distribution moving with uniform velocity 06 p1120 A70-17538

Uranium plasma design and characteristics, measuring emission and absorption coefficients as function of temperature and pressure [AIAA PAPER 70-43] 06 p1122 A70-18084

Spectrally and spatially resolved measurements on arc heated Ar plasma radiation for eliminating discrepancies in transition probabilities [AIAA PAPER 70-42] 06 p1122 A70-18187

Inhomogeneous plasma cylinder skin effect, surface impedance, radiation transport and mean noise temperature 07 p1347 A70-19107

Plasma polarization shift for resonance line of ionized He in shock tube due to negative space charge 07 p1348 A70-19273

Pulsed dense argon plasma arcs radiation spectra in visible and UV regions as function of current and pressure 07 p1349 A70-19652

Emission containment and working temperature reduction possibility in thermonuclear reactor by increasing plasma densities and introducing large atomic number contaminants 07 p1350 A70-19847

Electron density dependence on electron temperature during self and mutual interaction of electromagnetic waves in magnetoplasma, tabulating numerical results 07 p1351 A70-19968

Radio wave propagation in anisotropic plasma consisting of oxygen ions and protons, deriving expressions for radio wave refractive index 07 p1355 A70-20452

Plasma display system characteristics and history, discussing gas discharge cell construction and behavioral mechanisms 08 p1499 A70-21688

Fluidic logic elements to control firing and extinction of plasma matrix display system cells with constant electrical power supply 09 p1673 A70-22032

Thermal radiative transfer in nonuniform anisotropic magnetoactive plasma, correcting term of Zheleznyakov equation 09 p1734 A70-22514

Photon bremsstrahlung from relativistic hydrogen plasma determined by studying electron-positron pairing effect on plasma radiation intensity 09 p1735 A70-22986

Distortion of electromagnetic pulse undergoing total internal reflection in inhomogeneous isotropic plasmas in lower ionosphere 09 p1639 A70-23672

Fluidic logic elements for controlling selected cells extinction in hybrid plasma-fluidic display 09 p1738 A70-23758

Laser radiation conversion into kilovolt X rays using planar heated plasma, discussing electron temperature role 10 p1921 A70-23987

Radiative capacity measurement for plasmas produced from nonconducting materials by pulsed discharges in magnetic field 10 p1923 A70-24252

Continuum radiation of nitrogen plasma at atmospheric pressure at high temperatures 10 p1923 A70-24472

Stationary low pressure plasma enclosed in emitting surfaces calculated for spatial charge density distribution 10 p1923 A70-24539

Plasmas role in emission mechanisms active in celestial sources of radiation, discussing sun and quasars 10 p1948 A70-25027

Energy balance of self sustaining thermonuclear reaction with nonuniform magnetic field in wall-contained dense plasma, allowing for radiation losses 11 p2088 A70-25709

Microwave radiation from electron beam generated turbulent magnetoplasma measured, indicating enhancement near electron cyclotron harmonic frequencies 11 p2095 A70-26760

Stellar plasma neutrino pair emission, comparing photon neutrino coupling with current current coupling theory and white dwarf evolution 12 p2297 A70-26976

Radiative intensity calculations for carbon dioxide and carbon dioxide-nitrogen plasmas for various temperatures, densities and path lengths, computing UV and continuum spectra 12 p2275 A70-27170

Radiation emission and transfer in unsteady outer space plasmas, discussing turbulence mechanisms involving electron and ion motion, relativistic and non-relativistic electron beams, etc 12 p2305 A70-27854

Bremsstrahlung radiation emitted from homogeneous, field free, nonrelativistic plasma, deriving formulas 13 p2456 A70-28500

Incoherent scattering of radiation from collisionless plasma in quasi-stationary state, analyzing wave energy from spectral decomposition for given background distribution function 13 p2457 A70-28558

Far UV emission spectrum of plasma produced by laser beam impact on Al target observed as function of time, determining electron temperature 13 p2460 A70-28729

Gas discharge gap preionization by thin preheated tungsten wire ignition without explosion, resulting in plasma turbulence prevention and radiation density increase 13 p2462 A70-28986

Electron collision frequency effects on Cerenkov radiation from magnetoplasma, applying results to magnetosphere and ionosphere 13 p2465 A70-29546

Delayed ionospheric resonance echoes radiated from topside plasma after pulse sequence stimulation by Alouette 2 satellite 13 p2370 A70-29904

Emission resonances at harmonics of electron cyclotron frequency in laboratory plasmas, considering stellar optical radiation 13 p2467 A70-29915

Pulsar radiation emission by electrons and protons in close orbit taking into account density, energy and correlation in plasma 14 p2638 A70-30617

Time controllable continuous photon emission from plasma produced by pulsed laser vacuum spark applied to absorption spectroscopy in vacuum UV 15 p2734 A70-31757

Distant radiation from magnetic line source in moving isotropic plasma, discussing dependence on velocity 15 p2778 A70-31835

Two diaphragm combustion shock tube for plasma radiation energy transfer, describing development, performance, make-up and testing 15 p2779 A70-32019

Uranium plasma emission coefficients as function of DC arc operation, measuring intensity spectrum with scanning spectrometer
[AIAA PAPER 70-692] 16 p2950 A70-33554

Plasma wave radiation by electron stream in active solar corona, obtaining spectrum and growth rate 16 p2979 A70-34189

Oxygen, nitrogen and argon plasma total radiation measurement at various wavelengths and temperatures 17 p3139 A70-34547

Rayleigh-Gans-Born approximation application to the thermal radiation of reflecting convex plasma sphere, cylinder and ellipsoid 18 p3294 A70-36146

Regular and stochastic oscillations in plasma beam discharge produced by beam instability from observing time dependent variations in spectral line luminescence intensities 18 p3294 A70-36147

Radiation condition for unbounded anisotropic dispersive magnetoplasma 18 p3295 A70-36492

Radial profiles of emission and absorption coefficients and temperatures in cylindrically symmetric plasmas 19 p3475 A70-37551

Microwave diagnostics of electron density, temperature and light emission in self excited moving striations in hydrogen plasma 19 p3475 A70-37553

Particle flux diagnostics of nonisothermal low pressure plasma, using corpuscular passive method 19 p3476 A70-37556

Surface layer heating of solid body by dense gas discharge plasma radiation, comparing vaporization and reversible opacity onset times in quartz 19 p3482 A70-38733

Ball lightning model assuming radiation field within plasma dielectric region resonant at higher than collision frequency 22 p4016 A70-42780

Scattering indicatrix of electromagnetic radiation in plasma caused by electron-ion interactions 22 p3989 A70-43141

Laser light pulse interaction with solid targets, observing second harmonic generation in induced plasma from time resolved spectra 22 p4084 A70-43673

Atomic hydrogen plasma slab, calculating thermodynamic equilibrium deviations effect on resonance radiation 23 p4223 A70-43824

Hypervelocity impact flash resolved into submicrosecond continuum radiation pulse succeeded by slow rising long duration light pulse from neutral atomic line emission 23 p4227 A70-44553

X ray spectra from paraboloidal plasma focus devices, measuring electron energy produced by photoelectric effect and by Compton scattering 23 p4229 A70-44990

Expansion of laser produced plasma into uniform magnetic field, calculating electromagnetic radiation 24 p4382 A70-45108

Transition radiation due to charged particle moving in periodically stratified cold isotropic plasma 24 p4384 A70-45254

Anisotropic turbulent plasma EM emission due to density fluctuations, noting relationship to turbulence spectrum 24 p4384 A70-45256

Solar flare microwave spectra from coherent plasma emission mechanism 24 p4396 A70-45390

Microwave emission from Maxwellian magnetoplasma in uniform magnetic field 24 p4386 A70-45606

PLASMA RESONANCE

Conductivity and permittivity for ion and electron resonance region of ionospheric plasma model calculated in quasi-hydrodynamic approximation 01 p0082 A70-11528

Warm Maxwellian plasma stabilization of velocity-space instabilities, evaluating densities and temperatures for stabilizing resonant loss-cone modes 02 p0347 A70-12237

Surface wave attenuation in homogeneous plasma cylinder caused by resonance in transition layer between plasma and vacuum 03 p0447 A70-13286

Tonks-Dattner resonances peaks in rare gas plasmas, considering electron densities variations role 03 p0534 A70-14211

Magnetized resonantly sustained HF plasma column wave properties, obtaining above-critical density as function of static magnetic induction 04 p0728 A70-14999

Microwave cavity perturbation measurements of electron densities at electroacoustic resonances excited in afterglow plasma 04 p0728 A70-15004

Topside ray trajectories near upper hybrid resonance 04 p0650 A70-15119

Coupling between LF oscillations and third harmonic frequency resonances of bounded plasma capacitor system, discussing density profile variation 05 p0890 A70-16654

Plasma oscillations, resonances and wave propagation characteristics analyzed by radio pulse sounders for application to space measurements 06 p1115 A70-17360

Ionospheric observations of resonance oscillations using satellite-borne radio sounding instruments 06 p1115 A70-17361

Plasma resonances, considering unbounded and bounded uniform and nonuniform plasmas and nonlinear effects 06 p1116 A70-17365

Electrostatic oscillations in cylindrical column of laboratory plasmas excited by electromagnetic waves, investigating resonances by cold plasma theory 06 p1116 A70-17368

Quadrupole probe for ionospheric plasma resonances involving measurement of mutual impedance between pairs of electrodes 06 p1117 A70-17373

Satellite observations of VLF and ELF resonances related to ionospheric plasma singularities 06 p1118 A70-17375

Plasma polarization shift for resonance line of ionized He in shock tube due to negative space charge 07 p1348 A70-19273

Ion resonance instability in nonneutral plasmas, considering ions addition to low density electron cloud with low kinetic energy 07 p1352 A70-19991

Cold plasma approximation of whistler excitation of lower hybrid resonance at wake of body moving through ionosphere, comparing results with Alouette satellite observations 07 p1276 A70-20425

Longwave and shortwave mode transformation in resonant layer of inhomogeneous plasma 08 p1550 A70-20847

Discharge current effect on shape and position of resonance curves for electron concentrations during microwave oscillation conversion in magnetoactive plasma 08 p1551 A70-20866

Narrow band detector for polarized light in far UV based on plasma resonance 09 p1676 A70-22650

Ionospheric plasma lower hybrid resonance measurement and excitation via rocket-borne probe 09 p1670 A70-23319

Modulation coupling between electron and ion resonances in magnetoactive plasmas, discussing probeless feedback stabilization scheme 11 p2091 A70-26403

Plasma resonance excitation by small pulsed dipole in weakly inhomogeneous plasma determined using WKB solutions and stationary phase approximations 12 p2277 A70-27188

Resonant and nonresonant coupling between two coherent electron plasma waves propagating in opposite directions, considering parametric decay 12 p2279 A70-27780

Tonks-Dattner resonances in plasma columns, considering viscosity effect on radial oscillations in nonuniform plasmas 12 p2281 A70-27792

Energy loss radial dependence due to K resonance radiation for infinitely long plasma cylinder, using approximation method for integrals 13 p2461 A70-28731

Topside ionosphere structure deduced from resonance spikes on ionograms obtained by Alouette 2 satellite and electron density distributions 13 p2395 A70-29091

Alouette satellite antennas and receivers for detecting plasma resonances and VLF signals, noting ground station telemetry link 13 p2380 A70-29902

Alouette 1 plasma resonance observations, analyzing electron density measurements in sheath region and cyclotron harmonic resonant frequencies 13 p2466 A70-29903

Delayed ionospheric resonance echoes radiated from topside plasma after pulse sequence stimulation by Alouette 2 satellite 13 p2370 A70-29904

Floating resonance spike on Alouette 2 ionograms after sounder pulse transmission at half upper hybrid frequency, noting harmonic excitation role 13 p2370 A70-29905

Alouette plasma resonance stimulated perpendicularly to magnetic field by planar dipole charge sheet and permeable grids 13 p2467 A70-29907

Time decay of higher order cyclotron harmonic resonances with decreasing perpendicular wave number 13 p2467 A70-29908

Dispersion and group velocity characteristics of topside resonance oblique echoes near plasma frequencies observed by satellite 13 p2467 A70-29909

Local resonance at upper hybrid frequency from satellite observation, noting effects of electron plasma/cyclotron frequency ratio 13 p2370 A70-29911

Infinitesimal dipole moving through hot uniform electron plasma in magnetic field, investigating asymptotic time behavior of plasma resonance 13 p2467 A70-29912

Collision and motion effect on rocket-borne quadrupole probe transfer impedance near lower hybrid resonance in ionosphere 13 p2371 A70-29919

Bounded hot plasmas with/without steady magnetic field, discussing ion-electron resonances 15 p2779 A70-31997

Plasma resonance phenomena related to ionospheric plasma parameters using gyroplasma probe on Kappa 8-15 sounding rocket 17 p3077 A70-35307

Ionospheric sounding with gyro-plasma probe on Kappa 8-15 rocket, discussing electron density profiles and plasma resonance 17 p3079 A70-35638

Tonks-Dattner resonances in warm inhomogeneous plasma column, examining kinetic theory for waveform shapes and resonance location 19 p3475 A70-37534

Diffuse plasma resonance sequence observed on Alouette 2 ionograms, showing pattern similar to spread echo 20 p3620 A70-39335

Topside plasma frequency resonance below electron cyclotron frequency, discussing ray paths and delay times 20 p3620 A70-39336

Cold nonuniform plasma slab model for afterglow echoes at upper hybrid resonance in uniform magnetic field 20 p3679 A70-39664

Nonlinear resonance conditions for plasma three-wave interactions, considering wave propagation modes and constant magnetic field 20 p3682 A70-40137

Collisionless plasma shock wave instability, discussing resonance and energy dissipation through ion Landau damping 22 p4077 A70-42292

Slow wave propagation on conducting surface separated from plasma by ion sheath, observing resonances on cylindrical antenna 22 p4082 A70-43238

Magnetosonic resonance excitation in waveguide winding wrapped around plasma cylinder 22 p4082 A70-43380

Atomic hydrogen plasma slab, calculating thermodynamic equilibrium deviations effect on resonance radiation 23 p4223 A70-43824

LF resonances and potential in plane nonisothermal plasma layer, considering electromagnetic field interaction and ionic collisions 24 p4383 A70-45116

Resonant electrons interaction with turbulent ion-acoustic plasma oscillations consisting of superimposed three dimensional random phase wave packets 24 p4386 A70-45658

PLASMA RINGS

U TOROIDAL PLASMAS

PLASMA ROCKETS

U PLASMA ENGINES

PLASMA SHEATHS

Spherical and cylindrical electrostatic probe operation analyzed under conditions producing collision-dominated sheaths 01 p0149 A70-10105

Driving point admittance of infinite cylindrical antenna excited by uniform gap and immersed in lossy compressible isotropic plasma, discussing propagation constants 01 p0051 A70-11102

Equatorial patterns measurement of plasma covered axially slotted cylindrical antenna, describing discharge tube, facility and Langmuir probe survey of tube electron density 02 p0269 A70-12590

Microwave nonlinear effects including mixing, harmonic generation and current rectification observed in plasma sheath surrounding Langmuir probe using PIG discharge 05 p0852 A70-16992

Electromagnetic radiation patterns from aperture in conducting cylinder coated with moving isotropic plasma sheath, noting sheath velocity and plasma frequency influence 06 p1020 A70-17564

Reentry plasma RF noise temperature in-flight measurements by Trailblazer 2 compared with computed data 06 p1008 A70-17568

Boundary conditions and iterative procedures for plasma sheath problems, using matrix equation to represent differenced Poisson equation 06 p1123 A70-18295

Plasma sheath transition structure surrounding cylindrical probe in weak axial magnetic field on basis of moment equations

07 p1353 A70-20230

Low energy ions incidence angle effects on secondary electron emission from molybdenum cylinders in low pressure plasma, noting role of Langmuir sheath around target

07 p1355 A70-20356

Supersonic flight vehicle plasma sheath effect on effective range of onboard radar installation, discussing SNR

08 p1461 A70-20869

Plane electromagnetic wave scattering by perfectly conducting cylinder coated with moving dielectric or plasma sheath, using relativity theory, Lorentz transformations, etc

08 p1551 A70-21251

Thermal sheaths effect on cooled probes for stationary and flowing plasmas measurements at high pressure

08 p1497 A70-21528

Plasma sheath in quadrupole and hexapole geometries, investigating magnetic field variation, particle density and electrostatic potential in transition layer

08 p1552 A70-21530

Integrated electron density determination for plasma sheath on reentry vehicle based on power coupling change measurement

08 p1552 A70-21596

Electron density reduction in plasma surrounding reentry vehicle due to N atom removal by water droplets injection

09 p1737 A70-23237

Ion acoustic wave propagation near sheath at plasma-wall boundary in low pressure argon plasma measured by electron beam probe

10 p1921 A70-23965

Ion-burst excited by pulsed mesh grid in plasma in connection with sheath structure

10 p1922 A70-23989

Comets ionized shells, studying plasma expansion in corpuscular solar wind magnetic field

10 p1940 A70-24372

Surface waves excited by oscillating current in cold plasma surrounded by metallic sheath of infinite conductivity, deriving frequencies and growth rates

11 p2089 A70-25717

Stability of realistic inhomogeneous plasmas with sheaths, examining electron beam-stable Maxwellian plasma interaction

11 p2090 A70-26021

Sheath structure of plasma diode using kinetic theory model of plasma-sheath transition

13 p2376 A70-28642

Cylindrical electric dipole antenna in magnetoactive ionospheric plasma, noting ion sheath effect on input impedance and active length

13 p2399 A70-29402

Plasma sheath boundary as closed Mach surface, demonstrating Bohm criterion application to ion velocity component normal to sheath edge

13 p2464 A70-29465

Transition radiation in plasma sheet in vacuum assuming specular reflection of electrons at vacuum boundary

13 p2464 A70-29512

Radiation from electric dipole oriented normal to magnetostatic field in plasma column improving antenna transmission characteristic during reentry

13 p2467 A70-29913

Electric field intensity and extension of space charge sheath for ion extraction from nitrogen plasma

14 p2622 A70-30661

Container wall-collision plasma sheath model for charge carrier investigation using velocity distribution [DFVLR-SONDDR-51]

14 p2622 A70-30662

Low density collisionless plasma sheath in planar and cylindrical geometry under weak magnetic field, considering ion-electron pair generation

14 p2624 A70-31040

Steady state potential distributions near photoemitting plate immersed in plasma, noting overshoot effects role for sheaths around satellites in interplanetary plasma

15 p2778 A70-31906

Plasmopause motion in equatorial plane under sudden dawn-dusk field with constant solar wind-magnetosphere interaction

20 p3620 A70-39341

Radiation theory circular waveguide in dominant TE mode and flush mounted to infinite conducting flat ground plane covered by plasma or dielectric sheath

20 p3586 A70-39500

Positive ions energy dispersion effused from RF plasma, presenting ion extraction model for plasma sheath system and equivalent circuit

20 p3678 A70-39608

Ionospheric plasma sheath effect around floating cylindrical high power dipole antenna, obtaining electron, ion and potential profiles

20 p3589 A70-40466

Spacecraft sheath structure, potential and velocity effects on ion current measurements by traps and mass spectrometers

21 p3816 A70-41087

Continuous pseudoacoustic and ion waves excitation and damping in plasma sheath around grid, taking into account transit time effect on ion acceleration

21 p3858 A70-41710

Sheaths effect on capacitance of plane grid capacitor in plasma, discussing satellite aerials admittance

21 p3792 A70-42046

Plasma sheath boundary in anisotropic plasma taking into account ionization rate, momentum transferring collisions and finite ion temperature

22 p4077 A70-42291

Electron densities between inner edge plasma sheet and plasmasphere as function of geocentric radial distance fromOGO-3 electrostatic measurements

23 p4236 A70-43834

Dipole antenna in compressible lossy plasma, calculating sheath and absorptive surface effects on current distribution from boundary value problem formulation

23 p4228 A70-44963

Quasi-ambipolar diffusion in arc discharges in magnetic field, calculating ions and electrons density distributions between anode and cathode sheaths

24 p4384 A70-45148

PLASMA SLABS

Seasonal effect on F region midlatitude slab thickness diurnal variations during magnetic disturbances using monitoring VHF signals from geostationary satellites

02 p0290 A70-12160

Microwave transmission through afterglow of RF excited electrodeless He discharge approximating low collision frequency plasma slab of uniform electron density in magnetic field

03 p0530 A70-13152

Electromagnetic wave growth effect on wave field propagating along beam-plasma slab, showing Poynting vector component

04 p0651 A70-15293

Power reflection and transmission coefficients for polarized electromagnetic waves incident on plasma slab moving along magnetostatic field

06 p1008 A70-17566

Effective noise temperature of planar aperture antennas in lossy inhomogeneous plasma slabs calculated by computer

09 p1646 A70-22704

Electromagnetic scattering from underdense plasma slabs with randomly varying dielectric constant, calculating reflection coefficient

11 p2095 A70-26763

Small amplitude HF electromagnetic wave penetration in hot plasma slab, showing wave period/transit time ratio dependence of electromagnetic field distribution

14 p2551 A70-31037

Electromagnetic field transmission through plasma slab with specified electron density-collision frequency profiles, using integral derived from transmission and reflection coefficients

16 p2957 A70-32979

VLF wave generation due to nonlinear interaction of two microwaves with plasma slab under high DC field

22 p4077 A70-42294

Total electron content and equivalent slab thickness statistical data during magnetic disturbances from AT-3 satellite VHF transmission observations

22 p4020 A70-43162

Atomic hydrogen plasma slab, calculating thermodynamic equilibrium deviations effect on resonance radiation

23 p4223 A70-43824

Geomagnetic tail and plasma sheet hydromagnetic oscillations, deriving dispersion equations and stability conditions

23 p4184 A70-43829

PLASMA SOUND WAVES

U MAGNETOHYDRODYNAMIC WAVES

U PLASMA WAVES

PLASMA SPECTRA

Giant pulse Q switched lasers generated plasmas, noting VUV spectral line shifts, asymmetries and existence of satellite lines

02 p0345 A70-11894

Spectrum function in Booker scattering formula /first order Born approximation/ for dielectric constant fluctuations in hypersonic wake plasmas

03 p0529 A70-12908

Supersonic plasma jets studied spectroscopically, determining atomic levels populations, population inversion conditions, electron temperature and concentration distributions, etc

03 p0531 A70-13254

Plasma jet temperature and density determination from intensity ratio of H beta line and continuous spectrum

04 p0725 A70-14535

Vibrational relaxation and continuous spectrum transition during dissociation of diatomic low temperature plasma

04 p0721 A70-14539

Classical path methods for treating Stark spectral line broadening in plasmas illustrated by Lyman alpha line of hydrogen calculations

04 p0726 A70-14670

Visible light emission from nonequilibrium Cs plasma measured for spectral intensity distribution, suggesting excitation mechanism in terms of collision-radiation model

05 p0887 A70-16109

Transition probability and Stark profile of H alpha standards for absolute intensity calibration of spectroscopic data from thermal shock tube plasma

05 p0853 A70-17083

Plasma quasi-stationary turbulence spectrum determination from nonlinear equations for Langmuir waves interaction, considering fast particles effects

06 p1119 A70-17499

Calcium neutral and ionic lines broadening and shift by microfields measured by plasma flame observations

06 p1148 A70-18453

Turbulence spectra and generated power determined for plasma turbulence in objects with high electromagnetic radiation density /quasars and supernova shells/

07 p1384 A70-19412

Scalar potential nonlinear fluctuations in quasi-stationary plasma, deriving expressions for potential spectral function and Langmuir and ion-acoustic fluctuations spectral densities

08 p1550 A70-20844

Photoelectrons entry into F region detected at conjugate point during winter night by Thomson scatter observations of plasma lines appearing in signal spectrum

08 p1489 A70-21386

Convective-current instability in finite length plasma column, analyzing spectrum of unstable harmonics

08 p1554 A70-21802

Langmuir HF turbulence effect on anisotropic plasma oscillation spectra, determining instability conditions

08 p1554 A70-21809

Plasma electron density determination by number of extreme resolved line, considering broadening action by Doppler effect for Balmer, Lyman and Paschen series

09 p1734 A70-22731

High electron density plasma generation by ionized gaseous filament explosion, noting plasma frequency effect on spectral brightness

10 p1915 A70-23961

Plasma turbulence spectral theory, considering cascade processes in collisional and collisionless dissipation

11 p2095 A70-26756

Radiative intensity calculations for carbon dioxide and carbon dioxide-nitrogen plasmas for various temperatures, densities and path lengths, computing UV and continuum spectra

12 p2275 A70-27170

Turbulence spectrum due to density fluctuations in plasma with strong magnetic field, using hydrodynamic theory and Poisson equations

13 p2457 A70-28559

Radial ion temperature distribution in hydrogen arc within axial magnetic field measured spectroscopically by thermal Doppler effect

14 p2621 A70-30657

Plasma satellites near He I forbidden lines during turbulent heating

19 p3475 A70-37441

Coupling constant and binary collision expansions for ion motion in plasma line broadening

21 p3855 A70-40722

Steady state frequency spectra for Alfvén waves and MHD turbulence in collisionless plasma with nonlinear interaction by particle scattering

24 p4383 A70-45114

Clean shock tube maintaining high gas purity level for Ar plasma spectroscopy

24 p4388 A70-46271

PLASMA SPRAYING

Parameters effect on radius of dispersion during plasma and detonation spray coating process of niobium and zirconium carbides

06 p1076 A70-17849

Directional emissivity and thermal diffusivity of solids at 1000-3000 K by radiation comparison method, applying to sintered and plasma sprayed Mu, Ta and W

23 p4207 A70-44661

PLASMA STABILITY

U MAGNETOHYDRODYNAMIC STABILITY

PLASMA TEMPERATURE

Ionization instability in low temperature magnetized plasma, analyzing electron concentration perturbation caused by Joule heating during electron-ion collisions

01 p0153 A70-11598

Measurement techniques for determining density and temperature distributions along radius of plasma cylinder by electron cyclotron resonance, microwave refraction and acoustic resonance

02 p0349 A70-12758

P-n junction and microplasmas voltage temperature coefficients during avalanche breakdown
03 p0541 A70-13729

Electron temperature of hydrogen-oxygen flame plasma obtained by floating probe method compared to spectroscopic method results
03 p0608 A70-14380

Thin film heat gauge for measuring thermal transport from plasma to end wall of shock tube, discussing measurements in high temperature Ar
03 p0496 A70-14381

Plasma jet temperature and density determination from intensity ratio of H beta line and continuous spectrum
04 p0725 A70-14535

Excitation temperature functions calculated in rare gases spectrum lines to determine radial plasma temperature distribution
05 p0886 A70-15798

Laser produced plasma temperature measurements using method of X rays selective transmissions through different absorbing films
06 p1081 A70-17596

Solar wind temperature, using distribution function for solar wind ions in anisotropic Maxwell distribution form
06 p1135 A70-17895

Longitudinal spectral line intensity distributions measured for plasma temperature determination
06 p1074 A70-18601

Equivalent excited-state temperature of high pressure plasma calculated for unequal electron and gas temperature, considering ion and electron recombination
06 p1114 A70-18634

Plasma temperatures in magnetosphere, investigating ion energy balance, electron heating and agreement with rocket measurements
08 p1489 A70-21381

Alkali seeded plasma electron density and temperature enhancement by laser resonance pumping
08 p1552 A70-21576

Thermal and nonthermal plasmas for ion production, discussing gas pressure, voltage and discharge current effects on electron temperature
09 p1734 A70-22037

Plasma energy confinement time as function of discharge parameters for plasma thermal insulation in Tokamak-3
11 p2088 A70-25713

Thermal conductivity of argon, nitrogen and air plasmas at atmospheric pressure and 6500-16500 K range, discussing electric arc source
11 p2148 A70-25760

Nitrogen oxide ions mobility in air calculated at high plasma temperatures
12 p2276 A70-27845

Impurities and electrothermal instabilities effect on conductivity of two temperature nonequilibrium plasma
12 p2281 A70-27846

Variable temperature plasma with two ion species, noting rarefaction wave propagation during one dimensional expansion into vacuum
13 p2464 A70-29415

High argon plasma temperatures via pulsing constricted electric arc
14 p2621 A70-30504

Mars upper atmosphere refractivity, free electron number density and plasma temperature altitude profiles from Mariner 1969 radio occultation measurements
14 p2646 A70-31072

Plasma temperatures of X ray flux from laser induced breakdown plasmas in air, using absorption spectrometer
[ARL-70-0145] 15 p2750 A70-31753

Anisotropic temperature plasma susceptibility calculation based on velocity moment equations and circular polarized coordinates, compared to Vlasov equation solution
17 p3140 A70-34929

Ar plasma generation by focused Q switched ruby laser beam, measuring density and temperature by electro-optical spectroscopy
17 p3107 A70-35111

Spatial-temporal distribution of laser spark plasma electron density and temperature based on holographic interferometry
18 p3265 A70-36152

Shock layer microwave radiation measurements during reentry flight of spherical nose cone, determining effective plasma temperature
[AIAA PAPER 69-183] 18 p3208 A70-36694

Electronic excitation contribution to frozen properties and cut-off criteria of high temperature gas plasma
18 p3296 A70-36955

Radial profiles of emission and absorption coefficients and temperatures in cylindrically symmetric plasmas
19 p3475 A70-37551

Microwave diagnostics of plasma temperature and conductivity in streaming nitrogen arc with skin effect under atmospheric pressure
19 p3476 A70-37554

Ion temperatures and incident intensities in plasmas produced by solid target irradiation with Q switched laser beam
19 p3479 A70-37765

Soviet papers on transfer phenomena in low temperature plasmas
19 p3480 A70-38180

Emitting plasma probes floating potential, discussing emission rate dependence on probe temperature and surface coverage by seed
20 p3632 A70-39607

Spectral lines self rotation effects on plasma temperature and density measurement in MHD duct boundary layer
20 p3678 A70-39632

X ray emission of hot dense intergalactic plasma, discussing evolution equation for temperature and degree of gas ionization vs red shift
21 p3877 A70-40702

Low electron temperature plasma measurements by electrostatic planar guard ring probe with floating potential electrode, discussing electronic circuit
21 p3830 A70-42015

Probe technique for plasma electron temperature measurements at medium and high pressures, examining thermal boundary effects
22 p4078 A70-42362

Plasma generation by pulsed laser heating, investigating ionization effects on temperature
22 p4082 A70-43224

Temperature, densities and electric field strength of cascaded arcs burning in He under normal pressure
24 p4384 A70-45425

Translational temperature measurement of atoms and ions in plasma based on wavelength reduction by X ray spectroscopy
24 p4388 A70-46208

PLASMA THEORY U PLASMA PHYSICS

PLASMA TURBULENCE

LF electromagnetic waves theory for turbulent plasma based on expansion of particle collision and turbulent pulsation integrals
01 p0150 A70-10211

Particle distribution and plasma nonequilibrium field evolution with turbulence generation by microwave field, considering plasma kinetic instability
01 p0150 A70-10212

Kinetic equation of helicons interactions in electron-hole plasma, discussing turbulence spectrum and effect on current carrier drift velocity
03 p0531 A70-13407

Turbulent submerged plasma jet boundaries calculated theoretically and compared with experimental results from dynamic head profiles
03 p0532 A70-13515

Plasma turbulence theory formulated using averaging operators, obtaining nonlinear dispersion relation for turbulent diffusion coefficients
03 p0537 A70-14377

Turbulent-plasma electrons ballistic effects on solar wind magnetic field fluctuations in lunar vicinity
04 p0753 A70-15123

HF conductivity tensor of isotropic plasma, taking into account particle correlations describing weakly Langmuir turbulent plasma
05 p0889 A70-16532

Plasma quasi-stationary turbulence spectrum determination from nonlinear equations for Langmuir waves interaction, considering fast particles effects
06 p1119 A70-17499

Anisotropic plasma instability in nonlinear stage, studying turbulent relaxation of ion distribution by quasi-linear theory
06 p1119 A70-17501

Turbulence spectra and generated power determined for plasma turbulence in objects with high electromagnetic radiation density /quasars and supernova shells/
07 p1384 A70-19412

Scalar radiative transport equation solved iteratively for microwaves backscattering from turbulent plasma, deriving model for direct and cross polarized cross section
07 p1353 A70-19993

Plasma physics relating turbulence to cosmic rays covering oscillations, turbulent acceleration, subcosmic rays, langmuir turbulence spectra and acceleration, etc
07 p1371 A70-20332

Langmuir HF turbulence effect on anisotropic plasma oscillation spectra, determining instability conditions
08 p1554 A70-21809

Turbulent diffusion and ion heating in plasmas in presence of current instability
08 p1554 A70-21813

Nonlinear wave interactions in quiescent plasma column with external disturbance creating broadened frequency spectrum and weakly turbulent plasma
10 p1922 A70-24146

Cascade theory of turbulence, applying cascade decomposition resulting from Navier-Stokes application to hydrodynamic turbulence to Riemann equation for atmospheric and plasma turbulence
10 p1868 A70-24167

LF ion-acoustic wave nonlinear interaction with HF Langmuir waves in nonisothermal plasma, establishing criteria for ion plasma turbulence
10 p1925 A70-25103

Cascade mechanism of closure associated with nonlinear wave interactions between modes in turbulent plasmas, using hydrodynamical model
11 p2087 A70-25358

Turbulence of fluids and plasmas - Conference, New York, April 1968
11 p2093 A70-26751

Plasma turbulence stochastic processes, considering radiation, transport and acceleration mechanisms and relationships to fluid turbulence
11 p2094 A70-26752

Plasma turbulence theory, discussing particles stochastic acceleration in strong electric field
11 p2094 A70-26753

Thermal plasma devices with discrete modes, describing periodic pulling and transition to continuous noise spectrum characteristic of turbulence
11 p2094 A70-26754

Plasma turbulent diffusion across constant magnetic field, noting magnetic, kinetic energy and relaxation times ratio effects
11 p2094 A70-26755

Plasma turbulence spectral theory, considering cascade processes in collisional and collisionless dissipation
11 p2095 A70-26756

Neutral-dominated plasma turbulence, discussing space-time plasma probe correlation functions for electron density fluctuations measurements
11 p2095 A70-26757

Microwave radiation from electron beam generated turbulent magnetoplasma measured, indicating enhancement near electron cyclotron harmonic frequencies
11 p2095 A70-26760

Microwave scattering by turbulent plasma electron density fluctuations
11 p2096 A70-26765

Radar interferometry as diagnostic method for remote probing of turbulent plasma
11 p2096 A70-26766

Homogeneous plasma turbulence growth limits, determining bounds on density and electromagnetic field nonlinear fluctuations in thermodynamic terms
11 p2096 A70-26767

Turbulent flowing plasma, analyzing wavenumber frequency dependent spectral function and space-time correlation function
11 p2096 A70-26768

Plasma turbulence theory application to experimental phenomena using two stream instability example
11 p2096 A70-26769

Solar wind magnetic field power spectra and plasma velocity, discussing turbulence, viscosity and dissipation
11 p2106 A70-26770

Turbulence in incompressible electrically conducting fluid with uniform applied magnetic field, discussing nonlinear energy transfer mechanisms and magnetic effects
11 p2096 A70-26771

Gas and electron density fluctuations in weakly ionized turbulent wake behind hypersonic spheres and cones
11 p1978 A70-26773

Plasma turbulence due to nonlinear wave interaction, considering second sound LF oscillations propagation and plasmons scattering at ions
12 p2278 A70-27358

Diffusion coefficients measurements in velocity space from ion-ion collisions and ion wave microturbulence, supporting theoretical calculations and diffusion equations in plasma
12 p2279 A70-27777

Collisional drift-wave turbulence in Li Q-machine plasma far unstable regime, discussing power spectra variations of density fluctuations
12 p2280 A70-27784

Radiation emission and transfer in unsteady outer space plasmas, discussing turbulence mechanisms involving electron and ion motion, relativistic and non-relativistic electron beams, etc
12 p2305 A70-27854

Plasma turbulence in Van Allen belts, examining weak turbulent electromagnetic wave properties, with emphasis on trapped energetic particles radiation
13 p2486 A70-28555

Turbulence spectrum due to density fluctuations in plasma with strong magnetic field, using hydrodynamic theory and Poisson equations
13 p2457 A70-28559

Collisionless plasmas strong turbulence in terms of mixing length and Hamilton-Jacobi theories
13 p2458 A70-28562

Witness particle electric field as function of nonlinear conductivity of weakly turbulent anisotropic plasma by perturbation method
13 p2465 A70-29638

Stochastic particle acceleration by VLF in weakly turbulent plasmas in magnetic field, considering nonlinear cyclotron damping
13 p2468 A70-29935

PLASMA WAVES

Anisotropic plasma turbulence produced by two stream instability onset near light cylinder of rotating magnetic star for pulsar model 14 p2640 A70-30788

Weakly turbulent plasma dielectric constant nonlinear tensor for frequent Coulomb collisions, using hydrodynamic equations 15 p2781 A70-32824

Coherent wave propagation in warm turbulent plasma, using perturbation method for wave dispersion 16 p2860 A70-32945

Ion beam scattering at turbulent plasma oscillations in glass chamber containing low pressure air 16 p2958 A70-33253

Electron density fluctuations in transitional zone of turbulent plasma jet, using digital analysis of Langmuir probe signals [AIAA PAPER 70-731] 16 p2958 A70-33495

Correlation functions of weak quasi-steady plasma turbulence determined by plasmon interactions, using computerized integral equation 17 p3139 A70-34643

Mutual coherence function of light scattered by plasma turbulent electron density fluctuations, taking into account refractive index changes 17 p3137 A70-35722

Interplanetary plasma disturbances in Venus proximity from Venera measurements 18 p3312 A70-36172

Electron beam interaction with ionized K plasma, considering Langmuir waves instability, turbulence and electron heating 18 p3295 A70-36614

Relativistic electron spectra of cosmic rays accelerated by plasma turbulence, examining singularity in solution 18 p3322 A70-37127

Permittivity tensor of weakly turbulent magnetoactive cold electron plasma, calculating nonlinear currents 20 p3677 A70-39296

Electromagnetic waves scattering from dense turbulent plasma, calculating radar cross sections of inhomogeneous plasma for peak electron densities 20 p3586 A70-39459

Collisionless cylindrical Langmuir probe response in turbulent plasma for mean and statistical properties 20 p3684 A70-40258

Current driven ion wave plasma turbulence in collisionless shock, measuring frequency and wave number spectra by shock front light scattering 20 p3685 A70-40497

Temporal and spatial origin of hot ions in turbulent plasma heating, using particle analysis 21 p3855 A70-40824

Plasma turbulence statistical theory in magnetic field based on averaging operators, deriving nonlinear dispersion relation 21 p3857 A70-41386

Electromagnetic scattering power spectrum from underdense turbulent plasmas, deriving first and second moments 21 p3858 A70-41732

Collisionless magnetospheric plasma turbulent conductivities for weak and strong electric fields parallel to magnetic field 22 p4016 A70-42787

Plasma turbulence due to nonlinear wave interaction, considering second sound LF oscillations propagation and plasmons scattering at ions 22 p4084 A70-43599

Collisionless plasma weak turbulence theory derivation from Vlasov equations, considering interactions between oscillation modes 23 p4225 A70-44182

Turbulent collisionless plasma shocks formation, wave front steepness and explanation for earth bow shock 23 p4225 A70-44183

Ion beam scattering at turbulent plasma oscillations in glass chamber containing low pressure air 23 p4226 A70-44282

Scaling laws for turbulent plasma anomalous conductivity dependent on electrostatic fluctuation spectrum 23 p4227 A70-44796

Turbulent plasma without external magnetic field, observing low phase velocity ion wave mode 23 p4227 A70-44893

Anisotropic turbulent plasma EM emission due to density fluctuations, noting relationship to turbulence spectrum 24 p4384 A70-45256

Resonant electrons interaction with turbulent ion-acoustic plasma oscillations consisting of superimposed three dimensional random phase wave packets 24 p4386 A70-45658

PLASMA WAVES

NT ELECTROSTATIC WAVES

LF longitudinal waves propagation in DC gas discharge plasma, obtaining wave dispersion equation for various limiting cases 01 p0149 A70-10162

LF electromagnetic waves theory for turbulent plasma based on expansion of particle collision and turbulent pulsation integrals 01 p0150 A70-10211

Absorbed RF plasma wave noise spectrum in region of anomalous dispersion, noting peak in far IR region 01 p0150 A70-10286

Acoustic wave excitation and damping in cryogenic He plasma produced by HF pulse discharge, considering nonadiabatic heating and dissipation during reflection 03 p0529 A70-13056

Ion-cyclotron oscillations in plasmas, considering plasma waves and oscillation characteristics 03 p0530 A70-13065

Charged particles motion in isotropic weakly ionized plasma acoustic wave associated with difference in electrons and ions entrainment by neutral particles 03 p0530 A70-13087

Dispersive compression of plane frequency modulated waves in inhomogeneous plasma based on generalizing geometric optics approximation to unsteady quasi-harmonic processes 03 p0447 A70-13287

Van der Pol equation for finite amplitude ion-acoustic waves in unstable plasma propagating across weak magnetic field 03 p0531 A70-13404

Nonlinear drift wave buildup in inhomogeneous plasma faster than in linear approximation 03 p0531 A70-13509

MGD finite flow regions surrounded by nonconducting gas, considering wave behavior at boundary of conducting region and magnetic field influence 03 p0533 A70-13803

Solutions properties of initial and mixed initial-boundary value problems of wave equations 03 p0537 A70-14384

Collimated light beam enhanced scattering and anomalous absorption due to decay into plasma waves 04 p0727 A70-14996

Nonlinear propagation of electron plasma wave in cylindrical waveguide, discussing linear theory of electrostatic waves in cold plasma 04 p0728 A70-15000

Electrostatic field effects of electromagnetic wave propagation in anisotropic plasma 04 p0728 A70-15002

Critique of paper on transverse enhanced bremsstrahlung from supraluminous and subluminal longitudinal waves in isotropic homogeneous plasma 04 p0728 A70-15006

Scattering cone of hydromagnetic waves propagating along magnetic lines in magnetized plasma with oscillating electric dipole 04 p0683 A70-15738

Auroral radio reflections using two coherent bistatic radio systems, discussing ionoacoustic waves in auroral plasma 05 p0837 A70-16072

Plasma behind pressure front of shock wave investigated for ionization mechanism by microwave reflection and transmission, noting electron temperature distribution 05 p0887 A70-16110

Fields and power transfer for electromagnetic waves in hot plasma calculated using Fourier integral and Fourier series methods 05 p0888 A70-16165

Two dimensional propagation of transverse waves in plasma with embedded curl-free magnetic field, discussing cosmic ray acceleration and magnetic neutral sheet formation 05 p0888 A70-16437

Stability of nonlinear plasma waves set up by counterstreaming cold electron beams immersed in background of stationary ions 05 p0889 A70-16531

Whistler mode wave propagation in collisionless Vlasov plasma along nonuniform magnetic field 05 p0889 A70-16533

Thermal radiation effects on plane magnetoacoustic waves in semiinfinite expanse of radiating gas of perfect electrical conductivity 05 p0890 A70-16822

Induced Compton scattering of plasma and electromagnetic waves under astrophysical conditions, discussing HF radio emission spectra from cosmic objects and quasar 05 p0917 A70-16904

Relativistic plasma waves in uniform ambient magnetic field analyzed for growth rate to investigate plasma instabilities of streaming cosmic rays 05 p0904 A70-16931

Uniqueness and reciprocity theorems in elastic medium occupying infinite domain extended to electromagnetic wave propagation in plasma 05 p0890 A70-17097

Plasma waves in space and laboratory - NATO Conference, Norway, April 1968 06 p1114 A70-17359

Plasma oscillations, resonances and wave propagation characteristics analyzed by radio pulse sounders for application to space measurements 06 p1115 A70-17360

Plasma wave theory and experiments, emphasizing stable Maxwellian plasmas and transverse and longitudinal wave modes in zero and nonzero magnetic fields 06 p1116 A70-17366

Low altitude electric and magnetic measurements of plasma waves in space from OV3-3, Pioneer 8 andOGO 5 satellite observations 06 p1118 A70-17376

Plasma waves and instabilities, detailing linearized Vlasov-Maxwell equations solution appropriate to Landau problem 06 p1118 A70-17378

Linear transformation of waves in nonuniform magnetoactive plasma by solving wave equation with/without allowance for spatial dispersion 06 p1119 A70-17498

Heat transfer in dense high temperature plasma due to drift waves instability at trapped electrons 06 p1121 A70-17802

Kinetic theory of plasma waves in magnetic field, covering small amplitude waves in infinite homogeneous plasma, limiting cases, etc 06 p1121 A70-17902

Electron plasma wave damping by ion sound wave scattering using Vlasov equation 06 p1125 A70-18638

Waves and differential equations for electromagnetic field in nonuniform magnetized plasma described for all orders in electron and ion temperature 07 p1350 A70-19823

Dispersion of ion-acoustic waves in quiescent rare gas discharge plasmas, discussing model simulating ion waves generated by finite sine wave bursts 07 p1352 A70-19990

Asymptotic method for Vlasov equation formulated for weakly Landau damped monochromatic plasma wave in collisionless electron plasma 07 p1353 A70-20231

Asymptotic method for Vlasov equation of plasma wave reformulated in Eulerian representation 07 p1354 A70-20232

Diener kinetic theory for charged particles in EM field with Coulomb interactions taking into account transverse plasma waves 08 p1550 A70-20616

Longwave and shortwave mode transformation in resonant layer of inhomogeneous plasma 08 p1550 A70-20847

Plasma monochromatic wave propagation equilibrium state instability mechanisms, discussing stimulated scattering by thermal plasma particles and particle capture in wave potential well 08 p1551 A70-21422

Acoustic wave propagation in partially ionized gas in external electric field, solving differential equations by Laplace transformation 08 p1552 A70-21503

AM electromagnetic wave self modulation in magnetoplasma, considering self and mutual interaction of ordinary and extraordinary propagation modes 08 p1552 A70-21527

Weakly nonlinear dispersive cold plasma waves propagation by two time scale expansion, taking into account amplitude dispersion and coupling 08 p1553 A70-21613

Whistler type electromagnetic waves excitation by electron beam in plasma, noting intensity dependence on electron frequency 08 p1554 A70-21804

Tensor analysis of four photon interaction in rarefied plasma in magnetic field, determining cubic current of plasma wave self action 08 p1554 A70-21805

Pulse propagating in unstable plasma, determining characteristics by asymptotic expansion applied to Vlasov-Maxwell equations 09 p1734 A70-22684

Nonlinear effects related to plane electromagnetic wave propagation in weakly ionized plasma 09 p1735 A70-22842

Spontaneous echoes amplitude resulting from damped electronic plasma plane wave excitation in collisionless plasma 09 p1735 A70-22843

Fokker-Planck Coulomb collisions effect on plasma wave echoes 09 p1736 A70-23181

Wave dispersion relations in uniform magnetized plasma represented in single integral form, discussing model loss-cone and temperature anisotropy distributions 09 p1736 A70-23188

Amplitude modulation of microwave signals propagated through periodically varying plasma 09 p1639 A70-23673

Oblique E-mode electromagnetic wave in plane stratified collisionless plasma taking into account plasma temperature 09 p1639 A70-23674

Ion acoustic wave propagation near sheath at plasma-wall boundary in low pressure argon plasma measured by electron beam probe

10 p1921 A70-23965

Two-stream and cross-stream effects on nonlinear wave stability with shock in collisionless plasma

10 p1921 A70-23967

Ion-burst excited by pulsed mesh grid in plasma in connection with sheath structure

10 p1922 A70-23989

Fast magnetoacoustic wave propagation in cylindrical plasma column with constant current density, using geometric optics

10 p1923 A70-24229

Helicon wave dispersion in cold multicomponent plasma of n-type Si and Ge semiconductors in linear hydrodynamic approximation

10 p1928 A70-24832

Type I comet tails orientations dispersion attributed to nonradial plasma waves and discontinuities in interplanetary gas, calculating solar angular momentum loss rate

10 p1947 A70-24987

LF longitudinal waves propagation in DC gas discharge plasma, obtaining wave dispersion equation for various limiting gases

10 p1925 A70-25010

Microfluctuations frequency and wavelength of electromagnetic, electric and magnetic field distributions in plasma shock wave front found consistent with ion-acoustic origin hypothesis

10 p1925 A70-25031

Narrow band radiation from longitudinal plasma waves nonlinear interactions during solar bursts, comparing flux intensities for Corona single or double shock wave frequencies

10 p1934 A70-25272

Cascade mechanism of closure associated with nonlinear wave interactions between modes in turbulent plasmas, using hydrodynamical model

11 p2087 A70-25358

Long-time cross modulation field resulting from triggering electrostatic waves in one dimensional plasma, discussing supraluminous waves interactions

11 p2088 A70-25704

HF and LF plasma waves interaction in three wave approximation taking into account linear damping

11 p2089 A70-25714

Surface waves stability in cold bounded plasma against background of steady state electron oscillations, using nonlinear approximation

11 p2089 A70-25716

Surface waves excited by oscillating current in cold plasma surrounded by metallic sheath of infinite conductivity, deriving frequencies and growth rates

11 p2089 A70-25717

Chemical kinetic model for photoexcitation and photoionization of cold argon ahead of strong shock wave, predicting electron and excited atom concentrations

[ALAA PAPER 68-666]

11 p2090 A70-25953

Linear theory of density gradient drift waves in stable collision dominated plasma using external excitation method

11 p2090 A70-26019

Nonlinear parametric excitation of stable resonant drift waves by mode-mode coupling in potassium plasma of Q device

11 p2090 A70-26020

Refractive index profiles method for vertically polarized electromagnetic waves in horizontally stratified magneto-plasma extended to anisotropic media, noting relevance to ionospheric propagation

11 p2011 A70-26555

Wave propagation in solid state plasma with ferroelectric and ferromagnetic properties, deriving matrix equation allowing for nonlinearity of dielectric constant and magnetic permeability

12 p2283 A70-26970

Dispersion relations between wave frequency and vector obtained from matrix equation for wave propagation in solid state plasma with ferroelectric and ferromagnetic properties

12 p2283 A70-26971

Diluted plasma microinstabilities allowing for Langmuir waves propagation without magnetic field and Landau effects

12 p2277 A70-27057

Ionization instability of finite bounded plasma, investigating electrothermal waves in large disturbance domain by numerical simulation

12 p2163 A70-27065

Trumpet-type plane waves instability thresholds in plasma drifted by electric field, including calculation of thermodynamic equilibrium

12 p2184 A70-27236

Plasma turbulence due to nonlinear wave interaction, considering second sound LF oscillations propagation and plasmons scattering at ions

12 p2278 A70-27358

Spherical electroacoustic waves in drifting thermal plasma, describing ion acoustic perturbations

12 p2279 A70-27779

Resonant and nonresonant coupling between two coherent electron plasma waves propagating in opposite directions, considering parametric decay

12 p2279 A70-27780

Collisional drift-wave turbulence in Li Q-machine plasma far unstable regime, discussing power spectra variations of density fluctuations

12 p2280 A70-27784

Density gradient drift waves stabilization in collisionless plasma by stellarator type windings, observing oscillations amplitude reduction in shear magnetic field

12 p2280 A70-27785

Drift wave instabilities nonlinearities, discussing plasma growth rate and saturation coefficients, damping rate as function of amplitude and lower mode modification

12 p2280 A70-27786

Drift waves relation to anomalous cross field diffusion in fully ionized magnetoplasmas, introducing model predicting amplitude, correlation time, fluctuation spectrum and diffusion process

12 p2280 A70-27788

Parametric and Raman instabilities predicted by linear theory for plasma in electromagnetic field

13 p2458 A70-28563

Collisional theory of longitudinal wave propagation in partly ionized multitemperature gases

13 p2460 A70-28637

Inhomogeneous one dimensional plasma in electrostatic normal modes, considering interactions of waves and particles

13 p2460 A70-28638

Nonlinear drift wave buildup in inhomogeneous plasma faster than in linear approximation

13 p2460 A70-28652

Heat transfer in dense high temperature plasma due to drift waves instability at trapped electrons

13 p2460 A70-28653

Plane electrostatic shock waves propagation in plasma with electrons in potential equilibrium and collision free ions

13 p2461 A70-28730

Wave dispersion in lower exospheric multicomponent plasma, investigating mode group velocity frequency dependence at various altitudes

13 p2395 A70-28940

Hydrodynamic equations to obtain transformation coefficient for HF weakly damped waves in magnetoactive plasma, applying to solar corona

13 p2463 A70-29227

Plasma waves in space and laboratory - NATO Conference, Roros, Norway, April 1968

13 p2466 A70-29901

Electron temperature and concentration determined from longitudinal electron cyclotron harmonic waves in finite plasma column

13 p2467 A70-29916

Grid assemblies as electrostatic plasma wave antennas, computing driving point and transimpedances for approximating single pole impedance in heavy Landau damping regime

13 p2371 A70-29918

Polar ionosphere auroral oval position detection by satellite observations of naturally occurring VLF and man-made HF plasma waves

13 p2371 A70-29924

Trapped particle interactions with plasma waves, analyzing pitch angle scattering, oscillating electric field, transverse waves and resonance effects

13 p2468 A70-29929

Whistler mode wave packets propagation in hot inhomogeneous collisionless plasma immersed in nonuniform ambient magnetic field

13 p2468 A70-29931

Reverse flow in plasma generated in conical electromagnetic shock tube and reflected from downstream bulkhead, noting stabilization effects

13 p2469 A70-29974

Plasma wave particle interactions in outer magnetosphere, magnetosheath and solar wind, noting role of AC electric fields

13 p2483 A70-30085

Hydromagnetic wave velocity and space anisotropy instabilities in magnetosphere, using dispersion relation

13 p2483 A70-30086

Temporal wave echoes and Landau damping in collisionless plasma using signal averaging and time delay techniques

14 p2622 A70-30687

Scattering cone of hydromagnetic waves propagating along magnetic lines in magnetized plasma with oscillating electric dipole

14 p2575 A70-30822

Sideband instability and trapped particle charge density response of large periodic Bernstein-Greene-Kruskal waves in collisionless plasma

14 p2623 A70-31039

Normal wave propagation modes existence in magnetized plasma, deriving criteria for electrostatic approximation validity

14 p2624 A70-31045

Ordinary mode electromagnetic wave propagation instability in high beta plasma, determining lower bound on growth rate

14 p2624 A70-31048

Elastohydrodynamic monochromatic wave coupling in liquid filled container as model for Alfvén and magnetoacoustic waves transmission in plasma

14 p2625 A70-31356

Plasma waves with anisotropic pressure, discussing magnetoacoustic waves integral curves

15 p2777 A70-31476

Pioneer 8 wave and particle observations correlation showing broadband wave levels reduction during extended geomagnetic tail crossings

15 p2727 A70-31904

Low amplitude waves and substantial frequencies interaction by averaging method for hydrodynamics of waves in collisionless plasmas

15 p2720 A70-32114

Collisionless shock waves in magnetized plasma as function of Alfvén-Mach number, measuring electron temperature jump on wave front spectroscopically

15 p2779 A70-32116

Solar type 3 burst theory, considering plasma wave energy conversion into radio emission

15 p2802 A70-32484

Coherent wave propagation in warm turbulent plasma, using perturbation method for wave dispersion

16 p2860 A70-32945

Ion motion neglecting conditions for radio waves in plasma based on Ohm's law uncoupling from momentum transfer

16 p2957 A70-32980

Resonance excitation of high amplitude waves in plasma cylinder by HF azimuthal axially periodic current flowing through coil encircling plasma

16 p2957 A70-33194

Electron-acoustic, ion-acoustic and electromagnetic plane waves coupling at shock front in two fluid ionized viscous plasma

16 p2958 A70-33282

Resonant interaction and instability produced by nonlinear coupling of modulated wave and LF mode, stimulating self focusing of plasma waves

16 p2958 A70-33285

Plasma wave radiation by electron stream in active solar corona, obtaining spectrum and growth rate

16 p2979 A70-34189

Acoustic wave propagation through positive column of glow discharge of three component plasma, noting amplitudes dependence on excitation wave amplitude

17 p3140 A70-34872

Warm homogeneous magnetoplasma longitudinal cyclotron harmonic wave propagation perpendicular to static magnetic field, noting instabilities

17 p3140 A70-34927

Plasma waves parametric excitation by external electric field, using perturbation method of multimode scales

17 p3140 A70-34933

Cerenkov plasma waves generation by fast electron streams in solar corona and conversion into EM waves

17 p3173 A70-35768

OGO 5 observations of quasi-trapped electromagnetic waves in solar wind at 70 kHz

18 p3306 A70-36005

Nonlinear theory for surface waves propagating in bounded magnetoactive plasma

18 p3295 A70-36412

Nonlinear interactions of plasma waves with positive and negative energies producing explosive instability

18 p3295 A70-36420

Propagation constants in laminar plasma circular waveguides filled with anisotropic linear medium, using Galerkin-Ritz method

19 p3474 A70-37428

Higher order magnetic field-free temporal and spatial plasma wave echoes, solving collisionless Boltzmann equation by method of characteristics

19 p3476 A70-37557

Solid state plasmas waves and oscillations in metals, semimetals and semiconductors, noting applications for microwave devices

19 p3479 A70-37944

Synchrotron radiation emissivity function containment in dispersion equation for plane wave propagation in magnetoactive plasma

19 p3480 A70-38017

Slow wave propagation in plasma moving along external magnetic field, generalizing refractive index formula

19 p3417 A70-38592

Nonuniform finite amplitude plasma waves nonlinear decay and instability, discussing initial damping /or growth/ effect

20 p3678 A70-39660

Multidimensional control systems synthesized in accord with polyinvariance and coordinating couplings principles

20 p3604 A70-39837

Electrothermal mode wave propagation in nonequilibrium partially ionized gas, using model with finite ionization

20 p3680 A70-39984

Nonlinear resonance conditions for plasma three-wave interactions, considering wave propagation modes and constant magnetic field

20 p3682 A70-40137

Langmuir wave beam nonlinear transformation in isothermal plasma due to induced scattering by ions

20 p3684 A70-40385

Nonlinear resonant heating in magneto-plasma, calculating energy absorption by ions and plasma wave amplitude

20 p3685 A70-40467

Electromagnetic wave propagation in colloidal plasmas analyzed by kinetic approach, obtaining expressions for current density, DC and microwave conductivities, etc

20 p3685 A70-40502

Spread electron beam excitation of magnetoactive plasma waves in quasi-linear relaxation

21 p3855 A70-40948

Plasma wave echo, observing oscillatory behavior of perturbed distribution with different phases and amplitudes

21 p3858 A70-41389

Rotating cold plasma wave propagation modes including Coriolis effect in absence and presence of external magnetic field

21 p3860 A70-41924

Homogeneous plasma in uniform magnetic field, deriving theory for instabilities and LF wave propagation modes

22 p4079 A70-42370

Slow wave propagation on conducting surface separated from plasma by ion sheath, observing resonances on cylindrical antenna

22 p4082 A70-43238

Plasma turbulence due to nonlinear wave interaction, considering second sound LF oscillations propagation and plasmons scattering at ions

22 p4084 A70-43599

Solar type 3 burst theory, considering plasma wave energy conversion into radio emission

23 p4240 A70-43908

Plasmas kinetic theory, considering crossing from instability to stability, waves decay by collisional damping and emission by bremsstrahlung

23 p4224 A70-44178

Plane plasma waves in homogeneous conducting fluid with magnetic field, considering oscillations of two-fluid, cold and hot plasmas

23 p4224 A70-44179

Collisionless plasma shock wave structures from geophysical and astrophysical phenomena standpoint, describing tarantula experiment

23 p4225 A70-44184

Turbulent plasma without external magnetic field, observing low phase velocity ion wave mode

23 p4227 A70-44893

Partially ionized viscous plasma longitudinal wave propagation, formulating motion equations for electrons, ions and neutrals from Maxwell and Boltzmann equations

23 p4229 A70-44987

Bunched ion bursts amplitude modulation effects on nonlinear ion acoustic waves in grid plasma system

23 p4229 A70-44989

Ion acoustic wave propagation in collisionless gravity-supported plasma in static magnetic field calculated from linearized Vlasov equation

24 p4382 A70-45109

Electromagnetic waves nonlinear interaction at various threshold powers, inducing propagation in solid body plasma

24 p4388 A70-45201

LF electrostatic ion cyclotron wave energy resonant power absorption in plasma in axially nonuniform magnetic field

24 p4386 A70-45608

LF plasma waves amplification by beam-plasma interaction, considering electron and ion temperatures effects

24 p4387 A70-45797

Pressure gradient induced drift waves in collisionless hydrogen plasma in homogeneous magnetic field

24 p4388 A70-46209

PLASMA-ELECTROMAGNETIC INTERACTION

Transmission and reflection of electromagnetic waves by bounded moving plasma layer in slow wave space

01 p0042 A70-10167

Particle distribution and plasma nonequilibrium field evolution with turbulence generation by microwave field, considering plasma kinetic instability

01 p0150 A70-10212

LF electromagnetic waves interaction propagating in stream-magnetized cold plasma, discussing waves temporal growth and instability

02 p0262 A70-12603

Wave-wave coupling of two HF electromagnetic waves launched into warm plasma across constant

confining magnetic field, using Maxwell-Vlasov equations for electrons

02 p0349 A70-12757

Anomalous behavior of arc motion in high pressure cross-field plasma devices in terms of electromagnetic effects

03 p0529 A70-12938

Electromagnetic wave reflection on thin plasma layer with Epstein electron density profile, noting use in microwave diagnostics

03 p0529 A70-13016

Variable magnetic field effect on stability of Langmuir waves propagating in plasma in constant magnetic field

03 p0530 A70-13064

Van der Pol equation for finite amplitude ion-acoustic waves in unstable plasma propagating across weak magnetic field

03 p0531 A70-13404

Electromagnetic finite amplitude wave beams self action in magnetoactive plasma, noting nonlinear characteristics

03 p0448 A70-13411

Dynamic model for Martian ionosphere modification by solar wind, assuming negligible Mars magnetic moment and neutral atmosphere

04 p0753 A70-15103

Anomalous Doppler shift interaction between positive ions and right-hand polarized EM waves propagating at small angle to interplanetary magnetic field

05 p0905 A70-15761

Plasma behind pressure front of shock wave investigated for ionization mechanism by microwave reflection and transmission, noting electron temperature distribution

05 p0887 A70-16110

HF electromagnetic field penetration of plasma with finite conductivity and Hall constant for containment of hot plasmas, formulating nonlinear electrodynamic problem

05 p0889 A70-16490

Electrical conductivity calculation for plasma in spatially inhomogeneous magnetic field using small-gyroradius approximation to kinetic equation

05 p0889 A70-16491

Microwave nonlinear effects including mixing, harmonic generation and current rectification observed in plasma sheath surrounding Langmuir probe using PIG discharge

05 p0852 A70-16992

Propagation, reflection and dispersion equation for electromagnetic waves in longitudinally magnetized plasma filled coaxial waveguide using rotating coordinates

06 p1016 A70-17124

Light scattering at 90 deg from laser-induced breakdown plasmas in air, discussing origin

06 p1114 A70-17189

Electromagnetic wave scattering from finite plasma, discussing statistical measurement errors in degrees of freedom studies

06 p1007 A70-17464

Power reflection and transmission coefficients for polarized electromagnetic waves incident on plasma slab moving along magnetostatic field

06 p1008 A70-17566

Forward angle microwave scattering by plasma covered magnetized metallic sphere, calculating radial electron density distribution

06 p1008 A70-17576

Laboratory simulation of interactions between ionospheric plasma and diverse spacecraft systems

06 p1029 A70-18067

Solar wind interaction with moon derived for model and compared with satellite data

06 p1147 A70-18291

Numerical analysis of rarefied plasma flow interaction with charged conducting bodies of various forms and dimensions

06 p1123 A70-18298

Moving plasma column scattering of obliquely incident microwaves, assuming arbitrary polarization for incident plane wave

06 p1124 A70-18608

Microwave scattering from plasma column of low pressure discharge in Hg under free space conditions

06 p1125 A70-18609

Light scattering from free electrons in laboratory plasma, showing frequency spectrum equal to electron density fluctuations

07 p1347 A70-18899

Stress tensor for relativistic weakly ionized plasma in HF electromagnetic field taking into account collisions

07 p1348 A70-19197

Solar wind velocity anisotropy effect on interplanetary magnetic field inhomogeneity

07 p1366 A70-19443

Four satellite cluster laboratory in near-earth environment to investigate solar-terrestrial relationships, emphasizing interaction of solar wind and magnetosphere

07 p1387 A70-19711

Magnetic trap chamber walls adverse effect on plasma heating produced by electron beam injected at low hydrogen pressures

07 p1350 A70-19845

Electromagnetic wave scattering from charged particle in hot electron plasma in magnetic field, considering relativistic corrections for scattered radiation spectra

07 p1352 A70-19992

Surface oscillations of plasma in external HF field derived from hydrodynamics and Maxwell equations

07 p1355 A70-20367

S- and p-polarized electromagnetic wave incident on semiinfinite laminar plasma layers, analyzing reflection and absorption characteristics

08 p1456 A70-20504

TEM waves penetration into magnetoactive semibounded plasma using Vlasov and Maxwell equations, obtaining electric field for specular reflection of electrons

08 p1551 A70-21255

AM electromagnetic wave self modulation in magnetoplasma, considering self and mutual interaction of ordinary and extraordinary propagation modes

08 p1552 A70-21527

Whistler type electromagnetic waves excitation by electron beam in plasma, noting intensity dependence on electron frequency

08 p1554 A70-21804

Scattering cross sections of electromagnetic waves in rectangular plasma-filled waveguide based on reciprocity theorem

08 p1464 A70-21983

Thin linear antennas in plasma analyzed for radiation characteristics by linearized hydrodynamic theory, showing effect of feed points displacement

09 p1643 A70-22207

Pulsar model assuming magnetic dipole radiation by spinning neutron star interacting with nearby plasma

09 p1756 A70-22517

Ion-acoustic wave oscillations of weak collision plasma in strong electromagnetic field, discussing instability

09 p1736 A70-23198

Argon plasma interaction with RF electromagnetic field using MGD model, noting plasma-field coupling and plasma temperature exhibition of skin effect

09 p1737 A70-23433

Long radio wave propagation and effective refraction index in turbulent magnetoplasmas with stochastic density variation

10 p1832 A70-23962

Relativistic nonlinear coupled longitudinal-transverse propagation of intense laser beams in cold overdense plasma

10 p1921 A70-23968

Transmission and reflection of electromagnetic waves by bounded moving plasma layer in slow wave space

10 p1842 A70-25015

Nonlinear interaction between plasma and HF field near cyclotron frequency, studying plasma oscillations generation in strong magnetic field

10 p1925 A70-25102

Electromagnetic waves propagation in nonlinear medium, investigating polarized plane wave incident on vacuum-plasma interface in magnetic field

10 p1844 A70-25156

Laboratory simulation for shock waves around earth, moon and Venus based on artificial solar wind and magnetic dipole interaction study

10 p1948 A70-25182

Plasma production by solid hydrogen-giant pulse laser interaction, studying time dependent distributions of plasma density, temperature and velocity

10 p1902 A70-25222

Electromagnetic wave propagation through weakly inhomogeneous plasma layer with frequent electron-molecule collisions, noting applicability to ionosphere

11 p2003 A70-25530

Hall effect influence on HF traveling magnetic field penetration into solid cylinder plasma device compared to magnetically contained plasma

11 p2088 A70-25712

Ion-acoustic instability effect on HF EM field penetration into plasma taking into account nonlinear Ohm law

11 p2089 A70-25715

Microwave power absorption in plasma investigated by transmission cavity excited in TE mode, determining electron density and collision frequency

11 p2089 A70-25841

Alfven and cylindrical magnetoacoustic waves in homogeneous unbounded conducting plasma in non-homogeneous magnetic field, applying Weinberg method to propagation analysis

11 p2089 A70-25850

Polarization effects during HF EM wave interaction in plasma, discussing plasma scattering effects in polarization transport equations

11 p2004 A70-25937

RF interference emanating from satellite-borne pulse plasma thruster by measuring RF power at UHF antenna having plasma in near field

11 p2103 A70-26136

Radiation from electric dipole in moving isotropic plasma analyzed for plasma velocity effect on pattern and far fields 11 p2091 A70-26178

Electromagnetic scattering from underdense plasma slabs with randomly varying dielectric constant, calculating reflection coefficient 11 p2095 A70-26763

Microwave scattering by turbulent plasma electron density fluctuations 11 p2096 A70-26765

Radio wave scattering cross section in wake of body moving in ionosphere, using simplified procedure with asymptotic expressions 11 p2012 A70-26787

Electromagnetic wave penetration in plasma under uniform DC magnetic field, considering wave propagational direction and electric field 12 p2279 A70-27781

Electric dipole radiation field in homogeneous anisotropic compressible plasma, obtaining asymptotic expressions by saddle point integration method 12 p2282 A70-27970

Nonequilibrium solid state electronic plasma instabilities due to interactions with strong electric and magnetic fields 12 p2289 A70-28363

Parametric and Raman instabilities predicted by linear theory for plasma in electromagnetic field 13 p2458 A70-28563

Plasma properties investigation by laser beam probes, considering direct observation of oscillation mode 13 p2458 A70-28564

Macroscopic plasma response to absorption of high intensity laser radiation in one dimensional geometry 13 p2459 A70-28636

Inhomogeneous one dimensional plasma in electrostatic normal modes, considering interactions of waves and particles 13 p2460 A70-28638

LF electrostatic waves oblique to magnetic field in plasma, evaluating dispersion relation near ion cyclotron frequency 13 p2363 A70-28641

Laser radiation interaction with hot nonuniform plasma, determining thermal and electromagnetic forces for various temperatures and densities 13 p2460 A70-28643

Plane electromagnetic wave interaction with compressible plasma fluid moving with uniform velocity in vacuum, calculating reflection and transmission coefficients 13 p2462 A70-29101

Plane electromagnetic wave in moving conductive medium, analyzing without approximation of velocity limitation 13 p2462 A70-29104

HF electromagnetic forces on collisionless cold magnetoactive plasma-vacuum boundary using time-averaged stress tensor 13 p2462 A70-29127

Electron density and transverse electron temperature of magnetoactive plasma generated in circular waveguide by microwave signal with variable polarization 13 p2462 A70-29128

Plasma instability in TEM wave field, considering nonpotential HF oscillations buildup with frequency near external wave frequency 13 p2463 A70-29283

Q switched ruby laser pulses nonlinear absorption by partially ionized plasma behind reflected shock wavefront, observing absorptivity dependence on light intensity 13 p2429 A70-29420

RF admittance and electric field of plane grid capacitor in hot collision free magnetoplasma in parallel magnetic field dominated by Bernstein modes 13 p2467 A70-29910

Infinitesimal dipole moving through hot uniform electron plasma in magnetic field, investigating asymptotic time behavior of plasma resonance 13 p2467 A70-29912

Power absorption by microwave generated plasmas noting pressure effects 14 p2622 A70-30675

Light scattering from plasmas with nonMaxwellian electron velocity distribution function 14 p2622 A70-30694

Small amplitude HF electromagnetic wave penetration in hot plasma slab, showing wave period/transit time ratio dependence of electromagnetic field distribution 14 p2551 A70-31037

Comparative sets of higher order adiabatic motion equations for plasmas in electric and magnetic fields with slow variations 14 p2624 A70-31043

Em wave reflection and transmission at boundary between free space and semiinfinite anisotropic plasma 15 p2778 A70-31830

Gyrosynchrotron from accelerated electron, discussing effects of cold and collisionless magnetoplasma on far field and frequency spectra 15 p2728 A70-31989

Glass tube surrounded nonuniform plasma column interaction with TM microwave field of cylindrical cavity for electron density measurements 15 p2780 A70-32347

Plasma electron density measurement for microwave-excited pulsed discharges based on skin effect 15 p2780 A70-32367

Dipole and loop antennas in isotropic compressible plasma under wave incidence, using reciprocity theorem for receiving voltages and maximum powers 16 p2957 A70-32982

Refractive index equation for Whistler propagation in weakly drifting magnetoplasma 16 p2959 A70-34224

Hydrogen plasma refractive index and absorption constant for laser radiation frequencies as functions of electron temperature and atomic density 16 p2959 A70-34338

Antennas in plasma, investigating electromagnetic and electroacoustic waves and boundary value approach 17 p3045 A70-35076

Plasma induced radio frequency interferences from DC-DC converter to receiving antenna simulated for REXS satellite in space chamber 17 p3047 A70-35400

Electric field component of waves in auroral ionosphere measured by double Langmuir probe field detectors, discussing wave-particle interactions and turbulence 17 p3096 A70-35767

Relaxation properties of nonequilibrium electronic solid state plasma during nonlinear interaction with external fields, using kinetic equation 18 p3297 A70-36423

Solar wind velocity anisotropy effect on interplanetary magnetic field inhomogeneity 18 p3309 A70-36917

Homogeneous plasma electrostatic oscillations excitation by electromagnetic waves nonlinear interaction in magnetic field, deriving expression for density perturbation 19 p3475 A70-37536

Inhomogeneous plasma ellipsoid equilibrium in external HF field, assuming parabolic density distribution 19 p3479 A70-37739

Plane EM wave diffraction in cylindrical plasma-electron beam system 19 p3378 A70-37740

Ionization relaxation behind reflected luminous shock front in argon plasma flow interaction with magnetic fields, using spectroscopic and streak interferometric observations 19 p3479 A70-37814

Electric field component equations of electromagnetic wave traveling through stratified plasma, considering incident and reflected ordinary and extraordinary waves 19 p3379 A70-37863

Temporal echo in plasma for applied rectangular pulses, discussing ballistic approximation 19 p3480 A70-38174

Weakly ionized gas subjected to pulsed DC electric field, analyzing transient relaxation of electrons velocity distribution 19 p3482 A70-38899

Helium II line broadening in high temperature plasma, measuring profile for comparison with theoretical prediction 20 p3677 A70-39115

Electromagnetic waves scattering from dense turbulent plasma, calculating radar cross sections of inhomogeneous plasma for peak electron densities 20 p3586 A70-39459

Laboratory simulation of interactions between ionospheric plasma and diverse spacecraft systems [AIAA PAPER 70-169] 20 p3606 A70-39695

Large scale nonequilibrium linear MHD generator performance with rare gases under strong EM-gas dynamic interactions 20 p3681 A70-39993

Compressible plasma axisymmetric channel flow under electromagnetic forces and ohmic heating, noting velocity profiles and current density [AIAA PAPER 70-1098] 20 p3683 A70-40239

Plasma nonequilibrium state formation and light absorptivity variation under high power laser pulsed radiation 20 p3684 A70-40387

Shock waves formation in rarefied plasma investigated by Thomson scattering of ruby laser light 20 p3643 A70-40388

Electromagnetic waves and oscillations excited by magnetic current ring source around infinitely long compressible plasma column, deriving radiation field distribution 20 p3685 A70-40506

HF electromagnetic field effect on nonhomogeneous collisionless magnetized plasma stability, deriving dispersion equation for drift cyclotron oscillations 21 p3854 A70-40622

Anomalous electromagnetic wave absorption in collisionless plasma attributed to instability excitation causing ion density fluctuations 21 p3855 A70-40754

Electromagnetic wave propagation through weakly inhomogeneous plasma layer with frequent electron-molecule collisions, noting applicability to ionosphere 21 p3786 A70-41280

Electromagnetic scattering power spectrum from underdense turbulent plasmas, deriving first and second moments 21 p3858 A70-41732

Electromagnetic wave propagation through cold slowly varying plasma layers in absence of external magnetic field 21 p3860 A70-42000

VLF wave generation due to nonlinear interaction of two microwaves with plasma slab under high DC field 22 p4077 A70-42294

Space electric field considered for solar wind plasma drift origin and possible energy source for spacecraft propulsion, estimating intensity on lunar surface 22 p4100 A70-42789

Plasma-TEM wave nonlinear interactions in magnetosphere, discussing atmospheric occurrence 22 p4021 A70-43276

Solar wind intensity and direction correlated with intensity of earth surface magnetic disturbances and geomagnetic pi-2 type pulsations 22 p4022 A70-43284

EM wave second harmonic generation by plasma wave, discussing decay processes in inhomogeneous plasma layer 22 p4083 A70-43381

Ionospheric parametric amplification and frequency mixing due to polarized TEM waves nonlinear interaction with longitudinal electrostatic waves 23 p4185 A70-43838

Solar wind flux correlation with earth EM field pulsations, noting flare-generated shock front effects on magnetosphere 23 p4236 A70-44051

Laser light scattering in plasma for charged particle correlation function 23 p4225 A70-44187

External DC electric field effect on microwave absorption in plasma 23 p4226 A70-44372

Optimum input pulse signal synthesis for transmission through lossless homogeneous isotropic plasma, using matched filter theory 23 p4228 A70-44962

Dipolar resonant scattering of H-polarized plane waves by axially magnetized plasma column with perfectly conducting core 23 p4228 A70-44977

Expansion of laser produced plasma into uniform magnetic field, calculating electromagnetic radiation 24 p3482 A70-45108

LF resonances and potential in plane nonisothermal plasma layer, considering electromagnetic field interaction and ionic collisions 24 p4383 A70-45116

Acoustic plasma wave excitation by transverse electromagnetic wave beam, calculating LF instabilities and energy losses 24 p4384 A70-45149

Microwave propagation in circular waveguide with axially magnetized gas or solid state plasma/Faraday configuration/, calculating twist modes 24 p4318 A70-45213

Corotating magnetic field model of pulsar, using electromagnetic field equations of dipole radiation in low density plasma 24 p4413 A70-46137

PLASMA-PARTICLE INTERACTIONS

Quasi-linear relaxation of electron beam in plasma with concentration nonuniformities, noting electron velocity role 01 p0150 A70-10213

UHF signal amplification by electron beam-plasma interaction, defining amplification frequency ranges 01 p0043 A70-10658

Electron trapping effect on ion-wave instability in plasma, deriving expression for saturation energy spectrum 01 p0152 A70-11361

Inhomogeneous plasma containing weak electron beam using Vlasov equation, noting wave-wave coupling effect 02 p0345 A70-11882

Temporal and statistical characteristics of HF oscillations from electron beam interaction with plasma in magnetic field 03 p0532 A70-13524

Electron efflux effectiveness from discharge plasma into vacuum, investigating various electrodes influence 04 p0724 A70-14415

Galactic cosmic rays scattering by solar wind magnetic field fluctuations, considering energy and momentum transfer

04 p0739 A70-14596

Turbulent-plasma electrons ballistic effects on solar wind magnetic field fluctuations in lunar vicinity

04 p0753 A70-15123

Numerical solution for differential equations describing nonlinear beam-plasma interactions based on dispersion relation analysis

05 p0886 A70-15799

Ion-neutral coupling in plasma acceleration revealed by velocity disparities determined spectroscopically [ALAA PAPER 70-166]

06 p1133 A70-18219

Whistler amplification in magnetosphere for electron interaction with background plasma to produce wave growth, discussing stability of various anisotropic velocity distributions

06 p1059 A70-18533

Homogenous monoenergetic cylindrical electron beam interaction with homogeneous cold plasma, investigating system stability

06 p1125 A70-18615

Surface wave propagation and amplification by electron beam-plasma interaction, inapplicability of coupled mode theory and use for microwave amplifier

06 p1125 A70-18616

Synchrotron radiation negative reabsorption possibility for relativistic electrons dipped into and in absence of unrelativistic plasma

07 p1348 A70-19413

Electric and magnetic field perturbation at great distances behind body moving in collisionless magnetized plasma estimated from Fourier transform

07 p1385 A70-19447

Coupled mode method, analyzing interaction between slow space charge wave of electron beam and electroacoustic wave of lossless warm plasma

07 p1349 A70-19687

Quasi-linear feedback effect of enhanced ion-wave fluctuations on average electron distribution in current-carrying plasma

07 p1338 A70-19822

Plasma-electron beam system LF dispersion characteristics noting ion instability

08 p1549 A70-20505

Light ions acceleration to high energy by pulsed high intensity electron beams

08 p1553 A70-21694

Tensor analysis of four photon interaction in rarefied plasma in magnetic field, determining cubic current of plasma wave self action

08 p1554 A70-21805

Radial self focusing of low density electron beam by interaction with plasma in presence of beam plasma instability

08 p1554 A70-21818

Nonlinear wave scattering at plasma particles and weak plasma inhomogeneity effects on plasma current instability

08 p1554 A70-21819

Pinched plasma reversed current induction due to relativistic electron beam injection

09 p1736 A70-23183

Plasma charge transfer in unstable beam plasma in magnetic fields system allowing for electron discharge pump operation

09 p1737 A70-23334

Beam plasma system instability, studying anomalous diffusion toward vessel walls as function of generated oscillations

09 p1737 A70-23335

Cosmic rays diffusion through interstellar plasma noting microstabilities role

10 p1931 A70-23972

Electron-ion beam plasma system, using one dimensional quasi-linear equations for describing electron heating and stabilization

10 p1923 A70-24403

Stability of realistic inhomogeneous plasmas with sheaths, examining electron beam-stable Maxwellian plasma interaction

11 p2090 A70-26021

Electron beam-plasma interaction nonlinear development in time and space using computer simulation

11 p2095 A70-26758

Nonlinear effects in beam-plasma type interactions, studying particle redistribution under inhomogeneous oscillating electric field

11 p2095 A70-26759

Comet tail simulation by using fast acting gas valve to produce gas cloud for interaction with plasma stream

12 p2298 A70-27190

Spatial relaxation of electron gas colliding with positive ions from plasma velocity distributions, solving time independent Fokker-Planck boundary problem

12 p2280 A70-27791

Electron beam interaction with plasma in absence of magnetic field, discussing microwave radiation emission and incoherent scattering and instability spatial growth

13 p2459 A70-28569

Beam-plasma system mode coupling near electron cyclotron frequency, obtaining interference patterns

13 p2459 A70-28570

Electron beam interaction with Maxwellian plasma, investigating temperature effects on instabilities

13 p2460 A70-28639

Trapped particle interactions with plasma waves, analyzing pitch angle scattering, oscillating electric field, transverse waves and resonance effects

13 p2468 A70-29929

Whistler instability examined on gyrating electron beam interaction with cold background plasma propagating parallel to magnetic field

13 p2468 A70-29932

Perpendicular propagation of VLF waves from wave/ particle interaction in vicinity of lower hybrid resonance frequency in magnetosphere

13 p2468 A70-29934

Plasma wave particle interactions in outer magnetosphere, magnetosheath and solar wind, noting role of AC electric fields

13 p2483 A70-30085

Morphology of thermal and energetic particles in inner magnetosphere during geomagnetic disturbances and solar cycles

14 p2630 A70-30358

High energy electron temperature in beam plasma discharge pulsed laser measured by bremsstrahlung X radiation spectrum

15 p2752 A70-32194

Electrons, positrons and photon energy distribution inside hydrogen plasma injected with high energy electrons

15 p2781 A70-32429

Beam current instability and plasma heating by electron beam generated in linear discharge, discussing electron beam-cold plasma interactions

16 p2957 A70-33191

Ni particles induced quenching measured by probes in afterglow plasma of pulsed linear discharge, determining deionization rate

16 p2958 A70-33687

Spatial electric field variations and electron distribution for beam plasma amplification, using nonlinear approximation

16 p2959 A70-34336

HF oscillations excitation in decaying plasma-electron beam system, noting Coulomb collisions and nonlinear effects role

18 p3294 A70-36145

Electron beam interaction with ionized K plasma, considering Langmuir waves instability, turbulence and electron heating

18 p3295 A70-36614

Electric and magnetic field perturbation at great distances behind body moving in collisionless magnetized plasma estimated from Fourier transform

18 p3316 A70-36921

Charged particle interaction with fluctuation fields in nonequilibrium magnetoactive plasma

20 p3678 A70-39596

Ion heating during plasma instability due to interaction with electron beam in mirror magnetic trap

20 p3678 A70-39598

Langmuir wave beam nonlinear transformation in isothermal plasma due to induced scattering by ions

20 p3684 A70-40385

Energetic electron precipitation enhancement by cold plasma injection, discussing whistler mode turbulence, particle density and magnetosphere

21 p3818 A70-41105

Plasma and neutral gas collisionless interactions in magnetic field based on Alfvén critical velocity hypothesis, discussing electron energy distribution

21 p3857 A70-41383

Plasma and spiraling electron beam interactions, observing oscillations above integral multiples of electron cyclotron frequency

21 p3857 A70-41388

Charge separated and quasi-neutral solutions of electron heat transfer to spherical body in quiescent nonequilibrium plasma, noting diagnostic applications

21 p3860 A70-42080

Electron beam instability in cylindrical magnetically confined plasma column, calculating quasi-static spatial growth increments

22 p4080 A70-42403

Plasma-electron beam interaction instability transition from absolute to convective in hydrogen tube system at various pressures, considering electron collision effects

24 p4385 A70-45452

Resonant electrons interaction with turbulent ion-acoustic plasma oscillations consisting of superimposed three dimensional random phase wave packets

24 p4386 A70-45658

High resolution cylindrical capacitor observation of fine structure of distribution function of electron beam interacting with plasma

24 p4387 A70-45820

PLASMAGUIDES

Electromagnetic wave propagation in homogeneous plasma waveguide satisfying Appleton-Hartree approximation without collisions in presence of longitudinal magnetic induction

02 p0349 A70-12724

Electromagnetic wave propagation through stratified positive plasma column in waveguide, noting stratification travel effects on wave amplitude and phase shift

03 p0443 A70-13096

Electromagnetic wave diffraction effects on matching plasma waveguide to coaxial power extraction line

03 p0531 A70-13334

Anomalous H wave absorption in circular waveguide by dense collisionless plasma, connecting to instability excitation with subsequent plasma heating

03 p0537 A70-14379

Electromagnetic wave growth effect on wave field propagating along beam-plasma slab, showing Poynting vector component

04 p0651 A70-15293

Steady state plasma generation in metallic waveguide without dielectric container by cold cathode discharge in He

05 p0819 A70-15803

Propagation, reflection and dispersion equation for electromagnetic waves in longitudinally magnetized plasma filled coaxial waveguide using rotating coordinates

06 p1016 A70-17124

Scattering cross sections of electromagnetic waves in rectangular plasma-filled waveguide based on reciprocity theorem

08 p1464 A70-21983

Slow HF waves propagation under magnetic field effect in plasma waveguide surrounded by dielectrics or metal

10 p1843 A70-25106

Microwave field component distribution in plasma waveguide covered by metallic sheath in magnetic field, using counterbalanced antenna probes for field measurements

13 p2463 A70-29378

Circularly polarized waves in waveguide loaded with high density magnetoplasma, discussing propagation mode and plasma boundary

13 p2379 A70-29617

Electromagnetic wave diffraction effects on matching plasma waveguide to coaxial power extraction line

14 p2623 A70-30713

Plasma beam systems dispersion equation with allowance for electron collisions with heavy particles

15 p2779 A70-32117

Convolution equation for kinetic theory of EM field excitation in plasma waveguides

23 p4223 A70-43772

Microwave propagation in circular waveguide with axially magnetized gas or solid state plasma /Faraday configuration/, calculating twist modes

24 p4318 A70-45213

Circular waveguide with axially magnetized plasma, investigating twist mode propagation in InSb at 70 GHz

24 p4311 A70-45214

MPD experiments in inductive hydrodynamic shock tube with round cross section and radial magnetic field

24 p0000 A70-45798

PLASMAS [PHYSICS]

NT ARGON PLASMA

NT CESIUM PLASMA

NT COLD PLASMAS

NT COLLISIONLESS PLASMAS

NT COSMIC PLASMA

NT DEUTERIUM PLASMA

NT ELECTRON PLASMA

NT HELIUM PLASMA

NT HIGH TEMPERATURE PLASMA

NT HYDROGEN PLASMA

NT METALLIC PLASMAS

NT MICROPLASMAS

NT NITROGEN PLASMA

NT NONUNIFORM PLASMAS

NT RAREFIED PLASMAS

NT RELATIVISTIC PLASMAS

NT ROTATING PLASMAS

NT STELLAR WINDS

NT THERMAL PLASMAS

Cooling time estimation for white dwarf stars with ion component undergoing condensation, based on plasma thermodynamic properties

01 p0189 A70-11341

Whistlers paradoxical behavior in bounded magnetoplasmas, discussing double reflection and wave propagation

02 p0263 A70-12733

Rotary equilibrium of plasma ellipsoid in external HF fields in constant magnetic field, calculating revolution frequency and effective energy potential

03 p0530 A70-13085

Laser irradiation of RF plasmoid producing electron density increase, discussing resonance sustained RF discharges, mode locking, laser photodetachment, etc [ONERA-TP-751]

03 p0501 A70-13630

- Shock wave structure in quasi-neutral weakly ionized plasma using Mott-Smith functions
03 p0535 A70-14362
- Kinetic theory for calculating electron distribution function of weakly ionized plasmas in arbitrarily time dependent electromagnetic fields
05 p0886 A70-15800
- Plasma nature, properties and applications, discussing echoes, shocks, phase mixing and hot plasma containment
05 p0887 A70-16130
- Magnetic field fluctuations of interplanetary plasma, considering anisotropic temperature instabilities
05 p0915 A70-16750
- Electron distribution functions in weakly ionized plasmas by asymptotic analysis of boundary layer near wall
06 p1121 A70-17903
- Plasmapause observations by ion spectrometer aboard OGO-5 vehicle for early orbits, obtaining O, He and H ion concentration profiles for geomagnetic parameter
06 p1059 A70-18546
- Diffusion coefficient of charged particles in HF stabilization of current-convective instability measured in Ge semiconductor electron hole plasma
07 p1355 A70-20365
- Kinetic theory equations for completely ionized plasma taking into account Diener method
08 p1550 A70-20615
- Impedance radiation pattern and actual height of receiving dipole antenna in magnetoactive plasma calculated by electrodynamic reciprocity theorem
08 p1472 A70-20970
- Potential distribution outside ideally reflecting charged sphere immersed in resting plasma described by nonlinear integral equation, allowing for polarization
08 p1432 A70-21090
- Electrons velocity distribution function in homogeneous stationary weakly ionized Lorentz plasma in neon, investigating effect on mobility, collision frequency, diffusion and kinetic energy
11 p2089 A70-25871
- Radiation characteristics of ion acoustic waves from monopole and dipole antennas, observing patterns of longitudinal wave in isotropic plasma
12 p2279 A70-27778
- Bremsstrahlung radiation emitted from homogeneous, field free, nonrelativistic plasma, deriving formulas
13 p2456 A70-28500
- Magnetoplasmas nonlinear dielectric response function and parametric instabilities, discussing homogeneous pumping waves
13 p2459 A70-28568
- Electrostatic probe behavior in RF excited plasma, illustrating perturbation effect of potential drop on I-V characteristics
13 p2406 A70-28935
- Shot noise effect in antennas to measure electric charge density fluctuations in plasma, noting thermal equilibrium with Maxwellian distribution function
13 p2371 A70-29920
- BBGKY hierarchy pair correlation function for magnetoplasma under weak external force, using operator method and time periodic ansatz for distribution functions
14 p2623 A70-30697
- Electric and magnetic dipole VLF radiation patterns in lossy two component magnetoplasma
16 p2860 A70-32944
- Antennas in plasma, investigating electromagnetic and electroacoustic waves and boundary value approach
17 p3045 A70-35076
- Bremsstrahlung from weakly ionized plasma, discussing emission and absorption characteristics, electron-atom collisions and dispersive effects
18 p3294 A70-36347
- Temporal echo in plasma for applied rectangular pulses, discussing ballistic approximation
19 p3480 A70-38174
- Earth exospheric plasma distribution, relating solar eclipses effects to geophysical phenomenon
19 p3418 A70-38904
- Nonlinear resonant heating in magneto-plasma, calculating energy absorption by ions and plasma wave amplitude
20 p3685 A70-40467
- Plasma-air junction problem in parallel plate waveguide, obtaining discontinuity admittance expression
22 p3994 A70-42350
- Sparks channel resistance temporal variation, using resistivity of fully and singly ionized plasma
22 p4072 A70-42354
- Molecular vibrational temperature dependence on electron and neutral gas temperatures and degree of ionization for plasma excitation in nitrogen
22 p4078 A70-42358
- Optically thin plasma population and ionization equilibrium, taking into account heavy particle collisions
22 p4082 A70-43219
- Electron energy distribution in time-varying plasmas, using difference quotient circuits for Langmuir probe characteristics measurement
22 p4082 A70-43220
- Pulsed multipole magnetic field shaping short plasma blobs
22 p4083 A70-43389
- HF plasma propagation, discussing RF discharge by exciting axially symmetric mode of plasma column
22 p4084 A70-43671
- Electron distribution function in homogeneous ionized plasma under oscillating electric fields and steady magnetic fields, solving Boltzmann transport equation
23 p4226 A70-44248
- PLASMATRONS**
- Plasmatron generated rarefied helium plasma parameters in external magnetic field using hot-wire anemometer Langmuir probe
07 p1349 A70-19653
- Electric arc stability with descending static I-V characteristics in plasmatrons using direct Liapunov method
11 p2093 A70-26734
- Plasmatron geometrical parameters effect on electric arc I-V characteristics, using various gas vortex flows for arc stabilization
11 p2093 A70-26735
- Water cooled metallic diaphragm thermal stability effect on plasmatron electric arc characteristics stabilized by vortex air flow
11 p2093 A70-26736
- Heat exchange in linear vortex plasmatron with bilateral ejection, noting dependence on electrodes geometry and gas flow rates
11 p1984 A70-26737
- DC air flow plasmatron arc chamber operation with metal surfaces used for charge stabilization, obtaining I-V characteristics and gas flow parameters in quasi-limiting region
11 p1984 A70-26738
- Coaxial plasmatron pulsation on intensity of heat exchange between high temperature nitrogen jet and axisymmetric body near critical point region of spherical bluntness
11 p1984 A70-26739
- Flow dynamics effects on characteristics of high temperature plasmatron, describing plasma burner design and HF discharge plasma experiment
11 p1984 A70-26740
- Pulsed and CW microwave discharge plasmatrons design calculation, providing electrodeless plasma in metallic chamber and nonequilibrium plasma
11 p1984 A70-26741
- Ignitron converters for feeding power plasmatrons and arc reactors, describing circuit and operation
11 p1984 A70-26742
- Laminar Cu-W electrode erosion resistivity in single chamber electric arc hydrogen plasmatrons with gas vortex stabilization
15 p2780 A70-32130
- PLASMOIDS**
- U PLASMAS [PHYSICS]**
- PLASMONS**
- Inelastic scattering of electrons by surface plasma oscillation for low energy electron diffraction and photoemission, interpreting surface plasmon excitation
07 p1337 A70-19359
- Plasma turbulence due to nonlinear wave interaction, considering second sound LF oscillations propagation and plasmons scattering at ions
12 p2278 A70-27358
- Correlation functions of weak quasi-steady plasma turbulence determined by plasmon interactions, using computerized integral equation
17 p3139 A70-34643
- Plasmon decay by neutrinos emission in strong magnetic field, examining parallel and perpendicular propagation
18 p3305 A70-35936
- Plasma turbulence due to nonlinear wave interaction, considering second sound LF oscillations propagation and plasmons scattering at ions
22 p4084 A70-43599
- PLASTIC AIRCRAFT STRUCTURES**
- Boeing 707 B-epoxy composite forelap design, analysis, fabrication and flight testing
02 p0307 A70-11955
- Carbon fiber reinforced plastics /CFRP/ uses in commercial aircraft structural component
03 p0516 A70-13546
- Ti alloys, high strength steels and plastics for aircraft and spacecraft constructions, including aging behavior of lap joints and prepreg laminates in vacuum [DGLR-69-58]
04 p0699 A70-15162
- Boron-epoxy composite materials for secondary and primary aircraft structural components, discussing multidirectional laminates, joint analysis, etc
05 p0942 A70-16620
- Plastics applications in aircraft, missile systems, satellites, sounding rockets and manned spacecraft, discussing reinforced plastics and structural laminates
05 p0874 A70-16623
- Lightning protection development programs application to light aircraft plastic components, emphasizing structure and fuel systems designers awareness [SAE PAPER 700220]
11 p1980 A70-25892
- Boron epoxy composite structural parts for aerospace vehicles, discussing production times and cost reduction
12 p2240 A70-27076
- NDT methods for fiberglass, graphite and boron fiber composites for aircraft structures
12 p2243 A70-27465
- Tensile tests on wings and wing components of plastic engine-driven aircraft, discussing design, configurations and mechanical properties
14 p2656 A70-30250
- Foamed in place epoxy resins in aircraft composite structures
16 p2937 A70-33369
- Joint design for fiberglass reinforced plastic aircraft components regarding minimum weight and reliability [ASME PAPER 70-DE-56]
16 p2989 A70-33516
- Tungsten filled urethane in aircraft areas as balancing agent
17 p3126 A70-35418
- Composite compression tubes for VTOL aircraft components, describing weight parameters and mechanical properties [AIAA PAPER 70-898]
17 p3193 A70-35809
- Gliers made of glass fiber reinforced plastics, investigating thermostatic properties under solar irradiation and surrounding warm air
19 p3454 A70-37370
- Reinforced plastic for aircraft parts, investigating low viscosity polyester resins of styrene crosslinking type
20 p3656 A70-40028
- High thermal stability glass fibers alternatives improving stiffness-to-weight ratio of resin and Al-based composites used in F-111 boron epoxy wings
22 p4058 A70-42480
- PLASTIC ANISOTROPY**
- NT ELASTIC ANISOTROPY**
- Polymers yield criterion determination using Hill method exemplified by polyvinyl chloride, discussing effects of transversal anisotropy and rheological properties
02 p0320 A70-11740
- Plane-strain equations for deformation of weakly plastic anisotropic body analyzed by small parameter method
03 p0592 A70-13446
- Anisotropic fiberglass reinforced plastics creep properties under biaxial compression, showing compressive to tensile strain elimination or change
07 p1316 A70-19546
- Fiberglass reinforced anisotropic plastics heating during cyclic axial loading
16 p2934 A70-33215
- Anisotropic plasticity yield conditions, analyzing elastic to plastic deformation transition geometry
20 p3727 A70-39889
- PLASTIC COATINGS**
- Zinc and resin coated alkaline glass fibers tensile strength, describing test procedure
01 p0126 A70-10220
- Stress analysis based on observing birefringence effects in photoelastic surface coating
04 p0689 A70-14922
- Fluorocarbon polymer coatings, discussing role of fluorine content and carbon bond in chemical inertness, degradation resistance, thermal stability and low surface friction [SAE PAPER 690645]
05 p0868 A70-15842
- Series emittance thermal control coatings of polymeric dielectric films overlaying reflectors vacuum exposed to UV, X ray and proton radiation [AIAA PAPER 70-64]
06 p1106 A70-18069
- Atomic hydrogen maser wall shift determined by measurements on FEP Teflon coated storage bulbs, suggesting Teflon properties change as basis
07 p1301 A70-19973
- Plastic semiconductor devices encapsulation materials and fabrication techniques, considering device performance in various environments and military applications
08 p1468 A70-20626
- Performance characteristics of low density epoxy-water emulsion corrosion resistant coating for nonferrous alloys
08 p1526 A70-20648
- Axial flow compressor clearance control coatings at blade tip paths for efficiency [SAE PAPER 700330]
12 p2291 A70-27462
- Radiative heat transfer effects on polymeric combustion-inhibiting coatings in solid propellant rocket motors [AIAA PAPER 70-835]
16 p2971 A70-33930
- Basket weave fabrics for gliding descent decelerators with polyurethane and nylon coatings for tearing strength and pressure packing [AIAA PAPER 70-1180]
21 p3843 A70-41833

Book on plastic coatings for electronics covering chemical structure, properties, applications, manufacturing technology, etc

22 p4058 A70-42455

PLASTIC DEFORMATION

Combined aging and plastic deformation treatment effects on breaking point, yield stress, elongation and contraction of austenitic Fe-Ni-Ti alloy

01 p0115 A70-10064

Plastic deformation of wedge shaped model asperities influencing gas leakage between contacting surfaces, discussing critical contact pressure

01 p0060 A70-10267

Transformation induced plasticity steels tensile properties measurement indicating loss of ductility due to H embrittlement

01 p0118 A70-10729

Construction of formulas relating stresses and plastic deformations describing inelastic bodies behavior under complex loads

01 p0210 A70-11411

Bauschinger effects in repeated tensile and compressive strains in inelastic media under variable temperatures as function of load vector, using plastic yield

01 p0211 A70-11422

Alloying additions effect on plastic deformation anisotropy in GaAs single crystals, determining dislocation activation energies from creep tests

01 p0160 A70-11606

Constitutive equations and thermally activated dislocation processes in metals, noting temperature and strain rate relationship

02 p0316 A70-11737

Finite element technique extended for plastic buckling of flat plates, using Stowell theory

03 p0584 A70-12923

Thermodynamic constitutive equations for large dynamic plastic deformation problems

03 p0585 A70-12971

Plane-strain equations for deformation of weakly plastic anisotropic body analyzed by small parameter method

03 p0592 A70-13446

Flexible cylindrical shell elastoplastic state determined by theory of small elastoplastic deformations, utilizing material incompressibility in plastic state

03 p0593 A70-13500

Strain distribution measurement in plastically deformed region around crack tip in metals using moire grid and optical interference

03 p0513 A70-14019

Thin shells of revolution plastic collapse under axisymmetric loads on basis of Tresca-Nakamura yield criterion, using computer algorithm

03 p0598 A70-14238

Brittle composites /including fiber reinforced material/ deformability and plastic deformation effect on tensile strength, discussing pressure induction of sound flow

[ASME PAPER 69-WA/PROD-28]

04 p0705 A70-14834

Metals and alloys creep under tension and compression at elevated temperatures, considering plastic deformation equation applicability

04 p0707 A70-15265

Dynamic plastic response of finite bar subject to axial impact load noting reflected waves, stress-strain-time histories and residual strain

04 p0779 A70-15599

Biaxial prebuckling loading effect on compliance tensor in plastic buckling of square plates analyzed by local strain statistical theory

05 p0925 A70-15790

Unloading wave in elastic-plastic half space with rigid unloading for two parameter loads, discussing deformation body model

05 p0925 A70-15825

Plane deformation of plastic thin walled tubes under complex tensile and torsional load

05 p0935 A70-16233

Micromechanisms of fracture in metals and polymers before plastic deformation onset, discussing macroscopic polymer properties from microstructure and molecular structure

05 p0937 A70-16365

Test apparatus for investigating crystal defects influence on simultaneous measurement of metals thermal and electric conductivity under plastic deformation at cryogenic temperature

05 p0829 A70-16399

Elastoplastic thick layer with disk-shaped crack analyzed for stress and strain, determining width of plastic zone

05 p0939 A70-16482

Motion stability of ideally plastic medium flow in conical matrix, studying surface and velocity distribution for minimum plastic deformation energy

05 p0945 A70-16854

Small elastoplastic deformation effects on stress-strain state of rib-reinforced cylindrical shells

05 p0946 A70-16955

Work of plastic deformation in two dimensional rolling determined by energy dissipation function

05 p0857 A70-17017

Plastic deformation of refractory alloys during stress relaxation tests under vibrations, showing enhanced stability

05 p0866 A70-17033

Carrying capacity of machine parts under small numbers of cyclic plastic deformation, reviewing breakdown criteria relation to kinetics of stress-strain states

06 p1161 A70-17383

Plastic bodies stress-strain state under variable loads generalized to cases of cyclic loads and plasticity

06 p1162 A70-17384

Plastic flow theory applied to cyclic deformation of metals under complex cyclic loads

06 p1162 A70-17385

Copper specimens stress-strain diagrams under cyclic loads of various amplitudes, noting three stage process plastic deformation

06 p1162 A70-17386

Stress kinetics and breakdown time of hardening Al alloys and steels under cyclic loads, noting dependence on plastic deformation

06 p1162 A70-17391

Structural elements elastoplastic deformation regularities under repeated loadings, using adaptability theory

06 p1163 A70-17394

Shear and linear strain energy criteria for limiting stress state model of solid deformable bodies, considering uniaxial, biaxial and triaxial loading

06 p1166 A70-17657

Energy dissipation during torsional and flexural vibrations of steel and duralumin specimens subjected to plastic deformation, accounting for discrepancies due to methodical errors

06 p1166 A70-17658

Cyclic plastic deformation changes with load increase under uniform stress with normal loading and nonuniform stress with impact loading, considering fatigue limit

06 p1168 A70-17923

Plastic zone around propagating fatigue crack in Cu single crystals, using transmission electron microscopy and X ray topography

06 p1171 A70-18494

Plastic deformation effects on superconductivity of wire specimens of high purity Pb, In and Ti cold worked at liquid He and annealed

06 p1127 A70-18614

Plane elastic-relaxing plastic shock wave yielding of Fe numerically integrated by two step stable difference scheme without pseudoviscosity

06 p1172 A70-18618

Steels microstructural plastic deformation under pulsed laser irradiation

07 p1303 A70-18712

Elastic and plastic deformation zones stress-strain state under complex stresses, obtaining relation for stress and strain components

07 p1401 A70-18834

Surface mean deformation state under shot peening found equal to deformation under single indentation

07 p1292 A70-18835

Metallic adhesion produced by surfaces compression, discussing asperities plastic deformation and macrodeformation caused by contact area growth

07 p1292 A70-18939

Numerical analysis of axisymmetric elastoplastic deformation of circular plates under combined lateral load and membrane force

07 p1402 A70-18977

Rotating disk stability relation with stress distribution in plastic deformation of material

07 p1402 A70-19056

Plastic deformation of thin flexible axisymmetric shells under load, discussing tensile stresses

07 p1407 A70-19383

Rolling texture and recrystallization of Mo single crystals and deformation effect on texture formation using X ray transmission technique

07 p1309 A70-19613

Refractory metal monocarbide single crystal growth by plastic strain induced primary and secondary recrystallization

07 p1313 A70-19902

Thin walled metal cylinders residual deformation microstructures under internal impulsive loading

07 p1285 A70-19969

Abrasive wear of polymers subject to plastic and elastic deformation, considering papers, metal gauze and rough metal surfaces

07 p1296 A70-20003

Polycarbonate ductile fracture measured for strain energy release rates and plastic zone size and shapes to correlate with existing theories and experimental data

07 p1321 A70-20041

Axisymmetric elastoplastic deformation theory for elastic cylindrical shell using Saint Venant yield condition, obtaining expressions for strain components, longitudinal deformation, etc

07 p1415 A70-20185

Yield criterion for plastic bending of transversely anisotropic circular plates under plane stress

08 p1589 A70-21250

Energy equilibrium for crack growth in elastoplastic media, analyzing crack behavior during plastic deformation concentrated at edge of propagating crack

08 p1590 A70-21414

Thermal and athermal components of flow stress and deformation dynamics in Ti-Al alloy

08 p1521 A70-21578

Dynamic strain aging effect on Mo-Ti-C alloy creep, relating carbides precipitation during plastic deformation to mobile dislocations density

08 p1524 A70-21954

Plastic bodies plane flow Lagrangian description applied for prescribed deformation path of material fibers

09 p1769 A70-22251

Metals yield locus in strain hardening range in sigma-tau plane determined using slip theory, considering Bauschinger effects

09 p1771 A70-22395

Stressed state in region of strain raisers /round holes/ in plate subjected to two axial tension associated with plastic yield

09 p1771 A70-22464

Plastic growth of pressurized shell under cyclic thermal stresses superimposed on steady pressure load, investigating shake down using bending approximation

09 p1774 A70-22586

Cold and hot work deformation of aluminum alloys, discussing flow-stress dependence on strain rate, temperature and composition

09 p1692 A70-22642

Spherical and cylindrical cavities dynamic plastic expansion analysis by finite element method allowing for inertia forces

09 p1777 A70-22724

Particle fracture in oxide dispersed stainless steels during plastic deformation at room temperature

09 p1706 A70-22813

Nonisothermal loading model of polycrystalline material, investigating tangential stresses in slip direction and plastic deformation using linear strengthening law

09 p1779 A70-23102

Strain gages for static deformation measurement of fiberglass reinforced plastics at room and higher temperatures, discussing error sources and gage-specimen adhesive bonding

09 p1780 A70-23107

Plastic buckling of eccentrically stiffened circular cylindrical shells with multiple isotropic layers under combined axial and lateral pressure, deriving stability criterion

09 p1780 A70-23213

Power-law stress-strain relation in plastic complex stressed state, showing identical strain hardening curves for shear and tension

10 p1957 A70-24280

Rigid/plastic or rigid/perfectly plastic anisotropic plate under uniform bending, analyzing stress distribution

10 p1964 A70-25092

Residual stresses effect on strength and hardness of tungsten carbide-cobalt alloy by application of small plastic deformations, observing crack formation anisotropy

10 p1904 A70-25168

Strain tempering effects on upper and lower bainite, discussing strengthening and fracture toughness as function of temperature

10 p1905 A70-25173

Plastic strains buildup during thermal cycling, establishing relation between strain interval and cycles number to failure for strain hardening materials

10 p1965 A70-25293

Momentum theory of small elastic-plastic deformations, proving minimum potential energy, simple loading and elastic unloading theorems

11 p1218 A70-25387

Shells equilibrium with large plastic deformations, discussing stability under uniaxial/biaxial tension and physical models for material mechanical properties

11 p2130 A70-25569

Plastic strains at sharp notch roots in Perspex plates using interference patterns formed by gas laser monochromatic light beam for fracture initiation

11 p2131 A70-25594

Stress concentration in elastoplastic and creep deformations determined by approximate solution

11 p2134 A70-25845

Low cycle fatigue tests on stainless steel, discussing crack behavior dependence on temperature and plastic strain range

11 p2139 A70-26405

Thin cylindrical shells of perfectly plastic rigid material, analyzing dynamic plastic deformation under internal impulsive pressure

11 p2139 A70-26413

Metals low cycle fatigue resistance, discussing repeated plastic straining effect on mechanical properties

11 p2141 A70-26609

Energy principle providing upper bounds on plastic deformation in elastoplastic structures subjected to blast loading

11 p2144 A70-26670

Deformation theory for small elastic-plastic strains in orthotropic material and discretization and iterative solution techniques

11 p2144 A70-26684
Structural design for allowable plastic deformation under dynamic loads, deriving finite element representation of elastic-plastic plane frame beam

12 p2317 A70-27117
Thin walled tubes plastic instability under combined internal pressure and axial load for open and closed end conditions

12 p2322 A70-27216
Indentation pressures in rigid perfectly plastic solids correlated with ratio between indenter strain and material yield strain for various indenter geometries

12 p2322 A70-27232
Aluminum sheets anomalous plastic behavior under balanced biaxial and uniaxial tensions

12 p2324 A70-27398
Resistivity anomalies of nickel-chromium alloy with Al additions subjected to deformation and heating, studying K-state

12 p2254 A70-27496
Metallic cylindrical shells design reinforced with elastic glass fiber rings, considering elastoplastic deformation

12 p2324 A70-27530
Annealed stainless steel low cycle fatigue data analysis leading to method of characteristic slopes approach for correlating plastic strain range to fracture time

12 p2255 A70-27604
Superplasticity in physical metallurgy, comparing with metal deformation modes

12 p2257 A70-28145
Orthotropic fiberglass reinforced plastic deformation during stretching with allowance for binder breakdown in transverse layer

12 p2259 A70-28283
Polyurethane and metal surface layers deformation related during sliding friction in presence of liquid media, noting friction coefficient-deformation relation

12 p2244 A70-28284
Residual stress determination in flat strip elastoplastically deformed by finite bending

13 p2508 A70-28485
Plastic deformation in brittle and ductile fracture, discussing elastoplastic stress analysis of cracked bodies, plane strain deformation near cracks, etc

13 p2509 A70-28601
Plastic strain state effect on ductility and toughness of structural steels

13 p2432 A70-28675
Plastic symmetrical bending of freely supported beam under transverse local pulsed load, discussing deflection velocity fields during loading and unloading stages

13 p2514 A70-29307
Variational principles derivation for inelastically deformable body mixed boundary value problem, considering loading conditions with basic functions free of discontinuities

13 p2516 A70-29524
Plastic deformation of Mo-Re single crystals produced by electron beam zone refining, investigating lattice frictional stress, activation volume temperature variation, etc

13 p2436 A70-29562
High temperature dislocation model based on dislocation dynamics, rate theory and varying back stress ratio

13 p2436 A70-29563
Plastic deformation of Be single crystals under hydrostatic pressure, considering resolved shear stresses on glide systems

14 p2595 A70-30334
Pulsars crust plastic deformation leading to rotation damping, higher magnetic moments and rarer starquakes

14 p2638 A70-30672
Elastoplastic material mechanical theory, considering constitutive equations with plastic deformations and decompositions of total velocity-strain /stretching/

14 p2661 A70-31281
Pure Mo recrystallization deformed by cold rolling using transmission electron microscopy

14 p2597 A70-31284
Plastic deformation and aging effects on fatigue characteristics of steels until rupture under cyclic loads

15 p2755 A70-31540
Al-Zn eutectoid alloys defect structures and interactions in superplastic deformation process

15 p2756 A70-31567
Yield criteria for plastic deformation on glassy high polymers induced by stress field, noting crazing and shear yielding dependence on first stress invariant

15 p2764 A70-31787
Mechanical and morphological characteristics of overload and fatigue in dog ulnas, showing elastic and plastic deformation zones

15 p2682 A70-31935

Stress relaxation of Mo under plastic deformation controlled by diffusion of interstitial atoms and dislocations, determining activation energy

15 p2758 A70-32124
Shallow shells of revolution under axisymmetrical loads, analyzing plasticity and creep by integral equations algorithm

15 p2817 A70-32164
Axisymmetric elastoplastic deformation of compressible plate with arbitrary hardening under uniform load, solving in quadratures

15 p2817 A70-32167
Plane deformation of anisotropic plastic nonstrain-hardenable material, analyzing state equations for stresses and strain rates

15 p2818 A70-32184
Photoplastic material thickness change from mechanical and holographic measurements, showing correlation with isochromatics during plastic yielding

15 p2821 A70-32314
Size effects on impact energy disposition in plastically deformed thick steel specimens at shelf temperature, using similitude laws

15 p2760 A70-32332
Austenite strength effect on austenite-martensite transformation in alloy steels, measuring resistance to plastic deformation

15 p2760 A70-32376
Metal fiber multiple necking effect on uniaxial metal matrix composites ductility and plastic deformation behavior for brass-W model system

15 p2761 A70-32378
Alumina particles marker transport in Ag wires during early sintering as function of plastic deformation by slip

15 p2745 A70-32392
Work hardening properties of Ni single crystals of various orientations during intermittent and continuous plastic deformation

15 p2762 A70-32394
Metal property effects on deformation and strain energy distribution during hypervelocity projectile cratering

15 p2824 A70-32790
Metastability effects on plastically deformed Al, showing superplastic flow

15 p2764 A70-32902
Super plasticity in plastically deformed pure Al related to recrystallization

15 p2764 A70-32903
Superplastic deformation of thin circular diaphragms subjected to on-sided hydrostatic pressure, emphasizing thickness variations in bulged shapes

16 p2916 A70-32917
Titanium and Ti-Al single crystals microscopic plastic deformation features, slip modes and dislocation substructures

17 p3116 A70-34389
Commercial purity Ti athermal plastic deformation, showing anomalous behavior with temperature variations

17 p3116 A70-34392
Titanium hydride deformation assisted nucleation in alpha-beta titanium alloy, showing low strain rate embrittlement and stress corrosion crack propagation in aqueous environments

17 p3116 A70-34395
Hydrogen embrittlement of Ti and Ti alloys under plastic deformation and critical hydrogen concentration

17 p3117 A70-34397
Temperature cycling through phase transformation effects on plastic deformation of Ti and Ti-Al-V alloy under torsion and tension

17 p3117 A70-34400
Hot plasticity elongation of cast and wrought Ti-Al-V alloy as function of temperature and strain rate

17 p3117 A70-34401
Displacement bounding principle for finitely deforming rigid plastic structures exhibiting geometric stability, with application to cylindrical shell

17 p3184 A70-34906
Plastic deformation of two phase alloy with small nondeformable particles in ductile matrix, discussing cross slip, yield and flow stress, work hardening etc

17 p3126 A70-35460
Plastic deformation zones at crack tip considered as distributed heat sources, using stress and strain distribution solutions

17 p3191 A70-35463
Sapphire and ruby plastic deformation and fracture properties at room temperature, discussing sapphire base ceramics

18 p3278 A70-36046
Elastoplastic deformations during explosive extrusion of pipes of different materials with linear strain hardening law

18 p3335 A70-36132
Spherical shell of variable thickness, calculating stress-strain state around reinforced circular hole during elastoplastic deformation

18 p3336 A70-36138

Ti alloy prior plastic deformation effect on fatigue strength under bending, tension, torsion and rolling

18 p3275 A70-36141
Elastic and plastic cylindrical shells, investigating dynamic buckling under impulsive loads

18 p3338 A70-36436
Stress concentration in notched flat samples under plane plastic deformation

18 p3340 A70-36570
Cyclic plastic breakdown of thin cylindrical shell under ring shaped load in temperature field, using linear programming method

18 p3341 A70-36585
Loading history effect on work of plastic deformation in Ni and Cu pipes, taking into account stress and strain deviators deviation from similarity

18 p3344 A70-36945
Combined mechanical and cyclic thermal stresses effect on plastic deformation buildup in E1435 alloy preceding breakdown

19 p3449 A70-37349
Plastic deformation of melted Al-Mg single crystals, using dynamic tensile testing

19 p3450 A70-37374
Metal powder rolling process as compaction with plastic particle deformation, deriving pressure distribution on rollers

19 p3434 A70-37451
Superlattice stacking faults in plastically deformed nickel aluminate /gamma prime phase/ due to interaction of antiphase boundary /APB/ type dislocation pairs

19 p3451 A70-37704
Plastic deformation in Ni-Cr-Nb alloy precipitation hardened at different long terms of high temperature

19 p3451 A70-37706
Plasticity and strain hardening in sintered metals, considering pressure at pores and elastoplastic limit under small plastic deformation

20 p3644 A70-38962
Solid body nonelastic deformation in terms of thermodynamic principles of nonequilibrium processes

20 p3718 A70-39246
Elastoplastic deformation in strip with symmetrical semicircular notches simulating stress-strain-state on celluloid models by polarization-optical method

20 p3720 A70-39735
Elastoplastic deformation of thin circular plates under uniformly distributed transverse loads, using mixed type variational equation

20 p3721 A70-39776
Soviet papers on mechanics of solid deformed body covering elasticity and plasticity theories, shell stability, eigenvalue problems, etc

20 p3722 A70-39851
Low cycle metal fatigue under stress concentration, examining complex loading, cyclic strain, stress-strain state and plastic deformation

20 p3727 A70-39885
Anisotropic plasticity yield conditions, analyzing elastic to plastic deformation transition geometry

20 p3727 A70-39889
Thin circular plate clamped along edge, calculating large displacements and elastoplastic strains for comparison with measurement

21 p3935 A70-41406
Elastic-plastic deformation analysis at finite strain by two component thermodynamic model

21 p3937 A70-41431
Apollo 11 lunar soil and breccia shock metamorphism, examining plastic deformation structures in plagioclase, pyroxene and olivine

21 p3897 A70-41520
Compatibility equations in superelastic domain for permanent deformation hypotheses

22 p4114 A70-42611
Cylindrical cavity uniform expansion in compressible elastic plastic solid, calculating pressure by similarity solution

22 p4114 A70-42634
Spherical cavity nonuniform expansion in compressible elastic plastic solid, calculating velocity field and pressure by approximate similarity solution

22 p4114 A70-42635
Recrystallized and nitrided Mo alloy microstructure under plastic deformation by tension at high temperatures

22 p4038 A70-43122
Mo single crystals tensile properties at different orientations, noting asymmetric slip in plastic behavior

22 p4056 A70-43155
Alloy aging process after plastic deformation, examining relationship of phase distribution and mechanical and physical properties

22 p4056 A70-43340
Soviet bibliography on flexible plates covering elastic bending, elastoplastic state under transverse load and bending beyond elastic limit

22 p4119 A70-43710
Limiting pressure for isotropic plastic plates and spherical shells with stress dependent yield, using flow theory

22 p4120 A70-43717

- Precious metals, measuring tension, grinding and polishing induced surface plastic deformation effects on electron work function and exoemission
23 p4204 A70-43927
- Comparative load capacity of disk models of natural gas blowers of different designs under plastic strain
23 p4232 A70-43941
- Plastic postbuckling and imperfection sensitivity of spherical shells under axisymmetric bifurcation
23 p4272 A70-44714
- Plastic deformation dislocation motion and incompatibility relationship, describing strain rate, velocity and stresses
24 p4420 A70-45229
- Ti single crystals plastic deformation in axial compression at high temperatures
24 p4358 A70-45239
- Metal and alloy sheets, investigating deformation and failure under biaxial stretching tensile tests
24 p4358 A70-45240
- Plastic creep displacement and deformation bounds computation for simple redundant structures, using energy theorems
24 p4422 A70-45288
- Notch sensitivity dependence on plastic strain in Al alloy, heat resistant steels and Ni alloys under tensile tests at room temperature
24 p4360 A70-45827
- Isothermal plasticity thermodynamic foundation, deriving constitutive equations for various deformations
24 p4426 A70-45994
- Zn-Al alloy high velocity deformation characteristics, examining ductility and aging at various temperatures and heat treatments
24 p4363 A70-46194
- PLASTIC FILMS**
U POLYMERIC FILMS
PLASTIC FLOW
NT TRESKA FLOW
Strain rate, temperature and alloy content effects on plastic flow in binary substitutional alloys of bcc iron
01 p0119 A70-10735
- Plastic flow under biaxial stress, discussing data acquisition system and computer program for comparing test and theory
03 p0480 A70-12954
- Serrated plastic flow in stable austenitic stainless steels based on Fe/Ni, showing strength dependence on C and/or Cr presence
03 p0506 A70-13134
- Plastic flow failure of matrix of fiber reinforced composite sheet, discussing plane stress and simple tension
[ASME PAPER 69-APM-Z] 04 p0770 A70-14869
- Activation energy measurement using stress relaxation for plastic flow in commercially pure Al compared with creep and tensile method
04 p0777 A70-15495
- Motion stability of ideally plastic medium flow in conical matrix, studying surface and velocity distribution for minimum plastic deformation energy
05 p0945 A70-16854
- Plastic flow theory applied to cyclic deformation of metals under complex cyclic loads
06 p1162 A70-17385
- Plastic lubricants motion in circular pipes, determining drag and cross sectional velocity profile of laminar flows
07 p1290 A70-18652
- Elastic-plastic plane strain solutions in infinitesimal plastic flow theory with separable stress fields
[ASME PAPER 69-APMW-13] 08 p1592 A70-21470
- Fiber-reinforced composite sheet matrix failure by plastic flow, investigating two ply laminate in simple tension
08 p1592 A70-21471
- Interstitial solutes effect on athermal component of flow stress in alpha titanium
08 p1521 A70-21577
- Temperature effect on plastic flow in Ti-scavenged Fe, attributing microyielding to edge dislocations motion
08 p1525 A70-21959
- Cylindrical shells plastic flow buckling under radially inward impulsive loading, showing mode number dependence on shell length
11 p2140 A70-26486
- Athermal component of plastic flow stress in alpha titanium at room temperature using incremental unloading technique
12 p2257 A70-28100
- Metals and metal alloys ductility development, discussing plastic flow problem in metal working
12 p2327 A70-28144
- Circular cylinders torsion and plain strain analysis, completing statics by asymmetric shear and moment stresses according to Cosserat theory for plastic flow
13 p2508 A70-28492
- Metastability effects on plastically deformed Al, showing superplastic flow
15 p2764 A70-32902
- Plastic flow and failure of elastic fiber reinforced composite materials with noninteracting and interact-

ing discontinuities, obtaining stress distribution for various work hardening degrees
17 p3187 A70-34991

Pure Ni plastic flow threshold measurement under combined ultrasonic and static loadings, noting annealing
22 p4053 A70-42644

Moire technique application to fracture toughness tests on Zr alloys, measuring crack opening displacements and plastic flow beneath notch
23 p4208 A70-44914

Fe-Ni alloy plastic flow behavior during reversible austenite-martensite transformation under constant load
24 p4357 A70-45228

Plane flow of incompressible elastic perfectly plastic solid, deriving hyperbolic stress and velocity equations
24 p4427 A70-46043

PLASTIC MATERIALS

U PLASTICS

PLASTIC PROPELLANTS

Flame spreading theory for plastic fuels surfaces in nitrogen-oxygen mixtures, considering initial fuel temperature, pressure and mixture composition effects
02 p0396 A70-12015

Polyvinyl chloride plastisol propellants consisting of fine solid oxidizer and powdered metal, discussing composition, propellant flow, curing time and temperature dependence
07 p1360 A70-19908

Burning and degradation mechanism of polyester propellants correlated with mass regression rate dependent on surface temperature
11 p2099 A70-25990

Combustion rates acceleration of ammonium perchlorate mixtures with polystyrene and polymethyl methacrylate by KCl and LiF additions, forming molten layer on charge surface
18 p3299 A70-36248

PLASTIC PROPERTIES

NT ELASTOPLASTICITY

NT PHOTOPLASTICITY

NT THERMOPLASTICITY

NT VISCOPLASTICITY

NT YIELD POINT

Dissolved gases and carbon effect on transition temperature from plastic to brittle state of high melting metals including niobium and vanadium
01 p0124 A70-11615

Molybdenum cylinders strength and plasticity under various compression and cyclic tensile loads
02 p0315 A70-11662

Bounded region satisfying regularity necessary to Korn inequalities and Sobolev immersion theories, discussing plasticity theory operator monotony in Minty-Browder sense
02 p0387 A70-12109

Dislocation climb theories of creep and superplasticity derived, postulating strain hardening and recovery processes with independently determined rates
02 p0317 A70-12315

Thin simply supported circular rigid ideally plastic plate subjected to dynamic transverse load uniformly distributed over central circular region
02 p0389 A70-12668

Strain rates and stresses relations in plasticity theory for consolidatable orthotropic bodies having three elastic planes of symmetry
02 p0389 A70-12686

Rigid plastic body of material insensitive to strain rate under time dependent surface tension and time independent body forces
02 p0391 A70-12816

Elastoplastic media revised mathematical model with allowance for cumulative damages effect on elastoplastic property under variable loads
04 p0775 A70-15199

Plasticity theory of single crystals based on dislocations behavior, considering only plane and elastic strains
05 p0928 A70-16061

Testing equipment and methods for metallic materials selection for low temperature applications, characterizing plasticity by yield strength, tensile strength, elongation, etc
05 p0864 A70-16805

Finite element method for large displacement elastic-plastic analysis of plates and shells, using geometric stiffness matrices and stress-strain relationships
05 p0943 A70-16809

Continuous metal fiber composites tensile strength and ductility in terms of plastic instability
05 p0946 A70-16924

Dual model for describing brittleness and plasticity of solid elastic deformable body, formulating criteria for passage into inelastic state
06 p1166 A70-17656

Fabrication technique effect on tensile and plastic properties of semifinished sintered Al powder products at room temperature and 600 C
06 p1076 A70-17848

Oxidation behavior of metals concerning oxide plasticity role in connection with oxide film macro- and microstresses
07 p1305 A70-18968

Plastic symmetrical trough waveguides with metalized surfaces for hybrid millimeter-wave integrated circuit systems, discussing ferrite resonant isolator
07 p1243 A70-20151

Limiting equilibrium of rigid-plastic cylinder subjected to compression by concave stamps
08 p1583 A70-20533

Quenched and tempered steels ductile fracture with respect to plasticity, structure and crack development conditions using microfractography
08 p1515 A70-20922

Ultrasonic vibration effect on strength and plastic properties of metals undergoing torsion tests
08 p1520 A70-21499

Plastic properties of tungsten carbide single crystals at room temperature, determining slip system crystallographic orientations
08 p1520 A70-21557

Strength and plasticity criteria for anisotropic reinforced materials model taking into account material structure, components properties and behavior
09 p1768 A70-22119

Polarization-optical studies of large deformations in nonlinear theory of elasticity and plasticity, considering procedures based on photoelastic coatings and transparent models
09 p1768 A70-22120

Variational theorem for compatibility and plasticity for Mises solids based on stress functions
09 p1771 A70-22397

Finite deformations of flexible inelastic orthotropic shells of revolution for generalized plastic flow and deformation theories
10 p1955 A70-24079

Finite deflections theory applied to elastic-plastic arches, introducing coefficients depending on shape and degree of yielding of cross section
10 p1955 A70-24080

Interstitial and substitutional impurity effects on fracture strength, plastic properties and ductile-brittle transition temperature of vanadium determined from impact and tensile tests
11 p2066 A70-25913

Powder base superalloy with superplastic behavior, ascribing mechanism to migration of second phase gamma prime particles
12 p2252 A70-26889

Plastic properties of materials to elastic limit of pure metal and ionic solid crystals
12 p2283 A70-27055

Weather effects on plastic properties, discussing weathering interactions with plastics and polymer degradation
12 p2259 A70-27206

Stress-strain state effects on Cu and Ni tubular samples plasticity and strength using polarization-optical technique
12 p2323 A70-27341

Dispersion strengthened Ni-Cr alloys elastic and plastic properties at room temperature, studying preferred crystallographic orientation effect
12 p2255 A70-27609

Superplastic nickel superalloys fabrication by controlled densification during direct extrusion
12 p2257 A70-28020

Plasticity and superplasticity exploitation - Conference, Eastbourne, Sussex, England October 1969
12 p2327 A70-28143

Superplasticity in physical metallurgy, comparing with metal deformation modes
12 p2257 A70-28145

Engineering development role in metal forming industry expansion, discussing metals ductility or plasticity increase for extending processes
12 p2244 A70-28146

Elastoplastic continuum under specified rates of body forces, surface tractions and displacements, formulating minimum principle for solving boundary value problem
13 p2513 A70-29154

Al-Mg alloy sheets work hardened plastic properties, tensile strength and elongation
14 p2597 A70-30962

Elastoplastic torsion problems solution by strain theory of plasticity, describing torsion function in hypergeometric series form
14 p2661 A70-31329

Unloading shock waves propagation in elastoplastic medium, investigating strain hardening effect on shock strength decay, residual strains and radial stresses
15 p2815 A70-32002

Axissymmetric nonuniform initial thickness disk under pressure and twisting along interior surface of circular hole using incremental theory of plasticity for deformation analysis
15 p2816 A70-32004

Tapered cantilever Al plate load characteristics, determining elastic and plastic strain due to regular, reverse and second regular deflection sequence
15 p2821 A70-32307

Super plasticity in plastically deformed pure Al related to recrystallization 15 p2764 A70-32903

Book on structural mechanics with introduction to elasticity and plasticity 16 p2987 A70-32915

Metallic superplasticity and superplastic alloys in simple tension, forming tubes and sheets of superplastic Sn-Pb eutectic alloy by pressure forming techniques 16 p2916 A70-32916

Superplastic deformation of thin circular diaphragms subjected to oned-sided hydrostatic pressure, emphasizing thickness variations in bulged shapes 16 p2916 A70-32917

Lateral pressure bulging of superplastic alloy sheet, considering flat circular sheet and bulging into V grooves 16 p2916 A70-32918

Fiber reinforced prepreg properties measurements in high modulus graphite/epoxy and fiberglass/ epoxy prepreg sheets and tapes 16 p2938 A70-33386

Pressure forming Ti sheet alloy blanks in superplastic condition under controlled temperature and strain rate 17 p3117 A70-34402

Rate-sensitive perfectly plastic linear strain hardened rings and tubes, calculating response to impulsive loads 17 p3184 A70-34907

Plasticity limit theorems applicability extended without geometry change requirement, discussing load elastic buckling and fiber pullout from composite materials 17 p3186 A70-34977

Baron thermal diffusion effects on plastic of pure Mo subjected to recrystallization 17 p3102 A70-35408

Collection of papers on physics of strength and plasticity, covering flow mechanisms, stress fields, alloy hardening, crack structure and initiation, rock ductility, etc 17 p3190 A70-35451

Cyclic strain effects on creep for steel at elevated temperatures, discussing overload frequency effects on plastic strain buildup 17 p3127 A70-35719

Temperature changes minimization techniques in specimens during microplasticity tests, describing gage assembly for plastic strain measurement 18 p3272 A70-36030

Transformation induced plasticity (TRIP) high strength steels resistance to hydrogen embrittlement 18 p3273 A70-36047

Optimal distribution of plastic inhomogeneity of torsioned prismatic square bars under maximum loading 18 p3343 A70-36719

Polarization optical determination of plane stress plastic region, using celluloid model 18 p3343 A70-36723

Ti alloys low temperature strength and plasticity, noting twinning and additives effects 19 p3450 A70-37457

Strain transducer /optical diffraction grating/ for plastic wave propagation measurement along specimens subjected to impact 19 p3425 A70-37884

Molybdenum cylinders strength and plasticity under various compression and cyclic tensile loads 19 p3453 A70-38436

Continuum bodies strain subjected to shearing stresses in incremental form based on slip theory of metals plasticity 19 p3549 A70-38668

Ti-Nb-Zr alloys strength and plasticity at various temperatures, noting compositional effects on tensile and yield strength 19 p3453 A70-38712

Microstresses in plasticity theory, considering continuous elastic body model of crystal with dislocations 20 p3724 A70-39859

Stress-strain characteristics at high strain rates, obtaining materials dynamic plastic properties by thin wafer technique 21 p3932 A70-40543

Plastic zones between symmetric and collinear edge cracks in thin plexiglass strips, using He-Ne laser interferometry 21 p3939 A70-41967

Papers on thermoplastics covering types, properties and applications 22 p4060 A70-43624

Isothermal plasticity thermodynamic foundation, deriving constitutive equations for various deformations 24 p4426 A70-45994

Superplasticity, discussing strain rate-flow stress relationship and grain boundary sliding 24 p4363 A70-46218

PLASTIC TAPES

Fiber reinforced prepreg properties measurements in high modulus graphite/epoxy and fiberglass/ epoxy prepreg sheets and tapes 16 p2938 A70-33386

PLASTIC YIELDING

U PLASTIC DEFORMATION

PLASTICITY

U PLASTIC PROPERTIES

PLASTICS

NT ACRYLIC RESINS

NT EPOXY RESINS

NT NYLON [TRADEMARK]

NT PERSPEX [TRADEMARK]

NT PHENOLIC RESINS

NT POLYAMIDE RESINS

NT POLYBUTADIENE

NT POLYESTER RESINS

NT POLYETHER RESINS

NT POLYETHYLENES

NT POLYMETHYL METHACRYLATE

NT POLYPROPYLENE

NT POLYSTYRENE

NT POLYTETRAFLUOROETHYLENE

NT POLYVINYL CHLORIDE

NT REINFORCED PLASTICS

NT SYNTHETIC RESINS

NT TEFLON [TRADEMARK]

NT THERMOPLASTIC RESINS

NT THERMOSETTING RESINS

Electrically conductive plastics fabrication and applications limitations, discussing plastic matrix materials loaded with various conductive fillers 01 p0129 A70-10938

Quasi-brittle fracture of plastic materials based on Griffith theory and crack propagation, analyzing real surface energy and work of plastic strain 01 p0212 A70-11562

Nonsteady thermal decomposition of plastics subjected to large heat flows, introducing equations governing char layers and pyrolysis zones 02 p0397 A70-12021

Polymeric materials properties, discussing tensile stress disadvantage and compensation by reinforcement and polymer chain directional alignment 02 p0321 A70-12305

Complex Young modulus of plastics during flexural vibration, discussing deformation of viscoelastic bodies and test results of various plastics [ONERA-TP-715] 03 p0487 A70-13645

High speed photographic study of breakdown, crack formation, thermal explosions and molecular weight of transparent plastic dielectrics under laser beam 05 p0869 A70-16210

N-substituted tetrabromophthalimides prepared as fire retardant additives to PVC, polyester and epoxy resins 05 p0811 A70-16585

Handbook on fiberglass and advanced plastics composites covering raw materials, processing methods, design and applications 05 p0872 A70-16601

Precooling effect on load carrying capacity of heat resistant plastics subjected to unilateral heating 05 p0874 A70-17065

Heat resistant plastics stability subject to unilateral heating with allowance for mass removal, obtaining dimensionless stability characteristics for structures design 05 p0874 A70-17066

Test stand for endurance and creep testing of plastics, glazed ceramics and other brittle materials 06 p1028 A70-17665

Power series solution of Cauchy problem for axisymmetric state of ideally plastic body 07 p1405 A70-19288

Graphite-polyester plastic material with electrical resistance for eliminating static charges leading to explosions 07 p1295 A70-19764

Sand erosion of metals and plastics, discussing effects of impact conditions and impacting particles and target surface properties 07 p1314 A70-20004

Metals and plastics tensile strain rate sensitivity tested by drop weight tests, obtaining dynamic and static stress-strain curves 09 p1704 A70-22725

Dynamic photoelastic analysis of fracturing plastic plates, studying elastic and stress fields around propagating cracks 09 p1783 A70-23448

Macroscopic internal stresses in plastics surfaces, discussing stress effect on plastic moulding service life, Knoop hardness test and charts 11 p2132 A70-25597

Pinhole expansion in anisotropic plastic disks determined by obtaining solutions for Tresca and Mises yield functions, assuming plane stressed state 11 p2138 A70-26171

Charring ablative plastic thermal properties simultaneous measurement using modified heat transfer model and nonlinear regression analysis 12 p2333 A70-28111

Longitudinal stress waves propagation in polymeric optically active plastic bars using photoelasticity method 12 p2328 A70-28277

Fiberglass plastic cylindrical shells stability against creep under prolonged hydrostatic pressure, obtaining critical loading times 12 p3328 A70-28278

Strain induced in laminated orthotropic fiberglass plastic cylindrical shell by normal concentrated load, using equations free from rectilinear normals hypothesis 12 p3328 A70-28279

Structural strength of fiberglass plastics reinforced conical shells, using impregnation technique of dry package under pressure 12 p2328 A70-28280

Engineering properties and structure of plastics - Conference, New York, May 1970 13 p2438 A70-29251

Plastic encapsulated semiconductors reliability test programs with emphasis on accelerated humidity-temperature method 13 p2377 A70-29259

Simulated Venusian atmosphere effects on polymeric plastic and rubber materials, comparing with high temperature air and nitrogen exposures 14 p2640 A70-30781

Plastics - Conference, Washington, D.C., February 1970 16 p2934 A70-33351

Plastic structural components service life estimation based on creep diagrams and short time tests 16 p2941 A70-34323

Plastic materials Poisson ratio and Young modulus measurements by triaxial compression method 17 p3089 A70-35048

Nonlinear elasticity law for elastic moduli of plastics 18 p3344 A70-36947

Super heavy cosmic ray nuclei charge composition and track identification, using Lexan polycarbonate, cellulose triacetate (CTA) and nuclear emulsion 19 p3508 A70-38137

Complementary energy bounding theorem for statically loaded bodies composed of time independent plastic material 19 p3546 A70-38353

Plastic bodies rupture and crack growth under creep, considering tension of bar with symmetrical angular notches 20 p3727 A70-39882

Glass plastic composite electrically heated windshields for aircraft, discussing design, fabrication, qualification testing and service experience 21 p3750 A70-41137

Monolithic precision castings using photoetched plastic and lost-wax investment techniques [ASME PAPER 70-FLCS-8] 22 p4043 A70-42419

Plastic balloon platforms for atmospheric research and engineering applications, discussing design and use of unreinforced polyethylene and reinforced Mylar types 22 p3962 A70-43650

Dynamic deformation in thin walled axisymmetric plastic shells and filaments under time variable loads applied to high energy rate forming techniques 23 p4200 A70-44235

Plastic encapsulated IC for military environments, discussing cooker, corrosion and thermal shock tests 23 p4173 A70-44534

Approximation method for large deflection analysis of impulsively loaded rigid plastic circular plates and symmetric shells 23 p4275 A70-44943

Nondestructive examination for plastics, discussing transmission, microwave and ultrasonic tests 24 p4346 A70-45720

Papers on plastics, volume 1 covering materials, design, fabrication, applications, etc 24 p4368 A70-46223

PLASTISOLS

NT SMOKE

Slurry-cast filled nitrocellulose plastisols as solid propellants, discussing compositions, performance and applicability to beryllium fuel 07 p1360 A70-19907

Polyvinyl chloride plastisol propellants consisting of fine solid oxidizer and powdered metal, discussing composition, propellant flow, curing time and temperature dependence 07 p1360 A70-19908

PLATE [METAL]

U METAL PLATES

PLATE THEORY

Anisotropic shells and plates dynamic field equations derived, taking into account mechanical forces and nonuniform temperature field 01 p0200 A70-10553

Moments and shear forces in plate flexure represented by single valued stress functions of position, stating variational principle for compatibility 01 p0201 A70-10931

Longitudinal wave motion in rods, plates and shells based on three dimensional equations and asymptotic expansion 01 p0209 A70-11365

Plates and shells natural oscillations frequencies and modes, analyzing variational, asymptotic and numerical methods

01 p0210 A70-11412

Two asymptotic dimensional moment theory of elasticity, analyzing stress concentration at curvilinear holes and fluctuating boundary loads

01 p0212 A70-11563

Error estimates of stress concentration at free hole determined by two dimensional elasticity theory of thick plates

01 p0212 A70-11564

Triangular conforming plate bending element applied to static and dynamic problems, investigating convergence rates of finite element approximations

03 p0584 A70-12924

Monograph on buckling and postbuckling behavior of plates tapered in planform, comparing stability of tapered and rectangular plates

03 p0586 A70-13002

Stress-strain state equations of shallow spherical shells in rectangular and polar coordinates, discussing reduction to plate and Cauchy-Riemann equations

03 p0591 A70-13427

Elliptic system of twelfth order equations describing elastic equilibrium of plate with kinematic functions analyzed by integration procedure

03 p0600 A70-14306

Thermal stresses of semiinfinite plate with circular hole filled with elastic inclusion and subjected to uniform heat flow

03 p0601 A70-14317

Linear isothermal response of viscously damped thin homogeneous polygonal plates subjected to uniform dynamic loading, calculating forced solutions by numerical integration

03 p0601 A70-14318

Linear nonaxisymmetric bending of infinite plate coupled to elastic half space under concentrated loads using double Fourier transforms

04 p0766 A70-14480

Thin walled plate simply supported on three edges, studying behavior following local stability loss

04 p0772 A70-14923

Soviet monograph on numerical determination of dynamic characteristics of plates and shells by method of summary representations, covering oscillation and stability problems

04 p0773 A70-14954

Flat plates thermal buckling calculations with allowance for transverse shear deformation effect, using Rissner variational principle

04 p0773 A70-15091

Piston theory application to plates and shells stability in supersonic gas flows, considering critical velocities determination for asymmetric flows and oscillations

04 p0617 A70-15196

Biaxial prebuckling loading effect on compliance tensor in plastic buckling of square plates analyzed by local strain statistical theory

05 p0925 A70-15790

Soviet book on anisotropic plates theory, strength, stability and oscillations including corrections to classical theory

05 p0928 A70-16016

Dynamic response of simply supported rectangular plate under suddenly applied transverse load, comparing solutions of classical and improved plate theories

05 p0933 A70-16174

Stress distribution around crack tip of initially curved sheets

05 p0939 A70-16484

Green operator structure and eigenvalue approximation of boundary value problems regarding vibrations and buckling of clamped plates using orthogonal invariants

05 p0876 A70-16563

Finite element method for large displacement elastic-plastic analysis of plates and shells, using geometric stiffness matrices and stress-strain relationships

05 p0943 A70-16809

Modulus of rigidity and stress-strain state measured in square plate during shear produced by twisting

06 p1060 A70-17132

Rectangular and nonrectangular anisotropic plate bending and stability analysis by difference-differential technique, allowing for combined freely supported and clamped end conditions

06 p1167 A70-17864

Eigenvalue solutions convergence rates using two finite plate multidegrees of freedom bending elements

06 p1169 A70-17941

Numerical analysis of axisymmetric elastoplastic deformation of circular plates under combined lateral load and membrane force

07 p1402 A70-18977

Circular plates dynamic response to axisymmetric time dependent loads, analyzing transverse restraint effects on response maxima by plate theory

07 p1404 A70-19251

Governing equations solution for simply supported laminated anisotropic rectangular plate using Fourier series method

07 p1406 A70-19305

Unsteady heat conduction in plate, solid or hollow infinite cylinder and sphere with internal heat source and radiative heat transfer on surface

07 p1423 A70-19818

Elastic fields in bimaterial plate under uniform compressive and anti-plane shear loadings, finding stress distribution and induced interfacial shear stresses

07 p1412 A70-19957

Nonlinear thermodynamic theories of plates, elastic shells and rods derived from three dimensional theory of classical continuum mechanics

07 p1414 A70-20172

Transverse free molecular flow past broken plate of infinite span, determining aerodynamic coefficients

08 p1432 A70-21082

Thermoelastic characteristics of glass fiber reinforced plastic materials, determining temperature dependent deformation of composite plate

08 p1526 A70-21164

Thermoelastic state of plate near foreign circular inclusion, assuming heating by uniformly distributed sources and ideal plate-inclusion thermal contact

08 p1587 A70-21171

Variational problem of determining optimal heat transfer from gas flow to porous plate boundary layer

08 p1597 A70-21176

Biharmonic equation in polar coordinates solved for circular plates and plate sectors with various boundary conditions, using finite difference approximations

08 p1589 A70-21246

Two dimensional natural convection boundary layer on finite isothermal horizontal plate, examining upward facing cold plate and downward facing hot plate

08 p1598 A70-21580

Theorem for highest statically admissible multiplier for plates and shells, noting association with stress field satisfying yield equality at all cross sections

08 p1595 A70-21977

Nonuniqueness theorems for von Karman equations governing thin flat elastic plate deflections clamped at edges and subjected to normal and edge loading

09 p1768 A70-22063

Natural oscillation frequencies of subsonic gas flow past plate array, solving eigenvalue problem by splicing method

09 p1603 A70-22117

Nonorthotropic pinched plates deflections solution, demonstrating asymptotic convergence of small parameter method

09 p1769 A70-22151

Free incompressible oil jet interaction with mobile plate, discussing plate configuration, oil feed pressure and nozzle diameter, applications to electrohydraulic converter design, etc

09 p1613 A70-22825

Rectangular plate in unsteady temperature field, analyzing thermoplasticity problem by reducing solution to linear system with variable coefficients

09 p1779 A70-23098

Numerical analysis of forced parametrically excited plate vibration in plane supersonic flow, using digital computer

10 p1958 A70-24527

Transverse vibrations of rods, plates and shells based on hyperbolic, circular and Bessel functions

10 p1959 A70-24586

Temperature effect on plate damping by constrained viscoelastic layers, emphasizing transition and operating temperature compatibility

10 p1962 A70-25063

Noise-flutter interrelation in flight vehicle flexible plate and shell configurations immersed in fluid flow

11 p2132 A70-25726

Elastic bending of clamped and supported elliptic and parabolic plates under external pressure investigated by lines of equal deflection

11 p2133 A70-25839

Conforming plate bending solution with third degree polynomial deflection functions in triangular finite elements, using Lagrange multipliers as stress parameters

11 p2143 A70-26642

Stress concentration coefficients in multiply connected plates and bulky elements made of nonlinearly elastic materials

12 p2323 A70-27336

Critical equilibrium of plate under omnidirectional tension with radial rectilinear cracks

13 p2515 A70-29429

Isotropic plates weakened by circular holes, investigating bending by Ambartsumian plate theory

13 p2515 A70-29509

Plane stress state equations for micropolar elastic plates using complex potentials

13 p2517 A70-29629

Arbitrary planform plates with edge clamping and elastic beam spanwise support using Green function

14 p2655 A70-30182

Eigenvalues of membranes and plates, comparing asymptotic and numerical values

14 p2600 A70-31223

Rheological calculation of plate resistance and heat transfer in laminar flow of structurally viscous fluids

15 p2827 A70-32126

Axisymmetric elastoplastic deformation of compressible plate with arbitrary hardening under uniform load, solving in quadratures

15 p2817 A70-32167

Closed form difference equations for finite element models in structural mechanics, noting plate and grid applications

16 p2990 A70-33672

Infinite elastic plate with beam reinforced circular insert, using classical plate theory and Euler-Bernoulli hypothesis for beams

16 p2990 A70-33679

Transversely isotropic elastic plates vibrations without initial specification of field variables spatial dependence on thickness coordinate by two dimensional asymptotic theory

16 p2994 A70-34232

Three dimensional linear small deformation theory of elasticity solution for free vibration of simply supported homogeneous isotropic thick laminated rectangular plates

17 p3181 A70-34522

Matrix filtering method for stability solutions of shells and plates by finite difference method

18 p3341 A70-36580

Discrete element stress and displacement analysis of elastoplastic plates

18 p3342 A70-36686

Bent plates strain analysis using in-plane moire method for small and large deflections

19 p3535 A70-37383

Soviet book on theory of shell and plate type thin walled structural elements stability covering strength, boundary value problems, oscillations, design, etc

19 p3535 A70-37401

Linear micropolar elasticity theory of shells and plates, considering transverse shear and normal strains and rotary inertia

19 p3538 A70-37793

Open and multiply connected closed sections of varying thicknesses, solving for unrestrained torsion

19 p3545 A70-38339

Sandwich panels geometrically and physically nonlinear theory, obtaining equations of motion and boundary conditions consistent with strain displacement relations

19 p3547 A70-38360

Spherical shell equilibrium states dynamic calculation method applied to thin plates nonlinear theory statistical problems

20 p3725 A70-39871

Bending of rigidly fixed or simply supported parallelogram plates, using Ritz and Rubnov-Galerkin variational methods

21 p3933 A70-40742

Stress intensity factors for complicated crack configurations in finite plates, using finite element method with cracked elements

21 p3940 A70-42034

Symmetrical bending of isotropic elastic half-strip with free longitudinal edges and end displacements, indicating use for plate and shell theory

22 p4118 A70-43568

Cross ply laminated plates natural frequencies, approximating flexural vibration by classical theory

22 p4119 A70-43679

Limiting pressure for isotropic plastic plates and spherical shells with stress dependent yield, using flow theory

22 p4120 A70-43717

Stress concentration near holes in nonlinear viscoelastic plate, using elastic theory

23 p4266 A70-43989

Plate constituting doubly connected region bounded by outside curvilinear polygon and inside by eccentrically located circle, using series summation

24 p4424 A70-45636

PLATELETS

Platelet and lipid changes in thrombocytopenic and control rats subjected to bends producing technique in aerobolism

01 p0015 A70-10364

Human blood platelets volume measured in Coulter counter, noting relation to temperature

03 p0416 A70-13008

Platelet function in coronary artery disease and myocardial infarction, considering thrombosis, atherosclerosis, emboli in microcirculation, etc

04 p0635 A70-15458

Adhesive and aggregative properties of blood platelets in rats after beta irradiation linked to activity of serum factor

07 p1207 A70-19474

Platelet aggregation in whole blood, basing measurement method on filtration pressure with added adenosine diphosphate /ADP/

07 p1210 A70-19591

Blood platelets aggregation and release reaction in thromboembolic disease due to injury

17 p3032 A70-35471

PLATES

- Quasi-static thickness-shear approximation of radiation of electromagnetic energy accompanying oscillation of piezoelectric crystal plates 19 p3487 A70-37945
- Heat exchange and temperature distribution between two liquids divided by plate, discussing possible errors 20 p3737 A70-39634
- Plate temperature field and stress distribution under thermal pulses, evaluating critical heat load for damage 20 p3737 A70-39635
- Laminar boundary layer equations on plate with arbitrary catalytic properties in diatomic gas flow undergoing vibrational dissociative relaxation 20 p3611 A70-39802
- Plate temperature jump and heat flux in Knudsen layer using Bhatnagar-Gross-Krook model 24 p4429 A70-45997

PLATES (STRUCTURAL MEMBERS)

- NT ANISOTROPIC PLATES
- NT ANNULAR PLATES
- NT CANTILEVER PLATES
- NT CIRCULAR PLATES
- NT CORRUGATED PLATES
- NT ELASTIC PLATES
- NT END PLATES
- NT GIRDER WEBS
- NT ORTHOTROPIC PLATES
- NT PERFORATED PLATES
- NT POROUS PLATES
- NT REINFORCED PLATES
- Minimum weight sandwich plates complying with von Mises criterion, providing constant dissipated energy density 01 p0202 A70-10947
- Sandwich plates plastic buckling stability under uniaxial compressive loads from compressible theory viewpoint 01 p0204 A70-11137
- Sandwich panel equations derived from elasticity theory equations applicable to stress analysis in internal zone and edge effects analysis 01 p0210 A70-11409
- Stressed state of circular notched plate in tension under creep conditions 01 p0210 A70-11410
- Hologram interferometry accuracy, reliability, application to plate deformation and translation measurements, using moire method and correction factors 03 p0493 A70-13945
- Bending analysis of cracked plate with arbitrary stress distribution across thickness [ASME PAPER 69-WA/PVP-2] 04 p0768 A70-14791
- Fracture criteria in cracked plates under combined extension and cylindrical bending using Sih-Hartman theory [ASME PAPER 69-MET-L] 04 p0770 A70-14882
- Thin cylindrical circular shell and three layered plate, analyzing vibration and stability due to loads and temperature 05 p0926 A70-15916
- Simply supported skew plates calculated for buckling loads by Rayleigh-Ritz method using double Fourier series 05 p0940 A70-16514
- Radially nonsymmetric stress wave propagation from tip of moving crack in infinite plates, deriving minimal group velocity 05 p0941 A70-16516
- Time dependent creep and elastic strain interaction in plates and pressure vessels of cylindrical and spherical geometry 05 p0942 A70-16804
- Triangular plate bending elements with enforced compatibility, using cubic interpolation polynomial to describe element displacement [AIAA PAPER 70-136] 06 p1171 A70-18169
- Velocity fields and turbulent pulsations effects on heat transfer in gas flow past plate with rectangular protrusion using wind tunnel tests 07 p1254 A70-19063
- Optimal linear viscoelastic synthetic sandwich structures, investigating test/calculation agreement for simply supported beams and embedded plates [ONERA-TP-702] 07 p1404 A70-19137
- Buckling of clamped skew plates under uniform system of applied stress using Galerkin method 07 p1406 A70-19339
- Von Karman equations for rectilinear plate vibrations used for triangular plates, discussing amplitude/thickness effect and multimodal frequency formula 07 p1416 A70-20211
- Natural oscillation frequencies of three layer plates with rectangular planar form determined by integrated representations method 08 p1583 A70-20495
- Infinitely wide plate bending at small angle of attack in supersonic gas flow, obtaining critical flow rate equal to divergence rate 08 p1588 A70-21175

- Transient thermal stresses in plates with distributed heat source and heat exchange with arbitrary time dependent surroundings 08 p1593 A70-21623
- Four point supported square plate fundamental frequency by finite difference and energy methods 09 p1770 A70-22389
- Finite plates impact flow field analysis from isotropic one dimensional flow equations solution through hodograph transformation 09 p1776 A70-22721
- Thermoelastic stresses in plates and shells in random temperature fields, studying influence on service life 09 p1778 A70-23084
- Nonlinear flutter of three dimensional simply supported curved plates, employing quasi-steady supersonic aerodynamic theory 09 p1780 A70-23212
- Magnetophotoelastic model applied to plates bending stress analysis, deriving polarized light propagation equations 09 p1728 A70-23447
- Heat insulated plate compressible boundary layer energy equations approximate solutions in hypergeometric functions 10 p1966 A70-23867
- Nonautonomous boundary value problems for plates in plane and three dimensional supersonic flows, obtaining eigenfunctions of vibration by Laplace transform 10 p1956 A70-24118
- Plate bending triangular finite element for shell structure analysis, considering displacement functions, stiffness matrix and load vector 10 p1957 A70-24482
- Kinematic analysis of limit loads of equilateral triangular plates under various boundary conditions 10 p1958 A70-24517
- Stress, strain and acceleration spatial variation in plate structures under broad frequency band excitation using statistical energy method 10 p1962 A70-25065
- Convective-radiative heating of multilayer plate approximating temperature field by iteration 10 p1969 A70-25143
- Velocity fields and turbulent pulsations effects on heat transfer in gas flow past plate with rectangular protrusion using wind tunnel tests 10 p1871 A70-25214
- Multilayer plate vibrations calculated with allowance for energy dissipation in material, deriving equations of motion 10 p1965 A70-25297
- Nomograms for thermoelastic stress in plate determined as function of dimensions and heat transfer 10 p1965 A70-25300
- Crack propagation in tensioned plates subjected to sonically induced vibrations 11 p2133 A70-25731
- Temperature, stresses and deformations in melting plates of elastic perfectly plastic material, using penetration depth concept with heat balance approach 11 p2138 A70-26134
- Turbulent flow detachment in incompressible fluid around thick bodies, considering plate perpendicular to wind 11 p2037 A70-26466
- Finite element method solutions for plate bending, improving convergence based on error analysis 11 p2144 A70-26676
- Waffle plate structures least weight design under uniaxial, biaxial and multiple combined loading with various stiffening patterns, investigating pyramiding concept 12 p2318 A70-27133
- Plates elastic-plastic behavior under combined stretching and bending by finite element method 12 p2320 A70-27146
- Ideal weightless fluid jet flow past supercavitating plate at incidence using Tulin scheme 12 p2214 A70-28241
- Unsteady temperatures determination of integral plate consisting of skin with uniformly positioned longitudinal webs 13 p2518 A70-28478
- Plane flow problem for two hinged plates in motion toward each other with fluid displacement, discussing single vortex application to biomechanics 13 p2338 A70-28481
- Shear deformation of sandwich plate cross sections with hinged opposite edges, constructing transfer matrix for state variables 13 p2508 A70-28483
- Derivation procedure for dynamic flexibility matrix including material damping for triangular plate in bending, twisting and shear 13 p2509 A70-28540
- Viscoelastic plate crack growth analysis within continuum mechanics framework as analog to Griffith problem 13 p2510 A70-28671

- Soviet monograph on thermal conductivity of plates and bodies of revolution covering temperature and stress distributions, multilayer shells, etc 14 p2666 A70-30952
- Fourth order differential equations eigenfunctions construction and convergence of expansions in theory of flexure of sector plates 14 p2658 A70-30997
- Stress and deflection of nonisotropic assembled bar and plate composite structures, using computerized matrix displacement method 14 p2660 A70-31133
- Nondestructive bond inspection by interferometric holography of ultrasonically excited plates 14 p2588 A70-31166
- Complex plates free transverse oscillation modes and frequencies using Ritz method 15 p2818 A70-32183
- Stress analysis for plate with large displacements by multicamera photogrammetry, comparing results with numerical solution by finite differences 15 p2821 A70-32313
- Clamped skew plates influence coefficients, natural vibration frequencies and nodal patterns measurement, comparing to Galerkin method results 16 p2988 A70-33124
- Geometrically nonlinear theory for sandwich type plates symmetrically built of three elastically and thermally anisotropic layers, considering nonuniform temperature field 16 p2990 A70-33744
- Low aspect ratio plates flutter analysis for subsonic and supersonic models 16 p2991 A70-33888
- Sound wave phase fluctuations from ultrasonic waves traveling through turbulent wakes of circular cylinders and plates, using multichannel pulse height analysis 16 p2839 A70-34086
- Vibrations of shells, plates and membranes carrying dynamic systems at discrete points on surface, obtaining eigenfunction and eigenvalue equations 16 p2993 A70-34090
- Transonic flow around perpendicular plate, determining front side velocity and pressure from known stagnation point and transonic region 16 p2839 A70-34236
- Polycarbonate plate fatigue crack propagation, discussing length due to repetitions, striation number relationship to cycles, and stress intensity 16 p2941 A70-34335
- Stress intensity analysis method for plates with random cracks array under plane stress 17 p3187 A70-34997
- Natural vibrations of complex plates for combined free and clamped conditions 17 p3189 A70-35343
- Plates and rods tendency to warp and form nonsymmetrical stress systems during heat treatment 19 p3433 A70-37272
- Electromagnetic induction in plate with two dimensional conductivity distribution for case of E polarization, representing field by Green functions 19 p3408 A70-37314
- WKB or eikonal approximation for waves and vibrations in inhomogeneous Euler-Bernoulli beams and plates and Timoshenko beams 19 p3536 A70-37700
- Flexural vibrations of laminated composite plates, maintaining continuity of displacements and surface tractions at intersurfaces between reinforcing layers and composite matrix 19 p3537 A70-37790
- Book on thermoelasticity covering thermal stresses in disks, plates, shells and bodies of revolution under steady and unsteady temperature fields 19 p3541 A70-37974
- Book on structural analysis by finite difference calculus covering elastic and elastoplastic states, vibration and buckling of beams, gridworks, plates and shells 19 p3548 A70-38599
- Hydromagnetic flow past infinite impulsive motion plate, determining velocity and temperature fields distribution 19 p3482 A70-38934
- Vibrating plate thickness function, applying eigenvalue problem 20 p3726 A70-39877
- Finite deflection discrete element analysis of sandwich plates and cylindrical shells with unbalanced laminated faces 20 p3732 A70-40268
- Plate structural analysis by finite element method, obtaining geometric continuity by additional displacements and forces at corner nodes 21 p3932 A70-40553
- Stress-strain state of finite length elastic beam free of bending moments and coupled to semiinfinite plate 21 p3933 A70-40603
- Support elasticity role in axisymmetric plates bending, discussing Rayleigh-Ritz solution 21 p3937 A70-41739

- Accelerated supersonic motion of plate with attached shock wave at finite angle of attack in ideal gas, using perturbed nonstationary motion equations 21 p3748 A70-42209
- Aerodynamic noise scattering by semiinfinite compliant plate in turbulent flow, using Lighthill theory and Wiener-Hopf technique 23 p4179 A70-43968
- Finite element structural analysis /FESTRAN/ computer program predicting static structural response of plate and shell structures 23 p4272 A70-44717
- German monograph on stress-strain state in prestressed, rigidly supported flexible plates subjected to large deflections, using extended Wolmir solution 24 p4418 A70-45083
- Infinite plates and shallow shells stability under doubly periodic surface loadings, using nonlinear analysis 24 p4421 A70-45283
- German monograph on thermally induced elastic stress effects on crack formation and propagation in plates 24 p4422 A70-45524
- Periodically supported beams and plates free vibration, calculating natural frequency spectrum distribution and normal modes 24 p4427 A70-46070
- PLATFORMS**
- Mariner 4 scan platform structure and actuator design, development and performance 16 p2845 A70-34106
- PLATING**
- NT ELECTROPLATING
- NT NICKEL PLATE
- Hydrogen embrittlement of landing gear steels, discussing plating bath program additions for optimum safety conditions 07 p1294 A70-19349
- PLATINUM**
- Anions adsorption at platinum determined by ellipsometry, finding perchlorate and fluoride ions adsorption below detection limit 03 p0441 A70-14043
- Semitransparent Pt film reflectance in vacuum UV evaporated on glass, quartz, Al, Au and Cr on glass compared with opaque films 04 p0731 A70-15023
- Thermoelectric characteristics of graphite and titanium carbide compared with platinum after prolonged annealing at 2300 C 07 p1316 A70-19661
- Oxygen electrode ring and disk currents analysis, studying oxygen reduction on platinum via peroxy intermediates 10 p1829 A70-24453
- Pt resistance thermometers for low temperature measurements, discussing structural and mechanical characteristics 19 p3432 A70-38704
- Heat transfer measurement from Pt wire to carbon dioxide near critical pressure, discussing film boiling and free convection flows 21 p3953 A70-42167
- Hydrostatic and anisotropic piezoresistance in organometallic crystals, noting iridium and platinum complexes with maximum metal-metal interaction 22 p4086 A70-43021
- Various Frank loops in quenched and annealed Pt, examining dislocations with field ion microscopy and computer simulated approximations 23 p4230 A70-44758
- PLATINUM ALLOYS**
- Ultrahigh vacuum metal bonding by twist compression technique, reporting adhesion and friction coefficients for atomically ordered Pt-Co alloy 21 p3833 A70-41465
- PLENUM CHAMBERS**
- Nonlinear heaving motion of plenum-chamber air cushion vehicles induced by sinusoidal ground irregularity 22 p3961 A70-42280
- PLETHYSMOGRAPHY**
- Physiological signals of cardiovascular system transducing methods applied to vector ECG, heart sounds, peripheral pulse waves, chest microphone and pletismography 02 p0243 A70-12095
- Pletismographic investigation of myogenic load influencing sportsmen central nervous systems state, tabulating short and long distance running results 03 p0420 A70-13403
- Forced hyperventilation effect in human subject based on indices regarding changes in respiration rhythm, EEG and finger pletismogram 15 p2679 A70-31607
- Binocular fundus refectometry and pletismography in rabbits and man after dye injection and in patients with carotid occlusion 24 p4310 A70-46345
- PLEURAE**
- Pleural space of dogs investigated by spheres injection of varying density and diameter, discussing sedimentation velocities 03 p0429 A70-14160

- Position dependent variations in intrapericardial, pleural and esophageal pressures and cardiac output in thorax of dogs 13 p2356 A70-29946
- Topography of pleural surface pressure and vertical gradient of transpulmonary pressure above resting volume in relaxed animals as function of alveolar pressure 21 p3766 A70-42154
- PLEXIGLASS [TRADEMARK]**
- U POLYMETHYL METHACRYLATE
- PLIES**
- U LAYERS
- PLOTTERS**
- NT X-Y PLOTTERS
- Photogrammetric three dimensional control extension investigated by plotter and method of Independent Model Aerotriangulation 10 p1890 A70-24731
- Selenology by traverse method, discussing equipment and mapping procedure 11 p2111 A70-26043
- Plotter induced reconstruction errors minimization in computer generated binary Fourier transform holograms 15 p2737 A70-32044
- Computer generated holograms production, reducing memory size and plotter resolution 20 p3627 A70-39098
- PLOTTING**
- Radar primary plot extraction, suggesting signals summing technique in delay line 02 p0256 A70-11975
- Aircraft wing ribs tangents plotting procedure using Monge diagram 08 p1507 A70-21197
- Soviet book on aerial photo plotting of aerogeophysical routes and anomalies covering techniques, equipment, low altitude surveys, etc 19 p3410 A70-37408
- PLOTTING INSTRUMENTS**
- U PLOTTERS
- PLUG NOZZLES**
- Auxiliary inlet ejector and plug nozzle flight performance, describing design variation effects for high supersonic speeds 16 p2841 A70-33563
- [AIAA PAPER 70-701]
- Rocket attitude stabilization using exhaust gas flow spinning plug nozzle as gyroscopic mass 20 p3715 A70-39562
- [AIAA PAPER 70-67]
- Thrust deflector for VTOL aircraft fuselage mounted lift engines designed as isentropic plug nozzle, considering mass flow, pressure forces and Coanda effect 20 p3563 A70-40379
- [SAWE PAPER 841]
- PLUGS**
- Broadband RF filter/attenuator plug to replace plastic type plugs for protecting wire bridge electroexplosive devices against RF energy 03 p0495 A70-14130
- PLUM BROOK REACTOR**
- Precision machining and repair of radioactive Plum Brook Reactor core fuel grid 01 p0140 A70-10322
- Forced cooling water flow temporary loss accident at Plum Brook Reactor, discussing inspection and corrective action 01 p0140 A70-10323
- Optimum fuel utilization for Plum Brook Reactor, using criticality data for effects of neutron leakage and burnup uniformity in core point model 20 p3671 A70-39110
- PLUMBANE**
- U LEAD COMPOUNDS
- U METAL HYDRIDES
- PLUMES**
- NT ROCKET EXHAUST
- Plume-induced flow separation effect on thermal environment using Saturn 5 film and instrument data, attributing heating rate increase to recirculated exhaust gases 04 p0761 A70-14815
- [ASME PAPER 69-WA/HT-18]
- Plume-induced X band radar attenuation, AM and PM noise measured in aluminumized solid propellant motor firings 04 p0736 A70-15409
- Predicted and measured low density plume impingement effects on loads and heat transfer compared on orbiting Saturn 5 with oxygen-hydrogen burner engine 04 p0737 A70-15430
- Wind tunnel tests for engine jet plume effect on boatall pressure drag 06 p1038 A70-18050
- [AIAA PAPER 70-132]
- Exhaust plume from underexpanded sonic and supersonic nozzles including boundary mixing analyzed by approximate model to predict Mach disk location 06 p0972 A70-18135
- [AIAA PAPER 70-229]
- Mach disk in underexpanded exhaust plume predicted by dividing flow field into subregions 06 p0974 A70-18176
- [AIAA PAPER 70-231]
- Particle density of jet plumes exhausting in vacuum calculated for He, Ar and N 06 p1052 A70-18388

- Vertical plume velocity and temperature measurements by hot wire probe on turbulent free convection zones over model fires 07 p1282 A70-19582
- Contaminants formation during pulse mode operation of liquid bipropellant attitude control rocket engine, discussing exhaust plume effects 07 p1394 A70-19708
- [AIAA PAPER 69-574]
- Rocket plume effects impulsive ground test technique under simulated high altitude pressure conditions, discussing hardware simplifications 10 p1951 A70-24906
- [AIAA PAPER 70-399]
- Laminar natural convection plumes behavior above energy sources calculated by simplest variables, indicating optimum formulation of boundary value problem 12 p2332 A70-27700
- Carbon dioxide jet plumes condensation on model nozzle in vacuum chamber, noting particle size and growth rate 13 p2523 A70-29983
- Isolated convective plumes immersed in return flow turbulent downdraft 15 p2769 A70-31440
- Optical system measurement of density and rotational temperature in gaseous plume simulating auxiliary propulsion and oxygen hydrogen burner of S-4B 16 p2913 A70-34023
- Two phase plume at various incidence angles on flat plate, determining impinging particle mass flux, forces and damage 23 p4134 A70-44566
- PLUTO [PLANET]**
- Neptune and Pluto oblateness inferred from analogous similarities of mass, diameter and mean density with Uranus and Mars planets 09 p1750 A70-22096
- Pluto space probe using swingby technique with Jupiter, Saturn and Uranus gravitation fields for acceleration 21 p3886 A70-41073
- Pluto mass from Saturn, Uranus and Neptune masses 23 p4243 A70-44295
- Pluto albedo at various wavelengths from spectrophotometric measurements 24 p4399 A70-45129
- PLUTONIUM**
- NT PLUTONIUM ISOTOPES
- PLUTONIUM ISOTOPES
- Pu/U ratio in St. Severin meteorite at time of Xe retention beginning 13 p2488 A70-28723
- PLUVIOGRAPHS**
- U RECORDING INSTRUMENTS
- PNEUMATIC CIRCUITS**
- Pneumatic fluidic oscillator consisting of bistable multivibrator, analyzing feedback loop operation based on electropneumatic analog system 02 p0229 A70-12673
- Iterative solution to transmission lines termination problems 04 p0627 A70-14861
- [ASME PAPER 69-APM-M]
- Fluid flow at pneumatic network junction, considering junction pressure determination as boundary condition for all transmission lines meeting at junction 04 p0627 A70-14862
- [ASME PAPER 69-APM-N]
- Admittance calibration of short HF through flow pneumatic lines, using hot-wire anemometer 16 p2891 A70-33628
- [ASME PAPER 70-FE-10]
- PNEUMATIC CONTROL**
- Average pressure at downstream end of pipe discharging into reservoir with upstream end under pulsed flow, considering application to pneumatic control system 02 p0279 A70-12110
- Positive displacement low pressure air motors for Boeing 747 fan thrust reverser pneumatic actuators and controls 03 p0550 A70-12881
- Pneumatic line losses due to friction in pneumatic control systems 04 p0628 A70-15399
- Proportional controlled pneumatic servomechanisms analysis extended to include motion along stroke, considering position effect on stability 05 p0797 A70-15891
- Electropneumatic actuation systems for rocket engines in extreme environment applications involving high nuclear radiation levels and high and cryogenic temperatures 14 p2535 A70-31343
- Fluid thermal actuator for temperature control of ITOS /Improved Tiros Operational System/ meteorological satellite, discussing design and performance 16 p2846 A70-34129
- Flow control valve without moving parts used in ATS A and D, describing design, operation and theoretical performance 16 p2846 A70-34132
- Soviet book on fluidic theory covering jet elements, pneumatic throttles, chambers, communication channels, etc 19 p3357 A70-37469

Hydraulic and pneumatic controls construction and use in machine tools
19 p3359 A70-38725

Pneumatic actuator control system improvement, using invariance theory to compensate load variability and dynamic response of medium
20 p3564 A70-39848

Cryogenic fluid heat exchanger flow oscillation automatic feedback control, discussing design and simulation
23 p4280 A70-44370

Fluidically controlled aircraft fuel transfer system three-tank model construction, noting maintenance and fail safe operation
[SAE PAPER 700786]
24 p4294 A70-45858

PNEUMATIC EQUIPMENT
NT GAS VALVES
NT PNEUMATIC CIRCUITS
Pneumatic line losses due to friction in pneumatic control systems
04 p0628 A70-15399

Dynamic mathematical model of proportional electromagnetic transducer in pneumatic servomechanisms derived by Lagrange-Maxwell method assuming circuit linearity
07 p1195 A70-18750

Soviet book on pneumatic actuators theory and design, using digital computers to solve dynamic equations and to obtain diagrams and nomograms
08 p1440 A70-20752

Fluidic curved-wall electropneumatic converter optimization, presenting steady state, step and pulse mode responses for various positions and lengths of resistive heaters
09 p1614 A70-23691

Thermodynamic properties of periodically variable air volume in pneumatic pressure generator of pressure sensor calibration bench
10 p1863 A70-24027

Unmanned spacecraft landing shock absorption by hybrid pneumatic configuration having hard surfaced footpad with dual pneumatic bag attenuator
12 p2312 A70-27115

Fatigue life and long term strength of polycarbonate components in pneumatic pulsating pressure equipment described by power and exponential equations
13 p2440 A70-29784

Pneumatic suspension systems for air cushion skirts
16 p2841 A70-33759

Fluid thermal actuator for temperature control of ITOS /Improved Tيروس Operational System/ meteorological satellite, discussing design and performance
16 p2846 A70-34129

Working medium excess and absolute pressure effects on pneumatic elements characteristics
22 p3967 A70-43566

Fluidic logic devices compared with electric relay and hydraulic/pneumatic valve equivalents
24 p4293 A70-45429

Hydraulic and pneumatic components for logic circuits of automatic controls, considering amplifiers, interlocked systems and use of fluidics
24 p4293 A70-45618

Pneumatic actuator rod and piston head seals, examining materials at various temperatures, pressures and speeds
[SAE PAPER 700791]
24 p4294 A70-45855

Hydraulic and pneumatic dampers operation, analyzing force components
24 p4427 A70-46380

PNEUMATIC PROBES
Rotodynamic pumps energetic characteristics determination by pneumatic tests, describing air test results for various models
12 p2165 A70-27399

PNEUMATIC RESET
U PNEUMATIC CONTROL

PNEUMATICS
Pneumatic instability, capacity and rigidity of thrust and journal gas bearings with external air injection
18 p3264 A70-37072

PNEUMOGRAPHY
U PNEUMOGRAPHY
Radiorheopneumographic study of external respiration of office workers during mental and physical activity
07 p1204 A70-19142

Human lung closing and subdivision volume relationship to age and body position
12 p2169 A70-27657

Diaphragmatic muscle reactions and pneumogram changes in rats immediately after air passage obstruction
19 p3360 A70-37804

PNEUMOTHORAX
Aeroatelectasis and pneumothorax in fighter pilot postflight chest pains, noting decompression role
17 p3041 A70-35920

POCKELS EFFECT
U BIREFRINGENCE

PODS [EXTERNAL STORES]
Thrust follower force stability in pod mounted jet engine and nacelle whirl using multiple degrees of freedom model
10 p1930 A70-25070

POIKILOTHERMIA
NT FROGS
NT TURTLES

POINCARÉ PROBLEM
Poincaré invariance compatibility with general relativity, discussing Brandt groupoid, decomposition and local groups
06 p1106 A70-17540

Bounds in magnetofluidynamics for angular velocity of rotating fluid mass in relative equilibrium noting generalization of Poincaré theorem
13 p2463 A70-29153

POINCARÉ SPHERES
Poincaré sphere application to automatic polarization forms measurements and two/three dimensional photoelasticity by scattered light
11 p2142 A70-26633

Ellipsometry with Poincaré sphere representation, describing application to automatic two and three dimensional photoelasticity by scattered light
17 p3086 A70-35014

Interference-polarization light filter, calculating phase shifter errors effects on transmittance by Poincaré sphere method
22 p4072 A70-42505

POINT DEFECTS
NT FRENKEL DEFECTS
NT VACANCIES [CRYSTAL DEFECTS]
Stress intensity and strain energy release rate in elastic fiber-reinforced composites with different thermomechanical properties and imperfect bonding
[ASME PAPER 69-WA/APM-15]
04 p0771 A70-14913

Imperfect solid deformation, presenting formalism for elastic theory nonlinear aspects of continuous distributions of dislocations and point defects
17 p3190 A70-35456

POINT IMPACT
Small reentry vehicles roll motions and impact point dispersion due to spin reversal
15 p2813 A70-32522

Point mass impact on flexibly interconnected rigid bodies with tree structure and spherical joints without dry friction, discussing resulting velocity changes
21 p3849 A70-40552

POINT MATCHING METHOD [MATHEMATICS]
U BOUNDARY VALUE PROBLEMS

POINT SOURCES
Emission from broadband impulsive point source refracted by spherical interface between fluids with different acoustic velocities, showing emitted and inverse waveform disturbances
01 p0046 A70-11190

Compressible gas flow problem in point body gravitational field solved with reference to sun and interstellar gas
01 p0172 A70-11489

Ionospheric irregularities-diffraction patterns relative drifts, verifying point source effect for radio waves reflected from E and sporadic E layers
07 p1236 A70-20162

Strong point explosion in atmosphere with density dependent on height, obtaining numerical solutions for exact gas dynamic equations
09 p1658 A70-22112

Transient heat conduction of thin circular disk with uninsulated surfaces rotating past stationary point source by finite element method
09 p1787 A70-22269

Point source intensity fluctuations dependence on penetration depth of wave propagating in statistically homogeneous and isotropic media
09 p1636 A70-23133

Diffuse light transmission from point sources over horizontal paths in lower atmosphere, discussing effect of range
10 p1912 A70-24424

Shock propagation from point explosion energy source into cold exponential atmosphere with radiative heat transfer in rear of shock front
10 p1869 A70-24525

Multiwavelength laser beam propagation with point source transmitters, determining turbulence levels independently
13 p2426 A70-28837

Einstein-Maxwell equations for monopolar point electrical charge, calculating proper energy for electromagnetic and gravitational fields
13 p2451 A70-28956

Self similar dynamic problems in two dimensional elasticity theory for slot with point source in boundless body
13 p2517 A70-29763

Point heat source generation of thermal stresses in elliptical plate with circular hole, using functions of complex variable for stress field determination
15 p2818 A70-32182

POINTING CONTROL SYSTEMS
Hydromagnetic viscous flow of incompressible conducting fluid due to electric current radial divergence from point source
15 p2780 A70-32426

Holography without reference waves, describing image characteristics of spherical waves from point source
15 p2743 A70-32893

Direction finder for point source signals, discussing mathematical model for random noise in space, S/N performance and equipment design
17 p3042 A70-34586

Acoustical holography with single stationary point detector noting reciprocity between detector and point source illuminator
17 p3088 A70-35030

Integral equation for three dimensional Fourier transform applied to isotropic scattering of radiation from point source in finite spheroidal atmosphere
17 p3137 A70-35599

High energy cosmic gamma radiation detection from point source in Sagittarius, using balloon mounted spark chamber with Cerenkov telescope
19 p3500 A70-38078

Radio beam trajectory in Fresnel zones of isotropic laminarily inhomogeneous ionosphere, discussing point source field and wave propagation
19 p3381 A70-38569

Point source electric field over different sections of impedance piecewise inhomogeneous surface, calculating attenuation function near boundaries
19 p3381 A70-38570

Teleradiometer calibration in background radiation absence, using distant and finite point source method and collimator means
20 p3633 A70-39798

Self similar dynamic problems in two dimensional elasticity theory for slot with point source in boundless body
20 p3732 A70-40101

Microwave scintillations at sunrise indicating solar point sources at sunspot cycle peak and terrain configuration influence on ionospheric disturbances
20 p3591 A70-40493

Cygnus X-2 point X ray source, establishing as spectroscopic binary with peculiarities
21 p3875 A70-40682

Spherical shock from point explosion in medium with varying density, obtaining exact similarity solution for propagation
21 p3808 A70-41448

Tracking of point object in Fresnel zone from observation of amplitude-phase pattern in aperture plane
22 p4026 A70-42555

Photon flow delay regarding fluctuating source field in two points, applying correlation statistics by Pearson method of moments
22 p3988 A70-42564

Acoustic field scattering from multipole point sources by solid spherical surface
22 p4010 A70-42693

Radiation shielding calculations, discussing Monte Carlo concepts for point fluxes with random sampling of source distributions
23 p4217 A70-43810

Meteor trails isotropic diffusion in presence of moving point source of ionization with variable intensity, calculating plasma density on and near trajectory
23 p4240 A70-44084

Fourier hologram synthesis using laser point source and Wollaston birefringent prism
24 p4336 A70-45667

POINT TO POINT COMMUNICATIONS
Operational requirements of shipping for satellite communication systems, discussing distress cases, satellite navigation systems, information distribution traffic control, etc
03 p0522 A70-13605

Sirio satellite SHF transponder for experiments in atmospheric propagation and communication between ground stations
15 p2709 A70-32285

Point to point and radar return attenuation measurements at SHF through clear air and rain
16 p2858 A70-32928

POINTERS
U DIALS

POINTING CONTROL SYSTEMS
Attitude sensing and target pointing instrumentation in earth orbiting stellar telescopes in inertial space
16 p2905 A70-33155

Precision gimbaled sensor pointing system calibration data errors due to misalignments and inaccuracies in transducer readout
22 p4040 A70-43587

Pointing systems for balloon-borne telescopes in astronomical investigations
22 p4041 A70-43649

High performance reaction pointing control systems for sounding rockets, using proportional control of differential thrust and adaptive control of thrust magnitude
[SAE PAPER 700783]
24 p4415 A70-45861

POINTS

Close spaced material points motion stability in gravitational field of attractive center using Liapunov theorem, assuming nongravitational forces action on points

03 p0524 A70-13369

POINTS [MATHEMATICS]

NT INFLECTION POINTS

Optimal control problems concerning vector determination and trajectory of point motion toward target in n-dimensional phase space

01 p0053 A70-11028

Monograph on stochastic theory and cascade processes, discussing branching phenomena, point processes, electromagnetic cascades, extensive air showers, polarization, population growth, etc

01 p0134 A70-11327

Nonlinear differential equations analysis based on weighted linear approximation applied to singular points and trajectories in phase plane in friction problems

09 p1727 A70-22665

Geographic coordinates of intersection points determined directly on sphere, noting reduction on ellipsoid and adjustment for surplus intersections

09 p1670 A70-23441

Ill conditioned linear two point boundary value problems solved by Riccati transformation avoiding forward integration

10 p1909 A70-24059

Adjointness in nonadjoint boundary value problems, extending Neuberger symmetry study to obtain expansion theorem for nonself adjoint p-point problems

10 p1910 A70-24606

Rotating spherical galaxy evolution, using equations of motion for mass points representing mass distribution

13 p2492 A70-29385

Nonlinear differential equations solutions in power series with indefinite coefficients, determining type of singular points

20 p3658 A70-39766

Singular points in elasticity theory solved by correct boundary value problem and homogeneous solutions theorem

20 p3728 A70-39894

Equations of motion of mass points connected by inertialess elastic couplings

21 p3933 A70-40615

Interpolation and smooth curve fitting based on local procedures and piecewise function

24 p4369 A70-45162

POISEUILLE FLOW

U LAMINAR FLOW

POISONING [REACTION INHIBITION]

Low temperature fuel cell materials impurity effects on catalyst poisoning, stressing sulfur elimination from rubber molding

10 p1832 A70-25043

POISONING [TOXICOLOGY]

U TOXIC DISEASES

POISONS

NT PHOSGENE

NT URETHANES

POISSON DENSITY FUNCTIONS

Optical position estimation model based on defining photon density profile center of gravity in noise, using photon Poisson process theory

04 p0652 A70-15337

Perseids time distribution, based on observations during meteor showers, contradicting appearance of homogeneous Poisson process

09 p1750 A70-22099

One dimensional Poisson production process under costly surveillance, considering maximum attainable income rate approximation

09 p1653 A70-22347

Markov renewal processes sums convergence to multidimensional Poisson process, discussing convergence conditions

12 p2260 A70-26884

Poisson shot noise process relationship with continuous stochastic intensity as sample function

12 p2203 A70-27418

Skeletal muscle force generation stochastic model based on motor unit, discussing Poisson distribution and dynamic force response

21 p3769 A70-41199

Threshold distribution of time intervals between atmospheric contradicting Poisson law

23 p4190 A70-44082

POISSON EQUATION

Summary representation formulas for solving boundary value problems for Helmholtz and Poisson equations in rectangle

03 p0518 A70-13076

Programming system for Poisson series manipulation on computer, writing subroutines in machine language

05 p0817 A70-16342

Boundary conditions and iterative procedures for plasma sheath problems, using matrix equation to represent differenced Poisson equation

06 p1123 A70-18295

Mathematical model for finite-density non-homogeneous Newtonian cosmologies, approximating solutions using coupled Vlasov-Poisson equations

08 p1581 A70-21740

Inductive flow measurement history, considering Maxwell, material and Poisson equations

15 p2735 A70-31823

Boundary value problem of two dimensional Poisson equation solution procedure with Hockney formulas, applying to unsteady viscous incompressible flow past flat plate

16 p2943 A70-33737

Dynamic systems stability in sense of Poisson, relating motions commutative and stable families

19 p3472 A70-38936

Rayleigh wave scalar electric potential analysis on piezoelectric medium, using iterative techniques for Poisson equation

22 p4074 A70-42967

Poisson kinematic equations solution of symmetric gyrost in viscous medium for free rotor and constant angular speed, using perturbation technique

23 p4220 A70-44560

One dimensional collisionless electron-proton plasma, obtaining exact electrostatic shock solution to Vlasov and Poisson equations

24 p4382 A70-45107

POISSON PROCESS

U POISSON DENSITY FUNCTIONS

U STOCHASTIC PROCESSES

POISSON RATIO

Stresses in plane elastic bodies analyzed by generalizing biharmonic stress function equation in polar coordinates, assuming constant Poisson ratio and nonhomogeneity

01 p0206 A70-11152

Mixed boundary value problem for viscoelastic body with constant Poisson ratio solved by variables separation method, proving convergence

02 p0390 A70-12802

Photoelasticity extension to plane elastic problems with stress state depending on Poisson ratio, discussing multiple connected body with nonzero surface tractions on internal boundaries

[SESA PAPER 1570] 03 p0583 A70-12884

Poisson ratio of elastomers determination for defining compliant surface fluid film thrust bearings behavior, considering method and error analysis

[ASME PAPER 69-WA/LUB-7] 04 p0712 A70-14751

Displacements and stresses obtained for elastic half plane with variable Poisson ratio under certain traction boundary conditions, using Fourier transform method

05 p0940 A70-16512

Fiberglass reinforced plastics creep behavior under axial compression, studying time dependence of elasticity modulus and Poisson coefficient

08 p1526 A70-21174

Total Poisson ratio derivation from stress-strain relationship with known variations of elastic and plastic Poisson ratios for particular strain-hardening case

10 p1956 A70-24096

Hollow homogeneous polymer cylinder thermoelastic stressed state, analyzing radial temperature and Poisson Coefficient variations

12 p2325 A70-27532

Computer program for two body problem literal series expansions using Kepler functions with Bessel and Poisson series operation

14 p2638 A70-30702

Plastic materials Poisson ratio and Young modulus measurements by triaxial compression method

17 p3089 A70-35048

Poisson ratio of elastomers determination for defining compliant surface fluid film thrust bearings behavior, considering method and error analysis

[ASME PAPER 69-WA/LUB-7] 19 p3434 A70-37602

POLAND

Photographic plate reduction method at Polish Academy of Sciences based on sufficient reference stars, correcting x and y coordinates

11 p2007 A70-26194

Report to COSPAR on space exploration research in Poland including satellite tracking, geodesy, meteorology and aerospace medicine

15 p2830 A70-31721

POLAR AURORAS

U AURORAS

POLAR CAP ABSORPTION

Sudden cosmic noise absorption /SCNA/ in polar cap during 7 July 1966 solar proton flare, estimating SCNA latitudinal distribution and protons magnetic cut-off boundary

01 p0172 A70-11527

Time lag of commencement of PCA effect behind occurrence of Y-shaped phase of solar flares, tabulating data for several flares and particle effects

02 p0358 A70-12373

Microwave spectra of type 4 bursts at cm and dm waves compared to related PCA

02 p0359 A70-12774

Polar cap absorption midday recovery phenomenon analysis in northern and southern polar auroral regions showing increase in ionizing flux rigidity

04 p0682 A70-15729

High sensitivity particle spectrometer for onboard OV-1-18 satellite measurements of precipitating protons, electrons and alpha particles during PCA events

12 p2232 A70-27402

Polar cap absorption midday recovery phenomenon analysis in northern and southern polar auroral regions showing increase in ionizing flux rigidity

14 p2575 A70-30813

Ion effects on VLF propagation in earth-ionosphere waveguide during polar cap absorption events

16 p2859 A70-32933

Cosmic ray variations during PCA absorption, relating Forbush decreases to lower ionosphere ionization intensity increase

18 p3306 A70-36096

Polar cap absorption correlation with solar protons flux into magnetosphere, discussing diurnal and spatial variations and magnetic storm effects

19 p3411 A70-37492

Electron density measurements by rocket observation during PCA after solar flare of 25 February 1969, deriving effective loss rates in terms of recombination model

19 p3496 A70-37511

Earth surface pressure changes related to PCA of high energy protons

20 p3695 A70-39187

VLF signal phase and amplitude changes associated with PCA events and South Atlantic Geomagnetic Anomaly

22 p4023 A70-43292

VLF phase disturbances, HF absorption and solar protons in 1967 PCA events, using ionization model

24 p4314 A70-46128

POLAR CAPS

IR spectrometer on Mariner 7 Mars flyby recording sharp absorption near 3 microns at Martian southern polar cap

01 p0182 A70-10823

Geomagnetic perturbation coincidences observed at conjugate Polar Cap observatories, suggesting magnetospheric tail field lines convergence with plasma neutral layer

03 p0565 A70-13232

Ground observations synoptic distribution importance in studying magnetosphere, emphasizing polar caps

03 p0475 A70-13849

Jupiter observations /1966-1967/, discussing variations in size and position of polar caps and tropical belts

03 p0574 A70-13887

Martian polar cap spectra interpreted with laboratory measurements of water-carbon dioxide frost spectral reflectance

07 p1388 A70-19946

Polar cap magnetic field micropulsations simultaneous recordings at Greenland, Alaska, and Finland, noting seasonal variations

07 p1270 A70-20152

Geomagnetic perturbation coincidences observed at conjugate Polar Cap observatories, suggesting magnetospheric tail field lines convergence with plasma neutral layer

08 p1580 A70-21665

Magnetic spikes in polar cap region due to poleward shift of narrow westward electric current filament

08 p1491 A70-21716

Solar protons and electrons spatial and angular distributions over polar caps by USAF-OAR satellites 1966-70A, 1967-72D and 1968-59A

13 p2482 A70-30073

Auroral and polar cap ionospheric electric fields and tensor conductivity elements using ion clouds data of Ba release experiment

13 p2402 A70-30080

Polar cap elementary magnetic disturbance relationship to auroral electrojet

14 p2570 A70-30215

Solar proton structure across polar cap and anomalous latitude cut-off explained by local pitch angle variations

15 p2792 A70-31672

Polar cap disturbance of 7 June 1969 due to small proton enhancement, describing detection by transpolar VLF phase measurement

15 p2794 A70-32295

Martian soil thermal conditions at south pole, considering polar cap annual variations and carbon dioxide sublimation

15 p2802 A70-32492

Mars visual observations with colored glass filters during opposition, noting southern polar cap shape irregularity and Martian atmospheric transmittance

16 p2974 A70-33658

Solar particle observations over polar caps, considering spatial and angular distribution measurements

19 p3494 A70-37484

Solar protons distributions in 1-30 MeV range over northern polar cap during 25 February 1969 solar event by ESRO 1 satellite

19 p3496 A70-37508

Interplanetary magnetic field directional variation effect on polar caps geomagnetic field, discussing polarity reversals 22 p4022 A70-43285

Polar cap ionization processes in F region, discussing effects of particle precipitation, solar radiation, electromagnetic field drifts, atmospheric winds and magnetospheric tail distortion 22 p4024 A70-43309

Martian soil thermal conditions, considering polar cap annual variations and carbon dioxide sublimation 23 p4240 A70-43914

Polar cap elementary magnetic disturbance relationship to auroral electrojet 24 p4331 A70-46290

POLAR COORDINATES

Tangent plane method and polar coordinates for lifting surfaces, calculating normal velocity at field point on surface carrying doublet distribution for incompressible flow [AIAA PAPER 70-78] 06 p0975 A70-18195

Elasticity theory two dimensional problem solution for circular segment in polar coordinates, applying Lure symbolic notation and Prokopov minimum potential energy principle 09 p1782 A70-23291

Angular coordinate during multilevel quantization of radar signal reflected from scintillating body on Gaussian noise background, applying maximum probability method 11 p1996 A70-25347

Biased measurement of angular coordinates of phase modulated signals under meter input quantization 11 p2012 A70-26806

Solar wind structure as function of corotating coronal inhomogeneities determined using perturbation equations for spherical polar coordinate system 12 p2292 A70-27179

Superposed converter magnetic field intensity normal component distribution as function of polar coordinate 13 p2348 A70-28659

Orbit calculation based on first integrals of two body problem in spherical coordinates 15 p2797 A70-31620

Statistical test of Melchior laws governing Chandlerian motion of earth pole based on polar coordinates 15 p2732 A70-32497

Earth to planet radar signal time delay in general relativity expressed in relativistic spherical polar coordinates of earth and planet 15 p2806 A70-32801

Meteor trails angular coordinates, using phase difference in pairs of spaced antennas with unequal base lengths 19 p3433 A70-38789

Synoptic charts of polar magnetic fields plotted in polar coordinate system for consecutive solar rotations 20 p3711 A70-40408

Angular coordinate during multilevel quantization of radar signal reflected from scintillating body on Gaussian noise background, applying maximum probability method 20 p3589 A70-40459

Oscilloscope polar coordinate displays for multidimensional analog signals, noting human detection capability 21 p3823 A70-40853

Statistical test of Melchior laws governing Chandlerian motion of earth pole based on polar coordinates 23 p4187 A70-43918

POLAR GASES

Polar gas phase dielectric under conditions of power saturation interacting with microwave radiation field in waveguide 09 p1728 A70-22908

Self diffusion coefficient for gaseous ammonia at specific temperature range, applying polar gases theory 13 p2453 A70-29800

Approximate formula for viscosity of binary polar gas mixtures confirmed for unlike cross sections 16 p2996 A70-33055

Polar gas rotational relaxation time calculation, comparing volume viscosity and energy equation definitions 19 p3473 A70-38266

POLAR IONOSPHERE BEACON

U BEACON SATELLITES

POLAR METEOROLOGY

Stratospheric circulation and temperature variations periodicity, discussing midwinter warmings, polar vortex breakdown and relations to D region anomalies and solar events 01 p0072 A70-10580

POLAR ORBITS

Lyman alpha auroral emissions observations made with narrow band sky scanning photometer mounted on earth-oriented polar orbiting satellite 04 p0741 A70-15107

Navy navigation satellite passes predicted by equations for rise and set times, elevation and azimuth in plane circular polar orbit about spherical earth 04 p0764 A70-15431

Cosmic ray knee interpretation using polar orbiting ionization chambers data from OGO-2/4 15 p2793 A70-31903

Air densities from polar satellites orbit analysis 24 p4329 A70-45550

POLAR REGIONS

NT ANTARCTIC REGIONS

NT ARCTIC REGIONS

Jovian polar zones enhanced optical transparency causes, discussing thin clouds and difference in molecular optical depth between north and south poles 01 p0180 A70-10531

Ionospheric F layer in equatorial, mid and high latitude regions for various major phenomena including anomalies, neutral air winds, photoelectrons, etc 01 p0073 A70-10585

Polar magnetic disturbances during IQSY characterized by SP field superposed on Sq field generated by ionospheric dynamo 01 p0075 A70-10599

Polar thermosphere temperature measurements from artificial clouds indicating geophysical-associated variations, nocturnal decrease and annual variations 01 p0077 A70-11201

EEG investigation of cerebral biocurrents during polar night-day cycle, studying central nervous system nonspecific automatic control mechanism dependence on ecological factors 01 p0030 A70-11466

Polar geomagnetic disturbances global current systems representation by prototypes of equivalent current systems 01 p0084 A70-11557

Polar ionic exosphere electric field polarization, considering positive and negative charges escape fluxes, electric potential, mean ion velocity, etc 02 p0289 A70-12108

Winter diurnal behavior of northern high latitude ionospheric electron density using temperature data from Langmuir probes 03 p0478 A70-13993

Intermediate ionospheric layer at high latitudes, discussing relationship to geomagnetic and auroral activity and F region continuity 04 p0678 A70-14974

Plasma transport models of polar ionosphere, discussing physical processes involved and effects on electron concentration, ion composition and speeds 04 p0679 A70-15113

Polar lower ionosphere, using radar VLF step frequency sounding to determine reflection phase height at given propagation path 04 p0680 A70-15115

Band shaped polar auroras widths from photographs analysis, noting wider bands for midnight hours and winter solstice 04 p0682 A70-15732

Fragmentary arc and band-shaped polar aurora configurations associated with corpuscular rays penetration into upper atmosphere 04 p0684 A70-15749

Evening time latitudinal distribution of polar magnetic field perturbations compared with nighttime distribution, indicating evening electrojets 04 p0684 A70-15751

Ionospheric effect sudden commencement parameters of magnetic storm related to distance from origin in polar regions 05 p0841 A70-16737

Ionized gas height scale changes in polar ionosphere obtained assuming Chapman type ionization distribution 05 p0841 A70-16738

Correlation function of auroral reflection radio signals with allowance for polar ionospheric scattering and pulse signal transmission and reception 05 p0841 A70-16741

Polar auroral region displacement ascribed to distant magnetic field disturbances, proposing calculation method 05 p0842 A70-16745

Horizontal electric fields relations to charged particle fluxes in polar auroral ionosphere 05 p0842 A70-16756

Polar aurora rays mean length diurnal variations determined from photographic and visual observations in Tiksi bay 05 p0843 A70-16763

Magnetic storm /14 September 1966/ observation by Explorer 33 in geomagnetic tail and by polar stations, studying relation in magnetosphere and on earth 05 p0843 A70-16764

Sporadic electron flux contribution to high latitude geomagnetic disturbances at outer radiation belt boundary estimated from Elektron 1 and 2 observations 05 p0843 A70-16765

Three dimensional model current system with magnetospheric and ionospheric sections connected by

currents flowing along geomagnetic field lines proposed for polar magnetic substorms 06 p1059 A70-18535

Magnetospheric plasmopause-high latitude electron density trough relations using satellite topside ionograms, noting local time and magnetic disturbance effects 07 p1270 A70-20074

Polar ion-exosphere model with open geomagnetic field lines, calculating electrostatic field for region 07 p1270 A70-20077

Simultaneous riometer and ionosonde measurements at high latitude suggesting absorption events due to cosmic noise scattering by auroral sporadic E 07 p1271 A70-20165

Quasi-trapped electrons precipitating at high latitudes measured from low altitude polar orbiting satellite 08 p1562 A70-21382

Hydromagnetic emissions in high latitudes relationship to storm sudden commencements 08 p1491 A70-21715

Chapman-Vestine and Birkeland-Alfven electric current systems equivalence in ground geomagnetic effect explained for polar magnetic storms 08 p1491 A70-21719

Dual inertial navigation transpolar flight to North Pole aboard KC-135 airplane, discussing performance, installation, etc 09 p1719 A70-22189

Meteorological observations of Mars polar regions, surface activity and atmosphere with astronomical telescopes during Mariner 6 and 7 flyby 09 p1754 A70-22500

Two phase process for electron precipitation during polar substorm observed from balloon measurements of X rays produced by precipitated electrons in atmosphere 10 p1932 A70-24490

Scintillation sudden inception in Faraday rotation in Sodankyl and Oulu, noting diurnal north-south frontier movements in polar ionosphere 10 p1884 A70-25262

Polar ionosphere inhomogeneous electron concentration by analyzing satellite signal amplitude fluctuations received by spaced interferometers 11 p2042 A70-25528

Polar ionospheric current and interplanetary magnetic field directions related from mean diurnal values of solar wind velocity 11 p2044 A70-25551

Atmospheric activity centers movements dependence on latitudinal variation of deformation force horizontal component, noting earth poles motion 12 p2265 A70-28224

Monograph on polar aurora with emphasis on solar wind and interplanetary magnetic fields, discussing substorms, particle acceleration in current sheet, etc 13 p2395 A70-28983

Polar ionosphere auroral oval position detection by satellite observations of naturally occurring VLF and man-made HF plasma waves 13 p2371 A70-29924

Trapped and polar proton and electron flux observations during 9 June 1968 magnetic storm 13 p2482 A70-30072

Polar storm simultaneous onset and development, using observational data for geomagnetic field and aurorae 14 p2570 A70-30214

Subpolar ionosphere electron concentration measurements for both hemispheres during solar activity by Faraday effect signal recordings from satellites 14 p2570 A70-30223

Venus water presence from Venera 4 and Mariner 5 data suggesting polar seas and oceans saturated with hydrochloride and carbon dioxide as plant life source 14 p2637 A70-30365

Band shaped polar aurorae widths from photographs analysis, noting wider bands for midnight hours and winter solstice 14 p2575 A70-30815

Fragmentary arc and band-shaped polar aurora configurations associated with corpuscular rays penetration into upper atmosphere 14 p2576 A70-30833

Evening time latitudinal distribution of polar magnetic field perturbations compared with nighttime distribution, indicating evening electrojets 14 p2576 A70-30835

Polar ionospheric electron/ion density measurements by ESRO 1 satellite, observing dependence on Kp index 15 p2724 A70-31669

Polar peak F layer electron density around magnetic noon related to dayside aurora flux, comparing with soft particle precipitation 15 p2727 A70-31872

Quiettime cosmic ray ionization altitude dependence over polar regions from measurements by integrating ionization chamber on OGO-2 15 p2793 A70-31902

- Polar substorm activity associated with magnetopause position variation, using Imp 2 satellite observations 15 p2728 A70-31911
- Rocket measurements showing removal of electrons above mesopause in summer at high latitude 17 p3081 A70-35775
- High latitude magnetosphere structure, using two dipole model 18 p3312 A70-36168
- Temporal and spatial covariation of high latitude geophysical phenomena, using unified mechanism of solar plasma stream interaction with geomagnetic field 18 p3247 A70-36404
- F layer absence and nonuniform horizontal electron concentration of nighttime ionosphere at high latitudes, using Alouette 1 sounding 19 p3408 A70-37308
- High latitudes magnetospheric electric field structure, using electrostatic probes and artificial clouds 19 p3410 A70-37489
- Polar electrojet and VHF auroral radio wave backscattering correlation, discussing geomagnetic disturbances effect 19 p3376 A70-37498
- Trapped and precipitated electron observations at northern high latitudes in 45-450 keV range, using ESRO-1 satellite 19 p3496 A70-37515
- Geomagnetic field pulsations prior to polar magnetic disturbance onset, discussing solar wind role 19 p3416 A70-38588
- Polar stratospheric winter explosive warmings correlated with solar high energy charged particles injections 20 p3618 A70-39185
- Darkness adaptation of flight personnel in polar regions, discussing effects of physical and nervous strain, sickness and alcoholic intoxication 20 p3576 A70-40290
- Synoptic charts of polar magnetic fields plotted in polar coordinate system for consecutive solar rotations 20 p3711 A70-40408
- High latitude F region irregularity structure during magnetic storm from multistation scintillation observations of ATS 3 transmission 20 p3624 A70-40490
- Sporadic E layer ionization correlated with geomagnetic disturbances in northern auroral and polar regions 21 p3812 A70-40592
- Polar ionosphere inhomogeneous electron concentration by analyzing satellite signal amplitude fluctuations received by spaced interferometers 21 p3819 A70-41278
- Polar ionospheric current and interplanetary magnetic field directions related from mean diurnal values of solar wind velocity 21 p3819 A70-41301
- Synchronous satellites VHF signal fading attributed to high latitude scintillations, noting intensity at night and during magnetic storms 21 p3790 A70-41362
- Magnetotail magnetic field perturbations associated with polar magnetic substorms, using IMP-A and B satellite observations 21 p3882 A70-41720
- NO molecule gamma system in emission spectra of polar auroras in far UV by monochromator aboard Skylark rocket 21 p3821 A70-42261
- Ionospheric radio wave absorption above polar aurorae during solar activity minimum, discussing diurnal and annual behavior 23 p4162 A70-44058
- Polar ionosphere ion composition measurement by meteorological rocket-borne RF mass spectrometer 23 p4190 A70-44081
- High latitude geomagnetic secular variations determination by running 12-month means method, recommending data acquisition free of external sources effect 23 p4190 A70-44087
- FSRO satellites missions and payloads, emphasizing studies of earth magnetic and electric field environment and of polar region particle measurements 23 p4191 A70-44663
- Polar storm simultaneous onset and development, using observational data for geomagnetic field and aurorae 24 p4331 A70-46289
- Subpolar ionosphere electron concentration measurements for both hemispheres during solar activity by Faraday effect signal recordings from satellites 24 p4331 A70-46298
- POLARIMETERS**
- Electronic polarimeter using signal sampling technique and feedback to measure periodic retardation changes 02 p0297 A70-11918
- Polarimeter for atmospheric radiation with three optical channels enabling precision measurement of polarization 04 p0695 A70-15573
- Hertzian differential polarimeter-ellipsometer with single detector designed for multiwave oscillations analysis 10 p1888 A70-24477
- Solar magnetograph modified to simplify calibration, using polarimeter with special exit slit geometry 11 p2057 A70-26650
- Spectropolarimeter for measurements of polarization characteristics of atmospheric radiation in nanometer range 14 p2583 A70-30414
- Photographic polarimeter based on Savart and lambda/4 plates combination for linear polarization measurements of coronal and prominence emission lines during solar eclipse 20 p3627 A70-39092
- Battery operated electronic servo governed photoelectric polarimeter for airborne measurements of skylight polarization, discussing design and operation principles 23 p4199 A70-45006
- POLARIMETRY**
- Atmospheric pressure, optical thickness and Young particle size distribution of Mars atmosphere determined from polarization observations 07 p1385 A70-19421
- Integrated lunar disk wavelength dependence of polarization using photoelectric polarimeter, tabulating results 09 p1759 A70-22910
- Martian soil surface anomalies observed from polarimetric analysis of light diffused by Hellas region 10 p1943 A70-24708
- Magnetically sensitive Fe lines usefulness to solar polarimetry, observing absorption coefficient dependence on temperature variations 12 p2303 A70-27706
- Bragg reflecting crystals for spectroscopy and polarimetry in X ray astronomy 13 p2489 A70-28904
- Jupiter microwave spectrum from polarimetric observations and previous data 14 p2648 A70-31088
- Photoelectric and polarimetric observations of comet 1968 c Honda in BV system, noting dust scattering role in emission 19 p3515 A70-37657
- Triple polarizational astrophot observations of comet 1968 c Honda, noting dust component- Wolf number agreement 19 p3515 A70-37658
- Photoelectric polarimetry of dark unipolar type H sunspot in terms of value and direction of magnetic field vector 20 p3712 A70-40413
- POLARISCOPES**
- Warped wave front viewpoint in analyzing object plane resolution, contrast and location in polariscopes 07 p1280 A70-19236
- Stress analysis using transmitted light polariscope and Mach-Zehnder interferometer for frozen-stress slice 12 p2325 A70-27620
- Hologram interferometry with birefringent objects, showing advantages over polariscope and classical interferometers 17 p3086 A70-35013
- Isoclinic parameter determination from intersection points of secondary isochromatics lines in photoelastic analysis, discussing polariscope theory and imperfect quarter wave plates error effect 23 p4198 A70-44910
- POLARITY**
- Penumbra forms and magnetic polarity distribution relationship in sunspot groups 01 p0184 A70-10955
- Atmospheric space charge magnitude and polarity below 50 km based on rocket probes 04 p0675 A70-14437
- Atmospheric space charge magnitude and polarity below 50 km based on rocket probes 13 p2392 A70-28462
- Statistical heliographic latitude dependence of dominant polarity of interplanetary magnetic field, using photospheric synoptic chart 13 p2492 A70-29195
- Earth dipole field disk dynamo model, studying connection between polarity intervals and precession effects 14 p2638 A70-30619
- Geomagnetic activity dependence on angle between earth-sun and hourly averaged vectors of interplanetary magnetic field 24 p4405 A70-45523
- POLARIZATION**
- Second quantization exciton theory in amorphous disordered materials, discussing hamiltonian, boson annihilation operators and electronic polarization 14 p2627 A70-30693
- POLARIZATION [CHARGE SEPARATION]**
- NT ELECTROLYTIC POLARIZATION**
- Polar ionic exosphere electric field polarization, considering positive and negative charges escape fluxes, electric potential, mean ion velocity, etc 02 p0289 A70-12108
- Diffusive transport term in hydrodynamic equations describing flow over strongly ablating entry objects, discussing charge separation and pressure diffusion 03 p0405 A70-12926
- Slow electrons elastic scattering by diatomic hydrogen molecule, analyzing cross sections in two center prolate spheroidal coordinates emphasizing polarization effect 03 p0528 A70-14179
- Charge separation effects in boundary layer between cold streaming plasma and perpendicular magnetic field with relativistic electrons 04 p0727 A70-14997
- Potential distribution outside ideally reflecting charged sphere immersed in resting plasma described by nonlinear integral equation, allowing for polarization 08 p1432 A70-21090
- Electrode structural parameters effect on polarization characteristics of air-hydrogen cells to obtain optimum performance, reliability and service life 10 p1831 A70-24471
- Sideband instability and trapped particle charge density response of large periodic Bernstein-Greene-Kruskal waves in collisionless plasma 14 p2623 A70-31039
- Hall, polarization and Pedersen charged particle drift velocities in static magnetic and time dependent electric field 14 p2624 A70-31046
- Potential gradient effect on charge separation mechanism during interaction of polarized snow crystals with ice sphere 15 p2769 A70-31445
- Stress corrosion cracking of alpha-Ti alloys at room temperature, suggesting cathodic polarization promotion of film buildup 17 p3113 A70-34369
- Ferroelectric radiation detectors theory and applications, considering polarization changes due to temperature increase from absorbed radiation 17 p3082 A70-34649
- Electrical polarization effects on discharges in individual auditory nerve fibers following current application to cochlear partition 17 p3033 A70-35609
- Maxwell-Wagner migrational polarization resulting from free ions or electrons drift in dielectrics and semiconductors, considering relaxation time 18 p3298 A70-36595
- Polarization electric field in drifting ionospheric inhomogeneities, examining role of longitudinal currents 18 p3252 A70-36987
- Ionospheric electric field formation from polarization of electron density inhomogeneities under anisotropic conditions 18 p3252 A70-36988
- Ionospheric electric field origin theory in terms of charge separation due to neutral wind drag 22 p4016 A70-42785
- Planetary unipolar electric generator system theoretical model based on polarization charges deposition by solar wind 22 p4100 A70-42790
- Electrode and electrolyte additives effect on corrosion and polarization of alkaline zinc electrode 22 p3965 A70-43417
- Ni/sulfuric acid AC voltage polarization curves for anodic dissolution region 24 p4364 A70-46220
- POLARIZATION [SPIN ALIGNMENT]**
- Spin exchange theory for collisions between atoms extended to include target polarization 04 p0722 A70-14672
- Elastic and inelastic scattering of proton beam from Ne 20 measured for cross sections to interpret polarization data 04 p0723 A70-15636
- POLARIZATION [WAVES]**
- NT CIRCULAR POLARIZATION**
- NT ELLIPTICAL POLARIZATION**
- Geomagnetic field influence on extensive air shower radio emission, discussing frequency dependency and signal polarization 01 p0069 A70-10281
- Galactic water vapor radio sources spectral observation suggesting correlation between time variation and polarization 04 p0747 A70-14547
- Refractive index profile analysis for hypergeometric functions solutions for vertically polarized electromagnetic waves propagating in horizontally stratified isotropic media 04 p0647 A70-14616
- Parasitic cross polarization lobe elimination in radiation patterns of variable profile antennas by curved conductors, including confirmation for large radio telescope 05 p0820 A70-16253
- Monopulse radar signal detection efficiency with fully polarized reception taking into account target with fluctuating polarization 05 p0813 A70-16270

Satellite relay systems to provide polarization discrimination in antenna main beam to double spectrum for communications

05 p0815 A70-16661

Polarization insensitive phase shifter for phased array antennas, discussing limitations, design optimization and experimental results

06 p1019 A70-17508

Two port isotropic antenna excited by independent noise sources for uniform power radiation in all directions and polarizations

06 p1021 A70-17574

Polarization interference filter as laser resonator frequency selector, showing Q factor measurable within spontaneous emission line

06 p1082 A70-17771

Moving plasma column scattering of obliquely incident microwaves, assuming arbitrary polarization for incident plane wave

06 p1124 A70-18608

Polarization and absorption of radio waves in ionosphere using Appleton-Hartree equations, calculating LUF as function of sunspot number

07 p1229 A70-19160

Signal polarization and fading near LUF, describing spatial variations of wave amplitude in terms of angular spectrum

07 p1230 A70-19168

Field strength prediction for vertical horizontal broadside and horizontal end-on HF antennas, noting necessary polarization corrections

07 p1232 A70-19177

Crystals nonlinear permittivity related to temperature-time Green function for electromagnetic radiation, determining crystal polarizability by light-exciton method

07 p1335 A70-19868

Electrodynamic plasma accelerators fast particle generation mechanism during entrainment, studying polarization field potential structure

08 p1549 A70-20506

Faraday rotation in pulsars and in interstellar medium, discussing position angle drift, polarization changes and pulse fine structure

08 p1564 A70-20553

Plane E-polarized wave diffraction by slit in conducting screen using Fredholm integral equations of second kind

08 p1461 A70-21004

Polarization of interacting atoms resonance fluorescence and coherence transfer due to excitation exchange, considering electrostatic dipole-dipole and electromagnetic radiative interactions

08 p1548 A70-21341

Galactic latitude dependence of polarization and Faraday rotation of extragalactic radio sources at centimeter wavelengths

08 p1577 A70-21534

Radio sources linear polarization measurements at 6 cm wavelength, noting intensity changes with polarized flux and position angle

08 p1578 A70-21535

Laser display systems, discussing mechanical, diffractive and refractive beam deflection techniques, electro-optical polarization devices, holographic displays, etc

08 p1499 A70-21687

Polarization-optical studies of large deformations in nonlinear theory of elasticity and plasticity, considering procedures based on photoelastic coatings and transparent models

09 p1768 A70-22120

Polarization diversity reception effects on VHF telemetry signal from low altitude satellites

10 p1832 A70-23919

Helical propagation in multivalley semiconductors of n-Ge type, obtaining polarization anisotropy

10 p1928 A70-24842

Polarization regularities of Pc 1 oscillations interpreted from propagation along ionospheric waveguide centered at F 2 layer

11 p2043 A70-25543

Polarization effects during HF EM wave interaction in plasma, discussing plasma scattering effects in polarization transport equations

11 p2004 A70-25937

Solar microwave bursts polarization reversal mechanism, considering radiating electrons gyrosynchrotron absorption

11 p2106 A70-26617

Fluctuations of polarization induced fading periods in short wave transmissions of Soviet earth satellites, showing relation to ionospheric inhomogeneities

11 p2047 A70-26788

Very low frequency radio noise in ionosphere, magnetosphere and solar wind, using multiple receivers to measure mathematical relations between direction magnitude and polarization characteristics

12 p2184 A70-27574

Microwave solar bursts intensity and polarization measurements at 17 GHz, discussing chromospheric flares and X ray emission

12 p2293 A70-27592

Transmission coefficient for perforated screen related to orientation of rectangular and cross shaped narrow openings and field polarization during normal wave incidence

12 p2191 A70-28174

Pulsars linear polarization Stokes parameters measured, noting PSR 2045-16 radiation beamed into hollow cone centered on magnetic pole

13 p2487 A70-28631

Quasi-monochromatic radiation field polarization representation and transformation of state, including instrumental effects

13 p2451 A70-28829

Wave polarization effects on ionospheric HF radio wave transmission and reception in communication and broadcasting networks

14 p2550 A70-30650

Auroral echoes polarization with horizontal and vertical Yagis, discussing aerial patterns

14 p2578 A70-31240

Polarization role in radiation scattering by planetary atmosphere, considering luminance variation and Rayleigh scattering

14 p2651 A70-31302

Radar echo signal amplitude probability distribution during fully polarizational reception

15 p2696 A70-31517

Third harmonic generation using hot electron nonlinearity characteristics of semiconductors, considering plane-polarized electromagnetic wave nonlinear interaction with sample

15 p2783 A70-31970

Concentric polarization Fabry-Perot duochromator for spectral line displacement measurements applied to ion drifts in hollow cathode plasma

15 p2737 A70-32042

Faraday rotation in pulsars and in interstellar medium, discussing position angle drift, polarization changes and pulse fine structure

15 p2805 A70-32708

Backscattered radiation depolarization during illumination of aqueous medium by linearly polarized laser beam

15 p2753 A70-32861

Electromagnetic field intensity measurements in focal region of wide angle spherical reflector antenna illuminated by polarized plane wave

16 p2872 A70-32976

Radar and DC pulse signatures of multiple reflection from dry, damp and wet earth for vertical and horizontal polarization

16 p2861 A70-32977

Antenna system with linear polarization direction electronically changeable in microseconds

16 p2873 A70-33265

Pulse structure, polarization, time varying features and tight beam emission by pulsar model using finite thickness interfaces

17 p3153 A70-34532

Axially symmetric parabolic reflector with incident linearly polarized plane wave, determining Poynting vector behavior

17 p3043 A70-34615

Partially polarized wave with log-normal distribution law of component envelopes, investigating statistical characteristics of polarization parameters

18 p3228 A70-36624

Polarization splitting of EW and NS Alfvén oscillations in axisymmetric magnetosphere

19 p3409 A70-37319

Raman line coherence degree and polarization rate measurement, applying Wolf matrix

19 p3443 A70-37359

Radio polarization of quasars with and without absorption line spectra

19 p3523 A70-38605

Triangular ring laser polarization, using discharge tube with Brewster angle windows in optical circuit

20 p3639 A70-39084

Small angle of rotation measurement of coherent radiation polarization plane, discussing technique for increasing sensitivity and accuracy

20 p3643 A70-39759

Pulsar observational data and theories, discussing main pulse shape, wavelength, polarization, fine structure distance estimates, intensity and scintillations

20 p3706 A70-39935

Transmission line modal analysis for nonlinear polarizability in optical and quasi-optical waveguides

21 p3784 A70-40564

Polarization regularities of Pcl oscillations interpreted from propagation along ionospheric waveguide centered at F 2 layer

21 p3819 A70-41293

Wave polarization effects on ionospheric radio wave transmission and reception

21 p3790 A70-41361

Polarization of radiation reflected and transmitted by earth atmosphere, calculating scattering matrix for aerosol size distribution model

21 p3820 A70-41725

Stellar polarization measurements in Magellanic Clouds, tabulating position, magnitude, spectral type,

POLARIZATION CHARACTERISTICS

percentage polarization and electric vector position angle

21 p3922 A70-41979

Quasi-equispaced traveling wave slot arrays with below sidelobe crosspolarization, considering computer designed X band prototype

21 p3800 A70-42050

Micropulsations polarization characteristics from statistical spectrum analysis

23 p4185 A70-43837

Radar backscattering cross sections of horizontal and vertical polarizations for thin rectangular plate near grazing incidence

23 p4166 A70-44976

Pulsar radiation polarization, examining mean pulse profiles, frequency, position angle and rotational effects

24 p4403 A70-45404

POLARIZATION CHARACTERISTICS

Polarized and unpolarized impulsive solar centimetric radio bursts spectral peak interpretations

01 p0168 A70-10253

Radiometric method for calibrating loss of multimode antenna-feed components with linear or circular polarization, deriving calibration and error analysis equations

01 p0050 A70-10711

Jovian decimeter radiation polarization during 1966-1967 apparition compared with cyclotron model predictions

02 p364 A70-11793

Polarization characteristics of pulsars, noting stable average and time varying component

02 p3371 A70-12242

IR observations for position of hypothetical Seyfert-like nucleus explaining M82 polarization pattern

02 p3372 A70-12246

Multicolor Venus photography, discussing anomalous markings association with anomalous UV polarization

02 p3378 A70-12557

Total electron content (TEC), time delay and polarization errors on one way path through ionosphere, discussing measurements and predictions

02 p0293 A70-12568

Ionosonde spiral antenna for HF polarization studies

02 p0269 A70-12584

Spectral polarization characteristics phase variations used for classifying lunar surface features

03 p0565 A70-13234

Linearly polarized radiation in Na-glass laser obtained without energy loss by placing glass plates in resonator at Brewster angle to axis

03 p0499 A70-13257

Magnetic structure of type 4 solar outburst from continuous record of 80 MHz image and polarization

03 p0558 A70-13587

Polarization diversity provided to parallel plate antennas in airborne radar applications by orthogonal vector processing

03 p0452 A70-13967

Photoelectric polarimetry of samples of lunar maria, terra, lavas and chemicals for wavelength dependence of polarization, comparing to Mercury, Mars and asteroids

03 p0576 A70-14082

Helicone antenna /axial mode helix combined with conical horn/ compared to conical horn in pattern and polarization characteristics

04 p0655 A70-14662

Temporal isolation between pulsed orthogonal polarization state laser beams, showing selection dependence on sampling time

04 p0701 A70-15032

Polarization nature and changes evaluation of radio echo signals reflected from polar auroras

04 p0682 A70-15730

Nonlinear theory of elastic dielectrics with polarization gradients, obtaining jump conditions and field and constitutive equations by variational principle

05 p0882 A70-16092

Polarization transfer equations for electromagnetic waves propagating in inhomogeneous magnetized plasma solved analytically for homogeneous magnetized plasma

05 p0890 A70-16570

Flux densities from quasars 3C 273, 3C 279 and 3C 454.3 and Seyfert galaxy 3C 84, measuring linear polarization, discussing time variations in sources

05 p0918 A70-16926

Polarization loss for elliptically polarized antennas, using curves based on Hatkin equation

06 p1019 A70-17504

Polarization level of outgoing short wave radiation calculated along solar vertical in aerosol containing multiply scattering atmosphere

06 p1097 A70-17829

Geomagnetic micropulsation amplitudes and polarization along meridional profile analyzed from simultaneous ground station recording

07 p1268 A70-19463

Polarization anisotropy effect of laser cavity on neodymium glass laser output power

08 p1510 A70-20513

Red giants and supergiants intrinsic radiation polarization characteristics

08 p1569 A70-20826

Polarization of laser medium consisting of colliding two level molecules with velocity dependent mean free time

08 p1512 A70-20992

Pulsar NP 0532 average polarization parameters measured at 430 MHz, discussing variations of precursor and main pulse and flux of interpulse

08 p1578 A70-21549

Spectral polarization characteristics phase variations used for classifying lunar surface features

08 p1580 A70-21667

Vacuum-UV monochromators polarization and effective transmittance measurements, comparing characteristics of parallel and pyramidal biotite polarizers

08 p1546 A70-21791

Crab Nebula activity from telescopic plates, illustrating polarization structure on composite plate

09 p1750 A70-21999

Phase variations in polarization parameters of eclipsing binary Z Vul during polarimetric studies for interstellar polarization component

09 p1751 A70-22156

Elevation patterns of vertically polarized elements above circular finite ground screens directly on soil, discussing steering illumination

09 p1634 A70-22700

Solar eclipse coronal polarization and intensity measurements, discussing equipment, calibration, photometric reduction and results

09 p1757 A70-22736

Integrated lunar disk wavelength dependence of polarization using photoelectric polarimeter, tabulating results

09 p1759 A70-22910

Reflected solar radiation polarization over land, sea and cloud surfaces to determine atmospheric pollution

09 p1747 A70-23603

Pulsars pulse shapes and linear polarization measured, observing rapid change of polarization direction in double pulses

10 p1936 A70-23901

Metals, alloys and galvanic couples corrosion rates in synthetic seawater measured by polarization technique

10 p1887 A70-24044

Solar magnetic field measurement emphasizing circular and total polarization characteristics

10 p1939 A70-24275

Electrode structural parameters effect on polarization characteristics of air-hydrogen cells to obtain optimum performance, reliability and service life

10 p1831 A70-24471

Outer corona brightness and polarization during total solar eclipse from satellite photographs

10 p1947 A70-24988

Geomagnetic variations dominant polarization direction seasonal dependence based on magnetotelluric field observations, discussing micropulsations and LF cases

11 p2044 A70-25557

Icarus asteroid positions, UVB magnitude, brightness, colors, light curves and polarization, noting stony-iron composition

11 p2113 A70-26470

Poincare sphere application to automatic polarization forms measurements and two/three dimensional photoelasticity by scattered light

11 p2142 A70-26633

Polarization properties of radar channel with random parameters, relating observation range with transmitting-receiving antennas and target fluctuations

11 p2012 A70-26815

Resonant nonmonochromatic radiation effects on quantum system, deriving expressions for active medium nonlinear polarization, susceptibility and gain

12 p2245 A70-27304

Polarization of extragalactic radio sources and supernova remnants emphasizing instrumental effects

12 p2309 A70-27894

Hanle effect in single mode He-Ne laser, observing spontaneous emission on different spectral lines and estimating lifetimes of Ne excited states

13 p2424 A70-28598

Plane electromagnetic wave reflection at interface of two semiinfinite dielectric media in relative motion perpendicular to incidence plane, noting polarization change

13 p2365 A70-29102

Polarization of strong radio pulses from pulsar NP 0532 in Crab Nebula

13 p2492 A70-29269

Gas laser active medium nonlinear polarizability calculations with allowance for resonance emission capture effect on atomic velocity and population distributions

13 p2427 A70-29284

Radio waves attenuation anisotropy in sea ice by comparing vertically and horizontally polarized signals

14 p2546 A70-30132

Spectropolarimeter for measurements of polarization characteristics of atmospheric radiation in nanometer range

14 p2583 A70-30414

Polarization nature and changes evaluation of radio echo signals reflected from polar auroras

14 p2575 A70-30814

Venus radar anomalous features, examining rotation period, polarized and cross polarized scattering properties and topography

14 p2647 A70-31079

Visible polarization signature for remote sensing of soil surface moisture, noting invariance to partial shadowing in plowed or rough soils

15 p2724 A70-31667

Geomagnetic micropulsations horizontal polarization characteristics relationship between stations in southern and northern auroral zones

15 p2725 A70-31859

Polarization characteristics of solar radio waves reflected from coronal waves in meter wavelength range

15 p2802 A70-32485

Line formation in solar magnetic fields with allowance for absorption emission and scattering processes, discussing Hanle effect and atomic level polarization

15 p2804 A70-32617

Annular lasers energy, polarization, radiation loss and frequency characteristics dependence on phase shift due to anisotropic plate introduction

15 p2753 A70-32860

Earth magnetic field Pc 1 micropulsations polarization characteristics examined in narrow frequency bands

16 p2897 A70-33299

Radar mapping in heavy rain with orthogonal transmit and receive polarization, using backscatter and attenuation to define maximum operating altitude

16 p2863 A70-33434

Lunar millimeter wavelength thermal radiation measurement noting surface roughness effect on polarization

17 p3171 A70-35559

Partially polarized wave with log-normal distribution law of component envelopes, investigating statistical characteristics of polarization parameters

18 p3228 A70-36624

Geomagnetic micropulsation amplitudes and polarization along meridional profile analyzed from simultaneous ground station recording

18 p3250 A70-36937

Diurnal variations in polarization axis direction of Pc 1 pulsations

19 p3410 A70-37333

Photographic polarimeter based on Savart and lambda/4 plates combination for linear polarization measurements of coronal and prominence emission lines during solar eclipse

20 p3627 A70-39092

Electro-optical crystal resonator loss anisotropy, determining natural frequencies and polarizations

20 p3642 A70-39755

Geomagnetic variations dominant polarization direction seasonal dependence based on magnetotelluric field observations, discussing micropulsations and LF cases

21 p3820 A70-41307

Polarization characteristics of pulsar NP 0532 strong pulses at 430 MHz, using dual circularly polarized line feed

22 p4105 A70-43228

Micropulsation Pc-1 phase and polarization comparisons concerning L to R wave coupling in ionosphere

22 p4024 A70-43313

Antenna polarization and terrain depolarization effects on radar ground return, calculating echo pulse from smooth and rough terrains

22 p3990 A70-43327

Micropulsations polarization characteristics from statistical spectrum analysis

23 p4185 A70-43837

Polarization characteristics of solar radio waves reflected from coronal waves in meter wave length range

23 p4240 A70-43909

Polarization of short period oscillations Pc2-Pc4 dependence on time of day, oscillation type and geoelectromagnetic field activity

23 p4190 A70-44086

Continuum polarization at solar limb at various wavelengths, using source functions

23 p4246 A70-44754

Polarization properties of radar channel with random parameters, relating observation range with transmitting-receiving antennas and target fluctuations

24 p4311 A70-45187

SbSI semiconductor single crystal repolarization parameters temperature dependence, noting anoma-

lies in permittivity, spontaneous polarization and dielectric loss tangent

24 p4389 A70-45208

Circular polarization time evolution during solar microwave impulsive bursts

24 p4401 A70-45319

Solar flares X ray emission polarization measured by Thomson scattering instrument on Intercosmos-1 satellite

24 p4396 A70-45321

POLARIZATION CHARTS

U GRAPHS [CHARTS]

U POLARIZATION [WAVES]

POLARIZED ELASTIC WAVES

Single crystalline mercury elastic constants calculated from propagation velocity measurements of polarized sound waves

19 p3486 A70-37770

POLARIZED ELECTROMAGNETIC RADIATION

NT POLARIZED LIGHT

NT SYNCHROTRON RADIATION

X band radar with horizontally and vertically polarized antennas to compare sea clutter suppression by decorrelation and constant alarm rate receivers

03 p0451 A70-13935

Elliptically polarized microwave oscillations conversion to linearly polarized oscillations with polarization plane in original orientation

04 p0655 A70-14608

Faraday modulator for polarized laser radiation, eliminating analyzer by oblique magneto-optical active element, converting angular modulation into amplitude modulation

05 p0858 A70-16251

Polarization transfer equations for electromagnetic waves propagating in inhomogeneous magnetized plasma solved analytically for homogeneous magnetized plasma

05 p0890 A70-16570

Three dimensional electromagnetic scattering from thin walled conducting circular tube of finite length normally incident with E or H polarized plane wave

05 p0816 A70-16987

Mutual coupling between waveguides radiating through conducting ground planes with orthogonally polarized propagating modes described by first order analysis

06 p1020 A70-17562

Power reflection and transmission coefficients for polarized electromagnetic waves incident on plasma slab moving along magnetostatic field

06 p1008 A70-17566

Scattering and depolarization of plane horizontally polarized electromagnetic wave from slightly rough lossless dielectric layer, using small perturbation theory

06 p1010 A70-18019

Signal polarization and fading near LUF, describing spatial variations of wave amplitude in terms of angular spectrum

07 p1230 A70-19168

Polarized and unpolarized emission measurements of W 44 supernova remnant with radio telescope, showing results for eastern portion of source

07 p1383 A70-19405

Polarization structure of electromagnetic wave scattered by slanted two dimensional statistically rough surface of finite conductivity

08 p1456 A70-20573

Scattered field from rough ionospheric irregularities or earth surface for arbitrary polarization of incident wave

08 p1456 A70-20574

Electrical and magnetic polarizability coefficients in theory of diffraction at small apertures by formulating bilateral variational principles

09 p1631 A70-22150

Electromagnetic waves propagation in nonlinear medium, investigating polarized plane wave incident on vacuum-plasma interface in magnetic field

10 p1844 A70-25156

Refractive index profiles method for vertically polarized electromagnetic waves in horizontally stratified magneto-plasma extended to anisotropic media, noting relevance to ionospheric propagation

11 p2011 A70-26555

Discrete extragalactic radio sources integrated linear UHF polarization values, discussing optical identification and radio spectral index correlations

11 p2117 A70-26656

Polarized Lyman alpha radiation emitted in electron collisions with atomic and molecular hydrogen and by electric field quenching of metastable atom

13 p2455 A70-29221

Dipole antenna arrays feeds design and performance for spherical aberration correction, discussing polarization mismatch

16 p2871 A70-32955

Paraboloidal reflectors aperture fields from stereographic mapping of feed polarization pattern, illustrating electric and magnetic dipoles and Huygens sources

16 p2871 A70-32962

Partially polarized wave with log-normal distribution law of component envelopes, investigating statistical characteristics of polarization parameters 18 p3228 A70-36624

Thomson theory of arbitrarily intense elliptically polarized plane electromagnetic wave scattering by free electrons, solving electron equations of motion 18 p3267 A70-36649

Extragalactic radio sources polarization variations at 8 GHz based on expanding source type model, noting synchrotron self absorption depolarization 18 p3317 A70-37002

Polarized electromagnetic wave diffraction by semiinfinite symmetrical obstacles in rectangular waveguide, calculating transformation coefficients for wide frequency range 19 p3378 A70-37729

Double asymmetric grating with thin ideally conducting strips, describing incident E-polarized electromagnetic wave diffraction 19 p3378 A70-37744

Diffraction amplitudes in plane H-polarized electromagnetic wave incident obliquely on grating with closely spaced conducting rectangular bars, obtaining transmission coefficient 19 p3378 A70-37745

Optical activity of nonenantiomorphous biaxial crystals with mirror planes, investigating polarization plane rotation 21 p3850 A70-41934

B-V and U-B colors and B and V polarization calculation in single scattering for slab model reflection nebulae with dielectric or graphite grains 22 p4103 A70-42984

Intrinsic polarization from Thomson scattering in binary systems with tidal distortions, taking into account gray atmosphere, axial rotation, gravitational interaction and radiative interaction 22 p4103 A70-42988

Radar astronomical polarization measurements for lunar echoes by exploiting ionospheric Faraday rotation with linearly polarized antenna 23 p4165 A70-44964

Dipolar resonant scattering of H-polarized plane waves by axially magnetized plasma column with perfectly conducting core 23 p4228 A70-44977

POLARIZED LIGHT

Polarization level dependence of dye lasers emission on angles between direction of forced radiation and pumping laser resonator axis 01 p0113 A70-11037

Twilight sky polarization data in visible spectrum obtained by high altitude balloon-borne photoelectric photometers 01 p0079 A70-11219

Power losses in ruby laser with polarized spontaneous luminescence determined as function of laser parameters and light polarization 03 p0502 A70-13747

Thermodynamics of radiation and photosynthesis, discussing Ross-Calvin maximal efficiencies, Duysens method, light and dark conditions and polarized light 03 p0428 A70-14011

Lunar regolith and polarized component of earthlight observations by Surveyor 7 TV camera 04 p0752 A70-15061

Polarization effects of helium-neon laser emission at 3.39 micron wavelength investigated in longitudinal and transverse magnetic fields 04 p0702 A70-15227

Airglow and skylight polarization measurements at twilight compared for possible relationship 05 p0837 A70-15927

Successive small birefringences undergone by polarized light ray crossing photoelastic model represented by rotations in equatorial plane on Poincare sphere 06 p1168 A70-17918

Light intensity and polarization in twilight sky atmosphere at solar depressions 07 p1263 A70-19047

Fundus oculi in polarized light, investigating light intensity variations and polarization pattern in yellow spot 08 p1444 A70-20748

Polarized light study of fundus oculi facilitating early diagnosis of various optical nerve and yellow spot diseases 08 p1445 A70-20749

Polarized light electroreflection from GaAs single crystal, noting useful signal linear dependence on electric field 08 p1556 A70-21124

Narrow band detector for polarized light in far UV based on plasma resonance 09 p1676 A70-22650

Polarization-optical cinematographic method for study of mechanical stresses during dynamic loading 09 p1680 A70-23174

Magnetophotoelastic model applied to plates bending stress analysis, deriving polarized light propagation equations 09 p1728 A70-23447

Nb and Nb alloys activation in polarized light by etching technique, observing grain contrast improvement 10 p1906 A70-25229

Honda 1968c comet head light polarization measurements, noting correspondence to scattering on dust particles 12 p2300 A70-27499

Sky radiation scattering and polarization functions for various solar altitudes at Lomnitzer Peak observatory 12 p2294 A70-27674

Chandrasekhar polarization upper limit in early type stars noting effects of thermal absorption, wavelengths and effective temperature 12 p2303 A70-27675

Extragalactic objects polarization due to synchrotron radiation superimposed on stellar radiation, discussing Seyfert galaxies nuclei 12 p2307 A70-27869

Raman spectrum of lithium formate monohydrate single crystal in polarized He-Ne laser light, discussing crystal structure 13 p2425 A70-28714

Electronic heterodyne astronomical spectroscopy, using lasers for absolute monochromatic flux and polarization measurements on star-like objects 13 p2408 A70-29473

Autocorrelation of coherence characteristics of polarized components of light scattered at curved rough surface, showing nonadequate Kirchhoff approximation 15 p2749 A70-31555

Optical polarization, discussing radiation intensity and state measurement by two beam interferometer 15 p2736 A70-32035

Polarized light scattering angle relationship with Mueller matrix elements for polydisperse systems of irregular randomly oriented particles 15 p2775 A70-32040

Scattered light rosette using three polarized light beams intersecting at surface point to evaluate photoelastic stress data 15 p2739 A70-32320

Long period variable stars light polarization as function of brightness and wavelength, discussing molecular scattering and nonthermal emission 15 p2808 A70-32879

Solid state laser polarization mechanism, considering isotropic and anisotropic cavities 17 p3106 A70-35103

Planetary surface inhomogeneities detection by reflected and transmitted light polarimetry, using symmetry principles 18 p3319 A70-37057

Electronic absorption spectra of single crystal praseodymium acetate tetrahydrate in natural and polarized light 19 p3488 A70-38742

Light polarization during twilight at zenith from photoelectric recordings, noting intensity decrease with altitude 19 p3417 A70-38770

White dwarf star circular polarized light, indicating strong magnetic field 20 p3701 A70-39001

Laser interferometer system unwanted reflections elimination and intensities control in each arm by linear polarization method 21 p3823 A70-40820

Liquid crystal smectic C phase temperature dependent tilt angle, using conoscopic observation and circularly polarized light 21 p3862 A70-41322

Refractive index complex part effect on polarization and radiance of reflected and transmitted light for continental haze and nimbostratus cloud models 21 p3847 A70-41724

Low pressure supersonic wake measurement by differential interferometer in double pass polarized light (SMPT PREPRINT 95) 22 p4036 A70-43060

Laser light polarization and depolarization during backscattering from aqueous suspensions 23 p4215 A70-44271

Radiative transfer equation solution for polarized light in Rayleigh scattering atmosphere with absorption, using singular eigenfunction expansion technique 23 p4219 A70-44402

Battery operated electronic servo governed photoelectric polarimeter for airborne measurements of skylight polarization, discussing design and operation principles 23 p4199 A70-45006

POLARIZED RADIATION

NT POLARIZED ELASTIC WAVES

NT POLARIZED ELECTROMAGNETIC RADIATION

NT POLARIZED LIGHT

NT SYNCHROTRON RADIATION

Polarization of nonspherical plasma emission region in thermal X ray stars 02 p0357 A70-11787

Polarization observations of Saturn in UV and visible regions compared with Jupiter data, noting multiple scattering 02 p0368 A70-11818

High intensity pulsed laser radiation scattering by free electrons, studying linearly polarized incident radiation 02 p0312 A70-12276

Cosmic X ray observations by rockets and balloons noting polarization and line emissions of various sources 02 p0359 A70-12789

Linearly polarized radiation in Nd-glass laser obtained without energy loss by placing glass plates in resonator at Brewster angle to axis 03 p0499 A70-13257

Longitudinal magnetic field effect on output power and emission polarization of CW Ar laser employing Brewster windows 03 p0500 A70-13529

Flash lamp illuminated ruby laser operating with ordinary or extraordinary polarization, measuring gain or absorption 03 p0502 A70-13954

Interstellar polarization by graphite-silicate grain mixtures, observing variability in wavelength dependence of polarization for various models 03 p0577 A70-14218

Intensity, spectrum and polarization of gyrosynchrotron radiation from magnetosheath plasma electrons distribution 04 p0749 A70-14594

Anomalous Doppler shift interaction between positive ions and right-hand polarized EM waves propagating at small angle to interplanetary magnetic field 05 p0905 A70-15761

Cerenkov radiation in infinite anisotropic electron plasma linearly polarized in magnetic field having linear electron distribution moving with uniform velocity 06 p1120 A70-17538

Radiation from nonlinear polarization sideband in Ar lasers, discussing anomalous beat notes and mode locking phenomena 06 p1083 A70-17949

Plasma polarization shift for resonance line of ionized He in shock tube due to negative space charge 07 p1348 A70-19273

Solar protuberance radiation polarization in Ca I 4227 A line, discussing depolarization and electron- and photoexcitation 07 p1384 A70-19416

He-Ne single frequency laser output characteristics at various active medium pressures noting emission polarization 08 p1511 A70-20517

Red giants and supergiants intrinsic radiation polarization characteristics 08 p1569 A70-20826

Ionizer design for hydrogen atom beam ensuring storage of polarized protons, using electron beam for ionization 09 p1732 A70-22846

Polarized radiation transfer through inhomogeneous semiinfinite atmosphere by matrix perturbation method, giving nonlinear singular integral equation 10 p1933 A70-24985

Polarization of solar scattered radiation measured by radio probes for aerosol particle concentration and size distribution as function of altitude 10 p1884 A70-25253

Solar radio emissions of types I, II, III and IV activity and polarization during 18-26 May 1967 observed by narrow-band timesharing polarimeter 12 p2294 A70-27711

Cold variable stars intrinsic polarization model proposing light scattering in circumstellar dust shells 12 p2307 A70-27865

Polarization effect on radiant heat transfer between simply arranged smooth plate surfaces 13 p2523 A70-29993

Gas ring lasers, discussing optimal parameters, colliding waves interference, nonmutual effect and radiation polarization 15 p2749 A70-31451

Volcanic blankets aerological investigation by polarization and spectral techniques, determining brightness distribution of reflected solar light 15 p2803 A70-32495

Backscattered radiation depolarization during illumination of aqueous medium by linearly polarized laser beam 15 p2753 A70-32861

Transverse magnetic field effect on CW argon laser operation with linearly polarized radiation 15 p2754 A70-32866

Pyroelectric IR radiation detector based on materials polarization changes associated with temperature changes 16 p2905 A70-33154

Super and sub specular maxima in angular distribution of polarized radiation reflected from roughened dielectric surfaces [AIAA PAPER 70-861] 16 p2999 A70-33906

Taurus X-1 X ray emission polarization, using rocket-borne polarimeter 17 p3150 A70-34845

Radiation polarization measurements of natural underlying surfaces in centimeter range, noting dependence on sighting angle 18 p3250 A70-36967

Variable radio source linear polarization at 8 GHz, examining degree, position angle and flux density 18 p3317 A70-37001

Gas laser radiation depolarization coefficient as function of radiation energy, cavity anisotropy and operating transition type 19 p3444 A70-37445

Polarization in inverse Compton effect for arbitrary photon and electron distributions, discussing monochromatic photon beam 19 p3524 A70-38696

Optical emission conversion from solid state lasers into far IR region by nonlinear polarization with difference frequency generation 19 p3448 A70-38741

Thermally induced stress birefringence effect on linearly polarized CW YAG-Nd laser 21 p3834 A70-40566

Continuum polarization at solar limb at various wavelengths, using source functions 23 p4246 A70-44754

Linear polarization of sunlight scattered by Venus atmosphere, giving data for integrated disk and equatorial region 23 p4246 A70-44756

Polarized maser emission from interstellar hydroxyl and water related to nonlinear weak magnetoplasma 24 p4381 A70-45258

POLARIZERS

Vacuum-UV monochromators polarization and effective transmittance measurements, comparing characteristics of parallel and pyramidal biotite polarizers 08 p1546 A70-21791

Rectangular waveguide with cross shaped slot as polarizer ensuring circular polarization over wide frequency range 09 p1652 A70-23649

POLAROGRAPHS

U POLAROGRAPHY

POLAROGRAPHY

Polarographic probe for wall studies of turbulent flow velocity and direction by measuring maximum reduction current on redox compound microelectrode 01 p0062 A70-10664

POLES

Earth poles motion influence on latitude, longitude, azimuth and geocentric rectangular coordinates of points determinations on earth surface 03 p0473 A70-13187

Geomagnetic dipole field disturbances by trapped particles, calculating self consistent equilibrium configuration for ring current dipole moments 15 p2727 A70-31905

Feedback gains for repeated eigenvalues in Simon-Mitter pole allocation algorithm 16 p2941 A70-32986

Astronomically determined latitude longitude and azimuth reduction to common epoch, discussing secular nonperiodic pole motion due to crust drift 18 p3323 A70-37144

POLICIES

Future U.S. aerospace power in terms of military technology and defense policies and attitudes 05 p0960 A70-16633

POLISHED METALS

U METAL POLISHING

POLISHING

NT ELECTROPOLISHING

NT METAL POLISHING

Workpiece temperature during asymmetrical plane polishing by wheel face, deriving temperature distribution formulas for maximum heat source intensity 07 p1291 A70-18828

POLITICS

Aeronautics and astronautics sociopolitical aspects, discussing German scientific and industrial organization, American-European technology gap, taxation for research, etc [DGLR-69-1] 04 p0788 A70-15181

Midwestern political economy and federal R and D funds distribution, surveying bidding practices and NASA contracts for five year period 07 p1428 A70-19733

International legal and political aspects of earth resource surveying by satellite remote sensors, considering U.S. policy [AIAA PAPER 70-331] 09 p1793 A70-22862

Criticism of public administration aspect of Edwards Report, noting parliamentary and constitutional difficulties in some proposals 11 p2153 A70-25857

Earth Resources Satellites political background, investigating international implications 20 p3739 A70-39060

POLLUTANTS

U CONTAMINANTS

POLLUTION

NT AIR POLLUTION

NT WATER POLLUTION

Combustion research prospects, considering turbulence and flame stabilization, pollution control, flame self acceleration, subsonic/ supersonic flow combustion and flame diagnostics 11 p2150 A70-26376

High temperature energy systems with plasma reactors and inductive MPD converters, discussing spacecraft propulsion and ground based pollution-free power generation 15 p2791 A70-32278

Clean, rough vacuum, discussing cleanliness criteria and pollution avoidance via contaminant-free pump 19 p3358 A70-38494

POLYACRYLATES

U ACRYLIC RESINS

POLYAMIDE RESINS

Unlubricated wear characteristics of polyimide resin sliding against carbon steel in air, noting effects of surface temperature, bearing pressure and velocity 01 p0103 A70-10448

Solid glass sphere reinforced nylon resins properties, processing and applications, noting tensile and impact strength and heat distortion 01 p0128 A70-10772

Polystyrene and polyamide stress relaxation graphs, considering tensile stresses and temperature effects 04 p0712 A70-15101

Surface recession of low density phenolic nylon in arc heated air using stagnation point models, noting char removal processes 04 p0787 A70-15602

Polyamides chemical welding using HF heating to obtain optimum temperature distribution and to activate polymer reaction with crosslinking agents 06 p1091 A70-17316

Phenolic nylon ablative thermal effectiveness in arc heated nitrogen, air and nitrogen-carbon dioxide streams [AIAA PAPER 70-154] 06 p1183 A70-18233

Antifriction reinforced plastics based on polyamide fibers in epoxy phenolic resins, determining optimum ratios to obtain desired mechanical properties 09 p1710 A70-23675

Polyamides /nylons/ stress cracking by metal halides and halide-like salts, investigating effects of nylon temperature, moisture content, concentration, etc 10 p1907 A70-24224

Polyamide and secondary amide mode compounds stress cracking by metal halides using IR and nuclear magnetic resonance techniques 10 p1907 A70-24299

Nylon 6 polyamide tensile stress cracking by metal thiocyanates in aqueous and nonaqueous solutions, comparing results with cracking by metal halides 10 p1907 A70-24300

Quartz-polyimide for missile radome exhibiting low dielectric constant and thin wall for use over broader frequency range 13 p2417 A70-28664

Phenolic nylon ablative thermal effectiveness in arc heated nitrogen, air and nitrogen-carbon dioxide streams [AIAA PAPER 70-154] 23 p4282 A70-44520

Caprolon B mechanical properties, comparing properties to other polyamide resins for use in machine parts fabrication 24 p4367 A70-45503

POLYATOMIC GASES

NT DIATOMIC GASES

Radiative lifetimes and total transition probabilities measured in polyatomic gases using phase shift method and electron beam excitation 03 p0441 A70-14009

Nonlinear rarefied Couette flow with heat transfer in polyatomic gases, using kinetic theory of gases [ASME PAPER 69-WA/HT-39] 04 p0781 A70-14803

Coupled relaxation dependence on translational and vibrational temperature and number of modes in polyatomic gases, noting molecular dissociation 12 p2276 A70-27797

Quantum mechanical Boltzmann equation for atomic gas of composite particles, considering excited level degeneracy 14 p2619 A70-30651

Fluidic oscillator molecular weight of flowing mono- and polyatomic gases, discussing frequency dependence on pressure drop and temperature 17 p3081 A70-34515

Kinetic equation for rarefied polyatomic gases derived from Liouville equation 17 p3138 A70-35728

POLYATOMIC MOLECULES

NT DIATOMIC MOLECULES

NT TRIATOMIC MOLECULES

Matrix elements of nonadiabatic perturbation emphasized in semiempirical theory for evaluating polyatomic molecules radiationless rate constants in terms of electronic-vibrational state 04 p0722 A70-14699

Molecular vibration energy distributions of polyatomic molecules, formulating energy criterion valid for nth order general case 08 p1511 A70-20597

Polyatomic molecules radiationless transition rate statistical analysis, suggesting role of Franck-Condon principle in determination of nonradiative decay rates 16 p2858 A70-34014

Thermal diffusion of isotropic, nonisotropic and multicomponent mixtures with monatomic and polyatomic molecules, considering kinetic theory and experimental results 17 p3197 A70-35537

POLYBENZIMIDAZOLE

Polybenzimidazole /PBI/ resin-bonded solid film lubricants composed of molybdenum disulfide, antimony trioxide and PBI resins [ASME PAPER 69-LUB-15] 01 p0101 A70-10390

POLYBUTADIENE

Polybutadiene-ammonium perchlorate solid propellant microscopic failure analysis under uniaxial tension 09 p1741 A70-22424

Polybutadiene-ammonium perchlorate solid propellant BPT-1 mechanical properties viscoelastic analysis under constant strain rate tension 09 p1742 A70-22425

POLYCARBONATES

Constant stress creep and recovery behavior experiments of polycarbonate under combined tension and torsion stresses in weakly nonlinear range 01 p0130 A70-11083

Nonflammable coatings for polycarbonate to meet NASA safety standards, discussing alkali silicate and arc plasma deposition of glass and ceramic oxide [WSCI PAPER 69-34] 06 p1092 A70-17977

Polycarbonate ductile fracture measured for strain energy release rates and plastic zone size and shapes to correlate with existing theories and experimental data 07 p1321 A70-20041

Polycarbonate fatigue fracture surfaces and striation feature 12 p2259 A70-27168

Fiberglass content effects on reinforced polycarbonates long term dimensional stability during compression and tension creep tests 12 p2259 A70-28298

Fatigue life and long term strength of polycarbonate components in pneumatic pulsating pressure equipment described by power and exponential equations 13 p2440 A70-29784

Polycarbonate plate fatigue crack propagation, discussing length due to repetitions, striation number relationship to cycles, and stress intensity 16 p2941 A70-34335

Polycarbonate thin walled cylindrical shells mechanical and material stability under torsion 17 p3127 A70-34656

Graphite fiber reinforced polycarbonate composites interfacial adhesion improvement by controlled thermal treatment 20 p3652 A70-39168

POLYCRYSTALS

Polycrystalline rocks elastic constant and nonelastic behavior, discussing Voigt, Reuss and Hill averaging methods 01 p0071 A70-10446

Polycrystalline Mo ductility at low pressures in tension at ambient temperature, discussing H type embrittlement mechanism 01 p0121 A70-11234

Tensile tests of polycrystalline Nb-H alloys at low temperatures, noting cooling rate effect on ductility in terms of microstructure 01 p0122 A70-11240

Sputtering yield of amorphous and polycrystalline targets bombarded by energetic ions or recoil atoms calculated by integrodifferential equations derived from Boltzmann transport equation 02 p0343 A70-11885

Ingot and powder metallurgy polycrystalline Be flow and fracture behavior and microstructure pressure dependence at room temperature 02 p0317 A70-12318

Polycrystalline material tensile failure at high temperature, discussing intergranular cracking, shearing, etc 03 p0508 A70-13155

Polycrystalline Co strength and plastic properties tested at various temperatures and strain rates 03 p0510 A70-13352

Ductile-brittle transition temperature relation with grain size in polycrystalline Mo as function of annealing temperature 05 p0862 A70-15907

Structural changes in polycrystalline Al subjected to HF fatigue, using transmission electron microscopy 06 p1084 A70-17127

Fatigue crack growth in polycrystalline Mo at room temperature under cyclic loads observed along grain boundaries 07 p1314 A70-20013

- Structural elements reliability determination simulated by microinhomogeneous polycrystalline medium under thermal stresses and in stationary nonuniform temperature fields
09 p1778 A70-23085
- Nonisothermal loading model of polycrystalline material, investigating tangential stresses in slip direction and plastic deformation using linear strengthening law
09 p1779 A70-23102
- D-pattern changes of helium ions irradiated polycrystalline Mo and Ni specimens, observing line splitting
09 p1707 A70-23197
- Dispersion effect on accuracy of measuring polycrystalline samples electronograms by comparator using statistical method
09 p1682 A70-23392
- Ultrasonic vibrations effects on microstructure and mechanical properties of polycrystalline titanium during phase recrystallization
10 p1903 A70-23863
- Bi polycrystalline film grown by vacuum deposition on amorphous substrates investigated for electron microscope beam effects
12 p2285 A70-27261
- Polycrystalline molybdenum desorption of adsorbed hydrogen, oxygen and water by electron impact
12 p2182 A70-27679
- Polycrystalline lanthanides and metals resistance to deformation under compression and tension at different temperatures and strain rates
12 p2257 A70-28273
- Polycrystalline Al microstrain distribution nonuniformity under creep and static tension
14 p2595 A70-30173
- High temperature elastic moduli in polycrystalline Al rods from propagation velocity of elastic waves generated by Q switched laser [SESA PAPER 1641]
15 p2759 A70-32304
- Flow stress and dislocation density dependence on temperature in polycrystalline molybdenum
16 p2930 A70-33085
- Polycrystalline NaCl-KCl solid solution alloy, considering high temperature creep under constant compression stress
16 p2961 A70-33275
- Dislocation diffusion effects on strength of whiskers and fine grained polycrystals
16 p2934 A70-34327
- Unalloyed polycrystalline Ti fatigue tests, observing cyclic stresses effect on twinning
17 p3116 A70-34393
- Strain gage measurements of elastic properties of Ti sheet alloys, computing polycrystalline properties from single crystal values
17 p3121 A70-34433
- Crack initiation in wrought polycrystalline Be sheet, investigating three point loaded bend fractures of powder and ingot samples by optical and electron microscopy
17 p3122 A70-34551
- Temperature and strain rate effects on polycrystalline Al strength
17 p3124 A70-34655
- Single and polycrystalline indium arsenide preparation methods and quality control
17 p3143 A70-35119
- Electron impact desorption kinetics of ions and neutrals from polycrystalline W surfaces, using cylindrical magnetic spectrometer
18 p3225 A70-36321
- Microstructure effects on magnetic properties of polycrystalline MnZn ferrites with high permeability
19 p3484 A70-37565
- Crystal dislocations and microstructure effects on magnetic properties of polycrystalline MnZn ferrites with high permeability, noting eddy currents role
19 p3484 A70-37566
- Elastic-plastic behavior of fine grained fcc polycrystals based on single crystal slip data, satisfying displacement compatibility, equilibrium condition, etc
19 p3538 A70-37792
- Transparent ceramic armor fabrication using dense polycrystalline magnesia
19 p3437 A70-38422
- Nb single and polycrystalline thermal properties at high temperatures
20 p3648 A70-39639
- Solid bodies statistical creep analysis, assuming macroscopically homogeneous isotropic polycrystallinity
20 p3725 A70-39866
- Polycrystalline aluminas under thermal shock, investigating strength decrease and subcritical crack formation
22 p4059 A70-43413
- Stress-strain curves of polycrystalline metals and composites using single crystal elastoplastic model
24 p4425 A70-45779
- changes in creatine phosphate concentration and lactate/pyruvate ratio
02 p0232 A70-11717
- POLYESTER RESINS**
Unidirectional carbon and glass fiber reinforced polyester resins dynamic characteristics under torsional and flexural vibration, showing damping independence of cyclic stress amplitude
03 p0514 A70-13111
- Tetrabromophthalic anhydride (TBPA) in polyester and epoxy resins, studying fire retardant capabilities by comparative combustion tests
05 p0811 A70-16584
- Polyester resins characteristics, use, properties and manufacturing methods, discussing molded and reinforcing materials
05 p0811 A70-16602
- Compression strength of polyester resin reinforced with hard drawn and softened steel wires, discussing variations from predicted performance
07 p1320 A70-19954
- Flame-resistant trichloromethyl-containing polyester-styrene system, describing curing characteristics at room and higher temperatures
10 p1907 A70-24066
- Photoelastic stress analysis, discussing holographic interferometry for main stresses separation and polyester resins application to birefringence pattern superposition elimination
15 p2815 A70-31809
- Smooth surface polyester premix and sheet molding compound technology applied to reinforced plastics industry
16 p2917 A70-33364
- Reinforced plastic for aircraft parts, investigating low viscosity polyester resins of styrene crosslinking type
20 p3656 A70-40028
- Sources of variability in laboratory carbon arc weathering of light stabilized polyester resin
22 p4059 A70-43080
- POLYESTERS**
Linear aliphatic polyesters unit cell dimensions and crystalline densities
03 p0517 A70-13808
- Burning and degradation mechanism of polyester propellants correlated with mass regression rate dependent on surface temperature
11 p2099 A70-25990
- Gas and environmental temperatures, flow rate and sample geometry effects on limiting oxygen index in acrylonitril-butadiene-styrene copolymer, polystyrene and polyester
13 p2439 A70-29261
- Zero birefringent blend consisting of rigid and flexible polyesters with viscoelastic mechanical and optical response [SESA PAPER 1669]
15 p2765 A70-32318
- High temperature aromatic polyester Ekonol, discussing fabrication, properties and potential applications
21 p3842 A70-41136
- Linear aliphatic polyesters, calculating conformational contribution to heats and entropies of fusion
22 p3981 A70-42501
- Linear aliphatic polyesters melting point, fusion heat and entropy correlations to molecular parameters
22 p3982 A70-42502
- POLYETHER RESINS**
NT POLYMETHYL METHACRYLATE
Glass fiber reinforced polyether composites long time strength under plane stress
07 p1321 A70-20187
- POLYETHYLENES**
Polyethylene and polypropylene mechanical behavior under tensile and compressive loads and subject to hydrostatic pressure, obtaining tensile nominal stress-strain curves for various pressures
03 p0517 A70-14201
- Prestrain effect on waves propagation along slender low density unoriented polyethylene rod, indicating uniform phase velocity change over audio frequency range
07 p1248 A70-19237
- Thermal conductivities of glass reinforced polystyrene and polyethylene plastics measured over range of glass concentrations and sizes
07 p1320 A70-19958
- Polyethylene extended chain crystals melting process via electron microscopy and differential thermal analysis
12 p2258 A70-26896
- Longitudinal waves propagation in polyethylene bar using Boltzmann-Volterra equation, constructing dynamical stress-strain diagrams by viscous-elastic standard body model
12 p2328 A70-28276
- Diluent resins properties for blending with glass fiber reinforced high density polyethylene concentrate
16 p2935 A70-33353
- Mechanical properties of composite materials reinforced with ribbon fibers consisting of stainless steel and polyethylene ionomer resins
16 p2988 A70-33366
- Relative sensitivities of polyethylene shielded net radiometers, noting role of reflective white paint partial covering
18 p3261 A70-37087
- POLYGONIZATION**
Relieving microstrains in Ni powders by cold compaction at room temperature using X ray analysis, discussing polygonization process
01 p0117 A70-10161
- Polygonized and cellular Be structures formation, examining temperature, strain, annealing and material purity effects
15 p2758 A70-32122
- POLYGONS**
NT PARALLELOGRAMS
NT RECTANGLES
NT TRAPEZOIDS
NT TRIANGLES
Linear isothermal response of viscously damped thin homogeneous polygonal plates subjected to uniform dynamic loading, calculating forced solutions by numerical integration
03 p0601 A70-14318
- Optical polygon calibration by interferometric method using He-Ne laser light source
07 p1297 A70-19227
- POLYHEDRONS**
NT OCTAHEDRONS
NT PARALLELEPIPEDS
Duality theorem for complex quadratic programming over polyhedral cones
07 p1238 A70-19356
- Hidden-line determination for computer-drawn polyhedra using edge classification scheme for CRT display applications
09 p1641 A70-22966
- Surface, volume and body center temperature of convex polyhedrons under steady heat transfer
15 p2825 A70-31624
- POLYIMIDE RESINS**
Polyimide resins and composites state of cure determination by thermomechanical analysis (TMA)
11 p2069 A70-25807
- Low dielectric constant quartz-polyimide for radomes, considering curving methods
16 p2936 A70-33368
- Polyimide resin as matrix for glass fabric reinforced laminates
16 p2938 A70-33383
- Graphite fiber reinforced polyimide composites with low void content, high strength and modulus
16 p2938 A70-33384
- High strength graphite fiber reinforced polyimide resin composites fabrication
17 p3127 A70-34560
- Graphite-polyimide composites development for high temperature environments, discussing mechanical properties
19 p3455 A70-38425
- Polyimide resin vacuum thermal decomposition, using mass spectral and differential thermal analysis
21 p3783 A70-42133
- Thermally stable polyimide resins for carbon fiber composites, noting high temperature strength, oxidizing resistance and electrical insulation properties
22 p4058 A70-42478
- POLYIMIDES**
Cable involving woven multiconductor arrangement and aromatic polyimide insulations to connect thermal moon probe with transmitter for temperature measurements on lunar surface
05 p0798 A70-16034
- Polyimide prepreps reinforced with glass, carbon and graphite, describing processing characteristics, properties and applications
17 p3127 A70-35419
- Polyimideazopyrrolone films relative thermophysical properties, noting polymers thermal stability dependence on carbonyl groups percentage
21 p3783 A70-42132
- Book on polyimides covering synthesis and conversion processes, thermal and chemical stability, physical properties and applications
22 p4058 A70-42625
- POLYMER CHEMISTRY**
Ionene polymers, investigating cyclic and linear compounds and reaction products from tetramethyl-diaminoalkanes and dibromoalkanes using NMR, IR and mass spectroscopy
06 p1004 A70-17511
- Dicationic crosslinking agents isolation and characterization and formation of polymers with ionic crosslinks
06 p1004 A70-17512
- Air sample removal from hermetically sealed cavities during studies of toxic gas emanations from polymeric materials
07 p1221 A70-19516
- Gaseous pyrolysis products detection and identification during eruption from polymeric surfaces subjected to flash heating by time of flight mass spectrometer
07 p1319 A70-19887

POLYMER PHYSICS

- Propellants chemistry based on chemically cross-linked binder 07 p1360 A70-19909
- Extended chain polymer crystals temporary superheating before final melting, discussing hexagonal selenium crystals data 11 p2069 A70-25803
- Polymer structure and cross-link density effects on thermal analysis of phenol-formaldehyde polymers pyrolysis products 11 p2069 A70-25804
- Air sample removal from hermetically sealed cavities during studies of toxic gas emanations from polymeric materials 11 p1991 A70-26115
- Epoxide ring reactivity and crosslinking related to adjacent electrophilic and electronegative groups, considering epoxy resin technology 16 p2936 A70-33357
- Aromatic polymers synthesis for good thermal stability, describing single and double stranded chains 21 p3782 A70-42127
- Organic spiro polymers synthesis for thermal stability by condensation of aliphatic spiro tetraamines and aromatic dianhydrides 21 p3782 A70-42128
- Thermal stability of polymers based on aromatic diamines and isomeric dibenzoylbenzenes 21 p3782 A70-42129
- Thermally stable arylsulfonimide polymers incorporating 1, 2-disulfonimide group 21 p3782 A70-42130
- Heterocyclic polymer BBB properties, discussing IR absorption studies of structure 21 p3783 A70-42131
- Polyimide resin vacuum thermal decomposition, using mass spectral and differential thermal analysis 21 p3783 A70-42133
- Aromatic polysulfone thermomechanical behavior by torsional braid analysis, discussing structure, synthesis, thermal stability, radiation effects, etc 21 p3783 A70-42134
- Poly(perfluoroalkylene oxides) preparation and curing, considering molecular weight and thermal stability 21 p3783 A70-42145
- Book on polyimides covering synthesis and conversion processes, thermal and chemical stability, physical properties and applications 22 p4058 A70-42625
- Octadecatic anhydropolymers of amino acids, describing production by thermal condensation, heteropolymerization and panpolymerization 22 p3983 A70-42875
- IR absorption spectra of high-cis forms of deuterated polyisoprenes 23 p4157 A70-44274
- Photoelimination reactions of macromolecules, emphasizing intermediate pathways heuristic description via energy level diagrams 23 p4157 A70-44391
- POLYMER PHYSICS**
- Extended chain crystals of hexagonal Se temporary superheating before final melting, presenting melting equation 01 p0126 A70-10222
- Fluorocarbon polymer coatings, discussing role of fluorine content and carbon bond in chemical inertness, degradation resistance, thermal stability and low surface friction [SAE PAPER 690645] 05 p0868 A70-15842
- Frictional drag reducing polymer solution injection into boundary for turbulent pipe flow, discussing Reynolds number, injection rate, injection points and concentration 06 p1032 A70-17215
- Polyelectrolyte complexes formed from combined water soluble and negatively charged polyelectrolytes 06 p1005 A70-17513
- Long chain molecule additive effect on drag reduction in turbulent flow of aqueous polymeric solutions [ALAA PAPER 70-56] 06 p1037 A70-18030
- Matrix optimization of boron filament reinforced polymers for short duration high temperature aerospace applications 08 p1530 A70-21891
- Raman and IR spectrum analysis of polywater indicating impurities role in anomalous properties 11 p1994 A70-25655
- Viscoelastic polymeric materials tensile failure under multiaxial loading 12 p2321 A70-27205
- Weather effects on plastic properties, discussing weathering interactions with plastics and polymer degradation 12 p2259 A70-27206
- Microdefects as centers of disk shaped destructive cracks in polymer dielectrics under laser irradiation 13 p2437 A70-28621
- Polymer optical properties in terms of interaction matrix coupling monomers, applying to polypeptide alpha helix, beta sheets and polyproline helices 14 p2544 A70-30118
- Long chain molecule additive effect on drag reduction in turbulent flow of aqueous polymeric solutions 17 p3066 A70-34525

- Optical properties of amorphous polymers, considering one state calculations for flexible polypeptides in solution and disordered regions of films or proteins 21 p3780 A70-41702
- Heterocyclic polymer BBB properties, discussing IR absorption studies of structure 21 p3783 A70-42131
- Polymers low temperature relaxation behavior, discussing molecular structure, crystallinity, copolymerization, etc 21 p3844 A70-42135
- Amorphous and partly crystalline polymers low temperature thermal conductivity and heat capacity 21 p3844 A70-42136
- Polyvinyl alkyl ethers multiple transitions at low temperatures, using linear variable differential transformer 21 p3844 A70-42137
- Diluent molecules effect on polymers relaxation behavior at cryogenic temperatures from internal friction measurements, noting loss peaks shift 21 p3844 A70-42138
- Gaseous and liquid fluorine exposure effects on nitroso rubbers at ambient and cryogenic temperatures, using impact tests and IR spectroscopy 21 p3844 A70-42140
- Polymers as cryogenic adhesives, evaluating role of chain structure below glass transition temperature 21 p3783 A70-42142
- Isothermal kinetic rates of polymer swelling and dissolution, using thermomechanical analyzer 22 p4059 A70-43078
- Isothermal kinetic rates of penetration of polymer by spherical indenter, using thermomechanical analyzer 22 p4059 A70-43079
- POLYMERIC FILMS**
- NT MYLAR [TRADEMARK]
- Optical transmission spectra of polypeptide films showing exciton structure near 1600 A for alpha and polyproline II helices 02 p0345 A70-12723
- Plastic film precise perforation using carbon dioxide laser and optical tooling permitting double exposure to laser beam 03 p0497 A70-13565
- Thermoplastic polymers adhesion to glass fibers determined by measuring force necessary to pull fiber from flat film of polymer 06 p1091 A70-17317
- Series emittance thermal control coatings of polymeric dielectric films overlaying reflectors vacuum exposed to UV, X ray and proton radiation [ALAA PAPER 70-64] 06 p1106 A70-18069
- High purity pinhole free films /parylene/ applicability as barrier coating to keep semiconductor surface free from moisture, ions and contaminants 11 p2099 A70-26395
- Polyimidazopyrrolone films relative thermophysical properties, noting polymers thermal stability dependence on carbonyl groups percentage 21 p3783 A70-42132
- POLYMERIZATION**
- NT COPOLYMERIZATION
- NT DIMERIZATION
- Adiabatic calorimeter for exothermic chemical reactions determining heats of polymerization, curing rate and thermal decomposition rates as temperature function for high energy propellants 04 p0688 A70-14711
- Hydrogen sulfide participation in vinyl polymerization investigated for reaction mechanism 05 p0810 A70-16051
- Mechanical methods locking studs, discussing chemical locking based on hardening of resins by polymerization 06 p1076 A70-17437
- Peptide formation by stepwise tetramer-mediated condensation of alpha-amino acid as possible prebiotic process 07 p1204 A70-19202
- Two body collisions reaction mechanisms with small heats of reaction for Be and Al gaseous oxidation, noting low free energy properties of polymerization 10 p1928 A70-24089
- Polymerization reaction kinetics investigated with differential scanning calorimeter at isothermal conditions, determining heat of polymerization 11 p1994 A70-25810
- Methyl methacrylate and other vinyl monomers polymerization activation by low sulfur dioxide concentrations, noting inert solvents effect 14 p2544 A70-30246
- Amino acids asymmetric polymerization on clay minerals, discussing aspartic acid and kaolinite experiments 19 p3455 A70-38030
- Octadecatic anhydropolymers of amino acids, describing production by thermal condensation, heteropolymerization and panpolymerization 22 p3983 A70-42875

POLYMERS

- Temperature-time-variable stress-strain state of polymer structures, solving creep equation by linear model with rheological properties 01 p0211 A70-11426
- Polymers yield criterion determination using Hill method exemplified by polyvinyl chloride, discussing effects of transversal anisotropy and rheological properties 02 p0320 A70-11740
- Polymers development for ablative heat shields, aeroshell structures, antennas, insulators, electronic packaging, etc, to meet Mars and Venus atmospheric entry requirements 02 p0382 A70-12525
- Synthetic polymers properties and processing, discussing thermoplastics, elastomers, thermosets, etc 02 p0322 A70-12715
- Polymers application as engineering materials, discussing properties, physical states, etc 02 p0322 A70-12716
- Integral equation solution in viscoelasticity theory based on creep tests with polymer containing elastic inclusion, improving convergence of approximations method 02 p0390 A70-12801
- Interactions between adhesive polymers and fillers, emphasizing reinforced plastics composites properties [ONERA-TP-733] 03 p0516 A70-13644
- Variable strain bending form design for determining environmental craze resistance of polymers 04 p0713 A70-15375
- High temperature polymers including polybutadiene, polyphenylene sulfide, polysulfone, polybenzimidazole, etc 05 p0869 A70-16038
- Micromechanisms of fracture in metals and polymers before plastic deformation onset, discussing macroscopic polymer properties from microstructure and molecular structure 05 p0937 A70-16365
- Nontoxic method of immobilizing protozoan *Tetrahymena pyriformis* and bacterium *Escherichia coli* in acrylamide polymers, discussing microorganism viability 05 p0802 A70-16477
- Polymers with high temperature oxidation resistance, discussing problems caused by aromatic heterocyclic structures and manufacturing methods 05 p0873 A70-16604
- Pulsed supersonic plasma jets induced surface ablations and cracks in polymers, using X ray and IR analysis 06 p1091 A70-17763
- Crack self healing in aluminum foil-polyvinyl acetate sandwich structures 07 p1315 A70-18713
- Thickening of fluids with tetrafluoroethylene polymer to provide physically and chemically stable grease type lubricants for military applications 07 p1292 A70-18863
- Abrasive wear of polymers subject to plastic and elastic deformation, considering papers, metal gauze and rough metal surfaces 07 p1296 A70-20003
- Dynamic mechanical properties of filled polymers as function of filler concentration, particle agglomeration and ratio of particle to polymer modulus 08 p1527 A70-21335
- Polymeric materials flow at tube entrance, discussing pressure drop and flow birefringent patterns at tapered and sharp entrances 08 p1486 A70-21861
- Volatile toxic products outgassed by polymer construction materials, discussing physico-chemical classification of outgassing reduction methods 09 p1709 A70-22085
- Ammonium perchlorate-polymer mixtures combustion rates with/without cobalt oxide additions, studying ignition temperatures of stable flameless burning 09 p1787 A70-22108
- Temperature field and heat conduction equation for two layer polymer cylinder multiply heated from within, considering material decomposition 10 p1966 A70-23870
- Amorphous polymers thermal conductivity measured at 0.4-4 K, observing similar temperature dependences 10 p1906 A70-23979
- Velocity measurements with Pitot tubes in polymer solutions /polyethylene oxide/ in water, noting viscoelastic properties effect on measured pressure value 10 p1887 A70-24093
- Macrolon elastic-plastic strain model, studying stress-strain relationship and optico-mechanical properties 11 p2128 A70-25385
- Polywater electronic structure model, proposing hydrogen bonds resembling short strong bonds in FHF⁻/ions 11 p1994 A70-25656

Anomalous water /polywater/ dielectric constant and effective parallel conductance, suggesting hydrosol classification

11 p1994 A70-25657

Thermal Analysis - Conference Worcester, Mass., August 1968, Volume 1, Instrumentation, organic materials and polymers

11 p2069 A70-25801

Gruneisen ratios for polymeric materials, comparing values determined by ultrasonic and thermal studies

11 p2069 A70-25805

Polymeric materials thermal degradation kinetic parameters using combined mass spectrometric and thermogravimetric analysis /MS-TGA/

11 p2069 A70-25806

Thermal protection polymers ablator efficiency evaluation using high vacuum DTA cell coupled to high resolution mass spectrometer

11 p2070 A70-25813

Polymer shells lasting stability mathematical simulation, discussing similarity criteria of nonlinearly and hereditarily elastic materials

12 p2259 A70-27528

Hollow homogeneous polymer cylinder thermoelastic stressed state, analyzing radial temperature and Poisson Coefficient variations

12 p2325 A70-27532

Glass- and quartz-fabric reinforced polymers for high temperature microwave insulation, evaluating electrical and thermal aging properties

12 p2259 A70-28149

Polymer-metal adhesive joints rupture characteristics, considering polymer in solid or structurally fluid /elastic/ state during tests

12 p2244 A70-28341

Fracture kinetics model for polymers emphasizing quantum effects even at room temperature

13 p2510 A70-28670

Linear high polymers heat capacity measurements theory emphasizing simple mechanical systems and contribution of lattice vibrations

13 p2438 A70-28997

Teflon and fluoropolymers relative toxicity due to thermal degradation at 370 C, testing carboxy nitroso rubber, Kapton polyimide film, perfluorated polymers, etc

13 p2439 A70-29260

Transparent polymeric materials failure under neodymium-glass laser radiation in free generation mode

13 p2427 A70-29300

Polymer materials fatigue strength and deformability testing in vacuum, air and gas atmospheres at low and high temperatures, subjecting to cyclic loading

13 p2385 A70-29428

Turbulent flow theory of dilute linear polymer solutions in smooth and rough tubes based on Reynolds equation

15 p2719 A70-31491

Macromolecular polymer based heat resistant materials

15 p2765 A70-32264

Zero birefringent blend consisting of rigid and flexible polymers with viscoelastic mechanical and optical response

15 p2765 A70-32318

Volatile toxic products outgassed by polymer construction materials, discussing physico-chemical classification of outgassing reduction methods

15 p2766 A70-32681

Polymeric binders adhesion to glass fibers as function of type and chemical structure

16 p2938 A70-33379

Reinforced polymer composites design for aircraft structures [ASME PAPER 70-DE-67]

16 p2939 A70-33518

Polymeric materials fatigue tests, investigating correlation between crack propagation and stress intensity factor

17 p3127 A70-34624

Structural members of isotropic and anisotropic polymers, investigating creep behavior under simple stressed state

17 p3192 A70-35740

Polymers dynamic properties in hyperelastic and vitreous states as function of temperature, using torsion pendulum method

18 p3263 A70-36469

Polymers industrial applications in textiles, building materials, furniture, aviation, automobile industry and packaging

19 p3455 A70-38700

Thermoresistor parameters of organic semiconductor polymers with conjugated band system, plotting temperature and EV characteristics

20 p3595 A70-38966

Transparent polymers stress-strain state induced by elastic waves, using model with space and time dependence of laser beam

20 p3654 A70-39248

Smoke chamber measurements of opacity developed in polymer pyrolysis or combustion, including Materials Smoke Obscurity Index /MSOI/

20 p3736 A70-39404

Chemical and physical factors effect on smoke evolution from polymers

20 p3736 A70-39405

Toxicity problems from burning or heating of polymeric materials, discussing laboratory experiments and standardized toxicity testing procedures

20 p3579 A70-39406

High strength and stress corrosion resistant materials, considering Ti, Ni, Al alloys, metal-matrix composites and polymers

20 p3655 A70-39666

Polymeric materials yielding and fracture behavior under uniaxial and multiaxial fields, plotting octahedral shear stress

20 p3656 A70-39949

Thermally prepared poly-alpha-amino acids catalytic activity after long term dry state storage, suggesting enzyme activity role in biological evolution

21 p3772 A70-40713

Free vibrating reed apparatus for polymer low temperature internal friction and Young modulus measurements, discussing polystyrene properties

21 p3827 A70-41464

Holographic photopolymer recording systems, discussing sensitivity, reconstruction, fixing, etc

21 p3829 A70-41926

Polymers in space research - ACS Conference, Pasadena, July 1968

21 p3781 A70-42126

Carbon fiber reinforced polymer /CFRP/ failure mechanism, discussing nondestructive testing, destructive and cyclic loads

22 p4058 A70-42476

Dynamic melt properties of polymer blends, using orthogonal rheometer measurements

22 p4058 A70-43076

Dynamic elastic moduli of model two phase continuous composites, using polymer and metallic foams

22 p4059 A70-43077

Cyanoacrylate and anarobic polymer single component adhesives performance

22 p4046 A70-43120

High modulus carbon fibers production and properties describing polymer chains intermolecular structuring by pyrolysis and strength increase by fibers stretching at 2700 C

24 p4366 A70-45166

Polymers strength and stiffness properties, considering different molecular chain alignments as related to elastic modulus

24 p4366 A70-45173

Polymer crystal lattice defects and vacancies diffraction patterns observation and interpretation, using optical transformations

24 p4353 A70-45566

POLYMETHYL METHACRYLATE

Polymethylmethacrylate block breakdown under focused pulsed laser radiation in free emission regime, noting light absorption during crack development

02 p0314 A70-12813

Polymethyl methacrylate fuel for hypersonic air breathing propulsion systems, studying ablation, mixing and combustion processes

03 p0603 A70-12942

Transverse vibration of viscoelastic polymethyl methacrylate column with initial curvature under periodic axial load, determining amplitude- frequency curves

[ASME PAPER 69-WA/APM-13]

04 p0772 A70-14915

Transmission losses of plexiglass radome measured as function of frequency and antenna elevation angle, determining material dielectric constant

06 p1019 A70-17505

Transparent polymethylene methacrylate and polystyrene stressed state effect on failure characteristics under laser beam irradiation

08 p1526 A70-20936

Thermal decomposition of ammonium perchlorate and polymethylmethacrylate mixture thin layer between Ti plates in vacuum

09 p1741 A70-22109

Hypersonic wind tunnel testing of Plexiglas and nylon hemispheres instrumented with strain gages and thermocouples, comparing with calculated strain, temperature and ablation

13 p2520 A70-28727

Teflon and polymethyl methacrylate sublimation breakdown in plasma jets, using electric arc heated argon, nitrogen, air and oxygen

15 p2765 A70-32103

Shock propagation in Al fiber/polyethyl methacrylate composite, calculating pressure, densities, internal energies and particle velocities

17 p3182 A70-34556

Polymethyl methacrylate rupture during omnidirectional compression under laser radiation, showing pressure effect on microdefects and cracks

21 p3841 A70-40644

Polymethyl methacrylate glasses microcracks removal by dry friction

21 p3841 A70-40645

Compressive and rarefaction shock wave propagation in polymethyl methacrylate, fused silica and sapphire, using laser interferometer measurements

22 p4031 A70-43020

Specific heat of amorphous polymethyl methacrylate and polystyrene by pulse method below 4 K, comparing Debye and acoustic values

24 p4367 A70-45598

Fracture mechanics of craze growth of stressed polymethyl methacrylate in methanol

24 p4368 A70-45778

POLYMORPHISM

Polymorphic transformation effects on oxygen diffusion rate in alpha and beta phases of Ti, considering temperature effects and activation energy

04 p0707 A70-15211

Alloying elements effect on polymorphic alpha-beta transformation temperature of Ti systems, discussing heat resistance

07 p1307 A70-19555

Physical metallurgy, discussing metals, intermetallic compounds and polymorphic metals properties, single crystals production, etc

12 p2257 A70-28272

POLYNOMIALS

NT DYADICS

NT HERMITIAN POLYNOMIAL

Linear physical chains with Sturm-Liouville characteristic polynomials used for natural frequency determination of coupled harmonic oscillators or electrical analog

01 p0142 A70-10520

Mass action low-polynomial optimization analogy, illustrating optimal temperature determination in chemical reactors in series

01 p0143 A70-10925

Digital computers for calculating coefficients of electronic circuit functions polynomials, developing algorithm

04 p0659 A70-15205

Exact polynomial solution Saint Venant flexure of pretwisted rectangular plate treated as shallow hyperbolic paraboloidal shell

05 p0928 A70-16056

Algorithm for factorizing polynomials over finite fields usable with computer

05 p0876 A70-16312

Waveform-shaping transfer function rational polynomial approximation method with application to network problem in PCM communications

06 p1007 A70-17459

Finite element method using cubic polynomials over triangle as trial functions for solving second order boundary value problems in linear theory of elasticity

07 p1324 A70-19075

Algebraic criterion for polynomial with complex coefficients having all zeros in certain regions of complex plane

07 p1324 A70-19201

Geopotential fields expansion on 500 mb surface for hemisphere in terms of Chebyshev polynomials along meridian and trigonometric polynomials along latitude

07 p1329 A70-19648

Fourth order polynomial RC-RL decomposition conditions

07 p1326 A70-19686

Orthogonal polynomials in three dimensional contact problems without friction, discussing construction of kernels over finite and semiinfinite intervals

08 p1594 A70-21634

Polynomial force model supplementing reduced gravity model in determining accuracy of near equatorial, near synchronous and near circular satellite orbits

09 p1762 A70-23256

Three stage variable shift iteration algorithm for calculating zeros of polynomial with complex coefficients

09 p1712 A70-23419

Trigonometric interpolation of polynomials by Lagrangian type orthonormal functions, noting satellite geodesy applications

10 p1909 A70-24185

Simultaneous singular integral equations approximate solution in orthogonal polynomials

10 p1909 A70-24603

Asymptotic behavior of polynomial root locus in presence/absence of time lag, outlining procedures for constructing root locus diagrams

10 p1910 A70-24845

Polynomial model of uniform target motion for smoothing and extrapolating coordinates and parameters using independent radar range and velocity readings

10 p1843 A70-25136

Bessel generalized polynomial series convergence and summability on contour of convergence region

11 p2071 A70-25521

Coefficients for finite difference methods of numerical integration of products of Fourier and ordinary polynomials

11 p2074 A70-26848

Dynamic systems absolute stability, optimality and passivity algebraic criterion in terms of real even polynomial coefficients

12 p2261 A70-27412

Liapunov functions construction through conversion of differential equation with polynomial nonlinearities into auxiliary exact differential equation using algorithm

12 p2262 A70-28070

Algorithms based on Newton formula for polynomial interpolation and numerical differentiation

13 p2441 A70-29100

Bifurcation and stability analysis of point mappings with polynomial succession function, using parametric diagrams

13 p2383 A70-29751

Algorithm for improving approximate quadratic factor of polynomial with real coefficients using iterative method

14 p2600 A70-31227

Reduction procedure for determining sign definiteness and semidefiniteness of higher order real polynomials

17 p3129 A70-34954

Hurwitz matrix of real Hurwitzian polynomial, discussing relation between eigenvalues and zeros locations

18 p3279 A70-36062

Polynomial and logic theories of dynamic systems, explaining linear and nonlinear elements of automatic control systems

19 p3392 A70-37447

Ordinary differential equations piecewise polynomial approximation using subpartitioning to liquidate residuals

19 p3458 A70-38356

Elasticity theory equations polynomial solutions for use in boundary value problems

20 p3726 A70-39874

Polynomial tensor functions generated by vector functions in space of invariants, noting applicability to isotropic media

20 p3728 A70-39895

Polynomials with interval coefficients, presenting Newton Raphson algorithm for real roots error bounds

20 p3659 A70-40133

Recursive test for nonnegative polynomials using modified Routh scheme to determine real positive zeros

22 p4063 A70-43332

Linear methods for approximate solutions of ordinary differential equations and Fredholm integral equations by polynomials

23 p4211 A70-44249

Approximations by spline functions and polynomials, discussing modulus of continuity

24 p4369 A70-45126

Necessary and sufficient conditions on coefficients of real nonnegative polynomial p/ω , obtaining algebraic criterion for stability, optimality and passivity of dynamic linear systems

24 p4322 A70-46156

POLYPHENYL ETHER

Sliding wear of bearing Al lubricated with polyphenyl ethers in boundary region tested by pin and cylinder wear machine producing continuous record

05 p0854 A70-15910

POLYPROPYLENE

Glass-reinforced polypropylene for structural applications, investigating time/temperature dependent creep characteristics

01 p0128 A70-10773

Chemically coupled glass-reinforced polypropylene, studying short term physical properties, creep rupture and deformation, dynamic failure, etc

02 p0322 A70-12605

Polyethylene and polypropylene mechanical behavior under tensile and compressive loads and subject to hydrostatic pressure, obtaining tensile nominal stress-strain curves for various pressures

03 p0517 A70-14201

Small angle X ray scattering pattern of polypropylene drawn at various temperatures in closely spaced draw ratio values through neck region

03 p0517 A70-14202

Dynamic compressive properties of polypropylene, polystyrene bead and extruded polystyrene foams tested at given strain rate under room temperature

08 p1527 A70-21329

Polypropylene window proportional counter on board sounding rocket for cosmic soft X ray measurement

15 p2741 A70-32530

POLYSACCHARIDES

NT CELLULOSE

NT GLYCOSENS

UV radiation effects on mucopolysaccharide compounds in tears and on cornea epithelium of albino rabbits

01 p0037 A70-10860

Acid mucopolysaccharides in distal segments of medullary substance of kidneys of rodents under high ambient temperature, showing stable morphological characteristics

07 p1204 A70-19141

Ionizing X radiation influence in lethal and sublethal doses on cerebral hyaluronic acid in mice and guinea pigs

14 p2536 A70-30186

Biochemical heterogeneity of corneal mucopolysaccharides (glycosaminoglycans), using extraction without proteolytic enzymes

24 p4304 A70-46344

POLYSTYRENE

Liquid nitrogen evaporation in PSB foam polystyrene vessels compared with glass vessels for cryogenic application

02 p0305 A70-11875

Polystyrene and polyamide stress relaxation graphs, considering tensile stresses and temperature effects

04 p0712 A70-15101

Light collecting properties of polystyrene scintillator designed for counting particles of electron-photon showers generated by high energy cosmic ray particles

05 p0846 A70-15944

Thermal conductivities of glass reinforced polystyrene and polyethylene plastics measured over range of glass concentrations and sizes

07 p1320 A70-19958

Transparent polymethylene methacrylate and polystyrene stressed state effect on failure characteristics under laser beam irradiation

08 p1526 A70-20936

Dynamic compressive properties of polypropylene, polystyrene bead and extruded polystyrene foams tested at given strain rate under room temperature

08 p1527 A70-21329

Crystallite orientation distribution function refinement procedure, considering application to isotactic polystyrene

09 p1631 A70-23446

Gas and environmental temperatures, flow rate and sample geometry effects on limiting oxygen index in acrylonitril-butadiene-styrene copolymer, polystyrene and polyester

13 p2439 A70-29261

Stress analysis of polystyrene plate weakened by doubly periodic system of equal circular holes

15 p2817 A70-32166

Anthracene, polystyrene and stilbene for scintillation counters measuring cosmic ray protons, analyzing dosimetric properties

17 p3151 A70-35352

Specific heat of amorphous polymethyl methacrylate and polystyrene by pulse method below 4 K, comparing Debye and acoustic values

24 p4367 A70-45598

POLYSULFIDES

Tuned resonant test for measuring damping characteristics of lead and asbestos filled epoxy-polysulfide copolymer

08 p1527 A70-21336

POLYTETRAFLUOROETHYLENE

Polytetrafluoroethylene wear tested by rubbing cylindrical rod flat ends against glass plates, determining sliding contact pressure effects

06 p1077 A70-18403

Sliding friction and wear of polytetrafluoroethylene ball bearing filled with graphite investigated for irradiation effects

06 p1077 A70-18404

Thickening of fluids with tetrafluoroethylene polymer to provide physically and chemically stable grease type lubricants for military applications

07 p1292 A70-18863

Ablation products and high temperature boundary layer chemistry of polytetrafluoroethylene (Teflon) in arc jet streams using mass spectrometer

07 p1319 A70-19886

Stress relaxation in polytetrafluoroethylene (PTFE) at various compression deformations and temperatures, considering residual stresses degree

07 p1321 A70-20228

Silver/polytetrafluoroethylene water-repellant air-breathing cathodes for fuel cells with alkaline electrolytes, discussing pressure compatibility

10 p1829 A70-24454

Concorde engine bay thermal insulation combining stainless steel foil and polytetrafluoroethylene film, considering noise level, engine fire conditions and molten Ti globules penetration

18 p3346 A70-36345

POLYTROPES

Variational approach to structure of rotating polytrope with symmetry about axis of rotation in postNewtonian approximation of general relativity

02 p0338 A70-11778

Relativistic generalized gravity theory, studying polytropic models

09 p1754 A70-22458

Secular stability of rotating polytropes in relative equilibrium, isolating bifurcation point by calculating lowest sectorial modes for various sequences

10 p1937 A70-23946

Synchronous close binary stars primary component structure, using rapidly rotating polytrope method

23 p4250 A70-44816

Solar oblateness calculation based on Stockly differential rotation law application to polytropes

23 p4253 A70-44835

POLYTROPIC PROCESSES

Self similar wave solutions of continuity and momentum equations for two dimensional unsteady isentropic motion of polytropic gas

02 p0278 A70-11998

Radiation effects on polytropic atmosphere convective instability using method of disturbances

09 p1753 A70-22456

POLYURETHANE FOAM

Temperature dependence of diffusion coefficient for carbon dioxide filled rigid polyurethane foam, using Fick law

02 p0321 A70-12524

Foamed-in-place polyurethane for form fitting pilot helmet shock absorbing liner noting medical applications

07 p1218 A70-19015

Fire performance of spray applied rigid urethane foam applied as storage vessel insulation, noting continued functioning until destruction

09 p1710 A70-23345

Rigid fire-retardant polyurethane foams obtained from phosphonopropionate polyols, discussing physical properties and shelf stability tests

10 p1907 A70-24063

Solid and foam polyurethane creep stress, using multiplier for foam stress for comparison

11 p2141 A70-26601

Closed cell polyurethane foam for cryogenic insulation, determining thermal conductivity and net heat flow by analytical model and test

23 p4280 A70-44367

POLYURETHANE RESINS

Airline aircraft finishes for protection against corrosion, air pollution, discussing paint application and polyurethane technology

03 p0497 A70-14053

Polyurethane rubber time- and temperature-dependent visco- and photoviscoelastic coefficients using two dimensional strain and stress wave propagation photoviscoelastic analysis

03 p0599 A70-14243

Paint technology findings and recommendations for airline aircraft surface finishes emphasizing use of polyurethanes

05 p0869 A70-16106

Polyurethane propellant binders burning rate, studying siloxane moiety effects

07 p1358 A70-19330

Polyurethane-based solid rocket propellants, discussing catalyst modification, mix viscosities, moisture embrittlement, etc

07 p1360 A70-19910

Solid and foam polyurethane creep stress, using multiplier for foam stress for comparison

11 p2141 A70-26601

Polyurethane and metal surface layers deformation related during sliding friction in presence of liquid media, noting friction coefficient-deformation relation

12 p2244 A70-28284

Nonaggressive liquid media effect on residual strains and phase transformations initiation and development in polyurethane parts operating in lubricants, discussing wear resistance

13 p2439 A70-29431

Elastic and optical properties of polyurethane rubber under large deformation using natural stress concept derived from stress-strain linear relationship [SESA PAPER 1608]

15 p2821 A70-32319

Extinction pressures of polyurethane propellants increased by presence of AP, AP coated with silane and KP [AIAA PAPER 70-657]

16 p2963 A70-33619

Linear compressibility assumption incorporated into third order multiple integral representation of nonlinear creep of polyurethane, reducing time independent kernel functions

17 p1386 A70-34972

Polyurethane swelling in liquid media, measuring surface orientation effects during chemical machining on stress strain state

20 p3654 A70-39249

Epoxy and polyurethane adhesives stress-strain behavior in lap joints, examining bond thickness and cryogenic temperature effects

21 p3844 A70-42139

Polyurethane adhesives differential thermal analysis, rebound resilience and tensile properties at cryogenic temperatures

21 p3844 A70-42141

Resilience and tensile properties of polyurethane adhesive at cryogenic temperatures measured by differential thermal analysis

23 p4209 A70-44275

POLYVINYL CHLORIDE

Polymers yield criterion determination using Hill method exemplified by polyvinyl chloride, discussing effects of transversal anisotropy and rheological properties

02 p0320 A70-11740

Creep and recovery of polyvinyl chloride reinforced by oriented cotton fibers, considering roles of fiber density and stress magnitude

03 p0516 A70-13499

Polyvinyl chloride plastisol propellants consisting of fine solid oxidizer and powdered metal, discussing composition, propellant flow, curing time and temperature dependence

07 p1360 A70-19908

Thin circular cylindrical polyvinyl chloride plastic shells tested under axial compression and end-shortening conditions for buckling

12 p2324 A70-27473

Polyvinyl chloride sheet steel manufacture, properties and welding methods

22 p4045 A70-42479

Polyvinyl chloride /Novodur/ mechanical properties application to structural model testing

24 p4367 A70-45445

POLYWATER

Polywater properties, discovery and preparation

23 p4150 A70-44224

Venus polywater hydrosphere, discussing vapor phase, surface temperature, evolution, observations and model data

23 p4242 A70-44260

PONDEROMOTIVE FORCES

Ponderomotive meter for laser energy and power measurement, discussing mechanical design and elimination of radiometric and convection disturbances

03 p0500 A70-13481

Laser pulse energy ponderomotive meter using mechanical action exerted by light on movable sapphire plate in air at atmospheric pressure

09 p1700 A70-23657

Ponderomotive forces of plane electromagnetic wave incident at arbitrary angle on metal grating, based on diffraction results

19 p3377 A70-37723

PONTRYAGIN PRINCIPLE

Two point boundary value problem arising from Pontryagin maximum principle application in optimal control, describing solution based on combined existing methods

03 p0460 A70-13699

Pontryagin principle applied to minimum structural weight design problem in optimal control theory with state and control inequality constraints

[ASME PAPER 69-WA/AUT-1] 04 p0769 A70-14832

Law for time variations of modulus-restricted control action at trajectory end, two point boundary value problem solution and use of Pontryagin principle

04 p0661 A70-15011

Terminal states and time specifications influence on optimum control systems, using Pontryagin principle for boundary value problems application

05 p0824 A70-15874

Time-variable constrained control matrix optimization using Pontryagin principle applied to minimal time transfer, payoff and rotation maximization

07 p1247 A70-20024

Pontryagin principle for thin vibrating plates under mixed boundary conditions, examining optimal control

14 p2660 A70-31205

Pontryagin stability criterion interpretation for systems with time delay in parameter plane, using computer oriented method

16 p2882 A70-33046

Optimal control problem solution methods, comparing Euler-Lagrange equations, Pontryagin principle, dynamic programming and invariant imbedding

17 p3057 A70-35589

Noisy stochastic pattern recognition system, determining optimal measurement sequence by discrete Pontryagin maximum principle

18 p3234 A70-36337

Computerized Pontryagin stability analysis of nonlinear multiple delay systems

18 p3235 A70-36477

Pontryagin stability for distributed delay or parameter systems, using Brin criterion

18 p3235 A70-36478

Control error effect on performance index in Pontryagin principle calculation of optimum control

19 p3394 A70-38501

Sufficient condition for optimal control with continuous nonlinearities, using Pontryagin maximum principle

19 p3394 A70-38717

Optimal control problem for plant including dynamics and input constraints parameters treated by calculus of variations and Pontryagin maximum principle

21 p3801 A70-40899

Maximum principle for discrete systems of recurrence equations, applying Pontryagin principle

22 p4073 A70-42696

POPULATION INVERSION

Population inversion induced in middle channel of cascade gas laser, using probability method

01 p0106 A70-10059

He-Ne laser amplifier photon density, bandwidth and gain as functions of inversion and excited Ne atoms density

01 p0114 A70-11357

Atomic configurations population inversions of astrophysical interest, assuming excitation by electron

collisions, solving rate equations for level populations by computer

02 p0341 A70-11794

Steady state inversion coefficient for active substance in quantum paramagnetic amplifier with push-pull pumping determined by nonstationary methods

03 p0455 A70-13088

Supersonic plasma jets studied spectroscopically, determining atomic levels populations, population inversion conditions, electron temperature and concentration distributions, etc

03 p0531 A70-13254

Vibrational relaxation and optimum population inversion of carbon dioxide molecules under unsteady conditions during pulsed electron excitation, discussing laser output increase

03 p0528 A70-13408

Population inversion coefficient as function of optimal impurity concentrations and efficiency of ruby quantum paramagnetic amplifier in 3 cm range

03 p0499 A70-13457

Population inversion distribution effect on resonator losses of Nd-glass laser, showing threshold limits

03 p0500 A70-13527

Superfluorescence losses in large aperture disk laser systems using Monte Carlo method, determining maximum population inversion from enhanced photon flux density considerations

03 p0503 A70-14209

Pulsed Ar ion lasers at high currents, measuring plasma parameters, electrical conductivity, electron temperature and density for inversion mechanism

04 p0703 A70-15617

Operational characteristics, spectroscopy and inversion mechanisms of noble gas ion lasers in light of plasma theories and atomic data

[AIAA PAPER 70-82] 06 p1083 A70-18236

Unified model for pulsars involving electron population inversion and laser type transition

07 p1375 A70-18893

Argon ion CW lasers, discussing design, inverse population, plasma, radiative transition probabilities, pumping, frequency spectra and active medium

07 p1298 A70-19642

Upper cesium levels population inversion during cesium discharge plasma decay

08 p1550 A70-20848

Neodymium-glass laser under action of electron beam investigated for population inversion

08 p1512 A70-21204

Population inversion in neodymium glass impurities in four level laser dependent on electron beam intensity and energy

08 p1512 A70-21205

He-Ne laser investigated for He and Ne population inversion as function of discharge parameters

09 p1694 A70-22006

Mode coupling and intensity pulsations observed between two 6328 A He-Ne lasers through nonlinear gain characteristics of inverted population

09 p1699 A70-23363

Population inversion generation through gaseous oxides mixing with nitrogen flow thermally excited

09 p1700 A70-23569

Molecular densities and population inversion pulse shape in working gas in mixture with thermally excited auxiliary gas

10 p1920 A70-25112

Population inversions in rapidly expanded flows of nonequilibrium gases, discussing kinetic processes in cooled mixtures of shock heated nitrogen and carbon dioxide

11 p2041 A70-26572

Population inversion effect on angular divergence of neodymium glass laser radiation, observing energy independence for refractive index of medium surrounding active rod

12 p2250 A70-28154

Q switched CO-HE laser IR fluorescence, considering population inversion recovery by vibrational energy transfer

13 p2423 A70-28496

Energy resonances between laser levels of carbon dioxide and diatomic and triatomic molecular impurity species, discussing population inversion due to superelastic collisions

13 p2425 A70-28622

Carbon dioxide molecular vibrational energy levels above carbon monoxide-oxygen premixed flame, discussing vibration modes leading to population inversion and relaxation time variance

13 p2455 A70-29132

HF and DF continuous chemical lasers output power, obtaining population inversion by deuterium molecules diffusion into F atoms supersonic free jet

14 p2593 A70-30273

Chemical energy conversion in lasers, discussing vibrational inversions in diatomic and multiatomic molecules and chain reactions

16 p2927 A70-33233

Helium to electron excitation ratios for population inversion in helium-neon laser

19 p3445 A70-37758

Argon ion laser inversion saturation at large current densities due to upper working levels depletion

19 p3449 A70-38744

Convergent-divergent nonequilibrium nozzle flow numerical solution by time dependent technique, investigating rapid vibrational nonequilibrium supersonic expansion of gas mixture with population inversion

20 p3609 A70-39655

Metastable excitation levels in np/4 configuration for population inversion, discussing free electron collisions, forbidden line intensity and flow density pressure

20 p3642 A70-39751

Gas and semiconductor diode lasers construction and operation principles, discussing terminology, Boltzmann distribution function, excitation methods, population inversion, etc

20 p3643 A70-40535

Carbon monoxide vibrational population inversion in product molecule produced in free burning carbon disulfide/oxygen flame

21 p3950 A70-41708

Lasing transitions time delay in carbon monoxide laser under pulsed electrical excitation, attributing inversion to anharmonic decoupling

22 p4048 A70-42330

Approximate lasing condition from coupled rate and radiative transfer equations, determining population, energy density and power output

22 p4050 A70-43006

CW chemical lasers operation from partially inverted transitions of HCl, HF and DF molecules in subsonic flow

22 p4050 A70-43008

Al-27 NMR saturation effects on ruby electron cross relaxation and inversion

23 p4230 A70-43932

Flow-through carbon dioxide lasers population inversion relation to individual gas components and electron velocity distribution functions

24 p4352 A70-45458

POPULATIONS

Ar ion laser with high discharge current density observed for working level populations by simultaneously measuring power gain and spontaneous emission lines intensity

01 p0106 A70-10063

Slitless spectrograms of chromosphere obtained during 1962 eclipse to determine H level populations decrements, self absorption in Balmer lines and chromosphere model

01 p0175 A70-10245

Rotational temperature of molecular nitrogen Vegard-Kaplan bands determined from auroral spectra, including variations in vibrational levels populations

[AFCLR-69-0542] 01 p0076 A70-10873

Inter census population estimate by air photos, topographic maps and local and state census of population and housing

10 p1878 A70-24737

Census analysis and population data acquisition using aerial photography

14 p2576 A70-30978

Carbon monoxide-nitrogen system vibrational distribution of populations and kinetics in fundamental and harmonic regions, investigating vibroluminescence

21 p3837 A70-41718

PORES

U POROSITY

POROSITY

Rhenium powder sintering activated by palladium additions producing low porosity

01 p0117 A70-10158

Hydrogen, oxygen and nitrogen effects on gas shielded arc weld porosity of Ni, comparing MIG and TIG processes

02 p0310 A70-12543

Porosity in graphitized polycarbylonitrile-based carbon fibers determined from surface area increase during heat treatment in vacuum

04 p0711 A70-14400

Pyrolysis effect on infinite slab subjected to front heat flux, attributing increased porosity to mass loss

[WSCI PAPER 69-27] 06 p1178 A70-17978

Normal shock waves produced in argon and helium flow by holder with variable downstream porosity, measuring DC moments, component velocities and density

06 p1051 A70-18342

Prestrain effect on cavity formation at grain boundaries causing creep strength decrease

07 p1307 A70-19392

Mold canting effects on nonporosity of Al alloys flat castings noting decreased metal losses

08 p1517 A70-21134

Porosity formation in Al ingots made by semicontinuous casting, considering metal grade and purity, gas content and homogenization conditions

08 p1505 A70-21136

Weld porosity in TIG welding of technical Ni in ternary mixtures of Ar with H, O and N

08 p1518 A70-21345

Al weld metal compositions and hydrogen content effects on weld porosity, locating hydrogen in weld by radioactive tracers

08 p1507 A70-21485

Porosity and intergranular crack formation in tungsten fusion welds using electron fractography

11 p2059 A70-25666

Metals purity, gas content and porosity effects on nature and size of material zone affected by laser beam treatment

12 p2250 A70-28219

Early Precambrian chert porosity and permeability, investigating hydrocarbon content origin

13 p2400 A70-29863

Hydrogen oxygen fuel cells, demonstrating matching of power source and load, charge transfer, porosity, Nernst equation and electrochemical water synthesis

14 p2533 A70-30533

Argon-arc welds porosity mechanism in Ti welding

17 p3098 A70-34443

Effective pores size, volume and surface area in refractory materials, using impregnation rate measurement

18 p3277 A70-36467

Graphite modulus of elasticity as function of temperature, considering effects of moisture content in pores

18 p3278 A70-36470

Porosity effects on mechanical properties of high strength Al alloy weldments

18 p3265 A70-37204

Porosity effects on mechanical properties of Al alloy gas tungsten arc welds, noting strength loss proportional to cross sectional area loss

18 p3265 A70-37205

Porous matrix explosions during sublimation of dusty ice with nonvolatile particles

19 p3471 A70-37659

Metals purity, gas content and porosity effects on nature and size of material zone affected by laser beam treatment

20 p3643 A70-40094

Gas porosity in fusion welds of chemical vapor deposited W, noting formation of microfissures due to pore linkup

22 p4046 A70-43149

POROUS BOUNDARY LAYER CONTROL

Steady convective motions in horizontal fluid layer bounded by porous walls of various temperatures at supercritical Rayleigh numbers, noting nonlinear convection equations

04 p0673 A70-15237

Variational problem of determining optimal heat transfer from gas flow to porous plate boundary layer

08 p1597 A70-21176

Two layer model of burning in turbulent boundary layer on porous surface for carbon monoxide oxidation reaction

18 p3346 A70-36268

Steady incompressible turbulent boundary layer form on permeable curvilinear surface with uniform suction, assuming small pressure gradients

22 p4011 A70-42803

POROUS MATERIALS

Heat transfer coefficients for mesh simulating porous parachute cloth, measuring Nusselt number as function of sonic Reynolds number

01 p0004 A70-10292

Rarefied gas flow through ultrafine porous filtering media used to predict flow rate

04 p0666 A70-14755

Graphite foam reinforced by carbonized high polymers used for fabricating highly porous heat and corrosion resistant material

04 p0712 A70-15178

Low temperature oxide film effect on porous titanium carbide impregnation by liquid steel

07 p1311 A70-19805

Steel balls impact on polyurethane foam, porous rubber and fiber materials, noting effects on both pellets and targets

09 p1769 A70-22123

Massive blowing from porous cone with embedded shock wave in supersonic flow, assuming inviscid and conical injected flow field

09 p1662 A70-23216

Titanium sponge secondary structure obtained by magnesiothermal reduction of concentrated Ti-containing chloride melts, discussing temperature effect on porosity

09 p1709 A70-23783

Molecular, viscomolecular and laminar gas flows in tubes and porous bodies at low pressures

10 p1869 A70-24287

Hydrogen oxygen fuel cells with porous electrodes based on Elofflux principle, discussing diaphragms, electrolyte flow and heat removal

10 p1830 A70-24464

Catalytic load carrying capacity of porous carbon electrodes impregnated with nickel salt and nickel boride in anodic fuel cell hydrazine oxidation

10 p1831 A70-24469

Fuel cell electrolytes, describing porous tungsten carbide as catalyst

12 p2164 A70-27068

Porous hydrogen electrode performance with Ni skeleton catalyst, studying effects of temperature, active layer thickness, etc

12 p2182 A70-27759

Transpiration-cooled systems design with porous materials, considering mechanical and flow control/permeability/properties requirements

12 p2256 A70-27822

Inviscid, incompressible superposed fluids stability in presence of inhomogeneous porous media, noting motion with decaying amplitude

14 p2577 A70-30993

Marginal fluid flow stability in porous media taking into account inhomogeneity created by temperature

14 p2577 A70-31000

Erosion damage of porous sintered Fe in water or oil in test device with disk rotating near sample surface, noting relationship to metal fatigue

14 p2592 A70-31272

Carbon-graphite porous materials thermal conductivity at various temperatures

15 p2765 A70-32141

Human skull porous dipole layer shear and compressive properties, measuring static and dynamic strain rates

15 p2683 A70-32308

Flow dynamic lubrication equation for porous bearings under radial load with undefined axial dimension

15 p2745 A70-32442

Test stand based on Froude pendulum for measuring friction coefficients and oscillation parameters of porous bushings

16 p2924 A70-34298

Viscous fluid motion equations through anisotropic nonrigid porous solid, discussing blood flow in capillary vessels and extracellular fluid through interstitial space

21 p3768 A70-40776

Heat transfer in closed partially liquid filled steady state porous systems, testing linear flux force equation validity

21 p3952 A70-42081

Porous media MHD equations for general case, considering magnetized sphere surrounded by homogeneous envelope

24 p4384 A70-45367

Sodiumaluminumborosilicate fiber formation and extraction by leaching, obtaining high aluminate content temperature resistant porous fiber and insulation material

24 p4367 A70-45480

Jet engine noise propagation near porous surface, predicting anomalous LF dip from direct and reflected waves interference with phase delay

24 p4395 A70-46068

POROUS PLATES

Unsteady heat transfer from porous flat plate with impulsive motion and rising temperature, analyzing compressible boundary layer equations using Laplace transform

01 p0067 A70-11390

MHD laminar flow between parallel porous disks for large suction Reynolds number, solving equations of motion with singular perturbation technique

03 p0469 A70-14181

Hydromagnetic flow of viscous incompressible electrically conducting fluid near accelerated infinite porous flat plate with variable suction or injection

04 p0672 A70-15095

Transient one dimensional heat transfer analysis demonstrating infiltrant melting effect on self heat-releasing porous metal composite during surface melt layer formation

04 p0709 A70-15414

Fillers effect on thermal conductivity in porous cermet elements, investigating powdered Ti plates with air replaced by Hg, benzene, ethanol, ether and water vapor

05 p0957 A70-16291

Turbulent incompressible boundary layer on porous heat insulated plate with uniform suction, calculating ratio of friction drag coefficients

07 p1254 A70-19082

Boundary layers calculation for nonporous surface extended to porous with suction by replacing velocity distribution with longitudinal pressure gradient

07 p1254 A70-19083

Oscillatory flow in porous channel with suction and injection, using Laplace transform technique

13 p2389 A70-29538

Boundary layer retarded flow past porous surface with suction, using Runge-Kutta computerized integration of Falkner-Scan equation

15 p2720 A70-31586

Viscous incompressible fluid nonstationary flow boundary layer extension around porous plate at Prandtl number equal to unity

15 p2722 A70-32873

Inviscid film flow by fluid injection through bounding surface, considering porous plate inclination and power law injection rates

16 p2895 A70-34241

Unsteady laminar boundary layers on infinite porous plate, considering radiative heat transfer and transpiration cooling

17 p3067 A70-34632

Hydrodynamic entry length for laminar flow between parallel porous plates, using finite difference theory for flow equations

17 p3069 A70-34983

Elastoviscous incompressible electrically conducting oscillating free stream flow along infinite porous plate with suction in transverse magnetic field

20 p3685 A70-40508

Nonparallel viscous incompressible fluid flows in channel between parallel porous plates with suction and blowing respectively, calculating stability by numerical solution

21 p3811 A70-42216

Oscillating viscous conducting fluid laminar flow between parallel nonconducting infinite porous flat plates under suction in transverse magnetic field

24 p4383 A70-45146

POROUS WALLS

Fuel injections into supersonic air stream through isolated normal ports and porous wall, using interferometry, schlieren and high speed photography

02 p0354 A70-12044

Aerodynamic performance of cascade of porous gas turbine blades with cooling air effusion compared with solid noneffusing blades

02 p0355 A70-12311

Boundary layer calculation for semiinfinite plane turbulent jet on porous wall

02 p0287 A70-12691

Liquid heating in thin walled porous shells under various boundary conditions, deriving formulas for temperature fields

03 p0604 A70-13208

Porous wall material entrainment in turbulent boundary layer during supplementary inert gas injection, including nonisothermicity effects in heat and mass transfer equations

03 p0440 A70-13385

Mean volume heat transfer coefficient, mean thermal head and coolant temperature determined for gas flowing through porous wall with internal heat source

03 p0605 A70-13474

Flow stability of plane channel formed by incompressible viscous fluid injection through porous parallel walls

04 p0673 A70-15238

Heat and mass transfer in reacting laminar boundary layer over porous cylinder with propane injection in wind tunnel experiments

05 p0956 A70-16289

Flow characteristics of curved porous wall gas core reactors for nuclear rocket engines, visualizing simulated fuel flow with air-smoke combination

06 p1104 A70-17509

Turbulent boundary layers and wall jets development investigated for effect of mass injection through porous smooth and rough surfaces

06 p1034 A70-17679

Local heat transfer coefficients determined from temperature distribution on porous walls, deriving mathematical expressions for various surface geometries and transfer modes

06 p1184 A70-18555

Interference between body and porous walls of water tunnels by one dimensional solution for usable length of tunnel

07 p1248 A70-19078

Unsteady laminar boundary layers calculation for arbitrary velocity distributions at inner boundary in presence of suction/blowing through porous surface

07 p1254 A70-19080

Suction effect on thin film laminar flow past vertical wall, obtaining approximate solution for small porosity in accelerated region

08 p1484 A70-21309

Viscoelastic fluid steady flow in porous walled channel, examining mass flow solution continuity

08 p1485 A70-21639

Unsteady free convection laminar power-law fluid flow past porous vertical wall, studying similarity solution dependence on wall temperature and suction

08 p1486 A70-21765

Turbulent heat transfer in boundary layer at inlet of porous tube under nonisothermal conditions, studying velocity variations

09 p1787 A70-22169

Drag on sharp cones in hypersonic flow, studying effects of intense transverse mass injection through porous walls

09 p1603 A70-22441

Laminar boundary layer parameters on porous surface in presence of pressure gradient obtained for inner/wall/and outer regions

09 p1664 A70-23712

Externally pressurized porous journal gas bearings with solid sleeve parts for reducing porous media waviness and roughness effects

10 p1896 A70-25097

Two dimensional viscous incompressible conducting fluid flow between parallel porous walls in magnetic field, studying skin friction fluctuations
12 p2209 A70-27157

Transverse flow convective instability spectrum in vertical channel with porous walls, noting Peclet number effects
12 p2333 A70-28199

Ideal weightless fluid plane potential flow in channel with permeable wall, deriving expressions for dynamic characteristics
13 p2390 A70-29648

Inflow and pressure difference for mean flow in straight suction duct with porous walls, using elementary momentum analysis
13 p2392 A70-30020

Thermal boundary layer and heat and mass transfer at porous horizontal heated surface in presence of free convection, considering blowing and suction effects
15 p2827 A70-32133

Heat exchange in dissociating partly ionized gas flow over critical point on permeable surface with injection into laminar boundary layer
17 p3011 A70-35347

Turbulent boundary layer on porous surface with fluid injection into layer reexamined for causes of discrepancy with experimental results
17 p3072 A70-35547

Curved porous wall channels for noise suppression in power plants, ventilation systems, etc
18 p3216 A70-36302

Laminar flows with surface injection, calculating thermal boundary layer-porous wall coupling effects [ASME PAPER 70-GT-1]
18 p3243 A70-36860

Unsteady flow and heat transfer in viscous incompressible fluid due to infinite porous cylinder oscillations about axis with suction at surface
19 p3406 A70-38445

Unsteady viscous flow of incompressible fluid through porous straight channel under time varying pressure gradient, determining suction and injection effects
20 p3609 A70-39670

Divergent channel with porous walls, calculating effect of suction on laminar incompressible boundary layer by Runge-Kutta method
20 p3609 A70-39671

Transonic wind tunnel porous walls, investigating interference effects and aerodynamic characteristics
22 p3958 A70-42337

Transpiration cooling of porous constrictor walls of high intensity electric arc in plasma [ASME PAPER 70-HT-35]
22 p4122 A70-42432

Shock wave damping by perforated walls in gas channel, visualizing curved fronts with 24-spark HF camera [SMPT PREPRINT 104]
22 p4032 A70-43031

Porous tube inlet region, calculating fluid injection effect on laminar flow from integral form boundary layer equations
24 p4326 A70-45782

Temperature profiles for viscous fluid contained between two concentric rotating porous cylinders
24 p4327 A70-46005

Viscous flow stability between two concentric rotating porous cylinders, calculating critical Taylor numbers for wave numbers and velocity ratios
24 p4328 A70-46366

PORPHYRINS
NT CHLOROPHYLLS
Porphyrin in Fig Tree shale and Onverwacht chert from Swaziland System sediments, noting age of three billion years and importance in abiogenesis research
01 p0070 A70-10327

Gas chromatography and mass spectrometry applied to porphyrin microanalysis, studying homologous porphyrin series in ancient sediments and oils
02 p0252 A70-12516

Heme catabolism in untreated rats and in animals treated with phenobarbital or porphyrogenic drug, comparing bilirubin and Co production
20 p3583 A70-40450

Apollo 11 lunar fines porphyrin-like pigments content demonstrated by fluorescence spectrometry and analytical demetallation, suggesting rocket exhaust source
21 p3910 A70-41266

Organic solvent extracts of Apollo 11 bulk fine sample examined for porphyrins using spectrofluometry
21 p3780 A70-41635

Heme biosynthesis defect in vitamin E-deficient rats affecting bone marrow synthesis of delta-aminolevulinic acid and liver formation of porphobilinogen
24 p4304 A70-46146

PORTABLE EQUIPMENT
Transportable telemetry acquisition system (TTAS)/as mobile tracker featuring pseudomonopulse method
01 p0045 A70-11120

Ultrasonic wheel-type portable inspection device with internal coupling immersion fluid contained in silicone tier, allowing angle beam inspection without temperature correction
01 p0105 A70-11396

PKR portable xeroradiographic defectoscope for nondestructive testing of steel and Al alloys
02 p0301 A70-12486

Portable megaohmmeter for measuring insulation resistance of strain gauge ceramic installations
05 p0848 A70-16378

Portable unit for collection and analysis of toxic gas contaminants in enclosed aircraft and spacecraft cabin atmospheres
07 p1224 A70-20222

Portable optical communcator for voice transmission combining pulse position modulation and low power gallium arsenide diode
10 p1840 A70-24530

Portable low cost shearing interferometer for plasma and flow analysis and instruction aid
12 p2235 A70-27754

Preflight medical examination of flying personnel, describing portable device for recording systolic/diastolic pressure, body temperature and pulse rates
13 p2357 A70-29296

Portable autonomous EEG analyzer for processing brain biopotentials without use of computer hardware and qualified personnel
13 p2360 A70-29522

Portable MOS memory module with optical loading and electrical readout, using hybrid array of complementary silicon on sapphire chips
16 p2868 A70-33457

Ground based photographic experiments using portable equipment during 7 March 1970 solar eclipse in North Carolina
16 p2977 A70-33840

Lunar surface radiative balance and thermal environment measurement by portable meteorological station, considering lunar environment peculiarities for instruments design
19 p3514 A70-37631

Portable catapult and arresting gear analog instrumentation data acquisition system testing aboard aircraft carriers and at land-based facilities
19 p3384 A70-38533

Portable telescope for river and ocean vessels, discussing design and operation thermal stability and hermetization
20 p3629 A70-39311

Portable battery operated system for rapid measurements of blood plasma electrolytes during aeromedical evacuation
20 p3579 A70-39433

Transportable earth station for satellite communications system, describing antenna design and transportation modes
21 p3798 A70-41344

Batteries and fuel cells as portable and transportable electrochemical power sources
24 p4295 A70-46399

PORTABLE LIFE SUPPORT SYSTEMS
Open loop portable life support system containing light breathing vest within space suit
05 p0806 A70-16123

PORTS [OPENINGS]
Interferograms of window wave front deformations to measure angular deviations to line of sight
15 p2737 A70-32038

Perturbation method for stress-strain state of circular cylindrical shell with large curvilinear hole
20 p3734 A70-40442

POSITION [LOCATION]
NT SOLAR POSITION
Omega position location experiment applied to ship navigation, air traffic control and moving vehicle surveillance, noting daytime and night fixing accuracy
01 p0136 A70-10307

Pulsar PP 0943 properties, giving period, pulse characteristics and position
01 p0177 A70-10343

Spacecraft orientation from onboard stellar photographs, calculating absolute and relative elements, accuracy and camera parameters
01 p0198 A70-11512

Receiving station geodetic coordinates computed from Doppler curves of artificial satellite, using method of differential corrections
02 p0254 A70-11757

Stellar objects position accuracy with respect to reference stars improved by applying differential corrections methods to optical center coordinates of stellar photographs
02 p0362 A70-11759

Satellite tracking at several stations at synchronized time to obtain satellite positions, station coordinates and to improve orbital elements accuracy
02 p0254 A70-11760

Position determination for faint radio sources close to intense sources from radio astronomical maps
02 p0370 A70-12113

Position bound determination for objects ejected from space vehicle relative to vehicle trajectory position
03 p0562 A70-12932

Optical position estimation model based on defining photon density profile center of gravity in noise, using photon Poisson process theory
04 p0652 A70-15337

POSITION [LOCATION]
Reconnaissance uncertainty effect on precision of return to fixed point applied to circular error probable, drms calculations and Loran
04 p0652 A70-15345

Head movement effect on accuracy of visual and kinesthetic localization for free and fixed head conditions
05 p0803 A70-16669

X ray source position determination by balloon observations, estimating intensity in different energy ranges
05 p0904 A70-16978

Individual extensive air showers axes localized by measurement of charged particle densities, assuming age parameter
07 p1365 A70-18777

Flux deusities and positions for Southern Milky Way sources at 1410 MHz, determining spectral indexes
07 p1387 A70-19682

Position determination for compact radio sources in 3C catalog
08 p1577 A70-21490

Positions measurement for 4C radio sources between declinations of 4 and 20 degrees, noting RMS errors
08 p1577 A70-21533

Gradient method applied to onboard analysis of astronavigational bearings of spacecraft
09 p1719 A70-22165

Omega Position Location Experiment with synchronous satellite [ATS-3] as radio relay for merchant shipping, air traffic control and moving vehicle location and communication
09 p1720 A70-22193

Position determination from simultaneous observation of Paegeos and Geos 2 satellites, assuming known covariance matrix and applied corrections
09 p1754 A70-22499

Celestial positions and intensities of X ray sources in Sagittarius region obtained from rocket experiment
09 p1744 A70-22522

Orbit determination from two position vectors and periaipsis radius, introducing polar equation for conic to obtain solution
09 p1760 A70-22932

Satellite potential for long range air traffic control, discussing airline navigation requirements and ATC requirements for position determination
09 p1722 A70-23027

Reference ellipsoids mutual positions determination from observational data by satellites using triangulation points of two triangulations
09 p1763 A70-23327

Instrument localizing-resolving powers relationship as function of luminous source coherence
10 p1898 A70-23911

Stars identification on photographic plates and position computation in FORTRAN, using CONTROL DATA 6600 and IBM 1130 computers
11 p2113 A70-26183

Celestial object position determination, computing local errors for coordinate improvement
11 p2113 A70-26189

Satellite coordinates estimation precision by comparing artificial satellite positions obtained simultaneously by photographic cameras
11 p2008 A70-26199

Icarus asteroid positions, UBV magnitude, brightness, colors, light curves and polarization, noting stony-iron composition
11 p2113 A70-26470

Ring micrometer radius determination and application to right ascension changes in determining positions of comets, planets and planetary moons
11 p2057 A70-26675

Vertical tilt and horizontal position of antenna rotating device in radio astronomy and radar observations using photogrammetric methods
12 p2195 A70-27478

Lunar far side features position from Apollo 8 data, evaluating Apollo navigation system accuracy
12 p2309 A70-27949

Molonglo pulsars observations, using multiperiod integration technique for declinations, periods and positions
13 p2487 A70-28632

Radio sources positions on solar disk by 2800 and 408 MHz high resolution fan beams
13 p2491 A70-29161

SOFAR /sound fixing and ranging/ systems for location and recovery of reentry vehicles and missile cases and rescue of disabled transoceanic aircraft
13 p2449 A70-29169

Electronically lobed direction finder homing system for location and rescue of airmen downed on aircraft with emergency locator transmitter
13 p2449 A70-29170

Auroral oval position with trapping region phi s boundary compared with closed geomagnetic field lines phi c, using Alouette 2 satellite data
13 p2398 A70-29229

Extratropical planetary high altitude frontal zones statistical analysis and position forecasting by eigenfunction expansion

13 p2445 A70-29673

Latitude determination from observations of pairs of bright stars at equal altitudes, using computer ephemeris calculations

14 p2633 A70-30142

Satellite position fixing based on electromagnetic angle measurements from observation station, using least squares method

14 p2612 A70-30187

Free floating balloon position and velocity determination by satellite, using Kalman filter linear estimation theory

14 p2530 A70-30571

Soviet book on physical libration constants of moon based on visual and photographic observations of two craters by position angle method

14 p2642 A70-30959

Tabulation of minor planets positions observed by photographic equatorial at Bordeaux observatory

14 p2649 A70-31124

Tabulations of minor planets positions photographed at Besancon observatory

14 p2649 A70-31125

Balloon localization with transponder system, measuring payload distance by phase difference in ground transmitted and received CW signal

14 p2588 A70-31308

Statistical analysis of photogrammetrically surveyed three dimensional space points sets for aerospace vehicles and projectiles position location

15 p2733 A70-31550

Solar coronal streamers, considering disk locations, evolution, classification and morphological model

15 p2804 A70-32621

Radio source 3C279 position during October 1969 occultation by sun, determining SHF deflection in solar gravitational field

16 p2972 A70-33049

Position determination by range change method /RCM/, using pseudonoise modulated line of sight and one way ranging

16 p2948 A70-33453

Variable radio source linear polarization at 8 GHz, examining degree, position angle and flux density

18 p3317 A70-37001

Lunar limb tabular position angles accuracy, discussing Watt charts used for star occultation examination

18 p3321 A70-37124

Scorpid shower radiants measurement, discussing position, activity, physical properties and genetic relation with comet 1770 I

19 p3526 A70-38791

Position and velocity of geodetic drag free satellite in near circular orbit, including lunar-solar gravitational effects and zonal and tesseral harmonics

[AIAA PAPER 70-1054] 19 p3528 A70-38869

Second order approximations to velocity required concept for boundary value problems in guidance, deriving Riccati equation and position required concept

[AIAA PAPER 70-1015] 20 p3666 A70-39518

Cyg-X-1 X ray source angular size and position measurements by balloon-borne collimator

21 p3873 A70-40665

Position finding and navigation in space, air and sea - Conference, Hamburg, October 1969, Volume 1

21 p3847 A70-41126

Photographic determination of star positions at closed block plate adjustment, considering accuracy expectancy

21 p3889 A70-41146

Two dimensional position measurements of harmonic type 2 solar bursts, using 80 MHz observations

21 p3891 A70-41180

Detonation front position determination in explosive by photoelectric technique

22 p4121 A70-42341

Position experiments for navigation satellite system parameters determination, using satellite ATS-3 distance measurements

22 p4066 A70-42653

Nautical loci of constant azimuth of artificial satellite at corridor height in circular orbit at arbitrary inclination, using gyroscope and radio sextant

22 p4068 A70-42664

Aeolus A satellite for position fixing and automatic meteorological signal transmission in link with balloons for tropospheric observation

22 p4068 A70-42665

Thunderstorm frequencies related to lunar phase and declination for ground stations in eastern and central U.S.

22 p4018 A70-42909

X ray sources celestial positions in Sagittarius region, using rocket-borne rotating modulation collimator

22 p4094 A70-42928

Position finding and navigation in space, air and at sea - Conference, Hamburg, October 1969, Volume 2

23 p4162 A70-44227

Position fixing by distance measuring to geostationary satellites, discussing ATS-3 and ship experiment accuracy and orbit interference

23 p4215 A70-44232

Precise radio source positions from independent interferometer measurements in UK and U.S.

23 p4253 A70-44867

Minor planets, comets and natural satellites positions and motions, discussing orbit and ephemerides calculation, Icarus asteroid, etc

23 p4256 A70-45038

Position tracking of SOMEX superpressure balloons by solar angle method

24 p4372 A70-45423

Position experiments for navigation satellite parameters system using ATS-3 distance measurements

24 p4374 A70-46201

Stability solution of nonlinear differential equations in position determination on earth by inertial navigation

24 p4374 A70-46202

POSITION ERRORS

Precision and accuracy evaluation of convergence angles for measuring vertical and horizontal components of space position applicable to geodesy and flight measurement

[AAS PAPER 69-605] 04 p0676 A70-14634

Simultaneous maximum likelihood estimation and coordinate conversion for redundant hyperbolic lines of position in radio navigation

[AIAA PAPER 68-888] 04 p0717 A70-15545

Earth-ionosphere waveguide propagation variations effects on Omega navigation system position errors

08 p1541 A70-21564

Stars photographic position determination errors with NAFA-3C/25 camera, comparing films and plates

09 p1673 A70-22164

Hyperbolic navigation systems circular fixes derivation error analysis

09 p1719 A70-22191

Loran in range-range mode for computing user position based on remote clock synchronization, evaluating accuracy

09 p1719 A70-22192

ELDO rocket tracking error, considering guidance antenna angular precision and UHF circuit performance in signal comparison

09 p1720 A70-22649

Geodetic satellite positional problems taking into account parallax refraction

09 p1765 A70-22653

Error analysis of position finding techniques using analytical model composed of equations describing position error differential relationships

09 p1724 A70-23045

Schmidt photographs reduction, noting film bending during exposure and mean error of satellite position

11 p2007 A70-26195

Satellites photographic positions accuracy compared with stars based on stellar coordinates, investigating causes of difference

11 p2008 A70-26198

Multiple user satellite system for air navigation and traffic control, presenting comparative error analyses for position determination by spherical and hyperbolic ranging

12 p2270 A70-27925

Gyrostabilized platforms for astronomical observations, minimizing position errors

13 p2403 A70-28441

Meteors position angles determination during telescopic observations, discussing error due to angle reversion

13 p2491 A70-29043

Satellite time and position observations mean square error analysis using calculus of variations

13 p2367 A70-29528

Tracking error correction time and proprioceptive reaction time, suggesting role of central mechanism without sensory feedback

17 p3036 A70-34606

Neptune position errors by meridian observations compared with photoelectric observation of stellar occultation

19 p3518 A70-38008

Artificial satellite position visual estimates based on geometric relationship to reference stars pair accuracy

19 p3531 A70-38946

Onboard velocity sensors for VOR/DME navigation systems positional accuracy improvement, describing optimal and suboptimal data filtering

[AIAA PAPER 70-1024] 20 p3666 A70-39511

Tracking elevation/azimuth errors due to frame misalignment, presenting least squares procedure for determining true bias and misalignment angle and axis

23 p4215 A70-44518

Phase and tracking errors due to mutual scattering in phase monopulse phase-scanned antenna

24 p4315 A70-46135

POSITION INDICATORS

NT PLAN POSITION INDICATORS

NT RADIO DIRECTION FINDERS

NT SPACECRAFT POSITION INDICATORS

Onboard radio altimeter for position finding of research rockets and balloons used for aeronomic investigations

02 p0298 A70-12084

Omega position location equipment /OPLE/ experimental data analysis, obtaining quantitative measure of statistical performance of system

02 p0336 A70-12180

VLF radio wave propagation variations occurring in earth-ionosphere waveguide contributing to errors in OMEGA position lines used to obtain worldwide navigational fixes

03 p0523 A70-13614

Pitot boundary layer probes with position indicators using extensometric gages for boundary layers on wind tunnel test models

[ONERA-TP-754] 03 p0487 A70-13628

North seeking declination gyrocompass design and operation with directing moment induced through bifilar suspension

05 p0844 A70-15775

V/STOL Flight Profile Indicator display system development to present pilot situation information in vertical plane

[SAE PAPER 690694] 05 p0792 A70-15861

Radar digital indicators generating deflection signals for digital PPI display, discussing scale ranges, symbols and digital circuits application

05 p0828 A70-16191

Danjon astrolabe for star position and aberration constant determination with improved accuracy, discussing Mars observation

05 p0912 A70-16453

Optimum filter for aircraft inertial navigator and radio position fix data mixing using mathematical model of error propagation

[AIAA PAPER 70-35] 06 p1103 A70-18184

Range positioning system as automatic indicator in oceanography, aboard land vehicles and aircraft

08 p1541 A70-21360

Aeronautical satellite system for North Atlantic air traffic position monitoring, discussing simultaneous position display

09 p1723 A70-23040

Hyperbolic position finding with synchronous satellites having frequency conversion unit for operations at higher frequency satellite signals

09 p1724 A70-23044

Error analysis of position finding techniques using analytical model composed of equations describing position error differential relationships

09 p1724 A70-23045

Photoelectric devices for object position fixation and superposition of two images

09 p1684 A70-23635

Fluidic digital position sensor consisting of fluidic monostable amplifier, analyzing operation by characteristics method

09 p1614 A70-23689

VHF satellite transponders for ranging and position fixing, studying ionospheric and multipath effects

[AIAA PAPER 70-489] 11 p1999 A70-25433

VHF aeronautical communication satellites extended for use in aircraft position determination and surveillance, discussing accuracy and error source reduction

[AIAA PAPER 70-490] 11 p2002 A70-25487

Position location and aircraft communication equipment concept and Experimental PLACE System providing ATC two-way voice and digital data communications via geostationary satellites

12 p2269 A70-27921

Rarefied gas mixtures efflux from opening at various pressures, calculating component discharge coefficients for molecular flow conditions

15 p2721 A70-32137

SATRAM, multiple trajectory landing system for aircraft position indication within large airspace

18 p3289 A70-36948

DR-S Raydist radio location system in fixed wing aircraft for dynamic gravimetry

22 p4068 A70-43661

Flueric position and distance sensor characteristics

24 p4293 A70-45427

POSITION SERVOS

U SERVOMOTORS

POSITIONING

Programming device for positioning samples under X ray beam in testing welded seams and parts

02 p0301 A70-12488

Military pilots visual estimation of point location coordinates within rectangular area

13 p2357 A70-29121

POSITIONING DEVICES [MACHINERY]

NT BOOMS [EQUIPMENT]
Laser beam with small divergence angle kept in horizontal position by leveling instrument with automatic compensating device, discussing distortion effects on localization

09 p1699 A70-23442

Rarefied gas mixtures efflux from opening at various pressures, calculating component discharge coefficients for molecular flow conditions

15 p2721 A70-32137

Electromechanical surpenuator for positioning and handling of objects in weightless environment, discussing design and operations

16 p2919 A70-33720
Stepper motor for pointing Surveyor spacecraft TV transmitting antenna and solar panel at earth and sun
16 p2845 A70-34110
Orientation system for pointing balloon-borne X ray detector using flux gate magnetometer, DC amplifier and motor control relay circuit
21 p13831 A70-42249

POSITRON ANNIHILATION

Satellite recording of electron-positron annihilation gamma emission on Cosmos 135 artificial earth satellite relating to meteors antimatter nature
07 p1371 A70-20334
Positron annihilation in quenched Cd metal from radar backscatter intensities in aircraft model compared with anechoic chamber measurements
24 p4315 A70-46257

POSITRONS

Flux, energy spectrum and charge composition of primary cosmic ray electrons measured, determining energy spectrum of primary positrons above 220 Mev
04 p0739 A70-14595
Electron-positron pair formation in electromagnetic field created by coherent laser light focused into vacuum with ideal lens
08 p1513 A70-21411

Low energy positrons and gamma rays from large fluxes of galactic cosmic rays
09 p1746 A70-23477

Cosmic radiation low energy positrons flux estimation compared with calculation from solar modulation models
10 p1932 A70-24537

Primary cosmic rays electron-positron component, considering relative roles of collision-produced and directly accelerated electrons
12 p2292 A70-27382

Cosmic ray electron and positron differential energy spectra during solar quiet times from OGO- 5 satellite observations in interplanetary space
19 p3502 A70-38096

Interplanetary cosmic ray positrons energy spectral component with origin different from interstellar mesons decay
19 p3502 A70-38098

Galactic low energy cosmic ray positrons and gamma rays, considering production mechanism in interstellar space
19 p3503 A70-38099

Cosmic ray positrons and negatrons differential energy spectra and solar modulation, using balloon-borne magnetic spectrometer
19 p3503 A70-38100

Energy spectrum of primary cosmic ray electrons /negatron and positron/ in interstellar region observed near 1965 solar minimum
19 p3503 A70-38101

Cosmic ray positrons and negatrons differential intensities near north geomagnetic pole from balloon flight measurements, noting solar modulation effects
19 p3503 A70-38102

Positron fraction among primary cosmic ray low energy electrons, using pure emulsion stack exposed under residual atmosphere
19 p3504 A70-38109

Interstellar electron and positron intensity, observing pion production spectrum from nuclear collisions at machine energies
19 p3504 A70-38111

Collapsing or neutronizing stars detection by recording neutrino and antineutrino flux, calculating antineutrino-deuteron interaction cross section and positron energy and angular distribution
20 p3698 A70-39302

Low energy cosmic ray positrons arising from Co decay in Ni 56-Co 56-Fe 56 reaction chain in supernova Si burning shells
21 p3879 A70-40927

Apollo 11 lunar samples composition for Na 22, Al 26, Th and U, investigating positron activities
21 p3775 A70-41580

POSTFLIGHT ANALYSIS

Aircraft trajectory postflight reconstruction involving photographic starfield and landmark referenced to inertial navigator output, discussing optimal data smoothing technique
[AIAA PAPER 70-1022] 20 p3666 A70-39512

POSTURE

Posture and motion control for functional organizations of nervous systems, emphasizing reflexes and relation between suprasegmental structures and controlling organs
01 p0017 A70-10499

Posture effect on ballistocardiograms, considering ventricular ejection flow changes
02 p0248 A70-12684

Posture change effects on vasodilator responses in humans, studying reactive, postexercise and local heat hyperaemia in forearms of subjects lying and standing
07 p1211 A70-19596

Nine degree of freedom pitch axis model of human postural control system, deriving kinetic and potential energy expressions
11 p1990 A70-25675

Minnesota Impedance Cardiograph method evaluated by applying to cardiac output measurements in postural stress studies
17 p3031 A70-35431

Human postural control system response to mechanical torque disturbance, using second order differential equation with state dependent parameters for approximate analysis
22 p3979 A70-43494

Normal human postural control system reflex response to tendon jerk disturbance
22 p3979 A70-43495

Linear lumped parameter mechanical model of muscle spindle in postural control
22 p3979 A70-43496

POTABLE LIQUIDS

NT POTABLE WATER

Alcoholic beverages effect on positional nystagmus and Coriolis acceleration
11 p1993 A70-26520

POTABLE WATER

Potable water recovery from urine by vacuum distillation and vapor pyrolyzation
21 p3769 A70-40995

POTASSIUM

NT LIQUID POTASSIUM

Local contractures in K depolarized amphibian skeletal muscle fibers by intracellular injection or by microperfusion, discussing intracellular Ca ion concentration
02 p0234 A70-11728

Plasma camera photographs of K plasma spatial distribution with electric fields and density gradients perpendicular to magnetic field, observing rotating irregularities around edge
04 p0728 A70-15005

Rankine cycle two loop Li boiling Ka facility for nuclear turboplant simulation, studying alkali metal corrosion for operation with and without hot traps
[AIME PAPER F-69-1] 07 p1304 A70-18809

Scattering cross sections of K atoms on bromine molecules determined as function of particle energy using supersonic atomic beams
07 p1344 A70-20133

Sonic speed and damping in two phase potassium flow, discussing linear equations and propagation velocity
09 p1725 A70-22036

Ionized potassium plasma three body recombination coefficient measurements showing inverse temperature dependence
09 p1735 A70-22778

Lobster giant axon membrane steady state current fluctuations measured under voltage-clamp conditions, considering current potassium component
11 p1987 A70-26006

Nonlinear parametric excitation of stable resonant drift waves by mode-mode coupling in potassium plasma of Q device
11 p2090 A70-26020

Energy loss radial dependence due to K resonance radiation for infinitely long plasma cylinder, using approximation method for integrals
13 p2461 A70-28731

Current density distributions in Ar-K plasma streams through channel with segmented electrode array, measuring electron temperatures
13 p2461 A70-28732

Sodium and potassium daylong seasonal and diurnal variations using resonance cell technique and sky polarization effect
14 p2580 A70-31263

Solar potassium resonance line shape and gravitational red shift, using atomic beam technique
17 p3173 A70-35861

Projected nuclear MHD system conditions, examining electrical measurements in K vapor with diode at atmosphere pressure and high temperatures
20 p3681 A70-40006

Nuclear space power three stage potassium turbine erosion testing in stainless steel loop with various contamination levels
21 p3756 A70-41005

Spontaneous emission intensification at 6911 A in potassium to evaluate plasma local conditions, using low pressure arc and Q switched ruby laser
22 p4049 A70-42359

Lethal and sublethal radiation dosage effects on cellular Na and K distribution in rat brain, liver, kidneys and muscular tissues
23 p4145 A70-44314

POTASSIUM CHLORIDES

Oral potassium chloride usefulness and toxicity in EKG nonspecific T wave abnormality evaluation
01 p0014 A70-10274

KCl F centers isothermal annealing kinetics using EPR, considering electron irradiation levels effects
02 p0350 A70-12719

Li positive ions in KCl crystals, investigating internal strains effect on paraelectric resonance spectra
14 p2626 A70-30340

Third body coefficients of water and heavy water reactions in KCl coated and aged boric acid coated vessels with vibrational-vibrational exchanges
14 p2546 A70-31091

Polycrystalline NaCl-KCl solid solution alloy, considering high temperature creep under constant compression stress
16 p2961 A70-33275

Crack propagation at supersonic velocities in K Cl crystals, noting plasma induction within specimen by laser pulse
21 p3940 A70-42033

POTASSIUM COMPOUNDS

NT POTASSIUM CHLORIDES

NT POTASSIUM HYDROXIDES

NT POTASSIUM OXIDES

NT POTASSIUM PERCHLORATES

NT POTASSIUM PHOSPHATES

Potassium permanganate catalytic effects on ammonium perchlorate deflagration, studying catalyst dispersion degree role
07 p1358 A70-19329

Intense light effect on refractive index of potassium niobate crystals
09 p1698 A70-23317

Gas phase chemicals synthesis via AC diffuse discharge superimposed on propane-air flame seeded with potassium carbonate in electrically augmented flame burner
14 p2546 A70-31097

Safety characteristics of potassium chloratellactose mixtures as standard for comparing dangerousness of pyrotechnical compositions
15 p2786 A70-31848

Potassium salts thermal and chemical ionization in flames of hydrogen-oxygen-helium and hydrogen- air mixtures in constant volume vessels
18 p3345 A70-36243

Thermal decomposition of acetate ion in potassium halide matrices, using IR spectroscopy
22 p3981 A70-42453

Potassium acid phthalate crystal X ray spectrometric properties measurements, discussing parallel position rocking curves and reflection coefficients
23 p4230 A70-44420

POTASSIUM HYDROXIDES

Oxygen and hydrogen diffusion coefficients in aqueous potassium hydroxide electrolyte solutions at various temperatures and concentrations
12 p2181 A70-27575

POTASSIUM OXIDES

Closed circuit respiration studies on subjects at rest and work, demonstrating potassium superoxide as oxygen source in breathing apparatus
15 p2688 A70-31500

POTASSIUM PERCHLORATES

Extinction pressures of polyurethane propellants increased by presence of AP, AP coated with silane and KP
[AIAA PAPER 70-657] 16 p2963 A70-33619

Isomorphous mixed ammonium perchlorate and potassium perchlorate crystals structural homogeneity by X ray diffraction and differential thermal and thermogravimetric analyses
21 p3784 A70-42262

POTASSIUM PHOSPHATES

One piece KDP and AP reflector shutters used as laser Q switches, discussing compensation for working surfaces temperature displacement
01 p0106 A70-10060

Neodymium glass laser fundamental frequency spatial structure effects on KDP crystal second harmonic generation efficiency, describing optimal system for laser beam shaping
10 p1899 A70-24262

KDP crystal single cut for laser beam frequency conversion and tuning
12 p2245 A70-27302

Second harmonic emission from GaAs injection laser and from stimulated KDP crystal at room temperature
12 p2245 A70-27306

POTATOES

Sweet potatoes productivity and nutritive value as carbohydrates source in manned space flights
04 p0641 A70-14572

POTENTIAL ENERGY

NT BIOELECTRIC POTENTIAL

NT CONTACT POTENTIALS

NT COULOMB POTENTIAL

NT ELECTRIC POTENTIAL

NT GEOPOTENTIAL HEIGHT

NT IONIZATION POTENTIALS

NT PHOTOVOLTAGES

NT PLASMA POTENTIALS

NT SPIKE POTENTIALS

Periodic potential and residual Coulomb interaction effect on inelastic light scattering from electronic excitations in semiconductors, using diagrammatic perturbation theory
01 p0156 A70-10280

Semiempirical potential energy surface generation for triatomic hydrogen from London equation by evaluating Coulomb and exchange integrals taking into account effective orbital overlap
01 p0147 A70-10469

- Potential energy surface shapes for lowest states of temporary negative ions of nitrous oxide and carbon dioxide
03 p0441 A70-14008
- Kinetic, potential and dissipative energies computed in systems of randomly excited coupled oscillators, using Liapunov stability method
05 p0821 A70-16407
- Effective potential of electron screening of Coulomb nuclei field leading to thermonuclear reaction rate increase using self consistent field method
07 p1346 A70-20206
- Libration limits of satellite in Keplerian circular orbit, estimating potential energy of perturbing forces
08 p1582 A70-20967
- Energy equilibrium for crack growth in elastoplastic media, analyzing crack behavior during plastic deformation concentrated at edge of propagating crack
08 p1590 A70-21414
- Oscillatory transverse and longitudinal magnetostriiction in single crystal Bi, obtaining deformation potentials
08 p1557 A70-21838
- Variable modular elasticity theory demonstrated for anisotropic body subjected to plane stressed state, deriving expression for potential energy of deformation
09 p1769 A70-22152
- Resonance energy calculation and transmission coefficient estimate for quantum mechanical model of reactive scattering of three atoms in line
10 p1920 A70-25145
- High energy oxygen positive-ion reaction with molecular nitrogen, presenting semiempirical model with assumed crossing of potential energy surfaces
10 p1920 A70-25146
- Quantum mechanical inverse problem of elastic scattering theory, discussing Hylleberg solution for determining potential energy function from phase shift
12 p2274 A70-26899
- Potential energy curves for diatomic He molecules constructed by Rydberg-Klein-Rees procedures
14 p2618 A70-30112
- Stochastic medium mathematical model for loose medium motion in potential field of forces
15 p2821 A70-32342
- Curved finite elements for shell calculations, obtaining potential energy of internal forces
18 p3337 A70-36369
- Coordinates for diagonalizing kinetic energy of particle system relative motion, discussing potential energy surface
19 p3373 A70-37841
- Libration limits of satellite in Keplerian circular orbit, estimating potential energy of perturbing forces
20 p3713 A70-39388
- Base function selection for energy calculation optimal convergence conditions of frequencies and stresses in turbomachine blades vibrations
20 p3722 A70-39784
- ### POTENTIAL FIELDS
- Inertial gravitational fields described by Maxwell equations, showing potentials defining four vector velocity field of test particles
01 p0141 A70-10140
- Potential representation of vector fields effecting decoupling of vector wave equation of elasticity for radially heterogeneous isotropic media
01 p0208 A70-11189
- Kharlamova motion equations solution for solid body with fixed point in potential force field, assuming fixed center of gravity
01 p0145 A70-11432
- Kharlamov motion equations solution for solid body with fixed point subjected to zero-potential forces
01 p0145 A70-11433
- Electric potential fluctuations beyond long collisionless plasma cylinder in uniform magnetic field, noting thermal noise intensity
03 p0530 A70-13086
- Potential determination from gravity disturbances along fixed direction in analysis of residuals of Doppler tracking of Lunar Orbiter satellites for moon gravity field
03 p0577 A70-14177
- Ion and electron density, electron temperature and space potential measured in ion wake formed by Gemini spacecraft using sensors on Agena Target Vehicle
06 p1066 A70-18285
- Soviet book on nonperiodic processes in Northern Hemisphere stratosphere, discussing seasonal temperature fields, geopotential and circulation formation
07 p1261 A70-18733
- Potential and gravity distributions on lunar surface, showing presence of harmonics of all orders
07 p1385 A70-19425
- Motion of body with cavity completely filled with viscous fluid about center of mass in potential mass-force field, applying small parameter method
08 p1546 A70-21630
- Periodic orbits in highly perturbed dynamical systems, studying characteristic curves of various families in galactic-type potential
09 p1760 A70-22916
- Equations of motion integration for solid body in potential forces field induced by elastic springs
09 p1728 A70-23386
- Stability conditions of rotational motions of symmetrical solid body on vibrating base in potential force field
11 p2098 A70-25916
- Spherical harmonic coefficients of eccentric dipole potential and coinciding magnetic and mass center, noting geophysical prospecting applicability
11 p2047 A70-26571
- Oscillating infinite cylinder as acoustic waves source in homogeneous viscous medium, deriving scalar and vector potentials
12 p2274 A70-28240
- Euler potentials for magnetic fields field-line structure representation, discussing cross products of gradients of scalars in plasma physics
13 p2451 A70-29123
- Collisionless alkali plasma diode with two electrodes emitting electrons and ions with half-Maxwellian velocities, analyzing potential distribution
14 p2622 A70-30660
- Interstellar grains potential model, discussing plane electromagnetic waves scattering by infinite concentric homogeneous circular cylinders at oblique incidence
14 p2639 A70-30732
- Junction FET potential field and carrier distribution in channel investigated for current saturation mechanism
15 p2708 A70-31841
- Steady state potential distributions near photoemitting plate immersed in plasma, noting overshoot effects role for sheaths around satellites in interplanetary plasma
15 p2778 A70-31906
- Adiabatic corrections to long range Born-Oppenheimer interatomic potentials from rotationally coupled Schroedinger equations
17 p3138 A70-35199
- Gravitational force and potential within static metric spaces
17 p3136 A70-35597
- Potential calculation from given source distribution, including direct and iterative methods, error analysis, convergence, computer programs and applications in plasma physics
18 p3284 A70-36790
- Grid system with alternating filament potentials, deriving potential distribution for fields and electro-optical effect
21 p3835 A70-40632
- Dynamic potentials equations of guided electromagnetic wave propagating in laterally bounded plasma along magnetic field axis
21 p3860 A70-42005
- Axisymmetric potential problem of plane circular electrified disk in coplanar gap formulated in triple integral equation, obtaining Wiener-Hopf solution
22 p4080 A70-42632
- Magnetic vector potential of circular ring with current in Taylor series expansion for electromagnetic axisymmetric systems
23 p4189 A70-44069
- Microwave transmission systems, determining electric potential functions in inhomogeneous dielectrics by Earnshaw theorem and finite difference computation
24 p4318 A70-45217
- ### POTENTIAL FLOW
- #### NT EQUIPOTENTIALS
- Laminar airfoils for Reynolds numbers above 4,000,000, utilizing potential and boundary layer flow theories
01 p0063 A70-10930
- Irrational motions of relativistic ideal thermodynamic fluids fulfilling incompressibility conditions
01 p0063 A70-10948
- Two dimensional plane and axisymmetric free streamline flow problems solved by finite difference methods for supercavitating wedge in potential flows
01 p0065 A70-11127
- Potential triple traveling space waves in barotropic gas with arbitrary equation of state, analyzing adjacent and three dimensional self similar flows
01 p0068 A70-11582
- Integral method for computing two dimensional incompressible turbulent boundary layer development, including entrainment process of irrotational fluid
02 p0284 A70-12343
- Numerical method for attacking-lifting problems of general three dimensional wing executing arbitrary motion in potential flow
03 p0405 A70-12930
- Potential flow past plane theoretical airfoil lattices
03 p0407 A70-13448
- Surface singularities method for calculating incompressible potential flow about bodies of revolution with arbitrary thickness ratio and angle of attack
03 p0410 A70-14322
- Potential axisymmetric vortex flow interaction with stationary flat surface, using existing numerical analysis by transforming boundary value problem to Volterra integral equations
04 p0668 A70-14864
- Inviscid flow problems solution by partial differential equations, considering propagation processes, stratified media, potential, subsonic and three dimensional flows
04 p0672 A70-15170
- Singularity method applied to two and three dimensional potential flow described by Poisson, Helmholtz or related partial differential equations
05 p0832 A70-16114
- Potential flow over rocket contour containing bends calculated by polygonal distribution of singularities on axis of body of revolution, determining friction effects
06 p0964 A70-17239
- Separated incompressible flow around wing profile, considering calculation of separated potential flow generation with given separation point
06 p0966 A70-17253
- Ideal fluid planar potential flow, approximating stream function and velocity potential by matrix method
07 p1253 A70-18925
- Singular element technique effect on hydrodynamic and aerodynamic problems solutions, presenting potential flow problems and application to wings and propellers
07 p1188 A70-19133
- Plane rigid airfoil frequency response in incompressible potential flow using simple equivalent oscillator based on Theodorsen function
07 p1404 A70-19232
- Roshko model cavity solution based on Falkovich method application to two dimensional permanent irrotational flow of subsonic gas jet
07 p1258 A70-19571
- Circular turbulent air jet from flat plate into deflecting stream using potential flow model, noting applicability to V/STOL aircraft technology
07 p1190 A70-20406
- Pressure distribution on flat plate resulting from potential incompressible flow interaction between secondary jet and subsonic mainstream
07 p1190 A70-20415
- Potential vortex flow interaction with stationary surface calculation extended to Volterra equations by transforming boundary value problem, improving critical Reynolds number bounds
08 p1484 A70-21472
- Mixing region and potential cone of two dimensional jet, measuring velocity fluctuations
08 p1485 A70-21587
- Vortex and potential motions interactions in relativistic hydrodynamics, studying mutual generation
09 p1754 A70-22460
- Vortex and potential motions interactions in relativistic hydrodynamics, noting effects of gravitation equations nonlinearity
09 p1754 A70-22461
- Potential flow and boundary layer theory application as design tools in aerodynamics, basing calculations on digital computer methods
09 p1605 A70-22947
- Wake source model for two dimensional incompressible potential flow past bluff body, considering pressure distribution, flow separation, wake width, etc
09 p1607 A70-23681
- Blade inter-row distances upstream and downstream related to potential flow velocity disturbances created by cascade in turbomachines
09 p1607 A70-23734
- Equivalent oscillatory model defined from asymptotes of frequency response amplitude and cut-off frequency amplitude value of plane rigid airfoil in incompressible potential flow
10 p1953 A70-23841
- Potential flow resistance theory, deriving monoparameter wake formula for circular cylinder moving through viscous fluid
10 p1870 A70-24788
- Potential flow pertaining to motion of gas surrounding close binary systems generated by orbital motion of stars and matter outflow from stars
10 p1946 A70-24968
- Velocity distribution around isolated and cascaded airfoils in plane potential flows of incompressible fluid determined by use of nonsingular integrals
11 p1974 A70-25781
- Two and three dimensional potential flow analysis using finite element technique based on method of singularities
11 p2042 A70-26681
- Plasmopause form in equatorial plane in presence of magnetospheric tail subsonic potential convective flow
11 p2047 A70-26796
- Pressure distribution in two dimensional incompressible potential flow on Joukowski airfoils with normal upper surface spoilers, emphasizing potential flow theory
12 p2155 A70-27193

Transonic flow theory for two and three dimensional streamlined bodies in steady irrotational flow of inviscid perfect gas

12 p2158 A70-28201

Aerofoil free vibrations with fixed center of gravity in incompressible potential flow under representative previous histories effect

12 p2328 A70-28214

Two dimensional irrotational incompressible fluid motion bounded by flexible stretched and unstretched film, noting hydrodynamic shock for closed film

12 p2213 A70-28238

Compressible fluid two dimensional irrotational flow past Roshko model in channel, deriving exact solution by hodograph method

13 p2341 A70-29487

Incompressible ideal plane fluid flow complex potential caused by profile motion in presence of fixed infinite wall

13 p2390 A70-29632

Plane cavity geometry behind plate in incompressible potential flow, deriving geometrical functions to obtain desirable shapes

13 p2390 A70-29645

Ideal weightless fluid plane potential flow in channel with permeable wall, deriving expressions for dynamic characteristics

13 p2390 A70-29648

Steady plane relativistic flow small irrotational perturbation theory determining subsonic, transonic and supersonic approximation

14 p2566 A70-30472

Incompressible two dimensional potential flow analysis with compressibility effects for thick highly cambered multibodies in cascade, noting slotted compressor blade performance

[ASME PAPER 69-GT-6]

14 p2529 A70-31023

Incompressible fluid interaction of perfect irrotational flow through two blade wheels in relative motion, observing pressure variations at nozzle profile

16 p2836 A70-33755

German monograph on planar straight cascades in incompressible frictionless potential flow, basing method on singularity method integral equation reversal

16 p2839 A70-34081

Two dimensional cascades for incompressible plane potential flows with given velocity distribution

[ASME PAPER 70-GT-87]

18 p3209 A70-36880

Hodograph equations for relativistic irrotational steady plane flows, investigating transformation to physical plane

19 p3406 A70-38664

Boundary conditions on vector and scalar potentials in viscous three dimensional hydrodynamics, investigating compressible flow problems

20 p3612 A70-40115

Perfect gas irrotational isentropic nozzle flow by solving partial differential equations set

21 p3744 A70-41240

Hodography of compressible fluids three dimensional irrotational isentropic flow

21 p3808 A70-41439

Irrotational incompressible flow through two dimensional channel with asymmetric contraction

21 p3809 A70-41757

Perfect gas acyclic and cyclic, steady and irrotational motions in subsonic regime around convex profile with constant curvature variation by Chaplygin method

21 p3846 A70-42259

Fluid flow around plane plate system, basing model on potential flow theory and variational principle

22 p4009 A70-42606

Irrotational incompressible free falling jet, using asymptotic expansion solution for mixed boundary value potential problems

22 p4012 A70-42938

Potential flow around oscillating shell-plate structure subjected to supersonic gas flow at zero angle of attack, solving nonlinear aerostaticity problem

22 p4117 A70-43362

Lift determination of slender curved periodically recurring airfoils array in plane potential flow of inviscid incompressible fluid

23 p4133 A70-44158

Steady irrotational gas flow characteristics calculation from finite difference scheme for three dimensional method of characteristics, considering supersonic nozzle flow

23 p4133 A70-44308

Potential liquid flow in pulsating bulb applied to blood flow

23 p4155 A70-44847

Aerodynamic forces and torque on airfoil in potential jet from boundary asymptotes position, determining flow characteristics by electrical analogy

24 p4288 A70-45438

POTENTIAL GRADIENTS

Test setup to determine safe limits of atmospheric potential gradients in electroexplosive device initiation

03 p0549 A70-14136

Potential gradient radiosonde field distortion formula, deriving form factors

09 p1671 A70-23602

Thunderstorm detection and warning system, measuring vertical potential gradient and changes caused by lightning discharges

14 p2607 A70-30574

Potential gradient effect on charge separation mechanism during interaction of polarized snow crystals with ice sphere

15 p2769 A70-31445

Geomagnetic activity effect on potential gradient and air-earth conduction current density

19 p3413 A70-38000

Hollow cathode shape effect on glow discharge parameters and potential jump in cathode region, investigating I-V curves

22 p4078 A70-42357

POTENTIAL PROBLEMS

U POTENTIAL THEORY

POTENTIAL THEORY

Coulomb, Gaussian and harmonic oscillator potentials for particle pairs in three body system, using S wave expansion

01 p0147 A70-10519

Linearized potential theory application in aerodynamic design and analysis of supersonic aircraft emphasizing far field viewpoint

[AIAA PAPER 69-1132]

01 p0002 A70-10608

Geomagnetic potential optimal representation in frame of reference of eccentric inclined dipole using conversion formulas to determine harmonic coefficients

01 p0081 A70-11230

Symmetric Boolean function detection by method using potential concept, determining alpha numbers with potential values for canonical terms

02 p0324 A70-12188

De Sitter hydrostatic equations solution possible with help of boundary condition from external potential theory with/without assumed equilibrium in earth interior

04 p0678 A70-15051

Mixed boundary value potential theory problem numerical solution by integral equation invariant imbedding

06 p1171 A70-18511

Potential function of creep strain rates for incompressible nonstrengthening materials exhibiting different creep characteristics in tension and compression

09 p1769 A70-22122

Complex potentials used in semicomplex variable method for plane-strain problems in two dimensional linearized elasticity with couple stresses

13 p2508 A70-28494

Resonance energies of elastic scattering from one dimensional model potential containing barrier, using stabilization method

13 p2455 A70-29222

Potential stability theory for linear and nonlinear systems trajectory

16 p2943 A70-34042

Generalized Lagrange kinetic potentials, discussing force systems with ideal holonomic constraints

16 p2944 A70-34292

General potential function in triaxially ellipsoidal coordinates for Laplace equation, examining near earth satellites and Vinti potential

18 p3334 A70-37064

Boundary value problems in potential theory for electrical disk and spherical cap reduced to problems for two dimensional Laplace equation

20 p3657 A70-39446

Spoiler theory based on mathematical model, using two dimensional potential theory in conjunction with experimental data on wake phenomena

22 p3957 A70-42273

French book on strength of materials covering potential energy theory, cutoff and matrix methods, computer calculations, etc

22 p4119 A70-43623

Thin cylindrical shell flutter in linearized supersonic potential theory, considering Mach number, aspect ratio and pressure effects on critical wave number

24 p4420 A70-45263

POTENTIOMETERS

Shadow method for temperature field in potentiometer winding

19 p3420 A70-37264

POTENTIOMETERS (INSTRUMENTS)

Cryogenic temperature sensor calibration with automated data readout for spacecraft accuracy requirements, describing potentiometric system

03 p0486 A70-13561

Remote recording wind vane using continuous and step rotary switch potentiometers suitable for automatic weather stations

06 p1062 A70-17619

Structural and material design of contactless photopotentiometers operating in forward and reverse modes with given output characteristics

09 p1681 A70-23357

Random processes correlation coefficients and functions measured by quasi-compensator with potentiometer and digital/analog readout

12 p2235 A70-27770

Displacement and velocity measurements using strain gauges, linear potentiometers and seismic transducers

15 p2743 A70-32799

Potentiometer application to nondestructive tests of materials, operation principles, methodology and advantages

24 p4338 A70-45739

DC potentiometer for nondestructive tests of structural components, obtaining crack detection, depths and angles and wall thicknesses

24 p4338 A70-45740

POTENTIOMETERS (RESISTORS)

Output and frequency limitations of functional converter using photopotentiometer with shaped resistor

09 p1682 A70-23358

Low resistance multirange potentiometers, performing error analysis

19 p3432 A70-38706

POTENTIOMETRIC ANALYSIS

Potentiometric analysis for determining acidity and alkalinity in dark mineral oils with additives

05 p0810 A70-15898

Al-Zn-Mg alloys anodic corrosion behavior under various heat treatment regimes using potentiostatic method

06 p1090 A70-17922

POTENTIOMETRY

U POTENTIOMETRIC ANALYSIS

POTTING COMPOUNDS

Potting material applicability to attaching honeycomb sandwich assemblies to structures, describing pre- and postpotting methods

13 p2418 A70-28667

Rigid one component epoxy foam system mechanical, electrical and thermal properties for foamed-in-place electronic potting and encapsulation

13 p2439 A70-29263

One-component rigid epoxy foam system suitable for lightweight electronic potting, determining mechanical, electrical and thermal properties

20 p3652 A70-39167

POWDER (PARTICLES)

NT FINES

NT METAL POWDER

NT POWDERED ALUMINUM

Conformally plane solutions to Einstein equations derived with energy momentum tensor characteristics of pulverized material representing gravitational fields

01 p0193 A70-11629

Adsorption properties of pulverized silica gel, quartz, C and graphite under electron bombardment from low temperature plasma, showing surface and physicochemical influence

03 p0516 A70-13468

Terrestrial solid powdered rocks HF electrical properties measurements for lunar radar observation

04 p0678 A70-15054

Temperature dependence of thermal conductivity of granulated borazon powders measured in He and vacuum

07 p1319 A70-19803

Powder combustion on metal plate, investigating unburned layer thickness dependence on initial temperature

17 p3198 A70-35738

POWDER METALLURGY

Book on powder metallurgy treating characterization of powders, compaction, sintering and engineering considerations and applications

02 p0316 A70-11735

Prealloyed powders of Ni base alloys, made by inert gas atomization for improved strength and ductility

04 p0706 A70-14951

Mechanical property factors influencing selection of sintered uncorked refractory metals and alloys for structural applications

[AIME PAPER F-69-4]

07 p1290 A70-18810

Precision tungsten alloy tubing manufacture and properties, discussing direct conversion of metal powder to finished tubing with high temperature structural stability

07 p1292 A70-18928

Powder metallurgy all-inert processing method for producing nickel base superalloys forgings, discussing microstructure, reproducibility, mechanical properties, etc

09 p1701 A70-22553

Bibliography for powder metallurgy and related fields covering powder fabrication, compacting and sintering, refractory metals, hard materials, etc

10 p1904 A70-24387

Integrally stiffened structures made by hot isostatic pressing of metal powders followed by conventional rolling

12 p2242 A70-27109

Metal powder mixtures homogenization time calculation, using Fick equation and matrix model

13 p2433 A70-28845

Titanium alloys powder metallurgy, considering manufacturing methods and physical, chemical and mechanical properties

13 p2435 A70-29214

Powder metal parts induction sintering, comparing performance with conventional method
13 p2420 A70-29249

Powder metallurgy literature /1968-69/ covering metal powders, sintering, porous materials, etc
15 p2760 A70-32349

Mo powder compacting by hot pressing, determining activation energy
16 p2931 A70-33222

Ti-Be composite materials production by coextrusion of powders, investigating microstructure by microprobe analysis and X ray diffraction
20 p3649 A70-39945

Intergranular brittleness in powder metallurgy W by Auger Electron Emission Spectroscopy for fracture surfaces chemical analysis
22 p4053 A70-42733

Scorched aluminum powder /SAP/ materials, discussing fabrication, physical and mechanical properties, applications in aircraft structural components, etc
22 p4055 A70-43084

High purity Be preparation by Kroll process using Na as reductant, noting mechanical properties and ease of conversion to powder
24 p4341 A70-45242

Fe-Cr alloy powders obtained with thermodiffusive saturation from point sources, determining optimal mixture compositions and parameters
24 p4350 A70-46338

POWDERED ALUMINUM

Combustion time of Al powder, considering concentration, injection into gas flow, oxidizer composition and agglomeration
01 p0161 A70-11015

Al powder explosive compacting processing, equipment and tests noting heat treatment effect
05 p0894 A70-16324

Fatigue strength of sintered aluminum powder at room and elevated temperatures, discussing sensitivity to tensile loads misalignment
07 p1304 A70-18840

Scorched aluminum powder /SAP/ materials, discussing fabrication, physical and mechanical properties, applications in aircraft structural components, etc
22 p4055 A70-43084

POWDERED METALS

U METAL POWDER

POWER AMPLIFIERS

Supersonic fluid amplifier performance and design for use as power amplifier and high outlet leg differentials in vacuum environments
[ASME PAPER 69-WA/FLCS-7]
04 p0626 A70-14846

Three way power divider/summer fabricated symmetrically in stripline by resistive network transformation
05 p0821 A70-16386

UHF transistor power amplifier, discussing CW and pulse performance and power gain
08 p1477 A70-21294

Integrated CW UHF power amplifier modules using thin film lumped elements and UHF power transistor chips
10 p1846 A70-23884

S band CW high power broadband power source consisting of transistor amplifier-driven varactor doubler chains in hybrid integrated form
10 p1846 A70-23885

Solid state multistage high power avalanche amplifier at X band
10 p1847 A70-23890

Spacecraft S band power amplifier TWT electrical, environmental and life tests under saturated conditions
[AIAA PAPER 70-506]
11 p2016 A70-25468

Wideband high power output transistor amplifier design features and operational characteristics
12 p2199 A70-27980

S band CW power amplifier and varactor doubler module for airborne phased arrays
18 p3231 A70-36674

Hybrid integrated microwave power amplifiers, using high-Q thin film lumped passive elements
18 p3232 A70-36760

Microwave transistors for power generation and amplification, discussing packaging and pellet design
20 p3599 A70-40324

Local control loop model of multiphase rectifier used as power amplifier, considering extension to nonautonomous and discontinuous conduction systems
21 p3802 A70-42267

Diffusion effect on carbon dioxide Gaussian laser beam amplification, measuring gain saturation via pinhole method
22 p4051 A70-43335

Transistorized power amplifiers, frequency multipliers and parametric multipliers design for VHF and UHF ranges
23 p4170 A70-43876

POWER CONDITIONING

Liquid mercury /LM/ cathode thruster characteristics, power conditioning and control requirements
[AIAA PAPER 70-646]
16 p2965 A70-33536

Hollow cathode ion thruster and lightweight power conditioner of solar-electric propulsion system for unmanned deep space probes
[AIAA PAPER 70-648]
16 p2966 A70-33546

Power conditioning and control system prototype for Mercury spacecraft ion thruster, describing supply subsystems, circuit design, component selection and reliability
[AIAA PAPER 70-649]
16 p2970 A70-33615

Solid state switching effect on aerospace electric power conditioning equipment
[SAE PAPER 700306]
18 p3302 A70-36802

One millipound cesium ion thruster for synchronous ATS-F satellite, describing power conditioning and control logic subsystems
[AIAA PAPER 70-1149]
20 p3690 A70-40205

Power conditioning system for Hg ion thruster on SERT 2 spacecraft, considering performance, design, control circuits and arcing
[AIAA PAPER 70-1129]
20 p3568 A70-40216

Space compatible flight prototype ion engine power conditioning system design for Hg thruster using oxide cathode
21 p3867 A70-41006

Power conditioning - IEEE Conference, Greenbelt, Maryland, April 1970
21 p3757 A70-41206

Power conditioning systems for INTELSTAT satellites, describing methods for battery charging, charge control, voltage regulation and power management
21 p3757 A70-41207

Power conditioning requirements and specifications for spacecraft electric propulsion ion thruster
21 p3758 A70-41209

Solid state switching effect on aerospace electric power conditioning equipment
21 p3758 A70-41210

Integrated circuit requirements for space power conditioning equipment for ion thrusters
21 p3797 A70-41211

Integrated circuits for control and telemetry functions in oxide cathode ion thruster power conditioning system operating from solar panel
21 p3798 A70-41216

Solar cell array maximum power point in scientific satellites via closed loop conductance matching regulator
21 p3758 A70-41220

Electrical design of ferrite configuration high power rotary transformer for satellite slip ring replacement, minimizing transistor turn-off losses
21 p3759 A70-41222

High voltage solar array with integral power conditioning, discussing weight factors, panel design and layout, mechanization, performance prediction, etc
[AIAA PAPER 70-1158]
21 p3759 A70-41787

POWER CONVERSION

U ELECTRIC GENERATORS

POWER DENSITY

U FLUX DENSITY

POWER EFFICIENCY

GaAs and Si photocell batteries powered by solar radiation, investigating temperature dependence of efficiency I-V characteristics and optimal power
01 p0007 A70-10177

Electric power generators performance based on kinetic energy conversion of radioactive isotope decay products, noting space applications
01 p0140 A70-10217

Powered centrifugal separator for inlet filtering of rotary wing aircraft turbine engines, discussing efficiency and feasibility
01 p0164 A70-10683

High power pulsed lasers development compared to thermal light sources, discussing applications to nonlinear optics
02 p0312 A70-12070

Maximum power transfer theorem, discussing rotation symmetry with respect to optic axis and confocal optical resonators
02 p0339 A70-12454

Local criteria and geometric integration for stable transmitter power level selection in group of radio stations ensuring adequate SNR
03 p0446 A70-13237

Laser cavity structure for homogeneous transverse discharge in carbon dioxide-nitrogen-helium mixtures, discussing energy and power increase per unit volume
03 p0503 A70-14357

V/STOL power drive systems structural efficiency, comparing mechanical and pneumatic components from weight-optimal viewpoint
[ASME PAPER 69-WA/AV-7]
04 p0622 A70-14901

Light signals amplification efficiency, considering double-pass regenerative amplifier
04 p0702 A70-15225

High efficiency oscillator using avalanche square wave diode, considering case of silicon p-i-n diode
05 p0819 A70-15815

Doped beta-iron disilicide thermocouples measured for electrical characteristics and energy conversion efficiency at various temperatures
05 p0798 A70-16357

Improvement in power output of ramjet installed under wing using air compression
[ONERA-TP-783]
06 p1133 A70-18467

Static power processing efficiency illustrated by application to DC to DC converters
08 p1439 A70-20704

Flow turbulence effect on heat turbines efficiency using energy losses in blade cascades
08 p1432 A70-21073

Schottky barrier diodes microwave power rectification efficiency, developing diode losses theory based on back capacitance, series and front resistance and knee voltage
08 p1474 A70-21274

Optical devices for enhancement of semitransparent photocathode quantum efficiency applied to TV camera tubes, image intensifiers and other imaging detectors
09 p1682 A70-23502

Klystrons operation at millimeter band, using efficiently bunching drift fields for steady power output at critical wavelength
09 p1651 A70-23636

Millimeter band direct-transit klystrons oscillation and amplification at improved output power obtained by electron bunching in nonuniform drift fields
09 p1651 A70-23637

MHD generators optimum load selection by method of stepwise approach, noting agreement with pressure and density distributions to yield maximum power
10 p1923 A70-24156

Electrode shape and background resistance effects on power rationing between gas tungsten arc and electrode
10 p1897 A70-25314

Fuel cells power density improvement under pulsed loading at high current density and constant voltage
12 p2165 A70-27758

Low density Hall ion thruster with application to Van Allen probe and orbit-to-orbit transfer
[AIAA PAPER 69-281]
13 p2475 A70-29957

HF and DF continuous chemical lasers output power, obtaining population inversion by deuterium molecules diffusion into F atoms supersonic free jet
14 p2593 A70-30273

EGD energy converter system geometries for maximum power efficiencies, comparing slender conversion channels, abrupt expansion, free jet and divergent for operating characteristics
14 p2534 A70-30536

Bulk negative resistance microwave oscillators efficiency calculation by graphical method
17 p3056 A70-35876

Internal efficiency of turbine stages with long twist-varying blades
19 p3490 A70-37250

High power neodymium laser with aspherical lenses to focus photon beam for nuclear fusion experiments
19 p3447 A70-38165

Gas dynamic quantum amplifier improvement, discussing power utilization, photon distribution and radiation transport
21 p3836 A70-41418

CW gas laser improvement, discussing optimum efficiency and photon beam spatial distribution
21 p3836 A70-41419

Tunable high efficiency high peak power UHF avalanche diode oscillator
21 p3800 A70-42117

Turbomolecular pumps with uniformly distributed small plane blades, calculating rotor efficiency
22 p3964 A70-42604

Radiosonde receiver and transmitter system optimization, obtaining increased microwave power by appropriate oscillator operating modes
22 p4038 A70-43379

Scientific satellites nuclear experiments fast low power drain logic system, using AND and NAND gates, pulse generators, delays and bistables
23 p4143 A70-44299

Allison/Rolls-Royce TF41 turbofan engine improved power and reduced weight versions, comparing afterburning Model 912-B23 to nonafterburning TF41-A-2
23 p4234 A70-44596

Optimal load circuits number for maximum power extraction from Hall MHD generator with nonuniform gas flow along channel
23 p4143 A70-44900

POWER GAIN

Output power and gain saturation characteristics for high speed flowing gas molecular lasers, discussing electrically excited fluid mixing carbon dioxide laser
01 p0107 A70-10103

Gain, noise temperature and gain to noise temperature ratio measurement techniques for electrically large earth station antenna, recommending radio star technique
01 p0051 A70-11121

Unconditional stability criterion of active two port in scattering and admittance matrix notation equivalent to conjugate matching for maximum power gain with part impedances

02 p0271 A70-12820

Flash lamp illuminated ruby laser operating with ordinary or extraordinary polarization, measuring gain or absorption

03 p0502 A70-13954

Simple approximations for threshold current, gain and lasing frequency of GaAs injection laser at room temperature

03 p0503 A70-14085

Microwave transistors frequency and power characteristics and tradeoffs in relation to thermal and packaging design

06 p1023 A70-18390

CW high power operation of transferred-electron oscillators realized by low thermal resistance, describing fabrication

07 p1241 A70-19300

Parallel wire antenna arrays analysis and design, emphasizing directive power gain maximization and sidelobe reduction

08 p1471 A70-20789

Gain-to-noise temperature ratio G/T optimization by dish antenna shaping for nonuniform aperture field distribution

08 p1471 A70-20790

Gain stabilization of transistorized LF selective amplifiers in radiometric receivers, discussing two-frequency resonance system

08 p1473 A70-21061

UHF transistor power amplifier, discussing CW and pulse performance and power gain

08 p1477 A70-21294

Circuit allowing direct combining of power from several avalanche diodes, discussing CW power output, single and multiple diode oscillators, etc

08 p1477 A70-21295

Matrix method for maximizing radar antenna directive gain and simultaneously placing nulls in far field radiation patterns

08 p1477 A70-21758

Astronomical high power telescopes construction, discussing rough casting, forming, precision polishing, Foucaultage principle for spherical mirrors, thermal effects, etc

09 p1674 A70-22218

Low noise TWT, discussing dynamic range, gain and phase tracking, environmental performance, life behavior and noise factor interrelations

09 p1644 A70-22233

Transistor current gain measurement at HF by two channel method

09 p1632 A70-22234

Transverse mode distortions in high gain giant pulse laser oscillators associated with gain saturation effects

09 p1698 A70-23361

Multibeam O-type TWT characteristic equation analyzed for arbitrary space diversity, calculating gain for various velocity parameter values and electrical lengths

09 p1651 A70-23638

Single-pass multimode carbon dioxide laser amplifier power gain optimization

10 p1897 A70-23815

Silicon window with double carrier injection to achieve high power broadband microwave switching, obtaining power increase over p-i-n diodes

10 p1847 A70-23892

Semiconductor laser junction construction for increased gain making possible laser voice communication, optical intrusion alarms, laser pumping lamps and portable range finders

10 p1900 A70-24529

Carbon dioxide-neon-helium flowing lasers gain characteristics determined by transverse-discharge configuration

10 p1901 A70-24944

Sidelobe suppression for satellite reflector antennas by heavy taper, blockage compensation and active zone techniques, noting net antenna gain enhancement [AIAA PAPER 70-427]

11 p2016 A70-25476

RF amplifier design procedure for maximum stable gain with minimum noise figure

11 p2019 A70-26715

Carbon dioxide laser gain saturation measurements by intracavity Fresnel loss-plate technique, observing dependence on discharge current

12 p2249 A70-27715

Satellite pencil and shaped beam antennas, considering maximum gain conditions for various angles

12 p2197 A70-27929

Gain of optimal filter and predictor, using recursive estimation in discrete linear systems

13 p2381 A70-29063

On-axis pattern vector and power gain measurements by two identical antennas

15 p2698 A70-31955

Antenna pattern and power gain determination from near field measurements on electrically large horn lens, standard gain horn and measuring antenna duplicate

15 p2698 A70-31956

UHF ground communication dish antennas transmit and receive gains calibration by communication satellite repeater

16 p2872 A70-32967

Antenna gain, efficiency, half power bandwidth, sidelobe level and focal length for circularly polarized metallic lens antenna at X band frequencies

16 p2872 A70-32969

Lens antennas design for communication satellites, discussing power gain, beam width, sidelobe level, temperature distribution, etc

16 p2982 A70-33772

K-band high power Si avalanche diode oscillators, discussing decrease in pulse peak power output on basis of quenched plasma effect

16 p2880 A70-34260

Microwave receiving antenna, discussing directivity, cross section, power gain, equivalent circuit, etc

17 p3044 A70-35054

Nonlinear circuits with linear gain relations, examining input-output relations of two ports for analysis, synthesis and design

18 p3230 A70-36000

Fundamental microwave oscillator subharmonic phase locking for stable power, comparing with varactor frequency multipliers

19 p3386 A70-37689

Microwave power transistors, considering figure of merit, performance and packaging

19 p3386 A70-37691

Adiabatic microwave power meter design using sodium thiosulfate phase transformations

19 p3422 A70-37743

He-Ne laser with conical discharge tube, investigating transverse cross section geometry influence on power gain

19 p3449 A70-38745

He-Xe laser with pure Xe-136 gain cell inside cavity, observing enhanced Lamb dip in power output vs frequency curve

20 p3640 A70-39154

Infinite periodic phased array over ground plane with dipole elements in parallelogram lattice, calculating driving impedance and gain loss due to mismatch

23 p4172 A70-44004

Continuous channel electron multipliers /Channeltron/ gain improvement via blanking method avoid detection of unwanted particles

23 p4197 A70-44477

Nitrogen laser pumped exciplex 4-Methylumbelliferone and rhodamine 6G dye laser amplifier, measuring single pass power gain vs wavelength

24 p4355 A70-46088

POWER GENERATORS

U ELECTRIC GENERATORS

POWER LIMITERS

Hybrid ring microwave power divider /rat race/ for equal or unequal power splitting

13 p2377 A70-29061

POWER LINES

Conducted interference on input power lines of AC to DC power supplies with diode rectification and smoothing capacitors predicted by Fourier analysis

01 p0049 A70-10089

Multipolarized radar imagery for detecting high return linear cultural features in geographic areas including channel markers, bridges, railroad and power-line networks, etc

12 p2228 A70-26911

Electromagnetic interference filters design for equipment power lines from electromagnetic compatibility and reliability viewpoints

12 p2201 A70-28129

Connectors for superjet airliners, discussing butyl rubber grommet, power distribution collector, modular terminal blocks and passenger service connector

16 p2878 A70-33956

POWER PLANTS

Thermo-elastic analysis and optimum start-up in power plant, discussing transfer function for thermally loaded bodies with restricted boundary temperature

09 p1774 A70-22584

Rotary piston engine for powered gliders and light aircraft power source by modifying industrial Wankel engine

17 p3147 A70-34690

POWER SERIES

NT MACLAURIN SERIES

NT TAYLOR SERIES

Free vibrations of layer of micropolar continuum, analyzing displacements, microrotations and frequencies as wave number power series

04 p0777 A70-15498

Parametric interactions in three frequency TWT parametric amplifier, using power series

05 p0824 A70-16895

Shell shear strain determined by expanding displacement vectors into covariant power series of distance from middle surface [DFVLR-SONDDR-23]

05 p0955 A70-17078

Convergent power series solution for holonomous mechanical systems stability described by ordinary and partial differential equations

07 p1334 A70-19545

Plasma flow structure near frontal point in earth magnetosphere, using quasi-hydrodynamic two dimensional model to obtain power series solution

07 p1391 A70-20419

Point boundary value problem solution for differential equations with parameters in form of power series, considering Cauchy problem

09 p1712 A70-23383

Power series solution convergence of differential equations system, changing independent variable by conformal mapping

10 p1909 A70-24181

Nonlinear time-invariant lumped parameter dynamic systems, determining mathematical model by piecewise continuous power series expansions

15 p2768 A70-32576

Power series solutions to linear and nonlinear differential equations in region of asymptotic stability

18 p2379 A70-36155

Shell theory for shear deformations in covariant notation involving displacement power series expansion

18 p3337 A70-36371

Thin elastic conical shell axisymmetric solution for free vibration in terms of power series

19 p3545 A70-38335

Criterion for global asymptotic stability of system with power-law nonlinearity, reducing to Nyquist criterion for linear system cases

22 p4063 A70-43428

Heat conductivity problem of body with variable density and specific thermal conductivity reduced to differential equation via power series

23 p4277 A70-44340

POWER SPECTRA

Gas laser beams divergence at various laser power levels vs resonator nonconfocality

01 p0106 A70-10062

Noise power spectrum characteristics for He-Ne laser as function of discharge characteristics, measuring effect of cold vs hot cathodes

01 p0111 A70-10745

Fourier transform applied to power spectral distribution determination for two dimensional Fraunhofer holographic data of thin spherical lenses

01 p0090 A70-10907

Numerical solutions for laser-beam intensity focused by simple lenses with varying primary spherical aberration, demonstrating isophote nonuniformity role in biomedicine

01 p0114 A70-11650

Power spectrum of backscattered radiation from turbulent reentry wake illuminated by radar pulse train, discussing electron density decay and pulse shape effects

03 p0408 A70-13585

Power spectral density functions of vertical gust velocities, comparing theoretical results and C-141A flight test measurements

04 p0624 A70-15384

Power distribution in carbon dioxide laser resonator with external and internal mirror at different power levels

05 p0857 A70-15796

Power spectra of pulsar radiation intensity fluctuations, showing line structure

05 p0921 A70-16983

Photoelectric multislit micrometer for astronomical purposes, presenting stochastic variables mean error difference formula for arbitrary power spectrum

06 p1071 A70-18458

Pulsar short term pulse energy fluctuations presented in pulse amplitude histograms and power spectra

07 p1389 A70-20219

Radio wave reflection coefficient power spectra for three layer lunar surface models consistent with radar spectrum, calculating porous layer thickness

08 p1563 A70-20566

Electron paramagnetic resonance absorption curve influence on power transfer characteristics and maximum passband of multicavity maser

09 p1695 A70-22278

Power spectrum of light scattered by two level atom driven by monochromatic electric field obtained from atomic dipole moment correlation function

10 p1920 A70-24632

Airborne remote sensing automatic data processing for forest identification through pattern discrimination, utilizing power spectrum analysis

10 p1878 A70-24734

Power spectral density and autocorrelation functions of sinusoidal carrier amplitude modulated by split phase PCM and PSK

11 p2008 A70-26203

Solar wind magnetic field power spectra and plasma velocity, discussing turbulence, viscosity and dissipation

11 p2106 A70-26770

Cosmic ray intensity fluctuations at geomagnetic equator using power spectrum analysis on mu meson records, discussing solar photosphere and interplanetary magnetic field

12 p2291 A70-27176

- Green light laser using sodium fluorescein pumped by xenon pulse tubes, describing output power spectral characteristics 12 p2246 A70-27316
- Aircraft dynamic response to homogeneous isotropic atmospheric turbulence analyzed for power spectral density, taking into account spacewise variations in airframe loading [AIAA PAPER 70-544] 13 p2345 A70-29010
- He-Ne laser beam transmission through atmosphere, investigating intensity, spot size, polarization and power spectrum fluctuations 13 p2427 A70-29103
- Si solar cell power output and spectral response as function of angle illumination, eliminating atmospheric influence 14 p2533 A70-30337
- Wind gust data analysis for spacecraft design using power spectrum approach 14 p2607 A70-30580
- Atmospheric wind profiles and boundary layer turbulence power spectra for calculation of wind loads on space vehicles during prelaunch and launch 14 p2653 A70-30600
- Time autocorrelation and power spectrum of radar returns from underdense turbulent ionized gas as function of electron density decay 14 p2551 A70-31035
- Radio wave reflection coefficient power spectra for three layer lunar surface models consistent with radar spectrum, calculating porous layer thickness 15 p2805 A70-32721
- Laser energy and power measurement with thermal gradient radiometer 17 p3104 A70-35082
- Pi 2 pulsation power spectra change with magnetospheric substorm development, relating pulsations and electron precipitation 17 p3080 A70-35641
- Gain and loss processes in GaAlAs-GaAs heterostructure lasers as functions of current and cavity length 18 p3268 A70-36728
- Power spectrum analysis of division errors of graduated circles associated with meridian astronomy 19 p3523 A70-38686
- Pulsars CP 0834, AP 1237 and CP 1919 radiation intensity periodic variations, discussing power spectra fluctuations in circulating plasma model 20 p3701 A70-39007
- Electron density irregularities convected past space probe relationship to radio intensity power spectrum scintillations 20 p3703 A70-39023
- Simulated neutral atmospheric boundary layer measurements in wind tunnel, extending power spectral and correlation determinations 20 p3613 A70-40139
- Inner magnetosheath large amplitude hydromagnetic waves, discussing power spectrum, earth bow shock and solar wind 21 p3816 A70-41083
- Electromagnetic scattering power spectrum from underdense turbulent plasmas, deriving first and second moments 21 p3858 A70-41732
- Unipolar pulse frequency modulation system with white noise input, deriving output power spectral densities 21 p3793 A70-42225
- Electromagnetic radiation power spectrum scattered by relativistic particles, considering reflected waves resemblance to HF radio spectra of quasars 22 p4100 A70-42856
- Pulsars null pulse spacing significance, determining fluctuation power spectrum 23 p4238 A70-43814
- Antenna radiation pattern modeling by power optimization under constraints 23 p4175 A70-44800
- Sco XR-1 optical intensity power spectra oscillations searched for in pulsar frequencies and fundamental radial mode vibrations in white dwarfs and neutron stars 24 p4410 A70-45762
- Power spectrum of digital signals pulse modulated with random sequences, discussing phase modulation and z transform techniques 24 p4315 A70-46151
- POWER SUPPLIES**
- Conducted interference on input power lines of AC to DC power supplies with diode rectification and smoothing capacitors predicted by Fourier analysis 01 p0049 A70-10089
- Power sources - U.S. Army Conference, Atlantic City, May 1969 08 p1438 A70-20701
- Microwave sources power stabilization, control and noise reduction using feedback techniques 09 p1649 A70-23275
- Semiconductor power controllers for switching aircraft electrical power supplies [SAE PAPER 700308] 12 p2195 A70-27451
- Harrier fighter aircraft electrical supply system, considering generator design and installation 12 p2166 A70-27891
- Homopolar Inductor Alternators of minimum weight and maximum efficiency for aerospace power supplies 15 p2710 A70-32587
- Circuit design characteristics and reliability relationship in electronic power supplies for performance requirements 15 p2712 A70-32644
- Aircraft electric power generators performance, discussing transients, modulation and regulation of voltage and frequency 16 p2844 A70-33487
- Magnetomotive tools and power systems for maintenance, repair and assembly in space weightless environment 19 p3436 A70-37949
- Low noise requirements of DC current sources used in circuit design 21 p3797 A70-40854
- Propulsion control integration for aircraft power management [SAE PAPER 700818] 24 p4394 A70-45899
- Gas tight lead storage battery with negative plates for oxygen absorption 24 p4295 A70-46352
- Batteries and fuel cells as portable and transportable electrochemical power sources 24 p4295 A70-46399
- POWER SUPPLY CIRCUITS**
- Power supply equipment with automatic control for category 2 airport lighting, discussing reliability and economic efficiency 01 p0055 A70-10300
- Exponential pulse time converter investigated for effect of supply voltage variations on duration of generated pulses 08 p1474 A70-21232
- Stand-by power supply for emergency lighting of Hamburg airport, discussing circuit connections for generators 08 p1482 A70-21371
- Power sources, transfer and conditioning subsystems design, fabrication and testing for high power communication satellites [AIAA PAPER 70-433] 11 p2120 A70-25438
- Ignitron converters for feeding power plasmotrons and arc reactors, describing circuit and operation 11 p1984 A70-26742
- Hybrid ring microwave power divider /rat race/ for equal or unequal power splitting 13 p2377 A70-29061
- Hydrogen oxygen fuel cells, demonstrating matching of power source and load, charge transfer, porosity, Nernst equation and electrochemical water synthesis 14 p2533 A70-30533
- Switch controlled resonant current pulse modulation for power converters, noting integration with spacecraft ion propulsion engine 14 p2535 A70-31324
- Zener diodes as voltage transient suppressors for ground vehicle and aircraft power supplies 16 p2879 A70-34060
- Solid state multiplexed electrical power distribution system for future generation military and commercial airplanes [SAE PAPER 700301] 18 p3216 A70-36803
- Aircraft electrical system multiplexing, discussing design features and advantages over conventional hard wired systems [SAE PAPER 700303] 18 p3216 A70-36811
- Normal mode pulsed ruby laser system with Xe flash lamp pumping, trigger circuit and transistorized power supply 20 p3643 A70-40355
- Optimum junction area for maximum microwave output power of silicon IMPATT diodes for X band operation 23 p4167 A70-43775
- POWER TRANSMISSION**
- Gear ratios series determination for planetary reduction gear having positive and negative difference between number of gear teeth 05 p0856 A70-17007
- Quasi-optical power transmission in overmoded waveguides in interferometers, millimeter wave spectrometers, polarizers, etc 14 p2556 A70-30447
- Helicopter mechanical power transmission design, describing gearing, shaft bending, bearings, lubrication, weight factors, etc [SAE PAPER 700844] 20 p3563 A70-40367
- POYNTING THEOREM**
- Poynting flux direction for proton whistlers determined from Injun 5 observations, obtaining data on source region and propagation in ionosphere 03 p0477 A70-13987
- Axially symmetric parabolic reflector with incident linearly polarized plane wave, determining Poynting vector behavior 17 p3043 A70-34615
- Electromagnetic wave Poynting vector trajectories in absorbing inhomogeneous media, discussing reversibility and energy propagation of spherical and plane structures 18 p3293 A70-36144
- PPI [POSITION INDICATORS]**
- U PLAN POSITION INDICATORS
- PPM [MODULATION]**
- U PULSE POSITION MODULATION
- PRACTICES**
- U PROCEDURES
- PRANDTL NUMBER**
- Mixing length relationship in Prandtl theory for turbulent channel and pipe flow, deriving universal velocity distribution law 02 p0277 A70-11911
- Transient heat transfer in forced convection flow over curved wall with zero Prandtl number, applying to laminar boundary layer with variable free stream velocity 02 p0400 A70-12857
- Book on flow and thermal boundary layers covering laminar and turbulent flow velocity profiles, Prandtl equation, heat transfer problems, etc 03 p0465 A70-13015
- Laminar sublayer resistance to momentum and heat transfer, noting effects of Prandtl number and surface roughness using mathematical model and experiments 06 p1034 A70-17680
- Heat transfer from constant temperature and heat flux surfaces to viscous fluids with high Prandtl numbers, considering transient and steady state flow 06 p1176 A70-17687
- Temperature gradients, viscosity and conduction measurements in air stream between parallel plates, investigating limiting value of total Prandtl number 07 p1260 A70-19999
- Turbulent Prandtl number and eddy viscosity distribution in thermally stratified turbulent boundary layer of air shear flow dependent on wall distance and thermal stability 08 p1599 A70-21581
- Heat transfer coefficient to gas in tube under unsteady heat flow conditions, studying Nusselt number dependence on Reynolds and Prandtl numbers 09 p1787 A70-22173
- Thermal boundary layer similarity at extreme Prandtl numbers as series expansion, allowing for temperature distribution at wall 11 p2148 A70-25983
- Turbulent Prandtl number values for air with injection and suction obtained from velocity and temperature profile data 12 p2210 A70-27699
- Prandtl number effects on adiabatic wall temperature and pressure gradient at separation point for hypersonic compressible laminar boundary layer 14 p2566 A70-31027
- Laminar compressible flat plate boundary layer dependence on Prandtl number and viscosity- temperature relations 16 p2893 A70-33673
- Convective flow stability in rotating fluid layer under rigid boundary conditions, calculating critical Taylor number as function of Prandtl number 16 p2893 A70-33686
- Outer boundary conditions derivation from asymptotic form of similar boundary layer equations with unit Prandtl number 16 p2894 A70-33874
- Steady turbulent flow heat exchange in near wall region at large Prandtl numbers, plotting temperature distribution curves 20 p3612 A70-39811
- Turbulent heat exchange coefficient and Prandtl number in turbulent air flow through heated pipe with constant heat flux 23 p4183 A70-44740
- Unsteady incompressible thermal boundary layer flow past three dimensional obstacle for Prandtl numbers near unity 24 p4428 A70-45366
- PRANDTL-MEYER EXPANSION**
- NT THERMAL BUCKLING
- PRASEODYMIUM**
- Electronic absorption spectra of single crystal praseodymium acetate tetrahydrate in natural and polarized light 19 p3488 A70-38742
- PREAMPLIFIERS**
- X band electron paramagnetic resonance spectrometer with ruby maser preamplifier, correcting misinterpretation and noise figure analysis 01 p0114 A70-11196
- Low noise wideband uncooled preamplifier for small unattended satellite communication terminals, discussing theory, design and performance [AIAA PAPER 70-419] 11 p2016 A70-25485
- Parametric amplifier as preamplifier for microwave receivers in space probes, presenting block diagrams and test results 13 p2379 A70-29559

PRECAMBRIAN PERIOD

- Major and trace element concentration in contact zones of Precambrian diabase dikes from Wyoming ranges, showing dikes as continental tholeiites 03 p0472 A70-13148
- Early Precambrian chert porosity and permeability, investigating hydrocarbon content origin 13 p2400 A70-29863
- Precambrian cherts hydrocarbon and fatty acid concentrations and C and S stable isotope ratios, discussing biological evolution rate 18 p3244 A70-35969

PRECAUTIONS

U ACCIDENT PREVENTION

PRECESSION

NT LARMOR PRECESSION

- Precession motions of rigid body with variable mass, considering angular momentum and rotation stability 01 p0141 A70-10283

- Cyclic bending stress in disk type gyroscope rotor under steady precession, discussing solutions for modal functions and resonant frequencies [ASME PAPER 69-DE-A] 04 p0689 A70-14873

- Helicoidal precession in reentry problem found unstable in sense of Liapunov and Lagrange and asymptotically stable in sense of Poincare 04 p0765 A70-15666

- Deep freezing of nuclear precession magnetometer elements for improving instrument characteristics accuracy 05 p0851 A70-16769

- Precession of aircraft mounted astatic gyroscope under constant and periodic moments of external forces, discussing roll angle and rotor axis deviations from inertia axes 07 p1282 A70-19533

- Book on gyroscope couple stabilizing role on ships, satellites and stabilized platforms, discussing kinetic motion, gyroscopic precession, degrees of freedom, etc 07 p1283 A70-19665

- Cyclic bending stresses in web of precessing disk-type gyroscope rotor, considering fatigue failure and forced vibration response 09 p1770 A70-22270

- Planetary perihelion precession with velocity-dependent gravitational mass in terms of special relativity 09 p1765 A70-23800

- Spin axis motion of n-body coaxially mounted cluster of differentially spinning bodies, considering combined precession and nutation 11 p2123 A70-26128

- Pulsar theory of rotating and precessing neutron stars, rejecting relevance of forced precession to behavior 12 p2308 A70-27884

- Earth rotation perturbations, analyzing secular polar shift dependence on dimensions, depth and location of seismic event 13 p2400 A70-29604

- Earth dipole field disk dynamo model, studying connection between polarity intervals and precession effects 14 p2638 A70-30619

- Rigid body motion about fixed point with angular velocity vector parallel to fixed straight line plane in space and comoving plane 16 p2952 A70-33741

- Precession-nutation dependence on earth structure based on oscillations theory of ellipsoid with rotating fluid contained in rigid envelope 16 p2980 A70-34316

- Precessional stability of rigid body axial rotation in terms of Liapunov, Poincare and Lagrange concepts 17 p3131 A70-35318

- Correctable gyroscope stability estimation by energy method taking into account nutation and precession motions 22 p4039 A70-43556

- Earth quadrupole moment indirect effect on satellite gyroscope precession 23 p4217 A70-43799

- Celestial sphere scanning by spinning symmetric satellite with open loop magnetic control of precession 23 p4216 A70-44524

- Statistical estimates of precessional corrections, solar motion and galactic rotation from proper motions 23 p4246 A70-44752

- Rigid body rotation about fixed point under oscillatory precession and nutation due to noncentral attractive force, showing errors in Euler equations 23 p4247 A70-44792

- Gyroscope system steady states, showing dynamic couplings centering in finite angular precession rate case 24 p4335 A70-45630

PRECIOUS METALS

U NOBLE METALS

PRECIPITATION

- Condensed products of vaporized primordial terrestrial material accounting for moon formation, using single stage precipitation earth origin hypothesis 13 p2488 A70-28719

- Impulsive proton flux precipitation increase during auroral breakup observed by rocket 18 p3245 A70-36021

- Ti alpha alloys subjected to heating in beta region, investigating plate-like precipitates by electron transmission microscopy 20 p3645 A70-39042

- Auroral proton precipitation oval in antarctic winter based on H Balmer line radiation 21 p3882 A70-41091

PRECIPITATION [CHEMISTRY]

- Ni-Cb intermetallics phase precipitation during aging of Inconel alloy 718, composition, stability and structure 01 p0116 A70-10093

- Mo separation from W during chemical analysis of W in binary Mo-W alloys, using organic reagents for precipitation and extraction 03 p0504 A70-12982

- Thin film transmission electron microscopy study of precipitation in Fe-Ni-Cr-Mo alloy with added Be and specific thermoelastic properties 05 p0862 A70-16022

- Urinary calcium phosphate and carbonate precipitates reduction by protein and carbohydrate diet change to casein and sucrose in Macaca nemestrina 09 p1621 A70-23456

- Calcium phosphate crystals precipitation from nutrient gel to determine role of gelatinous ground substance in calcification 10 p1832 A70-25075

- Ti mechanical properties dependence on grain boundary size and hydride precipitation characteristics, considering transcrystalline and intercrystalline fracture 20 p3652 A70-40179

- Addition effects on lattice and electrophysical properties of trititanate prepared by Ba, Pb, Ca and Ti precipitation 22 p4087 A70-43134

- Silicon precipitation in nonrefined annealed Al, examining heat treatment effects 22 p4057 A70-43550

PRECIPITATION [METEOROLOGY]

NT DEW

NT HAIL

NT RAIN

NT SNOW

NT SNOW COVER

- Air flow in updraft through and around cloud region containing precipitation particles using numerical model, computing horizontal divergence 06 p1100 A70-18572

- X band Doppler radar observation of horizontal motion of precipitation particles in low levels of slow moving thunderstorm 06 p1101 A70-18580

- Microwaves scattering and attenuation in precipitations from raindrop size distribution curves analysis 08 p1462 A70-21096

- COMSAT measurement of precipitation scatter effects on propagation for frequency sharing with terrestrial radio relay terminals [ALAA PAPER 70-499] 11 p1997 A70-25413

- Geostrophic wind vector rotation correlated with precipitation and circulation in vertical solenoid field 11 p2076 A70-26074

- Radar measured precipitation increase from seeded cloud demonstrated by measurements, numerical cumulus model and physical reasoning 12 p2189 A70-28094

- Global weather prediction network economic benefits to key industries, discussing adverse weather effects on production schedules, fuel supplies, construction, harvesting, etc 14 p2610 A70-31143

- Clouds and precipitations radio brightness temperature contrasts taking into account underlying surface humidity 15 p2771 A70-32070

- Soviet book on aircraft electrification in clouds and precipitation during subsonic flight covering atmospheric electrical properties, flight dynamics modification, communications interference, etc 19 p3356 A70-38800

- Cetyl alcohol and water vapor growth by absorption and condensation on hygroscopic nuclei population in atmosphere under cooling 20 p3664 A70-40066

- Nighttime and daytime midlatitude magnetic bays statistical correlations with riometer-auroral absorption, suggesting precipitating particles role 22 p4018 A70-43107

PRECIPITATION HARDENING

- Coherent precipitates effect on explosive shock hardening of pure nickel and Inconel alloy sandwich assemblies determined from simultaneous shock loading at specific pressures 01 p0116 A70-10107

- Precipitation in Ni-base superalloy analysis with dark field electron microscopy and electron and X ray diffraction 01 p0119 A70-10730

- Intrinsic/extrinsic stacking fault pairs observed during creep of single crystals of gamma prime precipitation hardened Ni-base alloy, developing viscous slip model 01 p0119 A70-10731

- Strain field association with random TaC precipitate particles in austenitic stainless steel shown by electron microscope 01 p0123 A70-11242

- Ferrite and martensite precipitation hardening in Fe-Ni-Mo alloy, studying dislocation structure and aging kinetics 01 p0123 A70-11243

- Age hardening characteristics of maraging martensite stainless steels containing Mo and Co subjected to subzero treatment 01 p0125 A70-11641

- Embrittlement in martensitic and semiaustenitic precipitation hardening stainless steels upon exposure to high temperatures to determine causation and controlling means 03 p0506 A70-13132

- Ni-Nb intermetallic compound precipitation effect on various phase formations in strained samples of Alloy 718 (wrought Ni base alloy) 03 p0511 A70-13568

- Ni-V alloys precipitation behavior with 15.4/16.5 wt percent V content, observing tetragonal equilibrium theta phase precipitation 04 p0708 A70-15368

- Supersaturated Al alloy with Zr addition at high temperatures, showing tetragonal equilibrium phase and intermediate phase with cubic structure 04 p0708 A70-15369

- Ni dispersion-strengthened composites from ultrafine comminuted powders, describing forming techniques and test results 04 p0709 A70-15629

- Interrelation of precipitation state, mechanical properties and electrical conductivity of wrought aluminum age hardened alloy under varied heat treatment conditions 07 p1294 A70-19389

- Ternary Al-Mn alloys precipitation hardening with Cr, V and Ti, investigating ferro and ferrimagnetic phases 07 p1307 A70-19390

- Quadratic precipitate transformation into orthorhombic phase with conservation of maximal atomic density planes in Ni-Cr-Nb and Ni-Cr-Ta alloys during prolonged reheating 08 p1518 A70-21240

- Waspaloy gamma prime solvus temperature relationships as function of solution treatment and precipitation strengthening additives, discussing microstructure and tensile properties 08 p1520 A70-21555

- Dynamic strain aging effect on Mo-Ti-C alloy creep, relating carbides precipitation during plastic deformation to mobile dislocations density 08 p1524 A70-21954

- Precipitation in Fe-Ni-Co maraging alloys produced by austenite plates formation from martensite, discussing effects of Ti addition 08 p1524 A70-21955

- Strengthening mechanisms in dispersion hardened Nichrome /TDNiC/ analyzed in 70-2000 F range, discussing solid solution, dislocation substructure and grain refinement 08 p1525 A70-21961

- Hydrides precipitation in Ti-Al-Mo-V alloys using transmission electron microscopy, discussing crystal structure, activation energy, hydride-matrix phase interface, etc 08 p1525 A70-21964

- Vacuum rolling of high strength hard-workable dispersion-hardened Nb base alloys excluding recrystallization 09 p1692 A70-22756

- Alloying Ni, Cu and Nb effects on grain and strengthening of low carbon precipitation-hardenable ferritic steels 09 p1705 A70-22804

- Internal nitridation temperature effect on dispersion hardening of austenitic stainless Fe-Cr-Ni-Ti steels, investigating interparticle spacing and layer thickness effects 09 p1705 A70-22810

- Precipitation hardened nickel-base alloy microcracking during gas tungsten arc and electron beam welding, studying heat affected zone hardness, phases and grain size 10 p1897 A70-25311

- Hot shortness of molybdenum alloys under tensile testing due to molybdenum carbide precipitation on grain boundaries 11 p2066 A70-25914

- Carbide-strengthened Mo alloys dynamic strain aging processes 12 p2255 A70-27605

- Ni alloys hardening by solid solution precipitation and insoluble particles dispersion, emphasizing heat resistant alloys and mechanical properties 13 p2433 A70-28762

Age hardenable monolithic spring material composed of Ag-Pd-Cu alloys for make-break electrical contact

13 p2376 A70-28839

Carbide precipitation in metastable beta-Ti alloys, noting precipitations confinement to grain boundaries in alloys containing 15 percent Mo

13 p2434 A70-29083

Ti-8Al alloy embrittlement from ordered phase precipitation during aging using tensile, impact and hardness tests, optical and electron transmission microscopies

13 p2436 A70-29624

High temperature transformation of high speed steel low temper hardened in vacuum or atmosphere furnace

15 p2756 A70-31568

Omega phase embrittlement in aged Ti-V alloys, discussing precipitation effect on tensile properties

15 p2756 A70-31570

Cellular precipitation in lamellar eutectic and cast Ni-Cr alloys

15 p2761 A70-32383

Room temperature mechanical properties and structure of age hardened Ti-Cu alloys

15 p2761 A70-32384

Preprecipitation and reversion stages in Ni-Co-Mo steel, observing dislocation nucleated phase growth initiation by aging

16 p2929 A70-33047

Massive eutectic and fine gamma phases precipitation in cast nimonic 100 alloy at 900 C aging

16 p2930 A70-33083

Age hardening process in Ti-Cu alloy at 400 C, using electron diffraction

17 p3119 A70-34416

Solution heat treatment temperature effects on strength and age hardening of Ti alloys

17 p3120 A70-34419

Ti-Cu alloy sheet material age hardening, considering cold and warm work effects at various stages in aging cycle

17 p3121 A70-34430

Precipitation hardening Co-Cu-Mo stainless steels, determining martensitic structures free from delta ferrite and residual austenite

18 p3262 A70-35965

Ti-Al binary and Ti-Al-X ternary alloys grain boundary precipitation kinetics and correlation with mechanical properties

18 p3272 A70-36035

Carbide precipitation and grain boundary migration in solution annealed duplex stainless steel as function of aging time

18 p3274 A70-36050

High temperature reaging in Ni-Cr-Ti austenitic steel following reversion and interrupted quenching

18 p3274 A70-36054

Ti-Al alloys room temperature mechanical properties after age hardening

18 p3274 A70-36055

Dispersion hardened Co strength and plasticity temperature dependence, determining Ti and Nb carbides additives effects

19 p3450 A70-37350

Plastic deformation in Ni-Cr-Nb alloy precipitation hardened at different long terms of high temperature

19 p3451 A70-37706

Age hardening of Nb-Hf-C alloys investigated by metallography and X ray diffraction, discussing tests in various temperature ranges

19 p3452 A70-37826

Interstitial oxygen effect on properties and precipitation processes in pure V and V-Ti alloys, using electron microscope

19 p3454 A70-38812

Dispersion strengthened Ni-Cr alloys creep properties, investigating temperature, applied stress and thorium dioxide particles effects

20 p3644 A70-38984

Fe-Ni-C alloys austenite dispersion matrix effects on martensite structural characteristics

20 p3649 A70-39705

Mg-Al alloy beta phase precipitation, using metallography, hardness tests and electron microscopy

20 p3652 A70-40447

Stacking faults in gamma prime precipitation hardened high temperature Ni base alloys, relating fault energy to strength

22 p4053 A70-42728

Ni base superalloy for gas turbines, describing heat treatment for precipitation hardening

22 p4055 A70-43099

Ni-Fe-Cr-Nb alloy, investigating precipitation hardening of Ni3Nb phases by transmission electron microscopy

24 p4357 A70-45226

Superalloys dispersion strengthening and age hardening by mechanical alloying

24 p4341 A70-45246

Prestraining effect on cellular precipitation in Ni-Cr lamellar eutectic during creep testing

24 p4359 A70-45247

Heat treatment effects on dispersion strengthening of Ni alloys, showing enhanced long term creep strength at 1100 C

24 p4360 A70-45828

Fe-Ni-Co martensitic alloys isothermal age hardening, comparing bcc phase energy parameters of binary systems

24 p4362 A70-46182

Niobium nitride precipitation associated with stacking faults in Cr-Ni-Nb austenitic stainless steels, using electron microscopy

24 p4365 A70-46369

PRECIPITATION PARTICLE MEASUREMENT

Size distribution of Ni-Si particles precipitated from Si solid solution in Ni measured as function of concentration, aging time and temperature

02 p0317 A70-12320

Soviet collection of articles on physics of clouds modifications covering precipitations microstructure remote measurements, microwave scattering, etc

08 p1536 A70-21094

Precipitations microstructure remote measurements using Doppler method and attenuation coefficients measurements, estimating errors

08 p1536 A70-21095

Electro-optical technique for size distributions of cloud and precipitations particles using linear array of photodetectors

10 p1912 A70-23929

Atmospheric particles photographed in situ by cameras using microsecond flash lamps, discussing required mechanical motion compensation at aircraft speed

10 p1886 A70-23930

Airborne precipitation drop sampler imprint size relationship to water drop diameter

10 p1857 A70-23932

High sensitivity particle spectrometer for onboard OV-1-18 satellite measurements of precipitating protons, electrons and alpha particles during PCA events

12 p2232 A70-27402

Weather radar signal processing and data recording at National Severe Storms Laboratory /NSSL/, providing reduction in echo variations due to relative motion of precipitation elements

13 p2363 A70-28774

PRECONDITIONING

Precorrosion effects on strained Al alloy electrochemical response, examining strain test results graphically

19 p3451 A70-37780

Thermal preconditioning unit using radioactive isotope heat source for temperature control of inertial navigation system

20 p3671 A70-40059

PRECOOLING

Precooling effect on load carrying capacity of heat resistant plastics subjected to unilateral heating

05 p0874 A70-17065

Heat tolerance time extension due to prior body cooling observed in aircrew subjected to heat stresses

10 p1824 A70-24036

PREDICTION ANALYSIS TECHNIQUES

Selection of uncorrelated measurement composition ensuring optimal accuracy of space vehicle trajectory

10 p1939 A70-24301

Parameter estimates effectiveness from independent discrete and continuous navigation measurements of circular orbital plane

10 p1914 A70-24303

Flying accident liability predictions reliability from pilot trainee aptitude test performance at selection, discounting accident proneness theory

12 p2178 A70-27048

Coronal structure prediction for 7 March 1970 solar eclipse, using model for 22 September 1968 eclipse

12 p2304 A70-27718

Wind tunnel tests, analytical methods and fixed base simulation for predicting fighter aircraft spin characteristics

[AIAA PAPER 70-565]

13 p2346 A70-29030

Performance cost functions for reaction-jet controlled spacecraft during on-off-on limit cycle

13 p2382 A70-29072

Solar activity predictions for earth upper atmosphere models emphasizing linear repression method

14 p2638 A70-30565

Wing section pressure distributions, lift and drag in transonic mixed flow, considering prediction methods

14 p2529 A70-30866

Predicting retention rate of naval pilots and flight officers beyond initial obligated duty tour based on training performance

15 p2690 A70-31888

Filter parameter estimation in serially correlated measurement noise, using recursive least squares analysis

15 p2704 A70-32591

Broadband and narrowband pulse signal noise electromagnetic interference prediction techniques for filter or shielding parameters evaluation

16 p2862 A70-33065

Mechanical properties prediction analysis of boron filament wound reinforced composite structures verified by structural tests

16 p2937 A70-33370

Instantaneous burning rates prediction methods based on flame structure model and steady state burning rate data as pressure and initial temperature functions

[AIAA PAPER 70-667]

16 p2971 A70-33949

Optimal filters design predicting electronic systems parameters, preventing equipment failure due to wear and aging

17 p3055 A70-35744

Reliability figure of merit variations for predicted microwave radio system outages, using computer method

20 p3583 A70-38987

Aerodynamic heating prediction methods for delta body space shuttle orbiter, comparing with wind tunnel test data

21 p3744 A70-41016

State space method for small signal lumped IM-PATT diode model predicting small signal impedance

22 p3998 A70-43251

Sunspot number prediction from solar cycles statistical analysis

23 p4254 A70-44902

PREDICTIONS

NT IMPACT PREDICTION

NT LINEAR PREDICTION

NT PERFORMANCE PREDICTION

NT ROSKHO PREDICTION

Graphical display of diverse methods of flow predictions by various authors for turbulent boundary layers

02 p0287 A70-12363

Visual prediction accuracy in estimating point coincidence of two moving targets as function of viewing opportunity and length of period

03 p0428 A70-14084

Generalized approach for optimal corrector in mean squared sense for predictor-corrector filter structure, illustrating signal modes with nonlinear and linear dynamics

03 p0520 A70-14170

Stochastic predictor model for process, control, discussing multivariable search techniques and effect of forcing function and noise

10 p1856 A70-24872

Minimax one step and recursive nonlinear predictors for linear discrete time-invariant first order plant driven by unknown bounded forcing function

12 p2204 A70-28069

Choice prediction in partially repeatable decision situations, discussing phenomenological analysis

19 p3366 A70-38504

Modified McNish-Lincoln method for Zurich sunspot numbers prediction, adapting for computer operation

20 p3704 A70-39410

PREDICTORS

U PREDICTIONS

PREFLIGHT ANALYSIS

Shock tunnel preflight assessment of Apollo Block 2 command module base heating

07 p1394 A70-19722

Boeing 747 pretesting work including wind tunnel, components, engines and static structural tests, flight simulation, etc

08 p1437 A70-21730

Navigation correction systems for space missions, discussing prelaunch analysis, design and mission operations, hardware, etc

13 p2448 A70-28705

Apollo telescope mount postmanufacturing checkout under simulated mission environment, ensuring flight readiness

16 p2889 A70-33723

PREFORMS

Matched die molding technology working principles, mat materials, mold taper, preforms, etc

05 p0856 A70-16613

PREHEATERS

U HEATING EQUIPMENT

PREHEATING

U HEATING

PREIMPREGNATION

Bag molding process for molding laminates of reinforced preimpregnated material containing thermosetting resin

05 p0856 A70-16612

PRELAUNCH PROBLEMS

Saturn 5 Prelaunch Systems Simulation Model for launch opportunity containing multiple launch windows, considering last 26 hours of countdown

08 p1582 A70-20933

PRELAUNCH TESTS

NT STATIC FIRING

Prelaunch photometric calibration of Surveyor TV system for reconstruction of lunar terrain televised pictures permitting system lunar performance prediction

[AIAA PAPER 68-1138]

04 p0692 A70-15405

Computer aided on-line test generation for prelaunch checkout, describing interpretive test language for rapid man machine information transfer [AIAA PAPER 70-384] 10 p1846 A70-24921

Prelaunch dynamic response test parameter selection for control systems for space complexes with form of Nyquist locus 13 p2381 A70-28423

Spacecraft onboard computer for prelaunch targeting constants verification through checksum equation and error detection scheme, using generated number sequence [AIAA PAPER 69-946] 14 p2599 A70-30769

PRELOADING

U PRESTRESSING

PREMATURE OPERATION

Scout missile destruct charge system premature operational response to high temperature environment caused by combustion gas leak during stage separation 03 p0550 A70-14140

PREMIXED FLAMES

Premixed perchloric acid-methane two flame structure, measuring burning velocities, spectra, temperatures and burned gas compositions 02 p0352 A70-12034

Light scattering from thermally stable magnesium oxide particles in premixed turbulent flames used for measuring mean and fluctuating temperature values 02 p0398 A70-12039

Noise generation in turbulent premixed flames, turbulent diffusion flames and liquid-spray combustion of hydrocarbon fuels, using optical method 02 p0399 A70-12040

Cold ducted supersonic flow of premixed ethylene and air ignited by hot turbulent jet [AIAA PAPER 70-148] 06 p1131 A70-18057

Premixed compression initiated supersonic combustion, noting sensitivity to small perturbations in inlet flow variables [AIAA PAPER 68-995] 07 p1421 A70-19318

Premixed flames of methane with chlorine dioxide and perchloric acid, comparing properties with methane-oxygen flames, suggesting unified reaction mechanism 07 p1425 A70-20007

Ammonium perchlorate combustion catalysis, studying preflame heating and mixing effects on gas phase flame burning velocity 07 p1425 A70-20010

Monograph on convective heat flow in stagnation points of turbulent partly premixed free jet flames at cooled plates 08 p1598 A70-21343

Perfluoropropene, -cyclobutene and -cyclobutane mixing with atmospheric pressure oxygen to determine burning velocities 11 p2100 A70-26383

Carbon dioxide molecular vibrational energy levels above carbon monoxide-oxygen premixed flame, discussing vibration modes leading to population inversion and relaxation time variance 13 p2455 A70-29132

Microstructure and reaction kinetics of flat premixed fuel-rich hydrogen-oxygen-nitrogen flame at atmospheric pressure 16 p2998 A70-33900

Premixed laminar flames of hydrogen, oxygen and nitrogen burned on Meker burner, investigating diffusional effects on gas composition changes 20 p3739 A70-40469

Ion concentrations in premixed propane-air two dimensional laminar nozzle burner flames with seeding, discussing dependence on temperature and equivalence ratio 21 p3772 A70-40880

Book on stationary flame structure, radiation and temperature covering flow visualization, burning velocity, propagation, ionization, etc 22 p4121 A70-42325

Chemical equilibrium premixed flame composition at given temperature, pressure and mixture strength, using Newton-Raphson iteration technique for simultaneous nonlinear equations 23 p4157 A70-43892

PREPARATION

NT PRECONDITIONING

NT PRESTRESSING

NT PRETREATMENT

PREPOLYMERS

NT DIMERS

Low melt viscosity prepolymers of diallyl phthalate and isophthalate in mold encapsulation showing dimensional, electrical and mechanical stabilities under adverse environments 05 p0869 A70-16035

Butadiene prepolymers containing carboxyl functional groups used in binder matrix for solid composite propellants 07 p1360 A70-19911

Saturated hydrocarbon prepolymers for solid propellant elastomeric binders 21 p3865 A70-42144

Propellant binder prepolymers functionality distribution, examining solute concentration, solvent

type and temperature effects on number average molecular weight measurements 21 p3865 A70-42146

PRESBYOPIA

Near visual acuity requirements in flight deck from examination of presbyopic pilots, discussing instrument panel visibility 09 p1628 A70-23469

PRESENTATION

Presentation styles of passenger emergency evacuation briefing cards, noting preference for sequential action graphic displays with minimum key wording 23 p4141 A70-44486

PRESINTERING

U SINTERING

PRESSING [FORMING]

NT STAMPING

Press load prediction for deep drawing Ti-Al-V alloy, stainless steel and Inconel X under various lubrication conditions at room temperature [ASME PAPER 69-WA/PROD-15] 04 p0698 A70-14835

Ti alloy aircraft parts heavy press forging, considering mechanical properties, temperature effects, cost factors, etc 17 p3097 A70-34360

Matched-die compression molding of complex shape structures from composite materials [SAE PAPER 700751] 24 p4348 A70-45874

PRESSORS

U VASOCONSTRICTOR DRUGS

PRESSURE

NT ATMOSPHERIC PRESSURE

NT BASE PRESSURE

NT BLOOD PRESSURE

NT CRITICAL PRESSURE

NT DENSIFICATION

NT DYNAMIC PRESSURE

NT ELECTRON PRESSURE

NT GAS PRESSURE

NT HIGH PRESSURE

NT HIGH VACUUM

NT HYDROSTATIC PRESSURE

NT HYPERTENSION

NT HYPOTENSION

NT HYPOXEMIA

NT ILLUMINANCE

NT IMPACT LOADS

NT INLET PRESSURE

NT INTERNAL PRESSURE

NT INTRACRANIAL PRESSURE

NT INTRAOCULAR PRESSURE

NT LOW PRESSURE

NT LUMINANCE

NT LUMINOUS INTENSITY

NT OVERPRESSURE

NT OXYGEN TENSION

NT PARTIAL PRESSURE

NT RADIATION PRESSURE

NT SOUND PRESSURE

NT STAGNATION PRESSURE

NT STATIC PRESSURE

NT SUPERCRITICAL PRESSURES

NT SYSTOLIC PRESSURE

NT THRUST CHAMBER PRESSURE

NT TRANSIENT PRESSURES

NT ULTRAHIGH VACUUM

NT VACUUM

NT VAPOR PRESSURE

NT WALL PRESSURE

NT WATER PRESSURE

NT WIND PRESSURE

Hyperboloids and paraboloids in flow of Reynolds number 22-65000 and Mach number 10, discussing viscous interactions effects on pressure, drag and skin friction [AIAA PAPER 70-182] 06 p0976 A70-18240

Aeolian regime of Venus surface resulting from high surface temperature and pressure, discussing spurious radar echoes, dust and sand transport and deposition 21 p3885 A70-40929

Einstein-Maxwell fields in presence of matter and pressure, expressing existence conditions in terms of eigenvalues and eigenvectors of Ricci tensor 22 p4074 A70-43206

PRESSURE BREATHING

Control measurements to determine changes in lung volumes, intrapulmonary and intragastric pressure and breathing during submersion in water up to xiphoid process level 01 p0038 A70-10980

Positive pressure breathing effects on cerebral blood pressure and catecholamine content of hypothalamus and adrenal glands in dogs 16 p2849 A70-33997

PRESSURE CABINS

U PRESSURIZED CABINS

PRESSURE CHAMBERS

NT VACUUM CHAMBERS

Missile tracer mixture performance control facility noting chamber for pressure measurement during operation 03 p0544 A70-13758

EKG, EEG, pneumograms and X ray pictures showed no pathological effect after prolonged confinement in sealed chamber having artificial atmosphere with variable gas composition 05 p0810 A70-17121

Pressure chamber with inserted holder for adjusting Fabry-Perot interferometer 09 p1681 A70-23337

Gas transfer through silicone elastomer capillaries wall in variable pressure chamber 14 p2541 A70-30386

NERVA engine chamber pressure control, investigating replacement of TPCV with fluidic vortex valve [AIAA PAPER 70-658] 16 p2970 A70-33620

Instrumentation safety for physiological research in hyperbaric chamber environment, taking into account pressure, isolation, atmosphere, electricity and fire 18 p3222 A70-35939

Human respiration activity measurement in pressure chamber with different pressures and mixture compositions by spiograph equipment 20 p3581 A70-40175

Combustion velocity in high pressure chamber, determining fire mechanism in overpressure environment 24 p4393 A70-45447

Low and high chamber pressure concepts for space shuttle reaction control system [SAE PAPER 700802] 24 p4416 A70-45909

PRESSURE COEFFICIENT

U AERODYNAMIC COEFFICIENTS

PRESSURE DISTRIBUTION

Flow and pressure distribution for large normal injection along surface in supersonic stream solved numerically for two dimensional or axisymmetric body and wedge 01 p0001 A70-10336

Supersonic flow around thin warped delta wing, taking into account current separation at subsonic leading edges for pressure distribution and aerodynamic characteristics 01 p0002 A70-10546

Impingement pressure analysis associated with two phase cryogenic propellant venting to space environment [AIAA PAPER 69-571] 01 p0196 A70-10845

Inviscid surface pressures calculated on slender wedges and cones at low frequencies and large oscillation amplitudes in hypersonic flow 01 p0003 A70-10854

Turbulent boundary layer computations for flows with various pressure distributions 01 p0063 A70-10928

Linear structures response to pressure fields of deterministic excitation with input function spectra as meromorphic functions of wave number and frequency 01 p0208 A70-11191

Boundary conditions for equilibrium diamagnetic plasma in magnetic dipole having constant and isotropic pressure in system 01 p0153 A70-11631

Atmospheric transmittance line by line calculations along variable pressure and mixing ratio paths from 1.7-20 microns [AFCLR-70-0061] 02 p0289 A70-11908

Average pressure at downstream end of pipe discharging into reservoir with upstream end under pulsed flow, considering application to pneumatic control system 02 p0279 A70-12110

Rayleigh step journal bearings, considering pressure distribution, load capacity and attitude angle and optimal film thickness ratio for incompressible fluid lubrication 02 p0307 A70-12167

Walljet in crossflow, discussing characteristics and pressure field on plate, using flow visualization methods 03 p0465 A70-13004

Incompressible gas turbulent jet flow characteristics in subsonic wind tunnel, stressing pressure distribution in recirculation region for interpreting heat transfer in separated flows 03 p0593 A70-13495

Flow parameters of two interacting submerged turbulent jets from rectangular nozzles, determining total pressure profiles of coincident flow 03 p0466 A70-13504

Selectivity and pulsation sensitivity of electroacoustic transducers in turbulent flow under non-coherent reception of random pressure field 03 p0467 A70-13514

Turbulent reattachment of supersonic axisymmetric jet on cylindrical wall in air, investigating wall temperature effect on cavity pressure and heat flux [ONERA-TP-758] 03 p0467 A70-13643

Two dimensional cascade tests of turbine blade airfoil plotted by Legendre hodograph method, discussing pressure distribution measurements 03 p0410 A70-14272

PRESSURE DISTRIBUTION

Current stream function, Hall current density, force densities and pressure distribution for typical MPD thruster

03 p0552 A70-14372

Entrainment rate of ambient medium by MPD arc jet, discussing flow field in and around jet and pressure distribution along vacuum tank wall

03 p0553 A70-14373

Plane shock wave diffraction and reflection at slender wedge in linear approximation, proposing pressure distribution calculation formulas behind shock

04 p0665 A70-14493

Similarity of velocity profiles and pressure distribution of turbulent jet over inclined wall, indicating limitations of Glauert analysis
[ASME PAPER 69-WA/FLCS-1]

04 p0668 A70-14849

Fluid flow at pneumatic network junction, considering junction pressure determination as boundary condition for all transmission lines meeting at junction
[ASME PAPER 69-APM-N]

04 p0627 A70-14862

Static pressure distributions and velocity profiles for Hg flow through circular pipes in transverse magnetic field, studying laminar and turbulent flows

04 p0728 A70-15001

Mounted-above-wing jet engine effect on wing pressure distribution and elevator unit, using fluid mechanical model

[DGLR-69-34]

04 p0735 A70-15146

Unsteady pressure distributions on elastic swept wing upper and lower sides at high subsonic to transonic flow, investigating torsional and bending vibrations

[DGLR-69-31]

04 p0615 A70-15151

Unsteady pressure distributions measurement for oscillating rectangular wing, discussing test results for sub- and transonic velocities

[DGLR-69-32]

04 p0616 A70-15184

Heat fluxes, shear stresses and pressures distribution at spike on body in supersonic flow from asymptotic solutions of Navier-Stokes equations

04 p0673 A70-15232

Fluid mechanical problems with pressure distribution determined by interaction between external supersonic inviscid flow and inner laminar viscous layer

04 p0674 A70-15529

Entrance length and pressure drop in MHD parallel plate channel flow using one parameter Pohlhausen method

05 p0887 A70-15978

Pressure changes associated with surface friction and geostrophic drag coefficient related, discussing mass inflow and outflow

05 p0837 A70-16151

Gas pressure and pressure stratification in sunspot, using curve of growth analysis

05 p0911 A70-16432

Sound pressure field from stationary and moving jets determined from jet and aircraft trajectory parameters

05 p0834 A70-16781

Installed thrust vector for scarfed attitude control nozzles flush mounted with spacecraft cylindrical surface, predicting pressure distributions for internal thrust

06 p1154 A70-17167

Incompressible two dimensional turbulent boundary layer equations with arbitrary pressure distribution solved by weighted residual method
[AIAA PAPER 69-397]

06 p1032 A70-17214

Pressure distribution and drag measurements at flat triangular bodies and rectangular plates with blunt trailing edge in compressible flow

06 p0965 A70-17243

Pressure distribution at circular slender cone with 10 deg semiapex angle in hypersonic vacuum wind tunnel

06 p0966 A70-17251

Two dimensional wing model with harmonically oscillating control surface in transonic range, comparing theoretical with experimental results on unsteady pressure distribution

06 p0966 A70-17252

Laminar hypersonic blunt cone wakes, discussing flow fields and axial static pressure distributions

06 p0968 A70-17553

Gas phase reactions near solid-gas interface of deflagrating double base propellant causing abrupt changes in burning rate-pressure curve
[AIAA PAPER 70-124]

06 p1179 A70-18046

Boundary layer-induced pressures on flat plate in unsteady hypersonic flight calculated using tangent wedge approximation
[AIAA PAPER 70-184]

06 p1039 A70-18095

Pressure distributions prediction on blunt bodies at angle of attack, considering bodies of revolution and large angle cones
[AIAA PAPER 70-208]

06 p0971 A70-18104

Laminar boundary layer on cone at incidence in supersonic flow evaluated by pressure distribution technique, comparing heat transfer, pitot probe measurements, etc
[AIAA PAPER 70-48]

06 p0974 A70-18189

Wall pressure distribution, drag and lift measured on flat plates and wedges at Mach 8 rarefied gas flow for various leading edges

06 p0980 A70-18350

Circular cylinders drag and pressure distribution in hypersonic range between continuum and free molecular flow

06 p0983 A70-18376

Impact tube test to find empirical equation for correcting effect of shear in displacing effective pressure center in viscous flow

06 p1052 A70-18383

Transducer for pressure fluctuations measurement in wide frequency range based on piezoelectric microphones, discussing dynamic characteristics

06 p1071 A70-18472

Electret microphones application for pressure fluctuations measurements on thin aerodynamic profiles noting operation, vibration insensitivity, robustness and cost

06 p1071 A70-18473

Pressure history at end wall of electromagnetic shock tube measured during shock wave reflection by piezoceramic gage

06 p1031 A70-18505

Conical shells stability under uniform pressure, studying varying thickness influence by variational stress and bending equation

07 p1402 A70-19052

Pressure distribution measurement over profile by means of pneumatically activated inductive sensor

07 p1188 A70-19084

Shallow spherical caps elastic buckling under uniform pressure, considering symmetric and asymmetric deformation modes

07 p1405 A70-19252

Real gas behavior effect on shock tube temperature and pressure flow nonuniformity for range of Mach numbers

07 p1257 A70-19337

Viscoelastic perfectly plastic ring failure under uniform external pressure characterized by infinite strain rate occurring at finite value of ring deflection

07 p1416 A70-20300

Wave disturbances in tropical lower troposphere, discussing cross spectrum analysis of wind, temperature, relative humidity and surface pressure

07 p1275 A70-20304

Pressure distribution about finite axisymmetric nacelle determined using Douglas Neumann program for cowl surfaces and inlet external surface

07 p1190 A70-20412

Pressure distribution on flat plate resulting from potential incompressible flow interaction between secondary jet and subsonic mainstream

07 p1190 A70-20415

Laminar radial flow between parallel disks, estimating static wall pressure distribution perturbation caused by characteristic time

08 p1484 A70-21237

Surface roughness effects on measured cross spectral density of wall pressure fluctuations beneath turbulent boundary layer

08 p1486 A70-21859

Wave resistance of pressure field of hovercraft drifting over water surface determined as definite integral based on Wehausen expression

09 p1609 A70-22219

Endurance limit of momentless shells of revolution under uniform internal pressure, deriving differential equations based on aging and creep theories

09 p1779 A70-23096

Blast waves in low Mach number regime with assumption of power law density profile in rear, obtaining particle velocity and pressure distributions

09 p1661 A70-23214

Supersonic flow behind cone, studying bottom pressure and stagnation zone dependence on incident flow parameters and static pressure distribution

09 p1663 A70-23623

Axial tensile stress effects on stability of cylindrical shell under nonuniform external pressure

09 p1786 A70-23721

Pressure and velocity distribution within radial flow gas turbine rotor computed by two dimensional streamline curvature method

09 p1608 A70-23737

Pressure and velocity ratios and energy requirements dependence on flow parameters of cylindrical capsule in horizontal pipeline

09 p1665 A70-23747

Air shock tube driven by exploding mixture of propane and oxygen investigated for shock overpressure variation with distance

10 p1863 A70-23992

Wing in supersonic flow analyzed for surface pressure taking into account nonlinear effects of vibrations

10 p1798 A70-24119

Supersonic transports bow and rear shock pressure jump lower bounds for various physical constraints

10 p1805 A70-24558

Velocity and pressure distribution and flame front shape of confined flame in constant section duct

10 p1969 A70-24786

Extraterrestrial electrical and magnetic fields effect on meteorological observations, noting relationship between atmospheric pressure distribution and ionospheric developments

10 p1913 A70-25269

Pressure anisotropies contribution to solar wind corotation, discussing angular momentum and magnetic field

10 p1935 A70-25285

Monograph on numerical treatment method for harmonically oscillating flows covering pressure distributions, logarithmic singularity, etc

11 p1219 A70-25497

Critical load, force characteristics and pressure variation on blades of axial compressor under rotating stall

11 p1233 A70-25795

Aircraft multicell structures venting problem and pressure calculation

11 p1234 A70-25863

Eccentric cylinders with outer cylinder rotating measured for eccentricity and clearance ratios effects on pressure distribution and force on inner cylinder

11 p2060 A70-26409

Cavity pressure and velocities distributions of interfering two dimensional dual jets from parallel slot nozzles

11 p2037 A70-26419

Ring buckling under constant and centrally directed pressure, considering small displacement and inextensional deformation

11 p2141 A70-26492

Wind tunnel interference effect on fluttering airfoils and panels supersonic speeds, studying pressure distributions for various tunnel aspect ratios and roof conditions

12 p2155 A70-27103

Pressure distribution in two dimensional incompressible potential flow on Joukowski airfoils with normal upper surface spoilers, emphasizing potential flow theory
[AIAA PAPER 67-737]

12 p2155 A70-27193

Pressure fluctuations in acoustic field of boundary layer under slot suction, considering vortex formation and separation on edges

12 p2209 A70-27298

Dispersion relations for linearized Grad equations of three dimensional rarefied gas dynamics, including nonequilibrium pressure term for bulk viscosity

12 p2210 A70-27520

One dimensional perfect gas motion under spatial pressure distribution, investigating self similar solutions

12 p2212 A70-28189

Turbulent boundary layer and base pressure profiles of supersonic flow past conical models in wind tunnel

12 p2159 A70-28229

Pressure distribution over lateral surface of truncated cones in nonequilibrium flow, analyzing physicochemical transformations effect

12 p2159 A70-28246

Turbulent base flowfields in multinozzle configurations, considering adiabatic flow and determining base pressure distribution from reverse jet impingement
[AIAA PAPER 69-570]

13 p2338 A70-28511

Eulerian space-time correlations of velocity and pressure for universal homogeneous turbulence by separating kinematic convection effects of large eddies from velocity assumption

13 p2386 A70-28645

Pressure field equation derivation for hydrodynamic journal bearing in superlaminar regime, using turbulent Couette and screw flow friction correlations

13 p2418 A70-28742

Externally pressurized air journal bearing performance prediction, obtaining pressure distribution by numerical solution of Reynolds equation

13 p2418 A70-28743

Correction to Smyrl results for perturbation pressure in interaction field behind plane shock diffracted by supersonically moving thin yawed wedge

13 p2338 A70-28822

Pressure distributions and heat transfer at wall calculated to investigate supersonic laminar reattachment

13 p2338 A70-28953

Slender bodies surface pressure distribution under various aerodynamic loads, discussing cruciform wing, circular body-slender wing configuration, etc

13 p2341 A70-29749

Surface pressure and heat transfer over blunt conical body in hypersonic flow with uniform mass addition of various gases
[AIAA PAPER 69-716]

13 p2523 A70-29977

Pressure field due to control surface oscillation in subsonic flow, presenting numerical results for rectangular wing

14 p2528 A70-30295

Velocity and pressure distributions of tornado-like two cell vortices within boundary layer, using different assumptions for eddy diffusion coefficient

14 p2604 A70-30547

Wing section pressure distributions, lift and drag in transonic mixed flow, considering prediction methods

14 p2529 A70-30866

Gas kinetic pressure profile and mass density of propagating current sheet in argon pinch discharge, using piezoelectric transducer 14 p2624 A70-31041

Radial static pressure distribution of turbulent jet flow over rotating cylinder with constant curvature 14 p2567 A70-31399

Plasma waves with anisotropic pressure, discussing magnetoacoustic waves integral curves 15 p2777 A70-31476

Wind tunnel tests of flow past oblate ellipsoid of revolution incident on major axis, measuring pressure distribution 15 p2671 A70-31494

Pressure-flow relation for fluid in pipe obeying Casson equation, considering applicability to human blood 15 p2690 A70-31917

Upper troposphere pressure variations through 20 km separation layer, noting interdiurnal temperature changes 15 p2772 A70-32458

Kinetic energy and pressure distribution of three dimensional compressible fluid flow, using invariant transformation of Euler motion equation 16 p2890 A70-33073

F-111A airplane in-flight inlet pressure fluctuations for engine compressor surge, discussing average turbulence factor [AIAA PAPER 70-624] 16 p2840 A70-33543

Hypersonic internal flow investigation by differential equation numerical integration, determining shock shape and surface pressure 16 p2838 A70-33881

Reaction jets for control force generation in supersonic environment, analyzing downstream pressure distributions for two dimensional jet interactions 16 p2838 A70-33890

Pressurized gas bearing flow field, discussing velocity transversal component, pressure distribution and profile 16 p2924 A70-34237

Pressure distribution in moderately loaded self acting journal bearings with incompressible turbulent film, considering end leakage 17 p3101 A70-35147

Pressure distribution measurements on wedges in compressible flow at Mach 0.5-2.2, discussing wedge angle, Mach number and boundary layer thickness effects 17 p3013 A70-35923

Spherical gas lubricated sliding bearing with forced injection, determining pressure distribution by numerical integration 18 p3262 A70-36273

Previous history effect on parameters relation in similar turbulent boundary layers under pressure distributions 18 p3241 A70-36375

Pressure distribution shock pattern and impact wave resistance in frictionless plane parallel and source shaped supersonic flow 18 p3207 A70-36385

Equivalent bodies of revolution method extension for use in semiempirical approximation technique, calculating pressure distribution of nonaxisymmetric blunt bodies 18 p3208 A70-36569

Shallow conical shell stability under uniformly distributed pressure and concentrated force at apex for rigid and free clamping boundary conditions 18 p3341 A70-36589

Limit load of cylindrical shell with rigidly clamped edges under varying pressure and axial force, using Tresca yield condition 18 p3343 A70-36722

Pressure balanced rotor flow path design for mixed flow centrifugal compressors, calculating losses in rotor and diffuser section [ASME PAPER 70-GT-12] 18 p3209 A70-36863

Metal powder rolling process as compaction with plastic particle deformation, deriving pressure distribution on rollers 19 p3434 A70-37451

High temperature convective heat transfer in vortex chamber as function of Reynolds number and geometry, measuring pressure variations 19 p3552 A70-38186

Pressure and velocity distribution inside casing and around impeller of volute pumps, discussing flow at exit and in wedge shape space 19 p3437 A70-38225

Conical convergent nozzles discharge coefficient for varying pressure ratios 19 p3352 A70-38243

Pressure field behind plane shock wave interacting with curved boundary 19 p3406 A70-38447

MHD instability of homogeneous inviscid plasma with finite electrical conductivity and anisotropic pressure, obtaining dispersion equation for model 20 p3677 A70-39048

Pressure and temperature distribution in constant volume viscous Poiseuille gas flow velocity profile 20 p3608 A70-39121

Planetary wind field from observed pressure field by linearized balance equation, assuming solenoidal air motion 20 p3662 A70-39178

Modified linearized transonic flow theory application to pressure coefficient distribution on circular arc bodies of revolution 20 p3608 A70-39614

Cylindrical shells subjected by sectors to constant radial pressure, investigating stress state and deformation 20 p3719 A70-39620

Flow velocity and pressure profiles due to vortex ring confined in cylindrical channel, using electromagnetic analogy 20 p3609 A70-39651

Cylindrical gas suspension lubricating layer pressure distribution calculation by perturbation method, determining angular rigidity 20 p3637 A70-39818

Large MHD generator channel aerodynamics, discussing pressure distributions to stall and stagnation pressure loss 20 p3612 A70-40002

Hypersonic flat and biconvex conical wings, calculating yaw effects on shock shape and pressure distribution 21 p3761 A70-40918

Subcritical viscous flow around arbitrary airfoils, calculating boundary layer effect on pressure distribution from inviscid flow approximation 21 p3744 A70-40924

Dispersion relations for linearized Grad equations of three dimensional rarefied gas dynamics, including nonequilibrium pressure term for bulk viscosity 21 p3807 A70-41168

Rectangular wing with oscillating control surface, measuring induced unsteady pressure field for comparison with computations based on lifting surface theory 21 p3935 A70-41407

Liquid droplet shape effect flow field velocity and pressure distribution over windward surface in high speed gas streams 21 p3809 A70-41762

Axially reciprocating pump, calculating fluid over-flow effect on working cell pressure change 21 p3759 A70-41775

Stress distribution and shape in arbitrarily shaped gore parachute under unsteady pressure distribution during inflation and descent 21 p3752 A70-41819

Pressure field behind shock wave after interaction with nonuniform density region, describing shock front shape 21 p3810 A70-41964

Relative pressure and excitation induction transverse distribution relationship for MHD machine model, assessing dimensionless criteria effect on pressure peaks position 21 p3760 A70-42232

Unsteady supersonic flow around oscillating cross-shaped wing-fuselage system, determining perturbation velocities and pressure distributions 22 p3958 A70-42609

Cylindrical cavity uniform expansion in compressible elastic plastic solid, calculating pressure by similarity solution 22 p4114 A70-42634

Spherical cavity nonuniform expansion in compressible elastic plastic solid, calculating velocity field and pressure by approximate similarity solution 22 p4114 A70-42635

Optimum pressure distribution and airfoil profiles for maximum lift without separation in incompressible flow determined by second order theory 22 p3959 A70-42704

One dimensional perfect gas motion under spatial pressure distribution, investigating self similar solutions 22 p4012 A70-43314

Aerodynamic theory of pressure field induced on lifting surface by isotropic atmospheric turbulence, considering transfer function of Concorde aircraft [ICAS PAPER 70-30] 23 p4138 A70-44104

Pressure distribution, force and heat transfer measurements on varied-configurations of lifting reentry vehicles in hypersonic flow [ICAS PAPER 70-03] 23 p4132 A70-44117

Liquid lubricant unsteady motion and pressure distribution during pivot harmonic vibration in hydrodynamic bearing 23 p4200 A70-44163

Pressure distribution on thin nonlifting airfoils in steady two dimensional flow with freestream Mach number at or near unity 23 p4134 A70-44583

Rocket engine nozzle with wall-mounted obstacle, examining shock front shape, pressure distribution and side force characteristics 23 p4234 A70-44684

Five-moments approximation calculation of magnetoplasmadynamic hydrogen arc radial pressure 23 p4032 A70-10366

profile as function of ambient pressure and superimposed magnetic field 23 p4228 A70-44935

Magnetoplasmadynamic hydrogen arc radial pressure profile as function of ambient pressure and superimposed magnetic field, using thirteen- moments approximation 23 p4228 A70-44936

Pointed ogival body of revolution in supersonic flow field, investigating local pressure distributed by variational methods 23 p4136 A70-44992

Orography and friction effects on numerical forecast of atmospheric pressure variation 24 p4370 A70-45112

Incompressible Newtonian fluid flow between closely spaced corotating disks, showing radial pressure distribution similar to laminar flow 24 p4324 A70-45293

NonNewtonian fluids injection into boundary layer, comparing flow and pressure effects with water injection 24 p4324 A70-45364

PRESSURE DRAG

NT INTERREFERENCE DRAG

NT SUPERSONIC DRAG

NT WAVE DRAG

Wind tunnel tests for engine jet plume effect on boattail pressure drag [AIAA PAPER 70-132] 06 p1038 A70-18050

Circular cylinders drag and pressure distribution in hypersonic range between continuum and free molecular flow 06 p0983 A70-18376

Turbulent boundary layer interaction with wavy wall in wind tunnel, discussing wall pressure drag and surface waves interaction 11 p2039 A70-26538

Pressure distribution and drag for inviscid flow past slender sharp-nosed fuselages and afterbodies at arbitrary transonic Mach numbers [AIAA PAPER 70-556] 13 p2340 A70-29021

Heat transfer and pressure drag of axisymmetric body in hypersonic flow, obtaining minimum energy nose and leading edge shapes by Pontryagin principle [AIAA PAPER 70-825] 16 p3001 A70-33940

PRESSURE DROP

Slip flow of nitrogen gas through long circular tubes, measuring mass flow, pressure drop and cross sectional velocity profiles 06 p1051 A70-18368

Pressure drop at slender profile performing harmonic vibrations near interface between two media of different density solved by numerical method 07 p1254 A70-19079

Viscous fluid flow calculations in fine clearance eccentric annuli allowing for pressure losses in laminar or turbulent flows 07 p1293 A70-19120

Solid layer effect on laminar heat transfer and pressure drop in medium surrounding pipe with liquid flows below freezing point, discussing wall temperature effects 08 p1485 A70-21589

Tape-generated swirl flow of single phase water investigated for heat transfer and pressure drop characteristics [ASME PAPER 68-WA/HT-3] 08 p1600 A70-21829

Human lung and upper airway pressure drop and fluid flow regime of inspired air 12 p2170 A70-27660

Upstream wear of small metal orifices under large pressure drops in phosphate ester hydraulic fluids due to current driven electrochemical corrosion [ASME PAPER 70-FE-15] 16 p2919 A70-33629

Shock tube orifice effect on gas flow velocity and pressure drop, using pressure probes and Jenny friction formula 17 p3069 A70-34699

Axial flow compressor cascades, predicting total pressure losses for inlet relative Mach number greater than unity [ASME PAPER 70-GT-57] 18 p3209 A70-36872

Water and alkali metal boilers, predicting helical-flow-promoting inserts effect on pressure drop penalties by constant slip model 21 p3949 A70-41308

High velocity isothermal viscous compressible steam flow in circular tubes, measuring pressure drops 22 p4011 A70-42845

Jet engine combustion chamber pressure loss, flow velocity through flare tube holes and air supply calculation, noting adaptation for computer use 24 p4393 A70-45446

PRESSURE EFFECTS

Biophysical symptoms and clinical treatment of ailments resulting from pressure drop, considering exposure to higher and lower pressure changes [DVL-894] 01 p0011 A70-10036

Sea-level pressure interval to prevent decompression sickness in humans flying in commercial aircraft after diving 01 p0032 A70-10366

Externally pressurized air journal bearings load capacity, film stiffness, attitude-eccentricity locus and mass flow, studying supply pressure and shaft rotation effects

[ASME PAPER 69-LUB-29] 01 p0100 A70-10380
N atom recombination rate coefficient in static system pressure dependent at low pressure

01 p0147 A70-10450
Book on subatmospheric decompression sickness in man, covering raised intrapulmonary pressure effects and compensating pressure applications

[AGARDGRAPH-125] 01 p0019 A70-10514
Martensite start depressed temperatures vs pressure for steels, discussing hardness effects and microstructure

01 p0120 A70-10740
Thermal and pressure environments analysis in Saturn S-1C stage base during flight tests, noting base gas flowfield and heating

[AIAA PAPER 69-318] 01 p0195 A70-10833
Retinal vessels of humans at 11-2.0 atmosphere oxygen partial pressures, noting arterioles and venules dilation response to hypoxia and vasoconstriction response to hyperoxia

01 p0023 A70-10863
Elastic properties of thin curved cylindrical panels with constant mechanical properties subjected to thermal expansion and single face pressure

01 p0201 A70-10943
Pressure effects on burning rate of magnesium mixtures with solid oxygen containing organic compounds, determining charge density effect on mass velocity

01 p0218 A70-11021
Carbon dioxide refractivity measured under simulated Martian conditions and standard temperature and pressure, comparing results with radio occultation methods

01 p0186 A70-11085
Volterra equations for stresses, strains and displacements of viscoelastic tube with variable radius encased in shell under pressure and unsteady temperature field

02 p0384 A70-11663
Phase diagrams for binary mixtures at high pressures suggesting layered structures existence in Jupiter and Saturn atmospheres resulting from phase separations in hydrogen-helium mixture

02 p0368 A70-11819
Combustion instability of solid propellants using response to pressure perturbations for T and L burners

02 p0352 A70-12013
Hydrogen reactions with nitrogen dioxide, oxygen, and mixtures of oxygen and nitric oxide in adiabatic flow reactor measured as function of temperature and pressure

02 p0250 A70-12020
High pressure tests of primary zone flame radiation, flame and tube metal temperatures in aircraft combustion chambers, including oxygen and vitiated inlet air effects

02 p0355 A70-12051
Titanium thin films prepared in ultrahigh vacuum to determine low temperature/pressure oxidation kinetics, using electron microscopy and X ray diffraction

02 p0317 A70-12316
Ingot and powder metallurgy polycrystalline Be flow and fracture behavior and microstructure pressure dependence at room temperature

02 p0317 A70-12318
Acoustical resonators free oscillations and pressure effects on damping, amplification, decay decrement and relaxation time

02 p0304 A70-12772
Periodic shock fronted longitudinal pressure wave effect on instantaneous heat flux rates at tube end wall

02 p0400 A70-12860
Mathematical model for burning rates of solid propellant rocket motors during pressure transients, coupling conservation equations with mass balance equation

03 p0543 A70-12912
Internal hydrostatic or lateral pressure effect on deformations of infinitely long thin cylindrical isotropic shell subjected to equal concentrated radial loads

03 p0584 A70-12922
Pulse peak width of He-Ne laser with Ne filled absorbing cell in resonator found dependent on saturating field and Ne pressure in cell

03 p0498 A70-13089
Acoustic and shock waves propagation in multicomponent media, assuming uniform speed for components and complex density dependence of media on pressure

03 p0465 A70-13329
Axial compressive forces influence on steel and Al cylindrical shell stability under external pressure

03 p0593 A70-13472
Linearized steady state hydrodynamic equations describing solar wind meridional motions used for studying zonal pressure perturbations

03 p0558 A70-13599

Increased oxygen partial pressure effects on cerebral bioelectric activity from EEG recordings on unanesthetized dogs

03 p0422 A70-13690
He-Ne multimode laser radiation peak as function of pressure in methane-containing absorption cell installed in resonator

03 p0502 A70-13750
Transient creep analysis of simply supported circular cylindrical shells subjected to internal pressure based on strain and time hardening theories

03 p0595 A70-13813
Pressure changes in troposphere and lower stratosphere after strong solar flares analyzed statistically for Northern Hemisphere

03 p0476 A70-13909
Bleached eye pressure blinding at bleaching light termination during wavelength settings, discussing effect on interocular hue shifts

03 p0427 A70-13951
Negative O, NO and nitrous oxide ions formation by electron impact on nitrous oxide as function of pressure

03 p0441 A70-14007
Reduced ambient pressure effects on hot wire sensitivity of initiating materials of electroexplosive devices used in missiles

03 p0549 A70-14139
Vacuum UV flash photolysis of carbon suboxide, noting pressure dependent reaction rates of carbon atoms with various gases

04 p0645 A70-14391
Blood flow through veins and collapsible tubes simulated by physical model, downstream pressure effect and importance of collapse phenomena

04 p0641 A70-14631
Viscosity of nitrogen, hydrogen, Ar and He at high pressures measured by capillary flow viscometer with range extended to minus 100 C

04 p0718 A70-14697
Pressure and temperature sensitivity tests of fluoric oscillator for timer application, testing fluid relaxation oscillators using R-C-R feedback loops

[ASME PAPER 69-WA/FLCS-9] 04 p0626 A70-14844
Adiabatic elastic stiffness constants of single crystal forsterite measured as function of hydrostatic pressure and temperature, using pulse superposition technique

04 p0678 A70-15055
Energy supply for supersonic flight air suction propellant systems using external supersonic combustion, discussing Carat wing and pressure effect

04 p0785 A70-15160
Supersonic jet flow from diverging nozzle into space with given pressure or into supersonic slipstream, noting barrel shock formation inside jet

04 p0617 A70-15235
Hydrostatic pressure effects on DNA, RNA and protein synthesis and division in Escherichia coli cultures

04 p0637 A70-15475
Internal pressure deformed cruciform crack energy and stress intensity factor determined by linear equations

04 p0777 A70-15499
Material coupling in two layered orthotropic cylindrical shell subjected to normal external pressure

04 p0778 A70-15547
Wind tunnel testing technique innovations, reducing time and cost for low drag aircraft configurations by simultaneous force and pressure model transonic testing

[SAE PAPER 690677] 05 p0825 A70-15868
Stress factor-displacement relation in cruciform line crack deformation in elastic medium under arbitrary internal pressure

05 p0926 A70-15976
Equivalent pressure concept for breakdown processes and sparking voltage of gas moving at angle to electric field across uniformly stressed gap

05 p0881 A70-16000
Pressure sensitive components in cordwood modules noting temperature and pressure damaging stresses during encapsulation

05 p0855 A70-16037
Closed form solutions describing nonlinear motions of incompressible fluid flowing in thin walled tube buckled by uniform external pressure

05 p0832 A70-16090
Beryllium single crystals deformation under high pressures at room temperature similar to deformation under atmospheric pressure at elevated temperatures

05 p0863 A70-16203
Stress concentration of spherical hoop with discretely spaced meridional ribs under uniform pressure

05 p0935 A70-16229
Resistance strain gauge load cell for measuring compressive loads under high hydrostatic pressure, discussing gauge bonding

05 p0848 A70-16377
Fluid boundary at curved wall under pressure

05 p0834 A70-16680

Experimental and analytical work on structural panels vibratory response and acoustic radiation excited by turbulent boundary pressure fluctuations, evaluating applicability to noise research

05 p0835 A70-16789
Reinforced openings effect on burst strength of ductile circular plates subjected to pressure loads

05 p0943 A70-16810
Steady gravitational waves produced by variable pressure in fluid channel flow assuming small perturbed flow velocity components

05 p0836 A70-16969
External hydrostatic pressure effect on fiberglass-reinforced plastics strength under unilateral heating, analyzing stress distribution

05 p0875 A70-17067
Negative pressure gradients effects on wall heat flow and characteristic patterns for turbulent boundary layer profiles

06 p1033 A70-17231
White single-comb Leghorn chick embryonic development at increased pressures at various hyperbaric gas mixtures for ten day periods

06 p0991 A70-17296
High purity Ni fatigue in reversed bending as function of oxygen pressure and temperature

06 p1086 A70-17454
Electron recombination in inert gases at various pressures, studying electron density decrease in time by UHF and optical methods

06 p1109 A70-17495
Gaseous He measured for thermal conductivity along isotherms to observe pressure dependence

06 p1174 A70-17678
Time dependent pressure fluctuations effect on laminar film pool boiling on vertical flat plate by perturbation method to predict heat transfer

06 p1177 A70-17696
Low speed wind tunnel test results correction program, considering solid, wake blockage, lift, static pressure gradient and wall interference effects

06 p0968 A70-17934
Reaction heat for flameless combustion of double-base propellant using differential scanning calorimetry and thermogravimetric analysis, noting pressure effects

[AIAA PAPER 70-125] 06 p1179 A70-18045
Helmholtz resonator associated flow field analysis in nonlinear regime, considering external pressure, mean flow, velocity fluctuations and orifice flow

[AIAA PAPER 70-128] 06 p1038 A70-18065
Pressure interaction with slender cone in hypersonic flow

[AIAA PAPER 70-183] 06 p0972 A70-18126
Temperature and pressure effects as function of time in spectral and total normal emittance of metal coated refractory metals

[AIAA PAPER 70-68] 06 p1092 A70-18136
Thermal isolation characteristics of interstitial materials in vacuum environment, inserting materials between contacting metal surfaces at various pressures and temperatures

[AIAA PAPER 70-13] 06 p1181 A70-18143
Electron beam generated plasma behavior, showing electron pressure local anisotropy capability for generating supersonic-subsonic transitions

06 p1123 A70-18296
Polytetrafluoroethylene wear tested by rubbing cylindrical rod flat ends against glass plates, determining sliding contact pressure effects

06 p1077 A70-18403
Entropy fall in superheated liquid related to vapor bubble growth from finite so-called zero radius to critical radius, noting pressure effects

07 p1418 A70-18645
Perfusion pressure effect on myocardial oxygen consumption and coronary flow in stable nonworking rat heart

07 p1202 A70-18865
Elliptic cylinders buckling under normal pressure analyzed on polyvinyl chloride sheet models

07 p1406 A70-19304
Propellant sprays behavior in high pressure combustors, calculating jet breakup or atomization length

07 p1257 A70-19331
Microphone output level in airstream related to sound pressure and pressure fluctuations caused by turbulent flow

07 p1334 A70-19372
Pressure effects in predicting ablation velocities for gas-solid systems, assuming reactions and gaseous products reversible adsorption on solid surfaces

07 p1422 A70-19373
Wave numbers, intensity and half width of lines of vibration-rotation relative to carbon monoxide transition, noting band center displacement dependence on pressure

07 p1338 A70-19380
Lamellar magnetic core stacking pressure influence on core magnetic characteristics in variable magnetic field, noting effects on magnetic permeability

07 p1246 A70-19537

- Human physiological responses to lower body negative pressure /LBNP/, studying presence or absence of change for orthostatic tolerance as function of time
07 p1222 A70-19933
- Circular cylindrical shells buckling under lateral and hydrostatic pressure using Donnell and Flugge equations, assuming membrane stress state for prebuckling deformation
07 p1414 A70-20168
- Truncated conical shells buckling under hydrostatic pressure using Donnell equations, assuming membrane stress state for prebuckling deformation
07 p1414 A70-20170
- He-Ne single frequency laser output characteristics at various active medium pressures noting emission polarization
08 p1511 A70-20517
- Longitudinal modes competition in He-Ne laser, studying effects of active medium isotopic composition and pressure
08 p1511 A70-20518
- Visual analyzer physiology under effects of gravitation, atmospheric pressure, mechanical vibrations, etc
08 p1444 A70-20740
- Organic adhesives preparation and application to metal surface for bonding, examining time, pressure and temperature effects on curing
08 p1503 A70-20881
- Adhesive metal bonding, considering methods for application of pressure and heat
08 p1503 A70-20882
- Graphite molds compaction pressure effect on Ti castings nonporosity and surface layers carburization
08 p1506 A70-21143
- Free plasma column discharge in HF field in high pressure deuterium atmosphere, discussing high plasma temperature inside column and reliable thermonuclear reaction achievement
08 p1551 A70-21417
- Stiffeners inclination effects on instability of pressurized cylinder under bending by Ritz method, considering finite deflection and initial imperfections in strain-displacement relations
08 p1591 A70-21464
- Popping pressure of relief valve with helical spring under dynamic load noting frequency dependence
[ASME PAPER 69-VIBR-48] 08 p1441 A70-21479
- Atmospheric pressure-diameter relationship of common carotid artery in head and neck region of conscious men
08 p1447 A70-21508
- Zener diode used as hydrostatic pressure gauge, describing pressure effects on diode current/voltage characteristics
08 p1477 A70-21644
- Power output of sealed carbon dioxide-nitrogen-helium laser as function of gas composition and pressure
08 p1514 A70-21751
- Thoracic cage, heart and extirpated lung dimensions measurement for dogs before and after explosive decompression and after ground level recompression
08 p1448 A70-21793
- Magnetothermal oscillations in pressure-annealed pyrolytic graphite, relating period with angle between magnetic field and crystal c axis
08 p1557 A70-21839
- Long bone necrosis in response to reduced atmospheric pressure exposure, comparing lesions with caisson disease
08 p1449 A70-21944
- Pressure effects on melting temperature curves of solids, considering Van der Waals solids, metals and ionic compounds
09 p1665 A70-22056
- Alveolar ventilation and pulmonary circulation during application of negative pressure to lower part of human body
09 p1615 A70-22090
- Detonation mechanism in ammonium perchlorate ascribed to mechanical breakdown of charge occurring at pressure equal or above critical deformation of explosive
09 p1741 A70-22102
- Hypersonic spherical gas expansion into finite pressure region with transition from supersonic to subsonic flow in shock wave, discussing structure and pressure effects
09 p1658 A70-22116
- He-Ne laser emission modulation by varying discharge current, studying gas pressure effect and role of ballast resistor
09 p1695 A70-22411
- Axissymmetric nozzles flow regimes with subsonic ejection velocities analyzed by stabilization method, noting role of pressure in nozzle exit section
09 p1660 A70-22440
- Monatomic gas rarefaction wave structure in unsteady one dimensional flow from high to low pressure zones, describing numerical solution technique
09 p1604 A70-22449
- Diamagnetic plasma in nonuniform magnetic fields, determining equilibrium plasma configurations in and near neutral point for low and high pressure
09 p1734 A70-22478
- Magnesium solubility in titanium from X ray analysis of Mg distribution in diffusion zones at high temperature and pressures
09 p1703 A70-22567
- Plastic growth of pressurized shell under cyclic thermal stresses superimposed on steady pressure load, investigating shake down using bending approximation
09 p1774 A70-22586
- Laminar separation bubble in incompressible flow produced on flat plate by pressure gradients, correlating bursting with Reynolds number and pressure distribution
09 p1660 A70-22770
- Elastohydrodynamic lubrication of rollers relationship to pressure
09 p1693 A70-22978
- Cross hatching on various body surfaces due to periodic surface pressure fluctuations, discussing origin from counterrotating longitudinal vortices in boundary layer
[AIAA PAPER 69-11] 09 p1662 A70-23223
- Elastic cylindrical shells stability under uniform pressure, calculating critical transverse load by finite-difference computer program
09 p1781 A70-23287
- Shock deformation of single crystal biotite /lepidomelane/ imbedded in impedance matching NaI, relating kinking intensity to peak pressure and pulse duration
09 p1670 A70-23375
- Microwave-induced ionization oscillations in resonant plasma column excited by low pressure mercury DC discharge
10 p1922 A70-23988
- Sliding bearings with nonNewtonian lubricants, noting pressure gradient change effect caused by speed fluctuation and material constants
10 p1893 A70-24015
- Spectrum analysis of unsteady duct flow caused by pressure loss induced instability
10 p1863 A70-24026
- Wing in supersonic flow analyzed for surface pressure taking into account nonlinear effects of vibrations
10 p1798 A70-24119
- Heat sources effect on pressure and velocity of supersonic flow, discussing iteration procedure and asymptotic expansion
10 p1799 A70-24125
- Stress intensity and strain energy of pressurized line crack in cross form in thin elastic plate solved by Wiener-Hopf technique
10 p1956 A70-24192
- Graphite IR radiator for radiative capacity and flame temperature measurements investigated for life time dependence on ambient pressure and temperature
10 p1888 A70-24257
- Solar wind model with electrons, protons and alpha particles coupled by electric field and expanding due to pressure gradient and solar gravitation
10 p1931 A70-24433
- Small plane perturbations stability losses in uniform rectilinear motion of nonrigid deformable rocket, using slender bodies pressure theory
10 p1950 A70-24528
- Circular membrane creep under one-sided hydrostatic pressure, using governing equations for finite deformation
10 p1959 A70-24828
- Forced vibration of rib-skin structures under random pressure and heavy damping using wave group theory
10 p1963 A70-25060
- Transient creep analysis of pressurized circular cylindrical shells based on strain and time hardening theories
10 p1963 A70-25089
- Pressure loss in tubulature of oil-hydraulic drive mechanism, allowing for viscosity changes associated with oil temperature and pressure increases
10 p1809 A70-25209
- Pressure anisotropies contribution to solar wind corotation, discussing angular momentum and magnetic field
10 p1935 A70-25285
- Plasma cumulation, with and without shell under concentric pressure impulse using perfect gas theory, estimating critical parameters
10 p1926 A70-25322
- Thin cylindrical shell stresses and displacements enclosed in elastic casing under pressure band using classical theory of Flugge and Love functions
11 p2128 A70-25336
- Gas effect on natural frequency of electrostatically excited string vibrating between flat electrodes at medium pressures
11 p2048 A70-25582
- Explosion aerial blast wave for producing impulsive structural forced response, discussing spatial distribution method for increased wave duration
11 p2133 A70-25729
- Thermal conductivity coefficients of argon in 25-700 C range and up to 1200 bars pressure, using vertical concentric cylinder apparatus
11 p2147 A70-25754
- Tapered spherical shell under constant initial pressure calculated for strength, stiffness and durability on digital computer using numerical algorithm
11 p2134 A70-25846
- Working pressure effects on size and weight of aircraft hydraulic systems components, allowing for fluid properties change
11 p1982 A70-25865
- Buckled plates flutter at zero dynamic pressure, considering initial plate imperfections, including aerodynamic damping in quasi-steady supersonic approximation
11 p2135 A70-25988
- Fatigue life of Ni vibrated in reversed bending at 300 C in oxygen and in water vapor at various pressures
11 p2067 A70-26098
- Background pressure and magnetic field shape effect on MPD thruster performance, testing radiation cooled thrusters
[AIAA PAPER 69-243] 11 p2102 A70-26122
- Base pressure effects on cone angle of fixed length conical nozzle yielding maximum thrust
11 p1977 A70-26156
- Thermal control pressure sensitive adhesive tapes for spacecraft applications, discussing properties degradation due to simulated terrestrial and space environments
11 p2067 A70-26366
- Deep shells formation by high pressure methods, discussing fluid, mechanical edge pressure and friction aided extrusion techniques
[SME PAPER MF-69-147] 12 p2240 A70-27080
- Hot-electron cold-ion plasma with anisotropic electron velocity distribution function, discussing stability under finite pressure and unstable oscillation forms
12 p2277 A70-27314
- Low pressure burning rate of double base propellants at various initial temperatures in argon and in air
12 p2332 A70-27844
- Convergent-divergent nozzle operation at low pressure ratios causing separation of internal flow, discussing stability and flow field
12 p2157 A70-28084
- Pressure buckling values of rod and plate profiles with thicknesses graduated across pressure direction in presence of uniform and nonuniform stress distributions
13 p2507 A70-28477
- Film cavitation between flat annular surfaces in face seal resulting from hydrodynamic pressure generated by misalignment and surface waviness
13 p2417 A70-28613
- Slender cylindrical shell loaded by internal pressure analyzed using numerical procedure developed for digital computer
13 p2512 A70-28981
- Elastic constants pressure dependence of cubic crystals in NaCl and spinel structures using homogeneous static deformation method
13 p2396 A70-29172
- Methane and ethane hydrate number measurement, alleviating liquid water occlusion and evaluating pressure effect
13 p2362 A70-29212
- Stability loss of nonreinforced and reinforced cylindrical shells under external pressure
13 p2514 A70-29294
- Plane cylindrical and spherical explosion waves propagation in detonating gas mixtures with counter-pressure, calculating perturbed flow parameters by numerical method of integral relations
13 p2388 A70-29308
- Interstitial atoms arrangement in binary alloys with body centered lattice, describing pressure effects by statistical theory
13 p2435 A70-29321
- Initial pressure and pressure ratio effects on shock wave velocity evolution in shock tube
13 p2389 A70-29630
- Low pressure deflagration limit dependence on strand size in terms of cross section dimensions for composite ammonium chlorate propellant
[AIAA PAPER 69-144] 13 p2473 A70-29955
- Pure ammonium perchlorate single crystal self deflagration, determining energy transfer mechanisms from pressure effects, combustion characteristics and subsurface profile
[AIAA PAPER 69-142] 13 p2473 A70-29956
- Nucleate pool boiling, calculating sinusoidal and square wave pressure variations effect on heat flux for comparison with measurements
14 p2616 A70-30254
- Plastic deformation of Be single crystals under hydrostatic pressure, considering resolved shear stresses on glide systems
14 p2595 A70-30334
- Power absorption by microwave generated plasmas noting pressure effects
14 p2622 A70-30675
- Acoustic and shock waves propagation in multicomponent media, assuming uniform speed for components and complex density dependence of media on pressure
14 p2566 A70-30709

Ignition transients in solid propellant rocket engines, taking into consideration flame temperature changes with pressure and igniter secondary mass addition

14 p2628 A70-30778

Molecular beams formation from high pressures, discussing detection, diagnosis and applications in high temperature chemistry

14 p2545 A70-30904

Critical Mach numbers for transverse resistive shock waves as function of fluid/magnetic pressure ratio compared with cold plasma theory

14 p2623 A70-31036

Penning pump argon stability, noting influence of pressure and ion incidence angle on cathode surface

15 p2744 A70-31847

Positive ion composition in Cs plasma as function of normalized pressure

15 p2779 A70-31978

Axisymmetric nonuniform initial thickness disk under pressure and twisting along interior surface of circular hole using incremental theory of plasticity for deformation analysis

15 p2816 A70-32004

Rarefied gas mixtures efflux from opening at various pressures, calculating component discharge coefficients for molecular flow conditions

15 p2721 A70-32137

Alveolar ventilation and pulmonary circulation during application of negative pressure to lower part of human body

15 p2685 A70-32686

Superplastic deformation of thin circular diaphragms subjected to on-sided hydrostatic pressure, emphasizing thickness variations in bulged shapes

16 p2916 A70-32917

Lateral pressure bulging of superplastic alloy sheet, considering flat circular sheet and bulging into V grooves

16 p2916 A70-32918

Asymptotic relation between Thomas-Fermi-Dirac and Thomas-Fermi atom models for pressure with and without exchange, considering Coulomb contribution to energy

16 p2953 A70-33004

Pressure broadened line widths in electric field induced fundamental hydrogen spectral band, noting linear variation with density

16 p2954 A70-33276

Turbofan engine gross thrust dependence on nozzle pressure ratio and simulated flight Mach number, considering altitude chamber test data [AIAA PAPER 70-612]

16 p2969 A70-33608

Pressure effects on quantum yields of carbon trioxide formation in gas phase ozone photolysis with carbon dioxide

16 p2856 A70-33653

Additional inertia introduced by velocity profile gradient in flow direction effects on externally pressurized gas bearing

16 p2924 A70-34233

Al pressure-welded joints strength, investigating surface treatment role

16 p2924 A70-34340

Pressure forming Ti sheet alloy blanks in superplastic condition under controlled temperature and strain rate

17 p3117 A70-34402

High pressure ablation of plastic composites and graphites in arc heater, measuring erosion rate, shape change, surface roughness and physical characterization [AIAA PAPER 70-770]

17 p3193 A70-34482

Double acoustical resonators transient response to excitation by single sine wave, presenting pressure magnification factors as function of frequencies

17 p3135 A70-34521

Adhesive bond between steel wire and epoxy resin, investigating hydrostatic pressure effect on shear strength

17 p3123 A70-34623

Pressure and grain size effect on burnout velocity and combustion capacity of ammonium perchlorate

17 p3145 A70-34639

Pressure, subcooling and diameter effects on liquid nitrogen film boiling on thin horizontal wires, using high speed movies

17 p3194 A70-34742

Two dimensional hypersonic viscous flow, analyzing viscosity and bluntness induced pressure effects

17 p3010 A70-35034

Barometric pressure reduction effect on gaseous and volatile metabolic products elimination in men wearing oxygen-supplied rubberized suits

17 p3038 A70-35363

Ambient temperature effects on venous reactivity to hydrostatic stress, discussing posture changes and lower body negative pressure effects on index of compliance

17 p3031 A70-35426

Oxygen pressure effect on stainless steel cyclic hardening during vibration tests at resonant frequency

18 p3273 A70-36042

Hydrostatic pressurization effect on ductile-brittle transition temperature of polycrystalline chromium

18 p3274 A70-36053

Combustion rates and self ignition vs pressure and activity in ammonium perchlorate mixtures with Al and Mg powders compressed to maximum densities

18 p3299 A70-36249

Physiosorption isotherms for nitrogen on stainless steel at various temperatures and very low pressures

18 p3226 A70-36322

Two component warm plasma wave propagation along magnetic field, considering full pressure tensor equation with momentum and pressure relaxation mechanisms

18 p3294 A70-36405

Plane cross section hypothesis applied to fully developed creep in thin walled tube subjected to internal pressure and bending moments, calculating stress concentration

18 p3340 A70-36571

Argon and helium breakdown induced by ruby laser 50-picosec pulse at various pressures

18 p3267 A70-36616

Buzz-saw noise of transonic compressor due to rotating pressure field at supersonic blade tip speeds [ASME PAPER 70-GT-54]

18 p3303 A70-36838

Na I 5889 A pressure broadening by high temperature neutral He, allowing damping constant direct measurements

18 p3318 A70-37013

Long wave outgoing radiation angular distributions based on effective mass and Curtis-Godson methods of accounting for absorption pressure dependence

19 p3461 A70-37634

Omnidirectional dynamic stress gage as embedded elastic inclusion, discussing transient response to ground shock compression wave pressure

19 p3422 A70-37699

Hydrostatic pressure dependences of second order elastic constants of ZnTe and ZnSe at 295 K, using ultrasonic pulse echo method

19 p3486 A70-37762

Pressure dependence and high pressure limiting values of rate constants of gas phase reaction of monomethylamine and trimethylamine with boron trifluoride

19 p3373 A70-37775

Complete elastic spherical shell asymmetric buckling mode under pressure

19 p3539 A70-37801

Volterra equations for stresses, strains and displacements of viscoelastic tube with variable radius encased in shell under pressure and unsteady temperature field

19 p3547 A70-38437

Argon hydrostatic pressure effect on self diffusion coefficients and activation energy of Al and Be single crystals

20 p3644 A70-38961

Metallic surfaces vacuum electric spark alloying, investigating pressure effects on coating layer thickness and area

20 p3636 A70-39195

Carbon dioxide initial dissociation rates in glow discharges and gas mixtures at low pressures, using mass spectrometric sampling and plasma diagnostic methods

20 p3674 A70-39235

Cosmic ray beta neutron component barometric coefficients planetary distribution during IQSY, establishing latitude dependence for mountain and sea level equations

20 p3697 A70-39292

Sinusoidal vibrations effects on rats at different air pressures, discussing human vibration tolerances and resonant frequencies of thoraco-abdominal system

20 p3572 A70-39434

Unsteady viscous flow of incompressible fluid through porous straight channel under time varying pressure gradient, determining suction and injection effects

20 p3609 A70-39670

Choice reaction and movement time dependence on hypoxia induced by air pressure reduction inside decompression chamber, discussing adult human performance

20 p3573 A70-39714

Cylindrical shells dynamic stability under uniform radial pressure

20 p3722 A70-39786

Nonhomogeneous elastic cylinder under internal pressure with modulus in terms of Fermi-Dirac distribution function series, discussing fibers rigidity and modulus change

20 p3731 A70-40052

Ammonium perchlorate composite solid propellant pressure vs burning rate at various temperatures, discussing granular diffusion flame theory

20 p3694 A70-40266

Solid rocket propellants linear and nonlinear pressure coupled combustion instability behavior relationship to exothermic surface processes

20 p3694 A70-40274

Oxygen pressure effects on tracking control training for stable reactions, investigating muscles bioelectric activity changes during elevated pressure breathing

20 p3581 A70-40291

Ambient near vacuum pressure effect on blood circulation, examining thoracic aorta blood flow, pressures, gas expansion and water vaporization

20 p3576 A70-40326

Interplanetary plasma torque due to temperature and pressure anisotropy, considering solar wind angular velocity and sun angular momentum

20 p3712 A70-40423

Deflagration rate measurements by high speed cinematography of ammonium perchlorate single crystals under various ambient temperature and pressure conditions

20 p3688 A70-40468

LTE verification for argon plasma generated in free burning arc by measuring atomic line transition probability at various pressures

21 p3854 A70-40588

Polymethyl methacrylate rupture during omnidirectional compression under laser radiation, showing pressure effect on microdefects and cracks

21 p3841 A70-40644

Schrodinger equation for hydrogen solved for high pressure behavior of materials, applying to stellar atmospheres and laboratory plasmas

21 p3849 A70-40933

Pressure dependence and efficiency of carbon trioxide formation in Mars and Venus atmospheres

21 p3887 A70-41107

Ultrasonic machining of glass and cemented carbide, measuring ambient pressure effect on workpiece removal rate

21 p3833 A70-41253

Carbon steel thin walled cylinders creep fracture subjected to combined tension and internal pressure by large strain theory

21 p3840 A70-41438

Rhesus monkeys PCO₂ tolerance in low pressure environments, observing hyperthermia and heart and respiratory rates depression

21 p3765 A70-41486

Elastic-plastic axisymmetric shells of revolution, analyzing large deflection and yielding for internal and external pressures by finite element method

21 p3937 A70-41738

Interactions between components of turbulent flow velocity correlation tensor due to pressure fluctuations

21 p3810 A70-41956

Gas velocity and static pressure effects on evaporation rate of moving liquid fuel droplets

21 p3953 A70-42094

High output CW carbon dioxide laser design, using gas pressure variation and fast axial flow

22 p4048 A70-42322

Uranium plasma diagnostics, measuring emission and absorption coefficients as function of pressure and temperature

22 p4069 A70-42361

Probe technique for plasma electron temperature measurements at medium and high pressures, examining thermal boundary effects

22 p4078 A70-42362

High power plasma flow generation at variable pressure and rates, describing device characteristics and performance

22 p4079 A70-42367

Constricted arc characteristics in air and nitrogen at various pressures, considering spectral lines radiation transfer and electron, atom and ion temperature difference effects

22 p4079 A70-42369

Pressure role in inert gas shielded metal arc welding, discussing voltage-pressure relation, weld head profile, metal transfer, etc

22 p4043 A70-42383

Two dimensional incompressible flow, calculating strong suction effects on laminar boundary layer separation by linear model

22 p4010 A70-42630

Gaseous substances thermodynamic functions and chemical equilibrium constants logarithms dependence on temperature and pressure, deriving internally self consistent formulas

22 p4124 A70-42682

Pressure and temperature effects on large amplitude acoustic pulses propagating in stratified atmosphere

22 p4010 A70-42689

Hydrogen chloride self broadened fundamental vibration rotation band intensity variation with pressure investigated by absorption spectroscopy analysis

22 p3983 A70-42945

Silver fluorination kinetics, taking temperature and pressure effects into account

22 p3983 A70-43416

Cylindrical converging shock waves generation, propagation and structure at high pressures

22 p4012 A70-43431

Working medium excess and absolute pressure effects on pneumatic elements characteristics

22 p3967 A70-43566

Decompression sickness prevention in space flight, discussing suit and capsule pressure, extravehicular activity and alleviation of conditions

22 p3980 A70-43640

Carbon dioxide exposure limits of rhesus monkeys, examining body temperature, respiratory rate and pressure effects

22 p3973 A70-43642

Principle pressure vector components for liquid in moving V-shaped and U-shaped cross section tanks

23 p4180 A70-44164

Liquid nitrogen saturated film boiling from wire at pressures up to critical, discussing liquid-vapor interface configuration

23 p4279 A70-44362

Compressibility, viscosity and thermal conductivity of dense gases, examining high temperature and pressure effects

23 p4222 A70-44431

Spectral absorption of 2.7 micron water vapor band under various high temperature and pressure conditions, using black body radiation

23 p4220 A70-44444

Contoured nozzle shock tunnel condensation point, determining flow supercooling over specified pressure range

23 p4182 A70-44588

Pressure gradient effect on skin friction coefficients taking into account Mach, Reynolds and Stanton numbers

23 p4183 A70-44629

Static pressure effects on heat flux critical density for free convection and forced flow in circular pipes

23 p4282 A70-44726

Mammalian eardrum failure due to blast induced pressure variations, examining wave shape, character, magnitude and duration effects

23 p4148 A70-44839

Oxygen pressure effects on Ni oxidation kinetics at high temperatures

23 p4208 A70-44920

Rarefied binary gas mixture, determining temperature gradient effect under various pressures

23 p4284 A70-44984

Decompression disorders after exposures to safe pressure or altitude in cats, noting potential embolia from nongradual high-to-normal pressure passage

23 p4157 A70-45080

Cylindrical shells with unreinforced openings, determining limit pressures and deformation patterns

24 p4419 A70-45158

Shell of revolution /pressure vessel/ with meridional slope discontinuity, calculating pressurization effect on stresses by computer program

24 p4420 A70-45277

Plasma-electron beam interaction instability transition from absolute to convective in hydrogen tube system at various pressures, considering electron collision effects

24 p4385 A70-45452

Radiation pressure effects on artificial satellite motion, including earth shadow perturbation

24 p4408 A70-45554

Atmosphere and earth-reflected solar radiation pressure effects on high altitude satellite orbits

24 p4408 A70-45555

Pneumatic actuator rod and piston head seals, examining materials at various temperatures, pressures and speeds

24 p4294 A70-45855

Semifinite elastic medium under variable dynamic pressure on boundary, investigating couple stresses effect on stress distribution

24 p4426 A70-46006

Air and liquid filled excised lungs P-V hysteresis curves, determining surface tension in situ

24 p4302 A70-46104

Thermal constriction resistance due to nonuniform metal surface conditions, considering macroscopic contact resistance for nonuniform interface pressure distribution

24 p4429 A70-46177

Precompression and pressurization effects on ductile-brittle transition of polycrystalline cast Cr, W and Mo bcc transition metals

24 p4365 A70-46371

PRESSURE FIELDS

U PRESSURE DISTRIBUTION

PRESSURE GAGES

NT IONIZATION GAGES

NT KNUDSEN GAGES

NT MANOMETERS

NT PIEZOELECTRIC GAGES

NT VACUUM GAGES

Interactions between hypersonic neutral gas beam and orificed pressure gauge in spinning satellite noting dependence on angle of attack

06 p1159 A70-18290

Fluidic air gauge back pressure signal frequency response as function of time

[ASME PAPER 68-WA/FE-16] 08 p1441 A70-21316

Zener diode used as hydrostatic pressure gauge, describing pressure effects on diode current/voltage characteristics

08 p1477 A70-21644

Outgassing pressure variation with time near perigee in satellite-borne pressure gages, using Langmuir model of surface adsorption

13 p2408 A70-29202

Atmospheric density and temperature measurements by satellite- and rocket-borne pressure gages and mass spectrometers, considering error sources

15 p2731 A70-32092

Diaphragm pressure transducer interaction with solid propellant grain, superposing solutions to clamped circular plate and halfspace

16 p2992 A70-33987

Static pressure probes selection for measuring three dimensional flow at high velocities, considering sensitivity and errors

20 p3628 A70-39262

Vibrating ribbon pressure gauge sensitivity, discussing advantages

22 p4029 A70-42624

Ultravacuum measurement and calibration assembly for pressures down to one picotorr for vacuum gage standards

23 p4143 A70-44871

Oscillating vane and rotating disk pressure gage theory, considering gas damping and density variations

23 p4198 A70-44948

PRESSURE GAUGES

U PRESSURE GAGES

PRESSURE GRADIENTS

Pressure gradient required for self preserving of turbulent jets and wakes with small mean velocity variations compared with free stream velocity

02 p0223 A70-11860

Sealing mechanism theory with face seal applications, taking into account load carrying capacity and no leakage pressure gradient

[ASLE FICFS PREPRINT 18] 02 p0308 A70-12172

Modified Granville moment of momentum method used with integral equations in integral moment method for turbulent boundary layer flow, considering pressure gradient influence

02 p0282 A70-12334

Turbulent boundary layer response to sudden changes in surface conditions or pressure gradients, considering equilibrium attainment

02 p0287 A70-12360

Pressure gradient calculation in three dimensional laminar boundary layer, using method of local similarity

03 p0468 A70-13869

Incompressible viscous fluid rectilinear flow along arbitrary cross section duct under pressure gradients oscillating at large frequencies

03 p0468 A70-14147

Volumetric flow rate of rare gases, hydrogen and deuterium between parallel plates at various pressures and Knudsen numbers

04 p0665 A70-14414

Heaving and pitching motion analysis of wave action-induced pressure gradients in captured air bubble /CAB/ ship bubble chamber, discussing fan system design

[ASME PAPER 69-WA/AV-6] 04 p0622 A70-14902

Actively participating bounding surfaces effect on free molecule flow through slit or annular orifice situated in wall separating different pressure regions

[ASME PAPER 69-WA/APM-26] 04 p0668 A70-14906

Longitudinal pressure gradient measurement for DC discharges in He, Ne and Ar, investigating effects of gas purity, tube geometry, etc

04 p0671 A70-14995

Axial neutral gas pressure gradient calculated in cylindrical positive column of DC discharge due to driving volume force

04 p0671 A70-15003

Asymptotic expansion method to analyze laminar boundary layers with zero wall shear, large suction and adverse pressure gradients

04 p0674 A70-15563

Values measured on sharp flat plate in 10.4 Mach boundary layer induced pressure gradient, discussing effects of wall pressure and temperature gradients

04 p0621 A70-15609

First order pressure gradient microphone design based on electrostatic principle, using foil electrets to discriminate against airborne and solid-borne noises

05 p0821 A70-16402

Viscoelastic fluid flow through circular tube under time dependent pressure gradient superposed on steady Poiseuille flow

06 p1032 A70-17200

Negative pressure gradients effects on wall heat flow and characteristic patterns for turbulent boundary layer profiles

06 p1033 A70-17231

Sunspot temperature and pressure gradients from blue, red and IR photographs, deriving umbral depression and density scale height

06 p1143 A70-18000

Turbulent boundary layer control by wall jet, analyzing wall jets in adverse pressure gradients for two limiting cases

[AIAA PAPER 70-107] 06 p1041 A70-18160

Laminar boundary layer in hypersonic flow calculated by integral method, including effects of entropy gradient and induced pressure gradient

[ONERA-TP-784] 06 p0984 A70-18468

Steady turbulent boundary layer of compressible perfect gas on heat insulated surface with suction and longitudinal pressure gradient

07 p1254 A70-19081

Boundary layers calculation for nonporous surface extended to porous with suction by replacing velocity distribution with longitudinal pressure gradient

07 p1254 A70-19083

Ring seal elements structural parameters influence on fluid leakage at various shaft speeds and fluid pressures

07 p1294 A70-19123

Integral methods for predicting two dimensional incompressible turbulent boundary layers development in arbitrary pressure gradients, using momentum integral equation and wall friction relation

07 p1256 A70-19308

Nonsimilar laminar boundary layer solutions with negative pressure gradient compared to experimental boundary layer velocity profiles, momentum and displacement thicknesses

[AIAA PAPER 69-35] 07 p1256 A70-19312

Transverse pressure gradient effect on parameters of turbulent boundary layer on body rotating in axial flow

08 p1483 A70-21193

Hydrodynamic sealing action resulting from helical grooving machined into shaft or lip of radial seal, describing pressure gradients role

08 p1507 A70-21268

Static pressure gradient influence on turbulent shear stresses and energy production in asymmetric wall jet flow

08 p1484 A70-21314

Unsteady flow in circular tube of constant section with time dependent discharge, determining pressure gradient and velocity distribution

08 p1484 A70-21477

MHD flow between two parallel plates, noting pressure gradient and skin friction coefficient

08 p1554 A70-21774

Turbine pump systems operation in terms of liquid rocket engine combustion stability, noting altitude effects on pressure pulsations

08 p1559 A70-21849

Transparent gas radiation behind strong shock wave front with small pressure gradient due to energy losses

08 p1486 A70-21986

Laminar boundary layer in adverse pressure gradient calculated for momentum thickness from approximate equation, analyzing error

09 p1660 A70-22832

Two dimensional equations of boundary layer with arbitrary pressure gradient solved using successive approximations for numerical integration

09 p1605 A70-23168

Left ventricle pressure rise rate as function of heart contractility and hemodynamics

09 p1623 A70-23587

Laminar boundary layer parameters on porous surface in presence of pressure gradient obtained for inner /wall/ and outer regions

09 p1664 A70-23712

Boundary layer flow near flat plate trailing edge taking into account pressure gradient induced locally in external flow

10 p1862 A70-23846

Compressible turbulent boundary layer with adverse pressure gradients and crossflow over revolving bodies, integrating numerically three dimensional compressible integral equations

11 p2035 A70-25689

Pressure gradient, wind structure and shearing stress in atmospheric boundary layer related by formulation based on quasi- parallelism and boundary condition at Ekman layer top

11 p2076 A70-26071

Atmospheric pressure variations as function of vertical movements caused by friction and orography, considering numerical forecasting

11 p2076 A70-26073

Wall pressure fluctuations beneath turbulent boundary layers on flat plate and cylinder

11 p2038 A70-26529

Motion and shape of interface at separation of turbulent and nonturbulent regions in boundary layer with zero pressure gradient

11 p2040 A70-26539

Similar laminar boundary layer solutions exhibiting separation, pressure gradient and mass transfer

12 p2211 A70-27828

Boundary layer equations with pressure gradient for revolving slender body, examining transverse curvature influence on layer separation and integral characteristics

12 p2214 A70-28249

MHD boundary layer flow past walled flat plate in presence of pressure gradient, determining skin friction expansion terms

13 p2461 A70-28804

Two dimensional turbulent boundary layer with pressure gradient, calculating velocity distribution and local skin friction by Pohlhausen method

13 p2391 A70-29672

Aircraft altimeter measurement for vertical separation based on atmospheric pressure unit changes /Cayleys/ compared with linear measurements in meters and feet

13 p2411 A70-29778

Inflow and pressure difference for mean flow in straight suction duct with porous walls, using elementary momentum analysis

13 p2392 A70-30020

Mesoscale slope limits in constant pressure surfaces relation to g-forces on aircraft at SST altitude, using radiosonde measurements

14 p2530 A70-30607

Fluidic components downstream impedance calculation, using measured/monitored pressure ratio

14 p2534 A70-30680

Prandtl number effects on adiabatic wall temperature and pressure gradient at separation point for hypersonic compressible laminar boundary layer

14 p2566 A70-31027

Three dimensional boundary layer separation, noting necessity of streamlines perpendicular to pressure gradients near wall

15 p2719 A70-31488

Viscid-inviscid equations solution, describing flows with coupled mixing, combustion and lateral pressure gradients

[AIAA PAPER 69-166]

15 p2718 A70-32516

SST inlet steady state pressure defects and random pressure fluctuations determining TF30 engine/inlet compatibility

[AIAA PAPER 70-632]

16 p2834 A70-33530

Favorable pressure gradient effect on compressible two dimensional supersonic turbulent boundary, using temperature and pressure probes and shear balance

18 p3242 A70-36690

Boundary layer momentum thickness growth in channels with adverse pressure gradients by stepwise integration of Truckenbrodt equation and extending Gruschwitz-Schmidbauer separation criterion

[ASME PAPER 70-GT-12]

18 p3243 A70-36864

Two dimensional equations of boundary layer with arbitrary pressure gradient solved using successive approximations for numerical integration

19 p3406 A70-38390

One wavelength MHD induction generator, discussing field pressure gradients, fluid velocities, excitation and electrical output power

20 p3566 A70-40015

Pulsed coaxial plasma accelerator efficiency, examining high capacitance and axial propellant pressure gradients

[AIAA PAPER 70-1085]

20 p3693 A70-40250

Transformation theory for compressible turbulent boundary layer with arbitrary pressure gradient

[AIAA PAPER 69-160]

21 p3809 A70-41741

Stress distribution and shape in arbitrarily shaped gore parachute under unsteady pressure distribution during inflation and descent

[AIAA PAPER 70-1197]

21 p3752 A70-41819

Interactions between components of turbulent flow velocity correlation tensor due to pressure fluctuations

21 p3810 A70-41956

Cavitation characteristics of jet nozzles, formulating relationship between pressure differential and fluid flow rate

22 p3965 A70-43369

Neutral stability curve for flat plate boundary layer in zero pressure gradient with increasing thickness, giving critical Reynolds number

23 p4179 A70-43974

Nitrogen plasma viscosity measurements as function of velocity and axial static pressure gradient

23 p4226 A70-44439

Gas pressure differential across multilayer insulation blanket during rapid evacuation predicted, using one dimensional flow theory

[AIAA PAPER 69-608]

23 p4282 A70-44522

Pressure gradient effect on skin friction coefficients taking into account Mach, Reynolds and Stanton numbers

23 p4183 A70-44629

Atmospheric pressure surface sharp slopes at SST altitudes producing vertical acceleration based on temperature gradients inspection

24 p4372 A70-46050

Pressure gradient induced drift waves in collisionless hydrogen plasma in homogeneous magnetic field

24 p4388 A70-46209

PRESSURE HEADS

Stability region of hydraulic system containing centrifugal pump calculated from pressure head dependence on pump inlet pressure

09 p1607 A70-23622

Axial compressor stage head determination by measuring axial thrust, noting fluid velocity nonuniform distribution influence

13 p2474 A70-28892

MHD pressure head variations in Hg flow in square channel with conducting and insulating walls under transverse magnetic field

13 p2465 A70-29838

Aerothermopressor experiment in subsonic and supersonic gas flow compared with numerical solutions of equations

15 p2720 A70-31900

PRESSURE MEASUREMENTS

Microbarographic oscillations associated with geomagnetic activity during observation of infrasonic waves on geomagnetically disturbed days

01 p0081 A70-11298

Coordination technique for pressure, density and temperature measurements by probes during parachute reentry into planetary atmospheres, taking into account reentry dynamics

01 p0197 A70-11495

Ammonia red and green bands measured line positions, strengths and half widths applied to Jupiter atmospheric pressure determination

02 p0368 A70-11821

Nonequilibrium two phase forced convection flow, describing pressure, temperature and void fraction measurement techniques

02 p0305 A70-12838

Fixed mass fixed volume sinusoidal pressure generators for evaluation of transducers used in high pressure measurements

03 p0494 A70-14049

Longitudinal pressure gradient measurement for DC discharges in He, Ne and Ar, investigating effects of gas purity, tube geometry, etc

04 p0671 A70-14995

Pressure-volume-temperature measurements on H₂, calculating fugacity coefficients

04 p0719 A70-15057

Unsteady pressure distributions measurement for oscillating rectangular wing, discussing test results for sub- and transonic velocities

[DGLR-69-32]

04 p0616 A70-15184

Blood flow velocity and pressure measurements on conscious man with catheter-tip velocity probe

04 p0645 A70-15439

Lift forces and pressure on vibrating cylinders in plane perpendicular to air flow measured in wind tunnel

06 p0968 A70-17545

Atmospheric pressure measuring device based on hypsometer and mercury barometer principles for automatic weather stations or remote readout

06 p1066 A70-18247

Electret microphones application for pressure fluctuations measurements on thin aerodynamic profiles noting operation, vibration insensitivity, robustness and cost

06 p1071 A70-18473

Pressure distribution measurement over profile by means of pneumatically activated inductive sensor

07 p1188 A70-19084

Flat plate boundary layer induced pressures in unsteady hypersonic flight

07 p1257 A70-19327

Supersonic wind tunnel flow discontinuities effect on oscillatory pressures

07 p1257 A70-19338

Unsteady aerodynamic forces on helicopter rotors using pressure measurements and wind tunnel visualizations of smoke emission

[ONERA-TP-777]

08 p1434 A70-21847

Diastolic and systolic pressure measurement in acute and chronic experiments

09 p1627 A70-23302

Flow parameters behind shock waves calculated, determining amount of condensate evaporation and error in pressure measurements due to evaporation

09 p1607 A70-23711

Resultant of elementary aerodynamic pressures on profile with angular point of attachment

10 p1797 A70-23874

Temperature, pressure and electron density measurements behind reflected shocks in gas driven diaphragm shock tube compared with Rankine-Hugoniot predictions

10 p1967 A70-23960

Pulsating flow mean total pressure measurement accuracy in high turbulence regions, discussing standing and traveling acoustic waves produced at measuring system entrance

10 p1867 A70-24160

Shock pressure and impulse caused by Q switched laser light absorption, considering temperature dependence of EM radiation penetration depth

10 p1900 A70-24422

Vapor pressure of binary alloys with volatile components measured by combined Knudsen-torsion method, using thermal balance in vacuum

11 p2065 A70-25773

Methane oxidation behind reflected shock waves between 1350-1900 K, measuring pressure, chemiluminescence and 3067 A absorption of OH radical

11 p2150 A70-26380

Rarefied gas stream density measurements with electron beam fluorescence experiment, determining

pressures and densities behind plane shock wave and in supersonic nozzles

11 p2087 A70-26743

Air pressure, air density and gravity tables, including corrections for mercury barometer measurements

12 p2222 A70-27008

Indentation pressures in rigid perfectly plastic solids correlated with ratio between indenter strain and material yield strain for various indenter geometries

12 p3222 A70-27232

Omegatron for total and partial pressure measurement or mass spectrometer applications

12 p2231 A70-27262

Orbitron ion gauge experimental designs for low pressure applications

12 p2231 A70-27264

Lead azide detonation hazards and resulting pressure waves, evaluating protective glove material by dynamic pressure measurements

12 p2289 A70-27665

Pressure measurements and gas flow analysis during thermal vacuum tests of manned spacecraft indicating adequate space vacuum simulation

13 p2384 A70-28518

Conductive rubber pressure transducers for fluid flow measurement

14 p2584 A70-30503

Error measurements of sharpened edged circular static pressure hole normal to moving fluid boundary using flush transducers

15 p2722 A70-32374

Lifting body pressure and heat transfer measurements at various angles of attack in hypersonic flow [DGLR-70-029]

15 p2828 A70-32841

Liquid hydrogen axial flow pump inducer, describing suction pressure measurements, fluid conditions and flow rate

16 p2919 A70-33592

C-5A turbofan engine thrust determination using pressure and temperature values in exhaust nozzles

16 p2969 A70-33606

Wustite partial oxygen pressure measurements using emf in zirconia solid electrolyte

16 p2961 A70-33965

Transonic flow around perpendicular plate, determining front side velocity and pressure from known stagnation point and transonic region

16 p2839 A70-34236

Surface pressure and lift measurement on model lifting rotor blade as function of vortex interaction, using flush mounted pressure transducers

17 p3009 A70-34737

Measurement methods for forces, pressure and heat flow in hotshot hypersonic wind tunnels

17 p3057 A70-34773

Force-balance principle application to pressure and skin friction measuring instruments, discussing construction, operation and performance

17 p3089 A70-35171

Hypsometer design for accurate pressure measurements at high balloon altitudes

17 p3090 A70-35313

Dynamic force and pressure measurement on rocket nozzle during simulated stage separation, describing instrumentation and control system

17 p3061 A70-35478

Low pressure measuring system for aerodynamic models tested in Mach 12-14 wind tunnel, discussing transducers and high speed digital recording and data processing system

17 p3062 A70-35493

Pressure distribution measurements on wedges in compressible flow at Mach 0.5-2.2, discussing wedge angle, Mach number and boundary layer thickness effects

17 p3013 A70-35923

Ultrahigh vacuum pressure measurement by improved residual gas analysis mass spectroscopy with magnetic section

19 p3396 A70-37465

Residual gases partial pressure measurement in vacuum chamber by mass spectrometer with electromagnet scanner and electron multiplier, detecting electron current

19 p3421 A70-37466

Signal conditioner for expanded range pressure measurements from reentry vehicles via transducer zero shift suppression and output signal compression

19 p3426 A70-37899

Arterial pressure measurement by automatic control system based on external compression pressure for maximum amplitude intraarterial pressure pulse oscillations

19 p3370 A70-38215

Dynamic intravascular pressures measured in small vessels of frog lung using micropressure transducer inserted into vessel lumen

19 p3364 A70-38368

Reliability tests of blood carbon dioxide pressure measurement methods, indicating carbon dioxide-electrode method superiority

19 p3365 A70-38371

Static pressure probes selection for measuring three dimensional flow at high velocities, considering sensitivity and errors 20 p3628 A70-39262

Radio telemetry measurements of blood pressure and flow in unrestrained animals 20 p3579 A70-39370

Elastic bodies collision, determining temperature field variations and contact pressure 20 p3725 A70-39869

Rectangular wing with oscillating control surface, measuring induced unsteady pressure field for comparison with computations based on lifting surface theory 21 p3935 A70-41407

Pressure recording site localization in esophagus, discussing cardiac artifacts morphology and localization over esophagus length 21 p3765 A70-42152

Topography of pleural surface pressure and vertical gradient of transpulmonary pressure above resting volume in relaxed animals as function of alveolar pressure 21 p3766 A70-42154

High speed plasma jet propagation, obtaining time of arrival measurements, brightness temperature, pressure and impact data 22 p4012 A70-43014

Multiple tube manometer with selector switch for measuring flow channel wall pressures 23 p4194 A70-44000

Wave rider aerodynamic properties at small Reynolds numbers, using non-Weiler wing for flow field, pressure and force measurements at rarefied flow conditions [AVA-FB-7029] 23 p4135 A70-44668

Pressure measurements on harmonically vibrating sweptback wing with two control surfaces in incompressible flow 23 p4274 A70-44768

German monograph on three dimensional flow and blade pressure measurements at axial flow compressor casing wall, discussing test control and digital data processing 24 p4332 A70-45093

Indirect blood pressure measurements using motion artifact suppression circuit based on K-sound electrocardiography 24 p4296 A70-45335

Conscious rat systolic blood pressure measurement, using arterial pulse wave detection to occluding cuff by photoconductive cell 24 p4309 A70-46213

Thrustmeter for direct output reading from jet engines based on stream and total port pressures 24 p4340 A70-46328

PRESSURE MICROPHONES
U MICROPHONES

PRESSURE OSCILLATIONS

Pressure oscillograms and schlieren photographs of shock wave amplification during interaction of cellular flame of gas mixtures in cylindrical combustion chamber 01 p0217 A70-11014

Axial mode shock wave oscillations in end-burning solid rocket motor, obtaining periodic solutions for flow properties, solid temperature and burning rate 02 p0353 A70-12010

HF pressure oscillations during heat transfer to n-heptane at various flow rates and pressures, studying film or bubble boiling associated with oscillations 03 p0605 A70-13516

Dynamic response of solid propellant flame to oscillating pressure field using T-tube rocket motor, discussing entropy waves produced in oscillatory combustion [AIAA PAPER 68-499] 04 p0737 A70-15580

Pressure surges originated by tangential instabilities in solid propellant motors, using double base homogeneously compounded cylindrical grains 09 p1743 A70-22661

Pressure oscillations in LOX pump inducer of J-2 machine, using semianalytical first order model with retarded time mechanism 09 p1693 A70-23257

Entropy or material waves effects on HF pressure oscillations in liquid rocket combustor, assuming concentrated combustion zone and zero length nozzle 10 p1929 A70-24088

Turbulent gas nonresonant pressure pulsations effects on local convective heat transfer in tube flow 10 p1968 A70-24288

Field strength correlation with micropressure variations caused by internal gravity waves propagating in lower troposphere 10 p1883 A70-25252

Nucleate pool boiling, calculating sinusoidal and square wave pressure variations effect on heat flux for comparison with measurements 14 p2616 A70-30254

Acoustic measurement of surface pressure fluctuations in supersonic transitional boundary layers 17 p3092 A70-35482

Water cooled pressure probes for measuring rocket chamber HF pressure variations 17 p3093 A70-35485

Aft-end igniter design and placement for solid propellant rocket motors avoiding overpressurization and nozzle pressure oscillations 21 p3866 A70-40892

Elastic plate response to boundary layer pressure fluctuations, estimating vibration modes dependence on fluctuation convection velocity and response magnification as function of flow direction 22 p4007 A70-42283

Turbine blades aerodynamic forces theoretical and experimental investigation, noting cascade series interaction induced pressure pulsations 24 p4288 A70-45504

HF sinusoidal fluid pressure generators driven by electromagnetic vibrators for arterial applications 24 p4309 A70-46118

PRESSURE PROBES
U PRESSURE SENSORS

PRESSURE PULSES

Arterial pressure pulse waves mathematical analysis applied to variations in stroke volume in anesthetized dogs subjected to spine-to-breast accelerations 01 p0012 A70-10125

Pressure pulsations and velocity measurements in turbulent boundary layer without longitudinal gradient, analyzing Reynolds numbers, self similarity and structural characteristics 04 p0673 A70-15250

Plasma cumulation, with and without shell under concentric pressure impulse using perfect gas theory, estimating critical parameters 10 p1926 A70-25322

Thin cylindrical shells of perfectly plastic rigid material, analyzing dynamic plastic deformation under internal impulsive pressure 11 p2139 A70-26413

Nonstationary pressure pulse acting on body in liquid or gas, discussing flow with unperturbed parameters at infinity 12 p2213 A70-28239

Fatigue life and long term strength of polycarbonate components in pneumatic pulsating pressure equipment described by power and exponential equations 13 p2440 A70-29784

Circular elastic shell response to moving and simultaneous loads, using impulse simulation method 13 p2518 A70-29986

Severity comparisons of specified and actual impulse tests determining component reliability 14 p2563 A70-30867

Comparative arterial pressure pulse transmission velocity in dogs, relating wall elasticity with vascular disease 15 p2682 A70-31939

Error analysis of Corcos hypothesis concerning cross spectra of pseudoacoustic LF turbulent pressure pulsations on flat plate 18 p3241 A70-36305

First derivative of ventricular pressure recorded by conventional cardiac catheters, analyzing in terms of Fourier series 21 p3767 A70-40578

Vapor bubble response to sinusoidal pressure pulsation in water bulk and on metal wall 21 p3949 A70-41309

Circular cylindrical shell with annular orthotropic elastic core, analyzing stress wave propagation under pressure pulse 21 p3938 A70-41740

PRESSURE RECORDERS

Blood pressure indirect recording using ceramic crystal pick-up over brachial artery and under pneumatic cuff 06 p0992 A70-17299

PRESSURE RECOVERY

Pressure recovery for stagnation of underexpanded sonic air jet in chamber having transparent walls and containing nozzle and diffuser in coaxial positions 07 p1189 A70-19811

Pressure recovery and energy loss efficiencies of two dimensional diffusers with suction at entrance 11 p1977 A70-26418

Starting criterion for hypersonic inlets with large turbulent boundary layers, considering total pressure recovery from all shock and viscous losses 14 p2529 A70-30865

Mass flow rate and geometry effects on pressure recovery of conical diffusers with annular secondary injection at inlet [ASME PAPER 70-FE-18] 16 p2835 A70-33631

Conical diffuser-tailpipe system performance, discussing cone angle, area ratio, Reynolds number and velocity distribution effects on pressure recovery 20 p3559 A70-40082

Viscous gas flow through Laval nozzle, calculating velocity coefficient and pressure recovery in contracting and expanding parts 21 p3746 A70-41774

PRESSURE REDUCTION
NT EXPLOSIVE DECOMPRESSION

Sea-level pressure interval to prevent decompression sickness in humans flying in commercial aircraft after diving 01 p0032 A70-10366

Pressure drops in turbulent flow through circular or plane parallel section pipes, obtaining mean velocity expressions suitable for application to lubrication 02 p0277 A70-11912

Monograph on aircraft aerodynamic nozzle asymmetry effects for pressure drag reduction in critical conditions 03 p0465 A70-13003

Autonomic nervous system role in controlling body functions after rapid decompression, increasing tolerance to pressure gradients by physical training 04 p0630 A70-14575

Base bleed fluid injection effect on steady separated flow past two dimensional bluff body, studying streamline pattern near object 06 p0967 A70-17518

Gas bubbles formation in supersaturated solutions and body fluids during decompression 07 p1208 A70-19511

Flight maneuver for roll modulated lifting reentry vehicle to reduce deployment dynamic pressure 07 p1394 A70-19724

Viscoelasticity in shearing and accelerative flows by integral theory, discussing stress distribution and pressure drop 07 p1412 A70-20000

Hypoxia effect on retrograde amnesia /recent memory loss/ in albino rats subjected to shock and decompression treatments 08 p1441 A70-20477

Polymeric materials flow at tube entrance, discussing pressure drop and flow birefringent patterns at tapered and sharp entrances 08 p1486 A70-21861

Long bone necrosis in response to reduced atmospheric pressure exposure, comparing lesions with caisson disease 08 p1449 A70-21944

Alveolar ventilation and pulmonary circulation during application of negative pressure to lower part of human body 09 p1615 A70-22090

Shock impedance definition consistent with acoustic limit, considering use of impedance mismatch to reduce sonic boom overpressure 10 p1805 A70-24522

Pressure loss in tubulature of oil-hydraulic drive mechanism, allowing for viscosity changes associated with oil temperature and pressure increases 10 p1809 A70-25209

Pressure decay prediction improvement for venting and quenching processes of solid propellants using analytical method 11 p2101 A70-25683

Pressure peaks control in hydrazine propulsion system during static tests by controlling initial hydrazine injection 11 p2101 A70-25691

Stagnation pressure losses in radial vaneless diffusers to estimate compressor performance, noting one dimensional analysis 11 p1974 A70-25782

Gas bubbles formation in supersaturated solutions and body fluids during decompression 11 p1988 A70-26110

Incremental lower body negative pressure as assay method for human orthostatic tolerance 11 p1992 A70-26518

Monograph on acoustic theory for determining frictional pressure drop effect on gas state behind reflected wave in shock tube 12 p2209 A70-27000

Alveolar ventilation and pulmonary circulation during application of negative pressure to lower part of human body 15 p2685 A70-32686

Propellant flame temperature and emission spectra during depressurization by rarefaction waves, using rapid scanning spectrometer [AIAA PAPER 70-663] 16 p2962 A70-33570

Solid propellant extinguishment by rapid depressurization, investigating motor configuration effect, binder, burning rate catalyst, oxidizer, metal loading and exhaust pressure levels 16 p2962 A70-33572

Stable operating range of supersonic mixed compression inlet increase by air flow removal via throat bleed system [AIAA PAPER 70-686] 16 p2967 A70-33585

Barometric pressure reduction effect on gaseous and volatile metabolic products elimination in men wearing oxygen-supplied rubberized suits 17 p3038 A70-35363

Off-design pressure losses in single stage axial flow compressor, using test rotor in annular duct [ASME PAPER 70-GT-78] 18 p3210 A70-36886

Decompression hazards in manned orbiting systems, considering consciousness time, survival, pathological response, water vapor and denitrogenation effects and recompression rates 22 p3973 A70-43638

Rapid decompression due to pressure loss in space vehicle or suit, discussing fulminating hypoxia, mechanical trauma and ebullism

22 p3973 A70-43639

Combustion chamber flow visualization, obtaining information on pressure loss, velocity field, flow pattern and temperature gradients

24 p4393 A70-45444

PRESSURE REGULATORS

Crushable honeycomb regulating operating pressure of propellant actuated devices applied to recovery parachute catapult in F-111 crew module

03 p0546 A70-14108

Self contained remote sense remote control pressure regulator using pure fluid amplifiers, controlling large or small flow over wide pressure range

09 p1614 A70-23688

Human body homeostatic mechanisms autoregulation, discussing feedback control systems for blood pressure and flow regulation, bodily movements and postural control, etc

10 p1810 A70-24038

Nuclear rocket engine fluidic chamber pressure control, discussing design concepts for static and dynamic subsystems

[AIAA PAPER 70-1010] 20 p3688 A70-39585

Vortex pressure regulator with adjustable settings, discussing design, operation and test results

[ASME PAPER 70-FLCS-9] 22 p3964 A70-42418

Semifluidic proportional control systems for industrial controls involving oven temperature, remote hydraulic pressure regulation, drill bit pressure

24 p4293 A70-45432

PRESSURE RELIEF VALVES

U RELIEF VALVES

PRESSURE SENSORS

Frequency characteristics of air, water and blood filled pressure transducer systems using various needle and connecting tubing sizes

01 p0031 A70-10275

Shock tunnel type differential sensor for low range base pressure measurements on full scale flight reentry vehicles, discussing ground tests

01 p0089 A70-10843

Speed ratio of rarefied gas flows by molecular miniature pressure probes with orifice at thin cylindrical tube side, discussing LTE deviation regions

02 p0296 A70-11871

Silicon strain gage transducer for measurement of pressure between tongue and teeth, developing two types of temperature compensated strain gages

02 p0242 A70-12054

Moving contact pressure transducer for remote signaling

03 p0494 A70-14048

Fixed mass fixed volume sinusoidal pressure generators for evaluation of transducers used in high pressure measurements

03 p0494 A70-14049

Test method for inertial impact sensor switches subjected to multiple and varied shock inputs, using high energy detonators

03 p0494 A70-14128

Solid state digital pressure transducer incorporating Si diaphragm with piezoresistive sensing elements for computerized supersonic and subsonic data applications

03 p0496 A70-14194

Ultraminiature pressure sensor for continuous recording of hydrostatic pressure in renal tubules and blood capillaries

05 p0804 A70-15772

Thermomolecular pressure corrections in tubes and at orifices for errors in gaseous pressure measurements by temperature gradients

06 p1113 A70-18371

Shock wave profiles in rarefied gas expansion flows, using static and impact pressure probes

06 p1052 A70-18386

Transducer for pressure fluctuations measurement in wide frequency range based on piezoelectric microphones, discussing dynamic characteristics

06 p1071 A70-18472

Diffused diaphragm pressure sensors in impact probes used in wind tunnel tests of dynamic response of supersonic air induction systems

06 p1074 A70-18605

Pressure distribution measurement over profile by means of pneumatically activated inductive sensor

07 p1188 A70-19084

Miniature piezoresistive pressure transducers for catheter and external physiological measurements in small animals

07 p1220 A70-19297

Semiconductor compounds application as partial vapor pressure sensors of chemical elements, discussing electrical properties dependence

07 p1356 A70-19554

Velocity pulsations of hypersonic working flow in wind tunnel using miniature pressure transducers, discussing rms error

07 p1259 A70-19828

Flow noise measurement for boundary layer pressure fluctuations at rigid wall, analyzing effect of transducer size, shape and orientation on resolution

09 p1675 A70-22387

Acoustic pressure sensors positioning on bodies of revolution to determine laminar boundary layer stability loss during ideal liquid flow at nonzero angles of attack

09 p1660 A70-22479

Piezoelectric quartz and tourmaline pressure gages static calibration, evaluating errors

09 p1675 A70-22599

Thermodynamic properties of periodically variable air volume in pneumatic pressure generator of pressure sensor calibration bench

10 p1863 A70-24027

Capacitive pressure transducer with linearly coupled armatures for aerospace use

11 p2051 A70-26294

Digital air data system vibrating diaphragm pressure sensor

11 p1983 A70-26508

Conductive rubber pressure transducers for fluid flow measurement

14 p2584 A70-30503

Error measurements of sharply edged circular static pressure hole normal to moving fluid boundary using flush transducers

15 p2722 A70-32374

Holographic interferometry for evaluating bond between diaphragm and base in pressure transducer

16 p2904 A70-33138

Pressure transducer diaphragms displacement measurement by holographic interferometry

17 p3085 A70-35010

Laser interferometry for accelerometer and dynamic pressure transducer calibration and vibration measurement

17 p3089 A70-35124

Fast response transducer for measuring transient pressures due to shock interaction

17 p3093 A70-35484

Water cooled pressure probes for measuring rocket chamber HF pressure variations

17 p3093 A70-35485

Pressure transducers primary calibration to 10 kHz, using shock tube for step function excitation

17 p3093 A70-35486

Ultraminiature piezoelectric semiconductor pressure transducers for wind tunnel models

17 p3093 A70-35491

Ultraminiature pressure transducers for use in wind tunnel models

17 p3093 A70-35492

Low pressure measuring system for aerodynamic models tested in Mach 12-14 wind tunnel, discussing transducers and high speed digital recording and data processing system

17 p3062 A70-35493

Vibrating diaphragm gas pressure measuring system based on membrane damping, applying to prototype atmospheric entry probes

17 p3095 A70-35524

Pressure transducers, discussing characteristic parameters and properties, varieties and applications

18 p3258 A70-36350

Pressure sensors for large frequency and amplitude measurement, discussing calibration with square signal generator

18 p3262 A70-37210

Extradural sensor for continuous measurement and recording of human intracranial pressure in neurosurgical practice

19 p3367 A70-37353

Dynamic pressure transducer calibration system using fluidic pressure generators

19 p3358 A70-37897

Signal conditioner for expanded range pressure measurements from reentry vehicles via transducer zero shift suppression and output signal compression

19 p3426 A70-37899

Membrane attachment for pressure transducer with help of holographic interferometry, describing optical system

19 p3427 A70-38453

Launch and reentry vehicles pressure transducers, measuring propellant quantity, water systems, fuel, oxidizer, battery compartment and ascent engines, etc

19 p3430 A70-38519

Solid state, digital, Resonant Capsule Pressure Transducer based on natural frequency variation of aneroid capsules by pressure induced curvature changes

19 p3430 A70-38520

Piezoresistive Si pressure transducer design for Digital Air Data Computers, achieving optimum resistor matching and long term stability

19 p3430 A70-38521

Ultraminiature pressure transducer for airplane model and inlet/engine subsystem in wind tunnel tests, considering design, calibration, environments, etc

19 p3430 A70-38523

Sensing elements piezoresistive Si and indium antimonide film sensing elements for high sensitivity pressure transducers and accelerometers, discussing airborne telemetry applications

19 p3431 A70-38538

Miniature pressure transducers using piezoelectric or semiconductor elements

20 p3628 A70-39226

Probe connected to microphone membrane chamber by transmission tube for fluctuating pressure measurement at discrete point in air flow

20 p3635 A70-40509

Pressure sensor testing and calibrating at cryogenic temperatures, describing special test rig structural, insulation, fittings and materials requirements

23 p4178 A70-44846

Circuit design providing thermal compensation for atmospheric pressure sensor, using mercury barometer

24 p4340 A70-46403

PRESSURE SUITS

NT SPACE SUITS

Nonextension lines characteristic to human skin utilized to provide natural mobility and minimal ballooning in full pressure suits noting mapping, testing, construction, etc

[ASME PAPER 69-WA/AUT-22] 04 p0642 A70-14826

Apollo suit features applicable to operational or research program requiring pressure suits, discussing low torque constant volume joints

06 p1002 A70-17704

Pneumatic compression effects on canine cardiovascular dynamics after hemorrhage tested in G-suit inflation

11 p1988 A70-26516

Nonextension lines characteristic to human skin utilized to provide natural mobility and minimal ballooning in full pressure suits noting mapping, testing, construction, etc

17 p3036 A70-34951

G suit application to clinical therapeutics, noting intraabdominal bleeding control

21 p3767 A70-40737

G-suit hazards in lower extremity thrombophlebitis in pilots

24 p4307 A70-45347

PRESSURE SWITCHES

Fluidic membrane pressure wave switch with air control-action release, noting use in light signal control, conveyor belt counting, storage vessel level control, etc

21 p3759 A70-41425

PRESSURE TRANSDUCERS

U PRESSURE SENSORS

PRESSURE VESSEL DESIGN

Metal lined glass filament-wound pressure vessel performance at cryogenic temperatures, discussing fibers, resins and liners

06 p1091 A70-17615

PRESSURE VESSELS

Acoustic emission to monitor metal structures, pipes, pressure vessels and graphite shapes to detect structural deterioration before failure, emphasizing nuclear reactor pressure systems

01 p0054 A70-10015

Inconel 718 and Al 2219 alloys surface flawed specimens fracture toughness and flaw growth comparison for high pressure hydrogen vessel

01 p0114 A70-10029

Spherical pressure vessel fracture initiation and propagation from long flaws considered from theoretical and experimental approaches

01 p0199 A70-10264

Ductile-brittle fracture transition in steel pressure vessels suppressed by utilizing thin laminations

03 p0583 A70-12903

Pressure vessel deformation and stress analysis by matrix displacement method, considering solids and membrane shells under axisymmetric and asymmetric loading

[ASME PAPER 69-WA/PVP-3] 04 p0768 A70-14790

Torospherical heads attached to cylinders and under internal pressure as elastic and/or elastic-plastic shells, using finite element

[ASME PAPER 69-WA/PVP-7] 04 p0769 A70-14792

Flight type pressure vessels fabricated with quenched and tempered Ni-Cr-Mo-V structural steel, discussing fracture toughness, design, fabrication techniques

[SAE PAPER 690680] 05 p0853 A70-15866

Pressure vessel technology - Conference, Delft, Netherlands, September-October 1969

05 p0942 A70-16801

Failure prediction for arbitrary shape flawed pressurized vessels using structural geometry, crack length, ultimate and yield stresses and fracture toughness

05 p0942 A70-16803

Time dependent creep and elastic strain interaction in plates and pressure vessels of cylindrical and spherical geometry

05 p0942 A70-16804

Pressure vessel technology - Conference, Delft, Netherlands, September-October 1969, Part 1, Design and analysis

05 p0943 A70-16808

Lower bound limit analysis of symmetrically loaded thin shells of revolution having arbitrary meridional profiles, demonstrating methods for pressure vessel problems

05 p0944 A70-16815

Metal lined glass filament-wound pressure vessel performance at cryogenic temperatures, discussing fibers, resins and liners
06 p1091 A70-17615

Filament tensile strengths and pressure strain characteristics of high modulus boron filament wound/resin composite pressure vessels for cryogenic applications
08 p1509 A70-21909

Linear and nonlinear rupture mechanics applied to thick walled pressure vessels of high strength materials
09 p1769 A70-22184

Stress distributions in thin walled pressure vessels analyzed by scattered light photoelasticity technique compared to strain gage analysis
11 p2131 A70-25593

Saturn booster Ti alloy pressure vessel forging, heat treatment and welding, discussing machining, cleaning and tooling
[SME PAPER AD-70-733]
12 p2241 A70-27085

Stresses in cylindrical pressure vessels with heads formed by internal fluid pressure
13 p2509 A70-28532

Supercritical pressure system heat transfer characteristics for cryogenic space oxygen storage and supply
14 p2667 A70-31342

Instrumented Charpy impact test evaluating strain rate, alloying and irradiation effects on ductile-brittle transition temperature and fracture of pressure vessel steels
15 p2820 A70-32239

Stress corrosion cracking of Ti alloys in nitrogen tetroxide and methyl alcohol environments in Apollo spacecraft pressure vessels
17 p3199 A70-34453

Long orthotropic pressurized circular cylindrical shell under radial line loads along equally spaced generators, analyzing stresses and deflections by linearization
19 p3545 A70-38338

Pressure vessels charging procedure efficiency analysis
20 p3606 A70-39692

Cyclic thermal loading in viscoelastic spherical and cylindrical pressure vessels, investigating thermal frequency effect
21 p3937 A70-41430

Shell of revolution /pressure vessel/ with meridional slope discontinuity, calculating pressurization effect on stresses by computer program
24 p4420 A70-45277

Thermosetting glass reinforced plastics fabrication and use for pressure vessels, vacuum vessels and pipes
24 p4350 A70-46388

PRESSURE WAVES
U ELASTIC WAVES

PRESSURE WELDING
NT DIFFUSION WELDING
NT EXPLOSIVE WELDING
Cold pressure welding of space station tested on Soviet Soyuz spacecraft
06 p1078 A70-18503

Ultrahigh vacuum metal bonding by twist compression technique, reporting adhesion and friction coefficients for atomically ordered Pt-Co alloy
21 p3833 A70-41465

PRESSURIZED CABINS
Book on aircraft environmental control covering design, construction and operation of various systems
10 p1809 A70-25203

Harrier fighter aircraft cabin air conditioning and pressurization system
12 p2166 A70-27890

PRESSURIZING
NT FUEL TANK PRESSURIZATION
Externally pressurized journal bearing load tests, comparing load capacity data with analytical values
01 p0103 A70-10559

Equipment for cyclic biaxial stress states testing by simultaneous direct pressurization and axial loading of thin walled cylindrical specimens
03 p0462 A70-12966

Stiffness of multipad externally pressurized journal bearings with incompressible fluid feeding, comparing hydrodynamic and rolling bearings
15 p2745 A70-32445

Pressurized gas bearing flow field, discussing velocity transversal component, pressure distribution and profile
16 p2924 A70-34237

Pressure vessels charging procedure efficiency analysis
20 p3606 A70-39692

PRESTON TUBES
U PITOT TUBES
U SPEED INDICATORS

PRETRAINING
U PRESTRESSING

PRESTRESSING

Finite element bending stiffness matrices for deflections analysis of pretwisted cantilever plate subjected to static loads
02 p0384 A70-11858

Finite element method for calculating natural frequencies and mode shapes of pretwisted cantilever plates assembly of flat triangular elements
02 p0384 A70-11859

Elastic bending of pretwisted elliptical bars, showing stiffness response
02 p0387 A70-12216

Exact polynomial solution Saint Venant flexure of pretwisted rectangular plate treated as shallow hyperbolic paraboloidal shell
05 p0928 A70-16056

Prestrain effect on waves propagation along slender low density unoriented polyethylene rod, indicating uniform phase velocity change over audio frequency range
07 p1248 A70-19237

Prestrain effect on cavity formation at grain boundaries causing creep strength decrease
07 p1307 A70-19392

Steel strength under prolonged preliminary loading at elevated temperatures
08 p1515 A70-20934

Steel structure and mechanical properties under preliminary loading at elevated temperature and liquid Li at various exposure times
08 p1515 A70-20935

Prestressing in minimum weight design of statically indeterminate structures
09 p1781 A70-23231

High temperature creep of prestrained molybdenum single crystals as function of physical treatment and crystal orientation
10 p1902 A70-23860

Prestrain and mean stress effects on fatigue life using cumulative damage procedure based on Al alloy and aircraft quality steel tests
11 p2137 A70-26092

Tensile prestrain effect on yield locus of thin walled Al tubes from stress tests in torsion-tension space
13 p2431 A70-28536

Pretwisted slender beam coupled torsional and longitudinal vibrations under centrifugal force field, obtaining resonant frequency by Rayleigh Quotient method
20 p3719 A70-39601

Prestrained laminated media stability, discussing column buckling, standing waves, natural frequencies, wave propagation, stress-strain relations, motion equations and elastic moduli
20 p3731 A70-40049

Optimal load distribution for prestressed rod system, using Chebyshev solution of inequalities
22 p4121 A70-43725

Prestressed loadings on two layer fiberglass-reinforced plastic cylindrical shell under internal pressure
23 p4265 A70-43937

Prestraining effect on cellular precipitation in Ni-Cr lamellar eutectic during creep testing
24 p4359 A70-45247

PRETESTS

U TESTS

PRETREATMENT
NT PRESTRESSING
Solid film lubricants pretreatment and applications in aircraft and aerospace industries
06 p1075 A70-17341

PRETWISTING

U PRESTRESSING
U TWISTING

PREVENTION

NT ACCIDENT PREVENTION
NT CORROSION PREVENTION
NT FIRE PREVENTION
NT ICE PREVENTION

PRIMARY BATTERIES

NT ALKALINE BATTERIES
NT DRY CELLS
NT MAGNESIUM CELLS
NT METAL AIR BATTERIES
NT NICKEL ZINC BATTERIES

PRIMARY COSMIC RAYS

NT SOLAR COSMIC RAYS
Energy dependence of intensity ratio of Li, Be and B on C, N, O and F nuclei /L/M ratio in primary cosmic rays, analyzing data discrepancy
01 p0169 A70-10316

Primary cosmic ray nitrogen nuclei intensity and spectrum measured by balloons and Pioneer 8 space probe, obtaining abundance difference from solar atmosphere
01 p0169 A70-10319

Underground and surface telescope measurements of second harmonic of primary cosmic ray daily variation and upper solar modulation limit
01 p0170 A70-10405

High energy nuclear interactions defined by computerized determination of sea level lateral distribution of muons from primary cosmic ray air showers
01 p0171 A70-10667

Excess radiation in equatorial regions studied on-board Cosmos 137, noting contribution of primary particle multiplication to secondary radiation
01 p0192 A70-11542

High energy extensive air shower detection by Cerenkov receivers or liquid scintillators, considering 200 and 3000 MHz radio emission mechanisms
02 p0357 A70-12115

Primary cosmic ray proton energy spectrum determined using balloon-borne ionization spectrometer and spark chamber
02 p0360 A70-12844

Cosmic ray muon source implied from hadrons X pairs produced in primary cosmic ray collisions
02 p0360 A70-12845

Quiet time primary cosmic ray electron flux and energy spectrum from 10 to 200 Mev in interplanetary space observed byOGO 5 satellite
03 p0553 A70-12902

High energy primary cosmic ray and proton spectra measurements from Proton satellites
03 p0555 A70-13036

Primary protons energy estimated from energy ratio with maximum extremal distribution of electron numbers in lower half of atmosphere
03 p0527 A70-13054

Energy spectrum of cosmic radiation primary nuclei calculated from collisions against stellar light photons and 3 K black body radiation
03 p0561 A70-14185

Cerenkov radiation of electron-positron pair as moving radiating dipole in EAS, discussing emission effects of primary energy, production height and inclination angle
03 p0561 A70-14186

Superconducting magnetic system in magnetic analyzer of positrons and electrons in primary cosmic radiation tested on board Cosmos 213
04 p0685 A70-14443

Charged primary cosmic rays shield anisotropy generated diurnal/semidiurnal variations phase characteristics, using energy meson telescopes
04 p0738 A70-14513

Flux, energy spectrum and charge composition of primary cosmic ray electrons measured, determining energy spectrum of primary positrons above 220 Mev
04 p0739 A70-14595

Geomagnetic latitude survey by neutron multiplicity monitor covering threshold rigidity ranges at various elevations, relating data to primary cosmic ray rigidity spectrum
04 p0741 A70-15125

Very high energy cosmic rays disintegration and energy degradation by intense blue shifted photon fields of supernovae quasars and pulsar models
04 p0742 A70-15300

Light collecting properties of polystyrene scintillator designed for counting particles of electron-photon showers generated by high energy cosmic ray particles
05 p0846 A70-15944

Neutrinos production by primary cosmic rays in rarefied and dense media, calculating spectra
05 p0899 A70-15963

Pulsars as possible sources of superheavy nuclei in primary cosmic radiation, evaluating flux and mean power
05 p0901 A70-16314

Cerenkov light in extensive air shower observed at mountain altitude showing mixed primary cosmic rays in chemical composition
06 p1134 A70-17184

Relativistic magnetic monopoles detection in corpuscular primary cosmic rays, describing equipment and results
07 p1371 A70-20333

Ultrahigh energy primary cosmic rays model, considering galactic origin and energy spectrum
08 p1560 A70-20479

Cosmic ray air showers simulation, discussing high energy nuclear interaction and linear relation of primary particle energy to number
09 p1744 A70-22048

Pion and nucleon interactions, tabulating average multiplicity and inelasticity values for various primary cosmic ray energy levels
09 p1745 A70-22775

Primary cosmic ray particles location in photographic emulsions exposed to balloon elevations by spark chambers, noting stack alignment
09 p1679 A70-22990

Primary cosmic gamma-quanta fluxes measured using telescope consisting of Cerenkov counters
10 p1931 A70-24316

Cosmic ray particle abundance in upper atmosphere during minimum solar activity estimated by nuclear photographic emulsions on balloon flight
10 p1932 A70-24438

Energy spectra and composition of heavy nuclei in primary cosmic rays during low solar activity by nuclear emulsion stacks exposure in balloon flights
11 p2105 A70-26295

Highest energy primary cosmic ray particles, considering air shower characteristics and energy spectrum shape
12 p2292 A70-27381

Primary cosmic rays electron-positron component, considering relative roles of collision-produced and directly accelerated electrons 12 p2292 A70-27382

Primary cosmic ray proton and alpha particle spectral measurements by balloon flights 12 p2293 A70-27586

Penumbra and geomagnetic threshold effects on ionospheric electron production by primary cosmic rays 12 p2296 A70-28366

Superconducting magnetic system in magnetic analyzer of positrons and electrons in primary cosmic radiation tested on board Cosmos 213 13 p2403 A70-28468

Fireball role in N-N interactions at primary cosmic ray energies, using fireball model to explain particle production 13 p2476 A70-28913

Primary cosmic rays balloon-borne charge composition detector in 3-30 Z range 14 p2587 A70-31002

X rays and primary cosmic radiation intensity measurements near top of atmosphere, describing rocket payload and launch 14 p2632 A70-31307

Primary cosmic ray flux and p-carbon cross sections measurements by satellites showing heavy particle production at high energies 15 p2792 A70-31733

Relativistic cosmic rays primordial chemical composition above atmosphere from abundance data obtained with satellite-borne nuclear emulsion detector 15 p2793 A70-31735

Magnetic monopole flux limits in primary cosmic radiation derived from muon-poor shower data and inverse Compton scattering 16 p2972 A70-33050

Carbon isotopes abundance in primary cosmic radiation by nuclear emulsion stack exposure in high altitude balloon flight 17 p3151 A70-34914

Simultaneous primary energy spectrum, chemical composition and sidereal daily variation analysis for cosmic ray origin, using Proton measurements 19 p3500 A70-38080

High energy primary gamma quanta intensity limits from Proton-2 and Cosmos-208 measurements 19 p3502 A70-38092

Energetic primary gamma ray fluxes by satellite-borne spark chamber, isolating galactic radiation 19 p3502 A70-38093

Primary interplanetary electron energy spectrum, using Pioneer 8 measurements 19 p3502 A70-38094

Energy spectrum of primary cosmic ray electrons /negatron and positron/ in interstellar region observed near 1965 solar minimum 19 p3503 A70-38101

Primary cosmic ray electron flux, energy spectrum and east-west asymmetry, using balloon-borne spark chamber detector 19 p3503 A70-38104

High energy primary electron flux measurements by Cerenkov counter onboard ESRO 2 satellite 19 p3504 A70-38107

Positron fraction among primary cosmic ray low energy electrons, using pure emulsion stack exposed under residual atmosphere 19 p3504 A70-38109

Primary cosmic ray electron flux above 30 GeV, using nuclear emulsion plate chamber 19 p3504 A70-38110

Primary cosmic ray proton and alpha particle spectra measurements by balloon-borne equipment 19 p3505 A70-38118

Primary cosmic ray He nuclei rigidity measurement with magnetic spectrograph 19 p3505 A70-38119

Primary cosmic radiation singly charged component energy spectra by balloon-borne Cerenkov scintillation counter telescope 19 p3506 A70-38120

Primary cosmic rays energy spectra in interstellar space in relation to sunspot group number 19 p3506 A70-38121

Carbon isotopic composition in primary cosmic radiation by nuclear emulsions exposure in balloon flights 19 p3507 A70-38129

Primary cosmic rays above 4.5 GV, measuring charge composition from balloon flight 19 p3507 A70-38133

Rigidity spectra of primary cosmic ray nuclei groups from satellite-borne Cerenkov spectrometer 19 p3508 A70-38135

Highly charged cosmic ray heavy nuclei primaries, examining charge spectra and solar elements abundances 19 p3508 A70-38136

Primary cosmic ray particles with Z greater than 40 identified by tracks in balloon-borne nuclear emulsions and plastic detectors 19 p3508 A70-38138

Very heavy primary cosmic ray particles propagation calculation, using fragmentation parameters 19 p3508 A70-38139

High energy primary cosmic ray muons arrival directions examined for anisotropies underground 19 p3508 A70-38141

Primary cosmic ray proton energy spectra from satellite observation, presenting spectrum approximating function 19 p3510 A70-38153

Primary cosmic rays energy spectrum, investigating extensive air shower EAS, size spectrum in 2,000-1,000,000 eV range 19 p3510 A70-38154

Air shower radio pulse amplitude dependence on primary energy and core distance 19 p3581 A70-38607

Primary cosmic ray intensity variation during solar activity half cycle, expressing diffusion coefficient as function of sunspot group number 20 p3696 A70-39279

Primary cosmic rays nuclear transitions, determining fragmentation parameters 20 p3696 A70-39284

High energy charged particles equations of motion in quiet interplanetary magnetic field for primary cosmic ray distribution, calculating diurnal and semidiurnal variations 20 p3698 A70-39297

High transmission device for quark detection in primary cosmic rays 20 p3629 A70-39315

Recording device for gamma quanta in primary cosmic radiation 20 p3629 A70-39316

Primary cosmic rays spectrographic measurement, using hard muon component intensity variations data 20 p3629 A70-39320

Low energy cosmic ray heavy primary particles composition from nuclear emulsion stack observation 21 p3879 A70-40930

Rock particle tracks of primary cosmic rays, spallation recoil nuclei, nuclear fission and solar wind ions, observing time scale multiple soil orientation 21 p3914 A70-41652

Upper limit to primary deuteron flux and path length in space, using emulsion stack exposed near geomagnetic equator during minimum solar activity 22 p4093 A70-42673

Scattered photon effects on cosmic diffuse X ray spectrum at balloon altitude, noting overcorrection for absorption of primary X rays 23 p4237 A70-44794

Primary mass effects on extensive air shower characteristics, using Monte Carlo simulation 23 p4238 A70-44930

PRIMATES

Light synchronization of deep body temperature rhythms in Macaca nemestrina, investigating efficiency 03 p0416 A70-13013

Sensologic comparisons of carbonic anhydrases in human and other primate erythrocytes 13 p2355 A70-29805

GE-RESO primate life support subsystem design for NASA-ARC biosatellite program 17 p3174 A70-34766

PRIMERS [COATINGS]

Chemical and electrochemical corrosion resisting primers for Mg surface coatings in machine parts 14 p2598 A70-31293

PRINCETON SAILWINGS

U SAILWINGS

PRINTED CIRCUITS

NT LARGE SCALE INTEGRATION

IR microscope and digitally programmed mirror system for printed circuit inspection, allowing two dimensional scanning and magnetic tape reference 01 p0054 A70-10024

Printed circuit board connector selection techniques based on miniaturization reliability, cost and compatibility with intended application 02 p0268 A70-12473

Preamplifier-discriminator-gate generator in printed circuit for use with photomultipliers, noting pulse sensitivity and cost 09 p0676 A70-22987

Multiple wiring algorithm for automatic pattern design for AI interconnections and printed wiring in integrated circuits 15 p2715 A70-31842

Unidirectional tear drop radiation Archimedeian spiral broad band frequency independent antenna using printed circuit with cavity 21 p3801 A70-42246

Nondestructive measurement of elastic and plastic deformation in soldered joints and printed circuit boards by holographic interferometry 22 p4047 A70-43521

Printed circuit boards vibration control in dynamic environment, noting viscoelastic damping technique 22 p3999 A70-43675

Miniaturized VHF transmitter with bonded circular printed circuits for withstanding high shock loads, discussing design, production, packaging and testing 23 p4144 A70-44517

High performance military satellite missile command and control signal data processor modules, tremos packaging, using integrated and printed circuit modules 23 p4174 A70-44542

High density packaging of micrologic flatpacks using high interconnection method for r/o-side use of double-sided card in space flight applications 24 p4370 A70-45248

PRINTERS

NT PRINTERS [DATA PROCESSING]

Printers [DATA PROCESSING]
Digital color printer with opaque IBM card as filter for sea surface temperature and cloud vortex patterns display 16 p2907 A70-33180

Printing, electro etching and vacuum deposition stencil methods for preparing moire grids 19 p3432 A70-38721

PRINTING

Two inch high resolution vidicon for TV line processing of printed documents 16 p2906 A70-33173

PRINTOUTS

Instrumentation system for nuclear experiments on scientific satellites allowing highest priority event selection during telemetry sequence and periodic change of priority order 03 p0453 A70-13024

Real-time computer control system queueing model to optimize preemptible and nonpreemptible job priority assignment 05 p0817 A70-16414

Redundancy for spacecraft elements, describing various factors for priority establishment 15 p2712 A70-32643

PRISMATIC BARS

Saint Venant torsion and flexure of composite prismatic and cylindrical bars with circular and concentric interfaces 05 p0936 A70-16318

Prismatic pendularly supported beam load-forced vertical vibrations, critical load amplitude and force pulsation in case of stability loss 06 p1165 A70-17586

Elastoplastic torsion of combined prismatic bars with transverse distribution of constant properties solved by computer 07 p1415 A70-20189

Shear and cross sectional deformation of prismatic rectilinear rods with unicellular or multicellular thin walls, determining elastic behavior under arbitrary loads 10 p1955 A70-24055

Open cross section thin walled prismatic beam twisting and bending based on virtual displacements 13 p2511 A70-28744

Pyroceramics transient strength measurements on cylindrical and prismatic samples under static bending 15 p2764 A70-31545

Optimal distribution of plastic inhomogeneity of torsioned prismatic square bars under maximum loading 18 p3343 A70-36719

Prismatic isotropic homogeneous cantilever beams flexure for case of power series conformal mapping function 23 p4275 A70-44944

PRISMS

NT PRISMATIC BARS

Optimum prism angles and ultrasonic frequencies for detecting fatigue cracks 02 p0301 A70-12487

Ruby lasers simultaneous Q switching by single rotating prism, discussing possible differential frequency ranges 09 p1097 A70-22980

LiF prism spectrometer for space applications, discussing vacuum UV transmission and mechanical properties 10 p2049 A70-25609

Laser color TV display acousto-optic deflectors equalization using prisms 15 p2751 A70-32043

Pulsed laser alignment using pentaprisms-directec continuous laser light beam 15 p2752 A70-32047

Reflecting prism standards rotations effect on autocollimated images positions of optical instruments, investigating focusing method 16 p2915 A70-34214

Laser cavity design with total internal reflection quartz prisms, calculating prism angles tolerances 16 p2915 A70-34219

Prismatic adaptation under scotopic and photopic conditions in subjects, using transfer experiments 19 p3361 A70-38052

Optical telescope reflecting prism angle deviations effect on modulation transfer function and image quality 22 p4070 A70-42506

Prism film device coupling laser beam into thin film dielectric light guides, discussing operational theory 22 p4030 A70-42947

Prism film device for high efficiency laser beam coupling into light guiding thin film, deriving operation theory by plane wave analysis 22 p4030 A70-42948

Wollaston prism schlieren interferometer for quantitative density gradient measurements in air [SMPT PREPRINT 25] 22 p4034 A70-43050

Fourier hologram synthesis using laser point source and Wollaston birefringent prism 24 p4336 A70-45667

Interference fringes on gas laser beam reflected by total reflection prism 24 p4356 A70-46272

PRIVATE AIRCRAFT
U GENERAL AVIATION AIRCRAFT

PRIVATE AVIATION
U CIVIL AVIATION
U GENERAL AVIATION AIRCRAFT

PROBABILITY
U PROBABILITY THEORY

PROBABILITY DENSITY FUNCTIONS
NT NORMAL DENSITY FUNCTIONS
NT RAYLEIGH DISTRIBUTION
NT WEIBULL DENSITY FUNCTIONS

Signal discrimination from sequence of interference and noise by determining parameter value probability density using random process 01 p0044 A70-11024

Monograph on computation of density functions of parameters in stochastic systems, giving algorithms involving only matrix computations of fixed dimensionality 06 p1093 A70-17730

Superposition of dressed particles in plasma kinetic theory proved by using generalized stochastic equation for conditional probability density for one particle 06 p1124 A70-18500

Material inhomogeneity during high temperature fatigue tests taking into account probability density of random failure coordinate distribution 07 p1401 A70-18839

Statistical methods for characterizing interval sequences of ECG, treating interval distribution and joint probability density function of adjacent interval pairs 07 p1211 A70-19593

Phase coordinates conditional probability density statistical characteristics from continuous reception of random information, deriving differential equations 08 p1479 A70-20998

Probability density function of click duration in FM discriminator 11 p2018 A70-26270

Geometric and predictive methods for developing bounds on epsilon-entropy for infinity error norm constraint 11 p2014 A70-26306

Mathematical pattern recognition, using potential functions superposition methods for reconstructing probability density from samples 14 p2554 A70-30926

Optimum adaptive reception for binary sequences, using posteriori probability density function computing device synthesized from correlator, instantaneous nonlinearity and multiplier 14 p2552 A70-31188

System maintainability stochastic modeling using probability density functions 15 p2748 A70-32670

Probability density function of specularly fading signal plus noise for frequency shift keying and pulse radar systems 16 p2865 A70-34040

Search optimization for object drifting in outer space, considering approximate location and speed 17 p3172 A70-35668

Wind velocity fluctuation randomization signal probability density measurement, using statistical sampler 18 p3238 A70-36067

Ionospheric scatter communications channel phase frequency characteristics measuring method, considering probability density function 18 p3256 A70-36091

Density and distribution functions for quotient of ellipsoids of variance volumes, yielding probabilities and fractiles in three dimensional sets of points 19 p3382 A70-37835

Random vibration first threshold crossing probability density function for linear oscillator 19 p3427 A70-38038

Occupied bandwidth definition and measurement based on probability density function computation for radio transmitter spurious, harmonic and fundamental emissions 19 p3380 A70-38176

Dynamic plants optimal control, deriving algorithm for determining a posteriori probability density of generalized state vector 20 p3604 A70-39907

Output coordinates probability distribution density of nonlinear automatic control systems at fixed time, using multiple integrals 22 p4003 A70-42888

Monopulse radar excited by Gaussian signal and thermal noise in multiple targets, calculating angle error output probability density function for predicting tracking performance 22 p3992 A70-43593

PROBABILITY DISTRIBUTION FUNCTIONS
Nonparametric statistical pattern recognition conditions of finite probability distribution mixtures in non-supervised adaptive detection 03 p0454 A70-14078

Opacity-probability distributions for CO, computing theoretical spectra of line absorption coefficient, discussing effects of temperature and/or turbulent velocity 05 p0919 A70-16938

Probability distributions and error estimates for Monte Carlo solutions of radiation heat transfer problems, considering wavelength and direction of emitted photon bundles 06 p1175 A70-17683

Diatomic Br molecular vibration-rotation coupling effects on energy transfer during Br-Br collisions, determining probability distributions 07 p1339 A70-20054

Fatigue crack probability distributions under oscillatory stationary random loading, basing analysis on crack propagation model 09 p1776 A70-22683

Complex Gaussian processes with complex density functions, computing covariances and marginal distributions 10 p1915 A70-24057

Probability of given configuration and statistical distribution of peaks between mean crossings of broadband locally stationary and Gaussian processes [ONERA-TP-806] 10 p1805 A70-24546

Soviet book on discrete system for measuring multivariable probability distributions, covering automatic acquisition and reduction of statistical data 13 p2381 A70-28700

Cape Kennedy peak wind profile probabilities at 10-150 meters for various exposure times 14 p2607 A70-30581

Model probability distribution for hybrid phase locked loop derived by Fokker-Planck techniques, providing superior performance for all SNR 16 p2882 A70-33038

Closing method for turbulence equations of velocity field quantities joint probability distributions 21 p3811 A70-42075

Photon occurrence moments probability distribution in partially coherent light signals 22 p3988 A70-42563

PROBABILITY THEORY
Soviet monograph on transfer processes theory in statistical mechanical systems based on probabilistic approach to random particle walk 01 p0215 A70-10650

Probability selection of useful plants based on distribution of resolving statistics 01 p0053 A70-11023

Mathematical theory of time domain statistical description of random signals in terms of probability theory 01 p0044 A70-11042

Book on mathematical methods of reliability theory covering probability theory, statistics, Laplace transformation, set theory, testing, quality control, mass production, sampling, etc 01 p0133 A70-11308

Probabilities for cell survival after exposure to ionizing radiation obtained by two compartment model 01 p0028 A70-11370

Materials strength characteristics with respect to breakdown probability parameter by statistical fatigue stability analysis under unsteady loads and various distribution laws 01 p0211 A70-11424

N binomial events approximations to high probabilities of overall success for reliability situations and mission accomplishment, including operations research implications 01 p0134 A70-11475

Product reliability using statistical probability technology with product failure studies, discussing performance prediction accuracy 02 p0309 A70-12301

Nuclear reactor surface temperatures probability calculations allowing for some uncertainties and MTR type test reactor application 03 p0523 A70-12997

Cloud cover recurrence estimators from set of unconditional probabilities tested against sample of Northern Hemisphere diurnal variation data 03 p0521 A70-13164

Algorithm for optimal controls maximizing probability of linear time dependent control processes entering target manifold under random disturbances 03 p0460 A70-13580

Event probability and cost effects on performance in continuous motor task 03 p0436 A70-13771

Pulsed radar fluctuating echo digital-detection and false alarm probabilities assuming Rice signal distribution with noise 04 p0649 A70-15065

Probability theory for gimbal errors in directional gyroscopes under irregular rocking, using linearization of functions of random arguments 04 p0692 A70-15281

Radar false return probability relationship to noise, investigating moving window detectors 04 p0652 A70-15341

Rebuttal of criticisms on resonant structure hypothesis, giving probability value for chance stellar system formation similar to solar system 05 p0910 A70-16396

Solar system resonant structure probability analyzed by matrix methods 05 p0910 A70-16397

Monograph on probability of aircraft detection by ground visual observation using mathematical model based on Poisson process, considering laws of ocular physiology 05 p0794 A70-16558

Attenuation vs pathlength for given fading probability of microwaves by intense rain, evaluating dual parallel path diversity 05 p0815 A70-16575

Impression formation model extended to personality traits, noting curvilinear relationship between probability and liking ratings 05 p0803 A70-16670

Assignment problem for finite set elements pairing, discussing probabilistic formulations and applications to satellite communications problems 05 p0815 A70-16716

Hazards model for probabilistic prediction of casualties by exploding solid propellant rockets, deriving casualty expectation equation [AIAA PAPER 69-461] 06 p1154 A70-17169

Bounded approximations to average multirial detection probabilities over slowly fading radar target 06 p1013 A70-18627

Maximum probability estimates for satellite orbital plane, reducing computational labor by eliminating use of maximum likelihood principle in differential formulation 07 p1386 A70-19486

Fading effect on error probability of multi-hop PCM radio system, noting domination by worst hop 08 p1458 A70-20797

Optical coherence theory functional formalism developed in radiation field probability functional terms, noting role of P representation of density operator 08 p1545 A70-21254

Variables control charts based on sample means for determining in-control probability properties 09 p1691 A70-22575

Machine parts fatigue strength calculated from failure probability parameter during unsteady loading 09 p1776 A70-22622

Observational data smoothing method starting from Whittaker method based on probability, recommending use with high speed computer 09 p1669 A70-23057

Nonlinear utility f_{ns} effects on assessor probability forecasts, discussing psychological factors 10 p1912 A70-23934

Information theory as basis for statistical thermodynamics, discussing maximum entropy principle and probability as frequency in Gibbs ensemble 11 p2083 A70-25694

Bit error probability after decoding for binary perfect single error correcting codes 11 p2014 A70-26247

Stochastic dynamic prediction assuming deterministic laws for atmospheric behavior while seeking solutions corresponding to probabilistic statements of initial conditions 11 p2076 A70-26497

Mission oriented or time dependent systems reliability measures definitions in terms of probability 12 p2336 A70-28008

Complete sample estimation techniques for reparameterizations of Weibull density function to assign probabilities to components and systems lifetimes 12 p2243 A70-28012

Book on probabilistic systems analysis covering models, decision making, random processes, distribution functions, mass and density functions, etc 13 p2441 A70-29455

Computer program for system reliability prediction, using probability tree approach and block probabilities 13 p2373 A70-29565

Many body correlation and conditional probability functions of plasma shield clouds surrounding test particles 14 p2623 A70-31034

Decision directed receiver with unknown a priori probabilities, obtaining tight bound on runaway for binary and multiple signal detection 14 p2554 A70-31117

Nonsingular detection and likelihood ratio for random signals in white Gaussian noise

14 p2551 A70-31118

Probabilistic methods in aeronautical research and development

14 p2563 A70-31393

Earth and moon meteor fall probabilities calculation using hyperbolic encounters method and lunar near and far sides crater densities difference interpretation

15 p2798 A70-31658

Optimal search algorithm for stationary object hidden in one of N regions with a priori probability

15 p2767 A70-31843

Wolf numbers Zurich time series monthly values, evaluating mathematical expectation with probability smoothing by Whittaker operator

15 p2802 A70-32489

Moon shadow solar eclipse encounter probability for high altitude satellite in circular earth orbit

15 p2803 A70-32502

Maximum probability estimates for satellite orbital plane, reducing computational labor by eliminating use of maximum likelihood principle in differential formulation

15 p2805 A70-32731

Light scattering in one dimensional semiinfinite medium with moving boundary, deriving escape and reflection probability expressions

15 p2808 A70-32880

Maximum likelihood methods for aircraft identification problems, considering model types, flight disturbances and available data

16 p2885 A70-33326

Fifty percent coverage problem /Circular Error Probable/ of general bivariate Gaussian distribution from viewpoint of navigation systems error analysis

16 p2948 A70-33451

Probabilistic considerations relationship to failure free operation in product design

16 p2918 A70-33520

Probabilistic model for radiative transfer of photons in inhomogeneous infinite cylindrical shell medium, noting radiation intensity relation to scattering and transmission functions

16 p2952 A70-33785

Confidence limits on percent defective estimates for production processes characterized by two specification limits

16 p2921 A70-34025

Maximum likelihood estimates for setting confidence limits of Weibull percentiles and shape parameters

17 p3128 A70-34579

Book on stochastic tools in turbulence covering generalized functions, probability, moments, characteristic functions, Gaussian distribution, random functions and multidimensional fields

17 p3128 A70-34601

Learning scheme with probabilistic teacher for unclassified samples, establishing convergence, comparing with linear estimator

17 p3128 A70-34851

Error correcting decoders, investigating lower bounds on three complexity measures to meet error probability requirement

18 p3230 A70-35942

Wideband analog signal data transmission, evaluating messages accuracy in terms of error probability

18 p3228 A70-36623

Observation classification /image identification/ for two normal sets with common covariance matrix, investigating error probability asymptotic behavior

19 p3375 A70-37283

Book on optimization and probability in systems engineering covering mathematical models for reliability, repair, availability, Markov techniques and queueing

19 p3553 A70-37928

Psychological tests for ability to learn association between event and occurrence probability

19 p3363 A70-38319

Sporadic E layer occurrence probability over Dushanbe from ionospheric station data, discussing curves for diurnal and annual PE variations

19 p3417 A70-38785

Reliability analysis based on Bayesian subjective probability implemented by stored time sharing computer programs for engineering computations and operation analyses

19 p3441 A70-38818

Heisenberg uncertainty principle in communications technology, discussing variance products deficiencies and limits in carrier frequency pulses application

20 p3584 A70-39160

Uncertainty principle in optimum communication theory, discussing existence and value of minimum product of pulse duration in terms of calculus of variations and differential equations

20 p3584 A70-39161

Failure probability from finite sampling characteristics, emphasizing statistical safety factors to characterize structures strength reliability

20 p3724 A70-39856

Automatic stabilization of random noise mathematical expectancy and mean square deviation by feedback control system

20 p3593 A70-39916

Subjective probability estimation for R and D decision making, using analytical models incorporating risk and uncertainty

21 p3955 A70-41175

Bayes sequential detection test with constrained error probabilities, investigating properties of thresholds equations

21 p3787 A70-41333

Output probability of nonlinear systems from coupling moments for input random parameters, using equivalent perturbations method

22 p4003 A70-42885

PROBES

Electronic spray analyzers and conductance and capacitance probes for two phase flow studies, describing operation, characteristics and types of data obtainable

02 p0305 A70-12837

Flow mean velocity measurement using probe submerged in moving electrolyte and not requiring external power source

07 p1257 A70-19377

Temperature, pressure and flow direction probe in rotating fluid machines analysis

07 p1283 A70-19732

Transistorized pistol grip probe design, circuit and operation for testing wobble and asymmetry in rotating ring commutators of electric motors

12 p2165 A70-27495

PROBLEM SOLVING

NT ASYMPTOTIC METHODS

NT ITERATIVE SOLUTION

NT THEOREM PROVING

Restricted problem solving tasks /perceptual maze test/ formulated as multistage decision making, discussing use of dynamic programming and algorithms

02 p0246 A70-12321

Numerical methods of solving problems in mechanics of continuous media - Conference, Kiev, Ukrainian SSR, June-July 1966

04 p0669 A70-14956

Unsteady problems of gas dynamics solved by method of characteristics, Godunov method, difference methods, etc

04 p0670 A70-14958

Splitting procedures application to steady and unsteady problems of mathematical physics and predictor-corrector method application to unsteady problems

04 p0719 A70-14959

Small parameter method applied to numerical solution of conformal mapping and viscous fluid motion problems

04 p0719 A70-14960

Integral relations and finite difference methods application to problems of boundary layer equations in gas dynamics

04 p0670 A70-14962

Command control systems characterized as problem solving information processing systems, discussing information requirements specification prior to man-display design

05 p0806 A70-16177

Prandtl problem solution by reducing integrodifferential equation to linear differential equation in disk of complex variable, noting application to elliptical or rectangular wings

07 p1258 A70-19783

Solvability of linear problems with minimal smoothness constraints and of mixed problems for quasi-linear hyperbolic equations with coefficients and boundary conditions nonlinearities

09 p1712 A70-23120

Multipoint methods for two point boundary value problems with Banach space self mapped, proving convergence theorems for iterative solutions

09 p1712 A70-23420

Soviet monograph on method of functional equations for solving boundary value problems, discussing computer programs and various applications

09 p1712 A70-23548

Apollo Program mission evaluation and flight anomalies team to identify and understand unforeseen peculiarities and systems problems during spacecraft mission

09 p1768 A70-23708

Three phase code transformation task for human subjects, determining memory aid role in problem solving phase from factor analysis

13 p2361 A70-30019

Algorithm for fourth order stability equation

16 p2867 A70-32925

Nonlinear second order differential equations with periodic coefficients and solutions, examining stability by phase and amplitude plots by marginal range diagrams

18 p3282 A70-36356

Real cipher places in real function, describing interval analysis method with upper and lower bound indications

18 p3282 A70-36357

Human memory information structure, discussing pattern recognition, simultaneous attention, problem solving and logic

19 p3363 A70-38322

Initial value or boundary value problems in mathematical physics, solving by process of condition elimination

19 p3472 A70-38727

Soviet book on overshoot of random processes in problem solving covering application to radio engineering, length distribution, extremal values, etc

20 p3587 A70-39822

Control space properties of pareto-optimal and cooperative solutions for static continuous and differential games involving vector cost criteria

22 p4061 A70-42460

PROBLEMS

Book on classical astronomy and astrophysical problems covering time and longitude determination, calendar, precession, planetary motion, eclipses, gravitation, double stars, etc

01 p0191 A70-11376

PROCEDURES

NT FINITE ELEMENT METHOD

NT OPTICAL CORRECTION PROCEDURE

Air traffic control procedures pertaining to personnel, hardware and regulations

11 p2078 A70-25720

ATC procedures based on system error and aircraft accident probabilities, traffic flow and navigation control and controller manpower

11 p2078 A70-25721

PROCESSORS [COMPUTERS]

U CENTRAL PROCESSING UNITS

U COMPUTERS

PROCUREMENT

NASA Source Evaluation Board process for major contractor selection, discussing procurement practices and management techniques

03 p0610 A70-13962

DOD systems acquisition management tools and policies, emphasizing role of development concept paper and outside personnel dialogue in DOD decision making

05 p0959 A70-16460

Integrated USAF acquisition management systems approach engaging top management abilities available in government and industry

05 p0959 A70-16463

Procurement problems for U.S. Defense Department taking into account fighter F-15 development for USAF

07 p1428 A70-19672

DOD procurement practices for advanced weapon systems, discussing government errors in contracting policies

07 p1428 A70-19678

Program risk analysis by aerospace industry pursuant to Federal Government procurement requirements

16 p3003 A70-33427

PRODUCT DESIGN

U PRODUCT DEVELOPMENT

PRODUCT DEVELOPMENT

NT WEAPONS DEVELOPMENT

Failure mode evaluation techniques application to system design and product assurance activities, with examples of performance evaluation of components, circuits and systems

01 p0049 A70-10116

Magnetic components design, manufacturing and handling for use in space communication satellites, noting design group role in parts construction and quality control

02 p0267 A70-12057

Product reliability engineering analysis, discussing coordination, communication and data accumulation systems

02 p0309 A70-12302

Technology transfer between large company aerospace group and commercial products group

02 p0403 A70-12636

Intelsat communications /1963-1969/, discussing boosters, satellites, system characteristics and ground stations

03 p0451 A70-13840

Soviet aerospace manufacturing technologies development, considering forging, extrusion, metal working and joining, etc

05 p0853 A70-15826

AI casting design considering alloy materials selection and casting methods

06 p1076 A70-17602

Small penetration aid rocket motors fabrication, discussing axial- and tangential-thrust integral assembly, impulse levels, delay line convection for igniters, production evolution, etc

07 p1295 A70-19714

Strain gages design and development for small loads

08 p1493 A70-20586

Lead-acid and vented nickel cadmium batteries compared in redesign of military aircraft battery for cells reduction, low current density, etc

08 p1440 A70-20712

Coupling relations in product and systems development linking ideas to finished products

08 p1601 A70-20824

Oblique flow headers design for heat exchangers based on one dimensional momentum and continuity

08 p1598 A70-21482

Commercial thermoelectric generator design, applications and economics compared to batteries and small MG sets

- 10 p1808 A70-25033
- Automatic test equipment effect on product design, discussing test planning and quality control
- 13 p2422 A70-29678
- Soviet optical instrument industry development trend /1971-1975/, considering spectral, test, measuring, reading and microscopic equipment
- 13 p2412 A70-29864
- Reliability factors in design and development staging systems /DDSS/ for military and space exploration programs
- 15 p2747 A70-32639
- Reliability engineers role and responsibility in production process
- 15 p2832 A70-32640
- Glass drainline development and marketing, describing technology transfer role
- 20 p3740 A70-39100
- Cost and time optimization for complex aircraft development projects via network planning
- 20 p3740 A70-39644
- Translation gap between R and D and production occurring at design transmission to manufacturing
- 21 p3955 A70-40913

PRODUCTION

NT PRODUCTION PLANNING

PRODUCTION ENGINEERING

NT PRODUCTION PLANNING

- Optimum R and D organization in aircraft engine production illustrated on turbofan engine
- 01 p0161 A70-10080
- Product assurance concepts on corporate-wide scale from consumer point of view, discussing systems effectiveness, reliability, maintainability, human factors, product safety, etc
- 01 p0219 A70-10111
- Product reliability using statistical probability technology with product failure studies, discussing performance prediction accuracy
- 02 p0309 A70-12301
- Product reliability engineering, discussing product life cycle, operational reliability, failure analysis and design
- 02 p0309 A70-12303
- Two seater hovercraft development, considering lift system, fan, transmission and structural designs and construction steps to keep within automobile cost range
- 03 p0414 A70-14148
- Al fasteners design guidelines including material forming capabilities, cost consideration, applications, etc
- 04 p0697 A70-14722
- Steel welding processes in thicknesses useful to future booster production
- 04 p0700 A70-15652
- Airframe production factors involving choice of materials and fabrication methods, emphasizing weight reduction to increase payload
- 05 p0854 A70-15925
- Mechanized glycerine process for fibers and whiskers alignment on large scale at low cost
- 05 p0855 A70-16580
- Matched die molding technology working principles, mat materials, mold taper, preforms, etc
- 05 p0856 A70-16613
- TU-134 aircraft accessories assembly using fitting and aligning holes drilled into joined elements
- 05 p0857 A70-17019
- Process specifications to control manufacturing operations, describing contents, purposes and preparation, emphasizing three levels of control
- 06 p1184 A70-17601
- Al casting design considering alloy materials selection and casting methods
- 06 p1076 A70-17602
- Continuum mechanics equations for calculating strain energy in spherical bottoms production as function of radius and angle
- 06 p1077 A70-17870
- Precision tungsten alloy tubing manufacture and properties, discussing direct conversion of metal powder to finished tubing with high temperature structural stability
- 07 p1292 A70-18928
- Galvanoplasty process for parts for UHF circuits, discussing cost, safety and quality
- 08 p1468 A70-20611
- Soviet book on aircraft engines automated production including plant and machine automatic control, technical and economical factors, etc
- 08 p1502 A70-20767
- Laser systems application to automatic or semiautomatic materials processing in metal working and microelectronics, including hole drilling, silicon wafers scribing, etc
- 08 p1502 A70-20820
- Graphite shell molds for Al castings mass production
- 08 p1505 A70-21135

Carbon fiber composite materials production technology, physical properties and potential applications in aerospace

- 08 p1527 A70-21520
- Tubing materials for gas turbine engines covering fabrication, selection, etc
- 08 p1559 A70-21854
- Quality information equipment engineering including specifying, development, design, procurement, construction, installation, checkout, etc
- 09 p1792 A70-22569
- C-5 production engineering, discussing welding method for hydraulic stainless steel tubing, bonding of Al floor panels and painting preparation
- 10 p1893 A70-23853
- BAC 111 short/medium range jet airliner family status report on program activity
- 10 p1806 A70-24846
- Microwave converter system for ETV satellite reception, discussing characteristics and costs for mass production
- [AIAA PAPER 70-439]
- 11 p2017 A70-25493
- Complex organization-processing system of experimental production, noting work specialization in machine shops
- 11 p2060 A70-25936
- Computerized on-line industrial inspection involving automatic machine sequential control and product geometry error correction, discussing hardware and software requirements
- [SME PAPER IQ-70-712]
- 12 p2241 A70-27088
- Aerojet engine minimum weight design, suggesting use of welding and brazing instead of nut-and-bolt joints in component fabrication
- [SAE PAPER 700319]
- 12 p2243 A70-27457
- Foundry facilities for high strength nodular, pearlitic malleable and Cr-Mo gray iron and Al castings
- 13 p2420 A70-29250
- Corrective Action systems for identification, control and resolution of manufacturing, engineering and vendor problems
- 14 p2669 A70-31102
- Solar furnaces in space for treatment of high purity products in space vacuum, discussing design and operational problems
- 15 p2717 A70-31802
- Spark erosion milling machines adaptable to piece and mass production
- 15 p2744 A70-31899
- Filament winding reinforcement and resin noting production equipment and costs
- 15 p2744 A70-31932
- Carbon reinforcing fibers, discussing mechanical properties, production, cost reduction, etc
- 15 p2765 A70-32246
- Optimal control theory of asymptotically stable closed systems synthesis regarding product requirements
- 15 p2716 A70-32473
- Laser design for production tool applications, noting use of Nd-YAG and carbon dioxide laser
- [ASME PAPER 70-DE-1]
- 16 p2917 A70-33418
- Simulation devices in engineering feasibility studies emphasizing prototypes role
- [ASME PAPER 70-DE-50]
- 16 p2918 A70-33512
- Probabilistic considerations relationship to failure free operation in product design
- [ASME PAPER 70-DE-70]
- 16 p2918 A70-33520
- Aircraft design, development and production illustrating systems engineering functions, discussing control process model
- 16 p3004 A70-33676
- Space manufacturing in weightless environment, discussing unique processes, potential materials, product groups, planned experiments for Skylab Orbital Workshop mission, etc
- 16 p2888 A70-33716
- Materials preparation processes and improvements in space weightless environment, considering metals and ceramics melting, solidification, electromagnetic process control, etc
- 16 p2919 A70-33717
- Confidence limits on percent defective estimates for production processes characterized by two specification limits
- 16 p2921 A70-34025
- Candidate products for manufacturing on space station, emphasizing liquid solid transformations, bubbles and droplets, polymerization, and cost effectiveness
- [AAS PAPER 70-036]
- 17 p3041 A70-34791
- Complex control systems in integrated logic circuits and light laboratory materials production, discussing measurement equipment for quality control
- 17 p3090 A70-35416
- Aircraft engine production cost estimating techniques, discussing physical, thermodynamic and metallurgical characteristics
- [SAE PAPER 700271]
- 18 p3350 A70-36818
- Electron beam welding for instrument components including torsion shafts, heat sensing membranes, etc
- 19 p3436 A70-38074

Electron beam welding for thin copper, carbon and Cr-Ni steel sheets in precision mechanical and optical devices

- 19 p3436 A70-38075
- Cadmium telluride photocells, discussing performance and mass production
- 19 p3358 A70-38481
- Boeing 747 wing panels shot peening process, discussing machine, control technique and operational requirements
- 19 p3437 A70-38498
- Electronic components mass production for automatic control equipment, determining parameters probabilistic scatter
- 19 p3390 A70-38578
- Adhesive bonded aircraft structures, discussing methods and requirements for establishment and control of manufacturing procedures
- 19 p3438 A70-38594
- Reliability enforcement in design by competition and test program, using gyroscope example
- 19 p3433 A70-38842
- Soviet book on glass staple fibers covering classification, properties, composition, production, tests and industrial applications
- 20 p3655 A70-39399
- Al alloy products heat treatment, using synthetic quenchant for distortion control
- 20 p3650 A70-39967
- Design management by critical element objectives, correlating various engineering functions in production process
- [SAWE PAPER 868]
- 20 p3741 A70-40352
- Welding failure case histories, discussing design, materials and processes, fabrication and quality control integration
- 21 p3832 A70-40787
- Tooling concepts providing gas shielding in mechanized open air arc welding of Ti, evaluating effectiveness by various mechanical tests
- 21 p3832 A70-40788
- Programmable all-stored-logic numerical control system based on minicomputer, affording economy and adaptability in production tool applications
- 22 p3993 A70-42319
- Fluidic applications in missile components production, discussing various types of fluidic control and logic in relation to functional requirements
- [ASME PAPER 70-FLCS-11]
- 22 p3963 A70-42416
- Electronic packaging and production - Conference, Anaheim, California, February 1970 and New York, June 1970
- 23 p4173 A70-44532
- Digital computer codes for production finite element structural analysis, discussing input, output and engineering details
- 23 p4270 A70-44701
- Whiskers and filaments properties compared for fiber reinforcement applications in composite materials production
- 24 p4356 A70-45167
- Computer-aided production engineering involving numerically controlled machines for Rolls-Royce aircraft engines manufacture
- 24 p4341 A70-45299
- Aktion X program for production efficiency, mobilizing personnel in weak points monitoring
- 24 p4430 A70-45624

PRODUCTION METHODS

U PRODUCTION ENGINEERING

PRODUCTION PLANNING

- Equivalent linear programming in integer variables to solve production scheduling for N identical machines, minimizing changeover and inventory costs
- 10 p1895 A70-24662
- Translation gap between R and D and production occurring at design transmission to manufacturing
- 21 p3955 A70-40913

PRODUCTIVITY

- Hydrocarbon assimilating bacteria cultures selection, considering highest specific growth rate and maximum productivity
- 11 p1991 A70-25939
- Aircraft stretch efficiency factor as function of productivity and payload growth
- [SAWE PAPER 838]
- 20 p3563 A70-40369

PROFICIENCY MEASUREMENT

U HUMAN PERFORMANCE

U PERFORMANCE TESTS

PROFILES

- Propulsive and lifting motions of pointed profile in ideal incompressible fluid related to alternate vortices emission
- 08 p1433 A70-21234
- Diabatic mean profile forms in atmospheric surface layer, establishing profile relationships based on logarithmic analysis
- 08 p1540 A70-21973
- Resultant of elementary aerodynamic pressures on profile with angular point of attachment
- 10 p1797 A70-23874
- Incompressible ideal plane fluid flow complex potential caused by profile motion in presence of fixed infinite wall
- 13 p2390 A70-29632

- Aerodynamic pressures dependence on angle of incidence for profiles in adiabatic compressible flow
16 p2833 A70-33074
- Perturbation complex potential and aerodynamic forces determined for rectilinear profile motion under free surface, using linear theory
16 p2837 A70-33848
- Incompressible fluid flow past array of arbitrary profiles vibrating with arbitrary phase shift, taking into account blade displacement and vortex wake effect
18 p3206 A70-36277
- Pulling force during motion of sinusoidally deformable flat profile, taking into account trailing edge vortices
18 p3241 A70-36280
- Two dimensional steady inviscid incompressible flow past profiles in parallel flow with nonuniform velocity distribution
19 p3354 A70-38676

PROFILOMETERS

- Ball bearing performance prediction using analytical technique based on race profilometry data, considering torque variation
[ASME PAPER 69-WA/LUB-4] 04 p0698 A70-14769
- Airborne laser profilometer terrain roughness measurement and recording, considering error sources
12 p2244 A70-26938
- Laser profilometer for airborne ocean wave profile measurement
12 p2249 A70-28003
- Automatic profile measurement and recording, describing equipment and techniques
15 p2742 A70-32777
- He-Ne laser profile-tracing system for contour measurement, suggesting steps for error reduction
20 p3640 A70-39417

PROGNOSIS

- Ischemic heart disease /IHD/ prognosis using abnormal electrocardiographic stress test
10 p1820 A70-24940

PROGRAM MANAGEMENT

U PROJECT MANAGEMENT

PROGRAMMING

NT QUADRATIC PROGRAMMING

- Iterative computational procedure for generalized quadratic programming problem, formulating convergence theorem
03 p0460 A70-14165
- Space vehicle trajectories, discussing programming method to control motion for prescribed boundary conditions
17 p3173 A70-35700

PROGRAMMING [SCHEDULING]

NT THRUST PROGRAMMING

- Optimum balance between program and functional organizations to promote technology transfer
02 p0403 A70-12637
- Optimality criteria for selecting flight conditions for civil aviation helicopters, considering scheduled speed and efficiency, commercial load factor, wind rose, vertical separation, etc
06 p1185 A70-17874
- Stochastic programming models for flight scheduling within airlift system accounting for cargo uncertainties, using convex programming, linear programming codes, etc
08 p1600 A70-20605
- Numerically controlled gas tungsten arc welding, discussing tape programming, fixture design and fabrication for various welded metal joint configurations
11 p2058 A70-25661
- Automated programmed device for fatigue tests based on harmonic oscillator, presenting schematic diagram
16 p2900 A70-33068

PROGRAMS

- NT APOLLO APPLICATIONS PROGRAM
- NT APOLLO PROJECT
- NT CENTAUR PROJECT
- NT COMSAT PROGRAM
- NT DEFENSE PROGRAM
- NT EARTH RESOURCES PROGRAM
- NT EUROPEAN SPACE PROGRAMS
- NT GEMINI PROJECT
- NT LUNAR PROGRAMS
- NT MARINER PROGRAM
- NT MARS 69 PROJECT
- NT MARS 71 PROJECT
- NT MERCURY PROJECT
- NT NASA PROGRAMS
- NT RESEARCH PROJECTS
- NT ROVER PROJECT
- NT SCANNER PROJECT
- NT SKYLAB PROGRAM
- NT SPACE PROGRAMS
- NT SURVEYOR PROJECT
- NT SYNCHRONOUS COMMUNICATIONS
- NT SATELLITE PROJ
- NT TEKITE PROJECT
- NT TIROS PROJECT
- NT U.S.S.R. SPACE PROGRAM
- NT UNIVERSITY PROGRAM
- NT VOYAGER PROJECT

PROJECT MANAGEMENT

- HEOS 1 satellite project management, discussing costs, supervision problems and roles of experimenters, contractors, NASA and ESRO
01 p0221 A70-11112
- Analytical scoring model design for effective evaluation of competing research and development projects
02 p0402 A70-12634
- Surveyor project as basis for technology transfer management exemplified by planning and organization problems
02 p0403 A70-12639
- Decision model for R and D project selection
03 p0609 A70-12991
- Logic methods of efficient organization of satellite integration, considering project, physical components and program elements
03 p0609 A70-13842
- Decision analysis in R and D, discussing risk discounting and measure of value selection
03 p0610 A70-13956
- Project management systems failure analysis, discussing cost, products quality and project objectives
03 p0610 A70-13963
- Experiment selection in orbital program planning based on broad system synthesis, discussing identification and grouping of objectives, critical issues and experimental equipment requirements
04 p0749 A70-14652
- [AAS PAPER 69-580] Guiana Space Center for French space programs, describing launch complexes, measurement and control methods, safety methods, launch operation planning, etc
04 p0663 A70-14939
- Space projects quality assurance with allowance for technological trends, discussing product and system oriented organizational requirements, failure potentials, contractor performance, etc
04 p0699 A70-15138
- Swedish VIGGEN program for aircraft weapons system development emphasizing management methods
05 p0960 A70-16717
- Versatile avionics shop test /VAST/ Implementation Study recommendations on project management for automatic test equipment support system aboard attack aircraft carriers
08 p1601 A70-20663
- Management planning for French-British Martel /Missile Antiradar et Television/ project, emphasizing tasks of government agencies and contractors
08 p1601 A70-21038
- Program, test equipment and data reduction of aircraft prototype flight tests
08 p1438 A70-21865
- Optimal program selection using experience of applied technical research
08 p1601 A70-21872
- Multidiscipline systems analysis of satellite assisted information system improving earth resource management, developing User Decision Models
09 p1792 A70-22855
- Computer aided design programs as decision-making tool for fighter development projects technical management
09 p1611 A70-23024
- Apollo project hardware design and evaluation principles coupling simple design practice with stringent technical and administrative discipline
09 p1768 A70-23704
- Apollo mission planning process, discussing flight schedule evolution from panels, meetings and working groups
09 p1768 A70-23710
- Operational planning for earth resources surveys using spacecraft
09 p1672 A70-23762
- Models survey for evaluation and selection of research projects, discussing reasons for long range company
10 p1970 A70-24070
- Large scale project grading into stepwise decision stages exemplified by aircraft weapon system development program
10 p1971 A70-24596
- Prolonged hypodynamia effect on human organism, describing organizational and methodological principles for conducting investigations
10 p1813 A70-24667
- Space station program development requirements, describing ground and flight tests synthesis
10 p1952 A70-24926
- Industry role in sounding rocket program, highlighting activities in various areas
13 p2523 A70-28679
- DOD laser research and development contracts management
14 p2667 A70-30367
- BAC 111 commercial aircraft family development, discussing program management
14 p2532 A70-31334

- Project authority relationship concerning manager authority and influence in five organization models
15 p2828 A70-31571

- Reliability program planning and organization as part of integrated Development Risk Management System, considering task identification, assignment and accomplishment
15 p2747 A70-32628

- Program risk analysis by aerospace industry pursuant to Federal Government procurement requirements
16 p3003 A70-33427

- Effective R and D management working principles, discussing changing goals, policy and technology changes, environment, adequate reporting, etc
16 p3004 A70-33663

- Project management in aircraft manufacturing related to weapon system
17 p3200 A70-34918

- Project risk or cost estimation for antipollution, moon mining, tooling, burn-in test and warranties by theory of Takacs processes and correlated queues
19 p3554 A70-38598

- Project economic evaluation, discussing value analysis from market research recommendations
19 p3555 A70-38620

- Skylab test program taking into account program requirements, test management concepts and identification subsystems, status, performance review and control
19 p3441 A70-38820

- Predictive model for potential variance from planned schedule of R and D tasks to minimize risk in management
21 p3955 A70-41172

- Military program cost effectiveness and control, considering resources and products
21 p3955 A70-41173

- R and D programs engineering talent assignment case histories
21 p3955 A70-41174

- Subjective probability estimation for R and D decision making, using analytical models incorporating risk and uncertainty
21 p3955 A70-41175

- ELDO project planning and progress monitoring system for management provided by Central Planning and Progress Monitoring Service
21 p3956 A70-41497

- U.S. and Soviet space program administration and management
21 p3956 A70-41893

- Book on project management with critical path method and PERT, covering manual and computerized calculation of scheduling, networks, time-cost tradeoffs, etc
22 p4128 A70-43625

- MIL-STD-882 systems and subsystems and equipment safety requirements related to program management activities
22 p4048 A70-43730

- Project managers problems of anomalies and ambiguities in complex missions operation and implementation, discussing interactions with personnel
23 p4284 A70-43996

- International Space Research Organization /ISRO/ for space operations, considering political, economic, technical and scientific requirements
23 p4286 A70-44688

- Manned space flight programs management, discussing organizational aspects of projects including Apollo, space shuttle and space station
23 p4286 A70-44696

PROJECTED AREAS

U PROJECTIVE GEOMETRY

PROJECTILE CRATERING

- Mars surface, discussing craters, slump terraces, dry chutes, crater pair abundance, ballistic megacratering theory, etc
11 p2109 A70-25838

- Lunar surface erosion model by small projectiles impact for analytic representation of crater shape change as function of time
14 p2637 A70-30494

- Hypervelocity impact dynamics on copper cube targets imbedded with nickel wires, discussing terminal positions, Vickers hardness, flow fields, etc
14 p2657 A70-30765

- Hypervelocity impact theory, discussing Euler hydrodynamic codes, projectile cratering dimensional analysis, self similar solutions, etc
15 p2823 A70-32785

- Hypervelocity impact computerized calculations, considering material response, laminated meteor bumpers, hollowed projectiles and thick target cratering
15 p2823 A70-32787

- Metal property effects on deformation and strain energy distribution during hypervelocity projectile cratering
15 p2824 A70-32790

- Al spheres hypervelocity impact against dry quartz sand targets in light gas gun facility, discussing energy partitioning
18 p3344 A70-36769

PROJECTILE PENETRATION
U TERMINAL BALLISTICS
PROJECTILES

NT HYPERVELOCITY PROJECTILES

Artillery type projectiles field photography in flight in connection with service integrity evaluation of weapon components under real environment conditions

03 p0490 A70-13658

Meteoroid impacts as sources of seismic energy on moon, using projectile impact coupling to seismic waves in vacuum chamber experiment

04 p0751 A70-15056

Approximate time solutions to light antiaircraft projectiles velocity, altitude angles, gravity drop and downrange, reducing differential equations of motion to dimensionless forms

04 p0764 A70-15592

Ignition of cold premixed fuel by hot projectile, obtaining distance for ignition occurrence

[AIAA PAPER 70-150] 06 p1180 A70-18133

Cold combustible mixture ignition at forward stagnation region of hot projectile, calculating temperatures for propane-air mixture

07 p1422 A70-19577

Projectile acceleration under gas explosion calculated for velocity

09 p1777 A70-22723

Projectiles yawing and rolling over long flight paths, describing onboard solar aspect sensor and telemetry link to ground stations

[AIAA PAPER 70-538] 13 p2406 A70-29005

Helical engraving influence on aerodynamic stability of bullets at long range, discussing wind tunnel tests

[AIAA PAPER 70-557] 13 p2340 A70-29022

Subcaliber cylindrical boom at base of spin stabilized projectile shown to produce aerodynamic changes in static and Magnus moments

[AIAA PAPER 70-558] 13 p2340 A70-29023

Statistical analysis of photogrammetrically surveyed three dimensional space points sets for aerospace vehicles and projectiles position location

15 p2733 A70-31550

Projectile velocity measurement, using laser and Fabry-Perot interferometer for Doppler shift determination

[SMPE PREPRINT 29] 22 p4034 A70-43046

PROJECTION

Projection CRT with liquid-cooled phosphor faceplate, showing linear relationship between brightness and beam current

09 p1673 A70-22034

Instrumental measurement of projection center coordinates for aerial triangulation with independent models

18 p3248 A70-36780

Projection of integrating photometric spheres, discussing angular dependence on wall thickness, radiation losses and aperture dimensions

18 p3260 A70-36974

PROJECTIVE DIFFERENTIAL GEOMETRY

U DIFFERENTIAL GEOMETRY

U PROJECTIVE GEOMETRY

PROJECTIVE GEOMETRY

Variational methods in semigeodesic projections of analytic surfaces on plane surface, determining projections impossible by classical cartography

05 p0839 A70-16368

PROJECTORS

Light valve projectors and TV cameras, showing disparity between video information generation and large screen real time high brightness image presentation

01 p0088 A70-10811

Large wall display system for USAF command and control with central computer and seven color projector, discussing hardware and operational features

05 p0828 A70-16193

Dual cockpit wide angle visual cue simulator design, discussing sky-earth-sun projector with four axis gimbal drive

[AIAA PAPER 70-360] 10 p1857 A70-24204

Autofocus for variable magnification systems, discussing conjugate concepts and linkage and cam methods for enlargers and projectors

16 p2907 A70-33182

PROJECTS

NT APOLLO PROJECT

NT CENTAUR PROJECT

NT GEMINI PROJECT

NT MARS 69 PROJECT

NT MARS 71 PROJECT

NT MERCURY PROJECT

NT RESEARCH PROJECTS

NT ROVER PROJECT

NT SCANNER PROJECT

NT SURVEYOR PROJECT

NT SYNCHRONOUS COMMUNICATIONS

NT SATELLITE PROJ

NT THEMIS PROJECT

NT TIROS PROJECT

NT VOYAGER PROJECT

PROLATE SPHEROIDS

Left ventricle confocal prolate spheroid model taking into account physiologic variations of thickness

01 p0040 A70-11373

Stress differential equations of equilibrium for thick prolate spheroid /left ventricle/, yielding practical values for mean stresses in thick walled ventricles

03 p0434 A70-13571

Prolate spheroidal wave functions applied to detection Fredholm equation for band-limited noise and signals

09 p1640 A70-23803

Scalar plane wave LF scattering by prolate spheroid of revolution, obtaining iterative solution for Dirichlet problem

11 p2085 A70-26621

Scalar plane wave LF scattering by prolate spheroid of revolution, obtaining iterative solution for Neumann problem

11 p2085 A70-26622

Wave scattering by acoustically soft and hard prolate spheroids

15 p2700 A70-32411

Prolate and oblate wave functions for EM radiation from spheroidal antenna in surrounding inhomogeneous medium

17 p3044 A70-35063

Three dimensional boundary layer on lee- and wind-side of prolate spheroid, emphasizing separation and embedded streamwise vortices

20 p3608 A70-39359

PROMINENCES

NT SOLAR PROMINENCES

PROOFS

U PROVING

PROPAGATION

Book on vibration and propagation phenomena covering oscillations of linear and nonlinear systems with various degrees of freedom, propagation in solids and fluids, etc

07 p1335 A70-19904

PROPAGATION [EXTENSION]

NT CRACK PROPAGATION

NT FLAME PROPAGATION

Covariance propagation via differential equations for time-varying eigenvalues and eigenvectors

13 p2450 A70-29979

PROPAGATION MODES

Metal-nitride-oxide semiconductor /MNOS/ FET load devices by changing from enhancement to depletion through polarizing voltage

01 p0051 A70-10785

VLF energy propagation using ceramic dielectric model of earth-ionosphere waveguide

02 p0269 A70-12592

Field patterns of thin resonant and nonresonant antennas in warm plasma, using digital computer to evaluate propagation constant for current distribution

02 p0263 A70-12655

Natural modes and multiple beam interference in open resonators, taking into account centimeter wave experiments and computations

02 p0340 A70-12829

Energy modes nonlinear interactions in rarefied plasmas, presenting wave energy and momentum definitions and kinetic equations for mode density in wave number space

04 p0726 A70-14701

HF propagation losses from statistical measurement over north-south path found dependent on mode, day and night and high and low ray

04 p0649 A70-14968

Nonducted VLF walking trace whistlers and Doppler shifts in fixed frequency transmissions identified on OGO midlatitude spectrographic records

04 p0649 A70-15116

Transmission and reflection coefficients of propagating whistler modes for model ionosphere

05 p0837 A70-15880

Initial disturbances propagation in gas mixtures by asymptotic analysis, observing diffusely and viscously damped modes

05 p0833 A70-16404

Transient stress waves generated by spatially uniform distribution of transverse forces in laminated medium, using modal analysis

05 p0938 A70-16409

Small amplitude waves and collisionless shock waves within first order Chew-Goldberger-Low equations framework, presenting modes for propagation along applied magnetic field

05 p0889 A70-16534

Symmetrical and asymmetrical electromagnetic wave modes in conical waveguide calculated, relating critical cross section plane position to aperture angle

05 p0816 A70-16892

Plasma wave theory and experiments, emphasizing stable Maxwellian plasmas and transverse and longitudinal wave modes in zero and nonzero magnetic fields

06 p1116 A70-17366

Nonuniform plasma analyzed for parameters inhomogeneity effect on VLF propagation mode and instability

06 p1119 A70-17381

Mutual coupling between waveguides radiating through conducting ground planes with orthogonally polarized propagating modes described by first order analysis

06 p1020 A70-17562

Deep reflector antennas mode composition by graphic computer techniques for maximum efficiency feed matches

06 p1021 A70-17575

Eigenvalue corresponding to decaying modes for wave equation in exterior of obstacle investigated for dependence on obstacle geometry

06 p1095 A70-18474

Radio propagation characteristics and communication system performance, discussing concepts of MUF, LUF, error rate, communication system modeling, prediction techniques, etc

07 p1229 A70-19157

Signal strength of sky waves and noise levels near LUF, suggesting importance of changing mode structure

07 p1229 A70-19158

LUF for F layer propagation modes, discussing mode cut-off significance using computer ray tracing program

07 p1229 A70-19159

Field strength predictions for expected returns from backscatter ionospheric soundings, predicting ionospheric propagation modes and losses during sunspot minimum

07 p1229 A70-19161

Ray theory for determining short term and averaged characteristics of nonreciprocal HF ionospheric propagation paths for single magnetoionic waves transmitted between antennas

07 p1231 A70-19171

Lower ionosphere effects on HF propagation modes observed by pulse system, discussing propagation time, mode structure, transmission loss, etc

07 p1232 A70-19179

Ray tracing calculation and experimental observation for mode structure and absorption loss of oblique incidence HF radio wave propagation

07 p1234 A70-19217

OMEGA frequencies propagation characteristics measured to estimate navigation errors from multiple waveguide propagation modes close to transmitter, comparing day and night errors

07 p1330 A70-19222

Spherical hybrid modes in corrugated antenna conical horns, obtaining radiation pattern and gain with small flare angle

07 p1243 A70-20284

Longwave and shortwave mode transformation in resonant layer of inhomogeneous plasma

08 p1550 A70-20847

Field strength and interferential structure at different cross sections of inhomogeneous ionospheric channel calculated during bounce mode propagation of radio waves

08 p1461 A70-20969

Diffraction by single wire waveguide with obstacle, considering propagation phenomena of symmetrical modes

08 p1472 A70-21042

Multimode rectangular waveguide lateral surface opening, determining scattering matrix coefficients governing mode conversion characteristics

08 p1462 A70-21224

Circular dielectric waveguide modes self consistent description by asymptotic method, obtaining eigenvalues and eigenfunctions

08 p1476 A70-21288

Modal excitation and scattering in retinal receptors of human and insect visual systems investigated with dielectric rod uniform wave and irregularities

08 p1452 A70-21289

AM electromagnetic wave self modulation in magnetoplasma, considering self and mutual interaction of ordinary and extraordinary propagation modes

08 p1552 A70-21527

Earth-ionosphere waveguide propagation variations effects on Omega navigation system position errors

08 p1541 A70-21564

Electrical parameters approximate calculations for waveguides with complex cross sections by Schwarz alternating method, determining critical frequencies of fundamental modes

09 p1632 A70-22406

Standing wave measurements on radiating traveling wave dipole arrays with glide symmetric excitation, showing multimode propagation and effect on log periodic balancing

09 p1633 A70-22688

Open-sided shielded stripline and other parallel plate waveguide structures propagation modes

09 p1634 A70-22712

Radiation losses of tapered single mode dielectric slab waveguide for TE and TM modes

09 p1650 A70-23369

Waveguide windows for energy outlet in microwave devices analyzed by plane /Brillouin/ modes, discussing dielectric element reflection coefficient

09 p1651 A70-23646

Mode transducer and mode filter formed by rectangular and circular waveguide elements investigated by field expansion, calculating transmission coefficient and propagation constant

10 p1848 A70-24219

Wave amplification in semiconductors relationship to coupling between space charge wave and circuit wave based on coupled-mode theory

10 p1927 A70-24619

Wave propagation in finite length revolving shells, describing advantages of modal superposition method generated by finite element computer program

12 p2317 A70-27124

Electrostatic wave modes in inhomogeneous adiabatic plasma, discussing waves with gamma-fold ion and electron drift velocity

12 p2280 A70-27783

Seminfinite parallel plate waveguide modes reflection coefficients with propagation constants near cut-off and excited at open end for microwave-optical frequency range

12 p2198 A70-27959

Mode-scattering coefficients from ionospheric perturbations for sunrise and sunset propagation paths, comparing results with VLF radio measurements

12 p2189 A70-28053

Beam-plasma system mode coupling near electron cyclotron frequency, obtaining interference patterns

13 p2459 A70-28570

Electromagnetic waves extraordinary mode scattering by small diameter nonuniform plasma column in magnetic field

13 p2460 A70-28644

Quasi-pyramidal horn waveguide TE and TM modes eigenvalues computed by asymptotic formula

13 p2377 A70-29147

Circularly polarized waves in waveguide loaded with high density magnetoplasma, discussing propagation mode and plasma boundary

13 p2379 A70-29617

Whistler mode wave packets propagation in hot inhomogeneous collisionless plasma immersed in nonuniform ambient magnetic field

13 p2468 A70-29931

Magnetic field measurement of VLF wave propagating in whistler mode in magnetosphere by satellite FR-1

13 p2401 A70-30054

Trapped mode resonances, attenuation and launching tapers in overmoded rectangular waveguides

14 p2556 A70-30441

Surface wave excitation including PM and dipole modes and Sommerfeld waves

14 p2549 A70-30444

Optical and quasi-optical transmission of EM wave beams of type in directional antennas Fresnel region, examining free space and waveguide modes

14 p2549 A70-30445

Normal wave propagation modes existence in magnetized plasma, deriving criteria for electrostatic approximation validity

14 p2624 A70-31045

Ordinary mode electromagnetic wave propagation instability in high beta plasma, determining lower bound on growth rate

14 p2624 A70-31048

Plane parallel perfectly conducting grating by integral equation procedure, presenting equivalent network under multimode propagation conditions

14 p2562 A70-31317

False signal in scanning interferometer for helium-neon lasers in single and simultaneous TEM modes

15 p2749 A70-31557

Earth-ionosphere cavity resonances diurnal variations by considering different propagation characteristics of day and night hemispheres

15 p2728 A70-31910

Electromagnetic wave propagation in cylindrical guide containing anisotropic sheets, observing TE and TM modes existence

15 p2774 A70-31946

Paraboloidal and spherical reflectors focal region fields matching over corrugated waveguide open end propagating hybrid modes

16 p2861 A70-32966

Mode locked He-Ne laser nsec pulses propagation along multimode clad glass fibers

16 p2865 A70-34039

Attenuation characteristics for dominant hybrid mode in corrugated circular waveguide for antenna feed

16 p2879 A70-34041

Asymptotic analysis of wave propagation modes in circular solid elastic cylinder, obtaining displacement components and frequencies as dimensionless wave number power series

16 p2993 A70-34085

Microwave properties of uniformly magnetized slabs filling cross section of rectangular lossless waveguide operating in specific modes

17 p3050 A70-34584

Microwave properties of infinite lossless rectangular waveguide seminfinitely filled with magnetic material operating in specific modes

17 p3050 A70-34585

Acoustic wave propagation through positive column of glow discharge of three component plasma, noting amplitudes dependence on excitation wave amplitude

17 p3140 A70-34872

Traveling wave antennas, analyzing modal characteristics of various waveguiding structures

17 p3052 A70-35070

Heteroepitaxial ZnO film on anisotropic sapphire substrate, calculating dispersion for fundamental Rayleigh wave mode

17 p3144 A70-35908

Propagation constants in laminar plasma circular waveguides filled with anisotropic linear medium, using Galerkin-Ritz method

19 p3474 A70-37428

Waveguide transformer using rectangular waveguide permitting Galerkin method, determining scattering matrix

19 p3385 A70-37429

Traveling wave antenna array single lobe design using mode charts to reduce errors

19 p3376 A70-37688

Elastic particulate composite solid with microinclusions, deriving dispersion relations governing plane longitudinal wave propagation modes by analogy with continuum theory

19 p3540 A70-37942

Prime focus feeds performance for radiotelescopes, using one- or two-hybrid modes in circumferentially corrugated waveguides

19 p3388 A70-37967

Propagation mode conversion of Gaussian light beam due to random fluctuations of turbulent medium, discussing effect of aperture size and fluctuations anisotropy

20 p3585 A70-39451

Ionospheric VLF diurnal transmission loss differences on two long paths, analyzing values for first and second modes

20 p3585 A70-39455

Electrothermal mode wave propagation in nonequilibrium partially ionized gas, using model with finite ionization

20 p3680 A70-39984

Nonlinear resonance conditions for plasma three-wave interactions, considering wave propagation modes and constant magnetic field

20 p3682 A70-40137

Equatorial F layer irregularity extent from propagation path observations to synchronous satellites

20 p3624 A70-40485

Rotating cold plasma wave propagation modes including Coriolis effect in absence and presence of external magnetic field

21 p3860 A70-41924

Arbitrary mode launching on fiber-optical dielectric waveguides by spatial filtering technique

21 p3829 A70-41930

Acoustic surface waves phase velocity on lithium niobate with gold layer for propagation modes, predicting LF cut-off by substrate anisotropy

21 p3863 A70-42001

Optical communication waveguides with diffused boundaries, calculating modal propagation fields by perturbation theory

21 p3792 A70-42045

Maxwell equations for hybrid modes of shielded ring line with axial and coaxial region at cut-off and near cut-off conductivity

21 p3793 A70-42269

Homogeneous plasma in uniform magnetic field, deriving theory for instabilities and LF wave propagation modes

22 p4079 A70-42370

High level parametric upconverter for radio link using evanescent mode waveguide

22 p3997 A70-42925

Optical waveguides and resonators propagation modes detection and discrimination techniques evaluated for circular cylinder dielectrics/optical fibers

22 p4030 A70-42949

Nonradiating higher order modes on shielded slot lines for TM and TE cases, using series matching and Wiener-Hopf technique

22 p3990 A70-43420

Nonlinear frequency shift for electronic and ionic cyclotron modes in magnetospheric whistler and hydrodynamic propagation, using Vlasov equation

23 p4187 A70-43880

Multiphase modes for nonlinear dispersive waves under large scale interaction, extending Whitham theory

23 p4217 A70-43943

Energy rotation in electromagnetic wavefields, noting TE-MODE excitation in rectangular guides

23 p4164 A70-44384

Turbulent plasma without external magnetic field, observing low phase velocity ion wave mode

23 p4227 A70-44893

Microwave propagation in hollow conducting elliptical pipe waveguide, calculating successive modes cut-off wavelengths by numerical analysis

24 p4318 A70-45212

Microwave propagation in circular waveguide with axially magnetized gas or solid state plasma/Faraday configuration/, calculating twist modes

24 p4318 A70-45213

Circular waveguide with axially magnetized plasma, investigating twist mode propagation in InSb at 70 GHz

24 p4311 A70-45214

Wideband TEM quarter wave microwave coupler with continuously variable coupling range, employing even and odd mode characteristic impedance levels change

24 p4318 A70-45215

Microwave propagation in waveguides, investigating trapped and slightly leaky modes in multilayered or multiwave regions by ray-optical techniques

24 p4311 A70-45216

Microwave waveguide rotary joint using symmetrical excitation for mode conversion to oblate filters

24 p4318 A70-45221

Electromagnetic radiation propagation through resonant medium

24 p4378 A70-45260

Relativistic gas bulk motion nonrelativistic equations, demonstrating spatially random fluctuations damp suprathermal hydromagnetic perpendicular propagation mode to interstellar magnetic field

24 p4397 A70-45761

PROPAGATION VELOCITY

Flame propagation rate calculation methods, considering mass burning rate values

01 p0217 A70-11008

Pressure waves propagation velocity dependence on flow regime in gas-liquid mixtures

01 p0607 A70-11302

Crack propagation in pure alpha-Ti at room temperature using optical and electron microscopy, considering propagation rate relation to strain amplitude

01 p0125 A70-11643

Propagation velocity relation with time delay in human visual system, using various sets of line stimuli having different spatial distance

02 p0237 A70-12457

Gravitational finite propagation velocity effects in celestial mechanics, describing binary star motion studies

02 p0380 A70-12783

Flat flames in stationary gas in tubes useful for flame speed measurements without correction procedure

03 p0607 A70-13917

Gravitational wave propagation velocity determined by laboratory measurement of spin-spin coupling of two rotating masses

04 p0718 A70-14397

Crack propagation rate in aluminum alloy plates under cyclic tensile and transverse shear loadings, noting sliding mode increasing effect

[ASME PAPER 69-MET-1] 04 p0705 A70-14881

Effective wave propagation velocities, bulk and shear moduli of elastic heterogeneous solids approximated by self consistent method

04 p0777 A70-15496

Plasma gas jets high velocity propagation, studying radiation precursor and divergence and expansion chamber effects

04 p0675 A70-15594

Sonic waves induced by shock of laser produced brass and graphite vapor in air at atmospheric pressure using high speed shadowgraphs

05 p0857 A70-15802

Flame spreading velocity characteristics over solid fuel surfaces, discussing environmental pressure, chemical reactivity, pyrolysis, forced convection, etc [WSPCAPER 69-33]

06 p1178 A70-17979

Gas detonation in rough walled pipe, calculating Chapman-Jouguet detonation velocity, deriving existence criterion

07 p1419 A70-18752

Shear wave and plate velocity expressions derived for orthotropic elastic plate with shear coupling, considering propagation direction

07 p1412 A70-19961

Partial statistical description of turbulent flame interior and turbulent flame speed determination for effects of turbulence on flame propagation

08 p1485 A70-21607

Al alloys fatigue cracks propagation rate using electron microfractography

09 p1701 A70-22223

Electromagnetic wave deceleration in open cylindrical waveguide, noting guide action as bandpass filter

09 p1633 A70-22415

Current sheet velocity in coaxial plasma accelerator, noting drag due to insulator ablation and degassing [ALAA PAPER 69-265]

09 p1736 A70-23202

Flame spread rate across surface of liquid fuels, discussing effects of ignition mode, fuel purity and temperature, fuel container dimensions and material

10 p1929 A70-24090

Liquid phase convective heat transfer as rate controlling mechanism for flame propagation, analyzing surface tension driven liquid flow induced by temperature profile

10 p1929 A70-24091

Gas dynamics regarding velocity field excited by vibrations propagating over elastic wing surface at finite velocity

10 p1803 A70-24779

Energy methods applied to fatigue crack propagation rate under tensile mean stress

Small parameter structure and propagation velocity of ionization front in gas, applying nonequilibrium plasma model and electron equation

Fatigue crack propagation rate in sheet alloys with holes as stress concentrators related to duration of various development phases

Electromagnetic inductive shock tube design and wave velocity, electron temperature and plasma conductivity measurements

Initial pressure and pressure ratio effects on shock wave velocity evolution in shock tube

Nonviscous relativistic fluid energy momentum tensor modification to rule out sound wave propagation velocities above speed of light

Interplanetary shock wave properties in solar wind, determining propagation velocity, transit times proton density, proton and electron temperatures

Hydromagnetic wave velocity and space anisotropy instabilities in magnetosphere, using dispersion relation

High resistivity Si electron drift velocity measurement by exciting surface barrier diode with subnanosecond superradiant laser pulses

Distant radiation from magnetic line source in moving isotropic plasma, discussing dependence on velocity

High temperature elastic moduli in polycrystalline Al rods from propagation velocity of elastic waves generated by Q switched laser

Thermodynamically perfect fluids in general relativity, considering heat transmission paradox and wave propagation velocities

Elastoviscoplastic medium filled half space motion under pressure front moving along surface with time varying velocity, analyzing penetrating wave fronts form

S and SKS travel times for arc distances of 30-126 degrees

Elastic wave with discontinuities propagation, calculating decay velocities and stresses at leading wave front by theory of characteristics

Single crystalline mercury elastic constants calculated from propagation velocity measurements of polarized sound waves

Elastic wave propagation in isotropic homogeneous bodies, considering free vibrations and propagation velocity

Ne absorption cell and He-Ne gain cell pulse velocities compared with free space light velocity

Analytic shock front velocity as function of initial parameters in continuous inhomogeneous medium, verifying propagation through rarefaction wave

Magnetosphere Alfvén velocity profile relation to ELF chorus and hiss, indicating unstable wave generation by cyclotron resonance

PROPAGATORS

U PROPAGATION

PROPANE

Reactor surface and propylene role during vapor phase partial oxidation of propane in continuous flow tubular reactors

Propane oxidation reaction and ignition delay times

Temperature evolution of detonation products of Na seeded propane-oxygen mixtures, observing periodic variation for helicoidal cases

Gas mixture composition effect on bacteria growth oxidizing methane and propane, establishing proportional biomass concentration to hydrogen and oxygen in mixture

Methane and propane flames in rotating air flow fields generated by cylindrical rotating wire mesh screen, discussing flame lengths and blowoff velocities

Liquid propane turbojet exhaust simulator for wind tunnel propulsion testing, emphasizing nozzle jet properties

LPG use in fuel cells, discussing efficiency, weight and size

Low speed air-propane flame stability, examining holder diameter effects on vibration cutoff wavelength

PROPELLANT ACTUATED DEVICES

Crushable honeycomb regulating operating pressure of propellant actuated devices applied to recovery parachute catapult in F-111 crew module

Aerospace pyrotechnics applications, considering pressure controlled propellant actuated device for escape systems

PROPELLANT ADDITIVES

NT PROPELLANT BINDERS

NT SOLID ROCKET BINDERS

Metal particles additives behavior in solid rocket propellant combustion, using scanning electron microscope

Combustion stability effects of additives on hydrazine/nitrogen tetroxide propellant combination by measuring droplet burning rate

Composite propellant catalysts /copper chromate and chromite/ thermal decomposition using simultaneous thermogravimetric and differential thermal analysis

Acceleration effects on burning rates of double base propellants with and without Al additive

PROPELLANT BINDERS

NT SOLID ROCKET BINDERS

Composite propellants high pressure burning stability with various binders and oxidizers, showing ammonium perchlorate oxidized formulations susceptibility to instability

Polyurethane propellant binders burning rate, studying siloxane moiety effects

Butadiene prepolymers containing carboxyl functional groups used in binder matrix for solid composite propellants

Oxidizer particle size and binder type effects on nonacoustic combustion instability of solid propellants

Propellant binder prepolymers functionality distribution, examining solute concentration, solvent type and temperature effects on number average molecular weight measurements

PROPELLANT CASTING

Cast double base technique for free-standing and case-bonded propellant charges, discussing manufacturing and mathematical model of casting and curing

Solid propellant rocket motor, discussing manufacture, materials and configuration of 156 inch engine

Tempering stress in circular plates and cylinders in casting of solid propellants

PROPELLANT CHEMISTRY

Propellant condensation on surfaces near electric rocket exhaust, calculating particle arrival rates, backflow and desorption energies

Free gas formation in propellant systems and effects on attitude control systems

Propellants manufacture, hazards and testing - Conference, Miami Beach, April 1967

Propellants chemistry based on chemically cross-linked binder

Oxygen difluoride-diborane reaction measured for pressure-temperature relationships and gas composition dependence on time, noting possible applications as hypergolic rocket propellants

Book on chemical propellants performance covering properties and parameters effects, rocket performance, chemical thermodynamics, flame temperature, etc

Metallic fuels preparation by electric spark discharge process

Metalized solid propellant, calculating condensed phase distribution heterogeneity effect on performance

Solid propellant binders of saturated aliphatic hydrocarbons, describing microstructure, performance contribution, etc

Saturated hydrocarbon prepolymers for solid propellant elastomeric binders

Solid propellant ingredients and explosives differential thermal analyses, discussing thermogravimetry, isothermal or adiabatic constant volume decomposition, crystallographic phase changes, etc

PROPELLANT COMBUSTION

NT SOLID PROPELLANT IGNITION

Abnormal burning surface regression in rocket motor solid propellant detected with flash X ray exposures

Burning program for sounding rocket to reach maximum altitude with given initial and propellant masses, discussing numerical parameter optimization technique

Position control of burning solid nonmetalized propellant strand in combustion bomb using closed loop servomechanism

Nonlinear combustion instabilities in liquid propellant rockets, considering various combustion models and experimental techniques

Axial mode shock wave oscillations in end-burning solid rocket motor, obtaining periodic solutions for flow properties, solid temperature and burning rate

Premixed perchloric acid-methane two flame structure, measuring burning velocities, spectra, temperatures and burned gas compositions

Boron combustion in air augmented rockets, examining mixing and burning between subsonic air and supersonic fuel rich exhaust

Three dimensional combustion instability in liquid-propellant rocket engines, investigating dependence on design and operating parameters via boundary value problem analysis

Hybrid propellant combustion mechanisms, connecting surface reactions to melting mechanism and subsequent liquid flow

Transient response of heterogeneous solid propellant combustion surface determined by step technique regarding pressure buildup and drop conditions

Powder and solid propellant combustion, discussing heterogeneous and homogeneous systems, characteristics of foam, fizz and flame zones, etc

Energy supply for supersonic flight air suction propellant systems using external supersonic combustion, discussing Caret wing and pressure effect

Water or bromotrifluoromethane content required in propellant Aerozine-50 /A-50/ spill to inert against ignition in air, considering fire extinguishment

Optimum injector design for propellant spray mixing using nonreactive simulants and combustion efficiency model

Nonequilibrium initial condition combustion effects on propellant performance for hydrazine/ chlorine pentafluoride and hydrogen/fluorine with equilibrium, kinetic and frozen nozzle flow

Dynamic response of solid propellant flame to oscillating pressure field using T-tube rocket motor, discussing entropy waves produced in oscillatory combustion

Aluminized composite solid propellants burning rates in acceleration fields noting time dependent increase

Combustion model for temperature inhomogeneities effect on stability of solid fuels steady combustion

Combustion and pyrolysis of carbonaceous solids considered for hybrid rocket fuels, using integrating factors in Carathéodory multiple entropies

Heterogeneous ignition mechanism of solid fuels, deriving surface temperature history for time and nature of transition from weak to strong combustion mode

Reaction heat for flameless combustion of double-base propellant using differential scanning calorimetry and thermogravimetric analysis, noting pressure effects

Gas phase reactions near solid-gas interface of deflagrating double base propellant causing abrupt changes in burning rate-pressure curve

Aluminized solid propellant transient burning rate augmentation during acceleration loads

Combustion characteristics of blended droplets composed of monopropellant and diluent, using theoretical model to predict life histories
[AIAA PAPER 70-7] 06 p1180 A70-18141

Burning rates of monopropellant droplet evaluated by variable property models, discussing dimensionless mass flow rate
07 p1358 A70-18914

Liquid rocket motors with concentrated combustion, studying nonlinear longitudinal instabilities with shock waves in combustion chambers
07 p1362 A70-18917

LF nonacoustic instability of solid propellant rocket motors, using combustion model allowing flame temperature oscillations with chamber pressure
[AIAA PAPER 68-179] 07 p1421 A70-19319

Potassium permanganate catalytic effects on ammonium perchlorate deflagration, studying catalyst dispersion degree role
07 p1358 A70-19329

Preignition products from hydrazine propellants at simulated high altitude conditions using IR spectrophotometry, mass spectrometry and differential thermal analysis
07 p1358 A70-19579

Transverse and longitudinal combustion chamber oscillations in rocket motors with distributed mass and energy sources
07 p1364 A70-19581

Combustion of pure crystalline boron single particles injected into hot oxidizing gases streams at atmospheric pressure
[AIAA PAPER 69-562] 07 p1359 A70-19583

Burning rate for composite solid propellant, using model with specific gas phase combustion distribution
07 p1422 A70-19584

Heat transfer from composite propellant burning zone to regressing surface measured using microjet burner
07 p1359 A70-19587

Granular diffusion flame theory application to low pressure burning of composite solid AP propellants
07 p1361 A70-19914

Liquid rocket engine combustion processes determined by injector design using similarity principles
07 p1362 A70-19919

Detonation mechanism in ammonium perchlorate ascribed to mechanical breakdown of charge occurring at pressure equal or above critical deformation of explosive
09 p1741 A70-22102

Acoustic conductivity of burning solid propellant surface calculated, showing positive values or possible amplification at LF
09 p1741 A70-22113

Transient regimes of solid fuel diffusion combustion in channel with oxidizer fed in from outside, proposing finite difference scheme for integrating equations
09 p1741 A70-22114

Propellant extinction near powder-metal contact to study nonsteady combustion mechanism
09 p1742 A70-23228

Burning solid ammonium perchlorate composite propellants surface structure observation to assess heterogeneous or subsurface reactions, using scanning electron microscope
09 p1742 A70-23234

Burning and degradation mechanism of polyester propellants correlated with mass regression rate dependent on surface temperature
11 p2099 A70-25990

Ammonia-chlorine dioxide flame stabilization for simulating ammonium perchlorate combustion at high pressures
11 p2099 A70-25994

Grain configurations classification for solid propellant rockets by relative web thickness and mean vector direction of burning surface into topological continuum
11 p2100 A70-26288

Perfluoropropene, -cyclobutene and -cyclobutane mixing with atmospheric pressure oxygen to determine burning velocities
11 p2100 A70-26383

Regeneratively cooled stainless steel thrust chamber failure related to internal carburization by fuel decomposition and propellant combustion
12 p2290 A70-27111

Reissner variational theorem applied to stress analysis of vertically accelerated end burning solid propellant grain in studying elastic rocket launch failure
12 p2313 A70-27196

Low pressure burning rate of double base propellants at various initial temperatures in argon and in air
12 p2332 A70-27844

Solid propellant combustion - Conference, Novosibirsk, November 1965
13 p2519 A70-28576

Low pressure deflagration limit dependence on strand size in terms of cross section dimensions for composite ammonium chlorate propellant
[AIAA PAPER 69-144] 13 p2473 A70-29955

Monopropellant rocket combustion one dimensional theory with uniform velocity and size droplets injection, obtaining chamber length
14 p2629 A70-30773

Composite solid propellants surface structure and profile characteristics burning with various oxidizers and polyurethane binder by scanning electron microscopy
14 p2628 A70-30948

Biphase rockets combustion characteristics, comparing results with propellant vaporization and nonlinear instability models
14 p2665 A70-30950

Internal ballistics equations solution on basis of pressure index law of burning taking into consideration density approximation
15 p2786 A70-31849

Liquid rocket engine combustion analysis, discussing bipropellant spray mass distribution, drop size and velocity, spray evaporation interphase drag and ablative chambers
[AIAA PAPER 70-622] 16 p2997 A70-33527

Optimal water quench of solid rockets using injection normal to propellant surface
[AIAA PAPER 70-640] 16 p2968 A70-33598

Burning rate increase of nonmetalized composite propellants in acceleration field, assuming surface retention of ammonium perchlorate particles
16 p2963 A70-33861

Acceleration effects on burning rates of double base propellants with and without Al additive
16 p2963 A70-33883

Radiative heat transfer effects on polymeric combustion-inhibiting coatings in solid propellant rocket motors
[AIAA PAPER 70-835] 16 p2971 A70-33930

Extinction model of composite solid propellant combustion including wall and flame heat release zones
17 p3147 A70-34511

Thermal decomposition of perchlorates evaluated by mass spectrometer, with regard to composite propellants combustion processes
17 p3145 A70-34638

Solid propellant combustion, observing burning rate in spin acceleration environments
17 p3145 A70-35209

Rocket exhaust micro and mm waves attenuation attributed to low ionization potential metal particles in propellants
17 p3196 A70-35215

Pulsed laser holography for liquid rocket combustion studies, describing apparatus and techniques
17 p3092 A70-35477

Combustion instability due to narrow cavities in solid propellant engines
17 p3198 A70-35739

Al particles fusion during combustion of stoichiometric mixtures of ammonium and potassium perchlorate and polyformaldehyde
18 p3299 A70-36246

Combustion rates acceleration of ammonium perchlorate mixtures with polystyrene and polymethyl methacrylate by KCl and LiF additions, forming molten layer on charge surface
18 p3299 A70-36248

Ignition surges role in combustion economics
18 p3348 A70-36652

Flame propagation in narrow slit and fine hole of solid propellant grain
18 p3300 A70-36698

Premature exothermic decomposition suppression in propellant grade ammonium perchlorate, using differential thermal analysis
18 p3300 A70-36699

Nonsteady combustion analysis, using method of flame front penetration through fine metal layer in solid propellant
18 p3300 A70-36704

Internal ballistics of composite propellant charge in first stage of burning
19 p3489 A70-38373

Liquid rocket combustion instability due to velocity vector effect, showing importance in longitudinal and transverse modes
20 p3689 A70-40079

Liquid propellant rocket combustion instability, examining droplet vaporization, wake burning and chemical kinetics
20 p3689 A70-40080

Temperature measurements in gaseous reaction zone near surface of burning composite solid propellant, using modified line reversal pyrometer
20 p3694 A70-40273

Gas phase ignition theory with feedback of homogeneous propellant exposed to stagnant gas after shock reflection
[AIAA PAPER 69-559] 21 p3950 A70-41728

Integrated double oblique shock scramjet for supersonic combustion tests and instrumentation development, discussing fuel injection through sonic orifices, combustion data, etc
[AIAA PAPER 69-827] 21 p3867 A70-41752

Thermodynamic-kinetic analysis of fluorine/lithium/hydrogen tripropellant combustion efficiency, discussing liquid metal atomization, firings, facility and thrust chamber
[AIAA PAPER 68-618] 23 p4232 A70-44512

PROPELLANT DECOMPOSITION

Ammonium perchlorate decomposition, deflagration, sublimation, crystal growth and surface properties, using scanning electron microscope
07 p1358 A70-19576

Quasi-steady adiabatic vaporization and exothermic decomposition of monopropellant spherical droplet in inert and reactive environments
07 p1359 A70-19580

Turbulent heat and mass diffusion in catalytic reactors for hydrazine decomposition, developing computer program to calculate temperature and reactant concentration distributions
[AIAA PAPER 69-421] 07 p1365 A70-19706

Hydrazine decomposition in low pressure flame, investigating isotopic substitution effect on flame speed
14 p2628 A70-31094

Pressurization system for nitrogen generation based on hydrazine catalytic decomposition, describing metal membrane configuration, fuel additives, etc
[AIAA PAPER 70-682] 16 p2962 A70-33583

Liquid hydrazine decomposition by Shell 405 catalyst, determining gaseous products by gas chromatography and titrimetric analysis
[AIAA PAPER 70-606] 16 p2856 A70-33603

Proton transfer mechanism for thermal decomposition of ammonium perchlorate, discussing dissociation energy and decomposition products
21 p3864 A70-40883

PROPELLANT EVAPORATION

Heat exchange unit for low thrust attitude control propulsion system evaporator designed for converting liquid propellants to gas
[AICHE PREPRINT 25] 01 p216 A70-10969

Liquid fuel film vaporizing combustor for gas turbines, considering combustion efficiency and flame intensity
03 p0552 A70-14324

Quasi-steady adiabatic vaporization and exothermic decomposition of monopropellant spherical droplet in inert and reactive environments
07 p1359 A70-19580

LF unsteady behavior of liquid propellant rockets from droplets evaporation and combustion rates
[AIAA PAPER 70-620] 16 p2968 A70-33589

PROPELLANT GRAINS

Sensing device to measure radial stress induced at solid propellant grain-to-case bond interfaces during wide temperature variations, detailing instrumentation and operation
03 p0480 A70-12882

Pseudo two dimensional photoelastic test method applied to axisymmetric solid propellant rocket grains under pressure and thermal loads
[SESA PAPER 1482] 03 p0482 A70-12968

Two dimensional plane stress photoelastic models of star configurations in elastic case bonded solid propellant rocket motors under transverse body force loading
03 p0582 A70-14312

Stress analysis for nonlinear viscoelastic cylinder with ablating moving inner surface used to investigate propellant grain in solid fuel rocket under firing condition
[ASME PAPER 69-WA/APM-14] 04 p0771 A70-14914

Fragment fabrication of hybrid propellant solid grain emphasizing spherical shape and diameter uniformity
04 p0737 A70-15673

Cast double base technique for free-standing and case-bonded propellant charges, discussing manufacturing and mathematical model of casting and curing
07 p1360 A70-19906

Pressure surges originated by tangential instabilities in solid propellant motors, using double base homogeneously compounded cylindrical grains
09 p1743 A70-22661

Mandel adhesion and cure shrinkage impact on structural integrity of solid propellant grain
09 p1742 A70-23263

Grain configurations classification for solid propellant rockets by relative web thickness and mean vector direction of burning surface into topological continuum
11 p2100 A70-26288

Linear regression rate of spherical solid hybrid fuel grains oxidized in reducing gas flow
15 p2786 A70-32263

Diaphragm pressure transducer interaction with solid propellant grain, superposing solutions to clamped circular plate and halfspace
16 p2992 A70-33987

Pressure and grain size effect on burnout velocity and combustion capacity of ammonium perchlorate
17 p3145 A70-34639

Flame propagation in narrow slit and fine hole of solid propellant grain
18 p3300 A70-36698

Sensing device to measure radial stress induced at solid propellant grain-to-case bond interfaces during wide temperature variations, detailing instrumentation and operation

20 p3718 A70-39158

Wire reinforced solid rocket propellant grains mechanical properties and failure modes

20 p3689 A70-40050

PROPELLANT MASS RATIO

Nuclear light bulb engine critical fuel mass and design changes effects

[AIAA PAPER 68-571] 01 p0140 A70-10835

Europa 2 booster perigee stage engine design, discussing total and propellant masses, spin stabilization, materials, etc

23 p4234 A70-44672

PROPELLANT OXIDIZERS

U ROCKET OXIDIZERS

PROPELLANT PROPERTIES

NT PROPELLANT STORABILITY

Gas solubilities investigated for gaseous pressurization of propellants

01 p0160 A70-10840

Pulsed plasma transfer systems weight analysis, studying propellant density gradients effects on coaxial plasma gun performance

[AIAA PAPER 70-168] 06 p1133 A70-18231

Composite solid propellant ignition characteristics using arc imaging furnace for radiant energy source, discussing minimum initial pressure determined by binder thermal decomposition

09 p1742 A70-23226

Enthalpy-entropy, enthalpy-pressure and composition diagrams of fluorine-hydrogen system, noting possible applications to rocket propulsion systems

10 p1929 A70-25100

Book on chemical propellants performance covering properties and parameters effects, rocket performance, chemical thermodynamics, flame temperature, etc

12 p2289 A70-27350

Longitudinal temperature gradients effects on stress analysis in solid propellants, using viscoelastic data

14 p2627 A70-30755

Pulsed coaxial plasma accelerator efficiency, examining high capacitance and axial propellant pressure gradients

[AIAA PAPER 70-1085] 20 p3693 A70-40250

PROPELLANT SPRAYS

Liquid diethylocyclohexane /DECH/ sprays detonation propagation in gaseous oxygen, studying drop size effect on steady state development

02 p0351 A70-12003

Frozen wax measurement of droplet sizes and sprays from impinging injector elements, concerning like and unlike doublets and quintuplets

04 p0786 A70-15416

Optimum injector design for propellant spray mixing using nonreactive simulants and combustion efficiency model

04 p0737 A70-15419

Liquid propellant spray injection into high pressure gaseous environment noting geometric, dynamic and thermal characteristics

[AIAA PAPER 70-8] 06 p1182 A70-18211

Propellant sprays behavior in high pressure combustors, calculating jet breakup or atomization length

07 p1257 A70-19331

Liquid rocket engine combustion analysis, discussing bipropellant spray mass distribution, drop size and velocity, spray evaporation interphase drag and ablative chambers

[AIAA PAPER 70-622] 16 p2997 A70-33527

PROPELLANT STORABILITY

Solid tar deposits from hydrocarbon fuels oxidation during prolonged storage

12 p2289 A70-27494

Liquid rocket propellants tankage and components long term storage under extreme relative humidity and temperature conditions

[SAE PAPER 700800] 24 p4392 A70-45911

PROPELLANT STORAGE

Numerical analysis of low-g fluid flow and heating problems encountered with liquid propellant storage and supply

[AIAA PAPER 69-567] 07 p1394 A70-19719

Liquid oxygen usage inspection penetrant systems combining nonreactivity with flaw detection sensitivity

08 p1508 A70-21745

Payload optimization factors for orbital storage of liquid hydrogen, considering payload cost of agitation, tank pressure, pressurant weight, etc

[AIAA PAPER 69-1007] 09 p1767 A70-23262

Spacecraft propulsion development guidelines concerning rocket engines with storable propellants, rotating solid propulsion systems, cryogenic propellants, etc

15 p2790 A70-32256

Heat pipe cooled thrust chambers for space storable propellants, discussing design feasibility for radiation and regeneratively cooled concepts

[AIAA PAPER 70-942] 16 p2965 A70-33541

PROPELLANT TANKS

Structural support strut design for cryogenic propellant tanks to optimize load carrying capability and heat transfer characteristics

02 p0306 A70-11942

Liquid rocket technology for chemical engineers, discussing insulating tanks, flexible lines, turbopumps and combustion chamber

05 p0896 A70-16168

Dynamic instability of motion of rigid and elastic bodies with liquid filled cavities associated with practical problems of rocket technology

06 p1107 A70-18415

Thermally induced convective mixing motion in rotating cylindrical cryogen space storage tank model under heat flux, calculating critical Rayleigh number

07 p1257 A70-19320

Twin spool hydrogen turbopump performance at zero net positive suction pressure /NPSP/ saturated fluid in propellant tank, including steady state and simulated transient engine tests

[AIAA PAPER 69-550] 07 p1295 A70-19709

Simulated low gravity propellant sloshing in spherical, ellipsoidal and cylindrical tanks, discussing Bond number simulation and tank geometry effects

[AIAA PAPER 69-1004] 09 p1657 A70-23255

Expendable propellant tanks /Tip Tank Concept/ on lifting body reusable booster operations to reduce cost for low earth orbital transport mission

11 p2122 A70-26052

Spacecraft propellant tank development from Al alloy providing excellent weldability, propellant compatibility and strength to weight ratio

12 p2242 A70-27108

Cylindrical propellant tanks dynamic stability and parametric resonance, analyzing axial preload, liquid depth top impedance and ullage pressure by Donnell theory

14 p2657 A70-30764

Al alloys and stainless steels tensile properties and application in lightweight cryogenic propellant tank structures, discussing Ti alloys and reinforced composite materials tests

20 p3651 A70-40123

Third stage engine performance from mass properties data for space vehicles with side-by-side tanks

[SAWE PAPER 846] 20 p3717 A70-40378

Low and high chamber pressure concepts for space shuttle reaction control system

[SAE PAPER 700802] 24 p4416 A70-45909

Liquid rocket propellants tankage and components long term storage under extreme relative humidity and temperature conditions

[SAE PAPER 700800] 24 p4392 A70-45911

Orbit-to-orbit space shuttle toroidal propellant tank design, construction and testing for outflow and slosh characteristics

[AIAA PAPER 70-1325] 24 p4417 A70-45940

PROPELLANT TESTS

Preignition products from hydrazine propellants at simulated high altitude conditions using IR spectrophotometry, mass spectrometry and differential thermal analysis

07 p1358 A70-19579

Propellants manufacture, hazards and testing - Conference, Miami Beach, April, 1967

07 p1359 A70-19905

Solid propellant mechanical properties tests, failure and physical deterioration /aging/

07 p1361 A70-19913

Hazards in manufacturing solid propellants evaluated to design tests and suggest process conditions

07 p1361 A70-19915

Laboratory and field tests to evaluate liquid rocket propellant properties for tactical mission

07 p1362 A70-19918

Solid propellant technology, discussing manufacturing processes, sample testing, inspection, etc

08 p1557 A70-20690

Polybutadiene-ammonium perchlorate solid propellant microscopic failure analysis under uniaxial tension

09 p1741 A70-22424

Polybutadiene-ammonium perchlorate solid propellant BPT-1 mechanical properties viscoelastic analysis under constant strain rate tension

09 p1742 A70-22425

Burning solid ammonium perchlorate composite propellants surface structure observation to assess heterogeneous or subsurface reactions, using scanning electron microscope

09 p1742 A70-23234

Mandrel adhesion and cure shrinkage impact on structural integrity of solid propellant grain

09 p1742 A70-23263

Field test for microbiological contamination of jet fuel, discussing phosphates detection

18 p3299 A70-36344

Short duration tube wind tunnel supersonic testing, noting Saturn S-IC base heating and solid propellant rocket base burning tests

20 p3606 A70-39698

Electron bombardment Hg thruster with divergent magnetic fields, investigating performance dependence on configuration and propellant utilizations

[AIAA PAPER 70-1092] 20 p3692 A70-40243

Composite solid propellant thermal ignition from hot wire tests and model

21 p3942 A70-40877

Solid phosphorus triamide derivatives as ignition aids in hypergolic propellant systems, testing characteristics in interaction with oxidizers

21 p3865 A70-41404

Integrated double oblique shock scramjet for supersonic combustion tests and instrumentation development, discussing fuel injection through sonic orifices, combustion data, etc

[AIAA PAPER 69-827] 21 p3867 A70-41752

PROPELLANT TRANSFER

Propellant transfer unit for weapon or space vehicle systems, specifying aerospace ground equipment criteria

[SAE-AIR-1129] 07 p1248 A70-18806

Analytical model for liquid fluorine no-vent loading operations noting application to flightweight upper stage systems

[AIAA PAPER 69-579] 09 p1662 A70-23251

Capillary barriers to provide propellant positioning, expulsion capability and slosh dampening for spacecraft propulsion systems during rotational maneuvers

[AIAA PAPER 69-529] 11 p2123 A70-26119

Protective clothing for personnel handling toxic and corrosive liquid propellants in hot climatic conditions at Guyana Space Center

12 p2179 A70-28043

Orbital refueling techniques, discussing vapor-liquid interface stability, pressurant requirements, transfer line chilloff, propellant transfer dynamics, dielectrophoresis, suction speed estimating and system tradeoffs

[AIAA PAPER 69-564] 14 p2653 A70-30752

Vapor fraction dependence on liquid hydrogen propellant outflow during NERVA operation under stored gas or autogenous pressurization, using computer simulation

[AIAA PAPER 70-677] 16 p2950 A70-33578

Spacecraft propellant expulsion systems, comparing capillary with conventional techniques

[AIAA PAPER 70-685] 16 p2962 A70-33584

Saturn 5 S-2 stage propellant feedlines and J-2 engines simulating structural longitudinal oscillation by analog computer

[AIAA PAPER 70-626] 16 p2968 A70-33591

Dual bellows ball seat valve design for colloid thruster coupled to pressurized feed system, demonstrating thrust decay and flow regulation

[AIAA PAPER 70-615] 16 p2919 A70-33610

Zero gravity liquid ammonia propellant feed system, describing regulator/capillary tube assembly for propellant delivery pressure control

[AIAA PAPER 70-1151] 20 p3690 A70-40204

PROPELLANTS

NT AEROZINE

NT CASE BONDED PROPELLANTS

NT COLLOIDAL PROPELLANTS

NT COMPOSITE PROPELLANTS

NT CRYOGENIC ROCKET PROPELLANTS

NT DOUBLE BASE PROPELLANTS

NT DOUBLE BASE ROCKET PROPELLANTS

NT GASEOUS ROCKET PROPELLANTS

NT GELLED ROCKET PROPELLANTS

NT HIGH ENERGY PROPELLANTS

NT HYBRID PROPELLANTS

NT HYPERGOLIC ROCKET PROPELLANTS

NT LIQUID ROCKET PROPELLANTS

NT METAL PROPELLANTS

NT MONOPROPELLANTS

NT PENTOLITE

NT PLASTIC PROPELLANTS

NT RDX

NT ROCKET PROPELLANTS

NT SLURRY PROPELLANTS

NT SOLID PROPELLANTS

NT SOLID ROCKET PROPELLANTS

NT STORABLE PROPELLANTS

Digital control valve for high speed aerospace blending, considering propellant and cryogenics applications

06 p0989 A70-18602

PROPELLER BLADES

Vortex sheets pitch along constant aerodynamic pitched propeller blade at zero traction, discussing calculation, construction and wind tunnel testing

05 p0790 A70-16159

Wire dischargers at helicopter propeller blade tips reducing electrostatic RF interference, substituting stainless steel wire tufts for nichrome wire

05 p0848 A70-16320

Propeller noise research for achieving noise reductions in future propeller design

05 p0796 A70-16793

Laminar viscous flow on rotating propeller and helicopter rotor blades, studying crossflow and unsteady boundary layer effects, separation, transition, etc

[AIAA PAPER 70-50] 06 p0974 A70-18161

- Helicopter blade flapping torsion flutter behavior analysis showing stabilization effect in forward flight
10 p1958 A70-24559
- Slip-ringless propeller blade mounted measurement system for steady state and vibratory stresses from multiple strain-gage locations during flight and ground tests
11 p2051 A70-25891
[SAE PAPER 700223]
- Blade flexibility effects on static stability derivatives of prop/rotors in propeller flight mode
17 p3013 A70-34701
- Propeller blade aerodynamic characteristics at zero advance ratio, reducing singular integral equation to nonsingular form for computer solution
23 p4136 A70-44993
- Bending vibrations of propeller blades calculated by successive approximation
24 p4422 A70-45300

PROPELLER DRIVE

- NT HELICOPTER PROPELLER DRIVE
- Noise reduction for V/STOL aircraft operation by introducing quiet propellers, discussing variable camber propellers, propeller aerodynamics, etc
[AIAA PAPER 69-1038] 01 p0005 A70-10646
- Four-seat two-engine STOL propeller passenger and sport aircraft design and performance
19 p3355 A70-37371

PROPELLER EFFICIENCY

- V/STOL aircraft propellers featuring thrust augmenting air jet slits for increased lift
[DGLR-69-36] 04 p0616 A70-15175

PROPELLER FANS

- Sound generation by multibladed single stage fans operating in free field, deriving model as boundary value problem involving inhomogeneities due to quadrupole distribution
01 p0166 A70-11197
- H3-E Sprinter semicompound helicopter with pneumatic rotor drive and side mounted fans for forward flight
17 p3018 A70-35626

PROPELLER SYNCHRONIZERS

- U PROPELLERS
U SYNCHRONIZERS

PROPELLERS

- NT PROPELLER FANS
NT SHROUDED PROPELLERS
- Singular element technique effect on hydrodynamic and aerodynamic problems solutions, presenting potential flow problems and application to wings and propellers
07 p1188 A70-19133
- Flowfields in lifting-line approximation for finite bladed, lightly loaded propellers in axial cruise and heavily loaded propellers in static operation
07 p1190 A70-20411
- STOL touring aircraft propeller design and aerodynamics, discussing takeoff runs, landing runs, high lift, downwash, ground effects, etc
08 p1435 A70-20628
- Propeller in axial motion through homogeneous turbulence, studying forces and moments by statistical analysis
13 p2339 A70-29014
- German book on propeller theory covering airfoil theory, propeller flow and pressure fields, propeller vibrations, shrouded and tilted propellers, helicopter rotors, etc
23 p4180 A70-44097
- Optimal propeller selection for given aircraft and engine designs, considering aerodynamic and acoustic characteristics
24 p4393 A70-45441

PROPERTIES

- Remote sensing and privacy rights, noting political and social trends toward privacy protection
10 p1971 A70-24744

PROPHYLAXIS

- Acute gasoline poisoning toxicology and prophylaxis, manner of ingestion and effects on organs and systems
08 p1451 A70-20976
- Adenosine triphosphate and vitamins /amitetravit/ as prophylactics against radiation injuries in dogs during simulated space flight
17 p3038 A70-35351

PROPORTIONAL CONTROL

- Proportional controlled pneumatic servomechanisms analysis extended to include motion along stroke, considering position effect on stability
05 p0797 A70-15891
- Analog fluidic elements /operational amplifiers/ with beam deflector proportional amplifiers incorporated into close coupled circuit
12 p2164 A70-27072
- Semifluidic proportional industrial control systems using diaphragm summing junction including applications to temperature control, remote sensing and drill bit adaptive measurement
12 p2164 A70-27073
- Missile homing on moving target, assuming closing velocity vector angular rate proportional to line of sight
16 p2949 A70-34054

- Linear continuous feedback control system with dead time compensated by proportional plus integral controller, considering stability region variations
18 p3236 A70-36943

- Linear feedback control system with dead time compensated by proportional integral derivative action controller, evaluating stability by digital computer
18 p3236 A70-36944

- Phased locked AFC circuit, calculating internal harmonic noise reduction by proportionately integrating filter
23 p4161 A70-43960

- Jet interaction type proportional fluid amplifier as feedback oscillators, measuring frequency response
24 p4292 A70-45291

- Semifluidic proportional control systems for industrial controls involving oven temperature, remote hydraulic pressure regulation, drill bit pressure
24 p4293 A70-45432

PROPORTIONAL COUNTERS

- Gas flow proportional counter for measuring high emission rates of alpha particles, discussing design and operation
04 p0695 A70-15570

- Miniaturized proportional counter to measure radioactive Ar 37 ultramicroquantities, assessing errors
05 p0898 A70-15930

- Transistorized low impedance cascades as amplifiers for proportional counters in studying cosmic ray intensity variations
05 p0845 A70-15934

- Azimuthal telescope with proportional counters for underground recording of hard/soft cosmic ray components
05 p0846 A70-15937

- Cosmic rays meson component recording by proportional counters designed for use in large telescopes
05 p0846 A70-15939

- Wall effect on differential spectra distortions in cylindrical ionization chamber and proportional counter type detectors
05 p0900 A70-15971

- Solar soft X ray spectrum analyzed by OSO 4 proportional counter, discussing slowly varying component, corona active regions and impulsive event characteristics
07 p1369 A70-20289

- Laser beam ionization of gases, using proportional ionization counter
10 p1890 A70-24588

- Beryllium proportional counters for satellite X ray astronomy, noting long term stability and environmental resistance
12 p2232 A70-27403

- Polypropylene window proportional counter on board sounding rocket for cosmic soft X ray measurement
15 p2741 A70-32530

- Solar X-ray emission localization, examining spatial distribution by rocket-borne collimated proportional counter
17 p3151 A70-34864

- Extragalactic objects 3C 273 NGC 5128 and M87 X ray emission detection, using proportional counters on Aerobee 150 rocket
18 p3310 A70-37016

- Five-channel azimuthal underground cosmic ray telescope using proportional counters suitable for continuous recording
20 p3629 A70-39312

- X ray astronomy proportional counters sensitivity, reducing higher energy radiation background contribution
21 p3821 A70-40653

- Galactic plane scanned observation of X ray sources, using large area proportional counter rocket sounding
22 p4094 A70-42986

PROPORTIONAL LIMIT

- Nitrogen content effect on proportional limit and work hardening rate of austenitic stainless steel at 302 F
10 p1905 A70-25169

PROPRIOCEPTION

- Heart rate and skin conductance measurements during attention-direction tasks involving proprioceptive stimuli position on environmental acceptance and rejection continuum
01 p0026 A70-11166

- Flight simulators for pilot training, discussing need for aircraft motion cues
09 p1655 A70-22296

- Human motor functions changes following prolonged hypodynamia, including physical training and hypokinesia roles in standing and walking
10 p1815 A70-24682

- Human proprioceptive reflexes fluctuations correlation with spontaneous respiration and cardiovascular rhythms
13 p2350 A70-29323

- Human proprioceptive reflexes fluctuations during controlled respiration and voluntary apnea
13 p2351 A70-29324

PROPULSION

- NT ASCENT PROPULSION SYSTEMS
NT CHEMICAL PROPULSION
NT ELECTRIC PROPULSION
NT ELECTROMAGNETIC PROPULSION
NT ELECTROSTATIC PROPULSION
NT HYBRID PROPULSION
NT ION PROPULSION
NT JET PROPULSION
NT LOW THRUST PROPULSION
NT MAN OPERATED PROPULSION SYSTEMS
NT NUCLEAR ELECTRIC PROPULSION
NT NUCLEAR PROPULSION
NT PHOTONIC PROPULSION
NT PLASMA PROPULSION
NT SOLAR PROPULSION
NT SPACECRAFT PROPULSION

- Soviet book on physics of cosmic propulsion energy covering space vehicle propulsion systems, vehicle-medium interaction, etc
08 p1558 A70-20754

- Propulsive and lifting motions of pointed profile in ideal incompressible fluid related to alternate vortices emission
08 p1433 A70-21234

- Guidance and control and propulsion technology, discussing fluidic systems, digital computers and structural materials, solid and liquid propellant engines
17 p3179 A70-35284

PROPULSION CALCULATIONS

- U MATHEMATICAL MODELS
U PROPULSION

PROPULSION SYSTEM CONFIGURATIONS

- NT DESCENT PROPULSION SYSTEMS
- Interior ballistics of high-low propulsion system with fixed volume high pressure combustion chamber coupled to variable volume lower pressure action chamber
03 p0548 A70-14116

- High energy propulsion module utilizing F/H fuels for planet flyby, orbiter mission and injection of 24-hr satellites, discussing design and equipment
[DGLR-69-18] 04 p0736 A70-15176

- Pulsed MPD arc jet electric propulsion system requirements, examining physical constraints, pulse duration, duty cycle, power network structural details, etc
[AIAA PAPER 69-269] 04 p0737 A70-15424

- Development trends, design and gas dynamic characteristics of turbine engines for helicopter propulsion systems including pressure, turbofan and integral engines
05 p0896 A70-16350

- Satellite electric propulsion system and configuration for orbital transfer maneuvers, describing ELDO launcher, Black Arrow, orbital dynamics, sensor system, etc
06 p1130 A70-17648

- Air breathing launch vehicle for earth-orbit shuttle assessed in light of hypersonic propulsion and configuration development
[AIAA PAPER 70-269] 07 p1365 A70-20380

- V/STOL Do 231 design, discussing propulsion, control, safety, traffic control and economic factors
08 p1435 A70-20640

- Supersonic inlet role and nature in air breathing propulsion system, discussing inlet-engine matching by variable geometry
[AGARDOGRAPH-120] 08 p1434 A70-19128

- Air breathing engines for long range Mach 4 transport, discussing airplane mission profile- engine configuration interface
[AGARDOGRAPH-120] 08 p1560 A70-19134

- Soviet book on rocket structure mechanics covering acting loads and selection of tanks, stage segments, nose section and propulsion units
09 p1772 A70-22527

- Lift fan propulsion for VTOL passenger aircraft, discussing design, thrust augmentation, optimum element combination, engine-wing integrations and tests
[DGLR-70-007] 10 p1929 A70-24049

- Technological feasibility, economical and operational compatibility of subsonic aircraft nuclear propulsion /ANP/ compared with conventional propulsion systems
11 p2081 A70-26050

- Air deflection and modulation /ADAM/ turbofan propulsive wing V/STOL design
[AIAA PAPER 69-201] 12 p2162 A70-28087

- Airframe-propulsion system integration for Mach 6 transport and Mach 12 research airplane, examining off-design operation effects and interaction of aerodynamic forces
[AIAA PAPER 70-542] 13 p2345 A70-29009

- V/STOL propulsion for commercial needs, considering best tradeoff between propulsion size, weight, noise generation and fuel consumption
14 p2629 A70-31277

- Fighter engine capabilities in Mach 3 to 7 speed range, discussing propulsion system configurations
[AIAA PAPER 70-943] 16 p2965 A70-33542

- Solid propellant extinguishment by rapid depressurization, investigating motor configuration effect,

- binder, burning rate catalyst, oxidizer, metal loading and exhaust pressure levels 16 p2962 A70-33572
 - Low pressure ratio lift fan propulsion system for intercity VTOL transports, considering thrust, safety, noise, weight, components, speed, turbine and transmission [AIAA PAPER 70-670] 16 p2971 A70-33592
 - Propulsion system impact on military/commercial STOL transport aircraft commonality, taking into account augmented jet flap and externally blown flap powered lift wing concepts [SAE PAPER 700269] 18 p3214 A70-36819
 - V/STOL attitude control system as integral propulsion system part, analyzing design and weight tradeoffs [ASME PAPER 70-GT-31] 18 p3214 A70-36832
 - Electric propulsion systems design and performance, surveying various types 20 p3688 A70-39238
 - Electric propulsion systems integration into SERT 2 spacecraft, discussing launch imposed environment, thrust vector control, thruster breakdown, power conditioning, etc [AIAA PAPER 70-1123] 20 p3691 A70-40222
 - Electron bombardment Hg thruster with divergent magnetic fields, investigating performance dependence on configuration and propellant utilizations [AIAA PAPER 70-1092] 20 p3692 A70-40243
 - Mercury electron bombardment thruster, measuring effect of geometry and magnetic field inside pole piece region on discharge losses and propulsion efficiency [AIAA PAPER 70-1088] 20 p3693 A70-40247
 - Resistojet thrusters for spacecraft propulsion and control, discussing systems configurations, performance, weight, etc 21 p3866 A70-40986
 - Multimission solar electric spacecraft propulsion module design for Asteroid Belt, Jupiter and out-of-ecliptic missions, including thruster failure and power conditioning requirements [AIAA PAPER 70-1155] 21 p3868 A70-41785
 - Aircraft propulsion system test facilities, discussing altitude simulation, large subsonic and supersonic engines and component development [ICAS PAPER 70-45] 23 p4178 A70-44143
 - Two stream ejector type propelling nozzles for supersonic aircraft, investigating various configuration effects over range of secondary/primary air flow ratios [ICAS PAPER 70-48] 23 p4133 A70-44145
 - Energy transfer methods for hybrid air breathing ramjet propulsion systems with rocket motor S gas source [ICAS PAPER 70-61] 23 p4233 A70-44156
 - Entrainment theory for incompressible turbulent boundary layer velocity and drag on bodies of revolution employed in fuselage, submersible and cowings for propulsion design 23 p4182 A70-44400
 - Solar-electric ion propulsion mission analysis and spacecraft designs, discussing thruster, power conditioning, propellant storage and feed, etc 23 p4234 A70-44631
 - ELDO Europa 1 and 2 launchers configurations tendencies, discussing use of liquid propellant boosters, chemical, electrostatic or thermonuclear propulsion system, etc 23 p4263 A70-45002
 - Commercial STOL aircraft propulsion systems from airline viewpoint, emphasizing subsystem design, engine selection, thruster deterioration and maintainability [SAE PAPER 700810] 24 p4395 A70-45904
 - Hydrogen oxygen engine designs for space vehicle auxiliary propulsion systems, considering long life thrust chamber performance with compatible heat transfer characteristics [SAE PAPER 700803] 24 p4395 A70-45908
- PROPULSION SYSTEM PERFORMANCE**
- Airframe flow field effects on propulsion system performance in transonic flight, studying case of underwing aft mounted turbojet engine nacelles 01 p0004 A70-10321
 - Environmental effects on aircraft and propulsion systems - Conference, Bordentown, N.J., October 1969 01 p0162 A70-10678
 - Vaporization interaction liquid rocket performance model, discussing performance loss evaluation and test data 01 p0160 A70-10832
 - Performance boundaries of space propulsion systems containing nuclear electric stages [AIAA PAPER 69-249] 01 p0196 A70-10839
 - Boeing 747 nacelle development programs involving outdoor and ground test rigs, flying test bed, flight tests, etc [SAE PAPER 690389] 03 p0550 A70-12894
 - Annular combustion chamber for turboprop engines, analyzing design data and development stages, discussing performance characteristics 03 p0552 A70-13928
 - TV data transmitted by Iantar series automatic ionospheric laboratories released by geophysical rockets at 100-400 km, discussing plasma-ion propulsion system performance 04 p0735 A70-14936
 - Solid propellant motors relative performance as related to intermediate payload missions, considering reusable liquid strap-on stages for post-Saturn payloads 05 p0897 A70-16897
 - Nuclear and electric propulsion systems performance, considering applications in future European space activities 05 p0897 A70-16898
 - Steady state and dynamic performance of variable geometry free gas turbine using nomogram and analog simulation 06 p1129 A70-17143
 - Constant thrust electric propulsion systems performance with coast trajectories presented for 100 AU extracapsule missions [AIAA PAPER 68-546] 06 p1137 A70-17160
 - Aerobell extendible nozzle rocket engine design and performance, cold flow and simulated hot flow test results [AIAA PAPER 69-4] 06 p1129 A70-17168
 - Surveyor spacecraft vernier propulsion system survival in lunar environment, suggesting temperature resistant seal and valve seat material for fluid loss prevention 06 p1129 A70-17170
 - Resistojet design criteria for performance modeling of ammonia propellant thrusters and manned space stations using biowaste propellants [AIAA PAPER 70-211] 06 p1131 A70-18026
 - LES-6 satellite solid Teflon pulsed plasma thruster performance, determining energy balance, thrust and circuit parameters [AIAA PAPER 70-179] 06 p1132 A70-18206
 - Improvement in power output of ramjet installed under wing using air compression [ONERA-TP-783] 06 p1133 A70-18467
 - 30 cm diameter mercury bombardment low impulse thruster development for potential space applications, discussing performance and control [AIAA PAPER 69-238] 07 p1365 A70-19704
 - Kaufman thruster performance dependence on transmission of ion extraction optics and magnetic field shape [AIAA PAPER 69-257] 07 p1365 A70-19705
 - Interagency chemical rocket propulsion group method of treating measurement error for liquid rocket engine performance parameters, using uncertainty model [AIAA PAPER 69-734] 07 p1365 A70-19723
 - ICRPG liquid propellant thrust chamber performance evaluation methodology, reviewing imperfections and limitations [AIAA PAPER 69-468] 07 p1365 A70-19728
 - Aircraft engines development and reliability, discussing rejection causes, data retrieval, repair and salvage techniques 08 p1558 A70-21031
 - Soviet helicopter and aircraft engines characteristics covering designer, power, rpm limits, fuel consumption, weight, geometry and applications 08 p1559 A70-21366
 - F-106B aircraft in-flight study of airframes installation effects on propulsion system performance at transonic speeds 08 p1437 A70-21732
 - Supersonic burning ramjet /scramjet/ performances, discussing vehicle engine integration, superiority to ordinary ramjets at hypersonic speeds, combustion process-flow field interaction, etc [AGARDGRAPH-120] 08 p1600 A70-21930
 - Ammonia micropropulsion for geostationary satellites stabilization, discussing principle and working mode of thrusters 09 p1743 A70-22660
 - Turbojet engines departure from equilibrium performance during thermal soak transient attributed to heat absorption in turbine and compressor metals, observing thrust loss 09 p1744 A70-23739
 - Chemical rocket propulsion systems approximate calculation for characteristic velocity dependence on mixture ratio and pressure in combustion chamber [DFVLR-SONDDR-24] 10 p1929 A70-23842
 - Small turboprop engine development, flight tests, performance and weight reduction [SAE PAPER 700206] 11 p2102 A70-25878
 - Operating characteristics and performance of business aircraft jet engines compared with piston engine handling [SAE PAPER 700209] 11 p2102 A70-25880
 - Space charge sheath electric thruster principles, construction and performance using laboratory test model [AIAA PAPER 69-282] 11 p2102 A70-26121
 - Background pressure and magnetic field shape effect on MPD thruster performance, testing radiation cooled thrusters [AIAA PAPER 69-243] 11 p2102 A70-26122
 - NERVA nuclear rocket engine design for Saturn 5 third stage, comparing nuclear and chemical engines performance 12 p2270 A70-26871
 - Book on chemical propellants performance covering properties and parameters effects, rocket performance, chemical thermodynamics, flame temperature, etc 12 p2289 A70-27350
 - Sounding rockets impact dispersion associated with wind measurement errors and thrust misalignments, discussing correction via reduced aerodynamic stability and initial rocket spin 13 p2503 A70-28677
 - Agna propulsion system performance model for predicting propellant flow rate, mixture ratio, thrust time and specific impulse [AIAA PAPER 69-453] 14 p2629 A70-30754
 - Nuclear solid core rocket engine performance for interplanetary orbital launch of spacecraft by multi-orbit injection [AIAA PAPER 69-535] 14 p2616 A70-30767
 - Gas turbine performance dynamic modeling by analog and digital computer simulation providing clear picture of transient behavior 14 p2629 A70-30991
 - V/STOL propulsion for commercial needs, considering best tradeoff between propulsion size, weight, noise generation and fuel consumption 14 p2629 A70-31277
 - Discharge chamber plasma processes in electron bombardment ion thrusters, considering factors affecting thruster performance [AIAA PAPER 69-494] 15 p2791 A70-32501
 - Rocket engine thrust chambers and valves, discussing component lifetime extension and operational flexibility of reaction control systems [AIAA PAPER 70-603] 16 p2964 A70-33526
 - Unmanned electric propulsion spacecraft with external fuel and flashlight thermionic reactors, discussing thruster arrays, weight and performance for reference Jupiter orbiter mission [AIAA PAPER 70-644] 16 p2966 A70-33547
 - Oxygen difluoride/diborane propellant thrust chamber and injector technology, discussing engine duty cycles and performance [AIAA PAPER 70-717] 16 p2962 A70-33550
 - Aircraft propulsion control system accommodating transients and yielding higher steady state performance 16 p2966 A70-33557
 - Digital simulation for turbine engine propulsion system testing [AIAA PAPER 70-633] 16 p2869 A70-33593
 - Lunar flying vehicle propulsion system optimization, discussing weight, performance, engine life, reliability, etc [AIAA PAPER 70-605] 16 p2969 A70-33602
 - Jet engine combustion chamber design, discussing performance range and geometry 16 p2970 A70-33682
 - Shrouded propeller diffusers, considering diffusion effects on propulsion performance 16 p2970 A70-33754
 - Power plants development for air transport propulsion system economics, noting engine reliability, traffic delays, etc 16 p2841 A70-33770
 - Convertible fan-shaft engine for V/STOL tactical and transport aircraft, discussing design and performance 17 p3147 A70-34710
 - Aircraft gas turbine propulsion, discussing engine performance characteristics, thermodynamics, noise and installation [AIAA PAPER 70-873] 17 p3147 A70-34810
 - Power plant efficiency, size, maintenance and operating economics of propulsion systems for air transport 17 p3200 A70-34917
 - C-5A propulsion system onboard monitoring for malfunction detection, analysis and subsystem recording 17 p3148 A70-35497
 - On-line display of pulsed rocket engine performance data using hybrid computer 17 p3063 A70-35512
 - NERVA engine operational cycle and performance, discussing startup, thrust buildup and shutdown 17 p3135 A70-35653
 - Constant chamber pressure thrust throttling of expansion-deflection rocket nozzle, calculating wall static pressure and thrust by characteristic method, discussing performance [AIAA PAPER 69-435] 17 p3149 A70-35655
 - Low thrust high impulse nuclear and electric space propulsion systems, discussing performance capability for space missions 18 p3290 A70-36566
 - JT9D engine design and performance, describing operational problems [SAE PAPER 700288] 18 p3302 A70-36807
 - Military aircraft engines performance increase and cost reduction [SAE PAPER 700272] 18 p3302 A70-36817

Gas turbine engine dynamic performance simulation, using analog and digital techniques [ASME PAPER 70-GT-23] 18 p3237 A70-36830

Turbofan engine performance optimization by closed form solution of operating cycle parameter functions [ASME PAPER 70-GT-65] 18 p3303 A70-36840

Metalized solid propellant, calculating condensed phase distribution heterogeneity effect on performance 18 p3300 A70-37207

Europa 2 launcher fourth /perigee/ stage, describing trajectories, propulsion system design and performance, separation systems, etc 19 p3532 A70-37871

Gas turbine propulsion systems design, performance and applications for industrial and military uses, discussing sensors for measurement and control of critical engine parameters 19 p3424 A70-37881

Electric propulsion systems design and performance, surveying various types 20 p3688 A70-39238

Solar electric propulsion system performance consisting of thrusters with thrust vector aligning actuators, switching network and flight type power conditioner 20 p3688 A70-39687

RF plasma thrusters for synchronous satellites, estimating weights and efficiencies of various types 20 p3689 A70-40124

Electrothermal thruster with biowaste propellants, discussing design and performance with various propellant compositions [AIAA PAPER 70-1161] 20 p3567 A70-40201

SERT 2 spacecraft ion thruster ground tests and flight operation, tabulating performance data [AIAA PAPER 70-1125] 20 p3691 A70-40220

SERT 2 for testing ion thruster reliability and operational characteristics, discussing design and mission objectives [AIAA PAPER 70-1124] 20 p3716 A70-40221

Solar electric propulsion application to out-of-ecliptic mission for interplanetary fields and particles data, comparing performance with chemical systems [AIAA PAPER 70-1118] 20 p3691 A70-40225

Interplanetary solar electric spacecraft performance improvement by mission mode including earth swing-by maneuver in solar orbit inclined to ecliptic [AIAA PAPER 70-1117] 20 p3710 A70-40226

Primary solar electric propulsion for automated space transportation propulsion program, considering performance and technology readiness [AIAA PAPER 70-1115] 20 p3691 A70-40228

Colloid annular thruster performance, using low mass flow rate data and space charge formulas [AIAA PAPER 70-1113] 20 p3692 A70-40230

Colloid annular thrusters performance tests in vacuum chamber with LN cooled liner, using high speed analog to digital system to acquire time of flight /TOF/ data [AIAA PAPER 70-1112] 20 p3692 A70-40231

Colloid microthruster system life test, discussing design and steady state performance [AIAA PAPER 70-1110] 20 p3692 A70-40233

Colloid engine propellant mass flow distribution, determining beam current and specific charge effects on thrust, efficiency and specific impulse [AIAA PAPER 70-1109] 20 p3692 A70-40234

Critical components effect on small Hg electron bombardment thruster performance, considering glass coated accelerator grids, hollow cathodes and plasma bridge neutralizers [AIAA PAPER 70-1100] 20 p3692 A70-40238

Electron bombardment Hg thruster with divergent magnetic fields, investigating performance dependence on configuration and propellant utilizations [AIAA PAPER 70-1092] 20 p3692 A70-40243

SERT 2 Hg thrust ion extraction, loss, production and energy balance within ionization chamber [AIAA PAPER 70-1091] 20 p3693 A70-40244

Mercury electron bombardment thruster, measuring effect of geometry and magnetic field inside pole piece region on discharge losses and propulsion efficiency [AIAA PAPER 70-1088] 20 p3693 A70-40247

Low power MPD arc thruster performance with downstream cathode, using Xe propellant [AIAA PAPER 70-1084] 20 p3693 A70-40251

Cathode geometry effect on performance of radiation cooled MPD arc thruster in continuous mode [AIAA PAPER 70-1083] 20 p3693 A70-40252

Space shuttle with reusable launch system, discussing payload sensitivities regarding orbiter and booster weight and engine reliability [SAWE PAPER 849] 20 p3716 A70-40377

Third stage engine performance from mass properties data for space vehicles with side-by-side tanks [SAWE PAPER 846] 20 p3717 A70-40378

Solar electric propulsion systems technology development at JPL, discussing performance data and relationship to spacecraft requirements [AIAA PAPER 70-1153] 20 p3695 A70-40520

Repetitively pulsed MPD propulsion systems, considering thruster performance [AIAA PAPER 70-1093] 20 p3695 A70-40522

Drag-free satellite design and propulsion requirements, noting orbit perturbation mechanisms [AIAA PAPER 70-1145] 20 p3717 A70-40523

Optimal low thrust power plant for spacecraft payload-maneuver tradeoff 21 p3866 A70-40832

Resistojet thrusters for spacecraft propulsion and control, discussing systems configurations, performance, weight, etc 21 p3866 A70-40986

Nuclear rockets for interorbit transportation, discussing reuse economics, propulsion system performance, etc 21 p3866 A70-40987

OP-EX, optimal explicit guidance algorithm for powered flight outside atmosphere [AIAA PAPER 68-869] 21 p3848 A70-41734

Liquid metal /mercury/ cathode thruster system for operation at reduced beam voltages, discussing design and performance [AIAA PAPER 70-1103] 21 p3868 A70-41788

Rocket engines propulsion systems design and performance based on thermodynamical theory, involving expanding gas 21 p3869 A70-42038

Rocket motion and space propulsion systems, discussing exhaust velocity effect on payload 21 p3869 A70-42039

Solid propellant rocket motors performance, manufacture and hardware, discussing mechanical properties, storage, combustion, nozzle expansion, etc 21 p3869 A70-42040

Liquid propellant rocket engines performance and classification based on feed system, discussing heat transfer and thermochemical considerations 21 p3869 A70-42041

High and low thrust hybrid rocket propulsion systems involving combinations of chemical, nuclear, thermal and electric propellants for interplanetary flights 21 p3869 A70-42042

Spacecraft electric propulsion system performance, discussing exhaust velocity optimization 21 p3869 A70-42043

Nuclear rocket engines design and performance, discussing fission reactors, radiation leakage and shielding, heat transfer, etc 21 p3870 A70-42044

Quasi-hybrid rocket engines with solid propellant and liquid hydrogen injection, discussing performance in comparison with other propellant systems 22 p4089 A70-42498

Aircraft flight propulsion systems performance improvement via materials technology for gas turbine engine components 22 p4057 A70-43573

Analytical evaluation of secondary flow injection effects on rocket engine performance including cold flow and simulated hot flow data [AIAA PAPER 69-473] 23 p4233 A70-44516

Space vehicle for testing electric propulsion systems in space, powering by cluster of six electrostatic ion motors regulated by automatic thrust control 23 p4259 A70-44616

Iantar 1 automatic ionospheric laboratory flight tests results, investigating Ar ion engine performance 23 p4264 A70-45009

PROPULSIVE EFFICIENCY

NT PROPELLER EFFICIENCY

Propulsion efficiency in air and in space measured according to relativity concepts, including electric field inertia explanation 02 p0355 A70-12364

Experimental data to define idealized thruster discharge model power efficiency limits, computing probabilities for excitation, ionization, propellant escape and wall interception of ions [AIAA PAPER 70-177] 06 p1131 A70-18034

Colloid engine efficiency operating with pulsed positive voltages and square wave and sinusoidal voltages [AIAA PAPER 70-178] 06 p1132 A70-18158

Space electric rocket test /SERT/ II thruster system, discussing flight worthiness and mercury bombardment discharges [AIAA PAPER 67-700] 07 p1364 A70-19701

Supersonic and subsonic air breathing engines, discussing single and ducted fan turbojets, ramjets, turboprop engines and land based gas turbine engines 12 p2291 A70-28071

Propulsive efficiency definition deficiencies for bypass jet engines 15 p2791 A70-32769

Turbofan engine gross thrust dependence on nozzle pressure ratio and simulated flight Mach number, considering altitude chamber test data [AIAA PAPER 70-612] 16 p2969 A70-33608

Submillipound mercury electron bombardment ion thruster efficiency, noting cathode pole piece, baffle position and geometry influence on ion chamber performance [AIAA PAPER 70-616] 16 p2969 A70-33612

Helicopter engine rotor matching for tip propulsion efficiency, comparing with conventional shaft drive propulsion [ASME PAPER 70-GT-68] 18 p3215 A70-36842

Thrust measurements on pulsed vacuum-arc thruster, comparing specific impulse and efficiency with exhaust velocity measurements by ion collecting double probes [AIAA PAPER 70-1146] 20 p3567 A70-40207

Mercury electron bombardment thruster, measuring effect of geometry and magnetic field inside pole piece region on discharge losses and propulsion efficiency [AIAA PAPER 70-1088] 20 p3693 A70-40247

Pulsed coaxial plasma accelerator efficiency, examining high capacitance and axial propellant pressure gradients [AIAA PAPER 70-1085] 20 p3693 A70-40250

Thermodynamic-kinetic analysis of fluorine/lithium/hydrogen tripropellant combustion efficiency, discussing liquid metal atomization, firings, facility and thrust chamber [AIAA PAPER 68-618] 23 p4232 A70-44512

Single stage reusable ballistic space shuttle, featuring minimum payload mass ratios and high propulsive efficiency 23 p4262 A70-44686

Optimal propeller selection for given aircraft and engine designs, considering aerodynamic and acoustic characteristics 24 p4393 A70-45441

Radial inflow turbine optimum design geometry, calculating nozzle and rotor geometrical parameters efficiency 24 p4395 A70-46012

PROPYL COMPOUNDS

Combustion products of 280-400 C oxidation of ethyl acetate, methyl propionate and i-propyl acetate 21 p3864 A70-40882

Cellular irradiation sensitivity in tissue culture modified by propyl gallate as radical reactions inhibitor 21 p3767 A70-42242

PROPYLENE

Reactor surface and propylene role during vapor phase partial oxidation of propane in continuous flow tubular reactors 02 p0250 A70-12017

Propylene carbonate applications in nonaqueous electrolyte batteries, describing impurities identification by gas-liquid chromatographic analysis 12 p2164 A70-27069

Ethylene-propylene elastomers compatibility with hydrazine determined under ambient conditions from gas evolution rate by catalytic decomposition 13 p2472 A70-28669

PROSPECTING

U EXPLORATION

PROSTHETIC DEVICES

NT ARTIFICIAL EARS

Book on engineering in heart and blood vessels stressing technological aspects of artificial internal organs 06 p1001 A70-17649

Friction, wear and surface evaluation of alloys as bearing materials in prosthetic devices 09 p1690 A70-22044

PROTECTION

NT ACCELERATION PROTECTION

NT CIRCUIT PROTECTION

NT CORROSION PREVENTION

NT EYE PROTECTION

NT METEOROID PROTECTION

NT RADIATION PROTECTION

NT RADIATION SHIELDING

NT SOLAR RADIATION SHIELDING

NT THERMAL PROTECTION

PROTECTIVE CLOTHING

NT HELMETS

NT PRESSURE SUITS

NT SPACE SUITS

Thermal protection rating systems for clothing fabrics based on pain and blister effects in human skin 03 p0438 A70-14064

Physiological training programs and equipment for life support in transports, discussing changes in protective helmet and quick donning harness 06 p1002 A70-17708

Flotation dummy to simulate unconscious survivors characteristics analyzed for life jacket design 07 p1218 A70-19004

Fire resistant protective flight clothing program for USN airmen, presenting accident case histories 07 p1218 A70-19013

Lead azide detonation hazards and resulting pressure waves, evaluating protective glove material by dynamic pressure measurements 12 p2289 A70-27665

Protective clothing for personnel handling toxic and corrosive liquid propellants in hot climatic conditions at Guyana Space Center 12 p2179 A70-28043

Ergonomic and medicomilitary aspects of human adaptation to cold environments, discussing metabolic

and physical protective reactions, clothing and personnel selection

Cooling hood effect on physiological responses to work in hot environment, discussing body temperature
16 p2850 A70-34346
17 p3031 A70-35422
Near fatal crash in T-33 aircraft, discussing protective clothing, seat harnesses, bodily position and mental attitude
23 p4153 A70-44497

PROTECTIVE COATINGS

NT ANODIC COATINGS
NT CERAMIC COATINGS
NT PRIMERS [COATINGS]

Radiator selection for manned spacecraft, considering thermal coating degradation, structural design, micrometeorite protection, plume impingement, reliability and fabrication
[AIAA PAPER 69-1070] 01 p0215 A70-10631
Conflicting requirements for reflection reduction, thermal stabilization and radiation protection satisfied by three layer coatings on Si photocells
01 p0159 A70-10768

Annular metal specimens protection against oxidation during high temperature relaxation testing by covering specimens with Al powder thinned with alcohol
01 p0121 A70-11109

Silicide, aluminide and boride coatings transition temperature holdability, considering nitridation/oxidation protection for Cr alloys
01 p0122 A70-11241

Cr diffusion coating influence on fatigue life of Fe and steel, discussing residual stress measurement technique
02 p0320 A70-12848

Heat resistant coatings in high temperature gas flow, studying external layer deformation kinetics during shrinkage
03 p0483 A70-13250

Oxidation and sulfidation resistant diffusion coatings for superalloys, discussing processing methods, composition, properties and application
[SAE PAPER 690479] 03 p0509 A70-13266

Airline aircraft finishes for protection against corrosion, air pollution, discussing paint application and polyurethane technology
03 p0497 A70-14053

High temperature coatings in industrial, military and space applications, noting use in metal melting and working, furnace protection, propulsion systems, rocket engines, etc
04 p0709 A70-15630

X ray metallography methods applied to high temperature protective coating development, refractory alloys strengthening and metal fatigue studies
04 p0711 A70-15706

Paint technology findings and recommendations for airline aircraft surface finishes emphasizing use of polyurethanes
05 p0869 A70-16106

Soviet collection of papers on inorganic glassy coatings and materials
05 p0870 A70-16591

Heat resistant silicate enamel coatings to protect steels and alloys against high temperature gas corrosion, studying properties by various methods
05 p0872 A70-16600

Electrode surface bismuth coating selected for reducing electrostatic analyzers photocurrents
05 p0851 A70-16734

Heat resistant enamel coatings effect on vibration damping of cast steels for turbine blades
05 p0868 A70-17050

Metals mechanical properties with inorganic heat resistant coatings between 1900-2300 K in oxidizing medium, describing facility based on solar furnace
05 p0875 A70-17069

Computer optimization of spacecraft optical coatings for temperature control, using finite element analysis and matrix inversion
[AIAA PAPER 69-979] 06 p1172 A70-17180

Heat transfer boundary conditions determination in studying heat protective coatings effectiveness, discussing measurement methods for stagnation temperatures and heat fluxes from exhaust gases
06 p1173 A70-17662

Diffusion layer and protective oxide composition changed to increase chrome plated Mo heat resistance
06 p1089 A70-17742

Aluminosilicate coatings for increased Ni-Cr alloys heat resistance due to silicon properties
06 p1089 A70-17743

Nonflammable coatings for polycarbonate to meet NASA safety standards, discussing alkali silicate and arc plasma deposition of glass and ceramic oxide
[WSCI PAPER 69-34] 06 p1092 A70-17977

Coating and coating processes for superalloys in hot section components of gas turbine engines for aircraft, industrial, marine and vehicular applications
07 p1362 A70-18929

Silicide-coated columbium alloys reuse capabilities under flight conditions, considering coating local damage and emittance
[AIAA PAPER 70-279] 07 p1315 A70-20388

Heat transfer from inner wall of annular ducted cylindrical body cooled by liquid nitrogen, discussing effects of Teflon, asbestos and vaseline coating and thickness effects
08 p1596 A70-20577

Performance characteristics of low density epoxy-water emulsion corrosion resistant coating for nonferrous alloys
08 p1526 A70-20648

Epoxy-fenolic coatings effect on fatigue durability of bent steel samples
08 p1587 A70-21075

Thermal control coatings as solar reflectors for spacecraft heat dissipation
08 p1527 A70-21357

Passive film on stainless steels in boiling nitric medium studied by recording constant potential on sample subjected to polarizations
09 p1700 A70-22010

Nondestructive tests for diffusion-formed refractory alloy coatings used as oxidation protection for hypervelocity spacecraft and reusable systems
09 p1692 A70-22679

Silicon oxide films coated satellite aluminum surfaces solar absorptivity and thermal emissivity, noting suitability as temperature control coatings
09 p1613 A70-23514

Abradable and abrasive types thermal spray coatings application to jet engine parts
10 p1893 A70-23856

Consumable protective coat (silastene) application to reentry models to eliminate metallic pollution in hotshot wind tunnels for spectroscopic analysis
10 p1825 A70-24548

Insulation foils and surface coatings thermal properties effect on radiation properties for spacecraft thermal control systems
10 p1951 A70-24863

Nonisothermal dielectric coating on conductor surface, analyzing temperature distribution effect on thermal emission characteristics
11 p2148 A70-25975

Radiation stable refractory oxides in white spacecraft thermal control coatings, discussing photocatalysis application to degradation analysis
11 p2067 A70-26364

High purity pinhole free films (parylene) applicability as barrier coating to keep semiconductor surface free from moisture, ions and contaminants
11 p2099 A70-26395

Thermal coated extendable boom for space applications, describing construction and vacuum metalizing technique
12 p2242 A70-27266

Protective diffusion coatings for jet engine gas path parts, discussing repair procedures
[SAE PAPER 700332] 12 p2254 A70-27463

Inhibitive elastomeric sealing compounds and coating systems preventing aluminum alloy corrosion in aircraft
13 p2433 A70-28778

Diffuse coatings effect on strength characteristics and corrosion resistance of steels, analyzing structure, thickness and purity of surface layers
13 p2433 A70-28888

Preoxidation treatment alleviating silicide pest in protective coatings for refractory metals, discussing effectiveness against high temperature oxidation
13 p2434 A70-29082

Protective coatings with Si-Zr alloys for graphite, discussing wettability, spreading kinetics and impregnation
13 p2439 A70-29503

Corrosion resistant paint systems for aircraft structural parts under severe environmental conditions simulated in carrier test stand
14 p2598 A70-31292

Protective coatings for silicon photosensitive elements to reflect incident energy at wavelengths not participating in conversion into electricity
15 p2677 A70-31599

Surface recombination centers protecting against discoloration of thermal control coatings due to chemical changes induced by photoproduced holes and electrons in oxide pigments
[AIAA PAPER 70-830] 16 p2940 A70-33935

Metal oxides thermal control coatings, investigating mechanisms of interaction between constituents by luminescent technique
[AIAA PAPER 70-832] 16 p2940 A70-33936

UV irradiation effects on ZnO used as pigment for spacecraft thermal control coatings
[AIAA PAPER 70-829] 16 p2940 A70-33937

Space erectable boom with interlocked seam, perforations and coatings to provide torsional rigidity and thermal stability
16 p2986 A70-34143

Wear and fatigue of Ti-Mo-Al-Sn-Si (Hylite 50) alloy with resistant Mo or Cr coatings
17 p3099 A70-34447

Oxidation and atmospheric contamination protective coatings for high temperature materials, using burner ring tests
17 p3127 A70-34519

Spacecraft shape and thermal coating pattern optimization by computer program
17 p3178 A70-35251

Collection of papers on protective coatings on metals
17 p3101 A70-35390

Ni alloys with protective coatings for gas turbine blades, testing corrosion resistance in diesel fuel combustion products with intermittent salt water sprays
17 p3125 A70-35394

Collection of papers on protective coatings on metals, Volume 2
17 p3102 A70-35403

Diffusion during high temperature exposure of protective coatings on Mo, noting compact layers and carbide forming elements effect on thermal stability
17 p3125 A70-35404

Al effects on B and Cr diffusion in protective coating on Cr-Ni heat resistance alloy, noting thermochemical kinetics for homogeneous layers
17 p3125 A70-35405

Heat resistance evaluation of Zr S6-K alloy subjected to multicomponents surface diffusion
17 p3125 A70-35407

Temperature dependence of materials with protective coatings, emphasizing mechanical properties of Mo with various diffusive coatings
17 p3126 A70-35716

Concorde engine bay thermal insulation combining stainless steel foil and polytetrafluorethylene film, considering noise level, engine fire conditions and molten Ti globules penetration
18 p3346 A70-36345

Rocket engine with Teflon lined combustion chamber, considering design criteria and tests
18 p3301 A70-36662

Relative sensitivities of polyethylene shielded net radiometers, noting role of reflective white paint partial covering
18 p3261 A70-37087

Heat resistant coatings in high temperature gas flow, studying external layer deformation kinetics during shrinkage
19 p3428 A70-38468

Metallic shell with passive thermal protection coating, solving boundary value problem for high temperature heating with simplified mathematical model
20 p3739 A70-40296

Surface contamination and degradation effect on reflectance of evaporated vacuum UV mirrors and temperature control coatings under simulated space environments
21 p3842 A70-40815

Spacecraft thermal control coatings scale models, discussing temperature errors due to energy transport along surfaces
21 p3951 A70-41874

Molybdenum trisilicide-tantalum trisilicide and molybdenum trisilicide-tungsten trisilicide interdiffusion for molybdenum disilicide protective coating on Ta and W surfaces
21 p3840 A70-42056

Book on plastic coatings for electronics covering chemical structure, properties, applications, manufacturing technology, etc
22 p4058 A70-42455

Helicopter gas turbine engine protection against sand and dust erosion using particle separators, screens and coatings
[SAE PAPER 700705] 22 p4090 A70-42671

Sand and dust erosion reduction in gas turbine engines by coatings, sleeves and inserts
[SAE PAPER 700706] 22 p4090 A70-42672

Strain rate sensitivity and stress waves effects on dynamic response and adhesion failures of rain erosion resistant coatings
22 p4059 A70-43102

Thermochemical method for directional crystallization of wear-resistant alloy coatings on machine parts
23 p4205 A70-44043

Al alloy sheets with multicolor protective coatings, measuring surface temperature under solar radiation
24 p4428 A70-45434

Pyrolytic carbide protective coating deposition from gaseous phase on spherical particles in boiling layer
24 p4350 A70-46330

High temperature solar furnace for investigating heat resistant protective coatings thermal stability
24 p4350 A70-46331

Diffusive carbon redistribution in Mo during interaction with Ni and Cr protective coatings
24 p4364 A70-46334

Molybdenum disilicide and aluminum oxide coating sealing heat resistance tests
24 p4364 A70-46341

PROTECTORS

NT EAR PROTECTORS

Radar transmitters modulating circuits protection with microsec rapidly by power elimination, discussing electronic switches
21 p3792 A70-41987

PROTEIN METABOLISM

NT LIPID METABOLISM

Protein metabolism of mice exposed to compression of air-oxygen mixture containing 27 percent oxygen, showing relationship to food intake

01 p0028 A70-11363

Nucleic acid and protein synthesis dynamics in rat brain and heart during adaptation to high altitude hypoxia

07 p1209 A70-19518

Prolonged hypodynamia effect on human nutritional habits and protein metabolism, noting decrease in energy requirement and body weight

10 p1814 A70-24675

Altitude hypoxia adaptation effects on brain protein and RNA synthesis in rats, noting increase in memory resistance to environmental stress effects

17 p3030 A70-35359

Hypokinesia effects on rats protein synthesis rates, determining body and organ weights, muscle tissue nitrogen content and transaminase activity

20 p3575 A70-40187

Brain cortex protein metabolism alterations induced by anticipation stress and ACTH in rats

24 p4301 A70-45999

PROTEINOIDS

Membrane-like properties of synthetic proteinoid microparticulate systems, considering catalytic activities, size and ultrastructure

16 p2847 A70-33029

PROTEINS

NT ADENOSINE DIPHOSPHATE [ADP]

NT ADENOSINE TRIPHOSPHATE [ATP]

NT ALBUMINS

NT CARBONIC ANHYDRASE

NT CARBOXYHEMOGLOBIN

NT COENZYMES

NT FIBRIN

NT FIBRINOGEN

NT GAMMA GLOBULIN

NT GLOBULINS

NT KERATINS

NT LIPOPROTEINS

NT NUCLEOTIDES

NT OXIDASE

NT OXYHEMOGLOBIN

NT PEPTIDES

NT PROTEINOIDS

NT PYRIDINE NUCLEOTIDES

Tissue protein changes under visible and UV radiation noting denaturation, chemical bonds, protein configurations, clinical disease patterns, etc

01 p0022 A70-10856

Diet and feeding method effects on food intake and plasma amino acid concentrations of rats fed low protein diet with amino acid imbalance

02 p0231 A70-11707

Separate gamma irradiation effect of enzyme and hemoglobin-albumin-globulin substrates on proteolysis dynamics

03 p0419 A70-13308

Biophysics research, discussing supramolecular biological structures, synthesis of proteins, nucleic acids and genetic codes, biological membranes, coding in nervous system, etc

03 p0420 A70-13491

Whole body microwave irradiation effect on chromosomes and protein synthesis in Chinese hamsters

06 p0998 A70-17203

Hepatic polysome profiles and tyrosine transaminase activity daily rhythms in rats, studying dietary protein role

06 p0997 A70-18402

Flavor sweetening preference in high protein and high fat diets, basing human subjects experimental range on choice of formulas

07 p1216 A70-18948

LF ultrasound not producing irreversible denaturation of blood serum proteins but capable of modifying electrophoretic properties

07 p1206 A70-19470

Radial immunodiffusion for serum proteins quantitation adapted to capillary blood and compared with results for venous blood

07 p1214 A70-19932

Unicellular algae protein diet effects on animal and human enteric microflora composition

09 p1615 A70-22087

Fasting and postprandial serum amino acid patterns of human males fed protein-free or protein-sufficient diets

09 p1621 A70-23399

Biologically active fragments formation and functions in organism following liberation from inactive proteins via limited proteolysis

10 p1811 A70-24390

Butyl esters separation from protein amino acids, using acid washed Chromosorb W of various mesh sizes

10 p1828 A70-24397

Dietary protein and yeast RNA levels effect on uric acid metabolism in normal man

11 p1987 A70-26002

Hippocampus nerve cells protein fractions synthesis in rats, noting relation to learning process during transfer of handedness

12 p2172 A70-28217

Human gamma globulin and binary/ternary protein structures conformation transitions studied by UV difference spectra

12 p2173 A70-28346

High altitude effects on total protein content and composition in rats blood serum

13 p2352 A70-29346

Amino acid composition of protein in blue green algae *Stratostocot Linckia*

14 p2540 A70-30158

Xenon absorption by myoglobin at various temperatures and pressures, presenting evidence for H₂Xe formation

14 p2545 A70-30927

Unicellular algae protein diet effects on animal and human enteric microflora composition

15 p2685 A70-32683

Diffusion coefficient of dissolved oxygen in blood proteins aqueous solutions

15 p2686 A70-32848

Antigens existence shared by human blood serum and proteins of erythrocyte stroma established through RAHS absorption by stroma and subsequent micrommunoelectrophoresis of serum

15 p2687 A70-32900

Skeletal muscle proteins fractional composition in white rats during hypokinesia, noting water content changes

17 p3030 A70-35356

Melatonin or water deprivation effects on pituitary serotonin content in rats

17 p3034 A70-35625

Hydration and lipid-protein ionic interaction in stearic acid monolayers during conformation of poly-L-lysine films

19 p3373 A70-37840

Protein solutions and cell cultures changes by ruby and Nd lasers radiation, noting threshold energy

20 p3579 A70-39419

T4 phage proteins radioisotopic examination, determining quantitative analysis and molecular weight by autoradiography

20 p3583 A70-40325

Protein catabolism increase during high altitude exposure to hypoxia in rats, noting amino acid incorporation into tissue proteins

22 p3967 A70-42459

Gas-liquid chromatography studies of direct esterification of protein amino acids to n-butyl esters

22 p3984 A70-43525

Catalytic activities of thermal polyanhydro-alpha-amino acids for modeling enzymes and prebiotic protein

24 p4310 A70-45346

PROTON BEAMS

Gamma ray background near proton synchrotron beam degrader at NASA-LRC Space Radiation Effects Laboratory

02 p0275 A70-12268

Elastic and inelastic scattering of proton beams from magnesium and silicon isotopes, using optical model

04 p0723 A70-15637

PPi bursts interpreted as proton beams cyclotron instability in geomagnetic field

07 p1277 A70-20439

Ionizer design for hydrogen atom beam ensuring storage of polarized protons, using electron beam for ionization

09 p1732 A70-22846

Pc-1 pulsation production by Cerenkov emission of proton beam oscillating along magnetic field line

19 p3417 A70-38590

PROTON BELTS

Satellite radiation dose rates in inner Van Allen belt, correlating calculated and measured rates with proton environment model

06 p1134 A70-17264

Satellite observational data on time history of inner radiation belt /October 1963-December 1968/

09 p1746 A70-23488

Proton injection into radiation belt, comparing solar neutron decay /SND/ and cosmic ray albedo neutron decay /CRAND/ as proton sources

09 p1746 A70-23489

Topside sounder profiles interpretation, discussing ionosphere-protonosphere dynamic coupling

13 p2398 A70-29199

Proton distribution in radiation belt inner zone from radial diffusion addition to cosmic ray produced albedo-neutron decay and atmospheric collision loss

17 p3150 A70-34644

High energy radiation belt proton flux time dependence at low altitudes, examining atmospheric density influence

20 p3620 A70-39340

Cyclotron instability of high energy protons in magnetosphere with refraction of growing Alfvén waves

23 p4237 A70-44073

PROTON DAMAGE

Solar cell degradation by proton damage in synchronous orbit studied on LES-6 satellite [AIAA PAPER 70-600]

11 p2119 A70-25430

Low energy proton damage to silicon solar cells on INTEL-SAT II, F-4 and ATS-F-1, considering exposure area and radiation protection

15 p2677 A70-32419

Mice intestinal epithelium, investigating high energy protons irradiation effect on cells

23 p4149 A70-45028

PROTON DENSITY [CONCENTRATION]

Cosmic rays sudden intensity increases during proton flares of 28 January 1967 and 7 July and 2 September 1966, plotting proton density vs pressure

07 p1374 A70-20445

Trapped protons population explanation by combined pitch angle scattering and radial diffusion across L shells

13 p2484 A70-30097

HEOS 1 low energy proton measurements in interplanetary space, discussing particle direction during solar event and anisotropy time history

19 p3495 A70-37505

PROTON ENERGY

Primary cosmic ray proton energy spectrum determined using balloon-borne ionization spectrometer and spark chamber

02 p0360 A70-12844

High energy primary cosmic ray and proton spectra measurements from Proton satellites

03 p0555 A70-13036

Primary protons energy estimated from energy ratio with maximum extremal distribution of electron numbers in lower half of atmosphere

03 p0527 A70-13054

IMP F solid state detector data on 13 day solar proton event at low energy, considering cosmic rays anisotropy and interplanetary magnetic field

04 p0738 A70-14512

Very high energy cosmic rays disintegration and energy degradation by intense blue shifted photon fields of supernovae quasars and pulsar models

04 p0742 A70-15300

Response variation and detection efficiency of funnelled channel electron multipliers for low energy protons and Ar ions

06 p1021 A70-17623

Local time dependence of geomagnetic cut-offs for solar protons in 0.52-4.0 Mev range from satellite observations

06 p1136 A70-18529

High energy protons irradiation biological effects, noting qualitative and quantitative variations in radiation disease symptoms

07 p1208 A70-19508

Solar protons captured in earth dipole trap, discussing conditions for nonadiabatic escape

07 p1374 A70-20442

Solar modulation of low energy galactic cosmic ray protons, proposing diffusion-convection model with time dependent diffusion coefficient

08 p1561 A70-20906

Low energy proton distributions in interplanetary medium, correlating intensities with main-phase geomagnetic storm development

08 p1562 A70-21376

Electron and proton temperature differential near earth bow shock determined from plasma probe measurements by Vela 4B satellite

09 p1670 A70-23486

Low energy protons omnidirectional intensity contours in outer radiation zone at magnetic equator

09 p1747 A70-23491

Satellite-borne scintillation spectrometers for medium and high energy electron and proton measurements

10 p1931 A70-24315

High energy protons irradiation biological effects, noting qualitative and quantitative variations in radiation disease symptoms

11 p1987 A70-26107

Cosmos 137 proton spectra data obtained in inner radiation belt agreeing with Relay 1 data

11 p2106 A70-26786

Midlatitude upper atmospheric low energy proton intensity obtained from meteorological rocket data

12 p2296 A70-28265

Time comparative low energy proton measurements in inner radiation belt by Rubis rocket with detector telescopes and omnidirectional counters

13 p2475 A70-28572

Low energy protons penetration into magnetosphere between forbidden regions, using model of constant electric field with charge exchange as loss mechanism

13 p2477 A70-29183

Low energy protons in outer trapping region, discussing time variations and source and transport mechanisms

13 p2484 A70-30095

Low pressure nitrogen and air spectra excitation by low energy proton bombardment, using spectroscopic, photometric and microphotometric analyses

14 p2619 A70-30653

Fine structure of geomagnetic Pc 1 micropulsations by cyclotron instability due to anisotropic energetic proton velocity

19 p3410 A70-37334

Energy loss of fast protons in cold Li plasma confined by magnetic field, using precession around axis to develop large interaction length

19 p3474 A70-37364

Low energy solar protons temporal and spatial variations in magnetosphere by data comparison from polar orbiting satellite and Explorers 33 and 34

19 p3494 A70-37486

Cosmic ray electron and low energy proton fluxes by satellite-borne detector during solar flare of 25 February 1969

19 p3496 A70-37507

Solar protons distributions in 1-30 MeV range over northern polar cap during 25 February 1969 solar event by ESRO 1 satellite

19 p3496 A70-37508

Low energy electron and proton measurements by ESRO 1 satellite, discussing electron spectra, auroral zones and proton precipitation

19 p3412 A70-37516

Low energy solar protons observation by Esro 1 satellite during solar flare of 25 February 1969

19 p3497 A70-37520

Primary cosmic ray proton energy spectra from satellite observation, presenting spectrum approximating function

19 p3510 A70-38153

Stratospheric perturbation sources from atmospheric circulation as function of season, geographic latitude and altitude, suggesting high energy protons in atmosphere

20 p3618 A70-39183

Fermi momentum upper limit for universe neutrinos in cosmic ray propagation, determining maximum proton energy

20 p3700 A70-39592

Low energy solar protons penetration, examining geomagnetic cutoff latitude during magnetically disturbed period

21 p3881 A70-41077

Ionization rate and electron density height profiles for typical auroral proton energy spectrum, noting radio noise absorption, sporadic E and radio aurora

22 p4024 A70-43307

Proton energy angular distribution measurement by OV2-5 research satellite confirming model of shell splitting in geomagnetic field

23 p4236 A70-43832

Soft particle spectrometer in Isis-1 satellite using electrostatic deflection for differential energy spectra measurements for electrons and protons

23 p4197 A70-44468

Energy dependence of equatorial pitch angle distribution for protons trapped in radiation belt, based on adiabatic theory and observational data

23 p4192 A70-44923

PROTON FLUX DENSITY

Low energy proton flux in neighborhood of Moon measured by Luna 12 satellite indicating magnetized plasma region effect on burst

01 p0172 A70-11493

Low energy solar proton flux propagation model in interplanetary medium based on satellite data beyond earth magnetosphere

04 p0737 A70-14434

Satellite HEOS-1 S 73 experiment launched during solar maximum to determine flux and energy distribution of solar wind positive component

05 p0900 A70-16077

Redistribution of geomagnetically trapped 55 Mev protons by Starfish nuclear explosion, discussing hydromagnetic wave interactions and multiple reflections from magnetic field inhomogeneity

06 p1137 A70-18531

Solar particles penetration to lower ionospheric heights at low latitudes indicated from proton flux measurements by Explorer 33 satellite and Calcutta station

07 p1366 A70-18849

Solar proton flares radiometric measurement on-board Molniya 1 satellite, detecting intensities in outer regions of magnetosphere

07 p1366 A70-19428

Proton concentrations, magnetic field strength and temperatures distribution in interplanetary plasma flows as function of latitudinal distance from center of active region

07 p1391 A70-20420

Electron and proton precipitation measurements in auroral zone by soft particle spectrometer in ISIS-1 satellite

08 p1560 A70-20501

Plasma instabilities in solar wind for frequencies near proton gyrofrequency, driving instabilities by electron and proton thermal anisotropies

08 p1561 A70-21261

Solar proton flux increases associated with sudden commencements observed by geostationary ATS-1 satellite

08 p1562 A70-21378

Heliocentric longitude intensity profiles of protons associated with solar flare of 5 February 1965, discussing data from Mariner 4 and IMP 2

09 p1746 A70-23480

Extraterrestrial ring current proton intensities asymmetric increases in outer radiation belt during magnetic storms

09 p1747 A70-23490

Low energy protons omnidirectional intensity contours in outer radiation zone at magnetic equator

09 p1747 A70-23491

Midlatitude upper atmospheric low energy proton intensity obtained from meteorological rocket data

12 p2296 A70-28265

Low energy solar proton flux propagation model in interplanetary medium based on satellite data beyond earth magnetosphere

13 p2475 A70-28459

Time comparative low energy proton measurements in inner radiation belt by Rubis rocket with detector telescopes and omnidirectional counters

13 p2475 A70-28572

Trapped and polar proton and electron flux observations during 9 June 1968 magnetic storm

13 p2482 A70-30072

High energy proton flux variations in inner belt during solar cycle and magnetic storm, using satellite and balloon measurements

13 p2483 A70-30091

Trapped alpha particle and proton spectra from satellite measurements, considering magnetosphere injection

13 p2484 A70-30093

Trapped protons population explanation by combined pitch angle scattering and radial diffusion across L shells

13 p2484 A70-30097

X ray and proton flux measurement during solar flare of 29 September 1968 by balloon-borne detectors

14 p2633 A70-31310

Quiet time proton and alpha particle flux and differential energy spectra measured by cosmic ray detectors on OGO 3 satellite

15 p2793 A70-31795

German monograph on artificially accelerated proton measurements for ionization calorimeter calibration and cosmic radiation energy spectrum analysis during balloon flight

17 p3081 A70-34572

Impulsive proton flux precipitation increase during auroral breakup observed by rocket

18 p3245 A70-36021

Charge source density during interaction between atmosphere and electron/proton fluxes at prescribed boundary parameters

18 p3307 A70-36178

Solar proton flares radiometric measurement on-board Molniya 1 satellite, detecting intensities in outer regions of magnetosphere

18 p3309 A70-36902

Proton spectra and time history in interplanetary space during solar flare by satellite observation, investigating particle flux by shock waves

19 p3495 A70-37503

Cosmic ray electron and low energy proton fluxes by satellite-borne detector during solar flare of 25 February 1969

19 p3496 A70-37507

High energy radiation belt proton flux time dependence at low altitudes, examining atmospheric density influence

20 p3620 A70-39340

Solar proton intensity measurement during flare by satellite Proton 3 apparatus

20 p3700 A70-39729

Altitude spectrum of ion formation in interaction of proton flux with atmosphere, using Bragg dissipation function

21 p3878 A70-40846

PROTON IMPACT

Note on Bell-Kingston paper on Born total and differential cross sections for proton impact ionization of He

08 p1548 A70-21501

Inner-shell ionizations by proton impact calculated for cross section using impulse approximation model, comparing results with Born approximations

09 p1732 A70-22781

Electron and proton impact excitations of He using Born two and four state versions of impact parameter treatment

11 p2086 A70-25834

K shell X ray production by proton impact compared with binary encounter impulse approximation

14 p2620 A70-31362

Semiclassical collision theory for computing fine structure proton impact excitation rates and cross sections for positive ions, presenting excitation rate tables

14 p2652 A70-31383

PROTON IRRADIATION

Erythropoietic response in anesthetized dogs subjected to sublethal whole-body proton irradiation fol-

lowed by hypoxic hypoxia, discussing test procedure and results

01 p0027 A70-11300

Natural immunity characteristics in dogs after proton exposure, analyzing integumentary bactericidal activity, oral microflora and neutrophil phagocytic activity

03 p0423 A70-13707

Temporary mitotic activity depression with decrease in aberrant mitoses observed in mice in testicular epithelium cells after exposure to 50 Mev proton doses

03 p0423 A70-13708

Si-NP solar cell damage coefficient dependence on energy of irradiating electrons and protons, determining diffusion length from short circuit current

06 p1127 A70-18504

High energy protons irradiation biological effects, noting qualitative and quantitative variations in radiation disease symptoms

07 p1208 A70-19508

Micrococcus radiodurans and Sarcina flava radiation resistance from proton irradiation tests in carbonaceous chondrite Migei

08 p1441 A70-20550

Absorption spectra of n-type GaAs before and after proton irradiation, discussing dependence on wavelength

09 p1739 A70-22753

Therapeutic power of bone marrow transplanted from mice earlier irradiated by high energy protons into newly irradiated mice

09 p1619 A70-22814

Natural immunity characteristics in dogs after proton exposure, analyzing integumentary bactericidal activity, oral microflora and neutrophil phagocytic activity

11 p1985 A70-25507

Temporary mitotic activity depression with decrease in aberrant mitoses in mice intestinal epithelium cells after exposure to 50 Mev proton doses

11 p1985 A70-25508

F region magnetic disturbances due to low energy solar plasma penetration during proton bursts

11 p2104 A70-25535

High energy protons irradiation biological effects, noting qualitative and quantitative variations in radiation disease symptoms

11 p1987 A70-26107

Frenkel pairs and interstitial hydrogen atoms observed in thin silver films after proton bombardment

12 p2253 A70-27209

Radiation defects distribution in GaAs during proton irradiation, noting distribution dependence on proton energy and integral flux

12 p2287 A70-27488

Preplanetary matter irradiation by solar particles, noting isotopic abundances for evidence of nucleosynthesis induced by proton and alpha bombardment

13 p2486 A70-28619

Proton and electron irradiation producing oxygen vacancies in silicates, minerals and rocks, indicating similar processes in lunar surface materials erosion and transport

13 p2395 A70-28908

Electron paramagnetic resonance of Mn ions in single crystal and powder forsterite, testing heat treatment and proton irradiation effect on ordering

16 p2960 A70-33008

Satellite radiation dosage in space proton and electron environment

19 p3511 A70-38490

Earth surface pressure changes related to PCA of high energy protons

20 p3695 A70-39187

Proton irradiation effects on dogs with partial body protection

20 p3575 A70-40192

F region magnetic disturbances due to low energy solar plasma penetration during proton bursts

21 p3882 A70-41285

Apollo 11 rocks red luminescence and blue thermoluminescence under proton bombardment, discussing energy efficiency

21 p3913 A70-41644

Apollo 11 rocks spectral reflectance and albedo before/after proton irradiation and vitrification, investigating color differences for lunar surface dark and bright areas

21 p3913 A70-41645

Charge transfer of protons at electron capture in excited states, using proton beam and various target gases

23 p4221 A70-44209

PROTON MAGNETIC RESONANCE

Fine structure of excited P states of Li measured for magnetic fields in proton NMR frequency using level crossing and Zeeman effect

07 p1346 A70-20239

PROTON RESONANCE

Proton cyclotron echoes in topside ionograms from Alouette 2 satellite

13 p2396 A70-29092

Auroral protons and resonant concept of substorm, eliminating discrepancy between hydrogen emission spectroscopic and direct measurements
18 p3307 A70-36177

PROTON SATELLITES

NT PROTON 2 SATELLITE
NT PROTON 4 SATELLITE

Proton satellites measurements reconciliation with diurnal stellar variation data and cosmic rays origin models
06 p1135 A70-17885

PROTON SCATTERING

Elastic and inelastic scattering of proton beam from Ne 20 measured for cross sections to interpret polarization data
04 p0723 A70-15636

Redistribution of geomagnetically trapped 55 Mev protons by Starfish nuclear explosion, discussing hydromagnetic wave interactions and multiple reflections from magnetic field inhomogeneity
06 p1137 A70-18531

Proton-deuteron elastic large angle scattering cross sections, noting backward peak consistent with baryon exchange mechanism with resonance transfer
07 p1345 A70-20198

Cross sections measured for symmetric $p, 2p$ reactions on deuterium and He, discussing nonsymmetric $p, 2p$ events in He
08 p1548 A70-21233

High energy proton-He 3 elastic scattering cross section measurement, comparing result with Glauber model calculation
13 p2456 A70-29459

Ionic temperature difference from Arcicoba data indicated in Injun 3 and Alouette 1 sonograms of proton whistlers propagation time, noting Doppler shift role
13 p2372 A70-29928

Measuring instrument for total cross section of proton elastic scattering during sigma R reactions
16 p2908 A70-33210

Coupled channel calculation of inelastic proton scattering from Ne 20 using Hartree-Fock wave functions
17 p3137 A70-34517

Background gamma ray observations attributed to decay of pi-mesons produced by extragalactic cosmic ray protons collisions, noting radiation sources age
21 p3877 A70-40703

PROTON TELESCOPES

U PARTICLE TELESCOPES

PROTON 2 SATELLITE

Proton 2 satellite orientation and motion about center of mass determined from telemetric data analysis under aerodynamic moment
11 p2128 A70-26783

High energy primary gamma quanta intensity limits from Proton-2 and Cosmos-208 measurements
19 p3502 A70-38092

PROTON 4 SATELLITE

Soviet space activities /1969/, discussing Soyuz orbital flights, Venera probes, Zond lunar orbiters and Proton 4 space laboratory scientific results
05 p0917 A70-16862

PROTON-PROTON REACTIONS

Proton-proton cycle in star interior, calculating isotope concentrations, reaction duration and energy release as function of temperature and chemical composition
05 p0900 A70-15972

Cosmic gamma ray spectrum from secondary neutral pion production in $p-p$ interactions, discussing delta isobar, fireball and nuclear interactions effects
11 p2106 A70-26707

Stellar matter density and composition in proton-proton cycle, applying results to real solar model
20 p3698 A70-39308

PROTONS

NT SOLAR PROTONS

Interacting meson systems effective masses with/without secondary proton measured, detecting heavy boson resonances and fireballs, considering proton nuclear interactions
03 p0472 A70-13031

Electron and proton accelerators design characteristics, performance capabilities and specifications, emphasizing opposite-beam techniques for elementary particles interactions studies
03 p0527 A70-13045

Fast neutron spectrum produced by galactic cosmic ray protons in atmosphere, presenting Monte Carlo transport calculation results
04 p0742 A70-15130

Cosmic protons and high energy heavy nuclei interaction with radiation in expanding universe, including estimates of light radiation influence on cosmic ray spectra
05 p0904 A70-16903

Mass spectrometric determination of proton affinities of simple molecules determined from proton transfer and ion-molecule reactions
05 p0885 A70-17081

Highly variable component protons and alpha particles identified in low energy cosmic rays by IMP 4
07 p1369 A70-20199

Elementary processes cross sections in charged states changes during proton-hydrogen molecule interactions
08 p1549 A70-21817

Charge exchange probability in proton-hydrogen atom collisions computed with two state atomic orbital expansion
09 p1733 A70-23270

Venusian ionosphere thermal protons and/or deuterons source observed by radio occultation method, suggesting dominance at high altitudes
10 p1938 A70-24068

Methanol proton transfer reaction rate energy dependence
12 p2180 A70-26863

Particle spectrometer for Apollo measurements of trapped protons and electrons, using directional telescope composed of solid state and scintillation counters
12 p2232 A70-27404

Primary cosmic ray proton and alpha particle spectral measurements by balloon flights
12 p2293 A70-27586

Proton cyclotron echoes in topside ionograms using Alouette 2 satellite data
12 p2226 A70-28064

Hydrogen ion-molecule reactions analysis by flowing afterglow technique, noting application to proton affinity measurement
16 p2857 A70-34005

Periodic high energy gamma rays from pulsars, using night sky Cerenkov light receiver for proton showers
19 p3500 A70-38084

Primary cosmic ray proton and alpha particle spectral measurements by balloon-borne equipment
19 p3505 A70-38118

Cosmic ray electron and proton interaction, discussing hydromagnetic waves, synchrotron radiation, magnetic field effects and wave propagation
20 p3695 A70-39012

Ring current protons turbulent diffusion in magnetospheric plasmopause, considering ion cyclotron wave lifetime and geomagnetic storms
21 p3881 A70-41085

Auroral proton precipitation oval in antarctic winter based on H Balmer line radiation
21 p3882 A70-41091

NMR spin-spin coupling constants between vinyl protons in cyclopentadiene, 1,3-cyclohexadiene and 1,3-cyclooctadiene from spectrum analysis
21 p3780 A70-41704

Nike-Apache rocket aurora probes using proton detector to measure galactic cosmic ray intensity and relativistic electrons
23 p4192 A70-44879

P. JTOSTARS

NT T TAURI STARS

Protostars rapid contraction and flare up evolutionary phases, solving hydrodynamic equations of motion
01 p0190 A70-11344

Low mass protostar evolution in dynamic collapse, investigating opacity laws
01 p0190 A70-11345

PreHayashi phase of stellar evolution, discussing protostellar disks (stellisks) formation from flattened fragments of collapsed interstellar cloud under turbulent viscosity
01 p0190 A70-11346

Dynamic effect of radiation from massive protostar showing formation of transparent zone free of dust about star and gas density decrease until pressure equalization
06 p1148 A70-18400

Bright IR stars observed using photometry and spectroscopy, suggesting protostars presence
14 p2641 A70-30880

Upper main sequence and close early type binaries evolution by fission of rapidly rotating protostars
23 p4250 A70-44815

PROTOTYPES

Program, test equipment and data reduction of aircraft prototype flight tests
08 p1438 A70-21865

Simulation devices in engineering feasibility studies emphasizing prototypes role [ASME PAPER 70-DE-50]
16 p2918 A70-33512

PROTOZOA

NT AMOEBA

Nontoxic method of immobilizing protozoan Tetrahymena pyriformis and bacterium Escherichia coli in acrylamide polymers, discussing microorganism viability
05 p0802 A70-16477

PROTUBERANCES

Free molecular drag for flat plate with normal protuberance, determining flowfield distribution functions and stress components
06 p0981 A70-18357

Sting diameter and cylindrical protuberance length effects on axisymmetric body base pressure in turbulent supersonic flow [AIAA PAPER 70-585]
13 p2342 A70-29885

PROVING

NT THEOREM PROVING

Holographic motion measurement verification of constant velocity, sinusoidal vibration and both, using interferometer
17 p3087 A70-35022

PSEUDOMONAS

Enzymatic hydroxylation mechanism of p-hydroxybenzoate hydroxylase from Pseudomonas putidas, describing product separation and purification
02 p0236 A70-12100

Pure oxygen effect on amino acids uptake and metabolism of Pseudomonas saccharophila stationary cells
14 p2536 A70-30343

PSEUDONOISE

Pseudonoise phase shift keying /PN/PSK/ and frequency hopping /PN/FH/ modulation technique for low altitude satellite receiving /VHF/ transmissions [AIAA PAPER 70-496]
11 p1999 A70-25436

Pseudonoise sequence generation with 3-tap linear feedback binary shift registers, citing reduction theorems
11 p2025 A70-26224

Pseudonoise code command system for scientific satellite, describing added bits and decoder
17 p3046 A70-35276

PSEUDORANDOM SEQUENCES

Additive pseudorandom number generator with seminfinite sequence length, proposing statistical tests for randomness
11 p2074 A70-26325

Electron spin-echo device as programmable linear matched filter for PN modulated carrier waveforms detection
16 p2864 A70-33480

Algorithmic random process pseudorandom number generator composed of analog computer elements, evaluating stability
20 p3594 A70-39918

Fast pseudorandom number generators for digital computers
21 p3793 A70-40851

Soviet book on pseudorandom signals theory and application covering shape selection, generation, system noise, etc
22 p3985 A70-42456

PSYCHIATRY

Cliniconosographic criteria of flight phobia and differentiation from other psychopathologic syndromes, noting sociofamilial and operative factors
01 p0031 A70-10235

Aviation psychiatry role in pilots selection and treatment
24 p4296 A70-45124

PSYCHOACOUSTICS

Jet aircraft flyovers annoyance relationship to physical parameters of sound evaluated, using psychophysical method of constant stimulus differences
01 p0006 A70-11199

Collection of papers on human hearing, source book in psychoacoustics
06 p0995 A70-17822

Frequency function of sound localization in median plane measured psychoacoustically at both ears with narrow band signals
09 p1624 A70-22762

Loud and soft signal recognition task under information feedback of presentation schedules and sequence probabilities
16 p2854 A70-33974

Information theory of hearing, considering subjective properties of nonsteady sound signals and discernibility relations
23 p4155 A70-44700

PSYCHOLOGICAL EFFECTS

NT ILLUSIONS

NT MOON ILLUSION

NT OCULOGRAPHIC ILLUSIONS

Photointerpreters information extraction, studying psychological effects of image contrast and resolution on accuracy of target detection
02 p0300 A70-12459

Physical discomfort and miseries contribution to psychological deterioration during water survival tests on life raft
07 p1218 A70-19009

Somato-vegetative and behavioral reactions of rabbits to electric stimulation of hypothalamus after injecting aminazine
07 p1209 A70-19521

Prolonged hypodynamia /bed rest/ clinical observations, noting psychological and physical effects
10 p1813 A70-24668

Psychic state changes during prolonged bed rest, discussing effects of physical exercise and medicine
10 p1816 A70-24684

Psychic functions stability during prolonged hypodynamia, discussing memory, attention span, sensometer reactions, time estimating, etc
10 p1816 A70-24685

Hypodynamia effects on humans during prolonged bed rest, investigating immunological resistance, psychic disorders, myocardium changes, responses to pharmaceuticals, etc
10 p1817 A70-24696

Reaction time dependence on sound signal probability determined by temporal structure of signal presentation 10 p1818 A70-24713

Human reaction time study leading to promptness concept to embody quantitative and qualitative aspects of psychological behavior 10 p1818 A70-24716

Physiological and psychological human reactions during space flight concerning hypokinesia, space kinetosis, isolation and limited room conditions 11 p1986 A70-25707

Human reactions to confined interiors design, examining human-environment interactions present in aircraft [SAE PAPER 700234] 11 p1990 A70-25903

Pilots psychophysiological reactions to various aircraft types and flight maneuvers, considering recorded comments, blood pressure and heart rate 12 p2177 A70-27042

Psychophysiological characteristics of pilot activity during various landing approaches with different instrumentation levels, studying heart and respiratory rates 13 p2358 A70-29297

Human operators psychological response to unforeseen information received during routine activity in prolonged solitary isolation 17 p3038 A70-35362

Soviet book on man in aircraft control system covering engineering psychology, complex flight problems, human factors and instrument panels 19 p3367 A70-37236

Behavioral changes due to repeated low doses of rocket fuel monomethylhydrazine 21 p3771 A70-41485

Student pilot case diagnosis of hysterical neurosis with syncopal and epileptiform symptoms 21 p3771 A70-41493

Nervous inhibition effect on electroretinogram b wave during flash sequences 24 p4301 A70-45986

PSYCHOLOGICAL FACTORS

USAF visual flight simulation devices from engineering and psychological standpoints, discussing human factors considerations 01 p0057 A70-10808

Psychological aspects of unreliability sources in man machine systems for selection and training criteria of photoptical instruments users 01 p0036 A70-10821

Visual fatigue symptoms, causes, relation to general fatigue and psychological aspects, discussing testing for sensory and visual fatigue 01 p0022 A70-10857

Organic and psychological risk factors in myocardial infarction, presenting characteristic case history graphically 01 p0024 A70-10867

Human communication in pilots and in maintenance and administrative personnel, noting time factor influence 04 p0644 A70-14985

Psychosocial factors in myocardial infarction and sudden death, considering possible causes of fatal cardiac arrhythmia 04 p0635 A70-15462

Impression formation model extended to personality traits, noting curvilinear relationship between probability and liking ratings 05 p0803 A70-16670

Psychological factors in training and education of pilots and astronauts for optimal matching between human operator and vehicle control system 05 p0809 A70-16967

Book on human factor in aircraft accidents covering desire to please, fatigue, diurnal rhythm, psychology, etc 06 p0987 A70-18249

External environment changes effect on animal activity, considering reactions on molecular, physiological and behavioral levels 07 p1199 A70-18782

Survival psychology for civil aviation, discussing irrational behavior after forced landings resulting from exhaustion of mental resources and inappropriate activity 07 p1204 A70-19018

Display media development and implementation from engineering psychology viewpoint for information transfer in form compatible to sensory-perceptual capabilities 08 p1447 A70-21690

Flying safety and human factors from job dissatisfaction in Japan Air Self Defense Force 08 p1453 A70-21794

Nonlinear utility functions effects on assessor probability forecasts, discussing psychological factors 10 p1912 A70-23934

Psychological fitness capacity of students in pilot training, determining unfavorable traits for flight 11 p1985 A70-25670

Civilian pilot trainee stress level dependence on individual flying instructors, detecting psychophysiological variables by inflight recording 12 p2178 A70-27044

Mental blocking /incidental long reaction times/ during continuous serial performance using perceptual-selection and response theories 12 p2178 A70-27045

Bayesian probabilistic information processing in psychological decision making in air traffic control, discussing bookbag and poker-chip applications 12 p2178 A70-27047

Hunger, thirst and environmental stimuli roles in development and elicitation of stimulus bound eating and drinking in animals 13 p2355 A70-29806

Aircraft accident prevention via reduction of pilot attention distractions 15 p2692 A70-32226

Performance and response organization as uncertainty and structure function in pursuit tracking tasks 19 p3363 A70-38320

Panum phenomenon explained by projection, attraction and figure ground psychological theories 19 p3366 A70-38505

Interindividual differences in judging stimulus similarities, explaining unsatisfactory results obtained by average scalings 19 p3366 A70-38506

Age, grade, educational institution and attitude effects on pilot personality test performance 22 p3977 A70-42870

Near fatal crash in T-33 aircraft, discussing protective clothing, seat harnesses, bodily position and mental attitude 23 p4153 A70-44497

PSYCHOLOGICAL INDEXES

U PSYCHOLOGICAL TESTS

PSYCHOLOGICAL TESTS

NT RORSCHACH TESTS

Collection of articles on chimpanzee central nervous system and behavior 01 p0028 A70-11375

Scientifically oriented pilot selection objectives criteria taking into account data concerning accident causes [DVL-892] 02 p0242 A70-11684

Restricted problem solving tasks /perceptual maze test/ formulated as multistage decision making, discussing use of dynamic programming and algorithms 02 p0246 A70-12321

Experienced and naive subject evaluation of probabilistic data, data source determination and prediction of subsequent data in complex decision task 02 p0247 A70-12379

Human feedback and response mode in performing Bayesian decision task 02 p0237 A70-12382

SAS pilot selection system, discussing assessment variables, physiological examinations, psychological tests, recruiting procedure, etc 03 p0433 A70-13262

Recall and recognition memory in concept identification, discussing presentation time /PT/ 03 p0424 A70-13767

Relative slant judgments elicited by paired comparison methods from subjects viewing computer generated slides representing rotated regular dot patterns 03 p0435 A70-13769

Lines and letters identification and localization relationships to stimulus attributes in visual perception supporting hierarchical processing hypothesis 03 p0425 A70-13825

Flight personnel psychological fitness appraisal techniques, reviewing literature concerning test methods 06 p0995 A70-17668

Physical identity and name sameness matchings efficiency noting role of interpolated activity 07 p1203 A70-18942

Macaque monkey stereoscopic vision demonstrated behaviorally by combining random dot patterns with standard operant conditioning 07 p1205 A70-19277

Psychological measures in RAF operational aircrew to obtain details for comparison of flying anxiety casualties from same population 07 p1214 A70-19941

Discrete motor act short term retention measurement to investigate decay and interference effects 09 p1621 A70-23378

Aircraft pilot and captain selection system on basis of STANINE /standard nine/ method of psychological assessment 10 p1825 A70-24504

Psychological fitness capacity of students in pilot training, determining unfavorable traits for flight 11 p1985 A70-25670

Perceptual tuning in tachistoscopic identification task with alternatives provided after or before and after stimulus 11 p1986 A70-25829

Aviation psychological research - Conference, Zurich, September 1969 12 p2175 A70-27026

Short-time memory test based on model involving continuous information storage and reproduction [DFVLR-SONDDR-30] 12 p2175 A70-27027

Pilot training applicant test profiles, discussing difference between intelligent and intellectual candidates 12 p2176 A70-27028

Psychological tests of pilot adaptation to accident situation using photo display assessment 12 p2179 A70-27052

Nervous system response fluctuation measurement during perceptual and learning tasks in terms of signal to noise ratio of electrical and tactile stimuli 13 p2354 A70-29595

Psychophysiological tests involving programmed memory device evaluating human memorization process and sensorimotor reactions to light signals 17 p3040 A70-35676

Response bias of conservative human inference, using revised odds estimate experiments 19 p3361 A70-38055

Psychological tests for ability to learn association between event and occurrence probability 19 p3363 A70-38319

Visual vigilance task with standard, binary or rating procedures as response indicators based on signal detection theory, noting relationship to psychophysical procedures 21 p3761 A70-40743

Unitary and compound stimuli and role of response categories in decision time 21 p3767 A70-40751

Jet pilots psychological survey on troubles, frustrations and personality trends by questionnaire 22 p3978 A70-42876

Fixed-ratio performance patterns of pigeon key-peck responses to fractional punishments by electric shock 22 p3971 A70-43375

Preperceptual auditory image determination experiments by acoustic test tone pitch identification 22 p3971 A70-43402

Airline transport pilots selection based on psychiatric and psychological testing 22 p3981 A70-43697

Psychological training and selection of airline pilots for stress resistance [DFVLR-SONDDR-53] 24 p4310 A70-46413

PSYCHOLOGY

NT PSYCHOACOUSTICS

NT PSYCHOPHYSICS

Research problems resulting from observational methods in social-psychological studies, discussing categorization systems and coding reliability 05 p0802 A70-16668

Ballistographic psychological evaluation of heart and circulatory system by recording displacement, velocity, acceleration and total forces imparted during each beat 10 p1810 A70-24039

Applied psychology role regarding human factors in man machine systems, considering boredom, skills application, age and experience, etc 12 p2176 A70-27035

Flight doctor-pilot relationship, studying personal motivation 12 p2178 A70-27049

Imaginary axes effect of phenomenal space in contrast illusions of distance, discussing division of S field of vision by definite point fixation 20 p3573 A70-39764

PSYCHOMOTOR PERFORMANCE

NT PSYCHOSOMATICS

Voluntary control over velocity of smooth pursuits, discussing saccadic and saccade free modes and switching during tracking 01 p0026 A70-11056

Somatic motor unit spikes human biceps during posture holding, obtaining Markov chain and random variable behavior patterns 03 p0416 A70-13011

Postrest upswing or muscles warm-up in motor skill learning 05 p0803 A70-16671

High temperature effects on pilots psychomotor performance and physiological function, discussing measurements taken during complex tasks 06 p0999 A70-17290

Human motor functions changes following prolonged hypodynamia, including physical training and hypokinesia roles in standing and walking 10 p1815 A70-24682

Motor reactions and neural negative induction duration in male and female human subjects of different ages 12 p2174 A70-28356

Nervous system response fluctuation measurement during perceptual and learning tasks in terms of signal to noise ratio of electrical and tactile stimuli 13 p2354 A70-29595

Hand-eye coordination in altered gravitational fields, using mirror viewed target in reaching test 15 p2689 A70-31886

- Human tracking performance in position, rate and acceleration control systems under short term psychological stress induced by electric shocks
16 p2853 A70-33689
- Human acceleration resistance and psychomotor behavior under emergency flight conditions, including high temperature exposure and remaining in cino-static position
17 p3037 A70-35135
- Human operators psychological response to unforeseen information received during routine activity in prolonged solitary isolation
17 p3038 A70-35362
- Steering behavior during learning as function of self generated stimuli by movement compared with stimulus tracking
20 p3580 A70-39674
- Body surface cooling level and rate effects on psychomotor performance tested at various levels of mean weighted skin temperature /MWST/
20 p3573 A70-39675
- Rat neuron impulsive reactions and frequency response differences to varying sound signals, discussing time constant, signal intensity and frequencies
20 p3574 A70-40172
- Step and ramp input functions and pursuit and compensatory display modes effects on tracking performance
21 p3767 A70-40753
- Jet pilot EEG radio telemetry showing psychomotor stresses during takeoff and acceleration
22 p3978 A70-42877
- Human EEG alpha rhythm during surface-tapping test with rod at time-limited maximum frequency, noting slowdown to preferred frequency
24 p4301 A70-45987
- PSYCHOPHYSICS**
NT PSYCHOACOUSTICS
- Psychophysical and evoked potential correlates of changes in stimulus color and intensity compared with minimum subjective flicker conditions
12 p2171 A70-28035
- Steady state evoked potentials Fourier analysis from human scalp during psychophysical procedure of heterochromatic flicker photometry, obtaining spectral sensitivity curve
15 p2682 A70-32015
- Psychophysical adjustment methods effect on visual vertical orientation during head tilt
15 p2683 A70-32455
- Human monitoring behavior, discussing display, task and organismic variables effects
19 p3363 A70-38323
- PSYCHOPHYSIOLOGY**
- Collection of articles on chimpanzee central nervous system and behavior
01 p0028 A70-11375
- Astronauts physical training for space flight requirements
04 p0629 A70-14564
- High fidelity simulations for environmental stress evaluations, describing carbon dioxide effects on pilots simulated ground target tracking and reentry vehicle landing
06 p0999 A70-17291
- Psychophysiological regularities of nonlinear human color vision model, analyzing sensitivity curves, achromatic tints and hyperbolic position in perception space
08 p1443 A70-20728
- Human psychophysiological inability to avoid mid-air collisions investigated for aviation safety
09 p1611 A70-23465
- Accumulator model for psychophysical discrimination, discussing stimulus presentation and sampling, parameter values estimation, response latencies, etc
10 p1827 A70-24767
- Psychophysical metric for space perception visual cues measurement, describing applications to distance discrimination
10 p1827 A70-24768
- Psychovegetative and neurovegetative stress syndroms in flying personnel removed prematurely from active service as result of psychophysiological complementary diagnostics [DFVLR-SONDDR-31]
12 p2177 A70-27041
- Pilots psychophysiological reactions to various aircraft types and flight maneuvers, considering recorded comments, blood pressure and heart rate
12 p2177 A70-27042
- Book on psychophysical analysis of visual size-distance perception and physiological optics
15 p2688 A70-31575
- Psychophysiological tests involving programmed memory device evaluating human memorization process and sensorimotor reactions to light signals
17 p3040 A70-35676
- Medicopsychological and labyrinthic exploration of flight crew candidates aeronautical adaptation, using electronystagmographic method of swinging chair
17 p3041 A70-35918
- Attention direction role in auditory recognition, testing unwanted inputs attenuation hypothesis
19 p3362 A70-38317

Flight training quality prediction by multidimensional regression analysis, discussing relationship to candidates psychophysiological examinations
20 p3578 A70-38964

PSYCHOSES**NT PSYCHOTIC DEPRESSION****PSYCHOSOMATICS**

Myocardial infarct and other psychosomatic disturbances - Conference, Wiesbaden, West Germany, August 1967, Part 3
01 p0023 A70-10864

External environmental factors, life habits and personality structure effects on development of coronary artery disease, discussing psychosomatic aspects of myocardial infarction
01 p0023 A70-10866

Organic and psychological risk factors in myocardial infarction, presenting characteristic case history graphically
01 p0024 A70-10867

PSYCHOTHERAPY

Psychiatric disorder in civil aircrew leading to suspension or loss of licence, discussing physicians role and complications of treatments
07 p1223 A70-19940

PSYCHOTIC DEPRESSION

Psychiatric disorder in civil aircrew leading to suspension or loss of licence, discussing physicians role and complications of treatments
07 p1223 A70-19940

PSYCHROMETERS

Psychrometric chart for physiological research involving moist air thermodynamic properties
24 p4304 A70-46275

PTM (MODULATION)**U PULSE TIME MODULATION****PUBLICATIONS****U DOCUMENTS****PULLING**

Pulling force during motion of sinusoidally deformable flat profile, taking into account trailing edge vortices
18 p3241 A70-36280

PULMONARY CIRCULATION

Humans and dogs breathing CO in closed system, discussing distribution on blood, body stores and oxygen metabolism
02 p0234 A70-11727

Time varying blood flow in pulmonary capillaries affecting overall diffusing capacity and alveolar-arterial oxygen tension gradient
03 p0421 A70-13570

Vagotomy and carbon dioxide concentration effect on quiet and forced respiration rate, pleural pressure, tidal volume and lung ventilation in cats
03 p0422 A70-13694

Slope and shape of blood-gas dissociation curve as factor influencing pulmonary gas exchange in presence of ventilation-perfusion inequality
06 p0994 A70-17522

Pulmonary extravascular /PEV/ and intravascular /PBV/ fluid volumes measured at rest and exercise
07 p1211 A70-19595

Alveolar ventilation and pulmonary circulation during application of negative pressure to lower part of human body
09 p1615 A70-22090

Vertical distribution of pulmonary blood flow /DPBF/ in dogs without thoracotomy prone, supine, head-up, head-down and right and left decubitus positions
10 p1810 A70-24004

Pulmonary blood flow direction and distribution in dogs during near vacuum exposure and recompression
11 p1984 A70-25351

Intentional scolioses effect on intrapulmonary blood circulation, using photoelectrical cinedensigraphic technique
14 p2537 A70-30384

Alveolar ventilation and pulmonary circulation during application of negative pressure to lower part of human body
15 p2685 A70-32686

Distributed-lumped parameter model for impeded mass transfer and blood-gas maldistribution effects in human respiratory system
15 p2694 A70-32844

Weightlessness and gravitational effects on human pulmonary blood flow distribution, considering optimal gas exchange efficiency [ALAA PAPER 70-785]
17 p3035 A70-34472

Continuous murmur due to combination of rheumatic mitral stenosis and rare type of partial anomalous pulmonary venous drainage
17 p3032 A70-35473

Dynamic intravascular pressures measured in small vessels of frog lung using micropressure transducer inserted into vessel lumen
19 p3364 A70-38368

Mongrel dogs pulmonary and systemic circulatory responses to dopamine infusion
20 p3569 A70-38986

Pulmonary hypertension in congenital heart diseases as function of blood flow
20 p3571 A70-39367

Lung alveolar and capillary wall structure in mammals under normal conditions, transverse acceleration and mechanically changed pulmonary circulation
20 p3575 A70-40190

Body position effect on oxygen saturation of regional pulmonary venous blood and arterial-venous shunts in intact dogs
21 p3766 A70-42153

Pulmonary arterial and venous response to cooling, discussing role of sympathetic nervous system alpha receptors in hypothermia induced pulmonary constrictions in dogs
23 p4148 A70-44788

Pulmonary blood flow and ventilation distribution during forward acceleration by xenon 133 and lung scanning
24 p4302 A70-46105

Excised perfused dog lungs stratified dead space changes due to transpulmonary pressure and breathing frequency increase, considering pulmonary circulation
24 p4303 A70-46114

PULMONARY FUNCTIONS

Human pulmonary gas mixing between large airways and alveolar spaces, using argon bolus inhalation
01 p0024 A70-10976

Control measurements to determine changes in lung volumes, intrapulmonary and intragastric pressure and breathing during submersion in water up to xiphoid process level
01 p0038 A70-10980

Artificial pulmonary ventilation effects on carbonic anhydrase activity in human blood during hypoventilation and hyperventilation
01 p0025 A70-11029

Radiology instrument for examining pulmonary functions during deep inspiration, expiration and rest, describing material, components and assembly, mounting and radiogram development
01 p0040 A70-11401

Respiratory flow rate effect on emptying of lung regions, assessing regional and end-expiratory volumes
03 p0428 A70-14155

Vascular resistance and constriction and muscle mass related in pulmonary arteries of mice subjected to alveolar hypoxia
04 p0630 A70-14679

Energy converters and radio transmitters for physiological telemetry, using electric power converted from thermal and mechanical energy of human respiratory activity
04 p0644 A70-15276

Computer program for evaluating measured lung function values by comparison with accepted norms, using matrices containing regression coefficients
04 p0644 A70-15360

Ejection click of valvular pulmonic stenosis by external phonocardiograms and intracardiac pressure recordings during successive respiratory cycles
04 p0633 A70-15440

Inhaled air intrapulmonary distribution uniformity and alveolar N concentration using single breath method
05 p0802 A70-16496

Pulmonary CO diffusing capacity in young men during muscular exercise
06 p0993 A70-17432

Data analysis of compliance, resistance, inertance and natural frequency of chest-lung system, noting trend with body mass
06 p0993 A70-17521

Ventilation function, pulse rate and blood pressure measured for adaptation to vertical upright and head-down positions
07 p1201 A70-18794

Carbon dioxide effect on oxygen uptake during hyperventilation in normal man
07 p1205 A70-19294

Statistical analysis of pulmonary ventilation and gas exchange indices during orthostatic tests before and after water immersion
07 p1209 A70-19517

Static tensibility and vital capacity of lungs statistically analyzed in relation to sex and age
07 p1210 A70-19524

Respiratory neurons activity in respiratory center of medulla oblongata during suspension and forced recovery of respiratory motions
07 p1213 A70-19775

Electronic measurement of bronchial flow resistance in pulmonary function to determine impediment in inhaled and exhaled air passage
08 p1449 A70-20676

Orthogonal electrocardiograms of patients with pulmonary emphysema analyzed by computer, discussing diagnostic classification and correlation with physiologic parameters
09 p1616 A70-22276

Body temperature effect on pulmonary ventilation response to exercise
10 p1819 A70-24773

Human pulmonary ventilation during exercise in high altitude and sea level acclimated subjects
10 p1819 A70-24774

Physiology of oxygen transport in human organism and genesis of tissue hypoxia, discussing pulmonary

functions, blood transport properties and tissue blood flow and diffusion

10 p1821 A70-25077

Pulmonary functions disturbances producing hypoxia, discussing alveolar hypoventilation, arteriovenous admixing, blood distribution and oxygen diffusion disturbances

10 p1821 A70-25078

Oxygen transport after cardiopulmonary resuscitation from asystole and ventricular fibrillation in dogs

10 p1822 A70-25085

Statistical analysis of pulmonary ventilation and gas exchange indices during orthostatic tests before and after water immersion

11 p1988 A70-26116

Indicator dispersion model for cardio-pulmonary system based on continuity past sampling site, observing diffusion coefficient nonlinear increase with blood speed

12 p2174 A70-27019

Oxygen and carbon dioxide effects on airway smooth muscle following pulmonary vascular occlusion in dogs

13 p2356 A70-29943

Stress distribution and pressure distending air spaces in lungs, using mechanical pulmonary elasticity model

13 p2356 A70-29945

Pulmonary vital capacity measurements in young recruits for respiratory function, considering relationship to body weight and height

16 p2850 A70-34348

Upper pulmonary airways plastic conduit model, measuring laminar and turbulent flow velocity profiles by hot-wire anemometer

17 p3035 A70-34469

Intrapulmonary distribution of gases inhaled during positive and transverse accelerations

17 p3037 A70-35130

Pressure recording site localization in esophagus, discussing cardiac artifacts morphology and localization over esophagus length

21 p3765 A70-42152

Topography of pleural surface pressure and vertical gradient of transpulmonary pressure above resting volume in relaxed animals as function of alveolar pressure

21 p3766 A70-42154

Altered respiratory pattern effect on alveolar gas exchange in mechanically ventilated dogs after introducing end-inspiratory pause

21 p3766 A70-42156

Recording system errors for measuring pulmonary pressure-volume curves of excised lungs

24 p4309 A70-46122

PULMONARY LESIONS

Histopathological evidence for pulmonary emboli in experimental decompression sickness in dogs detected by radioisotopic lung scanning

06 p0991 A70-17295

Flying disability period due to coccidioidomycosis in southwestern U.S., giving recommendations for earlier return to flying duty

06 p1000 A70-17300

Altitude acclimatization protection against lung damage from exposure to oxygen at high partial pressures experimented on rats

12 p2170 A70-27659

Hyperbaric oxygen exposure produced hypertension and pulmonary edema, discussing carbon dioxide transport mechanism in blood

20 p3572 A70-39430

PULSARS

Pulsar CP 1919 radio emission observed on crossed wideband radio telescope in meter wavelength range, including pulse recordings

01 p0173 A70-10130

Pulsating very dense white dwarfs models noting general relativity

01 p0176 A70-10320

Pulsar PP 0943 properties, giving period, pulse characteristics and position

01 p0177 A70-10343

Bremsstrahlung radiation in intense magnetic fields rejected for pulsar radiation mechanism

01 p0169 A70-10344

Pulsed high energy X rays from Crab Nebula pulsar NP 0532 measured by balloon-borne X ray telescope

01 p0169 A70-10345

Pulsar synchrotron emission model, discussing elliptic polarization, pulse shape, duration and negative absorption /wave amplification/

01 p0183 A70-10897

Comparative diagrams for radio emission intensities of pulsar PP 0943 from observations by cross radio telescope

01 p0185 A70-11034

Pulsar distance and distribution estimation, considering galactic spiral structure and nature of interstellar medium

02 p0371 A70-12201

Random variations of terrestrial rotation rate effects on pulsar observations, discussing methods to minimize effects

02 p0371 A70-12203

Polarization characteristics of pulsars, noting stable average and time varying component

02 p0371 A70-12242

Optical and radio pulses from pulsars as test of light speed variation with frequency and photon mass possible existence

02 p0373 A70-12394

Electric fields in rotating magnetic relativistic neutron stars, analyzing static fields in corotating frame and pulsar emission

02 p0379 A70-12726

Secular increase in pulsar periods attributed to gravitational emission, velocity effects and galactic escape

03 p0564 A70-13219

Pulsars observed properties and interpretation based on oblique rotator model for neutron stars

03 p0577 A70-14099

X ray flux pulsations for pulsars near Crab Nebula observed in 2.5-30.0 kev range, determining pulsation profile

03 p0578 A70-14358

Pulsar research discoveries characteristics, detection techniques and origin theories

04 p0746 A70-14507

Cosmic ray origin theories, noting pulsars nature and properties may provide solution

04 p0738 A70-14517

Pulsed gamma radiation from pulsars searched for by Cerenkov air shower detection method

04 p0738 A70-14518

Analog techniques for pulse integration based on sonograph audio spectrum analyzer for pulsar observation by radio telescopes near Hobart, Tasmania

04 p0655 A70-14520

Crab Nebula pulsar light intensity fluctuations on very short time scale, noting negative observations

04 p0747 A70-14545

Pulsars pulse duration and shape as key to neutron stars linkage with supernova explosions

04 p0750 A70-14749

Power spectra, modulation indices, frequency distributions and decorrelation frequencies of intensity fluctuations of pulsar radiation consistent with interstellar scintillation theory

05 p0908 A70-16302

Pulsars as possible sources of superheavy nuclei in primary cosmic radiation, evaluating flux and mean power

05 p0901 A70-16314

Power spectra of pulsar radiation intensity fluctuations, showing line structure

05 p0921 A70-16983

Pulsars dispersions, setting upper limit to emission measure of dense plasma

05 p0921 A70-16984

Cosmological theories taking into consideration gravitational collapse, discussing pulsars, quasars and X ray stars evolution

06 p1140 A70-17584

Unified model for pulsars involving electron population inversion and laser type transition

07 p1375 A70-18893

Dense pulsating stellar core structure model for pulsars, discussing catastrophic collapse mechanism

07 p1380 A70-19278

Supernova pulsars parameters prediction based on Crab and Vela observations, discussing dispersion, period, flux density, etc

07 p1389 A70-20218

Pulsar short term pulse energy fluctuations presented in pulse amplitude histograms and power spectra

07 p1389 A70-20219

Pulsar slowdown by radiation field torques indicated by alignment torque in magnetized oblique sphere rotating in vacuum

07 p1389 A70-20220

Compton scattering of synchrotron radiation from parent electrons in pulsars, calculating Compton-synchrotron radiation from NP 0532 leads to lower limit for magnetic field

07 p1369 A70-20221

Pulsar magnetorelativistic model assuming neutron star with magnetic field

08 p1563 A70-20478

Faraday rotation in pulsars and in interstellar medium, discussing position angle drift, polarization changes and pulse fine structure

08 p1564 A70-20553

Supernova remnant luminosity dependence on central star rotation period, deriving parameters for pulsars in Cas A

08 p1570 A70-20897

Pulsar formation effect on orbits of preexisting planets and postformation planets effects on pulsar period and phase residuals

08 p1570 A70-20898

Pulsars pulse arrival time measured using cesium clock during weekly observations

08 p1570 A70-20899

Pulsars radio, optical and X ray emission spectrum analysis, suggesting oscillating current sheets as radiation source

08 p1561 A70-20914

Terrestrial rotation changes effects on pulsar period observations

08 p1575 A70-21260

Nonthermal mechanism for high energy radiation and particle emission from X-stars and pulsars

08 p1575 A70-21364

Pulsar CP 1919 radio emission observed on crossed wideband radio telescope in meter wavelength range, including pulse recordings

08 p1576 A70-21404

Pulsar clusters and associations within 1 kpc of sun and hot O-stars and supergiants, calculating radius of surrounding H II regions

08 p1577 A70-21493

Pulsar NP 0532 average polarization parameters measured at 430 MHz, discussing variations of precursor and main pulse and flux of interpulse

08 p1578 A70-21549

Secular increase in pulsar periods attributed to gravitational emission, velocity effects and galactic escape

08 p1580 A70-21652

Synchrotron emission of relativistic particle in magnetic field with radiative reaction force comparable to Lorentz force, emphasizing pulsar cosmic ray electron acceleration

09 p1731 A70-22273

Pulsar mathematical model accounting for pulse width, polarization and spectrum of emitted radiation

09 p1753 A70-22383

Pulsar NP 0532 synchrotron emission reinterpretation related to relativistic particles injection into Crab Nebula

09 p1756 A70-22516

Pulsar model assuming magnetic dipole radiation by spinning neutron star interacting with nearby plasma

09 p1756 A70-22517

Pulsars period distribution not related to decay of magnetic field in rotating neutron star

09 p1756 A70-22518

Pulsars high time-resolution studies revealing marching subpulse structures

09 p1756 A70-22519

Pulsars as tiny superdense neutron stars with spin to explain galactic cosmic rays and radiation from supernova remnants

09 p1756 A70-22631

Interstellar gas electron number density fluctuations effect on pulsar signals in terms of frequency dependent dispersion, noting long wavelength disturbances

09 p1764 A70-23609

X ray scattering from pulsar NP 0532 by interstellar grains

09 p1748 A70-23791

Universal X ray background as superposition of nascent pulsars in various galaxies, using Crab Nebula pulsar as guide

09 p1748 A70-23792

Periodic intensity fluctuations in pulsars from VHF phased array measurements

09 p1764 A70-23793

Frequency jumps and small amplitude wobble in pulsars

09 p1764 A70-23794

High energy pulsed gamma rays detection method for pulsars based on search for nanosecond duration Cerenkov light signals

09 p1748 A70-23795

Pulsars pulse shapes and linear polarization measured, observing rapid change of polarization direction in double pulses

10 p1936 A70-23901

Pulsars dynamic spectra in 110-420 MHz range, observing emission bandwidths to formulate power law

10 p1938 A70-24099

Pulsars in supernova remnants emitting X rays

10 p1933 A70-24627

Longitudinal electrical conductivity of relativistic gas in intense magnetic field

10 p1924 A70-24634

Wisps near Crab Nebula since September 1969 pulsar spin-up, suggesting dynamical changes in neutron star

10 p1947 A70-24994

Comparative diagrams for radio emission intensities of pulsar PP 0943 from observations by cross radio telescope

10 p1948 A70-25003

X ray scattering by interstellar grains in direction of Crab Pulsar and Sco XR-1

10 p1933 A70-25044

Pulsar radio emission reception with improved SNR based on periodic variation of average reception frequency with time

10 p1948 A70-25165

Bremsstrahlung radiation in intense magnetic field proposed as emission mechanism from pulsars, discussing absorption coefficient

11 p2104 A70-25697

Pulsars nature based on hypothesis for main energy of novae and supernovae bursts equaling gravitational energy of collapse

11 p2117 A70-26708

Pulsars properties and physical nature, considering state of matter not reproducible in terrestrial laboratories 12 p2297 A70-27056

Pulsar research, discussing possibilities in probing galactic medium 12 p2301 A70-27577

Pulsar properties association with neutron star rotation energy, discussing alternate pulsar theories 12 p2301 A70-27579

Pulsar theory of rotating and precessing neutron stars, rejecting relevance of forced precession to behavior 12 p2308 A70-27884

Dwarf and neutron stars as pulsar energy sources, considering Crab Nebula X ray emission and gravitational collapse 12 p2310 A70-27990

Pulsars starquakes frequency relationship to solid crust shear strength based on Ruderman model, considering Crab Nebula 12 p2310 A70-27998

Dissipation mechanism and period rate increase in neutron star pulsar model with neutrino emission from damping 12 p2312 A70-28368

Crab pulsar /neutron star NP 0532/ possible spherical asymmetry indicated by pulse arrival time anomalies 13 p2486 A70-28618

Pulsars linear polarization Stokes parameters measured, noting PSR 2045-16 radiation beamed into hollow cone centered on magnetic pole 13 p2487 A70-28631

Molonglo pulsars observations, using multiperiod integration technique for declinations, periods and positions 13 p2487 A70-28632

Polarization of strong radio pulses from pulsar NP 0532 in Crab Nebula 13 p2492 A70-29269

Pulsar CP 1919 X ray emission upper limits from balloon flight data, comparing to NP 0532 over entire electromagnetic spectrum 13 p2478 A70-29270

Pulsed gamma ray emission from Crab Nebula pulsar NP 0532 investigated by balloon-borne spark chamber detector 13 p2492 A70-29271

Molonglo pulsars H line absorption and dispersion in interstellar medium 13 p2495 A70-29788

Pulsar short period pulsations and emission patterns in meter wavelength range on crossed radio telescope 14 p2633 A70-30151

Pulsar radiation emission by electrons and protons in close orbit taking into account density, energy and correlation in plasma 14 p2638 A70-30617

Pulsars crust plastic deformation leading to rotation damping, higher magnetic moments and rarer starquakes 14 p2638 A70-30672

Planetary orbit after central star supernova explosion, discussing effect on pulsar period 14 p2640 A70-30787

Anisotropic plasma turbulence produced by two stream instability onset near light cylinder of rotating magnetic star for pulsar model 14 p2640 A70-30788

Runaway stars and pulsars near Crab Nebula, discussing binary system explosion and remnant motion 14 p2642 A70-30894

Coherent radio emission mechanisms of white dwarfs and neutron stars as magnetic pulsar models, discussing polarization 15 p2804 A70-32698

Faraday rotation in pulsars and in interstellar medium, discussing position angle drift, polarization changes and pulse fine structure 15 p2805 A70-32708

Pulsar formation mechanism, showing core collapse to neutron star state 15 p2806 A70-32773

Angular scattering of interstellar medium resulting in multipath dispersion of pulsar pulses, discussing NP0532 in Crab Nebula 16 p2972 A70-32988

Electronic pulsarium displaying flashing or beeping properties of pulsars 16 p2911 A70-33795

Pulsar gravitational waves detection by lunar mascons, discussing resonant standing vibrations 16 p2980 A70-34306

Pulsar observations based on magnetic dipole model, discussing turnoff time, emission characteristics, birth rate and scale height 17 p3153 A70-34531

Pulse structure, polarization, time varying features and tight beam emission by pulsar model using finite thickness interfaces 17 p3153 A70-34532

Optical search for CP 0328 and CP 0950 by photoelectric multichannel signal averaging 17 p3154 A70-34536

Critique of paper on Crab Nebula pulsar pulsed gamma ray emission, considering photon flux and statistical data analysis 17 p3149 A70-34565

Critique of paper on pulsed gamma rays detection from Crab Nebula pulsar by balloon flights, attributing pulsations to random fluctuations 17 p3149 A70-34566

Crab Nebula pulsar NP 0532, describing quasisinusoidal oscillation in arrival times of radio pulses 17 p3157 A70-34842

Pulsars MP 0031 and CP 1919 periodic variations in pulse intensity, considering radio emission models with plasma waves 17 p3157 A70-34843

Pulsars as cosmic ray sources, emphasizing time properties of acceleration mechanisms 17 p3151 A70-34913

Pulsar RF spectral fine structure in decimeter wave range 17 p3163 A70-35050

Radio observation of Crab Nebula radio pulsar NP 0532, discussing main and subpulse stability at optical and radio frequencies 17 p3164 A70-35116

Pulsars theories review, discussing geometrical model picturing pulsar as rotating neutron star with high magnetic field 17 p3164 A70-35117

Pulsars electrodynamics concerning EM emissions, discussing roles of rotation and magnetic field 17 p3172 A70-35591

Crab Nebula pulsar NP 0532 optical and X ray synchrotron radiation, explaining ratio of pulsar energy flux to nebula 17 p3152 A70-35747

Pulsars spatial distribution, comparing actual distribution to Monte Carlo computations 17 p3173 A70-35755

Pulsar models distinguishing by Huygens principle in flat space-time, describing electromagnetic propagation in Riemann space 17 p3173 A70-35757

Central pulsars effects on supernova envelopes, examining luminosity, energy input, shape and light curve 18 p3314 A70-36333

Pulsars PSR 1451-68, 1749-28 and 2045-16, discussing modulation effects associated with second periodicity 18 p3314 A70-36334

Pulsars period galactic equator concentration correlation, discussing period-radio luminosity relation and spatial distribution 18 p3314 A70-36335

Superheavy nuclei origin in primary cosmic rays, proposing neutron stars /pulsars/ as sources 18 p3308 A70-36403

Pulsars pulsation mechanism, using neutron star model with oblique rotation axis 18 p3319 A70-37048

Pulsar radio pulses structure and emission source theory based on synchrotron radiation and relativistic effect calculations 18 p3321 A70-37119

Physical processes in galactic and extragalactic sources of nonthermal radio emission, assuming pulsars as principal magnetic field and cosmic rays sources 18 p3321 A70-37126

Small angular diameter radio source in central Crab nebula association with pulsar NP 0532 based on spectra and pulse duration 18 p3322 A70-37128

Pulsar galactic longitudinal distribution, discussing observability impaired by high electron density in spiral 18 p3328 A70-37173

Pulsar distance calculation, assuming immersion in uniform average electron density medium 18 p3328 A70-37174

Pulsar studies, discussing periodicity, scintillations, interstellar plasma, etc 19 p3513 A70-37398

Guiding center theory for relativistic plasma embedded in strong magnetic field, discussing connection with pulsars emission dynamics 19 p3479 A70-37596

Pulsar radiation mechanisms, discussing magnetic field topology and current distribution estimation 19 p3518 A70-38022

Pulsar AP 2015 21 cm line absorption profile, indicating uniform density and temperature neutral H model invalid 19 p3518 A70-38026

High energy gamma rays detection from pulsars by fast night sky Cerenkov counter 19 p3500 A70-38083

Periodic high energy gamma rays from pulsars, using night sky Cerenkov light receiver for proton showers 19 p3500 A70-38084

Acceleration of high energy cosmic rays by pulsar LF electromagnetic radiation 19 p3501 A70-38085

Periodic cosmic gamma radiation from pulsars, using reflector detection of shower generated Cerenkov light 19 p3501 A70-38090

Pulsars postulated as supernova remnants sources of local cosmic rays 19 p3511 A70-38159

Critique of Ruderman theory of Crab pulsar LF wobble as long wavelength oscillation of superfluid vortex lattice 19 p3522 A70-38604

Pulsars CP 0834, AP 1237 and CP 1919 radiation intensity periodic variations, discussing power spectra fluctuations in circulating plasma model 20 p3701 A70-39007

Pulsar 1919 plus 21, discussing pulse intensity vs phase and number by statistical analysis of two dimensional data array 20 p3705 A70-39489

Pulsar observational data and theories, discussing main pulse shape, wavelength, polarization, fine structure distance estimates, intensity and scintillations 20 p3706 A70-39935

Pulsars subpulse intensities and shapes in magnetic field, noting drift speed sawtooth patterns 20 p3713 A70-40428

Neutron star superfluid turbulent state, applying dynamic model to conditions in pulsars 20 p3713 A70-40429

Pulsar NP 0535 X rays detection by ground based observations of upper air fluorescence 21 p3871 A70-40654

X ray emission from Crab Nebula pulsar by rocket-borne proportional counters, comparing with optical observations 21 p3874 A70-40674

Pulsed hard X and gamma rays from NP0532 pulsar in Crab Nebula, comparing with extrapolated optical data 21 p3874 A70-40675

Cosmic gamma radiation from pulsars, examining atmospheric Cerenkov light generated by energetic particle showers 21 p3874 A70-40676

Crab Nebula pulsar NP 0532 electromagnetic spectrum observations, examining radio, optical, IR and X ray emission 21 p3874 A70-40677

Rotating neutron stars, pulsars and cosmic X ray sources relationship, discussing stellar model with mass loss in presence of magnetic field 21 p3874 A70-40678

Pulsars and other discrete sources celestial gamma rays flux distribution calculation 21 p3878 A70-40745

Pulsar research review, discussing characteristics, neutron star theory and galactic origin 21 p3886 A70-41072

Optical pulsar search instrument in radio pulsar fields, showing performance on NP 0532 21 p3826 A70-41156

Secondary periodicities in energy spectrum of strong pulsars from 80 MHz radioheliograph observations 21 p3892 A70-41186

Galactic distribution of supernova remnants and association with pulsars and X ray sources 21 p3892 A70-41188

Pulsars discovery at low galactic latitudes, investigating dispersion, pulse shape and period 21 p3923 A70-41995

Pulsar short period pulsations and emission patterns in meter wavelength range on crossed radio telescope 21 p3923 A70-42073

Pulsar single pulse search at Jodrell Bank by on-line computer 21 p3923 A70-42102

Pulsars and neutron stars origin and properties, discussing superdense star angular velocity, blackholes, supernovae remnants, rotation, etc 21 p3923 A70-42171

Crab pulsar observations with refractor and on-line data acquisition, indicating optical pulse arrival times at variance with previously assumed 77 day periodic wobble 22 p4097 A70-42464

Pulsar pulse arrival time fluctuations, examining solar coronal nature by angular broadening, scintillation and turbulence spectrum 22 p4101 A70-42935

Crab Nebula pulsar NP 0532 optical timing, measuring frequency, arrival times and pulse interval 22 p4102 A70-42936

Pulsar emission mechanisms, discussing possible magnetospheric physics role and optical pulse generation 22 p4105 A70-43217

Crab Nebula pulsar optical polarization compared with surrounding nebula and radio polarization 22 p4105 A70-43227

Polarization characteristics of pulsar NP 0532 strong pulses at 430 MHz, using dual circularly polarized line feed

22 p4105 A70-43228

Pulsars null pulse spacing significance, determining fluctuation power spectrum

23 p4238 A70-43814

Crab Nebula X ray pulsation identified with pulsar NP 0532 by rocket measurements, noting implications for interstellar dust density

24 p4401 A70-45371

Neutron star or defunct pulsar accretion of interstellar matter, discussing effects on total luminosity and radiation spectrum

24 p4403 A70-45397

Pulsar radiation polarization, examining mean pulse profiles, frequency, position angle and rotational effects

24 p4403 A70-45404

Pulsar intensity variations, showing fine frequency structure by interstellar scintillation model

24 p4404 A70-45416

Current sheet motion and pulsar radio, optical and X ray emission, investigating finite thickness oscillating interface radiation with independent particle

24 p4397 A70-45760

Synchrotron source spectra natural frequency cut-off in absence of self absorption and electron energy cut-offs, discussing pulsar NP 0532

24 p4410 A70-45774

Pulsars correlation with stellar evolution using model, discussing distribution and formation rate in Milky Way galaxy

24 p4412 A70-45981

Pulsars radio evolution mechanism by phenomenological analysis, deriving time dependences of period, luminosity and emitting region size

24 p4412 A70-46101

Gravitational wave associated radio pulse observations using long baseline spaced receivers

24 p4412 A70-46136

Corotating magnetic field model of pulsar, using electromagnetic field equations of dipole radiation in low density plasma

24 p4413 A70-46137

Pulsar distributions without magnetic decay, concerning age dependence of surface field and radio luminosity of neutron stars

24 p4413 A70-46138

High energy electron proton and heavy nuclei absorption in pulsar vicinity, discussing implications for cosmic rays

24 p4398 A70-46170

PULSATING FLOW

U UNSTEADY FLOW

PULSE AMPLITUDE

Wide range pulse height discriminator with milliwatt power drain for use in nuclear experiments on scientific satellites

01 p0088 A70-10749

Pulsar synchrotron emission model, discussing elliptic polarization, pulse shape, duration and negative absorption /wave amplification/

01 p0183 A70-10897

Multistop time-to-pulse-height conversion unit to extend capability of pulse height analyzer for multichannel time analysis with narrow channel widths

02 p0271 A70-12749

Large amplitude wave trains in cosmic ray neutron intensity compared with diurnal variations, determining interplanetary space directional distribution from monitor data

03 p0559 A70-13912

Pulse amplitudes and delays measured for oblique absorption values during IGY over 1000 km transmission path for correlation with lower ionosphere model

07 p1228 A70-19155

Ionospheric reflection coefficients from vertical and oblique incidence pulse amplitude data, discussing night conditions effect on Ottawa pulse transmissions

07 p1232 A70-19176

Geomagnetic micropulsation amplitudes and polarization along meridional profile analyzed from simultaneous ground station recording

07 p1268 A70-19463

Pulsar short term pulse energy fluctuations presented in pulse amplitude histograms and power spectra

07 p1389 A70-20219

Forced vibrations amplitude of rotor mounted on elastically damping supports

08 p1588 A70-21181

Transient response analysis of nanosecond pulsed transistor amplifier having common-emitter configuration with negative feedback

08 p1474 A70-21229

Pi2-type pulsations in and near auroral zone observed for amplitude variation dependence on geomagnetic latitude and local time

10 p1885 A70-25280

Impact accelerations measurement for shock pulse amplitude and duration, describing system for direct reading

11 p2055 A70-26447

Solid state laser with traveling wave during steady state emission, determining pulse shape, duration and amplitude

12 p2247 A70-27497

Photomultipliers single electron response by measuring electron pulse height distribution

12 p2236 A70-27850

Finite amplitude stability of plasma column in weakly ionized gases and in semiconductor plasmas in longitudinal magnetic field

13 p2458 A70-28566

Paced respiration and selective attention effects on heart rate and finger pulse amplitude in adult females subjected to visual stimuli

13 p2350 A70-29241

Continuous differential energy pulse height spectra reduction to photon upper atmospheric spectra

15 p2694 A70-31800

Scientific satellites pulse height analyzer and associated threshold detection and logic circuitry

16 p2900 A70-33062

Optical and electronic components design for ruby lasers generating giant pulses

17 p3107 A70-35121

Gamma ray pulse height spectra during active and quiet solar periods from midlatitude balloon flights

17 p3152 A70-35774

Geomagnetic micropulsation amplitudes and polarization along meridional profile analyzed from simultaneous ground station recording

18 p3250 A70-36937

Giant pulses in passively Q switched laser oscillator, calculating time constant of light flux exponential increase

18 p3270 A70-36953

Finite difference time integration method for computing seismic ray intensities

19 p3412 A70-37837

Electric current pulses peak values measurement during aperiodic capacitor discharges, describing circuit with Rogowski coil, diode, capacitor and VTVM

19 p3426 A70-37938

Air shower radio pulse amplitude dependence on primary energy and core distance

19 p3381 A70-38607

Pulsar 1919 plus 21, discussing pulse intensity vs phase and number by statistical analysis of two dimensional data array

20 p3705 A70-39489

Polarization characteristics of pulsar NP 0532 strong pulses at 430 MHz, using dual circularly polarized line feed

22 p4105 A70-43228

Time analysis of pulsed activity of neurons, using amplitude analyzer with programmable control unit

22 p3972 A70-43551

Pulse height distributions due to terrestrial gamma rays, using NaI/Tl scintillation counter

23 p4187 A70-43899

Giant pulses by actively and passively Q-switched inorganic neodymium-liquid lasers with varying modulation due to mode coupling

23 p4202 A70-44937

Flaw echo height dependence on ultrasonic testing pulse frequency spectrum

24 p4336 A70-45688

Round pulsed jet diffusion rate from velocity measurements, considering Strouhal number and pulse amplitude

24 p4327 A70-46205

PULSE AMPLITUDE MODULATION

PWM-PAM and PTM-PAM systems analysis, deriving formulas for output signal shape determination

08 p1480 A70-21226

Holographic pulse compression technique employing amplitude modulation to circumvent need of matched filter in chirp process

08 p1498 A70-21593

Pulse duration, time and amplitude of pulse modulation, discussing device, detection circuit and statistical error analysis

09 p1639 A70-23697

PAM-FM modulation system optical receiver derivation, assessing threshold performance assuming uniformly distributed modulating signal

12 p2183 A70-27155

Phase recovery in vestigial sideband /VSB/ data transmission, deriving carrier acquisition time required to achieve satisfactory error rate for coherent demodulation of PAM

21 p3793 A70-42178

Pulse angle modulation and PTM-AM equivalence, examining noise effect on conversion

22 p3989 A70-42570

PULSE CODE MODULATION

NT DELTA MODULATION

FM data and telegraph signal transmission over PCM system analog channel, discussing adaptability to digital modulated signals

01 p0046 A70-11318

Azimuth information transmission by PCM signals with equal repetition and scanning frequencies, investigating antenna characteristics

02 p0270 A70-12619

PCM signal transmission testing over radio links with two level phase modulation

03 p0452 A70-14282

Baseband transmission system information transmission rate improvement, using multivalued PCM signals

06 p1007 A70-17461

PCM time division satellite multiple access communication system to increase time slot utility, considering individual earth station control and common signaling circuit features

06 p1011 A70-18409

Clock synchronization system design and test results for PCM time division multiple access satellite communication system

06 p1011 A70-18411

Multiple access channel control system operating in variable destination multiple access mode for application in PCM-TDMA satellite communication system

06 p1011 A70-18412

Fading effect on error probability of multi-hop PCM radio system, noting domination by worst hop

08 p1458 A70-20797

Binary, ternary and multilevel digital signals transmission codes emphasizing PCM signals

09 p1631 A70-22038

PCM-TDMA satellite communication system for maximum time slot utility without guard time slots

10 p1834 A70-24330

Multichannel PCM/TDMA INTELSAT network with time preassignment and time assignment speech interpolation features for field test

10 p1835 A70-24332

High speed PCM terminal with 600 channel capacity, evaluating feasibility for high speed PCM codec, examining STN degradation factors

10 p1835 A70-24337

Geostationary orbit capacity based on multichannel telephony, comparing digital and analog modulation techniques

10 p1836 A70-24343

Transmission performance of telephone calls routed through PCM satellite circuit between London and White Plains

10 p1837 A70-24349

PCM-TDMA satellite communication systems operation modes and applicability, considering efficient circuit utility, equipment cost and control complexity

10 p1837 A70-24352

FDMA and TDMA systems for demand assignment of satellite circuits noting PCM/TDM operation trends in satellite and ground communications

10 p1838 A70-24355

Book on principles of pulse code modulation covering analog to digital conversion, sampling, quantizing, coding, etc

10 p1841 A70-24775

Differential Pulse Code Modulation /DPCM/ system with quantizer separating slope overload and granular noise, using Fokker-Planck- Kolmogorov equation

10 p1844 A70-25204

Multiple-access and demand-assignment techniques, discussing compatibility of PCM-FDMA /SPADE/, PCM-TDMA, ATIC and INTELSAT 4 systems

11 p1997 A70-25415

Power spectral density and autocorrelation functions of sinusoidal carrier amplitude modulated by split phase PCM and PSK

11 p2008 A70-26203

Nonlinear estimation with quantized measurements, applying algorithms to PCM, predictive quantization and data compression

12 p2192 A70-27420

Sounding rocket telemetry systems, discussing use of PCM and thick film techniques

13 p2363 A70-28681

Statistical characteristics and energy spectra of pulse code signals in data transmission estimated by matrix methods

13 p2364 A70-28871

Wideband PCM/FM discriminator detection, predicting effects of predetection and postdetection filtering on system performance

14 p2558 A70-31192

DC-10 airborne flight test PCM data system, discussing capability, onboard operating characteristics and test results

17 p3093 A70-35498

PGM noisy high bit rate processing system, describing preprocessor, bit detector and synchronizer

19 p3379 A70-37903

PCM data transmission, considering baseband code and modulated carrier formats and spectral distributions

19 p3379 A70-37905

Optical communications system for transmission and detection of PCM word pattern at gigahertz rates, discussing optical and electrical modulation

21 p3788 A70-41339

Wideband high speed PCM/AM optical communication system using mode locked He-Ne laser, noting simultaneous signal transmission and bit rate

21 p3789 A70-41354

- Single channel per carrier PCM FDMA demand assignment satellite communication system, discussing digital encoding, quadrature PSK modulation, etc
21 p3791 A70-41367
- PCM/NRZ signal band-limiting effect on bit error probability, using sample detector
22 p3990 A70-43339
- High speed PCM Codec with maximum 600 channel capacity applied to Time Division Multiple Access (TDMA) system for satellite communication
23 p4166 A70-43774
- ### PULSE COMMUNICATION
- Pulse methods for measuring correlation function of incoherent scattered signal, calculating bit estimator errors for large and small SNR
01 p0045 A70-11088
- Message switching techniques in digital telecommunication networks, discussing automatic routing, operational and control facilities, etc
02 p0256 A70-11973
- Pulse signals optimal filtration in superregenerative receiver and resulting SNR effect
03 p0456 A70-13203
- Temporal position of pulse signals measured by multichannel storage devices, discussing interference immunity and required storage time
03 p0448 A70-13435
- Digital telemetry systems for geophysical satellites, describing onboard and ground systems design criteria and experimental results
03 p0451 A70-13837
- UHF radio telemetry system using pulse signal to measure and transmit sea waves amplitude and frequencies data to shore-based recorder
03 p0453 A70-14352
- Extremal statistics for signal and noise error probabilities estimation and computer simulation of digital feedback communication systems
08 p1459 A70-20800
- Circuit analysis of pulse integrator and square-law receiver used as optimal filter during incoherent radio pulse reception on background fluctuating noise
08 p1461 A70-20865
- Digital communications and circuits and components for GHz data rate capability, discussing modulation techniques and bit stream coding
08 p1462 A70-21258
- Pulse indicators using thermoelectric effect of hot carriers caused by nonuniform heating of electron gas in HF field
09 p1643 A70-22127
- Gigahertz rate circuits requirements for high speed digital data communication from component and system viewpoint, emphasizing coding and multiplexing techniques
09 p1633 A70-22605
- Sinusoidal modulated HF pulse signal, deriving parametric envelope and power density function
10 p1833 A70-24086
- Digital satellite communication - Conference, London, November 1969
10 p1833 A70-24326
- Error probability degradation for digital satellite communication systems, employing multiphase signal sets distorted by bandlimited filtering
10 p1836 A70-24342
- Interference problems arising during digital satellite communications, discussing PCM telephone system and PSK modulation
10 p1836 A70-24345
- Satellite relayed integrated digital multiple access systems, discussing traffic handling, satellite positioning, demand assignment, etc
10 p1839 A70-24369
- Pulsed system accuracy increment by increasing number of modulated signal parameters in addition to pulse duration modulation
10 p1843 A70-25137
- Satellite capacity utilization for mixed earth stations network using SPADE concept/digital satellite communication system employing demand assignment and voice-activated carrier techniques
11 p1996 A70-25404
- Review of 1969 London International Conference on Digital Satellite Communication session covering modulation, synchronization and coding
11 p1997 A70-25409
- Report on 1969 London International Conference on digital satellite communication session on operational requirements covering circuit operation modes, demand-assignment control, etc
11 p1997 A70-25412
- Report on Spectrum Utilization and System Constraints session of Intelsat/IEEE International Conference on Digital Satellite Communication, London, November 1969
11 p2002 A70-25486
- Digital satellite communications systems, discussing time division multiplexing, steerable beam antennas and satellite-to-satellite transmission
11 p2003 A70-25492
- Discrete sequential algorithms for bit synchronization implemented with digital computer for optimum data detection
12 p2184 A70-27249
- Reliable and optimum cost power sources design for long life electronic digital communication equipment
12 p2166 A70-27927
- Frequency modulated RF pulses compression with dispersive property of lossless, isotropic and homogeneous plasma used to enhance receiver transmission resolution
12 p2282 A70-27960
- Analog information transmission device using He-Ne laser radiation, discussing optical telemetric channel transfer characteristics for pulsed nanosecond analog signals
12 p2250 A70-28184
- Signal analysis from Russian Cosmos, Proton and Soyuz satellites, showing pulse width and pulse code telemetries
14 p2551 A70-30975
- Rank order statistics for optimum detection of binary pulsed signals in white noise and DC drift
14 p2551 A70-31122
- Wideband pulse signal synthesis and optimal filtration by dispersive ultrasonic delay lines, estimating potential noise stability for analog data transmission
15 p2696 A70-31502
- Lossless pulse-shaping active line for unipolar transmission, considering construction by loading two terminal Esaki diode to coaxial cable
15 p2697 A70-31827
- Stripline skin effect in digital equipment transmitting fast rising pulses
15 p2708 A70-31828
- Practical codes in digital space communication systems, reviewing Shannon information theory theorems
15 p2698 A70-31963
- Broadband and narrowband pulse signal noise electromagnetic interference prediction techniques for filter or shielding parameters evaluation
16 p2862 A70-33065
- Holographic recording of wideband pulsed carrier electric signals in Fourier transform, Fraunhofer, Fresnel and image formats
16 p2903 A70-33136
- Coherent digital communication systems optimal design based on unified theory, discussing tradeoffs between error rates, Doppler tracking capability and time and frequency division multiplexing
16 p2866 A70-34258
- Communication satellite UHF link with FSK or PSK modulation, considering coded digital transmissions
16 p2867 A70-34331
- Frequency synchronization channel pulse fluctuations effect on noise stability of binary signal reception
20 p3587 A70-40145
- Statistical pattern recognition and threshold learning in signal detection of noisy binary pulses
21 p3794 A70-41332
- Signal shape optimization by minimizing dispersion in temporal position estimates for radio pulse in presence of additive white noise
23 p4161 A70-43961
- Optimum input pulse signal synthesis for transmission through lossless homogeneous isotropic plasma, using matched filter theory
23 p4228 A70-44962
- Commercial satellite system circuit quality and reliability in digital communications, considering Automatic Digital Network Trans-Pac cable cut incident
24 p4311 A70-45223
- Power spectrum of digital signals pulse modulated with random sequences, discussing phase modulation and z transform techniques
24 p4315 A70-46151
- ### PULSE COMPRESSION
- Matched filter rectangular pulse compression nonlinear FM waveform design with low time sidelobes and zero mismatch loss due to spectral weighting
07 p1242 A70-20065
- Holographic pulse compression technique employing amplitude modulation to circumvent need of matched filter in chirp process
08 p1498 A70-21593
- Maser amplification in Chirp radar signals pulse paramagnetic compressors using electron spin echoes
09 p1637 A70-23321
- Optimal pulse compression time-invariant filter for signal reception with sidelobe constraints under white noise in radar and communications systems
11 p2025 A70-26218
- Frequency modulated RF pulses compression with dispersive property of lossless, isotropic and homogeneous plasma used to enhance receiver transmission resolution
12 p2282 A70-27960
- Pulse compression for geodesy satellite radar altimeter, considering tradeoff based on system accuracy, power and life
16 p2911 A70-33715
- Adaptive AC null detector with tuned compression amplifier used for oscilloscope display drive
21 p3828 A70-41469
- Intense laser light pulse longitudinal compression resulting from nonlinear intensity-dependent refractive index
22 p4050 A70-43221
- Compression of laser pulses reflected from periodic and zone plate gratings
22 p3990 A70-43337
- Linear FM radar pulse compression matched filter response calculated by computer evaluation of cross ambiguity function for design tradeoff between resolution and performance
22 p3992 A70-43589
- ### PULSE DIFFRACTION
- Diffraction shaped ruby laser monopulse during excitation of modulated ultrasonic traveling waves in phototropic Q switch
09 p1696 A70-22483
- Radio meteor orbit velocity and radiant measurements by pulse diffraction technique
18 p3315 A70-36603
- ### PULSE DOPPLER RADAR
- #### NT MONOPULSE RADAR
- #### NT PULSE RADAR
- Wind field-Doppler velocity field generalized correlation, describing horizontal velocity component measurement by single pulse Doppler radar technique
02 p0326 A70-12287
- Pulsed Doppler radar observation of thunderstorm uplift structure, noting vertical velocity perturbations
06 p1101 A70-18581
- Distributed ground clutter effects computation in airborne pulse Doppler radars, describing high PRF radar
07 p1236 A70-20063
- Coherent instrumentation radar for White Sands Missile Range, discussing system design emphasizing pulse Doppler capability
10 p1842 A70-24881
- Airborne pulse Doppler radar for tactical aircraft velocity vector measurement, improving navigation system performance
16 p2840 A70-33448
- Coding forms in radar signals in terms of ambiguity function trend, combining pulse compression with discriminating possibilities in Doppler frequency
21 p3792 A70-41988
- ### PULSE DURATION
- Pulsed arcs in argon and helium at superhigh pressures, noting plasma ionization and temperature and charged particle density
01 p0149 A70-10168
- Pulsar PP 0943 properties, giving period, pulse characteristics and position
01 p0177 A70-10343
- Pulse width and spectrum generated by ring laser mode locked by synchronously modulated absorber as function of modulator waveform curvature and active medium
01 p0109 A70-10430
- Picosecond on-off light gate based on Kerr cell design, using optical pulses to induce birefringence in liquids
01 p0111 A70-10571
- Frequency sweep /chirp/ and pulse width in externally mode locked laser with host dispersion obtained analytically using circulation pulse method
01 p0111 A70-10572
- Background luminance effect on flash brightness in eyes, measuring increment threshold and luminances required for various brightnesses
01 p0025 A70-11052
- Pulse propagation inside laser cavity containing amplifying medium and material displaying optical Kerr effect, predicting ultrashort pulses
01 p0113 A70-11177
- Electromagnetic pulse duration formed by spectral content in HF bandwidth received after ionospheric reflection
02 p0258 A70-12419
- High intensity short pulse flash lamps using quartz envelopes and wire electrodes for pumping high energy organic dye lasers
02 p0314 A70-12741
- Light pulse demodulator using zero crossing technique to eliminate photomultiplier bandwidth and sensitivity limitations
02 p0271 A70-12744
- Pulse peak width of He-Ne laser with Ne filled absorbing cell in resonator found dependent on saturating field and Ne pressure in cell
03 p0498 A70-13089
- Longitudinal and transverse mode locking in laser with passive filter, discussing giant pulse development and duration
03 p0502 A70-13746
- Pico-nanosecond light pulses from mode-locked Nd glass laser with spectral mode selector, noting correspondence between pulse duration and inverse bandwidth
03 p0503 A70-14210
- X ray flux pulsations for pulsars near Crab Nebula observed in 2.5-30.0 kev range, determining pulsation profile
03 p0578 A70-14358

Pulsars pulse duration and shape as key to neutron stars linkage with supernova explosions

04 p0750 A70-14749

Saturable Q switch of cryptocyanine used in ruby laser for pulse sharpening, describing dye sensitivity to solar radiation

04 p0701 A70-15035

Laser gain investigated for amplifications of short emission pulses in neodymium glass, discussing line broadening nonuniform mechanism

04 p0702 A70-15226

Transient molecular vibration excitation by picosecond laser pulses found dependent on shape of Stokes pulses in Raman scattering study

04 p0702 A70-15298

Ruby laser giant pulses time stretching and shaping using stimulated Raman scattering in liquid nitrogen cell inserted in laser resonator

05 p0857 A70-16076

Transient emissions on He I wavelength during breakup phase of auroral events, discussing observational interference by OH bands

05 p0907 A70-16277

Optical harmonic generation by doubling picosecond laser pulse frequency under nonstationary conditions

06 p1080 A70-17494

Spectral power distribution and ultrashort pulses limiting duration of ruby-neodymium laser with passive shutter

06 p1081 A70-17766

IR laser giant pulses duration and power measured by photomultiplier and lithium metaniobate

06 p1082 A70-17770

Pulse amplitudes and delays measured for oblique absorption values during IGY over 1000 km transmission path for correlation with lower ionosphere model

07 p1228 A70-19155

Step-recovery diodes to shape pulses with steep leading and trailing edges noting transient processes

07 p1241 A70-19734

Self mode locked pulses with rotating mirror Q switched carbon dioxide laser, attributing pulse shortness to saturation broadening of spectrum

07 p1301 A70-20018

Nitrogen molecules pulsed high energy beams transit time measurement by gated time of flight procedure and by multichannel analyzer

07 p1345 A70-20136

Optical pumping energy effects on lasing pulse duration during pulse excitation of alcohol solutions of rhodamine 6G

08 p1511 A70-20522

Pulse duration approximation in tunnel diode monostable multivibrator during low duty cycle operation

08 p1472 A70-20867

Pulsars pulse arrival time measured using cesium clock during weekly observations

08 p1570 A70-20899

Pulse characteristics of scintillator-photomultiplier-cathode ray tube channel for oscillographic recording of nanosecond pulses from neutron, gamma or X ray sources

08 p1496 A70-21218

Exponential pulse time converter investigated for effect of supply voltage variations on duration of generated pulses

08 p1474 A70-21232

Mode locked laser pulse chopping by interferometrically combined electro-optical frequency shifters

08 p1513 A70-21541

Pulsar NP 0532 average polarization parameters measured at 430 MHz, discussing variations of precursor and main pulse and flux of interpulse

08 p1578 A70-21549

Two photon interaction between ultrashort light pulse and medium, showing pulse propagation through medium without absorption

08 p1514 A70-21820

Longitude and latitude dependence of pc geomagnetic micropulsations related to local time, using analog spectral analysis

09 p1666 A70-22064

Subjective and objective measurement of sound impulses, pauses and intervals duration sensation, showing adjustment accuracy

09 p1618 A70-22763

Subnanosecond laser pulses for plasma production obtained via mode selecting uncoated flats inserted in laser cavity

09 p1699 A70-23364

Pulse-shaping transistor circuit analysis, considering circuit elements roles and temperature, pulse duration and leading and trailing edges durations effects

09 p1650 A70-23628

Q switched laser pulses lengthened using internal second harmonic generator

10 p1898 A70-23981

Time-bounded pulses with energy maximum in frequency band, solving integral equations for band-pass filters for maximum efficiency and optimum pulse shapes

11 p2004 A70-25799

Probability density function of click duration in FM discriminator

11 p2018 A70-26270

Impact accelerations measurement for shock pulse amplitude and duration, describing system for direct reading

11 p2055 A70-26447

Solid state laser with traveling wave during steady state emission, determining pulse shape, duration and amplitude

12 p2247 A70-27497

Molecular beam carbon dioxide laser Q switching by ethylene as saturating filter, reducing pulse duration by varying ethylene pressure and active mixture composition

12 p2248 A70-27509

Ruby crystal surface destruction by laser radiation, studying surface structural and optical properties effect and threshold power dependence on light pulses duration

12 p2248 A70-27541

Molongo pulsars observations, using multiperiod integration technique for declinations, periods and positions

13 p2487 A70-28632

CW mode locked lasers picosecond pulse widths and shapes measured, determining harmonics and Fourier expansion

13 p2425 A70-28794

Giant pulses composed of shorter pulse trains obtained in Q switched carbon dioxide laser with transverse modes

13 p2429 A70-29412

Transistorized voltage to pulse width converter based on constant current capacitor discharge

13 p2378 A70-29457

Strong short coherent light pulses with diffractive divergence generated by ruby lasers in series, showing pulse, emission and far field interferograms

13 p2430 A70-29762

Myocardium potential working capacity in relation to diastola duration of ventricles

13 p2355 A70-29767

Pulsar short period pulsations and emission patterns in meter wavelength range on crossed radio telescope

14 p2633 A70-30151

Radio echoes duration distribution from supercondensed meteoric trail emphasizing effects of recombination, adherence and turbulent diffusion

14 p2636 A70-30325

Multimode and dispersive distortion of short quasi-monochromatic pulses in earth-ionosphere VLF channel

16 p2858 A70-32930

Feedback system with combined pulse modulator incorporating pulse frequency and pulse width modulation laws

16 p2882 A70-33036

Q switched subnanosecond laser system with increased intensity, using pulse selection technique

16 p2927 A70-33163

Pulsars MP 0031 and CP 1919 periodic variations in pulse intensity, considering radio emission models with plasma waves

17 p3157 A70-34843

Long term geomagnetic pulsations /PC5/ with sinusoidal waveforms, using IGY data

17 p3080 A70-35642

Spectral and temporal characteristics of ruby laser operating with dielectric coated mirror scatterer

17 p3108 A70-35673

Laser mode locking theory, explaining subpicosecond structure and frequency chirp

18 p3266 A70-36315

Small angular diameter radio source in central Crab nebula association with pulsar NP 0532 based on spectra and pulse duration

18 p3322 A70-37128

Coupled fiber lasers maximum energy transfer between passive conductors, determining minimum pulse duration

19 p3443 A70-37286

Two photon absorption-fluorescence measurement of laser pulse width, using three level model of absorber

19 p3422 A70-37671

Strong short coherent light pulses with diffractive divergence generated by ruby lasers in series, showing pulse, emission and far field interferograms

19 p3447 A70-38394

Ultrashort light pulse generation by self mode locking laser, discussing power amplification problems

19 p3448 A70-38509

Heisenberg uncertainty principle in communications technology, discussing variance products deficiencies and limits in carrier frequency pulses application

20 p3584 A70-39160

Uncertainty principle in optimum communication theory, discussing existence and value of minimum product of pulse duration in terms of calculus of variations and differential equations

20 p3584 A70-39161

Giant pulse neodymium glass laser emission spectrum structure, showing cavity geometry effect on fine structure

20 p3641 A70-39450

Centimeter wave transmitting and receiving equipment for studying nanosecond pulse propagation

20 p3632 A70-39627

Multiphase relaxation oscillator with inductive coupling and common base resistor in feedback loop, determining circuit parameters effect on pulse length

20 p3598 A70-39791

Multimegawatt quasi-steady MPD arc accelerator in millisecond pulses, noting applicability to experiments requiring long exposure times

20 p3683 A70-40241

Pulsars subpulse intensities and shapes in magnetic field, noting drift speed sawtooth patterns

20 p3713 A70-40428

Single picosecond mode-locked laser pulse selection and multiple pass amplification device, obtaining high energy and signal to noise ratio

21 p3838 A70-42023

Pulsar short period pulsations and emission patterns in meter wavelength range on crossed radio telescope

21 p3923 A70-42073

Ultrabright nanosecond flash light generation technique, using superradiant light sources for shadowgraph photography in high resolution hyper-velocity field

22 p4037 A70-43070

Short pulse length X ray flash electro-optical recording equipment for explosive processes, describing technique, experimental setup, optical characteristics and information retrieval

22 p4037 A70-43071

Pulse duration dependent threshold intensity difference for sine tones related to dynamic properties of hearing

23 p4155 A70-44699

Pulsar radiation polarization, examining mean pulse profiles, frequency, position angle and rotational effects

24 p4403 A70-45404

Nd laser single picosecond pulse energy, duration and frequency width

24 p4354 A70-45664

Mode locked laser pulses picosecond structure predicted from theoretical model of Gaussian random radiation field with temporal envelope modulation

24 p4355 A70-46263

PULSE DURATION MODULATION

Pulse width modulated /PWM/ electrohydraulic servo response characteristics from modulator transfer characteristic determination by Fourier series analysis of PWM signal

[ASME PAPER 69-WA/AUT-2] 04 p0625 A70-14831

Pulse width modulation command code for German research satellite Azur control

04 p0653 A70-15662

PWM-PAM and PTM-PAM systems analysis, deriving formulas for output signal shape determination

08 p1480 A70-21226

Pulse repetition rate control and stabilization in passively Q switched carbon dioxide laser

09 p1699 A70-23537

Pulsed system accuracy increment by increasing number of modulated signal parameters in addition to pulse duration modulation

10 p1843 A70-25137

Signal transduction with differential pulse width modulation applied to data acquisition processes

13 p2405 A70-28812

DC-to-sinusoidal inverter employing PWM waveform, analyzing circuit parameters effect on harmonic content

19 p3358 A70-37854

Fluidic gyro compatible with PDM missile guidance system, discussing spherical gas bearing design

[AIAA PAPER 70-1008] 20 p3631 A70-39524

Spacecraft pulse width modulated attitude control system stability, using state space method

[AIAA PAPER 70-984] 20 p3714 A70-39545

PULSE FREQUENCY MODULATION

Neural pulse frequency modulation system stability, using feedback control model

17 p3056 A70-35553

Steady forced regime stability in pulse frequency modulated servosystems, using Liapunov method

18 p3234 A70-36071

Statistical characteristics of steady random signal of pulse frequency modulator, obtaining moments of output signal

18 p3234 A70-36072

Unipolar pulse frequency modulation system with white noise input, deriving output power spectral densities

21 p3793 A70-42225

Pulse angle modulation and PTM-AM equivalence, examining noise effect on conversion

22 p3989 A70-42570

PULSE FREQUENCY MODULATION TELEMETRY

FM telemetry channel noise effects on digital and analog accelerometer outputs accuracy, suggesting mean square error reduction methods

10 p1893 A70-25318

PULSE GENERATORS

Telemetric systems for moving machine elements tests, discussing seven channel PFM and FM/FM systems 11 p2056 A70-26451

PULSE GENERATORS

Superradiant traveling wave laser emission observed with polymethine cyanine dyes pumped by mode locked ruby laser for picosecond duration pulse generation 01 p0110 A70-10564

Pulse propagation inside laser cavity containing amplifying medium and material displaying optical Kerr effect, predicting ultrashort pulses 01 p0113 A70-11177

Longitudinal and transverse mode locking in laser with passive filter, discussing giant pulse development and duration 03 p0502 A70-13746

Leading edge phase shift of output pulse from threshold-type pulse shaping circuit determined as function of triggering threshold 06 p1009 A70-17675

Modulated high voltage pulse generator, using rectification of voltage obtained from HF oscillator 06 p1022 A70-17776

GaAs laser and laser array applications, discussing pulse generators, laser cooling, laser optics, detectors, etc 07 p1298 A70-19400

Radar coherent linear FM microwave generation with 14 microsecond pulse length and 1000 MHz bandwidth, discussing phase error and coherency 07 p1236 A70-20064

Step recovery frequency shift keyed retimer using Gunn effect FSK pulse regenerator for microwave communication 07 p1237 A70-20285

Exponential pulse time converter investigated for effect of supply voltage variations on duration of generated pulses 08 p1474 A70-21232

Short high current pulses generation by avalanche transistors in circuits suitable for investigating low impedance laser diode 09 p1642 A70-22035

Controllable generator of linearly stepped voltage pulse using avalanche transistors, controlling avalanche-transistor relaxation oscillator by gating storage condenser 09 p1643 A70-22130

Digital autopilot design using stochastic noise generator for synchronous random pulse sequence controlled by clock 09 p1720 A70-22418

Pulse-shaping transistor circuit analysis, considering circuit elements roles and temperature, pulse duration and leading and trailing edges durations effects 09 p1650 A70-23628

Electronic modulo-M counter driven by HF pulse generator used for generating random numbers sequence 10 p1848 A70-23976

Silicon L-band avalanche diodes as high power pulsed microwave sources, discussing fabrication, circuit requirements, radar applications, etc 10 p1852 A70-24893

Thyratron based fast pulse generator circuits noting applications 11 p2017 A70-25570

Soviet book on aircraft AC and DC relay pulse generators, emphasizing controllable frequencies and duty factors and neutral and polarized electromagnetic relays 12 p2194 A70-26874

Amplitude stabilization transient processes at output of four terminal network with arbitrary phase and amplitude characteristics by representing pulse transfer function in series 12 p2184 A70-27537

Electromagnetic pulse generator for simulation of EMP associated with nuclear explosions, describing electronic equipment vulnerability testing 12 p2208 A70-28135

Giant Stokes radiation pulse generation during stimulated combination scattering, emphasizing pulses traveling counter to pumping wave 12 p2250 A70-28288

Thyristor tetrode silicon controlled switches (SCS), considering unijunction transistors and pulse generator circuits 13 p2377 A70-29115

Intracranial pressure pulse waves formation mechanism mathematical model, estimating role of biomechanical factors 13 p2353 A70-29520

Ultrashort pulse generation by solid state Q switched lasers, discussing spontaneous emission effects, atomic polarization and populations variation 14 p2594 A70-30477

Multipurpose pulse generator design for 1 Hz-100 MHz frequency range and adjustable rise and fall times 14 p2557 A70-31162

High voltage gas laser trigger pulse generators featuring high pulse rate with semiconductor controlled rectifier 14 p2594 A70-31181

Giant pulse generation in ruby laser requiring no introduction of additional modulating elements into resonator 15 p2749 A70-31524

High power microwave pulse generation in SHF region, discussing use of boat-grown and epitaxial GaAs diodes 16 p2875 A70-33396

SHF pulsed Gunn effect GaAs oscillators for nsec pulse length radar applications 16 p2875 A70-33397

Multichannel time marker network synthesis device for physiological data assembly, transformation and processing, generating pulses 18 p3223 A70-36083

Avalanche transistor circuits for rectangular pulses generation, considering delay line for optimum results 18 p3233 A70-36774

Gunn effect pulse regenerators, describing random domain triggering rate voltage dependence comparison with Johnson noise predictions 19 p3387 A70-37820

Pulse shaper circuits with tunnel diodes and transistors, describing recovery time decrease 20 p3596 A70-38972

Pulse coding system for average evoked EEG potential data acquisition and analysis, describing pulse generation circuitry and computer implemented logic 20 p3578 A70-38985

Shock pulse reproduction on electrodynamic and hydraulic shakers for vibration testing, including SNAP 21 results 21 p3804 A70-40865

Book on pulse and switching circuits covering remote control, TV, computers, radar, telemetry and automation devices 21 p3798 A70-41324

Picosecond large amplitude pulse generating GaAs diode with nu-n structure 21 p3800 A70-42116

Discharge pulse generation and equivalent resistance of relaxation oscillator applied to avalanche transistor 24 p4319 A70-45639

PULSE HEATING

Rate and heat of vaporization of graphite filaments in 2500-3400 K range in vacuum and in He, using pulse heating techniques 03 p0517 A70-14004

Heat source temperature distribution on surface of infinite cylinder with zero temperature, presenting solution to boundary value problem 05 p0957 A70-16296

Heat conduction in anisotropic materials to measure thermophysical parameters, using pulsed point or line heat source 05 p0957 A70-16457

Transient heat conduction in dual-layer insulated plate exposed to pulse heating, discussing temperature response [ALAA PAPER 70-14] 06 p1180 A70-18120

Al and Be single particles combustion in various oxidizers, using pulsed Nd-glass laser and Xe flash heating device and scanning electron microscope 14 p2628 A70-30949

High speed photoelectric pyrometry of Ta heat capacity at high temperatures induced by pulse heating 23 p4207 A70-44441

PULSE HEIGHT

U PULSE AMPLITUDE

PULSE MODULATION

NT DELTA MODULATION

NT PULSE AMPLITUDE MODULATION

NT PULSE CODE MODULATION

NT PULSE DURATION MODULATION

NT PULSE FREQUENCY MODULATION

NT PULSE FREQUENCY MODULATION

TELEMETRY

NT PULSE POSITION MODULATION

NT PULSE TIME MODULATION

Corrective open-loop circuit, using delay elements for compensation of transient response in linear circuits with lumped parameters for pulse modulation transmissions 06 p1023 A70-17774

Step-recovery diodes to shape pulses with steep leading and trailing edges noting transient processes 07 p1241 A70-19734

Pulsed grid modulation for ion cyclotron resonance spectrometer 07 p1286 A70-19974

Silicon controlled diodes application to pulse modulation circuits of radar transmitters 09 p1631 A70-22016

Sinusoidal modulated HF pulse signal, deriving parametric envelope and power density function 10 p1833 A70-24086

Jupiter decametric emission modulation by planetary rotation and Io position, suggesting role of magnetic tail diurnal swings 10 p1940 A70-24434

Limit cycle oscillations in satellite attitude control system, producing control moment by pulse modulated controller 13 p2502 A70-28430

Frequency conversion during multiple phase modulation of supply voltage by pulse width technique 14 p2548 A70-30372

Switch controlled resonant current pulse modulation for power converters, noting integration with spacecraft ion propulsion engine 14 p2535 A70-31324

Feedback system with combined pulse modulator incorporating pulse frequency and pulse width modulation laws 16 p2882 A70-33036

Pulse modulated feedback control system, deriving sufficient condition theorem for input-output stability 16 p2884 A70-33099

Si controlled thyristors applied to pulse modulators in ionospheric stations 18 p3233 A70-37043

Signal modulation by pulse ratio variation in magnetic tape channel, discussing SNR characteristics 20 p3586 A70-39707

Pulse ratio modulation analysis based on information theory, emphasizing magnetic tape channel capacity optimal utilization in signal transmission 20 p3586 A70-39708

Solar radio pulsations, observing modulation of coronal microwave, X ray and type III emission 21 p3880 A70-40965

Weak noise and threshold effects on estimation error for nonlinear PM systems 24 p4312 A70-46053

Power spectrum of digital signals pulse modulated with random sequences, discussing phase modulation and z transform techniques 24 p4315 A70-46151

PULSE POSITION MODULATION

Frequency pulling and pulse position modulation of CW GaAs injection lasers by locking signal frequency variation 03 p0502 A70-13815

Pulse position modulation focused TWT for airborne electronic countermeasure broadband jamming, considering output power and thermal design 04 p0653 A70-15656

Narrow width pulse-position modulated optical communication system design, determining performance in terms of error probability and information rates 08 p1463 A70-21778

Noise threshold performance of optimum PPM telemetry receivers using slicer for detector 11 p2010 A70-26273

PULSE RADAR

NT MONOPULSE RADAR

Radar pulse scattering from ionized media including nuclear explosion fireballs and high speed reentry vehicle wakes, analyzing to retrieve backscattered pulse signal envelope 02 p0262 A70-12602

Variable RF signals in pulsed radar, examining circuits design for required functions 03 p0452 A70-14281

Tropospheric scattering ability investigation with radar transmitter emitting vertical pulses, considering implications for scatter propagation from backscattering detection 03 p0453 A70-14298

Feedback technique for frequency stability requirements of airborne radar systems, discussing non-coherent radar applications and cost comparison to power-amplifier approach 04 p0656 A70-14708

Pulsed radar fluctuating echo digital-detection and false alarm probabilities assuming Rice signal distribution with noise 04 p0649 A70-15065

Nonadaptive processor to detect coherent radar pulse trains with uniform amplitude in clutter-plus-noise environment 04 p0651 A70-15334

Pulse radar altimeter for measuring meteorological balloon altitude, using superregenerative RF stage 05 p0845 A70-15805

CW, pulsed and frequency modulated radar scatterometry, discussing flight, system, terrain and data processing parameters 06 p1012 A70-18594

Pulse radar altimeter design for balloon sounding, discussing flight tests, superregenerative stage, etc 07 p1286 A70-19996

Radar coherent linear FM microwave generation with 14 microsecond pulse length and 1000 MHz bandwidth, discussing phase error and coherency 07 p1236 A70-20064

Linear FM pulse compression radar system operating at 94 GHz, obtaining echoes from orbiting objects for identification 08 p1462 A70-21290

Radar target short pulse transient scattering response computation using fast Fourier transform algorithm 08 p1463 A70-21597

Silicon controlled diodes application to pulse modulation circuits of radar transmitters 09 p1631 A70-22016

Meteor astronomical parameters measurement by pulsed and CW radio methods, considering effects of wind, meteor trails, phase angle, etc 09 p1638 A70-23627

Pulsed Doppler radar technique for monitoring and diagnosing severe storms, obtaining wind velocity and direction within cloud 10 p1844 A70-25242

Short pulse radars application to range measurements, discussing technological and data analysis problems 11 p2005 A70-26041

Analog integrating moving window detector performance analysis for use with scanning pulse radar allowing for antenna radiation pattern and detection process dynamic characteristics 11 p2009 A70-26262

Ionospheric probing using pulsed radio waves at oblique incidence, discussing auroral radar, meteor radar, ground backscatter and variable frequency ionosondes techniques 12 p2224 A70-27728

Radar spectrum control based on two pulse shaping techniques using klystron transmitter 12 p2188 A70-27941

Optimal pulse allocation for radar array in simultaneous tracking of multiple targets, suggesting algorithms 13 p2365 A70-29068

Threshold sensitivity of pulsed optical radar with discrete signal storage, considering different operating modes 13 p2370 A70-29871

Probability density function of specularly fading signal plus noise for frequency shift keying and pulse radar systems 16 p2865 A70-34040

Digital logic techniques for pulse modulated radar systems, with application to controlling and timing waveforms for display 17 p3042 A70-34570

Linear FM radar pulse compression matched filter response calculated by computer evaluation of cross ambiguity function for design tradeoff between resolution and performance 22 p3992 A70-43589

Digital Doppler ambiguity resolution method for pulsed S-band radar, using integrating interval approach 22 p3992 A70-43592

Optimum pulse radar signal-receiver design, considering implementation errors for maximum target detectability in clutter 24 p4313 A70-46055

PULSE RATE

Short irregular geomagnetic pulsations repetitive characteristics relationship with magnetospheric cavity dimensions 01 p0081 A70-11229

Pulse counting frequency divider with discrete phasing device for use with quartz clock and electron beam chronoscope 04 p0694 A70-15492

Pulse rate techniques for signal processing and computation, considering feedback circuits, discussing stochastic rates, sampled systems and digital differential analyzer 06 p1027 A70-18510

Hypothermia effect at various temperatures and durations on nervous activity and vegetative functions of rats, discussing pulse and respiratory rates 07 p1197 A70-18696

Ventilation function, pulse rate and blood pressure measured for adaptation to vertical upright and head-down positions 07 p1201 A70-18794

Phasic aortic blood flow and left ventricular pressure measured at constant heart rates during pulsus alternans, discussing ejection duration and peak flow rate 07 p1210 A70-19588

German monograph on determination of blood velocity, pressure, pulse rate and vascular structure parameters using Doppler effect 08 p1452 A70-21297

Preamplifier-discriminator-gate generator in printed circuit for use with photomultipliers, noting pulse sensitivity and cost 09 p1679 A70-22997

Pulse repetition rate control and stabilization in passively Q switched carbon dioxide laser 09 p1699 A70-23537

Transistorized pulse repetition frequency bandpass and band elimination filters, using trigger circuit to improve pulse-edge steepness and critical frequency stability 09 p1650 A70-23630

Pulse signal transmission rate increase by transient processes compensator, discussing stability relation to signal to noise ratios 09 p1639 A70-23696

Pulse rate counter for randomly repetitive random processes, noting applications to lightning flash noise bursts in receivers 10 p1848 A70-23996

Transistorized pulsed activity converter for observing analog curve of change in pulse frequency 12 p2179 A70-28316

High voltage gas laser trigger pulse generators featuring high pulse rate with semiconductor controlled rectifier 14 p2594 A70-31181

Pulse activity records to investigate neuron functioning dynamics based on construction of frequency graph 15 p2679 A70-31601

High pulse repetition rate digital systems signal processing using Gunn effect diodes 15 p2710 A70-32583

Centrifugation effects on human peripheral arterial pulse behavior 17 p3037 A70-35126

Picosecond pulse frequency sweep measurement using time resolved spectroscopy 17 p3108 A70-35904

Carbon dioxide laser pulse shape, duration and power dependence on repetition rate during continuous pumping 21 p3835 A70-40634

Pulse velocity and mode pulling in inhomogeneously broadened laser with equally spaced modes, noting pulse shape time stability in presence of dispersion 21 p3838 A70-42008

Pulsars null pulse spacing significance, determining fluctuation power spectrum 23 p4238 A70-43814

HF pulsating air flow measuring technique with sharp edged orifice meter, discussing experimental setup and pulsation frequency and intensity effects 24 p4335 A70-45591

Nd laser single picosecond pulse energy, duration and frequency width 24 p4354 A70-45664

PULSE RECORDERS

U COUNTERS

PULSE TIME MODULATION

NT PULSE DURATION MODULATION

NT PULSE POSITION MODULATION

PWM-PAM and PTM-PAM systems analysis, deriving formulas for output signal shape determination 08 p1480 A70-21226

Pulse duration, time and amplitude of pulse modulation, discussing device, detection circuit and statistical error analysis 09 p1639 A70-23697

Pulse angle modulation and PTM-AM equivalence, examining noise effect on conversion 22 p3989 A70-42570

PULSE WIDTH

U PULSE DURATION

PULSE WIDTH MODULATION

U PULSE DURATION MODULATION

PULSED JET ENGINES

Pulsed MPD arc jet electric propulsion system requirements, examining physical constraints, pulse duration, duty cycle, power network structural details, etc [AIAA PAPER 69-269] 04 p0737 A70-15424

Dynamic I-V characteristics of megawatt pulsed MPD-ARC plasma thruster under various axial magnetic fields given for Ar and hydrogen propellants [AIAA PAPER 70-164] 06 p1131 A70-18092

LES-6 satellite solid Teflon pulsed plasma thruster performance, determining energy balance, thrust and circuit parameters [AIAA PAPER 70-179] 06 p1132 A70-18206

Pulsed plasma vacuum-arc thruster system incorporating throttle and thrust vector controls for long life satellite control applications [AIAA PAPER 70-180] 06 p1133 A70-18232

On-line display of pulsed rocket engine performance data using hybrid computer 17 p3063 A70-35512

Thrust measurements on pulsed vacuum-arc thruster, comparing specific impulse and efficiency with exhaust velocity measurements by ion collecting double probes [AIAA PAPER 70-1146] 20 p3567 A70-40207

Exhaust velocity, electron density and temperature of pulsed megawatt nitrogen MPD-ARC thruster, using Thomson scattering of pulsed laser light [AIAA PAPER 70-1081] 20 p3694 A70-40254

Repetitively pulsed MPD propulsion systems, considering thruster performance [AIAA PAPER 70-1093] 20 p3695 A70-40522

Pulsed plasma and low pressure detonator thrusters for long life secondary spacecraft propulsion, considering satellite stationkeeping and attitude control [AIAA PAPER 70-1147] 21 p3868 A70-41782

Round pulsed jet diffusion rate from velocity measurements, considering Strouhal number and pulse amplitude 24 p4327 A70-46205

PULSED LASERS

NT Q SWITCHED LASERS

Frequency sweep /chirp/ and pulse width in externally mode locked laser with host dispersion obtained analytically using circulation pulse method 01 p0111 A70-10572

Pulse propagation inside laser cavity containing amplifying medium and material displaying optical Kerr effect, predicting ultrashort pulses 01 p0113 A70-11177

Ballistic compressor performance as high intensity pulsed light source, discussing Xe gas heating and laser pumping 02 p0311 A70-11921

High power pulsed lasers development compared to thermal light sources, discussing applications to nonlinear optics 02 p0312 A70-12070

Q switched and high energy pulse laser devices for location of satellite photographed by night against background of stars, including optimization in noise [ONERA-TP-753] 02 p0313 A70-12369

Refractive index perturbation from energy absorbed from long pulsed and Q switched Nd doped glass lasers, observing sonic waves generated by Q switched laser 03 p0498 A70-13156

Thermoelastic stresses in diode of pulsed and CW injection lasers, showing energy parameter limitation 03 p0499 A70-13437

Nonlinear differential equations for determining radiation density of three level pulsed gas laser as function of power losses, active medium parameters and time 03 p0502 A70-13745

Atmospheric distortion effect on short laser pulses attributed to aerosols, using real time pulse comparison methods 04 p0701 A70-15020

Simultaneous recording of near and far field diffraction patterns at several exposures for single laser pulse 04 p0701 A70-15022

Temporal isolation between pulsed orthogonal polarization state laser beams, showing selection dependence on sampling time 04 p0701 A70-15032

Laser gain investigated for amplifications of short emission pulses in neodymium glass, discussing line broadening nonuniform mechanism 04 p0702 A70-15226

Pulsed Ar ion lasers at high currents, measuring plasma parameters, electrical conductivity, electron temperature and density for inversion mechanism 04 p0703 A70-15617

High power giant pulse YAG laser using nonlinear material to achieve complete second harmonic conversion in intracavity experiment 05 p0859 A70-16470

Pumping techniques, design and properties of pulsed and CW lasers based on Nd-glass, ruby, barium fluoride and calcium tungstate crystals 05 p0860 A70-16821

Double giant pulse ruby laser with 1.5 m coherence length for producing double exposure holograms of stress wave propagation in solids 05 p0861 A70-16850

Optical harmonic generation by doubling picosecond laser pulse frequency under nonstationary conditions 06 p1080 A70-17494

Oscillatory discharge properties of capacitance power storage circuit used for pumping pulse lasers 06 p1081 A70-17768

IR laser giant pulses duration and power measured by photomultiplier and lithium metaniobate 06 p1082 A70-17770

Time characteristics of pulsed calcium fluoride-dysprosium laser in single mode, observing constant emission and peak regime 06 p1082 A70-17808

Multiple beam interferometer coherence analyzer for temporal and spatial study of laser beams, emphasizing application to pulsed lasers, holography and nonlinear optics 07 p1297 A70-19145

Dye laser stimulation by pumping with pulsed nitrogen laser line to obtain entire visible spectrum 07 p1301 A70-20016

Front lid holograms of transient events and live subjects obtained with reflected light pulsed laser system 07 p1287 A70-20087

Holograms produced with pulsed argon-ion lasers operating in singly oscillating transverse modes 07 p1287 A70-20088

Kinetic model developed for Cl-HBr reaction pulsed chemical laser 08 p1513 A70-21337

Photodissociation of perfluoroalkylidides filler of pulsed laser operating cavity, discussing thermal

molecular dissociation and unexcited iodine atoms formation 08 p1513 A70-21418

Mode locked laser pulse chopping by interferometrically combined electro-optical frequency shifters 08 p1513 A70-21541

Pulsed nitrogen gas laser to obtain continuously tunable dye laser action to 3550 Å with output at 3771 Å in UV 08 p1513 A70-21553

Hydrodynamic processes during focusing of monopulse ruby laser emission into water, determining photohydrodynamic coefficient 09 p1694 A70-22111

Single-pulse laser radiation losses dependence on operation time length due to angular dispersion 09 p1694 A70-22140

Optimal adjusting of laser with instantaneously increasing Q without pumping and relaxation effects during pulse, using nonlinear differential equation 09 p1695 A70-22412

Output energies of Stokes components of stimulated combination scattering excited by pulsed laser 09 p1696 A70-22482

Time delay between pulses of discharge current and ionized argon laser power as function of current and discharge pressure 09 p1697 A70-22847

Pulse train transition in Nd-YAG and He-Ne lasers mode-locked by intracavity phase modulator 09 p1697 A70-22919

Self stabilization and narrowing of optical pulses from GaAs junction lasers by regenerative feedback of oscillations in injection current 09 p1697 A70-22921

Pulsed laser beams intensity fluctuations correlation functions dependence on propagation distance in turbulent atmosphere 09 p1636 A70-23135

Monopulse ruby lasers for moving object illumination during shadow photography, noting applications to ballistic studies 09 p1698 A70-23173

High resolution holography with pulsed radiation source, testing various emulsions for sensitivity and reciprocity behavior 09 p1681 A70-23175

He-Ne CW and pulsed lasers operation, design and technology, describing measurement methods for output, beam divergence and radiation spectrum distribution 09 p1698 A70-23303

Transverse mode distortions in high gain giant pulse laser oscillators associated with gain saturation effects 09 p1698 A70-23361

Subnanosecond laser pulses for plasma production obtained via mode selecting uncoated flints inserted in laser cavity 09 p1699 A70-23364

Pulse repetition rate control and stabilization in passively Q switched carbon dioxide laser 09 p1699 A70-23537

Atmospheric phase jitter for He-Ne locked laser measured by retroreflector for half mile round trip 09 p1699 A70-23539

Book on lasers, light amplifiers and oscillators covering optical resonators, optical pumping, pulsed lasers, etc 09 p1700 A70-23541

Ruby monopulse laser emission spectrum wavelength stabilization by frequency tuning of generated radiation using Fabry-Perot interferometer 10 p1898 A70-23970

Q switched laser pulses lengthened using internal second harmonic generator 10 p1898 A70-23981

Pulsed solid state laser power output stability in terms of kinetic theory noting laser action threshold role 10 p1899 A70-24254

Ruby monopulse laser with narrow emission line, describing two generator system 10 p1899 A70-24264

Plasma production by solid hydrogen-giant pulse laser interaction, studying time dependent distributions of plasma density, temperature and velocity 10 p1902 A70-25222

Mirror adjustment effect on transverse structure, time dependence and spatial coherence of pulsed UV molecular nitrogen laser emission 11 p2062 A70-25394

Pulsed laser holographic interferometry of density field created by high speed projectile motion in air [AIAA PAPER 69-347] 11 p2051 A70-25987

Ultrasonic effects on synchronization of ruby laser radiation, investigating emission pulse structure and peak sequence 12 p2245 A70-27297

Interferometric combinations of frequency-shifted mode-locked laser pulses achieved by optical modulation-demodulation methods 12 p2249 A70-27755

Raman scattering by oxygen and nitrogen in atmosphere observed by using pulsed nitrogen UV laser 12 p2189 A70-28093

Giant Stokes radiation pulse generation during stimulated combination scattering, emphasizing pulses traveling counter to pumping wave 12 p2250 A70-28288

Pulsed chemical laser output, considering increase in radiation energy 12 p2251 A70-28292

Pulsed CO₂ laser calculating upper level lifetime of carbon dioxide molecule with allowance for gas heating at relaxation 12 p2251 A70-28296

Thermoelastic stresses distribution in transmitting dielectric under short nonfocused laser pulses 12 p2251 A70-28327

CW mode locked lasers picosecond pulse widths and shapes measured, determining harmonics and Fourier expansion 13 p2425 A70-28794

Ar ion lasers investigated for effect of added He on pulse output intensity 13 p2426 A70-28809

Pulsed Ne laser superradiation spectrum fine structure, using Fabry-Perot interferometer 13 p2428 A70-29362

Pulse duration and beam diameter effects on threshold energy density in laser induced transparent dielectric breakdown 13 p2428 A70-29382

Crossed field nitrogen laser operation in second positive band to obtain high UV pulse output 13 p2429 A70-29669

Plasma ionization enhancement by laser line radiation matched to specific atomic transitions [AIAA PAPER 69-47] 13 p2468 A70-29958

Pulsed molecular and atomic gas laser sources design for submillimeter region 14 p2593 A70-30433

High temperature elastic moduli of slender polycrystalline aluminum rods with elastic waves generated by Q switched laser energy 14 p2595 A70-30638

Plasma production by irradiating solid hydrogen foils with intense pulse ruby laser 14 p2622 A70-30659

Injection semiconductor lasers emission characteristics, discussing gallium arsenide diodes, nonlinear losses in pulsed mode, laser interactions, etc 15 p2749 A70-31453

Luminescent line broadening effect on axial mode selectivity in pulsed neodymium lasers with Fabry-Perot resonator at above-threshold pumping power 15 p2749 A70-31554

Plasma temperatures of X ray flux from laser induced breakdown plasmas in air, using absorption spectrometer [ARL-70-0145] 15 p2750 A70-31753

Superradiant pulsed 5401 Å neon laser for interferograms of gas flow through nozzles in shock tunnel 15 p2750 A70-31763

Linear power scaling-mass flow relationship in multi-Joule pulsed carbon dioxide-nitrogen-helium laser, noting thermal effects role 15 p2751 A70-31977

Far IR second harmonic generation and frequency mixing in CdTe using pulsed water vapor laser 15 p2751 A70-31983

Pulsed laser alignment using pentaprism-directed continuous laser light beam 15 p2752 A70-32047

High energy electron temperature in beam plasma discharge pulsed laser measured by bremsstrahlung X radiation spectrum 15 p2752 A70-32194

Energetic ion production by giant pulse lasers measured on Al and Au foil targets 15 p2777 A70-32333

Solid state traveling medium laser pulsed emission characteristics and nonlinear intensity distribution 15 p2753 A70-32699

Pulsed carbon dioxide laser production with electron beam pumping, ascertaining beam effect on discharge parameters and output power 15 p2754 A70-32864

Turbulent wakes density fluctuations measurement using pulsed laser holographic interferometry in ballistic range [AIAA PAPER 70-727] 16 p2834 A70-33494

Coaxial gas laser generating high intensity pulses at constant pulse repetition rate, using singly ionized Ar and molecular nitrogen as active media 16 p2928 A70-33698

Mode locked He-Ne laser nsec pulses propagation along multimode clad glass fibers 16 p2865 A70-34039

Nd-glass laser operation in giant pulse mode with passive or optomechanical shutter, noting applications 16 p2929 A70-34211

Giant pulse periodic operation ruby laser with 50 MW power and 10 Hz frequency 16 p2929 A70-34217

Solid state giant pulse laser with small divergence angle, using polymethyl dye solution in nitrobenzene as Q switch 16 p2929 A70-34221

High speed pulsed ruby laser holography, discussing transmission-reflection holocameras and applications 17 p3085 A70-35007

Holographic measurement of transient behavior of structures under unsteady or impulsive loading, using pulsed lasers 17 p3085 A70-35008

Four dimensional recording using synchronous multiple pulse ruby laser holography 17 p3088 A70-35027

Time dependent characteristics of dense argon plasma formed by pulsed lasers, measuring shock wave front velocity with streak camera 17 p3104 A70-35083

Optical and electronic components design for ruby lasers generating giant pulses 17 p3107 A70-35121

German monograph on spectral emission behavior of pulsed ruby laser with regard to output intensity 17 p3107 A70-35369

Internally loss modulated multimode ring gas laser, showing pulse peak intensity with detuning for phase locking 17 p3107 A70-35475

Pulsed laser holography for liquid rocket combustion studies, describing apparatus and techniques 17 p3092 A70-35477

Time resolved measurements of ion and electron temperature in pulsed Ar ion laser discharge, observing heating 17 p3108 A70-35907

Spontaneous megawatt pulsing in ruby laser with output beam reflected back into cavity 17 p3108 A70-35909

Surface destruction of glass dielectric by pulsed laser beam, considering plasma clouds, shock waves, ablation and crack formation 18 p3266 A70-36153

He-Cd pulsed laser mode locking at 4416 and 3250 Å using intracavity acoustic loss modulator 18 p3266 A70-36314

Pulsed GaAs injection lasers second harmonic generation with nonlinear crystal alpha iodic acid phase matched by angular tuning 18 p3269 A70-36737

Pulsed laser holographic nondestructive testing optimization technique, monitoring honeycomb panel surface temperature during thermal stressing 18 p3259 A70-36754

Nd glass laser ultrashort light impulse optical rectification, presenting lower harmonics angular dependence 19 p3443 A70-37287

Subnanosecond jitter spark gap obtained with YAG-Nd pulsed laser triggered switching at moderate repetition rates 19 p3444 A70-37666

Two photon absorption-fluorescence measurement of laser pulse width, using three level model of absorber 19 p3422 A70-37671

Periodic resonant reflector with thin air intervals for YAG-Nd pulsed laser for retinal safety 19 p3445 A70-37673

Folded path transversely excited atmospheric pressure carbon dioxide laser using shower or brush discharges, measuring output pulse characteristics 19 p3445 A70-37674

Pulsed ruby laser holography with coherent light, discussing applications 19 p3425 A70-37886

Ultrashort light pulse generation by self mode locking laser, discussing power amplification problems 19 p3448 A70-38509

Pulsed laser emission at IR transitions of xenon and neon under electron beam pumping 19 p3449 A70-38743

Laser pulse amplification by stimulated thermal Rayleigh scattering in absorbing media by transient theory 20 p3640 A70-39113

Pulsed laser lidar measurements of atmospheric turbidity, diffusion, pollution, visibility and cloud physics 20 p3584 A70-39127

Pulsed argon ion laser output properties from electron temperatures and densities produced by He-Ar gas mixture 20 p3640 A70-39137

Giant pulse neodymium glass laser emission spectrum structure, showing cavity geometry effect on fine structure 20 p3641 A70-39450

Double holography on phase objects in diffused light using pulsed ruby laser 20 p3630 A70-39499

Pulsed composite laser performance with He-Ne active section and neodymium-glass power gain section 20 p3641 A70-39740

Pulsed ruby free emission mode laser spectrum narrowing, using diffraction lattice adjusted in resonator transversely to beam axis 20 p3643 A70-39757

Multidimensional control systems synthesized in accord with polyinvariance and coordinating couplings principles

20 p3604 A70-39837

Microwelding by pulsed ruby laser radiation, discussing characteristics and advantages

20 p3638 A70-40149

Normal mode pulsed ruby laser system with Xe flash lamp pumping, trigger circuit and transistorized power supply

20 p3643 A70-40355

Titanium powder compacts exothermic solid phase reaction ignition by focused laser pulse, obtaining temperature profile from mathematical model based on energy transport

20 p3639 A70-40473

Carbon dioxide laser pulse shape, duration and power dependence on repetition rate during continuous pumping

21 p3835 A70-40634

Reflected ruby, laser pulses from Apollo 11 laser ranging retro-reflector /LRRR/ with telescope, measuring round trip travel time of light

21 p3912 A70-41638

Pulsed ruby laser mass spectrometry technique for flash pyrolysis of ammonium perchlorate-catalyst mixtures

[ALAA PAPER 68-149] Acoustic waves in carbon dioxide at 2-25 torr initial pressures induced by heat from incident carbon dioxide laser pulses

21 p3837 A70-42003

Pulse velocity and mode pulling in inhomogeneously broadened laser with equally spaced modes, noting pulse shape time stability in presence of dispersion

21 p3838 A70-42008

Single picosecond mode-locked laser pulse selection and multiple pass amplification device, obtaining high energy and signal to noise ratio

21 p3838 A70-42023

Ne absorption cell and He-Ne gain cell pulse velocities compared with free space light velocity

22 p4048 A70-42329

Lasing transitions time delay in carbon monoxide laser under pulsed electrical excitation, attributing inversion to anharmonic decoupling

22 p4048 A70-42330

Cadmium sulfide pulsed laser spectrum analysis, discussing laser output stabilization by mode selection and electron beam scanning

22 p4049 A70-42405

Thin optically pumped pulsed CdSe platelet lasers, detecting mode jumping and tuning effects by time-resolved spectroscopy

22 p4049 A70-42946

Wavelength selective carbon dioxide laser using stationary grating to correlate pulses for high J values and line number

22 p4050 A70-43153

Argon laser for long pulse low duty cycle operation, discussing construction and performance

22 p4052 A70-43602

Pulsed laser radar tracking and ranging system for monitoring and directing TV camera at astronaut position on lunar surface

22 p3992 A70-43604

Solid state high energy light detector for pulsed ruby and glass lasers in long pulse mode

22 p4052 A70-43614

Laser applications in length measurement and holography, describing principles and techniques, modulated laser beams and pulse transit time

23 p4201 A70-43998

Nd-glass mode-locked laser with KDP crystal frequency doubling and pulse selection with Pockels cell

23 p4201 A70-44476

High power pulsed laser fog dispersal, calculating vaporization regimes of droplet interaction with laser radiation

23 p4201 A70-44592

Giant pulses by actively and passively Q-switched inorganic neodymium-liquid lasers with varying modulation due to mode coupling

23 p4202 A70-44937

Ruby laser in repetitive pulse operation, determining temperature, heat generation and transfer coefficient from spectrum shift measurement

23 p4203 A70-45071

Pulse area-pulse energy description of traveling-wave laser amplifier

24 p4351 A70-45257

Pulsed ruby laser radiation energy characteristics relation to crystal temperature distribution, thermal deformation and compensating lens focal length

24 p4352 A70-45460

Single mode ruby and Nd glass lasers axial mode selection by dye filters, noting radiation spectra and spatial coherence

24 p4352 A70-45462

Mode locked neodymium-glass pulsed laser stimulated picosecond time resolved light emission observation by cross beam technique

24 p4354 A70-45647

High pressure pulsed Xe laser obtained with transversely excited He-Xe discharge

24 p4355 A70-46087

Mode locked laser pulses picosecond structure predicted from theoretical model of Gaussian random radiation field with temporal envelope modulation

24 p4355 A70-46263

PULSED RADIATION

NT ELECTROMAGNETIC PULSES

Interferometer for compressing linearly FM light pulses and analyzing spectra of picosecond pulses

01 p0111 A70-10670

Acoustic transients in mammalian eye induced by normal and Q switched laser pulse absorption

02 p0313 A70-12325

Polymethylmethacrylate block breakdown under focused pulsed laser radiation in free emission regime, noting light absorption during crack development

02 p0314 A70-12813

Energetic and temporal characteristics of CW and pulse laser radiation measured using instrument with absolute sensor

03 p0500 A70-13480

Pulsed gamma radiation from pulsars searched for by Cerenkov air shower detection method

04 p0738 A70-14518

Crab Nebula pulsar light intensity fluctuations on very short time scale, noting negative observations

04 p0747 A70-14545

Self induced light pulses from GaAs injection lasers in pulse driven diodes at liquid nitrogen temperatures, noting pulse width and frequency

04 p0703 A70-15623

Pulsed gravitational radiation emitted by dense star clusters

05 p0921 A70-16977

Light pulse propagation in nonlinearly amplifying or absorbing medium, discussing coherent and non-coherent interaction between pulse and medium

07 p1296 A70-18745

Oblique incidence HF pulse ionospheric sounding, discussing propagation modes, seasonal and diurnal effects, frequency spectra, etc

07 p1233 A70-19182

Solar energy converter with shutter, determining light pulse power from solar light intensity and exposure time

07 p1196 A70-19624

Self pulsation in He-Cd laser, noting decreasing number of modes effect on beat frequency stability

07 p1301 A70-20017

Ionosphere absolute phase height measurement methods independent of virtual height, using fixed frequency CW emission and pulsed sounding

07 p1276 A70-20432

Faraday rotation in pulsars and in interstellar medium, discussing position angle drift, polarization changes and pulse fine structure

08 p1564 A70-20553

Modified diffusion approximation for spectral transfer of isotropic turbulent pulsation energy for temperatures with low Prandtl number

08 p1538 A70-21429

Two photon interaction between ultrashort light pulse and medium, showing pulse propagation through medium without absorption

08 p1514 A70-21820

Rectangular radio pulse sequence passage through narrow band filter, discussing transient process form as function of signal parameters

09 p1643 A70-22132

Fluorescence produced by resonant coherent light pulse passing through medium assuming infinite relaxation times and negligible pulse attenuation

09 p1726 A70-22321

Pulsed microwave spectrum analyzer using holography and Fourier spectroscopy compared with frequency methods

09 p1675 A70-22485

Pulsars high time-resolution studies revealing marching subpulse structures

09 p1756 A70-22519

Solar corona pulsating metric radio emissions, indicating phenomena as type 4 radiation phases

09 p1758 A70-22738

Cosmic ray air shower detection from radio pulses

09 p1745 A70-23276

High energy pulsed gamma rays detection method for pulsars based on search for nanosecond duration Cerenkov light signals

09 p1748 A70-23795

Pulsars pulse shapes and linear polarization measured, observing rapid change of polarization direction in double pulses

10 p1936 A70-23901

Cepheid type variable stars nuclear reaction and opacity pulsation excitation mechanisms

10 p1940 A70-24409

Shock pressure and impulse caused by Q switched laser light absorption, considering temperature dependence of EM radiation penetration depth

10 p1900 A70-24422

Coherent photon responses production in liquids and glasses by superposing trains of giant laser pulses,

achieving spatial separation of responses by combining pulse trains

10 p1900 A70-24564

Pulsed radio waves interactions during vertical propagation through perturbed ionosphere using cross modulation theory concepts, considering perturbation waves effects

11 p2003 A70-25531

Auroral pulsations photometric observation data, noting magnetic activity effects

11 p2043 A70-25540

Hard X-ray pulse identification with formation of brilliant kernel /11-12 September 1968/ flare by comparison with optical data

11 p2104 A70-25746

Ballistic pulsed photometer calibration without etalon light pulse using radiation sensitivity, oscillation period and galvanometer damping

12 p2238 A70-28179

Light pulse propagation in dispersive nonlinear dielectric analyzed on nonlinear Lorentz model

12 p2274 A70-28216

Resonant absorption in ruby crystal under combined acoustic and laser pulses, noting use for laser intensity measurements

12 p2251 A70-28331

Pulsar CP 1919 X ray emission upper limits from balloon flight data, comparing to NP 0532 over entire electromagnetic spectrum

13 p2478 A70-29270

Pulsating aurorae onset in magnetically conjugate points noting local nature of sources

14 p2572 A70-30241

Coaxial, inside-out and rising-sun magnetrons for millimeter waves generation under pulsed conditions, discussing tunability, frequency stability and weight

14 p2555 A70-30429

Electric space charge pulse density measurements near ground in sunny weather related to free convection

15 p2726 A70-31868

Coherent pulse propagation in inhomogeneously broadened attenuator, examining degeneracy influence and connection with self induced transparency /STI/ in nondegenerate system

15 p2699 A70-32395

Faraday rotation in pulsars and in interstellar medium, discussing position angle drift, polarization changes and pulse fine structure

15 p2805 A70-32708

Solid state spectrum centered receiver for eliminating externally generated pulse type interference between radar sets

16 p2862 A70-33066

Gas breakdown produced by long wave IR pulsed radiation of carbon dioxide laser

16 p2928 A70-33655

Critique of paper on Crab Nebula pulsar pulsed gamma ray emission, considering photon flux and statistical data analysis

17 p3149 A70-34565

Critique of paper on pulsed gamma rays detection from Crab Nebula pulsar by balloon flights, attributing pulsations to random fluctuations

17 p3149 A70-34566

Pulsar RF spectral fine structure in decimeter wave range

17 p3163 A70-35050

Crab Nebula X ray flux pulsations, analyzing spectra

17 p3152 A70-35756

Picosecond pulse frequency sweep measurement using time resolved spectroscopy

17 p3108 A70-35904

Picosecond light pulse measurement by two beam overlap technique using nonlinear photoelectric effect

17 p3097 A70-35912

Pulsed emission in midinfrared region at neutral atomic transitions of inert gases and mixtures, tabulating wavelengths, intensity, component ratios and optimal pressure

19 p3448 A70-38736

Pulse light amplification by stimulated thermal Rayleigh scattering measured as function of time, absorption coefficient and interaction length

20 p3640 A70-39114

Smooth periodic wavelength retuning in organic dye laser, using neodymium glass laser with YAG for pumping

20 p3642 A70-39742

Plasma nonequilibrium state formation and light absorptivity variation under high power laser pulsed radiation

20 p3684 A70-40387

Short light pulse coherent absorption in homogeneously broadened resonant medium, discussing influence of input pulse area and atomic coherence on propagation properties

21 p3784 A70-40565

Solar radio pulsations, observing modulation of coronal microwave, X ray and type III emission

21 p3880 A70-40965

- Light pulse propagation in nonlinearly amplifying or absorbing medium, discussing coherent and non-coherent interaction between pulse and medium
21 p3836 A70-41170
- Pulsed radio waves interactions during vertical propagation through perturbed ionosphere using cross modulation theory concepts, considering perturbation waves effects
21 p3786 A70-41281
- Auroral pulsations photometric observation data, noting magnetic activity effects
21 p3819 A70-41290
- Subnanosecond risetime milliohm Faraday cup for measuring electron beams from pulsed accelerators
21 p3799 A70-41466
- Pulsed signal synthesis from three dimensional function of indeterminacy, incorporating source distance, velocity and acceleration
22 p3988 A70-42562
- Pulsed eddy currents in metals nondestructive testing, discussing masked probes, reflection systems, correlation and filtering methods, etc
22 p4028 A70-42593
- Pulse counting and encoding system on rocket-borne spectrophotometer for starlight collected by primary telescope mirror
22 p4038 A70-43174
- Pulsed radio wave interactions with various lower ionosphere models, estimating cross modulation by computer calculation for comparison with measurements
23 p4162 A70-44080
- Hypervelocity impact flash resolved into sub-microsecond continuum radiation pulse succeeded by slow rising long duration light pulse from neutral atomic line emission
23 p4227 A70-44553
- Laser light pulse reflection by atmospheric boundary layer calculated on computer by Monte Carlo method, comparing results with full scale measurement
23 p4166 A70-45072
- Crab Nebula X ray pulsation identified with pulsar NP 0532 by rocket measurements, noting implications for interstellar dust density
24 p4401 A70-45371
- Ultrasonic pulse emitter with interference-free near field and sidelobe suppression for materials testing
24 p4343 A70-45685
- Pulsating aurorae onset in magnetically conjugate points noting local nature of sources
24 p4332 A70-46316
- PULSES**
NT ELECTRIC PULSES
NT ELECTROMAGNETIC PULSES
NT GEOMAGNETIC MICROPULSATIONS
NT GEOMAGNETIC PULSATIONS
NT MICROPULSATIONS
- Subjective measurement of sound level of impulses and pulses, investigating 1 kHz tone and selection of time length between sound events
05 p0882 A70-16344
- Ultrasonic pulses velocity and attenuation in fluids by coherent detection technique, measuring delay and decrease in amplitude due to transmission path length increase
16 p2913 A70-34084
- Effective reflection height measurement accuracy for pulsed vertical ionospheric sounding, using interference method
18 p3227 A70-36106
- Dynamic system modeling pulse test data reduction by digital computer and functional approximation for Fourier transform calculations
18 p3230 A70-36458
- Pulse superposition measurements of small ultrasonic waves velocity changes using automatic recording phase sensitive detection
21 p3827 A70-41468
- Space vehicle self oscillatory pulsed relay attitude control system with jet nozzles, determining angular motion
22 p4001 A70-42838
- Shock response of passive nonlinear elastic isolators under pulse excitation with viscous damping
22 p4117 A70-43249
- PULVERIZING**
U GRINDING [COMMINUTION]
- PUMP IMPELLERS**
Axial flow pump impellers suction performance and cavitation conditions
06 p1075 A70-17137
- Inducer tip clearance effect on centrifugal pump suction performance with velocity and total head distributions at outlet
14 p2592 A70-31332
- Centrifugal impellers primary and secondary flows velocity distributions, determining vorticity generation
18 p3243 A70-36871
- Pressure and velocity distribution inside casing and around impeller of volute pumps, discussing flow at exit and in wedge shape space
19 p3437 A70-38225

PUMP SEALS

- Helium gas shaft seal for spacecraft electrically driven LOX pump, noting advantages of floating carbon face seal type
[ASLE FICFS PREPRINT 24] 02 p0308 A70-12168
- Leakage in mechanical face seals with hydrodynamic films, noting misaligned seal theories for pumping with cavities and two fluids
[ASLE FICFS PREPRINT 19] 02 p0308 A70-12170
- Rarefied gas viscoelastic performance prediction by theoretical model, comparing results with experiment
[ASLE PREPRINT 70AM 5C-3] 19 p3439 A70-38806
- Power loss reduction from disk friction and gas leakage through rotor seals of low speed centrifugal pumps in aircraft hydraulic systems and liquid propellant rocket engines
22 p4091 A70-42806

PUMPING

- Titanium vacuum pump, discussing pumping speed, sticking factor and sorption coefficient for hydrogen
15 p2744 A70-31845

PUMPS

- NT AXIAL FLOW PUMPS
NT CENTRIFUGAL PUMPS
NT ELECTROMAGNETIC PUMPS
NT ION PUMPS
NT JET PUMPS
NT MOLECULAR PUMPS
NT TURBINE PUMPS
NT VACUUM PUMPS
- Rotodynamic pumps energetic characteristics determination by pneumatic tests, describing air test results for various models
12 p2165 A70-27399
- Hydraulic system pumps ratings, classification and selection
13 p2419 A70-29219
- Gear pumps for hydraulic systems, discussing costs, types and applications
14 p2590 A70-30302
- Liquid metals pump with cylindrical hydraulic coupling for actuating axial wheel, investigating cavitation and pumping effects on performance
14 p2535 A70-31012
- Penning pump argon stability, noting influence of pressure and ion incidence angle on cathode surface
15 p2744 A70-31847
- Thermally powered reciprocating piston pump for temperature control fluid transport on Thermoelectric Outer Planet Spacecraft (TOPS)
17 p3101 A70-34757
- Perfusion peristaltic pump for determining smooth muscle reaction in vascular bed, discussing applications to physiological and pharmacological investigations
19 p3372 A70-38958
- Plunger pump for aircraft hydraulic systems, measuring working fluid temperature effect on cavitation
22 p3965 A70-42817

PUNCHED CARDS

- Linked and fiber optic components, describing applications as punched card and tape reading, geometrical converters and sensing and scanning probes
16 p2904 A70-33145

PUNCHED TAPES

- Mathematical relations and procedures for automatic satellite tracking by four axis Zeiss camera, discussing motion along small circle approximation and punch tape criteria
02 p0255 A70-11770

PUNCHES

- Adhesive rocking and parallel translation contact for circular cylindrical punch indenting elastic half space solved using simultaneous equations
05 p0932 A70-16139

PUPIL SIZE

- Pupil diameter changes associated with constant change in accommodative stimulus as retinal illuminance varies
03 p0427 A70-13950
- Correction factors required for estimating influence of pupil area reduction on retinal illumination at oblique angles
05 p0801 A70-16449
- Age and retinal illumination influence on human pupillary near reflex investigated by photographic measurements
12 p2171 A70-28036

PUPILLOMETRY

- Critical duration for pupillary light reflexes measured with IR scanning pupillometer using various flash duration stimuli
02 p0237 A70-12458
- Transistorized circuit for automatic control of photographic studies of pupillary reaction transient states in rabbits subjected to light stimulus
07 p1216 A70-18731
- Age and retinal illumination influence on human pupillary near reflex investigated by photographic measurements
12 p2171 A70-28036

PUPILS

- Critical duration for pupillary light reflexes measured with IR scanning pupillometer using various flash duration stimuli
02 p0237 A70-12458
- Controllable light source for experiments on human pupillary servomechanism
04 p0642 A70-14633

PURGING

- Fuel cell cavities, analyzing fluid motion purge dynamics based on anisotropic porous media model
18 p3216 A70-36766

PURIFICATION

- NT AIR PURIFICATION
Differential melting for partial purification of chemically distinct region of chromosome mycoplasma sp. /Kid/
04 p0647 A70-15448
- Ammonium ions elimination from atmospheric moisture condensates by treatment with metal-exchange resins, discussing volume sorption capacity
13 p2362 A70-29339
- High purity V and V-Cr-Ti process, describing aluminothermic reduction and electron beam purification
15 p2761 A70-32387
- Al purification by subhalide reaction, discussing contamination sources and thermodynamics
24 p3439 A70-46187

PURIFIERS**U PURIFICATION****PURINES**

- NT CAFFEINE
NT URIC ACID
NT XANTHINES
- Ribonucleic acid polymerase model with initiating purine triphosphate binding to product terminus site and pyrimidine triphosphate engaging in exchange binds to substrate site
03 p0442 A70-14046

PURITY

- Purity requirements for oil in hydraulic systems of modern aircraft, discussing filtering devices and Swedish Air Force and SAAB specifications
01 p0130 A70-11359
- Population inversion coefficient as function of optimal impurity concentrations and efficiency of ruby quantum paramagnetic amplifier in 3 cm range
03 p0499 A70-13457
- Yield stress and work hardening properties of tension-deformed vanadium single crystals as function of purity
08 p1522 A70-21750
- Metals purity, gas content and porosity effects on nature and size of material zone affected by laser beam treatment
12 p2250 A70-28219
- Metals purity, gas content and porosity effects on nature and size of material zone affected by laser beam treatment
20 p3643 A70-40094
- Clean shock tube maintaining high gas purity level for Ar plasma spectroscopy
24 p4388 A70-46271

PURSUIT TRACKING

- Voluntary control over velocity of smooth pursuits, discussing saccadic and saccade free modes and switching during tracking
01 p0026 A70-11056
- Two step optimal motion of target and pursuer with thrust vector control in vacuum under arbitrary gravitational field, determining distance strategy
02 p0272 A70-12405
- Banked position and angle of attack changes in fighter aircraft sighting and attacking target, determining spatial zone of possible attack
02 p0227 A70-12406
- Approximate solutions to Cauchy problem describing controlled pursuit using approximate method of integrating Bellman equation
04 p0713 A70-14602
- Policies and controller design for pursuing vehicle developed in terms of pursuit-evasion differential games
06 p1025 A70-17955
- Linear-quadratic pursuit-evasion game with dynamics perturbed by additive white Gaussian noise, obtaining linear minimax solutions
06 p1025 A70-17957
- Differential game analysis of dynamic systems feedback control, presenting extremal aiming for successful pursuit completion
07 p1332 A70-18681
- Nonlinear pursuit problem solution taking into account drag and lift in pursuing object equations of motion
07 p1330 A70-18682
- Fixed target pursuit-evasion differential game based on pursuer-evader proximity as termination condition
11 p2073 A70-26242
- Human performance as controller evaluated in man machine control system, considering pursuit or compensatory tracking tasks
12 p2171 A70-27039

- Pursuit tracking during disturbance signal as function of human performance in man machine system
12 p2266 A70-27198
- Pursuit game problems with pursuer and target described by k-dimensional phase vectors, discussing evasion problems
13 p2452 A70-29276
- Extremal strategy to assure successful termination of pursuit at definite time, investigating sufficient conditions theorem
13 p2443 A70-29754
- Pursuit-evasion differential games involving two linear dynamic systems with state and control dependent thermal noise
16 p2881 A70-32985
- Discrete stochastic optimal control model of human operator for single loop compensatory/pursuit tracking
16 p2851 A70-33340
- Discrete stochastic optimal control model of human operator for single loop compensatory/pursuit tracking situation, considering application to manual control system design
16 p2852 A70-33463
- Missile homing on moving target, assuming closing velocity vector angular rate proportional to line of sight
16 p2949 A70-34054
- Performance and response organization as uncertainty and structure function in pursuit tracking tasks
19 p3363 A70-38320
- Pursuit evasion game with uncertain state-dependent measurements, modifying Brown-Robinson algorithm for behavior strategies computation
20 p3660 A70-40384
- Step and ramp input functions and pursuit and compensatory display modes effects on tracking performance
21 p3767 A70-40753
- Unilateral and minimax control with functional restrictions, including pursuit and evasion games
23 p4177 A70-44906
- PWM [MODULATION]**
U PULSE DURATION MODULATION
- PYLON MOUNTING**
U AIRCRAFT PRODUCTION
- PYRAMIDAL BODIES**
Friction drag on thin pyramidal lobed bodies in supersonic flow, analyzing detached shock region and body geometry function
09 p1606 A70-23612
- Metal surfaces contact with cones and pyramids asperities, analyzing surface roughness effects on dry friction
11 p2060 A70-26412
- PYRANOMETERS**
Abbot pyranometer as reference standard for calibration, reporting performance tests of time constant, cosine response and attitude
10 p1886 A70-23933
- Pyranometer with additional external glass cupola to eliminate temperature differences and heat exchange, discussing laboratory and field test results
20 p3626 A70-39034
- Phytoactinometers and phytopyranometer graduating methods, discussing measurement of photosynthetically active radiation
20 p3626 A70-39035
- PYRAZINES**
NT AZINES
- PYRIDINE NUCLEOTIDES**
Molecular respiratory reflex and fluorescent signal in rabbits during hypoxia, determining redox kinetics of intracellular pyridine nucleotides
14 p2539 A70-31346
- PYRIDINES**
Radioprotective action of pyridine derivatives in monkey heart and human epithelium cells exposed to gamma radiation evaluated by dioxiphenyl alpha-alanine oxidation
03 p0418 A70-13303
- PYRIDOXINE**
Aeroxine-50 toxicity therapeutic treatment by pyridoxine and phenobarbital resulting in 100 percent survival of mice
07 p1222 A70-19926
- PYRIMIDINES**
NT MITOCHONDRIA
NT THYMINE
NT THYMINE
Free radical formation in irradiated pyrimidines from ESR spectrum analysis of gamma irradiated single crystals of alloxantin, confirming radical stability
08 p1455 A70-20774
- Sunlight induced pyrimidine dimers formation in human cells in vitro, relating DNA lesions by 254 nm irradiation
24 p4304 A70-46139
- PYROCERAM [TRADEMARK]**
Pyroceramics transient strength measurements on cylindrical and prismatic samples under static bending
15 p2764 A70-31545
- PYROELECTRICITY**
Pyroelectric coefficient extrema measurement at constant stress in barium titanate ceramic at various temperature ranges for various transition points
03 p0513 A70-14205
- Laser pulse registration with pyroelectric detector, noting pyroelectric phenomenon inertia limiting effect on response time
05 p0858 A70-16250
- Pyroelectric IR radiation detector based on materials polarization changes associated with temperature changes
16 p2905 A70-33154
- PYROGRAPHALLOY**
U COMPOSITE MATERIALS
U PYROLYTIC GRAPHITE
U REFRACTORY MATERIALS
- PYROHELIOMETERS**
Angular and geometric properties of actinometers, pyroheliometers and photometers, measuring direct and scattered circumsolar radiation
20 p3625 A70-39028
- Correction procedures for measurement errors in actinometers and pyroheliometers caused by circumsolar radiation
20 p3625 A70-39029
- PYROLYSIS**
Initial pyrolysis kinetics of neopentane, showing decomposition rate tendency to equal formation rate at high temperature
01 p0215 A70-10706
- Nonsteady thermal decomposition of plastics subjected to large heat flows, introducing equations governing char layers and pyrolysis zones
02 p0397 A70-12021
- Amino acid stability in pyrolyzed Pleistocene Mercenaria shells, comparing decomposition rates for aqueous solution
03 p0472 A70-13150
- Bearing strength and rupture of reinforced plastic composites under intense one-sided electric heating and hydrostatic pressure due to pyrolysis of plastic bond
03 p0515 A70-13244
- Synthesis of 1-oxacyclopent-1-enyl cations from cyclopropyl ketones on heating in strong acids noting rearrangement rates
04 p0646 A70-15088
- Ammonium chlorate thermal decomposition products as function of temperature using mass spectrometry
05 p0895 A70-17082
- Combustion and pyrolysis of carbonaceous solids considered for hybrid rocket fuels, using integrating factors in Caratheodory multiple entropies
06 p1172 A70-17468
- Pyrolysis effect on infinite slab subjected to front heat flux, attributing increased porosity to mass loss [WSCI PAPER 69-27]
06 p1178 A70-17978
- Pueblo de Allemande chondrite unextractable carbon content using meteorite pyrolysis, obtaining aromatic hydrocarbons
07 p1380 A70-19204
- Fire extinguisher compounds /bromochloromethane and bromotrifluoromethane/ pyrolysis products inhalation toxicities for rats
07 p1219 A70-19223
- Gaseous pyrolysis products detection and identification during eruption from polymeric surfaces subjected to flash heating by time of flight mass spectrometer
07 p1319 A70-19887
- Refractory oxides synthesized using metal alkoxide thermal decomposition, comparing thermophysical properties with conventional ceramics
07 p1320 A70-19891
- Gas phase thermal decomposition of ammonium perchlorate at elevated temperatures using mass spectrometer
07 p1362 A70-20009
- Organic compounds chemical reactions during burning in laminar diffusive flames, describing technique for pyrolysis and combustion products sampling
09 p1787 A70-22107
- Thermal decomposition of ammonium perchlorate and polymethylmethacrylate mixture thin layer between Ti plates in vacuum
09 p1741 A70-22109
- Epoxy glass fiber composites pyrolyzates IR spectra as function of time, observing changes in fingerprint region
10 p1828 A70-24065
- Polymer structure and cross-link density effects on thermal analysis of phenol-formaldehyde polymers pyrolysis products
11 p2069 A70-25804
- Chemical kinetics of carbonyl fluoride thermal decomposition in argon and nitrogen diluent behind shock waves, using IR monitoring method
11 p1995 A70-25824
- Stannic oxide-chromium oxide catalyst effects on thermal decomposition and ignition of ammonium perchlorate /AP/, calculating activation energy
11 p2100 A70-26281
- Composite propellant catalysts /copper chromate and chromite/ thermal decomposition using simultaneous thermogravimetric and differential thermal analysis
11 p2100 A70-26382
- Thin films of vanadium niobium and tantalum obtained by vacuum thermal decomposition of metal iodides
12 p2253 A70-27210
- Thermogravimetric analysis /TGA/ of gadolinium-doped silver carbonate decomposition, obtaining activation energy, preexponential factor and reaction order
15 p2694 A70-32074
- Heating rate effect on Ti-V martensite decomposition, discussing elastic properties effects of partial tempering
16 p2931 A70-33256
- Reaction kinetics of gas phase pyrolysis of polydifluoroaminomethanes in various reactors, obtaining C-N bond cleavage as rate determining step
16 p2856 A70-33652
- Ammonium perchlorate pyrolysis, investigating exothermic surface reactions and gasification rates
16 p2963 A70-33873
- Thermal decomposition of perchlorates evaluated by mass spectrometer, with regard to composite propellants combustion processes
17 p3145 A70-34638
- Oxadiazolone pyrolytic and photolytic fragmentation, noting intramolecular cyclizations and intermediate azomethine nitrone production
17 p3041 A70-34771
- Aluminum particle combustibility in deflagration zone of ammonium perchlorate pellets, measuring combustion rate and pyrolytic behavior
17 p3145 A70-35208
- Phenolic nylon thermal decomposition, considering surface reradiation and physical parameters effects
17 p3196 A70-35242
- Pyrolyzed tetraethoxysilane for carburizing steels and Ti alloys at 850-1050 C
17 p3102 A70-35409
- Ethyl alcohol fuel diffusion flame, examining thermal decomposition pyrolysis and free electron concentration distribution
18 p3345 A70-36113
- Thermal decomposition mechanism of inorganic oxidizers, discussing reactivity of alkali and alkali earth salts
18 p3299 A70-36240
- Fe and Al impurities in bis-ethylbenzene chromium /BEBC/ and in chromium films obtained by thermally induced decomposition of metal organic compound
18 p3297 A70-36463
- Premature exothermic decomposition suppression in propellant grade ammonium perchlorate, using differential thermal analysis
18 p3300 A70-36699
- Thermal decomposition of nitrogen tetroxide and nitrogen dioxide induced by shock waves, examining temperature effects
19 p3373 A70-38265
- Bearing strength and rupture of reinforced plastic composites under intense one-sided electric heating and hydrostatic pressure due to pyrolysis of plastic bond
19 p3455 A70-38462
- Smoke chamber measurements of opacity developed in polymer pyrolysis or combustion, including Materials Smoke Obscurity Index /MSOI/
20 p3736 A70-39404
- Nucleation processes associated with thermal decomposition sites formation in ammonium perchlorate single crystals, using optical and electron microscopy
20 p3582 A70-39494
- Simultaneous mass spectrometric differential thermal analysis of low pressure decompositions of nitrate salts of monomethylhydrazine and methylamine
20 p3688 A70-40475
- Proton transfer mechanism for thermal decomposition of ammonium perchlorate, discussing dissociation energy and decomposition products
21 p3864 A70-40883
- Apollo 11 lunar samples organic carbon content analysis by pyrolysis hydrogen flame ionization detection
21 p3779 A70-41624
- Pulsed ruby laser mass spectrometry technique for flash pyrolysis of ammonium perchlorate-catalyst mixtures
21 p3781 A70-41729
- [AIAA PAPER 68-149]
Polyimide resin vacuum thermal decomposition, using mass spectral and differential thermal analysis
21 p3783 A70-42133
- Thermal decomposition of acetate ion in potassium halide matrices, using IR spectroscopy
22 p3981 A70-42453
- Semiconductor junctions passivation by silicon nitride insulation layers, discussing pyrolysis and cathode sputtering fabrication methods
22 p4087 A70-43444

- Thermal decomposition of fine-dispersion iron sulfate powders under continuous heating during ferrites manufacture 23 p4205 A70-44041
- Heating rate effect on Ti-V martensite decomposition, discussing elastic properties effects of partial tempering 23 p4206 A70-44285
- Charring ablative composites pyrolysis products composition determination, comparing chemical analysis techniques 23 p4158 A70-44519
- German monograph on soot formation and separation in turbulent diffusion flame in power plant combustion chamber, noting pyrolysis role 24 p4428 A70-45087
- Thermal decomposition of freeze dried Ta and mixed lithium-niobium oxalate, using surface area and electron micrographs 24 p4363 A70-46212

PYROLYTIC GRAPHITE

- Homogeneous Love-Reissner equations analytical solutions for noncircular pyrolytic graphite cylinders, using asymptotic expansion for transverse materials isotropy 01 p0206 A70-11551
- Reinforced graphite cloth composite for reentry heat shielding of SNAP 27 isotopic heat sources, describing structure, thermal and mechanical properties and ablative characteristics 07 p1332 A70-18933
- Pyrolytic C-TiC alloys obtained by precipitation from gaseous phase, discussing microstructural properties anisotropy 08 p1517 A70-21146
- Magnetothermal oscillations in pressure-annealed pyrolytic graphite, relating period with angle between magnetic field and crystal c axis 08 p1557 A70-21839
- Free vibrations of plates and beams of pyrolytic graphite type materials, analyzing transverse shear deformation and rotary inertia 09 p1780 A70-23210
- Thermoelectric power and Hall effect quantum resonances in pressure annealed pyrolytic graphite crystals for carrier locations evidence 11 p2097 A70-25616
- Pyrolytic graphite oxidation kinetics as function of temperature, air velocity and surface area 11 p2070 A70-25809
- Fe-Al and Fe-Si alloys strengthening by pyrolytic graphite fibers 14 p2595 A70-30543
- Temperature dependence of anisotropic reaction kinetics of oxygen with pyrolytic graphite 19 p3373 A70-37709
- Single crystal and pyrolytic graphite, examining spin split Landau levels, Fermi energy changes and anomalous g shifts 21 p3854 A70-42110

PYROLYTIC MATERIALS

- NT PYROLYTIC GRAPHITE
- Silicon-containing pyrocarbon, relating microhardness to microstructure 18 p3279 A70-37220
- Pyrolytic carbide protective coating deposition from gaseous phase on spherical particles in boiling layer 24 p4350 A70-46330

PYROMETERS

- NT RADIATION PYROMETERS
- Balanced ELF chemotron tetrode amplifiers with series-fed output circuits, showing characteristics calculations and use in pyrometric assembly 06 p1022 A70-17782
- Flame temperatures simultaneous measurement in two spectral regions, using photoelectric IR pyrometer 12 p2237 A70-28158
- Pyrometer for measuring temperature by ratio of radiation at two different wavelengths, eliminating spectral emissivity effect 15 p2736 A70-31824
- High speed photoelectric pyrometry of Ta heat capacity at high temperatures induced by pulse heating 23 p4207 A70-44441

PYROMETRY

U TEMPERATURE MEASUREMENT

PYROTECHNICS

- Aircraft seat ejection systems using SCID /small column insulated delay/ distribution system taking advantage of standard end devices 01 p0035 A70-10718
- Missile tracer mixture performance control facility noting chamber for pressure measurement during operation 03 p0544 A70-13758
- Electroexplosive devices - Conference, San Francisco, July 1969 03 p0544 A70-14101
- Apollo spacecraft pyrotechnics on lunar landing mission, considering standard initiator, modular cartridges, noninterchangeability of special purpose devices, postmanufacture indexing and data system 03 p0582 A70-14102

- Missile impact location visual identification by marker system using pyrotechnic aboard to produce dense white smoke detectable to unaided eye, including flight test 03 p0582 A70-14104

- Thermodynamics second law application to pyrotechnic systems, discussing solid-solid and reversible reactions 03 p0547 A70-14114

- Pyrotechnic thrusting devices output dynamics, describing testing for spacecraft applications 03 p0549 A70-14125

- Explosives and pyrotechnics information sources including government manuals, commercial publications, symposium proceeding, R and D programs 03 p0610 A70-14127

- Airborne pyrotechnic cloud seeding system development, testing and application, comparing rainfall from test and control clouds 10 p1886 A70-23931

- Safety characteristics of potassium chloratellactose mixtures as standard for comparing dangerousness of pyrotechnical compositions 15 p2786 A70-31848

- Flight behavior of pyrotechnic circuits in ELDO-EUROPA 1 booster for separating stages and autodestruction 15 p2709 A70-32288

- Combustion of decomposition products of Mg based pyrotechnic fuel in supersonic flow, obtaining heating device characteristics 20 p3736 A70-39266

- Aircraft auxiliary systems and spacecraft power supplies, considering fly-by-wire control actuators, pyrotechnics and stowable solar array 20 p3564 A70-39669

- Trajectory correction propulsion subsystem /TCPS/, attitude propulsion subsystem /APS/ and pyrotechnic subsystem of thermoelectric outer planet spacecraft /TOS/ 21 p3868 A70-41800

- Magnesium-sodium nitrate pyrotechnic flare spectral radiant energy comparison with radiative transfer theory data, considering Na resonance continuum formation 21 p3850 A70-41937

- Optimal color hierarchy for pyrotechnic markers and signals indicating red, violet and amber hues on top 23 p4146 A70-44459

- Apollo spacecraft pyrotechnic systems and devices functions during lunar exploration mission and in aborts [SAE PAPER 700833] 24 p4416 A70-45888

- Aerospace pyrotechnics applications, considering pressure controlled propellant actuated device for escape systems [SAE PAPER 700831] 24 p4295 A70-45889

PYROXENES

NT ENSTATITE

- Surveyor 5 lunar rock data from Mare Tranquillitatis compared with pyroxene gabbros, indicating gabbro or gabbroic anorthosite classification 01 p0181 A70-10575

- Abundance levels of K, Rb, Sr and Ba in pyroxenes, olivines and garnets of ultramafic rocks for upper mantle composition 03 p0472 A70-13149

- Synthetic pyroxenoid stability and crystallography, noting pyroxenite structure similar to yellow lunar mineral from Mare Tranquillitatis 12 p2226 A70-28022

- Majorite garnet in veinlet of Coorara meteorite suggesting transformation from pyroxene 13 p2492 A70-29267

- Fe ion, Mg order-disorder in natural orthopyroxenes as function of temperature 16 p2896 A70-33087

- Clinopyroxenes from Apollo 12 rocks studied by X ray diffraction and electron microprobe methods, noting phenocrysts, chemical composition and crystallization 19 p3519 A70-38033

- Apollo 11 lunar rock pyroxenes, examining band structure and magnetic ordering by high voltage electron microscopy and electron diffraction 21 p3898 A70-41523

- Plagioclases, pyroxenes and olivines in lunar soils and rocks, using X ray diffraction and Mossbauer effect 21 p3899 A70-41528

- Compositional zoning in pyroxenes from grained Apollo 11 microgabbros, implying supercooled magma origin 21 p3899 A70-41532

- Apollo 11 lunar rocks and fines, examining clinopyroxenes augite and pigeonite by single crystal X ray diffraction microprobe optical and electron optical techniques 21 p3902 A70-41549

- Fe 57 nuclear hyperfine splittings in clinopyroxenes from lunar igneous rocks, determining temperature dependent cation distribution 21 p3915 A70-41659

PYROXYLIN

U CELLULOSE NITRATE

PYRRHOTITE

NT TROILITE

- Orgueil C 1 carbonaceous meteorite mineral content, describing pyrrhotite identification by electron microprobe 24 p4411 A70-45792

PYRROLES

NT INDOLES

NT TRYPTOPHAN

- Polymidazopyrrolone films relative thermophysical properties, noting polymers thermal stability dependence on carbonyl groups percentage 21 p3783 A70-42132

Q

Q FACTORS

- Optimum automatic system for controlling helicopter formation flight, stressing transient response Q factor and transmission ratios 03 p0413 A70-13859

- Transistors used as UHF high-Q inductance active filters, utilizing internal phase shift and energy storage characteristics 03 p0458 A70-14033

- Wobblator measurement of Q factor of microwave resonator cavities using double modulated klystron signal 05 p0822 A70-16528

- Antenna reactive energies and modal quality factors by compact expressions given in terms of polynomials with positive coefficients not involving spherical Bessel functions 06 p1020 A70-17560

- Polarization interference filter as laser resonator frequency selector, showing Q factor measurable within spontaneous emission line 06 p1082 A70-17771

- TWT model with slow wave structure and realized negative depression coefficient and Q factor described by variational method 09 p1644 A70-22410

- Optimal adjusting of laser with instantaneously increasing Q without pumping and relaxation effects during pulse, using nonlinear differential equation 09 p1695 A70-22412

- Microwave Gunn oscillators loaded Q factors determined on basis of frequency changes resulting from constant-depth probe movement along output line 09 p1645 A70-22601

- Obstacle extinction cross section determination at microwave frequencies from Q factor of open resonator 09 p1637 A70-23307

- He-Ne laser Q factor modulator based on Fabry-Perot interferometer with alternating absorption 10 p1899 A70-24255

- Distributed-lumped-active network to produce transfer function with pair of high Q zero real part sensitivity poles 12 p2196 A70-27652

- Active RC bandpass filter with independent linear control of Q peak gain and frequency 13 p2376 A70-28801

- Electronic tuning range of solid state microwave oscillators, deriving equations in terms of tuning device Q factor and available power output 13 p2376 A70-28802

- Microstripline and balanced stripline, discussing parameters affecting maximum attainable Q in microwave integrated circuits 14 p2561 A70-30921

- Fluidic systems linear lumped components design with allowance for energy factor Q, investigating capacitance and inductance 15 p2678 A70-32675

- High Q reactance network realization for integrated microwave systems employing evanescent mode waveguide components 16 p2875 A70-33402

- Hybrid integrated microwave power amplifiers, using high-Q thin film lumped passive elements 18 p2322 A70-36760

- Microwave conductivity of thick film screen-printed microstrip circuits, measuring closed resonators SHF Q factors 19 p3388 A70-37964

- Selective inductorless amplifier design with four layered distributed RGC line in feedback loop, obtaining high Q factors in transfer function 19 p3390 A70-38674

- Microwave apparatus for resonant frequency change and loaded resonator Q measurement during DC discharge afterglow electron removal studies 20 p3679 A70-39715

- Active bandpass filter configurations with operational amplifiers, noting resonance frequency and Q factor variation relationship to amplifier gain-bandwidth product 21 p3796 A70-40561

High Q frequency stabilized cavity controlled microwave oscillator using Super Invar resonator 23 p4169 A70-43792

Q SWITCHED LASERS

One piece KDP and ADP reflector shutters used as laser Q switches, discussing compensation for working surfaces temperature displacement 01 p0106 A70-10060

Laser mode selection with slowly opened Q switches, discussing rotating prisms and Faraday rotators types, pulse buildup, far field spatial distribution, etc 01 p0108 A70-10427

Chirped pulses observation by heterodyning single frequency Q switched carbon dioxide laser with stable CW local oscillator and beat signal display on oscilloscope 01 p0109 A70-10433

Carbon dioxide lasers passive Q switching by gaseous methyl fluoride and phosphorus pentafluoride, presenting absorption coefficients 01 p0110 A70-10561

Semiconductors as optical limiters for Q switched lasers, reporting temperature values for nonlinear absorption coefficients of Si, CdSe, CdTe and GaAs 01 p0158 A70-10563

Q switching of continuously pumped Nd:YAG using double Fabry-Perot etalons to replace laser resonator output mirror 01 p0112 A70-10903

Oscillation and doubling of 0.946 micron line in Nd ion doped YAG, calculating optimum nonlinear coupling to internal Q switched laser 01 p0113 A70-11169

Optical parametric oscillator pumped by continuously repetitively Q switched Nd:YAG laser output 01 p0113 A70-11171

Ruby laser Q switching by chlorophyll d and derivatives, discussing peak output power 01 p0114 A70-11391

Giant pulse Q switched lasers generated plasmas, noting VUV spectral line shifts, asymmetries and existence of satellite lines 02 p0345 A70-11894

Q switched and high energy pulse laser devices for location of satellite photographed by night against background of stars, including optimization in noise [ONERA-TP-753] 02 p0313 A70-12369

Refractive index perturbation from energy absorbed from long pulsed and Q switched Nd doped glass lasers, observing sonic waves generated by Q switched laser 03 p0498 A70-13156

Opposing cavity modes interference effect on passive Q switched ruby laser energy yield 03 p0499 A70-13213

Chlorotrifluoroethylene and difluorodichloromethane saturable absorbers for wavelength extensions of passively Q switched carbon dioxide lasers 03 p0502 A70-13816

Saturable Q switch of cryptocyanine used in ruby laser for pulse sharpening, describing dye sensitivity to solar radiation 04 p0701 A70-15035

Wavelength selection in Q switched carbon dioxide laser by intracavity gas cell providing selective absorption 04 p0702 A70-15362

Bistable optical resonators with saturable absorbers, discussing hysteresis characteristics and Q switching applications 06 p1105 A70-17449

Breakdown of cryptocyanine dye in methanol solution by ruby laser pulses providing passive Q switching mechanism 06 p1083 A70-18524

Frequency calculation and measurement for acoustic waves produced by carbon dioxide Q switched lasers 06 p1084 A70-18620

Laser pulse power effect on edge absorption of glass filter used for Q switching applications 07 p1299 A70-19855

Self mode locked pulses with rotating mirror Q switched carbon dioxide laser, attributing pulse shortness to saturation broadening of spectrum 07 p1301 A70-20018

Uranyl ion luminescence and absorption cross section in silicate glass excited by high power light beam, considering Q switching action of ion 08 p1510 A70-20516

Tunable Q switched pulsed discharge carbon dioxide laser intensity dependence on time delay investigated for various vibrational/rotational lines and gas mixtures 08 p1512 A70-20618

Statistical characteristics of Q switched He-Ne laser emission gain during transient process from subthreshold to superthreshold value 08 p1514 A70-21814

Plasma discharge absorption coefficients measurement using Q switched ruby laser 09 p1694 A70-22139

Diffraction shaped ruby laser monopulse during excitation of modulated ultrasonic traveling waves in phototropic Q switch 09 p1696 A70-22483

Vitreous transparent solids emission after irradiation by Q switched laser, ascribing luminescence to multiphonic and excitonic phenomenon 09 p1710 A70-22836

Holographic recording of Q switched neodymium laser beam achieved through lens testing on reconstituted beam 09 p1697 A70-22845

Ruby lasers simultaneous Q switching by single rotating prism, discussing possible differential frequency ranges 09 p1697 A70-22989

Pulse repetition rate control and stabilization in passively Q switched carbon dioxide laser 09 p1699 A70-23537

Motion picture holography using continuously pumped ruby laser illumination system in repetitive Q switched mode 09 p1689 A70-23782

Q switched laser pulses lengthened using internal second harmonic generator 10 p1898 A70-23981

Shock pressure and impulse caused by Q switched laser light absorption, considering temperature dependence of EM radiation penetration depth 10 p1900 A70-24422

Plasma self Q switching in pulsed far IR lasers, discussing lens effect of plasma electrons delaying laser pulses 11 p2062 A70-25634

Electro-optical Q switches for generating laser radiation pulses 11 p2064 A70-26809

Monopulse laser operating on ruby and neodymium glass using quarter-wave electro-optical Q switch 11 p2064 A70-26810

Ruby laser with electro-optical Q switching, using polarization element for emission spectrum narrowing to single longitudinal mode 12 p2245 A70-27303

Molecular beam carbon dioxide laser Q switching by ethylene as saturating filter, reducing pulse duration by varying ethylene pressure and active mixture composition 12 p2248 A70-27509

Q switched CO-HE laser IR fluorescence, considering population inversion recovery by vibrational energy transfer 13 p2423 A70-28496

Laser field structure effect on spectrum of Q switched laser nonmonochromatic emission after amplitude modulation 13 p2426 A70-28872

Giant pulses composed of shorter pulse trains obtained in Q switched carbon dioxide laser with transverse modes 13 p2429 A70-29412

Ruby laser Q switching by chlorophyll thin film, discussing characteristics and mechanics 13 p2429 A70-29670

Repetitively Q switched Nd-YAG laser operated with intercavity second harmonic generator to produce one watt average power 13 p2430 A70-29831

Nitrous oxide and carbon dioxide laser Q switching by ammonia Stark effect 13 p2431 A70-29835

Radiation coherent enhancement of single frequency emission fields in Q modulated coupled ruby lasers 14 p2593 A70-30152

Ultrashort pulse generation by solid state Q switched lasers, discussing spontaneous emission effects, atomic polarization and populations variation 14 p2594 A70-30477

Mode controlled Q switched tuneable ruby laser, obtaining frequency scanning by temperature and pressure control 15 p2752 A70-32048

Glass disk calorimeter for measuring free running and Q switched laser pulses 15 p2742 A70-32545

Monopulse ruby laser with phototropic Q switch based on radiation density increase due to beam distribution 15 p2754 A70-32867

Q switched subnanosecond laser system with increased intensity, using pulse selection technique 16 p2927 A70-33163

Solid state giant pulse laser with small divergence angle, using polymethyl dye solution in nitrobenzene as Q switch 16 p2929 A70-34221

High-power Q switched solid state laser radiation intensity measurement methods for multi and single modes 17 p3105 A70-35094

Optical rectification/polarization/ and measurement of Q switched laser energy and time parameters, using crystals and parallel plate capacitor 17 p3105 A70-35098

QUADRANTID METEORIDS

Picosecond pulses in Q switched neodymium glass and ruby lasers, describing pulse measurement with fluorescence 17 p3108 A70-35623

Laser emission intensity oscillations during resonator Q sinusoidal variations 18 p3267 A70-36617

Q switched laser turn-on nonlinear dynamics, deriving field intensity distribution function 18 p3270 A70-36743

Nd-YAG Q switched laser using feedback loss control to increase switching speed for digital scanning 18 p3270 A70-36744

Laser pulse shaping using inducible absorption with Q switched time behavior controlled by nonlinearities within optical resonator 18 p3270 A70-36745

Carbon dioxide laser passive Q switching, using ethylene and methanol as saturable absorbers 18 p3270 A70-36749

Giant pulses in passively Q switched laser oscillator, calculating time constant of light flux exponential increase 18 p3270 A70-36953

Low jitter multiple high voltage spark gaps switching at 50 pps by Q spoiled YAG laser triggering 19 p3444 A70-37667

Ion temperatures and incident intensities in plasmas produced by solid target irradiation with Q switched laser beam 19 p3479 A70-37765

Single frequency ruby laser with electro-optical Q switching, selecting transverse and longitudinal modes by stepwise voltage application to shutter 19 p3448 A70-38737

Q switched lasers time dependent loss elimination from elastoplastic relaxation effect in lithium niobate and KDP Pockel cells 20 p3640 A70-39093

Q switching of nitrous oxide laser with Freon 12 and sulfurhexafluoride absorbers, comparing wavelengths with carbon dioxide laser outputs 21 p3834 A70-40567

Q switched free running mode-locked lasers with cavity mirror consisting of thin glass plates suitable for high power use 21 p3836 A70-40807

Radiation coherent enhancement of single frequency emission fields in Q modulated coupled ruby lasers 21 p3839 A70-42076

Breakdown mechanism in Q switched ruby laser triggered spark gap, noting pulse duration and power peak 22 p4049 A70-42352

Passive Q switching and mode locking of carbon dioxide laser with saturable absorbers and buffer gases, using electric pulse excitation 22 p4050 A70-43023

Rotating mirror hologram camera for high speed phenomena, using Q switched ruby laser pulses [SMPTE PREPRINT 7] 22 p4035 A70-43054

Electric strengths of liquid dielectrics during subjection to Q switched laser pulses, determining threshold currents for breakdown 22 p4051 A70-43338

Giant pulses by actively and passively Q-switched inorganic neodymium-liquid lasers with varying modulation due to mode coupling 23 p4202 A70-44937

Electro-optical Q switches for generating laser radiation pulses 24 p4351 A70-45181

Monopulse laser operating on ruby and neodymium glass using quarter-wave electro-optical Q switch 24 p4351 A70-45182

Carbon dioxide molecular vibration excitation by Q switched carbon dioxide laser, obtaining accommodation and diffusion coefficients by relaxation measurements 24 p4351 A70-45369

Spark gap triggering with Q switched laser, comparing performance with electrical method 24 p4353 A70-45560

Internal Q switching deviation in gallium aluminum arsenides-GaAs single heterojunction lasers attributed to loss reduction at current pulse end 24 p4354 A70-45815

Time evolution of instantaneous light intensity mean and variance for Q switched single mode laser near oscillation threshold 24 p4355 A70-46090

Gas ionization with Q switched carbon dioxide laser radiation, determining breakdown threshold or minimum power density requirement 24 p4355 A70-46261

QSO [RADIO SOURCES]

U QUASARS

QUADRANTID METEORIDS

Geminid and Quadrantid meteor shower densities observed on wave-channel-antenna radar 14 p2635 A70-30305

QUADRATIC EQUATIONS

Kharlamov conditions for existence of linear and quadratic invariant relationships between equations of motion of body about fixed point

01 p0145 A70-11435

Duality theorem for complex quadratic programming over polyhedral cones

07 p1238 A70-19356

Criteria for estimating errors in quadratic approximations to asymptotic stability involving Popov condition based on existence of quadratic Liapunov functions

16 p2941 A70-33045

Unified variational theory of quadratic forms, considering linear functional on real linear space and bilinear and quadratic functionals

17 p3129 A70-34867

Existence and uniqueness of optimal control for one dimensional linear system with distributed control parameter using input-output integral with quadratic functional

17 p3057 A70-35627

QUADRATIC PROGRAMMING

Quadratically convergent algorithms for function minimization, discussing unified method and applications to quadratic and nonquadratic functions

19 p3458 A70-38302

Book on theory of optimal control and mathematical programming covering linear, nonlinear, quadratic programmings, etc

21 p3845 A70-40891

Convex programming solution using quadratic approximation method with objective function

23 p4211 A70-44027

QUADRATURE APPROXIMATION

U QUADRATURES

QUADRATURES

Error estimation during application of Cauchy approximate integral formulas to numerical differentiation of analytic functions by quadrature

01 p0131 A70-10543

Iterative computational procedure for generalized quadratic programming problem, formulating convergence theorem

03 p0460 A70-14165

MHD boundary layer separation near rear stagnation point with magnetic field normal to wall solved by series expansion, calculating skin friction by numerical quadratures

03 p0469 A70-14182

Thermoelastic boundary value problems solutions in quadratures applicable to problems with given parameters on boundary sections

04 p0775 A70-15257

Transverse nonrecursive digital filters for Hilbert transformation, investigating ideal quadrature filters with Chebyshev approximation errors

05 p0822 A70-16772

Thermoelasticity boundary value problems solutions in quadratures based on symmetry property and Fourier integrals

05 p0947 A70-16971

Equations of motion for hypersonic friction layers integrated using quadrature procedures

[DVL-913] 06 p1033 A70-17230

Optimal quadrature formulae for numerical integration of 2 pi-periodic functions involving integrand derivative values at knots

06 p1093 A70-17582

Chebyshev quadrature formula weighting functions, presenting accuracy estimation method

07 p1321 A70-18659

Quadrature formulas with minimum remainder estimate for differentiable functions classes, considering piecewise polynomial /spline/ functions characteristic properties

09 p1711 A70-22147

One-step numerical integration of linear differential equations based on Labotto quadrature, including higher order applications and stability analysis

11 p2071 A70-25840

Numerical quadratures application to integral equations for radiative heat transfer computations, discussing validity for parallel and adjoint plates

12 p2332 A70-27840

Numerical integration or quadrature technique for evaluating Fourier integrals in theory of infinite cylindrical antenna

13 p2440 A70-29088

Numerical quadrature of singular functional equations, tabulating integral functions, Cauchy principle values and integral transformations for optimal error function

18 p3280 A70-36219

Quadratures asymptotic properties and convergence for continuous functions and function with singularity

19 p3456 A70-37415

Nonlinear two point boundary value problem, examining quadrature error effects in approximate numerical solutions by variational techniques

19 p3458 A70-37979

Elastic membrane axisymmetric deformations, reducing nonlinear equations system to quadratures

20 p3718 A70-39230

QUADRUPOLE NETWORKS

Quadrupole probe for ionospheric plasma resonances involving measurement of mutual impedance between pairs of electrodes

06 p1117 A70-17373

Inertialless nonlinear quadrupole output of oscillations modulated by normal noise, analyzing correlation functions

09 p1637 A70-23159

Algorithm for selective quadrupole parameter tolerance calculation, combining random search method with statistical testing

11 p2018 A70-25923

Voltage programmed RF oscillator /VPO/ for spaceborne quadrupole mass spectrometer, describing transistorized circuitry

20 p3630 A70-39487

QUADRUPOLES

Sound generation by multibladed single stage fans operating in free field, deriving model as boundary value problem involving inhomogeneities due to quadrupole distribution

01 p0166 A70-11197

Quadrupole moment matrix elements in adiabatic approximation for transition bands of hydrogen, HD and deuterium molecules in ground electronic state

02 p0342 A70-11822

Rotation-vibration matrix elements of quadrupole moments and absorption coefficients of ground electronic states of hydrogen, HD and deuterium

02 p0342 A70-11823

Variational and Z-expansion calculations for magnetic quadrupole transitions decay rates of He sequence

05 p0920 A70-16942

Noise and gain formulas for wideband distributed-gain amplifiers using quadrupole elements and transmission line configurations

08 p1472 A70-20863

Solar oblateness and gravitational quadrupole moment related under assumption of magnetic and velocity fields absence in surface layers, including rotation effects

08 p1570 A70-20902

Quadrupole coupling between single and double excitation channels in hydrogen-hydrogen collisions found ineffective due to energy defect between channels

09 p1733 A70-23268

Transfer impedance measurement for HF quadrupole probe immersed in hot magnetoplasma

10 p1877 A70-24709

Plasma column dynamic stability breakdown in quadrupole HF magnetic field in terms of violating stability criterion for long wave deformation

10 p1926 A70-25109

Ion line Stark broadening, considering electron-ion quadrupole excitation and electron resonant scattering

14 p2620 A70-31376

Solar quadrupole moment effect on secular perturbations of planetary orbital elements

18 p3313 A70-36325

Ion collision effect in quadrupole mass spectrometer, describing ion energy, total pressure in system and other parameters

19 p3421 A70-37411

Quadrupolar mass spectrometer design for lower thermosphere neutral composition measurement, discussing atmospheric physics, installation on rockets, etc

21 p3830 A70-41990

Nonzero electron temperature effect on mutual impedance of quadrupole probe in hot isotropic plasma

22 p4080 A70-42720

Space DC electric field measurement by quadrupole probe, discussing geomagnetic field and contact potential effects

22 p4029 A70-42792

Plasma injection and confinement in closed quadrupole magnetic trap

22 p4083 A70-43388

Earth quadrupole moment indirect effect on satellite gyroscope precession

23 p4217 A70-43799

QUALIFICATIONS

Qualification and testing procedures for Apollo Spacecraft Program components and systems, discussing vibration tests

09 p1693 A70-23705

QUALITY CONTROL

Collection of papers on RCA quality assurance

01 p0049 A70-10110

Product assurance concepts on corporate-wide scale from consumer point of view, discussing systems effectiveness, reliability, maintainability, human factors, product safety, etc

01 p0219 A70-10111

Dry lubricated instrument-size ball bearings operation in vacuum for long life and quality performance [ASME PAPER 69-LUB-21]

01 p0101 A70-10386

Magnetic components design, manufacturing and handling for use in space communication satellites, noting design group role in parts construction and quality control

02 p0267 A70-12057

Space projects quality assurance with allowance for technological trends, discussing product and system oriented organizational requirements, failure potentials, contractor performance, etc

04 p0699 A70-15138

Product assurance and large aircraft prototype testing in aircraft industry, discussing reliability testing [DGLR-69-031]

04 p0699 A70-15139

Contamination sources covering ball bearing contamination, relay contact failure, instrument window internal fogging, electronic circuit corrosion and air conditioning problems

05 p0809 A70-16712

Weld quality monitor for production testing of welding strength in electronic circuitry

05 p0856 A70-16722

Lasers for optical inspection of components and calibration of machine tools

05 p0860 A70-16823

Photoobjective and camera resolution tests regarding entire frame using two dimensional azimuth mark

05 p0852 A70-16864

Process specifications to control manufacturing operations, describing contents, purposes and preparation, emphasizing three levels of control

06 p1184 A70-17601

Nomograms for ultrasonic shadow defectoscope acoustic channel parameters calculation

06 p1065 A70-17921

Material Acquisition Division of Naval Air Systems Command, discussing engineering and testing functions in providing air weapons systems to operating forces

06 p1185 A70-17973

Correlations between 100 percent inspection by automatic equipment and quality control acceptance sampling in vacuum tube industry

06 p1077 A70-17986

Quality control manager role in aerospace company overall cost reduction

06 p1185 A70-17987

Apollo reliability and quality requirements, reviewing changes due to cost reductions in space program

06 p1065 A70-17988

Modulation type eddy current flaw detector with striding converter, considering envelope shape of carrier frequency oscillations

06 p1079 A70-18631

Equations for deep hole drilling errors calculations ensuring accuracy

07 p1291 A70-18826

Materials selection and simulated service testing to preclude failure, considering roles of design, fabrication and maintenance

07 p1248 A70-19235

Electron paramagnetic resonance for quality control of crystal structures in quantum electronics applications

07 p1356 A70-19479

Cooperation of NASA and DOD Quality Assurance personnel concerning Apollo 11, considering personnel training

07 p1428 A70-19674

Nondestructive testing of small metal tubing, discussing eddy current, ultrasonic and electromagnetic inspection and dye penetrants

08 p1509 A70-21748

Ceramic capacitors selection considering ionization, third harmonic and HF heating control properties

09 p1642 A70-22003

Quality control - Conference, Tokyo, October 1969

09 p1690 A70-22568

Quality information equipment engineering including specifying, development, design, procurement, construction, installation, checkout, etc

09 p1792 A70-22569

Quality planning for Japanese solid propellant sounding rocket motor production, discussing documentation, design, development and process controls, inspection and tests, etc

09 p1691 A70-22570

F-104 jet windshield components research concerning plate glass optical deviation problems to meet quality standards

09 p1691 A70-22571

V/STOL aircraft turbojet engine design and quality control for in-service reliability

09 p1743 A70-22572

Destructive and nondestructive tests optimum procedure for quality control based on information theory, decision statistics and cost optimization

09 p1691 A70-22573

Variables control charts based on sample means for determining in-control probability properties

09 p1691 A70-22575

Alkoxo-derived strontium zirconate and titanate preparation and characterization, considering purity control, crystallite size and ceramics synthesis

09 p1740 A70-22981

Oxygen index flammability test for polymeric materials, showing general applicability in quality control and research

09 p1710 A70-23346

- Aircraft maintenance, discussing trend toward increased use of quantified methods, failures reclassification, control techniques and check frequencies
09 p1693 A70-23371
- Compound semioaque thin films quality control for thickness uniformity by observing fringe patterns generated by optical data processing techniques
09 p1687 A70-23765
- TV test chart for evaluating Surveyor lunar spacecraft TV system covering resolution, photometric and colorimetric response and sun angular position [SMPT PAPER 105-71]
10 p1890 A70-24601
- Microwave equipment reliability achievement emphasizing tests and analyses on RF amplifiers, duplexers, antennas, etc
10 p1851 A70-24882
- Apollo Applications Program command and service module test requirements to achieve reliable hardware for extended missions
[AIAA PAPER 70-378]
10 p1952 A70-24925
- Book on integrated electronic systems covering integrated circuit design, device and material properties, quality control, applications, etc
10 p1853 A70-25049
- C-5A airframe composite materials fabrication, tooling, processing, quality assurance and nondestructive test methods
11 p2058 A70-25572
- Aerospace materials machining processes guidelines to minimize structural failures caused by lack of surface integrity
[ASTME PAPER MR-69-730]
12 p2239 A70-26988
- Electric discharge machining technology, discussing quality control factors
12 p2239 A70-26990
- Automatic in-process inspection testing of electronic products
[SME PAPER IQ-70-709]
12 p2241 A70-27083
- Economical inspection of numerical-control produced parts through critical dimensions determination and dimension measurement reduction
[SME PAPER IQ-70-710]
12 p2241 A70-27086
- Computerized on-line industrial inspection involving automatic machine sequential control and product geometry error correction, discussing hardware and software requirements
[SME PAPER IQ-70-712]
12 p2241 A70-27088
- Manufacturing error rate and inspection efficiency relevance to hardware product reliability
12 p2244 A70-28014
- Test and measuring equipment control systems analysis, discussing metrology and calibration requirements in overall quality assurance problem
13 p2416 A70-28374
- Nonlocalized ultrasonic defectoscopy resonance method for qualitative difference determination of small sized articles of complex form
13 p2417 A70-28662
- Glass fiber reinforced resin structures and equipment quality and physical/mechanical conditions determined by plastographic analysis
13 p2404 A70-28665
- Quality control technique for predicting exfoliation and stress corrosion resistance of Al alloy sheet and plate
13 p2435 A70-29175
- NDT techniques in manufacturing of Apollo command and service modules
13 p2420 A70-29243
- Quality control goals for manufactured products translated into manufacturing process inspection and investment costs terms
13 p2421 A70-29675
- Automatic test equipment effect on product design, discussing test planning and quality control
13 p2422 A70-29678
- Radio and electronic equipments production testing by automatic equipment combined with semiautomatic manual controller
13 p2379 A70-29680
- Automatic dynamic response system for testing logic and semiconductor devices
13 p2379 A70-29693
- Quality assurance of automatic testing in military or industrial equipment, including acceptance criteria and statistical proving
13 p2423 A70-29694
- Automatic laboratory or field testing equipment design requirements
13 p2423 A70-29695
- Quality control - ASQC Conference, Pittsburgh, May 1970
14 p2591 A70-31101
- Corrective Action systems for identification, control and resolution of manufacturing, engineering and vendor problems
14 p2669 A70-31102
- Apollo project overview and quality-cost effectiveness assurance requirements for future space programs
14 p2654 A70-31103
- Quality control role in configuration management, considering quality assurance organization of aircraft manufacturer
14 p2669 A70-31104
- Quality control variables optimization for maximum net revenue, using computerized simulation
14 p2592 A70-31105
- Quality evaluation surveys performance by contractors
14 p2669 A70-31106
- Quality control organization for miniature resistance welding of electronic equipment, examining planning phase and personnel training program
14 p2592 A70-31107
- Cost reduction and products reliability and quality maintenance by combining accurate cost reporting system with proper quality level control
14 p2669 A70-31108
- Quality control of electronic equipment using technical and management approach for attaining specified reliability
14 p2592 A70-31109
- Systems effectiveness equated to function of performance, availability, reliability, maintainability, quality control and manufacturing, emphasizing optimization
14 p2592 A70-31112
- Quality information system consisting of closed loop input/feedback methods insuring design requirements of Saturn S-2 stage
14 p2654 A70-31116
- Improved standard electrical equipment components development by test by use method, reducing cost and time
15 p2828 A70-31572
- Quality assurance R and D for product design and operational integrity in manned space flight, noting space developments application to aircraft safety
15 p2676 A70-32231
- High usage military system integrated circuit failure modes analysis for reliability improvement
15 p2713 A70-32650
- Electronic components prefailure analysis resulting in reduced failure rates, scrap and rework
15 p2832 A70-32652
- Reliability assurance of LSI components consisting of complex electronic functions fabricated by semiconductor technology on single chip
15 p2713 A70-32662
- Failure analysis in third generation reliability approach to IC product quality improvement, investigating Si-Al contact irregularity cause and effect
15 p2713 A70-32663
- Confidence limits on percent defective estimates for production processes characterized by two specification limits
16 p2921 A70-34025
- Precision components engineering inspection and sonic transducer surface vibration modes analysis by hologram interferometry
17 p3087 A70-35021
- Single and polycrystalline indium arsenide preparation methods and quality control
17 p3143 A70-35119
- Complex control systems in integrated logic circuits and light laboratory materials production, discussing measurement equipment for quality control
17 p3090 A70-35416
- Turbojet aircraft engine fuels quality control, considering chemical composition, physical properties and handling problems
18 p3299 A70-36550
- Precision electron beam welding for metal joints, discussing equipment and quality control factors
19 p3436 A70-38072
- Electronic equipment reliability improvement, based on reliability control group qualification, burn-in and diagnostic tests
19 p3554 A70-38401
- Nondestructive testing of diffusion bonded metals for quality assurance
19 p3437 A70-38423
- Military electronic equipment reliability limitations in terms of mean time to failure, considering quality control of components
19 p3390 A70-38596
- Semiconductor silicon power diodes nondestructive quality control, discussing optimal sampling procedures
20 p3595 A70-38969
- Superpure materials for low background radiation detectors, determining U, Th and Ca radioactive contamination by radiochemical activation analysis
20 p3629 A70-39317
- Optimum calibration intervals determination for obtaining instrument maintenance quality level at low cost
20 p3634 A70-40452
- Measuring and test equipment economic approach to quality levels and accuracy ratios, deriving cost tradeoffs in optimum inspection fidelity
20 p3634 A70-40453
- Lunar launch vehicles quality control and reliability, describing management procedures for test facilities, preproduction and purchased materials quality
22 p4126 A70-42384
- Fracture mechanics application to fusion weld
[ASME PAPER 70-MET-2]
22 p4043 A70-42424
- Fiber optic components quality control by image transmission intensity distribution measurement
22 p4045 A70-42513
- Defect grouping role in MIL-STD-105D inspection techniques, discussing costs and acceptance probabilities
22 p4048 A70-43727
- Industrial radiography for nondestructive control of products quality, discussing exposure time determination method
24 p4337 A70-45712
- Industrial radiography, discussing photographic emulsion layers granular structure formation due to ionizing radiation
24 p4337 A70-45714
- Equipment, sources and safety in neutron radiography for industrial quality control
24 p4376 A70-45747
- High current betatrons for defectoscopy of manufactured articles and materials compared with other radiation sources
24 p4348 A70-45846
- Quality control and reliability assurance in industrial supplier-customer relationship, emphasizing management role
24 p4431 A70-46386
- QUALITY FACTORS**
U Q FACTORS
QUANTITATIVE ANALYSIS
Quantitative separation of metastable and cubic chromium carbides in alloyed Cr steels utilizing hydrogen peroxide
03 p0504 A70-12981
- Quantitative method developed for photometric determination of B in nickel or titanium borides, using magnezon I reagent in alkaline solutions at various pH
03 p0504 A70-12983
- Surface active lipoproteins of lung, discussing quantitative determination and labeling on basis of per-bronchial wash-out procedure over trachea
15 p2680 A70-31725
- Quantitative analysis of nonmetallic inclusions in steels containing Ti after electrochemical anodic dissolution
18 p3277 A70-36464
- Quantitative and qualitative analysis of biochemically and radiobiologically important thiols and disulfides via gas-liquid chromatography
19 p3373 A70-37836
- T4 phase proteins radioisotopic examination, determining quantitative analysis and molecular weight by autoradiography
20 p3583 A70-40325
- Human body radioactive nuclides in vivo quantitative analysis by gamma ray spectra, considering matrix method accuracy
20 p3582 A70-40449
- Quantitative gas-liquid chromatography of histidine, using N-TFA n-butyl ester derivatives and histidine converted trimethylsilyl derivative
22 p3983 A70-43524
- Murchison and Lost City chondrites element abundance analysis by thermal neutron activation and wet chemical techniques, noting low oxygen content
24 p4411 A70-45790
- QUANTUM**
U MEASUREMENT
QUANTIZER
U COUNTERS
QUANTUM AMPLIFIERS
Regenerative quantum amplifiers with simple and complex resonators, discussing amplification coefficients and frequency characteristics
01 p0106 A70-10058
- Steady state inversion coefficient for active substance in quantum paramagnetic amplifier with push-pull pumping determined by nonstationary methods
03 p0455 A70-13088
- Population inversion coefficient as function of optimal impurity concentrations and efficiency of ruby quantum paramagnetic amplifier in 3 cm range
03 p0499 A70-13457
- Transient processes in ruby quantum paramagnetic amplifier during pumping, showing technique for saturation prevention and relaxation effects on population inversion
03 p0456 A70-13460
- Electron paramagnetic resonance for quality control of crystal structures in quantum electronics applications
07 p1356 A70-19479
- Spectroradiometer with paramagnetic traveling wave quantum amplifier applied to radio telescope, studying noise, temperature and fluctuation sensitivity at given time constant
08 p1495 A70-21054
- Stationary regime stability of one dimensional model of optical quantum traveling wave amplifier, determining trapping band of traveling wave laser
10 p1901 A70-25158
- Anomalous LF noise in receiving devices with traveling wave quantum paramagnetic amplifier
11 p2020 A70-26817

Molecular velocity influence of optically active medium in gas dynamic quantum amplifier on monochromatic radiation transport, using copropagating light model

15 p2721 A70-32356

Gas dynamic quantum amplifier improvement, discussing power utilization, photon distribution and radiation transport

21 p3836 A70-41418

Anomalous LF noise in receiving devices with traveling wave quantum paramagnetic amplifier

24 p4351 A70-45189

QUANTUM COUNTERS

Conical passive radiation coolers for quantum IR detectors on equatorial synchronous earth satellites, determining temperature excursions

16 p2915 A70-34314

Quantum detector with impinging EM field, discussing photoelectron counting distribution and signal with white noise

24 p4312 A70-46051

QUANTUM ELECTRODYNAMICS

Magnetic field effects on point Coulomb impurity charge static shielding by quantum electron plasma

01 p0151 A70-10449

Soviet book on quantum electrodynamics covering photon mechanics, electron relativistic mechanics, electromagnetic interactions, corrections to Green functions, particle interactions, etc

02 p0345 A70-12827

Bounded operator functionals used for deriving nonlocal interaction Hamiltonian of quantum electrodynamics corresponding to converging series for scattering matrix in perturbation theory

05 p0883 A70-16876

Bounded nonlocal operator used in deriving series of subtracting Hamiltonians representing S matrix in perturbation theory after transition to local limit

05 p0883 A70-16877

Optical devices for enhancement of semitransparent photocathode quantum efficiency applied to TV camera tubes, image intensifiers and other imaging detectors

09 p1682 A70-23502

Quantization of Wheeler-Feynman electrodynamics, discussing spontaneous emission and connection between quantum and classical interparticle action theories

11 p2108 A70-25700

Quantum-electrodynamics renormalization for electron charge in metal environment, using solid state many-body techniques

14 p2619 A70-30476

Maxwell field quantization theory for case of interaction with Dirac field, calculating S matrix for interacting electrons

19 p3473 A70-37413

Quantum gravity and UV infinities in quantum electrodynamics, describing constant gravitational length from nonperturbative calculations for self mass and self charge

19 p3473 A70-37575

QUANTUM GENERATORS

U STIMULATED EMISSION DEVICES

QUANTUM MECHANICS

NT QUANTUM ELECTRODYNAMICS

Hydrogen type exciton model applied to analysis of intermediate exciton state role in two quantum absorption in semiconductors

01 p0153 A70-10068

Particle trajectory and associated wave determined for nonclassical trajectory problem from nonprobabilistic point of view, discussing discontinuity arising from unbounded velocities

01 p0142 A70-10657

Atomic variables elimination technique applied to Markovian laser master equation, resulting in integrodifferential equations for field statistical operator

01 p0112 A70-10884

Neutrino in nonquantum and quantum gravitation theories, neutrino sea, etc, discussing classical neutrino dynamics

02 p0341 A70-11669

Semiconductor laser quantum mechanical rate equations derivation to determine temperature and current dependences of light output properties, indicating numerical calculations for GaAs

02 p0311 A70-11884

Laser amplifier electromagnetic field in arbitrary quantum mechanical state, deriving complex amplitude distribution function to calculate phase uncertainty

03 p0503 A70-14174

Rayleigh scattering cross sections of stellar He C, N and O computed by quantum defect method, discussing effects of wavelength dependent polarizabilities

04 p0723 A70-15692

Relativity theory and quantum mechanics relation concerning point charge velocity and motion at light speed, deriving elementary particle mass formula

06 p1106 A70-17833

Plasma dielectric tensor derived quantum mechanically, emphasizing similarity in classical and quantum

mechanical methods, discussing linear wave propagation, kinetic equations, etc

06 p1121 A70-17904

Co role in magnetic materials, discussing high magnetic moments in iron combinations, orbital angular momentum, quantum mechanics explanations, etc

07 p1306 A70-19074

Quantum mechanical form of Cramer-Rao inequality used to determined error lower bound for radiating object parameter observed by quantum-limited optical system

09 p1694 A70-22072

Singly ionized Mg resonance lines electron impact broadening quantum mechanical calculation

09 p1732 A70-22827

Resonance energy calculation and transmission coefficient estimate for quantum mechanical model of reactive scattering of three atoms in line

10 p1920 A70-25145

Digital filters response errors due to signal amplitude quantization, resulting from analog-to-digital conversion and arithmetic operations

11 p2029 A70-26333

Quantum mechanical inverse problem of elastic scattering theory, discussing Hylleraas solution for determining potential energy function from phase shift

12 p2274 A70-26899

Fracture kinetics model for polymers emphasizing quantum effects even at room temperature

13 p2510 A70-28670

Effective moment of inertia in quantum mechanical three body problem, applying specific decoupling to wave functions

13 p2452 A70-29478

Book on light and matter covering mathematical laser theory

13 p2429 A70-29574

Closed universe classical and quantum dynamics by ADM Hamiltonian treatment of Einstein equations for homogeneous cosmological models

13 p2495 A70-29812

Quantum mechanical model of electron scattering by homonuclear diatomic molecule at ground state, calculating differential and integral cross sections for elastic scattering

14 p2618 A70-30113

Fluid quantum corrections to viscosity, thermal conductivity and diffusion, expanding Wigner operator in Planck constant

14 p2665 A70-30655

Quantum mechanical communication system with thermal noise disturbance, analyzing reliability function and channel capacity

14 p2551 A70-31120

Photomultiplier tubes high quantum efficiency attainment by optical enhancement techniques

15 p2735 A70-31767

Absolute quantum efficiency of phosphor calcium tungstate-lead under monochromatic far UV illumination

15 p2729 A70-32017

Classical approach to quantum mechanics, emphasizing Schrodinger equations and starting from Hamilton-Jacobi equations

16 p2990 A70-33778

Gaseous diatomic molecules quantum mechanical treatment, calculating Hamiltonian matrix elements for interpretation of electron resonance spectra

16 p2955 A70-33799

Simultaneity in optical photon pairs parametric production, verifying quantum mechanical description of fluorescence

17 p3143 A70-35187

Quantum electronic space vehicle, discussing time reversing motor or inverse/anti-atomic engine

17 p3148 A70-35213

Quantum mechanical model of stimulated thermal, Brillouin and molecular excitation scattering of light due to absorption

18 p3266 A70-36409

Optically excited homogeneous bulk semiconductor lasers, examining quantum mechanical rate equations and monochromatic light field pump source

18 p3270 A70-36741

Multiquantum combination effects in ferrites at UHF frequencies

19 p3484 A70-37624

Electrons nonlinear interaction with field in traveling wave tube, using approximate quasi-classical quantum mechanics method

19 p3387 A70-37741

Three level gas laser amplifier theory, considering quantum mechanical atomic system in interaction with two monochromatic EM waves

19 p3446 A70-37829

Quantum mechanics classical equations for complex velocity variable, obtaining asymptotic series solution by applying modified WKB method

24 p4378 A70-45274

Relativistic and nonrelativistic generalizations of classical approach in quantum mechanics applied to equations of motion in electromagnetic field

24 p4378 A70-45275

Space three dimensionality compared with Huygens principle via quantum mechanics, discussing past and current theories and empirical arguments

24 p4380 A70-45643

QUANTUM NUMBERS

Synchrotron radiation rate from deexcitation of electrons in magnetic orbits of low quantum numbers, stressing electrons radiation in intense magnetic fields

06 p1108 A70-17183

Hydrogen atoms collisional excitation cross section expressed in terms of quantum numbers of levels and ratio of colliding electron energy to transition energy

07 p1338 A70-19410

Rotational quantum numbers from iodine molecule resonance fluorescence measurements during laser excitation using Fabry-Perot interferometer

23 p2402 A70-44938

QUANTUM STATISTICS

Thermodynamic properties of nonideal multicomponent gas mixtures including Fermi-Dirac statistics effect, discussing internal partition function for free and confined atoms

06 p1184 A70-18637

Quantum statistical decision theory for detection and estimation of signals in random noise

07 p1333 A70-18919

Superradiation signal stationary pulse excitation, describing quantum statistical theory of condensed media and gases, forced induction, signals and echoes

20 p3642 A70-39756

Statistical theory of electron-positron-photon vacuum in external magnetic field, noting magnetic activation effect at low temperatures

22 p4076 A70-43000

German monograph on quantum statistics for light propagation in laser-active fluctuating media

24 p4350 A70-45090

QUANTUM THEORY

NT BOHR THEORY

Book on quantum electronics covering energy levels of materials, matter-radiation interactions and laser theory and applications

01 p0112 A70-10876

Stellar X ray sources quanta fluxes estimation based on solar coronal emissions analysis

02 p0360 A70-12793

Book on quantum electronics, discussing dipole transitions, resonant processes, lasers, nonlinear effects in quantized media, field quantization, radiation-photon interactions, etc

05 p0893 A70-16800

Dielectronic recombination rate coefficient determined by quantum theory of resonance-collision processes, considering coupling, degeneracy and overlapping resonances

05 p0920 A70-16943

Hamiltonian methods applied to homogeneous cosmological models, obtaining Einstein equations, passing to quantum theory by imposing canonical commutation relations

07 p1336 A70-19921

Plasma finite DC resistivity quantum theory, considering electron-molecule collisions energy absorption, noise generation, etc

08 p1551 A70-21099

Radiation field photon density matrix for gas laser with ring resonator determined from double level atomic model, considering photon dispersion and wave reflection feedback

08 p1513 A70-21420

Tachyons /faster than light particles/ on basis of relativity theory, noting reaction with light speed particles and relation to quantum theory

10 p1916 A70-24385

Science of time considered with reference to quantum physics, special theory of relativity, directivity and symmetry and conditional probability, discussing clock designs

12 p2271 A70-27276

Thermal EM field as function of coherent states, outlining quantum theory for thermal radiation and solar energy

15 p2678 A70-32423

Laser beam scattering by free electrons in semiclassical radiation theory, discussing intensity dependent frequency shift

15 p2753 A70-32452

Microscopic quantum theory of liquid He isotopes emphasizing method of correlated basis functions

16 p2951 A70-32997

Quantum theory for spontaneous parametric light scattering, determining photon spectral distribution

16 p2951 A70-33196

Quantum gyroscopic theory for instrument design

16 p2927 A70-33229

Degenerate p-n diode junction capacitance calculation, taking into account quantum and temperature effects

20 p3596 A70-39117

M sub L alignment creation due to beam foil excitation process demonstrated with zero field quantum beats in He and H emission spectra

20 p3674 A70-39148

Quantum theory of inhomogeneously broadened laser, considering atomic motion-electromagnetic field interactions and detuning effects 22 p4048 A70-42293

Radiative transfer equations quantum theoretical deduction in spectral line regime, considering Planck law, Einstein coefficients and kinetic equations 22 p4072 A70-42339

Quantum noise in narrow-band ring laser, noting mode amplification of weak monochromatic signals 23 p4202 A70-45056

Relativistic two body system in circular orbits, examining quantum theory with massless and massive scalar fields and energy and angular momentum for bound system 24 p4379 A70-45521

QUARKS

Quarkian substance properties noting possibility of superconducting state at high densities 04 p0753 A70-15074

Quarks discovery in cores of energetic extensive air showers, discussing results evaluation and interpretation 04 p0722 A70-15299

Quark search in cores of air showers with four million GeV mean energy, deducing rough production rate 07 p1368 A70-19925

Nucleons split-up into quarks disregarded as energy source for quasars 08 p1547 A70-20583

Critical review of paper on evidence of quarks in air shower cores from cloud chamber tracks, explaining data by statistical fluctuations in particle fluxes 08 p1562 A70-21272

High energy and contemporaneous cosmic ray tracks in bubble chamber picture noting evidence of quarks 12 p2276 A70-27997

Quark search in cosmic radiation near sea level, using scintillation counter telescope 15 p2793 A70-31737

Cosmic ray experiment for detecting quarks in low density showers, using hodoscope of wire proportional counters 16 p2972 A70-33048

Quarks properties and observation methods, discussing reaction models with Coulomb potential barrier for energy due to participation in quasar dynamics 16 p2973 A70-33119

High transmission device for quark detection in primary cosmic rays 20 p3629 A70-39315

Criticism of evidence for cosmic ray quark passage through low density bubble chamber 20 p3701 A70-40499

Quark in stars, discussing electronic transitions and UV spectral lines 21 p3921 A70-41975

QUARRIES

U MINES [EXCAVATIONS]

QUARTZ

Quartz-Fiberfrax heat shield tests for Thor booster at high radiative heating rates, noting optimum material performance dependence on loose stitching 01 p0129 A70-10850

Statistical measurements of deformation structures and refractive indices in experimentally shock loaded quartz specimens with different crystallographic orientations 02 p0292 A70-12509

Temperature dependence of sputtering coefficient of quartz and chondrites at 2000 K and mass decrease prior to evaporation 03 p0569 A70-13357

Radiation effects on swept-synthetic quartz resonators and materials, discussing frequency shift measurements and defect studies 04 p0731 A70-14735

Correlation function procedure applied to quartz clock rate analysis, noting operating temperature control 04 p0693 A70-15487

Reinforced plastics high silica and quartz history, properties, uses, costs and pricing, tabulating sources and presenting product recommendations and cost comparisons 05 p0873 A70-16608

Quartz magnetometer design to measure horizontal component of geomagnetic field, observing stability of H/zero/ constant 07 p1281 A70-19467

Strain gage for measuring strain waves amplitude on surface of fused quartz to study electromagnetic waves interaction in Permalloy films 09 p1681 A70-23349

Axial mode selection and frequency stabilization of Nd-YAG laser by optimally designed crystal quartz etalon 10 p1900 A70-24943

Quartz and alkaline glasses fracture stability in water vapor and aqueous solutions with enhanced surface activity as function of time 11 p2068 A70-25379

Stimulated Mandelstam-Brillouin scattering and fracture of molten quartz and silicate glasses produced by laser giant pulse 11 p2061 A70-25380

Temperature dependence of sputtering coefficient of quartz and chondrites at 2000 K and mass decrease prior to evaporation 11 p2118 A70-26722

Quartz-polyimide for missile radome exhibiting low dielectric constant and thin wall for use over broader frequency range 13 p2417 A70-28664

High frequency tunnel diode quartz crystal oscillator circuits with inductive element compensating circuit capacitor 13 p2376 A70-28874

Synthetic autoclave grown quartz crystals with W and Ga impurities, discussing spectral properties and weak absorption bands after irradiation 14 p2625 A70-30154

Quartz floating component design, discussing magnetic sensitivity temperature dependence and microseismic noise rejection properties 14 p2582 A70-30245

Longitudinal and transverse hypersonic mm waves excitation in quartz single crystal at liquid helium temperature 16 p2952 A70-33258

Low dielectric constant quartz-polyimide for radomes, considering curving methods 16 p2936 A70-33368

Precambrian cherts hydrocarbon and fatty acid concentrations and C and S stable isotope ratios, discussing biological evolution rate 18 p3244 A70-35969

Quartz magnetometer design to measure horizontal component of geomagnetic field, observing stability of H/zero/ constant 18 p3260 A70-36941

Quartz magnetic variometer allowing simultaneous recording of magnetic field variations and suspension axis inclination changes 19 p3420 A70-37336

Quartz astatic galvanometer resistant to geomagnetic field variations, vibrations or microseismic noise 19 p3421 A70-37337

Quartz- and silicate-graphite mixtures carbothermal reduction in vacuum at 1400 C 20 p3583 A70-40425

Controlled self excited quartz triode oscillator, calculating flicker noise effect on frequency stability 23 p4171 A70-43959

Quartz Z-variometer for autonomous variation stations, describing construction and operation 23 p4194 A70-44089

Longitudinal and transverse hypersonic mm waves excitation in quartz single crystal at liquid helium temperature 23 p4218 A70-44281

Stable clock precision timing systems, discussing quartz crystal, rubidium, cesium and hydrogen oscillators 23 p4195 A70-44289

QUARTZ CRYSTALS

Chromite, zircon and quartz crystals in Muong Nong type tektites by X ray diffraction, discussing possible impact origin 20 p3709 A70-40088

QUARTZ TRANSDUCERS

Magnetosensitive quartz element with suspended magnet and two mirrors for recording magnetic variations 05 p0851 A70-16770

Quartz crystal particulate sensor instrument for terrestrial and Mars atmospheres 14 p2585 A70-30575

QUASARS

Quasar 3C 273 scintillation intensity, considering role of interplanetary plasma inhomogeneities 01 p0174 A70-10199

Quasars variability, distribution, absorption line characteristics, red shift peaks, physical models, cosmological problems, etc 01 p0177 A70-10341

Long baseline interferometry used to improve radio telescopes resolving power in measuring quasar diameters 01 p0183 A70-10885

Quasars emission and absorption red shifts distribution analysis suggesting cluster interpretation 01 p0183 A70-10895

Einstein-Friedman cosmology of vanishing constants assumed in deducing relations between antipodal radio sources red shifts and universe parameters 01 p0187 A70-11274

Quasar B264 observed with multichannel spectrometer attached to 200 inch telescope, comparing to N-type and Seyfert galaxies and other quasars 02 p0371 A70-12243

Quasars radio emission tabulated, showing quasar B264 as member of galactic cluster 02 p0372 A70-12244

Upper mass limit of quasar in galactic cluster from velocity dispersion of galaxies using generalized form of virial theorem, determining B264 mass 02 p0372 A70-12245

Radio source OQ208 characteristics observation suggesting possibility of quasi-stellar nature 02 p0377 A70-12492

Optical variations of quasars and other radio sources using photographic photometry, emphasizing bright optically violently variable (OVV) quasars properties 03 p0568 A70-13328

Quasar spectra interpretation, analyzing observational data and absorption lines correspondence to different red shifts 03 p0570 A70-13484

Periodic clustering of red shift values in quasi-stellar and unusual objects spectra, using power spectra 03 p0577 A70-14217

Long term behavior of blue photographic luminosity of Seyfert galaxy 3C 120 nucleus, considering similarity to quasar 3C 273B 04 p0748 A70-14589

Primordial cosmic ray sources evidence suggesting galaxies and quasars in initial stages of formation 05 p0897 A70-15921

Local theory alternative to cosmological quasar origin theories, considering red shifts properties 05 p0913 A70-16473

Secular variations in small quasar components, discussing compatibility with theory of expanding synchrotron sources 05 p0913 A70-16474

Electron ejections from nuclei of radio galaxies and quasars on basis of plasma stability, discussing role of relativistic electrons and resulting unstable pinch 05 p0917 A70-16901

Induced Compton scattering of plasma and electromagnetic waves under astrophysical conditions, discussing HF radio emission spectra from cosmic objects and quasar 05 p0917 A70-16904

Flux densities from quasars 3C 273, 3C 279 and 3C 454.3 and Seyfert galaxy 3C 84, measuring linear polarization, discussing time variations in sources 05 p0918 A70-16926

Particle acceleration during 1966-1967 radio burst of 3C 273, indicating breaking down of model of expanding source emitting synchrotron radiation 05 p0918 A70-16927

Cosmological theories taking into consideration gravitational collapse, discussing pulsars, quasars and X ray stars evolution 06 p1140 A70-17584

Statistical distribution of quasi-stellar objects with known red shifts over celestial sphere, observing symmetry over galactic equator 07 p1374 A70-18706

Absorption lines in quasars spectra indicating line formation close to quasar nucleus 07 p1383 A70-19402

Correlation function prediction of rapid brightness variations in quasar based on variable optical emission model including flares 07 p1383 A70-19403

Evolutionary effects associated with quasars listed in 3CR catalog using Schmidt method 07 p1389 A70-20209

Nucleons split-up into quarks disregarded as energy source for quasars 08 p1547 A70-20583

Seyfert galaxy NGC 4151 nucleus relation to quasars, discussing cloud structure and velocity and H line properties 08 p1568 A70-20617

Quasi-stellar objects absolute spectral energy distribution, considering electron temperature and photon density 08 p1572 A70-20916

Stellar formation and explosions in compact gas clouds to explain quasar phenomenon, discussing temporary star concept 08 p1578 A70-21548

Observational verification of cosmological models by examination of red shift discretization in quasars 09 p1750 A70-22098

Quasar-associated evolutionary effects, considering uniform distribution, constant optical luminosity and evolving radio luminosity 09 p1753 A70-22455

Quasar sky distribution as function of apparent magnitude for identification with galaxies of origin 09 p1759 A70-22909

X ray fluxes upper limits from quasars 3 C 196, 3 C 186 and 3C 380 measured by balloon flight experiments 09 p1745 A70-23271

Quasars photoionization of intergalactic high density hydrogen gas to interpret absorption features absence, noting gas temperature 10 p1942 A70-24628

Quasar spectra searched for intergalactic absorption lines, discussing red shift 10 p1947 A70-24998

Plasmas role in emission mechanisms active in celestial sources of radiation, discussing sun and quasars

10 p1948 A70-25027

Observational cosmology, discussing aspects of radio source and quasar counts, intergalactic medium and cosmic black body radiation

12 p2298 A70-27061

Radio galaxies and quasars radiated power, discussing red shift complicated by absorption lines discovery in spectra

12 p2298 A70-27064

Collection of papers on quasars and high energy astronomy covering radio galaxies, cosmic rays, gamma rays, galactic clusters, neutrino astronomy, gravitational collapse, etc

12 p2299 A70-27376

Quasar optical properties, red shift and models

12 p2299 A70-27379

Quasar model based on supermassive stars relaxation oscillations, considering energy requirements

12 p2300 A70-27380

Nonthermal radiation effects on emission line spectra of Seyfert galaxies and quasars determined from ionization equilibrium of gas envelope

12 p2293 A70-27585

Radiotelescope measurements for geodetic purposes, applying interferometric principles to quasar radiation

13 p2396 A70-29163

Flat emission spectra of quasars in 3CP catalog attributed to anisotropic relativistic electron fluxes

13 p2493 A70-29387

Quasars magnitude relation to red shift, discussing scatter in log cz vs m plane correlation with B-V color

13 p2495 A70-29797

Cosmogenic phenomena instability, discussing red shift, expanding universe, galactic nuclei and quasars

15 p2800 A70-32144

Intergalactic gas condensation rates in galactic nuclei, considering recurrent magnetoplasma cores and quasar-like phenomena

15 p2801 A70-32479

Electrodynamic-gravitational model of radio galaxies and quasars accounting for complex field, particle acceleration, angular momentum, luminosity and line emission

15 p2807 A70-32811

Quasars as protoclusters of galaxies, discussing hypothesis of dense matter cascading fragmentation with subsequent scattering in form dispersing stellar systems

15 p2808 A70-32881

Quasar 3C 298 angular dimensions and 3C 273 scintillating component at 60 MHz based on mean quasi-periods shifts of scintillations

15 p2808 A70-32885

Arp hypothesis regarding radio source ejection from galaxies tested for quasars

15 p2808 A70-32887

Quarks properties and observation methods, discussing reaction models with Coulomb potential barrier for energy due to participation in quasar dynamics

16 p2973 A70-33119

Quasar and radio galaxies, observing absorptions at red shifts close to emission line

17 p3157 A70-34846

Quasar 4C 05.34 absolute spectral energy distribution by multichannel photoelectric spectrometry

18 p3318 A70-37019

Radio polarization of quasars with and without absorption line spectra

19 p3523 A70-38605

Quasars and radio galaxies circular polarization at 49 cm wavelength, using radio telescope interferometer

19 p3523 A70-38606

Quasars PHL 5200 and RS 23 spectra absorption lines, examining resonance line transfer of radiation through differentially expanding atmosphere

20 p3701 A70-39006

Quasar red shift apparent magnitude data analysis, estimating deceleration parameter of universe

20 p3709 A70-40076

Blue stellar objects emission at 9.5 and 3.5 mm, suggesting quasi-stellar objects with small intrinsic radio luminosity

21 p3922 A70-41993

Electromagnetic radiation power spectrum scattered by relativistic particles, considering reflected waves resemblance to HF radio spectra of quasars

22 p4100 A70-42856

Extragalactic variable radio sources as clue for quasars and galactic nuclei energy, using long baseline interferometry

22 p4105 A70-43226

Intergalactic gas condensation rates in galactic nuclei, considering recurrent magnetoplasma cores and quasar-like phenomena

23 p4240 A70-43904

Extragalactic astronomy research covering quasars, Seyfert and related galaxies, cosmology, Magellanic Clouds, supernovae, etc

23 p4256 A70-45040

Quasars red shift distribution extrapolated from density evolution and luminosity function

24 p4402 A70-45386

Energy production of extragalactic radio sources, discussing objects associated with quasars

24 p4403 A70-45395

Ionized matter stability in intense radiation field opposed to gravitation, explaining quasar properties

24 p4398 A70-46162

Optical quasi-stellar objects radio emission observation for identification with radio sources

24 p4413 A70-46167

Extragalactic radio source optical identifications showing association with quasars or Seyfert galaxies nuclei

24 p4413 A70-46168

QUASI-STEADY STATES

Quasi-steady state plasma acceleration in coaxial electrode geometry during synchronized application of tailored pulses of mass flow and current

09 p1736 A70-23204

Spinning missile gravity induced angular motion for various trajectory portions, considering quasi-steady state assumption validity

20 p3715 A70-39561

Multimegawatt quasi-steady MPD arc accelerator in millisecond pulses, noting applicability to experiments requiring long exposure times

20 p3683 A70-40241

QUASI-STELLAR RADIO SOURCES

U QUASARS

QUASILINEARITY

U NONLINEARITY

QUATERNARY ALLOYS

Fe-Cr-Mn-Ni system studied to obtain high Mn austenite and establish boundaries in quaternary system

03 p0509 A70-13278

Al-Zn-Mg-Cu alloy corrosion cracking, studying effects of heat treatment, strain percent, blank parameters and grain size

03 p0512 A70-13734

Thin film transmission electron microscopy study of precipitation in Fe-Ni-Cr-Mo alloy with added Be and specific thermoelastic properties

05 p0862 A70-16022

Carbon-bearing materials for modification of Mg-Al-Zn-Mn alloys filtration processes

08 p1505 A70-21132

Austenitic Fe-Cr-Ni-Ti alloys at high temperature to determine activation energy for nitrogen diffusion, noting oxygen role

08 p1522 A70-21707

Ternary phase diagrams and quaternary excess free energy prediction using binary data, applied to Pb-Sn-Zn, Ag-Pd-Cu and Pb-Sn-Cd-Bi systems

12 p2254 A70-27475

Ti-Al-Sn-Zr system high temperature creep strength and ductility retention

17 p3120 A70-34424

Mn and Ti effects on hardening of Fe-Ni-Mn-Ti and Fe-Ni-Mn maraging martensitic steels

17 p3125 A70-35145

High temperature reaging in Ni-Cr-Ti austenitic steel following reversion and interrupted quenching

18 p3274 A70-36054

W-Mo-Nb-Ta system structure and properties at room and high temperature by microstructural analysis and hardness measurements, discussing Mo addition effects

19 p3453 A70-38713

W-Mo-Nb-Ta system with constant 30 percent W, discussing specific weight and hardness

19 p3453 A70-38714

Eutectic NiAl-Cr alloys, investigating quaternary additions effect on rod-plate transition to faceted microstructure

24 p4359 A70-45244

Simplex lattice mathematical models of solidus volume for quaternary Nb-W-Ti-Zr system

24 p4361 A70-45833

QUATERNIONS

Gravitational field equations in flat space, using quaternion representation of general relativity Riemannian space time in terms of spinors

01 p0141 A70-10279

Space vehicle digital control system attitude computations using quaternion matrix algebra to simplify control equations

07 p1393 A70-19302

Quaternion representation of general relativity applied to geodesic equation and planetary motion, noting difference from Einstein formulation

10 p1944 A70-24859

Initial quaternion for Cartesian time varying transformation matrix based on self alignment method of inertial analytic platform

11 p2072 A70-26150

Quaternion scheme for rigid body attitude determination, using Euler axis and angle

23 p4215 A70-44523

QUENCHING

Electron quench additives electrophilic effects in high temperature air plasma flow, simulating reentry flight conditions

04 p0664 A70-15561

Scattered Lyman alpha radiation intensities measured for mixtures of partially dissociated hydrogen in Ar, measuring quenching cross sections

06 p1053 A70-17327

Potassium iodide and paratoluidine fluorescent quenching effect on lasing threshold in rhodamine 6G alcohol solutions

09 p1696 A70-22487

Foreign gases effects on He-Ne lasers IR emission, describing quenching due to positive column electron temperature decrease

11 p2062 A70-25826

Quenching efficiency of molecular oxygen relative to nitrogen, carbon monoxide, carbon dioxide and argon, involving photolysis of gas mixtures

13 p2361 A70-28498

F region nightglow emissions rocket data, discussing rate coefficient for oxygen atoms quenching by molecular nitrogen

13 p2398 A70-29200

Laser excited atoms quenching by iodine molecules from light pulse induced photodissociation of perfluoropropyl iodide active media

24 p4352 A70-45467

Semiconductor solar energy converter, deriving conditions for occurrence of photoconductivity quenching

24 p4391 A70-46325

QUENCHING (COOLING)

Quenched Ti-Mn alloy omega transition phase microstructure characteristics by transmission electron microscopy using thin foils

01 p0125 A70-11639

Ti-Mn alloy quenched in brine and aged at high temperature studied for structural transformations using electron microscope

01 p0125 A70-11640

Al solidification in direct chilling molds effect on as-cast structure, analyzing heat removal, casting rate and application of water to outgoing ingot

02 p3116 A70-12298

Phase alteration quenching effects in Ni-Mo alloys, discussing high temperature alpha region, isothermal annealing below peritectoid temperature and metastable nickel molybdenide phase

03 p0508 A70-13143

Quenching temperature and deformation conditions for Ti alloy bars optimal mechanical properties emphasizing effect of primary structure

03 p0497 A70-13856

Pressure decay prediction improvement for venting and quenching processes of solid propellants using analytical method

11 p2101 A70-25683

Phase transformations in beta isomorphous Ti alloys, discussing effects on omega and alpha phases during quenching and aging and on martensite under stress

15 p2763 A70-32807

Quench hardening and Ni content relationship in Ti-Ni intermetallic compounds, investigating heat treatment effect on mechanical properties

16 p2930 A70-33084

Optimal water quench of solid rockets using injection normal to propellant surface

16 p2968 A70-33598

HEUS solid rocket motor impulse control, describing liquid quench concept development through full scale test firing

16 p2969 A70-33600

Ni particles induced quenching measured by probes in afterglow plasma of pulsed linear discharge, determining deionization rate

16 p2958 A70-33687

Titanium alloys quench hardenabilities, determining variations with distance from end of Jominy bars after annealing

17 p3119 A70-34415

Two phase Ti alloy subjected to quenching and annealing studied by diffraction electron microscope, discussing needles complex fine structure

20 p3645 A70-39043

Al alloy products heat treatment, using synthetic quenchant for distortion control

20 p3650 A70-39967

Pure Al thermal cycling tests, investigating effect of minimizing thermal stress during quenching on behavior of dislocations

24 p4360 A70-45518

Eutectic and hypereutectic Al-Si alloy quench modification by rapid solidification, investigating microstructure and mechanical properties

24 p4362 A70-46183

QUEUEING THEORY

Real time computer control system queueing model to optimize preemptible and nonpreemptible job priority assignment

05 p0817 A70-16414

Aircraft maintenance operations planning based on mathematical mass maintenance theory /queueing theory/

08 p1507 A70-21367

Computer-controlled single-server queueing system with constant access cycle and general service times,

- calculating mean size and waiting time at statistical equilibrium
14 p2553 A70-30518
- Project risk or cost estimation for antipollution, moon mining, tooling, burn-in test and warranties by theory of Takacs processes and correlated queues
19 p3554 A70-38598
- Satellite networks queueing analysis, examining graph-theoretic model based on stochastic inputs and time delay factors
20 p3589 A70-40338
- Queueing requirements in automatic radar target detection system operating with narrow bandwidth data link
22 p3990 A70-43489

R

RABBITS

- Phosphopentomutase activity in rabbit tissue, reporting probable PG-mutase subsidiary function and activity of previously unrecognized enzyme
01 p0012 A70-10091
- Indirect ADP deamination and reamination of corresponding deamino form of ionosine diphosphate in rabbit brain tissue
01 p0018 A70-10506
- Glutamine deamidation enhancement by N-acetyl-L-aspartic acid addition to mitochondrial preparations of rabbit brain incubated in Tris buffer
01 p0018 A70-10508
- NN dimethylguanidine for prevention of arterial lesions induced by cholesterol in rabbits
01 p0020 A70-10707
- UV radiation effects on mucopolysaccharide compounds in tears and on cornea epithelium of albino rabbits
01 p0037 A70-10860
- Chest, abdominal wall and diaphragm displacements of rabbits during partial and whole body exposure to shock waves produced by hexotol charges
02 p0231 A70-11704
- Direct links existence between rabbit temporal cortex neurons and neurons in each division of hippocampus, discussing topographic arrangement and axons quantity
03 p0417 A70-13071
- Biological hazards of laser radiation, noting eye injuries and cataract from transscleral exposure on rabbits
03 p0434 A70-13679
- Myocardial changes in rabbits after general chronic ionizing irradiation attributed to lower cardiac activity, hypotrophy and dystrophy
03 p0425 A70-13888
- Rabbits sensorimotor and visual cortical responses during defensive conditioning to rhythmic light
07 p1197 A70-18695
- Rabbits visual cortex evoked potential changes due to light flashes under different conditions
07 p1198 A70-18716
- Microwave irradiation effects on rabbit eye lenses, noting injury dependence on frequency
08 p1452 A70-21273
- Ophthalmological treatment of severe thermomechanical eye injuries investigated on radiant-energy burned rabbit eyelids
09 p1617 A70-22473

- Hydrogen peroxide infusion effect on skin remission following exposure to ionizing radiation on rabbit legs
09 p1619 A70-22791
- Autonomic effects on heart rate, portal, renal, cutaneous and muscle blood flows during arterial hypoxia in unanesthetized sham operated thalamic and pontine rabbits
12 p2170 A70-27899
- Gravity effect on positional alcohol nystagmus in man and rabbits, observing threshold value in weightless state
13 p2359 A70-29442
- Erythropoiesis inhibitor in blood from rabbit kidney vein during hyperoxia in nitrogen-oxygen atmosphere
14 p2535 A70-30155
- Electrophysiological characteristics of rabbit eye muscles tonic fibers, measuring postsynaptic and membrane rest potentials
15 p2679 A70-31604
- Visual cortical anomalous response to paired photic stimulus in rabbits with ablations in rostral part of brain stem
18 p3221 A70-37214
- Dehydrogenases activities in rabbit retina homogenates exposed to oxygen at high partial pressure for various time periods
21 p3765 A70-41487
- Water and salt metabolism changes during prolonged hypokinesia of rabbits, noting blood plasma dilution, hematocrit number and hemoglobin concentration reduction, etc
23 p4146 A70-44656

RACES

- 2000 meter race for endurance testing, using heart rate radiotelemetry before, during and after
14 p2543 A70-31173

RACON BEACONS

U RADAR BEACONS

RADAR

- NT COHERENT RADAR
NT CONTINUOUS WAVE RADAR
NT DOPPLER RADAR
NT METEOROLOGICAL RADAR
NT MONOPULSE RADAR
NT MOVING TARGET INDICATORS
NT OPTICAL RADAR
NT PULSE DOPPLER RADAR
NT PULSE RADAR
NT RADAR MEASUREMENT
NT RANGE AND RANGE RATE TRACKING
NT SATELLITE-BORNE RADAR
NT SEARCH RADAR
NT SECONDARY RADAR
NT SIDE-LOOKING RADAR
NT SURVEILLANCE RADAR
NT TRACKING RADAR
- Radar model of shower and hail clouds as two phase system of independently scattering spherical particles, stressing radar properties dependence on particle properties
08 p1536 A70-21097
- Radar handbook covering systems design, components, devices, measurements, applications, procurement, etc
13 p2367 A70-29601
- Book on random processes, communications and radar covering optimum filtering, detection, information theory, ergodic theory, probability and integration axioms, parameter estimation, coding, etc
17 p3043 A70-34602

RADAR ALTIMETERS

U RADIO ALTIMETERS

RADAR ANTENNAS

- Binary digital radar signal detectors optimization for radiation pattern of $\sin x/x$ radar antenna and for non-fluctuating target
02 p0255 A70-11899
- Radar system for air traffic control using twin beam antenna to improve performance with respect to ground and angel clutter
02 p0332 A70-11970
- Radar cross section computation for thin wires bent into circular arcs and V shapes using numerical method
02 p0262 A70-12597
- X band radar with horizontally and vertically polarized antennas to compare sea clutter suppression by decorrelation and constant alarm rate receivers
03 p0451 A70-13935
- Radio/radar antenna temperature measurement by phase principle insensitive to receiver gain fluctuations
05 p0819 A70-15804
- Helicopter all-visibility operation realized by using main rotor blade as scanning radar antenna
05 p0793 A70-16040
- Matrix method for maximizing radar antenna directive gain and simultaneously placing nulls in far field radiation patterns
08 p1477 A70-21758
- Electro-optical analogies application to sidelobe reduction of radar antenna illumination patterns and optics far field diffraction patterns in terrain image formation
09 p1631 A70-22009
- Backscattering from rough surface of nuclear fireball measured by two way directive radar antenna on reentry vehicle
09 p1634 A70-22703
- Airborne side-looking radar antenna optimal directional characteristics analysis from viewpoint of maximum surveillance range
10 p1843 A70-25139
- Polarization properties of radar channel with random parameters, relating observation range with transmitting-receiving antennas and target fluctuations
11 p2012 A70-26815
- Phased array radar for automatic random search using pseudorandom sequences to generate random phase characteristics of currents together with suitable gating
12 p2183 A70-26984
- Clutter signals in radar receiver antenna, determining autocorrelation function and spectral power density
15 p2701 A70-32466
- Search radar antennas for monopulse direction finding with radiation pattern for sum and difference operation
15 p2704 A70-32674
- C band radar antenna with pencil beam steered in plane by ferrite phase shifters
16 p2875 A70-33394
- High speed millimetric horn antenna with small azimuth and elevation beamwidths for airfield radar
16 p2876 A70-33407

Solid state phased array radar employing MIC modules in radiating elements, achieving reliability by redundancy
16 p2877 A70-33411

Antenna design for single engine light general aviation aircraft weather radar, reviewing attenuation and terrain return problems
16 p2864 A70-33471

Personnel danger zones demarcation around radar antennas, using beacons
17 p3040 A70-35913

Circular array radar antenna, describing feed systems, scanning switches and radiation patterns
21 p3799 A70-41360

Full-scanning random arrays with high resolution for space exploration, radio astronomy and long range radar
23 p4160 A70-43770

Phased array radar for missile defense, discussing development trends toward adaptive system logic control and microwave digital circuitry for signal processing
23 p4172 A70-44012

Step-scanned circular array radar antenna for operation over 20 percent bandwidth, discussing design, radiation patterns and performance advantages
23 p4175 A70-44951

Polarization properties of radar channel with random parameters, relating observation range with transmitting-receiving antennas and target fluctuations
24 p4311 A70-45187

RADAR APPROACH CONTROL

Helicopter radar approach aid for serving oil rigs
19 p3466 A70-38621

Aircraft onboard radar system with landing monitor perspective display of runway operating independently of ground based electronic equipment [ALAA PAPER 70-1336]
24 p4373 A70-45932

RADAR ASTRONOMY

Planetary information obtained from radar installations, discussing distance and orbit measurements, rotation periods, planetary surfaces, emphasizing Mercury and Venus
01 p0185 A70-11046

Radar probing of solar system noting contributions to knowledge on planets
01 p0192 A70-11485

Venus rotation period determination by radar observation of surface features
09 p1759 A70-22911

Mercury surface features from spectrograms of depolarized radar echoes
12 p2298 A70-27268

Lunar remote probing by IR and microwave thermal emission and by radar
14 p2644 A70-31056

Polarized and depolarized radar maps of moon, attributing anomalies and average diffuse component of echoes to scattering behavior of surface and subsurface rocks
14 p2645 A70-31060

Topographic variations in lunar surface from bistatic radar observations on Explorer 35
14 p2645 A70-31061

Venus and Mercury radio and radar studies concerning brightness temperature, surface reflectivity and planetary motion
14 p2647 A70-31074

Venus and Mercury surface height variations near equators, using radar time delay and Doppler observations
14 p2647 A70-31077

Mars surface topography and roughness from radar measurements
14 p2648 A70-31081

Mars radar results during 1969 opposition, presenting elevation and radar brightness as function of longitude
14 p2648 A70-31082

Radar astronomical polarization measurements for lunar echoes by exploiting ionospheric Faraday rotation with linearly polarized antenna
23 p4165 A70-44964

RADAR ATTENUATION

Plume-induced X band radar attenuation, AM and PM noise measured in aluminized solid propellant motor firings
04 p0736 A70-15409

Two frequency moving target indicator system overcoming clutter motion relative to radar
11 p2004 A70-25737

Point to point and radar return attenuation measurements at SHF through clear air and rain
16 p2858 A70-32928

Radar mapping in heavy rain with orthogonal transmit and receive polarization, using backscatter and attenuation to define maximum operating altitude
16 p2863 A70-33434

Antenna design for single engine light general aviation aircraft weather radar, reviewing attenuation and terrain return problems
16 p2864 A70-33471

RADAR BACKSCATTER

- Chemical kinetic and turbulent transport coefficients effects on afterburning rocket exhaust plumes and sea level transverse radar attenuations
[AIAA PAPER 70-733] 17 p3194 A70-34513
- RADAR BACKSCATTERING**
U BACKSCATTERING
U RADAR SCATTERING
- RADAR BEACONS**
VTOL steep descent beacon-guided landing systems
02 p0304 A70-12765
- Beacon identification-friend-foe/selective-identification-feature code-validation schemes for ATC, deriving expression for cumulative probability of validation on or within N interrogations
10 p1914 A70-24446
- Terminal automation system /ARTS/ digital computerized beacon tracking for future ATC facilities, noting add-on packages to increase system reliability
[SAE PAPER 700282] 12 p2206 A70-27441
- ATC radar beacon system, discussing interacting factors lowering reply reliability from transponder
12 p2267 A70-27639
- Radar beacon target processing system providing ATC information, noting target detecting and locating ability in noisy environment
12 p2268 A70-27640
- ATC radar beacon system, discussing narrow interrogator beams, siting and beam shaping, interrogation environment control, data link transmissions and message content
12 p2268 A70-27641
- Second generation radar beacon system for ATC using discrete address roll call
12 p2268 A70-27911
- Lunar based radar beacons for nearby spacecraft navigation, noting trajectory determination advantages
14 p2614 A70-30461
- Adaptive radar beacon forming, using conjugate reflections for propagation path errors compensation
16 p2865 A70-34061
- RADAR BEAMS**
Radar signals synthesis using steepest descent for minimizing Hermitian form
05 p0812 A70-16247
- Aperture antenna pattern beamwidth decrease in near field with increasing scan angle
21 p3796 A70-40559
- RADAR CHAFF**
U CHAFF
- RADAR CORNER REFLECTORS**
Luneberg lens application to construct multiple beam mechanically despun antenna for spin stabilized satellites, discussing temperature problems
17 p3055 A70-35663
- RADAR CROSS SECTIONS**
Radar observations of Icarus, using detected echoes to determine radar cross section, radius size and reflectivity
01 p0180 A70-10535
- Radar cross section computation for thin wires bent into circular arcs and V shapes using numerical method
02 p0262 A70-12597
- Geometrical optics method for obtaining radar cross section of perfectly conducting sphere with inhomogeneous dielectric coating
02 p0262 A70-12599
- Backscattering cross sections of metallic bodies of revolution, analyzing statistically echo pattern of complex targets
03 p0452 A70-14225
- Bistatic radar cross section measurements by pendulum method using modulated wave formed by target swing motion
09 p1634 A70-22698
- Radar cross section sea clutter model based on slightly rough surface superposition on swell structure
13 p2366 A70-29215
- Electromagnetic waves scattering from dense turbulent plasma, calculating radar cross sections of inhomogeneous plasma for peak electron densities
20 p3586 A70-39459
- Cavity radar cross section estimation by simplified models compared to semiempirical prediction with ray tracing procedure
22 p3992 A70-43583
- Subsonic jet engine intake duct radar cross section calculation using waveguide model
22 p3992 A70-43584
- Radar cross section and current distribution of dipole deformed into low pitch angle helix
23 p4166 A70-44974
- Radar cross section for thin dielectric plate and spherical and conical shells
23 p4166 A70-44975
- Radar backscattering cross sections of horizontal and vertical polarizations for thin rectangular plate near grazing incidence
23 p4166 A70-44976
- RADAR DATA**
Radar primary plot extraction, suggesting signals summing technique in delay line
02 p0256 A70-11975

- Radar data parameter determination method, discussing false alarm calculation
05 p0811 A70-15988
- Airborne and ground based radar data on thunderstorm echoes compared within framework of storm reflectivity model and radar theory
06 p1010 A70-18246
- Phased-array radars and parallel processing computers system in high target density environment, input-output, array steering and data storage and handling
07 p1236 A70-20150
- Angular coordinate during multilevel quantization of radar signal reflected from scintillating body on Gaussian noise background, applying maximum probability method
11 p1996 A70-25347
- Fighter-missile launch and control using direct radar information for guidance to reduce computation time and computer storage space
11 p2015 A70-26332
- Venus surface atmospheric conditions from radar and radio observations, including cross sections, microwave brightness spectrum and angular scattering law
16 p2974 A70-33645
- Radar data characteristics for extensive natural cumuli cloud evolution, noting use for precipitation forecasting
18 p3287 A70-37000
- Digital extraction of primary and secondary radar data for air traffic control
19 p3469 A70-38644
- Angular coordinate during multilevel quantization of radar signal reflected from scintillating body on Gaussian noise background, applying maximum probability method
20 p3589 A70-40459
- Discretization interval in discrete analog filters for optimal processing of complex radar signals, estimating systematic errors
22 p3984 A70-42393
- Radar information digital processing, deriving criterion for automatic lock-on of target trajectories
22 p3991 A70-43552
- ATC radar data processing and display systems equipment and operation, emphasizing economy
23 p4216 A70-45044
- RADAR DETECTION**
Kerr physical optics formula usefulness for calculation of radar reflectivity of metallic bodies of revolution in terms of electric and magnetic dipoles
02 p0262 A70-12598
- Book on radar design principles-signal processing and environment covering target detection in presence of noise, atmospheric effects, pulse techniques, etc
02 p0270 A70-12662
- Reliability of Doppler radar hail detection, discussing corrupting effects of turbulence and shear, size-sorting and vertical air motions
03 p0443 A70-13167
- Nonadaptive processor to detect coherent radar pulse trains with uniform amplitude in clutter-plus-noise environment
04 p0651 A70-15334
- Radar false return probability relationship to noise, investigating moving volume detectors
04 p0652 A70-15341
- Computer controlled radar guided tactical missile system using digital techniques in performing target detection, acquisition, tracking and illumination
05 p0814 A70-16328
- Linear FM pulse compression radar system operating at 94 GHz, obtaining echoes from orbiting objects for identification
08 p1462 A70-21290
- Clear air turbulence detection by radar equipped aircraft, considering reflection from refractive inhomogeneities
12 p2262 A70-26952
- Optimal noncoherent detector for fluctuating radar signals of noise background
13 p2369 A70-29727
- Optimal coherent radar detector for signals with unknown amplitude and background noise intensity
13 p2369 A70-29728
- Threshold sensitivity of pulsed optical radar with discrete signal storage, considering different operating modes
13 p2370 A70-29871
- Nonparametric rank tests detection performance for signals in Gaussian noise, considering radar application
14 p2551 A70-31119
- Radar detection range determination by parametric method based on SNR formula
16 p2866 A70-34062
- Scanning radar with feedback integration, calculating detection probabilities from antenna beam shape factor
16 p2888 A70-34063
- Airport bird detection equipment /ABDE/ radar to display airfield map for presence and magnitude of bird groups and vegetation on runway
18 p3226 A70-35998

- Meteoroid flux density from radar measurements, noting detectability dependence on initial ionized trail radius
19 p3515 A70-37660
- Range channel width effect on radar signal digital detector function and parameters optimal value
19 p3380 A70-38068
- Passive and cooperative active hologram radar extended from stationary coherent radar, considering use in airport surveillance of aircraft
21 p3792 A70-42119
- Queueing requirements in automatic radar target detection system operating with narrow bandwidth data link
22 p3990 A70-43489
- Radar information digital processing, deriving criterion for automatic lock-on of target trajectories
22 p3991 A70-43552
- Multiple range bin radar distribution-free detection procedure based on observation ranks without elaborate equipment
22 p3991 A70-43578
- RADAR DIRECTION FINDERS**
U RADIO DIRECTION FINDERS
- RADAR DISPLAYS**
U RADARSCOPES
- RADAR ECHOES**
NT ANGELS
NT CLUTTER
NT LUNAR RADAR ECHOES
NT SOLAR RADAR ECHOES
NT VENUS RADAR ECHOES
- Clear air layer type radar echoes intensities compared with refractive index variations in troposphere
01 p0043 A70-10331
- Moving targets automatic identification by radar signals digital processing, describing radar echoes properties, moving window detector system and circuits design
01 p0137 A70-10358
- Icarus radar and optical observations indicating surface smoothness differences between central and higher latitudes, radius size and radar reflectivity
01 p0180 A70-10534
- Radar observations of Icarus, using detected echoes to determine radar cross section, radius size and reflectivity
01 p0180 A70-10535
- Automatic aircraft tracking by returns from secondary surveillance radars, noting correlation of plots with track
02 p0332 A70-11966
- Compact range techniques using collimator for radar reflectivity and microwave antenna gain and pattern measurements
02 p0269 A70-12586
- Radar pulse scattering from ionized media including nuclear explosion fireballs and high speed reentry vehicle wakes, analyzing to retrieve backscattered pulse signal envelope
02 p0262 A70-12602
- Acoustooptical processing for amplification of weak radar echoes, describing design and operation of modulators, correlators, filters, etc
02 p0266 A70-12630
- Defruiter suppressing nonsynchronous responses /fruits/ in secondary surveillance radar systems, discussing effects on target detection probability
02 p0263 A70-12786
- Optimal radar resolution of objects during detection and measurements, giving diagrams of resolution characteristics vs echo signals parameters
03 p0448 A70-13453
- Backscattering cross sections of metallic bodies of revolution, analyzing statistically echo pattern of complex targets
03 p0452 A70-14225
- Pulsed radar fluctuating echo digital-detection and false alarm probabilities assuming Rice signal distribution with noise
04 p0649 A70-15065
- Polar lower ionosphere, using radar VLF step frequency sounding to determine reflection phase height at given propagation path
04 p0680 A70-15115
- Radar signal amplitude fluctuations reflected from disturbed sea water surface, noting wind induced waving stochastic nature influence
05 p0812 A70-16246
- Theoretical performance computation of on-line analyzer for radar echo detection by digital techniques
05 p0814 A70-16359
- Microwave frequency radar terrain echoes simulation concerning variation of echo delay, Doppler shift, random fine structure and time variation
06 p1008 A70-17482
- Short coherent laser radar detection of backscattered signal in measuring Doppler shift due to atmospheric temperature
07 p1297 A70-19368
- Linear FM pulse compression radar system operating at 94 GHz, obtaining echoes from orbiting objects for identification
08 p1462 A70-21290

Electron-to-ion temperature ratio determined from ion and plasma line components of radar Thomson scatter signal from ionosphere 08 p1489 A70-21389

Particle size distributions used in analyzing snow size spectra and radar reflectivity 11 p2004 A70-25651

Ionospheric electron and ion temperatures information extraction from Doppler broadening of radar returns based on correlation measurement 12 p2183 A70-27163

Mercury surface features from spectrograms of depolarized radar echoes 12 p2298 A70-27268

Weather radar signal processing and data recording at National Severe Storms Laboratory (NSSL), providing reduction in echo variations due to relative motion of precipitation elements 13 p2363 A70-28774

Altitude distribution of radar-signal-reflecting points and ionization in meteor trails 14 p2635 A70-30308

Time autocorrelation and power spectrum of radar returns from underdense turbulent ionized gas as function of electron density decay 14 p2551 A70-31035

Polarized and depolarized radar maps of moon, attributing anomalies and average diffuse component of echoes to scattering behavior of surface and subsurface rocks 14 p2645 A70-31060

Mars radar results during 1969 opposition, presenting elevation and radar brightness as function of longitude 14 p2648 A70-31082

Radar echo signal amplitude probability distribution during fully polarizational reception 15 p2696 A70-31517

Forward scattered radar reflections from various depths of rain volume, employing ultrasonic simulation 15 p2704 A70-32599

Earth to planet radar signal time delay in general relativity expressed in relativistic spherical polar coordinates of earth and planet 15 p2806 A70-32801

Venus radar backscattering properties indicating Muhleman theory applicability, noting radar echoes irregularity 15 p2806 A70-32802

Adaptive radar beacon forming, using conjugate reflections for propagation path errors compensation 16 p2865 A70-34061

Radar reflectivity correlations with lunar surface structure in Mare Imbrium, using delay-Doppler radar maps 17 p3154 A70-34568

Binary coded radar signal autocorrelation function main-to-sidelobe ratio improvement, using echo signal processed in mismatched filter 17 p3043 A70-34590

Radar receiving station equipment for studying upper atmosphere by radio meteor echoes 17 p3047 A70-35605

CAT at subsidence inversion in presence of strong wind shear, noting radar echo pattern as Kelvin-Helmholtz instability indicator 17 p3133 A70-35933

Atmospheric density from radar observations of meteor trails drift, using wind velocity semidiurnal components amplitudes 18 p3253 A70-36994

Meteor radar echoes of parallel and perpendicular polarization from ionized transient trails with linear electron densities 18 p3317 A70-36995

Radar tracking of meteors with slow drift velocity, improving accuracy via echo frequency multiplication 19 p3514 A70-37644

Meteor velocity determination by CW radar for constant phase angle, describing reflected signal processing 19 p3514 A70-37655

Electron photodetachment rate from meteor radar echo duration during night and daytime observations 19 p3515 A70-37664

Radar angels activity seasonal variation and height distribution statistical relationship to meteorological parameters 20 p3661 A70-39169

Antenna polarization and terrain depolarization effects on radar ground return, calculating echo pulse from smooth and rough terrains 22 p3990 A70-43327

Radar echo superrefraction and subrefraction concepts used with atmospheric waveguide model explaining extremal behavior and relations to atmospheric stratification 23 p4163 A70-44233

Modified time-domain reflectometer method for waveguide system evaluation, detecting and displaying radar echoes as function of time 24 p4315 A70-46234

RADAR EQUIPMENT
NT PLAN POSITION INDICATORS

NT RADAR ANTENNAS
NT RADAR BEACONS
NT RADAR CORNER REFLECTORS
NT RADAR FILTERS
NT RADAR RECEIVERS
NT RADAR REFLECTORS
NT RADAR TRANSMITTERS
NT RADARSCOPEs

Transversal equalizer for wideband radar systems distortion reduction 02 p0261 A70-12578

Tactical landing approach radar /TALAR/ guidance system for V/STOL aircraft steep angle approach and landing 02 p0336 A70-12767

Polarization diversity provided to parallel plate antennas in airborne radar applications by orthogonal vector processing 03 p0452 A70-13967

ABM perimeter acquisition radar effectiveness, discussing time limitation and burden on Missile Site Radar/Sprint combination 04 p0647 A70-15053

Lightweight Ka band magnetron for radar system use in missile fusing and airborne applications, discussing fixed frequency operation, anode and cathode, etc 04 p0655 A70-14622

Tradeoff methodology establishing evaluation criteria for comparing radar and laser systems to meet geodetic satellite altimeter performance requirements [AAS PAPER 69-604] 04 p0686 A70-14648

Feedback technique for frequency stability requirements of airborne radar systems, discussing non-coherent radar applications and cost comparison to power-amplifier approach 04 p0656 A70-14708

Display storage tubes /DST/ for radar systems, describing operating principles and characteristics 04 p0660 A70-15525

Radar and sonar data processing for display in command and control systems using digital technique, discussing processor configuration 05 p0828 A70-16189

Microwave applications in measuring and heating functions, describing battery operated radar for vibration and rotation measurements 05 p0816 A70-16824

Three frequency heterodyne system for acquisition and tracking of radar and communications signals, noting applicability in optical and microwave ranges 06 p1010 A70-17948

Phased-array radars and parallel processing computers system in high target density environment, input-output, array steering and data storage and handling 07 p1236 A70-20150

High resolution FM-CW radar sounder for tropospheric refractive index studies, describing equipment design and performance and clear air scatter observations 09 p1716 A70-22368

AM and FM CW Doppler radar by combined AM-FM waveform, noting automatic track while scan radar application 10 p1840 A70-24445

Phased array radar system synthesis, discussing small aperture systems, effects of solid state technology and role of data processing 10 p1842 A70-24877

Integrated circuit microwave phased array radar antenna systems for multiple frequency bands and multifunction operations to save cost and space 10 p1851 A70-24878

SAFEGUARD ballistic missile defense radars, discussing terminal defense concept, data processing system and microwave components 11 p2005 A70-26162

Automatic threshold regulation for radar applications, using feedback control device based on noise peak probabilities 11 p2012 A70-26717

Pipeline fast Fourier transform signal processor for digital spectrum analysis of wideband radars 12 p2186 A70-27904

Radar systems EM compatibility simulation, describing FORTRAN IV operational interference prediction program 12 p2193 A70-28139

Spurious output from C band radar magnetrons, discussing measurement procedures and noise reduction by waffle-iron waveguide filters 12 p2201 A70-28141

C band latching ring-and-post ferrite waveguide circulator for radar transmitting-receiving functions, presenting performance and design parameters 12 p2202 A70-28166

Radar handbook covering systems design, components, devices, measurements, applications, procurement, etc 13 p2367 A70-29601

Chirp radars energy spectra bounds calculation to insure electromagnetic compatibility 14 p2551 A70-31178

Ionospheric measurements from observations of incoherently scattered radio waves, describing radar installations specifications 15 p2731 A70-32096

Monolithic linear IC building blocks for radar systems circuit design 15 p2704 A70-32581

Acoustic and magnetic surface waves technologies for radar signal processing 16 p2874 A70-33390

Wideband varactor multipliers with flat output as microwave sources in radar systems 16 p2877 A70-33412

General purpose parallel processor design for avionics, considering radar signal processing 16 p2910 A70-33467

Lunar Module landing radar system design, discussing antenna and electronics assembly 16 p2865 A70-33681

Millimeter wave radar for high resolution aircraft landing aid, describing experiments to obtain backscatter data from airborne platform 17 p3133 A70-34721

Nationwide air traffic control, using radar network and real time computer flight information centers for air safety 17 p3135 A70-35880

Transmit only solid state radar module built with microstrip techniques for phased array systems operating at L and S dual bands 17 p3056 A70-35899

Recent radar developments covering ground and shipborne systems, clutter suppression and computer techniques 18 p3228 A70-36658

LM-Apollo rendezvous radar and transponder electronic assemblies packaging and mechanical design 18 p3232 A70-36762

Sea clutter tolerance comparison for frequency agile and fixed frequency radar 20 p3584 A70-39200

Radar consoles with various display components under different illumination levels to determine optimal operator performance, discussing push-button design recommendations 20 p3580 A70-39713

Airborne test computer for in-flight radar checkout featuring tape storage of computer program and cockpit mounted optical readout 22 p3993 A70-42320

Multiple range bin radar distribution-free detection procedure based on observation ranks without elaborate equipment 22 p3991 A70-43578

Synthetic aperture terrain-imaging radar systems, calculating tropospheric turbulence induced phase errors for comparison with microwave propagation experiment 22 p3991 A70-43579

Celestial radio source angle tracking techniques using monopulse antenna receiving system applied to angle tracking radar 22 p3991 A70-43582

Phased array radar systems microwave circuit modules packaging techniques, discussing interconnections, assembly, hermetic sealing and leak testing 23 p4173 A70-44535

RADAR FILTERS

Computerized statistical analysis of digital filters used to eliminate digital radar interference 05 p0822 A70-16530

Optimal pulse compression time-invariant filter for signal reception with sidelobe constraints under white noise in radar and communications systems 11 p2025 A70-26218

Digital range tracking, Doppler filtration and moving target selection in multichannel automatic surveillance radars 13 p2380 A70-29735

Solid state spectrum centered receiver for eliminating externally generated pulse type interference between radar sets 16 p2862 A70-33066

Fast Fourier digital processor for real time filtering of radar signals, discussing applications as Fourier transform system 16 p2870 A70-33738

Real time kalman filtering of Apollo LM/AGS rendezvous radar data [AIAA PAPER 70-957] 20 p3600 A70-39572

RADAR IMAGERY

K band SLR /side-looking radar/ imagery mapping tropical lowland vegetation compared to photographic coverage 10 p1879 A70-24747

Side-looking radar used to produce high resolution imagery of Panamanian province under persistent cloud cover 10 p1882 A70-25045

Radar observation of landscape regions, discussing dependence on recognition of variations in texture patterns on radar image 11 p2004 A70-25642

- Multipolarized radar imagery for detecting high return linear cultural features in geographic areas including channel markers, bridges, railroad and power-line networks, etc
12 p2228 A70-26911
- K band imagery of New England for evaluating size, shape and distribution of built-up areas
12 p2216 A70-26912
- Topographic shadow linear image enhancement by low angle illumination, describing pseudoradar technique for subcontinental sized fracture systems detection
12 p2221 A70-26960
- Radar look direction effects on geological features detectability, considering topographic relief and incidence angles roles in feature enhancement and suppression
12 p2221 A70-26962
- Book on synthetic aperture radar imaging systems theory and design covering SNR, optical data processing, phase and motion errors, ambiguity function, etc
13 p2368 A70-29603
- Synthetic array radar flying past flat plate, analyzing image relationship to flying path
14 p2552 A70-31193
- Radar imagery for crop discrimination, discussing sensor and data requirements and statistical analysis methods
14 p2578 A70-31237
- Snow field mapping with K band radar imagery determining signal return difference with surrounding terrain, noting role of volume scattering and old snow structure
14 p2578 A70-31238
- Pseudo three dimensional effect on monoscopic radar imagery for topographic relief differentiation, using offset superposition of transparencies
22 p4031 A70-42965
- Synthetic aperture terrain-imaging radar systems, calculating topographic turbulence induced phase errors for comparison with microwave propagation experiment
22 p3991 A70-43579
- ### RADAR MAPS
- #### NT. RADAR IMAGERY
- K band SLR /side-looking radar/ imagery mapping tropical lowland vegetation compared to photographic coverage
10 p1879 A70-24747
- Satellite coherent side-looking imaging radars producing radar maps with photographic-type quality
11 p2005 A70-26038
- Polarized and depolarized radar maps of moon, attributing anomalies and average diffuse component of echoes to scattering behavior of surface and subsurface rocks
14 p2645 A70-31060
- Venus radar mapping using fixed base line interferometer for hemispheric ambiguity resolution
14 p2647 A70-31078
- Monostatic and multistatic coherent radar techniques for target mapping, discussing measurements and inverse scattering
14 p2552 A70-31184
- Snow field mapping with K band radar imagery determining signal return difference with surrounding terrain, noting role of volume scattering and old snow structure
14 p2578 A70-31238
- Radar mapping in heavy rain with orthogonal transmit and receive polarization, using backscatter and attenuation to define maximum operating altitude
16 p2863 A70-33434
- Radar reflectivity correlations with lunar surface structure in Mare Imbrium, using delay-Doppler radar maps
17 p3154 A70-34568
- Signal processing antennas, discussing synthetic and multiplicative arrays for coherent radar airborne mapping
17 p3052 A70-35078
- Venus radar brightness map, using 40 km separation between range gates and comparable distances between Doppler slices
21 p3883 A70-40710
- ### RADAR MEASUREMENT
- Internal structure models of Mercury, Mars and Venus based on radar measurements of radius and mass, discussing two and three zone models
01 p0176 A70-10315
- Wind field-Doppler velocity field generalized correlation describing horizontal velocity component measurement by single pulse Doppler radar technique
02 p0326 A70-12287
- Power spectrum of backscattered radiation from turbulent reentry wake illuminated by radar pulse train, discussing electron density decay and pulse shape effects
03 p0408 A70-13585
- Ground clutter characteristics from moving receiver in bistatic radar system, developing method for performance prediction and problem analysis
03 p0449 A70-13586
- Rotation effects of two point scatterer on radar measurements of coherent acceleration
04 p0652 A70-15348
- Pulse radar altimeter for measuring meteorological balloon altitude, using superregenerative RF stage
05 p0845 A70-15805
- Ionospheric electron content, virtual height and profile measured by Faraday effect of satellite radio emissions compared with radar soundings
05 p0839 A70-16288
- Martian topographical radar ranging data correlated with surface features, discussing deserts, canals and maria topography
05 p0909 A70-16388
- X band Doppler radar observation of horizontal motion of precipitation particles in low levels of slow moving thunderstorm
06 p1101 A70-18580
- Pulsed Doppler radar observation of thunderstorm updraft structure, noting vertical velocity perturbations
06 p1101 A70-18581
- LF waves and irregularities in auroral ionosphere determined by radar measurements, suggesting role of plasma waves cross modulation
07 p1264 A70-19193
- Radar measurements of magnetic dip in E region compared with surface values and spherical harmonic models for dip angles
07 p1271 A70-20163
- Derived winds, wind shears and densities accuracies obtained by radar meteor trail technique
07 p1237 A70-20281
- Atmospheric turbulence parameters in meteor zone determined from simultaneous photographic and radar observations, determining turbulent diffusion coefficient dependence on height
08 p1563 A70-20546
- Martian surface radar observation results, discussing data processing method, backscattering behavior evaluation, relief and composition model, etc
08 p1456 A70-20643
- Potential refractive index mean vertical gradients role in turbulent mixing, noting applications to radar detection of CAT
09 p1716 A70-22365
- Laminar-turbulent regions boundary, discussing convective layer form and FM-CW microwave and acoustic radar measurement techniques
09 p1717 A70-22378
- Airport runway and slant visual ranges determination using single scanning lidar/laser radar/
09 p1696 A70-22490
- Oceanic wind and wave predictions by satellite radar radiometer using single receiver to determine wind velocity
09 p1668 A70-22877
- Ionospheric scintillations of lunar radar echo components isolation by CW Doppler shift or coherent pulse time delay techniques
10 p1841 A70-24802
- Radar interferometry as diagnostic method for remote probing of turbulent plasma
11 p2096 A70-26766
- Sea and sea ice remote sensing by four-frequency radar/4FR/ system in EC-121 aircraft
12 p2215 A70-26904
- Radar look direction effects on geological features detectability, considering topographic relief and incidence angles roles in feature enhancement and suppression
12 p2221 A70-26962
- Upper atmosphere probing based on light scattering from laser radar beam by atmospheric constituents
12 p2185 A70-27740
- Radar measured precipitation increase from seeded cloud demonstrated by measurements, numerical cumulus model and physical reasoning
12 p2189 A70-28094
- Radar meteorology in electromagnetic communications to provide storm systems data, noting clear air radar echoes
13 p2445 A70-28791
- Upper atmospheric wind evaluation in radar measurements by radio sounding technique, discussing equipment design
13 p2445 A70-29468
- Radar handbook covering systems design, components, devices, measurements, applications, procurement, etc
13 p2367 A70-29601
- Wind measurement with two spaced coherent-pulse radar stations for probing same region of meteor zone
14 p2582 A70-30317
- Meteor particle orbits, comparing inclined radio reflections with photographic and straight radar observations
14 p2636 A70-30322
- Balloon-radar soundings of horizontal wind profiles for booster vehicle design
14 p2653 A70-30588
- Laser radar measurements for atmospheric scattering properties, observing aerosol content, atmospheric density and composition
14 p2550 A70-30746
- Topographic variations in lunar surface from bistatic radar observations on Explorer 35
14 p2645 A70-31061
- Monostatic and multistatic coherent radar techniques for target mapping, discussing measurements and inverse scattering
14 p2552 A70-31184
- Alpha-beta and Kalman tracking filters with randomly interrupted data, evaluating transient responses as function of radar measurement accuracy and valid data acquisition probability
14 p2557 A70-31186
- Atmospheric turbulence parameters in meteor zone determined from simultaneous photographic and radar observations, determining turbulent diffusion coefficient dependence on height
15 p2796 A70-31455
- Radar meteor shower rate observation compared with direct cosmic dust measurements on satellites
15 p2798 A70-31682
- Long and short period internal gravity waves in atmosphere observed by high resolution radar, investigating generation mechanisms
17 p3075 A70-34609
- Meteor deceleration rates in atmosphere, using base line radar measurements
18 p3313 A70-36294
- High altitude clear air turbulence structure and evolution examined by high power radar and wind and temperature vertical soundings
18 p3228 A70-36483
- Optimal reception points for radar ranging measurement of angular coordinates of meteor trails, using central transmitter
19 p3515 A70-37665
- Pulsed laser lidar measurements of atmospheric turbidity, diffusion, pollution, visibility and cloud physics
20 p3584 A70-39127
- Radar for ionospherically propagated ground backscatter sounding, discussing two-sens aperture synthesis technique and optical spectrum data recording and processing
20 p3585 A70-39393
- Venus radius radar determination based on Mariner 5 and Veneras 5 and 6
21 p3883 A70-40714
- F region radar and optical temperature measurements, discussing Doppler and backscatter ion temperature
21 p3818 A70-41103
- Electron temperature incoherent scatter radar and satellite-borne Langmuir probe measurements discrepancy
21 p3825 A70-41104
- Adaptive tracking radar design, discussing ambiguity resolution problem in range and velocity dimensions
21 p3791 A70-41947
- CAT origin in unstable atmospheric shear and gravity waves, using ultrahigh resolution radar for observation of transition process
23 p4214 A70-44032
- Planetary masses determined from radar measurement data and radio tracking of space probes
24 p4407 A70-45535
- ### RADAR NAVIGATION
- Onboard radar self contained all-weather landing and taxiing /SALT/ system, discussing concept, requirements and results
01 p0138 A70-10641
- Airborne sidescan radar for fix-point navigation at low flight altitudes involving computerized sensing evaluated for operator performance
08 p1541 A70-21563
- Radar signal quick indication and extrapolation for terminal guidance control of Mars soft lander, reducing radar lock on loss sensitivity and engine spurious noise throttling
11 p2080 A70-26210
- Pilot landing aids for increasing air traffic, discussing Integrated Communication Navigation Identification
13 p2449 A70-29053
- Air traffic control, reviewing air navigation, communication systems and radar techniques
13 p2450 A70-29998
- LATA policy on future ATC development, discussing controlled airspace, communications and radar requirements
19 p3555 A70-38630
- ATC and general aviation growth, considering airport capacity, radars, navigation, National Airspace System, etc
19 p3467 A70-38631
- Radar inertial system flight evaluation, discussing V/STOL program for approach and landing by use of ground based radar for updating onboard inertial navigator
22 p4066 A70-42651
- Limiting effects of topographic quasi-optical radio propagation above 100 MHz in radar aircraft navigation, clear air disturbances detection and IR warning technique
23 p4163 A70-44230
- ### RADAR OBSERVATION
- #### U. RADAR TRACKING

RADAR PHOTOGRAPHY

- Terrain imaging radar applied to sensing earth resources
 - 02 p0298 A70-12181
- Anamorphic holograms in optical and radar holography and reconstruction, discussing formation and fundamentals
 - 02 p0298 A70-12182
- Aircraft range-only radar trial applications in stereotopographic surveys of difficult-access areas, discussing organizational problems
 - 07 p1282 A70-19632
- Radar flight configuration parameters effect on visual stereo model, expressing equivalent camera locations in terms of radar beams depression angles
 - 10 p1841 A70-24752

RADAR RANGE

- Compact range techniques using collimator for radar reflectivity and microwave antenna gain and pattern measurements
 - 02 p0269 A70-12586
- Electromagnetic-acoustic probe for remote wind velocity sensing and radar range performance
 - 06 p1071 A70-18509
- Supersonic flight vehicle plasma sheath effect on effective range of onboard radar installation, discussing SNR
 - 08 p1461 A70-20869
- Polynomial model of uniform target motion for smoothing and extrapolating coordinates and parameters using independent radar range and velocity readings
 - 10 p1843 A70-25136
- Airborne side-looking radar antenna optimal directional characteristics analysis from viewpoint of maximum surveillance range
 - 10 p1843 A70-25139
- Polarization properties of radar channel with random parameters, relating observation range with transmitting-receiving antennas and target fluctuations
 - 11 p2012 A70-26815
- Radar ducting effects on propagation at microwave frequencies, recording signal strength as function of transmitter to receiver range
 - 16 p2858 A70-32927
- Radar detection range determination by parametric method based on SNR formula
 - 16 p2866 A70-34062
- Multiple range bin radar distribution-free detection procedure based on observation ranks without elaborate equipment
 - 22 p3991 A70-43578
- Polarization properties of radar channel with random parameters, relating observation range with transmitting-receiving antennas and target fluctuations
 - 24 p4311 A70-45187

RADAR RECEIVERS

- Binary digital radar signal detectors optimization for radiation pattern of sin x/x radar antenna and for non-fluctuating target
 - 02 p0255 A70-11899
- Ground clutter characteristics from moving receiver in bistatic radar system, developing method for performance prediction and problem analysis
 - 03 p0449 A70-13586
- Amplitude scanning, multiple beam and dual baseline phase comparison direction finding receivers for installation in aircraft to locate and analyze radar signatures
 - 04 p0653 A70-15657
- Meteorological radar station reception equipment for increased radio telemetry channel reliability in complex radio sounding of atmosphere
 - 11 p2075 A70-25920
- High dynamic range low noise parametric microwave amplifier performance measurement for radar receivers
 - 12 p2183 A70-27166
- Radar receiving station equipment for studying upper atmosphere by radio meteor echoes
 - 17 p3047 A70-35605
- Synthetic aperture radar receivers, discussing cross-product term suppression in correlation detection for image distortion reduction
 - 20 p3585 A70-39392
- Digital radar receiver based on pseudo Bayes likelihood ratio algorithms
 - 21 p3789 A70-41353
- Optimum pulse radar signal-receiver design, considering implementation errors for maximum target detectability in clutter
 - 24 p4313 A70-46055

RADAR RECEPTION

- Acceleration influence on radar signal reception during range and velocity measurements
 - 13 p2366 A70-29301

RADAR REFLECTIONS

U RADAR ECHOES

RADAR REFLECTORS

- Radar target optimal detection algorithms in cloud of passive reflectors, noting space surveillance regularities
 - 15 p2696 A70-31516

RADAR RESOLUTION

- Air traffic control radar velocity resolution for eliminating ground, rain and angel clutter by optimizing wavelengths, pulse length and beam width
 - 02 p0332 A70-11969
- Target velocity effects on resolution of synthetic aperture side-looking radar
 - 02 p0268 A70-12582
- Optimal radar resolution of objects during detection and measurements, giving diagrams of resolution characteristics vs echo signals parameters
 - 03 p0448 A70-13453
- High resolution FM-CW radar sounder for tropospheric refractive index studies, describing equipment design and performance and clear air scatter observations
 - 09 p1716 A70-22366
- Side-looking radar used to produce high resolution imagery of Panamanian province under persistent cloud cover
 - 10 p1882 A70-25045
- Satellite coherent side-looking imaging radars producing radar maps with photographic-type quality
 - 11 p2005 A70-26038
- Subclutter visibility /SCV/, resolution and inter-clutter of MTI or Doppler search radars in land, sea and weather clutter
 - 12 p2188 A70-27940
- Tropospheric turbidity detection and measurements by lidar, considering performance limitations and thickness resolution vs range curve
 - 16 p2862 A70-33015
- Adaptive tracking radar design, discussing ambiguity resolution problem in range and velocity dimensions
 - 21 p3791 A70-41947
- Radar signal synthesis in noise with good range resolution for rapidly fluctuating targets, using ambiguity function
 - 22 p3988 A70-42566
- Digital Doppler ambiguity resolution method for pulsed S-band radar, using integrating interval approach
 - 22 p3992 A70-43592

RADAR SCANNING

- ATC surveillance radar for high density traffic, discussing optimum electronic scanning rates, 3D radar and MTI
 - 02 p0330 A70-11958
- Electronic scanning role in ATC radar, discussing combined search and track radar with elevation and azimuth scanning
 - 02 p0331 A70-11959
- Terrain imaging radar applied to sensing earth resources
 - 02 p0298 A70-12181
- Radar visual indicator used with scan converter and as synthetic indicator with computer controlled flight safety system
 - 02 p0263 A70-12700
- Helicopter all-visibility operation realized by using main rotor blade as scanning radar antenna
 - 05 p0793 A70-16040
- Analog integrating moving window detector performance analysis for use with scanning pulse radar allowing for antenna radiation pattern and detection process dynamic characteristics
 - 11 p2009 A70-26262
- Scanning radar with feedback integration, calculating detection probabilities from antenna beam shape factor
 - 16 p2888 A70-34063

RADAR SCATTERING

- Active AM scatterer /spiral antenna/ used as transponder in elementary CW radar system
 - 04 p0652 A70-15346
- Rotation effects of two point scatterer on radar measurements of coherent acceleration
 - 04 p0652 A70-15348
- Electromagnetic wave diffraction on absorbing black metallic and magnetic cylinders and strip, plotting radar scattering cross sections
 - 05 p0813 A70-16262
- Backscatter radar signal phase determination from amplitude data, measuring phase and amplitude in laboratory
 - 05 p0815 A70-16507
- CW, pulsed and frequency modulated radar scatterometry, discussing flight, system, terrain and data processing parameters
 - 06 p1012 A70-18594
- Radar target short pulse transient scattering response computation using fast Fourier transform algorithm
 - 08 p1463 A70-21597
- Atmospheric structure and turbulence relations to radar backscattering from clear air refractive index irregularities
 - 09 p1715 A70-22361
- Radar backscattering relationship to refractive index microstructure in turbulent clear atmosphere
 - 09 p1716 A70-22366
- He-Ne and argon lasers for measuring radar scattering cross sections of plane and three dimensional targets
 - 09 p1632 A70-22405

Turbulent ionized wakes Doppler radar scattering spectrum parameters in terms of wake characteristics using double convolution integral

- 11 p2010 A70-26271
- Astronomical, geometrical and physical selectivity factors of forward scattering radar observation concerning meteor weight
 - 14 p2635 A70-30310
- Monostatic and multistatic coherent radar techniques for target mapping, discussing measurements and inverse scattering
 - 14 p2552 A70-31194
- Forward scattered radar reflections from various depths of rain volume, employing ultrasonic simulation
 - 15 p2704 A70-32599
- Venus radar backscattering properties indicating Muhleman theory applicability, noting radar echoes irregularity
 - 15 p2806 A70-32802
- Millimeter wave radar for high resolution aircraft landing aid, describing experiments to obtain backscatter data from airborne platform
 - 17 p3133 A70-34721
- Ocean wave spectra from bistatic radar scatter data, using time delay Doppler-frequency map
 - 21 p4124 A70-43876
- Positron annihilation in quenched Cd metal from radar backscatter intensities in aircraft model compared with anechoic chamber measurements
 - 24 p4315 A70-46257

RADAR SIGNATURES

- Cirrus clouds signature analysis, discussing light scattering pertinent to lidar equation
 - 01 p0076 A70-10913
- Equivalence class technique to compute measure of similitude between two vehicles based on radar signature in terms of scattering matrix elements
 - 04 p0648 A70-14656
- Amplitude scanning, multiple beam and dual baseline phase comparison direction finding receivers for installation in aircraft to locate and analyze radar signatures
 - 04 p0653 A70-15657
- Radar signature analysis of convective precipitation, hailstorms, tornadoes, lightning, hurricanes and clear air echoes
 - 11 p2076 A70-26039
- Radar and IX pulse signatures of multiple reflection from dry, damp and wet earth for vertical and horizontal polarization
 - 16 p2861 A70-32977

RADAR TARGETS

- Optimal radar resolution of objects during detection and measurements, giving diagrams of resolution characteristics vs echo signals parameters
 - 03 p0448 A70-13453
- Pulsed radar fluctuating echo digital detection and false alarm probabilities assuming Rice signal distribution with noise
 - 04 p0649 A70-15046
- Radar false return probability relationship to noise, investigating moving window detectors
 - 04 p0652 A70-15341
- Monopulse radar signal detection efficiency with fully polarized reception taking into account target with fluctuating polarization
 - 05 p0813 A70-16270
- Bounded approximations to average multirad detection probabilities over slowly fading radar target
 - 06 p1013 A70-18627
- Radar target short pulse transient scattering response computation using fast Fourier transform algorithm
 - 08 p1463 A70-21597
- Atmospheric small scale turbulence observation by Doppler radar, noting role of tracers radial velocity spectrum
 - 09 p1716 A70-22364
- He-Ne and argon lasers for measuring radar scattering cross sections of plane and three dimensional targets
 - 09 p1632 A70-22405
- Bistatic radar cross section measurements by pendulum method using modulated wave formed by target swing motion
 - 09 p1634 A70-22699
- Polynomial model of uniform target motion for smoothing and extrapolating coordinates and parameters using independent radar range and velocity readings
 - 10 p1843 A70-25136
- Polarization properties of radar channel with random parameters, relating observation range with transmitting-receiving antennas and target fluctuations
 - 11 p2012 A70-26815
- Optimum binary digital detector of radar targets using confidence ratio as criterion of target presence
 - 12 p2182 A70-26896
- Radar beacon target processing system providing ATC information, noting target detecting and locating ability in noisy environment
 - 12 p2268 A70-27640

- Optimal pulse allocation for radar array in simultaneous tracking of multiple targets, suggesting algorithms 13 p2365 A70-29068
- Monostatic and multistatic coherent radar techniques for target mapping, discussing measurements and inverse scattering 14 p2552 A70-31184
- Radar target optimal detection algorithms in cloud of passive reflectors, noting space surveillance regularities 15 p2696 A70-31516
- Scattered fields evaluation due to creeping waves for smooth convex radar targets, using algebraic expressions 16 p2956 A70-32978
- Radar signal synthesis in noise with good range resolution for rapidly fluctuating targets, using ambiguity function 22 p3988 A70-42566
- Queueing requirements in automatic radar target detection system operating with narrow bandwidth data link 22 p3990 A70-43489
- Monopulse radar excited by Gaussian signal and thermal noise in multiple targets, calculating angle error output probability density function for predicting tracking performance 22 p3992 A70-43593
- Polarization properties of radar channel with random parameters, relating observation range with transmitting-receiving antennas and target fluctuations 24 p4311 A70-45187
- ### RADAR TRACKING
- PostNewtonian equations of Brans-Dicke scalar-tensor theory for n gravitating point masses, using obtained equations of motion for radar tracking 02 p0337 A70-11777
- Electronic scanning role in ATC radar, discussing combined search and track radar with elevation and azimuth scanning 02 p0331 A70-11959
- Automatic aircraft tracking by returns from secondary surveillance radars, noting correlation of plots with track 02 p0332 A70-11966
- Three dimensional radar system for automatic tracking all aircraft in terminal area to increase air traffic control system safety and capacity 02 p0332 A70-11967
- Book on radar design principles-signal processing and environment covering target detection in presence of noise, atmospheric effects, pulse techniques, etc 02 p0270 A70-12662
- Simplified aircraft instrument landing system (SAILS)/employing lightweight helicopter-borne radar for tracking radar beacon at touchdown point 02 p0337 A70-12768
- Bird strikes on aircraft, discussing airport control and environment alteration, radar tracking and link between migratory flights and weather conditions 03 p0411 A70-13075
- Interruptions influence in discrete information flow on characteristics of radar tracking system 03 p0446 A70-13198
- ABM perimeter acquisition radar effectiveness, discussing time limitation and burden on Missile Site Radar/Sprint combination 04 p0647 A70-14503
- Terrestrial solid powdered rocks HF electrical properties measurements for lunar radar observation 04 p0678 A70-15054
- Wideband transversal coaxial cable delay lines used for improving radar systems target recognition by eliminating misleading signals and distortion 05 p0822 A70-16723
- Atmospheric thermodynamic properties determined from radar studies of detonation waves from cesium-seeded explosive bursts in lower ionosphere 06 p1012 A70-18542
- Short wave radar tracking of comets, considering tail type criteria for signal reflection 07 p1379 A70-19040
- Navigational accuracy of two way Doppler tracking of interplanetary spacecraft during heliocentric and planetary encounter trajectory phases [AIAA PAPER 69-899] 07 p1331 A70-19727
- Forward looking airborne radar (FLAR)/moving target indicator for military helicopter mounting 08 p1462 A70-21358
- Soviet book on servo systems for radar automatic tracking and control stations covering static, dynamic and frequency characteristics, amplifiers and correction devices 09 p1654 A70-22597
- ELDO rocket tracking error, considering guidance antenna angular precision and UHF circuit performance in signal comparison 09 p1720 A70-22649
- Radar system for Safeguard ballistic missile system, detailing perimeter acquisition and data processing system 09 p1638 A70-23421
- Parabolic antenna for automatic tracking compared for characteristics between multimode and four horn feed systems 10 p1847 A70-23920
- Analog-digital real time data automatic acquisition and radar tracking system for air defense and air traffic control 11 p2014 A70-26313
- Vertical tilt and horizontal position of antenna rotating device in radio astronomy and radar observations using photogrammetric methods 12 p2195 A70-27478
- Horizontal wind velocity spectra at 80-100 km from radar meteor soundings 12 p2263 A70-27518
- Leonid meteor shower radar observation data, analyzing flux rates and particle size distribution 13 p2487 A70-28694
- Radar and optical meteor observations comparison, discussing luminosity function and angular velocity 13 p2490 A70-29042
- Optimal pulse allocation for radar array in simultaneous tracking of multiple targets, suggesting algorithms 13 p2365 A70-29068
- Geminid and Quadrantid meteor shower densities observed on wave-channel-antenna radar 14 p2635 A70-30305
- Time-amplitude characteristics and abundance in Leonid meteor shower from azimuthal radar observations 14 p2635 A70-30306
- Diurnal and seasonal variations of parameter s of meteor showers on celestial sphere, using radio echo amplitude distribution from radar observations 14 p2635 A70-30307
- Three-reception-point radar system for radiant and speed measurement of individual meteors in stream, using forward scattering 14 p2582 A70-30311
- Phase angle gauge measurement of meteor shower radiants, using radar observations of signal scattering in meteor trails 14 p2582 A70-30314
- Wind velocity determination by radar tracking of meteor trails, investigating errors 14 p2572 A70-30328
- Meteor radiant, drag and altitude via CW radar observation of meteor trails 15 p2800 A70-32150
- Parallel associative unstructured element computer design for real time radar track data processing 16 p2869 A70-33466
- Doppler radar frequency tracker with servomechanism applicable to velocity computation of aircraft for self contained navigation 18 p3226 A70-36063
- Automated radar terminal system, ARTS-III Beacon Tracking Level for continuous aircraft identity on controllers radar display 18 p3288 A70-36393
- Erroneous line of sight rates generation by radar radome refraction errors in aircraft tracking 18 p3231 A70-36457
- Relative effectiveness of radar and visual cloud observations 18 p3287 A70-36999
- Radar tracking of meteors with slow drift velocity, improving accuracy via echo frequency multiplication 19 p3514 A70-37644
- Meteor activity during IQSY by radar observations at 7.6 m wavelength 19 p3514 A70-37654
- Meteor velocity determination by CW radar for constant phase angle, describing reflected signal processing 19 p3514 A70-37655
- Laser radar tracking systems, calculating atmospheric turbulence effects on angular errors 19 p3379 A70-37857
- Ground based radar tracking data processing method for real time information concerning lunar module (LM)/position and velocity during Apollo 12 flight [AIAA PAPER 70-1020] 20 p3591 A70-39514
- Homing radar tracking accuracy improvement by glint reduction using frequency diversity [AIAA PAPER 70-992] 20 p3586 A70-39538
- Horizontal wind velocity spectra at 80-100 km from radar meteor soundings 21 p3846 A70-41166
- Monopulse radar excited by Gaussian signal and thermal noise in multiple targets, calculating angle error output probability density function for predicting tracking performance 22 p3992 A70-43593
- ### RADAR TRANSMISSION
- Book on radar design principles-signal processing and environment covering target detection in presence of noise, atmospheric effects, pulse techniques, etc 02 p0270 A70-12662
- Tropospheric fine structure influence on radio wave propagation, including atmospheric gases and precipitation effects and radar, navigation and TV applications 03 p0449 A70-13612
- Radar signals optimal synthesis characterized by ambiguity surfaces minimized over predetermined regions of ambiguity plane, noting weighted error criterion role 04 p0651 A70-15328
- Active AM scatterer/spiral antenna/used as transponder in elementary CW radar system 04 p0652 A70-15346
- Silicon controlled diodes application to pulse modulation circuits of radar transmitters 09 p1631 A70-22016
- Maser amplification in Chirp radar signals pulse paramagnetic compressors using electron spin echoes 09 p1637 A70-23321
- Radar transmission SNR formula concerning fluctuations with respect to working frequency 10 p1840 A70-24478
- Central sidelobes of multifrequency radar signals ambiguity functions, discussing code composition and auxiliary modulations 12 p2185 A70-27686
- Radar spectrum control based on two pulse shaping techniques using klystron transmitter 12 p2188 A70-27941
- Concorde aircraft radar signal transmission, describing modified Flexwell waveguide 13 p2379 A70-29561
- Binary coded radar signal autocorrelation function main-to-sidelobe ratio improvement, using echo signal processed in mismatched filter 17 p3043 A70-34590
- Airport and air route radar surveillance, beacon systems, microwave links and instrument landing systems, discussing transmission and reception problems 22 p4068 A70-43486
- Radar echo superrefraction and subrefraction concepts used with atmospheric waveguide model explaining extremal behavior and relations to atmospheric stratification 23 p4163 A70-44233
- ### RADAR TRANSMITTERS
- Radar transmitter waveforms for multifunction operation, emphasizing phase and frequency modulation for CW radars 12 p2188 A70-27939
- Mathematical models for radar transmitters emission spectra envelopes calculation, considering effects of pulse width, rise and fall times, corner smoothing and frequency modulation 12 p2189 A70-28136
- Radar transmitters modulating circuits protection with microsec rapidly by power elimination, discussing electronic switches 21 p3792 A70-41987
- ### RADARSCOPES
- #### NT PLAN POSITION INDICATORS
- Radar digital indicators generating deflection signals for digital PPI display, discussing scale ranges, symbols and digital circuits application 05 p0828 A70-16191
- Displayed cursor velocity effect on radar target acquisition time for subjects in simulated air defense environment 16 p2853 A70-33670
- ### RADIAL DISTRIBUTION
- Extensive air shower axis position determined using energy methods and radial distribution geometry of particle density 01 p0171 A70-11252
- Augmented small parameter gas film equation for squeeze film journal bearing solved in terms of radial displacement [ASME PAPER 69-WA/LUB-9] 04 p0697 A70-14766
- Charge carriers recombination and diffusion coefficients for confined gas discharge plasma obtained from data on radial particle distribution profile 05 p0888 A70-16330
- Spectroscopic determination of radial temperature distribution at various currents in negative glow of hollow cathode discharge, analyzing influence of gas pressure 05 p0888 A70-16358
- Helium and argon atoms number densities radial profiles in supersonic free jets of binary gas mixtures by molecular beam sampling 07 p1341 A70-20105
- Transient radial temperature distributions in cylindrical shells via Carslaw and Jaeger procedure involving binomial theorem and asymptotic expansions of Bessel function 08 p1599 A70-21588
- Algorithm for inversion of geomagnetic induction problem, determining earth radial conductivity distribution 09 p1669 A70-23305
- Radial distribution of plasma parameters for thermionic converters with electrode shielding by plane sapphire rings, showing lateral surface effect 10 p1808 A70-25124

Kaufman thruster with predominant radial field, noting electron mobility across ion extraction screen and advantages of uniform plasma distribution [ALAA PAPER 69-259] 11 p2102 A70-26120

Energy loss radial dependence due to K resonance radiation for infinitely long plasma cylinder, using approximation method for integrals 13 p2461 A70-28731

Three-reception-point radar system for radiant and speed measurement of individual meteors in stream, using forward scattering 14 p2582 A70-30311

Phase angle gauge measurement of meteor shower radiances, using radar observations of signal scattering in meteor trails 14 p2582 A70-30314

Radial ion temperature distribution in hydrogen arc within axial magnetic field measured spectroscopically by thermal Doppler effect 14 p2621 A70-30657

Radial distributions and escape of charged particles across magnetic field in hot cathode Penning discharge plasma with L F oscillations 15 p2780 A70-32191

Cosmic ray radial gradients and anisotropies, describing behavior in interplanetary medium 15 p2795 A70-32623

Radio meteor orbit velocity and radiant measurements by pulse diffraction technique 18 p3315 A70-36603

H 2 region and neutral gas spiral structure and radial distribution, using optical observations and radio continuum surveys 18 p3327 A70-37162

Radial profiles of emission and absorption coefficients and temperatures in cylindrically symmetric plasmas 19 p3475 A70-37551

Augmented small parameter gas film equation for squeeze film journal bearing solved in terms of radial displacement [ASME PAPER 69-WA/LUB-9] 19 p3435 A70-37609

Air shower radio pulse amplitude dependence on primary energy and core distance 19 p3381 A70-38607

Cylindrical shells subjected by sectors to constant radial pressure, investigating stress state and deformation 20 p3719 A70-39620

Radial distribution of plasma parameters for thermionic converters with electrode shielding by plane sapphire rings, showing lateral surface effect 20 p3568 A70-40517

Radiant dispersion, position, areas and orbital axis in meteor showers by double-station photographic observations, noting Apollo group detection 21 p3884 A70-40875

Low density gas jet from short circular cylindrical tube, calculating molecular flux radial density variation 22 p4076 A70-43430

Binary gas mixture separation effects by centrifugation in cylindrical tube, calculating maximum radial concentration difference between wall and axis by numerical integration 23 p4181 A70-44206

Saturn ring radial structure, discussing dynamic model, gravitational forces and perturbation of planetary satellites 23 p4241 A70-44253

Electric field radial distribution measured for stationary hydrogen arc with axial magnetic field 23 p4227 A70-44933

Five-moments approximation calculation of magnetoplasmadynamic hydrogen arc radial pressure profile as function of ambient pressure and superimposed magnetic field 23 p4228 A70-44935

Magnetoplasmadynamic hydrogen arc radial pressure profile as function of ambient pressure and superimposed magnetic field, using thirteen-moments approximation 23 p4228 A70-44936

Incompressible Newtonian fluid flow between closely spaced corotating disks, showing radial pressure distribution similar to laminar flow 24 p4324 A70-45293

RADIAL FLOW

Optical density measurements in high speed confined air vortex, discussing light deflection mapping of vortex density field at off axis positions [AIAA PAPER 68-694] 03 p0480 A70-12906

Radial outflow effect on fluid motion between rotating and stationary plane disks associated with rotor cooling in turbomachinery 05 p0833 A70-16503

Laminar steady radial flow of simple fluid of short memory between two parallel disks, demonstrating relation to Newtonian fluid 06 p1037 A70-17915

Turbulent-laminar transition in divergent radial flow between disks, relating velocity fluctuations to Reynolds number 08 p1483 A70-21235

Laminar radial flow between parallel disks, estimating static wall pressure distribution perturbation caused by characteristic time 08 p1484 A70-21237

Supersonic compressor applications for airborne vehicles propulsion systems, discussing axial flow compressors, three dimensional design methods, supersonic radial machines, etc [AGARDOGRAPH-120] 08 p1434 A70-21929

Navier-Stokes equation for plane unsteady axisymmetric rotation of viscous fluid in steady radial flow from source or sink 09 p1660 A70-22437

Two dimensional radial flow of inviscid infinitely conducting compressible fluid under influence of magnetic field 09 p1735 A70-22757

Pressure and velocity distribution within radial flow gas turbine rotor computed by two dimensional streamline curvature method 09 p1608 A70-23737

Swirl velocity and cavity stability in rotating container filled radially through porous cylindrical wall at constant and applied pressure 10 p1868 A70-24195

Radial flow impellers design for maximum machine performance, using straight cascade characteristics 15 p2672 A70-31825

Hydromagnetic viscous flow of incompressible conducting fluid due to electric current radial divergence from point source 15 p2780 A70-32426

German monograph on calculation and measurement of stress distribution in turbine rotors with radial flow, discussing differential equations for rotating disks 16 p2993 A70-34076

Computerized design for radial flow splitters in three dimensional fan exhaust nozzles 18 p3207 A70-36462

Gas turbine shrouded rotating disk system with radial outflow of air coolant, investigating fluid dynamics, pressure distribution and frictional moment [ASME PAPER 70-GT-6] 18 p3208 A70-36862

Monograph on radial flow between air cooled gas turbine rotating and stationary disk near stator covering turbulent boundary layer, velocity distribution, etc 19 p3404 A70-38007

Stellar wind theory and related steady radial flows, discussing gravitating point mass, heat conduction, shocks, viscosity, outflows and inflows 20 p3706 A70-39928

Flow parameters radial dependence of thin solar wind filament corotating with sun 21 p3881 A70-40972

Incompressible Newtonian fluid laminar radial flow between parallel stationary disks, obtaining integral solution for Navier-Stokes equation 22 p4007 A70-42302

Radial flow microturbines deflection and wave losses in circular nozzle ring oblique exit section 22 p3965 A70-43359

Variable geometry radial inflow turbine performance estimation based on one dimensional flow theory 22 p3960 A70-43738

Air circulation around radial flow machine rotor blades calculated without velocity distribution factor 23 p4183 A70-44774

Radial inflow turbine optimum design geometry, calculating nozzle and rotor geometrical parameters efficiency 24 p4395 A70-46012

RADIAL VELOCITY

Radial velocity profiles measured in plasma jet thrusters with thermal and self magnetic acceleration, discussing disturbances due to discharge current-magnetic field interactions 03 p0553 A70-14374

SS Cygni outburst origin in G type star indicated from radial velocity variations of hydrogen absorption lines during rising light 05 p0915 A70-16695

HR diagram calibration based on proper motions and radial velocities, deriving absolute magnitudes and statistical parallaxes 06 p1149 A70-18456

H I gas and H II regions kinematics, comparing radial velocities near galactic center 06 p1149 A70-18459

Equivalent line widths of anomalously fast stars of early spectral classes and reference stars, discussing binary nature and radial velocities of OB stars 08 p1569 A70-20828

Cygnus and Perseus symbiotic stars as binaries, studying radial velocities, relative emission line intensities and energy distribution 08 p1569 A70-20830

Internal radial velocities of diffuse emission nebulae in H II region, using photographic Fabry-Perot interferometer 08 p1581 A70-21952

Atmospheric small scale turbulence observation by Doppler radar, noting role of tracers radial velocity spectrum 09 p1716 A70-22364

Radial velocities tabulated for late B-type north and south of equator listed in Catalog of Bright Stars 09 p1763 A70-23452

Spectral lines and radial velocities of paired galaxies, noting red shift difference between emission and absorption lines 10 p1946 A70-24978

Electrons radial motion and beam focusing in linear accelerator allowing for perturbing forces, calculating particle trajectory 10 p1926 A70-25110

Radial velocities of supergiant distant stars in southern Milky Way regions of I Sco Association 11 p2113 A70-26465

Cygnus loop nebula H alpha line halfwidths and radial velocities 15 p2802 A70-32482

Radial velocities of neutral hydrogen in anticenter region of Galaxy 18 p3328 A70-37170

Galactic spiral structure from optical radial velocities of H II regions 18 p3329 A70-37179

O and B stars velocity dispersion, considering Oort terms and average residual radial velocity 18 p3330 A70-37188

Spectrum analysis of P Cygni star AG Carinae and derivation of mean radial velocities for different epochs 19 p3523 A70-38694

H II region radial velocity comparison to galactic spiral structure, using optical and radio investigations 19 p3524 A70-38698

B stars kinematic parameters determination from radial and tangential velocities 19 p3525 A70-38775

Nova Vulpeculae 1968 Number 1 medium dispersion spectra, using radial velocity line identification and line profile reductions 21 p3889 A70-41152

Planetary nebulae radial velocities using prime focus or coude spectra 21 p3889 A70-41157

BM Orionis eclipsing binary spectra, determining radial velocity curve 21 p3890 A70-41161

Beta CMa variable star HD 43818 spectral observations, discussing line profiles and radial velocities 22 p4100 A70-42853

Galactic rotation model derived from radial velocities and spectrophotometric distances of H II regions 22 p4101 A70-42864

Radial velocity-light amplitude ratios of grouped variable stars in continuous sequence, comparing pulsation prediction 23 p4247 A70-44793

Viscous conducting liquid forced vortex motion, considering radial velocity distribution and rotation effect on free surface shape 24 p4383 A70-45140

Sunspot penumbra velocity field spatial structure by filament spectrum analysis, plotting radial velocities relative to undisturbed photosphere 24 p4400 A70-45310

RADIANCE

Tungsten emissivity and radiance properties obtained at high surface temperatures 09 p1725 A70-22068

Cloud-free earth areas determined via reflected radiance measurements from ATS 3 cloud camera 17 p3133 A70-35930

Horizon sky UV spectral radiance, noting solar position and cloud cover effects 18 p3248 A70-36752

RADIANT COOLING

Radiation effects on postshock gas state, noting shock wave optical thickness dependence on radiative cooling and photon flight time 02 p0277 A70-11867

Passive radiant cooler design involving patch cone radiative coupling calculation based on specular image technique 07 p1425 A70-20091

Nonlinear steady state diffusion elliptic boundary value solutions exemplifying enzyme kinetics and radiation cooling 08 p1596 A70-20580

Solid radiating sphere cooling in space, determining transient temperature distribution by finite difference computing techniques 09 p1790 A70-23562

Multiband radiative cooling effect on enthalpy distribution behind incident wave in cylindrical shock tube for air, using differential approximation 14 p2663 A70-30268

Conical heat radiator system for cooling short cylinders 15 p2827 A70-32142

Passive radiative coolers role in utilizing IR detector systems for low temperature spacecraft applications.

describing staged radiator design, optimization and tests
[AIAA PAPER 70-854] 16 p2983 A70-33921
Conical passive radiation coolers for quantum IR detectors on equatorial synchronous earth satellites, determining temperature excursions 16 p2915 A70-34314
Cathode geometry effect on performance of radiation cooled MPD arc thruster in continuous mode [AIAA PAPER 70-1083] 20 p3693 A70-40252
Thermal protection system based on radiation cooling for high altitude cruising hypersonic flight, achieving zero net mass transfer 21 p3950 A70-41745
Thin plates radiant cooling with mutual irradiation in spacecraft radiators 22 p4122 A70-42518

RADIANT ENERGY

U RADIATION

RADIANT FLUX DENSITY

NT ELECTRON FLUX DENSITY

NT ILLUMINANCE

NT IRRADIANCE

NT LUMINANCE

NT LUMINOUS INTENSITY

NT NEUTRON FLUX DENSITY

NT PARTICLE FLUX DENSITY

NT PROTON FLUX DENSITY

NT RADIANCE

NT SOLAR CONSTANT

NT SOLAR FLUX DENSITY

Statistical relation between radiation power of radio source and distance of center from radio-galactic nucleus, investigating evolution of radio galaxies 01 p0174 A70-10196

Cosmic ray latitude survey in Canada using airport sites, noting ground snow effect on neutron monitor counting rate 01 p0167 A70-10227

Energy dependence of intensity ratio of Li, Be and B on C, N, O and F nuclei L/M ratio in primary cosmic rays, analyzing data discrepancy 01 p0169 A70-10316

Current-voltage characteristics of cascaded solar thermoelectric generator, determining optimum hot junction temperature as function of radiation concentration 01 p0000 A70-10752

Comparative diagrams for radio emission intensities of pulsar PP 0943 from observations by cross radio telescope 01 p0185 A70-11034

Interplanetary magnetic field sectoral structure effect on diurnal cosmic ray intensity and geomagnetic field, noting field direction influence 01 p0172 A70-11525

High altitude balloon measurements of secondary gamma quanta intensity vertical distribution, using scintillation counter with CsI/Tl crystal 01 p0172 A70-11544

Forward scattering by nonergodic system of identical particles, relating temporal correlation function of scattered radiation and intensity moments 02 p0255 A70-11919

Characteristic X radiation intensity in atmosphere calculated using irradiating electrons spatial and energy distribution data 02 p0358 A70-12156

Radio source ghost images in Lemaitre cosmological models, deriving luminosity functions and radio source ages 02 p0371 A70-12198

Ponderomotive meter for laser energy and power measurement, discussing mechanical design and elimination of radiometric and convection disturbances 03 p0500 A70-13481

Magnetic field effect on recombination radiation intensity under pinch effect in semiconductor non-degenerate electron hole plasma with recombination time exceeding carrier lifetime 03 p0540 A70-13508

Nonlinear differential equations for determining radiation density of three level pulsed gas laser as function of power losses, active medium parameters and time 03 p0502 A70-13745

He-Ne multimode laser radiation peak as function of pressure in methane-containing absorption cell installed in resonator 03 p0502 A70-13750

Cosmic ray increases during Forbush decrease onset stage in terms of transient spatial anisotropy 03 p0559 A70-13914

Forbush decrease recorded on 26-27 January 1968 showing large anisotropies in cosmic ray flux after SC magnetic storm 03 p0560 A70-13979

Radiative lifetimes and total transition probabilities measured in polyatomic gases using phase shift method and electron beam excitation 03 p0441 A70-14009

IR flux variations from Seyfert galaxy NGC 4151 nucleus, using telescope 03 p0562 A70-14221

Nonequilibrium zone radiation intensity profiles behind strong shock waves in air determined for specific wavelengths and shock velocities 03 p0535 A70-14364

Planetary nebulae with concordant and discordant radio and optical fluxes, discussing possible causes of discordances 04 p0747 A70-14516

VLF radio monitoring of celestial X ray fluxes from ground for long periods, discussing ionospheric D region conductivity 04 p0739 A70-14521

Intensity, spectrum and polarization of gyrosynchrotron radiation from magnetoactive plasma electrons distribution 04 p0749 A70-14594

Integrated intensity measurements of carbon dioxide bands in micron regions, using self-broadening method 04 p0690 A70-15025

Cosmic ray flux modulation in earth atmosphere produced by solar wind and geomagnetic variations, considering effects on atmospheric carbon 14 variations 04 p0680 A70-15114

Pencil beam survey of radio sources at 178 MHz, with tabulated flux densities compared to 4C interferometer data 04 p0757 A70-15693

Variable object BL Lacertae flux measurements using Schmidt telescope photography and radio study, comparing results with quasar 04 p0759 A70-15711

Cosmic ray energy spectrum variations possible effect on ray intensity amplitude intensity increases preceding Forbush decreases 04 p0743 A70-15719

Diurnal cosmic ray intensity variations first and second harmonics amplitudes during sudden phase variations diagrammed from neutron monitor data during IGY 05 p0898 A70-15936

Cosmic ray intensity decreases in relation to geomagnetic and F 2 region disturbances characterized by Forbush decreases from vertical sounding data 05 p0898 A70-15940

Gamma radiation integral fluxes and production rate evaluation from ground and neutron production in Plexiglas and Fe to calculate optimum recoil electron threshold 05 p0899 A70-15955

Electromagnetic structure of interplanetary space on basis of secondary cosmic ray intensity gradient annual variations as function of earth heliographic latitude 05 p0900 A70-15970

MM wave outbursts of 1 and 2 November 1968, discussing wavelength dependence of flux density 05 p0912 A70-16441

Cosmic ray intensity preceding Forbush effects as function of chromospheric flares solar longitude and solar wind velocity 05 p0903 A70-16730

Flux densities from quasars 3C 273, 3C 279 and 3C 454.3 and Seyfert galaxy 3C 84, measuring linear polarization, discussing time variations in sources 05 p0918 A70-16926

Brightness distributions and widths determined from monochromatic radiation intensity at earth during lunar occultation of RF source 05 p0920 A70-16941

Power spectra of pulsar radiation intensity fluctuations, showing line structure 05 p0921 A70-16983

Shear-free gravitational radiation described by Einstein equations, analyzing physical properties including energy, angular momentum, radiation flux and trapped surfaces 06 p1104 A70-17185

Time variations and angular collimation of radiation emitted by source with relativistic streaming 06 p1134 A70-17281

Solar flare H alpha brightness measurement from photograph taken through birefringent filter, deriving flare morphological changes from isophotes 06 p1135 A70-18004

Solar bursts of enhanced intensity at millimeter wavelengths suggested for limb brightening mechanism 06 p1153 A70-18545

Intense light beams self focusing in nonlinear media with quadratic Kerr effect, assuming spherical initial phase front after passing through condensing lens 07 p1296 A70-18720

Signal strength of sky waves and noise levels near LUF, suggesting importance of changing mode structure 07 p1229 A70-19158

Mass to luminosity relations in RF region derived from data for nearest galaxies 07 p1383 A70-19404

Turbulence spectra and generated power determined for plasma turbulence in objects with high elec-

tromagnetic radiation density /quasars and supernova shells/ 07 p1384 A70-19412

Cosmic ray intensity increase preceding Forbush effect using statistical correlation method 07 p1367 A70-19444

Specific radiant heat flow and spectral blackness degree of tungsten with different surface finish 07 p1309 A70-19662

Flux densities and positions for Southern Milky Way sources at 1410 MHz, determining spectral indices 07 p1387 A70-19682

Radiative heat transfer in radiant energy flux incident on plane surface of nonisothermal absorbing and dissipating layer 07 p1423 A70-19814

Galactic cosmic rays intensity long term modulation, studying roles of solar corona, solar wind and interplanetary electromagnetic field 07 p1369 A70-20075

Yearly fluctuations of Seyfert galaxy 3C 120 light curve, discussing effects of ambient temperature 08 p1563 A70-20498

Population inversion in neodymium glass impurities in four level laser dependent on electron beam intensity and energy 08 p1512 A70-21205

Solar microwave bursts with double structure, discussing single frequency observations and flare patrols, time variations of flux density and brightness 08 p1561 A70-21259

Center to limb variation of solar brightness measured at 5, 10 and 20 microns, discussing data collection and reduction and previous IR and UV measurements 08 p1562 A70-21396

Radio sources linear polarization measurements at 6 cm wavelength, noting intensity changes with polarized flux and position angle 08 p1578 A70-21535

Relative rotational lines intensities of carbon dioxide, considering sigma-sigma transitions for abundant isotopes 08 p1549 A70-21575

Celestial positions and intensities of X ray sources in Sagittarius region obtained from rocket experiment 09 p1744 A70-22522

Cosmic ray intensity variation correlated with amplitude changes in 27 day variation during solar cycle 18 09 p1745 A70-22740

Quasar sky distribution as function of apparent magnitude for identification with galaxies of origin 09 p1759 A70-22909

Non-Cerenkov radiation region produced by passage of oscillating electric dipole at uniform velocity 09 p1728 A70-22958

Photon bremsstrahlung from relativistic hydrogen plasma determined by studying electron-positron pairing effect on plasma radiation intensity 09 p1735 A70-22986

Point source intensity fluctuations dependence on penetration depth of wave propagating in statistically homogeneous and isotropic media 09 p1636 A70-23133

X ray fluxes upper limits from quasars 3C 196, 3C 186 and 3C 380 measured by balloon flight experiments 09 p1745 A70-23271

Periodic intensity fluctuations in pulsars from VHF phased array measurements 09 p1764 A70-23793

Gamma ray astronomy above 10 Mev, investigating intensity dependence on galactic latitude and radiation detection technology 10 p1931 A70-24067

Intense laser radiation effect on light absorption, gas breakdown and formation of spark at focus 10 p1899 A70-24154

Primary cosmic gamma-quanta fluxes measured using telescope consisting of Cerenkov counters 10 p1931 A70-24316

Comparative diagrams for radio emission intensities of pulsar PP 0943 from observations by cross radio telescope 10 p1948 A70-25003

Radio telescopic observations of Jupiter, Venus and radio source 3C 273 at 2 and 8 mm wavelengths, determining brightness temperatures and radiation flux densities 10 p1948 A70-25153

Narrow band radiation from longitudinal plasma waves nonlinear interactions during solar bursts, comparing flux intensities for Corona single or double shock wave frequencies 10 p1934 A70-25272

Solar flare videometer for measuring flare area and peak and integrated intensity in real time 11 p2104 A70-25744

Foreign gases effects on He-Ne lasers IR emission, describing quenching due to positive column electron temperature decrease 11 p2062 A70-25826

- Global distribution and intensity of solar radiation, determining radiation of satellites and other high altitude devices 11 p2105 A70-26010
- Celestial sources energy spectrum and absolute flux by rocket flights, attributing short lived outbursts to shock wave from nova expanding into circumstellar medium 11 p2113 A70-26297
- IR radiation intensity distribution in solar neighborhood from grain models of dirty ice, graphite and graphite core-dirty ice mantle 11 p2106 A70-26710
- Corpuscular radiation intensity measurements in upper atmosphere at midlatitudes by meteorological probe during geomagnetic storm, noting radio wave absorption 11 p2106 A70-26797
- Statistical properties of random intensity field during coherent laser radiation scattering by moving diffuse surface 11 p2064 A70-26812
- Radio galaxies and quasars radiated power, discussing red shift complicated by absorption lines discovery in spectra 12 p2298 A70-27064
- Radiative intensity calculations for carbon dioxide and carbon dioxide-nitrogen plasmas for various temperatures, densities and path lengths, computing UV and continuum spectra 12 p2275 A70-27170
- Cosmic ray intensity fluctuations at geomagnetic equator using power spectrum analysis on mu meson records, discussing solar photosphere and interplanetary magnetic field 12 p2291 A70-27176
- First harmonic of diurnal variation in pressure corrected cosmic ray neutron monitor rate, discussing amplitude variation with height and observed time dependence 12 p2291 A70-27177
- Lyman alpha intensity and hydrogen concentration at 5 to 19 earth radii determined fromOGO 3 spacecraft measurements 12 p2222 A70-27181
- Decameter radio sources flux density time variations, discussing possible causes and radio emission spectra 12 p2299 A70-27308
- Ruby laser illuminated Ge recombination radiation intensity measured at room temperature 12 p2286 A70-27369
- X ray source from Coma cluster of galaxies, interpreting observed flux on basis of missing mass suggested by Virial theorem 12 p2293 A70-27388
- Poisson shot noise process relationship with continuous stochastic intensity as sample function 12 p2203 A70-27418
- Vertical profiles of daytime and nighttime long wave radiation fluxes in atmosphere under stratus cloud conditions 12 p2264 A70-27521
- Intensity and photocounts statistical distribution of harmonic generated in nonlinear crystal by laser and thermal radiation 12 p2248 A70-27547
- Microwave solar bursts intensity and polarization measurements at 17 GHz, discussing chromospheric flares and X ray emission 12 p2293 A70-27592
- Solar plasma and energy and radiation fading during microwave bursts due to synchrotron radiation losses, determining magnetic field strength 12 p2294 A70-27593
- Earth radiation balance /net flux/ determination from satellite measurements of long wave radiance and reflected solar radiation in upper atmosphere 12 p2264 A70-28090
- Solar activity effects on midlatitude upper atmosphere corpuscular radiation intensity via rocket sounding 12 p2296 A70-28266
- Pulsed plasma jet radiant heat flux effect on celophane film coated, polished and etched metals, noting erosion destruction 12 p2282 A70-28287
- Pulsed chemical laser output, considering increase in radiation energy 12 p2251 A70-28292
- Sgr gamma-1 source, determining upper limit on soft X rays intensity 13 p2475 A70-28615
- Compton electron scattering generated galactic gamma ray flux effects on diffuse IR 13 p2476 A70-28630
- Threshold light flux densities for thin Al film breakdown by laser radiation 13 p2428 A70-29383
- Cosmic rays intensity frequency spectrum near earth, indicating relativistic electron energy spectra similarity in interstellar space and galactic particles existence 13 p2478 A70-29388
- Non Q switched Nd laser light intensity correlation function measurement, using optical gate for producing second harmonic light 13 p2430 A70-29706
- Integral radiation fluxes incident on sloping and horizontal surfaces compared under cloud covers of various intensities 14 p2603 A70-30408
- Cosmic ray energy spectrum variations possible effect on amplitude of intensity increases preceding Forbush decreases 14 p2632 A70-30803
- Cosmic ray shortest term regular intensity variations, measuring particle dispersion as time function 14 p2633 A70-31314
- Sun Lyman alpha emission line monitoring, describing intensity variations correlation with Zurich number 15 p2798 A70-31654
- Carbon dioxide-nitrogen and nitrous oxide-nitrogen laser systems, substituting diatomic N 15 for N 14 to investigate radiation intensity 15 p2750 A70-31761
- Optical polarization, discussing radiation intensity and state measurement by two beam interferometer 15 p2736 A70-32035
- Solar, clear sky and overall radiation characteristics, calculating incidence of light and radiation in room interiors 15 p2732 A70-32461
- Lasers and GaAs diode emitters near IR radiation intensity distributions, using IR films and IR display phosphors 15 p2753 A70-32607
- Power density fluctuations in emission peaks of ruby laser determined by splitting beam into two components and using photosensitive element and photomultiplier recording 15 p2754 A70-32874
- He II 3s and 3d states mean lives and initial population as function of energy, analyzing emitted radiation intensity 16 p2954 A70-33059
- High voltage photoelectric generator containing semiconductor plates with series- and parallel-connected p-n junctions forming solid circuit for super-high light flux concentrations 16 p2843 A70-33201
- Probabilistic model for radiative transfer of photons in inhomogeneous infinite cylindrical shell medium, noting radiation intensity relation to scattering and transmission functions 16 p2952 A70-33785
- Solar radiation intensity at Lyman alpha wavelength and X ray spectrum before and during solar eclipse of 7 March 1970 16 p2972 A70-33827
- Continuum radiative flux from nonisothermal stagnation shock layer of nonray atomic gases, employing ionization edges and bound free spectral forms [AIAA PAPER 70-837] 16 p3001 A70-33932
- Near equilibrium shock layers nonequilibrium radiant emission calculation, noting application to Mars entry conditions [AIAA PAPER 70-773] 17 p3007 A70-34481
- Solar X-ray spectrum and intensity and diffuse cosmic flux measurements, using polar orbiting satellite-borne instruments 17 p3149 A70-34534
- Omnidirectional cosmic gamma ray flux in 1-6 MeV range observed by ERS-18 satellite 17 p3149 A70-34539
- Galactic cosmic rays eleven year modulation, determining modulating region L depth from dynamical phase lag between changes in cosmic ray intensity and solar activity 17 p3150 A70-34833
- Solar X-ray flux measurements in selected emission lines, using curved crystal Bragg spectrometers in low altitude sounding rockets 17 p3150 A70-34834
- Orion stars far UV intensities, considering photometric data and electronographic spectra from rocket sounding 17 p3160 A70-34882
- Spectral densities of intensity and frequency fluctuations of single frequency He-Ne laser radiation 17 p3105 A70-35092
- High-power Q switched solid state laser radiation intensity measurement methods for multi and single modes 17 p3105 A70-35094
- Radiation measurements inside Apollo 4 and 6 command modules during passage through trapped radiation belts 17 p3040 A70-35645
- Optimum mounting angles for direct solar radiation flux on solar battery on circular orbit satellite 18 p3215 A70-36176
- Reciprocity law between radiation intensity and exposure time for photographic films in vacuum UV spectrum region, investigating departure at various wavelengths 18 p3257 A70-36281
- Giant E and SO galaxies, discussing radio spectra, emission characteristics and brightness distributions 18 p3313 A70-36332
- Long wave radiation fluxes calculation in troposphere based on principal radiant heat transfer components separation 18 p3285 A70-36632
- Cosmic ray intensity increase preceding Forbush effect using statistical correlation method 18 p3309 A70-36918
- Atmospheric layer attenuation of thermal radiation from water surface by airborne radiation thermometer measurements 18 p3260 A70-36969
- Atmospheric water vapor distribution by intensity measurements of outgoing radiation from satellites in carbon dioxide and water vapor spectral bands 18 p3287 A70-36971
- Log S /flux/-log Z /redshift/ diagram for radio galaxies, encouraging steady state cosmology 18 p3320 A70-37074
- Radio sources near 2 flux units at 408 MHz, presenting data on positions, optical identifications, angular size and flux densities 18 p3321 A70-37125
- Monograph on gas laser dynamics, emphasizing single mode intensity measurement as function of cavity loss in He-Ne laser 19 p3446 A70-37978
- High energy primary gamma quanta intensity limits from Proton-2 and Cosmos-208 measurements 19 p3502 A70-38092
- Energetic primary gamma ray fluxes by satellite-borne spark chamber, isolating galactic radiation 19 p3502 A70-38093
- Muon deficient showers intensity distribution as function of sidereal time, obtaining anisotropy upper limit by statistical analysis and Monte Carlo method 19 p3511 A70-38483
- Solar radio emission intensity distribution across disk during eclipse, constructing relative RF spectrum of uncovered region 19 p3522 A70-38556
- Solar radio flux variations prediction for various activity levels based on random functions theory 19 p3522 A70-38558
- Solar radio emission flux as activity index, analyzing permissible deviations from recommended wavelength 19 p3522 A70-38559
- Flux intensity measurements of radio sources at 10.69 GHz by radome protected telescope using cryogenically cooled parametric amplifier as receiver 19 p3524 A70-38750
- Radio source 3C 161 scintillating component angular dimensions and flux density at 60 MHz 19 p3524 A70-38760
- Radio sources right ascension and flux densities at 60 MHz 19 p3524 A70-38761
- Pulsars CP 0834, AP 1237 and CP 1919 radiation intensity periodic variations, discussing power spectra fluctuations in circulating plasma model 20 p3701 A70-39007
- Coherent light beam characteristics with Gaussian radial intensity variation during propagation along optical system axis, determining radius from diffraction theory 20 p3639 A70-39086
- Encircled energy calculation in optical systems with central obstruction, observing focus error, spherical aberration and central spot effects on image contrast 20 p3627 A70-39088
- Interplanetary magnetic field large scale structure from cosmic ray intensity secular variations during solar activity cycle 20 p3696 A70-39276
- Stratospheric cosmic ray intensity increases unassociated with chromospheric flares 20 p3696 A70-39278
- Primary cosmic ray intensity variation during solar activity half cycle, expressing diffusion coefficient as function of sunspot group number 20 p3696 A70-39279
- Cosmic ray 27 day variations during solar activity minimum, noting unipolar magnetic regions role 20 p3696 A70-39280
- Solar cosmic rays diurnal and semidiurnal variations modulation by noncoincidence between earth rotation axis and normal to ecliptic plane 20 p3697 A70-39289
- Atmospheric dynamic effect on cosmic ray intensity, showing extremum and seasonal variation at midlatitudes 20 p3697 A70-39291
- Cosmic ray intensity variation during maximum meteor showers periods detected on earth, noting relationship to solar activity 20 p3697 A70-39294
- Diurnal anisotropy variations of cosmic ray intensity, taking into account neutron monitors data 20 p3699 A70-39346

Object visibility limits when illuminated by laser beam with spatial selection method, discussing atmospheric conditions and light source radiation power 20 p3641 A70-39448

Light He isotope effect on He-Ne laser power output 20 p3641 A70-39737

High radiation intensity neodymium glass laser, describing installation for heating plasmas to high temperatures 20 p3643 A70-39758

Fluctuations in radiation power density of solid state laser near focal plane of convergent lens, using device for selecting and recording individual peaks 20 p3643 A70-40022

Flash lamp pumped organic dye laser intensity for dye solutions in contact with different argon-oxygen compositions, noting effect of oxygen partial pressure 21 p3834 A70-40569

X ray flux and energy spectrum of Cen-X2, Sco-X1 and Tau-X1 sources by rocket flight observation 21 p3872 A70-40659

Hard X ray sources energy spectra in 20-120 keV range by balloon flights, presenting Sco X-1 intensities 21 p3874 A70-40660

X ray intensity sudden changes in 29.9-52.3 keV range from Sco X-1, correcting for atmospheric attenuation 21 p3872 A70-40661

Stellar coronas X ray fluxes from models of convection zones and corresponding mechanical energy fluxes 21 p3875 A70-40681

Extragalactic gamma ray and X ray intensity with power law spectrum, comparing galactic plane and high latitude spectra 21 p3875 A70-40687

Galactic gamma ray intensity near Cygnus by OGO-5 spacecraft-borne telescope with acoustic spark chamber, discussing source intensity 21 p3876 A70-40691

Low energy, diffuse cosmic X radiation flux comparison with power law spectrum, observing asymmetry with respect to galactic latitude 21 p3876 A70-40692

High energy gamma rays detection by balloon flights, investigating flux and energy spectrum 21 p3876 A70-40696

Soft X ray background galactic absorption and intensity measurements indicating inverse relation to columnar atomic hydrogen density 21 p3877 A70-40698

Venus radar brightness map, using 40 km separation between range gates and comparable distances between Doppler slices 21 p3883 A70-40710

Pulsars and other discrete sources celestial gamma rays flux distribution calculation 21 p3878 A70-40745

Earth intrinsic radiation flux incident angular coefficient, examining effect on partially screened flat spacecraft elements 21 p3942 A70-40847

Optimum tube diameter for maximum radiation output of single and multimode He-Ne lasers 21 p3836 A70-40916

Beta Cephei star discovery criteria, examining mechanism theory by He and N overabundances, far UV flux, spectral line width and binary character 21 p3890 A70-41159

Strong newborn X ray source detection during balloon flight, showing softened low energy spectrum 21 p3892 A70-41190

Mode intensity fluctuations in unlocked multiple mode He-Ne laser related to LF noise 21 p3837 A70-41918

Monochromatic radiant flux angular distribution reflected from water and carbon dioxide cryodeposits, discussing incidence, deposit thickness and wavelengths [ASME PAPER 70-HT-34] 22 p4122 A70-42433

Solar type 4 event flux density and circular polarization radiopolarimetric recording, showing peculiar phases of short duration 22 p4095 A70-43263

Interplanetary magnetic field inhomogeneities structure from galactic cosmic rays intensity fluctuations observation 23 p4237 A70-44053

IR absorption bands absolute intensities determination method, giving special consideration to absorption band wings and precision 23 p4217 A70-44203

Ta spectral emissivity, using ratio of specimen surface and black body spectral radiant intensities 23 p4207 A70-44447

Radiant energy flux effect on atmospheric pressure burning rate of composite solid propellant 23 p4232 A70-44552

Unsteady radiating nongray gas diffuse boundary conditions, emphasizing monochromatic radiation slip and one dimensional radiant flux 23 p4282 A70-44593

Jupiter flux density changes at 2695 MHz correlated with 10.7 cm solar activity, suggesting magnetic anomaly explanation 23 p4246 A70-44751

Statistical properties of random intensity field during coherent laser radiation scattering by moving diffuse surface 24 p4351 A70-45184

CW laser beam power density distribution monitoring by self calibrating photographic dosimetry technique 24 p4307 A70-45343

Herculis 89 supergiant abnormal IR radiation flux originating in circumstellar shell of solid particles radiating at observed long wavelengths 24 p4410 A70-45772

Pulsar distributions without magnetic decay, concerning age dependence of surface field and radio luminosity of neutron stars 24 p4413 A70-46138

RADIANT HEATING

Quartz-Fiberfrax heat shield tests for Thor booster at high radiative heating rates, noting optimum material performance dependence on loose stitching 01 p0129 A70-10850

Corneal thermal response model for carbon dioxide laser radiation, computing temperature rise from power distribution and conducting air-cornea interface 11 p0262 A70-25635

Laser energy parameters measurement by calorimetric methods based on radiant heating effect 17 p3106 A70-35099

UV absorption lines in H I regions heated by cosmic rays, discussing possible detection by rocket or satellite spectroscopic observations 17 p3152 A70-35748

Heat conduction three dimensional problem in radiation heated thin crystalline plates with temperature dependent thermophysical characteristics 18 p3348 A70-36644

Radiant gas heater for Brayton cycle space power system [ASME PAPER 70-GT-36] 18 p3303 A70-36834

Interstellar gas thermal instability under cosmic ray heating, investigating perturbations causing transition to dense cool phase in pressure equilibrium with intercloud phase 18 p3309 A70-37003

Solid propellant radiant and hypergolic ignition, examining radiation absorption and surface reaction between fuel and gaseous oxidizer 20 p3689 A70-40081

Laminar flow of liquid in duct with zero heat resistance of walls, calculating temperature distribution during radiative convective heating 20 p3613 A70-40297

Acoustic waves in carbon dioxide at 2-25 torr initial pressures induced by heat from incident carbon dioxide laser pulses 21 p3837 A70-42003

Clamped parallelogram metal plate thermal deformation under single surface radiant heating 24 p4426 A70-46009

RADIANT INTENSITY

U RADIANT FLUX DENSITY

RADIATION

Cosmological constant role in closed universes with matter and radiation 13 p2490 A70-28936

Bremsstrahlung from weakly ionized plasma, discussing emission and absorption characteristics, electron-atom collisions and dispersive effects 18 p3294 A70-36347

Crab Nebula filamentary system, examining excitation conditions in terms of ionization and heating by HF radiation 20 p3702 A70-39011

TSF-SNAP reactor neutron radiation leakage, comparing Monte Carlo calculations with experimental and analytical determinations 20 p3671 A70-39156

RADIATION ABSORPTION

NT ATMOSPHERIC ATTENUATION

NT AURORAL ABSORPTION

NT ELECTROMAGNETIC ABSORPTION

NT MOLECULAR ABSORPTION

NT PHOTOABSORPTION

NT POLAR CAP ABSORPTION

NT SELF ABSORPTION

NT X RAY ABSORPTION

Combination absorption effect on Raman scattering and Stokes component gain in presence of pumping in antiStokes region, giving relation for radiation conversion 01 p0107 A70-10141

Mathematical model for saturable absorbers consisting of molecular gases for use in IR applied to carbon dioxide laser radiation absorption by sulfur hexafluoride 01 p0109 A70-10429

IR radiation absorption from carbon dioxide laser in supersonic gas jet, applying results to nitrogen-carbon dioxide gas dynamic laser action 01 p0148 A70-11123

Gas motion and heating by radiation behind shock wave front, noting ionization and radiation absorption occurrence 01 p0068 A70-11570

Absorption of EUV sunlight by Jupiter upper atmosphere, discussing photoelectron energy loss, thermal equilibrium and heating efficiencies 02 p0367 A70-11816

Quadruple microwave probe applied to phase and attenuation variations measurements of HF wave propagating through dielectric media 02 p0345 A70-11898

MK stellar spectral types in Monoceros, analyzing spatial distribution and interstellar absorption using slit spectrograms 02 p0369 A70-12063

Galactic interstellar absorption lower limit in selected Area 19 determined from Stellar spectra densities, using Schmidt camera 02 p0370 A70-12073

Two phase density and void fraction measurement using beta, gamma and X ray radiation, considering optimal accuracy and beam collimation 02 p0305 A70-12835

Wave numbers determined in waveguide formed by laminar inhomogeneous medium enclosed between homogeneous dielectric media, taking into account radiation losses through wall 03 p0447 A70-13290

Evidence disproving interstellar extinction by diamond crystals 03 p0572 A70-13818

Flash lamp illuminated ruby laser operating with ordinary or extraordinary polarization, measuring gain or absorption 03 p0502 A70-13954

Biological experiment on Zond 5 automatic station in earth-moon-earth trajectory determining cosmic radiation absorption and effects on plant seeds, turtles, larvae, etc 03 p0428 A70-14066

Spatial resonance capture rates for U-238 thick slabs to correct gamma ray attenuation errors in broad group shielding calculations 05 p0884 A70-16169

Pressure wave formation induced by absorption of radiation in oxygen, noting wave driving after radiation pulse decay by frozen dissociation energy 05 p0833 A70-16306

Satellite radiation dose rate experiment with simultaneous trapped particle and absorbed dose rate measurements, discussing proton spectra, material distribution, shielding effects, etc 06 p1061 A70-17263

Solar, albedo and earth thermal radiations absorbed by partially obscured spacecraft calculated on digital computer for various orbital positions 06 p1173 A70-17556

Radiation scattering during upper cloud altitude determination by satellite 06 p1097 A70-17790

Radio brightness distribution observation over Venus disk, investigating absorption of millimeter radio emission of hot surface by planetary atmosphere 06 p1141 A70-17801

Laser radiation increased absorption in opaque solid body attributed to vaporization, analyzing factors determining thermodynamic equilibrium between condensed and gaseous phases 06 p1083 A70-18563

Absorption cross sections for single and double molecules of oxygen and in UV region noting disagreement with Beer law 06 p1114 A70-18632

IR absorption properties of CO, HCl and sulfur dioxide measured for role in Venus greenhouse effect 08 p1579 A70-21567

Laser radiation absorption in xenon plasma, noting dependence on intensity due to atoms ionization 08 p1554 A70-21803

Temperature effects on IR absorption by water and carbon dioxide vapors measured in narrow spectral intervals 09 p1666 A70-22180

Temperature field and combined radiative-conductive heat flux in weakly absorbing cylindrical layer bounded by nonblack surfaces 10 p1966 A70-23866

Radiation scattering during upper cloud altitude determination by satellite 10 p1913 A70-25022

Cyclotron waves absorption study in bounded rarefied plasma having Larmor electron frequency exceeding plasma frequency 10 p1925 A70-25101

Solar radiation transmitted and reflected by earth atmosphere, solving absorption and scattering by computer programs 12 p2262 A70-26951

Cryogenic Ge bolometers sensitivity variation and noise, noting radiation absorption by sensor and by coating 12 p2237 A70-28151

Radio brightness distribution observation over Venus disk, investigating absorption of millimeter radio emission of hot surface by planetary atmosphere 13 p2487 A70-28651

Lower stratosphere ozone formation, suggesting origin in cosmic rays absorption 13 p2400 A70-29472

Solar radiation absorption by atmospheric ozone observations by ground stations for meteorological data 13 p2400 A70-29642

He-Ne laser radiation absorption in dense Li plasma, calculating absorptivity for bremsstrahlung and photoionization 13 p2465 A70-29710

Attenuation length of vacuum UV photoexcited electrons in evaporated metal films, observing lack of dependence on photon energy 13 p2472 A70-29711

Lunar horizontal and inclined surfaces net radiation and components, discussing surface temperature, thermal emission and absorbed solar radiation 14 p2634 A70-30194

Total Absorption Shower Cascade (TASC) detector for gamma ray astronomy space, discussing energy and angular resolution 14 p2587 A70-31004

Radiative transfer in scattering medium with nonuniform absorption 15 p2775 A70-32906

Extinction parameters of submicron carbon, tungsten and Si particles in hydrogen measured at various temperatures, discussing scattering amplitude functions and Monte Carlo calculations [AIAA PAPER 70-838] 16 p3001 A70-33933

Red shift absorption systems ions related to intergalactic medium properties in clusters of galaxies 17 p3153 A70-34526

UV interstellar extinction from comparison of epsilon and zeta Persei, noting graphite features 17 p3159 A70-34877

UV interstellar extinction, examining reddened and unreddened early stars with OAO satellite spectrophotometric scans 17 p3159 A70-34878

UV stellar spectra absorption, considering silicon and carbon opacity effect on Balmer discontinuity and Paschen continuum 17 p3159 A70-34880

Lyman alpha absorption by interstellar neutral hydrogen observed in O and B stars UV spectra 17 p3162 A70-34898

Lyman alpha radiation from gaseous hydrogen nebula model, taking into account absorption by dust and interstellar neutral hydrogen 17 p3163 A70-34904

Nonadiabatic self absorbing radiative flow of gray gas around sharp cornered blunt body at hyperbolic speed by integral relations method 17 p3010 A70-34974

Temperature dependent absorption, nonsteady beam propagation and laminar-turbulent transition in laser induced convection column, measuring turbulence onset by fine wire resistance thermometer [AIAA PAPER 70-800] 17 p3107 A70-35197

Hydrocarbon gas detection using He-Ne laser radiation absorption, discussing detector electronics 17 p3107 A70-35520

Solar and IR radiation distribution in multiple scattering and absorbing ground fog, obtaining intensities, fluxes and vertical divergence 18 p3284 A70-35943

Ionospheric cosmic noise absorption diurnal and seasonal variations at Alma-Ata during IQSY, noting chromospheric flares effects 18 p3306 A70-36089

Bremsstrahlung from weakly ionized plasma, discussing emission and absorption characteristics, electron-atom collisions and dispersive effects 18 p3294 A70-36347

Laser pulse shaping using inducible absorption with Q switched time behavior controlled by nonlinearities within optical resonator 18 p3270 A70-36745

IR absorption by water vapor in transmittance windows, considering continuous absorption coefficient dependence on window width 19 p3461 A70-37425

Long wave outgoing radiation angular distributions based on effective mass and Curtis-Godson methods of accounting for absorption pressure dependence 19 p3461 A70-37634

Nonactive absorption by silicate neodymium glasses at emission wavelength as function of pumping flash rate 19 p3448 A70-38739

Formaldehyde absorption coefficients measured photoelectrically in vacuum UV range 20 p3703 A70-39165

Cas A and SN 1572 supernova remnant radio sources X ray spectra, investigating absorption by interstellar medium 21 p3873 A70-40666

Soft X ray background galactic absorption and intensity measurements indicating inverse relation to columnar atomic hydrogen density 21 p3877 A70-40698

Atomic hydrogen emissions in dayglow, considering excitation by resonance absorption of solar radiation 21 p3812 A70-40728

Molecular oxygen density and vibrational distribution in lower atmosphere, observing solar UV radiation absorption by satellite OSO-4 21 p3816 A70-41066

Color-color diagram of M92, computing synthetic stellar spectra for line absorption effect 21 p3892 A70-41249

Apollo 11 rocks IR absorption properties, specific heat and thermal conductivity, discussing heat flow in surface layer 21 p3913 A70-41642

High resistivity single crystal silicon wafers induced IR absorption measurement, using Nd doped glass laser 21 p3837 A70-41916

Cosmic X ray extinction and halo by interstellar grains, applying to light elements identification 21 p3883 A70-42200

Ne absorption cell and He-Ne gain cell pulse velocities compared with free space light velocity 22 p4048 A70-42329

WC radiation damage by resonant absorption following Coulomb excitation observed from gamma ray spectra 23 p4231 A70-44888

Carbon ionization equilibrium in dense interstellar clouds, discussing grains and neutral atoms attenuation effects 24 p4402 A70-45387

High energy electron proton and heavy nuclei absorption in pulsar vicinity, discussing implications for cosmic rays 24 p4398 A70-46170

RADIATION BELTS

NT ARTIFICIAL RADIATION BELTS

NT INNER RADIATION BELT

NT OUTER RADIATION BELT

NT PROTON BELTS

Quasi-trapped particle currents having discontinuities on daytime and nighttime side of earth 01 p0171 A70-11487

Jupiter radio telescope observations at cm wavelengths, describing radiation belt emission characteristics and planetary brightness temperature spectrum 03 p0565 A70-13233

Azur satellite launching project by NASA and Germany, describing orbit for investigating earth inner radiation belt, auroral zone and solar flares 03 p0580 A70-13797

Satellite measurement of auroral particles and particles trapped in Van Allen belts 03 p0559 A70-13852

Particle flux and dose rates in Jupiter Van Allen belts based on assumed synchrotron radiation from trapped electrons in dipole magnetic field [AIAA PAPER 69-18] 04 p0742 A70-15543

Inhomogeneous fast electron clouds stability and perturbation dynamics captured in magnetosphere geomagnetic field described by hydrodynamic equations 04 p0743 A70-15721

Redistribution of geomagnetically trapped 55 Mev protons by Starfish nuclear explosion, discussing hydromagnetic wave interactions and multiple reflections from magnetic field inhomogeneity 06 p1137 A70-18531

Kinetic equation describing dynamics of inhomogeneous cloud of fast electrons and ions trapped in earth magnetic field 07 p1276 A70-20429

Solar protons captured in earth dipole trap, discussing conditions for nonadiabatic escape 07 p1374 A70-20442

Jupiter radio telescope observations at cm wavelengths, describing radiation belt emission characteristics and planetary brightness temperature spectrum 08 p1580 A70-21666

Ultrarelativistic electrons cone instability in Van Allen radiation belts, discussing distribution function, relativistic effects and electron lifetimes 11 p2104 A70-25529

Plasma turbulence in Van Allen belts, examining weak turbulent electromagnetic wave properties, with emphasis on trapped energetic particles radiation 13 p2486 A70-28555

Radiation belt and auroral primary ions, comparing origin possibilities of ionosphere and solar wind 13 p2481 A70-30063

Van Allen radiation belts energetic electrons injection and distribution due to magnetic storms, using satellite-borne spectrometers 13 p2483 A70-30090

Satellite observation of alpha particles trapped geomagnetically in radiation belts, including Injun 5 results 13 p2484 A70-30092

Radial diffusion role in radiation belt dynamics from flux profiles time variations observations or equilibrium states analysis 13 p2484 A70-30094

Inhomogeneous fast electron clouds stability and perturbation dynamics captured in magnetosphere geomagnetic field described by hydrodynamic equations 14 p2632 A70-30805

Magnetosphere survey, including solar wind flow theory, observational techniques, radiation belt theory, magnetic storms, etc 15 p2732 A70-32544

Plasma containment in adiabatic magnetic traps, discussing particles, Coulomb collisions, instabilities, cyclotron resonance masers, Van Allen belts, etc 16 p2958 A70-33232

Jovian decimeter radiation, discussing electron drift velocity in dipole field, characteristic time for energy loss and radiation belt dimensions 16 p2980 A70-34192

Radiation measurements inside Apollo 4 and 6 command modules during passage through trapped radiation belts 17 p3040 A70-35645

Ring current belt stability against LF electrostatic perturbations, including effects of finite electric field along magnetic lines of force 18 p3306 A70-36009

Cosmic ray and radiation belt data from vertical profile, determining instantaneous cross section of atmosphere 18 p3307 A70-36169

Van Allen electrons acceleration and precipitation during magnetospheric substorms in relation to auroral processes, discussing energy and pitch angle diffusion processes 19 p3411 A70-37495

Ultrarelativistic electrons cone instability in Van Allen radiation belts, discussing distribution function, relativistic effects and electron lifetimes 21 p3882 A70-41279

Electron loss by resonant interaction with whistlers in nonuniform magnetic field, taking Fokker-Planck equation as distribution function 23 p4237 A70-44052

Particle motions in magnetic field, demonstrating existence of adiabatic region in particle phase space for Van Allen belt region 23 p4238 A70-44898

Energy dependence of equatorial pitch angle distribution for protons trapped in radiation belt, based on adiabatic theory and observational data 23 p4192 A70-44923

RADIATION CONTROL

U RADIATION PROTECTION

RADIATION COUNTERS

NT CERENKOV COUNTERS

NT ELECTRON COUNTERS

NT GEIGER COUNTERS

NT NEUTRON COUNTERS

NT NEUTRON SPECTROMETERS

NT PARTICLE TELESCOPES

NT PROPORTIONAL COUNTERS

NT QUANTUM COUNTERS

NT SCINTILLATION COUNTERS

NT SPARK CHAMBERS

Gamma ray beam inspection of opposed arc weld with nugget penetration in Al-Cu alloy, including averaging circuit reducing counting statistics variation 01 p0054 A70-10020

Photomultiplier tubes for counting photoelectrons from photocathode, discussing pulse height distributions, SNR, quantum counting, statistical correlation and dark current properties 01 p0090 A70-10902

IMP F solid state detector data on 13 day solar proton event at low energy, considering cosmic rays anisotropy and interplanetary magnetic field 04 p0738 A70-14512

Solar neutrino spectroscopy using various radiochemical detectors for Be 7, N 13, O 15 and B 8 neutrino fluxes, noting Li 7 suitability for determining CNO cycle 05 p0898 A70-15949

Solar neutrinos detection from recording high energy electrons in reactions, using Li 7, Be 9 and B 11 as detectors 05 p0899 A70-15964

Environmental control underground low level radiation counting facility of Lunar Receiving Laboratory for gamma ray spectrometry, including radon adsorption system 05 p0829 A70-16707

Distribution function distortions produced in counting devices due to simultaneous arrival of particles, correcting errors 06 p1064 A70-17830

Ion counter circuit using second equivalent condenser for compensating background radiation current, assessing error 07 p1281 A70-19526

Radiation detector geometrical factor approximation for cylindrical bodies, observing convergence for right square and circular cylinders 07 p1286 A70-19971

- Longitudinal nuclear-electromagnetic cascade in ionization spectrometer simulated by Monte Carlo method, noting energy relationship to particle sum recording 08 p1500 A70-21743
- Spectrometer design for Helios solar probe using semiconductor detectors to identify particles separated by magnetic field 10 p1888 A70-24487
- Cosmic neutrinos detection, using inverse beta decay and elastic scattering by electrons to overcome solar neutrino problem 12 p2293 A70-27390
- Spaceborne logarithmic variable prescaling counters for automatic compression of particle measurement data, discussing statistical error 13 p2406 A70-28931
- Pioneer 8 wave and particle observations correlation showing broadband wave levels reduction during extended geomagnetic tail crossings 15 p2727 A70-31904
- Cosmic ray experiment for detecting quarks in low density showers, using hodoscope of wire proportional counters 16 p2972 A70-33048
- Low light intensities measured using photon counting method, comparing signal to noise ratio with lock-in method 16 p2911 A70-33524
- Flexible channel multiplier for particle counting with electron conductive polymer composition, discussing secondary electron emission, gain distribution and degradation 17 p3054 A70-35279
- Tiros solar proton monitor program, describing detector design, operational data processing and early warning network 17 p3180 A70-35304
- Solar neutrinos flux upper limit determination, describing detection equipment and procedures 19 p3511 A70-38486
- High transmission device for quark detection in primary cosmic rays 20 p3629 A70-39315
- ### RADIATION DAMAGE
- Local gamma irradiation effect on number of chromosome aberrations in lymphocytes of human blood of oncological patients after hysterectomy 01 p0013 A70-10137
- Probabilities for cell survival after exposure to ionizing radiation obtained by two compartment model 01 p0028 A70-11370
- Acoustic transients in mammalian eye induced by normal and Q switched laser pulse absorption 02 p0313 A70-12325
- Biological dosimetry techniques for irradiation damage evaluation 02 p0239 A70-12581
- Silicon solar cells I-V characteristics, spectral response and diffusion length measured after neutron irradiation 03 p0537 A70-13025
- Collection of Soviet papers on physicochemistry of radiation damage covering free radical processes in cellular organelles, protective action of pyridine derivatives, etc 03 p0418 A70-13301
- Postirradiation free radical processes in cellular organelles of rat liver exposed to gamma irradiation detected by graft copolymerization method 03 p0418 A70-13302
- Ultraweak luminescence intensity, radiation damage kinetics and spectral properties of cellular organelles of rat liver exposed to gamma radiation 03 p0419 A70-13304
- Graft copolymerization and chemiluminescence analysis of lipids complexes in animal and plant tissue homogenates exposed to gamma radiation 03 p0419 A70-13305
- Photodynamic damage in biological cells, discussing free radical originators and protective action of thiourea, mono and polyvinylpyrrolidone, cysteine and antibiotics 03 p0419 A70-13306
- Radiation damage recuperation process in living organisms and justified risk dose in prolonged space flights using Blair model 03 p0423 A70-13705
- Natural immunity characteristics in dogs after proton exposure, analyzing integumentary bactericidal activity, oral microflora and neutrophil phagocytic activity 03 p0423 A70-13707
- Neutron induced defect clusters in high field space charge region of Si p-n junctions, noting rate of volume damage dependence on electric field strength 04 p0730 A70-14728
- Chromium doping effect on ionizing radiation damage in MOS field effect transistors 04 p0658 A70-14744
- Specific heat and thermal EMF increase due to radiation damage in lattice of fast neutron bombarded Cu, Mo and W specimens 05 p0863 A70-16292
- Nonionizing radiation sources relationship to human targets, discussing damage threshold levels 06 p0998 A70-17201
- Si-NP solar cell damage coefficient dependence on energy of irradiating electrons and protons, determining diffusion length from short circuit current 06 p1127 A70-18504
- Antiradiation chemical substances for modifying radiation damage in peas during seed irradiation with fast neutrons 07 p1208 A70-19510
- Neutron irradiation damage in W, observing consistency of activation energy for self diffusion with vacancy mechanism 07 p1314 A70-20012
- Free radical destruction by gamma irradiation in organic solids at low temperature measured by electron spin resonance spectroscopy, noting dosage relationship 07 p1225 A70-20324
- Soviet book on radiation genetics problems covering radiation damage of chromosomes, sexual and somatic cells, postirradiation cell recovery, etc 08 p1445 A70-20761
- Biological effects of laser radiation on human eye, discussing damage caused by long term exposure to visible, IR and UV wavelengths 08 p1451 A70-21043
- Retinal damage thresholds by exposing rhesus monkey and human eyes to laser radiation, testing rabbit eyes for corneal thresholds 08 p1451 A70-21044
- Permeability disturbances in skin capillaries of rabbits and rats following exposure to Sr90-Y90 beta radiation 09 p1619 A70-22789
- Stimulated Mandelstam-Brillouin scattering and fracture of molten quartz and silicate glasses produced by laser giant pulse 11 p2061 A70-25380
- Radiation environmental model of synchronous communication satellite solar cell degradation by particle fluxes [ALAA PAPER 70-481] 11 p2103 A70-25411
- Radiation damage recuperation process in living organisms and justified risk dose in prolonged space flights using Blair model 11 p1985 A70-25505
- Natural immunity characteristics in dogs after proton exposure, analyzing integumentary bactericidal activity, oral microflora and neutrophil phagocytic activity 11 p1985 A70-25507
- Corneal thermal response model for carbon dioxide laser radiation, computing temperature rise from power distribution and conducting air-cornea interface 11 p2062 A70-25635
- Antiradiation chemical substances for modifying radiation damage in peas during seed irradiation with fast neutrons 11 p1988 A70-26109
- Radiation defects in Ge single crystals surface layers caused by low energy bombardment with He ions 12 p2287 A70-27486
- Radiation defects distribution in GaAs during proton irradiation, noting distribution dependence on proton energy and integral flux 12 p2287 A70-27488
- Ruby crystal surface destruction by laser radiation, studying surface structural and optical properties effect and threshold power dependence on light pulses duration 12 p2248 A70-27541
- Tungsten crystalline structure defects caused by alpha particles bombardment using helium ion projector at 78 K 12 p2255 A70-27544
- Microdefects as centers of disk shaped destructive cracks in polymer dielectrics under laser irradiation 13 p2437 A70-28621
- Alpha particles radiation damage effects in silicon surface barrier detector 14 p2584 A70-30511
- Chorioretinal damage thresholds spectral dependence of intense light sources, describing temporal, axial and radial temperature distributions 15 p2682 A70-32014
- Space radiation effects on secondary electron conduction /SEC/ image tube performance, observing temporary degradation and permanent damage 16 p2878 A70-33433
- Satellite-borne test instrument for determining mirror materials degradation due to long solar exposure 16 p2921 A70-34109
- Thermal-chemical damage to carbon particles in egg albumin under ruby laser irradiation, using chemical rate equations for protein denaturation 17 p3035 A70-34577
- Surface destruction of glass dielectric by pulsed laser beam, considering plasma clouds, shock waves, ablation and crack formation 18 p3266 A70-36153
- Thermal self focusing filaments observation in form of tracks in KDP and ADP crystals damaged by radiation from free emission mode laser 18 p3266 A70-36612
- Electronmicroscopical structure of laser irradiated Garding-Passy melanoma cell organelles, noting mitochondria damage 18 p3224 A70-36636
- Radiation flaws in semiconductors, examining effects of gamma quanta, fast electrons and neutrons and heavy charged particles 19 p3483 A70-37295
- Iron cyanide surface additives effect on photodamage to ZnO powder, using ESR method 19 p3372 A70-37543
- Electron radiation damage and stage 3 annealing effects on polycrystalline Mo properties 19 p3451 A70-37570
- Neutron irradiation effect on unijunction transistors and SCRs, developing damage prediction technique 19 p3388 A70-37848
- Soviet book on dynamics of postirradiation damage of biological objects covering dosage and protection effects on various animals 20 p3573 A70-39824
- Annealing properties of radiation damage in lithium-diffused silicon, formulating kinetic equation to describe processes associated with recovery and instability 20 p3687 A70-40165
- High energy electron irradiation generated defect centers in GaAs p-n electroluminescent diodes, using capacitance and thermally stimulated current measurements 21 p3863 A70-41914
- Threshold retinal damage by CW He-Ne lasers due to mode locking 21 p3771 A70-41997
- Laser radiation effects on lens lipid content in adult Rana temporaria frogs during cataract development 22 p3978 A70-43139
- Radiation-produced defects in silicon semiconductor devices, annealing gamma ray, electron and fast neutron damages 22 p4087 A70-43328
- Safety standards and biological effects of microwave radiation, investigating cataractogenesis and heart rate in rabbits 23 p4144 A70-43790
- Electron radiation damage Si, investigating p type defect concentration effect on isochronal temperature in annealing by fractionation experiment 23 p4231 A70-44887
- WC radiation damage by resonant absorption following Coulomb excitation observed from gamma ray spectra 23 p4231 A70-44888
- Optical damage center structural defects in transparent dielectrics under high energy ruby laser radiation, noting nontransparent inclusions and dislocation centers 24 p4351 A70-45209
- Sunlight induced pyrimidine dimers formation in human cells in vitro, relating DNA lesions by 254 nm irradiation 24 p4304 A70-46139
- ### RADIATION DETECTORS
- #### NT DOSIMETERS
- #### NT SILICON RADIATION DETECTORS
- #### NT THRESHOLD DETECTORS [DOSIMETERS]
- Radiation detectors for ionizing radiation onboard artificial satellites, considering weight and power supply constraints for ionization chamber, GM, proportional and scintillation counters, etc 01 p0093 A70-11254
- Long term storage effects on noise, leakage current and thickness of Li drifted Si surface barrier detectors 03 p0482 A70-13023
- Solar interior temperature measurement by Cl, Ga and Li isotopic detectors of solar neutrinos, discussing effectiveness and upper temperature bound 05 p0899 A70-15951
- Solar neutrino detectors calibration with artificial neutrino sources produced by reactors, electron and proton accelerators 05 p0846 A70-15953
- Gallium trichloride and aqueous solution of lithium chloride as solar neutrino detectors 05 p0899 A70-15956
- Experimental observations of neutrino in collapsing stars in Galaxy, showing detector capability of recording positrons or electrons from antineutrino-neutrino flux induced reactions 05 p0900 A70-15966
- Radiation data from manned orbital Mercury missions, correlating measurements from various additional sensors with main nuclear emulsion sensors 06 p1134 A70-17267
- Gemini spacecraft shielding configuration and radiation detectors, describing cabin radiation distributions 06 p0990 A70-17269
- Grating spectrometer with Ge-Cu detector used on balloon flights for studying variations of IR solar spectrum with altitude, emphasizing sunset features 06 p1152 A70-18523

Lepton charge and neutrino astrophysics, discussing oscillations role in solar neutrino detection difficulties

07 p1371 A70-20329

Relativistic magnetic monopoles detection in corpuscular primary cosmic rays, describing equipment and results

07 p1371 A70-20333

Statistics and coincidences of Argonne-Maryland gravitational radiation detector array with and without time delays

08 p1545 A70-21271

Time resolved photoelectric light detection, discussing photoelectric emission probability time dependence and radiation interaction with bound charge

09 p1726 A70-22232

Narrow band detector for polarized light in far UV based on plasma resonance

09 p1676 A70-22650

Cosmic ray air shower detection from radio pulses

09 p1745 A70-23276

High energy pulsed gamma rays detection method for pulsars based on search for nanosecond duration Cerenkov light signals

09 p1748 A70-23795

HF electromagnetic wave detector based on study of volt-ampere characteristics of luminescent plasma discharge

10 p1922 A70-24030

Gamma ray astronomy above 10 Mev, investigating intensity dependence on galactic latitude and radiation detection technology

10 p1931 A70-24067

Open magnetic electron multipliers /MEM/ with continuous dynode and field strips for satellite-borne detection systems, emphasizing extreme UV detectors

11 p2049 A70-25628

Isotropic cosmic background radiation detection in presence of earth and galactic radiation, discussing influence on steady state cosmology

11 p2106 A70-26673

Solar gamma ray lines search with high resolution balloon-borne directional spectrometer based on lithium-drifted germanium detector

12 p2292 A70-27178

Cosmic electron detection and measurement techniques, considering presence in solar system, interstellar space and metagalaxy and galactic continuum radio emission

12 p2293 A70-27572

X- and gamma-ray detectors design based on combination of solar batteries with scintillators, noting stability requirements

13 p2404 A70-28657

Gravity radiation detector insensitivity to cosmic rays

13 p2405 A70-28835

Standard sources and detectors for thermal radiation measurement

13 p2410 A70-29654

Automatic narrow band meter for continuous readout of frequency characteristics of radiation detectors

13 p2412 A70-29867

Energy balance in radiation detector cooling, analyzing refrigerator capacity and thermal load

13 p2412 A70-29870

Spectral characteristics of secondary emission alloys for photocathodes in extra atmospheric radiation open-type detectors in UV range

14 p2582 A70-30166

Light elements detection in interstellar grains by observing halo around X ray source arising from small angle scattering

14 p2631 A70-30539

Primary cosmic rays balloon-borne charge composition detector in 3-30 Z range

14 p2587 A70-31002

Superhigh energy particles detection by transition radiation, measuring Lorentz factor of emitted spectra

14 p2616 A70-31003

Total Absorption Shower Cascade /TASC/ detector for gamma ray astronomy space, discussing energy and angular resolution

14 p2587 A70-31004

Remote atmospheric temperature profile measurements, analyzing physical processes for radiation detection by earth pointing satellite-borne sensor

14 p2611 A70-31156

Single pulse ionospheric sounding system for detecting and identifying E region echoes

16 p2859 A70-32940

Pyroelectric IR radiation detector based on materials polarization changes associated with temperature changes

16 p2905 A70-33154

Radio receiving system for pulses detection from cosmic ray extensive air showers, discussing sensitivity and noise temperature

16 p2911 A70-33788

Pulsar gravitational waves detection by lunar mascons, discussing resonant standing vibrations

16 p2980 A70-34306

Ferroelectric radiation detectors theory and applications, considering polarization changes due to temperature increase from absorbed radiation

17 p3082 A70-34649

Extrinsic photoconductive detectors, comparing performance for microwave and DC bias based on gain bandwidth product and SNR analysis

18 p3232 A70-36746

Superpure materials for low background radiation detectors, determining U, Th and Ca radioactive contamination by radiochemical activation analysis

20 p3629 A70-39317

InAs pulsed injection laser at cryogenic temperature for measuring time constant of IR radiation detectors

20 p3630 A70-39449

Inverse beta decay thermonuclear reactions induced by neutrinos proposed for neutrino detection from solar interior

20 p3704 A70-39471

Thermal radiation detectors operation principles, design, specifications and applications

20 p3632 A70-39626

X ray astronomy instruments on sounding rockets, balloons and satellites, investigating sources distribution on celestial sphere

21 p3821 A70-40652

High energy gamma rays detection by balloon flights, investigating flux and energy spectrum

21 p3876 A70-40696

Orientation system for pointing balloon-borne X ray detector using flux gate magnetometer, DC amplifier and motor control relay circuit

21 p3831 A70-42249

High energy neutrinos generated by cosmic ray interactions with earth atmosphere, discussing detection, plotted energy spectrum and underground muons

22 p4093 A70-42310

Solid state high energy light detector for pulsed ruby and glass lasers in long pulse mode

22 p4052 A70-43614

Pioneer 8 and 9 cosmic ray detector system, discussing mechanical, electrical and data conditioning properties

23 p4195 A70-44300

Apollo command service module nondispersive X ray detection system for lunar composition map compilation, discussing design and performance

23 p4196 A70-44417

Secondary emission detector using linear signal to measure nonrepetitive microsecond ion bursts

23 p4197 A70-44475

Continuous channel electron multipliers /Channeltron/ gain improvement via blanking method avoid detection of unwanted particles

23 p4197 A70-44477

Gravitational radiation detectors design and components, discussing background noise and thermal fluctuations

23 p4198 A70-44850

Nike-Apache rocket aurora probes using proton detector to measure galactic cosmic ray intensity and relativistic electrons

23 p4192 A70-44879

Class 1b solar flare X ray examination, using rocket-borne liquid N cooled solid state detector

24 p4397 A70-45767

Solar X-ray flare temperature and emission measure profiles using OGO 5 satellite detector, interpreting energy dispersion of peak times

24 p4397 A70-45768

Radiative flow detection problems, calculating gamma radiation scattering

24 p4348 A70-45848

Radiation detectors with superconducting weak links response to single photons, considering Mercereau ring interferometer

24 p4391 A70-46256

RADIATION DISTRIBUTION

NT ANTENNA RADIATION PATTERNS

NT DIFFRACTION PATTERNS

NT RAINBOWS

NT SIDELOBES

Ruby ring lasers unidirectional emission obtained by using Faraday rotator with small polarization plane rotation angle

01 p0107 A70-10208

High energy nuclear interactions defined by computerized determination of sea level lateral distribution of muons from primary cosmic ray air showers

01 p0171 A70-10667

Successive approximations method for incorrectly posed problems in synthesis of radiating systems, discussing radiation patterns of linear emitter

01 p0044 A70-11036

Cerenkov radiation from electrons in magnetosphere and ionosphere, analyzing radiated power relationship with frequencies and latitudes

01 p0080 A70-11226

Soviet book on methods in laser design, Volume 2, covering pumping radiation in active rods, unsteady modes, ruby and Nd glass lasers

02 p0310 A70-11691

Evolution and entropy of partially ionized collision dominated plasmas interacting with radiation based on statistical analogs of irreversible thermodynamics

02 p0346 A70-11902

GaAs injection laser operated with external optical resonator for diffraction-limited radiation, considering peak power and quantum efficiency

02 p0311 A70-11920

Field pattern near paraboloid reflectors focus for low f/D ratios, considering vectorial character of electromagnetic field

02 p0268 A70-12474

Soviet collection of papers on radiation fluxes and ozone in atmosphere covering concentration, UV radiation scattering, etc

03 p0473 A70-13293

Converging series solutions for conducting circular disk in radiation field of vertical and horizontal magnetic dipoles to determine reemitted field

03 p0448 A70-13432

Laser with nonresonant feedback calculated for single mode and total radiation fields correlation functions from Heisenberg equations

03 p0503 A70-14175

Configuration factors independence on Lambert law in radiation from spheres and infinitely long cylinders [ASME PAPER 69-HT-1]

04 p0784 A70-14870

Axisymmetric radiating flow behind paraboloidal shock in ideal inviscid gas hypersonic stream, using differential approximation method for blunt body solution

04 p0669 A70-14937

Electromagnetic scattering from perfect conductors by numerical analysis, presenting far field pattern calculation for plane wave scattering from square cylinder

04 p0652 A70-15363

Fragmentary arc and band-shaped polar aurora configurations associated with corpuscular rays penetration into upper atmosphere

04 p0684 A70-15749

Solar cosmic rays diffusion enclosure in interplanetary space magnetic boundary suggested from balloon, satellite and ground observations of solar flare neutron component

05 p0904 A70-16753

Liquid fuel combustion luminous flame monochromatic radiation distribution, considering soot particle clouds effective emission thickness

06 p1172 A70-17142

Gemini spacecraft shielding configuration and radiation detectors, describing cabin radiation distributions

06 p0990 A70-17269

Radio emission distribution from supernova remnants and galactic magnetic field

06 p1139 A70-17323

Earth and atmosphere effect on solar radiation balance in Southern Hemisphere

06 p1054 A70-17413

Radiation patterns from finite conducting cone excited by quarter wave monopole protruding from center of base computed on digital computer

06 p1020 A70-17559

Backscattered field determination at edge on incidence from thin circular plates illuminated by plane waves

06 p1008 A70-17563

Electronic sine-cosine converters construction in devices for visual display of hydroacoustic transducers radiation patterns

06 p1064 A70-17773

Spatiotemporal correlation functions of random intensity field during diffuse scattering of coherent radiation by moving reflector

06 p1009 A70-17810

Pulsar slowdown by radiation field torques indicated by alignment torque in magnetized oblique sphere rotating in vacuum

07 p1389 A70-20220

Solar system cosmic ray time-space variations analysis based on simulation of meteorite nuclear processes

07 p1372 A70-20338

Solar corpuscular fluxes directional distribution time dependent changes effect on lower ionospheric electron production rates

07 p1373 A70-20344

Optical coherence theory functional formalism developed in radiation field probability functional terms, noting role of P representation of density operator

08 p1545 A70-21254

Radiation field photon density matrix for gas laser with ring resonator determined from double level atomic model, considering photon dispersion and wave reflection feedback

08 p1513 A70-21420

Dominant radiation field interaction with gas flow field using matched asymptotic expansion method

08 p1598 A70-21579

Radiation transfer in semifinite medium illuminated by parallel light beams assuming triinomial scattering indicatrix, deriving radiative effects and radiation field

09 p1751 A70-22154

Active element inhomogeneity effects on semiconductor injection lasers emission spectra and radiation intensity distribution

09 p1695 A70-22481

Non-Cerenkov radiation region produced by passage of oscillating electric dipole at uniform velocity

09 p1728 A70-22958

Polychromatic nonlinear light scattering in plane parallel layer solved by self consistent optical depths method

09 p1762 A70-23117

Polygonal-aperture antennas side radiation distribution

09 p1648 A70-23153

Plasma, Coulomb fields and radiation correlations obtained by relativistic kinetic equations, noting bremsstrahlung, synchrotron, cyclotron radiation, radiative and particle diffusion, etc

09 p1736 A70-23182

Fourier spectrum of chopped bivariate normal intensity distribution with coefficients calculated numerically by computer, verifying by chopped laser beam signal analysis

09 p1729 A70-23520

Successive approximations method for incorrectly posed problems in synthesis of radiating systems, discussing radiation patterns of linear emitter

10 p1842 A70-25006

Radiation fields of sources in plane stratified plasma medium calculated for amplitude transformation coefficient

10 p1843 A70-25155

Global distribution and intensity of solar radiation, determining radiation of satellites and other high altitude devices

11 p2105 A70-26010

Microwave illuminated aperture near radiation field mapped and processed for microwave hologram suitable for optical imaging for far field pattern simulation

11 p2051 A70-26025

Radiation from electric dipole in moving isotropic plasma analyzed for plasma velocity effect on pattern and far fields

11 p2091 A70-26178

CO vibration-rotation bands, calculating high resolution and temperature steradiance and spectral absorption coefficient

12 p2275 A70-27171

Gallium arsenide laser with external mirror excited by electron beam, measuring radiation patterns

12 p2247 A70-27482

Radiation profiles in ablating flat plate air-Teflon laminar boundary layer, discussing visible, UV and IR wavelengths

12 p2211 A70-27803

Electric dipole radiation field in homogeneous anisotropic compressible plasma, obtaining asymptotic expressions by saddle point integration method

12 p2282 A70-27970

Field distribution determination in holographic image space, obtaining ideal image and aberration terms

13 p2405 A70-28826

Emission field and Fermi quasi-levels distribution in injection laser with n-p heterojunction, determining frequency and threshold current temperature dependence

13 p2426 A70-28876

Focusing lens edge diffraction effect on angular distribution of laser radiation, considering zero mode field distribution

13 p2428 A70-29367

Transport equations for interaction between radiation and matter under arbitrarily large nonequilibrium in comoving system

13 p2521 A70-29414

Transition radiation in plasma sheet in vacuum assuming specular reflection of electrons at vacuum boundary

13 p2464 A70-29512

Mixed boundary value problems with radiation-type boundary conditions solved by complex Green function, discussing water waves in irrotational motion

13 p2452 A70-29536

Solar constant dependence on Wolf number and variations in transmission factor from balloon observations of radiation balance vertical distribution

14 p2568 A70-30126

Radiation coherent enhancement of single frequency emission fields in Q modulated coupled ruby lasers

14 p2593 A70-30152

Field characteristics of solar radiation reflected and scattered into outer space by earth atmosphere, discussing brightness and angular distribution of outgoing component

14 p2603 A70-30406

Fragmentary arc and band-shaped polar aurora configurations associated with corpuscular rays penetration into upper atmosphere

14 p2576 A70-30833

Self similar one dimensional flow behind plane shock propagating in exponentially decreasing atmosphere, considering radiation mean free paths and radiative heat transfer

14 p2567 A70-31032

Diffusely transmitted and reflected radiation fields for planetary isotropically scattering atmosphere bounded by Lambert law reflector

14 p2617 A70-31305

Electromagnetic wave diffraction by heterogeneous planar dielectric structures, showing field distributions by single variable Fredholm equations

15 p2695 A70-31436

Surface wave radiation from plane dielectric waveguide, considering phase constants, directional properties and optimal distance location

15 p2696 A70-31503

Opposing mode interaction effect on ring laser unidirectional emission instability, discussing homogeneous and inhomogeneous line broadening

15 p2749 A70-31552

Solar proton structure across polar cap and anomalous latitude cut-off explained by local pitch angle variations

15 p2792 A70-31672

Field correlation theorem for deducing Cassegrain antennas performance from internal field distributions, considering two reflector diffraction problems

15 p2698 A70-31953

Radiation fields structural characteristics of fronts, intertropical convergence zones and cyclone formations from radiation charts based on meteorological satellite observations

15 p2770 A70-32068

Electromagnetic waves scattering at circular cylinders in semibounded region, showing boundary influence on radiation pattern

15 p2698 A70-32174

Electric and magnetic dipole VLF radiation patterns in lossy two component magnetoplasma

16 p2860 A70-32944

Finite parallel plate waveguide arrays edge effects, comparing element radiation patterns and reflection coefficients vs scan

16 p2860 A70-32953

Paraboloidal and spherical reflectors focal region fields matching over corrugated waveguide open end propagating hybrid modes

16 p2861 A70-32966

Radiation pattern of conducting strip excited by linear slot parallel to strip edges, deriving asymptotic solution

16 p2863 A70-33239

Proton distribution in radiation belt inner zone from radial diffusion addition to cosmic ray produced albedo-neutron decay and atmospheric collision loss

17 p3150 A70-34644

Stellar mass loss, considering radiation field momentum transfer or coronal heating as mechanisms

17 p3157 A70-34841

Solar and IR radiation distribution in multiple scattering and absorbing ground fog, obtaining intensities, fluxes and vertical divergence

18 p3284 A70-35943

Simultaneous measurements of earth atmosphere radiation, comparing short and long wave data consistencies at various altitudes

18 p3286 A70-36963

Climatological maps of earth mean annual radiation balance compared with satellite data

18 p3286 A70-36966

Underlying surface inhomogeneity effect on radiation in presence of solid cloud cover

18 p3287 A70-36975

Stellar atmosphere radiation field quantity vs quality, deriving electron temperature as function of tau

18 p3309 A70-37007

Galactic radio corona existence, measuring northern galactic hemisphere sky brightness and cosmic ray distributions

18 p3322 A70-37129

Lunar surface radiative balance and thermal environment measurement by portable meteorological station, considering lunar environment peculiarities for instruments design

19 p3514 A70-37631

Long wave outgoing radiation angular distributions based on effective mass and Curtis-Godson methods of accounting for absorption pressure dependence

19 p3461 A70-37634

Diffraction radiation excitation by electron beam moving within resonant system formed by ribbon grating and metal plane, taking into account screen conduction losses

19 p3377 A70-37724

High energy primary cosmic ray muons arrival directions examined for anisotropies underground

19 p3508 A70-38141

High energy cosmic rays sidereal and solar anisotropy, using airborne Cerenkov telescope

19 p3510 A70-38151

Solar radio emission intensity distribution across disk during eclipse, constructing relative RF spectrum of uncovered region

19 p3522 A70-38556

Polarization in inverse Compton effect for arbitrary photon and electron distributions, discussing monochromatic photon beam

19 p3524 A70-38696

Solar spectral intensity distribution and ionizing radiation spatial emission patterns during eclipse, discussing effects on ionosphere

19 p3418 A70-38908

Resonance radiation transport in optically thick media, investigating complete frequency redistribution mathematical assumption

20 p3671 A70-39021

Atmospheric gamma rays vertical intensity dependence on spectrum and altitude from high altitude balloon studies

20 p3697 A70-39286

Inclined electromagnetic wave incidence on randomly inhomogeneous medium with changing mean dielectric permittivity, calculating reflected and scattered fields

20 p3587 A70-39726

Radiation field multidimensionality effect on radiating gas jet flow, taking into account radiative energy transfer by differential approximation

20 p3611 A70-39808

Electromagnetic waves and oscillations excited by magnetic current ring source around infinitely long compressible plasma column, deriving radiation field distribution

20 p3685 A70-40506

Pulsars and other discrete sources celestial gamma rays flux distribution calculation

21 p3878 A70-40745

Auroral UV night airglow radiation distribution over latitude range, using scanning spectrometer onboard Convair 990 aircraft

21 p3818 A70-41106

Gas dynamic quantum amplifier improvement, discussing power utilization, photon distribution and radiation transport

21 p3836 A70-41418

Radiation coherent enhancement of single frequency emission fields in Q modulated coupled ruby lasers

21 p3839 A70-42076

Relaxation behind shock waves in air, calculating radiation spectral distribution for comparison with shock tube experimental data

21 p3812 A70-42219

Radiation patterns and scattering cross sections of plane black disks excited by electromagnetic and acoustic waves

22 p3984 A70-42391

Fiber optic components quality control by image transmission intensity distribution measurement

22 p4045 A70-42513

Global solar radiation climatology of earth including direct and diffusive radiation

22 p4013 A70-42600

Ball lightning model assuming radiation field within plasma dielectric region resonant at higher than collision frequency

22 p4016 A70-42780

Approximate lasing condition from coupled rate and radiative transfer equations, determining population, energy density and power output

22 p4050 A70-43006

Two dimensional electromagnetic scattering body geometry reconstruction from given incident and scattered far field distributions

23 p4165 A70-44958

Electromagnetic scattering by two dimensional periodic arrays of conducting thin plates, calculating induced current and near field radiation distribution

23 p4165 A70-44961

Radiation and phase-scanning properties of planar array of parallel plate waveguides, using wedge diffraction theory

23 p4166 A70-44973

CW laser beam power density distribution monitoring by self calibrating photographic dosimetry technique

24 p4307 A70-45343

Ultrasonic angle probes with circular and rectangular transducers, discussing radiation field characteristics

24 p4336 A70-45686

Axial flow compressor fan discrete tone noise radiation directivity pattern measurement and theoretical explanation for cut-off effect, power and harmonics

24 p4380 A70-46069

Cerenkov light longitudinal distribution from extensive air showers, using near UV receivers

24 p4398 A70-46225

Confocal microwave Fabry-Perot interferometer resonator diffraction loss and field configuration measurements, noting agreement with theory

24 p4381 A70-46242

Mode locked laser pulses picosecond structure predicted from theoretical model of Gaussian random radiation field with temporal envelope modulation

24 p4355 A70-46263

RADIATION DOSAGE

Book on radiation protection, discussing atomic structure, nuclear transformations, effects on biological cells, total body exposures, somatic and genetic effects, etc

01 p0040 A70-11381

Radiation dosimetry and shielding onboard Cosmos 110 artificial satellite, noting earth belt proton radiation

01 p0198 A70-11518

Radiation damage recuperation process in living organisms and justified risk dose in prolonged space flights using Blair model

03 p0423 A70-13705

MOS devices radiation testing for estimating anticipated threshold voltage shift at various dose levels, including gate bias intermittent application during irradiation

04 p0658 A70-14745

Particle flux and dose rates in Jupiter Van Allen belts based on assumed synchrotron radiation from trapped electrons in dipole magnetic field

[ALAA PAPER 69-18] 04 p0742 A70-15543

Solar cosmic ray dose rate and total dose magnitude predictions based on Epeak and isotropic diffusion models

[ALAA PAPER 69-14] 04 p0742 A70-15584

Dose calculation by space radiation dose evaluation codes /SPARDEC/ for various space radiation environments

06 p0990 A70-17261

Space environment radiation dose monitoring systems requirements and implementation, discussing material distribution, dose equivalence, parameters accuracy, etc

06 p0990 A70-17262

Satellite radiation dose rate experiment with simultaneous trapped particle and absorbed dose rate measurements, discussing proton spectra, material distribution, shielding effects, etc

06 p1061 A70-17263

Satellite radiation dose rates in inner Van Allen belt, correlating calculated and measured rates with proton environment model

06 p1134 A70-17264

Solar proton flare dose rates, discussing tissue-equivalent-ionization-chamber /TEIC/ data usefulness in analyzing possible dose received by man behind shielding

06 p1134 A70-17265

Radiation dose measurements from satellite and space probe experiments, considering radiation and shielding characteristics, sensor orientation effects, etc

06 p0990 A70-17266

Accumulated dose and dose rate during Gemini 4 and 6 flights measured as function of elapsed time and position within spacecraft

06 p0990 A70-17270

Space radiation doses in inner Van Allen belt, comparing calculated and satellite measured rates

06 p0991 A70-17272

Spacecraft radiation environment, dosage and shielding problems, discussing high energy protons and electrons exposure hazards for astronauts and mission planning computer codes

06 p0991 A70-17273

Biological effects of laser radiation on human eye, discussing damage caused by long term exposure to visible, IR and UV wavelengths

08 p1451 A70-21043

USAF permissible human exposure levels for laser radiation established from monkey retina experiments

08 p1451 A70-21045

Premission planning and operational radiation dose limits for manned lunar and low earth orbit missions

08 p1454 A70-21940

Laser radiation cumulative effects compared to single dose in mice, using hair growth stoppage as test objective

09 p1624 A70-22817

Hormones excreted by adrenal cortex function in rhesus monkeys pathogenesis after irradiation by sublethal dose

09 p1620 A70-22822

Microwave radiation thermal and nonthermal biological effects, considering exposure limits

10 p1824 A70-24061

Radiation hazard to space vehicles by solar flare protons, calculating risk dose by computerized Monte Carlo simulation, applying importance sampling

10 p1934 A70-25190

Radiation damage recuperation process in living organisms and justified risk dose in prolonged space flights using Blair model

11 p1985 A70-25505

Permissible radiation exposure levels during prolonged space flights based on clinical data

13 p2351 A70-29336

Radiation measurements inside Apollo 4 and 6 command modules during passage through trapped radiation belts

17 p3040 A70-35645

Solar flare radiation protection requirements, considering bulk and plasma radiation shielding

17 p3040 A70-35647

Radiation dose estimates by biological and physical methods after radiation accident, discussing chromosome aberration counting

17 p3034 A70-35761

Crew radiation dosage from fission fragments in plume from gas core nuclear rocket

18 p3224 A70-36562

Satellite radiation dosage in space proton and electron environment

19 p3511 A70-38490

Soviet book on dynamics of postirradiation damage of biological objects covering dosage and protection effects on various animals

20 p3573 A70-39824

Supersonic transport radiation hazards to flight crew, passengers and population, discussing dosages, probabilities, solar cosmic ray encounters, warning systems, etc

20 p3700 A70-39923

Spurious photomultiplier response to short intense overexposure of atmospheric return using optical radar

21 p3828 A70-41474

Operational safety of nuclear rockets in orbit-to-orbit transportation in regard to radiation doses from plume and reactor, including malfunction condition

22 p4070 A70-43183

Lethal and sublethal radiation dosage effects on cellular Na and K distribution in rat brain, liver, kidneys and muscular tissues

23 p4145 A70-44314

RADIATION EFFECTS NT RADIATION INJURIES NT RADIOLYSIS

Book on radiation biochemistry covering effects on biological tissue, nucleic acids, proteins, carbohydrates, lipids, hormones, vitamins, living cells, metabolism and toxic substances formation

01 p0011 A70-10030

Radiation effect on enthalpy and velocity distributions of laminar compressible planar free jet

01 p0061 A70-10295

PbSe and GeTe cast and pressed samples thermoelectric properties before and after high energy gamma ray irradiation, using scintillation counter with photomultiplier

01 p0159 A70-10756

Tissue protein changes under visible and UV radiation noting denaturation, chemical bonds, protein configurations, clinical disease patterns, etc

01 p0022 A70-10856

Laser radiation effects on eye, quantifying light necessary for coagulation for retinal detachment surgery, discussing risks in laser surgery

01 p0037 A70-10859

UV radiation effects on mucopolysaccharide compounds in tears and on cornea epithelium of albino rabbits

01 p0037 A70-10860

High temperature ductility improvement in stainless steels containing He, analyzing lattice damage and interphase cavities after fast neutron irradiation

01 p0123 A70-11246

Probabilities for cell survival after exposure to ionizing radiation obtained by two compartment model

01 p0028 A70-11370

Book on radiation protection, discussing atomic structure, nuclear transformations, effects on biological cells, total body exposures, somatic and genetic effects, etc

01 p0040 A70-11381

Topically administered vitamin A radioprotective effect on postirradiation skin reactions

01 p0029 A70-11402

Keratinocyte development on epidermal surface of female patient exposed to cosmetic UV irradiation with quartz lamp

01 p0029 A70-11406

Numerical solutions for laser-beam intensity focused by simple lenses with varying primary spherical aberration, demonstrating isophote nonuniformity role in biomedicine

01 p0114 A70-11650

Book on photographic action of ionizing radiations in dosimetry and medical, industrial, neutron, auto- and microradiography, emphasizing photographic materials reaction to photons and particles

02 p0337 A70-11696

Radiation effects on postshock gas state, noting shock wave optical thinness dependence on radiative cooling and photon flight time

02 p0277 A70-11867

Space environment and radiation on Biosatellite 2 enhancing radiation effects in developing flour beetle Tribolium confusum

02 p0238 A70-12517

Interstellar space flight ramjet physical model, describing magnetic field funnel, radiation effects, relativistic effects, etc

02 p0379 A70-12822

Radiation hardened fiberglass reinforced plastics rupture, bending, compression and tensile strength and elastic modulus, considering gamma ray doses effect

02 p0323 A70-12811

Neutron bombardment effect on ordering and disordering state of alloys phase diagrams, noting temperature dependence

03 p0506 A70-13107

Superconducting properties of polycrystalline disordered cold worked Nb-Ti-V alloys showing unexpected sensitivity to fast neutron irradiation

03 p0508 A70-13144

Separate gamma irradiation effect of enzyme and hemoglobin-albumin-globulin substrates on proteolysis dynamics

03 p0419 A70-13308

Corpuscular sources geoeffectiveness related to position on solar disk at maximum flare activity

03 p0569 A70-13359

Nuclear environmental testing techniques, discussing radiation effects, measurements, instrumentation hardening, simulation source selection, dosimetry, noise sources and noise reduction, etc

03 p0523 A70-13540

Laser irradiation of RF plasmoid producing electron density increase, discussing resonance sustained RF discharges, mode locking, laser photodetachment, etc [ONERA-TP-751]

03 p0501 A70-13630

Peripheral blood, neutrophil myeloid hematopoiesis, phagocytic activity and serotonin level in gamma irradiated dogs

03 p0423 A70-13706

Myocardial changes in rabbits after general chronic ionizing irradiation attributed to lower cardiac activity, hypotrophy and dystrophy

03 p0425 A70-13888

Corneal epithelium chromosome rearrangements in gamma irradiated white adult mice, noting radiation dosage and duration

03 p0426 A70-13903

Numerical solution of physical equations describing temperature changes near ground fog-free air and in radiation fog

03 p0521 A70-13910

Biological experiment on Zond 5 automatic station in earth-moon-earth trajectory determining cosmic radiation absorption and effects on plant seeds, turtles, larvae, etc

03 p0428 A70-14066

Production rates determination for Na 24 and Mg 28 isotopes in Ar exposed to cosmic rays

03 p0561 A70-14092

Gamma radiation effects on membrane permeability of isolated nuclei from white rats thymus in sucrose-calcium buffer

04 p0629 A70-14460

Field effect transistors with controlled p-n junction and metal-dielectric-semiconductor transistors investigated for radiation effects on physical and electrical properties

04 p0730 A70-14500

Nuclear and space radiation effects - IEEE Conference, Pennsylvania State University, July 1969

04 p0656 A70-14726

Neutron irradiation effect on space charge limited current of electrons in high purity silicon, noting SCLC sensitivity in detecting traps and changes

04 p0731 A70-14730

Four layer semiconductor device triggering by X or gamma radiation calculated by transport equations for electron and hole distribution motion and electric field distribution

04 p0657 A70-14731

Complementary symmetry MOS/CMOS integrated circuit transient response to electron irradiation

04 p0657 A70-14733

Electron radiation-induced second breakdown in transistors indicated by time delay and failure by collector-to-emitter short

04 p0657 A70-14734

Radiation effects on swept-synthetic quartz resonators and materials, discussing frequency shift measurements and defect studies

04 p0731 A70-14735

Mathematical model based on equivalent electrical circuit for transient radiation analysis by computer /TRAC/ family of circuit analysis programs, simulating semiconductor devices

04 p0657 A70-14737

Computer modeling of operational amplifier integrated circuit in ionizing radiation environment, using RLC network and voltage transfer curve

04 p0658 A70-14740

Ionizing radiation response of integrated microcircuits with different circuit functions and manufactured by different methods

04 p0658 A70-14741

Integrated analog voltage regulator sensitivity to small signal transient radiation, discussing circuit hardening by diode compensation

04 p0658 A70-14742

Ion implantation for reducing space charge buildup in thermal oxides on silicon exposed to ionizing radiation

04 p0731 A70-14743

MOS devices radiation testing for estimating anticipated threshold voltage shift at various dose levels, including gate bias intermittent application during irradiation

04 p0658 A70-14745

Physical model to study coaxial or triaxial cable systems interaction with ionizing radiation fields, emphasizing effects governing induced signals
04 p0658 A70-14746

Ground-based biological experiments on insects and frog eggs to investigate effects of space flight weightlessness and radiation on mitosis and meiosis
04 p0631 A70-14942

Galactic mass loss by gravitational radiation, discussing galactic expansion and nucleus mass
04 p0752 A70-15068

Isomerization of isocyanide into azulene by irradiation and formation from biphenyl isothiocyanate, observing ring expansion and electrophilic carbenoid properties
05 p0811 A70-16055

Phase lock technique study of 10.6 micron radiation effect in carbon dioxide laser plasmas on 2.4 micron spontaneous emissions and plasma impedance
05 p0857 A70-16071

Specific heat and thermal EMF increase due to radiation damage in lattice of fast neutron bombarded Cu, Mo and W specimens
05 p0863 A70-16292

Pressure wave formation induced by absorption of radiation in oxygen, noting wave driving after radiation pulse decay by frozen dissociation energy
05 p0833 A70-16306

Transistor circuit design with junction compensation techniques to reduce transient gamma radiation effects
05 p0821 A70-16418

Flare radiation influence on high photospheric and low chromospheric lines in H alpha, H and K regions
05 p0902 A70-16439

Radiation environment in space and effect on man, discussing particulate and high energy electromagnetic radiation components
05 p0903 A70-16630

Thermal radiation effects on plane magnetoacoustic waves in semiinfinite expanse of radiating gas of perfect electrical conductivity
05 p0890 A70-16822

Q spoiled laser bombardment to obtain atomically clean surfaces in vacuum, noting damages
05 p0861 A70-16990

Whole body microwave irradiation effect on chromosomes and protein synthesis in Chinese hamsters
06 p0998 A70-17203

Solar proton flare dose rates, discussing tissue-equivalent-ionization-chamber (TEIC) data usefulness in analyzing possible dose received by man behind shielding
06 p1134 A70-17265

Soviet manned space flight radiation dosimetry evaluation, comparing U.S. and Soviet techniques for astronaut protection
06 p0990 A70-17271

Soviet monograph on radiobiological effects of ionizing radiation covering physicochemical and functional cellular changes, recovery mechanisms, etc
06 p0992 A70-17350

Nervous system influence on erythema radiation reactions from soft X ray irradiation, discussing blood supply effect
06 p0993 A70-17430

X rays from Sco XR-1 compared with galactic cosmic rays and solar Lyman alpha radiation to determine ionospheric ionization causing radio wave attenuation
06 p1134 A70-17443

X and UV radiation effects on *Escherichia coli* B/r in vacuum, noting irradiated cell inactivation and radiation sensitivity increases
06 p0995 A70-17750

Laser induced alloys erosion under various focusing conditions, determining optimal conditions for spectral studies
06 p1089 A70-17762

Heat radiation effect on set-up and scale of cellular convection in atmosphere
06 p1097 A70-17789

Acid soluble nucleotides content in normal and gamma irradiated rat spleens, presenting table
06 p0995 A70-17799

Previous radiation exposure effect on photographic film noting increased sensitivity at UV frequencies
06 p1065 A70-17890

Meyer-Neldel rule interpretation of distribution width parameter dependence on activation energy annealing of defects in irradiated Si
06 p1106 A70-17925

Space forecasting system to predict solar radiation bursts and effects on earth
06 p1136 A70-18023

Series emittance thermal control coatings of polymeric dielectric films overlaying reflectors vacuum exposed to UV, X ray and proton radiation [ALAA PAPER 70-64]
06 p1106 A70-18069

Sliding friction and wear of polytetrafluoroethylene ball bearing filled with graphite investigated for radiation effects
06 p1077 A70-18404

Electron irradiation for reducing thermal coefficient of resistance of Si strain gages, noting crystal orientation dependence of gage factor
06 p1070 A70-18442

Steels microstructural plastic deformation under pulsed laser irradiation
07 p1303 A70-18712

Canines conditioned reflex activity as function of cortex sections following head exposure to X ray irradiation
07 p1199 A70-18729

Peripheral blood and structural changes in hemopoietic organs of rabbits and mice exposed to microwave radiation
07 p1216 A70-18730

Radiobiological and radioecological aspects of radioactive pollution of earth atmosphere, considering international cooperation for preventive measures
07 p1199 A70-18781

Vacuum and radiation effects on *Escherichia coli*, noting role of cells water desorption in vacuum damage
07 p1203 A70-18962

Sialic acids metabolic behavior in cerebrum, liver, myocardium and blood plasma of rats after X ray irradiation
07 p1205 A70-19289

Numerical method of characteristics for unsteady radiation gas dynamics, discussing surface pressures and heat transfer rates
07 p1256 A70-19314

Geomagnetic field amplification near gamma radiation steady source, describing field displacement
07 p1367 A70-19446

Alpha irradiation effect on *Chlorella* survival, cell division and mutation
07 p1208 A70-19507

High energy protons irradiation biological effects, noting qualitative and quantitative variations in radiation disease symptoms
07 p1208 A70-19508

Radiation catastrophe in universe in terms of cosmological models
07 p1368 A70-19628

Spin decay from telemetered flight data of Explorer 20 compared with calculation based on solar influence theory
07 p1394 A70-19721

Radiation effect on heat transfer during film boiling in forced convection boundary layer of liquid flow past plate, noting vaporization temperature
07 p1423 A70-19812

Transparent semiconductor crystals breakdown under intense ruby laser radiation, noting threshold power correlation with forbidden region and pulse duration
07 p1357 A70-19856

Calf thymus DNA structural and functional changes following exposure to hydrogen atoms and gamma radiation
07 p1215 A70-20050

Radiation environments effect on logic circuitry constructed of MOS and bipolar transistors, discussing permanent and transient effects
07 p1242 A70-20149

Density gradient sedimentation of *Escherichia coli* populations irradiated with Co 60 gamma rays, showing correlation between DNA degradation and cell death
08 p1441 A70-20680

Escherichia coli cell division patterns, discussing generation times spread, gamma ray irradiation in nutrient broth, DNA damage and growing points, etc
08 p1441 A70-20681

Interkosmos-1 satellite for studying solar radiation and effects on ionization and molecular dissociation in atmosphere, weather and radio signals reception
08 p1582 A70-20714

Ionizing radiation effect on isolated frog retina using ERG recordings noting reduction of b wave
08 p1444 A70-20739

Free radical formation in irradiated pyrimidines from ESR spectrum analysis of gamma irradiated single crystals of alloxantin, confirming radical stability
08 p1455 A70-20774

DNA enzymatic breakdown in *Escherichia coli* as function of ionizing radiation and temperature
08 p1445 A70-20775

Transparent polymethylene methacrylate and polystyrene stressed state effect on failure characteristics under laser beam irradiation
08 p1526 A70-20936

Gamma radiation effects on emission time, excitation threshold and efficiency of four level Nd glass laser under multimode operation
08 p1512 A70-21209

UV radiation effects on pea plant chloroplasts photosynthesis at high altitudes, noting disruption of electron-transport chain reactions and cyclic phosphorylation
08 p1445 A70-21216

Cosmic rays induced Cerenkov light pulses effect on stellar intensity interferometer from measuring correlated pulses
08 p1497 A70-21492

IR absorption properties of CO, HCl and sulfur dioxide measured for role in Venus greenhouse effect
08 p1579 A70-21567

Solar radiation variations effect on earth climate, noting atmospheric transparency role in glaciation on thermal regime
08 p1539 A70-21919

Supernova fluorescent light excited by radiation impingement on material surrounding explosion site, assuming explosion time and UV energy
09 p1749 A70-21997

Chronic gamma irradiation effects on bone marrow mitotic activity and chromosome aberrations in dogs
09 p1614 A70-22083

Hydrodynamic processes during focusing of monopulse ruby laser emission into water, determining photohydrodynamic coefficient
09 p1694 A70-22111

Total body X irradiation effect on tyrosine hydroxylase and catecholamine levels in rats
09 p1616 A70-22318

Broad spectrum light sources effects on mammalian endocrine apparatus development and function determined in rats
09 p1617 A70-22335

Radiation effects on polytropic atmosphere convective instability using method of disturbances
09 p1753 A70-22456

Inert gas glow discharge current change under laser radiation, investigating dependence on discharge region, gas and electrode material and configuration
09 p1696 A70-22484

Gamma radiation effects on higher mammals nerve activity after chronic total body exposure
09 p1619 A70-22790

Hydrogen peroxide infusion effect on skin remission following exposure to ionizing radiation on rabbit legs
09 p1619 A70-22791

Ionizing radiation effects on tissues of developing cerebellar cortex of rats
09 p1619 A70-22815

Laser irradiation effects on mice skin and internal organs, observing inflammatory symptoms, hair follicles destruction and epithelial atrophy
09 p1624 A70-22816

Laser radiation cumulative effects compared to single dose in mice, using hair growth stoppage as test objective
09 p1624 A70-22817

X ray effects on central nervous system noting mutations in rats, guinea pigs, chickens, dogs and rabbits
09 p1620 A70-22821

Vitreous transparent solids emission after irradiation by Q switched laser, ascribing luminescence to multiphonon and excitonic phenomenon
09 p1710 A70-22836

Periodic solutions of restricted three body libration point perturbation due to fourth body gravitational and radiative influence using Huang model
09 p1761 A70-23053

Silicon monolithic integrated circuits technology for radiation environment near nuclear detonation
09 p1647 A70-23076

Atoms diffusion mobility enhancement in metal systems during irradiation suggested due to change in electrons energy states
09 p1707 A70-23192

D-pattern changes of helium ions irradiated polycrystalline Mo and Ni specimens, observing line splitting
09 p1707 A70-23197

Intense light effect on refractive index of potassium niobate crystals
09 p1698 A70-23317

Trapped Ag atoms production in silver nitrate ice by gamma irradiation, discussing reaction enhancement by fluoride ion
09 p1631 A70-23445

Gamma-neutron irradiation effect on miniature pig, observing incapacitation with severe convulsions and performance decrement
09 p1622 A70-23461

Fatigue effects of incident illumination on area sensitivity, dynode gain stability and anode output for end-on photomultipliers
09 p1683 A70-23511

Laser beam interaction with metals on basis of energy balance measurements, obtaining time dependent radiation reflectance
10 p1898 A70-23982

Microwave radiation thermal and nonthermal biological effects, considering exposure limits
10 p1824 A70-24061

Intense laser radiation effect on light absorption, gas breakdown and formation of spark at focus
10 p1899 A70-24154

Mercury arc injection lamp as radiation source for testing sunlight biological effects
10 p1888 A70-24388

Elastic stress-strain states in spherical reservoir and thick walled tube during nuclear radiation induced phase transformations
10 p1894 A70-24513

- Heat radiation effect on set-up and scale of cellular convection in atmosphere 10 p1882 A70-25021
- Adrenaline effects on rats peripheral blood leukocyte content used for X-irradiation sensitivity estimation 10 p1822 A70-25177
- Solar simulation laboratory test facility for extraterrestrial solar radiation effects on vehicles beyond earth atmosphere, emphasizing spectral filters 11 p2030 A70-25353
- Peripheral blood, neutrophil myeloid hematopoiesis, phagocytic activity and serotonin level in gamma irradiated dogs 11 p1985 A70-25506
- Thermal conductivity of neutron irradiated copper at low temperature noting lattice defects 11 p2148 A70-25757
- Alpha irradiation effect on *Chlorella* survival, cell division and mutation 11 p1987 A70-26106
- High energy protons irradiation biological effects, noting qualitative and quantitative variations in radiation disease symptoms 11 p1987 A70-26107
- Diffusion processes rate changes in metals and alloys resulting from radioactive emission, noting role in stress rupture strength mechanisms 11 p2068 A70-26595
- Energy deposition in cells by charged particles during ionizing radiation exposure, discussing RBE /relative biological effectiveness/ and dose-effect relation for neutrons 11 p1989 A70-26597
- Electron bombardment produced clustered displacements, paired vacancies and interstitial atoms in Si, discussing possible mechanism for developing defects 11 p2142 A70-26638
- Solar radiation effects on evaporation of dust with high latent heat of vaporization, considering particles in comets and zodiacal cloud 11 p2117 A70-26648
- Corpuscular sources geoeffectiveness related to position on solar disk at maximum flare activity 11 p2118 A70-26724
- Luminescence and destruction of gaseous boron trichloride by carbon dioxide laser radiation 11 p2064 A70-26818
- Light-induced electron paramagnetic resonance signal detected in *Anacystis Nidulans* 11 p1989 A70-26847
- Gamma irradiation effects on thermal stability and decomposition of ammonium perchlorate 12 p2289 A70-26870
- MOS structures and transistors emission-current degradation mechanism at heterojunction under ionizing radiation 12 p2194 A70-27165
- Resonant nonmonochromatic radiation effects on quantum system, deriving expressions for active medium nonlinear polarization, susceptibility and gain 12 p2245 A70-27304
- Intense laser radiation effect on electrons interactions with acoustic and optical phonons and ionized impurities in semiconductors 12 p2246 A70-27360
- Ruby laser illuminated Ge recombination radiation intensity measured at room temperature 12 p2286 A70-27369
- Cu doped GaAs n- to p-type transition after fast reactor neutron irradiation, measuring Hall effect and photoconductivity to determine Cu electrical activation 12 p2287 A70-27490
- Short wave radiation fluxes inclusion in hydrodynamic model of general atmospheric circulation based on aircraft sounding data and aerostatic observations 12 p2263 A70-27512
- Nonthermal radiation effects on emission line spectra of Seyfert galaxies and quasars determined from ionization equilibrium of gas envelope 12 p2293 A70-27585
- Radiation effects on viscous hypersonic low density stagnation flow using two layer model, calculating flow field and heat transfer coefficient 12 p2158 A70-28204
- Metals purity, gas content and porosity effects on nature and size of material zone affected by laser beam treatment 12 p2250 A70-28219
- Radiant shock layer in hypersonic air flow past blunt bodies, showing effects on temperature field and density 12 p2159 A70-28245
- Two-photon transitions effect on two-frequency generation threshold in media with line broadening, considering laser radiation effect on amplification in second channel 12 p2251 A70-28289
- Microwave radiation effects on radar operators myocardium functions 12 p2180 A70-28358
- Lunar rocks isotopic composition for Gd and variations due to low energy neutron capture produced by cosmic ray interactions 13 p2485 A70-28473
- Combined neutron and gamma ray irradiation effects on piezoresistive accelerometers 13 p2405 A70-28814
- X ray irradiation effects on phonocardiograms, EKGs, cardiac activity phases and Kunos-Garan mechanoelectrical coefficient in dogs 13 p2350 A70-28890
- Proton and electron irradiation producing oxygen vacancies in silicates, minerals and rocks, indicating similar processes in lunar surface materials erosion and transport 13 p2395 A70-28908
- Planar absorbing and emitting layer exposed to monochromatic collimated radiation, analyzing line or band shape effect on radiative transfer 13 p2451 A70-29135
- Transparent polymeric materials failure under neodymium-glass laser radiation in free generation mode 13 p2427 A70-29300
- Marrow granulocyte reserve restoration in dogs exposed to chronic gamma radiation, discussing leukocyte reaction to pyrogenic agent 13 p2351 A70-29326
- Hereditary UV luminescence of transplanted cancerous and lymphosarcomatous cells in mice and rats after ionizing radiation exposure 13 p2358 A70-29341
- Transport equations for interaction between radiation and matter under arbitrarily large nonequilibrium in comoving system 13 p2521 A70-29414
- Stimulated emission cut-off characteristics of laser based on crystals with Nd ions under UV irradiation 13 p2429 A70-29505
- Ag species paramagnetic relaxation in gamma-irradiated frozen aqueous solutions and in frozen methanol, relating spin-lattice relaxation to isotropic coupling 14 p2544 A70-30117
- Ionizing X radiation influence in lethal and sublethal doses on cerebral hyaluronic acid in mice and guinea pigs 14 p2536 A70-30186
- Radiation effects on heat transfer in turbulent channel flow for small optical depths and optically thin limit 14 p2665 A70-30548
- High temperature inviscid flow of ideal radiating gas, analyzing effects of radiation pressure and energy on flow field 14 p2666 A70-30999
- Gamma radiation effects on GaAs Gunn diodes, measuring Hall effect, low field resistance, output power and FM noise in X band cavity 14 p2558 A70-31322
- Gas ionization with hydrogen atoms in gravitational equilibrium at constant temperature in upper half space by instantaneous radiation burst in lower space 15 p2775 A70-31477
- Radiation planning nomogram to display radiobiological effects of dose, onset time and shielding factors for manned space vehicles 15 p2690 A70-31894
- Semiconducting gallium arsenide LF oscillations, considering domain behavior and illumination effects 15 p2783 A70-31972
- Radiation effects on large scale atmospheric air flows, accounting for role in global circulation by parameterization techniques 15 p2771 A70-32109
- Chronic gamma irradiation effects on bone marrow mitotic activity and chromosome aberrations in dogs 15 p2685 A70-32679
- Monograph on ionizing radiation effects on molecular biology of *Escherichia coli*, discussing cellular damage, DNA degradation and synthesis, incorporating radioactivity, mutations, etc 16 p2848 A70-33098
- Space radiation effects on secondary electron conduction /SEC/ image tube performance, observing temporary degradation and permanent damage 16 p2878 A70-33433
- Meteoroids origin and distribution, examining collisional and radiative processes effects 16 p2974 A70-33650
- Gas breakdown produced by long wave IR pulsed radiation of carbon dioxide laser 16 p2928 A70-33655
- Cryogenic multilayer insulation /MLI/, comparing radiation magnitudes, gas conduction and contact solid conduction to calorimeter and tank data [AIAA PAPER 70-850] 16 p2939 A70-33917
- Bidirectional reflectance and transmittance calculation for irradiated layer of monodisperse matrix suspended pigment particles [AIAA PAPER 70-839] 16 p2940 A70-33923
- UV irradiation effects on ZnO used as pigment for spacecraft thermal control coatings [AIAA PAPER 70-829] 16 p2940 A70-33937
- Calcium tungstate crystals, investigating electron paramagnetic resonance centers produced by neutrons and gamma rays to obtain information on lattice vacancies, defects, etc 16 p2961 A70-33963
- Void formation and creep during fast neutron irradiation of austenitic stainless steel based on thermodynamic approach, calculating nucleation and growth rates 17 p3123 A70-34626
- Low cycle fatigue and short term tensile behavior correlation for irradiated and unirradiated stainless steels 17 p3123 A70-34627
- Al single crystals hardening under low temperature reactor irradiation, emphasizing yield phenomenon associated with Luders bands 17 p3123 A70-34647
- Photolysis of 3-phenyl-oxadiazol-5-one by UV irradiation, eliminating carbon dioxide 17 p3041 A70-34772
- Neutron irradiation effects on stress corrosion susceptibility of Al alloy 17 p3124 A70-34822
- Post-Newtonian equations of hydrodynamics and radiation reaction in general relativity 17 p3156 A70-34828
- Radiation gas dynamics, investigating thermal radiation effects on flow field of high temperature gas 17 p3195 A70-35038
- Phenolic nylon thermal decomposition, considering surface reradiation and physical parameters effects 17 p3196 A70-35242
- Automated orbiting biosatellite program with reentry system, studying long term weightlessness and radiation effects 17 p3178 A70-35258
- Microelectronics in space environment, discussing circuit reliability, radiation effects, etc 17 p3053 A70-35269
- Radionuclides production rates in stratosphere from spallation reactions of cosmic rays with Ar 17 p3152 A70-35759
- Combined ultrasonic and ionizing radiation effects on electrophoretic mobility of tumor cells from albino mice 17 p3034 A70-35762
- MOS structure, measuring ionizing radiation effects on interface barrier energies by internal photoemission techniques 17 p3144 A70-35901
- Bird dispersal measure at airports, using behavioral and electrophysiological effects of high power microwave radiation 18 p3222 A70-35993
- Ultrasonic irradiation effects on steel hardenability and carbon diffusion rate during annealing, noting microstructure 18 p3273 A70-36049
- MOS devices, investigating laser radiation effects on electrical behavior 18 p3266 A70-36237
- Background thermal radiation veiling effect on IR photography extension into long wave spectrum 18 p2527 A70-36282
- Nuclear irradiation effect on embrittlement of Ti and Ti alloys at cryogenic temperature, determining radiation damage threshold as function of tensile properties changes 18 p3278 A70-36567
- Plane wall surface sublimation under radiation from shock wave heated gas 18 p3348 A70-36721
- Geomagnetic field amplification near gamma radiation steady source, describing field displacement 18 p3309 A70-36920
- Gliders made of glass fiber reinforced plastics, investigating thermostatic properties under solar irradiation and surrounding warm air 19 p3454 A70-37370
- Thermal radiation effect on plane shock wave propagation, using perturbation technique and method of characteristics 19 p3551 A70-37532
- ESR spectrum of gamma irradiated cyclohexatriene silver perchlorate, indicating free radicals and trapped electrons 19 p3374 A70-38272
- Ionizing radiation effects on endocrine system, studying ACTH metabolism in rats under X ray irradiation 19 p3372 A70-38723
- Materials jet-like ejection from metal surfaces under high density laser radiation action, investigating erosion and plasma spectrum 19 p3448 A70-38734
- Correction procedures for measurement errors in actinometers and pyrohelimeters caused by circum-solar radiation 20 p3625 A70-39029
- Temperature effect on radiation characteristics and cryogenic tensile properties of irradiated Be, Ti and Al alloys 20 p3647 A70-39111

RADIATION EMISSION

Radiation effect on heat transfer during film boiling in forced convection boundary layer of liquid food past plate, noting vaporization temperature
20 p3736 A70-39259

Protein solutions and cell cultures changes by ruby and Nd lasers radiation, noting threshold energy
20 p3579 A70-39419

Metals purity, gas content and porosity effects on nature and size of material zone affected by laser beam treatment
20 p3643 A70-40094

Heat conduction problems solved allowing for radiation on electrical models, using nonlinear resistance and composite circuit methods
20 p3738 A70-40178

Simulated space flight radiation effects on dogs DNA synthesis and bone marrow cell differentiation
20 p3575 A70-40191

Proton irradiation effects on dogs with partial body protection
20 p3575 A70-40192

Microwave radiation effects on maintenance personnel, investigating respiratory reaction, attention concentration, blood content of K, Ca, Na and proteins, etc
20 p3581 A70-40289

Plasma nonequilibrium state formation and light absorptivity variation under high power laser pulsed radiation
20 p3684 A70-40387

Flexible shallow shell with plastic inhomogeneity due to yield point-fast neutron flux relation, examining stability under uniform load
20 p3734 A70-40437

Radiation effects on dihydrothymine in frozen sulfuric acid solutions, detecting thymine after melting via low temperature UV absorption measurements
20 p3583 A70-40454

Radicals induced in thymine monohydrate single crystals by ionizing radiation
20 p3583 A70-40455

Polymethyl methacrylate rupture during omnidirectional compression under laser radiation, showing pressure effect on microdefects and cracks
21 p3841 A70-40644

Space travel genetic effects, discussing radiation, weightlessness, vibration and acceleration
21 p3761 A70-40842

Ionospheric D region electron production by cosmic X rays, noting Lyman radiation effects
21 p3882 A70-41099

Spherical radiation drive shock wave similarity solution, discussing time function, velocity, radial dependence and density
21 p3948 A70-41245

Tritium and Ar radioactivities attributable to galactic and solar cosmic ray interactions in Apollo 11 lunar rocks and soil
21 p3906 A70-41564

Apollo 11 lunar fines, investigating solar radiation effects on optical properties by standing and heating
21 p3915 A70-41660

Mammalian cells after X ray irradiation, showing two forms of DNA repair process
21 p3765 A70-42024

Self similar formulations for motion of radiating-absorbing perfect gas symmetric flow
21 p3954 A70-42202

Radiation induced free radicals in thymidine single crystals, attributing electron spin resonance spectral observations to nature of various radicals
22 p3981 A70-42348

Upper atmosphere electric field nature, considering solar radiation as major source of ionization
22 p4017 A70-42788

Peroxyacetyl nitrate decomposition products under continued and discontinued irradiations determined by IR spectral analysis
22 p3983 A70-42944

Neutron irradiation effect on elevated temperature fracture of various fcc alloys
22 p4054 A70-42957

Combined space and nuclear radiation effects in manned space flight
22 p3978 A70-43184

Electric strengths of liquid dielectrics during subjection to Q switched laser pulses, determining threshold currents for breakdown
22 p4051 A70-43338

Threshold parameters of liquid and gaseous helium breakdown caused by ruby laser beam, noting Mandelstam-Brillouin scattering in liquid phase
22 p4051 A70-43465

Lunar based vs orbiting astronomical observatories, discussing limitations imposed by geocorona
22 p4108 A70-43630

Mossbauer spectrum of submolecular changes of oxyhemoglobin in animal blood exposed to microwave irradiation
23 p4144 A70-43788

Multiphoton gas ionization by coherent radiation, showing electron transitions role with gas ionization model
23 p4201 A70-44205

Live skin tissue electrical parameters changes due to laser radiation, showing coagulative necrosis by histomorphological studies
23 p4150 A70-44313

High power pulsed laser fog dispersal, calculating vaporization regimes of droplet interaction with laser radiation
23 p4201 A70-44592

EM wave effects on radio receiver, using Maxwell equations without taking photons into account
23 p4221 A70-44798

Cosmos 110 satellite experiments concerning radiation effects on lysogenic bacteria and plants
23 p4149 A70-45030

Irradiation influence on emission power of GaAs laser excited by high energy electron beam
23 p4203 A70-45060

Spacecraft radioisotope thermoelectric generator interference in onboard instrument operation, using analytical models to determine necessary shielding
24 p4375 A70-45175

Luminescence and destruction of gaseous boron trichloride by carbon dioxide laser radiation
24 p4351 A70-45190

Light effect on cis-trans-isomerization of cinnamoyl-alpha-chymotrypsin, considering molecular modeling of visual reception
24 p4298 A70-45496

Satellite orbit perturbation due to earth reflected or reradiated solar radiation pressure
24 p4409 A70-45556

Lasers biomedical applications based on thermal and ionization effects on biological targets, considering eye surgery, tumor treatment, etc
24 p4308 A70-45568

Industrial radiography, discussing photographic emulsion layers granular structure formation due to ionizing radiation
24 p4337 A70-45714

Temperature induced humidity errors in military and Weather Bureau radiosondes carbon humidity element caused by solar irradiation
24 p4372 A70-46073

Ionized matter stability in intense radiation field opposed to gravitation, explaining quasar properties
24 p4398 A70-46162

Chromium ions isothermal annealing kinetics in X ray irradiated ruby crystals, using EPR method
24 p4382 A70-46253

RADIATION EMISSION

U RADIATION

RADIATION EXPOSURE

U RADIATION DOSAGE

RADIATION FIELDS

U RADIATION DISTRIBUTION

RADIATION HAZARDS

Precision machining and repair of radioactive Plum Brook Reactor core fuel grid
01 p0140 A70-10322

Biological hazards of laser radiation, noting eye injuries and cataract from transscleral exposure on rabbits
03 p0434 A70-13679

Annotated bibliography of laser eye hazards
03 p0434 A70-13680

Laboratory and field laser hazards control, noting beam termination in outdoor environment and optical density marking on protective eyewear
03 p0434 A70-13681

Collection of papers on spaceflight radiological problems experimentation covering satellite data, dosimetry, solar flares, etc
06 p0989 A70-17259

Spacecraft radiation environment, dosage and shielding problems, discussing high energy protons and electrons exposure hazards for astronauts and mission planning computer codes
06 p0991 A70-17273

Laser eye and skin hazard evaluation from viewpoints of threshold effect levels and worst case assumptions
07 p1219 A70-19224

Fission gases trapped in fuel particles, cladding and matrix of irradiated refractory metal-uranium oxide cermets determined by gamma counting
07 p1332 A70-19851

Particle properties and solar flare radiation hazards for passengers in supersonic flight
08 p1435 A70-20632

Laser safety programs in biomedical applications, discussing installations, techniques, hazards and protection
08 p1451 A70-21048

Microwave radiation exposure control program for biological hazards, particularly to eye lens
09 p1623 A70-22221

Health hazards of laser operations, considering laser and laser area physical characteristics, operating procedures and controls
10 p1824 A70-24062

Book on radiation protection covering hazards, detection and measurement, monitoring instruments, biological effects, permissible dosage, contamination control, etc
10 p1827 A70-24725

Radiation hazard to space vehicles by solar flare protons, calculating risk dose by computerized Monte Carlo simulation, applying importance sampling
10 p1934 A70-25190

Hazardous X ray bremsstrahlung from military radio electronic equipment, discussing radiation protection and operating safety standards
12 p2180 A70-28360

Personnel danger zones demarcation around radar antennas, using beacons
17 p3040 A70-35913

Commercial and industrial microwave hazards exposure criteria and survey techniques used in state and local governments
18 p3224 A70-36228

Crew radiation dosage from fission fragments in plume from gas core nuclear rocket
18 p3224 A70-36562

Supersonic transport radiation hazards to flight crew, passengers and population, discussing dosages, probabilities, solar cosmic ray encounters, warning systems, etc
20 p3700 A70-39923

RADIATION HEATING

U RADIANT HEATING

RADIATION INDICATORS

U DOSIMETERS

U INDICATING INSTRUMENTS

RADIATION INJURIES

Microwave irradiation effects on rabbit eye lenses, noting injury dependence on frequency [IMPI PAPER DA-4]
08 p1452 A70-21273

Microwave radiation exposure control program for biological hazards, particularly to eye lens
09 p1623 A70-22221

Ophthalmological treatment of severe thermomechanical eye injuries investigated on radiant-energy burned rabbit eyelids
09 p1617 A70-22473

Accident prevention in laser operation emphasizing eye protection
13 p2361 A70-30018

Adenosine triphosphate and vitamins /amitetravil/ as prophylactics against radiation injuries in dogs during simulated space flight
17 p3038 A70-35351

He-Ne laser beam hazard to human retina
19 p3371 A70-38309

Ruby laser radiation injury relationship to position and number of energy absorbing pigment particles in iris
20 p3579 A70-39425

Balloon-borne monkeys possible brain damage due to cosmic rays, discussing thindown tracks and acute vasculitis
21 p3764 A70-41476

RADIATION INTENSITY

U RADIANT FLUX DENSITY

RADIATION LAWS

NT KIRCHHOFF LAW OF RADIATION

NT STEFAN-BOLTZMANN LAW

RADIATION MEASUREMENT

Internal powers and effective temperatures of Jupiter and Saturn measured by aircraft mounted telescope, noting restraints on planetary structure and atmosphere models
01 p0173 A70-10045

Cosmic ray latitude survey in North America in summer using neutron and muon monitors operating near sea level and on mountains
01 p0167 A70-10226

Cosmic rays nucleon component measurements interpretation in terms of geomagnetic field model
01 p0169 A70-10354

Seasonal, solar diurnal and semidiurnal variations of cosmic ray soft component observed at sea over seven year period
01 p0170 A70-10467

Twilight and nightglow measurements with stratospheric balloons, discussing use for upper atmosphere exploration, meteoric influence and French network
01 p0079 A70-11217

Twilight brightness measurements with balloons, scattering coefficient and indicatrix for high altitudes and comparison with Rayleigh-Cabann theory
01 p0079 A70-11218

Elektron 4 satellite radio emission data transmitted from July to December 1964, noting month-to-month variations in mean radiation level
01 p0172 A70-11496

Excess radiation in equatorial regions studied on-board Cosmos 137, noting contribution of primary particle multiplication to secondary radiation
01 p0192 A70-11542

Constricted DC Arc arc with N or O additions calibrated as vacuum UV radiation standard for photon flux measurements
02 p0343 A70-11905

Grille spectrometer design for thermal IR measurements, discussing requirements to achieve optimum performance
02 p0296 A70-11917

Balloon measurements of cosmic ray alpha particle flux in upper atmosphere over Japan to obtain solar modulation effects data
02 p0357 A70-12122

- Stratospheric circulation model developed from radioactive element measurements, discussing large scale processes, seasonal variations, etc
02 p0291 A70-12291
- Cosmic ray neutrons energy spectrum and angular distribution at sea level based on measurement results
03 p0556 A70-13046
- Measured heat flux conversion into average radiation incident on convex satellite surfaces in test chambers
03 p0606 A70-13536
- Nuclear environmental testing techniques, discussing radiation effects, measurements, instrumentation hardening, simulation source selection, dosimetry, noise sources and noise reduction, etc
03 p0523 A70-13540
- Airborne optics control subsystem /AOCs/ in optical measurement program for radiation originating in reentry events in project PRESS /Pacific range electromagnetic signature study/
03 p0489 A70-13652
- Radiation level recordings during Soyuz manned orbital flights indicating safety standards maintenance
03 p0580 A70-13704
- D-2 experiments measuring atomic oxygen emission from terrestrial atmosphere and polarization rate and emission intensity from geocoronal hydrogen
03 p0559 A70-13828
- Equatorial ionosphere ionization and electron density measurements by San Marco 2 satellite
03 p0475 A70-13830
- Measurement method for second and third order photon intensity correlation functions, using optical field produced by gas laser operating near oscillation threshold
04 p0700 A70-14686
- Solar proton latitude profiles relation to outer radiation zone electron measurements by Alouette 2 satellite charged particle detectors during quiet magnetic conditions
04 p0740 A70-15105
- Hysteresis effect on cosmic ray modulation and gradient ionization near solar minimum from measurements made near earth with OGO 1 and 3 ion chambers
04 p0740 A70-15106
- Fast neutron spectrum produced by galactic cosmic ray protons in atmosphere, presenting Monte Carlo transport calculation results
04 p0742 A70-15130
- Gas flow proportional counter for measuring high emission rates of alpha particles, discussing design and operation
04 p0695 A70-15570
- Muon-electron ratio measurements in extensive air showers, showing anomaly due to chemical composition change of primary cosmic radiation
05 p0901 A70-16274
- Radiation fluxmeters involving black plates and sensor disk respectively for use in space simulation chambers
05 p0849 A70-16636
- Bolometric albedo of main sequence stars with deep convective envelopes in close binary systems derived as function of photometric proximity using entropy invariance
05 p0914 A70-16694
- Neutron flux measurements on Cosmos 53, equipment and calculation of secondary neutrons due to bombardment of satellite components
05 p0905 A70-17112
- Space radiation environment, discussing characteristics and measurement techniques of various radiation types and sources
06 p1134 A70-17260
- Radiation data from manned orbital Mercury missions, correlating measurements from various additional sensors with main nuclear emulsion sensors
06 p1134 A70-17267
- Accumulated dose and dose rate during Gemini 4 and 6 flights measured as function of elapsed time and position within spacecraft
06 p0990 A70-17270
- Scattered Lyman alpha radiation intensities measured for mixtures of partially dissociated hydrogen in Ar, measuring quenching cross sections
06 p1053 A70-17327
- Atmospheric temperature vertical profile reconstruction from ascending radiation observations using data regularization
06 p1097 A70-17793
- Anomalous dispersion measurements in IR range with multibeam sequential Fabry-Perot interferometers using photoelectric method
06 p1064 A70-17811
- Spherical cylindrical and toroidal electrostatic analyzers with symmetrical angular characteristics for solar wind investigations
06 p1135 A70-17896
- Rocket-borne spectrometer intensity measurements UV region of solar spectrum, noting agreement with IR observations of solar temperature minimum
06 p1143 A70-17998
- Emittance measurement by thermal decay integration method
06 p1184 A70-18597
- Antenna calibration by measuring emission of absorbing black disk positioned in Fresnel region
07 p1239 A70-18759
- Atmospheric X ray photons measured regularly by sounding balloons in U.S.S.R., discussing X ray photon flux relation to charged particle fluxes
07 p1367 A70-19445
- Volt-watt sensitivity of dilatocapacitor types of thermal radiation receivers, noting low natural noise levels
07 p1284 A70-19815
- Solar protons in subpolar stratosphere during solar activity minimum indicated from proton measurements at Tiksi Bay
07 p1374 A70-20444
- Electron and gamma quanta concentrations measurements by high altitude balloon, noting fluctuations at various altitudes
07 p1374 A70-20446
- Center to limb variation of solar brightness measured at 5, 10 and 20 microns, discussing data collection and reduction and previous IR and UV measurements
08 p1562 A70-21396
- Cosmos-261 satellite-borne scintillation electron proton spectrometers and lead shielded Geiger counter, measuring electron and proton energy spectra, pitch distributions, etc
08 p1501 A70-21799
- Solar constant measurement by Eppley normal incidence pyrheliometers on high altitude balloons
08 p1501 A70-21920
- Seasonal measurements of atmospheric transmittance spectra for horizontal near-earth paths in IR region under haze and clear weather
09 p1666 A70-22179
- Baseline measurements of Jupiter decametric radiation providing upper size limit to coherent and incoherent sources
09 p1755 A70-22512
- Photoemission energy distribution curves measuring circuit using AC retarding potential method, offering improved noise performance
09 p1679 A70-22996
- Amplitude measurement of plane light wave propagating in turbulent atmosphere, giving log amplitude dependence on dispersion of logarithm fluctuations
09 p1636 A70-23136
- He-Ne CW and pulsed lasers operation, design and technology, describing measurement methods for output, beam divergence and radiation spectrum distribution
09 p1698 A70-23303
- Fluorescent integrating sphere for absolute hemispherical reflectance measurements on imperfectly diffuse surfaces in vacuum UV, eliminating erroneous signals by filtering
09 p1729 A70-23527
- Reflected solar radiation polarization over land, sea and cloud surfaces to determine atmospheric pollution
09 p1747 A70-23603
- Stripline elements centimeter wavelength emission level determination by comparison with reference antenna radiation patterns
09 p1652 A70-23650
- Laser pulse energy ponderomotive meter using mechanical action exerted by light on movable sapphire plate in air at atmospheric pressure
09 p1700 A70-23657
- Radiative capacity measurement for plasmas produced from nonconducting materials by pulsed discharges in magnetic field
10 p1923 A70-24252
- Atmospheric temperature vertical profile reconstruction from ascending radiation observations using data regularization
10 p1913 A70-25024
- Radiation level recordings during Soyuz manned orbital flights indicating safety standards maintenance
11 p2121 A70-25504
- Solar neutrino flux measurement based on neutrino capture by large chlorine mass and subsequent Ar 37 decay in low noise environment
12 p2293 A70-27389
- Grating spectrometer performance in measuring earth IR radiance determined from balloon flights
12 p2235 A70-27752
- Hemispherical emissivity measurement in vacuum chamber for thermal testing of space satellite structural materials
12 p2332 A70-27984
- Earth radiation balance /net flux/ determination from satellite measurements of long wave radiance and reflected solar radiation in upper atmosphere
12 p2264 A70-28090
- Satellite measurement of water vapor height profiles using outgoing thermal radiation and solar radiation atmospheric absorption techniques
13 p2392 A70-28571
- Cosmic radiation yearly semidiurnal anisotropy characteristics based on worldwide neutron monitor stations data analysis
13 p2477 A70-29177
- Collection of papers on precision radiometry in geophysics covering radiation detectors and electromagnetic radiation measurements in atmosphere
13 p2409 A70-29651
- UV, visible and IR radiation measurement, discussing spectral distribution, thermopiles, monochromatic radiation and power measurements
13 p2410 A70-29653
- Standard sources and detectors for thermal radiation measurement
13 p2410 A70-29654
- Black bodies radiation properties and design for applications as absolute radiation standards
13 p2410 A70-29657
- Radiometric measuring techniques emphasizing transfer methods and data analysis
13 p2410 A70-29659
- Solar and terrestrial radiation measurements and computations in meteorology, considering diffuse radiation and radiative transfer in atmosphere
13 p2410 A70-29661
- Lower and upper atmospheric IR fluxes and equivalent radiation temperatures measurements, describing two- and four-sphere mean radiation temperature /MRT/ meter
13 p2410 A70-29662
- Thermal longwave radiation measurement applications to atmospheric radiation transfer and weather processes
13 p2411 A70-29663
- Spectrometer model for short wave radiation in atmosphere, measuring sky brightness, polarization and total solar flux
14 p2583 A70-30413
- Galactic cosmic rays high altitude measurements by balloon-borne Sparmo type multidirectional detectors, revealing azimuthal anisotropy
14 p2632 A70-31309
- Cosmic ray shortest term regular intensity variations, measuring particle dispersion as time function
14 p2633 A70-31314
- Solar X-rays measurements with spectroheliograph conducted on rocket flights
14 p2589 A70-31339
- Solar extreme UV radiation measurements over rotation period onboard satellite OSO-3, using atmospheric absorption correction
15 p2792 A70-31666
- Solar proton structure across polar cap and anomalous latitude cut-off explained by local pitch angle variations
15 p2792 A70-31672
- Report to COSPAR on Netherlands space research /1969/ including solar and stellar X radiation and UV spectrophotometry, cosmic ray measurements, satellite geodesy, etc
15 p2830 A70-31719
- Primary cosmic ray flux and p-carbon cross sections measurements by satellites showing heavy particle production at high energies
15 p2792 A70-31733
- Quark search in cosmic radiation near sea level, using scintillation counter telescope
15 p2793 A70-31737
- Quiet time proton and alpha particle flux and differential energy spectra measured by cosmic ray detectors on OGO 3 satellite
15 p2793 A70-31795
- Absolute radiometric reference scale, noting International Pyrheliometric Scale 1956 materialization by standard instruments
15 p2735 A70-31805
- Pyrometer for measuring temperature by ratio of radiation at two different wavelengths, eliminating spectral emissivity effect
15 p2736 A70-31824
- Cosmic ray knee interpretation using polar orbiting ionization chambers data from OGO-2/4
15 p2793 A70-31903
- Black body cavity type radiometers for high accuracy measurement of irradiance
15 p2737 A70-32036
- Ionospheric structure characteristics in D₁, intermediate D-E and E-F 2 regions using deflecting and nondeflecting radiation absorption measurements
15 p2730 A70-32085
- Electrostatic analyzer without fringe field effects for measuring low energy particles on spacecraft
15 p2740 A70-32432
- Polypropylene window proportional counter on board sounding rocket for cosmic soft X ray measurement
15 p2741 A70-32530
- Glass disk calorimeter for measuring free running and Q switched laser pulses
15 p2742 A70-32545
- Feed and terminal radiation patterns of surface wave antennas measured separately
16 p2861 A70-32973
- Electromagnetic field determination from oscillating vertical and horizontal electric dipoles above flat earth, demonstrating Sommerfeld formulation and dyadic Green function technique equivalence
16 p2861 A70-32974

Electron recording by shower counters, noting radiation length importance 16 p2908 A70-33211

Simultaneous measurement of optical and X ray emission from Scorpius X-1 and X ray diffuse background, using rocket-borne scintillation counter 17 p3157 A70-34831

Solar X-ray flux measurements in selected emission lines, using curved crystal Bragg spectrometers in low altitude sounding rockets 17 p3150 A70-34834

Lyman alpha emission from Comet Bennett observed with photometer on board OGO-5 satellite 17 p3163 A70-35049

Laser energy and power measurement with thermal gradient radiometer 17 p3104 A70-35082

High power Nd-glass solid state laser characteristics measured to improve beam properties 17 p3105 A70-35090

High-power Q switched solid state laser radiation intensity measurement methods for multi and single modes 17 p3105 A70-35094

Laser energy parameters measurement by calorimetric methods based on radiant heating effect 17 p3106 A70-35099

Submillimeter lasers radiation measurement with n-InSb detectors at liquid He temperature 17 p3107 A70-35109

Spectral radiation and polar distribution from high power Ar, Kr and Xe arcs 17 p3023 A70-35156

Lunar millimeter wavelength thermal radiation measurement noting surface roughness effect on polarization 17 p3171 A70-35559

Atmospheric X ray photons measured regularly by sounding balloons in U.S.S.R., discussing X ray photon flux relation to charged particle fluxes 18 p3309 A70-36919

Simultaneous measurements of earth atmosphere radiation, comparing short and long wave data consistencies at various altitudes 18 p3286 A70-36963

Angular structure of outgoing short wave radiation field measured from Cosmos satellite for clear and cloudy skies and various sun heights 18 p3286 A70-36965

Antenna calibration by measuring emission of absorbing black disk positioned in Fresnel region 18 p3233 A70-37103

Atmospheric moisture content vertical profile from terrestrial radiation measurements, using statistical regularization procedure 19 p3460 A70-37418

Spectral radiative capacity of lower level clouds in specific transmittance window, using airborne diffraction spectrometer measurements 19 p3461 A70-37424

Neutron flux measurement in nuclear reactors based on logarithmic techniques and digital approach, discussing temperature effects compensation 19 p3427 A70-37939

Primary cosmic ray proton and alpha particle spectra measurements by balloon-borne equipment 19 p3505 A70-38118

X rays measurement by spectrometer on satellite Cosmos 207 19 p3506 A70-38122

Cosmic ray nuclei charge composition of elements Ne to Ni, using emulsion stacks exposure in balloon flights 19 p3506 A70-38126

Cosmic X ray background measurements, describing ESRO R/73 experiment 19 p3512 A70-38491

Moon as standard radio source for eliminating earth atmosphere influence during solar radio radiation measurements 19 p3522 A70-38564

Angular and geometric properties of actinometers, pyroheliosimeters and photometers, measuring direct and scattered circumsolar radiation 20 p3625 A70-39028

Phytoactinometers and phytopyranometer graduating methods, discussing measurement of photosynthetically active radiation 20 p3626 A70-39035

Formaldehyde absorption coefficients measured photoelectrically in vacuum UV range 20 p3703 A70-39165

Cosmic ray intensity variation during maximum meteor showers periods detected on earth, noting relationship to solar activity 20 p3697 A70-39294

Recording device for gamma quanta in primary cosmic radiation 20 p3629 A70-39316

Light gathering nonuniformity in cylindrical plastic scintillator, analyzing detector signal amplitudes for various pulsed light source positions 20 p3629 A70-39318

Primary cosmic rays spectrographic measurement, using hard muon component intensity variations data 20 p3629 A70-39320

Low altitude cosmic rays dosimetric measurement by Cosmos 228 apparatus 20 p3700 A70-39728

Solar proton intensity measurement during flare by satellite Proton 3 apparatus 20 p3700 A70-39729

Balloon-borne measurements of hard X radiation from direction of Virgo 21 p3872 A70-40663

High energy galactic gamma rays search onboard OGO-5, tabulating results 21 p3876 A70-40690

Omnidirectional cosmic gamma ray flux near one MeV observed by ERS-18 satellite, plotting spectral energy distribution 21 p3876 A70-40697

Auroral X-ray radiation at magnetoconjugate points Kerguelen/archangel region, using balloon-borne spectrometers 21 p3813 A70-40839

Microsecond response bolometer for measuring thermal radiation fluxes in shock tube, discussing design, calibration and performance 21 p3824 A70-40859

Low energy cosmic ray heavy primary particles composition from nuclear emulsion stack observation 21 p3879 A70-40930

Galactic center region gamma radiation observations, discussing intensities, energy spectrum and decay 22 p4093 A70-42927

Exploding wire light source modification by immersing in transparent fluid to increase intensity, measuring spectral characteristics [SMPT PREPRINT 64] 22 p4032 A70-43037

Solar optical and radio activity observation in 1968, noting optical-radio data correlation 22 p4095 A70-43259

Solar type 4 event flux density and circular polarization radiopolarimetric recording, showing peculiar phases of short duration 22 p4095 A70-43263

Proton energy angular distribution measurement by OV2-5 research satellite confirming model of shell splitting in geomagnetic field 23 p4236 A70-43832

Contrail effects on atmospheric thermal radiation budget in heavy jet traffic regions from airborne IR and solar radiometric observations 23 p4214 A70-44033

Stratosphere radiation measurements by Nimbus 3 infrared spectrometer for 15 micron frequency, considering temperature variations 24 p4330 A70-46074

Esro 2 satellite instrument measuring soft solar X-rays 24 p4340 A70-46358

RADIATION MEASURING INSTRUMENTS

NT ACTINOMETERS

NT BOLOMETERS

NT DICKE RADIOMETERS

NT DOSIMETERS

NT FABRY-PEROT SPECTROMETERS

NT HODOSCOPES

NT INFRARED DETECTORS

NT INFRARED INSTRUMENTS

NT INFRARED SCANNERS

NT MICROWAVE RADIOMETERS

NT PYRANOMETERS

NT RADIATION DETECTORS

NT RADIOMETERS

NT RIOMETERS

NT SILICON RADIATION DETECTORS

NT SOLAR SPECTROMETERS

NT SPECTRORADIOMETERS

NT THRESHOLD DETECTORS [DOSIMETERS]

Cosmos 149 meteorological satellite telephotometer, radiometer and other electronic equipment for measuring atmosphere and underlying surfaces physical parameters 01 p0095 A70-11611

Cosmos 149 meteorological satellite telephotometers for measuring reflected solar radiation from earth 01 p0095 A70-11612

Nimbus 3 satellite observations of near UV solar flux intensity and variability, describing instrumentation and measurement of radiation producing molecular oxygen photodissociation 02 p0291 A70-12295

Radioactive nuclei alpha radiation investigation methods, discussing nuclear emulsions, scintillation spectrometry, ionization chambers, semiconductor counters and magnetic spectrographs 03 p0485 A70-13479

Energetic and temporal characteristics of CW and pulse laser radiation measured using instrument with absolute sensor 03 p0500 A70-13480

Cascade showers in horizontal flux of cosmic rays measured by ionization calorimeter 09 p1747 A70-23730

Heavy particles separation at sea level from overall flux of cosmic radiation, discussing method and device recording subrelativistic particles 09 p1684 A70-23732

Isootropic background radiation measured in ozone-sphere with balloon-borne far IR radiometer 10 p1917 A70-24630

Satellite radiometry, discussing vertical soundings, instruments, onboard calibration of interferometer, high spatial resolution, etc 13 p2411 A70-29664

Solar radiation and aureole measuring instruments composed of telescope, double monochromator, amplifier and recorder 15 p2735 A70-31807

Kirchhoff law validity for freely radiating metallic surfaces, using emissometer to measure hemispherical emittance 16 p2999 A70-33903

Solar radio bursts recording by spectrographs in 500-1500 MHz band, discussing sensitivity 18 p3307 A70-36109

Balloon-borne spectrophotometer with diffraction grating for upper atmospheric solar radiation attenuation measurement 19 p3422 A70-37639

Airborne optical scanning gyro for measuring sea surface radiation emission 22 p4039 A70-43558

RADIATION MEDICINE

NT RADIOBIOLOGY

Radioactive isotopes removal from respiratory tract, lungs and gastrointestinal tract by ion dilution and antagonism, blood transfusion and hemodialysis, etc 06 p0994 A70-17666

Whole body counters as standard measuring devices in nuclear medicine and radiation protection, using scintillation detector principles 09 p1624 A70-22819

RADIATION METERS

U RADIATION MEASURING INSTRUMENTS

RADIATION NOISE

U ELECTROMAGNETIC NOISE

RADIATION PRESSURE

NT ELECTRON PRESSURE

NT ILLUMINANCE

NT LUMINANCE

NT LUMINOUS INTENSITY

NT SOUND PRESSURE

Solar radiation pressure effects on zodiacal dust particle orbital velocity, computing Doppler shift of H-beta absorption line as function of elongation 01 p0070 A70-10348

Secular and short period perturbations calculation of satellite orbital elements under action of solar radiation pressure 02 p0362 A70-11763

Period changes of satellite 1963 53 A due to accelerations from atmospheric drag and solar radiation pressure 02 p0362 A70-11764

Earth shadow effect on solar radiation pressure induced short periodic perturbations of satellite orbits 09 p1761 A70-23054

Sun-pointing spinning spacecraft attitude control by solar radiation pressure using paddle arrangement without power, sensor and moving parts requirement 11 p1213 A70-26145

Light pressure induced secular effect contributing to planetary satellites and lunar orbits evolution calculated by numerical integration 11 p2118 A70-26777

One dimensional steady state flows and discontinuities in radiation gas dynamics, neglecting radiation pressure, viscosity and heat conduction 13 p2387 A70-28937

Stellar light pressure and gravitational force ratios for spherical water, quartz and graphite particles in interstellar space, considering refractive dependence on wavelength 13 p2493 A70-29396

Sun-planet-particle problem, considering solar radiation total pressure, Lagrangian solutions instability and differential equations of motion 13 p2494 A70-29400

Heliostationary spacecraft for solar observation near libration point between sun and earth, discussing attitude stabilization by solar pressure 17 p3178 A70-35254

Forced harmonic vibrations of clamped circular plate in inviscid fluid, calculating radiation pressure and power distributions 22 p4073 A70-42646

Radiation forces on flat plate in ecliptic earth orbit applicable to satellite attitude dynamics during pitching libration 22 p4125 A70-43437

Balloon satellite perturbations in orbital period involving air drag, lunar gravity and solar and terrestrial radiation pressures 24 p4414 A70-45358

Radiation pressure effects on artificial satellite motion, including earth shadow perturbation 24 p4408 A70-45554

Atmosphere and earth-reflected solar radiation pressure effects on high altitude satellite orbits
24 p4408 A70-45555

Satellite orbit perturbation due to earth reflected or reradiated solar radiation pressure
24 p4409 A70-45556

Echo 1 and PAGEOS 1 orbital elements variations, determining perturbing effects of earth albedo radiation pressure
24 p4409 A70-45558

RADIATION PROTECTION

NT RADIATION SHIELDING
NT SOLAR RADIATION SHIELDING

Conflicting requirements for reflection reduction, thermal stabilization and radiation protection satisfied by three layer coatings on Si photocells
01 p0159 A70-10768

Book on radiation protection, discussing atomic structure, nuclear transformations, effects on biological cells, total body exposures, somatic and genetic effects, etc
01 p0040 A70-11381

Radioprotective action of pyridine derivatives in monkey heart and human epithelium cells exposed to gamma radiation evaluated by dioxyphenyl alpha-alanine oxidation
03 p0418 A70-13303

Photodynamic damage in biological cells, discussing free radical originators and protective action of thiourea, mono and polyvinylpyrrolidone, cysteine and antibiotics
03 p0419 A70-13306

Radiation protective action of cystamin, cysteamine and aminoethyl in mice, noting equal decreases in redox potential
03 p0419 A70-13310

Dithiols protective effect against ionizing radiation in mice, noting oxygen pressure drop role
03 p0420 A70-13311

Laboratory and field laser hazards control, noting beam termination in outdoor environment and optical density marking on protective eyewear
03 p0434 A70-13681

Radiation level recordings during Soyuz manned orbital flights indicating safety standards maintenance
03 p0580 A70-13704

Experiments on frozen dogs to determine localized shielding effectiveness in astronauts protection from radiation
03 p0423 A70-13710

Radiation hardening of electronic systems for nuclear weapons using shielding, circuit design techniques and hardened components
04 p0657 A70-14738

Integrated analog voltage regulator sensitivity to small signal transient radiation, discussing circuit hardening by diode compensation
04 p0658 A70-14742

Heat stress due to microwave radiation, establishing reduction factor for radiation protection guide number under adverse thermal environments
06 p0998 A70-17202

Soviet manned space flight radiation dosimetry evaluation, comparing U.S. and Soviet techniques for astronaut protection
06 p0990 A70-17271

Experimental procedure for investigating radioprotective effectiveness of chemical compounds against X ray irradiation, discussing Cysteamine protection for golden hamsters and fetuses
06 p0993 A70-17429

Laser radiation protective goggle design, investigating retinal energy density levels and attenuation
08 p1451 A70-21046

Laser safety programs in biomedical applications, discussing installations, techniques, hazards and protection
08 p1451 A70-21048

Premission planning and operational radiation dose limits for manned lunar and low earth orbit missions
08 p1454 A70-21940

Microwave radiation exposure control program for biological hazards, particularly to eye lens
09 p1623 A70-22221

Whole body counters as standard measuring devices in nuclear medicine and radiation protection, using scintillation detector principles
09 p1624 A70-22819

Cholinegous muscarine-mechanism participation in radioprotective effect after cholinomimetics administration, reducing protective reactions against tissue irradiation and increasing mice survival rate
09 p1624 A70-22820

Book on radiation protection covering hazards, detection and measurement, monitoring instruments, biological effects, permissible dosage, contamination control, etc
10 p827 A70-24725

Radiation level recordings during Soyuz manned orbital flights indicating safety standards maintenance
11 p2121 A70-25504

Experiments on frozen dogs to determine localized shielding effectiveness in astronauts protection from radiation
11 p1985 A70-25510

Nuclear environments determination methodology for ground military equipment hardening, considering personnel and equipment responses to detonation in atmosphere
12 p2271 A70-27097

Low energy proton damage to silicon solar cells on INTELSAT II, F-4 and ATS-F-1, considering exposure area and radiation protection
15 p2677 A70-32419

Adenosine triphosphate and vitamins [amitetravit]/ as prophylactics against radiation injuries in dogs during simulated space flight
17 p3038 A70-35351

Personnel danger zones demarcation around radar antennas, using beacons
17 p3040 A70-35913

Skin simulation for thermal radiation protection studies, considering fused silica and epoxy resin filled with Al powder
18 p3225 A70-37093

Psychotropic drugs radioprotective effects in mice, noting oxygen consumption and body temperature decrease after X ray exposure
19 p3367 A70-37558

Soviet book on dynamics of postirradiation damage of biological objects covering dosage and protection effects on various animals
20 p3573 A70-39824

Proton irradiation effects on dogs with partial body protection
20 p3575 A70-40192

Safety factor estimation by nomographic techniques for eye protection against direct viewing of laser beam
21 p3768 A70-40761

RADIATION PYROMETERS

Radiation pyrometers development for in-flight measuring and controlling aircraft engine compressor blades temperature
03 p0480 A70-12900

Temperature measurement of products in solar furnace by IR pyrometers, considering interference filters, reflections parasitic effects, etc
15 p2740 A70-32424

Electric temperature sensors accuracy and stability, considering thermocouples, resistance thermometry, radiation and color pyrometry
15 p2743 A70-32798

RADIATION RESISTANCE

U RADIATION TOLERANCE

RADIATION SHIELDING

NT SOLAR RADIATION SHIELDING

Radiation dosimetry and shielding onboard Cosmos 110 artificial satellite, noting earth belt proton radiation
01 p0198 A70-11518

Nuclear environmental testing techniques, discussing radiation effects, measurements, instrumentation hardening, simulation source selection, dosimetry, noise sources and noise reduction, etc
03 p0523 A70-13540

Optimum radiation shield quantity assuring gas temperature measurement accuracy, using radiation transfer equations and shield-to-shield temperature estimations
03 p0486 A70-13556

Shield mass optimization of low thrust nuclear powered space vehicle for occupant shielding against reactor radiation
03 p0523 A70-13575

Experiments on frozen dogs to determine localized shielding effectiveness in astronauts protection from radiation
03 p0423 A70-13710

Spatial resonance capture rates for U-238 thick slabs to correct gamma ray attenuation errors in broad group shielding calculations
05 p0884 A70-16169

Positive effect of shielding and cystamin administration on tonic and evacuator functions of rats gastrointestinal tract after gamma irradiation
05 p0804 A70-17122

Satellite radiation dose rate experiment with simultaneous trapped particle and absorbed dose rate measurements, discussing proton spectra, material distribution, shielding effects, etc
06 p1061 A70-17263

Dosimetry data and personal radiation sensors from Apollo and Gemini flights, noting spacecraft geometry shielding effects
06 p1134 A70-17268

Spacecraft radiation environment, dosage and shielding problems, discussing high energy protons and electrons exposure hazards for astronauts and mission planning computer codes
06 p0991 A70-17273

Surface shielding from reentry radiation by injecting metal vapors into oxygen bearing boundary layer, calculating particle size distributions, optical depths and attenuation factors
06 p1041 A70-18163

Radiation Shielding Information Center computer code library for radiation transport or shielding calculations, listing programs available
07 p1239 A70-20364

Experiments on frozen dogs to determine localized shielding effectiveness in astronauts protection from radiation
11 p1985 A70-25510

Reusable nuclear shuttles /RNS/ for interorbital and escape missions, discussing alternate stage configurations, radiation shielding, subsystem options, etc [AIAA PAPER 70-678]
16 p2950 A70-33579

Thermal conductivity along parallel radiation shields, proposing calculation method for energy transport
16 p3000 A70-33914

Human body radiation shielding, describing development of computerized standing and seated model for space missions
17 p3036 A70-34794

Lead alloys as shielding materials in nuclear systems, discussing physical, chemical and metallurgical properties, fabrication and applications
19 p3469 A70-37833

Depleted uranium for gamma radiation shielding, discussing properties, alloys, fabrication and applications
19 p3469 A70-37834

Earth intrinsic radiation flux incident angular coefficient, examining effect on partially screened flat spacecraft elements
21 p3942 A70-40847

Spacecraft magnetic radiation shield optimization based on thickness criterion and system mass consideration
22 p3979 A70-43390

Energy attenuation parameters measurements for monoenergetic source neutrons in shielding materials, using Van de Graaff accelerator
23 p4216 A70-43807

Deep penetration radiation shielding calculations using discrete ordinates difference equations and computer program
23 p4216 A70-43808

Radiation shielding calculations using multidimensional Monte Carlo computer programs
23 p4217 A70-43809

Radiation shielding calculations, discussing Monte Carlo concepts for point fluxes with random sampling of source distributions
23 p4217 A70-43810

Radiation shield design and transport calculations, reviewing kernel methods development and relevant computer programs
23 p4217 A70-43811

NERVA Technology Reactor design integrated with Brayton cycle space power conversion systems, considering space bases and shielding analysis [AIAA PAPER 70-1226]
24 p4377 A70-45955

RADIATION SICKNESS

Adhesive and aggregative properties of blood platelets in rats after beta irradiation linked to activity of serum factor
07 p1207 A70-19474

High energy protons irradiation biological effects, noting qualitative and quantitative variations in radiation disease symptoms
07 p1208 A70-19508

Phase correlation of conditioned and electrophysiological postirradiation disturbances in central nervous system of monkeys
08 p1446 A70-21447

Laser irradiation effects on mice skin and internal organs, observing inflammatory symptoms, hair follicles destruction and epithelial atrophy
09 p1624 A70-22816

Hormones excreted by adrenal cortex function in rhesus monkeys pathogenesis after irradiation by sublethal dose
09 p1620 A70-22822

Thyroid gland function following radiation injury by measuring plasma protein bound iodine in irradiated rat blood
09 p1621 A70-23150

High energy protons irradiation biological effects, noting qualitative and quantitative variations in radiation disease symptoms
11 p1987 A70-26107

RADIATION SOURCES

NT MONOCHROMATORS

NT NEUTRON SOURCES

NT POINT SOURCES

Relativistic formulation of radiation for sources in uniformly moving isotropic dispersionless conducting medium in terms of Green functions
01 p0144 A70-11091

Celestial X rays from Cygnus XR-1 detected during high altitude balloon flight, noting compatibility with black body radiation or hot thin plasma
02 p0356 A70-11786

Polarization of nonspherical plasma emission region in thermal X ray stars
02 p0357 A70-11787

Compact 4 micron radiation band from high temperature air and gases measured on arc jet and shock tube, noting molecular O and N source
02 p0392 A70-11901

X ray source Sco XR-1 proper motion using photometry, suggesting association with Scorpius-Centaurus complex of young disk stars

02 p0372 A70-12248

X ray source GX341-6 with soft spectrum detected in Ara constellation by Aerobee rocket, including neighboring X ray sources in determining galactic coordinates, positions and fluxes

02 p0372 A70-12249

Cold cathode soft X ray source with discharge controlled by automatic pressure controller (APC/ or metering valve, noting applicability to radiography, luminescence, etc

02 p0271 A70-12743

Cosmic X ray observations by rockets and balloons noting polarization and line emissions of various sources

02 p0359 A70-12789

Cosmic X ray sources optically observed from ground, discussing identification, distribution, etc

02 p0359 A70-12790

Discrete galactic and extragalactic X ray and gamma ray sources observation, discussing energy spectra, emission mechanisms, properties and suggested models

02 p0360 A70-12791

Stellar X ray sources quanta fluxes estimation based on solar coronal emissions analysis

02 p0360 A70-12793

Cosmic x ray astronomy in near future for source detection concerning spectral bands, polarization, position, instrumentation, etc

02 p0304 A70-12794

Corpuscular sources geoeffectiveness related to position on solar disk at maximum flare activity

03 p0569 A70-13359

D layer radio absorption during solar eclipse of 22 September 1968 attributed to two solar X-ray sources

03 p0559 A70-13602

Poynting flux direction for proton whistlers determined from Injun 5 observations, obtaining data on source region and propagation in ionosphere

03 p0477 A70-13987

Solar wind-induced torque calculated considering special and general relativistic effects, extending method to pulsar rotational model

04 p0739 A70-14593

Primordial cosmic ray sources evidence suggesting galaxies and quasars in initial stages of formation

05 p0897 A70-15921

Cosmic gamma radiation sources above 50 Mev investigated by high altitude balloons in Northern Hemisphere with spark chamber system

05 p0904 A70-16930

Unusual IR object IRC plus 10216 interpreted as galactic source surrounded by optically thick dust shells, noting resemblance to black body energy distribution

05 p0920 A70-16976

X ray source position determination by balloon observations, estimating intensity in different energy ranges

05 p0904 A70-16978

Nonionizing radiation sources relationship to human targets, discussing damage threshold levels

06 p0998 A70-17201

Time variations and angular collimation of radiation emitted by source with relativistic streaming

06 p1134 A70-17281

Radiation from dipole in dispersive anisotropic magnetized plasmas using Fourier analysis

06 p1116 A70-17363

Wave focusing along static magnetic field from radiating VLF source immersed in cold magnetoplasma

06 p1120 A70-17577

Cosmic rays origin, discussing galactic theory of supernovae and formation mechanisms for energy spectra and composition of sources

07 p1371 A70-20327

Cosmic rays formation time and evolution in expanding universe, discussing high energy electrons, energy losses and spectra and metagalaxy cascade processes

07 p1371 A70-20328

Pulsars radio, optical and X ray emission spectrum analysis, suggesting oscillating current sheets as radiation source

08 p1561 A70-20914

Nonstellar 5 micron source in Orion nebula, noting intensity nonvariance and energy distribution calculation of temperature

08 p1575 A70-21375

Crab Nebula continuing energetic activity study indicating origin in nebula center and association with supernova remnant

09 p1750 A70-22000

Quantum mechanical form of Cramer-Rao inequality used to determined error lower bound for radiating object parameter observed by quantum-limited optical system

09 p1694 A70-22072

Baseline measurements of Jupiter decametric radiation providing upper size limit to coherent and incoherent sources

09 p1755 A70-22512

Angular size measurement for galactic X ray sources in Sagittarius region using modulation collimator aboard sounding rocket

09 p1744 A70-22521

Celestial positions and intensities of X ray sources in Sagittarius region obtained from rocket experiment

09 p1744 A70-22522

Electromagnetic radiation sources for remote sensing application to identification of water, moist soil and vegetation, discussing optical properties of diverse materials

09 p1667 A70-22851

Celestial X ray sources resolved against diffuse nearly isotropic background radiation by rocket and balloon experiments, noting brightness

09 p1745 A70-22895

Two beam Fraunhofer holography noting effect of spatially coherent source

09 p1678 A70-22968

Proton injection into radiation belt, comparing solar neutron decay (SND) and cosmic ray albedo neutron decay (CRAND) as proton sources

09 p1746 A70-23489

Gravitational waves and radiation study based on relativity theory, discussing outer space sources and antenna recording design and properties

10 p1916 A70-24384

IR radiation sources /irtrons/ accounting for energy releases by continuous matter and antimatter creation

10 p1947 A70-24997

Balloon observations of Cen XR-2 X ray emission decrease

10 p1948 A70-24999

Plasmas role in emission mechanisms active in celestial sources of radiation, discussing sun and quasars

10 p1948 A70-25027

X ray astronomy, discussing emission processes, radiation classification for intensity plot against energy, cosmic sources distribution, etc

11 p2111 A70-26035

Celestial sources energy spectrum and absolute flux by rocket flights, attributing short lived outbursts to shock wave from nova expanding into circumstellar medium

11 p2113 A70-26297

Corpuscular sources geoeffectiveness related to position on solar disk at maximum flare activity

11 p2118 A70-26724

Twin crystal X ray telescope principle, design and application, discussing radiation sources nature and measurement methods

11 p2057 A70-26824

Cosmic X ray sources, considering locations, fluxes and angular sizes from Aerobee rocket observations

12 p2292 A70-27384

Cosmic X ray sources searched for by Aerobee rockets, noting locations and distribution correlation with galactic novae

12 p2292 A70-27385

Night sky X ray sources at low galactic latitudes, describing rocket survey experiment

12 p2292 A70-27386

X ray source from Coma cluster of galaxies, interpreting observed flux on basis of missing mass suggested by Virial theorem

12 p2293 A70-27388

Gravitational forces accompanying radiation bursts of metric outside collapsing supernova core

12 p2300 A70-27393

Radiating objects localization and tracking by radiometer equipped with two antennas having slightly divergent beams

12 p2185 A70-27689

Sgr gamma-1 source, determining upper limit on soft X rays intensity

13 p2475 A70-28615

Quasi-monochromatic radiation field polarization representation and transformation of state, including instrumental effects

13 p2451 A70-28829

Catalog in tabular form of discrete celestial X ray sources in energy region above 2 kev

13 p2489 A70-28903

Cosmic rays and cosmic X rays, considering galactic and extragalactic sources, diffuse background, detection devices, etc

13 p2477 A70-29160

Standard sources and detectors for thermal radiation measurement

13 p2410 A70-29654

Black bodies radiation properties and design for applications as absolute radiation standards

13 p2410 A70-29657

Galactic X ray stars and X ray sources positions, appearance frequency and intensities

13 p2495 A70-29818

Scorpio X-1 and Taurus X-1 /Crab/ X ray flux effects on nighttime ionospheric radio transmission,

discussing ion production and resulting electron density

14 p2631 A70-30541

Pulsar radiation emission by electrons and protons in close orbit taking into account density, energy and correlation in plasma

14 p2638 A70-30617

Angular size of high energy X ray source in Crab Nebula from balloon-borne X ray modulation collimator

14 p2631 A70-30789

Cosmic IR radiation sources, discussing galactic and stellar masses

14 p2632 A70-30882

Electric and magnetic dipole VLF radiation patterns in lossy two component magnetoplasma

16 p2860 A70-32944

Chemiluminescent processes accounting for radiation from turbulent wake flows behind hypersonic spheres in air

[AIAA PAPER 70-729]

16 p2997 A70-33492

X and gamma ray astronomy instrumentation, point sources, continuum emission, line spectra, etc

16 p2976 A70-33721

Doppler shifted radiation production, using time and space dependent radiant energy sources

16 p2952 A70-34255

Sounding rocket X ray survey of Cassiopeia region for supernova remnants and galactic source distribution

17 p3153 A70-34528

Taurus X-1 X ray emission polarization, using rocket-borne polarimeter

17 p3150 A70-34845

Pulsars as cosmic ray sources, emphasizing time properties of acceleration mechanisms

17 p3151 A70-34913

Simple antenna sources, deriving far zone radiation field from arbitrary current distribution

17 p3043 A70-35052

Fluid transpiration arc radiation source based on forced convection effect on electric arc

17 p3023 A70-35153

Isotropic scattering of radiation from asymmetric spherical source in finite atmosphere

17 p3136 A70-35598

Superheavy nuclei origin in primary cosmic rays, proposing neutron stars /pulsars/ as sources

18 p3308 A70-36403

Diffraction radiation generator with CW operation in backward wave tube mode, discussing output power dependence on wavelength

18 p2321 A70-36410

Extragalactic objects 3C 273 NGC 5128 and M87 X ray emission detection, using proportional counters on Aerobee 150 rocket

18 p3310 A70-37016

Soft X ray extended source in Cygnus Loop, indicating supernova remnant

18 p3310 A70-37022

Information optical transmission parameters with electroluminescent GaAs diode as radiation source, calculating energy received over various distances

19 p3389 A70-38069

Metagalactic and galactic sources of cosmic rays, including composition, electron spectra and radio emission

19 p3500 A70-38077

Critique of metagalactic origin of high energy cosmic rays, reviewing neutrino hypothesis

19 p3500 A70-38082

Astronomical gamma ray emission measurement by balloon-borne spark chamber, presenting results for discrete and diffuse sources and albedo intensities

19 p3501 A70-38088

Cosmic gamma ray sources detection in 100-1000 GeV range by atmospheric Cerenkov radiation from energetic particle showers

19 p3501 A70-38091

High energy galactic gamma rays photons, suggesting two-component cosmic ray source model

19 p3505 A70-38115

Cosmic ray elements abundance at sources relative to carbon, comparing near-earth composition and solar photosphere

19 p3509 A70-38147

Pulsars postulated as supernova remnants sources of local cosmic rays

19 p3511 A70-38159

Cosmic rays relationship to cosmological parameters and galactic radiation source evolution

19 p3511 A70-38160

Solar simulation methods, discussing optical elements and artificial radiation sources suitability for thermal testing

19 p3398 A70-38282

Nebula K3-50 IR radiation source observation, noting energy distribution resembling NGC 7027 and W51-IRS 2

20 p3701 A70-39003

Short wave calibration system for net pyradiometers, using source with intensity and spectral distribution comparable to solar radiation

20 p3628 A70-39147

- Extrasolar X ray source optical observations, discussing identification method and individual characteristics 20 p3700 A70-39930
- Electromagnetic waves and oscillations excited by magnetic current ring source around infinitely long compressible plasma column, deriving radiation field distribution 20 p3685 A70-40506
- X ray astronomy instruments on sounding rockets, balloons and satellites, investigating sources distribution on celestial sphere 21 p3821 A70-40652
- COS-B satellite cosmic X ray experiment with high sensitivity and long pointing time for extragalactic sources discovery 21 p3871 A70-40655
- Galactic and extragalactic discrete cosmic X ray sources by rocket observation with narrow slit collimators 21 p3871 A70-40656
- Cosmic hard X ray sources spectra and time variations by balloons and OSO-3 satellite observations of Crab Nebula 21 p3872 A70-40657
- Virgo XR-1 rocket observations, discussing X rays due to synchrotron emission of relativistic electrons 21 p3872 A70-40658
- X ray flux and energy spectrum of Cen-X2, Sco-X1 and Tau-X1 sources by rocket flight observation 21 p3872 A70-40659
- Hard X ray sources energy spectra in 20-120 keV range by balloon flights, presenting Sco X-1 intensities 21 p3872 A70-40660
- X ray intensity sudden changes in 29.9-52.3 keV range from Sco X-1, correcting for atmospheric attenuation 21 p3872 A70-40661
- X ray sources location, distribution and spectral characteristics, investigating emission from supernova remnants 21 p3872 A70-40662
- Cosmic X ray spectra of Cyg XR-2 in 0.15-20 keV range by spinning rocket-borne detector, noting interstellar absorption 21 p3872 A70-40664
- Cyg-X-1 X ray source angular size and position measurements by balloon-borne collimator 21 p3873 A70-40665
- Optical photometric observations of nonsolar gamma and X ray sources WX Cen, NGC 5189 and GX3 plus 1 21 p3873 A70-40669
- X ray sources spectra, discussing distribution, supernova remnants, pulsars nebulae, optical spectra and general characteristics 21 p3873 A70-40670
- Magnitude-color relation for Cygnus X-2 and WX Centauri, indicating opposite correlation to Sco X-1 fluctuations 21 p3873 A70-40672
- Proper motion evidence for existence of X ray stars associated with Sco X-1 and Cen X-2, indicating formation by neutron stars 21 p3873 A70-40673
- Rotating neutron stars, pulsars and cosmic X ray sources relationship, discussing stellar model with mass loss in presence of magnetic field 21 p3874 A70-40678
- X ray emission mechanisms in galactic sources, considering black body, supernova remnants, synchrotron radiation, etc 21 p3874 A70-40679
- Discrete X ray and gamma ray sources theories, considering binary and gas stream models 21 p3874 A70-40680
- Galactic gamma ray intensity near Cygnus by OGO-5 spacecraft-borne telescope with acoustic spark chamber, discussing source intensity 21 p3876 A70-40691
- Gamma ray astronomical point sources by balloon flight and satellite observation, discussing detector system and telescope for flux and energy spectrum 21 p3821 A70-40694
- Innerbremsstrahlung of intergalactic protons colliding with electrons as source of cosmic background X rays, interpreting intensity and energy spectrum 21 p3877 A70-40700
- Solar wind X ray emission, investigating diffused cosmic ray origin and flow pattern models 21 p3878 A70-40708
- Sco X-1 extar high energy radiation production, discussing relativistic electron synchrotron emission and magnetic fluctuations spectrum 21 p3878 A70-40709
- Pulsars and other discrete sources celestial gamma rays flux distribution calculation 21 p3878 A70-40745
- X ray source population type optical observations, discussing interstellar matter and H II regions 21 p3882 A70-41117
- MI X ray emission, examining energy interval and power law spectral distribution 21 p3882 A70-41155
- Strong newborn X ray source detection during balloon flight, showing softened low energy spectrum 21 p3892 A70-41190
- Semiconductor junction diode spontaneous emission sources, considering frequency-energy characteristics relationship 22 p4085 A70-42504
- H alpha emission objects in Southern Milky Way, discussing positions, photometric data and relation to galactic structure 22 p4101 A70-42865
- X ray sources celestial positions in Sagittarius region, using rocket-borne rotating modulation collimator 22 p4094 A70-42928
- X ray sources identification with optical counterparts, noting lack of radio and pulsar type emissions 22 p4094 A70-42929
- Scorpius X-1 X ray line emission, discussing continuum and background counts and cosmic abundance of iron 22 p4094 A70-42931
- Galactic plane scanned observation of X ray sources, using large area proportional counter rocket sounding 22 p4094 A70-42986
- Simultaneous X ray and optical observations of Scorpius XR-1, comparing rocket data from various flights 22 p4094 A70-42987
- Secondary source distribution of EM field induced on ground-air interface by antenna 23 p4161 A70-43773
- Radiation shielding calculations, discussing Monte Carlo concepts for point fluxes with random sampling of source distributions 23 p4217 A70-43810
- Cosmic X ray sources astronomic observations and implications, considering Crab Nebula, galaxies, constellations, diffuse background radiation, etc 23 p4243 A70-44415
- High current betatrons for defectoscopy of manufactured articles and materials compared with other radiation sources 24 p4348 A70-45846
- RADIATION SPECTRA**
- NT ABSORPTION SPECTRA
- NT BALMER SERIES
- NT D LINES
- NT ELECTROMAGNETIC SPECTRA
- NT ELECTRONIC SPECTRA
- NT EMISSION SPECTRA
- NT FRAUNHOFER LINES
- NT H ALPHA LINE
- NT H BETA LINE
- NT H GAMMA LINE
- NT H LINES
- NT HERZBERG BANDS
- NT INFRARED SPECTRA
- NT K LINES
- NT LINE SPECTRA
- NT LYMAN SPECTRA
- NT MICROWAVE SPECTRA
- NT PASCHEN SERIES
- NT RADIO SPECTRA
- NT RAMAN SPECTRA
- NT RYDBERG SERIES
- NT SOLAR SPECTRA
- NT STELLAR SPECTRA
- NT TELLURIC LINES
- NT ULTRAVIOLET SPECTRA
- NT VIBRATIONAL SPECTRA
- Model explaining background X radiation spectral properties, assuming production by Compton scattering of radio, IR and optical quanta by relativistic electrons 01 p0171 A70-11124
- Fourier and perturbation methods applied to radiation from uniformly moving charge in inhomogeneous magnetoactive medium, deriving expressions for radiation spectrum and energy losses 03 p0531 A70-13285
- Thermal balance of radiosonde thermometric elements and radiation errors in atmospheric temperature measurements using spectra of radiation fluxes reflected from cloud cover 03 p0557 A70-13297
- Balloon-borne experiments with directional scintillators to measure low energy gamma radiation spectrum in midlatitude atmosphere for photons origin and gamma albedos investigation 03 p0561 A70-13996
- Intensity, spectrum and polarization of gyrosynchrotron radiation from magnetoactive plasma electrons distribution 04 p0749 A70-14594
- Cosmic ray electron spectrum above 200 Gev based on pure nuclear emulsion stack using horizontal sandwich assembly 06 p1135 A70-17473
- Flux densities and positions for Southern Milky Way sources at 1410 MHz, determining spectral indexes 07 p1387 A70-19682
- Phonon spectrum of mixed semiconductor crystals based on AIII-BV and AII-BVI compounds, studying frequency spectrum as function of crystal composition 07 p1300 A70-19867
- Signal to noise ratios and fluctuation spectrum of photomultiplier illuminated by laser passing through laser amplifier, noting population level effect 07 p1300 A70-19869
- Solid state lasers with strongly degenerated modes investigated for induced radiation spectral composition inertial properties 08 p1510 A70-20507
- Soviet book on celestial bodies radiation transfer and spectra covering light scattering, radiation fields, absorption, etc 08 p1568 A70-20768
- Fine structure morphology in dynamic spectra of Jupiter decametric radiation determined from spectral recordings 08 p1562 A70-21514
- Line strength and radiative lifetimes for Ne II determined from spontaneous emission data obtained from CW neon laser discharge 09 p1730 A70-22070
- Backscattered sun and skylight spectra from sea obtained from low flying aircraft as measure of chlorophyll concentration 09 p1666 A70-22250
- Radiation transport calculations based on approximate method restricted to X ray and low energy gamma ray region of electromagnetic spectrum 10 p1915 A70-23977
- Iostropic background radiation measured in ozonosphere by balloon-borne far IR radiometer 10 p1917 A70-24630
- Cosmic gamma ray spectrum from secondary neutral pion production in p-p interactions, discussing delta isobar, fireball and nuclear interactions effects 11 p2106 A70-26707
- Primordial radiation spectrum, discussing possible distortions due to energy injection before and after recombination 12 p2308 A70-27886
- Cosmic ray extensive air showers spectrum at high altitude, describing measuring equipment, techniques and results 12 p2295 A70-28048
- Pulsed Ne laser superradiation spectrum fine structure, using Fabry-Perot interferometer 13 p2428 A70-29362
- Trapped alpha particle and proton spectra from satellite measurements, considering magnetosphere injection 13 p2484 A70-30093
- Cosmic ray energy spectrum in absence of solar activity from eleven year ray variations, noting coincidence with galactic rays 14 p2630 A70-30204
- Entire functions for analysis and representation of distant atmospherics, using concentrated spectrum and zero coordinate readings 14 p2569 A70-30210
- Interstellar cosmic ray spectra from nonthermal radio background, obtaining electrons and protons modulation by diffusion-convection energy loss theory 14 p2631 A70-30673
- Galactic abundances and cosmic ray spectra by IMP-4 satellite, obtaining He ratio 15 p2793 A70-31794
- Volcanic blankets aerological investigation by polarization and spectral techniques, determining brightness distribution of reflected solar light 15 p2803 A70-32495
- Optical properties of electropolished cubic Nb-Ti alloys at cryogenic and room temperatures in visible and near IR spectral range 16 p2930 A70-33205
- Dynamic spectra of type 3 solar bursts from OGO-3 antenna/radiometer observations 17 p3150 A70-34835
- Ionization losses effect on spectrum of cosmic rays accelerated in solar chromosphere, interstellar space, supernovae, radiogalaxies, etc 18 p3308 A70-36425
- Long term variations of cosmic ray electron spectrum above 500 MeV from balloon and satellite observations, noting reduction during Forbush decreases 19 p3503 A70-38105
- Thermal radiation spectrum power of small spherical tin and lead particles 20 p3737 A70-39745
- Spontaneous and induced Cerenkov emission by charged particle in turbulent medium, discussing random fluctuations effect on radiation spectra 21 p3879 A70-40928
- Nd glass laser with smooth emission frequency scanning, giving block diagrams and radiation spectra 24 p4353 A70-45646
- Spectral anomalies due to inhomogeneous optical pumping in masked ruby laser, using mathematical model 24 p4355 A70-46264

- Cosmic ray energy spectrum in absence of solar activity from eleven year variations, noting coincidence with galactic rays 24 p4398 A70-46279
- Entire functions for analysis and representation of distant atmospheres, using concentrated spectrum and zero coordinate readings 24 p4330 A70-46285
- Ionized Ar laser developments, considering power output and radiation spectrum 24 p4356 A70-46324
- ### RADIATION THERAPY
- Therapeutic power of bone marrow transplanted from mice earlier irradiated by high energy protons into newly irradiated mice 09 p1619 A70-22814
- Therapeutic effects of hemopoietic tissue transplantations of bone marrow on irradiated rats, using diffusion chamber for resettlement prevention 13 p2354 A70-29753
- ### RADIATION TOLERANCE
- Erythropoietic response in anesthetized dogs subjected to sublethal whole-body proton irradiation followed by hypoxic hypoxia, discussing test procedure and results 01 p0027 A70-11300
- Radiation damage recuperation process in living organisms and justified risk dose in prolonged space flights using Blair model 03 p0423 A70-13705
- Survival rates of continuously cultivated *Chlorella* plants in air-carbon dioxide atmosphere after single exposure to gamma radiation, using microcolony counting technique 05 p0803 A70-17113
- Heat stress due to microwave radiation, establishing reduction factor for radiation protection guide number under adverse thermal environments 06 p0998 A70-17202
- Mice irradiation reactions determination from various metabolism indices including blood sugar level, leucocytes number, proteolytic processes rates, etc 07 p1198 A70-18714
- Micrococcus radiodurans* and *Sarcina flava* radiation resistance from proton irradiation tests in carbonaceous chondrite Migei 08 p1441 A70-20550
- Radiation hardened ICs development, discussing problem of dielectric isolation 08 p1468 A70-20627
- Dielectric coatings resistance to laser radiation, measuring rupture threshold of vacuum coatings consisting of zinc sulfide layers 10 p1901 A70-25111
- Radiation damage recuperation process in living organisms and justified risk dose in prolonged space flights using Blair model 11 p1985 A70-25505
- Global distribution and intensity of solar radiation, determining radiation of satellites and other high altitude devices 11 p2105 A70-26010
- Radiation stable refractory oxides in white spacecraft thermal control coatings, discussing photocatalysis application to degradation analysis 11 p2067 A70-26364
- Gravity radiation detector insensitivity to cosmic rays 13 p2405 A70-28835
- MOSFET integrated circuits radiation resistance measurements under electron irradiation, determining changes in threshold voltage, transconductance and on-resistance for applications in spacecraft 14 p2559 A70-31372
- VLF radiation resistance of short filamentary electric dipole at arbitrary angle to magnetic field in cold uniform plasma, using full wave theory 16 p2859 A70-32935
- Photoelectric conversion efficiency and radiation resistance of Li-doped Si solar cells, showing improved reliability over Li-free cells 17 p3023 A70-35311
- Microelectronic systems radiation resistance, examining logic IC gates for reactor neutron irradiation 18 p3233 A70-36783
- Square loop antenna radiation resistance in warm plasma, comparing theoretical results with measured values from Ariel 3 satellite antenna 21 p3796 A70-40562
- Cellular irradiation sensitivity in tissue culture modified by propyl gallate as radical reactions inhibitor 21 p3767 A70-42242
- Temperature effect on radiation tolerance of mice exposed to low dose rate gamma radiation, noting mortality delay in low temperature environment 23 p4148 A70-44789
- ### RADIATIVE HEAT TRANSFER
- Solid bodies unsteady thermal conductivity in presence of quasi-steady heat transfer under combined radiant and thermal fluxes, presenting thermodynamic nomograms 01 p0213 A70-10215
- Heat transfer in tube flow with forced convection, internal radiation exchange, axial wall heat conduction and arbitrary wall heat generation 01 p0214 A70-10294
- Radiant heat transfer in hypersonic aerodynamic heating, discussing radiant flux and carbon dioxide concentration in reentry problems 01 p0219 A70-11625
- Thermal protection systems (TPS) design criteria for maneuverable reentry spacecraft, comparing weight and cost for various alloy systems 02 p0392 A70-11940
- Radiative, conductive and convective combined heat transfer mechanism in nonisothermal atomic hydrogen plasma laminar flow 02 p0400 A70-12660
- Differential equation with associated boundary conditions constructed for radiative transfer with spherical symmetry, applying to gray gas between concentric black spheres 03 p0603 A70-12904
- Two dimensional approximate formulation for radiant heat flux applied to radiative equilibrium in gray gas 03 p0603 A70-12905
- Fracture and degree of material removal of glassy body in hypersonic gas flow, considering radiant heat conduction inside body 03 p0516 A70-13391
- Optimum radiation shield quantity assuring gas temperature measurement accuracy, using radiation transfer equations and shield-to-shield temperature estimations 03 p0486 A70-13556
- Transient and steady state radiation heat flux sensors calibration by developing and evaluating heat flux source 03 p0606 A70-13558
- Solid propellants ignition response to radiative and conductive heat transfer 03 p0544 A70-13921
- Radiation-convection interaction in plasma free jet, using two-thermal-domain model for enthalpy distribution determination [ASME PAPER 69-WA/HT-50] 04 p0781 A70-14798
- Approximate solutions for radiative heat transfer in shock layer, considering discontinuity role [ASME PAPER 69-WA/HT-48] 04 p0667 A70-14800
- Transport theory application to differential approximations for radiative transfer problems [ASME PAPER 69-WA/HT-45] 04 p0781 A70-14801
- Radiative heat transfer through dust clouds in radiative equilibrium and isothermal clouds between parallel plates measured with heat flowmeter [ASME PAPER 69-WA/HT-41] 04 p0781 A70-14802
- Radiative heat transfer from longitudinal rectangular conducting fins on plane wall involving mutual irradiation, using iterative method [ASME PAPER 69-WA/HT-22] 04 p0782 A70-14812
- Radiative heat flux between two parallel copper disks at cryogenic temperature, showing dependence on emitter temperature and spacing [ASME PAPER 69-WA/HT-7] 04 p0784 A70-14823
- Temperature distribution around radiating sphere in homogeneous gas medium with molecular heat transfer, solving energy transport equation 04 p0785 A70-15012
- Radiation view factor from differential area to conical surface determined using Stokes theorem and contour integration 04 p0787 A70-15598
- Absorption coefficient 5-step model applied to shock tube measurements of end wall radiative heat transfer behind reflected shock waves in air 04 p0787 A70-15606
- Surface roughness effects on radiant heat transfer rate of isolated plane surface with uniform temperature illuminated by collimated solar flux 06 p1172 A70-17178
- Probability distributions and error estimates for Monte Carlo solutions of radiation heat transfer problems, considering wavelength and direction of emitted photon bundles 06 p1175 A70-17683
- Atmospheric long wave radiation fluxes and energy balance and daytime radiative temperature variations calculated and compared with thermocell measurements 06 p1098 A70-17831
- Sunspot umbral dot models characteristics based on three dimensional radiative transfer analysis 06 p1144 A70-18003
- Viscous radiating flowfield coupled with ablation for computations on blunt body entering earth atmosphere at interplanetary return velocities [AIAA PAPER 70-128] 06 p0970 A70-18090
- Massive blowing effect on stagnation point radiative energy transfer of ablative heat shield during planetary entry at hypersonic velocities [AIAA PAPER 70-203] 06 p0971 A70-18101
- Convective and radiative heat fluxes measurement on charring ablative materials surface in rocket nozzle environment 06 p1070 A70-18444
- Stagnation point heating in hypersonic gas flow past blunt bodies, considering radiative transfer effects on shock wave temperature and density distribution, wave separation, etc 06 p0985 A70-18557
- Numerical method of characteristics for unsteady radiation gas dynamics, discussing surface pressures and heat transfer rates [AIAA PAPER 68-163] 07 p1256 A70-19314
- Convective and radiative heat transfer properties of two dimensional circular fin 07 p1421 A70-19316
- Perturbation solution for fins taking into consideration interaction of conduction with radiation and convection 07 p1422 A70-19333
- Radiative heat transfer in radiant energy flux incident on plane surface of nonisothermal absorbing and dissipating layer 07 p1423 A70-19814
- Radiative heating rates and gas environments effects on ablative material performance from tests at arc image facility 07 p1319 A70-19888
- Mathematical model for calculating radiative heat transfer from turbulent diffusion buoyant flame and predicting liquid fuel burning rate 07 p1425 A70-20008
- Wall material diathermy effects on critical thermal load under radiant transfer, comparing results for quartz glass and stainless steel tubes 08 p1597 A70-21186
- Radiative heat transfer in lunar and Mercurian surfaces, discussing radiative heat transfer in powders 08 p1579 A70-21569
- Nonequilibrium interaction of radiative and vibrational rate processes in IR-active diatomic gas using macroscopic equations 08 p1549 A70-21574
- Dominant radiation field interaction with gas flow field using matched asymptotic expansion method 08 p1598 A70-21579
- Radiant heat exchange for rectangular groove represented by integral equations using rapid iteration method 08 p1600 A70-21835
- Matrix multidimensional singular linear integral equation applied to electromagnetic radiation transfer through stratified atmosphere 09 p1711 A70-22349
- Thermal radiative transfer in nonuniform anisotropic magnetoactive plasma, correcting term of Zheleznyakov equation 09 p1734 A70-22514
- Temperature and stress fields in rotating thin tube exposed to stationary heat source with constant strength, considering materials 09 p1774 A70-22579
- Radiative heat transfer along adjacent layers of multilayer insulation blanket determined as energy transport mode 09 p1789 A70-23265
- Radiative transport in nongray cylindrical medium using total band absorptance 09 p1790 A70-23553
- One dimensional numerical solution for steady state thermal behavior of trapezoidal profile annular fins transferring heat by conduction and radiation [ASME PAPER 69-HT-6] 09 p1790 A70-23557
- Irradiance factor between perpendicular and arbitrarily positioned plane rectangles calculated by contour and numerical integration 09 p1791 A70-23619
- Thermal radiation shield influence on stationary radiative heat transfer in closed arbitrarily shaped two gray surface system 10 p1966 A70-23865
- Temperature field and combined radiative-conductive heat flux in weakly absorbing cylindrical layer bounded by nonblack surfaces 10 p1966 A70-23866
- Radiative transfer effect on thermal instability and critical Rayleigh number in gray transparent fluid layer heated from below 10 p1967 A70-23952
- Reflected shock wave structure and velocity at rigid wall, assuming radiative heat transfer as dissipative process 10 p1967 A70-24018
- Shock propagation from point explosion energy source into cold exponential atmosphere with radiative heat transfer in rear of shock front 10 p1869 A70-24525
- Radiant heat exchange local and angular coefficients determined allowing for absorbing and scattering medium between bodies 10 p1969 A70-25141
- Convective-radiative heating of multilayer plate approximating temperature field by iteration 10 p1969 A70-25143
- Radiative heat transfer due to radiation conductivity and transmission in low density glass fiber insulations by heat flowmeter for hot and cold surfaces 11 p2148 A70-25769

Radiation heat transfer around interior of long cylinder as function of surface emissivity
11 p2149 A70-26152

Radiant heat transfer predictions between isothermal plates based on diffuse plus specular directional property model
[AIAA PAPER 69-624] 11 p2149 A70-26157

Embossed/crinkled aluminized film multilayer insulation blankets with joints performance variation with temperature predicted by radiation heat transfer correlation
11 p2150 A70-26365

Radiative heat transfer in spherical space bounded by perpendicular annular rib system with gray diffuse and absolutely black body surfaces
12 p2331 A70-27554

Radiative energy transfer in hydrogen plasma having uniform heat source and bounded by parallel black plates
12 p2278 A70-27695

Steady state and transient heat transfer by radiation and conduction in absorbing medium bounded by infinite coaxial cylindrical surfaces
12 p2331 A70-27697

Transient heat transfer combining conduction and radiation in absorbing plane layer analyzed by differential approximation
12 p2332 A70-27801

Numerical quadratures application to integral equations for radiative heat transfer computations, discussing validity for parallel and adjoint plates
12 p2332 A70-27840

Resonance radiation transport in optically thick plane gas layer with two-level atoms
12 p2305 A70-27853

Airport runway to fog radiative heat transfer analysis by Monte Carlo method
12 p2333 A70-28115

Perturbation theory of supersonic steady anisotropic flow with radiative heat transfer using hyperbolic characteristic coordinates
12 p2334 A70-28203

Radiation effects on viscous hypersonic low density stagnation flow using two layer model, calculating flow field and heat transfer coefficient
12 p2158 A70-28204

Liquid film steady motion on ablating body surface allowing for radiative heat transfer from interior
12 p2334 A70-28244

One dimensional radiatively driven acoustic waves analysis by approximation for radiative heat addition, achieving better accuracy than substitute-kernel method
13 p2520 A70-28633

Surface emissivity effects on combined conduction, convection and radiation heat transfer in nonisothermal hydrogen plasma, discussing optically thin and thick solutions
13 p2521 A70-29134

Radiative heat transfer through gray gas in equilibrium between concentric spheres, using variational method
13 p2521 A70-29137

Thermal longwave radiation measurement applications to atmospheric radiation transfer and weather processes
13 p2411 A70-29663

Radiative heat transfer in channel with unsteady radiating medium temperature, assuming absolutely black walls with zero temperature
13 p2522 A70-29725

Polarization effect on radiant heat transfer between simply arranged smooth plate surfaces
13 p2523 A70-29993

Laminar or turbulent flow in parallel plate channels with combined forced convective and radiative heat transfer, determining gas temperature field and Nusselt numbers
14 p2663 A70-30253

Radiative heat transfer in optically thick gas between concentric spheres treated by matched asymptotic expansions, comparing results with Roseland approximation and numerical solution
14 p2663 A70-30266

Radiating gas flow about pointed bodies, investigating shock curvature at wedge or cone tip and straight shock waves flow field downstream
14 p2663 A70-30267

Radiant heat flux for standard model, dry and humid atmosphere, calculating temperature variations with altitude for entire IR spectrum
14 p2603 A70-30401

Thermal radiative transfer and magnetic field effects on hydromagnetic stability of hot electrically conducting fluid
14 p2623 A70-30996

Self similar one dimensional flow behind plane shock propagating in exponentially decreasing atmosphere, considering radiation mean free paths and radiative heat transfer
14 p2567 A70-31032

Boundary value problem of nonlinear one dimensional conduction in radiating heat shields, using perturbation and numerical methods
15 p2824 A70-31450

Conical heat radiator system for cooling short cylinders
15 p2827 A70-32142

Radiative properties of construction properties and working media, noting importance to radiative heat transfer calculation
15 p2827 A70-32143

Heat pipes design for rocket engines cooling, discussing connections to space radiator and to heat rejection device and heat transfer capability
[AIAA PAPER 69-582] 15 p2791 A70-32517

Minerals radiative thermal conductivity at high temperatures from IR measurement of absorption coefficient and refractive index
16 p2897 A70-33648

Diffuse specular rough surface measure for imperfect reflections in thermal radiation transfer through slot passages
[AIAA PAPER 70-860] 16 p2999 A70-33905

Viscous absorbing emitting shock layer in blunt body stagnation region, calculating skin friction and radiative heat transfer
[AIAA PAPER 70-868] 16 p2999 A70-33911

Radiation and conduction of open joint multilayer insulation systems, analyzing dependence on contact area by numerical methods
[AIAA PAPER 70-848] 16 p2939 A70-33915

Rocket exhaust gases radiant heat transfer prediction, using band models with computer program
[AIAA PAPER 70-841] 16 p3000 A70-33924

Radiative heat transfer effects on polymeric combustion-inhibiting coatings in solid propellant rocket motors
[AIAA PAPER 70-835] 16 p2971 A70-33930

Nonabsorbing gas effect in radiation-conduction heat transfer interaction, predicting magnitude and pressure trends by wideband gas model
[AIAA PAPER 70-836] 16 p3001 A70-33931

Correction techniques for thermal network lumped parameter inaccuracies with conduction and radiation coupling, considering temperature control system
[AIAA PAPER 70-821] 16 p3002 A70-33943

Mathematical model of heat flux absorbed by heated part in radiant heating reflector systems, considering shape, spectral, directional and polarizing effects
[AIAA PAPER 70-818] 16 p3002 A70-33945

Radiatively interacting adjoint plates in presence of collimated solar flux, considering surface roughness effects on equilibrium temperature distribution
[AIAA PAPER 70-817] 16 p3002 A70-33946

Radiative heat transfer between opaque interacting surfaces for equal temperature adjoint plates with one dimensional surface roughness profile
16 p3002 A70-34196

Diffuse-specular models for radiant heat interchange prediction for isothermal-adiabatic surface enclosure tested for steel and gold
16 p3003 A70-34197

Nongray radiant heat transfer corrections to thermal conductivity measurements for water vapor at atmospheric pressure
16 p3003 A70-34200

Flowfields behind reflected shock waves, predicting end-wall radiative heat transfer and radiative gas dynamic coupling effects
[AIAA PAPER 70-774] 17 p3065 A70-34480

Unsteady laminar boundary layers on infinite porous plate, considering radiative heat transfer and transpiration cooling
17 p3067 A70-34632

Radiation gas dynamics, investigating thermal radiation effects on flow field of high temperature gas
17 p3195 A70-35038

Thermal choking of channel flow by radiative transfer from upstream and application to shock waves generation
17 p3195 A70-35039

Meridional circulation velocities in Roche envelope of uniformly rotating star, using nonlocal equation for radiative heat transfer
17 p3171 A70-35560

Multiplying factors role in iterative solution of shock wave structures with large radiation-convection ratios
17 p3075 A70-35888

Long wave radiation fluxes calculation in troposphere based on principal radiant heat transfer components separation
18 p3285 A70-36632

Radiant heat transfer at vertex of adjoint flat plates separated by vacuum
18 p3243 A70-36711

Book on heat transfer covering conduction, convection, thermal radiation and heat exchange equipment
19 p3550 A70-37231

Venus atmosphere heat transfer processes from Venera 4, 5 and 6 probes data, evaluating radiative and convective motions model
19 p3520 A70-38256

Radiative gas dynamic equations similarity representation with spherical symmetry, constructing numerical examples for strong explosions and implosions
20 p3609 A70-39657

Heat conduction problems solved allowing for radiation on electrical models, using nonlinear resistance and composite circuit methods
20 p3738 A70-40178

High temperature gases radiative heat exchange, evaluating approximation methods
20 p3739 A70-40293

Radiative heat transfer between concentric spheres separated by absorbing-emitting medium with heat sources, deriving approximate solution
20 p3739 A70-40294

Steady one dimensional temperature field of cylindrical shell spacecraft, allowing for heat conduction and convective and radiative heat transfer within shell
21 p3942 A70-40841

Convective and radiative heat flux measurement incident on ablative surface in solid rocket nozzles
21 p3824 A70-40858

Radiation heat transfer from parallel plates with grooved surfaces for direction dependent radiation properties
21 p3944 A70-41021

Radiative propagation nondiffusive effects of thermal pulse in explosion, obtaining solutions for plane and spherical case by asymptotic expansion and numerical integration
21 p3950 A70-41379

Nonuniform radiation heat transfer between two coaxial cylinders, obtaining temperature distribution by Fourier series expansion
21 p3952 A70-42082

Constricted arc characteristics in air and nitrogen at various pressures, considering spectral lines radiation transfer and electron, atom and ion temperature difference effects
22 p4079 A70-42369

Ames Hypervelocity Free Flight Facility, discussing aerodynamic tunnel, radiation tunnel and light gas gun for reentry simulation
22 p4006 A70-42764

Gas turbine combustion chamber convective and radiant heat transmission, examining steam film cooling of flame tube
22 p4092 A70-43199

Nonlinear heat transport in structural elements due to radiative transfer, analyzing temperature field dynamics
22 p4125 A70-43360

Thermospheric heating by solar radiation in Schumann-Runge continuum, taking height and atmospheric components distribution into account
23 p4188 A70-44060

Spherical multilayer shell unsteady temperature fields, assuming mixed convective and radiative transfer at inner surface due to hot gas flow
23 p4276 A70-44165

One dimensional radiation transfer equation in non-homogeneous particle field, discussing spatial variations, particle number density, temperature, size distribution and optical properties
23 p4281 A70-44445

Spectral bidirectional reflectance measurements of rough metallic surfaces for reflected energy spatial distribution determination in radiative heat transfer problems
23 p4281 A70-44446

Radiative cooling of shock heated air in cylindrical shock tubes, calculating enthalpy profiles for nonadiabatic air flow
23 p4282 A70-44586

Steady state radiative heat transfer through gray gas in spherical cavity, solving transport equation by singular integral equations for uniform heat generation
23 p4283 A70-44784

Launch optimization of artificial satellites for minimizing thermal radiative heat input during low altitude orbit
23 p4264 A70-45047

Planetary atmosphere diffuse radiative transfer reflection and transmission, deriving reciprocity relations from integrodifferential equations
24 p4409 A70-45756

Surface constitutive assumptions restrictions for rigid heat conductor, accounting for radiative heat supply
24 p4429 A70-46032

RADIATIVE LIFETIME
Bowen levels of O III radiative lifetimes and transition probabilities measurements by beam-foil spectroscopy
10 p1936 A70-23909

Graphite IR radiator for radiative capacity and flame temperature measurements investigated for life time dependence on ambient pressure and temperature
10 p1888 A70-24257

API state lifetime of CO measured using molecular level crossing spectroscopy
10 p1920 A70-24629

Radiative lifetimes determination from beta-chi violet transition probabilities of CN
10 p1947 A70-24991

Radiative lifetime for atomic transitions in UV multiplts of zinc and cadmium atoms and ions measured using phase shift method
11 p2086 A70-25363

- Short term influences on sealed carbon dioxide laser action and lifetime, using mass spectrometry
15 p2750 A70-31752
- He II 3s and 3d states mean lives and initial population as function of energy, analyzing emitted radiation intensity
16 p2954 A70-33059
- Mean lives of excited levels in neutral He by beam foil method testing calculations for radiative transition probabilities
16 p2955 A70-33296
- Cosmic ray lifetime, investigating radioactive Be 10 nuclei decay effects on intensity ratios Be/B and Be/Li, suggesting nuclei confinement to galactic disk
19 p3509 A70-38148
- Weak predissociation effects of hydroxyl compounds electron state on radiative lifetime via phase shift method
19 p3374 A70-38270
- Galactic cosmic rays lifetime based on nuclei and matter interactions, discussing ionization losses effect
20 p3695 A70-38966
- H alpha chromospheric network lifetime from time lapse photographs
20 p3711 A70-40409
- Decay lifetimes and electron impact cross sections of vacuum UV O I and O II emission multiplets, using pulsed electron beam in low pressure gases
21 p3852 A70-40718
- Electronic transitions in B by beam foil technique for spectral lines in 450-5000 A range, measuring excited levels mean lives
21 p3781 A70-41932
- Recombination lifetime /laser/ states in Si doped GaAs light emitting diodes on p-type thin platelets
21 p3838 A70-42016
- Rhodamine 6G triplet lifetime under continuous pumping by Ar laser
22 p4050 A70-43225
- Atomic or molecular gases excited state lifetime measurements, using time to amplitude conversion and multichannel analyzer
23 p4198 A70-44946
- RADIATIVE RECOMBINATION**
- Pinch characteristics of simple band structure semiconductors and nondegenerate electron gas during bimolecular current carrier recombination, determining hole pairs spatial and recombination spectral distribution
03 p0538 A70-13062
- Variational model of collisional-radiative recombination of atomic ions in hydrogen and alkali plasmas
09 p1735 A70-22828
- Primordial radiation spectrum, discussing possible distortions due to energy injection before and after recombination
12 p2308 A70-27886
- Recombination radiation intensity current dependence and I-V characteristics p-n-n diode operating in double injection mode and electrons trapping
14 p2625 A70-30163
- InAs p-n junction laser electrical and optical characteristics during spontaneous and stimulated radiative recombination
18 p3269 A70-36739
- UV oxygen nightglow observation by OGO-4, examining ion-ion neutralization and radiative recombination production mechanisms
20 p3621 A70-39344
- RF spectral recombination lines from atomic level transitions, discussing populations, H lines, electron temperature, density and emission and formation
20 p3706 A70-39934
- Terminal compensation influence on radiative recombination in n- and p-type GaAs, observing emission band in photoluminescence and electroluminescence spectra
23 p4231 A70-45063
- Formation and radiative recombination of free excitonic molecules in CuCl single crystals via Q switched ruby laser excitation
24 p4353 A70-45604
- RADIATORS**
- High gain helix radiators for spacecraft phased arrays, measuring performance vs design parameters
15 p2678 A70-32600
- RADICALS**
- Radicals in low pressure supersonic free jets, investigating production by flash photolysis
07 p1343 A70-20126
- Cyclization of alkoxyl radicals, investigating 4-pentenoxy radical and entropy factors effect
08 p1455 A70-20975
- Upper atmosphere ammonia release experiments testing hypothetical mechanisms of radicals and ions formation in comets
20 p3708 A70-39962
- Radicals induced in thymine monohydrate single crystals by ionizing radiation
20 p3583 A70-40455
- RADII**
- Icarus radar and optical observations indicating surface smoothness differences between central and higher latitudes, radius size and radar reflectivity
01 p0180 A70-10534

- Radar observations of Icarus, using detected echoes to determine radar cross section, radius size and reflectivity
01 p0180 A70-10535
- Icarus surface reflectivity estimated from reflected light polarization, combining estimate with inferred absolute magnitude to obtain radius
01 p0180 A70-10537
- Ionized meteor trails initial radii statistical characteristics determined for two models
01 p0192 A70-11537
- Mass and radius relations for zero temperature spheres of chemical elements, using equation of state and numerical integration
04 p0749 A70-14599
- Critical radii of curvature in elastoplastic bending of rib-reinforced aircraft components from wafer panels determined using strain energy method
08 p1506 A70-21183
- Orbit determination from two position vectors and periapsis radius, introducing polar equation for conic to obtain solution
09 p1760 A70-22932
- Single and clad glass fibers radii and refractive indices measurements on basis of laser light scattering
09 p1699 A70-23444
- Coherent light beam characteristics with Gaussian radial intensity variation during propagation along optical system axis, determining radius from diffraction theory
20 p3639 A70-39086
- Venus radius radar determination based on Mariner 5 and Veneras 5 and 6
21 p3883 A70-40714
- RADIO ALTIMETERS**
- Onboard radio altimeter for position finding of research rockets and balloons used for aeronomic investigations
02 p0298 A70-12084
- Pulse radar altimeter for measuring meteorological balloon altitude, using superregenerative RF stage
05 p0845 A70-15805
- Pulse radar altimeter design for balloon sounding, discussing flight tests, superregenerative stage, etc
07 p1286 A70-19996
- Altimeter-telemetry system for small sounding rockets, discussing ground and flight test results
13 p2363 A70-28688
- Pulse compression for geodesy satellite radar altimeter, considering tradeoff based on system accuracy, power and life
16 p2911 A70-33715
- RADIO ANTENNAS**
- EMI /electromagnetic interference/ antennas relative received voltage vs height above ground as functions of effective length, impedance, etc
01 p0042 A70-10087
- Gain, noise temperature and gain to noise temperature ratio measurement techniques for electrically large earth station antenna, recommending radio star technique
01 p0051 A70-11121
- Multimirror illumination system for radio telescope antenna with reduced noise temperature, narrow radiation pattern and optimal specular cross section, noting sensitivity
03 p0455 A70-13082
- Radio telescope efficiency improved at 8 mm wavelength by quantum paramagnetic amplifier and multimirror antenna system
03 p0455 A70-13083
- Radio/radar antenna temperature measurement by phase principle insensitive to receiver gain fluctuations
05 p0819 A70-15804
- Structural and systems design of large orbital radio astronomy antenna /crossed H interferometer/ with astronaut participation in deployment, operation, maintenance and updating [AIAA PAPER 70-100]
06 p1156 A70-18058
- Radio astronomical antenna structure synthesis based on excitation of unshaded mirror surfaces with symmetrical caustics and virtual sources outside of focal axis
07 p1239 A70-18758
- Antenna calibration by measuring emission of absorbing black disk positioned in Fresnel region
07 p1239 A70-18759
- Mathematical models of vertical antennas of finite length and height, discussing signal strength and LUF determinations
07 p1240 A70-19167
- Transistor RF and IF amplifiers designed for 210-ft antenna of Australian National Radio Astronomy Observatory
07 p1243 A70-20350
- Deconvolution of barely resolved radio sources mapped with elliptical antenna beams, noting telescope brightness distribution and power polar diagram
12 p2309 A70-27897
- Spherical reflector antenna with Gregorian correctors, calculating gain, far field radiation pattern and

- efficiency as functions of subreflector and feed positions
12 p2200 A70-28052
- Monograph on analysis of reflector antennas covering electromagnetic field equations, computer aided design, etc
13 p2367 A70-29600
- Receiving antenna for ionospheric scatter lines, calculating input power versus height and energy flux density spreading for position optimization
18 p2330 A70-36094
- Radio astronomical antenna structure synthesis based on excitation of unshaded mirror surfaces with symmetrical caustics and virtual sources outside of focal axis
18 p2333 A70-37102
- Antenna calibration by measuring emission of absorbing black disk positioned in Fresnel region
18 p2333 A70-37103
- RADIO ASTRONOMY**
- Pulsar CP 1919 radio emission observed on crossed wideband radio telescope in meter wavelength range, including pulse recordings
01 p0173 A70-10130
- Extraterrestrial sources radiation including galactic, solar and magnetospheric radio emissions observed by RAE-1 satellite at long wavelengths [AIAA PAPER 69-1049]
01 p0170 A70-10603
- Long baseline interferometry used to improve radio telescopes resolving power in measuring quasar diameters
01 p0183 A70-10885
- Astronomical studies at millimeter wavelengths, describing radiometer and Fabry-Perot interferometer design for submillimeter range
01 p0185 A70-10975
- Optical and radioastronomical observations of 1966 solar eclipse, discussing data and instruments
01 p0191 A70-11472
- Position determination for faint radio sources close to intense sources from radio astronomical maps
02 p0370 A70-12113
- Jupiter radio telescope observations at cm wavelengths, describing radiation belt emission characteristics and planetary brightness temperature spectrum
03 p0565 A70-13233
- Magnetic structure of type 4 solar outburst from continuous record of 80 MHz image and polarization
03 p0558 A70-13587
- Pulsar research discoveries characteristics, detection techniques and origin theories
04 p0746 A70-14507
- Interstellar formaldehyde absorption from radio observations with parametric amplifier
04 p0747 A70-14515
- North Galactic Spur compared for edge, ridge and neck with previous results noting sharp temperature gradients
04 p0758 A70-15690
- Variable object BL Lacertae flux measurements using Schmidt telescope photography and radio study, comparing results with quasar
04 p0759 A70-15711
- Radio wave-ionosphere interaction effects on accuracy of radio astronomical observations from earth satellites
04 p0683 A70-15740
- Radio astronomical observations of shape and drift velocity of focusing ionospheric discontinuities
05 p0841 A70-16740
- Circular polarization measurements of Jovian decimeter radiation by 210-ft radio telescope at Goldstone, California
05 p0921 A70-16986
- Radio astronomy spacecraft /RAS/ engineering design, technology and flight results
06 p1153 A70-17151
- Radio astronomical observations in millimeter wavelength region, discussing sun, moon, planets, galactic and extragalactic sources, etc
06 p1139 A70-17417
- Structural and systems design of large orbital radio astronomy antenna /crossed H interferometer/ with astronaut participation in deployment, operation, maintenance and updating [AIAA PAPER 70-100]
06 p1156 A70-18058
- Spectral observations of radio sources including 3C461, 3C405, 3C84, 3C144 and 3C273
07 p1376 A70-18913
- Extra-atmospheric submillimeter astronomy, discussing emission observations between IR and RF region and astrophysical-cosmological applications
07 p1387 A70-19643
- Lunar surface chemical composition determination by radio astronomy, considering SHF electrical properties of silicate earth rocks
08 p1572 A70-20940
- Collection of Soviet papers on radio astronomical instruments and observations
08 p1472 A70-21051
- Solar wind velocity radioastronomical measurements, discussing radio wave fluctuations, telescope antenna designs, radiometers and observations
08 p1474 A70-21070

Pulsar CP 1919 radio emission observed on crossed wideband radio telescope in meter wavelength range, including pulse recordings

08 p1576 A70-21404

UHF telescopic survey of southern sky for studying galactic plane in absorption

08 p1578 A70-21536

Pulsar NP 0532 average polarization parameters measured at 430 MHz, discussing variations of precursor and main pulse and flux of interpulse

08 p1578 A70-21549

Jupiter radio telescope observations at cm wavelengths, describing radiation belt emission characteristics and planetary brightness temperature spectrum

08 p1580 A70-21666

Book on solar and planetary radio emission covering solar system physical characteristics, quiet Sun, thermal and nonthermal emission, etc

09 p1752 A70-22201

Spaceborne long wavelength radio astronomy, proposing lunar orbit and beyond Pluto observatories to reduce magnetospheric and interplanetary plasma effects

09 p1754 A70-22495

Saturn disk temperature obtained from centimeter wavelength, suggesting possibility of nonthermal radiation

09 p1759 A70-22912

Meteor astronomical parameters measurement by pulsed and CW radio methods, considering effects of wind, meteor trails, phase angle, etc

09 p1638 A70-23627

Jupiter brightness temperature values and standard deviations from EHF radio telescopic observations

09 p1765 A70-23809

Formaldehyde absorption profile in direction of Milky Way center observed using lunar occultation

10 p1936 A70-23905

Hydrogen 109 alpha recombination line emission in galactic H II regions surveyed at National Radio Astronomy Observatory

10 p1936 A70-23942

Cygnus X region surveyed with NRAO radio telescope, estimating visual absorption by comparing radio and H alpha emission

10 p1937 A70-23943

Hydrogen 21 cm emission line in Perseus region observed for motion of neutral hydrogen connected with II Per, discussing stellar radial velocity

10 p1937 A70-23944

Cosmic rays, particles and fields physics in relation to radio and X ray astronomy

10 p1931 A70-24410

Solar mapping using millimeter wave radio telescope, comparing results with H alpha photographs and magnetograms

10 p1945 A70-24963

Transitions in interstellar OH observed at National Radio Astronomy Observatory

10 p1948 A70-25000

Atomic frequency standards for phase calibration of large aerial arrays applied to radioheliograph

11 p2019 A70-26300

Beam switching Cassegrain antenna for millimeter wave radio astronomical measurements, describing RF and electronic systems

11 p2019 A70-26374

Aperture synthesis and spectral antenna characteristics in radio astronomy, considering Ryle systems, Mills-Christiansen crosses and variable interferometers

11 p2019 A70-26801

Vertical tilt and horizontal position of antenna rotating device in radio astronomy and radar observations using photogrammetric methods

12 p2195 A70-27478

Pulsar research, discussing possibilities in probing galactic medium

12 p2301 A70-27577

Milky Way large scale structure from radio recombination line surveys

12 p2301 A70-27580

Solar radio emission maps at 8.6 mm using parabolic antenna and TV camera for optical control

12 p2293 A70-27591

Cassiopeia A high resolution map at UHF revealing main source physical characteristics and enhanced emission compact components

12 p2309 A70-27976

Radio receiver bandwidth effect on lunar occultation observations

12 p2189 A70-27989

Submillimeter astronomy, discussing atmospheric absorption difficulties and principal areas of application

12 p2311 A70-28271

Galactic noise spectrum and solar radio bursts in hecto-decametric wave region observed by Alouette 2 satellite

13 p2491 A70-29093

Galactic continuum surveys at 8000 MHz by radio telescope, noting North American nebula and Cyg X region

13 p2491 A70-29096

Radio wave-ionosphere interaction effects on accuracy of radio astronomical observations from earth satellites

14 p2575 A70-30824

Water sources associated with W3, Orion Nebula, W49 and VY Canis Majoris observed with coherent interferometers having long baseline

14 p2642 A70-30892

Radio astronomical observations of lunar surface material EM properties compared with Surveyor 7 chemical analysis

14 p2645 A70-31059

Venus and Mercury radio and radar studies concerning brightness temperature, surface reflectivity and planetary motion

14 p2647 A70-31074

Lunar occultation observation of Jupiter by radio telescope, determining one dimensional strip brightness distribution

14 p2648 A70-31086

Book on nonthermal processes in galactic and extragalactic radio sources covering plasma behavior in magnetic field, energy redistribution in spectrum by electron scattering, etc

15 p2799 A70-31999

Lunar surface chemical composition determination by radio astronomy, considering SHF electrical properties of silicate earth rocks

15 p2805 A70-32752

Weak radio sources positions, structures and optical identifications from lunar occultation observations, tabulating radio and optical data

17 p3156 A70-34826

Synchronous oscillators of radio astronomical interferometer, discussing dephasing and servocoupling

17 p3090 A70-35415

Planar Tethered Orbiting Interferometer satellite for long wavelength solar and planetary radio astronomy, discussing deployment control and libration damping

18 p3333 A70-36230

Galactic center region lunar occultations in 21 cm neutral hydrogen line

18 p3313 A70-36328

Solar corona structure on 22 September 1968 using radio astronomical and optical eclipse data

18 p3315 A70-36607

Radio sources near 2 flux units at 408 MHz, presenting data on positions, optical identifications, angular size and flux densities

18 p3321 A70-37125

H I local spiral arm drift curves from radio telescope operation

18 p3328 A70-37171

Solar eclipse of 20 May 1966, analyzing radio observations

19 p3521 A70-38554

Solar eclipse of 22 September 1968, analyzing radio observations

19 p3521 A70-38555

Supernova remnants catalog based on radio surface brightness, deriving galactic distribution and testing theories for nonthermal radio sources evolution

20 p3709 A70-40077

Millimeter wave observation of sun, deriving empirical relationships between atmospheric attenuation, emission and water vapor

20 p3623 A70-40304

T, Y and ring microwave antenna array configurations for radio astronomy, comparing baseline distributions

20 p3599 A70-40317

Sc X-1 radio emission models, considering possible binary nature and thermal bremsstrahlung

21 p3875 A70-40685

Cold neutral atomic hydrogen in Taurus dust clouds from 21 cm line dips in radiotelescope observations

21 p3887 A70-41108

Carina nebula NGC 3372 continuum map at 5 GHz compared to optical photographs, discussing H alpha lines

21 p3887 A70-41109

Radio observations of limb darkening and structure of solar corona at 80 MHz

21 p3890 A70-41177

SHF-EHF region uses, discussing microwave radiometry and applications to radio astronomy and meteorology

21 p3799 A70-41421

Radio search for formaldehyde rotational transition and H 109 alpha recombination line in comet Bennett during perihelion passage

21 p3921 A70-41976

M87 radio observations at 5 GHz, examining central region components, optical nucleus and jet and X ray emission

21 p3923 A70-42103

Extragalactic radio astronomy development, describing source characteristics, distribution, spectra, brightness polarization, synchrotron radiation and evolution

22 p4098 A70-42580

Atomic hydrogen 21 cm line intensity distribution in Carina arm of Milky Way galaxy

22 p4100 A70-42851

Solar type 4 event flux density and circular polarization radiopolarimetric recording, showing peculiar phases of short duration

22 p4095 A70-43263

Solar radio burst observation before 7 March 1970 solar eclipse, tabulating spectrum data

22 p4095 A70-43266

H II regions density-size relationship, using emission measurements and radio data

22 p4109 A70-43746

Galactic plane continuum surveys at 8000 MHz, presenting radio contour map and sources list

22 p4109 A70-43747

Full-scanning random arrays with high resolution for space exploration, radio astronomy and long range radar

23 p4160 A70-43770

Structure and systems design of large gravity gradient stabilized orbiting tethered satellites structure for radio astronomy

23 p4259 A70-44603

Radio astronomy research covering solar radio emission, Milky Way radiation, molecular radio line spectra, etc

23 p4256 A70-45041

Optical quasi-stellar objects radio emission observation for identification with radio sources

24 p4413 A70-46167

RADIO ASTRONOMY EXPLORER SATELLITE

Tethered orbiting interferometer configurations for future Radio Astronomy Explorer satellites, discussing gravitational stabilization and delta launching into orbit as single payload

[AAS PAPER 69-255] 09 p1766 A70-22930

Radio astronomy explorer /RAE/ satellite main antenna array, describing elements, dispenser and take-up mechanisms, construction materials, etc

16 p2986 A70-34144

Radio Astronomy Explorer satellite boom deployment method resulting in gravity gradient capture, emphasizing role of predeployment attitude and antenna Vee angle

[AIAA PAPER 69-920] 21 p3931 A70-41856

Radio astronomy Explorer A attitude determination via disk-oriented programming ground support system for reducing and calibrating telemetry data, attitude prediction and command, etc

[AIAA PAPER 69-983] 21 p3795 A70-41857

RADIO ATTENUATION

Midlatitude ionospheric disturbances accompanied by auroral type radio absorption observed by radio astronomy and probes during 26 May 1967 storm

01 p0084 A70-11555

D layer radio absorption during solar eclipse of 22 September 1968 attributed to two solar X-ray sources

03 p0559 A70-13602

Interplanetary field influence on auroral radio absorption, considering sector structure of solar wind

03 p0476 A70-13915

VLF phase disturbances and HF absorption during solar proton events of 28 August and 2 September 1966 related to proton intensities, energies and cut-off latitudes

04 p0741 A70-15124

Ionospheric integral radio absorption measured by radio astronomical A2 method, including anomalous absorption during disturbances

04 p0650 A70-15283

Riometric data processing method for radio wave absorption measurement, considering nighttime cosmic radio emission intensity

05 p0842 A70-16742

Radio wave absorption coefficient in lower ionosphere related to total radiation absorption and electron concentration profile

05 p0843 A70-16761

Nighttime radio wave absorption in ionosphere during moderate solar activity based on echo observations

06 p1056 A70-17840

D and lower E region absorption of short waves, studying absorption distribution with height

07 p1263 A70-19153

Graphic method of calculating radio wave absorption in ionosphere and field strength at reception point with aid of vertical sounding data

07 p1235 A70-19437

Cosmic radio absorption nightly variations, considering ionospheric structure and composition and various scattering mechanisms

07 p1367 A70-19456

Radio wave absorption in Venusian ionosphere, estimating effective collision number

07 p1235 A70-19491

Frequency characteristics deviation of discrete cosmic radio emission sources from exponential law, analyzing radio wave absorption in galactic and intergalactic media and ionized hydrogen

07 p1370 A70-20315

Deviating and nondeviating absorption of radiowaves in ionosphere, deriving vertical distribution of particle collisions in E layer

08 p1490 A70-21431

- Sunspot cycle and ionospheric D and E layers daily radio wave absorption correlation, observing seasonal variation effect 10 p1885 A70-25267
- Auroral radio wave absorption in ionosphere at longitudinally opposite stations compared for appearance probability and variational properties 11 p2043 A70-25537
- Radio wave absorption at 2.2 MHz measured by vertical incidence pulse method, observing maxima in February and in September-October due to auroral activity 11 p2006 A70-26176
- Radio waves attenuation anisotropy in sea ice by comparing vertically and horizontally polarized signals 14 p2546 A70-30132
- Radio wave absorption in Venusian ionosphere, estimating effective collision number 15 p2705 A70-32736
- Attenuation characteristics for dominant hybrid mode in corrugated circular waveguide for antenna feed 16 p2879 A70-34041
- Transceiving system for recording D region radio signal absorption and reflection, describing component circuitry and operation 16 p2880 A70-34225
- Ozone content effect on presunrise fall in LF radio waves amplitude from Radio Tashkent to Delhi, noting UV light role 17 p3077 A70-34947
- Lower ionosphere electron density and winter anomaly in HF absorption 17 p3077 A70-34948
- Graphic method of calculating radio wave absorption in ionosphere and field strength at reception point with aid of vertical sounding data 18 p3229 A70-36911
- Cosmic radio absorption nightly variations, considering ionospheric structure and composition and various scattering mechanisms 18 p3309 A70-36930
- Ionospheric radio wave absorption and geomagnetic perturbations correlated with solar activity variations 18 p3250 A70-36931
- Point source electric field over different sections of impedance piecewise inhomogeneous surface, calculating attenuation function near boundaries 19 p3381 A70-38570
- Diurnal variations of sudden enhancements and decreases of ELF atmospherics, using mode theory 21 p3814 A70-40939
- Auroral radio wave absorption in ionosphere at longitudinally opposite stations compared for appearance probability and variational properties 21 p3819 A70-41287
- Ionospheric radio wave absorption above polar aurorae during solar activity minimum, discussing diurnal and annual behavior 23 p4162 A70-44058
- RADIO AURORAS**
- Radio waves propagation along polar auroras region, obtaining ionospheric parameters for magnetic disturbances based on penetration probability 05 p0842 A70-16744
- LF waves and irregularities in auroral ionosphere determined by radar measurements, suggesting role of plasma waves cross modulation 07 p1264 A70-19193
- Lunar periodicity detected from radio aurora data as possible cause of lunar interaction with magnetosphere 07 p1389 A70-20164
- Northern Hemisphere radar aurora latitude variation, considering magnetic activity effects 15 p2697 A70-31770
- VHF radio auroral scatter signal correlation analysis, determining scale size and drift velocity of scattered field 17 p3047 A70-35548
- Radio aurora model based on two stream, ion acoustic wave instability, investigating radar backscatter 20 p3623 A70-40465
- RADIO BEACONS**
- NT OMNIDIRECTIONAL RADIO RANGES**
- Beacon equipment as means of crashed or forced-landed aircraft locator to increase survival possibilities and reduce search cost 01 p0035 A70-10719
- Scanning beam radio guidance system for VTOL approach and landing 02 p0336 A70-12766
- Simplified aircraft instrument landing system /SAILS/ employing lightweight helicopter-borne radar for tracking radio beacon at touchdown point 02 p0337 A70-12768
- Electron density profiles along OGO 1 orbit portions calculated by measuring harmonic radio beacon transmissions differential Doppler frequencies and Faraday polarization rotation angle 04 p0741 A70-15118
- Design concept and operation of electronically lobed homing system providing commands to pilot for

flying aircraft directly to transmitting emergency beacon 06 p0987 A70-17725

Emergency equipment for aircraft accidents with dual channel radio beacons installed on life rafts, noting electronically conducted search 07 p1191 A70-19011

Lithium-cadmium fluoride battery for aircraft survival beacon radio receivers, considering voltage loss elimination by doping 08 p1439 A70-20708

Radio marker beacon-receiver design, tabulating technical data 09 p1684 A70-23574

Air traffic safety problems, discussing satellite radiobeacons applications to aerial navigation 22 p4066 A70-42652

Geometry and ionosphere effects on radio beacon operation for distress signal monitoring at sea, comparing night performance to daytime 23 p4163 A70-44229

RADIO BLACKOUT

U BLACKOUT [PROPAGATION]

RADIO BROADCASTING

U BROADCASTING

RADIO BURSTS

NT SOLAR RADIO BURSTS

NT TYPE 2 BURSTS

NT TYPE 3 BURSTS

NT TYPE 4 BURSTS

NT TYPE 5 BURSTS

MM wave outbursts of 1 and 2 November 1968, discussing wavelength dependence of flux density 05 p0912 A70-16441

Particle acceleration during 1966-1967 radio burst of 3C 273, indicating breaking down of model of expanding source emitting synchrotron radiation 05 p0918 A70-16927

Modulation lanes in fine structure of dynamic spectra of Jovian L bursts possibly due to ionosphere or magnetosphere 08 p1576 A70-21394

Receiver bandwidth effect on audible radio noise bursts parameters of quasi-peak value, burst duration and time interval 08 p1464 A70-21800

Flare star burst energy from radio telescope observations compared with solar flares 10 p1936 A70-23916

Jupiter decametric radio bursts observed by tape recording fringe interferometer 13 p2486 A70-28626

RADIO COMMUNICATION

NT PULSE FREQUENCY MODULATION

TELEMETRY

NT RADIO RELAY SYSTEMS

NT RADIO TELEMETRY

NT TELEPHONY

NT TELEPHOTOMETRY

Book on ionospheric scattering effects on long distance radio communication, considering Arctic ionosphere, scatter propagation, modulation, sporadic E, etc 01 p0046 A70-11305

Wave propagation problem, considering traffic control, surveying, tracking, navigation, etc 03 p0449 A70-13607

Ground station location, equipment and function for radio communication with German research satellites, noting NASA and ESRO cooperation 04 p0664 A70-15304

Adaptive frequency selection of optimum channels for radio communication on noninterference basis, discussing implementation and compatibility problems with nonadaptive systems 05 p0814 A70-16347

Optimal design of tropospheric scatter radio link between two localities, investigating power, antenna, diversity, frequency deviation and equipment 05 p0814 A70-16361

Ionospheric horizontal discontinuities of electron density distribution parameters effect on penetration frequency, skip distances and arrival angles 05 p0842 A70-16743

Polarization- and space-diversity reception techniques for radio links based on diffraction from ionized meteor trails 07 p1378 A70-18990

Geometrical and electrical characteristics of two mirror parabolic antenna for tropospheric radio relay communications lines in centimeter band, analyzing radiation patterns 07 p1240 A70-19125

Ray tracing in ionospheric HF communications, describing computational method for ray paths and ionospheric absorption 07 p1230 A70-19166

Radiometeorology research emphasizing interaction between troposphere and VHF waves to improve space and terrestrial radio communication 07 p1234 A70-19216

Stable moored ocean platforms providing reliable VHF communications and secondary surveillance

radar facilities for civil aviation operations over North Atlantic 09 p1723 A70-23035

Millimeter wave transmission, discussing atmospheric effects, system components and applications in terrestrial communication networks, synchronous satellites, etc 10 p1842 A70-24883

Electromagnetic pulse distortion with Gaussian envelope in longitudinally inhomogeneous anisotropic ionized media to investigate radio wave communication with ionospheric propagation 12 p2189 A70-27962

Inclined backscatter sounding of ionosphere in individual channels of multichannel radio link, analyzing data during minimum solar activity 14 p2547 A70-30149

Vaporization of small meteor particles with identical surface temperature, considering radio communication based on reflection from ionized trails 14 p2636 A70-30323

Wave polarization effects on ionospheric HF radio wave transmission and reception in communication and broadcasting networks 14 p2550 A70-30650

Trojan Relay system with satellites preceding and following Earth in solar orbit ensuring radio communication throughout solar system 15 p2698 A70-32061

Worldwide multichannel air communications system in 10 GHz to IR range by Quasi Laser Link modulation and satellites 19 p3378 A70-37855

RF communication signal to noise improvement by time variant tracking filter with high Q superconductive resonant cavity 19 p3391 A70-38892

Crystal controlled digital frequency setting for microwave oscillators in mobile FM radio links with remote handling 20 p3596 A70-39162

Satellites for direct radio and TV broadcasting, considering system quality and cost, network planning, frequency economy, etc 20 p3588 A70-40158

Deep space microwave and optical communications, describing grand tour requirements 21 p3784 A70-40546

RF requirements of deep space-outer planet spacecraft communications for Jupiter, Saturn, Uranus and Neptune flyby missions 21 p3791 A70-41369

Millimeter wave radio systems for relieving crowding at lower frequencies, discussing technology, atmosphere effects and applications 22 p3990 A70-43418

Binary data transmission via radio channel, discussing phase and frequency modulation and error probability as SNR function 23 p4159 A70-43756

Microwave communication - Conference, Budapest, April 1970, Volume 5, Microwave electronics, system measurements 23 p4170 A70-43793

RADIO CONTROL

Noise effects on joint operation of signal follow-up system with search device using semi-Markov random technique 08 p1461 A70-20864

Radio and inertial guidance of Europa 1 and 2 ELDO launch vehicles 08 p1542 A70-21870

Radio command guidance system for Mars probe ascent from surface to rendezvous with flyby vehicle on escape trajectory 13 p2447 A70-28421

Optimum filtering techniques for radio guidance of third stage of Europa 1 booster compared for effectiveness 13 p2381 A70-28437

RADIO DIRECTION FINDERS

UHF ranging system principles, discussing output proportional to approach angle 02 p0257 A70-12179

Coherent and incoherent interference effects on direction finding information derivation, using linear two channel principle 03 p0452 A70-14024

Angular resolution dependence on bearing ambiguities in radio direction finders based on interference measurement, using digital logic circuits 04 p0659 A70-15335

Simultaneous maximum likelihood estimation and coordinate conversion for redundant hyperbolic lines of position in radio navigation [AIAA PAPER 68-888] 04 p0717 A70-15545

Amplitude scanning, multiple beam and dual baseline phase comparison direction finding receivers for installation in aircraft to locate and analyze radar signatures 04 p0653 A70-15657

Direction finding characteristics of nonlinear antenna, including current determination and optimal angle for sidelobe level 06 p1023 A70-18561

Minimum performance standards for airborne radio receiving and direction finding equipment covering normal and environmental test procedures

13 p2365 A70-29000

Electronically lobed direction finder homing system for location and rescue of airmen downed on aircraft with emergency locator transmitter

13 p2449 A70-29170

Search radar antennas for monopulse direction finding with radiation pattern for sum and difference operation

15 p2704 A70-32674

Dual mode log periodic spiral DF antenna system, using monopulse to provide azimuth and bearing elevation data

16 p2863 A70-33450

Direction finder for point source signals, discussing mathematical model for random noise in space, S/N performance and equipment design

17 p3042 A70-34586

Radio direction finding of celestial bodies from moving platform, determining plane rotation effects on angle measurements

18 p3333 A70-36164

RADIO ECHOES

Lower ionosphere radio wave partial reflection strength relationship to electron density profiles measured by rocket probes

01 p0045 A70-11089

Spread F echoes occurrence variations over solar cycle, observing range and frequency splitting type during maximum and minimum sunspot years

01 p0080 A70-11222

Leonid meteoroids mass distribution law exponent evaluation based on unstable meteoric radio echo durations integral distribution

03 p0574 A70-13884

Ionospheric propagation experiments to measure radio echo height changes, observing correlation between LF signal reflection and MF transmitter power

04 p0650 A70-15132

Backscattered signal power density distribution along equivalent propagation path of delayed components, determining reflecting layers characteristics from echo signal phase

04 p0654 A70-15728

Polarization nature and changes evaluation of radio echo signals reflected from polar auroras

04 p0682 A70-15730

Auroral radio reflections using two coherent bistatic radio systems, discussing ionoacoustic waves in auroral plasma

05 p0837 A70-16072

Ionospheric observations of resonance oscillations using satellite-borne radio sounding instruments

06 p1115 A70-17361

Backscatter observations of F region field-aligned irregularities during IQSY, discussing diurnal variations of echoes

06 p1059 A70-18539

Ionization irregularities and drift in sporadic E layer determined using Mitra method for ground based radio reflection

06 p1012 A70-18543

Spread F echoes due to total reflection from large tilted ionized surfaces, using ionograms and airglow observations to study surface geometry

07 p1271 A70-20158

Long wave transmitter field strength calculation to 1000 km based on optical beam method and ionosphere model to account for radio wave reflection

10 p1840 A70-24495

Radio wave reflection from ionosphere, discussing suppression of magnetoionic component with fluctuating elliptical polarization

11 p2003 A70-25534

D region synoptic ionization changes investigated by radio waves partial reflection from lower ionosphere, relating wave amplitudes to height

12 p2224 A70-27732

Radio meteor train initial radius determination, discussing radio echo observation method

12 p2309 A70-27977

Proton cyclotron echoes in topside ionograms from Alouette 2 satellite

13 p2396 A70-29092

Lower ionosphere influence on radio reflection from sporadic E layer, determining diurnal variations of D region absorption for various frequencies

14 p2547 A70-30235

Lower ionosphere radio reflection during solar eclipse of 22 September 1968

14 p2571 A70-30237

Forward and backscattering meteor radio echo intensity variations during decay under molecular and turbulent diffusion, recombination and trapping

14 p2635 A70-30313

Meteoric radio reflections time variation based on observations at two frequencies, analyzing angular dimensions in reflecting regions

14 p2635 A70-30315

Radio wave scattering and echo intensity at inhomogeneous underdense meteor trail allowing for

electron density, trail formation time and diffusion coefficient

14 p2636 A70-30316

Ionized meteor trail radio signal reflections, observing duration and echo quantity random deviations and activity coefficient at specified times

14 p2636 A70-30318

Meteor radio reflections time-amplitude characteristics, discussing dependence on mirror point position in trail, wavelength, diffusion factor and initial radius

14 p2636 A70-30324

Radio echoes duration distribution from supercondensed meteoric trail emphasizing effects of recombination, adherence and turbulent diffusion

14 p2636 A70-30325

Radio wave reflection from ionized meteor trails, calculating propagation parameters by computer algorithm based on cylindrical approximation method

14 p2636 A70-30327

Errors estimation in wind velocity values by radio echo observations in meteor trails of different densities

14 p2572 A70-30330

Backscattered signal power density distribution along equivalent propagation path of delayed components, determining reflecting layers characteristics from echo signal phase

14 p2550 A70-30812

Polarization nature and changes evaluation of radio echo signals reflected from polar auroras

14 p2575 A70-30814

Single pulse ionospheric sounding system for detecting and identifying E region echoes

16 p2859 A70-32940

Reflection coefficient formula for principal radio wave reflected from thin long rod in middle of rectangular waveguide

16 p2878 A70-33800

Transceiving system for recording D region radio signal absorption and reflection, describing component circuitry and operation

16 p2880 A70-34225

Ionospheric radio wave absorption measurements, noting winter anomaly during maximum solar activity year

18 p3227 A70-36101

Electron concentration vertical profile in ionosphere as function of altitude of radio wave reflection and group refraction and velocity characteristics

19 p3409 A70-37329

Group delay times criterion of multibeam propagation of ionospheric radio echoes for communications systems

19 p3375 A70-37332

Free atmosphere turbulent diffusion coefficient determination, releasing dipole reflectors from helicopter for radio echo observation

19 p3461 A70-37423

Low elevation angle focusing of oblique radio waves after reflection from E and F layers

19 p3379 A70-37965

Ionospheric D region irregularities with partially reflected radio wave pulses, using phase path and drift measurements

21 p3814 A70-40941

Radio wave reflection from ionosphere, discussing suppression of magnetoionic component with fluctuating elliptical polarization

21 p3786 A70-41284

Lower ionosphere influence on radio reflection from sporadic E layer, determining diurnal variations of D region absorption for various frequencies

24 p4316 A70-46310

Lower ionosphere radio reflection during solar eclipse of 22 September 1968

24 p4332 A70-46312

RADIO ELECTRONICS

Equivalent radioelectric plan of ammoniac maser marginal type oscillator

18 p3265 A70-35946

Soviet book on operational tolerances in radio electronic equipment from reliability criteria

20 p3597 A70-39400

Radio electronic circuits precision, deriving relationship between frequency response and component variations solvable by linear programming

23 p4171 A70-43958

RADIO EMISSION

NT SOLAR RADIO BURSTS

NT SOLAR RADIO EMISSION

NT TYPE 2 BURSTS

NT TYPE 3 BURSTS

NT TYPE 4 BURSTS

NT TYPE 5 BURSTS

Rotation period of Jupiter based on decametric component of radio emission, suggesting anticorrelation with sunspot number for drift observed

01 p0173 A70-10044

Pulsar CP 1919 radio emission observed on crossed wideband radio telescope in meter wavelength range, including pulse recordings

01 p0173 A70-10130

Geomagnetic field influence on extensive air shower radio emission, discussing frequency dependency and signal polarization

01 p0069 A70-10281

Comparative diagrams for radio emission intensities of pulsar PP 0943 from observations by cross radio telescope

01 p0195 A70-11034

Elektron 4 satellite radio emission data transmitted from July to December 1964, noting month-to-month variations in mean radiation level

01 p0172 A70-11496

Radio sources emission separations statistical analysis, establishing little physical association in pairs of sources

02 p0370 A70-12112

High energy extensive air shower detection by Cerenkov receivers or liquid scintillators, considering 200 and 3000 MHz radio emission mechanisms

02 p0357 A70-12115

Quasars radio emission tabulated, showing quasar B264 as member of galactic cluster

02 p0372 A70-12244

Induced Compton scattering of plasma and electromagnetic waves under astrophysical conditions, discussing HF radio emission spectra from cosmic objects and quasar

05 p0917 A70-16904

Radio emission measurements of moon at 3.2 cm by artificial moon method, calculating radio temperature and phase amplitudes

05 p0918 A70-16919

Astrophysical plasmas radio emission interpreted as collective bremsstrahlung due to ultrarelativistic electron tails, discussing Crab Nebula, quasars and Jupiter

05 p0904 A70-16932

Radio emission distribution from supernova remnants and galactic magnetic field

06 p1139 A70-17323

Magnetospheric VLF emissions properties at frequencies below electron gyrofrequency

06 p1117 A70-17374

Vertical air density profile from satellite measurements of atmospheric oxygen radio emission at 40-70 km altitudes

06 p1056 A70-17788

Radio brightness distribution observation over Venus disk, investigating absorption of millimeter radio emission of hot surface by planetary atmosphere

06 p1141 A70-17801

Geophysical parameters of atmosphere and underlying surfaces from outgoing thermal radio emission measurements on Cosmos 243 satellite

07 p1261 A70-18724

Polarized and unpolarized emission measurements of W 44 supernova remnant with radio telescope, showing results for eastern portion of source

07 p1383 A70-19405

Atmospheric integral moisture content determination from thermal radio emission measurements by Cosmos 243 satellite

07 p1329 A70-19649

Frequency characteristics deviation of discrete cosmic radio emission sources from exponential law, analyzing radio wave absorption in galactic and intergalactic media and ionized hydrogen

07 p1370 A70-20315

Coherent and incoherent radio emission from extensive air showers simultaneously detected by radio telescope in VHF-UHF range

08 p1563 A70-20475

Zero radiospectrometer for spectral observations of radio emission of excited galactic hydrogen at centimeter wavelength, noting Omega nebula detection

08 p1495 A70-21063

Pulsar CP 1919 radio emission observed on crossed wideband radio telescope in meter wavelength range, including pulse recordings

08 p1576 A70-21404

Cygnus X region surveyed with NRAO radio telescope, estimating visual absorption by comparing radio and H alpha emission

10 p1937 A70-23943

Comparative diagrams for radio emission intensities of pulsar PP 0943 from observations by cross radio telescope

10 p1948 A70-25003

Vertical air density profile from satellite measurements of atmospheric oxygen radio emission at 40-70 km altitudes

10 p1882 A70-25020

Pulsar radio emission reception with improved SNR based on periodic variation of average reception frequency with time

10 p1948 A70-25165

Long wave cosmic radio background emission in circumlunar space by Luna 11 and 12 satellites, observing increase in earth magnetosphere tail

12 p2295 A70-28262

Electron beam interaction with plasma in absence of magnetic field, discussing microwave radiation emission and incoherent scattering and instability spatial growth

13 p2459 A70-28569

Radio brightness distribution observation over Venus disk, investigating absorption of millimeter radio emission of hot surface by planetary atmosphere 13 p2487 A70-28651

Whistler mode VLF emissions stimulation mechanism 13 p2401 A70-29930

Magnetospheric discrete VLF emission magnetic field intensity calculation by extending Helliwell theory to include electron density model and variable frequency waves 13 p2483 A70-30087

Pulsar short period pulsations and emission patterns in meter wavelength range on crossed radio telescope 14 p2633 A70-30151

M31 continuum radio emission produced by magnetic field aligned along arms, discussing field turbulence effects 14 p2642 A70-30891

Mars surface material properties from radio emission observations, considering daily temperature variations distribution 14 p2648 A70-31083

Thermal radio emission from major planets at mm and cm wavelengths and at decimeter wavelengths for Jupiter and Saturn 14 p2648 A70-31084

Jupiter decimeter radiation long term variations from flux density measurements, suggesting correlation with solar activity 14 p2648 A70-31087

Sea surface temperature and atmospheric moisture determination from satellite measurements of atmospheric thermal radio emission on quiet and cloudy windy days 15 p2770 A70-32069

Clouds and precipitations radio brightness temperature contrasts taking into account underlying surface humidity 15 p2771 A70-32070

Atmospheric humidity determination from satellite radio emission measurements at SHF 15 p2771 A70-32071

Coherent radio emission mechanisms of white dwarfs and neutron stars as magnetic pulsar models, discussing polarization 15 p2804 A70-32698

Neutron stars gamma and radio emission in gas accretion state, determining surface gravitational potential 15 p2808 A70-32883

Cosmic ray air showers UHF emission detection at 500 MHz 17 p3151 A70-34850

Giant E and SO galaxies, discussing radio spectra, emission characteristics and brightness distributions 18 p3313 A70-36332

Radio emission search from IR objects near IC 1805 18 p3318 A70-37018

Jupiter decametric radio emission modulation by Io simulated by DC circuit model 18 p3321 A70-37120

Milky Way galaxy continuous background radio emission observed at various longitude intervals 18 p3322 A70-37130

Radio wave emission from dust in H II region by dielectric grain photoelectric charging, rotation through stellar photons and rotating dipoles 19 p3518 A70-38024

Interstellar molecular radio frequency lines significance to galactic physics, noting abundance relation to constituent atoms indicating dust catalytic formation 19 p3521 A70-38496

Radio polarization of quasars with and without absorption line spectra 19 p3523 A70-38605

Air shower radio pulse amplitude dependence on primary energy and core distance 19 p3381 A70-38607

Sbc galaxy NGC 7320 radio emission and neutral H observations, showing improbability of physical association with Stephan Quintet by distance measurement 19 p3524 A70-38699

Pulsar short period pulsations and emission patterns in meter wavelength range on crossed radio telescope 21 p3923 A70-42073

Radio emission searched for X ray sources near Sagittarius 22 p4094 A70-42930

ELF emissions dependence on plasmapause location in magnetosphere indicated from OV-3 observations 23 p4186 A70-43847

Far field power of coherent Cerenkov radio emission from cosmic ray showers in turbulent atmosphere, using radio telescopes 23 p4247 A70-44791

Current sheet motion and pulsar radio, optical and X ray emission, investigating finite thickness oscillating interface radiation with independent particle 24 p4397 A70-45760

Delphini and Serpenti Novae radio emission in microwave spectra, noting consistency with thermal radiation of expanding ionized gas envelopes 24 p4410 A70-45771

Pulsars radio evolution mechanism by phenomenological analysis, deriving time dependences of period, luminosity and emitting region size 24 p4412 A70-46101

Optical quasi-stellar objects radio emission observation for identification with radio sources 24 p4413 A70-46167

RADIO ENERGY

U RADIANT FLUX DENSITY

U RADIO WAVES

RADIO EQUIPMENT

NT IONOSONDES

NT OMNIDIRECTIONAL RADIO RANGES

NT RADIO ANTENNAS

NT RADIO BEACONS

NT RADIO FILTERS

NT RADIO RECEIVERS

NT RADIO TELESCOPES

NT RADIO TRANSMITTERS

NT RADIOSONDES

NT RAWINSONDES

NT SPACECRAFT ANTENNAS

NT SUPERHETERODYNE RECEIVERS

NT TRANSMITTER RECEIVERS

NT TRANSPONDERS

NT VERY HIGH FREQUENCY RADIO EQUIPMENT

NT WHISTLER RECORDERS

AN/PRC-87 Pararecuse radio for hands free operation, using bone conduction microphone, voice operated transmitter, etc 06 p0986 A70-17723

Digital computer design of electric and radio equipment using secondary source method for field boundary calculation in inhomogeneous environment 07 p1241 A70-19480

Fading effect on error probability of multi-hop PCM radio system, noting domination by worst hop 08 p1458 A70-20797

Collection of Soviet papers on radio astronomical instruments and observations 08 p1472 A70-21051

Electronic radio equipment with encapsulated structure and natural ventilation, calculating heated zone and casing mean surface temperatures 09 p1648 A70-23147

Radio and automatic control electronic equipment reliability estimation by vibration testing, determining test stand simulation accuracy 09 p1650 A70-23632

Heating rate of radio electronic equipment with variable power shown dependent on initial dissipated power 10 p1853 A70-25134

Hazardous X ray bremsstrahlung from military radio electronic equipment, discussing radiation protection and operating safety standards 12 p2180 A70-28360

Radio and electronic equipments production testing by automatic equipment combined with semiautomatic manual controller 13 p2379 A70-29680

Ionospheric scatter channel amplitude frequency characteristics recording equipment, discussing design 18 p3256 A70-36090

Soviet book on aircraft electrical and radio systems manufacturing, assembling and testing methods, considering effectiveness and standardization 19 p3357 A70-37405

Lower ionospheric structure and electromagnetic resonance phenomena, describing radio equipment for solar activity effects studies 21 p3812 A70-40620

RADIO FILTERS

Ordinance circuit RF filter in backshell of standard connector, discussing design, physical-electrical specifications and tests 03 p0494 A70-14113

Broadband RF filter/attenuator plug to replace plastic type plugs for protecting wire bridge electroexplosive devices against RF energy 03 p0495 A70-14130

Circuit analysis of pulse integrator and square-law receiver used as optimal filter during incoherent radio pulse reception on background fluctuating noise 08 p1461 A70-20865

Rectangular radio pulse sequence passage through narrow band filter, discussing transient process form as function of signal parameters 09 p1643 A70-22132

Optimum filtering techniques for radio guidance of third stage of Europa 1 booster compared for effectiveness 13 p2381 A70-28437

Optimal synthesis of filters maximizing peak-sideobe ratio of arbitrary zone of mutual ambiguity function 13 p2369 A70-29734

Noise rejection during synchronous quasi-coherent radio signal reception with binary narrow band linear filter used for voltage shaping 13 p2369 A70-29737

Low level time truncated signals measurement by narrow bandwidth synchronous time notch filters, discussing sensitivity 19 p3380 A70-38177

VHF omnidirectional range /VOR/ receiver, considering noise reduction problem and active filter importance to signal improvement and system accuracy 22 p3992 A70-43586

RADIO FREQUENCIES

NT C BAND

NT EXTREMELY HIGH FREQUENCIES

NT EXTREMELY LOW RADIO FREQUENCIES

NT HIGH FREQUENCIES

NT LOW FREQUENCIES

NT MICROWAVE FREQUENCIES

NT SUPERHIGH FREQUENCIES

NT ULTRAHIGH FREQUENCIES

NT VERY HIGH FREQUENCIES

NT VERY LOW FREQUENCIES

Delay times elimination in pulse operated X band Gunn effect oscillators, using RF power injection 01 p0050 A70-10463

Wideband HF amplifier development for ionospheric radio sounding, describing various stages 02 p0255 A70-11895

RF holographic vision through rain, fog or darkness, discussing cholesterol ester-coated Mylar sheets and pyroelectric hot plates detectors and antenna sensory matrix 02 p0305 A70-12843

Planetary nebulae with concordant and discordant radio and optical fluxes, discussing possible causes of discordances 04 p0747 A70-14516

Carbon atom RF recombination lines evaluated for conditions in H II regions and planetary nebulae 04 p0748 A70-14587

Self contained and ground referenced radio systems combination for tactical air navigation, including Loran D and hybrid Loran /HYLO/ 04 p0716 A70-14628

Laser signal modulation at RF by subjecting emitting atoms of Xe-He laser amplifier to simultaneous DC and RF magnetic fields 06 p1079 A70-17191

Cesium clocks at fixed locations compared for precision and accuracy, noting influence of radio frequency diurnal variations 06 p1139 A70-17474

Circuit and operation of transistorized RF power attenuator with linear attenuation and binary code control by digital computer 06 p1022 A70-17777

Oblique radio ray tracing at 2-10 MHz and application to signal strength calculation, concentrating on digital techniques 07 p1230 A70-19162

Oblique incidence absorption measurements by pulse or CW signal strength observations or LOF data, comparing LUF to LOF 07 p1231 A70-19173

Lowest useful frequency /LUF/ prediction on long distance quasi-antipodal circuit, considering E layer blanketing 07 p1232 A70-19178

Lowest usable frequency /LUF/ measurement and prediction through synchronized oblique ionospheric sounding 07 p1233 A70-19181

Ionospheric auroral anomalous radio wave absorption frequency dependence index determined from cosmic radio emission intensity data 07 p1276 A70-20433

Radio waveguides with random inhomogeneities, studying mathematical models by orthogonalization method 08 p1457 A70-20723

Televar principle for radial radio coordinates production in all frequency bands, discussing ring antenna feeds 09 p1722 A70-23033

Electric bridge for measuring complex impedances and admittances in 60 kHz-30 MHz frequency range 09 p1650 A70-23402

Plasma instability in RF discharge in Ar in magnetic field 10 p1840 A70-24540

Channel separation in RF transponder for communication satellite achieved with RF multiplexers consisting of microwave filters and combiners with superior electrical performance [AIAA PAPER 70-509] 11 p2016 A70-25457

RF amplifier design procedure for maximum stable gain with minimum noise figure 11 p2019 A70-26715

Soviet book on radio frequency amplifiers covering vacuum tubes, transistors, tunnel diodes, TWT and low noise quantum paramagnetic and parametric devices 12 p2194 A70-26867

- Ionospheric parameters measurements by incoherent RF scattering, discussing current status of theory and observations 12 p2225 A70-27738
- Tantalum RF sputtered superconducting films structure and properties at various substrate temperatures, observing bcc, fcc and amorphous phases by electron microscopy 12 p2288 A70-27876
- Electrostatic probe behavior in RF excited plasma, illustrating perturbation effect of potential drop on I-V characteristics 13 p2406 A70-28935
- RF admittance and electric field of plane grid capacitor in hot collision free magnetoplasma in parallel magnetic field dominated by Bernstein modes 13 p2467 A70-29910
- Fluorine sensor for RF induced currents providing alternative to bridge wires as initiators of explosive charges 14 p2534 A70-30681
- RF floating double probe for plasma ionization density and electron temperature 15 p2778 A70-31755
- Voltage-frequency conversion technique using FM principle and RF oscillator beating with crystal oscillator output 15 p2705 A70-32705
- Computer controlled frequency surveillance system design and operation 16 p2871 A70-34052
- GaAs laser with inhomogeneous injection, noting instability of stimulated RF oscillations 17 p3108 A70-35631
- Radio frequency indigenous noise measurement in urban areas 18 p3228 A70-36568
- RF ion source for electrostatic spacecraft propulsion, discussing RIT-10 performance optimization and development [AIAA PAPER 70-1102] 20 p3692 A70-40236
- Taurus A 21 cm radiation anomalous frequency decrease during occultation by sun attributed to particle streams propagating in solar corona 21 p3886 A70-41064
- Oscillatory stability of selective RF transistor amplifiers, using stage dimensioning and gain graphs 22 p3996 A70-42818
- Linear IC for RF applications including multistage amplifiers, simulating by actual units 22 p3999 A70-42821
- RADIO FREQUENCY DISCHARGE**
- Laser irradiation of RF plasmoid producing electron density increase, discussing resonance sustained RF discharges, mode locking, laser photodetachment, etc [ONERA-TP-751] 03 p0501 A70-13630
- Stationary hydrogen RF plasma, using quadrupole mass analyzer for ion composition and extraction study 22 p4078 A70-42363
- HF plasma propagation, discussing RF discharge by exciting axially symmetric mode of plasma column 22 p4084 A70-43671
- RADIO FREQUENCY HEATING**
- Polyamides chemical welding using HF heating to obtain optimum temperature distribution and to activate polymer reaction with crosslinking agents 06 p1091 A70-17316
- Nonresonant electromagnetic absorption in high density plasma used for RF heating in magnetostatic field 09 p1735 A70-22923
- RF-sputtered CdS thin films structural and electrical characteristics from X ray diffractometer tracings, reflection electron diffraction and X ray double crystal spectrometry 13 p2470 A70-29201
- Numerical analysis of inductive electrodeless discharge of thermal Ar plasma column heated by RF axial magnetic field 21 p3859 A70-41902
- Maintenance voltage of RF argon thermal induction plasma at atmospheric pressure as function of ring probe 21 p3859 A70-41904
- RADIO FREQUENCY IMPEDANCE PROBES**
- RF probe admittance in ionosphere investigated for cold anisotropic and warm isotropic plasma diagnostics 06 p1117 A70-17370
- RF probe impedance variations with magnetic field strength in hot plasma for electron gyrofrequencies less than plasma frequency explained by model 06 p1117 A70-17371
- Plasma space potential measurement by RF characteristics of Langmuir probe 07 p1288 A70-20233
- Extraterrestrial electron density precision measurement using HF impedance probe with guard ring to remove ion sheath effects 10 p1892 A70-25255
- Ionospheric electron density profiles at various altitudes, using HF impedance probe method 12 p2227 A70-28261
- Ionospheric electron density measurements with high altitude rocket swept frequency RF impedance probe 13 p2400 A70-29906
- RADIO FREQUENCY INTERFERENCE**
- NT ATMOSPHERICS
- NT BLACKOUT [PROPAGATION]
- NT COSMIC NOISE
- NT CHORUS
- NT ELECTROMAGNETIC NOISE
- NT HISS
- NT IONOSPHERIC CROSS MODULATION
- NT IONOSPHERIC NOISE
- NT IONOSPHERICS
- NT SHOT NOISE
- NT SUDDEN ENHANCEMENT OF ATMOSPHERICS
- NT THERMAL NOISE
- NT WHISTLERS
- Atmospheric humidity effects on ionization and positive corona-current pulses development, discussing radio interference 02 p0258 A70-12425
- RF hazard measuring system for complete guided weapons electromagnetic compatibility tests with instrumented inert device replacing live igniter 03 p0495 A70-14132
- Linear phase detection using FM demodulation for Apollo S band communication system eliminating baseband voice interference with telemetry [AAS PAPER 69-610] 04 p0648 A70-14659
- Equation for disturbance of ILS localizer signals by reflection from flat hangar wall, discussing computer program 04 p0652 A70-15344
- Radio wave-ionosphere interaction effects on accuracy of radio astronomical observations from earth satellites 04 p0683 A70-15740
- Wire dischargers at helicopter propeller blade tips reducing electrostatic RF interference, substituting stainless steel wire tufts for nichrome wire 05 p0848 A70-16320
- Adaptive frequency selection of optimum channels for radio communication on noninterference basis, discussing implementation and compatibility problems with nonadaptive systems 05 p0814 A70-16347
- Noise mean duration in surface communications links due to communications satellites interference, discussing irradiation emission and termination 08 p1456 A70-20570
- Phase locked loop method for waveshaping rectangular wave frequency modulation signals in phase coherent VLF-FSK systems, reducing transient effects and adjacent channel interference 08 p1459 A70-20803
- Signal design for Gaussian noise and intersymbol interference immunity, discussing bandlimited signals and maximum likelihood detection technique 08 p1460 A70-20813
- Interference emission filtering in high power microwave transmitters, discussing spurious emissions removal or rejection by transmission line filters 08 p1474 A70-21257
- Multiple access PCM satellite communication system with minimum interference to earth radio links, using programmable switch for improved traffic handling and frequency coordination 10 p1837 A70-24346
- Ionospheric effects and transmitter characteristics observed on HF standard and time stations, discussing spurious emissions arising from frequency overcrowding 10 p1842 A70-25050
- Extraneous earth satellites interferences in ground communication line, determining combined duration and numbers average values 11 p1996 A70-25346
- COMSAT measurement of precipitation scatter effects on propagation for frequency sharing with terrestrial radio relay terminals [AIAA PAPER 70-499] 11 p1997 A70-25413
- RF interference emanating from satellite-borne pulse plasma thruster by measuring RF power at UHF antenna having plasma in near field 11 p2103 A70-26136
- RF EMI propagation between manned spaceflight network and Apollo 10 launch vehicle in translunar mission, considering cochannel interference possibilities 12 p2189 A70-28137
- Frequency selection in telemetry taking into account systems for minimum interference and crosstalk 13 p2366 A70-29216
- Radio wave-ionosphere interaction effects on accuracy of radio astronomical observations from earth satellites 14 p2575 A70-30824
- Plasma induced radio frequency interferences from DC-DC converter to receiving antenna simulated for REXS satellite in space chamber 17 p3047 A70-35400
- RFI measurements at X band on LES-7 prototype pulsed plasma thruster 17 p3149 A70-35669
- Optimal temporal and spatial-temporal resolution for unknown parameter of interfering signal on white noise background 17 p3048 A70-35680
- Short wave ionospheric scatter propagation, observing interference and crowding in 16-23 MHz and relationship to F2 layer maximum usable frequency 18 p3227 A70-36093
- Aircraft streamer /spark/ discharges formation, waveforms and RF noise levels, using mathematical model for electric field strength 19 p3380 A70-38179
- Sea clutter tolerance comparison for frequency agile and fixed frequency radar 20 p3584 A70-39200
- International Telecommunication Union /ITU/ legal recommendations on radio spectrum use, interference and frequency assignment problems 20 p3585 A70-39411
- Extraneous earth satellites interferences in ground communication line, determining combined duration and numbers average values 20 p3589 A70-40458
- FM transmission of multiplex telephone signals by communication satellites, deriving impulse noise due to adjacent channel interference 21 p3787 A70-41330
- Interference coupling between satellite ground station and radio relay station due to rain scattering at SHF 22 p3990 A70-43201
- Plasma-TEM wave nonlinear interactions in magnetosphere, discussing atmospheric occurrence 22 p4021 A70-43276
- Crosstalk error in binary phase modulated communications systems due to RFI and thermal noise 23 p4158 A70-43752
- RADIO FREQUENCY NOISE**
- U ELECTROMAGNETIC NOISE
- RADIO FREQUENCY RADIATION**
- U RADIO WAVES
- RADIO FREQUENCY SHIELDING**
- Shielded-cathode mode Gunn oscillators to eliminate constraints on operating frequency 12 p2200 A70-28056
- Nonradiating higher order modes on shielded slot lines for TM and TE cases, using series matching and Wiener-Hopf technique 22 p3990 A70-43420
- Electromagnetic interference reduction between communication satellite earth stations and microwave radio relay stations by pit shielding 22 p3991 A70-43577
- RADIO GALAXIES**
- Statistical relation between radiation power of radio source and distance of center from radio galactic nucleus, investigating evolution of radio galaxies 01 p0174 A70-10196
- Quasar B264 observed with multichannel spectrometer attached to 200 inch telescope, comparing to N-type and Seyfert galaxies and other quasars 02 p0371 A70-12243
- Emission lines origin in radio galaxies optical spectra explained by using energy gained from radioactive elements decay 03 p0563 A70-13214
- North Galactic Spur compared for edge, ridge and neck with previous results noting sharp temperature gradients 04 p0758 A70-15699
- Radio galaxy evolution in terms of analysis of relation to superluminous elliptical systems, deriving radio emission duration upper limits 04 p0759 A70-15715
- Physical conditions required to explain observations of radio galaxies through electrons of secondary origin, considering spectral characteristics and evolution 04 p0742 A70-15716
- Electron ejections from nuclei of radio galaxies and quasars on basis of plasma stability, discussing role of relativistic electrons and resulting unstable pinch 05 p0917 A70-16901
- Flux densities from quasars 3C 273, 3C 279 and 3C 454.3 and Seyfert galaxy 3C 84, measuring linear polarization, discussing time variations in sources 05 p0918 A70-16926
- Yearly fluctuations of Seyfert galaxy 3C 120 light curve, discussing effects of ambient temperature 08 p1563 A70-20498
- Seyfert galaxy NGC 4151 nucleus relation to quasars, discussing cloud structure and velocity and H line properties 08 p1568 A70-20617
- Varying flux density values measured at SHF for radio galaxy PK 0048-09 indicating recent origin of radio source 09 p1764 A70-23790
- Radio galaxy 3C 371 compact companions, studying luminous isophotes and red shift by long exposure plates with 200 inch telescope 10 p1936 A70-23908

- Radio galaxies and quasars radiated power, discussing red shift complicated by absorption lines discovery in spectra 12 p2298 A70-27064
- Gas with large radial velocity in radio galaxy NGC 1275, suggesting constitution of separate galaxy 12 p2308 A70-27870
- Electrodynamic-gravitational model of radio galaxies and quasars accounting for complex field, particle acceleration, angular momentum, luminosity and line emission 15 p2807 A70-32811
- Quasar and radio galaxies, observing absorptions at red shifts close to emission line 17 p3157 A70-34846
- Centaurus A radio galaxy X ray survey, implying upper limit of background radiation temperature 18 p3308 A70-36516
- Hydrogen line absorption at 21 cm from Centaurus A/NGC 5128/ radio galaxy 18 p3318 A70-37017
- Log S /flux-log Z /redshift/ diagram for radio galaxies, encouraging steady state cosmology 18 p3320 A70-37074
- Quasars and radio galaxies circular polarization at 49 cm wavelength, using radio telescope interferometer 19 p3523 A70-38606
- De Sitter nonempty static cosmological model, examining possibility by comparing integral luminosity function for cosmic radio sources to radio galaxies statistics 22 p4106 A70-43258
- RADIO INTERFERENCE**
- U RADIO FREQUENCY INTERFERENCE**
- RADIO INTERFEROMETERS**
- Long baseline interferometry used to improve radio telescopes resolving power in measuring quasar diameters 01 p0183 A70-10885
- Earth space signal propagation characteristics obtained by satellite-borne radio interferometer provide phase information in addition to amplitude for improving navigation accuracy 02 p0260 A70-12567
- Compact radio source in M87 nucleus observed with long base line interferometer composed of two telescopes, suggesting diameter 04 p0747 A70-14546
- Angular resolution dependence on bearing ambiguities in radio direction finders based on interference measurement, using digital logic circuits 04 p0659 A70-15335
- Structural and systems design of large orbital radio astronomy antenna /crossed H interferometer/ with astronaut participation in deployment, operation, maintenance and updating [AIAA PAPER 70-100] 06 p1156 A70-18058
- Radio telescopes relaying interferometers characteristics noting delay in IF channel and wideband performance 08 p1495 A70-21068
- Relaying interferometer design consisting of heterodyne frequency diversity antennas with coherent mixer, relaying transmitter and receiver 08 p1495 A70-21071
- Radio sources model brightness distribution and internal magnetic fields deduced from long baseline interferometer observation data 08 p1577 A70-21491
- Long baseline interferometer observations of radio sources for size determination, tabulating measured fringe visibility 08 p1578 A70-21547
- Satellite radio tracking systems noting interferometer most suitable for accuracy and maintenance 08 p1463 A70-21712
- Tethered orbiting interferometer configurations for future Radio Astronomy Explorer satellites, discussing gravitational stabilization and delta launching into orbit as single payload [AAS PAPER 69-255] 09 p1766 A70-22930
- Astronomical high resolution radio interferometers design with autonomous reception, analyzing sensitivity of data processing correlation devices 09 p1647 A70-23132
- Large-base radio interferometer with separate heterodyne receivers and electrical length automatic control, studying causes of phase errors 09 p1650 A70-23631
- Atmospheric refractive corrections in high accuracy radio interferometry 10 p1890 A70-24649
- Aperture synthesis and spectral antenna characteristics in radio astronomy, considering Ryle systems, Mills-Christiansen crosses and variable interferometers 11 p2019 A70-26801
- Discrete radio sources angular size determination by two antenna interferometry 12 p2299 A70-27378
- Jupiter decametric radio bursts observed by tape recording fringe interferometer 13 p2486 A70-28626

- Radiotelescope measurements for geodetic purposes, applying interferometric principles to quasar radiation 13 p2396 A70-29163
- Phased array monopulse autotracking, radiointerferometer and Doppler frequency methods for radio tracking systems for artificial satellite orbits 15 p2697 A70-31836
- Phase stability measurements at 2695 MHz with radio link interferometer, discussing atmospheric water content effect 16 p2861 A70-32959
- Synchronous oscillators of radio astronomic interferometer, discussing dephasing and servocoupling 17 p3090 A70-35415
- Planar Tethered Orbiting Interferometer satellite for long wavelength solar and planetary radio astronomy, discussing deployment control and libration damping 18 p3333 A70-36230
- Variable baseline interferometer installation for radio astronomy observatory, describing components and performance 20 p3605 A70-39240
- High resolution observation of compact radio sources at 13 cm, using long baseline dual antenna interferometer 22 p4102 A70-42976
- Aperture synthesis and spectral antenna characteristics in radio astronomy, considering Ryle systems, Mills-Christiansen crosses and variable interferometers 24 p4311 A70-45176

RADIO METEOROLOGY

- Radiometeorology research emphasizing interaction between troposphere and VHF waves to improve space and terrestrial radio communication 07 p1234 A70-19216
- Atmospheric fine-scale structure determination from forward scatter radio wave propagation, considering refractive index role 09 p1715 A70-22362
- Errors estimation in wind velocity values by radio echo observations in meteor trails of different densities 14 p2572 A70-30330
- Soviet collection of papers on radar meteorology 18 p3287 A70-36998
- SHF-EHF region uses, discussing microwave radiometry and applications to radio astronomy and meteorology 21 p3799 A70-41421

RADIO METEORS

- Horizontal wind velocity spectra at 80-100 km from radar meteor soundings 12 p2263 A70-27518
- Radio meteor train initial radius determination, discussing radio echo observation method 12 p2309 A70-27977
- Meteor radio path activity coefficient, reflections density distribution, characteristic heights and mean durations, noting meteor velocity effects 14 p2636 A70-30319
- Meteor radio reflections time-amplitude characteristics, discussing dependence on mirror point position in trail, wavelength, diffusion factor and initial radius 14 p2636 A70-30324
- Meteoric radio propagation for long trajectories, considering oblate scattering ellipsoid 14 p2636 A70-30326
- Radar receiving station equipment for studying upper atmosphere by radio meteor echoes 17 p3047 A70-35605
- Radio meteor orbit velocity and radiant measurements by pulse diffraction technique 18 p3315 A70-36603
- Meteor radar echoes of parallel and perpendicular polarization from ionized transient trails with linear electron densities 18 p3317 A70-36995
- Automatic meteor station jamming protection using ferrite diode logical elements 19 p3422 A70-37652
- Electron photodetachment rate from meteor radar echo duration during night and daytime observations 19 p3515 A70-37664
- Horizontal wind velocity spectra at 80-100 km from radar meteor soundings 21 p3846 A70-41166

RADIO NAVIGATION

- NT DECCA NAVIGATION
- NT HYPERBOLIC NAVIGATION
- NT LORAN
- NT LORAN C
- NT LORAN D
- NT TACAN
- NT VHF OMNIRANGE NAVIGATION
- Monograph on future air traffic control concerning radio navigation, color display and computer determined flight paths 01 p0136 A70-10090
- One way radio range measurements for surveying and navigation emphasizing McDonnell collision

avoidance and geophysical surveying systems, using Rb atomic clocks 01 p0136 A70-10306

Earth space signal propagation characteristics obtained by satellite-borne radio interferometer provide phase information in addition to amplitude for improving navigation accuracy 02 p0260 A70-12567

User problems in navigation methods, discussing Omega method, Navy Navigation Satellite System and VLF methods 03 p0522 A70-13603

Navy Shipboard Navigation Satellite System for worldwide all-weather navigation system, discussing shipboard system, receiver, stable oscillator and antenna 03 p0522 A70-13609

Quasi-optical propagation in frequency wave range above 100 MHz as user problem in VOR, ILS, navigation satellite and CAT detection and warning systems 03 p0523 A70-13613

Optimum filter for aircraft inertial navigator and radio position fix data mixing using mathematical model of error propagation [AIAA PAPER 70-35] 06 p1103 A70-18184

Radio air navigation systems by time separation signals with reference to anticollisional methods and ATC 08 p1541 A70-21019

Earth-ionosphere waveguide propagation variations effects on Omega navigation system position errors 08 p1541 A70-21564

Televor principle for radial radio coordinates production in all frequency bands, discussing ring antenna feeds 09 p1722 A70-23033

Doppler VOR offering increased course accuracy and allowing precise area coverage in conjunction with DME ground station 09 p1723 A70-23036

Seasonal variations in radio signal propagation from aircraft navigation system antenna located in dense forest, solving problem with Doppler-VOR installation 10 p1854 A70-25254

Pictorial display area navigation system for air traffic control in terms of cockpit utilization, interface with ground navigation aids, parallel multiple routes, etc [AIAA PAPER 69-798] 13 p2449 A70-29171

One way radio range measurements for surveying and navigation emphasizing McDonnell collision avoidance and geophysical surveying systems, using Rb atomic clocks 13 p2449 A70-29620

Combined radio and physical navigation systems, considering noise rejection and corrections of position and speed 15 p2772 A70-31623

Area navigation for aircraft guidance with radio aids, discussing advantages, airborne equipment, Dynamic Map Displays, etc 22 p4067 A70-42658

Radio navigation system using multiple satellite beacons /NAVSTAR/ for large area air and sea coverage 22 p4067 A70-42662

DR-S Raydist radio location system in fixed wing aircraft for dynamic gravimetry 22 p4068 A70-43661

Aircraft Doppler VHF omnidirectional radio range /DVOR/ performance test, noting improvement over VOR system 24 p4375 A70-46240

RADIO OBSERVATION

Random variations of terrestrial rotation rate effects on pulsar observations, discussing methods to minimize effects 02 p0371 A70-12203

Wave propagation problem, considering traffic control, surveying, tracking, navigation, etc 03 p0449 A70-13607

Small scale disturbances and radio wave scattering effects on signal transmission and radiophysical observations in ionosphere 04 p0653 A70-15723

Mars atmosphere refractivity, carbon dioxide condensation, temperature and surface pressure from Mariners 6 and 7 radio occultation measurements 05 p0908 A70-16301

Radioheliograph observations at 80 MHz of directive shock wave propagation in solar corona 06 p1144 A70-18007

Oblique incidence absorption measurements by pulse or CW signal strength observations or LOF data, comparing LUF to LOF 07 p1231 A70-19173

Oblique measurements in HF on Kiruna-Stockholm path with two fixed frequency pulsed transmitters, comparing results to ionosonde measurements 07 p1232 A70-19175

Ionospheric motions and irregularities effects on HF radio propagation using computer simulation involving ray tracing and ionosphere modeling 07 p1264 A70-19192

Winter anomaly ionization in lower ionosphere at medium latitudes from radio propagation observations, comparing wave absorption and phase height measurements

07 p1274 A70-20273
Collection of Soviet papers on radio astronomical instruments and observations

08 p1472 A70-21051
Terrestrial rotation changes effects on pulsar period observations

08 p1575 A70-21260
Atmospheric turbulence regarding refractive index fluctuations over UK measured by radio telescope, discussing effects on satellite communication

09 p1667 A70-22384
Ionospheric electron content from Doppler data and from Faraday observations of satellite S-66

10 p1884 A70-25256
Radio meteor train initial radius determination, discussing radio echo observation method

12 p2309 A70-27977
Orbital elements of small high velocity meteors, using oblique radio sounding

12 p2311 A70-28306
RF method for recording temperature dependence of electrical conductivity of solids, liquids and multicomponent plasma mixtures

13 p2459 A70-28583
Sporadic E layer space diversity reception data from stations 20 km apart, noting horizontal ionization gradient effect

14 p2571 A70-30234
Meteor trail radiant, velocity and altitude measurement by obliquely incident radio waves

14 p2635 A70-30309
Meteor particle orbits, comparing inclined radio reflections with photographic and straight radar observations

14 p2636 A70-30322
Ionospheric electron distribution by true height analysis of oblique incidence HF radio wave sounding data, applying to forward and ground backscatter

14 p2550 A70-30745
Lower ionospheric drift motions observed from VHF radio signal, relating to three paths near auroral zone during dark hours

14 p2574 A70-30749
Small scale disturbances and radio wave scattering effects on signal transmission and radiophysical observations in ionosphere

14 p2550 A70-30807
Radio observations of dense briefly visible Leonid meteor shower with fixed pencil beam antenna in coping with wave scattering in trails

15 p2796 A70-31511
Meteor orbit parameters and incident particle flux measurements by radio methods, eliminating backscatter radar sensitivity limitations

15 p2807 A70-32814
Venus surface atmospheric conditions from radar and radio observations, including cross sections, microwave brightness spectrum and angular scattering law

16 p2974 A70-33645
Radio observations of chromospheric brightness temperature distribution during solar eclipse of March 1970

16 p2977 A70-33846
Wolf-Rayet associated nebulae, presenting radio observations and mass determinations

16 p2980 A70-34193
Ionospheric drift measurement by 89 antennas array, testing validity of methods using three antennas

17 p3076 A70-34939
Radio observations of Crab Nebula and radio source, correlating optical and radio features

17 p3164 A70-35114
Radio observation of Crab Nebula radio pulsar NP 0532, discussing main and subpulse stability at optical and radio frequencies

17 p3164 A70-35116
Lunar rocks permittivity and density and surface roughness from radio wave scattering data

19 p3512 A70-37276
Weather occultation satellite orbit determination by radio wave measurements between master and slave satellites, formulating mathematical model [AIAA PAPER 70-1067]

19 p3529 A70-38880
Whistler VLF radio observations of sudden magnetic impulses in plasmasphere during storms, using ground based magnetometers

20 p3620 A70-39330
Heterodyne millimeter wave radiometric system for observing atmospheric attenuation due to water vapor, discussing design, development and initial measurements

20 p3588 A70-40308
Radioheliograph observations of solar outbursts involving MHD waves propagation along curved paths in corona at 80 MHz

21 p3891 A70-41178
Two dimensional positions of fundamental and harmonic type 2 solar bursts, using coronal streamer plasma and backward refracted radiation model

Two dimensional position measurements of harmonic type 2 solar bursts, using 80 MHz observations

21 p3891 A70-41180
Sporadic E layer space diversity reception data from stations 20 km apart, noting horizontal ionization gradient effect

24 p4331 A70-46309

RADIO PHYSICS

Radio science - Conference, Kleinheubach, West Germany, October 1968

10 p1882 A70-25251
Galactic spiral structure, discussing gravitational theory, pattern origin, radio and optical structure and magnetic field effects

18 p3332 A70-37201
Soviet book on overshoot of random processes in problem solving covering application to radio engineering, length distribution, extremal values, etc

20 p3587 A70-39822

RADIO PROBING

Horizontal ionospheric small scale inhomogeneity drift measurements at two closely spaced points, noting agreement with global network stations

04 p0684 A70-15747
Aerological radio thermometers random and systematic errors compared to network radio probe

05 p0848 A70-16206
Polarization of solar scattered radiation measured by radio probes for aerosol particle concentration and size distribution as function of altitude

10 p1884 A70-25253
Ionospheric probing using pulsed radio waves at oblique incidence, discussing auroral radar, meteor radar, ground backscatter and variable frequency ionosondes techniques

12 p2224 A70-27728
Ionospheric probing using continuous radio waves at oblique incidence, discussing HF Doppler, VHF forward scatter and radio aurora techniques

12 p2224 A70-27730
Ionospheric probing with LF/VLF/ELF radio waves, discussing measurement techniques and temporal and spatial resolutions

12 p2224 A70-27731
Ionospheric D region radio wave probing by cross modulation technique, obtaining electron densities and collision frequencies

12 p2224 A70-27733
Ionospheric absorption measurements by HF and VHF techniques, discussing electron density profiles, collision frequencies, anomalies and aeronomic and ionospheric implications

12 p2224 A70-27735
Millimeter-wave probing for vertical distribution of atmospheric water vapor, comparing ground, balloon and satellite observation techniques

13 p2394 A70-28785
Radio sounding of Van Allen inner belt from Antarctica, comparing American and Soviet deductions about magnetosphere structure

13 p2399 A70-29273
Collection of papers on precision radiometry in geophysics covering radiation detectors and electromagnetic radiation measurements in atmosphere

13 p2409 A70-29651
Horizontal ionospheric small scale inhomogeneity drift measurements at two closely spaced points, noting agreement with global network stations

14 p2576 A70-30831
Mariner 6 radio signals frequency changes analysis during occultation measurement for determining Mars surface pressure and temperature

14 p2646 A70-31071
Mariner 6/7 S band radio occultation probe of Mars atmosphere concerning surface pressure, temperature and existence of ionosphere

15 p2798 A70-31681
Polar cap disturbance of 7 June 1969 due to small proton enhancement, describing detection by transpolar VLF phase measurement

15 p2794 A70-32295
Atmospheric turbulence and wind velocity remote probing by millimeter waves, comparing results with conventional anemometer measurement

20 p3665 A70-40306
Clear lower atmosphere meteorological parameters remote sensing for weather forecasting, comparing optical, radio and acoustic radar techniques

21 p3785 A70-40802
Ionospheric layers critical frequencies recording, using automatic interplanetary station type probe

23 p4194 A70-44088
Ionospheric electron content measurement from Faraday effect of troposphere on beacon satellite Explorer 22 radio signals

23 p4163 A70-44231

RADIO PROPAGATION

U RADIO TRANSMISSION

RADIO RANGE

One way radio range measurements for surveying and navigation emphasizing McDonnell collision avoidance and geophysical surveying systems, using Rb atomic clocks

01 p0136 A70-10306

Televor principle for radial radio coordinates production in all frequency bands, discussing ring antenna feeds

09 p1722 A70-23033
One way radio range measurements for surveying and navigation emphasizing McDonnell collision avoidance and geophysical surveying systems, using Rb atomic clocks

13 p2449 A70-29620
Radio wave field intensity in middle frequency range, determining propagation curves for large distances

14 p2547 A70-30208
Long range tropospheric radio wave propagation, calculating signal impulse function and time lag between diffraction and reflection

17 p3048 A70-35678
Source antenna range length and aperture diameter, discussing length, frequency, aperture size and free space conditions

21 p3784 A70-40563
VHF geostationary satellite ranging and range correction systems, calculating second-order ionospheric delay effects on position error

22 p4068 A70-43590
Radio wave field intensity in middle frequency range, determining propagation curves for large distances

24 p4316 A70-46283

RADIO RANGES

U RADIO BEACONS

RADIO RECEIVERS

NT SUPERHETERODYNE RECEIVERS

NT TRANSMITTER RECEIVERS

NT WHISTLER RECORDERS

Signal detectability improvement by taking logical union of thresholded power of sensor outputs sum and thresholded power of sensor outputs difference

04 p0651 A70-15326
Cross modulation due to nonlinearity and linear cross modulation due to local oscillator pulling in FET FM receiver, discussing mixer operating points

08 p1460 A70-20818
Circuit analysis of pulse integrator and square-law receiver used as optimal filter during incoherent radio pulse reception on background fluctuating noise

08 p1461 A70-20865
Gain stabilization of transistorized LF selective amplifiers in radiometric receivers, discussing two-frequency resonance system

08 p1473 A70-21061
Large carrier to noise ratios in FM receivers as function of correlation between Gaussian and impulse shot noise /clicks/

08 p1463 A70-21776
Acousto-optic receiver and spectrum analyzer for electromagnetic signals in VHF-UHF range

08 p1463 A70-21780
Radio marker beacon-receiver design, tabulating technical data

09 p1684 A70-23574
Nomograms simplifying noise and natural loop bandwidth calculation for phase locked loop receiver, determining limiter suppression factor

10 p1844 A70-25244
FM/FM telemetry threshold carrier SNR and receiver IF bandwidth optimization through computer program

11 p2014 A70-26272
PAM-FM modulation system optimal receiver derivation, assessing threshold performance assuming uniformly distributed modulating signal

12 p2183 A70-27155
Radio receiver bandwidth effect on lunar occultation observations

12 p2189 A70-27989
Minimum performance standards established by Radio Technical Commission for Aeronautics for airborne radio marker receiving equipment operating on 75 MHz

13 p2364 A70-28999
Minimum performance standards for airborne radio receiving and direction finding equipment covering normal and environmental test procedures

13 p2365 A70-29000
Multilens quasi-optical transmission lines construction by determining lens profile for optimal conversion of source field into specified field at receiver end

13 p2366 A70-29403
Two signal selectivity and permissible noise level of FM receiver with linear cascades and detector non-linearity effects

15 p2696 A70-31506
Radio receiving system for pulses detection from cosmic ray extensive air showers, discussing sensitivity and noise temperature

16 p2911 A70-33788
Microwave radiometric receiver, analyzing video detector saturation effects on linearity

16 p2880 A70-34075
Receiver for artificial satellite transmission and optical tracking time signals, using crossed dipole directional antenna

16 p2867 A70-34303

Electron density measurements in lower ionosphere by narrow band VLF receiver flown in Tomahawk rocket during quiet daytime 17 p3076 A70-34938

Microwave receiving antenna, discussing directivity, cross section, power gain, equivalent circuit, etc 17 p3044 A70-35054

Centimeter wave transmitting and receiving equipment for studying nanosecond pulse propagation 20 p3632 A70-39627

VHF omnidirectional range /VOR/ receiver, considering noise reduction problem and active filter importance to signal improvement and system accuracy 22 p3992 A70-43586

Microelectronic phase lock microwave receiver packaging, discussing subassemblies interconnection minimization, shielding, RF interference, low loss and testing problems 23 p4164 A70-44536

EM wave effects on radio receiver, using Maxwell equations without taking photons into account 23 p4221 A70-44798

RADIO RECEPTION

Receiver bandwidth effect on audible radio noise bursts parameters of quasi-peak value, burst duration and time interval 08 p1464 A70-21800

Optimal amplitude modulated radio signal reception on white and narrow band background noise, using nonlinear filtration and phase locked control 09 p1633 A70-22416

Noise rejection for optimal reception of incoherent binary signals in one beam Rayleigh dispersion radio channel under ionospheric electron density fluctuations 13 p2369 A70-29738

Receiving antenna for ionospheric scatter lines, calculating input power versus height and energy flux density spreading for position optimization 18 p3230 A70-36094

RADIO REFLECTION

U RADIO ECHOES

RADIO RELAY SYSTEMS

Envelope delay and amplitude characteristics measurement of modulated carrier wave channel in radio relay link 02 p0258 A70-12475

Group delay characteristics curvature in radio relay systems, analyzing crosstalk in picture- sound and beamed multiplex signal transmission by nonlinear distortion method 05 p0815 A70-16774

Microwave radio refraction analysis for controlling interference between radio relay antenna and geostationary satellites 07 p1235 A70-19363

Relaying interferometer design consisting of heterodyne frequency diversity antennas with coherent mixer, relaying transmitter and receiver 08 p1495 A70-21071

Omega Position Location Equipment /OPLE/ system, testing operational feasibility of centralized global meteorological data collection system 09 p1722 A70-23030

Integral relay operations effectiveness based on random spatial distribution of aircraft under control of Army flight operations center 11 p2080 A70-26265

Broadband 2 GHz transhorizon radio relay system design and performance for transmission on four channel pairs 11 p2034 A70-26820

IF combinator for broadband transhorizon radio relay transmission improvement by providing optimum SNR 11 p2020 A70-26821

Broadband transhorizon radio relay system transmission improvement by applying switching equipment designed for protective channel 11 p2034 A70-26822

Cassegrain antenna with parabolic mirror and switch designed for broadband transhorizon radio relays, using antenna scale model to determine parameters and electrical properties 11 p2020 A70-26823

Decimeter waves propagation along overland path, considering tropospheric radio relay systems development 16 p2863 A70-33238

Interference coupling between satellite ground station and radio relay station due to rain scattering at SHF 22 p3990 A70-43201

Electromagnetic interference reduction between communication satellite earth stations and microwave radio relay stations by pit shielding 22 p3991 A70-43577

RADIO SCATTERING

Radio waves scattering in ionosphere, analyzing dependence on latitude, altitude, azimuth and polarization angle, considering anisotropy due to geomagnetic field 01 p0046 A70-11452

Ionospheric measurements of electron density, electron and ion temperature profiles from strength of incoherent radio wave scattering 01 p0082 A70-11530

Doppler spectrum and radio troposcatter beam swinging in thin homogeneous turbulent scatter layer as function of height, crosswind speed and refractivity 02 p0326 A70-12288

Specular reflections influence on bistatic tropospheric radio scatter from turbulent perturbations in refractivity 02 p0326 A70-12289

Crosspath wind motion measurement by dual arm noncoherent bistatic radio troposcatter link 02 p0326 A70-12290

Radio wave scattering and brightness on uneven interface, determining frequency spectrum of signal reflected from surface assuming uniformly moving receiver 05 p0813 A70-16261

Forward and backscattering meteor radio echo intensity variations during decay under molecular and turbulent diffusion, recombination and trapping 14 p2635 A70-30313

Radio wave scattering and echo intensity at inhomogeneous underdense meteor trail allowing for electron density, trail formation time and diffusion coefficient 14 p2636 A70-30316

VHF radio auroral scatter signal correlation analysis, determining scale size and drift velocity of scattered field 17 p3047 A70-35548

Electron density irregularities convected past space probe relationship to radio intensity power spectrum scintillations 20 p3703 A70-39023

Lunar surface specific effective radio signal scattering area measured by Luna 9 and 13, describing signal fluctuations 21 p3884 A70-40838

Radio sources minimum observable diameter attributed to interstellar scattering and synchrotron self absorption 22 p4101 A70-42862

RADIO SIGNAL ABSORPTION

U ELECTROMAGNETIC ABSORPTION

U RADIO TRANSMISSION

RADIO SIGNAL PROPAGATION

U RADIO TRANSMISSION

RADIO SIGNALS

Venus atmosphere ionization distribution, temperature and pressure profiles determined from amplitudes and differential Doppler of radio signals to Mariner 5 during occultation 01 p0186 A70-11084

Canary Bird synchronous satellite radio signal transmissions scintillations from recordings, noting diurnal scintillation pattern 02 p0260 A70-12573

Fluctuating radio signals optimal two step detection on Gaussian noise background applicable to coherent superposition of signals reception 03 p0448 A70-13454

Spectrum parameters analysis of signal in form of radio pulses sequence with harmonic angular modulation 03 p0448 A70-13511

CW and radar type RF signal effects on electroexplosive devices sensitivity in bridgewire heating mode 03 p0550 A70-14142

Variable RF signals in pulsed radar, examining circuits design for required functions 03 p0452 A70-14281

Doppler technique for HF ionospheric radio signal fading, observing frequency spreading during flutter fading conditions in low geomagnetic latitudes 07 p1231 A70-19169

Satellite signal scintillation phenomenon morphological study and relationship to ionospheric irregularities 07 p1234 A70-19194

Ionospheric inhomogeneities measured by Explorer 22 radio signals emphasizing satellite scintillation 07 p1265 A70-19195

Ionospheric distortion of linearly FM radio signals used for sounding, considering signal characteristics in distortion equations 07 p1268 A70-19459

Turbulent thermal flux in Venus atmosphere estimated from amplitude fluctuation dispersion of Venera 4 and Mariner 5 radio signals 07 p1390 A70-20305

Rectangular radio pulse sequence passage through narrow band filter, discussing transient process form as function of signal parameters 09 p1643 A70-22132

Cosmic ray air shower detection from radio pulses 09 p1745 A70-23276

Sinusoidal modulated HF pulse signal, deriving parametric envelope and power density function 10 p1833 A70-24086

Whistler activity continuous recording by autocorrelation method using electronic analog computation with fixed delay time 10 p1886 A70-25281

A priori initial phase distribution influence on optimal nonenergetic parameter estimation of rectangular narrow band radio signals on white noise background 13 p2369 A70-29730

Signal-arrival-time invariance and SNR resolution of discretely analog filters matched to complex radio signals 13 p2380 A70-29736

Sum envelope zero crossings determination for steady normal noise plus random amplitude signal 13 p2370 A70-29742

Ionospherically reflected HF radio signal frequency spread measurement involving phase difference crossings counting between antennas 14 p2550 A70-30743

Ionospheric distortion of linear FM radio signals used for sounding, considering signal characteristics in distortion equations 18 p3250 A70-36933

Random radio signals distributions properties with parameters subject to random variation 21 p3785 A70-40639

Cosmos 142 satellite measurements VLF radio signals transmitted through ionosphere by ground based stations 21 p3786 A70-40836

Radio signal source encoding, investigating error exponent 23 p4159 A70-43755

F region ionospheric disturbances size and shape from radio amplitude and phase scintillations in satellite transmission to ground stations 23 p4187 A70-43879

Signal shape optimization by minimizing dispersion in temporal position estimates for radio pulse in presence of additive white noise 23 p4161 A70-43961

RADIO SOURCES [ASTRONOMY]

NT CASSIOPEIA A

NT PULSARS

NT QUASARS

NT RADIO GALAXIES

NT RADIO STARS

Millimeter background discrete source model, deriving required source density from small scale anisotropy upper limit 01 p0173 A70-10041

Radiotelescope observations of position and motion of type 2 and 4 radio sources during flares based on proton model 01 p0168 A70-10256

Einstein-Friedman cosmology of vanishing constants assumed in deducing relations between antipodal radio sources red shifts and universe parameters 01 p0187 A70-11274

Fourth Cambridge catalogue radio sources observed for right ascensions using east-west arm of Molonglo radio telescope, presenting data analysis procedures 01 p0191 A70-11362

Radio sources emission separations statistical analysis, establishing little physical association in pairs of sources 02 p0370 A70-12112

Position determination for faint radio sources close to intense sources from radio astronomical maps 02 p0370 A70-12113

Radio source ghost images in Lemaitre cosmological models, deriving luminosity functions and radio source ages 02 p0371 A70-12198

Radio source OQ208 characteristics observation suggesting possibility of quasi-stellar nature 02 p0377 A70-12492

Cosmic X-ray background interpreted as Compton collisions between cosmic black body photons and relativistic electrons in radio sources 02 p0360 A70-12792

Radio telescopic observations at 408 and 5000 MHz in galactic plane, describing two sources 04 p0746 A70-14514

Compact radio source in M87 nucleus observed with long base line interferometer composed of two telescopes, suggesting diameter 04 p0747 A70-14546

Galactic water vapor radio sources spectral observation suggesting correlation between time variation and polarization 04 p0747 A70-14547

Angular diameter data from Cambridge radio telescope for sources with different flux densities for cosmological models red shift tests 04 p0757 A70-15691

Pencil beam survey of radio sources at 178 MHz, with tabulated flux densities compared to 4C interferometer data 04 p0757 A70-15693

Contour maps of radio sources structure in 3C catalog from radio telescope observations 04 p0758 A70-15698

Temporal behavior of NP 0532 in radio and optical bands compared for second derivative of period
05 p0906 A70-15893

Brightness distribution over source, discussing regularization algorithms for radio astronomical data reduction from crossed telescope
05 p0917 A70-16902

Right ascension and flux density of source in Crab Nebula measured at meter wavelengths, evaluating spectrum and relative position to binary star center
05 p0917 A70-16908

Brightness distributions and widths determined from monochromatic radiation intensity at earth during lunar occultation of RF source
05 p0920 A70-16941

Radio sources structure observations of Arecibo Ionospheric Observatory, discussing interplanetary scintillations of galaxies and quasars
06 p1138 A70-17216

Double radiosource W 49 hydrogen line absorption measurements revealing two H I clouds with different radial velocities
06 p1149 A70-18461

Cosmic evolution of radio sources, discussing observations and data interpretation
07 p1374 A70-18746

Galactic groups age considered in studying radio emission occurrence frequency
07 p1376 A70-18908

Phase switching method application to radio telescopic observations showing increase in reliability of radio source coordinates determination
07 p1240 A70-18909

Spectral observations of radio sources including 3C461, 3C405, 3C84, 3C144 and 3C273
07 p1376 A70-18913

Polarized and unpolarized emission measurements of W 44 supernova remnant with radio telescope, showing results for eastern portion of source
07 p1383 A70-19405

Flux densities and positions for Southern Milky Way sources at 1410 MHz, determining spectral indices
07 p1387 A70-19682

Frequency characteristics deviation of discrete cosmic radio emission sources from exponential law, analyzing radio wave absorption in galactic and intergalactic media and ionized hydrogen
07 p1370 A70-20315

Pulsars radio, optical and X ray emission spectrum analysis, suggesting oscillating current sheets as radiation source
08 p1561 A70-20914

Electrical axis adjustment of east-west antenna array of crossed radio telescope by statistical processing of discrete sources observations
08 p1473 A70-21067

Anomalous microwave recombination line at 11 cm detected in NGC 2024, Orion A, and IC 1795, discussing peak antenna temperature
08 p1576 A70-21399

Position determination for compact radio sources in 3C catalog
08 p1577 A70-21490

Radio sources model brightness distribution and internal magnetic fields deduced from long baseline interferometer observation data
08 p1577 A70-21491

Positions measurement for 4C radio sources between declinations of 4 and 20 degrees, noting RMS errors
08 p1577 A70-21533

Galactic latitude dependence of polarization and Faraday rotation of extragalactic radio sources at centimeter wavelengths
08 p1577 A70-21534

Radio sources linear polarization measurements at 6 cm wavelength, noting intensity changes with polarized flux and position angle
08 p1578 A70-21535

Cambridge one mile radio telescope observations of weak sources, extending radio source luminosity function and tabulating, graphing and mapping results
08 p1578 A70-21546

Long baseline interferometer observations of radio sources for size determination, tabulating measured fringe visibility
08 p1578 A70-21547

Supernovae remnants evolution, properties and galactic distribution, discussing criteria for catalog listing and remnants as X ray sources
09 p1749 A70-21990

Compact nonthermal radio sources in M87 giving rise to X ray source through Compton effect
09 p1744 A70-22520

Cosmic radio waves discrete sources spectra measured in decametric wavelength range, discussing wave generation and absorption
09 p1762 A70-23189

Varying flux density values measured at SHF for radio galaxy PK 0048-09 indicating recent origin of radio source
09 p1764 A70-23790

Galactic sources H109 alpha line and continuum surveys, showing thermal continuum spectrum for sources with radio recombination lines
10 p1936 A70-23903

Galactic radio sources examined for hydroxyl lines associated with H II regions, making observations in absorption and emission
10 p1936 A70-23904

Sagittarius sources A and B2 O18H absorption lines measured at microwave frequencies, determining oxygen isotopes abundance ratios
10 p1936 A70-23907

Galactic radio source W 31 distance from sun determined from measurements of OH, H I and formaldehyde absorption lines
10 p1937 A70-23949

Radio spectra formation mechanisms in discrete sources within framework of synchronous emission theory
10 p1934 A70-25152

Radio telescopic observations of Jupiter, Venus and radio source 3C 273 at 2 and 8 mm wavelengths, determining brightness temperatures and radiation flux densities
10 p1948 A70-25153

Solar flares period, core and physical nature of areas by measurements at millimeter wavelengths, discussing radio source center
10 p1934 A70-25277

Evolutionary cosmological models for radio sources at large red shifts, considering source counts, luminosity functions, etc
11 p2117 A70-26655

Discrete extragalactic radio sources integrated linear UHF polarization values, discussing optical identification and radio spectral index correlations
11 p2117 A70-26656

Continuum spectra of well-resolved thermal and nonthermal galactic sources compared with H-alpha recombination line
12 p2296 A70-26898

Decameter radio sources flux density time variations, discussing possible causes and radio emission spectra
12 p2299 A70-27308

Extragalactic radio sources evolution, discussing energy requirements of hollow-shell models
12 p2299 A70-27377

Discrete radio sources angular size determination by two antenna interferometry
12 p2299 A70-27378

Polarization of extragalactic radio sources and supernova remnants emphasizing instrumental effects
12 p2309 A70-27894

Deconvolution of barely resolved radio sources mapped with elliptical antenna beams, noting telescope brightness distribution and power polar diagram
12 p2309 A70-27897

Radio sources scintillation due to scattering medium with refractive index irregularities under detection of finite bandwidth receiver
13 p2365 A70-29148

Radio sources positions on solar disk by 2800 and 408 MHz high resolution fan beams
13 p2491 A70-29161

Cosmic microwave radiation origin based on discrete source models
13 p2479 A70-29787

Solar wind turbulence, demonstrating radio source interplanetary scintillation consistent with plasma density correlation
14 p2642 A70-30888

Radio sources spectroscopy, discussing central density and mass of elliptical galaxy NGC 3998 and red shifts of radio galaxies
14 p2642 A70-30893

Galactic hydroxyl emission sources right ascensions, presenting coordinates and antenna temperature measurements
15 p2796 A70-31594

Book on nonthermal processes in galactic and extragalactic radio sources covering plasma behavior in magnetic field, energy redistribution in spectrum by electron scattering, etc
15 p2799 A70-31999

Arp hypothesis regarding radio source ejection from galaxies tested for quasars
15 p2808 A70-32887

Radio source 3C279 position during October 1969 occultation by sun, determining SHF deflection in solar gravitational field
16 p2972 A70-33049

Field classifications for southern extragalactic radio sources with available optical observations, identifying 21 objects
16 p2980 A70-34194

Weak radio sources positions, structures and optical identifications from lunar occultation observations, tabulating radio and optical data
17 p3156 A70-34826

Radio observations of Crab Nebula and radio source, correlating optical and radio features
17 p3164 A70-35114

Large anisotropy observed for gravitational radiation detector intensity as function of sidereal time, suggesting source from galactic center
17 p3137 A70-35725

Radio sources angular broadening by solar wind turbulence used for solar corona probe
18 p3311 A70-36003

Planetary nebula K3-50 microwave observations, determining composite source radio spectrum
18 p3313 A70-36326

Planetary nebula NGC 7027 radio component, determining brightness temperature from fringe amplitude
18 p3313 A70-36327

Variable radio source linear polarization at 8 GHz, examining degree, position angle and flux density
18 p3317 A70-37001

Extragalactic radio sources polarization variations at 8 GHz based on expanding source type model, noting synchrotron self absorption depolarization
18 p3317 A70-37002

Extragalactic radio source counts analysis, suggesting luminosity evolution as dominating influence
18 p3320 A70-37073

Pulsar radio pulses structure and emission source theory based on synchrotron radiation and relativistic effect calculations
18 p3321 A70-37119

Radio sources near 2 flux units at 408 MHz, presenting data on positions, optical identifications, angular size and flux densities
18 p3321 A70-37125

Physical processes in galactic and extragalactic sources of nonthermal radio emission, assuming pulsars as principal magnetic field and cosmic rays sources
18 p3321 A70-37126

Continuum source counts in galactic plane
18 p3327 A70-37165

Galactic plane hard X ray emission measurements, considering gamma and X ray origin from Compton scattering of photons by galactic electrons
19 p3497 A70-38023

Interstellar molecular radio frequency lines significance to galactic physics, noting abundance relation to constituent atoms indicating dust catalytic formation
19 p3521 A70-38496

Antenna systems with minimum angular resolving power for solar limb radio sources recording, using data from solar meridian passage
19 p3522 A70-38563

Moon as standard radio source for eliminating earth atmosphere influence during solar radio radiation measurements
19 p3522 A70-38564

Radio sources with opaque microwave spectra near galactic equator
19 p3522 A70-38603

Spectral intensity distribution of extragalactic radio sources, comparing spectral deviations from simple power law to radio emission from relativistic electrons in magnetic field
19 p3524 A70-38749

Flux intensity measurements of radio sources at 10.69 GHz by radome protected telescope using cryogenically cooled parametric amplifier as receiver
19 p3524 A70-38750

Radio source 3C 161 scintillating component angular dimensions and flux density at 60 MHz
19 p3524 A70-38760

Radio sources right ascension and flux densities at 60 MHz
19 p3524 A70-38761

Radio sources angular dimensions estimation based on shifts in histograms of scintillation quasi-periods
19 p3525 A70-38766

Radio sources flux density and variability at microwave wavelengths
20 p3703 A70-39025

Optical identification of Parkes Catalog radio sources at declinations below minus 45 degrees, using Cordoba Observatory photographs
20 p3704 A70-39476

Supernova remnants catalog based on radio surface brightness, deriving galactic distribution and testing theories for nonthermal radio sources evolution
20 p3709 A70-40077

Radio source counts from Ohio State University observations, noting faint sources decrease relative to uniform Euclidean universe
20 p3713 A70-40427

Radio source master catalog giving name, coordinates, flux density and frequency of observation
20 p3713 A70-40539

Cas A and SN 1572 supernova remnant radio sources X ray spectra, investigating absorption by interstellar medium
21 p3873 A70-40666

Extragalactic cosmic X ray background source models for intensity and energy spectrum, noting Compton scattering of black body photons by relativistic electrons
21 p3877 A70-40699

- Galactic gamma ray sources model with magnetic fields concentration in expanding shell, suggesting production by neutral pion decays in supernova remnants 21 p3877 A70-40701
- Taurus A 21 cm radiation anomalous frequency decrease during occultation by sun attributed to particle streams propagating in solar corona 21 p3886 A70-40704
- Extragalactic radio sources observable and intrinsic properties relationship for distance estimates, considering surface brightness, diameter, luminosity, etc 21 p3889 A70-41145
- Optical pulsar search instrument in radio pulsar fields, showing performance on NP 0532 21 p3826 A70-41156
- Cosmic evolution of radio sources, discussing observations and data interpretation 21 p3890 A70-41171
- Position scatter of 80 MHz sources of type 3 solar bursts reflecting outer corona structure 21 p3891 A70-41182
- Radiobeliograph observations of coronal broadening of Crab Nebula at 80 MHz, noting radial scattering and intensity irregularities 21 p3891 A70-41184
- Extended extragalactic bright radio sources with complex structure, comparing radio to optical field 21 p3892 A70-41189
- Laboratory measurement and low noise search in W OH for microwave emission lines in excited rotational level of interstellar OH 21 p3922 A70-41977
- Catalog 4C radio sources optical identification, determining distribution, coordinates and radio luminosities 21 p3922 A70-41978
- Radio source count formula in zero pressure model universe for background radiation differential density evolution 21 p3923 A70-42104
- Extragalactic radio source count interpretation of cosmological model and evolution, discussing luminosity, electron scattering and red shifts effects 21 p3923 A70-42105
- Extragalactic radio astronomy development, describing source characteristics, distribution, spectra, brightness polarization, synchrotron radiation and evolution 22 p4098 A70-42380
- Radio sources minimum observable diameter attributed to interstellar scattering and synchrotron self absorption 22 p4101 A70-42862
- Radio emission searched for X ray sources near Sagittarius 22 p4094 A70-42930
- High resolution observation of compact radio sources at 13 cm, using long baseline dual antenna interferometry 22 p4102 A70-42976
- Weak scattering limit in thin screen model of interplanetary scintillations of radio sources involving solar wind fluctuations at Fresnel scale 22 p4104 A70-42996
- Extragalactic variable radio sources as clue for quasars and galactic nuclei energy, using long baseline interferometry 22 p4105 A70-43226
- De Sitter nonempty static cosmological model, examining possibility by comparing integral luminosity function for cosmic radio sources to radio galaxies statistics 22 p4106 A70-43258
- Celestial radio source angle tracking techniques using monopulse antenna receiving system applied to angle tracking radar 22 p3991 A70-43582
- Galactic hydroxyl emission sources right ascensions, presenting coordinates and antenna temperature measurements 22 p4242 A70-44277
- Discrete radio sources absolute spectra in 10-5000 MHz range, discussing data disagreement and measurement errors 22 p4247 A70-44795
- Precise radio source positions from independent interferometer measurements in UK and US 22 p4253 A70-44867
- Energy production of extragalactic radio sources, discussing objects associated with quasars 24 p4403 A70-45395
- Gravitational wave associated radio pulse observations using long baseline spaced receivers 24 p4412 A70-46136
- Extragalactic radio source optical identifications showing association with quasars or Seyfert galaxies nuclei 24 p4413 A70-46168
- Physical conditions required to explain observations of radio galaxies through electrons of secondary origin, considering spectral characteristics and evolution 04 p0742 A70-15716
- Satellite relay systems to provide polarization discrimination in antenna main beam to double spectrum for communications 05 p0815 A70-16661
- Right ascension and flux density of source in Crab Nebula measured at meter wavelengths, evaluating spectrum and relative position to binary star center 05 p0917 A70-16908
- Galactic longitude interval region radio telescope observations, obtaining isophotes of brightness distribution of RF spectral line of neutral H and continuous spectrum 08 p1564 A70-20551
- Radio spectra formation mechanisms in discrete sources within framework of synchronous emission theory 10 p1934 A70-25152
- Lightning discharge slow tail atmospheric relation to return stroke, using VLF spectra and frequency analysis 15 p2727 A70-31871
- Galactic longitude interval region radio telescope observations, obtaining isophotes of brightness distribution of RF spectral line of neutral H and continuous spectrum 15 p2805 A70-32706
- Pulsar RF spectral fine structure in decimeter wave range 17 p3163 A70-35050
- Orion nebula core radio recombination line intensities, showing variations in mean electron temperatures and physical conditions 18 p3313 A70-36329
- Giant E and SO galaxies, discussing radio spectra, emission characteristics and brightness distributions 18 p3313 A70-36332
- Synchrotron model limitation for nonthermal spectra, demonstrating restriction to small pitch angles and strong fields 18 p3318 A70-37024
- Small angular diameter radio source in central Crab nebula association with pulsar NP 0532 based on spectra and pulse duration 18 p3322 A70-37128
- Electron density irregularities convected past space probe relationship to radio intensity power spectrum scintillations 20 p3703 A70-39023
- International Telecommunication Union (ITU) legal recommendations on radio spectrum use, interference and frequency assignment problems 20 p3585 A70-39411
- RF spectral recombination lines from atomic level transitions, discussing populations, H lines, electron temperature, density and emission and formation 20 p3706 A70-39934
- Solar active region radio spectrum during 12 November 1966 eclipse, discussing flux, magnetic field effects, temperature and electron density 21 p3886 A70-40961
- Complex burst of 2 September 1966, comparing dynamic radio spectra from Culgoora and Weissenau 21 p3880 A70-40968
- Jupiter RF spectrum in 80 to 10,000 MHz range for dipolar model, noting independent synchrotron component 21 p3891 A70-41185
- Secondary periodicities in energy spectrum of strong pulsars from 80 MHz radiobeliograph observations 21 p3892 A70-41186
- Electromagnetic radiation power spectrum scattered by relativistic particles, considering reflected waves resemblance to HF radio spectra of quasars 22 p4100 A70-42856
- Pulsar pulse arrival time fluctuations, examining solar coronal nature by angular broadening, scintillation and turbulence spectrum 22 p4101 A70-42935
- Discrete radio sources absolute spectra in 10-5000 MHz range, discussing data disagreement and measurement errors 23 p4247 A70-44795
- Solar VHF radio spectra indicating type 4 burst activity associated with type 3 formation 24 p4401 A70-45318
- UV Ceti type variable flare stars, observing radio and optical spectral regions for X ray production 24 p4397 A70-45763
- Synchrotron source spectra natural frequency cut-off in absence of self absorption and electron energy cut-offs, discussing pulsar NP 0532 24 p4410 A70-45774
- RADIO SPECTROSCOPY**
Zero radiospectrometer for spectral observations of radio emission of excited galactic hydrogen at centimeter wavelength, noting Omega nebula detection 08 p1495 A70-21063
- RADIO STARS**
NT PULSARS
- Radio star and satellite scintillation observation, considering diurnal, seasonal and latitude variations and relationship to magnetic and solar activity 01 p0181 A70-10590
- Focusing and saturation effects in radio star and satellite signal scintillations based on diffraction and refraction theories 07 p1271 A70-20157
- OH radio emission from IR stars, discussing spectra, polarization properties and red giant star model with expanding atmosphere 14 p2641 A70-30881
- RADIO TELEMETRY**
NT PULSE FREQUENCY MODULATION TELEMETRY
FM/FM telemetry systems waveform distortion measurement technique based on minimum rms error between input and output signals 01 p0044 A70-10941
- Radio telemetry of athlete hearts, noting strenuous physical stress induction of transient serum potassium increase, metabolic acidosis, T-wave amplitudes, etc 02 p0230 A70-11694
- UHF radio telemetry system using pulse signal to measure and transmit sea waves amplitude and frequencies data to shore-based recorder 03 p0453 A70-14352
- Earth resources satellites capabilities and requirements emphasizing orbit parameters, remote sensing, data handling and telemetry systems [AAS PAPER 69-587] 04 p0760 A70-14642
- AM baseband telemetry system for wideband signal transmission emphasizing SSB, DSB and quadrature multiplexed DSB modulation techniques 06 p1007 A70-17435
- Physiological reactions detection, transmission and data evaluation of aircraft pilots subjected to various stress environments, using radio telemetry 09 p1626 A70-23009
- Terrestrial surface radiometric imaging by sensing thermal radiation at centimeter wavelengths to reduce atmospheric scattering attenuation 09 p1687 A70-23763
- Polarization diversity reception effects on VHF telemetry signal from low altitude satellites 10 p1832 A70-23919
- Meteorological radar station reception equipment for increased radio telemetry channel reliability in complex radio sounding of atmosphere 11 p2075 A70-25920
- Mechanical parameters measurement by radio telemetry during aircraft and motor vehicles tests, noting onboard recording methods 11 p2056 A70-26452
- Time constant, steady state and tracking error of AGC loops at input/output of FM link in AM-FM telemetry system 12 p2184 A70-27250
- Sounding rocket telemetry systems, discussing use of PCM and thick film techniques 13 p2363 A70-28681
- Solar probe Helios data processing and transmission system, describing block diagram, PCM/PSK/PM telemetry and transmitter 13 p2367 A70-29558
- Signal analysis from Russian Cosmos, Proton and Soyuz satellites, showing pulse width and pulse code telemetries 14 p2551 A70-30975
- S band telemetric signals reception transmitted by Apollo 12 during occultation behind lunar disk, discussing lunar surface reflectivity 15 p2699 A70-32290
- Miniature wireless strain and temperature radio telemetry transmitters for measurements in areas inaccessible to direct wire connections 15 p2738 A70-32301
- FM/FM radio telemetry system for transmitting strain and temperature data from rotating parts 15 p2739 A70-32330
- UHF radio telemetry for transmissometers measuring airport runway visibility 16 p2889 A70-34222
- S band telemetry antenna with electronic tracking and polarity diversity for remote location missile testing 19 p3388 A70-37901
- Automatic calibration verification of subcarrier telemetry discriminators with selective channel readjustment 19 p3383 A70-37902
- Dynamic radio telemetry in physiology and medicine, discussing recordable parameters, multichannel systems, automatic data processing, etc 19 p3370 A70-38216
- Four channel FM radio telemetry for exercise physiology, measuring EKG, respiration rate and pulmonary ventilation 23 p4151 A70-44380
- RADIO TELESCOPES**
Long baseline interferometry used to improve radio telescopes resolving power in measuring quasar diameters 01 p0183 A70-10885

Monograph on radio telescopes covering developments from simple parabolic reflectors to computer based image forming instruments
01 p0046 A70-11250

Reflector radio telescope of Pulkovo Astronomical Observatory noting high resolution
01 p0094 A70-11585

Phase measuring scheme for large radio telescope array, describing constant-phase calibration signal production
02 p0269 A70-12583

Multimirror illumination system for radio telescope antenna with reduced noise temperature, narrow radiation pattern and optimal specular cross section, noting sensitivity
03 p0455 A70-13082

Radio telescope efficiency improved at 8 mm wavelength by quantum paramagnetic amplifier and multimirror antenna system
03 p0455 A70-13083

Subcritical wavelengths processing of solar radio emission, allowing for antenna radiation pattern distortion due to surface defects
04 p0745 A70-14498

Radio telescopic observations at 408 and 5000 MHz in galactic plane, describing two sources
04 p0746 A70-14514

Analog techniques for pulse integration based on sonograph audio spectrum analyzer for pulsar observation by radio telescopes near Hobart, Tasmania
04 p0655 A70-14520

Contour maps of radio sources structure in 3C catalog from radio telescope observations
04 p0758 A70-15698

Parasitic cross polarization lobe elimination in radiation patterns of variable profile antennas by curved conductors, including confirmation for large radio telescope
05 p0820 A70-16253

Phase switching method application to radio telescopic observations showing increase in reliability of radio source coordinates determination
07 p1240 A70-18909

Statistical characteristics of random wind effects on radio telescopes tracking cosmic object
08 p1586 A70-21062

Discrete diode phase inverter for meter wavelengths providing north-south antenna control of radio telescope by diffraction method
08 p1473 A70-21064

Radiometers with low noise parametric amplifiers at centimeter wavelengths for radio telescope, discussing design, performance and Venus observations
08 p1495 A70-21065

Parametric amplifier for spectral radiometer of U.S.S.R. astronomical telescope, showing improved sensitivity observations of neutral H emission
08 p1473 A70-21066

Electrical axis adjustment of east-west antenna array of crossed radio telescope by statistical processing of discrete sources observations
08 p1473 A70-21067

Radio telescopes relaying interferometers characteristics noting delay in IF channel and wideband performance
08 p1495 A70-21068

Antenna exciter of crossed radio telescope, discussing design, performance and increased wide band sensitivity
08 p1473 A70-21069

Solar wind velocity radioastronomical measurements, discussing radio wave fluctuations, telescope antenna designs, radiometers and observations
08 p1474 A70-21070

Cambridge one mile radio telescope observations of weak sources, extending radio source luminosity function and tabulating, graphing and mapping results
08 p1578 A70-21546

Cross type radio telescope beam forming and steering system, describing switched delay lines and phasing circuits
08 p1477 A70-21823

Beam delay line for introducing variable gradients in Molonglo radio telescope, discussing circuits and performance
08 p1478 A70-21824

Reflector focus location for variable profile antenna of radio telescope determined by modified Hartmann method in optics field
09 p1648 A70-23164

Radio telescope construction, discussing early planning decisions, site selection, structural compensation for built-in elastic deformation, foundation, telescope mount, etc
12 p2207 A70-27578

Radiotelescope measurements for geodetic purposes, applying interferometric principles to quasar radiation
13 p2396 A70-29163

SHF radio telescope for solar radio wave observation, describing design and performance
15 p2717 A70-31897

Steerable 100 meter radio telescope, discussing foundations, azimuth towers, reflector, assembly, electric motors, steering and receivers
16 p2888 A70-33656

Highly directive radio telescope antenna parameters in near zone, using focusing at minimum distance
17 p3055 A70-35679

Neutral hydrogen distribution in galactic region surveyed with radiotelescope
18 p3328 A70-37169

Pulsar galactic longitudinal distribution, discussing observability impaired by high electron density in spiral
18 p3328 A70-37173

Parabolic antennas for satellite communications network and radio telescopes, investigating surface utilization coefficient
19 p3395 A70-37267

Prime focus feeds performance for radiotelescopes, using one- or two-hybrid modes in circumferentially corrugated waveguides
19 p3388 A70-37967

Canadian HF T array radio telescope at Dominion Radio Astrophysical Laboratory, discussing design and performance
19 p3397 A70-38275

Sun role in radio telescope radiation patterns analysis and adjustment, allowing for solar radio source finite dimensions and nonuniform brightness
19 p3390 A70-38560

Algorithm for radio telescope antenna pattern reconstruction from solar transit and radiation distribution data
19 p3390 A70-38561

Flux intensity measurements of radio sources at 10.69 GHz by radome protected telescope using cryogenically cooled parametric amplifier as receiver
19 p3524 A70-38750

RADIO TRACKING
Statistical characteristics of random wind effects on radio telescopes tracking cosmic object
08 p1586 A70-21062

Satellite radio tracking systems noting interferometer most suitable for accuracy and maintenance
08 p1463 A70-21712

Mariner 7 preencounter anomaly in radio tracking data and trajectory investigated by computerized simulation
19 p3534 A70-38878

Global upper atmosphere circulation pattern by daytime tracking of high altitude rocket vapor trail, using differential radiometer
23 p4214 A70-44039

Planetary masses determined from radar measurement data and radio tracking of space probes
24 p4407 A70-45535

RADIO TRANSMISSION
NT DOUBLE SIDEBAND TRANSMISSION
NT IONOSPHERIC F-SCATTER PROPAGATION
NT IONOSPHERIC PROPAGATION
NT MICROWAVE TRANSMISSION
NT MULTIPATH TRANSMISSION
NT SHORT WAVE RADIO TRANSMISSION
NT SINGLE SIDEBAND TRANSMISSION
NT TRANSEQUATORIAL PROPAGATION

Tropospheric parameters determination using combinations of measurement and transhorizon radio signals propagation techniques
01 p0044 A70-11086

HF radio waves propagation between antipodal transmitter and receiver, discussing diurnal variations and reception over polar caps and water
01 p0045 A70-11103

VLF energy propagation using ceramic dielectric model of earth-ionosphere waveguide
02 p0269 A70-12592

Wave propagation problem, considering traffic control, surveying, tracking, navigation, etc
03 p0449 A70-13607

Tropospheric fine structure influence on radio wave propagation, including atmospheric gases and precipitation effects and radar, navigation and TV applications
03 p0449 A70-13612

VLF radio wave propagation variations occurring in earth-ionosphere waveguide contributing to errors in OMEGA position lines used to obtain worldwide navigational fixes
03 p0523 A70-13614

Global satellite VLF propagation system for investigating mesospheric ionization
03 p0475 A70-13827

Radio wave propagation in linear, isotropic homogeneous medium with irregular boundaries solved by expanding Helmholtz integral
04 p0648 A70-14965

Direction fluctuations in radio wave scattering in turbulent gyrotropic medium using Einstein-Fokker-Kolmogoroff equation
04 p0653 A70-15722

Ionospheric probe for simultaneous measurement of radio signal reflection coefficient and amplitude-frequency characteristics
04 p0684 A70-15746

Radio waves propagation along polar auroras region, obtaining ionospheric parameters for magnetic disturbances based on penetration probability
05 p0842 A70-16744

Radio wave propagation in stratified media consisting of periodically stacked dielectric slabs solved for boundary condition by reducing Maxwell equations to Hill equation
06 p1007 A70-17463

VHF propagation variations relationship to changes in interplanetary plasma associated with interplanetary space sectorial structure rotation
07 p1226 A70-18757

LUF/lowest useful frequency/ prediction for HF sky wave communication, emphasizing prediction methods using computers
07 p1229 A70-19156

Radio propagation characteristics and communication system performance, discussing concepts of MUF, LUF, error rate, communication system modeling, prediction techniques, etc
07 p1229 A70-19157

Ray tracing techniques applied to night sky wave medium frequency propagation, modifying program for absorption and polarization coupling losses
07 p1230 A70-19164

Ionospheric radio transmission field strength calculation for given electron density and collision frequency profiles, considering electron variations along transmission path
07 p1230 A70-19165

Ray tracing calculation and experimental observation for mode structure and absorption loss of oblique incidence HF radio wave propagation
07 p1234 A70-19217

Radio signal reception beyond normal horizon by partial reflection from elevated layer in troposphere calculated by computer
07 p1234 A70-19218

Ionospheric electron content and concentration variations analysis based on data of radio waves propagating from satellite, considering Doppler shift and Faraday effect
07 p1237 A70-20427

Radio wave propagation in anisotropic plasma consisting of oxygen ions and protons, deriving expressions for radio wave refractive index
07 p1355 A70-20452

Field strength and interferential structure at different cross sections of inhomogeneous ionospheric channel calculated during bounce mode propagation of radio waves
08 p1461 A70-20969

Fossil turbulence /three dimensional quasi-isotropic refractive index microstructure left behind during turbulence patch decay/ effects on radio wave propagation
09 p1717 A70-22377

Radio wave propagation equations, applying stationary phase method for finite limits of dimensionless line integral
09 p1638 A70-23662

Geomagnetic field orientation effects on VLF nighttime propagation, checking computer program predictions
09 p1639 A70-23664

Long range radio wave propagation and effective refraction index in turbulent magnetoplasmas with stochastic density variation
10 p1832 A70-23962

MF signals sky wave propagation, studying roles of geomagnetic dip and propagation direction at various latitudes
10 p1832 A70-23997

Millimeter wave transmission, discussing atmospheric effects, system components and applications in terrestrial communication networks, synchronous satellites, etc
10 p1842 A70-24883

Seasonal variations in radio signal propagation from aircraft navigation system antenna located in dense forest, solving problem with Doppler-VOR installation
10 p1854 A70-25254

Ionospheric changes from field intensity and phase data of long distance propagation of long waves, determining electron concentration
10 p1884 A70-25258

Italian SIRIO SHF experiment for study of atmospheric effects on satellite link, discussing system design and performance
11 p1999 A70-25442

Pulsed radio waves interactions during vertical propagation through perturbed ionosphere using cross modulation theory concepts, considering perturbation waves effects
11 p2003 A70-25531

Broadband 2 GHz transhorizon radio relay system design and performance for transmission on four channel pairs
11 p2034 A70-26820

Rocket measurement of ionospheric electron density based on radio propagation effects involving Doppler frequency shift, Faraday rotation, wave absorption, etc
12 p2224 A70-27736

Ionospheric parameters measurements by incoherent RF scattering, discussing current status of theory and observations 12 p2225 A70-27738

Radio propagation over sea water path, predicting transmission loss by computer programs 12 p2188 A70-27936

Atmospheric difference measurements interpretation in terms of radio refractive index spectra at single point based on corresponding frequency component ratio 13 p2394 A70-28790

Radio wave transmission through magnetized plasma layer as function of electron concentration and collision frequency, using coaxial accelerator 13 p2366 A70-29377

Millimeter and submillimeter radio waves propagation, outlining molecular and aerosol attenuation in real atmosphere together with transmitters and receivers 13 p2366 A70-29401

Radiation from electric dipole oriented normal to magnetostatic field in plasma column improving antenna transmission characteristic during reentry 13 p2467 A70-29913

Radio waves attenuation anisotropy in sea ice by comparing vertically and horizontally polarized signals 14 p2546 A70-30132

Radio wave field intensity in middle frequency range, determining propagation curves for large distances 14 p2547 A70-30208

Meteor radio path activity coefficient, reflections density distribution, characteristic heights and mean durations, noting meteor velocity effects 14 p2636 A70-30319

Meteor radio propagation for long trajectories, considering oblate scattering ellipsoid 14 p2636 A70-30326

Radio wave reflection from ionized meteor trails, calculating propagation parameters by computer algorithm based on cylindrical approximation method 14 p2636 A70-30327

UHF propagation measurement over sea for varying surface refractivity and meteorological conditions, noting diurnal variations 14 p2549 A70-30513

Radio wave propagation obstacle gain changes with varying distance between obstacle and path terminal 14 p2549 A70-30514

Direction fluctuations in radio wave scattering in turbulent gyrotropic medium using Einstein-Fokker-Kolmogoroff equation 14 p2550 A70-30806

Ionospheric probe for simultaneous measurement of radio signal reflection coefficient and amplitude-frequency characteristics 14 p2576 A70-30830

Ionospheric electron density profiles between two locations calculated from oblique incidence ionograms, plotting radio path for ground range 15 p2726 A70-31861

Sudden phase anomaly /SPA/ in VLF radio wave propagation during Proton Flare Project, noting corresponding solar X-ray flux intensity enhancement 15 p2794 A70-32294

Negative sudden phase anomaly /SPA/ in VLF radio transmission, noting solar X ray flux intensity and zenith angle effects 15 p2699 A70-32297

Decimeter waves propagation along overland path, considering tropospheric radio relay systems development 16 p2863 A70-33238

Sounding rocket instrumentation for ionospheric VLF radio noise measurement and recording 17 p3090 A70-35398

Ionospheric radio noise measurements with VLF wideband receivers onboard rocket 17 p3046 A70-35399

Long range tropospheric radio wave propagation, calculating signal impulse function and time lag between diffraction and reflection 17 p3048 A70-35678

VHF propagation variations relationship to changes in interplanetary plasma associated with interplanetary space sectorial structure rotation 18 p3229 A70-37101

Radio beam trajectory in Fresnel zones of isotropic laminarly inhomogeneous ionosphere, discussing point source field and wave propagation 19 p3381 A70-38569

Pulsed radio waves interactions during vertical propagation through perturbed ionosphere using cross modulation theory concepts, considering perturbation waves effects 21 p3786 A70-41281

Optimal nonlinear filtration for continuous automatic data transmission with radio signal under white, narrow band and Markov noise 22 p4004 A70-42891

High level parametric upconverter for radio link using evanescent mode waveguide 22 p3997 A70-42925

Magnetosphere radio propagation from ground based measurements for HF, ULF and VLF 22 p4021 A70-43280

Coherent reflection waves produced by radio wave propagating through entire earth atmosphere 23 p4159 A70-43757

Phase and group velocity variations of LF transmission compared against crystal oscillator 23 p4163 A70-44228

Limiting effects of topographic quasi-optical radio propagation above 100 MHz in radar aircraft navigation, clear air disturbances detection and IR warning technique 23 p4163 A70-44230

Radio wave field intensity in middle frequency range, determining propagation curves for large distances 24 p4316 A70-46283

RADIO TRANSMITTERS

NT IONOSONDES

NT OMNIDIRECTIONAL RADIO RANGES

NT RADIO BEACONS

NT RADIOSONDES

NT RAWINSONDES

NT TRANSMITTER RECEIVERS

Airborne UHF transmitters, discussing data on designs, performance, packaging and limiting factors of solid state devices for RF utilization 02 p0267 A70-12183

Local criteria and geometric integration for stable transmitter power level selection in group of radio stations ensuring adequate SNR 03 p0446 A70-13237

Energy converters and radio transmitters for physiological telemetry, using electric power converted from thermal and mechanical energy of human respiratory activity 04 p0644 A70-15276

FM spectral density model with applications to radio transmitter bandwidth estimation and interference analysis 08 p1456 A70-20473

Relaying interferometer design consisting of heterodyne frequency diversity antennas with coherent mixer, relaying transmitter and receiver 08 p1495 A70-21071

Interference emission filtering in high power microwave transmitters, discussing spurious emissions removal or rejection by transmission line filters 08 p1474 A70-21257

Long wave transmitter field strength calculation to 1000 km based on optical beam method and ionosphere model to account for radio wave reflection 10 p1840 A70-24495

Ionospheric effects and transmitter characteristics observed on HF standard and time stations, discussing spurious emissions arising from frequency overcrowding 10 p1842 A70-25050

Solar probe Helios data processing and transmission system, describing block diagram, PCM/PSK/PM telemetry and transmitter 13 p2367 A70-29558

Occupied bandwidth definition and measurement based on probability density function computation for radio transmitter spurious, harmonic and fundamental emissions 19 p3380 A70-38176

Soviet book on radio transmitting equipment, covering vacuum tube and transistorized devices, amplifier stages, AM transmitters, oscillator circuits, etc 20 p3597 A70-39599

Centimeter wave transmitting and receiving equipment for studying nanosecond pulse propagation 20 p3632 A70-39627

Miniaturized VHF transmitter with bonded circular printed circuits for withstanding high shock loads, discussing design, production, packaging and testing 23 p4164 A70-44537

RADIO WAVE REFRACTION

Microwave radio refraction analysis for controlling interference between radio relay antenna and geostationary satellites 07 p1235 A70-19363

Radio wave refraction and field strength in model Venus atmosphere for various spacecraft trajectories 07 p1235 A70-19492

Focusing and saturation effects in radio star and satellite signal scintillations based on diffraction and refraction theories 07 p1271 A70-20157

Radio wave propagation in anisotropic plasma consisting of oxygen ions and protons, deriving expressions for radio wave refractive index 07 p1355 A70-20452

Atmospheric fine-scale structure determination from forward scatter radio wave propagation, considering refractive index role 09 p1715 A70-22362

Long radio wave propagation and effective refraction index in turbulent magnetoplasmas with stochastic density variation 10 p1832 A70-23962

Temperature and ion effect on refractive index of VLF radio waves in quiet and disturbed ionospheric conditions 11 p2004 A70-25842

Atmospheric optical thickness from radio telescopic measurements of wave absorption at millimeter wavelengths, showing dependence on lower atmospheric moisture content 14 p2546 A70-30127

UHF propagation measurement over sea for varying surface refractivity and meteorological conditions, noting diurnal variations 14 p2549 A70-30513

Radio wave refraction and field strength in model Venus atmosphere for various spacecraft trajectories 15 p2705 A70-32737

Radar ducting effects on propagation at microwave frequencies, recording signal strength as function of transmitter to receiver range 16 p2858 A70-32927

Erroneous line of sight rates generation by radar radome refraction errors in aircraft tracking 18 p3231 A70-36457

Ionospheric refraction during radio wave propagation using space diversity recordings of Faraday and Doppler effects for coherent signals from geophysical rockets 19 p3407 A70-37306

RADIO WAVES

NT DECA-METRIC WAVES

NT DECIMETER WAVES

NT EXTRATERRESTRIAL RADIO WAVES

NT GALACTIC RADIO WAVES

NT LONG WAVE RADIATION

NT MICROWAVES

NT MILLIMETER WAVES

NT RADIO EMISSION

NT SHORT WAVE RADIATION

NT SKY WAVES

NT SOLAR RADIO BURSTS

NT SOLAR RADIO EMISSION

NT SUBMILLIMETER WAVES

NT TYPE 2 BURSTS

NT TYPE 3 BURSTS

NT TYPE 4 BURSTS

NT TYPE 5 BURSTS

Horizontal gradients below satellite orbit effect on reduced and minimum difference in Doppler frequency shifts of coherent radio waves from satellite in inhomogeneous ionosphere 01 p0046 A70-11517

Vertical probe observations of short radio waves propagation through sporadic E at various frequencies and path lengths 01 p0084 A70-11553

Data collection for ionospheric disturbances, geomagnetic field, radio wave intensity, cosmic rays and solar activity 02 p0290 A70-12125

Phase distortion and Faraday rotation of wideband radio waves propagating through ionosphere 03 p0449 A70-13584

VLF radio monitoring of celestial X ray fluxes from ground for long periods, discussing ionospheric D region conductivity 04 p0739 A70-14521

Helmholtz integral for radio waves scattering from surfaces expanded for reflection from terrain or atmospheric layers 04 p0648 A70-14964

Error correction for previous derivation of radio propagation of wave-hop series for anisotropic ionosphere resulting in improved nighttime field strength accuracy 04 p0649 A70-14967

Radio wave scattering increase in moving body wake near caustic in vertically inhomogeneous ionosphere 04 p0653 A70-15725

Correlation function of auroral reflection radio signals with allowance for polar ionospheric scattering and pulse signal transmission and reception 05 p0841 A70-16741

Oblique ionospheric radio wave propagation at frequencies near lowest usable HF - NATO/AGARD Conference, Leicester, England, July 1966 07 p1227 A70-19151

Polarization and absorption of radio waves in ionosphere using Appleton-Hartree equations, calculating LUF as function of sunspot number 07 p1229 A70-19160

Reflection coefficient for radio wave pulse reflected from ionosphere with large scale fluctuations in electron density, compared to empirical data for reflecting surface irregularities 07 p1231 A70-19170

Ionospheric radio wave /auroral/ absorption during substorm investigated for longitudinal and latitudinal variations by multistation riometer measurements, inferring electron precipitation characteristics 07 p1269 A70-20030

Ionospheric data of local and integral electron concentration obtained by measuring phase shift of satellite emitted coherent radio waves 07 p1276 A70-20422

Scattering cross sections of radio waves at wake of vertically moving body near reflecting ionospheric layer, noting wave sphericity influence

07 p1237 A70-20423

Radio wave sphericity influence on scattering at moving body wake in ionosphere, determining scattering cross section principal maximum

07 p1237 A70-20424

Perturbed ionospheric regions acting as radio wave focusing lens, discussing frequency, power and pattern selection

07 p1237 A70-20448

Radio wave reflection coefficient power spectra for three layer lunar surface models consistent with radar spectrum, calculating porous layer thickness

08 p1565 A70-20566

Tropospheric electrical path length estimated by microwave radiometry using atmospheric models

09 p1640 A70-23806

Loran C radio wave field intensity diurnal variations measurements, investigating ionospheric waves characteristics

10 p1832 A70-23921

F region electrons collision frequency from short radio waves amplitude and group path relationship

10 p1876 A70-24535

Radio wave reflection spectra from plane surfaces, determining physical properties and composition

10 p1843 A70-25154

Atmospheric refractivity role in range errors from ground station to stationary satellite and in range rate measurement

12 p2189 A70-28058

Radio wave propagation obstacle gain changes with varying distance between obstacle and path terminal

14 p2549 A70-30514

Reflection and conversion coefficients of model ionospheres for VLF and LF radio waves

14 p2573 A70-30735

Radio wave scattering increase in moving body wake near caustic in vertically inhomogeneous ionosphere

14 p2550 A70-30809

Radio wave reflection coefficient power spectra for three layer lunar surface models consistent with radar spectrum, calculating porous layer thickness

15 p2805 A70-32721

Ion motion neglecting conditions for radio waves in plasma based on Ohms law uncoupling from momentum transfer

16 p2957 A70-32980

Refractive index gradients effect on scattering of radio waves perturbing ionosphere or passing through perturbed region

16 p2863 A70-33259

VLF and ELF radio wave propagation with mode coupling in inhomogeneous stratified ionosphere

17 p3047 A70-35402

Ionospheric VLF radio waves observations via wideband receiver on K-9M-26 rocket, determining electron density profiles

17 p3047 A70-35639

Radio wave absorption dependence on ionospheric sounding frequency at vertical incidence, using pulse method

18 p3255 A70-37038

Pulsar radio pulses structure and emission source theory based on synchrotron radiation and relativistic effect calculations

18 p3321 A70-37119

Radio wave holography with unequal reference to signal frequency, recording linear object with superheterodyne receiver

19 p3420 A70-37290

Skin effect for unsteady radio waves emitted into homogeneous nonmagnetic isotropic half space, calculating electric field

19 p3381 A70-38571

Radio wave propagation over inhomogeneous terrains, determining perturbing effects of details on wave characteristics

19 p3381 A70-38573

X ray star effects on ionospheric LF radio wave field strength, examining absorption and ionization in D region

21 p3873 A70-40668

Wave polarization effects on ionospheric radio wave transmission and reception

21 p3790 A70-41361

Radio wave reflection properties in 16-3000 kHz range calculated from D and E region models for comparison with measurement

22 p3989 A70-43164

Pulsed radio wave interactions with various lower ionosphere models, estimating cross modulation by computer calculation for comparison with measurements

23 p4162 A70-44080

RADIOACTIVE AGE DETERMINATION

Re 187 to Os 187 nuclear decay rate variability, discussing earth age, temperature and ionization effects

01 p0178 A70-10349

Three mode galactic age model for nucleosynthesis of solar radioisotopic material produced by r-processes

01 p0182 A70-10720

Age and initial strontium for Guarena chondrite, determining differential evolution of Rb/Sr systems involving simple metamorphism of closed systems or multistage processes

03 p0576 A70-14088

Age data on high sodium tektites from Australia showing distinct fall

03 p0576 A70-14089

Pb isotope data from young mantle derived volcanics suggesting mantle evolution and lunar capture

04 p0743 A70-14396

I-Xe dating of Abee enstatite chondrite by combined neutron activation and mass spectrometric analysis

05 p0915 A70-16829

Earth oxygen atmosphere age estimated from sulfur isotope composition of geological phlogopite and lazurite deposits from South Baikal region

06 p1056 A70-17798

Dating method for stone meteorites feldspar phase based on time interval between solar nebula Al 26 production and decay into Mg 26

06 p1150 A70-18479

Rb 87-Sr 87 age determination of carbonaceous chondrites, showing agreement among petrological classification types

06 p1150 A70-18480

Uranium abundance in hypersthene chondrites determined by homogenized fission track analysis, comparing age estimation with iron meteorite event occurrence

07 p1391 A70-20354

Stone meteorites age determination from decay of cosmic ray produced Kr 81 and 78, comparing production rate to He 3 ages

08 p1563 A70-20499

Age dating of earth and universe emphasizing methods based on radioactivity, discussing stellar evolution, galactic age and assessment of cosmic time

08 p1568 A70-20633

Australite fall age determination from in situ radioactive carbon and standard geological dating methods

09 p1750 A70-22055

Radioactive dating of meteorites based on high temperature release of iodine-correlated Xe129 and Xe128

10 p1949 A70-25328

Archeomagnetic measurements showing westward drift of geomagnetic intensity and correlation of magnetic earth moment with radiocarbon production

11 p2044 A70-25599

Australasian and Ivory Coast deep sea microtektites fission track ages compared to deposition ages from paleomagnetic data

12 p2310 A70-28021

Rb-Sr internal isochrons of crystalline lunar rocks from Tranquility Sea for moon age estimation

13 p2485 A70-28472

Middle Miocene hiatus in volcanic activity of Western U.S., discussing K-Ar dates for Tertiary rock of Great Basin area

13 p2393 A70-28718

Tektites age from fission track method, discussing elimination technique for strain caused spurious tracks

13 p2488 A70-28721

Enstatite chondrites K, Rb and Sr concentrations, measuring ages from Sr87/Sr86 ratios

16 p2974 A70-33649

Rb-Sr internal isochron ages from Ocean of Storms, discussing analytical results of two texturally and mineralogically distinct crystalline rocks from Apollo 12

16 p2975 A70-33659

Apollo 11 lunar rocks and dust from Tranquility Sea measured for age by Rb-Sr and K-Ar methods

18 p3320 A70-37082

Meteorite I-Xe 129, demonstrating cold assembly of unequilibrated chondrite

19 p3519 A70-38036

Middle Devonian Tioga Bentonite age from Rb, Sr and Sr isotopes in weathered whole rock samples

20 p3615 A70-38989

Apollo 11 lunar rocks, breccias and fines age and chemistry, major element, trace element and rare earth abundances, texture, crystallization and meteoritic effects

21 p3906 A70-41563

Apollo 11 lunar material isotopic age determination, discussing rock crystallization, radiogenic dust, lead isotope data and moon origin

21 p3907 A70-41576

Apollo 11 lunar rock Rb-Sr isotopic age relationships, discussing magmatic fractionation of Rb relative to Sr in moon primordial material

21 p3908 A70-41585

Lead and thallium isotopic compositions of Apollo 11 fines compared with meteorites and earth for lunar surface age determination

21 p3775 A70-41588

Apollo 11 lunar rock and soil bombardment produced radionuclide patterns, discussing solar flare

protons and alphas, age determination and astronomical models

21 p3777 A70-41604

Apollo 11 lunar rocks, breccia and fines U, Th and Pb isotopes systematics, considering implications for lunar history

21 p3909 A70-41605

Cosmic ray exposure age of lunar surface material by radioactive isotopes Ar 37 and 39 measurement, investigating temperature dependence

21 p3909 A70-41607

Lunar surface material age and post-crystallization from isotopic investigation of Apollo 11 samples of U-Th-Pb systematics

21 p3909 A70-41608

Apollo 11 crystalline rocks chemical analysis by argon 40/argon 39 dating techniques

21 p3778 A70-41613

Age determination of Apollo 11 samples from isotopic composition measurements by isotope dilution techniques, comparing to terrestrial and meteoritic values

21 p3778 A70-41616

Allende meteorite age determination, probing K, U and rare gases in whole rock and chondrule samples

21 p3920 A70-41939

Chondritic meteorite thermal histories based on K-Ar dating using Ar 39/40 method

21 p3921 A70-41974

Crystalline rocks from Mare Tranquillitatis and Oceanus Procellarum, determining K-Ar ages

23 p4238 A70-43803

RADIOACTIVE CONTAMINANTS

Seasonal variation of vertical profiles of atmospheric radioactivity concentration between stratosphere and troposphere due to meridional zonal wind distribution caused by eddy diffusion

08 p1539 A70-21923

Atmospheric dust natural radioactivity effect on tropospheric Pb 210 mean residence time determination for Pb210 and Ra226 fallout in rain near Moscow

14 p2630 A70-30131

German monograph on radioactive gases and decomposition products mass transport in turbulent atmospheric boundary layer, noting Boussinesq approximation and Reynolds decomposition

24 p4324 A70-45094

RADIOACTIVE DATING

U RADIOACTIVE AGE DETERMINATION

RADIOACTIVE DEBRIS

Tropopause role in stratospheric-tropospheric exchange processes for radioactive debris transport

03 p0476 A70-13908

Crew radiation dosage from fission fragments in plume from gas core nuclear rocket

18 p3224 A70-36562

RADIOACTIVE DECAY

NT ALPHA DECAY

NT NEUTRON EMISSION

Electric power generators performance based on kinetic energy conversion of radioactive isotope decay products, noting space applications

01 p0140 A70-10217

Re 187 to Os 187 nuclear decay rate variability, discussing earth age, temperature and ionization effects

01 p0178 A70-10349

Extensive air shower models, noting role of nuclear active component energy decay rate

03 p0556 A70-13038

Emission lines origin in radio galaxies optical spectra explained by using energy gained from radioactive elements decay

03 p0563 A70-13214

Radioactive nuclei alpha radiation investigation methods, discussing nuclear emulsions, scintillation spectrometry, ionization chambers, semiconductor counters and magnetic spectrographs

03 p0485 A70-13479

Radiative lifetimes and total transition probabilities measured in polyatomic gases using phase shift method and electron beam excitation

03 p0441 A70-14009

Atmospheric ionization by beta particles due to fission product decay, showing diagram for magnetic shell parameters and postfission periods

04 p0743 A70-15739

Cytosine-thymine transitions from cytosine-5-H3 decay in bacteriophage S13 DNA, discussing coding change efficiency

05 p0803 A70-16948

Melting zone evolution in thermal history of earth, investigating upper mantle heat transfer effect on layer motion due to radioactive decay

06 p1056 A70-17804

Extinct radioactive isotopes of solar system, discussing decay during nuclear synthesis and planetary formation periods

09 p1762 A70-23126

Isotopic ratio anomaly of Re and detection at nanogram level in solar wind using decay curves of Re source from lunar specimen

10 p1932 A70-24532

Atmospheric ionization by beta particles due to fission product decay, showing diagram for magnetic shell parameters and postfission periods
14 p2632 A70-30823

Cosmic ray lifetime, investigating radioactive Be 10 nuclei decay effects on intensity ratios Be/B and Be/Li, suggesting nuclei confinement to galactic disk
19 p3509 A70-38148

Solar B8-Be8 decay neutrinos energy spectrum and absorption cross sections calculation
20 p3698 A70-39307

Inverse beta decay thermonuclear reactions induced by neutrinos proposed for neutrino detection from solar interior
20 p3704 A70-39471

Low energy cosmic ray positrons arising from Co decay in Ni 56-Co 56-Fe 56 reaction chain in supernova Si burning shells
21 p3879 A70-40927

Isotopic decay rates, solving time dependent atmospheric turbulent dispersion from steady state measurements
22 p4093 A70-42915

Kapoeta howardite Xe abundance and isotopic composition for indications of extinct Pu 244 and I 129 decay
24 p4402 A70-45380

RADIOACTIVE ELEMENTS

U RADIOACTIVE ISOTOPES

RADIOACTIVE FALLOUT PARTICLES

U FALLOUT

U PARTICLES

RADIOACTIVE ISOTOPES

NT BERYLLIUM 9
NT BERYLLIUM 10
NT CARBON 14
NT IODINE 131
NT KRYPTON 85
NT PLUTONIUM ISOTOPES
NT RUBIDIUM 86
NT SODIUM 22
NT SODIUM 24
NT TRITIUM
NT URANIUM 233
NT URANIUM 238
NT XENON 133

Thermal preconditioning using radioisotope heat source to eliminate inertial sensor warmup time by maintaining aircraft navigation system at constant temperature
01 p0140 A70-10310

Cr 51 osteotropic properties for osseous system studies, discussing binding to bones, experiments on rats and rabbits, applications for human osseous system diagnosis, etc
01 p0029 A70-11403

Stratospheric circulation model developed from radioactive element measurements, discussing large scale processes, seasonal variations, etc
02 p0291 A70-12291

Emission lines origin in radio galaxies optical spectra explained by using energy gained from radioactive elements decay
03 p0563 A70-13214

Diffusion categories and propagation of radioactive elements in lower atmosphere determined with respect to measured radiation balance, temperature gradient and wind
03 p0521 A70-14290

Thermal steady state characterization of isotope radioisotope thermoelectric generator, discussing design features and heat transfer models for operating temperatures and output performance
[ASME PAPER 69-WA/ENER-12]
04 p0717 A70-14897

Allende carbonaceous chondrite radionuclide composition and concentration determined by nondestructive gamma ray spectrometry
04 p0754 A70-15275

Miniaturized proportional counter to measure radioactive Ar 37 ultramicroquantities, assessing errors
05 p0898 A70-15930

Block diagrams of three stage device for extracting radioactive Ar from perchloroethylene considered for solar nucleus studies
05 p0845 A70-15933

Meteorological parameters influence on diurnal variations of radionuclide activity and resulting global air pollution
05 p0903 A70-16662

Radioactive isotopes removal from respiratory tract, lungs and gastrointestinal tract by ion dilution and antagonism, blood transfusion and hemodialysis, etc
06 p0994 A70-17666

Radioactive sodium and potassium diffusion in single crystal and polycrystalline Mo and Nb at various temperatures, calculating activation energies and coefficients
06 p1089 A70-17745

Earth central region chemical exploration using antineutrino flux produced by natural radioactive isotopes
09 p1761 A70-22985

Extinct radioactive isotopes of solar system, discussing decay during nuclear synthesis and planetary formation periods
09 p1762 A70-23126

Radioactive Mn 54 with high specific activity for short distance gamma radiography
13 p2404 A70-28658

Solar flare proton induced radioactivity in Apollo 11 lunar surface material compared with stony meteorite data, noting cobalt 56 concentration
13 p2489 A70-28910

Coating thickness measurement and analysis by radioisotope techniques including beta-particle, X or gamma ray backscatter and X ray fluorescence and absorption
15 p2742 A70-32780

Radionuclides production rates in stratosphere from spallation reactions of cosmic rays with Ar
17 p3152 A70-35759

Depth distribution of radioactive nuclei generated by cosmic rays in asteroidal sized bodies, calculating primary and secondary surface layer particle fluxes
20 p3698 A70-39295

Stony meteorites radionuclides gamma emission measurement, determining specific activity ratios
20 p3703 A70-39322

Thermal preconditioning unit using radioactive isotope heat source for temperature control of inertial navigation system
20 p3671 A70-40059

Human body radioactive nuclides in vivo quantitative analysis by gamma ray spectra, considering matrix method accuracy
20 p3582 A70-40449

Vacuum distillation vapor filtered catalytic oxidation water recovery system, using radioisotopes for thermal energy supply
21 p3769 A70-40994

Dosso stony meteorite gamma emitters radioactivity by nondestructive spectroscopy, obtaining quantitative analysis by least squares method
21 p3893 A70-41446

Apollo 11 lunar rocks and fines cosmic ray produced radioisotopes, considering surface exposure to high energy component flux
21 p3906 A70-41562

Apollo 11 lunar material actinide element abundance and isotopic composition, examining Th, U and transuranium elements by mass spectrometric and radiometric techniques
21 p3774 A70-41569

Apollo 11 lunar rock and fines primordial radionuclide abundances and concentration gradients by gamma ray spectrometry at Lunar Receiving Laboratory
21 p3776 A70-41595

Cosmogenic and primordial radionuclides in Apollo 11 lunar soil and rocks, using nondestructive gamma ray spectral measurements
21 p3776 A70-41599

Apollo 11 lunar rock and soil bombardment produced radionuclide patterns, discussing solar flare protons and alphas, age determination and astronomical models
21 p3777 A70-41604

Lunar samples and terrestrial materials isotopic analyses, discussing mineralogical and chemical compositions for lunar origin
22 p4098 A70-42574

Aircraft engine diagnostics and defectoscopy, considering radioactive isotopes testing for component wear and performance
22 p4046 A70-43083

Radioisotope thrusters for space propulsion, considering thermal heating methods and direct recoil
22 p4070 A70-43185

RADIOACTIVE MATERIALS

Computer method to combine autofluoroscope data to produce three dimensional display of absorbed radioactive material from multiview images
04 p0686 A70-14563

Satellite studies geoactive particles and photoelectrons, including interactions with earth atmosphere
10 p1874 A70-24312

Gaseous radioactive penetrant inspections for early low cycle fatigue in aircraft engine materials, discussing impact on maintainability
19 p3441 A70-38828

Superpure materials for low background radiation detectors, determining U, Th and Ca radioactive contamination by radiochemical activation analysis
20 p3629 A70-39317

RADIOACTIVE NUCLIDES

U RADIOACTIVE ISOTOPES

RADIOACTIVITY

Scinticamera resolving power in radioactivity measurements, discussing mathematical principle of division of radioisotope concentration in biological experiments
01 p0040 A70-11404

Radiobiological and radioecological aspects of radioactive pollution of earth atmosphere, considering international cooperation for preventive measures
07 p1199 A70-18781

Half life of Mn53 calculated from measured activity in sample from Fe meteorite and isotopic ratio Mn53/Mn55
07 p1337 A70-19226

Lunar surface alpha radioactivity at Surveyor 5, 6 and 7 landing sites
11 p2104 A70-25658

Diffusion processes rate changes in metals and alloys resulting from radioactive emission, noting role in stress rupture strength mechanisms
11 p2068 A70-26595

Environmental surveillance associated with ground tests of nuclear rocket engine prototypes, determining statistical nature of radioactive effluent
19 p3470 A70-38013

Apollo 11 lunar rock samples alpha particle activity in polished thin sections, using autoradiography and electron microprobe
21 p3901 A70-41546

Auger spectra characteristics obtained with X rays and electrons from radioactive alpha sources
23 p4222 A70-44421

RADIOBIOLOGY

Soviet monograph on radiobiological effects of ionizing radiation covering physicochemical and functional cellular changes, recovery mechanisms, etc
06 p0992 A70-17350

Radiobiological and radioecological aspects of radioactive pollution of earth atmosphere, considering international cooperation for preventive measures
07 p1199 A70-18781

Oxygen enhancement ratio and relative biological effectiveness of accelerated helium nuclei on mouse tumor cells, discussing applicability in radiation therapy
09 p1617 A70-22336

Radiation planning nomogram to display radiobiological effects of dose, onset time and shielding factors for manned space vehicles
15 p2690 A70-31894

RADIOCHEMISTRY

Solar neutrino spectroscopy using various radiochemical detectors for Be 7, N 13, O 15 and B 8 neutrino fluxes, noting Li 7 suitability for determining CNO cycle
05 p0898 A70-15949

Nucleon spectra, particle multiplicities and radiochemical cross sections following stopped-pion absorptions by complex nuclei, comparing calculated and experimental data
14 p2618 A70-30341

Radiochemical neutron activation analysis of In, Cd, Y and rare earth elements in rocks
24 p4310 A70-46375

RADIOCHEMICAL MATERIALS

Induced nuclear processes role in radiogenic Ne-21 production in earth atmosphere
12 p2227 A70-28367

RADIOGRAPHY

NT AUTORADIOGRAPHY

He camera with reduced linear absorption coefficient for contact microradiography, relating exposure, X ray wavelength and atmosphere
01 p0084 A70-10013

Aircraft nondestructive testing, discussing radiography requirements, ultrasonic bond testing technique, etc
01 p0104 A70-11319

PKR portable xeroradiographic defectoscope for nondestructive testing of steel and Al alloys
02 p0301 A70-12486

Computer evaluation of photographic imagery of left ventricle volume obtained by cineangiography, including densitometric measurements
03 p0434 A70-13678

Neutron radiography for visual nondestructive failure analysis and production inspection of ordnance components compared with X ray radiography
03 p0494 A70-14122

Nondestructive testing of Apollo CSM /Command and Service Module/ spacecraft arm explosive devices by indirect and direct neutron radiography
03 p0494 A70-14123

Black and white roentgenograms conversion to full color and three dimensional CRT radiograph displays, incorporating electronic data processing circuitry
04 p0641 A70-14560

Three dimensional X ray imaging technique from conventional radiograph set photoetched and projected by special purpose imaging system
04 p0686 A70-14561

Computer processing role in film scanning and digitizing for enhancing X ray and radioisotope scanner images in medical radiographs, discussing image noise reduction
04 p0654 A70-14562

High energy neutron accelerator as fast neutron radiography source, comparing contrasts with gamma and X radiography
05 p0844 A70-15779

Percentage changes in X ray calibration wedge mass equivalency to actual changes in bone Ca content
06 p0997 A70-18015

Acceleration effects on chest organs by X ray studies noting heart shape changes, pulmonary areas, diaphragm position, etc

07 p1201 A70-18791
Radioheopneumographic study of external respiration of office workers during mental and physical activity

07 p1204 A70-19142
Nondestructive betatron radiographic testing techniques for Ti billets, evaluating various lead screen, film and geometry combinations

08 p1508 A70-21746
Pathogenic mechanisms of fatal injuries during supersonic ejection determinable by radiography

09 p1627 A70-23114
Color radiography with photographic negative film exposed to X rays, obtaining same thickness latitude with improved detail sensitivity on single emulsion line

10 p1887 A70-24168
X ray laminography for nondestructive testing based on synchronous rotation of source, sample and image forming planes

10 p1895 A70-24577
Radioactive Mn 54 with high specific activity for short distance gamma radiography

13 p2404 A70-28658
Dimensional measurements of nuclear fuel cylindrical specimens by scanning neutron radiographic negative with microdensitometer, taking into account specimen geometry and neutron cross section

15 p2735 A70-31769
Radiograph images digital processing by linear and nonlinear position invariant techniques, obtaining contrast enhancement

15 p2706 A70-32569
Type 3 solar bursts classification, measuring diameter, lifetime and position

17 p3151 A70-35581
Neutron radiography in cold, resonance or epithermal, and fast neutron energy ranges, discussing converter materials for direct exposure or transfer method

22 p4028 A70-42590
High speed X ray flash motion picture installation for ballistic photography [SMPT PREPRINT 76]
Nondestructive testing - Conference, Hanover, June 1970, Radiography

24 p3435 A70-45706
Radiography using projective magnification from X ray tube with small focal spot, describing equipment and applications

24 p3437 A70-45707
Monochrome radiography for contrast strengthening to increase color images detectability by human eye

24 p3437 A70-45708
Radiography for nondestructive tests, considering image quality specification and choice of geometric progression for determining visibility

24 p3437 A70-45709
X ray films sensitometric investigation in medical and industrial radiography, evaluating HVL and ISO methods for X ray quality

24 p3437 A70-45710
Gamma ray nondestructive tests for materials defects, discussing cinematic, geometric and radiological factors effects on detection

24 p3437 A70-45711
Industrial radiography for nondestructive control of products quality, discussing exposure time determination method

24 p3437 A70-45712
Wire and hole type penetrometers minimum perceptible image contrast level on radiograph, considering X ray quality and films effects

24 p3437 A70-45713
Industrial radiography, discussing photographic emulsion layers granular structure formation due to ionizing radiation

24 p3437 A70-45714
Photographic paper as emulsion film substitute in industrial radiography, evaluating sensitivity and image contrast

24 p3437 A70-45715
Radiography using photo-nuclear reaction emulsion to improve picture contrast by eliminating scattered photons in sample

24 p3437 A70-45716
High speed radiographic observation of electric arc movement and metal transfer during submerged arc welding

24 p3422 A70-45724
Aircraft structures service life estimation, using Ir-192 and Tm-170 gamma ray radiography

24 p3436 A70-45725
Reactor, isotropic and accelerator neutron sources for thermal neutron radiography

24 p3435 A70-45746
Equipment, sources and safety in neutron radiography for industrial quality control

24 p3437 A70-45747
Image contrast enhancement on neutron radiograph by energy tailored beams

24 p3437 A70-45748

Fast neutron radiography, considering sources and transfer and scintillator-film detectors

24 p4376 A70-45749
Scintillator-film neutron radiography converter combinations efficiency gain for small sources by cooling

24 p4376 A70-45751
Thermal neutron radiography with small accelerators using optimized collimator and fission increased flux

24 p4376 A70-45752
Thermal neutron radiography with 2.5 MeV Van de Graaff accelerator

24 p4376 A70-45753
Fluoroscopes for radiographic examination of materials and products with X ray and hard bremsstrahlung radiation

24 p4348 A70-45847
Betatron monoenergetic electron beams in radiometric, spectrometric and radiographic testing of composite materials

24 p4339 A70-45850
Fast neutrons for radiogenic nondestructive material testing, describing defectoscope performance, sensitivity and cost efficiency

24 p4377 A70-45851

RADIOISOTOPE BATTERIES

NT SNAP 19

NT SNAP 27

Electric power generators performance based on kinetic energy conversion of radioactive isotope decay products, noting space applications

01 p0140 A70-10217
Guidebook on application of space nuclear power systems covering radioisotope and reactor systems, static and dynamic systems, power system suppliers and users, etc

01 p0140 A70-10942
Radioisotope fueled organic Rankine power system with weight dependence on operations depth [AIAA PAPER 70-520]

13 p2349 A70-29037
Deep space spacecraft radioisotope thermoelectric generators, discussing testing and evaluating for future missions

18 p3215 A70-36229
Vacuum distillation vapor filtered catalytic oxidation for water reclamation from human waste, using radioisotopes for thermal energy

20 p3579 A70-39437
Multiple revolution lunar module reentry problem, analyzing isotopic systems trajectory, reentry environment, thermal response and ablation [AIAA PAPER 70-989]

20 p3714 A70-39540
Reentry protection for radioisotope heat sources, using thermal switch of composite ceramic foam with metal impregnants

22 p4054 A70-42958
Radioisotope thermoelectric generator with lead telluride converter, discussing intact reentry and impact capability, refractory construction and reliability

22 p4072 A70-43196

RADIOLOGY

Radiology instrument for examining pulmonary functions during deep inspiration, expiration and rest, describing material, components and assembly, mounting and diagram development

01 p0040 A70-11401
Collection of papers on spaceflight radiological problems experimentation covering satellite data, dosimetry, solar flares, etc

06 p0989 A70-17259
Radiological studies of young adult spines for selecting aircrew personnel and collecting data to compile reference dossiers in case of accidents

12 p2171 A70-28039
Image intensifier systems for direct view radiological systems

22 p4028 A70-42589

RADIOLYSIS

Trapped Ag atoms production in silver nitrate ice by gamma irradiation, discussing reaction enhancement by fluoride ion

09 p1631 A70-23445

RADIOMETERS

NT DICKE RADIOMETERS

NT INFRARED DETECTORS

NT INFRARED SCANNERS

NT MICROWAVE RADIOMETERS

NT SPECTRORADIOMETERS

Radiometric method for calibrating loss of multimode antenna-feed components with linear or circular polarization, deriving calibration and error analysis equations

01 p0050 A70-10711
Image intensifiers to improve telescope system sensitivity and spectral resolution in radiometric measurements of reentry vehicles

03 p0489 A70-13654
Lidar and IR radiometer mobile laboratory for atmospheric optics research, including construction details and support equipment

03 p0463 A70-13677
Schottky barrier diodes design for wideband radiometer mixers to obtain optimum noise per-

formance and broadband operation by DC bias application

03 p0457 A70-13968
Rocket stability monitoring by temporal radiometry, using exhaust radiance measurement to detect frequencies in thrust chamber combustion pressure [AIAA PAPER 69-580]
Radiometric investigation of energy brightness distribution over clear, cloudy and variable sky at micron wavelengths

06 p1056 A70-17835
Radiometers with low noise parametric amplifiers at centimeter wavelengths for radio telescope, discussing design, performance and Venus observations

08 p1495 A70-21065
Solar wind velocity radioastronomical measurements, discussing radio wave fluctuations, telescope antenna designs, radiometers and observations

08 p1474 A70-21070
Nimbus high resolution IR radiometer /HRIR/ data processed by color display enhancement system, demonstrating meteorological, oceanographic and geomorphological applications

11 p2049 A70-25636
Switched self balancing comparison radiometer with coupling between channels, showing measurement errors due to coupling correctable by phase switching

11 p2018 A70-26269
Gain-stabilization of SHF traveling wave maser radiometer, using thermal noise from neon discharge tube

12 p2228 A70-26881
Atmospheric stability sensing by millimeter wave radiometry, discussing thermal radiation emitted and absorbed by oxygen molecules

12 p2263 A70-26955
Low noise temperature radiometer to study solar radio emission, measuring atmospheric absorption

12 p2184 A70-27235
Radiating objects localization and tracking by radiometer equipped with two antennas having slightly divergent beams

12 p2185 A70-27689
Brightness temperature of earth atmospheric emission in submillimeter band at 35 km, describing airborne radiometer

12 p2265 A70-28171
Collection of papers on precision radiometry in geophysics covering radiation detectors and electromagnetic radiation measurements in atmosphere

13 p2409 A70-29651
Precision radiometry of electromagnetic energy transfer in atmospheric and space physics emphasizing solar and terrestrial radiative fluxes measurements

13 p2409 A70-29652
UV, visible and IR radiation measurement, discussing spectral distribution, thermopiles, monochromatic radiation and power measurements

13 p2410 A70-29653
Standard sources and detectors for thermal radiation measurement

13 p2410 A70-29654
Black body design for radiometry, discussing error sources in calibration

13 p2410 A70-29658
Radiometric measuring techniques emphasizing transfer methods and data analysis

13 p2410 A70-29659
System design for IR imaging radiometer from synchronous altitude satellite, considering spacecraft dynamics, detectors and cooling

14 p2586 A70-30974
Nomogram for true and apparent radiometric temperatures of remote graybodies in presence of atmosphere

14 p2577 A70-31231
Absolute radiometric reference scale, noting International Pyrheliometric Scale 1956 materialization by standard instruments

15 p2735 A70-31805
Radiometers calibration equipment maintaining radiation standards, investigating long and short waves by digital voltmeter coupled to paper tape punch

15 p2735 A70-31806
Black body cavity type radiometers for high accuracy measurement of irradiance

15 p2737 A70-32036
Radiometer employing frequency domain coding of noise-like signal spectrum, comparing with Dicke system

16 p2871 A70-32926
Solid state logarithmic radiometer, measuring radiation within narrow portions of optical spectrum

16 p2905 A70-33160
IR optical radiometer for jet engine turbine blade temperature measurement, comparing with junction wire thermocouple

16 p2905 A70-33168
IR radiometer for Mariner Mars 1971 project providing surface brightness temperatures

16 p2913 A70-34028
Surveyor Canopus sensor and Project Scanner dual IR radiometer mechanical design

16 p2914 A70-34107

- Laser energy and power measurement with thermal gradient radiometer 17 p3104 A70-35082
- Weak narrow band noise measurements using FM radiometer insensitive to gain fluctuations 17 p3053 A70-35278
- Relative sensitivities of polyethylene shielded net radiometers, noting role of reflective white paint partial covering 18 p3261 A70-37087
- Cardioid condenser as radiometer mirror objective in low temperature radiometry, describing optical characteristics 19 p3420 A70-37261
- Diffraction effects on radiometer field of view with rectangular primary and secondary apertures and field stop 20 p3627 A70-39087
- Short wave calibration system for net pyrriadiometers, using source with intensity and spectral distribution comparable to solar radiation 20 p3628 A70-39147
- Teleradiometer calibration in background radiation absence, using distant and finite point source method and collimator means 20 p3633 A70-39798
- Double resonator ruby maser for observing transitions of interstellar hydroxyl, noting incorporation in modulation radiometer of astronomical telescope 21 p3835 A70-40641
- Communications satellite carrier instrumentation, using computer controlled frequency shift radiometer for power monitoring 21 p3826 A70-41345
- Quiet sun and new moon brightness temperature measurements at 3.3 and 5.7 mm wavelengths, giving radiometric maps 23 p4241 A70-44254
- Atmospheric temperature profiles using Nimbus 4 selective chopper radiometer 23 p4192 A70-44865
- Analog and digital low pass filters for radiometric postdetector filtering 24 p4321 A70-45622
- Mm wavelength radiometer for recording solar activity and radiation attenuation in atmosphere as function of time 24 p4315 A70-46236
- Airborne radiometer slim multibeam millimetric antenna, describing design, construction and performance 24 p4316 A70-46320
- RADIONUCLIDES**
- U RADIOACTIVE ISOTOPES
- RADIOPROTECTIVE AGENTS**
- U ANTIRADIATION DRUGS
- RADIOSENSITIVITY**
- U RADIATION TOLERANCE
- RADIOSONDES**
- NT IONOSONDES
- NT RAWINSONDES
- Thermal balance of radiosonde thermometric elements and radiation errors in atmospheric temperature measurements using spectra of radiation fluxes reflected from cloud cover 03 p0557 A70-13297
- Meteorological data from radiosonde and radar wind observations during Indian Ocean expedition of research vessel Meteor 07 p1329 A70-19350
- Potential gradient radiosonde field distortion formula, deriving form factors 09 p1671 A70-23602
- Meteorological radar station reception equipment for increased radio telemetry channel reliability in complex radio sounding of atmosphere 11 p2075 A70-25920
- Barium fluoride film hygrometer elements for radiosondes, discussing manufacturing and testing methods 13 p2408 A70-29470
- Time constant equations for hair and film radiosonde hygrometers, allowing for inertial errors in humidity and cloud boundary measurements 14 p2603 A70-30412
- Balloon flight measurements clarifying Arcasonde sensor bias over radiosonde atmospheric temperature data 14 p2585 A70-30570
- Balloon-borne optical dew point hygrometer and radiosonde measurements of atmospheric range refractive index 14 p2585 A70-30573
- Meteorological transponder rocketsonde instrumentation system evolution and data error analysis 14 p2585 A70-30579
- Noise rejection characteristics of ionospheric radiosondes via phase-code modulated signals, noting nonoptimal filter role in power loss 18 p3229 A70-37042
- Radiosonde technique for locating atmospheric turbulence regions and estimating vertical air movement component in associated gusts 19 p3427 A70-38246
- Radiosonde receiver and transmitter system optimization, obtaining increased microwave power by appropriate oscillator operating modes 22 p4038 A70-43379
- Radiosonde errors in temperature and pressure height determination using paired AN/GMD-1 probe flights 24 p4371 A70-46047
- Temperature induced humidity errors in military and Weather Bureau radiosondes carbon humidity element caused by solar irradiation 24 p4372 A70-46073
- RADIOTHERAPY**
- U RADIATION THERAPY
- RADIUS**
- U RADII
- RADOME MATERIALS**
- Quartz-polyimide for missile radome exhibiting low dielectric constant and thin wall for use over broader frequency range 13 p2417 A70-28664
- Low dielectric constant quartz-polyimide for radomes, considering curving methods 16 p2936 A70-33368
- RADOMES**
- Transmission losses of plexiglass radome measured as function of frequency and antenna elevation angle, determining material dielectric constant 06 p1019 A70-17505
- Computer predicted horn antenna radiation patterns through aircraft radome compared with measured values 09 p1645 A70-22689
- Antenna characteristics and parameters as function of position and orientation in radome by automatic system consisting of electromechanical and programming device 10 p1848 A70-23971
- Missile radome design optimization, considering compromise between conflicting aerodynamic, thermal and structural aspects 11 p2134 A70-25862
- Angular aberrations produced by airborne radomes calculated by computer, allowing optimal parameters selection and knowledge of radio properties 12 p2195 A70-27274
- RADON**
- German monograph on atmospheric turbulence by Rn 220 as tracer, relating concentration to various meteorological parameters 16 p2946 A70-34080
- Atmospheric radon concentration ratios diurnal and vertical variations used for turbulent exchange and washout study 17 p3132 A70-34611
- RAE-1**
- U EXPLORER 38 SATELLITE
- RAFTS**
- NT LIFE RAFTS
- RAIL TRANSPORTATION**
- Dynamic characteristics of systems consisting of train and air in tunnel using one dimensional incompressible fluid description [AIAA PAPER 70-141] 06 p1042 A70-18216
- Multipolarized radar imagery for detecting high return linear cultural features in geographic areas including channel markers, bridges, railroad and power-line networks, etc 12 p2228 A70-26911
- Short haul transportation needs in multimodal transportation systems planning, discussing modeling in Northeast Corridor Project [AIAA PAPER 70-1265] 24 p4431 A70-45925
- RAILS**
- Ultrasonic surface waves detection of transverse fatigue crack initiation in rails under load, applying results to fatigue life determination 06 p1168 A70-17924
- Missile and rail launching structure combined dynamic response determined by discrete element dynamic analysis 12 p2312 A70-27116
- RAIN**
- Attenuation vs pathlength for given fading probability of microwaves by intense rain, evaluating dual parallel path diversity 05 p0815 A70-16575
- Cloud base updraft field, three dimensional reflectivity pattern and rain and hailfall pattern for thunderstorms in Alberta, discussing shear 06 p1099 A70-18569
- Hot-film anemometers for measuring storm turbulence in presence of heavy rain 10 p1887 A70-23940
- Communication satellite repeater design requirements to achieve adequate SNR for varying rain and cloud attenuation [AIAA PAPER 70-498] 11 p1998 A70-25425
- Atmospheric water effect on satellite communications in UHF region and above, discussing signal attenuation 13 p2364 A70-28782
- Electromagnetic radiation attenuation in rain at cm and mm wavelengths, determining rainfall rates and drop size distribution 13 p2364 A70-28783
- Extraterrestrial magnetic spherules concentration in relation to meteor shower activity and rainfall probability 14 p2640 A70-30740
- Forward scattered radar reflections from various depths of rain volume, employing ultrasonic simulation 15 p2704 A70-32599
- Radar mapping in heavy rain with orthogonal transmit and receive polarization, using backscatter and attenuation to define maximum operating altitude 16 p2863 A70-33434
- Atmospheric aerosols, fog and rain effects on signal transmittance and backscatter at 3400-10600 Å 18 p3248 A70-36751
- Rain sampling by Varsity aircraft, determining reliability of droplet sampling instruments above aircraft top surface 19 p3463 A70-38947
- Rainfall effects on EM wave propagation at centimeter and millimeter wavelengths 20 p3588 A70-40310
- Artificial rain erosion effects on missile and spacecraft recorded via high speed photography 20 p3635 A70-40531
- Interference coupling between satellite ground station and radio relay station due to rain scattering at SHF 22 p3990 A70-43201
- RAIN EROSION**
- U WATER EROSION
- RAIN IMPACT DAMAGE**
- Photo-optical instrumentation for temperature estimates of nose cone in simulated reentries, using rocket monorail sleds and artificial rainfalls for rain erosion effects 09 p1688 A70-23778
- Water drop-solid surface collision experiments to study rain impact erosion process, using gas gun projectiles, high speed photography, photomicrography and profilometry techniques 22 p4116 A70-43096
- Strain rate sensitivity and stress waves effects on dynamic response and adhesion failures of rain erosion resistant coatings 22 p4059 A70-43102
- RAINBOWS**
- Differential elastic scattering cross section of Ar nozzle beam in nitrogen considered with rainbow effect in determining intermolecular potential well depth 02 p0344 A70-12722
- RAINDROPS**
- Cloud particles growth and interactions, discussing water vapor condensation, ice phase nucleation, rain droplet growth rate, etc 07 p1262 A70-18897
- Approximate formulas for disperse attenuation and scattering coefficients for water drops in visible and IR spectrum 18 p3260 A70-36973
- Computerized simulation of raindrop effects on initiation of cloud-to-ground lightning strokes 24 p4371 A70-45978
- RAINSTORMS**
- NT THUNDERSTORMS
- RAMAN EFFECT**
- U RAMAN SPECTRA
- RAMAN SCATTERING**
- U RAMAN SPECTRA
- RAMAN SPECTRA**
- Combination absorption effect on Raman scattering and Stokes component gain in presence of pumping in antiStokes region, giving relation for radiation conversion 01 p0107 A70-10141
- Light Raman scattering in semiconductors under constant magnetic field, studying electron-phonon spectrum characteristics 01 p0155 A70-10183
- Raman effect liquid laser power as function of cavity length, using Q switched ruby laser beam focused by cylindrical lens for optical pump 01 p0111 A70-10674
- Focal length-to-aperture ratio for maximizing collection of scattered light at right angles to illuminating laser beam used in Raman spectroscopy 02 p0311 A70-11888
- Molecular rotations and kinetics from spectral features of molecular Raman spectra, using light scattering spectroscopy 02 p0343 A70-12077
- Partial coherence in spontaneous Raman effect, using He-Ne laser source 02 p0313 A70-12465
- Transverse mode controlled hydrogen Stokes laser oscillator optically pumped by pulsed ruby laser 03 p0498 A70-13153
- Raman spectra of lead titanate, sodium tantalate/potassium tantalate and potassium tantalate/potassium niobate solid solutions at various temperatures 03 p0542 A70-13824

External optical phonon modes in ammonium and deuterioammonium halides phase transitions as function of temperature, using IR and Raman spectra

04 p0646 A70-14695

Raman backscatter of frequency doubled ruby laser beam by water vapor in atmosphere observed by optical radar, calculating water vapor mixing ratio profile

04 p0677 A70-14950

Collapsing beam transition into self focusing light channel numerically analyzed allowing for Kerr effect saturation, multiphoton absorption and stimulated Raman scattering

04 p0650 A70-15285

Transient molecular vibration excitation by picosecond laser pulses found dependent on shape of Stokes pulses in Raman scattering study

04 p0702 A70-15298

Ruby laser giant pulses time stretching and shaping using stimulated Raman scattering in liquid nitrogen cell inserted in laser resonator

05 p0857 A70-16076

Laser atmospheric backscatter measurements using frequency shifted Raman scatter and Rayleigh components for separating returns due to gaseous and aerosol components

05 p0859 A70-16476

Raman and IR spectra of unsymmetrical dimethylhydrazine and unsymmetrical dimethylhydrazine-d2 recorded in liquid and gaseous states

06 p1128 A70-17329

Laser induced Raman scattering as diagnostic technique for measuring specie concentrations in gas mixtures

06 p1066 A70-18214

Raman effect in liquid nitrogen resonator with light from Q modulated Nd laser pumped into resonator at small angle to axis

07 p1303 A70-20366

Organic dyes investigated for amplification characteristics of Raman emission stimulated by Q switched ruby laser

09 p1694 A70-22134

Transient stimulated rotational and vibrational Raman scattering in gases using mode locked ruby laser

09 p1700 A70-23568

Atmospheric water vapor profiles remote measurements using Raman component of high powered Q switched laser backscatter

10 p1886 A70-23938

Raman scattering by oxygen and nitrogen in atmosphere observed by using pulsed nitrogen UV laser

12 p2189 A70-28093

Parametric and Raman instabilities predicted by linear theory for plasma in electromagnetic field

13 p2458 A70-28563

Thermospectrometric investigation of stimulated Raman lines in benzene to identify generation modes, observing optical sideband effect at 8050 Å

13 p2425 A70-28714

Raman spectrum of lithium formate monohydrate single crystal in polarized He-Ne laser light, discussing crystal structure

13 p2425 A70-28714

Raman scattering cross sections in solid state semiconductor plasma in magnetic field from phonon fluctuations

14 p2621 A70-30485

Three level molecular coherence effects in stimulated Raman scattering, considering molecular relaxation and field inhomogeneity

15 p2752 A70-32350

Laser Raman scatter process applied to atmospheric probing

16 p2925 A70-33017

IR Raman and vibrational spectra and structure of gaseous and liquid 1-pyrazoline

16 p2857 A70-34007

IR and Raman spectra of gaseous and liquid germylcyclopentane, determining torsional barriers and skeletal ring atom symmetry

16 p2858 A70-34008

Self phase modulation of stimulated Raman light in carbon disulfide, discussing Stokes and anti-Stokes spectrum regions

18 p3266 A70-36422

Raman line coherence degree and polarization rate measurement, applying Wolf matrix

19 p3443 A70-37359

Inlet optics modification in Raman laser spectrometer, discussing high pressure gas storage and support plate enlargement

19 p3443 A70-37361

Light combinatorial scattering by longitudinal photons with frequency near forbidden zone width, calculating Raman scattering cross sections

19 p3444 A70-37444

Solid para hydrogen IR and Raman spectra frequency analysis, examining lattice vibration effects

21 p3853 A70-41721

Frequency modulated gas laser communication system, discussing Raman-Nath effect, Doppler shifting phase grating, monochromatic light, pseudostanding wave, optical heterodyne detector, etc

22 p3989 A70-42966

Laser radiation hyper Raman scattering intensity enhancement via resonance processes, using density matrix method

22 p4075 A70-43233

Graphite and carbon fiber surfaces, correlating Raman spectrum and shear strength of composite

22 p4060 A70-43680

GaAs crystal surface Raman scattering from phosphorus impurities localized modes, using Ar ion laser line

24 p4391 A70-46255

RAMAN SPECTROSCOPY

Laser light investigations of atoms, molecules and plasmas, considering Raman molecular spectroscopy, acoustic phonons interactions and plasma diagnostics by light scattering

12 p2245 A70-27063

Ultrafast laser-Raman spectroscopy, comparing Scan and No-Scan techniques

14 p2593 A70-30361

Remote Raman spectroscopy of air contaminants, considering electro-optical technology and data processing

16 p2900 A70-33018

Semiremote laser Raman spectroscopy application in pipes, reactors, hot cells, jet and rocket engines and air pollution studies, discussing LIDAR model for chemical analysis

16 p2926 A70-33161

Raman spectrochemical system design based on laser radiation as parent source, discussing relay optics and photon counting detector system

16 p2913 A70-33979

Laser Raman spectroscopy, discussing scattering from vibrational modes in solid and from phonons above optical gap

17 p3081 A70-34599

Raman spectroscopy with lidar for remote mapping of air pollutants and concentrations

20 p3627 A70-39126

Spectroscopic detection of sulfur dioxide and carbon dioxide molecules and concentrations in polluted atmosphere by laser-Raman radar technique

20 p3640 A70-39389

RAMJET ENGINES

NT SUPERSONIC COMBUSTION RAMJET ENGINES

NT TURBORAMJET ENGINES

Optimum performance for Mach 3 to 7 fixed geometry ramjet with successive subsonic and supersonic combustion, noting lifting wing conjunction

02 p0355 A70-12365

Interstellar space flight ramjet physical model, describing magnetic field funnel, radiation effects, relativistic effects, etc

02 p0379 A70-12782

Ramjet engines combustion chamber and air intake design for velocities between Mach 2 to 7

06 p1130 A70-17932

Improvement in power output of ramjet installed under wing using air compression

[ONERA-TP-783]

Supersonic and subsonic air breathing engines, discussing single and ducted fan turbojets, ramjets, turboprop engines and land based gas turbine engines

12 p2291 A70-28071

Aircraft engine design combining turbojet and ramjet features to ensure optimum performance

20 p3690 A70-40148

Hybrid combustion ram rocket drives, discussing booster initial acceleration, exhaust gas use as fuel and payload gain

[ICAS PAPER 70-50]

23 p4233 A70-44147

Energy transfer methods for hybrid air breathing ramjet propulsion systems with rocket motor S gas source

[ICAS PAPER 70-61]

23 p4233 A70-44156

RAMJET MISSILES

Two stage rocket booster-ram rocket launcher combination compared to single and two stage rockets

11 p2126 A70-26287

RAMP FUNCTIONS

Step and ramp input functions and pursuit and compensatory display modes effects on tracking performance

21 p3767 A70-40753

RAMPS [STRUCTURES]

M 3.5 two dimensional mixed compression inlet system with self restart using flexible variable ramp system

[AIAA PAPER 69-447]

22 p3959 A70-42707

RAMSAUER EFFECT

Electric field structure at shock wave front propagating in weakly ionized gas under Ramsauer effect

10 p1871 A70-25121

Electric field structure at shock wave front propagating in weakly ionized gas under Ramsauer effect

20 p3685 A70-40514

RANDOM DISTRIBUTIONS

U STATISTICAL DISTRIBUTIONS

RANDOM ERRORS

Satellite optical tracking data in space geodesy, determining stations position from minimum number of stations and observations with time errors

03 p0446 A70-13195

Optimal trajectory measurement program for orbit parameter determination, assuming random errors and nondegenerate weighting matrix of normal equations

10 p1940 A70-24302

Regression analysis of linear statistical model experiments with stationary Gaussian error of slowly varying spectral density

11 p2073 A70-26249

Arithmetic mean, least squares method and standard deviation concepts in random error analysis of measurement data

11 p2117 A70-26674

Experimental model for random phase errors caused by surface irregularities in paraboloid reflector antennas

19 p3388 A70-37927

Bayes sequential detection test with constrained error probabilities, investigating properties of thresholds equations

21 p3787 A70-41333

RANDOM LOADS

NT GUST LOADS

Service life analysis at randomly varying load - Conference, Muelheim-Ruhr, Germany, April 1969

[DFVLR-SONDDR-4]

Fatigue testing facilities and methods with emphasis on consumable load, randomized serviceability and random process tests, examining closed loop control servohydraulic appliances

02 p0276 A70-12853

Aircraft structures service life estimation, comparing results of serviceability tests, solo flight tests, programmed random load tests and linear defect buildup hypothesis

02 p0391 A70-12854

Periodic biharmonic stress cycling determination of load influence of fatigue failure used for random load serviceability tests

02 p0391 A70-12855

Nonlinear stochastic differential equations formulated during random loading processes generation, designing testing devices with stable performance parameters

03 p0598 A70-14236

Amsler Vibrophore machine modifications to permit narrow band random fatigue tests

05 p0826 A70-15887

Unsteady vibrations of cylindrical thin walled elastic closed shell under random loads, using correlation method

05 p0937 A70-16371

Thin walled cylindrical shell stability under stochastic lateral and axial compression loads using Liapunov method

[AIAA PAPER 70-104]

Minimum weight beams and frames calculation for random loads taking into account material carrying capacity

07 p1400 A70-18821

Minimum weight reliable beams and frames calculation for random loads, using one degree of freedom system to obtain closed form solution

07 p1401 A70-18825

Dynamic calculation of oscillating liquid filled elastic cavity on elastic kinematic system under random load, using random signals transmission theory

07 p1416 A70-20194

Fatigue crack probability distributions under oscillatory stationary random loading, basing analysis on crack propagation model

09 p1776 A70-22683

Transient process statistical calculation in discrete elastic mechanical system possessing energy dissipation under time dependent cross correlated random forces

09 p1729 A70-23595

Sinusoidal and random loading response of age hardening aluminum alloy determined by fatigue testing

11 p2133 A70-25732

Fatigue life tests of Al alloy under narrow and broad band random loads based on number of peaks to failure

11 p2066 A70-26095

Programmed and randomized loading flight-by-flight tests for fatigue life, noting stress cycles

11 p2138 A70-26096

Vibration of thin elastic plates under random driving forces simulated digitally, using power residue method for pseudorandom number generation

11 p2139 A70-26277

Materials fatigue lifetime estimation under irregular loads by simultaneous use of random programming for testing machines and computing equipment

12 p2315 A70-26873

Materials fatigue life dependence on statistical characteristics of random loads obtained from energy balance equation solution

12 p2323 A70-27339

- Liapunov type analysis of linear structural dynamic system excited by stochastic parametric load, discussing radially loaded thin circular plates 14 p2657 A70-30763
- Safety, microdamages and lifetime of elastic structures under random Poisson pulsed loads 16 p2996 A70-34328
- Randomized load sequence simulating narrow band Gaussian process for predicting fatigue strength, assuming crack propagation mechanism 17 p3183 A70-34660
- Structural fatigue testing by computer control of random force cycles 17 p3062 A70-35505
- Elastic plate vibration with damping under random load, calculating linear response by harmonic analysis 18 p3334 A70-35958
- Multidimensional discrete control for fatigue testing under random loads, discussing model 18 p3234 A70-36074
- Aluminum alloys subjected to random loading, comparing fatigue life with predictions based on linear accumulation of damage hypothesis 20 p3647 A70-39157
- Hydraulic load loops with random force signal for aircraft structures endurance testing 20 p3593 A70-39913
- Orthotropic shells under arbitrary loads, deriving approximation equations 20 p3734 A70-40436
- Survival probability of randomly excited structures, using maximum entropy principle 23 p4270 A70-44582
- Lightly damped second order linear system mean square response to nonstationary random load excitation 24 p4421 A70-45280
- Continuous structural systems stability under random load excitation from linear partial differential equations of motion 24 p4421 A70-45281

RANDOM NOISE

NT RANDOM SIGNALS

- Rms error for reproduction of satellite signal transmitted through continuous Gaussian channel assessed by numerical calculation 01 p0046 A70-11513
- Sinusoidal signal detection in Gaussian noise band by zero crossing method, discussing signal frequency position and SNR 04 p0648 A70-14705
- Linear-quadratic pursuit-evasion game with dynamics perturbed by additive white Gaussian noise, obtaining linear minimax solutions 06 p1025 A70-17957
- Optimal signal detection with random phase on Gaussian noise background, estimating error probabilities 07 p1226 A70-18685
- Optimal receiver synthesis for signal detection on Gaussian noise resulting from nonlinear filtration of Gaussian noise 07 p1226 A70-18760
- Quantum statistical decision theory for detection and estimation of signals in random noise 07 p1333 A70-18919
- Digital data transmission over discrete time Gaussian channel with noisy feedback, investigating error-exponent/reliability/ and finite SNR 07 p1235 A70-19362
- Digital autopilot design using stochastic noise generator for synchronous random pulse sequence controlled by clock 09 p1720 A70-22418
- Coding and decoding efficiency in data transmission over Gaussian channels, comparing error probability, power, bandwidth and equipment complexity 09 p1637 A70-23320
- Memoryless input discrete noisy channels essential equivalence to white Gaussian channel for rates above capacity using extreme value theory 11 p2010 A70-26326
- First excursion failure survival probability of randomly excited structures, considering single degree of freedom linear oscillator under Gaussian white noise 12 p2327 A70-27819
- Differential equations of controller providing optimum transient response for plant with indeterminate parameters, allowing for nonadditive random noise 13 p2382 A70-29278
- Nonsingular detection and likelihood ratio for random signals in white Gaussian noise 14 p2551 A70-31118
- Nonparametric rank tests detection performance for signals in Gaussian noise, considering radar application 14 p2551 A70-31119
- Stochastic linearized state estimator for nonlinear dynamic systems with Markovian noise, using digital simulation 15 p2715 A70-31975
- Optimum decision rule/likelihood ratio/ algorithm for random signals detection in Gaussian noise, using pseudo Bayes approach 15 p2703 A70-32560

- Vector valued Gaussian random processes with Gaussian measurement noise, estimating phase and time delay parameters by maximum likelihood theory 15 p2704 A70-32593
- Prediction of polynomial signals in white Gaussian noise, using discrete data 16 p2866 A70-34065
- Direction finder for point source signals, discussing mathematical model for random noise in space, S/N performance and equipment design 17 p3042 A70-34586
- Sine wave discrete components detection from complex spectrum with random noise, evaluating errors 17 p3059 A70-35168
- Noisy stochastic pattern recognition system, determining optimal measurement sequence by discrete Pontryagin maximum principle 18 p3234 A70-36337
- Optimal receiver synthesis for signal detection on background noise resulting from nonlinear filtration of Gaussian noise 18 p3229 A70-37104
- Two dimensional phase distribution function of mixture of Gaussian noise with amplitude modulated signal 18 p3229 A70-37110
- Pulsed signal amplitude and delay time measurement in presence of interfering/reverberated/ signals and steady noise 19 p3375 A70-37285
- Plasma lasers, investigating striation oscillations and excess noise phenomena and generation mechanisms 19 p3446 A70-37858
- Automatic stabilization of random noise mathematical expectancy and mean square deviation by feedback control system 20 p3593 A70-39916
- Objective and subjective laser speckle noises in holography, discussing causes and methods of elimination 21 p3835 A70-40716
- Two probe electron energy distribution measurements in gaseous discharges with random and coherent oscillations, giving xenon results at low pressures 21 p3828 A70-41471
- Shot, thermal, induced gate and flicker noise in various solid state devices and lasers 21 p3792 A70-42112
- Wideband detection of frequency uncertain M-ary frequency shift-keyed/MFSK/ transmission in Gaussian noise, deriving symbol error rate for limiting SNR cases 21 p3792 A70-42177
- Optimal binary and ternary signal system synthesis by information divergence procedure for communication channels with colored Gaussian noise 22 p3985 A70-42491
- Random signal detection on uncorrelated Gaussian noise background with unknown intensity, discussing detector performance 22 p3986 A70-42553
- Signal accuracy prediction in nonlinear steady or unsteady continuous and discrete automatic control systems in random noise, using statistical linearization 22 p4003 A70-42883
- Dynamic characteristics of autooscillatory nonlinear self adaptive systems under random noise, using statistical and harmonic linearization 22 p4003 A70-42884
- Quantitative reduction of statistical nodes for nonlinear automatic control system with random noise, using minimal approximating polynomials 22 p4003 A70-42887
- Coherent radar backscatter, calculating autocorrelation and power spectrum of spuri noise from periodic random phase injections for filter design to eliminate noise 22 p3992 A70-43591
- Monopulse radar excited by Gaussian signal and thermal noise in multiple targets, calculating angle error output probability density function for predicting tracking performance 22 p3992 A70-43593
- Controlled self excited quartz triode oscillator, calculating flicker noise effect on frequency stability 23 p4171 A70-43959
- Optimum finite memory model for sequential minimum-mean-square-error estimation of random variable in added noise 24 p4317 A70-46052
- Estimation errors of multilevel modified digital correlator using auxiliary random noise for unbiased output 24 p4312 A70-46054

RANDOM NUMBERS

- Electronic modulo-M counter driven by HF pulse generator used for generating random numbers sequence 10 p1848 A70-23976
- Additive pseudorandom number generator with semifinite sequence length, proposing statistical tests for randomness 11 p2074 A70-26325

- Random values statistical characteristics by digital methods, deriving errors as function of quantization parameters 19 p3432 A70-38705
- Random values analog sensors classification based on physical, algorithmic and data reproduction techniques 20 p3593 A70-39917
- Fast pseudorandom number generators for digital computers 21 p3793 A70-40851

RANDOM PROCESSES

- Reentry trajectory dispersions due to atmospheric uncertainties determined using continuous differential equations based on atmospheric random processes method 01 p0183 A70-10846
- Nonlinear system under random excitation, discussing analytic solution method and statistical properties 01 p0206 A70-11149
- Random variations of terrestrial rotation rate effects on pulsar observations, discussing methods to minimize effects 02 p0371 A70-12203
- Random function theory for determining influence of system oscillation characteristics on load distribution 02 p0324 A70-12852
- Correlation function estimate of random process represented by sum of steady distributed and independent arbitrary processes 03 p0518 A70-13081
- Simple harmonic oscillator vibrations due to local random processes in spacecraft launching, calculating oscillator displacement variance 04 p0774 A70-15102
- Prediction errors lower bound for accuracy in predicting future position of randomly accelerating target 04 p0652 A70-15342
- Statistical description of geomagnetic field as random vector field, presenting correlation functions from empirical estimates from geomagnetic charts 05 p0842 A70-16748
- Randomly perturbed linear differential equation involving first derivative of n-vector function of real variable 05 p0878 A70-17096
- Slowly varying component filtration from multiplicative mixture of two random processes by statistical analysis 06 p1009 A70-17670
- Suboptimal closed-loop controller design based on quadratic equivalence for linear time varying process with minimum probability of inequality constraints violation 06 p1024 A70-17951
- Algorithm applied to specific classes of random processes for calculating minimum channel capacity required by transmission system for sources in each class 06 p1012 A70-18621
- Nonstationary correlation function for cross correlation of sample records from random processes, discussing minimum mean square error and weighting method 07 p1238 A70-19250
- Kinetic processes in plasma subjected to randomly fluctuating electric field, obtaining chain of single particle distribution functions 07 p1349 A70-19553
- Ergodic steady random functions measurement and analysis in terms of statistical properties [ONERA-TP-720] 07 p1411 A70-19825
- Random synchronization errors in PN and PSK systems reduce input signal power and introduce additional self noise 07 p1236 A70-20069
- Time block pooling of atmospheric noise data, basing randomness conclusion on observations correlation 07 p1236 A70-20161
- Nonenergetic parameter estimation of signal during optimal reception with random amplitude fluctuation in normal background noise using maximum probability function 08 p1461 A70-20868
- Phase coordinates conditional probability density statistical characteristics from continuous reception of random information, deriving differential equations 08 p1479 A70-20998
- Pulse neurons random homogeneous networks macroscopic description, considering operation modes in terms of input frequencies and output pulse sequences 08 p1451 A70-21000
- Spectral densities of phase coordinates of nonlinear automatic systems in steady states at random disturbances determined by statistic linearization 08 p1480 A70-21016
- Random perturbation procedure for control variable functions optimization using hybrid computer method for analog solutions and digital storage 08 p1467 A70-21783

Correlation function of oscillation modulated in amplitude, phase and frequency by random processes causing spectral density maximum shift away from carrier frequency

09 p1633 A70-22409

Refractive index variation regions and mapping along propagation path in random medium, noting application to solar wind electron density structures measurements

09 p1634 A70-22699

Initial value problem of macroscopic disorder-order transformation in random thermal convection phase of fluid heated from below

09 p1791 A70-23679

Random process noncommutative transformations and correlation functions in linear form of time functions

09 p1655 A70-23695

Pulse rate counter for randomly repetitive random processes, noting applications to lightning flash noise bursts in receivers

10 p1848 A70-23996

Monte Carlo method research development covering techniques for variance reduction, linear equations solutions and use of various random sequences

10 p1910 A70-24844

Group Method of Data Handling based on heuristic self organization for solving complex system problems, with applications to random processes prediction

10 p1845 A70-24869

Random process represented in canonical expansion form simulated by method of prognosis of reliability

11 p2022 A70-25344

Minimum fuel control for discrete time Gaussian processes, applying results to spacecraft midcourse guidance for earth-Mars mission

11 p2079 A70-25958

Maxima increases without limit in damped linear oscillator response to random wideband excitation interpreted by heuristic explanation

11 p2085 A70-26694

Wave propagation in continuous random media solved by partial differential equations with random coefficients, describing perturbation methods for obtaining solutions statistical properties

11 p2085 A70-26761

Satellite trajectory parameters estimation by maximum likelihood method applied to continuous satellite observations assuming random Gaussian process as measurement error

11 p2081 A70-26780

Random processes correlation functions determined by stochastic differential equations applied to lunar surface statistical characteristics determination

11 p2118 A70-26785

Nonlinear panel flutter for random excitation and linear/nonlinear aerodynamic loading, using Rayleigh-Ritz approximation to Hamilton variational principle

12 p2316 A70-27105

Cylindrical shell response to random acoustic excitation, considering single point transfer functions and equivalent force power spectral densities

12 p2317 A70-27125

Random processes correlation coefficients and functions measured by quasi-compensator with potentiometer and digital/analog readout

12 p2235 A70-27770

Random fields entropy estimation technique taking into account higher than immediately adjacent spatial dependencies

12 p2192 A70-27771

Random-input describing function as linear approximation to instantaneous nonlinearity in terms of minimum mean-squared error

13 p2382 A70-29070

Turbulent diffusion random model of foreign substance, investigating latent parameters existence

13 p2387 A70-29211

Random reversible failures effect on linear automatic control systems precision treated as randomly varying structure, proposing statistical characteristics calculation

13 p2382 A70-29279

Noise level influence on optimal recognition of non-stationary random processes in white noise

13 p2369 A70-29729

Turbulent boundary layer loading function for use with finite element structural analysis system applied to elastic aircraft structures random vibration [AIAA PAPER 69-20]

14 p2658 A70-30853

Alpha-beta and Kalman tracking filters with randomly interrupted data, evaluating transient responses as function of radar measurement accuracy and valid data acquisition probability

14 p2557 A70-31186

Kinetic processes in plasma subjected to randomly fluctuating electric field, obtaining chain of single particle distribution functions

15 p2777 A70-31460

Search duration distribution of two stage lock-on indicator scanning signal search systems, using regenerative random process and integral recovery equation

15 p2696 A70-31501

Earth satellite motion about center of mass, examining effects of random variations in atmospheric density, geomagnetic intensity and solar radiation

15 p2809 A70-31650

Vector valued Gaussian random processes with Gaussian measurement noise, estimating phase and time delay parameters by maximum likelihood theory

15 p2704 A70-32593

Variance reduction technique for hybrid computer generated random walk solutions of partial differential equations, comparing to analytical solution

16 p2942 A70-33731

Critique of paper on pulsed gamma rays detection from Crab Nebula pulsar by balloon flights, attributing pulsations to random fluctuations

17 p3149 A70-34566

Book on random processes, communications and radar covering optimum filtering, detection, information theory, ergodic theory, probability and integration axioms, parameter estimation, coding, etc

17 p3043 A70-34602

Gaussian source model of image, deriving rate distortion function under mean square error criterion

17 p3049 A70-34857

Monograph on state variable approach to continuous estimation of random processes with applications to analog communication theory

17 p3045 A70-35189

Observation space transforming for synthesis of automatic optimization systems with memory tracking randomly walking extremum

18 p3234 A70-36073

Strain gradient theory for random media, considering equations for response to forcing field

19 p3456 A70-37382

Forecasted algorithms to predict random processes, using mathematical statistics

19 p3382 A70-37450

Data processing systems functions and composition for random data reduction during aircraft flight tests based on analog and digital techniques

19 p3430 A70-38524

Solar radio emission slowly varying component, analyzing random aspects, correlation functions and relationship to spot groups

19 p3521 A70-38552

Propagation mode conversion of Gaussian light beam due to random fluctuations of turbulent medium, discussing effect of aperture size and fluctuations anisotropy

20 p3585 A70-39451

Nonstationary random processes prediction by numerical method

20 p3673 A70-39762

Soviet book on overshoot of random processes in problem solving covering application to radio engineering, length distribution, extremal values, etc

20 p3587 A70-39822

Extremal dynamic controlled plant with random input signals, identifying components weighting functions by statistical approximation

20 p3604 A70-39908

Nonstationary inhomogeneous random vector fields linear prediction, determining minimum mean square approximation error

20 p3604 A70-39911

Generator for modeling random processes with given statistical parameters

20 p3593 A70-39915

Algorithmic random process pseudorandom number generator composed of analog computer elements, evaluating stability

20 p3594 A70-39918

Digital correlation system for stationary and nonstationary random processes, estimating mathematical expectations and cross- and autocorrelation function

20 p3594 A70-39920

Statistical analysis of random oscillations excited in electron beam-plasma system based on signal recording data

21 p3855 A70-40631

Random radio signals distributions properties with parameters subject to random variation

21 p3785 A70-40639

Heat transfer in laminar channel flow with random velocity variations, using Monte Carlo technique

21 p3949 A70-41312

Unipolar pulse frequency modulation system with white noise input, deriving output power spectral densities

21 p3793 A70-42225

Coherent beam propagation through turbulent atmosphere, discussing limiting resolving power due to random fluctuations of refractive index

22 p4072 A70-42290

Random ergodic process extremal behavior, determining mean time to reach maximum or minimum for first time

22 p3985 A70-42400

Steady random process intensity estimation, using iterative probability algorithm

22 p3987 A70-42559

Statistically optimal nonlinear automatic control systems synthesis in presence of random perturbations, using gradient or steepest descent methods

22 p4003 A70-42889

Gyro drift rate mathematical modeling based on stationary and nonstationary time series analysis techniques with random process reduction to white noise residuals

[AIAA PAPER 69-838] 23 p4197 A70-44557

Particle motion in constant density dynamic viscosity random translational velocity fluid

24 p4324 A70-45139

Turbulent flow mechanics heuristic exposition, discussing random processes, instability, nonlinear interactions, energy exchange, intermittency dependence on Reynolds number, fluid properties and boundary conditions effects, etc

[AIAA PAPER 70-1308] 24 p4326 A70-45948

Optical wave propagation through random atmospheric turbulence, deriving wave equation power series solution for homogeneous random refractive index field

24 p4314 A70-46126

RANDOM SAMPLING

Analytical design of optimum linear multivariable control systems with randomly sampled stationary random signals, evaluating matrix complex convolution integral using Laplace transforms

02 p0272 A70-12610

Randomly sampled linear systems stability with linear or nonlinear feedback loops, using stochastic Liapunov function method

02 p0272 A70-12727

Variables control charts based on sample means for determining in-control probability properties

09 p1691 A70-22575

Alias-free randomly timed sampling of stochastic processes, considering spectrum recovery by linear operation

12 p2204 A70-27419

Wind velocity fluctuation randomization signal probability density measurement, using statistical sampler

18 p3238 A70-36067

Semiconductor silicon power diodes nondestructive quality control, discussing optimal sampling procedures

20 p3595 A70-38969

Aircraft design fatigue life and cumulation damage problems, discussing information value of programmed load and random tests

20 p3720 A70-39622

Random values analog sensors classification based on physical, algorithmic and data reproduction techniques

20 p3593 A70-39917

Critical values tables for Wilcoxon rank sum test in randomized blocks

22 p4064 A70-43729

Radiation shielding calculations, discussing Monte Carlo concepts for point fluxes with random sampling of source distributions

23 p4217 A70-43810

RANDOM SIGNALS

Mathematical theory of time domain statistical description of random signals in terms of probability theory

01 p0044 A70-11042

Linear system response to random signal inputs, deriving SNR and noise figure equations using autocorrelation and spectral analysis concepts

02 p0257 A70-12193

Analytical design of optimum linear multivariable control systems with randomly sampled stationary random signals, evaluating matrix complex convolution integral using Laplace transforms

02 p0272 A70-12610

Autocorrelation function distortion in pseudorandom signal with limited spectrum at RC filter output

03 p0446 A70-13202

Nonlinear complexing problem in measuring random signal, proposing optimal data processing algorithm with minimum error variance criterion

09 p1654 A70-22542

Statistical linearization technique for nonlinear control systems with feedback and zero memory under random input excitation evaluated for output signal characteristics

09 p1654 A70-22960

Nonsingular detection and likelihood ratio for random signals in white Gaussian noise

14 p2551 A70-31118

Optimum decision rule/likelihood ratio/algorithm for random signals detection in Gaussian noise, using pseudo Bayes approach

15 p2703 A70-32560

Plane wave random signals arrival angle maximum likelihood estimation for multiple antenna systems

15 p2704 A70-32594

Transient response of self adaptive systems subjected to determinate or random signal mixed with additive noise

16 p2882 A70-33234

Dynamics of continuously operating linear servosystems stimulated by stochastic signals, using vectorial equation and impulse response matrix

16 p2944 A70-34295

Servosystems with random input signals, obtaining optimal transfer function by variational calculus

17 p3056 A70-34617

Wind velocity fluctuation randomization signal probability density measurement, using statistical sampler 18 p3238 A70-36067

Statistical characteristics of steady random signal of pulse frequency modulator, obtaining moments of output signal 18 p3234 A70-36072

Random signal nonlinear transformations using relations between Laplace and Fourier transforms 20 p3583 A70-39123

Extremal dynamic controlled plant with random input signals, identifying components weighting functions by statistical approximation 20 p3604 A70-39908

Random signal detection on uncorrelated Gaussian noise background with unknown intensity, discussing detector performance 22 p3986 A70-42553

Optimal transducers distribution for estimating random field values in presence of additive noise 22 p4005 A70-43562

RANDOM VARIABLES

Automatic control nonlinear systems with random inputs, determining phase coordinates probability densities 02 p0272 A70-12414

Service life analysis at randomly varying load - Conference, Muelheim-Ruhr, Germany, April 1969 [DFVLR-SONDDR-4] 02 p0391 A70-12851

Monte Carlo methods for calculating simple and multiple integrals and random variables characteristics, noting applications to Europa 2 booster 03 p0454 A70-13535

Time optimal control of system variable with bounded controlling input and arbitrary disturbances, deriving necessary conditions using maximum principle [ASME PAPER 69-WA/AUT-7] 04 p0661 A70-14827

Linear transformation for random-data vector z reduction to smaller dimension vector 04 p0714 A70-15066

Incoherent reception of wideband signals transmitted through multibeam channel with changing random parameters 05 p0812 A70-16248

Photoelectric multislit micrometer for astronomical purposes, presenting stochastic variables mean error difference formula for arbitrary power spectrum 06 p1071 A70-18458

Convolution formulas for Cauchy and standard normal random variable distributions derived from geometry of circular symmetric distribution on plane 07 p1323 A70-18946

Suboptimal computational algorithm for terminal control of random linear dynamical system, noting increasing optimality with random variations degeneration to deterministic quantities 07 p1324 A70-19091

Fatigue life cyclic sensitivity threshold with random nature statistically estimated on basis of maximum likelihood principle 09 p1776 A70-22618

Independent identically distributed random variables sequence, obtaining asymptotic expansion for large deviations of distribution function 10 p1910 A70-24799

Limiting distributions of sums of random variables coupled in homogeneous Markov chain with finite number of states 12 p2261 A70-27551

Book on probabilistic systems analysis covering models, decision making, random processes, distribution functions, mass and density functions, etc 13 p2441 A70-29455

Random data analysis application to aircraft inlet diagnostics [AIAA PAPER 70-597] 13 p2375 A70-29878

Optimal control stochastic problem with initial conditions treated as random variables, using matrix minimum principle 15 p2716 A70-32563

Limiting theorems for sums of random variables linked in Markovian chain, applying probabilistic and analytical methods 19 p3456 A70-37235

Output probability of nonlinear systems from coupling moments for input random parameters, using equivalent perturbations method 22 p4003 A70-42885

Algorithm for fast digital computer recursive estimation of mean of random variable 22 p3993 A70-43074

RANDOM VIBRATION

Random vibration of interconnected systems, analyzing power flow and energy levels in linear oscillator interacting with environments, using Thevenin-Norton representations 01 p0207 A70-11161

Optimal control of continuous and discrete observations described by linear differential and recurrent algebraic equations in presence of random perturbations 03 p0447 A70-13341

Spectrum deductions from profile excited random vibration response, considering single profile imposed displacements 03 p0600 A70-14250

Randomly oriented vibration effect on noncompensated three degree of freedom gyroscope with displaced center of gravity 04 p0692 A70-15278

Unsteady vibrations of cylindrical thin walled elastic closed shell under random loads, using correlation method 05 p0937 A70-16371

Random vibrations of linear system with viscous damping excited by stochastically acting force with monotonically varying frequency, using correlation method 05 p0882 A70-16372

Vibration theory damping using mathematical model emphasizing controlling response under steady state resonance and random excitation 09 p1769 A70-22238

Stress peak distribution effects on fatigue life of test specimen excited to bending by Gaussian random vibrations 11 p2137 A70-26093

Random vibration isolation for two degrees of freedom model system investigated statistically, assuming wide band white noise 11 p2139 A70-26416

Rotor blade random vibrations in response to turbulence [AIAA PAPER 70-548] 13 p2339 A70-29013

Optimal control of continuous and discrete observations described by linear differential and recurrent algebraic equations in presence of random perturbations 14 p2561 A70-30717

Pendulous integrating gyro accelerometer float excursions minimization in random vibration environment [Saturn 5 launch] by statistical technique 14 p2589 A70-31344

Equivalent linearization for random vibration, considering stationary statistics of bilinear hysteretic one degree of freedom oscillator response 14 p2661 A70-31428

Drift of two platform gyroazimuth with stabilized base under harmonic or random vibrations 15 p2734 A70-31622

Monograph on harmonic and random vibrations filtering, discussing objects protection from ground vibrations produced by mechanical source 15 p2774 A70-31693

Electromechanical velocity feeder redesign for functional performance in random vibration environments [ASME PAPER 70-DE-25] 16 p2917 A70-33425

Random vibration test for quasi-flexible specimens with each mounting point subjected to different vibration levels and spectrum shapes 16 p2889 A70-34022

Linear, nonlinear and random vibrations - Conference, Poznan, Poland, April 1968 16 p2994 A70-34276

Mechanical system random excitation, evaluating parameters to satisfy conditions for statistical characteristics of steady state output processes 16 p2953 A70-34296

Astatic gyroscope subjected to steady random translational vibration, optimizing parameters by mathematical model 18 p3257 A70-36136

Probability theory of stresses during random vibrations of flat panel in acoustic field of jet engine exhaust 18 p3301 A70-36301

Covariance matrix of mean square response in structural systems under white noise 19 p3536 A70-37702

Random vibration first threshold crossing probability function for linear oscillator 19 p3427 A70-38038

Vibration signals analysis in random and periodic modes, presenting analyzers block diagrams 19 p3430 A70-38526

Thin cylindrical shell under nonaxisymmetric concentrated stationary radial loading, calculating random responses and stability 21 p3940 A70-42051

Gyro pendulum mounted on randomly vibrating platform, calculating stability of rotor axis vertical position 22 p4039 A70-43557

Electrodynamic and electrohydraulic vibrators for frequency sweep, wideband random and sweep random vibration test methods 23 p4195 A70-44333

Cantilever plate random vibration response, calculating eigenvectors and natural frequencies by finite element method 23 p4270 A70-44591

RANEY NICKEL
U CATALYSTS
U NICKEL

RANGE

Disposable load drop effect on aircraft range, using Breguet equations for graphic determination of bombing range 21 p3750 A70-40868

RANGE (EXTREMES)

NT FREQUENCY RANGES
NT PROPORTIONAL LIMIT
NT RADIO RANGE
NT ROCHE LIMIT

Terminal state control systems efficiency from determining permissible range of control parameter variation for steady and unsteady linear dynamic systems 01 p0052 A70-10982

Position bound determination for objects ejected from space vehicle relative to vehicle trajectory position 03 p0562 A70-12932

Error probability upper and lower bounds determined for self synchronized binary PSK communications systems, presenting maximum-likelihood and Monte Carlo computer simulation 08 p1463 A70-21777

Geometric and predictive methods for developing bounds on epsilon-entropy for infinity error norm constraint 11 p2014 A70-26306

Energy principle providing upper bounds on plastic deformation in elastoplastic structures subjected to blast loading 11 p2144 A70-26670

Error probability bounds for systematic convolutional codes 12 p2192 A70-27422

Extrema of functions of many variables in presence of constraints from modified simplex method with variable search step 13 p2382 A70-29277

Temperature, pressure and density extremes between 30 and 80 km, extrapolating estimates to all latitudes 14 p2608 A70-30591

Computer program for limit analysis of rotationally symmetric shells, generating yield point load upper and lower bounds and velocity profile 15 p2822 A70-32351

Mariner attitude control system limit cycle operation during cruise, noting variation from ideal case to single side operation [AIAA PAPER 69-844] 15 p2812 A70-32507

Controlled libration point satellite limit cycle motion, deriving solution in infinite series by harmonic analysis 17 p3181 A70-35752

Nonlinear second order differential equations with periodic coefficients and solutions, examining stability by phase and amplitude plots by marginal range diagrams 18 p3282 A70-36356

Real cipher places in real function, describing interval analysis method with upper and lower bound indications 18 p3282 A70-36357

Signal conditioner for expanded range pressure measurements from reentry vehicles via transducer zero shift suppression and output signal compression 19 p3426 A70-37899

Statistically nonhomogeneous fields by variational principles of elasticity, obtaining bounds of average displacement for hollow sphere under pressure 20 p3732 A70-40112

Cracked brittle body limiting equilibrium, determining critical loads for two half spaces with various circular rib couplings 20 p3733 A70-40432

Limit surface behavior equations for structural membrane elements in terms of number, orientation and limit load of constituent fibers by limit theorems 21 p3934 A70-40778

RANGE AND RANGE RATE TRACKING

Optimal control of elevation and azimuth of automatic tracking device carrying pulse laser and receiving telescope [ONERA-TP-785] 06 p1011 A70-18469

Wideband stochastic signals for radar range and velocity measurements using polarity coincidence correlation technique 12 p2188 A70-27942

Atmospheric refractivity role in range errors from ground station to stationary satellite and in range rate measurement 12 p2189 A70-28058

Digital range tracking, Doppler filtration and moving target selection in multichannel automatic surveillance radars 13 p2380 A70-29735

Adaptive tracking radar design, discussing ambiguity resolution problem in range and velocity dimensions 21 p3791 A70-41947

Error analysis of satellite orbits obtained by synchronous satellites range and range rate measurements 24 p4407 A70-45539

RANGE CONTROL

U TRAJECTORY CONTROL

RANGE ERRORS

Refraction-induced range and tracking errors estimation in exponential model atmosphere by closed functions

01 p0044 A70-11087

Range of ground station to stationary satellite and range rate measurement errors induced by atmospheric refractive index fluctuation

13 p2365 A70-29095

VHF geostationary satellite ranging and range correction systems, calculating second-order ionospheric delay effects on position error

22 p4068 A70-43590

RANGE FINDERS

NT LASER RANGE FINDERS

NT OPTICAL RANGE FINDERS

UHF ranging system principles, discussing output proportionality to approach angle

02 p0257 A70-12179

Coherent instrumentation radar for White Sands Missile Range, discussing system design emphasizing pulse Doppler capability

10 p1842 A70-24881

Short pulse radars application to range measurements, discussing technological and data analysis problems

11 p2005 A70-26041

RANGE INDICATORS

U INDICATING INSTRUMENTS

U RANGE FINDERS

RANGE MEASUREMENT

U RANGEFINDING

RANGE SAFETY

Range safety philosophy and practice concerning malfunctioning missile and space vehicle launch and flight

[AIAA PAPER 70-249] Enhanced real time operational impact and casualty analysis [ERIOCA] for range safety, discussing computer-driven CRT display and missile flight parameters selection

07 p1250 A70-20369

[AIAA PAPER 70-247] Missile and space vehicle range safety policies and practices using past statistical performance data and cost consideration

07 p1251 A70-20371

[AIAA PAPER 70-246] Sounding rockets safe operation and handling, examining ground and flight factors

16 p2981 A70-32923

Apollo digital Range Safety Command System for signal-crowded communications channels

20 p3605 A70-39497

Enhanced real time operational impact and casualty analysis for range safety, discussing computer-driven CRT display and missile flight parameters selection

23 p4178 A70-44517

RANGEFINDING

NT SOUND RANGING

One way radio range measurements for surveying and navigation emphasizing McDonnell collision avoidance and geophysical surveying systems, using Rb atomic clocks

01 p0136 A70-10306

Runway visibility measuring techniques, discussing RVR measurement limitations

02 p0336 A70-12226

Q switched and high energy pulse laser devices for location of satellite photographed by night against background of stars, including optimization in noise [ONERA-TP-753]

02 p0313 A70-12369

Ruby laser experiment in illuminating satellites equipped with retroreflectors to determine satellite position in space from range and photographic data

03 p0450 A70-13674

Hypersonic orbital glider range maximization, analyzing optimal angle of attack by use of rectangular velocity components

07 p1393 A70-19341

Airport runway and slant visual ranges determination using single scanning lidar/laser radar

09 p1696 A70-22490

VHF satellite transponders for ranging and position fixing, studying ionospheric and multipath effects [AIAA PAPER 70-489]

11 p1999 A70-25433

Binary-coded sequential acquisition spacecraft ranging system operating at weak signals using HF digital logic

11 p2009 A70-26252

Multipath tolerant ranging and data acquisition for air-ground-air links in ATC based on mathematical scattering theory

12 p2268 A70-27642

Range of ground station to stationary satellite and range rate measurement errors induced by atmospheric refractive index fluctuation

13 p2365 A70-29095

Acceleration influence on radar signal reception during range and velocity measurements

13 p2366 A70-29301

One way radio range measurements for surveying and navigation emphasizing McDonnell collision

avoidance and geophysical surveying systems, using Rb atomic clocks

13 p2449 A70-29620

Earth-satellite range measurements using broadband pseudonoise modulation and delay lock tracking method

15 p2705 A70-32724

Position determination by range change method (RCM), using pseudonoise modulated line of sight and one way ranging

16 p2948 A70-33453

Range and velocity components for ray paths between tracking and data relay satellite and user communication satellite

16 p2866 A70-34073

Soviet book on complex signals in ranging, navigation and communications, discussing correlation and ambiguity functions and bandwidth effect

20 p3587 A70-39723

Airborne computerized time frequency systems for aircraft range and velocity determination, using stable clocks with ambiguity resolution

22 p4067 A70-42659

RANGER LUNAR PROBES

Ranger lunar photographic evidence for volcanic hypothesis, considering fracture systems, Caldera analogy, common walls, crater size, etc

12 p2297 A70-26985

Lunar surface fine structure and geological analysis from Ranger 7, 8 and 9 photographs

14 p2644 A70-31052

RANGER SATELLITES

U RANGER LUNAR PROBES

RANGES (FACILITIES)

NT BALLISTIC RANGES

NT MISSILE RANGES

NT TEST RANGES

Turbulent wakes in Canadian Armament Research and Development Establishment free flight ranges measured for mean and fluctuating properties

11 p1978 A70-26774

RANGING

U RANGEFINDING

RANK TESTS

Multivariate linear model and robust estimators of parameters based on rank tests

07 p1323 A70-19027

Nonparametric rank tests detection performance for signals in Gaussian noise, considering radar application

14 p2551 A70-31119

Rank order statistics for optimum detection of binary pulsed signals in white noise and DC drift

14 p2551 A70-31122

RANKINE CYCLE

Rankine cycle technology concerning high temperature, refractory alloy and liquid metal experience, showing applicability to nuclear Brayton and thermionic power systems

02 p0229 A70-12513

Liquid metal pump design and performance in SNAP 8 Mercury Rankine and Advanced Rankine fluid power systems, including containment materials and corrosion effects

04 p0718 A70-15641

Rankine cycle two loop Li boiling Ka facility for nuclear turbopump simulation, studying alkali metal corrosion for operation with and without hot traps [AIME PAPER F-69-1]

07 p1304 A70-18809

Fluorocarbon fluid Rankine cycle system utilizing gas turbine exhaust heat for environmental control [SAE PAPER 700160]

11 p1982 A70-25371

Reciprocating Rankine-cycle engine with organic working fluids, noting piston speed and efficiency [SAE PAPER 700162]

11 p1982 A70-25372

Rankine 10 MWe nuclear electric space power system design, discussing reactor power, fuel, coolant, structural material, control system, shield, etc

11 p2082 A70-26123

Radioisotope fueled organic Rankine power system with weight dependence on operations depth [AIAA PAPER 70-520]

13 p2349 A70-29037

Brayton, Hg, organic-Rankine and potassium-Rankine dynamic space power systems for use with nuclear energy sources

13 p2450 A70-29492

Metal corrosion effects in Rankine cycle lithium-boiling potassium test loop simulating working fluids of spacecraft nuclear turbopump propulsion system

16 p2933 A70-34204

Brayton, Hg, organic-Rankine and potassium-Rankine dynamic space power systems for use with nuclear energy sources

22 p4071 A70-43189

RANKINE TEMPERATURE SCALE

U TEMPERATURE SCALES

RANKINE-HUGONIOT RELATION

Ion density profile across shock in partially ionized gas measured in plasma jet wind tunnel for comparison with Rankine-Hugoniot relation

09 p1662 A70-23235

Temperature, pressure and electron density measurements behind reflected shocks in gas driven

diaphragm shock tube compared with Rankine-Hugoniot predictions

10 p1967 A70-23960

Velocity and temperature distribution behind shock waves in hydrogen plasma measured to determine factors responsible for discrepancies in Rankine-Hugoniot conditions

10 p1867 A70-24149

RANKING

Aircrewmen work credit under Flying Time system to determine rank order for mission scheduling, noting legitimate functions performance

21 p3771 A70-41483

RAPCON [CONTROL]

U RADAR APPROACH CONTROL

RAPID EYE MOVEMENT STATE

Postcaloric nystagmus clinical evaluation by analog computer measuring fast-phase eye displacement in Vestibular Function laboratory

08 p1448 A70-21942

Sleep intensity and stages from EEG studies concerning rapid eye movements, vegetative nervous system, heart/respiration rate, blood pressure, body temperature and stomach motility

15 p2680 A70-31743

Nocturnal headache relationship to REM sleep stage from EEG, EOG and EMG data

20 p3569 A70-38994

Desynchronized sleep phase in cats, discussing activation and hippocampal theta and hippocampal delta rhythm predominance stages

20 p3574 A70-40171

Prolonged REM sleep deprivation effect on gamma-aminobutyric acid concentration in mice

23 p4146 A70-44658

RAPID TRANSIT SYSTEMS

High speed ground tube vehicle transportation system aerodynamics, presenting drag coefficients and static wall pressure measurements

16 p2839 A70-34264

RARE EARTH ALLOYS

NT NEODYMIUM ALLOYS

RARE EARTH COMPOUNDS

NT NEODYMIUM COMPOUNDS

NT SCANDIUM OXIDES

Absorption transition fine structure measurements for bulk rare earth garnets single crystals using reflectivity techniques [IEEE PAPER 19.6]

05 p0894 A70-16998

RARE EARTH ELEMENTS

NT CERIUM

NT DYSPROSIUM

NT EUROPIUM

NT GADOLINIUM

NT HOLMIUM

NT LANTHANUM

NT NEODYMIUM

NT PRASEODYMIUM

NT TERBIUM

NT YTTERBIUM

NT YTTRIUM

Rare earth elements effects on microstructures and mechanical properties of cast Al, Al-Si and Al-Si-Mg alloys

08 p1516 A70-21127

Excitation energy transfer processes in oxide glasses containing trivalent Tb ions in combination with other rare earth activators

09 p1738 A70-22137

Polycrystalline lanthanides and metals resistance to deformation under compression and tension at different temperatures and strain rates

12 p2257 A70-28273

Rare earth energy band structure effect on RKKY magnetic interaction between atomic spins

13 p2472 A70-29799

Strontium titanates ceramics containing various trivalent rare earth ions, observing dielectric relaxation

19 p3486 A70-37755

Submarine basalt sea water alteration effects, examining Sr and rare earth concentrations, Ba enrichments or depletions and trace element data

19 p3413 A70-38015

Allende Type III carbonaceous chondrite, examining rare earth and other elemental abundances

19 p3519 A70-38028

Electrophysical properties of refractory and rare earth metallic single crystals, discussing work function, transition temperature, resistivity and superconductivity

19 p3454 A70-38731

Rare earth and trace element abundances for Apollo 11 lunar samples by neutron activation, comparing with Bruderheim chondrite and submarine basalts

21 p3907 A70-41578

Apollo 11 lunar rock K, Rb, Sr, Ba and rare earth element concentrations, examining relationship to terrestrial and chondritic levels

21 p3776 A70-41600

Lanthanide zinc intermetallic compounds magnetic characteristics in 4-300 K range, observing Curie-Weiss behavior

22 p4085 A70-42482

- Light rare earth metals improving Mg alloys, Al alloys, Cu alloys and superalloys 22 p4057 A70-43575
- Rare earth metals-ruthenium Laves phases solid solutions superconducting transition temperature measurement 23 p4231 A70-44885
- Radiochemical neutron activation analysis of In, Cd, Y and rare earth elements in rocks 24 p4310 A70-46375
- RARE GAS COMPOUNDS**
- Rare gas diatomic ions reactions with molecules and rare gas atoms, measuring rate coefficients and product channels by flowing afterglow technique 15 p2776 A70-31726
- Rare gas diatomic and hydride ions reactions with hydrogen, determining rate coefficients and product channels by flowing afterglow technique 15 p2776 A70-31727
- RARE GASES**
- NT ARGON
- NT ARGON ISOTOPES
- NT HELIUM
- NT HELIUM ATOMS
- NT HELIUM FILM
- NT HELIUM ISOTOPES
- NT LIQUID HELIUM
- NT NEON
- NT NEON ISOTOPES
- NT RADON
- NT XENON
- NT XENON ISOTOPES
- NT XENON 129
- NT XENON 133
- Coherent light scattering disturbance in level-crossing signals of Rb 85 and Rb 87 second excited state by noble gas atoms 02 p0311 A70-11851
- Ionized Ne, Ar and Kr first excited p states lifetime and transition probabilities, tabulating energy levels and mixing coefficients 02 p0343 A70-11887
- Differential elastic scattering cross section of Ar nozzle beam in nitrogen considered with rainbow effect in determining intermolecular potential well depth 02 p0344 A70-12722
- Physiological equivalents of air with rare gases and H substitutes for nitrogen in inhaled gas mixtures providing normal oxygen intake 02 p0249 A70-12798
- Well depth determination for weak intermolecular potentials based on dimerization enthalpy measurement of rare gas atoms by mass spectrometry 03 p0527 A70-13299
- Diffusivities of argon, krypton and xenon determined in olive oil by curve-fitting analysis of sorption curves 03 p0429 A70-14159
- Tonks-Dattner resonances peaks in rare gas plasmas, considering electron densities variations role 03 p0534 A70-14211
- Volumetric flow rate of rare gases, hydrogen and deuterium between parallel plates at various pressures and Knudsen numbers 04 p0665 A70-14414
- Noble gases breathing effects on free amino acid pool increase in rat brains, considering O mixtures with He, Ar and Ne 04 p0632 A70-15086
- Excitation temperature functions calculated in rare gases spectrum lines to determine radial plasma temperature distribution 05 p0886 A70-15798
- He and Ne adsorption and desorption on field ion microscope tip, determining minimum required field strengths of gas films at different temperatures 05 p0891 A70-15975
- Bronzite, hypersthene and amphibole chondrites examined by X ray diffraction for inert gas retention ages relationship to shock and reheating 05 p0912 A70-16448
- Polyamide fabric burning rates in oxygen-inert gas mixtures, studying damping effects of density, thermal conductivity, molecular constants and mass flow 06 p1090 A70-17284
- Electron recombination in inert gases at various pressures, studying electron density decrease in time by UHF and optical methods 06 p1109 A70-17495
- Critical Hall parameter indicating instability in alkali-seeded noble gases in nonequilibrium MHD generators [AIAA PAPER 70-40] 06 p1122 A70-18107
- Operational characteristics, spectroscopy and inversion mechanisms of noble gas ion lasers in light of plasma theories and atomic data [AIAA PAPER 70-82] 06 p1083 A70-18236
- Three dimensional model for high energy scattering of inert gas atoms from solid surfaces, calculating trapping, accommodation and flux and velocity distributions 06 p1110 A70-18261

- Inert gases scattering from Ni {111} plane as function of beam temperature and angle of incidence compared to Au and Ag 06 p1110 A70-18263
- Molecular He and Ar nozzle-type beams scattering from room temperature LiF crystal surfaces, measuring particles flux and speed distributions 06 p1111 A70-18267
- Angular distributions of fast scattered particles resulting from noble gases collision with metal surfaces 06 p1112 A70-18271
- Rare gas scattering from Ag surfaces calculated up to earth satellite energy values 06 p1112 A70-18275
- Dispersion of ion-acoustic waves in quiescent rare gas discharge plasmas, discussing model simulating ion waves generated by finite sine wave bursts 07 p1352 A70-19990
- Molecular N rotational temperature effect on rare gases scattering cross section 07 p1344 A70-20134
- Inert gases and nitrogen determined at high temperature, discussing revision of existing functions representing intermolecular energy 08 p1598 A70-21525
- Ionization of rare gases /H and N/ by nitrogen ions, determining cross sections of formation of slow ions and electrons 08 p1549 A70-21801
- Electron ion recombination role in atomic collision process in rare gases ionization path, considering scintillation mechanism 08 p1549 A70-21815
- Inert gas glow discharge current change under laser radiation, investigating dependence on discharge region, gas and electrode material and configuration 09 p1696 A70-22484
- Rare gases abundance patterns on earth and in chondrites, proposing chemical adsorption mechanism at planetesimal stage during accretion 09 p1764 A70-23610
- Electrons thermodiffusion and energy transport coefficients in noble gases at mean reduced electric field intensities, obtaining distribution functions 11 p2089 A70-25868
- Inert gas plasma jets diagnostics in accelerator by spectroscopy, determining flow velocities, excitation and gas temperatures 11 p2093 A70-26744
- Shock-heated noble gases total ionization times, considering recombination and atom-atom and atom-electron collisions 12 p2274 A70-26856
- Translational spectral bands of compressed rare gas binary mixtures, considering mass and temperature effects 12 p2275 A70-27172
- Hydrogen and inert gas atoms collisional excitation cross sections calculated by multistate impact parameter approximation 12 p2276 A70-27878
- Inert gas absorption from tissue cavities in body, using models with different wall distribution patterns of capillaries and diffusion resistance 12 p2171 A70-28025
- DC plasma arc jet excitation and emission characteristics for solution analysis with economical inert gas flow rates 13 p2362 A70-29107
- Inert gas ionization behind shock wave at high Mach numbers, using electrical conductivity and continuum emission measurements 13 p2388 A70-29380
- He, Ne, Ar and Xe in plagioclase concentrate separated from Serra de Mage meteorite feldspar 13 p2497 A70-29855
- Spectral irradiances of inert gases and mixtures for laboratory solar simulation 15 p2717 A70-32028
- High temperature plasmas of mixtures of nitrogen with rare gases, calculating equilibrium thermodynamic properties 17 p3195 A70-34932
- Spectral radiation and polar distribution from high power Ar, Kr and Xe arcs 17 p3023 A70-35156
- Mass spectrometric analysis of lunar rocks for rare gases of solar wind, determining relative abundance, isotopic composition, rock age, exposure time, etc 18 p3320 A70-37083
- Apollo 12 rock and dust analyses, discussing modifications to conclusions from Apollo 11 samples with reference to rare gas concentrations 18 p3321 A70-37085
- Monoatomic inert gas molecules interaction with continuous elastic solid of alkaline and nonalkaline metals, calculating energy exchange 19 p3373 A70-37816
- Alkali metal vapors diffusion coefficients in inert gases, determining atomic interaction parameters 19 p3473 A70-38190
- Pulsed emission in midinfrared region at neutral atomic transitions of inert gases and mixtures, tabulat-

- ing wavelengths, intensity, component ratios and optical pressure 19 p3448 A70-38736
- Carbonaceous chondrites noble gases measurement by mass spectroscopy, discussing compositional trends and origins 20 p3703 A70-39323
- Cesium beam velocity attenuation by He, Kr and Xe, determining scattering cross sections from gas pressure and density measurements 20 p3675 A70-39618
- Large scale nonequilibrium linear MHD generator performance with rare gases under strong EM-gas dynamic interactions 20 p3681 A70-39993
- Molecular and noble gas rotational collision numbers from thermal transpiration measurements 20 p3738 A70-39995
- Noble gas mixture large shock tunnel driven linear MHD generator, examining electron density, operating characteristics and electrical properties 20 p3682 A70-40012
- Rare gas ions recombination with electrons, describing microwave cavity method and light and mass spectrometer techniques 20 p3676 A70-40155
- Apollo 11 lunar fines trapped noble gas elemental and isotopic abundances, suggesting solar wind origin 21 p3906 A70-41565
- Rare gas analysis of Apollo 11 lunar soil and breccia for surface layer history 21 p3906 A70-41571
- Radiogenic and cosmogenic inert gases and isotopic ratios in Tranquility Base fines indicating solar wind saturation 21 p3775 A70-41581
- Apollo 11 lunar matter rare gas, H and N concentrations and isotopic abundances, discussing solar wind, gas diffusion loss from silicates and spallation component 21 p3908 A70-41583
- Trapped and cosmogenic rare gases from stepwise heated Apollo 11 lunar dust and crystalline rocks, using mass spectrometry 21 p3908 A70-41584
- Rare gas distribution in grain surfaces of lunar soil, breccias and rocks originating from solar wind, using microhelium probe 21 p3908 A70-41587
- Apollo 11 lunar soil irradiation history from solar wind rare gas abundances and cosmic ray spallation products 21 p3908 A70-41590
- Apollo 11 lunar fines, breccia and crystalline rocks rare gas data, emphasizing trapped and spallation Ne, Kr and Xe isotopic compositions 21 p3909 A70-41598
- Molecular size dependent steric effects in translation-vibration energy transfer by velocity dispersions in cyclopropane-inert mixtures 21 p3780 A70-41706
- Slow and fast ionization waves in inert gas or molecular gas plasma columns, describing striation formation in neon discharge by hydrodynamic equations 22 p4079 A70-42371
- Plasma positive column impedance in low current noble gas discharges, using Boltzmann equation for electrons 24 p4387 A70-45796
- RAREFACTION**
- Monatomic gas rarefaction wave structure in unsteady one dimensional flow from high to low pressure zones, describing numerical solution technique 09 p1604 A70-22449
- RAREFACTION WAVES**
- U ELASTIC WAVES**
- RAREFIED GAS DYNAMICS**
- Hydrodynamic equations and Grad transport coefficients for nonequilibrium rarefied monatomic gases developed for molecular collisions 01 p0068 A70-11567
- Speed ratio of rarefied gas flows by molecular miniature pressure probes with orifice at thin cylindrical tube side, discussing LTE deviation regions 02 p0296 A70-11871
- Equilibrium temperature and heat transfer of sphere in supersonic flow of rarefied air 03 p0409 A70-13874
- Maximum entropy principle used in rarefied gas dynamics for optimal representation of distribution function, examining difficulties associated with constraints on boundary conditions 04 p0718 A70-14492
- Rarefied gas flow through ultrafine porous filtering media used to predict flow rate [ASME PAPER 69-WA/PID-8] 04 p0666 A70-14755
- Thermal recovery factors at hemispheric probe stagnation point in low density supersonic jets of He-Ar and H-N mixtures [ASME PAPER 69-WA/HT-27] 04 p0782 A70-14810
- Entrance shape effects on tube rarefied flow in transition regime, noting role of Reynolds number in shape selection 04 p0675 A70-15593

- Hypersonic glider performance in mesosphere entry using models located in rarefied gas flow at Mach 8
05 p0789 A70-15811
- Rarefied H, He, air, carbon dioxide and water vapor flow rates between parallel optically flat glass surfaces measured, giving flow equation describing channel flow
05 p0833 A70-16525
- Soviet collection of papers on numerical methods in rarefied gas theory
06 p1035 A70-17751
- Rarefied gas dynamics - Conference, Cambridge, Mass., July 1968, Volume 2
06 p0976 A70-18251
- Electron beam fluorescence in rarefied air flow at low static temperature used to study influence of secondary electron emission on rotational temperature measurements
06 p1123 A70-18300
- Rotational and vibrational temperatures measured in hypersonic nonequilibrium rarefied gas flow field of cooled circular cylinder by electron beam technique
06 p1123 A70-18304
- Rarefied gas dynamics - Conference, Cambridge, Mass., July 1968, Volume 1
06 p1044 A70-18309
- Statistical models in kinetic theory for describing gases ranging from gas with no internal degrees of freedom to multicomponent reacting mixtures
06 p1047 A70-18312
- Rarefied gas shear flow over infinite plane wall, using Boltzmann-Krook-Welander equation to determine compressibility effect on Knudsen layer
06 p1048 A70-18327
- Asymptotic behavior /for small mean free path/ of rarefied gas steady flow over smooth solid boundary
06 p1048 A70-18328
- Rarefied gas flows and heat transfer between parallel plates, concentric cylinders and spheres in presence of fractionally accommodating boundaries
06 p1049 A70-18330
- Normal shock waves produced in argon and helium flow by holder with variable downstream porosity, measuring DC moments, component velocities and density
06 p1051 A70-18342
- Normal shock wave structure in binary gas mixtures of chemically inert monatomic molecules, using kinetic theory moment method
06 p1051 A70-18343
- Least squares method to determine shock thickness at arbitrary Mach number from Boltzmann equation for rigid sphere rarefied gas
06 p1051 A70-18345
- Wall pressure distribution, drag and lift measured on flat plates and wedges at Mach 8 rarefied gas flow for various leading edges
06 p0980 A70-18350
- Hypersonic rarefied argon and nitrogen flows over flat plate, investigating flow field and surface measurements from merged layer into transition regime
06 p0981 A70-18355
- Kinetic theory of rarefied supersonic flow over finite plate, calculating molecular velocity distribution functions for flowfield
06 p0981 A70-18356
- Drag coefficients of sharp and blunt cones in rarefied supersonic flow for bluntness ratios and angles of attack
06 p0981 A70-18360
- Hypersonic rarefied merged layer flow over sharp slender cones, using strong interaction theory and free molecular flow to analyze surface pressures
06 p0982 A70-18363
- Orifice effect investigated for sharp flat plate in hypersonic rarefied flow, measuring surface pressure
06 p0982 A70-18366
- Pipe orifice conductance for rarefied gas flow measured for specific Knudsen numbers and pressure ratios
06 p1052 A70-18370
- Drag and heat transfer predicted by kinetic theory for rarefied gas flow over sphere at low Mach numbers, analyzing flow field
06 p0984 A70-18381
- Hypersonic rarefied gas flow near stagnation point investigated to predict drag on sphere in high speed gas stream with densities in transition regime
06 p0984 A70-18382
- Velocity profile at entrance of two dimensional channel immersed in rarefied slow moving uniform flow with slip at walls
06 p1052 A70-18384
- Shock wave profiles in rarefied gas expansion flows, using static and impact pressure probes
06 p1052 A70-18386
- Cylinder wakes in rarefied gas flow at Mach 20, obtaining density profile data from electron gun, impact pressure and cooled film probe measurements
06 p0984 A70-18387
- Rarefied gas flow past sphere, using integral iteration method for Krook equation
07 p1187 A70-18675
- Similarity model for spherically symmetrical flow following explosion in rarefied atmosphere satisfying hydrodynamic energy conservation equation
07 p1260 A70-19981
- Stable flow distribution of sonic jet exhausting counter to low density supersonic airstream
07 p1189 A70-19982
- Molecular beam approximation introduced in Boltzmann equation to investigate high speed rarefied flows
07 p1261 A70-20130
- Density profiles of sphere wake in rarefied hypersonic flow compared to free molecular flow calculations
08 p1431 A70-20591
- Atomic gas particles interactions with self and solid surfaces based on rarefied gas dynamics and classical mechanics
08 p1547 A70-21077
- Aerodynamic characteristics of bodies in rarefied gases calculated using surface momentum flow dependence on local angle of attack
08 p1432 A70-21091
- Magnetic field and conducting walls effect on laminar steady MHD Couette flow of electrically conducting incompressible viscous rarefied gas in slip regime
08 p1553 A70-21764
- Heat transfer in MHD channel flow of viscous incompressible rarefied gas with slip flow and temperature jump boundary conditions
08 p1554 A70-21769
- Supersonic air jet structure in central shock wave region affected by both Mach number and flow rarefaction
09 p1734 A70-22185
- Aerodynamic characteristics of cooled blunt spherical bodies in low density hypersonic gas flow, discussing heat flux representation for different body surface temperatures
09 p1604 A70-22447
- Drag on cylinder in transverse rarefied gas flow varying from free molecular to almost continuum
09 p1604 A70-22448
- Monatomic gas rarefaction wave structure in unsteady one dimensional flow from high to low pressure zones, describing numerical solution technique
09 p1604 A70-22449
- Rarefied gas flow past arbitrary three dimensional body using variational principles based on linearized BGK equation, considering constant and adiabatic wall temperature
09 p1605 A70-23178
- Transition regime of rarefied gas dynamics using kinetic theory of gases, discussing Couette and Poiseuille flow, heat transfer and time dependent problems
10 p1919 A70-24141
- Electron beam fluorescence probes for rarefied gas flow, describing local density and temperature measurement methods
10 p1888 A70-24399
- Electron beam probe applied to flow visualization in rarefied gas wind tunnels
10 p1860 A70-24549
- Rarefied hypersonic axisymmetric blunt body, examining bow shock and viscous layer upstream merging
10 p1804 A70-24823
- Molecular reflection effects on aerodynamic characteristics of rarefied gas flow past plate
11 p1973 A70-25386
- Velocity profile and volume flow rate for rarefied gas flowing isothermal parallel plates, solving linearized Boltzmann equation by BGK model
11 p2037 A70-26168
- Rarefied gas stream density measurements with electron beam fluorescence experiment, determining pressures and densities behind plane shock wave and in supersonic nozzles
11 p2087 A70-26743
- Dispersion relations for linearized Grad equations of three dimensional rarefied gas dynamics, including nonequilibrium pressure term for bulk viscosity
12 p2210 A70-27520
- Dilute gas transport properties calculation, investigating numerical techniques to minimize computation time to prescribed accuracy
13 p2441 A70-29089
- Supersonic rarefied flow over sharp flat plate with merged shock layer and free molecular-continuum transition, using electron beam fluorescence
14 p2529 A70-31028
- Rarefied gas flow past sphere, using integral iteration method for Krook equation
15 p2671 A70-31467
- Rarefied gas slip flow coefficients calculations at nonuniformly heated surface, demonstrating relationship between temperature and isothermal slip coefficients
15 p2776 A70-31478
- Convective heat transfer in Cu spherical shell and plate in supersonic rarefied gas flow at zero angle of attack from wind tunnel experiments
15 p2824 A70-31497
- Heat flux measurements in hypersonic rarefied gas flow by thin film surface thermometer
15 p2825 A70-31820
- Boltzmann equation for Knudsen layer and outer region of weakly rarefied gas flow
15 p2777 A70-32131
- Rarefied gas mixtures efflux from opening at various pressures, calculating component discharge coefficients for molecular flow conditions
15 p2721 A70-32137
- Stationary gas flows continuous to rarefied transition analysis based on mean free path anisotropy
15 p2721 A70-32139
- Book on aerodynamics of bodies of revolution covering hypersonic flow parameters effects, method of characteristics, slender body drag, blunt bodies, rarefied gas aerodynamics, etc
16 p2834 A70-33271
- Flow and diffusion phenomena in rarefied gas mixtures associated with separation nozzle process, using molecular pressure probe and mass spectrometer
16 p2893 A70-33699
- Aerodynamic wake structure of cylinders and spheres in hypersonic rarefied gas flow as function of Mach and Knudsen numbers
16 p2836 A70-33756
- Rarefied binary gas mixture transient Couette flow, considering nonlinear case of plate with equal temperature accelerated impulsively
17 p3067 A70-34546
- Modified discrete ordinate approach in rarefied gas dynamics tested on linearized Couette flow between concentric cylinders, using integral iteration
17 p3067 A70-34548
- Soviet book on rarefied gas dynamics involving methods and approaches for kinetic description of gas behavior, emphasizing Boltzmann equation
17 p3067 A70-34604
- Shock wave and viscous layer structures ahead of blunt body in rarefied hypersonic flow, using continuum theory
17 p3009 A70-34698
- Low speed rarefied slip flow over wedge by asymptotic method of boundary layer equations integration, obtaining velocity profiles for various angles
17 p3010 A70-34973
- Rarefied gas dynamics at different Knudsen numbers, discussing elements of kinetic theory and analyzing free molecular and slip flows
17 p3070 A70-35037
- Dihedra placed at angle of attack in hypersonic rarefied gas flow, investigating base flow and near wakes
17 p3010 A70-35047
- Hypersonic rarefied gas flow around flat plate with sharp leading edge and circular cylinder in transition region
17 p3011 A70-35241
- Dilute gas transport expressions experimental substantiation, emphasizing nonequilibrium thermodynamics as macroscopic theory rather than empirical postulate
17 p3072 A70-35536
- Kinetic equation for rarefied polyatomic gases derived from Liouville equation
17 p3138 A70-35728
- ONERA low pressure wind tunnel equipped with electron beam probing device to visualize flows too rarefied for optical methods
18 p3210 A70-37208
- Dispersion relations for linearized Grad equations of three dimensional rarefied gas dynamics, including nonequilibrium pressure term for bulk viscosity
21 p3807 A70-41168
- Rarefied gas flow over plane wall, considering boundary layer thickness of order of mean free path
21 p3809 A70-41715
- Exhaust plume rarefaction from sonic orifice, considering continuum to transitional behavior for perfect gas
21 p3745 A70-42118
- [AIAA PAPER 69-657]
Minimum entropy production in kinetic theory of rarefied gases described by Boltzmann equation
21 p3745 A70-42118
- Wall recombination heat transfer in rarefied flow with velocity slip near leading edge
21 p3952 A70-42083
- Sphere and axisymmetric body with spherical blunting in low density gas flow, measuring local heat transfer flux
21 p3748 A70-42218
- Wave rider aerodynamic properties at small Reynolds numbers, using non-Weiler wing for flow field, pressure and force measurements at rarefied flow conditions
23 p4135 A70-44668
- [AVA-FB-7029]
Rarefied gas heat conduction between concentric cylinders in slip regime, obtaining perturbed temperature and density variations
23 p4284 A70-44985
- Rarefied gas plane Couette flow, calculating upper and lower bounds on shear stress
24 p4325 A70-45600

RAREFIED GASES
NT COSMIC GASES
NT INTERPLANETARY GAS

NT INTERSTELLAR GAS

Maximum plasma decay rate in heterogeneous medium determined from ionization process in rarefied gases

03 p0536 A70-14369

Free molecular mass flow rate through vacuum seal separating two rarefied gas environments, using coupled integral equations formulated on kinetic theory [ASME PAPER 69-WA/FE-18] 04 p0625 A70-14779

Nonlinear rarefied Couette flow with heat transfer in polyatomic gases, using kinetic theory of gases [ASME PAPER 69-WA/HT-39] 04 p0781 A70-14803

Interpolation method for predicting and correlating heat transfer in rarefied gases, yielding correct limiting results in free molecular and continuum regimes [ASME PAPER 69-WA/HT-30] 04 p0782 A70-14808

Nonlinear boltzmann equation for heat transfer in rarefied gases between parallel plates at different temperatures using Monte Carlo method [ASME PAPER 69-WA/HT-23] 04 p0782 A70-14811

Rarefied gas heat conduction between concentric cylinders at small Knudsen number and temperature gradient, using integral equations obtained from Krook equation [ASME PAPER 69-WA/HT-19] 04 p0783 A70-14816

Distribution functions for solving moment equations of Maxwell-Boltzmann equation used in studying heat conduction through rarefied gases within concentric cylinders and spheres [ASME PAPER 69-WA/HT-17] 04 p0783 A70-14817

Neutrinos production by primary cosmic rays in rarefied and dense media, calculating spectra 05 p0899 A70-15963

Mathematical models describing interactions between rarefied gas atoms and solid surfaces 06 p1036 A70-17759

Boltzmann equation for binary mixtures of rarefied gases solution involving specific expansion of distribution functions 06 p1047 A70-18311

Pipe bounding walls effect on sound waves dispersion in rarefied gas, deriving integral equations showing frequency range decrease with container size 06 p1107 A70-18315

Surface pressures and shock wave shapes on sharp flat plates and wedges in rarefied hypersonic transition flow with emphasis on merged layer regime 06 p0982 A70-18362

Free molecular heat transfer from sphere at rest in rarefied monatomic gas solved for Krook model of Boltzmann equation 06 p1183 A70-18375

Maser-like stimulated OH emission regions observed in interstellar rarefied gas 06 p1148 A70-18391

Aerodynamic coefficients for blunt cones in rarefied gas calculated as functions of angle of attack using empirical formulas 08 p1432 A70-21092

Aerodynamic forces acting on circular plates in rarefied gases, calculating coefficients as functions of angle of attack 08 p1433 A70-21093

Acoustic velocity in rarefied argon and nitrogen using Brillouin scatter and Burnett equations 09 p1698 A70-23314

Heat transfer from circular cylinder in rarefied gas flow at low Mach number, using B-G-K model of Boltzmann equation 09 p1791 A70-23582

Linear heat propagation in rarefied and non-homogeneous atmospheres, considering Green function behavior and various boundary and initial value problems 11 p2107 A70-25542

Rarefied gas flow in slip regime through cylindrical tube assuming parabolic velocity profile 14 p2565 A70-30263

Dilute gases kinetic theory, discussing microscopic explanation of macroscopic properties under intermolecular forces 17 p3072 A70-35533

Rarefied gas viscoseals performance prediction by theoretical model, comparing results with experiment [ASLE PREPRINT 70AM 5C-3] 19 p3439 A70-38806

Linear heat propagation in rarefied and non-homogeneous atmospheres, considering Green function behavior and various boundary and initial value problems 21 p3892 A70-41292

Intermolecular forces at close approach distances in calculating thermodynamic and transport properties of high temperature dilute gases, using molecular beam methods 23 p4222 A70-44430

Rarefied binary gas mixture, determining temperature gradient effect under various pressures 23 p4284 A70-44984

RAREFIED PLASMAS

Plane model of magnetosphere shape and structure, considering rarefied plasma flow past two dimensional magnetic dipole with dynamic and static boundary pressure, using conformal mapping 04 p0675 A70-14435

Energy modes nonlinear interactions in rarefied plasmas, presenting wave energy and momentum definitions and kinetic equations for mode density in wave number space 04 p0726 A70-14701

Rarefied ionospheric plasma flow around rockets and satellites, studying electric field effect on ion motion by kinetic equation and similarity law 04 p0680 A70-15188

Rarefied plasma motion in geomagnetic dipole equatorial plane near magnetosphere symmetry axis deriving approximate solution to quasi-hydrodynamic equations 04 p0681 A70-15717

Electric field determination from charged particle concentration in wake of body moving in rarefied plasma, noting hydrodynamics similarity 05 p0915 A70-16754

Multiple electrode probe characteristics in rarefied plasma flow created by ion source, noting electrode potential role 06 p1064 A70-17886

Single and double cylindrical Langmuir probe responses in highly expanded low density flowing Ar plasma [AIAA PAPER 70-85] 06 p1066 A70-18207

Numerical analysis of rarefied plasma flow interaction with charged conducting bodies of various forms and dimensions 06 p1123 A70-18298

Current collected by cylindrical Langmuir probe immersed in rarefied collisionless plasma streaming with high velocity 06 p1124 A70-18307

Collective interactions and low density plasma instability in high current gas discharge showing influence on neutral gas breakdown in interelectrode space 07 p1354 A70-20317

Particle flux densities in electric field near spherical body moving in rarefied plasma 07 p1355 A70-20368

Rarefied plasma flow past bodies, considering determination of aerodynamic coefficients, charged states, electric and magnetic fields and plasma parameters 08 p1432 A70-21087

Aerodynamic drag coefficients and moments for axisymmetric bodies of revolution in rarefied plasma derived for limiting case of delta flux 08 p1432 A70-21088

Aerodynamic coefficients for axisymmetric bodies moving in rarefied plasma, calculating corrections for thermal ion velocities 08 p1432 A70-21089

Cyclotron waves absorption study in bounded rarefied plasma having Larmor electron frequency exceeding plasma frequency 10 p1925 A70-25101

Plane model of magnetosphere shape and structure, considering rarefied plasma flow past two dimensional magnetic dipole with dynamic and static boundary pressure, using conformal mapping 13 p2392 A70-28460

Variable temperature plasma with two ion species, noting rarefaction wave propagation during one dimensional expansion into vacuum 13 p2464 A70-29415

Rarefied plasma motion in geomagnetic dipole equatorial plane near magnetosphere symmetry axis by deriving approximate solution to quasi-hydrodynamic equations 14 p2575 A70-30801

Low density collisionless plasma sheath in planar and cylindrical geometry under weak magnetic field, considering ion-electron pair generation 14 p2624 A70-31040

Nonlinear electrostatic vibrations in colliding antiparallel flows of rarefied plasma 17 p3141 A70-35335

Ti alloys thermomdiffusion impregnation with rarefied nitrogen and oxygen plasma, determining optimal gas pressure and temperature conditions and magnetic field frequency effects 17 p3101 A70-35391

Supersonic flow of rarefied plasma around plane bodies, allowing for electric field effect on ion motion 19 p3351 A70-37302

Rarefied plasma flute oscillation stabilization in magnetic field, using controlled electron beams 20 p3677 A70-39173

Shock waves formation in rarefied plasma investigated by Thomson scattering of ruby laser light 20 p3643 A70-40388

Slightly rarefied and electrically conducting gas, calculating effects of applied magnetic field on steady laminar low speed plane Couette flow 20 p3685 A70-40504

Rarefied ionospheric plasma flow around rockets and satellites, studying electric field effect on ion motion by kinetic equation and similarity law 21 p3819 A70-41169

Electromagnetic scattering power spectrum from underdense turbulent plasmas, deriving first and second moments 21 p3858 A70-41732

Microwave characteristics in plasma of short discharges in low pressure cesium and mercury vapors, noting spectral and spatial distribution of microwave power and intensities 22 p4083 A70-43392

Inertia effect on low density plasma losses in toroidal MHD equilibrium in model stellarator field 24 p4383 A70-45115

RASERS

U MASERS

RATE METERS

U MEASURING INSTRUMENTS

RATES (PER TIME)

NT ACCELERATION [PHYSICS]

NT ACOUSTIC VELOCITY

NT AIRSPEED

NT ANGULAR ACCELERATION

NT ANGULAR VELOCITY

NT ARRHYTHMIA

NT BRADYCARDIA

NT BURNING RATE

NT COLLISION PARAMETERS

NT COLLISION RATES

NT CRITICAL VELOCITY

NT CURRENT DENSITY

NT DECAY RATES

NT DECELERATION

NT DRIFT RATE

NT ELECTRON DECAY RATE

NT ELECTRON FLUX DENSITY

NT ESCAPE VELOCITY

NT EVAPORATION RATE

NT EXHAUST VELOCITY

NT FLOW VELOCITY

NT FLUX [RATE]

NT FLUX DENSITY

NT GROUND SPEED

NT GROUP VELOCITY

NT HEART RATE

NT HEAT FLUX

NT HIGH ACCELERATION

NT HIGH SPEED

NT HYPERSONIC SPEED

NT ILLUMINANCE

NT IMPACT ACCELERATION

NT ION PRODUCTION RATES

NT IRRADIANCE

NT LANDING SPEED

NT LIGHT SPEED

NT LOADING RATE

NT LOW SPEED

NT LUMINANCE

NT LUMINOUS INTENSITY

NT MAGNETIC FLUX

NT MASS FLOW RATE

NT NEUTRON FLUX DENSITY

NT ORBITAL VELOCITY

NT PARTICLE ACCELERATION

NT PARTICLE FLUX DENSITY

NT PHASE VELOCITY

NT PHOTON DENSITY

NT PLASMA ACCELERATION

NT PROPAGATION VELOCITY

NT PROTON FLUX DENSITY

NT PULSE RATE

NT RADIAL VELOCITY

NT RADIANCE

NT RADIANT FLUX DENSITY

NT RECOMBINATION COEFFICIENT

NT RELATIVISTIC VELOCITY

NT RESPIRATORY RATE

NT ROTOR SPEED

NT SIGNAL FADING RATE

NT SOLAR CONSTANT

NT SOLAR FLUX

NT SOLAR FLUX DENSITY

NT SOLAR VELOCITY

NT SOUND INTENSITY

NT SPIN REDUCTION

NT STRAIN RATE

NT SUBSONIC SPEED

NT SUPERSONIC SPEEDS

NT SYSTOLE

NT TACHYCARDIA

NT TERMINAL VELOCITY

NT TIP SPEED

NT TRANSONIC SPEED

NT WIND VELOCITY

NT ZERO SOUND

Motion equations for vibratory two degrees of freedom spring mass system subjected to rotation, discussing use for small rates of turn measurement 01 p0199 A70-10266

Tactile control in man machine systems using feed-forward loops to provide rate information, noting unmanned aircraft and machine-tool applications [ASME PAPER 69-WA/BHF-14] 04 p0642 A70-14855

Instantaneous corrosion rate measurement, comparing coupon, resistance and polarization methods 24 p4365 A70-46390

RATINGS

Cooper aircraft handling rating scale on basis of test pilot experience 06 p1003 A70-18018

Ultrasonics for steel cleanliness rating, considering advantages and fatigue life 15 p2743 A70-31768

RATIONAL FUNCTIONS

Consistent dependence of best rational Chebyshev Lp approximator on given function 23 p4210 A70-44025

RATINGS

NT SPACE RATINGS

RATIOS

NT ASPECT RATIO
NT DIMENSIONLESS NUMBERS
NT FINENESS RATIO
NT FROUDE NUMBER
NT FUEL-AIR RATIO
NT GRASHOF NUMBER
NT HARTMANN NUMBER
NT HIGH ASPECT RATIO
NT INDEXES [RATIOS]
NT LAVAL NUMBER
NT LEWIS NUMBERS
NT LIFT DRAG RATIO
NT LOW ASPECT RATIO
NT MACH NUMBER
NT MASS RATIOS
NT NUSSELT NUMBER
NT OPTICAL REFLECTION
NT PAYLOAD MASS RATIO
NT PECLET NUMBER
NT PERVEANCE
NT POISSON RATIO
NT PRANDTL NUMBER
NT PROPELLANT MASS RATIO
NT RAYLEIGH NUMBER
NT REYNOLDS NUMBER
NT RICHARDSON NUMBER
NT SCALE [RATIO]
NT SCHMIDT NUMBER
NT SIGNAL TO NOISE RATIOS
NT STANDING WAVE RATIOS
NT STRESS RATIO
NT STROUHAL NUMBER
NT THICKNESS RATIO
NT THRUST-WEIGHT RATIO
NT VOID RATIO

RATS

Platelet and lipid changes in thrombocytopenic and control rats subjected to bends producing technique in aeroembolism 01 p0015 A70-10364

Male rats locomotor activity responses to altered photoperiods during exposure to varied-light artificial days 01 p0015 A70-10367

Cerebral histamine distribution in rat brains, noting highest concentrations in hypothalamus and thalamus 01 p0020 A70-10708

Skin and hypothalamic temperature inputs for behavioral regulation of hypothalamic temperature of rats 01 p0020 A70-10725

Conditioned suppression after differential training, discussing shock tests on rats with safe and danger signals 01 p0036 A70-10794

Dibutyltryl cyclic adenosine monophosphate stimulation of melatonin and serotonin synthesis from C-14 labeled tryptophan by rat pineals in organ culture 01 p0022 A70-10824

Rats sympathoadrenomedullary response to increased oxygen tensions, measuring catecholamines, norepinephrine and epinephrine in adrenal gland, hypothalamus, serum and urine 01 p0024 A70-10979

Rodents hypoxia tolerance following adaptation to hypercapnia by recording time of useful consciousness /TUC/ in repeated sloped surface clinging tests 01 p0026 A70-11249

Appetitive behavior of rats following cessation of hypothalamic stimulation, observing eating and drinking inhibition 01 p0027 A70-11275

Rat water intake and urine output during chronic centrifugation at resultant inertial fields of 1.7 and 3.0 g 02 p0231 A70-11705

Diet and feeding method effects on food intake and plasma amino acid concentrations of rats fed low protein diet with amino acid imbalance 02 p0231 A70-11707

Alpha-aminoisobutyric acid accumulation by soleus and plantaris muscles of rat in vivo during work induced growth, showing amino acid transport variation with work level 02 p0232 A70-11711

Rats decreased muscular work and denervation effects on alpha-aminoisobutyric acid uptake by skeletal muscle 02 p0232 A70-11712

Ambient temperature effects on rats excretion of epinephrine, norepinephrine and major metabolites 02 p0232 A70-11714

Polycythemia and hypercapnia effects on apparent oxygenation of rat brain during acute hypoxia by changes in creatine phosphate concentration and lactate/pyruvate ratio 02 p0232 A70-11717

Stainless steel micropipettes implantation in rat amygdala to study role in gastric secretion 02 p0234 A70-11729

Starvation effect on intestinal amino acid absorption of rats, noting protein synthesis reduction 02 p0234 A70-11731

Object carrying behavior of rats, using electrical stimulation of hypothalamic structures 02 p0237 A70-12395

Brain norepinephrine synthesis rate in gonadectomized and control rats treated with alpha-methyl paratyrosine 03 p0416 A70-12987

Physicochemical properties of hypothalamic secretions responsible for coronary dilatation in rats, cattle and pigs, using analytical techniques 03 p0417 A70-13215

Ultraweak luminescence intensity, radiation damage kinetics and spectral properties of cellular organelles of rat liver exposed to gamma radiation 03 p0419 A70-13304

Free radical antioxidant reactions in lipids from blood, liver, spleen, brain and intestines of rats exposed to ionizing radiation 03 p0419 A70-13309

Vascular electrical activity in cats and rats by inserting glass microelectrode into blood vessel, showing blood flow conditioning effect on activity 03 p0422 A70-13691

Conditioned reflexes, respiration and heart beat rates changes in white rats under hypothermia 03 p0424 A70-13717

Fraction of Chlorella and Scenedesmus biomass, noting changes in adrenal cortex and renal glomerus 03 p0425 A70-13889

Antihypoxic preparations protective effect on white mice and rats subjected to gravitational accelerations 03 p0425 A70-13890

Vestibular reactions in rats under hypothermal conditions by measuring postrotatory nystagmus beats number and duration, respiration rates and rectal temperature 03 p0425 A70-13893

Rats ability to discriminate slow rotation speeds, suggesting otolith organs and proprioceptors sensitivity role in discrimination 03 p0439 A70-14296

Gamma radiation effects on membrane permeability of isolated nuclei from white rats thymus in sucrose-calcium buffer 04 p0629 A70-14460

High altitude environmental effects on adrenal glands and hypothalamic neurosecretion in rats 04 p0629 A70-14568

Calcium isotopes tracer migration in caged rats in metabolism study 04 p0630 A70-14571

Hyperbaric oxygenation effects on metabolism, comparing protective agents for rats exposed to 5 absolute oxygen pressures 04 p0631 A70-14681

Chloride and sulfhydryl activators in glucagol degradation and secretion by purified rat liver dipeptidyl aminopeptidase I/Cathepsin C/ 04 p0631 A70-14682

Noble gases breathing effects on free amino acid pool increase in rat brains, considering O mixtures with He, Ar and Ne 04 p0632 A70-15086

Acidosis effects on anoxic rat heart cardiac performance and anaerobic energy generation 04 p0635 A70-15461

Nutritive value of mycelium of Cantharellus cibarius mushroom on rats compared with eggs and fresh and sour milk 05 p0809 A70-17111

Rat survival rate after prolonged gradually decreased body temperature without motion restraint or kept in fixed position 05 p0804 A70-17115

Cerebellar cortex reactions to sciatic nerve stimulation in rats under transverse accelerations in centrifuge 05 p0804 A70-17116

Positive effect of shielding and cystamin administration on tonic and evacuator functions of rats gastrointestinal tract after gamma irradiation 05 p0804 A70-17122

Red blood cell mechanical fragility independence from cell age in rats 06 p0989 A70-17221

Hematologic changes in rats under hypergravity, effects of vitamin B12, folic acid and return to 1 g 06 p0991 A70-17283

Acid soluble nucleotides content in normal and gamma irradiated rat spleens, presenting table 06 p0995 A70-17799

Hypothermia effect at various temperatures and durations on nervous activity and vegetative functions of rats, discussing pulse and respiratory rates 07 p1197 A70-18696

Oxygen tension change effects on rats smooth vascular muscles electrical and contractile properties 07 p1198 A70-18715

Rat body fluids displacement during positive centripetal accelerations by radioisotope tracer compounds, freezing rats in liquid nitrogen to fix hemodynamic changes 07 p1202 A70-18796

Extraction, analysis and properties of rat prolactin isolated from pituitary glands 07 p1203 A70-18895

Sialic acids metabolic behavior in cerebrum, liver, myocardium and blood plasma of rats after X ray irradiation 07 p1205 A70-19289

Adhesive and aggregative properties of blood platelets in rats after beta irradiation linked to activity of serum factor 07 p1207 A70-19474

Succinic dehydrogenase activity in white rats cerebrum and liver under hypothermia and after warming 07 p1207 A70-19475

Vascular and dystrophic disturbances in rat parenchymatous organs in hyperbaric pure oxygen atmospheres, observing increased tissue eosinophilia 07 p1207 A70-19504

Hypokinesia effects on cellular and humoral indices of antibody formation in rats, noting exposure time role 07 p1208 A70-19509

Adaptive reactions in thyroidectomized rats blood and brain during adaptation to hypoxia compared with intact animals 07 p1214 A70-19794

Hyperoxia effects on red blood cell/RBC/ survival in rats on normal diets, noting relatively normal erythropoiesis after long term exposure 07 p1214 A70-19935

Hypoxia effect on retrograde amnesia /recent memory loss/ in albino rats subjected to shock and decompression treatments 08 p1441 A70-20477

Time course of changes in rat brain norepinephrine levels after olfactory bulb lesions, discussing automatic and biological mechanisms 08 p1448 A70-21841

Decompression rates effect on altitude tolerance of white rats, discussing hypoxia influence on cardiovascular, respiratory, circulatory, thermal control and central nervous systems 09 p1614 A70-22084

Central nervous system activity of white rats during hypokinesia, observing organism shifts and long time effects on functions 09 p1615 A70-22093

Total body X irradiation effect on tyrosine hydroxylase and catecholamine levels in rats 09 p1616 A70-22318

Amino acid metabolism time dependent variations, studying tyrosine transaminase rhythm in rat liver 09 p1618 A70-22525

Glycogen accumulation in astroglia following brain trauma caused by partial transection of cerebral hemisphere in rats 09 p1620 A70-22898

Electromagnetic flowmeter for cardiac output changes in unanesthetized rats, discussing construction, form and associated electronic equipment of implanted probe 09 p1627 A70-23267

Vasoactive agent effects on decompression sickness in rats, noting increased severity of bends by serotonin and platelet role 10 p1811 A70-24176

High altitude acclimatization effect on tissue capillary, investigating physiological evidence in rats by tissue diffusing capacity measurement 10 p1823 A70-25220

Conditioned reflexes, respiration and heart beat rate changes in white rats under hypothermia 11 p1985 A70-25517

Rats heart rate change during running at simulated altitude, discussing respiratory-circulatory training effect 11 p1985 A70-25671

Hypoxia tolerance of albino rats in He-oxygen and Ar-oxygen environments in heat-pressure chamber, discussing He-oxygen mixture cooling effect 11 p1987 A70-26103

Hypokinesia effects on cellular and humoral indices of antibody formation in rats, noting exposure time role 11 p1988 A70-26108

Mathematical model for rats nonlinear time-varying glucocorticoid secretion control mechanism, obtaining time dependent characteristics of hypothalamic-hypophyseal complex 12 p2174 A70-26893

Altitude acclimatization protection against lung damage from exposure to oxygen at high partial pressures experimented on rats

12 p2170 A70-27659

Rats myocardial contractility depression by free fatty acids during hypoxia or anoxia, noting mechanical performance improvement by glucose

12 p2170 A70-27898

Rats cardiac aerobic and anaerobic pathways response to hyperbaric oxygen exposure

13 p2349 A70-28833

Electrode placement ancillary technique for obtaining stereotaxic atlas of infant rat hypothalamus

13 p2350 A70-29322

Somatotropic hormone and esculamine injection effects on rat survival rates under acceleration, noting sex linked differences

13 p2352 A70-29345

Hypoxia tolerance in white rats after exposure in hypercapnic medium

13 p2355 A70-29757

Single and combined hypoxia and hypercapnia effects on growing rats, discussing body weights, blood and histological measurements

13 p2357 A70-29948

Intraocular tension due to muscular fatigue in overheated albino rats, determining Na and K content in eye tissue

14 p2535 A70-30159

Chronic hypoxia exposure effect on development and maintenance of renal hypertension in rats

14 p2539 A70-30956

Rats under constant environmental conditions exhibiting circadian rhythmicity in rate of bar pressing with hypothalamic and septal reinforcing brain electrical stimulation

14 p2539 A70-30986

Prolonged hyperoxia effect on red blood cell survival and hemolysis in rats on normal diet

15 p2681 A70-31786

Radial acceleration effects on tissue carbohydrate in starved female rats, observing blood glucose increase and muscle glycogen levels decrease

15 p2684 A70-32536

Decompression rates effect on altitude tolerance of white rats, discussing hypoxia influence on cardiovascular, respiratory, circulatory, thermal control and central nervous systems

15 p2685 A70-32680

Central nervous system activity of white rats during hypokinesia, observing organism shifts and long time effects on functions

15 p2685 A70-32689

Electrical stimulation in rostral medulla hypothalamus effects on thermogenesis of juvenile rats, calculating heat transfer at trunk

16 p2849 A70-33696

Integrating influence of medio-rostral hypothalamic structures upon temperature regulation of juvenile rat based on Area praoptica medialis stimulation

16 p2849 A70-33697

Long term weightlessness effects on cardiovascular system of rats using miniaturized pump oxygenator

16 p2854 A70-33999

Plasma free fatty acids and glucose relative role in contribution to metabolic state and energy production in partially hepatectomized rats

16 p2850 A70-34319

Dietary amino acids combination allowing maximum growth in rat

16 p2850 A70-34320

Rat neuron impulsive reactions and frequency response differences to varying sound signals, discussing time constant, signal intensity and frequencies

20 p3574 A70-40172

Hypokinesia effects on rats protein synthesis rates, determining body and organ weights, muscle tissue nitrogen content and transaminase activity

20 p3575 A70-40187

Myocardial Na and K content of rats exposed to high altitude, preparing isolated right ventricular strip

20 p3577 A70-40541

Fasting plasma glucose concentration in rats after chronic hypoxia

20 p3577 A70-40542

Click-evoked potentials in rat auditory cortex, medial geniculate body, reticulate formation and hippocampus during natural sleep and waking

21 p3761 A70-40917

L-dihydroxyphenylalanine intraperitoneal injection effect on S-adenosylmethionine concentration in rat brain

21 p3764 A70-41269

Growth and caloric intake of rats exposed to high altitude dependence on high carbohydrate, protein and fat diets

22 p3967 A70-42458

Protein catabolism increase during high altitude exposure to hypoxia in rats, noting amino acid incorporation into tissue proteins

22 p3967 A70-42459

Tranquilizers and hypnotics from rats organs analyzed by thin layer chromatography

22 p3978 A70-42879

Inherited hypertension genetic and autonomic factors, discussing rats crossbreeding for genetic contribution ratio in males vs females, age effects, etc

24 p4299 A70-45806

Conscious rat systolic blood pressure measurement, using arterial pulse wave detection to occluding cuff by photoconductive cell

24 p4309 A70-46213

RAWINSONDES

Mesoscale rawinsonde network for convective process resolution, describing reduction and analysis techniques for thunderstorm wind, temperature and moisture data

03 p0521 A70-13165

Right-moving thunderstorm characteristics from mesonetwork rawinsonde updraft observations, considering hydrostatic pressure and cyclonic rotation

19 p3462 A70-38260

RAY TRACING

Ray-optical analysis of electromagnetic scattering in plane and circular waveguides, giving formulas for modal reflection and coupling coefficients

03 p0452 A70-14034

Topside ray trajectories near upper hybrid resonance

04 p0650 A70-15119

Polar aurora rays mean length diurnal variations determined from photographic and visual observations in Tiksi bay

05 p0843 A70-16763

Variational ray path calculation method for HF electromagnetic wave in anisotropic inhomogeneous lossless ionospheric plasma

06 p1055 A70-17592

Successive small birefringences undergone by polarized light ray crossing photoelastic model represented by rotations in equatorial plane on Poincare sphere

06 p1168 A70-17918

LUF for F layer propagation modes, discussing mode cut-off significance using computer ray tracing program

07 p1229 A70-19159

Oblique radio ray tracing at 2-10 MHz and application to signal strength calculation, concentrating on digital techniques

07 p1230 A70-19162

Three dimensional ray tracing computer program in Fortran for determining radio paths in ionosphere

07 p1230 A70-19163

Ray tracing techniques applied to night sky wave medium frequency propagation, modifying program for absorption and polarization coupling losses

07 p1230 A70-19164

Ray tracing in ionospheric HF communications, describing computational method for ray paths and ionospheric absorption

07 p1230 A70-19166

Ray theory for determining short term and averaged characteristics of nonreciprocal HF ionospheric propagation paths for single magnetoionic waves transmitted between antennas

07 p1231 A70-19171

Ray tracing calculation and experimental observation for mode structure and absorption loss of oblique incidence HF radio wave propagation

07 p1234 A70-19217

Qualitative analysis and comparison of hypothesis versions of Martian point flare observed by Maeda, considering solar ray reflection from ice cloud or vertical surface object

07 p1385 A70-19420

Optical resonators formed by spherical mirrors, deriving mode density-output power relationship by ray analysis

09 p1729 A70-23521

Solar energy exchange with radiator surface recessed within specular axisymmetric cylindrical spinning cavity, using deterministic ray tracing scheme

11 p2150 A70-26353

Two dimensional ray tracing analysis for plume attenuation coefficient calculation using flame diagnostic data

15 p2695 A70-32608

Plane wave reflection from stratified isotropic medium using ray tracing in complex space, noting agreement with phase integral method

19 p3380 A70-38404

Magnetoionic component of entire N/z profile on incomplete ionospheric traces, including invisible part of ionogram

19 p3419 A70-38957

Space-time rays relation to plane wave dispersion surfaces in radiation and diffraction problems, using ray tracing diagrams

20 p3671 A70-39220

Diffraction theory relationship to ray optics for coherent light propagation through lens systems

21 p3829 A70-41929

Cavity radar cross section estimation by simplified models compared to semiempirical prediction with ray tracing procedure

22 p3992 A70-43583

Ray theory of diffraction from open-ended parallel plate waveguides, using Wiener-Hopf technique

23 p4219 A70-44404

Microwave propagation in waveguides, investigating trapped and slightly leaky modes in multilayered or multiwave regions by ray-optical techniques

24 p4311 A70-45216

RAYLEIGH DISTRIBUTION

Rayleigh and m fading signals spectral location in additive white Gaussian noise, allowing predetermined or variable channel observation time

11 p2010 A70-26268

Ferromagnetic cylindrical specimens eddy current density distribution under influence of field strength dependent permeability corresponding to Rayleigh law

24 p4344 A70-45695

RAYLEIGH EQUATIONS

Rayleigh method convergence for linear development of perturbations in unsteady plane parallel flow of ideal fluid, formulating and proving theorem

01 p0064 A70-11032

Kinetic theory treatment of linearized Rayleigh problem using wall boundary condition models

06 p1049 A70-18329

Rayleigh method convergence for linear development of perturbations in unsteady plane parallel flow of ideal fluid, formulating and proving theorem

10 p1871 A70-25001

Suction velocity effects on Rayleigh problem in MHD of flat nonmagnetic nonconducting plate, solving for velocity distribution and skin friction

19 p3481 A70-38448

RAYLEIGH NUMBER

Steady convective motions in horizontal fluid layer bounded by porous walls of various temperatures at supercritical Rayleigh numbers, noting nonlinear convection equations

04 p0673 A70-15237

Thermally induced convective mixing motion in rotating cylindrical cryogen space storage tank model under heat flux, calculating critical Rayleigh number

07 p1257 A70-19320

Vertical heat transfer in silicone oil by single row convection cells, correlating cell number to transport rate and Rayleigh number

09 p1612 A70-22052

Rayleigh number effects on convection in planetary mantles, considering conservation equations of mass, energy and momentum

09 p1752 A70-22312

Radiative transfer effect on thermal instability and critical Rayleigh number in gray transparent fluid layer heated from below

10 p1967 A70-23952

Angular dependence of instability and Rayleigh number of natural convection flow on inclined flat plates, using electrochemical flow visualization

18 p3345 A70-36190

Sufficient conditions for confined fluids stability, defining critical and modified Rayleigh numbers

21 p3810 A70-41952

RAYLEIGH SCATTERING

Atmospheric penetration of UV and visible solar radiation during twilight, oxygen and ozone absorption, Rayleigh scattering and atmosphere refraction

02 p0357 A70-12155

Rayleigh scattering cross sections of stellar He C, N and O computed by quantum defect method, discussing effects of wavelength dependent polarizabilities

04 p0723 A70-15692

Laser atmospheric backscatter measurements using frequency shifted Raman scatter and Rayleigh components for separating returns due to gaseous and aerosol components

05 p0859 A70-16476

Rayleigh phase matrix solutions and albedo values for imperfect Rayleigh scattering in semiinfinite planetary atmosphere

06 p1149 A70-18460

Day sky Fraunhofer lines filling-in /Ring effect/ considered from analogous effects in surface albedo, suggesting role of Rayleigh wings

10 p1947 A70-24992

Light scattering by atom generalized for multilevel system, showing additional coherent spontaneous scattering and incoherent stimulated combination scattering

12 p2272 A70-27549

Noise rejection for optimal reception of incoherent binary signals in one beam Rayleigh dispersion radio channel under ionospheric electron density fluctuations

13 p2369 A70-29738

Polarization role in radiation scattering by planetary atmosphere, considering luminance variation and Rayleigh scattering

14 p2651 A70-31302

Rayleigh scattering in atmosphere, determining brightness dependence on altitude, latitude and season

18 p3251 A70-36979

Relaxation theory of Rayleigh scattering of light by isotropic continuous medium, deriving spectral densities via fluctuation dissipation theorem

19 p3470 A70-37446

Laser pulse amplification by stimulated thermal Rayleigh scattering in absorbing media by transient theory

20 p3640 A70-39113

Pulse light amplification by stimulated thermal Rayleigh scattering measured as function of time, absorption coefficient and interaction length

20 p3640 A70-39114

Atmospheric scattering governed by Rayleigh phase function with absorption, calculating radiative transfer by numerical solution of Chandrasekhar integral equations

22 p4072 A70-42340

Daytime near horizon atmospheric luminescence measurement by Cosmos 224 satellite, discussing contributions of nitrogen and aerosol and Rayleigh scatterings

23 p4188 A70-44061

Radiative transfer equation solution for polarized light in Rayleigh scattering atmosphere with absorption, using singular eigenfunction expansion technique

23 p4219 A70-44402

RAYLEIGH WAVES

Plane harmonic Rayleigh wave propagation in piezoelectric semiconductor GaAs crystals, using successive approximation procedure

01 p0154 A70-10131

Rayleigh and Lamb waves propagating on solid and hollow elastic cylinders immersed in water, noting correspondence to symmetric and antisymmetric vibrations in shell

05 p0938 A70-16410

Plane harmonic Rayleigh wave propagation in piezoelectric semiconductor GaAs crystals, using successive approximation procedure

08 p1556 A70-21407

Rayleigh and Love wave phase velocities for great circle paths from ordinary seismograms of World Wide Standard Seismographic Network /WWSSN/ stations

09 p1672 A70-23702

Electron amplification and phase velocity of plane harmonic Rayleigh wave in gallium arsenide crystals under constant electric field

12 p2285 A70-27294

Stimulated light scattering by capillary waves on incompressible fluid surface or by Rayleigh waves on surface of isotropic solid body with small opticoelastic moduli

16 p2951 A70-33195

Interdigital Rayleigh wave transducers piezoelectric coupling coefficient from bulk constants, permitting equivalent circuit parameters prediction

17 p3055 A70-35875

Heteroepitaxial ZnO film on anisotropic sapphire substrate, calculating dispersion for fundamental Rayleigh wave mode

17 p3144 A70-35908

Rayleigh wave scalar electric potential analysis on piezoelectric medium, using iterative techniques for Poisson equation

22 p4074 A70-42967

RAYLEIGH-RITZ METHOD

Simply supported skew plates calculated for buckling loads by Rayleigh-Ritz method using double Fourier series

05 p0940 A70-16514

Bending stress concentrations in elastic square plate with central hole under uniform load, using finite element solutions of modified Rayleigh-Ritz method

06 p1168 A70-17940

Free vibration analysis of elastic structures using Rayleigh-Ritz method and finite element methods

10 p1961 A70-25055

Natural frequencies of thin cantilever cylindrical shells, using Flugge equations of motion and Rayleigh-Ritz method

11 p2146 A70-26704

Pivoted plane pad bearings, calculating design variables from inner products of two vectors and Rayleigh-Ritz matrix function

[ASME PAPER 69-LUB-1]

19 p3435 A70-37612

Assumed vibration modes generation method in beams with arbitrary boundary conditions, applied to cantilevered beams, using modified Rayleigh-Ritz analysis

21 p3934 A70-40923

Support elasticity role in axisymmetric plates bending, discussing Rayleigh-Ritz solution

21 p3937 A70-41739

Iterative Rayleigh-Ritz method for eigenvalue determination in natural vibration problems

23 p4270 A70-44580

RAYON

Wool felt based carbon and graphite composite materials for orthogonally isotropic high shear strength compared with rayon felt based composites

13 p2437 A70-28776

RAZOR BLADES

Razor blade calibration and measurement of wall jet flow shear stress in turbulent boundary layer with secondary injection

05 p0833 A70-16504

RELATIVE BIOLOGICAL EFFECTIVENESS [RBE]

RC CIRCUITS

Autocorrelation function distortion in pseudorandom signal with limited spectrum at RC filter output

03 p0446 A70-13202

Three dimensional RC network simulating temperature fields in IC at different heat source power dissipation laws, discussing harmonic heat source field

09 p1643 A70-22128

Distributed RC notch filter normalized constants for dominant and nondominant transmission zero

09 p1654 A70-23025

Active RC bandpass filter with independent linear control of Q peak gain and frequency

13 p2376 A70-28801

Root locus of active distributed RC circuit for synthesis of magnitude response of parabolic filters

14 p2562 A70-31323

Active RC bandpass filter for space fluxgate magnetometer, using state variable synthesis

17 p3054 A70-35526

Low pass linear phase active feedback circuit synthesis using distributed RC networks to realize flat magnitude response

19 p3392 A70-37707

Optimal synthesis of linear active RC filters with controlled source, using feedforward and feedback weighted signals

20 p3596 A70-39163

Ga-as Gunn diodes small signal admittance in dipole oscillation mode, analyzing RC model

20 p3598 A70-40062

Transistorized LF RC filter circuit design for desired frequency response characteristics

23 p4171 A70-43962

Multivibrator designs incorporating distributed R-C-NR thin film structures

24 p4321 A70-46395

Multivibrators with improved stability and frequency-division capacity, using distributed R-C-NR structures

24 p4321 A70-46396

LF narrow band-pass amplifiers with distributed RC structures

24 p4321 A70-46397

RC NETWORKS

U RC CIRCUITS

RDX

Performance characteristics of RDX-metal sheath systems, using high speed motion picture photography for missile design applications

03 p0550 A70-14141

REACTANCE

Reactance filters for matching circuits design with optimum transforming performance

09 p1650 A70-23404

Circuitry for phase modulated synchronized electronic oscillators for measuring minor reactance changes during remote sensing

11 p2052 A70-26373

MIS varactors applications as nonlinear reactances, discussing charge-voltage characteristics and minority carriers effect

12 p2196 A70-27685

High Q reactance network realization for integrated microwave systems employing evanescent mode waveguide components

16 p2875 A70-33402

High speed homopolar inductor alternators with minimum leakage reactance, using geometric programming for objective function optimization

16 p2879 A70-34059

High speed aerospace homopolar alternator, calculating end zone three dimensional magnetic flux distribution and leakage reactance

22 p3999 A70-43585

REACTION CONTROL

Rocket engine thrust chambers and valves, discussing component lifetime extension and operational flexibility of reaction control systems

[AIAA PAPER 70-603]

16 p2964 A70-33526

Monopropellant hydrazine RCS rocket engine module, discussing operating conditions, development, thermal control and valve internal leakage

[AIAA PAPER 70-654]

16 p2965 A70-33544

Boron and boron carbide coatings formation on graphite by vapor deposition, determining optimum parameters for reaction control

19 p3455 A70-38250

High performance reaction pointing control systems for sounding rockets, using proportional control of differential thrust and adaptive control of thrust magnitude

[SAE PAPER 700783]

24 p4415 A70-45861

Warm gas reaction control thrusts via solid propellant exhaust products for ballistic missiles attitude control

[SAE PAPER 700780]

24 p4295 A70-45863

Low and high chamber pressure concepts for space shuttle reaction control system

[SAE PAPER 700802]

24 p4416 A70-45909

REACTION JET ATTITUDE CONTROL

U ATTITUDE CONTROL

U JET THRUST

REACTION JET BACKPACKS

U SELF MANEUVERING UNITS

REACTION JETS

U JET FLOW

U JET THRUST

REACTION KINETICS

Diffusion flame structure in boundary layer with fuel injection from wall, analyzing expansions with single step reversible chemical kinetics, including nonequilibrium case

01 p0214 A70-10334

Initial pyrolysis kinetics of neopentane, showing decomposition rate tendency to equal formation rate at high temperature

01 p0215 A70-10706

Mass action law-polynomial optimization analogy, illustrating optimal temperature determination in chemical reactors in series

01 p0143 A70-10925

Combustion time of Al powder, considering concentration, injection into gas flow, oxidizer composition and agglomeration

01 p0161 A70-11015

Ti-Al-Co alloys reactions in solid phase in Ti-rich region, using optical microscopy and X ray diffraction analysis

01 p0125 A70-11645

Hydrogen reactions with nitrogen dioxide, oxygen and mixtures of oxygen and nitric oxide in adiabatic flow reactor measured as function of temperature and pressure

02 p0250 A70-12020

Chemical kinetics in reaction zone of shock heated hydrogen-carbon monoxide-oxygen mixtures, measuring density field behind normal shock wave by optical interferometry

02 p0250 A70-12022

Gas detonation dynamics associated with shock tube self ignition kinetics, noting chemokinetic factors role

02 p0397 A70-12024

Detonation of gaseous systems with marginal compositions, showing sensitivity to physicochemical factors

02 p0251 A70-12025

Reaction analysis of acetylene-oxygen flames with known concentrations and temperature profiles, integrating one dimensional flame equations numerically

02 p0251 A70-12035

Volumetric reaction rates and mass transport coefficients as function of position for ducted two dimensional turbulent hydrogen-air diffusion flame

02 p0398 A70-12036

Book on gas kinetics, treating experimental methods, reaction theories, transition state theories, complex processes, etc

02 p0251 A70-12058

Internal nitriding kinetics of W-base alloys containing Hf, investigating morphology of resulting Hf nitride dispersion

02 p0317 A70-12319

Synthetic molybdenum diselenide oxidation kinetics between 375-530 C, determining isothermally reaction rate constants in dry air

[ASLE PREPRINT 69-LC-8]

02 p0321 A70-12537

KCl F centers isothermal annealing kinetics using EPR, considering electron irradiation levels effects

02 p0350 A70-12719

Chemiluminescent reaction rates measurements for emission of diatomic oxygen molecules Herzberg bands in oxygen and oxygen-inert-gas afterglows

03 p0440 A70-13579

Parietal ablation in phenolic resins using chemical kinetics

[ONERA-TP-734]

03 p0606 A70-13634

Bimolecular transfer reactions activation energies for multivalent gaseous compounds estimated by bond energy method avoiding use of adjustable parameters

03 p0441 A70-14045

Vacuum UV flash photolysis of carbon suboxide, noting pressure dependent reaction rates of carbon atoms with various gases

04 p0645 A70-14391

Temperature dependence of reaction rate for dissociative recombination in vibrationally excited gases, using electronic threshold law for diatomic ions

04 p0722 A70-14669

Life fraction hypothesis equation in creep testing derived on basis of chemical reaction rate theory

[ASME PAPER 69-MET-A]

04 p0705 A70-14875

Time-to-rupture dependence on temperature and stress related to chemical reaction rate equation in creep testing

[ASME PAPER 69-MET-B]

04 p0770 A70-14877

Synthesis of 1-oxacyclopent-1-enyl cations from cyclopropyl ketones on heating in strong acids noting rearrangement rates

04 p0646 A70-15088

Hydrogen sulfide participation in vinyl polymerization investigated for reaction mechanism

05 p0810 A70-16051

Alpha- and beta-styryl azides catalyzed reactions in ethanolic sulfuric acid

05 p0810 A70-16053

Dicyanostilbene formation from phenylethynyl azide and isocyanate

05 p0811 A70-16054

He to carbon fusion reaction rate enhancement in dense matter by inelastic scattering processes, discussing C 12 deexcitation to ground state
05 p0885 A70-16934

Silane coupling agents glass-catalyzed hydrolysis without presence of acid, discussing reaction kinetics
06 p1091 A70-17599

Shear wave interaction in infinite homogeneous reacting fluid, using Fourier and Taylor series for velocity, temperature, density, pressure and composition
[AIAA PAPER 70-146] 06 p1040 A70-18154

Supersonic free jets condensation, examining kinetics of reactions in mono- or diatomic gases
06 p1044 A70-18282

Chemical reaction rates corresponding to initial molecules fixed internal energy levels determinable for multitemperature Maxwell-Boltzmann distribution as function of reagent temperatures
07 p1224 A70-18769

Angular distribution of nonreactively scattered molecules in reactive collision, analyzing relation to reaction probability using gray sphere optical model
07 p1225 A70-18903

Preignition heat release rate profile in ethylene-air mixture flow against hot surface, determining temperature and velocity distribution optically
07 p1420 A70-19263

W oxidation kinetics as function of ribbon temperature and absorption time using flash technique with sweep pulse mass spectrometer
07 p1306 A70-19275

Kinetics of attack of SiC in monoatomic mixtures of N and O generated by microwave discharge dissociation
07 p1421 A70-19332

Isothermal reaction rate determination at given temperature from nonisothermal data illustrated on Knudsen cell vaporizations
07 p1424 A70-19901

Atomic oxygen and chlorine attack on refractory materials studied for kinetics of chemical reactions of free radicals and atoms
07 p1313 A70-19903

Mass spectra of 1,2-cyclohexanediol and deuterium labeled analogs data recorded and mechanistic rationalizations of degradation processes given
07 p1225 A70-20200

Kinetics of homogeneous nitrogen dioxide-carbon monoxide atom transfer reaction in single pulse shock tube, carrying out product analysis by vapor phase chromatography
08 p1455 A70-21263

Kinetic model developed for Cl-HBr reaction pulsed chemical laser
08 p1513 A70-21337

Transition kinetics during linear to parabolic oxidation of Cr in water-hydrogen gas mixture measured thermogravimetrically
08 p1521 A70-21558

Forward and backward rate constants for diatomic recombination and dissociation in dilute gas
09 p1730 A70-22231

Oxide spinel formation kinetics and reaction mechanisms with emphasis on Ni and Co chromites, discussing cation diffusion
09 p1739 A70-22307

Water vapor high temperature dissociation kinetics in dilute mixtures with argon in shock waves
09 p1629 A70-22319

Kinetic model for acid catalyzed Delrin decomposition, testing for Delrin-citric acid system and predicting thermograms with nonlinear regression analysis
09 p1630 A70-22896

Aeronomic neutral reaction rates, describing ozone excited state photochemistry
10 p1872 A70-23824

Plane exponential reactive shock waves following piston impact on gamma-law gas solved by similarity method, including Whitham conditions and shock acceleration
10 p1967 A70-24194

Flowing afterglow system below 300 K for rate constants of certain gases association with helium third body, investigating oxygen cluster ions formation and reactions
10 p1920 A70-25144

Ionospheric reaction rate coefficients based on electron concentration curves, discussing maximum number and accuracy obtainable
11 p2043 A70-25538

Polymeric materials thermal degradation kinetic parameters using combined mass spectrometric and thermogravimetric analysis (MS-TGA)
11 p2069 A70-25806

Thermal analysis - Conference, Holy Cross College, August 1968, Volume 2, Inorganic materials and physical chemistry
11 p2070 A70-25808

Pyrolytic graphite oxidation kinetics as function of temperature, air velocity and surface area
11 p2070 A70-25809

Polymerization reaction kinetics investigated with differential scanning calorimeter at isothermal conditions, determining heat of polymerization
11 p1994 A70-25810

Thermal dissociation kinetics in chlorine pentafluoride over high temperature range
11 p1994 A70-25823

Chemical kinetics of carbonyl fluoride thermal decomposition in argon and nitrogen diluent behind shock waves, using IR monitoring method
11 p1995 A70-25824

Chemical kinetic model for photoexcitation and photoionization of cold argon ahead of strong shock wave, predicting electron and excited atom concentrations
[AIAA PAPER 68-666] 11 p2090 A70-25953

Reagent translational energy effect on dynamics of ionic and atomic reactions, using nuclear recoil and chemical accelerator methods
11 p1995 A70-26005

Mechanism and kinetics of intermetallic layers formation and growth in welded joints of unlike metals
11 p2067 A70-26594

Hydrogen-air reaction by singular perturbation methods for temperature and pressure values of supersonic combustion, changing reaction velocity by initial stoichiometry
11 p1995 A70-26624

CO dissociation kinetics in Ar and mixtures of O in Ar by shock tube study using vacuum UV absorption
12 p2180 A70-26857

Methyl fluoride calculated for ion-molecule reaction rate constants from ion cyclotron resonance spectra
12 p2180 A70-26862

Methanol proton transfer reaction rate energy dependence
12 p2180 A70-26863

Reaction rate constants in heated mixture of hydrogen, carbon dioxide and Ar behind shock waves measured by IR spectroscopy
12 p2274 A70-26891

Low temperature oxidation of metals, discussing logarithmic kinetics of slow growth of oxides
12 p2257 A70-28006

Vacuum annealing treatments effect on oxidation rate of Co-Cr alloy at high temperatures
12 p2257 A70-28007

Reaction rates temperature dependence for artificial carbographites of various densities in oxidizing gas media
13 p2519 A70-28577

Collision coefficients of reaction and inverse reaction for nonequilibrium processes with variable distribution functions and cross sections
13 p2461 A70-28920

High temperature kinetics of pyrolytic silicon carbide oxidation and nitridation in dissociated gases
13 p2361 A70-29077

CaO reaction rate with ZrC in effusion cells as function of reactant ion diffusion through product layer
13 p2362 A70-29496

Free jet expansions in molecular beam sampling systems, using Sherman equations and chemical kinetic equations
[WSCI PAPER 70-12] 13 p2389 A70-29608

Oxygen difluoride-diborane reaction kinetics and boron fluoride formation rate
[WSCI PAPER 70-11] 13 p2362 A70-29611

Shock slip analysis of merged layer stagnation point air ionization, clarifying effects of reaction rates, species diffusion, etc
13 p2343 A70-29987

Differential thermal analyzer coupled to mass spectrometer for kinetics of reactions giving volatile products at high temperature, considering ablative materials
14 p2664 A70-30292

Molecular respiratory reflex and fluorescent signal in rabbits during hypoxia, determining redox kinetics of intracellular pyridine nucleotides
14 p2539 A70-31346

Rare gas diatomic ions reactions with molecules and rare gas atoms, measuring rate coefficients and product channels by flowing afterglow technique
15 p2776 A70-31726

Rare gas diatomic and hydride ions reactions with hydrogen, determining rate coefficients and product channels by flowing afterglow technique
15 p2776 A70-31727

Ketene and diazomethane flash photolytic measurement of reaction rates of singlet-triplet methylene deactivation
15 p2694 A70-31729

Linear regression rate of spherical solid hybrid fuel grains oxidized in reducing gas flow
15 p2786 A70-32263

Oxygen-hemoglobin reaction rate constants in red cells obtained by applying in vitro blood data to solutions of differential equations describing intracellular oxygen transport
15 p2686 A70-32846

High temperature reaction kinetics between oxygen difluoride and CO in shock tube, discussing carbon dioxide formation
16 p2855 A70-33010

Thermal energy negative ion-molecule reactions in photoionized NO-water vapor mixtures, determining rate constants by stationary afterglow system
16 p2954 A70-33280

Reaction kinetics of gas phase pyrolysis of polydifluoroaminomethanes in various reactors, obtaining C-N bond cleavage as rate determining step
16 p2856 A70-33652

Far wake properties of reentry body in hypersonic air flow calculated with or without chemical kinetics, using finite difference method
16 p2836 A70-33753

Microstructure and reaction kinetics of flat premixed fuel-rich hydrogen-oxygen-nitrogen flame at atmospheric pressure
16 p2998 A70-33900

Ionic collision processes in water vapor by high pressure single source mass spectrometry, examining reaction rates as function of primary ion translational energy
16 p2857 A70-34004

Molecular oxygen role in photolytic decomposition of ozone by intermediate quantum yield method, presenting rate constants
16 p2858 A70-34009

Thermal-chemical damage to carbon particles in egg albumin under ruby laser irradiation, using chemical rate equations for protein denaturation
17 p3035 A70-34577

Benzoyl cyanide deoxygenation, describing reaction kinetics and products
17 p3041 A70-34750

Post-Newtonian equations of hydrodynamics and radiation reaction in general relativity
17 p3156 A70-34828

Reaction rate kinetics characteristics from isothermal data, investigating relationship to activation energy distribution
17 p3042 A70-35330

Siliconizing of Mo in medium with silicon chloride, comparing reaction probabilities for various heating methods
17 p3102 A70-35392

NO in earth atmosphere, describing theory of formation for explaining observed density distribution
18 p3245 A70-36019

Niobium oxychloride conversion to niobium pentachloride by vapor phase chlorination with phosgene, examining reaction kinetics
18 p3272 A70-36031

Sodium sulfate induced accelerated oxidation of Ni and superalloys, investigating thermodynamics and reaction mechanism
18 p3272 A70-36037

Chemical kinetics effect on combustion rates of fuel plate in turbulent oxidizer flow, deriving conservation equations in boundary layer and diffusion equation
18 p3346 A70-36245

F 2 layer maximum electron concentration diurnal variations dependence on ionization intensity and dissociative recombination and ion-molecular reactions rate coefficients
18 p3255 A70-37039

Indeterminacy interval reduction for ionospheric reaction rate constants by imposing supplementary condition on NO/oxygen molecular ion concentrations ratio
19 p3408 A70-37309

Refractory metals interaction with boron during vacuum boronizing, investigating kinetics and optimal process conditions
19 p3434 A70-37452

Temperature dependence of anisotropic reaction kinetics of oxygen with pyrolytic graphite
19 p3373 A70-37709

Pressure dependence and high pressure limiting values of rate constants of gas phase reaction of monomethylamine and trimethylamine with boron trifluoride
19 p3373 A70-37775

Sulfidation kinetics and scale morphology of Cr and Cr-Mo alloys at high temperatures in hydrogen/hydrogen sulfide atmosphere
19 p3452 A70-37827

Book on thermal radiative properties of air, Volume 2, covering reaction rates, photons and charged particles interactions with air molecules, secondary air excitation, etc
19 p3552 A70-38010

Elementary chemical reaction kinetics effect on electrophysical parameters of low temperature plasma jets, calculating relaxation time for C fuels
19 p3481 A70-38184

Chemical reactions of ions and neutral particles in D region, discussing photochemistry of atomic oxygen and ozone and reaction rate constants
19 p3418 A70-38905

Hydrogen negative ion thermal energy reactions with oxygen, nitric oxide, carbon monoxide and nitrous oxide, determining rate constants
20 p3583 A70-39616

Homogeneous opaque reactive solid heating and ignition by constant energy flux, examining physical and chemical parameters at critical conditions
20 p3738 A70-40078

Slow ions mobility, diffusion and reactions in gases by drift tubes, developing mathematical analysis of drifting ion swarm space-time behavior
20 p3676 A70-40152

- Hypokinesia effects on rats protein synthesis rates, determining body and organ weights, muscle tissue nitrogen content and transaminase activity
20 p3575 A70-40187
- Hydrogen-oxygen flames recombination rates measurements analysis, taking into account reverse reaction rates
20 p3583 A70-40470
- Multicomponent fuels combustion in air, deriving simplified flame sheet model
21 p3942 A70-40881
- Ionospheric reaction rate coefficients based on electron concentration curves, discussing maximum number and accuracy obtainable
21 p3819 A70-41288
- Shock tube measurements of bimolecular reaction rates in branched chain hydrogen-carbon monoxide-oxygen system, monitoring flame band emission
21 p3773 A70-41314
- Turbulent boundary layers produced by nonuniform shock tube flow, considering effects on chemical kinetic measurements
21 p3807 A70-41315
- Electron attachment rate to sulfur hexafluoride in He buffered flowing afterglow
21 p3853 A70-41394
- Thermonuclear rate constant for deuterium atom recombination, using orbiting resonance theory
21 p3781 A70-41886
- Nucleic acids constituents reactions with singlet oxygen, determining oxidation mechanism in photodynamic processes
21 p3781 A70-42025
- EPR method for elementary reaction kinetics of vapor phase oxygen atoms interacting with molecular hydrogen
22 p3983 A70-43349
- Silver fluorination kinetics, taking temperature and pressure effects into account
22 p3983 A70-43416
- Differential scanning calorimetry and thermogravimetric analysis combination for thermochemical kinetic measurements, matching analytical and experimental curves for data accuracy
23 p4196 A70-44429
- Thermodynamic-kinetic analysis of fluorine/lithium/hydrogen tripropellant combustion efficiency, discussing liquid metal atomization, firings, facility and thrust chamber
[AIAA PAPER 68-618] 23 p4232 A70-44512
- Reacting gas supersonic flow over two dimensional base, examining reaction rate effects on base pressure
23 p4135 A70-44626
- Reaction kinetics of microbial sterilization in ultrahigh vacuum and in outer space
23 p4148 A70-44841
- Oxygen pressure effects on Ni oxidation kinetics at high temperatures
23 p4208 A70-44920
- Convective diffusion limited oxidation of Mo, measuring kinetics up to 2000 K by rotating disk method
24 p4358 A70-45233
- Air revitalization chemicals reactions with water vapor and gaseous carbon dioxide, describing apparatus for kinetic studies
24 p4307 A70-45348
- Chemical diffusion kinetics of zirconium silicates formation during sintering under pressure, noting activation energy estimation
24 p4367 A70-45479
- Numerical analysis of fuel combustion in supersonic stationary flows of hydrogen air mixture past bodies by two-component reaction kinetics model
[ICAS PAPER 70-52] 24 p4428 A70-45500
- Laser kinetics based on exothermal chemical reactions for electron transition stimulation, emphasizing single mode operation
24 p4354 A70-45656
- Cold boundary layer effect on chemical kinetic parameters behind reflected shocks in single-pulse shock tube
24 p4323 A70-46044
- Photosystem II and oxygen evolution kinetics
24 p4305 A70-46411
- REACTION TIME**
Visual stimuli duration effect on saccades precision and reaction time in peripheral field in normal subjects
01 p0026 A70-11055
- Synthetic molybdenum diselenide oxidation kinetics between 375-530 C, determining isothermally reaction rate constants in dry air
[ASLE PREPRINT 69-1C-8] 02 p0321 A70-12537
- Human perceptual and response biases in choice reaction time tasks involving visual and auditory stimuli
02 p0239 A70-12624
- Mean signal response time relationship to nonaging foreperiod
02 p0239 A70-12627
- Propane oxidation reaction and ignition delay times
[AIAA PAPER 68-633] 03 p0603 A70-12909
- Reaction time task to examine relationship between preparatory intervals and auditory stimulus intensity in experimental designs
03 p0424 A70-13764
- Auditory and visual ready signal intensity effects on reaction time, considering roles of practice and individual differences
03 p0436 A70-13772
- Mathematical model building for temporal human motor responses/reaction, movement, manipulation/by response surface technology and statistical experimental design
[ASME PAPER 69-WA/BHF-5] 04 p0642 A70-14851
- Interindividual reaction time using target speed anticipation test and relationship with manifest anxiety scale
04 p0643 A70-14978
- Classical human reaction time as function of high and low auditory signal rates in vigilance setting, supporting inhibition theory of vigilance decrement
04 p0640 A70-15646
- Critical discreteness interval of visual analyzer, investigating dependence on stimulus location, flare brightness and adaptation
08 p1443 A70-20734
- Reduced visual perception time in patients under X ray treatment of diencephalo-hypophyseal region
08 p1443 A70-20736
- F region ion-molecule reaction rate constants laboratory measurements, observing reactions energy dependence
10 p1872 A70-23825
- Motor performance effects on averaged sensory-evoked potentials in reaction time tasks
10 p1811 A70-24226
- Attention and reaction time - Conference, Eindhoven, Netherlands, July-August 1968
10 p1825 A70-24710
- Human movement speed and accuracy as function of age in pencil tapping between paper-drawn targets
10 p1817 A70-24711
- Speed-accuracy interrelationship in human performance as operating characteristic for reaction time under variety of task conditions
10 p1826 A70-24712
- Reaction time dependence on sound signal probability determined by temporal structure of signal presentation
10 p1818 A70-24713
- Information hypothesis and repetition hypothesis concerning human reaction time to visual stimulus information
10 p1826 A70-24714
- Numerical payoff influence on reaction time to second stimulus in subjects receiving successive signals at short intervals
10 p1818 A70-24715
- Human reaction time study leading to promptness concept to embody quantitative and qualitative aspects of psychological behavior
10 p1818 A70-24716
- Reaction time in determining visual transient response at frequencies above flicker fusion
10 p1818 A70-24717
- Verbal information recall latencies as function of time interval from initial memory storage and retrieval repetitions
10 p1818 A70-24718
- Auditory and visual warning signals effects as reaction stimulus in time-uncertainty situation
10 p1826 A70-24719
- Visual stimuli intensity influence on delay in reaction to second of pair of visual stimuli
10 p1818 A70-24721
- Neurophysiological mechanism of motor activity during simple reaction time situation performance
10 p1818 A70-24724
- Choice reaction time task involving right or left hand button pressing in monocular and binocular visual response to directional commands by colored lights
11 p1990 A70-25830
- Mental blocking/incidental long reaction times/ during continuous serial performance using perceptual-selection and response theories
12 p2178 A70-27045
- Continuous active work effects on human sensorimotor performance, comparing latency distributions in mass and spaced practice groups
12 p2178 A70-27046
- Food ingestion initiation, investigating role of hyposmotic solutions from observation of rats under water deprivation
13 p2353 A70-29495
- Human temporal motor response models relating reaction, movement and manipulation time to stimulus, movement and manipulation information
14 p2540 A70-30248
- Human operator ocular tracking and decay time stimulation response measurements using information, statistical, point process and random analysis
14 p2537 A70-30388
- Gas mass diffusivity measurements in plasma and reaction velocity constant in human and dog blood
15 p2692 A70-32311
- Display-control relationships in visual display information processing, considering spatial incompatibility effects on reaction time
16 p2852 A70-33661
- Decision theory model evaluation based on experimental findings concerning relationship between stimulus intensity and reaction time
17 p3036 A70-34605
- Tracking error correction time and proprioceptive reaction time, suggesting role of central mechanism without sensory feedback
17 p3036 A70-34606
- Heat stress effects on serial reaction time in subjects performing visual tasks
19 p3361 A70-38053
- Human response time to visual stimulus preceding or following auditory stimulus as function of interstimulus interval
19 p3362 A70-38311
- Reaction time intersensory facilitation relationship to single channel theories of attention and human performance
19 p3362 A70-38312
- Preliminary taxonomy for errors in serial, self-paced choice reaction time experiments, discussing speed-error tradeoff
19 p3362 A70-38313
- Choice reaction and movement time dependence on hypoxia induced by air pressure reduction inside decompression chamber, discussing adult human performance
20 p3573 A70-39714
- Unitary and compound stimuli and role of response categories in decision time
21 p3767 A70-40751
- Carbon dioxide-atomic oxygen reaction rate constant to investigate Martian ionosphere, discussing reactions involving oxygen, nitrogen molecular ions and NO
21 p3886 A70-41067
- Longitudinal vibration effects on human reaction time and motor performance involving toggle switch and manual knob control in different working positions
22 p3977 A70-42871
- Hypoxia effects on voluntary response time to peripherally located visual stimuli
24 p4302 A70-46107
- REACTION WHEELS**
Suboptimal attitude control system for Nimbus satellite using motor-driven inertia wheels as control torque source for three dimensional control
07 p1331 A70-20027
- Three axis attitude control of earth oriented non-spinning synchronous communications satellite, using gimbal-mounted momentum wheel and pulsed plasma thrusters
[AIAA PAPER 70-456] 11 p2119 A70-25431
- Hybrid satellite attitude control system deformation model, utilizing pivoted flexible boom with tip mass as actuator and inertia wheels to dampen gravity induced librations
11 p2123 A70-26127
- Freely spinning satellites gimbal and momentum wheel system, determining stable equilibrium states by analog computer simulations
[AIAA PAPER 70-982] 20 p3714 A70-39547
- Magnetic desaturation of inertia flywheels of satellite in equatorial or slightly inclined orbit, discussing satellite stabilization
22 p4110 A70-42488
- REACTIVITY**
Angular distribution of nonreactively scattered molecules in reactive collision, analyzing relation to reaction probability using gray sphere optical model
07 p1225 A70-18903
- Hydrocarbon fuel components relative reactivities in direct electrochemical oxidation on platinum black/Teflon electrodes in phosphoric acid
12 p2182 A70-27762
- Thermal decomposition mechanism of inorganic oxidizers, discussing reactivity of alkali and alkali earth salts
18 p3299 A70-36240
- REACTOR CHEMISTRY**
U RADIOCHEMISTRY
REACTOR CORES
Precision machining and repair of radioactive Plum Brook Reactor core fuel grid
01 p0140 A70-10322
- Nuclear rocket engine core thermal and neutronic transient and steady state dynamics digital simulation, showing advantages over lump model analysis
[ASME PAPER 69-WA/NE-3] 04 p0717 A70-14757
- Gas core nuclear reactors feasibility based on gas core hydrodynamics, heat transfer and neutronics development, noting spacecraft weight and trip time reduction potential
04 p0717 A70-15639
- Constant flux gas core nuclear rocket acoustic instabilities, presenting idealized physical model with gas dynamic field perturbed by wave phenomena
09 p1725 A70-23227
- Gas-core nuclear rocket engine simulation by induction coupled plasma torch, determining gas flow patterns
[AIAA PAPER 70-691] 16 p2950 A70-33555

Turbulent coaxial flow analysis predicting fuel volume fraction in gas core nuclear rocket reactor cavity, using free-jet computer code and eddy viscosity equation 18 p3290 A70-36560

Open cycle gas core nuclear rocket reactor, evaluating critical mass for U isotopes 18 p3290 A70-36564

Optimum fuel utilization for Plum Brook Reactor, using criticality data for effects of neutron leakage and burnup uniformity in core point model 20 p3671 A70-39110

Gas core nuclear rocket engine light and heavy species centrifugal separation by MHD-driven rotating flow, discussing fluid dynamic simulation results 20 p3671 A70-40256

Nuclear light bulb and coaxial flow gaseous core nuclear rocket reactors based on energy transfer via thermal radiation 22 p4070 A70-43182

Aeromechanical characteristics of colloidal fuel core nuclear reactor in relation to cavity geometry and propellant gas injection [AIAA PAPER 70-1222] 24 p4377 A70-45958

REACTOR DESIGN

Controlled thermonuclear power generation, considering fusion reactors feasibility and reactor energy balance improvement 04 p0717 A70-14528

Rankine 10 MWe nuclear electric space power system design, discussing reactor power, fuel, coolant, structural material, control system, shield, etc 11 p2082 A70-26123

Controllable thermonuclear reactor with free-floating HF discharge plasma in deuterium 12 p2271 A70-27351

Ground test reactor design based on colloid fueled reactor concept [AIAA PAPER 70-688] 16 p2950 A70-33587

Controllable thermonuclear reactor with free-floating HF discharge plasma in deuterium 22 p4084 A70-43595

NERVA Technology Reactor design integrated with Brayton cycle space power conversion systems, considering space bases and shielding analysis [AIAA PAPER 70-1226] 24 p4377 A70-45955

REACTOR FUELS

U NUCLEAR FUELS

REACTOR MATERIALS

Material evaluation and selection for compact nuclear reactor control bearings operating at high temperature in vacuum [ASME PAPER 69-WA/LUB-11] 04 p0697 A70-14765

Metal corrosion product dissolution in reactor cooling deionized water, investigating Cu, W and Cd using chemical analyses 10 p1904 A70-24398

Book on refractory metal properties covering nuclear reactor use, atomic, electronic and crystal structures, thermal and electrical characteristics irradiation effects, nuclear properties, etc 16 p2931 A70-33268

Solid core nuclear reactor engine variables, considering specific impulse, engine weight, operating life and engine thrust 22 p4070 A70-43181

Refractory metal alloys tensile and creep rupture properties for reactor fuel jackets 24 p4364 A70-46347

REACTOR PHYSICS

Reactor gamma in-pile effects on thermionic diodes simulated in electron accelerator, noting ion production insufficient to support saturation currents 04 p0717 A70-14948

REACTOR SAFETY

Forced cooling water flow temporary loss accident at Plum Brook Reactor, discussing inspection and corrective action 01 p0140 A70-10323

TSF-SNAP reactor neutron radiation leakage, comparing Monte Carlo calculations with experimental and analytical determinations 20 p3671 A70-39156

Operational safety of nuclear rockets in orbit-to-orbit transportation in regard to radiation doses from plume and reactor, including malfunction condition 22 p4070 A70-43183

Space nuclear power system design and operation related to safety, discussing SNAP flights 22 p4071 A70-43192

REACTOR TECHNOLOGY

Freezing-mixing model for predicting plasma jet flow reactor yield development from analyses of thermochemical equilibrium, chemical reaction freezing and turbulent mixing 07 p1351 A70-19893

NERVA nuclear rocket reactors, considering NRX and XE technology tests 22 p4069 A70-43178

Solid core nuclear reactor engine variables, considering specific impulse, engine weight, operating life and engine thrust 22 p4070 A70-43181

REACTORS

Dwell time boundary and mean values for laminar flows through channel and tube reactors, obtaining field representation from streamline network and isochrones 16 p2893 A70-33745

READERS

Word organized photodetector array design for holographic read-only optical memories 07 p1288 A70-20148

Electromechanical graph digital reader for records of cardiovascular studies 07 p1224 A70-20197

Alphanumeric solid state displays with vertically stacked character rows for text format reading, using injection electroluminescence technology 10 p1846 A70-23882

Character recognition methods applied to reading machines transforming printed material into forms acceptable to blind 13 p2360 A70-29809

Linked and fiber optic components, describing applications as punched card and tape reading, geometrical converters and sensing and scanning probes 16 p2904 A70-33145

High speed digital computer input device for reading data from magnetic tape, discussing design and operation principles 18 p3230 A70-36095

READING

Automated Readability Index for technical materials weighting word and sentence length in multiple regression equation 24 p4308 A70-45510

Readability of segmented numerals under critical accuracy and limited exposure time, comparing with conventional displays 24 p4308 A70-45514

READING MACHINES

U READERS

READJUSTMENT

U ADJUSTING

READOUT

Multichannel ionization calorimeter data readout into electronic computer using short circuit coil magnetic storage 05 p0816 A70-15947

Quasi-logarithmic readout of conventional binary scaler provided by reduced logic system following generalized equations 05 p0851 A70-16844

Digital computers structural and operational address format dependence on number of storage readouts expressible with aid of linear function 05 p0818 A70-17004

Real time angular readout system for declination axis of U.S. Naval Observatory six inch transit circle, using Inductosyn as basic transducer 16 p2906 A70-33176

Digital readout test equipment characteristics and parameters for electrical properties measurement, proposing pulse counting analog-digital conversion technique 19 p3432 A70-38701

Seven segment in-line digital readout circuit for binary-quinary decade counter, using resistance transistor logic 21 p3793 A70-40763

REAL GASES

Similarity laws in hypersonic flow of real gas around slender blunted bodies, particularly bodies with rough lateral surface 03 p0409 A70-13866

Hypersonic blunt body heat transfer prediction, including coupled effects of real gas behavior and slip boundary conditions [ASME PAPER 69-WA/HT-28] 04 p0614 A70-14809

Real gas properties effect on base pressure of blunt nosed vehicle flying through atmosphere at high velocities 04 p0764 A70-15556

Real gas behavior effect on shock tube temperature and pressure flow nonuniformity for range of Mach numbers 07 p1257 A70-19337

Hypersonic flow past blunted cylinder at Mach number of infinity, investigating real gas effect using Lighthill ideal dissociating gas model 08 p1431 A70-20646

Transformed thermodynamics equations derived automatically by substitution codes, noting exceptions for real gas and discharge flow 08 p1597 A70-20918

Thermodynamic properties of real gases estimated using Hirschfelder equation of state 08 p1598 A70-21363

Plane, cylindrical and spherical blast waves structure with ionization at local thermodynamic equilibrium analyzed using successive approximation to non-similar solution 10 p1967 A70-23991

Shock and thermodynamic phenomena of real gases near critical points, discussing specific volume and specific enthalpy increases 10 p1867 A70-24136

Real gas adiabatic lapse rate applied to Venus atmosphere assumed to consist of pure carbon dioxide 11 p2107 A70-25646

Monograph on relaxation processes at high temperatures for thrust nozzle calculation and optimization covering real gas effects, reaction kinetics, heat transfer, etc 11 p2103 A70-26475

Real hydrogen driver performance, analyzing intermolecular forces effects under high compression and heat 16 p2998 A70-33889

Real gas effects in blowdown analysis of leakage through choked nozzle in air flask 17 p3073 A70-35670

Real gas transonic flow transition through critical velocity in Laval nozzle, examining reasons for increment of viscosity and heat conduction effects 18 p3239 A70-36217

Binary Boltzmann operator for quantum statistical second virial coefficient for real gases and plasmas in two-particle scattering problem involving Jost function 22 p4081 A70-42824

REAL NUMBERS

NT INTEGERS

Real cipher places in real function, describing interval analysis method with upper and lower bound indications 18 p3282 A70-36357

Polynomials with interval coefficients, presenting Newton Raphson algorithm for real roots error bounds 20 p3659 A70-40133

Recursive test for nonnegative polynomials using modified Routh scheme to determine real positive zeros 22 p4063 A70-43332

REAL TIME OPERATION

Mark III airborne Omega system designed as receiver-computer to demonstrate real time operation, discussing flight test results 01 p0136 A70-10302

Computer applications in French missile testing center, describing real and delayed time equipment and computations 01 p0057 A70-10798

Light valve projectors and TV cameras, showing disparity between video information generation and large screen real time high brightness image presentation 01 p0088 A70-10811

Digital real time simulation for training and evaluating ATC controllers, discussing system hardware, software, design and implementation 02 p0274 A70-11977

Optimum numerical integration with application to real time digital simulation of continuous systems, deriving three step methods 03 p0455 A70-14173

Shooting method for real time optimization of multiple burn rocket flights, presenting analysis, algorithm and test results 04 p0761 A70-14932

Integrated flight test data acquisition and processing system with real time graphic display, discussing ground station function [SAE PAPER 690678] 05 p0793 A70-15867

Gigacycle correlator involving sampling oscilloscopes for real time display of correlation functions over adjustable time interval, discussing design and performance 05 p0847 A70-16066

Real time large screen display systems operation, brightness, accuracy, resolution, contrast ratio, data rates, reliability, fail-safe and management functions 05 p0828 A70-16190

Flight plans monitoring in real time with on-line computer for optimal route, fuel consumption and speed 05 p0817 A70-16362

Real time computer control system queueing model to optimize preemptible and nonpreemptible job priority assignment 05 p0817 A70-16414

Special purpose computer organized as time-shared digital filter for real time applications with adaptable coefficients, programming and multiplexing scheme 05 p0818 A70-16415

Color CRT system to display engineering data based on real time analysis, discussing performance requirements 06 p1061 A70-17349

Apollo 11 premission planning, real time situation and postflight analysis for lunar descent and ascent phases, providing navigation correction capability for Apollo 12 [AIAA PAPER 70-25] 06 p1159 A70-18227

Multichannel correlator for turbulent signal processing in real time scale using natural delay 07 p1284 A70-19832

Digital cross correlator design for impulse response determination in linear systems, noting real time operation without software and storage problems 07 p1236 A70-20068

- ATC real time simulation exercises in Brussels Upper Information Region 07 p1250 A70-20227
- Computer program /SAFETE/ for evaluating missile launch risk on near real time basis [AIAA PAPER 70-248] 07 p1250 A70-20370
- Enhanced real time operational impact and casualty analysis /ERIOCA/ for range safety, discussing computer-driven CRT display and missile flight parameters selection 07 p1251 A70-20371
- Real time simulation of air traffic control problems in Brussels upper information region /UIR/ 08 p1541 A70-21361
- Computer system for real time data acquisition and servicing of asynchronous inertial guidance system test stations 08 p1467 A70-21591
- Airborne real time IR imagery of thermal anomalies for geophysical exploration of water resources 09 p1674 A70-22262
- Real time hologram-interferometry application to optical aspheric surfaces testing explained by geometrical optics 09 p1676 A70-22717
- Multispectral point scan camera system as remote sensor for Earth Resources Satellite, noting real time automatic data processing and interpretation [AIAA PAPER 70-319] 09 p1677 A70-22867
- IR holograms real time visual reconstruction by frequency stabilized carbon dioxide lasers 09 p1684 A70-23534
- Real time opto-triangulation by cinehologolites for data acquisition used in rocket impact prediction 09 p1640 A70-23779
- Swedish real time IR imaging system, discussing airborne applications in locating fresh water springs and defining irrigation patterns 10 p1879 A70-24743
- Launch vehicle automatic checkout methods emphasizing guidance and control equipment performance in real time operations [AIAA PAPER 70-393] 10 p1952 A70-24912
- Solar flare videometer for measuring flare area and peak and integrated intensity in real time 11 p2104 A70-25744
- Spacecraft launch computerized simulator, discussing operational characteristics applicable to on-line real time process control 11 p2013 A70-26217
- Analog-digital real time data automatic acquisition and radar tracking system for air defense and air traffic control 11 p2014 A70-26313
- Empennage loads on T tail transport determined for combined vertical and lateral gust loads using real time analog-digital computer simulation 12 p2160 A70-27113
- Real time 2000 line TV camera with 40 MHz bandwidth, 1600 line vertical resolution and 1000 line horizontal resolution [SMPT PAPER 105-73] 12 p2235 A70-27663
- Computer controlled system for real time measurement and analysis of electromagnetic interference and compatibility with economy of time, manpower and cost 12 p2201 A70-28133
- Real time signal processor for correlation and spectrum analysis, displaying results on cathode ray oscilloscope 13 p2370 A70-29817
- Time shared computer system providing real time service to multiple laboratory instrumentation, discussing high speed channel, computer control and data abstracting techniques 13 p2375 A70-29830
- Ground support real time operating system 360 for manned spaceflight, discussing system features and performance 13 p2375 A70-29937
- Real time sonic information input/output computer system for acoustic signals and speech synthesis, concerning man machine communication 14 p2553 A70-30425
- Apollo 9 scientific multispectral photography mission, discussing meteorological support aspect of real time planning 14 p2610 A70-30614
- Real time Apollo PCM telemetry data compression and transmission using zero order predictor 14 p2550 A70-30768
- Real time Apollo lunar module thermal mission data analysis using computer programs 14 p2653 A70-30774
- Book on space flight simulation systems examining real time and real performance requirements, mathematical models and various simulation programs 14 p2563 A70-30955
- Vibration modes real time observation of complex surfaces with matt finish using changes in laser speckle 15 p2750 A70-31762
- Real time analog simulation of helicopter rotor, calculating lift and drag coefficients along blade 15 p2672 A70-31775
- Rockets trajectories recording on real time at Guiana Space Center using IR pointing deviation meter 15 p2698 A70-31960
- Passive optical crossed beam detection systems monitoring meteorological parameters in rocket or aircraft environments, noting real time display 15 p2736 A70-32032
- Metabolic Rate Monitor for measuring continuous oxygen consumption during changes in work in real time 15 p2741 A70-32540
- Real time computer algorithm for achieving optimal position of tracking antenna with nonlinear control system 15 p2703 A70-32575
- Real time variable range digital filter design in suitable form for LSI realization, satisfying reduced dead-band requirement for input interface element 16 p2882 A70-33040
- Encapsulated liquid crystal screens for IR laser beam imaging detectors with high thermal sensitivity and real time viewing in bright light 16 p2927 A70-33167
- Real time angular readout system for declination axis of U.S. Naval Observatory six inch transit circle, using Inductosyn as basic transducer 16 p2906 A70-33176
- Apollo 10 color TV camera for real time scenes, describing configuration performance and total system operation 16 p2907 A70-33187
- Optimal interceptor-target allocation and guidance for linear interception and rendezvous using real time and storage computer 16 p2947 A70-33311
- Real time recording systems design for increased writing speeds on photochromic films 16 p2910 A70-33435
- Real time video data display at visual and thermal IR wavelengths, demonstrating performance improvement for target recognition 16 p2910 A70-33436
- Parallel associative unstructured element computer design for real time radar track data processing 16 p2869 A70-33466
- Remote real time simulation, using CDC 6600 computers, peripheral equipment and wideband communication link 16 p2870 A70-33732
- Real time simulation of space vehicle and ground support equipment by digital computer for launch programs checkout 16 p2870 A70-33733
- Fast Fourier digital processor for real time filtering of radar signals, discussing applications as Fourier transform system 16 p2870 A70-33738
- Materials real time strain measurements by optical correlation techniques, noting sensitivity 16 p2913 A70-33980
- Real time swept sine wave spectrum analyzer using time compression to change filter bandwidth as function of control signal 17 p3059 A70-35166
- Real time data processing and display for spacecraft thermal vacuum testing, using hybrid computer 17 p3059 A70-35176
- Nuclear rocket engine testing, monitoring reactor and facility performance with real time digital computer 17 p3135 A70-35212
- Real time hybrid computer simulation of guided and controlled rocket flight, noting correlation with digital simulation 17 p3060 A70-35285
- Real time computer complex /RTCC/ supporting role in Project Apollo, describing mission control center data interfaces, equipment configuration, software, etc 17 p3060 A70-35295
- Real time computers design tradeoffs in avionics systems 17 p3050 A70-35510
- Gyro test package, dynamic test facility and real time attitude algorithm to investigate operational capabilities of strapdown inertial attitude package 17 p3134 A70-35652
- Nationwide air traffic control, using radar network and real time computer flight information centers for air safety 17 p3135 A70-35880
- Real time holographic reconstruction by electro-optic light modulation through crystal 18 p3258 A70-36312
- Real time analog display inputs for electronic computers and tracking in physiological control circuits, describing various manual controls 19 p3367 A70-37564
- Real time narrow band vibration spectrum analysis techniques, discussing application to failure prediction and flight and wind tunnel tests 19 p3430 A70-38528
- Operational analysis and real time computer simulation models in ATC development 19 p3468 A70-38637
- Signal automatic air traffic control system /SATCO/ for flight plan processing, using multi-processing real time computer, electronic displays and software facilities 19 p3469 A70-38646
- Holographic ultrasonic imager using liquid surface detector for real time imaging of test objects moving through viewfield, discussing nondestructive test applications 19 p3433 A70-38829
- Frank orthogonal vectorcardiograms on humans during acceleration, using beat-by-beat real time analog-digital computer technique 20 p3572 A70-39435
- Ground based radar tracking data processing method for real time information concerning lunar module /LM/ position and velocity during Apollo 12 flight [AIAA PAPER 70-1020] 20 p3591 A70-39514
- Real time kalman filtering of Apollo LM/AGS rendezvous radar data [AIAA PAPER 70-957] 20 p3600 A70-39572
- Real time network support simulation allowing network configuration for nominal or perturbed trajectory for Saturn vehicles, applicable to any flight azimuth [AIAA PAPER 69-936] 20 p3591 A70-39684
- Computer time sharing system for real time mass properties measurements [SAWE PAPER 853] 20 p3595 A70-40374
- Aerospace computers design, considering real time operation and reliability requirements 21 p3794 A70-41686
- Real time global temperature and geopotential height profiles acquisition from satellite spectrometer measurements by least squares regression method 21 p3820 A70-42121
- Combined hypersensitization and rapid in situ processing for time-average observation in real time hologram interferometry 22 p4025 A70-42321
- Real time holographic interferometry for flame propagation research, using high speed camera [SMPT PREPRINT 9] 22 p4035 A70-43053
- Real time contourgraphic electrocardiographic display determining heart rate from CRT face on beat-by-beat basis 23 p4150 A70-44377
- Spectral and real time computation for acoustic absorbers with nonlinear material characteristics 23 p4219 A70-44393
- Enhanced real time operational impact and casualty analysis for range safety, discussing computer-driven CRT display and missile flight parameters selection [AIAA PAPER 70-247] 23 p4178 A70-44517
- Acoustic holographic system producing two dimensional picture in real time, using stationary linear transducer arrays 24 p4339 A70-46080

REAL VARIABLES

NT ABEL FUNCTION
NT ASYMPTOTES
NT ASYMPTOTIC SERIES
NT BESSEL FUNCTIONS
NT BETHE-SALPETER EQUATION
NT BIHARMONIC EQUATIONS
NT BLASIUS EQUATION
NT BURGER EQUATION
NT CALCULUS OF VARIATIONS
NT CAUCHY-RIEMANN EQUATIONS
NT CHANDRASEKHAR EQUATION
NT COPLANARITY
NT CUBIC EQUATIONS
NT DELTA FUNCTION
NT DIFFERENTIAL EQUATIONS
NT DUFFING DIFFERENTIAL EQUATION
NT EINSTEIN EQUATIONS
NT ELLIPTIC DIFFERENTIAL EQUATIONS
NT EXISTENCE THEOREMS
NT EXTREMUM VALUES
NT FALKNER-SKAN EQUATION
NT FOKKER-PLANCK EQUATION
NT FOURIER SERIES
NT FUNCTIONAL INTEGRATION
NT GAUSS EQUATION
NT GREEN FUNCTION
NT HANKEL FUNCTIONS
NT HELMHOLTZ VORTICITY EQUATION
NT HYPERBOLIC FUNCTIONS
NT HYPERPLANES
NT INTEGRAL CALCULUS
NT JACOBI INTEGRAL
NT KERNEL FUNCTIONS
NT LAME WAVE EQUATIONS
NT LIAPUNOV FUNCTIONS
NT LIMITS (MATHEMATICS)
NT LINEAR EQUATIONS
NT LIOUVILLE EQUATIONS
NT LIPSCHITZ CONDITION
NT MACLAURIN SERIES
NT MAXIMA
NT MEASURE AND INTEGRATION
NT MINIMA
NT MONGE-AMPERE EQUATION
NT NEUMANN PROBLEM
NT NONLINEAR EQUATIONS

NT NUMERICAL INTEGRATION
NT PARABOLIC DIFFERENTIAL EQUATIONS
NT PARTIAL DIFFERENTIAL EQUATIONS
NT PERIODIC FUNCTIONS
NT POISSON EQUATION
NT POWER SERIES
NT QUADRATIC EQUATIONS
NT RUNGE-KUTTA METHOD
NT SERIES [MATHEMATICS]
NT STIELTJES INTEGRAL
NT STURM-LIOUVILLE THEORY
NT TANGENTS
NT TAYLOR SERIES
NT TRIGONOMETRIC FUNCTIONS
NT VECTOR ANALYSIS
NT VLASOV EQUATIONS
NT VORTICITY
NT WEIGHTING FUNCTIONS
NT WHITTAKER FUNCTIONS
Differential properties of class of functions of many real variables

01 p0132 A70-11067
Book on integrals and elliptic functions in real domain, solving fourth degree Hermitian equation and integral reduction

02 p0323 A70-11897
Geometrical determination of real roots of equations applied to linear oscillator and gyroscope in gimbal suspension

03 p0484 A70-13374
Randomly perturbed linear differential equation involving first derivative of n -vector function of real variable

05 p0878 A70-17096
Real nonnegative function representing transmittance of computer synthesized Fourier transform hologram displayed on flying spot scanner and recorded on film

11 p2049 A70-25631
Reduction procedure for determining sign definiteness and semidefiniteness of higher order real polynomials

17 p3129 A70-34954
Real cipher places in real function, describing interval analysis method with upper and lower bound indications

18 p3282 A70-36357
Nonlinear discrete uniform approximation of real valued functions by gradient method

19 p3459 A70-38677
Real functions and sets representation theorems derivation and application to nonlinear programming, using Bellman quasi-linearization technique

24 p4370 A70-46099
Necessary and sufficient conditions on coefficients of real nonnegative polynomial $p(\omega)$, obtaining algebraic criterion for stability, optimality and passivity of dynamic linear systems

24 p4322 A70-46156

REATTACHED FLOW

Turbulent reattachment of supersonic axisymmetric jet on cylindrical wall in air, investigating wall temperature effect on cavity pressure and heat flux [ONERA-TP-758]

03 p0467 A70-13643
Laminar flow separation, reattachment and transition over downstream step, including visual observations of smoke filaments, velocity fluctuation measurements and velocity profiles

[ASME PAPER 69-WA/FE-5] 04 p0667 A70-14784
Gas dynamics of intense explosion with expanding inner contact surface in Newtonian limit, discussing shock layer reattachment

04 p0619 A70-15322
Reattachment of supersonic jet with turbulent shear boundary layer abruptly expanding into axisymmetric parallel diffuser, using surface flow technique

04 p0619 A70-15323
Isoenergetic mixing and reattachment processes of two dimensional supersonic turbulent separated flow, modeling mixing process by constant pressure theory [AIAA PAPER 70-108]

06 p1037 A70-18039
Soviet book on unsteady attached turbulent flow in turbine lattices, studying blade aeroleastic vibrations onset and attenuation in compressible and incompressible fluids

07 p1189 A70-19602
Pressure distributions and heat transfer at wall calculated to investigate supersonic laminar reattachment

13 p2338 A70-28953
Transonic scaling effects for shock boundary layer interaction on circular and two dimensional airfoil models, discussing separation and reattachment [AIAA PAPER 70-541]

13 p2339 A70-29008
Boundary layer flow between nodal and saddle points of attachment, comparing matched series and finite difference methods

14 p2565 A70-30281
Convective heat transfer at solid boundaries in separated and reattached subsonic and supersonic flows, considering booster base heating

17 p3007 A70-34484
Laminar incompressible separating and reattaching flows, correlating finite difference solutions with experimentation [AIAA PAPER 70-763]

17 p3008 A70-34488

Flow field, heat transfer rates and reattachment surface wall temperature of planar supersonic turbulent flow

21 p3744 A70-41036
Jet flow reattachment to walls of various shapes, measuring undeveloped velocity profiles at nozzle exit [ASME PAPER 70-FLCS-2]

22 p4008 A70-42429
Frequency dependent effects of applied acoustic fields on attached jet flows for Reynolds numbers over curved surfaces

[ASME PAPER 70-FLCS-1] 22 p4008 A70-42430
Wing lift increase by spanwise blowing along upper surface, causing flow reattachment on wing and vortex induced effective aerodynamic camber increase [ICAS PAPER 70-09]

23 p4132 A70-44120
Two dimensional aperture flow with downstream asymmetric pressure distribution due to jet reattachment to boundary, simulating flows in hydraulic spool valves and fluidic devices

24 p4325 A70-45582

REATTACHMENT

U ATTACHMENT

REBREATHING

Pulmonary artery blood sampled before or during rebreathing of carbon dioxide in nitrogen mixtures, at rest and during exercise, discussing oxygen pressure changes

01 p0020 A70-10652

RECEIVERS

NT LOGARITHMIC RECEIVERS

NT SUPERHETERODYNE RECEIVERS

NT TELEVISION RECEIVERS

IF optimum bandwidth for maximizing output SNR in FM receiver with barrier to noise ratio below discriminator threshold

01 p0051 A70-11119
Microelectronic L-band phase-lock loop receiver for data transmission between earth stations and satellites

06 p1017 A70-17338
Maximum likelihood receiver /MLR/ to detect pulsed signal propagated through turbulent medium, assuming optical propagation over long path in atmosphere

07 p1227 A70-19146
UHF satellite receiver for binary FSK data collection system using matched integrate and dump filter detectors

08 p1459 A70-20804
FM feedback demodulator performance model using mixer-correlator, showing cross correlation receiver design

08 p1479 A70-20810
Satellite TV broadcast requirements impact on high power transmitter design, permitting low cost terrestrial receiving systems

[AIAA PAPER 70-434] 11 p1999 A70-25450
Dual conversion receiver for remote frequency control in satellite TV distribution system

[AIAA PAPER 70-414] 11 p2002 A70-25482
Phase noise and cycle slip optimization of steady state digital data transition tracking loop used as bit synchronizer in phase-coherent receiver

11 p2024 A70-26202
Noise stability of optimal binary detection receiver of rectangular-pulse and discrete pseudorandom signals under nonideal synchronization

13 p2364 A70-28869
Side scattered light effects on atmospheric transmittance measurements, showing influence on total receiver illumination

14 p2603 A70-30411
Millimeter and submillimeter wave receivers, describing detectors, mixers, low noise amplifiers and radiometers

14 p2549 A70-30448
Injection laser communication link for high data rate transmission, discussing design and construction of transmitter and receiver

16 p2862 A70-33139
Optimal receiving systems for satellite broadcasting, considering costs, power requirements, service area, etc

17 p3046 A70-35272
Multiple remote control systems design, emphasizing transmitter and receiver characteristics matching to overall network parameters

18 p3235 A70-36426
Frequency discrimination circuits for multiple remote control receiver systems with high harmonic noise levels

18 p3235 A70-36428
Coherent receiver as hybrid carrier tracking loop consisting of standard phase locked and modified Costas loop

21 p3802 A70-41351
Radiosonde receiver and transmitter system optimization, obtaining increased microwave power by appropriate oscillator operating modes

22 p4038 A70-43379
Low noise dual receiver system for satellite communication earth station using parametric and transistor amplifiers

23 p4169 A70-43791

RECEIVING SYSTEMS

U RECEIVERS

RECEPTACLES [CONTAINERS]

U CONTAINERS

RECEPTORS [PHYSIOLOGY]

Integrated static discharge frequencies of cat lingual cold receptors measured as function of constant temperature

01 p0017 A70-10472
Nerve cell response to change in chemical constitution of surroundings used to investigate animal periphery sensory mechanisms

01 p0033 A70-10497
Color vision forms, investigating sensitivity of human retinal receptors and combinations of spectral functions

08 p1443 A70-20731
Modal excitation and scattering in retinal receptors of human and insect visual systems investigated with dielectric rod uniform wave and irregularities

08 p1452 A70-21289
Retinal receptors physiology involved in transforming visible radiant energy into sensory message

12 p2172 A70-28105
Vibration effects on receptors in frog toe muscles at various frequencies

12 p2179 A70-28344
Skin receptors afferent discharge characteristics during vibrotactile stimulation

13 p2354 A70-29594
Pulmonary arterial and venous response to cooling, discussing role of sympathetic nervous system alpha receptors in hypothermia induced pulmonary constrictions in dogs

23 p4148 A70-44788

RECIPROCAL THEOREMS

Uniqueness and reciprocity theorems in elastic medium occupying infinite domain extended to electromagnetic wave propagation in plasma

05 p0890 A70-17097
Micropolar homogeneous and anisotropic elastic solids linear dynamic theory, deriving reciprocity and variational theorems

06 p1172 A70-18512
Reciprocity principle for biased and two component compressible plasmas

12 p2282 A70-27971
Reciprocity law between radiation intensity and exposure time for photographic films in vacuum UV spectrum region, investigating departure at various wavelengths

18 p3257 A70-36281
Reciprocity theorem for stresses and strains in medium under creep and temperature field

19 p3548 A70-38582
Elastomechanical system reciprocity relation principles using differential equations for bar with forces in two places

20 p3735 A70-40537
Electromagnetic scattering by homogeneous gyrotropic cylinder, discussing matrix equations formulation and solution by reciprocity theorem

23 p4165 A70-44959
Planetary atmosphere diffuse radiative transfer reflection and transmission, deriving reciprocity relations from integrodifferential equations

24 p4409 A70-45756
Variational principle and reciprocity theorem for initial value problems associated with wave equations, discussing solution uniqueness conditions

24 p4380 A70-46037

RECIPROCATING ENGINES

U PISTON ENGINES

RECIRCULATION

U CIRCULATION

RECIRCULATIVE FLUID FLOW

Roll control method using recirculating base flow reaction against oriented blades or fins attached to reentry vehicle base to produce rolling moments

01 p0003 A70-10847
Free recirculation areas in wake of flame holders used for flame stabilization at bluff bodies in supersonic flow

06 p0965 A70-17244
Residence time of foreign gas injected into recirculation region of wake behind slender body in axisymmetric supersonic flow

[AIAA PAPER 70-111] 06 p0968 A70-18040
Heat transfer from impinging gas jets on enclosed concave surface, noting self recirculation currents within cavity

07 p1425 A70-20413
Turbulent flames bluff-body stabilization model, measuring recirculation zone concentrations and temperatures for methane and propane-air mixtures

10 p1967 A70-24092
Turbulent viscous flow with gas-liquid interface, using recirculation loop for gas ingestion reduction [ASLE PREPRINT 70AM 5C-4]

19 p3439 A70-38804
Jet curtain flow recirculation model based on air-bubble flow visualization technique, determining minimum power for air cushion vehicle

22 p3957 A70-42278

RECLAMATION
NT MATERIALS RECOVERY
NT WATER RECLAMATION
RECOGNITION
NT CHARACTER RECOGNITION
NT PATTERN RECOGNITION
NT SPEECH RECOGNITION
NT TARGET RECOGNITION
NT TIMBER IDENTIFICATION
Optimal strategies for observation system subject to recognition using data transmission along symmetrical channel
04 p0647 A70-14401
Electronic camera instrumental profile, information capacity and object recognition
14 p2583 A70-30363
RECOIL ATOMS
Sputtering yield of amorphous and polycrystalline targets bombarded by energetic ions or recoil atoms calculated by integrodifferential equations derived from Boltzmann transport equation
02 p0343 A70-11885
RECOMBINATION COEFFICIENT
N atom recombination rate coefficient in static system pressure dependent at low pressure
01 p0147 A70-10450
Auroral light emission and electron density simultaneous measurements by rocket flights into auroral glow, deriving recombination rates
01 p0171 A70-10872
Static atmosphere model above 120 km, assuming oxygen atoms and molecules and nitrogen molecules presence to determine diffusion velocity and recombination coefficient
02 p0327 A70-12385
Dissociative recombination coefficients temperature dependence in molecular neon and argon ions measured under equal gas, ion and electron temperature
04 p0722 A70-14668
NO ion dissociative recombination rate coefficient determined in high temperature air plasma from electron temperature and number density measurements
04 p0675 A70-15583
Dissociative recombination coefficient ratio between O ion and nitrogen oxide ion in ionosphere using rocket data
04 p0683 A70-15743
Charge carriers recombination and diffusion coefficients for confined gas discharge plasma obtained from data on radial particle distribution profile
05 p0888 A70-16330
Electron temperature dependence of molecular neon ions recombination with electrons using microwave afterglow/mass spectrometer, obtaining recombination coefficient
05 p0885 A70-16468
Dielectronic recombination rate coefficient determined by quantum theory of resonance-collision processes, considering coupling, degeneracy and overlapping resonances
05 p0920 A70-16943
Seasonal variations of maximum electron concentration in stratified E-F region, including E 2 layer recombination coefficient and F layer characteristics probability
06 p1057 A70-17842
Excitation, ionization and recombination rates for charged ions during collisions with electrons in solar corona assuming Maxwellian electron distribution
07 p1384 A70-19409
Diurnal variations of lower F region ion composition and recombination coefficient based on numerical modeling of continuity equations for electrons and molecular species
07 p1265 A70-19431
Nighttime ionospheric F region velocity component and recombination coefficient computer calculation
07 p1277 A70-20449
Numerical solutions of one dimensional expanding flow of dissociating gas initially in frozen state for variations in recombination rate
08 p1484 A70-21531
Forward and backward rate constants for diatomic recombination and dissociation in dilute gas
09 p1730 A70-22231
Ionized potassium plasma three body recombination coefficient measurements showing inverse temperature dependence
09 p1735 A70-22778
Dissociative-recombination rate coefficient measured for dissociative recombination reaction in inviscid nozzle flow of reflected shock tunnel, using high temperature and pressure nitrogen
09 p1737 A70-23225
Electron temperature diurnal variations data from rocket soundings used for determining recombination coefficient in E region
11 p2044 A70-25550
Oxygen cation electron dissociative recombination rate coefficient measurement during expanding oxygen flow in nozzle
12 p2276 A70-27802
Electron density profiles interpretation for quiet daytime D region, noting role of electron-positive ion recombination coefficient
13 p2397 A70-29192
Dissociative recombination coefficient ratio between O ion and nitrogen oxide ion in ionosphere using rocket data
14 p2576 A70-30827
Ionization-neutralization processes and recombination coefficient in F and E regions, using radiophysical measurements
15 p2730 A70-32083
D region electron density rocket measurements implying recombination coefficient
16 p2896 A70-32939
Diurnal variations of lower F region ion composition and recombination coefficient based on numerical modeling of continuity equations for electrons and molecular species
18 p3249 A70-36905
E layer electron concentrations, effective recombination coefficient and ionization sources during solar eclipse, noting soft X radiation intensity
19 p3408 A70-37310
Electron density measurements by rocket observation during PCA after solar flare of 25 February 1969, deriving effective loss rates in terms of recombination model
19 p3496 A70-37511
Electron temperature diurnal variations data from rocket soundings used for determining recombination coefficient in E region
21 p3819 A70-41300
Lower E region recombination coefficients from electron density and flux measurements in glow aurora by Nike-Apache rocket
22 p4020 A70-43163
Oxidized Si surface recombination rate measurement by electric field effect, noting electron bombardment effects on electrical properties
22 p3998 A70-43443
Three body recombination and dissociation rate coefficients of nitrogen in Ar atoms heat bath, using modified phase-space theory
23 p4221 A70-44008
Partially ionized gas electron-ion recombination rate coefficients calculation methods compared with Ar plasma data
23 p4226 A70-44436
RECOMBINATION REACTIONS
NT ATOMIC RECOMBINATION
NT ELECTRON RECOMBINATION
NT ELECTRON-ION RECOMBINATION
NT HYDROGEN RECOMBINATIONS
NT ION RECOMBINATION
NT OXYGEN RECOMBINATION
NT RADIATIVE RECOMBINATION
Recombination instabilities in plasmas and gases undergoing density changes through volumetric processes, solving linearized and nonlinear cases by simplified fluid mechanics equations
02 p0348 A70-12238
Recombination emission of InSb semiconductor at low temperature during pinch effect with electron gas degeneration, calculating spectral distribution and effective temperature vs current
03 p0539 A70-13406
Carbon atom RF recombination lines evaluated for conditions in H II regions and planetary nebulae
04 p0748 A70-14587
Temperature dependence of reaction rate for dissociative recombination in vibrationally excited gases, using electronic threshold law for diatomic ions
04 p0722 A70-14669
Attractive potential effects on free and bound particles distribution in dissociating gas, studying recombination reaction effects on gas kinetic structure
06 p1044 A70-18280
Recombination processes in comet atmospheres listing ion, atom and electron reactions, cross sections and resonance defects
07 p1379 A70-19037
CO vertical distribution near tropopause from photochemical atmospheric model with CO recombination with OH for stratospheric sink
07 p1265 A70-19282
GaAs solar cells performance as function of doping levels, ascribing poor efficiencies to surface recombinations
08 p1557 A70-21721
Dissociative-recombination rate coefficient measured for dissociative recombination reaction in inviscid nozzle flow of reflected shock tunnel, using high temperature and pressure nitrogen
09 p1737 A70-23225
Metastable level populated by dissociative recombination mechanism, estimating efficiencies of various processes
09 p1745 A70-23438
Ionospheric loss rates from rocket observation during auroral absorption interpreted by two ion model of recombination
10 p1881 A70-24813
Alpha recombination line emission from galactic center detected, discussing possible origins in continuum source or interstellar medium
10 p1947 A70-24995
Electron density decrease in F 2 layer ascribed to 9 July 1962 thermonuclear explosion, noting dissociative recombination role
11 p2047 A70-26791
Temperature effects on base and surface currents of plane bipolar transistors, testing validity of surface recombination process model
11 p2021 A70-26832
Continuum spectra of well-resolved thermal and nonthermal galactic sources compared with H-alpha recombination line
12 p2296 A70-26898
Electroluminescence recombination emission spectra during avalanche breakdown in AlGaAs n-p and p-n heterojunctions
12 p2286 A70-27367
Ruby laser illuminated Ge recombination radiation intensity measured at room temperature
12 p2286 A70-27369
Milky Way large scale structure from radio recombination line surveys
12 p2301 A70-27580
Thermal feedback theory of flicker noise generation in transistors and temperature fluctuations effect in vicinity of recombination centers
12 p2196 A70-27687
Partially ionized plasma stability with allowance for ionization and recombination processes, discussing ion-acoustic oscillations
15 p2781 A70-32823
Surface recombination centers protecting against discoloration of thermal control coatings due to chemical changes induced by photoproducts holes and electrons in oxide pigments
16 p2940 A70-33935
Frequency multipliers with charge storage diodes, examining recombination and hysteresis effects on performance
17 p3050 A70-34588
Supersonic conductive gas recombination fronts for arbitrarily oriented magnetic field, allowing for dissipative coefficients
18 p3294 A70-36255
Orion nebula core radio recombination line intensities, showing variations in mean electron temperatures and physical conditions
18 p3313 A70-36329
Pinch effect in degenerate and nondegenerate electron hole plasma in semiconductors during bimolecular bulk recombination
18 p3298 A70-36620
Ionization-recombination parameters based on diurnal variations of electron concentration in F 2 layer maximum, discussing latitudinal variations
18 p3254 A70-37033
Ionization-recombination parameters variation as function of season and solar activity, using diurnal changes of F 2 layer maximum electron concentration
18 p3254 A70-37034
F 2 layer maximum electron concentration diurnal variations dependence on ionization intensity and dissociative recombination and ion-molecular reactions rate coefficients
18 p3255 A70-37039
CdS crystals luminescence spectrum excitation by UV light of ruby laser, noting excitons and phonons recombination
19 p3444 A70-37368
Nitrogen dioxide continuous visible emission under thermal and recombination excitation, examining spectral characteristics
19 p3374 A70-38267
Nonequilibrium recombination in supersonic nozzle of dissociated combustion products of hydrogen in air, investigating initial system and rate constants effect
20 p3582 A70-39269
Tropical UV nightglow measurement by Ogo-4 spectrometer, considering ionospheric recombination excitation mechanism
20 p3620 A70-39338
Current distribution and interband recombination emission in bipolar semiconductor crystal under pinch effect produced by external magnetic field
20 p3677 A70-39590
Recombination lifetime /laser/ states in Si doped GaAs light emitting diodes on p-type thin platelets
21 p3838 A70-42016
Hydrogen and air nonequilibrium chemical recombination effects in two dimensional exhaust nozzles, using Bray freezing criterion
22 p3982 A70-42760
Recombination model of diurnal variation of electron density in midlatitude D region, assuming NO ionization by solar Lyman-alpha radiation
22 p4020 A70-43158
Current oscillations in external circuits of semiconductor with low surface recombination in parallel electromagnetic field
23 p4231 A70-45062
RECOMPRESSION
U COMPRESSING

RECONNAISSANCE

NT AERIAL RECONNAISSANCE
NT PHOTORECONNAISSANCE
NT SPECTRAL RECONNAISSANCE
Reconnaissance uncertainty effect on precision of
return to fixed point applied to circular error probable,
drms calculations and Loran

04 p0652 A70-15345

RECONNAISSANCE AIRCRAFT

NT CL-84 AIRCRAFT
NT EARTH RESOURCES SURVEY AIRCRAFT
NT G-91 AIRCRAFT
V/STOL supersonic fighter VJ 101, transport Do 31
and VTOL fighter/reconnaissance VAK 191 develop-
ment in West Germany, discussing control and sta-
bilization during hovering

03 p0413 A70-13794

Oxygen equipment design for USN patrol and at-
tack aircraft, considering masks, regulators, helmets
and hoses

07 p1191 A70-19005

Remote control turboprop drone aircraft for long
unmanned electronic intelligence or tactical commu-
nications relay missions

08 p1435 A70-20625

Avionics on military combat-reconnaissance air-
craft, discussing automatic systems testing and cost
effectiveness model

13 p2380 A70-29698

VAK 191 B VTOL aircraft fitting NATO Basic Mil-
itary Requirements for low level reconnaissance-
fighter operations developed from Fiat G-91

17 p3017 A70-34992

Armor airframed helicopter for aerial armored
reconnaissance vehicle, noting design, fabrication and
weight

23 p4137 A70-44095

RECONNAISSANCE DRONE AIRCRAFT

U DRONE AIRCRAFT

U RECONNAISSANCE AIRCRAFT

RECONNAISSANCE SPACECRAFT

NT MIDAS 4 SATELLITE

RECONSTRUCTION

NT WAVE FRONT RECONSTRUCTION

RECORDING

NT DATA RECORDING

NT DATA SMOOTHING

NT MAGNETIC RECORDING

NT PHOTOGRAPHIC RECORDING

RECORDING INSTRUMENTS

NT BATHYTHERMOGRAPHS

NT FLIGHT LOAD RECORDERS

NT FLIGHT RECORDERS

NT LUNAR SEISMOGRAPHS

NT OSCILLOGRAPHS

NT PLOTTERS

NT PRESSURE RECORDERS

NT SEISMOGRAPHS

NT WEATHER DATA RECORDERS

NT WHISTLER RECORDERS

NT X-Y PLOTTERS

Real time recording and permanent display, using
high power energy density focused Ar laser beam for
ink transfer

01 p0111 A70-10782

Continuous measurement and automatic recording
of metals electrical resistance during fatigue testing in
vacuum at elevated temperatures

01 p0092 A70-11108

Algorithm for determining readings dispersion dur-
ing cosmic rays variability, statistical nature and in-
strument errors

01 p0172 A70-11526

Gas pressure differences and diffusion rates record-
ing using He-Ne laser interferometer, discussing
aerodynamic applications and avionic instrumentation
problems

02 p0299 A70-12272

Ionospheric critical frequency recorder develop-
ment for continuous recording of frequency variations
with time

02 p0303 A70-12736

Frequency amplitude-threshold EEG analyzer with
automatic distribution of filter signals over recording
levels

03 p0434 A70-13695

Monitoring and recording of physiological param-
eters, discussing heart, muscle, brain potentials, blood
pressure, respiration measurements and instrumenta-
tion

03 p0439 A70-14267

Schlieren recorder and Erdmann field absorption
methods applied to qualitative and quantitative flow
process studies in high velocity wind tunnel

04 p0689 A70-14925

High altitude observatory solar magnetograph in-
stallation modifications including computer control,
improved Zeeman effect observation instrument, etc

04 p0691 A70-15037

Transistorized photoelectric star transit recorder
operable in ambient media with large temperature
variations ensuring low zero point drift

04 p0694 A70-15490

Ultraminiature pressure sensor for continuous
recording of hydrostatic pressure in renal tubules and
blood capillaries

05 p0804 A70-15772

Cosmic ray intensity variations recording device
adaptable to computer forming centralized data
processing system

05 p0845 A70-15932

Spectral intensity recording facility design for high
energy electrons and hard gamma quanta in upper
layer and beyond atmosphere

05 p0846 A70-15959

Azimuthal telescope for recording cosmic rays in-
tensity, noting statistical error for vertical and oblique
incident component

05 p0846 A70-15967

Amplification and contactless recording device with
ferroresonant servomotor controlled by low DC
signals

05 p0848 A70-16364

Scientific equipment on Cosmos 237 satellite for
recording extraterrestrial radiation data, discussing
specifications, operation and mission purpose

05 p0851 A70-16733

Test stand design and automatic recording of tur-
bine blade fatigue test data, including statistical
evaluation

05 p0953 A70-17054

Multichannel magnetograph display for pattern
recognition of solar feature morphology compared
with spectroheliograms

06 p1142 A70-17993

Versatile recorder for experimental studies with dif-
fering requirements

07 p1283 A70-19670

Holography without reference beam for two and
three dimensional interferential wave front recording
and reconstruction

07 p1285 A70-19858

Recording apparatus design and operation for
characteristics of electromagnetic waves generated by
weather discharges, discussing electromagnetic per-
turbations propagation

08 p1468 A70-20467

Electronic recording of cyclic strain diagrams of
metals in wide loading frequency range using dynamic
hysteresis method

08 p1585 A70-20987

Simultaneous recording of fast and slow precision
manual movements with electroencephalogram and
electromyogram

08 p1452 A70-21438

Visual recordings of cardiac rhythm obtained from
flashes of miniature indicator tube, describing circuit
filter function

08 p1452 A70-21439

Micromotor torsion moment-speed characteristic
curve obtained by automatic recording apparatus

09 p1672 A70-22026

High speed instrumentation camera system for
recording rapid motions during Apollo landing impact

09 p1688 A70-23770

Medical thermograph with modified image-pickup
device characteristics and additional thermal analysis
equipment

10 p1828 A70-25307

Precise sweep calibrations and simultaneous spec-
trum recording for high resolution nuclear magnetic
resonance spectroscopy

11 p2052 A70-26375

Vibration test instrument with automatic plotting of
vibrating system amplitude-frequency characteristics

11 p2032 A70-26440

Transistorized pulsed activity converter for observ-
ing analog curve of change in pulse frequency

12 p2179 A70-28316

RF method for recording temperature dependence
of electrical conductivity of solids, liquids and mul-
ticomponent plasma mixtures

13 p2459 A70-28583

Holographic recording of wideband pulsed carrier
electric signals in Fourier transform, Fraunhofer,
Fresnel and image formats

16 p2903 A70-33136

Real time recording systems design for increased
writing speeds on photochromic films

16 p2910 A70-33435

Photoelectric device for recording plant rhythmic
leaf movements in space

16 p2849 A70-33998

Semiautomatic ionospheric absorption recorder,
describing components circuitry and operation

16 p2915 A70-34223

Aircraft onboard maintenance recording system,
discussing design and effectiveness

17 p3094 A70-35516

European requirements for aircraft accident and
maintenance recording systems

17 p3094 A70-35517

Ionospheric scatter channel amplitude frequency
characteristics recording equipment, discussing design

18 p3256 A70-36090

Recording instrumental noise resolution of standard
algorithm for cosmic ray stations

18 p3307 A70-36100

Solar radio bursts recording by spectrographs in
500-1500 MHz band, discussing sensitivity

18 p3307 A70-36109

Quartz magnetic variometer allowing simultaneous
recording of magnetic field variations and suspension
axis inclination changes

19 p3420 A70-37336

Instrumentation magnetic recorders in aerospace in-
dustry in relation to new components and techniques
development, investigating airborne recorder as flight
test tool

19 p3429 A70-38516

Multichannel cosmic ray recorder providing input to
computer memory

20 p3629 A70-39313

Automatic cosmic ray station for recording nucleon
and meson components

20 p3629 A70-39314

Recording device for gamma quanta in primary
cosmic radiation

20 p3629 A70-39316

Magneto-optic rotation and hysteresis recording in-
strument for thin magnetic films as function of tem-
perature and wavelength, using Faraday effect

21 p3826 A70-41452

Pulse superposition measurements of small ul-
trasonic waves velocity changes using automatic
recording phase sensitive detection

21 p3827 A70-41468

Pulse counting photoelectric photometer for lunar
occultation recording of stars, discussing design, as-
sociated equipment and operation principles

22 p4030 A70-42860

High speed holographic recording of transient
events by single shot ruby and Nd-doped pulsed
lasers, applying to shock tubes and wind tunnels

22 p4035 A70-43056

Short pulse length X ray flash electro-optical
recording equipment for explosive processes, describ-
ing technique, experimental setup, optical charac-
teristics and information retrieval

22 p4037 A70-43071

Visual system recording neuron pulse potential spa-
tial and temporal responses to sinusoidal stimuli

23 p4144 A70-43922

Ionospheric layers critical frequencies recording,
using automatic interplanetary station type probe

23 p4194 A70-44088

Digital recording system for body temperature
telemetry from small animals, using FM transmitter
implanted in peritoneal cavities

23 p4151 A70-44381

Solar activity research, discussing optical facilities,
photoelectric magnetographs, magnetic field measure-
ment, solar cycles and flares, etc

23 p4256 A70-45034

RECORDS

International Aeronautical Federation space
records, discussing record classification for subor-
bital, earth orbital and lunar and planetary missions

15 p2831 A70-32245

RECOVERABILITY

Linear time-varying control process with bounded
control amplitudes and rates, deriving conditions for
recoverability

11 p2028 A70-26314

Recoverability for amplitude and rate bounded op-
timal control of linear time varying systems

14 p2562 A70-31203

RECOVERABLE LAUNCH VEHICLES

Reusable air breathing launch vehicle for earth orbit
shuttle, comparing performance, costs and operation
with rocket powered systems

[AIAA PAPER 70-270]

07 p1396 A70-20381

Launch vehicle first stage cost reduction, consid-
ering weight factors, mass production, recoverability,
etc

11 p2126 A70-26285

Suborbital space transports problem solution by
recoverable jet orbital or jet assisted aircraft,
discussing implications of Concorde supersonic flight

18 p3350 A70-36663

RECOVERABLE SATELLITES

U RECOVERABLE SPACECRAFT

RECOVERABLE SPACECRAFT

NT APOLLO SPACECRAFT

NT GEMINI SPACECRAFT

NT MARS [MANNED SPACECRAFT]

NT MERCURY SPACECRAFT

NT REUSABLE SPACECRAFT

NT SPACE SHUTTLES

Aerodynamic braking for returning high speed
recoverable space tug to low earth orbit

23 p4259 A70-44611

Recoverable stages for satellites low to stationary
orbital transfer, taking costs into account

23 p4245 A70-44671

RECOVERY

Dislocation network recovery kinetics of cold
worked undoped powder metallurgical W wires by
electrical resistivity measurements, determining ac-
tivation energy

21 p3839 A70-40797

RECOVERY PARACHUTES

- Crushable honeycomb regulating operating pressure of propellant actuated devices applied to recovery parachute catapult in F-111 crew module
03 p0546 A70-14108
- Aircrew parachute with low speed-low altitude capability, considering static on-the-deck recovery, pack volume, weight, escape envelope spectrum, etc
07 p1191 A70-19014
- Pilot Airborne Recovery Device (PARAD) using hot air ballute, noting capability to ascend or descend by flow control valve controlling butane burner
07 p1192 A70-19019
- RESY parachute recovery for payloads launched by Skylark high altitude sounding rocket, noting flotation system and location aids
13 p2505 A70-28771
- Parachute recovery system for surveillance drone and landing bag subsystem
[AIAA PAPER 68-935] 14 p2531 A70-30858
- Tractor rocket powered escape system of 600 knot extraction capability using drogue parachute and barometric time delay device
[AIAA PAPER 70-1209] 21 p3751 A70-41809

RECOVERY TEMPERATURE

U SKIN TEMPERATURE [NON-BIOLOGICAL]

RECOVERY ZONES

- Space rescue requirements for earth-returning astronauts recovery under emergency conditions, discussing recovery zones determination by space flight mission control
04 p0761 A70-14929
- Spacecraft or escape capsule rescue, discussing design, recovery planning, forces and sites
17 p3180 A70-35301
- Rescue waiting time relation to number of communication and return sites for emergency astronaut return, considering day vs day/night recovery
23 p4245 A70-44639

RECREATION

- Spacecrew candidates leisure time preferences, discussing off-duty concepts for long space missions
16 p2853 A70-33709
- Active recreation in motor function regulation in aging individuals
22 p3968 A70-42897

RECRYSTALLIZATION

- Recrystallization diagrams of commercially pure Mo and Mo alloyed with Fe, Co or Fe plus Ni, noting additions effect on recrystallized grain size
01 p0124 A70-11616
- Al and Ti single additions effects on recrystallization of Ni-Cr alloys, noting phase transformation and hardness variations
03 p0513 A70-14300
- Recrystallization annealing third stage of cold worked polycrystalline niobium by measuring electrical resistance at liquid nitrogen temperature
05 p0863 A70-16204
- Recrystallization behavior of Al alloy containing Mg and Si subjected to maximum aging before cold working
06 p1085 A70-17418
- Ni-Fe alloys texture formation, studying strong deoxidizers role in secondary recrystallization
06 p1088 A70-17614
- High melting point oxides effects on niobium alloys recrystallization temperature and grain growth
07 p1303 A70-18741
- Chemical composition and heat treatment effects on deformation resistance of nonaging aluminum alloys during hot working, noting quenching effect on recrystallization
07 p1294 A70-19388
- Molybdenum rolling-deformed single crystals recovery and recrystallization using diffraction electron spectroscopy
07 p1307 A70-19550
- Rolling texture and recrystallization of Mo single crystals and deformation effect on texture formation using X ray transmission technique
07 p1309 A70-19613
- Refractory metal monocarbide single crystal growth by plastic strain induced primary and secondary recrystallization
07 p1313 A70-19902
- Compatibility of single metal coated carbon fibers, discussing structural recrystallization in contact with Ni or Co matrix by dissociation/diffusion/precipitation mechanism
07 p1315 A70-20048
- Recrystallization in austenite phases of vanadium and columbium HSLA steel alloys determined in high temperature deformation tests
08 p1521 A70-21704
- Anomalous grain growth kinetics and recrystallization in electron beam annealed nickel determined by microstructural and radiographic study, noting annealing time dependence
11 p2068 A70-26596
- Compacted titanium carbide powder coarsening recrystallization within homogeneous region, determining relation between initial activation energy and carbide composition
12 p2254 A70-27284

- Recrystallization effect on 3-D graphite orientation in carbon fibers under high temperature heat treatment
12 p2259 A70-27720
- Pure Mo recrystallization deformed by cold rolling using transmission electron microscopy
14 p2597 A70-31284
- Super plasticity in plastically deformed pure Al related to recrystallization
15 p2764 A70-32903
- Ti alloys crack formation during oxidation under stress, considering annealing and recrystallizing effects
17 p3114 A70-34374
- Baron thermal diffusion effects on plastic of pure Mo subjected to recrystallization
17 p3102 A70-35408
- Nb-based Ti-Zr alloy surface phase recrystallization characteristics, using field emission microscope
18 p3276 A70-36309
- Al-Mg alloys recrystallization, investigating heating rate and annealing time effects on sheet grain size
19 p3450 A70-37372
- Deformed single crystals of high purity Al of different orientation with respect to growth during recrystallization
19 p3450 A70-37373
- Recrystallization kinetics and microstructure of low carbon Ti stabilized steel cold rolled and annealed in 800-1750 F range
22 p4053 A70-42730
- Recrystallized and overrecrystallized Al alloys, investigating factors controlling anisotropy of mechanical properties
22 p4056 A70-43126
- Gas bubbles effect on recovery and recrystallization in W sheet deposited from tungsten fluoride vapor
24 p3458 A70-45243
- German monograph on sintered molybdenum silicide recrystallization following high temperature heating in oxidizing atmosphere
24 p4367 A70-45575
- Pure Ni recrystallization, noting stacking faults and parallel sided and thin annealed twins formation during boundary migration
24 p4363 A70-46192
- Grain growth abnormality in Al-Mg ingots with small amounts of Mn and Cr during secondary recrystallization
24 p4363 A70-46197

RECTANGLES

- Summary representation formulas for solving boundary value problems for Helmholtz and Poisson equations in rectangle
03 p0518 A70-13076
- Adhesive or frictionless compression/or extension/under axial load of elastic rectangle between two identical elastic half spaces in condition of plane strain
05 p0931 A70-16132

RECTANGULAR BEAMS

- Rectangular anisotropic beam torsion using Green function combined with wide step numerical method
03 p0593 A70-13471
- Monograph on shear lag measurement in rectangular section beam subjected to bending or torque free from axial restraint, using inductance probe sensors
03 p0603 A70-14351
- Thermal and mechanical stresses in rectangular composite beams, considering effects of temperature and reinforcing fiber orientation
06 p1164 A70-17503
- Anticlastic bending effect on rectangular beam curvature, presenting deflection equations
07 p1414 A70-20175
- Rigid rectangular box with supported flexible wall analyzed for internal acoustostructural mode coupling factors and corresponding modal average radiation efficiency
09 p1770 A70-22393
- Beams torsion problems solution by variational method of variables separation, obtaining values for torsional rigidity and stress function
09 p1773 A70-22547
- Rectangular beam creep rupture time under bending moment and axial tensile force, using power series to solve integral equations
11 p2142 A70-26635
- Reference stress evaluated by numerical analysis techniques, discussing rectangular beam in pure bending
16 p2987 A70-32921
- Maximum secondary principal stress axis and isotropic points determination in scattered light photoelastic analysis, considering bar in uniaxial tension and rectangular beam
19 p3546 A70-38345
- Torsion of composite rectangular cross section beam consisting of isotropic media, using Green function and Fourier expansion
20 p3732 A70-40334
- Third isotropic point in rectangular beam under bending stresses by Hertzian load, using Stokes-Wilson method and photoelastic comparison
21 p3941 A70-42265

- Fiber-reinforced narrow rectangular beam flexural strain analysis by birefringent coating technique, deriving isochromatic and isoclinic patterns
23 p4275 A70-44915

RECTANGULAR GUIDES

- Multimode excitation of large aperture horn antennas to produce electronic deflections of directional pattern
01 p0046 A70-11454
- Input impedance of monopole antenna in rectangular waveguide assuming sinusoidal current distribution, noting accuracy limitation to specific monopole lengths
03 p0457 A70-13698
- Reflection coefficients of circular posts in rectangular waveguides computed by Green function and method of moments
05 p0820 A70-16384
- Rectangular waveguides broad wall longitudinal slot equivalent networks, noting series/parallel function dependence on slot length
07 p1240 A70-19221
- Multimode rectangular waveguide lateral surface opening, determining scattering matrix coefficients governing mode conversion characteristics
08 p1462 A70-21224
- Scattering cross sections of electromagnetic waves in rectangular plasma-filled waveguide based on reciprocity theorem
08 p1464 A70-21983
- Thin resistive layers located in rectangular waveguide assuming constant and surface variable conductivity and permittivity
09 p1644 A70-22279
- Rectangular waveguides filled with magnetized ferrite with/without dielectric, calculating phase shift and attenuation by Ritz method
09 p1645 A70-22548
- Equivalent circuit for radiation admittance of infinite planar array of phased rectangular waveguide apertures
09 p1646 A70-22692
- Open cut-off rectangular resonator calculated for frequency dependence on reflection coefficient and relative length
09 p1648 A70-23165
- Rectangular coaxial waveguide with internal conductor contained between inhomogeneous magneto-dielectric bars, deriving computer algorithm for natural mode fields
09 p1638 A70-23645
- Rectangular waveguide with cross shaped slot as polarizer ensuring circular polarization over wide frequency range
09 p1652 A70-23649
- Relative permittivity of small thickness dielectric substrate plates determined from reflection coefficient in rectangular waveguides
11 p2011 A70-26603
- Transverse electric field distribution in multilayered dielectric loaded rectangular guides determined by ray optics and residue calculus
12 p2199 A70-28051
- Electric field distribution in rectangular waveguide loaded with magnetized n-InSb at room temperature obtained by solving boundary value problem by variational method
12 p2202 A70-28163
- Microwave transmission through thin film screens with apertures placed in transverse plane of X band rectangular guides
12 p2202 A70-28164
- Attenuation, resistivity and surface roughness measurements in rectangular waveguides
14 p2555 A70-30440
- Trapped mode resonances, attenuation and launching tapers in overmoded rectangular waveguides
14 p2556 A70-30441
- Reflection coefficient formula for principal radio wave reflected from thin long rod in middle of rectangular waveguide
16 p2878 A70-33800
- Microwave properties of uniformly magnetized slabs filling cross section of rectangular lossless waveguide operating in specific modes
17 p3050 A70-34584
- Microwave properties of infinite lossless rectangular waveguide semiinfinitely filled with magnetic material operating in specific modes
17 p3050 A70-34585
- Waveguide transformer using rectangular waveguide permitting Galerkin method, determining scattering matrix
19 p3385 A70-37429
- Rectangular waveguide EM radiation into plane parallel region through asymmetrical longitudinal slot
19 p3386 A70-37727
- Polarized electromagnetic wave diffraction by semiinfinite symmetrical obstacles in rectangular waveguide, calculating transformation coefficients for wide frequency range
19 p3378 A70-37729

- Linear equations for wave diffraction in rectangular waveguides with step-shaped inhomogeneities
19 p3378 A70-37730
- Dispersion characteristics of electronically tunable periodic rectangular waveguides, using external DC magnetic field
23 p4168 A70-43781
- Stepped termination design for rectangular waveguides achieving minimum length and maximum reflection coefficient
23 p4169 A70-43783
- Energy rotation in electromagnetic wavefields, noting TE-MODE excitation in rectangular guides
23 p4164 A70-44384
- Dielectric covered narrow radiating slots in rectangular waveguide broad face, calculating impedance from equivalent circuits
23 p4175 A70-44952
- RECTANGULAR PANELS**
- Rectangular clamped panel flutter characteristics at various oncoming flow angles of attack
03 p0590 A70-13382
- Energy method for analyzing rectangular panels buckling under nonuniform in-plane loading, considering stability under uniform compression
05 p0931 A70-16117
- Transient heat flow in three dimensional rectangular panels, developing criterion for problem dimensionality [AIAA PAPER 70-16]
06 p1182 A70-18212
- Shallow rectangular shell panels nonsymmetric nonlinear deflection states computed by finite difference equations iteration, discussing snap-through buckling loads
09 p1780 A70-23209
- RECTANGULAR PLANFORMS**
- NT RECTANGULAR PANELS
- NT RECTANGULAR PLATES
- NT RECTANGULAR WINGS
- Shallow orthotropic shell of rectangular planform with edges under dynamic load, studying forced vibrations by anisotropic shell theory
07 p1403 A70-19057
- Natural oscillation frequencies of three layer plates with rectangular planar form determined by integrated representations method
08 p1583 A70-20495
- Rectangular planform shallow cylindrical shell parametric vibrations using method applied to large bending vibrations of plates
08 p1588 A70-21212
- RECTANGULAR PLATES**
- Rectangular plates deformation under uniaxial compression, studying postcritical buckling behavior in presence of creep
01 p0201 A70-10937
- Elastic support effect on bending of clamped circular, elliptical, rectangular and skewed plates, using variational method and small perturbation technique
01 p0205 A70-11144
- Stiffeners reinforced rectangular plates parametric stability under dynamic load, deriving equilibrium equations and boundary conditions by averaging stiffener effects
01 p0205 A70-11146
- Stress-strain analysis of rectangular plates under concentrated load, noting sealed liquid compressibility effect on deflections and bending moments
02 p0388 A70-12499
- Monograph on buckling and postbuckling behavior of plates tapered in planform, comparing stability of tapered and rectangular plates
03 p0586 A70-13002
- Plane elasticity solution for differential expansion stresses on interface of laminated elastic rectangular strip
03 p0586 A70-13114
- Cylindrical bending in laminated plates displaying bending-extensional coupling approximating behavior of rectangular laminated plates with high length-to-width ratio
03 p0587 A70-13125
- Rib-reinforced rectangular plate flutter in gas flow, considering shell stability, rib torsional rigidity, etc
03 p0593 A70-13498
- Finite difference method for obtaining free vibrations natural frequencies and mode shapes for rectangular plates of varying stiffnesses
03 p0595 A70-13812
- Structural analysis of rectangular plates simply supported on two edges subjected to free edge uniform moments
03 p0602 A70-14332
- Sound attenuation rate of rectangular flat steel plates contact and branch point relation to velocity difference and absorption length
03 p0526 A70-14353
- Elastic equilibrium of quasi-completely regular rectangular parallelepiped with rigidly clamped lateral faces, obtaining Lamé equations in double Fourier series
04 p0765 A70-14418
- Rectangular waffle plates minimum-weight design efficiency with multiple rib sizes in stiffening direction compared to honeycomb core sandwich construction
04 p0777 A70-15526
- Exact polynomial solution Saint Venant flexure of pretwisted rectangular plate treated as shallow hyperbolic paraboloidal shell
05 p0928 A70-16056
- Dynamic response of simply supported rectangular plate under suddenly applied transverse load, comparing solutions of classical and improved plate theories
05 p0933 A70-16174
- Fiberglass reinforced rectilinear plastic plates bending under various edge loads, noting shear pliability
05 p0934 A70-16220
- Elastoplastic bending of rectangular plates by finite difference and variational methods assuming homogeneity in elastic region
05 p0946 A70-16962
- Pressure distribution and drag measurements at flat triangular bodies and rectangular plates with blunt trailing edge in compressible flow
06 p0965 A70-17243
- Rectangular and nonrectangular anisotropic plate bending and stability analysis by difference-differential technique, allowing for combined freely supported and clamped end conditions
06 p1167 A70-17864
- Rectangular plates with symmetrical cracks, studying bending under various crack distributions
07 p1399 A70-18662
- Equilibrium forms of prolonged rectangular plate in gas flow in terms of nonlinear boundary problem, emphasizing plate with hinged supports
07 p1187 A70-18679
- Rectangular three layer plate bending with load carrying central layer obeying Kirchhoff-Love hypotheses and external layers obeying Noeth hypothesis
07 p1403 A70-19117
- Governing equations solution for simply supported laminated anisotropic rectangular plate using Fourier series method
07 p1406 A70-19305
- Flexural elastic behavior of rectangular plates with boundary restraint acting on same side using finite differences method
07 p1406 A70-19348
- Rectangular bidirectional composites and sandwich plates three dimensional elasticity solutions
07 p1412 A70-19952
- Elastoplastic bending of inhomogeneous rectangular plates with modulus of elasticity and yield stress varying over plate thickness
08 p1583 A70-20530
- Rectangular plate girder webs buckling under partial edge loadings, using finite element method for flange-web interaction
08 p1589 A70-21247
- Rectangular thin plates in small deformation transient creep bending, using finite element method in iterative procedure
08 p1590 A70-21356
- Green function for stress intensity factors of rectangular plate edge cracks, noting application to thermal stresses [ASME PAPER 68-WA/MET-19]
08 p1591 A70-21457
- Simply supported rectangular plate investigated for effect of thermal gradient on transverse vibrational frequencies
08 p1595 A70-21976
- Rectangular plate in unsteady temperature field, analyzing thermoplasticity problem by reducing solution to linear system with variable coefficients
09 p1779 A70-23098
- Free vibrations of plates and beams of pyrolytic graphite type materials, analyzing transverse shear deformation and rotary inertia [AIAA PAPER 69-55]
09 p1780 A70-23210
- Kantorovich variational method extended to thermoelastic plane stress problem of rectangular plates
09 p1781 A70-23278
- Failure compression tests of flat rectangular Al alloy panels presented in unitary form, adopting structural load index for solution from weight standpoint
09 p1782 A70-23376
- Irradiance factor between perpendicular and arbitrarily positioned plane rectangles calculated by contour and numerical integration
09 p1791 A70-23619
- Bending of homogeneous orthotropic rectangular plate of variable thickness supported on opposite edges, obtaining solution as Fourier series
10 p1955 A70-24083
- Large amplitude free vibration of rectangular plates subjected to aerodynamic heating with different boundaries and temperature distribution, deriving Duffing nonlinear differential equation
10 p1957 A70-24417
- Rectangular sandwich plates stability under combined loads, deriving equations for determining critical loads
11 p2129 A70-25563
- Boundary conditions effect on bending, vibrations and buckling of unsymmetrically laminated rectangular plates
11 p2136 A70-26079
- Thin rectangular plates transverse natural frequencies, deriving equations of motion and boundary conditions in bending moment terms by vibrational principle
11 p2143 A70-26645
- Iteration procedures for boundary value problem of orthotropic rectangular plate under bending loads, discussing convergence of procedures
12 p2325 A70-27552
- Supersonic flutter solutions using finite elements, analyzing rectangular plate bending elements, square simply supported and clamped panels, low aspect ratio configurations, etc
12 p2327 A70-27823
- Transverse bending of isotropic rectangular plate with symmetric crack under uniformly distributed load, considering corrections for stress-strain state near cracks
13 p2516 A70-29516
- Tensile test on perforated Al-filled rectangular plate of photoelastic material, obtaining stress concentration at hole by photoelastic visualization
13 p2516 A70-29628
- Postbuckling of flat variable thickness rectangular plates with unloaded transverse edges, using dynamic relaxation method
13 p2518 A70-30024
- Clamped orthotropic rectangular sandwich plates bending using approximate solution
14 p2661 A70-31429
- Equilibrium forms of prolonged rectangular plate in gas flow in terms of nonlinear boundary problem, emphasizing plate with hinged supports
15 p2671 A70-31471
- Plane rectangular plate in acoustic field of jet engine exhaust, calculating surface stresses
15 p2819 A70-32186
- Semiclamped strut supported rectangular plate deflection determined holographically, mechanically and analytically [SESA PAPER 1650]
15 p2740 A70-32331
- Three dimensional linear small deformation theory of elasticity solution for free vibration of simply supported homogeneous isotropic thick laminated rectangular plates
17 p3181 A70-34522
- Failure prediction for interlaminar shear stress in filament wound rectangular plate
17 p3188 A70-35228
- Homogeneous orthotropic cantilevered rectangular plate with reinforcing ribs, calculating flutter in supersonic gas flow
18 p3336 A70-36140
- Creep bending of rectangular plates with stress-strain and strain displacement nonlinearities
18 p3343 A70-36703
- Optimal rectangular plates with adaptability, using convex programming
19 p3535 A70-37344
- Waveform changes in postbuckling behavior of thin rectangular plates under axial compression
19 p3535 A70-37380
- Edge distribution of transverse reactive forces of rectangular plate with nonuniform flexural rigidity at buckling load
19 p3541 A70-38042
- Rectangular plates free and forced vibrations, including rotary inertia and shear deformation effects in dynamic response analysis
19 p3544 A70-38327
- Rectangular plate with three clamped edges, analyzing free vibration by Ritz method with deflection functions
19 p3544 A70-38328
- Harmonic forced transverse vibrations effects on rectangular plates with cross braces, deriving motion stability equations
20 p3725 A70-39867
- Structural synthesis concept in optimal design of composite material structural systems, considering failure modes of rectangular fiber composite plate
20 p3731 A70-40044
- Elastoplastic flexure and critical loading of isotropic rectangular plates of constant and variable thickness, using Lagrange principle with numerical integration
22 p4115 A70-42810
- Elastic bending, vibration and buckling of simply supported thick orthotropic rectangular plates and laminates
22 p4116 A70-43205
- Rectangular plates natural vibration problem, using straight line method with approximate separation of variables
23 p4265 A70-43982
- Rigid and elastic rectangular plates vibration under uniformly distributed dynamic load, investigating bending behavior by Galerkin method
23 p4268 A70-44170

Fluttering isotropic rectangular flat plate fatigue life estimation, taking into account stress, dynamic pressure, frequency, Mach number and plate thickness
23 p4270 A70-44577

Radar backscattering cross sections of horizontal and vertical polarizations for thin rectangular plate near grazing incidence
23 p4166 A70-44976

RECTANGULAR WINGS
Harmonically oscillating semiinfinite rectangular wing perturbation velocity potential in unsteady transonic flow without heat exchange
02 p0279 A70-12118

Ground proximity effect on rectangular wing, studying lift and pitching coefficients dependence on angle of attack
03 p0407 A70-13493

Unsteady pressure distributions measurement for oscillating rectangular wing, discussing test results for sub- and transonic velocities
[DGLR-69-32] 04 p0616 A70-15184

Nonlinear theory extended to slender triangular and rectangular wings with symmetric profile, taking into account finite wing thickness
06 p0966 A70-17254

Air compressibility effects on aerodynamic characteristics of slender rectangular wings moving at subsonic speed near earth surface approximated by lifting surface theory
10 p1801 A70-24276

Pressure field due to control surface oscillation in subsonic flow, presenting numerical results for rectangular wing
14 p2528 A70-30295

Nonlinear bearing surface of symmetrical rectangular edge wings without slipping in incompressible flow, using oblique horseshoe vortex model
15 p2673 A70-32128

Ackeret theory for infinite aspect ratio, rectangular and trapezoidal constant cord wings with arbitrary spanwise variation of profile in supersonic flow
16 p2836 A70-33748

Rectangular wing with oscillating control surface, measuring induced unsteady pressure field for comparison with computations based on lifting surface theory
21 p3935 A70-41407

Aerodynamic lift, drag and momentum coefficients in supersonic regime for rectangular and trapezoidal wings with spanwise variable profile
22 p3958 A70-42615

RECTIFICATION
Modulated high voltage pulse generator, using rectification of voltage obtained from HF oscillator
06 p1022 A70-17776

Nd glass laser ultrashort light impulse optical rectification, presenting lower harmonics angular dependence
19 p3443 A70-37287

RECTIFIERS
NT AVALANCHE DIODES
NT CRYSTAL RECTIFIERS
NT GERMANIUM DIODES
NT IGNITRONS
NT THYRATRONS
NT THYRISTORS
Rectennas design, construction and power output
04 p0660 A70-15649

Schottky barrier diodes microwave power rectification efficiency, developing diode losses theory based on back capacitance, series and front resistance and knee voltage
08 p1474 A70-21274

Low power semiconductor diode rectifying test apparatus for analysis of fusing and shaping effects on dynamic current-volt and frequency characteristics
09 p1649 A70-23355

High voltage gas laser trigger pulse generators featuring high pulse rate with semiconductor controlled rectifier
14 p2594 A70-31181

Thermal contact resistance, discussing behavior at cryogenic temperatures and directional or thermal rectifying effect
17 p3197 A70-35541

Multiple remote control systems effectiveness increased via controlled rectifier as even voltage harmonics generator
18 p3235 A70-36427

Cyclotron wave rectifier with Cuccia coupler for converting microwave power into DC or LF AC
21 p3756 A70-40730

Local control loop model of multiphase rectifier used as power amplifier, considering extension to nonautonomous and discontinuous conduction systems
21 p3802 A70-42267

RECTUM
Human rectal temperature cooling rate during refrigeration in mortuary, applying Newton law
01 p0017 A70-10471

Tympanic membrane and rectal temperatures compared over wide range of ambient environments as indicators of deep body temperature
17 p3029 A70-35332

RECUPERATORS
U REGENERATORS
RECURSION FORMULAS
U RECURSIVE FUNCTIONS
RECURSIVE FUNCTIONS
Nonlinear networks computer analysis by recursive decomposition, discussing network graphs construction rules
04 p0662 A70-15451

Perturbation theory based on Lie transforms, reducing Deprit equation to generate general recursion formulas
05 p0908 A70-16336

Error propagation in linear first order difference equations studied to improve accuracy of derivative recursive computation
07 p1328 A70-20249

Planar restricted three body problem in Thiele coordinates, developing recurrence formulas for coefficients in Taylor series expansions of solution
10 p1938 A70-24178

Minimax one step and recursive nonlinear predictors for linear discrete time-invariant first order plant driven by unknown bounded forcing function
12 p2204 A70-28069

Gain of optimal filter and predictor, using recursive estimation in discrete linear systems
13 p2381 A70-29063

Semiwideband and adaptive noise variance recursive estimation techniques applicable to spacecraft trajectory analysis
15 p2803 A70-32586

State estimation for nonlinear discrete time systems with quantized measurements, obtaining recursive algorithm through boundary value problem linearization
16 p2867 A70-33305

Recursive estimation and Kalman filtering for space vehicle trajectory tracking, using Doppler shift measurements
16 p2866 A70-34071

Recursive digital filters for flight control system airborne computer, considering quantization effects and eigenvalue sensitivity
[AIAA PAPER 70-953] 20 p3601 A70-39575

Recursive formulas for stability tests and quadratic loss functions evaluation for linear discrete time dynamical systems
20 p3659 A70-40114

Recursive differential equation for moments of time-to-cycle slip in first and second order phase lock loops
21 p3802 A70-41350

Recursive signal detection scheme, obtaining SNR by derivative approximation
22 p3984 A70-42317

Algorithm for fast digital computer recursive estimation of mean of random variable
22 p3993 A70-43074

Recursive test for nonnegative polynomials using modified Routh scheme to determine real positive zeros
22 p4063 A70-43332

Aircraft maintenance cost statistical analysis recursive regression model for aircraft failure and manhour cost data
24 p4292 A70-46125

RECYCLING
U CIRCULATION
RED ARCS
Electron temperature and density data obtained during Alouette satellite passage over middle latitude red arc, noting influence of intersecting magnetic field lines
03 p0476 A70-13911

Photometric and interferometric observations of midlatitude stable auroral red arc, determining structure, intensity and position
11 p2047 A70-26570

Stable auroral red /SAR/ arcs, discussing radiation, orientation, etc
13 p2397 A70-29188

Stable auroral red /SAR/ arc alignment-movement relationship, suggesting dominant local time control
13 p2397 A70-29193

Stable midlatitude red arc observation by Alouette 2 satellite for electron temperature and density structure measurement, calculating intensity and extent
20 p3620 A70-39333

F region heating by magnetic storms, discussing electron temperature, ring current conduction and red arcs
21 p3817 A70-41095

RED BLOOD CELLS
U ERYTHROCYTES
RED SHIFT
Gravitational theories scheme combining tetrad field with bimetric theories, including general relativity, space-time dependent Lorentz rotations, red shift and light deflection
01 p0141 A70-10232

Quasars variability, distribution, absorption line characteristics, red shift peaks, physical models, cosmological problems, etc
01 p0177 A70-10341

Quasars emission and absorption red shifts distribution analysis suggesting cluster interpretation
01 p0183 A70-10895

Einstein-Friedman cosmology of vanishing constants assumed in deducing relations between antipodal radio sources red shifts and universe parameters
01 p0187 A70-11274

Emission spectrum characteristic distortion in scattering of background X rays at large red shifts by metagalactic electrons, considering photon scattering effect
02 p0358 A70-12491

Quasar spectra interpretation, analyzing observational data and absorption lines correspondence to different red shifts
03 p0570 A70-13484

Periodic clustering of red shift values in quasi-stellar and unusual objects spectra, using power spectra
03 p0577 A70-14217

Angular diameter data from Cambridge radio telescope for sources with different flux densities for cosmological models red shift tests
04 p0757 A70-15691

Local theory alternative to cosmological quasar origin theories, considering red shifts properties
05 p0913 A70-16473

Statistical distribution of quasi-stellar objects with known red shifts over celestial sphere, observing symmetry over galactic equator
07 p1374 A70-18706

Distance between objects in Friedmann cosmological model determined on basis of red shift, determining relationship between observed and emitted wavelengths
07 p1377 A70-18945

O star red shift considering gravitation interpretation effects on stellar masses
07 p1391 A70-20465

Orbiting clock experiment for measuring gravitational red shift of earth by comparing ground based and satellite-borne hydrogen maser clocks
08 p1501 A70-21950

Observational verification of cosmological models by examination of red shift discretization in quasars
09 p1750 A70-22098

Radio galaxy 3C 371 compact companions, studying luminous isophotes and red shift by long exposure plates with 200 inch telescope
10 p1936 A70-23908

Spectral lines and radial velocities of paired galaxies, noting red shift difference between emission and absorption lines
10 p1946 A70-24978

Quasar spectra searched for intergalactic absorption lines, discussing red shift
10 p1947 A70-24998

Solar charge effects on Mercury perihelion motion, relativistic light deflection and gravitational red shift, using Reissner-Nordstrom solution
11 p2107 A70-25395

Evolutionary cosmological models for radio sources at large red shifts, considering source counts, luminosity functions, etc
11 p2117 A70-26655

Radio galaxies and quasars radiated power, discussing red shift complicated by absorption lines discovery in spectra
12 p2298 A70-27064

Quasar optical properties, red shift and models
12 p2299 A70-27379

Stark-broadened neutral atomic line widths and shifts, determining electron densities from H beta profiles and pressure-temperature data
13 p2455 A70-29220

Quasars magnitude relation to red shift, discussing scatter in log cz vs m plane correlation with B-V color
13 p2495 A70-29797

Water vapor in sunspots, taking into account red shift between telluric and intrinsic sunspot HOH lines
14 p2641 A70-30790

Radio sources spectroscopy, discussing central density and mass of elliptical galaxy NGC 3998 and red shifts of radio galaxies
14 p2642 A70-30893

Cosmogonic phenomena instability, discussing red shift, expanding universe, galactic nuclei and quasars
15 p2800 A70-32144

Red shift absorption systems ions related to intergalactic medium properties in clusters of galaxies
17 p3153 A70-34526

Quasar and radio galaxies, observing absorptions at red shifts close to emission line
17 p3157 A70-34846

Solar potassium resonance line shape and gravitational red shift, using atomic beam technique
17 p3173 A70-35861

Log S /flux/-log Z /redshift/ diagram for radio galaxies, encouraging steady state cosmology
18 p3320 A70-37074

Spiral galaxy NGC 4319 arms high red shift Seyfert nucleus, discussing UV continua of Markarian 205
20 p3701 A70-39005

REDUCED GRAVITY

Relativistic gas spheres and collisionless star cluster models with large red shifts, showing radial perturbation stability

20 p3703 A70-39175

Quasar red shift apparent magnitude data analysis, estimating deceleration parameter of universe

20 p3709 A70-40076

X ray emission of hot dense intergalactic plasma, discussing evolution equation for temperature and degree of gas ionization vs red shift

21 p3877 A70-40702

Stability conditions for relativistic stars, discussing mass-energy density distribution, Taylor instability, Schwarzschild criterion, Newtonian stellar model, gravitational red shift, etc

22 p4104 A70-42999

Quasars red shift distribution extrapolated from density evolution and luminosity function

24 p4402 A70-45386

REDUCED GRAVITY

Reduced gravity simulators for studies of human mobility in space and lunar missions

01 p0037 A70-10958

Reduced traction effects on human work performance in weightless and lunar gravity environment

01 p0037 A70-10959

Prototype lunar gravity simulator for studies of reduced gravity effects on human self locomotive capability, using magnetic air bearings and body support system

01 p0037 A70-10960

Human factors research with simulated reduced gravity conditions by parabolic flight technique with aircraft

[AMRL-TR-69-16]

01 p0037 A70-10962

Water immersion technique to simulate zero and partial gravity conditions for investigation of astronaut capability to execute extravehicular work procedures

01 p0038 A70-10963

Earth model based on free air gravity anomaly with condensed topography for eliminating gravity reduction difficulties, noting use in Vening-Meins formula

05 p0840 A70-16640

Numerical analysis of low-g fluid flow and heating problems encountered with liquid propellant storage and supply

[AIAA PAPER 69-567]

07 p1394 A70-19719

Venous pressure of man in space, investigating return to heart in absence of gravity and distention by hydraulic pressure

08 p1448 A70-21943

Simulated low gravity propellant sloshing in spherical, ellipsoidal and cylindrical tanks, discussing Bond number simulation and tank geometry effects

[AIAA PAPER 69-1004]

09 p1657 A70-23255

Polynomial force model supplementing reduced gravity model in determining accuracy of near equatorial, near synchronous and near circular satellite orbits

09 p1762 A70-23256

Reduced gravity effect on nucleate boiling using drop tower method with high speed motion pictures and telemetry

10 p1969 A70-25096

Test machine for partial gravity environment simulation for aerospace subsystem testing in vacuum chamber

17 p3060 A70-35181

Negative g Drone aircraft surface tension fuel system preventing air inclusion in turbojet engine fuel by tank filters/screens/

[AIAA PAPER 70-910]

17 p3019 A70-35822

Heated surface orientation and reduced gravity effects on Freon 113 nucleate

21 p3948 A70-41204

Xanthine dehydrogenase activity in Drosophila and Habrobracon under hypogravity conditions onboard Biosatellite

23 p4144 A70-43863

Low gravity fuel sloshing in axisymmetric rigid tank, calculating oscillations by modified Galerkin method

24 p4324 A70-45292

REDUCTION [CHEMISTRY]

NT DEOXIDIZING

NT HYDROGENATION

Reduction temperature effects on molybdenum powders sinterability noting dispersion role

08 p1517 A70-21145

Oxygen reduction reaction mechanism and catalysis, considering metal electrode surfaces and substrates, hydrogen peroxide role, adsorption, metal-oxygen bonds, etc

10 p1829 A70-24452

Oxygen electrode ring and disk currents analysis, studying oxygen reduction on platinum via peroxy intermediates

10 p1829 A70-24453

Oxygen reduction in sulfuric acid with phthalocyanine-carbon catalysts

10 p1829 A70-24456

Electrocatalytic activity of oxides in redox reactions without adsorption, noting application to hydrogen oxidation in acid medium

10 p1831 A70-24470

Gold alloys electrocatalytic activity in cathodic reduction of oxygen in potassium hydroxide

12 p2182 A70-27760

High purity V and V-Cr-Ti process, describing aluminothermic reduction and electron beam purification

15 p2761 A70-32387

Optically active amino acids synthesis by reduction of Schiff bases with sodium borohydride

17 p3041 A70-34748

Quartz- and silicate-graphite mixtures carbothermal reduction in vacuum at 1400 C

20 p3583 A70-40425

Chemical composition and reducing capacity of Apollo 11 igneous rocks, breccia and soil fines, using semimicro X ray fluorescence

21 p3777 A70-41602

Gas reducers transient processes, analyzing valve equations of motion

22 p3965 A70-43357

Metal phthalocyanin catalyzed oxidation by oxygen of vanadium and iron couples in externally regenerated redox fuel cell cathode

22 p3966 A70-43536

High purity Be preparation by Kroll process using Na as reductant, noting mechanical properties and ease of conversion to powder

24 p4341 A70-45242

REDUNDANCY

Integrity monitoring of redundant multiplex control systems for aircraft autoland operations, discussing Triplex autopilot

02 p0329 A70-11833

Redundancy optimization based on partial failure modes effect on system reliability to reduce cost

12 p2243 A70-28010

Redundant variable errors in weather prediction, specifying initial conditions for time integration of hydrothermodynamic equations for atmospheric motion

15 p2771 A70-32368

REDUNDANCY ENCODING

Fixed information bit rate approach to coding over space channel introducing redundancy and check digits for error probability

11 p2014 A70-26223

Q-ary /n, k/ cyclic code and subcode generations and weight distributions relationship

14 p2554 A70-31123

Fibonacci codes polarized and partial error detection and correction capabilities

15 p2707 A70-32702

Nonbinary redundant error correcting codes for improving TV transmission speed and fidelity

22 p3985 A70-42493

Picture transmitting systems noise rejection enhancement via redundancy, discussing video coding and decoding and signal filtration

23 p4159 A70-43760

Unit distance redundant counting code for single error correction or double error detection with digital equipment simplicity advantages

24 p4316 A70-45104

REDUNDANT COMPONENTS

Computer program for automatically selecting redundant parts and redundancy types for various aerospace systems characteristics

01 p0103 A70-10488

Redundant components optimal quantity determination for maximizing reliability of series system subject to multiple resource restrictions

01 p0104 A70-11383

Comparator design for triplicated attitude indicator instrumentation system in aircraft to achieve reliability, discussing system failure characteristics

02 p0224 A70-11844

Optimal redundancy for maximizing systems reliability of mixed series and parallel network consisting of N modules including I module with specified reliability cost function

03 p0585 A70-12995

Digital network reliability with redundancy to mask logic modules failure for asymmetric failure modes

03 p0454 A70-14022

Twinjet helicopter design for business transport, emphasizing redundant systems for safety and bad weather flight capability

07 p1191 A70-18844

Apollo service module engine design for maximum pilot safety, noting components redundancy

11 p2103 A70-26289

Redundant threshold logic elements synthesis based on von Neumann multiplexing principle for automatic error correction

13 p2376 A70-29940

Redundant amplifier /RAMP/ for reliability improvement

15 p2708 A70-31961

Computerized optimal redundancy analysis, considering cost, size, weight, volume, etc

15 p2712 A70-32642

Redundancy for spacecraft elements, describing various factors for priority establishment

15 p2712 A70-32643

Maintenance vs redundancy for manned space station economy, considering costing structure and time increase for maintenance

15 p2713 A70-32666

Mathematical reliability model for quasi-redundant electronic system with two failure modes for each component

15 p2769 A70-32827

Solid state phased array radar employing MIC modules in radiating elements, achieving reliability by redundancy

16 p2877 A70-33411

Design and reliability of digital systems for hard cores of fault tolerant computers /hybrid-redundant systems/, discussing advantages over multiplexed systems

[JPL-TR-32-1490]

16 p2887 A70-33734

Apollo lunar module rendezvous radar redundant gyro system for reliability enhancement, discussing principles and logic

16 p2983 A70-34066

Systems consisting of redundant and different modules, deriving vector and matrix expressions for effectiveness

17 p3099 A70-34581

Large complex system with standby components, approximating reliability by simple model substitution

17 p3099 A70-34582

Computerized metropolitan air transit system, discussing system redundancy for safety level maintenance and all-weather dependability

17 p3199 A70-34730

High reliability release mechanism with mechanical redundancy on SERT 2 satellite

17 p3174 A70-34759

Apollo ordnance systems design and reliability, stressing redundant components role

17 p3179 A70-35263

Automatic landing system assurance of DH 121 aircraft schedule all-weather regularity through high safety level via redundancy

17 p3022 A70-35856

Redundant systems reliability under wearout conditions for active and standby units, including failure rates of sensing and switching devices

19 p3438 A70-38597

All-weather Autoland control system using inertial smoothing, discussing required redundancy, fault detection, ground beam anomalies compensation, etc

19 p3469 A70-38821

Reliability of redundant repairable systems with preventive maintenance, determining mean time between failures

20 p3638 A70-40181

Optimum automatic selection of redundancies, discussing weighting and pivot choice and rigid element incorporation

20 p3732 A70-40264

Digital systems reliability improvement by redundancy at circuit and system levels

21 p3797 A70-40762

Ultrasurvivable and maintainable computer design involving redundant spare modules and own tester for aerospace applications

21 p3795 A70-41695

Strapdown inertial system mechanization and modularized instrument packaging with self contained failure isolation, temperature control and redundant components

[AIAA PAPER 70-1027]

22 p4066 A70-42315

Stochastic behavior of failed standby redundant electronic equipment with imperfect switching and opportunistic repairs

24 p4319 A70-46016

Reliability characteristics of standby redundant electronic equipment with imperfect switching and sensing

24 p4319 A70-46017

REDUNDANT STRUCTURES

REUNDANT COMPONENTS

REENTRY

NT HYPERSONIC REENTRY

NT MANNED REENTRY

NT SPACECRAFT REENTRY

REENTRY ANGLE

U ANGLES [GEOMETRY]

U REENTRY TRAJECTORIES

REENTRY BODIES

U REENTRY VEHICLES

REENTRY COMMUNICATION

Reentry plasma RF noise temperature in-flight measurements by Trailblazer 2 compared with computed data

06 p1008 A70-17568

High altitude telemetry plasma attenuation for hypersonic blunt nose slender reentry bodies

[AIAA PAPER 70-220]

06 p1010 A70-18088

Electron beam density probe calibration for earth atmospheric reentry vehicles communication

12 p2230 A70-26982

REENTRY EFFECTS

Boundary layer research during past decade covering crosshatching during reentry, transition, drag reduction by LFC or compliant surfaces

08 p1483 A70-21040

Upper stratosphere-mesosphere monthly-mean charts from reentry heating and atmospheric model based on hydrodynamics

14 p2608 A70-30590

Shock layer microwave radiation measurements during reentry flight of spherical nose cone, determining effective plasma temperature

18 p3208 A70-36694

Long range infrasound from rockets, showing two wave groups generated by launch and first stage reentry

19 p3531 A70-37694

REENTRY GLIDERS

U LIFTING REENTRY VEHICLES

REENTRY GUIDANCE

Optimal space vehicle reentry control ensuring minimum scattering of landing points based on accelerometer and free pitch-angle gyroscope data

04 p0760 A70-14431

Reentry targeting philosophy for Apollo missions emphasizing premission planning activities and real time targeting decisions, discussing Apollo 10 post-flight results

06 p1158 A70-18149

Subsonic glide landing approach guidance for unpowered lifting vehicles, using perturbation feedback and approximation of heading and position coordinates

09 p1725 A70-23253

Mathematical model for determining optimal control of spacecraft reentry into atmosphere

10 p1940 A70-24318

Reentry control algorithm for prescribed landing point of space vehicle entering earth atmosphere at parabolic velocity, discussing double-dip reentry and digital simulation

13 p2499 A70-28376

Self contained optimal control synthesis for spacecraft entering atmosphere at first cosmic speed, considering landing spots dispersion component decrease

13 p2500 A70-28407

Optimal space vehicle reentry control ensuring minimum scattering points based on accelerometer and free pitch-angle gyroscope data

13 p2503 A70-28456

Temperature rate flight control system (TRFCS) for lifting reentry vehicles control and guidance

14 p2614 A70-30464

Optimal control solution for dynamic entry vehicle along planar trajectory, using hybrid computer simulation

16 p2981 A70-33443

Optimum guidance and control law for lifting reentry bodies, investigating plane descent trajectories for minimum structural heating

16 p2982 A70-33774

Scientific satellite reentry guidance algorithms for inertial system, discussing controllability, onboard computer, gyros, accelerometers, jet actuators, terminal guidance, glide trajectory, etc

23 p4216 A70-44667

REENTRY PHYSICS

Coordination technique for pressure, density and temperature measurements by probes during parachute reentry into planetary atmospheres, taking into account reentry dynamics

01 p0197 A70-11495

Power spectrum of backscattered radiation from turbulent reentry wake illuminated by radar pulse train, discussing electron density decay and pulse shape effects

03 p0408 A70-13585

Airborne optics control subsystem (AOCS) in optical measurement program for radiation originating in reentry events in project PRESS /Pacific range electromagnetic signature study/

03 p0489 A70-13652

Electron quench additives electrophilic effects in high temperature air plasma flow, simulating reentry flight conditions

04 p0664 A70-15561

Helicoid precession in reentry problem found unstable in sense of Liapunov and Lagrange and asymptotically stable in sense of Poincare

04 p0765 A70-15666

Ablation of heat shielding materials subjected to superorbital reentry conditions, noting dependence on heating rate to surface

06 p0970 A70-18100

Three dimensional ablation calculated for reentry sphere-cone taking into account shape changes and internal heat conduction

06 p1181 A70-18150

Lifting reentry dynamic stability of flare stabilizers and flap controls

09 p1766 A70-23242

Mathematical model of microwave probe for reentry plasma, using variational method to calculate reflection coefficient

12 p2230 A70-26983

Terminal constraints affecting matrices comprising linear impulsive guidance law for earth approach, discussing Mars mission

13 p2447 A70-28516

Plasma diagnostic data from onboard Langmuir probes, reflectometers, antenna VSWR and beacon and telemetry attenuation for blunt body reentry flow field

17 p3008 A70-34495

Ablating nose equilibrium shape in laminar hypersonic flow during reentry

18 p3208 A70-36707

Multiple revolution lunar module reentry problem, analyzing isotopic systems trajectory, reentry environment, thermal response and ablation

20 p3714 A70-39540

Nonequilibrium radiation from stagnation region of high velocity spherical gas cap traveling through air

22 p4124 A70-42758

Astronautics - IAF Conference, New York, October 1968, Volume 3, Propulsion reentry physics

23 p4234 A70-45017

REENTRY RANGE

Spacecraft longitudinal control during reentry of Lunar Orbiter into atmosphere, analyzing final range prediction, trajectory tracking and accelerometers performance

01 p0197 A70-11497

Spacecraft range control algorithm during reentry at parabolic velocity into atmosphere with varying parameter distributions

01 p0197 A70-11498

REENTRY SHIELDING

Spacecraft thermal control during reentry, considering heat absorption, cooling by gas injection, radiant heat removal and shielding

04 p0780 A70-14407

Surface shielding from reentry radiation by injecting metal vapors into oxygen bearing boundary layer, calculating particle size distributions, optical depths and attenuation factors

06 p1041 A70-18163

Reinforced graphite cloth composite for reentry heat shielding of SNAP 27 isotopic heat sources, describing structure, thermal and mechanical properties and ablative characteristics

07 p1332 A70-18933

Reentry thermal protection materials technology, discussing thermophysical, thermomechanical and kinetic effects, noting interdisciplinary approach

07 p1319 A70-19878

Reentry vehicles development, discussing systems analysis and design, vehicle aerodynamics, aerodynamic heating and shielding, and flight mechanics and control

13 p2506 A70-29055

Apollo thermal protection system noting low density ablation, flight and ground tests

15 p2813 A70-32514

Static aerodynamic characteristics of slender ablating reentry vehicle, discussing coupling between flow field and thermochemical analyses of heat shield materials response

16 p3001 A70-33939

Stress wave propagation based on elasticity theory for reentry heat shield composites reinforced with unidirectional high strength high modulus fibers

19 p3537 A70-37788

Two-layer slab under aeroheating, solving bondline temperature graphically

20 p3737 A70-39693

Composite structural materials for thermal protection in reentry vehicles applications, evaluating fused quartz yarns, silicone rubber and phenolic resins

20 p3656 A70-40031

Reentry protection for radioisotope heat sources, using thermal switch of composite ceramic foam with metal impregnants

22 p4054 A70-42958

REENTRY TRAJECTORIES

Reentry trajectory dispersions due to atmospheric uncertainties determined using continuous differential equations based on atmospheric random processes method

01 p0183 A70-10846

Reentry trajectories from lunar surface and orbit obtained by computer with allowance for initial data spread

01 p0191 A70-11476

Integration time reduction for equations of motion of vehicle center of mass during parabolic reentry, using Runge principle

01 p0134 A70-11483

Spacecraft reentry trajectory optimization, considering minimum coolant weight requirement in internal cooling system

02 p0381 A70-12416

Optimum impulsive velocity calculation for three dimensional deorbit from elliptical orbits to achieve specified reentry angle

06 p1152 A70-18496

Lunar swingby trajectory analysis with atmospheric reentry, characteristics of geocentric portions of earth-moon and moon-earth transfers

10 p1940 A70-24306

Staging along reentry trajectory in atmosphere, discussing parent body and separation point influence on aerodynamic loading and heating of ejected body

11 p2124 A70-26151

Controlled missile reentry trajectory through dense atmosphere, describing digital computer solution of differential equations of motion

12 p2314 A70-27768

Spacecraft reentry trajectory reconstruction using accelerometer and onboard navigation data from Apollo flights

13 p2485 A70-28378

Stochastic optimal trajectory control for spacecraft reentry at supercircular velocity, deriving computer algorithm

13 p2499 A70-28382

Angle of attack for nearly circular reentry motion, deriving expression for lateral rates frequencies

14 p2654 A70-30779

Heating and g forces on rockets and space vehicles in descent trajectories as function of reentry velocity, achieving control by attack angle variation

15 p2812 A70-32361

Initial reentry body motion effects on angle of attack envelope value throughout trajectory, including altitude of maximum transient amplification

16 p2982 A70-33892

Lunik 16 lunar probe recovery technique, using steep angle and high deceleration reentry trajectory for unmanned capsule

23 p4257 A70-44096

Hypersonic viscous effects on space shuttle entry trajectory, measuring lift and drag in free flight regime

23 p4258 A70-44526

REENTRY VEHICLES

NT APOLLO SPACECRAFT

NT BOOSTGLIDE VEHICLES

NT GEMINI SPACECRAFT

NT LIFTING REENTRY VEHICLES

NT MARK 3 REENTRY BODY

NT MARS [MANNED REUSABLE

SPACECRAFT]

NT MERCURY SPACECRAFT

NT RECOVERABLE SPACECRAFT

NT REUSABLE SPACECRAFT

Earth and planetary entry vehicle designs for manned and unmanned space missions, noting thermal protection, environmental control requirements and communication systems

01 p0195 A70-10826

Shock tunnel type differential sensor for low range base pressure measurements on full scale flight reentry vehicles, discussing ground tests

01 p0089 A70-10843

Roll control method using recirculating base flow reaction against oriented blades or fins attached to reentry vehicle base to produce rolling moments

01 p0003 A70-10847

Radiant heat transfer in hypersonic aerodynamic heating, discussing radiant flux and carbon dioxide concentration in reentry problems

01 p0219 A70-11625

Thermal protection systems /TPS/ design criteria for maneuverable reentry spacecraft, comparing weight and cost for various alloy systems

02 p0392 A70-11940

Liquid film stability relation to angle of attack oscillations during reentry body deceleration

03 p0406 A70-12939

Optical telescope spectrograph to obtain radiometric and spectrographic data on vehicles reentering atmosphere, discussing performance criteria and tests

03 p0489 A70-13653

Image intensifiers to improve telescope system sensitivity and spectral resolution in radiometric measurements of reentry vehicles

03 p0489 A70-13654

Reentry body aerodynamic heating and thermal insulation system design, discussing analytical procedure taking into account complex geometrical configurations

04 p0616 A70-15186

Anomalous roll behavior of spinning ballistic reentry vehicles with compound aerodynamic asymmetry consisting of lateral offset combined with trim angle of attack

04 p0763 A70-15411

Acoustic technique for flow transition detection on hypersonic ablating reentry vehicles, presenting supersonic wind tunnel test results

04 p0620 A70-15531

Roll acceleration influence on angle of attack convergence and windward meridian rotation rate of rolling reentry vehicles

04 p0764 A70-15546

Real gas properties effect on base pressure of blunt nosed vehicle flying through atmosphere at high velocities

04 p0764 A70-15556

Multiple time scaling analysis of reentry roll rate and angle of attack for missiles with center of gravity and aerodynamic trim asymmetries

04 p0764 A70-15597

Thermal stresses in transversely isotropic hollow circular cylinder, applying formulas derived to reentry vehicles aerodynamic heating

04 p0779 A70-15608

Transonic dynamic stability of free flight half angle cones in wind tunnel for high drag planetary entry vehicles, discussing Mars entry trajectories [AIAA PAPER 69-105] 06 p1154 A70-17164

Dynamic stability loss on ablating vehicles ascribed to boundary layer transition effect from turbulent aft body heating [AIAA PAPER 69-106] 06 p0961 A70-17166

Estimated aerodynamic coefficients of reentry body compared with coefficients derived from Antares and Berenice flights 06 p0966 A70-17248

Porous matrix flow, surface liquid layer and hot gaseous boundary layer interactions at nose tip of reentry vehicle 06 p1037 A70-18028

Ballistic reentry vehicle roll related to trim angles caused by inertia asymmetries 06 p1156 A70-18074 [AIAA PAPER 70-204]

Viscous radiating flowfield coupled with ablation for computations on blunt body entering earth atmosphere at interplanetary return velocities [AIAA PAPER 70-128] 06 p0970 A70-18090

Aerodynamic heating of blunt-nosed reentry bodies noting effects of angles of attack [DGLR-69-0401] 07 p1392 A70-18983

Numerical methods for computing solutions in optimal control of variable lift reentry spacecraft, applying digital computer techniques 07 p1245 A70-19093

Streamwise directed vortices and crosshatched surface roles in heat transfer and ablation processes of reentry vehicles 07 p1394 A70-19729

Crew visibility requirements for rendezvous, docking and earth landing of reusable reentry vehicles [AIAA PAPER 70-262] 07 p1399 A70-20398

Integrated electron density determination for plasma sheath on reentry vehicle based on power coupling change measurement 08 p1552 A70-21596

Backscattering from rough surface of nuclear fireball measured by two way directive radar antenna on reentry vehicle 09 p1634 A70-22703

Electron density reduction in plasma surrounding reentry vehicle due to N atom removal by water droplets injection 09 p1737 A70-23237

Boundary layer transition measurements on flight tests of experimental 22 degree conical reentry vehicle with Be heat shield and graphite nose [AIAA PAPER 68-1152] 09 p1606 A70-23243

Consumable protective coat /silastene/ application to reentry models to eliminate metallic pollution in hotshot wind tunnels for spectroscopic analysis 10 p1825 A70-24548

Minuteman 3 Reentry System real time laboratory aging and surveillance test program to evaluate long-term storage effects on equipment behavior [AIAA PAPER 70-395] 10 p1952 A70-24910

Low cost launch and reentry vehicles, surveying technology and economics of spacecraft 11 p2126 A70-26286

Electron beam density probe calibration for earth atmospheric reentry vehicles communication 12 p2230 A70-26982

Reentry vehicles dynamic stability analysis involving pitch, yaw and roll motions modes coupled by asymmetries [AIAA PAPER 70-561] 13 p2341 A70-29027

Blunt heat shield effectiveness for trailing payload in reentry capsules, discussing dynamic instability effect [AIAA PAPER 70-563] 13 p2341 A70-29028

Reentry vehicles development, discussing systems analysis and design, vehicle aerodynamics, aerodynamic heating and shielding, and flight mechanics and control 13 p2506 A70-29055

Rolling reentry body velocity as function of roll, pitch, yaw rates and angle of attack 13 p2343 A70-29991

Small reentry vehicles roll motions and impact point dispersion due to spin reversal 15 p2813 A70-32522

Optimal adaptive digital autopilot design for reentry vehicle flight path control 16 p2946 A70-33307

Linearization error bound analysis in solution of equations of motion of reentry vehicle 16 p2974 A70-33319

Reentry vehicles fluidically controlled hydrazine rocket engine modules for roll rate control [AIAA PAPER 70-650] 16 p2970 A70-33617

Far wake properties of reentry body in hypersonic air flow calculated with or without chemical kinetics, using finite difference method 16 p2836 A70-33753

Static aerodynamic characteristics of slender ablating reentry vehicle, discussing coupling between flow field and thermochemical analyses of heat shield materials response [AIAA PAPER 70-826] 16 p3001 A70-33939

Reliable collet release mechanism design for separation and ejection of reentry vehicle payload from booster 16 p2922 A70-34118

Analytic theory of unsteady separated flow effects on dynamics of heat sink type reentry bodies and elastic launch vehicles [AIAA PAPER 70-762] 17 p3008 A70-34489

Free flight wind tunnel test for feasibility of hypersonic drogue deployment into reentry vehicle wake [AIAA PAPER 70-587] 17 p3060 A70-35195

Acoustic measurement for transition localization on reentry vehicles, describing apparatus and techniques 17 p3093 A70-35483

Nonpenetrative reentry vehicle nose thickness ablation sensor using gamma radiation backscatter 17 p3094 A70-35519

Signal conditioner for expanded range pressure measurements from reentry vehicles via transducer zero shift suppression and output signal compression 19 p3426 A70-37899

Launch and reentry vehicles pressure transducers, measuring propellant quantity, water systems, fuel, oxidizer, battery compartment and ascent engines, etc 19 p3430 A70-38519

Spinning blunt entry vehicles dynamic stability tests in terminal regime, discussing dependence on angle of attack [AIAA PAPER 70-988] 20 p3714 A70-39541

Asymmetric boundary layer transition effects on slender reentry vehicle motion by changing static stability characteristics [AIAA PAPER 70-987] 20 p3557 A70-39542

Liquid jets aerodynamic atomization at orifice exit in reentry vehicle into gaseous crossflow, investigating critical Weber number variation with Knudsen number 20 p3610 A70-39701

Reentry bodies of revolution subsonic and supersonic aerodynamic characteristics 20 p3558 A70-39704

Reinforced plastic composites thermal protection and ablative performance in high temperature environments for reentry vehicle applications 20 p3656 A70-40029

Reentry vehicle with multicomponent gas mixture injection, calculating heat and mass transfer correlations for stagnation point flow 21 p3945 A70-41033

Ballistic reentry vehicle roll-pitch coupling, showing influence of nose asymmetries [AIAA PAPER 69-101] 21 p3930 A70-41736

Reentry vehicle recovery deployment initiation, comparing performances of conical wake drogue and body attached spoilers hypersonic deceleration devices [AIAA PAPER 70-1207] 21 p3752 A70-41811

REFERENCE ATMOSPHERES

Variable atmospheric attenuation of 5 mm wavelength band, considering oxygen absorption spectrum and attenuation for reference atmosphere 02 p0260 A70-12570

Sonic boom wave shapes and amplitudes determination in still stratified atmosphere, comparing U.S. standard atmosphere results to various atmospheric models 03 p0411 A70-12927

REFERENCE SYSTEMS

North American datum related to geocentric satellite reference system, using Lambek method for geodetic parameters 05 p0841 A70-16644

Cosmological gravitation theory for uniformly expanding universe model providing fundamental reference frame and acceleration field 08 p1563 A70-20497

Selenodetic control systems orientation based on lunar features correlation with reference stars, considering ephemeris times corrections 08 p1572 A70-20941

Selenocentric coordinate system originating at center of mass, determining lunar figure center from photographs with reference stars 08 p1572 A70-20942

Liapunov direct method for synthesizing self adaptive model reference control system with simultaneously used passive /signal/ and active /parameter/ adjustment loops 08 p1480 A70-21018

Schwarzschild metric properties in synchronous reference system, using succession of Schwarzschild interval holonomic transformations as function of gravitational radius 08 p1545 A70-21406

Multipole analysis applied to 1965 International Geomagnetic Reference Field, separating secular variation field into drifting and nondrifting components 09 p1666 A70-22065

Televor principle for radial radio coordinates production in all frequency bands, discussing ring antenna feeds 09 p1722 A70-23033

Satellite navigation method for locating Mars landmark or target point for exploration by roving vehicle located as center of coordinate system 11 p2080 A70-26213

Reference systems for two dimensional visual indications as correction device for pilot guidance errors associated with rotation effects 12 p2177 A70-27036

Einstein equations derivation in comoving reference frame for spatially homogeneous gravitational fields 12 p2310 A70-28221

Visual display reference system rotation effect on control quality and tracking error compensation using stick signal control 14 p2540 A70-30249

Selenodetic control systems orientation based on lunar features correlation with reference stars, considering ephemeris times corrections 15 p2806 A70-32753

Selenocentric coordinate system originating at center of mass, determining lunar figure center from photographs with reference stars 15 p2806 A70-32754

Holographic device for satellite attitude determination, providing three axis reference information in analog or digital form from single star field sampling 16 p2946 A70-33158

Satellite equations of motion in noninertial instantaneous astronomical system, taking into account perturbation equations terms 17 p3155 A70-34684

Piezoelectric accelerometer reference systems calibration by function separation 17 p3089 A70-35173

Weak nonlinear one dimensional wave propagation in nonequilibrium flow, using governing system characteristics for reference coordinates 17 p3071 A70-35468

Computer program transforming spherical harmonic coefficients into arbitrarily tilted coordinate systems, tabulating coefficients of International Geomagnetic Reference Field 1965 in dipole coordinate system 20 p3621 A70-39353

Einstein equations derivation in comoving reference frame for spatially homogeneous gravitational fields 20 p3710 A70-40096

Hybrid fluidic heading reference system with negative feedback servo loop around vortex rate sensor [ASME PAPER 70-FLCS-10] 22 p3963 A70-42417

Varian HA-100 spectrometer eliminating phase change by compensation network in synchronous audio detector reference signals 23 p4199 A70-44949

REFERENCES [STANDARDS]

U STANDARDS

REFINING

NT ELECTROREFINING

NT ELECTROSLAG REFINING

Grain refining of continuously cast Al by additions of B and Ti 02 p0309 A70-12299

Small high temperature rotary plasma-heated furnace for refractory material high purity processing, discussing design and operation 22 p4005 A70-42368

REFLECTANCE

Icarus surface reflectivity estimated from reflected light polarization, combining estimate with inferred absolute magnitude to obtain radius 01 p0180 A70-10537

Optical measurements of mirrors reflectance and solar radiation transmittance to solve problems specific to solar energy engineering by standard optical equipment 01 p0010 A70-10765

Ionospheric reflection coefficients calculations by two full wave theory, using related monoenergetic and collisional frequency profiles and 10-100 kHz frequencies 01 p0076 A70-10870

Reflection coefficient of electromagnetic wave reflected from thin ionization layer, using frequency dependence of amplitude to estimate ionospheric layer thickness 01 p0083 A70-11532

Doppler radar spectrum mean and variance derived for reflectivity gradients combined with linear wind shear velocity gradient 02 p0328 A70-12508

Kerr physical optics formula usefulness for calculation of radar reflectivity of metallic bodies of revolution in terms of electric and magnetic dipoles 02 p0262 A70-12598

Transmission and reflection coefficients of propagating whistler modes for model ionosphere 05 p0837 A70-15880

Normal incidence reflectance of BeO single crystals, analyzing data by Kramers-Kronig inversion for dielectric function and energy loss function 05 p0891 A70-16047

Reflection coefficients of circular posts in rectangular waveguides computed by Green function and method of moments 05 p0820 A70-16384

- Reflection of clean and fluoride coated aluminum surfaces in vacuum UV 05 p0883 A70-16590
- Reflection coefficients, radiation patterns and surface wave excitation calculated from aperture electric field obtained for waveguide radiating through dielectric slab 06 p1020 A70-17561
- Transmission and reflection coefficients calculated for electromagnetic waves incident on inhomogeneous absorbing layer applicable to ionosphere, plasma and p-n junction 06 p1009 A70-17834
- Reflection coefficient for radio wave pulse reflected from ionosphere with large scale fluctuations in electron density, compared to empirical data for reflecting surface irregularities 07 p1231 A70-19170
- Ionospheric reflection coefficients from vertical and oblique incidence pulse amplitude data, discussing night conditions effect on Ottawa pulse transmissions 07 p1232 A70-19176
- Time variations of reflectance measured for carbon dioxide laser beam splitters 07 p1302 A70-20095
- Radio wave reflection coefficient power spectra for three layer lunar surface models consistent with radar spectrum, calculating porous layer thickness 08 p1565 A70-20566
- Solar radiation reflection function for plane-parallel atmosphere with isotropic phase function calculated by successive scattering method, noting application to planetary atmospheres 08 p1571 A70-20909
- Open cut-off rectangular resonator calculated for frequency dependence on reflection coefficient and relative length 09 p1648 A70-23165
- Waveguide master short circuit devices reflection coefficient measurements by microcalorimeter 09 p1638 A70-23322
- Fluorescent integrating sphere for absolute hemispherical reflectance measurements on imperfectly diffuse surfaces in vacuum UV, eliminating erroneous signals by filtering 09 p1729 A70-23527
- Diffraction of plane cylindrical and spherical waves in wedge-shaped regions with reflecting edge, using asymptotic expansions 10 p1911 A70-25186
- Particle size distributions used in analyzing snow size spectra and radar reflectivity 11 p2004 A70-25651
- Bidirectional reflectance of three dimensional surfaces described by diffuse triangular subareas network for spacecraft thermal design, giving numerical technique 11 p2084 A70-26354
- Relative permittivity of small thickness dielectric substrate plates determined from reflection coefficient in rectangular waveguides 11 p2011 A70-26603
- Electromagnetic scattering from underdense plasma slabs with randomly varying dielectric constant, calculating reflection coefficient 11 p2095 A70-26763
- Cotton leaf light reflectance and transmittance changes with maturity 12 p2218 A70-26919
- Mathematical model of microwave probe for reentry plasma, using variational method to calculate reflection coefficient 12 p2230 A70-26983
- Semiinfinite parallel plate waveguide modes reflection coefficients with propagation constants near cut-off and excited at open end for microwave optical frequency range 12 p2198 A70-27959
- Bragg reflecting crystals for spectroscopy and polarimetry in X ray astronomy 13 p2489 A70-28904
- Ice radiation and reflection characteristics in IR spectral region at certain Brewster angles 14 p2568 A70-30133
- Reflectivity measurement in near IR using black bodies near room temperature for light sources 14 p2588 A70-31210
- Reflection of single leaves and field plots of cotton, determining Cycocel treatment effects on aerial IR photography 14 p2577 A70-31233
- Visual reflectance of wet soils, attributing darkening to internal reflection of radiation in water layer enveloping soil particles 14 p2577 A70-31236
- Radio wave reflection coefficient power spectra for three layer lunar surface models consistent with radar spectrum, calculating porous layer thickness 15 p2805 A70-32721
- Finite parallel plate waveguide arrays edge effects, comparing element radiation patterns and reflection coefficients vs scan 16 p2860 A70-32953
- Reflection coefficient formula for principal radio wave reflected from thin long rod in middle of rectangular waveguide 16 p2878 A70-33800
- Monochromatic radiation angular distribution surface reflectance measurement using photographic reflectometer [ALAA PAPER 70-859] 16 p2912 A70-33904
- Bidirectional reflectance and transmittance calculation for irradiated layer of monodisperse matrix suspended pigment particles [ALAA PAPER 70-839] 16 p2940 A70-33923
- Synchronous measurements of reflection coefficient and frequency characteristics of sporadic E layer by ionospheric sounding 18 p3247 A70-36293
- Electromagnetic wave scattering on resonant dielectric sphere in rectangular waveguide, using reflection coefficient 18 p3227 A70-36419
- Reflectivity effect on external quantum efficiency of Fabry-Perot type GaAs injection lasers 18 p3268 A70-36731
- Reflectance measurements of directional spectral emittance of black body cavities with specific geometries, using laser source and integrating hemi-ellipsoid 20 p3627 A70-39091
- Reflectivity index meter for materials at room temperature under oblique light incidence 20 p3632 A70-39638
- Optical reflection measurement at grazing incidence from shock front at Mach 1.94 in air at atmospheric pressure 20 p3674 A70-40167
- Plane wave diffraction by periodic array at boundary between two media, discussing asymptotic behavior of reflection and transmission coefficients 21 p3806 A70-40614
- Surface contamination and degradation effect on reflectance of evaporated vacuum UV mirrors and temperature control coatings under simulated space environments 21 p3842 A70-40815
- Script-F radiative interchange matrix for enclosures with arbitrary surface emission and reflection characteristics 21 p3944 A70-41020
- Lunar rocks mineralogy and visible and near IR reflectivity, discussing depression in telescopic curve 21 p3912 A70-41637
- Total reflectance of composite light diffuser with nonuniform absorption by two beam model, noting application to photochemistry 21 p3829 A70-41936
- Lunar crater Plato optical reflectance photoelectric measurements, discussing absorption and luminescent features, radiance factors, phase angles color variations and brightness 21 p3922 A70-41983
- Visible and near IR radiation reflectance from vegetation, discussing incident solar radiation plant structures, leaf areas shadows and absorption by chlorophylls 22 p4014 A70-42767
- Stepped termination design for rectangular waveguides achieving minimum length and maximum reflection coefficient 23 p4169 A70-43783
- Millimeter band electromagnetic scattering from weakly doped GaAs, calculating reflection coefficient and phase angle 23 p4229 A70-43926
- Electroreflectance at CdS-electrolyte interface, noting field strength effect on relaxation time 23 p4230 A70-43930
- Potassium acid phthalate crystal X ray spectrometric properties measurements, discussing parallel position rocking curves and reflection coefficients 23 p4230 A70-44420
- Planar conducting screen with periodic rectangular perforations, determining transmission and reflection coefficients and aperture field distribution 24 p4311 A70-45219
- Light reflectance from optically inhomogeneous medium due to space charge near semiconductor surface 24 p4390 A70-45661
- REFLECTED RADIATION**
- U REFLECTED WAVES**
- REFLECTED RAYS**
- U REFLECTED WAVES**
- REFLECTED WAVES**
- Reflected solar energy measurements by ATS satellites applied to meteorological research, emphasizing high area resolution and dynamic range of cameras 01 p0094 A70-11297
- Cosmos 149 meteorological satellite telephotometers for measuring reflected solar radiation from earth 01 p0095 A70-11612
- Solar UV radiation reflected from Echo satellites measured and compared with UV fluxes from Lyrae 01 p0095 A70-11614
- Electrical conductivity of air behind incident and reflected shock wave fronts as function of temperature and Mach numbers measured by electrode method 01 p0095 A70-11622
- Arc phenomena for producing interaction effects, discussing reflected shocks rarefaction waves and gas dynamics 02 p0345 A70-11863
- Visible radiation reflection, transmission and inside intensities of terrestrial clouds calculated by Monte Carlo program utilizing scattering phase function 02 p0326 A70-12286
- Forward air cushion performance of tracked hovercraft entering tunnel, determining arrival of reflected expansion wave at vehicle front 02 p0226 A70-12313
- Whistlers paradoxical behavior in bounded magnetoplasmas, discussing double reflection and wave propagation 02 p0263 A70-12733
- Interference wave formula for multiple reflections from smooth inhomogeneous region with arbitrary boundary 03 p0442 A70-13093
- Energy transfer formula and scattering of electromagnetic waves at ideally reflecting bodies in inhomogeneous medium using geometrical optics approximation 03 p0442 A70-13094
- Shadow optical raster method for quantitative investigation of dynamic stress states in two dimensional transparent or reflecting bodies 03 p0496 A70-14215
- Reflected shock wave velocity, boundary layer disturbance and wall ionization measurements using thin film resistance thermometers 04 p0666 A70-14537
- Flow fields construction for normal shock waves with nonequilibrium chemical reactions reflected from shock tube end wall [ALAA PAPER 68-732] 04 p0674 A70-15537
- Absorption coefficient 5-step model applied to shock tube measurements of end wall radiative heat transfer behind reflected shock waves in air 04 p0787 A70-15606
- Impact against elastoplastic blank allowing for base and striker compressibility, giving solution in region of plane wave first reflection from base 05 p0947 A70-17016
- Reflected waves development during shock waves collision and during shock collision with constant temperature wall, using Monte Carlo method 06 p1109 A70-17520
- Laser radiation diffuse reflection from rough surfaces, considering surface specularly and reflected waves polarization and spatial structure 09 p1696 A70-22630
- Reflection patterns of solar radiation from cloud, water and land surfaces measured by airborne radiometer, observing anisotropy 09 p1671 A70-23523
- Antenna array circular polarization adjustment using reflections from horn radiator and mirror 09 p1650 A70-23633
- Temperature, pressure and electron density measurements behind reflected shocks in gas driven diaphragm shock tube compared with Rankine-Hugoniot predictions 10 p1967 A70-23960
- Reflected shock wave structure and velocity at rigid wall, assuming radiative heat transfer as dissipative process 10 p1967 A70-24018
- Test model thermal balance in space simulator, measuring effects of solar simulator irradiance reflected from carbon dioxide cryopanel deposits [ALAA PAPER 69-1012] 11 p2149 A70-26153
- Monograph on acoustic theory for determining frictional pressure drop effect on gas state behind reflected wave in shock tube 12 p2209 A70-27000
- Reflected light directional diagram effects on scintillating surface luminescence yield, considering scattering function gradient 12 p2231 A70-27310
- Sun glitter on sea surface from space photographs, considering wind and sea conditions effect on shape and brightness of patterns 14 p2572 A70-30345
- Field characteristics of solar radiation reflected and scattered into outer space by earth atmosphere, discussing brightness and angular distribution of outgoing component 14 p2603 A70-30406
- Sonic boom incident and ground reflected waves action on exterior wall, calculating arrival time as functions of aircraft speed and altitude and wall slope 14 p2566 A70-30861
- Monograph on nozzle design effect on starting process initiated by plane shock wave in reflected shock tunnel 15 p2672 A70-31692

- Polarization characteristics of solar radio waves reflected from coronal waves in meter wavelength range 15 p2802 A70-32485
- Laser beam photography by multiple reflections from partially reflecting mirrors 16 p2913 A70-33985
- Reflected shock waves generation by shock produced plasma flow interaction with strong magnetic fields, determining electron density and ionization relaxation times [ALAA PAPER 70-761] 17 p3139 A70-34490
- Ionospheric D region irregularities with partially reflected radio wave pulses, using phase path and drift measurements 21 p3814 A70-40941
- Plasma heating by ionizing shock waves reflected by transverse magnetic field barrier, discussing discontinuity resolution 21 p3857 A70-41381
- Spurious photomultiplier response to short intense overexposure of atmospheric return using optical radar 21 p3828 A70-41474
- Ultrasonic Rayleigh critical angle reflectivity of liquid-solid interface energy, detecting near-surface properties changes 22 p4027 A70-42585
- Starting shock and contact surface measurement reflection nozzle, using HF spark camera and interference techniques [SMPTF PREPRINT 89] 22 p3959 A70-43064
- Remote sensing of returning reflected and diffracted seismic waves illuminating layered rocks subsurface, discussing data visual display 22 p4018 A70-43085
- Coherent reflection waves produced by radio wave propagating through entire earth atmosphere 23 p4159 A70-43757
- Polarization characteristics of solar radio waves reflected from coronal waves in meter wave length range 23 p4240 A70-43909
- Anomalous multiple reflections from ionosphere showing concave surface focusing 23 p4164 A70-44374
- Local thermal equilibrium validity for electron temperature and density determination in reflected shock waves in He plasma, comparing laser scattering and spectroscopic methods 23 p4229 A70-44986
- Atmosphere and earth-reflected solar radiation pressure effects on high altitude satellite orbits 24 p4408 A70-45555
- Satellite orbit perturbation due to earth reflected or reradiated solar radiation pressure 24 p4409 A70-45556
- Cold boundary layer effect on chemical kinetic parameters behind reflected shocks in single-pulse shock tube 24 p4323 A70-46044
- ### REFLECTING TELESCOPES
- Lund astronomical observatory, describing Cassegrain-Nasmyth reflector and attached electrophotometer for stellar measurements 02 p0275 A70-12061
- Photometric measurements in Cygnus, analyzing formulas used for conversion to standard UVB system for Javan reflector Sweden 02 p0297 A70-12065
- Cassegrainian liquid He cooled IR telescope for rocket-borne IR astronomy, discussing optical, cryogenic and electronic designs 04 p0689 A70-15017
- Telescopic paraboloid mirrors optical distortion from surface deformation due to gravity loads 07 p1281 A70-19254
- Solar observatory at San Fernando Valley, describing evacuated aperture reflecting telescope function and design, data recording cameras, etc 09 p1688 A70-23772
- Temperature insensitive telescope with metallic mirror at Milan-Merate Observatory 10 p1889 A70-24584
- Dynamic stability of multipoint servocontrol system actuating thin deformable primary mirror of orbiting telescope 12 p2203 A70-27413
- Size and cost of Al mirror IR photometric telescopes optimized for scientific information acquisition 14 p2586 A70-30896
- Shemakha observatory telescope main mirror spherical aberration, coma, astigmatism and light concentration, describing support system and adjustment and control mechanisms 15 p2738 A70-32203
- Reflecting X ray telescopes with glancing incidence mirror, discussing design, manufacture and testing 16 p2904 A70-33150
- Primary mirror development problems for large orbiting telescopes 17 p3083 A70-34873
- 1620 Geographos observations using Ritchey-Chretien reflector and Curtis Schmidt telescope 17 p3171 A70-35446
- X ray source optical identification, discussing reflector optics, photometry and spectrography 21 p3873 A70-40671
- Tilted-component corrected off-axis telescope design based on third-order aberration theory 21 p3822 A70-40818
- Optical telescope reflecting prism angle deviations effect on modulation transfer function and image quality 22 p4072 A70-42506
- Spheroidal three mirror telescopes distortion involving dioptrics combination 23 p4194 A70-44213
- ### REFLECTION
- NT INFRARED REFLECTION
- NT RETROREFLECTION
- NT SIGNAL REFLECTION
- NT SPECULAR REFLECTION
- NT ULTRAVIOLET REFLECTION
- NT WAVE REFLECTION
- Near IR reflection spectra of artificial cumulus clouds with progressive droplet sizes 01 p0076 A70-10911
- Reflected molecular beam intensity distribution interpreted in terms of disturbances in boundary layer between gas and solid 07 p1343 A70-20122
- Crystalline structure effect on molecular beam reflection from rough polycrystalline Au surfaces 07 p1343 A70-20123
- Electron density measurements by partial reflection and rocket techniques during 20 May 1966 solar eclipse, showing agreement below 82 km height 15 p2726 A70-31869
- Plasma reflection edge in thin film InAs semiconductors, calculating refractive index and extinction coefficient from free charge parameters 15 p2783 A70-31966
- Monte Carlo model of V groove surface roughness effects on directional reflections in plane of incidence, employing energy localization circle [ALAA PAPER 70-820] 16 p3002 A70-33944
- Atomic oxygen beams interaction with various surfaces at low pressure, discussing reflection probability and recombination reactions 18 p3225 A70-36187
- ### REFLECTION COEFFICIENT
- U REFLECTANCE
- ### REFLECTIVITY
- U REFLECTANCE
- ### REFLECTOMETERS
- IR region spectral hemispherical emittance of surfaces measured by bihemispherical reflectometer [ALAA PAPER 70-820] 06 p1107 A70-18205
- Near IR reflectance spectrometer integrated into environmental chamber to study frost spectral properties 06 p1072 A70-18522
- IR reflectometer system using Fourier transform spectrometer and ellipsoidal mirror, describing design, construction and performance 16 p2905 A70-33171
- Monochromatic radiation angular distribution surface reflectance measurement using photographic reflectometer [ALAA PAPER 70-859] 16 p2912 A70-33904
- Reflectivity index meter for materials at room temperature under oblique light incidence 20 p3632 A70-39638
- Modified time-domain reflectometer method for waveguide system evaluation, detecting and displaying radar echoes as function of time 24 p4315 A70-46234
- ### REFLECTOR SATELLITES
- U PASSIVE SATELLITES
- ### REFLECTORS
- NT PARABOLIC REFLECTORS
- NT PARABOLOID MIRRORS
- NT RADAR CORNER REFLECTORS
- NT RADAR REFLECTORS
- NT SOLAR REFLECTORS
- Reflector radio telescope of Pulkovo Astronomical Observatory noting high resolution 01 p0094 A70-11585
- Modified Smith-type reflector for long laser cavities using etalon without coatings instead of usual beam splitter, discussing output characteristics 03 p0501 A70-13648
- French laser reflectors for lunar telemetry functioning with ruby laser, discussing applications to lunar orbital parameters, continental drift, gravity constant secular variations, etc 04 p0700 A70-14609
- Mode patterns and losses for laser resonator with identical tilted spherical rectangular reflectors in stable and unstable configurations 04 p0701 A70-15021
- Carbon dioxide laser resonator design and operation, discussing performance with dish reflector made of leucosapphire 05 p0859 A70-16272
- Antenna noise temperature of large aperture reflectors from feed system RF characteristics, discussing spillover and blockage factors 06 p1008 A70-17506
- Deep reflector antennas mode composition by graphic computer techniques for maximum efficiency feed matches 06 p1021 A70-17575
- Spatiotemporal correlation functions of random intensity field during diffuse scattering of coherent radiation by moving reflector 06 p1009 A70-17810
- Paraboloidal- and spherical-reflector antennas efficiency optimization obtained from optimum combination of amplitude and phase of hybrid modes propagating in guide 07 p1240 A70-19220
- End reflectors effects on ruby lasers emission spectra and kinetics 07 p1300 A70-19873
- Low pass filter structure of focusing reflectors designed for quasi-optical system, noting energy absorption 08 p1476 A70-21287
- Aberration-correcting line source feed for spherical reflector using linearly polarized light waveguide array 09 p1646 A70-22694
- Square Van Atta reflector with/without conducting plate used for mounting antenna half wave dipoles, considering scattering cross sections 09 p1646 A70-22695
- Reflector focus location for variable profile antenna of radio telescope determined by modified Hartmann method in optics field 09 p1648 A70-23164
- Aluminized epoxy integrating hemiellipsoidal reflector, discussing fabrication, focusing properties and selection of detector size 09 p1683 A70-23530
- Wide angle emitter images transformation into circular by reflecting cone and lens system, describing photographic and photoelectric methods 12 p2237 A70-28157
- Electromagnetic field intensity measurements in focal region of wide angle spherical reflector antenna illuminated by polarized plane wave 16 p2872 A70-32976
- Mathematical model of heat flux absorbed by heated part in radiant heating reflector systems, considering shape, spectral, directional and polarizing effects [ALAA PAPER 70-818] 16 p3002 A70-33945
- Antenna reflectors of evolution and double curvature optimization by iteration method 16 p2866 A70-34267
- Reflector antennas analysis, design principles and uses, with emphasis on paraboloidal and spherical reflecting surface types 17 p3052 A70-35068
- Periodic resonant reflector with thin air intervals for YAG-Nd pulsed laser for retinal safety 19 p3445 A70-37673
- Gratings as laser wavelength-selective end reflectors, noting application to carbon dioxide and dye lasers 20 p3639 A70-39083
- Millimeter wave reflector antennas, considering various system designs, performance, pointing capabilities, limitations and applications 20 p3599 A70-40309
- Initial value transport of monoenergetic neutrons migrating in slab with infinite reflectors for isotropic scattering as function of material properties 21 p3854 A70-41999
- Reflectors group mean effective scattering cross section measurement by far field criterion 22 p3995 A70-42387
- Near field vector evaluation of Fresnel zone field for microwave reflector antennas 23 p4161 A70-43771
- Octave bandwidth unidirectional circularly polarized reflector antenna, using crossed conical dipoles near second resonance 23 p4176 A70-44970
- Reflector materials flow size and orientation using ultrasonic spectral frequency analysis 24 p4335 A70-45573
- ### REFLEXES
- NT CAROTID SINUS REFLEX
- NT RESPIRATORY REFLEXES
- Temporary interneuron connections mechanisms during conditioned reflexes development 01 p0025 A70-11040
- Critical duration for pupillary light reflexes measured with IR scanning pupillometer using various flash duration stimuli 02 p0237 A70-12458
- Conditioned reflexes, respiration and heart beat rates changes in white rats under hypothermia 03 p0424 A70-13717
- Complex conditioned reflexes to three component visual-acoustic-tactile stimulus in dogs analyzed by secretory and thermoelectrical techniques 04 p0638 A70-15504

Human unloading reflex, using experimental setup unloading muscle without tension increase
06 p1000 A70-17450

Pavlovian conditioned reflexes theory reappraisal, discussing cortex-subcortical formations interrelations models
07 p1197 A70-18694

Amysyl effects on conditioned passive avoidance reflexes development and reinforcement in white mice under electric shock
07 p1198 A70-18717

Anticerebral cytotoxic serum effect on white rats conditioned reflex activity
07 p1199 A70-18727

Canines conditioned reflex activity as function of cortex sections following head exposure to X ray irradiation
07 p1199 A70-18729

Delayed trace reaction under stable and unstable pauses in apes and monkeys, noting independence of conditioned reflex
08 p1446 A70-21446

Nervous control of unconditioned cardiovascular reflexes during ontogenesis in children, observing sympathetic and vagal tonicity
08 p1446 A70-21449

Bioelectrical activity of brain during conditioned motor reflex system operation modes in response to stimulating light pulses
08 p1447 A70-21450

Conditioned reflexes, respiration and heart beat rate changes in white rats under hypothermia
11 p1985 A70-25517

Human blinking reflex recorded by electromyography, studying latent period in response to stimulation by air stream
12 p2168 A70-27346

Age and retinal illumination influence on human pupillary near reflex investigated by photographic measurements
12 p2171 A70-28036

Electrical activity of visual cortex, subcortical structures and reticular formations in cats during conditioned reflex stimulation by light
12 p2173 A70-28351

Dynamic interaction between stored and active memory images in apes and monkeys with conditioned alimentary motor reflexes stimulated by visual signals
12 p2173 A70-28352

Threshold excitation of cutaneous analyzer in man under vascular conditioned reflexes in response to acoustic signals with shock
12 p2173 A70-28353

Human proprioceptive reflexes fluctuations correlation with spontaneous respiration and cardiovascular rhythms
13 p2350 A70-29323

Human proprioceptive reflexes fluctuations during controlled respiration and voluntary apnea
13 p2351 A70-29324

Conditioned reflex type fear reaction by electric stimulation of hippocampus in cats
14 p2535 A70-30184

Vestibular nystagmus evocation by conditioned reflexes technique after pure tone stimulation
14 p2538 A70-30910

Thermoregulatory vasodilation conditioned reflexes developed by combination of prolonged physical and acoustic stimuli
15 p2679 A70-31606

Human and animal adaptation and responses to time intervals and temporal activity cycles, discussing conditioned reflexes in terms of physiological factors
15 p2687 A70-32869

Spinal reflex activity in normal and altitude exposed cats before, during and after acute hypoxia
17 p3031 A70-35430

Human muscular function in conditioned and unconditioned thermoregulatory reflex changes of gaseous metabolism during repeated cooling
18 p3218 A70-36528

Latent period of human motor reflex in telegraph key press testing in response to oral command
18 p3222 A70-37218

Soviet monograph on secondary signaling system role in development of speech, thought, conditioned and unconditioned reflexes, human will and hypnosis, noting salivary gland function
19 p3359 A70-37407

Normal human postural control system reflex response to tendon jerk disturbance
22 p3979 A70-43495

Mammal and human acoustic reflex for impulsive sound, investigating immunization effectiveness
24 p4297 A70-45373

REFRACTED RADIATION
U REFRACTED WAVES
REFRACTED RAYS
U REFRACTED WAVES
REFRACTED WAVES

Emission from broadband impulsive point source refracted by spherical interface between fluids with different acoustic velocities, showing emitted and inverse waveform disturbances
01 p0046 A70-11190

HF cylindrical waves propagation by line source in stratified medium, investigating refraction and diffraction at plane boundary using mathematical and ray methods
07 p1335 A70-19683

Doppler-effect-like phenomena of waves or pulses reflected and refracted at moving boundary layers
09 p1728 A70-23072

Seismic refraction profiles of ash flow in Valley of Ten Thousand Smokes, Alaska, obtaining P wave velocities
14 p2573 A70-30493

Plasma refractive index determination by propagation method allowing simultaneous electron concentration and density measurements by reflected damped wave
14 p2622 A70-30658

Shock wave nonlinear refraction by upstream disturbances in two dimensional steady nonuniform flow
20 p3608 A70-39354

REFRACTING TELESCOPES

Chromatic aberrations of Poltava observatory AVR-2 refractor
08 p1496 A70-21161

Large photographic telescope characteristics for stellar and planetary observations, noting differential refraction influence on plate scale factors
18 p3259 A70-36608

Mercury drawings from refractor observations during 1964-1967
18 p3315 A70-36611

REFRACTION

NT ATMOSPHERIC REFRACTION

NT BIREFRINGENCE

NT RADIO WAVE REFRACTION

Book on electromagnetic waves in stratified media covering reflection, propagation, waveguide mode theory, superrefraction and tropospheric ducting
20 p3586 A70-39604

REFRACTIVE INDEX

U REFRACTIVITY

REFRACTIVITY

Clear air layer type radar echoes intensities compared with refractive index variations in troposphere
01 p0045 A70-10331

Focusing factor dependence on range in spherically stratified medium with linearly varying refractive index profile, including earth atmosphere
01 p0142 A70-10490

Carbon dioxide refractivity measured under simulated Martian conditions and standard temperature and pressure, comparing results with radio occultation methods
01 p0186 A70-11085

Thermodynamic aspects of ray invariance of spectral brightness ratio to square of local index of refraction compared to black body power radiation
01 p0144 A70-11293

Specular reflections influence on bistatic tropospheric radio scatter from turbulent perturbations in refractivity
02 p0326 A70-12289

CuCl single crystal refractive index measurement at room temperature using V-block refractometer
02 p0350 A70-12453

Quantitative interpretation of three dimensional weakly refractive phase objects using holographic interferometry, determining index of refraction
02 p0300 A70-12464

Statistical measurements of deformation structures and refractive indices in experimentally shock loaded quartz specimens with different crystallographic orientations
02 p0292 A70-12509

Superrefractive layer development at 3000 ft during radio refractive index profile measurements by microwave refractometer carried on aircraft, producing enhanced signals
02 p0261 A70-12591

Refractive index perturbation from energy absorbed from long pulsed and Q switched Nd doped glass lasers, observing sonic waves generated by Q switched laser
03 p0498 A70-13156

Three dimensional structure determination for weakly scattering semitransparent objects from holographic data, discussing inverse scattering problem and refractive index calculation
03 p0487 A70-13647

Scattered light photoelastic stress analysis using doubly refracting materials and lasers
03 p0594 A70-13657

Refractive index profile analysis for hypergeometric functions solutions for vertically polarized electromagnetic waves propagating in horizontally stratified isotropic media
04 p0647 A70-14616

Integrodifferential equation solved for plane wave reflection and transmission by random medium assuming homogeneous background refractive index
04 p0649 A70-14970

Solid carbon dioxide measured for complex index of refraction at IR wavelengths
04 p0719 A70-15036

Phase and amplitude level of plane light wave propagation in medium with randomly discontinuous refractive index, discussing wave phase dependence on dielectric constant
04 p0650 A70-15288

Saturation induced wave front distortions effect on beam divergence and frequency modulation in laser amplifiers, discussing refractive index changes
04 p0703 A70-15620

Density, refractivity, thermal expansion coefficient, softening point and soaking stability for glass containing barium, lead, boron, bismuth and titanium oxides
05 p0871 A70-16594

Telescope resolution limit dependence on refractive index mean square fluctuation and effective aperture in turbulent medium
06 p1067 A70-18396

Refractive index variations effect on backscattering, scattering and attenuation cross sections of ice sphere at various low temperatures
08 p1536 A70-21098

Atmospheric structure and turbulence relations to radar backscattering from clear air refractive index irregularities
09 p1715 A70-22361

Atmospheric fine-scale structure determination from forward scatter radio wave propagation, considering refractive index role
09 p1715 A70-22362

Tropospheric refractive index homogeneity from beam-swinging experiments, noting relationship to meteorological parameters and height
09 p1715 A70-22363

Potential refractive index mean vertical gradients role in turbulent mixing, noting applications to radar detection of CAT
09 p1716 A70-22365

Radar backscattering relationship to refractive index microstructure in turbulent clear atmosphere
09 p1716 A70-22366

High resolution FM-CW radar sounder for tropospheric refractive index studies, describing equipment design and performance and clear air scatter observations
09 p1716 A70-22368

Refractive index chart for scattered electromagnetic fields from sphere, evaluating modal coefficient for lossy materials
09 p1633 A70-22697

Refractive index variation regions and mapping along propagation path in random medium, noting application to solar wind electron density structures measurements
09 p1634 A70-22699

Turbulent medium refractive index fluctuations effect on parameters of focused plane light wave, calculating diffraction patterns center of gravity
09 p1636 A70-23138

Intense light effect on refractive index of potassium niobate crystals
09 p1698 A70-23317

Single and clad glass fibers radii and refractive indices measurements on basis of laser light scattering
09 p1699 A70-23444

Grand tour space probe optics for observation of objects on planet, considering atmospheric refraction indices effect
09 p1700 A70-23768

Eye spherical, cylindrical and spherocylindrical refractive errors incidence at various visual acuity levels, tabulating standards
10 p1810 A70-24035

Carbon dioxide dissociation effects on refractive index gradients and decay rates in pulsed carbon dioxide-nitrogen laser mixture
10 p1900 A70-24602

Interferometric stress analysis in three dimensional photoelasticity, including practical measurements and analysis in terms of refractive index
12 p2326 A70-27621

Servocontrolled IR optometer providing electrical signal proportional to refractive power of human eye
12 p2237 A70-28123

Balloon-borne measurement of troposphere refractive index vertical distribution using spaced-cavity refractometer
13 p2394 A70-28789

Atmospheric difference measurements interpretation in terms of radio refractive index spectra at single point based on corresponding frequency component ratio
13 p2394 A70-28790

Savart interferometer for high sensitivity measurements of refractive index gradients using double exposure technique
14 p2583 A70-30400

Plasma refractive index determination by propagation method allowing simultaneous electron concentration and density measurements by reflected damped wave
14 p2622 A70-30658

Obliquely incident spherical wave amplitude and phase fluctuations, deriving formulae to compare vari-

ances behavior for refractive index fluctuation autocorrelation functions 14 p2574 A70-30750

Book on microwave propagation physics covering unbonded homogeneous medium, terrain effects, uniform refractivity gradient, nonstandard refractivity, fading, etc 14 p2551 A70-30953

Air cell optical phase shifter for holography based on refractive index variation with air pressure 15 p2741 A70-32439

Microwave propagation refractive index over India, showing influence of humidity and vapor pressure 15 p2701 A70-32470

Refractive index and group velocity in moving dispersive half space /cold plasma or dielectric/ under incident wave from vacuum 16 p2859 A70-32936

Troposphere effects on microwave and optical signals, correlating refractive index and dispersion variabilities 16 p2862 A70-33020

Refractive index gradients effect on scattering of radio waves perturbing ionosphere or passing through perturbed region 16 p2863 A70-33259

Refractive index equation for Whistler propagation in weakly drifting magnetoplasma 16 p2959 A70-34224

Hydrogen plasma refractive index and absorption constant for laser radiation frequencies as functions of electron temperature and atomic density 16 p2959 A70-34338

Pulsed plasmas refractive index measurement by two-wavelength He-Ne laser interferometry, estimating effects of heavy atoms and neutral gas density 17 p3107 A70-35110

Mutual coherence function of light scattered by plasma turbulent electron density fluctuations, taking into account refractive index changes 17 p3137 A70-35722

Clear air turbulence /CAT/ remote sensing feasibility by optical signal covariance measurement, taking into account refractive index fluctuations 17 p3132 A70-35723

Atmospheric turbulence effects on light propagation, measuring refractive index variations by high speed temperature sensors 18 p3285 A70-36961

Tantalum oxide thin films electro-optical effects due to refractivity changes 19 p3488 A70-38203

Slow wave propagation in plasma moving along external magnetic field, generalizing refractive index formula 19 p3417 A70-38592

Gaseous media absorption coefficient and refractive index in field of two nonmonochromatic radiation streams quasi-resonant with neighboring atoms and molecules transitions 19 p3448 A70-38740

Lower atmosphere refractive index vertical distribution and fluctuations, using airborne refractometer 20 p3619 A70-39191

Heat transfer measurements based on optical methods with temperature dependence of refractive index making temperature field visible 21 p3826 A70-41373

Refractive index complex part effect on polarization and radiance of reflected and transmitted light for continental haze and nimbostratus cloud models 21 p3847 A70-41724

Carbon dioxide and water cryodeposits refractive indices and densities, using thin film interference technique [ASME PAPER 70-HT-33] 22 p4122 A70-42434

Single and crossed light beam techniques for optical measurement of fluid turbulence with refractive index fluctuations 22 p4011 A70-42694

Spectral radiation extinction at atmospheric aerosol particles, discussing particles complex refractive indices and size distributions 22 p4065 A70-43171

Weak EM transmission through resonant medium of two-level atoms in presence of intense monochromatic wave, obtaining absorption coefficient and refractive index 22 p4075 A70-43473

Plasma diagnostics based on light beam refractivity, considering laser interferometry and holographic methods 23 p4225 A70-44188

Zi and Ze smallness effect on complex refractive index of ionosphere for VLF propagation 23 p4164 A70-44373

REFRACTOMETERS

Spectroscopic parameters for attenuation and dispersion caused by 22 GHz water vapor line, using differential microwave refractometer 13 p2393 A70-28784

REFRATORIES

Automatic TV radioscopic X ray control for mass NDT of refractories and grinding wheels 24 p4368 A70-45723

REFRACTORY MATERIALS

NT MOLYBDENUM

NT MOLYBDENUM ALLOYS

NT NIOBIUM

NT NIOBIUM ALLOYS

NT REFRATORIES

NT REFRACTORY METAL ALLOYS

NT REFRACTORY METALS

NT RENE 41

NT RHENIUM

NT RHENIUM ALLOYS

NT RHENIUM ISOTOPES

NT TANTALUM

NT TANTALUM ALLOYS

NT TUNGSTEN

NT TUNGSTEN ALLOYS

Refractory and heat resistant materials thermal diffusivity coefficient, discussing theoretical basis and technical implementation for measurement at high temperature 01 p0085 A70-10178

Projector with paraboloid mirror solar radiation condensing lens for studying heat resistant materials mechanical properties at high temperatures 01 p0055 A70-10179

Cascaded thermoelements with high figure of merit for increasing solar thermoelectric generator efficiency, noting high temperature materials effect 01 p0158 A70-10754

Fiber reinforced composites emphasizing refractory fibers, preparation methods, properties and fabrication 01 p0129 A70-10939

Collection of Soviet papers on chemical properties and analytical methods of refractory compounds 03 p0504 A70-12977

Oxidation resistance of mixed silicon nitride and silicon carbide refractory materials at high temperatures 03 p0514 A70-12979

Complexonometric analysis of alloys containing Mo without component separation, treating molybdenum aluminides, zirconium boride-molybdenum silicide, molybdenum carbide in Ti, etc 03 p0504 A70-12980

Durability of refractory tubes of small thickness under creep with account of scale factor and unsteady conditions, tabulating experimental and theoretical values 03 p0508 A70-13247

Ceramic, cermet and metallic high temperature coatings development and applications, discussing time and cost saving procedures [SAE PAPER 690478] 03 p0515 A70-13267

Machine for refractory crystals creep testing in thermal vacuum or inert protective medium 03 p0493 A70-13959

High temperature coatings in industrial, military and space applications, noting use in metal melting and working, furnace protection, propulsion systems, rocket engines, etc 04 p0709 A70-15630

Torsion testing apparatus for refractory materials at 2400 C, measuring applied torsion moment, twisting angle and second order modulus of elasticity 05 p0825 A70-15881

High temperature polymers including polybutadiene, polyphenylene sulfide, polysulfone, polybenzimidazole, etc 05 p0869 A70-16038

Refractory materials deformation and failure analysis based on relations between stresses, strains and irreversible energy absorption per cycle in thermal cyclic fatigue testing 05 p0867 A70-17042

Scale dependence and optimal sample dimensions for strength tests of brittle refractory materials 05 p0955 A70-17064

Microhardness measurements of carbides, borides and nitrides in wide temperature range, considering indentation load selection 06 p1089 A70-17661

Surface energy data calculated for bcc and hcp metals and high melting point compounds 06 p1090 A70-17845

Heat resistant fibers fabrication and properties for composite materials, noting metal whiskers, C, B, Be and alumina 07 p1318 A70-19802

High temperature techniques, measurement and data methodology noting refractory materials 07 p1312 A70-19877

Reentry thermal protection materials technology, discussing thermophysical, thermomechanical and kinetic effects, noting interdisciplinary approach 07 p1319 A70-19878

Laser characteristics and applications in high temperature research including metal heating, welding, machining, surface particle emission and plasma production 07 p1301 A70-19881

Single crystal carbides as high temperature structural materials, noting titanium carbide properties and strength-to-density ratio of B-doped crystals 07 p1312 A70-19883

Refractory oxides synthesized using metal alkoxide thermal decomposition, comparing thermophysical properties with conventional ceramics 07 p1320 A70-19891

Atomic oxygen and chlorine attack on refractory materials studied for kinetics of chemical reactions of free radicals and atoms 07 p1313 A70-19903

Boride composites with high strength and thermal resistance suitable as nose cap and leading edge materials for reusable lifting reentry systems [AIAA PAPER 70-278] 07 p1312 A70-20387

Composite materials in Co or Fe matrix for solid rotor core materials applications at high temperature and stress, discussing magnetic properties 08 p1524 A70-21908

High temperature vacuum dilatometer for continuous photographic recording of expansion curves for refractory materials, determining thermal expansion coefficient 09 p1675 A70-22565

Refractory oxide submillimeter spherical particle preparation by focused emission from carbon dioxide laser 09 p1697 A70-22984

Thermal cyclic loads effects on heat resistant materials strength during strain hardening, considering role of time factors in durability 09 p1779 A70-23104

Solid electrolyte high temperature fuel cells electrode materials, investigating various metal oxides 10 p1830 A70-24461

Glass- and quartz-fabric reinforced polymers for high temperature microwave insulation, evaluating electrical and thermal aging properties 12 p2259 A70-28149

Book on high temperature, transition and hydrated ceramics covering nomenclature, natural occurrence, mechanical, thermal, sonic, electrical, magnetic and chemical properties 13 p2436 A70-29781

High temperature molecules matrix isolation in saturated vapor over refractory solids, discussing optical spectroscopy of VO, metal oxide and halide molecules 14 p2545 A70-30903

Macromolecular polymer based heat resistant materials 15 p2765 A70-32264

High service temperature glass reinforced premix compound on Glastic grade electrical laminate, discussing optimum molding and applications 16 p2936 A70-33356

Thermal conductivity of multilayer and mixed powder high temperature insulation systems over wide temperature range and vacuum conditions [AIAA PAPER 70-637] 16 p2997 A70-33596

Oxidation and atmospheric contamination protective coatings for high temperature materials, using burner ring tests 17 p3127 A70-34519

Effective pores size, volume and surface area in refractory materials, using impregnation rate measurement 18 p3277 A70-36467

Thermal stability test assembly for refractory materials cylindrical specimens, using argon plasma jet 19 p3395 A70-37351

Soviet reference book on highly refractory elements and compounds covering crystalline, chemical, thermodynamic, thermophysical, electrical, optical and nuclear properties 19 p3451 A70-37470

Durability of refractory tubes of small thickness under creep with account of scale factor and unsteady conditions, tabulating experimental and theoretical values 19 p3453 A70-38465

Composite technology effects on engineering design, emphasizing carbon-carbon materials for aircraft structural weight reduction, performance improvement and high temperature applications 20 p3653 A70-39202

Small high temperature rotary plasma-heated furnace for refractory material high purity processing, discussing design and operation 22 p4005 A70-42368

German monograph on refractory materials softening under bending and compression at high temperatures 22 p4061 A70-43742

Ceramic composite materials structural application, improving brittleness and thermal shock resistance via reinforcing refractory fibers [ICAS PAPER 70-40] 23 p4267 A70-44138

Columnar grain and Ni alloy single crystal gas turbine engine components resistant to high temperatures produced by precision casting, using directional solidification 23 p4207 A70-44857

High melting point fibrous composites, discussing fiber-matrix systems for high temperature applications as in gas turbine blades 24 p4357 A70-45168

Sodiumalumoborosilicate fiber formation and extraction by leaching, obtaining high aluminate content temperature resistant porous fiber and insulation material 24 p4367 A70-45480

German monograph on use of Ge as oxidation resistant refractory materials alloy component covering base materials, test samples processing methods and apparatus, etc 24 p4367 A70-45525

Refractory materials surface behavior under friction, discussing microscopic nature of wear and surface deterioration due to thermal fatigue, fusion and material transfer, etc 24 p4342 A70-45595

REFRACTORY METAL ALLOYS

NT MOLYBDENUM ALLOYS

NT NIOBIUM ALLOYS

NT RENE 41

NT RHENIUM ALLOYS

NT TANTALUM ALLOYS

NT TUNGSTEN ALLOYS

Loads effects on refractory alloy fatigue strength and life at high temperatures, describing aircraft turbine blade tests 01 p0115 A70-10069

Creep deformation modes of Ni-base austenitic superrefractory alloy as function of test temperature 01 p0118 A70-10704

Tantalum base alloy T-111 creep tests in vacuum at elevated temperature suggesting diffusion controlled microcreep mechanism 01 p0120 A70-10738

Chromium refractory alloys, discussing production difficulties, mechanical properties, engineering applications, etc 02 p0320 A70-12760

Monograph on elevated temperature strength data for wrought austenitic stainless steels, considering yield, tensile, creep and rupture strengths for allowable stresses 03 p0510 A70-13300

Refractory metals in rocket propulsion devices, applying tungsten in uncooled rocket nozzles and tungsten and rhenium to electrothermal propulsion 03 p0512 A70-13617

Metals and alloys creep under tension and compression at elevated temperatures, considering plastic deformation equation applicability 04 p0707 A70-15265

Welding atmosphere purity effects on Li corrosion resistance of refractory metals in space power systems 04 p0709 A70-15627

X ray metallography methods applied to high temperature protective coating development, refractory alloys strengthening and metal fatigue studies 04 p0711 A70-15706

Diffusion rates in refractory metal alloys for thermionic emitters as function of time and temperature [GA-9495] 05 p0892 A70-16075

Thermophysical characteristics of annealed Ta and Mo alloy welded joints under electron beam and ray heating, noting use for short term tests 05 p0865 A70-17028

Refractory Ni alloys defects accumulation under creep and cyclic temperature variations assessed by relative lifetime additive method 05 p0866 A70-17032

Plastic deformation of refractory alloys during stress relaxation tests under vibrations, showing enhanced stability 05 p0866 A70-17033

Thermocyclic creep and rupture strength of Nb, Ta and Mo refractory alloys under temperature and load variations, showing failure dependence on cycle parameters 05 p0867 A70-17043

Heating influence on circular bending fatigue strength of refractory steel and alloys, using radiative and HF inductive heating 05 p0868 A70-17059

Metals mechanical properties with inorganic heat resistant coatings between 1900-2300 K in oxidizing medium, describing facility based on solar furnace 05 p0875 A70-17069

Refluxing capsule tests of refractory metal alloys-boiling alkali metals corrosion compatibility, noting role of capsule geometry 06 p1087 A70-17510

Heat pipe structural alloys compatibility with different working fluids using capsule tests at high temperatures, noting corrosion behavior [AIME PAPER F-69-2] 07 p1304 A70-18812

Thermal conductivities and total emittance of Ta, W, Re and alloys at high temperatures compared with NBS values 07 p1313 A70-19894

Simultaneous titration of gases, metalloids and metals in steels and refractory alloys by far UV vacuum spectrometry [ONERA-TP-765] 08 p1455 A70-21842

Nondestructive tests for diffusion-formed refractory alloy coatings used as oxidation protection for hypervelocity spacecraft and reusable systems 09 p1692 A70-22679

Unidirectional-solidification casting of superalloys of refractory metals in turbine blade production 15 p2757 A70-31811

Refractory alloys Li corrosion resistance, examining effects of oxygen contamination during welding 16 p2924 A70-34205

Liquid metal corrosion of heat pipe refractory alloys at high temperatures, noting oxygen role 16 p2933 A70-34208

Refractory metal alloys tensile and creep rupture properties for reactor fuel jackets 24 p4364 A70-46347

REFRACTORY METALS

NT MOLYBDENUM

NT NIOBIUM

NT RHENIUM

NT RHENIUM ISOTOPES

NT TANTALUM

NT TUNGSTEN

Annular metal specimens protection against oxidation during high temperature relaxation testing by covering specimens with Al powder thinned with alcohol 01 p0121 A70-11109

Rockwell hardness tester attachment design for studying temperature dependence in various multiphase alloys at high temperature 01 p0121 A70-11110

Dissolved gases and carbon effect on transition temperature from plastic to brittle state of high melting metals including niobium and vanadium 01 p0124 A70-11615

Refractory metal-oxygen systems phases and phase relations 02 p0318 A70-12640

Ta-V-Cb and Ta-V-Ti alloys used as brazing fillers for refractory metals bonding, noting wetting and flow characteristics, shear strength, remelt temperatures, etc 02 p0319 A70-12753

Carbon effect on high temperature elasticity modulus and long term hardness of Nb, indicating diffusion enhancement and counteractive Zr addition 03 p0509 A70-13252

Deformation and failure of refractory metals at high temperatures under constant and variable thermal loads concerning turbomachine components 05 p0865 A70-17027

Refractory metal structural elements stress rupture strength in vacuum and inert gas tested up to 2000 K 05 p0829 A70-17071

Temperature and pressure effects as function of time in spectral and total normal emittance of metal coated refractory metals [AIAA PAPER 70-68] 06 p1092 A70-18136

Mechanical property factors influencing selection of sintered uncorked refractory metals and alloys for structural applications [AIME PAPER F-69-4] 07 p1290 A70-18810

Soviet collection of articles on single crystals of rare and high melting point metals 07 p1307 A70-19606

Thermal conductivities and total emittance of Ta, W, Re and alloys at high temperatures compared with NBS values 07 p1313 A70-19894

Refractory metals electrical resistivity as function of density near critical point, using exploding wire 07 p1335 A70-19899

Refractory metal monocarbide single crystal growth by plastic strain induced primary and secondary recrystallization 07 p1313 A70-19902

Zr, Ti, Nb and Ta carbides deposition from metal chloride, methane, hydrogen and argon mixture, studying gas concentration and temperature effects on deposition rate 08 p1517 A70-21147

Solid Mo, Ni, Ta and W surface energies determined by multiphase equilibration technique 08 p1522 A70-21749

Vacuum melting and heat treating equipment for high melting point metals from phase equilibria studies viewpoint 09 p1655 A70-22562

Boron carbonitride soldering with refractory metals by molybdenum disilicide as solder, analyzing electrical resistance and gas tightness 09 p1707 A70-23123

Rhenium alloying effect on room temperature ductility of Cr, Mo and W, measuring lattice parameters by Debye-Scherrer method 12 p2256 A70-27616

Preoxidation treatment alleviating silicide pest in protective coatings for refractory metals, discussing effectiveness against high temperature oxidation 13 p2434 A70-29082

Specific heat and enthalpy of body centered cubic refractory metals at high temperatures 15 p2757 A70-31943

Book on refractory metal properties covering nuclear reactor use, atomic, electronic and crystal structures, thermal and electrical characteristics irradiation effects, nuclear properties, etc 16 p2931 A70-33268

Ablative composites containing in situ reaction formed refractory metal carbides 16 p2937 A70-33371

Refractory metals penetration by liquid alkali metals along grain boundaries and crystallographic planes, considering threshold oxygen concentration 16 p2932 A70-34203

Molten contaminated Li effects on microstructure, tensile strength and stress corrosion of stainless steels and refractory metals 16 p2933 A70-34206

Surface alloying of high melting points in Al melts, noting prior oxidation enhancement and simplifying of calorizing techniques 17 p3102 A70-35406

Ti, Nb and Mo solubility during surface doping in Al melts containing various metals, discussing melt lattice structure effects 18 p3276 A70-36208

Soviet monograph on bimetal and refractory metals production by rolling in vacuum or inert media 19 p3433 A70-37402

Refractory metals interaction with boron during vacuum boronizing, investigating kinetics and optimal process conditions 19 p3434 A70-37452

Carbon effect on high temperature elasticity modulus and long term hardness of Nb, indicating diffusion enhancement and counteractive Zr addition 19 p3453 A70-38470

Electrophysical properties of refractory and rare earth metallic single crystals, discussing work function, transition temperature, resistivity and superconductivity 19 p3454 A70-38731

High temperature specific heat terms for refractory metals and ceramics from room temperature to near-melting point 23 p4207 A70-44440

W, Ta and Mo components economical fabrication by plasma spraying for rocket nozzles, susceptors and crucibles 24 p4350 A70-46355

REFRASIL [TRADEMARK]

U FIBERS

U SILICON DIOXIDE

REFRIGERATING

Human rectal temperature cooling rate during refrigeration in mortuary, applying Newton law 01 p0017 A70-10471

Experiments on frozen dogs to determine localized shielding effectiveness in astronauts protection from radiation 03 p0423 A70-13710

Experiments on frozen dogs to determine localized shielding effectiveness in astronauts protection from radiation 11 p1985 A70-25510

Polarized Co59 target using He3-He4 dilution refrigerator, analyzing fast neutron scattering 14 p2584 A70-30508

REFRIGERATING MACHINERY

NT REFRIGERATORS

Superconducting magnetometers and cryogenic refrigeration techniques, discussing liquid helium refill systems, Joule-Thompson expansion, etc 13 p2414 A70-30027

REFRIGERATORS

Airline passenger food service, discussing public health measures, low temperature and cryogenic galley cooling [SAE PAPER 690674] 05 p0804 A70-15833

Vortex refrigerators characteristics, examining configurations with cylindrical and conical hot ends with and without diffuser 06 p0988 A70-17855

Cryogenic refrigeration below 20 K, analyzing cycles using similarities of work and heat exchange mechanisms 09 p1726 A70-22290

U.S. cryogenic refrigerators specifications in tabular form 09 p1655 A70-22291

Energy balance in radiation detector cooling, analyzing refrigerator capacity and thermal load 13 p2412 A70-29870

Optimum low temperature two circuit vortex refrigerator using compressed air precooled in heat exchanger 22 p3965 A70-42808

Three-stage Gifford-MacMahon cycle regenerative refrigerator in 6.5 K region, using lead shot matrices for coldest regenerators 23 p4280 A70-44371

REFUELING

NT AIR TO AIR REFUELING

Optimal motion control of spacecraft refueling during flight by liquefying atmospheric gas along prescribed trajectory under constant thrust 01 p0197 A70-11502

Superjets demands on airport fuel handling facilities [SAE PAPER 690559] 03 p0463 A70-13263
Orbital refueling techniques, discussing vapor-liquid interface stability, pressurant requirements, transfer line chilldown, propellant transfer dynamics, dielectrophoresis, suction speed estimating and system tradeoffs 14 p2653 A70-30752
Boeing 747 aircraft pressure fueling system, describing tanks, feed system, refueling and electrostatic charge minimization 18 p3214 A70-36816 [SAE PAPER 700276]
Jet fuels ground handling at airfields, describing flow monitors, filters, fueling techniques, etc 22 p4006 A70-43093

REGENERATION [ENGINEERING]

Regenerative quantum amplifiers with simple and complex resonators, discussing amplification coefficients and frequency characteristics 01 p0106 A70-10058
Sand and dust environmental test of T-63 regenerative engine, discussing performance depreciation, recuperator inspection and comparison with non-regenerative t63-a-5a engine 01 p0164 A70-10685
Granular amine used as regenerable absorbent in cycling two bed system for carbon dioxide removal 01 p0038 A70-10972

Regenerative life support system development for multiman crews on extended space missions, considering maintainability, reliability and automation [SAE PAPER 690637] 05 p0804 A70-15845
Surface photovoltage regeneration mechanism in GaAs dependent on free carrier concentration, space charge density and minority carriers 15 p2783 A70-31951
Integrated regenerative life support manned tests for space laboratory design and development 23 p4154 A70-44632
Space cabin atmosphere regeneration by unicellular algae photosynthesis, discussing *Chlorella* cultivation procedures and additional functions in life support systems 23 p4154 A70-44655
Manned space flight regenerative life support systems requirements, considering weight, volume, power, cost effectiveness and integration problems 23 p4156 A70-45023
Closed loop life support system employing algae and bacteria cultures to recycle water in addition to atmospheric regeneration 23 p4156 A70-45024

REGENERATION [PHYSIOLOGY]
Dark adaptation correlated with in vivo visual pigments regeneration as function of bleaching during monomolecular time course 08 p1447 A70-21722
Monograph on measurement and regeneration of water vapor loss of human skin, studying protective qualities of horny layer 10 p1812 A70-24598
Mammalian tissues metabolic and genetic alteration during weightlessness, relating rats liver regeneration delay to centrifuging intensity following hepatectomy 23 p4146 A70-44617

REGENERATIVE COOLING
Regeneratively cooled stainless steel thrust chamber failure related to internal carburization by fuel decomposition and propellant combustion 12 p2290 A70-27111
Heat transfer in Z shaped regenerative heat exchangers with/without air mixing, determining parameters defining thermal efficiency 13 p2520 A70-28857
Heat pipe cooled thrust chambers for space storable propellants, discussing design feasibility for radiation and regeneratively cooled concepts 16 p2965 A70-33541 [AIAA PAPER 70-942]
Heat transfer between wall and liquid and vapor films in internal regenerative cooling of thrust chambers 21 p3867 A70-41027
Three-stage Gifford-MacMahon cycle regenerative refrigerator in 6.5 K region, using lead shot matrices for coldest regenerators 23 p4280 A70-44371

REGENERATIVE CYCLES
U REGENERATION [ENGINEERING]
REGENERATIVE FUEL CELLS
Materials for separator matrix of rechargeable hydrogen oxygen fuel cell, noting use of composite potassium titanate 09 p1612 A70-22045
Regenerative hydrogen-oxygen secondary fuel cells as rechargeable battery for communication satellites 21 p3756 A70-41007
Metal phthalocyanin catalyzed oxidation by oxygen of vanadium and iron couples in externally regenerated redox fuel cell cathode 22 p3966 A70-43536

REGENERATORS
NT THERMOSIPHONS
Low Reynolds number laminar flow gas turbine regenerators, investigating manufacturing tolerances effects on heat transfer and flow friction behavior 14 p2629 A70-31022
Transient heat and mass transfer in adiabatic regenerator, solving mathematical model in terms of Green functions 17 p3197 A70-35542
Three-stage Gifford-MacMahon cycle regenerative refrigerator in 6.5 K region, using lead shot matrices for coldest regenerators 23 p4280 A70-44371

REGIONS

NT ANTARCTIC REGIONS
NT ARCTIC REGIONS
NT AUROREAL ZONES
NT BRILLOUIN ZONES
NT FRESNEL REGION
NT GUTENBERG ZONE
NT LUMBAR REGION
NT NULL ZONES
NT PELAGIC ZONE
NT POLAR REGIONS
NT TEMPERATE REGIONS
NT TROPICAL REGIONS
Intelsat compatibility with independent regional telecommunication satellite systems 22 p4111 A70-43514

REGISTERS [COMPUTERS]

NT ACCUMULATORS [COMPUTERS]
NT SHIFT REGISTERS
REGRESSION [STATISTICS]
U REGRESSION ANALYSIS
REGRESSION ANALYSIS
NT REGRESSION COEFFICIENTS
Stability characteristics from flight test results using regression analysis 04 p0623 A70-15155
Linear statistical forecast accuracy and optimal predictor dimensionality based on multiple regression equation 04 p0715 A70-15251
Multidimensional Kiefer-Wolfowitz stochastic approximation algorithm modified to locate regression function minimum 07 p1247 A70-20028
Regression analysis of linear statistical model experiments with stationary Gaussian error of slowly varying spectral density 11 p2073 A70-26249
Gravitational and magnetic anomaly interpretation by regression analysis including geological field discrimination, inverse gravimetry and magnetometry, etc 12 p2223 A70-27348
Loran C coordinates bias function determination by regression analysis using observed time differences 14 p2615 A70-31195
Nonlinear regression techniques for statistical simultaneous measurement of thermal properties including convergence criterion 16 p2998 A70-33859
Pilot induced oscillation rating regression analysis, examining time delay, slope after and time to first peak and stick force per g 18 p3213 A70-36444
Flight training quality prediction by multidimensional regression analysis, discussing relationship to candidates psychophysiological examinations 20 p3578 A70-38964
Stepwise linear regressions method for estimating black body surface radiances from model atmospheres and corresponding simulated Nimbus 2 window-channel radiances 22 p4013 A70-42617
Parallelism of two regression lines, suggesting distribution free signed rank test 22 p4064 A70-43526
Multidimensional integral Monte Carlo evaluation applying regression analysis to linear unbiased estimators 24 p4370 A70-46100

REGRESSION COEFFICIENTS
Linear regression equations to relate atmospheric precipitable water to surface dew point, sky cover and weather 03 p0520 A70-13163
Nozzle throat ablative materials for controlled high regression rates in tactical rocket motors, primarily nylon reinforced thermosetting resins [AIAA PAPER 69-423] 04 p0713 A70-15428

REGULARITY

Regularization techniques for optimal control problems in polynomial algorithms of data handling by groups 16 p2867 A70-33236

REGULATION

U CONTROL
REGULATIONS
Flight characteristics differences between VTOL and conventional transport aircraft, recommending differences consideration in regulations 03 p0414 A70-14095
Collision safety standards in helicopter services for shore-to-ship transportation of pilots, stores and spares 06 p1103 A70-17639

Low visibility aircraft landing problem concerning pilot instrument and visual cue and federal regulations governing operational approval [AIAA PAPER 70-936] 17 p3134 A70-35845
Air transport regulatory system, considering operational, technological and economic factors 21 p3954 A70-40579
Juridical problems in satellite direct TV broadcasting, discussing regulation proposals submitted to UN and educational applications 24 p4430 A70-45596

REGULATORS

NT AUTOMATIC FREQUENCY CONTROL
NT CURRENT REGULATORS
NT FLOW REGULATORS
NT FREQUENCY CONTROL
NT FUEL FLOW REGULATORS
NT OXYGEN REGULATORS
NT PRESSURE REGULATORS
NT RELIEF VALVES
NT SPEED REGULATORS
NT THERMOSTATS
NT VOLTAGE REGULATORS
Linear regulator optimal for exponentially time-weighted quadratic performance indices, using cost equivalence concept in infinite terminal time solution 04 p0663 A70-15604
Information transfer for quantitative relationships to error- and cause-controlled regulations 07 p1216 A70-18859
Automatic threshold regulation for radar applications, using feedback control device based on noise peak probabilities 11 p2012 A70-26717
Optimal control of processes with lags, including linear analytical regulator problem 19 p3395 A70-38718

REHEATING

U HEATING

REIGNITION

U IGNITION

REINFORCED MATERIALS

U COMPOSITE MATERIALS

REINFORCED PLASTICS

Graphite fiber-epoxy resin composites interfacial bonding, describing various surface treatments for increased interlaminar shear strength 01 p0127 A70-10477
Fiber-polymer matrix interfacial tensile and shear strengths evaluation methods, including data correlation from various tests 01 p0087 A70-10478
Water effect on glass fiber-resin bonds in interphase region, discussing initial stiffening and long term effects 01 p0127 A70-10484
Interfacial equilibrium free surface energies between glass fibers, coupling agent and resin matrix, considering wetting, absorption and bonding 01 p0128 A70-10486
Reinforced thermoplastics - Conference, Hartford, October 1969 01 p0128 A70-10769
Glass fiber-fortified thermoplastics development, properties and applications, considering ionomer, polyimide, chlorinated trifluoroethylene polymer, polymethylpentene, polybutylene, polyaryl ether and nylon 01 p0128 A70-10770
Fiber glass reinforcement effect on flammability properties of thermoplastics 01 p0128 A70-10771
Solid glass sphere reinforced nylon resins properties, processing and applications, noting tensile and impact strength and heat distortion 01 p0128 A70-10772
Glass-reinforced polypropylene for structural applications, investigating time/temperature dependent creep characteristics 01 p0128 A70-10773
Reinforcement of thermoplastic resins, considering single crystal whisker and carbon fibers and microspheres 01 p0129 A70-10774
Glass fiber-reinforcing techniques of polymers, discussing coating and compounding processes 01 p0104 A70-10775
Boron fiber reinforced epoxy fatigue life dependence on reinforcing fibers aspect ratio 01 p0129 A70-11082
Ultrasonic image superposition technique for visualization of impact fractures in glass reinforced plastics 01 p0059 A70-11101
Mechanical properties of asbestos as reinforcing material for fiber filled thermoplastics compared with glass fiber 02 p0320 A70-11677
High strength high modulus carbon fibers for use in structural reinforced plastics, describing carbonizing and pyrolysis processes 02 p0320 A70-11856

Fortified thermoplastic compounds for increased flame retardancy, environmental resistance and toughness

02 p0320 A70-11865

Design allowable curves based on laminate test data for high modulus graphite fiber and resin systems, considering Wagner cantilever beam specimens

02 p0387 A70-11954

Boeing 707 B-epoxy composite forelap design, analysis, fabrication and flight testing

02 p0307 A70-11955

B and C fiber unidirectionally reinforced plastic composites, discussing mechanical properties, fabrication and testing

02 p0321 A70-12082

Chemically coupled glass-reinforced polypropylene, studying short term physical properties, creep rupture and deformation, dynamic failure, etc

02 p0322 A70-12605

Reinforced epoxy resin performance prediction from correlation between unfilled resin and laminates mechanical properties

02 p0322 A70-12606

Reinforced plastics creep rupture strength under compression along elastic symmetry axes

02 p0322 A70-12805

Reinforced plastics models for determining internal stress, temperature and electromagnetic fields of multicomponent reinforced plastics

02 p0323 A70-12806

Mechanical losses in fiberglass reinforced textile converted into thermal energy during cyclic tension and compression

02 p0323 A70-12807

Fiberglass reinforced plastic shells stability analysis, assuming weak shear resistance of shell material

02 p0390 A70-12808

Radiation hardened fiberglass reinforced plastics rupture, bending, compression and tensile strength and elastic modulus, considering gamma ray doses effect

02 p0323 A70-12811

Stress concentration in optically active fiberglass reinforced plastics during static loading determined by optical polarization method

02 p0390 A70-12812

Component proportion and porosity effect on fiberglass reinforced plastics properties, establishing relation between bending strength and thermal conductivity coefficient

02 p0323 A70-12814

Fiberglass reinforced textile fatigue characteristics under impact tensile loads, noting different characteristics under cyclic sinusoidal loads

02 p0323 A70-12815

Unidirectional carbon and glass fiber reinforced polyester resins dynamic characteristics under torsional and flexural vibration, showing damping independence of cyclic stress amplitude

03 p0514 A70-13111

Interlaminar shear stress and fabrication of high modulus graphite-reinforced epoxy matrix composites

03 p0515 A70-13119

Graphite fiber content determination technique for plastic composites based on epoxy, polyimide and phenolic resins, using concentrated sulfuric acid

03 p0515 A70-13123

Bearing strength and rupture of reinforced plastic composites under intense one-sided electric heating and hydrostatic pressure due to pyrolysis of plastic bond

03 p0515 A70-13244

Creep and recovery of polyvinyl chloride reinforced by oriented cotton fibers, considering roles of fiber density and stress magnitude

03 p0516 A70-13499

Carbon fiber reinforced plastics /CFRP/ uses in commercial aircraft structural component

03 p0516 A70-13546

Interactions between adhesive polymers and fillers, emphasizing reinforced plastics composites properties [ONERA-TP-733]

03 p0516 A70-13644

Electron bombardment effects on epoxy based textiles mechanical properties, studying structural changes spectroscopically

03 p0516 A70-13735

Elasticity theory of orthotropic materials applied to steady rotation of long cylindrical tubes of filament reinforced plastics

03 p0602 A70-14331

Compression failure of unidirectional fiberglass reinforced plastics

04 p0712 A70-14487

Plastic flow failure of matrix of fiber reinforced composite sheet, discussing plane stress and simple tension [ASME PAPER 69-APM-Z]

04 p0770 A70-14869

Fiberglass reinforced plastics energy dissipation during fatigue failure phases, studying mechanical-to-thermal energy transformation under cyclic strain

04 p0713 A70-15263

Carrying capacity and deformation susceptibility of anisotropic fiberglass reinforced conical and cylindrical plastic shells under axial compression

05 p0933 A70-16209

Stability, critical load and strength algorithm for fiberglass reinforced cylindrical plastic shells under external load allowing for shear stresses

05 p0933 A70-16211

Stability and critical loads of transversally isotropic reinforced plastic annular plates with weak shear resistance under axisymmetrical buckling

05 p0933 A70-16213

Statistical stress distribution of breakdown during scaling of wound fiberglass reinforced plastics, noting relation between critical stress and defects

05 p0870 A70-16214

Statistical stability of cylindrical fiberglass reinforced plastic shells under axial compression, showing breakdown loads vs radius/thickness ratio

05 p0933 A70-16215

Residual stress variations in ring shaped fiberglass reinforced plastic shells produced by winding due to elastic modulus decrease and filler/binder contraction

05 p0934 A70-16216

Three layer plate of elastic fiber glass reinforced plastic outer layers and metallic plastic filler, studying elastoplastic stability

05 p0934 A70-16218

Fiberglass reinforced rectilinear plastic plates bending under various edge loads, noting shear pliability

05 p0934 A70-16220

Stress distribution in restrained hyperelastic sphere based on elastomer reinforcement theory by carbon black

05 p0940 A70-16510

Carbon fiber-reinforced plastics fabrication, discussing leaky mold, prepeg and filament winding methods

05 p0855 A70-16581

Glass filled thermoplastics fabrication techniques and composites, discussing molding compounds and processes, reinforced thermoplastics properties and applications

05 p0873 A70-16605

Reinforced plastics high silica and quartz history, properties, uses, costs and pricing, tabulating sources and presenting product recommendations and cost comparisons

05 p0873 A70-16608

Graphite yarn, cloth and fiber composites physical properties tabulated, discussing multiply laminates for graphite-epoxy composites

05 p0873 A70-16610

Whiskers and whisker products physical characteristics, available forms and types and compositing methodology, discussing utilization in plastics

05 p0873 A70-16611

Bag molding process for molding laminates of fiber-reinforced preimpregnated material containing thermosetting resin

05 p0856 A70-16612

Preimpregnated materials processing, discussing molding, resin-reinforcement, unidirectional materials, ablative applications, mechanical data and air-frame uses

05 p0874 A70-16614

Mechanical fastening, adhesive bonding and machining methods for laminated fiberglass reinforced plastic materials

05 p0856 A70-16618

Reinforced plastics destructive and nondestructive testing including standard methods, equipment and procedures applicable to materials and parts

05 p0874 A70-16621

Plastics applications in aircraft, missile systems, satellites, sounding rockets and manned spacecraft, discussing reinforced plastics and structural laminates

05 p0874 A70-16623

External hydrostatic pressure effect on fiberglass-reinforced plastics strength under unilateral heating, analyzing stress distribution

05 p0875 A70-17067

Fiberglass reinforced plastics load carrying capacity under unsteady unilateral heating described by thermal similarity criteria

05 p0955 A70-17070

Fatigue life of unidirectionally glass fiber reinforced composites subjected to low cycle loading, using linear elastic body model for cyclic deformation process

06 p1091 A70-17408

Glass fiber reinforced thermoplastics fatigue behavior during and after cyclic loading

06 p1091 A70-17600

Thin walled glass fiber reinforced plastics beams strength analysis combined with results from elasticity theory of anisotropic bodies

06 p1167 A70-17913

Anisotropic fiberglass reinforced plastics creep properties under biaxial compression, showing compressive to tensile strain elimination or change

07 p1316 A70-19546

Crack formation in resin matrix and effect on fiberglass reinforced composites behavior under loading

07 p1318 A70-19754

Fiberglass reinforced plastics bonding, discussing structure fabrication and use as material

07 p1295 A70-19759

Rupture safety in fiberglass reinforced plastics using variation coefficient illustrated in vessel design

07 p1410 A70-19760

Fiberglass plastics structure safety design using time dependent limiting states with wear allowance

07 p1410 A70-19761

Reinforced plastics underframe design based on hooks law, noting middle layer loaded laminates and shell advantages

07 p1410 A70-19762

Electrostatic ignition discharge prevention on fiberglass reinforced depot tanks, noting ground connection safeguard

07 p1295 A70-19763

Air bubble free glass fiber-plastic laminates fabricated by wet-winding method using vacuum, noting void free filament woumpies

07 p1295 A70-19766

Interlaminar shear strength determination methods taking into account plastics composition, considering polyester and epoxy plastics, glass and graphite fiber reinforcing materials

07 p1410 A70-19767

Transverse stress failure analysis of reinforced extruded plastic laminates taking into account cohesive and adhesive failure

07 p1410 A70-19768

Tensile and compressive stress cycles effect on short term strength of glass fiber plastic laminates

07 p1411 A70-19769

Fabrication and properties of carbon fibers and carbon fiber reinforced epoxy resins

07 p1318 A70-19772

Cycloaliphatic epoxy resins for glass and carbon fiber reinforced plastics and laminates

07 p1318 A70-19773

Compression strength of polyester resin reinforced with hard drawn and softened steel wires, discussing variations from predicted performance

07 p1320 A70-19954

Thermal conductivities of glass reinforced polystyrene and polyethylene plastics measured over range of glass concentrations and sizes

07 p1320 A70-19958

Creep and stress relaxation tests to investigate time dependent fracture strength of unidirectional glass fiber reinforced epoxy composites

07 p1321 A70-19962

Glass fiber reinforced polyether composites long time strength under plane stress

07 p1321 A70-20187

Elastic and optical properties anisotropy in fiberglass reinforced epoxy plates using photoelastic method

07 p1416 A70-20295

Modulus of elasticity of fiber glass reinforced plastic under transverse bending as function of length-to-height ratio in laminates

08 p1526 A70-20532

Glass filament reinforced plastics characteristics, considering filament protection during manufacture

08 p1526 A70-20717

Distilled water and mineral oils heated to 50-80 C studied for effect on residual stresses in fiberglass reinforced plastics

08 p1526 A70-20925

Thermoelectric characteristics of glass fiber reinforced plastic materials, determining temperature dependent deformation of composite plate

08 p1526 A70-21164

Fiberglass reinforced plastics creep behavior under axial compression, studying time dependence of elasticity modulus and Poisson coefficient

08 p1526 A70-21174

Fiber-reinforced composite sheet matrix failure by plastic flow, investigating two ply laminate in simple tension

08 p1592 A70-21471

Test specimen shapes for determining tensile, compressive and edge-wise shear properties of reinforced plastic laminates

08 p1529 A70-21878

Mechanical properties characterization of unidirectional high modulus carbon fiber reinforced epoxy matrix composite

08 p1530 A70-21883

Matrix optimization of boron filament reinforced polymeric for short duration high temperature aerospace applications

08 p1530 A70-21891

Adhesion characteristics in composites, investigating correlation between short beam and torsion shear tests in glass and graphite reinforced epoxy materials

08 p1531 A70-21892

Creep and rupture of graphite-epoxy composites under unidirectional state of stress and controlled temperature environment, extrapolating long term loading behavior

08 p1531 A70-21897

Glass fiber reinforced epoxy laminate specimens tests in tension and flexure at various strain rates to determine geometry effect on strength

08 p1532 A70-21898

Graphite fiber/resin matrix composites for airframe structures, studying tensile, compressive and in-plane shear strengths 08 p1532 A70-21901

Laminated anisotropic rectangular plates of boron-epoxy composite material, studying shear stability by potential energy and Ritz method 08 p1595 A70-21903

Fiberglass-epoxy laminates mechanical behavior under biaxial loading, describing test equipment and procedures 08 p1532 A70-21904

Structural analysis of boron filament-epoxy composite laminate tubes for use as spacecraft long column members 08 p1595 A70-21911

Failure mode in shear loaded graphite filament reinforced epoxy composites dependent on interfacial bond strength 08 p1533 A70-21915

Electrical and photographic methods for measuring microcracking in fiber reinforced plastics 08 p1501 A70-21916

Fiberglass reinforced plastic laminates shear characteristics determination, giving expressions for shear modulus and tangential stress 09 p1709 A70-22300

Failure analysis of unidirectionally reinforced fiberglass composites due to winding, using critical stress distribution function 09 p1710 A70-22462

Strain gages for static deformation measurement of fiberglass reinforced plastics at room and higher temperatures, discussing error sources and gage-specimen adhesive bonding 09 p1780 A70-23107

Antifriction reinforced plastics based on polyamide fibers in epoxy phenolic resins, determining optimum ratios to obtain desired mechanical properties 09 p1710 A70-23675

Temperature fields and thermal stresses in FN fiberglass reinforced textolite under nonstationary unilateral heating, determining stress as function of time and heating rate 09 p1710 A70-23724

Fiberglass reinforced textolite creep strains as function of stress, temperature and time, noting correlation with theory to 200 C 09 p1710 A70-23725

Fibrillated asbestos dispersed in thermoplastic ionomer lattices, precipitated, dried and compression molded into bars, testing for flexural modulus, flexural stress and Vicat softening temperature 10 p1906 A70-24024

Epoxy glass fiber composites pyrolyzates IR spectra as function of time, observing changes in fingerprint region 10 p1828 A70-24065

Glass-epoxy composites failure mode dependence on matrix characteristics and fiber orientation, observing flexural strength increase with strain rate 10 p1908 A70-25174

Thermoplastics reinforcement with glass and asbestos fibers taking into account fiber properties 11 p2070 A70-25825

Two dimensional photoelastic investigation of crack propagation in fiber-reinforced composites consisting of glass and polyester resin layers 11 p2136 A70-26078

Resonant frequencies and Young's/shear moduli of unidirectional graphite epoxy composite beams under high modes of vibration 11 p2136 A70-26082

Wire sheet reinforcement for resin matrices, discussing mechanical properties, fabrication, bonding, wetting, etc 11 p2071 A70-26346

Boron epoxy composite structural parts for aerospace vehicles, discussing production times and cost reduction [ASTME PAPER EM-69-143] 12 p2240 A70-27076

Filament reinforced composites tested under dynamic compression loads for determining relations among strain rate, constituent properties, stress-strain behavior, fracture energy and mode 12 p2253 A70-27119

Elastic moduli and damping coefficients for glass- and boron-epoxy beams determined from resonant frequencies and bandwidths during lateral forced vibrations 12 p2253 A70-27120

Filament winding process for boron modified phenolic resin tape used in high temperature applications 12 p2242 A70-27204

Glass-plastic thin cylindrical shells carrying capacity dependence under axial and external loads on combinations of longitudinal and transverse reinforcing layers 12 p2259 A70-27527

Glass fiber reinforced thin rectilinear orthotropic plastic plates bending using finite difference method with allowance for creep 12 p2324 A70-27531

Residual stresses levels in glass fiber reinforced plastic components after production by compression or winding 12 p2325 A70-27534

Orthotropic fiberglass reinforced plastic deformation during stretching with allowance for binder breakdown in transverse layer 12 p2259 A70-28283

Fiberglass plastic reinforced high pressure balloons design and fabrication with oblated ellipsoid of revolution, discussing deformability, strength and cyclic loadings resistance 12 p2328 A70-28285

Stress concentration in fiberglass reinforced plastic composite cantilever cylindrical shell in round hole region subjected to concentrated load on free supported end 12 p2328 A70-28286

Molding procedure to orient filaments relative to loads for optimizing structural component/compressor blades/ of filament reinforced composite 13 p2417 A70-28663

Glass fiber reinforced resin structures and equipment quality and physical/mechanical conditions determined by plastographic analysis 13 p2404 A70-28665

Planar reinforced plastic resins strength and stiffness, considering mechanics of film, flake and ribbon reinforcements 13 p2438 A70-29206

Tensile tests on wings and wing components of plastic engine-driven aircraft, discussing design, configurations and mechanical properties 14 p2656 A70-30250

Cutting speed, feed parameters and tool tip curvature effects on machined surface roughness of turned fiberglass reinforced epoxy laminates 14 p2590 A70-30873

Fibre reinforced polymers fatigue life under cyclic stresses, obtaining data from rotary cantilever tests 15 p2764 A70-31933

Dangerous plane stressed state surfaces for fiberglass reinforced plastic pipes, using fourth degree polynomial 15 p2766 A70-32852

Stress rupture shear strength of fiberglass reinforced plastics under monotonic, prolonged and cyclic loading 15 p2766 A70-32853

Anisotropic glass fiber reinforced plastics strength and deformability under cyclic axial loads 15 p2766 A70-32897

Fiberglass reinforced anisotropic plastics heating during cyclic axial loading 16 p2934 A70-33215

Material data file and retrieval system for designers in automotive, equipment and appliance industries, discussing applications to other FRP markets 16 p2935 A70-33352

Diluent resins properties for blending with glass fiber reinforced high density polyethylene concentrate 16 p2935 A70-33353

Friction properties of internally lubricated and glass-fortified thermoplastic resins for gears and bearings 16 p2935 A70-33354

Low cost flame retardant high service temperature glass reinforced electrical grade laminate tested for continuous use 16 p2935 A70-33355

High service temperature glass reinforced premix compound on Glastic grade electrical laminate, discussing optimum molding and applications 16 p2936 A70-33356

Chemical structure and room temperature tensile, flexural and compressive properties of metaphenylenediamine cured castings for graphite fiber reinforced epoxy resin matrices 16 p2936 A70-33358

Glass fiber reinforced resin structures evaluation by plastographic analysis using visual, macrographic, stereomicroscopic, and scanning electron microscope methods 16 p2908 A70-33361

Cold forming of thermoset-thermoplastic laminate consisting of reinforced epoxy core sandwiched between thermoplastic face sheets 16 p2916 A70-33362

Thickeners and low shrink additives for premix and sheet molding compounds/SMC/ 16 p2936 A70-33363

Smooth surface polyester premix and sheet molding compound technology applied to reinforced plastics industry 16 p2917 A70-33364

Carbon fiber reinforced plastics potential as fatigue resistant materials 16 p2936 A70-33367

Shear and tensile joint strength measurements at fiber-polymer matrix interface, using pull-out test and debonding methods 16 p2937 A70-33372

Moisture induced failure of glass-resin composites at interface, discussing water adsorption, crack

propagation, wet strength and nonsilicate reinforcement 16 p2937 A70-33373

Reinforced plastics adhesion to hydrophilic mineral surfaces by using silane coupling agents 16 p2937 A70-33374

Free radical coupling of silyl peroxides in reinforced plastics, laminates and adhesives 16 p2937 A70-33377

Interfacial chemistry of glass fiber reinforced thermoplastics, discussing matrix resin- reinforcement bond 16 p2937 A70-33378

Solvents and chemicals resistant thermosetting resin producing high strength glass reinforced laminates based on polyanhydride crosslinked with monoepoxide 16 p2938 A70-33382

Polyimide resin as matrix for glass fabric reinforced laminates 16 p2938 A70-33383

Creep and tensile fatigue behavior of notched and unnotched graphite/epoxy composites [ASME PAPER 70-DE-32] 16 p2938 A70-33503

Joint design for fiberglass reinforced plastic aircraft components regarding minimum weight and reliability [ASME PAPER 70-DE-56] 16 p2989 A70-33516

Lamellar and fibrous Be-reinforced epoxy resin and metal matrix composites, describing preparation and properties 16 p2939 A70-33693

High pressure ablation of plastic composites and graphite in arc heater, measuring erosion rate, shape change, surface roughness and physical characterization [ALAA PAPER 70-770] 17 p3193 A70-34482

Shock propagation in Al fiber-polyethyl methacrylate composite, calculating pressure, densities, internal energies and particle velocities 17 p3182 A70-34556

High strength graphite fiber reinforced polyimide resin composites fabrication 17 p3127 A70-34560

Adhesive bond between steel wire and epoxy resin, investigating hydrostatic pressure effect on shear strength 17 p3123 A70-34623

Flexural creep deflections of glass fiber reinforced polycarbonate and Nylon thermoplastics 17 p3127 A70-34657

Fiberglass reinforced plastics fatigue properties, describing electric model and nondestructive testing 17 p3183 A70-34658

Temperature and constant compressive loading effects on mechanical characteristics of fiberglass reinforced plastics 17 p3127 A70-35341

Graphite-epoxy resin cross-ply composites fabrication, analyzing residual thermal stresses role in cracking [ASME PAPER 70-GT-84] 18 p3279 A70-36828

Anisotropic composite materials comprised of B and graphite fibers in polymer matrix, discussing precision molding technologies [ASME PAPER 70-GT-126] 18 p3264 A70-36852

Gliders made of glass fiber reinforced plastics, investigating thermoplastic properties under solar irradiation and surrounding warm air 19 p3454 A70-37370

Glass fiber reinforced cross ply and quasi-isotropic plastics, considering notches effect on fatigue behavior for comparison with metals 19 p3455 A70-37951

Graphite-polyimide composites development for high temperature environments, discussing mechanical properties 19 p3455 A70-38425

Bearing strength and rupture of reinforced plastic composites under intense one-sided electric heating and hydrostatic pressure due to pyrolysis of plastic bond 19 p3455 A70-38462

Graphite fiber reinforced polycarbonate composites interfacial adhesion improvement by controlled thermal treatment 20 p3652 A70-39168

Unidirectional carbon fiber reinforced plastics /CFRP/ interlaminar shear strength measurements using short beam shear, notch overlap and solid rod torsion methods 20 p3653 A70-39203

Shearing strain in oriented fiberglass reinforced plastics under torsion, obtaining creep curves 20 p3655 A70-39768

Fiberglass reinforced plastics fatigue life, analyzing structural factors role 20 p3655 A70-39891

Reinforced plastic for aircraft parts, investigating low viscosity polyester resins of styrene crosslinking type 20 p3656 A70-40028

Reinforced plastic composites thermal protection and ablative performance in high temperature environments for reentry vehicle applications 20 p3656 A70-40029

Glass reinforced plastics /GRP/ mechanical properties degradation by water, discussing effects of temperature, pressure, environment, etc

20 p3656 A70-40056

Fiber reinforced plastics /FRP/ composites applications in Japanese aircraft production and aerospace industries

20 p3657 A70-40057

Contact shaped fiberglass-reinforced plastic tensile creep tests, showing strain property linearity dependence on direction

21 p3841 A70-40642

Unidirectional fiberglass-reinforced plastic, investigating binder content and porosity effects on strength

21 p3841 A70-40647

Thin walled fiberglass-reinforced plastic cylinders in torsion, calculating load carrying capacity as function of temperature

21 p3841 A70-40648

Orthotropic fiberglass-reinforced plastic cylindrical shell with allowance for material creep, calculating stress-strain state during bending under external pressure

21 p3842 A70-40649

Textolite and fiberglass-reinforced plastics relaxation parameters tabulation for viscoelasticity boundary value problems solution

21 p3842 A70-40650

Boron vs carbon fiber reinforced plastics, discussing layer and panel structures, molded and mechanical sections, prepregmentation, cost and structural concepts

21 p3842 A70-41263

Carbon fiber reinforced polymer /CFRP/ failure mechanism, discussing nondestructive testing, destructive and cyclic loads

22 p4058 A70-42476

Joint strength of three layer fiberglass reinforced plastic panels with bilateral adhesive patches under linear axial force

22 p4115 A70-42812

Deformational characteristics of unidirectional glass epoxy composites with ductile and brittle matrices evaluated in flexure

22 p4059 A70-43101

Glass-epoxy composites, measuring embedding filaments effect on time-temperature relationship under ultimate stress conditions

22 p4118 A70-43549

Boron-epoxy composites rectangular reinforcing arrays spacing aspect ratios, considering matrix stress concentrations and stiffness estimates

22 p4119 A70-43688

Transverse bending of orthotropic glass fiber reinforced plastic plates under uniformly distributed loads

22 p4120 A70-43720

Prestressed loadings on two layer fiberglass-reinforced plastic cylindrical shell under internal pressure

23 p4265 A70-43937

Stress-strain diagrams for oriented fiberglass-reinforced plastic under tension taking into account temperature and anisotropy effects

23 p4209 A70-43938

Fiberglass reinforced plastic strength and deformation properties under creep and stress relaxation, investigating temperature effects and load duration

23 p4209 A70-43980

Saturn Orbital Workshop experiment for testing chemically rigidized expandable materials and structures for space applications, discussing resin impregnated glass fiber cloth

23 p4264 A70-45012

German monograph on glass fiber reinforcement effect on soft thermoplastics strength, adhesion and slip properties

24 p4366 A70-45088

Thermosetting glass reinforced plastics fabrication and use for pressure vessels, vacuum vessels and pipes

24 p4350 A70-46388

REINFORCED PLATES

Stiffeners reinforced rectangular plates parametric stability under dynamic load, deriving equilibrium equations and boundary conditions by averaging stiffener effects

01 p0205 A70-11146

Elastic ring reinforced annular plate of uniform thickness, heated nonuniformly along radius, discussing axisymmetric and asymmetric stability losses

01 p0210 A70-11415

Stress-strain state of epoxy resin plates with single or paired wire reinforcement, using polarization-optical method

02 p0384 A70-11664

Hole reinforcement providing stressed state beyond hole equivalent to plate stress without hole, reducing problem to annulus region mapping

03 p0590 A70-13378

Equivalent rigidity of doubly periodic symmetrically perforated infinite plate strengthened by elastic ring under isotropic tension

03 p0595 A70-13754

Stability and critical loads of transversally isotropic reinforced plastic annular plates with weak shear resistance under axisymmetrical buckling

05 p0933 A70-16213

Three layer plate of elastic fiber glass reinforced plastic outer layers and metallic plastic filler, studying elastoplastic stability

05 p0934 A70-16218

Reinforced openings effect on burst strength of ductile circular plates subjected to pressure loads

05 p0943 A70-16810

Galerkin method to formulate buckling problem of homogeneous and fiber reinforced anisotropic plates simply supported under uniform membrane loads

06 p1160 A70-17313

Stressed state of plate with reinforced circular hole under tension and bending using Airy stress functions

07 p1407 A70-19540

Unsteady temperature field and thermal stresses in reinforced anisotropic plate strengthened at rim by thin isotropic rod

07 p1408 A70-19543

Hole reinforcement in flat plate under uniaxial load with high stress region at boundary, resulting in weight savings

07 p1414 A70-20174

Elastic and optical properties anisotropy in fiberglass reinforced epoxy plates using photoelastic method

07 p1416 A70-20295

Vibration insulation of rib estimated with respect to diffuse flexural wave field in reinforced plate

08 p1586 A70-21010

Stress concentration in elastic plate reinforced at edge by straight rib analyzed in finite form by Cauchy integrals and Fourier transforms

08 p1594 A70-21635

Free and forced vibrations of three layer freely suspended plate with allowance for energy dissipation

09 p1772 A70-22468

Stress concentrations and load transfer around cutouts in fiber reinforced laminates, discussing boron epoxy plates with circular holes

09 p1710 A70-22793

Stress concentration in plate with hole reinforced by elastic cylinder described by equations of three dimensional elasticity theory

09 p1784 A70-23592

Sandwich plates stability in conducting compressible fluid flow under magnetic field

09 p1785 A70-23621

Equivalent rigidity of doubly periodic symmetrically perforated infinite plate strengthened by elastic ring under isotropic tension

10 p1960 A70-25009

Glass fiber reinforced thin rectilinear orthotropic plastic plates bending using finite difference method with allowance for creep

12 p2324 A70-27531

Stress concentrations and optimum shape minimum-weight reinforcement of circular holes in plates determined by polarization-optical technique

13 p2512 A70-28864

Reinforced shallow shells and plates stability beyond elastic limit, obtaining optimal parameters under compressive loads

15 p2816 A70-32159

Infinite elastic plate with beam reinforced circular insert, using classical plate theory and Euler-Bernoulli hypothesis for beams

16 p2990 A70-33679

Homogeneous orthotropic cantilevered rectangular plate with reinforcing ribs, calculating flutter in supersonic gas flow

18 p3336 A70-36140

Rib stiffened elliptical and circular plate vibrations, determining fundamental frequencies by variational techniques

19 p3536 A70-37693

Stress-strain state of epoxy resin plates with single or paired wire reinforcement, using polarization-optical method

19 p3547 A70-38438

Thermomechanical contact and heat transfer on reinforced edge in plates butt joined by curvilinear closed rigidity rib

22 p4120 A70-43718

Fatigue strength of stiffened aircraft panels subjected to repeated buckling by compression loads

23 p4267 A70-44132

REINFORCED SHELLS

Boundary conditions at reinforced edge of shell by separating solution into zero moment stress and edge effect solutions

01 p0209 A70-11407

Thin circular elastic ribs strengthened shallow shells, obtaining solutions in single series

01 p0210 A70-11408

Supercritical strains and buckling in rib-reinforced cylindrical shells under axial compression using strain-energy method

04 p0766 A70-14478

Damping factor of fiberglass-reinforced cylindrical shells, concerning dependence on wave number and

energy losses due to medium resistance and acoustic radiation

04 p0712 A70-14488

Elastic orthotropic fiberglass reinforced plastic shells stability under axial compression, analyzing shear modulus influence

04 p0712 A70-14490

Free vibrations of reinforced elastic shell structures subject to constraints imposed by reinforcing elements, utilizing equivalent models without reinforcing elements

[ASME PAPER 69-WA/APM-25]

04 p0770 A70-14907

Carrying capacity and deformation susceptibility of anisotropic fiberglass reinforced conical and cylindrical plastic shells under axial compression

05 p0933 A70-16209

Stability, critical load and strength algorithm for fiberglass reinforced cylindrical plastic shells under external load allowing for shear stresses

05 p0933 A70-16211

Statistical stability of cylindrical fiberglass reinforced plastic shells under axial compression, showing breakdown loads vs radius/thickness ratio

05 p0933 A70-16215

Residual stress variations in ring shaped fiberglass reinforced plastic shells produced by winding due to elastic modulus decrease and filler/binder contraction

05 p0934 A70-16216

Strain parameters and equilibrium equation of rib-reinforced thin shells, analyzing length, curvature and torsion variations using smooth shell analogy

05 p0935 A70-16230

Circular cylindrical shells stiffened by rings and stringers and subjected to periodic axial force, analyzing parametric instability

05 p0940 A70-16513

Digital computer program for analyzing axisymmetrically loaded ring-stiffened segmented composite elastic shells of revolution, giving vibration frequencies

05 p0944 A70-16814

Small elastoplastic deformation effects on stress-strain state of rib-reinforced cylindrical shells

05 p0946 A70-16955

Hydrodynamic coefficients of algebraic equations for boundary value problems in disturbed motion of body with rib-reinforced liquid filled cavity

05 p0836 A70-16956

Membrane reinforced thin walled cylindrical shells stability as asymmetric contact problem in shell and plate theory

05 p0947 A70-17011

Dynamics of composite, sandwich and stiffened shell type structures with various geometries

06 p1160 A70-17158

Segmented elastic shells of revolution supported by rings, studying buckling and vibration by matrix method

07 p1405 A70-19257

Limiting equilibrium of axisymmetric shells consisting of alternating reinforcement layers separated by layers of homogeneous isotropic material

07 p1415 A70-20184

Rib-reinforced cylindrical shells stability under longitudinal compressive loading, studying stress-strain state using network method

08 p1583 A70-20528

Strain energy method applied to stability analysis of short longitudinally reinforced cylindrical shells under axial compression

08 p1584 A70-20536

Buckling of elastic cylinders with rectangular cutouts and reinforcements under axial or lateral loading, using modified Newton method

09 p1780 A70-23208

Free vibration of rib stiffened freely supported circular cylindrical shells, verifying rib eccentricity importance to natural frequencies by numerical solutions

09 p1780 A70-23211

Plastic buckling of eccentrically stiffened circular cylindrical shells with multiple isotropic layers under combined axial and lateral pressure, deriving stability criterion

09 p1780 A70-23213

Stress analysis for cylindrical shells with reinforced circular holes by collocation method

09 p1781 A70-23280

Reinforced cylindrical shells stress-strain state under concentrated longitudinal loads, considering ribs of variable rigidity

09 p1782 A70-23289

Stress concentration at elliptical hole of arbitrary eccentricity in shallow sandwich shells with hard and soft fillers

09 p1783 A70-23385

Contour immobility effect on load carrying capacity of rigid plastic thin shells of revolution, establishing minimum reinforcement value for edge

09 p1783 A70-23388

Ribs reinforced shells of revolution designs calculations by approximate numerical method, considering surface geometry and cyclic temperature loads effect

09 p1784 A70-23589

Elastic ribs reinforced thin cylindrical shells stress-strain state under arbitrary load distribution allowing for rib spacing discreteness

09 p1784 A70-23590

Stress distribution in rib reinforced cylindrical shells under concentrated forces calculated using finite difference scheme

09 p1791 A70-23718

Reinforcing ribs eccentricity effect on closed circular cylindrical shell stability using strain energy method

09 p1786 A70-23720

Truncated, structurally orthotropic and round conical shell oscillations taking into account reinforcing ribs eccentricity

10 p1964 A70-25195

Eccentrically stiffened thin cylindrical shell stability under torsion emphasizing exact finite formula derivation

11 p2129 A70-25561

Rectangular conical shells reinforced along ribs by belts under tension/compression calculated by initial functions method

11 p2130 A70-25568

Stiffened cylindrical shells under internal pressure numerically analyzed based on C-5A fuselage material parameters

11 p2135 A70-25961

Inplane and rotary inertia effects on free vibration frequencies of circular cylindrical shells eccentrically stiffened by orthogonal set of stringers and/or rings

11 p2135 A70-25993

Asymmetric stiffened shell structure analysis by finite element method, introducing constant transverse shear model concept

11 p2144 A70-26677

Automated optimum structural design by variable step direct search algorithm, noting application to stiffened cylindrical shells

12 p2319 A70-27138

Stiffened fiber composite cylindrical shells minimum weight design, discussing configuration and material parameters

12 p2319 A70-27139

Stiffened cylindrical shells buckling under axial compression, obtaining imperfections and prebuckling growth mappings

12 p2319 A70-27141

Stability analysis of ring-stiffened orthotropic, multilayered shells of revolution under axisymmetric torsionless loads by digital computer

12 p2320 A70-27143

Thermal buckling theory for multilayered stiffened cylindrical shells under various combined loads

12 p2321 A70-27149

Axially stiffened and barreled cylindrical shells elastic postbuckling behavior, considering effects of stringer and load eccentricities

12 p2321 A70-27175

Glass-plastic thin cylindrical shells carrying capacity dependence under axial and external loads on combinations of longitudinal and transverse reinforcing layers

12 p2259 A70-27527

Structural strength of fiberglass plastics reinforced conical shells, using impregnation technique of dry package under pressure

12 p2328 A70-28280

Laminated glass fiber reinforced cylindrical shell stability resting on hinged supports under axial compression

13 p2514 A70-29285

Stability loss of nonreinforced and reinforced cylindrical shells under external pressure

13 p2514 A70-29294

Eccentrically stiffened orthotropic cylinders with intermittently attached stiffeners under bending and axial load, analyzing instability and buckling

13 p2518 A70-29966

Linear compressive orthotropic stability theory for shallow-stiffened cylinders

13 p2518 A70-30022

Reinforced shells of revolution carrying capacity upper limit subjected to internal adiabatic ideal gas flow

15 p2814 A70-31534

Strength and critical load determination for spherical shells with reinforced hole under internal pressure based on stress-strain state analysis during deformations

15 p2814 A70-31543

Cylindrical shells with longitudinal rib reinforcements, deriving yield surface from strain mapping and collapse under pressure

15 p2816 A70-32006

Reticulated shell structure buckling using approximate equivalent shell and discrete analysis of individual beams

15 p2816 A70-32007

Reinforced shallow shells and plates stability beyond elastic limit, obtaining optimal parameters under compressive loads

15 p2816 A70-32159

Spherical shell of variable thickness, calculating stress-strain state around reinforced circular hole during elastoplastic deformation

18 p3336 A70-36138

Stability of circular cylindrical shell reinforced by elastic rings at edges under longitudinal compression

18 p3341 A70-36581

Stiffened thin walled circular cylinders buckling and postbuckling behavior under axial compression or external hydrostatic pressure

[DFVL-SONDDR-59] 20 p3719 A70-39621

Structurally closed orthotropic circular cylindrical reinforced shell stability, developing approximate method to obtain various boundary conditions

20 p3727 A70-39886

Thin cylindrical shells optimum design with symmetrically paired spiral type stiffeners under uniform axial compressible load and lateral pressure

20 p3732 A70-40287

Circular rib reinforced cylindrical shells, analyzing error due to Kirchhoff-Love hypothesis

20 p3734 A70-40435

Buckling analysis of stiffened noncircular cross section cylindrical shells constructed by circular arcs and straight line segments

21 p3934 A70-40922

Circular cylindrical orthotropic fiberglass-reinforced shell buckling under longitudinal impact, assuming initial surface imperfections

22 p4117 A70-43347

Ring-stiffened thin circular cylindrical shells, calculating free vibration natural frequencies and mode shapes by finite element method

24 p4427 A70-46067

REINFORCEMENT

Polyimide preregs reinforced with glass, carbon and graphite, describing processing characteristics, properties and applications

17 p3127 A70-35419

REINFORCEMENT [PSYCHOLOGY]

Human subjects performances on fixed interval reinforcement schedules, emphasizing effects of instruction

01 p0035 A70-10793

Pigeon response to concurrent variable interval reinforcement schedules, investigating relative and changeover rates regarding key color

05 p0800 A70-16126

Human macrosaccadic eye movements related to four dial display conditioned by concurrent variable interval schedules of signals

05 p0800 A70-16127

Amphetamine effects on observing and monitoring performance in squirrel monkeys, investigating lever and key responses using food reinforcements

05 p0806 A70-16128

Stochastic reinforcement learning model synthesizing control and pattern recognition systems with learning attributes

13 p2374 A70-29584

REINFORCEMENT [STRUCTURES]

Beaded-doubler reinforced skin design concept for Improved HAWK Missile wing, considering compression stress, weight, cost and field service characteristics

02 p0380 A70-11946

Soviet book on experimental investigation of thin walled structures elastoplastic work with complex reinforcement, outlining test procedures

03 p0585 A70-12985

Structural reinforcement for existing airport pavements, discussing construction procedures

03 p0462 A70-13174

Hole reinforcement providing stressed state beyond hole equivalent to plate stress without hole, reducing problem to annulus region mapping

03 p0590 A70-13378

Mechanical behavior of cylinders with alternating layers of reinforcing and matrix materials derived from governing equations, including equations of motion

[ALAA PAPER 70-134] 06 p1169 A70-18051

Stress analysis of composite materials reinforced with glass ribbons embedded in epoxy matrix by photoelastic technique, discussing perturbation effect

08 p1594 A70-21862

Stress-strain characteristics of reinforced elastoplastic layer using mathematical model

09 p1769 A70-22183

Reinforced epoxy models as precursor to prototype design and analysis of aircraft structures, discussing stress analysis methods

12 p2318 A70-27129

Structural strength of fiberglass plastics reinforced conical shells, using impregnation technique of dry package under pressure

12 p2328 A70-28280

Optimal design for composite material structure, considering internal and external reinforcement

15 p2816 A70-32005

Boron-epoxy stiffener reinforced metal wings, examining structural efficiency of multiweb beam aluminum cover skins and Z stiffened panels

16 p2994 A70-34230

German monograph on creep in statically indeterminate reinforced concrete beams with graduated cross sections

19 p3548 A70-38473

Overbraced frame loaded at joints, limiting elastic buckling examinations to geometrically perfect structures

20 p3717 A70-38973

Composite materials physical properties based on linearly reinforced media models and complex variable functions theory

20 p3655 A70-39860

Multicomponent composite materials, discussing fiber reinforced structures, clad metals and bulk materials

20 p3650 A70-39947

Mechanical behavior of cylinders with alternating layers of reinforcing and matrix materials derived from governing equations, including equations of motion

20 p3732 A70-40267

Aerial retrieval webbing performance characteristics, discussing structure, type of material, finishing and strength levels

[ALAA PAPER 70-1181] 21 p3843 A70-41832

REINFORCEMENT RINGS

Elastic ring reinforced annular plate of uniform thickness, heated nonuniformly along radius, discussing axisymmetric and asymmetric stability losses

01 p0210 A70-11415

Equivalent rigidity of doubly periodic symmetrically perforated infinite plate strengthened by elastic ring under isotropic tension

03 p0595 A70-13754

Structural vibration of ring stiffened and mass-attached hemispherical shells

08 p1593 A70-21618

Eccentricity and clamping effects on stability and critical pressure of ring-reinforced cylindrical shells under internal pressure

10 p1956 A70-24248

Equivalent rigidity of doubly periodic symmetrically perforated infinite plate strengthened by elastic ring under isotropic tension

10 p1960 A70-25009

Metallic cylindrical shells design reinforced with elastic glass fiber rings, considering elastoplastic deformation

12 p2324 A70-27530

Shallow circular cylindrical shell with rigid collar on lateral surface, calculating stress under axial tension and internal pressure loading

19 p3534 A70-37245

REINFORCING FIBERS

Graphite fiber-epoxy resin composites interfacial bonding, describing various surface treatments for increased interlaminar shear strength

01 p0127 A70-10477

Fiber-polymer matrix interfacial tensile and shear strengths evaluation methods, including data correlation from various tests

01 p0087 A70-10478

Fiber-matrix interface mechanics in composites, considering shear strength, stress distribution, fiber strength effects, etc

01 p0127 A70-10479

Fiber-composite materials fracture, noting interface mechanical strength effects on composite properties under tension and shear

01 p0127 A70-10481

Tensile tests of heat treated silicon carbide coated B filament reinforced metals, discussing fiber strength and interfacial stability

01 p0117 A70-10483

Fiber composite cylinder tensile performance improvement through mechanical residual stress relief by axial straining

01 p0120 A70-10737

Reinforcement of thermoplastic resins, considering single crystal whisker and carbon fibers and microspheres

01 p0129 A70-10774

Glass fiber-reinforcing techniques of polymers, discussing coating and compounding processes

01 p0104 A70-10775

Fiber reinforced composites emphasizing refractory fibers, preparation methods, properties and fabrication

01 p0129 A70-10939

Glass reinforced and unreinforced thermoplastics HF fatigue failure modes, discussing isothermal and nonisothermal test procedure

01 p0129 A70-11081

Boron fiber reinforced epoxy fatigue life dependence on reinforcing fibers aspect ratio

01 p0129 A70-11082

Plane sinusoidal wave propagation through material reinforced with parallel fibers, using integral formulation for multiple scattering in infinite slab

01 p0130 A70-11187

Reinforced metals properties and applications including fibers and lamination, notch sensitivity, brittle fracture, failure and heat resistance characteristics

01 p0124 A70-11619

Stress-strain state of epoxy resin plates with single or paired wire reinforcement, using polarization-optical method

02 p0384 A70-11664

Mechanical properties of carbon fiber reinforced Al, Cu and Ni, noting rope and wire applications

02 p0384 A70-11676

High strength high modulus carbon fibers for use in structural reinforced plastics, describing carbonizing and pyrolysis processes

02 p0320 A70-11856

Boron-polyimide composite reinforced Ti fuselage stringers design and test program for SST

02 p0387 A70-11950

Composite fibrous materials applicability to V/STOL rotor blades design and fabrication confirmed by structural analysis

02 p0225 A70-11953

Design allowable curves based on laminate test data for high modulus graphite fiber and resin systems, considering Wagner cantilever beam specimens

02 p0387 A70-11954

B and C fiber unidirectionally reinforced plastic composites, discussing mechanical properties, fabrication and testing

02 p0321 A70-12082

Polymeric materials properties, discussing tensile stress disadvantage and compensation by reinforcement and polymer chain directional alignment

02 p0321 A70-12305

Fiber reinforced composites fabrication, properties and industrial applications, discussing modulus of elasticity and tensile strength equations, bonding and temperature applicability

02 p0322 A70-12713

Bending strength analysis for high strength beam with thin and long fibers embedded in matrix of viscoelastic material noting maximum stress

03 p0584 A70-12934

Reversed bending fatigue tests on stainless steel fibermetal with porous structure to investigate effects of density, thickness, wire diameter, screen stiffening, etc

03 p0481 A70-12957

Fiber composites dimensional changes, stresses and plastic flow during component allotropic transformation, studying temperature variations effects

03 p0585 A70-12973

Unidirectional carbon and glass fiber reinforced polyester resins dynamic characteristics under torsional and flexural vibration, showing damping independence of cyclic stress amplitude

03 p0514 A70-13111

Interlaminar shear stress and fabrication of high modulus graphite-reinforced epoxy matrix composites

03 p0515 A70-13119

Graphite fiber content determination technique for plastic composites based on epoxy, polyimide and phenolic resins, using concentrated sulfuric acid

03 p0515 A70-13123

Failure mechanisms in notched or damaged fiber reinforced composite materials determined from analysis of axial tensile strength and broken fibers

03 p0515 A70-13124

Laminate approximation model of randomly oriented fibrous composites estimating stiffness and thermal and expansional strains

03 p0587 A70-13126

Unidirectional composite materials properties, discussing stiffer filaments effect on Young modulus and shear coupling constant relating shear strain to longitudinal strain

03 p0587 A70-13128

Stiffness and expansion properties of oriented short fiber composites, discussing longitudinal modulus and expansion strain dependence on aspect ratio

03 p0587 A70-13129

Mechanical properties, optimum deformation and rupture of W wire reinforced Ni and Ti metal composites obtained by hot rolling in vacuum

03 p0508 A70-13245

Rational design of structurally anisotropic plane multilayer plates with weak binder, suggesting strengthening fibers orientation in internal stresses direction

03 p0516 A70-13379

Carbon fiber reinforced plastics /CFRP/ uses in commercial aircraft structural component

03 p0516 A70-13546

Composite materials possible applications, considering metal matrices reinforced by high strength metallic or nonmetallic fibers

03 p0512 A70-13857

Al and Sn composites reinforced by E glass and silicon dioxide glass fibers compared for tensile strength, noting difference due to resistivity

03 p0514 A70-14314

Brittle composites /including fiber reinforced material/ deformability and plastic deformation effect on tensile strength, discussing pressure induction of sound flow

[ASME PAPER 69-WA/PROD-28]

04 p0705 A70-14834

Plastic flow failure of matrix of fiber reinforced composite sheet, discussing plane stress and simple tension

[ASME PAPER 69-APM-Z] 04 p0770 A70-14869

Stress intensity and strain energy release rate in elastic fiber-reinforced composites with different thermomechanical properties and imperfect bonding

[ASME PAPER 69-WA/APM-15]

Ceramic fibers formation by particles mechanical deformation by extrusion in W matrix, describing grain structure of various extruded metal oxides

04 p0699 A70-15643

Axisymmetric elasticity problem for straight fiber imbedded into infinite matrix, noting homogeneous temperature changes causing residual stresses, tractions at infinity and fiber pulling

05 p0931 A70-16088

Continuum model for plastic-elastic behavior of fiber reinforced composite material, formulating yield condition and constitutive equations

05 p0931 A70-16131

Composite materials use in nonload bearing and heavily stressed materials, considering applications in aircraft industry and high strength fibers role

05 p0870 A70-16576

High modulus fibers as reinforcing fillers in thermoplastic matrices, discussing cost compensation in low fiber loadings

05 p0870 A70-16578

Mechanized glycerine process for fibers and whiskers alignment on large scale at low cost

05 p0855 A70-16580

Carbon fiber-reinforced plastics fabrication, discussing leaky mold, prepreg and filament winding methods

05 p0855 A70-16581

Rotary machine for classifying reinforcing fibers and whiskers with respect to length

05 p0855 A70-16583

Chrysotile-type asbestos reinforcing fiber properties and applications, tabulating asbestos fiber types for commercial reinforced plastics

05 p0873 A70-16607

Boron and other high performance reinforcements made by vapor plating process, discussing boron filament atomic structure and morphology

05 p0873 A70-16609

Whiskers and whisker products physical characteristics, available forms and types and compositing methodology, discussing utilization in plastics

05 p0873 A70-16611

Filament winding methods of aerospace industry based on motor case winding, emphasizing reinforcing materials, winding geometry and finished composite evaluation methods

05 p0856 A70-16615

Micro and macromechanics for design and mechanical properties prediction of laminated fibrous composites for airframes and space structures

05 p0941 A70-16619

Boron-epoxy composite materials for secondary and primary aircraft structural components, discussing multidirectional laminates, joint analysis, etc

05 p0942 A70-16620

Continuous metal fiber composites tensile strength and ductility in terms of plastic instability

05 p0946 A70-16924

Thermal conductivity and aperiodic temperature distribution in microstructure of composite materials reinforced with solid and hollow fibers

05 p0958 A70-16952

Fibers random curvature effect on thermoelastic properties of unidirectionally reinforced fibrous materials

05 p0946 A70-16953

Fatigue life of unidirectionally glass fiber reinforced composites subjected to low cycle loading, using linear elastic body model for cyclic deformation process

06 p1091 A70-17408

Thin walled glass fiber reinforced plastics beams strength analysis combined with results from elasticity theory of anisotropic bodies

06 p1167 A70-17913

Arbeitsgemeinschaft Verstärkte Kunststoffe - Conference, Freudenstadt, West Germany, September-October 1969

07 p1316 A70-17953

Sizing and design of large vessels of fiberglass reinforced composites based on minimum cost

07 p1409 A70-17957

Fiberglass reinforced materials characteristics under stress evaluated by ring test in form of split disk or hydraulic tests

07 p1410 A70-17958

Boron and carbon fiber reinforced composites mechanical properties compared with fiberglass reinforced composites

07 p1318 A70-17970

Boron fiber reinforced composites structure and loading capacity, describing network-like fiber winding technique for light reinforced structures

07 p1318 A70-17971

Fabrication and properties of carbon fibers and carbon fiber reinforced epoxy resins

07 p1318 A70-19772

Heat resistant fibers fabrication and properties for composite materials, noting metal whiskers, C, B, Be and alumina

07 p1318 A70-19802

Tensile strength test and clamping of epoxy impregnated fiber strands

07 p1250 A70-19959

Fiber reinforcement of metals, considering strength of boron, alumina, graphite, silicon carbide and silica glass fibers

08 p1514 A70-20471

Distilled water and mineral oils heated to 50-80 C studied for effect on residual stresses in fiberglass reinforced plastics

08 p1526 A70-20925

Fiber-reinforced composite sheet matrix failure by plastic flow, investigating two ply laminate in simple tension

08 p1592 A70-21471

Residual stresses in continuous fiber reinforced composites with unknown strain history determined by empirical methods

08 p1520 A70-21498

Aluminum-base reinforced material synthesis by liquid impregnation, investigating transition layer dependence on holding time and fiber/matrix microhardness

08 p1520 A70-21500

Carbon fiber composite materials production technology, physical properties and potential applications in aerospace

08 p1527 A70-21520

Axial constant load creep and strength rupture measurements of B-coated and silicon carbide-coated B filament reinforced Al alloys

08 p1521 A70-21702

Composite materials shear strength test problems with high modulus fibers

08 p1529 A70-21877

Mechanical properties characterization of unidirectional high modulus carbon fiber reinforced epoxy matrix composite

08 p1530 A70-21883

Mechanical testing of metal matrix high modulus B-A filament composites, using unidirectional and multidirectional reinforcement

08 p1523 A70-21894

Fibrous reinforced composites influence in aircraft structural design based on DOD industry development programs, investigating interlaminar shear

08 p1595 A70-21899

Graphite fiber/resin matrix composites for airframe structures, studying tensile, compressive and in-plane shear strengths

08 p1532 A70-21901

Unidirectional filamentary composites failure theory for uniaxial and combined stress, considering constituent material properties and fabrication processes

08 p1532 A70-21902

Fiber composites-Ti alloy adhesive, rivet and combined joints for aircraft applications, noting fiber orientation role in joint tensile strength

08 p1509 A70-21905

Tungsten alloy fiber reinforced Ni-base superalloy composites evaluated for high temperature turbojet engine applications, considering stress-rupture strength, oxidation and impact resistance

08 p1523 A70-21907

Fracture processes in homogeneous anisotropic fiber composite materials, describing microcrack initiation, growth and unstable propagation at critical stress level

08 p1532 A70-21912

Composite material tensile strength, discussing statistical scatter in fiber strength and local fiber overstress caused by fiber discontinuities

08 p1532 A70-21914

Electrical and photographic methods for measuring microcracking in fiber reinforced plastics

08 p1501 A70-21916

Longitudinal strength characteristics of filament reinforced composites, discussing bond strength effect on filament fracture

08 p1533 A70-21918

Cold rolling characteristics of unidirectionally reinforced Al-B fiber composites, measuring hardness and tensile properties

08 p1524 A70-21957

Metal matrix fiber reinforced materials bonding, discussing brazing and fusion and diffusion welding

[ASM PAPER W9-23.2] 09 p1690 A70-22557

Tungsten fiber reinforced aluminum composites tensile strength aspect ratio using foil metallurgy technique

09 p1703 A70-22627

Carbon fibers and fiber-reinforced composites fabrication, structural properties and uses

09 p1710 A70-22758

Fiber-reinforced composite alloys prepared by controlled dissociation of Au-Ni and Al-Zn solid solutions

10 p1902 A70-23814

Fibrillated asbestos dispersed in thermoplastic ionomer lattices, precipitated, dried and compression molded into bars, testing for flexural modulus, flexural stress and Vicat softening temperature

10 p1906 A70-24024

Filament-reinforced metallic composites corrosion control by specificity of environment and galvanic interactions between components

10 p1904 A70-24651

Thermoplastics reinforcement with glass and asbestos fibers taking into account fiber properties

11 p2070 A70-25825

Two dimensional photoelastic investigation of crack propagation in fiber-reinforced composites consisting of glass and polyester resin layers

11 p2136 A70-26078

Elastic moduli of fiber reinforced composites calculated, deriving reinforcement factor in Halpin-Tsai equation from volume fraction

11 p2070 A70-26087

Silicon carbide whiskers properties and applications compared with other reinforcing fibers

11 p2070 A70-26340

Ultrasonic pulse technique for measuring fiber reinforced composites elastic constants

11 p2052 A70-26341

Wire sheet reinforcement for resin matrices, discussing mechanical properties, fabrication, bonding, wetting, etc

11 p2071 A70-26346

Anisotropic fiber reinforced composites elastic moduli determined by analytical matrix method

11 p2141 A70-26488

Fiber reinforced composites under longitudinal shear loading, noting orthotropic nature and shear moduli assuming circular fibers

11 p2141 A70-26489

Steady state creep of composite material with short fibers, discussing effects of fiber/aspect ratio, fiber volume fraction and distribution

11 p2144 A70-26671

Elastic stiffness of unidirectional glass reinforced epoxy fiber composite determined from ultrasonic velocity measurements

11 p2071 A70-26692

Fiber reinforced Al alloys fabrication by thin sheet metallurgy techniques

12 p2252 A70-26887

Boron fibrous composite panels machining methods including drilling, routing, band sawing and reaming [ASTM PAPER EM-69-141]

12 p2240 A70-27077

Wide goods fabrication of boron composites, discussing mechanical properties and cost effectiveness

[ASTM PAPER EM-69-142]

12 p2240 A70-27078

Filament winding process for boron modified phenolic resin tape used in high temperature applications

12 p2242 A70-27204

Interfacial tractions between matrix and fiber in elastic composite materials reinforced with elastic fibers

12 p2322 A70-27230

Stress and strain in matrix of fiber reinforced material within elastic region, calculating interface shear stress for rectangular fiber

12 p2322 A70-27231

Composite materials fabrication with glass, boron and graphite fibers reinforcement, discussing matrix and binder materials

12 p2253 A70-27267

NDT methods for fiberglass, graphite and boron fiber composites for aircraft structures

12 p2243 A70-27465

High modulus carbon fibers low angle X ray diffraction correlation to physical properties

12 p2259 A70-28050

Fiberglass content effects on reinforced polycarbonates long term dimensional stability during compression and tension creep tests

12 p2259 A70-28298

Fiber diameter effects on metal matrix composites strength from proposed model

12 p2329 A70-28370

Stress concentration in fiber reinforced materials resulting from thermal self straining, using finite element method and photoelastic analysis

13 p2509 A70-28533

Molding procedure to orient filaments relative to loads for optimizing structural component /compressor blades/ of filament reinforced composite

13 p2417 A70-28663

Glass fiber reinforced resin structures and equipment quality and physical/mechanical conditions determined by plastographic analysis

13 p2404 A70-28665

Aircraft structure fabrication combining unidirectional strength and stiffness of B composite with metal, including test and weight/cost data

13 p2418 A70-28777

Ductile fracture in Al matrix composite reinforced with unidirectional stainless steel fibers described by critical crack tip displacement and fracture strain criteria

13 p2512 A70-28917

Fiberglass reinforcement effects on injection molded thermoplastics physical properties, noting role of binder and glass content

13 p2438 A70-29204

Unidirectional composite with transversely isotropic fibers, calculating elastic stiffness constants by modified point-matching technique

13 p2515 A70-29466

Stainless steel fiber reinforced Sn-Pb eutectic alloy composite mechanical properties, noting tensile strength and rupture behavior

13 p2436 A70-29625

Filament reinforced metal matrix composites fabrication and engineering uses

14 p2590 A70-30542

Fe-Al and Fe-Si alloys strengthening by pyrolytic graphite fibers

14 p2595 A70-30543

Metallic base fiber and particulate composites, emphasizing silicon carbide, sapphire, boron and graphite filaments

14 p2597 A70-31168

Book on high modulus fibers and composites providing data for preparation, microstructure, structure and properties

14 p2598 A70-31315

Filament orientation and fabrication variables effect on Ag matrix-W fiber composite mechanical properties

15 p2756 A70-31569

Beryllium fibers and Al matrix interactions at high temperatures and various durations, investigating diffusion by X ray diffraction, electron microscope and microprobe analysis

15 p2757 A70-31812

Filament winding reinforcement and resin noting production equipment and costs

15 p2744 A70-31932

Fibre reinforced polymers fatigue life under cyclic stresses, obtaining data from rotary cantilever tests

15 p2764 A70-31933

Fiber reinforced viscoelastic composites complex elastic moduli derivation

15 p2816 A70-32003

Stress distribution in fiberglass unidirectionally reinforced composite material under uniaxial tension

15 p2765 A70-32180

Carbon reinforcing fibers, discussing mechanical properties, production, cost reduction, etc

15 p2765 A70-32246

Metal fiber multiple necking effect on uniaxial metal matrix composites ductility and plastic deformation behavior for brass-W model system

15 p2761 A70-32378

Statistical theory of material strength applied to composite materials reinforced with whiskers and noncontinuous fibers

15 p2763 A70-32833

Mechanical properties of composite materials reinforced with ribbon fibers consisting of stainless steel and polyethylene ionomer resins

16 p2988 A70-33366

Carbon fiber reinforced plastics potential as fatigue resistant materials

16 p2936 A70-33367

Shear and tensile joint strength measurements at fiber-polymer matrix interface, using pull-out test and debonding methods

16 p2937 A70-33372

Interfacial chemistry of glass fiber reinforced thermoplastics, discussing matrix resin- reinforcement bond

16 p2937 A70-33378

Polyimide resin as matrix for glass fabric reinforced laminates

16 p2938 A70-33383

Graphite fiber reinforced polyimide composites with low void content, high strength and modulus

16 p2938 A70-33384

Fiber reinforced prepreg properties measurements in high modulus graphite/epoxy and fiberglass/ epoxy prepreg sheets and tapes

16 p2938 A70-33386

Glass reinforced laminates fatigue characteristics, discussing differences from metals due to composites anisotropic structure

16 p2989 A70-33420

Lamellar and fibrous Be-reinforced epoxy resin and metal matrix composites, describing preparation and properties

16 p2939 A70-33693

Elastic constants for plates of unidirectional fiber reinforced anisotropic composite material determined by ultrasonic wave propagation

16 p2991 A70-33847

Constitutive equation for fiber reinforced viscoelastic materials, using continuum theory of mixtures

16 p2994 A70-34231

Shock propagation in Al fiber-polyethyl methacrylate composite, calculating pressure, densities, internal energies and particle velocities

17 p3182 A70-34556

High strength graphite fiber reinforced polyimide resin composites fabrication

17 p3127 A70-34560

Optimum fiber orientation for minimum weight boron/epoxy shear panel design

17 p3182 A70-34562

Optimum filament orientation for maximum strength in composite with combined normal and shear stresses

17 p3183 A70-34563

Longitudinal shear modulus of unidirectional fibrous composite, involving series solution of Laplace equation

17 p3183 A70-34564

Fiberglass reinforced plastics fatigue properties, describing electric model and nondestructive testing

17 p3183 A70-34568

Circular inclusion interface separation in matrix under incident compressive waves interpreted for fiber reinforced composites

17 p3185 A70-34963

Plastic flow and failure of elastic fiber reinforced composite materials with noninteracting and interacting discontinuities, obtaining stress distribution for various work hardening degrees

17 p3187 A70-34991

Metal matrix alloys with base of Co, Fe or Ni reinforced by transition metal carbide fibers, discussing deformation tests at various temperatures

17 p3124 A70-35142

Fiber reinforced composite with ductile matrix, discussing fatigue life prediction from strain hardening characteristics

17 p3128 A70-35465

Composite wing section design and fabrication utilizing unidirectional glass reinforcement [AIAA PAPER 70-919]

17 p3193 A70-35813

Honeycomb panels with fiber reinforced facings, obtaining acoustic fatigue design criteria [AIAA PAPER 70-897]

17 p3064 A70-35814

Deformation behavior of continuous W and B fibers reinforced Al alloy matrix composites, monitoring stress-strain characteristics by X ray diffraction

18 p3272 A70-36036

Buckling of fiber reinforced composite orthotropic plates

18 p3343 A70-36706

Fiber-metal matrix composites for gas turbine blades, discussing stress rupture strength, modulus of elasticity, fabrication, etc [ASME PAPER 70-GT-133]

18 p3302 A70-36827

Boron composites development for aircraft structures compared with titanium [ASME PAPER 70-GT-120]

18 p3344 A70-36851

Anisotropic composite materials comprised of B and graphite fibers in polymer matrix, discussing precision molding technologies

[ASME PAPER 70-GT-126]

18 p3264 A70-36852

Fiber reinforced materials with oriented arming, calculating stress strain state under transverse shear

19 p3454 A70-37348

Tungsten fiber reinforced copper based composite material, investigating moulding and sintering conditions effect on mechanical properties

19 p3450 A70-37454

Stress wave propagation based on elasticity theory for reentry heat shield composites reinforced with unidirectional high strength high modulus fibers

19 p3537 A70-37788

Stress and displacement within internally pressurized composite cylinders having continuous fiber reinforcement in circumferential direction, using finite element method

19 p3538 A70-37797

Fiber reinforced solid material, determining swelling or temperature change induced dilatation by micromechanics and physical chemistry

19 p3540 A70-37943

Glass fiber reinforced cross ply and quasi-isotropic plastics, considering notches effect on fatigue behavior for comparison with metals

19 p3455 A70-37951

Unidirectional composites subjected to free vibration and axial end loading, considering longitudinal stress wave propagation in fiber direction

19 p3540 A70-37954

Micropolar mechanics application to stress and displacement within separate components of fibrous composite material

19 p3541 A70-37961

Stress-strain state of epoxy resin plates with single or paired wire reinforcement, using polarization-optical method

19 p3547 A70-38438

Mechanical properties, optimum deformation and rupture of W wire reinforced Ni and Ti metal composites obtained by hot rolling in vacuum

19 p3453 A70-38463

Strain measurement on filament-wound structural members, incorporating electric resistance wire as strain gage within windings

19 p3550 A70-38719

Soviet book on fiber reinforced composites covering strength, rheologic and elastic properties, thermal conductivity, diffusion processes, etc

19 p3456 A70-38795

Hydrofoil and hovering craft design by fiber technology, discussing composite materials, whisker

mechanical properties, polycrystalline fibers, matrix materials, etc

19 p3456 A70-38941

Duplex eutectic with Ni-Be fibers embedded in Ni-Cr solid solution matrix, discussing solidification conditions, optimum composition, heat treatment, mechanical properties and oxidation

20 p3647 A70-39107

Graphite fiber reinforced polycarbonate composites interfacial adhesion improvement by controlled thermal treatment

20 p3652 A70-39168

Unidirectional carbon fiber reinforced plastics /CFRP/ interlaminar shear strength measurements using short beam shear, notch overlap and solid rod torsion methods

20 p3653 A70-39203

High modulus graphite fiber tensile strength and structure, using X ray diffraction

20 p3653 A70-39205

Graphite filament composite structure shear strength decrease with modulus increase, examining fiber microstructure effect on interlaminar properties by short beam shear test

20 p3654 A70-39206

Chemical vapor deposition of carbon matrix material in fiber structure, investigating thermodynamic fundamentals in processes

20 p3654 A70-39207

Carbon fiber/carbon matrix composites fabrication by isotropic casting, flock and spray lay-up and pulp molding, describing physical and mechanical properties

20 p3636 A70-39208

Short graphite fiber classification and orientation control in matrix by electrostatic methods

20 p3654 A70-39215

Multicomponent composite materials, discussing fiber reinforced structures, clad metals and bulk materials

20 p3650 A70-39947

Filamentary composite materials for space vehicles structural design, noting mass reduction, strength, foldability, formability, etc

20 p3656 A70-40030

Fiber reinforced composite shell structures stress-strain relations, noting membrane and flexural variables coupling in constitutive relations

20 p3729 A70-40034

Strains and stresses along interfaces and near fiber ends in composite structures made of reinforced matrix, using photoelastic methods

20 p3730 A70-40035

Dynamic theories for wave propagation in laminated and fiber reinforced composites, using dispersion curves for transverse and longitudinal motions

20 p3730 A70-40036

Thermoelasticity of fiber reinforced materials, considering stress concentration in beams and reinforcing fibers buckling under thermal loading

20 p3730 A70-40037

Structural mechanics of continuous fiber reinforced composites, discussing bending and stretching of cylinders, pressure vessels, plates and beams

20 p3730 A70-40039

Uniaxial fiber composites tensile strength models, including failure analysis

20 p3731 A70-40046

Tungsten wire reinforced copper matrix composite, determining fibers pull-out contribution to fracture work

20 p3651 A70-40047

Unidirectional fiber reinforced composites strength, obtaining limit load bounds from plasticity analysis

20 p3731 A70-40051

Fiber reinforced plastics /FRP/ composites applications in Japanese aircraft production and aerospace industries

20 p3657 A70-40057

Contact shaped fiberglass-reinforced plastic tensile creep tests, showing strain property linearity dependence on direction

21 p3841 A70-40642

Multilayer three dimensionally woven fiberglass-reinforced materials, measuring strength and deformation under tension, compression, bending, torsion and shear tests

21 p3841 A70-40646

Unidirectional fiberglass-reinforced plastic, investigating binder content and porosity effects on strength

21 p3841 A70-40647

Textolite and fiberglass-reinforced plastics relaxation parameters tabulation for viscoelasticity boundary value problems solution

21 p3842 A70-40650

Bond stresses between fiber and matrix of fiber reinforced composite materials determined by numerical method based on superposition

21 p3934 A70-41252

Boron vs carbon fiber reinforced plastics, discussing layer and panel structures, molded and mechanical sections, preimpregnation, cost and structural concepts

21 p3842 A70-41263

Composites reinforced with weakened fibers, investigating weak points effect on fracture toughness by fiber pullout and tensile tests

21 p3843 A70-41889

Fracture toughness and surface energy of fibrous reinforced composites as function of fiber content, strength, diameter, modulus and matrix flow stress

21 p3843 A70-41890

Hot pressed zirconia-zirconia ceramic fiber reinforced ceramic matrix composites, discussing mechanical properties and failure modes

22 p4057 A70-42285

Ceramic fiber technology, forming processes and matrix composites fabrication, discussing chemical and physical compatibility factors, plastic forming, slip casting, cold pressing, etc

22 p4045 A70-42477

High thermal stability glass fibers alternatives improving stiffness-to-weight ratio of resin and Al-based composites used in F-111 boron epoxy wings

22 p4058 A70-42480

Load transfer to elastic fiber in infinite elastic matrix, determining fiber force distribution

22 p4113 A70-42539

Composites made by unidirectional solidification of eutectics with transition metal carbide fibers embedded in metal matrix, discussing tensile tests [ONERA-TP-853]

22 p4057 A70-43457

Graphite fiber oxidation prevention in metal matrix composites, examining various thermodynamic parameters

22 p4126 A70-43676

Graphite and carbon fiber surfaces, correlating Raman spectrum and shear strength of composite

22 p4060 A70-43680

Unidirectional fiber reinforced composite longitudinal shear deformation, deriving effective shear modulus

22 p4060 A70-43681

Boron-Al composite filament fracture behavior and postimpact tensile strength, examining shock loading and impact velocity effects

22 p4060 A70-43682

Specific strength of unidirectional fiber reinforced metal matrix composites, using volume ratio-transfer coefficient diagrams

23 p4209 A70-43939

Ceramic composite materials structural application, improving brittleness and thermal shock resistance via reinforcing refractory fibers [ICAS PAPER 70-40]

23 p4267 A70-44138

Fiber-reinforced narrow rectangular beam flexural strain analysis by birefringent coating technique, deriving isochromatic and isoclinic patterns

23 p4275 A70-44915

German monograph on glass fiber reinforcement effect on soft thermoplastics strength, adhesion and slip properties

24 p4366 A70-45088

Whiskers and filaments properties compared for fiber reinforcement applications in composite materials production

24 p4356 A70-45167

High melting point fibrous composites, discussing fiber-matrix systems for high temperature applications as in gas turbine blades

24 p4357 A70-45168

Unimodal and bimodal distribution of fiber composite properties at different stress levels using quantitative metallography

24 p4359 A70-45250

Composite materials tensile strength dependence on reinforced fibers with dispersed tensile strength, using model to predict crack propagation from fiber rupture

24 p4427 A70-46270

REISSNER THEORY

Homogeneous Love-Reissner equations analytical solutions for noncircular pyrolytic graphite cylinders, using asymptotic expansion for transverse materials isotropy

01 p0206 A70-11151

Finite element method for thin shells using specialized form of Reissner variational principle for stresses and displacements

01 p0208 A70-11184

Einstein-Maxwell equations solutions relation to Robinson and Robinson metrics compared with Reissner-Nordstrom solution relation to Schwarzschild

07 p1333 A70-18961

Reissner-Sagoci transient mixed boundary value problem concerning displacement of infinite half space of isotropic elastic material, deriving surface displacement and reactive torque

09 p1784 A70-23571

Reissner variational theorem applied to stress analysis of vertically accelerated end burning solid propellant grain in studying elastic rocket launch failure

12 p2313 A70-27196

REJECTION

Phonocardiographic and ultrasound observations of acute rejection following cardiac transplantation, considering rejection treatment at early stage

03 p0415 A70-12888

RELATIVE BIOLOGICAL EFFECTIVENESS (RBE)

Energy deposition in cells by charged particles during ionizing radiation exposure, discussing RBE /relative biological effectiveness/ and dose-effect relation for neutrons

11 p1989 A70-26597

RELATIVISTIC EFFECTS

Irrotational motions of relativistic ideal thermodynamic fluids fulfilling incompressibility conditions

01 p0063 A70-10948

Geodesic motion of massless particles inside static sphere of small volume, analyzing relativistic effect of energy accumulation and release

02 p0339 A70-12117

Interstellar space flight ramjet physical model, describing magnetic field funnel, radiation effects, relativistic effects, etc

02 p0379 A70-12782

Relativistic phase of stellar system evolution caused by inelastic stellar collisions, discussing thermal relaxation rate, obtaining distribution function

03 p0564 A70-13226

Hydrostatic equilibrium in self gravitating core of rotating relativistic star, considering Newton and Einstein gravitation theories

05 p0914 A70-16648

Relativistic phase of stellar system evolution caused by inelastic stellar collisions, discussing thermal relaxation rate, obtaining distribution function

08 p1580 A70-21659

Solar charge effects on Mercury perihelion motion, relativistic light deflection and gravitational red shift, using Reissner-Nordstrom solution

11 p2107 A70-25395

Space probe trajectory near second order integration under influence of solar oblateness and gravitation

14 p2635 A70-30288

Red giant model, investigating inclusion of semirelativistic partially degenerate gas characteristics by perturbatory technique

14 p2651 A70-31290

Earth/moon mass ratio and Mars mass and ephemeris from Mariners range and Doppler tracking data, noting relativistic time delay measurement possibility

15 p2798 A70-31652

Earth to planet radar signal time delay in general relativity expressed in relativistic spherical polar coordinates of earth and planet

15 p2806 A70-32801

Relativistic solutions to model stellar wind, discussing equation of radial momentum

17 p3153 A70-34530

Stellar atmosphere radiation field quantity vs quality, deriving electron temperature as function of tau

18 p3309 A70-37007

Pulsar radio pulses structure and emission source theory based on synchrotron radiation and relativistic effect calculations

18 p3321 A70-37119

Relativistic effects for MHD Riemann waves in electrically conducting fluid

19 p3478 A70-37583

WKB method for asymptotic oscillatory solutions of nonlinear equations of relativistic fluid mechanics

19 p3403 A70-37587

Energy and impulse tensor of nonviscous relativistic fluid, excluding sound velocity greater than light velocity

19 p3404 A70-37593

Geometrical appearances at relativistic speeds for celestial sphere with multiple constellations, spherical surface features at observer proximity and rectangular box train

19 p3520 A70-38273

Relativistic gas spheres and collisionless star cluster models with large red shifts, showing radial perturbation stability

20 p3703 A70-39175

Relativistic observer in rotational motion relative to inertial observer, imposing velocity onto perfect relativistic fluid

21 p3851 A70-42096

Relativistic and nonrelativistic generalizations of classical approach in quantum mechanics applied to equations of motion in electromagnetic field

24 p4378 A70-45275

RELATIVISTIC PARTICLES

Bremsstrahlung emission from thermal plasma coexisting with relativistic electron tails, noting enhancement at electron plasma frequency harmonics

02 p0348 A70-12240

Solar wind-induced torque calculated considering special and general relativistic effects, extending method to pulsar rotational model

04 p0739 A70-14593

Charge separation effects in boundary layer between cold streaming plasma and perpendicular magnetic field with relativistic electrons

04 p0727 A70-14997

Relativistic solar proton propagation fluctuation effects in interplanetary magnetic field during cosmic ray intensity increase

05 p0903 A70-16731

Astrophysical plasmas radio emission interpreted as collective bremsstrahlung due to ultrarelativistic electron tails, discussing Crab Nebula, quasars and Jupiter

05 p0904 A70-16932

Time variations and angular collimation of radiation emitted by source with relativistic streaming

06 p1134 A70-17281

Synchrotron radiation negative reabsorption possibility for relativistic electrons dipped into and in absence of unrelativistic plasma

07 p1348 A70-19413

Inverse Compton collisions of relativistic electrons with universal black body photons for diffuse component of cosmic X rays

07 p1369 A70-20166

Relativistic magnetic monopoles detection in corpuscular primary cosmic rays, describing equipment and results

07 p1371 A70-20333

Relativistic particles formation associated with supernovae outbursts estimated to determine relativistic electrons mechanism in Crab Nebula

08 p1564 A70-20552

Supernovae remnants X ray emission associated with explosion process generating relativistic particles, indicating Crab Nebula as X ray object

09 p1749 A70-21998

Synchrotron emission of relativistic particle in magnetic field with radiative reaction force comparable to Lorentz force, emphasizing pulsar cosmic ray electron acceleration

09 p1731 A70-22273

Electrical conductivity and conductive opacity for relativistic electron gas in presence of ions taking into account ion-ion interaction

09 p1727 A70-22509

Pulsar NP 0532 synchrotron emission reinterpretation related to relativistic particles injection into Crab Nebula

09 p1756 A70-22516

Pinched plasma reversed current induction due to relativistic electron beam injection

09 p1736 A70-23183

Heavy particles separation at sea level from overall flux of cosmic radiation, discussing method and device recording subrelativistic particles

09 p1684 A70-23732

Ultrarelativistic electrons cone instability in Van Allen radiation belts, discussing distribution function, relativistic effects and electron lifetimes

11 p2104 A70-25529

Flat emission spectra of quasars in 3CP catalog attributed to anisotropic relativistic electron fluxes

13 p2493 A70-29387

Cosmic rays intensity frequency spectrum near earth, indicating relativistic electron energy spectra similarity in interstellar space and galactic particles existence

13 p2478 A70-29388

Relativistic particles formation associated with supernovae outbursts estimated to determine relativistic electrons mechanism in Crab Nebula

15 p2805 A70-32707

Nitrogen and air bombardment by relativistic electrons, determining absolute fluorescence intensity of nitrogen molecular ion first negative band

16 p2954 A70-33279

Charge spectrum of heavy relativistic cosmic ray nuclei, using tracks from balloon-borne photographic emulsions

18 p3308 A70-36781

Degenerate relativistic electrons in intense magnetic field, computing transverse electrical conductivity

18 p3296 A70-36896

Relativistic electron spectra of cosmic rays accelerated by plasma turbulence, examining singularity in solution

18 p3322 A70-37127

Relativistic cosmic rays nuclei abundances from Gemini 11 flight

19 p3509 A70-38144

Ultrarelativistic electrons cone instability in Van Allen radiation belts, discussing distribution function, relativistic effects and electron lifetimes

21 p3882 A70-41279

High power pulsed relativistic annular electron beam production and focusing by injection gun using magnetic field control

21 p3827 A70-41461

Electromagnetic radiation power spectrum scattered by relativistic particles, considering reflected waves resemblance to HF radio spectra of quasars

22 p4100 A70-42856

Plasma inhomogeneity and drift effects on synchrotron radiation from relativistic charged particles in magnetoplasma

22 p4082 A70-43254

Nonlinear collective ionic acceleration by relativistic electron beam, assuming blob dimensions of plasma wavelength

22 p4077 A70-43471

Nike-Apache rocket aurora probes using proton detector to measure galactic cosmic ray intensity and relativistic electrons

23 p4192 A70-44879

Relativistic two body system in circular orbits, examining quantum theory with massless and massive scalar fields and energy and angular momentum for bound system

24 p4379 A70-45521

Relativistic cosmic ray LH nuclei abundance via Cerenkov scintillator telescope on polar orbiting OV1-10 satellite

24 p4397 A70-45522

RELATIVISTIC PLASMAS

Relativistic plasma waves in uniform ambient magnetic field analyzed for growth rate to investigate plasma instabilities of streaming cosmic rays

05 p0904 A70-16931

Relativistic electron low beta plasma oscillations in external magnetic field using covariant dispersion relations

06 p1120 A70-17542

Stress tensor for relativistic weakly ionized plasma in HF electromagnetic field taking into account collisions

07 p1348 A70-19197

Relativistic electrons synchrotron radiation by calculating magnetoactive plasma permittivity tensor, determining normal waves polarization characteristics

08 p1554 A70-21812

Photon bremsstrahlung from relativistic hydrogen plasma determined by studying electron-positron pairing effect on plasma radiation intensity

09 p1735 A70-22986

Plasma, Coulomb fields and radiation correlations obtained by relativistic kinetic equations, noting bremsstrahlung, synchrotron, cyclotron radiation, radiative and particle diffusion, etc

09 p1736 A70-23182

Relativistic nonlinear coupled longitudinal-transverse propagation of intense laser beams in cold overdense plasma

10 p1921 A70-23968

Dissipative parameters determination for relativistic gas within kinetic theory framework based on particle interaction model, assuming constant differential effective interaction cross section

10 p1867 A70-24148

Boltzmann collisionless transport equation for relativistic plasma solved by expanding distribution function in terms of unnormalized spherical harmonics

10 p1923 A70-24228

Computer models simulating plasma motion applied to sheet pinch stability, investigating relativistic and nonrelativistic regimes

14 p2623 A70-30696

Guiding center theory for relativistic plasma embedded in strong magnetic field, discussing connection with pulsar emission dynamics

19 p3479 A70-37596

RELATIVISTIC THEORY

Relativistic formulation of radiation for sources in uniformly moving isotropic dispersionless conducting medium in terms of Green functions

01 p0144 A70-11091

Book on unitary relativistic theory of universe covering conservation and quantization axioms, general relativity equations, applications to corpuscular, electromagnetic and gravitational phenomena, etc

02 p0337 A70-11686

Universe oscillating closed model dynamics emphasizing conditions of collapse by contraction in terms of relativity theory

02 p0370 A70-12114

Relativistic tensor theories of gravitation in flat space with Neumann and Newton forms of gravitational potential, deriving expressions to estimate differences perceived by observer

03 p0526 A70-14305

Relativistic simple shear of slab of neo-Hookean material

05 p0929 A70-16067

Infinite-dimensional relativistic wave equations for mass spin dependence

07 p1333 A70-18959

Monograph on relativistic and steady state cosmology covering optical and radio astronomy, matter and galaxies origin, etc

07 p1379 A70-19101

Electromagnetic wave scattering from charged particle in hot electron plasma in magnetic field, considering relativistic corrections for scattered radiation spectra

07 p1352 A70-19992

Electromagnetic fields interaction with nonconducting neutral elastic solid, formulating relativistic variational principle for balance laws and constitutive equations

08 p1545 A70-21252

Relativistic gravity theories testing, discussing experimental tools and relativistic effects in solar system

09 p1750 A70-22059

Baryon configurations in relativistic generalized theory of gravitation, discussing field equation transformations, mass distribution, central pressure, etc

09 p1753 A70-22454

Relativistic generalized gravity theory, studying polytropic models

09 p1754 A70-22458

Cosmological solutions of Jordan-Dicke relativistic scalar-tensor theory, giving qualitative analysis of homogeneous isotropic problem at zero pressure

09 p1754 A70-22459

Vortex and potential motions interactions in relativistic hydrodynamics, studying mutual generation

09 p1754 A70-22460

Prime formulas for studying perfect relativistic fluids with spin

09 p1728 A70-22840

First vorticity theorem of Helmholtz derived in general relativistic and covariant differential form, proving invariant kinematical identity

10 p1916 A70-24498

Black body radiation properties with temperature important only in rest frame, using transformation formulas for coherence and spectral parameters

10 p1968 A70-24631

Homogeneous open anisotropic relativistic world model with negative space curvature, observing shear decrease with time and magnitude reciprocal variation with function R/t

11 p2109 A70-25866

Cauchy problem for relativistic heat equation for unbounded domain generated by streamlines of future oriented vector field

13 p2451 A70-28709

Einstein-Maxwell equations for monopolar point electrical charge, calculating proper energy for electromagnetic and gravitational fields

13 p2451 A70-28956

Complex vector parametrization of Lorentz group in relativistic kinematics, discussing Wigner rotation, Lorentz transformation and particles classification during scattering

13 p2453 A70-29722

Elasticity theory in general relativity formulated from classical nonlinear three dimensional theory, discussing thermodynamics and weak field limit

15 p2774 A70-31734

Relativistic gravitation theory and experimentation, surveying literature on gravity waves, EM propagation, gyroscopic precession, etc

16 p2973 A70-33230

Newtonian gravity law in light of relativistic theories, considering deviations of quasars and red shift deviations from Newton theory

16 p2976 A70-33722

Model classification for relativistic universes containing noninteracting matter and radiation by cosmological constant and density parameters

16 p2979 A70-34190

Relativistic three force transformation showing no contraction in static conditions

17 p3136 A70-34823

Relativistic thermal equilibrium conditions in external gravitational field, considering heat with inertial and gravitational mass

18 p3291 A70-36552

Ideal relativistic fluids adiabatic flow, investigating heat exchange effects within framework of special relativity

18 p3347 A70-36554

Thermodynamics of thermoviscous fluids based on Riemannian space time notions and balance laws of general theory of relativistic continuum mechanics

18 p3347 A70-36557

Classical and relativistic MHD - Conference, Lille, France, June 1969

19 p3476 A70-37576

Existence theorem for piecewise-continuous solutions of waves and shocks in relativistic MHD, using Riemann manifold

19 p3477 A70-37579

Boltzmann equation for relativistic gas, adapting Grad solution method

19 p3403 A70-37584

Cauchy problem for linearized relativistic Boltzmann equation near equilibrium, using functional analysis

19 p3403 A70-37585

Boltzmann equation for relativistic gas without dissipation, solving for relaxation time and elastic collisions

19 p3403 A70-37586

Relativistic and nonrelativistic fluid dynamic equations, deriving limiting procedure leading to fluid magnetodynamic Lundquist equations

19 p3478 A70-37590

Relativistic kinetic theory of gases, considering phase space quantum statistics, Liouville equation, Boltzmann equation, conservation laws, kinematics, equilibrium distributions, etc

19 p3404 A70-37594

Stable hyperon star existence in general relativity, discussing state equations for baryon matter, radial pulsation and superlumina and ultrabaric conditions

21 p3888 A70-41116

Stability conditions for relativistic stars, discussing mass-energy density distribution, Taylor instability,

Schwarzschild criterion, Newtonian stellar model, gravitational red shift, etc

22 p4104 A70-42999

Electron energies correlation in relativistic theory of atoms applied to multielectron atoms energy levels

22 p4076 A70-43470

Relativistic gas bulk motion nonrelativistic equations, demonstrating spatially random fluctuations damp suprathermal hydromagnetic perpendicular propagation mode to interstellar magnetic field

24 p4397 A70-45761

Earth-moon laser distance measurements, examining relationship between Newtonian and relativistic field coordinates

24 p4413 A70-46160

Gravitational relativistic theory tests using tracking data from interplanetary spacecraft, orbiters and landers

[AIAA PAPER 70-1317]

24 p4414 A70-46326

RELATIVISTIC VELOCITY

Solar system various natural members examination for suitability to relativistic pericentum motion investigation

02 p0373 A70-12255

Photon propulsion with constant power in exhaust beam and intragalactic travel in force free space from solving relativistic rocket equations

[AIAA PAPER 70-215]

06 p1132 A70-18105

Pulsar magnetorelativistic model assuming neutron star with magnetic field

08 p1563 A70-20478

Nonlinear relativistic wave velocity distribution within spherical nucleus bounded by shock wave in supersonic gas determined by Cauchy problem

08 p1484 A70-21403

Minimum time interstellar trajectories for thrust limited rockets by applying Pontryagin maximum principle to relativistic rocket equations of motion

09 p1760 A70-22933

Steady plane relativistic flow small irrotational perturbation theory determining subsonic, transonic and supersonic approximation

14 p2566 A70-30472

Charged particles focusing and sorting in bispiral systems, deriving differential equations for relativistic trajectories

15 p2707 A70-31520

Gravitational bremsstrahlung for small mass with relativistic velocity passing large mass in unbound trajectory, calculating energy flux of emitted waves

17 p3136 A70-34596

Interstellar drag resulting from relativistic rocket elastic collisions with interstellar matter, discussing effects on minimum time acceleration limited relativistic trajectories

17 p3155 A70-34752

Geometrical appearances at relativistic speeds for celestial sphere with multiple constellations, spherical surface features at observer proximity and rectangular box train

19 p3520 A70-38273

Macroscopic equations of motion established by Maxwell transport equations for relativistic perfect gas

22 p4011 A70-42716

RELATIVITY

Gravitational theories scheme combining tetrad field with bimetric theories, including general relativity, space-time dependent Lorentz rotations, red shift and light deflection

01 p0141 A70-10232

Gravitational field equations in flat space, using quaternion representation of general relativity Riemannian space time in terms of spinors

01 p0141 A70-10279

Pulsating very dense white dwarfs models noting general relativity

01 p0176 A70-10320

Mass point motion in inertial reference system of special relativity, finding motion equations analogous to relative motion equations in classical mechanics

01 p0145 A70-11442

Motion equations of material point in general relativity theory found analogous to equations in classical mechanics for metric in introduced physical space

01 p0146 A70-11443

Lagrange and Hamilton equations of motion of mass point in physical space of general theory of relativity based on least action principle

01 p0146 A70-11444

Equations of state for continuous media, using variational principles within framework of relativity theory

01 p0146 A70-11593

Book on unitary relativistic theory of universe covering conservation and quantization axioms, general relativity equations, applications to corpuscular, electromagnetic and gravitational phenomena, etc

02 p0337 A70-11686

Equations of hydrodynamics governing perfect fluid in second postNewtonian approximation to general relativity, deriving energy momentum tensor equation

02 p0337 A70-11776

PostNewtonian equations of Brans-Dicke scalar-tensor theory for n gravitating point masses, using obtained equations of motion for radar tracking

02 p0337 A70-11777

Variational approach to structure of rotating polytrope with symmetry about axis of rotation in postNewtonian approximation of general relativity

02 p0338 A70-11778

Brans-Dicke cosmological gravitational instability using Lagrangian gauge for galaxy formation, discussing density contrast growth in time

03 p0577 A70-14154

Light emission from collapsing nonrotating gas in general relativity, noting restrictions on range and frequency shift

04 p0719 A70-14702

Binary star formation using singular solution of Kepler problem in general theory of relativity

04 p0755 A70-15355

Relative motion of two spheroidal homogeneous rigid bodies of isolated binary system, obtaining potential energy

05 p0880 A70-15760

Relativistic length contraction, time dilation and classical electrodynamics formulated in terms of special relativity using Galilean transformations

05 p0881 A70-15875

Gravitational radiation damping effect on motion of two bodies, evaluating field components in approximation by Einstein-Infeld-Hoffman method

05 p0882 A70-16308

Relativistic stellar structure equations for spherically symmetric configurations in slow motion, using Einstein gravitational field and conservation equations

05 p0912 A70-16454

Transverse Doppler effect of laser beam retroreflected from artificial satellite predicted by special relativity theory, noting transformations

05 p0860 A70-16653

Lorentz principle application to general relativity freeing formalism from inconsistencies to derive expressions for Christoffel symbols and Riemann-Christoffel tensor

06 p1105 A70-17537

Poincare invariance compatibility with general relativity, discussing Brandt groupoid, decomposition and local groups

06 p1106 A70-17540

Artificial satellites in short period highly eccentric solar orbits of arbitrary inclination for solar gravitational quadrupole moment measurement to test general relativity

06 p1139 A70-17552

Relativity theory and quantum mechanics relation concerning point charge velocity and motion at light speed, deriving elementary particle mass formula

06 p1106 A70-17833

General relativity taking into account astronomical and laboratory tests, cosmology and theoretical studies /1967 to 1969/

07 p1334 A70-19102

Collapse-anticollapse transition near Schwarzschild radius in multitime universe with arbitrary number of time-similar dimensions

07 p1381 A70-19286

Gravitational waves in general relativity theory, discussing Kaigorodov exact solution to Einstein equations

08 p1545 A70-20993

Momentum vector and spin tensor definitions for extended body moving in arbitrary gravitational and electromagnetic fields, considering test body in de Sitter universe

08 p1545 A70-21352

General relativity equations of gravitation consistent with empirical data, discussing curvature tensor, scalar gravitational waves and solar mass difference

08 p1577 A70-21419

Einstein power transfer theory used for demonstrating energy transfer rate by gravitational radiation from emitter to absorber

08 p1546 A70-21742

Relativistic gravity theories testing, discussing experimental tools and relativistic effects in solar system

09 p1750 A70-22059

Vortex and potential motions interactions in relativistic hydrodynamics, noting effects of gravitation equations nonlinearity

09 p1754 A70-22461

General relativistic expressions for angular momentum and rotational kinetic energy of slowly rotating stars

09 p1764 A70-23608

Planetary perihelion precession with velocity-dependent gravitational mass in terms of special relativity

09 p1765 A70-23800

Maxwell electromagnetism analogy to Einstein gravitation inferred from asymptotic studies of electromagnetic and gravitational radiation

10 p1915 A70-24029

Gravitational waves and radiation study based on relativity theory, discussing outer space sources and antenna recording design and properties

10 p1916 A70-24384

Tachyons /faster than light particles/ on basis of relativity theory, noting reaction with light speed particles and relation to quantum theory

10 p1916 A70-24385

Time dilation in space travels at light velocity under influence of special theory of relativity

10 p1943 A70-24760

Quaternion representation of general relativity applied to geodesic equation and planetary motion, noting difference from Einstein formulation

10 p1944 A70-24859

Electromagnetic radiation frequency shift during passage by sun or earth not caused by electrostatic or magnetic fields

10 p1917 A70-24860

Soviet book on physical fields in general relativity theory

10 p1917 A70-25200

Energy concept in cosmology based on relativistic considerations, indicating universal time by synchronous clocks system

11 p2109 A70-25870

Milne special relativistic cosmology consistency with Birkhoff flat space gravitation theory, calculating red shift correction in galactic light

11 p2114 A70-26549

Oscillating gyroscopes in satellite testing general relativity and earth gravitational field relation to stars

11 p2057 A70-26706

Rotation effect on singularities in general relativity from local observer standpoint, inquiring into gravitational collapse in ideal fluid

12 p2271 A70-26978

Gravitational collapse of star and general relativity role, considering Schwarzschild solution to Einstein vacuum equations

12 p2298 A70-27058

Science of time considered with reference to quantum physics, special theory of relativity, directivity and symmetry and conditional probability, discussing clock designs

12 p2271 A70-27276

Clock synchronization in general relativity theory, investigating temporal and spatial relations in four dimensional continuum using simultaneous hypersurface

12 p2272 A70-27357

General relativistic hydrodynamics near equilibrium, discussing velocity and kinetic energy increase spherically symmetric large masses as function of radius change

12 p2300 A70-27392

Singular and nonsingular cosmological models validity for general relativity allowing for cosmic dust

12 p2300 A70-27394

Book on electromagnetic fields and waves covering electrostatic and magnetic fields, relativity, vectors, Maxwell equations and propagation

12 p2273 A70-28150

General relativity integral conservation laws of system of bodies in curved space-time obtained from symmetrical energy-momentum tensor

12 p2274 A70-28222

Oscillatory perturbed motion of elastic body in general relativity space time, discussing energy tensor, unitary speed vector and density

13 p2451 A70-28954

Rigid solid replacement by elastic body in relativistic mechanics

13 p2451 A70-28955

Kerr-Schild space-time manifolds with electromagnetic field, solving Einstein equations

13 p2451 A70-29166

Delayed moment of force relativistic definition within reference of inertia, discussing lever bent at right angles

13 p2452 A70-29635

Energy and canonical momentum relationship in relativistic mechanics, discussing particle production and annihilation

13 p2453 A70-29721

Frequency dependence of gravitational-electromagnetic fields interaction assumption inconsistent with general relativity and consistent with data on deflection of radiation by massive bodies

14 p2573 A70-30616

Thermodynamically perfect fluids in general relativity, considering heat transmission paradox and wave propagation velocities

16 p2997 A70-33103

Celestial mechanics experiment for Mariner Mars 1971 to test general relativity theory and improve Martian ephemeris

16 p2978 A70-34031

Post-Newtonian equations of hydrodynamics and radiation reaction in general relativity

17 p3156 A70-34828

Relativistic thermodynamics, developing relativity theories in nonvacuo regimes and discussing covariant scalars and formalisms

18 p3291 A70-36553

General relativistic equations for stationary axially symmetric rotating perfect fluid in comoving coordinate system

18 p3292 A70-36900

Variational principle application to relativistic MHD, deriving Einstein field equations, Maxwell equations and equations of motion for self gravitating charged fluid

19 p3478 A70-37591

Gravitationally induced (Machian) magnetic field by rotating mass-shell with centrally located stationary charged sphere, using linearized relativity theory

19 p3471 A70-37815

Hodograph equations for relativistic irrotational steady plane flows, investigating transformation to physical plane

19 p3406 A70-38664

Relativistic high temperature gas asymptotic solutions with or without body force, comparing flow field with photon gas

20 p3673 A70-39654

General relativity integral conservation laws of system of bodies in curved space-time obtained from symmetrical energy-momentum tensor

20 p3673 A70-40097

Time travel and cosmological model based on Einstein relativity theory, considering hypothetical motor design, energy supply, tachyons and four dimensional orbits implications

20 p3710 A70-40132

Einstein theory of length contraction and time dilation relative to ether regarding slowness of clocks in motion

21 p3849 A70-40550

Invariance principle in mechanics of deformable continua connecting three dimensional and relativistic space-time formulation

21 p3940 A70-42097

Chronometrically invariant formulation of Petrov gravitational fields algebraic classification at space-time fixed point in general relativity

21 p3851 A70-42239

Astrophysics and general relativity - Waltham, Mass., June-July 1968, Volume I

22 p4098 A70-42576

Newtonian hydrodynamic analogies for homogeneous anisotropic models in general relativity

22 p4075 A70-43472

Clock synchronization in general relativity theory, investigating temporal and spatial relations in four dimensional continuum using simultaneous hypersurface

22 p4075 A70-43598

Nonlinear Lagrangians in relativistic cosmology of open oscillating world model

24 p4404 A70-45409

Faster-than-light particles impossibility in causal loops using nonquantum special relativity framework, considering tachyons

24 p4378 A70-45424

Einstein-Rosen matter concept given by space-time with isomeric domains, discussing hypersurface derivatives

24 p4379 A70-45486

Einstein equations internal solution other than Schwarzschild for case of central symmetry and static source

24 p4379 A70-45628

Rarita-Schwinger fields in general relativity, extending equations for Fermion motion in linearized gravitational field to higher spin particles

24 p4380 A70-45818

RELAXATION

Models of partially relaxed stellar disks in galaxies, discussing gravitational instability and stellar velocities

04 p0748 A70-14588

RELAXATION (MECHANICS)

NT SPIN-LATTICE RELAXATION

NT STRESS RELAXATION

Relaxation in gas-particle flow, analyzing thermodynamic properties, interactions, single particles and one dimensional flow equations

01 p0062 A70-10805

Moving gas with thermodynamic relaxation process, discussing bulk viscosity and application to shock structure calculations

01 p0063 A70-10927

Cardiac relaxation mechanics from isolated preparation of cat papillary muscle, noting inotropic influences role

02 p0231 A70-11709

Averaging analysis of oscillations attenuation of relaxing one dimensional linear viscoelastic systems under external force at resonance applied to nonlinear multidimensional systems

05 p0933 A70-16208

Molecular beams and particle adsorbing surfaces interactions in state of relaxation, determining reflection parameters as function of gas characteristics

08 p1547 A70-21078

Molecular beams and particle adsorbing surfaces interaction with allowance for deposited atoms relaxation, determining reflected flux

08 p1547 A70-21079

Radiative relaxations of chromospheric oscillations generated by granule, assuming isothermal atmosphere and linearizing equations of motion

08 p1576 A70-21395

Monograph on relaxation processes at high temperatures for thrust nozzle calculation and optimization covering real gas effects, reaction kinetics, heat transfer, etc

11 p2103 A70-26475

GaAs relaxation and hybrid modes properties and formation conditions

11 p2099 A70-26827

Spatial relaxation of electron gas colliding with positive ions from plasma velocity distributions, solving time independent Fokker-Planck boundary problem

12 p2280 A70-27791

Relaxation function of linear viscoelastic body, defining mechanical deformation process using Stieltjes integral

12 p2327 A70-28046

Zirconium additions effect on Ni internal friction behavior and relaxation spectrum

13 p2435 A70-29498

Linearized gas mixture nonequilibrium flow fields, analyzing consequences of multiplicity of principal relaxation frequencies

14 p2566 A70-30474

Relaxations from anelastic and dielectric measurements of fused silica and soda-silica glasses at low temperatures ascribed to vibration modes exceeding Debye spectrum

16 p2960 A70-32996

Delayed rupture and relaxation in Ti alloys during cyclic deformation, comparing fatigue tests results for continuous and discontinuous cyclic loadings

16 p2931 A70-33209

Monograph on steady shock waves in one dimensional frictionless gas flows with thermodynamic relaxation, using continuum mechanics

16 p2891 A70-33294

Transport and relaxation processes prediction for turbulent fluid, noting similarities to Fourier integral representation of flow field

16 p2895 A70-33969

Krook gas particle collision model for relaxation from nonequilibrium to equilibrium Boltzmann distribution in spatially uniform gases

17 p3068 A70-34697

Two component warm plasma wave propagation along magnetic field, considering full pressure tensor equation with momentum and pressure relaxation mechanisms

18 p3294 A70-36405

Relaxation theory of Rayleigh scattering of light by isotropic continuous medium, deriving spectral densities via fluctuation dissipation theorem

19 p3470 A70-37446

Seismic wave attenuation mechanisms emphasizing partial melting, grain boundary relaxation and high temperature internal friction background

19 p3416 A70-38440

Textolite and fiberglass-reinforced plastics relaxation parameters tabulation for viscoelasticity boundary value problems solution

21 p3842 A70-40650

Polymers low temperature relaxation behavior, discussing molecular structure, crystallinity, copolymerization, etc

21 p3844 A70-42135

Relaxation behind shock waves in air, calculating radiation spectral distribution for comparison with shock tube experimental data

21 p3812 A70-42219

Thermal relaxation effect on thermal contact of two semiinfinite walls, showing existence of dynamic contact resistance

22 p4125 A70-43243

RELAXATION (PHYSIOLOGY)

Activity and rest alternation effect on fatigue and rehabilitation behavior of trained athletes, discussing muscle performance characteristics

04 p0639 A70-15510

Physiological examination of healthy human beings, considering repose situation abnormal

15 p2691 A70-31923

Contractile mechanics of cat papillary muscle during hypoxia and reoxygenation recovery

15 p2686 A70-32836

RELAXATION METHOD (MATHEMATICS)

Relaxation method for inverse radiative transfer equation solution, determining temperature profiles and atmospheric parameters

23 p4214 A70-44036

Plasma kinetic theory, applying Boltzmann equation, Lorentz gas model and relaxation method

23 p4224 A70-44177

RELAXATION OSCILLATORS

Controllable generator of linearly stepped voltage pulse using avalanche transistors, controlling avalanche-transistor relaxation oscillator by gating storage condenser

09 p1643 A70-22130

Threshold and frequency relaxational radiation detectors, discussing operation and sensitivity of p-n-p-n

silicon photodiode and luminosity dependent devices

09 p1649 A70-23356

Quasar model based on supermassive stars relaxation oscillations, considering energy requirements

12 p2300 A70-27380

Regular relaxation oscillations of ruby laser by moving resonator mirrors

18 p3271 A70-36954

Nonlinear LC circuit with p-n junction capacitance, examining relaxation vibrations during automatic biasing

20 p3596 A70-38970

Low power thyristors in relaxation oscillation circuits, considering static and dynamic characteristics in large signal mode

20 p3596 A70-38971

Multiphase relaxation oscillator with inductive coupling and common base resistor in feedback loop, determining circuit parameters effect on pulse length

20 p3598 A70-39791

Discharge pulse generation and equivalent resistance of relaxation oscillator applied to avalanche transistor

24 p4319 A70-45639

RELAXATION TIME

Relaxation time approximation formulas for galvanomagnetic effects in graphite based on energy spectrum model

01 p0126 A70-10181

Nitrogen and helium collisional effect on rotational relaxation rate of carbon dioxide upper laser level, noting thermalization

01 p0110 A70-10567

Vibrational relaxation times in carbon dioxide and carbon dioxide-argon mixtures at 360-3000 K, using shock tube and laser schlieren method

01 p0148 A70-11355

Weak shock waves relaxation time and amplitude and acoustic velocity as functions of thermorelaxing media

01 p0068 A70-11588

Stellar systems evolutionary stages, considering gravitational instability in rotating expanding gas, relaxation, viscosity, transition to metastable state and drift effect on geometry

02 p0376 A70-12445

Acoustical resonators free oscillations and pressure effects on damping, amplification, decay decrement and relaxation time

02 p0304 A70-12772

Dynamic time constants for specific transition and relaxation times of hydrogen maser, noting coupling between hyperfine differences and atomic polarization

03 p0498 A70-13007

Formation of Maxwell and nonMaxwellian energy distribution in gases, noting reduction of time reversible to time irreversible equations

03 p0606 A70-13861

Shock tube measurements of ionization relaxation times behind shock waves in air at shock Mach numbers from 8 to 17

03 p0471 A70-14360

Electron relaxation in shock heated Ar plasma estimated by measuring radiation intensity at various frequencies

03 p0535 A70-14363

Semiconductors low temperature photoconductivity fluctuations occurrence during energy relaxation probability by optical phonons

04 p0730 A70-14413

Rotational relaxation times for low density hypersonic nitrogen free jet, comparing measured and predicted impact pressures

06 p1043 A70-18279

Spatial and temporal relaxation problems approximate solution in kinetic theory, making calculations for Maxwellian molecules and hard spheres

06 p1047 A70-18318

Time dependent relaxation model for heat flux in metals from quantum mechanical form of Boltzmann transport equation, yielding damped wave equation for temperature

06 p1090 A70-18612

Relaxation time calculation for ground and excited states of H atoms and H-like ions in optically thin and thick plasmas, considering electron density role

07 p1353 A70-20058

Minority carriers lifetime following CdS and ZnTe spontaneous luminescence relaxation after electron beam excitation

07 p1302 A70-20318

Electric field effects on electrification of colliding ice spheres, discussing relaxation time of sphere charges and charge exchange

08 p1538 A70-21114

Diatomic gases, describing rotational distribution function evolution by diffusion equation approximation, discussing apparent relaxation times

08 p1548 A70-21521

Relaxation time influence on mass output calculation errors for gases in small diameter sonic nozzles

09 p1604 A70-22841

Spin-lattice NMR and EPR relaxation time measurements, using train signals and free induction decays
09 p1679 A70-22995

Rotational-translational energy transfer in collisions between homonuclear diatomic molecules and rotational relaxation time in diatomic gases
10 p1918 A70-23956

Solid state plasma drift velocity effect on helicon propagation constant assuming isotropic momentum relaxation time and effective mass
10 p1928 A70-24831

Dispersion function model based on mixed second order kinetics with distributed relaxation times
11 p2086 A70-25831

Relaxation functions of one dimensional viscoelastic linear and nonlinear materials having monotone decreasing time properties
11 p2141 A70-26556

Vibrational relaxation time and transition probability in bromine collisions with He, Ne, Ar, Xe atoms determined by shock wave method
12 p2275 A70-27353

Free carriers effective mass and relaxation time in semiconductors determined from IR spectra of light reflection
12 p2285 A70-27362

Electromagnetic energy propagation through absorbing single resonant frequency dielectric, deriving transport velocity and relaxation time
13 p2452 A70-29464

Extrinsic photoconductor with reduced background under uniform illumination, describing frequency response as function of recombination and dielectric relaxation times and load resistances
14 p2586 A70-30989

Thermal relaxation rate in one and two dimensional electron plasma models with positive background, using particle in cell simulation
14 p2624 A70-31047

Sphere slow motion in viscous fluid with solid particle suspension, considering Stokes flow pattern small relaxation time perturbation
16 p2896 A70-34272

Reflected shock waves generation by shock produced plasma flow interaction with strong magnetic fields, determining electron density and ionization relaxation times
17 p3139 A70-34490

Chamber solution of Boltzmann time dependent equation in relaxation time approximation
17 p3136 A70-35596

Photoconductivity relaxation kinetics of low resistivity n- and p-type GaAs, showing nonradiative recombination
17 p3143 A70-35703

Relaxation properties of nonequilibrium electronic solid state plasma during nonlinear interaction with external fields, using kinetic equation
18 p3297 A70-36423

Maxwell-Wagner migrational polarization resulting from free ions or electrons drift in dielectrics and semiconductors, considering relaxation time
18 p3298 A70-36595

Relaxation time for nitrogen molecule vibration temperature in ionosphere due to thermal electron collisions
19 p3409 A70-37324

HD molecule nuclear relaxation time in liquid state as function of temperature, discussing various mechanisms
19 p3473 A70-37367

Boltzmann equation for relativistic gas without dissipation, solving for relaxation time and elastic collisions
19 p3403 A70-37586

Strontium titanates ceramics containing various trivalent rare earth ions, observing dielectric relaxation
19 p3486 A70-37755

Ionization relaxation behind reflected luminous shock front in argon plasma flow interaction with magnetic fields, using spectroscopic and streak interferometric observations
19 p3479 A70-37814

Polar gas rotational relaxation time calculation, comparing volume viscosity and energy equation definitions
19 p3473 A70-38266

Weakly ionized gas subjected to pulsed DC electric field, analyzing transient relaxation of electrons velocity distribution
19 p3482 A70-38899

Globular cluster relaxation time using nonMaxwellian velocity distribution and polytropic spatial distribution
22 p4109 A70-43744

Electroreflectance at CdS-electrolyte interface, noting field strength effect on relaxation time
23 p4230 A70-43930

Level relaxation constants measurements by three-level laser spectroscopy, using line shape of stimulated shifted resonance scattering in gas
24 p4354 A70-45821

RELAY

Relay control design for model-tracking system with parameter uncertainties and disturbances using semidefinite Liapunov function
07 p1247 A70-20026

Radio telescopes relaying interferometers characteristics noting delay in IF channel and wideband performance
08 p1495 A70-21068

Delayed feedback for LF periodic conditions/autoscillations/ in relay systems of cosmic flying apparatus stabilization
11 p2119 A70-25342

Third order dynamic relay control system, determining periodic motion and motion stability
13 p2507 A70-29719

Rotary relay for solar array space power transfer using clutch of low moment of inertia capable of recycling once each orbit
17 p3101 A70-34765

RELAY SATELLITES

Solar phenomena effect on VHF communications between synchronous satellite relay and earth ground stations
02 p0259 A70-12566

Satellite relay systems to provide polarization discrimination in antenna main beam to double spectrum for communications
05 p0815 A70-16661

Broad beam Tracking Data Relay Satellite (TDRS) for manned and automated spacecraft using VHF bands
06 p1006 A70-17345

Coding and signal selection for data relay satellite interrogation channel serving many low- powered unattended user terminals
06 p1006 A70-17347

Geometrical and electrical characteristics of two mirror parabolic antenna for tropospheric radio relay communications lines in centimeter band, analyzing radiation patterns
07 p1240 A70-19125

Satellite relayed integrated digital multiple access systems, discussing traffic handling, satellite positioning, demand assignment, etc
10 p1839 A70-24369

S band communications repeater using retrodirective phased array on synchronous altitude data relay satellite (DRS) for intersatellite and ground links
11 p2001 A70-25472

Controlled digital data relay satellite system to provide multiple access between central station and user terminals, noting computer time sharing operation
11 p2008 A70-26230

Digital river and rainfall data automatic transmission from remote hydrologic platforms via ATS-1, studying system economic and technological feasibility
12 p2205 A70-26939

Transmission delay and echo effects in long distance satellite relay telephony links, describing echo suppression and speech quality
12 p2183 A70-27004

Earth resources satellite real time wideband relay communication link to ground station
13 p2368 A70-29614

Geostationary tracking and data relay satellites (tdrs), discussing system design and advantages
14 p2615 A70-31182

Trojan Relay system with satellites preceding and following earth in solar orbit ensuring radio communication throughout solar system
15 p2698 A70-32061

Range and velocity components for ray paths between tracking and data relay satellite and user communication satellite
16 p2866 A70-34073

Tracking and data relay satellite system in low altitude synchronous orbit
24 p4311 A70-45085

Tracking and data relay satellite system performance by ATS and Nimbus spacecraft for range and range rate tracking and command and data transmission
24 p4374 A70-45949

[AIAA PAPER 70-326]

[AIAA PAPER 70-1305]

[AIAA PAPER 70-1306]

[AIAA PAPER 69-1080]

[AIAA PAPER 70-1080]

[AIAA PAPER 70-1080]

[AIAA PAPER 70-1080]

[AIAA PAPER 70-1080]

[AIAA PAPER 70-1080]

[AIAA PAPER 70-1080]

Kolmogoroff partial differential equations for non-Markovian stochastic processes, noting applications to reliability theory
07 p1323 A70-18938

Manufacturing error rate and inspection efficiency relevance to hardware product reliability
12 p2244 A70-28014

Inter-Range Instrumentation Group (IRIG) document regarding meteorological data reliability, defining measuring process accuracy and errors
14 p2606 A70-30567

Project acquisition based on consideration of logistic effects /ABLE/ for tool measuring logistic consequences of reliability and maintainability
15 p2832 A70-32634

Numerically controlled /N/C/ machines reliability program based on organized failure reporting and analysis system for cost effectiveness and downtime reduction
15 p2747 A70-32635

Reliability physics role in kinetic studies of physical and chemical degradation and failure mechanisms in semiconductor devices
15 p2713 A70-32661

Software reliability program development, functional analysis and error sources
15 p2742 A70-32667

Reliability - ASQC Conference, Los Angeles, May 1970
19 p3438 A70-38593

Long life reliability measurement for reentry and recovery systems, noting applicability to program monitoring, optimum resources allocation, etc
19 p3442 A70-38832

Airborne electronic equipment guarantees, discussing USAF experience with full life, maximum failure rate and failure free plans
19 p3391 A70-38843

Optimal burn-in testing of repairable equipment, improving reliability by decreasing failure rate with age under operating conditions
23 p4199 A70-43923

Deterministic vs stochastic signals for equipment and installations short cycle reliability tests over service life during changing environments
23 p4166 A70-44332

Computer program for systems reliability approximation, giving algorithm for cut and tie sets identification
20 p3594 A70-40060

Nonrepairable elements reliability under external influences, discussing linear damage accumulation hypothesis
20 p3638 A70-40180

Reliability of redundant repairable systems with preventive maintenance, determining mean time between failures
20 p3638 A70-40181

Reliability of redundant repairable systems with preventive maintenance, determining mean time between failures
20 p3638 A70-40181

Reliability of redundant repairable systems with preventive maintenance, determining mean time between failures
20 p3638 A70-40181

Reliability of redundant repairable systems with preventive maintenance, determining mean time between failures
20 p3638 A70-40181

Reliability of redundant repairable systems with preventive maintenance, determining mean time between failures
20 p3638 A70-40181

Reliability of redundant repairable systems with preventive maintenance, determining mean time between failures
20 p3638 A70-40181

Reliability of redundant repairable systems with preventive maintenance, determining mean time between failures
20 p3638 A70-40181

Reliability of redundant repairable systems with preventive maintenance, determining mean time between failures
20 p3638 A70-40181

Reliability of redundant repairable systems with preventive maintenance, determining mean time between failures
20 p3638 A70-40181

Reliability of redundant repairable systems with preventive maintenance, determining mean time between failures
20 p3638 A70-40181

Reliability of redundant repairable systems with preventive maintenance, determining mean time between failures
20 p3638 A70-40181

Reliability of redundant repairable systems with preventive maintenance, determining mean time between failures
20 p3638 A70-40181

Reliability of redundant repairable systems with preventive maintenance, determining mean time between failures
20 p3638 A70-40181

Reliability of redundant repairable systems with preventive maintenance, determining mean time between failures
20 p3638 A70-40181

Reliability of redundant repairable systems with preventive maintenance, determining mean time between failures
20 p3638 A70-40181

Reliability of redundant repairable systems with preventive maintenance, determining mean time between failures
20 p3638 A70-40181

Reliability of redundant repairable systems with preventive maintenance, determining mean time between failures
20 p3638 A70-40181

Reliability of redundant repairable systems with preventive maintenance, determining mean time between failures
20 p3638 A70-40181

Reliability of redundant repairable systems with preventive maintenance, determining mean time between failures
20 p3638 A70-40181

Reliability of redundant repairable systems with preventive maintenance, determining mean time between failures
20 p3638 A70-40181

Product reliability engineering, discussing product life cycle, operational reliability, failure analysis and design

02 p0309 A70-12303

Safe-life and fail-safe structural design philosophies in fatigue damage and operating lifetime control

02 p0389 A70-12615

Optimal redundancy for maximizing systems reliability of mixed series and parallel network consisting of N modules including 1 module with specified reliability cost function

03 p0585 A70-12995

Design reliability of through-bulkhead initiator explosive train using parametric test program data, discussing shock transmission and acceptor charge sensitivity energy balance

03 p0549 A70-14124

Design and economic concepts of Lockheed L-1011 wide body trijets, discussing airport and airway congestion alleviation, passenger appeal, etc

[RAES PAPER 15]

04 p0623 A70-15044

Product assurance and large aircraft prototype testing in aircraft industry, discussing reliability testing

[DGLR-69-031]

04 p0699 A70-15139

Reliability optimization of information systems with discrete time resource output and measured efficiency control

04 p0661 A70-15195

Reliability engineering related to general and professional levels, discussing space program methods and Concerto program for electronic components

05 p0853 A70-15810

Apollo spacecraft propulsion systems design and operational requirements, emphasizing use of redundant components and system backups to achieve reliability

[SAE PAPER 690704]

05 p0923 A70-15858

Apollo reliability and quality requirements, reviewing changes due to cost reductions in space program

06 p1065 A70-17988

Monograph on models of failure covering mathematical system reliability determination and relationship to physical nature of failures

06 p1171 A70-18394

Book on mathematical bases of industrial reliability covering components, parts stocking, Poisson distribution, redundancy, etc

07 p1290 A70-18700

Efficiency of terminal state control systems defined, relating efficiency, random parameters and reliability

07 p1246 A70-19528

Onboard modular computer research in strapdown guidance technology for computational ability and long term reliability of unmanned missions

07 p1238 A70-20062

Ground and onboard electronics systems for space shuttle vehicles, discussing role in equipment reliability and maintainability, life cycle costs, management control, etc

[AIAA PAPER 70-261]

07 p1398 A70-20391

Analytical structural design reliability, discussing static test failures of wings, fuselage, horizontal and vertical stabilizer and landing gear

07 p1417 A70-20400

Soviet collection of papers on apparatus for meteorological measurements covering error analysis, reliability engineering, use of computers, etc

08 p1494 A70-20771

Ti alloys failure-safe design developing procedures for incorporation of stress-corrosion cracking characterizations into ratio analysis diagram system

08 p1519 A70-21456

Design allowables and factors of safety for filamentary composite materials, discussing reliability

08 p1595 A70-21900

Reliability estimations precision evaluated by Monte Carlo simulation, analyzing causes of data inaccuracy

09 p1689 A70-22019

Apportionment optimization of reliability and maintainability by Lagrange multipliers and dynamic programming, discussing maintainability cost model and computerized simulation

09 p1792 A70-22211

V/STOL aircraft turbojet engine design and quality control for in-service reliability

09 p1743 A70-22572

Reliability engineering for complex systems of multiple repairable parts based on analysis involving signal flow graphs and Markov renewal processes

09 p1691 A70-22574

Electric propulsion design, considering effects of weight, impedance matching, beam voltage regulation and operating point variations in formulating system mass and reliability

09 p1743 A70-23248

Whirl effect on heat exchanger efficiency and reliability, discussing tests with transparent models and defective filling of circuits by feeding system

[ONERA-TP-768]

10 p1968 A70-24400

System with recovery consisting of n elements, discussing reliability and solution to steady state problem

10 p1855 A70-24798

Microwave equipment reliability achievement emphasizing tests and analyses on RF amplifiers, duplexers, antennas, etc

10 p1851 A70-24882

Complex microwave solid state subsystems designs for specialized systems

10 p1852 A70-24889

Maintainable electronic equipment requirements for long duration manned space missions

10 p1852 A70-24895

Integrated planning and testing for systems reliability improvement

[AIAA PAPER 70-391]

10 p1896 A70-24914

Hardware and system testing mathematical model assuming stochastic design and manufacturing defects detection and nondetection probability equations analogous to reliability function

[AIAA PAPER 70-390]

10 p1896 A70-24915

Reliability model for analyzing operational phase test programs developed from R and D phase models, processing data according to test scope

[AIAA PAPER 70-389]

10 p1896 A70-24916

Apollo Applications Program command and service module test requirements to achieve reliable hardware for extended missions

[AIAA PAPER 70-378]

10 p1952 A70-24925

Integrated Test Program for S-3A Weapon System, detailing test sequence flow and interfaces to assure vehicle and avionics systems reliability and maintainability

[AIAA PAPER 70-370]

10 p1959 A70-24931

Nickel cadmium battery for aircraft jet engine starting, discussing selection for optimum service life and reliability under maintenance and environmental conditions

[SAE PAPER 700211]

11 p1980 A70-25883

Interplanetary space systems, analyzing failure factors to assure reliability

11 p2112 A70-26051

Nuclear environments determination methodology for ground military equipment hardening, considering personnel and equipment responses to detonation in atmosphere

12 p2271 A70-27097

Telecommunication satellite system operation reliability taking into account maintenance and economics, discussing spacecraft acceptance and performance tests

12 p2313 A70-27470

First excursion failure survival probability of randomly excited structures, considering single degree of freedom linear oscillator under Gaussian white noise

12 p2327 A70-27819

Reliable and optimum cost power sources design for long life electronic digital communication equipment

12 p2166 A70-27927

Mission oriented or time dependent systems reliability measures definitions in terms of probability

12 p2336 A70-28008

Redundancy optimization based on partial failure modes effect on system reliability to reduce cost

12 p2243 A70-28010

Weibull process with unknown scale and shape parameters analyzed by Bayesian decision making model, with application to component reliability problem

12 p2243 A70-28011

Complete sample estimation techniques for reparameterizations of Weibull density function to assign probabilities to components and systems lifetimes

12 p2243 A70-28012

On-line optimization of maintenance and verification schedules for complex system safety insurance

12 p2244 A70-28013

Electromagnetic interference filters design for equipment power lines from electromagnetic compatibility and reliability viewpoints

12 p2201 A70-28129

Onboard computers automatic reliability control with implementation of self repair, modeling by Markov processes nonhomogeneous in time

13 p2372 A70-28438

Plastic encapsulated semiconductors reliability test programs with emphasis on accelerated humidity-temperature method

13 p2377 A70-29259

System reliability and effectiveness - Conference, Beverly Hills, February 1969

13 p2524 A70-29564

Computer program for system reliability prediction, using probability tree approach and block probabilities

13 p2373 A70-29565

Reliability relation to mean time between failures /MTBF/ relation for long life repairable equipment with limited life components

13 p2421 A70-29567

Beneficial and detrimental effects of value engineering change proposals on system reliability, relating cost improvement and performance factors

13 p2524 A70-29568

Reliability prediction techniques accuracy and optimal timing including true and project control predictions

13 p2524 A70-29569

Reliability guarantee vs cost of capital, analyzing contract compliance delay and discounted penalty expenditures

13 p2525 A70-29570

Quality control goals for manufactured products translated into manufacturing process inspection and investment costs terms

13 p2421 A70-29675

Failure prediction testing and elements replacement at field maintenance level for increasing equipment reliability

13 p2423 A70-29697

Guidance system cost and reliability by Monte Carlo analysis of failure statistics

14 p2614 A70-30462

Cost reduction and products reliability and quality maintenance by combining accurate cost reporting system with proper quality level control

14 p2669 A70-31108

Quality control of electronic equipment using technical and management approach for attaining specified reliability

14 p2592 A70-31109

System effectiveness apportionment for constraints existing on accountable factors using Lagrange multiple method

14 p2669 A70-31111

Systems effectiveness equated to function of performance, availability, reliability, maintainability, quality control and manufacturing, emphasizing optimization

14 p2592 A70-31112

Approximating hazard rate function parameters estimation from failure data, using computer program

14 p2592 A70-31113

Availability assurance using computerized spare allocation model for optimal selection of sufficient spares to achieve required protection against system failures

14 p2592 A70-31114

Quality information system consisting of closed loop input/feedback methods insuring design requirements of Saturn S-2 stage

14 p2654 A70-31116

Quantum mechanical communication system with thermal noise disturbance, analyzing reliability function and channel capacity

14 p2551 A70-31120

Precision reliability indices for automatic dimensional control vibration-contact sensor

15 p2714 A70-31582

Redundant amplifier /RAMP/ for reliability improvement

15 p2708 A70-31961

Cost effective reliability prediction techniques, discussing precision gyros procurement by NASA

15 p2736 A70-31964

State transitions and couplings in reliability of complex systems, using logic algebra suitable for computer

15 p2709 A70-32132

Reliability - IEEE Conference, Los Angeles, February 1970

15 p2745 A70-32626

Mission analysis in system evolution, determining subtasks sequence to accomplish performance goals

15 p2804 A70-32627

Reliability program planning and organization as part of integrated Development Risk Management System, considering task identification, assignment and accomplishment

15 p2747 A70-32628

Reliability criteria documents updating, discussing input vs output, experience retention, tradeoffs, etc

15 p2747 A70-32630

Optimum reliability programs, suggesting simulation to provide cost effectiveness basis for systems design configurations evaluation as alternative to demonstration testing

15 p2831 A70-32631

Long term storage effects on systems reliability, emphasizing tradeoffs regarding availability, reliability and costs

15 p2712 A70-32637

Reliability factors in design and development staging systems /DDSS/ for military and space exploration programs

15 p2747 A70-32639

Reliability engineers role and responsibility in production process

15 p2832 A70-32640

Integrated test program including proper timing for various testing levels, discussing environmental effects and sample size determination

15 p2747 A70-32641

Computerized optimal redundancy analysis, considering cost, size, weight, volume, etc

15 p2712 A70-32642

Circuit design characteristics and reliability relationship in electronic power supplies for performance requirements

15 p2712 A70-32644

High usage military system integrated circuit failure modes analysis for reliability improvement

15 p2713 A70-32650

- Subcontracting for cost optimal parts screening, discussing negotiations and reliability requirements 15 p2747 A70-32651
- Practical electronic components criteria accommodating reliability engineer and circuit designer 15 p2832 A70-32653
- Interrelated computer programs and comprehensive parts data bank /REACT/ for reliability assurance analysis 15 p2706 A70-32654
- System failure rate estimation as function of age using incomplete field reliability data 15 p2748 A70-32660
- Reliability assurance of LSI components consisting of complex electronic functions fabricated by semiconductor technology on single chip 15 p2713 A70-32662
- Failure analysis in third generation reliability approach to IC product quality improvement, investigating Si-Al contact irregularity cause and effect 15 p2713 A70-32663
- Personnel subsystem reliability through empirical approach, determining relations of man-hardware-procedure systems 15 p2804 A70-32665
- Nonparametric reliability application to numerical data involving failure distribution, using mathematical model 15 p2748 A70-32669
- System maintainability stochastic modeling using probability density functions 15 p2748 A70-32670
- Satellite reliability, discussing quality control, contractual matters, mathematical models, project management, failure modes, etc 15 p2813 A70-32826
- Mathematical reliability model for quasi-redundant electronic system with two failure modes for each component 15 p2769 A70-32827
- Reliability test facilities for military shipboard electronic equipment, subjecting equipment to combined thermal shock and vibration cycles 16 p2888 A70-33125
- Electrical, electronic, electromechanical, pneumatic and hydraulic subsystems failure pattern determination, discussing sensing techniques in signature analysis [ASME PAPER 70-DE-34] 16 p2917 A70-33505
- Reliability-cost model to determine optimum failure rate for minimization of systems total life cycle cost [ASME PAPER 70-DE-43] 16 p3004 A70-33507
- Probabilistic considerations relationship to failure free operation in product design [ASME PAPER 70-DE-70] 16 p2918 A70-33520
- NERVA rocket engine program reliability, design, performance and managerial approaches [AIAA PAPER 70-711] 16 p2950 A70-33568
- Reliability life tests preventing sliding electrical contacts failure in space vehicles, discussing data dissemination 16 p2920 A70-33806
- NERVA flight engine operating characteristics and reliability requirements for missions, noting conditioning, startup shutdown, reactor cooldown, fuel consumption, etc [AIAA PAPER 70-676] 16 p2951 A70-33951
- Systems subject to failure and repair cycles, describing performance and reliability by stochastic processes in terms of excess time 17 p3099 A70-34580
- Systems consisting of redundant and different modules, deriving vector and matrix expressions for effectiveness 17 p3099 A70-34581
- Large complex system with standby components, approximating reliability by simple model substitution 17 p3099 A70-34582
- Combined environments testing to reveal potential flight failure modes 17 p3059 A70-35165
- Solid oxygen generator for oxygen gas production from sodium chlorate decomposition, discussing reliability, safety and maintenance 18 p3225 A70-36211
- Wideband analog signal data transmission, evaluating messages accuracy in terms of error probability 18 p3228 A70-36623
- Book on optimization and probability in systems engineering covering mathematical models for reliability, repair, availability, Markov techniques and queueing 19 p3553 A70-37928
- Systems reliability numerical prediction 19 p3389 A70-38205
- Cost effective spacecraft testing in terms of statistical reliability, program effectiveness and equipment costs 19 p3554 A70-38293
- Electronic equipment reliability improvement, based on reliability control group qualification, burn-in and diagnostic tests 19 p3554 A70-38401
- Optimum reliability level in terms of economic benefits and external constraints 19 p3554 A70-38595
- Military electronic equipment reliability limitations in terms of mean time to failure, considering quality control of components 19 p3390 A70-38596
- Redundant systems reliability under wearout conditions for active and standby units, including failure rates of sensing and switching devices 19 p3438 A70-38597
- Soviet book on statistical algorithms for reliability covering repairable and first failure systems with ideal and imperfect switching 19 p3395 A70-38798
- Reliability and maintainability - Conference, Detroit, July 1970, Volume 9, Assurance technology spinoffs 19 p3440 A70-38815
- Reliability analysis based on Bayesian subjective probability implemented by stored time sharing computer programs for engineering computations and operation analyses 19 p3441 A70-38818
- Test data interpretation by design margin techniques in poststorage reliability of high quality gyro assemblies 19 p3441 A70-38822
- Condition Monitored Maintenance program for turbine engines eliminating total overhauls at specified time, using NDT 19 p3441 A70-38830
- Weapon systems effective reliability analysis, using degraded mode evaluation and deterministic computer program 19 p3442 A70-38833
- SUREFIRE /system for utilization of remote equipment for failure investigation and reliability evaluation/ monitoring reliability in closed loop failure reporting and corrective action system 19 p3555 A70-38834
- Avionics hardware operational effectiveness assessment method, considering inertial navigation system LN-12D 19 p3442 A70-38837
- Hazard functions, renewal and peril rates for reliability models of nonrepairable parts, sockets and repairable systems 19 p3442 A70-38839
- Economics of reliability relating risks of failure and cost of failure prevention 19 p3555 A70-38841
- Reliability enforcement in design by competition and test program, using gyroscope example 19 p3433 A70-38842
- Integrated structural analysis for reliability prediction of solid propellant rocket motors 19 p3489 A70-38844
- Large scale array /LSA/ MOS devices failure rate prediction model, determining reliability 19 p3391 A70-38847
- Fatigue strength distributions at specific cycles of finite life with given cycles-to-failure, calculating reliability 19 p3550 A70-38851
- Soviet book on operational tolerances in radio electronic equipment from reliability criteria 20 p3597 A70-39400
- Prior distributions computer aided selection for generating Monte Carlo confidence bounds on system reliability 20 p3658 A70-39641
- Failure rate and MTBF in reliability engineering, clarifying ambiguous terminology 20 p3638 A70-40061
- Digital systems reliability improvement by redundancy at circuit and system levels 21 p3797 A70-40762
- Accelerated life testing, discussing accumulated damage for graphical procedure in normal conditions [ASME PAPER 70-PROD-10] 21 p3832 A70-40871
- Statistical data for optimum fatigue reliability design for dynamic and rotary machinery, considering static strength, cycle-to-failure and stress-to-failure distributions 21 p3833 A70-41004
- Aerospace computers design, considering real time operation and reliability requirements 21 p3794 A70-41686
- Ultrasurvivable and maintainable computer design involving redundant spare modules and own tester for aerospace applications 21 p3795 A70-41695
- Phase recovery in vestigial sideband /VSB/ data transmission, deriving carrier acquisition time required to achieve satisfactory error rate for coherent demodulation of PAM 21 p3793 A70-42178
- MIL-STD-882 systems and subsystems and equipment safety requirements related to program management activities 22 p4048 A70-43730
- NERVA nuclear rocket engine design technology program, discussing probabilistic techniques for reliability engineering [SAE PAPER 700801] 24 p4377 A70-45910
- Quality control and reliability assurance in industrial supplier-customer relationship, emphasizing management role 24 p4431 A70-46386
- RELIEF MAPS**
- Universal Automatic Map Compilation Equipment /UNAMACE/ for terrain altitudes determination on uniform and dense grid in stereo model to obtain orthophotographic projection 11 p2051 A70-26042
- Soviet collection of lunar geological and morphological maps and relief tracings, showing tectonic features, craters and surface characteristics 19 p3518 A70-38011
- Pseudo three dimensional effect on monoscopic radar imagery for topographic relief differentiation, using offset superposition of transparencies 22 p4031 A70-42965
- RELIEF VALVES**
- Stability conditions for relief valves assumed to be part of closed hydraulic line simulating receiving part 05 p0797 A70-15899
- Popping pressure of relief valve with helical spring under dynamic load noting frequency dependence [ASME PAPER 69-VIBR-48] 08 p1441 A70-21479
- REMAGNETIZATION**
- U MAGNETIZATION**
- REMANENCE**
- Apollo 11 rocks natural remanence and induced magnetism by triaxial magnetic gradiometer at Lunar Receiving Laboratory 21 p3914 A70-41650
- Apollo 11 type C breccia sample remanent magnetism, observing viscous component with several hours time constant 21 p3914 A70-41651
- Remanence and saturation methods for magnetic-particle flaw detection 24 p4346 A70-45726
- REMETLING**
- U MELTING**
- REMOTE CONSOLES**
- Automatic multiple station test system for manufacturing plants, considering centrally controlled vs free standing and intelligent vs nonintelligent remote stations 08 p1470 A70-20655
- Remote real time simulation, using CDC 6600 computers, peripheral equipment and wideband communication link 16 p2870 A70-33732
- Heat transfer and viscous flow pedagogy, discussing classroom use of remote time sharing computer terminals 23 p4166 A70-44642
- REMOTE CONTROL**
- NT RADIO CONTROL**
- Unmanned teleoperator spacecraft /UTS/ for future orbital demonstration, discussing manipulators, multi-function viewing, stabilization, human factors, etc [AIAA PAPER 69-1067] 01 p0195 A70-10649
- Man machine system consisting of manned station controlling distant spacecraft via wideband radio link 02 p0229 A70-12145
- Programming device for positioning samples under X ray beam in testing welded seams and parts 02 p0301 A70-12488
- Physician-monitored central control facility communicating with remote site facilities staffed by paramedical personnel for public health care, based on aerospace experience 04 p0644 A70-15357
- Dynamic mathematical model of proportional electromagnetic transducer in pneumatic servomechanisms derived by Lagrange-Maxwell method assuming circuit linearity 07 p1195 A70-18750
- Remote control turboprop drone aircraft for long unmanned electronic intelligence or tactical communications relay missions 08 p1435 A70-20625
- Self contained remote sense remote control pressure regulator using pure fluid amplifiers, controlling large or small flow over wide pressure range 09 p1614 A70-23688
- Remote control telescope for deployment in hazardous locations, discussing design criteria, operation and test results 09 p1640 A70-23777
- State space models of remote manipulation problem applied to human supervised or autonomous computer manipulators 10 p1828 A70-25230
- Dual conversion receiver for remote frequency control in satellite TV distribution system [AIAA PAPER 70-414] 11 p2002 A70-25482
- Remote controlled diaphragm exploding device associated with shock tube for MHD generator 11 p2090 A70-26170
- Remote signal measurement and analysis in hazardous environment by command terminal utilizing manual or computerized control 12 p2201 A70-28134

Ground controlled remote manipulator spacecraft system through wideband radio link for satellite maintenance and repair

15 p2810 A70-31780

Tactical aircraft performance, discussing electro-optical devices, weaponry, communication and navigational networks, information displays and real time remotely manned control systems

17 p3013 A70-34672

Multiple remote control systems design, emphasizing transmitter and receiver characteristics matching to overall network parameters

18 p3235 A70-36426

Multiple remote control systems effectiveness increased via controlled rectifier as even voltage harmonics generator

18 p3235 A70-36427

Frequency discrimination circuits for multiple remote control receiver systems with high harmonic noise levels

18 p3235 A70-36428

Caterpillar remote controlled unmanned lunar exploration vehicle, describing construction and scientific missions

18 p3237 A70-36512

Automatic weight analysis by calculation and orientation of mass properties /COMP/ program, using remote terminal time sharing computer system [SAWE PAPER 824]

20 p3595 A70-40353

Pulse-time multistable state elements for automatic and remote control constructed from pulse sequence interactions with multiple frequency relations

22 p4005 A70-43567

Free flight remote controlled teleoperator system applications in manned orbital space station/space shuttle program

23 p4260 A70-44644

Unmanned Luna 16 landing mission, discussing launching and automatic mission control via onboard computer and earth-radioed data

24 p4412 A70-45982

REMOTE HANDLING

Computer controlled remote manipulator development, operation, components and applications, describing system programs consisting of executive control programs and subroutines

08 p1465 A70-20817

Crystal controlled digital frequency setting for microwave oscillators in mobile FM radio links with remote handling

20 p3596 A70-39162

REMOTE SENSORS

CAT remote sensing for advance aircraft warning, using IR instrument to detect turbulence-associated temperature preceding aircraft

01 p0087 A70-10697

Remote sensors to determine atmospheric characteristics and underlying earth surface structure, using electromagnetic and acoustic waves as signal carriers

01 p0093 A70-11266

Martian orbital photographic missions objectives and sensors realizable capabilities, discussing relationships between orbital parameters and imaging systems constraints

03 p0490 A70-13663

Remote sensing system for earth resources surveys temporal information employing human interpreter and machine for spatial and spectral data processings

03 p0491 A70-13668

Aircraft multispectral IR scanning systems for earth resources remote sensing, discussing capabilities

03 p0491 A70-13670

Moving contact pressure transducer for remote signaling

03 p0494 A70-14048

University/industry team project Bonanza conducting aircraft flight over Colorado to investigate earth resources remote sensing techniques

[AAS PAPER 69-574]

04 p0788 A70-14637

Remote sensing application to agriculture, forestry and range resources in terms of human priority over monetary benefits, noting high altitude aircraft use

[AAS PAPER 69-583]

04 p0788 A70-14638

Remote sensor capability in land use, urban and soil moisture analysis data acquired by NASA Earth Resources Program

[AAS PAPER 69-575]

04 p0676 A70-14641

Earth resources satellites capabilities and requirements emphasizing orbit parameters, remote sensing, data handling and telemetry systems

[AAS PAPER 69-587]

04 p0760 A70-14642

Orbital spacecraft/sensor systems for earth resource surveys and measurement, considering agriculture, forestry, geology, mineralogy, hydrology, etc

[AAS PAPER 69-584]

04 p0761 A70-14643

Remote sensing aerial and space surveys application to agriculture, forestry and water resources, discussing imaging systems and information acquisition and analysis techniques

05 p0838 A70-16164

Earth resources remote sensing investigations from spacecraft and aircraft, noting Gemini and Apollo

photography, hydrological surveys and radar techniques

05 p0849 A70-16450

Remote sensing advantages and limitations of various wavelength bands, resolutions and time spans, discussing instrumentation and environmental limitations

05 p0850 A70-16684

Optical crossbeam technique for remote sensing of wind speeds, relating light fluctuations to convective wind velocity by space-time correlation methods

05 p0850 A70-16688

Geostationary mode application to earth sensing, examining resolution requirements for earth scanning tracking telescope

06 p1154 A70-17152

Balloon flights for remote sensor systems tests, describing return-beam vidicon and tracking telescope experiments

06 p1061 A70-17153

Blood pressure indirect recording using ceramic crystal pick-up over brachial artery and under pneumatic cuff

06 p0992 A70-17299

Earth resources and meteorological data collection from in situ sensors via satellite, discussing system considerations

06 p1006 A70-17343

Remote recording wind vane using continuous and step rotary switch potentiometers suitable for automatic weather stations

06 p1062 A70-17619

Atmospheric difficulties in earth surface remote sensing by satellites, describing absorption, emission and scattering as wavelength functions

[ALAA PAPER 70-193]

06 p1057 A70-18083

Climatological cloud type statistics for simulating earth sensing mission data output as function of sensor field of view and spatial resolution

[ALAA PAPER 70-196]

06 p1065 A70-18098

Remote sensing of winds and atmospheric turbulence by cross correlation of passive optical signals, discussing results for power spectrum of fluctuations and winds

06 p1072 A70-18553

Remote sensors for measurement and mapping of ocean color variations, discussing Wierdange Image Spectrophotometer and Water Color Spectrometer

06 p1073 A70-18592

Spatial resolution and repetition intervals for optimum utilization of space-derived remotely sensed data of ocean surface features

06 p1060 A70-18593

Remote sensors application to direct and indirect fish detection in fishery research, using aerial and Gemini photography

07 p1262 A70-18957

Inductive sensor design and circuitry for measuring rapidly rotating shaft bending deflections at various vibration frequencies

07 p1279 A70-19115

Return Beam Vidicon /RBV/ system compatibility with requirements for Earth Resources Observation Satellite /EROS/, featuring high resolution image sensor for decreasing signal noise

07 p1280 A70-19231

Airborne real time IR imagery of thermal anomalies for geophysical exploration of water resources

09 p1674 A70-22262

Broadband remote sensing magnetometer for measuring fast-rising pulsed magnetic fields

09 p1676 A70-22716

Electromagnetic radiation sources for remote sensing application to identification of water, moist soil and vegetation, discussing optical properties of diverse materials

09 p1667 A70-22851

Spacecraft conditions influencing remote imaging sensor performance, discussing altitude, temperature and moisture at sensor, air turbulence, vehicle motion, etc

[ALAA PAPER 70-291]

09 p1677 A70-22853

Earth resources observation satellite /EROS/ program, describing remote sensor data acquisition, processing, dissemination and utilization

[ALAA PAPER 70-332]

09 p1667 A70-22861

International legal and political aspects of earth resource surveying by satellite remote sensors, considering U.S. policy

[ALAA PAPER 70-331]

09 p1793 A70-22862

Multispectral point scan camera system as remote sensor for Earth Resources Satellite, noting real time automatic data processing and interpretation

[ALAA PAPER 70-319]

09 p1677 A70-22867

Remote sensing data applications to agricultural statistics, discussing policy and standards for aggregate data release, confidentiality, error analysis, etc

[ALAA PAPER 70-312]

09 p1793 A70-22868

Microwave radiometric techniques for continuous all-weather remote sensing of sea conditions from satellites, discussing foam and surface ripple effects

[ALAA PAPER 70-318]

09 p1677 A70-22869

Specifications nomographs for earth resources IR radiometers, considering ground resolution, aperture diameters, detector arrays, etc

[ALAA PAPER 70-317]

09 p1677 A70-22870

Earth resources sensor integration into satellite or aircraft, discussing cost effectiveness

[ALAA PAPER 70-316]

09 p1677 A70-22871

Multiband high resolution spaceborne imagery telemetry with optical mechanical scanners from earth orbiting satellites in earth resource applications

[ALAA PAPER 70-314]

09 p1677 A70-22873

Satellite monitoring of air pollution, discussing sulfur dioxide measurement in UV, optical correlation techniques, IR and visible spectra, stratospheric balloon tests, etc

[ALAA PAPER 70-305]

09 p1668 A70-22875

Remote sensing systems for vegetation analysis, discussing machine-aided photointerpretation methods for data analysis

[ALAA PAPER 70-308]

09 p1678 A70-22879

Satellite remote sensors for oceanographic applications, estimating resolution requirements for temperature, spatial interval, roughness patterns, wind speeds, etc

[ALAA PAPER 70-306]

09 p1668 A70-22880

ERTS satellite role in resource policy, management and remote sensing

[ALAA PAPER 70-304]

09 p1668 A70-22881

Philosophy and technology of spacecraft-borne sensors for earth resource surveys, noting ERTS-A satellite

[ALAA PAPER 70-302]

09 p1668 A70-22883

Coastal areas remote sensing instrumentation and techniques, discussing data handling and analysis and ground verification of color and multispectral imagery

[ALAA PAPER 70-299]

09 p1669 A70-22885

Ground truth calibration for aircraft and spacecraft earth resource sensors, discussing ground truth instrumentation, procurement procedures, reduction techniques, etc

[ALAA PAPER 70-296]

09 p1678 A70-22887

Remote sensors for earth resources observation by satellites, discussing electromagnetic spectrum, device operation, atmospheric transmission, measuring instruments, etc

[ALAA PAPER 70-288]

09 p1718 A70-22893

Information extraction efforts using imaging sensors on earth resources satellites compared to data processing for environmental satellite imaging sensors

[ALAA PAPER 70-284]

09 p1669 A70-22894

High resolution Fourier interference near IR spectrometer for aircraft, balloon and spacecraft remote sensing applications

[ALAA PAPER 70-292]

09 p1678 A70-22891

Atmospheric limitations on remote sensors using visible sunlight, noting applications to Earth Resources Technology Satellite and human vision

[ALAA PAPER 70-288]

09 p1718 A70-22893

Information extraction efforts using imaging sensors on earth resources satellites compared to data processing for environmental satellite imaging sensors

[ALAA PAPER 70-284]

09 p1669 A70-22894

High resolution Fourier interference near IR spectrometer for aircraft, balloon and spacecraft remote sensing applications

[ALAA PAPER 70-292]

09 p1678 A70-22891

IR thermometers in situ calibration, analyzing maximum error due to reflection effect

[ALAA PAPER 70-292]

09 p1684 A70-23536

Self contained remote sense remote control pressure regulator using pure fluid amplifiers, controlling large or small flow over wide pressure range

[ALAA PAPER 70-284]

09 p1614 A70-23688

Fluidic digital position sensor consisting of fluidic monostable amplifier, analyzing operation by characteristics method

[ALAA PAPER 70-292]

09 p1614 A70-23689

ESRO 4 satellite design, listing basic requirements of experiments in terms of orbital maneuvers and sensor locations

[ALAA PAPER 70-292]

09 p1767 A70-23700

Multipurpose multiband photographic system used for aerial remote sensing of earth resources

[ALAA PAPER 70-292]

09 p1686 A70-23755

Sea surface temperature measurement over large areas using IR remote sensing system mounted on airborne platform

[ALAA PAPER 70-292]

09 p1686 A70-23756

Earth horizon signal sensors on spin stabilized satellites using micron filters for cloud signal rejection

[ALAA PAPER 70-292]

09 p1686 A70-23757

Earth resources program function of early orbital manned space station in remote sensing

[ALAA PAPER 70-292]

09 p1687 A70-23760

Aerial remote sensing package for Earth Resources Program

[ALAA PAPER 70-292]

09 p1687 A70-23761

Terrestrial surface radiometric imaging by sensing thermal radiation at centimeter wavelengths to reduce atmospheric scattering attenuation

[ALAA PAPER 70-292]

09 p1687 A70-23763

Equidensity film advantages in photointerpretation relating to remote sensing in hydrology and land use

[ALAA PAPER 70-292]

10 p1889 A70-24502

High energy neutron activation method for remote extraterrestrial in situ rock surface constituents analysis

[ALAA PAPER 70-292]

10 p1932 A70-24614

Remote sensor input radiation at aperture, signals within and sensed data processing by computer techniques, noting automatic image interpretation

10 p1841 A70-24733

Airborne remote sensing automatic data processing for forest identification through pattern discrimination, utilizing power spectrum analysis

10 p1878 A70-24734

Oil pollution remote sensing by aircraft, utilizing 9-14 micron IR mapper, 19.35 GHz microwave radiometer, aerial cameras and multiband video system

10 p1878 A70-24740

Water depth determination by remote measurement of near IR reflectance of underwater plants, discussing effects of water path length changes

10 p1878 A70-24741

Remote sensing techniques for water resources evaluation and hydrobiological features mapping with multiband scanner imagery

10 p1879 A70-24742

Remote sensing and privacy rights, noting political and social trends toward privacy protection

10 p1971 A70-24744

Circuitry for phase modulated synchronized electronic oscillators for measuring minor reactance changes during remote sensing

11 p2052 A70-26373

Sensor selection and telemetry measurement of physical parameters

11 p2011 A70-26453

Atmospheric temperature and pressure profiles remote measurement using airborne microwave radiometer

11 p2056 A70-26502

Radar interferometry as a diagnostic method for remote probing of turbulent plasma

11 p2096 A70-26766

Environmental remote sensing - Conference, Ann Arbor, October 1969, Volume 2

12 p2214 A70-26901

Microwave radiometer as passive satellite sensor for observing ocean surface properties

12 p2228 A70-26902

Microwave radiometric temperature measurements generating curves relating sea state and surface temperature

12 p2215 A70-26903

Sea and sea ice remote sensing by four-frequency radar /4FR/ system in EC-121 aircraft

12 p2215 A70-26904

Passive remote sensing in microwave spectra for oceanographic applications including sea state, pollution and sea ice properties

12 p2216 A70-26905

Urban development detection by remote sensing imagery of highway and rail linkage

12 p2216 A70-26908

Slope failure erosional and mass wastage forms identification, characteristics and distribution based on large scale aerial photography depicted by remote sensor returns

12 p2217 A70-26913

Remote sensing from aircraft and satellites of chlorophyll concentrations for monitoring of biological productivity of sea

12 p2217 A70-26915

Water depth determination by various remote sensing techniques, discussing bottom reflection, wave analysis, thermal anomalies and laser ranging by time difference

12 p2217 A70-26916

Aerial IR film optical density related to preharvest crop yield indicators in micro experiments with remote sensors

12 p2217 A70-26918

Plant leaves discrimination by multispectral reflectance indicated in transmittance measurements via remote sensing from aircraft and spacecraft

12 p2218 A70-26920

Multistage sampling of space and aircraft remote sensor imagery for forest inventory

12 p2228 A70-26921

Remote photometric and spectrometric measurements for plant structure and productivity of grass and shrub vegetation in desert environments

12 p2218 A70-26923

Remote sensing of lunar photometric function at small phase angles by Apollo 8 command service module

12 p2297 A70-26926

Remote environmental sensing - Conference, Ann Arbor, October 1969, Volume 1

12 p2218 A70-26929

Wheat fields recognition, mapping and acreage measurement by multispectral scanning with real time analog data processing, considering seasonal and observation altitude effects

12 p2219 A70-26930

Spectral discrimination technique for crops remote sensing, comparing statistical irradiance model with airborne multispectral scanner data

12 p2219 A70-26931

Remote sensing techniques for earth resources inventory, describing image enhancement role in multiband space photography

12 p2220 A70-26936

Multispectral color aerial photography, describing instrumentation, oceanographic and agricultural applications, atmospheric effects on images, etc

12 p2220 A70-26937

Nonimaging remote sensor data display in spatial registration with ground scene to determine sensor boresight position accuracy

12 p2229 A70-26940

Two dimensional remote sensing displays based on diffraction patterns generated by coherent light, discussing optical processing of photographs, drawings, maps, etc

12 p2229 A70-26944

Lidar ground-based sensing of atmospheric density, temperature, moisture content, discussing scattering theory and technique

12 p2183 A70-26945

IR sensor for detecting clear air turbulence, discussing design, installation, supporting equipment and inflight test results

12 p2229 A70-26946

IR remote temperature gradient sensor as clear air turbulence detector, presenting inflight test results

12 p2229 A70-26947

Remote monitoring of atmospheric wind and turbulence by cross correlation passive techniques, measuring heat and humidity fluxes

12 p2230 A70-26948

Remote measurement of CAT associated temperature gradients, comparing monochromatic and finite bandpass models

12 p2262 A70-26949

Air pollution measured from high altitude balloons and satellites by remote sensing of diffused atmospheric gases, using solar illumination

12 p2221 A70-26950

Atmospheric stability sensing by millimeter wave radiometry, discussing thermal radiation emitted and absorbed by oxygen molecules

12 p2263 A70-26955

Luminescing materials remote sensing during daylight by Fraunhofer line depth method with sun as excitation source

12 p2221 A70-26958

Microwave radiometry assumptions relating to absorptivity, emissivity and reflectivity data for earth resources remote sensing applications

12 p2230 A70-26959

Radiophase and induced pulse transient /input/ remote sensor systems for geological mapping, describing data acquisition and reduction techniques

12 p2221 A70-26961

Meteorological data acquisition by navigational aids, satellites and surface based indirect sensors for computer forecasting

13 p2405 A70-28773

Tactical aid displays /TAD/ for lightweight multi-sensor airborne ASW localization missions, discussing mission planning, avionics design, operator direction airborne tactical decision structures, etc [AIAA PAPER 70-517]

13 p2407 A70-29036

Magnetic moment measurement of satellite in near earth orbit, using data transmitted by rectangular magnetic sensors

13 p2454 A70-30032

Air photographs or imagery linear features, assessing sensors performance and developing interpretation criteria in photogeological research

14 p2573 A70-30641

Land use classification system of photointerpretation from remote sensor imagery

14 p2576 A70-30976

Lunar remote probing by IR and microwave thermal emission and by radar

14 p2644 A70-31056

Remote atmospheric temperature profile measurements, analyzing physical processes for radiation detection by earth pointing satellite-borne sensor

14 p2611 A70-31156

Cloud cover statistical data applied to planning remote satellite-borne sensing missions, using Monte Carlo method

14 p2611 A70-31232

Remote sensors applied to classification of aerial data concerning housing quality at different scales, using variables observation

14 p2577 A70-31234

Radar imagery for crop discrimination, discussing sensor and data requirements and statistical analysis methods

14 p2578 A70-31237

Book on geomagnetic micropulsations covering dynamic processes of magnetically trapped particles and micropulsations usability in remote sensing of magnetosphere

14 p2581 A70-31325

Visible polarization signature for remote sensing of soil surface moisture, noting invariance to partial shadowing in plowed or rough soils

15 p2724 A70-31667

Orbital earth resources sensors, outlining user oriented method of determining measurement requirements

15 p2735 A70-31777

Remote Raman spectroscopy of air contaminants, considering electro-optical technology and data processing

16 p2900 A70-33018

Target signature concept of spectral, spatial, temporal, and polarization effects to develop electromagnetic signatures against background, considering remote sensor system design

16 p2910 A70-33437

Optimal use of remotely sensed data from NASA Earth Resources Program by matching user models with capabilities of aircraft/satellite remote sensing system

16 p3004 A70-33708

Day/night thermal IR imagery detection of moisture stress of girdled trees in upland forest

16 p2898 A70-34047

Surveyor Canopus sensor and Project Scanner dual IR radiometer mechanical design

16 p2914 A70-34107

Airborne multispectral sensing, describing multichannel scanners, pattern recognition techniques and equipment, etc

17 p3083 A70-34874

Remote sonic monitoring system for Saturn V noise measurement and recording

17 p3094 A70-35521

Remote sensing in ecology - Conference, Madison, Wisconsin, June 1968

17 p3078 A70-35611

Remote sensing experiment demonstrating utility of multispectral color aerial photography for detection of differences among vegetative species

17 p3095 A70-35615

Photographic and multisensor imagery augmented by field survey for mapping vegetation boundaries and density differences within and between plant communities

17 p3079 A70-35616

Remote multispectral sensing of environmental and vegetative gradients in Yellowstone National Park by intercomparison of thermal IR and visible band imagery

17 p3079 A70-35617

Remote sensing of plankton and matter in sea by determining spectral changes in scattered light measured with radiometer

17 p3079 A70-35619

Multispectral remote sensing for detection and mapping of ecological objects and energy budget parameters measurement

17 p3079 A70-35622

Clear air turbulence /CAT/ remote sensing feasibility by optical signal covariance measurement, taking into account refractive index fluctuations

17 p3132 A70-35723

Meteorological satellites, discussing observation continuity, orbital characteristics onboard memory capacity and sensing methods

19 p3460 A70-37386

Atmospheric ozone remote sensing by high resolution IR interferometer spectrometer /IRIS/ aboard Nimbus 3 satellite

19 p3414 A70-38262

SUREFIRE /system for utilization of remote equipment for failure investigation and reliability evaluation/ monitoring reliability in closed loop failure reporting and corrective action system

19 p3555 A70-38834

Earth resources satellite orbits and imaging sensors, discussing multispectral spin scanner design

20 p3626 A70-39053

Earth resources data from man operated airborne/spaceborne sensors and data handling systems, examining Apollo Applications Program

20 p3616 A70-39056

Earth resources ground data processing in image formats from sensors in aerospace platforms, discussing collection control, image storage, retrieval, etc

20 p3591 A70-39058

Space acquired hydrological cycle data relating to water occurrence and movement in atmosphere and earth surface mantle

20 p3616 A70-39063

Water management decision model using earth resources information system with satellite-based remote sensors, evaluating costs and benefits by systems analysis

20 p3616 A70-39066

Aircraft/spacecraft assisted agricultural resource information system design concerning nongovernmental user and remote sensing needs

20 p3740 A70-39067

Lidar technique for remote detection and mapping of atmosphere based on weather radar and optical scattering concepts

20 p3660 A70-39079

CAT detection by IR radiation, remotely detecting atmospheric horizontal temperature gradients

20 p3626 A70-39080

Raman spectroscopy with lidar for remote mapping of air pollutants and concentrations

20 p3627 A70-39126

- Mariner spacecraft roll control star sensors and trackers design and flight performance
20 p3665 A70-39239
- Ultrasonic sensor for detecting altitude and vertical velocity of aircraft near ground, applying to helicopter hovering flight or conventional airplane takeoff and landing
[AIAA PAPER 70-1031] 20 p3631 A70-39506
- Air polluting sulfur dioxide and nitrogen dioxide remote sensing based on radiation molecular absorption using long line correlation spectrometer
20 p3633 A70-39793
- Automatic measurement of drainage networks for lengths and areas by copper plate etching or flying spot scanner on transparencies or radar images
20 p3633 A70-39794
- Earth resources observation satellite program and organization for acquiring, processing, utilizing and disseminating remote sensor data
20 p3741 A70-39944
- Lunar environment diagnostic features enhancement on IR emission spectra, making moon excellent target for remote sensing
20 p3709 A70-39979
- Atmospheric turbulence and wind velocity remote probing by millimeter waves, comparing results with conventional anemometer measurement
20 p3665 A70-40306
- Thermistor and dew cell as remote air temperature and dewpoint measurement at airports
21 p3822 A70-40760
- Remote sensing of atmosphere with emphasis on earth orbiting operational and research satellites
21 p3785 A70-40801
- Clear lower atmosphere meteorological parameters remote sensing for weather forecasting, comparing optical, radio and acoustic radar techniques
21 p3785 A70-40802
- Remote digital mean wind speed indicator with numerical display, using photoanemometer for airport application
21 p3831 A70-42247
- Remote sensing of returning reflected and diffracted seismic waves illuminating layered rocks subsurface, discussing data visual display
22 p4018 A70-43085
- Meteorological TV imaging systems development in last decade, including low and synchronous altitude camera, sensors, orthicons, etc
23 p4193 A70-43963
- Microwave radiometry and applications as material composition and temperature sensors for aircraft navigation, landing aids, pollution surveillance, meteorology and oceanology
23 p4198 A70-44648
- Solar stimulated terrestrial materials luminescence remote detection by Fraunhofer line depth method using UV grating spectrometer
23 p4199 A70-45007
- Ocean currents and sea surface temperature remote sensing by Nimbus 2 High Resolution IR Radiometer
24 p4332 A70-46400
- REMS**
- U RAPID EYE MOVEMENT STATE**
- RENAL FUNCTION**
- Renal and hepatic glutamine synthetase distribution in mammals, studying relation between glutaminase and urinary activities/ammonia metabolism/
02 p0232 A70-11710
- Renal hemodynamics and clearances alterations in owl monkey, using hemorrhagic shock procedure
02 p0234 A70-11732
- Ultraminiature pressure sensor for continuous recording of hydrostatic pressure in renal tubules and blood capillaries
05 p0804 A70-15772
- Human renal function, electrolyte and water metabolism during bed rest with daily leg exercise
07 p1223 A70-19937
- Sodium balance effect on intrarenal distribution of blood flow in normal man determined with Xe washout method
10 p1810 A70-24005
- Systemic hypoxia effect on renal tubule sodium reabsorption in anesthetized mongrel dogs
[AMRL-TR-69-135] 13 p2353 A70-29435
- Chronic hypoxia exposure effect on development and maintenance of renal hypertension in rats
14 p2539 A70-30956
- Unanesthetized dogs renal hemodynamic response to negative centrifugal acceleration
15 p2681 A70-31883
- Human renal response to various exercise rates, measuring endogenous creatinine clearance, urine volume, solutes, acid, elements and protein excretion
15 p2684 A70-32534
- Human water-salt metabolism following exposure to transverse accelerations, discussing diuresis and Cl-K excretion
17 p3038 A70-35364
- Renal lithiasis frequency among flight crews during aeronautical activity, noting role of rich food intake
17 p3040 A70-35917

- Renal hemodynamic response of unanesthetized dogs to positive accelerations within physiological tolerance range, measuring pressure and blood flow velocity
20 p3577 A70-40332
- Desoxycorticosterone action on human kidneys and sweat glands as function of temperature tested with various DOCA and NaCl doses
24 p4301 A70-45988
- Hypothermia and body rewarming effects on renal hemodynamics in anesthetized dogs
24 p4301 A70-45998
- RENDEZVOUS**
- NT EARTH ORBITAL RENDEZVOUS
- NT LUNAR ORBITAL RENDEZVOUS
- NT ORBITAL RENDEZVOUS
- NT SPACE RENDEZVOUS
- RENDEZVOUS GUIDANCE**
- Manned vehicles rendezvous missions in space and hydrospace, proposing functional structure involving concurrent ship control, navigation, perception, communication and prehension
[AIAA PAPER 69-1102] 01 p0034 A70-10615
- Automatically controlled rendezvous and docking for orbital assembly of spacecraft, deriving motion equations for mass centers
07 p1393 A70-19481
- Space rendezvous navigation and guidance based on optical sightings with hand-held sextant entered into and processed by small digital computer
07 p1331 A70-20061
- Rendezvous control law for spacecraft moving in central gravitational field along trajectory representing target vehicle Keplerian orbit
08 p1582 A70-21636
- Optimal longitude rendezvous for geostationary satellite by using inertially fixed orientation thrust for performing final positioning
[ONERA-TP-801] 10 p1941 A70-24541
- Manual spacecraft rendezvous system based on handheld instruments and manual computations, considering error analysis and simulation
13 p2357 A70-28392
- Manual control systems for spacecraft stabilization in rendezvous, midcourse correction, landing, etc
13 p2357 A70-28394
- Radio command guidance system for Mars probe ascent from surface to rendezvous with flyby vehicle on escape trajectory
13 p2447 A70-28421
- Automatically controlled rendezvous and docking for orbital assembly of spacecraft, deriving motion equations for mass centers
15 p2813 A70-32726
- Optimal interceptor-target allocation and guidance for renal interception and rendezvous using real time and storage computer
16 p2947 A70-33311
- Manned Mars lander launch-to-rendezvous analysis, using subsequent Venus swingby for mission velocity requirement reduction
[AIAA PAPER 70-1075] 19 p3530 A70-38887
- Differential rendezvous game theory with non-separated control inputs on right side of equations of motion applied to guidance problem
22 p4063 A70-43346
- RENDEZVOUS SPACECRAFT**
- Optimal rendezvous maneuver of two spacecraft in circular orbits with minimum fuel consumption, taking into account propelled vehicle control program and flight path
01 p0193 A70-10424
- Optimal rendezvous between satellite and spacecraft, determining power and time optimal coplanar rendezvous in circular orbit
01 p0139 A70-11479
- Rendezvous control law for spacecraft moving in central gravitational field along trajectory representing target vehicle Keplerian orbit
08 p1582 A70-21636
- RENDEZVOUS TRAJECTORIES**
- Rendezvous trajectory control problems solution by regularization techniques, emphasizing equations of motion in gravitational field
13 p2446 A70-28380
- Comet de Arrest 1976 opportunity mission analysis, considering flyby and rendezvous trajectories and guidance problems
[AIAA PAPER 70-1073] 19 p3513 A70-37426
- RENE 41**
- Postweld heating cycle for circular patch test to predict strain age cracking susceptibility in welded Rene 41
04 p0700 A70-15654
- Rene 41 resistance to strain-age cracking during postweld heat treatment
18 p3277 A70-36523
- Rene 41 ductility reduction by environmental oxygen promoting intergranular cracking at high temperatures
18 p3277 A70-36524
- REPAIRING**
- U MAINTENANCE**

REPEATERS

- Traveling wave tubes used in electronic counter-measure chain or repeater for deception jammer, discussing design and performance
04 p0653 A70-15658
- Communication satellite repeater design requirements to achieve adequate SNR for varying rain and cloud attenuation
[AIAA PAPER 70-498] 11 p1998 A70-25425
- S band communications repeater using retrodirective phased array on synchronous altitude data relay satellite /DRS/ for intersatellite and ground links
[AIAA PAPER 70-424] 11 p2001 A70-25472
- Multiple access to communication satellite by limiting repeater, considering model of n signals plus band limited white Gaussian noise in zero memory device
11 p2008 A70-26229
- Trends in military communication satellite repeaters, noting influence by increased payload size, weight and complexity
11 p2009 A70-26258
- Carrier synchronization system for PSK signals, using direct regenerative repeater and phase locked loop /DR-PLL/
15 p2697 A70-31826
- Repeater and antennas for space telecommunications onboard ELDO STV-F9 satellite, describing tests and measurements
15 p2811 A70-32282
- UHF ground communication dish antennas transmit and receive gains calibration by communication satellite repeater
16 p2872 A70-32967
- Tactical communications satellite /TACSAT/ design, emphasizing communications repeater characteristics
16 p2983 A70-34051
- REPETITION**
- Information hypothesis and repetition hypothesis concerning human reaction time to visual stimulus information
10 p1826 A70-24714
- REPLENISHMENT**
- MHD power generation, investigating replenishment of zirconia electrodes from plasma in open flame and duct configurations
14 p2534 A70-30535
- REPRESENTATIONS**
- Meteorological fields objective representation by numerical analysis, discussing statistical parameters and analytic errors checking
21 p3847 A70-41400
- REPRODUCTION**
- Chlorella reproduction rates at steady and variable illumination intensity levels, determining productivity autocorrelation function by statistical analysis
17 p3030 A70-35355
- REPRODUCTION [COPYING]**
- NT XEROGRAPHY
- Display devices using electrostatic forces, discussing electrostatic printing, magnetic display system, etc
08 p1499 A70-21686
- Diazo compounds purity effect on photosensitive photographic film quality, determining color image reproduction density
24 p4334 A70-45498
- Photo copying in diapositive form, using ruby laser light on IR film
24 p4352 A70-45559
- REPRODUCTIVE SYSTEMS**
- NT OVARIES
- NT TESTES
- REPTILES**
- NT TURTLES
- REPUBLIC MILITARY AIRCRAFT**
- U MILITARY AIRCRAFT**
- REPULSION**
- U FORCE**
- RESCUE OPERATIONS**
- Aircrew escape/rescue capability /AERCAB/ flying ejection seat design and test programs, noting rotary wing, fixed wing and parawing feasibility
01 p0035 A70-10714
- Beacon equipment as means of crashed or forced-landed aircraft locator to increase survival possibilities and reduce search cost
01 p0035 A70-10719
- Astronaut rescue and return of objects launched into space, discussing U.S.S.R. and U.S. proposals
03 p0612 A70-14263
- Space rescue requirements for earth-returning astronauts recovery under emergency conditions, discussing recovery zones determination by space flight mission control
04 p0761 A70-14929
- Three man space escape system, describing emergency situations, parachute descent, life raft design, rescue operations and engineering tests
[AIAA PAPER 68-936] 04 p0763 A70-15403
- Electronic search and rescue system developed for West German Air Force, consisting of personal trans-

ceiver and automatic distress signal transmitter unit, etc

05 p0793 A70-15904
Helicopters usefulness in rescue service via test flights, discussing rescue cars and centers for emergency patients

05 p0806 A70-16325
Optimal colors for target and rescue markers, discussing influence on signal detection, response and identification

06 p1002 A70-17713
Air crash rescue operations by helicopter ambulances of U.S. Army Medical Department, discussing postcrash fire suppression and injured personnel removal, emergency treatment and evacuation

06 p1002 A70-17714
AN/PRC-87 Pararescue radio for hands free operation, using bone conduction microphone, voice operated transmitter, etc

06 p0986 A70-17723
Spacecraft incorporated emergency rescue systems, discussing design of nonseparable crew escape compartment and separable capsule

07 p1218 A70-19010
Search and rescue (SAR) concepts behind advanced Navy systems, emphasizing flying ejection seat (AER-CAB) for air to air self rescue

07 p1192 A70-19024
Blind flight and helicopter navigation during prolonged maritime survival operations

07 p1193 A70-19132
Helicopter hoist rescue system, considering helicopter power, cable length, pilot visibility, etc

09 p1610 A70-22341
Aircraft crash fire fighting equipment and tactics for future airport needs

12 p2160 A70-27433
SOFAR/sound fixing and ranging/ systems for location and recovery of reentry vehicles and missile cases and rescue of disabled transoceanic aircraft

13 p2449 A70-29169
Electronically lobed direction finder homing system for location and rescue of airmen downed on aircraft with emergency locator transmitter

13 p2449 A70-29170
Space rescue probabilities, considering spacecraft emergency returns from orbit to earth surface and time sequences

14 p2654 A70-30780
Spacecraft or escape capsule rescue, discussing design, recovery planning, forces and sites

17 p1810 A70-35301
Aircraft-borne and descent systems performance and weight optimized for midair retrieval

[AIAA PAPER 70-1201] 21 p3751 A70-41805
Pilot airborne recovery device (PARAD) midair rescue system, discussing buoyancy, midair pickup, seat ejection energy absorber, homing avionics and human factors

[AIAA PAPER 70-1206] 21 p3752 A70-41812
Geometry and ionosphere effects on radio beacon operation for distress signal monitoring at sea, comparing night performance to daytime

23 p4163 A70-44229
Global rescue alarm net (GRAN) using satellites for relaying distress signals, eliminating current line of sight restrictions

23 p4143 A70-44455
Helicopter automatic approach and hover coupler systems, discussing cockpit display devices, handling qualities, pilot workload and fatigue and external load stabilization

23 p4140 A70-44464
Smoke, chaff and flare distress signals design and operation for search and rescue operations

23 p4143 A70-44494
Space rescue operations in orbit during heavy traffic of spacecraft with large passenger loadings, noting role of space shuttles and tugs

23 p4260 A70-44619
Space vehicle personnel escape/rescue/ survivability capabilities, considering on board, prepositioned aid and earth launched concepts

23 p4260 A70-44620
Rescue waiting time relation to number of communication and return sites for emergency astronaut return, considering day vs day/night recovery

23 p4245 A70-44639
Astronaut biological parameters monitored under prolonged space flight conditions for rescue operations

23 p4146 A70-44678
Apollo 13 flight rescue operation as function of flight crew performance and Mission Control Center [AIAA PAPER 70-1260] 24 p4412 A70-45968

RESEARCH

NT CRITICAL PATH METHOD
NT DYNAMIC PROGRAMMING
NT GAME THEORY
NT HIGH TEMPERATURE RESEARCH
NT LINEAR PROGRAMMING
NT MINIMAX TECHNIQUE
NT NONLINEAR PROGRAMMING
NT NUCLEAR RESEARCH
NT OPERATIONS RESEARCH

NT SADDLE POINTS (GAME THEORY)

Research problems resulting from observational methods in social-psychological studies, discussing categorization systems and coding reliability

05 p0802 A70-16668
Monograph on hypersonic flow boundary layers research conducted by European countries, determining pressures, velocity and temperature profiles, skin friction, heat transfer, displacements, etc

[ONERA-TP-770] 08 p1601 A70-21844
Radar signature analysis of convective precipitation, hailstorms, tornadoes, lightning, hurricanes and clear air echoes

11 p2076 A70-26039

RESEARCH AIRCRAFT

NT AVRO 707 AIRCRAFT
NT B-70 AIRCRAFT
NT X-15 AIRCRAFT
NT X-22 AIRCRAFT
NT X-22A AIRCRAFT
NT XV-4 AIRCRAFT
NT XV-5 AIRCRAFT

RESEARCH AND DEVELOPMENT

Optimum R and D organization in aircraft engine production illustrated on turbofan engine

01 p0161 A70-10080
NASA Technology Utilization Program extending space exploration and upper atmosphere R and D to X ray pictures, safer highways, TV cameras, etc

01 p0220 A70-10282
Military aeronautical R and D contributions to civil aviation since 1905, discussing jet engine and supersonic aircraft introduction, air traffic control, etc

[AIAA PAPER 69-1114] 01 p0005 A70-10614
UK aeronautics R and D, attributing competitive technology lag in military and subsonic civil fields to failure in aims and targets and program cost justification

02 p0402 A70-12306
Analytical scoring model design for effective evaluation of competing research and development projects

02 p0402 A70-12634
Decision model for R and D project selection

03 p0609 A70-12991
Decision analysis in R and D, discussing risk discounting and measure of value selection

03 p0610 A70-13956
R and D effect on aircraft engine business, considering aircraft operating cost, funds allocation, etc

04 p0787 A70-14390
German research institutes activities in fluid mechanics, structural materials, propulsion, flight control and electronics, space physics and medicine

05 p0829 A70-16374
Shock tube research covering shock structure, atomic and molecular physics, radiation, plasma flows, shock waves in solids and boundary layers

06 p1028 A70-17517
R and D laboratories quality and performance evaluation techniques, describing Apstein-modified Pelz technique

06 p1185 A70-17603
Team hiring of research scientists by industrial and academic organizations, discussing causes and influence on R and D organizations management and design

07 p1427 A70-19002
V/STOL R and D, comparing civil aviation in U.S. and Europe, discussing system approach

07 p1194 A70-19679
30 cm diameter mercury bombardment low impulse thruster development for potential space applications, discussing performance and control

[AIAA PAPER 69-238] 07 p1365 A70-19704
Midwestern political economy and federal R and D funds distribution, surveying bidding practices and NASA contracts for five year period

07 p1428 A70-19733
Coupling relations in product and systems development linking ideas to finished products

08 p1601 A70-20824
Civil engineering research needs in air transportation, discussing information sources and processing and industry estimates of manpower, facilities and funding

08 p1481 A70-21305
CRT display devices and R and D, discussing electron generation, luminescent materials, resolution, brightness, etc

08 p1498 A70-21680
Laser technology, discussing activation types, applications and commercial development for data processing, voice communication, medical equipment, etc

09 p1695 A70-22338
Government environment challenges to government sponsored big technology management illustrated by space nuclear engine research program

09 p1792 A70-22494
French microwave semiconductor technology in terms of basic research, technology studies, reliability and integrated circuits

09 p1739 A70-22602

RESEARCH AND DEVELOPMENT

Federal contract research centers objectives, characteristics, crucial issues and future

09 p1793 A70-22971
R and D idea flow studies, analyzing liaison, interface, coupling and technology transfer (LINCOTT/

09 p1794 A70-23410
Technology transfer or coupling from corporate viewpoint, discussing organizational responses to literature mushrooming, time compression of technological advance, etc

09 p1794 A70-23411
R and D resources allocation model based on correlated Navy technological forecast (NTF) and exploratory development goals (EDG/

09 p1794 A70-23412
Weapon systems combat effectiveness measurements, stressing need for proper data acquisition from early R and D through obsolescence

09 p1794 A70-23414
Technological forecasting for R and D planning including project selection and resource allocation decision making

09 p1794 A70-23416
Resource allocation model with cost-effectiveness relationship for Army long range R and D

09 p1795 A70-23417
Technology or Research Quantitative Utility Evaluation (TORQUE) system genesis and operation, with implications affecting R and D

09 p1795 A70-23418
Optical equipment development at Jet Propulsion Laboratory, discussing flight TV systems and associated digital image processing laboratory, planetary spectroscopy, spacecraft guidance, etc

09 p1657 A70-23505
Optical tools in aeronautical and space research at Langley Research Center, discussing schlieren photography of aeronautical and space models in wind tunnels

09 p1657 A70-23510
Marshall Space Flight Center optical research programs technology base for launch vehicle development support, discussing Apollo Telescope Mount

09 p1657 A70-23518
Models survey for evaluation and selection of research projects, discussing reasons for long range company

10 p1970 A70-24070
Earth resources satellite systems synthesis, describing analytical techniques in R and D preceding operational status

12 p2334 A70-26942
Computerized automation of R and D engineering, discussing critical effects of generalization and oversimplification

12 p2334 A70-27006
Personnel and organizational policies for university research management

12 p2336 A70-27750
Automatic computation at SNECMA for turbomachines R and D, emphasizing digital computer for scientific calculation and analog simulator for engine regulation

12 p2193 A70-28073
DOD laser research and development contracts management

14 p2667 A70-30367
International cooperation in military aviation emphasizing cost effectiveness in R and D, production and export prospects

14 p2669 A70-30939
R and D impact on transport aircraft design economics

14 p2669 A70-30945
Probabilistic methods in aeronautical research and development

14 p2563 A70-31393
Decision making role in management contribution towards success of research and development based on statistical decision theory

15 p2828 A70-31573
Quality assurance R and D for product design and operational integrity in manned space flight, noting space developments application to aircraft safety

15 p2676 A70-32231
Space propulsion research with emphasis on tripropellant mixtures, discussing increased combustion pressure, nozzle design, reusable orbital transporter, etc

15 p2789 A70-32252
Effective R and D management working principles, discussing changing goals, policy and technology changes, environment, adequate reporting, etc

16 p3004 A70-33663
Air safety R and D and future safety standards

16 p2842 A70-33816
Chemical rocket propellant research covering composite liquid monopropellants, lateral thrust in solid propellant rockets, ELDO third stage, friction losses, etc

17 p3148 A70-35211
Optimal R and D planning from estimated efficiency of research projects or national programs

20 p3740 A70-39646

RESEARCH FACILITIES

- Translation gap between R and D and production occurring at design transmission to manufacturing
21 p3955 A70-40913
- Lunar module systems design, describing R and D program and landing mission
21 p3928 A70-40977
- Predictive model for potential variance from planned schedule of R and D tasks to minimize risk in management
21 p3955 A70-41172
- R and D programs engineering talent assignment case histories
21 p3955 A70-41174
- Subjective probability estimation for R and D decision making, using analytical models incorporating risk and uncertainty
21 p3955 A70-41175
- TOPS /thermoelectric outer planet spacecraft/ project integrating R and D for specific space missions
21 p3920 A70-41793
- Papers on research techniques in nondestructive testing covering acoustic emission, ultrasonic spectroscopy, imaging systems angle reflectivity and holography, optical methods, etc
22 p4026 A70-42581
- European hypersonic aerodynamic research activities, describing Eurohyp program
22 p4127 A70-43507
- NASA safety related research programs based on technology transfer involving information summarizing, indexing and storage from global aerospace research and development
23 p4285 A70-44457

RESEARCH FACILITIES

- Rumanian book on shock tubes covering facility construction, gas flow, electronic measuring equipment, etc
01 p0059 A70-11379
- Lidar and IR radiometer mobile laboratory for atmospheric optics research, including construction details and support equipment
03 p0463 A70-13677
- Transonic wind tunnel of aerodynamic research station in Goettingen, Germany, taking into account fixed nozzle replacement by flexible nozzle
03 p0463 A70-13799
- Czechoslovakian Aeronautical Research and Test Institute history, organization, activities, equipment and achievements
03 p0464 A70-13925
- Aerospace laboratories organization concepts, discussing dependence on product, size, location and technological trends
03 p0612 A70-14313
- German Research Establishment for Air and Space Navigation covering aerodynamics, aircraft design, flight mechanics, guidance and jet propulsion
07 p1249 A70-19671
- Monograph on research by Japanese Institute of Plasma Physics covering theta pinch, plasma heating, flow, diagnostics, etc
07 p1350 A70-19843
- Onboard modular computer research in strapdown guidance technology for computational ability and long term reliability of unmanned missions
07 p1238 A70-20062
- Lewis Research Center applications of optics to research in flight propulsion and space power generation, discussing gas density visualization, radiative heat transfer, etc
09 p1657 A70-23522
- Canada/U.S. scientific sounding rocket program, describing facilities and projects at Churchill Research Range
11 p2032 A70-26292
- Report to COSPAR on Indian space research describing organizational structure, facilities, experiments and international cooperation
15 p2830 A70-31715
- Low speed wind tunnel design and construction for laboratory experiments and research projects, describing test sections
16 p2889 A70-33769
- Space law teaching and study facilities
17 p3204 A70-35801
- Solar eclipse of 7 March 1970 in Mexico, discussing characteristics, research program, equipment and photographs
18 p3318 A70-37046
- Space environment simulation in terrestrial laboratories, discussing test instruments and procedures
19 p3398 A70-38279
- Optical solar observatory for investigation of solar activity and impact on earth environment, discussing site selection and equipment
22 p4005 A70-42349
- Hypersonic wind tunnel facility for hypersonic aircraft and recoverable booster systems development [DFVLR-SONDDR-19]
23 p4178 A70-44799
- Manned earth orbital space astronomy instruments, facilities and research objectives
24 p4415 A70-45825

RESEARCH PROJECTS

- NASA research studies supporting tracked air cushion vehicle /TACV/ program illustrating aerospace technology application to ground transportation [AAS PAPER 69-565]
04 p0622 A70-14639
- Decision trees application to research projects selection, cost stages, probable return on investment and control device
07 p1427 A70-19001
- AEROS satellite A2 launching to investigate aeronomic processes in outer atmospheric layers, discussing scientific research program, mission data, satellite and ground station equipment [DGLR-69-050]
07 p1393 A70-19149
- Optimal program selection using experience of applied technical research
08 p1601 A70-21872
- Long range army budget forecasting model based on research projects cost distributions and parameters, describing computer program
09 p1794 A70-23415
- Management planning for global atmospheric research program /GARP/ applied to climatology and weather forecasting
09 p1795 A70-23545
- Canada/U.S. scientific sounding rocket program, describing facilities and projects at Churchill Research Range
11 p2032 A70-26292
- Report to COSPAR on Indian space research describing organizational structure, facilities, experiments and international cooperation
15 p2830 A70-31715
- Si and CdS solar cell research at COSMAT laboratories, discussing proton and electron irradiations and thermal cycling
15 p2677 A70-31804
- Lunar exploration program based on U.S. antarctic research experience, considering man role, environment, logistics, transportation, economics, etc
15 p2800 A70-32058
- Phased arrays, discussing ground based, shipboard and airborne research programs for military
16 p2863 A70-33264
- Small rocket systems research programs, discussing Apollo-Pacemaker and planetary entry parachute flight tests
17 p3177 A70-35203
- FAA research activities on eliminating birds at airports and improving aircraft components resistance to impact, including interagency committee functions on hazard problems
18 p3349 A70-35982
- Electric propulsion research involving MPD thrusters, current sheets and neutral-ion motion coupling [ALAA PAPER 70-1086]
20 p3683 A70-40249
- International Space Research Organization /ISRO/ for space operations, considering political, economic, technical and scientific requirements
23 p4286 A70-44688
- NACA/NASA rotating wing aircraft research history 1915-1970, Part 2, autogyro flight test experiences, rotor blade dynamics research, interest in helicopters, etc
23 p4142 A70-44852
- NACA/NASA rotary wing aircraft research history 1915-1970, Part 3, covering rotor and helicopter theory, related flight and wind tunnel testing, etc
23 p4142 A70-44853
- NACA/NASA rotating wing aircraft research history 1915-1970, Part 3, covering rotor dynamics and flying qualities, hovering tests, rotor flow, loads, etc
23 p4142 A70-44856

RESEARCH VEHICLES

- Lunar surface mobility systems designs based on terrestrial transporters or mission requirements consideration, comparing capabilities
13 p2384 A70-28416

RESERVOIRS

- Chimikuran reservoir algae life and physicochemical characteristics
09 p1627 A70-23148

RESIDUAL GAS

- Fission gases trapped in fuel particles, cladding and matrix of irradiated refractory metal-uranium oxide cermets determined by gamma counting
07 p1332 A70-19851
- Residual gas effects on critical load and brittleness of pure and molybdenum-coated niobium bars after annealing in vacuum
12 p2258 A70-28324
- Residual atmosphere analysis and application to ion pumping on Al alloy high pressure chamber of differential vacuum system
19 p3434 A70-37464
- Ultrahigh vacuum pressure measurement by improved residual gas analysis mass spectroscopy with magnetic section
19 p3396 A70-37465
- Residual gases partial pressure measurement in vacuum chamber by mass spectrometer with elec-

tromagnetic scanner and electron multiplier, detecting electron current
19 p3421 A70-37466

RESIDUAL STRESS

- Fiber composite cylinder tensile performance improvement through mechanical residual stress relief by axial straining
01 p0120 A70-10737
- Residual stress determination in elastoplastic body with known plastic strains, using Hilbert space for symmetric tensor fields
01 p0209 A70-11399
- WC-Co alloys noting polishing and grinding effects on residual stress and crack resistance
03 p0508 A70-13145
- Light alloys cold hardening effect and fatigue strength estimation, considering residual stress variability with time
03 p0587 A70-13239
- Residual stresses in cylindrical shells eliminated by local heat treatment, determining temperature field in elastic strain regions
03 p0497 A70-13739
- Residual stress distribution in butt joints during welding of sheet Nb measured by extensometer, noting annealing temperature effect on stress relieving
03 p0513 A70-14072
- Residual stress variations in ring shaped fiberglass reinforced plastic shells produced by winding due to elastic modulus decrease and filler/binder contraction
05 p0934 A70-16216
- Residual strains determination in rotating disks from photoelastic coatings interference
05 p0955 A70-17063
- X ray elastic constants measured in cementite phase in high carbon tool steel following plastic deformation at tension, noting residual stresses increase and balance
06 p1084 A70-17126
- X rays of surface residual stresses produced during fatigue process of annealed low carbon steel and copper
06 p1084 A70-17128
- Thin walled metal cylinders residual deformation microstructures under internal impulsive loading
07 p1285 A70-19969
- Distilled water and mineral oils heated to 50-80 C studied for effect on residual stresses in fiberglass reinforced plastics
08 p1526 A70-20925
- Interaction between boundary layer and internal stressed state of thin elastic shell by formulating two dimensional linear theory
08 p1585 A70-20955
- Ti alloy band polished surfaces properties, obtaining required residual stresses by process control
08 p1507 A70-21198
- Residual stresses in continuous fiber reinforced composites with unknown strain history determined by empirical methods
08 p1520 A70-21498
- Al and Ti alloys residual stress determination by X ray diffraction
09 p1704 A70-22796
- Internal stresses and substructures dependence on thermomechanical histories of stainless steel during creep, noting subgrain orientation
09 p1705 A70-22805
- Dynamic stresses during abrupt temperature changes of medium, showing internal stress waves amplitude incompressibility by suitable internal stress source selection
09 p1778 A70-23089
- Residual stresses effect on strength and hardness of tungsten carbide-cobalt alloy by application of small plastic deformations, observing crack formation anisotropy
10 p1904 A70-25168
- Heat resistant alloys low cycle fatigue tests between 20-800 C, establishing residual strain change patterns as function of stress and temperature
10 p1906 A70-25294
- Macroscopic internal stresses in plastics surfaces, discussing stress effect on plastic moulding service life, Knoop hardness test and charts
11 p2132 A70-25597
- Continually changing residual stress patterns effect defined for predicting cumulative damage in structural fatigue
11 p2137 A70-26090
- Residual macrostress measurement by X ray diffractometer methods
11 p2058 A70-26839
- Residual stresses levels in glass fiber reinforced plastic components after production by compression or winding
12 p2325 A70-27534
- Residual stresses in cylindrical shell made of two component solid solution under thermal diffusion
12 p2329 A70-28323
- Residual stress determination in flat strip elastically deformed by finite bending
13 p2508 A70-28485

- Internal stresses in transfer molding of electronic modules by photoelastic technique, discussing component failure 13 p2420 A70-29254
- Nonaggressive liquid media effect on residual strains and phase transformations initiation and development in polyurethane parts operating in lubricants, discussing wear resistance 13 p2439 A70-29431
- Li positive ions in KCl crystals, investigating internal strains effect on piezoelectric resonance spectra 14 p2626 A70-30340
- Residual stress measurement in anodic film on duraluminum as function of film thickness and cyclic loadings in air and corrosive media 15 p2757 A70-31635
- Residual stresses near weld in spherical rocket motor casing constructed from maraging steel sheet, discussing moire measurement and reduction treatments 15 p2744 A70-31926
- Pure iron and low carbon steel macroscopic stress measurements, determining correlation between residual stress, fatigue damage and fatigue life 15 p2759 A70-32322
- Glass bead blast induced residual stress and surface cold work effects on Ni base superalloy fatigue crack initiation and propagation 15 p2761 A70-32381
- Thermoelectric power measurement of thin Au films, relating results to transport parameters and internal stresses 15 p2785 A70-32582
- Phenomenological theory of transient high temperature creep, considering internal back stress 15 p2763 A70-32809
- Steady state high temperature creep theory, including internal back stress and temperature dependencies 15 p2763 A70-32810
- Weld cracks in welded joints of Ni-Cr base alloys due to residual stresses during aging, recommending annealing for prevention 16 p2930 A70-33051
- Residual stress concentration at fatigue crack tip, using oscillating crystal X ray microbeam diffraction photographic method 17 p3183 A70-34652
- Microscopic residual stress in crystals at fatigue crack tip in notched specimen in terms of flow stress and dislocation density 17 p3183 A70-34653
- Graphite-epoxy resin cross-ply composites fabrication, analyzing residual thermal stresses role in cracking [ASME PAPER 70-GT-84] 18 p3279 A70-36828
- Thermal expansion anisotropy in graphite-epoxy composites causing residual stresses [ASME PAPER 70-GT-129] 18 p3279 A70-36855
- Residual stress of electrodeless nickel deposits on beryllium from bow deformation measurements, noting role of phosphorus content 19 p3451 A70-37708
- Internal residual stress relaxation theory in dielectric aging in tetragonal solid solutions of calcium titanate in barium titanate 19 p3486 A70-37776
- Composite body with free surface under plane deformation, analyzing residual, thermal and dislocation stresses dependence on elastic constants 19 p3544 A70-38332
- Light alloys cold hardening effect and fatigue strength estimation, considering residual stress variability with time 19 p3548 A70-38457
- Bcc metals and alloys stress relaxation, internal stress and work hardening, discussing temperature dependence and dislocation motion 20 p3647 A70-39108
- Interaction between boundary layer and internal stressed state of thin elastic shell by formulating two dimensional linear theory 20 p3719 A70-39378
- Atmospheric environment effect on residual shear stress corrosion cracking of commercial Al-Zn-Mg alloys subjected to heat treatment regimes 22 p4052 A70-42307
- Mechanical properties and internal stress fields in composite materials reinforced by glass fibrous filler under transverse shear 22 p4061 A70-43724
- Bcc metals, measuring correlation between residual stress level and fatigue damage by X ray diffraction analysis 23 p4207 A70-44422
- Residual stress measurement using programmed horizontal X ray diffractometer 24 p4425 A70-45729
- RESIDUES**
- Difference set D of k distinct residues, extending Hall search with negative results, discussing multipliers, polynomial congruence, etc 01 p0132 A70-11073
- RESILIENCE**
- Resilience coefficient of intermediate elements of threaded connection related to transverse and axial nut dimensions by least squares method 05 p0856 A70-17012
- Polyurethane adhesives differential thermal analysis, rebound resilience and tensile properties at cryogenic temperatures 21 p3844 A70-42141
- Resilience and tensile properties of polyurethane adhesive at cryogenic temperatures measured by differential thermal analysis 23 p4209 A70-44275
- RESIN BONDING**
- Polybenzimidazole (PBI)/resin-bonded solid film lubricants composed of molybdenum disulfide, antimony trioxide and PBI resins [ASME PAPER 69-LUB-15] 01 p0101 A70-10390
- Load, speed and coating thickness effect on near life of resin bonded solid lubricant, using oscillating motion and low pressure blocks [ASLE PREPRINT 69-AM-5C-3] 01 p0103 A70-10447
- Graphite fiber-epoxy resin composites interfacial bonding, describing various surface treatments for increased interlaminar shear strength 01 p0127 A70-10477
- Water effect on glass fiber-resin bonds in interphase region, discussing initial stiffening and long term effects 01 p0127 A70-10484
- Resin bonding material suitable for IR detectors noting transmission properties 02 p0321 A70-11926
- Particle, resin and inorganic bonding of solid lubricant to surface and dry lubricant film performance 05 p0855 A70-16043
- Bonding and sealing of fluid amplifiers with epoxy resin dry-film adhesive, noting low rejects rate 12 p2164 A70-27075
- Fluid urethane laminating resin for bonding nylon and glass fabrics, giving physical properties as function of room temperature curing time 16 p2938 A70-33381
- Conducting epoxy shielding and bonding efficiency and bulk resistivity at high frequencies for bonding cover onto compartmentalized module 23 p4170 A70-43866
- RESINS**
- NT ACRYLIC RESINS
- NT EPOXY RESINS
- NT ION EXCHANGE RESINS
- NT NYLON [TRADEMARK]
- NT PHENOLIC RESINS
- NT POLYAMIDE RESINS
- NT POLYESTER RESINS
- NT POLYETHER RESINS
- NT POLYIMIDE RESINS
- NT POLYMETHYL METHACRYLATE
- NT POLYURETHANE RESINS
- NT SYNTHETIC RESINS
- NT THERMOPLASTIC RESINS
- NT THERMOSETTING RESINS
- Planar reinforced plastic resins strength and stiffness, considering mechanics of film, flake and ribbon reinforcements 13 p2438 A70-29206
- Resin systems for encapsulation of microelectronic packages, using thermal expansion dilatometer and gravimetric and differential analyses 13 p2439 A70-29258
- Filament winding reinforcement and resin noting production equipment and costs 15 p2744 A70-31932
- Resinous compounds content determination in jet fuels using ice cold acetic acid for desorbent to improve accuracy 16 p2961 A70-33203
- Microelectronic packages encapsulation by resin systems with emphasis on thermal expansion, discussing effects of curing temperature, reactive diluents, etc 20 p3655 A70-39444
- High temperature organic resin binders and solid lubricant thermal and oxidative behavior examined by thermogravimetric analysis [ASME PAPER 70-HT-30] 22 p4058 A70-42436
- Solidified polyglycol maleinate resin optical and mechanical properties under tensile stress creep, using hereditary photoelasticity 22 p4121 A70-43723
- RESISTANCE**
- Input conductance variation for common-emitter triode distributed-gain wideband amplifier, deriving energy equations improving tube characteristics 08 p1472 A70-20862
- Microwave conductance tensor in crystals with non-parabolic carrier energy dissipation under crossed constant electric and magnetic fields 12 p2288 A70-28326
- Ultrahigh precision microminiature bearing resistance moment measurement with inductive sensors 18 p3264 A70-37069
- RESISTANCE COEFFICIENTS**
- U COEFFICIENTS
- U RESISTANCE**
- RESISTANCE HEATING**
- Heat transmission by current carriers to cryogenic region, ascribing heat flux to Joule effect in conductor 05 p0881 A70-16025
- Aircraft skin heating by lightning, discussing possibility of exceeding jet fuel vapor ignition temperature 07 p1195 A70-20402
- Metals thermal conductivity at high temperatures determined by direct electrical heating method, considering specimen geometry effects on radiation losses 08 p1497 A70-21526
- Fluidic curved-wall electropneumatic converter optimization, presenting steady state, step and pulse mode responses for various positions and lengths of resistive heaters 09 p1614 A70-23691
- Heating rate of radio electronic equipment with variable power shown dependent on initial dissipated power 10 p1853 A70-25134
- Ionosphere dynamo region thermal input by Joule heating and solar radiation and coupling to various thermotidal modes, observing semidiurnal and semianual effects 11 p2047 A70-26569
- Infrasonic waves generated by pulsating aurora, using Joule heating and Lorentz force coupling 13 p3399 A70-29236
- Flat plate and cylinder with periodic Joulian heating from time dependent heat source, analyzing transient temperature distribution 14 p2664 A70-30269
- Heating rate effect on parameters of resistance wire strain gages subjected to temperature gradients 15 p2733 A70-31536
- Graphite Shore hardness measurement at high temperature on Joule heated specimens, describing apparatus and procedure 15 p2764 A70-31944
- Metal matrix composite resistance spot welding, discussing value of nondestructive tests 17 p3100 A70-34636
- Compressible plasma axisymmetric channel flow under electromagnetic forces and ohmic heating, noting velocity profiles and current density [AIAA PAPER 70-1098] 20 p3683 A70-40239
- Direct electrical heating for high temperature thermal conductivity measurements of pure W, giving results for graphite 21 p3850 A70-42057
- Compressible plasma flow in axisymmetric channels under EM body forces and Joule heating 23 p4228 A70-44934
- RESISTANCE THERMOMETERS**
- Constant temperature hot-wire anemometer to compensate for thermal lag of wire/film resistance thermometer within useful frequency range 03 p0492 A70-13761
- Atmospheric wind velocity and temperature oscillations measurement using acoustic anemometer, resistance thermometer and multichannel signal spectrum analyzer 07 p1284 A70-19833
- Measurement physics of resistance wire temperature sensing system used in Skua rocket sounding system 07 p1396 A70-20262
- Transient heat flux measurement with surface thermocouples, thin film resistance thermometers and mathematical computation programs 11 p2065 A70-25768
- Electric temperature sensors accuracy and stability, considering thermocouples, resistance thermometry, radiation and color pyrometry 15 p2743 A70-32798
- Cryogenic temperature measurement including metallic and semiconductor resistance thermometers, thermocouples and bibliography 17 p3082 A70-34740
- Time constants of low inertia resistance thermometers by heating with alternating AC and DC currents 19 p3420 A70-37263
- Thermocouples and resistance thermometers comparison for low temperature measurements 19 p3432 A70-38703
- Pt resistance thermometers for low temperature measurements, discussing structural and mechanical characteristics 19 p3432 A70-38704
- Heat conduction errors in immersion thermocouples and resistance temperature sensors, using mathematical model 21 p3823 A70-40856
- In thin film resistance thermometers fabrication by vapor deposition in vacuum, considering electrical properties dependence on temperature 22 p4039 A70-43446
- RESISTIVITY**
- U ELECTRICAL RESISTIVITY**
- RESISTOJET ENGINES**
- Chemical engineering problems of resistojets, pulsed plasma, ion bombardment and colloid thrusters 01 p0166 A70-10974

Electric thrusters for putting communications satellite into synchronous orbit analyzed for mission performance, finding hydrogen resistojets as attractive compromise between payload and transfer time

05 p0897 A70-16899

Resistojet design criteria for performance modeling of ammonia propellant thrusters and manned space stations using biowaste propellants

[AIAA PAPER 70-211] 06 p1131 A70-18026

Long term life test and vacuum tests of high temperature resistojets using ammonia and hydrogen propellants

[AIAA PAPER 70-1136] 20 p3567 A70-40212

Parameterized design data and selection criteria of biowaste resistojets for orbit keeping and control moment gyro desaturation of manned space station

[AIAA PAPER 70-1132] 20 p3567 A70-40213

Environmental control-life support systems /ECLSS/ waste methane gas utilization in low thrust resistojets for manned space applications

[AIAA PAPER 70-1131] 20 p3568 A70-40214

Integrated environmental control-life support resistojets systems, surveying NASA programs

[AIAA PAPER 70-1130] 20 p3690 A70-40215

Communication satellites low thrust transfer to synchronous orbit by two-stage operation using hydrogen resistojets and Hg ion motors

[AIAA PAPER 70-1116] 20 p3691 A70-40227

Concentric tube resistojets life tested on hydrogen and ammonia propellants for use with biowaste propellants

[AIAA PAPER 70-1133] 20 p3568 A70-40521

Resistojet thrusters for spacecraft propulsion and control, discussing systems configurations, performance, weight, etc

21 p3866 A70-40986

Thermal efficiency of ceramic and metal heat exchangers for biowaste resistojets thrusters

[AIAA PAPER 70-1135] 21 p3868 A70-41779

Low thrust trajectory transfer from low to synchronous orbit, examining hydrogen resistance jet and mercury bombardment ion thruster

22 p4089 A70-42487

High temperature acceleration of propellants in electrothermal thrusters including resistojets, arcjet, thermionic and plasma configurations

22 p4091 A70-42763

RESISTOJETS

U RESISTOJET ENGINES

RESISTORS

NT POTENTIOMETERS (RESISTORS)

NT THERMISTORS

Three way power divider/summer fabricated symmetrically in stripline by resistive network transformation

05 p0821 A70-16386

Tin oxide film resistors reliability test based on measurement of resistance nonlinearity by third harmonic voltage

09 p1689 A70-22005

Evanohm alloy resistance wire for applications in magnetic field, illustrating percentage change at 4.2 K

09 p1679 A70-22998

Optoelectronic devices for variable resistors controlled by electrical signal, investigating decoupling, capacitance and DC resistance

09 p1649 A70-23353

Carbon composition resistors investigated for cause of resistance dependence on thermal pulses, suggesting application as stabilization process

10 p1849 A70-24617

Evaporated Au-Ni-Cr alloy resistor films physical and electrical characteristics, noting dependence on composition

14 p2625 A70-30285

Nonlinear resistance element with square law I-V characteristics for electrical analogs of hydraulic systems

19 p3359 A70-38707

Electric resistance adjustment of thick and thin film resistors on ceramic substrate, using laser for material evaporation

20 p3640 A70-39416

Traveling wave antenna arrays with resistance elements for coupling, measuring noise elimination capabilities

20 p3598 A70-40146

Carbon resistors negative magnetoresistance measurement near absolute zero temperature by helium cryostat, noting anisotropy

20 p3687 A70-40168

Cryogenic fluid multipoint level sensing detector circuit using carbon resistors

24 p4339 A70-46200

RESOLUTION

NT ANGULAR RESOLUTION

NT HIGH RESOLUTION

NT RADAR RESOLUTION

Phased array antennas bandwidth and range resolution, discussing delay elements and antenna size affecting radiation patterns

01 p0042 A70-10262

CRT resolution measurements by double slit method, relating light spot response to slit width

01 p0093 A70-11278

Scinticamera resolving power in radioactivity measurements, discussing mathematical principle of division of radioisotope concentration in biological experiments

01 p0040 A70-11404

Photointerpreters information extraction, studying psychological effects of image contrast and resolution on accuracy of target detection

02 p0300 A70-12459

Threshold visibility of uniformly moving colored gratings, noting chromaticity discrimination dependence on spatial and temporal frequencies

02 p0237 A70-12460

Photoobjective and camera resolution tests regarding entire frame using two dimensional azimuth mark

05 p0852 A70-16864

Telescope resolution limit dependence on refractive index mean square fluctuation and effective aperture in turbulent medium

06 p1067 A70-18396

Spatial resolution and repetition intervals for optimum utilization of space-derived remotely sensed data of ocean surface features

06 p1060 A70-18593

Resolution, contrast and gray scale performance of CRT displays compared to dot matrix displays

08 p1500 A70-21763

Satellite remote sensors for oceanographic applications, estimating resolution requirements for temperature, spatial interval, roughness patterns, wind speeds, etc

[AIAA PAPER 70-306] 09 p1668 A70-22880

Photoemission analyzer with finite emitter in spherically symmetric retarding field with magnetic field present, analyzing energy resolution

09 p1679 A70-22988

Airborne camera resolution degradations/window losses/ introduced by multiglazing wedge, irregularity and structural deformation

09 p1687 A70-23767

Instrument localizing-resolving powers relationship as function of luminous source coherence

10 p1898 A70-23911

Channel electron multipliers design and operation, investigating parameters influencing amplification, resolving power and response probability

10 p1888 A70-24484

Hologram resolution and information storage along depth of reconstructed image related to maximum track density of bubble chamber

10 p1892 A70-25113

Real time 2000 line TV camera with 40 MHz bandwidth, 1600 line vertical resolution and 1000 line horizontal resolution

[SMPTE PAPER 105-73] 12 p2235 A70-27663

Microwave holography with artificial reference wave and receiver multiplier, improving linear resolution in image

13 p2408 A70-29407

Noise level influence on optimal recognition of nonstationary random processes in white noise

13 p2369 A70-29729

Statistical estimation of resolvability of incoherently radiating object sampled at aperture field of observing optical instrument, using Cramer-Rao inequality

13 p2453 A70-29823

Speckle patterns Fourier transform analysis for diffraction limited resolution attainment in large telescopes

14 p2589 A70-31382

Three dimensional holographic optical imaging system, examining resolution factors

15 p2734 A70-31595

Retention times and gas chromatographic conditions for resolution of galactonic and gluconic acid derivatives

16 p2855 A70-33064

Recording instrumental noise resolution of standard algorithm for cosmic ray stations

18 p3307 A70-36100

Photographic images formation mechanism, examining streaks resolving power and total densities

20 p3632 A70-39747

Photographic materials resolving power for lines and points

20 p3633 A70-39750

Coherent beam propagation through turbulent atmosphere, discussing limiting resolving power due to random fluctuations of refractive index

22 p4072 A70-42290

Three dimensional holographic optical imaging system, examining resolution factors

23 p4195 A70-44279

Ground temperature effects on thermal gradients resolution in IR line scan imagery

24 p4334 A70-45363

Image forming performance in photographic system design, considering Cobb chart resolution as figure of merit

24 p4334 A70-45449

Cobb chart resolution in photographic system including independent sources of image spread and single source of granularity

24 p4334 A70-45450

RESOLVENTS

U PROBLEM SOLVING

RESOLVING POWER

U RESOLUTION

RESONANCE

NT CYCLOTRON RESONANCE

NT ELECTRON

RESONANCE

NT FERROMAGNETIC RESONANCE

NT MAGNETIC RESONANCE

NT MAGNETOSONIC RESONANCE

NT MICROWAVE RESONANCE

NT NUCLEAR MAGNETIC RESONANCE

NT OPTICAL RESONANCE

NT PARAMAGNETIC RESONANCE

NT PLASMA RESONANCE

NT PROTON MAGNETIC RESONANCE

NT PROTON RESONANCE

NT RESONANT VIBRATION

NT SPIN RESONANCE

Critique of double resonance theory in gaseous lasers, including correction regarding saturation parameter for small RF perturbations and line width dependence

01 p0109 A70-10432

Ultraharmonic resonance excited by centrifugal force in system with Duffing restoring force characteristic using Ritz method

05 p0925 A70-15886

Critique of solar system resonant structure hypothesis based on planetary orbital frequencies errors

05 p0910 A70-16394

Critique of resonant structure of solar system noting chance effects possibility

05 p0910 A70-16395

Rebuttal of criticisms on resonant structure hypothesis, giving probability value for chance stellar system formation similar to solar system

05 p0910 A70-16396

Solar system resonant structure probability analyzed by matrix methods

05 p0910 A70-16397

Resonance in restricted three body problem applied to asteroidal motion in asteroid-Jupiter-sun system

06 p1152 A70-18492

Ritz method applied to second order nonlinear differential-difference equations subjected to sinusoidal driving functions, studying stability criteria and resonance properties

07 p1327 A70-20023

Singly ionized Mg resonance lines electron impact broadening quantum mechanical calculation

09 p1732 A70-22827

Nonlinear oscillations averaging method applied to resonant interactions of acoustic gravity waves

09 p1729 A70-23666

Periodic orbits for reduced problem of conservative Hamiltonian system with two degrees of freedom, discussing emergence from resonant equilibrium

10 p1939 A70-24187

Thermoelectric power and Hall effect quantum resonances in pressure annealed pyrolytic graphite crystals for carrier locations evidence

11 p2097 A70-25616

Fermi triplet resonance between fundamental molecular vibrations possible in presence of harmonic or composite tone of same symmetry

12 p2275 A70-27502

Finned configurations with nonlinear aerodynamic properties, obtaining solutions for angular motion at and near resonance

[AIAA PAPER 70-535] 13 p2506 A70-29026

Parametric resonances at zero field crossing levels of optically pumped atoms on alkali vapors, noting applications to weak magnetic measurements

13 p2456 A70-30034

Crossing level resonances of magnetometer in optically pumped Rb87 atoms applied to weak field measurement

13 p2454 A70-30035

Li positive ions in KCl crystals, investigating internal strains effect on paraelectric resonance spectra

14 p2626 A70-30340

Resonance ignition technique for gaseous oxygen and hydrogen rocket propellants

14 p2627 A70-30776

Monograph on nonlinear oscillation equations resonance solutions and solution stability, considering Green matrix, differential equations reduction to integrodifferential equations, etc

14 p2618 A70-31417

Diffraction grating systems resonance properties, obtaining transcendental equations for natural slow wave and radiation modes

19 p3377 A70-37717

Interstellar molecular H Lyman resonance-absorption bands in far UV spectrum using rocket observation

20 p3701 A70-39002

Resonant and nonresonant satellite eccentric orbits for determination of high order terms in geopotential 20 p3709 A70-40073
Boundary layer problems with resonance solved by matched asymptotic expansions and WKBJ method 23 p4179 A70-43945

RESONANCE CHARGE EXCHANGE

Proton-deuteron elastic large angle scattering cross sections, noting backward peak consistent with baryon exchange mechanism with resonance transfer 07 p1345 A70-20198
Low energy proton-hydrogen collisions, computing differential cross sections for direct elastic scattering, resonant charge exchange and direct and exchange excitation 24 p4382 A70-46226

RESONANCE PROBES

High temperature thermometer using pulsed excitation ultrasonic resonance with ruthenium sensor, discussing resonator types, transmission lines and transducer 02 p0300 A70-12468
Electron temperature resonance probe to eliminate effects of geomagnetic field, rocket velocity and random noise 09 p1675 A70-22422
Inductive effect in C-Cl chemical bonds in chloroalkenes, using nuclear quadrupole resonance frequencies shifts 09 p1630 A70-22903
Ionospheric plasma lower hybrid resonance measurement and excitation via rocket-borne probe 09 p1670 A70-23319
High sensitivity conditions for rapid electronic spin resonance magnetometer 13 p2415 A70-30049
Planar resonance probe in free molecular arc heated flowing plasma, examining shift nature in measured frequency position of minimum drawn current 22 p4081 A70-43013

RESONANCE SCATTERING

Resonance scattering and drift motion of electrons in gases under pressure, determining ion state lifetime and mean electron-molecule collision frequency for trapping collisions 02 p0342 A70-11883
Rotational compound state resonances in subthreshold atom-diatom scattering determined for lowest state molecular hydrogen and deuterium model systems scattered by Xe 03 p0526 A70-13006
Dielectronic recombination rate coefficient determined by quantum theory of resonance-collision processes, considering coupling, degeneracy and overlapping resonances 05 p0920 A70-16943
Geocoronal glow as resonant scattering of solar Lyman-alpha-radiation by H atoms in upper atmosphere 07 p1270 A70-20032
Resonant and foreign gas broadening using Schrodinger equations for collision problems 07 p1346 A70-20244
Scattering matrix for resonance lines with arbitrary level splitting in magnetic field 09 p1753 A70-22452
Resonance energy calculation and transmission coefficient estimate for quantum mechanical model of reactive scattering of three atoms in line 10 p1920 A70-25145
Resonance energies of elastic scattering from one dimensional model potential containing barrier, using stabilization method 13 p2455 A70-29222
Dipolar resonant scattering of H-polarized plane waves by axially magnetized plasma column with perfectly conducting core 23 p4228 A70-44977
Level relaxation constants measurements by three-level laser spectroscopy, using line shape of stimulated shifted resonance scattering in gas 24 p4354 A70-45821

RESONANCE TESTING

Tuned resonant test for measuring damping characteristics of lead and asbestos filled epoxy-polysulfide copolymer 08 p1527 A70-21336
HF shaker for accelerometer calibration and resonance evaluation, discussing construction materials, accuracy and test results 16 p2889 A70-34021
Data acquisition and processing in structural modal characteristics analysis during ground resonance tests [ICAS PAPER 70-36] 23 p4267 A70-44133
Wall thickness measurement by supersonic testing method based on resonance 24 p4336 A70-45681
Thickness measurement and internal defects inspection by ultrasonic resonance technique 24 p4343 A70-45683

RESONANT FREQUENCIES

Vibration frequencies and modal shapes for square and rhombic cantilever plates with diamond cross section, including commercial resonance test system 01 p0199 A70-10122
Linear physical chains with Sturm-Liouville characteristic polynomials used for natural frequency determination of coupled harmonic oscillators or electrical analog 01 p0142 A70-10520
Gaseous He bubbles injection into liquid propellant launch vehicle fuel lines to reduce vehicle pogo oscillations by lowering feed system natural frequencies 01 p0196 A70-10851
Optimal structural design including service requirements on strength, buckling and natural frequency stated as optimal control problem 01 p0207 A70-11158
Plates and shells natural oscillations frequencies and modes, analyzing variational, asymptotic and numerical methods 01 p0210 A70-11412
Natural oscillation frequencies of closed circular orthotropic cylindrical shells having freely supported end faces, particularly with stringers 01 p0210 A70-11413
Finite element method for calculating natural frequencies and mode shapes of pretwisted cantilever plates assembly of flat triangular elements 02 p0384 A70-11859
Field patterns of thin resonant and nonresonant antennas in warm plasma, using digital computer to evaluate propagation constant for current distribution 02 p0263 A70-12655
Natural mode shapes of longitudinal oscillations and resonant frequencies of thin rods of constant curvature and rings with slit, noting use for crack determination 03 p0588 A70-13283
Natural oscillation frequencies of partially liquid-filled cylindrical shells determined by resonance method 03 p0592 A70-13444
Natural oscillation frequencies lower bounds of orthotropic plates determined as coupled elastic systems 03 p0592 A70-13451
Finite difference method applied to solving equations of motion for computing natural torsional vibration frequencies of pretwisted cantilever beams 03 p0595 A70-13811
Finite difference method for obtaining free vibrations natural frequencies and mode shapes for rectangular plates of varying stiffnesses 03 p0595 A70-13812
Natural frequency calculation accuracy for coupled beam bending vibrations shown dependent on connection stiffness determination 03 p0595 A70-13929
Large dielectric constant with small loss determined as function of frequency from resonant frequencies measurement 03 p0493 A70-14039
Sputter machining thickness reduction methods for VHF resonant piezoelectric transducers 03 p0496 A70-14207
Tonks-Dattner resonances peaks in rare gas plasmas, considering electron densities variations role 03 p0534 A70-14211
Aircraft structural weight optimization for given fundamental vibration frequency obtained by aeroelastic constraints 03 p0598 A70-14231
Frequency equation for flexural vibration of simply supported beam, considering tabular procedure for cantilever beam 03 p0602 A70-14330
Natural circular frequencies of small axisymmetric vibrations of shells of revolution of arbitrary shape, using Rutishauser algorithm for eigenvalues 04 p0767 A70-14525
Inhomogeneous plasma oscillations in counterstreaming plasmas analyzed for electric fields and resonant frequencies from Vlasov equation 04 p0726 A70-14671
Equivalent circuit for acoustoelectric oscillator providing practical device analog, discussing oscillation suppression and resonant frequency changes under reactive load 04 p0656 A70-14719
Lumped model formulated for dynamics of proportional fluidic amplifiers, describing flow visualization experiments for resonances and instabilities mechanisms [ASME PAPER 69-WA/FLCS-3] 04 p0627 A70-14848
Cyclic bending stress in disk type gyroscope rotor under steady precession, discussing solutions for modal functions and resonant frequencies [ASME PAPER 69-DE-A] 04 p0689 A70-14873
Resonant compression waves in geomagnetic tail estimated for frequency and spatial distribution by single layered two dimensional model 04 p0680 A70-15127

Nonlinear systems periodic oscillations with resonance from differential equations solutions 04 p0720 A70-15258
Circular sandwich plates fundamental natural frequencies, considering face members membrane characteristics and thickness, face and core isotropy, etc 04 p0778 A70-15559
Natural vibrational frequencies of trapezoidal, triangular, circular and elliptical isotropic flat plates with different edge conditions tabulated 05 p0936 A70-16319
Torsional vibrations of four cell tube, deriving cross sectional constants and natural frequencies 05 p0936 A70-16321
Resonance effects on satellite orbits due to tesseral harmonics in potential field 05 p0908 A70-16335
Natural frequencies upper and lower bounds of elastic clamped vibrating curved beams (arcs) determined on basis of differential operator theory 05 p0937 A70-16405
Eigenvalues upper and lower bounds of vibrating anisotropic material with multiple elastic constants, predicting free vibration frequencies by bounding isotropic moduli 05 p0937 A70-16408
Coupling between LF oscillations and third harmonic frequency resonances of bounded plasma capacitor system, discussing density profile variation 05 p0890 A70-16654
Magnetron amplifiers with ferrite circulators for synchronizing natural frequency, obtaining I-V characteristics and gain vs bandwidth curves 05 p0823 A70-16886
Ionospheric observations of resonance oscillations using satellite-borne radio sounding instruments 06 p1115 A70-17361
Apparent resonance frequencies of earth-ionosphere cavity excited by single dipole source, noting dependence on source-observer separation 06 p1058 A70-18414
Dynamic elastic modulus of graphites and composites measured as function of temperature using thin rod resonance method 06 p1070 A70-18447
VLF noise phenomena observed with satellite electric dipole antennas compared with lower hybrid resonance frequency of ionospheric medium in vicinity 06 p1011 A70-18534
Elastic bars self excited oscillations at audible frequencies, determining natural frequencies from analyzing sound 07 p1401 A70-18847
Vibrational overloads development in turboprop engines ascribed to natural vibrations mode shape frequency approaching rotor revolutions number 07 p1363 A70-19110
Complex elastic system coupled flexural vibrations resonant frequencies determined with allowance for friction 07 p1363 A70-19111
Parametric vibrations onset and resonance regions boundaries determined for feed line system with flexible compensator 07 p1403 A70-19114
Circular plates with optimal natural frequency of transverse vibrations, discussing boundary conditions 07 p1405 A70-19256
Size reduction and low noise temperature in receiving antennas obtained by transistor integration and resonance frequency modulation 07 p1241 A70-19353
Geomagnetic tail natural oscillations, studying magnetospheric substorms role 07 p1268 A70-19499
Torsional vibrations of nonhomogeneous anisotropic finite circular tube, computing natural frequencies for various parameters 07 p1414 A70-20173
Natural oscillation frequencies determined for shallow shells with hinged and clamped edges 08 p1583 A70-20484
Natural oscillation frequencies of three layer plates with rectangular planar form determined by integrated representations method 08 p1583 A70-20495
Boundary conditions effect on natural vibration frequencies of unloaded components and components loaded with concentrated masses, obtaining frequency equations 08 p1584 A70-20698
Resonant oscillations of coupled physical pendulums, investigating phase trajectories by Struble method 08 p1544 A70-20964
Periodic and almost periodic solutions to vibrations of quasi-linear nonautonomous systems in presence of resonance, determining principal amplitudes 08 p1544 A70-20966
Thin shells of revolution natural oscillation frequencies approximation based on shell subdivision into series of cylindrical shells 08 p1588 A70-21194

Boundary value contact problems in thermoelastic oscillations theory found to have unique solutions for any frequency

08 p1591 A70-21440

Eigenfrequencies of thin barrel shaped shells on simple supports, noting correspondence of ratio of radius to shell wall thickness

08 p1592 A70-21474

Natural frequencies and electromagnetic field distributions in rectilinear and cylindrical dielectric resonators used in microwave circuits

09 p1644 A70-22280

Multispan horizontally curved beams natural frequencies determination illustrated by developing frequency equation

09 p1770 A70-22388

Four point supported square plate fundamental frequency by finite difference and energy methods

09 p1770 A70-22389

Electromagnetic wave diffraction by sphere and spheroid at resonance frequencies with incident wavelength comparable to bodies dimensions

09 p1632 A70-22402

Free vibration of rib stiffened freely supported circular cylindrical shells, verifying rib eccentricity importance to natural frequencies by numerical solutions

09 p1780 A70-23211

Natural bending vibrations of circular plates with allowance for stress tensor asymmetry, deriving transcendental frequency equation

09 p1782 A70-23292

Vibration decrement of nonlinear elastic system from resonance peak width of displacement amplitude curve of perturbing force

09 p1782 A70-23295

Centrifugal forces and nonuniform heating effect on natural vibration frequencies of circular plates using lumped parameter method

09 p1784 A70-23588

Sectorial and circular strip resonators natural oscillation modes and freely propagating waves of uniformly bent stripline

09 p1651 A70-23644

Neodymium glass laser fundamental frequency spatial structure effects on KDP crystal second harmonic generation efficiency, describing optimal system for laser beam shaping

10 p1899 A70-24262

Uniform beams flexural vibration natural frequencies approximate calculation showing effect of shear flexibility and rotary inertia

10 p1959 A70-24562

Shell dynamics equations role in natural frequencies, determining dynamic response with damping allowance

10 p1960 A70-25052

Natural frequencies and mode shapes of vibrating shells and shell combinations determined using variational finite difference method in conjunction with Hamilton principle

10 p1961 A70-25056

Equations of motion, modal vectors and natural frequencies of n-degree of freedom structurally damped linear system determined directly from test data

10 p1961 A70-25058

Undamped natural modes intercoupling resulting from arbitrary linear damping addition to linear dynamic system

10 p1962 A70-25061

Natural frequency of paramagnetic amplifier retuned by coupling Cr ions doped silver coated ruby resonator to passive resonator

10 p1901 A70-25138

Thin elastic plates and shells parametric resonance amplitudes by solving nonlinear differential equations, considering dynamic stability

11 p2129 A70-25523

Gas effect on natural frequency of electrostatically excited string vibrating between flat electrodes at medium pressures

11 p2048 A70-25582

Inplane and rotary inertia effects on free vibration frequencies of circular cylindrical shells eccentrically stiffened by orthogonal set of stringers and/or rings

11 p2135 A70-25993

Resonant frequencies and Young/shear moduli of unidirectional graphite epoxy composite beams under high modes of vibration

11 p2136 A70-26082

Device for measuring turbine blades natural frequencies by converting vibrations to electric current at same frequency

11 p2033 A70-26443

Thin rectangular plates transverse natural frequencies, deriving equations of motion and boundary conditions in bending moment terms by vibrational principle

11 p2143 A70-26645

Natural frequencies of thin cantilever cylindrical shells, using Flugge equations of motion and Rayleigh-Ritz method

11 p2146 A70-26704

Elastic moduli and damping coefficients for glass and boron-epoxy beams determined from resonant

frequencies and bandwidths during lateral forced vibrations

12 p2253 A70-27120

Limited frequency range analytical model for predicting mass and stiffness changes effect on natural frequencies and normal modes

12 p2317 A70-27121

Three dimensional variational dynamic and static large deformation equations solutions for stability and natural frequencies and wave propagation in bodies under initial strains

12 p2322 A70-27331

Elastic beam vibration under constant amplitude and varying frequency periodic forces during passage through resonance

12 p2326 A70-27798

Free elastic rotating beam with tip masses and inertia, developing solutions for flexible modes and natural frequencies of H-type configuration

12 p2273 A70-27820

Nonlocalized ultrasonic defectoscopy resonance method for qualitative difference determination of small sized articles of complex form

13 p2417 A70-28662

Hydroelastic oscillations natural frequencies in incompressible and nonviscous liquid in circular cylinder with free surface, demonstrating wall elasticity effects

13 p2512 A70-28832

Initial thermal stresses effect on natural oscillation frequencies of thin cylindrical elastic shells, obtaining linearized equations of motion and boundary conditions

13 p2514 A70-29286

Electromagnetic energy propagation through absorbing single resonant frequency dielectric, deriving transport velocity and relaxation time

13 p2452 A70-29464

Laminated composite materials dynamic elastic properties, outlining resonant frequency effect on apparent Young modulus

13 p2515 A70-29467

Perpendicular propagation of VLF waves from wave/particle interaction in vicinity of lower hybrid resonance frequency in magnetosphere

13 p2468 A70-29934

GaAs epitaxial layered wafer natural CW R band oscillations in LSA mode

14 p2550 A70-30688

Dynamic stiffness, natural frequencies and mode shapes of prismatic and thin walled open grids, including warping and shear flange deformation

14 p2659 A70-31132

Numerical method for roots of algebraic equations, computing continuous beam lateral vibrations natural frequencies

14 p2600 A70-31330

Nutation damper for dual-spin spacecraft, considering various two degree of freedom systems with two natural frequencies

14 p2655 A70-31367

Natural vibrations frequency of tubular cantilever pipe with fluid flow, solving differential equation of motion by Ritz method

14 p2567 A70-31426

Natural oscillation frequencies in rectangular shallow shells weakened by cuts, using summary representations method for eigenvalues determination

15 p2814 A70-31585

Natural oscillation frequencies of shallow shells with mixed boundary conditions on clamped edges, using summary representations method

15 p2814 A70-31590

Earth-ionosphere cavity resonances diurnal variations by considering different propagation characteristics of day and night hemispheres

15 p2728 A70-31910

Complex plates free transverse oscillation modes and frequencies using Ritz method

15 p2818 A70-32183

Geomagnetic tail natural oscillations, studying magnetospheric substorms role

15 p2732 A70-32744

Clamped skew plates influence coefficients, natural vibration frequencies and nodal patterns measurement, comparing to Galerkin method results

16 p2988 A70-33124

Optimal design of structures with constraints on strength and natural frequency, developing steepest descent boundary value method

16 p2991 A70-33854

Embedded damped sandwich beams, determining equations for resonant frequency, loss factor and modal roots

16 p2992 A70-34018

Free oscillations of Euler-Bernoulli and Timoshenko cantilever beams of variable cross section, obtaining approximate modes and natural frequencies bounds

16 p2994 A70-34234

Statistically indeterminate Timoshenko beams oscillations natural frequencies and modes by lumping properties of linear and rotary inertia at discrete points

16 p2994 A70-34235

Linear and nonlinear systems natural frequency and stability determination, using theorems for degenerate systems

16 p2944 A70-34284

Time-average holographic interferometry applied to HF transverse vibrations of uniform cantilever beam, noting correlation with Timoshenko beam theory

17 p3083 A70-34961

Natural frequencies and corresponding mode shapes for free flexural vibrations of circular plates, extending to elastic support cases

17 p3186 A70-34980

Accelerometer installation resonant frequency, discussing mounting methods, structure material, geometry and total mass

17 p3089 A70-35174

Laser emission intensity oscillations during resonator Q sinusoidal variations

18 p3267 A70-36617

Gravitational field effect on natural frequencies of rotating ring laser, using general relativity and electromagnetic fields theories in continuous media

18 p3267 A70-36622

Microwave self modulating GaAs diode laser, showing coupled external cavity resonator influence on intrinsic resonance frequency

18 p3269 A70-36733

Plane galactic orbits near spiral field particle resonance, calculating numerically for ring orbits librating near maxima at Lagrangian points

18 p3331 A70-37193

Rib stiffened elliptical and circular plate vibrations, determining fundamental frequencies by variational techniques

19 p3536 A70-37693

Diffraction grating systems resonance properties, obtaining transcendental equations for natural slow wave and radiation modes

19 p3377 A70-37717

Diffraction radiation excitation by electron beam moving within resonant system formed by ribbon grating and metal plane, taking into account screen conduction losses

19 p3377 A70-37724

Coupled open plane resonators system self oscillation intrinsic frequencies solution by numerical method, obtaining algorithm for characteristic equation roots

19 p3387 A70-37737

Transmitter-antenna matching, using Pi-filter for resonance transformation

19 p3389 A70-38071

HF ballistocardiograms resonance distortions correction, using electrical selective filters

19 p3369 A70-38210

Solid state, digital, Resonant Capsule Pressure Transducer based on natural frequency variation of aneroid capsules by pressure induced curvature changes

19 p3430 A70-38520

Sound vibrations resonant frequency relation to jet internal structure in gas jet stem radiator

19 p3354 A70-38658

Gunn effect devices with concentric cylindrical electrodes, examining oscillation natural frequency-applied voltage relation

19 p3392 A70-38900

Resonance radiation transport in optically thick media, investigating complete frequency redistribution mathematical assumption

20 p3671 A70-39021

Lower hybrid resonance frequency propagation ducts in multilayer open ionosphere, showing association with VLF hiss bands

20 p3584 A70-39331

Resonant oscillations of coupled physical pendulums, investigating phase trajectories by Struble method

20 p3672 A70-39386

Ulnar resonant frequency reproducibility as objective measure of skeletal status, discussing forearm and hand positioning effect

20 p3579 A70-39432

Time and power dependent Lamb shift resonance shapes measurement with circular polarized RF field in beam foil excited H atoms

20 p3675 A70-39498

Pretwisted slender beam coupled torsional and longitudinal vibrations under centrifugal force field, obtaining resonant frequency by Rayleigh Quotient method

20 p3719 A70-39601

Liquid fuel behavior in right circular cylindrical tank inclined to earth gravitational field, computing fundamental sloshing frequency

20 p3610 A70-39694

Microwave apparatus for resonant frequency change and loaded resonator Q measurement during DC discharge afterglow electron removal studies

20 p3679 A70-39715

Electro-optical crystal resonator loss anisotropy, determining natural frequencies and polarizations

20 p3642 A70-39755

Low speed air-propane flame stability, examining holder diameter effects on vibration cutoff wavelength 20 p3738 A70-40281

Natural flexural vibration frequencies of bars with periodic thickness variations, comparing Hamilton principle, matrix approach and experimental investigations 20 p3735 A70-40536

Active bandpass filter configurations with operational amplifiers, noting resonance frequency and Q factor variation relationship to amplifier gain-bandwidth product 21 p3796 A70-40561

Linearly elastic skeletal structures, calculating natural frequencies of undamped vibration by computer program 21 p3935 A70-41254

Tethered parachutes vibration modes, determining fundamental frequencies from canopy/lines mass ratio and materials elastic properties [AIAA PAPER 70-1169] 21 p3755 A70-41844

Transfer function optimization for linear follow-up frequency filter with controlled resonance, analyzing noise band performance 22 p3985 A70-42402

Multifrequency autooscillatory systems, comparing reflex klystron with He-Ne laser 22 p3995 A70-42404

Linear elastomechanical systems natural vibration parameters by harmonic excitation method 22 p4116 A70-43200

Laser radiation hyper Raman scattering intensity enhancement via resonance processes, using density matrix method 22 p4075 A70-43233

Automatic frequency control device for power klystron with two cavities, obtaining stabilization at natural frequency of crystal-containing cavity 22 p3998 A70-43236

Electronic damped plasma oscillations eigenfrequency in presence of external electric field 22 p4082 A70-43253

Cross ply laminated plates natural frequencies, approximating flexural vibration by classical theory 22 p4119 A70-43679

Resonant frequencies of microwave dielectric resonator in magnetic wall waveguide 23 p4169 A70-43784

Thin circular cylindrical shells with clamped-clamped and fixed-fixed edges, calculating natural frequencies of nonsymmetrical free vibrations 23 p4266 A70-43997

Frequency dependence of Gunn oscillator maximum negative conductance 23 p4172 A70-44198

Single-frequency oscillations mode in nonlinear catenary systems, considering factors promoting stabilization and uniformity 23 p4218 A70-44344

Automatic resonance tuning of transmitting and receiving antennas by electronic control for use in mobile communications 23 p4172 A70-44385

Iterative Rayleigh-Ritz method for eigenvalue determination in natural vibration problems 23 p4270 A70-44580

Cantilever plate random vibration response, calculating eigenvectors and natural frequencies by finite element method 23 p4270 A70-44591

Antiferromagnetic and ferrimagnetic resonance frequencies, determining temperature dependence by spin wave theory 24 p4388 A70-45132

Electromagnetic radiation propagation through resonant medium 24 p4378 A70-45260

Natural frequencies of elastic bodies with variable properties, using external forcing function and continued fractions approximation 24 p4422 A70-45295

Frequency equations derived for cylindrical panels with surface loading, comparing free vibration natural frequencies of panels with attached mass at centers 24 p4422 A70-45297

Elastic orthotropic plates vibration analysis by finite strip method via eigenvalue matrix, obtaining natural frequencies and modal vectors by small computer 24 p4423 A70-45579

Synchrotron source spectra natural frequency cut-off in absence of self absorption and electron energy cut-offs, discussing pulsar NP 0532 24 p4410 A70-45774

Coriolis acceleration effect on inplane vibration resonant frequencies of rotating disks 24 p4425 A70-45780

Ring-stiffened thin circular cylindrical shells, calculating free vibration natural frequencies and mode shapes by finite element method 24 p4427 A70-46067

Periodically supported beams and plates free vibration, calculating natural frequency spectrum distribution and normal modes 24 p4427 A70-46070

RESONANT VIBRATION

Natural oscillation modes two dimensional resonator determined in form of superimposed uniform plane waves with arbitrary coefficients of wave reflection 01 p0140 A70-10057

Machine element materials damping properties, determining energy dissipation during steady resonant vibrations 01 p0211 A70-11423

Resonant energy transfer of trivalent Yb into trivalent Eb for optical pumping improvement for fluorophosphate glass lasing 02 p0314 A70-12725

N degree of freedom pendulum with suspension point vibrating vertically, determining conditions for parametric resonance occurrence 03 p0524 A70-13368

Resonance oscillations onset by initial conditions in dynamic system described by hyperbolic equation containing independent time lag variable 04 p0718 A70-14485

Topological analysis of lumped mechanical vibration systems using mathematical induction, considering linear graphs properties 04 p0773 A70-15077

Amplitude and phase frequency characteristics relations established by analyzing forced resonant oscillations in nonlinear circuit operating at power source frequency 04 p0662 A70-15207

Turbine blade materials resonant vibration resistance criterion dependence on temperature and cyclic and static stresses amplitude 04 p0776 A70-15262

Holographic interferometry applied to amplitude measurement of periodic mechanical surface vibration 06 p1069 A70-18436

Nonsymmetric planform cantilever plate apparent mass, material properties and geometrical changes effect on vibration frequency 07 p1403 A70-19058

Nonlinear system oscillations analysis based on small parameter method and difference equations, including resonant case and stability criterion for periodic solutions 08 p1546 A70-21629

Vibration theory damping using mathematical model emphasizing controlling response under steady state resonance and random excitation 09 p1769 A70-22238

Combination resonance in two degree of freedom dissipative nonlinear system using small parameter and Ritz-Galerkin methods 09 p1727 A70-22667

Dynamic stresses, temperature and displacements fields in thin circular disk under transient heat sources, considering mechanical resonance vibration 10 p1958 A70-24518

Aerospace vehicles structural vibration environments prediction methods emphasizing vibration sensor mounting resonances [AIAA PAPER 70-402] 10 p1959 A70-24903

Natural vibrations of truss systems of four circular cylinders hinged along walls, using linear group representation 11 p2132 A70-25605

Resonant oscillations of passive Fabry-Perot resonator in optically anisotropic medium, using parabolic equations for wave vector amplitudes polarized components 11 p2063 A70-25869

Energy dissipation effect on complex parametric resonance and stability of two rotor gyrocompass on ship in motion 13 p2408 A70-29295

Book on vibrations covering natural oscillations, damped and undamped oscillations, energy sources, forced vibrations, resonance and multiple degree of freedom systems 13 p2515 A70-29452

Turboengine blade resonance vibration measurement by ELURA device, assuming one degree of freedom system 13 p2411 A70-29714

Cylindrical propellant tanks dynamic stability and parametric resonance, analyzing axial preload, liquid depth top impedance and ullage pressure by Donnell theory 14 p2657 A70-30764

Gravity stabilized gyrostatt satellites internal angular momentum effect on nonlinear resonant attitude motions 15 p2810 A70-31785

Hingeless rotor helicopter airborne and ground resonance characteristics, noting feedback stability control interference with rotors aerodynamic damping 17 p3015 A70-34733

Natural vibrations of complex plates for combined free and clamped conditions 17 p3189 A70-35343

Longitudinal wave absorbers attenuating resonance vibrations in rods and plates 18 p3337 A70-36304

RESONATORS

Gravitational effects on impact damper performance, discussing dynamic stability and kinematically viable periodic motion and resonant conditions 20 p3717 A70-38975

Long thin circular cylindrical shell resonance velocities in steady response to fluid motion 20 p3727 A70-39884

Elastic quasi-stationary waves, discussing waveforms and resonance phenomena 20 p3727 A70-39890

Shock and bump testing for dynamic mechanical environments effects encountered by vehicle equipment and components 23 p4195 A70-44331

Accelerated vibration equipment testing for reducing test time, discussing vibration environment simulation 23 p4269 A70-44336

Vibration loads in turbomachinery blading, examining blade detuning effects on resonant response levels and fatigue life 24 p4392 A70-45157

RESONATORS

NT CAVITY RESONATORS

NT MULTIMODE RESONATORS

Natural oscillation modes two dimensional resonator determined in form of superimposed uniform plane waves with arbitrary coefficients of wave reflection 01 p0140 A70-10057

Regenerative quantum amplifiers with simple and complex resonators, discussing amplification coefficients and frequency characteristics 01 p0106 A70-10058

Equivalent circuit for trapped energy resonators and calculations of capacitances ratios for straight crested waves 01 p0088 A70-10777

GaAs injection laser operated with external optical resonator for diffraction-limited radiation, considering peak power and quantum efficiency 02 p0311 A70-11920

Acoustical resonators free oscillations and pressure effects on damping, amplification, decay decrement and relaxation time 02 p0304 A70-12772

Natural modes and multiple beam interference in open resonators, taking into account centimeter wave experiments and computations 02 p0340 A70-12829

Quasi-optical design methods applied to mm microwave resonators characterized by high Q and low spectral densities 04 p0655 A70-14623

Radiation effects on swept-synthetic quartz resonators and materials, discussing frequency shift measurements and defect studies 04 p0731 A70-14735

Mode patterns and losses for laser resonator with identical tilted spherical rectangular reflectors in stable and unstable configurations 04 p0701 A70-15021

Spatial distribution of field intensities of resonators, using diffraction gratings and prisms 04 p0651 A70-15289

Optical resonator reaction to coupled laser frequency, attributing differences between theory and experiment to errors in mirror reflection efficiency measurement 05 p0859 A70-16354

Frequency reaction of optical resonator to coupled laser in mismatch case, measuring laser and resonator axes displacements 05 p0859 A70-16355

Tuning range slope steepness as criterion for evaluating microwave resonators tuning range 05 p0824 A70-16893

Caustic surface of spherical resonator with external mirrors used to calculate light angular divergence and spectral properties 07 p1299 A70-19859

Broadbanding method for microwave reflection type amplifiers using additional resonators 09 p1645 A70-22604

Open cut-off rectangular resonator calculated for frequency dependence on reflection coefficient and relative length 09 p1648 A70-23165

Obstacle extinction cross section determination at microwave frequencies from Q factor of open resonator 09 p1637 A70-23307

Resonator system frequency spectrum in coaxial inverted magnetron with stepped interaction space 09 p1651 A70-23643

Resonant oscillations of passive Fabry-Perot resonator in optically anisotropic medium, using parabolic equations for wave vector amplitudes polarized components 11 p2063 A70-25869

Composite resonator for semiconductor laser to increase single mode power generation, determining optimal length of passive part 12 p2247 A70-27484

- Two mirror astigmatic resonator mode fields and stability determined by writing Fredholm equation suitable to geometrical optics approximation
13 p2424 A70-28596
- Laser with telescopic resonator, examining characteristics at different Fresnel zones and emission losses with geometric optics approximation
13 p2427 A70-29280
- Light transmission losses in optical resonators partially filled with inhomogeneous dielectric, specifying optimal geometrical parameters
13 p2378 A70-29404
- Fabry resonator X band model with step or slope rimmed mirrors, noting periodical trend of power losses
14 p2558 A70-31320
- Filter circuits composed of stripline resonators, determining input impedance and attenuation by digital computer
15 p2701 A70-32468
- Double acoustical resonators transient response to excitation by single sine wave, presenting pressure magnification factors as function of frequencies
17 p3135 A70-34521
- Single gap klystron output resonator optimization, showing maximum electronic efficiency during bunched beam excitation
17 p3055 A70-35681
- Hemispherical open resonators with plane mirror partially coated by reflecting diffraction grating
18 p3231 A70-36411
- Spatial signal transmission through open resonator determination based on resonator integral equation, extending to dielectric lens with finite Fresnel diffraction number
18 p3259 A70-36480
- Coupled open plane resonators system self oscillation intrinsic frequencies solution by numerical method, obtaining algorithm for characteristic equation roots
19 p3387 A70-37737
- Slot type oscillations electrodynamic suppression in coaxial magnetrons resonator systems, calculating long wave oscillation frequencies
19 p3387 A70-37738
- Pulsed ruby free emission mode laser spectrum narrowing, using diffraction lattice adjusted in resonator transversely to beam axis
20 p3643 A70-39757
- Resonant frequencies of microwave dielectric resonator in magnetic wall waveguide
23 p4169 A70-43784
- Directional periodic linear Yagi-Uda arrays application for open low pass or bandpass filters and open resonators
23 p4166 A70-44971
- Confocal microwave Fabry-Perot interferometer resonator diffraction loss and field configuration measurements, noting agreement with theory
24 p4381 A70-46242
- RESOURCES**
NT EARTH RESOURCES
NT EXTRATERRESTRIAL RESOURCES
R and D resources allocation model based on correlated Navy technological forecast (NTF) and exploratory development goals (EDG)
09 p1794 A70-23412
- Resource allocation model with cost-effectiveness relationship for Army long range R and D
09 p1795 A70-23417
- RESPIRATION**
NT HIGH ALTITUDE BREATHING
NT PRESSURE BREATHING
Analog time delay device for returning respiratory flow signal to correct time
01 p0035 A70-10654
- Human pulmonary gas mixing between large airways and alveolar spaces, using argon bolus inhalation
01 p0024 A70-10976
- Radiology instrument for examining pulmonary functions during deep inspiration, expiration and rest, describing material, components and assembly, mounting and radiogram development
01 p0040 A70-11401
- Endtidal oxygen and carbon dioxide partial pressures, oxygen uptake and carbon dioxide after apnea and during apneic diving
02 p0235 A70-12089
- Pleural space of dogs investigated by spheres injection of varying density and diameter, discussing sedimentation velocities
03 p0429 A70-14160
- Ego strength relationship to respiration in response to sound and light stimulation tested in subjects balanced for alertness-drowsiness by EEG criteria
09 p1616 A70-22331
- Hypoxemia and acidosis avoidance during respiration cessation in halothane anesthesia
10 p1822 A70-25086
- Brain tissular respiration and oxygen consumption in rats during hypothermia
12 p2168 A70-27345

- Nitrogen respiratory elimination by human lung, analyzing expired air by mass spectrometry and volume displacement in closed systems
13 p2351 A70-29325
- Inhalation in functional respiratory exploration, describing equipment for aerosol volume measurement in contact with bronchopulmonary effectors
14 p2541 A70-30377
- Ventilating flowmeter tests with jet deflection for respiration measurement in patient
14 p2541 A70-30380
- Closed circuit respiration studies on subjects at rest and work, demonstrating potassium superoxide as oxygen source in breathing apparatus
15 p2688 A70-31500
- Ventilatory response to carbon dioxide in goats during acute and chronic hypoxia
15 p2684 A70-32539
- Human phasic right ventricular blood velocity, examining respiration, rhythm disturbances and Valsalva maneuver influence by radiotelemetry
16 p2850 A70-33111
- Intermittent forced inspirations or expirations effects on venous tone and blood flow in human skin vessels
17 p3024 A70-34595
- Tissue respiration measurement with membrane-covered oxygen electrode, discussing effects of electrode deterioration and diffusion artifacts on accuracy
17 p3026 A70-35186
- Cardiac rhythm, respiration and rhythmical processes of alimentary tract, using digital data device
19 p3370 A70-38214
- Respiration rhythm mechanism from medulla oblongata electric shock stimulation in cats, considering inspiration-expiration phase shift relation to neuron fatigue
24 p4297 A70-45493

RESPIRATORY DISEASES

- NT EMPHYSEMA
Respiratory syncope with cardiac ineffectiveness and numerous complications during and after flight at high altitude clinically observed for causes
12 p2171 A70-28040
- Pursed lips breathing effects on ventilation and blood gas exchange in patients with chronic airway obstruction
15 p2684 A70-32538
- Air transportation of respiratory failure patients, considering medical equipment adaptation for aircraft use
20 p3580 A70-39440
- Obstructive lung diseases clinical, radiological and functional diagnosis in legal medicine
24 p4296 A70-45122

RESPIRATORY IMPEDANCE

- Electronic measurement of bronchial flow resistance in pulmonary function to determine impediment in inhaled and exhaled air passage
08 p1449 A70-20676
- Minute hyperventilation of human lungs causing expiratory suppression of respiration
12 p2173 A70-28315
- Spirometers for ventilation measurement of separate lungs, recording impedance changes during respiratory cycle
14 p2541 A70-30378
- Thoracic impedance changes in premature infants respiration monitoring, noting Respiratory distress syndrome /Rds/ physiopathology
14 p2541 A70-30382
- Circulatory phenomenon and deep thoracic impedance changes of ventilatory origin
14 p2537 A70-30385

RESPIRATORY PHYSIOLOGY

- Chemical and physical adsorption of gaseous oxygen contaminants to maintain purity for respiratory purposes, noting trichlorethylene and carbon tetrachloride
01 p0031 A70-10236
- Positive Na and K ion effects on mitochondrial respiratory control, O uptake and adenosine triphosphate activity in rat liver
01 p0026 A70-11063
- Respiratory muscles neuromotor units activity as function of volley from electric discharge features study on dogs and cats
03 p0417 A70-13068
- Respiratory center functional organization established as automatism with negative feedback, based on experimental data of dogs and cats artificial respiration and hypocapnic apnea
03 p0417 A70-13069
- Commercial pilots susceptibility to emphysema and respiratory impairment in hypobaric environment, discussing flying disability implications
03 p0438 A70-14068
- Energy converters and radio transmitters for physiological telemetry, using electric power converted from thermal and mechanical energy of human respiratory activity
04 p0644 A70-15276

- Muscle temperature variations and respiratory activity of athletes under various exercise regimens, outlining optimal weight lifting training programs
04 p0639 A70-15507
- Inhaled air intrapulmonary distribution uniformity and alveolar N concentration using single breath method
05 p0802 A70-16496
- Data analysis of compliance, resistance, inertance and natural frequency of chest-lung system, noting trend with body mass
06 p0993 A70-17521
- Respiration behavior of men during inhalation of various gas mixtures, observing spontaneous changes in breathing rates
07 p1206 A70-19471
- Static tensibility and vital capacity of lungs statistically analyzed in relation to sex and age
07 p1210 A70-19524
- Respiratory neurons pulsating activity in medulla oblongata of anesthetized cats during imposed rhythm
07 p1213 A70-19774
- Minute volume changes under acoustic excitation of mice for measuring respiratory process without strain on organs
07 p1214 A70-19824
- Thoracic cage, heart and extirpated lung dimensions measurement for dogs before and after explosive decompression and after ground level recompression
08 p1448 A70-21793
- Body temperature effect on pulmonary ventilation response to exercise
10 p1819 A70-24773
- Human pulmonary ventilation during exercise in high altitude and sea level acclimated subjects
10 p1819 A70-24774
- External respiration, hemodynamics, oxygen transport and consumption in lungs during static load tests
10 p1822 A70-25176
- Cold air inhalation effect on vital physiological functions of dogs, describing heat exchange simulator of upper respiratory tract
11 p1985 A70-25672
- Dogs respiratory response to arterial hydrogen ions at different carbon dioxide pressure levels during hypoxia or hyperoxia, discussing acid-base balance effects
11 p1986 A70-25674
- Anterior lobe role of brain limbic region in analysis of afferent pulses arising in receptors of respiratory system
11 p1987 A70-25942
- Cardio-respiratory functions preceding syncope induced by combined lower body negative pressure and head-up tilt
11 p1988 A70-26510
- Open circuit gas washout test of lungs under inspiration-expiration transmission symmetry, using Hilbert-Schmidt operators
12 p2175 A70-27021
- Human lung closing and subdivision volume relationship to age and body position
12 p2169 A70-27657
- Anaerobic and aerobic oxidation efficiency in muscular work performance before and after achieving oxygen steady state consumption
12 p2169 A70-27658
- Minute hyperventilation of human lungs causing expiratory suppression of respiration
12 p2173 A70-28315
- Human respiratory responses to gas mixtures with different oxygen content under rarefied atmospheric conditions
13 p2353 A70-29521
- Gravity dependent lung region emptying sequence effects on alveolar Xe 133 and nitrogen plateaus in pivoted subjects
13 p2356 A70-29944
- Inspired carbon dioxide pressure effects on human response to physical exercise, noting dyspnea and intercostal muscle pain
13 p2360 A70-29949
- Iterative weighted nonlinear least squares parameter estimation for human respiratory control system by transfer function modeling, comparing results with visual curve fitting
16 p2851 A70-33322
- Pulmonary vital capacity measurements in young recruits for respiratory function, considering relationship to body weight and height
16 p2850 A70-34348
- Oxygen uptake capacity, ventilation, heart rate and acid base values during bicycle ergometer exercise
17 p3036 A70-34594
- Intrapulmonary distribution of gases inhaled during positive and transverse accelerations
17 p3037 A70-35130
- Arterial blood carbon dioxide tension effects on rhythmic volley activity of respiratory medulla oblongata neurons in cats
17 p3030 A70-35354
- Extreme heating effects on polypnea reaction in aquatic birds
18 p3219 A70-36537

Adaptive recession of gas metabolism in rats during multiple high temperature exposures
18 p3220 A70-36545

Respiratory activity of internal organs and skeletal muscles in rats exposed to long term heat and cold
18 p3220 A70-36546

Respiratory gas metabolism of liver, heart, brain and muscle tissues in birds exposed to various ambient temperatures for long periods
18 p3220 A70-36547

Respiratory gas metabolism, tissue respiration and enzyme distribution in white rats skeletal muscles following long term cold acclimatization
18 p3220 A70-36548

Chloride ion shift of respiration occurring between plasma and erythrocytes as function of carbon dioxide, using rapid filtration method
19 p3364 A70-38366

Human sensory perception associated with breathing, comparing physical stimulus intensity with judgement of magnitude
19 p3365 A70-38370

Skeletal muscles static tension influence on dog respiratory center functional properties, showing increased frequency volume and sensitivity under stimulation
20 p3574 A70-40174

Expiratory gas flow oscillations during forced vital capacity maneuvers in atmospheres of various composition and pressure
22 p3981 A70-43702

Mathematical model simulating human respiratory physiopathology, based on hypothetical stable auto-oscillations dependence on ventilation/ pulmonary exchange system
23 p4155 A70-44859

Vagus nerve blockage effect on arterial carbon dioxide tension and breathing regulation in dogs
24 p4303 A70-46112

RESPIRATORY RATE
Artificial pulmonary ventilation effects on carbonic anhydrase activity in human blood during hypoventilation and hyperventilation
01 p0025 A70-11029

Accelerative and decelerative heart rate responses in human subjects given differential conditioning trials by auditory and electric shock stimuli under paced respiration
02 p0239 A70-12628

Vagotomy and carbon dioxide concentration effect on quiet and forced respiration rate, pleural pressure, tidal volume and lung ventilation in cats
03 p0422 A70-13694

Conditioned reflexes, respiration and heart beat rates changes in white rats under hypothermia
03 p0424 A70-13717

Photosynthesis and respiration rate in vegetables in controlled temperature, humidity, illumination levels, carbon dioxide and oxygen contents
03 p0425 A70-13892

Vestibular reactions in rats under hypothermal conditions by measuring postrotatory nystagmus beats number and duration, respiration rates and rectal temperature
03 p0425 A70-13893

Respiratory flow rate effect on emptying of lung regions, assessing regional and end-expiratory volumes
03 p0428 A70-14155

Diurnal variations of phase coupling between heart beat and respiration under resting conditions and modification by quantitatively regulated physical effort
03 p0431 A70-14294

Hypothermia effect at various temperatures and durations on nervous activity and vegetative functions of rats, discussing pulse and respiratory rates
07 p1197 A70-18696

Radioreopneumographic study of external respiration of office workers during mental and physical activity
07 p1204 A70-19142

Conditioned reflexes, respiration and heart beat rates changes in white rats under hypothermia
11 p1985 A70-25517

Respiratory gas exchange, heart rate, arterial acidemia and hypocapnia responses to physical work in hyperbaric environments and hyperoxia conditions
12 p2169 A70-27655

Paced respiration and selective attention effects on heart rate and finger pulse amplitude in adult females subjected to visual stimuli
13 p2350 A70-29241

Human proprioceptive reflexes fluctuations correlation with spontaneous respiration and cardiovascular rhythms
13 p2350 A70-29223

Human proprioceptive reflexes fluctuations during controlled respiration and voluntary apnea
13 p2351 A70-29324

Actoballistocardiography based on piezoelectricity for biorythmic activity, respiratory movements and heart rate of small animals
14 p2543 A70-31321

Sleep intensity and stages from EEG studies concerning rapid eye movements, vegetative nervous system, heart/respiration rate, blood pressure, body temperature and stomach motility
15 p2680 A70-31743

Sheep cardiac rate, respiration rate, hematocrit, erythrocytes per cubic mm and hemoglobin concentration responses to elevated ambient carbon dioxide
17 p3030 A70-35421

Human respiration activity measurement in pressure chamber with different pressures and mixture compositions by spiograph equipment
20 p3581 A70-40175

Pressure recording site localization in esophagus, discussing cardiac artifacts morphology and localization over esophagus length
21 p3765 A70-42152

Altered respiratory pattern effect on alveolar gas exchange in mechanically ventilated dogs after introducing end-inspiratory pause
21 p3766 A70-42156

Carbon dioxide exposure limits of rhesus monkeys, examining body temperature, respiratory rate and pressure effects
22 p3973 A70-43642

Miniature respiratory minute volume and rate sensor as pilot personal equipment in flight environment
23 p4155 A70-44840

RESPIRATORY REFLEXES
Control measurements to determine changes in lung volumes, intrapulmonary and intragastric pressure and breathing during submersion in water up to xiphoid process level
01 p0038 A70-10980

Respiratory neurons activity in respiratory center of medulla oblongata during suspension and forced recovery of respiratory motions
07 p1213 A70-19775

Molecular respiratory reflex and fluorescent signal in rabbits during hypoxia, determining redox kinetics of intracellular pyridine nucleotides
14 p2539 A70-31346

RESPIRATORY SYSTEM
NT BRONCHI
NT BRONCHIAL TUBE
NT DIAPHRAGM [ANATOMY]
NT LUNGS
NT NOSE [ANATOMY]
NT PHARYNX
NT TRACHEA
Respiratory mass spectrometer design specifications, considering sampling and vacuum systems
01 p0041 A70-11649

Dielectrocardiograph for studying cardiovascular and respiratory activities by recording hyperemia-evoked permittivity variations in localized body areas
03 p0435 A70-13714

Alveolar ventilation difference in nasal and oral breathing in hyperventilation due to work
05 p0802 A70-16492

Radioactive isotopes removal from respiratory tract, lungs and gastrointestinal tract by ion dilution and antagonism, blood transfusion and hemodialysis, etc
06 p0994 A70-17666

Respiratory waves formation of intracranial pressure in anesthetized cats and dogs, studying various contributing factors
07 p1213 A70-19792

Prolonged hypodynamia effect on human external respiration, arterial blood oxygenation, circulation rate and gas exchange under various physical stress conditions
10 p1814 A70-24674

Dielectrocardiograph for studying cardiovascular and respiratory activities by recording hyperemia-evoked permittivity variations in localized body areas
11 p1990 A70-25514

Anterior lobe role of brain limbic region in analysis of afferent pulses arising in receptors of respiratory system
11 p1987 A70-25942

Cycloergometer with powder type electromagnetic brake for respiratory and circulatory measurements and functional rehabilitation
14 p2541 A70-30379

Cardiac and respiratory cycles phase coincidence detection device, making photographic plates under physiological conditions
14 p2541 A70-30381

Distributed-lumped parameter model for impeded mass transfer and blood-gas maldistribution effects in human respiratory system
15 p2694 A70-32844

Coulometric microrespirometer for long term numerical recording of oxygen consumption in respiratory chamber under sterile conditions
19 p3371 A70-38372

Occupational and age composition of working population of U.S.S.R., comparing cardiovascular and respiratory systems
22 p3969 A70-42904

Physical training effects on blood circulation, respiratory and muscular functions in aging persons
22 p3970 A70-42905

Computer photokymographic recording of gravitational-inertial force environment effects on cardiovascular and respiratory systems on centrifuge
22 p3976 A70-43709

Continuous flow requirements in aircraft passenger oxygen systems using phased dilution principle, discussing breathing mask efficiencies
23 p4141 A70-44483

Hypodynamic effects on human external respiratory function and cardiovascular state under various microclimatic conditions
23 p4149 A70-45078

Pulmonary blood flow and ventilation distribution during forward acceleration by xenon 133 and lung scanning
24 p4302 A70-46105

RESPIROMETERS
Automatic recording respirometer for industrial wastes, discussing design and advantages
14 p2543 A70-31164

Coulometric microrespirometer for long term numerical recording of oxygen consumption in respiratory chamber under sterile conditions
19 p3371 A70-38372

Miniature respiratory minute volume and rate sensor as pilot personal equipment in flight environment
23 p4155 A70-44840

RESPONDERS
U TRANSPONDERS
RESPONSE BIAS
Human perceptual and response biases in choice reaction time tasks involving visual and auditory stimuli
02 p0239 A70-12624

Two degrees of freedom differentiating gyroscope response time decrease and phase and amplitude error reduction, using differential feedback
05 p0853 A70-17003

Time variations in human spectral response, considering sequential gain and phase estimates formation by Gabor elementary signals theory
10 p1823 A70-23895

Response bias of conservative human inference, using revised odds estimate experiments
19 p3361 A70-38055

RESPONSE TIME [COMPUTERS]
Response times in deciding same or different between successive visual stimuli
10 p1826 A70-24722

Information processing stages by reaction time measurements permitting discovery, property assessment and separate testing of stage durations additivity and stochastic independence
10 p1826 A70-24723

RESPONSES
NT DYNAMIC RESPONSE
NT FREQUENCY RESPONSE
NT GALVANIC SKIN RESPONSE
NT HEMODYNAMIC RESPONSES
NT MODAL RESPONSE
NT PHYSIOLOGICAL RESPONSES
NT TIME RESPONSE
NT TRANSIENT RESPONSE
NaI scintillation spectrometer response function matrices semiautomatic generation, using standard source spectra to obtain normalized Compton continua
14 p2587 A70-31006

REST
NT BED REST
Diurnal variations of phase coupling between heart beat and respiration under resting conditions and modification by quantitatively regulated physical effort
03 p0431 A70-14294

Left ventricular wall motion in normal man at rest and after exercise using echocardiogram
07 p1210 A70-19573

Hypercapnic atmosphere effect on human organisms found tolerable in state of rest or performing light labor
09 p1615 A70-22094

Resting concentrations of fibrinogen, plasminogen and levels of euglobulin fibrinolitic activity, plasmin inhibitors and urokinase in blood in inactive and exercising men
13 p2356 A70-29942

Rest periods assignment on long distance air travel of passengers based on physiological stress factor
15 p2690 A70-31892

Hypercapnic atmosphere effect on human organisms found tolerable in state of rest or performing light labor
15 p2685 A70-32690

Exercise and rest of humans under hypoxia and hyperoxia, determining blood acid-base state, ventilation and carbon dioxide partial pressure
16 p2849 A70-34256

RESTARTABLE ROCKET ENGINES
S-IVB liquid rocket engine and propellant feed systems restart shutdown in orbital operations [AIAA PAPER 70-672]
16 p2967 A70-33574

Solid rocket motors, investigating thrust magnitude and stop-restart control
17 p3148 A70-35207

European rocket engine technology, discussing liquid rockets, reliability, restart capability, performance, cryogenic engine, components, facilities and U.S. cooperation

22 p4092 A70-43509

RESTORATION

Blurred photographic image restoration by combining computer generated holographic phase and photographic amplitude filters

12 p2230 A70-26981

Holographic method for recovery of complete image /ghost/ from partial hologram and entire diffraction picture

12 p2238 A70-28186

Sequential and combined gradient restoration algorithms for functional minimization in control theory

15 p2716 A70-32574

RESTRAINTS

U CONSTRAINTS

RESTRICTIONS

U CONSTRAINTS

RESULTS

Resultant of elementary aerodynamic pressures on profile with angular point of attachment

10 p1797 A70-23874

RESUSCITATION

Respiratory neurons activity in respiratory center of medulla oblongata during suspension and forced recovery of respiratory motions

07 p1213 A70-19775

Oxygen transport after cardiopulmonary resuscitation from asystole and ventricular fibrillation in dogs

10 p1822 A70-25085

Extracellular spontaneous sequences of action potentials of thalamic neurons during asphyxia in rats under artificial respiration

19 p3361 A70-38306

RETARDERS [DEVICES]

Mars lander atmospheric entry digital simulation for deceleration system design, discussing ballistic coefficient, aeroshell diameter, parachute size and deployment altitude, etc

08 p1582 A70-20932

Parachute recovery system for surveillance drone and landing bag subsystem [AIAA PAPER 68-935]

14 p2531 A70-30858

RETENTION [PSYCHOLOGY]

Recall and recognition memory in concept identification, discussing presentation time /PT/

03 p0424 A70-13767

Retroactive and proactive inhibition in verbal discrimination learning, using paradigms characteristic of paired-associate retention studies

03 p0435 A70-13768

Cats trained for visual form discrimination tested for retention and reversal performance, studying oxygen deprivation influence

04 p0633 A70-15443

Retroactive interference stimuli effects on pitch discrimination in short term recognition memory task

07 p1215 A70-20046

Divided attention utility for monitoring information processing during encoding, retention and recall of words

07 p1224 A70-20047

Discrete motor act short term retention measurement to investigate decay and interference effects

09 p1621 A70-23378

Verbal information recall latencies as function of time interval from initial memory storage and retrieval repetitions

10 p1818 A70-24718

Preperceptual auditory image demonstration experiments by acoustic test tone pitch identification

22 p3971 A70-43402

RETINA

NT FOVEA

Motion perception sensitivity measurement in various portions of retina for operation accuracy of photooptical systems of simulation

01 p0036 A70-10820

Space or atmospheric flight caused or aggravated ophthalmic lesions, noting retinal and conjunctival hemorrhages from barometric pressure fall and rapid acceleration and deceleration

01 p0022 A70-10858

Laser radiation effects on eye, quantifying light necessary for coagulation for retinal detachment surgery, discussing risks in laser surgery

01 p0037 A70-10859

Retinal vessels of humans at .11-2.0 atmosphere oxygen partial pressures, noting arterioles and venules dilation response to hypoxia and vasoconstriction response to hyperoxia

01 p0023 A70-10863

Flash blinding of cats using Q switched laser beam, discussing ERG response and retina changes

01 p0113 A70-10920

Perceived size relation to retinal size under reduced observation conditions compared with size-distance invariance hypothesis for binocular and monocular observations

01 p0025 A70-11051

Acoustic transients in mammalian eye induced by normal and Q switched laser pulse absorption

02 p0313 A70-12325

Pupil diameter changes associated with constant change in accommodative stimulus as retinal illuminance varies

03 p0427 A70-13950

Degenerate retinal fibers in duck photoreceptor path connecting to supraoptical hypothalamic region detected following optic nerve dissection

03 p0427 A70-13955

Rod-cone interaction in cat S potentials, analyzing effect of wavelength and intensity upon dark adapted responses

05 p0801 A70-16380

Guinea pigs visual analyzer during stimulations by diffuse light, nonspecific thalamic nuclei and microelectrodes polarization, determining A- neuron activity

07 p1213 A70-19788

Operator analysis of electroretinograms, investigating eye reaction dependence on stimulation using amplitude-phase-frequency characteristics

08 p1450 A70-20730

Color vision forms, investigating sensitivity of human retinal receptors and combinations of spectral functions

08 p1443 A70-20731

Cortical induction phases estimated by retinal mobility index concerning activity of acoustic, olfactory and cutaneous analyzers

08 p1443 A70-20735

Direct anatomical couplings between retina and hypothalamus via centripetal and centrifugal fibers by investigating light evoked potentials in rabbits brains

08 p1444 A70-20737

Ionizing radiation effect on isolated frog retina using ERG recordings noting reduction of b wave

08 p1444 A70-20739

USAF permissible human exposure levels for laser irradiation established from monkey retina experiments

08 p1451 A70-21045

Laser radiation protective goggle design, investigating retinal energy density levels and attenuation

08 p1451 A70-21046

Modal excitation and scattering in retinal receptors of human and insect visual systems investigated with dielectric rod uniform wave and irregularities

08 p1452 A70-21289

Retinal temperature increases produced by intense light absorption described by heat conduction equation

09 p1614 A70-22075

Dogs breathing air or oxygen during slow and rapid decompression, measuring intraocular and cardiovascular pressure changes and retinal responses

09 p1621 A70-23460

Different retinal regions simultaneous stimulation, describing evoked potentials measurement method

10 p1811 A70-24227

Stimuli eliciting vergence eye movements and stereopsis, discussing retinal disparity locations and limits due to form, spatial position, luminance, contrast and onset

12 p2171 A70-28034

Age and retinal illumination influence on human pupillary near reflex investigated by photographic measurements

12 p2171 A70-28036

Retinal receptors physiology involved in transforming visible radiant energy into sensory message

12 p2172 A70-28105

Neuron processing of retinal activity in estimating distances and sizes of objects in field of vision

12 p2172 A70-28312

Chorioretinal damage thresholds spectral dependence of intense light sources, describing temporal, axial and radial temperature distributions

15 p2682 A70-32014

He-Ne laser beam hazard to human retina

19 p3371 A70-38309

Photoperiodism in animal organism, discussing retinal epithelium photosensitive substance accumulation and retino-hypothalamo-hypophyseal mechanism of pigmentation

19 p3365 A70-38413

Plasma tocopherol concentrations and vitamin E deficiency in dogs, noting pathologic changes in smooth muscle, central nervous system, skeletal muscle and retina

20 p3569 A70-38991

Dehydrogenases activities in rabbit retina homogenates exposed to oxygen at high partial pressure for various time periods

21 p3765 A70-41487

Threshold retinal damage by CW He-Ne lasers due to mode locking

21 p3771 A70-41997

Human retinal detachment treatment by centrifugation

22 p3975 A70-43699

Isochromic change in bleaching of rhodopsin, showing additional intermediate without detectable color change

23 p4147 A70-44776

Spatial aspects of sensitization effect properties compared to background light fields, lowering rod threshold at center by light addition to surrounding angular region

23 p4147 A70-44779

Time dependent visual perception probability under prolonged testing at eccentricities, using observer exposed to flashed stimulus with dark-adapted retina

23 p4147 A70-44782

Systolic and diastolic pressure in central artery of retina in deep-sea divers during oxygen inhalation at atmospheric pressure

23 p4150 A70-45081

Photographic representation of localization center of anomalous retinal correspondence

24 p4310 A70-46343

RETINAL ADAPTATION

NT DARK ADAPTATION

NT LIGHT ADAPTATION

Mathematical model for vestibular nystagmus adaptation to subjective sensation of rotation, noting time constants

01 p0032 A70-10362

Human size-selective neurons indicated by aftereffect from successive viewing of striped patterns with different spatial frequencies

01 p0035 A70-10724

Time delay between ocular movement and retinal input by yoking visual target to eye movement using real time computer systems

05 p0805 A70-16094

Rod and cone contributions to S potentials from cat retina using spectral sensitivity observation

05 p0801 A70-16379

Rod aftereffect relationship to percent rhodopsin bleached in S potentials from cat retina

05 p0801 A70-16381

Correction factors required for estimating influence of pupil area reduction on retinal illumination at oblique angles

05 p0801 A70-16449

Corpus callosum damage effects on human depth perception implying interhemispheric link for binocular integration in central vision

09 p1618 A70-22670

Flashtube photostimulators for examining human physiological response, discussing design and calibration

09 p1624 A70-22673

Prismatic adaptation under scotopic and photopic conditions in subjects, using transfer experiments

19 p3361 A70-38052

RETINAL IMAGES

Human and cat visual neuron properties, discussing encoding orientation and dimensions of retinal images

01 p0028 A70-11360

Scaling and refractoriness effect in neutral-pulse train transmission on eye incremental sensitivity, discussing applicability as intraretinal mechanism concept

02 p0247 A70-12466

Visual threshold elevation for test flash perception determined by retinal image displacement in saccadic fashion

07 p1205 A70-19283

Evoked potential /EP/ correlate of binocular depth perception in man, discussing responses to horizontal and vertical changes in retinal disparity

07 p1205 A70-19284

Human eye accommodation system, discussing blur detection on retina

13 p2360 A70-29671

Retinal images smearing during voluntary saccadic eye movements, obtaining thresholds for horizontal and vertical stimuli bands

19 p3366 A70-38927

Visual suppression linear dependence on angular size of voluntary saccadic eye movements, observing percentage of trials for stimulus perception

19 p3367 A70-38928

Temporal and spatial distribution of visual suppression during voluntary saccadic eye movement on different places of retina

19 p3367 A70-38929

Geometrical figure fragmentation produced by intermittent illumination, examining dependence on presentation frequency and temporal factors

20 p3580 A70-39491

Spatial summation of retinal neurons receptive field centers excitation from single optic tract fibers action potential in light-adapted cats

22 p3971 A70-43403

Retinal image tracking movement effect on discriminatory perceptibility of orifice orientations of Landolt ring

23 p4147 A70-44778

Perceptual suppression of retinal emissive afterimages by rapid eye movements

23 p4147 A70-44780

- RETINENE**
Topically administered vitamin A radioprotective effect on postirradiation skin reactions
01 p0029 A70-11402
- RETRACTABLE LANDING GEAR**
U LANDING GEAR
- RETRIEVAL**
NT DATA RETRIEVAL
NT INFORMATION RETRIEVAL
Aerial retrieval webbing performance characteristics, discussing structure, type of material, finishing and strength levels
[AIAA PAPER 70-1181] 21 p3843 A70-41832
- RETROACTION**
U RETROTHRUST
- RETROFIRING**
Retrorocket jet size and structure for scientific instruments soft Mars landing, estimating off-optimum supersonic jet interaction with quiescent atmosphere
17 p3011 A70-35660
- RETROREFLECTION**
Transverse Doppler effect of laser beam retroreflected from artificial satellite predicted by special relativity theory, noting transformations
05 p0860 A70-16653
Laser ranging systems used with retroreflecting satellites in geodetic and geophysical applications
05 p0815 A70-16691
Apollo 11 laser ranging retro reflector measurements from McDonald Observatory confirming thermal design analysis performance prediction
06 p1011 A70-18482
Atmospheric phase jitter for He-Ne locked laser measured by retroreflector for half mile round trip
09 p1699 A70-23539
Apollo 11 lunar laser reflector for earth-moon distance measurement
10 p1898 A70-23847
Mathematical-physical parametric model of satellite geodetic laser range accuracy, false alarm and count probabilities, correlating with retroreflector signal strength
16 p2863 A70-33166
Mechanical design and mounting technique of Apollo 11 fused silica laser ranging retroreflector array at Tranquility Base
17 p3082 A70-34763
Reflected ruby, laser pulses from Apollo 11 laser ranging retro-reflector (LRRR) with telescope, measuring round trip travel time of light
21 p3912 A70-41638
- RETROROCKET ENGINES**
Retrorocket effects on aerodynamic stability and drag of conical aeroshell planetary entry vehicles, discussing supersonic wind tunnel tests and jet shock interaction
[AIAA PAPER 70-219] 06 p0974 A70-18166
Spacecraft landing gear shock attenuation systems using crushable honeycomb, draw-die tubes and retrorocket skirt jet
23 p4262 A70-44695
- RETROSEQUENCING**
U RETROFIRING
U SEQUENTIAL CONTROL
- RETROTHRUST**
Fuel-optimal retrothrust control in state dependent retarding force fields, taking into consideration synthesis for vertical trajectory system configuration
11 p2126 A70-26321
- RETURN BEAM VIDICONS**
Multispectral scanner for Earth Resources Technology Satellite, discussing agriculture applications and advantages over return beam vidicon
03 p0493 A70-13957
Balloon flights for remote sensor systems tests, describing return-beam vidicon and tracking telescope experiments
06 p1061 A70-17153
Return Beam Vidicon (RBV) system compatibility with requirements for Earth Resources Observation Satellite (EROS), featuring high resolution image sensor for decreasing signal noise
07 p1280 A70-19231
Multispectral photography in earth resources research, noting three return beam vidicons for technology satellites
20 p3628 A70-39128
High resolution electron return beam vidicon cameras, comparing transfer functions and SNR with photographic films
20 p3630 A70-39496
- RETURN TO EARTH SPACE FLIGHT**
Reusable earth-moon and deep space return transportation, assuming extraterrestrial nuclear rocket propellant source
14 p2653 A70-30766
Optimal angle of attack transition trajectories for space shuttle from atmospheric entry to cruising flight for conventional airport landing
[AIAA PAPER 70-1018] 20 p3713 A70-39515
Aerodynamic braking for returning high speed recoverable space tug to low earth orbit
23 p4259 A70-44611
- Apollo 13 flight rescue operation as function of flight crew performance and Mission Control Center
[AIAA PAPER 70-1260] 24 p4412 A70-45968
- REUSABLE SPACECRAFT**
NT MARS [MANNED SPACECRAFT] REUSABLE
Manned reusable space transportation system technology requirements and vehicle types
[AIAA PAPER 69-1116] 01 p0194 A70-10613
Reusable airbreathing launcher for manned space station ferry operations, considering nozzles, intakes, thrust, acceleration, flight plan, weight analysis, etc
02 p0381 A70-12502
Saturn launch vehicle systems in terms of design, operating characteristics and potential applications, showing need for reusable space shuttle systems
[SAE PAPER 690703] 05 p0922 A70-15830
Reusable lifting entry vehicle flight tests, investigating handling qualities and subsonic-transonic aerodynamics of M2-F2/M2-F3, HL-10 and X-24A
[SAE PAPER 690662] 05 p0792 A70-15840
Reusable booster rocket heat protection system design, discussing ablation and insulation methods
05 p0958 A70-16635
Reusable space shuttle employing two stages resembling subsonic aircraft for carrying passengers and cargo between earth surface and orbit
07 p1392 A70-18873
Reusable lifting reentry bodies subsonic and hypersonic aerodynamic characteristics, considering viscosity effects
[DGLR-69-038] 07 p1392 A70-18984
Low operating cost space shuttle system for cargo and personnel transportation to earth orbiting stations involving reusable winged vehicles
[AIAA PAPER 70-242] 07 p1396 A70-20376
Structural composite materials for thermal protection of reusable weight-saving vehicles in space transportation system
07 p1397 A70-20382
Reusable metallic and nonmetallic thermal protection materials for space shuttle applications
[AIAA PAPER 70-273] 07 p1397 A70-20383
Space transportation system booster and orbiter development ground and flight tests, considering vehicle size and reusability requirements
[AIAA PAPER 70-276] 07 p1397 A70-20385
Refurbishable ablative thermal protection for reusable lifting reentry vehicles
[AIAA PAPER 70-277] 07 p1397 A70-20386
Boride composites with high strength and thermal resistance suitable as nose cap and leading edge materials for reusable lifting reentry systems
[AIAA PAPER 70-278] 07 p1315 A70-20387
Abort and staging separation maneuvers of two equal size reusable lifting entry vehicles in wind tunnel tests
[AIAA PAPER 70-260] 07 p1397 A70-20389
Strap-on ferry package for reusable spacecraft and launch vehicles subsonic lift/drag increase
[AIAA PAPER 70-259] 07 p1397 A70-20390
Reusable space transportation vehicle design evolution, considering staging, aerodynamic shapes, etc
[AIAA PAPER 70-265] 07 p1398 A70-20395
Crew visibility requirements for rendezvous, docking and earth landing of reusable reentry vehicles
[AIAA PAPER 70-262] 07 p1399 A70-20398
Reusable passenger and cargo shuttle system based on integral launch and reentry vehicle (ILRV), considering propulsion systems, aerodynamic and structural configurations, aerothermal characteristics, etc
08 p1582 A70-20689
Rocket sled launching for reusable single stage-to-orbit ballistic transport system, noting increased payload capacity and global application
09 p1767 A70-23434
Ground based simulation for hypersonic reusable lifting reentry vehicle design with pilot-in-loop, discussing six degree of freedom simulation
[AIAA PAPER 70-385] 10 p1861 A70-24920
Reusable ballistic orbital-global transportation systems using rocket sled-assist-takeoff compared to SST systems in terms of effectiveness and cost
11 p2122 A70-26048
Expendable propellant tanks /Tip Tank Concept/ on lifting body reusable booster operations to reduce cost for low earth orbital transport mission
11 p2122 A70-26052
Single stage reusable launch vehicle /project BETA/ feasibility, considering orbit, payload, reentry, cost, etc
13 p2505 A70-28902
Reusable earth-moon and deep space return transportation, assuming extraterrestrial nuclear rocket propellant source
14 p2653 A70-30766
Hypersonic aircraft technology, discussing long range transport, reusable launch vehicles and propulsion systems
15 p2673 A70-31851
Two stage reusable space shuttle consisting of booster and orbiter
15 p2789 A70-32255
- Scramjets for recoverable booster transporting payloads into earth orbits
15 p2811 A70-32258
- Reusable ferry spacecraft program, discussing space shuttles, cost reduction and nuclear propulsion for deep space missions
15 p2791 A70-32300
- Space based reusable manned/unmanned tug, discussing potential missions, system requirements and auxiliary hydrogen oxygen propulsion system
[AIAA PAPER 70-719] 16 p2964 A70-33533
- Materials technology for reuse capability of space shuttle, discussing normal and stress corrosion, hydrogen embrittlement and flammability
16 p2987 A70-34228
- Reusable nuclear shuttle /RNS/ for space program providing low cost transportation beyond earth orbit
[AIAA PAPER 70-679] 17 p3174 A70-34512
- Future manned planetary missions with reusable nuclear shuttles, comparing operating modes in terms of propellant requirement, costs, complexity, etc
[AAS PAPER 70-040] 17 p3155 A70-34781
- Logistic support reusable earth to orbit space shuttle design, noting weight penalties, payloads and development time
[AAS PAPER 70-042] 17 p3175 A70-34782
- Propulsion requirements for reusable space shuttle, discussing engine development program
[AAS PAPER 70-044] 17 p3147 A70-34784
- Cost reduction in designing space shuttle system using reusable winged vehicles, suggesting airline operations method
[AAS PAPER 70-043] 17 p3175 A70-34785
- Space shuttle weight, reliability and reuse cost factors, discussing Phase A ILRV project reducing cost per pound of payload to orbit
[AAS PAPER 70-046] 17 p3175 A70-34786
- Space shuttle atmospheric maneuvers, examining booster and orbiter entry, flyback and abort
[AAS PAPER 70-047] 17 p3175 A70-34787
- Reusable rocket engine for space shuttle, discussing propellants, configuration, design, combustion cycle and size
20 p3689 A70-40084
- Technological and economic problems of reusable aeroballistic and ballistic launch vehicles
20 p3562 A70-40150
- Space shuttle with reusable launch system, discussing payload sensitivities regarding orbiter and booster weight and engine reliability
[SAWE PAPER 849] 20 p3716 A70-40377
- Two stage reusable shuttle for space transportation, discussing aerodynamic characteristics, thermal protection system, performance requirements, etc
21 p3929 A70-40981
- Reusable space shuttle technology, discussing vehicle configurations, system growth capability, thermal protection, cryogenics, integrated avionics, etc
21 p3929 A70-40985
- Nuclear rockets for interorbit transportation, discussing reuse economics, propulsion system performance, etc
21 p3886 A70-40987
- Reusable space transporter predicted applications evolution from earth circling to space bases and space colonies for deep space missions
21 p3930 A70-41495
- Strap-on ferry package for reusable spacecraft and launch vehicles subsonic lift/drag increase
[AIAA PAPER 70-259] 21 p3931 A70-41867
- Nuclear rocket applications in Nuclear Flight Propulsion Module /NFPM/ and Reusable Nuclear Shuttle /RNS/
22 p4070 A70-43180
- Reusable earth surface-to-orbit shuttle, discussing cost and performance design considerations
23 p4260 A70-44618
- Space shuttle for low cost transportation, discussing reusable vehicles, payload, design, orbital inclination, mission capabilities and international participation
23 p4261 A70-44676
- Single stage reusable ballistic space shuttle, featuring minimum payload mass ratios and high propulsive efficiency
23 p4262 A70-44686
- International participation in U.S. post-Apollo program involving reusable space transportation system and multipurpose space station
24 p4431 A70-46123
- REUSE**
Silicide-coated columbium alloys reuse capabilities under flight conditions, considering coating local damage and emittance
[AIAA PAPER 70-279] 07 p1315 A70-20388
- REUSABLE SPACECRAFT**
NT SPACE SHUTTLES
- REVERBERATION**
Release adiabats and recentered Hugoniot curves determination by shock reverberation techniques for compressible nonlinear materials, presenting results for epoxy resin and porous tuff
01 p0198 A70-10106

Localization of lunar acoustic energy, discussing long reverberation time measured at Apollo 12 site after module explosion 18 p3319 A70-37053

REVERSE TIME

U REACTION TIME

REVERSED FLOW

Dipolar fluid effect on back flow between parallel plates, considering generalized Couette flow 01 p0062 A70-10545

Compressible swirling inviscid nozzle flows approximate solution showing changed choking at throat, axial velocity distributions and reversing in subsonic region 01 p0003 A70-11128

Axial flow reversal in swirling incompressible tube flow, discussing static pressure, velocity profiles and turbulent Navier-Stokes equation 03 p0465 A70-13017

Reverse flow in plasma generated in conical electromagnetic shock tube and reflected from downstream bulkhead, noting stabilization effects 13 p2469 A70-29974

Reverse hydromagnetic shock in solar wind as discontinuity of plasma density, proton temperature and magnetic field density, using spacecraft data 22 p4093 A70-42474

REVERSING

Circular polarization time dependent reversals during simultaneous microwave solar bursts at different plages, considering relations to coincident flares 10 p1932 A70-24626

REYNOLDS EQUATION

Spherical radial bearing with gas lubricant, solving Reynolds equation by small parameter method 09 p1690 A70-22450

Pressurized gas bearing analysis, using finite difference method for solving Reynolds equation for pressures in lubricant layer 09 p1690 A70-22545

Externally pressurized air journal bearing performance prediction, obtaining pressure distribution by numerical solution of Reynolds equation 13 p2418 A70-28743

Turbulent flow theory of dilute linear polymer solutions in smooth and rough tubes based on Reynolds equation 15 p2719 A70-31491

Free turbulent incompressible jet, analyzing pulsating characteristics and energy balance with Reynolds stress equations 18 p3240 A70-36264

REYNOLDS LAW

U REYNOLDS EQUATION

REYNOLDS NUMBER

Laminar airfoils for Reynolds numbers above 4,000,000, utilizing potential and boundary layer flow theories 01 p0063 A70-10930

Water tunnel experiments with slender cones to investigate frequency of vortex shedding at low Reynolds number controlled by local diameter 01 p0003 A70-11098

Forced convection of hot wire in hypersonic flow, determining Nusselt-Reynolds number relationship for hot-wire anemometers 02 p0223 A70-12101

Turbulent boundary layer development calculation by shear work integral method involving Reynolds number introduction procedure 02 p0283 A70-12336

Computer application to Navier-Stokes equations numerical integration for incompressible viscous fluid deflected flow with large Reynolds number 02 p0287 A70-12376

Ablation effects on transition Reynolds number of hypersonic boundary layer on slender cones 03 p0465 A70-12945

Viscous inlet flow into straight channels, studying velocity profiles at low Reynolds numbers [ASME PAPER 69-APM-Q] 04 p0668 A70-14863

Instability of viscous laminar plane jet of incompressible fluid, finding minimum critical Reynolds number for various assumptions of parallelism 04 p0670 A70-14990

Pressure pulsations and velocity measurements in turbulent boundary layer without longitudinal gradient, analyzing Reynolds numbers, self similarity and structural characteristics 04 p0673 A70-15250

Wake behind axisymmetric bluff body in steady laminar flow, noting role of Reynolds number 04 p0619 A70-15392

Wall and total temperature variations effects on transition Reynolds number in hypersonic He tunnel, noting sound mode dominance 04 p0620 A70-15560

Magnetohypersonic boundary layer interactions, discussing boundary layer thickness relationship to Hartmann and Reynolds numbers 04 p0729 A70-15564

Low Reynolds number flow of variable property gas past infinite heated circular cylinder at large temperature differences, measuring drag on cylinder 05 p0789 A70-16014

Constitutive equations for Reynolds fluxes in large scale transversely isotropic turbulent mixing using gradients of mean quantities 05 p0836 A70-17103

Longshot free-piston wind tunnel for very high Reynolds number hypersonic flows, describing piston cycle, supply conditions, real gas effects on nozzle flow, etc 06 p1027 A70-17245

Induced drag dependence on Reynolds number for wings without camber and warping 06 p0967 A70-17257

Time dependent transport equations for full Reynolds stress tensor and turbulence decay function using flux approximations and relaxation model [AIAA PAPER 70-3] 06 p1038 A70-18080

Cylindrical tubes steady axisymmetric inlet flow at lower Reynolds numbers, applying results to blood vessels entry flow 07 p1205 A70-19244

Conducting fluids flow instabilities characterized by incipience at critical electric Hartmann number and convection rate proportional to electric Reynolds number 07 p1348 A70-19265

Circular nozzle contraction and Reynolds number effects on turbulent pulsation damping, measuring longitudinal and transverse components 07 p1259 A70-19830

Orifice diameter for low Reynolds number flowmeter dependent on pipeline diameter tolerances 08 p1482 A70-20684

Very small diameter laminar flow orifice coefficient calculation as function of Reynolds number 08 p1484 A70-21321

Potential vortex flow interaction with stationary surface calculation extended to Volterra equations by transforming boundary value problem, improving critical Reynolds number bounds 08 p1484 A70-21472

Shock front stability under free flow in electromagnetically driven shock tubes, determining critical hydrodynamic Reynolds number 08 p1482 A70-21529

Airfoil research in S-10 French wind tunnel for two dimensional flow, noting Reynolds and Mach number ranges [ONERA-TP-766] 08 p1433 A70-21843

Trisonic high pressure wind tunnel simulating flow conditions on large transonic aircraft, noting high Reynolds number capability 09 p1655 A70-22023

Heat transfer coefficient to gas in tube under unsteady heat flow conditions, studying Nusselt number dependence on Reynolds and Prandtl numbers 09 p1787 A70-22173

Incompressible anisotropic fluid flow around semiinfinite plate at large Reynolds numbers, using interlocked asymptotic expansions and deformed coordinates to obtain boundary layer equations 09 p1663 A70-23390

Local Nusselt numbers beyond abrupt circular channel expansion tested for Reynolds numbers with air as working fluid 09 p1790 A70-23554

Compressor blade performance dependence on Reynolds number, turbulence intensity and axial velocity ratio, considering wind tunnel tests with porous side walls 09 p1609 A70-23748

Two dimensional MHD flow past solid body at large Reynolds numbers, treating boundary layer transition 10 p1922 A70-24011

Vorticity distribution influence on inviscid laminar jet boundary layer instability investigated for large Reynolds numbers, using shear flow and linearized theory [DFVLR-SONDDR-14] 10 p1868 A70-24163

MHD flow turbulence suppression at small magnetic Reynolds numbers, considering MHD interaction parameter role 10 p1924 A70-24575

Adiabatic flow coefficient in supersonic nozzle with choked flow conducted over throat Reynolds number range 11 p1976 A70-25999

Steady state two dimensional flow velocity profiles at low Reynolds numbers of homogeneous incompressible viscous liquid in straight channel inlet region 11 p2037 A70-26476

Turbulent three dimensional Poiseuille channel flow at large Reynolds numbers, investigating eddy shapes and energy balance 11 p2041 A70-26546

Stick-slip problem for motion of free jet at low Reynolds numbers by Wiener-Hopf technique, considering two dimensional Newtonian jet without gravity 11 p2041 A70-26554

Quasi-steady devices design to investigate high Reynolds number flows for flight vehicles, noting test time 11 p2041 A70-26573

Heat transfer at low Reynolds and Grashof numbers determined using constant temperature anemometric wire 13 p2521 A70-28952

Transonic aircraft testing capabilities and limitations, considering tunnel wall interference and Reynolds number effects [AIAA PAPER 70-580] 13 p2348 A70-29876

Cone boundary layer transition location and Reynolds number as function of nose bluntness combined effect with Ar, air and He mass injection [AIAA PAPER 69-706] 13 p2343 A70-29954

Correction factor for free stream Reynolds number errors resulting from low temperature viscosity in He wind tunnels 13 p2385 A70-29985

Reynolds momentum and mass transport at velocity half radius of coaxial jet compared to eddy viscosity models 14 p2564 A70-30260

Graphical plotting of critical Preston tube diameter, allowing for Mach and Reynolds numbers effects and introducing limiting line 14 p2586 A70-30871

Spherical liquid drop deformation time dependence in unbound fluid at low Reynolds number, investigating effects of temperature, pressure, velocity and size 15 p2722 A70-32795

High Reynolds number flow in moving corner, observing vortex motion at piston and cylinder wall interface by flow visualization techniques 16 p2895 A70-34240

Low Reynolds number flow inside Delaval nozzle, examining gas density and rotational temperatures by electron beam techniques [AIAA PAPER 70-810] 17 p3065 A70-34454

Laminar boundary layer transition on sharp cone at zero yaw in supersonic wind tunnels, correlating aerodynamic noise disturbances with transition Reynolds numbers [AIAA PAPER 70-799] 17 p3006 A70-34462

Turbulent gas flows shear turbulence structure at various Reynolds numbers in nonconducting channels with and without heat transfer under transverse magnetic field 17 p3141 A70-35245

Fluid turbulence unified heuristic model, defining determinate solutions for Navier-Stokes equations numerical integration at high Reynolds numbers 17 p3074 A70-35884

Steady incompressible flow past circular cylinder at Reynolds numbers up to 100, using finite difference solutions of motion equations 18 p3238 A70-36191

Horizontal boundary layers development on flat plate in nondiffusive stratified flow characterized by Reynolds and Russell numbers 18 p3239 A70-36192

Plane stationary supersonic flows with laminar separation zones at large subcritical Reynolds numbers 18 p3206 A70-36257

Viscous hypersonic flow around nonslender bodies with mass supply at small Reynolds numbers, using thin shock layer model 18 p3206 A70-36259

Energy dissipation and viscosity effects on isotropic turbulence in extreme short wave region at large Reynolds numbers 18 p3239 A70-36263

Nonequilibrium ionized hypersonic flow over blunt body at low Reynolds number, using thin shock layer assumption in analysis 18 p3208 A70-36689

Laminar two dimensional wall jet with small natural disturbances, examining flow stability at various Reynolds numbers 19 p3402 A70-37526

Turbulent boundary layer characteristics on unblown flat plate at low Reynolds numbers, extending to cases with blowing and suction 19 p3405 A70-38020

High Reynolds number isotropic homogeneous turbulence fine scale structure heuristic model, relating spatial intermittency to vorticity generation 20 p3609 A70-39665

Conical diffuser-tailpipe system performance, discussing cone angle, area ratio, Reynolds number and velocity distribution effects on pressure recovery 20 p3559 A70-40082

Turbulent gas boundary layer at finite Reynolds numbers, investigating relative changes in friction and heat transfer coefficients and temperature factor 20 p3614 A70-40390

Laminar fluid flow in pipes of rectangular cross section, determining critical Reynolds numbers and maximum instability locations 20 p3614 A70-40400

Tube heat transfer augmentation by helical vane inserts, noting Reynolds number and mass flow rate effects 21 p3949 A70-41318

Steady viscous flow past oblique flat plate at high Reynolds number, using Oseen linearized approximation 21 p3809 A70-41714

Free stream disturbances influence on hypersonic boundary layer transition Reynolds number in heated and unheated flows [AIAA PAPER 69-704] 21 p3809 A70-41744

Drag estimation for circular cylinders at subcritical Reynolds numbers and subsonic speeds, using Karman vortex street theory for wake 23 p4131 A70-43894

Neutral stability curve for flat plate boundary layer in zero pressure gradient with increasing thickness, giving critical Reynolds number 23 p4179 A70-43974

Tollmein-Schlichting waves in flat plate Blasius boundary layer, comparing experimental and theoretical critical Reynolds number 23 p4179 A70-43975

Mass transfer between sphere and liquid flow at small Reynolds numbers 23 p4276 A70-44219

Wave rider aerodynamic properties at small Reynolds numbers, using non-Weiler wing for flow field, pressure and force measurements at rarefied flow conditions [AVA-FB-7029] 23 p4135 A70-44668

Low Reynolds number gas flow past heated circular cylinder, considering Stokes region transport properties 23 p4284 A70-44978

Spherical shape gas or liquid drop steady motion at large Reynolds numbers, examining buoyancy forces and velocity gradients 24 p4326 A70-45996

RF-8 AIRCRAFT
U F-8 AIRCRAFT

RH-2 HELICOPTER
U UH-1 HELICOPTER

RHENIUM
NT RHENIUM ISOTOPES
Rhenium powder sintering activated by palladium additions producing low porosity 01 p0117 A70-10158

Low energy electron diffraction pattern from surface steps and facets resulting from recrystallization of Re single crystal 08 p1557 A70-21602

Rhenium single crystals basal plane surface properties using LEED and Auger electron spectroscopy, describing gas adsorption studies 09 p1739 A70-22526

Tungsten-rhenium thermocouple for high temperature measurement of samples under unsteady heating processes, analyzing instrument error sources 09 p1789 A70-23108

Carbon monoxide adsorption on rhenium and ruthenium HCP metals emphasizing surface migration, work function increments and desorption 12 p2181 A70-27676

Oxygen interaction on rhenium filament, considering sticking probability as function of temperature 12 p2181 A70-27677

Nitrous oxide chemisorption by rhenium filament at low pressures at various temperatures, determining sticking probability 12 p2181 A70-27678

Calorimetric measurements for Re specific heat in normal and superconducting states, comparing to theoretical calculation 14 p2626 A70-30478

Substrate and thickness dependence of electrical and superconductivity properties of rhenium and molybdenum films prepared by electron beam evaporation 19 p3485 A70-37684

Solar search for neutral rhenium lines using low noise, high resolution photometric tracings of Fraunhofer spectrum 20 p3711 A70-40406

RHENIUM ALLOYS
Refractory metals in rocket propulsion devices, applying tungsten in uncooled rocket nozzles and tungsten and rhenium to electrothermal propulsion 03 p0512 A70-13617

Dilatometric diagrams of phase transformations at low temperatures in Re steels, studying dilatation coefficient behavior 05 p0862 A70-16201

Polycrystalline W-Re alloy creep tests in tension, investigating dislocation substructure formation as function of stress, temperature and strain 12 p2255 A70-27606

Rhenium alloying effect on room temperature ductility of Cr, Mo and W, measuring lattice parameters by Debye-Scherrer method 12 p2256 A70-27616

Plastic deformation of Mo-Re single crystals produced by electron beam zone refining, investigating lattice frictional stress, activation volume temperature variation, etc 13 p2436 A70-29562

W-3 percent Re-W-25 percent Re thermocouple reliability and stability, describing emf vs temperature table in 0-2400 C range 18 p3257 A70-36200

RHENIUM ISOTOPES
Isotopic ratio anomaly of Re and detection at nanogram level in solar wind using decay curves of Re source from lunar specimen 10 p1932 A70-24532

RHEOELECTRICAL SIMULATION
Electrical analog simulation of cardiovascular system, determining blood flow rate and pressure in aorta and peripheral vessels 03 p0420 A70-13490

Heat conduction problems solved allowing for radiation on electrical models, using nonlinear resistance and composite circuit methods 20 p3738 A70-40178

RHEOENCEPHALOGRAPHY
Antigravitation suit effects on rheoencephalography changes during Valsalva maneuver and horizontal-passive orthostatism transition in humans 07 p1212 A70-19738

Rheoencephalographic recording of healthy persons during rest and mental tension in expectation of stimulus 18 p3222 A70-37219

RHEOGRAPHY
U RECORDING INSTRUMENTS
U RHEOMETERS

RHEOLOGY
Biomechanics of microcirculation, discussing rheological characteristics of blood, erythrocyte and vessel wall, hydrodynamics of erythrocyte-shaped bodies mathematical models, etc 01 p0039 A70-11160

Unsaponifiable, molecular weight acids, alcohols and esters effect on rheological properties of lithium lubricants based on synthetic fatty acids 06 p1076 A70-17800

Rheological factors effect on deformation behavior of thin walled spherical shell made of strongly extensible elastically hereditary material and subjected to internal pressure 08 p1587 A70-21168

High speed testing - Conference, Boston, March 1969, Volume 7, Rheology of solids 08 p1526 A70-21326

Rheological calculation of plate resistance and heat transfer in laminar flow of structurally viscous fluids 15 p2827 A70-32126

Solid state mechanics of deformable media, surveying development trends with emphasis on rheology and dislocation theory 15 p2818 A70-32176

Thermorheologically simple model for viscoelastic materials stochastic behavior in random temperature fields, introducing reduced time scale 16 p3003 A70-34238

Rheology and structure formation in three dimensional and two dimensional bulk phase and pigmented systems in surface layers and films, including paints and varnishes 24 p4368 A70-46141

Inertia effects and suspension rheology for incompressible Newtonian fluid shear flow around neutrally buoyant rigid sphere 24 p4327 A70-46243

RHEOMETERS
Radiorheopneumographic study of external respiration of office workers during mental and physical activity 07 p1204 A70-19142

Complex viscosity relationship to steady state shearing in Maxwell Orthogonal Rheometer 11 p2041 A70-26560

Dynamic melt properties of polymer blends, using orthogonal rheometer measurements 22 p4058 A70-43076

RHEUMATIC DISEASES
Autoimmunity to heart tissues in cardiac diseases, reviewing immune mechanisms in rheumatic fever, postcardiotomy and postinfarction syndromes 01 p0016 A70-10438

Continuous murmur due to combination of rheumatic mitral stenosis and rare type of partial anomalous pulmonary venous drainage 17 p3032 A70-35473

RHODIUM
Clean Ru/0001/ and Rh/111/ surface properties by LEED and Auger electron spectroscopy, discussing gas adsorption 19 p3483 A70-37546

RHODIUM ALLOYS
Phase diagram of Nd-Rh system determined by powder X ray diffraction, metallography and differential thermal analysis methods 08 p1522 A70-21711

Ni alloys with Ir and Rh using X ray diffraction and microscopy, exhibiting continuous solid solutions 09 p1708 A70-23423

Thorium phosphide anti-type microstructure of La-Rh system by X ray diffraction, discussing bcc structure, lattice constants, etc 15 p2695 A70-32549

RHOMBIC ANTENNAS

Parameter optimization of V and rhombic antennas with sloped wires, determining radiation angle from radiation pattern 09 p1649 A70-23336

RHYTHM [BIOLOGY]

NT CIRCADIAN RHYTHMS

Reciprocal rhythm occurring with impulses of atrial or atrioventricular /A-V/ nodal or ventricular origin, noting role of A-V nodal pathways 01 p0016 A70-10442

Biological rhythm disturbances of astronauts during air and space travel, discussing sleeping habits, alertness under weightlessness conditions, etc 02 p0241 A70-12763

Autocorrelation and cross correlation analysis of slow EEG potentials in rhythm of movement as cortical activity pattern of cerebral hemispheres during work 03 p0421 A70-13687

Evidence supporting concept of His bundle and not A-V node as pacemaker site in nodal rhythms using electrode catheter technique 03 p0424 A70-13774

Immobilization effects on alpha rhythm, locomotor coordination and visual alimentary motor reflexes of cats 04 p0629 A70-14570

Diurnal and seasonal variations of mortality due to cardiac and circulatory failure using model representing daylight regulation of human organism 05 p0802 A70-16663

Human motor reactions rhythmic system, relating reaction-skin-galvanic reflex to formation of successive conditioned connections 07 p1197 A70-18697

Periodic components distribution of human cardiac activity rhythm noting slow waves 07 p1210 A70-19556

Respiratory neurons pulsating activity in medulla oblongata of anesthetized cats during imposed rhythm 07 p1213 A70-19774

P wave and P loop changes during transvenous pacing of specific locations in coronary sinus and left atrium in dogs and man 08 p1445 A70-21266

Visual recordings of cardiac rhythm obtained from flashes of miniature indicator tube, describing circuit filter function 08 p1452 A70-21439

Amino acid metabolism time dependent variations, studying tyrosine transaminase rhythm in rat liver 09 p1618 A70-22525

Period length calculation method for physiological rhythms by digital computer 10 p1811 A70-24380

Rhesus monkeys tolerance to graded increase in closed environment carbon dioxide, examining heart rate and cardiac rhythm 11 p1988 A70-26517

Pilots EEG characteristics, noting alpha and beta rhythms prevalence 13 p2358 A70-29342

Sleep-wakefulness cycle electroencephalogram of auditory and visual portions of neocortex and hippocampus activity in cats, using spectral analysis and integration 14 p2536 A70-30185

Circannual rhythm in levels, amplitudes and acrophases of serum corticosterone in mice compared with phase shift after change of lighting regime 14 p2537 A70-30725

Stochastic processes for physiological analysis of cardiac rhythm dynamics during work 15 p2680 A70-31609

Human phasic right ventricular blood velocity, examining respiration, rhythm disturbances and Valsalva maneuver influence by radiotelemetry 16 p2850 A70-33111

Biological satellite experiment, considering long term weightlessness effects on metabolism and biological rhythms of medical leech 16 p2854 A70-33993

Photoelectric device for recording plant rhythmic leaf movements in space 16 p2849 A70-33998

Electrophysiological characteristics of man during disorders in rhythmic system of conditioned motor reactions 18 p3221 A70-37217

Alpha rhythm phase coherence during photic blocking, examining pacemaker model 19 p3368 A70-37811

Cardiac rhythm, respiration and rhythmical processes of alimentary tract, using digital data device 19 p3370 A70-38214

Statistical analysis of short periodic time series in biological rhythms including cosinor, periodic regression, harmonic and synchronization analyses 19 p3365 A70-38412

Photoperiodism in animal organism, discussing retinal epithelium photosensitive substance accumulation and retino-hypothalamo-hypophyseal mechanism of pigmentation 19 p3365 A70-38413

Long rhythms of periodic disparate heritable diseases in man 19 p3365 A70-38414

Cardiac contraction rhythm autocorrelation and spectral analysis in healthy subjects and patients with disturbed sinus node functional states 20 p3578 A70-38963

Respiration rhythm mechanism from medulla oblongata electric shock stimulation in cats, considering inspiration-expiration phase shift relation to neuron fatigue 24 p4297 A70-45493

Vascular smooth muscle contraction regulation, discussing contractile protein, energy metabolism, excitation-contraction coupling, spontaneous rhythmicity, response to stimulants, etc 24 p4299 A70-45807

RIBBONS

Stress analysis of composite materials reinforced with glass ribbons embedded in epoxy matrix by photoelastic technique, discussing perturbation effect 08 p1594 A70-21862

Stress distribution in infinite strip of finite thickness under symmetric edge loading analyzed by linear couple stress theory using Fourier transforms 10 p1954 A70-24017

Mechanical properties of composite materials reinforced with carbon fibers consisting of stainless steel and polyethylene ionomer resins 16 p2988 A70-33366

RIBONUCLEIC ACIDS

Thyroidin influence on RNA content and nucleotide composition in hypothalamus, cortex and phenolic fractions of cerebral hemispheres resulting in accelerated protein biosynthesis 01 p0019 A70-10511

Methylating agents and nitrosoguanidine actions on polynucleotides, including ribonucleic acid 03 p0440 A70-13550

Ribonucleic acid polymerase model with initiating purine triphosphate binding to product terminus site and pyrimidine triphosphate engaging in exchange binds to substrate site 03 p0442 A70-14046

Differential melting for partial purification of chemically distinct region of chromosome mycoplasma sp./Kid/ 04 p0647 A70-15448

Orthorhombic form of crystalline formylmethionine transfer RNA, obtaining Patterson function from three dimensional X ray diffraction data 05 p0803 A70-16947

Human metabolic study showing effect of yeast RNA and allopurinol on serum and urinary uric acid formation 08 p1454 A70-20679

Alternating copolymer of guanylic and cytidylic residues synthesized in RNA polymerase-catalyzed reaction 09 p1630 A70-23274

Dietary protein and yeast RNA levels effect on uric acid metabolism in normal man 11 p1987 A70-26002

Partial nucleotide sequences for fragments isolated from ribonuclease digests of tobacco mosaic virus RNA, suggesting genetic duplication possibility 13 p2363 A70-29798

Nucleated organisms divergence from bacteria compared to nucleated organisms divergence into separate kingdoms by analysis of genetic changes in cytochrome c and transfer RNA 16 p2846 A70-32990

Altitude hypoxia adaptation effects on brain protein and RNA synthesis in rats, noting increase in memory resistance to environmental stress effects 17 p3030 A70-35359

RIBS [SUPPORTS]

Thin circular elastic ribs strengthened shallow shells, obtaining solutions in single series 01 p0210 A70-11408

Stress concentration of spherical hoop with discretely spaced meridional ribs under uniform pressure 05 p0935 A70-16229

Strain parameters and equilibrium equation of rib-reinforced thin shells, analyzing length, curvature and torsion variations using smooth shell analogy 05 p0935 A70-16230

Vibration insulation of rib estimated with respect to diffuse flexural wave field in reinforced plate 08 p1586 A70-21010

Critical radii of curvature in elastoplastic bending of rib-reinforced aircraft components from wafer panels determined using strain energy method 08 p1506 A70-21183

Aircraft wing ribs tangents plotting procedure using Monge diagram 08 p1507 A70-21197

Stress concentration in elastic plate reinforced at edge by straight rib analyzed in finite form by Cauchy integrals and Fourier transforms 08 p1594 A70-21635

Free vibration of rib stiffened freely supported circular cylindrical shells, verifying rib eccentricity importance to natural frequencies by numerical solutions 09 p1780 A70-23211

Reinforcing ribs eccentricity effect on closed circular cylindrical shell stability using strain energy method 09 p1786 A70-23720

Forced vibration of rib-skin structures under random pressure and heavy damping using wave group theory 10 p1963 A70-25066

Radiative heat transfer in spherical space bounded by perpendicular annular rib system with gray diffuse and absolutely black body surfaces 12 p2331 A70-27554

Wing rib structure transient thermal stresses analysis using photothermoelastic method 12 p2327 A70-27982

Cylindrical shells with longitudinal rib reinforcements, deriving yield surface from strain mapping and collapse under pressure 15 p2816 A70-32006

Homogeneous orthotropic cantilevered rectangular plate with reinforcing ribs, calculating flutter in supersonic gas flow 18 p3336 A70-36140

Rib stiffened elliptical and circular plate vibrations, determining fundamental frequencies by variational techniques 19 p3536 A70-37693

Circular rib reinforced cylindrical shells, analyzing error due to Kirchhoff-Love hypothesis 20 p3734 A70-40435

Thermomechanical contact and heat transfer on reinforced edge in plates butt joined by curvilinear closed rigidity rib 22 p4120 A70-43718

RICCATTI EQUATION

Algorithm for algebraic matrix Riccati equation, using Fletcher-Powell reformulation of Davidson function minimization 02 p0324 A70-12604

Riccati equation role in solving finite dimensional time invariant transport equations based on equivalent coupled linear equations 02 p0324 A70-12667

Navier-Stokes equation approximation for non-homogeneous case obtained by relating Burgers equation to Riccati equation through similarity transformation 09 p1711 A70-22613

Ill conditioned linear two point boundary value problems solved by Riccati transformation avoiding forward integration 10 p1909 A70-24059

Gain determination from dynamic /on line/ solutions to Riccati equation for model reference adaptive control applicable to multiple input/output or stochastic systems 11 p2029 A70-26339

Riccati-like linear functional differential equation with quadratic cost, analyzing feedback control solution existence and uniqueness 14 p2600 A70-31204

Feedback regulator synthesis for linear time invariant dynamic system with quadratic performance index, using computer algorithm for algebraic Riccati matrix equation 19 p3395 A70-38937

Second order approximations to velocity required concept for boundary value problems in guidance, deriving Riccati equation and position required concept [AIAA PAPER 70-1015] 20 p3666 A70-39518

State-space method of parameter tracking for adaptive control, using Riccati equation and Kalman filtering 23 p4177 A70-44675

Sufficient condition for bounded solution of matrix Riccati differential equation 23 p4212 A70-44896

RICHARDSON NUMBER

Sheared frontal zones structure and stability, studying Richardson number limiting role in free atmosphere 08 p1492 A70-21971

Turbulent boundary layer instability on rotating cylinder in axial stream, correlating mixing length to Richardson number 15 p2722 A70-32372

Atmospheric temperature fluctuation spectrum determination by energy budget solution, considering spectral density dependence on Richardson number 15 p2732 A70-32542

Richardson turbulence criterion computation from measurements during and after winter anomaly 17 p3077 A70-34945

CAT as mechanism relieving wind and temperature discontinuities, maintaining Richardson number at limiting value by turbulent energy dissipation 20 p3663 A70-39373

RICHARDSON-DUSHMAN EQUATION

U TEMPERATURE EFFECTS
U THERMIONIC EMISSION

RIDGES

Major and trace element concentration in contact zones of Precambrian diabase dikes from Wyoming ranges, showing dikes as continental tholeiites 03 p0472 A70-13148

Lunar volcanic ridges features from interpretation of photographs by telescopes and satellites 19 p3518 A70-37992

RIEMANN INTEGRAL

U MEASURE AND INTEGRATION

RIEMANN MANIFOLD

Gravitational field equations in flat space, using quaternion representation of general relativity Riemannian space time in terms of spinors 01 p0141 A70-10279

Motion equations of material point in general relativity theory found analogous to equations in classical mechanics for metric in introduced physical space 01 p0146 A70-11443

Riemann tensor symbolic computation by compact method using differential forms, discussing advantages due to antisymmetry 05 p0818 A70-16681

Compatibility conditions of theory of micromorphic elastic solids using Riemann theorem 06 p1164 A70-17530

Time-similar and isotropic geodetic curves simulating paths of test bodies in Riemann space corresponding to gravitational field 06 p1107 A70-18564

Riemann invariants, discussing method of characteristics in physical and hodograph space applications and multidimensional hyperbolic systems 10 p1865 A70-24103

Asymptotic model for stationary radiative stationary transitions using Newman-Penrose spin coefficient approach to gravitational radiation for Riemann spacetime 11 p2084 A70-26547

Thermodynamics of thermoviscous fluids based on Riemannian space time notions and balance laws of general theory of relativistic continuum mechanics 18 p3347 A70-36557

Existence theorem for piecewise-continuous solutions of waves and shocks in relativistic MHD, using Riemann manifold 19 p3477 A70-37579

Space-time Riemann metric for scalar-tensor gravitational theories with arbitrary omega parameter 22 p4104 A70-42991

RIEMANN PROBLEM

U CAUCHY PROBLEM

RIEMANN SPACE

U RIEMANN MANIFOLD

RIEMANN WAVES

Relativistic effects for MHD Riemann waves in electrically conducting fluid 19 p3478 A70-37583

RIGID BODIES

U RIGID STRUCTURES

RIGID ROTOR HELICOPTERS

NT CH-3 HELICOPTER

NT F-28 HELICOPTER

High speed compound helicopters with rigid and hinged rotors noting features, advantages and construction 05 p0794 A70-16351

Bolkow BO-105 twin turbine rigid rotor helicopter flight tests 08 p1437 A70-21731

RIGID ROTORS

Dynamic unbalance effects in rigid body rotors, discussing lubricant temperature changes and instability hysteresis [ASME PAPER 69-LUB-14] 01 p0101 A70-10391

Lateral vibrations of rigid rotating shaft in viscous fluid using inner and outer expansions method, considering small amplitude vibration and fast rotation 04 p0769 A70-14865

Helicopter rotor, discussing conventional, semirigid, gyro and ABC systems in relation to roll balance and control 13 p2344 A70-28849

Hingeless rotor helicopter airborne and ground resonance characteristics, noting feedback stability control interference with rotors aerodynamic damping 17 p3015 A70-34733

Dynamic unbalance effects in rigid body rotors, discussing lubricant temperature changes and instability hysteresis [ASME PAPER 69-LUB-14] 19 p3435 A70-37606

RIGID STRUCTURES

NT RIGID ROTORS

NT RIGID WINGS

Precession motions of rigid body with variable mass, considering angular momentum and rotation stability 01 p0141 A70-10283

Coriolis effects in spherical Einstein universe perturbed by rigid body rotation of shell with finite thickness 01 p0186 A70-11272

Time dependence of contact zone radius of rigid sphere pressed against viscoelastic half space by normal force 02 p0384 A70-11738

Rigid support properties effect on deformation of ULF ballistocardiogram for quality of recorded curves 02 p0248 A70-12679

Rigid plastic body of material insensitive to strain rate under time dependent surface tension and time independent body forces

02 p0391 A70-12816

Shells of revolution having arbitrary stiffness distribution and subjected to arbitrary loads and temperatures

03 p0583 A70-12916

Rigid and flexible pavements response to jumbo jets load using elastic theory

03 p0462 A70-13175

Penetration depth calculation of high speed non-deformable sphere into massive body, approximating force on sphere by ideal incompressible fluid cavitating flow

04 p0776 A70-15269

Longitudinal stability derivatives prediction for rigid and elastic airplanes, using influence coefficient method

[AIAA PAPER 69-131]

04 p0624 A70-15383

Nonlinear connected oscillations of vibrator and rigid bodies, analyzing plane-parallel and spatial motions, including elastic beams self excited oscillations

04 p0720 A70-15446

Forced torsional vibration of elastic stratum produced by rigid circular disk approximated by Fredholm equations

04 p0777 A70-15497

Relative motion of two spheroidal homogeneous rigid bodies of isolated binary system, obtaining potential energy

05 p0880 A70-15760

Motion equations of rigid vehicle derived in terms of body axes noncoinciding with mass center applied to ships and aircraft

05 p0881 A70-15883

Stress-strain state of drawn and bent circular plate made of rigid viscoplastic work hardened material

05 p0946 A70-16958

Limiting equilibrium of rigid-plastic cylinder subjected to compression by concave stamps

08 p1583 A70-20533

Rotating parabolic mirror /antenna/ cantilever suspension rigidity with emphasis on rigidity of central bushing

08 p1586 A70-21056

Longitudinal vibrations propagation in nonlinear inelastic beam under harmonic kinematic disturbance solved by harmonic linearization method

09 p1773 A70-22541

Torsional vibrations frequency calculations for multibranched system exhibiting linear rigidity and viscous damping, constructing algorithm for digital computer

09 p1783 A70-23409

Rigid body mode of viscous incompressible fluid flow response to small perturbations of rotating spheroidal container, applying torque interaction

10 p1868 A70-24196

Rigid/plastic or rigid/perfectly plastic anisotropic plate under uniform bending, analyzing stress distribution

10 p1964 A70-25092

Integrally stiffened structures made by hot isostatic pressing of metal powders followed by conventional rolling

12 p2242 A70-27109

Rigid and stretch yo-yo device equations of motion for despinning rotating rigid body derived for two and three dimensional model

12 p2271 A70-27228

Axissymmetrical stress tensor singularity convergence of rigidly clamped circular plate, showing identity of plane stressed state transcendental equations

12 p2325 A70-27558

Adaptive flight control systems utilization to compensate for variations in aerospace vehicle rigid body dynamics, noting control system performance requirements

[AIAA PAPER 68-970]

12 p2204 A70-28076

Rigid solid replacement by elastic body in relativistic mechanics

13 p2451 A70-28955

Thermal stresses dependence on temperature field during axisymmetric heating of rigid cylindrical shells

13 p2421 A70-29426

Rigid cylinder acceleration within elastic shell-core structure under pressure pulse distribution over shell semicircumference

13 p2518 A70-29984

Rigid body motion about fixed point with angular velocity vector parallel to fixed straight line plane in space and comoving plane

16 p2952 A70-33741

Optimal orientation of axisymmetric spin stabilized rigid bodies as function of moments of inertia ratios, using single jet for alignment

[DFVLR-SÖNDDR-50]

16 p2976 A70-33773

Space erectable boom with interlocked seam, perforations and coatings to provide torsional rigidity and thermal stability

16 p2986 A70-34143

Linear systems with two degrees of freedom modeled as rigid beam on elastic supports, considering vibration damping

16 p2996 A70-34291

Displacement bounding principle for finitely deforming rigid plastic structures exhibiting geometric stability, with application to cylindrical shell

17 p3184 A70-34906

Precessional stability of rigid body axial rotation in terms of Liapunov, Poincare and Lagrange concepts

17 p3131 A70-35318

Rocket vehicle flight optimization for model including rigid body degrees of freedom in boundary layer approximation to attitude transients

17 p3180 A70-35664

Stable equilibrium positions for satellite consisting of many rigid bodies in circular orbit about center of gravity, using numerical method

18 p3332 A70-35963

Spinning body with rigid and elastic parts, using Liapunov direct method for attitude stability analysis

18 p3292 A70-36677

Stiffness matrix correction for curved element deficient in rigid body motion

18 p3342 A70-36687

Point mass impact on flexibly interconnected rigid bodies with tree structure and spherical joints without dry friction, discussing resulting velocity changes

21 p3849 A70-40552

Aircraft, rocket or other rigid or flexible structure, computing inertial constants based on measurements of generalized masses of natural modes

21 p3935 A70-41408

Static and dynamic longitudinal stability of semirigid parafoil gliding descent system in pitching motion

[AIAA PAPER 70-1191]

21 p3753 A70-41825

Rigid circular cylindrical inclusion elastic bedding dynamic loading, calculating stresses in interface

22 p4112 A70-42345

Light rigid civil aircraft response to continuous atmospheric turbulence estimated using two rigid body degrees of freedom method for vertical and lateral gusts

[AIAA PAPER 69-766]

22 p3961 A70-42703

Rigid and elastic rectangular plates vibration under uniformly distributed dynamic load, investigating bending behavior by Galerkin method

23 p4268 A70-44170

Point accelerations on semirigid body spacecraft from accelerometer data with structural vibration noise at landing

23 p4200 A70-44387

Quaternion scheme for rigid body attitude determination, using Euler axis and angle

23 p4215 A70-44523

Rigid body with external torque acting along one principal axis, deriving Euler equations of motion

23 p4221 A70-44572

Satellites with many flexibly coupled rigid bodies, calculating libration upper bounds for predicting perturbation and stability

23 p4262 A70-44682

Approximation method for large deflection analysis of impulsively loaded rigid plastic circular plates and symmetric shells

23 p4275 A70-44943

German monograph on stress-strain state in prestressed, rigidly supported flexible plates subjected to large deflections, using extended Wolmir solution

24 p4418 A70-45083

RIGID WINGS

Equivalent oscillatory model defined from asymptotes of frequency response amplitude and cut-off frequency amplitude value of plane rigid airfoil in incompressible potential flow

10 p1953 A70-23841

Rigid wing subsonic and supersonic civil and military aircraft utilizing aerodynamic lift at takeoff and landing

13 p2344 A70-28543

Deformable and rigid wings aerodynamic characteristics with subsonic leading and trailing edges, calculating action of gust

15 p2671 A70-31486

RIGIDITY

Low temperature tempering effects on steel transformations and axial rigidity of radial thrust ball bearings in aircraft

12 p2243 A70-27568

Cylindrical gas suspension lubricating layer pressure distribution calculation by perturbation method, determining angular rigidity

20 p3637 A70-39818

RILLS

U VALLEYS

RIMS

Lunar maria absolute age from lunar craters rim height changes via isostatic settling and small craters quantity

14 p2649 A70-31213

Lava thickness measurement in lunar maria from projecting rim width of partially buried craters

23 p4242 A70-44292

RING CURRENTS

Magnetospheric ring current model from ground stations data to interpret observed magnetic field disturbances

01 p0082 A70-11515

Magnetic lines of force penetration into magnetosphere accompanied by plasma insertion generating ring current responsible for main phase of magnetic storm

01 p0083 A70-11543

Temporal behavior of energy injection into geomagnetic ring current found burst-like and similar to Dp at all magnetic levels

04 p0679 A70-15108

Earth magnetosphere physics, considering solar plasma flow, ring currents, charged particles during magnetic storms, solar wind energy transfer, etc

06 p1060 A70-18552

Extraterrestrial ring current proton intensities asymmetric increases in outer radiation belt during magnetic storms

09 p1747 A70-23490

Model current system for magnetospheric substorm accounting for distribution of geomagnetic disturbance field vectors on earth surface and auroral electrons and protons

13 p2481 A70-30062

Magnetosphere topology in presence of time independent ring current symmetrical with respect to earth dipole field axis

14 p2578 A70-31242

Geomagnetic dipole field disturbances by trapped particles, calculating self consistent equilibrium configuration for ring current dipole moments

15 p2727 A70-31905

Ring current belt stability against LF electrostatic perturbations, including effects of finite electric field along magnetic lines of force

18 p3306 A70-36009

Geomagnetic fluctuations relationship to magnetospheric ring current and plasmopause during magnetic storm

20 p3619 A70-39328

Ring current protons turbulent diffusion in magnetospheric plasmopause, considering ion cyclotron wave lifetime and geomagnetic storms

21 p3881 A70-41085

F region heating by magnetic storms, discussing electron temperature, ring current conduction and red arcs

21 p3817 A70-41095

Turbulent plasma heating by adiabatic magnetic compression with longitudinal ring current

21 p3857 A70-41387

Virial theorem for magnetospheric dynamics, discussing boundary and ring currents and densities and geomagnetic sudden impulses and commencement

23 p4184 A70-43830

Magnetic vector potential of circular ring with current in Taylor series expansion for electromagnetic axisymmetric systems

23 p4189 A70-44069

RING DISCHARGE

Multiple narrow beam antenna system with plasma column and electromagnetic wave ring source, discussing radiation pattern and electronic scannability

18 p3294 A70-36346

RING LASERS

Ruby ring lasers unidirectional emission obtained by using Faraday rotator with small polarization plane rotation angle

01 p1017 A70-10208

Optical paths inequality of nonuniform power opposing waves in ring lasers

01 p1017 A70-10209

Solid state ring laser properties as oscillator, waveguide, interferometer and mechanical gyro considered for potential as rate gyro

01 p1018 A70-10417

Pulse width and spectrum generated by ring laser mode locked by synchronously modulated absorber as function of modulator waveform curvature and active medium

01 p1019 A70-10430

CW visible ring cavity parametric oscillator, discussing pump depletion, conversion efficiency and improved stability resulting from optical isolation

01 p0052 A70-11173

He-Ne ring lasers with plane mirrors investigated for amplitude and frequency characteristics at high gain operation at 3.39 microns

02 p0312 A70-12099

Electromagnetic field spectrum and spatial distribution in ring laser, considering transverse modes influence

03 p0500 A70-13462

Discharge tube rotation effects on ring laser polarization, Q factor and radiation frequency

03 p0501 A70-13744

Amplitude and frequency characteristics of gas ring laser with optical feedback between oppositely moving waves amplified by reflecting mirrors

06 p1081 A70-17497

Ring laser frequency characteristics at two longitudinal modes emphasizing intermodal pulse frequencies

06 p1081 A70-17769

- Laser resonator with concave mirrors and ring aperture as radiation outlet, calculating natural oscillations by wave equation
08 p1510 A70-20508
- Radiation field photon density matrix for gas laser with ring resonator determined from double level atomic model, considering photon dispersion and wave reflection feedback
08 p1513 A70-21420
- Single mode He-Ne ring laser lock-in threshold and output power relationships to frequency
08 p1514 A70-21692
- Auto-oscillatory regimes in annular gas laser under coupling due to scattering, considering mode competition
11 p2064 A70-26811
- Single mode TW ruby laser with ring resonator, analyzing emission spectral characteristics by Fabry-Perot etalon
12 p2246 A70-27356
- Local losses distribution effect on intensity and opposing waves generation in ring gas laser analyzed in approximation of noninteracting modes
12 p2248 A70-27510
- Annular gas laser, considering external periodic perturbation effect on difference frequency of oppositely moving waves
12 p2251 A70-28291
- Gas ring lasers, discussing optimal parameters, colliding waves interference, nonmutual effect and radiation polarization
15 p2749 A70-31451
- Frequency locked noise effect on beat frequency measurement of angular velocity with ring laser, comparing gyroscope and phase methods
15 p2749 A70-31551
- Opposing mode interaction effect on ring laser unidirectional emission instability, discussing homogeneous and inhomogeneous line broadening
15 p2749 A70-31552
- Atomic collision effect on frequency range of opposing traveling wave modes in gas ring laser, using density matrix equation
15 p2749 A70-31553
- Natural fluctuations sources intensity in annular lasers taking into account field strength dependence
16 p2927 A70-33197
- Internally loss modulated multimode ring gas laser, showing pulse peak intensity with detuning for phase locking
17 p3107 A70-35475
- Beat and synchronization modes of opposed waves in rotating gas ring laser, examining frequency response asymptotic behavior
17 p3108 A70-35683
- Amplitude and phase fluctuations of opposing waves in ring laser with allowance for waves coupling due to backscattering
18 p3267 A70-36618
- Gravitational field effect on natural frequencies of rotating ring laser, using general relativity and electromagnetic fields theories in continuous media
18 p3267 A70-36622
- Triangular ring laser polarization, using discharge tube with Brewster angle windows in optical circuit
20 p3639 A70-39084
- Ring lasers design and performance, measuring angular velocity by interferometry
20 p3641 A70-39418
- Ring laser gyro angular rate sensor for strapdown inertial systems
[AIAA PAPER 70-1025] 20 p3631 A70-39510
- Ring lasers loss lock-in, attributing frequency synchronization between oppositely directed traveling waves to mutual coupling
21 p3838 A70-42007
- Quantum noise in narrow-band ring laser, noting mode amplification of weak monochromatic signals
23 p4202 A70-45056
- Auto-oscillatory regimes in annular gas laser under coupling due to scattering, considering mode competition
24 p4351 A70-45183
- RING STRUCTURES**
- NT REINFORCEMENT RINGS**
- Piezoelectric transducer for photoelastic analysis of HF stress waves in thick ring subjected to transient loads
02 p0389 A70-12500
- T and L spiral waves existence in disk galaxies, noting helical and ring structures formation near center from standing waves onset
03 p0564 A70-13223
- Natural mode shapes of longitudinal oscillations and resonant frequencies of thin rods of constant curvature and rings with slit, noting use for crack determination
03 p0588 A70-13283
- Dispersion equation and coupling impedance of two dimensionally periodic slow wave structure of cellular cylinder type with parallel perpendicular diaphragms
03 p0456 A70-13438
- Residual stress variations in ring shaped fiberglass reinforced plastic shells produced by winding due to elastic modulus decrease and filler/binder contraction
05 p0934 A70-16216
- Mixed boundary value problems of isotropic elastic half space with ring shaped separation region
05 p0935 A70-16232
- Uniform cross section rings creep characteristics testing method, proposing relations for calculating stresses and strains
05 p0952 A70-17037
- Energy methods used in thermoelastic analysis of thermal stresses and deflections in thin rings
07 p1401 A70-18935
- Temperature stress in ring-like plate caused by point heat source, discussing thermoelastic problem
07 p1413 A70-20147
- Viscoelastic perfectly plastic ring failure under uniform external pressure characterized by infinite strain rate occurring at finite value of ring deflection
07 p1416 A70-20300
- Fourth Saturn ring detection equipment and procedures, discussing negatives revealing small weak zones near globe equatorial east and west edges
08 p1567 A70-20600
- Membrane stress in thin circular viscoelastic ring under impulsive loads and internal heat, using stress-strain relation for linear Maxwell material model
08 p1589 A70-21311
- Free in-plane flexural vibrations of circular rings, developing equation of motion to include shear deformation and rotatory inertia effects
08 p1592 A70-21473
- T and L spiral waves existence in disk galaxies, noting helical and ring structures formation near center from standing waves onset
08 p1580 A70-21656
- Dynamic buckling of thin circular ring subjected to radially directed impulsive load, investigating in-plane and out-of-plane modes
08 p1596 A70-21978
- Saturn globe, rings and satellites observations (1968-1969)
09 p1751 A70-22198
- Standing wave ratio frequency dependence in miniature stripline power dividers and ring structure hybrid junction
09 p1652 A70-23653
- Meteoroidal bombardment effects on material loss or gain in Saturn rings
11 p2113 A70-26471
- Ring buckling under constant and centrally directed pressure, considering small displacement and inextensional deformation
11 p2141 A70-26492
- Radiative heat transfer in spherical space bounded by perpendicular annular rib system with gray diffuse and absolutely black body surfaces
12 p2331 A70-27554
- Contact stresses and radial displacements in circular rings with loaded inner and outer boundaries
13 p2515 A70-29506
- Thermally self induced laser beam phase modulation resulting in far field aberrational rings, describing structure and profile
13 p2431 A70-29834
- Computerized analysis of shear failure at initial fragment collision during trifragment rotor disk interaction with containment rings
14 p2563 A70-30870
- Secular variations in osculating orbital elements of particle in Saturn ring gravitational field, considering motion in both external and internal space
16 p2973 A70-33226
- Space collector ring systems surface physics, discussing dry thin film lubricants, smoothness, service life, etc
16 p2917 A70-33485
- Slip ring assemblies for spacecraft devices, evaluating sliding electrical contact industry technological capabilities
16 p2920 A70-33811
- Sandwich rings inplane transient response to concentrated radial impulsive loads based on Timoshenko type theory, noting dependence on extensional to shear stiffness ratio
16 p2993 A70-34093
- Accelerated vacuum testing of ball bearings and slippings at 30-130 F, considering dry lubricated brush/slipping material combinations
17 p3101 A70-34762
- Rate-sensitive perfectly plastic linear strain hardened rings and tubes, calculating response to impulsive loads
17 p3184 A70-34907
- Impulse loading of rings using magnetically accelerated flyer plates
17 p3187 A70-35163
- Anisotropic disk compressed by isotropic ring of smaller radius, considering elastic equilibrium
18 p3336 A70-36134
- Al alloys missile splice rings fabrication, discussing extrusion, draw forming, flash butt welding and stretch sizing
18 p3264 A70-37112
- Stellar rings and galactic structure, examining prolate ellipsoidal star aggregate diameter constancy
18 p3330 A70-37187
- Ring and cylindrical structures comparative stress relaxation at room temperature
19 p3535 A70-37341
- Stress relaxation in rings and rods, discussing errors possible in data correlation
19 p3535 A70-37342
- Saturn ring photometric properties, discussing multiple scattering and Seeliger principal photometric theory deviation
21 p3885 A70-40932
- Euler buckling of inflated toroidal drag bodies, including packaging and load deflection tests for Mylar, dacron-neoprene and stainless steel-silicone fabrics [AIAA PAPER 70-1198]
21 p3938 A70-41818
- Maxwell equations for hybrid modes of shielded ring line with axial and coaxial region at cut-off and near cut-off conductivity
21 p3793 A70-42269
- Stress analysis of anisotropic circular ring with pressed-in solid disk, using sectionally holomorphic functions
22 p4119 A70-43686
- Saturn ring radial structure, discussing dynamic model, gravitational forces and perturbation of planetary satellites
23 p4241 A70-44253
- Stability of elastic stretched ring on thin spherical shell under critical loads
23 p4268 A70-44318
- Elastic circular sandwich beams optimal design for minimum compliance and given weight, considering rings and semicircular arches
24 p4420 A70-45276
- RINGS**
- Back-up rings and special sealing devices performance qualification testing specifications [SAE-ARP-979]
07 p1290 A70-18802
- Saturn ring atmosphere absorption spectrum observation during earth passage through ring plane
09 p1754 A70-22497
- Saturn observation by astronomers of various countries during earth passage through plane of rings, measuring rings thickness
12 p2298 A70-27279
- Saturn rings observations during earth passage through ring plane by Abastuman observatory telescope, describing photometric processing and data reduction
15 p2797 A70-31619
- RINGS [MATHEMATICS]**
- Nonlinear free boundary value problems involving region bounded by curvilinear ring consisting of smooth curves, reducing problem to nonlinear equations in Banach space
23 p4212 A70-44342
- RIOMETERS**
- Riometric data processing method for radio wave absorption measurement, considering nighttime cosmic radio emission intensity
05 p0842 A70-16742
- Large scale horizontal gradients in auroral radio absorption and effects on absorption height measurement by multifrequency riometry
06 p1055 A70-17595
- Auroral cosmic noise absorption, discussing east-west motion, conjugate magnitudes and breakdown
16 p2899 A70-34191
- RIOMETRY**
- U MEASUREMENT**
- U RIOMETERS**
- RISK**
- Risk-reducing information role in decision making using Marschak bidding procedure
07 p1203 A70-18964
- Decision rules for incomplete a priori data, deriving informational risk estimates for Markov processes and optimal control problems
09 p1653 A70-22144
- Radiation hazard to space vehicles by solar flare protons, calculating risk dose by computerized Monte Carlo simulation, applying importance sampling
10 p1934 A70-25190
- Program risk analysis by aerospace industry pursuant to Federal Government procurement requirements
16 p3003 A70-33427
- Cost effective reliability apportionment in spacecraft subsystems, allocating failure-risk goals by mathematical model
17 p3101 A70-35160
- Risk interpretation of prior distributions in acceptance sampling by Bayesian analysis
19 p3440 A70-38817
- Optimal flight route selection with respect to meteorological prediction errors, using decision under risk and Monte Carlo method
22 p4067 A70-42656
- Space shuttle economic risk analysis, using computer program as design and management tool
23 p4261 A70-44674

RITZ AVERAGING METHOD

Equilibrium of thin curved cylindrical panels subjected to thermal expansion and pressure numerically analyzed by Ritz method

01 p0201 A70-10945

Ultraharmonic resonance excited by centrifugal force in system with Duffing restoring force characteristic using Ritz method

05 p0925 A70-15886

Ritz method applied to second order nonlinear differential-difference equations subjected to sinusoidal driving functions, studying stability criteria and resonance properties

07 p1327 A70-20023

Three dimensional elasticity by Ritz method, using coordinate system orthonormalized in energy metric of operator to avoid precision loss

10 p1957 A70-24511

Classical and elastically restrained boundary conditions requirements for anisotropic plates Ritz solution

11 p2135 A70-26076

Ritz procedure for problems with eigenvalues in boundary conditions

18 p3336 A70-36222

Asymptotic, averaging and Ritz methods for steady state periodic vibrations of nonlinear systems with many degrees of freedom

18 p3338 A70-36437

Rectangular plate with three clamped edges, analyzing free vibration by Ritz method with deflection functions

19 p3544 A70-38328

Undamped forced two degree of freedom system with one linear and one nonlinear spring, analyzing subharmonic vibrations by Ritz averaging method

19 p3544 A70-38329

RIVERS

Aerial photography analysis of drainage basin discharge properties, discussing surface runoff, sub-surface flow and underground water movement

10 p1879 A70-24750

River bed channel flow instantaneous velocities described by logarithmic law, determining turbulent energy dissipation

12 p2265 A70-28336

Microwave radiometric airborne measurement of salinity of Mississippi River outflow, using P3A aircraft

24 p4330 A70-45979

RIVETS

Centrally cracked sheet, calculating riveted and uniformly spaced stringers effect on stress intensity factor

23 p4270 A70-44549

RL CIRCUITS

NT LC CIRCUITS

NT RLC CIRCUITS

RLC CIRCUITS

Fourth order polynomial RC-RL decomposition conditions

07 p1326 A70-19686

LC circuit with time dependent resistance containing wire explosion physics, solving differential equation of discharge circuit

09 p1726 A70-22492

Selective inductorless amplifier design with four layered distributed RGC line in feedback loop, obtaining high Q factors in transfer function

19 p3390 A70-38674

Asynchronous delta modulation channels with RLC integrators in feedback circuit, measuring articulation in presence and absence of noise

20 p3587 A70-40144

RLC networks and microwave components design by applying optimization technique

22 p3997 A70-43175

Microwave p-i-n diode RLC equivalent circuit parameters experimental determination

23 p4171 A70-43956

RLC NETWORKS

U RLC CIRCUITS

RNA

U RIBONUCLEIC ACIDS

ROADS

NT HIGHWAYS

ROBIN BALLOONS

ROBIN superpressure mylar spherical falling balloon deployed from sounding rocket apogee for density and wind measurements via radar tracking

07 p1194 A70-20260

ROBOTS

Humanoid unmanned reconnaissance and assault vehicle maneuvers, describing cover-seeking and obstacle-avoidance functions from physiological and engineering viewpoint

01 p0033 A70-10495

Robot motion optimal control in partially unknown environment, using dynamic programming and heuristic methods

14 p2543 A70-31413

ROCHE LIMIT

Dynamic stability of Jeans spheroid and Roches ellipsoid using small perturbations method

09 p1759 A70-22749

Meridional circulation velocities in Roche envelope of uniformly rotating star, using nonlocal equation for radiative heat transfer

17 p3171 A70-35560

ROCKET BOOSTERS

U BOOSTER ROCKET ENGINES

ROCKET CATAPULTS

Rocket catapult design, development and qualification for Advanced Concept Ejection Seat System /ACES/

06 p0987 A70-17724

ROCKET CHAMBERS

U COMBUSTION CHAMBERS

U THRUST CHAMBERS

ROCKET COMBUSTORS

U COMBUSTION CHAMBERS

U THRUST CHAMBERS

ROCKET ENGINE CASES

Radial bond stresses in case/liner bond line of full-scale rocket motor measured, describing instrumentation, motor design and thermal cycling test sequence

[AIAA PAPER 68-510] 04 p0736 A70-15407

Fracture mechanics applications in stress analysis and structural design, considering rocket motor case failure

09 p1786 A70-23799

Residual stresses near weld in spherical rocket motor casing constructed from maraging steel sheet, discussing moire measurement and reduction treatments

15 p2744 A70-31926

High strength low-alloyed steel for solid propellant rocket engine case, discussing high temperature production and test methods

23 p4208 A70-45046

ROCKET ENGINE CONTROL

Optimization of control forces in rocket nozzles produced by multiport secondary gaseous injection

05 p0923 A70-15889

Contaminants formation during pulse mode operation of liquid bipropellant attitude control rocket engine, discussing exhaust plume effects

[AIAA PAPER 69-574] 07 p1394 A70-19708

Soviet book on liquid rocket engines dynamics, emphasizing computational engineering methods and engines automatic control

08 p1558 A70-20757

Electropneumatic actuation systems for rocket engines in extreme environment applications involving high nuclear radiation levels and high and cryogenic temperatures

14 p2535 A70-31343

Nerva nuclear subsystem diagnostics and control instrumentation, discussing transducers

16 p2949 A70-33551

Reentry vehicles fluidically controlled hydrazine rocket engine modules for roll rate control

[AIAA PAPER 70-650] 16 p2970 A70-33617

Control systems synthesis with parametric invariance for spacecraft boosters

17 p3177 A70-35219

Satellite launching rocket guidance and control based on implicit measurement

17 p3133 A70-35283

Rocket attitude stabilization using exhaust gas flow spinning plug nozzle as gyroscopic mass

[AIAA PAPER 70-67] 20 p3715 A70-39562

Saturn 5 suboptimal continuous guidance design, eliminating discontinuous control encountered in SA-502 flight

[AIAA PAPER 70-965] 20 p3600 A70-39564

ROCKET ENGINE DESIGN

Vaporization interaction liquid rocket performance model, discussing performance loss evaluation and test data

01 p0160 A70-10832

ELDO booster rocket third stage design and construction, including pictures of parts and devices

03 p0580 A70-13795

Ion thruster with hollow cathode electron source, discussing operation principles, experimental characteristics, etc

03 p0552 A70-14150

Radial bond stresses in case/liner bond line of full-scale rocket motor measured, describing instrumentation, motor design and thermal cycling test sequence

[AIAA PAPER 68-510] 04 p0736 A70-15407

Nozzle throat ablative materials for controlled high regression rates in tactical rocket motors, primarily nylon reinforced thermosetting resins

[AIAA PAPER 69-423] 04 p0713 A70-15428

Sounding rocket Vera 15 design with emphasis on operation safety, discussing payload capacity

04 p0765 A70-15669

Modern astronautics, discussing postwar rocket motors and ballistic missiles construction, ELDO program, moon and planetary photographs and space walk, etc

05 p0960 A70-16627

Aerobell extendible nozzle rocket engine design and performance, cold flow and simulated hot flow test results

[AIAA PAPER 69-4] 06 p1129 A70-17168

Soviet book on thermodynamic and ballistic fundamentals of designing solid propellant rocket engines

06 p1130 A70-17421

Heat transfer to hydrogen calculated with reference to design of cooled rocket nozzles and combustion chambers

06 p1174 A70-17677

Fluid controlled solid rocket motors design for Mars mission with acceleration level as parameter, discussing mission specifications, system design and component considerations

[AIAA PAPER 69-446] 07 p1365 A70-19707

Small penetration aid rocket motors fabrication, discussing axial- and tangential-thrust integral assembly, impulse levels, delay line convection for igniters, production evolution, etc

[AIAA PAPER 69-520] 07 p1295 A70-19714

Apollo service module engine design for maximum pilot safety, noting components redundancy

11 p2103 A70-26289

NERVA nuclear rocket engine design for Saturn 5 third stage, comparing nuclear and chemical engines performance

12 p2270 A70-26871

Europa 3 launch vehicle liquid propellant engine design and performance data, discussing West German research in high pressure rocket engines

13 p2473 A70-28447

SR-1 hybrid propellant engine for sounding rockets, describing design and operating characteristics

13 p2474 A70-28689

Petrel sounding rocket design and performance

13 p2504 A70-28692

Turbopump-fed rocket engine for satellite launchers, discussing gas cooling, fuel tank pressurization, etc

13 p2474 A70-29138

Balloon-radar soundings of horizontal wind profiles for booster vehicle design

14 p2653 A70-30588

Soviet book on rocket engine theory covering liquid and solid propellants, combustion physics, nozzle and thrust chamber geometry, etc

14 p2628 A70-30628

Heat pipes design for rocket engines cooling, discussing connections to space radiator and to heat rejection device and heat transfer capability

[AIAA PAPER 69-582] 15 p2791 A70-32517

FLOX methane propellant rocket engines, describing operating conditions, injectors, thrust chambers fabrication and cooling, engine cycles, turbomachinery, etc

[AIAA PAPER 70-718] 16 p2965 A70-33540

Rocket engine prototype for Mariner Mars 71 spacecraft, describing performance test results and response, thermal and throttling characteristics

[AIAA PAPER 70-716] 16 p2966 A70-33545

Throttleable thruster system for Mars soft landing, selecting catalytic decomposition engine from system weight and performance studies

[AIAA PAPER 70-652] 16 p2966 A70-33549

Motor design parameters effects on solid propellant extinguishment predicted from mathematical combustion model

16 p2962 A70-33571

Reusable nuclear shuttles /RNS/ for interorbital and escape missions, discussing alternate stage configurations, radiation shielding, subsystem options, etc

[AIAA PAPER 70-678] 16 p2950 A70-33579

Low, medium and high specific impulse microthrusters development in France, using cold gases, subliming solids, hydrazine, ammonia and cesium ions

[AIAA PAPER 70-617] 16 p2969 A70-33613

R-4D multiapplication rocket engine for Apollo spacecraft reaction control, discussing design, performance, quality assurance and tests

17 p3178 A70-35259

Hybrid rocket engine with solid oxidizer, noting applications as apogee or perigee motor

18 p3301 A70-36655

Rocket engine with Teflon lined combustion chamber, considering design criteria and tests

18 p3301 A70-36662

Nuclear rocket engine fluidic chamber pressure control, discussing design concepts for static and dynamic subsystems

[AIAA PAPER 70-1010] 20 p3688 A70-39585

Reusable rocket engine for space shuttle, discussing propellants, configuration, design, combustion cycle and size

20 p3689 A70-40084

Electrothermal thruster with biowaste propellants, discussing design and performance with various propellant compositions

[AIAA PAPER 70-1161] 20 p3567 A70-40201

Aft-end igniter design and placement for solid propellant rocket motors avoiding overpressurization and nozzle pressure oscillations

21 p3866 A70-40892

Nuclear rocket engines design and performance, discussing fission reactors, radiation leakage and shielding, heat transfer, etc

21 p3870 A70-42044

- European rocket engine technology, discussing liquid rockets, reliability, restart capability, performance, cryogenic engine, components, facilities and U.S. cooperation 22 p4092 A70-43509
- Hybrid combustion ram rocket drives, discussing booster initial acceleration, exhaust gas use as fuel and payload gain [ICAS PAPER 70-50] 23 p4233 A70-44147
- Spacecraft trajectory control rockets design and operational characteristics, discussing various propellant types, control valve designs, etc 24 p4393 A70-45640
- Rocket engines with high chamber pressure for reusable spacecraft [SAE PAPER 700798] 24 p4395 A70-45912
- ROCKET ENGINE NOISE**
- Titan 3C launch environmental hazards including noise and exhaust cloud content 07 p1393 A70-19225
- Remote sonic monitoring system for Saturn V noise measurement and recording 17 p3094 A70-35521
- ROCKET ENGINES**
- NT BOOSTER ROCKET ENGINES
- NT ELECTRIC ROCKET ENGINES
- NT ELECTROSTATIC ENGINES
- NT F-1 ROCKET ENGINE
- NT HOT WATER ROCKET ENGINES
- NT HYBRID PROPELLANT ROCKET ENGINES
- NT HYDRAZINE ENGINES
- NT HYDROGEN OXYGEN ENGINES
- NT J-2 ENGINE
- NT LIQUID PROPELLANT ROCKET ENGINES
- NT MICROROCKET ENGINES
- NT NUCLEAR ENGINE FOR ROCKET VEHICLES
- NT NUCLEAR ROCKET ENGINES
- NT RESTARTABLE ROCKET ENGINES
- NT RETROCKET ENGINES
- NT SOLID PROPELLANT ROCKET ENGINES
- Apollo spacecraft contamination control, describing Rocketdyne programs for rocket engines 01 p0059 A70-11078
- Radiation from flames in gas turbines and rocket engines, discussing effects of soot formation fuel chemical composition, combustor operating conditions, etc 02 p0354 A70-12050
- ELDO-PAS apogee motor prequalification test to determine specifications for constructing units for qualification testing 03 p0581 A70-13854
- Pyrotechnic thrusting devices output dynamics, describing testing for spacecraft applications 03 p0549 A70-14125
- Fluoric altitude insensitive thruster based on two way gas flow diversion valve developed for VTOL aircraft and missile hot gas attitude control systems [ASME PAPER 69-WA/FLCS-10] 04 p0626 A70-14843
- High altitude simulation installations design for rocket motors starting tests under long term high vacuum exposure 04 p0736 A70-15179
- Flight performance prediction for throttling bipropellant rocket engine utilizing ablative combustion chamber throat, discussing lunar module descent engine [AIAA PAPER 69-452] 06 p1130 A70-17176
- Colloid engine efficiency operating with pulsed positive voltages and square wave and sinusoidal voltages [AIAA PAPER 70-178] 06 p1132 A70-18158
- Strain gage high temperature performance in rocket engines tested by spot welding to turbine manifold, noting installation and position influence 06 p1069 A70-18440
- Transverse and longitudinal combustion chamber oscillations in rocket motors with distributed mass and energy sources 07 p1364 A70-19581
- Space electric rocket test /SERT/ II thruster system, discussing flight worthiness and mercury bombardment discharges [AIAA PAPER 67-700] 07 p1364 A70-19701
- Chemical rocket propulsion systems approximate calculation for characteristic velocity dependence on mixture ratio and pressure in combustion chamber [DFVLR-SONDDR-24] 10 p1929 A70-23842
- Rocket plume effects impulsive ground test technique under simulated high altitude pressure conditions, discussing hardware simplifications [AIAA PAPER 70-399] 10 p1951 A70-24906
- RF interference emanating from satellite-borne pulse plasma thruster by measuring RF power at UHF antenna having plasma in near field 11 p2103 A70-26136
- Pilot chamber initiated thermal decomposition reactor concept for monopropellant thruster, discussing thrust levels and throttling ratios [AIAA PAPER 69-420] 13 p2473 A70-28507

- Upper atmospheric sounding rocket Skylark engine, attitude control and payload components modifications for increasing versatility and performance 13 p2503 A70-28678
- Ion thrusters and sources in space propulsion, discussing power supply level, efficiency and service lifetime [ONERA-TP-739] 15 p2787 A70-31808
- Rocket engine thrust chambers and valves, discussing component lifetime extension and operational flexibility of reaction control systems [AIAA PAPER 70-603] 16 p2964 A70-33526
- Stress and vibration analysis of rocket engine turboprop inducer blades, using finite element method [AIAA PAPER 70-630] 16 p2964 A70-33529
- Liquid mercury /LM/ cathode thruster characteristics, power conditioning and control requirements [AIAA PAPER 70-646] 16 p2965 A70-33536
- Hydraulic characteristics of flow through miniature slot orifices for rocket engine injectors, observing stability of effluent liquid streams [AIAA PAPER 70-706] 16 p2891 A70-33566
- Dual bellows ball seat valve design for colloid thruster coupled to pressurized feed system, demonstrating thrust decay and flow regulation [AIAA PAPER 70-615] 16 p2919 A70-33610
- Supersonic cylindrical ejectors without induced flow for rocket engine studies 16 p2837 A70-33763
- High response thrust measurement system for pulsed attitude control rocket engines 17 p3061 A70-35479
- Water cooled pressure probes for measuring rocket chamber HF pressure variations 17 p3093 A70-35485
- On-line display of pulsed rocket engine performance data using hybrid computer 17 p3063 A70-35512
- RFI measurements at X band on LES-7 prototype pulsed plasma thruster 17 p3149 A70-35669
- Rocket engine tests dynamic data oscillographic presentation and digital processing 19 p3490 A70-37916
- Thruster exhaust effluent characteristics relating to spacecraft contamination [AIAA PAPER 70-1143] 20 p3690 A70-40208
- Colloid annular thruster performance, using low mass flow rate data and space charge formulas [AIAA PAPER 70-1113] 20 p3692 A70-40230
- Colloid annular thrusters performance tests in vacuum chamber with LN cooled liner, using high speed analog to digital system to acquire time of flight /TOF/ data [AIAA PAPER 70-1112] 20 p3692 A70-40231
- Colloid engine propellant mass flow distribution, determining beam current and specific charge effects on thrust, efficiency and specific impulse [AIAA PAPER 70-1109] 20 p3692 A70-40234
- Parameters influence on mercury hollow cathode neutralizers for Kaufman ion thruster [AIAA PAPER 70-1090] 20 p3693 A70-40245
- Pulsed plasma and low pressure detonator thrusters for long life secondary spacecraft propulsion, considering satellite stationkeeping and attitude control [AIAA PAPER 70-1147] 21 p3868 A70-41782
- Papers on rocket propulsion, discussing motors thermodynamics, solid and liquid propellant engines, electric and nuclear/thermal propulsion, etc 21 p3869 A70-42037
- Rocket engines propulsion systems design and performance based on thermodynamical theory, involving expanding gas 21 p3869 A70-42038
- Radioisotope thrusters for space propulsion, considering thermal heating methods and direct recoil 22 p4070 A70-43185
- Energy transfer methods for hybrid air breathing ramjet propulsion systems with rocket motor S gas source [ICAS PAPER 70-61] 23 p4233 A70-44156
- Analytical evaluation of secondary flow injection effects on rocket engine performance including cold flow and simulated hot flow data [AIAA PAPER 69-473] 23 p4233 A70-44516
- ROCKET EXHAUST**
- Propellant condensation on surfaces near electric rocket exhaust, calculating particle arrival rates, backflow and desorption energies [AIAA PAPER 69-270] 01 p0166 A70-10836
- High altitude scale model experiment to evaluate rocket plume impingement effects on Manned Orbital Workshop pressures, heating rates, forces and moments 03 p0579 A70-13646
- Rocket exhaust plume size determined from schlieren photographs during wind tunnel tests, noting agreement with Hill-Habert theory 04 p0736 A70-15417
- Rocket stability monitoring by temporal radiometry, using exhaust radiance measurement to detect frequencies in thrust chamber combustion pressure [AIAA PAPER 69-580] 04 p0737 A70-15429

- Supersonic exhaust plume/boundary layer interactions, developing integral method and extending to turbulent interactions [AIAA PAPER 70-230] 06 p1040 A70-18117
- Titan 3C launch environmental hazards including noise and exhaust cloud content 07 p1393 A70-19225
- Rocket exhaust plume flow fields studied for vehicle effects taking into account nozzle boundary layer, coalescence shock and nonisentropic flow [AIAA PAPER 69-569] 09 p1743 A70-23246
- Electrostatic rocket exhaust condensation on spacecraft solar electric panels cover glasses, noting deleterious effects [AIAA PAPER 69-271] 11 p2103 A70-26131
- Stagnation point electrostatic probe for measuring local electrical properties of solid propellant rocket exhausts [AIAA PAPER 69-573] 13 p2475 A70-29960
- Toxicity and downwind diffusion of Be rocket exhaust product measurements, using ADOBE experiment and AFRPL micromet meteorological data system 14 p2628 A70-30611
- Upper atmosphere turbulence spectra of passive contaminants deposited by rockets from radiometrically calibrated photographs of chemical trails 15 p2725 A70-31688
- Two dimensional ray tracing analysis for plume attenuation coefficient calculation using flame diagnostic data 15 p2695 A70-32608
- Rocket exhaust gases radiant heat transfer prediction, using band models with computer program [AIAA PAPER 70-841] 16 p3000 A70-33924
- Titan 3C solid rocket motor exhaust plumes thermal radiation analysis for designing Stage I engines and components thermal protection [AIAA PAPER 70-842] 16 p3000 A70-33925
- ATS-C satellite rocket exhaust plume convective heating measurements of VHF whip antennas, discussing nozzle flow and heating rate [AIAA PAPER 70-843] 16 p3000 A70-33926
- Liquid rocket propellant engine exhaust plume flow field, discussing mathematical models for combustion chamber, throat region and nozzle [AIAA PAPER 70-844] 16 p3001 A70-33927
- Chemical kinetic and turbulent transport coefficients effects on afterburning rocket exhaust plumes and sea level transverse radar attenuations [AIAA PAPER 70-733] 17 p3194 A70-34513
- Rocket exhaust micro and mm waves attenuation attributed to low ionization potential metal particles in propellants 17 p3196 A70-35215
- Crew radiation dosage from fission fragments in plume from gas core nuclear rocket 18 p3224 A70-36562
- Atmospheric ions interaction with rocket exhaust gas water molecules, using sounding rocket mass spectrometric data 18 p3293 A70-36982
- Thruster exhaust effluent characteristics relating to spacecraft contamination [AIAA PAPER 70-1143] 20 p3690 A70-40208
- Cs and Hg electrostatic thruster effluents effects on spacecraft materials, describing chemical, metallurgical and thermophysical experiments [AIAA PAPER 70-1144] 20 p3652 A70-40519
- Radar backscattering from turbulent rocket exhaust plumes [AIAA PAPER 69-71] 21 p3791 A70-41730
- Exhaust plume rarefaction from sonic orifice, considering continuum to transitional behavior for perfect gas [AIAA PAPER 69-657] 21 p3745 A70-41742
- Rocket motion and space propulsion systems, discussing exhaust velocity effect on payload 21 p3869 A70-42039
- Spacecraft electric propulsion system performance, discussing exhaust velocity optimization 21 p3869 A70-42043
- Temperature measurement on thin steel shield subjected to hydrogen peroxide motor exhaust heating at cryogenic temperatures in space 23 p4280 A70-44389
- ROCKET FIRING**
- NT RETROFIRING
- High altitude simulation installations design for rocket motors starting tests under long term high vacuum exposure 04 p0736 A70-15179
- Plume-induced X band radar attenuation, AM and PM noise measured in aluminized solid propellant motor firings 04 p0736 A70-15409
- Meteorological rocket system Meteor 1 firing procedure 07 p1395 A70-20254
- Petrel sounding rocket performance and facilities, describing rocket firings at Hebrides range 13 p2504 A70-28693
- First pulse vacuum startup measurements of monopropellant hydrazine thrust reactors with spon-

aneous catalyst, simulating spacecraft control dynamics 14 p2628 A70-30753

ROCKET FLIGHT

Optimum flight paths of energy and power limited rockets with generalized thrust characteristic, considering vertical, horizontal, rectilinear, zero drag and vacuum trajectories 01 p0193 A70-10425

Soviet book on flight vehicle trajectories covering equations of motion, flight mechanics, reference systems, etc., for rockets and spacecraft 03 p0410 A70-12871

Soviet book on rocket motion and flight theory covering equations of motion, launching and flight optimization, data acquisition and correction, etc. 03 p0579 A70-12872

Flight test results of attitude control device for TACTIC rocket probe to explore solar disk and neighborhood [ONERA-TP-762] 03 p0523 A70-13626

Hazards model for probabilistic prediction of casualties by exploding solid propellant rockets, deriving casualty expectation equation [AIAA PAPER 69-461] 06 p1154 A70-17169

Normal force component distribution and aerodynamic pressure position on rocket bodies at supersonic and hypersonic velocities 06 p0964 A70-17238

Estimated aerodynamic coefficients of reentry body compared with coefficients derived from Antares and Berenice flights 06 p0966 A70-17248

Optimum rocket climbing regime in dense atmospheric layers, including gravitational acceleration investigation in outside layers 06 p1155 A70-17626

Photon propulsion with constant power in exhaust beam and intragalactic travel in force free space from solving relativistic rocket equations [AIAA PAPER 70-215] 06 p1132 A70-18105

Rocket rectilinear motion, comparing Meshcherskii and Gantmacher-Levin equations in light of contact interaction hypothesis 07 p1392 A70-19087

Dynamical characteristics of variable-mass flexible spinning rocket with internal flow, investigating rigid body motion, elastic displacements and vibrations 09 p1767 A70-23252

Real time opto-triangulation by cinetheodolites for data acquisition used in rocket impact prediction 09 p1640 A70-23779

Different gravitational force fields effecting optimal rocket trajectories and queried validity of Newtonian law 10 p1943 A70-24820

Accelerated gradient projection method applied to rocket trajectory optimization for minimizing fuel required for placing payload in circular orbits 13 p2485 A70-28395

Petrel payloads taking into consideration rocket stability after launch and compartment design 13 p2503 A70-28683

Rockets trajectories recording on real time at Guiana Space Center using IR pointing deviation meter 15 p2698 A70-31960

Real time hybrid computer simulation of guided and controlled rocket flight, noting correlation with digital simulation 17 p3060 A70-35285

Electrical power supply systems for meteorological sounding rockets under vibration, acceleration and temperature variation conditions during flight 18 p3215 A70-36251

Integrals of motion for minimum fuel rocket trajectories in inverse square field calculated for constant power and constant exhaust rockets 18 p3316 A70-36678

Aircraft and rocket guidance systems navigation error analysis, discussing numerical integration techniques and computer program [AIAA PAPER 70-1004] 20 p3667 A70-39527

Rocket course correction by lateral air expulsion /ram air control/, deriving model for performance prediction [AIAA PAPER 70-90] 20 p3715 A70-39559

Sounding rockets dispersion, considering deviations from predicted point of impact due to wind effects, thrust vector errors and manufacturing inaccuracies 23 p4262 A70-44845

ROCKET FUEL TANKS

U PROPELLANT TANKS

ROCKET LAUNCHERS

NT ROCKET CATAPULTS

Light weight integrated spin-up launch mechanism for rocket propelled payload 16 p2845 A70-34113

ROCKET LAUNCHING

NT ORBITAL LAUNCHING

Unified Flight Analysis System processing post-flight data from Saturn 5 launches, discussing system components, support programs and performance 02 p0264 A70-12127

Soviet book on rocket motion and flight theory covering equations of motion, launching and flight optimization, data acquisition and correction, etc. 03 p0579 A70-12872

Unconventional gyros, discussing nuclear magnetic resonance, induction, cryogenic, electrostatic and laser technology 03 p0481 A70-12960

Time history of spin and forward motion accuracy of rocket launched from smoothbore, using analytical model and motion coupling through dynamic friction coefficient 03 p0582 A70-14311

Guiana Space Center for French space programs, describing launch complexes, measurement and control methods, safety methods, launch operation planning, etc. 04 p0663 A70-14939

Wind compensation for wind effects with elevation angle in ballistic rocket launching problems 07 p1394 A70-19718

Saturn 5 Prelaunch Systems Simulation Model for launch opportunity containing multiple launch windows, considering last 26 hours of countdown 08 p1582 A70-20933

Reissner variational theorem applied to stress analysis of vertically accelerated end burning solid propellant grain in studying elastic rocket launch failure 12 p2313 A70-27196

Wide range wind compensated launcher settings for unguided rockets using wind-weighting model and iterative procedure requiring real time computation 13 p2503 A70-28528

ESRange-high altitude sounding rocket range for European space research, discussing location, safety, equipment, instrumentation, staff and programs 13 p2523 A70-28690

Pendulous integrating gyro accelerometer float excursions minimization in random vibration environment /Saturn 5 launch/ by statistical technique 14 p2589 A70-31344

Juridical status and sovereignty of rocket launching and cosmic stations in international law 17 p3202 A70-35786

Long range infrasound from rockets, showing two wave groups generated by launch and first stage reentry 19 p3531 A70-37694

ROCKET LININGS

Radial bond stresses in case/liner bond line of full-scale rocket motor measured, describing instrumentation, motor design and thermal cycling test sequence [AIAA PAPER 68-510] 04 p0736 A70-15407

F-1 rocket engine acoustic liner, reevaluating damping data for combustion stability improvement 16 p2968 A70-33588

ROCKET MOTOR CASES

U ROCKET ENGINE CASES

ROCKET NOSE CONES

Attitude control system for pointing rocket nose cone at sun examined by digital computer simulation 13 p2501 A70-28419

Rocket nose cone optimal turn into horizontal ballistic trajectory after separation from booster, using dynamic programming 22 p3962 A70-43351

ROCKET NOZZLES

Fatigue life of rocket nozzle coolant tubes under thermal cycling environmental conditions, considering design formulas for thermal buckling prediction 03 p0579 A70-12963

Refractory metals in rocket propulsion devices, applying tungsten in uncooled rocket nozzles and tungsten and rhenium to electrothermal propulsion 03 p0512 A70-13617

Graphite rocket engine nozzles chemical erosion at various temperatures, comparing reaction and diffusion rates 03 p0516 A70-13619

Annular nozzle shapes established via method of straight line characteristics, noting flow patterns at various regions 03 p0409 A70-13872

Rocket nozzle originated oblique shock waves effect on near-field plume impingement flows, heat transfer and pressure distribution 04 p0737 A70-15421

Optimization of control forces in rocket nozzles produced by multiport secondary gaseous injection 05 p0923 A70-15889

Aerobell extendible nozzle rocket engine design and performance, cold flow and simulated hot flow test results [AIAA PAPER 69-4] 06 p1129 A70-17168

Liquid propellant rocket nozzle configurations maximum stress and stability limits using computer program for composite ring-stiffened shells of revolution [AIAA PAPER 70-138] 06 p1014 A70-18053

Structural analysis of Titan 3 Stage 2 ablative nozzle extension made of composite material 08 p1595 A70-21910

Configurations stress stability liquid propellant rocket nozzle analysis by BOSOR 3 digital program, describing mathematical model construction 13 p2508 A70-28509

Free flow field from underexpanded rocket motor nozzle and impingement effects of pressure and heat transfer to flat plate [AIAA PAPER 69-568] 13 p2473 A70-28510

Rocket motor combustion chamber lining thickness distribution matching to effusor by designing effusor as multiple nozzle made of circular graphite plate 15 p2790 A70-32271

Nuclear rocket nozzle cooling passages, discussing heat transfer and friction correlations for single-phase hydrogen turbulent flow [AIAA PAPER 70-661] 16 p2950 A70-33622

Nonequilibrium combustion products and condensables containing reactive multiphase rocket nozzle flows and exhaust plumes characterization using generalized kinetics streamtube program /MGKS/ [AIAA PAPER 70-845] 16 p3001 A70-33928

Dynamic force and pressure measurement on rocket nozzle during simulated stage separation, describing instrumentation and control system 17 p3061 A70-35478

Constant chamber pressure thrust throttling of expansion-deflection rocket nozzle, calculating wall static pressure and thrust by characteristic method, discussing performance [AIAA PAPER 69-435] 17 p3149 A70-35655

Convective and radiative heat flux measurement incident on ablative surface in solid rocket nozzles 21 p3824 A70-40858

Gaseous film cooling effect on adiabatic wall temperature distribution in rocket nozzle with gas injection 21 p3867 A70-41028

Rocket roll control by secondary compressed air injection via slender fins inserted into nozzle convergent 21 p3931 A70-41953

Rocket engine nozzle with wall-mounted obstacle, examining shock front shape, pressure distribution and side force characteristics 23 p4234 A70-44684

Low cost fabrication for solid rocket nozzles using carbon or graphite reinforcements in throat inserts [SAE PAPER 700796] 24 p4349 A70-45897

ROCKET OXIDIZERS

NT FLOX

Composite propellants high pressure burning stability with various binders and oxidizers, showing ammonium perchlorate oxidized formulations susceptibility to instability [AIAA PAPER 69-438] 01 p0160 A70-10852

Hydrogen peroxide oxidizer for higher characteristic mixture ratio in hybrid propulsion systems with hypergolic reactions ignition [ONERA-TP-773] 02 p0352 A70-12209

Fuel and oxidizer selection for liquid bipropellant system, considering dependence on vehicle, propulsion system and propellant requirements 07 p1361 A70-19916

Transient regimes of solid fuel diffusion combustion in channel with oxidizer fed in from outside, proposing finite difference scheme for integrating equations 09 p1741 A70-22114

Hybrid rocket engine with solid ammonium perchlorate oxidizer, discussing equilibrium conditions and engine performance 15 p2786 A70-32272

Hybrid rocket engine with solid oxidizer based on ammonium perchlorate and Al, studying performance with FORTRAN 5 program 15 p2787 A70-32273

Hybrid rocket motor with solid oxidizer in ammonium nitrate additive, determining stable combustion conditions 15 p2790 A70-32274

Solid propellant extinguishment by rapid despressurization, investigating motor configuration effect, binder, burning rate catalyst, oxidizer, metal loading and exhaust pressure levels 16 p2962 A70-33572

ROCKET PLANES

NT X-15 AIRCRAFT

ROCKET PROPELLANT TANKS

U PROPELLANT TANKS

ROCKET PROPELLANTS

NT AEROZINE

NT CRYOGENIC ROCKET PROPELLANTS

NT DOUBLE BASE ROCKET PROPELLANTS

NT GASEOUS ROCKET PROPELLANTS

NT GELLED ROCKET PROPELLANTS

NT HYPERGOLIC ROCKET PROPELLANTS

NT LIQUID ROCKET PROPELLANTS

NT METAL PROPELLANTS

NT MONOPROPELLANTS

NT SLURRY PROPELLANTS

NT SOLID ROCKET PROPELLANTS

Flight performance prediction for throttling bipropellant rocket engine utilizing ablative combustion chamber throat, discussing lunar module descent engine [AIAA PAPER 69-452] 06 p1130 A70-17176

Book on chemical propellants performance covering properties and parameters effects, rocket performance, chemical thermodynamics, flame temperature, etc. 12 p2289 A70-27350

Lunar resources classified as rocket fuel, construction and life support materials, discussing implications for manned surface exploration missions

14 p2634 A70-30198

Rocket engine propellants flame temperature measurement by spectral line intensity comparison method

15 p2786 A70-32270

Chemical rocket propellant research covering composite liquid monopropellants, lateral thrust in solid propellant rockets, ELDO third stage, friction losses, etc

17 p3148 A70-35211

Electrothermal thruster with biowaste propellants, discussing design and performance with various propellant compositions

[AIAA PAPER 70-1161]

20 p3567 A70-40201

Behavioral changes due to repeated low doses of rocket fuel monomethylhydrazine

21 p3771 A70-41485

Papers on rocket propulsion, discussing motors thermodynamics, solid and liquid propellant engines, electric and nuclear/thermal propulsion, etc

21 p3869 A70-42037

Nonequilibrium gasdynamic and thermodynamic properties of chemically reacting gas mixtures in high expansion subsonic and supersonic nozzles for selected rocket propellants

22 p3982 A70-42761

Monomethylhydrazine /MMH/ missile propellant toxicity, describing symptoms and effects on blood and intellectual capacity

24 p4306 A70-45125

Spacecraft trajectory control rockets design and operational characteristics, discussing various propellant types, control valve designs, etc

24 p4393 A70-45640

ROCKET PROPELLED SLEDS

Rocket sled launching for reusable single stage-to-orbit ballistic transport system, noting increased payload capacity and global application

09 p1767 A70-23434

Photo-optical instrumentation for temperature estimates of nose cone in simulated reentries, using rocket monorail sleds and artificial rainfields for rain erosion effects

09 p1688 A70-23778

Reusable ballistic orbital-global transportation systems using rocket sled-assist-takeoff compared to SST systems in terms of effectiveness and cost

11 p2122 A70-26048

Laser velocity measuring system /LVMS/ for high speed rocket sleds, tracking supersonic sleds through shock front

16 p2926 A70-33142

ROCKET SONDES

U SOUNDING ROCKETS

ROCKET SOUNDING

Global meteorological sounding network requirements, restraints and sensors, considering gun launched meteorological probe role

01 p0054 A70-10082

Rocket and satellite studies of geomagnetic field during IQSY, confirming ionospheric currents responsible for magnetic diurnal variations

01 p0075 A70-10596

Near limb solar IR brightness distribution observed during total solar eclipse of 12 November 1966 in Argentina by sounding rocket photometers

01 p0186 A70-11271

Diurnal variations of intensity and height profile of diatomic O concentration from photometric rocket measurements compared with balloon data

02 p0297 A70-12066

Extrasolar far IR background radiation observed with liquid He cooled telescope carried by Aerobee rocket

02 p0358 A70-12197

Gyrostabilized attitude reference platform for high altitude rotating research rocket payload alignment with preselected star

03 p0579 A70-13606

Uniform stratified layers in equatorial E region determined from Centaur rocket capacitance probe electron density observations, suggesting internal atmospheric gravity waves mechanism

03 p0478 A70-14222

Daytime midlatitude ionosphere composition and electron concentration profile measured by synchronized satellites and rocket, investigating discrepancy

04 p0741 A70-15110

Intensity and spectral distribution measurement techniques for nonvisible extraterrestrial radiation, discussing rocket spectroscopy results

04 p0757 A70-15648

Sco X-1 line spectra search in X ray spectrum by rocket-borne proportional counters, noting iron line emission

05 p0904 A70-16979

Magnus effects on Apache sounding rocket at supersonic speeds, discussing spinning model and static tests

[AIAA PAPER 70-207]

06 p1157 A70-18103

Rocket measurement techniques for electron density profiles in D region, giving results from auroral zone disturbed and midlatitude quiet D region

07 p1263 A70-19152

Midlatitude upper atmosphere soft electron energy flux nighttime measurements by sounding rocket

07 p1368 A70-19500

Upper atmospheric horizontal sounding, discussing satellites uses in atmospheric structure studies

07 p1268 A70-19603

ARCAS meteorological rocket system designed for upper atmospheric soundings to provide thermodynamic and wind data, discussing payloads

07 p1395 A70-20256

Rocket sounding to obtain thermistor temperature profiles of 30-65 km atmospheric region, discussing error correction equation

07 p1288 A70-20261

Meteorological rocket sounding data for Eurasia in mean profiles, time and lateral cross sections, discussing temperature and wind variations

07 p1274 A70-20270

Planetary scale disturbances in winter stratospheric circulation during sudden warming using rocket observations

07 p1274 A70-20272

Stratospheric and mesospheric circulation during winter, investigating wind fluctuations using meteorological rocket observations

07 p1274 A70-20274

Plasma temperatures in magnetosphere, investigating ion energy balance, electron heating and agreement with rocket measurements

08 p1489 A70-21381

Microparticle collection experiments during 1966 Orionid and Leonid meteor showers accomplished by Luster and ALARR /air launched-air recovered rocket/ instruments

08 p1575 A70-21393

Vertical water vapor profile in strato-, meso- and thermospheres measured in rocket and satellite experiments by mass spectroscopy, spectral analysis and thermal sensometry

09 p1666 A70-22187

Rocketborne cryogenic sampler using shock diffuser inlet for air collection at supersonic speeds during rocket ascent

10 p1949 A70-23937

Auroral green line rocket measurements, showing roles of atomic and molecular oxygen dissociative recombinations

10 p1874 A70-24432

Electron temperature diurnal variations data from rocket soundings used for determining recombination coefficient in E region

11 p2044 A70-25550

Sound speed and horizontal wind velocity components determined in upper atmosphere from measured data of Rocket Grenade Experiment

11 p2121 A70-25678

Project HARP gun-launched projectiles as vertical sounding probes for upper atmospheric meteorological and geophysical measurements, discussing payloads development for high acceleration

11 p2122 A70-26047

Canada/U.S. scientific sounding rocket program, describing facilities and projects at Churchill Research Range

11 p2032 A70-26292

UV flash spectra of total solar eclipse of 7 March 1970 obtained by Aerobee 150 rocket

12 p2304 A70-27717

Rocket measurement of ionospheric electron density based on radio propagation effects involving Doppler frequency shift, Faraday rotation, wave absorption, etc

12 p2224 A70-27736

Probe rocket Tacite 02 head attitude gyrorestoration for IR horizon analysis, using stellar sensor and signal measurements

13 p2500 A70-28408

Time comparative low energy proton measurements in inner radiation belt by Rubis rocket with detector telescopes and omnidirectional counters

13 p2475 A70-28572

Skylark sounding rocket telemetry data reduction system providing attitude analysis

13 p2363 A70-28680

Bora-Sond rocket for cost effective upper atmospheric sounding, discussing Li-Al-O systems performance

13 p2504 A70-28684

Probe diagnostic techniques for ionospheric electron density and temperature measurement, describing results from P53H firing

13 p2404 A70-28691

RESY parachute recovery for payloads launched by Skylark high altitude sounding rocket, noting flotation system and location aids

13 p2505 A70-28771

F region nightglow emissions rocket data, discussing rate coefficient for oxygen atoms quenching by molecular nitrogen

13 p2398 A70-29200

Ionospheric electron density measurements with high altitude rocket swept frequency RF impedance probe

13 p2400 A70-29906

Collision and motion effect on rocket-borne quadrupole probe transfer impedance near lower hybrid resonance in ionosphere

13 p2371 A70-29919

Low and high apogee satellite and rocket magnetometers for space measurements, discussing self oriented fluxgate, proton, quantum cesium and three component types

13 p2415 A70-30047

Vertical ionospheric electron concentration profiles, horizontal gradients and integral component from Doppler and Faraday signal recording on geophysical rockets, using diversity reception

14 p2569 A70-30205

Statistical mesosphere temperature, density and wind profiles models based on rocket soundings

14 p2608 A70-30593

Solar eclipse of March 1970 observation by sounding rockets, discussing ionospheric and meteorological measurements

14 p2586 A70-30800

Solar X-rays measurements with spectroheliograph conducted on rocket flights

14 p2589 A70-31339

Mesospheric levels wind oscillations in Spanish range of Arenosillo measured by meteorological rockets during February 1970

15 p2723 A70-31653

D region rocket sounding at geomagnetic equator, measuring electron density, collision frequency, current, temperature, etc

15 p2724 A70-31668

Langmuir probe comparison to electron temperature probe measurements of ionospheric electron temperature during rocket flights

15 p2734 A70-31674

E region ion composition from rocket-borne mass spectrometer data

15 p2725 A70-31689

Report to COSPAR on Swedish space research /1969/ including rocket-borne auroral particle experiments, plasma physics, atmospheric, solar, cosmic radiation, etc

15 p2830 A70-31722

Electron density measurements by partial reflection and rocket techniques during 20 May 1966 solar eclipse, showing agreement below 82 km height

15 p2726 A70-31869

Electric field measurements in ionosphere using satellite and rocket experiments

15 p2729 A70-32082

Ionospheric radio wave propagation from rocket and satellite signal transmission using Faraday and Doppler effects, phase delay and refraction measurements

15 p2698 A70-32095

Midlatitude upper atmosphere soft electron energy flux nighttime measurements by sounding rocket

15 p2795 A70-32745

Coronal observations from Aerobee 150 rocket after total solar eclipse of 7 March 1970 in Mexico, combining coronagraph flight record with ground photography

16 p2977 A70-33839

Sounding rocket X ray survey of Cassiopeia region for supernova remnants and galactic source distribution

17 p3153 A70-34528

Simultaneous measurement of optical and X ray emission from Scorpius X-1 and X ray diffuse background, using rocket-borne scintillation counter

17 p3157 A70-34831

Orion stars far UV intensities, considering photometric data and ultraviolet spectra from rocket sounding

17 p3160 A70-34882

Rocket spectroscopy of zeta Puppis below 1100 A

17 p3160 A70-34886

High resolution solar spectrum at 2000-2200 A from sunpointing Skylark rocket flight, noting detectable absorption lines

17 p3162 A70-34896

Electron density measurements in lower ionosphere by narrow band VLF receiver flown in Tomahawk rocket during quiet daytime

17 p3076 A70-34938

Nighttime E region structure variations observed by Wallops Island rocket flights, obtaining electron density profiles by Langmuir probe during ascent

17 p3076 A70-34941

Sounding rocket instrumentation for ionospheric VLF radio noise measurement and recording

17 p3090 A70-35398

Ionospheric radio noise measurements with VLF wideband receivers onboard rocket

17 p3046 A70-35399

Ionospheric VLF radio waves observations via wideband receiver on K-9M-26 rocket, determining electron density profiles

17 p3047 A70-35639

- Rocket measurements showing removal of electrons above mesopause in summer at high latitude
17 p3081 A70-35775
- Impulsive proton flux precipitation increase during auroral breakup observed by rocket
18 p3245 A70-36021
- Meteoritic dust collection in upper atmosphere by sounding rocket, discussing efficiency of sampling configurations for inertial impaction
18 p3316 A70-36768
- Optimal separation height of instrument container in atmospheric gas composition mass spectrometric studies
18 p3260 A70-36996
- Atmospheric temperatures from thin walled ballistic rocket surface measurements with high sensitivity photometer
18 p3261 A70-36997
- Ionospheric rocket measurements during solar eclipse of 12 November 1966, observing electron and ion density decrease
19 p3418 A70-38907
- D region electron densities during 20 May 1966 solar eclipse, using partial reflection and rockets
19 p3419 A70-38914
- Anomalous IR auroral emission observation during rocket flight, indicating unknown energy sources of oxygen excitation
20 p3621 A70-39350
- Virgo XR-I rocket observations, discussing X rays due to synchrotron emission of relativistic electrons
21 p3872 A70-40658
- X ray emission from Crab Nebula pulsar by rocket-borne proportional counters, comparing with optical observations
21 p3874 A70-40674
- Cosmic X ray background measurements at 25-200 keV onboard ESO Skylark rocket, plotting results against galactic latitude
21 p3876 A70-40695
- Ionospheric transition and ozone correction from D region sunrise auroral rocket flight
21 p3814 A70-40935
- Electron temperature diurnal variations data from rocket soundings used for determining recombination coefficient in E region
21 p3819 A70-41300
- Auroral zone electric field measurements from rocket-borne instruments
22 p4017 A70-42794
- Neutral air density and composition at 150 km, comparing satellite drag data to rocket measurements results
23 p4185 A70-43843
- Global upper atmosphere circulation pattern by daytime tracking of high altitude rocket vapor trail, using differential radiometer
23 p4214 A70-44039
- Polar ionosphere ion composition measurement by meteorological rocket-borne RF mass spectrometer
23 p4190 A70-44081
- Solar L alpha absorption in upper atmosphere, using rocket-borne ionization chamber
23 p4191 A70-44270
- Electron density measurements in ionosphere along rocket trajectory, using sweep frequency RF impedance probe with guard ring
23 p4192 A70-44877
- High altitude cosmic dust observations with microphonic impact detector onboard L-3H-6 sounding rocket
23 p4257 A70-45049
- Vertical ionospheric electron concentration profiles, horizontal gradients and integral component from Doppler and Faraday signal recording on geophysical rockets, using diversity reception
24 p4330 A70-46280
- ROCKET TEST FACILITIES**
Short duration tube wind tunnel supersonic testing, noting Saturn S-1C base heating and solid propellant rocket base burning tests
20 p3606 A70-39698
- ROCKET THRUST**
NT RETROTHRUST
Small penetration aid rocket motors fabrication, discussing axial- and tangential-thrust integral assembly, impulse levels, delay line convection for igniters, production evolution, etc
[AIAA PAPER 69-520] 07 p1295 A70-19714
- Composite programming of vertical ascending rocket with constant thrust phase followed by acceleration and coasting phases, discussing burnout altitude and fuel consumption
08 p1582 A70-21775
- Injection induced swirl effect on thrust and mass flow through nozzle in spinning rocket, discussing internal and exhaust flow measurements and visualization
09 p1606 A70-23247
- Rockets angular motion due to thrust with ramp input, presenting graphs for different inputs and inertia ratios
11 p2123 A70-26125
- Electron bombardment ion engine thrust variations, considering effects of electrode misalignment and ion current changes
12 p2291 A70-27808
- Agema propulsion system performance model for predicting propellant flow rate, mixture ratio, thrust time and specific impulse
[AIAA PAPER 69-453] 14 p2629 A70-30754
- NERVA engine operational cycle and performance, discussing startup, thrust buildup and shutdown
17 p3135 A70-35653
- Constant chamber pressure thrust throttling of expansion-deflection rocket nozzle, calculating wall static pressure and thrust by characteristic method, discussing performance
[AIAA PAPER 69-435] 17 p3149 A70-35655
- Rocket vehicle flight optimization for model including rigid body degrees of freedom in boundary layer approximation to attitude transients
17 p3180 A70-35664
- High and low thrust hybrid rocket propulsion systems involving combinations of chemical, nuclear, thermal and electric propellants for interplanetary flights
21 p3869 A70-42042
- Minimum fuel thrust limited transfer trajectories computation for coplanar elliptic orbits
[AIAA PAPER 69-914] 23 p4244 A70-44558
- Minimum-time transfer trajectories between close planar orbits, using single stage thrust-limited rocket
23 p4244 A70-44624
- Lawden intermediate rocket thrust arcs numerical integration and Kelley-Contensou optimality in Newton central force field
[ONERA TP-869] 23 p4245 A70-44657
- Europa III SLV payload for geostationary equatorial orbit, describing engine thrust and propellant capacity for high energy second stage
24 p4414 A70-46357
- ROCKET VEHICLES**
NT AEROBEE ROCKET VEHICLE
NT AGENA D ROCKET VEHICLE
NT AGENA ROCKET VEHICLES
NT ANTARES ROCKET VEHICLE
NT APACHE ROCKET VEHICLE
NT ARCAS ROCKET VEHICLES
NT ATLAS CENTAUR LAUNCH VEHICLE
NT ATLAS LAUNCH VEHICLES
NT BERENICE ROCKET VEHICLE
NT BLACK KNIGHT ROCKET VEHICLE
NT BLUE STREAK LAUNCH VEHICLE
NT CENTAUR LAUNCH VEHICLE
NT DIAMANT LAUNCH VEHICLE
NT ELDO LAUNCH VEHICLE
NT JAVELIN ROCKET VEHICLE
NT METEOR 1 ROCKET VEHICLE
NT MULTISTAGE ROCKET VEHICLES
NT SATURN LAUNCH VEHICLES
NT SATURN S-1C STAGE
NT SATURN S-2 STAGE
NT SATURN S-4B STAGE
NT SATURN STAGES
NT SATURN IB LAUNCH VEHICLES
NT SATURN 5 LAUNCH VEHICLES
NT SCOUT LAUNCH VEHICLE
NT SINGLE STAGE ROCKET VEHICLES
NT SKUA ROCKET VEHICLES
NT SKYLARK ROCKET VEHICLE
NT SOUNDING ROCKETS
NT THOR DELTA LAUNCH VEHICLE
NT THOR LAUNCH VEHICLES
NT TITAN LAUNCH VEHICLES
NT TITAN 3 LAUNCH VEHICLE
NT X-15 AIRCRAFT
- ASTRID two axis stabilization system for rocket payloads, aligning optical axis of experiment with star [DGLR-69-42] 04 p0762 A70-15161
- Soviet book on rocket structure mechanics covering acting loads and selection of tanks, stage segments, nose section and propulsion units
09 p1772 A70-22527
- Rocket and supersonic aircraft weapon systems, discussing missile delivery and interception
13 p2507 A70-30000
- Aircraft, helicopters and rockets aviation systems design and components service life problems, emphasizing maintenance intervals
17 p3100 A70-34686
- Small rocket systems research programs, discussing Apollo-Pacemaker and planetary entry parachute flight tests
17 p3177 A70-35203
- Flush mounted lightweight antennas for rockets, discussing construction radiation patterns, input impedance, etc
17 p3053 A70-35273
- Rocket vehicle flight optimization for model including rigid body degrees of freedom in boundary layer approximation to attitude transients
17 p3180 A70-35664
- Ablative heat transfer to nonstagnation surfaces of high speed rocket vehicle in continuum atmosphere, using finite difference theory
22 p4125 A70-43433
- ROCKET-BORNE INSTRUMENTS**
Far IR night sky emission above 120 km over millimeter range, using rocket-borne telescope
01 p0069 A70-10040
- Solar Mg II doublet and XUV images obtained by Fabry-Perot interferometer mounted in Skylark spectrograph
01 p0177 A70-10339
- Monk-Gillieson convergent beam dispersion method applied to rocket-borne photoelectric spectrophotometer for far UV stellar spectra observation
01 p0090 A70-10904
- Rocket telescope spectrometer precision pointing achieved by servocontrolling secondary mirror, discussing use for planetary atmospheres far UV spectrum studies
02 p0296 A70-11916
- Onboard radio altimeter for position finding of research rockets and balloons used for aeromic investigations
02 p0298 A70-12084
- Spectral index for diffuse X ray sky background within specific band determined from rocket observations with wide angle telescope
03 p0479 A70-14223
- Rocket-borne differential capacity probe measuring electron densities in upper atmosphere, reducing errors caused by temperature and composition variations
[AAS PAPER 69-567] 04 p0686 A70-14649
- Cassegrainian liquid He cooled IR telescope for rocket-borne IR astronomy, discussing optical, cryogenic and electronic designs
04 p0689 A70-15017
- Far IR extrinsic photoconductive detectors for rocket-borne liquid He-cooled IR telescope, discussing limiting noise factor
04 p0689 A70-15018
- Miniature fluxgate magnetometer for sounding rocket measurements of two orthogonal components of external magnetic field, predicting performance by linear mathematical model
05 p0851 A70-16690
- Rocket-borne spectrometer intensity measurements UV region of solar spectrum, noting agreement with IR observations of solar temperature minimum
06 p1143 A70-17998
- UV rocket-borne up-down photometer measuring zenith and nadir intensities for auroral profile studies
06 p1072 A70-18518
- D region positive ion composition measurements by rocket-borne quadrupole mass spectrometer, discussing downleg and upleg data
06 p1137 A70-18537
- Seasonal variation of F 1 region ion composition measured by rocket-borne mass spectrometer, noting altitude dependence of electron and ion temperatures
06 p1059 A70-18540
- Rocket-borne radar chaff wind sensor synoptic application above 65 km, describing low fall velocity
07 p1237 A70-20258
- Parachute wind sensors used in Arcas and Loki sounding rocket systems for stratospheric sounding, describing position data acquisition via radar tracking
07 p1395 A70-20259
- ROBIN superpressure mylar spherical falling balloon deployed from sounding rocket apogee for density and wind measurements via radar tracking
07 p1194 A70-20260
- Measurement physics of resistance wire temperature sensing system used in Skua rocket sounding system
07 p1396 A70-20262
- Arcas rocket-borne chemiluminescent ozonesonde for measuring ozone concentration after deployment above stratosphere level
07 p1396 A70-20263
- Rocket-borne sampler for collecting noctilucent cloud particles in mesopause, describing collection and analysis methods and protection against tropospheric contamination
07 p1273 A70-20266
- Omegatron mass spectrometer for rocket measurements of molecular nitrogen density and temperature in middle thermosphere
07 p1289 A70-20308
- Stellar spectrophotometry by rocket-borne equipment, describing instrumentation, rocket assembly, calibration and spectra obtained
09 p1755 A70-22505
- Upper atmosphere research by U.S.S.R. mass spectrometers onboard French rocket probes, discussing design, payloads and equipment tests
09 p1766 A70-22658
- Ionospheric irregularities investigated by rocket- and satellite-borne transmitters, obtaining ionization profiles from amplitude, phase and polarization of radio waves
09 p1669 A70-23273
- Ionospheric plasma lower hybrid resonance measurement and excitation via rocket-borne probe
09 p1670 A70-23319
- Solar x-ray flare of 17 August 1966, describing rocket-borne instruments and measurements
09 p1746 A70-23479

Auroral ion composition and chemistry from rocket-borne mass spectrometer measurements, investigating oxygen density and green line excitation

10 p1874 A70-24431

Rocket- and projectile-borne microwave miniature solid state transmitters, discussing transistor oscillator-multiplier, hybrid integrated circuits, bulk effect devices, etc

10 p1852 A70-24887

Solar outer corona brightness distribution from rocket observation with scanning devices during solar eclipse, estimating error

11 p2107 A70-25397

Meteorological transponder rocketsonde instrumentation system evolution and data error analysis

14 p2585 A70-30579

Stratospheric and mesospheric ozone diurnal variation by rocket-borne ozonesonde in January 1968

14 p2577 A70-31170

Ionospheric electron concentration and temperature measurements by cylindrical Langmuir probe on rockets and satellites, emphasizing error sources

15 p2723 A70-31657

D region electron concentration and collision frequency in slowly varying plasma, using rocket-borne probe for ground emitted wave detection

15 p2778 A70-31673

E region ion composition from rocket-borne mass spectrometer data

15 p2725 A70-31689

Atmospheric density and temperature measurements by satellite- and rocket-borne pressure gages and mass spectrometers, considering error sources

15 p2731 A70-32092

Polypropylene window proportional counter on board sounding rocket for cosmic soft X ray measurement

15 p2741 A70-32530

Nerva nuclear subsystem diagnostics and control instrumentation, discussing transducers [AIAA PAPER 70-659]

16 p2949 A70-33551

Solar UV flash spectrum by spectroheliographs flown aboard Aerobee 170 mission during total solar eclipse

16 p2977 A70-33838

Taurus X-1 X ray emission polarization, using rocket-borne polarimeter

17 p3150 A70-34845

Solar X-ray emission localization, examining spatial distribution by rocket-borne collimated proportional counter

17 p3151 A70-34864

Plasma resonance phenomena related to ionospheric plasma parameters using gyroplasma probe on Kappa 8-15 sounding rocket

17 p3077 A70-35307

Winter ionosphere electron density profile from rocket-borne gyro-plasma probe observations

17 p3078 A70-35308

Sounding rocket instrumentation for ionospheric VLF radio noise measurement and recording

17 p3090 A70-35398

Ionospheric radio noise measurements with VLF wideband receivers onboard rocket

17 p3046 A70-35399

Ionospheric sounding with gyro-plasma probe on Kappa 8-15 rocket, discussing electron density profiles and plasma resonance

17 p3079 A70-35638

Meteoritic dust collection in upper atmosphere by sounding rocket, discussing efficiency of sampling configurations for inertial impaction

18 p3316 A70-36768

Upper atmospheric neutral components temperature determination by rocket-borne mass spectrometers

18 p3252 A70-36983

Upper atmospheric layers neutral composition by rocket-borne mass spectrometers, indicating gravitational separation of argon from molecular nitrogen

18 p3252 A70-36984

Gyroplatform for controlling rocket motion during rotation about longitudinal axis

19 p3420 A70-37258

Protons and alpha particles energy spectra during 25 February 1969 solar event from Centaur rocket measurements

19 p3496 A70-37509

Protons and alpha particles energy spectra following solar flares of 24-25 February 1969 from rocket measurements, estimating proton mean free path

19 p3496 A70-37510

D region positive ion density during solar proton event by Arcas rocket-borne cylindrical electrostatic probe

19 p3411 A70-37512

Voltage programmed RF oscillator (VPO) for spaceborne quadrupole mass spectrometer, describing transistorized circuitry

20 p3630 A70-39487

Solar outer corona brightness distribution from rocket observation with scanning devices during solar eclipse, estimating error

20 p3710 A70-40089

Galactic and extragalactic discrete cosmic X ray sources by rocket observation with narrow slit collimators

21 p3871 A70-40656

Cosmic X ray spectra of Cyg XR-2 in 0.15-20 keV range by spinning rocket-borne detector, noting interstellar absorption

21 p3872 A70-40664

Rocket-borne double probe electric field detector design and operation, discussing error sources

22 p4030 A70-42793

Auroral zone electric field measurements from rocket-borne instruments

22 p4017 A70-42794

Pulse counting and encoding system on rocket-borne spectrophotometer for starlight collected by primary telescope mirror

22 p4038 A70-43174

Auroral electrojet, arcs, electric and magnetic fields relationship investigated by rocket-borne magnetometers and photometers

23 p4184 A70-43835

Aerobee rocket-borne cryogenic air samplers heat exchanger design by mathematical model and computer solution

23 p4280 A70-44365

Cactus high sensitivity accelerometer flight tests, discussing operation and experimental conditions [ONERA-TP-875]

23 p4198 A70-44660

Nike-Apache rocket aurora probes using proton detector to measure galactic cosmic ray intensity and relativistic electrons

23 p4192 A70-44879

Class 1b solar flare X ray examination, using rocket-borne liquid N cooled solid state detector

24 p4397 A70-45767

ROCKET-BORNE PHOTOGRAPHY

Rocket-borne spectroheliograph for taking X ray and monochromatic pictures of sun in Mg II line

03 p0570 A70-13594

Auroral pulsation observed by Aerobee rocket instruments and ground multichannel photometer indicating primarily temporal fluctuation

09 p1671 A70-23497

Orbital photography interpretation from test rockets and Apollo-Gemini spacecraft, considering environmental applications

20 p3634 A70-40321

Solar X-ray corona during eclipse of 7 March 1970, using Aerobee rocket photographs

20 p3713 A70-40430

ROCKETRY

U ROCKETS

ROCKETS

Potential flow over rocket contour containing bends calculated by polygonal distribution of singularities on axis of body of revolution, determining friction effects

06 p0964 A70-17239

ROCKS

NT ANORTHOSITE

NT ATAXITE

NT BASALT

NT BRECCIA

NT CARBONACEOUS ROCKS

NT ENSTATITE

NT IGNEOUS ROCKS

NT LAVA

NT LIMESTONE

NT LUNAR ROCKS

NT MAGMA

NT MOLDAVITE

NT OLIVINE

NT PYROXENES

NT QUARTZ

NT SEDIMENTARY ROCKS

NT SHALES

Worldwide data inventory of rock features associated with meteorite impact structures, including photomicrographs of petrographic features

01 p0069 A70-10223

Polycrystalline rocks elastic constant and nonelastic behavior, discussing Voigt, Reuss and Hill averaging methods

01 p0071 A70-10446

Lherzolite, anorthosite, Gabbro and basalt dredged from Mid-Indian Ocean Ridge noting geological and geophysical features

04 p0675 A70-14422

Terrestrial solid powdered rocks HF electrical properties measurements for lunar radar observation

04 p0678 A70-15054

Surveyor 5, 6, 7 missions alpha-scattering experiments, lunar rocks chemical composition compared with earth rocks and chondritic meteorites

04 p0752 A70-15062

Surveyor 7 highland landing soil mechanical properties and rock diameter similar to previous sites

04 p0752 A70-15063

Surveyor 7 lunar surface sampler, obtaining soil and rock data

04 p0752 A70-15064

Chemical abundance data of lunar surface rocks, suggesting basaltic achondrites and eucrites origin from moon

06 p1137 A70-17196

Finite element method applied to potential distribution and stress analysis in earth sciences, determining elastic response of rock layer using structural matrix analysis

06 p1055 A70-17606

Bottom rock structure and composition of young lunar craters compared with Kamchatka volcanic morphological analogs

07 p1385 A70-19424

Color and black-and-white photomicrographs and photomicrographs of Apollo 11 moon rock sample consisting of spongy gray mass of pumice-like material

07 p1288 A70-20224

Lunar science - NASA Conference, Houston, January 1970, covering moon rock composition, magnetic, electrical and physical properties, etc

08 p1565 A70-20587

Laboratory irradiation of rock samples for solar wind flux effects on IR reflectivity of lunar rocks

08 p1579 A70-21565

Gaseous species in equilibrium with Apollo 11 holocrystalline rocks during crystallization

09 p1758 A70-22744

Photographic and IR multiband spectral discrimination for rock and soil mapping from orbiting ERTS satellites

09 p1668 A70-22882

High energy neutron activation method for remote extraterrestrial in situ rock surface constituents analysis

10 p1932 A70-24614

Oceanic ridge volcanic rocks alkali metal, alkaline earth, rare earth, nickel and major element content, observing partial melting

10 p1877 A70-24648

Physicomaterial properties of tuff rock based on similarity to lunar surface rock, determining natural density, porosity and compression strength

11 p2119 A70-26798

Lunar rocks types determination by mass spectrometry, describing results of terrestrial rocks tests

11 p2119 A70-26799

Mass distribution of Sikhote Alin meteorite fragmentation, noting similarity to terrestrial rocks

13 p2490 A70-28916

Total nitrogen content determination in silicate samples of rocks, synthetic silicate standards, NBS steels and meteorites using inert carrier-gas extraction-gas chromatography

13 p2362 A70-29497

Cretaceous rock paleomagnetism from Israel lava fields, determining original magnetization directions

19 p3413 A70-38034

Microorganisms metabolic activity effects on rocks and minerals, observing solubilization and altered IR absorption in Si-oxygen vibration region during penicillium simplicissimum growth

21 p3761 A70-40712

Sequential instrumental activation analysis for trace elements in rocks and stony meteorites, comparing with silicate method

24 p4310 A70-46407

ROCKWELL HARDNESS

Martensite start depressed temperatures vs pressure for steels, discussing hardness effects and microstructure

01 p0120 A70-10740

Rockwell hardness tester attachment design for studying temperature dependence in various multiphase alloys at high temperature

01 p0121 A70-11110

RODENTS

NT GROUND SQUIRRELS

NT GUINEA PIGS

NT HAMSTERS

NT MICE

NT RABBITS

NT RATS

Neuron activity in somatosensory cortex region of guinea pigs and rats with intracortical connections severed by circular incision

01 p0030 A70-11470

Time course of end bulb material formation in vitro in rodent myelinated nerve fibers, confirming elastic capillary concept

02 p0233 A70-11725

Acid mucopolysaccharides in distal segments of medullary substance of kidneys of rodents under high ambient temperature, showing stable morphological characteristics

07 p1204 A70-19141

Long term helium-oxygen atmosphere effects on rats and mice, investigating biochemical and metabolic changes

16 p2849 A70-33996

RODS

Longitudinal wave motion in rods, plates and shells based on three dimensional equations and asymptotic expansion

01 p0209 A70-11365

Elastic curve deformation of rod in equilibrium under end loads, using equations analogous to Kharlamov kinematic equations and Chaplygin solution

01 p0094 A70-11440

- Kirchhoff kinematic analogy applied to solution of gyrostat motion, noting elastic rod deformation under torsion, using Kharlamov equations
01 p0094 A70-11441
- Boundary conditions of heat conduction in systems of vessels connected by rods with given heat capacity and unknown temperature
02 p0400 A70-12674
- Heat equation prediction, considering insulated uniform rod with unknown temperature distribution
03 p0604 A70-12993
- Stress cycle asymmetry effects on energy dissipation in rods under torsional vibration
03 p0588 A70-13249
- Natural mode shapes of longitudinal oscillations and resonant frequencies of thin rods of constant curvature and rings with slit, noting use for crack determination
03 p0588 A70-13283
- Rotational stability of spacecraft with hinged inelastic rods determined in first approximation from motion equations
04 p0759 A70-14426
- Parametric oscillations of unclamped rod under variable longitudinal force applied to end, approximating resonance boundaries and instability regions
05 p0934 A70-16226
- Elastoplastic rod systems under repeated variable loads, calculating carrying capacity from plastic failure considerations
06 p1163 A70-17395
- Rotation of circular cross sectioned continuous rod with constant bending moment, assuming linear strengthening with fixed cyclic strain diagram
06 p1163 A70-17396
- Stress-strain state of curved rod made of anisotropic material under bending loads applied to end face cross sections
07 p1399 A70-18661
- Soviet monograph on theory and calculations of impact systems covering solid body collisions, elasticity, wave mechanics and nonflat rod applications
07 p1400 A70-18732
- Calibrating rods design for vibrating components stress measurement gauges
07 p1400 A70-18822
- Prestrain effect on waves propagation along slender low density unoriented polyethylene rod, indicating uniform phase velocity change over audio frequency range
07 p1248 A70-19237
- Nonlinear thermodynamic theories of plates, elastic shells and rods derived from three dimensional theory of classical continuum mechanics
07 p1414 A70-20172
- Natural oscillations of three dimensional bundle of parallel strapped rods with variable elastic mass parameters determined by Hamilton-Ostrogradskii variational principle
08 p1583 A70-20485
- Single frequency oscillations of variable cross section rods with random perturbations using asymptotic methods of nonlinear mechanics, discussing wedge oscillations
08 p1583 A70-20487
- Stress-strain analysis for rod-shaped structural elements under combined tensile and bending loads
08 p1588 A70-21191
- Curved thin rods torsional and flexural waves propagation equations, considering geometry and shear and Young moduli
08 p1588 A70-21201
- Elastic body equilibrium forms bifurcation solution for uniform strain applied to cylindrical rod and shell under compressive strain
09 p1773 A70-22539
- Longitudinal vibration of finite viscoelastic rod with changing boundaries under time-variant force, analyzing impulse response by transform calculus
09 p1777 A70-22833
- Thermoacoustic waves formation and propagation in metallic rods by light pulses, studying pulse rise time influence on waves shape and amplitude
09 p1778 A70-23090
- Buckling stability of slender knife-edge suspended rods subjected to compression end loads
10 p1955 A70-24053
- Transverse vibrations of rods, plates and shells based on hyperbolic, circular and Bessel functions
10 p1959 A70-24586
- Capacity bounds in microwave filters computed for periodic cylindrical rods between parallel ground planes using variational principles
10 p1850 A70-24834
- Thermal conductivity on coupled heat conducting rods calculated by implicit difference scheme on finite graphs
10 p1969 A70-25189
- Frequency equation for harmonic waves propagating in composite circular-cylindrical rods consisting of circular core and circular casing of different material
11 p2145 A70-26693
- Rotational stability of spacecraft with hinged inelastic rods determined in first approximation from motion equations
13 p2503 A70-28451
- Pressure buckling values of rod and plate profiles with thicknesses graduated across pressure direction in presence of uniform and nonuniform stress distributions
13 p2507 A70-28477
- Composite cylindrical laser rods end region stress and optical pathlength change with thermal expansion or contraction between core and cladding
13 p2429 A70-29703
- Torsion of variable diameter rods based on moment theory of elasticity, solving integral equations system
13 p2517 A70-29774
- High temperature elastic moduli of slender polycrystalline aluminum rods with elastic waves generated by Q switched laser energy
14 p2595 A70-30638
- Energy dissipation during independent flexural-torsional vibrations of rods, noting alternating shear stress superposition effect on damping
15 p2813 A70-31530
- Differential equation for longitudinal vibrations of rod at high temperature, giving asymptotic solution
15 p2814 A70-31589
- Rarefaction wave analytical construction by successive approximation, solving hyperbolic equations for longitudinal vibrations of rods
15 p2815 A70-31644
- Reflection coefficient formula for principal radio wave reflected from thin long rod in middle of rectangular waveguide
16 p2878 A70-33800
- One dimensional analysis of stress and strain concentration resulting from longitudinal impact of viscoelastic rods
17 p3185 A70-34965
- One dimensional elastoplastic wave propagation in rate-sensitive viscoplastic rod with thermal gradient
17 p3185 A70-34966
- Mass distribution role in stability theory of rods under nonconservative buckling load
18 p3335 A70-35961
- Critical loads for notched square Al alloy rods under tension
18 p3343 A70-36718
- Plates and rods tendency to warp and form nonsymmetrical stress systems during heat treatment
19 p3433 A70-37272
- Stress relaxation in rings and rods, discussing errors possible in data correlation
19 p3535 A70-37342
- Stress cycle asymmetry effects on energy dissipation in rods under torsional vibration
19 p3548 A70-38467
- Rod surface roughness effect on eddy sound frequency and intensity and on aerodynamic resistance
19 p3353 A70-38654
- Laser rod faces parallelism measurement by interferometric method for Brewster or square ended rods
20 p3640 A70-39095
- Oscillation harmonics in rods under loads, giving inequalities to obtain algorithm for determination of overtones
20 p3721 A70-39781
- Isotropic homogeneous elastic cylindrical rods, investigating nonlinear longitudinal dispersive waves corresponding to water wave theory analogs
22 p4115 A70-42952
- Heavy homogeneous material free elastic rod dynamic stability under distributed scanning load, investigating plane transverse vibrations by differential equations
22 p4121 A70-43722
- Optimal load distribution for prestressed rod system, using Chebyshev solution of inequalities
22 p4121 A70-43725
- Exponential compression wave propagation in conical rod with smooth tapering cross section
22 p4121 A70-43726
- Fundamental error in Galerkin method application to bending problem of elastic rods
23 p4268 A70-44172
- Torsion in rods with rectangular and trapezoidal cross sections, using functional-analytic iterative method
23 p4268 A70-44241
- Perturbation effects on nonlinear first order wave equations discontinuous solutions decay, discussing boundary value problem for stress wave propagation in rod with viscous damping
24 p4426 A70-46026
- Ballistic reentry vehicle roll related to trim angles caused by inertia asymmetries
06 p1156 A70-18074
- Aircraft roll rate response and aileron step input matching in terms of modal parameters with flight test records by analog computer program
08 p1465 A70-20781
- Airborne simulator program for evaluation of motion and visual cue effects on pilot performance in roll, using compensatory tracking tasks
10 p1857 A70-24202
- Cone roll dynamics-ablation patterns coupling in hypersonic wind tunnels
13 p2340 A70-29025
- Aircraft optimal roll stabilization control system design using performance index with weighting matrix
14 p2532 A70-31395
- Ballistic reentry vehicle roll-pitch coupling, showing influence of nose asymmetries
21 p3930 A70-41736
- Aircraft rolling motion /eigenmotion/ in flight at small angle of attack following initial disturbance, discussing response to control action
22 p3961 A70-42515
- ROLL CONTROL
U LATERAL CONTROL
- ROLLER FORMING
Roller machine adjustment parameters determination by analytical relations allowing for intermediary zone
07 p1292 A70-18837
- Rolling texture and recrystallization of Mo single crystals and deformation effect on texture formation using X ray transmission technique
07 p1309 A70-19613
- Earing during rolling of high purity aluminum on broad hot-strip mill, investigating thickness, temperature and composition relationship
09 p1692 A70-22641
- Integrally stiffened structures made by hot isostatic pressing of metal powders followed by conventional rolling
12 p2242 A70-27109
- Metal powder rolling process as compaction with plastic particle deformation, deriving pressure distribution on rollers
19 p3434 A70-37451
- ROLLER BEARINGS
Roller bearing endurance dependence on shaft speed, surface finish and elastohydrodynamic lubricants temperature, viscosity and film thickness
01 p0101 A70-10387
- Hybrid boost bearing applied to jet engines thrust bearing life extension and to land turbine equipment for providing high overload capacity
01 p0101 A70-10389
- Inertia effects in squeeze film between two curved surfaces and in externally pressurized bearing with converging lubricant film
01 p0104 A70-11388
- Roller bearings convex conical surfaces grinding using centerless grinder
08 p1506 A70-21192
- Elastohydrodynamic lubrication of rollers relationship to pressure
09 p1693 A70-22978
- Turbine technology application to high speed roller bearing design, considering reduction of roller skidding and skewing
13 p2419 A70-28918
- Rolling element bearings fatigue life prediction and extension, using elastohydrodynamic lubrication theory
16 p2917 A70-33423
- Rolamite low friction suspension system, describing components, force generation and applications
16 p2923 A70-34165
- Hybrid boost bearing with long life and free starting, stopping and oil system failure characteristics of rolling element bearing
19 p3435 A70-37605
- Jet engine roller bearings retainer candidate cage materials and coatings evaluation on test rig simulating engine conditions
19 p3439 A70-38805
- Gas turbine engine compressor rotor roller bearing operation conditions analysis by computer calculation of thermal regime
21 p3834 A70-41777
- ROLLING
Work of plastic deformation in two dimensional rolling determined by energy dissipation function
05 p0857 A70-17017
- Strain rate effects in cold metal working processes involving rolling and drawing
08 p1590 A70-21327
- Hot rolling and warm working effects on microstructure and mechanical properties of Ni-Cu-Cb steel, noting optimum austenite plus ferrite phase field
15 p2756 A70-31566
- Soviet monograph on bimetal and refractory metals production by rolling in vacuum or inert media
19 p3433 A70-37402

Succession of passes in rolling and hot shaping of thin walled angle steel

22 p0405 A70-42813

Strained state of Ti and steel sheets during unsymmetric rolling, constructing deformed metal particles displacements rates field based on ideal fluid motion equations

22 p0405 A70-42814

ROLLING CONTACT BEARINGS

U ANTIFRICTION BEARINGS

ROLLING CONTACT LOADS

Creep and wear due to microslip under dry rolling contact conditions

05 p0854 A70-15890

Bearing materials rolling contact fatigue life, describing three ball-cone test machine

09 p1702 A70-22555

Fractography of spall cavities and crack growth in ball rolling contact fatigue, using scanning electron microscope

15 p2745 A70-32444

Crack initiation and propagation in rolling contact fatigue, emphasizing electrochemical effects in ball bearing failure

16 p2931 A70-33509

ROLLING MOMENTS

Gyrocompass composed of angular velocity integrators and interconnected by correction amplifiers, analyzing behavior during roll on vessel, determining error components

03 p0484 A70-13371

Roll acceleration influence on angle of attack convergence and windward meridian rotation rate of rolling reentry vehicles

[AIAA PAPER 69-100] 04 p0764 A70-15546

Roll induced cross coupling evaluation in two dimensional homing systems based on defining roll transfer matrix

11 p2122 A70-25681

Low aspect ratio wings calculated for roll-damping derivatives, investigating load distribution

12 p2157 A70-27983

Nonlinear rolling motion of four-finned missile, investigating function of angle of attack and cubic damping

13 p2503 A70-28531

Asymmetrical slender planetary entry vehicle roll dynamics, analyzing steady state angular motion

[AIAA PAPER 70-560] 13 p2339 A70-29003

Projectiles yawing and rolling over long flight paths, describing onboard solar aspect sensor and telemetry link to ground stations

[AIAA PAPER 70-538] 13 p2406 A70-29005

Slender wings leading edge vortex flow effect on roll damping at subsonic speeds

[AIAA PAPER 70-540] 13 p2339 A70-29007

Missile roll rate from yawing motion frequencies determined by epicyclic theory

[AIAA PAPER 70-536] 13 p2506 A70-29075

Aircraft lateral and longitudinal motion stability in steady rolling, deriving inertia cross coupled stability criterion

13 p2347 A70-29445

Rudder control of aircraft nullifying yawing and sideslip angles, analyzing rolling response to proportional control by ailerons

13 p2348 A70-29450

Rolling reentry body velocity as function of roll, pitch, yaw rates and angle of attack

13 p2343 A70-29991

Small reentry vehicles roll motions and impact point dispersion due to spin reversal

15 p2813 A70-32522

Cruciform-finned missiles dynamic stability investigation by nonlinear differential equations of motion, considering roll lock-in, resonance instability and catastrophic yaw

[AIAA PAPER 70-969] 20 p3715 A70-39560

ROOM TEMPERATURE

Beryllium single crystals deformation under high pressures at room temperature similar to deformation under atmospheric pressure at elevated temperatures

05 p0863 A70-16203

Fabrication technique effect on tensile and plastic properties of semifinished sintered Al powder products at room temperature and 600 C

06 p1076 A70-17848

Reflectivity measurement in near IR using black bodies near room temperature for light sources

14 p2588 A70-31210

High power CW CO laser operation at room temperature by introducing mercury vapor into discharge

15 p2751 A70-31979

Thermal exposure effect on room temperature mechanical properties of Ti alloys, noting diffusion bonding, hot forming and heat treatment

17 p3120 A70-34422

Ring and cylindrical structures comparative stress relaxation at room temperature

19 p3535 A70-37341

ROOMS

NT CLEAN ROOMS

NT DARKROOMS

Coupled panel-cavity vibrations analysis, emphasizing sonic boom excitation of large window-room combinations

11 p2133 A70-25728

ROOT-MEAN-SQUARE ERRORS

FM/FM telemetry systems waveform distortion measurement technique based on minimum rms error between input and output signals

01 p0044 A70-10941

Rms error for reproduction of satellite signal transmitted through continuous Gaussian channel assessed by numerical calculation

01 p0046 A70-11513

Generalized approach for optimal corrector in mean squared sense for predictor-corrector filter structure, illustrating signal modes with nonlinear and linear dynamics

03 p0520 A70-14170

Statistical analysis for personal variations contribution to total mean square error in time determinations

05 p0914 A70-16649

Optimal synthesis of linear steady multidimensional systems with common output ensuring minimum rms error in reproducing control action

08 p1480 A70-21497

F 2 layer critical frequencies rms deviations approximate dependences on latitude and solar activity for computer calculation of long-range ionospheric forecasts

11 p2043 A70-25549

Phase locked loop damping characteristics optimization based on input rms error rate minimization and transient error integral square value limitation

15 p2704 A70-32604

Adaptive linear estimator for stationary time series, evaluating asymptotic mean square error bound

17 p3128 A70-34852

Gaussian source model of image, deriving rate distortion function under mean square error criterion

17 p3049 A70-34857

Statistical accuracy of standard muon azimuthal semicubic telescope for solar cosmic rays, discussing rms error

18 p3256 A70-36103

RMS spectrum analysis system for wideband acoustic data processing, using analog method with digital output

19 p3397 A70-37910

Mean square error for measurement series with unknown error distribution law, specifying necessary number of terms

19 p3390 A70-38583

Nonstationary inhomogeneous random vector fields linear prediction, determining minimum mean square approximation error

20 p3604 A70-39911

Automatic stabilization of random noise mathematical expectancy and mean square deviation by feedback control system

20 p3593 A70-39916

F 2 layer critical frequencies rms deviations approximate dependences on latitude and solar activity for computer calculation of long-range ionospheric forecasts

21 p3819 A70-41299

Monthly and annual root-mean-square deviations of ionosphere radio wave absorption

24 p4312 A70-45485

ROOTS

Structural fatigue strength model tests for turbine blade root connections, using asymmetric load cycle and working temperature

19 p3547 A70-38433

ROOTS OF EQUATIONS

Self excited oscillators zero crossing times distribution for Markov process formulated as boundary value problem involving Kolmogoroff backward equation

01 p0143 A70-10891

Zero crossings of signal harmonic function with normal phase distribution, deriving relations with spectrum and modulating process parameters

03 p0447 A70-13289

Geometrical determination of real roots of equations applied to linear oscillator and gyroscope in gimbal suspension

03 p0484 A70-13374

Sinusoidal signal detection in Gaussian noise band by zero crossing method, discussing signal frequency position and SNR

04 p0648 A70-14705

Stability and limiting frequency of analog computer solutions of differential equations with root shifts caused by resolver imperfection

07 p1321 A70-18689

Flugge characteristic equation approximate roots for closed cylindrical shell compared with Donnell equation solution

08 p1593 A70-21625

Solar system planetary mean motions calculation from characteristic equations roots at equilibrium points of restricted three body problem, using Taylor series solution

09 p1760 A70-22915

Asymptotic splitting of system of linear differential equations with slowly varying coefficients in cases with characteristic equation having multiple roots

09 p1712 A70-23119

Root-locus approximation technique extended for complex plane analysis of equations with quadratic term in variable parameter for linear multivariable feedback systems

10 p1855 A70-24449

Asymptotic behavior of polynomial root locus in presence/absence of time lag, outlining procedures for constructing root locus diagrams

10 p1910 A70-24845

Stability of multiconnected nonlinear controlled systems with nonsingle equilibrium position, representing lumped parameter system with characteristic equation having complex roots

11 p2021 A70-25338

Root loci construction for differential equations with quadratic free parameters applied to aircraft motion with roll control

11 p2071 A70-25393

Characteristic equation roots for circular cylindrical shells deformation under edge load

11 p2135 A70-25960

Dimensional stability derivatives from XV-4B aircraft simulator varied in computer program for extracting roots of lateral-directional characteristic equation

[AIAA PAPER 70-551] 13 p2346 A70-29016

Sum envelope zero crossings determination for steady normal noise plus random amplitude signal

13 p2370 A70-29742

Root locus of active distributed RC circuit for synthesis of magnitude response of parabolic filters

14 p2562 A70-31323

Numerical method for roots of algebraic equations, computing continuous beam lateral vibrations natural frequencies

14 p2600 A70-31330

Single input control system design for specified roots using output feedback

17 p3057 A70-35554

Automatic control systems synthesis based on root locus trajectories theory

19 p3392 A70-37808

Multiparameter systems with dominant complex roots constrained by degrees of freedom to construct reduced characteristic equation

19 p3392 A70-37824

Feedback control system characteristic equation generalized root locus following technique using straight line approximation

20 p3659 A70-40121

Polynomials with interval coefficients, presenting Newton Raphson algorithm for real roots error bounds

20 p3659 A70-40133

Intrinsic equations with roots for optimal two-impulse transfer between given positions

23 p4246 A70-44698

RORSCHACH TESTS

Pilot trainees psychological screening, correlating Rorschach test parameters with subsequent training performance

24 p4306 A70-45123

ROSETTE SHAPES

Strain gauge data obtainable on rosettes used for measuring test component stresses at 550 F in inert atmosphere

03 p0482 A70-12965

Scattered light rosette using three polarized light beams intersecting at surface point to evaluate photoelastic stress data

15 p2739 A70-32320

ROSHKO PREDICTION

Compressible fluid two dimensional irrotational flow past Roshko model in channel, deriving exact solution by hodograph method

13 p2341 A70-29487

ROSSBY REGIMES

Two layer truncated harmonic model of Rossby wave dynamo for solar cycle, accounting for maintenance and reversal of magnetic fields

01 p0174 A70-10238

Vorticity number derivation for rotational flows, discussing reciprocal of kinematic Rossby number and vorticity measures

01 p0061 A70-10541

Geostrophic baroclinic flow with zonal magnetic field in beta plane channel, analyzing instability, phase velocities, Alfvén-Rossby waves and Eady problem

02 p0291 A70-12284

Swirling flow through axisymmetrically deformed tube without consideration of viscosity and compressibility, noting wall flow for critical Rossby number values

03 p0468 A70-13788

Solar differential rotation relation to Rossby waves in upper convection zone based on energy conversion rate estimates

06 p1144 A70-18010

Jupiter geostrophy indicated by circulation, vorticity and Rossby number determined from Great Red Spot observations

08 p1580 A70-21573

Rosby wave critical level time dependent behavior on latitudinally varying flow 19 p3414 A70-38259

Solar photosphere negative viscosity phenomenon, examining Rossby wave on differentially rotating isothermal spherical shell of nonconducting inviscid ideal gas 22 p4109 A70-43748

Stationary disturbances in winter Northern Hemisphere stratosphere considered as upward propagating Rossby waves, assuming zonal winds profile 23 p4213 A70-44030

ROTARY DRIVES

U MECHANICAL DRIVES

ROTARY GYROSCOPES

Rotational motion of self excited symmetric gyroscopes applied to attitude control and nutation damping of space vehicles 01 p0143 A70-10929

Cyclic bending stress in disk type gyroscope rotor under steady precession, discussing solutions for modal functions and resonant frequencies [ASME PAPER 69-DE-A] 04 p0689 A70-14873

Rotor-driven vibrational gyroscope device dynamic characteristics, stability, transient delta function, signal response and sensitivity assessment 05 p0848 A70-16222

Wave functions of asymmetric gyroscope in rotating coordinate system, presenting quantum equation of motion solution 06 p1105 A70-17500

Directional gyroscopes with accelerated rotors on moving bases, deriving gyro errors as base motion functions 09 p1680 A70-23145

Two rotor gyrocompass unperturbed motion nonasymptotic stability as function of vessel speed and cruising latitudes 09 p1681 A70-23299

Energy dissipation effect on complex parametric resonance and stability of two rotor gyrocompass on ship in motion 13 p2408 A70-29295

Damping by hemispheric torquing to control spin axis in gyroscope rotor while remaining unchanged with respect to case fixed reference 15 p2741 A70-32505

Free rotor air bearing gyros active damping evaluated through experimental studies [AIAA PAPER 67-590] 15 p2741 A70-32506

Two body torque free gyrostat equations of rotational motion, relating rotational, spin and precession angular velocities 16 p2912 A70-33877

Variable mass body rotational motion stability in central Newtonian field with gyroscope on symmetry axis 21 p3849 A70-40616

Poisson kinematic equations solution of symmetric gyrostat in viscous medium for free rotor and constant angular speed, using perturbation technique 23 p4220 A70-44560

ROTARY STABILITY

NT GYROSCOPIC STABILITY

Precession motions of rigid body with variable mass, considering angular momentum and rotation stability 01 p0141 A70-10283

Externally pressurized gas lubricated journal bearings zero load rotating stability, using digital computer [ASME PAPER 69-LUB-27] 01 p0100 A70-10382

Spinning top motion stability in homogeneous incompressible ideal resting fluid, using stability derivative for body of revolution 01 p0145 A70-11438

Stability and dynamics of dielectrophoretic equilibria, considering circular cylindrical column of inviscid liquid with rigid body rotation 03 p0525 A70-13784

Stability analysis of rotors consisting of disks on massless shaft mounted in unsymmetrical flexible bearings, considering free and forced vibrations with damping neglected 03 p0599 A70-14248

Elasticity theory of orthotropic materials applied to steady rotation of long cylindrical tubes of filament reinforced plastics 03 p0602 A70-14331

Rotational stability of spacecraft with hinged inelastic rods determined in first approximation from motion equations 04 p0759 A70-14426

Aircraft engine support system dynamic loads induced by fan unbalance analyzed by coupling pylon and engine vibration modes 05 p0895 A70-15850

Helicopter dynamics structural model extended to LF longitudinal motions by including stabilizing feedback loop representing forward velocity influence on main rotor 06 p0987 A70-17910

Forced and free vibrations of shaft carrying unsymmetrical rotor, studying effects of distributed shaft mass and nonlinear shaft stiffness 07 p1401 A70-18976

Unstable vibrations in rotating flat shaft with unsymmetrical flexibility carrying unsymmetrical rotor in four degrees of freedom 07 p1402 A70-18978

Dioscures project satellites design, considering use of rotation stabilization 07 p1392 A70-18989

Anisotropically elastic rotor vibrations stability analysis allowing for damper mass and internal/external friction, determining regions of steady and unsteady motions 07 p1403 A70-19059

Equilibrium state instability of radial gas bearing accompanied by oscillations, examining bearing dynamics and nonlinear film reaction characteristics 07 p1295 A70-19536

Bladed wheels stability in centrifugal compressors, calculating natural vibration frequencies of rotors 07 p1364 A70-19634

Forced vibrations amplitude of rotor mounted on elastically damping supports 08 p1588 A70-21181

Magnetothermal instability and radiative effects on incipient fragmentation of rotating gravitating interstellar fluid forming condensations 08 p1578 A70-21545

Navier-Stokes equation for plane unsteady axisymmetric rotation of viscous fluid in steady radial flow from source or sink 09 p1660 A70-22437

Secular stability of rotating polytropes in relative equilibrium, isolating bifurcation point by calculating lowest sectorial modes for various sequences 10 p1937 A70-23946

Instability of Godel rotating universe, discussing stability to perturbations in rotation plane and unstable density perturbations along rotation axis 10 p1937 A70-23973

Stability conditions of rotational motions of symmetrical solid body on vibrating base in potential force field 11 p2098 A70-25916

Transistorized pistol grip probe design, circuit and operation for testing wobble and asymmetry in rotating ring commutators of electric motors 12 p2165 A70-27495

Rotational stability of spacecraft with hinged inelastic rods determined in first approximation from motion equations 13 p2503 A70-28451

Numerical solution of satellite rotational damping by onboard motors using Euler equations, local variations and finite control time 13 p2505 A70-28963

Oscillations and stability of rotating masses for axisymmetric equilibrium configurations with toroidal magnetic field based on virial equations 14 p2642 A70-30886

Ellipsoidal plasmoid equilibrium in external HF field, calculating rotation rate and potential energy 15 p2779 A70-32113

Spherical shaped rotor unbalance effect on electrostatic gyroscope runout time, discussing energy dissipation 15 p2738 A70-32152

Continuous elastic turboshaft flexible journal bearings, analyzing radial misalignment effects on operation [ASME PAPER 70-DE-71] 16 p2918 A70-33521

Rotor blade flutter in forward flight accounting for wake unsteady aerodynamic effect 17 p3184 A70-34727

Precessional stability of rigid body axial rotation in terms of Liapunov, Poincare and Lagrange concepts 17 p3131 A70-35318

Spinning body with rigid and elastic parts, using Liapunov direct method for attitude stability analysis 18 p3292 A70-36677

Sliding friction effects of nonlinear asymmetric supports on turbine engine rotor-shaft stability [SAE PAPER 700320] 18 p3301 A70-36799

Rotational stability of heavy horizontal shaft supported on plain lubricated bearings with cavitation in lubricant 19 p3438 A70-38669

Variable mass body rotational motion stability in central Newtonian field with gyroscope on symmetry axis 21 p3849 A70-40616

Differentially rotating stellar interiors nonaxisymmetric perturbation stability in toroidal and poloidal magnetic fields 24 p4413 A70-46165

ROTARY WING AIRCRAFT

NT AUTOGYROS

NT BO-105 HELICOPTER

NT CH-3 HELICOPTER

NT CH-46 HELICOPTER

NT CH-47 HELICOPTER

NT CH-54 HELICOPTER

NT COMPOUND HELICOPTERS

NT F-28 HELICOPTER

NT HELICOPTERS

NT MILITARY HELICOPTERS

NT OH-6 HELICOPTER

NT RIGID ROTOR HELICOPTERS

NT SA-330 HELICOPTER

NT UH-1 HELICOPTER

U.S. rotorcraft research regarding materials and engine technologies of conventional and compounded helicopters 02 p0226 A70-12314

Rotor propelled aircraft development in West Germany, analyzing military and civil demand for rotor aircraft, light helicopters and V/STOL transports 03 p0413 A70-13793

Complex integrated avionics computer system design for navigation, guidance and control of rotary wing aircraft, emphasizing microelectronic modular assembly 06 p1014 A70-17353

Rotorcraft design and aerodynamics, discussing structural vibrations and all-weather operation 13 p2344 A70-28545

NACA/NASA rotating wing aircraft research history 1915-1970, Part 2, autogyro flight test experiences, rotor blade dynamics research, interest in helicopters, etc 23 p4142 A70-44852

NACA/NASA rotary wing aircraft research history 1915-1970, Part 3, covering rotor and helicopter theory, related flight and wind tunnel testing, etc 23 p4142 A70-44853

NACA/NASA rotating wing aircraft research history 1915-1970, Part 3, covering rotor dynamics and flying qualities, hovering tests, rotor flow, loads, etc 23 p4142 A70-44856

ROTARY WINGS

NT LIFTING ROTORS

NT RIGID ROTORS

NT TILTING ROTORS

NT TIP DRIVEN ROTORS

Test chamber to simulate helicopter rotor downwash for engine inlet air particle separator optimization 01 p0056 A70-10676

Turbojet aircraft engine performance correlation with relative humidity, noting air density effect on rotor performance resulting from moisture content 01 p0165 A70-10689

Flight tests conducted in artificial and natural icing conditions, using CH-3C helicopter with rotor blades equipped with polyethylene antiicing tape 01 p0006 A70-10695

Blade forces of helicopter rotor in forward flight calculated by unsteady lifting-line theory 01 p0004 A70-11366

Composite fibrous materials applicability to V/STOL rotor blades design and fabrication confirmed by structural analysis 02 p0225 A70-11953

Helicopter engineering covering structure, rotor systems, aerodynamics, vibration and applicability to fixed wing aircraft 02 p0225 A70-12309

Electron beam welding of AH-56A helicopter rotor hubs outside of vacuum chamber, discussing modifications of machine 04 p0699 A70-15651

Helicopter all-visibility operation realized by using main rotor blade as scanning radar antenna 05 p0793 A70-16040

Wire dischargers at helicopter propeller blade tips reducing electrostatic RF interference, substituting stainless steel wire tufts for nichrome wire 05 p0848 A70-16320

High speed compound helicopters with rigid and hinged rotors noting features, advantages and construction 05 p0794 A70-16351

Sound radiated by fluctuating forces on helicopter rotor analyzed, predicting noise output variation as function of helicopter design parameters 05 p0796 A70-16792

Matrix method for calculating aerodynamic loads, shearing forces, bending moments, torques, etc, in hinged main rotor helicopter blades during hover and vertical flight 06 p1167 A70-17914

Rotation and forward flight effects on separation line of laminar incompressible boundary layer along helicopter blade of airfoil shape [AIAA PAPER 70-49] 06 p0973 A70-18151

Laminar viscous flow on rotating propeller and helicopter rotor blades, studying crossflow and unsteady boundary layer effects, separation, transition, etc 06 p0974 A70-18161

Lifting line with arbitrary motion represented by line of acceleration doublets for unsteady aerodynamics of helicopter blades [ONERA-TP-787] 06 p0984 A70-18471

Unsteady aerodynamic forces on helicopter rotors using pressure measurements and wind tunnel visualizations of smoke emission [ONERA-TP-777] 08 p1434 A70-21847

Tuft position on rotating helicopter blade in hovering and forward flight, calculating tip path plane and tuftlines 08 p1438 A70-21868

ROTATING

Mathematical model with straight wake airfoil to determine aerodynamic forces on oscillating rotor blades in hovering flight

09 p1605 A70-23222

Blade torsional degree of freedom effects on stability and flapping response of rotors operating at high advance ratios

13 p2507 A70-28444

Helicopter rotor, discussing conventional, semirigid, gyro and ABC systems in relation to roll balance and control

13 p2344 A70-28849

Dual controlled elastically twisting rotor blade performance during flight with azimuthal and collective variations compared to direct control rotor

13 p2345 A70-29012

Electrothermal helicopter rotor blade deicing system, discussing design, operation and solutions for mechanical and reliability problems

13 p2348 A70-29552

Bifilar pendulum type absorber for helicopter main rotor vibration reduction

13 p2348 A70-29827

Real time analog simulation of helicopter rotor, calculating lift and drag coefficients along blade

15 p2672 A70-31775

Helicopter aerodynamic problems, discussing rotor performance improvement for increased cruising speed

16 p2841 A70-33758

Helicopter rotors flow conditions by digital computer, investigating slipstream configuration

16 p2836 A70-33761

CH-47C helicopter fiberglass main rotor blade, discussing composite materials impact on design

17 p3013 A70-34702

Composite tail rotor driveshaft for next generation helicopter, discussing materials, fabrication and tests

17 p3100 A70-34703

Helicopter rotor blades flapwise bending moments prediction by transfer function/superposition techniques

17 p3013 A70-34704

Helicopter blade sections dynamic stall characteristics, considering accelerated flow generation by nonzero pitch rate

17 p3014 A70-34718

Rotor blade flutter in forward flight accounting for wake unsteady aerodynamic effect

17 p3184 A70-34727

Helicopter rotors noise intensity prediction for high tip Mach number, including compressibility and thickness effects

17 p3015 A70-34729

Helicopter rotor blade stall flutter response prediction based on NACA 0012 airfoil aerodynamic data

17 p3009 A70-34734

Swept tip rotor blade design, discussing wind tunnel-whirl stand correlations

17 p3015 A70-34736

Helicopter rotor blade differential pressure and structural load characteristics in transient and steady state maneuvers

17 p3016 A70-34739

IR NDT bond inspection system for helicopter rotor blade honeycomb box assemblies, using closed circuit slow scan video system to detect bondline voids

17 p3101 A70-35184

Convertible helicopter rotor technology, discussing materials, blade configurations and variable diameter concept

17 p3018 A70-35550

Optimum adaptation of propulsion gas generators to power jet driven rotors with blown flap control, considering jet engine, fanjet and engine driven compressor

17 p3024 A70-35661

Aerodynamics theory for separated flow effects on helicopter lift-drag capability, taking into account three dimensional flow and blade aeroelasticity

18 p3205 A70-35956

Cross section deformation effect on helicopter rotor blade torsional vibration, using differential equations of vibrating beam

18 p3334 A70-35959

Model testing for helicopters, considering scaling, ditching and rotor performance

19 p3402 A70-38610

AERCAB (Aircrew Escape/Rescue Capability)/ flying ejection seat, considering rotary wings, fixed wings and parawings

21 p3751 A70-41806

Rotor drive systems for rotary wing aircraft, indicating mechanical hub drive advantages over reaction blade drive

21 p3755 A70-41850

Aerodynamic characteristics of elliptical airfoils with jet circulation control for VTOL rotors including dual jets and cyclic results

22 p3959 A70-42705

Aerodynamic problems due to mixed subsonic and supersonic/ transonic flows on swept wings, nacelle lips and helicopter rotor blades

23 p4132 A70-44125

Helicopter rotors fatigue testing using small scale models of full scale components

[ICAS PAPER 70-34] 23 p4267 A70-44131

Helicopter rotor tests in large wind tunnel for increased flight speed, noting pressure and noise measurements

[ICAS PAPER 70-44] 23 p4132 A70-44142

Low disk loading rotors in high speed VTOL aircraft for economical vertical payload lift

[ICAS PAPER 70-57] 23 p4139 A70-44153

Main rotor wake adverse effects on tail rotor directional control in low velocity wind

23 p4140 A70-44323

Dynamic systems stability with periodically varying parameters analyzed by Hill type infinite determinant, exemplifying helicopter rotor aeroelastic stability in forward flight

23 p4220 A70-44556

ROTATING

U ROTATION

ROTATING BODIES

NT COMPRESSOR ROTORS

NT FLYWHEELS

NT IMPELLERS

NT LIFTING ROTORS

NT PUMP IMPELLERS

NT RIGID ROTORS

NT ROTARY WINGS

NT ROTATING CYLINDERS

NT ROTATING DISKS

NT ROTATING SPHERES

NT ROTORS

NT TILTING ROTORS

NT TIP DRIVEN ROTORS

NT TURBINE WHEELS

Precession motions of rigid body with variable mass, considering angular momentum and rotation stability

01 p0141 A70-10283

Squeeze film investigation between rotating plane annuli, considering inertia due to centrifugal effect

[ASME PAPER 69-LUB-6] 01 p0102 A70-10396

Free convection to rotating central plate in synchronously rotating surroundings with and without consideration of Coriolis forces

[AICHE PREPRINT 9] 01 p0216 A70-10968

Characteristics method for calculating steady supersonic flow of burning gas mixture past wedge and rotating cones

01 p0218 A70-11018

Coriolis effects in spherical Einstein universe perturbed by rigid body rotation of shell with finite thickness

01 p0186 A70-11272

Geometrical interpretation of motion of body about fixed point in Hess case based on Kharlamov kinematic equations, using special coordinates system

01 p0144 A70-11428

Lagrange solution to differential equations of motion of body with fixed point, deriving directrices of mobile and fixed hodograph

01 p0144 A70-11429

Kharlamova solution for solid body motion in Newtonian force field represented as rolling, without slipping, of mobile hodograph of angular velocity vector

01 p0145 A70-11431

Kharlamova motion equations solution for solid body with fixed point in potential force field, assuming fixed center of gravity

01 p0145 A70-11432

Kharlamov motion equations solution for solid body with fixed point subjected to zero-potential forces

01 p0145 A70-11433

Euler-Poisson equations application to motion of heavy solid body about fixed point to determine kinetic momentum vector relative to fixed reference system

01 p0145 A70-11434

Kharlamov conditions for existence of linear and quadratic invariant relationships between equations of motion of body about fixed point

01 p0145 A70-11435

Canonic equations of motion of heavy solid body with fixed point

01 p0145 A70-11436

Motion of body with fixed point reduced to single second-order differential equation, analyzing special cases of gyrostatic motion

01 p0145 A70-11437

Variational approach to structure of rotating polytrope with symmetry about axis of rotation in postNewtonian approximation of general relativity

02 p0338 A70-11778

Elastic couplings applied as sliding contact-free continuous junction between permanently rotating and fixed parts in rotating coil magnetometer

02 p0298 A70-12214

Bubnov-Galerkin approximations convergence in problem of thin plate nonlinear vibrations, allowing for inertial forces due to rotation

03 p0593 A70-13470

Nonlinear theory for thin elastic shells with small strains and rotations, analyzing nonzero Gaussian curvature

03 p0594 A70-13622

Time optimal attitude control for alignment of spin stabilized sounding rocket, discussing feedback control system

03 p0580 A70-13805

Gravitational wave propagation velocity determined by laboratory measurement of spin-spin coupling of two rotating masses

04 p0718 A70-14397

Translational-rotational motion of long dumbbell in Newtonian central force field, analyzing plane center of mass trajectory with perpendicular kinetic moment vector

04 p0744 A70-14427

MHD Stokes flow for magnetized bodies of revolution, rotating with steady motion in viscous conducting fluid at rest at infinity

04 p0726 A70-14615

Rotation effects of two point scatterer on radar measurements of coherent acceleration

04 p0652 A70-15348

Cold flow-porous plate simulation of swirling flow-field in spinning end-burning rocket chamber, noting vortex generation and flow characteristics

04 p0764 A70-15541

Optimal stabilization of spinning body motion about dynamic symmetry axis by controllable gyroscope

05 p0923 A70-16221

Linearized MHD equations for motion of solids in viscous and electrically conducting fluids

06 p1120 A70-17532

Heat transfer coefficients for heat exchangers rotating in air at various velocities computed from skin friction coefficients in laminar and turbulent flow regime

06 p1177 A70-17701

Three dimensional boundary value problems for bodies of revolution rotating in fluid at rest and for bodies at rest in rotating fluids

07 p1252 A70-18709

Lagrange rotational motion stability of heavy symmetrical body attached at point to platform moving forward using Liapunov theorem

07 p1334 A70-19641

Cross coupled rotational motions of free solid body carrying nutation-damping pendulums

07 p1335 A70-19808

Time optimal control for rotation of solid supporting body with aid of pendulum, obtaining motion equations by algorithm

07 p1337 A70-20299

Material particles unrealizability of periodic motion near libration points of triaxial ellipsoid rotating steadily about polar axis

08 p1543 A70-20491

Transverse pressure gradient effect on parameters of turbulent boundary layer on body rotating in axial flow

08 p1483 A70-21193

Heat transfer in axially symmetric laminar viscous boundary layer flow due to rotating bodies of revolution, obtaining temperature distribution

08 p1485 A70-21698

Frequency change for coupled vibrations of slender rotating beam due to hub radius change determined in centrifugal force field by perturbation method

08 p1594 A70-21772

Motion equations and decay of rotating equal mass triple systems for random configuration integrated numerically on computer

09 p1751 A70-22160

Gravitating bodies quasi-stationary rotating systems, giving equations of state and evolution

09 p1753 A70-22457

Secular stability of rotating polytropes in relative equilibrium, isolating bifurcation point by calculating lowest sectorial modes for various sequences

10 p1937 A70-23946

Membrane deformations in second order rotating surfaces with positive Gaussian curvature investigated for external couple loaded spherical shells

10 p1958 A70-24515

MHD boundary layer on rotating body in viscous incompressible conducting fluid, studying magnetic field effects on time-to-separation

10 p1924 A70-24572

Heat transfer from gas to gas turbine buckets, determining angle of attack and rotation influences by extending transfer equation

10 p1930 A70-25140

Torsional vibration of rotating tapered and twisted turbomachine blade, constructing digital computer program for convergence and boundary conditions

11 p2128 A70-25373

Solid body control moments ensuring braking from rotational motion, finite orientation and angular velocity under minimum energy constraint

11 p2023 A70-25609

Flow characteristics of airfoil rotating cascades in variable width channel in incompressible liquid

11 p1975 A70-25789

Stability conditions of rotational motions of symmetrical solid body on vibrating base in potential force field

11 p2098 A70-25916

Passive coupling of spatial six-element mechanical mixer with rotary pairs as function of element axial position and dimensions

11 p1983 A70-25933

Spin axis motion of n-body coaxially mounted cluster of differentially spinning bodies, considering combined precession and nutation

11 p2123 A70-26128

Newtonian fluid laminar throughflow between coaxial corotating cones, applying solution for flow between disks

11 p2038 A70-26491

Rigid and stretch yo-yo device equations of motion for despinning rotating rigid body derived for two and three dimensional model

12 p2271 A70-27228

Moving object angles of rotation averaging during single measurement of geomagnetic field vector components by quantum magnetometer

12 p2234 A70-27566

Thermal boundary layer equations solved for compressible gas at rotating axisymmetric surface with viscosity as linear function of temperature

12 p2331 A70-27698

Free elastic rotating beam with tip masses and inertia, developing solutions for flexible modes and natural frequencies of H-type configuration

12 p2273 A70-27820

Translational-rotational motion of long dumbbell in Newtonian central force field, analyzing plane center of mass trajectory with perpendicular kinetic moment vector

13 p2485 A70-28452

Logarithmic and Coles velocity profiles validity for turbulent boundary layers on radial rotating impeller blades

14 p2527 A70-30176

Axisymmetric bodies slow rotation or rotary oscillation in hydrodynamics and MHD using boundary value problems solutions

14 p2527 A70-30276

FM/FM radio telemetry system for transmitting strain and temperature data from rotating parts

15 p2739 A70-32330

Boundary value problem of elastic isotropic material, obtaining pointwise bounds of Cosserat continuum, considering couple stresses and constrained rotation of particles

15 p2821 A70-32340

Computer program for limit analysis of rotationally symmetric shells, generating yield point load upper and lower bounds and velocity profile

15 p2822 A70-32351

Free solid body time optimal rotation about fixed central axis under action of external control moment vector, assuming zero initial and terminal angular velocity

15 p2775 A70-32447

Hard wire hermetically sealed two degrees of freedom rotating coupling design for continuous soldered wire connections between spacecraft and oriented solar array

16 p2924 A70-34172

Skin friction variation and boundary layer separation for rotating axisymmetric body, using two layer model

17 p3011 A70-35240

Kinetic instability of elastic cantilever beam under excitation by rotating masses, relating bending and torsional vibrations to masses angular velocity

18 p3334 A70-35960

Gravitational field effect on natural frequencies of rotating ring laser, using general relativity and electromagnetic fields theories in continuous media

18 p3267 A70-36622

Spinning body with rigid and elastic parts, using Liapunov direct method for attitude stability analysis

18 p3292 A70-36677

Gyroplatform for controlling rocket motion during rotation about longitudinal axis

19 p3420 A70-37258

Squeeze film investigation between rotating plane annuli, considering inertia due to centrifugal effect [ASME PAPER 69-LUB-6]

19 p3435 A70-37608

Gravitationally induced/Machian/magnetic field by rotating mass-shell with centrally located stationary charged sphere, using linearized relativity theory

19 p3471 A70-37815

Galactic rotation law parameters determination, considering effect of random and systematic errors on accuracy

19 p3525 A70-38774

Rotating mechanical components reliability under complex fatigue, presenting design data

19 p3442 A70-38845

Spinning missile gravity induced angular motion for various trajectory portions, considering quasi-steady state assumption validity [AIAA PAPER 70-968]

20 p3715 A70-39561

Heat transfer from gas to gas turbine buckets, determining angle of attack and rotation influences by extending transfer equation

20 p3694 A70-40345

Asymmetric rotating bodies mass properties measurement on Dynamic Balancing Machine, taking into account aerodynamic forces [SAWE PAPER 818]

20 p3634 A70-40351

Lense-Thirring effect in test masses approaching in same orbit around rotating body, noting correction dependence on central body geometry and angular velocity

21 p3926 A70-42240

Multipurpose transistorized tachometer for rotating body speed measurement, control and recording, using electronic integrator and magnet pickup

21 p3831 A70-42245

Coupled rotational vibration system dynamic behavior near critical speed, using graphs of autonomous two degree of freedom system on reduced phase plane

22 p4112 A70-42271

Dual spin bodies stability, controlling nutation by passive damper fitted to despin platform

22 p4110 A70-42486

Rotating flexible cable-connected space station dynamic scale model, describing suspension system and artificial gravity generation

23 p4258 A70-44528

Rigid body with external torque acting along one principal axis, deriving Euler equations of motion

23 p4221 A70-44572

Spinning cold-flow rocket motor, studying rotation effects on chamber flow velocity field

23 p4233 A70-44579

Rigid body rotation about fixed point under oscillatory precession and nutation due to noncentral attractive force, showing errors in Euler equations

23 p4247 A70-44792

Holographic interference pattern interpretation, measuring object rotation

24 p4336 A70-45666

ROTATING CONES

U CONICAL BODIES

U ROTATING BODIES

ROTATING CYLINDERS

Turbulent heat transfer on heated horizontal circular cylinder rotating freely in space, discussing dimensionless numbers relations and frictional heating

01 p0215 A70-10926

Torque upper bounds in Couette flow between concentric rotating cylinders, considering dissipation integral and boundary and continuity conditions validity

03 p0468 A70-13787

Thermoelastic stresses in rotating circular cylinder, analyzing temperature effect on angular velocity for neo-Hookean material using finite deformation theory

05 p0930 A70-16080

Free molecular flow through long circular tube rotating with constant angular velocity about axis, discussing rotation speed effect on mass flow

05 p0836 A70-16994

Three dimensional stress-strain analysis of rotating finite hollow cylinder, emphasizing wall thickness effect on stress and strain distribution

06 p1160 A70-17130

Viscous frictional torque on inner cylinder of eccentrically rotating concentric cylinders measured from laminar to turbulent flow

06 p1074 A70-17134

Time dependent stability of viscous rotational Couette flow induced by impulsively started rotating inner cylinder, using dye injection and motion pictures

07 p1255 A70-19209

Thermally induced convective mixing motion in rotating cylindrical cryogen space storage tank model under heat flux, calculating critical Rayleigh number

07 p1257 A70-19320

Aerodynamic characteristics of rotating transverse cylinder in subsonic normal flow from analysis of cylinder vortex system, discussing friction drag coefficient

08 p1431 A70-20720

Acoustic radiation produced in response to harmonically oscillating circular cylinder rotating in viscous fluid solved within Lighthill-Curle formalism for aerodynamically generated sound

09 p1726 A70-22391

Temperature and stress fields in rotating thin tube exposed to stationary heat source with constant strength, considering materials

09 p1774 A70-22579

Rotating cylinder stress-strain state under steady and unsteady creep, using Lagrange variational principle for differential equations

09 p1779 A70-23100

Rotating degenerate gravitating fluid cylinders equilibrium configuration

10 p1917 A70-25208

Eccentric cylinders with outer cylinder rotating measured for eccentricity and clearance ratios effects on pressure distribution and force on inner cylinder

11 p2060 A70-26409

Incompressible boundary layers velocity distributions on cylinders rotating in axial flow, considering centrifugal force effects, momentum thicknesses, local shearing stress, etc

11 p2038 A70-26477

Liquids relative rotary motion in vertical rotating cylinders under large amplitude axial vibrations and angular velocities

12 p2209 A70-27213

Unstable Ekman boundary layer vortex structure analysis by generating similar flow in liquid filled rotating cylinder

14 p2604 A70-30545

Radial static pressure distribution of turbulent jet flow over rotating cylinder with constant curvature

14 p2567 A70-31399

Turbulent boundary layer instability on rotating cylinder in axial stream, correlating mixing length to Richardson number

15 p2722 A70-32372

Annular fluids hydrodynamic mass and damping effects on long rotating cylinders vibrations, discussing theory of fluid friction and forces, vortex and turbulent flows, etc [ASME PAPER 70-FE-30]

16 p2892 A70-33636

Annular fluids hydrodynamic mass and damping effects on long rotating cylinders vibrations, analyzing test results [ASME PAPER 70-FE-31]

16 p2892 A70-33637

Couette flow stability between coaxial rotating cylinders, calculating eigenvector in first approximation small perturbation equations

17 p3073 A70-35695

Solid or hollow anisotropic elastic cylinders rotating with variable angular velocity, determining dynamic response by Hankel and Laplace transforms

18 p3338 A70-36433

Rigid cylinder rotation and flexible shaft torsion observation by holographic interferometry

21 p3822 A70-40813

Spinning cylindrical spicule model with radial and axial gradients in electron number and temperature forming Ca II K line

21 p3879 A70-40955

Temperature distribution in rotating thin cylindrical shell with line conduction discontinuity under solar heating, evaluating tubular elements thermal bending on spinning spacecraft

21 p3951 A70-41875

Buoyancy effects on transient free convection heat transfer in revolving tube for zero to 100 g centrifugal acceleration [ASME PAPER 70-HT-10]

22 p4122 A70-42437

Poiseuille-Couette spiral flow stability between concentric rotating cylinders

22 p4010 A70-42691

Temperature profiles for viscous fluid contained between two concentric rotating porous cylinders

24 p4327 A70-46005

Viscous flow stability between two concentric rotating porous cylinders, calculating critical Taylor numbers for wave numbers and velocity ratios

24 p4328 A70-46366

ROTATING DISKS

Thermal conditions and graph-analytic solution of laminar boundary layer combustion of disk rotating in free atmosphere and plate in Couette flow

01 p0218 A70-11017

Elastic stability of Coriolis-coupled oscillations of thin rotating disk under influence of centrifugal forces

02 p0389 A70-12650

Centrally clamped spinning circular disk free transverse vibration analysis within accuracy of numerical computations

03 p0584 A70-12931

Finite element method applied to finite dimensional state variable formulation of transient heat conduction with surface diffusion of thin circular rotating disk [ASME PAPER 69-DE-B]

04 p0785 A70-14874

Gas turbine rotating disks failure analysis, studying strength as function of material properties, thermal stresses and hole dimensions

04 p0775 A70-15260

Radial outflow effect on fluid motion between rotating and stationary plane disks associated with rotor cooling in turbomachinery

05 p0833 A70-16503

Self similar problems of anisotropic fluid boundary layer involving infinite disk rotation and fluid flow near stagnation point

05 p0835 A70-16857

Analog to Burger model applied to rotating disk creep problem solution and stress-strain state of plane sample with hyperbolic groove

05 p0952 A70-17038

Creep and strength criteria reliability for turbomachine disks, determining stresses, destructive rotations and strength margin

05 p0953 A70-17056

Residual strains determination in rotating disks from photoelastic coatings interference

05 p0955 A70-17063

Bursting speed and mode of high speed rotating disk with rim, boss and blades, noting influence of boss thickness

06 p1129 A70-17129

Load capacity of rotating field MHD hydrostatic thrust bearing increased by rotating axial magnetic field

06 p1076 A70-17527

Rotating disk stability relation with stress distribution in plastic deformation of material

07 p1402 A70-19056

Outside-matching functioning of single rotating disk of axial compressor, investigating critical disengagement and rotary detachment

[ONERA-TP-701] 07 p1193 A70-19127

Perturbed gyroscopic system consisting of disk hinged by rigid weightless rod, investigating stability condition at axial and equatorial inertia moments

08 p1496 A70-21210

Rotating circular disk under angular acceleration, analyzing stress and deformation distributions

08 p1596 A70-21980

Thermal conditions and graph-analytic solution of laminar boundary layer combustion of disk rotating in free atmosphere and plate in a Couette flow

09 p1787 A70-22266

High speed rotating disks design and stress analysis [ASME PAPER 69-DE-1]

09 p1770 A70-22268

Transient heat conduction of thin circular disk with uninsulated surfaces rotating past stationary point source by finite element method

09 p1787 A70-22269

Elastoplastic stressed state of variable thickness disk under combined effects of nonuniform heating, repeated centrifugal and surface tensile loads

09 p1778 A70-23091

Elastoplastic stress state of variable thickness disk under combined effect of nonuniform heating and centrifugal forces, applying flow theory to stress component determination

09 p1779 A70-23095

Rotating cantilever beams mounted on disk periphery, analyzing forced and free vibrations characteristics

09 p1781 A70-23283

Metal probes friction coefficient and impact temperature during impingement onto rotating chromium steel disk related to speed under various atmospheres

09 p1708 A70-23425

Elastic shaft with central unbalanced disk, deriving equation of motion for rotation in flexible bearings

10 p1958 A70-24520

Asymptotic eigensolutions for equations governing flow between oppositely rotating infinite plane disks in inviscid limit

10 p1870 A70-24607

Two-disk flexible rotor balancing method based on shaft vibration and bearing forces analysis

10 p1896 A70-25093

Naphthalene rotating disk with confronting stationary disk, investigating heat and mass transfer dependence on shroud dimensions, measuring flow types

11 p2060 A70-26410

Transient heat transfer considered for thermal boundary layer over rotating disk following temperature change

13 p2519 A70-28493

Rotating disk service life and structural failure under creep, using Tresca yield and maximum stress criterion

13 p2514 A70-29290

Incompressible, viscous and electrically conducting fluid flow due to rotating disk in uniform magnetic field, discussing hydromagnetic interaction effect on velocity and friction

13 p2465 A70-29544

Spiral structure of disk galaxies as nonaxisymmetric perturbations in density, using pressure free hydrodynamical equations

14 p2639 A70-30731

Soviet book on bearing capacity of turbomachine rotor elements covering testing methods, stress analysis, design factors on stability, etc

14 p2658 A70-30958

Disk elements perpendicular mounting by rotation on vibrating shaft, obtaining orientation by centrifugal force

15 p2733 A70-31580

Conducting incompressible fluid laminar flow between rotating disks in transverse magnetic field with source at center

15 p2779 A70-31915

Monograph on temperature dependent material properties effect on elastic stress distribution in thin rotating disks of arbitrary profile

15 p2823 A70-32700

Transverse vibration of thin circular elastic turbine disk of variable thickness rotating axially at constant angular velocity

16 p2916 A70-32994

Unsteady hydromagnetic flow of viscous electrically conducting incompressible fluid due to rotating disk under perpendicular magnetic field

16 p2958 A70-33297

German monograph on calculation and measurement of stress distribution in turbine rotors with radial flow, discussing differential equations for rotating disks

16 p2993 A70-34076

German monograph on stress calculation for rotating elliptical rimmed and notched turbine disks using Weinel integral equations and cascade computer procedure

16 p2993 A70-34079

Disk forced vibration mounted on rotating shaft with ball bearings, assuming nonlinear elastic characteristic of system

16 p2996 A70-34293

Anisotropy and variable thickness effects on elastic stress distribution in rotating disks, discussing limiting cases

17 p3185 A70-34912

Similarity equations for rotating flow near disk, using Navier-Stokes equations for case of complicated boundary conditions

18 p3239 A70-36223

Nonlinearized exact solution of Navier-Stokes equations for fluid motion between two coaxial circular disks rotating at equal velocity

18 p3241 A70-36381

Gas turbine shrouded rotating disk system with radial outflow of air coolant, investigating fluid dynamics, pressure distribution and frictional moment

[ASME PAPER 70-GT-6] 18 p3208 A70-36862

Heat transfer characteristics of flows between high speed rotating disk and parallel stationary shroud, discussing experimental facility and procedures

[ASME PAPER 70-GT-20] 18 p3349 A70-36865

Stress measurements in rotating plane disks with notched disturbed symmetry, using stroboscopic photoelasticity and numerical methods

[ASME PAPER 70-GT-26] 18 p3344 A70-36867

Tightly wound spiral nonlinear density waves in pressureless self gravitating disk with external gravitational field, examining solid body and differential rotation

18 p3331 A70-37192

Stellar isolated disks spiral structure, examining large numbers of point masses self consistent motion in galactic plane

18 p3331 A70-37195

Monograph on radial flow between air cooled gas turbine rotating and stationary disk near stator covering turbulent boundary layer, velocity distribution, etc

19 p3404 A70-38007

External and material damped three dimensional rotating elastic shaft-disk system, using energy technique and nonlinear model

19 p3542 A70-38062

Viscous incompressible electrically conducting fluid steady flow between parallel coaxial rotating disks with transverse magnetic field

19 p3481 A70-38446

Rotating Ti disk in liquid Co flow, investigating titanium carbide dissolution kinetics

20 p3648 A70-39245

Rotating shaft system consisting of variable cross sections, disks and journal bearings, calculating unbalance vibration by numerical method

21 p3832 A70-40898

Optimal weight design of axisymmetric rotating elastic disks for specific edge radial displacement

22 p4112 A70-42463

Unsteady compressible boundary layer formation on rotating disk, assuming uniform fluid rotation

22 p4009 A70-42616

Incompressible Newtonian fluid flow between closely spaced corotating disks, showing radial pressure distribution similar to laminar flow

24 p4324 A70-45293

Coriolis acceleration effect on inplane vibration resonant frequencies of rotating disks

24 p4425 A70-45780

ROTATING ELECTRICAL MACHINES

Nonsliding rotary electrical connector for conducting current and signals from satellite solar panel

[AIAA PAPER 70-458] 11 p2016 A70-25453

Brush current collectors for strain measurements in rotating machine parts, discussing acceptance testing

11 p1983 A70-26438

Electrical design of ferrite configuration high power rotary transformer for satellite slip ring replacement, minimizing transistor turn-off losses

21 p3759 A70-41222

ROTATING ENVIRONMENTS

Free convection to rotating central plate in synchronously rotating surroundings with and without consideration of Coriolis forces

[AIChE PREPRINT 9] 01 p0216 A70-10968

Thermal instability of uniformly rotating self gravitating homogeneous medium with perturbations in plane perpendicular to rotation axis

04 p0745 A70-14471

Dispersion relation governing hydromagnetic gravity waves propagation in rotating nonisotropic medium, discussing effects of constant entropy gradient

04 p0745 A70-14473

Adaptation to Coriolis accelerations associated adaptation schedule to with 1-rpm increments developed for preventing motion sickness in slow rotating environment

07 p1223 A70-19938

Shear and rotation limits on universe from X ray background, using Euclidean shear and vorticity models with open and closed geometries

08 p1561 A70-20901

Quantification of subjective estimates of well-being during onset and remission of motion sickness symptomatology in slow rotation room

08 p1448 A70-21941

Antimotion sickness drugs evaluated for effectiveness under standardized stress conditions in slow rotation room

20 p3572 A70-39439

Reflex vestibular disturbances and motion sickness prevention in artificial gravity of rotating space base, by incremental adaptation tests and drugs

23 p4154 A70-44625

Head movement role in motion sickness as function of angular velocity, discussing prediction of human tolerance in space station

24 p4297 A70-45341

ROTATING FLUIDS

NT ROTATING LIQUIDS

Cauchy problem solution asymptotic behavior for linearized system of rotating compressible fluid at time approaching infinity

01 p0064 A70-11031

Incompressible viscous fluid flow in contact with infinite plate and rotating in perpendicular magnetic field, obtaining flow characteristics by Laplace transform

01 p0067 A70-11138

Adiabatic disturbances propagating as transverse waves in inviscid fluid rotating as Rankine vortex about cylindrical container axis, discussing harmonics

03 p0467 A70-13779

Stability and dynamics of dielectrophoretic equilibria, considering circular cylindrical column of inviscid liquid with rigid body rotation

03 p0525 A70-13784

Laminar and turbulent flows of compressible media in rotating pipes, analyzing velocity distribution, angular velocity and Coriolis effects using Abel equation

04 p0672 A70-15159

Computer program to calculate ideal rotating fluid flow in arbitrary airfoil lattice on axisymmetric stream surface in variable thickness layer

04 p0617 A70-15239

Equilibrium shapes of rotating weightless fluid with surface tension in absence of external force field obtained by boundary layer theory

04 p0673 A70-15241

Motion generated by spherical body moving along axis of uniformly rotating fluid, measuring particle velocities ahead of and behind body

05 p0789 A70-16013

Theory for describing rotating fluid planets external geometry in state of hydrostatic equilibrium, noting role of equipotential surfaces

06 p1153 A70-18559

Three dimensional boundary value problems for bodies of revolution rotating in fluid at rest and for bodies at rest in rotating fluids

07 p1252 A70-18709

Temperature, pressure and flow direction probe in rotating fluid machines analysis

07 p1283 A70-19732

Damped turbulent whirling tube flow friction characteristics and heat exchange, solving equation of maximum tangential flow rate

07 p1261 A70-20464

Finite amplitude effects on MHD thermal convection in rotating layer of conducting fluid, discussing subcritical instability

08 p1563 A70-20472

Magnetothermal instability and radiative effects on incipient fragmentation of rotating gravitating interstellar fluid forming condensations

08 p1578 A70-21545

Motion of body with cavity completely filled with viscous fluid about center of mass in potential mass-force field, applying small parameter method

08 p1546 A70-21630

Cauchy problem solution for linearized Navier-Stokes equations of incompressible rotating viscous fluid, discussing velocity and angular momentum effect on asymptotic behavior

09 p1659 A70-22326

Poiseuille and Couette fluid flow with internal rotation in flat channel

09 p1660 A70-22436

Navier-Stokes equation for plane unsteady axisymmetric rotation of viscous fluid in steady radial flow from source or sink

09 p1660 A70-22437

Nonlinear equations for large fluid oscillations in axisymmetric rotating cavities with radial partitions

09 p1660 A70-22438

Uniformly rotating gas disk large scale spiral structure analysis, studying density waves due to gravitational disturbance by supersonic particle

09 p1755 A70-22503

Flow field around and drag on sphere rising axially through rotating viscous fluid

09 p1663 A70-23676

Forced inertial oscillations in rotating processing fluid-filled cylindrical cylinder

09 p1664 A70-23682

Transonic aerodynamics problems concerning plane and spatial rotational flows of perfect gas, discussing analytical and numerical methods

10 p1800 A70-24132

Swirl velocity and cavity stability in rotating container filled radially through porous cylindrical wall at constant and applied pressure

10 p1868 A70-24195

Rigid body mode of viscous incompressible fluid flow response to small perturbations of rotating spheroidal container, applying torque interaction

10 p1868 A70-24196

Elongated rotating configuration evolution by gravitational radiation and secular instability using homogeneous figures of Maclaurin and Jacobi

10 p1916 A70-24404

Rotating degenerate gravitating fluid cylinders equilibrium configuration

10 p1917 A70-25208

Linear viscous theory of steady rotating fluid flows with nonlinear modification of boundary layers, considering inertial modifications

11 p2036 A70-26011

Temperature profiles in upper symmetric regime of heated rotating water annulus convection obtained by thermocouple probe, noting flow field disturbance and correction

11 p2046 A70-26499

Liquids relative rotary motion in vertical rotating cylinders under large amplitude axial vibrations and angular velocities

12 p2209 A70-27213

Bounds in magnetofluidynamics for angular velocity of rotating fluid mass in relative equilibrium noting generalization of Poincare theorem

13 p2463 A70-29153

Convective flow stability in rotating fluid layer under rigid boundary conditions, calculating critical Taylor number as function of Prandtl number

16 p2893 A70-33686

Stratified-rotating fluids mathematical analogy, examining flow constraints, parameters and variables

17 p3068 A70-34664

Similarity equations for rotating flow near disk, using Navier-Stokes equations for case of complicated boundary conditions

18 p3239 A70-36223

Spatially periodic dynamos, analyzing homogeneous conducting fluid motions and magnetic field forms

18 p3291 A70-36407

General relativistic equations for stationary axially symmetric rotating perfect fluid in comoving coordinate system

18 p3292 A70-36900

Velocity profiles in steady and unsteady rotating flows for impulsive slow down and acceleration in cylindrical chamber

19 p3403 A70-37527

Boundary layer oscillatory flow interaction with nonuniformly rotating lamina, calculating velocity distribution and transitional frequencies

19 p3406 A70-38443

Weak stratification and geometry effect on steady mechanically driven motion of contained rotating viscous fluid

20 p3608 A70-39357

Gas core nuclear rocket engine light and heavy species centrifugal separation by MHD-driven rotating flow, discussing fluid dynamic simulation results

20 p3671 A70-40256

Unsteady compressible boundary layer formation on rotating disk, assuming uniform fluid rotation

22 p4009 A70-42616

Ducted propeller subsonic rotational flow with free boundaries, presenting second-order partial differential equation solution without linearizing assumptions

24 p4287 A70-45269

Sphere rotating in viscous fluid at rest, investigating surrounding flow field from creeping flow to turbulent boundary layer

24 p4326 A70-45989

Nonlinear effects of oscillatory disturbances produced by viscous excitations in rotating fluid inside of cylindrical tank

13 p2386 A70-28819

Helical vortex generation in rotating flow in straight tube having angular momentum flux sufficiently large relative to linear momentum flux

14 p2565 A70-30277

Figure of gravitating inhomogeneous rotating liquid, applying results to Jupiter and Saturn model construction

15 p2805 A70-32713

Viscous conducting liquid forced vortex motion, considering radial velocity distribution and rotation effect on free surface shape

24 p4383 A70-45140

ROTATING MATTER

Finite rotating universe model construction not possessing Goedel cosmos pathological properties, discussing relation to Mach principle

01 p0191 A70-11358

Oscillations and stability of rotating masses for axisymmetric equilibrium configurations with toroidal magnetic field based on virial equations

14 p2642 A70-30886

Surface temperature distribution over rotating nucleus of comet deficient in volatiles

18 p3319 A70-37058

Einstein field equations for spatially homogeneous spaces, considering rotating matter model in regularized Euler-Lagrange form

23 p4219 A70-44406

ROTATING MIRRORS

Broad bandwidth electronic analysis of high resolution photographic film using flying spot CRT or rotating mirror devices

02 p0302 A70-12613

Self mode locked pulses with rotating mirror Q switched carbon dioxide laser, attributing pulse shortness to saturation broadening of spectrum

07 p1301 A70-20018

Rotating parabolic mirror /antenna/ on multisupported suspension analyzed for static rigidity, determining elastic deformation under mirror weight

08 p1586 A70-21055

Rotating parabolic mirror /antenna/ cantilever suspension rigidity with emphasis on rigidity of central bushing

08 p1586 A70-21056

Control system for high speed photographic diagnostics based on rotating mirror action

09 p1679 A70-22993

Systematic errors in rotating mirror framing cameras and film records for quantitative high speed motion analysis

17 p3095 A70-35632

High speed camera rotating mirror dynamic surface deformations, discussing reflected waves, astigmatism, gas turbulence and pressure effects [SMPT PREPRINT 34]

22 p4033 A70-43043

Partial frame shutter for high speed rotating mirror camera, using explosively driven opaque dust cloud [SMPT PREPRINT 33]

22 p4033 A70-43044

Rotating mirror hologram camera for high speed phenomena, using Q switched ruby laser pulses [SMPT PREPRINT 7]

22 p4035 A70-43054

ROTATING PLASMAS

Transverse Kelvin-Helmholtz instability in rotating thermally ionized alkali metal plasmas /Q machines/, analyzing LF drift wave edge oscillation using dispersion equation

02 p0348 A70-12239

Rotary equilibrium of plasma ellipsoid in external HF fields in constant magnetic field, calculating revolution frequency and effective energy potential

03 p0530 A70-13085

Axial and rotational velocity profiles of plasma jet from Doppler shift of spectral lines [DFVLR-SONDDR-27]

04 p0729 A70-15612

Rotating plasma in nonuniform magnetic field analyzed for interchange instability based on MHD fluid and charged particle treatments

10 p1924 A70-24800

Solar thermal convection model, examining effects of rotation about vertical axis

13 p2496 A70-29839

Rotating plasma disturbances onset in MPD arc, determining magnetic field dependence on mass flow, background pressure and propellant [AIAA PAPER 69-232]

13 p2475 A70-29961

Ar arc discharge magnetically induced retrograde rotation dynamics, using high speed photography

19 p3475 A70-37533

Inhomogeneous plasma ellipsoid equilibrium in external HF field, assuming parabolic density distribution

19 p3479 A70-37739

Fully ionized magnetized rotating plasma interaction with neutral gas blanket, discussing plasma decay and velocity field

19 p3481 A70-38489

Rotating cold plasma wave propagation modes including Coriolis effect in absence and presence of external magnetic field

21 p3860 A70-41924

Low beta surface ionized rotating streaming plasma column, determining low magnetic field effects on density and stability

23 p4229 A70-44988

ROTATING SHAFTS

NT SHAFTS [MACHINE ELEMENTS]

NT TURBOSHAFTS

Externally pressurized air journal bearings load capacity, film stiffness, attitude-eccentricity locus and mass flow, studying supply pressure and shaft rotation effects

[ASME PAPER 69-LUB-29] 01 p0100 A70-10380

Static deformation of radially polarized inhomogeneous rotating cylindrical shaft of barium titanate using elasticity, electric field and constitutive equations for piezoelectric materials

01 p0118 A70-10549

Mathematical model for studying three dimensional whirling shaft stability as function of angular to critical velocity ratio, using Liapunov method for equations of motion

01 p0143 A70-10889

Step thrust self acting gas bearing without feed grooves for two directions of shaft rotation, determining geometric, gas and speed parameter characteristics

02 p0307 A70-12164

Photoelastic stress analysis of shouldered shafts with keyways in shanks under direct loading and torsion, including keyway and shoulder fillet stresses

02 p0388 A70-12496

Lateral vibrations of rigid rotating shaft in viscous fluid using inner and outer expansions method, considering small amplitude vibration and fast rotation

04 p0769 A70-14865

Shaft misalignment effect on accuracy of precision digital shaft angle encoders, using test fixture and optical methods

05 p0844 A70-15769

Rotation of circular cross sectioned continuous rod with constant bending moment, assuming linear strengthening with fixed cyclic strain diagram

06 p1163 A70-17396

Lip and face seal lubrication used on rotating shafts operating in compartments with fluids under pressure

07 p1293 A70-18955

Forced and free vibrations of shaft carrying unsymmetrical rotor, studying effects of distributed shaft mass and nonlinear shaft stiffness

07 p1401 A70-18976

Unstable vibrations in rotating flat shaft with unsymmetrical flexibility carrying unsymmetrical rotor in four degrees of freedom

07 p1402 A70-18978

Inductive sensor design and circuitry for measuring rapidly rotating shaft bending deflections at various vibration frequencies

07 p1279 A70-19115

Hydrostatic journal bearing calculation for case of shaft misalignment, deriving linear inhomogeneous equations with symmetrical matrix for pressure

07 p1293 A70-19119

Rotating rotor with mass distributed along shaft analyzed for nonlinear flexural and torsional vibrations, determining dynamic instability ranges

08 p1584 A70-20694

Rotating shaft vibrations on assembly designed to balance rotor in magnetic field, eliminating bearings effect on shaft to determine internal friction

01 p1584 A70-20697

Rigid rotating cylindrical shaft vibrations along diameter in viscous fluid using inner and outer expansions method [ASME PAPER 69-APM-S]

08 p1589 A70-21307

Self excited vibrations in balanced vertical shaft running on plain lubricated bearings, making numerical analysis of small perturbation transition to fully developed swirl

09 p1690 A70-22399

Elastic shaft with central unbalanced disk, deriving equation of motion for rotation in flexible bearings

10 p1958 A70-24520

Rotating shaft model with slight curvature for estimating maximum bending moment through Fourier series analysis

13 p2416 A70-28372

Dynamic instability of multirecess hydrostatic journal bearings at critical shaft rotation velocity

13 p2418 A70-28745

Temperature measurement of rotating shafts under cyclic loading, using thermistor as thermal radiation sensor

15 p2734 A70-31581

Disk forced vibration mounted on rotating shaft with ball bearings, assuming nonlinear elastic characteristic of system

16 p2996 A70-34293

Magnetostrictive measurements of torque from high speed rotating shafts

17 p3093 A70-35501

External and material damped three dimensional rotating elastic shaft-disk system, using energy technique and nonlinear model

19 p3542 A70-38062

Rotational stability of heavy horizontal shaft supported on plain lubricated bearings with cavitation in lubricant 19 p3438 A70-38669

Closed loop automatic speed control system for working shaft of two stage alternating current electric servomotor, using invariance principle 20 p3564 A70-39849

Rotating elastic shafts rectangular shape stability under creep conditions, considering single mass rotor 20 p3727 A70-39883

Rotating shaft system consisting of variable cross sections, disks and journal bearings, calculating unbalance vibration by numerical method 21 p3832 A70-40898

Three-lobe fluid film bearing configuration for gas turbine concentric rotating shafts/spool shafts/[ASME PAPER 70-LUBS-10] 22 p4045 A70-42450

Viscoelastic continuous shaft whirling motion, discussing boundary conditions and internal linear viscous damping 22 p4012 A70-42939

Elastoplastic bending of rotating circular shaft with constant end cross section force couple, assuming small deformations of linearly hardening materials 22 p4118 A70-43570

ROTATING SPHERES

Thin liquid film equilibrium on rotating sphere, determining conditions for detachment as function of angular velocity 01 p0068 A70-11578

Pulsar slowdown by radiation field torques indicated by alignment torque in magnetized oblique sphere rotating in vacuum 07 p1389 A70-20220

Moon rotational constants determination allowing for crater Moesting A coordinate errors 08 p1574 A70-21156

Viscous incompressible fluid secondary steady state flow due to rotating spheroid, considering acceleration terms in Stokes linear equation solution 11 p2034 A70-25390

Swirling and meridional flow induced by steady rotation of gravitating sphere in compressible monatomic gas, considering compressibility effects and surface layer [ASTME PAPER MR-69-714] 11 p1978 A70-26690

Convective heat transfer from rotating Al spheres in air at rest, investigating structure and boundary layer changes by schlieren method 14 p2665 A70-30398

Transparent spherical rotor spin axis orientation by measuring Fresnel drag effect of optical beam inside ring laser cavity 19 p3445 A70-37669

Viscous incompressible fluid flow between two rotating concentric spheres, calculating stability 21 p3811 A70-42217

Nonaxisymmetric convection of rotating spherical shell in Herring approximation, noting applicability to sun 22 p4104 A70-42994

Spherical celestial bodies anomalous rotation problem, noting sunspots zonal character 22 p4106 A70-43261

Gravitating sphere high speed rotation in monatomic gas, discussing viscous and thermal boundary layers, velocity fields, temperature effects and fluid motion 23 p4131 A70-43944

Rotating spherical shell equations as initial value problem, noting maximum convective heat transport at equator 23 p4249 A70-44805

Laminar boundary layer on uniformly rotating sphere studied by momentum integral method, imposing zero vorticity condition 23 p4184 A70-44981

Magnetized conducting sphere steady rotation in viscous conducting liquid, solving for fluid velocity and induced magnetic field 24 p4386 A70-45609

Two spherical particles rotation and slow motion about axis of circular cylinder in direction perpendicular to line of centers, considering fluid flow characteristics 24 p4325 A70-45781

Sphere rotating in viscous fluid at rest, investigating surrounding flow field from creeping flow to turbulent boundary layer 24 p4326 A70-45989

Conducting sphere MHD rotation in viscous conducting fluid under uniform magnetic field 24 p4387 A70-46028

ROTATING STALLS

Axial flow compressor blade rings interaction effect on angular speed of rotating stall zones 11 p1974 A70-25780

Critical load, force characteristics and pressure variation on blades of axial compressor under rotating stall 11 p2133 A70-25795

Axial-flow compressors stall characteristics measurement using water as working fluid 13 p2341 A70-29446

Rotating stall in axial compressors, using finite difference method 17 p3011 A70-35450

ROTATING VEHICLES

U ROTATING BODIES
U VEHICLES

ROTATION

NT AUTOROTATION
NT EARTH ROTATION
NT MOLECULAR ROTATION
NT PLANETARY ROTATION
NT SATELLITE ROTATION
NT SOLAR ROTATION
NT STELLAR ROTATION

Integral formulas of thermoelasticity theory for calculating displacements and rotations caused by temperature field action in micropolar Cosserat and Hooke media 02 p0391 A70-12817

Discharge tube rotation effects on ring laser polarization, Q factor and radiation frequency 03 p0501 A70-13744

Illusions of rotation perception with oscillating trapezoid and oscillation perception with rotating trapezoid, correlating magnitudes 05 p0807 A70-16673

Whirl effect on heat exchanger efficiency and reliability, discussing tests with transparent models and defective filling of circuits by feeding system [ONERA-TP-768] 10 p1968 A70-24400

Vestibular adaptation to heat and rotary stimulation in animals and men 11 p1986 A70-25822

Galaxies rotation, applying optical and radio data to statistical analysis of angular velocities and periods 13 p2492 A70-29386

Reflecting prism standards rotations effect on autocollimating images positions of optical instruments, investigating focusing method 16 p2915 A70-34214

Small angle of rotation measurement of coherent radiation polarization plane, discussing technique for increasing sensitivity and accuracy 20 p3643 A70-39759

Asymmetric micropolar thermoelasticity, deriving integral expressions for strains, rotations and temperatures in finite body 20 p3726 A70-39878

Galactic rotation model derived from radial velocities and spectrophotometric distances of H II regions 22 p4101 A70-42864

Atmospheric vorticity and dust devil rotation direction relationship, suggesting shear in horizontal flows associated with convective activity in unstable atmosphere 22 p4065 A70-42912

Energy rotation in electromagnetic wavefields, noting TE-MODE excitation in rectangular guides 23 p4164 A70-44384

ROTATIONAL FLOW

U FLUID FLOW
U VORTICES

ROTONS

Velocity distribution of atoms evaporating from superfluid He II at low temperatures, noting roton shifting and multiexcitation processes 06 p1108 A70-18639

ROTOR AERODYNAMICS

Helicopter engineering covering structure, rotor systems, aerodynamics, vibration and applicability to fixed wing aircraft 02 p0225 A70-12309

Air cooling with radial and jet blowing on gas turbine stage, discussing influence on aerodynamic characteristics 03 p0551 A70-13486

Helicopter tail rotors aerodynamic characteristics, using statistical methods for planning experiments and interpreting results 05 p0793 A70-15900

Laminar viscous flow on rotating propeller and helicopter rotor blades, studying crossflow and unsteady boundary layer effects, separation, transition, etc [AIAA PAPER 70-50] 06 p0974 A70-18161

Lifting line with arbitrary motion represented by line of acceleration doublets for unsteady aerodynamics of helicopter blades [ONERA-TP-787] 06 p0984 A70-18471

STOL touring aircraft propeller design and aerodynamics, discussing takeoff runs, landing runs, high lift, downwash, ground effects, etc 08 p1435 A70-20628

Static tank visualizations obtained in two dimensional flow and on rotors hovering or in transition in ONERA hydrodynamic tunnel [ONERA-TP-777] 08 p1434 A70-21846

Unsteady aerodynamic forces on helicopter rotors using pressure measurements and wind tunnel visualizations of smoke emission [ONERA-TP-777] 08 p1434 A70-21847

Dual flow turbojet engine rotor slip constraints during turning, investigating turbine blade strength, thrust deviation, fuel consumption and compressor stability 10 p1930 A70-24285

Helicopter rotor, discussing conventional, semirigid, gyro and ABC systems in relation to roll balance and control 13 p2344 A70-28849

Propeller in axial motion through homogeneous turbulence, studying forces and moments by statistical analysis [AIAA PAPER 70-549] 13 p2339 A70-29014

Soviet book on practical aerodynamics of Mi 6 helicopter covering engine/rotor power balance, control, flight characteristics and solutions to in-flight emergencies 14 p2532 A70-31414

Axial compressor aerodynamics investigation methods concerning compressor flow for efficiency improvement 16 p2836 A70-33757

Helicopter aerodynamic problems, discussing rotor performance improvement for increased cruising speed 16 p2841 A70-33758

Helicopter rotor blades flapwise bending moments prediction by transfer function/superposition techniques 17 p3013 A70-34704

Soviet book on vibration and balancing of aircraft engine rotors covering structural deformation and dynamics of turbine engines and compressors 19 p3489 A70-37237

German book on propeller theory covering airfoil theory, propeller flow and pressure fields, propeller vibrations, shrouded and tilted propellers, helicopter rotors, etc 23 p4180 A70-44097

NACA/NASA rotating wing aircraft research history 1915-1970, Part 3, covering rotor dynamics and flying qualities, hovering tests, rotor flow, loads, etc 23 p4142 A70-44856

ROTOR BLADES

Discrete noise generation and propagation due to fan engine rotor forcing excitation and interaction with downstream stator 05 p0896 A70-16791

Rotor blades structural fatigue strength tested on gas dynamic test stand under cyclic thermal loading and static tensile load 05 p0954 A70-17058

Rotor blade random vibrations in response to turbulence [AIAA PAPER 70-548] 13 p2339 A70-29013

CH-47C helicopter fiberglass main rotor blade, discussing composite materials impact on design 17 p3013 A70-34702

Helicopter rotor blade stall flutter response prediction based on NACA 0012 airfoil aerodynamic data 17 p3009 A70-34734

Shock wave radiation from supersonic ducted rotor, determining sound power at blade passing harmonic frequency 19 p3353 A70-38614

NACA/NASA rotating wing aircraft research history 1915-1970, Part 2, autogyro flight test experiences, rotor blade dynamics research, interest in helicopters, etc 23 p4142 A70-44852

ROTOR BLADES [TURBOMACHINERY]

Cascade tests to investigate nature of flow in rotor blade channels of axial flow turbines with partial admission 01 p0162 A70-10329

Fan rotors aerodynamic noise tonal annoyance reduction by blade unequal circumferential spacing, noting sound-pressure wave shape determination [ASME PAPER 69-WA/FE-23] 04 p0614 A70-14776

Packing rub effect on rotating machinery produced by unstable vibration generated by friction and heat of rubbing rotor in sliding contact 05 p0854 A70-15908

Wear resistance of turbine rotor blade stabilizing elements in form of bolts connecting overlapping leading and trailing edges of adjacent tips 09 p1768 A70-22095

Pressure and velocity distribution within radial flow gas turbine rotor computed by two dimensional streamline curvature method 09 p1608 A70-23737

Three dimensional incompressible turbulent boundary layer detachment on rotating blading of axial impellers 11 p1975 A70-25793

Incompressible inviscid fluid flow behind impeller blades, determining velocity profiles, flow-off angle and stable operation limits 11 p1977 A70-26349

Turboengine blade resonance vibration measurement by ELURA device, assuming one degree of freedom system 13 p2411 A70-29714

Logarithmic and Coles velocity profiles validity for turbulent boundary layers on radial rotating impeller blades 14 p2527 A70-30176

Rotor wakes and diffuser blades interactions visualization using hydraulic setup 14 p2528 A70-30297

German monograph on stress-strain state determination for rotors of turbomachines covering strain equations, partial differential equations, boundary conditions, etc 16 p2971 A70-34078

Gas turbine aero engines damage due to bird strikes, emphasizing rig testing and simulation at first stage rotor blading 18 p3236 A70-35995

Buzz-saw noise of transonic compressor due to rotating pressure field at supersonic blade tip speeds [ASME PAPER 70-GT-54] 18 p3303 A70-36838

Rotor wakes intrastator transport effects on high Mach number axial flow compressors performance, considering stagnation temperature profile and rotor blade loss factor [ASME PAPER 70-GT-39] 18 p3209 A70-36869

Discrete components formation in noise spectra of axial turbocompressor intake, considering relationship between blades and rotor disk 19 p3353 A70-38652

Air circulation around radial flow machine rotor blades calculated without velocity distribution factor 23 p4183 A70-44774

ROTOR DISKS

U TURBINE WHEELS

ROTOR HUBS

U HUBS

U ROTORS

ROTOR LIFT

Lifting line with arbitrary motion represented by line of acceleration doublets for unsteady aerodynamics of helicopter blades [ONERA-TP-787] 06 p0984 A70-18471

ROTOR SPEED

Optimal damping of flexibly mounted rotor by providing system with additional degrees of freedom and applying damping to additional masses 01 p0199 A70-10121

High speed rotor supported by air lubricated foil bearings subjected to periodic unidirectional excitation by vibrator, noting stability at high speeds [ASME PAPER 69-LUB-E] 01 p0099 A70-10376

Air lubricated foil bearing support design with external pressurization for high speed rotor in high temperature turbomachinery [ASME PAPER 69-LUB-D] 01 p0100 A70-10377

Photochronographic measurements of high speed rotor vibrations, showing precision and nutation components 01 p0093 A70-11268

Bursting speed and mode of high speed rotating disk with rim, boss and blades, noting influence of boss thickness 06 p1129 A70-17129

Thin gas turbine disk strength under axisymmetric flexural vibrations, noting agreement of calculated and experimental rotor rpm danger zone 06 p1166 A70-17654

Ring seal elements structural parameters influence on fluid leakage at various shaft speeds and fluid pressures 07 p1294 A70-19123

Machine-plotted pseudo three dimensional turbocharger rotor whirl display, discussing amplitude and frequency 08 p1496 A70-21300

Cavitation in centrifugal pumps, predicting breakdown and inception points variation with temperature and speed 15 p2744 A70-32097

High powered high speed helicopters autorotation entry characteristics, noting capability of meeting control time delay requirement 17 p3014 A70-34715

High speed photographic recording of bursting rotor in fragment control device 17 p3063 A70-35523

Time of acceleration to rated speed for three-phase asynchronous gyroengine rotor 19 p3420 A70-37259

Forced vibrations of rotor with variable rotating speed, investigating inertia terms effect 19 p3542 A70-38221

Critical rotation rates of gas turbine rotors disk-drum designs, describing initial parameters of model in matrix form 20 p3721 A70-39782

Gas lubricated three-foil bearing for high speed rotor support, considering dynamic and static behavior in zero gravity environment [ASME PAPER 70-LUBS-18] 22 p4044 A70-42443

ROTORCRAFT

U ROTARY WING AIRCRAFT

ROTORCRAFT

NT COMPRESSOR ROTORS

NT FLYWHEELS

NT IMPELLERS

NT LIFTING ROTORS

NT PUMP IMPELLERS

NT RIGID ROTORS

NT ROTARY WINGS

NT TILTING ROTORS

NT TIP DRIVEN ROTORS

NT TURBINE WHEELS

Stability analysis of rotors consisting of disks on massless shaft mounted in unsymmetrical flexible bearings, considering free and forced vibrations with damping neglected 03 p0599 A70-14248

Axial misalignment control of gimbal pivots and rotors in gyroscopes 04 p0692 A70-15282

High speed helicopter with fixed wings and longitudinal axis tail rotor 05 p0794 A70-16349

Forced and free vibrations of shaft carrying unsymmetrical rotor, studying effects of distributed shaft mass and nonlinear shaft stiffness 07 p1401 A70-18976

Flexural vibrations of rotor resting on nonlinear elastic bearings under action of exciting forces harmonics using variational method based on Hamilton principle 07 p1403 A70-19112

Rotating rotor with mass distributed along shaft analyzed for nonlinear flexural and torsional vibrations, determining dynamic instability ranges 08 p1584 A70-20694

Central equilibrium position stability of gas bearing supported rotor allowing for inertia and lubricant compressibility 08 p1502 A70-20695

Stable equilibrium of rotor in pressurized gas bearing, considering perturbed rotor motion equation together with Reynolds equations for pressures in lubricant layer 09 p1690 A70-22544

Error analysis in calculating periodic limiting state of rotor motion 09 p1727 A70-22624

Two-disk flexible rotor balancing method based on shaft vibration and bearing forces analysis 10 p1896 A70-25093

Moments equations for electrostatic gyroscope drift caused by rotor asphericity 11 p2048 A70-25559

Balanced rotor with radial sliding bearing bushings, studying lubricant gas restoring force effect on stability with allowance for bushings translational movements 11 p2058 A70-25581

Vertical position stability of gyropendulum mounted on vibrating platform, showing foundation induced gimbal rotor parametric vibrations 12 p2233 A70-27563

Electromagnetic single-coil suspension for cryogenic gyroscope with superconducting sphere rotor, calculating suspension force characteristics 12 p2234 A70-27565

Satellite stationary motions stabilization using rotors with axes fixed inside spacecraft 13 p2499 A70-28389

Brushless DC motor consisting of permanent magnet rotor, wound stator and optical rotor position sensing 16 p2843 A70-33000

Mechanical stresses effect on Vicalloy rotor packets magnetic properties 19 p3357 A70-37265

Three dimensional flow through rotor of axial vortex flow fan, using airfoil method for design 19 p3352 A70-38248

Nonspinning symmetrical satellite in circular orbit, analyzing laterally oriented rotor effect on attitude stability 19 p3533 A70-38340

Tail rotor thrust increase for yaw control via increased blade area, higher tip speeds and cambered airfoils 23 p4140 A70-44324

ROUGHNESS

NT SEA ROUGHNESS

NT SURFACE ROUGHNESS

ROUND TRIP TRAJECTORIES

NT CIRCUMLUNAR TRAJECTORIES

Atrophic changes in tortoises during roundtrip to moon on Zond 5 ascribed to hunger and space flight factors 07 p1207 A70-19496

Atrophic changes in tortoises during roundtrip to moon on Zond 5 ascribed to hunger and space flight factors 15 p2685 A70-32741

Circumlunar trajectories with return to earth atmosphere, comparing various methods 18 p3312 A70-36165

Travel time for trips to Neptune, calculating earth gravitational field escape hyperbola and waiting time before return 23 p4245 A70-44653

ROUNDED LEADING EDGES

U LEADING EDGES

ROUTES

Long range air transport routes, predicting equipment and expenditures modifications 22 p4128 A70-43533

ROVER PROJECT

Transport ratio for I-131 air to milk concentrations, determining mean value and statistical variation from Project Rover data 19 p3361 A70-38012

RUBBER

NT CHLOROPRENE RESINS

NT ELASTOMERS

NT SYNTHETIC RUBBERS

Inertial damping of soft rubber under forced torsional vibrations, discussing viscoelastic body linear model 04 p0712 A70-15100

Atomic bond rupture rate in rubber subjected to uniaxial tensile strain in ozone environment monitored by electron paramagnetic resonance measurements 08 p1527 A70-21454

Conductive rubber pressure transducers for fluid flow measurement 14 p2584 A70-30503

Simulated Venusian atmosphere effects on polymeric plastic and rubber materials, comparing with high temperature air and nitrogen exposures 14 p2640 A70-30781

Colloidal filler /carbon black/ reinforced rubber for various applications, noting fabrication into composite material 15 p2764 A70-31930

Elastic and optical properties of polyurethane rubber under large deformation using natural stress concept derived from stress-strain linear relationship [SESA PAPER 1608] 15 p2821 A70-32319

Connectors for superjet airliners, discussing butyl rubber grommet, power distribution collector, modular terminal blocks and passenger service connector 16 p2878 A70-33956

Gaseous and liquid fluorine exposure effects on nitroso rubbers at ambient and cryogenic temperatures, using impact tests and IR spectroscopy 21 p3844 A70-42140

Carbon dioxide laser adapted for high speed drilling of fine holes in thin rubber sheeting 23 p4201 A70-44474

RUBBER COATINGS

Hotshot wind tunnel performance improvement by coating arc chamber with silastene to retard heat loss and metal pollution 17 p3057 A70-34774

RUBIDIUM

NT RUBIDIUM ISOTOPES

NT RUBIDIUM 86

Crossed molecular beam study of reactive asymmetry of oriented methyl iodide molecules reacting with Rb, accounting for observations with hard sphere model 07 p1225 A70-20051

RUBIDIUM COMPOUNDS

Solid state batteries based on highly conducting solid electrolyte rubidium silver iodide, testing discharge performance 22 p3966 A70-43543

RUBIDIUM ISOTOPES

NT RUBIDIUM 86

Coherent light scattering disturbance in level-crossing signals of Rb 85 and Rb 87 second excited state by noble gas atoms 02 p0311 A70-11851

Age and initial strontium for Guarena chondrite, determining differential evolution of Rb/Sr systems involving simple metamorphism of closed systems or multistage processes 03 p0576 A70-14088

Atomic clock reproducibility short and long term stability, weight and power consumption characteristics, noting Rb gas cell for collision avoidance systems 04 p0688 A70-14724

Frequency shift in Rb-87 atomic frequency standards dependence on filter temperature interpreted for optical pumping radiation improvement 05 p0859 A70-16269

Crossing level resonances of magnetometer in optically pumped Rb87 atoms applied to weak field measurement 13 p2454 A70-30035

Optically pumped Rb laser theory, taking into account superfine and Zeeman structure of atoms 15 p2749 A70-31521

Rb-Sr internal isochron ages from Ocean of Storms, discussing analytical results of two texturally and mineralogically distinct crystalline rocks from Apollo 12 16 p2975 A70-33659

Rubidium-85 maser, discussing continuous oscillation in low magnetic field 19 p3446 A70-37769

Middle Devonian Tioga Bentonite age from Rb, Sr and Sr isotopes in weathered whole rock samples 20 p6165 A70-38989

Apollo 11 lunar rock Rb-Sr isotopic age relationships, discussing magmatic fractionation of Rb relative to Sr in moon primordial material 21 p3908 A70-41585

- Magnetic field-independent optically pumped Rb 85 maser oscillator power output 22 p4049 A70-42334
- RUBIDIUM 86**
- Myocardial blood flow in patients with acute myocardial infarction determined from measuring effective capillary flow /ECF/ by direct counting of rubidium 86 uptake 04 p0636 A70-15468
- RUBY**
- Ruby green /U/ absorption band magnetic circular dichroism calculations in linear approximation, considering spin-orbital interaction constant and magnetic field strength 01 p0156 A70-10188
- Electron-phonon interaction model of temperature dependence of luminescence produced by multiphonon nonradiative transitions in Cr ions of ruby crystal, deriving transition probability 03 p0538 A70-13058
- Temperature dependence of luminescence quantum yields and lifetimes in transitions during excitation of ruby crystal atoms 03 p0538 A70-13059
- Magnetic field effects on ruby absorption in R-line region 08 p1555 A70-20543
- Ruby crystal surface destruction by laser radiation, studying surface structural and optical properties effect and threshold power dependence on light pulses duration 12 p2248 A70-27541
- Temperature influence on luminosity centers and line darkening in synthetic ruby powder with chromium concentration 15 p2782 A70-31558
- Doubly pumped ruby maser operating in conjunction with superconducting magnet 18 p3265 A70-35953
- Sapphire and ruby plastic deformation and fracture properties at room temperature, discussing sapphire base ceramics 18 p3278 A70-36046
- RUBY LASERS**
- Difference frequency generation by resonant three photon process during optical mixing in ruby laser medium with simultaneous emission of optical transitions 01 p0108 A70-10350
- Frequency control of ruby laser pumped lithium niobate singly resonant parametric oscillator by radiation injection of CW Nd-YAG laser 01 p0110 A70-10566
- Electrical supply and control of monopulse 6.25 Hz ruby laser for use in optical radar, high speed photography, etc 01 p0114 A70-11270
- Ruby laser Q switching by chlorophyll d and derivatives, discussing peak output power 01 p0114 A70-11391
- Banana self focusing in water of laser beams with nonmonotonic intensity distribution, noting ruby laser experiment 02 p0312 A70-12260
- Ruby laser light wavelength temperature dependence measurement using Fabry-Perot etalon 02 p0313 A70-12440
- Ruby laser emission wavelength temperature dependence measured spectrographically 02 p0313 A70-12441
- Book on ruby laser output power calculation as function of pumping efficiency, considering energy density distribution, absorption, induced emission and excited Cr ions 02 p0314 A70-12692
- Population inversion coefficient as function of optimal impurity concentrations and efficiency of ruby quantum paramagnetic amplifier in 3 cm range 03 p0499 A70-13457
- Transient processes in ruby quantum paramagnetic amplifier during pumping, showing technique for saturation prevention and relaxation effects on population inversion 03 p0456 A70-13460
- Ruby laser experiment in illuminating satellites equipped with retroreflectors to determine satellite position in space from range and photographic data 03 p0450 A70-13674
- Power losses in ruby laser with polarized spontaneous luminescence determined as function of laser parameters and light polarization 03 p0502 A70-13747
- Flash lamp illuminated ruby laser operating with ordinary or extraordinary polarization, measuring gain or absorption 03 p0502 A70-13954
- Pumping energy distribution over cross section of active ruby laser elements in relation to smoothly polished, roughly polished and dull lateral cylindrical surfaces 04 p0700 A70-14607
- Raman backscatter of frequency doubled ruby laser beam by water vapor in atmosphere observed by optical radar, calculating water vapor mixing ratio profile 04 p0677 A70-14950

- Ruby laser giant pulses time stretching and shaping using stimulated Raman scattering in liquid nitrogen cell inserted in laser resonator 05 p0857 A70-16076
- Double giant pulse ruby laser with 1.5 m coherence length for producing double exposure holograms of stress wave propagation in solids 05 p0861 A70-16850
- Breakdown of cryptocyanine dye in methanol solution by ruby laser pulses providing passive Q switching mechanism 06 p1083 A70-18524
- Ohmic contacts to n- and p-type semiconductors obtained by ruby laser, noting linear current-voltage characteristics 07 p1299 A70-19797
- Emission kinetics variations of ruby laser due to aging attributed to inhomogeneity of active medium developing simultaneously with color centers 07 p1300 A70-19872
- End reflectors effects on ruby lasers emission spectra and kinetics 07 p1300 A70-19873
- Two photon photoconductivity of CdS crystals stimulated by ruby laser, showing emission self focusing during pumping 07 p1302 A70-20322
- Coherence improvement of ruby laser emission in free mode using corrective holograms in resonator 07 p1303 A70-20323
- Ruby laser energy threshold dependence on partial shielding of rod by stainless steel tubing 09 p1694 A70-22136
- Diffraction shaped ruby laser monopulse during excitation of modulated ultrasonic traveling waves in phototropic Q switch 09 p1696 A70-22483
- Ruby lasers simultaneous Q switching by single rotating prism, discussing possible differential frequency ranges 09 p1697 A70-22989
- Transient stimulated rotational and vibrational Raman scattering in gases using mode locked ruby laser 09 p1700 A70-23568
- Motion picture holography using continuously pumped ruby laser illumination system in repetitive Q switched mode 09 p1689 A70-23782
- Ruby monopulse laser emission spectrum wavelength stabilization by frequency tuning of generated radiation using Fabry-Perot interferometer 10 p1898 A70-23970
- Ruby monopulse laser with narrow emission line, describing two generator system 10 p1899 A70-24264
- Divergence measurement of beam emitted by ruby laser in relaxation mode as function of cavity length and excitation voltage 11 p2063 A70-26462
- Ultrasonic effects on synchronization of ruby laser radiation, investigating emission pulse structure and peak sequence 12 p2245 A70-27297
- Ruby laser with electro-optical Q switching, using polarization element for emission spectrum narrowing to single longitudinal mode 12 p2245 A70-27303
- Single mode TW ruby laser with ring resonator, analyzing emission spectral characteristics by Fabry-Perot etalon 12 p2246 A70-27356
- Ruby laser beam used to trigger high voltage spark discharge in vacuum, studying auxiliary photoionization during firing delay or failure 12 p2249 A70-27999
- Triple passage crystal amplifier of single frequency ruby laser emission, noting radiation structure and coherence 12 p2250 A70-28183
- Ruby and He-Ne laser radiation attenuation found due to scattering by gas molecules and aerosols from atmospheric spectral transparency fine structure studies 12 p2191 A70-28294
- Resonant absorption in ruby crystal under combined acoustic and laser pulses, noting use for laser intensity measurements 12 p2251 A70-28331
- Ruby laser output calculated as function of pumping power, taking into account pumping energy density spatial distribution and laser level depopulation 13 p2427 A70-28985
- Ruby laser radiation frequency control by birefringent calcite plate and KDP electro-optical Q switch 13 p2428 A70-29363
- Interference holograms of low temperature nitrogen plasma jet using fundamental and second harmonic ruby laser emissions 13 p2464 A70-29384
- Ruby laser Q switching by chlorophyll thin film, discussing characteristics and mechanics 13 p2429 A70-29670

- Strong short coherent light pulses with diffractive divergence generated by ruby lasers in series, showing pulse, emission and far field interferograms 13 p2430 A70-29762
- Small angle light scattering indicatrices in ruby crystals approximated by Gauss type function 13 p2431 A70-29869
- Radiation coherent enhancement of single frequency emission fields in Q modulated coupled ruby lasers 14 p2593 A70-30152
- Giant pulse generation in ruby laser requiring no introduction of additional modulating elements into resonator 15 p2749 A70-31524
- CW nonspiking single mode ruby laser operation by end pumping ruby with CW argon ion laser output 15 p2751 A70-31981
- Mode controlled Q switched tuneable ruby laser, obtaining frequency scanning by temperature and pressure control 15 p2752 A70-32048
- Mirror damage problem with mode locked ruby laser system solved by rough stack mirror fabricated from microscope coverslips 15 p2753 A70-32546
- Ruby laser spatial and temporal characteristics improvement with bleachable dye filter, using local negative feedback 15 p2754 A70-32865
- Monopulse ruby laser with phototropic Q switch based on radiation density increase due to beam distribution 15 p2754 A70-32867
- Power density fluctuations in emission peaks of ruby laser determined by splitting beam into two components and using photosensitive element and photomultiplier recording 15 p2754 A70-32874
- Peak emission currents from tungsten under ruby laser focused radiation, describing integral emission by heat conduction theory and Richardson equation 15 p2754 A70-32875
- Free generation regime of ruby laser studied by electro-optical method of smoothing spatial inversion inhomogeneities 16 p2927 A70-33192
- Ruby laser second harmonic radiation generation efficiency, using cylindrical lens beam forming optical system 16 p2929 A70-34212
- Giant pulse periodic operation ruby laser with 50 MW power and 10 Hz frequency 16 p2929 A70-34217
- High speed pulsed ruby laser holography, discussing transmission-reflection holocameras and applications 17 p3085 A70-35007
- Four dimensional recording using synchronous multiple pulse ruby laser holography 17 p3088 A70-35027
- Optical and electronic components design for ruby lasers generating giant pulses 17 p3107 A70-35121
- German monograph on spectral emission behavior of pulsed ruby laser with regard to output intensity 17 p3107 A70-35369
- Spectral and temporal characteristics of ruby laser operating with dielectric coated mirror scatterer 17 p3108 A70-35673
- Spontaneous megawatt pulsing in ruby laser with output beam reflected back into cavity 17 p3108 A70-35909
- Nonequidistant structure of axial mode spectrum of ruby laser with plane dielectric mirrors 18 p3266 A70-36418
- Regular relaxation oscillations of ruby laser by moving resonator mirrors 18 p3271 A70-36954
- Holographic interferometry of rapid phase objects by two wavelengths from ruby laser and KDP crystal filter, noting application to dense plasmas 19 p3422 A70-37650
- Pulsed ruby laser holography with coherent light, discussing applications 19 p3425 A70-37886
- Strong short coherent light pulses with diffractive divergence generated by ruby lasers in series, showing pulse, emission and far field interferograms 19 p3447 A70-38394
- Single frequency ruby laser with electro-optical Q switching, selecting transverse and longitudinal modes by stepwise voltage application to shutter 19 p3448 A70-38737
- Ruby laser radiation injury relationship to position and number of energy absorbing pigment particles in iris 20 p3579 A70-39425
- Double holography on phase objects in diffused light using pulsed ruby laser 20 p3630 A70-39499
- Pulsed ruby free emission mode laser spectrum narrowing, using diffraction lattice adjusted in resonator transversely to beam axis 20 p3643 A70-39757

- Microwelding by pulsed ruby laser radiation, discussing characteristics and advantages 20 p3638 A70-40149
- Normal mode pulsed ruby laser system with Xe flash lamp pumping, trigger circuit and transistorized power supply 20 p3643 A70-40355
- Ruby giant pulse laser produced plasmas from aluminum and copper surfaces, measuring electron and ion energies by time of flight and retarding potential techniques 21 p3860 A70-41925
- Radiation coherent enhancement of single frequency emission fields in Q modulated coupled ruby lasers 21 p3839 A70-42076
- Breakdown mechanism in Q switched ruby laser triggered spark gap, noting pulse duration and power peak 22 p4049 A70-42352
- Ruby laser mode excitation, spatial coherence and free emission kinetics investigated by high speed camera scanning 22 p4051 A70-43461
- Optical transmission and reflection gratings formed by standing light waves evaporation of thin metallic films in ruby laser cavity 23 p4200 A70-43817
- Al-27 NMR saturation effects on ruby electron cross relaxation and inversion 23 p4230 A70-43932
- Ruby laser in repetitive pulse operation, determining temperature, heat generation and transfer coefficient from spectrum shift measurement 23 p4203 A70-45071
- Pulsed ruby laser radiation energy characteristics relation to crystal temperature distribution, thermal deformation and compensating lens focal length 24 p4352 A70-45460
- Photo copying in diapositive form, using ruby laser light on IR film 24 p4352 A70-45559
- Ruby laser second harmonics generation in low loss lithium iodate crystal with high conversion efficiency 24 p4355 A70-46085
- Spectral anomalies due to inhomogeneous optical pumping in masked ruby laser, using mathematical model 24 p4355 A70-46264
- Ruby laser application to air humidity measurement via hygrometric method 24 p4356 A70-46401
- RUDDERS**
- NT AERIAL RUDDERS**
- Natural frequencies and modes of tapered swept back rudder fin of aircraft using vibration analysis 07 p1417 A70-20417
- Flutter suppression in elastic finned beams in supersonic flow controlled automatically by rudder deflection according to flexural strain 09 p1785 A70-23615
- F-4 Be rudders design and tests compared to Al structure [ASM PAPER W70-12.4] 15 p2676 A70-32336
- RULES**
- NT FLIGHT RULES**
- NT INSTRUMENT FLIGHT RULES**
- NT PALMGREN-MINER RULE**
- NT SUM RULES**
- NT WHITHAM RULE**
- RUMANIA**
- Tabulated corrections of data concerning reduction of photographs of small planets obtained at Bucharest Astronomical Observatory 06 p1139 A70-17549
- RUMBLE INSTABILITY**
- U ACOUSTIC INSTABILITY**
- RUN TIME [COMPUTERS]**
- Speed convergence of hybrid vs digital computer synthesis of optimal boost vehicle controller, considering fuel consumption and pitch dynamics 16 p2981 A70-33442
- Computer hardware and software technology for complex problems, discussing switching speeds and parallel and pipeline designs 23 p4167 A70-44716
- RUNGE-KUTTA METHOD**
- Runge-Kutta method with position dependent optimal parameter alpha for initial value problem solution to minimize total error 01 p0134 A70-11364
- Complete solution of fifth order Runge-Kutta equations in condensed matrix form, considering coefficients of linear dependence 04 p0714 A70-15047
- Numerical solution of transient heat conduction with radiating surface, imposing Runge-Kutta type integration on surface 04 p0787 A70-15613
- ALGOL algorithm for Runge-Kutta type numerical integration of simultaneous differential equations, using Merson method for step length determination 10 p1845 A70-24405
- Boundary layer retarded flow past porous surface with suction, using Runge-Kutta computerized integration of Falkner-Scan equation 15 p2720 A70-31586
- Divergent channel with porous walls, calculating effect of suction on laminar incompressible boundary layer by Runge-Kutta method 20 p3609 A70-39671
- Runge-Kutta formulas with multiple nodes for differential equations solution 24 p4369 A70-45163
- Fifth-order pseudo-Runge-Kutta methods for numerical solution of ordinary differential equations, determining optimal parameters 24 p4369 A70-45163
- RUNNING**
- Plethysmographic investigation of myogenic load influencing sportsmen central nervous systems state, tabulating short and long distance running results 03 p0420 A70-13403
- Blood lactate changes during prolonged exhaustive running at varied intensities and durations 10 p1809 A70-24001
- Rats heart rate change during running at simulated altitude, discussing respiratory-circulatory training effect 11 p1985 A70-25671
- 2000 meter race for endurance testing, using heart rate radiotelemetry before, during and after 14 p2543 A70-31173
- Serum enzymes lactate dehydrogenase, creatine phosphokinase and isoenzymes in conditioned male after marathon run, noting little myocardial damage 21 p3766 A70-42158
- Human leg blood flow distribution between deep and superficial veins during alternate treadmill work-rest periods 21 p3767 A70-42160
- Electrolyte changes after marathon running noting increase in serum sodium and serum potassium 24 p4302 A70-46108
- RUNUP**
- U ENGINE TESTS**
- RUNWAY CONDITIONS**
- Runway visibility measuring techniques, discussing RVR measurement limitations 02 p0336 A70-12226
- Lift-dump system for Hawker Siddeley DH 125, combining aerodynamic drag increase with lift reduction to improve deceleration 02 p0225 A70-12266
- Airport fog attenuation systems design and operation consisting of power and communication cables linking diffusers to central control and command 05 p0830 A70-17092
- Accelerate-stop distance problem in takeoff refusal due to critical engine failure, emphasizing runway limited length hazards 08 p1436 A70-21270
- Airport runway and slant visual ranges determination using single scanning lidar/laser radar/ 09 p1696 A70-22490
- Video role in air transport safety, describing runway visual range (RVR)/ measurement using TV camera and spaced lights 10 p1889 A70-24507
- Slush and water hazards on runways, discussing investigation and amelioration methods 11 p2030 A70-25356
- Airport runway slipperiness rating, predicting and alleviating to reduce aircraft accidents [SAE PAPER 700265] 12 p2206 A70-27434
- Collision and missed approach risks in high capacity airport landing operations, discussing parallel runways spacing and aircraft longitudinal separation 12 p2207 A70-27629
- Wing tip trailing vortices hazard reduction on closely spaced parallel runways by suction application, discussing power requirements 12 p2207 A70-27631
- Jet transport wakes resulting from high engine thrusts considered hazardous to following aircraft, discussing multiple-instrumented runways for measuring visibility 12 p2162 A70-27995
- Wet runway operations in air traffic control, discussing viscous, reverted rubber and dynamic hydroplaning 13 p2348 A70-29779
- Aircraft tires tread design for improved adhesion under wet runway conditions 14 p2532 A70-31336
- UHF radio telemetry for transmissometers measuring airport runway visibility 16 p2889 A70-34222
- Runway visual range assessment using automatic transmissometer-reflector measurements 17 p3132 A70-34641
- Aircraft landing and takeoff difficulties and dangers due to mud and water on runways, discussing coping methods 17 p3057 A70-34692
- Fog dissipation on aircraft runways, using aircraft jet engine exhaust heat and mixing properties 17 p3133 A70-35929
- Airport bird detection equipment (ABDE)/ radar to display airfield map for presence and magnitude of bird groups and vegetation on runway 18 p3226 A70-35998
- Runway low visibility and ceilings frequency and duration at German airports, using 1949-1967 statistical data 19 p3462 A70-37925
- RUNWAY LIGHTS**
- Liverpool airport lighting emphasizing beacons, approach, runway and taxiway high intensity lighting installations 10 p1857 A70-24000
- Video role in air transport safety, describing runway visual range (RVR)/ measurement using TV camera and spaced lights 10 p1889 A70-24507
- RUNWAYS**
- Flexible pavements for commercial jet planes representative of current and future aircraft 03 p0462 A70-13173
- Structural reinforcement for existing airport pavements, discussing construction procedures 03 p0462 A70-13174
- Rigid and flexible pavements response to jumbo jets load using elastic theory 03 p0462 A70-13175
- Runway acceptance rate improvements to alleviate air traffic congestion metropolises areas, using approach and landing sequence model for conventional jet aircraft [AIAA PAPER 70-74] 06 p1029 A70-18078
- Control system, operational procedures, aircraft guidance and runway design for increasing runway capacity, noting roles of automation and reduced separation [SAE PAPER 700280] 12 p2206 A70-27440
- Urban airport runway capacity increase via reduced aircraft separation, additional parallels and improved terminal traffic control, discussing design for acceptable safety levels 12 p2207 A70-27627
- Airport capacity increase via electronic aids enhancing guidance, flight control, reduced aircraft separation, ATC automation and runway configurations 12 p2208 A70-27914
- Longer runways for increased airport safety indicated from data concerning overruns, undershoots and veering, discussing certification testing during takeoff and landing 12 p2208 A70-27994
- Airport runway to fog radiative heat transfer analysis by Monte Carlo method 12 p2333 A70-28115
- Commercial aircraft launching and arresting systems for airport runway length reduction, discussing safety factors [SAE PAPER 700264] 18 p3237 A70-36821
- ATC systems safety, capacity and delay, discussing terminal operations, runway capacity and aircraft spacing 19 p3465 A70-38228
- Maximum throughput-rate capacity for runway and final approach path airspace involving multiple IFR landings 19 p3465 A70-38235
- Airport capacity analysis for terminal areas, using simulation for alternatives to parallel runway operation 19 p3397 A70-38236
- ATC airborne surveillance, communication and control system functioning as CAS after error or failure, discussing minimum parallel runway separation 19 p3466 A70-38241
- RUPTURING**
- Bearing strength and rupture of reinforced plastic composites under intense one-sided electric heating and hydrostatic pressure due to pyrolysis of plastic bond 03 p0515 A70-13244
- Life fraction hypothesis equation in creep testing derived on basis of chemical reaction rate theory [ASME PAPER 69-MET-A] 04 p0705 A70-14875
- Time-to-rupture dependence on temperature and stress related to chemical reaction rate equation in creep testing [ASME PAPER 69-MET-B] 04 p0770 A70-14877
- Carbide rupture energy in wear resistant alloys during abrasion, considering metallographic data and energy parameters 04 p0707 A70-15212
- Polycrystalline metals strength factors in aircraft and aerospace construction as relation between rupture time and embrittled grain boundary at high temperatures 04 p0779 A70-15671
- Creep rupture effect on fatigue damage of structural material, constructing nondimensional stress range diagrams 05 p0943 A70-16806
- Traumatic rupture of aortic arch and descending thoracic aorta resulting from abrupt linear body deceleration 07 p1206 A70-19295

Rupture safety in fiberglass reinforced plastics using variation coefficient illustrated in vessel design
07 p1410 A70-19760

Dimensionless strength parameter in determining bursting pressure of ductile metal diaphragms in square section shock tubes
08 p1481 A70-21034

Atomic bond rupture rate in rubber subjected to uniaxial tensile strain in ozone environment monitored by electron paramagnetic resonance measurements
08 p1527 A70-21454

Ni-Fe base superalloy notch and rupture properties as function of thermal and chemical changes, using electron microscopy
13 p2437 A70-29829

Al-Zn-Mg alloys aging kinetics and rupture mechanism, discussing stress corrosion, welded structures stability, activation energy, etc
14 p2597 A70-30965

Al alloy welded joints delayed rupture tendency, describing constant load test method
14 p2591 A70-30969

Al-Zn-Mg alloy welds delayed rupture under constant uniaxial load in distilled water or aqueous salt solution
14 p2591 A70-30970

Al-Zn-Mg high strength weldable alloys rupture characteristics, analyzing crack distribution, stress raisers and weld defects
14 p2591 A70-30971

Delayed rupture and relaxation in Ti alloys during cyclic deformation, comparing fatigue tests results for continuous and discontinuous cyclic loadings
16 p2931 A70-33209

High speed photographic recording of bursting rotor in fragment control device
17 p3063 A70-35523

Bearing strength and rupture of reinforced plastic composites under intense one-sided electric heating and hydrostatic pressure due to pyrolysis of plastic bond
19 p3455 A70-38462

Plastic bodies rupture and crack growth under creep, considering tension of bar with symmetrical angular notches
20 p3727 A70-39882

Deformable bodies rupture condition formulation by melting analogy, comparing results to experimental data
20 p3733 A70-40394

Longitudinal shear crack propagation in random internal stress field, examining quasi-brittle rupture theory and cyclic loading
20 p3733 A70-40396

Polymethyl methacrylate rupture during omnidirectional compression under laser radiation, showing pressure effect on microdefects and cracks
21 p3841 A70-40644

Slip, fracture and rupture in sintered and cast ductile and brittle polycrystalline Mo under tension, using optical and electron microscopy
23 p4204 A70-43884

RUTHENIUM

Carbon monoxide adsorption on ruthenium and ruthenium HCP metals emphasizing surface migration, work function increments and desorption
12 p2181 A70-27676

Clean Ru/0001/ and Rh/111/ surface properties by LEED and Auger electron spectroscopy, discussing gas adsorption
19 p3483 A70-37546

RUTHENIUM ALLOYS

Nb-Ru equiatomic alloys reversible phase transformations, using electrical resistivity, hot stage optical metallography, X ray diffraction and magnetic susceptibility measurements
23 p4208 A70-44858

Rare earth metals-ruthenium Laves phases solid solutions superconducting transition temperature measurement
23 p4231 A70-44885

RUTILE

Maser amplifier with nonoriented Fe-doped rutile powder as active material, observing broad absorption bands under magnetic field
12 p2249 A70-27649

RYAN AIRCRAFT

NT XV-5 AIRCRAFT

RYAN MILITARY AIRCRAFT

U MILITARY AIRCRAFT

RYDBERG SERIES

Atomic Ar absorption spectrum in vacuum UV region, observing Rydberg series interactions as perturbations and autoionizations
21 p3781 A70-41933

S

S BAND

U SUPERHIGH FREQUENCIES

U ULTRAHIGH FREQUENCIES

A-1548

S GLASS

S glass fibers strength characteristics at quasi-static strain rates, considering temperature effects on elastic modulus
13 p2439 A70-29707

S MATRIX THEORY

Unconditional stability criterion of active two port in scattering and admittance matrix notation equivalent to conjugate matching for maximum power gain with part impedances
02 p0271 A70-12820

Reduced multipoint equivalent scattering parameters derivation by matrix method, determining load reflection coefficients effect on signal attenuation and phase shift
03 p0458 A70-14038

Intrinsic noise of passive waveguide multipoint with losses, obtaining mean values and wave correlation functions using scattering matrix
04 p0655 A70-14402

Equivalence class technique to compute measure of similitude between two vehicles based on radar signature in terms of scattering matrix elements
04 p0648 A70-14656

Bounded operator functionals used for deriving nonlocal interaction Hamiltonian of quantum electrodynamics corresponding to converging series for scattering matrix in perturbation theory
05 p0883 A70-16876

Bounded nonlocal operator used in deriving series of subtracting Hamiltonians representing S matrix in perturbation theory after transition to local limit
05 p0883 A70-16877

Scattering matrix noniterative integral solutions applied to singlet and triplet s-wave Hartree-Fock phase shifts for electron-H-atom scattering
06 p1108 A70-17486

Noniterative integral solutions of scattering equations extended to coupled channels using matrix notation
06 p1108 A70-17487

Optical activity theory based on Kirkwood independent group model using scattering matrix
07 p1334 A70-19264

Probability of three photon band-band excitation of electron in semiconductors using S-matrix formalism, calculating absorption coefficient for two band approximation
07 p1356 A70-19795

Multimode rectangular waveguide lateral surface opening, determining scattering matrix coefficients governing mode conversion characteristics
08 p1462 A70-21224

Numerical calculation of S matrices for Stark broadening of Lyman-alpha line based on straight line classical path model
09 p1730 A70-22228

Scattering matrix for resonance lines with arbitrary level splitting in magnetic field
09 p1753 A70-22452

Computerized design of microwave circuits with S matrix
11 p2019 A70-26714

Wave scattering by statistical distributions of discrete obstacles, deriving various functions for diagnostic applications
11 p2086 A70-26762

Microwave parametric amplifiers with nonideal circulators, deriving gain via scattering matrix theory and signal flow graphs
16 p2874 A70-33389

Maxwell field quantization theory for case of interaction with Dirac field, calculating S matrix for interacting electrons
19 p3473 A70-37413

Waveguide transformer using rectangular waveguide permitting Galerkin method, determining scattering matrix
19 p3385 A70-37429

Two dimensional electromagnetic fields in presence of cylindrical objects of arbitrary physical properties and cross sections, using scattering matrix approximation
19 p3471 A70-37778

Diatom molecules inelastic collision cross sections for specific rotational transitions, discussing S matrix energy requirements for statistical analysis
19 p3474 A70-38268

Polarization of radiation reflected and transmitted by earth atmosphere, calculating scattering matrix for aerosol size distribution model
21 p3820 A70-41725

Scattering matrix for external coupling effects in dielectric covered phased array
23 p4160 A70-43766

Strong coupled rotational excitation problem in atom-diatom molecule scattering system, discussing transition probability matrices statistical analysis
23 p4212 A70-44600

S WAVES

Shear velocity variation with depth in upper mantle for Basin and Range province of western North America, using S waves measurements
02 p0292 A70-12505

Shear wave interaction in infinite homogeneous reacting fluid, using Fourier and Taylor series for velocity, temperature, density, pressure and composition
06 p1040 A70-18154

Electron scattering from diatomic molecular systems including coupling of partial waves in fixed-nuclei approximation
06 p1114 A70-18633

Shear wave and plate velocity expressions derived for orthotropic elastic plate with shear coupling, considering propagation direction
07 p1412 A70-19961

Dynamic response of joined elastic quarter spaces of solids to time varying free surface shear tractions parallel to plane of juncture
08 p1591 A70-21467

Alfvén shear waves collisionless damping from finite Larmor radius coupling to ion acoustic mode, observing longitudinal electric field existence
10 p1921 A70-23966

First order scattering formulae for s- and p-light reflected and transmitted by rough plane surface using perturbation theory
11 p2086 A70-26840

Upper critical field dependence on s- and p-wave scattering of Frenkel effects in electron irradiated niobium
13 p2471 A70-29535

CDs high field domain modes generation for C parallel to E described by interaction between drift carriers and off-axis shear wave
15 p2784 A70-31984

S and SKS travel times for arc distances of 30-126 degrees
16 p2898 A70-33975

Brittle elastic material with wedge shaped void, calculating shear stresses during crack propagation generated by horizontally polarized shear wave
21 p3932 A70-40547

Phase velocity and attenuation of shear waves in gases from sampled-CW ultrasonic crystal resonator reflection measurement
21 p3827 A70-41457

Apollo 11 lunar sample elastic wave velocities at high pressures, examining P and S waves, Q value and geophysical implications
21 p3916 A70-41666

CAT origin in unstable atmospheric shear and gravity waves, using ultrahigh resolution radar for observation of transition process
23 p4214 A70-44032

S-N DIAGRAMS

S/N fatigue life gage for nondestructive evaluation of cumulative damage, discussing calibration and two step, block and random tests
01 p0053 A70-10009

Turbine blades durability and fatigue characteristics, plotting fatigue diagram from statistical tests
01 p0105 A70-11418

Overstress cycles sensitivity for welded specimens on basis of French fatigue damage line and Wohler S-N line
05 p0941 A70-16520

Heat resistant steel and nickel alloys stress rupture strength at operating temperatures, discussing endurance diagrams under cyclic bending loads
05 p0868 A70-17047

Cylindrical Al, high strength pig iron and heat resistant steels elastoplastic deformation diagrams for cyclic compression tension loads
06 p1084 A70-17387

Fatigue resistance of high yield strength steel weldments under uniaxial loading, describing cyclic behavior by S-N curve
18 p3278 A70-37114

S-6 SATELLITE

U EXPLORER 17 SATELLITE

S-16 SATELLITE

U OSO-1

S-17 SATELLITE

U OSO-B

S-18 SATELLITE

U OAO

S-27 SATELLITE

U ALOUETTE 1 SATELLITE

S-49 SATELLITE

U OGO-A

S-64 HELICOPTER

U CH-54 HELICOPTER

SA-330 HELICOPTER

SA.330 Puma tactical support helicopter design and performance
14 p2530 A70-30286

SAAB AIRCRAFT

NT SAAB 37 AIRCRAFT

SAAB 37 AIRCRAFT

Canard and variable geometry aircraft designs noting SAAB 37 Viggen performance
10 p1805 A70-24764

Flight simulation in SAAB AJ37 aircraft development, describing analog and digital computers, cockpit simulators, automatic pilots, control and display devices
23 p4178 A70-44140

[ICAS PAPER 70-42]

Viggen aircraft testing for flight properties, discussing measuring instruments, analog and digital recording, preprogrammed control, etc 24 p4317 A70-46228

Sapuc-Salut system for evaluating test data measured onboard Viggen aircraft 24 p4339 A70-46229

SACCHARIDES
U CARBOHYDRATES
SACCHAROMYCES
3-O-methyl-mannose neutral sugar indentification as constituent of fungal polysaccharide 20 p3572 A70-39625

Homogeneous magnetic fields effects on growth rate of *Saccharomyces cerevisiae* and *Micrococcus denitrificans* 24 p4306 A70-45102

SADDLE POINTS (GAME THEORY)
Steady burning process equations numerical solution for boundary conditions prescribed at saddle point singularity 01 p0218 A70-11019

Two dimensional supersonic turbulent near wake saddle point singularity during recompression analyzed by including transverse momentum integral equation [AIAA PAPER 70-228] 06 p1039 A70-18106

Saddle point existence in determinate integrodifferential games with variable delay, assuming given control function over time interval 10 p1911 A70-25183

Stationary saddle points phase method for wave diffraction problems in inhomogeneous medium, deriving asymptotic expansion for surface integrals 22 p3984 A70-42390

SAFETY
NT AIRCRAFT SAFETY
NT FLIGHT SAFETY
NT INDUSTRIAL SAFETY
NT RANGE SAFETY
NT REACTOR SAFETY
SAFETY DEVICES
NT ABORT APPARATUS
NT ARRESTING GEAR
NT EJECTION SEATS
NT ESCAPE CAPSULES
NT ESCAPE ROCKETS
NT HELMETS
NT SEAT BELTS
NT SPACE SUITS
Transistorized lightning protected VHF ground antenna for air traffic communication providing high operational safety standards 03 p0459 A70-14297

Fire safety in hyperbaric systems isolated from environment by gas tight barrier [ASME PAPER 69-WA/SAF-2] 04 p0784 A70-14836

Air traffic control problems in avoiding midair collisions, satellite utilization in transatlantic flight control and anticollision devices and procedures 04 p0623 A70-15350

Static electricity suppression for textile materials by blending conducting metal fibers into yarn 05 p0870 A70-16299

Emergency in-flight evacuation concepts adapted from military experience considered for application to commercial aircraft 06 p0986 A70-17722

Spacecraft incorporated emergency rescue systems, discussing design of nonseparable crew escape compartment and separable capsule 07 p1218 A70-19010

Laser safety programs in biomedical applications, discussing installations, techniques, hazards and protection 08 p1451 A70-21048

Lightning protection development programs application to light aircraft plastic components, emphasizing structure and fuel systems designers awareness [SAE PAPER 700220] 11 p1980 A70-25892

Aircraft crash fire fighting equipment and tactics for future airport needs 12 p2160 A70-27433

Static charge reducer for aircraft fuels handling safety, discussing performance factors [SAE PAPER 700277] 18 p3263 A70-36808

Tractor rocket powered escape system of 600 knot extraction capability using drogue parachute and barometric time delay device 21 p3751 A70-41809

Pilot airborne recovery device /PARd/ midair rescue system, discussing buoyancy, midair pickup, seat ejection energy absorber, homing avionics and human factors [AIAA PAPER 70-1206] 21 p3752 A70-41812

Aircraft crash protection with preinflated air bag added to conventional seat/lap belt tested with human sled subjects 23 p4140 A70-44456

Emergency life saving instant exits for transport aircraft, using electromechanical confined transfer shaped explosive device 23 p4141 A70-44487

Testing laboratory for safety, survival and life support equipment concerning parachutes, aircrew protective helmets and maintenance manuals 23 p4141 A70-44488

Information handling for safety design concerning standards, criteria and requirements 23 p4153 A70-44493

Modularized multiple use SIIS-3 ejection seat escape system, discussing weight, envelope and low cost 23 p4143 A70-44499

SAFETY FACTORS
Marine safety aspects of helicopters with flotation equipment, considering effects of severe winds and waves, aircraft abandonment procedure, etc 01 p0007 A70-11316

Materials selection and Apollo command module atmosphere design considerations, discussing fire extinguisher system, equipment design changes, etc 03 p0437 A70-14058

Electroexplosive devices /EED/ in electromagnetic environments, discussing principles of warship safety 03 p0549 A70-14129

Static electricity generation and discharge in human beings due to clothing layers, analyzing body capacitance, resistance and inductance for ordnance and fuels safety 03 p0439 A70-14133

Test setup to determine safe limits of atmospheric potential gradients in electroexplosive device initiation 03 p0549 A70-14136

Space station damage containment and control, emphasizing safety problems and guidelines 04 p0762 A70-14933

Flammability control requirements and related hazards in avionics systems materials and components, using systems approach [SAE PAPER 690712] 05 p0956 A70-15854

NASA aerospace system safety program implementation and supporting organization with emphasis on background, concepts, constraints, methods and results [SAE PAPER 690710] 05 p0792 A70-15856

Safety analysis of VTOL aircraft for passenger transport based on accidental failures caused by technical defects, human error, weather, sabotage, etc 05 p0794 A70-16348

Rupture safety in fiberglass reinforced plastics using variation coefficient illustrated in vessel design 07 p1410 A70-19760

Fiberglass plastics structure safety design using time dependent limiting states with wear allowance 07 p1410 A70-19761

Computer program /SAFETE/ for evaluating missile launch risk on near real time basis [AIAA PAPER 70-248] 07 p1250 A70-20370

Missile and space vehicle range safety policies and practices using past statistical performance data and cost consideration [AIAA PAPER 70-246] 07 p1251 A70-20372

Design allowables and factors of safety for filamentary composite materials, discussing reliability 08 p1595 A70-21900

Safety characteristics of potassium chloratellactose mixtures as standard for comparing dangerousness of pyrotechnical compositions 15 p2786 A70-31848

Aircraft ground damage during maintenance and servicing 15 p2675 A70-32210

Flight safety standards, criteria and requirements, stressing accident prevention shift from accident investigation 15 p2831 A70-32212

C-5 aircraft failures and system safety program, noting landing gear, pressure equalization, visor nose, crosswind computer, nacelle separation and propulsion design 15 p2675 A70-32215

Airplane design safety considerations covering turbine cooling, liquid methane fuel, turbine wheel burst damage and lightning hazards 15 p2676 A70-32230

Sounding rockets safe operation and handling, examining ground and flight factors 16 p2981 A70-32923

Safety, microdamages and lifetime of elastic structures under random Poisson pulsed loads 16 p2996 A70-34328

Evolution and current status of Apollo crew safety, discussing hazard aspects, program approach and measures and activities incorporated in project [AAS PAPER 70-051] 17 p3176 A70-34790

Manned space station safety, discussing hazards identification and elimination, rescue/escape systems, etc [AAS PAPER 70-056] 17 p3016 A70-34792

Tektite II program safety planning for ambient pressure habitat under saturation diving conditions [AAS PAPER 70-053] 17 p3036 A70-34796

Aircraft accident prevention and investigation, noting economic factors as deterrent to safety measures implementation 17 p3022 A70-35860

Instrumentation safety for physiological research in hyperbaric chamber environment, taking into account pressure, isolation, atmosphere, electricity and fire 18 p3222 A70-35939

Solid oxygen generator for oxygen gas production from sodium chlorate decomposition, discussing reliability, safety and maintenance 18 p3225 A70-36211

Safety factor limit analysis for anisotropic non-homogeneous solids by variational method, exemplifying by four layer rectangular beam 19 p3547 A70-38355

Safety program effectiveness based on evaluation activity for monitoring field installations 19 p3555 A70-38848

Failure probability from finite sampling characteristics, emphasizing statistical safety factors to characterize structures strength reliability 20 p3724 A70-39856

Safety factor estimation by nomographic techniques for eye protection against direct viewing of laser beam 21 p3768 A70-40761

MIL-STD-882 systems and subsystems and equipment safety requirements related to program management activities 22 p4048 A70-43730

Safety standards and biological effects of microwave radiation, investigating cataractogenesis and heart rate in rabbits 23 p4144 A70-43790

Man-rated chamber facilities at Manned Spacecraft Center /MSC/, discussing safety requirements and criteria, environmental test chamber design and test results 23 p4152 A70-44458

Equipment, sources and safety in neutron radiography for industrial quality control 24 p4376 A70-45747

SAFETY HAZARDS
U HAZARDS
SAGITTARIUS CONSTELLATION
Angular size measurement for galactic X ray sources in Sagittarius region using modulation collimator aboard sounding rocket 09 p1744 A70-22521

Celestial positions and intensities of X ray sources in Sagittarius region obtained from rocket experiment 09 p1744 A70-22522

Formaldehyde absorption profile in direction of Milky Way center observed using lunar occultation 10 p1936 A70-23905

Sagittarius sources A and B2 018H absorption lines measured at microwave frequencies, determining oxygen isotopes abundance ratios 10 p1936 A70-23907

Sgr gamma-1 source, determining upper limit on soft X rays intensity 13 p2475 A70-28615

Neutral hydrogen observations in Sagittarius and Scutum spiral arms, examining circular galactic rotation by density wave theory kinematic models 18 p3331 A70-37197

High energy cosmic gamma radiation detection from point source in Sagittarius, using balloon mounted spark chamber with Cerenkov telescope 19 p3500 A70-38078

Gamma ray background anisotropy effects of Sgr A flux arising from Compton scattering and neutral pion decay, discussing complex radio and IR structure 21 p3878 A70-40926

X ray sources celestial positions in Sagittarius region, using rocket-borne rotating modulation collimator 22 p4094 A70-42928

Radio emission searched for X ray sources near Sagittarius 22 p4094 A70-42930

SAHA EQUATIONS
Ionization equilibrium of atoms and hydrogen-like ions in nonthermal plasma, transforming into Saha formula for high electron densities 11 p2086 A70-25836

Statistical mechanics of partially ionized hydrogen plasma, deriving Saha equation to calculate ionization degree and potential for various electron densities and temperature 12 p2281 A70-27882

Observational evidence concerning validity of Saha and Boltzmann laws in O, B and A stellar atmospheres 17 p3170 A70-35387

SAILPLANES
U GLIDERS
SAILS
NT SAILWINGS
NT SOLAR SAILS
SAILWINGS
Flying ejection seat providing capability for leaving hostile area before vertical descent by parachute, using Princeton Sailing and bypass fanjet 07 p1192 A70-19020

Hi-glide personnel canopy /Para-Foil, Parawing, Sailing, Volplane/ technology capability requirements identification from performance parameters tradeoffs [AIAA PAPER 70-1194] 21 p3753 A70-41822

- Water ballast loadings on sailplane Cobra 17, considering wing, aileron, tailplane, fuselage and landing gear 22 p3962 A70-42962
- SAINT VENANT FLEXURE PROBLEM**
U SAINT VENANT PRINCIPLE
SAINT VENANT PRINCIPLE
 Astatic equilibrium loadings in Saint Venant principle for linear elasticity, analyzing physical distinction from self equilibrated loadings to explain smaller long range stresses 04 p0769 A70-14860
 Compression test for ductile materials based on Saint Venant principle of plasticity to reduce friction effects on deformation by lubricant pressurization 04 p0776 A70-15373
 Saint Venant torsion problem using finite element method, establishing direct matrix relation between forces and displacements 04 p0778 A70-15527
 Exact polynomial solution Saint Venant flexure of pretwisted rectangular plate treated as shallow hyperbolic paraboloidal shell 05 p0928 A70-16056
 Saint Venant torsion and flexure of composite prismatic and cylindrical bars with circular and concentric interfaces 05 p0936 A70-16318
 Axially uniform stress and strain in cylindrical shells, discussing Saint Venant torsion and displacement relations 07 p1405 A70-19255
 Saint Venant principle in cantilever sandwich beams under two statically equivalent load systems, considering Young moduli effects 07 p1406 A70-19328
 Strain and stress compatibility from extension of Saint Venant and Beltrami-Mitchell equations for physically and geometrically linear to nonlinear media 08 p1585 A70-20962
 Integration of Saint Venant equations of deformation continuity for region occupied by elastic medium 08 p1587 A70-21166
 Astatic equilibrium in Saint Venant principle applied to surface of linear elastic body, discussing stress field produced by boundary loading 08 p1591 A70-21463
 Flexural rigidity of thin walled beams, analyzing relationship between loads and displacements taking into account Saint Venant torsional resistance 10 p1955 A70-24052
 Saint Venant principle in linear isotropic viscoelasticity of Toupin estimates for body of arbitrary shape to allow integration by parts 13 p2513 A70-28990
 Saint Venant principle treating Neumann problem with nonthin two dimensional domain 15 p2767 A70-31855
 Book on elasticity theory covering end effects, Saint Venant principle, edge and screw dislocations, moire method, thermoelasticity, cavity and inclusion effects, Muskhelishvili methods, etc 17 p3183 A70-34603
 Stress decay rates in Saint Venant boundary region in truncated semiinfinite elastic cone, using Papkovitch-Neuber functions for eigenfunctions formulation 18 p3339 A70-36489
 Strain and stress compatibility from extension of Saint Venant and Beltrami-Mitchell equations for physically and geometrically linear to nonlinear media 20 p3719 A70-39384
 Medium thickness shells under thermal creep using Saint Venant semiinverse method 20 p3722 A70-39787
- SALINITY**
 Cotton plant leaves from high saline soil area, observing chlorophyll content on color photographs 14 p2576 A70-30977
 Sea water temperature and salinity effects on smooth ocean surface radiation in centimeter range 18 p3250 A70-36968
 Microwave radiometric airborne measurement of salinity of Mississippi River outflow, using P3A aircraft 24 p4330 A70-45979
- SALIVA**
 Thermoregulatory salivary responses of dog to various ambient temperatures, emphasizing hypothalamic temperature, threshold and proportionality constant 01 p0017 A70-10465
- SALIVARY GLANDS**
 Hypoxia and parotid secretion in humans exposed to angular accelerations 17 p3038 A70-35137
 Human mental stress evaluation through chemical analysis of 17-hydrocorticosteroid level in parotid fluid 24 p4308 A70-45509
- SALT BATHS**
 High temperature oxidation of Ni-Cr alloys and stainless steels in molten salt, observing grain boundary corrosion with electron probe 15 p2757 A70-31875

SALT SPRAY TESTS

- Ni alloys with protective coatings for gas turbine blades, testing corrosion resistance in diesel fuel combustion products with intermittent salt water sprays 17 p3125 A70-35394
 Alloying elements effects on corrosion resistance of Mg ingot in NaCl aqueous solution 24 p4363 A70-46198

SALTS

- Polyamides /nylons/ stress cracking by metal halides and halide-like salts, investigating effects of nylon temperature, moisture content, concentration, etc 10 p1907 A70-24224
 Nylon 6 polyamide tensile stress cracking by metal thiocyanates in aqueous and nonaqueous solutions, comparing results with cracking by metal halides 10 p1907 A70-24300
 Electrodeless electrolysis of solid ionic conductors and fused salts without contact leads, using electron beams and glow discharge 13 p2361 A70-28929
 Human water-salt metabolism following exposure to transverse accelerations, discussing diuresis and Cl-K excretion 17 p3038 A70-35364
 Inorganic liquid lasers, discussing Nd salts solution preparation and handling methods 23 p4201 A70-44929

SAMPLED DATA

- U DATA SAMPLING**
SAMPLED DATA SYSTEMS
U DATA SAMPLING

SAMPLERS

- Microbiological evaluation of modified vacuum probe surface sampler for handling and fallout contamination compared with swab-rinse technique 05 p0807 A70-16574
 Vacuum probe sampler to monitor particle contamination on surfaces within clean environments 05 p0808 A70-16703
 Vacuum probe as effective device for sampling surface contamination of airborne microorganisms 05 p0808 A70-16704
 Vacuum probe sampler to monitor particle contamination on surfaces within clean environments 09 p1623 A70-22340
 Airborne precipitation drop sampler imprint size relationship to water drop diameter 10 p1857 A70-23932
 Rocketborne cryogenic sampler using shock diffuser inlet for air collection at supersonic speeds during rocket ascent 10 p1949 A70-23937
 Atmospheric aerosols optical and microphysical measurements comparison, evaluating sample collection equipment, errors, etc 19 p3421 A70-37637
 Rain sampling by Varsity aircraft, determining reliability of droplet sampling instruments above aircraft top surface 19 p3463 A70-38947
 Aerobee rocket-borne cryogenic air samplers heat exchanger design by mathematical model and computer solution 23 p4280 A70-44365

SAMPLES

- Free jet expansions in molecular beam sampling systems, using Sherman equations and chemical kinetic equations [WSCI PAPER 70-12] 13 p2389 A70-29608
 Apollo 11 mafic crystalline rocks and mineral assemblages, discussing collection, classification and sample environments 21 p3894 A70-41502

SAMPLING

- NT AIR SAMPLING**
NT CORE SAMPLING
NT DATA SAMPLING
NT RANDOM SAMPLING
 Probability selection of useful plants based on distribution of resolving statistics 01 p0053 A70-11023
 Stationary Gaussian stochastic processes sample functions properties and local times 02 p0324 A70-12504
 Automated mars surface sample return /AMSSR/ mission, discussing Saturn 5 chemical and nuclear approach [AIAA PAPER 69-1066] 04 p0764 A70-15626
 Duration measurements for sampling function in dynamic crossed field photomultiplier 05 p0849 A70-16655
 Rocket-borne sampler for collecting noctilucent cloud particles in mesopause, describing collection and analysis methods and protection against tropospheric contamination 07 p1273 A70-20266
 Multistage sampling of space and aircraft remote sensor imagery for forest inventory 12 p2228 A70-26921
 Data system obtaining sampling rate for cardiac volume measurement via fast biplane cineangiography 15 p2691 A70-31922

- Sample images division into teaching and checking sequences in pattern recognition problems, determining coefficients based on statistical properties of set 19 p3382 A70-37449

- Risk interpretation of prior distributions in acceptance sampling by Bayesian analysis 19 p3440 A70-38817

SAMPLING DEVICES**U SAMPLERS****SAN MARCO SATELLITE**

- Global and European geodetic satellite network, discussing San Marco equatorial satellite and observation stations 03 p0581 A70-13829

SAN MARCO SATELLITES**NT SAN MARCO 2 SATELLITE****SAN MARCO 2 SATELLITE**

- Equatorial ionosphere ionization and electron density measurements by San Marco 2 satellite 03 p0475 A70-13830

SANDS

- Sand and dust environmental test of T-63 regenerative engine, discussing performance depreciation, recuperator inspection and comparison with non-regenerative t63-a-5a engine 01 p0164 A70-10685
 Sand erosion of metals and plastics, discussing effects of impact conditions and impacting particles and target surface properties 07 p1314 A70-20004
 Erosion by solid particles, discussing impacting velocity effects, natural sand quartz particle size distribution and composition, artificial industrial abrasives, etc 17 p3126 A70-35600
 Sand bed stability under shear flow of low Froude number 24 p4330 A70-45980

SANDWICH CONSTRUCTION**U SANDWICH STRUCTURES****SANDWICH PLATES****U PLATES [STRUCTURAL MEMBERS]****U SANDWICH STRUCTURES****SANDWICH STRUCTURES**

- Coherent precipitates effect on explosive shock hardening of pure nickel and Inconel alloy sandwich assemblies determined from simultaneous shock loading at specific pressures 01 p0116 A70-10107
 Minimum weight sandwich plates complying with von Mises criterion, providing constant dissipated energy density 01 p0202 A70-10947
 Sandwich plates plastic buckling stability under uniaxial compressive loads from compressible theory viewpoint 01 p0204 A70-11137
 Buckling of orthotropic sandwich plates derived for sixth order governing differential equation by variational theorem 01 p0204 A70-11139
 Sandwich panel equations derived from elasticity theory equations applicable to stress analysis in internal zone and edge effects analysis 01 p0210 A70-11409
 Mathematical model for local postbuckling strength of flat truss core sandwich panels loaded in compression, considering application to Ti structures 02 p0386 A70-11948
 Sandwich structures nondestructive testing by holographic interferometry, discussing system operation, specimen stressing, acoustic vibration, etc 02 p0309 A70-12274
 Cylindrical two layer shells stability under compression and radial pressure, calculating compression and transverse shear strains in carrying layer and filler 03 p0592 A70-13443
 DC electrical conduction in In and In-Pb alloy foils sandwich structures, discussing size effect and Pb diffusion rate 03 p0540 A70-13624
 Complex uncoupled modes to analyze forced vibrations of three layer damped sandwich beam with arbitrary boundary conditions, discussing orthogonality 04 p0773 A70-15076
 Shear modulus of sandwich structure tubular core derived by virtual work principle and matrix approach, comparing results with honeycomb core [DGLR-69-64] 04 p0774 A70-15156
 Orthotropic sandwich cylinders buckling under axial compression, presenting linear theory approximate design equations 04 p0776 A70-15381
 Rectangular waffle plates minimum-weight design efficiency with multiple rib sizes in stiffening direction compared to honeycomb core sandwich construction 04 p0777 A70-15526
 Circular sandwich plates fundamental natural frequencies, considering face members membrane characteristics and thickness, face and core isotropy, etc 04 p0778 A70-15559

- Thin cylindrical circular shell and three layered plate, analyzing vibration and stability due to loads and temperature 05 p0926 A70-15916
- Three layer plate of elastic fiber glass reinforced plastic outer layers and metallic plastic filler, studying elastoplastic stability 05 p0934 A70-16218
- Honeycomb and sandwich construction design, discussing optimal material selection, filament wound technology, panels fabrication, destructive and non-destructive test methods, etc 05 p0941 A70-16616
- Dynamics of composite, sandwich and stiffened shell type structures with various geometries 06 p1160 A70-17158
- Transient heat flow in three dimensional rectangular panels, developing criterion for problem dimensionality [AIAA PAPER 70-16] 06 p1182 A70-18212
- Crack self healing in aluminum foil-polyvinyl acetate sandwich structures 07 p1315 A70-18713
- Vibration damping by sandwich structure consisting of viscoelastic layer between two high Youngs modulus metal sheets 07 p1401 A70-18845
- Tensile and shear properties of blind fixed, blind floating and through types of bonded sandwich inserts, noting geometry and temperature effects 07 p1401 A70-18934
- Shallow spherical sandwich shells under concentrated forces, obtaining inhomogeneous equations solution by integral Hankel transforms 07 p1402 A70-19053
- Rectangular three layer plate bending with load carrying central layer obeying Kirchhoff-Love hypothesis and external layers obeying Noeth hypothesis 07 p1403 A70-19117
- Optimal linear viscoelastic synthetic sandwich structures, investigating test/calculation agreement for simply supported beams and embedded plates [ONERA-TP-702] 07 p1404 A70-19137
- Shell elastic constants for multilayered sandwich cylinders using Donnell approximation 07 p1406 A70-19326
- Saint Venant principle in cantilever sandwich beams under two statically equivalent load systems, considering Young moduli effects 07 p1406 A70-19328
- Minimum weight design of elastic sandwich beams with deflection constraints using n-dimensional space of discretized bending stiffness 07 p1407 A70-19358
- Rectangular bidirectional composites and sandwich plates three dimensional elasticity solutions 07 p1412 A70-19952
- Stability equations of three layer panels with allowance for rigid filler transverse deformations 07 p1415 A70-20186
- Elastic-plastic work hardening sandwich arch under given loading rate analyzed for stress rates using integral equation [ASME PAPER 69-APM-21] 08 p1593 A70-21616
- Stresses and strains in multilayer systems of viscoelastic materials showing aging solved by quadratures and Volterra equations, noting dependence on time 08 p1594 A70-21672
- Combustion rates and temperature distribution in condensed and gaseous phases of ammonium perchlorate sandwich with synthetic resin middle layer 09 p1741 A70-22105
- Stress concentration at elliptical hole of arbitrary eccentricity in shallow sandwich shells with hard and soft fillers 09 p1783 A70-23385
- Sandwich plates stability in conducting compressible fluid flow under magnetic field 09 p1785 A70-23621
- Equipment container with sandwich type structure for packing delicate parts 10 p1852 A70-24899
- Convective-radiative heating of multilayer plate approximating temperature field by iteration 10 p1969 A70-25143
- Multilayer plate vibrations calculated with allowance for energy dissipation in material, deriving equations of motion 10 p1965 A70-25297
- Rectangular sandwich plates stability under combined loads, deriving equations for determining critical loads 11 p2129 A70-25563
- Vibration equations for closed and open sandwich cylindrical shell with thickness-shear deformation in core and face layers compared with membrane theory 11 p2145 A70-26697
- Axisymmetric and unsymmetric free vibrational modes of right-circular conical or cylindrical sandwich shells with free edges, discussing Rayleigh-Ritz solution 11 p2145 A70-26700
- Supersonic aerial target wing synthesis using sandwich construction with graphite-epoxy laminate skins bonded to Al honeycomb, achieving significant weight reduction 12 p2160 A70-27118
- Thermal stresses in temperature dependent multilayered cylindrically anisotropic hollow cylinders 12 p2321 A70-27203
- Sandwich beams elastoplastic stability, determining critical load 12 p2323 A70-27342
- Shear deformation of sandwich plate cross sections with hinged opposite edges, constructing transfer matrix for state variables 13 p2508 A70-28483
- Potting material applicability to attaching honeycomb sandwich assemblies to structures, describing pre- and postpotting methods 13 p2418 A70-28667
- Vibration control by alternate layers of high damping viscoelastic material, discussing damping and loss factors, beams design and attachment 13 p2513 A70-29079
- Thermoelastic equations for circular sandwich plates bending due to asymmetric temperature distribution 13 p2518 A70-29976
- Thin film sandwich Ag/Ni/Cu, demonstrating multiple electron diffraction 14 p2627 A70-30724
- Photographic enhancement by slightly offset film sandwiching 14 p2586 A70-30979
- Clamped orthotropic rectangular sandwich plates bending using approximate solution 14 p2661 A70-31429
- Core shear deformations effects on stress, deflection and buckling load calculations for sandwich panels 15 p2815 A70-31931
- Sandwich wire planar antenna array design, noting electrical performance, ruggedness, volume and weight 16 p2877 A70-33416
- Geometrically nonlinear theory for sandwich type plates symmetrically built of three elastically and thermally anisotropic layers, considering nonuniform temperature field 16 p2990 A70-33744
- Embedded damped sandwich beams, determining equations for resonant frequency, loss factor and modal roots 16 p2992 A70-34018
- Sandwich rings inplane transient response to concentrated radial impulsive loads based on Timoshenko type theory, noting dependence on extensional to shear stiffness ratio 16 p2993 A70-34093
- Core flexibility effects on deformation of uniformly loaded clamped parallelogrammic sandwich panels using linear theory 17 p3185 A70-34920
- Optimal design of elastic sandwich, solid beam and plate structures under dynamic harmonically varying loads 18 p3336 A70-36220
- Thickness determination of external elastic plates in freely supported three layer structures of uniform strength under perpendicular loads 18 p3343 A70-36717
- Minimum weight thermoelastic design of sandwich beam for given deflection, using potential energy principle 19 p3541 A70-38044
- Minimum weight design of sandwich beams with elementwise constant cross section for prescribed compliances under alternative loads 19 p3543 A70-38303
- Circular sandwich arc subject to central concentrated load and symmetrically applied edge couple, obtaining shakedown interaction curve 19 p3546 A70-38354
- Sandwich panels geometrically and physically nonlinear theory, obtaining equations of motion and boundary conditions consistent with strain displacement relations 19 p3547 A70-38360
- Ti sandwich structures low temperature brazing with Al alloy, describing fabrication process and mechanical properties 20 p3638 A70-39969
- Finite deflection discrete element analysis of sandwich plates and cylindrical shells with unbalanced laminated faces 20 p3732 A70-40268
- Stress distribution at hole in orthotropic cylindrical sandwich shell under internal pressure 20 p3734 A70-40440
- Closed circular cylindrical shell nonlinear problem solvability extended to anisotropic sandwich shell, using mean deflection theory 21 p3933 A70-40601
- Solid and sandwich beams lateral vibrations under transverse shear, rotary inertia and variable midplane stretching 21 p3938 A70-41761
- Weight-optimal sandwich beam design for given static deflection, using energy approach 22 p4113 A70-42535
- Joint strength of three layer fiberglass reinforced plastic panels with bilateral adhesive patches under linear axial force 22 p4115 A70-42812
- Sandwich multilayer structures temperature fields and heat transfer characteristics at high temperature [ICAS PAPER 70-38-BIS] 23 p4276 A70-44136
- Elastic circular sandwich beams optimal design for minimum compliance and given weight, considering rings and semicircular arches 24 p4420 A70-45276
- Holographic interferometry for NDT inspection of adhesive bonded honeycomb sandwich aerospace structures 24 p4338 A70-45754
- Sandwich structures in aerospace hardware, considering joining methods, materials and geometries [SAE PAPER 700859] 24 p4425 A70-45879
- Bonded honeycomb sandwich structure fastening techniques in aerospace design, noting application to aircraft and spacecraft structures [SAE PAPER 700850] 24 p4425 A70-45882
- SAPPHIRE Schottky barrier FET fabrication using epitaxial growth of single crystal GaAs on insulating sapphire substrate 04 p0660 A70-15364
- Epitaxial beta-SiC films formation on sapphire by chemical conversion 06 p1127 A70-17946
- Sapphire whisker-Al composites fabrication methods using air elutriation techniques and semiautomatic methods for fiber alignment, discussing elastic modulus, tensile strength, etc 07 p1314 A70-19956
- C-axis single crystalline sapphire filament tensile and fracture tests 08 p1514 A70-20647
- Laser pulse energy ponderomotive meter using mechanical action exerted by light on movable sapphire plate in air at atmospheric pressure 09 p1700 A70-23657
- Metallic base fiber and particulate composites, emphasizing silicon carbide, sapphire, boron and graphite filaments 14 p2597 A70-31168
- ZnO epitaxial layers deposition by chemical vapor transport on sapphire single crystal substrates 15 p2784 A70-31982
- Hydrogen effect on impurity redistribution in heteroepitaxial Si layers on sapphire substrate 15 p2785 A70-32529
- Sapphire and ruby plastic deformation and fracture properties at room temperature, discussing sapphire base ceramics 18 p3278 A70-36046
- Compressive and rarefaction shock wave propagation in polymethyl methacrylate, fused silica and sapphire, using laser interferometer measurements 22 p4031 A70-43020
- SARCOMA U CANCER SAS-A Variable parameter nutation damper SAS-A dual spin satellite, discussing design and expected in-flight performance by digital simulation [AIAA PAPER 70-972] 20 p3669 A70-39557
- SATAN (SENSOR) U TERRAIN ANALYSIS SATELLITE ANTENNAS Solar radiation influence on Alouette satellite spin behavior with long flexible antennae, taking into account sunlight/shadow history and solar vector inclination 02 p0380 A70-11852
- Satellite mounted mm wave parabolic dish antenna for tracking communication satellite in synchronous orbit 02 p0392 A70-11933
- Structural and systems design of large orbital radio astronomy antenna /crossed H interferometer/ with astronaut participation in deployment, operation, maintenance and updating [AIAA PAPER 70-100] 06 p1156 A70-18058
- TV system for satellite antenna boom position monitoring, describing camera system and programming, imaging techniques, position calibration, etc 10 p1891 A70-24898
- Air traffic control system using ground controlled satellite-borne phased array antenna to overcome UHF downlink path loss [AIAA PAPER 70-497] 11 p2077 A70-25421
- Attitude stabilization of synchronous communications satellites employing multiple narrow beam antennas [AIAA PAPER 70-457] 11 p2119 A70-25422

Orbit utilization, discussing sharing of satellite communication frequency bands and use of multiple earthward antenna beams
[AIAA PAPER 70-468] 11 p1999 A70-25428

VHF aerosol antenna design and system interactions, analyzing impact of spacecraft dynamics, control system, power supply and propulsion
[AIAA PAPER 70-486] 11 p2120 A70-25439

Low cost earth station and antenna for Canadian domestic satellite, bringing color TV to northern territories
[AIAA PAPER 70-432] 11 p2000 A70-25458

Multiple feed waveguide lens in variable coverage communications antenna for geostationary LES-7 satellite
[AIAA PAPER 70-423] 11 p2016 A70-25461

S band communications repeater using retrodirective phased array on synchronous altitude data relay satellite /DRS/ for intersatellite and ground links
[AIAA PAPER 70-424] 11 p2001 A70-25472

Sidelobe suppression for satellite reflector antennas by heavy taper, blockage compensation and active zone techniques, noting net antenna gain enhancement
[AIAA PAPER 70-427] 11 p2016 A70-25476

X band mechanically despun antenna system with RF and motor drive assembly developed for earth coverage communications satellite
[AIAA PAPER 70-422] 11 p2001 A70-25481

Digital satellite communications systems, discussing time division multiplexing, steerable beam antennas and satellite-to-satellite transmission
[AIAA PAPER 70-491] 11 p2003 A70-25492

RF interference emanating from satellite-borne pulse plasma thruster by measuring RF power at UHF antenna having plasma in near field
11 p2103 A70-26136

Satellite pencil and shaped beam antennas, considering maximum gain conditions for various angles
12 p2197 A70-27929

Ultrahigh strength stainless steel for light gage springs and satellite antennas
13 p2420 A70-29248

Alouette satellite antennas and receivers for detecting plasma resonances and VLF signals, noting ground station telemetry link
13 p2380 A70-29902

Alouette spikes decrease with time equivalent to antenna transient response during hot plasma immersion
13 p2371 A70-29921

Repeater and antennas for space telecommunications onboard ELDO STV-F9 satellite, describing tests and measurements
15 p2811 A70-32282

Counterrotating antenna onboard Italian satellite in synchronous equatorial orbit for microwave propagation experiment
15 p2709 A70-32287

Multibeam array antenna performance improvement by shaping beam for optimum earth coverage from stabilized synchronous satellites
16 p2860 A70-32952

Lens antennas design for communication satellites, discussing power gain, beam width, sidelobe level, temperature distribution, etc
16 p2982 A70-33772

ATSC satellite rocket exhaust plume convective heating measurements of VHF whip antennas, discussing nozzle flow and heating rate
[AIAA PAPER 70-843] 16 p3000 A70-33926

Radio astronomy explorer /RAE/ satellite main antenna array, describing elements, dispenser and take-up mechanisms, construction materials, etc
16 p2986 A70-34144

Brushless despun mechanical drive and control system design and performance for orientation of high gain communications antenna from spin stabilized satellite
16 p2986 A70-34161

Canister for protecting DC motors in Isis 1 antenna unit, noting pressure monitoring device and shaft seal
17 p3100 A70-34753

Electronically despun antenna for spin stabilized medium altitude satellites
17 p3179 A70-35270

Plasma induced radio frequency interferences from DC-DC converter to receiving antenna simulated for REXS satellite in space chamber
17 p3047 A70-35400

Complex impedance measurements for monopole antenna for electron densities in/out of OGO satellite wake in upper ionosphere
17 p3080 A70-35771

Directional solar thermal field /sunlight/ effect on coupled nonplanar transverse and torsional vibrations of satellite cylindrical antennas in orbit
20 p3720 A70-39676

Square loop antenna radiation resistance in warm plasma, comparing theoretical results with measured values from Ariel 3 satellite antenna
21 p3796 A70-40562

Multiple beam antenna system for regional communications satellite directing high radiated power toward specific earth areas
21 p3790 A70-41358

Single multiple access satellite communication system requirements for worldwide, trunked and local operations, considering transponder allocation and antennas
21 p3790 A70-41365

Radio Astronomy Explorer satellite boom deployment method resulting in gravity gradient capture, emphasizing role of predeployment attitude and antenna Vee angle
[AIAA PAPER 69-920] 21 p3931 A70-41856

Satellite-borne loop antenna resistive and reactive impedance measurements in topside ionosphere
22 p4019 A70-43112

SATELLITE ATTITUDE CONTROL

Heat exchange unit for low thrust attitude control propulsion system evaporator designed for converting liquid propellants to gas
[AICHE PREPRINT 25] 01 p0216 A70-10969

HEOS 1 satellite for interplanetary space exploration, describing eccentric orbit, structure, power supply, attitude measurement and control, spin rate control, telemetry and telecommand systems
01 p0196 A70-11114

Satellite attitude control, discussing passive, active and hybrid stabilization methods including spin, gravity gradient and magnetic stabilization
01 p0197 A70-11264

Hydrodynamic journal-thrust bearing system for satellite attitude control flywheel, discussing bearing stability, grease lubricant seal, power consumption, etc
[ASLE PREPRINT 69-1C-22] 02 p0309 A70-12532

Satellites gravity-gradient stabilization by flywheels in elliptical orbits, designing control system for orientation and optimal motion damping
03 p0582 A70-14321

Spacecraft orientation control without measuring vehicle angular velocity based on transient response and oscillations damping effectiveness
04 p0760 A70-14428

Electrostatic charged particle acceleration and ion thruster function in geostationary satellite station-keeping and attitude control, orbital transfer and drag compensation
[ONERA-TP-764] 04 p0735 A70-14934

Satellite orbit and attitude determination and planetary gravity and astronomical constants from earth-based radio Doppler and orbital photogrammetric observations
04 p0750 A70-14938

ESRO 1 satellite attitude stabilization in launching, transition and stabilized phases
[DGLR-69-14] 04 p0762 A70-15168

Free gas formation in propellant systems and effects on attitude control systems
[AIAA PAPER 69-434] 04 p0763 A70-15418

Dodge satellite postlaunch attitude stabilization and flight data comparison with digital simulation, underlining simulation use in design analyses
04 p0765 A70-15674

Semiactive gravity gradient attitude stabilization system /SAGS/ providing active pitch control and semipassive roll/yaw control, discussing design, development and testing
[SAE PAPER 690691] 05 p0923 A70-15863

Pulsed plasma and ion microthrusters providing satellite attitude and position control
05 p0896 A70-16119

Magnetic torquers consisting of permanent magnets or coils for attitude stabilization of earth satellites in geomagnetic field
[IEEE PAPER 27.1] 05 p0924 A70-17000

Attitude performance of GEOS 2 gravity gradient spacecraft, discussing prelaunch design and post-launch analyses
06 p1154 A70-17162

Capture and gravity gradient stabilization of LIDOS satellite in eccentric orbit
[AIAA PAPER 69-921] 06 p1154 A70-17175

Satellite launch vehicle attitude control stability study including fuel sloshing and body bending effects
06 p1155 A70-17320

Jet engine risetime effect on spacecraft orientation control system performance, assuming monotonic or extremal thrust mode
06 p1103 A70-17883

Hybrid coordinate formulation for flexible space vehicle attitude control system design
[AIAA PAPER 70-20] 06 p1158 A70-18180

Aeros satellite active magnetic position control system of axis and spin noting design and operation
[DGLR-69-056] 07 p1393 A70-19148

Suboptimal attitude control system for Nimbus satellite using motor-driven inertia wheels as control torque source for three dimensional control
07 p1331 A70-20027

Active and passive geomagnetic rate dampers for attitude control systems of geomagnetically, gravitationally or spin stabilized spacecraft
09 p1766 A70-22936

Nonspinning satellite orbit eccentricity effect on attitude stability
09 p1766 A70-23229

Satellite attitude and orbit control systems based on electrically heated ammonia or hydrazine
09 p1767 A70-23432

Ionosphere sounding satellite attitude variation dependence on transverse moments of inertia
10 p1949 A70-23918

Gravity gradient satellites equilibrium attitude error analysis showing relative effects of error sources
10 p1951 A70-24825

Star tracker linear and nonlinear model selection influence on satellite attitude stability
10 p1953 A70-25231

Attitude stabilization of synchronous communications satellites employing multiple narrow beam antennas
[AIAA PAPER 70-457] 11 p2119 A70-25422

Communications and attitude control on Phase 2 satellite for Defense Satellite Communication System
[AIAA PAPER 70-493] 11 p1998 A70-25427

Three axis attitude control of earth oriented non-spinning synchronous communications satellite, using gimbal-mounted momentum wheel and pulsed plasma thrusters
[AIAA PAPER 70-456] 11 p2119 A70-25431

Despin ball bearing assemblies performance data for TACSAT and Intelsat 4, discussing technology needed for accelerated testing, higher precision, failure detection and lubricants
[AIAA PAPER 70-459] 11 p2058 A70-25471

LES 5 and 6 feasibility demonstration of satellite communications at VHF/UHF to mobile terminals and as test beds, emphasizing stationkeeping and attitude control
[AIAA PAPER 70-494] 11 p2121 A70-25474

Ammonia micropropulsion operation modes and performance for stabilizing synchronous communication satellite, noting advantages over chemical and ion propulsions
11 p2122 A70-25817

Hybrid attitude attitude control system deformation model, utilizing pivoted flexible boom with tip mass as actuator and inertia wheels to dampen gravity induced librations
11 p2123 A70-26127

Sun-pointing spinning spacecraft attitude control by solar radiation pressure using paddle arrangement without power, sensor and moving parts requirement
11 p2123 A70-26145

Spin stabilized satellite attitude and orbital maneuvers computation, considering required accuracy and computer time in numerical integration procedures
11 p2125 A70-26278

Roll and pitch attitude control for long range station-keeping mission of synchronous flywheel stabilized communication satellite, discussing constraints on on-board equipment and technology
11 p2126 A70-26279

Ground testing apparatus with three degrees of freedom for artificial satellites attitude control systems, establishing mathematical model by digital and analog techniques
11 p2031 A70-26290

Kalman filter modifications for spinning satellite attitude determination in elliptical orbit prior to apogee maneuver, using sun and IR earth sensors
11 p2028 A70-26304

Experimental IR earth horizon profiles measured by satellite in F region, discussing spectral channels and attitude control
12 p2225 A70-27751

Molniya 1 communication satellite attitude control involving automatic solar panel and antenna orientation, using powered gyroscopic stabilizers
13 p2499 A70-28387

Synchronous satellite attitude acquisition and keeping, proposing roll and pitch control law for simulation
13 p2500 A70-28409

Attitude-translation motion coupling effect on stability of gravity-stabilized drag-free satellites
13 p2501 A70-28424

Suboptimal satellite attitude control using ionic microthrusters operating by large modulated amplitude impulses caused by electrostatic deflection of beam
13 p2501 A70-28426

Limit cycle oscillations in satellite attitude control system, producing control moment by pulse modulated controller
13 p2502 A70-28430

Symphonic communication satellite orbit and attitude stabilization systems components, operation and accuracy requirements
13 p2502 A70-28432

Spinning sun oriented satellite using magnetic coil around spin axis for attitude control, detailing design
13 p2502 A70-28439

Thermal interface between edge of planetary disk and space for providing attitude reference during orbiting of planet
13 p2403 A70-28442

Spacecraft orientation control without measuring vehicle angular velocity based on transient response and oscillations damping effectiveness
13 p2503 A70-28453

Simultaneous satellite attitude control and flywheel desaturation using external torque
13 p2503 A70-28527

- Azur satellite flight results, noting trajectory accuracy telemetry reception, yo-yo triggering and attitude control 13 p2505 A70-28766
- Satellite orientation control and stabilization by gyro with statically and dynamically balanced rotors, showing steady motions and stability region augmentation 13 p2507 A70-29769
- Gravity gradient stabilization systems for earth-pointing satellites, noting long term reliability and accuracy 13 p2507 A70-29769
- Nimbus weather satellite as laboratory for sensors collecting data for global weather system, describing launching, attitude control systems and cameras 14 p2654 A70-31149
- Satellite feedback attitude control system resulting in high accuracy earth pointing motions in elliptic orbits 14 p2654 A70-31172
- Nutation damper for dual-spin spacecraft, considering various two degree of freedom systems with two natural frequencies 14 p2655 A70-31367
- Earth-pointing satellites joined by tether, discussing reel back and drag brake orbital deployment techniques and dynamic behavior 15 p2799 A70-31776
- OGO spacecraft structures, thermal control systems, attitude control, weight and power supplies 15 p2810 A70-31782
- Gravity stabilized gyrostatt satellites internal angular momentum effect on nonlinear resonant attitude motions 15 p2810 A70-31785
- Satellite attitude control via optical-inertial stabilization, using Bucy-Kalman linear statistical filtering 15 p2811 A70-32265
- Microthrusters for geostationary satellites attitude and position control 15 p2791 A70-32279
- IR radiating bodies angular displacement determination by vacuum evaporated thermocouple radiation detectors, describing stationary communication satellite attitude control 15 p2740 A70-32422
- Mariner attitude control system limit cycle operation during cruise, noting variation from ideal case to single side operation [AIAA PAPER 69-844] 15 p2812 A70-32507
- Motion and stability characteristics of dual spin satellite system with pendulous type nutation dampers, noting mass unbalance effect [AIAA PAPER 69-857] 15 p2812 A70-32508
- Magnetic hysteresis dynamic model for digital simulation of stabilized satellite attitude motions 15 p2812 A70-32509
- Star tracker rigidly connected to spacecraft frame for attitude determination by star field correlation 16 p2946 A70-33157
- Spacecraft gravity gradient stabilization by damping out oscillatory motions by energy dissipation, using combined eddy current and hysteresis dampers /Combination Passive Damper/ 16 p2985 A70-34133
- ATS attitude stabilization boom packages, describing torque transmission, drum synchronization, electrical isolation, lubrication, etc 16 p2846 A70-34145
- Hydrodynamic journal-thrust bearing system for satellite attitude control flywheel, discussing bearing stability, grease lubricant seal, power consumption, etc 17 p3099 A70-34630
- Bearing assembly energy dissipation effects on dual spin spacecraft attitude stability, explaining satellite motion anomalies 17 p3100 A70-34756
- Heliostationary spacecraft for solar observation near libration point between sun and earth, discussing attitude stabilization by solar pressure 17 p3178 A70-35254
- Spin stabilized satellite reorientation, using magnetic dipole interaction with geomagnetic field 17 p3179 A70-35287
- Steady state off-on attitude control strategy for minimizing propellant consumption and thrust ignitions of satellite in presence of environmental disturbance torques 17 p3180 A70-35556
- Spacecraft wide angle attitude control system stability analysis, using air bearing table simulation 17 p3134 A70-35651
- Spinning symmetric satellite attitude stability in hyperbolic orbit on flyby mission, examining by numerical integrations of equations of motion 17 p3181 A70-35753
- Spacecraft simulator using air bearing technique to simulate low friction aspect of environment, considering application to satellite attitude control 18 p3236 A70-36064
- Japanese scientific satellite magnetic attitude and spin rate control system design and computer simulation 18 p3332 A70-36065
- Optimal orientation control of axisymmetric rotating space vehicle, using cyclic sliding mode theory 18 p3332 A70-36162
- Constraint torque elimination from vector equations canonical system for attitude dynamics of satellite consisting of arbitrarily interconnected rigid bodies [AIAA PAPER 69-923] 18 p3316 A70-36679
- Control moment gyros for spinning satellite stabilization and attitude control 18 p3289 A70-36714
- Gravity stabilized gyrostatt satellite attitude motion stability, using three dimensional diagram and Liapunov functions 18 p3334 A70-37061
- Magnetic perturbations effect neutralization for satellite attitude stabilization by real time simulation of satellite angular motion in magnetic field 19 p3399 A70-38286
- Space motion simulators for Azur satellite, considering satellite attitude related to sun 19 p3400 A70-38296
- Gravity gradient attitude control for satellites near lunar far side libration point [AIAA PAPER 70-1053] 19 p3528 A70-38868
- Interactive hybrid simulation of TRIAD satellite motions, describing attitude control system with magnetic hysteresis damping [AIAA PAPER 70-994] 20 p3714 A70-39536
- Magnetic compensation for attitude control of gravity gradient stabilized satellite using environmental torques and momentum gyro damping [AIAA PAPER 70-993] 20 p3668 A70-39537
- Turbofan engine aerodynamic interactions, cryogenic space storable propellants, space station attitude control biowaste resistojets and long burning time solid propellants 20 p3688 A70-39667
- Satellite steady state motion and relative equilibrium position optimal stabilization by additional forces application 21 p3849 A70-40606
- Digital orbital clock and telemetry adapter for TDIA satellite attitude stabilization, describing mechanical structure 21 p3798 A70-41272
- Ion thrust vectoring systems for satellite attitude control and stationkeeping, discussing deflection techniques [AIAA PAPER 70-1150] 21 p3868 A70-41783
- Three axis attitude ion thrust vector control mechanism for solar electric propulsion spacecraft, discussing gimbal and translation actuators, array and cabling [AIAA PAPER 70-1156] 21 p3759 A70-41784
- Radio astronomy Explorer A attitude determination via disk-oriented programming ground support system for reducing and calibrating telemetry data, attitude prediction and command, etc [AIAA PAPER 69-983] 21 p3795 A70-41857
- Attitude and orbit control electric propulsion systems for long term space stations, discussing resistojets and electron bombardment and contact ionization ion thrusters 22 p4092 A70-43654
- Earth quadrupole moment indirect effect on satellite gyroscope precession 23 p4217 A70-43799
- Attitude control of artificial gravity mass-unbalanced axisymmetric orbital space stations 23 p4258 A70-44502
- Ion micropropulsion for geostationary satellites time optimal attitude control 23 p4261 A70-44669
- Magnetically stabilized satellites passive roll control, discussing resonance solutions by variational approach 23 p4262 A70-44690
- Adaptive time optimum inertial satellite attitude control using air jet 23 p4265 A70-45048
- SATELLITE ATTITUDE DISTURBANCE**
- U ATTITUDE STABILITY
- U SPACECRAFT STABILITY
- SATELLITE COMMUNICATIONS**
- U SPACECRAFT COMMUNICATION
- SATELLITE CONFIGURATIONS**
- Satellite electric propulsion system and configuration for orbital transfer maneuvers, describing ELDO launcher, Black Arrow, orbital dynamics, sensor system, etc 06 p1130 A70-17648
- Tethered orbiting interferometer configurations for future Radio Astronomy Explorer satellites, discussing gravitational stabilization and delta launching into orbit as single payload [AAS PAPER 69-255] 09 p1766 A70-22930
- Optimum sequence integration and ground testing of Defense Communication System Phase II Satellite, considering vibration, shock, space simulation, spin/despin, RF and acoustic requirements [AIAA PAPER 70-447] 11 p2030 A70-25444
- Three-nodes analysis for thermal design of spinning spherical satellite using heat transfer equations in mathematical model 12 p2332 A70-28061
- Automatic rendezvous and mooring-coupling of spin stabilized satellites, discussing configuration, guidance and dynamics model 13 p2499 A70-28397
- Equilibrium configurations, considering aerodynamic forces for axisymmetric satellites attitude stability using infinitesimal analysis and Liapunov method 15 p2809 A70-31779
- Earth gravity deforming effect on flexible crossed-dipole satellite configuration, considering dynamic stability and spin stabilization 22 p4110 A70-43434
- Earth gravity effect on spin vector attitude stability of flexible crossed dipole satellite configuration 22 p4110 A70-43435
- Satellites with many flexibly coupled rigid bodies, calculating libration upper bounds for predicting perturbation and stability 23 p4262 A70-44682
- Dynamics of spin-stabilized flexible satellites of long crossed dipoles or slender beams, noting Alouette and ISIS-1 spacecraft 24 p4415 A70-45549
- SATELLITE CONTROL**
- NT SATELLITE ATTITUDE CONTROL**
- Optimum thrust control of satellite along given trajectory to rendezvous at zero velocity with orbited satellite 01 p0197 A70-11500
- Continuous and pulsed parameter stabilization for circular orbits of navigation and communication satellites under perturbing effects of oblateness and atmospheric drag 02 p0374 A70-12402
- Intelsat satellites telemetry and telecontrol /TTC/, describing Fucino plant design and operation 02 p0263 A70-12647
- Pulse width modulation command order for German research satellite Azur control 04 p0653 A70-15662
- Pulsed plasma vacuum-arc thruster system incorporating throttle and thrust vector controls for long life satellite control applications [AIAA PAPER 70-180] 06 p1133 A70-18232
- Angular motion of deformable earth satellite as solid-elastic system with distributed masses, applying automatic control transfer function 10 p1914 A70-24308
- UK UHF telemetry command station capabilities for Skynet satellites control, discussing equipment [AIAA PAPER 70-415] 11 p2030 A70-25420
- Visible light sensors application in LES control system for circular near equatorial orbits [AIAA PAPER 70-477] 11 p2107 A70-25432
- Satellite stationkeeping by ground command, self contained or combined methods compared for networks of synchronous satellites 11 p2121 A70-25463
- Satellite rendezvous programmed control with allowance for thrust limitation by free trajectories method, determining impulse duration, magnitude and time 12 p2314 A70-28257
- Spin stabilized nonrigid satellite dynamics, considering liquid propellant behavior effect 13 p2499 A70-28401
- Satellite stabilization one-axis control system using earth magnetic torquer 13 p2500 A70-28405
- Electromagnetic control system for spin rate and axis orientation of ISIS ionospheric research satellites, describing design parameters 13 p2501 A70-28414
- Circular orbit gravitationally stabilized satellite oscillation damping by changes of moments of inertia 13 p2501 A70-28420
- Minimum time control for placing circular orbit satellite in gravitationally stable position 13 p2502 A70-28440
- Satellite spin stabilization by Cs contact ion microthrusters with beam deflection, investigating performance obtained by optimal and suboptimal laws 13 p2506 A70-29143
- Two axis eddy current and single axis gravity gradient dampers for satellite stabilization 16 p2985 A70-34135
- PCM telemetry transmitters, command receiver and ground control for German research satellite Azur 16 p2890 A70-34349
- Intelsat IV command and control system, describing ground stations, control center, telemetry data handling and acquisition, etc 17 p3046 A70-35275
- Dynamic flexible artificial earth satellites with mass distribution, considering control systems design principles 17 p3180 A70-35294
- Controlled libration point satellite limit cycle motion, deriving solution in infinite series by harmonic analysis 17 p3181 A70-35752

Planar Tethered Orbiting Interferometer satellite for long wavelength solar and planetary radio astronomy, discussing deployment control and libration damping
18 p3333 A70-36230

Radio Astronomy Explorer satellite boom deployment method resulting in gravity gradient capture, emphasizing role of predeployment attitude and antenna Vee angle
[AIAA PAPER 69-920] 21 p3931 A70-41856

SATELLITE DESIGN

Delta boosted electrically raised high power synchronous satellite for communication tasks
[AIAA PAPER 69-1104] 01 p0194 A70-10617

Manned space station power systems design and selection problems, discussing requirements based on impacts on space station design and operations
[AIAA PAPER 69-1081] 01 p0008 A70-10625

Weather satellites performance emphasizing designs for geostationary altitude and hydrological, oceanographic and earth science applications
[AIAA PAPER 69-1082] 01 p0135 A70-10648

Unmanned teleoperator spacecraft (UTS) for future orbital demonstration, discussing manipulators, multifunction viewing, stabilization, human factors, etc
[AIAA PAPER 69-1067] 01 p0195 A70-10649

ESRO 4 satellite as ESRO 2 design modification, describing experiments involving topside ionosphere ions, mass spectrometry, auroral particles distribution, solar and trapped particle fluxes
02 p0381 A70-12503

German-French communication satellite project Symphonie for radio, TV, telephone, teletype and data transmission, discussing objectives, organization and technical problems
[DVL-910] 03 p0580 A70-13796

Logic methods of efficient organization of satellite integration, considering project, physical components and program elements
03 p0609 A70-13842

European Ultra-Violet Astronomical Satellite (U-VAS) to replace Large Astronomical satellite (LAS) to reduce cost while maintaining scientific objectives
03 p0582 A70-14343

TD-1 satellite design and scientific payload
[DGLR-69-11] 04 p0762 A70-15142

Mission objectives and technical realization of AZUR research satellite and Symphonie communication satellite
04 p0763 A70-15303

Structural and systems design of large orbital radio astronomy antenna [crossed H interferometer] with astronaut participation in deployment, operation, maintenance and updating
[AIAA PAPER 70-100] 06 p1156 A70-18058

Dioscures project satellites design, considering use of rotation stabilization
07 p1392 A70-18989

Monograph on OAO design, experiments, testing, mission operations and history
07 p1393 A70-19100

Lightweight mirror blanks of titanium silicate for OAO-4 providing thermal and dimensional stability
09 p1678 A70-22952

Navy Navigation Satellite System program development and present status, discussing satellite design and system accuracy-geodesy connection
09 p1723 A70-23039

TD-1 satellite design and scientific payload
09 p1767 A70-23429

ESRO 4 satellite design, listing basic requirements of experiments in terms of orbital maneuvers and sensor locations
09 p1767 A70-23700

Pages 1 satellite characteristics, design, structure and orbital elements
10 p1941 A70-24585

Tiros M requirements for earth resources sensor systems, discussing spacecraft structure, dynamics, power, command and communications subsystems
10 p1950 A70-24638

Franco-German telecommunication satellite Symphonie mission objectives and system design
[AIAA PAPER 70-406] 11 p1996 A70-25401

Power sources, transfer and conditioning subsystems design, fabrication and testing for high power communication satellites
[AIAA PAPER 70-433] 11 p2120 A70-25438

Linearized equations of motion solved for stability of dual spin satellite with two dampers, comparing to Floquet analysis
[AIAA PAPER 70-431] 11 p2120 A70-25440

Titan 3C boost phase inertia loads on payload estimated for satellite design, using frequency and interface acceleration methods
[AIAA PAPER 70-485] 11 p2120 A70-25446

TACSAT 1 communication satellite design, dual-spin stabilization principles and dynamic characteristics, noting nutation behavior
[AIAA PAPER 70-455] 11 p2120 A70-25447

Initial Defense Communication Satellite Program/augmentation satellite design and mission, on-board communications equipment, control subsystems, American-British cooperation, etc
[AIAA PAPER 70-492] 11 p2121 A70-25449

Equations of motion for dynamic stability of flexible freely spinning Alouette-type satellite with crossed dipole configuration
12 p2312 A70-27194

Three-nodes analysis for thermal design of spinning spherical satellite using heat transfer equations in mathematical model
12 p2332 A70-28061

Onboard satellite information processing systems for bandwidth compression using digital filters and error correcting coding
13 p2381 A70-28431

Aeros aeronomic satellite mission, orbit and design for upper atmosphere observations, noting braking field analyzer for ion and electron speed measurement
13 p2505 A70-28767

Astronomical Netherlands Satellite (ANS) for carrying out stellar UV and X ray emission experiments
13 p2506 A70-28989

Magnetic field simulator for investigating magnetic properties of satellites designed for magnetometric experiments
13 p2385 A70-29556

Syncom and Early Bird systems development, launch procedure and operation, discussing common components
14 p2654 A70-31144

Equilibrium configurations, considering aerodynamic forces for axisymmetric satellites at attitude stability using infinitesimal analysis and Liapunov method
15 p2809 A70-31779

Small satellites for scientific technological and operational missions, discussing piggyback launching, command, battery storage, telemetry and attitude control systems
15 p2810 A70-31781

Satellite reliability, discussing quality control, contractual matters, mathematical models, project management, failure modes, etc
15 p2813 A70-32826

Tactical communications satellite (TACSAT)/design, emphasizing communications repeater characteristics
16 p2983 A70-34051

Dual spin satellites considered as deformable flexible gyrostats, obtaining stability criteria
17 p3177 A70-35234

Nonlinear three nodes analysis for thermal design of spinning spherical satellite
17 p3177 A70-35249

Satellite temperature distribution prediction from digital simulation
17 p3177 A70-35250

Automated orbiting biosatellite program with reentry system, studying long term weightlessness and radiation effects
17 p3178 A70-35258

OGOs design evolution with respect to scientific mission requirements
17 p3180 A70-35303

Alouette and ISIS experiments programs and design
17 p3180 A70-35305

Stable equilibrium positions for satellite consisting of many rigid bodies in circular orbit about center of gravity, using numerical method
18 p3332 A70-35963

Space environment simulation and thermal vacuum tests for satellite thermal balance during development
19 p3401 A70-38300

Torque free spinning satellite with flexible appendages, investigating design parameters effects on nutational stability
[AIAA PAPER 70-1046] 19 p3534 A70-38861

Space environment simulation chamber for testing of equipment temperature and satellite thermal model
19 p3402 A70-38897

Variable parameter nutation damper SAS-A dual spin satellite, discussing design and expected in-flight performance by digital simulation
[AIAA PAPER 70-972] 20 p3669 A70-39557

Drag-free satellite design and propulsion requirements, noting orbit perturbation mechanisms
[AIAA PAPER 70-1145] 20 p3717 A70-40523

Baseline satellite design for U.S. domestic communications, discussing structural weight, transponders and bandwidth, antennas, etc
21 p3790 A70-41356

Scientific satellites evolution during past decade and future development possibilities in conjunction with space shuttles and stations
23 p4260 A70-44621

Multipurpose earth resource satellites design, emphasizing land use factors and data reduction problems
23 p4286 A70-45005

ATS 6 and 7 satellite design features, operational characteristics and experiments objectives
[AIAA PAPER 70-1307] 24 p4415 A70-45375

SATELLITE DRAG

Atmospheric density variations in thermosphere determined from braking satellite data, discussing correlation with solar activity and temperature variations
01 p0077 A70-11202

Thermospheric structure and variations obtained from satellite drag data analysis, discussing gas density, temperature and atmospheric composition
01 p0077 A70-11203

Jacchia 1965 model discrepancies in solar and geomagnetic activity and semiannual effects observed in satellite drag measurements at 150-200 km and 700-1500 km
01 p0077 A70-11204

Period changes of satellite 1963 53 A due to accelerations from atmospheric drag and solar radiation pressure
02 p0362 A70-11764

Statistical analysis of satellite drag data for characteristic time of thermal fluctuations in upper atmosphere caused by soft solar X-rays
03 p0472 A70-13179

Statistical model based on kinetic and probability theories to determine drag coefficient of orbiting satellites
06 p1159 A70-18289

Satellite wake in ionosphere simulated in cold ion plasma without magnetic field, observing complex far wake structure and peculiar electrostatic probes response
06 p1147 A70-18297

Artificial satellites MHD drag, noting altitude and temperature effects
10 p1921 A70-23834

Satellite orbit prediction using computer program based on first order secular node-to-node drag perturbations
10 p1943 A70-24822

Atmospheric density estimation from observation of satellite drag-induced energy dissipation
13 p2400 A70-29530

Artificial satellite around Venus, investigating orbital lifetime based on atmospheric drag effect on periaapsis height
14 p2637 A70-30563

Steady state plasma wind tunnel for flow around ionospheric satellites, studying wakes of cylinders and spheres
16 p2837 A70-33866

Planetary orbiter parameters long term variations under central body oblateness, solar and atmospheric drag perturbations
[AIAA PAPER 70-1055] 19 p3528 A70-38870

Gravity stabilized drag free satellites attitude instabilities due to coupling between attitude and translational motions
[AIAA PAPER 70-995] 20 p3714 A70-39535

Drag-free satellite design and propulsion requirements, noting orbit perturbation mechanisms
[AIAA PAPER 70-1145] 20 p3717 A70-40523

Monoenergetic nitrogen free molecule beam impingement on solid surface, calculating satellite drag coefficients from momentum transfer measurements
21 p3745 A70-41743

Satellite drag and lift from spatial impulsive surface interaction model
[ICAS PAPER 70-05] 23 p4132 A70-44116

Balloon satellite perturbations in orbital period involving air drag, lunar gravity and solar and terrestrial radiation pressures
24 p4414 A70-45358

Echo 1 satellite orbital acceleration correlated with solar activity, determining atmospheric density from drag observations using PERLO computer program
24 p4408 A70-45552

Balloon satellites orbital accelerations, considering effects due to air drag, solar radiation pressure and spin
24 p4409 A70-45557

SATELLITE GROUND SUPPORT

Postlaunching operations putting HEOS 1 satellite into orbit, verifying subsystem functions, starting experiments and tracking for data recovery
01 p0197 A70-11117

Telemetry tracking and command antenna array of Central German Ground Station for satellite communication
[DFVLR-SONDDR-52] 11 p2017 A70-25800

Azur satellite ground control, describing system organization to measure scientific and data information for entire satellite lifetime
13 p2384 A70-28976

Transmission power formula for satellite to ground station and slant ranges calculations
21 p3785 A70-40755

Fences and pits effectiveness for shielding satellite earth stations from local terrestrial facilities interference
21 p3789 A70-41342

SATELLITE GROUND TRACKS

Terrestrial satellites ground tracks by FORTRAN IV computer program, investigating orbital parameters effects
21 p3892 A70-41325

SATELLITE GUIDANCE

Automatic simulator for guidance system installed on cartographic satellite in circular orbit at 600 km,

discussing weightlessness and vacuum simulation devices 03 p0464 A70-13834

French guided satellite space flight simulator developed in search for suitable three axial onboard guidance systems 06 p1028 A70-17933

Civil aviation satellites for aircraft communication, navigation and traffic control, discussing technical, political and administrative problems 10 p1842 A70-24974

Satellite optimal guidance, discussing gyroscope application for stabilization and orientation control 17 p1381 A70-35691

Low thrust station keeping guidance scheme for gravity gradient stabilized 24-hour satellite, solving equations of motion for near circular equatorial orbit 18 p3289 A70-36676

Guidance and navigation system design for automatic stationkeeping one earth orbiting vehicle with respect to other [AIAA PAPER 70-1005] 20 p3667 A70-39526

Scientific satellite reentry guidance algorithms for inertial system, discussing controllability, onboard computer, gyros, accelerometers, jet actuators, terminal guidance, glide trajectory, etc 23 p4216 A70-44667

SATELLITE INSTRUMENTS

NT LASER ALTIMETERS

High power TV broadcast satellite subsystems technologies requirements, considering transmitters, power conditioners, solar arrays and component reliability [AIAA PAPER 69-1069] 01 p0194 A70-10632

Wide range pulse height discriminator with milliwatt power drain for use in nuclear experiments on scientific satellites 01 p0088 A70-10749

Radiation detectors for ionizing radiation onboard artificial satellites, considering weight and power supply constraints for ionization chamber, GM, proportional and scintillation counters, etc 01 p0093 A70-11254

Cosmos 149 meteorological satellite telephotometer, radiometer and other electronic equipment for measuring atmosphere and underlying surfaces physical parameters 01 p0095 A70-11611

Cosmos 149 meteorological satellite telephotometers for measuring reflected solar radiation from earth 01 p0095 A70-11612

Rb-75 adapted reconnaissance cameras error sources on basis of processed Echo 2 satellite photographs 02 p0294 A70-11772

Instrumentation system for nuclear experiments on scientific satellites allowing highest priority event selection during telemetry sequence and periodic change of priority order 03 p0453 A70-13024

Meteorological spaceborne IR instruments associated with NASA satellites, discussing various Tiros and Nimbus instruments 03 p0491 A70-13666

IR equipment on Tiros and Nimbus 1 and 2 satellites, describing vertical atmospheric sounding 03 p0492 A70-13833

Synchronous satellite attitude measurement during early flight and operating conditions, describing PAS satellite attitude sensor configurations 03 p0581 A70-13844

Superconducting magnetic system in magnetic analyzer of positrons and electrons in primary cosmic radiation tested on board Cosmos 213 04 p0685 A70-14443

Tradeoff methodology establishing evaluation criteria for comparing radar and laser systems to meet geodetic satellite altimeter performance requirements [AAS PAPER 69-604] 04 p0686 A70-14648

In-flight radiometric calibration of low brightness OGO 4 airglow photometer 04 p0696 A70-15645

Onboard digital data acquisition instrumentation system for scientific satellites, combining existing functional blocks to obtain different configurations and performances 05 p0818 A70-16587

Thermal and dynamic considerations of materials choice for satellite mounted telescope mirrors noting Be and silica properties 06 p1064 A70-17781

Mass spectrometer design and calibration for ionic composition measurements on ionosphere sounding satellite, noting effects of satellite velocity and attitude 06 p1065 A70-17908

French guided satellite space flight simulator developed in search for suitable three axial onboard guidance systems 06 p1028 A70-17933

Mirror material for satellite-borne telescopes, considering Be and CER-VIT or ULE silica thermal and mechanical properties 07 p1279 A70-19000

Monograph on balloon and satellite borne spark chambers for cosmic gamma radiation energy and direction determination, discussing relativistic electrons multiple scattering 07 p1368 A70-19617

Satellite-borne experiments of neutral molecular beam-solid surface interactions, describing Molsink chamber, densitometer, sphere and paddlewheel satellites 07 p1344 A70-20128

Thermistors used in temperature measurements aboard satellites, discussing results of electrical and mechanical tests 08 p1493 A70-20612

IR technology in aircraft, satellite and rocket electronics, discussing photography, scanners, search and pursuit devices, guided rockets, pilot warning devices, etc 08 p1494 A70-20687

Liquid helium cryostat for onboard satellite storing designed with allowance for overloads and vibrations during powered flight 08 p1440 A70-21220

Cosmos-261 satellite-borne scintillation electron proton spectrometers and lead shielded Geiger counter, measuring electron and proton energy spectra, pitch distributions, etc 08 p1501 A70-21799

Orbiting clock experiment for measuring gravitational red shift of earth by comparing ground based and satellite-borne hydrogen maser clocks 08 p1501 A70-21950

Satellite remote sensors for oceanographic applications, estimating resolution requirements for temperature, spatial interval, roughness patterns, wind speeds, etc [AIAA PAPER 70-306] 09 p1668 A70-22880

Orbiting satellite-borne instruments for scientific observation of earthquakes, volcanic eruptions, atmospheric phenomenon, cyclones, floods and soil erosion 09 p1763 A70-23377

ESRO 4 satellite design, listing basic requirements of experiments in terms of orbital maneuvers and sensor locations 09 p1767 A70-23700

Earth horizon signal sensors on spin stabilized satellites using micron filters for cloud signal rejection 09 p1686 A70-23757

PSK distortion spectra generated in satellite transponders by interactions of FDMA PSK modulated carriers, developing computer programs for multichannel FDMA PSK modulated systems 10 p1839 A70-24364

Satellite mounted device for detecting and recording 20-110 Mev solar neutrons 10 p1889 A70-24488

Pseudonoise phase shift keying /PN/PSK/ and frequency hopping /PN/FH/ modulation technique for low altitude satellite receiving /VHF/ transmissions [AIAA PAPER 70-496] 11 p1999 A70-25436

Nimbus high resolution IR radiometer /HRIR/ data processed by color display enhancement system, demonstrating meteorological, oceanographic and geomorphological applications 11 p2049 A70-25636

Plate measurement on comparators in satellite geodesy, discussing optics, magnification, mark selection and error elimination 11 p2051 A70-26181

Fluid sphere gyro satellite nutation sensor 11 p2057 A70-26504

Oscillating gyroscopes in satellite testing general relativity and earth gravitational field relation to stars 11 p2057 A70-26706

Microwave radiometer as passive satellite sensor for observing ocean surface properties 12 p2228 A70-26902

Intercoms 2 equipment for measurement of positive ion concentration, electron temperature and energy distribution, electron concentration between satellite and ground reception points, etc 12 p2207 A70-27500

Ionospheric probing by ground based and satellite-borne vertical incidence sounders 12 p2224 A70-27729

Elektron 2 and 4 satellites orientation based on on-board solar and magnetic sensors 12 p2314 A70-28256

Superconducting magnetic system in magnetic analyzer of positrons and electrons in primary cosmic radiation tested on board Cosmos 213 13 p2403 A70-28468

Outgassing pressure variation with time near perigee in satellite-borne pressure gages, using Langmuir model of surface adsorption 13 p2408 A70-29202

Satellite radiometry, discussing vertical soundings, instruments, onboard calibration of interferometer, high spatial resolution, etc 13 p2411 A70-29664

Reliability and environmental testing of residual magnetic field measurements of satellite HEOS-A1 electronic equipment, using Rb vapor magnetometers 13 p2380 A70-30031

Remote atmospheric temperature profile measurements, analyzing physical processes for radiation detection by earth pointing satellite-borne sensor 14 p2611 A70-31156

Ionization measurements by OV-3-6 satellite cold cathode ionization gage of Redhead inverted magnetron type in near circular polar orbit 15 p2723 A70-31660

Photometric calibration changes in EUV solar satellite instruments during orbital operation 15 p2737 A70-32045

Ionospheric probe designs and measurement errors due to perturbations by satellite carriers 15 p2731 A70-32094

Sirio satellite SHF transponder for experiments in atmospheric propagation and communication between ground stations 15 p2709 A70-32285

Low energy proton damage to silicon solar cells on INTELSAT II, F-4 and ATS-F-1, considering exposure area and radiation protection 15 p2677 A70-32419

Scientific satellites pulse height analyzer and associated threshold detection and logic circuitry 16 p2900 A70-33062

Electrostatic near wake model for ionospheric satellites, using low speed fluid dynamic blunt body similarities [AIAA PAPER 69-674] 16 p2837 A70-33867

Nimbus weather satellites mechanical devices and subsystems, including solar array drive, fluid thermal control sensors, horizon scanners and hydraulic dampers 16 p2921 A70-34105

Satellite-borne test instrument for determining mirror materials degradation due to long solar exposure 16 p2921 A70-34109

Lunar Orbiter photo subsystem mechanisms, discussing film transport, vacuum and mechanical clamps, focal plane shutter, processor-dryer and optical mechanical scan 16 p2914 A70-34146

High reliability release mechanism with mechanical redundancy on SERT 2 satellite 17 p3174 A70-34759

Satellite-borne instruments for thermal sounding of troposphere, noting information limitation due to atmospheric effects 17 p3132 A70-35338

Optimum mounting angles for direct solar radiation flux on solar battery on circular orbit satellite 18 p3215 A70-36176

Satellite use for forest fire detection in Italy, discussing forest distribution and measuring instruments 18 p3248 A70-36669

Satellite electrometer for weak DC currents due to charged particle flux 19 p3428 A70-38485

UV photometry from OAO-2, describing Wisconsin instrumentation and equipment 20 p3624 A70-39009

Michelson IR interferometer spectrometer /IRIS/ design calibration and performance onboard Nimbus 3 satellite, demonstrating data reduction and inflight calibration 20 p3626 A70-39078

Remote sensing of atmosphere with emphasis on earth orbiting operational and research satellites 21 p3785 A70-40801

Satellite-borne sensor for ionospheric ions velocity measurement, describing design and principles of operation 21 p3813 A70-40834

Electron temperature incoherent scatter radar and satellite-borne Langmuir probe measurements discrepancy 21 p3825 A70-41104

Digital orbital clock and telemetry adapter for TD1A satellite attitude stabilization, describing mechanical structure 21 p3798 A70-41272

Low noise FET amplifier for satellite magnetometer, measuring interplanetary fields 21 p3799 A70-41923

Pioneer 8 and 9 cosmic ray detector system, discussing mechanical, electrical and data conditioning properties 23 p4195 A70-44300

Soft particle spectrometer in Isis-I satellite using electrostatic deflection for differential energy spectra measurements for electrons and protons 23 p4197 A70-44468

Helios solar observation satellite equipment design study for solar plasma low energy particles onboard measurements 23 p4262 A70-44844

Atmospheric temperature profiles using Nimbus 4 selective chopper radiometer 23 p4192 A70-44865

Esro 2 satellite instrument measuring soft solar X-rays 24 p4340 A70-46358

SATELLITE LAUNCHING
U SPACECRAFT LAUNCHING

SATELLITE LIFETIME

- Long life subsystems design and testing for orbital space station programs, considering nuclear generation, electromechanical equipment, positive expulsion of fluids, instrumentation, etc
[AIAA PAPER 69-1080] 01 p1013 A70-10626
- Azur satellite ground control, describing system organization to measure scientific and data information for entire satellite lifetime
13 p2384 A70-28976
- Atmospheric density effect on satellite lifetime and position prediction, utilizing data from Cannon Ball and SPADES low altitude density research satellites
14 p2653 A70-30562
- Artificial satellite around Venus, investigating orbital lifetime based on atmospheric drag effect on periapsis height
14 p2637 A70-30563
- Nonrecoverable Cosmos satellites lifetimes comparison with last stage rockets
14 p2638 A70-30690
- Ten year NASA manned space station in low earth orbit, grouping experiments in functional program elements/FPE/
[AAS PAPER 70-033] 17 p3156 A70-34802
- Practical stability of highly eccentric orbits quasi-normal to ecliptic, discussing lunar effects on orbital lifetime
23 p4243 A70-44510

SATELLITE MANEUVERS

U SPACECRAFT MANEUVERS

SATELLITE NAVIGATION SYSTEMS

- Satellite navigation efficiency compared with inertial and Omega navigation techniques
01 p0139 A70-11263
- Algorithm for solving autonomous artificial satellite orbital elements, using successive approximations
01 p0139 A70-11503
- User problems in navigation methods, discussing Omega method, Navy Navigation Satellite System and VLF methods
03 p0522 A70-13603
- Operational requirements of shipping for satellite communication systems, discussing distress cases, satellite navigation systems, information distribution traffic control, etc
03 p0522 A70-13605
- Navy Shipboard Navigation Satellite System for worldwide all-weather navigation system, discussing shipboard system, receiver, stable oscillator and antenna
03 p0522 A70-13609
- Satellite potential for long range air traffic control, discussing airline navigation requirements and ATC requirements for position determination
09 p1722 A70-23027
- Navy Navigation Satellite System program development and present status, discussing satellite design and system accuracy-geodesy connection
09 p1723 A70-23039
- Aeronautical satellite system for North Atlantic air traffic position monitoring, discussing simultaneous position display
09 p1723 A70-23040
- SPOT navigation satellite system for near instantaneous fixes or continuous tracks providing height, velocity and automatic guidance and control signals
09 p1723 A70-23041
- Navigation satellite system with 10-meter accuracy, continuous coverage, rapid position determination, simultaneous service and interference immunity achieved by synchronous satellites
09 p1723 A70-23042
- Hyperbolic position finding with synchronous satellites having frequency conversion unit for operations at higher frequency satellite signals
09 p1724 A70-23044
- Error sensitivity to measurement uncertainties and satellite geometry of satellite linked hyperbolic navigation systems
09 p1724 A70-23046
- Navigation-traffic control satellite system application to transoceanic traffic surveillance
[AIAA PAPER 70-487] 11 p2000 A70-25462
- VHF aeronautical communication satellites extended for use in aircraft position determination and surveillance, discussing accuracy and error source reduction
[AIAA PAPER 70-490] 11 p2002 A70-25487
- Satellite navigation method for locating Mars landmark or target point for exploration by roving vehicle located as center of coordinate system
11 p2080 A70-26213
- Low altitude satellite system for aircraft navigation, considering cost factors, military applications, traffic control capabilities, etc
12 p2270 A70-27922
- Midaltitude satellite system for continuous three dimensional navigation, considering elevation angles, constellations and orbits
12 p2270 A70-27923
- Satellite system for air traffic control providing data links for aircraft position determination for U.S. in 1990s using 24-hour inclined elliptical orbits
12 p2270 A70-27926

Hard wired modular multipurpose global navigation system using cluster noncoplanar synchronous satellites
13 p2446 A70-28385

Aircraft/ship navigation system using three synchronous satellites positioned over equator for Pacific applications
17 p3134 A70-35302

Application satellites, discussing uses in communications, meteorology, earth survey and navigation
18 p3333 A70-36348

Optimum altitudes for passive ranging satellite navigation systems, using electronic clocks in satellite and navigator receiver
21 p3883 A70-40724

Dioscures project for ATC over Atlantic Ocean, describing distance measurement by simultaneous use of two geostationary satellites
21 p3848 A70-41258

Air traffic safety problems, discussing satellite radiobeacons applications to aerial navigation
22 p4066 A70-42652

Dioscures satellite navigation system for aircraft and ships, discussing coverage, radio links, project costs, etc
22 p4067 A70-42657

Nautical loci of constant azimuth of artificial satellite at corridor height in circular orbit at arbitrary inclination, using gyroscope and radio sextant
22 p4068 A70-42664

SATELLITE NETWORKS

- TV broadcast satellite system operating with home receivers or special receivers, evaluating technological and cost factors
[AIAA PAPER 68-1061] 01 p0044 A70-10831
- Satellite international system chain consisting of down path, receiving earth station and domestic receiver for Europe, North Africa and Middle East TV distribution
02 p0258 A70-12420
- Aeronautical satellite system for civil flight safety, discussing operational, technical and economic aspects
03 p0522 A70-13610
- Global and European geodetic satellite network, discussing San Marco equatorial satellite and observation stations
03 p0581 A70-13829
- Channels demand assignment between earth terminals of international satellite communication systems, examining multiple access problems
03 p0453 A70-14323
- Meghdoot program for satellite network communications technology applications to national goals in India
04 p0757 A70-15670
- Satellite communications influence on ground stations design, describing steerable antenna and receive and transmit configurations for domestic station
05 p0811 A70-16095
- Four satellite cluster laboratory in near-earth environment to investigate solar-terrestrial relationships, emphasizing interaction of solar wind and magnetosphere
07 p1387 A70-19711
- Digital record message communication satellite network system involving synchronous satellites and small earth terminals
10 p1834 A70-24327
- Worldwide telephone network optimum interoperation including communication satellites complementation
10 p1834 A70-24328
- Satellite communication system using delta modulation for telephone service to large number single channel earth stations
10 p1834 A70-24329
- PCM-TDMA satellite communication system for maximum time slot utility without guard time slots
10 p1834 A70-24330
- Multichannel PCM/TDMA INTELSAT network with time preassignment and time assignment speech interpolation features for field test
10 p1835 A70-24332
- Message traffic problems in satellite telephone network, considering traffic distribution characteristics, interarrival mean time, bidirectional traffic, etc
10 p1839 A70-24367
- Satellite relayed integrated digital multiple access systems, discussing traffic handling, satellite positioning, demand assignment, etc
10 p1839 A70-24369
- Satellite system applicability to earth resources data collection from in situ sensors, discussing synoptic, local time, emergency and demand data collection
10 p1840 A70-24371
- Numerical weather forecasting for several weeks based on global meteorological satellite network observation
10 p1913 A70-25241
- Communication satellites geostationary orbit sharing problem, considering system design and utilization criteria
[AIAA PAPER 70-441] 11 p1998 A70-25419

Orbit utilization, discussing sharing of satellite communication frequency bands and use of multiple earthward antenna beams
[AIAA PAPER 70-468] 11 p1999 A70-25428

Satellite stationkeeping by ground command, self contained or combined methods compared for networks of synchronous satellites
[AIAA PAPER 70-479] 11 p2121 A70-25463

Instructional communication system for U.S. using synchronous satellites over 15 regions
[AIAA PAPER 70-450] 11 p2000 A70-25465

Global commercial communications satellite system arrangements, considering evolutionary political, economic and technological developments within IN-TELSAT context
[AIAA PAPER 70-446] 11 p2152 A70-25478

Communications satellite systems for developing nations, considering educational TV, economic growth, cost estimates, etc
[AIAA PAPER 70-475] 11 p2152 A70-25479

TATS Master tactical communication satellite network controller with modems and digital computer for semiautomatic control over terminals
[AIAA PAPER 70-412] 11 p2002 A70-25491

Symphonic satellite telecommunication network for multiple access telephone, telegraph, data transmission, radio and TV dissemination
11 p2005 A70-26008

Satellite communication systems optimal utilization achievable through supervisory control system
11 p2009 A70-26261

Earth resources satellite systems synthesis, describing analytical techniques in R and D preceding operational status
12 p2334 A70-26942

Multipurpose domestic satellite system design for TV distribution, discussing frequency sharing, synchronous orbit and system model
12 p2183 A70-26998

Air traffic control surveillance and data system using synchronous satellites in inclined elliptical orbits for communications and aircraft position determination
12 p2268 A70-27644

North Atlantic air traffic control system using aeronautical satellites, discussing flight levels, surveillance and positioning, terminals, etc
12 p2268 A70-27645

Navigation systems using 24-hour orbit satellites, discussing system concept options for U.S., Western Hemisphere and global coverage
12 p2270 A70-27924

Multiple user satellite system for air navigation and traffic control, presenting comparative error analyses for position determination by spherical and hyperbolic ranging
12 p2270 A70-27925

Hard wired modular multipurpose global navigation system using cluster noncoplanar synchronous satellites
13 p2446 A70-28385

Cost optimal carrier rocket system for European satellite TV, communication, navigation and earth survey networks
13 p2502 A70-28448

Geostationary tracking and data relay satellites /tdrs/, discussing system design and advantages
14 p2615 A70-31182

Trojan Relay system with satellites preceding and following earth in solar orbit ensuring radio communication throughout solar system
15 p2698 A70-32061

GaAs injection lasers for optical communication, synthesizing high bit rate data link between synchronous relay satellites
16 p2865 A70-33710

Multiple access discrete address system for satellite networks
16 p2865 A70-33729

Satellite broadcasting frequency resources, discussing interference, frequency sharing, antenna transmitting and receiving patterns, etc
17 p3046 A70-35271

Legal problems of space telecommunications, discussing world juridical regime, United Nations work and satellite systems broadcasting
17 p3201 A70-35777

Legal aspects of telecommunications by satellite systems, discussing international organization, Intelsat integration and direct broadcasting
17 p3202 A70-35781

Worldwide communication satellite network cost optimization and application, discussing Intelsat role
18 p3228 A70-36510

Small earth stations to link isolated areas with Intelsat network, discussing costs
18 p3229 A70-36957

Soviet communication satellites orbit and design characteristics, operational uses and ground stations, discussing Molniya 1 series transmitting television, multichannel radio, telephone and telegraphy
18 p3230 A70-37225

U.S. nationwide satellite network for multichannel community antenna TV /CATV/ operated at 12 GHz band
19 p3382 A70-38891

Telecommunication, ATC and navigation satellite systems, examining economic bases for aeronautical and maritime space systems
20 p3740 A70-39407

Communication satellites systems for civil application, considering ground stations design, regional communication, ATC and maritime communications and navigation
20 p3585 A70-39409

Satellite-based air traffic control system for North Atlantic, applying stochastic optimal control theory [ALAA PAPER 70-966]
20 p3669 A70-39563

SKYNET PCM telemetry and command station, discussing system design, pseudomonopulse feed, command and computer subsystems, etc
20 p3589 A70-40322

Satellite networks queueing analysis, examining graph-theoretic model based on stochastic inputs and time delay factors
20 p3589 A70-40338

Global integrated communications satellite system, discussing International Telecommunication Union regulatory functions, etc
21 p3955 A70-40625

Monograph on communicating by satellite covering INTELSAT system design, pricing, procurement, broadcasting, international community responsibilities, etc
21 p3955 A70-40739

Aeronautical satellite system for civil flight safety, discussing operational, technical and economic aspects
21 p3848 A70-41131

Multiple access communication satellite systems providing reliable speech communication for low density use in remote areas [JPL-TR-32-1501]
21 p3791 A70-41368

Italian Sirio satellite with local and foreign ground stations network measuring SHF wave propagation variables
23 p4158 A70-43753

Global rescue alarm net /GRAN/ using satellites for relaying distress signals, eliminating current line of sight restrictions
23 p4143 A70-44455

Worldwide common satellite network for sea and air navigation, discussing cost estimate and economics
23 p4216 A70-44608

Tracking and data relay satellite system in low altitude synchronous orbit [ALAA PAPER 70-1305]
24 p4311 A70-45085

Commercial satellite system circuit quality and reliability in digital communications, considering Automatic Digital Network Trans-Pac cable cut incident
24 p4311 A70-45223

Tracking and data relay satellite system performance by ATS and Nimbus spacecraft for range and range rate tracking and command and data transmission [ALAA PAPER 70-1306]
24 p4374 A70-45949

SATELLITE OBSERVATION

Solar X ray flare regions size, structure and localization from Cosmos 166 and 230 heliograph observations
01 p0168 A70-10252

Spatial characteristics of magnetosheath magnetic field observed simultaneously by Explorer satellites, showing zero order agreement with prediction of MGD theory
01 p0071 A70-10410

Micrometeoroid experiments on OGO 2 and OGO 4 satellites, measuring velocity, masses and particle orbits in earth dust cloud
01 p0086 A70-10444

Earth gravity field intensity variations measured by orbiting two geometrically identical satellites, discussing sensitivity and cost
01 p0087 A70-10445

Alpha particle emissivity measurement of moon by Explorer 35 spacecraft for U 238 abundance in outer crust
01 p0181 A70-10573

Radio star and satellite scintillation observation, considering diurnal, seasonal and latitude variations and relationship to magnetic and solar activity
01 p0181 A70-10590

Rocket and satellite studies of geomagnetic field during IQSY, confirming ionospheric currents responsible for magnetic diurnal variations
01 p0075 A70-10596

Earth resources satellites use in agriculture, considering materials reflectance and emittance, electromagnetic spectrum wavelengths identification and data accuracy standards [ALAA PAPER 69-1083]
01 p0220 A70-10624

Cosmic dust particle direction, velocity and mass from ionization and momentum measurements by dust sensor during impact on Pioneer 8 satellite
01 p0088 A70-10748

Venus atmosphere ionization distribution, temperature and pressure profiles determined from amplitudes

and differential Doppler of radio signals to Mariner 5 during occultation
01 p0186 A70-11084

Satellite observations of semiannual density variations in upper atmosphere
01 p0077 A70-11205

Ionosphere total electron content diurnal and seasonal variations at midlatitudes, based on data analysis from Explorer 22 in polar orbit
01 p0080 A70-11223

Reflected solar energy measurements by ATS satellites applied to meteorological research, emphasizing high areal resolution and dynamic range of cameras
01 p0094 A70-11297

Elektron 4 satellite radio emission data transmitted from July to December 1964, noting month-to-month variations in mean radiation level
01 p0172 A70-11496

Venusian atmospheric pressure and temperature measurements by Venera 4 probe, noting agreement with Mariner 5 observations
01 p0192 A70-11505

Greenhouse effect in Venusian atmosphere, discussing cause of vertical temperature distribution established by Venera 4 probe
01 p0192 A70-11506

Venus atmosphere optical properties on basis of Venera 4 data, proposing models for measured rotational temperature and subcloud atmosphere radiative equilibrium
01 p0192 A70-11507

Fast charged particles measurements by Cerenkov counter in Cosmos 137 satellite, noting hard electron flux and cosmic ray radiation spectrum
01 p0172 A70-11509

High latitude capture region boundary for electrons in upper radiation belt determined relative to current electrojets in ionosphere from satellite observations
01 p0172 A70-11516

Excess radiation in equatorial regions studied on-board Cosmos 137, noting contribution of primary particle multiplication to secondary radiation
01 p0192 A70-11542

Collection of articles on satellite observations, Number 8
02 p0361 A70-11751

Satellite triangulations scale and orientation control, describing terrestrial methods of geodetic bases determination
02 p0254 A70-11755

Doppler observations of D1 A satellite, discussing dispersion of data, mean point displacement and resonance harmonics
02 p0362 A70-11756

Receiving station geodetic coordinates computed from Doppler curves of artificial satellite, using method of differential corrections
02 p0254 A70-11757

Ground station geocentric coordinates from intersection of spatial directions in Baker- Nunn network determined by satellites
02 p0254 A70-11758

Solar activity indices and upper atmospheric density interrelationship from Explorer 1 satellite observations, showing statistical variations
02 p0356 A70-11762

Orbital period determination for satellite from single station visual observations, assuming known orbit inclination, ascending node length and node precession
02 p0254 A70-11765

Air density variations calculated by visual satellite observations processing, comparing results of INTEROBS and average anomalies methods
02 p0288 A70-11766

Cosmos 44 quasi-draconic period analytical and graphical determination, comparing moments of meridian intersection with INTEROBS observations
02 p0363 A70-11767

Satellite rotation periods determination accuracy from photometric observation data improved by determining initial and terminal moments of maximum brightness
02 p0255 A70-11769

Azimuth between two stations of triangulation net determined by simultaneous observation of two satellites, discussing mathematical principles and applications in Europe
02 p0289 A70-11797

Pioneer 6 radio signal spectrograms during solar occultation, noting solar event effects on bandwidth
02 p0369 A70-12060

Solar mean magnetic field relation to sector structure of interplanetary magnetic field, discussing Explorer 33 and 35 observations
02 p0371 A70-12206

Satellite measurement of mean temperature in atmospheric layers to determine vertical temperature distribution
02 p0291 A70-12279

Nimbus 3 satellite observations of near UV solar flux intensity and variability, describing instrumentation and measurement of radiation producing molecular oxygen photodissociation
02 p0291 A70-12295

Solar activity effect on ionospheric total electron content via Explorer 22 observations, discussing relationship to solar elevation angle
02 p0292 A70-12561

Ionospheric electron density vertical distribution calculation starting from satellite measurements of total electron content
02 p0293 A70-12575

UV photometry from OAO, observing planets, gaseous nebulae, X ray source, quasars, Crab Nebula, extragalactic nebulae, etc
02 p0303 A70-12705

Faraday rotation observations on Explorer 22 signals at two receiving stations, discussing comparative evaluation procedures and results
03 p0472 A70-12874

Quiet time primary cosmic ray electron flux and energy spectrum from 10 to 200 Mev in interplanetary space observed by OGO 5 satellite
03 p0553 A70-12902

High energy primary cosmic ray and proton spectra measurements from Proton satellites
03 p0555 A70-13036

Geodetic treatment of satellite observation - Conference, Tashkent, Uzbek SSR, November 1968
03 p0444 A70-13182

Earth satellites optical observations accuracy for geodetic purposes based on errors in station position determinations
03 p0445 A70-13183

Simultaneous ground and space triangulation procedures, recommending use of satellite photographic observations for error reduction
03 p0445 A70-13185

Satellite observations for determining earth shape and gravitational field zonal harmonics, using dynamic methods
03 p0473 A70-13188

Earth potential errors from gravity and satellite motion measurements, discussing sectoral, tesseral and zonal harmonics with large and small second indices
03 p0473 A70-13190

Space triangulation net using direction and distance measurements from satellite photographic and Doppler observations, including tracking data leveling
03 p0446 A70-13194

Undiscovered satellites of solar system major planets, predicting Jupiter satellites
03 p0569 A70-13360

Solar wind discontinuity surfaces observed by spacecraft magnetometers determined from measured time delays and solar wind speed
03 p0558 A70-13600

ESSA system operation, describing applications of satellite meteorological data
03 p0454 A70-13667

Ruby laser experiment in illuminating satellites equipped with retroreflectors to determine satellite position in space from range and photographic data
03 p0450 A70-13674

Satellite observations used to construct coordinate system referred to earth center of mass and axis of rotation
03 p0474 A70-13733

Azur satellite launching project by NASA and Germany, describing orbit for investigating earth inner radiation belt, auroral zone and solar flares
03 p0580 A70-13797

Libration clouds reality possibility from satellite dust counting experiments
03 p0572 A70-13819

Earth exploration and service by satellites - Conference, Rome, March 1969
03 p0572 A70-13826

Global satellite VLF propagation system for investigating mesospheric ionization
03 p0475 A70-13827

Equatorial ionosphere ionization and electron density measurements by San Marco 2 satellite
03 p0475 A70-13830

Geomagnetic tail observations by Pioneer 8 probe
03 p0475 A70-13851

Satellite measurement of auroral particles and particles trapped in Van Allen belts
03 p0559 A70-13852

Electron temperature and density data obtained during Alouette satellite passage over middle latitude red arc, noting influence of intersecting magnetic field lines
03 p0476 A70-13911

Interplanetary magnetic field measurements from Mariner and OGO satellites at various paths, regions and intervals, finding dominant polarity effect dependent on sun latitude
03 p0575 A70-13980

Geomagnetic tail observations by Pioneer 8 at 500 earth radii, analyzing time-averaged magnetic field data
03 p0575 A70-13983

Ionogram conjugate echoes observed at Singapore longitudes by Alouette 2 topside sounder, attributing sequential occurrence to field-aligned irregularities in magnetosphere
03 p0477 A70-13986

Poynting flux direction for proton whistlers determined from Injun 5 observations, obtaining data on source region and propagation in ionosphere
03 p0477 A70-13987

Explorer observations of large temporal variations of midlatitude outer zone energetic electron intensities interpreted as redistribution during geomagnetic disturbances
03 p0560 A70-13989

Interplanetary magnetic field during solar cycle rise and minimum based on Explorer 33 magnetometer measurements
03 p0575 A70-13999

Nimbus 3 satellite carrying IR spectrometer to measure spectral radiances and retrieve atmospheric temperature profiles
04 p0675 A70-14393

Low energy solar proton flux propagation model in interplanetary medium based on satellite data beyond earth magnetosphere
04 p0737 A70-14434

Magnetograms by Venera 4 and Mariner 5 compared to determine interplanetary magnetic field nature in Venus proximity
04 p0744 A70-14438

Three dimensional characteristic of light scattered by lunar surface determined for various incidence angles and azimuths from Zond 3 photometric measurements
04 p0744 A70-14441

Magnetospheric magnetic field disturbance due to abrupt solar wind parameters change, using Explorer 26 data
04 p0738 A70-14444

IMP F solid state detector data on 13 day solar proton event at low energy, considering cosmic rays anisotropy and interplanetary magnetic field
04 p0738 A70-14512

Interplanetary dust measurements near earth compared to theories predicting dust characteristics, discussing concentration, flux, impact rate and solar radiation pressure
04 p0749 A70-14619

Satellite observation of energetic particles and magnetic fields, discussing radiation belts, magnetosphere, galactic cosmic rays, etc
04 p0740 A70-14620

Satellite surveillance in cloud and weather modification, considering area selection for cloud seeding, atmospheric energy redistribution, etc
[AAS PAPER 69-621] 04 p0677 A70-14645

Earth photographs for geotectonic research from manned orbiting spacecraft, describing Apollo and Gemini belts
[AAS PAPER 69-579] 04 p0677 A70-14663

Satellite orbit and attitude determination and planetary gravity and astronomical constants from earth-based radar Doppler and orbital photogrammetric observations
04 p0750 A70-14938

Explorer 31 Langmuir probe data for electron temperature at conjugate point, tracing magnetic field line passing through spacecraft to earth
04 p0000 A70-14971

Ionosphere beacon satellites BeB and BeC transmits for field alignment of small ionospheric irregularities
04 p0678 A70-14975

Lyman alpha auroral emissions observations made with narrow band sky scanning photometer mounted on earth-oriented polar orbiting satellite
04 p0741 A70-15107

Daytime midlatitude ionosphere composition and electron concentration profile measured by synchronized satellites and rocket, investigating discrepancy
04 p0741 A70-15110

Alouette 2 Langmuir probe measurements analyzed for size and amplitude of electron concentration fine structure irregularities in topside ionosphere, discussing F spread
04 p0679 A70-15111

Magnetospheric observations of whistler mode emissions byOGO 1 satellite over VLF and LF ranges
04 p0649 A70-15117

Atmospheric density measurements from Explorer 17 satellite by density gage and drag techniques resolved for difference by calibration and systematic errors considerations
04 p0691 A70-15120

Interplanetary magnetic field fluctuations stimulated by lunar wake, using Explorer 35 satellite measurements
04 p0753 A70-15122

Solar Lyman-alpha radiation observed byOGO 4 spacecraft showing short term fluctuations superposed with monthly variation
04 p0741 A70-15128

Satellite multispectral photometry data in airglow bands correlated with cloud characteristics and surface albedo variations
04 p0715 A70-15522

Radio wave-ionosphere interaction effects on accuracy of radio astronomical observations from earth satellites
04 p0683 A70-15740

Ionospheric air density profiles revision based on satellite orbits analysis
05 p0839 A70-16287

Ionospheric electron content, virtual height and profile measured by Faraday effect of satellite radio emissions compared with radar soundings
05 p0839 A70-16288

Upper ionospheric electron density variations at low magnetic activity times observed with Alouette 2 satellite
05 p0901 A70-16307

Weighting coefficient matrix parameters for European satellite triangulation determined, considering sequence of separate points shown by photographs instead of single point
05 p0839 A70-16345

Computerized method for processing photographic earth satellite observation results, transforming coordinates by nonconformal approximation of polynomial function
05 p0814 A70-16367

Lyman alpha flux observed by satellite-borne ion chambers during solar flare of 20 March 1966
05 p0902 A70-16442

North American datum related to geocentric satellite reference system, using Lambeck method for geodetic parameters
05 p0841 A70-16644

Tangential solar wind discontinuity observed by Vela 2A satellite, producing ground magnetic disturbances conjunctively with magnetospheric, ground and ionospheric currents
05 p0903 A70-16727

Night airglow variations observed during Cosmos satellite orbits, determining atmospheric albedo wavelength dependence for solid and medium cloudiness and clear skies
05 p0841 A70-16728

Error correction for correlation coefficient between satellite data of earth radiation intensity and satellite vision field shift
05 p0841 A70-16729

Magnetic storm /14 September 1966/ observation by Explorer 33 in geomagnetic tail and by polar stations, studying relation in magnetosphere and on earth
05 p0843 A70-16764

Sporadic electron flux contribution to high latitude geomagnetic disturbances at outer radiation belt boundary estimated from Elektron 1 and 2 observations
05 p0843 A70-16765

Lunar structure and evolution based on satellite measurements of mass distribution, radius moments of inertia, gravity anomalies and topographic irregularities
05 p0920 A70-16945

Satellite IR measurements of surface horizontal temperature structure of Gulf Stream compared with ship and aircraft data
05 p0844 A70-17104

Neutron flux measurements on Cosmos 53, equipment and calculation of secondary neutrons due to bombardment of satellite components
05 p0905 A70-17112

Geostationary mode application to earth sensing, examining resolution requirements for earth scanning tracking telescope
06 p1154 A70-17152

Earth resources observation satellite /EROS/ program, discussing geologic terrain and land-use planning maps
[SPE PAPER 2703] 06 p1053 A70-17155

Satellite determination of underlying surface temperature by IR spectroscopy, measuring emitted radiation in atmospheric windows
06 p1061 A70-17205

Atmospheric circulation in tropics using weather satellite data
06 p1095 A70-17220

Radiation dose measurements from satellite and space probe experiments, considering radiation and shielding characteristics, sensor orientation effects, etc
06 p0990 A70-17266

Space radiation doses in inner Van Allen belt, comparing calculated and satellite measured rates
06 p0991 A70-17272

Earth resources and meteorological data collection from in situ sensors via satellite, discussing system considerations
06 p1006 A70-17343

Ionospheric resonances observed by swept frequency Alouette topside sounders, discussing plasma non-linearity
06 p1115 A70-17362

Satellite observations of VLF and ELF resonances related to ionospheric plasma singularities
06 p1118 A70-17375

Low altitude electric and magnetic measurements of plasma waves in space from OV3-3, Pioneer 8 andOGO 5 satellite observations
06 p1118 A70-17376

Simultaneity circle for calculating spatial direction of straight line joining satellite observation stations, noting time factor role
06 p1139 A70-17548

Spatial direction Riga-Cairo determined using simultaneous photographic observations of Pageos A satellite
06 p1054 A70-17550

Thermal sounding of atmosphere from satellites under cloudy conditions, plotting temperature profiles
06 p1097 A70-17787

Vertical air density profile from satellite measurements of atmospheric oxygen radio emission at 40-70 km altitudes
06 p1056 A70-17788

Radiation scattering during upper cloud altitude determination by satellite
06 p1097 A70-17790

Proton satellites measurements reconciliation with diurnal stellar variation data and cosmic rays origin models
06 p1135 A70-17885

Nighttime F 2 region temperature distribution under geomagnetically calm and disturbed conditions calculated from Alouette 1 satellite data
06 p1057 A70-17887

Solar X-ray flux from Explorer 33 and 35 observations, presenting catalog of tabular and graphical data
06 p1135 A70-18006

Atmospheric difficulties in earth surface remote sensing by satellites, describing absorption, emission and scattering as wavelength functions
[ALAA PAPER 70-193] 06 p1057 A70-18083

Passive microwave observation from space of sea surface degraded by atmosphere
[ALAA PAPER 70-197] 06 p1010 A70-18087

Atmospheric effects on passive microwave sensing in EHF region under all-weather conditions on global scale using satellites
[ALAA PAPER 70-198] 06 p1010 A70-18099

Ion and electron density, electron temperature and space potential measured in ion wake formed by Gemini spacecraft using sensors on Agena Target Vehicle
06 p1066 A70-18285

Surface-particle interaction and atmospheric parameters measurements by paddlewheel satellites, discussing angular distribution of re-emitted molecules and accommodation coefficients
06 p1067 A70-18287

Solar wind interaction with moon derived for model and compared with satellite data
06 p1147 A70-18291

Electric field in earth magnetotail via Explorer 33 and 35 satellite observation of solar electrons above 50 keV energy
06 p1058 A70-18528

Local time dependence of geomagnetic cut-offs for solar protons in 0.52-4.0 MeV range from satellite observations
06 p1136 A70-18529

Magnetic activity effect on magnetospheric plasmopause position, measuring ion concentrations as function of local time fromOGO 5 observations
06 p1058 A70-18530

Satellite observations of equatorial erosion and defocusing of VLF waves propagating at low magnetic latitudes
06 p1058 A70-18532

VLF noise phenomena observed with satellite electric dipole antennas compared with lower hybrid resonance frequency of ionospheric medium in vicinity
06 p1011 A70-18534

Plasmopause observations by ion spectrometer aboardOGO-5 vehicle for early orbits, obtaining O, He and H ion concentration profiles for geomagnetic parameter
06 p1059 A70-18546

Tornado producing thunderstorms, using conventional surface and upper air data combined with ATS-III data, discussing mesoscale disturbances and momentum exchange
06 p1102 A70-18583

Satellite observed characteristics of severe local storms in central and eastern U.S., noting potential use for storm forecasting
06 p1102 A70-18584

Data reduction from D1A satellite VHF and UHF Doppler measurements to attempt geodetic link between Nice and Beirut
07 p1262 A70-18941

Book on space observatories covering rocket mounted telescopes for atmospheric structure, opaque wall, air diffusion, clouds and refraction, particle bombardment, meteorite melting, etc
07 p1379 A70-19099

Monograph on OAO design, experiments, testing, mission operations and history
07 p1393 A70-19100

Outer ionosphere magnetoionic and MHD waves, combining electromagnetic and plasma kinetic theory with reference to satellite observations
07 p1264 A70-19188

Solar proton flares radiometric measurement onboard Molniya 1 satellite, detecting intensities in outer regions of magnetosphere
07 p1366 A70-19428

- Mariner 4 and 5 and Venera 4 data used for comparing terrestrial planets ionospheres 07 p1386 A70-19488
- Charged particles and He nuclei spatial distribution from recordings in cosmic ray equator region by Cerenkov counter mounted on Proton 2 satellite 07 p1367 A70-19490
- Micrometeor flux in near-earth space measured by satellite-borne low noise acoustic detectors 07 p1386 A70-19493
- Upper atmospheric horizontal sounding, discussing satellites uses in atmospheric structure studies 07 p1268 A70-19630
- Harmonic ion cyclotron resonances associated with proton whistlers observed from OGO-4 satellite VLF recordings 07 p1268 A70-19630
- Atmospheric integral moisture content determination from thermal radio emission measurements by Cosmos 243 satellite 07 p1329 A70-19649
- Four satellite cluster laboratory in near-earth environment to investigate solar-terrestrial relationships, emphasizing interaction of solar wind and magnetosphere 07 p1387 A70-19711
- Topside ionosphere morphology during IQSY, emphasizing plasma scale height diurnal and latitudinal variations role in satellite data interpretation 07 p1270 A70-20073
- Magnetospheric plasmopause-high latitude electron density trough relations using satellite topside ionograms, noting local time and magnetic disturbance effects 07 p1270 A70-20074
- Highly variable component protons and alpha particles identified in low energy cosmic rays by IMP 4 07 p1369 A70-20199
- Solar soft X ray spectrum analyzed by OSO 4 proportional counter, discussing slowly varying component, corona active regions and impulsive event characteristics 07 p1369 A70-20289
- Ionospheric data of local and integral electron concentration obtained by measuring phase shift of satellite emitted coherent radio waves 07 p1276 A70-20422
- Cold plasma approximation of whistler excitation of lower hybrid resonance at wake of body moving through ionosphere, comparing results with Alouette satellite observations 07 p1276 A70-20425
- Electron and proton precipitation measurements in auroral zone by soft particle spectrometer in ISIS-1 satellite 08 p1560 A70-20501
- Interkosmos-1 satellite for studying solar radiation and effects on ionization and molecular dissociation in atmosphere, weather and radio signals reception 08 p1582 A70-20714
- Satellites for meteorological and geographical studies using information from TV and IR pictures 08 p1487 A70-20716
- Space research in terms of earth environment in space, discussing near-earth spacecraft role in solar, magnetospheric and ionospheric studies 08 p1488 A70-21344
- Solar proton flux increases associated with sudden commencements observed by geostationary ATS-1 satellite 08 p1562 A70-21378
- Magnetic field measurements in geomagnetic tail from Explorers 33 and 35 indicating depressed field region centered on neutral sheet 08 p1488 A70-21379
- Magnetic equator ELF noise examined with OGO 3 magnetometer, indicating unique signals in plasmasphere 08 p1488 A70-21380
- Quasi-trapped electrons precipitating at high latitudes measured from low altitude polar orbiting satellite 08 p1562 A70-21382
- Electron wake measurements on Explorer 8 and 31 and Ariel 1, discussing order of magnitude discrepancy 08 p1497 A70-21392
- Optimal atmospheric transmittance windows for underlying surface and cloud temperature determination from satellites 08 p1538 A70-21426
- Critique of blue haze negative hypothesis in preliminary Mariner 6 data report 08 p1578 A70-21556
- Statistical correlation between polar magnetic disturbances and magnetospheric energetic electron flux increase from IMP-1 satellite observations 08 p1491 A70-21714
- Geoeffective low energy particles and fresh photoelectrons interactions with upper atmosphere observed by satellite Cosmos 261 08 p1492 A70-21796
- Auroral electrons and photoelectrons spatial, energy and angular distributions measurements using low energy electron spectrometer onboard satellite Cosmos-261 08 p1500 A70-21797
- Low energy ion spectrum and spatial distribution measurements in auroral zones by Cosmos-261 satellite spectrometer 08 p1492 A70-21798
- Abstracts with references to literature sources on oceanography from space and aircraft 09 p1665 A70-22014
- Vertical water vapor profile in strato-, meso- and thermospheres measured in rocket and satellite experiments by mass spectroscopy, spectral analysis and thermal sensometry 09 p1666 A70-22187
- TIROS, Nimbus, ESSA and ATS weather satellites configurations, onboard equipment and cloud photographs 09 p1765 A70-22227
- Energy distribution of solar wind alpha particles in magnetosheath observed by Heos A satellite 09 p1744 A70-22305
- Moon gravity field model derived from long-arc analysis of Lunar Orbiters tracking data, considering lunar mass distribution role 09 p1752 A70-22309
- Spaceborne long wavelength radio astronomy, proposing lunar orbit and beyond Pluto observatories to reduce magnetospheric and interplanetary plasma effects 09 p1754 A70-22495
- Position determination from simultaneous observation of Pagesos and Geos 2 satellites, assuming known covariance matrix and applied corrections 09 p1754 A70-22499
- Solar wind heating, determining roles of various energy sources from Explorer 34 observations 09 p1755 A70-22511
- Ionospheric electron content and distribution determination from Explorer 22 satellite signal amplitude recordings, considering wave propagation and polarization and Faraday effect 09 p1633 A70-22530
- Atmospheric density in thermosphere observed by satellites, noting daily and semiannual variations related to solar and geomagnetic activities 09 p1667 A70-22626
- Solar equatorial XUV limb brightening for resonance lines of Li-like ions from OSO-4 observations interpreted by coronal model 09 p1757 A70-22732
- Solar low energy X ray bursts using data from OSO-4 proportional counter spectrometer 09 p1745 A70-22739
- Earth resources data transmission, describing picture reception and reproduction equipment [AIAA PAPER 70-328] 09 p1634 A70-22856
- Communications satellite technology for earth resources data collection 09 p1634 A70-22857
- Earth resources data exploitation, describing potential organizational structures for data handling and various political, economic and technological problems [AIAA PAPER 70-344] 09 p1793 A70-22859
- Earth resources observation satellite /EROS/ program, describing remote sensor data acquisition, processing, dissemination and utilization [AIAA PAPER 70-332] 09 p1667 A70-22861
- International legal and political aspects of earth resource surveying by satellite remote sensors, considering U.S. policy [AIAA PAPER 70-331] 09 p1793 A70-22862
- Microwave radiometric techniques for continuous all-weather remote sensing of sea conditions from satellites, discussing foam and surface ripple effects [AIAA PAPER 70-318] 09 p1677 A70-22869
- Synthetic aperture radar in earth resource monitoring by satellite, determining topography and surface nature from spatial patterns 09 p1635 A70-22872
- Satellite monitoring of air pollution, discussing sulfur dioxide measurement in UV, optical correlation techniques, IR and visible spectra, stratospheric balloon tests, etc [AIAA PAPER 70-305] 09 p1668 A70-22875
- Oceanic wind and wave predictions by satellite radar radiometer using single receiver to determine wind velocity [AIAA PAPER 70-310] 09 p1668 A70-22877
- Satellite remote sensors for oceanographic applications, estimating resolution requirements for temperature, spatial interval, roughness patterns, wind speeds, etc [AIAA PAPER 70-306] 09 p1668 A70-22880
- ERTS satellite role in resource policy, management and remote sensing [AIAA PAPER 70-304] 09 p1668 A70-22881
- Satellite high resolution IR imagery for arctic sea ice mapping, describing sensor design and day and nighttime operation in film-strip format [AIAA PAPER 70-301] 09 p1669 A70-22884
- Remote sensors for earth resources observation by satellites, discussing electromagnetic spectrum, device operation, atmospheric transmission, measuring instruments, etc 09 p1678 A70-22888
- EROS program earth imaging models characteristics, describing airborne and spaceborne film return and global and geosynchronous space data transmission [AIAA PAPER 70-294] 09 p1678 A70-22889
- Artificial earth satellites photographic observation without chronometric recording aids, determining location and time by single indicator 09 p1635 A70-23055
- Solar wind magnitude and variability effects on geomagnetic activity and cosmic ray intensity modulation from satellite observations 09 p1745 A70-23272
- Reference ellipsoids mutual positions determination from observational data by satellites using triangulation points of two triangulations 09 p1763 A70-23327
- Azimuth determination by Vector method based on satellite observations compared to Popovich method, discussing discrepancy 09 p1670 A70-23329
- Orbiting satellite-borne instruments for scientific observation of earthquakes, volcanic eruptions, atmospheric phenomenon, cyclones, floods and soil erosion 09 p1763 A70-23377
- Heliocentric longitude intensity profiles of protons associated with solar flare of 5 February 1965, discussing data from Mariner 4 and IMP 2 09 p1746 A70-23480
- Electron and proton temperature differential near earth bow shock determined from plasma probe measurements by Vela 4B satellite 09 p1670 A70-23486
- Satellite observational data on time history of inner radiation belt /October 1963-December 1968/ 09 p1746 A70-23488
- Auroral arcs far UV observations by OGO 4, discussing luminosity, morphology, position, etc 09 p1670 A70-23493
- Ion cyclotron whistler in Injun 5 satellite VHF radio noise data 09 p1638 A70-23499
- Layered cloud amounts, cloud bases and tops heights analyses based on satellite TV and IR data 10 p1912 A70-23936
- Intertropical convergence zone /ITCZ/ movements, analyzing data obtained by ship and ESSA satellite cloud photography 10 p1912 A70-23939
- Spectral, angular and spatial evolution of earth twilight aureole brightness pattern from visual observation and spectrophotometry on Soyuz 5 spacecraft 10 p1873 A70-24270
- Satellite studies geoeffective particles and photoelectrons, including interactions with earth atmosphere 10 p1874 A70-24312
- Satellite-borne spectrometer for low energy electrons measurement, describing virgin photoelectrons equilibrium energy spectrum for different latitudes and pitch angles 10 p1874 A70-24313
- Satellite-borne spectrometer for low energy ion measurement 10 p1874 A70-24314
- Satellite-borne scintillation spectrometers for medium and high energy electron and proton measurements 10 p1931 A70-24315
- Magnetopause boundary between shocked streaming solar plasma and geomagnetic tail observed at lunar orbit by magnetometer on Explorer 35 10 p1941 A70-24436
- Visual observations of Molniya satellite during low perigee, determining air density 10 p1875 A70-24443
- Plate coordinate measurements obtained with Zeiss precision monocomparator at satellite observation station 10 p1889 A70-24501
- Earth Observation Satellites - BIS-NATO Conference, Cambridge, England, July 1969 10 p1950 A70-24635
- Manned and unmanned earth resources observation satellite program, noting international cooperation 10 p1971 A70-24636
- Manned and unmanned earth observation satellite programs technology gains, discussing atmospheric temperature, pressure, winds, clouds and moisture 10 p1876 A70-24637
- Ozone measurement from satellite by direct beam and scattered light methods employing UV sunlight attenuation 10 p1890 A70-24639
- Lunar cratering and erosion from Orbiter 5 photographs, observing crater densities, highland and maria regions, etc 10 p1942 A70-24643
- Simple layer model of geopotential from satellite-borne Baker-Nunn camera observations 10 p1876 A70-24645

ESRO satellite projects, studying interplanetary magnetic field, ionosphere, relations between sun and earth, gamma radiation sources, particle flow, electric fields, etc 10 p1951 A70-24867

Vertical air density profile from satellite measurements of atmospheric oxygen radio emission at 40-70 km altitudes 10 p1882 A70-25020

Radiation scattering during upper cloud altitude determination by satellite 10 p1913 A70-25022

Soviet cameras for photographic observation of artificial celestial bodies, noting equatorial platform mount, mirror lenses and installations 10 p1892 A70-25128

Numerical weather forecasting for several weeks based on global meteorological satellite network observation 10 p1913 A70-25241

Ionospheric electron content from Doppler data and from Faraday observations of satellite S-66 10 p1884 A70-25256

Satellite solar wind observations concerning interplanetary magnetic field direction and strength, proton distribution, solar wind velocity, density and direction 10 p1935 A70-25286

VHF aeronautical communication satellites extended for use in aircraft position determination and surveillance, discussing accuracy and error source reduction [AIAA PAPER 70-490] 11 p2002 A70-25487

Open magnetic electron multipliers /MEM/ with continuous dynode and field strips for satellite-borne detection systems, emphasizing extreme UV detectors 11 p2049 A70-25628

Gravitational field signatures for planetary fine structure analysis, describing lunar orbiter, selenodesy experiment and gravity field and earth gravity field satellite observation 11 p2111 A70-26029

Gravity waves structure simultaneous determination from airborne ozone and temperature sensors and satellite observations data 11 p2076 A70-26072

Solar wind correlation with geomagnetic activity, comparing Vela 3 and 4 observations with Mariner 2 measurements 11 p2105 A70-26075

Satellite observations reduction, determining continuous transformation over whole field of photograph by local transformations 11 p2007 A70-26187

U.S. Coast and Geodetic Survey satellite triangulation data reduction methods, discussing data acquisition system, plate preparation, etc 11 p2046 A70-26190

Spatial geodesy calculations based on photographs of satellites against star background, recommending ECHO type satellites 11 p2046 A70-26191

Passive satellite coordinates correlations to instants of observation in U.S.S.R. ground stations, reducing quasi-synchronous observations by interpolation 11 p2007 A70-26192

Schmidt photographs reduction, noting film bending during exposure and mean error of satellite position 11 p2007 A70-26195

Photographic satellite plates reduction by astrometric method at geodetic institute at Potsdam, discussing star coordinates, astronomic refraction, etc 11 p2008 A70-26200

Oblique shock initiated by 7 July 1966 proton flare in solar wind observed by satellite magnetometers outside magnetosphere 11 p2105 A70-26562

Undiscovered satellites of solar system major planets, predicting Jupiter satellites 11 p2118 A70-26725

Satellite trajectory parameters estimation by maximum likelihood method applied to continuous satellite observations assuming random Gaussian process as measurement error 11 p2081 A70-26780

Cosmos 137 proton spectra data obtained in inner radiation belt agreeing with Relay 1 data 11 p2106 A70-26786

Radial velocity data monitored during Venera 4 descent used for determining vertical and horizontal atmospheric flows velocities 11 p2118 A70-26792

Geopedological features derivation from satellite measurements, discussing Nimbus 2 data and grid point maps 12 p2217 A70-26914

Remote sensing from aircraft and satellites of chlorophyll concentrations for monitoring of biological productivity of sea 12 p2217 A70-26915

Worldwide crop calendar development from repetitive satellite observation to perform agricultural change detection 12 p2218 A70-26922

Remote sensing techniques for earth resources inventory, describing image enhancement role in multiband space photography 12 p2220 A70-26936

ERTS multispectral scanner with optimal sensitivity and resolution for agricultural scenes signature analysis 12 p2229 A70-26941

Atmospheric temperature determination by satellite IR spectrometer /SIRS-A/, describing data analysis and instrument design, calibration and performance 12 p2263 A70-26954

Energetic electron layer near magnetopause attributed to geomagnetic activity from satellite observations of fluxes 12 p2292 A70-27180

Lyman alpha intensity and hydrogen concentration at 5 to 19 earth radii determined from OGO 3 spacecraft measurements 12 p2222 A70-27181

Broadband and highpass LF noise in distant magnetosphere detected by VLF/LF experiment on OGO 1 satellite 12 p2222 A70-27183

Quasi-sinusoidal fluctuations of magnetic field during geomagnetic storms measured by ATS 1 in synchronous equatorial orbit 12 p2223 A70-27192

Mascons in lunar maria depressions observed by Lunar Orbiter 5 on basis of two layer model of crust 12 p2299 A70-27281

Low energy electron flux as interplanetary radiation primary component, considering data from IMP-1 observations 12 p2292 A70-27383

Beryllium proportional counters for satellite X ray astronomy, noting long term stability and environmental resistance 12 p2232 A70-27403

Ultra low frequency waves features in magnetosphere, considering geomagnetic pulsations, magnetic data from Explorer 33 and bounce resonance 12 p2233 A70-27573

Lunar limb shock wave observed by Explorer 35 satellite defined with respect to solar wind flow direction, discussing formation mechanism 12 p2302 A70-27594

Ionospheric probing by ground based and satellite-borne vertical incidence sounders 12 p2224 A70-27729

Ionospheric electron content calculations based on satellite measurements of Faraday rotation and phase path length variations 12 p2294 A70-27739

Meteorological research potential of manned orbiting spacecraft, discussing electromagnetic sensing instrumentation development, specialized observing programs, etc 12 p2225 A70-27744

Terrain spectral imagery from satellites for natural resources investigations 12 p2235 A70-27745

Oceanographic potential of spacecraft, discussing synoptic scanning, International Decade of Ocean Exploration, etc 12 p2225 A70-27746

Earth resource observation from orbiting spacecraft, discussing photo-image map construction for continents and continental shelves, terrain analysis, delta formation, etc 12 p2225 A70-27747

Experimental IR earth horizon profiles measured by satellite in F region, discussing spectral channels and attitude control 12 p2225 A70-27751

Ionospheric electron content at temperate latitudes during solar cycle increasing phase by radio beacon satellite, discussing diurnal, seasonal and latitudinal variations 12 p2225 A70-27892

Topside ionosphere structural analysis, considering electron density profiles deduced from Alouette 2 satellite data 12 p2226 A70-28062

Topside ionosphere nighttime structure over Japan deduced from Alouette 2 satellite plasma frequency measurements 12 p2226 A70-28063

Proton cyclotron echoes in topside ionograms using Alouette 2 satellite data 12 p2226 A70-28064

Galactic noise and solar type 3 bursts using Alouette 2 satellite HF receiver voltage recordings 12 p2226 A70-28065

F 2 region critical frequency from Alouette 2 satellite data compared with ground based measurement 12 p2226 A70-28066

Plasmasphere ion concentration measurements on-board Elektron 2 and 4 satellites, observing dependence on geomagnetic activity 12 p2295 A70-28260

Long wave cosmic radio background emission in circumlunar space by Luna 11 and 12 satellites, observing increase in earth magnetosphere tail 12 p2295 A70-28262

Low energy solar proton flux propagation model in interplanetary medium based on satellite data beyond earth magnetosphere 13 p2475 A70-28459

Magnetograms by Venera 4 and Mariner 5 compared to determine interplanetary magnetic field nature in Venus proximity 13 p2485 A70-28463

Three dimensional characteristic of light scattered by lunar surface determined for various incidence angles and azimuths from Zond 3 photometric measurements 13 p2485 A70-28466

Magnetospheric magnetic field disturbance due to abrupt solar wind parameters change, using Explorer 26 data 13 p2475 A70-28469

Satellite measurement of water vapor height profiles using outgoing thermal radiation and solar radiation atmospheric absorption techniques 13 p2392 A70-28571

Clouds upper height boundary relation with radiation temperature field from satellite data, noting cirrus clouds influence 13 p2444 A70-28589

Shutter thermal control for Helios solar observation satellite, considering closed and open conditions 13 p2505 A70-28769

Astronomical Netherlands Satellite /ANS/ for carrying out stellar UV and X ray emission experiments 13 p2506 A70-28989

Topside ionosphere structure deduced from electron density profiles observed by Alouette 2 satellite 13 p2395 A70-29090

Topside ionosphere structure deduced from resonance spikes on ionograms obtained by Alouette 2 satellite and electron density distributions 13 p2395 A70-29091

Galactic noise spectrum and solar radio bursts in hecto-decmetric wave region observed by Alouette 2 satellite 13 p2491 A70-29093

F 2 critical frequencies from Alouette 2 satellite ionogram data compared with ground-based sounding results 13 p2396 A70-29094

Magnetosheath plasma measurements by Pioneer 6 during outbound passage in dusk meridian, comparing results with various predictions 13 p2396 A70-29180

Geomagnetic tail structure and magnetic field fluctuations from IMP 3 satellite measurements, showing enhancement during/after SSC and sudden impulses /SI/ 13 p2396 A70-29182

Northern auroral regions low energy electron fluxes survey by Injun 4 satellite during minimum solar activity 13 p2477 A70-29184

Triaxial earth ellipsoid best fitting parameters for geoidal surface radius vector by spherical harmonics with coefficients computed from satellite observations 13 p2398 A70-29207

Harmonic functions defining geopotential and gravity derived from satellite orbit dynamics, applying to earth shape parameters 13 p2398 A70-29208

Universal triaxial instrument with AT-1 telescope for visual observation of satellites, discussing applications and accuracy 13 p2408 A70-29274

Refraction errors and anomalies effects on satellite observation, using atmospheric model 13 p2449 A70-29275

Martian terrain features and atmospheric activity observation by Mariner 6 and 7 13 p2494 A70-29526

Satellite time and position observations mean square error analysis using calculus of variations 13 p2367 A70-29528

Geodetic systems relative positions determination based on satellite synchronous observation 13 p2400 A70-29529

Atmospheric density estimation from observation of satellite drag-induced energy dissipation 13 p2400 A70-29530

Satellite radiometry, discussing vertical soundings, instruments, onboard calibration of interferometer, high spatial resolution, etc 13 p2411 A70-29664

Alouette 1 plasma resonance observations, analyzing electron density measurements in sheath region and cyclotron harmonic resonant frequencies 13 p2466 A70-29903

Dispersion and group velocity characteristics of topside resonance oblique echoes near plasma frequencies observed by satellite 13 p2467 A70-29909

Local resonance at upper hybrid frequency from satellite observation, noting effects of electron plasma/cyclotron frequency ratio 13 p2370 A70-29911

Polar ionosphere auroral oval position detection by satellite observations of naturally occurring VLF and man-made HF plasma waves 13 p2371 A70-29924

Low and high apogee satellite and rocket magnetometers for space measurements, discussing self oriented fluxgate, proton, quantum cesium and three component types

13 p2415 A70-30047

Solar wind parameters time variations influence on geomagnetic activity from measurements by electrostatic analyzers on Vela satellites

13 p2481 A70-30065

Electron and positive ion velocity distributions measurements near earth bow shock by electrostatic analyzer on Vela 4B satellite

13 p2481 A70-30068

Spatial distribution and directional anisotropies of tail plasma sheet energetic electrons from measurements by electrostatic analyzer and energetic particle experiments on Vela 4

13 p2482 A70-30071

Plasmapause position and density profile from ion concentration measurements by OGO-5, determining reaction to magnetic variations

13 p2482 A70-30074

Geomagnetic tail structure and shape from Explorer 33 and 35 and Pioneer 8 observation data, examining field lines divergence with distance from earth

13 p2402 A70-30075

Geomagnetic field distortion in high beta magnetospheric regions from OGO observations for quiet and slightly disturbed conditions

13 p2402 A70-30076

Geomagnetic field distant fluctuations during substorm from ATS 1 magnetometer data on abrupt recoveries of H component

13 p2482 A70-30077

Ionospheric DC electric fields long period oscillations at high latitudes observed by polar orbiting Injun 5 satellite

13 p2403 A70-30081

Van Allen radiation belts energetic electrons injection and distribution due to magnetic storms, using satellite-borne spectrometers

13 p2483 A70-30090

Satellite observation of alpha particles trapped geomagnetically in radiation belts, including Injun 5 results

13 p2484 A70-30092

Trapped alpha particle and proton spectra from satellite measurements, considering magnetosphere injection

13 p2484 A70-30093

Cloud cover photographs in deep occluded cyclone by Soyuz 4 spacecraft

14 p2602 A70-30139

Subpolar ionosphere electron concentration measurements for both hemispheres during solar activity by Faraday effect signal recordings from satellites

14 p2570 A70-30223

Earth radiation balance climatological characteristics based on satellite and published data, analyzing earth-atmosphere albedo on global scale

14 p2603 A70-30402

Free floating balloon position and velocity determination by satellite, using Kalman filter linear estimation theory

14 p2530 A70-30571

Satellite scintillation index variation with zenith angle and azimuth at ground station

14 p2574 A70-30739

Radio wave-ionosphere interaction effects on accuracy of radio astronomical observations from earth satellites

14 p2575 A70-30824

Ion temperature sensitive end effect in long cylindrical Langmuir probe response in high speed collisionless plasma flow at ionospheric satellite conditions

14 p2577 A70-31038

Topographic variations in lunar surface from bistatic radar observations on Explorer 35

14 p2645 A70-31061

Spacecraft measurements revealing hot dense Venusian and cold thin Martian carbon dioxide atmospheres

14 p2646 A70-31066

Numerical weather prediction requirements for global satellite observing systems using atmospheric models

14 p2610 A70-31152

Satellite probing method for transmission absorption spectroscopy of planetary atmospheres

14 p2650 A70-31230

Cloud cover statistical data applied to planning remote satellite-borne sensing missions, using Monte Carlo method

14 p2611 A70-31232

Harmonic analysis of digital data from satellite measurements of periodic phenomena with unknown periodicity

14 p2554 A70-31415

Gravitational field representation in satellite geodesy by simple layer potential, comparing with geopotential expansion in spherical harmonics

15 p2722 A70-31548

Atomic hydrogen distribution in upper atmosphere and solar system obtained during spin operation of OGO 5 with Lyman alpha photometer

15 p2798 A70-31655

Ionospheric electron concentration and temperature measurements by cylindrical Langmuir probe on rockets and satellites, emphasizing error sources

15 p2723 A70-31657

VLF wave propagation direction observation by satellite after passage through magnetosphere at low and mid latitudes

15 p2697 A70-31659

Solar extreme UV radiation measurements over rotation period onboard satellite OSO-3, using atmospheric absorption correction

15 p2792 A70-31666

Polar ionospheric electron/ion density measurements by ESRO 1 satellite, observing dependence on Kp index

15 p2724 A70-31669

Atmospheric density near 180 km /1968-1969/ from orbit of satellite 1967-31A /ATS 2/, noting weak dependence on solar activity and correlations to geomagnetic disturbances

15 p2724 A70-31680

Radar meteor shower rate observation compared with direct cosmic dust measurements on satellites

15 p2798 A70-31682

Ionospheric density profiles measurement by accelerometers on SPADES and Cannon Ball 1 satellites, comparing results with prediction from atmospheric model

15 p2724 A70-31686

Atmospheric vertical temperature sounding from geosynchronous satellite, discussing instrumentation, cloud cover and wind effects, etc

15 p2809 A70-31690

Report to COSPAR on space research in Bulgaria, considering ionospheric physics, cosmic rays, satellite observations, meteorology and space communications

15 p2829 A70-31704

Report to COSPAR on Austrian space research covering picture transmissions, solar activity, satellite observation, etc

15 p2829 A70-31707

Report to COSPAR on Hungarian space research including satellite observations, upper atmosphere, geomagnetic effect, geodesy, cosmic rays, etc

15 p2830 A70-31713

Report to COSPAR on space research in Pakistan, covering rocket, satellite and ground based investigations, etc

15 p2830 A70-31718

Relativistic cosmic rays primordial chemical composition above atmosphere from abundance data obtained with satellite-borne nuclear emulsion detector

15 p2793 A70-31735

Orbital earth resources sensors, outlining user oriented method of determining measurement requirements

15 p2735 A70-31777

Quiet time proton and alpha particle flux and differential energy spectra measured by cosmic ray detectors on OGO 3 satellite

15 p2793 A70-31795

Quietest cosmic ray ionization altitude dependence over polar regions from measurements by integrating ionization chamber on OGO-2

15 p2793 A70-31902

Cosmic ray knee interpretation using polar orbiting ionization chambers data from OGO-2/4

15 p2793 A70-31903

Pioneer 8 wave and particle observations correlation showing broadband wave levels reduction during extended geomagnetic tail crossings

15 p2727 A70-31904

Neutral particle and electron density measurements by Explorer 32 proving thermospheric gravity waves association with wave-like structure in F region electron density

15 p2727 A70-31907

Polar substorm activity associated with magnetopause position variation, using Imp 2 satellite observations

15 p2728 A70-31911

Soviet collection of articles on satellite meteorology covering atmospheric cellular convection, cloud cover, wind field analysis, etc

15 p2769 A70-32063

Wind field reduction from satellite cloud structure data

15 p2770 A70-32066

Atmospheric radiation and heat fluxes calculations comparison with satellite and ground station actinometric measurements

15 p2770 A70-32067

Sea surface temperature and atmospheric moisture determination from satellite measurements of atmospheric thermal radio emission on quiet and cloudy windy days

15 p2770 A70-32069

Atmospheric humidity determination from satellite radio emission measurements at SHF

15 p2771 A70-32071

Earth surface temperature, emissivity and dielectric constant from satellite measurements of SHF radiation

15 p2771 A70-32072

Electric field measurements in ionosphere using satellite and rocket experiments

15 p2729 A70-32082

Atmospheric density and temperature measurements by satellite- and rocket-borne pressure gauges and mass spectrometers, considering error sources

15 p2731 A70-32092

Prolonged upper ionospheric observations from Sputnik 3, Transit 4A and Explorer 22 signals Faraday fading and phase shifts, showing electron content dependence on solar activity

15 p2731 A70-32093

Intercomcos 1 satellite for observing solar UV and X-ray emission in solar flares prediction

15 p2738 A70-32145

Equatorial atmospheric density during geomagnetic storm and quiet days by satellite observation

15 p2811 A70-32284

Solar radio burst satellite observation during Proton Flare Project, giving dynamic spectra

15 p2794 A70-32293

OGO 5 satellite scientific observations, payloads, parameters and objectives

15 p2812 A70-32364

Mariner 4 and 5 and Venera 4 data used for comparing terrestrial planets ionospheres

15 p2805 A70-32733

Charged particles and He nuclei spatial distribution from recordings in cosmic ray equator region by Cerenkov counter mounted on Proton 2 satellite

15 p2795 A70-32735

Micrometeor flux in near-earth space measured by satellite-borne low noise acoustic detectors

15 p2805 A70-32738

Spatial vectors determination by two laser measurements and one optical observation of artificial satellite

16 p2926 A70-33118

Thermal atmospheric sounding from satellites based on Fredholm integral equations, obtaining vertical temperature profiles

16 p2896 A70-33257

Twilight colorimetry from horizon spectra obtained by Soyuz 5, computing chromaticity coefficients for purely scattering molecular atmosphere

16 p2896 A70-33260

Satellite communication/navigation/surveillance systems for domestic and transoceanic ATC

16 p2949 A70-33479

Oceanographic phenomena inference from satellite cloud photographs, developing seasonal cloud climatology for Peru Current area

16 p2897 A70-33713

Gravity wave generation during solar eclipse confirmed by satellite observation on Faraday rotation angle of ionospheric VHF transmissions

16 p2898 A70-33836

Mars evolution observation by gamma ray spectrometer in Martian orbit, transmitting information to earth as pulse height distribution

16 p2912 A70-33978

Solar X-ray spectrum and intensity and diffuse cosmic flux measurements, using polar orbiting satellite-borne instruments

17 p3149 A70-34534

Omnidirectional cosmic gamma ray flux in 1-6 MeV range observed by ERS-18 satellite

17 p3149 A70-34539

Galactic gamma rays from OSO-3 observations attributed to decay of neutral pions produced by cosmic rays interaction with interstellar gas nucleons

17 p3150 A70-34567

Earth gravity field from successive satellite passages, introducing direction and range observations of first passage

17 p3154 A70-34683

Dynamic spectra of type 3 solar bursts from OGO-3 antenna/radiometer observations

17 p3150 A70-34835

UV interstellar extinction, examining reddened and unreddened early stars with OAO satellite spectrophotometric scans

17 p3159 A70-34878

Early-type star spectral scan analysis from OAO observation, comparing model atmosphere calculations

17 p3161 A70-34887

Solar UV spectrum variations due to flares and solar activity diurnal variations from satellite spectrometry

17 p3161 A70-34894

Night sky brightness in UV and visible region by photoelectric photometers on Cosmos 51 and 213 satellites

17 p3163 A70-34901

Ionospheric irregularities properties from San Marco 2 and BE-B satellites recordings, deriving height variation of irregularity size and occurrence

17 p3076 A70-34942

Lyman alpha emission from Comet Bennett observed with photometer on board OGO-5 satellite

17 p3163 A70-35049

Heliostationary spacecraft at L2 point for solar wind observation, describing mission, instrumentation and spacecraft design

17 p3168 A70-35252

OGO-4 observations of hydrogen Lyman-alpha air-glow surrounding earth, measuring dependence on solar zenith angle
17 p3080 A70-35764

Space legal problems involving earth resource survey (ERS) satellites and weather modification
17 p3203 A70-35799

OGO 5 observations of quasi-trapped electromagnetic waves in solar wind at 70 kHz
18 p3306 A70-36005

Plasmasphere bulge region morphology from hydrogen ion concentration measurement by mass spectrometer on OGO 5 satellite
18 p3312 A70-36014

Magnetospheric electric field configuration from trapped particle flux asymmetries, using Explorer 14 electron data
18 p3306 A70-36024

Large amplitude irregular magnetic fluctuations during expansion phase of magnetic substorms, using ATS 1 observations
18 p3312 A70-36025

High energy electrons in near space excess radiation from high altitude balloon and satellite data
18 p3307 A70-36170

Nimbus 3 satellite-borne Michelson interferometer IR spectrometer for spectrum measurement, obtaining temperature, water vapor and ozone vertical distribution
18 p3257 A70-36175

Satellite based systems for aircraft surveillance, discussing satellite power and bandwidth conservation, pulse techniques and interrogators
18 p3288 A70-36391

British X 3 satellite for investigating thermal control surface finishes stability, ultrathin solar cells, electronic systems reliability and micrometeoroid flux measurement
18 p3333 A70-36511

Brightness field spatial structure of solar radiation reflected from earth by Cosmos 149 satellite, discussing homogeneity and isotropy
18 p3247 A70-36629

Earth radiation measurement at 10-12 microns by Cosmos 243 satellite-borne radiometer, comparing temperatures for boundary air layers in cloudless conditions
18 p3247 A70-36630

Proton magnetometer measurements from satellite Cosmos 49, observing residual and broad magnetic anomalies
18 p3248 A70-36770

Solar proton flares radiometric measurement on-board Molniya 1 satellite, detecting intensities in outer regions of magnetosphere
18 p3309 A70-36902

Soviet papers on atmospheric radiation processes and satellite meteorology
18 p3285 A70-36962

Climatological maps of earth mean annual radiation balance compared with satellite data
18 p3286 A70-36966

Atmospheric water vapor distribution by intensity measurements of outgoing radiation from satellites in carbon dioxide and water vapor spectral bands
18 p3287 A70-36971

Electron temperature in 500-1000 km range during minimum solar activity based on Alouette satellite data and atmospheric model, observing latitudinal variation
18 p3254 A70-37029

Meteorological satellites, discussing observation continuity, orbital characteristics onboard memory capacity and sensing methods
19 p3460 A70-37386

Satellite observations of earth by human or automatic methods, discussing principle applications of Earth Resources Technological Satellite
19 p3410 A70-37387

Intercorrelated satellite observations related to solar events - ESRO Conference, Noordwijk, Netherlands, September 1969
19 p3491 A70-37471

Solar cosmic rays satellite observation, considering flare associated, recurrent and storm particle events and active center associated energetic particles
19 p3493 A70-37474

Solar wind disturbances associated with solar activity observed by spacecraft probing interplanetary space, considering geomagnetic activity classes
19 p3494 A70-37478

Solar wind fluxes observed onboard Venera 2 and 6 compared with earth electromagnetic field pulsations and short period disturbances
19 p3494 A70-37479

Low energy solar protons temporal and spatial variations in magnetosphere by data comparison from polar orbiting satellite and Explorers 33 and 34
19 p3494 A70-37486

Geomagnetic storms at ATS 1 in 1967, discussing storm-time disturbance field and associated pulsations
19 p3410 A70-37488

Interplanetary plasma observations by Vela satellites in solar wind and plasma sheet of magnetotail during magnetic storm
19 p3410 A70-37490

ESRO-1, ESRO-2 and HEOS-1 simultaneous observation of solar event of 25 February 1969, describing satellite and experiments
19 p3531 A70-37496

Solar flare of 25 February 1969 ground observations comparison to satellite data, measuring magnetic fields, radio emission, sunspots, ionospheric effects, etc
19 p3513 A70-37497

Solar flare of 25 February 1969 at soft X ray frequencies by ESRO 2 satellite observation
19 p3495 A70-37499

Interplanetary magnetic field during solar particle event of 25 February 1969 from Heos 1 measurements
19 p3495 A70-37500

Solar wind discontinuity during solar flare from Heos A measurements, observing shock wave propagation
19 p3495 A70-37502

Proton spectra and time history in interplanetary space during solar flare by satellite observation, investigating particle flux by shock waves
19 p3495 A70-37503

Solar cosmic ray protons and electrons increase during 25 February-5 March 1969 observed by Venus 5 and 6 space probes, discussing interplanetary medium disturbance
19 p3495 A70-37504

Solar protons directional and omnidirectional measurements during particle event of 25 February 1969 by Heos 1 spacecraft, indicating particle diffusion in interplanetary space
19 p3496 A70-37506

Solar protons distributions in 1-30 MeV range over northern polar cap during 25 February 1969 solar event by ESRO 1 satellite
19 p3496 A70-37508

Magnetospheric thermal plasma electron density measurement during solar flare by OGO-5 satellite
19 p3411 A70-37513

Ionospheric electron density and temperature variation measurements after solar proton event of 25 February 1969, using ESRO 1 satellite
19 p3411 A70-37514

ESRO 1 satellite and ground observations of energetic auroral electrons angular distribution during solar event, using Geiger counters
19 p3412 A70-37519

Low energy solar protons observation by Esro 1 satellite during solar flare of 25 February 1969
19 p3497 A70-37520

High energy solar electrons observed by HEOS-A1 satellite, discussing semitransparent barrier existence at distance from sun
19 p3497 A70-37521

Electron intensity long term variations above 500 MeV by OGO-5 satellite-borne cosmic ray electron detector, supporting diffusion-convection theory of solar modulation
19 p3497 A70-37522

Future space missions for observing solar events, magnetospheric problems, cosmic rays and low energy plasma, considering use of multiple satellites
19 p3513 A70-37523

Simultaneous primary energy spectrum, chemical composition and sidereal daily variation analysis for cosmic ray origin, using Proton measurements
19 p3500 A70-38080

Extraterrestrial gamma radiation from Cygnus region of galactic disk, using OGO-5 observations
19 p3501 A70-38087

High energy gamma ray flux enhancement towards galactic plane from OSO-3 particle telescope observations
19 p3501 A70-38089

Energetic primary gamma ray fluxes by satellite-borne spark chamber, isolating galactic radiation
19 p3502 A70-38093

Quiet time intensity increases and long term solar modulation of interplanetary low energy electrons, using IMP observations
19 p3502 A70-38097

Electron energy spectra range from HEOS A1 satellite mounted Cerenkov counter with shower telescope
19 p3503 A70-38103

High energy charged particle observations on OSO 3 at various rigidities
19 p3505 A70-38117

X rays measurement by spectrometer on satellite Cosmos 207
19 p3506 A70-38122

Galactic cosmic ray energy spectra of light and medium nuclei from IMP-4 satellite measurements, investigating L/M ratio
19 p3506 A70-38124

Cosmic ray heavy nuclei charge composition from satellite-borne emulsion stacks exposure
19 p3507 A70-38134

Rigidity spectra of primary cosmic ray nuclei groups from satellite-borne Cerenkov spectrometer
19 p3508 A70-38135

Relativistic cosmic rays nuclei abundances from Gemini 11 flight
19 p3509 A70-38144

Primary cosmic ray proton energy spectra from satellite observation, presenting spectrum approximating function
19 p3510 A70-38153

Venus atmospheric temperature, pressure and density measurements by Venera 5 and 6 space probes, developing model
19 p3520 A70-38255

Venus atmosphere heat transfer processes from Venera 4, 5 and 6 probes data, evaluating radiative and convective motions model
19 p3520 A70-38256

Atmospheric ozone remote sensing by high resolution IR interferometer spectrometer /IRIS/ aboard Nimbus 3 satellite
19 p3414 A70-38262

Simultaneous hydrogen ion composition measurements by upper ionospheric polar orbiting OGO 4 and eccentric orbiting magnetospheric OGO 3 at midlatitude
19 p3520 A70-38377

Jovian continuum radiation observation by RAE-1 during lunar occultations
19 p3512 A70-38608

Auroral photographic and visual observations, discussing satellite results and substorm development
19 p3417 A70-38730

Artificial satellites photographic observation by camera, describing sighting system, tracking adjustments and shutter controls
19 p3433 A70-38793

Ionospheric electron content measurements during 20 May 1966 solar eclipse by Beacon S-66 satellite
19 p3419 A70-38915

Vertical electron concentrations in upper F region during solar eclipses in South Atlantic from satellite observation
19 p3419 A70-38920

Free air temperature by onboard satellite IR spectrometer /SIRS/, measuring earth spectral radiance in carbon dioxide 15 micrometer band
20 p3660 A70-39077

Cosmic ray albedo neutron flux latitude and altitude dependence, using OGO-6 polar orbiting satellite
20 p3698 A70-39326

Stable midlatitude red arc observation by Alouette 2 satellite for electron temperature and density structure measurement, calculating intensity and extent
20 p3620 A70-39333

Tropical UV nightglow measurement by Ogo-4 spectrometer, considering ionospheric recombination excitation mechanism
20 p3620 A70-39338

Vertical motion determination from satellite cloud pictures based on canonical correlation of initial fields
20 p3664 A70-39401

Atmospheric effects on passive microwave sensing in EHF region under all-weather conditions on global scale using satellites
20 p3586 A70-39703

Global meteorological parameters measurement by satellites, discussing IR instruments
20 p3664 A70-39711

Low altitude cosmic rays dosimetric measurement by Cosmos 228 apparatus
20 p3700 A70-39728

Solar proton intensity measurement during flare by satellite Proton 3 apparatus
20 p3700 A70-39729

Nighttime lightning activity observations by orbiting solar satellite OSO-B, determining thunderstorms positions by optical radiation detection
20 p3623 A70-39978

Cloud motions from IR measurements within overlap region of adjacent Nimbus II orbits compared with wind vectors from constant pressure charts
20 p3665 A70-40068

Millimeter wave propagation measurements by ATS-5 satellite, observing attenuation dependence on meteorological parameters for communication data link performance prediction
20 p3589 A70-40311

Solar soft X ray flare spectra of 16 November 1967, examining electron temperatures and emission lines by OSO-4
20 p3700 A70-40419

OSO far UV solar spectroheliograms atlas, describing instrumentation, data acquisition, etc
20 p3713 A70-40540

COS-B satellite cosmic X ray experiment with high sensitivity and long pointing time for extragalactic sources discovery
21 p3871 A70-40655

High energy galactic gamma rays search onboard OGO-5, tabulating results
21 p3876 A70-40691

Galactic gamma ray intensity near Cygnus by OGO-5 spacecraft-borne telescope with acoustic spark chamber, discussing source intensity
21 p3876 A70-40691

Gamma ray astronomical point sources by balloon flight and satellite observation, discussing detector system and telescope for flux and energy spectrum 21 p3821 A70-40694

Omnidirectional cosmic gamma ray flux near one MeV observed by ERS-18 satellite, plotting spectral energy distribution 21 p3876 A70-40697

Atmospheric temperature and water vapor profiles from iterative solution of radiative transfer equation for comparison with spectral radiance observation from Nimbus satellites 21 p3846 A70-40803

Satellite-borne sensor for ionospheric ions velocity measurement, describing design and principles of operation 21 p3813 A70-40834

Ionospheric ions drift velocity horizontal and vertical components distribution, using satellite-borne sensor 21 p3813 A70-40835

Cosmos 142 satellite measurements VLF radio signals transmitted through ionosphere by ground based stations 21 p3786 A70-40836

Geostationary beacon satellite recording of gravity wave influence on ionospheric electron content 21 p3815 A70-40943

Solar X-ray bursts correlation with H alpha flares and microwave bursts observed by Explorer 34 experiment 21 p3880 A70-40970

Near earth solar UV flux measurement by Spades satellite, discussing nonrandom variations and Ca plage regions 21 p3881 A70-41078

Large scale flare associated solar wind disturbances observed by Vela satellites, noting prolonged elevated flow speed after shock 21 p3881 A70-41080

Solar wind proton properties examined by Vela 3, observing density distribution, flow speed and direction, thermal anisotropy, magnitude and orientation 21 p3881 A70-41081

EROS program earth imaging models characteristics, describing airborne and spaceborne film return and global and geosynchronous space data transmission [AIAA PAPER 70-294] 21 p3829 A70-41871

Real time global temperature and geopotential height profiles acquisition from satellite spectrometer measurements by least squares regression method 21 p3820 A70-42121

Sea surface temperature determination from satellite high resolution IR window radiation measurements by statistical histogram inference method 21 p3820 A70-42122

Ephemerides for lunar-orbiting observation of dust clouds in earth-moon system libration points L4 and L5 by observer orbiting over lunar equator 22 p4097 A70-42308

Dual satellite magnetic field and plasma measurements of earth bow shock pulsation shock by Vela 3A and Explorer 33 22 p4013 A70-42470

Global thunderstorm activity location found by measuring differences between time of arrival of electromagnetic energy at three satellites 22 p4016 A70-42779

F region electron content day-to-day changes observation by Early Bird satellite, determining cross correlation with magnetic indices 22 p4020 A70-43161

Total electron content and equivalent slab thickness statistical data during magnetic disturbances from AT-3 satellite VHF transmission observations 22 p4020 A70-43162

Geostationary satellites for magnetosphere and ionosphere sounding, discussing specific observational capabilities 22 p4024 A70-43397

Outer zone electrons radial diffusion coefficients and lifetimes determined as functions of magnetic shell parameter, based on satellite measurement following geomagnetic storm 23 p4236 A70-43831

Proton energy angular distribution measurement by OV2-5 research satellite confirming model of shell splitting in geomagnetic field 23 p4236 A70-43832

High altitude outer radiation zone boundary region electron energy measurement by satellite Injun 3, noting angular distribution dependence on local time, latitude, etc 23 p4236 A70-43833

Ionospheric ion temperature measurements by retarding potential analyzer on OGO-6 satellite 23 p4185 A70-43840

Neutral air density and composition at 150 km, comparing satellite drag data to rocket measurements results 23 p4185 A70-43843

ELF emissions dependence on plasmopause location in magnetosphere indicated from OV-3 observations 23 p4186 A70-43847

Ionospheric electron trough and magnetospheric plasmopause movements from satellite observations, showing statistical correlation with geomagnetic field 23 p4186 A70-43854

Daytime near horizon atmospheric luminescence measurement by Cosmos 224 satellite, discussing contributions of nitrogen and aerosol and Rayleigh scatterings 23 p4188 A70-44061

Ionospheric electron content measurement from Faraday effect of troposphere on beacon satellite Explorer 22 radio signals 23 p4163 A70-44231

Ozone vertical distribution from satellite IR data, discussing Fredholm equations for radiation transfer 23 p4191 A70-44269

Celestial sphere scanning by spinning symmetric satellite with open loop magnetic control of precession 23 p4216 A70-44524

FSRO satellites missions and payloads, emphasizing studies of earth magnetic and electric field environment and of polar region particle measurements 23 p4191 A70-44663

Geopotential zonal spherical harmonics coefficients revised values determined from reduced Baker-Nunn observations for satellites 24 p4407 A70-45537

Tesseral harmonics of geopotential and station coordinates from combined Baker-Nunn, laser and range data from satellites 24 p4407 A70-45538

Error analysis of satellite orbits obtained by synchronous satellites range and range rate measurements 24 p4407 A70-45539

GEOS 1 satellite short arc optical observations over North American network to improve survey coordinates of tracking stations 24 p4312 A70-45542

Doppler satellite measurements in semidynamic geodesy using data from Mediterranean ground stations 24 p4312 A70-45543

Dynamical and geometrical geodesy on European datum, comparing data from Doppler, laser and photographic satellite measurements 24 p4312 A70-45544

Geodetic parameters estimated from satellite dynamic and geometric solutions and Mariner 4 and 5 missions 24 p4312 A70-45545

Satellite data acquisition and dissemination functions of National Space Science Data Center (NSSDC) 24 p4322 A70-45615

Earth Resources Technology Satellites (ERTS) providing high resolution image data regarding agriculture, geology, hydrology, geography, etc 24 p4416 A70-45869

D2A satellite optical experiments, examining atmospheric atomic H and solar and extraterrestrial 1216 A emission 24 p4339 A70-46094

Subpolar ionosphere electron concentration measurements for both hemispheres during solar activity by Faraday effect signal recordings from satellites 24 p4331 A70-46298

SATELLITE ORBIT CALCULATION
U ORBIT CALCULATION
SATELLITE ORBITS
 NT PARKING ORBITS
 NT POLAR ORBITS
 NT STATIONARY ORBITS
 NT TWENTY-FOUR HOUR ORBITS
 Periodic motion of satellite with magnetic damper along circular orbit, assuming small value of damping coefficient 01 p0197 A70-11481

Horizontal gradients below satellite orbit effect on reduced and minimum difference in Doppler frequency shifts of coherent radio waves from satellite in inhomogeneous ionosphere 01 p0046 A70-11517

Satellite orbital elements optical determination accuracy by differential corrections, presenting computations for data distributed along small arc 02 p0254 A70-11754

Satellite tracking at several stations at synchronized time to obtain satellite positions, station coordinates and to improve orbital elements accuracy 02 p0254 A70-11760

Cosmos 44 quasi-draconic period analytical and graphical determination, comparing moments of meridian intersection with INTEROBS observations 02 p0363 A70-11767

Three-body gravity gradient satellite orbital plane motion analysis, studying transient damping of proposed tethered orbiting interferometer/TOI/ 02 p0383 A70-12781

Steady motions stability of gyrostat satellite in central Newtonian gravitational field 03 p0579 A70-13343

Azur satellite launching project by NASA and Germany, describing orbit for investigating earth inner radiation belt, auroral zone and solar flares 03 p0580 A70-13797

ESRO German-built satellite HEOS 1 planned scientific space measurements, required orbit and technical concepts 03 p0580 A70-13798

Generalized Keplerian orbits for large cylindrical satellites noting orbit stability 03 p0578 A70-14252

Relative satellite motion equations derived in generalized parameters, obtaining expressions for coefficients of correcting impulses sensitivity to measurement errors 04 p0760 A70-14430

Earth resources satellites capabilities and requirements emphasizing orbit parameters, remote sensing, data handling and telemetry systems [AAS PAPER 69-587] 04 p0760 A70-14642

Prediction accuracies of atmospheric models investigated for medium altitude satellites during disturbed geomagnetic conditions, discussing solar flux and geomagnetic indices as input data [AAS PAPER 69-617] 04 p0677 A70-14647

Satellite orbit and attitude determination and planetary gravity and astronomical constants from earth-based radio Doppler and orbital photogrammetric observations 04 p0750 A70-14938

Navy navigation satellite passes predicted by equations for rise and set times, elevation and azimuth in plane circular polar orbit about spherical earth 04 p0764 A70-15431

Resonance effects on satellite orbits due to tesseral harmonics in potential field 05 p0908 A70-16335

Error analysis of resonant orbits for geodesy, discussing high order geopotential coefficient recovery by resonance and gravity model errors 05 p0909 A70-16341

Earth figure parameters from satellite orbit dynamics, including potential on geoidal surface and scale factor for lengths 05 p0840 A70-16638

Geodetic vertical and geoidal height deflection calculated by gravimetric method, considering satellite orbits data 05 p0841 A70-16643

Satellites and space probes orbital parameters calculation, considering circular and elliptical trajectories and rendezvous maneuver example 06 p1140 A70-17583

Electrically charged earth satellite motion under action of Lorentz force produced by geomagnetic field interaction, relating field trajectories to acceleration 06 p1142 A70-17879

Relative motion of two bodies linked by flexible weightless tether in artificial earth satellite orbit, simulating extravehicular walk 06 p1142 A70-17882

Gyrostat satellite equilibrium positions in circular equatorial orbit under action of gravitational magnetic and aerodynamic moments based on gyrostatized satellite equations of motion 06 p1155 A70-17884

Balloon satellite orbital time and eccentricity correlated, investigating earth shadow and solar radiation effects 06 p1142 A70-17892

Satellite temperature determination in earth orbit, testing mathematical thermal model in simulation chamber 06 p1155 A70-17935

Baseline length and orientation of closely co-orbiting satellites estimated by combined onboard sensor and ground tracking data [AIAA PAPER 70-39] 06 p1146 A70-18186

Eccentric and inclined motions of satellite of spheroidal planet in planet centered coordinate system, applying formulas to Jupiter motion 07 p1374 A70-18693

Satellite orbit using analytic partial derivatives of perturbed motion based on state transition matrices 07 p1381 A70-19301

Maximum probability estimates for satellite orbital plane, reducing computational labor by eliminating use of maximum likelihood principle in differential formulation 07 p1386 A70-19486

Satellite circular orbital plane rotation by jet thrust, minimizing fuel for fixed time 07 p1393 A70-19497

Winds above 200 km measured from vapor trail observations compared to winds deduced from satellite orbital changes and theoretical models 07 p1269 A70-19950

Libration limits of satellite in Keplerian circular orbit, estimating potential energy of perturbing forces 08 p1582 A70-20967

Earth satellite orbit determined by small separated optical observations at two stations 09 p1751 A70-22162

Spherical coordinate intermediaries for calculating satellite orbits 09 p1760 A70-22914

Satellite orbital characteristics selection techniques, tools and methods for mission objectives and constraints
[AAS PAPER 68-136] 09 p1761 A70-22937

Center of mass small displacement effects on satellite orbits by solving variational equations for scalar potential function employing matrix formalism
09 p1761 A70-22938

Nonspinning satellite orbit eccentricity effect on attitude stability
09 p1766 A70-23229

Polynomial force model supplementing reduced gravity model in determining accuracy of near equatorial, near synchronous and near circular satellite orbits
09 p1762 A70-23256

Satellite attitude and orbit control systems based on electrically heated ammonia or hydrazine
09 p1767 A70-23432

Material elasticity effects on librational motion of arbitrary shaped satellite
10 p1950 A70-24177

Satellite orbit prediction formulas for Vinti dynamic model with three coordinates expressed in terms of independent variable
10 p1939 A70-24188

Satellite orbit prediction using computer program based on first order secular node-to-node drag perturbations
10 p1943 A70-24822

Variations after one revolution in semimajor axis, period and eccentricity computed for orbit using variable drag coefficient involving satellite and air thermal speeds
10 p1951 A70-24824

Communication satellites geostationary orbit sharing problem, considering system design and utilization criteria
[AIAA PAPER 70-441] 11 p1998 A70-25419

Orbit utilization, discussing sharing of satellite communication frequency bands and use of multiple earthward antenna beams
[AIAA PAPER 70-468] 11 p1999 A70-25428

Visible light sensors application in LES control system for circular near equatorial orbits
[AIAA PAPER 70-477] 11 p2107 A70-25432

ATS-3 hydrazine orbit control system efficiency evaluation statistical method, considering stationkeeping maneuvers
[AIAA PAPER 70-460] 11 p2121 A70-25464

Systematic errors of reference star catalogs in satellite geodesy, discussing influence on orbit predictability
11 p2045 A70-26180

Satellite trajectory parameters estimation by maximum likelihood method applied to continuous satellite observations assuming random Gaussian process as measurement error
11 p2081 A70-26780

Satellite motion initial phase vector estimation for calculating satellite motion from selection of complete or increasing volume of measurements
11 p2118 A70-26781

Orbital perturbations earth satellite due to zonal and tesseral earth gravitational harmonics and external body fields
12 p2302 A70-27671

Aerodynamic moment on satellite with asymmetrically positioned solar cell platforms, analyzing motion around center of mass for diffuse scattering flow
12 p2314 A70-28254

Ground stationed automatic orbital operations system /AOOSY/ for satellites and space probes, discussing flow diagram and Siemens computer programming
13 p2372 A70-28398

Nondimensional aerodynamic forces and moments coefficients independent of air density and acting on satellites in low orbits
13 p2500 A70-28403

Low altitude operational meteorological and navigation spacecraft, discussing need for orbit adjustment by dynamic control
13 p2500 A70-28404

Symphonic communication satellite orbit and attitude stabilization systems components, operation and accuracy requirements
13 p2502 A70-28432

Relative satellite motion equations derived in generalized parameters, obtaining expressions for coefficients of correcting impulses sensitivity to measurements errors
13 p2503 A70-28455

Atmospheric density effect on satellite lifetime and position prediction, utilizing data from Cannon Ball and SPADES low altitude density research satellites
14 p2653 A70-30562

Steady motions stability of gyrostat satellite in central Newtonian gravitational field
14 p2653 A70-30718

Synchronous satellite orbits determination using mathematical model for simulating gravitational perturbations induced by terrestrial globe and foreign bodies
14 p2651 A70-31279

Earth-pointing satellites joined by tether, discussing reel back and drag brake orbital deployment techniques and dynamic behavior
15 p2799 A70-31776

Synergetic plane change maneuver optimal control, combining aerodynamic and propulsive flight phases for efficiency
15 p2715 A70-31784

Moon shadow solar eclipse encounter probability for high altitude satellite in circular earth orbit
15 p2803 A70-32502

Maximum probability estimates for satellite orbital plane, reducing computational labor by eliminating use of maximum likelihood principle in differential formulation
15 p2805 A70-32731

Satellite circular orbital plane rotation by jet thrust, minimizing fuel for fixed time
15 p2813 A70-32742

Satellite equations of motion in noninertial instantaneous astronomical system, taking into account perturbation equations terms
17 p3155 A70-34684

Intermediate elliptical orbits for planetary satellites with small inclination to equatorial plane
18 p3312 A70-36174

Artificial satellite theory main problem for small and moderate eccentricities, using perturbation techniques based on Lie transforms for computer programming
18 p3334 A70-37062

General potential function in triaxially ellipsoidal coordinates for Laplace equation, examining near earth satellites and Vinti potential
18 p3334 A70-37064

Satellite orbit theory error bounds and initialization, investigating first order von Zeipel method in axisymmetric force field
18 p3320 A70-37067

Position and velocity of geodetic drag free satellite in near circular orbit, including lunar-solar gravitational effects and zonal and tesseral harmonics
[AIAA PAPER 70-1054] 19 p3528 A70-38869

Orbital and physical parameters of calibration satellites launched into right circular cylinder and right circular cone
19 p3382 A70-38894

Earth resources satellite orbits and imaging sensors, discussing multispectral spin scanner design
20 p3626 A70-39053

Libration limits of satellite in Keplerian circular orbit, estimating potential energy of perturbing forces
20 p3713 A70-39388

Guidance and navigation system design for automatic stationkeeping one earth orbiting vehicle with respect to other
[AIAA PAPER 70-1005] 20 p3667 A70-39526

German monograph on satellite orbit synergetic plane change maneuver optimal control by entry into denser atmosphere
20 p3705 A70-39924

Resonant and nonresonant satellite eccentric orbits for determination of high order terms in geopotential
20 p3709 A70-40073

Global geoid sections determined by satellite orbit dynamics, using best fitting ellipses
21 p3812 A70-40591

Optimum altitudes for passive ranging satellite navigation systems, using electronic clocks in satellite and navigator receiver
21 p3883 A70-40724

Computer algorithm for optimal linear impulse corrections to satellite orbit under inequality type constraints
21 p3801 A70-40828

Perturbation of body motion in vicinity of smallest primary according to Huang model of restricted four body problem, discussing near lunar satellite application
21 p3884 A70-40874

Magnetic desaturation of inertia flywheels of satellite in equatorial or slightly inclined orbit, discussing satellite stabilization
22 p4110 A70-42488

Radiation forces on flat plate in ecliptic earth orbit applicable to satellite attitude dynamics during pitching libration
22 p4125 A70-43437

Baseline length and orientation of closely coorbiting satellites estimated by combined onboard sensor and ground tracking data
[AIAA PAPER 70-39] 23 p4243 A70-44505

Recoverable stages for satellites low to stationary orbital transfer, taking costs into account
23 p4245 A70-44671

Parameter optimization of gravity gradient stabilized satellite in circular orbit, considering minimum transition time and eccentricity oscillation
23 p4264 A70-45014

Rapid satellite orbit prediction program by numerical integration including oblateness squared and radiation pressure effects over long time spans
24 p4406 A70-45528

Satellite orbital element values and perturbation parameters from incomplete element system, using maximum likelihood principle
24 p4406 A70-45529

Satellite orbital elements determination by differential correction procedure, considering observation stations distribution influence on accuracy
24 p4406 A70-45530

Satellite orbital elements calculation using ellipsoidal harmonics for geopotential representation
24 p4406 A70-45531

Lunar mass and gravitational fields determined from lunar satellite dynamics
24 p4407 A70-45533

GEOS A and OGO-4 satellite orbits and trajectory analysis using Definitive Orbit Determination System, discussing tracking stations error role
24 p4407 A70-45536

Error analysis of satellite orbits obtained by synchronous satellites range and range rate measurements
24 p4407 A70-45539

Resonant satellites geodesy, determining orbit perturbation and gravity constant via mean Kepler elements high speed analysis
24 p4408 A70-45540

Echo 1 satellite orbital acceleration correlated with solar activity, determining atmospheric density from drag observations using PERLO computer program
24 p4408 A70-45552

Upper atmosphere diurnal, annual and solar activity induced density variations effects on satellite orbits
24 p4408 A70-45553

Atmosphere and earth-reflected solar radiation pressure effects on high altitude satellite orbits
24 p4408 A70-45555

Balloon satellites orbital accelerations, considering effects due to air drag, solar radiation pressure and spin
24 p4409 A70-45557

Echo 1 and PAGEOS 1 orbital elements variations, determining perturbing effects of earth albedo radiation pressure
24 p4409 A70-45558

SATELLITE ORIENTATION

Satellite triangulations scale and orientation control, describing terrestrial methods of geodetic bases determination
02 p0254 A70-11755

Synchronous satellite attitude measurement during early flight and operating conditions, describing PAS satellite attitude sensor configurations
03 p0581 A70-13844

Satellites gravity-gradient stabilization by flywheels in elliptical orbits, designing control system for orientation and optimal motion damping
03 p0582 A70-14321

Spacecraft orientation control without measuring vehicle angular velocity based on transient response and oscillations damping effectiveness
04 p0760 A70-14428

Pulsed plasma and ion microthrusters providing satellite attitude and position control
05 p0896 A70-16119

Attitude performance of GEOS 2 gravity gradient spacecraft, discussing prelaunch design and post-launch analyses
06 p1154 A70-17162

Solar, albedo and earth thermal radiations absorbed by partially obscured spacecraft calculated on digital computer for various orbital positions
06 p1173 A70-17556

Instantaneous and integral solar irradiance of earth oriented satellite surface, noting solar illumination nomogram representation
06 p1155 A70-17893

Baseline length and orientation of closely co-orbiting satellites estimated by combined onboard sensor and ground tracking data
[AIAA PAPER 70-39] 06 p1146 A70-18186

Aeros satellite active magnetic position control system of axis and spin noting design and operation
[DGLR-69-056] 07 p1393 A70-19148

Stationary satellite perturbed motion calculations, assuming small initial orbital eccentricity and inclination and revolution period close to that of earth
07 p1386 A70-19485

Optimal longitude rendezvous for geostationary satellite by using inertially fixed orientation thrust for performing final positioning
[ONERA-TP-801] 10 p1941 A70-24541

Gravity gradient satellites equilibrium attitude error analysis showing relative effects of error sources
10 p1951 A70-24825

Satellite orientation by determining rotation parameters about centers of mass with respect to certain coordinates
11 p2128 A70-26782

Proton 2 satellite orientation and motion about center of mass determined from telemetric data analysis under aerodynamic moment
11 p2128 A70-26783

- Satellite aerodynamic characteristics, considering orbital position and attitude of cylindrical body and separate plate
11 p1218 A70-26795
 - Artificial earth satellites orientation determined by onboard telemetric measurements, constructing model for rotational motion around center of mass
12 p2314 A70-28255
 - Elektron 2 and 4 satellites orientation based on onboard solar and magnetic sensors
12 p2314 A70-28256
 - Electromagnetic control system for spin rate and axis orientation of ISIS ionospheric research satellites, describing design parameters
13 p2501 A70-28414
 - Spacecraft orientation control without measuring vehicle angular velocity based on transient response and oscillations damping effectiveness
13 p2503 A70-28453
 - Orbiting gyrostats equilibrium orientations under gravitational torques, considering internal angular momentum effects
14 p2655 A70-31364
 - Attitude dynamics of slowly spinning axisymmetric satellites under influence of gravity gradient torques, using analytical and numerical techniques
15 p2809 A70-31778
 - Spin stabilized Project Scanner spacecraft attitude determination by star mapping technique, describing optics, photomultiplier, reticle, electronics and sun shield
15 p2772 A70-31791
 - Stationary satellite perturbed motion calculations, assuming small initial orbital eccentricity and inclination and revolution period close to that of earth
15 p2805 A70-32730
 - Holographic device for satellite attitude determination, providing three axis reference information in analog or digital form from single star field sampling
16 p2946 A70-33158
 - Scanning celestial attitude determination system /SCADS/, providing triaxial information for earth stabilized satellites
16 p2946 A70-33159
 - Manned and unmanned orbital space facilities pointing and stability requirements, noting application to stellar and solar astronomy, earth observations, etc
16 p2979 A70-34068
 - Spin stabilized satellite reorientation, using magnetic dipole interaction with geomagnetic field
17 p3179 A70-35287
 - Satellite optimal guidance, discussing gyroscope application for stabilization and orientation control
17 p3181 A70-35691
 - Optimal orientation control of axisymmetric rotating space vehicle, using cyclic sliding mode theory
18 p3332 A70-36162
 - Nonspinning symmetrical satellite in circular orbit, analyzing laterally oriented rotor effect on attitude stability
19 p3533 A70-38340
 - Spacecraft principal inertial axis orientation estimation, comparing tangent 2 theta method with eigenvalue solution
20 p3660 A70-40361
 - Space vehicles dimensions effects on working fluid mass and power required for orientation
21 p3927 A70-40826
 - Artificial earth satellite orbit perigee motion, calculating perturbation effect due to gravitational and magnetic fields on orientation and rotation
21 p3884 A70-40843
 - Baseline length and orientation of closely co-orbiting satellites estimated by combined onboard sensor and ground tracking data
23 p4243 A70-44505
- SATELLITE PERTURBATION**
- Collection of articles on satellite observations, Number 8
02 p0361 A70-11751
 - Secular and short period perturbations calculation of satellite orbital elements under action of solar radiation pressure
02 p0362 A70-11763
 - Geomagnetic field influence on satellite motion for various angles between field vector and satellite angular velocity vector
03 p0563 A70-13180
 - Geopotential zonal harmonic coefficients determined from satellite orbit perturbations, using spherical harmonics orthogonality
05 p0840 A70-16639
 - Second order secular perturbations formulas of distant earth satellite motion valid for nearly circular orbits with small inclination to ecliptic plane
06 p1141 A70-17823
 - Stochastic Liapunov stability of satellite motion influenced by aerodynamic and gravity gradient torques, considering atmospheric density uncertainty
06 p1159 A70-18185
 - Stationary satellite perturbed motion calculations, assuming small initial orbital eccentricity and inclination and revolution period close to that of earth
07 p1386 A70-19485
 - Planetary satellites perturbation by sun for elliptical solar orbit, applying Zeipel method to equations of motion
09 p1754 A70-22480
 - Earth shadow effect on solar radiation pressure induced short periodic perturbations of satellite orbits
09 p1761 A70-23054
 - Satellite motion in lunar orbit by von Zeipel method, considering perturbations due to nonspherical lunar gravity field and earth and solar attraction
10 p1939 A70-24186
 - Geopotential resonance effects on low altitude satellites orbit determination, analyzing GEOS 2 orbit variations to determine even-degree coefficients
10 p1939 A70-24189
 - Small plane perturbations stability losses in uniform rectilinear motion of nonrigid deformable rocket, using slender bodies pressure theory
10 p1950 A70-24528
 - Satellite orbit prediction using computer program based on first order secular node-to-node drag perturbations
10 p1943 A70-24822
 - Diffusion processes on multidimensional cylindrical phase space for studying stochastic processes for physical systems with angular measurements, developing model for satellite under torque
12 p2273 A70-28067
 - Aerodynamic moment on satellite with asymmetrically positioned solar cell platforms, analyzing motion around center of mass for diffuse scattering flow
12 p2314 A70-28254
 - Tesseral and sectorial harmonics effect on satellite perturbations using numerical integration
13 p2494 A70-29531
 - First order node to node satellite orbital elements perturbations due to arbitrary zonal geopotential harmonic, determining computation methods and time
14 p2638 A70-30703
 - Synchronous satellite orbits determination using mathematical model for simulating gravitational perturbations induced by terrestrial globe and foreign bodies
14 p2651 A70-31279
 - Stationary satellite perturbed motion calculations, assuming small initial orbital eccentricity and inclination and revolution period close to that of earth
15 p2805 A70-32730
 - Artificial planetary satellites long term orbital evolution under strong perturbations, considering solar and lunar gravitational effects
17 p3155 A70-34779
 - Satellite structural vibration damping material and methods, discussing high polymer synthetics and viscoelastic laminae and damping systems data
19 p3533 A70-38291
 - Artificial earth satellite orbit perigee motion, calculating perturbation effect due to gravitational and magnetic fields on orientation and rotation
21 p3884 A70-40843
 - Satellites with many flexibly coupled rigid bodies, calculating libration upper bounds for predicting perturbation and stability
23 p4262 A70-44682
 - Balloon satellite perturbations in orbital period involving air drag, lunar gravity and solar and terrestrial radiation pressures
24 p4414 A70-45358
 - Short period lunar perturbation on satellites by computer program with Fortran statements, considering errors, program output and table driven algebraic processors
24 p4406 A70-45532
 - Solar and terrestrial perturbations on lunar satellite calculated by Brown theory
24 p4407 A70-45534
 - Geophysical parameters from artificial earth satellite orbital elements evolution data, discussing atmospheric density and zonal harmonics
24 p4330 A70-45551
 - Upper atmosphere diurnal, annual and solar activity induced density variations effects on satellite orbits
24 p4408 A70-45553
 - Radiation pressure effects on artificial satellite motion, including earth shadow perturbation
24 p4408 A70-45554
 - Satellite orbit perturbation due to earth reflected or reradiated solar radiation pressure
24 p4409 A70-45556
- SATELLITE RENDEZVOUS**
- U ORBITAL RENDEZVOUS**
- SATELLITE ROTATION**
- Gyro stabilized satellite steady state motions in Newtonian force field having displaced satellite center of mass orbital plane relative to center of attraction
01 p0198 A70-11577
 - Satellite 1965-11-4 /Cosmos 54 rocket/ braking, rotation periods and revolution from INTEROBS and SPIN observations, comparing K-index and solar activity parameters
02 p0363 A70-11768
 - Satellite rotation periods determination accuracy from photometric observation data improved by determining initial and terminal moments of maximum brightness
02 p0255 A70-11769
 - Solar radiation influence on Alouette satellite spin behavior with long flexible antennae, taking into account sunlight/shadow history and solar vector inclination
02 p0380 A70-11852
 - Artificial satellite rotation study on basis of SPIN program photometric data - Conference, Kishinev, Moldavian SSR, September 1968
03 p0443 A70-13176
 - Rotational stability of spacecraft with hinged inelastic rods determined in first approximation from motion equations
04 p0759 A70-14426
 - Optimal iterative weighted least squares estimation of rotation-coupled flexural oscillations of boom stabilized satellites in earth orbits
04 p0763 A70-15413
 - Single degree of freedom nutation damper motion instability on dual spin stabilized spacecraft ascribed to parametric excitation by transverse angular rates
04 p0764 A70-15585
 - Magnetic damping of homogeneous cylindrical satellite rotation about transverse axis
05 p0924 A70-16751
 - Spin decay from telemetered flight data of Explorer 20 compared with calculation based on solar influence theory
07 p1394 A70-19721
 - Libration limits of satellite in Keplerian circular orbit, estimating potential energy of perturbing forces
08 p1582 A70-20967
 - Nutation damping in gyrostat stabilization for multispin satellites in terms of energy momentum and damping torque arguments
11 p2119 A70-25357
 - Capillary barriers to provide propellant positioning, expulsion capability and slosh damping for spacecraft propulsion systems during rotational maneuvers
11 p2123 A70-26119
 - Errors in determining controlled satellite rotation periods, proposing scheme for corrected trajectory calculation of small eccentricity orbits
11 p2118 A70-26779
 - Satellite orientation by determining rotation parameters about centers of mass with respect to certain coordinates
11 p2128 A70-26782
 - Proton 2 satellite orientation and motion about center of mass determined from telemetric data analysis under aerodynamic moment
11 p2128 A70-26783
 - Motion stability of rapidly spinning satellite, discussing elastic booms effect
11 p2128 A70-26784
 - Linear periodic coefficient differential equations stability analysis by infinite determinate method, considering applications to damped mechanical systems motion and dual spin satellite
12 p2261 A70-27813
 - Aerodynamic moment on satellite with asymmetrically positioned solar cell platforms, analyzing motion around center of mass for diffuse scattering flow
12 p2314 A70-28254
 - Artificial earth satellites orientation determined by onboard telemetric measurements, constructing model for rotational motion around center of mass
12 p2314 A70-28255
 - Spinning sun oriented satellite using magnetic coil around spin axis for attitude control, detailing design
13 p2502 A70-28439
 - Rotational stability of spacecraft with hinged inelastic rods determined in first approximation from motion equations
13 p2503 A70-28451
 - Earth satellite motion about center of mass, examining effects of random variations in atmospheric density, geomagnetic intensity and solar radiation
15 p2809 A70-31650
 - Attitude dynamics of slowly spinning axisymmetric satellites under influence of gravity gradient torques, using analytical and numerical techniques
15 p2809 A70-31778
 - Book on celestial mechanics covering perturbation methods, two body problems, astronomical coordinates, orbital mechanics, satellite rotation, gravitational effects, etc
15 p2799 A70-31998
 - Ball in tube nutation damper for spinning satellite, describing design, testing and fabrication techniques for achieving low friction level
16 p2985 A70-34136
 - Balloon satellites brightness change from rotation effects, analyzing light curves
16 p2980 A70-34317
 - Dual spin satellites considered as deformable flexible gyrostats, obtaining stability criteria
17 p3177 A70-35234
 - Nonlinear three nodes analysis for thermal design of spinning spherical satellite
17 p3177 A70-35249

Japanese scientific satellite magnetic attitude and spin rate control system design and computer simulation 18 p3332 A70-36065

Liapunov stability analysis of dynamic systems described by simultaneous ordinary and partial differential equations of motion, applying to satellite spin stabilization [AIAA PAPER 70-1045] 19 p3472 A70-38860

Torque free spinning satellite with flexible appendages, investigating design parameters effects on nutational stability [AIAA PAPER 70-1046] 19 p3534 A70-38861

Libration limits of satellite in Keplerian circular orbit, estimating potential energy of perturbing forces 20 p3713 A70-39388

Freely spinning satellites gimbal and momentum wheel system, determining stable equilibrium states by analog computer simulations [AIAA PAPER 70-982] 20 p3714 A70-39547

Motion and stability of rotating connected two body space station satellite system, developing Lagrangian equations of motion and optimizing damping system parameters [AIAA PAPER 69-919] 20 p3716 A70-39678

Magnetic damper motions in rapidly spinning satellite 21 p3927 A70-40833

Artificial earth satellite orbit perigee motion, calculating perturbation effect due to gravitational and magnetic fields on orientation and rotation 21 p3884 A70-40843

Comparative stability of freely spinning satellites for arbitrary number of flexible booms in rotation plane 22 p4111 A70-43440

Spacecraft thin walled tubular booms thermal curvature time constants in relation to solar induced despin of satellites 23 p4258 A70-44521

Rotating cable-connected orbital space stations deployment dynamics, considering cable mass and motion equation 23 p4258 A70-44529

Dynamic systems stability with periodically varying parameters analyzed by Hill type infinite determinant, exemplifying helicopter rotor aeroelastic stability in forward flight 23 p4220 A70-44556

Optimal moments of inertia of rigid satellite in circular orbit by generalization of Beletskij concept, discussing libration boundaries 23 p4261 A70-44677

Freely spinning gyrostatt satellites with dissipation, deriving rotational motion equations by osculating elements method 23 p4261 A70-44681

Lunar libration amplitude estimation, using stochastic process theory 23 p4247 A70-44771

Artificial satellite motion about center of mass, considering gravitational and magnetic effects, resonance effects, motion stability, etc 24 p4415 A70-45548

Dynamics of spin-stabilized flexible satellites of long crossed dipoles or slender beams, noting Alouette and ISIS-1 spacecraft 24 p4415 A70-45549

SATELLITE TELEVISION

High power TV broadcast satellite subsystems technologies requirements, considering transmitters, power conditioners, solar arrays and component reliability [AIAA PAPER 69-1069] 01 p0194 A70-10632

TV broadcast satellite system operating with home receivers or special receivers, evaluating technological and cost factors [AIAA PAPER 68-1061] 01 p0044 A70-10831

Future phase of satellite TV programs distribution in Europe 02 p0403 A70-12645

Ranger, Surveyor and Lunar Orbiter televised and reconstructed picture quality, suggesting improvements in existing photographic systems 03 p0490 A70-13656

Satellites for meteorological and geographical studies using information from TV and IR pictures 08 p1487 A70-20716

Earth resources satellite TV cameras operating on different spectral bands, discussing data preprocessing for correlation with topographic maps 09 p1674 A70-22259

Satellite applications to TV broadcasting for developed and developing areas, considering national and international telecommunications policies 09 p1633 A70-22634

Satellite TV transmission economic, technical and practical feasibility, describing direct transmission system 09 p1634 A70-22766

Direct domestic reception of TV signals from satellites, discussing microwave components, economics and reliability 10 p1840 A70-24448

TV system for satellite antenna boom position monitoring, describing camera system and programming, imaging techniques, position calibration, etc 10 p1891 A70-24898

Software production for Brazilian Advanced Educational Technology System 11 p2152 A70-25403

Satellite distribution of TV signal over earth surface as alternative to terrestrial linkups, overcoming rain attenuation by high power spot beam [AIAA PAPER 70-454] 11 p1997 A70-25410

TV network distribution in Canada by communications satellite and terrestrial microwave links, discussing signal to noise ratios and picture quality [AIAA PAPER 70-430] 11 p1998 A70-25417

ACME hybrid airborne satellite TV and communications system for India, using airborne TV transmitters [AIAA PAPER 70-472] 11 p1998 A70-25418

Educational satellite TV for developing countries, giving model relating economic development to education and applied technology [AIAA PAPER 70-514] 11 p2152 A70-25429

Satellite ETV/ITV broadcast system, discussing frequency, receiver population, channel number, beam number, minimum cost solutions, etc [AIAA PAPER 70-452] 11 p1999 A70-25437

Satellite TV broadcast requirements impact on high power transmitter design, permitting low cost terrestrial receiving systems [AIAA PAPER 70-434] 11 p1999 A70-25450

Low cost earth station and antenna for Canadian domestic satellite, bringing color TV to northern territories [AIAA PAPER 70-432] 11 p2000 A70-25458

High power transmitters for satellites, discussing optimum configurations, supporting power subsystems, breakdown problems in space environments, etc [AIAA PAPER 70-436] 11 p2000 A70-25459

Frequency sharing between satellite-transmitted FM TV signals and terrestrially transmitted AM-VSB TV signals [AIAA PAPER 70-438] 11 p2001 A70-25467

Communications satellite for Alaska and Mountain States TV defined using computerized synthesis program [AIAA PAPER 70-453] 11 p2001 A70-25473

Dual conversion receiver for remote frequency control in satellite TV distribution system [AIAA PAPER 70-414] 11 p2002 A70-25482

Ground frequency converters for reception of NTSC color TV transmission from synchronous communication satellites, tabulating cost estimates [AIAA PAPER 70-440] 11 p2002 A70-25490

Microwave converter system for ETV satellite reception, discussing characteristics and costs for mass production [AIAA PAPER 70-439] 11 p2017 A70-25493

Multipurpose domestic satellite system design for TV distribution, discussing frequency sharing, synchronous orbit and system model 12 p2183 A70-26998

Heavy squalls observations by satellite TV and radar, considering wave disturbances at cold front 13 p2444 A70-28585

Monograph on troposphere pressure, temperature and humidity and satellite TV photographs interpretation 13 p2446 A70-29786

Meteorological satellites TV pictures processing for hydrological information, emphasizing snow photographs interpretation 14 p2601 A70-30138

TIROS weather satellite TV system providing observations to ground stations via ESSA satellites 14 p2654 A70-31148

Space research cost effectiveness in weather forecasting, TV broadcasting, space biology and medicine, geodesy, aerial and maritime navigation, earth resources, etc 15 p2811 A70-32283

Celestee TV photometer system operation on-board OAO by mathematical simulation 16 p2906 A70-33174

Earth resources technology satellite /ERTS-A/ for Eros program, producing telemetric imagery spatially correlated to earth surface 16 p2898 A70-34046

Earth resources satellite /ERS/ TV camera configurations, return beam vidicon camera characteristics and devices for TV picture reproduction on film 16 p2915 A70-34312

UN space committee discussion on rules governing direct TV broadcasting by satellite, taking into account frequency allocation, geostationary orbits, etc 17 p3201 A70-35779

International norms establishment for direct TV broadcast by satellites 17 p3201 A70-35780

Legal problems in satellite communications, emphasizing copyright, satellite television legality and protection of transmission and broadcasts 17 p3203 A70-35800

Satellite-borne UV TV system for photometric investigations of UV stars 19 p3428 A70-38456

Satellite TV cloud picture digital representation, deriving algorithms for statistical analysis of geometrical features 19 p3463 A70-38755

U.S. nationwide satellite network for multichannel community antenna TV /CATV/ operated at 12 GHz band 19 p3382 A70-38891

Earth resources satellite missions TV systems design, using vidicon as sensing element 20 p3626 A70-39052

Space law aspects of direct broadcasting satellites for TV and sound transmission 20 p3740 A70-39408

Satellites for direct radio and TV broadcasting, considering system quality and cost, network planning, frequency economy, etc 20 p3588 A70-40158

Low cost microwave receiver and antenna for instructional satellite TV broadcasting in developing nations 21 p3789 A70-41355

Ground TV station network operating with communication satellites in remote areas 23 p4159 A70-43758

SECAM video and audio color TV transmission over Molniia satellite relay path 23 p4162 A70-44091

Educational TV system via satellite, discussing social benefits for Spanish speaking countries in South America 23 p4285 A70-44602

ITOS-1 second generation meteorological satellite launched with Delta N booster, providing direct APT global readout and AVCS TV data recording for playback 23 p4259 A70-44615

Low cost microwave antenna-receiver for satellite FM TV signal reception at SHF and conversion for standard sets 23 p4164 A70-44645

TV broadcast satellites program distribution direct to home by network and by community 23 p4164 A70-44646

Juridical problems in satellite direct TV broadcasting, discussing regulation proposals submitted to UN and educational applications 24 p4430 A70-45596

OAO 2 satellite Telescope astronomical TV system, describing various developmental problems for future guidelines 24 p4415 A70-45824

SATELLITE TRACKING

Postlaunching operations putting HEOS 1 satellite into orbit, verifying subsystem functions, starting experiments and tracking for data recovery 01 p0197 A70-11117

European Space Operations Center activities in observing HEOS 1 satellite, discussing launch, data processing and S-11 experiment involving ionized Ba cloud creation 01 p0197 A70-11118

Satellite tracking antennas servo design including adaptive and compensation methods and digital computer applications 01 p0011 A70-11453

Least squares method adjusting observation functions in satellite triangulation with correlated observations 01 p0082 A70-11455

Collection of articles on satellite observations, Number 8 02 p0361 A70-11751

Satellite positions from simultaneous measurement by laser along geocentric arc usable for determining earth mass center position 02 p0253 A70-11752

Space triangulation equations based on simultaneous measurements of satellite topocentric coordinates and distances between tracking station and satellite 02 p0254 A70-11753

Satellite tracking at several stations at synchronized time to obtain satellite positions, station coordinates and to improve orbital elements accuracy 02 p0254 A70-11760

Mathematical relations and procedures for automatic satellite tracking by four axis Zeiss camera, discussing motion along small circle approximation and punch tape criteria 02 p0255 A70-11770

Automatic four axle satellite tracking camera design and operational principle, examining lens aberration 02 p0294 A70-11771

Satellite topocentric equatorial coordinates determination from photographic observations 02 p0363 A70-11773

Automatic camera theodolite at Sophia satellite tracking station, discussing instrument constants 02 p0273 A70-11774

Satellite mounted mm wave parabolic dish antenna for tracking communication satellite in synchronous orbit

02 p0392 A70-11933

Laser position finding of satellites fitted with corner reflectors, discussing atmospheric attenuation and applications to global triangulation and gravitational field measurements

02 p0256 A70-12083

Laser range finding by mobile missile station compared with geodesic satellite telemetry by ground station

02 p0312 A70-12212

Q switched and high energy pulse laser devices for location of satellite photographed by night against background of stars, including optimization in noise

[ONERA-TP-753] 02 p0313 A70-12369

Digital onboard telecommunications and tracking equipment based on Dioscures two satellite system for L band operation

03 p0442 A70-12990

Visual photometric tracking data obtained in SPIN program for satellites 1965-II-4 and 1965-53-6 at Kishinev station

03 p0444 A70-13181

Earth satellite tracking data reduction for determining geodetic ground nets, examining errors in triangulation procedures

03 p0445 A70-13184

Gravimetric and satellite tracking data reduction for determining coefficients in mathematical expansion representing earth gravitational field

03 p0473 A70-13189

Satellite surveys and astronomic-geodetic nets for joint terrestrial, space triangulation and gravimetric measurements, including laser distance determination

03 p0445 A70-13191

Great circle vector formula in space triangulation, discussing topocentric and geocentric position of satellite and tracking stations and absolute distance determination

03 p0445 A70-13193

Space triangulation net using direction and distance measurements from satellite photographic and Doppler observations, including tracking data leveling

03 p0446 A70-13194

Satellite optical tracking data in space geodesy, determining stations position from minimum number of stations and observations with time errors

03 p0446 A70-13195

Ruby laser experiment in illuminating satellites equipped with retroreflectors to determine satellite position in space from range and photographic data

03 p0450 A70-13674

Directional transponders for telemetry command, tracking and communications in retrodirective communication satellites

03 p0457 A70-13838

Potential determination from gravity disturbances along fixed direction in analysis of residuals of Doppler tracking of Lunar Orbiter satellites for moon gravity field

03 p0577 A70-14177

Laser ranging systems used with retroreflecting satellites in geodetic and geophysical applications

05 p0815 A70-16691

Triaxial universal astrometric instrument for tracking artificial satellite path with eyepiece crosswire, considering instrument errors

05 p0851 A70-16698

Gravity anomalies of moon mapped by time differentiation of Doppler-tracked satellite velocities, noting isostatic equilibrium

05 p0915 A70-16827

Baseline length and orientation of closely co-orbiting satellites estimated by combined onboard sensor and ground tracking data

[AIAA PAPER 70-39] 06 p1146 A70-18186

Satellite radio tracking systems noting interferometer most suitable for accuracy and maintenance

08 p1463 A70-21712

SPOT navigation satellite system for near instantaneous fixes or continuous tracks providing height, velocity and automatic guidance and control signals

09 p1723 A70-23041

Sequential collation of range/SECOR/ satellite tracking system using electronic phase comparison for measuring ground station-satellite distance

09 p1724 A70-23047

Satellite photograph equatorial coordinates dependence on magnitude of evaluated region, objective distortion and transformation methods

09 p1679 A70-23056

Satellites equatorial topocentric coordinates determination from photographic observations

09 p1763 A70-23328

Short arc method and spatial fitting of orbit in satellite triangulation, establishing sequential order between methods

09 p1670 A70-23440

Telemetry tracking and command antenna array of Central German Ground Station for satellite communication [DFVLR-SONDDR-52]

11 p2017 A70-25800

Satellites photographic positions accuracy compared with stars based on stellar coordinates, investigating causes of difference

11 p2008 A70-26198

Satellite position fixing based on electromagnetic angle measurements from observation station, using least squares method

14 p2612 A70-30187

French EOLE tracking satellite-balloon network for global atmospheric data, describing satellite and electronic instrument package

14 p2611 A70-31154

Report to COSPAR on space research covering satellite tracking telemetry, Apt, meteorology, cosmic rays, solar activity and international cooperative programs, etc

15 p2829 A70-31709

Report to COSPAR on Czechoslovakian space research /1969/ covering satellite telemetry and tracking, proton flares, aeronomy, etc

15 p2829 A70-31710

Report to COSPAR on space exploration research in Poland including satellite tracking, geodesy, meteorology and aerospace medicine

15 p2830 A70-31721

Phased array monopulse autotracking, radiointerferometer and Doppler frequency methods for radio tracking systems for artificial satellite orbits

15 p2697 A70-31836

Earth-satellite range measurements using broadband pseudonoise modulation and delay lock tracking method

15 p2705 A70-32724

Laser range finding to satellite equipped with retroreflectors, noting accuracy dependence on signal strength

16 p2925 A70-33021

Automatic speech recognition and tracking techniques of moving objects, considering applicability to processing data from earth resources satellites

16 p2871 A70-34313

Scientific satellites orbit determination and improvement procedures for tracking system based on Doppler frequency and angular measurements

17 p3046 A70-35280

Weather occultation satellite orbit determination by radio wave measurements between master and slave satellites, formulating mathematical model

[AIAA PAPER 70-1067] 19 p3529 A70-38880

Orbit determination accuracy in synchronous satellite tracking analysis, using weighted least squares method

[AIAA PAPER 70-1068] 19 p3529 A70-38881

Artificial satellite position visual estimates based on geometric relationship to reference stars pair accuracy

19 p3531 A70-38946

Timing systems using Cs frequency standard for satellite tracking

21 p3828 A70-41697

Satellite tracking camera lens-distortion coefficient from comparison of standard stellar and measured X-Y coordinates

22 p4029 A70-42596

Nautical loci of constant azimuth of artificial satellite at corridor height in circular orbit at arbitrary inclination, using gyroscope and radio sextant

22 p4068 A70-42664

VHF geostationary satellite ranging and range correction systems, calculating second-order ionospheric delay effects on position error

22 p4068 A70-43590

Baseline length and orientation of closely co-orbiting satellites estimated by combined onboard sensor and ground tracking data

[AIAA PAPER 70-39] 23 p4243 A70-44505

Laser measurements in semidynamic space geodesy on D1-D satellite using Mediterranean stations

24 p4352 A70-45541

SATELLITE TRANSMISSION

High power TV broadcast satellite subsystems technologies requirements, considering transmitters, power conditioners, solar arrays and component reliability

[AIAA PAPER 69-1069] 01 p0194 A70-10632

Numeric keyboard CRT display for weather data acquisition from ships at sea, utilizing ATS-3 satellite as transmission medium

01 p0048 A70-11279

Ionospheric electron concentration irregularities via satellite signal scintillation analysis, using radio wave diffraction theory

02 p0258 A70-12562

Magnetoionic mode coupling in satellite transmissions through ionosphere near transverse region, showing diurnal variations and error of electron content

02 p0259 A70-12563

Application of atmospheric studies to satellite transmissions - Conference, Bedford, Mass., September 1969

02 p0259 A70-12564

Channel constraints on multiple access systems obtained from airborne propagation tests via satellites, studying disparities in received signal strength

02 p0260 A70-12569

Canary Bird synchronous satellite radio signal transmissions scintillations from recordings, noting diurnal scintillation pattern

02 p0260 A70-12573

Wideband satellites bandwidth and aperture limits direct measurement based on ground monitoring of CW signals, taking into account ionospheric dispersion

02 p0261 A70-12577

Future phase of satellite TV programs distribution in Europe

02 p0403 A70-12645

Traveling ionospheric disturbances from signatures left in columnar electron content records obtained by measuring signal Faraday rotation angle from geostationary satellite

03 p0477 A70-13991

Data transmission from automatic space stations on Mars and Venus, considering relaying via artificial planet satellite or direct transmission to ground station

04 p0648 A70-14931

Electron density profiles along OGO 1 orbit portions calculated by measuring harmonic radio beacon transmissions differential Doppler frequencies and Faraday polarization rotation angle

04 p0741 A70-15118

Magnetoionic mode coupling in satellite transmissions through ionosphere near transverse region, using electron concentration profiles for night and daytime estimates

04 p0650 A70-15131

ESRO 1 thermal behavior, discussing trajectory effects, onboard temperature measurement, data storage, data transmission, telemetered data and data comparison

04 p0762 A70-15164

Frequency bandwidth reduction for geophysical data transmission from satellites or lunar stations by time correlation of signal and transmission channel band changes

05 p0847 A70-15968

Second antenna at Pleumeur-Bodou /France/ for satellite transmissions reception in Intelsat network program

05 p0826 A70-15981

Weather data communication, discussing transmission of radar, polar satellite and ATS satellite data to processing center and forecasts dissemination to public media

05 p0814 A70-16327

Microelectronic L-band phase-lock loop receiver for data transmission between earth stations and satellites

06 p1017 A70-17338

Wideband transmission of photographic reconnaissance information over long distances using Initial Defense Communication Satellite Program satellites

06 p1006 A70-17346

Rate of change of radio ray path length for transionospheric satellite VHF signals determined from Doppler and Faraday effect analyses

06 p1008 A70-17578

Ionosphere disturbances due to high altitude thermonuclear explosions, discussing experimental proof by cosmos satellites short wave transmitter radio signal scintillation statistical evaluation

06 p1057 A70-17888

Satellite signal scintillation phenomenon morphological study and relationship to ionospheric irregularities

07 p1234 A70-19194

Ionospheric inhomogeneities measured by Explorer 22 radio signals emphasizing satellite scintillation

07 p1265 A70-19195

Focusing and saturation effects in radio star and satellite signal scintillations based on diffraction and refraction theories

07 p1271 A70-20157

Ionospheric electron content and concentration variations analysis based on data of radio waves propagating from satellite, considering Doppler shift and Faraday effect

07 p1237 A70-20427

Ionospheric electron content estimated from measurements of Faraday rotation of VHF signals from geostationary satellite

08 p1489 A70-21388

Signal properties of VHF satellite-to-aircraft communications link, discussing results of ATS tests

08 p1463 A70-21779

Earth resources program data management system, discussing mission control, processing and distribution of data from satellite vidicon cameras and multispectral line sensors

[AIAA PAPER 70-321] 09 p1792 A70-22854

Multiband high resolution spaceborne imagery telemetry with optical mechanical scanners from earth orbiting satellites in earth resource applications

[AIAA PAPER 70-314] 09 p1677 A70-22873

Aircraft and ship position surveillance by satellites system with independent capability and undelayed voice and digital communication

09 p1723 A70-23043

Ionospheric irregularities investigated by rocket- and satellite-borne transmitters, obtaining ionization

profiles from amplitude, phase and polarization of radio waves

09 p1669 A70-23273

Polarization diversity reception effects on VHF telemetry signal from low altitude satellites

10 p1832 A70-23919

SNR and system error rate prediction for coherent nonlinear satellite channels based on bounding techniques

10 p1836 A70-24341

Cost analysis for satellite data system determined for bit rates range and break-even distances

10 p1838 A70-24361

Soviet book on satellite communication systems for telephone and TV transmission covering orbit selection, signal level calculation, channel characteristics for frequency bands, etc

10 p1840 A70-24378

Ionospheric electron content diurnal, latitudinal variations and equivalent slab thickness determined from observing satellite signals Faraday fading

10 p1874 A70-24426

Plasmaspheric columnar electron content determination up to plasmapause by ATS-3 beacon transmitter and combining differential Doppler frequency and Faraday rotation angle methods

10 p1874 A70-24430

Direct domestic reception of TV signals from satellites, discussing microwave components, economics and reliability

10 p1840 A70-24448

Ionospheric irregularities showing dispersive motions from systematic skewness in cross correlation functions for satellite scintillations at spaced receivers

10 p1881 A70-24810

Direct broadcast voice satellite for educational system improvement, discussing lesson formatting, ground receiver/programmer, multichannel capacity, etc

11 p1998 A70-25423

Digital satellite communications systems, discussing time division multiplexing, steerable beam antennas and satellite-to-satellite transmission

11 p2003 A70-25492

Polar ionosphere inhomogeneous electron concentration by analyzing satellite signal amplitude fluctuations received by spaced interferometers

11 p2042 A70-25528

Fixed information bit rate approach to coding over space channel introducing redundancy and check digits for error probability

11 p2014 A70-26223

Fluctuations of polarization induced fading periods in short wave transmissions of Soviet earth satellites, showing relation to ionospheric inhomogeneities

11 p2047 A70-26788

Low latitude scintillations from satellite transmission scintillations correlation with solar activity spread F, electron content and ionospheric irregularities

13 p2397 A70-29189

Satellite scintillation index variation with zenith angle and azimuth at ground station

14 p2574 A70-30739

Electronically tracking antenna system for satellite reception in VHF range suitable for unmanned receiving stations

14 p2558 A70-31196

Prolonged upper ionospheric observations from Sputnik 3, Transit 4A and Explorer 22 signals Faraday fading and phase shifts, showing electron content dependence on solar activity

15 p2731 A70-32093

Ionospheric radio wave propagation from rocket and satellite signal transmission using Faraday and Doppler effects, phase delay and refraction measurements

15 p2698 A70-32095

Ionospheric electron content measurement during solar eclipse of 7 March 1970, using VHF radio waves from geostationary satellites

16 p2897 A70-33830

Ionospheric electron density during solar eclipse of 7 March 1970, using Faraday rotation measurements of geostationary satellites VHF transmissions

16 p2898 A70-33831

F region integrated electron density response during solar eclipse of 7 March 1970, using Faraday rotation of linearly polarized signals from ATS 3

16 p2898 A70-33835

Range and velocity components for ray paths between tracking and data relay satellite and user communication satellite

16 p2866 A70-34073

Receiver for artificial satellite transmission and optical tracking time signals, using crossed dipole directional antenna

16 p2867 A70-34303

Satellite broadcasting frequency resources, discussing interference, frequency sharing, antenna transmitting and receiving patterns, etc

17 p3046 A70-35271

Atmospheric studies application to satellite transmissions - USAF Conference, Boston, September 1969

20 p3589 A70-40476

Faraday rotation of radio beacon satellite signals during traveling ionospheric disturbances simulated for spaced ground stations

20 p3590 A70-40481

Satellite wideband transmission of ionosphere data, monitoring amplitude and phase of phase-coherent CW signals from geostationary satellite

20 p3590 A70-40483

Ionosphere and magnetosphere total electron content from beacon method of measuring difference-differential-doppler (DDD) and Faraday effects via synchronous satellite signal frequencies

20 p3590 A70-40484

Scintillation LF observations with synchronous satellite radio signals at low latitude station, noting magnetic activity effects on night and day scintillations

20 p3590 A70-40488

High scintillation indices associated with vertical spreading of sporadic E layer from minute-by-minute ionograms and signal amplitude recordings from Explorer 22 satellite

20 p3624 A70-40489

High latitude F region irregularity structure during magnetic storm from multistation scintillation observations of ATS 3 transmission

20 p3624 A70-40490

Ionospheric electron density disturbance heights measured via radio signal scintillation from earth satellite, using spaced receiver method

20 p3590 A70-40491

Ionospheric disturbances heights at subauroral latitude from Explorer 22 satellite beacon signals recorded at spaced receivers

20 p3624 A70-40492

Long range low loss earth-detached propagation paths in lower ionosphere indicated via OV4-1 satellite experiment on guided ionospheric propagation

20 p3591 A70-40494

Ionospheric ducting of satellite beacon signals observed on Orbis Cal satellite experiment

20 p3591 A70-40495

Polar ionosphere inhomogeneous electron concentration by analyzing satellite signal amplitude fluctuations received by spaced interferometers

21 p3819 A70-41278

Communications satellite carrier instrumentation, using computer controlled frequency shift radiometer for power monitoring

21 p3826 A70-41345

ATS-5 spacecraft L band propagation performance, describing up and downlink test methods

21 p3790 A70-41363

Aeolus A satellite for position fixing and automatic meteorological signal transmission in link with balloons for tropospheric observation

22 p4068 A70-42665

F region ionospheric disturbances size and shape from radio amplitude and phase scintillations in satellite transmission to ground stations

23 p4187 A70-43879

SATELLITE-BORNE PHOTOGRAPHY

Photogeological mapping at medium to small scales, comparing satellite transparencies with aerial photographs

02 p0298 A70-12202

Simultaneous ground and space triangulation procedures, recommending use of satellite photographic observations for error reduction

03 p0445 A70-13185

Martian orbital photographic missions objectives and sensors realizable capabilities, discussing relationships between orbital parameters and imaging systems constraints

03 p0490 A70-13663

Earth resources applications of Apollo 6 photography, describing camera system and photographic coverage

03 p0474 A70-13672

Land use mapping of southwestern U.S. using photographs from Apollo and Gemini missions

[AAS PAPER 69-576] 04 p0676 A70-14640

Earth photographs for geotectonic research from manned orbiting spacecraft, describing Apollo and Gemini belts

[AAS PAPER 69-579] 04 p0677 A70-14663

Geological contribution of satellite photography, discussing synoptic surveyability of vast areas and reduced scale maps of little known remote territories

05 p0837 A70-16073

Sea surface sunglint pattern irregularities in earth orbiting satellite photographs, observing dark patches

05 p0838 A70-16152

Spiral cloud vortex model in occluded extratropical cyclone constructed using atmospheric dynamics equations and satellite photographs

05 p0879 A70-16642

Phobos and Deimos photographic reconnaissance feasibility during 1971 orbiter and 1973 Viking missions, studying trajectory

[AIAA PAPER 70-60] 06 p1146 A70-18191

Remote sensors application to direct and indirect fish detection in fishery research, using aerial and Gemini photography

07 p1262 A70-18957

Three vector coplanarity equations for space geodetic triangulation grid, discussing role of satellite photographic observation

09 p1667 A70-22488

Multispectral point scan camera system as remote sensor for Earth Resources Satellite, noting real time automatic data processing and interpretation

[AIAA PAPER 70-319] 09 p1677 A70-22867

Satellite photographs for geological mapping and research assessed against interpretation of field data and conventional aerial photographs

10 p1876 A70-24640

Simple layer model of geopotential from satellite-borne Baker-Nunn camera observations

10 p1876 A70-24645

Photogrammetric map compilation from orbital satellite photographs, with fictitious and ground coordinates generated by electronic computer, discussing error sources

10 p1890 A70-24728

Cloud cover effect on earth photographing space missions by Monte Carlo computer simulation, using worldwide cloud statistics

11 p2075 A70-25600

Satellite photographic plate reduction - COSPAR Conference, Prague, April 1968

11 p2006 A70-26179

Classical astronomical photographic methods for reducing satellite photographs taking into account linear and nonlinear methods, analyzing random errors

11 p2006 A70-26184

Reduction of satellite photographic data using transformation functions

11 p2007 A70-26186

Plate reduction method for Schmidt satellite camera, considering satellite position, distortion parameters, etc

11 p2007 A70-26193

Data compression for telemetry transmission with sample choice based on time-varying stream slope thresholds illustrated for Ranger photograph

11 p2010 A70-26305

Lunar surface mapping and far side gravity field probing by satellite photogrammetry

12 p2308 A70-27874

Earth global photography by satellites, discussing photointerpretation

12 p2227 A70-28270

Cyclone cloud vortex evolution from satellite photographs, examining reasons for onset and disintegration

13 p2444 A70-28588

Satellite photographs interpretation for cloud types and patterns with allowance for transmission characteristics, image cut-off at corners and sun angle and glint

13 p2394 A70-28786

System design for IR imaging radiometer from synchronous altitude satellite, considering spacecraft dynamics, detectors and cooling

14 p2586 A70-30974

Lunar soil and rocks photometric and polarimetric properties from high resolution Surveyor pictures

14 p2644 A70-31054

Long term effects model evaluation of meteoritic impact against lunar surface compared with analyses of Lunar Orbiter photographs

14 p2645 A70-31062

Cloud distribution and optimal satellite picture foreshortening for global meteorological analysis of atmosphere, using Zond 7 photograph

15 p2771 A70-32110

Onboard IR receiver and ground photorecorder for Meteor satellite cloud tracking, using computer processed data

15 p2738 A70-32112

Anomalous dark areas in sunglint patterns from ATS photographs, considering water temperature effect on ocean surface conditions

16 p2897 A70-33725

ATS spin scan cloud cameras mechanical design and operation

16 p2914 A70-34149

Shallow water bottom biota, sediments and morphology determination by aerial and satellite photography

17 p3079 A70-35620

Surveyor 7 TV system in photon integration mode, analyzing slow scan vidicon storage characteristics and dark current limitations

[SMPTE PAPER 105-72] 17 p3095 A70-35635

Cloud-free earth areas determined via reflected radiance measurements from ATS 3 cloud camera

17 p3133 A70-35930

Satellite-borne UV TV system for photometric investigations of UV stars

19 p3428 A70-38456

Multispectral photography in earth resources research, noting three return beam vidicons for technology satellites

20 p3628 A70-39128

Synoptic surface and upper air analysis and APT mosaics of meridional circulation over Mediterranean by remote satellite images

21 p3846 A70-41399

Ocean swell wavelength and propagation direction measurements, using Fourier optical analysis of Apollo 7 space photography

22 p4029 A70-42766

Ocean roughness determination from satellite photographs sunglint patterns, indicating surface wind speeds

22 p4014 A70-42770

Phobos and Deimos photographic reconnaissance feasibility during 1971 Orbiter and 1973 Viking missions, studying trajectory

23 p4243 A70-44507

North Carolina continental shelf discolored water origin, movement and dissipation from Apollo 9 photograph interpretation

24 p4329 A70-45361

SATELLITE-BORNE RADAR

Satellite coherent side-looking imaging radars producing radar maps with photographic-type quality

11 p2005 A70-26038

Pulse compression for geodesy satellite radar altimeter, considering tradeoff based on system accuracy, power and life

16 p2911 A70-33715

SATELLITES

NT ACTIVE SATELLITES
NT AEROS SATELLITE
NT ALOUETTE SATELLITES
NT ALOUETTE 1 SATELLITE
NT ALOUETTE 2 SATELLITE
NT APPLICATIONS TECHNOLOGY SATELLITES

NT ARIEL SATELLITES
NT ARIEL 3 SATELLITE
NT ARTIFICIAL SATELLITES
NT ATS 1
NT ATS 3
NT ATS 5

NT AZUR SATELLITE
NT BEACON SATELLITES
NT BIOSATELLITES
NT COMMUNICATION SATELLITES
NT COSMOS SATELLITES
NT COSMOS 5 SATELLITE
NT COSMOS 44 SATELLITE
NT COSMOS 110 SATELLITE
NT COSMOS 149 SATELLITE

NT D-1 SATELLITE
NT DEIMOS
NT DIADEME SATELLITE
NT DODGE SATELLITE
NT EARLY BIRD SATELLITES

NT EARTH RESOURCES TECHNOLOGY SATELLITES
NT EARTH SATELLITES
NT ECHO SATELLITES
NT ECHO 1 SATELLITE
NT ECHO 2 SATELLITE
NT ELEKTRON 2 SATELLITE
NT ELEKTRON 4 SATELLITE

NT ENVIRONMENTAL RESEARCH SATELLITES
NT EOSS
NT ESRO 1 SATELLITE
NT ESRO 2 SATELLITE
NT ESSA SATELLITES
NT ESSA 9 SATELLITE

NT EXPLORER 1 SATELLITE
NT EXPLORER 4 SATELLITE
NT EXPLORER 17 SATELLITE
NT EXPLORER 19 SATELLITE
NT EXPLORER 20 SATELLITE
NT EXPLORER 22 SATELLITE
NT EXPLORER 31 SATELLITE
NT EXPLORER 32 SATELLITE
NT EXPLORER 33 SATELLITE
NT EXPLORER 38 SATELLITE
NT EXPLORER 40 SATELLITE

NT GEODETIC SATELLITES
NT GEOPHYSICAL SATELLITES
NT GEOS 1 SATELLITE
NT GEOS 2 SATELLITE
NT GRAVITY GRADIENT SATELLITES
NT HEOS A SATELLITE
NT HEOS SATELLITES

NT IMP
NT INTELSAT SATELLITES
NT ISIS SATELLITES
NT ISIS-A
NT LINCOLN EXPERIMENTAL SATELLITES

NT LUNAR ORBITER
NT LUNAR SATELLITES
NT METEOROLOGICAL SATELLITES
NT MIDAS 4 SATELLITE
NT MOON

NT NATURAL SATELLITES
NT NAVIGATION SATELLITES
NT NIMBUS SATELLITES
NT NIMBUS 2 SATELLITE
NT NIMBUS 3 SATELLITE
NT NIMBUS 4 SATELLITE

NT OAO
NT OGO
NT OGO-A
NT OGO-B

NT OGO-D
NT OGO-E
NT OGO-F
NT ORBIS CAL SATELLITE
NT ORBITAL WORKSHOPS
NT OSO
NT OSO-B
NT OSO-1
NT OUTER PLANETS EXPLORERS
NT PAGEOS SATELLITE
NT PASSIVE SATELLITES
NT PHOBOS
NT PROTON SATELLITES
NT PROTON 2 SATELLITE
NT PROTON 4 SATELLITE
NT RADIO ASTRONOMY EXPLORER SATELLITE

NT RELAY SATELLITES
NT SAN MARCO SATELLITE
NT SAN MARCO 2 SATELLITE
NT SCIENTIFIC SATELLITES
NT SMALL ASTRONOMY SATELLITES
NT SYNCHRONOUS SATELLITES
NT SYNCOM SATELLITES
NT TD-1 SATELLITE
NT TIROS SATELLITES
NT TRANSIT SATELLITES
NT VELA SATELLITES
NT VENERA SATELLITES

Measured heat flux conversion into average radiation incident on convex satellite surfaces in test chambers

03 p0606 A70-13536

Space temperature determination, discussing planet or satellite absorption and radiation rate dependence on surface characteristics, solar radiation, planet albedo and thermal radiation

05 p0914 A70-16629

Monograph on ionosphere-satellite interactions, discussing ionosphere layers, plasma sheaths and wakes, electromagnetic wave propagation, spacecraft antennas, etc

10 p1944 A70-24900

Magnetic moment measurement of satellite in near earth orbit, using data transmitted by rectangular magnetic sensors

13 p2454 A70-30032

Nonrigid satellites dynamical equations derivation in modeling by generalized coordinates

18 p3333 A70-36702

Satellite dynamics - Conference, Prague, May 1969

24 p4405 A70-45526

SATURATED HYDROCARBONS U LKANES SATURATION

Critique of double resonance theory in gaseous lasers, including correction regarding saturation parameter for small RF perturbations and line width dependence

01 p0109 A70-10432

Emission saturation in Ar CW laser at high discharge current densities under different pressures and tube channel parameters

08 p1511 A70-20542

Carbon dioxide laser saturated gain constant calculated for low and high electron densities based on thermodynamic approach

13 p2425 A70-28793

Regenerative semiconductor parametric amplifier saturation in forward current mode, assuming harmonic voltages /signal, pumping and difference frequencies/ action at p-n junction

15 p2708 A70-31522

Junction FET potential field and carrier distribution in channel investigated for current saturation mechanism

15 p2708 A70-31841

Single mode gas laser with large saturation and dispersion effects, discussing resonator alignment to spectral line frequency

15 p2752 A70-32196

Conditionally stable feedback control systems with saturation, comparing large signal stabilization methods

16 p2884 A70-33313

Microwave radiometric receiver, analyzing video detector saturation effects on linearity

16 p2880 A70-34075

Saturated nitrogen vapors condensing coefficients measurement by cryostat, comparing results with theoretical prediction

23 p4218 A70-44364

Remanence and saturation methods for magnetic-particle flaw detection

24 p4346 A70-45726

Steel surface diffusive saturation with elements of chlorides, noting role of iron chloride phase in promoting coating uniformity

24 p4350 A70-46332

Carbon steel diffusion saturation with Ti and B, investigating layer depth, weight gain and microhardness dependence on powdered mixture composition

24 p4364 A70-46336

SATURN WORKSHOPS

NT SATURN I WORKSHOP

SATURN [PLANET]

Internal powers and effective temperatures of Jupiter and Saturn measured by aircraft mounted telescope, noting restraints on planetary structure and atmosphere models

01 p0173 A70-10045

Atlas of near IR spectra of Venus, Mars, Jupiter and Saturn obtained by Fourier spectroscopy, discussing observational procedures, data recording and processing

01 p0173 A70-10078

Jupiter and Saturn near IR spectra for relative abundances of atmospheric constituents and distribution with altitude, noting rough solar composition

01 p0179 A70-10526

Atmospheric models of deep atmosphere thermal emission and ionosphere free-free emission used for studying Saturn microwave spectrum

01 p0180 A70-10533

Giant planets structure, calculating Jupiter and Saturn densities using Russell solar mixture and internal heat from central core radioactivity

01 p0181 A70-10663

Methane and ammonia absorption bands and possible structure of Jupiter and Saturn cloud layers by spectrophotometric observations

02 p3666 A70-11807

Polarization observations of Saturn in UV and visible regions compared with Jupiter data, noting multiple scattering

02 p3668 A70-11818

Phase diagrams for binary mixtures at high pressures suggesting layered structures existence in Jupiter and Saturn atmospheres resulting from phase separations in hydrogen-helium mixture

02 p3668 A70-11819

Figure of gravitating inhomogeneous rotating liquid, applying results to Jupiter and Saturn model construction

08 p1564 A70-20558

Fourth Saturn ring detection equipment and procedures, discussing negatives revealing small weak zones near globe equatorial east and west edges

08 p1567 A70-20600

Jupiter and Saturn IR reflection spectra observed with Michelson interferometer-spectrometer, eliminating effects of terrestrial atmospheric absorption, solar spectral lines, etc

08 p1570 A70-20895

Saturn globe, rings and satellites observations /1968-1969/

09 p1751 A70-22198

Saturn ring atmosphere absorption spectrum observation during earth passage through ring plane

09 p1754 A70-22497

Planet Saturn right ascensions tabulation /1967, 1968/

09 p1756 A70-22651

Saturn disk temperature obtained from centimeter wavelength, suggesting possibility of nonthermal radiation

09 p1759 A70-22912

Bode law development from dynamical relaxation suggested from comparison of Jupiter, Saturn and Uranus inner satellite systems with planetary system

09 p1765 A70-23796

Saturn ring IR spectrum, discussing resemblance and discrepancies of ammonia and water frost spectra

10 p1935 A70-23813

Motion of negligible mass body near large mass body affected by larger third body applied to Phoebe-Saturn-sun system

10 p1945 A70-24960

Meteoroidal bombardment effects on material loss or gain in Saturn rings

11 p2113 A70-26471

Saturn observation by astronomers of various countries during earth passage through plane of rings, measuring rings thickness

12 p2298 A70-27279

Saturn rings observations during earth passage through ring plane by Abastumant observatory telescope, describing photometric processing and data reduction

15 p2797 A70-31619

Figure of gravitating inhomogeneous rotating liquid, applying results to Jupiter and Saturn model construction

15 p2805 A70-32713

Secular variations in osculating orbital elements of particle in Saturn ring gravitational field, considering motion in both external and internal space

16 p2973 A70-33226

Uranus and Saturn reciprocal mass determination based on astronomical observations of Saturn and Jupiter respectively

20 p3705 A70-39477

Saturn ring photometric properties, discussing multiple scattering and Seeliger principal photometric theory deviation

21 p3885 A70-40932

Saturn ring radial structure, discussing dynamic model, gravitational forces and perturbation of planetary satellites

23 p4241 A70-44253

SATURN LAUNCH VEHICLES

NT SATURN 1B LAUNCH VEHICLES
NT SATURN 5 LAUNCH VEHICLES
Apollo spacecraft contamination control, discussing Boeing responsibility for engineering, facilities, materials, etc, for Saturn rocket

01 p0058 A70-11077
Saturn launch vehicle systems in terms of design, operating characteristics and potential applications, showing need for reusable space shuttle systems [ALAA PAPER 690703] 05 p0922 A70-15830
Apollo-Saturn Launch Vehicle Targeting Program for Lunar Landing Missions, describing functions of integrated digital computer programs [ALAA PAPER 70-172] 06 p145 A70-18093
Saturn ULLAGE solid propellant rocket motor vibration test evaluation

07 p1365 A70-20039
Test program effectiveness for Saturn Instrument Unit (IU), summarizing objectives, costs and results [ALAA PAPER 70-379] 10 p1891 A70-24924
Real time network support simulation allowing network configuration for nominal or perturbed trajectory for Saturn vehicles, applicable to any flight azimuth [ALAA PAPER 69-936] 20 p3591 A70-39684
Jmsphere wind profiles gust variance and spectrum densities for horizontal wind speeds viewed by Saturn vehicle

21 p3847 A70-41878

SATURN S-1C STAGE

Thermal and pressure environments analysis in Saturn S-1C stage base during flight tests, noting base gas flowfield and heating [ALAA PAPER 69-318] 01 p0195 A70-10833
Temperature profiles and frequency driftings of VHF telemetry transmitters for Saturn S-1C stage, using IR radiation data

12 p2196 A70-27725
Systems operation hybrid simulator for computer checkout of Saturn S-1C stage

17 p3061 A70-35489
Short duration tube wind tunnel supersonic testing, noting Saturn S-1C base heating and solid propellant rocket base burning tests

20 p3606 A70-39698

SATURN S-2 STAGE

Quality information system consisting of closed loop input/feedback methods insuring design requirements of Saturn S-2 stage

14 p2654 A70-31116
Saturn S-2 stage propellant feedlines and J-2 engines simulating structural longitudinal oscillation by analog computer [ALAA PAPER 70-626] 16 p2968 A70-33591

SATURN S-4B STAGE

Apollo spacecraft contamination control, describing McDonnell Douglas role in S-4B stage production

01 p0059 A70-11079
Spent Saturn S-4B stage conversion into orbital workshop in Apollo Applications Program 11 p2122 A70-26044
Seismic echo produced by jettisoned Apollo 12 S-4B stage impact at lunar surface analyzed by multiscade scattering theory

12 p2298 A70-27280
S-IVB liquid rocket engine and propellant feed systems restart shutdown in orbital operations [ALAA PAPER 70-672] 16 p2967 A70-33574
Optical system measurement of density and rotational temperature in gaseous plume simulating auxiliary propulsion and oxygen hydrogen burner of S-4B

16 p2913 A70-34023

SATURN STAGES

NT SATURN S-1C STAGE
NT SATURN S-2 STAGE
NT SATURN S-4B STAGE
NASA automatic checkout systems for Saturn 5 stages and instrument units

21 p3803 A70-40770

SATURN 1 WORKSHOP

Deployable meteoroid shield for Saturn 1 workshop, describing design and hardware kinematics

23 p4257 A70-44386

SATURN 1B LAUNCH VEHICLES

Saturn 1B Orbital Workshop solar array thermal and performance analysis for various vehicle orientations and orbital conditions, emphasizing modeling and data handling

11 p2127 A70-26357

SATURN 5 LAUNCH VEHICLES

Apollo/Saturn 5 space vehicle supporting and restraining mechanisms design and operation, discussing holddown assemblies

01 p0055 A70-10468
Saturn 5 launch vehicle design, role in exploration and anomalous structural vibration and oscillation [ALAA PAPER 69-1094] 01 p0194 A70-10620

Unified Flight Analysis System processing post-flight data from Saturn 5 launches, discussing system components, support programs and performance

02 p0264 A70-12127
Saturn 5 thru-bulkhead initiator for solid propellant rocket motor ignition, discussing transfer design, pressure output and postfire leakage

03 p0546 A70-14105

Predicted and measured low density plume impingement effects on loads and heat transfer compared on orbiting Saturn 5 with oxygen-hydrogen burner engine

04 p0737 A70-15430
Saturn 5 program status to meet mission requirements for manned lunar exploration, space station/base programs and outer planet exploration with unmanned probes [SAE PAPER 690715] 05 p0922 A70-15852

Nuclear propulsion requirements for manned landing mission to Mars assuming Saturn 5-based operation

07 p1375 A70-18874
Saturn 5 Prelaunch Systems Simulation Model for launch opportunity containing multiple launch windows, considering last 26 hours of countdown

08 p1582 A70-20933
Launch load simulation on scaled vibration model concerning Saturn 5 structural integrity and flight failure

10 p1953 A70-25072
Cylindrical shell segments supersonic flutter boundaries engineering estimates related to Saturn 5 booster, obtaining thickness requirement as function of panel geometry [ALAA PAPER 68-284] 11 p2134 A70-25959

NERVA nuclear rocket engine design for Saturn 5 third stage, comparing nuclear and chemical engines performance

12 p2270 A70-26871
Saturn 5 launch vehicle navigation system design, discussing configurations, implementation schemes, system tradeoffs and performance

14 p2613 A70-30453
German monograph on heavy space probes for solar system investigation covering systems analysis, mission success, flight programs, Saturn 5 launch vehicle, etc

17 p3168 A70-35378
Remote sonic monitoring system for Saturn V noise measurement and recording

17 p3094 A70-35521
Saturn 5 launch vehicle targeting methods for lunar missions, solving earth departure variables via iterative process [ALAA PAPER 70-1052] 19 p3528 A70-38867

Saturn 5 suboptimal continuous guidance design, eliminating discontinuous control encountered in SA-502 flight [ALAA PAPER 70-965] 20 p3600 A70-39564
NASA automatic checkout systems for Saturn 5 stages and instrument units

21 p3803 A70-40770
Saturn 5 Apollo booster stages oscillations induced by coupling between vehicle structure and engine thrust corrected within existing systems [ALAA PAPER 70-1236] 24 p4417 A70-45954

SAWTOOTH WAVEFORMS

Sawtooth waveform generator using linear discharge of capacitor

15 p2714 A70-32701
Simple high level shock machine producing trapezoidal and terminal peak sawtooth pulses with Al honeycomb impact material

19 p3396 A70-37832
Pulsars subpulse intensities and shapes in magnetic field, noting drift speed sawtooth patterns

20 p3713 A70-40428

SCALARS

Isotropic incompressible three dimensional turbulence representation by wave vector scalar functions, discussing maximum functions number determination

02 p0277 A70-11878
Scalar potential nonlinear fluctuations in quasi-stationary plasma, deriving expressions for potential spectral function and Langmuir and ion-acoustic fluctuations spectral densities

08 p1550 A70-20844
Scalar-tensor theory in canonical form, discussing neutral particle and electron self energy problem

15 p2773 A70-31439
Magnetic scalar potential of circular loop represented by toroidal coordinate system, solving boundary value problems determining fields of coils and toroidal magnetic conductors

18 p3215 A70-36295
Relativistic thermodynamics, developing relativity theories in nonvacuo regimes and discussing covariant scalars and formalisms

18 p3291 A70-36553
Rayleigh wave scalar electric potential analysis on piezoelectric medium, using iterative techniques for Poisson equation

22 p4074 A70-42967
Polynomial approximation process for scalar nonlinear equation solution, applying to Cauchy problem

22 p4064 A70-43482
Static spherically symmetric charged mass distribution exact solutions derived for electrons in scalar tensor theory of gravity by Hamilton-Jacobi method

23 p4222 A70-44403
Relativistic two body system in circular orbits, examining quantum theory with massless and massive

scalar fields and energy and angular momentum for bound system

24 p4379 A70-45521
Beltrami flows on spherical surfaces, using scalar equations from kinematic conditions

24 p4326 A70-45990

SCALE [CORROSION]

Chemical composition of scale formation in jet engine injectors for various fuel types tabulated, noting buildup levels in transport aircraft and subsonic jets

07 p1362 A70-18651
High temperature scaling of Ni, investigating role of oxide microstructure and growth stresses

15 p2762 A70-32388
Sulfidation kinetics and scale morphology of Cr and Cr-Mo alloys at high temperatures in hydrogen/hydrogen sulfide atmosphere

19 p3452 A70-37827

SCALE [RATIO]

Generalized multiple scales method for solving linear differential equations with variable coefficients applied to Liouville-Green approximation

03 p0518 A70-12994
Acoustic intensity determined from time, length and velocity scales in mixing region of jet from nozzle with turbulent boundary layers

05 p0834 A70-16779
Optimal scale selection for aerial surveys by analyzing aerial photography data

07 p1278 A70-18690
Absolute radiometric reference scale, noting International Pyrheliometric Scale 1956 materialization by standard instruments

15 p2735 A70-31805

SCALE EFFECT

Stress rupture strength dependence on specimen geometry /scale effect/ from analyzing metals failure under prolonged loads

02 p0383 A70-11655
Scaling and refractoriness effect in neutral-pulse train transmission on eye incremental sensitivity, discussing applicability as intraretinal mechanism concept

02 p0247 A70-12466
Scale factor effect on crack development in blanks and structure elements undergoing linear and complex stressed states under cyclic thermal loads

05 p0867 A70-17045
Fatigue limits distribution functions of full-scale machine parts estimated by rupture similarity criterion, discussing stress concentration and scale factor effects

09 p1776 A70-22616
Hollow cylindrical sample scale effect on accuracy of testing heat resistance of brittle materials

10 p1965 A70-25301
Transonic scaling effects for shock boundary layer interaction on circular and two dimensional airfoil models, discussing separation and reattachment [ALAA PAPER 70-541] 13 p2339 A70-29008

Similarity and scaling between atmospheric and wind tunnel simulated shear flows near earth surface

14 p2602 A70-30369
Stress rupture strength dependence on specimen geometry /scale effect/ from analyzing metals failure under prolonged loads

19 p3547 A70-38428
Scale factor effect on brittle fracture resistance for Ti and Al alloys and high strength steels

23 p4265 A70-43936

SCALE HEIGHT

High resolution photometry near planetary limb yielding scale height and optical depth applied to Mariner 4 Mars observations

05 p0909 A70-16387
Gas pressure and pressure stratification in sunspot, using curve of growth analysis

05 p0911 A70-16432
Ionized gas height scale changes in polar ionosphere obtained assuming Chapman type ionization distribution

05 p0841 A70-16738
Topside ionosphere morphology during IQSY, emphasizing plasma scale height diurnal and latitudinal variations role in satellite data interpretation

07 p1270 A70-20073
Topside ionospheric plasma scale height, showing influence of magnetic activity level

14 p2569 A70-30207
Pulsar observations based on magnetic dipole model, discussing turnoff time, emission characteristics, birth rate and scale height

17 p3153 A70-34531
Mean molecular mass determination method for upper atmosphere based on Nicolet equation for scale height, using satellite orbit and spin decay data

17 p3138 A70-35773
Lower chromosphere shock wave heating, analyzing density scale height effects

22 p4105 A70-43001
Topside ionospheric plasma scale height, showing influence of magnetic activity level

24 p4330 A70-46282

SCALE MODELS

Flow profiles in models of human bronchial tree typical junctions, visualizing inspiration and expiration patterns for various Reynolds numbers

01 p0034 A70-10653

High altitude scale model experiment to evaluate rocket plume impingement effects on Manned Orbital Workshop pressures, heating rates, forces and moments

03 p0579 A70-13646

Tower influence of wind speed and direction measurements, comparing 150 meter meteorological tower and scale wind tunnel model

09 p1661 A70-22964

Launch load simulation on scaled vibration model concerning Saturn 5 structural integrity and flight failure

10 p1953 A70-25072

Reinforced epoxy models as precursor to prototype design and analysis of aircraft structures, discussing stress analysis methods

12 p2318 A70-27129

Transonic scaling effects for shock boundary layer interaction on circular and two dimensional airfoil models, discussing separation and reattachment [AIAA PAPER 70-541]

13 p2339 A70-29008

Modeling techniques based on Froude scaling laws for helicopter ditching and flotation stability characteristics

17 p3016 A70-34738

Wind tunnel balance for measuring small aerodynamic loads on scale models, describing three component construction

17 p3062 A70-35490

Buoyant Venus station balloon for deployment and inflation during parachute descent into Venus atmosphere tested with scale model balloons in wind tunnels

17 p3063 A70-35658

Structurally similar models, investigating space vehicles dynamic characteristics

18 p3332 A70-36161

Model testing for helicopters, considering scaling, ditching and rotor performance

19 p3402 A70-38610

Thermal scale modeling of heat pipe in deep space, using material and heat flux preservation techniques

21 p3946 A70-41048

Multilayer insulation thermal scale modeling, discussing surface control techniques

21 p3951 A70-41865

Spacecraft thermal control coatings scale models, discussing temperature errors due to energy transport along surfaces

21 p3951 A70-41874

Helicopter rotors fatigue testing using small scale models of full scale components [ICAS PAPER 70-34]

23 p4267 A70-44131

High bypass model jet noise study, describing test setup and noise measurement results as function of secondary/primary flow velocity ratio

23 p4233 A70-44394

Tycho crater northeast rim scale relief model including lava lakes in outer walls

23 p4253 A70-44881

Polyvinyl chloride /Novodur/ mechanical properties application to structural model testing

24 p4367 A70-45445

SCALERS

Quasi-logarithmic readout of conventional binary scaler provided by reduced logic system following generalized equations

05 p0851 A70-16844

SCALING

Scaling and angular resolution for sequential type holographic stereogram, comparing results with conventional hologram

04 p0695 A70-15574

Missile oscillations in plane during pitching moment hysteresis, discussing test coefficients suitability for predicting motion

09 p1606 A70-23258

Interindividual differences in judging stimulus similarities, explaining unsatisfactory results obtained by average scalings

19 p3366 A70-38506

SCALING LAWS

Scaling laws for nose bluntness effects on hypersonic aerodynamics of bodies of revolution [AIAA PAPER 68-1158]

04 p0620 A70-15530

Critical regions equilibrium thermodynamic properties of fluids and magnets using scaled equation of state

07 p1421 A70-19298

Modeling techniques based on Froude scaling laws for helicopter ditching and flotation stability characteristics

17 p3016 A70-34738

Scaling relations showing effects of ballistic coefficient, flight path angle and inverse atmospheric scale height on heating of ballistic entry bodies

17 p3012 A70-35667

Scaling laws for turbulent plasma anomalous conductivity dependent on electrostatic fluctuation spectrum

23 p4227 A70-44796

Cosmic ray events angular distribution from scaling hypothesis

23 p4238 A70-44894

SCANDIUM COMPOUNDS

NT SCANDIUM OXIDES

SCANDIUM OXIDES

Partition functions and equilibrium constants for ScO, YO and LaO computed for 1000-8000 K, assuming doublet ground electronic state

10 p1946 A70-24970

SCANNER PROJECT

Spin stabilized Project Scanner spacecraft attitude determination by star mapping technique, describing optics, photomultiplier, reticle, electronics and sun shield

15 p2772 A70-31791

SCANNERS

NT HORIZON SCANNERS

NT INFRARED SCANNERS

NT OPTICAL SCANNERS

Scanning beam radio guidance system for VTOL approach and landing

02 p0336 A70-12766

Pencilbeam scanning observations of solar bursts revealing recognizable postincrease phase

03 p0558 A70-13588

Airborne multispectral sensing based on modified AN/AAS-5/XE-2/ scanners mounted in C47 aircraft, discussing applications

03 p0491 A70-13669

Projection display methods using scanned and modulated multicolor laser beams, discussing beam generation, modulation and scanning

05 p0858 A70-16188

Laser beam trajectory equation in scanning ultrasonic cell for nonzero incidence angle, relating input and output beam divergence

07 p1300 A70-19865

Soviet book on automatic scanning information systems, discussing equipment, system parameters, scanning methods, etc

10 p1840 A70-24376

Computer program for flying spot scanner pattern recognition, analyzing human chromosome contour

12 p2170 A70-27938

Scanning technique for allowing whole vibration cycles storage on one hologram

15 p2738 A70-32052

Bicylindrical microwave lenses, discussing collimating, virtual line source and point fed scanning lenses design

16 p2876 A70-33405

Scan platform servomechanical actuator for Mariner Mars 1969 spacecraft, emphasizing gear arrangement and train dynamics

16 p2845 A70-34108

Lens with radial symmetry for mm wave scanning antenna

20 p3598 A70-40307

ERTS line scanning system for cartographic data of water, snow, vegetation and cultural areas

22 p4037 A70-43090

Full-scanning random arrays with high resolution for space exploration, radio astronomy and long range radar

23 p4160 A70-43770

SCANNING

NT FREQUENCY SCANNING

NT PANORAMIC SCANNING

NT RADAR SCANNING

Duty factor and contrast in scanned displays, discussing light modulator and emitting displays

01 p0043 A70-10780

Computer processing role in film scanning and digitizing for enhancing X ray and radioisotope scanner images in medical radiographs, discussing image noise reduction

04 p0654 A70-14562

Aperture dissection scheme to reduce transit time of Bragg angle acousto-optical scanning of laser beam

05 p0860 A70-16657

Holography by fixing detector and scanning source based on reciprocity theorem for diffraction field

05 p0849 A70-16677

Dispersion function and measured line profile distortion by rectangular detector slit of order scanning Fabry-Perot spectrometer

06 p1063 A70-17622

Phase interpolation circuits for scanning phased array antennas, using doublers and frequency multipliers

09 p1646 A70-22701

Photosensitivity and scanning of planar Si photodiode image detector arrays, using most ring counter and shift register

10 p1846 A70-23881

Laser-light spatial-domain scanning function for deconvolution of blurred photographs using point-spread and holographic Fourier transform division filter

11 p2050 A70-25832

Track-while-scan algorithm, considering probabilistic interpretation of linear recursive least squares filter for velocity variations

11 p2029 A70-26319

Microwave scanning beam landing system providing aircraft radio approach guidance

12 p2269 A70-27918

Maximum mode selection tuning of scanning interferometer with spherical mirrors applied to He-Ne laser spectrum analysis

12 p2250 A70-28182

Ultrafast laser-Raman spectroscopy, comparing Scan and No-Scan techniques

14 p2593 A70-30361

Search duration distribution of two stage lock-on indicator scanning signal search systems, using regenerative random process and integral recovery equation

15 p2696 A70-31501

Lens antennas for performing radiation collimating function through refraction, discussing solid and artificial dielectrics lens design, beam scanning applications, etc

17 p3052 A70-35069

Apollo black and white TV scan converter design and operation

17 p3095 A70-35636

High speed electro-optic spectral scanning in UV, visible and IR regions, using monochromator deflection of dispersed light

20 p3671 A70-39090

Pilot scanning dwell times and control workload in simulated instrument approach, using eye-point-of-regard/EPR/ measurements

20 p3580 A70-39532

High velocity source and receiver scanning effect on holographic image, observing rotation and distortion

21 p3829 A70-41928

Galactic plane scanned observation of X ray sources, using large area proportional counter rocket sounding

22 p4094 A70-42986

Radiation and phase-scanning properties of planar array of parallel plate waveguides, using wedge diffraction theory

23 p4166 A70-44973

SCANNING DEVICES

U SCANNERS

SCATTER PROPAGATION

NT IONOSPHERIC F-SCATTER PROPAGATION

Pulse methods for measuring correlation function of incoherent scattered signal, calculating bit estimator errors for large and small SNR

01 p0045 A70-11088

Book on ionospheric scattering effects on long distance radio communication, considering Arctic ionosphere, scatter propagation, modulation, sporadic E, etc

01 p0046 A70-11305

Tropospheric scattering ability investigation with radar transmitter emitting vertical pulses, considering implications for scatter propagation from backscattering detection

03 p0453 A70-14298

Daylight ionospheric scatter propagation and absorption during energetic electron precipitation event in auroral zone using bremsstrahlung observations at balloon altitude

07 p1271 A70-20154

Comparative passband of optimal and fixed frequency systems in ionospheric scatter communications during nighttime

14 p2547 A70-30239

Ionospheric measurements from observations of incoherently scattered radio waves, describing radar installations specifications

15 p2731 A70-32096

Ionospheric scatter channel amplitude frequency characteristics recording equipment, discussing design

18 p3256 A70-36090

Ionospheric scatter communications channel phase frequency characteristics measuring method, considering probability density function

18 p3256 A70-36091

Comparative passband of optimal and fixed frequency systems in ionospheric scatter communications during nighttime

24 p4316 A70-46314

SCATTERERS

U SCATTERING

SCATTERING

NT ACOUSTIC SCATTERING

NT ATMOSPHERIC SCATTERING

NT BACKSCATTERING

NT COHERENT SCATTERING

NT COMPTON EFFECT

NT ELASTIC SCATTERING

NT ELECTROMAGNETIC SCATTERING

NT ELECTRON SCATTERING

NT FORWARD SCATTERING

NT INCOHERENT SCATTERING

NT ION SCATTERING

NT IONOSPHERIC F-SCATTER PROPAGATION

- NT LIGHT SCATTERING
 NT MICROWAVE SCATTERING
 NT MIE SCATTERING
 NT NEUTRON SCATTERING
 NT NUCLEAR SCATTERING
 NT PROTON SCATTERING
 NT RADAR SCATTERING
 NT RAMAN SPECTRA
 NT RAYLEIGH SCATTERING
 NT RESONANCE SCATTERING
 NT REVERBERATION
 NT TROPOSPHERIC SCATTERING
 NT WAVE SCATTERING
 NT X RAY SCATTERING
- Metastable diatomic N beam scattering from Teflon and Cu surfaces measured for velocity and angular distributions
 06 p1112 A70-18273
- Ar beam scattering and UV radiation from glass target surface with adsorbed gas layer
 06 p1112 A70-18274
- Open region waveguide radiation and scattering solved using impedance surfaces of related closed region convergence
 09 p1640 A70-23807
- Nozzle source design for high intensity thermal energy molecular beam with small dispersion in velocity suitable for scattering experiments
 11 p2086 A70-25973
- Chandrasekhar H function approximation for isotropic scattering, calculating absorption line contours
 22 p4109 A70-43750
- SCATTERING AMPLITUDE**
 Backscatter radar signal phase determination from amplitude data, measuring phase and amplitude in laboratory
 05 p0815 A70-16507
- Scattered field amplitude and phase determined from hologram light intensity distribution, noting biological applications
 08 p1500 A70-21786
- Intensity and velocity distributions of thermal energy argon atoms scattered from silver (111) face, using time of flight methods
 16 p2953 A70-33007
- Electromagnetic field amplitude and phase scattering diagrams analysis for shape information capacity
 21 p3785 A70-40637
- SCATTERING COEFFICIENTS**
 Twilight brightness measurements with balloons, scattering coefficient and indicatrix for high altitudes and comparison with Rayleigh-Cabann theory
 01 p0079 A70-11218
- Plane and spherical albedos of planet surrounded by infinite optical thickness atmosphere, with application to Venusian atmosphere
 01 p0193 A70-11591
- Twilight atmospheric brightness calculation for models of vertical distribution of aerosol scattering coefficient, using numerical data
 06 p1056 A70-17828
- Gas stream-elastic solid surface scattering characteristics, calculating trajectories, particle flux angular distributions, velocities, transfer coefficients, etc
 06 p1111 A70-18265
- High energy Ar atomic beams scattering from single crystal face of W measured for distribution pattern
 06 p1112 A70-18270
- Visibility, atmospheric light scattering coefficient and aerosol mass concentration related by integrating nephelometer measurements
 07 p1328 A70-18923
- Mode-scattering coefficients from ionospheric perturbations for sunrise and sunset propagation paths, comparing results with VLF radio measurements
 12 p2189 A70-28053
- Approximate formulas for disperse attenuation and scattering coefficients for water drops in visible and IR spectrum
 18 p3260 A70-36973
- Binary Boltzmann operator for quantum statistical second virial coefficient for real gases and plasmas in two-particle scattering problem involving Jost function
 22 p4081 A70-42824
- SCATTERING CROSS SECTIONS**
 Differential elastic and rotational excitation cross sections for electron-hydrogen scattering in close coupling approximation with electron exchange neglected
 02 p0342 A70-11880
- Hydrogen-hydrogen double excitation collision cross sections computed by impact parameter method, using Born and two state approximations
 02 p0342 A70-11881
- Differential elastic scattering cross section of Ar nozzle beam in nitrogen considered with rainbow effect in determining intermolecular potential well depth
 02 p0344 A70-12722
- Triggered spark source for multiply charged carbon ions applied to collision cross section measurements
 02 p0303 A70-12747
- Slow electrons elastic scattering by diatomic hydrogen molecule, analyzing cross sections in two

- center prolate spheroidal coordinates emphasizing polarization effect
 03 p0528 A70-14179
- Backscattering cross sections of metallic bodies of revolution, analyzing statistically echo pattern of complex targets
 03 p0452 A70-14225
- Electron-electron and electron-atom bremsstrahlung, giving graphical expressions for one and two electron atoms cross sections
 04 p0721 A70-14667
- Elastic and inelastic scattering of proton beam from Ne 20 measured for cross sections to interpret polarization data
 04 p0723 A70-15636
- Rayleigh scattering cross sections of stellar He C, N and O computed by quantum defect method, discussing effects of wavelength dependent polarizabilities
 04 p0723 A70-15692
- Experimental determination of solar neutrino activity from interaction cross section between neutrinos and target nuclei
 05 p0900 A70-15965
- Electromagnetic wave diffraction on absorbing black metallic and magnetic cylinders and strip, plotting radar scattering cross sections
 05 p0813 A70-16262
- Molecule spatial and velocity distributions of supersonic molecular beams, measuring scattering cross sections of He and Ar on noncondensable gases
 06 p1043 A70-18252
- Particle, momentum and energy flux spatial distributions of molecules scattered in collisions of low energy Ar atoms with mica and Ag surfaces
 06 p1111 A70-18268
- Collision cross sections direct measurement for determining macroscopic reaction rates in inelastic molecular collision processes in gas dynamics
 06 p1113 A70-18276
- Hydrogen atoms collisional excitation cross section expressed in terms of quantum numbers of levels and ratio of colliding electron energy to transition energy
 07 p1338 A70-19410
- Wall boundary condition model modification applied to molecular beam-solid surface scattering, noting qualitative agreement with observed distributions
 07 p1342 A70-20118
- Intermolecular potential of atoms and/or molecules determined from scattering cross sections of supersonic He and/or Ar atomic beams
 07 p1344 A70-20132
- Scattering cross sections of K atoms on bromine molecules determined as function of particle energy using supersonic atomic beams
 07 p1344 A70-20133
- Molecular N rotational temperature effect on rare gases scattering cross section
 07 p1344 A70-20134
- Ar-Kr integral collision cross sections based on density measurements of Ar beam passed through liquid nitrogen cooled Kr filled scattering chamber
 07 p1344 A70-20135
- Energy dependence of elastic total collision cross section of identical He molecules, using velocity selected primary beams at low target temperature
 07 p1345 A70-20137
- Proton-deuteron elastic large angle scattering cross sections, noting backward peak consistent with baryon exchange mechanism with resonance transfer
 07 p1345 A70-20198
- Time dependent matrix elements for multistate impact-parameter calculations for atom-atom inelastic cross sections
 07 p1346 A70-20242
- Scattering cross sections of radio waves at wake of vertically moving body near reflecting ionospheric layer, noting wave sphericity influence
 07 p1237 A70-20423
- Radio wave sphericity influence on scattering at moving body wake in ionosphere, determining scattering cross section principal maximum
 07 p1237 A70-20424
- Refractive index variations effect on backscattering, scattering and attenuation cross sections of ice sphere at various low temperatures
 08 p1536 A70-21098
- Cross sections measured for symmetric p , $2p$ reactions on deuterium and He, discussing nonsymmetric p , $2p$ events in He
 08 p1548 A70-21233
- Scattering cross sections of electromagnetic waves in rectangular plasma-filled waveguide based on reciprocity theorem
 08 p1464 A70-21983
- Photon scattering by Ar in vacuum UV measured for cross sections
 09 p1730 A70-22071
- He-Ne and argon lasers for measuring radar scattering cross sections of plane and three dimensional targets
 09 p1632 A70-22405

- Square Van Atta reflector with/without conducting plate used for mounting antenna half wave dipoles, considering scattering cross sections
 09 p1646 A70-22695
- Scattering equations and cross sections for rotational excitation in collisions of rigid diatomic molecules interacting through soft potential
 09 p1732 A70-22901
- Obstacle extinction cross section determination at microwave frequencies from Q factor of open resonator
 09 p1637 A70-23307
- Plane electromagnetic wave scattering by conducting circular cylinder/wire in air/vacuum, computing scattering cross sections by Wiener-Hopf method
 09 p1638 A70-23347
- Dissipative parameters determination for relativistic gas within kinetic theory framework based on particle interaction model, assuming constant differential effective interaction cross section
 10 p1867 A70-24148
- Plane electromagnetic waves scattering from radially inhomogeneous cylindrical structure, deriving expressions for far field and cross section for both polarizations
 10 p1841 A70-24856
- Ar ions excitations by low energy electron collisions, noting excitation functions and cross sections of lines and levels by optical methods
 12 p2278 A70-27501
- Axial incidence HF backscattering cross section for absorbing flat based cone assumed to obey impedance boundary condition
 12 p2185 A70-27716
- Hydrogen and inert gas atoms collisional excitation cross sections calculated by multistate impact parameter approximation
 12 p2276 A70-27878
- Helium excitation from ground to excited state by electron impact, determining differential and integral scattering cross sections
 12 p2276 A70-27879
- Cross sections for electron impact excitation of positive helium and hydrogen ions, using non-relativistic Coulomb-Born-Oppenheimer reactance matrices
 13 p2455 A70-28988
- High energy proton-He 3 elastic scattering cross section measurement, comparing result with Glauber model calculation
 13 p2456 A70-29459
- Quantum mechanical model of electron scattering by homonuclear diatomic molecule at ground state, calculating differential and integral cross sections for elastic scattering
 14 p2618 A70-30113
- Elastic scattering of electrons by hydrogen as function of vibrational excitation, discussing intensities and cross sections
 14 p2618 A70-30114
- Differential cross sections for electron scattering by hydrogen with and without vibrational excitation, discussing inelastic processes
 14 p2618 A70-30115
- Raman scattering cross sections in solid state semiconductor plasma in magnetic field from phonon fluctuations
 14 p2621 A70-30485
- Electron impact excitation cross sections of oxygen ion first negative bands, considering relationship to oxygen ionization cross section
 14 p2620 A70-31363
- Semiclassical collision theory for computing fine structure proton impact excitation rates and cross sections for positive ions, presenting excitation rate tables
 14 p2652 A70-31383
- EM and acoustic scattering by simple shapes covering Maxwell equations, boundary and radiation conditions, radar cross sections, EM potentials, etc
 15 p2700 A70-32402
- Wave scattering from circular cylindrical body, considering plane wave primary source, line source, point and dipole source
 15 p2700 A70-32403
- Measuring instrument for total cross section of proton elastic scattering during sigma R reactions
 16 p2908 A70-33210
- NO and oxygen ions vibrational excitation due to inelastic scattering from He, calculating scattering angle variation
 16 p2955 A70-34010
- Scattering cross sections for monoenergetic Ar beams on epitaxial Ag films
 16 p2956 A70-34013
- Excitation cross sections for Ar I and He I spectral lines in low energy He ion-Ar collisions
 17 p3138 A70-34642
- Total cross sections for production of free electrons in collisions of low energy negative atomic oxygen ions with molecular nitrogen
 18 p3292 A70-36188
- Electron correlations and solar neutrino counts, correcting frequency independent Thomson cross section
 18 p3308 A70-36485

Finite size particle physics for plasma computerized simulation, considering longitudinal oscillations, scattering cross sections, diffusion coefficients, etc
18 p3296 A70-36791

Na D lines emission cross sections measurement from ionic and neutral gases collisions at simulated meteor conditions
18 p3318 A70-37014

Light combinatorial scattering by longitudinal photons with frequency near forbidden zone width, calculating Raman scattering cross sections
19 p3444 A70-37444

Closed coupled partial wave calculation of cross section for fine structure transitions in Na in collisions with He
19 p3372 A70-37541

Diatomic molecules inelastic collision cross sections for specific rotational transitions, discussing S matrix energy requirements for statistical analysis
19 p3474 A70-38268

Deep inelastic lepton-hadron scattering cross sections universality properties based on Wilson theory
20 p3674 A70-39150

Emission cross sections of nitrogen in vacuum UV by electron impact
20 p3675 A70-39617

Cesium beam velocity attenuation by He, Kr and Xe, determining scattering cross sections from gas pressure and density measurements
20 p3675 A70-39618

Decay lifetimes and electron impact cross sections of vacuum UV O I and O II emission multiplets, using pulsed electron beam in low pressure gases
21 p3852 A70-40718

High energy alpha particle beam exposed to plastic scintillators, determining spallation cross section for C12/alpha, alpha/C11
21 p3852 A70-41138

Numerical molecular rotational transition probabilities and cross sections in HCN-HCN and ICN-ICN collisions, using perturbation theory and multipole potentials
21 p3853 A70-41391

Electron excitation cross sections for light atoms using Slater wave functions and Born-Bethe approximations
21 p3853 A70-41393

Reflectors group mean effective scattering cross section measurement by far field criterion
22 p3995 A70-42387

Radiation patterns and scattering cross sections of plane black disks excited by electromagnetic and acoustic waves
22 p3984 A70-42391

Elastic wave diffraction by rigid inclusion, calculating far field displacement and cross section by integral equation method
22 p4073 A70-42636

Differential elastic cross sections of 42 MeV alpha particles scattering from He 3, using optical model with spin-orbit potential
22 p4076 A70-42722

Effective collision cross section for reaction resulting in Cs ions neutralization in thermal Cs plasma calculated from measured ion currents
22 p4082 A70-43374

Low energy proton-hydrogen collisions, computing differential cross sections for direct elastic scattering, resonant charge exchange and direct and exchange excitation
24 p4382 A70-46226

SCATTERING FUNCTIONS

Book on scattering of light and other electromagnetic radiation, treating scattering by spheres, cylinders, liquids, Rayleigh-Debye scattering, particle size analysis, etc
02 p0337 A70-11689

Visible radiation reflection, transmission and inside intensities of terrestrial clouds calculated by Monte Carlo program utilizing scattering phase function
02 p0326 A70-12286

Sky brightness distribution data to determine shape of aerosols scattering as function of wavelength
02 p0292 A70-12435

Scattering functions from sky light spectra measurements on high mountain for various sun altitudes, obtaining color value functions
02 p0359 A70-12776

Mie scattering and polarization functions of atmospheric aerosols determined on basis of logarithmic Gaussian distributions
05 p0879 A70-16664

Noniterative integral solutions of scattering equations extended to coupled channels using matrix notation
06 p1108 A70-17487

Thermally emitted photons of atmospheric molecules and aerosols and planetary surface followed by Monte Carlo method, using anisotropic single scattering functions
09 p1719 A70-23524

Radiant heat exchange local and angular coefficients determined allowing for absorbing and scattering medium between bodies
10 p1969 A70-25141

Wave scattering by statistical distributions of discrete obstacles, deriving various functions for diagnostic applications
11 p2086 A70-26762

Sky radiation scattering and polarization functions for various solar altitudes at Lomnitzer Peak observatory
12 p2294 A70-27674

Single and multistage parametric amplifiers for broadband communications, noting nonideal circular characteristics by scattering parameter and signal flow graph
12 p2197 A70-27933

Scattering function and image quality in sharp edge holography using single mode laser, analyzing coherent and diffuse light
15 p2733 A70-31556

Noniterative homogeneous solutions of integral equations for coupled open channel and coupled eigenvalue scattering
19 p3473 A70-38264

Interstellar spherical dust particles from meteoritic silicates and dirty ice, calculating optical properties and scattering functions
21 p3889 A70-41147

Convergent numerical method for principal value integrals in dispersion relations of coupled channel scattering problem involving wave phase shifts
22 p4062 A70-42748

Absorption line multiple scattering in thick planetary atmosphere, using successive scattering method for single-scattering phase function based on line profile and equivalent width
23 p4222 A70-44550

SCATTERING MATRIX

U S MATRIX THEORY

SCENEDESMUS

Fraction of Chlorella and Scenedesmus biomass, noting changes in adrenal cortex and renal glomerus
03 p0425 A70-13889

SCF

U SELF CONSISTENT FIELDS

SCHEDULES

Automatic landing system assurance of DH 121 aircraft schedule all-weather regularity through high safety level via redundancy
17 p3022 A70-35856

Central passenger traffic schedule role in air traffic control, discussing computer solutions, aircraft optimal use, etc
18 p3289 A70-36397

SCHEDULING

NT PREDICTION ANALYSIS TECHNIQUES

Flights best day pair and weekly leg schedules concept based on decision making model for traffic volume estimation in airline operations
02 p0403 A70-12787

Cost/schedule planning and control system /C/SPCS/ providing early exposure of inadequacies in work execution and initial planning
05 p0959 A70-16461

Linear programming for aircraft takeoff and landing schedules for traffic control on airport runway, using simplex technique for proposed algorithm
08 p1540 A70-20872

Pilot and copilot task distribution schedules adopted by European civil aviation for landing approaches under poor weather conditions
08 p1542 A70-21850

Dynamic programming successive approximation method application to airline scheduling, reviewing real time dispatching, operations, schedule and fleet planning
11 p2013 A70-26209

Tradeoff decision processes scheduling maintenance frequencies for commercial transport aircraft [SAE PAPER 700328]
12 p2243 A70-27461

Reliability prediction techniques accuracy and optimal timing including true and project control predictions
13 p2524 A70-29569

Space station experiments, payloads and activity planning
16 p2983 A70-34067

Predictive model for potential variance from planned schedule of R and D tasks to minimize risk in management
21 p3955 A70-41172

Schedule theory problem with redundancy and technological constraints reduced to optimal control problem by penalty function, making maximum principle applicable
23 p4177 A70-44304

Critical supersaturation vs phase equilibration of tissue in computing decompression schedules from depth and exposure time
24 p4301 A70-45983

SCHALKUNOFF PRINCIPLE

Excited circular cylindrical dielectric rod antenna radiation patterns derivation by Schelkunoff equivalence principle
16 p2872 A70-33121

SCHLEICHER AIRCRAFT

Schleicher AS-W15 glider wing span, weight, wing loading capacity and speed range, noting performance in international competition
05 p0793 A70-15905

SCHLIENEN PHOTOGRAPHY

Holographic color schlieren flow visualization system for three dimensional photography, variable focus shadowgraph, knife edge schlieren, etc
01 p0091 A70-10908

Metal film graded filter fabrication for schlieren photographic system with laser light source and framing camera, using vacuum evaporation
01 p0113 A70-10921

Inexpensive schlieren system for medical ultrasonic research, discussing equipment and application to short wave transducer beam patterns used in ophthalmology
02 p0300 A70-12472

Schlieren photograph intensity variations correlated with statistical parameters for turbulent flow density variations
03 p0464 A70-12941

Displacement interferograms and schlieren pictures of optical inhomogeneities in transparent media obtainable from single exposure hologram, using nonmonochromatic and laser light for reconstruction
03 p0483 A70-12358

Schlieren recorder and Erdmann field absorption methods applied to qualitative and quantitative flow process studies in high velocity wind tunnel
04 p0689 A70-14925

Semifocusing color schlieren systems for quantitative investigations of flows in fluid mechanics and heat transfer, including photographs of boundary layers
04 p0690 A70-15029

Rocket exhaust plume size determined from schlieren photographs during wind tunnel tests, noting agreement with Hill-Habert theory
04 p0736 A70-15417

Schlieren system modification using diffraction grating to produce color applied to airfoil flowfield analysis
06 p1029 A70-18165

Optical tools in aeronautical and space research at Langley Research Center, discussing schlieren photography of aeronautical and space models in wind tunnels
09 p1657 A70-23510

Duplex schlieren optical system with one channel for data recording and second channel for visual monitoring
09 p1687 A70-23766

Color schlieren photography with complete spectrum displayed in single photograph, discussing filter matrix
10 p1857 A70-23913

Gas dynamic processes insufficiency for triggering transition to detonation obtained from laser schlieren records of nonsteady flow field ahead of accelerating turbulent flame
11 p2150 A70-26378

Lambda type pseudoshock /shock during supersonic flow deceleration to subsonic in duct/, investigating mechanism by schlieren photography
11 p2037 A70-26408

Backward facing separated step boundary layer flow at Mach 2.25 investigated by diffraction grating interferometer and color schlieren technique [AIAA PAPER 70-571]
13 p2343 A70-29898

Schlieren optical method for measuring He jet penetration into supersonic flow
15 p2741 A70-32520

Self focusing schlieren observation in gas breakdown, discussing cubic polarizability of excited atoms in electron cascade due to laser pulses
21 p3835 A70-40594

Schlieren method application in plasma diagnostics, obtaining density change of neutral, ion and electron gases
21 p3825 A70-40950

Gas velocity measurement by high speed schlieren observation of laser induced breakdown phenomena [SMPE PREPRINT 27]
22 p4034 A70-43048

Wollaston prism schlieren interferometer for quantitative density gradient measurements in air [SMPE PREPRINT 25]
22 p4034 A70-43050

Supersonic wakes visualization and photographic measurement by schlieren techniques, using amplitude subtraction and He-Ne laser [SMPE PREPRINT 94]
22 p4036 A70-43061

Color filter schlieren photography for visualization of wind tunnel shock and pressures, liquid mixing and convection currents [SMPE PREPRINT 86]
22 p4036 A70-43065

SCHMIDT CAMERAS

Planetary faint nebulae containing northern Milky Way portion in direction of galactic anticenter observed with spectral Schmidt camera, noting stellar appearance
09 p1761 A70-23051

Plate reduction method for Schmidt satellite camera, considering satellite position, distortion parameters, etc
11 p2007 A70-26193

- Schmidt photographs reduction, noting film bending during exposure and mean error of satellite position
11 p2007 A70-26195
- Optical Schmidt system shortening with spherical, ellipsoidal and flattened spherical mirrors
19 p3433 A70-38767

SCHMIDT METHOD

- Evolutionary effects associated with quasars listed in 3CR catalog using Schmidt method
07 p1389 A70-20209

SCHMIDT NUMBER

- Prandtl mixing length and effective Schmidt number distributions from wall jet and wake data to predict film cooling
06 p1035 A70-17688

- Mass transfer and velocity gradient fluctuations at wall in two dimensional or rotational flow for large Schmidt numbers
23 p4181 A70-44210

SCHOTTKY EFFECT

U WORK FUNCTIONS

SCHREIBERSITE

- Enstatite chondrites and achondrites electron microprobe analysis for Si, P and Ni in metal grains and associated schreibersite and perryite
10 p1935 A70-23849

SCHROEDINGER EQUATION

- Coupled Schroedinger equations for diatomic molecules internal motion solved using best adiabatic approximation to obtain energy correction to Born-Oppenheimer method
08 p1548 A70-21522

- Operator originated by Schroedinger equation having inhomogeneous boundary conditions on portion of boundary of Hilbert spaces orthogonal sum, defining region of self conjugation
13 p2442 A70-29514

- Radial Schrodinger equation bound state eigenvalues and properties by iterative method, calculating Coulomb potentials
14 p2600 A70-31360

- Classical approach to quantum mechanics, emphasizing Schroedinger equations and starting from Hamilton-Jacobi equations
16 p2990 A70-33778

- Coupled simple harmonic oscillators with almost degenerate energy levels, comparing partitioning perturbation techniques with Rayleigh-Schroedinger approach
16 p2955 A70-34002

- Adiabatic corrections to long range Born-Oppenheimer interatomic potentials from rotationally coupled Schroedinger equations
17 p3138 A70-35199

- Schroedinger equation for hydrogen solved for high pressure behavior of materials, applying to stellar atmospheres and laboratory plasmas
21 p3849 A70-40933

- Stark effect in hydrogen atoms for nonuniform electric fields, considering correction of energy eigenvalues of Schroedinger equation by WKB method
23 p4221 A70-44401

SCHUMANN-RUNGE BANDS

- Transition probabilities for diatomic oxygen Schumann-Runge bands determined from shock tube emission studies
02 p0344 A70-12658

- Thermospheric heating by solar radiation in Schumann-Runge continuum, taking height and atmospheric components distribution into account
23 p4188 A70-44060

SCHWARTZ METHOD

- Generalized boundary value problems solution for elliptic differential equations by Schwarz method, proposing algorithm
18 p3283 A70-36573

SCHWARTZ-CHRISTOFFEL TRANSFORMATION

- Stress distribution around moving cracks in finite width strip, obtaining solutions for boundary conditions by Schwarz-Christoffel transformation and complex functions theory
22 p4116 A70-43025

SCHWARZSCHILD METRIC

- Einstein equations for five dimensional spherically symmetric space solved using gravitational constant without singularities on Schwarzschild sphere
05 p0880 A70-15793

- Einstein-Maxwell equations solutions relation to Robinson and Robinson metrics compared with Reissner-Nordstrom solution relation to Schwarzschild
07 p1333 A70-18961

- Collapse-anticollapse transition near Schwarzschild radius in multitime universe with arbitrary number of time-similar dimensions
07 p1381 A70-19286

- Circular and radial trajectories in Schwarzschild field applied to isolated metagalaxy with charged central body and nonzero cosmological constant
07 p1385 A70-19426

- Schwarzschild metric properties in synchronous reference system, using succession of Schwarzschild interval holonomic transformations as function of gravitational radius
08 p1545 A70-21406

- Schwarzschild exterior metric stability against perturbations from asymptotic behavior of Einstein field equations solution in Kruskal coordinates
18 p3291 A70-36650

- Differential equations for odd and even parity Regge-Wheeler perturbations on Schwarzschild metric
19 p3457 A70-37573

- Schwarzschild solution singularity elimination using Lorentz transform
20 p3673 A70-39998

- Gravitational radiation scattering by Schwarzschild horizon, discussing odd parity waves of angular momentum
21 p3878 A70-40731

- Optical point characteristics of static spherically symmetric space-times of de Sitter universe, Einstein universe and exterior Schwarzschild field
23 p4239 A70-43821

SCHWASSMANN-WACHMANN COMET

- Comet Schwassmann-Wachmann I brightness variations due to interplanetary shock waves in solar wind
22 p4097 A70-42475

SCIATIC NERVE

- Cerebellar cortex reactions to sciatic nerve stimulation in rats under transverse accelerations in centrifuge
05 p0804 A70-17116

- Bioelectrical reactions in anesthetized cats cortical zones in response to stimulation of contralateral sciatic nerve
07 p1199 A70-18722

- Thalamic N.VPL role in distributing afferent flux in anesthetized cats cortex, using stimulating contralateral sciatic nerve
07 p1199 A70-18723

- Hypothalamus influence on potentials and recovery cycles of mesencephalic reticular formation in response to sciatic nerve stimulation in anesthetized rabbits
07 p1204 A70-19138

SCIENTIFIC SATELLITES

NT APPLICATIONS TECHNOLOGY SATELLITES

NT ATS 1

NT ATS 3

NT ATS 5

NT ENVIRONMENTAL RESEARCH SATELLITES

NT ORBITAL SATELLITE

- HEOS-1 satellite development for ESRO to investigate interplanetary magnetic fields, cosmic radiation, solar wind outside magnetosphere and earth shock wave
02 p0382 A70-12646

- Instrumentation system for nuclear experiments on scientific satellites allowing highest priority event selection during telemetry sequence and periodic change of priority order
03 p0453 A70-13024

- ESRO German-built satellite HEOS 1 planned scientific space measurements, required orbit and technical concepts
03 p0580 A70-13798

- European Ultra-Violet Astronomical Satellite (U-VAS) to replace Large Astronomical satellite (LAS) to reduce cost while maintaining scientific objectives
03 p0582 A70-13434

- Pulse width modulation command coder for German research satellite Azur control
04 p0653 A70-15662

- Onboard digital data acquisition instrumentation system for scientific satellites, combining existing functional blocks to obtain different configurations and performances
05 p0818 A70-16587

- HEOS-A2 project development plan for investigating unexplored interplanetary space in eccentric orbit
05 p0923 A70-16588

- Scientific equipment on Cosmos 237 satellite for recording extraterrestrial radiation data, discussing specifications, operation and mission purpose
05 p0851 A70-16733

- Four satellite cluster laboratory in near-earth environment to investigate solar-terrestrial relationships, emphasizing interaction of solar wind and magnetosphere
07 p1387 A70-19711

- Orbiting satellite-borne instruments for scientific observation of earthquakes, volcanic eruptions, atmospheric phenomenon, cyclones, floods and soil erosion
09 p1763 A70-23377

- Italian Sirio project, describing SHF propagation and communication, cosmic ray and confined plasma experiments
11 p2011 A70-26604

- Diamant B satellite launcher testing and construction, discussing DIAL/WIKA scientific satellite launch
12 p2314 A70-28299

- Azur satellite ground control, describing system organization to measure scientific and data information for entire satellite lifetime
13 p2384 A70-28976

- Astronomical Netherlands Satellite (ANS) for carrying out stellar UV and X ray emission experiments
13 p2506 A70-28989

- Atmospheric density effect on satellite lifetime and position prediction, utilizing data from Cannon Ball and SPADES low altitude density research satellites
14 p2653 A70-30562

- Scientific satellites history, projects, technology, coordination and international collaboration
14 p2655 A70-31416

- Small satellites for scientific technological and operational missions, discussing piggyback launching, command, battery storage, telemetry and attitude control systems
15 p2810 A70-31781

- American-German solar probe HELIOS mission parameters for interplanetary and close proximity solar research, discussing spacecraft building and launching
15 p2801 A70-32281

- Space program planning for scientific and application earth satellites, stressing image sensors development
15 p2812 A70-32289

- OGO 5 satellite scientific observations, payloads, parameters and objectives
15 p2812 A70-32364

- Scientific satellites pulse height analyzer and associated threshold detection and logic circuitry
16 p2900 A70-33062

- Sliding electrical contacts for unmanned scientific satellites, discussing Nimbus AVCS camera iris motors
16 p2920 A70-33809

- Mariner Mars 1971 scientific experiments, describing onboard equipment, mission objectives, etc
16 p2983 A70-34026

- ESRO organization, program, locations, establishments and operational and future scientific satellites
17 p3200 A70-35204

- Japanese sounding rockets for space research, discussing missions, launchings, flight tests, etc, of Kappa and MT-135 rockets and M-45 launch vehicle
17 p3177 A70-35205

- UK space program, describing scientific satellites, Black Arrow launch vehicle and sounding rockets
17 p3167 A70-35206

- Heliostationary spacecraft at L2 point for solar wind observation, describing mission, instrumentation and spacecraft design
17 p3168 A70-35252

- Pseudonoise code command system for scientific satellite, describing added bits and decoder
17 p3046 A70-35276

- Scientific satellites orbit determination and improvement procedures for tracking system based on Doppler frequency and angular measurements
17 p3046 A70-35280

- Japanese scientific satellite magnetic attitude and spin rate control system design and computer simulation
18 p3332 A70-36065

- Apollo Command and Service Modules for lunar orbital science missions, discussing spacecraft-experiment integration
21 p3928 A70-40978

- Small scientific satellite design objectives, structural and electrical requirements, components integration, instrumentation, antennas, spin rates, vibrations, sealing, reliability, etc
22 p4110 A70-42497

- Geostationary satellites for magnetosphere and ionosphere sounding, discussing specific observational capabilities
22 p4024 A70-43397

- Scientific satellites nuclear experiments fast low power drain logic system, using AND and NAND gates, pulse generators, delays and bistables
23 p4143 A70-44299

- Scientific satellites evolution during past decade and future development possibilities in conjunction with space shuttles and stations
23 p4260 A70-44621

- Scientific satellite reentry guidance algorithms for inertial system, discussing controllability, onboard computer, gyros, accelerometers, jet actuators, terminal guidance, glide trajectory, etc
23 p4216 A70-44667

SCIENTISTS

- Correlations between organizational factors and individual engineer performance, analyzing stability of relationships and time lags in measurement
02 p0246 A70-12378

- Aerospace scientific and engineering work force movement between geographical areas and resource location
07 p1426 A70-18799

- Team hiring of research scientists by industrial and academic organizations, discussing causes and influence on R and D organizations management and design
07 p1427 A70-19002

SCINTILLATION

Quasar 3C 273 scintillation intensity, considering role of interplanetary plasma inhomogeneities 01 p0174 A70-10199

Radio star and satellite scintillation observation, considering diurnal, seasonal and latitude variations and relationship to magnetic and solar activity 01 p0181 A70-10590

Optical scintillation measurements applied to turbulence diagnostics, inferring spatial spectrum of turbulent scatterers, using Monte Carlo numerical procedure 02 p0296 A70-11892

Ionospheric electron concentration irregularities via satellite signal scintillation analysis, using radio wave diffraction theory 02 p0258 A70-12562

Canary Bird synchronous satellite radio signal transmissions scintillations from recordings, noting diurnal scintillation pattern 02 p0260 A70-12573

Power spectra, modulation indices, frequency distributions and decorrelation frequencies of intensity fluctuations of pulsar radiation consistent with interstellar scintillation theory 05 p0908 A70-16302

Radio sources structure observations of Arecibo Ionospheric Observatory, discussing interplanetary scintillations of galaxies and quasars 06 p1138 A70-17216

Ionosphere disturbances due to high altitude thermonuclear explosions, discussing experimental proof by cosmos satellites short wave transmitter radio signal scintillation statistical evaluation 06 p1057 A70-17888

Satellite signal scintillation phenomenon morphological study and relationship to ionospheric irregularities 07 p1234 A70-19194

Ionospheric inhomogeneities measured by Explorer 22 radio signals emphasizing satellite scintillation 07 p1265 A70-19195

Diffraction pattern drift velocity increase with temporal frequency of Fourier components by dispersion analysis of interplanetary scintillation, noting solar wind structure 07 p1388 A70-20076

Focusing and saturation effects in radio star and satellite signal scintillations based on diffraction and refraction theories 07 p1271 A70-20157

Electron ion recombination role in atomic collision process in rare gases ionization path, considering scintillation mechanism 08 p1549 A70-21815

Stellar scintillation saturation at large zenith angles interpreted in terms of combined dispersion and aperture filtering 09 p1726 A70-22073

Ionospheric scintillations of lunar radar echo components isolation by CW Doppler shift or coherent pulse time delay techniques 10 p1841 A70-24802

F region irregularity model to include field-aligned columns and sheets and frontal irregularity shapes effect on radio star and satellite scintillations 10 p1841 A70-24805

Ionospheric irregularities showing dispersive motions from systematic skewness in cross correlation functions for satellite scintillations at spaced receivers 10 p1881 A70-24810

Scintillation sudden inception in Faraday rotation in Sodankyl and Oulu, noting diurnal north-south frontier movements in polar ionosphere 10 p1884 A70-25262

Angular coordinate during multilevel quantization of radar signal reflected from scintillating body on Gaussian noise background, applying maximum probability method 11 p1996 A70-25347

Satellite signal scintillation spectrum analysis by digital filtering of magnetic tape recording 11 p2012 A70-26718

Radio sources scintillation due to scattering medium with refractive index irregularities under detection of finite bandwidth receiver 13 p2365 A70-29148

Low latitude scintillations from satellite transmission scintillations correlation with solar activity spread F, electron content and ionospheric irregularities 13 p2397 A70-29189

Satellite scintillation index variation with zenith angle and azimuth at ground station 14 p2574 A70-30739

Solar wind turbulence, demonstrating radio source interplanetary scintillation consistent with plasma density correlation 14 p2642 A70-30888

Quasar 3C 298 angular dimensions and 3C 273 scintillating component at 60 MHz based on mean quasi-periods shifts of scintillations 15 p2808 A70-32885

Coherent light propagation through turbulent atmosphere observed by applying He-Ne lasers to simultaneous measurements of scintillation effects over homogeneous optical paths 17 p3108 A70-35721

Radio source 3C 161 scintillating component angular dimensions and flux density at 60 MHz 19 p3524 A70-38760

Radio sources angular dimensions estimation based on shifts in histograms of scintillation quasi-periods 19 p3525 A70-38766

Angular coordinate during multilevel quantization of radar signal reflected from scintillating body on Gaussian noise background, applying maximum probability method 20 p3589 A70-40459

Low latitude F region irregularities from scintillations of beacon satellite signals 20 p3624 A70-40486

Scintillation LF observations with synchronous satellite radio signals at low latitude station, noting magnetic activity effects on night and day scintillations 20 p3590 A70-40488

High scintillation indices associated with vertical spreading of sporadic E layer from minute-by-minute ionograms and signal amplitude recordings from Explorer 22 satellite 20 p3624 A70-40489

High latitude F region irregularity structure during magnetic storm from multistation scintillation observations of ATS 3 transmission 20 p3624 A70-40490

Ionospheric electron density disturbance heights measured via radio signal scintillation from earth satellite, using spaced receiver method 20 p3590 A70-40491

Microwave scintillations at sunrise indicating solar point sources at sunspot cycle peak and terrain configuration influence on ionospheric disturbances 20 p3591 A70-40493

Low latitude observations of spread F echoes and stationary satellite scintillations, correlating with ionospheric disturbances and geomagnetic activity 21 p3818 A70-41097

Synchronous satellites VHF signal fading attributed to high latitude scintillations, noting intensity at night and during magnetic storms 21 p3790 A70-41362

Weak-scattering limit in thin screen model of interplanetary scintillations of radio sources involving solar wind fluctuations at Fresnel scale 22 p4104 A70-42996

Scintillation index correlation with mean wind velocity of jet streams 22 p4020 A70-43262

F region ionospheric disturbances size and shape from radio amplitude and phase scintillations in satellite transmission to ground stations 23 p4187 A70-43879

SCINTILLATION COUNTERS

Scintillation resolving power in radioactivity measurements, discussing mathematical principle of division of radioisotope concentration in biological experiments 01 p0040 A70-11404

Scintillation counters hodoscope system for studying spatial distribution of muon and muon-number fluctuations in extensive air showers 03 p0482 A70-13042

Light-gathering amplitude and intrinsic resolution of large-area flat scintillation detectors used for cosmic rays-nuclear interaction experiments at high energies 03 p0484 A70-13466

Light collecting properties of polystyrene scintillator designed for counting particles of electron-photon showers generated by high energy cosmic ray particles 05 p0846 A70-15944

Deuteron splitting by solar neutrinos for neutrino detection, describing deuterium scintillation detector characteristics 05 p0899 A70-15954

Scintillation spectrometer design for mass and energy spectra of elementary particles, discussing block diagram 05 p0846 A70-15962

Pulse characteristics of scintillator-photomultiplier-cathode ray tube channel for oscillographic recording of nanosecond pulses from neutron, gamma or X ray sources 08 p1496 A70-21218

Whole body counters as standard measuring devices in nuclear medicine and radiation protection, using scintillation detector principles 09 p1624 A70-22819

Satellite-borne scintillation spectrometers for medium and high energy electron and proton measurements 10 p1931 A70-24315

Cosmic ray muons continuous recordings, describing design and performance of plastic scintillators with photomultipliers 10 p1889 A70-24489

Cosmic gamma rays observation by balloon flight and satellite with scintillation detector, tabulating counting rates in pulse height channels relative to Crab Nebula 12 p2292 A70-27387

Particle spectrometer for Apollo measurements of trapped protons and electrons, using directional telescope composed of solid state and scintillation counters 12 p2232 A70-27404

Muon intensity meter for cosmic ray muon flux underground using scintillation telescope consisting of two coincidence counters 12 p2295 A70-28176

Scintillation and semiconductor counters - IEEE Conference, Washington, D.C., March 1970 14 p2586 A70-31001

Photomultiplier tubes for liquid scintillation equipment, emphasizing detection efficiency and coincidence background 14 p2587 A70-31005

NaI scintillation spectrometer response function matrices semiautomatic generation, using standard source spectra to obtain normalized Compton continua 14 p2587 A70-31006

Anthracene, polystyrene and stilbene for scintillation counters measuring cosmic ray protons, analyzing dosimetric properties 17 p3151 A70-35352

Liquid scintillator neutron spectrometer using pulse shape discrimination and two parameter analyzer 18 p3290 A70-36563

Light gathering nonuniformity in cylindrical plastic scintillator, analyzing detector signal amplitudes for various pulsed light source positions 20 p3629 A70-39318

Organic liquid scintillators with high transparency, describing optical and chemical properties 20 p3629 A70-39319

Scintillator-film neutron radiography converter combinations efficiency gain for small sources by cooling 24 p4376 A70-45751

SCINTILLATION SPECTROMETERS
U SCINTILLATION COUNTERS
U SPECTROMETERS
SCINTILLATORS
U SCINTILLATION COUNTERS
SCINTILLOMETERS
U SCINTILLATION COUNTERS
SCISSION
U CLEAVAGE
SCORING
Analytical scoring model design for effective evaluation of competing research and development projects 02 p0402 A70-12634

SCORPIO CONSTELLATION
U SCORPIUS CONSTELLATION
SCORPIUS CONSTELLATION
X ray line emission from Sco X-1 using Monte Carlo estimates of spectral distribution of scattered photons in terms of Fe line and cosmic abundance 01 p0169 A70-10338

Sco X-1 high energy X ray emission intensity changes observed by balloon-borne telescope 01 p0169 A70-10346

Radial velocities determined from prism spectrograms for O and B stars in Milky Way field in Scorpius 02 p0369 A70-12062

X ray source Sco XR-1 proper motion using photometry, suggesting association with Scorpius-Centaurus complex of young disk stars 02 p0372 A70-12248

X rays from Sco XR-1 compared with galactic cosmic rays and solar Lyman alpha radiation to determine ionospheric ionization causing radio wave attenuation 06 p1134 A70-17443

Sco X-1 simultaneous X ray and optical flares correlation and X ray enhancements 08 p1561 A70-20900

Elongated neutral-hydrogen emission feature in Sco-Oph region, comparing with interstellar sodium lines for distance from sun 10 p1945 A70-24966

X ray scattering by interstellar grains in direction of Crab pulsar and Sco XR-1 10 p1933 A70-25044

Radial velocities of supergiant distant stars in southern Milky Way regions of I Sco Association 11 p2113 A70-26465

Scorpio X-1 and Taurus X-1 /Crab/ X ray flux effects on nighttime ionospheric radio transmission, discussing ion production and resulting electron density 14 p2631 A70-30541

Hard X rays from Sco X-1, discussing high energy excess with large temporal variations 15 p2795 A70-32772

Simultaneous measurement of optical and X ray emission from Scorpius X-1 and X ray diffuse background, using rocket-borne scintillation counter 17 p3157 A70-34831

H 2 regions in Sc galaxies NGC 628, 4254 and 5194 18 p3327 A70-37159

Sco X-1 X ray source properties in 16-111 keV energy interval, using balloon-borne detectors 19 p3505 A70-38116

Hard X ray sources energy spectra in 20-120 keV range by balloon flights, presenting Sco X-1 intensities 21 p3872 A70-40660

X ray intensity sudden changes in 29.9-52.3 keV range from Sco X-1, correcting for atmospheric attenuation 21 p3872 A70-40661

Sco X-1 X ray emission data from rocket-borne measurement, indicating Fe K-emission from high ionization states 21 p3873 A70-40667

Sco X-1 radio emission models, considering possible binary nature and thermal bremsstrahlung 21 p3875 A70-40685

Sco X-1 extar high energy radiation production, discussing relativistic electron synchrotron emission and magnetic fluctuations spectrum 21 p3878 A70-40709

Scorpius X-1 X ray line emission, discussing continuum and background counts and cosmic abundance of iron 22 p4094 A70-42931

Simultaneous X ray and optical observations of Scorpius XR-1, comparing rocket data from various flights 22 p4094 A70-42987

Daytime ionospheric effect of X ray flare from SCO XR-1, discussing LF radio wave intensity decrease 22 p4095 A70-43165

Interstellar matter in Scorpius constellation, discussing star counting, gas identification, etc 23 p4254 A70-44901

Sco XR-1 optical intensity power spectra oscillations searched for in pulsar frequencies and fundamental radial mode vibrations in white dwarfs and neutron stars 24 p4410 A70-45762

SCOUT LAUNCH VEHICLE
Scout missile destruct charge system premature operational response to high temperature environment caused by combustion gas leak during stage separation 03 p0550 A70-14140

SCR [RECTIFIERS]
U SILICON CONTROLLED RECTIFIERS

SCRAMBLING [COMMUNICATION]
Optimum interleavers realization procedure for reordering contiguous symbols sequence to satisfy minimum distance requirement for improving communication system performance 14 p2554 A70-31121

SCRAMJET ENGINES
U SUPERSONIC COMBUSTION RAMJET ENGINES

SCRAMJETS
U SUPERSONIC COMBUSTION RAMJET ENGINES

SCREEN EFFECT
Reflection and transmission characteristics of screens in duct obstructing shock propagating in unsteady compressible fluid, describing theoretical models and experimental detection 01 p0060 A70-10224

Vertical electric dipole transient response over circular ground screen, studying low angle radiation patterns 06 p1021 A70-17573

Effective potential of electron screening of Coulomb nuclei field leading to thermonuclear reaction rate increase using self consistent field method 07 p1346 A70-20206

Electric dipole emission near ideally conducting screen with variable surface impedance parallel strips, analyzing radiation pattern 09 p1636 A70-23140

Granularity spectrum of diffusing screen uniformly illuminated by normally incident coherent light, basing study on long and short distance visual observations 10 p1899 A70-24031

Asymmetric cross correlation functions in D and lower E region drift measurements interpreted in terms of moving screens 10 p1881 A70-24811

Radiation patterns of slots in flat and curved screens using open waveguide emission theory 13 p2378 A70-29305

Sound passage through rigid screen of arbitrary wave thickness with apertures, using linear algebraic equations 18 p3291 A70-36306

SCREENING
Subcontracting for cost optimal parts screening, discussing negotiations and reliability requirements 15 p2747 A70-32651

SCREENS
Vertical Hertzian doublet with large circular screen placed above earth, calculating radiation pattern, directive gain, efficiency and radiation resistance 09 p1637 A70-23152

Diffraction effects for bilinear screen with irregular apertures determined using correction weighting function for solution 09 p1639 A70-23668

Transmission coefficient for perforated screen related to orientation of rectangular and cross shaped

narrow openings and field polarization during normal wave incidence 12 p2191 A70-28174

Dielectric layer and screen heat loss effects on diffraction radiation in resonant waveguide 19 p3377 A70-37725

Planar conducting screen with periodic rectangular perforations, determining transmission and reflection coefficients and aperture field distribution 24 p4311 A70-45219

SCREW DISLOCATIONS

Shear moduli and lattice parameters effect on screw dislocation equilibrium in bimetallic medium of soft and hard phases 03 p0587 A70-13117

Steady creep process microscopic mechanisms, discussing creep due to glide of jogged screw dislocations, climbing of edge dislocations and stress directed vacancy diffusion 08 p1593 A70-21519

Double ended dislocation pileups and elastic cracks at bimaterial interface under screw, edge and shear modes 15 p2756 A70-31561

Elastic properties of dislocations in Ti basal, prismatic and pyramidal slip systems, discussing dilatational fields of edge and screw dislocations 17 p3115 A70-34385

Isotropic body screw dislocations, using finite elasticity approach 17 p3190 A70-35453

Elastic properties of complex screw dislocation arrays from equations for stress fields of dislocation segments 17 p3190 A70-35455

Superlattice stacking faults in plastically deformed nickel aluminate [gamma prime phase] due to interaction of antiphase boundary /APB/ type dislocation pairs 19 p3451 A70-37704

Half plane with stress-free surface deformed by protrusions or notches, deriving edge force or screw dislocation by linear elastic analysis 21 p3939 A70-42028

Stress fields of screw and edge dislocations in linearly elastic isotropic Cosserat continuum using stress functions 23 p4266 A70-44022

Cross slip between screw dislocations coplanar arrays in Ti-Al alloy, noting fringe pattern and bowing absence 24 p4359 A70-45248

SCREWS

Differential screw gauge for determining micrometer screw periodic errors and error components in level triers, using Rydberg method 04 p0693 A70-15488

SCRIBING**U SCORING****SCUTUM CONSTELLATION**

Delta Scuti stars, determining consistent absolute magnitudes by Stromgren intermediate band colors and Crawford photoelectric H beta indices 17 p3171 A70-35443

Neutral hydrogen observations in Sagittarius and Scutum spiral arms, examining circular galactic rotation by density wave theory kinematic models 18 p3331 A70-37197

SDP [COMPUTERS]**U SITE DATA PROCESSORS****SEA KNIGHT HELICOPTER****U CH-46 HELICOPTER****SEA ROUGHNESS**

Sun glitter on sea surface from space photographs, considering wind and sea conditions effect on shape and brightness of patterns 14 p2572 A70-30345

SEA STATES

Microwave radiometric temperature measurements generating curves relating sea state and surface temperature 12 p2215 A70-26903

Passive remote sensing in microwave spectra for oceanographic applications including sea state, pollution and sea ice properties 12 p2216 A70-26905

State of sea definition for hovercraft performance purposes, recommending Hovercraft Coastal Wind Wave Code 13 p2347 A70-29126

Criticism of theory for cosmogenic tritium produced oceanic He 3 excess 21 p3920 A70-41883

Sea surface temperature determination from satellite high resolution IR window radiation measurements by statistical histogram inference method 21 p3820 A70-42122

SEA WATER

Wind velocity longitudinal profile measurements in atmospheric boundary layer over rough sea surface using floating beacon and statistical analysis of airflow perturbations 04 p0715 A70-15253

Radar signal amplitude fluctuations reflected from disturbed sea water surface, noting wind induced waving stochastic nature influence 05 p0812 A70-16246

Electric and magnetic fields of waterspouts measured by instrumented U.S. Navy aircraft 06 p1101 A70-18582

Microwave radiometric techniques for continuous all-weather remote sensing of sea conditions from satellites, discussing foam and surface ripple effects [AIAA PAPER 70-318] 09 p1677 A70-22869

Sea surface temperature measurement over large areas using IR remote sensing system mounted on airborne platform 09 p1686 A70-23756

Metals, alloys and galvanic couples corrosion rates in synthetic seawater measured by polarization technique 10 p1887 A70-24044

PH variation effect on sea water on stress corrosion cracking behavior of Ti alloys 13 p2435 A70-29174

Radio waves attenuation anisotropy in sea ice by comparing vertically and horizontally polarized signals 14 p2546 A70-30132

Sea water temperature and salinity effects on smooth ocean surface radiation in centimeter range 18 p3250 A70-36968

Submarine basalt sea water alteration effects, examining Sr and rare earth concentrations, Ba enrichments or depletions and trace element data 19 p3413 A70-38015

SEALANTS**U SEALERS****SEALERS**

Defects development in cermet materials sealing elements in high O content gas flows of turboprop and turbojet engines 01 p0161 A70-10160

Chemical composition of cermet material for radial sealing of high temperature gas turbines, ensuring structural stability and oxidation resistance 01 p0124 A70-11621

Thermal stability of turbine sealant mica-ceramic materials containing boron nitride 04 p0712 A70-14467

Bonding and sealing of fluid amplifiers with epoxy resin dry-film adhesive, noting low rejects rate 12 p2164 A70-27075

Elastomeric seals and sealants selection for SST, describing tests in air, fuel vapors and hydraulic fluids at elevated temperatures 13 p2418 A70-28668

Inhibitive elastomeric sealing compounds and coating systems preventing aluminum alloy corrosion in aircraft 13 p2433 A70-28778

SEALING**NT SELF SEALING**

Sealing mechanism theory with face seal applications, taking into account load carrying capacity and no leakage pressure gradient [ASLE FICFS PREPRINT 18] 02 p0308 A70-12172

Load support and leakage from microasperity lubricated face seals, developing hydrodynamic lubricant films [ASLE FICFS PREPRINT 21] 02 p0308 A70-12174

Hydrodynamic sealing action resulting from helical grooving machined into shaft or lip of radial seal, describing pressure gradients role 08 p1507 A70-21268

Fluid sealing - ASLE-ASME Conference, Philadelphia, May 1969 13 p2416 A70-28609

Controlled leakage sealing of hydrodynamic bearing lubrication systems for space vehicles in synchronous orbit 16 p2923 A70-34158

One-step closure sealing of pressurized stainless steel capillary tubes by resistance pinch welding 21 p3832 A70-40789

Molybdenum disilicate and aluminum oxide coating sealing heat resistance tests 24 p4364 A70-46341

SEALS [STOPPERS]**NT HERMETIC SEALS****NT O RING SEALS****NT PLUGS****NT PUMP SEALS**

Electrical lead sealing in hydrostatic high pressure systems with gaseous pressure transmitting medium, considering piston cone seals, frozen oil seals, epoxy seals, etc 01 p0104 A70-10744

Spiral grooved turbulent screw seal /viscoseal/ analysis, combining results of spiral grooved journal bearing study with turbulent fluid film theory [ASLE FICFS PREPRINT 32] 02 p0308 A70-12169

Misalignment and eccentricity effect on face seal, discussing leakage dependence on phase angle [ASLE FICFS PREPRINT 15A] 02 p0308 A70-12171

Sealing mechanism theory with face seal applications, taking into account load carrying capacity and no leakage pressure gradient
[ASLE FICFS PREPRINT 18] 02 p0308 A70-12172

Lubrication and leakage control mechanics of face seals, considering liquid to vapor boundary within interface
[ASLE FICFS PREPRINT 22] 02 p0308 A70-12173

Noncontacting minimum leakage dynamic seals requiring liquid-vapor interface with leakage tolerance
[ASLE FICFS PREPRINT 40] 02 p0308 A70-12175

Eccentric face seal with tangentially varying film thickness, analyzing leakage flow proportional to eccentricity and surface waviness
[ASLE FICFS PREPRINT 15B] 02 p0308 A70-12176

Free molecular mass flow rate through vacuum seal separating two rarefied gas environments, using coupled integral equations formulated on kinetic theory
[ASME PAPER 69-WA/FE-18] 04 p0625 A70-14779

Allowable leakage guidelines for in-service aircraft hydraulic components, discussing causes and measurements, tabulating rates for static and dynamic seals
05 p0797 A70-15776

Back-up rings and special sealing devices performance qualification testing specifications
[SAE-ARP-979] 07 p1290 A70-18802

Lip and face seal lubrication used on rotating shafts operating in compartments with fluids under pressure
07 p1293 A70-18895

Hydrodynamic sealing action resulting from helical grooving machined into shaft or lip of radial seal, describing pressure gradients role
08 p1507 A70-21268

Sputtering method used for applying metalizing layer to ceramics in producing ceramic to metal seals
10 p1895 A70-24555

Model testing gas flow calculation in system emitting electron beam into atmosphere through supersonic gas seal
10 p1895 A70-24590

Hydromechanics and thermodynamics in mechanical radial face seal design
11 p2059 A70-25792

Book on mechanical seals design covering temperature and pressure effects, leakage and wear problems, etc
12 p2238 A70-26851

Hydraulic seals for fire resistant fluids in hydraulic equipment, describing computerized designs
13 p2416 A70-28610

Mechanical seals ringing sound relationship with heat transfer and interfacial conditions, noting sliding surfaces temperature effect
13 p2417 A70-28611

Thermohydrodynamic seals design, properties and performance compared with standard mechanical seals
13 p2417 A70-28612

Film cavitation between flat annular surfaces in face seal resulting from hydrodynamic pressure generated by misalignment and surface waviness
13 p2417 A70-28613

Self energized hydrostatic shaft seal operating with incompressible fluid in laminar flow regime, using general lubrication theory
13 p2417 A70-28614

Elastomeric seals and sealants selection for SST, describing tests in air, fuel vapors and hydraulic fluids at elevated temperatures
13 p2418 A70-28668

Friction and wear effects on leakage path in sliding seal interface
16 p2916 A70-33078

Dynamic seal effectiveness prediction, considering bearing and sealing pressure distributions, friction coefficient, flow characteristics, etc
[ASME PAPER 70-DE-53] 16 p2918 A70-33514

Liquid fluorine feed system valves, seals and seats, discussing design criteria for flight weight components
[AIAA PAPER 70-705] 16 p2844 A70-33564

Teflon bucket and Be-Cu cap seal against hydrostatic pressure, discussing applications for high pressure superconductivity measurements
18 p3262 A70-37097

Turbulent viscoseal with gas-liquid interface, using recirculation loop for gas ingestion reduction
[ASLE PREPRINT 70AM 5C-4] 19 p3439 A70-38804

Oil seals service life as function of friction horsepower
[ASLE PREPRINT 70AM 5C-1] 19 p3439 A70-38807

Postmechanical interface separation in elastically supported rotary face seals under input excitation
[ASLE PREPRINT 70AM 3C-3] 19 p3439 A70-38808

Dry face mechanical shaft seal operating on self generated graphitic film without boundary fluid lubrication
[ASLE PREPRINT 70AM 3C-2] 19 p3439 A70-38809

Low friction seal for axial loading piston in triaxial soil testing cells
23 p4199 A70-43873

Pneumatic actuator rod and piston head seals, examining materials at various temperatures, pressures and speeds
[SAE PAPER 700791] 24 p4294 A70-45855

SEAMS [JOINTS]
Bar butt current penetration welding, using HF continuous current seam welding process for joining finite length pieces
22 p4046 A70-43148

Materials for glass-metal compressed joints, tabulating stress and thermal expansion coefficients
22 p3999 A70-43447

SEAPLANES
Water tests with N 300 Naviplanes confirming flexible skirt concept regarding speeds and stability
08 p1435 A70-20622

Passenger seaplanes virtues and drawbacks, discussing bases, servicing, refueling, passenger conveyance, prospects, etc
23 p4137 A70-43887

SEARCH PROFILES
Correction method for single frequency search in extremal control of continuous quick response multivariable plants
04 p0662 A70-15434

Search optimization for object drifting in outer space, considering approximate location and speed
17 p3172 A70-35668

Optimal control of coordinate space cells inspection order during search for unknown number of objects
22 p3999 A70-42552

SEARCH RADAR
Phased array radar for automatic random search using pseudorandom sequences to generate random phase characteristics of currents together with suitable gating
12 p2183 A70-26984

Subclutter visibility /SCV/, resolution and interclutter of MTI or Doppler search radars in land, sea and weather clutter
12 p2188 A70-27940

Search radar antennas for monopulse direction finding with radiation pattern for sum and difference operation
15 p2704 A70-32674

SEARCHING
NT SEARCH PROFILES
Optimal strategy for searching for object hidden in box involving use of optimal return function
05 p0877 A70-16715

Search and rescue /SAR/ concepts behind advanced NAV systems, emphasizing flying ejection seat /AER-CAB/ for air to air self rescue
07 p1192 A70-19024

Noise effects on joint operation of signal follow-up system with search device using semi-Markov random technique
08 p1461 A70-20864

Visual search activity decrease observed as function of time-on-task for skilled and unskilled helicopter pilots, recording eye movements and blinks
09 p1628 A70-23463

Search duration distribution of two stage lock-on indicator scanning signal search systems, using regenerative random process and integral recovery equation
15 p2696 A70-31501

Optimal search algorithm for stationary object hidden in one of N regions with a priori probability
15 p2767 A70-31843

Eye movements during visual search and meaningless pattern discrimination
19 p3361 A70-38054

Iterative adaptation algorithms, using automatic search techniques for single and multiparameter systems
19 p3394 A70-38163

SEARCHLIGHTS
Xenon arc lamp searchlight performance and application during Apollo 8 launch
12 p2207 A70-27662

Vertical tropospheric turbidity distribution determination from intensity measurements of inclined searchlight beams
13 p2445 A70-29471

SEAS
NT MEDITERRANEAN SEA
Passive microwave observation from space of sea surface degraded by atmosphere
[AIAA PAPER 70-197] 06 p1010 A70-18087

Fraunhofer line discriminator /FLD/ used for airborne fluorometer applicable to marine and estuarine studies
09 p1681 A70-23350

SEASONAL VARIATIONS
U ANNUAL VARIATIONS
SEASONS
NT SUMMER
NT WINTER

Favorable air mass type and season for long cross country soaring flights over eastern U.S. determined from record analysis
09 p1718 A70-23062

Physiological reactions of humans to orthostatic heat tolerance and natural acclimatization in summer and winter using tilt-table test and bicycle ergometer
12 p2169 A70-27656

SEAT BELTS
Aircraft passenger tie-down failure, comparing injury patterns in various accidents to aid reconstruction
17 p3039 A70-35572

Aircraft crash protection with preinflated air bag added to conventional seat/lap belt tested with human sled subjects
23 p4140 A70-44456

Near fatal crash in T-33 aircraft, discussing protective clothing, seat harnesses, bodily position and mental attitude
23 p4153 A70-44497

SEATS
NT EJECTION SEATS
Radiography of spine in seated position, discussing aircraft seats, aeronautical ergonomics, etc
05 p0804 A70-15765

General aviation aircraft styling and interior developments, describing seat construction role in personalized aircraft production costs
[SAE PAPER 700232] 11 p1980 A70-25901

SECANTS
U TRIGONOMETRIC FUNCTIONS
SECONDARY AIR
U AIR
SECONDARY COSMIC RAYS
Secondary corpuscular stream effect on diurnal variations in cosmic ray intensity obtained from statistical analysis
01 p0172 A70-11524

Excess radiation in equatorial regions studied on-board Cosmos 137, noting contribution of primary particle multiplication to secondary radiation
01 p0192 A70-11542

High altitude balloon measurements of secondary gamma quanta intensity vertical distribution, using scintillation counter with CsI/Tl crystal
01 p0172 A70-11544

Angular distribution and production probability of secondary shower particles produced by high energy cosmic ray muons using scintillation counter facility
05 p0899 A70-15957

Electromagnetic structure of interplanetary space on basis of secondary cosmic ray intensity gradient annual variations as function of earth heliographic latitude
05 p0900 A70-15970

Cosmic gamma ray spectrum from secondary neutral pion production in p-p interactions, discussing delta isobar, fireball and nuclear interactions effects
11 p2106 A70-26707

Vertical secondary cosmic gamma spectra from primary nucleon and electron spectra, discussing effects of solar cycle and geomagnetic cut-off
18 p3308 A70-36500

Secondary cosmic ray muon inelasticity in high energy neutrino interactions for deep mine experiments, using lepton current
21 p3845 A70-41139

SECONDARY EMISSION
Spacecraft surface secondary electron emission effects on electron trap measurements in magnetosphere and solar wind, noting agreement with positive ion densities
03 p0561 A70-13994

Physical conditions required to explain observations of radio galaxies through electrons of secondary origin, considering spectral characteristics and evolution
04 p0742 A70-15716

Neutron flux measurements on Cosmos 53, equipment and calculation of secondary neutrons due to bombardment of satellite components
05 p0905 A70-17112

Secondary electron emission coefficients and energy distributions to investigate interaction between positive ions and Cu/Be dynodes of electron multiplier
07 p1344 A70-20127

Low energy ions incidence angle effects on secondary electron emission from molybdenum cylinders in low pressure plasma, noting role of Langmuir sheath around target
07 p1355 A70-20356

Fireball detection and discovery, investigating angular distribution of secondary particles using Van Hove and Amati theory
09 p1747 A70-23729

Foil decarbonization process monitored by mass spectrometry of secondary carbon ion emission
12 p2254 A70-27311

Pulsed electron beam irradiated dielectrics secondary electron emission in vacuum, emphasizing inelastic scattering
13 p2471 A70-29409

Solar Monitoring Experiment program, observing solar activity relation to large enhancements of lower stratosphere secondary radiation

15 p2792 A70-31656

Open type secondary electron multipliers, discussing circuitry, emission recording, component materials and performance

16 p2873 A70-33231

SECONDARY FLOW

Secondary velocities analysis in turbulent boundary layer in dihedral interior based on turbulence anisotropy and effects on wall pressure gradient

03 p0471 A70-14354

Secondary vortex generation in near wake of circular cylinders under forced oscillation, analyzing motion dependent transition regimes using hydrogen bubbles flow visualization

[AIAA PAPER 69-755] 06 p1032 A70-17212

Hydraulic loss and secondary circulation of fluid flow in three dimensional bend commercial conduits, discussing relationship to velocity distribution

10 p1871 A70-25094

Viscous incompressible fluid secondary steady state flow due to rotating spheroid, considering acceleration terms in Stokes linear equation solution

11 p2034 A70-25390

Wall shear stress distribution in rectangular ducts, discussing secondary currents and main flow prediction

11 p2035 A70-25779

Centrifugal impellers primary and secondary flows velocity distributions, determining vorticity generation

18 p3243 A70-36871

Secondary flow model for planetary boundary layer, considering flow as finite perturbation

21 p3813 A70-40904

Rocket roll control by secondary compressed air injection via slender fins inserted into nozzle convergent

21 p3931 A70-41953

Injection slot geometry effect on gas film cooling, discussing effect of secondary stream acceleration

21 p3952 A70-42084

Analytical evaluation of secondary flow injection effects on rocket engine performance including cold flow and simulated hot flow data

23 p4233 A70-44516

SECONDARY HARMONIC GENERATION

U HARMONIC GENERATIONS

SECONDARY INJECTION

Optimization of control forces in rocket nozzles produced by multipoint secondary gaseous injection

05 p0923 A70-15889

Pressure distribution on flat plate resulting from potential incompressible flow interaction between secondary jet and subsonic mainstream

07 p1190 A70-20415

Injectant stagnation temperature and molecular weight variation effect on flow field generated from secondary gas injection into supersonic stream

[AIAA PAPER 69-1] 09 p1733 A70-23217

Secondary peripheral air injection effects on subsonic airflow through slotted tube, discussing primary flow, flow separation, static and stagnation pressures and temperature changes

11 p2036 A70-26140

Flow disturbances and side forces in supersonic rocket nozzle due to gaseous secondary injection analyzed by semiempirical models

14 p2629 A70-30756

Mass flow rate and geometry effects on pressure recovery of conical diffusers with annular secondary injection at inlet

[ASME PAPER 70-FE-18] 16 p2835 A70-33631

Two dimensional sonic secondary fluid jet interaction with uniform primary supersonic stream in wind tunnel

[ASME PAPER 70-FE-33] 16 p2835 A70-33638

Turbine engine combustion chambers with various frontal devices, investigating burnout mechanism and heat yield in secondary air flow injection zone

19 p3489 A70-37246

SECONDARY RADAR

Secondary surveillance radar to operate autonomously with digital techniques and digital handling systems, discussing design and ATC applications

02 p0266 A70-11957

Defruiter suppressing nonsynchronous responses /fruits/ in secondary surveillance radar systems, discussing effects on target detection probability

02 p0263 A70-12786

Secondary radar application to assist ATC achieving air to ground communications reduction

08 p1541 A70-21020

Stable moored ocean platforms providing reliable VHF communications and secondary surveillance radar facilities for civil aviation operations over North Atlantic

09 p1723 A70-23035

SECONDARY WAVES

U S WAVES

SECRECTIONS

NT ENDOCRINE SECRECTIONS

NT HORMONES

NT INSULIN

NT SWEAT

Mathematical model for rats nonlinear time-varying glucocorticoid secretion control mechanism, obtaining time dependent characteristics of hypothalamic-hypophyseal complex

12 p2174 A70-26893

Structure and function of juxtaglomerular apparatus of kidneys controlling synthesis and secretion of renin

24 p4305 A70-46392

SECULAR PERTURBATION

U LONG TERM EFFECTS

SEDATIVES

Differential effect of hypobaric hypoxia on depressive characteristics of sodium barbital, sodium pentobarbital and chloral hydrate in rats and mice

04 p0631 A70-14680

SEDIMENTARY ROCKS

NT CARBONACEOUS ROCKS

NT LIMESTONE

NT SHALES

Hydrocarbon contents of two sediments from Scottish Carboniferous Formation, examining isoprenoid alkanes abiogenesis

01 p0041 A70-10038

Australasian microtektite compositional trends compared with critical plots enabling distinction between rocks formed by igneous sedimentary and vapor fractionation processes

06 p1150 A70-18477

Lunar seismogram response behavior in terms of power law model of sedimentary earth rock anelasticity

13 p2497 A70-29856

Lateral compression of rocks and global shells multilayers, using equations for buckling of single free stratum

18 p3255 A70-37076

Remote sensing of returning reflected and diffracted seismic waves illuminating layered rocks subsurface, discussing data visual display

22 p4018 A70-43085

SEDIMENTS

Reworking of deep-sea sediments as indicated by vertical dispersion of Australasian and Ivory Coast microtektite horizons, implying years of deposition

01 p0178 A70-10474

Gas chromatography and mass spectroscopy study of fatty acids and hydroxy acids in 5000 year sediment from English Lake District

02 p0252 A70-12507

Hydrocarbons and fatty acids distribution in living organisms, fossils, sediments and crude oils, discussing slow thermal maturation role and geological applications

02 p0252 A70-12520

Gas chromatographic-mass spectrometric identification of aliphatic hydroxy acids in plants and sediments

02 p0252 A70-12521

Erythrocyte sedimentation rate in chicken blood predictable by Stokes equation

02 p0238 A70-12547

Fatty acids and aliphatic hydrocarbons in 3.4 billion year old metamorphosed sediment, suggesting biological origin

03 p0475 A70-13820

Pleural space of dogs investigated by spheres injection of varying density and diameter, discussing sedimentation velocities

03 p0429 A70-14160

Hydrocarbon distribution of various algae and bacteria, discussing hydrocarbons diagenesis and biological transformations in sediments

06 p0997 A70-18401

Three dimensional unsteady and steady sediment distribution obtained by Monte Carlo simulation method, using stochastic hydrodynamics model for transport

07 p1255 A70-19103

Shallow water bottom biota, sediments and morphology determination by aerial and satellite photography

17 p3079 A70-35620

SEEBECK COEFFICIENT

U SEEBECK EFFECT

SEEBECK EFFECT

Metallic thermoelectric materials, measuring electrical resistivities and Seebeck coefficients of binary Ni alloys

14 p2533 A70-30530

SEEDING (INOCULATION)

U INOCULATION

SEEDS

Antiradiation chemical substances for modifying radiation damage in peas during seed irradiation with fast neutrons

07 p1208 A70-19510

Spaceflight effects on dry crepis capillaris seeds in five day orbit, showing chromosome rearrangements and increased mutagenic sensitivity

10 p1811 A70-24323

Orbital space flight effects on dry barley seeds, noting increased intracellular rearrangements

10 p1811 A70-24324

Antiradiation chemical substances for modifying radiation damage in peas during seed irradiation with fast neutrons

11 p1988 A70-26109

Wheat seedlings cellular response to weightlessness during NASA Biosatellite II flight compared with simulated weightlessness effects

15 p2688 A70-31662

SEEKERS

U HOMING DEVICES

SEGREGATION

U SEPARATION

SEISMIC ENERGY

Meteoroid impacts as sources of seismic energy on moon, using projectile impact coupling to seismic waves in vacuum chamber experiment

04 p0751 A70-15056

Lunar elastic waves anomalous propagation, considering Apollo seismographic records and earth rocks specific dissipation function measurements

13 p2486 A70-28617

Vacuum effect on explosive coupling seismic energy considered in lunar geophysical experiment

16 p2896 A70-33092

Thermoelastic seismic-energy release as source mechanism for volcanic earthquakes, describing thermal microfracture tests

20 p3619 A70-39217

Isotropic finite strain expressions for compressional and shear velocities, noting no discrepancy with ultrasonic and seismic data

20 p3619 A70-39218

SEISMIC WAVES

NT LOVE WAVES

NT MICROSEISMS

NT RAYLEIGH WAVES

Optical wave front reconstruction principles applied to sonic and seismic wave holography for mapping earth subsurface structure

05 p0850 A70-16685

Seismic refraction profiles of ash flow in Valley of Ten Thousand Smokes, Alaska, obtaining P wave velocities

14 p2573 A70-30493

Body waves in lunar models, calculating travel times and amplitudes

14 p2638 A70-30674

Observational errors effects on surface waves resolution, describing shear velocity determination in crust and mantle from observed waves

16 p2897 A70-33647

Ionospheric acoustic wave propagation from seismic waves of Kurile Islands earthquake on 11 August 1969

17 p3075 A70-34569

Finite difference time integration method for computing seismic ray intensities

19 p3412 A70-37837

Seismic wave attenuation mechanisms emphasizing partial melting, grain boundary relaxation and high temperature internal friction background

19 p3416 A70-38440

Seismic measurements at inertial test facilities, considering vibration environment relevant to single degree of freedom gyroscope performance tests

[AIAA PAPER 70-951] 20 p3606 A70-39576

Seismic signal by Apollo 12 lunar module impact indicating deep layer of powder by signal propagation

21 p3920 A70-41894

Remote sensing of returning reflected and diffracted seismic waves illuminating layered rocks subsurface, discussing data visual display

22 p4018 A70-43085

Computer-based seismic data acquisition system using digital vibroseis process for eliminating low signal to noise ratio characteristics

22 p4038 A70-43092

SEISMOGRAPHS

NT LUNAR SEISMOGRAPHS

Displacement and velocity measurements using strain gauges, linear potentiometers and seismic transducers

15 p2743 A70-32799

Phase delay of solid earth tide, minimizing ocean and atmosphere loading by strain seismograph measurement

18 p3255 A70-37077

SEISMOLOGY

Neutron star vulcanism and seismicity, discussing neutron star volcano size and shape possibilities

04 p0753 A70-15070

Seismology as tool for investigation of planets, discussing earth rigidity, tides and long period oscillations

11 p2111 A70-26040

Seismic measurements of sonic boom induced ground vibrations for hazard to structures

12 p2227 A70-28078

Lunar seismogram response behavior in terms of power law model of sedimentary earth rock anelasticity

13 p2497 A70-29856

Anelasticity in lunar seismology, discussing low Q regolith layer model from Apollo 12 LP seismogram

13 p2497 A70-29857

SEISMOMETERS

U SEISMOGRAPHS SEIZURES

Low body temperature effects on convulsive activity elicited by hyperbaric oxygen in unrestrained unanesthetized rats
04 p0629 A70-14448

SELECTION

NT PERSONNEL SELECTION NT PILOT SELECTION

Computer program for automatically selecting redundant parts and redundancy types for various aerospace systems characteristics

01 p0103 A70-10488
Optimal selection of subsystems, minimizing mathematical expectation of output losses considering malfunctions

03 p0460 A70-13429
Nondestructive screen test efficiency, determining potential failures of electric components by Bayes theorem

15 p2748 A70-32659
Visual sensory storage item selection efficiency
19 p3363 A70-38321
Ni-Cd cell plates screening and selection by weight for reliability and uniformity improvement
21 p3760 A70-42147

SELECTIVE FADING

Frequency-time coded multichannel communication system error probability bounds to investigate frequency selective fading effect on performance
12 p2184 A70-27416

SELECTIVITY

Selectivity and pulsation sensitivity of electroacoustic transducers in turbulent flow under non-coherent reception of random pressure field

03 p0467 A70-13514
Solar installations optical properties selectivity increase by light-collecting surfaces mechanical treatment, describing plate grinding with abrasive powders
07 p1196 A70-19625

Umkehr observation days selectivity effects on calculated mean ozone distributions in layers 2 and 3
08 p1492 A70-21970
Two signal selectivity and permissible noise level of FM receiver with linear cascades and detector non-linearity effects
15 p2696 A70-31506

SELECTORS

Multiple tube manometer with selector switch for measuring flow channel wall pressures
23 p4194 A70-44000

SELENIDES

NT CADMIUM SELENIDES NT GALLIUM SELENIDES NT LEAD SELENIDES NT ZINC SELENIDES

Synthetic molybdenum diselenide oxidation kinetics between 375-530 C, determining isothermally reaction rate constants in dry air
[ASLE PREPRINT 69-LC-8] 02 p0321 A70-12537

Composition dependence of optical energy gap and diffuse reflectance in MnSe-CdSe solid solutions
16 p2960 A70-33094
Transition metal disulfides and selenides as solid lubricants, investigating sliding friction characteristics [ASLE PREPRINT 70AM 6E-1]
19 p3438 A70-38801

SELENIUM

Extended chain crystals of hexagonal Se temporary superheating before final melting, presenting melting equation

01 p0126 A70-10222
Selenium additions effect on structural steels transverse mechanical properties, emphasizing plasticity, shock resistance and machinability
07 p1310 A70-19750

Extended chain polymer crystals temporary superheating before final melting, discussing hexagonal selenium crystals data
11 p2069 A70-25803

Switching circuit with Se diode, comparing I-V characteristics with Se rectifiers
17 p3054 A70-35411

Photometric determination of Ti with diantipyrilmethane in steels containing Se
18 p3277 A70-36465

SELENIUM ALLOYS

Cd-Se and Cd-Te systems phase diagrams based on regular solutions theory, discussing molecular interaction energy dependence on composition
22 p4085 A70-42678

Amorphous semiconductor alloys in As-Se system, measuring DC and AC electrical conductivity dependence on temperature
24 p4390 A70-45657

SELENIUM COMPOUNDS

NT CADMIUM SELENIDES NT GALLIUM SELENIDES NT LEAD SELENIDES NT SELENIDES NT ZINC SELENIDES

Phase equilibria in Mn-S, Mn-Se and MnS-MnSe systems by X ray diffraction after preparation by annealing
02 p0249 A70-11652

SELENOGRAPHY

Selenodetic investigations based on lunar photographs with background stars, converting equatorial coordinates to orbital using Cracovian formulas
08 p1564 A70-20560

Selenodetic control systems orientation based on lunar features correlation with reference stars, considering ephemeris times corrections
08 p1572 A70-20941

Selenocentric coordinate system originating at center of mass, determining lunar figure center from photographs with reference stars
08 p1572 A70-20942

Selenodetic control system, considering photogrammetric networks, Apollo landing site, topographical maps, lunar photographs, etc
10 p1890 A70-24732

Selenodetic investigations based on lunar photographs with background stars, converting equatorial coordinates to orbital using Cracovian formulas
15 p2805 A70-32715

Selenodetic control systems orientation based on lunar features correlation with reference stars, considering ephemeris times corrections
15 p2806 A70-32753

Selenocentric coordinate system originating at center of mass, determining lunar figure center from photographs with reference stars
15 p2806 A70-32754

Lunar geomorphological charts of Mare Nubium northern part, considering structural features in equatorial band
19 p3517 A70-37984

Lunar geomorphological charts in Archimedes crater and Appenine and Haemus mountain region, examining duration and stages in Mare Imbrium depression development
19 p3517 A70-37986

Lunar maria distribution, explaining origin and characteristics by surface brightness
19 p3517 A70-37987

Small lunar crater structural characteristics and distribution
19 p3517 A70-37989

Lunar crater number and density vs diameter graph, showing rhythmical deviations from mean asymmetrical cosine curve
19 p3517 A70-37990

Lunar surface selenographic reference points tabulation, considering suitability for selenodetic measures
23 p4247 A70-44773

SELENOLOGY

Solar IR light brightness distribution reflected by volcanic covers compared with lunar observation data
04 p0744 A70-14439

Lunar density gradient, free oscillation and tides study inferring lunar atomic number similarity to Si and earth mantle
05 p0908 A70-16316

Enstatite luminescence response for bulk specimens, powders and individual grains, considering selenological implications
05 p0909 A70-16391

Mathematical techniques for selenodesy computer simulation program, solving problems arising from infinite series of spherical harmonics for lunar gravitational potential
06 p1152 A70-18498

Lunar interior electrical conductivity estimated using lunar interaction with solar wind and interplanetary electric and magnetic fields
06 p1153 A70-18544

Lunar origin and history, discussing evolution temperature, large and small craters and association with solar system evolution
08 p1581 A70-21822

Moon observation in megalithic times by means of menhirs
09 p1751 A70-22194

Soviet book on lunar physics covering exploration, topography, internal structure, etc
09 p1756 A70-22528

Lunar sinuous rilles formation by fluid flow mechanisms, discussing evidence for lava and rille formation by lava tube collapse
09 p1759 A70-22799

Selenology by traverse method, discussing equipment and mapping procedure
11 p2111 A70-26043

Book on moon covering motion, earth-moon system, internal structure, hydrostatic equilibrium, thermal history, global form, gravitation, topography, etc
12 p2298 A70-27096

Lunar physics expansion stemming from physical, geophysical and chemical experiments and measurements by manned and unmanned space flight
12 p2302 A70-27583

Solar light brightness distribution reflected by volcanic covers compared with lunar observation data
13 p2485 A70-28464

Lunar libration constants determination from Bessel to present, discussing data reduction methods, international cooperation and impact of lunar exploration
13 p2490 A70-28946

SELF ADAPTIVE CONTROL SYSTEMS

Book on stratigraphic view of lunar geology covering lunar craters and terrestrial analogs, remote sensing, material ages, surface interpretations and Apollo mission results
13 p2491 A70-29060

Lunar surface material composition in terra region from alpha scattering data on Surveyor 7, noting Si Na abundance
13 p2492 A70-29265

Lunar dimple craters formation by meteoritic erosion of concentric impact craters
15 p2807 A70-32850

Moon Surface Basic Points catalogs differences, estimating position dispersion by residuals of transformations
18 p3323 A70-37143

Apollo 11 lunar science - Conference, Houston, January 1970, Volume 2, Chemical and isotope analyses
21 p3903 A70-41560

Papers on lunar geology covering Tycho northeast rim, multiphase eruptions, basalt melts in simulated lunar environment and lava tubes in New Mexico
23 p4253 A70-44880

Lunar research via direct exploration, discussing lunar geology, cartography, selenodesy, gravific potential, rotation, etc
23 p4256 A70-45037

Book on lunar rocks covering pre-Apollo lunar scientific knowledge, apollo and future lunar mission planning, lunar mineralogy, petrology and geochemistry, etc
24 p4412 A70-46025

SELF ABSORPTION

Radio sources minimum observable diameter attributed to interstellar scattering and synchrotron self absorption
22 p4101 A70-42862

SELF ADAPTIVE CONTROL SYSTEMS

Control system main and self adaptive loops structural synthesis
01 p0053 A70-11043

Optimal use of adaptive renewal capability determined for first order time varying linear systems with quadratic performance index by exponential model of component failure
02 p0273 A70-12729

Soviet book on nonsearching gradient self adjusting system for determining error function gradient, using Liapunov method to study stability
04 p0661 A70-14677

Self adaptive servosystems operating with incomplete input signal information, proposing schemes for parameter adjustment by employing differential circuit containing frequency filters
07 p1239 A70-18734

Motion of second order autonomous quasi-linear system with disturbances, obtaining criterion for recognition of random forced and self oscillations
07 p1247 A70-20180

Liapunov direct method for synthesizing self adaptive model reference control system with simultaneously used passive /signal/ and active /parameter/ adjustment loops
08 p1480 A70-21018

Soviet papers on complex control systems covering hierarchical structures, accuracy and stability analysis, optimal and self adjusting control, etc
11 p2022 A70-25601

Asymptotic stability of multivariable autonomous control systems used Liapunov vector function method
11 p2083 A70-25606

Statistical linearization synthesis of nonlinear self adjusting systems with frequency filters and input signal under white noise
14 p2559 A70-30156

Transient response of self adaptive systems subjected to determinate or random signal mixed with additive noise
16 p2882 A70-33234

Frequency filters in nonlinear self adaptive system design for noncorrelated input and noise signals
18 p3234 A70-36119

Self adaptation algorithm of optimally fast acting system for variable parameter plant control
18 p3234 A70-36120

Sensitivity functions use in parametrically invariant self adjusting control systems
20 p3602 A70-39828

Self adaptive system with standard model, using direct loop amplification factor as controlled parameter
20 p3603 A70-39832

Self adjusting autopilot system based on invariance principle for stabilization against wind gusts
20 p3670 A70-39840

High performance aircraft self adaptive feedback control system, using airborne digital computer with inputs of elevator deflection and pitch rate for effectiveness identification
20 p3605 A70-40119

SELF ALIGNMENT

Harmonic linearization for nonsearching self adaptive automatic control systems described by nonlinear differential equations

22 p4001 A70-42835

Dynamic characteristics of autooscillatory nonlinear self adaptive systems under random noise, using statistical and harmonic linearization

22 p4003 A70-42884

Optimal self adaptive control systems with incomplete input information, ensuring minimum error dispersion

22 p4004 A70-42890

SELF ALIGNMENT

Initial quaternion for Cartesian time varying transformation matrix based on self alignment method of inertial analytic platform

11 p2072 A70-26150

Laser Doppler-shift velocimeter with self aligning optics, discussing performance parameters

16 p2926 A70-33143

Self alignment for gimballless inertial navigation system fixed base by generating computer programs from error signals derived from inertial sensors

16 p2946 A70-33302

Commercial aircraft strapdown inertial navigation systems, examining initial self alignment techniques

18 p3289 A70-36442

SELF BIAS

U BIAS

SELF CONSISTENT FIELDS

Self consistent field method to calculate effective dynamic characteristics of elastic media with filler for plane longitudinal wave propagation

02 p0388 A70-12485

Integral Hellman-Feynman formula applied to binding energy of molecular H and LiH, using SCF wavefunctions for atomic states

12 p2276 A70-27570

Iteration method for calculating self consistent fields in semiconductor surface inversion layers

22 p4085 A70-42745

SELF DEPLOYING SPACE STATIONS

U SELF ERECTING DEVICES

U SPACE STATIONS

SELF DIFFUSION

U DIFFUSION

SELF ERECTING ANTENNAS

U ANTENNAS

U SELF ERECTING DEVICES

SELF ERECTING DEVICES

Gearhead DC/AC electric motors with wet/dry lubricants, discussing selection criteria for spacecraft boom deployment

16 p2846 A70-34139

SELF EXCITATION

Self excited oscillators zero crossing times distribution for Markov process formulated as boundary value problem involving Kolmogoroff backward equation

01 p0143 A70-10891

Rotational motion of self excited symmetric gyroscopes applied to attitude control and nutation damping of space vehicles

01 p0143 A70-10929

Two degree of freedom gyroscopes stability with hydrodynamic grooved rotor bearings, describing parallel and conical whirling rotor oscillations

02 p0307 A70-12163

Frequency response linearity for self excited microwave oscillators with complimentary cavity derived, proposing parameters selection for widening voltage tunable frequency range

05 p0824 A70-16891

Stationary ring vortices in unbounded conducting fluid, investigating self excitation of magnetic field by vortices

13 p2461 A70-28965

Self excited cavity oscillators with tunnel and parametric diodes and nonequilibrium medium, noting single and multimodes, energy capabilities and frequency interactions

13 p3366 A70-29405

He-Ne laser memory, discussing induced oscillation excitation with radiation fed back to resonator by moving reflecting mirror

13 p2429 A70-29572

Self excited electron-phonon-spin spontaneous oscillations generation, deriving dispersion equation

16 p2878 A70-33779

Self excited systems limiting states with traveling wave, analyzing oscillator moving along string under tension

16 p2990 A70-33781

Mechanical systems spontaneous oscillation due to different critical velocities with and without arbitrarily small damping

18 p3338 A70-36430

Microwave self modulating GaAs diode laser, showing coupled external cavity resonator influence on intrinsic resonance frequency

18 p3269 A70-36733

Plasma anomalous diffusion relation to self excited LF oscillations

19 p3480 A70-38016

SELF FOCUSING

Argon CW lasers stationary thermal self focusing in various absorbing crystals and glasses

01 p0107 A70-10207

Gas laser beams short time constant and thermal self defocusing following small spot focusing on thin dye sample

01 p0109 A70-10431

Banana self focusing in water of laser beams with nonmonotonic intensity distribution, noting ruby laser experiment

02 p0312 A70-12260

Electromagnetic finite amplitude wave beams self action in magnetoactive plasma, noting nonlinear characteristics

03 p0448 A70-13411

Collapsing beam transition into self focusing light channel numerically analyzed allowing for Kerr effect saturation, multiphoton absorption and stimulated Raman scattering

04 p0650 A70-15285

Single mode neodymium laser second harmonic radiation self focusing resulting in filamentary fractures in solid dielectrics

06 p1080 A70-17496

Intense light beams self focusing in nonlinear media with quadratic Kerr effect, assuming spherical initial phase front after passing through condensing lens

07 p1296 A70-18720

Two photon photoconductivity of CdS crystals stimulated by ruby laser, showing emission self focusing during pumping

07 p1302 A70-20322

Self focusing antennas directive gain losses reduction for wave with jagged phase front impinging on linear array having passed through inhomogeneous atmosphere

09 p1648 A70-23163

Self focusing of ruby laser radiation in CdS single crystal, considering effect on crystal photoconductivity

12 p2248 A70-27540

Argon CW laser blue beam self focusing in methylene iodide, iodine and liquids under steady state conditions

12 p2248 A70-27545

Autofocus for variable magnification systems, discussing conjugate concepts and linkage and cam methods for enlargers and projectors

16 p2907 A70-33182

Resonant interaction and instability produced by nonlinear coupling of modulated wave and LF mode, stimulating self focusing of plasma waves

16 p2958 A70-33285

Thermal self focusing filaments observation in form of tracks in KDP and ADP crystals damaged by radiation from free emission mode laser

18 p3266 A70-36612

Self focusing schlieren observation in gas breakdown, discussing cubic polarizability of excited atoms in electron cascade due to laser pulses

21 p3835 A70-40594

Self focusing in nonlinear optics, discussing physical processes of wave propagation in dielectrics

22 p4074 A70-43207

SELF INDUCED VIBRATION

NT PANEL FLUTTER

NT SUBSONIC FLUTTER

NT SUPERSONIC FLUTTER

NT TRANSONIC FLUTTER

Nonlinear connected oscillations of vibrator and rigid bodies, analyzing plane-parallel and spatial motions, including elastic beams self excited oscillations

04 p0720 A70-15446

Self excited vibrations in balanced vertical shaft running on plain lubricated bearings, making numerical analysis of small perturbation transition to fully developed swirl

09 p1690 A70-22399

Parametric effect maser developed by maintaining self oscillations in static amplitude modulated magnetic field, noting application as magnetometer

11 p2063 A70-25947

Mechanical systems vibrations comprising tension couplings compensating misalignment between non-coaxial shafts

11 p2060 A70-26348

Self excited lateral vibration of poppet valve under positive and negative damping effects

11 p1983 A70-26420

Self induced intensity pulsations frequency stabilization and narrowing in continuously operating GaAs injection lasers

18 p3269 A70-36734

Self induced sustained light pulsations from GaAs injection lasers with tandem double section stripe geometry based on repetitively Q switched model

18 p3269 A70-36735

SELF LUBRICATION

Dry face mechanical shaft seal operating on self generated graphitic film without boundary fluid lubrication

[ASLE PREPRINT 70AM 3C-2]

19 p3439 A70-38809

SELF MANEUVERING UNITS

Extravehicular activity maneuvering devices, describing design and performance of Gemini project unit

21 p3929 A70-41075

SELF ORGANIZING SYSTEMS

Heuristic principles for self organization algorithm of cognitive automation system with active learning strategy

08 p1466 A70-20874

Automatic test equipment for different type of planes and relation to self organizing systems, considering airport implantation

10 p1970 A70-24476

Group Method of Data Handling based on heuristic self organization for solving complex system problems, with applications to random processes prediction

10 p1845 A70-24869

Adaptive extremal control systems operational stability, defining optimal convergence coefficient values for identifier and perceptron

14 p2559 A70-30175

Learning self learning relationship in image recognition, analyzing resolving function with minimum probability for erroneous recognition

14 p2553 A70-30420

Stochastic control optimization, examining self organizing approach for performance adaptive controller with asymptotic optimal properties

22 p4005 A70-43733

Heuristic self organizing systems role in technical cybernetics

24 p4321 A70-45645

SELF OSCILLATION

Second order dynamic systems stability, analyzing nonlinear and self excited oscillations by using two differential equations

01 p0146 A70-11604

Stability characteristics of two degree of freedom gyroscope having hydrodynamic grooved journal rotor bearings, discussing frequency of self excited oscillation

04 p0689 A70-14872

[ASME PAPER 69-LUB-H] Elastic bars self excited oscillations at audible frequencies, determining natural frequencies from analyzing sound

07 p1401 A70-18847

Motion of second order autonomous quasi-linear system with disturbances, obtaining criterion for recognition of random forced and self oscillations

07 p1247 A70-20180

Charged particle self oscillatory motion in plane condenser field, applying results to electrical measuring instruments theory

09 p1680 A70-23144

Steady state analysis of harmonic oscillations in HF synchronized transistor autooscillators, considering transistor inertial properties

09 p1649 A70-23341

Correlation functions of nonlinear auto-oscillatory system under nonstationary conditions determined by statistic linearization

11 p2022 A70-25341

Delayed feedback for LF periodic conditions/auto-oscillations/ in relay systems of cosmic flying apparatus stabilization

11 p2119 A70-25342

Readjustment algorithm for auto-oscillatory adaptive control system with variable structure, using harmonic linearization

11 p2022 A70-25343

Auto-oscillatory regimes in annular gas laser under coupling due to scattering, considering mode competition

11 p2064 A70-26811

Book on vibrations covering natural oscillations, damped and undamped oscillations, energy sources, forced vibrations, resonance and multiple degree of freedom systems

13 p2515 A70-29452

First harmonic precision improvement of dual input describing function, applying to self oscillation of nonlinear systems

14 p2560 A70-30625

Coupled open plane resonators system self oscillation intrinsic frequencies solution by numerical method, obtaining algorithm for characteristic equation roots

19 p3387 A70-37737

Self oscillatory operation of laser with bleachable light filters, solving power balance equations by computer algorithm

20 p3641 A70-39738

LF self excited oscillations in inhomogeneous afterglow magnetoplasma measured by Langmuir probe, noting dissipative drift instabilities

22 p4079 A70-42372

Multifrequency autooscillatory systems, comparing reflex klystron with He-Ne laser

22 p3995 A70-42404

Harmonic linearization equations for frequency and amplitude of self oscillations in nonlinear automatic control systems

22 p4001 A70-42832

Harmonic linearization method for nonlinear automatic control systems with finite automata, discussing self oscillating modes of operation

22 p4001 A70-42836

Self oscillations and dead zones of automatic control systems with variable structures, using harmonic linearization

22 p4001 A70-42837

Periodic solutions to complex nonlinear automatic control systems with initial deviations, considering system stability and self oscillation conditions

22 p4002 A70-42839

Dynamic characteristics of autooscillatory nonlinear self adaptive systems under random noise, using statistical and harmonic linearization

22 p4003 A70-42884

S band tunable free running high Q triode oscillator phase and frequency instability measurement based on delay lines applications

23 p4170 A70-43796

Auto-oscillatory regimes in annular gas laser under coupling due to scattering, considering mode competition

24 p4351 A70-45183

SELF REGULATING

U AUTOMATIC CONTROL

SELF REPAIRING DEVICES

Thermoelectric outer planet spacecraft (TOPS) project incorporating adaptable data handling system and self testing and repairing computer with triple redundancy subsystems

11 p1996 A70-25368

Onboard computers automatic reliability control with implementation of self repair, modeling by Markov processes nonhomogeneous in time

13 p2372 A70-28438

SELF SEALING

Crack self healing in aluminum foil-polyvinyl acetate sandwich structures

07 p1315 A70-18713

SELF STIMULATION

Rats under constant environmental conditions exhibiting circadian rhythmicity in rate of bar pressing with hypothalamic and septal reinforcing brain electrical stimulation

14 p2539 A70-30986

Steering behavior during learning as function of self generated stimuli by movement compared with stimulus tracking

20 p3580 A70-39674

SELSYNS [TRADEMARK]

U SERVOMOTORS

SEMICIRCULAR CANALS

Astronaut vestibular fitness determined from threshold labyrinthine tests on isolated horizontal and vertical semicircular canals

03 p0437 A70-14059

Vestibular semicircular canal excitation thresholds of experienced and candidate pilots for imposed angular accelerations

07 p1201 A70-18795

Oculogyral illusion provoked by angular accelerations during flying stationary and spiral turns in jet aircraft, considering semicircular canals stimulation

11 p1992 A70-26512

Vestibular threshold dependence on gravity, considering linear accelerations effect on canals sensitivity

14 p2539 A70-30916

Mathematical model for short term adaptation effects in human semicircular canal response to rotation, discussing nystagmus

18 p3216 A70-35940

Nystagmic response to directional inert shift of endolymph in semicircular canals in frontal plane head subject rotation

18 p3220 A70-36635

Electrokinetic model for semicircular canal transduction, focusing IR beam on exposed ampullae from posterior canals of Rana pipiens

21 p3765 A70-41696

Semicircular canals dynamic cross coupled responses to rotational movement, discussing mechanical model applicability

22 p3981 A70-43703

Semicircular canals-otoliths interactions for antagonistic and synergistic information

22 p3976 A70-43704

SEMICONDUCTING FILMS

Epitaxial PbSe films formation mechanism-defect structure relation using moire rotation method, discussing elastic strains, dislocations, boundary formation, etc

01 p0155 A70-10182

Book on thin film transistors microelectronics covering semiconductor physics, fabrication, analysis, applications and comparison with MOS transistors

01 p0052 A70-11329

Electrical conductivity of GaSe thin films developed in vacuum by electron bombardment as function of temperature

03 p0540 A70-13686

Ge films crystallinity deposited on Ge substrates in vacuum as function of deposition rate, substrate tem-

perature and thermal treatment and background O pressure

03 p0543 A70-14204

Vacuum deposited thin cadmium sulfide films semiconducting properties, discussing captured free carriers effects on temperature dependence of dark and photo current

05 p0893 A70-16543

Thin n-type Ge film electrical conductivity effect on ferromagnetic barium titanate single crystals as function of magnitude and sign of polarizing field

11 p2097 A70-25383

Nucleation and heteroepitaxial GaAs film growth on sapphire using electrical measurements, reflection diffraction and electron microscopy

11 p2098 A70-26393

Semiconductor diamond films electrical conductivity obtained by injecting various ions during isochronal stepwise annealing, studying activation energy values

12 p2286 A70-27479

Hall constant and carrier mobility in semiconductor diamond films doped by boron ion injection, observing temperature dependence of mobility

12 p2287 A70-27480

Piezoelectric field effect strain gage with semiconducting film for extremely small strains in electrically noisy background

[SESA PAPER 1676]

15 p2739 A70-32317

Thin film solar cells photosensitivity improvement by semiconductors with graded energy gap, describing construction techniques and electrical properties

15 p2678 A70-32420

Amorphous boron arsenide films deposited on Si substrates, measuring current voltage characteristics

15 p2785 A70-32584

Solar cells based on homogeneous diffusion p-n junctions in epitaxial GaAs films grown on Ge single crystal substrate

16 p2843 A70-33202

Surface growth morphology and crystallographic orientation of beta-SiC films formed by chemical conversion and heating

17 p3142 A70-34678

Adsorption influence on electrical and photoelectrical properties of CdSse thin films

17 p3143 A70-35674

Electrical properties of n-type GaAs epitaxial films grown by gas transport method

17 p3144 A70-35706

Electrical conductivity of thin semiconductor films for FETs, investigating excessive conductivity scattering

19 p3389 A70-38067

Thin films for semiconductor integrated circuits and solid state devices

19 p3389 A70-38195

Deformation effects on metallic and semiconductor thin films conductivity

19 p3488 A70-38199

Cadmium sulfide photocell development, noting plastic support base, film deposition and interconnection

19 p3358 A70-38480

Sensing elements piezoresistive Si and indium antimonide film sensing elements for high sensitivity pressure transducers and accelerometers, discussing airborne telemetry applications

19 p3431 A70-38538

Impurity distribution in diffused p-n junction in thin epitaxial film, calculating space charge region width and junction capacitance

20 p3685 A70-38967

SEMICONDUCTOR DEVICES

NT AVALANCHE DIODES

NT GALLIUM ARSENIDE LASERS

NT GERMANIUM DIODES

NT JUNCTION DIODES

NT JUNCTION TRANSISTORS

NT METAL OXIDE SEMICONDUCTORS

NT MIS [SEMICONDUCTORS]

NT PARAMETRIC DIODES

NT PHOTODIODES

NT PHOTOTRANSISTORS

NT PHOTOVOLTAIC CELLS

NT SEMICONDUCTOR LASERS

NT SILICON TRANSISTORS

NT THERMISTORS

NT THYRISTORS

NT TRANSISTOR AMPLIFIERS

NT TRANSISTORS

NT VARACTOR DIODES

Scanned laser microscope producing shadowgraph displays of IR transmittance variations attributed to defects in polished Si and GaAs semiconductor wafers

01 p0105 A70-10025

Output voltage stabilizers for thermal compensation in semiconductor power generating circuits, using stabilitor reference source

01 p0049 A70-10139

Planar Gunn effect devices using various surface electrode configurations, discussing limitations by breakdown on Ga arsenide exposed surface

01 p0049 A70-10287

Soviet papers on semiconductor solar energy converters covering design and tests for thermoelectric, thermionic and photoelectric units, properties, materials, etc

01 p0008 A70-10750

Hot junctions nonuniform heating influence on thermoelectric generator efficiency, taking into account temperature dependence of thermoelement materials properties

01 p0009 A70-10753

Light emission by solids, discussing injection lasers, luminescence semiconductor diodes, group 2 and 6 compounds, etc

01 p0160 A70-11288

Microwave generation and amplification using Gunn effect semiconductor devices

01 p0160 A70-11289

Book on GaAs components technology covering properties, fabrication and applications of GaAs semiconductor elements in electronics

02 p0350 A70-11734

Phase detector with two value output and pulsed input for measurement and control circuits, noting construction with semiconductor elements

02 p0266 A70-11900

Time sharing computer systems for data reduction from semiconductor strain gauges applied to FORTRAN IV programs

03 p0453 A70-12969

Generation-recombination noise theory extension to nonlinear devices applied to double injection diode in various operation modes

03 p0458 A70-14028

Semiconductors and devices for sensor applications, development history, materials requirements and future prospects

03 p0542 A70-14189

Photocell uses in semiconductor integrated circuit, discussing scanned arrays applications and economics

03 p0459 A70-14265

Four layer semiconductor device triggering by X or gamma radiation calculated by transport equations for electron and hole distribution motion and electric field distribution

04 p0657 A70-14731

Mathematical model based on equivalent electrical circuit for transient radiation analysis by computer /TRAC/ family of circuit analysis programs, simulating semiconductor devices

04 p0657 A70-14737

Semiconductor electronic devices applications in microelectronics, optical/dielectric electronics and photography and electron-acoustical phenomena and negative differential conductivity

05 p0822 A70-16863

Subminiature sensor element integrated with silicon semiconductor strain gages for simultaneous three dimensional measurement of acceleration components

06 p1069 A70-18434

Silicon semiconductor irradiated strain gages for precision measurement of low level strain

06 p1069 A70-18441

Electron irradiation for reducing thermal coefficient of resistance of Si strain gages, noting crystal orientation dependence of gage factor

06 p1070 A70-18442

Instability of semiconductor circuit with nonlinear current-voltage characteristics, showing potential negative differential conductivity effect

07 p1240 A70-19274

Plastic semiconductor devices encapsulation materials and fabrication techniques, considering device performance in various environments and military applications

08 p1468 A70-20626

Spatially inhomogeneous semiconductor structures dynamic characteristics, obtaining equations

08 p1474 A70-21207

Negative differential conductivity effects in Gunn domain GaAs semiconductors, discussing physical properties and microwave applications

08 p1556 A70-21303

Semiconducting components reliability test involving electrical parameters measurement following thermomechanical stresses

09 p1689 A70-22002

French microwave semiconductor technology in terms of basic research, technology studies, reliability and integrated circuits

09 p1739 A70-22602

Low power semiconductor diode rectifying test apparatus for analysis of fusing and shaping effects on dynamic current-volt and frequency characteristics

09 p1649 A70-23355

Broad band power amplification with Gunn effect diodes, describing frequency response and saturation characteristics and FM/AM noise spectrum measurements for reflection amplifier in X band

10 p1847 A70-23886

Silicon window with double carrier injection to achieve high power broadband microwave switching, obtaining power increase over p-i-n diodes

10 p1847 A70-23892

Spectrometer design for Helios solar probe using semiconductor detectors to identify particles separated by magnetic field

10 p1888 A70-24487

Electronic switching effects in amorphous semiconductors emphasizing mass memory for computers based on thin films of chalcogenides

11 p2017 A70-25524

Semiconductor strain gages/tensometers/ materials, fabrication and properties

11 p2054 A70-26429

Tensodiode effect in long plate-shaped semiconductors, noting bend direction effects on I-V characteristics

12 p2195 A70-27312

Semiconductor power controllers for switching aircraft electrical power supplies [SAE PAPER 700308]

12 p2195 A70-27451

HF quenched-domain mode (Q mode) Gunn effect oscillator in single frequency operation using signal analysis, obtaining instantaneous I-V transfer characteristics

12 p2202 A70-28162

Water contaminating effects on thin thermal oxide passivated silicon planar devices

13 p2361 A70-28930

Automatic dynamic response system for testing logic and semiconductor devices

13 p2379 A70-29693

Nd laser drilling and welding tool for microminiature electronic device fabrication

14 p2594 A70-30639

Scintillation and semiconductor counters - IEEE Conference, Washington, D.C., March 1970

14 p2586 A70-31001

GaAs Gunn devices oscillatory modes under various operating conditions

14 p2557 A70-31158

Regenerative semiconductor parametric amplifier saturation in forward current mode, assuming harmonic voltages /signal, pumping and difference frequencies/ action at p-n junction

15 p2708 A70-31522

GaAs slices efficiency as transferred electron devices, correlating impurity profiles with microwave performance

15 p2708 A70-31957

Thermal loads on semiconductors in solid state converters during short circuit and overload

15 p2709 A70-32205

Reliability physics role in kinetic studies of physical and chemical degradation and failure mechanisms in semiconductor devices

15 p2713 A70-32661

Semiconductor image detectors in photodiode and photoconductor forms, describing construction and operation modes

15 p2714 A70-32673

Ion implantation doping for MOS devices, discussing improved HF performance, integrated circuitry and threshold voltage selection

16 p2872 A70-33054

Mercury cadmium telluride photodetectors, analyzing gain, signal current and radiation limits

16 p2905 A70-33153

High sawtooth voltage generator with semiconductor triodes, giving circuit parameters and diagrams

16 p2873 A70-33212

Ultraminiature piezoelectric semiconductor pressure transducers for wind tunnel models

17 p3093 A70-35491

Microwave oscillator performance of InP three level transferred electron devices

17 p3048 A70-35874

Holographic projection to print etching patterns on semiconductor wafers, discussing development, basic principles and uses

18 p3233 A70-36773

B and P ions bombardment techniques for Si doping of multilayered transistor structures

19 p3385 A70-37268

Soviet papers on physics of semiconductors and semiconductor devices covering kinetic equation, electrical conductivity anisotropy, thermal emf, current carrier recombination, radiation flaws, etc

19 p3482 A70-37292

Four-terminal p-n-p-n small signal semiconductor tetrode amplifier operation principle and linear circuit applications

19 p3390 A70-38305

Miniature pressure transducers using piezoelectric or semiconductor elements

20 p3628 A70-39226

Semiconductor diodes, discussing characteristics and applications of Schottky barrier, varactor, tunnel, Gunn and field effect diodes, etc

20 p3600 A70-40500

Unmodulated microwave oscillations power stabilizer with semiconductor attenuator

21 p3796 A70-40635

Subminiature three directional cantilever beam accelerometer using semiconductor strain gages

21 p3824 A70-40861

Computer storage technology, discussing magnetic films, semiconductor cells, content addressable and read-only memories, etc

21 p3795 A70-41693

Double tunneling electrothermal initiation of threshold electronic switching in semiconducting glasses, discussing temperature profile and current density saturation effects

21 p3864 A70-42019

Iteration method for calculating self consistent fields in semiconductor surface inversion layers

22 p4085 A70-42745

Reprogrammable read-mostly memory (RMM)/ using integrated circuit array of amorphous and crystalline semiconductor devices, discussing design and applications

22 p3996 A70-42772

Semiconductor storage unit with decoding circuit, memory matrix and read-out amplifiers

22 p3996 A70-42847

Radiation-produced defects in silicon semiconductor devices, annealing gamma ray, electron and fast neutron damages

22 p4087 A70-43328

Semiconductor thermometer for skin temperature differences using resistance bridge, transistor amplifier and thermistors

23 p4150 A70-44317

Wideband wattmeter for measurement and analysis of power dissipation in semiconductor switching devices, considering occurrence of peaks, frequency dependency of average dissipation, etc

23 p4174 A70-44597

Electrical and electronic semiconductor device failures from metallurgical viewpoint

23 p4175 A70-44746

Current oscillations in external circuits of semiconductor with low surface recombination in parallel electromagnetic field

23 p4231 A70-45062

Soviet book on modulation-type frequency converters based on electromagnetic and semiconductor elements covering modulators static and dynamic characteristics, optimal operating conditions, etc

24 p4319 A70-45626

Si crystal microdefects influence on semiconductor device performance and reliability

24 p4391 A70-46015

IC metallization systems in semiconductor devices fabrication and packaging, assessing metals alternate to Al for electromigration difficulties avoidance

24 p4319 A70-46075

Semiconductor solar energy converter, deriving conditions for occurrence of photoconductivity quenching

24 p4391 A70-46325

Two-cascade amplifying circuits with current and voltage feedback for semiconductor precision devices

24 p4321 A70-46394

SEMICONDUCTOR JUNCTIONS

NT JOSEPHSON JUNCTIONS

NT N-N JUNCTIONS

NT N-P-N JUNCTIONS

NT P-I-N JUNCTIONS

NT P-N JUNCTIONS

NT P-N-P JUNCTIONS

NT P-N-P-N JUNCTIONS

NT SILICON JUNCTIONS

Current dependence of integral brightness and electroluminescence spectrum of ZnS-GaAs heterojunctions obtained by I vapor reaction in H flow

01 p0155 A70-10142

Electric characteristics and impurity distribution in GaAs-Ge heterojunctions obtained by deposition on p-type Ge

01 p0155 A70-10143

Semiconductor solar thermoelectric generator allowing thermoelement replacement during service including construction, bridging methods and characteristics

01 p0009 A70-10751

Current-voltage characteristics of cascaded solar thermoelectric generator, determining optimum hot junction temperature as function of radiation concentration

01 p0000 A70-10752

Current-voltage and current-temperature characteristics of alloyed p Ge-n Si heterojunctions, discussing current flow process complexity

02 p0350 A70-11667

Coordinate-sensitive photocells with heterojunctions between wideband semiconductors, noting increased longitudinal photovoltage

03 p0541 A70-13722

Low threshold injection lasers in IR and visible spectrum at room temperature employing AlAs-GaAs heterojunctions, noting use for CW mode

03 p0501 A70-13723

Piezojunction effect and applications in transducers, showing needle and mesa configurations as most promising methods

03 p0496 A70-14193

Center frequency shift prediction model for non-linear collector junction capacitance in transistor Class C amplifiers

04 p0660 A70-15343

Fabrication and electrical properties of p-ZnTe/n-InAs heterojunctions obtained by interface alloying, suggesting p-i-n structure from characteristics and capacitance behavior

06 p1125 A70-17123

Free current carriers activity in indirect magnetooptical junctions in quantized magnetic field

06 p1126 A70-17817

UHF and VHF stacked ferrite loaded junction circulators construction, improving cost to power performance

08 p1476 A70-21292

Electron tunneling into amorphous Ge films using Al-aluminum sesquioxide-germanium tunnel junctions, observing conductance dependence on bias voltage

09 p1739 A70-22918

Volt-ampere characteristics of metal-semiconductor contacts for Schottky barrier diodes, investigating suppression of minority carriers and frequency response

09 p1741 A70-23352

Semiconductor laser junction construction for increased gain making possible laser voice communication, optical intrusion alarms, laser pumping lamps and portable range finders

10 p1900 A70-24529

Germanium, silicon and gallium arsenide point contact and Schottky barrier diodes as submillimetric wavelength detectors and mixers

11 p2017 A70-25736

Epitaxial surface morphology layer electrical properties and autodoping at GaAs-Ge heterojunctions as function of substrate temperature, orientation and HCl concentration

11 p2098 A70-26392

Current flow across metal-semiconductor contacts via electron tunneling

12 p2285 A70-27254

Electroluminescence recombination emission spectra during avalanche breakdown in AlGaAs n-p and p-n heterojunctions

12 p2286 A70-27367

Minority carrier diffusion lengths on sides of copper sulfide-cadmium sulfide heterojunctions measured by light microprobes

13 p2471 A70-29709

Junction and contact regions in electronic devices using X ray microanalysis and electron probe

14 p2590 A70-30355

Metal-Ge n-type semiconductor tunnel junctions, discussing Sb and As doped units and conductance and barrier heights air cleavage effects

14 p2626 A70-30482

CW GaAs junction lasers bistable operation above delay transition temperature based on double acceptor trap theory

18 p3268 A70-36729

GaAs lasers with light propagation along curved junctions, discussing threshold current density variation with radius of curvature

18 p3269 A70-36738

Four-terminal p-n-p-n small signal semiconductor tetrode amplifier operation principle and linear circuit applications

19 p3390 A70-38305

Collection efficiency and spectral response calculations for semiconductor heterojunction solar cells

21 p3861 A70-40623

Heat treatment and photovoltaic properties of copper disulfide-cadmium sulfide heterojunctions, measuring I-V characteristics, capacitance and spectral response

21 p3862 A70-41911

Temperature and bias voltage dependence of zero bias tunneling structure in p-type GaAs-Au Schottky junctions

21 p3863 A70-41917

Semiconductor junction diode spontaneous emission sources, considering frequency-energy characteristics relationship

22 p4085 A70-42504

Semiconductor junctions passivation by silicon nitride insulation layers, discussing pyrolysis and cathode sputtering fabrication methods

22 p4087 A70-43444

Electron recombination effect on current transmission through insulator-semiconductor junction with large diffusion length of minority carriers

24 p4390 A70-45634

Thin film BiSb-oxide-BiSb tunneling junction I-V characteristics anomalies as function of temperature, magnetic field and bias voltage

24 p4390 A70-45662

SEMICONDUCTOR LASERS

NT GALLIUM ARSENIDE LASERS

Semiconductor laser active element radiation absorbing inhomogeneities effect on I-V characteristics, considering oscillation modes excitation

01 p0106 A70-10095

Semiconductor laser excitation by bremsstrahlung from electrons and gamma radiation from nuclear reactor

01 p0107 A70-10187

Semiconductor laser quantum mechanical rate equations derivation to determine temperature and current dependences of light output properties, indicating numerical calculations for GaAs

02 p0311 A70-11884

Kr, Xe and W-iodine lamps efficiencies for pumping Nd-doped YAG compared for use in high continuous power lasers

02 p0311 A70-11922

Refractive index perturbation from energy absorbed from long pulsed and Q switched Nd doped glass lasers, observing sonic waves generated by Q switched laser

03 p0498 A70-13156

Semiconductor injection laser modes, considering inhomogeneous lasing action levels over p-n junction area

03 p0499 A70-13410

Semiconductor laser-photodiode system used as optical logic elements for electronic circuits describing storage elements, dynamic trigger and multivibrator

03 p0499 A70-13456

Photostability of Nd-activated glass elements as function of dopant concentration and laser mode operation

05 p0858 A70-16266

Emission modulation in multifunctional injection laser-photodiode system used as optical memory, pulse generator, multivibrator and trigger

05 p0859 A70-16268

Semiconductor injection laser with large emitting area, discussing light absorption, waveguide channel formation as factors obstructing laser action

06 p1082 A70-17821

Injection laser theory taking into account radiative emission rates and spectral dependence, using two band semiconductor model

07 p1298 A70-19395

Exciton spectrum in semiconductor laser emission, investigating location in Brillouin zone and temperature dependence

07 p1298 A70-19478

Laser oscillation conditions for CdS crystal pumped by electron beam, using energy loss per unit length for calculations

07 p1298 A70-19681

Kinetic theory of laser emission on direct band-band semiconductor transitions

07 p1299 A70-19853

Doped semiconductor unsteady stimulated emission, solving kinetic reactions in multimodal approximation

07 p1357 A70-19862

Semiconductor laser signals coupling into thin optical platelet waveguides

07 p1301 A70-20019

Neodymium-doped glass bars laser amplification efficiency increased by using conical bar and divergent beam

07 p1302 A70-20096

Neodymium-tytrofluorite crystal laser free and Q switched operating characteristics

08 p1511 A70-20523

Dispersive resonator for near IR frequency control of neodymium-silicate glass laser

08 p1512 A70-20850

Neodymium-glass laser under action of electron beam investigated for population inversion

08 p1512 A70-21204

Unsaturable frequency discriminator influence in semiconductor laser feedback loop on laser emission spectrum

08 p1514 A70-21821

Semiconductor injection laser, analyzing light absorption by free carriers and gain characteristics

09 p1694 A70-22133

Neodymium/YAG laser emission characteristics, studying spectral selection at various excitation energy levels and output-pumping power relationship

10 p1899 A70-24261

Semiconductor laser junction construction for increased gain making possible laser voice communication, optical intrusion alarms, laser pumping lamps and portable range finders

10 p1900 A70-24529

Composite resonator for semiconductor laser to increase single mode power generation, determining optimal length of passive part

12 p2247 A70-27484

Temperature effects on injection semiconductor lasers optical gain and threshold current using energy spectrum model

12 p2247 A70-27485

Fabry-Perot resonator mirrors with local reflecting inhomogeneities within perimeter of single crystal wafer for application in optically coupled semiconductor lasers

13 p2427 A70-28884

Tunable diode laser for high resolution IR spectroscopy of sulfur hexafluoride absorption near carbon dioxide laser lines

13 p2430 A70-29832

Semiconductor laser emission at band-band transitions with free carriers participation under quantizing magnetic field, using kinetic equations

15 p2749 A70-31627

Optically pumped cadmium phosphide laser, obtaining IR coherent oscillation from Q switched Nd doped YAG laser excitation

15 p2751 A70-31985

Semiconductor lasers - IEEE Conference, Mexico City, December 1969

18 p3267 A70-36726

Semiconductor laser frequency modulation by ultrasonic waves, noting pressure variation effect on sideband resolution

18 p3269 A70-36736

InAs p-n junction laser electrical and optical characteristics during spontaneous and stimulated radiative recombination

18 p3269 A70-36739

Optically excited homogeneous bulk semiconductor lasers, examining quantum mechanical rate equations and monochromatic light field pump source

18 p3270 A70-36741

Electron gun for high current density electron bombardment of semiconductor lasers

20 p3641 A70-39482

Gas and semiconductor diode lasers construction and operation principles, discussing terminology, Boltzmann distribution function, excitation methods, population inversion, etc

20 p3643 A70-40535

Semiconductor platelet laser stimulated emission visual observation in unwanted reflected modes

21 p3838 A70-42022

Cadmium sulfide pulsed laser spectrum analysis, discussing laser output stabilization by mode selection and electron beam scanning

22 p4049 A70-42405

Thermoelectrically cooled GaAlAs injection laser illuminator, discussing optical-electronic interface problems and design and performance characteristics

22 p4052 A70-43603

Irradiation influence on emission power of GaAs laser excited by high energy electron beam

23 p4203 A70-45060

Threshold characteristics of injection and electron excitation semiconductor lasers having photoluminescence properties of n-type GaAs single crystals

23 p4203 A70-45065

Spectral and threshold emission from optically pumped semiconductor lasers as function of carrier type and concentration in GaAs single crystals

23 p4203 A70-45069

Internal Q switching deviation in gallium aluminum arsenides-GaAs single heterojunction lasers attributed to loss reduction at current pulse end

24 p4354 A70-45815

Pb-Sn-Te junction diodes prepared by Sb diffusion, investigating spontaneous and laserlike emission

24 p4355 A70-46086

SEMICONDUCTORS [MATERIALS]

NT ACCEPTOR MATERIALS

NT DONOR MATERIALS

NT METAL OXIDE SEMICONDUCTORS

NT MIS (SEMICONDUCTORS)

NT N-TYPE SEMICONDUCTORS

NT ORGANIC SEMICONDUCTORS

NT P-TYPE SEMICONDUCTORS

NT PHOTOCONDUCTORS

Electronic materials nondestructive evaluation techniques, describing analytic tests for chemical, structural, electrical and optical characteristics determination

01 p0085 A70-10023

Hot photoelectrons in semiconductor assuming short lived photoexcited current carriers, deriving expressions for energy distribution function of semiconductor current carriers

01 p0153 A70-10066

Frequency dependence of intraband absorption of electromagnetic waves by free current carriers in doped semiconductors

01 p0153 A70-10067

Hydrogen type exciton model applied to analysis of intermediate exciton state role in two quantum absorption in semiconductors

01 p0153 A70-10068

Glass formation region of chalcogenide semiconductor arsenic triselenide-antimony triselenide system and vitreous-crystalline transformation, investigating electrical and optical properties

01 p0153 A70-10085

Double injection in semiconductors at high current densities, discussing procedure yielding space charge and field distribution and voltage drop

01 p0154 A70-10123

Electrical properties of Si-doped GaAs p-n structures obtained by liquid phase epitaxy, considering charge buildup

01 p0155 A70-10132

SEMICONDUCTORS [MATERIALS]

Complex formation mechanisms and effects on impurity diffusion profiles in semiconductors

01 p0155 A70-10180

Light Raman scattering in semiconductors under constant magnetic field, studying electron-phonon spectrum characteristics

01 p0155 A70-10183

Energy spectrum of electrons and holes in semiconductors under strong electromagnetic wave field, calculating electron-phonon interaction Green function

01 p0155 A70-10184

Electron-hole pair quasi-linear fluctuations at recombination boundary in semiconductor crystal under crossed electric and magnetic fields

01 p0156 A70-10191

Gallium found suitable for doping cadmium/tin arsenide semiconductor, exhibiting hole-type conductivity

01 p0156 A70-10214

Periodic potential and residual Coulomb interaction effect on inelastic light scattering from electronic excitations in semiconductors, using diagrammatic perturbation theory

01 p0156 A70-10280

Space charge barriers AC impedance modification at metal/semiconductor contacts due to trapping

01 p0157 A70-10296

Electron mobility in single component aromatic hydrocarbons, considering crystals structures and electrical properties, energy dissipation and fluctuation, etc

01 p0158 A70-10517

Semiconductors as optical limiters for Q switched lasers, reporting temperature values for nonlinear absorption coefficients of Si, CdSe, CdTe and GaAs

01 p0158 A70-10563

Solution crystallization method to obtain gallium indium phosphide semiconductor alloys, discussing optical absorption thresholds and transitions

01 p0158 A70-10661

PbSe and GeTe cast and pressed samples thermoelectric properties before and after high energy gamma ray irradiation, using scintillation counter with photomultiplier

01 p0159 A70-10756

Bridging joints resistance effect on thermoelement efficiency, describing W and Co coatings deposition on GeTe based thermoelectric alloys

01 p0159 A70-10757

Variational methods for investigation of thermal and electrical properties of semiconducting materials, noting accuracy

01 p0159 A70-10759

Diamond-like glassy semiconductor compound of cadmium germanium arsenide, determining optical lattice vibrations from IR reflection spectra

01 p0160 A70-11599

Electrical domain instability in homogeneous hot electron semiconductors, discussing boundary conditions application to fluctuations

02 p0350 A70-11697

Book on GaAs components technology covering properties, fabrication and applications of GaAs semiconductor elements in electronics

02 p0350 A70-11734

Vacuum cleavage device for producing small area evaporated metal semiconductor contacts free from oxygen or other contamination

02 p0304 A70-12748

Energy distributions of emitted electrons from Si, GaP and ZnS semiconductors, determining relative core levels and Si valence band states optical density

03 p0537 A70-12879

Pinch characteristics of simple band structure semiconductors and nondegenerate electron gas during bimolecular current carrier recombination, determining hole pairs spatial and recombination spectral distribution

03 p0538 A70-13062

Current density and electron concentration fluctuations in semiconductors under electric field, obtaining theory of light scattering at hot electrons

03 p0539 A70-13405

Semiconductors low temperature electron energy losses due to inelastic electron scattering at neutral impurity donors shown to exceed scattering losses at phonons

03 p0539 A70-13423

Voltage-power sensitivity, response time, frequency limit and minimum registered power of hot carrier thermoelectric detectors calculated from characteristic semiconductor parameters

03 p0540 A70-13436

Magnetic field effect on recombination radiation intensity under pinch effect in semiconductor nondegenerate electron hole plasma with recombination time exceeding carrier lifetime

03 p0540 A70-13508

Electromagnetic wave propagation in semiconductors, considering effects of electric field, energy dissipation law and band structure

03 p0540 A70-13719

Onset conditions for galvanothermal current instability of Ge semiconductors as function of electric

field oscillations, carrier concentration and carrier-lattice temperature

03 p0541 A70-13724

Interband transitions and optical absorption edge analysis in indium telluride using dependence on photon energy

03 p0541 A70-13725

Low molecular weight organic semiconductors photoelectron UV emission spectra, studying electron energy distribution and optical ionization, dark bulk conductivity, etc

03 p0541 A70-13728

Semiconductors and devices for sensor applications, development history, materials requirements and future prospects

03 p0542 A70-14189

AsSbSI crystal production technology concerning substitution-type solid solution structure and photoconducting ferroelectric properties

04 p0729 A70-14409

Semiconductors low temperature photoconductivity fluctuations occurrence during energy relaxation probability by optical phonons

04 p0730 A70-14413

Electromagnetic waves amplification in semiconductor plasma with high electron concentration, analyzing equations describing waves drift instability

04 p0731 A70-15216

Memory exchange between pairs of electrodes amorphous semiconductors, discussing switch-on and unlocking

04 p0732 A70-15687

Vapor deposited GaN single crystals tested for electrical and optical properties, determining band gap energy, electron concentration, etc

04 p0732 A70-15688

Phenomenology theory on conduction and switching behavior of amorphous semiconductor diodes

05 p0891 A70-16021

Soviet book on microwave devices employing semiconductor diodes design and synthesis covering electric field effects, optimality criteria, tabular data, etc

06 p1019 A70-17536

Cascade capture of carriers in semiconductors with negatively charged dislocation explained by diffusion-type equation

06 p1126 A70-17818

P-n junction depth in semiconductors, using electron beam of scanning electron microscope

06 p1127 A70-17820

Hall effect measurements in liquid semiconductors and metals

06 p1127 A70-17919

Possible pairing without superconductivity at low carrier concentrations in bulk and thin film superconducting semiconductors

06 p1127 A70-18641

Excess titanium dioxide effect on electric resistance of semiconductive barium titanate ceramics suitable for posistors

07 p1355 A70-18654

Semiconductor compounds application as partial vapor pressure sensors of chemical elements, discussing electrical properties dependence

07 p1356 A70-19554

Probability of three photon band-band excitation of electron in semiconductors using S-matrix formalism, calculating absorption coefficient for two band approximation

07 p1356 A70-19795

Transparent semiconductor crystals breakdown under intense ruby laser radiation, noting threshold power correlation with forbidden region and pulse duration

07 p1357 A70-19856

Phonon spectrum of mixed semiconductor crystals based on AIII-BV and AII-BVI compounds, studying frequency spectrum as function of crystal composition

07 p1300 A70-19867

Hall effect and electric conductivity of cadmium arsenide at high temperatures as function of carrier concentration dependence on temperature and phase transformation

07 p1357 A70-20314

Diffusion coefficient of charged particles in HF stabilization of current-convective instability measured in Ge semiconductor electron hole plasma

07 p1355 A70-20365

Absorption and luminescence in complex molecules and semiconductors, describing particle distribution and Fermi quasi-levels dependence on temperature and excitation intensity

08 p1555 A70-20510

Literature on IV-VI semiconducting Pb compounds PbTe, PbSe, PbS and PbO, discussing PbTe-SnTe and PbSe-SnSe solid solutions

08 p1555 A70-20584

Switching and memory phenomena in semiconducting glasses, thin films and variable threshold metal-oxide-nitride-semiconductor MNOS transistor

08 p1556 A70-21304

Electrical properties of Si-doped GaAs p-n structures obtained by liquid phase epitaxy, considering charge buildup

08 p1556 A70-21408

Threshold switching and thermal filaments in thick specimen of amorphous semiconductors using IR spectrum viewer

08 p1477 A70-21540

Te nuclear magnetic resonance in amorphous semiconducting sample cycled between conducting and nonconducting states

08 p1557 A70-21697

Electron mobility transition in infinite system of random hard core scatterers relation to switching effect in semiconductors

08 p1549 A70-21840

Book on solar cells U.S. patent literature, discussing Si semiconductors, panel fabrication techniques, photoemissive devices, Cd, Ga and organic compounds, etc

09 p1612 A70-22050

Ion accelerator for doping semiconductors, discussing electronic bombardment of low pressure vapors, electrostatic extraction, focusing and mass spectrometer

09 p1649 A70-23325

Light-emitting integrated circuit semiconductor display devices with inherent memory permitting logic and optical output functions performed on surface

10 p1846 A70-23883

Wave amplification in semiconductors relationship to coupling between space charge wave and circuit wave based on coupled-mode theory

10 p1927 A70-24619

Silicon avalanche diodes contingencies effect on material choice

10 p1850 A70-24622

GeTe, SnTe and strontium titanate transition into superconducting state including induced superconductivity

10 p1928 A70-25028

Coulomb interaction during optical transitions between Landau subbands of Ge semiconductor valence and conduction bands in magnetic field, observing diamagnetic excitons

10 p1928 A70-25029

Acoustic wave amplification and generation in piezoelectric semiconductors and semimetals by superionic carrier drift currents

10 p1925 A70-25030

Phase equilibria and maximum melting compositions determinations for compound semiconductors by differential thermal analysis compared with vapor and high pressure techniques

11 p2098 A70-25812

High purity pinhole free films (parylene) applicability as barrier coating to keep semiconductor surface free from moisture, ions and contaminants

11 p2099 A70-26395

Metal-semiconductor transition in magnetite described on band model with electrons breaking symmetry by ordering in self induced Coulomb potential

12 p2283 A70-27239

Intense laser radiation effect on electrons interactions with acoustic and optical phonons and ionized impurities in semiconductors

12 p2246 A70-27360

Impurity centers thermal and autoionization and effective capture cross section dependent on free carrier concentration in GaAs under electric field, allowing for plasma shielding

12 p2285 A70-27361

Free carriers effective mass and relaxation time in semiconductors determined from IR spectra of light reflection

12 p2285 A70-27362

Doped semiconductors electronic state density in forbidden band, assuming fluctuations in impurities in form of homogeneous spheres with varying charges and radii

12 p2286 A70-27363

Light absorption coefficient frequency dependence related to interband transitions in highly doped semiconductors

12 p2287 A70-27487

Low resistance small area contacts on semiconducting metal oxides

12 p2288 A70-28057

Temperature dependence of electrical conductivity and optical properties of strontium titanate semiconductor single crystals doped with Ce and Nb

12 p2288 A70-28328

Finite amplitude stability of plasma column in weakly ionized gases and in semiconductor plasmas in longitudinal magnetic field

13 p2458 A70-28566

Electromagnetic waves propagation in semiconductors, allowing for nonlinear effects from field heating of carriers

13 p2469 A70-28877

Interband Faraday effect in doped semiconductors by quasi-classical approximation

13 p2469 A70-28878

Electromotive force appearance in fissionable material semiconductor during thermal neutrons irradiation

13 p2469 A70-28879

Free carriers mobility and concentration in microwave semiconductors measurable by two mode resonator over temperature ranges and magnetic fluxes

13 p2470 A70-28881

Plastic encapsulated semiconductors reliability test programs with emphasis on accelerated humidity-temperature method

13 p2377 A70-29259

Piezoelectric scattering effects on electron temperature and mobility in IIB-VIA semiconductor compounds with nonparabolic conduction band

13 p2471 A70-29373

Impurities effects on UV absorption in semiconductors, deriving kinetic type equation for two particle Green function

13 p2471 A70-29511

Degenerate pinch in bipolar electron-hole plasma in semiconductors

13 p2472 A70-29760

Landau and Doppler-shifted cyclotron damping effects on helicon-like and plasma excitations of many-valley semiconductors

13 p2472 A70-30016

Ionized impurity scattering in polar semiconductors by strong electric fields, using energy and momentum conservation equations in electron temperature approximation

13 p2472 A70-30017

Switching initiation in Ovonic, discussing temperature profile in semiconducting sandwiches as function of time and thermally forced double tunneling

14 p2626 A70-30333

Raman scattering cross sections in solid state semiconductor plasma in magnetic field from phonon fluctuations

14 p2621 A70-30485

Semiconductors as igniter material for ignitrons, tabulating electrical characteristics

14 p2590 A70-30640

Nickel-doped p- and n-type Ge hot electrons recombination characteristics in strong electric fields, examining electron capture cross section

15 p2782 A70-31628

Artificial B-doped semiconductor diamond crystals resistance temperature dependence, determining conductivity and luminescence spectra

15 p2782 A70-31630

IR photography extension into long wave region of spectrum, discussing contact sensitized and electrically controlled semiconductor photographic systems

15 p2734 A70-31632

Equilibrium and steady state Hall and thermoelectric effects in inhomogeneous semiconductor materials

15 p2783 A70-31760

Plasma reflection edge in thin film InAs semiconductors, calculating refractive index and extinction coefficient from free charge parameters

15 p2783 A70-31966

Third harmonic generation using hot electron nonlinearity characteristics of semiconductors, considering plane-polarized electromagnetic wave nonlinear interaction with sample

15 p2783 A70-31970

Semiconducting gallium arsenide LF oscillations, considering domain behavior and illumination effects

15 p2783 A70-31972

Energy bands shape effect on fluctuations in nonequilibrium low resistance semiconductor plasma

15 p2784 A70-32192

Electric conductivity, thermal emf and EPR spectra of oxide semiconductor glasses based on vanadium and phosphorus oxides, correlating unpaired electron and charge carrier concentrations

15 p2784 A70-32201

Semiconductors surface energy levels based on conductivity, metal-dielectric-semiconductor capacity and optics

15 p2785 A70-32765

Semiconductor surfaces electrical equilibrium, considering statistical occupation of surface energy and Fermi levels for given doping of bulk material

15 p2786 A70-32766

Fermi level for crystal with slowly changing impurity determinable by solving Poisson equation and by condition of electroneutrality

15 p2786 A70-32899

Nonisothermal measurement in semiconductors in presence of thermoelectric, thermomagnetic and galvanomagnetic effects

16 p2960 A70-32920

High voltage photoelectric generator containing semiconductor plates with series- and parallel-connected p-n junctions forming solid circuit for super-high light flux concentrations

16 p2843 A70-33201

Impurities solubility in semiconducting indium telluride with stoichiometric vacancies, verifying thermodynamic model by phase diagrams

16 p2960 A70-33224

Magneto-optics of semiconductors, taking into account intraband and interband effects with Faraday and Voigt field configurations

18 p3297 A70-35951

Band model of switching effects between conducting and high resistance states of amorphous semiconductors

18 p3297 A70-35952

Homogeneity criteria for semiconductor materials, considering variation coefficient, goodness factor and overshot density

18 p3298 A70-36468

Maxwell-Wagner migrational polarization resulting from free ions or electrons drift in dielectrics and semiconductors, considering relaxation time

18 p3298 A70-36595

Pinch effect in degenerate and nondegenerate electron hole plasma in semiconductors during bimolecular bulk recombination

18 p3298 A70-36620

Soviet papers on physics of semiconductors and semiconductor devices covering kinetic equation, electrical conductivity anisotropy, thermal emf, current carrier recombination, radiation flaws, etc

19 p3482 A70-37292

Kinetic equation in strong electric fields, describing current carrier behavior in semiconductors

19 p3483 A70-37293

Multivalley semiconductors electrical conductivity anisotropy, discussing redistribution and electron transfer under strong electric field

19 p3483 A70-37294

Radiation flaws in semiconductors, examining effects of gamma quanta, fast electrons and neutrons and heavy charged particles

19 p3483 A70-37295

Semiconductor capture level parameter determination, using thermostimulated conductivity

19 p3483 A70-37296

Ge and Si surface electrical properties, discussing conductivity, field effect, work function, current carriers, photoconductivity, photocurrent carrier capture, etc

19 p3483 A70-37297

Surface atom bonding configuration energy in two-center theory of large surface unit cells on semiconductors

19 p3483 A70-37544

High efficiency semitransparent III-V semiconductor photocathodes fabrication and operation

19 p3486 A70-37756

Carrier diffusion effect in large signal analysis of semiconductor avalanches in quasi-static approximation

19 p3387 A70-37768

Iron phosphate semiconducting glasses, determining electrical and magnetic properties dependence on thermal treatment

19 p3487 A70-37861

Solid state plasmas waves and oscillations in metals, semimetals and semiconductors, noting applications for microwave devices

19 p3479 A70-37944

Frequency dependent reversible switching characteristics of glass semiconductors, assuming current control

19 p3389 A70-38070

Photovoltaic effects in p-n junction semiconductors, discussing conduction and electro-optical mechanism in thermal equilibrium

19 p3488 A70-38476

Photovoltaic effects in semiconductors, considering excess load carrier transport and I-V characteristics

19 p3488 A70-38477

Ultrasonic surface waves amplification in piezoelectric crystal-Si semiconductor system, observing dependence on permittivity

19 p3488 A70-38675

Electrical conductivity of semiconductor diamonds made by alloying with Al under high pressure and temperature

19 p3488 A70-38728

InSb semiconductor, measuring small signal microwave conductivity for hot electron region at 9.4 GHz in high electric DC fields

19 p3488 A70-38747

Gunn effect in two-valley semiconductors with traps explained by model, assuming field-dependent trapping times and field-independent carrier generation rates

20 p3686 A70-39116

Semiconductors, ferrites and segnetoelectrics automatic temperature stabilization problem based on heat source energy conversion

20 p3597 A70-39255

Current fluctuations in polar semiconductors in strong electric field, taking into account semiconductor band structure

20 p3686 A70-39589

Current distribution and interband recombination emission in bipolar semiconductor crystal under pinch effect produced by external magnetic field

20 p3677 A70-39590

Transverse impedance in semiconductor surface layer, taking into account charge in diffusion region

20 p3686 A70-39594

Temperature dependence of titanium-zirconium oxide semiconductor compounds growth, using samples arc melted in purified He

20 p3687 A70-39631

Multiphoton absorption coefficient for semiconductors, using interband absorption method

20 p3687 A70-40020

Liquid and solid semiconductors thermal emf and electrical and heat conductivities measurement over wide temperature range

20 p3634 A70-40300

Wave instabilities in avalanche diode bulk semiconductors with negative field dependent drift velocity and carrier temperature, noting validity for gas plasma

21 p3863 A70-41915

Antiferro-, ferri- and ferromagnetic semiconductors properties, discussing narrow band electron correlation, electrostatic and magnetic polarons formation, etc

21 p3864 A70-42254

Current-controlled negative resistance and conductive memory state in Si-doped single crystal YIG wafers

22 p4085 A70-42331

Amorphous semiconductors optical absorption, thermoelectric effects and switching mechanisms characterized by energy band structure model

22 p4086 A70-42773

Current oscillations produced in finite-length electron hole semiconductors by strong electric and magnetic fields, discussing HF stabilization

22 p4084 A70-43469

Gunn oscillation stabilization in layered semiconductors based on space charge growth reduction via two-stream interaction between GaAs diode and passive bias semiconductor

23 p4230 A70-44196

Cubic monocrystalline semiconductor upper critical magnetic field, using correlation function method

23 p4231 A70-44926

Terminal compensation influence on radiative recombination in n- and p-type GaAs, observing emission band in photoluminescence and electroluminescence spectra

23 p4231 A70-45063

Ultrasonic absorption in SbSI segnetoelectric semiconductor as function of temperature, illumination and constant electric field strength, noting absorption coefficient rise near Curie point

24 p4389 A70-45207

SbSI semiconductor single crystal repolarization parameters temperature dependence, noting anomalies in permittivity, spontaneous polarization and dielectric loss tangent

24 p4389 A70-45208

Helicons and transverse optical phonons coupling in degenerate polar semiconductors investigated from electromagnetic linear response theory and field method

24 p4390 A70-45603

Amorphous semiconductor alloys in As-Se system, measuring DC and AC electrical conductivity dependence on temperature

24 p4390 A70-45657

Semiconductors with bipolar conductivity under electron-hole scattering, calculating plasma pinch effect on I-V characteristics

24 p4390 A70-45659

Light reflectance from optically inhomogeneous medium due to space charge near semiconductor surface

24 p4390 A70-45661

Solubility isotherms of alloying elements in Ge-Al-P semiconductor-acceptor-donor system at high temperatures

24 p4391 A70-46143

Hot electrons Faraday effect in many-valley semiconductors, considering constant energy surface ellipsoidal form

24 p4392 A70-46360

Franz-Keldysh and hot electron effects in interband absorption of semiconductors in external electric field

24 p4392 A70-46361

SEMIEMPIRICAL EQUATIONS

Mean stress effect on low cycle fatigue strength, deriving expression for completely reversed stress cycling

10 p1964 A70-25091

Viscous transonic flow past cascades by semiempirical approach, discussing pressure distribution, boundary layer parameters and compression shock

22 p4088 A70-42343

SEMIMETALS

U METALLOIDS

SENDER

U TRANSMITTERS

SENSATIONS

U PERCEPTION

SENSE ORGANS

- NT BARORECEPTORS
- NT CHOROID MEMBRANES
- NT COCHLEA
- NT CORNEA
- NT CORTI ORGAN
- NT EAR
- NT EARDRUMS

NT EYE (ANATOMY)

NT FOVEA

NT LABYRINTH

NT MIDDLE EAR

NT OCULOMOTOR NERVES

NT OTOLITH ORGANS

NT PHOTORECEPTORS

NT PUPILS

NT RETINA

NT SEMICIRCULAR CANALS

NT THERMORECEPTORS

NT VESTIBULES

SENSES

U SENSORY PERCEPTION

SENSIBILITY

U SENSITIVITY

SENSING

U DETECTION

SENSITIVITY

NT IMPACT RESISTANCE

NT LIGHT ADAPTATION

NT NOTCH SENSITIVITY

NT PHOTOSENSITIVITY

NT PHOTOTROPISM

NT RADIATION TOLERANCE

Sensitivity analysis of discrete filtering and smoothing algorithms, noting in-track motion of circular orbit satellite and marine inertial navigation

[AIAA PAPER 68-824] 03 p0459 A70-12913

Dominant and small parameters determination through sensitivity coefficients in heat transfer problem

[ASME PAPER 69-WA/AUT-4] 04 p0713 A70-14829

Two degree of freedom gyroscope sensitivity threshold during gimbal vibration with respect to casing

04 p0692 A70-15279

Sensitivity functions of nonlinear circuits obtained by calculation of dependent linear model responses, topologically equivalent to original circuit

05 p0824 A70-16125

Subjects sensitivity to differences in statistical distributions of locally defined element density and shape, using stochastically textured visual patterns

06 p0998 A70-17223

Open and closed loop time optimal systems compared with respect to sensitivity measure represented by terminal error norm

06 p1026 A70-17969

Haematocrit variations effect on electromagnetic blood flowmeter sensitivity, discussing blood specific impedance changes

07 p1217 A70-18951

Volt-watt sensitivity of dilatocapacitor types of thermal radiation receivers, noting low natural noise levels

07 p1284 A70-19815

Increasing sensitivity of tuning fork gyroscope by parametric signal amplification

07 p1289 A70-20297

Multibeam interferometer sensitivity restrictions due to diffraction effects on interference patterns near transparent inhomogeneities

08 p1493 A70-20540

Radiometers sensitivity increaseable by combining quasi-zero method with compensation circuits

08 p1495 A70-21053

Equivalent transformations method for minimizing electronic equipment sensitivity to circuit components value variations during operation

08 p1474 A70-21221

Monopole mass spectrometer mass range extension by voltage method, discussing sensitivity and mass scan time

08 p1497 A70-21537

Algorithm for evaluating nth order partial derivatives of network functions and corresponding sensitivity functions

08 p1467 A70-21643

Algorithm for controlled plant parameters determination based on sensitivity function calculation

09 p1653 A70-22145

Fatigue life cyclic sensitivity threshold with random nature statistically estimated on basis of maximum likelihood principle

09 p1776 A70-22618

Sensitivity of nondiffuse double exposure holographic interferometry with transparent medium increased via multiple beam passage through medium placed in optical cavity

09 p1682 A70-23360

Human operator transinformation sensitivity to display gain and forcing function bandwidth in rate control tracking task

10 p1823 A70-23896

Scalar measure of system sensitivity to plant parameter variations applied to design of linear lumped stationary multivariable feedback control systems

10 p1856 A70-25233

Linear systems optimal control problems with sensitivity considerations for restriction to linear feedback of output variables

11 p2026 A70-26235

Vector-matrix differential equation for second order sensitivity coefficients applied to trajectory optimization, modeling and compensation and guidance and control

11 p2029 A70-26324

Connecting wires length effect on sensitivity and current-voltage characteristics of sensors for dynamic values measurement, deriving integral electrical parameters

11 p2055 A70-26445

Cross sensitivity errors effect on stress determination by free-filament wire strain gages used at high temperature

11 p2058 A70-26838

Cryogenic Ge bolometers sensitivity variation and noise, noting radiation absorption by sensor and by coating

12 p2237 A70-28151

Rocket-borne flight testing of sensitive accelerometer developed to measure small forces applied to satellite or space probe surface

13 p2403 A70-28433

Magnetic induction sensors sensitivity for magnetotelluric surveying in geophysics

13 p2415 A70-30048

Savart interferometer for high sensitivity measurements of refractive index gradients using double exposure technique

14 p2583 A70-30400

Multivariable feedback control system, minimizing mean squared error and error sensitivity to random perturbations

14 p2560 A70-30622

SCAMP 2 program for statistical analysis of electronic circuit sensitivity to variations in parameters and DC input values

14 p2560 A70-30665

Output feedback control systems design, considering closed loop system sensitivity to plant parameters based on linear optimal control problem

16 p2885 A70-33324

Initial condition sensitivity functions in bang-bang and optimal control, considering discontinuous functions, perturbation equations, iteration algorithms terminal states, cost functions, etc

16 p2885 A70-33325

Relative sensitivities of polyethylene shielded net radiometers, noting role of reflective white paint partial covering

18 p3261 A70-37087

Grille spectrometer design, fabrication and adjustments, noting increased IR sensitivity over slit devices

19 p3421 A70-37358

Simultaneous generation of sensitivity functions for linear automatic control system with known characteristic differential equation

19 p3394 A70-37867

Low level time truncated signals measurement by narrow bandwidth synchronous time notch filters, discussing sensitivity

19 p3380 A70-38177

IMPATT diode microwave oscillator with modulated bias current, discussing amplitude and frequency modulation sensitivity, thermal effects and load parameters

19 p3390 A70-38363

Optimal control systems sensitivity analysis, discussing trajectory tracking

19 p3394 A70-38716

Automatic control system stability error analysis, discussing sensitivity and statistical dispersion analysis

[AIAA PAPER 70-985]

20 p3668 A70-39544

Sensitivity optimization for linear optimal control systems design, describing aircraft lateral-directional control case study

[AIAA PAPER 70-962]

20 p3600 A70-39567

Kalman filter sizing for air-launched tactical missile via covariance sensitivity matrix

[AIAA PAPER 70-954]

20 p3601 A70-39574

Small angle of rotation measurement of coherent radiation polarization plane, discussing technique for increasing sensitivity and accuracy

20 p3643 A70-39759

Sensitivity functions use in parametrically invariant self adjusting control systems

20 p3602 A70-39828

X ray astronomy proportional counters sensitivity, reducing higher energy radiation background contribution

21 p3821 A70-40653

Vibrating ribbon pressure gage sensitivity, discussing advantages

22 p4029 A70-42624

Holographic interferometry sensitivity augmentation by use of nonlinear properties of photoemulsion

22 p4038 A70-43140

Spectral sensitivity of freely moving human eye by determining threshold energy for correct choice between two monochromatically illuminated stimulus patches

22 p3972 A70-43412

Cactus high sensitivity accelerometer flight tests, discussing operation and experimental conditions

[ONERA-TP-875]

23 p4198 A70-44660

Closed loop synthesis algorithm and comparison to sensitivity of open loop system, noting applicability to optimal control

24 p4322 A70-46013

SENSITIZING

Photodecomposition of 1,4-dichlorobutane sensitized by n, pi singlet state of acetone as chemical process

04 p0646 A70-15319

SENSOR-AIRBORNE TERRAIN ANALYSIS

U SENSORS

U TERRAIN ANALYSIS

SENSORIMOTOR PERFORMANCE

NT PSYCHOMOTOR PERFORMANCE

NT PSYCHOSOMATICS

Male rats locomotor activity responses to altered photoperiods during exposure to varied-light artificial days

01 p0015 A70-10367

Mathematical models for perception and skilled action in man or machine, noting sensorimotor theory

01 p0034 A70-10498

Soviet book on higher cortical functions of man and disorders due to local brain injuries, describing methods for neuropsychological studies of motor functions

01 p0017 A70-10503

Neuron activity in somatosensory cortex region of guinea pigs and rats with intracortical connections severed by circular incision

01 p0030 A70-11470

Event probability and cost effects on performance in continuous motor task

03 p0436 A70-13771

Work and exercise conditions effect in early training stages of learning sensorimotor skill, considering different body positions

03 p0432 A70-14295

Mathematical model building for temporal human motor responses (reaction, movement, manipulation/ by response surface technology and statistical experimental design

[ASME PAPER 69-WA/BHF-5]

04 p0642 A70-14851

Biological model describing spacecraft operator sensorimotor activity in response to various spacecraft control stimuli, outlining computer algorithm

05 p0810 A70-17118

Rabbits sensorimotor and visual cortical responses during defensive conditioning to rhythmic light

07 p1197 A70-18695

Human motor reactions rhythmic system, relating reaction-skin-galvanic reflex to formation of successive conditioned connections

07 p1197 A70-18697

Symmetrical motor centers inequality significance in humans during interaction under conditions of successive innervations during exercise

07 p1213 A70-19790

Dogs spinal cord bioelectric activity monitoring by implanted electrodes, noting interelectrode resistances after prolonged operation

09 p1615 A70-22091

Monograph on systematically disturbed sensorimotor coordination, studying various parameters effects on eye-hand system recorelation

09 p1618 A70-22529

Air traffic vibration effects on human organs and sensations, considering blood circulation, lungs, eyes and muscles

09 p1625 A70-23007

Illusory visual signals experienced by pilots ascribed to aerodynamic forces interference with normal functional relationships between sensory systems

09 p1627 A70-23131

Human sensory-motor adaptation and aftereffects of exposure to accelerative forces using hand-eye coordination measurements

09 p1628 A70-23466

Startle auditory stimuli effects on motor performance and recovery characteristics from heart rate and skin conductance recordings

09 p1628 A70-23577

Motor performance effects on averaged sensory-evoked potentials in reaction time tasks

10 p1811 A70-24226

Transverse g-force tolerance and stability after prolonged hypodynamia in bed rest, noting effects of pharmaceuticals, physical exercise and prophylactic measures

10 p1817 A70-24695

Human movement speed and accuracy as function of age in pencil tapping between paper-drawn targets

10 p1817 A70-24711

Neurophysiological mechanism of motor activity during simple reaction time situation performance

10 p1818 A70-24724

Choice reaction time task involving right or left hand button pressing in monocular and binocular visual response to directional commands by colored lights

11 p1990 A70-25830

Aircraft pilot candidates reactions under simulated flight conditions tested using precision coordination

analyzer /PCA II/ and instrument coordination analyzer /ICA/

12 p2176 A70-27034

Continuous active work effects on human sensorimotor performance, comparing latency distributions in mass and spaced practice groups

12 p2178 A70-27046

Human temporal motor response models relating reaction, movement and manipulation time to stimulus, movement and manipulation information

14 p2540 A70-30248

Dogs spinal cord bioelectric activity monitoring by implanted electrodes, noting interelectrode resistances after prolonged operation

15 p2685 A70-32687

Physiological tests of sampled data hypothesis in human motor control system

16 p2851 A70-33323

Psychophysiological tests involving programmed memory device evaluating human memorization process and sensorimotor reactions to light signals

17 p3040 A70-35676

Evoked potentials in dogs sensorimotor cortex during defensive instrumental conditioning

18 p3221 A70-37213

Cerebrum electrical activity and myogenic tonus relation in subjects performing tasks in response to visual and acoustic stimuli

18 p3221 A70-37216

Electrophysiological characteristics of man during disorders in rhythmic system of conditioned motor reactions

18 p3221 A70-37217

Latent period of human motor reflex in telegraph key press testing in response to oral command

18 p3222 A70-37218

Heat stress effects on serial reaction time in subjects performing visual tasks

19 p3361 A70-38053

Reaction time intersensory facilitation relationship to single channel theories of attention and human performance

19 p3362 A70-38312

Longitudinal vibration effects on human reaction time and motor performance involving toggle switch and manual knob control in different working positions

22 p3977 A70-42871

Labyrinthine and sensory information role in driving, discussing car simulator, driver tests with impaired inputs, age factors, etc

22 p3976 A70-43708

Forebrain participation in motor response suppression reaction during stimulation of caudate nucleus in rats and cats, noting brain damage effects

24 p4299 A70-45836

SENSORS

Airborne sensor simulator using recorded imagery for target detection and recognition problems, discussing closed circuit TV

01 p0088 A70-10810

Terrain imaging radar applied to sensing earth resources

02 p0298 A70-12181

Meteorological satellite TV cameras development, discussing image sensors and tabulating characteristics

03 p0491 A70-13665

Semiconductors and devices for sensor applications, development history, materials requirements and future prospects

03 p0542 A70-14189

Meteor particles spatial density and energy characteristics on space vehicles, using luminescent sensors coupled with photomultiplier

04 p0744 A70-14445

Fluid oscillators for sensing and missile control, discussing performance, design, frequency variation and applications

[ASME PAPER 69-WA/FLCS-8]

04 p0626 A70-14845

Blood flow sensors based on electrical conductivity dependence on flow rate, discussing system instrumentation and experimental results

04 p0644 A70-15295

Laser alignment sensors for measurement and control of five degrees of freedom with increased sensitivity, faster recording and remote meter readout

06 p1083 A70-18591

Rectilinear oblique harmonic vibration effect on gyrocompass with torsional suspension

07 p1278 A70-18737

Temperature, pressure and flow direction probe in rotating fluid machines analysis

07 p1283 A70-19732

Sensors design for studying temperature fields and stressed state of structures

09 p1680 A70-23106

Systems engineering study of sensors in fighter aircraft avionics

11 p2081 A70-26501

Fluid sphere gyro satellite nutation sensor

11 p2057 A70-26504

Automated Weather Network and Environmental Survey Satellite /ESSA 9/ global weather sensing systems 11 p2033 A70-26505

Differential equations of motion of manometers in log instrument systems with allowance for viscous liquid in sensor and pulse line 12 p2234 A70-27567

Waveform estimation by adaptive combination of analog and hardlimited sensor signals 12 p2187 A70-27906

Meteor particles spatial density and energy characteristics on space vehicles, using luminescent sensors coupled with photomultiplier 13 p2485 A70-28470

Free nuclear precession sensor with rotating sample for performing measurements in nonuniform magnetic field 14 p2582 A70-30218

Flueric sensor for RF induced currents providing alternative to bridge wires as initiators of explosive charges 14 p2534 A70-30681

Displacement sensor based on interference fringes counting by laser interferometry 14 p2594 A70-30683

Contactless electromagnetic level sensor for liquid metal using eddy currents 14 p2587 A70-31011

Electro-optical sensor night time capabilities with laser illuminator, determining current per unit area from photocathode 16 p2907 A70-33183

Nonpenetrative reentry vehicle nose thickness ablation sensor using gamma radiation backscatter 17 p3094 A70-35519

Adiabatic calorimeter for heat flux sensor contact calibration, describing operational principles and design 18 p3257 A70-36115

Random values analog sensors classification based on physical, algorithmic and data reproduction techniques 20 p3593 A70-39917

Airborne integrated computerized ASW system, describing navigation, flight control, display and sensor subsystems 21 p3821 A70-40575

Flow difference sensor for aircraft hydraulic systems damage vulnerability reduction, discussing design, operation and flight tests results 21 p3750 A70-40786

Precision gimbaled sensor pointing system calibration data errors due to misalignments and inaccuracies in transducer readout 22 p4040 A70-43587

High pressure hydraulic fluidic vortex rate sensor feasibility, considering variable geometry sensor design, fabrication and tests [SAE PAPER 700788] 24 p4294 A70-45857

Spacecraft sensor trends from space station research and technology requirements regarding astronomy, biomedicine and biology, earth resources, etc [AIAA PAPER 70-1291] 24 p4418 A70-45974

Cryogenic fluid multipoint level sensing detector circuit using carbon resistors 24 p4339 A70-46200

Free nuclear precession sensor with rotating sample for performing measurements in nonuniform magnetic field 24 p4339 A70-46293

SENSORY DEPRIVATION

Visual restriction effects on critical flicker fusion threshold, loudness and pitch discrimination determined using reticular activating system 09 p1622 A70-23576

Sensory deprivation induced EEG changes, discussing duration effect on postisolation occipital alpha frequency 13 p2350 A70-29242

Mental performance changes due to extended exposure of man to sensory deprivation environment, discussing prevention and treatment methods 21 p3770 A70-41479

SENSORY DISCRIMINATION

NT BRIGHTNESS DISCRIMINATION

NT TACTILE DISCRIMINATION

NT VISUAL DISCRIMINATION

Comfort and thermal sensations and associated physiological responses during exercise at various ambient temperatures, noting effects on sensory estimates 01 p0031 A70-11648

Rats ability to discriminate slow rotation speeds, suggesting otolith organs and proprioceptors sensitivity role in discrimination 03 p0439 A70-14296

Acceleration cues removal effects on vehicular velocity perception, using movie technique to control visual cues 05 p0806 A70-16143

Subjective and objective measurement of sound impulses, pauses and intervals duration sensation, showing adjustment accuracy 09 p1618 A70-22763

Accumulator model for psychophysical discrimination, discussing stimulus presentation and sampling, parameter values estimation, response latencies, etc 10 p1827 A70-24767

Aged pilots hearing acuity using speech audiometry, noting discrimination loss for HF verbal sounds 11 p1990 A70-25669

All-or-none hypothesis of selective sensory attention, discussing simple stimuli, target detectability and switching time 15 p2681 A70-31790

Human vigilance paradigm and physiology, discussing relationships between vigilance, signal detection and animal discrimination 19 p3364 A70-38324

SENSORY FEEDBACK

Receptive fields in visual systems, discussing characteristics, size, geometry, adaptation effects, sensory interactions, etc 02 p0236 A70-12304

Human feedback and response mode in performing Bayesian decision task 02 p0237 A70-12382

Biological model describing spacecraft operator sensorimotor activity in response to various spacecraft control stimuli, outlining computer algorithm 05 p0810 A70-17118

Retinal receptors physiology involved in transforming visible radiant energy into sensory message 12 p2172 A70-28105

Tracking error correction time and proprioceptive reaction time, suggesting role of central mechanism without sensory feedback 17 p3036 A70-34606

Visual sensory storage item selection efficiency 19 p3363 A70-38321

Fluidically augmented artificial feel system for fighter and attack aircraft control, discussing improved handling qualities [SAE PAPER 700785] 24 p4294 A70-45859

SENSORY PERCEPTION

NT AUDITORY PERCEPTION

NT CONSCIOUSNESS

NT CRITICAL FLICKER FUSION

NT KINESTHESIA

NT OLFACTORY PERCEPTION

NT PROPRIOCEPTION

NT SPACE PERCEPTION

NT TACTILE DISCRIMINATION

NT TASTE

NT VERTICAL PERCEPTION

NT VIBRATION PERCEPTION

NT VISUAL DISCRIMINATION

NT VISUAL PERCEPTION

Mathematical models for perception and skilled action in man or machine, noting sensorimotor theory 01 p0034 A70-10498

Sensory and muscular factors interaction in space perception via empirical test of summative hypothesis derived from sensory tonic field theory 02 p0239 A70-12626

Perceptual selection and integration of sensory data conveyed to brain, explaining various optical illusions 10 p1827 A70-24766

Feline hypersexuality, aggression and perceptual disorientation resulting from p-chlorophenylalanine administration 12 p2167 A70-27271

Sensory function in multimodal signal detection forced choice experiment involving auditory, visual and auditory-visual stimuli 14 p2539 A70-31167

Thermal thermesthesiometer for skin heat sensitivity studies 19 p3368 A70-37806

Human sensory perception associated with breathing, comparing physical stimulus intensity with judgement of magnitude 19 p3365 A70-38370

Semicircular canals-otoliths interactions for antagonistic and synergistic information 22 p3976 A70-43704

Labyrinthine and sensory information role in driving, discussing car simulator, driver tests with impaired inputs, age factors, etc 22 p3976 A70-43708

SENSORY STIMULATION

Nerve cell response to change in chemical constitution of surroundings used to investigate animal periphery sensory mechanisms 01 p0033 A70-10497

Object carrying behavior of rats, using electrical stimulation of hypothalamic structures 02 p0237 A70-12395

Evoked potentials arising in entorhinal cortex of rabbits in response to stimulation of somatic nerves, light and sound 03 p0417 A70-13070

Somatosensory cortex removal effect on blocking action of skin stimulation on associative response to light flash in cats 03 p0420 A70-13430

Complex conditioned reflexes to three component visual-acoustic-tactile stimulus in dogs analyzed by secretary and thermoelectrical techniques 04 p0638 A70-15504

Human blinking reflex recorded by electromyography, studying latent period in response to stimulation by air stream 12 p2168 A70-27346

Skin receptors afferent discharge characteristics during vibrotactile stimulation 13 p2354 A70-29594

Nervous system response fluctuation measurement during perceptual and learning tasks in terms of signal to noise ratio of electrical and tactile stimuli 13 p2354 A70-29595

Vibrotactile display operational skill acquisition, discussing stimuli quality and spacing effects on lumen of temporal ordering of sensory events in haptic space 13 p2354 A70-29596

Antidiuresis associated with oral cavity stimulation during food ingestion by rats 13 p2355 A70-29813

Perception threshold in rapidly changing circumstances, discussing stimulus signals recognition 15 p2687 A70-32872

Visual and auditory reactions in dogs to alimentary stimuli before and after partial removal of cerebellum, noting complete recovery within month 15 p2687 A70-32892

Decision theory model evaluation based on experimental findings concerning relationship between stimulus intensity and reaction time 17 p3036 A70-34605

Vestibular thermal stimulation method using distilled water injected into ear, discussing nystagmus appearance and duration 19 p3367 A70-37355

Soviet monograph on secondary signaling system role in development of speech, thought, conditioned and unconditioned reflexes, human will and hypnosis, noting salivary gland function 19 p3359 A70-37407

Human spatio-temporal visual evoked response characteristics, showing potential gradient rotation in same period as input stimulus 19 p3360 A70-37845

Reaction time intersensory facilitation relationship to single channel theories of attention and human performance 19 p3362 A70-38312

Human sensory perception associated with breathing, comparing physical stimulus intensity with judgement of magnitude 19 p3365 A70-38370

Vestibular sinusoidal stimulation effects on compensatory tracking under various postures and display conditions 22 p3976 A70-43706

Peripheral stimulations of various modalities effect on neurons impulse activity in hippocamp dorsal area of rabbits, noting excitation and latent periods 23 p4145 A70-44311

Alpha and beta reciprocal hunger regulating systems localized in rats hypothalamus areas by varying injection sites of alpha and beta adrenergic drugs 24 p4304 A70-46233

SENTENCES

NT WORDS [LANGUAGE]

Automated Readability Index for technical materials weighting word and sentence length in multiple regression equation 24 p4308 A70-45510

SENTINEL SYSTEM

U.S. Safeguard plan suitability as hardpoint missile defense system, discussing technical controversy over Sentinel components 04 p0760 A70-14502

SEPARATED FLOW

NT BOUNDARY LAYER SEPARATION

Time dependent behavior of separated and un-separated unsteady flow of incompressible viscous and inviscid fluids without heat transfer 01 p0067 A70-11162

Supersonic flow separation at antisymmetrical delta wing edges, noting eddy layer and vertical velocity fields effects on aerodynamic characteristics 02 p0224 A70-12625

Cyclic changes in concentration produced in fluid flowing through fixed bed of solid adsorbent, governing separation by beds wave propagation properties 04 p0780 A70-14712

Laminar flow separation, reattachment and transition over downstream step, including visual observations of smoke filaments, velocity fluctuation measurements and velocity profiles [ASME PAPER 69-WA/FE-5] 04 p0667 A70-14784

Plume-induced flow separation effect on thermal environment using Saturn 5 film and instrument data, attributing heating rate increase to recirculated exhaust gases [ASME PAPER 69-WA/HT-18] 04 p0761 A70-14815

Vortex separation effects on elliptic bodies lift distribution, analyzing separated flow pattern

04 p0619 A70-15385

Hypersonic laminar separation of slip flow on slender cone with attached compression flares, using surface pressure measurements and Pitot surveys [DFVLR-SONDDR-26]

04 p0620 A70-15577

Three dimensional flow separations on upswept rear fuselages, using flow visualization and pressure measurement

05 p0790 A70-16097

Separated incompressible flow around wing profile, considering calculation of separated potential flow generation with given separation point

06 p0966 A70-17253

Base bleed fluid injection effect on steady separated flow past two dimensional bluff body, studying streamline pattern near object

06 p0967 A70-17518

Flow separation angle and loss coefficient in cascades with small aspect ratio blades under secondary vortex pair expansion over channel

06 p1130 A70-17858

Isoenergetic mixing and reattachment processes of two dimensional supersonic turbulent separated flow, modeling mixing process by constant pressure theory [AIAA PAPER 70-108]

06 p1037 A70-18039

Supersonic flow separation over rearward facing step, measuring upstream boundary layer, lip shock and shear layer formation by pitot probe and surface pressure survey

06 p0973 A70-18153

Laminar to turbulent boundary layer transition and separation on circular cylinder measured by heated end-window film sensor applicable to water flow

07 p1259 A70-19831

Diffusive separation of Ar 36 and 40 and He in axisymmetric supersonic jet taking into account pressure diffusion

08 p1431 A70-21027

Numerical techniques and solutions for compressible and incompressible laminar separated flows using time dependent finite difference equations

11 p2035 A70-25972

Off-centerline heating on lee surface of supersonic delta wing with separation and vortex initiation at leading edge

11 p1976 A70-25996

Convergent-divergent nozzle operation at low pressure ratios causing separation of internal flow, discussing stability and flow field

12 p2157 A70-28084

Hydrodynamic forces by oscillating foils in ideal incompressible fluid turbulent flow with stream separation

13 p2390 A70-29649

Blunt base heat transfer in axisymmetric supersonic separated flow in axisymmetric near wake tunnel, comparing to previous data

13 p2523 A70-29989

Book on flow separation covering steady/unsteady, turbulent and incompressible flows, base pressure, thermal effects, etc

16 p2833 A70-32913

Reactive stream separation high speed color photography for impinging streams of nitrogen tetroxide and hydrazine

16 p2998 A70-33605

Two dimensional incompressible isothermal laminar separation of Newtonian fluid in steady flow, obtaining velocity profiles

16 p2892 A70-33635

Vortices in axisymmetrically separated flows, comparing results of various experiments

16 p2894 A70-33895

Convective heat transfer at solid boundaries in separated and reattached subsonic and supersonic flows, considering booster base heating

17 p3007 A70-34484

Transitional flow separation upstream of compression corner at trailing edge of sharp leading edge flat plate

17 p3007 A70-34487

Laminar incompressible separating and reattaching flows, correlating finite difference solutions with experimentation

17 p3008 A70-34488

Analytic theory of unsteady separated flow effects on dynamics of heat sink type reentry bodies and elastic launch vehicles

17 p3008 A70-34489

Aerodynamics theory for separated flow effects on helicopter lift-drag capability, taking into account three dimensional flow and blade aerelasticity

18 p3205 A70-35956

Mathematical model of three dimensional separated flows with applications to small aspect ratio delta wing and flat plate

18 p3207 A70-36438

Axial flow compressor stage efficiency under rotary separation conditions, investigating dependence on flow rate

19 p3490 A70-37252

Hypersonic aerodynamic characteristics of sharp slender right circular cones at angles of attack, using

Newtonian impact theory modified for flow separation effects

[AIAA PAPER 70-979] 20 p3558 A70-39550

Supersonic flows with imbedded separated regions, emphasizing cavities with recompression against solid boundary layer

21 p3745 A70-41372

Transitional flow separation upstream of compression corner for two dimensional model relationship to attached flow and boundary layer transition on plate

21 p3746 A70-41864

Unsteady aerodynamic forces at stall flutter, applying vortex sheet theory to separated flow field around thin airfoil at high angle of attack

22 p3957 A70-42284

Twisted incompressible viscous fluid flow in conical diffuser described by differential equation system, considering flow velocity field and separation point

23 p4133 A70-44159

Two dimensional incompressible air flow past circular cylindrical body, investigating separation point control by suction and jet injection

24 p4288 A70-46010

Jet momentum for flow separation control of air past circular cylindrical surface

24 p4288 A70-46011

SEPARATION

Hydride segregation in Ti alloy weldments made with unalloyed Ti filler-metal, determining effect on mechanical properties

14 p2591 A70-30932

Solidification theory application to Ti alloys, predicting microsegregation in binary alloys

17 p3112 A70-34352

SEPARATORS

NT AIR FILTERS

NT DUST COLLECTORS

NT EVAPORATORS

NT FLUID FILTERS

Test chamber to simulate helicopter rotor downwash for engine inlet air particle separator optimization

01 p0056 A70-10676

Design parameter importance in centrifugal axial flow particle separator tubes performance from separator tube development program data

01 p0163 A70-10680

Hydrophobic-hydrophilic zero gravity liquid-gas phase separator for Apollo 11 flight life support system

[SAE PAPER 690638] 05 p0804 A70-15844

Materials for separator matrix of rechargeable hydrogen oxygen fuel cell, noting use of composite potassium titanate

09 p1612 A70-22045

Gravity effect on conical vortex separator, predicting body force effect on heavy fluid boundary layer flow for limiting condition determination

13 p2391 A70-29978

Water separation index modified /WSIM/ test for jet fuel surface active materials in relation to filter/separator performance

18 p3300 A70-36815

Liquid-gas separator design with reduced friction loss for MHD generators using two phase convergent-divergent nozzles

20 p3612 A70-40014

SEQUENCING

Loud and soft signal recognition task under information feedback of presentation schedules and sequence probabilities

16 p2854 A70-33974

Successful application development and implementation of data processing system, noting sequence, magnitude, manpower and time required

17 p3200 A70-35507

Sample images division into teaching and checking sequences in pattern recognition problems, determining coefficients based on statistical properties of set

19 p3382 A70-37449

Coordinate sequences for regions with complex geometries and various boundary conditions, using linear operators

19 p3460 A70-38940

Test selecting and sequencing for adaptive checkout processes, determining malfunctions

20 p3659 A70-40106

SEQUENTIAL ANALYSIS

Multichannel sequential detection of stationary signal, deriving analytical expressions for probabilities of erroneous solutions and mean duration of tests

07 p1227 A70-18762

DICAP system to analyze digital sequential switching circuits, studying simulation technique range and limitations of applicability

10 p1845 A70-24236

Discrete calculus of variations for optimal control involving use of discrete time sequence and functionals

10 p1910 A70-24702

Space vehicle on-line tracking with impulsive thrust maneuver by sequential estimation scheme, reducing radius measurement error

11 p2008 A70-26237

Binary-coded sequential acquisition spacecraft ranging system operating at weak signals using HF digital logic

11 p2009 A70-26252

Discrete sequential algorithms for bit synchronization implemented with digital computer for optimum data detection

12 p2184 A70-27249

Optimal singular controls made nonsingular for decreasing epsilon values by adding integral quadratic functional of control to cost functional

13 p2382 A70-29066

Gradient algorithm for sequential identification of features in dynamic linear systems

13 p2383 A70-29582

Adaptive optimization methods involving minimization of unknown function, determining new input location via sequential search

13 p2383 A70-29583

Quasi-optimal sequential detection of phase modulated signal of varying frequency on white noise background, using Markov theory

13 p2369 A70-29732

Maximum convergence function in image recognition using dynamic programming and sequential optimization

14 p2553 A70-30419

Sequential gradient restoration algorithm for optimal control requiring state, control and parameter to satisfy vector differential equation, initial and final conditions

14 p2561 A70-31099

Convolutional code decoder modeled as autonomous stochastic sequential machine, considering finite Markov chain theory for error probability

17 p3049 A70-34854

Multichannel sequential detection of stationary signal, deriving analytical expressions for probabilities of erroneous solutions and mean duration of tests

18 p2229 A70-37106

Bayes sequential detection test with constrained error probabilities, investigating properties of thresholds equations

21 p3787 A70-41333

Sequential experiments design and model discrimination, comparing Chernoff and Box-Hill approaches

22 p4064 A70-43527

Hologram rapid sequence recording, using scatter plate holographic system

23 p4198 A70-44947

Sequential decoder program for low weight codewords in binary convolutional code over one-half constraint length

24 p4313 A70-46065

Suboptimum sequential algorithm for recovery decoding errors in convolutional codes, using Hamming distance criterion

24 p4314 A70-46066

SEQUENTIAL COMPUTERS

Permanent memory faults effects on sequential machines finite-state behavior, considering masking role in synthesis of fault-tolerant sequential networks

11 p2072 A70-26220

Automatic ground based aircraft collision avoidance using combined associative processor- sequential computers

16 p2948 A70-33468

Sequential logic circuit synthesis using truth table, minimizing by Quine-McCluskey method

23 p4167 A70-44861

SEQUENTIAL CONTROL

Terminal area approach control sequencing, using digital computer to allocate identification mode and landing time slot

02 p0332 A70-11971

Optimal guaranteeing control for single switching representable in form of two different successive stages in time, ensuring invariance with respect to motion perturbations

07 p1332 A70-18664

Electronic modulo-M counter driven by HF pulse generator used for generating random numbers sequence

10 p1848 A70-23976

Statistical methods for feature selection and ordering, mode estimation and pattern classification in pattern recognition, describing sequential decision model

13 p2374 A70-29578

Spacecraft onboard computer for prelaunch targeting constants verification through checksum equation and error detection scheme, using generated number sequence

[AIAA PAPER 69-946] 14 p2599 A70-30769

Sequential circuit specification in terms of input/output pair strings, allowing programmed translation algorithm for automation of flow table construction

15 p2711 A70-32605

Linear sequential Kalman filter for time correlated noise without state augmenting and measurement differencing demanding less computer sizing

16 p2887 A70-33350

Dynamical theorems to control number of collisions for sequences in generalized Boltzmann equation, discussing binary collisions involving three molecules
21 p3852 A70-40946

Automatic and command multiple sequencer for spacecraft solar cell battery charger, providing switching logic by integrated circuits design
21 p3758 A70-42128

Pulse-time multistable state elements for automatic and remote control constructed from pulse sequence interactions with multiple frequency relations
22 p4005 A70-43567

SEQUENTIAL DETECTION
U SEQUENTIAL ANALYSIS

SERIES [MATHEMATICS]
NT ASYMPTOTIC SERIES
NT FOURIER SERIES
NT MACLAURIN SERIES
NT POWER SERIES
NT TAYLOR SERIES

Atmospheric dynamics nonlinear equations reduction to spectral form using generalized spherical functions series
01 p0135 A70-12023

Two variable expansion method applied to ordinary differential equation and two wave propagation problems, comparing results with matched asymptotic expansions and coordinate stretching methods
01 p0132 A70-11072

F 2 layer state prediction as function of solar activity by series expansion for describing space-time variations of monthly F 2 medians critical frequencies
01 p0083 A70-11547

Incompressible viscous fluid plane flow using series expansion
02 p0277 A70-11910

One dimensional diffusion equation serial solution implementation by hybrid computation, using equivalence between differential and integral equations
02 p0324 A70-12259

Coefficients of Legendre polynomial expansion of earth gravitational potential, using Stokes problem solution
03 p0474 A70-13344

Converging series solutions for conducting circular disk in radiation field of vertical and horizontal magnetic dipoles to determine reemitted field
03 p0448 A70-13432

HF expansions of harmonic solutions concentrated at waves propagating in inhomogeneous medium to dynamic equations in elasticity theory
04 p0767 A70-14499

Spherical harmonics expansion for earth surface and outer space geopotential by mapping earth surface onto sphere
05 p0837 A70-15926

Programming system for Poisson series manipulation on computer, writing subroutines in machine language
05 p0817 A70-16342

Series expanding velocity profile in parabolic cylinder functions describing nonlinear evolution of steady laminar incompressible wake from arbitrary initial profile
10 p1802 A70-24418

Adjointness in nonadjoint boundary value problems, extending Neuberger symmetry study to obtain expansion theorem for nonself adjoint p-point problems
10 p1910 A70-24606

Independent identically distributed random variables sequence, obtaining asymptotic expansion for large deviations of distribution function
10 p1910 A70-24799

Bessel generalized polynomial series convergence and summability on contour of convergence region
11 p2071 A70-25521

Thermal boundary layer similarity at extreme Prandtl numbers as series expansion, allowing for temperature distribution at wall
11 p2148 A70-25983

Arbitrary function expansion into series of Legendre functions by generalizing Weyl-Lebedev-Skalskaia integral transform
13 p2441 A70-29312

Boundary layer flow between nodal and saddle points of attachment, comparing matched series and finite difference methods
14 p2565 A70-30281

Computer program for two body problem literal series expansions using Kepler functions with Bessel and Poisson series operation
14 p2638 A70-30702

Coefficients of Legendre polynomial expansion of earth gravitational potential, using Stokes problem solution
14 p2573 A70-30719

Orthogonal expansion of multivalued functions for weights in threshold function realization
15 p2767 A70-31838

Series expansions convergence of solutions to boundary value problem for Navier-Stokes equations, introducing small parameter in boundary conditions
16 p2890 A70-33243

Linear system under ergodic random processes, determining optimal dynamic characteristics by approximation of spectral density by Laguerre series
16 p2944 A70-34280

Controlled libration point satellite limit cycle motion, deriving solution in infinite series by harmonic analysis
17 p3181 A70-35752

F 2 region critical frequency diurnal variation forecasting, using series expansion of natural orthogonal components
19 p3409 A70-37327

Center fed cylindrical half wavelength dipole antenna, computing radiation pattern by trigonometric expansion approximation for current distribution
19 p3388 A70-37869

Terrestrial ELF electromagnetic wave fields strength variation with distance over earth surface, using residue series zero-order term
19 p3380 A70-38405

German book on functional theory, Volume 6, tabulating theta and elliptic functions for application to applied physics, potential theory, fluid dynamics and oscillation theory
19 p3459 A70-38600

Kahan Babuska summation method variant in Triplex-ALGOL 60 for reducing roundoff errors in finite series calculation
19 p3385 A70-38678

Lunar ephemeris computerized analytical solution, considering literal expansions generation
20 p3705 A70-39479

Thin plane bars elasticity theory, constructing integrals of equations by asymptotic series expansion
20 p3726 A70-39881

Microwave antenna near field patterns analysis by spherical harmonic expansion, discussing validity conditions and convergence
21 p3796 A70-40556

Harmonic mixed boundary value problem with singularity, deriving approximate solution by dual series technique with conformal transformation and finite difference method
22 p4062 A70-42642

QUANTUM MECHANICS
SERIES EXPANSION
U SERIES [MATHEMATICS]
SERT [ROCKET TESTS]
U SPACE ELECTRIC ROCKET TESTS

SERT 2 SPACECRAFT
SERT 2 solar array power system in sun synchronous orbit, considering power conditioning and deployment technique
20 p3567 A70-40202

Power conditioning system for Hg ion thruster on SERT 2 spacecraft, considering performance, design, control circuits and arcing
20 p3568 A70-40216

SERT 2 spacecraft surface contamination by Hg ion thruster effluents, using solar cell sensors
20 p3690 A70-40217

SERT 2 measurements for spacecraft and ion beam potential as function of thruster and orbital parameters, using hot wire emissive probes
20 p3691 A70-40218

In-flight thrust measurement methods on SERT 2 ion thrusters, using accelerometer, electrical parameters and orbit change
20 p3691 A70-40219

SERT 2 spacecraft ion thruster ground tests and flight operation, tabulating performance data
20 p3691 A70-40220

SERT 2 for testing ion thruster reliability and operational characteristics, discussing design and mission objectives
20 p3716 A70-40221

Electric propulsion systems integration into SERT 2 spacecraft, discussing launch imposed environment, thrust vector control, thruster breakdown, power conditioning, etc
20 p3691 A70-40222

SERT 2 Hg thrust ion extraction, loss, production and energy balance within ionization chamber
20 p3693 A70-40244

SERUMS
Serologic evidence of immune mechanisms, including heart muscle antibodies in patients with idiopathic cardiomyopathy, showing no autoimmune disease in majority
01 p0014 A70-10276

Adrenocortical responses of military recruits to sub-tropical climate, making serum and urinary 17-OHCS measurements on subjects fasting, inactive and at thermoneutrality
01 p0032 A70-10359

LF ultrasound not producing irreversible denaturation of blood serum proteins but capable of modifying electrophoretic properties
07 p1206 A70-19470

Radial immunodiffusion for serum proteins quantitation adapted to capillary blood and compared with results for venous blood
07 p1214 A70-19932

Idiopathic myocardial disease patients investigated for serological anomalies and markers of immunopathology
09 p1621 A70-23301

Fasting and postprandial serum amino acid patterns of human males fed protein-free or protein-sufficient diets
09 p1621 A70-23399

Antigens existence shared by human blood serum and proteins of erythrocyte stroma established through RAHS absorption by stroma and subsequent microimmunoelectrophoresis of serum
15 p2687 A70-32900

Serum enzymes lactate dehydrogenase, creatine phosphokinase and isoenzymes in conditioned male after marathon run, noting little myocardium damage
21 p3766 A70-42158

Electrolyte changes after marathon running noting increase in serum sodium and serum potassium
24 p4302 A70-46108

SERVICE LIFE
Loads effects on refractory alloy fatigue strength and life at high temperatures, describing aircraft turbine blade tests
01 p0115 A70-10069

Dielectric overcoatings effect on Al interconnections electromigration in IC metallization, noting longer intervals between failures
01 p0153 A70-10083

Life-test sampling plan for electron tubes based on exponential failure distribution for reliability demand of military specifications
01 p0099 A70-10112

Hybrid boost bearing applied to jet engines thrust bearing life extension and to land turbine equipment for providing high overload capacity
01 p0101 A70-10389

Bonded solid lubricant films wear life equation for low contact stress conditions, determining optimal film thickness
01 p0102 A70-10397

Cost reductions achieved by space payload life extension through manned maintenance and increased transportation economies via refueling and improved space propulsion
01 p0196 A70-10844

Turbine blades durability and fatigue characteristics, plotting fatigue diagram from statistical tests
01 p0105 A70-11418

Machine parts fatigue behavior and service life, studying endurance margin under load cycles spectra below initial endurance limit
02 p0383 A70-11657

F-8 wing service life extension design techniques, emphasizing fatigue design curves and procedures
02 p3886 A70-11939

Safe-life and fail-safe structural design philosophies in fatigue damage and operating lifetime control
02 p3889 A70-12615

Service life analysis at randomly varying load - Conference, Muelheim-Ruhr, Germany, April 1969 [DFVLR-SONDDR-4]
02 p3931 A70-12851

Aircraft structures service life estimation, comparing results of serviceability tests, solo flight tests, programmed random load tests and linear defect buildup hypothesis
02 p0391 A70-12854

Sealed-off He-Cd laser construction, describing life test, noise, Cd transport characteristics and transverse magnetic field effect
03 p0501 A70-13582

Boeing 707 aircraft operational efficiency optimization by modification program to extend wing life
03 p0497 A70-14052

Nondestructive test procedures for maintaining and determining serviceability of penetrant inspection materials during use
05 p0844 A70-15780

Solar energy as spacecraft power source emphasized in operating life comparison with chemical, electrochemical and nuclear energy, discussing silicon solar cells
05 p0799 A70-17023

Molybdenum disulfide solid film lubricant with increased wear life developed from in situ conversion of electrodeposited molybdenum trioxide
06 p1091 A70-17339

SERT 2 thruster system performance over expected mission parameters, noting operational lifetime excess over mission requirements
07 p1364 A70-19702

Nickel-cadmium batteries rapid deterioration due to destructive demand pulse charging methods
08 p1439 A70-20706

Composite materials fatigue determinations providing curves of stress-strain magnitude vs usable life or time to failure, considering environmental effects in service for design criteria
08 p1531 A70-21895

Low noise TWT, discussing dynamic range, gain and phase tracking, environmental performance, life behavior and noise factor interrelations
09 p1644 A70-22233

Current-voltage characteristics and lifetime of thin film diodes on chalcogenide glass substrate with symmetrical and asymmetrical electrodes

09 p1647 A70-22751

Thermoelastic stresses in plates and shells in random temperature fields, studying influence on service life

09 p1778 A70-23084

Electrode structural parameters effect on polarization characteristics of air-hydrogen cells to obtain optimum performance, reliability and service life

10 p1831 A70-24471

Expansion bellows fatigue strength based on load and displacement measurements performed during low cycle model tests

10 p1965 A70-25299

Traveling wave tube amplifier performance in numerous orbiting communication satellites, emphasizing life test data

[AIAA PAPER 70-507] 11 p2015 A70-25406

TWT, obtaining life performance data from spacecraft, discussing distortion characteristics

[AIAA PAPER 70-505] 11 p2017 A70-25494

Molybdenum disulfide dry film lubricant wear life as film sintering process dependent on binder, additive or atmosphere chemical effects

11 p2058 A70-25571

Macroscopic internal stresses in plastics surfaces, discussing stress effect on plastic moulding service life, Knoop hardness test and charts

11 p2132 A70-25597

Components life determination from calculating cumulative damage using empirical stress amplitude distributions

11 p2133 A70-25844

Low cycle fatigue problems, environmental influence of operational differences on component life, life limits and controls for safe operation of jet engines [SAE PAPER 700207] 11 p2102 A70-25879

Generator regulator for Ni-Cd batteries capable of sensing temperature, reducing charge rate and limiting output to increase batteries life

[SAE PAPER 700212] 11 p1983 A70-25884

Service life and friction coefficient of molybdenum disulfide-silicon lubricating coating as function of load, sliding rate and vacuum level

11 p2060 A70-25943

Complex airframe design for economic and safe operation and long life using fatigue and fracture mechanics

[AIAA PAPER 70-512] 12 p2324 A70-27466

Space station design for long duration operation, considering optimum mix of redundancy, maintainability and checkout

12 p2313 A70-27743

First excursion failure survival probability of randomly excited structures, considering single degree of freedom linear oscillator under Gaussian white noise

12 p2327 A70-27819

Reliable and optimum cost power sources design for long life electronic digital communication equipment

12 p2166 A70-27927

Materials life estimation under irregular load sequences, discussing computational and graphical method, applications and test and computer equipment

13 p2513 A70-29162

Rotating disk service life and structural failure under creep, using Tresca yield and maximum stress criterion

13 p2514 A70-29290

Reliability relation to mean time between failures /MTBF/ relation for long life repairable equipment with limited life components

13 p2421 A70-29567

Turboprop aircraft engine service life extension, correcting deficiencies via accelerated tests based on relation between failure rate and usage

15 p2787 A70-31535

Decreasing failure rate /DFR/ with time in electronic systems operating in avionics applications

15 p2712 A70-32646

Wearout life and reliability of rate gyros from field service test data

15 p2748 A70-32668

Reliability-cost model to determine optimum failure rate for minimization of systems total life cycle cost [ASME PAPER 70-DE-43] 16 p3004 A70-33507

Life and confidence tests of miniature self contained flexure pivots in critical mechanisms

[ASME PAPER 70-DE-76] 16 p2918 A70-33522

Reliability life tests preventing sliding electrical contacts failure in space vehicles, discussing data dissemination

16 p2920 A70-33806

Space suit thermal insulation properties, wear durability and nonflammability improvements, reflecting techniques in fabricating cryogenic multilayer insulation systems

[AIAA PAPER 70-851] 16 p2939 A70-33918

Hazard plotting methods for analyzing service life data with different failure modes

16 p2921 A70-34024

Plastic structural components service life estimation based on creep diagrams and short time tests

16 p2941 A70-34323

Aircraft, helicopters and rockets aviation systems design and components service life problems, emphasizing maintenance intervals

17 p3100 A70-34686

Materials and noncontacting design for 50,000 hour lifetime electromechanical components, noting magnetically suspended motor

17 p3100 A70-34754

Boeing 747 aircraft JT9D engine deflections and removals during early service experience and maintenance

[AIAA PAPER 70-890] 17 p3019 A70-35807

Machine parts fatigue behavior and service life, studying endurance margin under load cycles spectra below initial endurance limit

19 p3547 A70-38430

Contact-relay circuits failure free operation probability, taking into account coil winding breakage

19 p3390 A70-38579

Redundant systems reliability under wearout conditions for active and standby units, including failure rates of sensing and switching devices

19 p3438 A70-38597

Oil seals service life as function of friction horsepower

[ASLE PREPRINT 70AM 5C-1] 19 p3439 A70-38807

Binder wetting relation to solid film lubricant wear life

[ASLE PREPRINT 70AM 5A-3] 19 p3439 A70-38810

Computer program for assessment and modification of mechanical component life predictions by discrete formulation of Bayes theorem

19 p3440 A70-38816

Long life reliability measurement for reentry and recovery systems, noting applicability to program monitoring, optimum resources allocation, etc

19 p3442 A70-38832

Long term life test and vacuum tests of high temperature resistojets using ammonia and hydrogen propellants

[AIAA PAPER 70-1136] 20 p3567 A70-40212

Colloid microthruster system life test, discussing design and steady state performance

[AIAA PAPER 70-1110] 20 p3692 A70-40233

Accelerated life testing, discussing accumulated damage for graphical procedure in normal conditions

[ASME PAPER 70-PROD-10] 21 p3832 A70-40871

Helicopter parts and assemblies fatigue life estimation and testing, discussing loading spectra, service conditions, etc

22 p4046 A70-43119

Aircraft turbine engines durability estimated from rotor blade minimum tip clearance measurements

22 p4092 A70-43529

Ni-Zn high energy secondary battery cycle life and discharge capability

22 p3966 A70-43540

German monograph on fiberglass, matrix and filler effect on service life of composites with low fiberglass content

24 p4365 A70-45084

Chemically treated rolled hard properties following long term use in air hygrometers

24 p4333 A70-45138

NDT for aircraft service life extension, discussing fatigue tests and crack detection

24 p4346 A70-45719

Aircraft structures service life estimation, using Ir-192 and Tm-170 gamma ray radiography

24 p4346 A70-45725

SERVICE MODULES

Nondestructive testing for Apollo Command and Service Module, describing requirements added to quality control scope

01 p0098 A70-10026

Apollo spacecraft hardware, command, service and lunar modules, discussing design factors and tests contributing to spacecraft reliability

[AIAA PAPER 69-1095] 01 p0194 A70-10618

Fuel cell assemblies as primary electrical source for Apollo command and service modules, discussing heat removal, water vapor control and transient performance

08 p1439 A70-20702

Apollo command and service modules from metallurgical viewpoint

09 p1766 A70-22792

Apollo service module engine design for maximum pilot safety, noting components redundancy

11 p2103 A70-26289

Apollo command and service modules environmental control system, discussing redesign of faulty hardware

[SAE PAPER 690618] 12 p2167 A70-27948

NDT techniques in manufacturing of Apollo command and service modules

13 p2420 A70-29243

Apollo service module retrograde motion due to propellants reorientation after reentry jettison predicted by digital simulation

[AIAA PAPER 70-1047] 19 p3534 A70-38862

SERVICES

Airfreight carriers secondary services from legal viewpoint

07 p1427 A70-18889

Computerized air transportation service including passenger name record, fare quotation, ticketing, etc

17 p3199 A70-34688

SERVO LOOPS

U FEEDBACK CONTROL

U SERVOCONTROL

SERVOACTUATORS

U ACTUATORS

U SERVOMOTORS

SERVOAMPLIFIERS

Soviet book on servo systems for radar automatic tracking and control stations covering static, dynamic and frequency characteristics, amplifiers and correction devices

09 p1654 A70-22597

Hydraulic regenerative servoamplifier system for electrohydraulic actuator design, discussing specifications and test results

09 p1614 A70-23686

SERVOCONTROL

Satellite tracking antennas servo design including adaptive and compensation methods and digital computer applications

01 p0011 A70-11453

Optimal servocontrol via nonquadratic performance index and linear plant dynamics obtainable as nonlinear function of error between controllable states and input vector

02 p0273 A70-12732

Servo systems for analog automatic reduction of time dependent photomechanical model materials fringe data in stress analysis

03 p0482 A70-12967

Static and dynamic characteristics of inertia load driving systems using electrohydraulic pressure and flow control servovalves

[ASME PAPER 69-WA/FLCS-15] 04 p0626 A70-14842

Weighting function of optimal correctable gyroscopic servosystem in random narrow band noise

05 p0880 A70-16225

Laboratory Electronic Servo Controller for structural fatigue tests, aircraft material tests, model position and velocity control in wind tunnels

06 p0989 A70-18606

Servo systems for analog automatic reduction of time dependent photomechanical model materials fringe data in stress analysis

07 p1286 A70-20040

Soviet book on servo systems for radar automatic tracking and control stations covering static, dynamic and frequency characteristics, amplifiers and correction devices

09 p1654 A70-22597

Procedures for conducting fatigue studies at high temperatures on servocontrolled testing machines using stress, axial, transverse or plastic strains

11 p2033 A70-26612

Telescope servocontrol system with low pointing error and drift rate, permitting extended time exposure photography of star or deep space probe

12 p2202 A70-26869

High temperature compressive creep tests at constant stress, describing strain measurement techniques and servocontrolled compressive equipment

12 p2206 A70-27214

Dynamic stability of multipoint servocontrol system actuating thin deformable primary mirror of orbiting telescope

12 p2203 A70-27413

Servocontrolled IR optometer providing electrical signal proportional to refractive power of human eye

12 p2237 A70-28123

Nonlinear servo system stability criteria based on plus or minus controlled data theory

13 p2381 A70-28939

Servocontrolled laser strainmeter based on Michelson-Morley interferometer, determining dynamic characteristics dependence on feedback loop filter type

16 p2925 A70-33022

Desensitized linear servo model following feedback control systems design using specific optimal control concepts

16 p2884 A70-33315

High strain fatigue machine with axial loading and servocontrol for short endurance testing

17 p3063 A70-35586

Steady forced regime stability in pulse frequency modulated servosystems, using Liapunov method

18 p3234 A70-36071

Hybrid fluidic heading reference system with negative feedback servo loop around vortex rate sensor

[ASME PAPER 70-FLCS-10] 22 p3963 A70-42417

- Amplitude instability in vibration testing systems, noting effects of bandpass filters in feedback loop of amplitude servo 22 p4006 A70-43250
- SERVOMECHANISMS**
NT SERVOAMPLIFIERS
NT SERVOMOTORS
 Position control of burning solid nonmetallized propellant strand in combustion bomb using closed loop servomechanism 01 p0215 A70-10830
 Satellite tracking antennas servo design including adaptive and compensation methods and digital computer applications 01 p0011 A70-11453
 Triple mode control strategy to provide near optimal stable transient response in variably loaded electrohydraulic servomechanisms 02 p0272 A70-12728
 Slide and sleeve type servovalves used in Boeing aircraft possessing chip shearing capability of 200 pounds axial force 02 p0229 A70-12863
 Harmonic equilibrium method applied in dynamic properties analysis of autopilot electrohydraulic servomechanisms stability 03 p0415 A70-13930
 Controllable light source for experiments on human pupillary servomechanism 04 p0642 A70-14633
 Pulse width modulated (PWM) electrohydraulic servo response characteristics from modulator transfer characteristic determination by Fourier series analysis of PWM signal [ASME PAPER 69-WA/AUT-2] 04 p0625 A70-14831
 Proportional controlled pneumatic servomechanisms analysis extended to include motion along stroke, considering position effect on stability 05 p0797 A70-15891
 Self adaptive servosystems operating with incomplete input signal information, proposing schemes for parameter adjustment by employing differential circuit containing frequency filters 07 p1239 A70-18734
 Dynamic mathematical model of proportional electromagnetic transducer in pneumatic servomechanisms derived by Lagrange-Maxwell method assuming circuit linearity 07 p1195 A70-18750
 Band polishing machines slave mechanisms and programmed controllers, describing helicopter longrons finishing process 07 p1291 A70-18829
 Simulator servo drive system dynamic requirements for single-axis manual control task using pilot models and computer [AIAA PAPER 70-355] 10 p1858 A70-24208
 Electrohydraulic fast response servosystem design and operation, describing nonlinear model based on component limitations 10 p1807 A70-24578
 Hydraulic piston-valve-type slave mechanism oscillations with rigid feedback and inertial load at actuated shaft, using harmonic linearization method 12 p2167 A70-28340
 Adaptive hydraulic servomechanism control systems synthesis by Liapunov direct method, noting parameter compensation effect on state error reduction 14 p2534 A70-30621
 Bang-bang control of electrohydraulic servomechanisms, approximating optimal control by quasi-optimal controls 16 p2887 A70-33685
 Scan platform servomechanical actuator for Mariner Mars 1969 spacecraft, emphasizing gear arrangement and train dynamics 16 p2845 A70-34108
 Solar power panel orientation servomechanism using passive elements without power consumption 16 p2846 A70-34130
 Dynamics of continuously operating linear servosystems stimulated by stochastic signals, using vectorial equation and impulse response matrix 16 p2944 A70-34295
 Servosystems with random input signals, obtaining optimal transfer function by variational calculus 17 p3056 A70-34617
 Doppler radar frequency tracker with servomechanism applicable to velocity computation of aircraft for self contained navigation 18 p3226 A70-36063
 High order servosystems approximation characterized by gain, time constant and dead time, discussing application to response prediction 19 p3394 A70-38503
 Electrochemical dimensional machining of complex profile components, using servosystem with feedback for interelectrode gap control 20 p3636 A70-39196
 Multichannel iterative servosystems operators for useful signals reproduction 20 p3603 A70-39836
- Hydraulic servomechanism stability and step response, considering unequal oil volume on either side of jack 24 p4292 A70-45159
- SERVOMOTORS**
 Approximate determination of termination hydraulic servomotors frequency characteristics with four way valves using piecewise straight lines on Bode diagram 01 p0007 A70-10034
 Servoactuator simulating vertical acceleration in F-104 simulator, duplicating other forces conventionally 02 p0229 A70-12864
 Amplification and contactless recording device with ferromagnetic servomotor controlled by low DC signals 05 p0848 A70-16364
 Electromechanical start-up time, inertia and synchronous electromagnetic moment of wave-type electric servomotor calculated by energy method 10 p1809 A70-25202
 F-111 aircraft wings unstable fore and aft oscillations in swept forward position ascribed to actuator motor drive rate variations 12 p2160 A70-27112
 Dynamic stability of multipoint servocontrol system actuating thin deformable primary mirror of orbiting telescope 12 p2203 A70-27413
 Parameters optimization of nonlinear electric servo actuator on basis of statistical criteria 14 p2559 A70-30157
 Stepper motor for pointing Surveyor spacecraft TV transmitting antenna and solar panel at earth and sun 16 p2845 A70-34110
 Servoactuator for stick force augmentation on light turboprop STOL aircraft at high angles of attack [AIAA PAPER 70-909] 17 p3019 A70-35821
 Closed loop automatic speed control system for working shaft of two stage alternating current electric servomotor, using invariance principle 20 p3564 A70-39849
 Liquid metal hydraulic servoactuation packages for flight control in high temperature environments without coolant systems 21 p3750 A70-40785
 Automated aircraft flight safety, concerning probabilities and onboard elimination of servomotor failures in hydraulic system due to fuel contamination 22 p3361 A70-42804
 Amplitude-phase characteristics of relay slave mechanisms with AC and DC motors under dynamic braking, using harmonic linearization 22 p4002 A70-42842
 Thyristor-servomotor temperature control unit, describing circuit and applications 22 p3996 A70-42850
- SERVO**
U SERVOMOTORS
SERVOSTABILITY CONTROL
U SERVOCONTROL
SET THEORY
NT EQUIVALENCE
NT THRESHOLD LOGIC
 Difference set D of k distinct residues, extending Hall search with negative results, discussing multipliers, polynomial congruence, etc 01 p0132 A70-11073
 Classical mechanics and thermodynamics principles restated using functions of sets, material sets and reciprocal actions between material sets 02 p0339 A70-11896
 Covering properties of topological space as function of set density 07 p1323 A70-18963
 Invariant set existence inside submanifold convex to flow established from vector field properties on submanifold boundary 07 p1324 A70-19198
 Invariance and stability of subsets in metric state-time dynamical polysystems 07 p1324 A70-19200
 Differential calculus for multifunctions using Radstrom embedding theorem for convex sets 09 p1710 A70-22060
 Class of spaces containing class of order totally paracompact spaces, deriving invariance theorem 09 p1712 A70-22774
 Optimal control of systems with time transitions described by finite state stationary Markov chain, noting resetting control 13 p2382 A70-29065
 Seminormality and upper semicontinuity of variable sets in optimal control 22 p4061 A70-42461
 Binary codes linear metric properties description reduced to finite set determination by convex programming procedure 22 p3993 A70-42494
 Combinatorial optimization problems design on permutation set, considering applicability of variants successive analysis method 24 p4321 A70-45472
- Linear operator convex closed set, considering range-domain or output-input implications 24 p4369 A70-46023
 Real functions and sets representation theorems derivation and application to nonlinear programming, using Bellman quasi-linearization technique 24 p4370 A70-46099
- SEWAGE**
 Sewage water flowmeter calibration, analyzing error propagation and tolerance 09 p1672 A70-22027
- SEX**
 Feline hypersexuality, aggression and perceptual disorientation resulting from p-chlorophenylalanine administration 12 p2167 A70-27271
- SEX GLANDS**
NT OVADS
NT OVARIES
NT TESTES
SEXTANTS
 Space rendezvous navigation and guidance based on optical sightings with hand-held sextant entered into and processed by small digital computer 07 p1331 A70-20061
- SERICS**
U ATMOSPHERICS
SHADOWGRAPH PHOTOGRAPHY
NT SCHLIERN PHOTOGRAPHY
 Holographic color schlieren flow visualization system for three dimensional photography, variable focus shadowgraph, knife edge schlieren, etc 01 p0091 A70-10908
 Shadow optical raster method for quantitative investigation of dynamic stress states in two dimensional transparent or reflecting bodies 03 p0496 A70-14215
 Nonequilibrium processes behind shock wave in shock tube supersonic air and nitrogen flow, using photoelectrical shadow method 06 p1053 A70-18562
 Monopulse ruby lasers for moving object illumination during shadow photography, noting applications to ballistic studies 09 p1698 A70-23173
 Grid shadow moire method to measure displacement contours of large plates, discussing sensitivity changes 11 p2131 A70-25589
 Planview shadowgraph method for observing disturbances generated by spark discharges into laminar boundary layer 13 p2385 A70-29982
 Shadow photography applied to Mach reflections in argon, carbon dioxide and Freon 12 in shock tube, using Huygens principle for transfer mechanism 18 p3205 A70-36148
 Turbulent flows shadowgraph analysis, solving electromagnetic equations for optical response 18 p3242 A70-36692
 Shadow method for temperature field in potentiometer winding 19 p3420 A70-37264
 Stereo synchroballistic shadowgraph system for explosively projected shock wave, using streak camera [SMPT PREPRINT 114] 22 p4031 A70-43027
 Spark photography of models in free flight in hypersonic shock tunnel [SMPT PREPRINT 99] 22 p4032 A70-43035
 Spark tracing in gaseous flows in flames, wind tunnels, nozzles and pneumatic valves, using pulse transformer [SMPT PREPRINT 41] 22 p4033 A70-43041
 Laser and flash X ray shadowgraph techniques in hypervelocity ablation/erosion investigations in hyperballistics range 22 p4034 A70-43047
 Starting shock and contact surface measurement reflection nozzle, using HF spark camera and interference techniques 22 p3959 A70-43064
 Ultrabright nanosecond flash light generation technique, using superradiant light sources for shadowgraph photography in high resolution hypervelocity field [SMPT PREPRINT 74] 22 p4037 A70-43070
- SHADOWGRAPHS**
U SHADOWGRAPH PHOTOGRAPHY
SHADOWS
NT LUNAR SHADOW
NT PENUMBRAS
 Sunspot group of July 1966, studying umbrae structures relation to magnetic field 08 p1569 A70-20835
 Photometric profiles of Jupiter shadows cast by large natural satellites used as upper atmosphere probes 08 p1579 A70-21571
 Eckert shadow technique for radiation view factors applied to toroid inside shadow hemisphere 08 p1546 A70-21832
 Earth shadow effect on solar radiation pressure induced short periodic perturbations of satellite orbits 09 p1761 A70-23054

Earth shadow enlargement during 13 April 1968 lunar eclipse, discussing craters exit and entry in umbra

HOH lines existence in sunspot umbral spectrum

Peripheric umbra photometric analysis during lunar eclipses based on homogeneous observational material, revealing luminescence excited by solar corpuscular radiation

Cassegrain antennas design parameters using graphs for minimum blockage condition

Photoelectric spectra of photosphere and sunspot umbra and penumbra ranging from 3900 to 8000 Å

Large sunspot umbra continuum intensity, examining visible spectra

Umbral flash as magnetoacoustic wave, examining Ca II K line variations formation during adiabatic compression

Sunspot umbras and penumbras magnetically nonsplit lines measured photographically by spot contrast discriminator

SHAFTS [MACHINE ELEMENTS]

NT TURBOSHAFTS

Book on vibrational motions of straight and curved shafts, covering dynamic analysis for noncircular cross sections, applications to machine tools and vehicles design, etc

Elastoplastic stress concentrations calculations in notched strips and shafts under tension, bending and torsion, using approximate method

Mechanical systems vibrations comprising tension couplings compensating misalignment between non-coaxial shafts

Monograph on critical speeds of nonzero mass shaft supported at both ends by bearings with nonlinear elastic displacements

Self energized hydrostatic shaft seal operating with incompressible fluid in laminar flow regime, using general lubrication theory

Contour notch position effects on stress concentration in taper section of dumbbell shafts, using photoelastic shaft models and cyclic tests

Disk elements perpendicular mounting by rotation on vibrating shaft, obtaining orientation by centrifugal force

Axial stress at notch root of shafts under axially symmetric loading, utilizing integrated birefringent patterns in transmitted light at room temperature [SESA PAPER 1970]

Shear stress distribution in axially nonuniform circular shaft subjected to torsion, using finite difference approximations

Composite tail rotor driveshaft for next generation helicopter, discussing materials, fabrication and tests [AHS PREPRINT 451]

German monograph on form factors and torsion at shafts with longitudinal keyways under pure torsion

Dry face mechanical shaft seal operating on self generated graphitic film without boundary fluid lubrication [ASLE PREPRINT 70AM 3C-2]

Rigid cylinder rotation and flexible shaft torsion observation by holographic interferometry

SHAKERS

Single or repetitive shock pulses produced on electrodynamic and hydraulic shakers for shock testing on vibration machines

Electrohydraulic vibrators and shakers for testing aircraft systems, diesel engines and structural joints, describing design and operation

HF shaker for accelerometer calibration and resonance evaluation, discussing construction materials, accuracy and test results

Multiple head shaker systems theory as application of linear algebra, noting open loop control system with computer control of frequency, amplitude and phase

Digital electrodynamic vibration exciter control for sinusoidal, random and shock spectrum testing of aircraft, missiles and satellites

Aeroelastic test equipment for Concorde SST using harmonic method and electromagnetic shakers

Shock pulse reproduction on electrodynamic and hydraulic shakers for vibration testing, including SNAP 21 results

SHALES

Steranes and triterpanes identification from Green River shale by capillary gas liquid chromatography and mass spectrometry

Nitrogenous compounds from Colorado Green River Formation oil shale using high resolution mass spectrometry

SHALLOW SHELL EQUATIONS

Thin circular elastic ribs strengthened shallow shells, obtaining solutions in single series

Shallow shell theory, discussing equation kernels, reduction of boundary value problems to integral equations, potential theory application and transformation into Fourier series

Stress-strain state of perforated shallow shells with arbitrary curvature using Green matrices

Integral equations for antisymmetric shallow shell stress-strain state with crack, obtaining asymptotic solution in form of power series

Stress-strain state equations of shallow spherical shells in rectangular and polar coordinates, discussing reduction to plate and Cauchy-Riemann equations

Shallow flexible shells similarity conditions derived in dimensionless form, assessing error

Shallow elliptical planform shell under uniformly distributed normal load calculated with 'ritz and Bubnov-Galerkin variational methods

Donnell shallow circular cylindrical shell equation, obtaining approximate solution for stresses in infinitely long circular cylindrical shell with circular hole subjected to edge loading

Stress-strain state under bending of shallow spherical shell having form of circular rectangle with clamped edges

Clamped and simply supported shallow spherical shells buckling using computer programs

Thin elastic shallow shell static problem solved using numerical integration of differential equation

Heated isotropic shallow shells results extended to solving nonlinear problem in bending theory of orthotropic shallow shells clamped, heated and under pressure

Exact polynomial solution Saint Venant flexure of pretwisted rectangular plate treated as shallow hyperbolic paraboloid shell

Stressed state of shallow spherical shells of revolution undergoing large displacements reduced to Karman equation, solved by small parameter method

Stability and critical load algorithm for flexible shallow spherical and conical shells of revolution derived from variational equation

Shallow spherical shells stability under combined loading, hinging and edge clamping conditions, deriving strain energy expressions

Shallow spherical shell subjected to arbitrarily located concentrated normal force, discussing boundary effects on resulting stress distribution

Thermal stresses in shell with spherical and circular cylindrical sections, using thin shell approximations and shallow shell theory

Stress and buckling measurement of shallow cylindrical steel shells linked to thin plate using resistant strain gauges and high precision indicators

Revolving shallow shells steady creep equations solved by approximation adaptable to computer

Shallow spherical sandwich shells under concentrated forces, obtaining inhomogeneous equations solution by integral Hankel transforms

Shallow orthotropic shell of rectangular planform with edges under dynamic load, studying forced vibrations by anisotropic shell theory

Shallow spherical caps elastic buckling under uniform pressure, considering symmetric and asymmetric deformation modes

Nonlinear spinning shallow spherical shell equations solved for equilibrium stress and displacement distributions, discussing inertia loading

Shallow shells of variable thickness and curvature calculated using small parameter method based on functional analysis

Natural oscillation frequencies determined for shallow shells with hinged and clamped edges

Stress concentration on isotropic elastic circular cylindrical shallow shell using plane waves and spherical means method, obtaining periodic solutions convergence

Variable coefficient equations for free oscillations of shallow shells of variable thickness in Vlasov moment theory

Dynamic stability of shallow shells, taking into account longitudinal inertial forces and nonlinear geometry

Rectangular planform shallow cylindrical shell parametric vibrations using method applied to large bending vibrations of plates

Pairs existence of symmetrical equilibrium forms in nonlinear shallow shell under load applicable to nonshallow shells equilibrium

Shallow rectangular shell panels nonsymmetric nonlinear deflection states computed by finite difference equations iteration, discussing snap-through buckling loads

Partially loaded clamped plastic shallow spherical caps collapse loads and stress and velocity distributions

Carrying capacity of shallow shells of revolution, determining buckling stress and limiting equilibrium of shells with varying thickness under transverse load

Lower critical load for shallow rigidly convex shell expression refined by considering effect of rigid clamping of shell edge on buckling boundary deformation

Solutions existence for nonlinear partial differential equations describing orthotropic and nonlinear shallow shells under loads and temperature effects

Creep deflections and collapse times for supported thin shallow spherical shells under uniform pressure predicted using variational theorem

Finite element method using shallow shell stiffness matrix extended to cylindrical shell solution

Shallow spherical shells stress-strain state in multiply connected regions resting on Winklerian base

Clamped shallow spherical cap elastic buckling and initial postbuckling behavior under uniformly distributed load over circular region centered at apex

Shallow shell solutions complete with respect to finite simply connected surface region applied to circular cylindrical shells

Shallow shell theory partial differential equations, obtaining integral representations of general solutions

Linear compressive orthotropic stability theory for shallow-stiffened cylinders

Shallow shell theory, discussing equation kernels, reduction of boundary value problems to integral equations, potential theory application and transformation into Fourier series

Thermal stability of simply supported bimetallic shallow spherical shell, considering rotationally symmetric deflection modes

Natural oscillation frequencies in rectangular shallow shells weakened by cuts, using summary representations method for eigenvalues determination

Natural oscillation frequencies of shallow shells with mixed boundary conditions on clamped edges, using summary representations method

Reinforced shallow shells and plates stability beyond elastic limit, obtaining optimal parameters under compressive loads

Shallow shells displacement theory, representing solution in terms of analytical functions

Shallow shells of revolution under axisymmetrical loads, analyzing plasticity and creep by integral equations algorithm

15 p2817 A70-32164

Stability characteristics of elastic shallow shells of revolution in temperature field and under compression, reducing variational equation of bending by Ritz method

15 p2817 A70-32169

Nonlinear dynamic analysis of shells of revolution under symmetric and asymmetric loads, obtaining solutions for shallow cap buckling

16 p2994 A70-34229

Shallow shell finite element of triangular shape, noting application to static problems

17 p3184 A70-34908

Singular solutions to concentrated loads on shallow shell equations with quadratic middle surface

17 p3186 A70-34968

Solutions for normal and tangential displacements and concentrated forces on shallow cylindrical shells

17 p3186 A70-34969

Coupled integral equations for cutouts in shallow shells

17 p3186 A70-34970

Shallow shell theory boundary value problems, calculating stress concentration for domes and shells with holes

17 p3192 A70-35694

Critical load of shallow shell of revolution as function of geometric and material parameters

17 p3192 A70-35717

Dynamic axisymmetrical loading of thin elastic shallow spherical rigidly clamped dome, using variational method

18 p3341 A70-36582

Shallow conical shell stability under uniformly distributed pressure and concentrated force at apex for rigid and free clamping boundary conditions

18 p3341 A70-36589

Shallow spherical shell dynamics nonlinear problems solution with algorithm permitting use of straight lines method

18 p3341 A70-36590

Shallow shell solutions complete with respect to finite simply connected surface region applied to circular cylindrical shells

19 p3547 A70-38396

Stress concentration on isotropic elastic circular cylindrical shallow shell using plane waves and spherical means method, obtaining periodic solution convergence

20 p3719 A70-39385

Shallow shell theory partial differential equations, obtaining integral representations of general solutions

20 p3732 A70-40102

Flexible shallow shell with plastic inhomogeneity due to yield point-fast neutron flux relation, examining stability under uniform load

20 p3734 A70-40437

Donnell-Vlasov shallow shell equations error analysis

20 p3734 A70-40441

Stresses around circular hole in shallow conical shell under torsional load, using perturbations in parameters for curvature and cone angle

21 p3934 A70-40779

Infinite plates and shallow shells stability under doubly periodic surface loadings, using nonlinear analysis

24 p4421 A70-45283

Shallow arch clamped at ends and subjected to uniform lateral load, deriving nonunique equilibrium stability states

24 p4426 A70-46038

SHANKS

U JOINTS (JUNCTIONS)

SHANNON INFORMATION THEORY

U INFORMATION THEORY

SHAPED CHARGES

Pentolite spherical charge gaseous explosion products expansion into vacuum, using Taylor similarity solution for flow in detonation wave

15 p2774 A70-31764

SHAPES

NT CONVEXITY

NT ELLIPTICITY

NT LINE SHAPE

NT ROSETTE SHAPES

NT T SHAPE

Curved cylindrical panel flutter in presence of uniform compressive load, taking into account relationship between actual and ideal shape

01 p0202 A70-10946

Shape optimization of elastic rod compressed by force directed toward point on undeformed rod axis, deriving optimal bending line

05 p0937 A70-16373

Test specimen shapes for determining tensile, compressive and edge-wise shear properties of reinforced plastic laminates

08 p1529 A70-21878

Optimizing shape of elastic bar compressed by polar force obtained by determining functional extremum representing volume of bar at constant critical force

09 p1769 A70-22252

Heat treatment induced shape distortions measurements in maraging steel bars, plates and sheets, noting dependence on number of anneals and product form

14 p2595 A70-30544

Shadow moire method for comparing diffusely reflecting component against holographically recorded master shape, noting turbine blade measurement

17 p3088 A70-35025

Stiffness matrix correction for curved element deficient in rigid body motion

18 p3342 A70-36687

Electromagnetic field amplitude and phase scattering diagrams analysis for shape information capacity

21 p3785 A70-40637

SHARING

U COORDINATION

SHARP LEADING EDGES

Leading edge suction analogy for predicting low speed lift and drag-due-to-lift characteristics of sharp edge delta and related wing planforms

[AIAA PAPER 69-1133] 01 p0002 A70-10607

Convective heat transfer rates measured on cooled sharp leading edge flat plates at various angles of attack in hypersonic merged flow

[ASME PAPER 69-WA/HT-21] 04 p0614 A70-14813

Finite difference analysis of partial differential equations derived from Navier-Stokes equations in hypersonic leading edge problem in merged gas flow-layer regime

06 p0980 A70-18349

Nitrogen hypersonic transitional flow at adiabatic sharp flat plate leading edge, presenting density, flow-field shape and local rotational temperature for various regions

06 p0982 A70-18361

Surface pressures and shock wave shapes on sharp flat plates and wedges in rarefied hypersonic transition flow with emphasis on merged layer regime

06 p0982 A70-18362

Surface temperature effects on low Reynolds number hypersonic shock layer development over flat plate sharp leading edge

06 p0982 A70-18364

Continuum to free molecule hypersonic flow near flat plate sharp leading edge, studying Knudsen, Reynolds and Mach numbers effects

06 p0982 A70-18365

Kinetic theory applied to model of interaction between two gas flows colliding at sharp leading edge at different hypersonic speeds

10 p1800 A70-24139

Low Mach number aerodynamic sound generation by turbulent flow at sharp edged thin scattering half plane solved with Green function

10 p1802 A70-24521

Flow near leading edge of sharp insulated and cooled flat plates, using Monte Carlo direct molecular simulation

11 p1975 A70-25968

Electromagnetic field singularities near sharp edge relating to geometry scatter using for treating singularities in current distribution integral equations

12 p2183 A70-26977

Hypersonic near free molecule flow over flat plate with sharp leading edge, using linearized kinetic B-K-G equation for small thermal accommodation coefficient

15 p2673 A70-32796

Aerodynamic characteristics of thick sharp edged cropped delta and gothic wings, giving low lift-dependent drag

19 p3353 A70-38615

Slender wings of low aspect ratio and sharp leading edges, predicting inviscid maximum lift

21 p3743 A70-40585

SHATTERING

U FRAGMENTATION

SHEAR

Observational errors effects on surface waves resolution, describing shear velocity determination in crust and mantle from observed waves

16 p2897 A70-33647

SHEAR CREEP

Monograph on shear lag measurement in rectangular section beam subjected to bending or torque free from axial restraint, using inductance probe sensors

03 p0603 A70-14351

Flat plates thermal buckling calculations with allowance for transverse shear deformation effect, using Rieissner variational principle

04 p0773 A70-15091

Free in-plane flexural vibrations of circular rings, developing equation of motion to include shear deformation and rotatory inertia effects

08 p1592 A70-21473

Novozhilov complex transformation method extended to Timoshenko theory of elastic shells constructed with allowance for transverse shear deformation

21 p3941 A70-42237

SHEAR DISTURBANCES

U S WAVES

SHEAR FATIGUE

U SHEAR STRESS

SHEAR FLOW

Pitot tube measurements of mixing zone of turbulent shear flow, discussing velocity gradient effects

01 p0066 A70-11134

Nonlinear waves in parallel shear flows, discussing laminar flow breakdown due to free stream disturbances

02 p0277 A70-11876

Energy reversal zones in turbulent shear flows with asymmetric mean velocity distribution, implying zones of opposing shear

02 p0279 A70-12228

Integral method for turbulent shear flow based on momentum and moment-of-momentum equations and Cole velocity profile family, determining shear stress integral

02 p0282 A70-12329

Governing equations determined for turbulent boundary layer and quasi-parallel turbulent shear flows, taking into account effects of convection, diffusion, pressure, etc

02 p0285 A70-12348

Wave packet dynamics recapitulation and tentative application to turbulent shear flow

02 p0287 A70-12362

Shear velocity variation with depth in upper mantle for Basin and Range province of western North America, using S waves measurements

02 p0292 A70-12505

Statistical model of turbulent chemically reacting shear flows, analyzing wave number fluctuations effect and Couette flow

03 p0464 A70-12928

Shear moduli and lattice parameters effect on screw dislocation equilibrium in bimetallic medium of soft and hard phases

03 p0587 A70-13117

Velocity structure associated with motion of interface between turbulent and nonturbulent fluid at turbulent boundary layer edge, considering shear flows

03 p0470 A70-14240

Couette problem for Krook kinetic equation solution, considering shear stress variation at high plate velocities

04 p0672 A70-15228

Shear-dependent nearly isotropic turbulence energy spectrum theory, considering effects of viscous loss, shear production and inertial and velocity gradient transfer

04 p0674 A70-15520

Rotta differential equation for turbulent boundary layer flow with fixed profiles of length scale, shear stress and kinetic energy

06 p1035 A70-17694

Conservation equation for thermal energy in turbulent shear flow, including turbulence kinetic energy equation terms

[WSCI PAPER 69-43] 06 p1179 A70-17983

Shear generated atmospheric clear air turbulence growth and dependence on atmospheric instabilities calculated numerically by invariant model

[AIAA PAPER 70-55] 06 p1098 A70-18031

Aerodynamic forces for boundary layer profiles of flexible plate under transient motion in shear flow using computer programs

[AIAA PAPER 70-76] 06 p0972 A70-18122

Rarefied gas shear flow over infinite plane wall, using Boltzmann-Krook-Welander equation to determine compressibility effect on Knudsen layer

06 p1048 A70-18327

Turbulent shear flow kinematic characteristics determined by photographic method and flow visualization using vortex model

07 p1259 A70-19827

Viscoelasticity in shearing and accelerative flows by integral theory, discussing stress distribution and pressure drop

07 p1412 A70-20000

Turbulent Prandtl number and eddy viscosity distribution in thermally stratified turbulent boundary layer of air shear flow dependent on wall distance and thermal stability

08 p1599 A70-21581

Sheared frontal zones structure and stability, studying Richardson number limiting role in free atmosphere

08 p1492 A70-21971

Stably stratified atmospheric turbulent shear flow governing spectral equations asymptotic solutions for buoyancy subrange

09 p1659 A70-22372

Turbulent jet injection from circular opening into unbounded transverse shear flow, determining velocity distribution along axis

09 p1659 A70-22427

Shear flow of inviscid incompressible fluid past sphere, calculating secondary vorticity and upstream velocity distribution

09 p1664 A70-23680

Landau damping and stability of low density crossed field electron beams using analogy with inviscid shear flows

10 p1918 A70-23964

Plasma stabilizing effect of shear and magnetic flux minimum in asymmetric conductors and currents in helical stellarator winding

11 p2088 A70-25711

Shear flow near walls through cascade of untwisted blades, observing variation in lift coefficient across span

11 p1975 A70-25788

Nearly homogeneous turbulent shear flow for flow field structure, determining pressure/velocity tensor using wind tunnel

11 p2039 A70-26530

Momentum transport bounds in turbulent shear flow using variational methods

11 p2039 A70-26535

Nonlinear viscoelastic turbulence model with monotone increasing time scale to predict behavior in homogeneous shear and in pure strain

11 p2040 A70-26544

Complex viscosity relationship to steady state shearing in Maxwell Orthogonal Rheometer

11 p2041 A70-26560

Turbulent shear flow energy spectrum theory for unstratified fluid with arbitrary eddies-mean velocity gradient interaction

12 p2214 A70-28364

Crack extension by alternating shear indicated from slip line flow field comparison at sharp crack tip and blunted crack

13 p2432 A70-28606

Turbulent shear flow direct interaction equations simplification to differential equations amenable to computation

13 p2389 A70-29463

Cylinders and airfoils drag tests and simulation in two dimensional sheared flow, considering shapes optimization

13 p2342 A70-29893

Lower stratosphere temperature and wind periodic variations associated with shear flow gravity waves

14 p2601 A70-30124

Similarity and scaling between atmospheric and wind tunnel simulated shear flows near earth surface

14 p2602 A70-30369

Low aspect ratio wing aerodynamic characteristics in shear flow, noting forces dependence on flow velocity gradients

14 p2529 A70-31274

Viscometric Poiseuille or Couette flow kinematics, considering nonuniform shear rate

14 p2567 A70-31282

Shear flow turbulence effect on chemical reactions, considering two dimensional low speed turbulent mixing layer between high velocity cold gas and air at rest [AIAA PAPER 70-721]

16 p2855 A70-33493

Diffusion flame development in homologous turbulent shear flow, investigating flame structure and chemical reaction by statistical theory

16 p2997 A70-33499

Normalized Reynolds stress tensor in upstream region of fully developed turbulent shear flow as function of position, using inviscid linear model [ASME PAPER 70-FE-2]

16 p2891 A70-33626

Shear flow perturbations in inviscid incompressible stratified fluid of given density, comparing stability characteristics with jet flow

16 p2895 A70-34243

Turbulent shear flow asymptotic theory, discussing channel, pipe and two dimensional boundary layers

16 p2895 A70-34244

Electrostatic probe measurements of vortex streets growth in plasmas bounded shear flow [AIAA PAPER 70-758]

17 p1319 A70-34493

Turbulent gas flows shear turbulence structure at various Reynolds numbers in nonconducting channels with and without heat transfer under transverse magnetic field

17 p3141 A70-35245

Variational principle for turbulent shear flow between parallel plates, taking into account isothermal flow and Malkus theory

17 p3073 A70-35595

Aerofoil section characteristics in shear flows of arbitrary velocity profile calculated by Glauert image method

18 p3205 A70-35957

Turbulent shear flow velocity and kinetic energy distributions in tunnel

18 p3241 A70-36383

Initial condition effects on weak homogeneous turbulence with uniform shear, studying energy transfer and dissipation

19 p3403 A70-37537

Stability of thermal and inertial perturbations superimposed on unstably stratified plane parallel flow with variable vertical shear

19 p3462 A70-37753

Steady two dimensional incompressible shear flow, correlating velocity profiles with resistance distribution

19 p3406 A70-38350

Small viscosity and heat conductivity in solutions to critical layer in stratified shear flow

20 p3608 A70-39447

Trajectory equations for plane and three dimensional gas jets with arbitrary injection hole shapes in subsonic shear flow

22 p3960 A70-43365

Shear flow distribution equations in prismatic shells under constant shear loading

23 p2465 A70-43891

Miles-Howard theorem extension to gravitationally stratified compressible fluid containing parallel shear flow, considering stability against adiabatic perturbations

23 p4179 A70-43976

Rotational two dimensional steady shear flows of perfect incompressible fluid, considering channel flow characteristics for various wave modes

23 p4181 A70-44202

Laminar boundary layer wall shear and velocity profiles by N parameter integral method, using exponential

23 p4182 A70-44567

Inertia effects and suspension rheology for incompressible Newtonian fluid shear flow around neutrally buoyant rigid sphere

24 p4327 A70-46243

Two point hydrodynamic equation for molecular fluctuations divergent growth in classical shear flow via B-B-G-K-Y procedure and double series moment expansion

24 p4382 A70-46254

SHEAR LAYERS

Incompressible inviscid free shear layer stability with respect to spatially growing three and two dimensional disturbances, considering hyperbolic tangent velocity profile

03 p0468 A70-13786

Linearized velocity profiles for turbulent free shear layers using transverse shift and longitudinal motion equation [ASME PAPER 69-WA/APM-28]

04 p0668 A70-14904

Boundary layer momentum integral equations to predict shear layer behavior, developing method to avoid nonphysical constraint appearance [ASME PAPER 69-WA/APM-11]

04 p0669 A70-14916

Reattachment of supersonic jet with turbulent shear boundary layer abruptly expanding into axisymmetric parallel diffuser, using surface flow technique

04 p0619 A70-15323

Steady MHD shear layer velocity profiles using hot film anemometry

05 p0887 A70-15924

Supersonic flow separation over rearward facing step, measuring upstream boundary layer, lip shock and shear layer formation by pitot probe and surface pressure survey

06 p0973 A70-18153

Projectile penetration of Al alloys, noting melting during intense shear band formation

08 p1522 A70-21710

Dynamic shear modulus and depth of dominant layer of vibrating elastic medium, assuming foundation as isotropic stratum on rigid bed

10 p1957 A70-24481

Vibration equations for closed and open sandwich cylindrical shell with thickness-shear deformation in core and face layers compared with membrane theory

11 p2145 A70-26697

Mathematical model for describing flow in Hele-Shaw cell, predicting attached viscous shear layers in lifting body wake

13 p2338 A70-28818

Laminar incompressible free shear layers by method of weighted residuals for turbulent jets, obtaining velocity profiles for similarity and physical planes

20 p3613 A70-40286

SHEAR PROPERTIES

NT SHEAR STRENGTH

Fatigue crack propagation in metals exhibiting initial crystallographic shear mode followed by noncrystallographic tensile mode

01 p0198 A70-10101

Elastic orthotropic fiberglass reinforced plastic shells stability under axial compression, analyzing shear modulus influence

04 p0712 A70-14490

Shear modulus of sandwich structure tubular core derived by virtual work principle and matrix approach, comparing results with honeycomb core [DGLR-69-64]

04 p0774 A70-15156

Effective wave propagation velocities, bulk and shear moduli of elastic heterogeneous solids approximated by self consistent method

04 p0777 A70-15496

Shear testing and data reduction based on torsion analysis to obtain elastic shear constants of thin orthotropic Be sheets

04 p0664 A70-15552

Neutral sheet instabilities in magnetotail from collisionless plasma instabilities from shear magnetic field

05 p0887 A70-15911

Relativistic simple shear of slab of neo-Hookean material

05 p0929 A70-16067

Antiplane strain deformation problems concerning crack extension along circular interface separating materials with different shear moduli

05 p0931 A70-16091

Tensile and shear properties of blind fixed, blind floating and through types of bonded sandwich inserts, noting geometry and temperature effects

07 p1401 A70-18934

Internal friction and shear modulus of Co under dynamic and steady state conditions, discussing peak at alpha-epsilon transformation

07 p1306 A70-19073

Three dimensional finite element method for quasi-homogeneous laminate moduli, discussing interlaminar and in-plane shear properties

07 p1321 A70-19966

Shear and rotation limits on universe from X ray background, using Euclidean shear and vorticity models with open and closed geometries

08 p1561 A70-20901

Test specimen shapes for determining tensile, compressive and edge-wise shear properties of reinforced plastic laminates

08 p1529 A70-21878

Test methods for evaluating tensile, compressive, interlaminar shear and bearing strength properties of carbon yarns and flat and tubular composites

08 p1529 A70-21881

Split ring load test method for determining shear modulus of isotropic and composite materials

08 p1530 A70-21888

Rotatory inertia and shear deformation effects on structural vibrations of Timoshenko beams and frameworks using matrix formulation

09 p1770 A70-22257

Fiberglass reinforced plastic laminates shear characteristics determination, giving expressions for shear modulus and tangential stress

09 p1709 A70-22300

Free vibrations of plates and beams of pyrolytic graphite type materials, analyzing transverse shear deformation and rotary inertia [AIAA PAPER 69-55]

09 p1780 A70-23210

Contact stresses in elastic half plane with boundary connected to rod and moment applied at arbitrary point

10 p1965 A70-25324

Resonant frequencies and Young/shear moduli of unidirectional graphite epoxy composite beams under high modes of vibration

11 p2136 A70-26082

Shear buckling and uniaxial compression dependence on mechanical properties of clamped orthotropic plates, using Ritz method to compute bifurcation type loads

12 p2326 A70-27817

Cylindrical shells stability under axial compression by two dimensional Kirchhoff-Love applied theories, calculating critical stresses

12 p2328 A70-28282

Tantalum single crystals elastic constants temperature dependence, considering compressibility and shear properties

14 p2596 A70-30841

Human skull porous dipole layer shear and compressive properties, measuring static and dynamic strain rates

15 p2683 A70-32308

Composite beam testing concepts and interpretation under three and four point loading, noting shear deformation effect

16 p2989 A70-33385

Shear coupling effect in cylindrical bending of anisotropic composite laminates

17 p3182 A70-34558

Optimum fiber orientation for minimum weight boron/epoxy shear panel design

17 p3182 A70-34562

Longitudinal shear modulus of unidirectional fibrous composite, involving series solution of Laplace equation

17 p3183 A70-34564

Band structure contributions to elastic shear constants of hexagonal close packed metals, using optimized model potential

21 p3839 A70-40600

Unidirectional fiber reinforced composite longitudinal shear deformation, deriving effective shear modulus

22 p4060 A70-43681

Thin metal matrix composite rods elastic properties, examining Al-W system by Young and shear modulus measurements

22 p4061 A70-43687

SHEAR STRAIN

Unidirectional composite materials properties, discussing stiffer filaments effect on Young modulus and shear coupling constant relating shear strain to longitudinal strain

03 p0587 A70-13128

- Cylindrical two layer shells stability under compression and radial pressure, calculating compression and transverse shear strains in carrying layer and filler
03 p0592 A70-13443
- Shell shear strain determined by expanding displacement vectors into covariant power series of distance from middle surface
[DFVLR-SONDDR-23] 05 p0955 A70-17078
- Isotropic shells with shear deformations, investigating stress-strain relations in Cosserat continuum applied to plates
[DFVLR-SONDDR-23] 07 p1404 A70-19233
- Beam vibration eigenfunctions with allowance for shear compliance used to determine beams dynamic stability under pulsating axial load
09 p1785 A70-23600
- Aluminum and aluminum-copper alloys dislocation damping at high strain rates using impact shear tests
10 p1903 A70-23983
- Uniform beams flexural vibration natural frequencies approximate calculation showing effect of shear flexibility and rotatory inertia
10 p1959 A70-24562
- Asymmetric stiffened shell structure analysis by finite element method, introducing constant transverse shear model concept
11 p2144 A70-26677
- Thin shells stiffness matrix and shear by finite curved triangular elements based on discrete Kirchhoff hypothesis
14 p2659 A70-31129
- Grain boundary sliding model subjected to shear strain, discussing effect on mechanical properties
16 p2932 A70-33789
- Shell theory for shear deformations in covariant notation involving displacement power series expansion
18 p3337 A70-36371
- Shearing strain in oriented fiberglass reinforced plastics under torsion, obtaining creep curves
20 p3655 A70-39768
- SHEAR STRENGTH**
- Graphite fiber-epoxy resin composites interfacial bonding, describing various surface treatments for increased interlaminar shear strength
01 p0127 A70-10477
- Fiberglass reinforced plastic shells stability analysis, assuming weak shear resistance of shell material
02 p0390 A70-12808
- Interlaminar shear strength determination methods taking into account plastics composition, considering polyester and epoxy plastics, glass and graphite fiber reinforcing materials
07 p1410 A70-19767
- Composite materials application to structural members, considering bond or adhesive shear strength
08 p1594 A70-21855
- Transverse and shear strengths of Al-B composite materials used in F-111 aircraft components, investigating cold work, thermal treatments and steel wire addition effects
08 p1509 A70-21857
- Composite materials shear strength test problems with high modulus fibers
08 p1529 A70-21877
- Geometry effect on short beam tests for interlaminar shear strength of composite materials
08 p1529 A70-21882
- Inplane shear stress-strain response determined for unidirectional composites, using uniaxial test method for laminated plates
08 p1530 A70-21884
- Adhesion characteristics in composites, investigating correlation between short beam and torsion shear tests in glass and graphite reinforced epoxy materials
08 p1531 A70-21892
- Laminated anisotropic rectangular plates of boron-epoxy composite material, studying shear stability by potential energy and Ritz method
08 p1595 A70-21903
- Failure mode in shear loaded graphite filament reinforced epoxy composites dependent on interfacial bond strength
08 p1533 A70-21915
- Al-B composites mechanical properties, using heat treatments and transverse steel wires to increase matrix shear and transverse tensile strengths
09 p1701 A70-22551
- Thin shell design for minimum bending stresses and transverse shear for composite materials with low interlaminar shear strength
11 p2141 A70-26490
- Pulsars starquakes frequency relationship to solid crust shear strength based on Ruderman model, considering Crab Nebula
12 p2310 A70-27998
- Wool felt based carbon and graphite composite materials for orthogonally isotropic high shear strength compared with rayon felt based composites
13 p2437 A70-28776
- Stress rupture shear strength of fiberglass reinforced plastics under monotonic, prolonged and cyclic loading
15 p2766 A70-32853
- Shear and tensile joint strength measurements at fiber-polymer matrix interface, using pull-out test and debonding methods
16 p2937 A70-33372
- Ti explosive bonding and forming, examining peel and shear strengths on Ti clad steel plate
17 p3098 A70-34446
- Adhesive bond between steel wire and epoxy resin, investigating hydrostatic pressure effect on shear strength
17 p3123 A70-34623
- Unidirectional carbon fiber reinforced plastics /CFRP/ interlaminar shear strength measurements using short beam shear, notch overlap and solid rod torsion methods
20 p3653 A70-39203
- Graphite filament composite structure shear strength decrease with modulus increase, examining fiber microstructure effect on interlaminar properties by short beam shear test
20 p3654 A70-39206
- Hydraulic fluids and lubrication oils resistance to mechanical shear forces by ultrasonic method based on acoustically induced cavitation effects
20 p3655 A70-39718
- Composite material engineering problems, discussing tensile, compressive and shear strengths, design approaches, unidirectional properties and substance characterizations
20 p3651 A70-40027
- Directional dependence of elastic shear stiffness on cubic axes for Si, Cu and Mo, making polar plots of shear stiffness coefficients
21 p3850 A70-41909
- Internal friction and shear modulus of thin glass fibers of sodium silicate, aluminosodium silicate and nonalkaline aluminoborosilicate
22 p4059 A70-43135
- Graphite and carbon fiber surfaces, correlating Raman spectrum and shear strength of composite
22 p4060 A70-43680
- SHEAR STRESS**
- NT TORSIONAL STRESS**
- Elongation and combined shear stresses in incompressible creeping plane flows of viscoelastic lubrication for squeeze-film bearings
[ASME PAPER 69-LUB-22] 01 p0101 A70-10385
- Moments and shear forces in plate flexure represented by single valued stress functions of position, stating variational principle for compatibility
01 p0201 A70-10931
- Nonlinear dynamic beam response for classical and shear deformation theories, comparing stresses and deflections using traveling wave approach with finite difference schemes
01 p0206 A70-11147
- Growth rate and shear stress parameter of symmetric, turbulent, two dimensional and axisymmetric self preserving wakes and jets in streaming flow
02 p0223 A70-11861
- Integral method for turbulent shear flow based on momentum and moment-of-momentum equations and Cole velocity profile family, determining shear stress integral
02 p0282 A70-12329
- Turbulent boundary layers behavior prediction by strip integral momentum equation method, considering velocity profiles and shear stresses
02 p0282 A70-12332
- Extended mixing length method for computing turbulent shear stress distribution required in calculating two dimensional incompressible turbulent boundary layer
02 p0282 A70-12333
- Turbulent boundary layer development calculation by shear work integral method involving Reynolds number introduction procedure
02 p0283 A70-12336
- Shear stress transport equation derivation from turbulent energy equation based on properties of turbulent velocity fluctuations
02 p0284 A70-12346
- Three dimensional turbulent boundary layers on high aspect ratio bodies /swept wings/, discussing shear stress direction determination
02 p0286 A70-12354
- Static and cyclic stress distributions in buckling shear panel comprising flat plate of clad Cu-Al alloy
02 p0388 A70-12497
- Interlaminar shear stress and fabrication of high modulus graphite-reinforced epoxy matrix composites
03 p0515 A70-13119
- Microstructure of turbulent jet in concurrent flow, analyzing wake parameter and measuring profiles of pulsation velocity components and Reynolds shear stresses
03 p0409 A70-13871
- Stress distribution of thin walled structure of open section, considering warping and torsional bending, using calculus of variations
03 p0596 A70-14030
- Swenson shear fatigue crack model expanded to include mean stress effect on cyclic shear crack growth
[ASME PAPER 69-WA/APM-8] 04 p0772 A70-14918
- Fatigue crack incremental propagation under cyclic shear loading, developing discrete dislocation model for crack and plastic zones
[ASME PAPER 69-WA/APM-7] 04 p0772 A70-14919
- Couette problem for Krook kinetic equation solution, considering shear stress variation at high plate velocities
04 p0672 A70-15228
- Heat fluxes, shear stresses and pressures distribution at spike on body in supersonic flow from asymptotic solutions of Navier-Stokes equations
04 p0673 A70-15232
- Stress distributions in infinite elastic solids for shear loadings prescribed over coplanar circular regions, solving integral equations iteratively for coplanar penny-shaped cracks
05 p0928 A70-16057
- Geometrically linear anisotropic shell deformation under transverse shear applied to stability analysis of orthotropic shells of revolution sustaining axisymmetric stresses
05 p0933 A70-16212
- Static-geometric analogy of Kirchhoff-Love shell theory applied to Timoshenko complex equations allowing for transverse shear deformation
05 p0934 A70-16219
- Razor blade calibration and measurement of wall jet flow shear stress in turbulent boundary layer with secondary injection
05 p0833 A70-16504
- Static buckling load for beam with pinned ends and Wiegardt-type elastic foundation, considering shear stresses effect
05 p0955 A70-17105
- Modulus of rigidity and stress-strain state measured in square plate during shear produced by twisting
06 p1060 A70-17132
- Free molecular drag for flat plate with normal protuberance, determining flowfield distribution functions and stress components
06 p0981 A70-18357
- Cantilever cylindrical shell stability under shearing stresses created by transverse force applied to free end
07 p1403 A70-19116
- Blood-endothelial surface shear stress in artery inlet, considering asymmetric and radially symmetric plugging effects
07 p1220 A70-19248
- Elastic fields in bimaterial plate under uniform compressive and anti-plane shear loadings, finding stress distribution and induced interfacial shear stresses
07 p1412 A70-19957
- Geometrical-mechanical properties in terms of interlaminar shear stress of composite cantilever beams under end load
07 p1412 A70-19965
- Shear stress distribution in metal adhesive joints, discussing methods for calculating
08 p1504 A70-20892
- Shear stress in thick cylindrical closed shells subjected to plastic torsion determined from displacement distribution over thickness and generatrix
08 p1588 A70-21182
- Static pressure gradient influence on turbulent shear stresses and energy production in asymmetric wall jet flow
08 p1484 A70-21314
- End plugs bending moment and shear loads reduction during compression tests of composite orthotropic cylinders
08 p1594 A70-21889
- Fibrous reinforced composites influence in aircraft structural design based on DOD industry development programs, investigating interlaminar shear
08 p1595 A70-21899
- Calibration of shear sensitive cholesteric liquid crystals film, measuring shearing forces and scattering light intensity
09 p1656 A70-22992
- Gamma prime phase structure ordering effect on critical shear stresses of aging Ni-Al alloys and nimonic
09 p1707 A70-23195
- Turbulent three dimensional incompressible wall jets issuing into quiescent air ambient, tangent to and at surface of flat plate, investigating shear stress and flow field
09 p1661 A70-23215
- Irreversible viscosity decrease and thermal stability in polymer-containing lubricating oils under shearing forces effect
09 p1693 A70-23408
- Power-law stress-strain relation in plastic complex stressed state, showing identical strain hardening curves for shear and tension
10 p1957 A70-24280
- Lines of influence of bending moments and cutting force for straight beam using differential equation integration
10 p1959 A70-24777
- Wall shear stress distribution in rectangular ducts, discussing secondary currents and main flow prediction
11 p2035 A70-25779

Transient bending and shear stresses at clamped support of orthotropic circular cylindrical shells

11 p2135 A70-25985

Pressure gradient, wind structure and shearing stress in atmospheric boundary layer related by formulation based on quasi-parallelism and boundary condition at Ekman layer top

11 p2076 A70-26071

Interlaminar shear stresses analysis for laminated composites under generalized plane stress

11 p2136 A70-26080

Elastic-plastic shear cracks propagation in two phase composite materials using dislocation model, determining critical fracture strength

11 p2136 A70-26081

Air and salt water tensile and shear mode cracking of titanium alloy sheets examined with electron fractographs

11 p2067 A70-26099

Stress concentration around elastic spheroidal inclusions in isotropic elastic body under shear

11 p2140 A70-26483

Fiber reinforced composites under longitudinal shear loading, noting orthotropic nature and shear moduli assuming circular fibers

11 p2141 A70-26489

Elastic wedge under spatially uniform but time dependent shear tractions, studying shear stress and transient wave propagation

11 p2142 A70-26629

Mechanical properties in solids under dynamic incremental shear loading, discussing wave propagation tests on steel, Cu and Al

11 p2143 A70-26669

Wall shear stress distribution in noncircular ducts with steady incompressible fluid flow

12 p2209 A70-27217

Stress and strain in matrix of fiber reinforced material within elastic region, calculating interface shear stress for rectangular fiber

12 p2322 A70-27231

Secondary crack growth direction from preexisting crack under longitudinal shear loading

13 p2510 A70-28674

Preston tube errors in pipe flow wall shear stress determination due to velocity distribution deviations

13 p2387 A70-28848

Stress concentration coefficient around hole in isotropic nonlinear plate under shear, reducing solution to integrating fourth order differential equation

13 p2516 A70-29510

Computerized analysis of shear failure at initial fragment collision during trifragment rotor disk interaction with containment rings

14 p2563 A70-30870

Stress distribution in anisotropic cylindrical shell due to shearing force varying linearly and quadratically with depth on inner boundary

14 p2658 A70-30994

Incompressible turbulent boundary layer calculation based on shearing stress hypothesis, considering layer at flat plate, boundary conditions and velocity profiles

15 p2719 A70-31490

Energy dissipation during independent flexural-torsional vibrations of rods, noting alternating shear stress superposition effect on damping

15 p2813 A70-31530

Double ended dislocation pileups and elastic cracks at bimaterial interface under screw, edge and shear modes

15 p2756 A70-31561

Core shear deformations effects on stress, deflection and buckling load calculations for sandwich panels

15 p2815 A70-31931

Riemann-Hilbert problem for discontinuous coefficient solving mixed boundary value problems in infinite elastic strip, discussing shear stress along whole boundary

15 p2822 A70-32355

Shear stress distribution in axially nonuniform circular shaft subjected to torsion, using finite difference approximations

16 p2988 A70-33001

Optimum filament orientation for maximum strength in composite with combined normal and shear stresses

17 p3183 A70-34563

Failure prediction for interlaminar shear stress in filament wound rectangular plate

17 p3188 A70-35228

Axisymmetric mixed boundary problem for elastic infinite cone, obtaining solution by assuming zero shearing stresses

17 p3192 A70-35698

Energy dissipation in material under complex vibrations, noting role of summary shear stress

19 p3535 A70-37347

Fiber reinforced materials with oriented armoring, calculating stress strain state under transverse shear

19 p3454 A70-37348

Velocity distribution and shear stress measurements in three dimensional turbulent boundary layer approaching separation

19 p3405 A70-38021

Continuum bodies strain subjected to shearing stresses in incremental form based on slip theory of metals plasticity

19 p3549 A70-38668

Shear stress and velocity profiles in three dimensional mixing layer between grazing perpendicular streams

20 p3608 A70-39356

Polymeric materials yielding and fracture behavior under uniaxial and multiaxial fields, plotting octahedral shear stress

20 p3656 A70-39949

Turbulent shear stress correlation with turbulent kinetic energy for wake and circular jet flow conditions

20 p3613 A70-40277

Longitudinal shear crack propagation in random internal stress field, examining quasi-brittle rupture theory and cyclic loading

20 p3733 A70-40396

Wall jet turbulent flow regions with shear stress and mean velocity gradient of opposite sign, considering theoretical explanation

20 p3615 A70-40501

Brittle elastic material with wedge shaped void, calculating shear stresses during crack propagation generated by horizontally polarized shear wave

21 p3932 A70-40547

Impurity dependent critical resolved shear stress of magnesium oxide single crystals, using compression testing

21 p3862 A70-41910

Crack propagation in antiplane shear by opening semipenny shaped cracks straddling front at 45 deg

21 p3940 A70-42035

Turbulent heat/mass transfer from solid boundary with shear stress dependent on wall distance for various Schmidt or Prandtl numbers

21 p3953 A70-42088

Linear corrections formulas for shear stress and heat transfer coefficients associated with boundary layer blowing in binary gas mixture

21 p3748 A70-42207

Atmospheric environment effect on residual shear stress corrosion cracking of commercial Al-Zn-Mg alloys subjected to heat treatment regimes

22 p4052 A70-42307

Mechanical properties and internal stress fields in composite materials reinforced by glass fibrous filler under transverse shear

22 p4061 A70-43724

Two dimensional turbulent wake theory, considering shear stress and velocity distribution behind flat plate and circular cylinder

23 p4134 A70-44575

Finite beam element in bending, deriving shear deflection terms in stiffness matrix based on stress assumption

23 p4274 A70-44909

Rarefied gas plane Couette flow, calculating upper and lower bounds on shear stress

24 p4325 A70-45600

SHEAR WAVES

U S WAVES

SHEARING STRESS

U SHEAR STRESS

SHEATHS

NT ION SHEATHS

NT PLASMA SHEATHS

SHEEP

Enzyme beta-hydroxybutyrate dehydrogenase concentration in mitochondria from bovine and sheep liver

03 p0430 A70-14198

Sheep cardiac rate, respiration rate, hematocrit, erythrocytes per cubic mm and hemoglobin concentration responses to elevated ambient carbon dioxide

17 p3030 A70-35421

SHEET METAL

U METAL SHEETS

SHEETS

Fiber-reinforced composite sheet matrix failure by plastic flow, investigating two ply laminate in simple tension

08 p1592 A70-21471

SHELL STABILITY

Axially compressed cylindrical shells with edge constraints, determining critical load from inelastic behavior considerations

01 p0205 A70-11141

Thin shells of revolution torsional vibration including bending terms and thickness considerations

01 p0205 A70-11142

Thin elastic shells parallel surface nonlinear tangential strains derived in terms of midsurface tangential and bending strain components

01 p0205 A70-11143

Thick walled incompressible hyperelastic dielectric sphere periodic oscillations, noting dielectric properties influence on amplitude and period

01 p0209 A70-11386

Plates and shells natural oscillations frequencies and modes, analyzing variational, asymptotic and numerical methods

01 p0210 A70-11412

Natural oscillation frequencies of closed circular orthotropic cylindrical shells having freely supported end faces, particularly with stringers

01 p0210 A70-11413

Carrying capacity of shells of revolution obtained with threads spun around metallic shell, including stresses during spinning process

01 p0210 A70-11414

Fiberglass reinforced plastic shells stability analysis, assuming weak shear resistance of shell material

02 p0390 A70-12808

Orthotropic cylindrical shell with initial deflection under long term effect of external hydrostatic pressure, solving bending problem

02 p0390 A70-12809

Internal hydrostatic or lateral pressure effect on deformations of infinitely long thin cylindrical isotropic shell subjected to equal concentrated radial loads

03 p0584 A70-12922

Cylindrical shells buckling under biaxial compression and transverse loads, examining critical loads dependence on shell parameters, end conditions and elastic properties

03 p0590 A70-13380

Cylindrical two layer shells stability under compression and radial pressure, calculating compression and transverse shear strains in carrying layer and filler

03 p0592 A70-13443

Natural oscillation frequencies of partially liquid-filled cylindrical shells determined by resonance method

03 p0592 A70-13444

Axial compressive forces influence on steel and Al cylindrical shell stability under external pressure

03 p0593 A70-13472

Rib-reinforced rectangular plate flutter in gas flow, considering shell stability, rib torsional rigidity, etc

03 p0593 A70-13498

Nonlinear flexural vibration properties of thin circular cylindrical shells with simply supported ends assuming deflection mode

03 p0594 A70-13549

High speed photography for instability onset and subsequent buckling process in photoelastic circular cylindrical shells under axial compression

03 p0594 A70-13659

Stress-strain state of arbitrarily cracked cylindrical shell under symmetric and asymmetric loading

03 p0594 A70-13736

Radial vibration of cylindrical shell of transversely isotropic material determined using finite Hankel transform

03 p0595 A70-13904

Thin shells of revolution plastic collapse under axisymmetric loads on basis of Tresca-Nakamura yield criterion, using computer algorithm

03 p0598 A70-14238

Far nonlinear postbuckling behavior of noncircular cylindrical shell under axial compression

03 p0598 A70-14241

Natural oscillations and flutter of three layer cylindrical shell in supersonic gas flow analyzed by semimomentless theory, discussing boundary value problems, damping effects, etc

03 p0600 A70-14301

Elastic orthotropic fiberglass reinforced plastic shells stability under axial compression, analyzing shear modulus influence

04 p0712 A70-14490

Natural circular frequencies of small axisymmetric vibrations of shells of revolution of arbitrary shape, using Rutishauser algorithm for eigenvalues

04 p0767 A70-14525

Pressure vessel deformation and stress analysis by matrix displacement method, considering solids and membrane shells under axisymmetric and asymmetric loading

[ASME PAPER 69-WA/PVP-3] 04 p0768 A70-14790

Elastic postbuckling behavior of axially stiffened and barreled cylindrical shells

[ASME PAPER 69-APM-U] 04 p0769 A70-14866

Free vibrations of reinforced elastic shell structures subject to constraints imposed by reinforcing elements, utilizing equivalent models without reinforcing elements

[ASME PAPER 69-WA/APM-25] 04 p0770 A70-14907

Thin orthotropic composite circular cylindrical shells buckling under axial and radial loads, satisfying end boundary conditions for clamped and simply supported shells

[ASME PAPER 69-WA/APM-21] 04 p0771 A70-14910

Stress analysis of shell loaded at free edge by concentrated forces and moments

04 p0772 A70-14920

Orthotropic axially compressed conical shell stability, evaluating lower critical load and postbuckling state

04 p0772 A70-14921

Thin walled plate simply supported on three edges, studying behavior following local stability loss

04 p0772 A70-14923

Soviet monograph on numerical determination of dynamic characteristics of plates and shells by method

of summary representations, covering oscillation and stability problems

Spherical shells axisymmetric equilibrium properties under uniformly distributed external compression

Initial deflection effect on elastic cylindrical shell stability under compression, finding critical load by determining limiting point in successive loading

Piston theory application to plates and shells stability in supersonic gas flows, considering critical velocities determination for asymmetric flows and oscillations

Thermal buckling of elliptic cylindrical shells assuming tangential temperature, constant axial pressure and conservation of elastic properties

Principal instability region of hinged cylindrical shell under dynamic loading

Clamped and simply supported shallow spherical shells buckling using computer programs

Circular cylindrical shells with axisymmetric imperfections tested under axial compressive load, studying imperfection amplitude and wavelength effects on minimum buckling load

Buckling of toroidal shells with reasonably uniform thickness distribution manufactured by casting epoxy resin material

Thin cylindrical circular shell and three layered plate, analyzing vibration and stability due to loads and temperature

Pseudocylindrical concave polyhedral shells proposed from postbuckling configurations analysis, considering rigidity and structural applications

Buckling equations for neutral equilibrium of arbitrary elastic shells specialized to uniformly loaded circular cylindrical shell with accuracy

Carrying capacity and deformation susceptibility of anisotropic fiberglass reinforced conical and cylindrical plastic shells under axial compression

Stability, critical load and strength algorithm for fiberglass reinforced cylindrical plastic shells under external load allowing for shear stresses

Geometrically linear anisotropic shell deformation under transverse shear applied to stability analysis of orthotropic shells of revolution sustaining axisymmetric stresses

Statistical stability of cylindrical fiberglass reinforced plastic shells under axial compression, showing breakdown loads vs radius/thickness ratio

Static-geometric analogy of Kirchhoff-Love shell theory applied to Timoshenko complex equations allowing for transverse shear deformation

Stability of clamped, hinged and elastically supported circular cylindrical shells under critical combined torsional and transverse pressure

Static and continuity equations of equilibrium of axisymmetric and periodic stressed states of rectilinear helicoidal shell derived for elasticity relations

Strain parameters and equilibrium equation of rib-reinforced thin shells, analyzing length, curvature and torsion variations using smooth shell analogy

Buckling of three layer cylindrical shells under steady creep conditions, deriving axisymmetric deformation

Stressed state of shallow spherical shells of revolution undergoing large displacements reduced to Karmann equation, solved by small parameter method

Stability and critical load algorithm for flexible shallow spherical and conical shells of revolution derived from variational equation

Revolving shells local stability developing boundary effect under normal and bending external loads solved by computer program

Shallow spherical shells stability under combined loading, hinging and edge clamping conditions, deriving strain energy expressions

Compressive forces eccentricity influence on circular cylindrical shell stability noting relation to bending moments

Isotropic elastic cylindrical shell stability under combined compressive and axisymmetric local loads, using equilibrium equations for shallow shells

Circular cylindrical shells stiffened by rings and stringers and subjected to periodic axial force, analyzing parametric instability

Asymmetric deformation of shells of revolution with variable thickness solved by asymptotic method in form of higher Fourier series harmonics

Membrane reinforced thin walled cylindrical shells stability as asymmetric contact problem in shell and plate theory

Thin shell buckling stressing maximum applied loads analysis for circular cylindrical shells with imperfect walls under axial compression

Stability analysis of deflected shallow thin walled elastic noncircular conical and cylindrical orthotropic shells using straight lines method

Thin walled cylindrical shells design for axisymmetric impulsive loads, calculating strains due to explosive forming in water

Displacement hybrid finite element models for analyzing shells with distributed loads

Nonlinear postbuckling equilibrium of thin cylindrical shell and axisymmetric buckling pressure of imperfect spherical shell calculated by Rayleigh-Ritz method

Thin walled cylindrical shell stability under stochastic lateral and axial compression loads using Liapunov method

Liquid propellant rocket nozzle configurations maximum stress and stability limits using computer program for composite ring-stiffened shells of revolution

Local axisymmetric dimple imperfection effects on buckling load of circular cylindrical shell under axial compression

Buckling-critical composite shell structures, describing pseudo T-rib stiffening and integrated composite design concepts

Thin circular cylindrical shells elastic equilibrium under loads producing deflection, elongation or contraction described by integrating equilibrium equations with constant coefficient

Stress-strain state equations for axisymmetrically loaded shells of revolution made of materials with variable moduli

Thin walled cylindrical shell stability with hollow filler under distributed external loads, determining critical loads

Conical shells stability under uniform pressure, studying varying thickness influence by variational stress and bending equation

Cantilever cylindrical shell stability under shearing stresses created by transverse force applied to free end

Notched cylindrical shells of nonuniform thickness using two dimensional photoelastic models mounted on elastic foundations

Shallow spherical caps elastic buckling under uniform pressure, considering symmetric and asymmetric deformation modes

Circular cylindrical shells creep buckling under nonuniform external loads, considering thermal effects and initial imperfections

Axially uniform stress and strain in cylindrical shells, discussing Saint Venant torsion and displacement relations

Segmented elastic shells of revolution supported by rings, studying buckling and vibration by matrix method

Plastic deformation of thin flexible axisymmetric shells under load, discussing tensile stresses

Natural vibration frequencies and mode shapes for laminated orthotropic shells of revolution using finite element method

Green matrices construction for joint shells by method of arbitrary constants variation, considering strained state symmetrical with joint lines

Circular cylindrical shells buckling under lateral and hydrostatic pressure using Donnell and Flugge equations, assuming membrane stress state for prebuckling deformation

Truncated conical shells buckling under hydrostatic pressure using Donnell equations, assuming membrane stress state for prebuckling deformation

Limiting equilibrium of axisymmetric shells consisting of alternating reinforcement layers separated by layers of homogeneous isotropic material

Initial perturbation effect of smooth cylindrical shells stability under critical axial compression noting deflection factor

Equilibrium of torque-free cylindrical shell vertically positioned and partly filled with liquid, obtaining solution for biaxial stress

Limiting equilibrium of shells of revolution with different yield points under tension and compression

Rib-reinforced cylindrical shells stability under longitudinal compressive loading, studying stress-strain state using network method

Strain energy method applied to stability analysis of short longitudinally reinforced cylindrical shells under axial compression

Soviet book on free, forced and parametric vibrations of thin walled shells containing liquid, gas and continuous elastic medium

Elastic body with incompressible fluid filled cavities, studying motion and stability by deriving motion equations starting from principle of least action

Rheological factors effect on deformation behavior of thin walled spherical shell made of strongly extensible elastically hereditary material and subjected to internal pressure

Stress-strain state of shells with positive Gaussian curvature under concentrated tangential loads, basing fundamental solution on two dimensional Fourier transform

Dynamic stability of shallow shells, taking into account longitudinal inertial forces and nonlinear geometry

Toroidal metallic shells stability under static loads, determining snap-through pressures in pressure chamber with nitrogen working gas

Rectangular planform shallow cylindrical shell parametric vibrations using method applied to large bending vibrations of plates

Prismatic thin walled shells with box type cross section under torsion using Vlasov variational method in conjunction with transfer matrices

Elastic/perfectly plastic hollow cylinder unloading under monotonic twist during torsion, considering sandhill-membrane analog validity

Circular cylindrical shell supported along generator under arbitrary forces using finite Fourier transform, simplifying results by Euler sum formula

Pairs existence of symmetrical equilibrium forms in nonlinear shallow shell under load applicable to nonshallow shells equilibrium

Eigenfrequencies of thin barrel shaped shells on simple supports, noting correspondence of ratio of radius to shell wall thickness

Cylindrical shells buckling under axial surface tensions using Donnell stability equations

Plastic growth of pressurized shell under cyclic thermal stresses superimposed on steady pressure load, investigating shake down using bending approximation

Temperature fields in cylindrical shell under axisymmetric heating, ensuring optimal stressed state

Algorithm for stress-strain state calculation of nonuniformly heated cylinder weakened by star-shaped cavity

Endurance limit of momentless shells of revolution under uniform internal pressure, deriving differential equations based on aging and creep theories

Layered conical shell creep under axisymmetric load and time dependent temperature field by iterating boundary integral equation

Buckling and postbuckling equilibrium behavior of fiber reinforced cylindrical shell under uniform axial compression

09 p1780 A70-23207

Buckling of elastic cylinders with rectangular cut-outs and reinforcements under axial or lateral loading, using modified Newton method
[AIAA PAPER 69-92]

09 p1780 A70-23208

Shallow rectangular shell panels nonsymmetric nonlinear deflection states computed by finite difference equations iteration, discussing snap-through buckling loads

09 p1780 A70-23209

Plastic buckling of eccentrically stiffened circular cylindrical shells with multiple isotropic layers under combined axial and lateral pressure, deriving stability criterion

09 p1780 A70-23213

Partially loaded clamped plastic shallow spherical caps collapse loads and stress and velocity distributions

09 p1781 A70-23230

Stress distribution in shells of revolution with variable elastic moduli, considering material rigidity and strain state

09 p1781 A70-23286

Elastic cylindrical shells stability under uniform pressure, calculating critical transverse load by finite-difference computer program

09 p1781 A70-23287

Carrying capacity of shallow shells of revolution, determining buckling stress and limiting equilibrium of shells with varying thickness under transverse load

09 p1781 A70-23288

Reinforced cylindrical shells stress-strain state under concentrated longitudinal loads, considering ribs of variable rigidity

09 p1782 A70-23289

Stress concentration at elliptical hole of arbitrary eccentricity in shallow sandwich shells with hard and soft fillers

09 p1783 A70-23385

Contour immobility effect on load carrying capacity of rigid plastic thin shells of revolution, establishing minimum reinforcement value for edge

09 p1783 A70-23388

Cylindrical shell critical load boundaries under uniform external stress and small torsion

09 p1783 A70-23389

Elastic ribs reinforced thin cylindrical shells stress-strain state under arbitrary load distribution allowing for rib spacing discreteness

09 p1784 A70-23590

Lower critical load for shallow rigidly convex shell expression refined by considering effect of rigid clamping of shell edge on buckling boundary deformation

09 p1784 A70-23594

Three dimensional deformation of finite circular cylindrical shell under plane shock wave solved in linear form

09 p1785 A70-23618

Axisymmetric free vibrations of orthotropic cylindrical shell loaded on ends by constant axial force, investigating nonlinear elasticity

09 p1785 A70-23625

Stress distribution in rib reinforced cylindrical shells under concentrated forces calculated using finite difference scheme

09 p1791 A70-23718

Asymmetric deformation of spherical shell by solving homogeneous differential equation in spherical functions, assessing approximation error

09 p1786 A70-23719

Reinforcing ribs eccentricity effect on closed circular cylindrical shell stability using strain energy method

09 p1786 A70-23720

Axial tensile stress effects on stability of cylindrical shell under nonuniform external pressure

09 p1786 A70-23721

Cylindrical shell stability under combined torsion and internal pressure, noting yield point effect on critical load, obtaining buckling-internal pressure relationship

09 p1786 A70-23722

Spherical isotropic shells motion equations solved in terms of associated Legendre functions, considering surface loads and body forces

10 p1953 A70-23876

Solutions existence for nonlinear partial differential equations describing orthotropic and nonlinear shallow shells under loads and temperature effects

10 p1954 A70-24019

Finite deformations of flexible inelastic orthotropic shells of revolution for generalized plastic flow and deformation theories

10 p1955 A70-24079

Eccentricity and clamping effects on stability and critical pressure of ring-reinforced cylindrical shells under internal pressure

10 p1956 A70-24248

Energy dissipation in free oscillations of multilayer shells consisting of alternating rigid elastic layers and soft fillers, deriving equations of motion

10 p1956 A70-24249

Transverse vibrations of rods, plates and shells based on hyperbolic, circular and Bessel functions

10 p1959 A70-24586

Natural frequencies and mode shapes of vibrating shells and shell combinations determined using variational finite difference method in conjunction with Hamilton principle

10 p1961 A70-25056

Forced vibrations of cylindrically curved multispan shell structures, using transfer matrix methods

10 p1962 A70-25062

Rapid expansion of thin walled aluminum alloy cylinders under pulsed magnetic field pressure using high speed streak camera oscillography

10 p1964 A70-25120

Truncated, structurally orthotropic and round conical shell oscillations taking into account reinforcing ribs eccentricity

10 p1964 A70-25195

Homogeneous boundary value problems in stability theory of circular cylindrical shells axisymmetric equilibrium state

11 p2129 A70-25396

Eccentrically stiffened thin circular cylindrical shell stability under torsion emphasizing exact finite formulas derivation

11 p2129 A70-25561

Random displacement fields in thin circular cylindrical shells with initial imperfections under axial compression using statistical analysis

11 p2129 A70-25562

Stability loss in cylindrical shell under axial compression, noting critical load reduction by local axisymmetric depression

11 p2130 A70-25566

Clamping edges effect on critical parameters of cylindrical orthotropic shell under axial compression using undetermined Lagrange multipliers

11 p2130 A70-25567

Shells equilibrium with large plastic deformations, discussing stability under uniaxial/biaxial tension and physical models for material mechanical properties

11 p2130 A70-25569

Tapered spherical shell under constant initial pressure calculated for strength, stiffness and durability on digital computer using numerical algorithm

11 p2134 A70-25846

Load carrying capacity of isotropic rigid-plastic shells of revolution with different yield points under tension and compression applied to spherically coupled cylinders

11 p2134 A70-25932

Characteristic equation roots for circular cylindrical shells deformation under edge load

11 p2135 A70-25960

Stiffened cylindrical shells under internal pressure numerically analyzed based on C-5A fuselage material parameters

11 p2135 A70-25961

Creep deflections and collapse times for supported thin shallow spherical shells under uniform pressure predicted using variational theorem

11 p2135 A70-25963

Initial geometric imperfections effect on buckling and postbuckling behavior of laminated composite cylindrical shells under axial compression, considering reinforcing fiber orientations

11 p2135 A70-25986

Dynamic buckling of shell or arch structure determined from response of two degrees of freedom structure to step load application

11 p2138 A70-26158

Stresses and displacements determinations in spherical shells under concentrated loads, considering transverse shear deformation effect

11 p2139 A70-26347

Buckling load calculations for axially compressed circular cylindrical shells under relaxed boundary conditions

11 p2140 A70-26484

Cylindrical shells plastic flow buckling under radially inward impulsive loading, showing mode number dependence on shell length

11 p2140 A70-26486

Stability analysis of ring-stiffened orthotropic, multilayered shells of revolution under axisymmetric torsionless loads by digital computer

12 p2320 A70-27143

Shells of revolution under combined thermal and mechanical loading, presenting analytical basis of BOSOR 3 digital stress analysis program

12 p2320 A70-27144

Thermal buckling theory for multilayered stiffened cylindrical shells under various combined loads

12 p2321 A70-27149

Axially stiffened and barreled cylindrical shells elastic postbuckling behavior, considering effects of stringer and load eccentricities

12 p2321 A70-27175

Thin walled tubes plastic instability under combined internal pressure and axial load for open and closed end conditions

12 p2322 A70-27216

Blunted spherical shells stability under hydrostatic pressure by reducing equilibrium equations to differential

12 p2322 A70-27333

Thin cylindrical shells elastic buckling under uniform axial compression, considering Kirchhoff-Love hypotheses in critical stress determinations

12 p2324 A70-27396

Glass-plastic thin cylindrical shells carrying capacity dependence under axial and external loads on combinations of longitudinal and transverse reinforcing layers

12 p2259 A70-27527

Polymer shells lasting stability mathematical simulation, discussing similarity criteria of nonlinearly and hereditarily elastic materials

12 p2259 A70-27528

Transversely isotropic shells stability with respect to subcritical deformation under axial compression using three dimensional linearized equations, determining critical loads

12 p2324 A70-27529

Clamped shallow spherical cap elastic buckling and initial postbuckling behavior under uniformly distributed load over circular region centered at apex

12 p2326 A70-27814

Fiberglass plastic cylindrical shells stability against creep under prolonged hydrostatic pressure, obtaining critical loading times

12 p2328 A70-28278

Structural strength of fiberglass plastics reinforced conical shells, using impregnation technique of dry package under pressure

12 p2328 A70-28280

Transversely isotropic hollow spherical shell with elastic filler, analyzing stability

12 p2328 A70-28281

Cylindrical shells stability under axial compression by two dimensional Kirchhoff-Love applied theories, calculating critical stresses

12 p2328 A70-28282

Laminated glass fiber reinforced cylindrical shell stability resting on hinged supports under axial compression

13 p2514 A70-29285

Critical loads and stability of isotropic cylindrical shells under uniformly distributed longitudinal compression loads based on network method

13 p2514 A70-29287

Stability loss of nonreinforced and reinforced cylindrical shells under external pressure

13 p2514 A70-29294

Elastic material filled cylindrical, segmented toroidal and conical shells thermal stability, allowing for stiffer eccentricity

13 p2516 A70-29523

Linear compressive orthotropic stability theory for shallow-stiffened cylinders

13 p2518 A70-30022

Thermal stability of simply supported bimetallic shallow spherical shell, considering rotationally symmetric deflection modes

14 p2657 A70-30845

Thin spherical shell postbuckling behavior with constrained rigid boundary under edge load, using deep and shallow shell theory

14 p2658 A70-30848

Curved finite element for shells of revolution based on minimum potential energy principle, discussing stiffness and equilibrium of domed and branched shells

14 p2659 A70-31130

Stress distribution in spirally corrugated shell under torsional deformation, calculating twisting moment for stiffness

14 p2661 A70-31327

Reinforced shells of revolution carrying capacity upper limit subjected to internal adiabatic ideal gas flow

15 p2814 A70-31534

Strength and critical load determination for spherical shells with reinforced hole under internal pressure based on stress-strain state analysis during deformations

15 p2814 A70-31543

Natural oscillation frequencies in rectangular shallow shells weakened by cuts, using summary representations method for eigenvalues determination

15 p2814 A70-31585

Shells of revolution zero moment stressed state calculation by analytical functions, solving boundary value problem for edge loading

15 p2814 A70-31587

Stress-strain state of catenoid, cylindrical and spherical shells of revolution, emphasizing catenoid shell bending problem

15 p2815 A70-31648

Elastic shells of revolution stability and critical loads, discussing moment stress state and edge effect

15 p2816 A70-32158

- Reinforced shallow shells and plates stability beyond elastic limit, obtaining optimal parameters under compressive loads 15 p2816 A70-32159
- Bifurcation stability in geometrically nonlinear shells of revolution under transverse loads, considering tension and compression deformation 15 p2817 A70-32168
- Stability characteristics of elastic shallow shells of revolution in temperature field and under compression, reducing variational equation of bending by Ritz method 15 p2817 A70-32169
- Cylindrical shells upper critical loads calculation based on linearization of nonlinear shell theory equations 15 p2818 A70-32181
- Computer program for limit analysis of rotationally symmetric shells, generating yield point load upper and lower bounds and velocity profile 15 p2822 A70-32351
- Cylindrical shells under axial compression, using elastic stability analysis for critical loads prediction 15 p2822 A70-32512
- Gravitational instability and collapse of thin spherical shell of charged fluid, using energy conservation law 16 p2952 A70-33787
- Combined internal pressure and axial loading influence on aeroelastic stability of thin walled cylindrical shell in supersonic flow field 16 p2991 A70-33851
- Stability analysis of anisotropic cylindrical shells under combined loadings using inverse operators 16 p2994 A70-34246
- Polycarbonate thin walled cylindrical shells mechanical and material stability under torsion 17 p3127 A70-34656
- Solutions for normal and tangential displacements and concentrated forces on shallow cylindrical shells 17 p3186 A70-34969
- In-plane boundary conditions effect on axially compressed conical shell stability under low buckling loads, using linear Donnell-type theory 17 p3186 A70-34971
- Radial vibration frequency variation with wall thickness in hollow spherical shells, tabulating and plotting results 17 p3186 A70-34978
- Membrane and bending stresses at crack tip in cylindrical shell weakened by elliptic hole with major axis perpendicular to shell axis 17 p3186 A70-34981
- Axially loaded cylindrical shells prebuckling deformation behavior measurement by holographic interferometry 17 p3086 A70-35012
- Double curved shell membrane stress calculation under arbitrary load, using stress functions 18 p3338 A70-36373
- Stress-strain equilibrium of thin isotropic elastic shells of revolution loaded along meridian 18 p3340 A70-36577
- Matrix filtering method for stability solutions of shells and plates by finite difference method 18 p3341 A70-36580
- Stability of circular cylindrical shell reinforced by elastic rings at edges under longitudinal compression 18 p3341 A70-36581
- Shallow conical shell stability under uniformly distributed pressure and concentrated force at apex for rigid and free clamping boundary conditions 18 p3341 A70-36589
- Thin circular cylindrical shell stability subjected to axisymmetric thermal pulse, describing buckling process by mathematical model 18 p3342 A70-36641
- Thin walled cylindrical shell stability under axial compression edge load beyond limit of proportionality 19 p3534 A70-37243
- Carrying capacity of nonshallow rectangular shells, showing corner dependent collapse 19 p3535 A70-37345
- Core-filled thin cylindrical shell under radial ring and band pressure loads, using Boussinesq-Neuber stress function and Flugge shell theory 19 p3543 A70-38247
- Blast loaded cylindrical shell collapse hinge dynamic instability prediction by mathematical model 19 p3545 A70-38334
- Clamped spherical shells under concentrated, distributed and ring loadings, analyzing large axisymmetric deflections for prebuckled and postbuckled states 19 p3545 A70-38336
- Straight thin walled elliptical cylindrical shells stability in pure bending, solving boundary value problem 19 p3550 A70-38683
- Elastic body with incompressible fluid filled cavities, studying motion and stability by deriving motion equations starting from principle of least action 20 p3672 A70-39376
- Radial and shearing stresses in hollow composite sphere due to thermoelastic strain nucleus 20 p3719 A70-39602
- Cylindrical shells dynamic stability under uniform radial pressure 20 p3722 A70-39786
- Thin shells of revolution static and dynamic stability under symmetric loads, presenting eigenvalue algorithm for boundary value problems 20 p3725 A70-39863
- Elastic shell stability criterion during short duration dynamic loading 20 p3725 A70-39864
- Spherical shell equilibrium states dynamic calculation method applied to thin plates nonlinear theory statistical problems 20 p3725 A70-39871
- Stability loss in linear approximation by thin elastic shell of revolution with negative Gaussian curvature 20 p3726 A70-39872
- Structurally closed orthotropic circular cylindrical reinforced shell stability, developing approximate method to obtain various boundary conditions 20 p3727 A70-39886
- Homogeneous boundary value problems in stability theory of circular cylindrical shells axisymmetric equilibrium state 20 p3732 A70-40100
- Flexible shallow shell with plastic inhomogeneity due to yield point-fast neutron flux relation, examining stability under uniform load 20 p3734 A70-40437
- Rapid expansion of thin walled aluminum alloy cylinders under pulsed magnetic field pressure using high speed streak camera oscillography 20 p3735 A70-40513
- Circular cylindrical shell stability under axial compressive load, analyzing buckling process by high speed photographic recording of photoelastic isoclinic pattern changes 20 p3735 A70-40528
- Concentrated lateral loads effect on elastic stability and moment carrying capacity of circular cylindrical shells in bending 21 p3932 A70-40544
- Dynamic stability of cylindrical shell with small curvature under static or periodically variable axial pressure loads 21 p3932 A70-40554
- Vibration of combined cylindrical shells via Lagrangian minimization regarding unknown boundary values 21 p3934 A70-40897
- Elastic-plastic axisymmetric shells of revolution, analyzing large deflection and yielding for internal and external pressures by finite element method 21 p3937 A70-41738
- Circular cylindrical shell with annular orthotropic elastic core, analyzing stress wave propagation under pressure pulse 21 p3938 A70-41740
- Thin cylindrical shell under nonaxially symmetric concentrated stationary radial loading, calculating random responses and stability 21 p3940 A70-42051
- Nonlinear flexural vibration of thin circular cylindrical shells with clamped ends, using method of averaging for stability 22 p4112 A70-42517
- Axisymmetric vibrations of cylindrical shell with concentric circular plates at each end, obtaining Lagrangian of combined system 22 p4115 A70-42843
- Transient elastic vibrations of air and liquid filled cylindrical shells under radial impact, using shadow-optical cinematography [SMPT PREPRINT 107] 22 p4031 A70-43030
- Circular cylindrical shell with varying thickness under circumferential load and radial pressure, calculating critical load 22 p4117 A70-43354
- Flutter of elastic current-carrying shell containing incompressible inviscid nonconducting fluid flow 22 p4117 A70-43383
- Limiting pressure for isotropic plastic plates and spherical shells with stress dependent yield, using flow theory 22 p4120 A70-43717
- Spherical shell nonaxisymmetrical deformation under varying loads, relating parameters, Poisson coefficient and complex function 23 p4267 A70-44168
- Cylindrical shell stability under off-center compression loads applied to end faces, determining collapse conditions 23 p4268 A70-44169
- Thin walled shells structural vibration, buckling and stress analysis by computer methods, discussing shell theory and design 23 p4271 A70-44704
- Gradient minimization and higher order discrete elements application to shell buckling and vibration eigenproblems, using 48 degree of freedom Bogner cylindrical panel element 23 p4271 A70-44705
- Rectangular and triangular grids with variably sized mesh elements for finite difference analysis of shell structures 23 p4272 A70-44709
- Plastic postbuckling and imperfection sensitivity of spherical shells under axisymmetric bifurcation 23 p4272 A70-44714
- Second approximation for limit loads due to imperfection sensitivity of axisymmetric elastic shell structures with unique harmonic buckling modes 23 p4273 A70-44720
- Computer program for geometrical nonlinear static and dynamic structural analysis of arbitrarily loaded shells of revolution 23 p4273 A70-44724
- Stress, buckling and vibration analysis of shells of revolution by numerical integration and finite difference methods, summarizing computer programs 23 p4273 A70-44725
- Approximation method for large deflection analysis of impulsively loaded rigid plastic circular plates and symmetric shells 23 p4275 A70-44943
- Curved element approximation of orthotropic axisymmetric thin shells under axial loads 24 p4419 A70-45152
- Axisymmetrically imperfect spherical thin shell stability analysis, comparing results with theory of initial postbuckling behavior 24 p4421 A70-45282
- Infinite plates and shallow shells stability under doubly periodic surface loadings, using nonlinear analysis 24 p4421 A70-45283
- Truncated spherical shells nonlinear axisymmetric buckling calculation from equilibrium equations 24 p4421 A70-45284

SHELL THEORY

- Interior shell equations compared with classical shell theory, considering helicoidal, spherical and circular cylindrical geometry 01 p0200 A70-10542
- Anisotropic shells and plates dynamic field equations derived, taking into account mechanical forces and nonuniform temperature field 01 p0200 A70-10553
- Finite element method for thin shells using specialized form of Reissner variational principle for stresses and displacements 01 p0208 A70-11184
- Longitudinal wave motion in rods, plates and shells based on three dimensional equations and asymptotic expansion 01 p0209 A70-11365
- Boundary conditions at reinforced edge of shell by separating solution into zero moment stress and edge effect solutions 01 p0209 A70-11407
- Rotating compressor vanes vibration frequencies and modes using shell theory, considering Coriolis forces and rotation rates effects 01 p0211 A70-11427
- Green function type solutions of shell equations by small parameter technique for case of free terms consisting of Dirac delta function 01 p0212 A70-11565
- Nonlinear boundary value problem algorithm in shell theory 01 p0212 A70-11566
- Asymptotic dynamic theory for elastic cylindrical shells incorporating thickness effects, considering longitudinal wave propagation in infinite length shell 02 p0385 A70-11877
- Shells of revolution having arbitrary stiffness distribution and subjected to arbitrary loads and temperatures 03 p0583 A70-12916
- Zero-moment theory boundary value problem of shells of revolution with negative curvature under tangential static and geometrical conditions imposed on ends 03 p0589 A70-13337
- Shallow shell theory, discussing equation kernels, reduction of boundary value problems to integral equations, potential theory application and transformation into Fourier series 03 p0589 A70-13338
- Nonlinear theory for thin elastic shells with small strains and rotations, analyzing nonzero Gaussian curvature 03 p0594 A70-13622
- Thin elastic laminar shells nonlinear physical theory assuming Love-Kirchhoff hypothesis validity, rigidly connected layers and nonlinear mechanical behavior 04 p0765 A70-14419
- Nonlinear thin shell theory kinematics generalized in terms of physical strain and surface deformation and geometry 04 p0766 A70-14450
- Shell theory resolving equations transformation to second order partial differential equations suited for solution by numerical algorithms of network method 04 p0767 A70-14495

Spherical caps axisymmetric static and dynamic buckling under load, using axisymmetric nonlinear elastic shell theory approximation and finite difference equations
[AIAA PAPER 69-89] 04 p0778 A70-15587

Static-geometric analogy of Kirchhoff-Love shell theory applied to Timoshenko complex equations allowing for transverse shear deformation
05 p0934 A70-16219

Finite element method for large displacement elastic-plastic analysis of plates and shells, using geometric stiffness matrices and stress-strain relationships
05 p0943 A70-16809

Stress analysis of curved tubes capable of accounting for all end effects based on shell theory equations
05 p0944 A70-16811

Lower bound limit analysis of symmetrically loaded thin shells of revolution having arbitrary meridional profiles, demonstrating methods for pressure vessel problems
05 p0944 A70-16815

Axisymmetric deformation of shells of revolution with variable thickness solved by asymptotic method in form of higher Fourier series harmonics
05 p0945 A70-16853

Shell shear strain determined by expanding displacement vectors into covariant power series of distance from middle surface
[DFVLR-SONDDDR-23] 05 p0955 A70-17078

Dynamics of composite, sandwich and stiffened shell type structures with various geometries
06 p1160 A70-17158

Buckling behavior of elliptical cylinders under normal pressure using linear thin shell theory and Galerkin method, compared with test results
[AIAA PAPER 70-105] 06 p1169 A70-18038

Hybrid finite element analysis for combination of axisymmetric shell and linear displacement triangular ring elements
[AIAA PAPER 70-137] 06 p1169 A70-18052

Seminfinite simply supported cylindrical shell transient response due to axisymmetrically engulfing step pressure wave, investigating moving load critical velocity
[AIAA PAPER 70-18] 06 p1170 A70-18063

Equations for general shells of revolution reduced to simultaneous fourth order ordinary differential equations for stress and displacement functions
07 p1401 A70-18892

Uniform thickness thin helicoidal shell stress-strain state with middle surface in asymptotic lines, assuming parameters governed by one dimensional law
07 p1402 A70-19055

Isotropic shells with shear deformations, investigating stress-strain relations in Cosserat continuum applied to plates
[DFVLR-SONDDDR-23] 07 p1404 A70-19233

Elliptic cylinders buckling under normal pressure analyzed on polyvinyl chloride sheet models
07 p1406 A70-19304

Shell elastic constants for multilayered sandwich cylinders using Donnell approximation
07 p1406 A70-19326

Nonlinear thermodynamic theories of plates, elastic shells and rods derived from three dimensional theory of classical continuum mechanics
07 p1414 A70-20172

Axisymmetric elastoplastic deformation theory for elastic cylindrical shell using Saint Venant yield condition, obtaining expressions for strain components, longitudinal deformation, etc
07 p1415 A70-20185

Natural axisymmetric vibrations of cylindrical shell with hollow filler, analyzing motion by shallow shell and elasticity theory dynamic equations
07 p1415 A70-20191

Shallow shells of variable thickness and curvature calculated using small parameter method based on functional analysis
07 p1416 A70-20193

Variable coefficient equations for free oscillations of shallow shells of variable thickness in Vlasov moment theory
08 p1586 A70-21011

Thin shells of revolution natural oscillation frequencies approximation based on shell subdivision into series of cylindrical shells
08 p1588 A70-21194

Cylindrical and flat shells equilibrium equations representation using stress, deflection or tangential displacement functions
08 p1591 A70-21442

Transient radial temperature distributions in cylindrical shells via Carslaw and Jaeger procedure involving binomial theorem and asymptotic expansions of Bessel function
08 p1599 A70-21588

Flügge characteristic equation approximate roots for closed cylindrical shell compared with Donnell equation solution
08 p1593 A70-21625

Theorem for highest statically admissible multiplier for plates and shells, noting association with stress field satisfying yield equality at all cross sections
08 p1595 A70-21977

Linearly exact displacement and strain variations in transverse coordinate within shell structure
09 p1781 A70-23233

Elastic shell theory, deriving dynamic bidimensional equations from tridimensional elasticity equations asymptotic integration
10 p1959 A70-24793

Shell dynamics equations role in natural frequencies, determining dynamic response with damping allowance
10 p1960 A70-25052

Axisymmetric elasticity theory problem solution for hollow finite cylinder with symmetrical end loading, employing stress function
11 p2128 A70-25388

Noise-flutter interrelation in flight vehicle flexible plate and shell configurations immersed in fluid flow
11 p2132 A70-25726

First order differential equations for unsymmetrical bending of shells of revolution
11 p2135 A70-25978

Free vibration characteristics of circular cylindrical shells of finite length, utilizing Flügge equations
11 p2135 A70-25997

Finite element method using shallow shell stiffness matrix extended to cylindrical shell solution
11 p2138 A70-26159

Monograph on shells of revolution and prismatic shells of arbitrary cross sectional shape with arbitrary load covering partial shells, programs, boundary condition methods, etc
11 p2141 A70-26600

Nonlinear thin shell theory equations reduced to equations in unknowns with boundary conditions
11 p2143 A70-26653

Asymmetric stiffened shell structure analysis by finite element method, introducing constant transverse shear model concept
11 p2144 A70-26677

Axisymmetrically loaded shells of revolution with displacement behavior defined by fourth order differential equations, discussing finite difference method suitability for solution
11 p2144 A70-26679

Large deflection analysis of elastic-plastic shells of revolution by computer program based on nonlinear theory and multisection method of numerical integration
12 p2320 A70-27147

Polymer shells lasting stability mathematical simulation, discussing similarity criteria of nonlinearly and hereditarily elastic materials
12 p2259 A70-27528

Equilibrium equations for thin multilayer shells with variable thickness, assuming simultaneous work without friction under loads
12 p2325 A70-27556

Slender cylindrical shell loaded by internal pressure analyzed using numerical procedure developed for digital computer
13 p2512 A70-28981

Discretized linear theory of arbitrary shell forms
13 p2513 A70-29151

Geometrical theory of nonlinearly elastic inhomogeneous flexible shells, deriving variational equation in terms of displacement component and stress function
13 p2514 A70-29288

Shallow shell solutions complete with respect to finite simply connected surface region applied to circular cylindrical shells
13 p2517 A70-29758

Shallow shell theory partial differential equations, obtaining integral representations of general solutions
13 p2517 A70-29764

Zero-moment theory boundary value problem of shells of revolution with negative curvature under tangential static and geometrical conditions imposed on ends
14 p2657 A70-30715

Shallow shell theory, discussing equation kernels, reduction of boundary value problems to integral equations, potential theory application and transformation into Fourier series
14 p2657 A70-30716

Shell homogeneity theory, considering uniform states, spheres and circular cylinders
14 p2600 A70-31280

Reticulated shell structure buckling using approximate equivalent shell and discrete analysis of individual beams
15 p2816 A70-32007

Sinusoidal stress and strain in elastic shells of revolution, reducing linear theory to simultaneous second order differential equations
15 p2816 A70-32008

Shallow shells displacement theory, representing solution in terms of analytical functions
15 p2817 A70-32160

Closed spherical shell, demonstrating effects of concentrated forces at poles
15 p2818 A70-32170

Addition theorems for cylindrical functions, discussing applications to shell stress analysis and three dimensional elasticity theory
15 p2819 A70-32187

Zero moment/membrane/ theory for anisotropic thin walled shells, deriving expressions for stress-strain states and displacements under torsion
15 p2824 A70-32894

Normally intersecting closed cylindrical shells subjected to internal hydrostatic pressure, using Donnell shell theory
16 p2990 A70-33678

Membrane stresses on nonspherical domes with axisymmetric loads
16 p2990 A70-33743

Shells of revolution nonlinear finite element analysis by matrix displacement method, including higher order strain energy terms
16 p2991 A70-33885

Strain compatibility equations for continuous shells from physical and mathematical considerations
16 p2991 A70-33893

Stability analysis of anisotropic cylindrical shells under combined loadings using inverse operators
16 p2994 A70-34246

Canonical variational principle for boundary condition contractions in elastic shell theory
17 p3182 A70-34545

Turbine blades vibrations based on thick curved shell theory, deriving element from isoparametric solid
17 p3187 A70-34989

Thin elastic shells linear theory, examining three dimensional stress distribution and displacement field
17 p3191 A70-35608

Axisymmetric torsion by terminal loads of elastic shells of revolution, investigating energy inequalities for assessing quality of approximate solution of thin shell problem
18 p3335 A70-36058

Curved finite elements for shell calculations, obtaining potential energy of internal forces
18 p3337 A70-36369

Shell theory for shear deformations in covariant notation involving displacement power series expansion
18 p3337 A70-36371

Zero moment theory for stress-strain state of thin walled anisotropic shells with nonuniform moduli under simultaneous torsion and tension
18 p3340 A70-36578

Shallow spherical shell dynamics nonlinear problems solution with algorithm permitting use of straight lines method
18 p3341 A70-36590

Soviet book on theory of shell and plate type thin walled structural elements stability covering strength, boundary value problems, oscillations, design, etc
19 p3535 A70-37401

Linear micropolar elasticity theory of shells and plates, considering transverse shear and normal strains and rotary inertia
19 p3538 A70-37793

Anisotropic axisymmetric elastic shell theory including transverse stress effects, with application to orthotropic cylinder
19 p3545 A70-38337

Open and multiply connected closed sections of varying thicknesses, solving for unrestrained torsion
19 p3545 A70-38339

Shallow shell solutions complete with respect to finite simply connected surface region applied to circular cylindrical shells
19 p3547 A70-38396

Nonhomogeneous shell theory, considering load carrying surfaces with constitutive equations independent of shell curvature
20 p3719 A70-39619

Medium thickness shells under thermal creep using Saint Venant semiinverse method
20 p3722 A70-39787

Optimal variable shell thickness, describing numerical solution as function of forces, moments and thickness
20 p3725 A70-39865

Thin shell theory elastic coupling conditions, discussing stress-strain and edge effect states
20 p3726 A70-39875

Hollow shell theory equations for complex stress-strain states, using complex transform method
20 p3726 A70-39880

Circular cylindrical shells theory based on Novozhilov equation, deriving auxiliary formulas for strain and displacement characteristics in terms of stress function
20 p3727 A70-39888

Thin elastic shells displacement vector and strain boundary conditions determination from stress-strain relations
20 p3728 A70-39896

Fiber reinforced composite shell structures stress-strain relations, noting membrane and flexural variables coupling in constitutive relations
20 p3729 A70-40034

Shallow shell theory partial differential equations, obtaining integral representations of general solutions
20 p3732 A70-40102

Circular rib reinforced cylindrical shells, analyzing error due to Kirchhoff-Love hypothesis
20 p3734 A70-40435

Donnell-Vlasov shallow shell equations error analysis
20 p3734 A70-40441

Closed circular cylindrical shell nonlinear problem solvability extended to anisotropic sandwich shell, using mean deflection theory
21 p3933 A70-40601

Buckling analysis of stiffened noncircular cross section cylindrical shells constructed by circular arcs and straight line segments
21 p3934 A70-40922

Membrane theory of shells, reducing equilibrium equations to single second order partial differential equation through transformation in terms of stress function derivatives
21 p3939 A70-42031

Novozhilov complex transformation method extended to Timoshenko theory of elastic shells constructed with allowance for transverse shear deformation
21 p3941 A70-42237

Hollow spheres and hemispheres nonlinear axisymmetric deformation, using shell theory reduced to two point boundary value problem for differential equations
22 p4112 A70-42288

Nonlinear shell theory formulated in Lagrangian stress and moment resultants, deriving equilibrium equations
22 p4118 A70-43545

Circular cylindrical shell under longitudinal line load, deriving closed form solution in Fourier series
22 p4118 A70-43547

Symmetrical bending of isotropic elastic half-strip with free longitudinal edges and end displacements, indicating use for plate and shell theory
22 p4118 A70-43568

Shear flow distribution equations in prismatic shells under constant shear loading
23 p4265 A70-43891

Two dimensional shell equations derivation from three dimensional elasticity theory, considering rotationally symmetric bending of shells of revolution
23 p4265 A70-43942

Simplified Sanders-Koiter linear thin shell equations with uncoupled stress-strain relations for arbitrary, nonzero Gaussian curvature, catenoidal and helicoidal midsurface geometries
23 p4269 A70-44399

Arbitrary shells large deflection transient response, using finite difference computer program
23 p4272 A70-44710

Thin shell structural analysis by doubly curved arbitrary quadrilateral finite element, using Kirchhoff theory and cubic polynomial for membrane displacements
23 p4272 A70-44711

Numerical methods for mixed boundary value problem of axisymmetric shells of revolution, using truncated series expansion and finite difference expressions
23 p4272 A70-44712

Mixed formulations for finite element shell analysis based on flat and curved elements
23 p4272 A70-44713

Shell analysis based on discretization into one, two and three dimensional configurations, comparing finite difference, numerical integration and finite element methods
23 p4272 A70-44715

Nonlinear material and geometric behavior of shell structures studied by Eulerian and Lagrangian approaches
23 p4273 A70-44718

Nonlinear shell analysis by finite difference energy method, using BOSOR3 and STAGS computer programs
23 p4273 A70-44723

Rotating spherical shell equations as initial value problem, noting maximum convective heat transport at equator
23 p4249 A70-44805

Corrugated plates, closed cylinders and developable shells nonlinear elastic analysis, deriving boundary conditions
23 p4275 A70-44913

Matrix-vector computer program for three dimensional perspective projection and shell analysis in FORTRAN IV
24 p4419 A70-45155

SHELLS [STRUCTURAL FORMS]
NT ANISOTROPIC SHELLS
NT CIRCULAR SHELLS
NT CONICAL SHELLS
NT CORRUGATED SHELLS

NT CYLINDRICAL SHELLS
NT DOMES [STRUCTURAL FORMS]
NT ELASTIC SHELLS
NT HEMISPHERICAL SHELLS
NT LIQUID FILLED SHELLS
NT METAL SHELLS
NT ORTHOTROPIC SHELLS
NT RADOMES
NT REINFORCED SHELLS
NT SPHERICAL CAPS
NT SPHERICAL SHELLS
NT THIN WALLED SHELLS
NT TOROIDAL SHELLS

Shells with holes using Neumann method, obtaining Fredholm alternative for singular integral equations
03 p0589 A70-13347

Computer programs for numerical analysis of shell structures, considering series expansion, numerical integration, finite differences and finite elements
04 p0768 A70-14787

Shell directional antennas operational behavior at 2 and 4 GHz and mechanical properties
04 p0660 A70-15661

Thermoelastic stresses in plates and shells in random temperature fields, studying influence on service life
09 p1778 A70-23084

Monograph on shells of revolution and prismatic shells of arbitrary cross sectional shape with arbitrary load covering partial shells, programs, boundary condition methods, etc
11 p2141 A70-26600

Stress analysis of plane, shell and three dimensional structures using finite element method
12 p2315 A70-26886

Deep shells formation by high pressure methods, discussing fluid, mechanical edge pressure and friction aided extrusion techniques
12 p2240 A70-27080

Wave propagation in finite length revolving shells, describing advantages of modal superposition method generated by finite element computer program
12 p2317 A70-27124

Mechanics of solid structures including shells and beams, considering three dimensional behavior laws in plasticity and creep
14 p2656 A70-30294

Shells with holes using Neumann method, obtaining Fredholm alternative for singular integral equations
14 p2657 A70-30721

Curved finite element for shells of revolution based on minimum potential energy principle, discussing stiffness and equilibrium of domed and branched shells
14 p2659 A70-31130

Positive/negative curvature shells local stresses due to concentrated loads and heat sources, deriving approximate solutions
15 p2817 A70-32161

Arbitrary shaped shell structures analysis by finite element method, using curved shell elements approach
16 p2988 A70-33289

Pressurized shells of revolution loaded axisymmetrically, formulating equations for calculation of displacements, forces and stresses
18 p3338 A70-36406

Book on thermoelasticity covering thermal stresses in disks, plates, shells and bodies of revolution under steady and unsteady temperature fields
19 p3541 A70-37974

Book on structural analysis by finite difference calculus covering elastic and elastoplastic states, vibration and buckling of beams, gridworks, plates and shells
19 p3548 A70-38599

General purpose computer programs for shell structural analysis, using finite element modeling and displacement methods
23 p4271 A70-44707

Finite element structural analysis/FESTRAN/ computer program predicting static structural response of plate and shell structures
23 p4272 A70-44717

SHELTERS
NT Nonsteady flow past duct junctures, investigating ventilation system of underground bomb shelter for blast wave passage prevention
11 p2036 A70-26139

SHIELDING
NT ELECTROMAGNETIC SHIELDING
NT ELECTROSTATIC SHIELDING
NT HEAT SHIELDING
NT MAGNETIC SHIELDING
NT RADIATION SHIELDING
NT RADIO FREQUENCY SHIELDING
NT REENTRY SHIELDING
NT SOLAR RADIATION SHIELDING
NT SPACECRAFT SHIELDING

Screening devices to control heat supplied to spacecraft, discussing mathematical model to determine effective emission
07 p1392 A70-18816

Bumper materials effect on two component hypervelocity impact shields performance, noting material density influence
07 p1310 A70-19713

Radial distribution of plasma parameters for thermionic converters with electrode shielding by plane sapphire rings, showing lateral surface effect
10 p1808 A70-25124

Radial distribution of plasma parameters for thermionic converters with electrode shielding by plane sapphire rings, showing lateral surface effect
20 p3568 A70-40517

SHIFT REGISTERS
Beam-lead substrate package for six stage TTL shift register, discussing metallization systems for interconnections and beams
02 p0271 A70-12846

Pseudonoise sequence generation with 3-tap linear feedback binary shift registers, citing reduction theorems
11 p2025 A70-26224

Integrated analog shift register circuits computer aided design, using insulated gate field effect transistor/IGFET/
15 p2711 A70-32597

Analog shift register for use as delay line and digital filter, discussing applications to radio astronomy
18 p3261 A70-37088

SHIMS
U COMPENSATORS

SHIPS
NT AIRCRAFT CARRIERS
NT SUBMARINES

Operational requirements of shipping for satellite communication systems, discussing distress cases, satellite navigation systems, information distribution traffic control, etc
03 p0522 A70-13605

Electroexplosive devices (EED) in electromagnetic environments, discussing principles of warship safety
03 p0549 A70-14129

Integrated man machine shipboard maintenance systems design, describing computerized model based on information flow network
08 p1465 A70-20665

Energy dissipation effect on complex parametric resonance and stability of two rotor gyrocompass on ship in motion
13 p2408 A70-29295

SHOCK
Blood volume and circulation rate in dogs subjected to traumatic shock and hemorrhage under high mountain conditions
07 p1198 A70-18708

Oxygen transport, arterial resistance and consumption in normovolemic and hypovolemic dogs in hemorrhagic shock
24 p4302 A70-46106

SHOCK ABSORBERS
Thermal damping in gas-filled composite materials during impact loading due to heat transport, discussing role in impact energy dissipation
04 p0712 A70-14867

Vibration damping of oil hydraulic system using bladder type accumulator composed of rubber, measuring frequency response of shock absorber
06 p0988 A70-17140

Foamed-in-place polyurethane for form fitting pilot helmet shock absorbing liner noting medical applications
07 p1218 A70-19015

Optimum control for shock absorber of elastic body solved by graph analytic method
09 p1727 A70-22535

Shock absorbing forces for absorber with one degree of freedom optimized for given acceleration during periodic disturbances by variational method
09 p1727 A70-22537

Optimum damping and stiffness in nonlinear single degree of freedom systems, discussing protection from ground and velocity shock during landing impact
11 p2145 A70-26695

Unmanned spacecraft landing shock absorption by hybrid pneumatic configuration having hard surfaced footpad with dual pneumatic bag attenuator
12 p2312 A70-27115

Honeycomb shock absorbers, noting landing gear applications
13 p2512 A70-28772

Surveyor spacecraft landing shock absorbers design and performance assessment by digital computer simulation
16 p2922 A70-34123

Passive shock isolation, describing environments, excitation types, equations of motion, etc
21 p3934 A70-40915

Parachute decelerator towline energy absorber shock attenuation characteristics, discussing drop test results
21 p3752 A70-41815

Rubber mount vibration and shock isolation problems, discussing dynamic response to reaction forces and force concentration
23 p4269 A70-44330

Spacecraft landing gear shock attenuation systems using crushable honeycomb, draw-die tubes and retrorocket skirt jet
23 p4262 A70-44695

SHOCK DIFFUSERS
U DIFFUSERS

SHOCK DISCONTINUITY

U SHOCK WAVE ATTENUATION SHOCK DISCONTINUITY

Oblique unsteady shock wave structure propagating at large Mach numbers in plasma cylinder under steady magnetic field, showing particle velocity profile discontinuity

01 p0064 A70-10999

Monograph on MHD waves covering theories for weak discontinuities, wave propagation in inhomogeneous media and behavior in magnetic fields

06 p1114 A70-17275

Progressive shock waves propagation, reflection and transmission through sudden changes in pipe cross sectional area, obtaining boundary conditions for quasi-steady junction flow

09 p1664 A70-23738

Quasi-transverse constant profile wave in finite elasticity with isothermal shock at discontinuity compared to Whitham breakdown

10 p1956 A70-24191

Stagnation point position as function of gas thermodynamic state behind detached shock for spherical segment at incidence in three dimensional hypersonic flow

12 p2159 A70-28247

One dimensional steady state flows and discontinuities in radiation gas dynamics, neglecting radiation pressure, viscosity and heat conduction

13 p2387 A70-28937

Time and spatial evolution of shock and expansion wave evolution from density discontinuity for gas with repulsive delta function interaction between particles

13 p2388 A70-29224

Hydromagnetic shock waves structure, investigating resistive, viscous and thermal conduction dissipation effects on discontinuities

17 p3140 A70-34928

Viscous heat-conducting one dimensional piston driven gas flow, assuming sharp shock discontinuity

17 p3075 A70-35890

Jump relations for shocks in anisotropic collisionless magnetized plasma

21 p3856 A70-41267

Plane parallel transonic flow with curved compression shock discontinuity in supersonic region, obtaining solution by indeterminate coefficients and hypergeometric functions

21 p3748 A70-42212

SHOCK FRONTS

Multiple pulsations mechanism during detonation spherical wavefront propagation in channels with various cross sections, noting volume effect

01 p0060 A70-10135

Critical detonation diameter as function of concentration and dimensions of inhomogeneities in explosive, assuming chemical reaction generated behind detonation front

01 p0217 A70-11005

Gas motion and heating by radiation behind shock wave front, noting ionization and radiation absorption occurrence

01 p0068 A70-11570

Electrical conductivity of air behind incident and reflected shock wave fronts as function of temperature and Mach numbers measured by electrode method

01 p0095 A70-11622

Detonation front macroscopic properties, Mach configurations, shock spacing, etc, considering effects of tube walls and nonlaminar flow

02 p0278 A70-12026

Transient energy transfer during expansion of plane layer of radiating gas bounded by strong shock, assuming LTE and perfect inviscid nonconducting gas

02 p0279 A70-12230

Adiabatic invariance of action integral for motion in nonregular fields, explaining charged particles motion through magnetic shock front in interplanetary space

02 p0359 A70-12788

Periodic shock fronted longitudinal pressure wave effect on instantaneous heat flux rates at tube end wall

02 p0400 A70-12860

Vibrational energy exchange between molecules during collision behind normal shock front as function of wave velocity

03 p0468 A70-13873

Ionization study of gas discharge parameters behind shock wave front produced by moving plasma pulse interaction with immovable gas discharge plasma

03 p0535 A70-14361

Detonation front structure stability in gases, discussing spin detonation, transverse waves, perturbation, etc

07 p1418 A70-18751

Shock front stability under free flow in electromagnetically driven shock tubes, determining critical hydrodynamic Reynolds number

08 p1482 A70-21529

Transparent gas radiation behind strong shock wave front with small pressure gradient due to energy losses

08 p1486 A70-21986

Accelerating shock wave fronts by detonating passive triethyl and hexogen using high speed photography

09 p1658 A70-22103

Carbon dioxide molecules dissociation along tube length, measuring temperature drop behind shock front at various pressures and 4300 K

09 p1730 A70-22172

Plane one dimensional motion of shock wave with moving inner boundary investigated for given shock wave front position and gas mass and energy

09 p1659 A70-22432

Shock wavefront configurations before inclined obstacles in supersonic flow, studying inclination angle role

09 p1604 A70-22443

Spectroscopic technique measuring OH concentrations behind shock waves by measuring absorption of OH lines, using water cooled RF powered lamp

09 p1683 A70-23512

Ionization front interactions in interstellar gas, investigating expanding planar H II region and contact discontinuity in H I region

10 p1937 A70-23975

Hydrodynamic energy flow down horizontal tunnel from nuclear explosive detonated underground, recording shock front luminosity and time of arrival

10 p1857 A70-23985

Microfluctuations frequency and wavelength of electromagnetic, electric and magnetic field distributions in plasma shock wave front found consistent with ion-acoustic origin hypothesis

10 p1925 A70-25031

Electron temperature distribution behind strong shock wavefront in air measured by electrostatic probe and compared to results of spectral line inversion method

10 p1871 A70-25114

Electric field structure at shock wave front propagating in weakly ionized gas under Ramsauer effect

10 p1871 A70-25121

Distance separating shock wave front of contact surface between motor and target gases in electromagnetic shock tube, discussing surface instabilities

11 p1977 A70-26467

Ionization kinetics of Ar, Xe and Hg monatomic gas behind shock wave front at high temperatures

12 p2210 A70-27319

Vertical propagation of short acoustic waves from harmonic source in inhomogeneous atmosphere, calculating shock front width and heating rate

12 p2264 A70-27519

Stellar upper atmospheric shock wave motion, discussing emission spectra interpretation and temperature gradients

13 p2493 A70-29395

Shock waves structure in radiating gases at high temperatures, taking into account radiation anisotropy in shock front

15 p2720 A70-31645

Shock wave front propagation instability in decreasing density medium, applying to stellar structure

16 p2890 A70-33200

Electron-acoustic, ion-acoustic and electromagnetic plane waves coupling at shock front in two fluid ionized viscous plasma

16 p2958 A70-33282

Elastoviscoplastic medium filled half space motion under pressure front moving along surface with time varying velocity, analyzing penetrating wave fronts form

16 p2990 A70-33780

Attenuation, refraction and multiple reflection effects on light reflection from shock front at near grazing incidence

16 p2953 A70-34271

Plane normal shock front diffraction along free interface between half planes of homogeneous fluids at rest, using method of characteristics and Whitham technique

17 p3074 A70-35886

Magnetic probes effectiveness study of electron heating behind shock wave front in plasma, measuring electron temperature

18 p3294 A70-36149

Supersonic conductive gas recombination fronts for arbitrarily oriented magnetic field, allowing for dissipative coefficients

18 p3294 A70-36255

Electron temperature and concentration profiles behind shock front from IR emission and absorption simultaneous measurement, applying method to xenon ionization and recombination processes

19 p3402 A70-37443

Optical reflection measurement at grazing incidence from shock front at Mach 1.94 in air at atmospheric pressure

20 p3674 A70-40167

Solar wind flow behind shock fronts from Mariner 5 and Explorer 34 spacecraft

20 p3701 A70-40422

Electric field structure at shock wave front propagating in weakly ionized gas under Ramsauer effect

20 p3685 A70-40514

Vertical propagation of short acoustic waves from harmonic source in inhomogeneous atmosphere, calculating shock front width and heating rate

21 p3818 A70-41167

Axisymmetric detached shock before blunt body in hypersonic monatomic gas flow, obtaining radiative ionization patterns in cold precursor

21 p3950 A70-41731

Pressure field behind shock wave after interaction with nonuniform density region, describing shock front shape

21 p3810 A70-41964

Ionization kinetics of Ar, Xe and Hg monatomic gas behind shock wave front at high temperatures

21 p3854 A70-42061

Detonation front position determination in explosive by photoelectric technique

22 p4121 A70-42341

Analytic shock front velocity as function of initial parameters in continuous inhomogeneous medium, verifying propagation through rarefaction wave

22 p4010 A70-42687

Turbulent collisionless plasma shocks formation, wave front steepness and explanation for earth bow shock

23 p4225 A70-44183

SHOCK HEATING

Solar corona heating by shock waves, considering chromosphere and solar wind physical properties, heat flow channeling, etc

02 p0361 A70-11750

Chemical kinetics in reaction zone of shock heated hydrogen-carbon monoxide-oxygen mixtures, measuring density field behind normal shock wave by optical interferometry

02 p0250 A70-12022

Propane oxidation reaction and ignition delay times [AIAA PAPER 68-633]

03 p0603 A70-12909

Electron relaxation in shock heated Ar plasma estimated by measuring radiation intensity at various frequencies

03 p0535 A70-14363

Thermochemical relaxation influence on shock heated plasma gases via heat transfer experiments on ionized Ar, molecular nitrogen and carbon dioxide

03 p0536 A70-14366

High temperature thermal transport and ionization relaxation in Ar from measurements by thin film surface thermometer in high pressure shock tube end wall

04 p0787 A70-15607

Bronzite, hypersthene and amphibole chondrites examined by X ray diffraction for inert gas retention ages relationship to shock and reheating

05 p0912 A70-16448

Stagnation point heating in hypersonic gas flow past blunt bodies, considering radiative transfer effects on shock wave temperature and density distribution, wave separation, etc

06 p0985 A70-18557

Shock heated molecular beams of argon, oxygen and mixtures with helium, measuring particle velocities and gas dissociation

09 p1733 A70-23180

Temperature, pressure and electron density measurements behind reflected shocks in gas driven diaphragm shock tube compared with Rankine-Hugoniot predictions

10 p1967 A70-23960

Shock-heated noble gases total ionization times, considering recombination and atom-atom and atom-electron collisions

12 p2274 A70-26856

Primitive earth prebiological organic synthesis via amino acids shock heating in atmosphere-simulating gas mixture, suggesting energy sources from atmospheric entry

12 p2167 A70-27269

Vertical propagation of short acoustic waves from harmonic source in inhomogeneous atmosphere, calculating shock front width and heating rate

12 p2264 A70-27519

Multiband radiative cooling effect on enthalpy distribution behind incident wave in cylindrical shock tube for air, using differential approximation

14 p2663 A70-30268

Hypersonic flow of shock heated plasma past axisymmetric blunt body and onboard magnetic source, using numerical method

17 p3008 A70-34491

Magnetic probes effectiveness study of electron heating behind shock wave front in plasma, measuring electron temperature

18 p3294 A70-36149

Plane wall surface sublimation under radiation from shock wave heated gas

18 p3348 A70-36721

Heat fluxes from shock-heated gas to shock tube wall and wedge surface as function of Mach number, using platinum resistance thermometers

20 p3613 A70-40343

Vertical propagation of short acoustic waves from harmonic source in inhomogeneous atmosphere, calculating shock front width and heating rate

21 p3818 A70-41167

Plasma heating by ionizing shock waves reflected by transverse magnetic field barrier, discussing discontinuity resolution
21 p3857 A70-41381

Shock waves strength and frequency in solar atmosphere heating deduced by empirical model, integrating radiative losses over height
21 p3925 A70-42188

Heating and extension of solar chromosphere and corona via shock waves generated by piston below convection zone surface
21 p3925 A70-42189

Energy deposition in solar corona associated with momentum transfer from heating wave in transition region, discussing wave pressures
21 p3925 A70-42190

Fluid dynamics nonlinear equations for thermally driven motions in compressible, isothermal gravitational solar atmosphere, considering flow discontinuities and heat conduction
21 p3925 A70-42191

Lower chromosphere shock wave heating, analyzing density scale height effects
22 p4105 A70-43001

Radiative cooling of shock heated air in cylindrical shock tubes, calculating enthalpy profiles for nonadiabatic air flow
23 p4282 A70-44586

SHOCK LAYERS

Modified shock layer theory for predicting hypersonic internal flow in axisymmetric converging duct with attached shock at leading edge
02 p0276 A70-11854

Approximate solutions for radiative heat transfer in shock layer, considering discontinuity role
[ASME PAPER 69-WA/HT48] 04 p0667 A70-14800

Gas dynamics of intense explosion with expanding inner contact surface in Newtonian limit, discussing shock layer reattachment
04 p0619 A70-15322

Viscous shock layer at hypersonic blunt body stagnation point, applying finite difference and nonlinear overrelaxation methods to seven species air model
04 p0620 A70-15539

Inviscid hypersonic blunt body flow of hydrogen-oxygen mixtures in shock layer stagnation region
06 p0968 A70-17555

Surface temperature effects on low Reynolds number hypersonic shock layer development over flat plate sharp leading edge
06 p0982 A70-18364

Shock layer thickness in supersonic inviscid gas flow past blunt bodies, calculating boundary layer near stagnation point
09 p1603 A70-22442

Friction drag on thin pyramidal lobed bodies in supersonic flow, analyzing detached shock region and body geometry function
09 p1606 A70-23612

Electric arc shape moving at hypersonic speed investigated by Newtonian pressure distribution for thin shock layer
11 p2090 A70-25992

Solid particle motions in dusty gas in inviscid hypersonic shock layers of slender wedges and cones and stagnation regions of cylinders and spheres
12 p2156 A70-27827

Interplanetary shock waves layer formation in collisionless medium, using bulk transport parameters for dissipation requirement
12 p2308 A70-27885

Radiant shock layer in hypersonic air flow past blunt bodies, showing effects on temperature field and density
12 p2159 A70-28245

Transonic scaling effects for shock boundary layer interaction on circular and two dimensional airfoil models, discussing separation and reattachment
[AIAA PAPER 70-541] 13 p2339 A70-29008

Viscous shock layer equations of laminar hypersonic flow past blunt body at moderate to high Reynolds numbers
13 p2343 A70-29952

Shock slip analysis of merged layer stagnation point air ionization, clarifying effects of reaction rates, species diffusion, etc
13 p2343 A70-29987

Supersonic rarefied flow over sharp flat plate with merged shock layer and free molecular-continuum transition, using electron beam fluorescence
14 p2529 A70-31028

Blockage ratio effect on supersonic zone with shock layer interaction on nonlifting circular arc airfoils at transonic speeds in wind tunnels
16 p2835 A70-33674

Experimental and numerical nonequilibrium shock layer around cones in hypersonic pure oxygen flows with simultaneous rotational, vibrational and dissociation relaxation
[AIAA PAPER 69-136] 16 p2894 A70-33858

Electron concentration profiles in blunt nose vehicle shock layer during atmospheric near orbital entry at high altitudes, using finite rate chemistry
16 p2837 A70-33865

Inviscid air nonequilibrium shock layer properties correlation based on plenum entropy, predicting composition of downstream converging-diverging nozzle expanding air flow
[AIAA PAPER 70-866] 16 p2838 A70-33909

Viscous absorbing emitting shock layer in blunt body stagnation region, calculating skin friction and radiative heat transfer
[AIAA PAPER 70-868] 16 p2999 A70-33911

Continuum radiative flux from nonisothermal stagnation shock layer of nongray atomic gases, employing ionization edges and bound free spectral forms
[AIAA PAPER 70-837] 16 p3001 A70-33932

Nonreacting and chemically reacting laminar flows, calculating equilibrium, nonequilibrium and ideal gas laminar boundary and viscous shock layers over hyperboloid
[AIAA PAPER 70-808] 17 p3005 A70-34456

Near equilibrium shock layers nonequilibrium radiation emission calculation, noting application to Mars entry conditions
[AIAA PAPER 70-773] 17 p3007 A70-34481

Nonequilibrium air ionization in hypersonic viscous shock layers in flow about axisymmetric blunt bodies
17 p3008 A70-34501

Shock layer and combustion in supersonic flows about conical bodies at various angles of attack
17 p3012 A70-35894

Viscous hypersonic flow around nonslender bodies with mass supply at small Reynolds numbers, using thin shock layer model
18 p3206 A70-36259

Nonuniform external flow near blunt body stagnation point in diverging hypersonic thin shock layer
18 p3206 A70-36267

Nonequilibrium ionized hypersonic flow over blunt body at low Reynolds number, using thin shock layer assumption in analysis
18 p3208 A70-36689

Shock layer microwave radiation measurements during reentry flight of spherical nose cone, determining effective plasma temperature
[AIAA PAPER 69-183] 18 p3208 A70-36694

Thin radiating shock layer about axisymmetric blunt bodies, investigating energy-momentum transport coupling
21 p3950 A70-41746

Radiative transfer upstream absorption effect on inviscid stagnation region shock layer radiation
23 p4133 A70-44551

Inviscid rotational supersonic flow near three dimensional stagnation point, examining solutions for compatibility with vortical shock layer boundary conditions
23 p4183 A70-44692

SHOCK LOADS

NT BLAST LOADS

Coherent precipitates effect on explosive shock hardening of pure nickel and Inconel alloy sandwich assemblies determined from simultaneous shock loading at specific pressures
01 p0116 A70-10107

Dynamic response to step transverse loads of viscoelastic annulus of constant Poisson ratio in plane strain, analyzing work and spring-dashpot model
[ASME PAPER 69-LUB-23] 01 p0101 A70-10384

Al double crystals mechanical properties improvement after shock loading, studying surface and dislocation structures and active slip planes number
01 p0124 A70-11449

Naturally and artificially shocked iron meteorites, analyzing microstructure and alterations induced by pressure wave and high temperatures
02 p0377 A70-12506

Statistical measurements of deformation structures and refractive indices in experimentally shock loaded quartz specimens with different crystallographic orientations
02 p0292 A70-12509

Mechanical responses and residual defect structures in brass and stainless steel following explosive shock loading and cold reduction by rolling
03 p0507 A70-13139

Shock wave compression of single olivine crystals and specimens from chondritic meteorites, observing planar deformation microstructures
07 p1391 A70-20353

Static and shock kink bands in biotite deformed by metamorphism, meteorite impact, nuclear explosion and laboratory experiments
09 p1665 A70-22053

Interaction between bodies and spherical detonation wave, measuring force pulse transfer to immobile cylinder and flow patterns past flying blunt body
09 p1659 A70-22186

Uniaxial strain pulse propagation through various materials loaded uniformly with step function pressure by gas dynamic shock wave reflection
09 p1783 A70-23449

Three dimensional deformation of finite circular cylindrical shell under plane shock wave solved in linear form
09 p1785 A70-23618

Supersonic axial flow compressors, studying shocks shared by rotor and stator to obtain high efficiency
11 p2101 A70-25819

Unmanned spacecraft landing shock absorption by hybrid pneumatic configuration having hard surfaced footpad with dual pneumatic bag attenuator
12 p2312 A70-27115

Shock deformation effects on strengthening and microstructure of Ti and Ti-Mo alloys
17 p3120 A70-34420

Impulsive loading of structures via light-initiated sprayed explosives
17 p3059 A70-35162

Impulse loading of rings using magnetically accelerated flyer plates
17 p3187 A70-35163

Dynamic response to step transverse loads of viscoelastic annulus of constant Poisson ratio in plane strain, analyzing work and spring-dash model
[ASME PAPER 69-LUB-23] 19 p3435 A70-37607

Erasure fission tracks in soda-lime glass, tektite, biotite and apatite by shock loading, determining dynamic pressure and associated temperature effects
19 p3414 A70-38035

Dynamic response of distended carbon materials to shock loading defined by measuring equation of state, unloading behavior and spallation strength
20 p3657 A70-40263

Apollo 11 lunar soil and breccia shock metamorphism, examining plastic deformation structures in plagioclase, pyroxene and olivine
21 p3897 A70-41520

Shock metamorphism, grain size and mineralogy of lunar surface regolith materials
21 p3901 A70-41543

Shock metamorphism in lunar microbreccias and loose regolith materials, assuming crater formation by meteorite impacts
21 p3902 A70-41551

Preferred disorder and shock histories of chemical group 4A meteorites from metallographic and X ray diffraction, discussing preterrestrial shock loading
21 p3920 A70-41940

Annealing response of explosively shock loaded Ni, thoria-Ni, Chromel-A, Inconel 600 and thoria-Chrome, noting activation temperature inverse relation with stacking fault free energy
23 p4204 A70-43883

Solid cloth personnel parachutes opening forces, discussing loading conditions, flight path shock parameters, mass ratio variations and elasticity of system
[AIAA PAPER 70-1167] 23 p4137 A70-43992

SHOCK MEASURING INSTRUMENTS

Manganin piezoresistive shock gauge constant current supply using inductor and termination technique eliminating shunting
02 p0303 A70-12737

Mechanical shock accelerometer calibration by light frequency Doppler shift measurement using laser interferometer and single sideband carrier insertion circuit
08 p1493 A70-20602

Impact accelerations measurement for shock pulse amplitude and duration, describing system for direct reading
11 p2055 A70-26447

Shock wave and surface velocity measurements in exploding foil testing by streak photography with image converter camera
21 p3824 A70-40863

Optical FM system with laser interferometer and sideband carrier circuit for measuring mechanical shock by Doppler shift
23 p4193 A70-43964

SHOCK RESISTANCE

NT IMPACT RESISTANCE

Design reliability of through-bulkhead initiator explosive train using parametric test program data, discussing shock transmission and acceptor charge sensitivity energy balance
03 p0549 A70-14124

Bioelectronic equipment shock hazards reduction by current limiting diodes use in signal and ground leads
06 p0998 A70-17285

Selenium additions effect on structural steels transverse mechanical properties, emphasizing plasticity, shock resistance and machinability
07 p1310 A70-19750

Elastic post stability under longitudinal impact on rigid support, considering loading/unloading phases for calculating shock half wave length and critical rate
08 p1591 A70-21443

Materials selection for vibration or shock control based on cost, resonance frequency, strength, weight, etc
13 p2513 A70-29218

Ruggedized spacecraft mechanisms for severe shock environments
16 p2922 A70-34121

Ceramic composite materials structural application, improving brittleness and thermal shock resistance via reinforcing refractory fibers
[ICAS PAPER 70-40] 23 p4267 A70-44138

SHOCK SENSITIVITY

U SHOCK RESISTANCE

SHOCK SIMULATORS

Flight Impact Simulator for simulating bird strikes and bird-proofing of aircraft

16 p2888 A70-33290

Simple high level shock machine producing trapezoidal and terminal peak sawtooth pulses with Al honeycomb impact material

19 p3396 A70-37832

SHOCK SPECTRA

Transition probabilities for diatomic oxygen Schumann-Runge bands determined from shock tube emission studies

02 p0344 A70-12658

High speed sampling used with digital computer providing response shock spectrum data

08 p1481 A70-20610

Dynamic structures design optimization subject to shock spectrum, describing conversational type computer program

16 p2989 A70-33501

Equipment shock test model, using impedance method for spectrum analysis

16 p2992 A70-33988

Shock function response and Fourier spectra relationship, using Fourier transform for equation of motion solution

19 p3456 A70-37381

Shock waves strength and frequency in solar atmosphere heating deduced by empirical model, integrating radiative losses over height

21 p3925 A70-42188

SHOCK TESTS

Conditioned suppression after differential training, discussing shock tests on rats with safe and danger signals

01 p0036 A70-10794

Laser beam technique applied to thermal shock testing of metal disks, using solid state laser, compared to predicted results

01 p0113 A70-11058

Test method for inertial impact sensor switches subjected to multiple and varied shock inputs, using high energy detonators

03 p0494 A70-14128

Design and qualification test criteria for components derived by enveloping peaks of shock response spectra in ground tests of missile stages explosive separation

05 p0922 A70-15849

Impact tube test to find empirical equation for correcting effect of shear in displacing effective pressure center in viscous flow

06 p1052 A70-18383

Single or repetitive shock pulses produced on electrodynamic and hydraulic shakers for shock testing on vibration machines

06 p1030 A70-18438

Hypoxia effect on retrograde amnesia / recent memory loss/ in albino rats subjected to shock and decompression treatments

08 p1441 A70-20477

Force controlled vibration for shock tests, discussing feasibility and merits for simulation testing

12 p2205 A70-27099

Equipment shock test model, using impedance method for spectrum analysis

16 p2992 A70-33988

Shock pulse reproduction on electrodynamic and hydraulic shakers for vibration testing, including SNAP 21 results

21 p3804 A70-40865

Shock and bump testing for dynamic mechanical environments effects encountered by vehicle equipment and components

23 p4195 A70-44331

SHOCK TUBES

NT SHOCK TUNNELS

Rumanian book on shock tubes covering facility construction, gas flow, electronic measuring equipment, etc

01 p0059 A70-11379

Strong shocks and high temperature gases production using multistage gaseous detonation driven shock tube

02 p0274 A70-11855

Shock tube measurements of ionization relaxation times behind shock waves in air at shock Mach numbers from 8 to 17

03 p0471 A70-14360

Plasma unsteady one dimensional flow behind shock wave front in shock tube MGD channel, deriving differential gas dynamics equations

04 p0726 A70-14540

Air-glass particle suspensions flows in shock tubes, deriving effective drag coefficients from simultaneous particle concentration and pressure measurements

04 p0667 A70-14778

Flow fields construction for normal shock waves with nonequilibrium chemical reactions reflected from shock tube end wall

04 p0674 A70-15537

Precursor electron densities measured in nitrogen and air ahead of shock waves, noting shock tube wall reflectivity

04 p0694 A70-15565

Absorption coefficient 5-step model applied to shock tube measurements of end wall radiative heat transfer behind reflected shock waves in air

04 p0787 A70-15606

Shock tube research covering shock structure, atomic and molecular physics, radiation, plasma flows, shock waves in solids and boundary layers

06 p1028 A70-17517

Shock tube chemistry including ideal and nonideal behavior, instrumentation techniques, etc

06 p1005 A70-17727

Free electron formation ahead of strong shock waves traveling into nitrogen-oxygen mixtures in shock tube, observing electron densities

[AIAA PAPER 70-83] 06 p1065 A70-18029

Light emission and gas phase ignition of homogeneous solid propellants under shock tube conditions

[AIAA PAPER 70-120] 06 p1128 A70-18042

Impact tube test to find empirical equation for correcting effect of shear in displacing effective pressure center in viscous flow

06 p1052 A70-18383

Pressure history at end wall of electromagnetic shock tube measured during shock wave reflection by piezoceramic gage

06 p1031 A70-18505

Free piston compression with sonic flow outlet for determining orifice size by matching with bounce parameters

07 p1249 A70-19334

Real gas behavior effect on shock tube temperature and pressure flow nonuniformity for range of Mach numbers

07 p1257 A70-19337

Heat transfer measurement in ionized high temperature gas flows with discharge shock tube and thermal sensors

07 p1283 A70-19663

Carbon dioxide gas dynamic layer in shock tube facility, measuring shape, time, output energy, beam diameter, etc

07 p1301 A70-20021

Dimensionless strength parameter in determining bursting pressure of ductile metal diaphragms in square section shock tubes

08 p1481 A70-21034

Kinetics of homogeneous nitrogen dioxide-carbon monoxide atom transfer reaction in single pulse shock tube, carrying out product analysis by vapor phase chromatography

08 p1455 A70-21263

Shock front stability under free flow in electromagnetically driven shock tubes, determining critical hydrodynamic Reynolds number

08 p1482 A70-21529

Ternary detonation wave configurations calculated by shock polar method using methane-oxygen and hydrogen-oxygen mixtures in shock tubes

09 p1658 A70-22101

Current diffusion from magnetic piston into postshock gas upstream observed in electromagnetic shock tube

09 p1736 A70-23185

Laminar boundary layers behavior in shock tube flows behind primary moving shock wave using perturbation method

09 p1662 A70-23281

Kerr cell-shuttered high speed stigmatic spectrograph for shock tube electron density distribution measurement

09 p1682 A70-23503

Air shock tube driven by exploding mixture of propane and oxygen investigated for shock overpressure variation with distance

10 p1863 A70-23992

Gas viscosity high temperature measurement method in shock tube using boundary layer equations for velocity and static temperature distributions

10 p1867 A70-24151

High intensity shock wave propagation and generation of high enthalpy hypersonic flow studied to determine IMF-2 hypersonic shock tube performance limit

10 p1871 A70-24795

Time dependence of shock wave attenuation at multiple reflection in shock tube after diaphragm burst, using damped vibration solution

11 p2034 A70-25495

Remote controlled diaphragm exploding device associated with shock tube for MHD generator

11 p2090 A70-26170

Distance separating shock wave front of contact surface between motor and target gases in electromagnetic shock tube, discussing surface instabilities

11 p1977 A70-26467

CO dissociation kinetics in Ar and mixtures of O in Ar by shock tube study using vacuum UV absorption

12 p1810 A70-26857

Optimal conditions for obtaining dense low temperature cesium plasma in shock tube with heating calculated by Debye theory

12 p2278 A70-27327

Electromagnetic inductive shock tube design and wave velocity, electron temperature and plasma conductivity measurements

12 p2206 A70-27400

Shock ionized xenon electrical conductivity measurement at high temperatures as function of Mach number, noting equilibrium effects

12 p2281 A70-27807

Flush-mounted electrostatic probes behavior in shock tube over wide range of freestream conditions and bias voltage

12 p2236 A70-27810

Electromagnetic shock tube demonstrations of electrode spark breakdown, strong shock behavior, plasma conductivity and hypersonic shock flow over blunt body

13 p2404 A70-28623

Hypersonic test equipment, describing flight simulating hypervelocity wind tunnels, firing tunnels and shock wave tubes

13 p2384 A70-28927

Reverse flow in plasma generated in conical electromagnetic shock tube and reflected from downstream bulkhead, noting stabilization effects

13 p2469 A70-29974

Turbulent mixing at contact surface in driven shock wave in shock tube with bursting diaphragm for He-Ar test gas mixtures

14 p2566 A70-31030

Two diaphragm combustion shock tube for plasma radiation energy transfer, describing development, performance, make-up and testing

15 p2779 A70-32019

Electromagnetic diaphragm for use in shock tubes, describing construction and operation

15 p2741 A70-32440

Shock tube orifice effect on gas flow velocity and pressure drop, using pressure probes and Jenny friction formula

17 p3069 A70-34699

Pressure histories of burning modes in combustion driven shock tube using ignition of stoichiometric hydrogen-oxygen mixture with He dilution

17 p3195 A70-34922

Forcing time functions prediction for structures under shock tube test, relating aerodynamic parameters to mechanics terminology

17 p3060 A70-35180

Shock tube flow of dissociating oxygen with chemical relaxation using Lax method

17 p3070 A70-35243

Film condensation rates of vaporized substance in shock tube during passage of shock wave, formulating quasi-one dimensional problem

18 p3239 A70-36244

Unsteady two dimensional gas flow calculation axisymmetric shock tube of variable cross section, using numerical method

18 p3240 A70-36275

Heat transfer rates in short flow duration facilities /shock tubes/ from surface temperature measurement of solid exposed to flow

18 p3348 A70-36715

Carbon monoxide oxidation by molecular oxygen in incident shock waves, accounting for chain branching in shock tubes

19 p3374 A70-38271

Event-triggered high speed spectrograph shutter, studying shock tube plasmas

20 p3630 A70-39484

Shock tube high temperature air viscosity from laminar boundary layer heat exchange data

20 p3608 A70-39633

Shock tube with diffuser in low shock wave Mach number range, considering gas flow models to relate wave intensity to initial conditions in chambers

20 p3606 A70-39820

Shock tube facility with high explosive driver for reentry flow conditions simulation of manned planetary flights

21 p3804 A70-40849

Microsecond response bolometer for measuring thermal radiation fluxes in shock tube, discussing design, calibration and performance

21 p3824 A70-40859

Shock tube measurements of bimolecular reaction rates in branched chain hydrogen-carbon monoxide-oxygen system, monitoring flame band emission

21 p3773 A70-41314

Turbulent boundary layers produced by nonuniform shock tube flow, considering effects on chemical kinetic measurements

21 p3807 A70-41315

Optimal conditions for obtaining dense low temperature cesium plasma in shock tube with heating calculated by Debye theory

21 p3860 A70-42068

Computerized nonequilibrium thermochemical gas dynamic solutions for nozzle, shock tube and stream tube flow with arbitrary species and kinetic reactions numbers

22 p3982 A70-42762

Image orthicon detection and recording system adapted for spectroscopic measurements in shock tube emission studies

23 p4197 A70-44469

- Subsonic Ludwig/simple expansion/tube as shock tube for aerodynamic testing, examining flow characteristics 23 p4182 A70-44578
- MPD experiments in inductive hydrodynamic shock tube with round cross section and radial magnetic field 24 p4322 A70-45798
- Clean shock tube maintaining high gas purity level for Ar plasma spectroscopy 24 p4388 A70-46271
- SHOCK TUNNELS**
- Wall roughness effects on model heat transfer in high Reynolds number shock tunnel milliseconds flow using thick film fast response calorimeter 06 p1070 A70-18446
- Simultaneous high speed shock tunnel data acquisition system using single tape recorder, analog or digital readout and computerized reduction 06 p1031 A70-18604
- Shock tunnel preflight assessment of Apollo Block 2 command module base heating 07 p1394 A70-19722
- Dissociative-recombination rate coefficient measured for dissociative recombination reaction in inviscid nozzle flow of reflected shock tunnel, using high temperature and pressure nitrogen 09 p1737 A70-23225
- Arc driven shock tunnel operation with expansive area change at main diaphragm, evaluating flow characteristics 09 p1657 A70-23279
- Superradiant pulsed 5401 A neon laser for interferograms of gas flow through nozzles in shock tunnel 15 p2750 A70-31763
- Hypersonic nozzle ignition phenomenon in reflected shock wind tunnel 19 p3352 A70-38170
- Noble gas mixture large shock tunnel driven linear MHD generator, examining electron density, operating characteristics and electrical properties 20 p3682 A70-40012
- Combustion driven shock tunnel applied to tailored interface operating conditions, controlling mass flow into tube by throttling plates 22 p4006 A70-42765
- Contoured nozzle shock tunnel condensation point, determining flow supercooling over specified pressure range 23 p4182 A70-44588
- SHOCK WAVE ATTENUATION**
- Plane double front detonation wave attenuation by pursuing rarefaction waves, analyzing oscillations, onset mechanism and stability during transition to Chapman-Jouguet mode 08 p1485 A70-21633
- Time dependence of shock wave attenuation at multiple reflection in shock tube after diaphragm burst, using damped vibration solution 11 p2034 A70-25495
- Shock wave extinction point within plane steady upstream flow with uniform entropy and limit velocity 21 p3808 A70-41441
- Shock wave damping by perforated walls in gas channel, visualizing curved fronts with 24-spark HF camera [SMPT PREPRINT 104] 22 p4032 A70-43031
- Plane shock wave decay by interaction with simple wave, solving nonisentropic equations of gas dynamics 23 p4179 A70-43969
- SHOCK WAVE CONTROL**
- Supersonic transport sonic boom theory and effect reduction, discussing Whitham rule, bow shock, overpressure, engine and aircraft design and shock wave control 16 p2843 A70-34263
- SHOCK WAVE GENERATORS**
- NT SHOCK TUBES**
- NT SHOCK TUNNELS**
- Strong shocks and high temperature gases production using multistage gaseous detonation driven shock tube 02 p0274 A70-18555
- Pressure wave formation induced by absorption of radiation in oxygen, noting wave driving after radiation pulse decay by frozen dissociation energy 05 p0833 A70-16306
- Sonic bang simulation by linearly distributed explosives, creating blast waves with wide range of shapes and durations 05 p0796 A70-16796
- Explosive blast wave effects on flight vehicle in supersonic flow, using conical blast generator and short duration supersonic wind tunnel [ALAA PAPER 70-221] 06 p0972 A70-18127
- Monte Carlo simulation for shock wave formation by specularly reflecting piston, discussing reflection from specularly reflecting wall 06 p1049 A70-18334
- Book on sonic boom effects covering shock waves generation and propagation, elastic structures response to dynamic loads, structural damage, etc 09 p1609 A70-22203
- Shock wave formation and propagation analyzed by hydrodynamic model of two directional traffic flow based on continuity equations and velocity-density empirical relations 12 p2212 A70-28196
- In-flight shock cell noise generation by static jets, discussing frequency prediction formula 13 p2347 A70-29078
- Reflected shock waves generation by shock produced plasma flow interaction with strong magnetic fields, determining electron density and ionization relaxation times 17 p3139 A70-34490
- Thermal choking of channel flow by radiative transfer from upstream and application to shock waves generation 17 p3195 A70-35039
- Simple high level shock machine producing trapezoidal and terminal peak sawtooth pulses with Al honeycomb impact material 19 p3396 A70-37832
- Piston problem numerical solution by Boltzmann collision integral, considering shock waves and thermal disturbances evolution at gas-solid interfaces 21 p3808 A70-41378
- Mach effect on cylinders, tracking triple point of shock interaction using 25-spark camera [SMPT PREPRINT 103] 22 p4032 A70-43032
- Shock wave formation and propagation analyzed by hydrodynamic model of two directional traffic flow based on continuity equations and velocity-density empirical relations 22 p4012 A70-43321
- Resonant fixtures utilization attaining high amplitude in shock synthesis testing, discussing test specifications [SAE PAPER 700848] 24 p4322 A70-45886
- SHOCK WAVE INTERACTION**
- Combustion chamber traveling oscillating shock wave as driving mechanism of high amplitude axial mode solid rocket combustion instability 02 p0353 A70-12009
- Hydrodynamic structure of multifront detonation waves produced in gases by primary shock interaction with transverse disturbances 02 p0278 A70-12027
- Combustor geometry and heat release effects on supersonic combustor thrust efficiency, considering shock-free, normal and oblique shock situations 02 p0354 A70-12043
- Atomic and electron densities measurements in shock wave interactions with magnetic fields, using interferometric and spectroscopic method 03 p0529 A70-12876
- Thin elastic cylindrical panel motion induced by plane acoustic shock wave analyzed by integrating nonlinear motion equations using finite difference scheme 03 p0524 A70-13377
- Reaction of three dimensional shock wave with turbulent boundary layer in supersonic flow around plate 03 p0409 A70-13876
- Interface instability between gases due to shock wave increased linearly with time 04 p0673 A70-15245
- Rocket nozzle originated oblique shock waves effect on near-field plume impingement flows, heat transfer and pressure distribution 04 p0737 A70-15421
- Numerical results for perturbed downstream flow field resulting from entropy wave interaction with normal shock and oblique shock generated by wedge flow 05 p0835 A70-16788
- Reflected waves development during shock waves collision and during shock collision with constant temperature wall, using Monte Carlo method 06 p1109 A70-17520
- Far and near field solutions of plane steady transonic flow past thin airfoil including imbedded shock waves using small disturbance theory [ALAA PAPER 70-188] 06 p0969 A70-18056
- Combustion processes and ignition criteria in shock wave ignition of liquid fuel drop in oxidizing atmosphere 06 p1180 A70-18142
- Static pressure, temperature profiles, heat transfer and optical data for turbulent boundary layer-shock interaction with/without injection [ALAA PAPER 70-91] 06 p1042 A70-18210
- Cone bluntness effect on merging onset and downstream flow in merged region at Mach 8 and various Reynolds numbers 06 p0980 A70-18352
- Supersonic oblique shock wave reflection on turbulent boundary layer, considering layer separation and pressure effects 07 p1255 A70-19210
- Hydromagnetic wave interaction with magnetopause and bow shock, considering solar wind turbulence and magnetopause tail stability 07 p1270 A70-20070
- Interaction between bodies and spherical detonation wave, measuring force pulse transfer to immobile cylinder and flow patterns past flying blunt body 09 p1659 A70-22186
- Water vapor high temperature dissociation kinetics in dilute mixtures with argon in shock waves 09 p1629 A70-22319
- Interaction shock shape prediction for gaseous and liquid injection in supersonic flow, using solid body and complementary models 09 p1662 A70-23244
- Laminar boundary layers behavior in shock tube flows behind primary moving shock wave using perturbation method 09 p1662 A70-23281
- Shock deformation of single crystal biotite /lepidomelane/ imbedded in impedance matching NaI, relating kinking intensity to peak pressure and pulse duration 09 p1670 A70-23375
- Shock wave interactions effect on propagation in ducts with gradual or sudden change in cross section, using schlieren spark photography 09 p1664 A70-23735
- Shock wave initiated two dimensional time dependent ducted flows in nonuniform regions using fluid-in-cell method, discussing density, pressure and energy distributions 09 p1665 A70-23740
- Upstream influence distance estimation associated with critical pressure rise in two dimensional shock-boundary layer interactions based on Lighthill subsonic inner boundary layer concept 10 p1862 A70-23840
- Initial blast wave axisymmetric shock-on-shock interaction for blunt bodies moving supersonically at zero angle of attack solved in Taylor series 10 p1797 A70-23954
- Gas stream velocity field produced by shock wave impinging against wing moving at supersonic speed 10 p1799 A70-24124
- Plane shock wave interaction with supersonic blunt body, considering pressure-time studies for stagnation point of flow 10 p1801 A70-24145
- Strong shock wave reflection from rigid wall at high shock velocities, studying effect on flow structure 10 p1922 A70-24152
- Oblique blast wave interaction with small bend along plane wall analyzed for diffraction using conformal transformation and complex variable techniques 10 p1869 A70-24524
- Solar cosmic rays interaction with interplanetary shock waves, discussing chromospheric eruptions 13 p2476 A70-28959
- Inert gas ionization behind shock wave at high Mach numbers, using electrical conductivity and continuum emission measurements 13 p2388 A70-29380
- Shock wave interaction with burning liquid fuel droplets in gaseous oxygen atmosphere, observing wave amplification due to mass combustion rate increase 13 p2522 A70-29424
- Solar wind interaction with earth, moon, planets and comets, using hypersonic fluid analog involving shock wave interactions 14 p2631 A70-30360
- Shock and simple wave interactions, using quasi-linear equations for forward facing wave overtaking forward facing shock 14 p2567 A70-31283
- Collisionless shocks structure in turbulent wave-particle interactions, obtaining ion distribution function 16 p2959 A70-33970
- Hypersonic cruise vehicles viscous interactions areas, examining compression corners, shock interactions, laminar and turbulent flow, boundary layer separation, etc [ALAA PAPER 70-781] 17 p3007 A70-34475
- Cloud droplet agglomeration by weak shock waves, discussing growth mechanism 17 p3067 A70-34549
- German monograph on shock wave diffraction at spheres and cylinders 17 p3071 A70-35377
- Fast response transducer for measuring transient pressures due to shock interaction 17 p3093 A70-35484
- Cumulative jets during shock induced collapse of air cavities in thin fluid layers, using high speed motion picture photography 17 p3074 A70-35742
- Shock wave diffraction by moving thin wing over flat terrains, discussing aircraft blast encounter 18 p3205 A70-36195
- Conical shock wave-turbulent boundary layer interaction data obtained for adiabatic wall conditions at supersonic free stream Mach numbers, including suction effects 18 p3241 A70-36448
- Shock wave attenuation and reflection effects on turbulent hypersonic wakes in ballistic ranges 18 p3237 A70-36708
- Thermal decomposition of nitrogen tetroxide and nitrogen dioxide induced by shock waves, examining temperature effects 19 p3373 A70-38265

- Pressure field behind plane shock wave interacting with curved boundary
19 p3406 A70-38447
- Supersonic boundary layer interaction with shock wave produced by wedge slope
20 p3557 A70-39139
- Flow rate, momentum and energy perturbations during gas motions through shock wave, discussing acoustic waves impinging from supersonic region
20 p3612 A70-39815
- Manganin in wire and thin foil geometries, measuring shock piezoresistance coefficient as function of deformation
20 p3687 A70-40166
- Large scale flare associated solar wind disturbances observed by Vela satellites, noting prolonged elevated flow speed after shock
21 p3881 A70-41080
- Loads induced by terminal shock boundary layer interaction on cone-cylinder bodies, discussing angle of attack effect
21 p3746 A70-41863
- Pressure field behind shock wave after interaction with nonuniform density region, describing shock front shape
21 p3810 A70-41964
- Elastic cylindrical shell transient response to plane acoustic shock wave traveling through light fluid medium
22 p4114 A70-42647
- Heat transfer from turbulent boundary layer interacting with shock and expansion waves in supersonic flow
23 p4134 A70-44573

SHOCK WAVE LUMINESCENCE

- Strong radiating shock wave structure and reflection at rigid wall, investigating flow velocity, density and temperature changes
05 p0956 A70-15788
- Transparent gas radiation behind strong shock wave front with small pressure gradient due to energy losses
08 p1486 A70-21986
- Radiant shock layer in hypersonic air flow past blunt bodies, showing effects on temperature field and density
12 p2159 A70-28245
- Ionization relaxation behind reflected luminous shock front in argon plasma flow interaction with magnetic fields, using spectroscopic and streak interferometric observations
19 p3479 A70-37814

SHOCK WAVE PROFILES

- Chapman-Enskog expansion for Boltzmann equation solution, using PLK method to obtain higher approximations for shock wave structure
01 p0063 A70-10923
- Moving gas with thermodynamic relaxation process, discussing bulk viscosity and application to shock structure calculations
01 p0063 A70-10927
- Topological properties of plane flow in subsonic region behind smooth shock wave in uniform supersonic flow, discussing shock wave convexity
01 p0068 A70-11580
- Shock wave structure determination in simple monatomic gas, using statistical counting and successive approximation algorithm
01 p0068 A70-11601
- Shock wave shapes in hypersonic flow past blunt conical nosed circular cylinders, using analogy with Savic perturbed hypersonic blast wave theory
02 p0277 A70-11862
- Shock wave shapes over axisymmetric power law bodies in hypersonic flow, noting asymptotic flow theory implications
03 p0406 A70-12946
- Ionization and electron temperature dependence on shock wave structure in partially ionized hydrogen plasma allowing for luminescent energy losses
03 p0465 A70-13060
- Shock wave structure in quasi-neutral weakly ionized plasma using Mott-Smith functions
03 p0535 A70-14362
- Sound wave propagation in liquid containing gas bubbles allowing for relative motion of bubbles and liquid, deriving steady shock wave structure
04 p0671 A70-14991
- Shock wave width and temperature expressions for argon-helium mixture
04 p0672 A70-15223
- Rocket exhaust plume size determined from schlieren photographs during wind tunnel tests, noting agreement with Hill-Habert theory
04 p0736 A70-15417
- Strong radiating shock wave structure and reflection at rigid wall, investigating flow velocity, density and temperature changes
05 p0956 A70-15788
- Gas dynamics theory with nonequilibrium radiative and collisional ionization applied to strong normal shock wave structure
05 p0831 A70-15870
- Second order wave structure theory for shock wave system from body in supersonic flight analyzed for planar flows
05 p0790 A70-16797

- Weak shock thicknesses with turbulent scattering as dissipative mechanism compared with magnitude in sonic boom flight tests and explosions
[AIAA PAPER 70-54] 06 p1042 A70-18190
- Molecular beam continuum model to determine structure of shock waves in diatomic gases, comparing calculated profiles with measurements in nitrogen
06 p1050 A70-18338
- Kinetic theory study of shock wave structure in rotationally relaxing diatomic gases
06 p1050 A70-18339
- Kinetic model equation for shock structures in rotationally relaxing gas with internal degrees of freedom
06 p1050 A70-18340
- Normal hypersonic shock wave structure in diatomic gas, measuring density by electron beam fluorescence technique
06 p1050 A70-18341
- Normal shock wave structure in binary gas mixtures of chemically inert monatomic molecules, using kinetic theory moment method
06 p1051 A70-18343
- Shock structure in binary gas mixture, discussing governing equations and Chapman-Enskog procedure
06 p1051 A70-18344
- Least squares method to determine shock thickness at arbitrary Mach number from Boltzmann equation for rigid sphere rarefied gas
06 p1051 A70-18345
- Shock wave structure in He-Ar mixture velocity and temperature profiles based on kinetic model equations
06 p1051 A70-18346
- Surface pressures and shock wave shapes on sharp flat plates and wedges in rarefied hypersonic transition flow with emphasis on merged layer regime
06 p0982 A70-18362
- Shock wave profiles in rarefied gas expansion flows, using static and impact pressure probes
06 p1052 A70-18386
- Uniform supersonic flow with receding shock wave past smooth profile
07 p1187 A70-18674
- Liquid rocket motors with concentrated combustion, studying nonlinear longitudinal instabilities with shock waves in combustion chambers
07 p1362 A70-18917
- One dimensional steady neutral shock wave structure, using expanding Boltzmann equation distribution function in terms of Hermite polynomials
07 p1260 A70-19984
- Hydromagnetic ionizing shock wave structure in electromagnetic fields, using model composed of strong adiabatic shock to translational equilibrium followed by ionization initiation
07 p1351 A70-19985
- Shock wave structure in binary mixture of monoatomic gases based on integral kinetic equations, using iteration process
08 p1483 A70-21086
- Hypersonic spherical gas expansion into finite pressure region with transition from supersonic to subsonic flow in shock wave, discussing structure and pressure effects
09 p1658 A70-22116
- Shock wavefront configurations before inclined obstacles in supersonic flow, studying inclination angle role
09 p1604 A70-22443
- Shock wave configurations across compression cascades in transonic approach flow
09 p1604 A70-22657
- Shock wave structure nonequilibrium kinetic model using Boltzmann and Navier-Stokes equations
09 p1662 A70-23306
- Plane, cylindrical and spherical blast waves structure with ionization at local thermodynamic equilibrium analyzed using successive approximation to non-similar solution
10 p1967 A70-23991
- Reflected shock wave structure and velocity at rigid wall, assuming radiative heat transfer as dissipative process
10 p1967 A70-24018
- Bidimensional curved weak shock wave structure, deducing transonic equation from Navier-Stokes equations
10 p1800 A70-24138
- Vibrational and dissociation relaxation effects on plane shock wave structure and supersonic flow around blunt bodies
10 p1801 A70-24150
- Quasi-transverse constant profile wave in finite elasticity with isothermal shock at discontinuity compared to Whitham breakdown
10 p1956 A70-24191
- Plane exponential reactive shock waves following piston impact on gamma-law gas solved by similarity method, including Whitham conditions and shock acceleration
10 p1967 A70-24194
- Expanding arch structure of type 2 solar radio burst observed with Culgoora radioheliograph
11 p2105 A70-25749

- High purity beryllium dynamic tests determining Hugoniot equation of state, shock profile and spall threshold/onset of microcracking/ for elastic pulses
[AIAA PAPER 69-360] 11 p2066 A70-25964
- Thermal shock waves structure and effective temperature in stellar atmospheres taking into account absorption effects and possible isothermicity
12 p2306 A70-27861
- Shock patterns for simple caret wings generating specific flow patterns
13 p2509 A70-28542
- Satellite plasma diagnostics for electric and magnetic fields and fine structure of collisionless shocks in solar wind plasma flows and interplanetary shocks
13 p2481 A70-30069
- Radiating gas flow about pointed bodies, investigating shock curvature at wedge or cone tip and straight shock waves flow field downstream
14 p2663 A70-30267
- Strong shock waves profiles in monatomic perfect gases by Monte Carlo simulation, obtaining maximum density slope thicknesses
14 p2567 A70-31031
- Uniform supersonic flow with receding shock wave past smooth profile
15 p2671 A70-31466
- Periodic shock waves amplitudes and profiles, investigating longitudinal nonlinear oscillations of gas excited in closed tube
15 p2719 A70-31482
- Shock waves structure in radiating gases at high temperatures, taking into account radiation anisotropy in shock front
15 p2720 A70-31645
- Collisionless shock waves in magnetized plasma as function of Alfvén-Mach number, measuring electron temperature jump on wave front spectroscopically
15 p2779 A70-32116
- Transonic compression grid functions, considering shock wave configurations
16 p2836 A70-33752
- Hypersonic internal flow investigation by differential equation numerical integration, determining shock shape and surface pressure
16 p2838 A70-33881
- Mach disk structure in free low density expanding supersonic jet from static pressure probe measurements
17 p3068 A70-34696
- Shock wave and viscous layer structures ahead of blunt body in rarefied hypersonic flow, using continuum theory
17 p3009 A70-34698
- Hydromagnetic shock waves structure, investigating resistive, viscous and thermal conduction dissipation effects on discontinuities
17 p3140 A70-34928
- Normal shock structure in thermally perfect gas, using perturbation methods
17 p3070 A70-35244
- Multiplying factors role in iterative solution of shock wave structures with large radiation-convection ratios
17 p3075 A70-35888
- Electrostatic turbulence in bow shock magnetic structures observed by OGO 5, explaining turbulence as ion acoustic or Buneman mode due to two stream instability
18 p3311 A70-36006
- Pressure distribution shock pattern and impact wave resistance in frictionless plane parallel and source shaped supersonic flow
18 p3207 A70-36385
- Viscoplastic solids, computing plane shock wave propagation structure from nonlinear constitutive relations
18 p3338 A70-36435
- Explosive phase of solar flares in nonuniform atmosphere, determining explosion energy and shock wave front shape for various times
20 p3699 A70-39463
- Entropy layer in hypersonic flows, determining body configuration from shock wave shape described by coordinates power function
21 p3743 A70-40610
- Hypersonic flat and biconvex conical wings, calculating yaw effects on shock shape and pressure distribution
21 p3761 A70-40918
- Collisionless shock wave geometry, determining dispersion relation for ion acoustic waves propagating in plasma
21 p3856 A70-41082
- Shock waves and solitons structure propagating oblique to magnetic field in warm plasma based on two-fluid equations
21 p3857 A70-41382
- Dual satellite magnetic field and plasma measurements of earth bow thick pulsation shock by Vela 3A and Explorer 33
22 p4013 A70-42470
- Time dependent shock wave structure, considering shock tube flow as initial and boundary value problem
22 p4009 A70-42516

- Large scale magnetic field and spiral shock pattern of Galaxy, using density-wave theory 22 p4103 A70-42981
- Numerical model of light diffraction on plane shock waves at optical phase jump region for shadow and schlieren techniques [SMPT PREPRINT 97] 22 p4035 A70-43058
- Cylindrical converging shock waves generation, propagation and structure at high pressures 22 p4012 A70-43431
- Relaxation gas dynamics, discussing vorticity and drag generation by relaxation, linearized theory and shock waves structure 23 p4178 A70-43889
- Two dimensional steady flow around slender profiles at free transonic stream with curved compression shocks, approximating by hodographic method 23 p4131 A70-44023
- Collisionless plasma shock wave structures from geophysical and astrophysical phenomena standpoint, describing tarantula experiment 23 p4225 A70-44184
- Heat transfer and shock wave shapes about blunt slender cones in viscous-inviscid coupling hypersonic flow 23 p4134 A70-44569
- Shock curvature at wedge or cone tip in radiating gas flow, noting differences between radiative and chemically coupled gas dynamics 23 p4135 A70-44638
- Rocket engine nozzle with wall-mounted obstacle, examining shock front shape, pressure distribution and side force characteristics 23 p4234 A70-44684
- Upstream gas photoionization caused precursor ionization effects on MHD switch-on shock structure 24 p4382 A70-45106
- Normal shock waves structured by nonequilibrium radiative and electron-atom collisional ionization, using generalized radiation model 24 p4324 A70-45290
- Shock wave structure calculation in liquids containing gas bubbles, taking into account compression wave steepening by convection 24 p4326 A70-45783
- ## SHOCK WAVE PROPAGATION
- Multiple pulsations mechanism during detonation spherical wavefront propagation in channels with various cross sections, noting volume effect 01 p0060 A70-10135
- Shock wave structure in two phase media with temperature and velocity gradients and possible phase transitions 01 p0060 A70-10147
- Reflection and transmission characteristics of screens in duct obstructing shock propagating in unsteady compressible fluid, describing theoretical models and experimental detection 01 p0060 A70-10224
- Steady one dimensional flow in gas filled cylindrical tube, studying shock induced compression wave generated by sudden piston acceleration 01 p0062 A70-10804
- Pressure oscillograms and schlieren photographs of shock wave amplification during interaction of cellular flame of gas mixtures in cylindrical combustion chamber 01 p0217 A70-11014
- Calorimetric measurement of electron temperature in collisionless shock wave propagating in plasma column, discussing role of H beta line Stark broadening 01 p0153 A70-11589
- Arc phenomena for producing interaction effects, discussing reflected shocks rarefaction waves and gas dynamics 02 p0345 A70-11863
- Radiation effects on postshock gas state, noting shock wave optical thinness dependence on radiative cooling and photon flight time 02 p0277 A70-11867
- Axial mode shock wave oscillations in end-burning solid rocket motor, obtaining periodic solutions for flow properties, solid temperature and burning rate 02 p0353 A70-12010
- Interstellar media under action of supernova or nova, solving Navier-Stokes equations of hydrogen plasma for motion during shock wave formation 03 p0564 A70-13221
- Acoustic and shock waves propagation in multicomponent media, assuming uniform speed for components and complex density dependence of media on pressure 03 p0465 A70-13329
- Ionizing shock wave propagation into magnetic field from Ar gas flow characteristics in electromagnetic shock tube 03 p0532 A70-13548
- Nonequilibrium zone radiation intensity profiles behind strong shock waves in air determined for specific wavelengths and shock velocities 03 p0535 A70-14364
- Reflected shock wave velocity, boundary layer disturbance and wall ionization measurements using thin film resistance thermometers 04 p0666 A70-14537
- Flow viscosity and heat conduction effects on shock wave propagation in bent channel with weak Mach reflection 04 p0671 A70-15013
- Solar flare duration effect on propagation and modification of forward-reverse shock pair between sun and 1 AU, using equations of motion for spherically symmetric flow 04 p0740 A70-15104
- Precursor electron densities measured in nitrogen and air ahead of shock waves, noting shock tube wall reflectivity 04 p0694 A70-15565
- Sonic boom propagation in still atmosphere with vertical temperature gradient, using graphical method of determining rays for aircraft motion 05 p0791 A70-15786
- Sonic boom research, considering exposure pattern development, propagation in inhomogeneous atmosphere and effects on structural responses 05 p0796 A70-16795
- Doppler shift of laser beam reflected from shock wave measuring velocity through optical mixing 05 p0852 A70-16993
- Self similar flow patterns arising during cylindrical shock and detonation waves propagation in gas at rest, considering MGD shock waves 06 p1119 A70-17516
- Kinetic relaxation and Boltzmann equations for studying shock waves propagating in gas composed of rigid ideally elastic spherical molecules without internal degrees of freedom 06 p1036 A70-17756
- Radioheliograph observations at 80 MHz of directive shock wave propagation in solar corona 06 p1144 A70-18007
- Free electron formation ahead of strong shock waves traveling into nitrogen-oxygen mixtures in shock tube, observing electron densities [AIAA PAPER 70-83] 06 p1065 A70-18029
- Pressure-time history in spherical shock waves flow field at low ambient pressures recorded with piezoelectric transducers, showing shock strength decrease 06 p1052 A70-18385
- Single or repetitive shock pulses produced on electrodynamic and hydraulic shakers for shock testing on vibration machines 06 p1030 A70-18438
- Pressure history at end wall of electromagnetic shock tube measured during shock wave reflection by piezoceramic gage 06 p1031 A70-18505
- Sonic booms propagation in nonhomogeneous atmosphere, outlining effects on intensity and range for transport and military fighter aircraft 07 p1190 A70-18779
- Strong explosion model for analyzing shock wave propagation after chromospheric flare allowing for quasi-radial motion of unperturbed solar wind 07 p1367 A70-19489
- Gaseous detonation transverse wave propagation and measurement from smoked foil records 07 p1424 A70-20006
- Interstellar media under action of supernova or nova, solving Navier-Stokes equations of hydrogen plasma for motion during shock wave formation 08 p1580 A70-21654
- Two temperature gasdynamics for binary gas mixtures of differing molecular weight components, analyzing ultrasound and shock wave propagation 08 p1486 A70-21808
- Accelerating shock wave fronts by detonating passive trotyl and hexogen using high speed photography 09 p1658 A70-22103
- Plane shock wave stability propagating in external magnetic field determined by temperature dependence of medium electrical conductivity 09 p1658 A70-22168
- Laser heating of plasma, motion pattern and shock wave parameters during absorption burst in solid body vapor, using numerical analysis 09 p1695 A70-22181
- Book on sonic boom effects covering shock waves generation and propagation, elastic structures response to dynamic loads, structural damage, etc 09 p1695 A70-22203
- Shock wave interactions effect on propagation in ducts with gradual or sudden change in cross section, using schlieren spark photography 09 p1664 A70-23735
- Progressive shock waves propagation, reflection and transmission through sudden changes in pipe cross sectional area, obtaining boundary conditions for quasi-steady junction flow 09 p1664 A70-23738
- Longitudinal shock wave oblique reflection in nonlinear harmonic elastic material in terms of wave propagation 10 p1956 A70-24097
- Shock wave and gas flow structure at constant Mach number past three dimensional blunt bodies, applying method for unsteady flow 10 p1799 A70-24127
- Super sonic booms occurrence and propagation, discussing aircraft operating conditions for prevention of effect on ground 10 p1805 A70-24130
- Symmetrical, asymmetrical and three dimensional sonic flows past finite obstacle, investigating regions upstream and downstream from shock waves for airflow 10 p1800 A70-24134
- Velocity and temperature distribution behind shock waves in hydrogen plasma measured to determine factors responsible for discrepancies in Rankine-Hugoniot conditions 10 p1867 A70-24149
- Shock propagation from point explosion energy source into cold exponential atmosphere with radiative heat transfer in rear of shock front 10 p1869 A70-24525
- High intensity shock wave propagation and generation of high enthalpy hypersonic flow studied to determine IMF-2 hypersonic shock tube performance limit 10 p1871 A70-24795
- Electric field structure at shock wave front propagating in weakly ionized gas under Ramsauer effect 10 p1871 A70-25121
- Cylindrical shock wave two dimensional propagation in conducting plasma in magnetic field, assuming isentropic flow along streamline 11 p2091 A70-26174
- Shock wave reflection into ideal gas flow with linear density variation analyzed for flow field 12 p2211 A70-27832
- Interplanetary shock waves layer formation in collisionless medium, using bulk transport parameters for dissipation requirement 12 p2308 A70-27885
- Shock wave formation and propagation analyzed by hydrodynamic model of two directional traffic flow based on continuity equations and velocity-density empirical relations 12 p2212 A70-28196
- Piston formed weak steady shock wave propagation in relaxing gases, investigating via characteristics method [DFVLR-SONDDR-38] 12 p2212 A70-28206
- Plane acoustic shock wave vertical propagation in gravity-stratified atmosphere with temperature gradient, using homogeneous perturbation velocity [DFVLR-SONDDR-35] 12 p2212 A70-28209
- Heat transfer and flow stabilization dependence on initial shock wave reflection from conducting wall 12 p2213 A70-28228
- Plane electrostatic shock waves propagation in plasma with electrons in potential equilibrium and collision free ions 13 p2461 A70-28730
- Shock wave multiple ionization in hydrogen with impurities, discussing intensity and duration effects on electron temperature profile and ion concentrations 13 p2388 A70-29369
- Adiabatic index effect on shock waves reflection, emphasizing critical angle dependence on incident wave intensity 13 p2388 A70-29416
- Initial pressure and pressure ratio effects on shock wave velocity evolution in shock tube 13 p2389 A70-29630
- Interplanetary shock wave properties in solar wind, determining propagation velocity, transit times proton density, proton and electron temperatures 13 p2481 A70-30066
- Acoustic and shock waves propagation in multicomponent media, assuming uniform speed for components and complex density dependence of media on pressure 14 p2566 A70-30709
- Self similar one dimensional flow behind plane shock propagating in exponentially decreasing atmosphere, considering radiation mean free paths and radiative heat transfer 14 p2567 A70-31032
- Critical Mach numbers for transverse resistive shock waves as function of fluid/magnetic pressure ratio compared with cold plasma theory 14 p2623 A70-31036
- Monograph on nozzle design effect on starting process initiated by plane shock wave in reflected shock tunnel 15 p2672 A70-31692
- Unloading shock waves propagation in elastoplastic medium, investigating strain hardening effect on shock strength decay, residual strains and radial stresses 15 p2815 A70-32002
- Shock wave propagation during moving pulsed plasma interaction with stationary gas discharge plasma 15 p2780 A70-32197

- Strong explosion model for analyzing shock wave propagation after chromospheric flare allowing for quasi-radial motion of unperturbed solar wind
15 p2795 A70-32734
- Hypervelocity impact generated shock propagation based on governing differential equations, using fluid mechanical model for perfect gas and real fluid
15 p2824 A70-32788
- Equation of state of solids measured by shock wave techniques, considering elastic-plastic flow in plane wave geometry
15 p2824 A70-32789
- Shock wave front propagation instability in decreasing density medium, applying to stellar structure
16 p2890 A70-33200
- Shock wave propagation through giant star atmosphere, using approximate analytical method
16 p2980 A70-34305
- Shock propagation in Al fiber-polyethyl methacrylate composite, calculating pressure, densities, internal energies and particle velocities
17 p3182 A70-34556
- Shock wave response of metals and nonmetals under high strain rates
17 p3188 A70-35223
- Film condensation rates of vaporized substance in shock tube during passage of shock wave, formulating quasi-one dimensional problem
18 p3239 A70-36244
- Viscoplastic solids, computing plane shock wave propagation structure from nonlinear constitutive relations
18 p3338 A70-36435
- Solar wind discontinuity during solar flare from Heos A measurements, observing shock wave propagation
19 p3495 A70-37502
- Thermal radiation effect on plane shock wave propagation, using perturbation technique and method of characteristics
19 p3551 A70-37532
- Thermodynamics and velocity of MHD shock waves in perfect conducting fluid, using compressibility conditions and relativistic Hugoniot equation
19 p3477 A70-37580
- Intersecting shock waves propagation, deriving equations for aircraft sonic boom intensity
19 p3355 A70-38484
- Shock wave radiation from supersonic ducted rotor, determining sound power at blade passing harmonic frequency
19 p3353 A70-38614
- Shock wave nonlinear refraction by upstream disturbances in two dimensional steady nonuniform flow
20 p3608 A70-39354
- Metallurgical changes induced by planar shock wave propagation through metals and alloys, describing shock-hardened metals macro and substructure
20 p3652 A70-40142
- Electric field structure at shock wave front propagating in weakly ionized gas under Ramsauer effect
20 p3685 A70-40514
- High speed shock wave propagation in deuterium gas, observing neutron production
21 p3806 A70-40744
- Spherical shock from point explosion in medium with varying density, obtaining exact similarity solution for propagation
21 p3808 A70-41448
- Gas phase ignition theory with feedback of homogeneous propellant exposed to stagnant gas after shock reflection
21 p3950 A70-41728
[AIAA PAPER 69-559]
- Shock waves formation and dynamic characteristics in transition region response to infalling material from solar flares
21 p3883 A70-42193
- Collisionless plasma shock wave instability, discussing resonance and energy dissipation through ion Landau damping
22 p4077 A70-42292
- Reverse hydromagnetic shock in solar wind as discontinuity of plasma density, proton temperature and magnetic field density, using spacecraft data
22 p4093 A70-42474
- Analytic shock front velocity as function of initial parameters in continuous inhomogeneous medium, verifying propagation through rarefaction wave
22 p4010 A70-42687
- Compressive and rarefaction shock wave propagation in polymethyl methacrylate, fused silica and sapphire, using laser interferometer measurements
22 p4031 A70-43020
- Shock wave propagation studies by grating spectrograph with high speed camera, computing equilibrium detonation gases temperature from emitted light
22 p4035 A70-43057
[SMPT PREPRINT 98]
- Starting shock and contact surface measurement reflection nozzle, using HF spark camera and interference techniques
22 p3959 A70-43064
[SMPT PREPRINT 89]
- Shock response of passive nonlinear elastic isolators under pulse excitation with viscous damping
22 p4117 A70-43249
- Shock wave formation and propagation analyzed by hydrodynamic model of two directional traffic flow based on continuity equations and velocity-density empirical relations
22 p4012 A70-43321
- Cylindrical converging shock waves generation, propagation and structure at high pressures
22 p4012 A70-43431
- Strong shocks propagation in atmosphere of variable density at rest, obtaining numerical solution of similarity flow behind shocks
23 p4182 A70-44599
- Shock wave electrical precursor measurements in weakly ionized gas, describing approximate electrostatic probe theory and high sensitivity gages
23 p4184 A70-44995
- Coronal shock growth as source of thermal solar X ray bursts associated with optical events
24 p4401 A70-45320
- ### SHOCK WAVES
- #### NT DETONATION WAVES
- #### NT MACH CONES
- #### NT NORMAL SHOCK WAVES
- #### NT OBLIQUE SHOCK WAVES
- #### NT RIEMANN WAVES
- #### NT SONIC BOOMS
- Nondestructive testing and fatigue life analysis of cyclically loaded mechanism, determining dynamic responses to velocity shocks by computer techniques
01 p0053 A70-10010
- Release adiabats and recentered Hugoniot curves determination by shock reverberation techniques for compressible nonlinear materials, presenting results for epoxy resin and porous tuff
01 p0198 A70-10106
- Stable geomagnetic pulsations related to plasma density shock position in magnetosphere and to magnitude of diurnal variations
01 p0082 A70-11508
- Weak shock waves relaxation time and amplitude and acoustic velocity as functions of thermorelaxing media
01 p0068 A70-11588
- Electrical conductivity of air behind incident and reflected shock wave fronts as function of temperature and Mach numbers measured by electrode method
01 p0095 A70-11622
- Carbon dioxide temperature distribution, absorption and concentration as functions of molecular dissociation behind shock wave determined by measuring IR bands intensity
01 p0069 A70-11623
- Oxygen molecules dissociation by molecular and atomic collisions in shock tube from measuring molecular O concentration behind shock wave front
01 p0149 A70-11632
- Two armed spiral galactic shock waves as triggering mechanism for gravitational collapse leading to star formation, considering gaseous disk motion using Schmidt model
02 p0363 A70-11781
- Shock and detonation waves stability in arbitrary media, noting overdriven and underdriven waves
02 p0397 A70-12023
- Blast wave model for galaxy M82 explosion using Sedov self similar solutions, indicating line excitation mechanism origin in shock wave heating and compression
02 p0372 A70-12247
- Explosion analogy to study hypersonic flow region behind shock wave including boundary layer at blunt body surface
03 p0406 A70-13332
- Shock wave diffraction at wedge moving at supersonic velocity, solving Hilbert space formulated for constant parameter flow
03 p0406 A70-13333
- Atomic oxygen reaction with carbon dioxide and carbon dioxide dissociation in shock waves, using nitrous oxide decomposition for oxygen source
03 p0440 A70-13578
- Two dimensional and axisymmetric bodies shapes providing minimum wave drag to supersonic flow of perfect gas, considering bodies around which flow causes bound shock waves
03 p0409 A70-13863
- Supersonic unsteady state three dimensional flow around blunted bodies with detached shock wave
03 p0409 A70-13864
- Supersonic unsteady gas flow around bodies at low Strouhal numbers, noting angle of attack amplitude and leading edge shock wave
03 p0409 A70-13865
- Shock wave research in plasma physics, discussing classical gas dynamic shock wave theory, detonation waves, collisional shocks, relativistic velocity shock waves, etc
03 p0533 A70-14017
- Hydromagnetic normal ionizing shock wave properties in H and D mixtures and pure gases in SUPPER 2 shock wave tube
03 p0536 A70-14365
- Hypersonic flow over blunt bodies, discussing Mach number, specific heat and blast wave limits
04 p0613 A70-14454
- Plane shock wave diffraction and reflection at slender wedge in linear approximation, proposing pressure distribution calculation formulas behind shock
04 p0665 A70-14493
- Discharges in Ar flow in membrane shock tube at Mach 5, discussing plasma compression, shock wave position and effect on electrode region
04 p0725 A70-14534
- Plasma unsteady one dimensional flow behind shock wave front in shock tube MGD channel, deriving differential gas dynamics equations
04 p0726 A70-14540
- Structural strength under impact loading with allowance for shock waves, comparing various strength calculation methods
04 p0774 A70-15098
- Supersonic jet flow from diverging nozzle into space with given pressure or into supersonic slipstream, noting barrel shock formation inside jet
04 p0617 A70-15235
- Electron beam technique to measure density profiles of strong shock waves in argon
04 p0692 A70-15325
- Ideal equivalent gas method for studying thermodynamic properties in supersonic gas flows behind shock wave
05 p0831 A70-15872
- Plasma behind pressure front of shock wave investigated for ionization mechanism by microwave reflection and transmission, noting electron temperature distribution
05 p0887 A70-16110
- Small amplitude waves and collisionless shock waves within first order Chew-Goldberger-Low equations framework, presenting modes for propagation along applied magnetic field
05 p0889 A70-16534
- Earth bow shock and magnetopause oscillatory motions with respect to positions assumed under quiet solar wind conditions, discussing satellite observations
05 p0840 A70-16586
- MHD equations including energy dissipation terms applied to irreversible processes occurring in fast hydromagnetic shock waves in solar chromosphere
06 p1143 A70-17999
- Inviscid transonic approximation theory, calculating mixed flow field around nonlifting slender ogive body, accounting for shock wave generation, strength and location
06 p0972 A70-18132
[AIAA PAPER 70-189]
- Monte Carlo method applied to solving nonlinear Boltzmann equation for plane shock waves in elastic sparse gases
06 p1050 A70-18335
- Moment methods for calculating modeled diffusion gas mixture shock waves using Monte Carlo method, discussing distribution function and flow pattern
06 p1050 A70-18336
- Solar flare induced interplanetary shock and helium enriched driver gas observed on 13 February 1967, discussing wind velocity and plasma acceleration
06 p1152 A70-18526
- Nonequilibrium processes behind shock wave in shock tube supersonic air and nitrogen flow, using photoelectrical shadow method
06 p1053 A70-18562
- Plane elastic-relaxing plastic shock wave yielding of Fe numerically integrated by two step stable difference scheme without pseudoviscosity
06 p1172 A70-18618
- Soviet monograph on theory and calculations of impact systems covering solid body collisions, elasticity, wave mechanics and nonflat rod applications
07 p1400 A70-18732
- Three dimensional hypersonic flow past body solved assuming developable surface head shock wave
07 p1187 A70-18767
- Unipolar induction to calculate moon interior electric field profiles, noting magnetic back pressure as limb shock wave and interaction with solar wind
07 p1377 A70-18970
- Shock wave amplitude found strongest influence in explosives initiation to detonation by shock
07 p1359 A70-19675
- Two dimensional flow field behind shock wave resulting from boundary layer growth in driven gas of shock tube
07 p1260 A70-19983
- Skimmer interaction influences on nozzle beam production explaining intensity maxima, proposing model assuming normal shock across skimmer mouth
07 p1341 A70-20103
- Solid surface roughness influence on reflection of thermal energy molecular jets, showing shock determined by incidence angle
07 p1343 A70-20121

- Anodic precursors of convergent cylindrical shock wave of z-pinch discharges in He and Ar
07 p1261 A70-20357
- Turbulence in quiescent prominences relationship to shock waves in upper atmosphere
08 p1570 A70-20840
- Tungusk meteorite atmospheric shock waves obtained from simulation experiments based on forest damage
08 p1572 A70-20944
- Perfect fluid sonic flows around weakly lifting three dimensional bodies downstream of shock wave, proving existence of lifting boundary layer
08 p1433 A70-21238
- Shock ionized Ar flow properties estimation using alignment charts
08 p1551 A70-21324
- Water vapor dissociation in dilute mixtures with Ar behind shock waves, studying OH concentrations using flash-absorption technique
08 p1548 A70-21355
- Initial deceleration of solar wind positive ions upstream of earth bow shock determined fromOGO 5 high time resolution plasma measurements
08 p1562 A70-21377
- Nonlinear relativistic wave velocity distribution within spherical nucleus bounded by shock wave in superdense gas determined by Cauchy problem
08 p1484 A70-21403
- Supernovae hydrodynamics, discussing early light curves energy requirements and shock wave dynamics in terms of neutrino diffusion
09 p1749 A70-21992
- Supersonic air jet structure in central shock wave region affected by both Mach number and flow rarefaction
09 p1734 A70-22185
- Massive blowing from porous cone with embedded shock wave in supersonic flow, assuming inviscid and conical injected flow field
09 p1662 A70-23216
- Inviscid hypersonic small disturbance theory applied to flow behind concave and convex exponential shock waves, determining supporting two dimensional airfoil surfaces
09 p1605 A70-23220
- Lunar limb weak solar wind shock due to conducting crust-interplanetary magnetic field interaction
09 p1764 A70-23485
- Electron and proton temperature differential near earth bow shock determined from plasma probe measurements by Vela 4B satellite
09 p1670 A70-23486
- Charged particles velocity profile across shock determined by induction velometry, considering eddy currents effects on induced potential gradient
09 p1738 A70-23677
- Flow parameters behind shock waves calculated, determining amount of condensate evaporation and error in pressure measurements due to evaporation
09 p1607 A70-23711
- Blast wave eigenvalues in asymptotic expansions approximation for hypersonic flows past blunt bodies
10 p1797 A70-23953
- Two-stream and cross-stream effects on nonlinear wave stability with shock in collisionless plasma
10 p1921 A70-23967
- One dimensional fluid flows with shock waves described by constructing discontinuous solution for gas dynamic equations, using successive approximation
10 p1866 A70-24113
- Shock and thermodynamic phenomena of real gases near critical points, discussing specific volume and specific enthalpy increases
10 p1867 A70-24136
- Radiating shock wave reflection from rigid wall studied for velocity and structural changes, assuming unsteady and one dimensional flow
10 p1867 A70-24140
- Shock pressure and impulse caused by Q switched laser light absorption, considering temperature dependence of EM radiation penetration depth
10 p1900 A70-24422
- Supersonic transports bow and rear shock pressure jump lower bounds for various physical constraints
10 p1805 A70-24558
- Stationary collisionless shock waves in hot initial plasma produced by theta pinch discharge, discussing magnetic field, density and electron temperature profiles
10 p1924 A70-24697
- Head wave distance from body determined for slender pointed profile in subsonic region of transonic flow
10 p1803 A70-24780
- Auroral motions determined by absorption onsets pattern and infrasonic wave morphology
10 p1880 A70-24803
- Laboratory simulation for shock waves around earth, moon and Venus based on artificial solar wind and magnetic dipole interaction study
10 p1948 A70-25182
- Chemical kinetics of carbonyl fluoride thermal decomposition in argon and nitrogen diluent behind shock waves, using IR monitoring method
11 p1995 A70-25824
- Chemical kinetic model for photoexcitation and photoionization of cold argon ahead of strong shock wave, predicting electron and excited atom concentrations
[AIAA PAPER 68-666] 11 p2090 A70-25953
- Laminar boundary layer behind normal shock wave with vaporization and combustion, obtaining profiles on analog computer
11 p2148 A70-25967
- Gas passing through shock wave, investigating constitutive relations for stress and heat flux using Maxwell moment method
11 p2036 A70-26015
- Trans-Alfvénic ionizing shock waves stability in absorption of rotational Alfvén disturbances
11 p2090 A70-26023
- Modified laser Michelson interferometer for probing highly transient plasmas occurring behind incident shock waves in shock tubes
11 p2052 A70-26369
- Plasma density and velocity required for simulating solar wind flow over magnetosphere /bow shock/ in plasma wind tunnel
11 p2032 A70-26372
- Methane oxidation behind reflected shock waves between 1350-1900 K, measuring pressure, chemiluminescence and 3067 Å absorption of OH radical
11 p2150 A70-26380
- Lambda type pseudoshock /shock during supersonic flow deceleration to subsonic in duct/, investigating mechanism by schlieren photography
11 p2037 A70-26408
- Shock waves in unsteady aortic blood flow at systole beginning, considering aorta elastic properties and shock formation distances
11 p1992 A70-26479
- Reaction rate constants in heated mixture of hydrogen, carbon dioxide and Ar behind shock waves measured by IR spectroscopy
12 p2274 A70-26891
- Monograph on acoustic theory for determining frictional pressure drop effect on gas state behind reflected wave in shock tube
12 p2209 A70-27000
- Central shock and target displacement of underexpanded supersonic jets with obstacle at nozzle exit, using Toepler schlieren photographs
12 p2156 A70-27293
- Lunar limb shock wave observed by Explorer 35 satellite defined with respect to solar wind flow direction, discussing formation mechanism
12 p2302 A70-27594
- Vibrational dissociation relaxation effects on chemical reactions, molecular energy and thermal quanta in air flow behind direct shock wave
12 p2213 A70-28232
- Electromagnetic shock tube demonstrations of electrode spark breakdown, strong shock behavior, plasma conductivity and hypersonic shock flow over blunt body
13 p2404 A70-28623
- Correction to Smyrn results for perturbation pressure in interaction field behind plane shock diffracted by supersonically moving thin yawed wedge
13 p2338 A70-28822
- Collisionless electrostatic shock generation conditions, simulating homogeneous counterstreaming plasmas by computer
13 p2462 A70-29110
- Fast time-resolved spectra of earth bow shock electrostatic turbulence based on broadband analog electric data fromOGO-5
13 p2396 A70-29111
- Shock waves in partially ionized gas discharge argon plasma, recording potential jump at wavefront
13 p2388 A70-29419
- Q switched ruby laser pulses nonlinear absorption by partially ionized plasma behind reflected shock wavefront, observing absorptivity dependence on light intensity
13 p2429 A70-29420
- High Mach number viscous flow past cylinder with cylindrical shock wave
13 p2391 A70-29970
- Simultaneous equations for motion location, speed and direction in acoustic tracking of supersonic objects, recording shock wave times of arrival with microphone system
13 p2450 A70-29988
- Electron and positive ion velocity distributions measurements near earth bow shock by electrostatic analyzer on Vela 4B satellite
13 p2481 A70-30068
- Explosion analogy to study hypersonic flow region behind shock wave including boundary layer at blunt body surface
14 p2528 A70-30711
- Shock wave diffraction at wedge moving at supersonic velocity, solving Hilbert space formulated for constant parameter flow
14 p2528 A70-30712
- Turbulent mixing at contact surface in driven shock wave in shock tube with bursting diaphragm for He-Ar test gas mixtures
14 p2566 A70-31030
- Solar wind interaction with planetary ionosphere, considering flow behavior across bow MHD shock
14 p2647 A70-31073
- Internal shock waves in axisymmetric flowfield of perfect gas past blunt cone, noting roles of Mach number and cone half angle
15 p2672 A70-31592
- Type 2 and 4 solar radio emission, showing bursts exciting by common shock wave ejected from flare region
15 p2794 A70-32620
- Tungusk meteorite atmospheric shock waves obtained from simulation experiments based on forest damage
15 p2806 A70-32756
- Ions energy spectra in plasma heated by shock wave, using passive corpuscular diagnostic technique
15 p2781 A70-32821
- Collisionless shock waves model in solar wind plasma, discussing instability and energy dissipation
15 p2795 A70-32825
- Hemisphere model flow field investigations in low density plasma wind tunnel, considering flow regimes of transition and shock formation
15 p2673 A70-32838
- High temperature combustion wind tunnels for investigating gas and liquid fuel combustion stabilized by shock waves in supersonic flow
16 p2996 A70-32991
- Shock wave stability in plane steady flow at uniform entropy and limiting velocity
16 p2890 A70-33101
- Monograph on steady shock waves in one dimensional frictionless gas flows with thermodynamic relaxation, using continuum mechanics
16 p2891 A70-33294
- Axisymmetric detached shock preceding blunt body immersed in hypersonic monatomic gas flow, considering radiative ionization in cold precursor by differential approximation
16 p2839 A70-34252
- Flowfields behind reflected shock waves, predicting end-wall radiative heat transfer and radiative gas dynamic coupling effects
17 p3065 A70-34480
- Time dependent characteristics of dense argon plasma formed by pulsed lasers, measuring shock wave front velocity with streak camera
17 p3104 A70-35083
- Automatic shock spectrum synthesizer/analyzer for shock testing of field environments
17 p3059 A70-35175
- Shock waves in supersonic conical nozzle flow due to secondary gas injection, using conical lens for flow visualization
17 p3011 A70-35236
- Solar atmosphere shock waves frequency and strength, computing radiative energy losses of chromospheric models
17 p3174 A70-35865
- Electrostatic turbulence in bow shock magnetic structures observed byOGO 5, explaining turbulence as ion acoustic or Buneman mode due to two stream instability
18 p3311 A70-36006
- Shadow photography applied to Mach reflections in argon, carbon dioxide and Freon 12 in shock tube, using Huygens principle for transfer mechanism
18 p3205 A70-36148
- Thermal dissociation mechanism of diatomic molecules in inert diluent behind shock wave, assuming distribution function described by Fokker-Planck equation
18 p3292 A70-36242
- Radiative energy loss and wall sublimation effects on gas flow parameters behind reflected strong plane shock wave, taking into account small disturbances
18 p3348 A70-36673
- Disk shaped galaxy stationary spiral shock pattern, examining gas cloud gravitational collapse for star formation
18 p3331 A70-37198
- Plasma properties across bow shock and in magnetosheath as function of supersonic solar wind
19 p3494 A70-37481
- Solar energetic charged particles interaction with earth bow shock and magnetopause
19 p3494 A70-37482
- Magnetic and electric field changes across earth bow shock and magnetosheath, discussing Pioneer 8 andOGO-5 data
19 p3494 A70-37483
- Interplanetary shock wave of 26 February 1969, discussing association with solar flares
19 p3513 A70-37517
- Energetic storm particle events observation, noting association with solar protons and interplanetary shock waves
19 p3496 A70-37518

Existence theorem for piecewise-continuous solutions of waves and shocks in relativistic MHD, using Riemann manifold

19 p3477 A70-37579

Cosmic rays shock from small mass supernovae explosions

19 p3507 A70-38128

Low temperature underexpanded supersonic gas plasma jets behind shock wave, analyzing rarefaction and viscosity effects on parameters distribution

19 p3352 A70-38185

Heat transfer behind shock wave in air, oxygen or carbon dioxide flow past wedge, determining thermal fluxes vs wave velocity

19 p3405 A70-38188

Carbon monoxide oxidation by molecular oxygen in incident shock waves, accounting for chain branching in shock tubes

19 p3374 A70-38271

Steady sub and supersonic flow calculations behind receding shock wave, using finite difference scheme

20 p3611 A70-39803

Shock tube with diffuser in low shock wave Mach number range, considering gas flow models to relate wave intensity to initial conditions in chambers

20 p3606 A70-39820

Wedge angle large amplitude slow oscillations in hypersonic and supersonic flows, examining attached bow shock

20 p3559 A70-40288

Weak steady shock waves formation in relaxing binary gas mixture, discussing vibrational specific heat temperature dependence

20 p3614 A70-40350

Shock waves formation in rarefied plasma investigated by Thomson scattering of ruby laser light

20 p3643 A70-40388

Current driven ion wave plasma turbulence in collisionless shock, measuring frequency and wave number spectra by shock front light scattering

20 p3685 A70-40497

Hypersonic flow pattern past windward side of triangular wing with supersonic leading edges, joining potential and vortex regions behind shock wave

21 p3743 A70-40609

Magnetosheath turbulence generation by hydromagnetic waves amplification carried by solar wind through earth bowshock, computing refracted and incident energy fluxes ratio

21 p3815 A70-41059

Inner magnetosheath large amplitude hydromagnetic waves, discussing power spectrum, earth bow shock and solar wind

21 p3816 A70-41083

Shock wave excitation of type 2 and moving type 4 solar bursts from Culgoora radioheliograph and spectrograph recording

21 p3891 A70-41181

Spherical radiation drive shock wave similarity solution, discussing time function, velocity, radial dependence and density

21 p3948 A70-41245

Shock and expansion waves formation by moving piston based on kinetic theory of gases, solving Bhatnagar-Gross-Krook equation by numerical method

21 p3808 A70-41377

Ion sound system one dimensional hydrodynamic equations, examining formation and interaction of nonlinear ion acoustic shock waves

21 p3857 A70-41384

Plane stationary shock wave reflection from rigid concave wall at low Mach numbers

21 p3811 A70-42204

Accelerated supersonic motion of plate with attached shock wave at finite angle of attack in ideal gas, using perturbed nonstationary motion equations

21 p3748 A70-42209

Relaxation behind shock waves in air, calculating radiation spectral distribution for comparison with shock tube experimental data

21 p3812 A70-42219

Hot electrons bunch spread deceleration in collisionless plasma, discussing stationary moving jump formation similar to shock wave

22 p4077 A70-42299

Comet Schwassmann-Wachmann I brightness variations due to interplanetary shock waves in solar wind

22 p4097 A70-42475

Stereo synchrotronic shadowgraph system for explosively projected shock wave, using streak camera

[SMPT PREPRINT 114] 24 p4031 A70-43027

Interferometric investigation of rapidly variable frequency dependent phase objects, using ruby laser waves

[SMPT PREPRINT 26] 22 p4034 A70-43049

Curved shock waves regular and Mach reflection in steady supersonic flow at plane wall

[ICAS PAPER 70-11] 23 p4180 A70-44122

Plane transonic flow around airfoils, using hodograph based methods for shock free flow and finite difference methods for flow with shock waves

[ICAS PAPER 70-12] 23 p4132 A70-44123

Turbulent collisionless plasma shocks formation, wave front steepness and explanation for earth bow shock

23 p4225 A70-44183

Internal shock waves in axisymmetric flow field of perfect gas past blunt cone, noting poles of Mach number and cone half angle

23 p4133 A70-44276

Local thermal equilibrium validity for electron temperature and density determination in reflected shock waves in He plasma, comparing laser scattering and spectroscopic methods

23 p4229 A70-44986

One dimensional collisionless electron-proton plasma, obtaining exact electrostatic shock solution to Vlasov and Poisson equations

24 p4382 A70-45107

Finite amplitude longitudinal shock waves in nonlinear hyperelastic materials, deriving solutions for various shock types in accordance with second law of thermodynamics and Lax stability criterion

24 p4420 A70-45265

Type 2 solar radio burst shock wave exciter velocity from dynamic spectrograms, relating correction to shock strength gradient

24 p4401 A70-45322

Time dependent inviscid transonic flow past two dimensional and axisymmetric bodies, presenting numerical procedures including imbedded shock waves as discontinuities

[AIAA PAPER 70-1322] 24 p4288 A70-45943

Contact region structure with viscosity, conduction and radiative transfer effects applied to plane shock wave reflection from heat conducting wall

24 p4326 A70-46001

Cold boundary layer effect on chemical kinetic parameters behind reflected shocks in single-pulse shock tube

24 p4323 A70-46044

SHOOTING STAR AIRCRAFT

U T-33 AIRCRAFT

SHORT CIRCUITS

Waveguide master short circuit devices reflection coefficient measurements by microcalorimeter

09 p1638 A70-23322

Thermal loads on semiconductors in solid state converters during short circuit and overload

15 p2709 A70-32205

Insulator wall temperature effect on supersonic nonequilibrium MHD generator channel under open and short circuit conditions

20 p3681 A70-39994

SHORT HAUL AIRCRAFT

V/STOL aircraft for short haul transportation, discussing speed, noise, reliability, economy, etc

[SAE PAPER 700333] 18 p3214 A70-36797

V/STOL short haul air transportation program in western U.S., assessing public acceptance and economic viability

[AIAA PAPER 70-888] 19 p3552 A70-37394

Yak-40 business jet design and flight characteristics

21 p3755 A70-42174

Short haul jet transport aircraft design, discussing Computer Aid Design, Airline System Simulator and Traffic Demand Predictor computer programs

[ICAS PAPER 70-28] 23 p4284 A70-44105

Short haul intercity center facilities air transportation traffic alleviation by VTOL aircraft, emphasizing performance, ground facilities, system operation and economics

[AIAA PAPER 70-1243] 24 p4290 A70-45914

U.S. western region short haul air transportation, discussing demand, modal split, STOL and VTOL aircraft, avionics and ground systems

[AIAA PAPER 70-1284] 24 p4322 A70-45915

Short haul transportation needs in multimodal transportation systems planning, discussing modeling in Northeast Corridor Project

[AIAA PAPER 70-1265] 24 p4431 A70-45925

Short haul metropolitan air transportation, considering systems engineering as unifying technology

[AIAA PAPER 70-1281] 24 p4373 A70-45927

ATC, air navigation facilities and airport design requirements for short haul transportation system

[AIAA PAPER 70-1288] 24 p4323 A70-45973

SHORT TAKEOFF AIRCRAFT

STOL aircraft configurations optimization including cost effectiveness, considering propulsive lift systems

[AIAA PAPER 69-1131] 01 p0162 A70-10609

Area navigation and automatic data communications in air traffic control proposed for New York area STOL aircraft operations and Boeing 747 aircraft

[AIAA PAPER 69-1054] 01 p0138 A70-10640

Turbobfan VTOL or STOL intercity transports noting lift engines, noise, aircraft design and interior

[AIAA PAPER 69-1039] 01 p0005 A70-10645

STOL ports in city environments, discussing elevated building design, assisted takeoff and landing equipment and Navy operational safety potential

01 p0057 A70-10715

Three dimensional navigation and guidance system for transport aircraft to alleviate operational problems, noting application to STOL aircraft

02 p0334 A70-11983

Touring aircraft, discussing vibration and noise reduction, instrumentation, STOL aircraft, etc

02 p0227 A70-12663

STOL in northeast corridor, discussing technology applications, economics, requirements for progress, industry, government regulations and decision making

[SAE PAPER 690418] 03 p0608 A70-12897

VTOL technical problems relating to military and civil transport applications, discussing sensitivity to mission requirement variations including design costs, noise levels, etc

05 p0797 A70-17077

California future transport complex, considering STOL and ESTOL /extremely short takeoff landing aircraft/ design requirements

06 p0985 A70-17197

STOL/VTOL airports design, location and complementary ground access transport

06 p1028 A70-17324

High lift devices design and operation problems in short and vertical takeoff

07 p1189 A70-19874

VSTOL and STOL transport development concerning aircraft types, air traffic control and navigation, airports, etc

07 p1194 A70-20250

STOL touring aircraft propeller design and aerodynamics, discussing takeoff runs, landing runs, high lift, downwash, ground effects, etc

08 p1435 A70-20628

Harrier engine nozzle actuation system role in short ground takeoff run facility, discussing pneumatic system, air motor servo unit and pilot control

09 p1610 A70-22606

Hybrid simulation, determining vehicle and performance parameters on longitudinal flying qualities of STOL transport in power approach configuration

[AIAA PAPER 70-387] 10 p1806 A70-24918

Air transport and European cooperation involving supersonic transports, jumbo jets and STOL aircraft

12 p2334 A70-26966

Jet powered Ultra STOL aircraft engine selection, considering effects of engine size, wing loading, thrust loading, etc

[SAE PAPER 700266] 12 p2161 A70-27435

Economic factors in developing STOL and VTOL metroflight service, proposing evolutionary process beginning with short term demonstration

[SAE PAPER 700313] 12 p2335 A70-27454

STOL aircraft noise level certification based on aircraft type, landing and takeoff paths and airports

[SAE PAPER 700325] 12 p2161 A70-27459

American Airlines-McDonnell Douglas intermetropolitan STOL evaluation tests, noting microwave landing guidance system

[SAE PAPER 700336] 12 p2161 A70-27464

Harrier short takeoff fighter aircraft cockpit design, describing layout, lighting, warning and escape systems, etc

12 p2162 A70-27888

VTOL and STOL design and operation, discussing noise and vibration reduction

13 p2344 A70-28544

Servoactuator for stick force augmentation on light turboprop STOL aircraft at high angles of attack

[AIAA PAPER 70-909] 17 p3019 A70-35821

STOL takeoff trajectory optimization for heavily loaded helicopter, using optimal control theory

17 p3021 A70-35841

STOL navigation systems, evaluating Vector Analog Computer, Decca Omnitrac IIB and inertial system

18 p3289 A70-36513

STOL systems 1975 technical and economic characteristics in terms of passenger market, aircraft design, terminal facilities and ATC capability

[SAE PAPER 700311] 18 p3350 A70-36812

Propulsion system impact on military/commercial STOL transport aircraft commonality, taking into account augmented jet flap and externally blown flap powered lift wing concepts

[SAE PAPER 700269] 18 p3214 A70-36819

Four-seat two-engine STOL propeller passenger and sport aircraft design and performance

19 p3355 A70-37371

Avionics role in STOL air transportation operational capabilities in congested air traffic environment

19 p3466 A70-38238

STOL system traffic analysis simulation model for interurban transportation system as tool for flight hardware evaluation

22 p4007 A70-43731

Wheel force and roll moment nonlinearities effect on light STOL aircraft handling qualities during approach

[ICAS PAPER 70-55] 23 p4139 A70-44151

STOL operations from city centers, discussing safety requirements, navigation and guidance systems, airport criteria, etc

23 p4140 A70-44174

STOL aircraft augmentor wing concept, examining noise suppression, flight research vehicle program and application to turboprop production aircraft

[SAE PAPER 700812] 24 p4290 A70-45903

Commercial STOL aircraft propulsion systems from
airline viewpoint, emphasizing subsystem design, en-
gine selection, thrust deterioration and maintainability
[SAE PAPER 700810] 24 p4395 A70-45904

Satellite based navigation/air traffic control infor-
mation systems for short range STOL air carrier air-
craft
[AIAA PAPER 70-1338] 24 p4373 A70-45930

STOL aircraft guidance and control, discussing area
navigation utilization, multiple airways, data links and
ground ATC computers
[AIAA PAPER 70-1334] 24 p4373 A70-45934

STOL aircraft low speed handling characteristics
described via approach and landing profiles, power
requirements, wind effects, etc
[AIAA PAPER 70-1332] 24 p4291 A70-45936

STOL aircraft FAA airworthiness standards and
certification rules, examining noise, control systems,
all weather operation, fire protection, handling qual-
ities and performance
[AIAA PAPER 70-1331] 24 p4291 A70-45937

Commercial STOL aircraft takeoff and landing
physical parameters relationships based on wind tun-
nel and flight tests
[AIAA PAPER 70-1238] 24 p4292 A70-45959

STOL aircraft field length, terminal area per-
formance and minimum handling qualities require-
ments for safe and efficient operations
[AIAA PAPER 70-1240] 24 p4292 A70-45960

Highlift and blown wing types slow speed STOL air-
craft, comparing pilot training requirements with jet
airline flying
[AIAA PAPER 70-1282] 24 p4292 A70-45971

STOL aircraft operational constraints, considering
economics, short haul market characteristics, com-
munity acceptance, speed, propulsion system,
takeoff/landing performance and maneuverability
[AIAA PAPER 70-1283] 24 p4374 A70-45972

SHORT WAVE RADIATION
NT DECIMETER WAVES
NT MICROWAVES
NT MILLIMETER WAVES
NT SUBMILLIMETER WAVES
Coherent short wave and UV radiation generation
using continuous ion gas laser, discussing efficiency,
stability and feedback effects 01 p0108 A70-10356

Polarization level of outgoing short wave radiation
calculated along solar vertical in aerosol containing
multiply scattering atmosphere 06 p1097 A70-17829

Short wave radar tracking of comets, considering
tail type criteria for signal reflection 07 p1379 A70-19040

D and lower E region absorption of short waves,
studying absorption distribution with height 07 p1263 A70-19153

Field strength determination at reception point for
long range short wave paths, taking into account mul-
tiple ray paths and antenna radiation patterns 07 p1237 A70-20435

Short wave radiation model of single layer stratus
and stratocumulus cloud based on actinometric
soundings of lower troposphere 08 p1537 A70-21104

Vertical short wave albedo profiles in lower tropo-
sphere under cloudiness and clear sky using ac-
tinometric sounding 08 p1537 A70-21105

Short wave radiation fluxes inclusion in
hydrodynamic model of general atmospheric circula-
tion based on aircraft sounding data and aerostatic ob-
servations 12 p2263 A70-27512

Soviet book on solar short wave radiation effects on
ionosphere, covering solar atmosphere and spectra,
ionospheric ion concentration vertical distribution, etc
13 p2487 A70-28649

Thermospheric heating and conversion efficiency of
short wave radiation as functions of solar radiation
spectral flux, atmospheric components concentration
and elementary processes cross sections 14 p2569 A70-30212

Spectrometer model for short wave radiation in at-
mosphere, measuring sky brightness, polarization and
total solar flux 14 p2583 A70-30413

Angular structure of outgoing short wave radiation
field measured from Cosmos satellite for clear and
cloudy skies and various sun heights 18 p3286 A70-36965

Short wave calibration system for net pyrriadiome-
ters, using source with intensity and spectral distribu-
tion comparable to solar radiation 20 p3628 A70-39147

Short radio wave propagation over single jump lines
in F sub zero F 2 gradient presence, examining max-
imum usable frequency increase 23 p4162 A70-44076

Thermospheric heating and conversion efficiency of
short wave radiation as functions of solar radiation
spectral flux, atmospheric components concentration
and elementary processes cross sections 24 p4331 A70-46287

SHORT WAVE RADIO TRANSMISSION
Vertical probe observations of short radio waves
propagation through sporadic E at various frequencies
and path lengths 01 p0084 A70-11553

Normal mode helical antennas performance in medi-
um and short wave regions, discussing advantage over
log periodic antennas and maximum radiation angle
achieved by phase shift 02 p0270 A70-12735

Short wave signal field strength measurement errors
by frame antenna, outlining correction procedure 11 p2003 A70-25552

Mutual correlation coefficients for signal level
changes during short wave space diversity reception
and radio wave propagation over two midlatitude
paths 14 p2546 A70-30145

F 2 layer effects on ionospheric short wave scatter-
ing lines for operating frequencies above MUF 14 p2547 A70-30231

Tetrode for single sideband short wave transmitter,
discussing design, characteristics and intermodulation
distortion reduction 17 p3054 A70-35412

Short wave propagation above F2 maximum usable
frequency, observing field intensity and SNR seasonal
and diurnal variations 18 p3226 A70-36092

Short wave ionospheric scatter propagation, observ-
ing interference and crowding in 16-23 MHz and rela-
tionship to F 2 layer maximum usable frequency 18 p3227 A70-36093

Short wave signal field strength measurement errors
by frame antenna, outlining correction procedure 21 p3786 A70-41302

F 2 layer effects on ionospheric short wave scatter-
ing lines for operating frequencies above MUF 24 p4316 A70-46306

SHOT NOISE
Poisson shot noise process relationship with con-
tinuous stochastic intensity as sample function 12 p2203 A70-27418

Shot noise effect in antennas to measure electric
charge density fluctuations in plasma, noting thermal
equilibrium with Maxwellian distribution function 13 p2371 A70-29920

Shot, thermal, induced gate and flicker noise in var-
ious solid state devices and lasers 21 p3792 A70-42112

SHOT PEENING
Shot delivery per second per unit area from ejector
nozzle during shot peening, determining ideal delivery
rates for shot of various sizes 07 p1291 A70-18830

Surface mean deformation state under shot peening
found equal to deformation under single indentation 07 p1292 A70-18835

Boeing 747 wing panels shot peening process,
discussing machine, control technique and operational
requirements 19 p3437 A70-38498

SHOULDERS
Photoelastic stress analysis of shouldered shafts
with keyways in shanks under direct loading and tor-
sion, including keyway and shoulder fillet stresses 02 p0388 A70-12496

SHRINKAGE
Heat resistant coatings in high temperature gas
flow, studying external layer deformation kinetics dur-
ing shrinkage 03 p0483 A70-13250

Alloy specimen shortening due to aging during
stress relaxation under vibration 07 p1304 A70-18820

Computer analysis of degree of constraint against
butt joint transverse shrinkage, using finite element
method for stress analysis 12 p2239 A70-26854

Heat resistant coatings in high temperature gas
flow, studying external layer deformation kinetics dur-
ing shrinkage 19 p3428 A70-38468

SHROUDED BODIES
U SHROUDS
SHROUDED PROPELLERS
Ducted propellers design with flow accelerating and
retarding nozzle analyzed by impulse theory 12 p2155 A70-26876

Shrouded propeller diffusers, considering diffusion
effects on propulsion performance 16 p2970 A70-33754

Fenestron shrouded tail rotor for SA 341 Gazelle
helicopter eliminating ground contact during approach
and landing 23 p4140 A70-44322

Ducted propeller subsonic rotational flow with free
boundaries, presenting second-order partial dif-
ferential equation solution without linearizing assump-
tions 24 p4287 A70-45269

SHROUDED TURBINES
Turbine rotor and stator blades twist inaccuracies in
assembly due to shroud induced stresses and blade
root mountings clearances 07 p1291 A70-18827

Centrifugal force induced stressed state in gas tur-
bine blades using photoelastic analysis, emphasizing
stress distribution at shroud holes 07 p1403 A70-19118

Shrouded aircraft engine turbine blades vibration
stresses found minimum by setting up paired blades
with fixed tension along shroud 10 p1964 A70-25288

Gas turbine shrouded rotating disk system with rad-
ial outflow of air coolant, investigating fluid dynamics,
pressure distribution and frictional moment
[ASME PAPER 70-GT-6] 18 p3208 A70-36862

SHROUDS
Compression spring mechanisms for separation of
spacecraft and shrouds, summarizing design charac-
teristics 16 p2921 A70-34116

Heat transfer characteristics of flows between high
speed rotating disk and parallel stationary shroud,
discussing experimental facility and procedures
[ASME PAPER 70-GT-20] 18 p3349 A70-36865

SHUNTS
U BYPASSES
U CIRCUITS
SHUTDOWNS
NERVA engine operational cycle and performance,
discussing startup, thrust buildup and shutdown 17 p3135 A70-35653

SHUTTERS
Solar energy converter with shutter, determining
light pulse power from solar light intensity and expo-
sure time 07 p1196 A70-19624

Electro-optical shutter for optical pumping experi-
ments using Kerr cell controlled by high voltage modu-
lator 07 p1286 A70-19972

Shutter thermal control for Helios solar observation
satellite, considering closed and open conditions 13 p2505 A70-28769

Nd-glass laser operation in giant pulse mode with
passive or optomechanical shutter, noting applications
16 p2929 A70-34211

SIC [COEFFICIENT]
U STRUCTURAL INFLUENCE COEFFI-
CIENTS
SICKNESSES
NT ALTITUDE SICKNESS
NT DECOMPRESSION SICKNESS
SID [IONOSPHERIC DISTURBANCES]
U SUDDEN IONOSPHERIC DISTURBANCES
SIDE-LOOKING RADAR
NT RADAR IMAGERY
Holographic relationship of coherent optical
processing applications to coherent or side- looking
radar, discussing seismic holography concept 01 p0086 A70-10414

Microwave holography, discussing zone plate lens
design, coherent side-looking radar, large antennas,
three dimensional radar display applications 01 p0086 A70-10415

Target velocity effects on resolution of synthetic
aperture side-looking radar 02 p0268 A70-12582

Synthetic aperture airborne side-looking radar using
coherent optical data processor, discussing system
configuration and operation 02 p0263 A70-12632

Airborne sidescan radar for fix-point navigation at
low flight altitudes involving computerized sensing
evaluated for operator performance 08 p1541 A70-21563

K band SLR /side-looking radar/ imagery mapping
tropical lowland vegetation compared to photographic
coverage 10 p1879 A70-24747

Side-looking radar used to produce high resolution
imagery of Panamanian province under persistent
cloud cover 10 p1882 A70-25045

Airborne side-looking radar antenna optimal
directional characteristics analysis from viewpoint of
maximum surveillance range 10 p1843 A70-25139

Satellite coherent side-looking imaging radars
producing radar maps with photographic-type quality
11 p2005 A70-26038

SIDEBANDS
Radiation from nonlinear polarization sideband in
Ar lasers, discussing anomalous beat notes and mode
locking phenomena 06 p1083 A70-17949

Thermospectrometric investigation of stimulated
Raman lines in benzene to identify generation modes,
observing optical sideband effect at 8050 A 13 p2425 A70-28712

Semiconductor laser frequency modulation by ul-
trasonic waves, noting pressure variation effect on
sideband resolution 18 p3269 A70-36736

- Sideband frequency disturbances at analog data magnetic storage using frequency modulation
20 p3586 A70-39706
- Diffraction theory of sideband holography with transmission objects, discussing geometrical construction of image location and disappearance conditions
21 p3830 A70-41998
- Phase recovery in vestigial sideband /VSB/ data transmission, deriving carrier acquisition time required to achieve satisfactory error rate for coherent demodulation of PAM
21 p3793 A70-42178

SIDELOBE REDUCTION

- Radiation patterns of scanning antenna using digital phase shifters to obtain suitable phase distribution to move sidelobes into invisible region
05 p0822 A70-16676
- Circular antenna arrays synthesis, minimizing peak sidelobe level by dynamic programming
06 p1022 A70-18021
- Parallel wire antenna arrays analysis and design, emphasizing directive power gain maximization and sidelobe reduction
08 p1471 A70-20789
- Electro-optical analogies application to sidelobe reduction of radar antenna illumination patterns and optics far field diffraction patterns in terrain image formation
09 p1631 A70-22009
- Linear antenna array synthesis by variational calculus, minimizing sidelobe level for fixed input powers and field strengths
09 p1644 A70-22404
- Sidelobe suppression for satellite reflector antennas by heavy taper, blockage compensation and active zone techniques, noting net antenna gain enhancement [AIAA PAPER 70-427]
11 p2016 A70-25476
- Radiation patterns of phased array scanning antenna using digital phase shifter, reducing peak sidelobe level
13 p2380 A70-29785
- Asymmetrical element spacings in thinned antenna arrays, obtaining symmetrical radiation patterns with low sidelobe levels
14 p2556 A70-30689
- Linear and circular apertures sum and difference radiation patterns for minimum sidelobe power
19 p3375 A70-37280
- Optical aperture tapering for attenuating sidelobe impairing LF signals detection
20 p3639 A70-39089
- Ultrasonic pulse emitter with interference-free near field and sidelobe suppression for materials testing
24 p4343 A70-45685

SIDELOBES

- Direction finding characteristics of nonlinear antenna, including current determination and optimal angle for sidelobe level
06 p1023 A70-18561
- Polygonal-aperture antennas side radiation distribution
09 p1648 A70-23153
- Line source antenna arrays containing random dissimilarities in waveguide cross section analyzed for phase errors to determine sidelobe deterioration
11 p2018 A70-26177
- Optimal pulse compression time-invariant filter for signal reception with sidelobe constraints under white noise in radar and communications systems
11 p2025 A70-26218
- Pencil-beam antenna idealized patterns derived from maximum gains and operating wavelengths, discussing sidelobes
12 p2195 A70-27247
- Central sidelobes of multifrequency radar signals ambiguity functions, discussing code composition and auxiliary modulations
12 p2185 A70-27686
- Optimum synthesis of complex signals, using autocorrelation function side peak level effect on false alarm probability
13 p2369 A70-29733
- Optimal synthesis of filters maximizing peak-sidelobe ratio of arbitrary zone of mutual ambiguity function
13 p2369 A70-29734
- Amplitude distribution selection in antenna aperture in presence of phase amplitude errors from relation between sidelobe level probabilistic and phase amplitude errors characteristics
16 p2873 A70-33241
- Binary coded radar signal autocorrelation function main-to-sidelobe ratio improvement, using echo signal processed in mismatched filter
17 p3043 A70-34590
- Quasi-equispaced traveling wave slot arrays with below sidelobe crosspolarization, considering computer designed X band prototype
21 p3800 A70-42050

SIDERITE METEORITES

U IRON METEORITES

SIDESLIP

- NT EARTH ORBITAL RENDEZVOUS
NT LUNAR ORBITAL RENDEZVOUS
NT ORBITAL RENDEZVOUS
NT SPACECRAFT DOCKING

SIGHT
U VISUAL PERCEPTION
SIGNAL ANALYSIS

- Geomagnetic field influence on extensive air shower radio emission, discussing frequency dependency and signal polarization
01 p0069 A70-10281
- Electronic polarimeter using signal sampling technique and feedback to measure periodic retardation changes
02 p0297 A70-11918
- Ionspheric electron concentration irregularities via satellite signal scintillation analysis, using radio wave diffraction theory
02 p0258 A70-12562
- Book on microwave theory and applications covering transmission line theory, microwave measurement, signal sources and analysis, network analysis, etc
03 p0455 A70-13001
- Zero crossings of signal harmonic function with normal phase distribution, deriving relations with spectrum and modulating process parameters
03 p0447 A70-13289
- Spectrum parameters analysis of signal in form of radio pulses sequence with harmonic angular modulation
03 p0448 A70-13511
- Sampled signal and associated sequence with identical Fourier transforms, noting applications to digital spectral analysis onboard spacecraft
03 p0449 A70-13538
- CW and radar type RF signal effects on electroexplosive devices sensitivity in bridgewire heating mode
03 p0550 A70-14142
- Limits on signal amplitude, spectrum, derivatives and modulus of variations
03 p0453 A70-14283
- Read theory application to LF operation of avalanche diodes under large signal conditions
04 p0656 A70-14720
- Signal amplitude and Doppler shift statistical characteristics calculated from sounding data on scattering at lower ionospheric discontinuities
04 p0650 A70-15284
- Backscattered signal power density distribution along equivalent propagation path of delayed components, determining reflecting layers characteristics from echo signal phase
04 p0654 A70-15728
- Radar signals synthesis using steepest descent for minimizing Hermitian form
05 p0812 A70-16247
- Complex control follow-up systems in transient modes, suggesting synthesis for transfer function of control signal coupling
06 p1023 A70-17775
- Statistical analysis of dynamic plant based on steady signal, showing numerical determination of operator by least squares method
07 p1226 A70-18726
- Hilbert transform as operator in function space defined on harmonic analysis groups, noting application to noise stability, modulation and signal detection
07 p1235 A70-19644
- Noise effects on joint operation of signal follow-up system with search device using semi-Markov random technique
08 p1461 A70-20864
- Optimal control frequency signals for automatic spacecraft docking
08 p1582 A70-21180
- PWM-PAM and PTM-PAM systems analysis, deriving formulas for output signal shape determination
08 p1480 A70-21226
- Ionspheric electron content estimated from measurements of Faraday rotation of VHF signals from geostationary satellite
08 p1489 A70-21388
- Signal properties of VHF satellite-to-aircraft communications link, discussing results of ATS tests
08 p1463 A70-21779
- Multilevel quantum systems interaction with electromagnetic fields at frequencies near quantum transitions using small signal analysis
09 p1695 A70-22256
- Quasi-linear estimator algorithms to achieve both optimal nonlinear filtration and signal interpolation resulting in significant gain of estimate accuracy
09 p1633 A70-22408
- Ionspheric electron content and distribution determination from Explorer 22 satellite signal amplitude recordings, considering wave propagation and polarization and Faraday effect
09 p1633 A70-22530
- Nonlinear phase distortion measurement in microwave limiters under dynamic conditions using two tone test signal
09 p1647 A70-22714
- Signal properties and measurement accuracy of noncontacting optical heterodyne velocity sensing method used in differential Doppler velocity measurements
09 p1678 A70-22926

Vertical incidence /VI/ F layer ionograms, magnetograms and signal amplitude data obtained during annular eclipse of 23 November 1965

- 09 p1671 A70-23494
- Synchronous harmonics generation of sinusoidal signal with given frequency for vibration analysis of linear and nonlinear structures
10 p1860 A70-24550
- Remote sensor input radiation at aperture, signals within and sensed data processing by computer techniques, noting automatic image interpretation
10 p1841 A70-24733
- Functional model of signal analysis and pulse sequence conversion in nervous system at periphery of hearing
10 p1827 A70-25127
- Polar ionosphere inhomogeneous electron concentration by analyzing satellite signal amplitude fluctuations received by spaced interferometers
11 p2042 A70-25528
- Signal amplitude and intensity fluctuations after laser amplification, considering P representation for density operator
11 p2063 A70-25867
- Atmospheric turbulent boundary layer velocity signals correlation with lognormal distribution
11 p2076 A70-26531
- Steady state large signal computer model for junction-gate field effect transistors below pitch-off
11 p2019 A70-26711
- Satellite signal scintillation spectrum analysis by digital filtering of magnetic tape recording
11 p2012 A70-26718
- Seismic analysis of lunar module impact and missile-earth impact, comparing recorded signal parameters
11 p2118 A70-26748
- Steady state EPR signal I kinetic behavior in wild type Chlamydomonas reinhardtii and in mutant strain AC-206 lacking cytochrome 53
12 p2168 A70-27468
- Waveform estimation by adaptive combination of analog and hardlimited sensor signals
12 p2187 A70-27906
- HF quenched-domain mode /Q mode/ Gunn effect oscillator in single frequency operation using signal analysis, obtaining instantaneous I-V transfer characteristics
12 p2202 A70-28162
- Output signal spectrum analysis for nonlinear active element in presence of distorted modulating voltage
12 p2191 A70-28342
- Statistical characteristics and energy spectra of pulse code signals in data transmission estimated by matrix methods
13 p2364 A70-28871
- Signal decoder for barium USA Germany /BUG/ project command reception system, discussing Ba ion cloud propagation and expansion along geomagnetic field
13 p2367 A70-29557
- A priori initial phase distribution influence on optimal nonenergetic parameter estimation of rectangular narrow band radio signals on white noise background
13 p2369 A70-29730
- Optimum synthesis of complex signals, using autocorrelation function side peak level effect on false alarm probability
13 p2369 A70-29733
- Signal-arrival-time invariance and SNR resolution of discretely analog filters matched to complex radio signals
13 p2380 A70-29736
- Entire functions for analysis and representation of distant atmospherics, using concentrated spectrum and zero coordinate readings
14 p2569 A70-30210
- Backscattered signal power density distribution along equivalent propagation path of delayed components, determining reflecting layers characteristics from echo signal phase
14 p2550 A70-30812
- Signal analysis from Russian Cosmos, Proton and Soyuz satellites, showing pulse width and pulse code telemetries
14 p2551 A70-30975
- Search duration distribution of two stage lock-on indicator scanning signal search systems, using regenerative random process and integral recovery equation
15 p2696 A70-31501
- False signal in scanning interferometer for helium-neon lasers in single and simultaneous TEM modes
15 p2749 A70-31557
- IMPATT microwave diodes small signal characterization by equivalent circuit using iterative computer procedure
15 p2708 A70-31971
- Dynamic spectral characteristics of LF whistler signals for outer ionosphere electron profile determination, using satellite observation
15 p2729 A70-32081

- Prediction of polynomial signals in white Gaussian noise, using discrete data
16 p2866 A70-34065
- Frequency and stability measurements of IF signals generated by laser far IR radiations and conventional oscillators
17 p3104 A70-35084
- IR heterodyne signal statistics, discussing receiver characteristics and design
17 p3105 A70-35096
- VHF radio auroral scatter signal correlation analysis, determining scale size and drift velocity of scattered field
17 p3047 A70-35548
- Statistical characteristics of steady random signal of pulse frequency modulator, obtaining moments of output signal
18 p3234 A70-36072
- Simultaneous optimal detection and parameter estimation of signals in noise, considering multiple solution, learning and image recognition
18 p3228 A70-36597
- EEG analysis for poststimulus events, examining contingent negative variation and late positive wave of average evoked potential
19 p3368 A70-37813
- Small signal oscillation and growth for microwave loaded avalanche diodes with drift and ionization allowance
19 p3389 A70-37968
- Signal spectral parameters for reducing VLF atmospheric data from analyzer observations
19 p3412 A70-37998
- Vibration signals analysis in random and periodic modes, presenting analyzers block diagrams
19 p3430 A70-38526
- Frequency discriminators output voltages under action of fluctuating signal and noise with arbitrary energy spectrum
20 p3584 A70-39254
- Electronic correlation signal analysis for localizing noise sources, detecting signals against background noise
20 p3601 A70-39650
- Soviet book on complex signals in ranging, navigation and communications, discussing correlation and ambiguity functions and bandwidth effect
20 p3587 A70-39723
- Amplitude-phase data from gathering receiving antenna array, obtaining Doppler frequency spectrum as arrival angle function
20 p3599 A70-40319
- Low latitude F region irregularities from scintillations of beacon satellite signals
20 p3624 A70-40486
- Scintillation LF observations with synchronous satellite radio signals at low latitude station, noting magnetic activity effects on night and day scintillations
20 p3590 A70-40488
- High scintillation indices associated with vertical spreading of sporadic E layer from minute-by-minute ionograms and signal amplitude recordings from Explorer 22 satellite
20 p3624 A70-40489
- Ionospheric electron density disturbance heights measured via radio signal scintillation from earth satellite, using spaced receiver method
20 p3590 A70-40491
- Ionospheric disturbances heights at subauroral latitude from Explorer 22 satellite beacon signals recorded at spaced receivers
20 p3624 A70-40492
- Polar ionosphere inhomogeneous electron concentration by analyzing satellite signal amplitude fluctuations received by spaced interferometers
21 p3819 A70-41278
- Electro-optical modulation lock-in techniques for minimizing statistical fluctuations and eliminating internal noise in sampling of light signals
21 p3827 A70-41462
- Cosmic ray signal anisotropy around 0900 h sidereal time and 30-60 degree declination, investigating muon events in liquid scintillator
21 p3882 A70-41994
- Unipolar pulse frequency modulation system with white noise input, deriving output power spectral densities
21 p3793 A70-42225
- System parameters identification from short-term signal observations, using Bayesian approach
21 p3802 A70-42253
- Photon occurrence moments probability distribution in partially coherent light signals
22 p3988 A70-42563
- State space method for small signal lumped IMPATT diode model predicting small signal impedance
22 p3998 A70-43251
- Multibeam communication channel identification from output signal autocorrelation function analysis
23 p4159 A70-43761
- Secondary emission detector using linear signal to measure nonrepetitive microsecond ion bursts
23 p4197 A70-44475
- Bayesian identification of system parameters for observable and nonobservable input signals
24 p4316 A70-45474
- Reflector materials flaw size and orientation using ultrasonic spectral frequency analysis
24 p4335 A70-45573
- Signal flow graphs for selectively invariant autonomous multichannel control systems design
24 p4321 A70-45641
- Sequential decoder program for low weight codewords in binary convolutional code over one-half constraint length
24 p4313 A70-46065
- Entire functions for analysis and representation of distant atmospherics, using concentrated spectrum and zero coordinate readings
24 p4330 A70-46285
- SIGNAL ANALYZERS**
- Multistop time-to-pulse-height conversion unit to extend capability of pulse height analyzer for multichannel time analysis with narrow channel widths
02 p0271 A70-12749
- Frequency amplitude-threshold EEG analyzer with automatic distribution of filter signals over recording levels
03 p0434 A70-13695
- Closed loop frequency response analyzer with steepest descent computing procedure to obtain in-phase and quadrature signal components in linear or nonlinear systems
[ASME PAPER 69-WA/AUT-3] 04 p0688 A70-14830
- Theoretical performance computation of on-line analyzer for radar echo detection by digital techniques
05 p0814 A70-16359
- Atmospheric wind velocity and temperature oscillations measurement using acoustic anemometer, resistance thermometer and multichannel signal spectrum analyzer
07 p1284 A70-19833
- Acousto-optic receiver and spectrum analyzer for electromagnetic signals in VHF-UHF range
08 p1463 A70-21780
- Comparator for measuring relative phase difference between identical frequency signals within microwave octave band
09 p1647 A70-22715
- Physiological data analyzer modification for simultaneously estimating scaled interval histograms/SIHs/written in one memory subgroup
14 p2542 A70-30799
- Scientific satellites pulse height analyzer and associated threshold detection and logic circuitry
16 p2900 A70-33062
- Real time swept sine wave spectrum analyzer using time compression to change filter bandwidth as function of control signal
17 p3059 A70-35166
- Mechanical and acoustic vibrations signals analyzer, noting automatic or manual operation
17 p3054 A70-35417
- Portable hybrid automatic sleep analyzer for on-line EEG and EOG processing
17 p3040 A70-35606
- Digital correlator errors due to quantization by levels, designing analyzer of slow processes
20 p3594 A70-39922
- SIGNAL DETECTION**
- NT CORRELATION DETECTION**
- Chirped pulses observation by heterodyning single frequency Q switched carbon dioxide laser with stable CW local oscillator and beat signal display on oscilloscope
01 p0109 A70-10433
- He-Ne gas laser simultaneous oscillation detection based on output power modulation due to variable path length element placed in cavity
01 p0109 A70-10434
- Signal discrimination from sequence of interference and noise by determining parameter value probability density using random process
01 p0044 A70-11024
- Intermittent vs continuous noise effects on signal detection measures during audio visual checking task performance
01 p0039 A70-11167
- Atmospheric density profiles based on laser radar return from ruby laser detected by photomultiplier
01 p0079 A70-11220
- Subjects trained in visual monitoring task with autoinstructional device, showing higher signal detection rate than group trained by practice alone
02 p0247 A70-12380
- Transient response role in limiter-discriminator detection of binary FSK signals, comparing resulting and optimum error probabilities
02 p0258 A70-12421
- Azimuth information transmission by PCM signals with equal repetition and scanning frequencies, investigating antenna characteristics
02 p0270 A70-12619
- Detection efficiency compared for system containing clipper circuit and quasi-optimal linear system for video pulse signal with additive noise background
03 p0446 A70-13201
- Temporal position of pulse signals measured by multichannel storage devices, discussing interference immunity and required storage time
03 p0448 A70-13435
- Fluctuating radio signals optimal two step detection on Gaussian noise background applicable to coherent superposition of signals reception
03 p0448 A70-13454
- Third harmonic generation detection for strongly absorbing media in reflection with neodymium-glass mode-locked laser, measuring nonlinear susceptibilities of semiconductors and metals
03 p0501 A70-13649
- Signal detection theory analysis indicating within-session changes in human willingness to respond in visual monitoring task, considering optimal decision behavior
03 p0435 A70-13766
- Slitless system using interference filter, fixed Fabry-Perot etalon and automatically controlled etalon for recording spectral information for efficient light detection
04 p0685 A70-14523
- Sinusoidal signal detection in Gaussian noise band by zero crossing method, discussing signal frequency position and SNR
04 p0648 A70-14705
- Pulsed radar fluctuating echo digital-detection and false alarm probabilities assuming Rice signal distribution with noise
04 p0649 A70-15065
- Signal detectability improvement by taking logical union of thresholded power of sensor outputs sum and thresholded power of sensor outputs difference
04 p0651 A70-15326
- Light signals frequency converters and amplifiers applied to detection problems
05 p0813 A70-16264
- Monopulse radar signal detection efficiency with fully polarized reception taking into account target with fluctuating polarization
05 p0813 A70-16270
- Coding and signal selection for data relay satellite interrogation channel serving many low-powered unattended user terminals
06 p1006 A70-17347
- Optical heterodyne quantum detector response, calculating signal to noise ratios
06 p1008 A70-17524
- Lateralization and detection of signals under antiphasic noise masking measured at various SNR levels
06 p1106 A70-17597
- Optimal colors for target and rescue markers, discussing influence on signal detection, response and identification
06 p1002 A70-17713
- Three frequency heterodyne system for acquisition and tracking of radar and communications signals, noting applicability in optical and microwave ranges
06 p1010 A70-17948
- Optimal nonparametric amplitude and phase methods for synthesizing signal detection systems invariant to noise distribution and noise-signal combination
07 p1226 A70-18684
- Optimal signal detection with random phase on Gaussian noise background, estimating error probabilities
07 p1226 A70-18685
- Optimal receiver synthesis for signal detection on background noise resulting from nonlinear filtration of Gaussian noise
07 p1226 A70-18760
- Multichannel sequential detection of stationary signal, deriving analytical expressions for probabilities of erroneous solutions and mean duration of tests
07 p1227 A70-18762
- Quantum statistical decision theory for detection and estimation of signals in random noise
07 p1333 A70-18919
- Maximum likelihood receiver [MLR] to detect pulsed signal propagated through turbulent medium, assuming optical propagation over long path in atmosphere
07 p1227 A70-19146
- Short coherent laser radar detection of backscattered signal in measuring Doppler shift due to atmospheric temperature
07 p1297 A70-19368
- Optical data processing systems with spatial filters for two dimensional signals detection, using film nonlinearities to record Fourier transform hologram
07 p1287 A70-20094
- Frequency locked loop optimization, showing advantages in frequency shift keying detection and FM signal demodulation
08 p1460 A70-20808
- Threshold extension techniques using impulse noise detection and elimination implemented at phase lock loop demodulator output
08 p1460 A70-20811

Time resolved photoelectric light detection, discussing photoelectric emission probability time dependence and radiation interaction with bound charge
09 p1726 A70-22232

Two stage detection effectiveness in presence of signal fluctuations in partly dependent or independent stages
09 p1633 A70-22417

Pulse duration, time and amplitude of pulse modulation, discussing device, detection circuit and statistical error analysis
09 p1639 A70-23697

Prolate spheroidal wave functions applied to detection Fredholm equation for band-limited noise and signals
09 p1640 A70-23803

Differential luminance sensitivity of human eye using signal detection theory, correlating discrimination and detection results with electrophysiological data
10 p1812 A70-24599

System configuration requirements and detectability performance characteristics analysis for optimizing array reception of multipath
11 p2018 A70-26264

Rayleigh and m fading signals spectral location in additive white Gaussian noise, allowing predetermined or variable channel observation time
11 p2010 A70-26268

Signal selection for phase coherent and incoherent additive noise channels to maximize receiver correct decision probability
11 p2010 A70-26327

Light-induced electron paramagnetic resonance signal detected in *Anacystis nidulans*
11 p1989 A70-26847

Signal transduction with differential pulse width modulation applied to data acquisition processes
13 p2405 A70-28812

Radio sources scintillation due to scattering medium with refractive index irregularities under detection of finite bandwidth receiver
13 p2365 A70-29148

Asymptotically optimal signal detection algorithms for statistical systems synthesis
13 p2369 A70-29726

Noise level influence on optimal recognition of non-stationary random processes in white noise
13 p2369 A70-29729

Quasi-optimal sequential detection of phase modulated signal of varying frequency on white noise background, using Markov theory
13 p2369 A70-29732

Book on millimeter and submillimeter waves covering generation, transmission, components and detection
14 p2548 A70-30426

Temporal wave echoes and Landau damping in collisionless plasma using signal averaging and time delay techniques
14 p2622 A70-30687

Decision directed receiver with unknown a priori probabilities, obtaining tight bound on runaway for binary and multiple signal detection
14 p2554 A70-31117

Nonsingular detection and likelihood ratio for random signals in white Gaussian noise
14 p2551 A70-31118

Nonparametric rank tests detection performance for signals in Gaussian noise, considering radar application
14 p2551 A70-31119

Rank ordered statistics for optimum detection of binary pulsed signals in white noise and DC drift
14 p2551 A70-31122

Sensory function in multimodal signal detection forced choice experiment involving auditory, visual and auditory-visual stimuli
14 p2539 A70-31167

Wideband PCM/FM discriminator detection, predicting effects of predetection and postdetection filtering on system performance
14 p2558 A70-31192

Hard limiting bandpass limiter output signal to noise ratio in PM signal detection calculated using probability density function
14 p2552 A70-31194

Optimum decision rule/likelihood ratio/algorithm for random signals detection in Gaussian noise, using pseudo Bayes approach
15 p2703 A70-32560

Digital data detection in presence of noise and double sided intersymbol interference, deriving error rates for known and stochastic signals
15 p2703 A70-32561

Plane wave random signals arrival angle maximum likelihood estimation for multiple antenna systems
15 p2704 A70-32594

Perception threshold in rapidly changing circumstances, discussing stimuli signals recognition
15 p2687 A70-32872

Angle modulated carrier acquisition and demodulation, developing baseband model for behavior of output signal from phase lock loop
16 p2864 A70-33481

Loud and soft signal recognition task under information feedback of presentation schedules and sequence probabilities
16 p2854 A70-33974

Incoherent Manchester coded FSK system performance based on optimal signal detection theory, plotting instantaneous frequency vs time
16 p2866 A70-34074

Digital simulation of linear filter, investigating noise and rounding errors effects on decoding signals from lunar and interplanetary probes
17 p3049 A70-34612

Cosmic ray air showers UHF emission detection at 500 MHz
17 p3151 A70-34850

Binary data system parameters sudden change detection by noisy observation based on Bayes criterion
17 p3056 A70-34856

Sine wave discrete components detection from complex spectrum with random noise, evaluating errors
17 p3059 A70-35168

Monaural detection and filtering of sinusoidal signals in noise, using amplitude model
17 p3033 A70-35610

Simultaneous optimal detection and parameter estimation of signals in noise, considering multiple solution, learning and image recognition
18 p3228 A70-36597

Optimal receiver synthesis for signal detection on background noise resulting from nonlinear filtering of Gaussian noise
18 p3229 A70-37104

Multichannel sequential detection of stationary signal, deriving analytical expressions for probabilities of erroneous solutions and mean duration of tests
18 p3229 A70-37106

Optical aperture tapering for attenuating sidelobe impairing LF signals detection
20 p3639 A70-39089

Frequency discriminators output voltages under action of fluctuating signal and noise with arbitrary energy spectrum
20 p3584 A70-39254

Amplitude modulated optical band signal detection, comparing optimal direct photodetection and super-heterodyne receivers sensitivities
21 p3785 A70-40633

Visual vigilance task with standard, binary or rating procedures as response indicators based on signal detection theory, noting relationship to psychophysical procedures
21 p3761 A70-40743

Statistical pattern recognition and threshold learning in signal detection of noisy binary pulses
21 p3794 A70-41332

Bayes sequential detection test with constrained error probabilities, investigating properties of thresholds equations
21 p3787 A70-41333

FM threshold extension for system performance improvement, comparing impulse noise elimination, correlation detection and delta modulation signal processing techniques implemented at demodulator output
21 p3787 A70-41334

Optical communications system for transmission and detection of PCM word pattern at gigahertz rates, discussing optical and electrical modulation
21 p3788 A70-41339

Wideband detection of FSK transmissions in three component two path channel, obtaining channel bit error probability
21 p3792 A70-42176

Wideband detection of frequency uncertain M-ary frequency shift-keyed (MFSK) transmission in Gaussian noise, deriving symbol error rate for limiting SNR cases
21 p3792 A70-42177

Recursive signal detection scheme, obtaining SNR by derivative approximation
22 p3984 A70-42317

One, two and three dimensional array receiving systems, determining signal detectability characteristics by spatial filtering variation
22 p3986 A70-42527

Random signal detection on uncorrelated Gaussian noise background with unknown intensity, discussing detector performance
22 p3986 A70-42553

Fluctuating light pulse packet detection by inertialess photodetector, deriving optimal algorithm
22 p3987 A70-42554

Optimal heterodyne receiver for laser signals element-by-element wavefront detection
22 p3987 A70-42558

Fluctuating light pulses detection and arrival time estimation for heterodyne reception
22 p3987 A70-42560

Light signals detection on noise background, comparing algorithms based on nonparametric statistics
22 p3989 A70-42569

Adaptive channel equalization approach leading to adaptive detector for slowly time varying channel
22 p3989 A70-43172

Multilevel FSK system with limiter discriminator followed by low pass filter as demodulator, calculating error rates for comparison with other analyses
23 p4161 A70-44003

Varian HA-100 spectrometer eliminating phase change by compensation network in synchronous audio detector reference signals
23 p4199 A70-44949

SIGNAL DETECTORS

Telemetry signal processor for diversity signals for performing as optimum maximal ratio predetection combiner
02 p0266 A70-11747

Binary digital radar signal detectors optimization for radiation pattern of $\sin x/x$ radar antenna and for non-fluctuating target
02 p0255 A70-11899

Transmission channel nonlinearity effect on signal detector performance for signal received by synthesized antenna indicating SNR change
04 p0659 A70-15287

Divided photoelectric cell position sensitive detectors in laser alignment systems, obtaining independent signals for displacements in orthogonal directions
06 p1081 A70-17624

Atmospheric pressure waves generated by high energy disturbance in South Pacific, using ionospheric Doppler signals correlated with ground-level pressure signals
08 p1490 A70-21646

Earth horizon signal sensors on spin stabilized satellites using micron filters for cloud signal rejection
09 p1686 A70-23757

Analog integrating moving window detector performance analysis for use with scanning pulse radar allowing for antenna radiation pattern and detection process dynamic characteristics
11 p2009 A70-26262

Noise threshold performance of suboptimum PPM telemetry receivers using slicer for detector
11 p2010 A70-26273

Analog computer simulation of command signal detectors for reconstruction of transmitted binary character from noisy binary coded signal
13 p2385 A70-29560

FM detector without normalization useful for low S/N reception of FSK and PSK in telemetry systems
13 p2367 A70-29589

Optimal noncoherent detector for fluctuating radar signals of noise background
13 p2369 A70-29727

Optimal coherent radar detector for signals with unknown amplitude and background noise intensity
13 p2369 A70-29728

Millimeter and submillimeter wave receivers, describing detectors, mixers, low noise amplifiers and radiometers
14 p2549 A70-30448

FM optical signals detection, using Fabry-Perot interferometer with air gap between mirrors
15 p2733 A70-31523

Heterodyne conversion transducer large signal internal parameters dependence on heterodyne, signal amplitudes and intermediate voltage
16 p2873 A70-33240

Electron spin-echo device as programmable linear matched filter for PN modulated carrier waveforms detection
16 p2864 A70-33480

Radio receiving system for pulses detection from cosmic ray extensive air showers, discussing sensitivity and noise temperature
16 p2911 A70-33788

Microwave radiometric receiver, analyzing video detector saturation effects on linearity
16 p2880 A70-34075

Frequency locking and control of autodyne oscillating NMR detector for signal averaging
21 p3827 A70-41454

Adaptive AC null detector with tuned compression amplifier used for oscilloscope display drive
21 p3828 A70-41469

Optimal detectors for two signals with fluctuating amplitudes and arbitrary mutual coherence, discussing distribution function processing
22 p3987 A70-42556

Nd-glass mode-locked laser with KDP crystal frequency doubling and pulse selection with Pockels cell
23 p4201 A70-44476

SIGNAL DISCRIMINATORS

U SIGNAL DETECTORS

SIGNAL DISTORTION

FM/FM telemetry systems waveform distortion measurement technique based on minimum rms error between input and output signals
01 p0044 A70-10941

Rms error for reproduction of satellite signal transmitted through continuous Gaussian channel assessed by numerical calculation
01 p0046 A70-11513

Nonlinear distortion in switching transistor mixer predicted by modifying analysis used for diode modulator and mixer circuitry
02 p0268 A70-12423

Ionospheric electron concentration irregularities via satellite signal scintillation analysis, using radio wave diffraction theory

02 p0258 A70-12562

Transversal equalizer for wideband radar systems distortion reduction

02 p0261 A70-12578

Rate distortion function for class of sources, proving positive and negative sides of Shannon encoding theorem for noisy channels

02 p0266 A70-12611

Microwave holography using probe scanning, analyzing causes of distortion and effects on image reconstruction

02 p0302 A70-12618

Autocorrelation function distortion in pseudorandom signal with limited spectrum at RC filter output

03 p0446 A70-13202

Troposphere effects on low incident Explorer 22 satellite signal amplitude, noting role of diffraction

03 p0449 A70-13611

Transistor behavior prediction at threshold of large signal conditions, using nomographs to evaluate maximum drive levels before distortion onset

03 p0452 A70-13966

Narrow bandwidth FM signal distortion during multiplication in lossless varactor multiplier calculated, using equivalent circuit of frequency doubler

03 p0452 A70-14040

Vertical gyroscope with nonlinear compensation circuit under random distortion of signal spectral composition

05 p0880 A70-16223

Wideband transversal coaxial cable delay lines used for improving radar systems target recognition by eliminating misleading signals and distortion

05 p0822 A70-16723

Distribution function distortions produced in counting devices due to simultaneous arrival of particles, correcting errors

06 p1064 A70-17830

Ionospheric distortion of linearly FM radio signals used for sounding, considering signal characteristics in distortion equations

07 p1268 A70-19459

Signal design for Gaussian noise and intersymbol interference immunity, discussing bandlimited signals and maximum likelihood detection technique

08 p1460 A70-20813

Matched filter SNR behavior under time and frequency domains distortion and random distortion, deriving design equations for energy loss coefficients

08 p1474 A70-21223

Nonlinear circuits reducing nonlinear distortions in amplifiers, discussing wideband nonlinear distortion compensating circuits

09 p1643 A70-22131

Distortion-compensation circuit theory, considering voltage-frequency characteristics and varactor controlled oscillator nonlinearities of frequency modulators

09 p1632 A70-22235

Distortion of electromagnetic pulse undergoing total internal reflection in inhomogeneous isotropic plasmas in lower ionosphere

09 p1639 A70-23672

Error probability degradation for digital satellite communication systems, employing multiphase signal sets distorted by bandlimited filtering

10 p1836 A70-24342

Geometric distortions in ESSA 7, Surveyor 7 and Mariner 4 TV systems caused by scale distortion, discussing stability of systematic component in magnitude and shape

10 p1890 A70-24727

TWT, obtaining life performance data from spacecraft, discussing distortion characteristics [ALAA PAPER 70-505]

11 p2017 A70-25494

Pursuit tracking during disturbance signal as function of human performance in man machine system

12 p2266 A70-27198

Electromagnetic pulse distortion with Gaussian envelope in longitudinally inhomogeneous anisotropic ionized media to investigate radio wave communication with ionospheric propagation

12 p2189 A70-27962

Output signal spectrum analysis for nonlinear active element in presence of distorted modulating voltage

12 p2191 A70-28342

Binary code distortion in relative phase telegraphy signals under wideband and correlated noise

13 p2364 A70-28870

Wideband FM signals transionospheric propagation, calculating output spectrum, signal to distortion ratios and signal to noise ratios

13 p2367 A70-29588

Off-axis nonlinear holograms, defining spurious distortion and SNR

14 p2588 A70-31206

Multimode and dispersive distortion of short quasinonochromatic pulses in earth-ionosphere VLF channel

16 p2858 A70-32930

Image distortion in reconstructions from phase only holograms, noting savings in collection and processing of acoustic holographic data

16 p2915 A70-34324

Gaussian source model of image, deriving rate distortion function under mean square error criterion

17 p3049 A70-34857

Tetrode for single sideband short wave transmitter, discussing design, characteristics and intermodulation distortion reduction

17 p3054 A70-35412

Ionospheric distortion of linear FM radio signals used for sounding, considering signal characteristics in distortion equations

18 p3250 A70-36933

HF ballistocardiograms resonance distortions correction, using electrical selective filters

19 p3369 A70-38210

Synthetic aperture radar receivers, discussing cross-product term suppression in correlation detection for image distortion reduction

20 p3585 A70-39392

Low latitude F region irregularities from scintillations of beacon satellite signals

20 p3624 A70-40486

Frequency division multiple access satellite communication system, calculating bandwidth variations effects on intermodulation distortion

21 p3787 A70-41328

Triangle and sine waveforms generation, discussing reduced peak and crossover distortion and extended frequency operation

22 p3989 A70-42923

Adaptive channel equalization approach leading to adaptive detector for slowly time varying channel

22 p3989 A70-43172

VLF signal phase and amplitude changes associated with PCA events and South Atlantic Geomagnetic Anomaly

22 p4023 A70-43292

Signal and noise properties of degenerate and quasidegenerate nonreciprocal parametric amplifiers without circulators

22 p3990 A70-43423

Microwave transmission over elevated line-of-sight path, measuring phase front distortion between pairs of paths

22 p3991 A70-43580

Line-by-line and two dimensional image processing performance, considering transmission rates and distortion

23 p4160 A70-43762

Intermodulation distortion reduction in four frequency parametric converter by low impedance path

23 p4169 A70-43785

Time varying signals sampling, noting role of frequency in distortion

24 p4311 A70-45433

Signal distortion dependence on sampling frequency during continuous signals restoration

24 p4312 A70-45440

SIGNAL ENCODING

Digital log-linear companding technique for nonuniform quantization of speech and image signals

01 p0044 A70-10784

Coding and signal selection for data relay satellite interrogation channel serving many low-powered unattended user terminals

06 p1006 A70-17347

Divided attention utility for monitoring information processing during encoding, retention and recall of words

07 p1224 A70-20047

Physical formula for information content in communication signals based on receiver observation concept, noting role of channel properties and encoding

10 p1844 A70-25223

Optimum symbol sequence interleavers realization taking into account storage capacity and encoding delay

11 p2014 A70-26246

THEMIS source encoding systems research program to investigate inherent quantizing noise and degradation of analog to digital conversion

11 p2014 A70-26255

Pattern recognition with time interval modulation information coding /TIMIC/, considering channel capacity of switching device, similarity with nervous system, etc

11 p2010 A70-26267

Fourier and Hadamard transformation codings for multidimensional data channel noise immunity and bandwidth reduction

11 p2011 A70-26329

Frequency-time coded multichannel communication system error probability bounds to investigate frequency selective fading effect on performance

12 p2184 A70-27416

Central sidelobes of multifrequency radar signals ambiguity functions, discussing code composition and auxiliary modulations

12 p2185 A70-27686

Digital signals transmission codes comparison for transient response by reducing channel bandwidth to obtain error probability

13 p2372 A70-28899

Q-ary /n, k/ cyclic code and subcode generations and weight distributions relationship

14 p2554 A70-31123

Practical codes in digital space communication systems, reviewing Shannon information theory theorems

15 p2698 A70-31963

Fibonacci codes polarized and partial error detection and correction capabilities

15 p2707 A70-32702

Incoherent Manchester coded FSK system performance based on optimal signal detection theory, plotting instantaneous frequency vs time

16 p2866 A70-34074

Data transmission from information sources over communication channels with limit imposed on attainable reliability, discussing coding theorem of information theory

16 p2871 A70-34259

Pulse coding system for average evoked EEG potential data acquisition and analysis, describing pulse generation circuitry and computer implemented logic

20 p3578 A70-38985

Coding forms in radar signals in terms of ambiguity function trend, combining pulse compression with discriminating possibilities in Doppler frequency

21 p3792 A70-41988

Information transmission and coding theory - Conference, Tashkent, Uzbek SSR, September - October 1969, Section 1, Data transmission theory, Methods of coding and decoding

22 p3985 A70-42490

Information transmission techniques by discrete amplitudes and increments, comparing effectiveness for noise rejection

22 p3986 A70-42495

Pulse counting and encoding system on rocket-borne spectrophotometer for starlight collected by primary telescope mirror

22 p4038 A70-43174

Radio signal source encoding, investigating error exponent

23 p4159 A70-43755

Line-by-line and two dimensional image processing performance, considering transmission rates and distortion

23 p4160 A70-43762

SIGNAL FADEOUT

U SIGNAL FADING

SIGNAL FADING

NT SELECTIVE FADING

Book on communication and information theories application to fading dispersive communication channels, discussing tropospheric scatter, HF ionospheric links, moon bounds, etc

02 p0253 A70-11700

High altitude telemetry plasma attenuation for hypersonic blunt nose slender reentry bodies [AIAA PAPER 70-220]

06 p1010 A70-18088

Oblique radio ray tracing at 2-10 MHz and application to signal strength calculation, concentrating on digital techniques

07 p1230 A70-19162

Signal polarization and fading near LUF, describing spatial variations of wave amplitude in terms of angular spectrum

07 p1230 A70-19168

Doppler technique for HF ionospheric radio signal fading, observing frequency spreading during flutter fading conditions in low geomagnetic latitudes

07 p1231 A70-19169

Effective LUF fade-out and fade-in times seasonal and diurnal variations for oblique ionospheric propagation paths, noting sunspot number effects

07 p1233 A70-19180

Winter midlatitude electron density trough from length fluctuation of Faraday signal fading period of satellite Explorer 22, noting characteristic seasonal variation

07 p1270 A70-20034

Time-frequency correlation function for fading communication channel between transmitter and receiver sites, using AM transmissions as probing signals

08 p1458 A70-20796

Fading effect on error probability of multi-hop PCM radio system, noting domination by worst hop

08 p1458 A70-20797

Intermodulation noise performance of FM FDM trunk radio systems in two path fading situations, calculating noise/power ratio and baseband enhancements

09 p1632 A70-22237

Two stage detection effectiveness in presence of signal fluctuations in partly dependent or independent stages

09 p1633 A70-22417

Microwave signal fading in Venus atmosphere due to turbulence, discussing atmospheric dielectric permittivity variance

09 p1764 A70-23484

Interstellar gas electron number density fluctuations effect on pulsar signals in terms of frequency dependent dispersion, noting long wavelength disturbances

09 p1764 A70-23609

Ionospheric electron content diurnal, latitudinal variations and equivalent slab thickness determined from observing satellite signals Faraday fading

10 p1874 A70-24426

Signal attenuation and bandwidth limitations imposed by atmospheric hydrometeors on communications satellite systems above 10 GHz, discussing Comsat measurement programs

11 p1997 A70-25408

Rayleigh and m fading signals spectral location in additive white Gaussian noise, allowing predetermined or variable channel observation time

11 p2010 A70-26268

Stratospheric water vapor measurement by submillimeter wave sounding, considering signal fluctuations due to scattering by high cirrus clouds

11 p2077 A70-26619

Fluctuations of polarization induced fading periods in short wave transmissions of Soviet earth satellites, showing relation to ionospheric inhomogeneities

11 p2047 A70-26788

Atmospheric water effect on satellite communications in UHF region and above, discussing signal attenuation

13 p2364 A70-28782

Mutual correlation coefficients for signal level changes during short wave space diversity reception and radio wave propagation over two midlatitude paths

14 p2546 A70-30145

Forward and backscattering meteor radio echo intensity variations during decay under molecular and turbulent diffusion, recombination and trapping

14 p2635 A70-30313

Book on microwave propagation physics covering unbounded homogeneous medium, terrain effects, uniform refractivity gradient, nonstandard refractivity, fading, etc

14 p2551 A70-30953

Prolonged upper ionospheric observations from Sputnik 3, Transit 4A and Explorer 22 signals Faraday fading and phase shifts, showing electron content dependence on solar activity

15 p2731 A70-32093

Probability density function of specularly fading signal plus noise for frequency shift keying and pulse radar systems

16 p2865 A70-34040

Optimal incoherent signal reception in discrete information transmission systems with fluctuation and concentration noise, including Rayleigh fading

18 p3228 A70-36600

SHF and EHF waves simultaneous propagation over slant line-of-sight overwater path, comparing phase variations and fading for signal coherence

20 p3588 A70-40301

Correlation distance of VHF fading from irregularities in equatorial ionosphere, using NASA STADAN in Chile

20 p3590 A70-40487

Synchronous satellites VHF signal fading attributed to high latitude scintillations, noting intensity at night and during magnetic storms

21 p3790 A70-41362

Optical communication in turbulent media, investigating error rate for binary single path fading channels by photocount detection

21 p3837 A70-41935

SIGNAL FADING RATE

Rapid fading intensity distribution formula for analysis of aperture phase and amplitude errors influence on antenna arrays directional characteristics

03 p0456 A70-13463

Field amplitude distribution parameter in long distance tropospheric communications based on fading depth

15 p2696 A70-31512

SIGNAL FLOW GRAPHS

Signal flow graph, obtaining numeric and symbolic expressions for network function in terms of component parameters and sensitivity coefficients

06 p1026 A70-18420

Loops and paths in Mason signal flow graph of linear systems using algorithm with remote time shared digital computation

07 p1238 A70-18842

Matrix graph concept to unify signal-flow, flow- and N-graph technique approaches to representation and evaluation of matrices and linear algebraic equations

07 p1238 A70-19676

Reliability engineering for complex systems of multiple repairable parts based on analysis involving signal flow graphs and Markov renewal processes

09 p1691 A70-22574

SIGNAL GENERATORS

NT FREQUENCY SYNTHESIZERS

NT FUNCTION GENERATORS

Radar signals optimal synthesis characterized by ambiguity surfaces minimized over predetermined regions of ambiguity plane, noting weighted error criterion role

04 p0651 A70-15328

Signal format for eight station Omega network, considering integrating /DR/ receiver and concept combining time multiplex and frequency multiplex signals

09 p1722 A70-23031

Error functional minimization in class of current distribution relay functions noting applications to linear antennas and FM signals synthesis

09 p1637 A70-23154

Carbon dioxide laser frequency stabilization, using plasma tube impedance variations generating error signal

10 p1901 A70-24946

Pseudonoise sequence generation with 3-tap linear feedback binary shift registers, citing reduction theorems

11 p2025 A70-26224

Sum and difference frequency signals generated and propagated by mixing carbon dioxide laser and millimeter wave klystron outputs in GaAs loaded waveguide

12 p2250 A70-28098

Optimum synthesis of complex signals, using autocorrelation function side peak level effect on false alarm probability

13 p2369 A70-29733

Multipurpose pulse generator design for 1 Hz-100 MHz frequency range and adjustable rise and fall times

14 p2557 A70-31162

Sawtooth waveform generator using linear discharge of capacitor

15 p2714 A70-32701

Optical quantum amplifier frequency characteristics dependence on broad spectral composition amplified signal intensity and resonator parameters

15 p2754 A70-32862

Microwave IC methods applied to solid state signal sources design, using varactor tuned transistor oscillators, resistive isolation pads, amplifiers and frequency multipliers

16 p2872 A70-33069

CRT symbol generators design for high speed computer data display as function of electro-optical and human operator constraints

16 p2850 A70-33133

Silicon avalanche transit time diodes as CW microwave generators and amplifiers

16 p2876 A70-33404

Transient signal generation during large amplitude ultrasonic pulse propagation through carbon tetrachloride

16 p2952 A70-34097

Unrestrained oscillator under action of external synchronous signal, deriving differential synchronization equation

17 p3051 A70-34614

Pressure sensors for large frequency and amplitude measurement, discussing calibration with square signal generator

18 p3262 A70-37210

Thyristor circuit for storing or generating digital control signals, considering reliability at high noise levels

19 p3385 A70-37377

Algorithmic random process pseudorandom number generator composed of analog computer elements, evaluating stability

20 p3594 A70-39918

Pulsed signal synthesis from three dimensional function of indeterminacy, incorporating source distance, velocity and acceleration

22 p3988 A70-42562

Linear differential equation solution associated with FM signal generation, presenting analytical methods for FM and AM components

22 p4063 A70-43209

Spectrum generator with step recovery diode multiplier, discussing line spacing, energy and phase coherence

22 p3990 A70-43485

Klystron microwave signal generator power stabilization using compact low consumption integrated circuits

23 p4170 A70-43797

SIGNAL MEASUREMENT

Pulse methods for measuring correlation function of incoherent scattered signal, calculating bit estimator errors for large and small SNR

01 p0045 A70-11088

Phase fluctuations measurements of obliquely incident signal reflected from ionosphere performed over distance of 1300 km, showing amplitude dependence

01 p0046 A70-11533

Backscatter radar signal phase determination from amplitude data, measuring phase and amplitude in laboratory

05 p0815 A70-16507

Wobbulator measurement of Q factor of microwave resonator cavities using double modulated klystron signal

05 p0822 A70-16528

Large scale ionospheric inhomogeneities anisotropy, dimensions and drift velocities from simultaneously measured irregular refraction

05 p0841 A70-16739

Acoustic impedance method for nondestructive testing exploiting phase defect of signal from piezoelectric transducer

06 p1074 A70-18629

Nonlinear complexing problem in measuring random signal, proposing optimal data processing algorithm with minimum error variance criterion

09 p1654 A70-22542

Ionospheric fine structure from signal broadening measurements on ionograms, including scattering region algorithm

11 p2044 A70-25553

Biased measurement of angular coordinates of phase modulated signals under meter input quantization

11 p2012 A70-26806

DC signals measurement in automatic control circuits, ensuring transformer isolation by use of transistorized amplifier

12 p2196 A70-27682

Wideband stochastic signals for radar range and velocity measurements using polarity coincidence correlation technique

12 p2188 A70-27942

Sinusoidal signal harmonics measurement to determine nonlinear resistance junction I-V equation, discussing applications to circuit analysis

12 p2204 A70-28132

Remote signal measurement and analysis in hazardous environment by command terminal utilizing manual or computerized control

12 p2201 A70-28134

Subpolar ionosphere electron concentration measurements for both hemispheres during solar activity by Faraday effect signal recordings from satellites

14 p2570 A70-30223

Asymmetrical transient attenuation effects of bridge circuit phase discriminator on accuracy of phase difference measurements

15 p2707 A70-31508

Radar ducting effects on propagation at microwave frequencies, recording signal strength as function of transmitter to receiver range

16 p2858 A70-32927

Point to point and radar return attenuation measurements at SHF through clear air and rain

16 p2858 A70-32928

Mathematical-physical parametric model of satellite geodetic laser range accuracy, false alarm and count probabilities, correlating with retroreflector signal strength

16 p2863 A70-33166

Actuating signal at sampling instants determined in phase plane by Mullin-Jury method for sampled data feedback containing quantizer and zero order hold circuit

16 p2886 A70-33336

Intensity interferometer for weak noise-like signal power measurement in presence of additive Gaussian noise

17 p3089 A70-35265

Spectral densities of input and output signals of discretely continuous systems as function of comparison moment

18 p3233 A70-36069

Ionospheric scatter communications channel phase frequency characteristics measuring method, considering probability density function

18 p3256 A70-36091

Effective reflection height measurement accuracy for pulsed vertical ionospheric sounding, using interference method

18 p3227 A70-36106

Pulsed signal amplitude and delay time measurement in presence of interfering /reverberated/ signals and steady noise

19 p3375 A70-37285

Ionospheric refraction during radio wave propagation using space diversity recordings of Faraday and Doppler effects for coherent signals from geophysical rocks

19 p3407 A70-37306

Occupied bandwidth definition and measurement based on probability density function computation for radio transmitter spurious, harmonic and fundamental emissions

19 p3380 A70-38176

Low level time truncated signals measurement by narrow bandwidth synchronous time notch filters, discussing sensitivity

19 p3380 A70-38177

Signal measurement and processing in thermal vacuum and space simulation tests of Azur and Dial satellites

19 p3400 A70-38298

Phase shift direct and balance measurement procedures between signals over wide frequency range classified by conversion schemes
19 p3391 A70-38702

Lunar surface specific effective radio signal scattering area measured by Luna 9 and 13, describing signal fluctuations
21 p3884 A70-40838

Ionospheric fine structure from signal broadening measurements on ionograms, including scattering region algorithm
21 p3819 A70-41303

Threshold SNR for signal frequency meter based on zero number count method, determining reliability
22 p3985 A70-42401

Radio wave reflection properties in 16-3000 kHz range calculated from D and E region models for comparison with measurement
22 p3989 A70-43164

Deterministic vs stochastic signals for equipment and installations short cycle reliability tests over service life during changing environments
23 p4166 A70-44332

Photon-coupled biomedical amplifier for measuring and recording physiological signals
23 p4155 A70-44848

X band horn antennas precision phase center measurement technique for high resolution system applications
23 p4176 A70-44966

Subpolar ionosphere electron concentration measurements for both hemispheres during solar activity by Faraday effect signal recordings from satellites
24 p4331 A70-46298

SIGNAL MIXING

Frequency measurement for HCN laser at 0.357 and 0.311 mm wavelength by mixing signal with backward wave tube harmonics
03 p0500 A70-13464

Two frequency electron beam modes produced by O-type TWT at simultaneous input of HF signals of different amplitudes and frequencies
05 p0824 A70-16894

Microwave mixer design to increase dynamic range applied to communications and video systems
07 p1243 A70-20216

Optical and electronic mixing in avalanche photodiode during variable amplitude signal demodulation in optical heterodyne receiver, considering conversion losses
07 p1243 A70-20282

FM feedback demodulator performance model using mixer-correlator, showing cross correlation receiver design
08 p1479 A70-20810

Resistive parametric mixing in GaAs oscillators at microwave frequencies resulting in negative mobility at signal frequency
10 p1849 A70-24231

IF combinator for broadband transhorizontal radio relay transmission improvement by providing optimum SNR
11 p2020 A70-26821

Sum envelope zero crossings determination for steady normal noise plus random amplitude signal
13 p2370 A70-29742

Far IR second harmonic generation and frequency mixing in CdTe using pulsed water vapor laser
15 p2751 A70-31983

Nonlinear effects of harmonic generation and mixing in lithium niobate microwave acoustic surface wave delay lines measured using laser light deflection
19 p3485 A70-37698

Harmonic generation and small signal mixing in thin magnetic films subjected to static and time varying fields, generating output voltage expressions
21 p3864 A70-42012

SIGNAL NOISE

U SIGNAL TO NOISE RATIOS

SIGNAL PROCESSING

Moving targets automatic identification by radar signals digital processing, describing radar echoes properties, moving window detector system and circuits design
01 p0137 A70-10358

Flying spot scanners evaluation as image processing devices, discussing scan patterns effect on video signal
01 p0089 A70-10817

Observation process optimization in system described by linear differential equations of motion reducible to optimal control problem
01 p0047 A70-11574

Telemetry signal processor for diversity signals for performing as optimum maximal ratio predetection combiner
02 p0266 A70-11747

Acoustooptical processing for amplification of weak radar echoes, describing design and operation of modulators, correlators, filters, etc
02 p0266 A70-12630

Book on radar design principles-signal processing and environment covering target detection in presence of noise, atmospheric effects, pulse techniques, etc
02 p0270 A70-12662

Signal waveform algorithmic construction with optimal autocovariance properties, using isosum integer partitions, applied to clustered multipath distribution measurement
02 p0263 A70-12773

Demodulation of signals modulated with respect to wave period, deriving spectral width of pulsed period modulation
03 p0446 A70-13200

Pulse signals optimal filtration in superregenerative receiver and resulting SNR effect
03 p0456 A70-13203

Electronic transistorized harmonic signal integrator operating in connection with static-dynamic bridge
03 p0493 A70-13975

Subcritical wavelengths processing of solar radio emission, allowing for antenna radiation pattern distortion due to surface defects
04 p0745 A70-14498

Nonadaptive processor to detect coherent radar pulse trains with uniform amplitude in clutter- plus-noise environment
04 p0651 A70-15334

Differential equations for minimum variance linear filter separating signals from additive correlated noise, using discrete time optimum formulas
04 p0663 A70-15586

[AIAA PAPER 69-73]

Optimum signals for phase locked or delay locked loops determined as function of signal to noise ratio
06 p1023 A70-17523

Pulse rate techniques for signal processing and computation, considering feedback circuits, discussing stochastic rates, sampled systems and digital differential analyzer
06 p1027 A70-18510

Clutter symmetry as indication of matching optimum signal filter pair, comparing mismatched and matched systems
06 p1013 A70-18626

Equivalent scheme for tunnel diode oscillator operating mode and parameters effect on LF modulating signal phase correlations
07 p1241 A70-19287

Multichannel correlator for turbulent signal processing in real time scale using natural delay
07 p1284 A70-19832

Signal processor with ratio-squared predetection combining for adaptive antenna array, discussing radiation patterns for coherent and incoherent signal and noise sources
07 p1242 A70-20066

Discrete analog filters circuits for optimal noncoherent processing of phase manipulated signals
08 p1456 A70-20571

Phase locked loop method for waveshaping rectangular wave frequency modulation signals in phase coherent VLF-FSK systems, reducing transient effects and adjacent channel interference
08 p1459 A70-20803

Signal design for Gaussian noise and intersymbol interference immunity, discussing bandlimited signals and maximum likelihood detection technique
08 p1460 A70-20813

Linear signal converter analysis using topological method and coordinate transformation
08 p1480 A70-21231

Compatible single sideband transmission realized using iterative signal processing method and ideal band limited channels
08 p1464 A70-21781

LSI Mark 3 airborne Omega system with computerized signal processing for navigation parameters, discussing system features and flight test results
09 p1719 A70-22190

Nonlinear complexing problem in measuring random signal, proposing optimal data processing algorithm with minimum error variance criterion
09 p1654 A70-22542

Optimal inertialess nonlinear filters synthesis with various optimality criteria for signal distributions differing from normal
09 p1654 A70-22543

Optical signal processing using circular array and spatial frequency filtering to yield azimuthal distribution of sources
09 p1678 A70-22969

Optical processing of signals from circular aerial arrays involving use of spatial filter
09 p1678 A70-22970

Tape recorder performance characteristics relevant to signal types handled, considering phase response and envelope delay
09 p1679 A70-22975

Vacuum tube signal frequency converters for meteorological telemetry measurements including blocking oscillators, multivibrator and fantastron
09 p1718 A70-23332

Digital image processing applied to picture generation, intensity and geometric manipulation, spatial frequency operations and image analysis
09 p1682 A70-23507

[JPL-TR-32-1482]

Signal converter for centimeter band-DC voltage transformation, noting applications to microwave power measurement by digital computers
09 p1650 A70-23629

SIGNAL PROCESSING

Textured gray-scale imagery by computer simulating lunar display
09 p1642 A70-23771

Collection of papers on digital signal processing covering digital filter synthesis, Fourier transforms, algorithms, etc
11 p2003 A70-25575

Surface acoustic wave delay lines using interdigital transducers based on piezoelectrics with applications in VHF and UHF signal processing
11 p2005 A70-26165

Radar signal quick indication and extrapolation for terminal guidance control of Mars soft lander, reducing radar lock on loss sensitivity and engine spurious noise throttling
11 p2080 A70-26210

Processing system for tape recorded signals with nonelectrical varying parameters
11 p2056 A70-26456

Optimal phase-manipulated signals synthesis from autocorrelation function using algorithm
11 p2012 A70-26804

Superlayer structure in turbulent boundary layer on flat plate obtained by statistical processing of signals from hot-wire probes
12 p2209 A70-27226

Pipeline fast Fourier transform signal processor for digital spectrum analysis of wideband radars
12 p2186 A70-27904

Navigation satellite systems, analyzing error sources in signal processing and propagation developing computer programs
13 p2447 A70-28429

Weather radar signal processing and data recording at National Severe Storms Laboratory (NSSL), providing reduction in echo variations due to relative motion of precipitation elements
13 p2363 A70-28774

Air-damped capacitance accelerometers and velocimeters in data acquisition systems using signal processing
13 p2405 A70-28813

Earth colorimetry data improvement by separating signals of each bandwidth on one photographic emulsion or TV tube
13 p2406 A70-28987

Portable autonomous EEG analyzer for processing brain biopotentials without use of computer hardware and qualified personnel
13 p2360 A70-29522

Sum envelope zero crossings determination for steady normal noise plus random amplitude signal
13 p2370 A70-29742

Real time signal processor for correlation and spectrum analysis, displaying results on cathode ray oscilloscope
13 p2370 A70-29817

Threshold sensitivity of pulsed optical radar with discrete signal storage, considering different operating modes
13 p2370 A70-29871

Physical signals continuous to discrete transformation by analog to digital conversion, considering coding process and transfer functions
14 p2554 A70-30679

Microwave channelizing filters input ports interconnection techniques for signals sorting into contiguous frequency bands
14 p2558 A70-31319

Wideband pulse signal synthesis and optimal filtration by dispersive ultrasonic delay lines, estimating potential noise stability for analog data transmission
15 p2696 A70-31502

Noise rejection and spurious reception probability in optimal channel for continuous sequenced signal with undetermined arrival and overlapping spectra
15 p2696 A70-31509

Digital sampled data demodulation, discussing methods of obtaining quadrature channels from single signal
15 p2703 A70-32579

High pulse repetition rate digital systems signal processing using Gunn effect diodes
15 p2710 A70-32583

Optimal perturbation signal waveform linearizing nonlinear transfer characteristic of image sensing receptor array
15 p2705 A70-32725

Holographic recording of wideband pulsed carrier electric signals in Fourier transform, Fraunhofer, Fresnel and image formats
16 p2903 A70-33136

Drosograph high brilliance display device for rapid line-pattern projections and optical signal processing
16 p2906 A70-33179

Upper bound determination for errors due to signal quantization in multirate digital control system through state variable or z transform formulations
16 p2867 A70-33306

Acoustic and magnetic surface waves technologies for radar signal processing
16 p2874 A70-33390

Optimum carrier phase delay estimation for one way ranging aircraft navigation, investigating receiver signal processing

16 p2947 A70-33449

General purpose parallel processor design for avionics, considering radar signal processing

16 p2910 A70-33467

Walsh functions and spectrum for signal processing, discussing computer compatibility

16 p2864 A70-33483

Fast Fourier digital processor for real time filtering of radar signals, discussing applications as Fourier transform system

16 p2870 A70-33738

Binary coded radar signal autocorrelation function main-to-sidelobe ratio improvement, using echo signal processed in mismatched filter

17 p3043 A70-34590

Signal processing antennas, discussing synthetic and multiplicative arrays for coherent radar airborne mapping

17 p3052 A70-35078

Optimal temporal and spatial-temporal resolution for unknown parameter of interfering signal on white noise background

17 p3048 A70-35680

Discrete signals synthesis optimal with respect to given criterion, determining ambiguity function extremum

19 p3374 A70-37270

Radio wave holography with unequal reference to signal frequency, recording linear object with superheterodyne receiver

19 p3420 A70-37290

Radar tracking of meteors with slow drift velocity, improving accuracy via echo frequency multiplication

19 p3514 A70-37644

DC-to-sinusoidal inverter employing PWM waveform, analyzing circuit parameters effect on harmonic content

19 p3358 A70-37854

Signal conditioner for expanded range pressure measurements from reentry vehicles via transducer zero shift suppression and output signal compression

19 p3426 A70-37899

PGM noisy high bit rate processing system, describing preprocessor, bit detector and synchronizer

19 p3379 A70-37903

Signal measurement and processing in thermal vacuum and space simulation tests of Azur and Dial satellites

19 p3400 A70-38298

Signal processing by differential data and common mode amplifiers and active filters, emphasizing low level transducers

19 p3431 A70-38529

Optimal synthesis of linear active RC filters with controlled source, using feedforward and feedback weighted signals

20 p3596 A70-39163

Multichannel iterative servosystems operators for useful signals reproduction

20 p3603 A70-39836

Uncontrolled plant dynamic characteristics analysis based on signal recordings, using black box without input method

20 p3705 A70-39909

Analog communication optimal nonlinear modulation scheme design for large SNR through transformation into inner product functions

20 p3587 A70-39973

Satellite wideband transmission of ionosphere data, monitoring amplitude and phase of phase-coherent CW signals from geostationary satellite

20 p3590 A70-40483

FM threshold extension for system performance improvement, comparing impulse noise elimination, correlation detection and delta modulation signal processing techniques implemented at demodulator output

21 p3787 A70-41334

Strapdown redundant experimental sensor inertial navigation package containing gyros and accelerometers, discussing signal real time processing by digital computer

[AIAA PAPER 69-851]

21 p3849 A70-41858

Digital filtering of sampled narrowband sinusoidal signal embedded in wideband white noise, assessing hard clipping effect on performance by simulation on digital computer

21 p3791 A70-41948

Discretization interval in discrete analog filters for optimal processing of complex radar signals, estimating systematic errors

22 p3984 A70-42393

Optico-acoustic autocorrelator for linear FM signals spatial compression, discussing design and performance

22 p3984 A70-42398

Multichannel correlation filter devices for processing periodic fluctuating signals in noise background

22 p3987 A70-42557

Recurrent adaptive methods for verification of multialternative hypotheses in stepwise signal processing

22 p3993 A70-42565

Multiparameter eddy current test methods, describing test coil output signal amplification, demodulation and recombination

22 p4028 A70-42592

Harmonic linearization method for periodic regimes in discrete nonlinear automatic control systems performing signal quantization with respect to level or time

22 p4001 A70-42833

Active filter operation, examining angle modulated signal at input by various approximation methods

22 p3997 A70-43130

Coherent reference for demodulating double sideband suppressed carrier (DSB-SC) signals in presence of frequency detuning, using squaring or Costas loop

22 p3990 A70-43326

PCM/NRZ signal band-limiting effect on bit error probability, using sample detector

22 p3990 A70-43339

Multiple range bin radar distribution-free detection procedure based on observation ranks without elaborate equipment

22 p3991 A70-43578

Vestibular message flow regulation by central nervous system, describing afference, inhibition and copy formation

22 p3976 A70-43705

Varied-frequency signals separation using bridge circuits for splitting process resulting in unchanged phase ratio and changed amplitude ratio

23 p4159 A70-43759

Signal processing methods application to myoelectric studies of muscular fatigue, employing surface electrodes

23 p4151 A70-44378

Electronic equipment automatic testing systems signal routing and switching trees and matrices design, emphasizing modular approach

23 p4173 A70-44540

High performance military aircraft missile command and control signal data processor microelectronics packaging, using integrated and printed circuit modules

23 p4174 A70-44542

Low cost microwave antenna-receiver for satellite FM TV signal reception at SHF and conversion for standard sets

23 p4164 A70-44645

Time varying signals sampling, noting role of frequency in distortion

24 p4311 A70-45433

Signal distortion dependence on sampling frequency during continuous signals restoration

24 p4312 A70-45440

Analog three dimensional electrical signal multiplier circuit based on Hall effect, considering division and square root extraction

24 p4319 A70-45484

Multifunction programmable digital filter design performing bandpass, bandstop, comb, nonlinear phase and matched filtering of signals

24 p4319 A70-46082

Digital to analog converters for signal processing in CRT character and sweep generation, programmable power supplies, resolver positioning, shaft angle conversion, etc

24 p4326 A70-46083

SIGNAL RECEPTION

NT SYMBOLS

NT TELEVISION RECEPTION

EMI /electromagnetic interference/ antennas relative received voltage vs height above ground as functions of effective length, impedance, etc

01 p0042 A70-10087

HF radio waves propagation between antipodal transmitter and receiver, discussing diurnal variations and reception over polar caps and water

01 p0045 A70-11103

Ionospheric discontinuities drift velocities from diversity reception data indicating no dependence on solar activity

01 p0083 A70-11531

Channel constraints on multiple access systems obtained from airborne propagation tests via satellites, studying disparities in received signal strength

02 p0260 A70-12569

Mean signal response time relationship to nonaging foreperiod

02 p0239 A70-12627

Recognition problem in multipositional symmetrical channel solved by special separation of observational space with preference to signal arriving at reception point

03 p0446 A70-13197

Pulse signals optimal filtration in superregenerative receiver and resulting SNR effect

03 p0456 A70-13203

Fluctuating radio signals optimal two step detection on Gaussian noise background applicable to coherent superposition of signals reception

03 p0448 A70-13454

Transmission channel nonlinearity effect on signal detector performance for signal received by synthesized antenna indicating SNR change

04 p0659 A70-15287

Horizontal atmospheric surface layer propagation path for 3370 A UV signal, studying reception distances for given SNR

05 p0812 A70-16242

Incoherent reception of wideband signals transmitted through multibeam channel with changing random parameters

05 p0812 A70-16248

Signal parameter quasi-optimal estimation during reception on background of normal noise with unknown correlation function

06 p1009 A70-17671

Optimal receiver synthesis for signal detection on background noise resulting from nonlinear filtration of Gaussian noise

07 p1226 A70-18760

Continuous signal a posteriori distribution density formed on basis of learning sequence with no a priori information about signal and noise statistics

07 p1226 A70-18761

Polarization- and space-diversity reception techniques for radio links based on diffraction from ionized meteor trails

07 p1378 A70-18990

Narrow band limiter influence on SNR at FM reception output by computer simulation using threshold pulse model

07 p1227 A70-19124

Radio signal reception beyond normal horizon by partial reflection from elevated layer in troposphere calculated by computer

07 p1234 A70-19218

Nonenergetic parameter estimation of signal during optimal reception with random amplitude fluctuation in normal background noise using maximum probability function

08 p1461 A70-20868

Phase coordinates conditional probability density statistical characteristics from continuous reception of random information, deriving differential equations

08 p1479 A70-20998

Acousto-optic receiver and spectrum analyzer for electromagnetic signals in VHF-UHF range

08 p1463 A70-21780

Astronomical high resolution radio interferometers design with autonomous reception, analyzing sensitivity of data processing correlation devices

09 p1647 A70-23132

Polarization diversity reception effects on VHF telemetry signal from low altitude satellites

10 p1832 A70-23919

Transient analysis of transistor under large input signal accounting for minority carrier life and base collector capacity

10 p1849 A70-24383

Reaction time dependence on sound signal probability determined by temporal structure of signal presentation

10 p1818 A70-24713

Numerical payoff influence on reaction time to second stimulus in subjects receiving successive signals at short intervals

10 p1818 A70-24715

Pulsar radio emission reception with improved SNR based on periodic variation of average reception frequency with time

10 p1948 A70-25165

Physical formula for information content in communication signals based on receiver observation concept, noting role of channel properties and encoding

10 p1844 A70-25223

Signal frequency capture probability vs frequency search rates and AFC loop parameters determined in phase locked oscillator

11 p1996 A70-25349

Optimal pulse compression time-invariant filter for signal reception with sidelobe constraints under white noise in radar and communications systems

11 p2025 A70-26218

System configuration requirements and detectability performance characteristics analysis for optimizing array reception of multipath

11 p2018 A70-26264

Signal selection for phase coherent and incoherent additive noise channels to maximize receiver correct decision probability

11 p2010 A70-26327

Emission spectrum of neon-helium laser receiving Doppler shifted signal from moving mirror, showing memory effect due to beat harmonics

12 p2246 A70-27352

Dynamic tracking filter response analysis for FM reception using equivalent circuit method

12 p2200 A70-28054

Noise stability of optimal binary detection receiver of rectangular-pulse and discrete pseudorandom signals under nonideal synchronization

13 p2364 A70-28869

Satellite based random Doppler environmental measurement technique for Global Atmospheric Research

Program /GARP/, receiving signals from balloons, buoys and land stations 13 p2407 A70-29176

Nonlinear optimal filtration and adaptive quasi-coherent reception of Markov signals on white noise background 13 p2369 A70-29731

Noise rejection during synchronous quasi-coherent radio signal reception with binary narrow band linear filter used for voltage shaping 13 p2369 A70-29737

AM signal reception on strong AM noise background, describing theoretical receiver design 13 p2370 A70-29740

Mutual correlation coefficients for signal level changes during short wave space diversity reception and radio wave propagation over two midlatitude paths 14 p2546 A70-30145

Vertical ionospheric electron concentration profiles, horizontal gradients and integral component from Doppler and Faraday signal recording on geophysical rockets, using diversity reception 14 p2569 A70-30205

Sporadic E layer space diversity reception data from stations 20 km apart, noting horizontal ionization gradient effect 14 p2571 A70-30234

Correlation characteristics of turbulent motions in atmospheric meteor region, discussing diversity and single point reception methods 14 p2572 A70-30329

Correlation apparatus for ionospheric drift measurement by spaced receivers using closed loop of magnetic tape 14 p2550 A70-30741

Optimum adaptive reception for binary sequences, using posteriori probability density function computing device synthesized from correlator, instantaneous nonlinearity and multiplier 14 p2552 A70-31188

Electronically tracking antenna system for satellite reception in VHF range suitable for unmanned receiving stations 14 p2558 A70-31196

Noise rejection and spurious reception probability in optimal channel for continuous sequenced signal with undetermined arrival and overlapping spectra 15 p2696 A70-31509

Radar echo signal amplitude probability distribution during fully polarizational reception 15 p2696 A70-31517

Clutter signals in radar receiver antenna, determining autocorrelation function and spectral power density 15 p2701 A70-32466

Dipole and loop antennas in isotropic compressible plasma under wave incidence, using reciprocity theorem for receiving voltages and maximum powers 16 p2957 A70-32982

Laser range finding to satellite equipped with retroreflectors, noting accuracy dependence on signal strength 16 p2925 A70-33021

Discrete signals optimal reception by lowering synchronization requirements for communications or radar purposes 16 p2863 A70-33242

Multiple sensor arrays phase difference estimation, assuming Gaussian signal and noise statistics 16 p2866 A70-34064

Optimal incoherent signal reception in discrete information transmission systems with fluctuation and concentration noise, including Rayleigh fading 18 p3228 A70-36600

Optimal receiver synthesis for signal detection on background noise resulting from nonlinear filtration of Gaussian noise 18 p3229 A70-37104

Continuous signal a posteriori distribution density formed on basis of learning sequence with no a priori information about signal and noise statistics 18 p3229 A70-37105

Frequency synchronization channel pulse fluctuations effect on noise stability of binary signal reception 20 p3587 A70-40145

Signal frequency capture probability vs frequency search rates and AFC loop parameters determined in phase locked oscillator 20 p3589 A70-40461

Wave polarization effects on ionospheric radio wave transmission and reception 21 p3790 A70-41361

Information transmission and coding theory - Conference, Tashkent, September-October 1969, Section 2, Statistical theory of signals and noise, Optimal reception methods 22 p3986 A70-42551

Optimal reception of phase manipulated signal on noise background with unknown statistics and information parameter a priori probabilities 22 p3987 A70-42561

Algorithms for analog wideband signals optimal reception in presence of strong Gaussian noise 22 p3988 A70-42568

Emission spectrum of neon-helium laser receiving Doppler shifted signal from moving mirror, showing memory effect due to beat harmonics 22 p4052 A70-43596

Low cost microwave antenna-receiver for satellite FM TV signal reception at SHF and conversion for standard sets 23 p4164 A70-44645

Vertical ionospheric electron concentration profiles, horizontal gradients and integral component from Doppler and Faraday signal recording on geophysical rockets, using diversity reception 24 p4330 A70-46280

Sporadic E layer space diversity reception data from stations 20 km apart, noting horizontal ionization gradient effect 24 p4331 A70-46309

SIGNAL REFLECTION

Phase fluctuations measurements of obliquely incident signal reflected from ionosphere performed over distance of 1300 km, showing amplitude dependence 01 p0046 A70-11533

Ionospheric propagation experiments to measure radio echo height changes, observing correlation between LF signal reflection and MF transmitter power 04 p0650 A70-15132

Equation for disturbance of ILS localizer signals by reflection from flat hangar wall, discussing computer program 04 p0652 A70-15344

Polarization nature and changes evaluation of radio echo signals reflected from polar auroras 04 p0682 A70-15730

Ionospheric probe for simultaneous measurement of radio signal reflection coefficient and amplitude-frequency characteristics 04 p0684 A70-15746

Radio wave scattering and brightness on uneven interface, determining frequency spectrum of signal reflected from surface assuming uniformly moving receiver 05 p0813 A70-16261

Correlation function of auroral reflection radio signals with allowance for polar ionospheric scattering and pulse signal transmission and reception 05 p0841 A70-16741

Electromagnetic-acoustic probe for remote wind velocity sensing and radar range performance 06 p1071 A70-18509

Short wave radar tracking of comets, considering tail type criteria for signal reflection 07 p1379 A70-19040

Reflection coefficient for radio wave pulse reflected from ionosphere with large scale fluctuations in electron density, compared to empirical data for reflecting surface irregularities 07 p1231 A70-19170

Ionospheric reflection coefficients from vertical and oblique incidence pulse amplitude data, discussing night conditions effect on Ottawa pulse transmissions 07 p1232 A70-19176

Recording technique for measuring short period variations of radio signal reflections altitudes from ionosphere applicable to fast ionospheric processes 07 p1277 A70-20454

Polarized light electroreflection from GaAs single crystal, noting useful signal linear dependence on electric field 08 p1556 A70-21124

Angular coordinate during multilevel quantization of radar signal reflected from scintillating body on Gaussian noise background, applying maximum probability method 11 p1996 A70-25347

Meteor trail angular dimensions determined by frequency scanning method involving minimum points on reflected signal characteristics 11 p2107 A70-25556

True height of reflection determination for oblique sounding data interpretation, considering method error 14 p2547 A70-30230

Ionized meteor trail radio signal reflections, observing duration and echo quantity random deviations and activity coefficient at specified times 14 p2636 A70-30318

Ionospherically reflected HF radio signal frequency spread measurement involving phase difference crossings counting between antennas 14 p2550 A70-30743

Polarization nature and changes evaluation of radio echo signals reflected from polar auroras 14 p2575 A70-30814

Ionospheric probe for simultaneous measurement of radio signal reflection coefficient and amplitude-frequency characteristics 14 p2576 A70-30830

Snow field mapping with K band radar imagery determining signal return difference with surrounding

terrain, noting role of volume scattering and old snow structure 14 p2578 A70-31238

S band telemetric signals reception transmitted by Apollo 12 during occultation behind lunar disk, discussing lunar surface reflectivity 15 p2699 A70-32290

Speech signals reflection in nervous system, constructing functional perception model for signals conversion into phonetic patterns 15 p2687 A70-32870

Radar and DC pulse signatures of multiple reflection from dry, damp and wet earth for vertical and horizontal polarization 16 p2861 A70-32977

Long range tropospheric radio wave propagation, calculating signal impulse function and time lag between diffraction and reflection 17 p3048 A70-35678

External SHF signal effects on multifrequency spectrum of reflex klystron coupled with long waveguide 17 p3055 A70-35682

Delay time between beams reflected from different parts of meteor trail, using phase invariant and frequency scanning methods 19 p3512 A70-37313

Angular coordinate during multilevel quantization of radar signal reflected from scintillating body on Gaussian noise background, applying maximum probability method 20 p3589 A70-40459

Meteor trail angular dimensions determined by frequency scanning method involving minimum points on reflected signal characteristics 21 p3892 A70-41306

Two echo complex signature in group path vs time records by ionospheric traveling disturbances 21 p3820 A70-42243

E region electron concentration profiles, using ground sounding equipment allowing accurate signal reflection altitude measurements 23 p4190 A70-44078

Atmospheric horizontal stratification and UV transmittance by signal reflection from satellites 23 p4191 A70-44268

True height of reflection determination for oblique sounding data interpretation, considering method error 24 p4316 A70-46305

SIGNAL STABILIZATION

Signal stabilization and performance of nonlinear sampled data systems, suggesting oscillations injection at input 06 p1026 A70-17970

Two mode gas laser behavior under external signal action showing mode locking possibility by combination frequencies due to medium nonlinearity 07 p1296 A70-18764

Terrestrial interface at SPADE terminals for converting international telephone exchange differences into common signaling format [ALAA PAPER 70-413] 11 p1997 A70-25407

Conditionally stable feedback control systems with saturation, comparing large signal stabilization methods 16 p2884 A70-33313

Two mode gas laser behavior under external signal action showing mode locking possibility by combination frequencies due to medium nonlinearity 18 p3271 A70-37108

SIGNAL TO NOISE RATIOS

IF optimum bandwidth for maximizing output SNR in FM receiver with barrier to noise ratio below discriminator threshold 01 p0051 A70-11119

CW laser ranging systems power and signal to power ratio characteristics, finding possible advantages over pulsed systems 01 p0114 A70-11321

Error probability, signal to noise ratio and average signal level for coherent heterodyne and photon limited laser communication systems, using Poisson distributions 02 p0255 A70-11914

Signal to noise ratio for optical heterodyne with inhomogeneous partially coherent signal and local oscillator fields, using phase-quadrature description 02 p0255 A70-11915

Linear system response to random signal inputs, deriving SNR and noise figure equations using autocorrelation and spectral analysis concepts 02 p0257 A70-12193

Multielement active/passive antenna systems maximum SNR value obtained by determining conditions satisfied by parameters 03 p0456 A70-13092

Detection efficiency compared for system containing clipper circuit and quasi-optimal linear system for video pulse signal with additive noise background 03 p0446 A70-13201

Pulse signals optimal filtration in superregenerative receiver and resulting SNR effect 03 p0456 A70-13203

Local criteria and geometric integration for stable transmitter power level selection in group of radio stations ensuring adequate SNR

03 p0446 A70-13237

Binary systems noise resistance with various cross correlation functions and indefinite moment of arrival

03 p0448 A70-13512

Intrinsic noise of passive waveguide multipoint with losses, obtaining mean values and wave correlation functions using scattering matrix

04 p0655 A70-14402

Phase feedback demodulation technique to analyze telemetry performance degradation caused by voice interference in modes of Apollo communication system, providing linear detection scheme

[AAS PAPER 69-609] 04 p0648 A70-14660

Sinusoidal signal detection in Gaussian noise band by zero crossing method, discussing signal frequency position and SNR

04 p0648 A70-14705

Transmission channel nonlinearity effect on signal detector performance for signal received by synthesized antenna indicating SNR change

04 p0659 A70-15287

Radar false return probability relationship to noise, investigating moving window detectors

04 p0652 A70-15341

Differential equations for minimum variance linear filter separating signals from additive correlated noise, using discrete time optimum formulas

[AIAA PAPER 69-73] 04 p0663 A70-15586

Horizontal atmospheric surface layer propagation path for 3370 A UV signal, studying reception distances for given SNR

05 p0812 A70-16242

SNR for IR photovoltaic semiconductor cell generalized for astronomical case, noting stars approximation to black body radiators

05 p0849 A70-16645

Optimum signals for phase locked or delay locked loops determined as function of signal to noise ratio

06 p1023 A70-17523

Optical heterodyne quantum detector response, calculating signal to noise ratios

06 p1008 A70-17524

Lateralization and detection of signals under antiphasic noise masking measured at various SNR levels

06 p1106 A70-17597

Output autocorrelation properties of ideal limiters driven by binary deterministic signal plus stationary zero-mean Gaussian noise

06 p1013 A70-18625

Optimal nonparametric amplitude and phase methods for synthesizing signal detection systems invariant to noise distribution and noise-signal combination

07 p1226 A70-18684

Optimal signal detection with random phase on Gaussian noise background, estimating error probabilities

07 p1226 A70-18685

Continuous signal a posteriori distribution density formed on basis of learning sequence with no a priori information about signal and noise statistics

07 p1226 A70-18761

Quantum statistical decision theory for detection and estimation of signals in random noise

07 p1333 A70-18919

Narrow band limiter influence on SNR at FM reception output by computer simulation using threshold pulse model

07 p1227 A70-19124

Return Beam Vidicon (RBV) system compatibility with requirements for Earth Resources Observation Satellite (EROS), featuring high resolution image sensor for decreasing signal noise

07 p1280 A70-19231

Digital data transmission over discrete time Gaussian channel with noisy feedback, investigating error-exponent/reliability and finite SNR

07 p1235 A70-19362

Magnetic field filtration into time-variable and constant parts, using signal to noise analogies

07 p1266 A70-19440

Signal to noise ratios and fluctuation spectrum of photomultiplier illuminated by laser passing through laser amplifier, noting population level effect

07 p1300 A70-19869

Delay locked closed loop system with and without signal clipping in noisy /Gaussian/ environment applied to radar, sonar and seismic propagation

07 p1242 A70-19997

Signal processor with ratio-squared predetection combining for adaptive antenna array, discussing radiation patterns for coherent and incoherent signal and noise sources

07 p1242 A70-20066

Phase and amplitude modulated signals transmission over band limited channel disturbed by additive white Gaussian noise

07 p1237 A70-20195

Gain-to-noise temperature ratio /G/T/ optimization by dish antenna shaping for nonuniform aperture field distribution

08 p1471 A70-20790

Extremal statistics for signal and noise error probabilities estimation and computer simulation of digital feedback communication systems

08 p1459 A70-20800

White noise and nonlinear effects in telemetry RF links, analyzing received process to phase coherent receiver

08 p1460 A70-20823

Noise effects on joint operation of signal follow-up system with search device using semi-Markov random technique

08 p1461 A70-20864

Circuit analysis of pulse integrator and square-law receiver used as optimal filter during incoherent radio pulse reception on background fluctuating noise

08 p1461 A70-20865

Supersonic flight vehicle plasma sheath effect on effective range of onboard radar installation, discussing SNR

08 p1461 A70-20869

Matched filter SNR behavior under time and frequency domains distortion and random distortion, deriving design equations for energy loss coefficients

08 p1474 A70-21223

Large carrier to noise ratios in FM receivers as function of correlation between Gaussian and impulse shot noise /clicks/

08 p1463 A70-21776

Threshold characteristics of compression line demodulator obtained from output SNR

09 p1631 A70-22017

Pulse signal transmission rate increase by transient processes compensator, discussing stability relation to signal to noise ratios

09 p1639 A70-23696

Signal detection in correlated noise with two stage prewhitening and matched filter system

10 p1833 A70-24220

SNR and system error rate prediction for coherent nonlinear satellite channels based on bounding techniques

10 p1836 A70-24341

Radar transmission SNR formula concerning fluctuations with respect to working frequency

10 p1840 A70-24478

Pulsar radio emission reception with improved SNR based on periodic variation of average reception frequency with time

10 p1948 A70-25165

Angular coordinate during multilevel quantization of radar signal reflected from scintillating body on Gaussian noise background, applying maximum probability method

11 p1996 A70-25347

Communication satellite repeater design requirements to achieve adequate SNR for varying rain and cloud attenuation

[AIAA PAPER 70-498] 11 p1998 A70-25425

Optical heterodyning of Doppler shifted signal with minimal instrumental spectral broadening and high SNR, applying to turbulence structure measurement by CW laser

11 p2062 A70-25630

Multiple access to communication satellite by limiting repeater, considering model of n signals plus band limited white Gaussian noise in zero memory device

11 p2008 A70-26229

Rayleigh and m fading signals spectral location in additive white Gaussian noise, allowing predetermined or variable channel observation time

11 p2010 A70-26268

FM/FM telemetry threshold carrier SNR and receiver IF bandwidth optimization through computer program

11 p2014 A70-26272

Phase velocity and direction estimation of unknown signal propagating across two dimensional array in dispersive waveguide, showing dependence on SNR

11 p2018 A70-26274

Optimum transmitter strategy and receiver gain for linear feedback communication in nonstationary additive noise

11 p2011 A70-26328

Digital filters response errors due to signal amplitude quantization, resulting from analog-to-digital conversion and arithmetic operations

11 p2029 A70-26333

RF amplifier design procedure for maximum stable gain with minimum noise figure

11 p2019 A70-26715

Multiplicative modulation noise of helium-neon traveling wave laser amplifier at micron wavelength

11 p2020 A70-26816

IF combinator for broadband transhorizonal radio relay transmission improvement by providing optimum SNR

11 p2020 A70-26821

Electromagnetic differential flowmeter design and performance, considering SNR

12 p2231 A70-27162

Performance characteristics of quadriphase PSK communication system with noisy reference signal, formulating error probability

12 p2187 A70-27907

Noise stability of optimal binary detection receiver of rectangular-pulse and discrete pseudorandom signals under nonideal synchronization

13 p2364 A70-28869

Binary code distortion in relative phase telegraphy signals under wideband and correlated noise

13 p2364 A70-28870

Delta modulation with slope-overload prediction, showing signal to noise ratio improvement from computer simulation

13 p2365 A70-29146

Computer modeling of nonlinear phase automatic frequency control systems under noise and oscillating disturbance

13 p2383 A70-29303

Analog computer simulation of command signal detectors for reconstruction of transmitted binary character from noisy binary coded signal

13 p2385 A70-29560

Wideband FM signals transionospheric propagation, calculating output spectrum, signal to distortion ratios and signal to noise ratios

13 p2367 A70-29588

FM detector without normalization useful for low S/N reception of FSK and PSK in telemetry systems

13 p2367 A70-29589

Stationary phase error variance for second order phase locked loop for low signal to noise ratios

13 p2383 A70-29590

Digital transition tracking symbol synchronizer improving SNR without lowering loop bandwidth

[JPL-TR-32-1488] 13 p2367 A70-29591

Optimal coherent radar detector for signals with unknown amplitude and background noise intensity

13 p2369 A70-29728

Signal-arrival-time invariance and SNR resolution of discretely analog filters matched to complex radio signals

13 p2380 A70-29736

Noise rejection during synchronous quasi-coherent radio signal reception with binary narrow band linear filter used for voltage shaping

13 p2369 A70-29737

Noise rejection for optimal reception of incoherent binary signals in one beam Rayleigh dispersion radio channel under ionospheric electron density fluctuations

13 p2369 A70-29738

Noise effect on single band modulation receiver using phase automatic frequency control for carrier wave at arbitrary SNR

13 p2370 A70-29739

AM signal reception on strong AM noise background, describing theoretical receiver design

13 p2370 A70-29740

Statistical linearization synthesis of nonlinear self adjusting systems with frequency filters and input signal under white noise

14 p2559 A70-30156

FM limiter-discriminator followed with ideal bandpass filter, deriving output signal to noise ratio

14 p2558 A70-31189

Hard limiting bandpass limiter output signal to noise ratio in PM signal detection calculated using probability density function

14 p2552 A70-31194

Off-axis nonlinear holograms, defining spurious distortion and SNR

14 p2588 A70-31206

Coherent or spatially incoherent light recordings of Fourier transform holograms, investigating resolution cells film grain and signal to noise ratio

14 p2588 A70-31207

Demodulators threshold performance for satisfying carrier to noise ratios requirement of Intelsat 4 system

14 p2552 A70-31352

Two signal selectivity and permissible noise level of FM receiver with linear cascades and detector nonlinearity effects

15 p2696 A70-31506

Hologram superposition on photosensitive surface for multiimage successive recording, examining resolution, SNR, etc

15 p2734 A70-31596

Cascade digital filter computerized design with favorable signal to noise ratio, considering round-off errors

15 p2709 A70-32465

Digital data detection in presence of noise and double sided intersymbol interference, deriving error rates for known and stochastic signals

15 p2703 A70-32561

Filter parameter estimation in serially correlated measurement noise, using recursive least squares analysis

15 p2704 A70-32591

Augmented state variable method of nonlinear discrete system identification with noise corrupted input observations

15 p2704 A70-32592

- Radiometer employing frequency domain coding of noise-like signal spectrum, comparing with Dicke system
16 p2871 A70-32926
- Model probability distribution for hybrid phase locked loop derived by Fokker-Planck techniques, providing superior performance for all SNR
16 p2882 A70-33038
- Broadband and narrowband pulse signal noise electromagnetic interference prediction techniques for filter or shielding parameters evaluation
16 p2862 A70-33065
- Solid state spectrum centered receiver for eliminating externally generated pulse type interference between radar sets
16 p2862 A70-33066
- Laser ranging and tracking for high velocity targets, discussing SNR considerations, ambiguity resolution, error analysis, measurement centroid and target acquisition
16 p2862 A70-33165
- Airborne electro-optical imaging sensor subsystems performance optimization, comparing mathematical and graphical methods for providing maximum SNR
16 p2906 A70-33172
- Low light intensities measured using photon counting method, comparing signal to noise ratio with lock-in method
16 p2911 A70-33524
- Probability density function of specularly fading signal plus noise for frequency shift keying and pulse radar systems
16 p2865 A70-34040
- Radar detection range determination by parametric method based on SNR formula
16 p2866 A70-34062
- Direction finder for point source signals, discussing mathematical model for random noise in space, S/N performance and equipment design
17 p3042 A70-34586
- Intensity interferometer for weak noise-like signal power measurement in presence of additive Gaussian noise
17 p3089 A70-35265
- Loudspeaker optimal arrangement for speech intelligibility in aircraft crew compartments, discussing apparent SNR improvement
17 p3039 A70-35564
- Monaural detection and filtering of sinusoidal signals in noise, using amplitude model
17 p3033 A70-35610
- Optimum spectral control of nonlinear plant, using Newton iteration and linear programming
18 p3234 A70-36075
- Frequency filters in nonlinear self adaptive system design for noncorrelated input and noise signals
18 p3234 A70-36119
- Asymptotic transmitting capacity of continuous channel with intense independent and additive noise
18 p3228 A70-36598
- Lower reliability estimates for block codes of binary channels with feedback noise
18 p3235 A70-36599
- Threshold extension capabilities of phase lock loop and FM feedback demodulators, calculating output SNR for broadband systems
18 p3229 A70-36784
- Magnetic field filtration into time-variable and constant parts, using signal to noise analogies
18 p3249 A70-36914
- Signal to noise ratios for metastable and ion detection of excited neutral molecules in beam
18 p3262 A70-37096
- Continuous signal a posteriori distribution density formed on basis of learning sequence with no a priori information about signal and noise statistics
18 p3229 A70-37105
- Two dimensional phase distribution function of mixture of Gaussian noise with amplitude modulated signal
18 p3229 A70-37110
- Mechanical parametric amplification, improving SNR of acoustic systems in hostile environments
19 p3422 A70-37695
- Signal processing by differential data and common mode amplifiers and active filters, emphasizing low level transducers
19 p3431 A70-38529
- RF communication signal to noise improvement by time variant tracking filter with high Q superconductive resonant cavity
19 p3391 A70-38892
- Electronic correlation signal analysis for localizing noise sources, detecting signals against background noise
20 p3601 A70-39650
- Signal modulation by pulse ratio variation in magnetic tape channel, discussing SNR characteristics
20 p3586 A70-39707
- Analog communication optimal nonlinear modulation scheme design for large SNR through transformation into inner product functions
20 p3587 A70-39973
- Angular coordinate during multilevel quantization of radar signal reflected from scintillating body on Gaussian noise background, applying maximum probability method
20 p3589 A70-40459
- Two dimensional and volume diffuse signal beam dielectric holograms, calculating and measuring diffraction efficiency and signal to noise ratio
21 p3835 A70-40717
- Statistical confidence levels for frequency analysis, detecting peak sinusoid for desired signal to noise ratio
21 p3825 A70-40867
- Digital filtering of sampled narrowband sinusoidal signal embedded in wideband white noise, assessing hard clipping effect on performance by simulation on digital computer
21 p3791 A70-41948
- Single picosecond mode-locked laser pulse selection and multiple pass amplification device, obtaining high energy and signal to noise ratio
21 p3838 A70-42023
- Wideband detection of frequency uncertain M-ary frequency shift-keyed /MFSK/ transmission in Gaussian noise, deriving symbol error rate for limiting SNR cases
21 p3792 A70-42177
- Dynamic noise performance equivalence of phase locked or double superheterodyne tracking loops, using noise free external generator
21 p3793 A70-42180
- Transient behavior of first order phase locked loop in presence of noise, solving Fokker-Planck equation for loop dynamics by numerical integration
21 p3802 A70-42181
- Photographic processing methods for high efficiency low noise phase holograms on silver halide emulsions
22 p4025 A70-42286
- Recursive signal detection scheme, obtaining SNR by derivative approximation
22 p3984 A70-42317
- Threshold SNR for signal frequency meter based on zero number count method, determining reliability
22 p3985 A70-42401
- Random signal detection on uncorrelated Gaussian noise background with unknown intensity, discussing detector performance
22 p3986 A70-42553
- Multichannel correlation filter devices for processing periodic fluctuating signals in noise background
22 p3987 A70-42557
- Optimal reception of phase manipulated signal on noise background with unknown statistics and information parameter a priori probabilities
22 p3987 A70-42561
- Radar signal synthesis in noise with good range resolution for rapidly fluctuating targets, using ambiguity function
22 p3988 A70-42566
- Signal accuracy prediction in nonlinear steady or unsteady continuous and discrete automatic control systems in random noise, using statistical linearization
22 p4003 A70-42883
- Optimal nonlinear filtration for continuous automatic data transmission with radio signal under white, narrow band and Markov noise
22 p4004 A70-42891
- Computer-based seismic data acquisition system using digital vibroseis process for eliminating low signal to noise ratio characteristics
22 p4038 A70-43092
- Signal and noise properties of degenerate and quasi-degenerate nonreciprocal parametric amplifiers without circulators
22 p3990 A70-43423
- VHF omnidirectional problem /VOR/ receiver, considering noise reduction problem and active filter importance to signal improvement and system accuracy
22 p3992 A70-43586
- Signal shape optimization by minimizing dispersion in temporal position estimates for radio pulse in presence of additive white noise
23 p4161 A70-43961
- Multiplicative noise reduction during transmission of analog signals over tropospheric microwave relay links
23 p4162 A70-44090
- Hologram superposition on photosensitive surface for multimage successive recording, examining resolution, SNR, etc
23 p4195 A70-44280
- Communication system signal to noise ratio requirements, determining minimum signal power level
23 p4163 A70-44297
- Quantum noise in narrow-band ring laser, noting mode amplification of weak monochromatic signals
23 p4202 A70-45056
- Multiplicative modulation noise of helium-neon traveling wave laser amplifier at micron wavelength
24 p4317 A70-45188
- SNR of moving diffuser illuminated by laser light, considering image plane and Fresnel field observations
24 p4354 A70-45670
- Quantum detector with impinging EM field, discussing photoelectron counting distribution and signal with white noise
24 p4312 A70-46051
- Weak noise and threshold effects on estimation error for nonlinear PM systems
24 p4312 A70-46053
- Optimal noiseless linear information feedback estimation for additive white Gaussian noise channels, applicable to digital transmission
24 p4313 A70-46064
- Output signal/quantization noise ratio, dynamic range and transmission error effects for syllabically companded delta-sigma modulator systems
24 p4320 A70-46152

- SIGNAL TRANSMISSION
- NT AUTOMATIC PICTURE TRANSMISSION
- NT BIOTELEMETRY
- NT DATA TRANSMISSION
- NT DOUBLE SIDEBAND TRANSMISSION
- NT IONOSPHERIC F-SCATTER PROPAGATION
- NT IONOSPHERIC PROPAGATION
- NT MICROWAVE TRANSMISSION
- NT MULTIPATH TRANSMISSION
- NT PCM TELEMETRY
- NT PULSE FREQUENCY MODULATION TELEMETRY
- NT RADAR TRANSMISSION
- NT RADIO TELEMETRY
- NT RADIO TRANSMISSION
- NT SATELLITE TRANSMISSION
- NT SHORT WAVE RADIO TRANSMISSION
- NT SINGLE SIDEBAND TRANSMISSION
- NT TELEMETRY
- NT TELEVISION TRANSMISSION
- NT TRANSEQUATORIAL PROPAGATION
- Dual frequency ranging within narrow bandwidth of VHF communications satellite repeater for transmitted signals correction of ionospheric refraction error
01 p0043 A70-10781
- Rms error for reproduction of satellite signal transmitted through continuous Gaussian channel assessed by numerical calculation
01 p0046 A70-11513
- Electrical signaling civil aircraft systems, discussing design and integrated maneuver demand controls
02 p0224 A70-11835
- Earth space signal propagation characteristics obtained by satellite-borne radio interferometer provide phase information in addition to amplitude for improving navigation accuracy
02 p0260 A70-12567
- Wideband satellites bandwidth and aperture limits direct measurement based on ground monitoring of CW signals, taking into account ionospheric dispersion
02 p0261 A70-12577
- Superrefractive layer development at 3000 ft during radio refractive index profile measurements by microwave refractometer carried on aircraft, producing enhanced signals
02 p0261 A70-12591
- Airplane navigation based on VHF ranging between aircraft and geostationary satellite, examining errors by unknown propagation characteristics of signal in ionosphere
02 p0262 A70-12594
- Radar pulse scattering from ionized media including nuclear explosion fireballs and high speed reentry vehicle wakes, analyzing to retrieve backscattered pulse signal envelope
02 p0262 A70-12602
- Signal orientation insensitive filter for pattern recognition
02 p0266 A70-12701
- Faraday rotation observations on Explorer 22 signals at two receiving stations, discussing comparative evaluation procedures and results
03 p0472 A70-12874
- Optimal selection of centralized communication network of combined radial and linear structures minimizing disconnected peripheral points
03 p0446 A70-13238
- Reduced multipoint equivalent scattering parameters derivation by matrix method, determining load reflection coefficients effect on signal attenuation and phase shift
03 p0458 A70-14038
- PCM signal transmission testing over radio links with two level phase modulation
03 p0452 A70-14282
- Physical model to study coaxial or triaxial cable systems interaction with ionizing radiation fields, emphasizing effects governing induced signals
04 p0658 A70-14746
- Integrodifferential equation solved for plane wave reflection and transmission by random medium assuming homogeneous background refractive index
04 p0649 A70-14970
- Small scale disturbances and radio wave scattering effects on signal transmission and radiophysical observations in ionosphere
04 p0653 A70-15723

Transmission equipment of Pleumeur-Bodou space communication installation including modulators, converters and amplifiers for telephone and TV carriers
05 p0819 A70-15986

Current carrier motion and diffusion capacity in p-n junctions with highly doped regions under large variable signal
05 p0892 A70-16197

Horizontal atmospheric surface layer propagation path for 3370 A UV signal, studying reception distances for given SNR
05 p0812 A70-16242

Group delay characteristics curvature in radio relay systems, analyzing crosstalk in picture- sound and beamed multiplex signal transmission by nonlinear distortion method
05 p0815 A70-16774

Rate of change of radio ray path length for transionospheric satellite VHF signals determined from Doppler and Faraday effect analyses
06 p1008 A70-17578

HF signals propagation through auroral curtain investigated for scattering or blanketing effects, discussing ground scatter echo cut-off caused by sporadic E layer
06 p1011 A70-18538

Communication satellite transponders design, cost, reliability, manufacturing, testing and future developments
07 p1241 A70-19620

Monograph on time measurements covering time scales, intervals, natural and artificial clocks, frequency standards, time and time signal transmission
07 p1283 A70-19664

Dynamic calculation of oscillating liquid filled elastic cavity on elastic kinematic system under random load, using random signals transmission theory
07 p1416 A70-20194

Phase and amplitude modulated signals transmission over band limited channel disturbed by additive white Gaussian noise
07 p1237 A70-20195

Time-frequency correlation function for fading communication channel between transmitter and receiver sites, using AM transmissions as probing signals
08 p1458 A70-20796

Binary, ternary and multilevel digital signals transmission codes emphasizing PCM signals
09 p1631 A70-22038

Inertialess nonlinear quadrupole output of oscillations modulated by normal noise, analyzing correlation functions
09 p1637 A70-23159

Amplitude modulation of microwave signals propagated through periodically varying plasma
09 p1639 A70-23673

Time correlation telemetering systems design, describing structural scheme
11 p2004 A70-25929

Digital computer simulation of Bake concept as related to tropospheric CW signal scatter measurement
11 p2009 A70-26240

Phase velocity and direction estimation of unknown signal propagating across two dimensional array in dispersive waveguide, showing dependence on SNR
11 p2018 A70-26274

Memoryless input discrete noisy channels essential equivalence to white Gaussian channel for rates above capacity using extreme value theory
11 p2010 A70-26326

Atmospheric turbulence effects on line-of-sight electromagnetic wave propagation, deriving signal statistics for nonvalid weak scattering solutions case
11 p2012 A70-26764

Large capacity long distance transmission by circular waveguides, describing artery frequency modulation and equipment for multiplexed telephone messages transmission
12 p2194 A70-27233

Microwave signals covariance and spectra calculation for amplitude and phase fluctuations propagated over line-of-sight path through turbulent atmosphere
12 p2189 A70-27963

Navigation satellite systems, analyzing error sources in signal processing and propagation developing computer programs
13 p2447 A70-28429

Digital signals transmission codes comparison for transient response by reducing channel bandwidth to obtain error probability
13 p2372 A70-28899

Analog computer simulation of command signal detectors for reconstruction of transmitted binary character from noisy binary coded signal
13 p2385 A70-29560

Wideband FM signals transionospheric propagation, calculating output spectrum, signal to distortion ratios and signal to noise ratios
13 p2367 A70-29588

Small scale disturbances and radio wave scattering effects on signal transmission and radiophysical observations in ionosphere
14 p2550 A70-30807

Quantum mechanical communication system with thermal noise disturbance, analyzing reliability function and channel capacity
14 p2551 A70-31120

Mean first passage signal time in one shot electronic system as function of threshold level
14 p2552 A70-31198

Control and guidance theories for biological problems, discussing signal transfer of linear control units and mathematical approaches
15 p2689 A70-31741

High power TWT for satellite communications ground stations, including Intelsat experience
17 p3054 A70-35282

Spatial signal transmission through open resonator determination based on resonator integral equation, extending to dielectric lens with finite Fresnel diffraction number
18 p3259 A70-36480

Asymptotic transmitting capacity of continuous channel with intense independent and additive noise
18 p3228 A70-36598

Atmospheric aerosols, fog and rain effects on signal transmittance and backscatter at 3400-10600 A
18 p3248 A70-36751

Gas flow velocity measurement by thermal signal emitted from thin wire fed with modulated known frequency current
19 p3406 A70-38673

Centimeter wave transmitting and receiving equipment for studying nanosecond pulse propagation
20 p3632 A70-39627

Pulse ratio modulation analysis based on information theory, emphasizing magnetic tape channel capacity optimal utilization in signal transmission
20 p3586 A70-39708

Superradiation signal stationary pulse excitation, describing quantum statistical theory of condensed media and gases, forced induction, signals and echoes
20 p3642 A70-39756

Transmission power formula for satellite to ground station and slant ranges calculations
21 p3785 A70-40755

Cosmos 142 satellite measurements VLF radio signals transmitted through ionosphere by ground based stations
21 p3786 A70-40836

Triboelectric noise in mechanically flexed low level signal cables for piezoelectric transducers with high gain amplifiers
21 p3825 A70-40866

Optical communications system for transmission and detection of PCM word pattern at gigahertz rates, discussing optical and electrical modulation
21 p3788 A70-41339

Wideband high speed PCM/AM optical communication system using mode locked He-Ne laser, noting simultaneous signal transmission and bit rate
21 p3789 A70-41354

Seismic signal by Apollo 12 lunar module impact indicating deep layer of powder by signal propagation
21 p3920 A70-41894

Noise effect on signal parameter control in linear measurement devices
22 p3984 A70-42394

Global rescue alarm net /GRAN/ using satellites for relaying distress signals, eliminating current line of sight restrictions
23 p4143 A70-44455

Optimum input pulse signal synthesis for transmission through lossless homogeneous isotropic plasma, using matched filter theory
23 p4228 A70-44962

Carrier frequency transfer of amplitude modulated signal at two coupled transitions in traveling wave gas laser
23 p4202 A70-45055

Output signal/quantization noise ratio, dynamic range and transmission error effects for syllabically companion delta-sigma modulator systems
24 p4320 A70-46152

SIGNALS

Signaling system for communication satellites demand assignment, considering error control, unit negative acknowledgement, system parameters selection, control signals, etc
10 p1837 A70-24347

Soviet book on pseudorandom signals theory and application covering shape selection, generation, system noise, etc
22 p3985 A70-42456

SIGNATURE ANALYSIS

Gravitational field signatures for planetary fine structure analysis, describing lunar orbiter, selenodyssey experiment and gravity field and earth gravity field satellite observation
11 p2111 A70-26029

Signature theory application to space mission planning and archeological project
11 p2051 A70-26034

ERTS multispectral scanner with optimal sensitivity and resolution for agricultural scenes signature analysis
12 p2229 A70-26941

Overpressure, rise time and wave period of sonic boom signatures at ground level from unaccelerated supersonic overflights
14 p2530 A70-30608

Visible polarization signature for remote sensing of soil surface moisture, noting invariance to partial shadowing in plowed or rough soils
15 p2724 A70-31667

Target signature concept of spectral, spatial, temporal, and polarization effects to develop electromagnetic signatures against background, considering remote sensor system design
16 p2910 A70-33437

Electrical, electronic, electromechanical, pneumatic and hydraulic subsystems failure pattern determination, discussing sensing techniques in signature analysis
16 p2917 A70-33505

Secondary effect signatures for potential failure detection in jet aircraft engine compressor blades
16 p2918 A70-33517

Ecological potentials in spectral signature analysis, using laboratory leaf and soil spectral reflectance data
17 p3078 A70-35612

Vortex signature recognition from radial velocity field by Doppler radar
20 p3664 A70-40067

Two echo complex signature in group path vs time records by ionospheric traveling disturbances
21 p3820 A70-42243

Nondestructive tests for performance levels, discussing signature analysis as methodology
24 p4338 A70-45736

SIGNALS

NT MAGNETIC SIGNATURES

NT RADAR SIGNATURES

NT SPECTRAL SIGNATURES

SIGNS (SYMBOLS)

U SYMBOLS

SIGNS AND SYMPTOMS

NT ASPHYXIA

NT BRADYCARDIA

NT HEADACHE

NT VERTIGO

Wolff-Parkinson-White syndrome simulation of myocardial infarction, indicating false positive tests for exercise electrocardiograms
09 p1622 A70-23468

Psychovegetative and neurovegetative stress syndroms in flying personnel removed prematurely from active service as result of psychophysiological complementary diagnostics
12 p2177 A70-27041

Involuntary vectorcardiographic signs of right ventricular hypertrophy
17 p3025 A70-34859

Single ventricle and hypoplastic left and right heart syndromes, investigating with reflected ultrasound
17 p3032 A70-35472

Wolff-Parkinson and White syndrome applicability in aeromedical appraisal for aircrew selection, noting effects of paroxysmal tachycardia
17 p3040 A70-35916

Avionics maintenance effectiveness logistics, discussing symptom pattern observation technique /SPOT/ for in-flight data
19 p3554 A70-38399

Neurotic syndromes in aviation medicine, discussing acute reactions, anxiety, depressions, structured syndromes and psychosomatic disorders
21 p3771 A70-41490

Flying personnel fitness, discussing Wolff-Parkinson-White syndrome
22 p3975 A70-43695

Cinecoronary arteriographic investigation of chest pain patients, establishing correlations of clinical symptoms, coronary artery narrowing, arterial lesions, serum cholesterol levels, etc
23 p4145 A70-43948

SIKORSKY AIRCRAFT

NT CH-3 HELICOPTER

NT CH-54 HELICOPTER

SIKORSKY MILITARY HELICOPTERS

U MILITARY HELICOPTERS

SIKORSKY S-64 HELICOPTER

U CH-54 HELICOPTER

SILANES

Silane coupling agents glass-catalyzed hydrolysis without presence of acid, discussing reaction kinetics
06 p1091 A70-17599

Reinforced plastics adhesion to hydrophilic mineral surfaces by using silane coupling agents
16 p2937 A70-33374

Pyrolyzed tetraethoxysilane for carburizing steels and Ti alloys at 850-1050 C
17 p3102 A70-35409

Photoelectron spectra of methane, silane, germane, methyl fluoride, difluoromethane and trifluoromethane, describing electron spectrometer with double focusing electrostatic plates
19 p3374 A70-38269

SILENCERS

Airport noise silencers for aircraft engines, discussing design, operation and damping efficiency
05 p0829 A70-16353

SILICA
U SILICON DIOXIDE
SILICA GLASS
 Amplification cross section of 1.06 micron transition of trivalent Nd ion in alkaline silicate glass host material, based on three level energy level diagram 02 p0312 A70-12111
 Time-temperature relation necessary to fine Libyan desert glass and remove gas bubbles calculated by viscosity determination at various temperatures 05 p0843 A70-16833
 Be atoms effect on lattice structure of three component sodium oxide-beryllia-silicate glasses using IR absorption spectra 07 p1315 A70-18704
 Stimulated Mandelstam-Brillouin scattering and fracture of molten quartz and silicate glasses produced by laser giant pulse 11 p2061 A70-25380
 Impact crater cross section in fused silica, describing photomicrographic technique for distinguishing hypervelocity from low energy impacts [AIAA PAPER 69-367] 11 p2138 A70-26133
 Relaxations from anelastic and dielectric measurements of fused silica and soda-silica glasses at low temperatures ascribed to vibration modes exceeding Debye spectrum 16 p2960 A70-32996
 Compositional variation effect on low silica glass formation based on calcium aluminates 16 p2934 A70-33273
 Nonactive absorption by silicate neodymium glasses at emission wavelength as function of pumping flash rate 19 p3448 A70-38739
 Laser characteristics of Nd doped lithium germanate and silicate glasses, discussing spectroscopic properties 21 p3838 A70-42010

SILICATES
NT ALUMINUM SILICATES
NT CALCIUM SILICATES
NT ENSTATITE
NT FELDSPARS
NT FORSTERITE
NT GARNETS
NT KAOLINITE
NT PYROXENES
NT SODIUM SILICATES
NT YTTRIUM-ALUMINUM GARNET
NT YTTRIUM-IRON GARNET
 Chondrite-normalized lanthanide pattern of silicate inclusion of Woodbine iron meteorite, showing differences from mesosiderite phase and chondrite 01 p0177 A70-10340
 Oxides and silicates universal equations of state based on experimental data including elastic properties, density, mean atomic weight relations and geophysics interpretations 02 p0294 A70-12778
 Interstellar polarization by graphite-silicate grain mixtures, observing variability in wavelength dependence of polarization for various models 03 p0577 A70-14218
 Silicate enamel coating formulas for application on titanium exhibiting adequate adhesion 05 p0872 A70-16599
 Heat resistant silicate enamel coatings to protect steels and alloys against high temperature gas corrosion, studying properties by various methods 05 p0872 A70-16600
 Silicates thermal conductivity-Debye temperature relationship from thermal conductivity and acoustic data, applying to earth conductivity measurements 09 p1665 A70-22054
 Synthetic silicate liquid viscosity with lunar rock composition compared with volcanic rock on earth 10 p1938 A70-24074
 Crystal-chemical and geophysical implications concerning earth mantle phase transitions from beta magnesium silicate crystal structure 11 p1994 A70-25333
 Composition and monoclinic parameters of chromium sulfide mineral brezniaite in metal matrix and silicate inclusions of Tuscon meteorite using electron microprobe 11 p2110 A70-26004
 Total nitrogen content determination in silicate samples of rocks, synthetic silicate standards, NBS steels and meteorites using inert carrier-gas extraction-gas chromatography 13 p2362 A70-29497
 Weekeroo Station iron meteorite silicate inclusions chemical composition compared to chondrites 13 p2497 A70-29858
 Comet Bennett 1969i photometric observations, showing blackbody-like continuum at short wavelengths with sharp peak due to silicate grains 14 p2642 A70-30895
 Lunar, meteoritic and terrestrial silicate rock chemical individuality based on atomic ratios 15 p2799 A70-31896
 Metal-silicate rock friction in ultrahigh vacuum of lunar environment 17 p3101 A70-34760

Interstellar silicate absorption in IR spectra, discussing existing observations 17 p3157 A70-34840
 Thermal release profiles and retention coefficients of injected argon ions for silicates and iron simulating meteoritic materials 19 p3474 A70-38601
 Silicate inclusions in iron meteorites analyzed by microprobe and classified according to phase assemblages, compositions and textures 20 p3701 A70-38981
 Quartz- and silicate-graphite mixtures carbothermal reduction in vacuum at 1400 C 20 p3583 A70-40425
 Interstellar silicate absorption bands four color photometric observations in galactic direction, using metal mirror telescope 20 p3713 A70-40431
 Interstellar spherical dust particles from meteoritic silicates and dirty ice, calculating optical properties and scattering functions 21 p3889 A70-41147
 Lunar crystalline rock static and dynamic deformation, examining regolith and silicates textures and structures 21 p3897 A70-41515
 Trace phyllosilicates in Apollo 11 soil sample and rock, using electron microscopy and diffraction studies 21 p3897 A70-41518
 Lunar petrology of silicate melt inclusions from Apollo 11 rock samples, discussing heating experiments 21 p3902 A70-41548
 Earth-moon system formation theory, discussing condensation from terrestrial hot extended silicate atmosphere 22 p4098 A70-42548
 Weak superstructure line patterns of ternary phases with TiFeSi and ordered iron phosphides by single crystal, Guinier powder and diffractometer techniques 24 p3459 A70-45249
 Neutron activation determined concentrations of Ni, Ga, Ge and Ir in iron meteorites with silicate inclusions 24 p4401 A70-45376
 Hydrus Cu-Ca silicate mineral (kinoite) from Arizona occurring as single crystals and veinlets 24 p3429 A70-45459
 Chemical composition and degree of thermodynamic equilibrium reflected in ferromagnesian silicates of chondrites 24 p4411 A70-45793
 Molybdenum disilicate and aluminum oxide coating sealing heat resistance tests 24 p4364 A70-46341

SILICIDES
 Free energies of formation determined for tantalum silicides from EMF measurements on cells with solid thorium-yttria electrolytes 01 p0041 A70-10084
 Silicide-coated columbium alloys reuse capabilities under flight conditions, considering coating local damage and emittance [AIAA PAPER 70-279] 07 p1315 A70-20388
 Ti tetrachloride, Si tetrachloride and hydrogen gas mixtures flow over heated graphite substrates, describing Ti silicides formation 09 p1703 A70-22646
 Preoxidation treatment alleviating silicide pest in protective coatings for refractory metals, discussing effectiveness against high temperature oxidation 13 p2434 A70-29082
 Molybdenum trisilicide-tantalum trisilicide and molybdenum trisilicide-tungsten trisilicide interdiffusion for molybdenum disilicide protective coating on Ta and W surfaces 21 p3840 A70-42056
 German monograph on sintered molybdenum silicide recrystallization following high temperature heating in oxidizing atmosphere 24 p4367 A70-45575

SILICON
NT SILICON ISOTOPES
 Scanned laser microscope producing shadowgraph displays of IR transmittance variations attributed to defects in polished Si and GaAs semiconductor wafers 01 p0105 A70-10025
 Si cleaved crystal nature on basis of Auger spectra, discussing impurity stabilization 01 p0159 A70-11175
 High energy dopant ion implants into silicon, discussing implantation profiles and electrical conductivity for use in type conversion and electrical junctions 04 p0730 A70-14727
 Silicon effect on stress corrosion resistance of low alloy high strength steels in NaCl solution for different tensile strength ranges 04 p0707 A70-15272
 Electron microprobe determinations of Si concentrations in metal of iron meteorites, showing weak evidence for Si presence in earth core 05 p0921 A70-17094

Meyer-Neldel rule interpretation of distribution width parameter dependence on activation energy annealing of defects in irradiated Si 06 p1106 A70-17925
 Reactive scattering from solid surfaces, discussing atom beam reaction of O with heated Ge and Si single crystals 07 p1342 A70-20117
 Integrated circuit film and hybrid technologies in microelectronics, discussing role of monolithic Si arrays 09 p1645 A70-22632
 Relative transition probabilities of Si I and II determined from emission spectra obtained by injecting SiCl₄ vapor into argon plasma jet 09 p1737 A70-23315
 Silicon window with double carrier injection to achieve high power broadband microwave switching, obtaining power increase over p-i-n diodes 10 p1847 A70-23892
 Silicon avalanche diodes contingencies effect on material choice 10 p1850 A70-24622
 Planar Ge and Si diodes application in pulsed bridge elements, investigating current-voltage and resistance-voltage characteristics 11 p2015 A70-25350
 Dopant effect on dislocation mobility in elastically loaded silicon crystal using internal friction and modulus defect measurements 11 p2099 A70-26394
 Electron bombardment produced clustered displacements, paired vacancies and interstitial atoms in Si, discussing possible mechanism for developing defects 11 p2142 A70-26638
 Epitaxial Ge deposits on Si control by Kikuchi pseudolines, considering surface polish, crystallinity and substrate orientation 13 p2470 A70-28957
 Silicon and alpha-alumina support interface reactions during nucleation-coalescence and after epitaxial growth, investigating electrical properties 13 p2470 A70-28958
 Gold impurity photovoltaic effect in silicon, determining optical cross section for transition 14 p2627 A70-30528
 B, In or Ga doped Si photosensitivity dependence on sample temperature, supply voltage and illumination intensity, determining optimal operating conditions 15 p2782 A70-31631
 Ge and Si hemispherical emittance, showing doping and temperature effects 15 p2784 A70-32055
 Average triton energy required to produce electron-hole pair in silicon measured, describing precision charge calibration of amplifier system 15 p2784 A70-32396
 Hydrogen effect on impurity redistribution in heteroepitaxial Si layers on sapphire substrate 15 p2785 A70-32529
 Micro-Hall device as tool for evaluating epitaxial silicon in integrated circuit processing 15 p2710 A70-32573
 K-band high power Si avalanche diode oscillators, discussing decrease in pulse peak power output on basis of quenched plasma effect 16 p2880 A70-34260
 Cone crack closure in brittle solids, discussing optical and X ray studies on glass and silicon during unloading 17 p3183 A70-34621
 UV stellar spectra absorption, considering silicon and carbon opacity effect on Balmer discontinuity and Paschen continuum 17 p3159 A70-34880
 Lithium-like line spectra in Mg, Al and Si observed with grazing incidence spectrometer and low inductance microfarad spark source 17 p3138 A70-35720
 Silicon elastic constant measurement by Debye-Sears effect, using He-Ne laser source 18 p3298 A70-36952
 Silicon-containing pyrocarbon, relating microhardness to microstructure 18 p3279 A70-37220
 Ge and Si surface electrical properties, discussing conductivity, field effect, work function, current carriers, photoconductivity, photocurrent carrier capture, etc 19 p3483 A70-37297
 Heavy cosmic ray abundance attributed to thermal nucleosynthesis during silicon burning at high temperature and density 19 p3507 A70-38132
 Si photocells fabrication, reliability and energy conversion efficiency 19 p3358 A70-38479
 Epitaxially grown Si contact for area reduction of MOS transistor circuits 20 p3596 A70-39099
 Ionospheric Si and SiO ions equilibrium interconversion during Leonid meteor shower 20 p3621 A70-39351

- Mo-Si system phase diagram by X ray, microstructural and thermal differential analyses, identifying eutectic, peritectic and eutectoid equilibria
20 p3649 A70-39773
- Lithium-diffused silicon, investigating heat treatment and electron irradiation effects on electrical resistivity at high temperatures
20 p3687 A70-40164
- Annealing properties of radiation damage in lithium-diffused silicon, formulating kinetic equation to describe processes associated with recovery and instability
20 p3687 A70-40165
- Helium-like resonance, intercombination and forbidden transitions of Ca, Si and S lines during 3b solar flare decay
20 p3700 A70-40420
- Planar Ge and Si diodes application in pulsed bridge elements, investigating current-voltage and resistance-voltage characteristics
20 p3600 A70-40462
- Apollo 11 lunar rocks and fines oxygen, Si and Al content determination by neutron activation analysis
21 p3774 A70-41566
- Apollo 11 lunar rocks and soil hydrogen, C and Si concentration and isotopic composition
21 p3774 A70-41568
- High resistivity single crystal silicon wafers induced IR absorption measurement, using Nd doped glass laser
21 p3837 A70-41916
- Holographic recording on n-type Si single crystal surface by photoanodic engraving
22 p4026 A70-42332
- Silicon line collisional broadening by electrons and hydrogen atoms, discussing Stark effect and van der Waal interactions
22 p4076 A70-42861
- Rb and Cs ions implanted Si analyzed by Hall effect and sheet resistivity measurements and channeling techniques
22 p4087 A70-43143
- Radiation-produced defects in silicon semiconductor devices, annealing gamma ray, electron and fast neutron damages
22 p4087 A70-43328
- Silicon precipitation in nonrefined annealed Al, examining heat treatment effects
22 p4057 A70-43550
- Electron radiation damaged Si, investigating p type defect concentration effect on isochronal temperature in annealing by fractionation experiment
23 p4231 A70-44887
- Si crystal microdefects influence on semiconductor device performance and reliability
24 p4391 A70-46015
- Si-carbide composites electrical conductivity from temperature and thickness dependence, obtaining volt-ampere characteristics via computer method
24 p4391 A70-46154
- SILICON ALLOYS**
- Size distribution of Ni-Si particles precipitated from Si solid solution in Ni measured as function of concentration, aging time and temperature
02 p0317 A70-12320
- Cracks development in hydrogenated silicon iron, investigating plastic strain relation and brittle rupture propagation
06 p1165 A70-17580
- Ce-Ni-Si system X ray and microstructural analysis, constructing phase diagram for Ce contents of 0-33.3 wt percent
08 p1555 A70-21115
- Silicon containing alpha matrix Ti alloy with high creep strength and stability at elevated temperatures, studying processing and heat treatment effects on properties
08 p1509 A70-21853
- Si-Ge air-vacuum thermocouples for thermoelectric conversion, describing construction materials, mechanical and electrical properties, radiative heat transfer operation, etc
10 p1807 A70-24896
- Thermoelectric generators design, discussing Si-Ge air-vac thermocouple configurations, compression modules, thermal losses, etc
10 p1808 A70-24897
- Protective coatings with Si-Zr alloys for graphite, discussing wettability, spreading kinetics and impregnation
13 p2439 A70-29503
- Ti-Si eutectic alloys unidirectional solidification by zone melting
19 p3450 A70-37375
- Phase diagrams and nonvariant equilibria points of Ti-Si alloys subjected to prior annealing, determining phase transformations, decomposition and other properties as function of temperature
22 p4057 A70-43350
- Self flammability temperature of binary alloy Al-Si powders in aerosol state as function of chemical and phase compositions
23 p4205 A70-44046
- Eutectic and hypereutectic Al-Si alloy quench modification by rapid solidification, investigating microstructure and mechanical properties
24 p4362 A70-46183
- Si content and chip treatment effects on drilling machinability of Al-Si alloys
24 p4349 A70-46199
- SILICON CARBIDES**
- Tensile tests of heat treated silicon carbide coated B filament reinforced metals, discussing fiber strength and interfacial stability
01 p0117 A70-10483
- Oxidation resistance of mixed silicon nitride and silicon carbide refractory materials at high temperatures
03 p0514 A70-12979
- Mechanical properties of Al composites reinforced with alpha-silicon carbide sintered whiskers, discussing voids, fiber breakage and orientation effects
03 p0506 A70-13113
- N-type layer formation with ion implanted nitrogen or Sb in p-type alpha-SiC, evaluating electrical characteristics, discussing junction devices formed
04 p0732 A70-15685
- Kinetics of attack of SiC in monoatomic mixtures of N and O generated by microwave discharge dissociation
07 p1421 A70-19332
- Silicon carbide whiskers end structure using field emission patterns
08 p1528 A70-21551
- Al alloy matrix composites with beta-SiC whiskers reinforcement, evaluating tensile and fatigue properties
08 p1523 A70-21856
- Crystal growth of 2H silicon carbide showing temperature profile along susceptor as affecting factor
09 p1739 A70-22498
- Al-Si and Cu-Ti eutectic alloys showing good ohmic contacts to SiC
10 p1927 A70-23990
- Silicon carbide whiskers properties and applications compared with other reinforcing fibers
11 p2070 A70-26340
- High temperature kinetics of pyrolytic silicon carbide oxidation and nitridation in dissociated gases
13 p2361 A70-29077
- Metallic base fiber and particulate composites, emphasizing silicon carbide, sapphire, boron and graphite filaments
14 p2597 A70-31168
- Boron, silicon carbide and graphite fibers surface properties
16 p2937 A70-33376
- Surface growth morphology and crystallographic orientation of beta-SiC films formed by chemical conversion and heating
17 p3142 A70-34678
- Epitaxial beta SiC film formation on SiC by reactive evaporation or sputtering at low temperature
17 p3144 A70-35906
- Electrical conduction and surface properties of beta-SiC films obtained by heating Si wafer in presence of hydrocarbon
19 p3485 A70-37685
- SiC whiskers X ray diffraction studies of crystal structure, suggesting single crystal permanent deformation at ambient temperatures
19 p3455 A70-37941
- Temperature effect on friction coefficient of boron and silicon carbides, using similar wear pairs in vacuum
23 p4205 A70-44044
- High cutoff negative resistance silicon carbide diodes, noting temperature independent current-voltage curve
23 p4176 A70-45067
- SILICON COMPOUNDS**
- NT ALUMINUM SILICATES
NT CALCIUM SILICATES
NT ENSTATITE
NT FELDSPARS
NT FORSTERITE
NT GARNETS
NT KAOLINITE
NT MUSCOVITE
NT ORGANIC SILICON COMPOUNDS
NT PYROXENES
NT QUARTZ
NT SILANES
NT SILICATES
NT SILICIDES
NT SILICON CARBIDES
NT SILICON DIOXIDE
NT SILICON NITRIDES
NT SILICON OXIDES
NT SODIUM SILICATES
NT YTTRIUM-ALUMINUM GARNET
NT YTTRIUM-IRON GARNET
- SiH molecular absorption lines in solar disk spectrum, determining maximum equivalent widths and oscillator strength
06 p1143 A70-17996
- Ti tetrachloride, Si tetrachloride and hydrogen gas mixtures flow over heated graphite substrates, describing Ti silicides formation
09 p1703 A70-22646
- Protective coatings for silicon photosensitive elements to reflect incident energy at wavelengths not participating in conversion into electricity
15 p2677 A70-31599
- Free radical coupling of silyl peroxides in reinforced plastics, laminates and adhesives
16 p2937 A70-33377
- SILICON CONTROLLED RECTIFIERS**
- Silicon controlled diodes application to pulse modulation circuits of radar transmitters
09 p1631 A70-22016
- Si controlled thyristors applied to pulse modulators in ionospheric stations
18 p3233 A70-37043
- Neutron irradiation effect on unijunction transistors and SCRs, developing damage prediction technique
19 p3388 A70-37848
- SILICON DIOXIDE**
- NT QUARTZ
- Reinforced plastics high silica and quartz history, properties, uses, costs and pricing, tabulating sources and presenting product recommendations and cost comparisons
05 p0873 A70-16608
- Luminescence of powdered silica and basalt bombarded by atomic hydrogen, relating spectral distributions dependence on ion energy to luminescence
10 p1942 A70-24647
- Selective optical coatings of alternate Ni and silicon dioxide layers, describing optical and spectral characteristics of black mirror
12 p2272 A70-27307
- Position sensitive planar photocells based on silicon-silicon dioxide systems, discussing photoelectromotive force generation mechanism, light intensity and load characteristics
18 p3297 A70-36236
- Silica marker motion in sintering of loose spherical copper powder aggregates
20 p3647 A70-39109
- Compressive and rarefaction shock wave propagation in polymethyl methacrylate, fused silica and sapphire, using laser interferometer measurements
22 p4031 A70-43020
- SILICON FILMS**
- Mo-Si epitaxial planar Schottky barrier diodes, describing reverse I-V characteristics improvement by edge leakage effects elimination
01 p0052 A70-11174
- Two step B vacuum diffusion from boron oxide into Si surface using evacuated tube and N atmosphere
05 p0891 A70-15791
- Epitaxial beta-SiC films formation on sapphire by chemical conversion
06 p1127 A70-17946
- Service life and friction coefficient of molybdenum disulfide-silicon lubricating coating as function of load, sliding rate and vacuum level
11 p2060 A70-25943
- Surface field effect, contact potential and photoconductivity measurements on p- and n-type heteroepitaxial single crystal silicon films on sapphire
13 p2470 A70-29372
- Surface growth morphology and crystallographic orientation of beta-SiC films formed by chemical conversion and heating
17 p3142 A70-34678
- Photon capture cross sections for surface silicon electronic states using IR photoconductivity measurements
17 p3144 A70-35707
- SILICON ISOTOPES**
- Elastic and inelastic scattering of proton beams from magnesium and silicon isotopes, using optical model
04 p0723 A70-15637
- Critique of paper on diffusion in Si isotopes and excess vacancies generation by motions of diffusion induced dislocations
08 p1553 A70-21696
- Inverted coexistence possibility of spherical and deformed states in Si 28 and S 32 nuclei
17 p3137 A70-34518
- SILICON JUNCTIONS**
- MOS structure electrical characteristics dependence on silicon/silicon dioxide interfacial energy and electric charges, considering fabrication difficulties
02 p0350 A70-12541
- HF admittance and noise in forward-biased majority carrier Ge-Si n-n heterojunctions and Schottky barrier
03 p0539 A70-13159
- Solid state digital pressure transducer incorporating Si diaphragm with piezoresistive sensing elements for computerized supersonic and subsonic data applications
03 p0496 A70-14194
- Silicon photodiode arrays with total active area noting element isolation
03 p0459 A70-14195

- Neutron induced defect clusters in high field space charge region of Si p-n junctions, noting rate of volume damage dependence on electric field strength
04 p0730 A70-14728
- Resistivity, temperature and injection level dependence of minority carrier lifetime in neutron irradiated p- and n-type Si
04 p0730 A70-14729
- Neutron irradiation effect on space charge limited current of electrons in high purity silicon, noting SCLC sensitivity in detecting traps and changes
04 p0731 A70-14730
- Gas discharge avalanche breakdown in Si semiconductor, analyzing microplasmas, ionization coefficients, p-n junction voltage, electron and light emissions
04 p0731 A70-15494
- High efficiency oscillator using avalanche square wave diode, considering case of silicon p-i-n diode
05 p0819 A70-15815
- Photosensitivity and scanning of planar Si photodiode image detector arrays, using most ring counter and shift register
10 p1846 A70-23881
- Silicon diodes pulse operated in avalanche resonance pumped modes for producing stable microwave amplification
10 p1847 A70-23889
- Silicon L-band avalanche diodes as high power pulsed microwave sources, discussing fabrication, circuit requirements, radar applications, etc
10 p1852 A70-24893
- Ionization gage with reverse biased silicon carbide p-n junction hot electron emitter as source
12 p2231 A70-27263
- Thyristor tetrode silicon controlled switches (SCS), considering unijunction transistors and pulse generator circuits
13 p2377 A70-29115
- High resistivity Si electron drift velocity measurement by exciting surface barrier diode with subnanosecond superradiant laser pulses
14 p2594 A70-30924
- Position sensitive planar photocells based on silicon-silicon dioxide systems, discussing photoelectromotive force generation mechanism, light intensity and load characteristics
18 p3297 A70-36236
- Etching effects on mesa profiles and edge breakdown of silicon avalanche diodes at high power and temperatures, using scanning electron microscope
19 p3389 A70-37971
- Semiconductor silicon power diodes nondestructive quality control, discussing optimal sampling procedures
20 p3595 A70-38969
- Crystal orientation dependence of thermal resistance and gage factor in electron irradiated n-type silicon strain gages
21 p3824 A70-40862
- Optimum junction area for maximum microwave output power of silicon IMPATT diodes for X band operation
23 p4167 A70-43775
- SILICON NITRIDES**
Oxidation resistance of mixed silicon nitride and silicon carbide refractory materials at high temperatures
03 p0514 A70-12979
- Memory technology based on electrically alterable nonvolatile silicon nitride variable threshold transistor
16 p2868 A70-33458
- MIS structures with silicon nitride film deposited by RF glow discharge, observing doping increase in epitaxial substrate
17 p3055 A70-35873
- Semiconductor junctions passivation by silicon nitride insulation layers, discussing pyrolysis and cathode sputtering fabrication methods
22 p4087 A70-43444
- SILICON OXIDES**
NT MUSCOVITE
NT QUARTZ
NT SILICON DIOXIDE
Ion implantation for reducing space charge buildup in thermal oxides on silicon exposed to ionizing radiation
04 p0731 A70-14743
- Silicon oxide films coated satellite aluminum surfaces solar absorptivity and thermal emissivity, noting suitability as temperature control coatings
09 p1613 A70-23514
- Water contaminating effects on thin thermal oxide passivated silicon planar devices
13 p2361 A70-28930
- Spectrum of bright IR object VY Canis Majoris, noting absorption feature attributed to SiO molecules in stellar atmosphere
17 p3154 A70-34540
- Ionospheric Si and SiO ions equilibrium interconversion during Leonid meteor shower
20 p3621 A70-39351
- Oxidized Si surface recombination rate measurement by electric field effect, noting electron bombardment effects on electrical properties
22 p3998 A70-43443
- Low temperature stars SiO IR spectral band identification based on rotation-vibration spectrum calculation
24 p4411 A70-45777
- SILICON POLYMERS**
NT SILICONES
NT SILOXANES
SILICON RADIATION DETECTORS
Threshold and frequency relaxational radiation detectors, discussing operation and sensitivity of p-n-p silicon photothyristor and luminosity dependent devices
09 p1649 A70-23356
- Silicon high resistivity surface barrier detectors fabrication for nondestructive tests, discussing long term sensitivity and calibration
10 p1893 A70-24169
- Alpha particles radiation damage effects in silicon surface barrier detector
14 p2584 A70-30511
- SILICON RECTIFIERS**
U CRYSTAL RECTIFIERS
SILICON SOLAR CELLS
U SOLAR CELLS
SILICON TRANSISTORS
Noise source model of Si planar diffused bipolar IC transistors in operational amplifiers, noting base-emitter junction burst noise
02 p0257 A70-12192
- Burst noise in forward biased silicon diodes and transistors, discussing measurements on gate controlled devices
03 p0458 A70-14029
- Silicon bipolar transistors primary photocurrent calculation using manufacturers data
04 p0657 A70-14736
- Microwave Si transistors with overlay and interdigital geometries and integrated circuit design considerations for power amplifiers, power oscillators and frequency multipliers
05 p0819 A70-16149
- Silicon monolithic integrated circuits technology for radiation environment near nuclear detonation
09 p1647 A70-23076
- Double diffused epitaxial silicon bipolar microwave transistor design, fabrication and performance evaluation, including scattering parameters vs frequency for common-emitter amplifier
13 p2379 A70-29592
- Hysteresis in MOS transistors attributed to trapped charge carriers on oxide near silicon oxide interface
14 p2555 A70-30338
- UHF Si p-n-p transistors with low noise and high gain for small signal applications
14 p2557 A70-31161
- Memory technology based on electrically alterable nonvolatile silicon nitride variable threshold transistor
16 p2868 A70-33458
- B and P ions bombardment techniques for Si doping of multilayered transistor structures
19 p3385 A70-37268
- High voltage MOST silicon integrated circuits, using dielectric isolation and field plate techniques
21 p3798 A70-41214
- Reverse curvature silicon transistor linearizer for hot-wire and thin-film constant temperature anemometers for aorta blood flow velocity measurements
21 p3827 A70-41458
- Metal nitride oxide silicon (MNOS) integrated circuit transistor, reviewing characteristics, operation mechanisms and applications
21 p3800 A70-42113
- Silicon MOSTs LF noise model, discussing noise and gate voltages and trapping efficiency of surface states
22 p3996 A70-42916
- SILICONE RUBBER**
Elastomeric silicone ablator reinforced by carbon cloth or fibers for Venus entry heat protection [AIAA PAPER 70-201]
06 p1157 A70-18086
- SILICONES**
NT SILOXANES
Phenolics and silicones characteristics, history, chemical composition, available forms, impregnation process, manufacture, productivity, electrical applications and temperature resistance
05 p0873 A70-16603
- Temperature distribution in heated horizontal layer of high Prandtl number silicone fluids at high Rayleigh numbers confined between rigid parallel conducting plates
07 p1418 A70-18647
- Vertical heat transfer in silicone oil by single row convection cells, correlating cell number to transport rate and Rayleigh number
09 p1612 A70-22052
- Silicone products with low outgassing characteristics for spacecraft applications, discussing fluids, compounds and elastomers
10 p1906 A70-23914
- Gas transfer through silicone elastomer capillaries wall in variable pressure chamber
14 p2541 A70-30386
- Synthetic fluids as lubricants, examining physicochemical properties of polyglycols, silicones and esters
16 p2917 A70-33421
- Hotshot wind tunnel performance improvement by coating arc chamber with silastene to retard heat loss and metal pollution
17 p3057 A70-34774
- SILICONIZING**
Siliconizing of Mo in medium with silicon chloride, comparing reaction probabilities for various heating methods
17 p3102 A70-35392
- SILOXANES**
Polysiloxanes morphology crystallized isothermally from melt using electron microscopy, noting fracture ease increment with molecular weight decrease
03 p0517 A70-14203
- Polyurethane propellant binders burning rate, studying siloxane moiety effects
07 p1358 A70-19330
- Lunar fines hydrochloric acid hydrolyses examination by gas-liquid chromatography indicating presence of organosiloxanes
21 p3779 A70-41627
- Temperature and long term effects on volatility of perfluoroalkyl ether and polysiloxane greases [ASME PAPER 70-HT-31]
22 p4058 A70-42435
- SILVER**
Rare gas scattering from Ag surfaces calculated up to earth satellite energy values
06 p1112 A70-18275
- Trapped Ag atoms production in silver nitrate ice by gamma irradiation, discussing reaction enhancement by fluoride ion
09 p1631 A70-23445
- Epitaxy of Ag deposited on Ni, observing irreversible crystallographic order transition from metastable nominal orientation by LEED
10 p1927 A70-24076
- Silver/polytetrafluoroethylene water-repellant air-breathing cathodes for fuel cells with alkaline electrolytes, discussing pressure compatibility
10 p1829 A70-24454
- Oscillations of longitudinal magnetostriiction in silver and copper single crystals at low temperature
11 p2098 A70-25619
- Frenkel pairs and interstitial hydrogen atoms observed in thin silver films after proton bombardment
12 p2253 A70-27209
- Annealed compressed ground synthetic mica and silver dust composite materials, analyzing physicomechanical properties
12 p2260 A70-28319
- Ag species paramagnetic relaxation in gamma-irradiated frozen aqueous solutions and in frozen methanol, relating spin-lattice relaxation to isotropic coupling
14 p2544 A70-30117
- Filament orientation and fabrication variables effect on Ag matrix-W fiber composite mechanical properties
15 p2756 A70-31569
- Alumina particles marker transport in Ag wires during early sintering as function of plastic deformation by slip
15 p2745 A70-32392
- Cu and Ag low alloying effect on Al single crystals elastic limits and first deformation stages
20 p3644 A70-38960
- Crystal growth in polycrystalline Au, Ag and Au-Ag thin films annealing, observing by electron microscopy and electron diffraction
24 p4391 A70-45672
- Thin epitaxial Ag films on mica, measuring electrical resistivity strain dependence
24 p4391 A70-46266
- SILVER ALLOYS**
Age hardenable monolithic spring material composed of Ag-Pd-Cu alloys for make-break electrical contact
13 p2376 A70-28839
- Phase relations in system Ag-Fe-S in 700-1200 C range at various vapor pressures by quenching and differential thermal analysis, observing liquid-immiscibility fields
22 p4053 A70-42732
- SILVER COMPOUNDS**
NT SILVER HALIDES
NT SILVER IODIDES
NT SILVER NITRATES
Thermogravimetric analysis (TGA) of gadolinium-doped silver carbonate decomposition, obtaining activation energy, preexponential factor and reaction order
15 p2694 A70-32074
- ESR spectrum of gamma irradiated cycloheptatriene silver perchlorate, indicating free radicals and trapped electrons
19 p3374 A70-38272
- Silver fluorination kinetics, taking temperature and pressure effects into account
22 p3983 A70-43416
- SILVER HALIDES**
NT SILVER IODIDES

SILVER IODIDES

- High resolution silver halide photoemulsions by holographic resolvemetry using Ne-He laser to obtain interference patterns
01 p0095 A70-11633
- Computer generated displays and USAF equipment design for operational command and control systems, discussing Ag halide film technique
05 p0847 A70-16185
- Photolytic reactions mechanism in photochromic glass with silver halide crystals formed during glass manufacture, discussing properties and applications
08 p1499 A70-21683
- Efficiency, low noise and photochromic effects suppression in bleached silver halide holography with various films
20 p3627 A70-39097

SILVER IODIDES

- Ice nucleating properties of dust particles above 80 km compared with soil and AgI particles
01 p0081 A70-11296
- Complex dielectric constant of alpha-AgI measured in microwave region and far IR, noting sample positioning
16 p2960 A70-33225
- Solid state batteries based on highly conducting solid electrolyte rubidium silver iodide, testing discharge performance
22 p3966 A70-43543

SILVER NITRATES

- Trapped Ag atoms production in silver nitrate ice by gamma irradiation, discussing reaction enhancement by flouride ion
09 p1631 A70-23445

SILVER OXIDE ZINC BATTERIES

U SILVER ZINC BATTERIES

- High impact Ag-Zn cell design for space missions instrument package landing, considering heat sterilization and minimum operational capability
21 p3757 A70-41013

SIMICOR (IMAGE CORRELATOR)

U IMAGE CORRELATORS

SIMILARITIES

U ANALOGIES

SIMILARITY THEOREM

- NT LAGRANGE SIMILARITY HYPOTHESIS
Shallow flexible shells similarity conditions derived in dimensionless form, assessing error
03 p0592 A70-13450

- Pressure gradient calculation in three dimensional laminar boundary layer, using method of local similarity
03 p0468 A70-13869

- Structural similarity hypothesis for fully developed turbulence in smooth circular tubes, using intensity correction procedure
04 p0665 A70-14453

- Kinetic theory of thermal conduction in collisionless Knudsen gas in arbitrary closed systems with various geometries, establishing similarity law
[ASME PAPER 69-WA/HT-20] 04 p0783 A70-14814
- Turbulent boundary layer model using two region characterization for eddy viscosity and similarity solution taking into account interfacial conditions
[ASME PAPER 69-WA/AFM-27] 04 p0668 A70-14905

- Boundary layer equations closed form similarity solutions for laminar jet of compressible pseudoplastic fluid, discussing velocity transverse behavior
04 p0671 A70-15053

- Von Karman transonic similarity law applied to flow through plane turbine blade cascades
[DGLR-69-24] 04 p0616 A70-15183

- Small disturbance theory for internal conical inlet hypersonic flows, using method of characteristics for similarity law verification
[AIAA PAPER 70-127] 06 p0969 A70-18048

- Liquid rocket engine combustion processes determined by injector design using similarity principles
07 p1362 A70-19919

- Atmospheric boundary layer wind and temperature analysis according to similarity scheme for mathematical modeling of atmosphere
08 p1540 A70-21974

- Self similarity concept relevance to atmospheric turbulence demonstrated from ground and airborne observational data
09 p1717 A70-22373

- Thermal boundary layer similarity at extreme Prandtl numbers as series expansion, allowing for temperature distribution at wall
11 p2148 A70-25983

- Harmonic fields with boundary flow losses, discussing similarity on basis of dimensional analysis and pi theorem
12 p2271 A70-26877

- Similarity theory in design of isofunctional electric converters, relating input-output criteria
14 p2533 A70-30374

- Similarity equations for rotating flow near disk, using Navier-Stokes equations for case of complicated boundary conditions
18 p3239 A70-36223

- Power law fluid flow past suddenly accelerated wall, applying group theory to similarity solutions
19 p3406 A70-38444

- Radiative gas dynamic equations similarity representation with spherical symmetry, constructing numerical examples for strong explosions and implosions
20 p3609 A70-39657

- Self similar formulations for motion of radiating-absorbing perfect gas symmetric flow
21 p3954 A70-42202

- Two dimensional transonic cascade flow, using Von Karman similarity law
22 p4089 A70-42347

- Similarity rules for sinusoidal gust loads on thin two dimensional wing in nonstationary subsonic flows
23 p4131 A70-43970

- Incompressible laminar swirling jet flow, obtaining similarity solution for Navier-Stokes equations
23 p4184 A70-44982

- Stability of self-similar flows of second kind near critical point
24 p4327 A70-46004

SIMILITUDE LAW

- Similarity laws in hypersonic flow of real gas around slender blunted bodies, particularly bodies with rough lateral surface
03 p0409 A70-13866

- Equivalence class technique to compute measure of similitude between two vehicles based on radar signature in terms of scattering matrix elements
[AAS PAPER 69-607] 04 p0648 A70-14656

- Small disturbance and similitude applicability to internal hypersonic conical flows in edge shock and Busemann inlets
09 p1606 A70-23245

SIMULATED ALTITUDE

- Human alveolar-arterial oxygen differences during rest, sleep and exercise in initial hypoxia induced by simulated high altitude exposure
03 p0429 A70-14161

SIMULATION

- NT ACOUSTIC SIMULATION
NT ALTITUDE SIMULATION
NT ANALOG SIMULATION
NT ATMOSPHERIC ENTRY SIMULATION
NT COMPUTERIZED SIMULATION
NT CONTROL SIMULATION
NT DIGITAL SIMULATION
NT ENVIRONMENT SIMULATION
NT EXHAUST FLOW SIMULATION
NT FLIGHT SIMULATION
NT LANDING SIMULATION
NT RHEOELECTRICAL SIMULATION
NT SOLAR SIMULATION
NT SPACE ENVIRONMENT SIMULATION
NT THERMAL SIMULATION
NT WEIGHTLESSNESS SIMULATION

- Image quality effects on human performance in simulation, discussing time sharing strategies and task difficulty factors
01 p0036 A70-10809

- Visual simulation limitations, discussing parallax error correction in display system, wraparound system, image generation, TV and motion picture film systems
01 p0036 A70-10813

- Climatological cloud type statistics for simulating earth sensing mission data output as function of sensor field of view and spatial resolution
[AIAA PAPER 70-196] 06 p1065 A70-18098

- Time-similar and isotropic geodetic curves simulating paths of test bodies in Riemann space corresponding to gravitational field
06 p1107 A70-18564

- Model characteristics selection for dynamic system behavior simulation, studying characteristics variability extent without changing trajectory behavior dependence on parameter space
08 p1544 A70-20953

- Earth storable liquid propellants combustion products simulation by combustion of gaseous fuel and oxidizer combination, discussing elemental composition and thermodynamic considerations
08 p1557 A70-21622

- Cosmic ray air showers simulation, discussing high energy nuclear interaction and linear relation of primary particle energy to number
09 p1744 A70-22048

- Traffic simulation in telephone network via communication satellite with presassigned and demand assigned circuits
10 p1838 A70-24356

- Random process represented in canonical expansion form simulated by method of prognosis of reliability
11 p2022 A70-25344

- Simulation studies for first GARP global experiment, discussing data redundancy, measured and derived data, sampling, etc
18 p3285 A70-36785

SIMULATOR TRAINING

U TRAINING SIMULATORS

SIMULATORS

- NT COCKPIT SIMULATORS
NT CONTROL SIMULATION
NT ENVIRONMENT SIMULATORS
NT FLIGHT SIMULATORS
NT HIGH VACUUM ORBITAL SIMULATOR
NT LUNAR GRAVITY SIMULATOR

NT LUNAR ORBIT AND LANDING SIMULATORS

- NT SHOCK SIMULATORS
NT SOLAR SIMULATORS
NT SPACE SIMULATORS
NT SPACECRAFT CABIN SIMULATORS
NT TRAINING SIMULATORS
NT VIBRATION SIMULATORS

- Photooptical techniques in simulators - Conference, South Fallsburg, N.Y., April 1969
01 p0057 A70-10807

- U.S., U.S.S.R. and European space environment simulation chambers accommodating assembled spacecraft for thermal tests, describing design and characteristics
07 p1249 A70-19659

- Deterministic and stochastic simulation models for obtaining optimal solution in operations research by trial and error
08 p1464 A70-20579

- U.S., U.S.S.R. and European space environment simulation chambers accommodating assembled spacecraft for thermal test, describing design and characteristics
15 p2718 A70-32696

- Simulation devices in engineering feasibility studies emphasizing prototypes role
[ASME PAPER 70-DE-50] 16 p2918 A70-33512

- Space motion simulators for Azur satellite, considering satellite attitude related to sun
19 p3400 A70-38296

- Airfreighters maintenance and reliability simulation, modeling specific aircraft designs via input data selection
19 p3357 A70-38835

- Myocardium bioelectric activity electrocardiogram simulator, describing block diagram and operation
22 p3979 A70-43553

SIMULTANEOUS EQUATIONS

- Simultaneous equations of longitudinal impact bending, introducing temporal and spatial transformations regarding dispersive wave characteristics in elastic rod
03 p0591 A70-13428

- Computational methods of homogeneous ill-conditioned and singular simultaneous linear equations
04 p0714 A70-15096

- Least squares iterative method for solving simultaneous linear equations having singular coefficient matrix
04 p0714 A70-15450

- Equations for general shells of revolution reduced to simultaneous fourth order ordinary differential equations for stress and displacement functions
07 p1401 A70-18892

- Simultaneous partial integrodifferential equations for transverse oscillations of uniform short beams
07 p1406 A70-19306

- Mixed system of simultaneous linear differential equations under general boundary conditions, deriving numerical solution in Chebyshev series
09 p1711 A70-22288

- Simultaneous singular integral equations approximate solution in orthogonal polynomials
10 p1909 A70-24603

- Simultaneous equations for motion location, speed and direction in acoustic tracking of supersonic objects, recording shock wave times of arrival with microphone system
13 p2450 A70-29988

- Linear second order equation systems decoupling transformation, noting applications to structural feedback, flutter and control systems
16 p2943 A70-33891

- Iterative solutions for systems of nonlinear equations and discretization of elliptic differential equations
21 p3845 A70-40736

- Nonlinear differential equations system under small perturbation, considering uniqueness for autonomous unperturbed system
22 p4062 A70-42969

- Nonlinear differential equation systems overall stability, using qualitative methods
23 p4211 A70-44092

- Differential equation systems with Jordan form block-triangular matrix, discussing homeomorphic mapping
23 p4211 A70-44093

- Differential equations with integrable coefficients, proposing asymptotic integration for second order system
24 p4370 A70-46031

SIMULTANEOUS IMAGE CORRELATOR

U IMAGE CORRELATORS

SINE

U TRIGONOMETRIC FUNCTIONS

SINE WAVES

- Dynamic stability of simply supported column of linear viscoelastic materials under sinusoidal loading
01 p0206 A70-11148

- Plane sinusoidal wave propagation through material reinforced with parallel fibers, using integral formulation for multiple scattering in infinite slab
01 p0130 A70-11187

Sinusoidal signal detection in Gaussian noise band by zero crossing method, discussing signal frequency position and SNR

04 p0648 A70-14705

Digital microcircuits for one kva three phase DC-AC inverter control to generate sinusoidal 400 Hz output using HF bridge chopper techniques

04 p0628 A70-15340

Linear damping of sinusoidal oscillation in plasma, solving linearized Vlasov equation by integration along particle trajectories

05 p0888 A70-16304

Sinusoidal modulated HF pulse signal, deriving parametric envelope and power density function

10 p1833 A70-24086

Force input and thoraco-abdominal strain due to sinusoidal motion of electrohydraulic shake table over 2-14 Hz range imposed on human body

13 p2359 A70-29438

Wheatstone structure impedance bridges, describing balancing method in sinusoidal alternating regime

16 p2872 A70-35106

Double acoustical resonators transient response to excitation by single sine wave, presenting pressure magnification factors as function of frequencies

17 p3135 A70-34521

Real time swept sine wave spectrum analyzer using time compression to change filter bandwidth as function of control signal

17 p3059 A70-35166

Sine wave discrete components detection from complex spectrum with random noise, evaluating errors

17 p3059 A70-35168

Long term geomagnetic pulsations (PC5) with sinusoidal waveforms, using IGY data

17 p3080 A70-35642

Pulling force during motion of sinusoidally deformed flat profile, taking into account trailing edge vortices

18 p3241 A70-36280

Long period duration digital sinusoidal voltage generator, presenting schematic diagram and theoretical and operational characteristics

19 p3385 A70-37376

Statistical confidence levels for frequency analysis, detecting peak sinusoid for desired signal to noise ratio

21 p3825 A70-40867

Transistorized DC to AC converter providing sinusoidal output to power automatic spacecraft control devices via pulse width modulation

22 p3994 A70-42309

Quasi-harmonic friction induced near sinusoidal form vibration, calculating amplitude dependence on sliding velocity

22 p4044 A70-42445

Triangle and sine waveforms generation, discussing reduced peak and crossover distortion and extended frequency operation

22 p3989 A70-42923

SINGLE CRYSTALS

NT WHISKERS [SINGLE CRYSTALS]

Nonlinear optical properties of lithium niobate single crystals, considering optically induced index inhomogeneity and second harmonic generation

01 p0157 A70-10422

Intrinsic/extrinsic stacking fault pairs observed during creep of single crystals of gamma prime precipitation hardened Ni-base alloy, developing viscous slip model

01 p0119 A70-10731

Stress-strain effect on dislocation densities of cylindrical Mg single crystals deformed by torsion basal slip compared to tension test

01 p0122 A70-11236

Alloying additions effect on plastic deformation anisotropy in GaAs single crystals, determining dislocation activation energies from creep tests

01 p0160 A70-11606

Temperature effects on tensile deformation mechanism of Mo single crystals, investigating stress-strain characteristics and slip geometry

02 p0316 A70-11699

CuCl single crystal refractive index measurement at room temperature using V-block refractometer

02 p0350 A70-12453

Epitaxial growth of Cu vapor deposited on W single crystal /110/ surface using low energy diffraction, Auger electron and work function techniques

03 p0538 A70-13100

Strain hardening on single crystals of aging Ni-based alloys with ordered separated phase

03 p0505 A70-13104

GaAs n-type single crystals thermoreflectance spectra at various energies

03 p0541 A70-13721

Electrical properties thermally induced irreversible changes in CdSb single crystals measured as function of current intensity and flow

03 p0542 A70-13751

Niobium ditelluride single crystals production with purity dependent on initial materials, discussing X ray structural and chemical analysis and electrical properties

03 p0542 A70-13753

Schottky barrier FET fabrication using epitaxial growth of single crystal GaAs on insulating sapphire substrate

04 p0660 A70-15364

Vapor deposited GaN single crystals tested for electrical and optical properties, determining band gap energy, electron concentration, etc

04 p0732 A70-15688

Normal incidence reflectance of BeO single crystals, analyzing data by Kramers-Kronig inversion for dielectric function and energy loss function

05 p0891 A70-16047

Plasticity theory of single crystals based on dislocations behavior, considering only plane and elastic strains

05 p0928 A70-16061

Beryllium single crystals deformation under high pressures at room temperature similar to deformation under atmospheric pressure at elevated temperatures

05 p0863 A70-16203

Single crystal Ge surface etching characteristics using laser beam reflection pattern

05 p0860 A70-16656

Electrical properties of unipolar barium titanate single crystals involving hysteresis loops plotting

05 p0894 A70-17024

Electron transmission diffraction patterns of thin monocrystal films using Ar laser

06 p1080 A70-17444

Niobium single crystals annealed in ultrahigh vacuum, studying stress-strain behavior, secondary slip geometry and slip line morphology

06 p1090 A70-18493

Plastic zone around propagating fatigue crack in Cu single crystals, using transmission electron microscopy and X ray topography

06 p1171 A70-18494

Absorption spectra of single crystals TbAlG and DyAlG garnets, investigating Verdet constant dependence on ion concentration

07 p1355 A70-18705

Molybdenum rolling-deformed single crystals recovery and recrystallization using diffraction electron spectroscopy

07 p1307 A70-19550

Soviet collection of articles on single crystals of rare and high melting point metals

07 p1307 A70-19606

Carbides content determination in Mo single crystals by metallographic method, establishing relation between brittle-ductile transition temperature and carbon content

07 p1308 A70-19607

Vanadium single crystals substructure on different planes to growth direction using X ray diffraction

07 p1308 A70-19608

Cylindrical Mo single crystals during cyclic heating, studying characteristic dislocation changes at various stages of thermal fatigue

07 p1308 A70-19609

Oriented single crystals properties obtained from Mo powder subjected to compacting, annealing in hydrogen and electron beam zone melting

07 p1308 A70-19610

Size effect on structure and mechanical properties of thin wire made of Mo single crystals deformed in recrystallized state

07 p1308 A70-19611

Structure and mechanical properties of Mo single crystals grown from gas phase using metallographic and X ray analysis

07 p1308 A70-19612

Rolling texture and recrystallization of Mo single crystals and deformation effect on texture formation using X ray transmission technique

07 p1309 A70-19613

Molybdenum single crystals orientation effect on thermal resistance to argon plasma flow

07 p1309 A70-19614

Tracks shape associated with dislocation motion during etching of Mo single crystals

07 p1309 A70-19639

Single crystal carbides as high temperature structural materials, noting titanium carbide properties and strength-to-density ratio of B-doped crystals

07 p1312 A70-19883

Synthesis procedure for single crystal transition metal diborides, using high pressure capability in controlling stoichiometry

07 p1313 A70-19895

Dislocation velocity-stress exponent for Nb single crystals calculated from strain rate sensitivity measurements of effective flow stress

07 p1314 A70-20011

Gruneisen parameter for metal and semiconductor single crystals obtained from measuring one dimensional thermoelastic response during exposure to pulsed electron beam

07 p1357 A70-20020

Reactive scattering from solid surfaces, discussing atom beam reaction of O with heated Ge and Si single crystals

07 p1342 A70-20117

N-type InAs single crystals optical properties with various carrier concentrations at 1-6 mu wavelengths and 300-78 K temperatures, studying absorption spectra

08 p1555 A70-20512

C-axis single crystalline sapphire filament tensile and fracture tests

08 p1514 A70-20647

Gadolinium ions in zinc tungstate single crystals, studying low symmetry effects on EPR spectrum

08 p1556 A70-21120

Plastic properties of tungsten carbide single crystals at room temperature, determining slip system crystallographic orientations

08 p1520 A70-21557

Low energy electron diffraction pattern from surface steps and facets resulting from recrystallization of Re single crystal

08 p1557 A70-21602

Subboundary migration in Mo, W and W-Re alloy single crystals subjected to cyclic heating, using metallographic technique involving electrolytic polishing and special etching

09 p1701 A70-22297

Rhenium single crystals basal plane surface properties using LEED and Auger electron spectroscopy, describing gas adsorption studies

09 p1739 A70-22526

Creep deformation in single crystals of gamma prime precipitation hardened nickel base alloys at intermediate temperatures

09 p1705 A70-22809

Transverse Dember effect in elastically bent Ge single crystal illuminated by light beam, considering EMF distribution and photocell application

09 p1740 A70-23191

Shock deformation of single crystal biotite /lepidomelane/ imbedded in impedance matching NaI, relating kinking intensity to peak pressure and pulse duration

09 p1670 A70-23375

Mo single crystals creep behavior temperature and stress dependences using X ray analysis

09 p1708 A70-23543

Mo single crystals dislocation substructure strain dependence after creep using etch pitting techniques

09 p1708 A70-23544

Nb-W single crystal low temperature thermally activated deformation, observing slope change in temperature dependence curves of flow stress and strain rate sensitivity

09 p1708 A70-23572

High temperature creep of prestrained molybdenum single crystals as function of physical treatment and crystal orientation

10 p1902 A70-23860

Oscillations of longitudinal magnetostriction in silver and copper single crystals at low temperature

11 p2098 A70-25619

Chemisorption on Mo single crystal surfaces observed by LEED techniques, discussing bcc planes and adsorbed gases

12 p2181 A70-27256

Self focusing of ruby laser radiation in CdS single crystal, considering effect on crystal photoconductivity

12 p2248 A70-27540

Cleavage cracks initiation and propagation in basal plane of Be single crystals, determining propagation energy as function of temperature, purity and alloying

12 p2256 A70-27614

Ohmic contacts for gallium arsenide single crystals, describing fabrication technique and IV characteristics

12 p2202 A70-28187

Raman spectrum of lithium formate monohydrate single crystal in polarized He-Ne laser light, discussing crystal structure

13 p2425 A70-28714

Deformation, mechanical properties and processes during recrystallization annealing of nickel and alloys single crystals

13 p2433 A70-28761

Nonoriented cadmium silicon arsenide single crystals optical properties, determining spectral distribution of IR absorptivity for various photon energies

13 p2470 A70-28883

Fabry-Perot resonator mirrors with local reflecting inhomogeneities within perimeter of single crystal wafers for application in optically coupled semiconductor lasers

13 p2427 A70-28884

Lead ion effects on single crystal zinc dissolution and electrodeposition in alkaline solutions investigated microscopically

13 p2361 A70-28928

Surface field effect, contact potential and photoconductivity measurements on p- and n-type heteroepitaxial single crystal silicon films on sapphire

13 p2470 A70-29372

Plastic deformation of Mo-Re single crystals produced by electron beam zone refining, investigating

ing lattice frictional stress, activation volume temperature variation, etc

13 p2436 A70-29562

Nb single crystal faces electron work functions and comparison of thermionic emission patterns with Ba-Nb system

14 p2625 A70-30162

Plastic deformation of Be single crystals under hydrostatic pressure, considering resolved shear stresses on glide systems

14 p2595 A70-30334

Au films nucleation and growth on single crystal graphite substrates in ultrahigh vacuum, using transmission electron microscopy for examination

14 p2627 A70-30499

Bulk n-type InP single crystal transferred-electron oscillators, investigating current instabilities

14 p2556 A70-30686

Methyl-nitroazobenzene-sulphenyl cyanide unit cell dimensions and space group by single crystal oscillation, rotation and Weissberg X ray diffraction photographs

14 p2581 A70-31300

Single crystal W and W alloys dislocation structures as function of strain, temperature and dilute alloys addition, using electron microscopy

15 p2756 A70-31563

Artificial B-doped semiconductor diamond crystals resistance temperature dependence, determining conductivity and luminescence spectra

15 p2782 A70-31630

Twinned lamella formation in Nb single crystals, examining slip and shear roles in surface tilt formation

15 p2761 A70-32382

Work hardening properties of Ni single crystals of various orientations during intermittent and continuous plastic deformation

15 p2762 A70-32394

Yield strength of Nb-O single crystal solid solutions as function of temperature

15 p2763 A70-32808

Fermi level for crystal with slowly changing impurity determinable by solving Poisson equation and by condition of electroneutrality

15 p2786 A70-32899

GaAs microwave devices including diffused varactor, Schottky barrier and Gunn diode, discussing single crystals preparation and epitaxial growth layers

16 p2873 A70-33293

Metallographic observations on slow crack growth in Be monocrystals suggesting explanation for transition regions

16 p2933 A70-34275

Beta-Ti and Ti-Cr single crystals elastic moduli, determining A ratio temperature dependence

17 p3115 A70-34380

Titanium and Ti-Al single crystals microscopic plastic deformation features, slip modes and dislocation substructures

17 p3116 A70-34389

Single and polycrystalline indium arsenide preparation methods and quality control

17 p3143 A70-35119

Barium fluorides single crystals compression, investigating stress-strain behavior and dislocation mobility

19 p3483 A70-37339

Deformed single crystals of high purity Al of different orientation with respect to growth during recrystallization

19 p3450 A70-37373

Plastic deformation of melted Al-Mg single crystals, using dynamic tensile testing

19 p3450 A70-37374

Ferrite single crystals physical properties - Conference, Krasnoyarsk, U.S.S.R., June-July 1969

19 p3484 A70-37621

Ferrite single crystals physical properties - Conference, Krasnoyarsk, U.S.S.R., June-July 1969

19 p3485 A70-37626

Single crystal ferrite thin film microwave parameters measurement, examining susceptibility in weak magnetic fields and ferromagnetic resonance

19 p3485 A70-37628

Single crystal yttrium ferrite garnet intrinsic electromagnetic radiation as function of coupling coefficient between specimen and waveguide

19 p3485 A70-37630

High vacuum effects on creep properties of single crystal low carbon nickel base superalloy

19 p3451 A70-37705

Elastic constants of ZnTe and ZnSe single crystals over 77-300 K range, using ultrasonic pulse echo method

19 p3486 A70-37761

Hydrostatic pressure derivatives of adiabatic elastic moduli of single crystal zirconium, noting high temperature Gruneisen-thermal expansion deviation

19 p3486 A70-37763

CdS conversion by cation exchange to single crystal CuS, examining phases structural relationship

19 p3486 A70-37766

Single crystalline mercury elastic constants calculated from propagation velocity measurements of polarized sound waves

19 p3486 A70-37770

Elastic-plastic behavior of fine grained fcc polycrystals based on single crystal slip data, satisfying displacement compatibility, equilibrium condition, etc

19 p3538 A70-37792

Phase equilibrium of Fe-rich Fe-Al alloys using single crystal X ray diffraction

19 p3452 A70-37838

Fe rich Fe-Al alloys single crystals, determining three dimensional order and atomic displacements coefficients by X ray diffuse scattering

19 p3452 A70-37839

Electrophysical properties of refractory and rare earth metallic single crystals, discussing work function, transition temperature, resistivity and superconductivity

19 p3454 A70-38731

Electronic absorption spectra of single crystal praseodymium acetate tetrahydrate in natural and polarized light

19 p3488 A70-38742

Cu and Ag low alloying effect on Al single crystals elastic limits and first deformation stages

20 p3644 A70-38960

Solidification and composition model of macroscopic freckles in nickel base superalloys single crystals

20 p3646 A70-39101

Nb-Ta and Nb-Mo alloys single crystal solid solution strengthening as function of composition, temperature and strain rate

20 p3646 A70-39105

Creep resistant Ni-base superalloys ductility and thermal shock resistance improvement by precision casting technique, producing columnar grain and single crystal structures

20 p3648 A70-39415

Nucleation processes associated with thermal decomposition sites formation in ammonium perchlorate single crystals, using optical and electron microscopy

20 p3582 A70-39494

Nb single and polycrystalline thermal properties at high temperatures

20 p3648 A70-39639

Radicals induced in thymine monohydrate single crystals by ionizing radiation

20 p3583 A70-40455

Deflagration rate measurements by high speed cinematography of ammonium perchlorate single crystals under various ambient temperature and pressure conditions

20 p3688 A70-40468

Sn and tetraethylammonium ions effects on Zn electrodeposition on Zn single crystals in aqueous KOH, using scanning electron microscopy

21 p3772 A70-40726

Crystallography of euhedral single crystals from lunar troilite indicating hexagonal forms consistent with high temperature NiAs type structure

21 p3898 A70-41522

Apollo 11 lunar rock plagioclases crystallography, obtaining single crystal X ray diffraction patterns by Buerger precession method

21 p3903 A70-41555

Hydrogen adsorption and coadsorption with oxygen on W single crystal surface measured by mass spectroscopy and low energy electron diffraction method

21 p3862 A70-41887

Impurity dependent critical resolved shear stress of magnesium oxide single crystals, using compression testing

21 p3862 A70-41910

High resistivity single crystal silicon wafers induced IR absorption measurement, using Nd doped glass laser

21 p3837 A70-41916

Electron tunneling through p-type GaAs point contacts on Pb single crystals at liquid He temperatures

21 p3864 A70-42017

Single crystal and pyrolytic graphite, examining spin split Landau levels, Fermi energy changes and anomalous g shifts

21 p3854 A70-42110

Orientation and applied stress effects on pure Nb-6W bcc single crystals yield stress, discussing thermal activation strengthening and crystal dislocations

22 p4052 A70-42318

Current-controlled negative resistance and conductive memory state in Si-doped single crystal YIG wafers

22 p4085 A70-42331

Radiation induced free radicals in thymidine single crystals, attributing electron spin resonance spectral observations to nature of various radicals

22 p3981 A70-42348

Mo single crystals tensile properties at different orientations, noting asymmetric slip in plastic behavior

22 p4056 A70-43155

Superconductivity and crystalline structure of laminar solid solutions of niobium-selenide-niobium-telluride single crystals

22 p4088 A70-43464

Short range order and Fermi surface effects in copper-rich Cu-Al alloys single crystals from X ray scattering measurements

23 p4204 A70-43886

YIG single crystals piezo-optical effect and magnetic double refraction, describing stress measurement technique

23 p4230 A70-43931

Columnar grain and Ni alloy single crystal gas turbine engine components resistant to high temperatures produced by precision casting, using directional solidification

23 p4207 A70-44857

Cubic monocrystalline semiconductor upper critical magnetic field, using correlation function method

23 p4231 A70-44926

Threshold characteristics of injection and electron excitation semiconductor lasers having photoluminescence properties of n-type GaAs single crystals

23 p4203 A70-45065

Spectral and threshold emission from optically pumped semiconductor lasers as function of carrier type and concentration in GaAs single crystals

23 p4203 A70-45069

SbSI semiconductor single crystal polarization parameters temperature dependence, noting anomalies in permittivity, spontaneous polarization and dielectric loss tangent

24 p4389 A70-45208

Ti single crystals plastic deformation in axial compression at high temperatures

24 p4358 A70-45239

Stress dependent creep rate in nickel based superalloy single crystals

24 p4359 A70-45289

Single crystal piezoelectric materials growth characteristics and wave propagation properties for surface acoustic wave applications

24 p4367 A70-45399

Formation and radiative recombination of free excitonic molecules in CuCl single crystals via Q switched ruby laser excitation

24 p4353 A70-45604

Vanadium carbide single crystals superconductivity from upper limit on electron phonon interactions at 30 mK

24 p4391 A70-46252

Solid solution hardening of single crystal Ta base alloys, measuring critical shear stress at various temperatures

24 p4365 A70-46370

SINGLE SIDEBAND DEMODULATION

U SINGLE SIDEBAND TRANSMISSION

SINGLE SIDEBAND MODULATION

U SINGLE SIDEBAND TRANSMISSION

SINGLE SIDEBAND RECEIVERS

U SINGLE SIDEBAND TRANSMISSION

SINGLE SIDEBAND TRANSMISSION

Flight configured single sideband telemetry accuracy determined by digitally computed frequency response

06 p1012 A70-18600

Compatible single sideband transmission realized using iterative signal processing method and ideal band limited channels

08 p1464 A70-21781

Noise effect on single band modulation receiver using phase automatic frequency control for carrier wave at arbitrary SNR

13 p2370 A70-29739

Tetrode for single sideband short wave transmitter, discussing design, characteristics and intermodulation distortion reduction

17 p3054 A70-35412

SINGLE STAGE ROCKET VEHICLES

NT AGENA D ROCKET VEHICLE

NT AGENA ROCKET VEHICLES

NT ARCAS ROCKET VEHICLES

NT BLACK KNIGHT ROCKET VEHICLE

Rocket sled launching for reusable single stage-to-orbit ballistic transport system, noting increased payload capacity and global application

09 p1767 A70-23434

Minimum-time transfer trajectories between close planar orbits, using single stage thrust-limited rocket

23 p4444 A70-44624

Single stage reusable ballistic space shuttle, featuring minimum payload mass ratios and high propulsive efficiency

23 p4262 A70-44686

SINGLE-PHASE FLOW

Single phase flow problem in heated vertical prismatic channel, using dimensional analysis from conservation equations with boundary layer approximation

21 p3954 A70-42170

SINGULAR INTEGRAL EQUATIONS

Singular integral equation applied to elasticity theory of composite beam with or without cavity under torsion

04 p0765 A70-14416

Three dimensional elastostatics problems solution method using singular integral equations solvable numerically for surface tractions and displacements of fully mixed boundary value problem 05 p0926 A70-15912

Inverse boundary value problems for supercavitating bodies, deriving singular integral equations using Prandtl acceleration potential method 07 p1254 A70-19076

Direct boundary value problem for supercavitating profile with finite cavity, deriving singular integral equations by Prandtl acceleration potential method 07 p1254 A70-19077

Stress rate boundary value problem formulation for elastoplastic body by singular integral equations 07 p1405 A70-19258

Elastic contact between bodies in presence of friction or adhesion by reducing singular integral equations to Fredholm equation 08 p1585 A70-20958

Matrix multidimensional singular linear integral equation applied to electromagnetic radiation transfer through stratified atmosphere 09 p1711 A70-22349

Second order elliptic differential equations solution involving Dirichlet problem reduced to equivalent singular integral equations 10 p1908 A70-23923

Simultaneous singular integral equations approximate solution in orthogonal polynomials 10 p1909 A70-24603

Jacobi conditions for singular optimization problems by transforming singular accessory minimum problem into nonclassical nonsingular form, considering optimal control theory applicability 16 p2885 A70-33331

Numerical quadrature of singular functional equations, tabulating integral functions, Cauchy principle values and integral transformations for optimal error function 18 p3280 A70-36219

Singular integral equations of elasticity theory, formulating boundary value problem for discontinuous plane stresses 18 p3337 A70-36370

Singular integral equation formulation for torsion from membrane analogy, obtaining boundary value problem solution by computer program 20 p3718 A70-39000

Elastic contact between bodies in presence of friction or adhesion by reducing singular integral equations to Fredholm equation 20 p3719 A70-39381

Steady state radiative heat transfer through gray gas in spherical cavity, solving transport equation by singular integral equations for uniform heat generation 23 p4283 A70-44784

Propeller blade aerodynamic characteristics at zero advance ratio, reducing singular integral equation to nonsingular form for computer solution 23 p4136 A70-44993

SINGULARITY [MATHEMATICS]

Elliptic restricted three body problem singularities dynamical meaning and character, presenting regularization transformations for equations of motion 03 p0576 A70-14074

Two dimensional wave diffraction problems involving discontinuity line, analyzing instability behavior of geometrically induced singularities by applying integral transform on Helmholtz equations 03 p0525 A70-14199

Surface singularities method for calculating incompressible potential flow about bodies of revolution with arbitrary thickness ratio and angle of attack 03 p0410 A70-14322

Computational methods of homogeneous ill-conditioned and singular simultaneous linear equations 04 p0714 A70-15096

Singularities arising during collisions in restricted n-body problem elimination, discussing Jacobi integral and finite-mass body configuration 04 p0714 A70-15354

Binary star formation using singular solution of Kepler problem in general theory of relativity 04 p0755 A70-15355

Least squares iterative method for solving simultaneous linear equations having singular coefficient matrix 04 p0714 A70-15450

Singularity method applied to two and three dimensional potential flow described by Poisson, Helmholtz or related partial differential equations 05 p0832 A70-16114

Motion near collision singularity in perturbed two body problem, applying method to boundedness proof for Sperting cluster energy 05 p0909 A70-16339

Correctness of Meixner assumption of scattered light field singularity near grating edge due to diffraction 05 p0816 A70-16879

Potential flow over rocket contour containing bends calculated by polygonal distribution of singularities on axis of body of revolution, determining friction effects 06 p0964 A70-17239

Optimality conditions determined for control involving trajectory with singular component equations of motion 06 p1024 A70-17813

Singular element technique effect on hydrodynamic and aerodynamic problems solutions, presenting potential flow problems and application to wings and propellers 07 p1188 A70-19133

Cosmological solution of Einstein gravitational equations with singularity in time 07 p1381 A70-19361

Dynamic characteristics approximation in transfer functions class with singularity at infinity 07 p1327 A70-19806

Singularity for absolute zero of time suggested for beginning of universe by Einstein relativity theory 07 p1336 A70-19922

Space-time singularities of gravitational collapse and cosmology indicated by timelike or null geodesic incompleteness 08 p1575 A70-21353

Einstein gravitational equations general solution having physical singularity with respect to time 08 p1546 A70-21424

Self similar and steady state flows near singularities, studying flow stability by partial differential equations 10 p1863 A70-24071

Physical singularity reduced to imaginary by introducing arbitrary function in form of perturbation into gravitational equations general solution 10 p1917 A70-25032

Two and three dimensional potential flow analysis using finite element technique based on method of singularities 11 p2042 A70-26681

Regularity domain and singularity location of stream function of transonic two dimensional compressible fluid flow, using integral operators 12 p2260 A70-26972

Electromagnetic field singularities near sharp edge relating to geometry scatter used for treating singularities in current distribution integral equations 12 p2183 A70-26977

Rotation effect on singularities in general relativity from local observer standpoint, inquiring into gravitational collapse in ideal fluid 12 p2271 A70-26978

Singular and nonsingular cosmological models validity for general relativity allowing for cosmic dust 12 p2300 A70-27394

Axisymmetrical stress tensor singularity convergence of rigidly clamped circular plate, showing identity of plane stressed state transcendental equations 12 p2325 A70-27558

Singularities of boundary layer conditions on parabolic cylinder in homogeneous incompressible viscous flow with leading edge, using Weyl integral equation 12 p2210 A70-27559

Optimal singular controls made nonsingular for decreasing epsilon values by adding integral quadratic functional of control to cost functional 13 p2382 A70-29066

Uniform function defined throughout plane with isolated singularities at finite distance, obtaining solution uniqueness proof 13 p2389 A70-29626

Singular perturbation problems in theory of differential equations with almost periodic coefficients 14 p2599 A70-30847

German monograph on planar straight cascades in incompressible frictionless potential flow, basing method on singularity method integral equation reversal 16 p2839 A70-34081

Singular solutions to concentrated loads on shallow shell equations with quadratic middle surface 17 p3186 A70-34968

Stress concentration on axisymmetric annular wings calculated using method of singularities 18 p3207 A70-36377

Damped vibrations of single-mass elastic systems, determining E function singularity effect on dynamic characteristics 18 p3341 A70-36587

Singularities of solutions of partial differential equations, discussing smallest convex set in manifold with differential operator 19 p3457 A70-37680

Nonlinear differential equations solutions in power series with indefinite coefficients, determining type of singular points 20 p3658 A70-39766

Singular points in elasticity theory solved by correct boundary value problem and homogeneous solutions theorem 20 p3728 A70-39894

Schwarzschild solution singularity elimination using Lorentz transform 20 p3673 A70-39998

Boundary value problems for linear ordinary differential equations with singularities, determining eigenvalues by computer oriented method 20 p3659 A70-40134

Jacobi-type conditions for singular optimization problems obtained by transformation to nonsingular form adaptable to linear quadratic optimal control theory 20 p3659 A70-40262

Equal thickness singularity interference fringe networks behavior in singularities region of photoelasticity 21 p3941 A70-42260

Harmonic mixed boundary value problem with singularity, deriving approximate solution by dual series technique with conformal transformation and finite difference method 22 p4062 A70-42642

Systematic approach to construction of finite elements, discussing choice of generalized coordinates useful in problems involving singularities 22 p4116 A70-43208

Gravitational equations with oscillatory physical singularity, noting Bianchi type IX homogeneous metric 22 p4063 A70-43477

Metric evolution in oscillatory mode of approach to singularity in homogeneous cosmological models in asymptotic region, showing Kasner epoch dependence on perturbation 22 p4075 A70-43478

Dirichlet problem with singularities for plane with cutouts along circumference, determining analytical function 23 p4211 A70-44239

Singular and nonsingular optimal control problems, deriving sufficient conditions for nonnegativity of second variation 23 p4213 A70-44908

German monograph on airfoil and wings aerodynamic coefficients calculations, showing advantages of analog computers based on singularity theory and distance functions 24 p4287 A70-45097

SINKS

NT HEAT SINKS

SINTERED ALUMINUM POWDER

Fabrication technique effect on tensile and plastic properties of semifinished sintered Al powder products at room temperature and 600 C 06 p1076 A70-17848

SINTERING

Rhenium powder sintering activated by palladium additions producing low porosity 01 p0117 A70-10158

Book on powder metallurgy treating characterization of powders, compaction, sintering and engineering considerations and applications 02 p0316 A70-11735

Titanium carbide sintering under continuous heating in Ar atmosphere, studying ultrasonic waves effects on compaction process 04 p0696 A70-14463

Optimal temperature for sintering of compact titanium carbide in Ar atmosphere 04 p0697 A70-14468

Residual free energy effects on ferrites density and structure after sintering, using powders obtained by thermal decomposition of solid solutions of salts 07 p1355 A70-18703

Reduction temperature effects on molybdenum powders sinterability noting dispersion role 08 p1517 A70-21145

Yttrium iron garnet sintering and grain growth rates dependence on yttrium/iron ratio [ACS PAPER 16-BE-68F] 09 p1740 A70-22982

High intensity ultrasonics for changing solids properties, discussing effects on metal powder sintering, yield strength, fatigue life, crystallization rate, etc 09 p1728 A70-23348

Molybdenum disulfide dry film lubricant wear life as film sintering process dependent on binder, additive or atmosphere chemical effects 11 p2058 A70-25571

Isotropic Be billet fabrication by gas pressure consolidation and pressureless sintering techniques 12 p2252 A70-26888

Porous Ti powder sintering process activation energy determination, noting influence of oxides solution in surface layer of Ti particles 12 p2254 A70-27283

Sintering processes using boundary porosity in welded Nb bicrystal for model of final stages 13 p2434 A70-29081

Powder metal parts induction sintering, comparing performance with conventional method 13 p2420 A70-29249

Alumina particles marker transport in Ag wires during early sintering as function of plastic deformation by slip 15 p2745 A70-32392

Tungsten fiber reinforced copper based composite material, investigating moulding and sintering conditions effect on mechanical properties 19 p3450 A70-37454

Silica marker motion in sintering of loose spherical copper powder aggregates 20 p3647 A70-39109

SINUSES

- Dry and water-saturated sintered fiber metal wick thermal conductivity, obtaining semiempirical correlations for solid and fluid phases and void fraction 21 p3945 A70-41041
- Photoelastic stress measurement of metal powder particles during sintering, using two dimensional models 21 p3935 A70-41410
- Sintered boron-alloyed Mo electron beam welding behavior examined by texture-revealing color etching method 21 p3833 A70-41411
- Titanium diboride particles contact surface increase during sintering in vacuum as function of temperature 23 p4205 A70-44042
- Chemical diffusion kinetics of zirconium silicates formation during sintering under pressure, noting activation energy estimation 24 p4367 A70-45479
- German monograph on sintered molybdenum silicide recrystallization following high temperature heating in oxidizing atmosphere 24 p4367 A70-45575
- Sintered material density-sound velocity relation, deriving ultrasonic wave propagation time dependence 24 p4360 A70-45731

SINUSES

- Arrhythmia resembling atrial flutter simulated in dogs by coronary sinus and left atrial pacing and in man by coronary sinus pacing 02 p0240 A70-12696

SINUSOIDS

U SINE WAVES

SITE DATA PROCESSORS

- Flight test programs site selection method using computer program analysis of magnetic tape weather records [AIAA PAPER 70-397] 10 p1806 A70-24908

SITES

- NT LANDING SITES
- NT LAUNCHING SITES
- NT LUNAR LANDING SITES
- Big Bear Solar Observatory, discussing site selection, observatory construction and telescope optical system 12 p2205 A70-26864

SITTING POSITION

- Forward and rearward facing passenger seats effects in postdecompression emergency descent of high speed high altitude aircraft 03 p0437 A70-14061
- Radiography of spine in seated position, discussing aircraft seats, aeronautical ergonomics, etc 05 p0804 A70-15765
- Human nostril airflow resistance during supported sitting and lateral recumbency and crutch pressure, discussing ipsilateral nasal congestion mechanisms 08 p1448 A70-21874
- Vertebral injury prediction of seated human subjected to caudocephalad acceleration, suggesting consideration for head and torso forward flexion and external restraints effects 09 p1627 A70-23462
- Heart rate variations due to influence of body position rapid changes, emphasizing oxygen consumption in crouching position 17 p3024 A70-34591

SIZE (DIMENSIONS)

- Far and near side lunar crater chains regularities in distribution and size 03 p0574 A70-13879
- Gravity and size effects on film boiling from horizontal cylinders, recommending formulas for wavelength and minimum heat flux predictions [ASME PAPER 69-WA/HT-12] 04 p0784 A70-14821
- Tektite size restricted by thermal stress limit on diameter and aerodynamic load limit on length 05 p0916 A70-16831
- Moon illusion on basis of perceived size relativity, discussing dependence on objective characteristics of visual field 09 p1752 A70-22248
- Frequency-size distribution of Martian and lunar craters and oases, suggesting common mode of origin 09 p1765 A70-23810
- Oxidizer particle size and binder type effects on nonacoustic combustion instability of solid propellants [AIAA PAPER 69-175] 12 p2332 A70-27804
- Low pressure deflagration limit dependence on strand size in terms of cross section dimensions for composite ammonium chlorate propellant [AIAA PAPER 69-144] 13 p2473 A70-29955
- Size effects on impact energy disposition in plastically deformed thick steel specimens at shelf temperature, using similitude laws 15 p2760 A70-32332
- Lunar fragmental debris physics from Surveyor observations, examining size-frequency distribution 20 p3707 A70-39956
- Electrode size effects on combustion driven MHD generator performance, examining voltage losses, gas boundary layer temperature and surface conditions 20 p3566 A70-40005

- Design component size index as function of various system demands, using Monte Carlo method 21 p3846 A70-41870

SIZE DETERMINATION

NT PRECIPITATION PARTICLE MEASUREMENT

- Human size-selective neurons indicated by aftereffect from successive viewing of striped patterns with different spatial frequencies 01 p0035 A70-10724
- Long baseline interferometry used to improve radio telescopes resolving power in measuring quasar diameters 01 p0183 A70-10885
- Perceived size relation to retinal size under reduced observation conditions compared with size-distance invariance hypothesis for binocular and monocular observations 01 p0025 A70-11051
- Vertical concentration and size distribution determinations for aerosols in stratosphere, suggesting volcanic origin 02 p0294 A70-12842
- Venusian cloud layer radius, discussing error in determination of occultation level height of regulus by venus 03 p0574 A70-13881
- Scanned CRT display optimum spot size in relation to raster pitch, assuming Gaussian luminance distribution 04 p0691 A70-15136
- Solar powered communications spacecraft weight, electrical power and communication capacity models for optimizing size and launch vehicle fractionation 04 p0763 A70-15347
- Optimum second stage sizes for Blue Streak first stage for maximum payload injection into various orbits, tabulating sizes and payloads 05 p0924 A70-16589
- Liquids particulate contamination sizing and counting by membrane filtration, specifying procedures and apparatus used [SAE-ARP-598A] 07 p1195 A70-18804
- Orifice diameter for low Reynolds number flowmeter dependent on pipeline diameter tolerances 08 p1482 A70-20684
- Long baseline interferometer observations of radio sources for size determination, tabulating measured fringe visibility 08 p1578 A70-21547
- Baseline measurements of Jupiter decametric radiation providing upper size limit to coherent and incoherent sources 09 p1755 A70-22512
- Angular size measurement for galactic X ray sources in Sagittarius region using modulation collimator aboard sounding rocket 09 p1744 A70-22521
- Electro-optical technique for size distributions of cloud and precipitations particles using linear array of photodetectors 10 p1912 A70-23929
- Ultrasonic echography for ventricular size determination, calculating stroke volume and valvular regurgitation severity 10 p1820 A70-24938
- Heart dimension measurement by miniature implantable ultrasonic sonomicrometer, describing system design and operation 12 p2174 A70-26897
- Discrete radio sources angular size determination by two antenna interferometry 12 p2299 A70-27378
- Radio meteor train initial radius determination, discussing radio echo observation method 12 p2309 A70-27977
- Angular size of high energy X ray source in Crab Nebula from balloon-borne X ray modulation collimator 14 p2631 A70-30789
- Book on psychophysical analysis of visual size-distance perception and physiological optics 15 p2688 A70-31575
- Quasar 3C 298 angular dimensions and 3C 273 scintillating component at 60 MHz based on mean quasi-periods shifts of scintillations 15 p2808 A70-32885
- Optical heterodyne interferometer for stellar diameter measurements 16 p2925 A70-33025
- Jovian planets polar and equatorial diameters and lateral dimensions of Saturn rings by optical measurements 16 p2979 A70-34034
- Fraunhofer holography for recording small particles to determine size distribution without disturbing sample 17 p3086 A70-35016
- Physical and electrical sizes in large antennas, discussing paraboloid reflectors, arrays, slot antennas, etc 17 p3053 A70-35079
- Vortex core diameters calculation methods for axisymmetric angular momentum flows 17 p3074 A70-35750

- Vesta diameter and albedo determination by IR emission measurements, allowing for roughness and rotation 17 p3173 A70-35758

- Constrained viscoelastic layer optimal length for vibration damping of metallic structures 19 p3536 A70-37696
- Equidistance effects on human size and distance perception in visual alley 19 p3368 A70-37771
- Radio sources angular dimensions estimation based on shifts in histograms of scintillation quasi-periods 19 p3525 A70-38766
- Water droplet size measurement by forward light scatter holography, evaluating reconstructed wave front by Fresnel transform 20 p3628 A70-39132
- Ultrasonic pulse echo flaw detection, relating defect size to echo amplitude 20 p3636 A70-39192
- Kalman filter sizing for air-launched tactical missile via covariance sensitivity matrix [AIAA PAPER 70-954] 20 p3601 A70-39574
- Cyg-X-1 X ray source angular size and position measurements by balloon-borne collimator 21 p3873 A70-40665
- Total energies of stars with velocities perpendicular to galactic plane, examining absolute luminosities, galaxy size and local gravitational potential 21 p3890 A70-41162
- Tank collection and spectrophotometric tests in determining aluminum oxide particle size produced by small rocket engine 21 p3867 A70-41727
- Solar radio to optical radius ratio calculated from residual flux measurements during 7 March 1970 solar eclipse 22 p4097 A70-42466
- Radio sources minimum observable diameter attributed to interstellar scattering and synchrotron self absorption 22 p4101 A70-42862
- H II regions density-size relationship, using emission measurements and radio data 22 p4109 A70-43746
- Defect size estimation, using ultrasonic angle beam probes and distance-gain-size/DGS/ diagram 24 p4343 A70-45689
- Photographic measurement of droplets size, velocity and number during sprayed liquid fuel combustion, using Xe flash bulbs 24 p4429 A70-46008

SIZE PERCEPTION

U SPACE PERCEPTION

SIZE SEPARATION

- Dispersion/peak broadening/in gel chromatography measured with nonporous and porous column packings, suggesting diffusion controlled separation with linear permeation isotherm 12 p2181 A70-27474

SIZING [SEPARATION]

U SIZE SEPARATION

SIZING [SHAPING]

- Electrical discharge machining showing close tolerance sizing capability on honeycomb panels 02 p0310 A70-12665
- Hard alloy mixture shaping by free vibrational compacting of powders 07 p1296 A70-19801

SKELETON

U MUSCULOSKELETAL SYSTEM

SKEWNESS

- Clamped skew plates of orthotropic material under transverse load analyzed by stationary potential energy method and compared with isotropic case 01 p0205 A70-11140

SKID LANDINGS

- Recommended design practices to assure good brake system performance with compatibility for skid control equipped aircraft 01 p0007 A70-11457

- Steerable landing gear system consisting of freely castoring corotating wheel nose gear, tiltable axle and main gear skids for lifting body spacecraft [AIAA PAPER 69-790] 13 p2344 A70-28514

SKIDDING

- Turbine technology application to high speed roller bearing design, considering reduction of roller skidding and skewing 13 p2419 A70-28918

- Fluid film lubricated, thrust loaded, angular contact ball bearing high speed performance, predicting skidding by isothermal Newtonian behavior in ball to raceway contact [ASME PAPER 70-LUBS-7] 22 p4045 A70-42452

SKIN [ANATOMY]

NT EPIDERMIS

NT EPITHELIUM

- Typically administered vitamin A radioprotective effect on postradiation skin reactions 01 p0029 A70-11402
- Skin sensitivity representation in cats cerebellar cortex during electrocutaneous stimulation in chronic experiment, providing information on afferent system 03 p0417 A70-13216

Somatosensory cortex removal effect on blocking action of skin stimulation on associative response to light flash in cats

03 p0420 A70-13430

Thermal protection rating systems for clothing fabrics based on pain and blister effects in human skin

03 p0438 A70-14064

Nonextension lines characteristic to human skin utilized to provide natural mobility and minimal ballooning in full pressure suits noting mapping, testing, construction, etc

[ASME PAPER 69-WA/AUT-22]

04 p0642 A70-14826

Nervous system influence on erythema radiation reactions from soft X ray irradiation, discussing blood supply effect

06 p0993 A70-17430

Laser eye and skin hazard evaluation from viewpoints of threshold effect levels and worst case assumptions

07 p1219 A70-19224

Esthesiometric analysis of cutaneous thermoreceptors reaction dependence on heat production rates of human organisms

07 p1206 A70-19472

Permeability disturbances in skin capillaries of rabbits and rats following exposure to Sr90-Y90 beta radiation

09 p1619 A70-22789

Hydrogen peroxide infusion effect on skin remission following exposure to ionizing radiation on rabbit legs

09 p1619 A70-22791

Monograph on measurement and regeneration of water vapor loss of human skin, studying protective qualities of horny layer

10 p1812 A70-24598

Skin receptors afferent discharge characteristics during vibrotactile stimulation

13 p2354 A70-29594

Skin and tissue mechanical characteristics response to vibratory stimulation, considering effects on physiological and psychophysical tactile sensitivity measurements

13 p2354 A70-29598

Intermittent forced inspirations or expirations effects on venous tone and blood flow in human skin vessels

17 p3024 A70-34595

Nonextension lines characteristic to human skin utilized to provide natural mobility and minimal ballooning in full pressure suits noting mapping, testing, construction, etc

17 p3036 A70-34951

Skin simulation for thermal radiation protection studies, considering fused silica and epoxy resin filled with Al powder

18 p3225 A70-37093

Isopotential surface maps for body surface potential relation to ECG and Frank vectorcardiogram during QRS stages in children

20 p3571 A70-39368

Body composition and weight changes estimation after physical exercise by prediction equations based on skinfold and girth measurements

21 p3766 A70-42155

Live skin tissue electrical parameters changes due to laser radiation, showing coagulative necrosis by histomorphological studies

23 p4150 A70-44313

SKIN [STRUCTURAL MEMBER]

Beaded-doubler reinforced skin design concept for Improved HAWK Missile wing, considering compression stress, weight, cost and field service characteristics

02 p0380 A70-11946

Fatigue life of stiffened skin panels under acoustic loading of wideband frequencies to achieve structural resistance optimization

[DGLR-69-63]

04 p0774 A70-15140

Aircraft skin heating by lightning, discussing possibility of exceeding jet fuel vapor ignition temperature

07 p1195 A70-20402

Forced vibration of rib-skin structures under random pressure and heavy damping using wave group theory

10 p1963 A70-25066

Corrugated skins solar absorbance and IR emittance computed for spacecraft thermal design, analyzing other nondiffusive radiative enclosures

11 p2150 A70-26352

Moving skin boundary layer control on airfoil achieved by moving wetted surface in streamwise direction

[AIAA PAPER 70-881]

17 p3010 A70-34808

Airframe skin panels adhesive bonding in wide-bodied jet transports, emphasizing fuselage fatigue and corrosion resistance

[SAE PAPER 700863]

24 p4349 A70-45875

SKIN FRICTION

NT AERODYNAMIC DRAG

NT FRICTION DRAG

NT SUPERSONIC DRAG

NT VISCIOUS DRAG

Density and heat transfer effects on compressible turbulent boundary layers used to investigate velocity and temperature profiles, skin friction, Mach number and Reynolds number

01 p0003 A70-10936

Local skin friction measurement on model in blow-down hypersonic wind tunnels using floating element transducer, giving results for flat plate and wedge

[ONERA-TP-756]

03 p0463 A70-13629

MHD boundary layer separation near rear stagnation point with magnetic field normal to wall solved by series expansion, calculating skin friction by numerical quadratures

03 p0469 A70-14182

Suction influence on skin friction fluctuations of MHD flow along infinite flat wall using Navier-Stokes equations

05 p0886 A70-15787

Friction on fuselage surface layer under static and instantaneous loads without allowance for oscillation

05 p0856 A70-17015

Skin friction law for compressible boundary layer allowing calculation of coefficient of friction for isothermal walls with heat transfer

06 p1033 A70-17232

Air floated skin friction balance adaptable for cylindrical and plane surfaces

06 p1076 A70-17625

Skin friction and heat transfer on flat plate in high velocity laminar motion with mass transfer for any free stream and injected gas combination

06 p1176 A70-17689

Unheated solid starting length effect on skin friction and heat transfer characteristics in incompressible transpired laminar boundary layer on flat plate

06 p1035 A70-17691

Heat transfer coefficients for heat exchangers rotating in air at various velocities computed from skin friction coefficients in laminar and turbulent flow regime

06 p1177 A70-17701

Hyperboloids and paraboloids in flow of Reynolds number 22-65000 and Mach number 10, discussing viscous interactions effects on pressure, drag and skin friction

[AIAA PAPER 70-182]

06 p0976 A70-18240

Laminar viscous flow past semfinite flat plate parallel to uniform stream, solving Navier-Stokes equation to determine local skin friction coefficient

09 p1663 A70-23581

Skin friction near flat plate trailing edge at high Reynolds number by linearizing velocity profile

10 p1801 A70-24159

Boundary layer transition detection at supersonic speeds using thin film gages to infer local laminar and turbulent supersonic skin friction

11 p2035 A70-25970

Coupled effects of transverse curvature and pseudoplasticity on skin friction characteristics of slender circular cylinder in laminar power law fluids

11 p2038 A70-26493

MHD boundary layer flow past yawed flat plate in presence of pressure gradient, determining skin friction expansion terms

13 p2461 A70-28804

Two component piezoelectric skin friction force transducer for hypersonic flow tunnel

13 p2405 A70-28815

Two dimensional turbulent boundary layer with pressure gradient, calculating velocity distribution and local skin friction by Pohlhausen method

13 p2391 A70-29672

Supersonic skin friction measurements in grit type boundary layer transition trips with zero heat transfer

13 p2343 A70-29969

Viscous absorbing emitting shock layer in blunt body stagnation region, calculating skin friction and radiative heat transfer

[AIAA PAPER 70-868]

16 p2999 A70-33911

Force-balance principle application to pressure and skin friction measuring instruments, discussing construction, operation and performance

17 p3089 A70-35171

Skin friction variation and boundary layer separation for rotating axisymmetric body, using two layer model

17 p3011 A70-35240

Local skin friction law for turbulent boundary layers in incompressible flow, applying rule for compressible flow conditions

17 p3075 A70-35922

Free convection boundary layer on two dimensional or axisymmetric body with sudden temperature increase, determining skin friction and heat transfer coefficients

18 p3346 A70-36487

Skin friction measurement in supersonic flows by thin film heated element method, describing thermal boundary layer properties

18 p3243 A70-36710

Two dimensional turbulent boundary layer computation using two parameter family of velocity profiles and skin friction law

21 p3806 A70-40921

Heat transfer and skin friction in quasi-steady axisymmetric turbulent pipe flow of incompressible fluid with variable physical properties

21 p3808 A70-41375

Slender axisymmetric power-law missile bodies with minimum ballistic factor, using Newton-Busemann centrifugal theory with skin friction

21 p3746 A70-41756

Time-mean velocity and skin friction of laminar boundary layer near two dimensional stagnation point with oscillating oncoming flow

22 p4010 A70-42686

Pressure gradient effect on skin friction coefficients taking into account Mach, Reynolds and Stanton numbers

23 p4183 A70-44629

SKIN FRICTION DRAG

U FRICTION DRAG

SKIN RESISTANCE

Heart rate and skin conductance measurements during attention-direction tasks involving proprioceptive stimuli position on environmental acceptance and rejection continuum

01 p0026 A70-11166

Inhomogeneous plasma cylinder skin effect, surface impedance, radiation transport and mean noise temperature

07 p1347 A70-19107

Stripline skin effect in digital equipment transmitting fast rising pulses

15 p2708 A70-31828

SKIN TEMPERATURE [BIOLOGY]

Skin and hypothalamic temperature inputs for behavioral regulation of hypothalamic temperature of rats

01 p0020 A70-10725

Human thermoregulatory responses as function of peripheral thermoreceptors during imposed negative heat load in different ambient environments

01 p0024 A70-10977

Spinal cord and skin temperature effects on tension-extension diagrams in cats red and pale muscles

02 p0236 A70-12092

Thermal comfort in disparate environments, discussing human subjects skin mean temperature and body water loss

03 p0429 A70-14158

Cardiovascular responses to sustained high skin temperature in resting men noting dizziness, impaired vision and extracutaneous vasodilatation

03 p0429 A70-14162

Human skin temperature variations in supramuscular areas under physical activity and rest

04 p0638 A70-15505

Synchronous variations in skin and muscle temperatures of musculus gastrocnemius and flexor carpi in human subjects performing intermittent physical exercises

04 p0639 A70-15506

Skin-muscle temperatures ratio variations in dogs during periods of activity and rest

04 p0639 A70-15508

Physical exercise and rest regime evaluation by thermoelectric method recording skin temperature above gastrocnemius muscle

04 p0640 A70-15513

Human finger tips skin temperature periodical variations process and influencing factors using electronic analog model

10 p1823 A70-25306

Blood flow redistribution during sustained high skin temperatures of men in supine position

12 p2169 A70-27654

Thermal thermesthesiometer for skin heat sensibility studies

19 p3368 A70-37806

Cutaneous liquid crystal temperature sensors for thermographic patterns of angina pectoris induced by treadmill exercise

19 p3364 A70-38361

Body surface cooling level and rate effects on psychomotor performance tested at various levels of mean weighted skin temperature [MWST]

20 p3573 A70-39675

Human peripheral blood flow rewarming in cold ambient temperature, examining skin, rectal and tympanic membrane and oxygen uptake

20 p3576 A70-40327

Mean skin temperatures of human body by 10 point method, using cold and hot exposure data

22 p3978 A70-42874

Semiconductor thermometer for skin temperature differences using resistance bridge, transistor amplifier and thermistors

23 p4150 A70-44317

SKIN TEMPERATURE [NON-BIOLOGICAL]

Aircraft skin heating by lightning, discussing possibility of exceeding jet fuel vapor ignition temperature

07 p1195 A70-20402

Unsteady temperatures determination of integral plate consisting of skin with uniformly positioned longitudinal webs

13 p2518 A70-28478

Thin walled spherical shell spacecraft solar heating in planetary surface proximity, considering skin temperature distribution

21 p3944 A70-41019

SKIRTS

Multiple skirt air cushion vehicle /ACV/ pitch and heave dynamic characteristics, describing mathematical modeling and analog computer simulation

04 p0624 A70-15389

Water tests with N 300 Naviplanes confirming flexible skirt concept regarding speeds and stability

08 p1435 A70-20622

SKUA ROCKET VEHICLES

Skua meteorological rocket system for synoptic stratospheric sounding, describing system, launch preparation, firing and flight characteristics

07 p1395 A70-20253

Measurement physics of resistance wire temperature sensing system used in Skua rocket sounding system

07 p1396 A70-20262

SKULL

NT CRANIUM

Mechanical properties of human skull specified for construction of physical and mathematical models

02 p0243 A70-12097

Vibration mode response and impact time sensitivity of mechanical impedance of human skull, relating head injury factors

15 p2682 A70-31934

Human skull porous dipole layer shear and compressive properties, measuring static and dynamic strain rates

15 p2683 A70-32308

SKY

NT NIGHT SKY

SKY BRIGHTNESS

Sky brightness distribution data to determine shape of aerosols scattering as function of wavelength

02 p0292 A70-12435

Scattering functions from sky light spectra measurements on high mountain for various sun altitudes, obtaining color value functions

02 p0359 A70-12776

Sky background brightness temperature measurement at 408 MHz by pyramidal horn antenna

03 p0496 A70-14344

Altitude variation of mesospheric daytime sky brightness from earth based measurements of twilight sky brightness, noting inconsistency in calculations based on standard atmospheres

06 p1053 A70-17207

Radiometric investigation of energy brightness distribution over clear, cloudy and variable sky at micron wavelengths

06 p1056 A70-17835

Illumination of zenith region of sky before and during solar eclipse of September 1968 measured by luxometer

08 p1573 A70-20950

Absolute sky brightness temperatures measured with horn antennas and Dicke receivers, indicating spectrum change due to galactic nonthermal radiation

12 p2309 A70-27893

Night sky visible brightness at minus 19 degrees declination from July 1965-June 1966 in Tsumeb, South West Africa

14 p2581 A70-31390

Illumination of zenith region of sky before and during solar eclipse of September 1968 measured by luxometer

15 p2806 A70-32762

Earth atmosphere transmission coefficients determination by relation between transparency and daytime sky brightness, noting limits of applicability

16 p2899 A70-34180

Automatic spectroelectrophotometer for measuring sky spectrum brightness at 6910-4040 Å, determining point of minimum brightness

16 p2899 A70-34182

Atmosphere spectral transparency and stability spectrophotometric studies based on measuring solar aureole brightness

16 p2899 A70-34183

Twilight sky brightness measurements at 5200 Å for estimating upper atmospheric dust component, discussing error rates

16 p2899 A70-34184

Night sky brightness in UV and visible region by photoelectric photometers on Cosmos 51 and 213 satellites

17 p3163 A70-34901

Upper atmosphere temperatures from vapor cloud diffusion, eliminating errors from bright sky background at twilight

17 p3076 A70-34940

Sky brightness scattering indicatrix in effective atmospheric layer free from underlying surface multiple scattering and reflection distortions

18 p3248 A70-36634

Horizon sky UV spectral radiance, noting solar position and cloud cover effects

18 p3248 A70-36752

Rayleigh scattering in atmosphere, determining brightness dependence on altitude, latitude and season

18 p3251 A70-36979

Earth aerosol layer formation mechanism, giving atmospheric brightness measurements in terms of dust particles density and size

18 p3251 A70-36981

Zodiacal light observations at elongation angles from sun, examining surface brightness, color index and polarization degree by balloon-borne instruments

18 p3318 A70-37012

Galactic radio corona existence, measuring northern galactic hemisphere sky brightness and cosmic ray distributions

18 p3322 A70-37129

Daylight sky brightness at different wavelengths by airborne photometer, investigating statistical characteristics

19 p3460 A70-37419

Atmospheric scattering indicatrices from daytime sky brightness balloon measurements in presence of cloud cover

19 p3460 A70-37420

SKY RADIATION

NT AIRGLOW

NT DAYGLOW

NT GEOCORONAL EMISSIONS

NT NIGHTGLOW

NT TWILIGHT GLOW

Absorption band observation near 0.43 mu in solar spectra and scattered radiation of sky, determining nontelluric origin

01 p0084 A70-11613

Depth and shape of 0.94 micron water vapor absorption band for clear and cloudy skies, noting radiation distortion for dark dense clouds

04 p0690 A70-15024

Solar and sky far IR radiation in upper atmosphere, estimating precipitable water quantities and low absorption regions

04 p0681 A70-15521

Light intensity and polarization in twilight sky atmosphere at solar depressions

07 p1263 A70-19047

Vertical short wave albedo profiles in lower troposphere under cloudiness and clear sky using actinometric sounding

08 p1537 A70-21105

UHF telescopic survey of southern sky for studying galactic plane in absorption

08 p1578 A70-21536

Day sky Fraunhofer lines filling-in /Ring effect/ considered from analogous effects in surface albedo, suggesting role of Rayleigh wings

10 p1947 A70-24992

Sky radiation scattering and polarization functions for various solar altitudes at Lomnitzer Peak observatory

12 p2294 A70-27674

Atmospheric sodium concentration in twilight and daytime sky from D1 and D2 line intensities in twilight

13 p2399 A70-29239

Circumsolar sky radiation effect on pyrheliometric measurements, considering atmospheric scattering and turbidity

13 p2400 A70-29660

Polar auroral hydrogen emission intensity dependence on K index of geomagnetic activity

14 p2569 A70-30213

Solar, clear sky and overall radiation characteristics, calculating incidence of light and radiation in room interiors

15 p2732 A70-32461

Multispectral UV sky mapping and heavenly body intensity measurement onboard OAO 2 satellite

17 p3179 A70-35264

Galactic or extragalactic origin of diffuse X ray background, reporting sky survey results

21 p3875 A70-40688

Diffuse background of 2-20 keV X rays over Scorpius to North Galactic Pole sky band by rocket measurements

21 p3876 A70-40693

Mechanical passive cone angle amplifier for spinning sounding rockets for IR sky scanning, solving equations of motion for system

21 p3931 A70-41905

Lyman alpha sky background measurements by Mariner 6 UV spectrometer

22 p4094 A70-42932

OAO 2 for UV telescope sky mapping and spectrophotometric measurements of celestial bodies

23 p4261 A70-44666

Battery operated electronic servo governed photoelectric polarimeter for airborne measurements of skylight polarization, discussing design and operation principles

23 p4199 A70-45006

Polar auroral hydrogen emission intensity dependence on K index of geomagnetic activity

24 p4331 A70-46288

SKY WAVES

LUF /lowest useful frequency/ prediction for HF sky wave communication, emphasizing prediction methods using computers

07 p1229 A70-19156

Signal strength of sky waves and noise levels near LUF, suggesting importance of changing mode structure

07 p1229 A70-19158

Ray tracing techniques applied to night sky wave medium frequency propagation, modifying program for absorption and polarization coupling losses

07 p1230 A70-19164

MF signals sky wave propagation, studying roles of geomagnetic dip and propagation direction at various latitudes

10 p1832 A70-23997

Sky wave amplitudes analysis recorded at D region height by loop and short whip antennas during 7 March 1970 solar eclipse

16 p2898 A70-33833

D region LF and VLF sky waves opposite phase perturbation behavior

23 p4162 A70-44006

SKYCRANE HELICOPTER

U CH-54 HELICOPTER

SKYLAB PROGRAM

Skylab test program taking into account program requirements, test management concepts and identification subsystems, status, performance review and control

19 p3441 A70-38820

Skylab scientific space station, discussing crew living quarters and supplies, artificial atmosphere and manned solar observatory

20 p3713 A70-39481

Post Apollo space research, discussing Saturn Workshop /Skylab/, Nerva nuclear rocket engine and international cooperation

21 p3956 A70-41496

Skylab Orbital Workshop fabrication experiments under space environment conditions, discussing weightlessness and vacuum effects on various manufacturing techniques

22 p4046 A70-43075

Life support systems for biological flight experiments on Biosatellite project and Skylab A mission

23 p4154 A70-44665

Apollo and Skylab photographic systems, describing equipment and missions

24 p4333 A70-45360

Skylab experiments, spacecraft facilities and project status, discussing operations, crew functions and weight of structure, systems, consumables and related storage

24 p4416 A70-45913

Skylab mission in 1972, describing orbital workshop configuration and three man crew integration for operational experiments

24 p4417 A70-45939

SKYLARK

U SKYLARK ROCKET VEHICLE

SKYLARK ROCKET VEHICLE

Thrust vector control application to Skylark vehicle to eliminate wind and thrust misalignments effects

13 p2503 A70-28676

Upper atmospheric sounding rocket Skylark engine, attitude control and payload components modifications for increasing versatility and performance

13 p2503 A70-28678

Skyark sounding rocket telemetry data reduction system providing attitude analysis

13 p2363 A70-28680

Three axis star pointing attitude control system for stabilized Skylark sounding rocket program

13 p2447 A70-28687

RESY parachute recovery for payloads launched by Skylark high altitude sounding rocket, noting flotation system and location aids

13 p2505 A70-28771

Atmospheric temperature vertical distribution measurement using sounding balloon and Skylark rocket

15 p2725 A70-31846

SLABS

Relativistic simple shear of slab of neo-Hookean material

05 p0929 A70-16067

Transient thermal stresses in restrained-in-bending slab with surfaces heated and cooled with finite heat transfer coefficients

10 p1964 A70-25095

Isotropic slab with implanted elastic circular disk, analyzing stress-strain state due to torsional and bending moments

15 p2824 A70-32895

Microwave properties of uniformly magnetized slabs filling cross section of rectangular lossless waveguide operating in specific modes

17 p3050 A70-34584

Slab melting under hot spots, obtaining starting solutions

18 p3346 A70-36491

- Thermoelastic stresses in infinite anisotropic slab due to temperature field variations along thickness and length
19 p3539 A70-37872
- Passive type stable test platforms /slabs/ covering configurations, foundations, vibration isolation, environmental effects, etc
[AIAA PAPER 70-960] 20 p3605 A70-39569
- Initial value transport of monoenergetic neutrons migrating in slab with infinite reflectors for isotropic scattering as function of material properties
21 p3854 A70-41999
- SLAGS**
Elastoplastic properties of welded joints containing slag inclusions defects, determining sizes radiographically
24 p4347 A70-45734
- SLANT**
U SLOPES
SLANT PERCEPTION
U SPACE PERCEPTION
SLATER ORBITALS
One and two center Coulomb, hybrid and exchange integrals contributing to orbit-orbit interaction in diatomic molecules evaluated for Slater orbitals combinations
03 p0528 A70-14010
- Energy levels predicted for various electron orbital configurations in Fe V by Slater parameters
10 p1944 A70-24953
- Threshold photoionization cross sections for homonuclear diatomic N molecules calculated from Slater orbitals and Coulomb waves
11 p2086 A70-25833
- Molecular orbital wave functions for water molecule, using minimum set of Slater orbitals
14 p2544 A70-30119
- Electron excitation cross sections for light atoms using Slater wave functions and Born-Bethe approximations
21 p3853 A70-41393
- SLEDS**
NT ROCKET PROPELLED SLEDS
SLEEP
NT HYPNOSIS
Synchronizing and desynchronizing systems for cerebral electrical activity, noting roles in sleep and wakefulness mechanisms
03 p0417 A70-13073
- Unrestrained chimpanzees cortical and subcortical electrical activity during sleep recorded by telemetry and compared with human beings and other mammals
03 p0432 A70-14347
- Wake-sleep rhythm of spacecrews for operational capacity to maintain constant watch of spacecraft, suggesting recreation of terrestrial time cycle in space
05 p0799 A70-15766
- Sleep biphasic paradoxical stage in cats, correlating brain structures electroencephalographic data with various somatic and vegetative signs
12 p2173 A70-28345
- Sleep-wakefulness cycle electroencephalogram of auditory and visual portions of neocortex and hippocampus activity in cats, using spectral analysis and integration
14 p2536 A70-30185
- Collection of articles on fatigue, sleep and dreams covering mechanisms, biochemistry, pathological physiology, etc
15 p2680 A70-31743
- Sleep intensity and stages from EEG studies concerning rapid eye movements, vegetative nervous system, heart/respiration rate, blood pressure, body temperature and stomach motility
15 p2680 A70-31743
- Portable hybrid automatic sleep analyzer for on-line EEG and EOG processing
17 p3040 A70-35606
- Human sleep pattern changes due to acute sleep-waking cycle reversal
20 p3569 A70-38990
- Nocturnal headache relationship to REM sleep stage from EEG, EOG and EMG data
20 p3569 A70-38994
- Desynchronized sleep phase in cats, discussing activation and hippocampal theta and hippocampal delta rhythm predominance stages
20 p3574 A70-40171
- Click-evoked potentials in rat auditory cortex, medial geniculate body, reticulate formation and hippocampus during natural sleep and waking
21 p3761 A70-40917
- EEG dynamics during normal and altered human sleep-wakefulness regimens
22 p3971 A70-43137
- Automatic detection of K-complex waveforms in sleep electroencephalograms, using pattern recognition
23 p4151 A70-44379
- Human cortisol intermittent secretion during early morning sleep and sleep-wake cycle, examining adrenal activity
24 p4305 A70-46410
- SLEEP DEPRIVATION**
Prolonged wakefulness effect on human work capacity in isolated chamber, determining physical, intellectual and sensory capacities
05 p0809 A70-17117
- Airline pilots sleep patterns during worldwide east-west routes, considering modification by irregular duty periods and time zone adaptation
15 p2689 A70-31882
- Prolonged REM sleep deprivation effect on gamma-aminobutyric acid concentration in mice
23 p4146 A70-44658
- Sleep patterns during double aircrew continuous flying operations, suggesting 3-day maximum mission duration
24 p4306 A70-45327
- SLENDER BODIES**
NT **SLENDER CONES**
Two velocity hydrodynamic scheme for describing dynamic behavior of two phase supersonic flow past slender body
01 p0003 A70-10995
- Navier-Stokes hypersonic weak interaction theory for viscous heat conducting compressible fluid flow past slender axisymmetric body
01 p0003 A70-11097
- Surface catalysis and variable transport properties effects on chemically frozen dissociated hypersonic air flow boundary layers enveloping flat plates and slender wedges
01 p0067 A70-11179
- Slender bodies optimum aerodynamic shape for supersonic velocities, discussing minimum wave drag and total drag two step analysis using calculus of variations
03 p0408 A70-13801
- Supersonic unsteady gas flow around bodies at low Strouhal numbers, noting angle of attack amplitude and leading edge shock wave
03 p0409 A70-13865
- Similarity laws in hypersonic flow of real gas around slender blunted bodies, particularly bodies with rough lateral surface
03 p0409 A70-13866
- Axisymmetric sonic flow around slender body, determining boundary regions for slender body approximation and Guderley expansion utility
03 p0409 A70-14233
- Trailing edge flow of slender aerodynamic shapes terminating in cusp or wedge, analyzing boundary layer reactions
04 p0613 A70-14457
- Boundary layer equations for axial laminar and turbulent incompressible flows over slender bodies of revolution solved by finite difference method
[ASME PAPER 69-WA/FE-2] 04 p0667 A70-14786
- Slender wings and fuselages resistance at zero lift in supersonic flow, using Karman and Moore linear theory
[DGLR-69-28] 04 p0616 A70-15154
- Transonic flow about slender profiles computed for flow velocities slightly below and above Mach 1
04 p0616 A70-15185
- Hypersonic viscous gas flow past power law bodies under viscous interaction between boundary layer and inviscid flow extended to slender bodies
04 p0618 A70-15240
- Unsteady pressure at slender blunt body surface in three dimensional hypersonic gas flow
04 p0618 A70-15244
- Vortex separation effects on elliptic bodies lift distribution, analyzing separated flow pattern
04 p0619 A70-15385
- Mass transfer and viscous interaction combined effects on axisymmetric hypersonic flow of perfect gas over slender bodies
[AIAA PAPER 68-717] 04 p0675 A70-15576
- Hypersonic far wake mean flow properties behind two dimensional slender body wind tunnel models at zero angle of attack
[AIAA PAPER 68-700] 04 p0621 A70-15578
- Residence time of foreign gas injected into recirculation region of wake behind slender body in axisymmetric supersonic flow
[AIAA PAPER 70-111] 06 p0968 A70-18040
- Base mass injection effects of various gases on slender body supersonic near wake stability, diffusion and cooling
[AIAA PAPER 70-110] 06 p0970 A70-18075
- High altitude telemetry plasma attenuation for hypersonic blunt nose slender reentry bodies
[AIAA PAPER 70-220] 06 p1010 A70-18088
- Flow model for steady asymmetric vortex system shed from slender body of revolution in coning motion
[AIAA PAPER 70-52] 06 p0971 A70-18118
- Inviscid transonic approximation theory, calculating mixed flow field around nonlifting slender ogive body, accounting for shock wave generation, strength and location
[AIAA PAPER 70-189] 06 p0972 A70-18132
- Slender body theory for steady state aerodynamic characteristics of high speed ground vehicles with arbitrary cross sections, discussing side wind
[AIAA PAPER 70-139] 06 p0973 A70-18155
- Pressure drop at slender profile performing harmonic vibrations near interface between two media of different density solved by numerical method
07 p1254 A70-19079
- Slender body approximation for shape determination of nonslender hypersonic body of revolution with minimum convective heat transfer rate
09 p1788 A70-22931
- Shape of minimum drag slender body of revolution in Newtonian flow for given volume, length and maximum cross section determined by stochastic optimality principle
10 p1802 A70-24278
- Small plane perturbations stability losses in uniform rectilinear motion of nonrigid deformable rocket, using slender bodies pressure theory
10 p1950 A70-24528
- Head wave distance from body determined for slender pointed profile in subsonic region of transonic flow
10 p1803 A70-24780
- Coupled effects of transverse curvature and pseudoplasticity on skin friction characteristics of slender circular cylinder in laminar power law fluids
11 p2038 A70-26493
- Slender body transonic wave drag double integral, describing computer program for numerical evaluation
11 p1977 A70-26644
- Boundary layer equations with pressure gradient for revolving slender body, examining transverse curvature influence on layer separation and integral characteristics
12 p2214 A70-28249
- Slender cylindrical shell loaded by internal pressure analyzed using numerical procedure developed for digital computer
13 p2512 A70-28981
- Asymmetrical slender planetary entry vehicle roll dynamics, analyzing steady state angular motion
[AIAA PAPER 70-560] 13 p2339 A70-29003
- Pressure distribution and drag for inviscid flow past slender sharp-nosed fuselages and afterbodies at arbitrary transonic Mach numbers
[AIAA PAPER 70-556] 13 p2340 A70-29021
- Wind tunnel interference for inviscid compressible conducting fluid on slender body of revolution, discussing disturbance potential
13 p2464 A70-29449
- Unitary solution to incompressible and nonviscous fluids in presence of slender profile
13 p2464 A70-29542
- Slender bodies surface pressure distribution under various aerodynamic loads, discussing cruciform wing, circular body-slender wing configuration, etc
13 p2341 A70-29749
- Radiating gas flow about pointed bodies, investigating shock curvature at wedge or cone tip and straight shock waves flow field downstream
14 p2663 A70-30267
- Differential equations for coupled bending and torsional vibrations of slender beam in centrifugal force field
14 p2661 A70-31226
- Static aerodynamic characteristics of slender ablating reentry vehicle, discussing coupling between flow field and thermochemical analyses of heat shield materials response
[AIAA PAPER 70-826] 16 p3001 A70-33939
- German monograph on supersonic flows calculation past slender bodies of revolution using perturbation approach based on Poincare-Lighthill-Kuo method
16 p2839 A70-34082
- Wedge and cylinder high supersonic wakes stability and transition at various Reynolds numbers
17 p3006 A70-34465
- Two dimensional supersonic wake behind heated slender flat plate, considering flow properties in transition zone
17 p3006 A70-34466
- Steady state laminar flow model for near wake of slender body in supersonic flow
17 p3006 A70-34467
- Hypersonic flow past slender bodies, discussing inviscid flows, outer edge singularity of boundary layer and three dimensional interaction on needle-like bodies
17 p3010 A70-35035
- Flow field on suction side of slender body of revolution with/without wings, investigating by directional probe in wind tunnel
17 p3013 A70-35924
- Compression and expansion characteristics of steady supersonic flow passing along yawing slender body of rotation, linearizing differential equations
18 p3207 A70-36382
- Slender hypersonic airfoil shape optimization for maximum lift to drag ratio for given profile area, chord and free stream conditions
19 p3352 A70-38304
- Asymmetric boundary layer transition effects on slender reentry vehicle motion by changing static stability characteristics
[AIAA PAPER 70-987] 20 p3557 A70-39542

- Electrically conducting gas flow past slender body of arbitrary cross section in presence of crossed magnetic field by MHD Stokes approximation 20 p3558 A70-39613
- Supersonic flow past slender bodies in presence of strong blowing, extending solution by expansion at leading edge of thin plate 20 p3559 A70-39771
- Aerodynamics of steady, inviscid transonic flows around slender bodies and wing-body combinations at free stream Mach number one [AIAA PAPER 70-798] 20 p3559 A70-39900
- Slender axisymmetric power-law missile bodies with minimum ballistic factor, using Newton-Busemann centrifugal theory with skin friction 21 p3746 A70-41756
- Conducting fluid supersonic flow past slender body of revolution in circular wind tunnel under inclined magnetic field, investigating MHD interference problem 22 p3958 A70-42669
- Two dimensional steady flow around slender profiles at free transonic stream with curved compression shocks, approximating by hodographic method 23 p4131 A70-44023
- Iterative method based on slender body approximation applied to axisymmetric sonic flow fields, splitting differential equation into coupled parabolic equations [ICAS PAPER 70-13] 23 p4132 A70-44124
- Optimum thickness ratio and minimum drag of slender bodies in hypersonic viscous flow as function of altitude 23 p4134 A70-44571
- Nonrigidly supported ballast effects on dynamic characteristics of slender body during atmospheric entry 23 p4258 A70-44594
- Hypersonic three dimensional flow past elliptic cross section slender bodies, discussing disturbance equations, pressure, velocity and density distributions and shock shape [DFVLR-70-27] 23 p4135 A70-44633
- Two dimensional laminar near wake of slender body in supersonic flow at high Reynolds number 23 p4135 A70-44693
- Viscous heat conducting compressible fluid flow past slender axisymmetric body, presenting Navier-Stokes hypersonic strong interaction theory 24 p4289 A70-46020
- SLENDER CONES**
- Inviscid surface pressures calculated on slender wedges and cones at low frequencies and large oscillation amplitudes in hypersonic flow 01 p0003 A70-10854
- Water tunnel experiments with slender cones to investigate frequency of vortex shedding at low Reynolds number controlled by local diameter 01 p0003 A70-11098
- Ablation effects on transition Reynolds number of hypersonic boundary layer on slender cones 03 p0465 A70-12945
- Hypersonic laminar separation of slip flow on slender cone with attached compression flares, using surface pressure measurements and Pitot surveys [DFVLR-SONDDR-26] 04 p0620 A70-15577
- Pressure distribution at circular slender cone with 10 deg semiapex angle in hypersonic vacuum wind tunnel 06 p0966 A70-17251
- Rectangular-slot antenna pair self and mutual admittances in inhomogeneous plasma layer on slender conical body, calculating VSWR and isolation 06 p1020 A70-17565
- Axial profile characteristics of hypersonic near wake of slender circular cone based on pitot pressure, static pressure and stagnation temperature measurements 06 p0968 A70-17916
- Nose bluntness, angle of attack and oscillation amplitude effect on hypersonic unsteady aerodynamics of slender cones [AIAA PAPER 70-216] 06 p0969 A70-18059
- Pressure interaction with slender cone in hypersonic flow [AIAA PAPER 70-183] 06 p0972 A70-18126
- Full scale R/V flight test base pressure data for slender cones with ablative heat shields, considering mass flow and addition effects 06 p0973 A70-18148
- Drag of diffusely reflecting and cool slender cone in hypersonic flow, using nonlinear Boltzmann equation for hard spheres 06 p0981 A70-18359
- Drag coefficients of sharp and blunt cones in rarefied supersonic flow for bluntness ratios and angles of attack 06 p0981 A70-18360
- Hypersonic rarefied merged layer flow over sharp slender cones, using strong interaction theory and free molecular flow to analyze surface pressures 06 p0982 A70-18363
- Sphere and sharp slender cone drag coefficients in hypersonic transitional flow measured by flow modulation technique 06 p0984 A70-18389

- Low density hypersonic flow over slender cone using air and He test gases 07 p1188 A70-19309
- Mangler displacement thickness correction for slender cones 08 p1590 A70-21320
- Drag on sharp cones in hypersonic flow, studying effects of intense transverse mass injection through porous walls 09 p1603 A70-22441
- Free flight static, dynamic stability and drag data for 10 degree semiangle cone obtained at 8-16 Mach numbers [AIAA PAPER 69-133] 09 p1605 A70-23218
- Drag coefficients for spheres and sharp cones in rarefied hypersonic air flow obtained in shock tunnel using free flight technique 09 p1605 A70-23221
- Hypersonic viscous interactions on insulated slender cone with mass injection assuming perfect gas flow and negligible transverse curvature effects 10 p1803 A70-24821
- Ballistic range tests to study ablation effects on aerodynamic characteristics of ablating and nonablating slender cones [AIAA PAPER 69-179] 11 p2148 A70-25976
- Aerodynamic effects of bluntness on slender cones in free flight tests at Mach 17 [AIAA PAPER 70-554] 13 p2340 A70-29019
- Spatial distribution of three dimensional laminar boundary layer transition zone on sharp half angle cone from hypersonic wind tunnel tests [AIAA PAPER 69-12] 13 p2343 A70-29953
- Hypersonic low density transitional flow over slender conical vehicle, calculating drag coefficient and density profiles 14 p2529 A70-31365
- Transpiration and film cooling effects on aerodynamic characteristics of slender cone in hypersonic flow tested in hypervelocity wind tunnel using mass injection 16 p2837 A70-33857
- Hypersonic aerodynamic characteristics of sharp slender right circular cones at angles of attack, using Newtonian impact theory modified for flow separation effects [AIAA PAPER 70-979] 20 p3558 A70-39550
- Full scale R/V flight test base pressure data for slender cones with ablative heat shields, considering mass flow and addition effects [AIAA PAPER 70-109] 21 p3745 A70-41753
- Heat transfer and shock wave shapes about blunt slender cones in viscous-inviscid coupling hypersonic flow 23 p4134 A70-44569
- Free jet flow axial gradient effects on drag coefficient measurement of slender blunted cones at zero attack angle 23 p4135 A70-44584
- SLENDER WINGS**
- Research program to improve performance of high lift devices on wings having small sweepback and high aspect ratio 01 p0001 A70-10047
- Contour, pressure distribution and aerodynamic parameters calculations of slender highly cambered parawings in symmetric and asymmetric inviscid flow 03 p0408 A70-13800
- Lift effectiveness of slender wings with streamwise root gaps and fences, obtaining lift curve slope variation with fence height 04 p0621 A70-15611
- Slender wing with blunted leading edge to reduce thermal stresses at supersonic speed studied for aerodynamic characteristics in hypersonic flow 05 p0791 A70-17001
- Nonlinear theory extended to slender triangular and rectangular wings with symmetric profile, taking into account finite wing thickness 06 p0966 A70-17254
- Air compressibility effects on aerodynamic characteristics of slender rectangular wings moving at subsonic speed near earth surface approximated by lifting surface theory 10 p1801 A70-24276
- Supersonic flow around slender polygonal wings with nonsymmetrically distributed incidence using method for conical flow around angular wings 10 p1803 A70-24797
- Low speed buffet intensity under pressure fluctuations on slender wing aircraft at vortex breakdown, using wind tunnel model 10 p1963 A70-25067
- Slender wings leading edge vortex flow effect on roll damping at subsonic speeds [AIAA PAPER 70-540] 13 p2339 A70-29007
- Steady isentropic weakly perturbed supersonic flows past arbitrary slender tapered wings with subsonic leading edges 16 p2838 A70-33971
- Slender wings of low aspect ratio and sharp leading edges, predicting inviscid maximum lift 21 p3743 A70-40585

SLEWING

- Pendulous integrating gyro accelerometer gas bearing wheel characteristics at high slew rates monitored by differential varmeter [ASME PAPER 69-WA/LUB-3] 04 p0698 A70-14770
- Pendulous integrating gyro accelerometer gas bearing wheel characteristics at high slew rates monitored by differential varmeter [ASME PAPER 69-WA/LUB-3] 19 p3436 A70-37618

SLIDES

U CHUTES

SLIDING

- Strain component determination for grain boundary sliding influence in creep of alpha iron 20 p3735 A70-40446

SLIDING CONTACT

- Frictional traction-sliding speed relation in elastohydrodynamic lubrication in Barlow-Lamb model of viscoelastic liquid, discussing oscillatory and continuous shear 09 p1691 A70-22600
- Sliding electrical contacts in vacuum and space - Conference, Virginia Polytechnic Institute, September-October 1969 16 p2919 A70-33805
- Reliability life tests preventing sliding electrical contacts failure in space vehicles, discussing data dissemination 16 p2920 A70-33806
- Literature review of sliding electrical contacts in space vehicles, covering heavy aromatic hydrocarbons, molybdenum disulfide and other lubrication materials 16 p2920 A70-33807
- Sliding electrical contacts for unmanned scientific satellites, discussing Nimbus AVCS camera iris motors 16 p2920 A70-33809
- Slip ring assemblies for spacecraft devices, evaluating sliding electrical contact industry technological capabilities 16 p2920 A70-33811
- Heat conduction from sliding solids, discussing restrictions effect on temperature field near interface 17 p3197 A70-35543
- Sliding bodies contact surfaces stable roughness magnitude by molecular-mechanical friction and wear fatigue theories 24 p4341 A70-45489

SLIDING FRICTION

- Sliding friction and adhesion mechanisms theories based on thermodynamics, noting frictional heat and adhesive joints [ASME PAPER 69-LUB-4] 01 p1013 A70-10398
- Unlubricated wear characteristics of polyimide resin sliding against carbon steel in air, noting effects of surface temperature, bearing pressure and velocity 01 p1013 A70-10448
- Inertia effect of electrically conducting lubricant on load capacity of hydromagnetic inclined slider bearing under magnetic field 01 p1014 A70-11389
- Friction and surface damage between clean metal hemispheres and flats at low sliding speeds and 25 K room temperature range 01 p1015 A70-11393
- Sliding steel specimens anomalous friction behavior in vacuum, noting friction-time plot dependence on oxide film rupture, load, environmental pressure, etc 02 p0321 A70-12534
- Calculus of variations used for determining optimum one dimensional MHD slider bearing with bounded control variables [ASME PAPER 69-WA/LUB-2] 04 p0698 A70-14771
- Optimum one dimensional Rayleigh gas slider bearing, calculating step location, pressure and load capacity for range of bearing numbers [ASME PAPER 69-WA/LUB-1] 04 p0698 A70-14772
- Sliding wear of bearing Al lubricated with polyphenyl ethers in boundary region tested by pin and cylinder wear machine producing continuous record 05 p0854 A70-15910
- Polytetrafluoroethylene wear tested by rubbing cylindrical rod flat ends against glass plates, determining sliding contact pressure effects 06 p1077 A70-18403
- Sliding friction and wear of polytetrafluoroethylene ball bearing filled with graphite investigated for irradiation effects 06 p1077 A70-18404
- Lubricating oils viscosity deterioration during sliding motion in machines determined by quantitative evaluation 09 p1693 A70-23407
- Sliding bearings with nonNewtonian lubricants, noting pressure gradient change effect caused by speed fluctuation and material constants 10 p1893 A70-24015
- Stress measurement in discontinuous layered medium subjected to perpendicular load under sliding friction, using photoelastic interferometric models 11 p2131 A70-25587

Hydraulic driving system stick-slip prevention by acceleration and transient velocity feedback compensation techniques

11 p2060 A70-26407

Surface sliding friction interactions in aluminum alloys friction welding

12 p2239 A70-26855

Fretting and fretting fatigue in metal-metal contacts, showing friction as important parameter

12 p2253 A70-27110

Friction and wear of Ni sliding on Ni, Cu on Cu and Au on Au tested in vacuum at room temperature with constant load

12 p2242 A70-27229

Polyurethane and metal surface layers deformation related during sliding friction in presence of liquid media, noting friction coefficient- deformation relation

12 p2244 A70-28284

Sliding rigid conical indenter friction experiments over work hardenable metal flats in high adhesion conditions, observing forces, stresses and deformation modes

13 p2421 A70-29548

Oxygen interlayer diffusion effects on wear change during gliding friction of normalized steel samples

15 p2743 A70-31636

Antifriction and wear properties of iron fluoride materials and white cast iron under sliding friction in air and vacuum

15 p2743 A70-31637

Gas formation by sliding friction of self lubricating Teflon with carbon black on steel in ultrahigh vacuum, using mass spectrometry

15 p2745 A70-32446

Friction and wear effects on leakage path in sliding seal interface

16 p2916 A70-33078

Sliding friction effects of nonlinear asymmetric supports on turbine engine rotor-shaft stability

18 p3301 A70-36799

Optimum one dimensional Rayleigh gas slider bearing, calculating step location, pressure and load capacity for range of bearing numbers

19 p3436 A70-37617

Calculus of variations used for determining optimum one dimensional MHD slider bearing with bounded control variables

19 p3436 A70-37620

Transition metal disulfides and diselenides as solid lubricants, investigating sliding friction characteristics

19 p3438 A70-38801

Quasi-harmonic friction induced near sinusoidal form vibration, calculating amplitude dependence on sliding velocity

22 p4044 A70-42445

Sliding bodies contact surfaces stable roughness magnitude by molecular-mechanical friction and wear fatigue theories

24 p4341 A70-45489

Energy absorption and dissipation in friction brakes, investigating brake lining polymer binder contribution through molecular reorientation, crystallinity increase and entropy decrease

24 p4342 A70-45585

Refractory materials surface behavior under friction, discussing microscopic nature of wear and surface deterioration due to thermal fatigue, fusion and material transfer, etc

24 p4342 A70-45595

SLIP

Mo single crystals tensile properties at different orientations, noting asymmetric slip in plastic behavior

22 p4056 A70-43155

SLIP BANDS

U EDGE DISLOCATIONS

SLIP FLOW

Navier-Stokes equations for compressible gas, generalizing viscous channel flow of heat conducting gas to slip flow of rarefied gas

01 p0068 A70-11579

Magnetic boundary layer equations applied to flow past stationary circular cylinder and sphere, showing graphical variation of slip velocity with angle

03 p0471 A70-14334

Hypersonic blunt body heat transfer prediction, including coupled effects of real gas behavior and slip boundary conditions

04 p0614 A70-14809

Hypersonic laminar separation of slip flow on slender cone with attached compression flares, using surface pressure measurements and Pitot surveys

04 p0620 A70-15577

Axisymmetric motion of viscous heat conducting gas by constructing indirect analog of Poiseuille gas flow, applying results to slip flow regime

06 p1048 A70-18325

Thermal slip velocity of gas in infinite temperature gradient tangential to solid wall, basing calculation on linearized Boltzmann kinetic equation

06 p1049 A70-18332

Surface diffusion slip velocity in binary gas mixture above solid surface, basing calculation on distribution functions determined from Boltzmann equation

06 p1049 A70-18333

Meksyn asymptotic method of integrating boundary layer equations applied to ordinary differential equations for slip flow past seminfinit plate

06 p0979 A70-18348

Slip flow of nitrogen gas through long circular tubes, measuring mass flow, pressure drop and cross sectional velocity profiles

06 p1051 A70-18368

Velocity profile at entrance of two dimensional channel immersed in rarefied slow moving uniform flow with slip at walls

06 p1052 A70-18384

Temperature dependence of microplastic yield and flow stress and transient creep responses of gamma prime phase

08 p1522 A70-21709

Magnetic field and conducting walls effect on laminar steady MHD Couette flow of electrically conducting incompressible viscous rarefied gas in slip regime

08 p1553 A70-21764

Dual flow turbojet engine rotor slip constraints during turning, investigating turbine blade strength, thrust deviation, fuel consumption and compressor stability

10 p1930 A70-24285

Rarefied gas flow in slip regime through cylindrical tube assuming parabolic velocity profile

14 p2565 A70-30263

Rarefied gas slip flow coefficients calculations at nonuniformly heated surface, demonstrating relationship between temperature and isothermal slip coefficients

15 p2776 A70-31478

Low speed rarefied slip flow over wedge by asymptotic method of boundary layer equations integration, obtaining velocity profiles for various angles

17 p3010 A70-34973

Rarefied gas dynamics at different Knudsen numbers, discussing elements of kinetic theory and analyzing free molecular and slip flows

17 p3070 A70-35037

Kinetic effects of Barnett equations and slip conditions for continuous dense gas flows at small Knudsen numbers

18 p3239 A70-36256

Two dimensional MHD couette flow in slip regime, considering constant suction on stationary plate to determine transverse magnetic effects

20 p3677 A70-39047

Steady compressible supersonic planar flow of viscous heat conducting fluid under linearization freestream conditions, describing slip flow past finite flat plate

20 p3557 A70-39228

Local heat transfer between heated circular cylinder and air in transverse slip flow at low Reynolds and Mach numbers

21 p3945 A70-41035

Wall recombination heat transfer in rarefied flow with velocity slip near leading edge

21 p3952 A70-42083

Rarefied gas heat conduction between concentric cylinders in slip regime, obtaining perturbed temperature and density variations

23 p4284 A70-44985

SLIPSTREAMS

Axisymmetric helium jet transition to turbulent flow in air slipstream, measuring temperature and velocity profiles

09 p1660 A70-22439

Helicopter rotors flow conditions by digital computer, investigating slipstream configuration

16 p2836 A70-33761

SLITS

Stress-strain relations for rigidly sealed orthotropic planes with finite number of slits

03 p0592 A70-13447

Electromagnetic field sources in two dimensional problem of diffraction by slit

03 p0526 A70-14355

Actively participating bounding surfaces effect on free molecule flow through slit or annular orifice situated in wall separating different pressure regions

[ASME PAPER 69-WA/APM-26]

04 p0668 A70-14906

Plane E-polarized wave diffraction by slit in conducting screen using Fredholm integral equations of second kind

08 p1461 A70-21004

Stress-strain state of infinite isotropic plate weakened by curvilinear slit

13 p2514 A70-29293

Elastoplastic equilibrium of thin infinite plate with periodic slit system along straight line under tension, investigating localized plastic deformation domains

20 p3721 A70-39769

Light intensity distributions within successive slits imaged by transmission gratings, using theory for spatial moire fringe blurring

23 p4217 A70-43819

Plane wave diffraction by infinite strips and slitte planes, obtaining asymptotic expansions valid for HF

24 p4426 A70-46019

SLOPES

NT GLIDE PATHS

Slopes distribution over finite span on planetary surface excavated by primary impact craters, including typical lunar mare crater densities

01 p0178 A70-10443

Noontime ground surface temperature relationship to exposure and slope angle for meadows and woodland, using airborne IR pyrliometer

06 p1054 A70-17415

Slope failure erosional and mass wastage forms identification, characteristics and distribution based on large scale aerial photography depicted by remote sensor returns

12 p2217 A70-26913

Wind velocity components on nonuniformly heated plane slope with linear periodic temperature function

14 p2602 A70-30165

Integral radiation fluxes incident on sloping and horizontal surfaces compared under cloud covers of various intensities

14 p2603 A70-34048

Macaulay method extended for slope and deflection of statically indeterminate beams, rewriting design equations into index notation for computer programming

[ASME PAPER 70-DE-2]

16 p2989 A70-33419

SLOSHING

U LIQUID SLOSHING

SLOT ANTENNAS

Monograph on radio telescopes covering developments from simple parabolic reflectors to computer based image forming instruments

01 p0046 A70-11250

UHF shallow-cavity crossed-slot aircraft antenna for satellite to air communications

02 p0269 A70-12585

Equatorial patterns measurement of plasma covered axially slotted cylindrical antenna, describing discharge tube, facility and Langmuir probe survey of tube electron density

02 p0269 A70-12590

Antenna biasing with DC field to improve power handling capacity tested on U-slot and helical antennas

02 p0269 A70-12595

Surface function and impedance distribution for unilateral surface wave antenna excitation by slot emitter above surface impedance segment

04 p0655 A70-14403

Aperture electric field bounds presented for TE, TM and TE/TM excitation over azimuthally symmetric slotted cylinder subject to constraint of specified radiated power

04 p0649 A70-14969

Variational principle used in microwave breakdown predictions for rectangular aperture antenna

05 p0824 A70-16988

Rectangular-slot antenna pair self and mutual admittances in inhomogeneous plasma layer on slender conical body, calculating VSWR and isolation

06 p1020 A70-17565

Element pattern derived for circular arrays of axial slits on large perfectly conducting cylinders, comparing properties with planar arrays

06 p1021 A70-17571

Rectangular waveguides broad wall longitudinal slot equivalent networks, noting series/parallel function dependence on slot length

07 p1240 A70-19221

Far field synthesis for calculating excitation pattern of waveguide-excited aperture antenna arrays

07 p1243 A70-20325

Equivalent circuit for radiation admittance of infinite planar array of phased rectangular waveguide apertures

09 p1646 A70-22692

Bounds on near electric field outside rectangular slot in conducting ground plane applied to microwave breakdown limitation

09 p1646 A70-22696

Effective noise temperature of planar aperture antennas in lossy inhomogeneous plasma slabs calculated by computer

09 p1646 A70-22704

Waveguide slot antenna with electrical control of field polarization from linear to circular and beam scanning over wide sector

09 p1652 A70-23652

Solid dielectrics permittivity measurement using beam deflection phenomenon in multislot waveguide antenna

09 p1652 A70-23656

Variational principle in electromagnetics to produce linear algebraic equations with Rayleigh-Ritz procedure for application to dielectrically coated slot antenna

12 p2198 A70-27957

Impedance in coaxial line generated by tee-fed waveguide slot antenna, using equivalent circuit

12 p2198 A70-27966

Waveguide slot array operation in different frequency bands generating independent radiation patterns, utilizing orthogonal dominant modes propagation 12 p2199 A70-27967

Leaky waveguide radiation patterns with periodic loading slots along axis 13 p2377 A70-29105

Radiation patterns of slots in flat and curved screens using open waveguide emission theory 13 p2378 A70-29305

Radiation pattern theory for primary aperture antenna with two secondary radiators 13 p2378 A70-29547

Aperture antennas planar finite array, calculating excitation pattern for prescribed surface current distribution 14 p2557 A70-31160

Asymmetric phase error in antenna circular apertures, emphasizing beam squint resulting from distortion of paraboloidal reflector 16 p2859 A70-32942

Admittance measurements of rectangular or circular waveguide fed aperture antennas illuminating displaced metal plate 16 p2872 A70-32963

Wedge diffraction analyses of TE sub 10 mode slot radiation characteristics on circular and elliptical cylinder, considering boundary value solutions existence 16 p2861 A70-32965

Amplitude distribution selection in antenna aperture in presence of phase amplitude errors from relation between sidelobe level probabilistic and phase amplitude errors characteristics 16 p2873 A70-33241

Radiation from simple slots in moving dispersionless dielectric, using Minkowski electrodynamics 17 p3043 A70-34984

Microwave antenna with aperture in infinite conducting plane, analyzing radiation patterns, scattering and diffraction 17 p3043 A70-35053

Continuous line source, array or aperture antennas of linear rectangular or circular shape, discussing radiation patterns synthesis methods 17 p3044 A70-35057

Radiation patterns and impedance properties of slot antenna in ground plane, slot on cylinder and sphere and waveguide slot arrays 17 p3051 A70-35064

Physical and electrical sizes in large antennas, discussing paraboloid reflectors, arrays, slot antennas, etc 17 p3053 A70-35079

Shadow current method for asymptotic solution to two dimensional problem of electromagnetic wave far diffraction field on ideally conducting plane with infinite rectilinear slot 18 p3227 A70-36142

Open plane slotted waveguide excitation by current carrying filament, using long wave approximation 19 p3377 A70-37726

Electromagnetic wave propagation perpendicular to slots of plane dielectric filled waveguide used as slow wave system and antenna 19 p3386 A70-37728

Microwave aperture antenna in finite size ground plane, calculating radiation pattern distortion by superposition of boundary value and wedge diffraction solutions 20 p3599 A70-40314

Aperture antennas admittance calculation, considering upper bound on error involved in approximating finite ground plane conductivity by perfect conductivity 20 p3599 A70-40316

Aperture antenna pattern beamwidth decrease in near field with increasing scan angle 21 p3796 A70-40559

Quasi-equispaced traveling wave slot arrays with below sidelobe crosspolarization, considering computer designed X band prototype 21 p3800 A70-42050

Cylindrical slot antennas radiation patterns in plane perpendicular to axis, discussing field emission and angular position of each slot for phase multiplier 22 p3997 A70-43131

Nonradiating higher order modes on shielded slot lines for TM and TE cases, using series matching and Wiener-Hopf technique 22 p3990 A70-43420

Dielectric covered narrow radiating slots in rectangular waveguide broad face, calculating impedance from equivalent circuits 23 p4175 A70-44952

Annular aperture /slot/ antenna driven by coaxial line, calculating input admittance and complete near field radiation distribution 23 p4176 A70-44954

Planar conducting screen with periodic rectangular perforations, determining transmission and reflection coefficients and aperture field distribution 24 p4311 A70-45219

SLOTS
NT WING SLOTS

Foreign gas injection and slot geometry influencing film cooling effectiveness 01 p0219 A70-11182

Ideal fluid flow past sphere in rectangular duct and slot solved in series form in spherical functions 04 p0666 A70-14605

Liquid flow through cylindrical slot of constant and variable thickness, calculating flow variations 06 p1034 A70-17630

Slot burner laminar flame front stability loss ascribed to increased slot dimensions and angles between velocity vector and flame front 08 p1598 A70-21208

Slot line wavelength, impedance, transitions and tolerances measured at S band using different dielectric constant materials 08 p1475 A70-21282

Slot transmission line applicability to miniature ferrite phase shifter design exploiting elliptically polarized H field existence 08 p1475 A70-21283

Laminar boundary layer separation noting effect of mass slot suction 09 p1662 A70-23236

Plane turbulent wall jet from small slot, investigating velocity distribution dependence on slot inclination 13 p2388 A70-29448

Self similar dynamic problems in two dimensional elasticity theory for slot with point source in boundless body 13 p2517 A70-29763

Supersonic slot cooling for surface protection at hypersonic speeds using contoured axisymmetric nozzle with streamlined body 14 p2663 A70-30257

MHD induction generator efficiency, investigating winding slot finite spacing and width effects 14 p2533 A70-30531

Incompressible two dimensional potential flow analysis with compressibility effects for thick highly cambered multibodies in cascade, noting slotted compressor blade performance 14 p2529 A70-31023

Radiation pattern of conducting strip excited by linear slot parallel to strip edges, deriving asymptotic solution 16 p2863 A70-33239

Hydraulic characteristics of flow through miniature slot orifices for rocket engine injectors, observing stability of effluent liquid streams 16 p2891 A70-33566

MHD induction generator efficiency reduction due to finite winding slots spacing and width 20 p3565 A70-39987

Self similar dynamic problems in two dimensional elasticity theory for slot with point source in boundless body 20 p3732 A70-40101

SLOTTED ANTENNAS U SLOT ANTENNAS SLOTTED WIND TUNNELS

Upwash interference on oscillating wing in slotted wall wind tunnels, analyzing acceleration and velocity potentials using small wing theory 04 p0621 A70-15605

Optimal V/STOL wind tunnel interference study of slotted tunnel walls, including porosity and height to width ratio effects 07 p1251 A70-20407

V/STOL testing wind tunnel section with solid vertical and slotted horizontal zero interference walls 18 p2327 A70-36461

Calibration tests in transonic wind tunnel with two and four sided perforation section 19 p3353 A70-38475

Low speed airfoil two dimensional testing in wind tunnel with slotted wall, examining lift, drag and pitching moments 23 p4132 A70-44119

SLOW NEUTRONS U THERMAL NEUTRONS SLUDGE

Sludge removal from electrolyte in electrochemical machining by settling system, discussing temperature control, flow requirements, concentration control and balance system 10 p1893 A70-23859

SLURRY PROPELLANTS

Slurry-cast filled nitrocellulose plastisols as solid propellants, discussing compositions, performance and applicability to beryllium fuel 07 p1360 A70-19907

SLUSH

Liquid and slush hydrogen gravimetric flow calibration system for research in slush generation, slush fluid mechanics and flow instrumentation 06 p1031 A70-18449

Slush and water hazards on runways, discussing investigation and amelioration methods 11 p2030 A70-25356

Hydrogen slush characteristics, discussing advantages of liquid-solid mixture over liquid hydrogen, production methods, aging effects, transfer and pumping losses, storage, instrumentation, etc 23 p4232 A70-45075

SLV (SOFT LANDING VEHICLES) U SOFT LANDING SPACECRAFT SM-65 MISSILE

U ATLAS LAUNCH VEHICLES
SMALL ASTRONOMY SATELLITES
Small Astronomy Satellite /SAS/ program providing Explorer class Scott launched satellite capability for astronomical observations 08 p1581 A70-20608

SMALL PERTURBATION FLOW

Small amplitude perturbations in interstellar medium, discussing order of magnitude estimates of properties of cosmic rays, thermal gas, dust and magnetic field 03 p0575 A70-14016

Premixed compression initiated supersonic combustion, noting sensitivity to small perturbations in inlet flow variables 07 p1421 A70-19318

[AIAA PAPER 68-995]
Small disturbance and similitude applicability to internal hypersonic conical flows in edge shock and Busemann inlets 09 p1606 A70-23245

Small linear disturbance and stability of potential unsteady motion of finite mass of liquid with free boundary 10 p1866 A70-24111

Rigid body mode of viscous incompressible fluid flow response to small perturbations of rotating spherical container, applying torque interaction 10 p1868 A70-24196

Plane Couette oscillating flow stability to small disturbances under composed unsteady velocity at high Reynolds number 10 p1868 A70-24197

Small plane perturbations stability losses in uniform rectilinear motion of nonguided deformable rocket, using slender bodies pressure theory 10 p1950 A70-24528

Inviscid incompressible conducting fluid flow past body in aligned magnetic field at low magnetic Reynolds number, discussing small perturbations evolution 11 p2041 A70-26623

Two phase convex corner flows of particle imbedded inviscid incompressible fluid using small perturbations method 14 p2565 A70-30279

Steady plane relativistic flow small irrotational perturbation theory determining subsonic, transonic and supersonic approximation 14 p2566 A70-30472

Integral equation for transonic small disturbance flow applied to plane flows over lifting airfoils 15 p2673 A70-32768

Three dimensional inviscid small perturbation compressible flow past lifting axial compressor rotor at subsonic and transonic speeds 18 p3208 A70-36691

Viscous dielectric incompressible fluid cylinder capillary stability under small axisymmetric disturbances and axial electric field, deriving perturbed fluid flow equations 19 p3406 A70-38351

Boundary layer transition under small trim-dimensional perturbations interacting with excitations from wall 24 p4327 A70-46206

SMEAR

Edge smear in far field holography as function of interference orders, using short-cut trace technique 09 p1684 A70-23532

SMELL

U OLFACTORY PERCEPTION SMITH CHART

Microwave transistors parameters measurement by scattering /S/ parameter method for characterizing noise, gain and dynamic range, reading input and output impedances from Smith chart 19 p3386 A70-37692

SMOKE

Smoked-foil technique for transverse wave quantitative study in condensed-phase explosives 03 p0606 A70-13814

Standard method for aircraft engine exhaust smoke measurement for air pollution control 12 p2290 A70-27429

[SAE PAPER 700250]
Smoke chamber measurements of opacity developed in polymer pyrolysis or combustion, including Materials Smoke Obscurity Index /MSOI/ 20 p3736 A70-39404

Chemical and physical factors effect on smoke evolution from polymers 20 p3736 A70-39405

Aircraft gas turbine engine smoke emission measurement, discussing test equipment and procedure standardization 20 p3689 A70-39720

Aerodynamic holder stabilized smoke flames to avoid intermittent flaming and thick puffs for incinerator air pollution reduction 21 p3942 A70-40887

SMOKE ABATEMENT

- Flammability resistance and smoke emission characteristics of aircraft interior fire retardant materials under ambient and increased temperature and zero ventilation conditions
[AIAA PAPER 70-400] 10 p1908 A70-24905
- Aircraft smoke emission reduction and elimination by engine modifications 14 p2628 A70-30190
- Reduced smoke combustion chambers for jet aircraft engines tested in full scale JT8D engine 24 p4396 A70-46387

SMOKE TRAILS

- Missile impact location visual identification by marker system using pyrotechnic aboard to produce dense white smoke detectable to unaided eye, including flight test 03 p0582 A70-14104
- Three camera method for studying upper atmosphere winds via smoke trails providing wind velocity, earth coordinate data and error indication 14 p2607 A70-30572
- Lagrange time scale of air turbulence from photographic measurements of smoke aerosol particle dispersion in horizontal direction across mean wind 19 p3460 A70-37416
- Smoke, chaff and flare distress signals design and operation for search and rescue operations 23 p4143 A70-44494

SMOOTHING

- NT DATA SMOOTHING
- SMU [MANEUVERING UNITS]
- U SELF MANEUVERING UNITS

SNAKING

- U LATERAL OSCILLATION

SNAP

- NT SNAP 8
- NT SNAP 19
- NT SNAP 27
- NT SPACE POWER UNIT REACTORS
- SNAP reactor control system mechanisms development for operation in space environment 16 p2951 A70-34163
- TSE-SNAP reactor neutron radiation leakage, comparing Monte Carlo calculations with experimental and analytical determinations 20 p3671 A70-39156
- Space nuclear power system design and operation related to safety, discussing SNAP flights 22 p4071 A70-43192

SNAP 8

- Liquid metal pump design and performance in SNAP 8 Mercury Rankine and Advanced Rankine fluid power systems, including containment materials and corrosion effects 04 p0718 A70-15641
- Al radiator with thin stainless steel tube liner using liquid metal coolant tested for heat rejection system of SNAP-8 Rankine cycle power system [AIAA PAPER 70-855] 16 p3000 A70-33922
- Ta oxygen concentration effects on corrosion resistance to NaK in SNAP 8 boilers 16 p2932 A70-34202

SNAP 19

- SNAP 19 radioisotope fueled thermoelectric power supply orbital performance on Nimbus 3, ascribing power output decrease to decreasing generator output currents [AIAA PAPER 70-480] 11 p2120 A70-25435
- SNAP 19 radioisotope thermoelectric generator module for Viking Lander and Pioneer applications, discussing design requirements, environmental and mission constraints, life, performance and reliability characteristics, etc 22 p4071 A70-43195

SNAP 27

- Reinforced graphite cloth composite for reentry heat shielding of SNAP 27 isotopic heat sources, describing structure, thermal and mechanical properties and ablative characteristics 07 p1332 A70-18933
- Apollo lunar surface experiment package-SNAP 27 program, discussing mission profile, design and performance characteristics 22 p4071 A70-43194
- SNAP 27 thermoelectric generator for Apollo Lunar Surface Experiments Package [ALSEP/ 24 p4377 A70-46385

SNATCHING

- U SPACECRAFT RECOVERY

SNOW

- Localized numerical weather forecasts via interpolation from primitive equation model outputs, analyzing winter season results in terms of snow prediction 06 p1098 A70-18241
- Particle size distributions used in analyzing snow size spectra and radar reflectivity 11 p2004 A70-25651
- Potential gradient effect on charge separation mechanism during interaction of polarized snow crystals with ice sphere 15 p2769 A70-31445

SNOW COVER

- Meteorological satellites TV pictures processing for hydrological information, emphasizing snow photographs interpretation 14 p2601 A70-30138
- Snow field mapping with K band radar imagery determining signal return difference with surrounding terrain, noting role of volume scattering and old snow structure 14 p2578 A70-31238

SNOWPLOW EFFECT

- U PLASMA DYNAMICS

SOAPS

- Thin soap membranes shape determined by photogrammetric method, using stereo camera and fluorescent light 10 p1891 A70-24735

SOARING

- Favorable air mass type and season for long cross country soaring flights over eastern U.S. determined from record analysis 09 p1718 A70-23062
- Glider pilots flight above cloudstreets in clear sky, discussing situation for wave soaring over flat ground 10 p1805 A70-24583

SOCIAL FACTORS

- Psychosocial factors in myocardial infarction and sudden death, considering possible causes of fatal cardiac arrhythmia 04 p0635 A70-15462
- Research problems resulting from observational methods in social-psychological studies, discussing categorization systems and coding reliability 05 p0802 A70-16668
- Impression formation model extended to personality traits, noting curvilinear relationship between probability and liking ratings 05 p0803 A70-16670
- National Space Program relevance to human society, discussing solar system exploration, applications in meteorology, communication, etc 09 p1792 A70-22041
- Remote sensing and privacy rights, noting political and social trends toward privacy protection 10 p1971 A70-24744
- Communication satellite technology impacts on potential socio-economic developments of emerging nations of Asia, Africa and South America [AIAA PAPER 70-473] 11 p2152 A70-25426
- Global commercial communications satellite system arrangements, considering evolutionary political, economic and technological developments within INTELSAT context [AIAA PAPER 70-446] 11 p2152 A70-25478
- Elementary flight training study in Royal Netherlands Air Force for improving pilot selection, discussing instructor and social science roles 12 p2176 A70-27030
- Aerospace technology and system analysis application possibilities to urban social and economic planning problems 14 p2670 A70-31191
- Educational TV system via satellite, discussing social benefits for Spanish speaking countries in South America 23 p4285 A70-44602
- Wide-bodied and SST aircraft impact on airport design based on economic, social and environmental considerations [AIAA PAPER 70-1269] 24 p4323 A70-45970

SOCIAL ISOLATION

- Time sense in human subjects kept in caisson or cave isolation determined as function of upper brain stem paraconsciousness 01 p0041 A70-11474
- Cardiovascular system, neuromuscular activity and mental fitness of subjects performing physical and mental assignments with prescribed work-rest schedule during confinement 03 p0425 A70-13895
- Closed life support systems tests, describing effects of long term /one year/ confinement of three human subjects 04 p0641 A70-14565
- Sensory deprivation induced EEG changes, discussing duration effect on postisolation occipital alpha frequency 13 p2350 A70-29242
- Human operators psychological response to unforeseen information received during routine activity in prolonged solitary isolation 17 p3038 A70-35362

SOCIOLOGY

NT SOCIAL FACTORS

- Aeronautics and astronautics sociopolitical aspects, discussing German scientific and industrial organization, American-European technology gap, taxation for research, etc [DGLR-69-1] 04 p0788 A70-15181
- Systems analysis approach to problem solving, discussing application to sociological and educational considerations 17 p3130 A70-35297

SODALITE

- Sodalites color centers creation by electron beam, discussing application in dark trace cathode ray storage display tubes 19 p3379 A70-38048
- Inorganic photochromic and cathodochromic recording materials, examining transition metal doped strontium titanates, rare earth doped calcium fluorides and Fe or S doped sodalite 22 p4088 A70-43601

SODIUM

- NT LIQUID SODIUM
- NT SODIUM ISOTOPES
- NT SODIUM VAPOR
- NT SODIUM 22
- NT SODIUM 24
- H ion increased activity effect on sodium transport across short circuited turtle bladder 02 p0234 A70-11730
- Age data on high sodium tektites from Australia showing distinct fall 03 p0576 A70-14089
- Antarctic twilight Na emission abundance and concentration in lower E region, discussing meteor ablation models 05 p0836 A70-15819
- Na abundance in terrestrial upper atmosphere, solving steady state continuity and momentum equations for Na atoms and ions 05 p0840 A70-16475
- Dye laser tuned to sodium D line used for measuring ionospheric atomic sodium 08 p1492 A70-21757
- Sodium night airglow analyzed by Chapman mechanism, considering nocturnal intensity seasonal behavior and location in upper atmosphere 10 p1873 A70-23829
- Sodium balance effect on intrarenal distribution of blood flow in normal man determined with Xe washout method 10 p1810 A70-24005
- Atmospheric sodium concentration in twilight and daytime sky from D1 and D2 line intensities in twilight 13 p2399 A70-29239
- Systemic hypoxia effect on renal tubule sodium reabsorption in anesthetized mongrel dogs [AMRL-TR-69-135] 13 p2353 A70-29435
- Thermal and electrical resistances of Na at low temperatures measured by germanium thermometers and galvanometer amplifier 14 p2617 A70-31021
- Sodium dayglow seasonal and diurnal variations observed with Zeeman cell photometer 14 p2579 A70-31253
- Sodium and potassium dayglow seasonal and diurnal variations using resonance cell technique and sky polarization effect 14 p2580 A70-31263
- Na I 5889 A pressure broadening by high temperature neutral He, allowing damping constant direct measurements 18 p3318 A70-37013
- Closed coupled partial wave calculation of cross section for fine structure transitions in Na in collisions with He 19 p3372 A70-37541
- Sodium line in meteor spectrum, determining electron temperature and number of atoms as velocity and height function 19 p3514 A70-37600
- Atmospheric free Na atoms layer measurement during twilight and throughout night by laser radar 19 p3413 A70-37999
- Sodium behavior in young and old late type stars, examining relation to iron abundance in F, G and K dwarf and giant stars 21 p3887 A70-41114
- Nightglow Na-D lines excitation, attributing emission to Chapman mechanism 22 p4023 A70-43294
- Lethal and sublethal radiation dosage effects on cellular Na and K distribution in rat brain, liver, kidneys and muscular tissues 23 p4145 A70-44314
- High purity Be preparation by Kroll process using Na as reductant, noting mechanical properties and ease of conversion to powder 24 p4341 A70-45242

SODIUM ALLOYS

- High temperature gas turbine blades cooling by liquid Na-K alloy [ONERA-TP-872] 22 p4125 A70-43458

SODIUM CHLORIDES

- Q switched ruby laser light effect on absorption spectra of NaCl crystals 10 p1902 A70-25221
- Interstitial Cl molecule formation in NaCl lattice, computing strain field and energetics by energy minimization technique based on point ion lattice model 14 p2544 A70-30352
- Vaporization characteristics of solids for relationship between chemical bonding and sublimation mechanism emphasizing NaCl, CdS and GaAs 14 p2545 A70-30906

Polycrystalline NaCl-KCl solid solution alloy, considering high temperature creep under constant compression stress 16 p2961 A70-33275

SODIUM COMPOUNDS

NT SODIUM CHLORIDES

NT SODIUM IODIDES

NT SODIUM SILICATES

Ferroelectric sodium nitrite single crystals LF linear electro-optical coefficients as function of temperature 01 p0154 A70-10104

Oxygen uptake increase following sodium L-lactate isomer infusion into anesthetized dogs 02 p0233 A70-11721

NaLi molecular and ionic electronic states, discussing valence formulation, Hartree-Fock calculations, wave functions, excited state potential, etc 15 p2776 A70-31728

Sodium oxybutyrate effects on brain tissue oxidation during hypoxia in mice 15 p2686 A70-32851

Adiabatic microwave power meter design using sodium thiosulfate phase transformations 19 p3422 A70-37743

Ni base alloys sulfidation kinetics, examining roles of sodium/sulfur compounds-substrate interactions in accelerated oxidation 20 p3651 A70-40072

SODIUM COOLING

High temperature gas turbine blades cooling by liquid Na-K alloy [ONERA-TP-872] 22 p4125 A70-43458

SODIUM D-LINE

U D LINES

SODIUM IODIDES

NaI scintillation spectrometer response function matrices semiautomatic generation, using standard source spectra to obtain normalized Compton continua 14 p2587 A70-31006

SODIUM ISOTOPES

NT SODIUM 22

NT SODIUM 24

Production rates determination for Na 24 and Mg 28 isotopes in Ar exposed to cosmic rays 03 p0561 A70-14092

SODIUM SILICATES

Sodiumalumoborosilicate fiber formation and extraction by leaching, obtaining high aluminate content temperature resistant porous fiber and insulation material 24 p4367 A70-45480

SODIUM VAPOR

Na heat pipe with wick structure consisting of wire rods observed for ease of wick rewetting, dryout limit reproducibility, etc [AICHE PREPRINT 7] 01 p0216 A70-10967

Lower E region turbulence interpretation based on high resolution photographs of artificial sodium vapor trails 03 p0476 A70-13913

Laser emission generation on sodium lines, studying pulsed discharge mechanism involving ion-ion recombination in sodium vapor and hydrogen mixture 13 p2425 A70-28600

Ion-ion potential for sodium vapor for second virial coefficient as function of temperature at 1200-1700 K 24 p4381 A70-45649

SODIUM 22

Apollo 11 lunar surface fine material and rocks cosmogenic radio nuclides Al 26 and Na 22 concentrations determination by gamma ray spectroscopy 21 p3910 A70-41618

SODIUM 24

Short lived cosmic ray produced nuclides as lower atmospheric motion tracers, studying Na 24 characteristics and activity in rain water 07 p1373 A70-20355

SOFT LANDING

Spacecraft horizontal maneuvers in homogeneous gravitational field to achieve soft landing on planetary surface, including optimal liftoff and orbital transfer 01 p0197 A70-11501

Radar signal quick indication and extrapolation for terminal guidance control of Mars soft lander, reducing radar lock on loss sensitivity and engine spurious noise throttling 11 p2080 A70-26210

Retrorocket jet size and structure for scientific instruments soft Mars landing, estimating off-optimum supersonic jet interaction with quiescent atmosphere 17 p3011 A70-35660

SOFT LANDING AIRCRAFT

NT SURVEYOR 5 LUNAR PROBE

SOFT LANDING SPACECRAFT

NT APOLLO SPACECRAFT

NT GEMINI SPACECRAFT

NT LANDING MODULES

NT LUNAR LANDING MODULES

NT LUNAR MODULE

NT MARS EXCURSION MODULE

NT MERCURY SPACECRAFT

NT SURVEYOR LUNAR PROBES

NT SURVEYOR 5 LUNAR PROBE

Earth-moon-earth flight characteristics, discussing spacecraft trajectory, velocity and corrections for close distance placement and return for soft landing 03 p0569 A70-13483

Insulation materials selection for Martian soft lander to meet mission environmental conditions based on tests [AIAA PAPER 70-11] 06 p1182 A70-18224

Multispectral imaging from lander for Martian surface constituents discrimination 11 p2051 A70-26000

Subsystem weight trade-offs for design optimization of out-of-orbit Mars soft lander, using atmosphere and surface environmental Monte Carlo model 11 p2124 A70-26215

Throttleable thruster system for Mars soft landing, selecting catalytic decomposition engine from system weight and performance studies [AIAA PAPER 70-652] 16 p2966 A70-33549

Terminal guidance for Mars softlander utilizing Doppler and range radar for steering and propulsive control 17 p3133 A70-35286

SOFT RECOVERY

U SOFT LANDING

SOFTENING

Solid solution softening in bcc Ta-Re alloy system attributed to substitutional-interstitial interaction 07 p1310 A70-19736

Softening of cold worked alloy by high speed electrical heating, noting supersaturation before natural aging 08 p1520 A70-21496

Austenitic steels and alloys high temperature softening under conditions of stress relaxation and creep, noting hardening action of plastic deformation 09 p1709 A70-23785

Strain rate effect on cyclic behavior of materials with hardening and softening characteristics 17 p3187 A70-34988

German monograph on refractory materials softening under bending and compression at high temperatures 22 p4061 A70-43742

SOFTWARE (COMPUTERS)

U COMPUTER PROGRAMS

U COMPUTER SYSTEMS PROGRAMS

SOIL MAPPING

Soil characteristics influence on soil thermal regime related to thermal IR imagery and subsurface soil conditions 03 p0474 A70-13555

Photographic and IR multiband spectral discrimination for rock and soil mapping from orbiting ERTS satellites [AIAA PAPER 70-303] 09 p1668 A70-22882

Crop species and soil conditions identification from space by comparison of multivase and multiemulsion photography, assigning standard signature to optical fields 10 p1879 A70-24745

Geopedological features derivation from satellite measurements, discussing Nimbus 2 data and grid print maps 12 p2217 A70-26914

Engineering soils mapping by multispectral techniques, describing image interpretation by visual means, densitometric measurements and automatic spectral response classification 12 p2220 A70-26932

Soil characteristics determination from black and white, color and IR aerial photographs 14 p2577 A70-30980

Map making for Soviet soil fertilization, discussing map symbols and scale 19 p3407 A70-37275

SOIL MECHANICS

Ice nucleating properties of dust particles above 80 km compared with soil and AgI particles 01 p0081 A70-11296

Surveyor 7 lunar surface sampler, obtaining soil and rock data 04 p0752 A70-15064

Lunar surface mechanical properties from Surveyor spacecraft interactions with soil/exclusive of surface sampler/ 14 p2644 A70-31055

Apollo 11 lunar rock and soil mechanical behavior and physical characteristics, discussing color, specific gravity, density, shapes and adhesive and cohesive properties 21 p3913 A70-41646

Sand bed stability under shear flow of low Froude number 24 p4330 A70-45980

SOIL SCIENCE

Nitrification reactions in soil with constant ammonium solution entry rate and nitrifying organisms, considering ion concentrations as functions of time and distance 02 p0252 A70-12518

Photoelectric polarimetry of samples of lunar maria, terra, lavas and chemicals for wavelength dependence

of polarization, comparing to Mercury, Mars and asteroids 03 p0576 A70-14082

Remote sensor capability in land use, urban and soil moisture analysis data acquired by NASA Earth Resources Program [AAS PAPER 69-575] 04 p0676 A70-14641

Aerial photographs interpretation methodology based on soil sciences taking into consideration reference level of photointerpreter 07 p1284 A70-19778

Ground wave electric field intensity prediction model in EMC applications, discussing soil conditions and polarization effects 07 p1336 A70-20217

Geopedological features derivation from satellite measurements, discussing Nimbus 2 data and grid print maps 12 p2217 A70-26914

Dipole and monopole antenna radiation patterns, considering effects of soil conductivity and elevation above ground 12 p2199 A70-27979

Cotton plant leaves from high saline soil area, observing chlorophyll content on color photographs 14 p2576 A70-30977

Visual reflectance of wet soils, attributing darkening to internal reflection of radiation in water layer enveloping soil particles 14 p2577 A70-31236

Sampling error origin and magnitude during soil temperature measurements, noting dependence on weather character and season 15 p2731 A70-32459

Martian soil thermal conditions at south pole, considering polar cap annual variations and carbon dioxide sublimation 15 p2802 A70-32492

Lunar soil characteristics, analyzing sample from Apollo 11 mission 18 p3316 A70-36892

Assay procedures for extraction and determination of N-acetylglucosamine in soil 18 p3226 A70-36959

Physical model of lunar soil prior to Apollo 11 landing, discussing meteoritic shock formation of powdery soil 18 p3320 A70-37080

Apollo 11 and 12 results tabulated for soil packing characteristics, composition and rare gas analysis data 18 p3332 A70-37223

P32 labeled organic phosphate esters in water extracts of soil 20 p3615 A70-38979

Soil science and climatology in Central Europe archeological site location by aerial photography 21 p3826 A70-41402

Tranquility Base lunar soil origin, establishing component nature, size distribution, density, mineralogy, constructional or destructional history 21 p3897 A70-41519

Lunar soil sample preparation and monitoring for viable microorganisms presence 22 p3978 A70-42973

Low friction seal for axial loading piston in triaxial soil testing cells 23 p4199 A70-43873

Martian soil thermal conditions, considering polar cap annual variations and carbon dioxide sublimation 23 p4240 A70-43914

SOILS

NT CLAYS

NT LUNAR DUST

NT LUNAR SOIL

NT SANDS

Soil characteristics influence on soil thermal regime related to thermal IR imagery and subsurface soil conditions 03 p0474 A70-13555

Martian soil surface anomalies observed from polarimetric analysis of light diffused by Hellas region 10 p1943 A70-24708

Visible polarization signature for remote sensing of soil surface moisture, noting invariance to partial shadowing in plowed or rough soils 15 p2724 A70-31667

Radar and DC pulse signatures of multiple reflection from dry, damp and wet earth for vertical and horizontal polarization 16 p2861 A70-32977

Ecological potentials in spectral signature analysis, using laboratory leaf and soil spectral reflectance data 17 p3078 A70-35612

SOLAR ACTIVITY

NT FACULAE

NT SOLAR FLARES

NT SOLAR PROMINENCES

NT SOLAR STORMS

NT SPICULES

NT SUNSPOTS

Interplanetary space investigation by HEOS 1 satellite during maximum solar activity, discussing orbital apogee, mission and technical requirements 01 p0186 A70-11113

- Jacchia 1965 model discrepancies in solar and geomagnetic activity and semiannual effects observed in satellite drag measurements at 150-200 km and 700-1500 km
01 p0077 A70-11204
- Solar activity indices and upper atmospheric density interrelationship from Explorer 1 satellite observations, showing statistical variations
02 p0356 A70-11762
- Data collection for ionospheric disturbances, geomagnetic field, radio wave intensity, cosmic rays and solar activity
02 p0290 A70-12125
- F region irregularity drift, morphology and generation in magnetosphere, discussing ionospheric structure at different latitudes and solar activity association
02 p0293 A70-12572
- Electron gyrofrequencies computed from split pair bursts in 1966 compared with results from type II bursts in 1967
04 p0738 A70-14510
- Long range solar flare forecasting noting correlation between planetary conjunctions and proton events [AAS PAPER 69-624]
04 p0740 A70-14658
- Forbush effect on intensity of neutron component of cosmic rays during quiet sun period
05 p0897 A70-15795
- Solar and geomagnetic activity daily parameters persistence, discussing autocorrelation function, variance spectra, sunspot numbers, radiation flux, etc
05 p0906 A70-15877
- Solar particle events 1966 /August-September/ in McMath region 8461
05 p0901 A70-16426
- Solar activity centers life history in terms of radio emission and Ca plage intensity, noting radio emission decay faster than plage intensity
05 p0911 A70-16440
- IQSY 27-day recurrence sequence for 1964 solar and terrestrial activity, considering geomagnetic, auroral and ionospheric disturbances correlation with plage
05 p0841 A70-16646
- Solar activity study based on solar X ray spectra observation, considering flare mechanism
05 p0903 A70-16719
- Flares and fast processes interrelation with active region stationary filaments, filament field magnetic envelope explosion stimulation of surges, plasma stream ascents, etc
05 p0904 A70-16910
- Periodicities in solar activity variation from correlation spectral analysis, establishing monotonically decreasing component and secular variations in activity
05 p0918 A70-16913
- NASA solar particle alert network /SPAN/ operated by Manned Spacecraft Center giving 24 hr coverage of solar activity at optical and radio frequencies
06 p1029 A70-18013
- Solar activity model for simulating scheduling of observation experiments for Apollo Telescope Mount missions [AIAA PAPER 70-32]
06 p1145 A70-18121
- Horizontal ionospheric drift over Northern Hemisphere during low solar activity, studying spatiotemporal distribution patterns of drift parameters
07 p1266 A70-19438
- East-west dissymmetry in solar activity center births for solar cycles XII-XIX, noting independence of latitude and invariance throughout last eight cycles
08 p1567 A70-20599
- Contraction and expansion in solar region producing synchrotron emission of relativistic electrons to explain solar burst behavior
08 p1560 A70-20841
- Solar meter wave emissions enhancement or emission centers, comparing radio and optical coronal enhancements
08 p1576 A70-21402
- Corona green /5303 A/ and red /6374 A/ lines during minimum solar activity in 1964, discussing N-S and E-W asymmetries and intensities
09 p1750 A70-22100
- Solar activity forecasting using normalized sunspot curves deduced from 200 years of observations, discussing parameters of running 11 year cycle
10 p1949 A70-25287
- Solar active regions in chromosphere and corona observed by EUV spectroheliometer aboard OSO-4 spacecraft, discussing ion formation and temperatures
12 p2303 A70-27705
- Toroidal solar field emergence to surface forming magnetic field of active region
13 p2493 A70-29392
- Electron density, characteristic dimensions and vertical density gradient of coronal enhancements in white light, observing elliptical cross section
13 p2479 A70-30004
- Solar activity predictions for earth upper atmosphere models emphasizing linear repression method
14 p2638 A70-30565
- Planetary tidal force effect on solar activity cycle, showing amplitude proportionality to solar and gravity center deviation
14 p2649 A70-31199
- Solar activity during Proton Flare Project Retrospective Interval 1969, discussing empirical flare forecasting methods
15 p2794 A70-32292
- Orbiting solar telescope design for solar disturbances location and monitoring in H alpha line
16 p2907 A70-33188
- Type 3 solar bursts classification, measuring diameter, lifetime and position
17 p3151 A70-35581
- Horizontal ionospheric drift over Northern Hemisphere during low solar activity, studying spatiotemporal distribution patterns of drift parameters
18 p3249 A70-36912
- Wolf numbers monthly fluctuations, giving histogram of fluctuation amplitude distribution
18 p3323 A70-37137
- Interrelated satellite observations related to solar events - ESRO Conference, Noordwijk, Netherlands, September 1969
19 p3491 A70-37471
- ESRO-1, ESRO-2 and HEOS-1 simultaneous observation of solar event of 25 February 1969, describing satellite and experiments
19 p3531 A70-37496
- Whistler density variability correlated with solar activity during IQSY
19 p3462 A70-37924
- Temperature and radio brightness distributions in active regions and upper chromosphere during minimum activity periods
19 p3522 A70-38557
- Solar radio flux variations prediction for various activity levels based on random functions theory
19 p3522 A70-38558
- Solar radio emission flux as activity index, analyzing permissible deviations from recommended wavelength
19 p3522 A70-38559
- Soviet papers on solar activity covering solar stations, flares, coronal data, etc
20 p3699 A70-39460
- Supergranular network time and shape changes, examining correlations with solar rotation, activity and cycles
21 p3885 A70-40954
- Solar active regions at millimeter wavelengths, discussing brightness temperature, background radiation, electron density, optical thickness, polarization and chromospheric magnetic fields
21 p3886 A70-40960
- Solar active region radio spectrum during 12 November 1966 eclipse, discussing flux, magnetic field effects, temperature and electron density
21 p3886 A70-40961
- Solar X-ray spectra of active regions, examining emission lines, fluxes electron temperature and density and transitions
21 p3879 A70-40963
- Oso-4 far UV observations of solar chromosphere and corona active regions
21 p3925 A70-42187
- Solar optical and radio activity observation in 1968, noting optical-radio data correlation
22 p4095 A70-43259
- Solar X-ray data from rocket and satellites, discussing hot dense plasmas and correlation with H alpha flares, calcium plages and microwave emission
22 p4096 A70-43300
- Geomagnetic Sq variation examination, using field expansion into natural orthogonal component series
23 p4188 A70-44063
- Quiet sun and new moon brightness temperature measurements at 3.3 and 5.7 mm wavelengths, giving radiometric maps
23 p4241 A70-44254
- Sunspot number prediction from solar cycles statistical analysis
23 p4254 A70-44902
- Solar activity research, discussing optical facilities, photoelectric magnetographs, magnetic field measurement, solar cycles and flares, etc
23 p4256 A70-45034
- Solar VHF radio spectra indicating type 4 burst activity associated with type 3 formation
24 p4401 A70-45318
- Mm wavelength radiometer for recording solar activity and radiation attenuation in atmosphere as function of time
24 p4315 A70-46236
- SOLAR ACTIVITY EFFECTS**
- Hypothetical magnetic configurations in presence of Coriolis forces from convective cell hydromagnetic activity in solar plasma, considering dynamos with increasing magnetic field
01 p0173 A70-10133
- Upper atmosphere temperature lag behind solar decimeter flux 27 day variation maximum attributed to varying solar EUV heating
01 p0070 A70-10404
- Underground and surface telescope measurements of second harmonic of primary cosmic ray daily variation and upper solar modulation limit
01 p0170 A70-10405
- Geomagnetic micropulsations relation to magnetospheric boundary location on sun-earth line, noting influence of solar wind pressure variations
01 p0071 A70-10412
- Hydrodynamic explanation of upper atmosphere perturbation effects on tropospheric circulation, discussing experiments for solar activity effects on atmospheric dynamics
01 p0073 A70-10582
- Atmospheric density variations during solar maximum and minimum, discussing solar corpuscular stream and EUV radiation
01 p0075 A70-10594
- Sq data acquisition and analysis, noting automatic standard observatories using nuclear magnetometers and ionospheric current information from instrumented rockets
01 p0075 A70-10597
- Polar magnetic disturbances during IQSY characterized by SP field superposed on Sq field generated by ionospheric dynamo
01 p0075 A70-10599
- Regular/irregular micropulsations variations during solar cycle, noting possible magnetospheric contraction and solar wind velocity influence
01 p0075 A70-10600
- Atmospheric density variations in thermosphere determined from braking satellite data, discussing correlation with solar activity and temperature variations
01 p0077 A70-11202
- Exospheric temperature variations by Thompson scatter technique, considering solar and geomagnetic activity effects
01 p0078 A70-11209
- Spread F echoes occurrence variations over solar cycle, observing range and frequency splitting type during maximum and minimum sunspot years
01 p0080 A70-11222
- Mariner 2 measurements of geomagnetic field and interplanetary plasma parameters, analyzing interaction between interplanetary medium and magnetosphere during decreased solar activity
01 p0192 A70-11520
- Ionospheric discontinuities drift velocities from diversity reception data indicating no dependence on solar activity
01 p0083 A70-11531
- Geomagnetic micropulsations fluctuations during solar activity cycle showing changes in excitation frequency with change in corpuscular fluxes parameters
01 p0083 A70-11539
- F 2 layer state prediction as function of solar activity by series expansion for describing space-time variations of monthly F 2 medians critical frequencies
01 p0083 A70-11547
- Geomagnetic field pulsations frequency changes in relation to geomagnetic and solar activity level
01 p0084 A70-11559
- Hydrodynamic approximation to interplanetary gas motion influenced by solar flare caused perturbations
01 p0192 A70-11586
- Transient Faraday rotation of S-band telemetry carrier observed during Pioneer 6 occultation by solar corona, correlating with decametric solar radio bursts
02 p0369 A70-12059
- Pioneer 6 radio signal spectrograms during solar occultation, noting solar event effects on bandwidth
02 p0369 A70-12060
- Balloon measurements of cosmic ray alpha particle flux in upper atmosphere over Japan to obtain solar modulation effects data
02 p0357 A70-12122
- Cosmic ray protons, He nuclei and electrons solar modulation by betatron deceleration mechanism during interplanetary space passage
02 p0357 A70-12123
- Solar eclipse effects in equatorial F region electron density, noting data analysis method for reexamining existing measurements
02 p0290 A70-12157
- Solar activity effect on ionospheric total electron content via Explorer 22 observations, discussing relationship to solar elevation angle
02 p0292 A70-12561
- Solar phenomena effect on VHF communications between synchronous satellite relay and earth ground stations
02 p0259 A70-12566
- Corpuscular sources geoeffectiveness related to position on solar disk at maximum flare activity
03 p0569 A70-13359
- Visible solar hemisphere circumstances for 28 January 1967 and ground level cosmic rays enhancement not preceded by intense H alpha flares
03 p0558 A70-13590
- Pressure changes in troposphere and lower stratosphere after strong solar flares analyzed statistically for Northern Hemisphere
03 p0476 A70-13909

Secular variation in F region ionization response to sunspot number, noting dominant component as cosine term equal to four sunspot cycles

04 p0678 A70-14972

Solar flare duration effect on propagation and modification of forward-reverse shock pair between sun and 1 AU, using equations of motion for spherically symmetric flow

04 p0740 A70-15104

Hysteresis effect on cosmic ray modulation and gradient ionization near solar minimum from measurements made near earth with OGO 1 and 3 ion chambers

04 p0740 A70-15106

Solar and geomagnetic effects on variations in physiological tests using alimentary reflex of dogs

04 p0639 A70-15512

Tropospheric periodic responses to chromospheric flares, analyzing stations atmospheric pressure power spectra

04 p0742 A70-15524

Magnetic storms frequency and levels coincidence with solar activity variations

04 p0682 A70-15734

Diurnal fluctuations of quiet F 2 region intensity at midlatitude based on vertical probe observations during solar activity minimum

04 p0684 A70-15745

Cosmic rays neutron component solar-diurnal variations as function of solar activity using magnetically quiet data

05 p0898 A70-15941

Geophysical-solar phenomenological interrelationships, considering earth rotation and nutation, sunspot area, earthquake energy, etc

06 p1056 A70-17636

Nighttime radio wave absorption in ionosphere during moderate solar activity based on echo observations

06 p1056 A70-17840

Solar asymmetries associated with sun motion toward apex related to formation of N-S asymmetries of geomagnetic storms

06 p1144 A70-18011

Spatial properties of solar wind during maximum and minimum activity inferred from sodium D-line emissions for cometary nuclei

06 p1136 A70-18012

Space forecasting system to predict solar radiation bursts and effects on earth

06 p1136 A70-18023

Spectral characteristics of B and S components of solar radio emission from statistical data, investigating dependence on 11-yr cycle and minimum solar activity

07 p1378 A70-19031

Polarization and absorption of radio waves in ionosphere using Appleton-Hartree equations, calculating LUF as function of sunspot number

07 p1229 A70-19160

Field strength predictions for expected returns from backscatter ionospheric soundings, predicting ionospheric propagation modes and losses during sunspot minimum

07 p1229 A70-19161

LOF observations of long distance transequatorial step frequency radio circuits in Pacific Area during sunspot minimum period

07 p1232 A70-19174

Midlatitude F 2 perturbations from vertical sounding stations data during solar activity minimum, discussing F 2 region critical frequency variation

07 p1266 A70-19450

F 2 small scale inhomogeneities drift relation to current systems of dynamo region, discussing solar activity effects on ionospheric conductivity

07 p1267 A70-19452

Ionospheric radio wave absorption and geomagnetic perturbations correlated with solar activity variations

07 p1267 A70-19457

Electron production in lower ionosphere by solar cosmic rays, calculating rates by computer as function of nuclear charge number, energy spectrum and height

07 p1373 A70-20348

Geomagnetic storms data compilation (1957-1964), showing solar activity effect on solar corpuscular stream velocity

07 p1373 A70-20436

Solar modulation of low energy galactic cosmic ray protons, proposing diffusion-convection model with time dependent diffusion coefficient

08 p1561 A70-20906

E layer atmospheric circulation model for meteor zone, noting solar thermal radiation role

08 p1575 A70-21215

Hypothetical magnetic configurations in presence of Coriolis forces from convective cell hydromagnetic activity in solar plasma, considering dynamos with increasing magnetic field

08 p1576 A70-21409

Atmospheric regions interactions concerning stratosphere, mesosphere, troposphere, etc, noting solar activity effects

08 p1490 A70-21428

Diurnal vertical shifts of constant electron concentration levels in D region, considering effects of chromosphere, nuclear explosions, solar eclipses, etc

08 p1490 A70-21430

Solar wind and Venus topside ionosphere interaction, discussing charged particle density, temperature and pressure distribution

08 p1578 A70-21550

Solar continually changing features / brightenings, darkenings, condensations and groupings/ associated with solar activity, emphasizing sunspot number formulas

09 p1751 A70-22197

Solar activity analysis emphasizing sunspots, magnetic disturbances and bursts data

09 p1752 A70-22199

Cosmic ray intensity variation correlated with amplitude changes in 27 day variation during solar cycle 18

09 p1745 A70-22740

Solar wind magnitude and variability effects on geomagnetic activity and cosmic ray intensity modulation from satellite observations

09 p1745 A70-23272

Solar corpuscular streams effect on meteoric particles behavior in circular orbit around sun, determining lifetime on basis of mass loss due to pulverization

09 p1763 A70-23382

Soviet book on solar activity influence on earth natural processes covering atmospheric circulation and pressure, air temperature, precipitations and hydrological changes

09 p1719 A70-23471

Predawn enhancement morphology and variations of 6300 A airglow, discussing solar declination and activity effect

10 p1873 A70-23831

Neutral atomic oxygen auroral and nebular emissions in twilight airglow, suggesting photodissociation of molecules by sunlight

10 p1873 A70-23832

Cosmic ray particle abundance in upper atmosphere during minimum solar activity estimated by nuclear photographic emulsions on balloon flight

10 p1932 A70-24438

Daily horizontal intensity spectrum for equatorial observatories, computing power densities near 27 day variation during high, moderate and low solar activity

10 p1875 A70-24440

Geomagnetic field secular variation and cyclic components amplitudes separation by digital filters, observing seasonal and solar activity effects

10 p1880 A70-24808

Seasonal changes in thermospheric composition in middle latitudes, investigating molecular oxygen density and solar activity effects

10 p1881 A70-24817

Midlatitude sporadic E layer critical frequencies dependence on solar activity using vertical ionospheric sounding data, observing ionization correlation

10 p1882 A70-25197

Cosmic layer in lower ionosphere investigated by 164 kHz frequency absorption at night, discussing solar activity effects

10 p1934 A70-25198

Nocturnal E layer electron density profile dependence on solar activity

10 p1885 A70-25265

Nocturnal F layer electron density profile and temperature dependence on solar activity

10 p1885 A70-25266

Air and solar activity electrical parameters relationship, observing ionizing radiation increase in upper atmosphere during solar activity

10 p1885 A70-25268

Ionospheric waves positive phases and disturbances related to solar activity variations and cosmic ray modulations

10 p1885 A70-25270

Dawn chorus frequency relation to solar activity, showing correlation to mean geomagnetic activity

10 p1886 A70-25282

F 2 layer midday ionization level annual variation gradient, noting gradient latitudinal distribution dependence on solar activity level

11 p2042 A70-25532

F 2 layer critical frequencies rms deviations approximate dependences on latitude and solar activity for computer calculation of long-range ionospheric forecasts

11 p2043 A70-25549

Sun effect on anomalous frequency shift in 21 cm absorption spectrum in Taurus A

11 p2108 A70-25659

Solar active centers interaction effects on spot growth and proper motion

11 p2109 A70-25743

Mars upper atmosphere semiempirical model, reducing density uncertainties by allowing for solar cyclic variations

11 p2111 A70-26031

Energy spectra and composition of heavy nuclei in primary cosmic rays during low solar activity by nuclear emulsion stacks exposure in balloon flights

11 p2105 A70-26295

Corpuscular sources geoeffectiveness related to position on solar disk at maximum flare activity

11 p2118 A70-26724

Ozonosphere heating between 20-60 km during high solar activity, determining positive heating rate gradient directions and maximum heating altitude

12 p2223 A70-27514

Solar and lunar daily geomagnetic variations, correcting harmonic components calculated values

12 p2303 A70-27673

Long term ionospheric absorption measurements in Japan from IGY through IQSY using A1 method, discussing annual and diurnal variations correlation with solar activity

12 p2226 A70-28059

Long term ionospheric absorption measurements in Northern Hemisphere from IGY through IQSY, discussing annual and diurnal variations correlation with solar activity

12 p2226 A70-28060

Interplanetary magnetic field intensity and geomagnetic activity level correlation with 27-day solar activity cycle based on Venera 4 and Mariner 5 data comparison

12 p2310 A70-28263

Low latitude atmospheric vertical density variations, comparing solar and geomagnetic activities effects

12 p2227 A70-28264

Solar activity effects on midlatitude upper atmosphere corpuscular radiation intensity via rocket sounding

12 p2296 A70-28266

Soviet book on solar short wave radiation effects on ionosphere, covering solar atmosphere and spectra, ionospheric ion concentration vertical distribution, etc

13 p2487 A70-28649

Oxygen 18 concentration in Greenland ice core correlation to solar activity index, indicating earth temperature control by solar activity

13 p2489 A70-28909

Solar flare proton induced radioactivity in Apollo 11 lunar surface material compared with stony meteorite data, noting cobalt 56 concentration

13 p2489 A70-28910

Pc-periods dependence on geomagnetic latitude during active sun years, using IGY data

13 p2395 A70-28943

Visual aurora properties attributed to magnetic storm following solar flare, using multiple channel photometer measurements

13 p2478 A70-29231

Solar wind effect on structure of magnetic field in magnetosphere and interplanetary space, noting interaction with moon

13 p2498 A70-30051

Inclined backscatter sounding of ionosphere in individual channels of multichannel radio link, analyzing data during minimum solar activity

14 p2547 A70-30149

Subpolar ionosphere electron concentration measurements for both hemispheres during solar activity by Faraday effect signal recordings from satellites

14 p2570 A70-30223

Solar activity variations effects on equation parameters, describing nighttime F2 ionization levels dependence on geographical latitude

14 p2570 A70-30224

Geomagnetic field influence on annual F 2 layer longitudinal ionization at midlatitudes, relating solar activity level

14 p2570 A70-30225

Geomagnetic storm intensity nonuniform relationship to 27 day and 11 year cycles

14 p2571 A70-30240

Book on thermal and gravitational atmospheric tides covering solar oscillations, lunar air tides, upper air data, ozone radiation absorption, etc

14 p2573 A70-30633

Lunar tide in ionospheric D region absorption near magnetic equator, noting annual variation relationship to sunspots

14 p2574 A70-30747

Carbon and sulfur reactions with solar hydrogen atoms in Apollo 11 lunar samples accounting for isotopic composition of fine-grained basaltic rocks

14 p2545 A70-30791

Magnetic storms frequency and levels coincidence with solar activity variations

14 p2575 A70-30818

Diurnal fluctuations of quiet F 2 region intensity at midlatitude based on vertical probe observations during solar activity minimum

14 p2576 A70-30829

Jupiter decimeter radiation long term variations from flux density measurements, suggesting correlation with solar activity

14 p2648 A70-31087

Solar Monitoring Experiment program, observing solar activity relation to large enhancements of lower stratosphere secondary radiation

15 p2792 A70-31656

Magnetospheric protons and electron energy spectra time and magnetic activity dependence during solar maximum

15 p2792 A70-31671

Atmospheric density near 180 km /1968-1969/ from orbit of satellite 1967-31A /ATS 2/, noting weak dependence on solar activity and correlations to geomagnetic disturbances

15 p2724 A70-31680

Superposed effects in solar quiet daily variations of geomagnetic horizontal component, using Lerwick and Eskdalemuir data

15 p2728 A70-31991

F 2 layer afternoon and evening ionization maxima dependence on season, zenith angle and solar activity

15 p2730 A70-32084

F 1 layer formation and ion production rates related to F layer stratification, atomic oxygen, zenith angle and solar activity periods

15 p2730 A70-32086

Proton Flare Project 1969, reporting synoptic observations of sun and solar terrestrial effects

15 p2794 A70-32291

Polar cap disturbance of 7 June 1969 due to small proton enhancement, describing detection by trans-polar VLF phase measurement

15 p2794 A70-32295

Solar Proton Flare Project 1969, summarizing observations and solar activity-terrestrial event correlation for June retrospective interval

15 p2794 A70-32296

Negative sudden phase anomaly /SPA/ in VLF radio transmission, noting solar X ray flux intensity and zenith angle effects

15 p2699 A70-32297

Atmospheric transmission variability related to solar constant variations

15 p2801 A70-32371

Galactic cosmic rays eleven year modulation, determining modulating region L depth from dynamical phase lag between changes in cosmic ray intensity and solar activity

17 p3150 A70-34833

Ionospheric E layer formation, investigating role of solar X ray control by electron production rate and density calculations

17 p3151 A70-34943

Radio sources angular broadening by solar wind turbulence used for solar corona probe

18 p3311 A70-36003

Ionospheric cosmic noise absorption diurnal and seasonal variations at Alma-Ata during IQSY, noting chromospheric flares effects

18 p3306 A70-36089

Electric fields in lower ionosphere during solar activity minimum above magnetic equator, using vertical profiles of ionospheric current magnetic fields and electron concentration

18 p3246 A70-36098

Ionospheric radio wave absorption measurements, noting winter anomaly during maximum solar activity year

18 p3227 A70-36101

Periodic cosmic ray variations near Southern magnetic pole related to chromospheric flares

18 p3307 A70-36102

Vertical secondary cosmic gamma spectra from primary nucleon and electron spectra, discussing effects of solar cycle and geomagnetic cut-off

18 p3308 A70-36500

Midlatitude F 2 perturbations from vertical sounding stations data during solar activity minimum, discussing F 2 region critical frequency variation

18 p3249 A70-36924

F 2 small scale inhomogeneities diff relation to current systems of dynamo region, discussing solar activity effects on ionospheric conductivity

18 p3249 A70-36926

Ionospheric radio wave absorption and geomagnetic perturbations correlated with solar activity variations

18 p3250 A70-36931

Residual solar modulation of relativistic cosmic ray nuclei in galaxy over eleven years, observing magnitude at solar activity minima

18 p3309 A70-37009

Electron temperature in 500-1000 km range during minimum solar activity based on Alouette satellite data and atmospheric model, observing latitudinal variation

18 p3254 A70-37029

F 1 layer occurrence probability as function of mean monthly WU numbers at midlatitudes, noting solar activity effect

18 p3254 A70-37032

Ionization-recombination parameters variation as function of season and solar activity, using diurnal changes of F 2 layer maximum electron concentration

18 p3254 A70-37034

Solar activity sudden perturbations effect on earth pressure field and atmospheric circulation

19 p3460 A70-37315

Ionization rate experimental profiles during maximum solar activity compared with calculations, showing additional source of ionization in E region

19 p3409 A70-37322

Global diurnal variations in F 2 layer seasonal anomaly during high and low solar activity, noting corpuscular radiation role

19 p3491 A70-37326

Vertical electron density profile variations during ionospheric perturbations in years of solar activity maximum and minimum

19 p3409 A70-37328

Solar flares associated interplanetary and terrestrial phenomena by satellite, space probe and rocket observation, investigating solar wind disturbances, geomagnetic storms, ionospheric effects, etc

19 p3493 A70-37472

Solar wind disturbances associated with solar activity observed by spacecraft probing interplanetary space, considering geomagnetic activity classes

19 p3494 A70-37478

Trapped particle population changes associated with solar events, discussing solar wind discontinuity effects on magnetosphere

19 p3495 A70-37487

Interplanetary magnetic field measurements by Pioneer 8 during 25 February 1969 solar activity, discussing geomagnetic storms, cosmic rays, shock fronts and ionospheric disturbances

19 p3513 A70-37501

Energetic storm particle events observation, noting association with solar protons and interplanetary shock waves

19 p3496 A70-37518

ESRO 1 satellite and ground observations of energetic auroral electrons angular distribution during solar event, using Geiger counters

19 p3412 A70-37519

Cosmic ray electron and positron differential energy spectra during solar quiet times from OGO- 5 satellite observations in interplanetary space

19 p3502 A70-38096

Quiet time intensity increases and long term solar modulation of interplanetary low energy electrons, using IMP observations

19 p3502 A70-38097

Cosmic ray positrons and negatrons differential energy spectra and solar modulation, using balloon-borne magnetic spectrometer

19 p3503 A70-38100

Cosmic ray positrons and negatrons differential intensities near north geomagnetic pole from balloon flight measurements, noting solar modulation effects

19 p3503 A70-38102

Pc-1 pulsations during solar activity maximum and minimum, discussing diurnal, seasonal and cyclic variations

19 p3416 A70-38586

Solar UV radiation contributing to ionization in higher ionospheric layer over Dushanbe during partial solar eclipse of 20 May 1966

19 p3417 A70-38786

Solar eclipse effects on E and F layers, discussing photoionization rate, electron density and temperature, plasma diffusion, electric fields, etc

19 p3418 A70-38903

Annular solar eclipse of 20 May 1966 effects on ionosphere, discussing regions virtual heights, critical frequency variations, ion production rates, etc

19 p3419 A70-38917

Soviet papers on relations between earth troposphere phenomena and solar activity covering geomagnetic and stratosphere perturbations, warmings and circulation, solar cycles, etc

20 p3618 A70-39181

Explosive and diffuse stratospheric warmings over Arctic attributed to solar activity and stratospheric circulation

20 p3618 A70-39184

Polar stratospheric winter explosive warmings correlated with solar high energy charged particles injections

20 p3618 A70-39185

Solar activity effects on Northern Hemisphere atmospheric temperature, mapping gradients for 11 year solar cycle

20 p3662 A70-39188

Twenty two year solar activity cycle effect on earth climate, plotting odd and even 11 year cycle curves for pressure and temperature

20 p3662 A70-39189

Solar activity effects on mean anomalies in repeatability of types of atmospheric circulation epochs and stages

20 p3662 A70-39190

Primary cosmic ray intensity variation during solar activity half cycle, expressing diffusion coefficient as function of sunspot group number

20 p3696 A70-39279

Cosmic ray 27 day variations during solar activity minimum, noting unipolar magnetic regions role

20 p3696 A70-39280

Cosmic ray intensity decreases and Forbush effects energy spectra during various solar activity periods

20 p3696 A70-39281

Midlatitude atmospheric neutron density height dependence during minimum solar activity

20 p3697 A70-39285

Cosmic ray neutron semidiurnal variations day and night components with respect to geomagnetic and solar activity

20 p3697 A70-39288

Cosmic ray intensity variation during maximum meteor showers periods detected on earth, noting relationship to solar activity

20 p3697 A70-39294

Lyman alpha geocoronal emission rate as function of altitude at midnight during solar minimum, solving radiative transfer equations

20 p3619 A70-39329

Neutral atmosphere continuity equation of ionization and equation of motion in F 2 region for different seasons in various solar activity epochs

20 p3623 A70-40478

Solar activity effects on ionospheric total electron content seasonal variations over Tortosa, using BE-B satellite data

20 p3624 A70-40482

Lower ionospheric structure and electromagnetic resonance phenomena, describing radio equipment for solar activity effects studies

21 p3812 A70-40620

Anomalous nighttime ionospheric total electron content increases seasonal and solar cycle dependences attributed to ionization sources due to electrodynamic drifts

21 p3815 A70-41061

Atmospheric neutron flux increase during solar proton event, measuring flux and energy spectrum of particles by balloon sounding

21 p3881 A70-41076

Solar wind free electron number density measurement by Pioneer 6 spacecraft after solar proton flare, constructing plasma cloud models

21 p3881 A70-41079

Pc 1 geomagnetic micropulsation statistics for middle latitudes, discussing solar cycle and annual variations in occurrence rates

21 p3817 A70-41088

F 2 layer midday ionization level annual variation gradient, noting gradient latitudinal distribution dependence on solar activity level

21 p3819 A70-41282

F 2 layer critical frequencies rms deviations approximate dependences on latitude and solar activity for computer calculation of long-range ionospheric forecasts

21 p3819 A70-41299

Optical solar observatory for investigation of solar activity and impact on earth environment, discussing site selection and equipment

22 p4005 A70-42349

Solar wind properties correlated with geomagnetic activity, discussing interplanetary discontinuities, shock waves, flare associated disturbances and geomagnetic activity sequences

22 p4022 A70-43288

Solar and geomagnetic events for maximum solar activity year 1968, correlating magnetic storms

22 p4022 A70-43290

E region winds response to solar radiation variations, including geomagnetism role

23 p4186 A70-43848

Cosmic ray 11-year variation pattern change in 19th and 20th solar activity cycles determined by latitude expeditions spectrum analysis

23 p4237 A70-44071

E region additional ionization source during solar activity maximum, analyzing ion production function and electron concentration

23 p4190 A70-44077

Jupiter flux density changes at 2695 MHz correlated with 10.7 cm solar activity, suggesting magnetic anomaly explanation

23 p4246 A70-44751

Lyman alpha radiation scattering intensity during solar radiation period, discussing dependence of interstellar hydrogen density in interplanetary space on solar EUV

23 p4237 A70-44753

Solar flare effects in ionosphere observed at Lindau, collating with heavy geomagnetic storm

23 p4237 A70-44876

Jupiter red spot darkness parameter and solar activity as clue to Jupiter-solar relationship

24 p4402 A70-45391

Solar corpuscular flux and visible solar spot area correlation with geomagnetic planetary index for 27-day intervals, considering relationship to earth satellites motion

24 p4408 A70-45547

Echo 1 satellite orbital acceleration correlated with solar activity, determining atmospheric density from drag observations using PERLO computer program

24 p4408 A70-45552

Cosmic ray electrons solar modulation, considering diffusion-convection theory

24 p4397 A70-45769

Subpolar ionosphere electron concentration measurements for both hemispheres during solar activity by Faraday effect signal recordings from satellites

24 p4331 A70-46298

Solar activity variations effects on equation parameters, describing noontime F 2 ionization levels dependence on geographical latitude

24 p4331 A70-46299

- Geomagnetic field influence on annual F 2 layer longitudinal ionization at midlatitudes, relating solar activity level 24 p4331 A70-46300
- Geomagnetic storm intensity nonuniform relationship to 27 day and 11 year cycles 24 p4332 A70-46315
- ### SOLAR ATMOSPHERE
- Velocity distribution and optical depth of line formation in solar atmosphere using blue and red wing filtergram and numerical experiment 01 p0175 A70-10241
- Angular momentum conservations for solar gas confined by closed field lines or outflowing along open magnetic field lines 01 p0176 A70-10251
- MHD model for microwave solar circular polarization bursts interpretation, suggesting Alfvén wave disturbances in solar atmosphere 01 p0168 A70-10254
- Coarse structure of solar atmosphere from observations of quiet sun, discussing contradictions with existing models 03 p0570 A70-13592
- One dimensional magnetograph scans studying photospheric velocity oscillations and supergranulation, noting downward flows coincident with chromospheric network 03 p0570 A70-13593
- Zeeman-split Fraunhofer line profiles for pure absorption lines determined taking into account solar atmosphere elliptical birefringence 03 p0570 A70-13595
- Solar photospheric Fe abundance determined from IR supermultiplet line spectra, considering LTE effects 04 p0749 A70-14597
- Heat transport conduction mode and earth as heat sink in solar atmosphere, discussing mesopause coldest region, turbulence and solar plasma-earth electromagnetic interactions 04 p0677 A70-14644
- Solar atmospheric structure near sunspots by spectrophotometry, presenting observational and theoretical sunspot magnetic and velocity field data 04 p0754 A70-15351
- Solar limb brightening in various ranges, suggesting obtaining temperature distribution during solar eclipse 05 p0911 A70-16436
- Solar atmosphere granular convective velocity field determination methods, using realistic assumptions for typical granulation size and seeing parameter 06 p1142 A70-17990
- Solar Cd abundance, using spectrograph and synthetic spectral line computer program 06 p1143 A70-17995
- Electromagnetic acceleration and energy losses of charged chromospheric-coronal plasma electrons and protons in unsteady magnetic fields of sunspots 07 p1384 A70-19417
- Turbulence in quiescent prominences relationship to shock waves in upper atmosphere 08 p1570 A70-20840
- Effective depths of formation of absorption lines in solar atmosphere used for magnetic field recording 08 p1570 A70-20842
- Nitrogen dioxide presence in solar atmosphere from balloon-borne spectrometer observations, presenting graph of sunset solar spectrum 08 p1575 A70-21262
- Radiative relaxations of chromospheric oscillations generated by granule, assuming isothermal atmosphere and linearizing equations of motion 08 p1576 A70-21395
- Fe abundance in solar photosphere, evaluating various determination methods 09 p1753 A70-22382
- Europium isotope ratio in solar atmosphere equal to terrestrial using spectral line profiles analysis 09 p1757 A70-22727
- Homogeneous model solar photosphere in strict radiative equilibrium with depth-dependent line blanketing by neutral and ionized metals 09 p1757 A70-22728
- Small scale motions in solar photosphere and chromosphere using solar spectrograms 09 p1757 A70-22729
- Solar chromosphere dark and bright mottles mean lifetime from photographs, identifying with spicules 09 p1757 A70-22733
- Solar and solar system planetary atmospheres including interplanetary space filled with solar wind 10 p1942 A70-24611
- Supergranules /convective cells/ development shown in quiet sun filtergrams of H alpha chromospheric network taken above Arctic Circle 11 p2109 A70-25741
- Rotation law and circulation velocities in solar hydrogen convection zone under anisotropic turbulent velocity 12 p2302 A70-27588
- Violet K2 emission in H and K line cores of solar calcium ions using atmospheric model in state of motion 12 p2303 A70-27701
- Soviet book on solar short wave radiation effects on ionosphere, covering solar atmosphere and spectra, ionospheric ion concentration vertical distribution, etc 13 p2487 A70-28649
- Radiative energy transport effect on temperature distribution in conduction heated plane layer applied to solar chromosphere 13 p2488 A70-28716
- Chromospheric flares electron concentration and structure from half widths and Balmer lines numbers 13 p2493 A70-29394
- Solar thermal convection model, examining effects of rotation about vertical axis 13 p2496 A70-29839
- Solar chromospheric fine structure from high resolution photographs 13 p2497 A70-29849
- Venus spin-orbit resonance resulting in consistent inferior conjunction with earth, suggesting solar atmosphere tidal influence 14 p2650 A70-31216
- Hydrogen abundance in Jupiter atmosphere quadrupole line used in comparing jupiter and solar atmosphere C/H ratios 14 p2650 A70-31221
- Gravitational atmosphere thermally driven motions, noting expansion towards lower density regions in solar chromosphere 15 p2804 A70-32619
- Coronal structures' relationship to chromospheric features in H alpha and Ca II K 16 p2977 A70-33843
- Solar atmosphere structure and chemical composition by UV spectrum analysis 17 p3161 A70-34892
- Temperature distribution of solar atmosphere, discussing solar models 17 p3169 A70-35382
- Chromospheric spicules fine structure recorded on H alpha spectrograms and filtergrams from high altitude coronagraph 17 p3174 A70-35863
- Solar atmosphere shock waves frequency and strength, computing radiative energy losses of chromospheric models 17 p3174 A70-35865
- Ba II emission lines in solar chromosphere, examining excitation and ionization equilibrium and resonance line intensities by eclipse observations 18 p3317 A70-37010
- Solar envelope unstable gravitational mode model, considering spherical harmonics by numerical integration and asymptotic representation 19 p3523 A70-38688
- Solar atmospheric hydrodynamic response to stationary random forces homogeneous over horizontal planes, discussing common energy argument, various models and photospheric oscillation 19 p3523 A70-38690
- Solar chromospheric Fe abundance, considering f-value effects 19 p3524 A70-38697
- Non-LTE line blanketed solar model atmospheres with various temperature distributions 20 p3703 A70-39020
- Solar atmosphere vortex ring observation in H alpha light /2 December 1969/ 20 p3703 A70-39022
- Explosive phase of solar flares in nonuniform atmosphere, determining explosion energy and shock wave front shape for various times 20 p3699 A70-39463
- Particle ejections in solar atmosphere and chromosphere structure, discussing dark halo exhibited by H alpha line in active region 20 p3699 A70-39464
- H alpha chromospheric network lifetime from time lapse photographs 20 p3711 A70-40409
- Supergranular network time and shape changes, examining correlations with solar rotation, activity and cycles 21 p3885 A70-40954
- Oso-4 far UV observations of solar chromosphere and corona active regions 21 p3925 A70-42187
- Shock waves strength and frequency in solar atmosphere heating deduced by empirical model, integrating radiative losses over height 21 p3925 A70-42188
- Heating and extension of solar chromosphere and corona via shock waves generated by piston below convection zone surface 21 p3925 A70-42189
- Fluid dynamics nonlinear equations for thermally driven motions in compressible, isothermal gravitational solar atmosphere, considering flow discontinuities and heat conduction 21 p3925 A70-42191
- Solar chromosphere spicules acceleration via supersonic jet formed by magnetic field under gravity and Melon seed effect 21 p3925 A70-42192
- Shock waves formation and dynamic characteristics in transition region response to infalling material from solar flares 21 p3883 A70-42193
- Solar chromosphere elements abundances methods, suggesting Fe differences origin in Fe I and Fe II inconsistencies 21 p3925 A70-42194
- Solar spectra isodentitraces indicating transition zones between and on sides of spicules in sheaths 21 p3926 A70-42197
- Solar atmosphere three dimensional microstructure observation, considering hypothesis linking flares to magnetic field 22 p4107 A70-43450
- Solar photosphere negative viscosity phenomenon, examining Rossby wave on differentially rotating isothermal spherical shell of nonconducting inviscid ideal gas 22 p4109 A70-43748
- Solar atmosphere radiation and structure, discussing continuum and line spectra, solar rotation, chromosphere, spicules, etc 23 p4256 A70-45035
- Solar center-limb observations of line brightness and Doppler shift fluctuations for Mg b lines 24 p4399 A70-45302
- Solar chromosphere model convective instability, considering temperature and magnetic field effects 24 p4399 A70-45303
- Giant cell regular structures in solar atmosphere, using magnetic synoptic charts of solar activity 24 p4400 A70-45305
- Vertical supergranular motions in solar atmosphere from multichannel magnetograph observations 24 p4400 A70-45306
- Nonspherical wave excitation in solar atmosphere in presence of toroidal magnetic field 24 p4400 A70-45312
- ### SOLAR AZIMUTH
- ### U AZIMUTH
- ### SOLAR POSITION
- ### SOLAR CELLS
- GaAs and Si photocell batteries powered by solar radiation, investigating temperature dependence of efficiency I-V characteristics and optimal power 01 p0007 A70-10177
- Si solar cells for powering artificial satellites on-board equipment, discussing fabrication and substitute materials 01 p0011 A70-11253
- Deployment systems for extending large area lightweight flexible solar arrays in space, tabulating estimated design weights including power-weight ratios 02 p0228 A70-11932
- Structural design experience in developing large area Be solar array for Mars flyby mission, describing configurations, requirements, material and manufacturing 02 p0228 A70-11935
- Solar cell array fabrication methods extending operating temperature by pulsed spot welding techniques and deletion of adhesives 02 p0228 A70-12080
- Silicon solar cells I-V characteristics, spectral response and diffusion length measured after neutron irradiation 03 p0537 A70-13025
- Solar power system of ELDO F-9 satellite boosted into polar orbit by EUROPA 1, discussing cell placement 03 p0573 A70-13847
- Performance characteristics analysis of large area roll-up solar arrays based on support structure size and weight [ASME PAPER 69-WA/ENER-11] 04 p0770 A70-14898
- Performance degradation in cadmium sulfide solar cells, discussing cause identification technique, I-V curve parameter changes, etc 04 p0628 A70-15329
- Silicon solar cell panels, studying roles of solder, interconnector metals and substrate materials in failures under thermal cycling 04 p0628 A70-15333
- Solar cell for improved performance during extreme temperature fluctuations, discussing wraparound contact 05 p0799 A70-16724
- Solar energy as spacecraft power source emphasized in operating life comparison with chemical, electrochemical and nuclear energy, discussing silicon solar cells 05 p0799 A70-17023
- Si-NP solar cell damage coefficient dependence on energy of irradiating electrons and protons, determining diffusion length from short circuit current 06 p1127 A70-18504
- GaAs solar cells performance as function of doping levels, ascribing poor efficiencies to surface recombinations 08 p1557 A70-21721

- Book on solar cells U.S. patent literature, discussing Si semiconductor, panel fabrication techniques, photoemissive devices, Cd, Ga and organic compounds, etc 09 p1612 A70-22050
- ESRO 1, ESRO 2 and HEOS 1 satellites solar arrays orbital performance 09 p1765 A70-22648
- Radiation environmental model of synchronous communication satellite solar cell degradation by particle fluxes [AIAA PAPER 70-481] 11 p2103 A70-25411
- Solar cell degradation by proton damage in synchronous orbit studied on LES-6 satellite [AIAA PAPER 70-600] 11 p2119 A70-25430
- Oriented flexible rolled-up solar array /FRUSA/ for spacecraft electric power generation, describing orientation and deployment mechanisms, solar panel, system operation, etc [AIAA PAPER 70-738] 11 p2119 A70-25434
- Electrostatic rocket exhaust condensation on spacecraft solar electric panels cover glasses, noting deleterious effects [AIAA PAPER 69-271] 11 p2103 A70-26131
- Saturn IB Orbital Workshop solar array thermal and performance analysis for various vehicle orientations and orbital conditions, emphasizing modeling and data handling 11 p2127 A70-26357
- Azur satellite p- and n-type Si solar cell system providing both power supply and storage battery charging 13 p2506 A70-29553
- Design requirements for solar cells and arrays as function of illumination, orbit, geometry and type of stabilization, space environment, etc 13 p2349 A70-29554
- Space environment simulators and test facilities for solar cells and arrays, describing solar and magnetic field simulators and universal battery charger 13 p2385 A70-29555
- Si solar cell power output and spectral response as function of angle illumination, eliminating atmospheric influence 14 p2533 A70-30337
- Si solar cell configurations for balloons and satellites, discussing critical design constraints for weather balloon power systems 14 p2670 A70-31139
- Solar cell power supplies for weather balloon and satellite systems 14 p2535 A70-31146
- Si and CdS solar cell research at COSMAT laboratories, discussing proton and electron irradiations and thermal cycling 15 p2677 A70-31804
- Low energy proton damage to silicon solar cells on INTELSAT II, F-4 and ATS-F-1, considering exposure area and radiation protection 15 p2677 A70-32419
- Thin film solar cells photosensitivity improvement by semiconductors with graded energy gap, describing construction techniques and electrical properties 15 p2678 A70-32420
- CdS and CdTe thin film solar cells R and D survey, describing construction and electrical properties 15 p2678 A70-32421
- Solar cells based on homogeneous diffusion p-n junctions in epitaxial GaAs films grown on Ge single crystal substrate 16 p2843 A70-33202
- Thermal response of passive heliotrope solar array orientation device using rotating bimetallic helix, performing energy balance analysis for helix temperature distribution 17 p3082 A70-34761
- Rotary relay for solar array space power transfer using clutch of low moment of inertia capable of recycling once each orbit 17 p3101 A70-34765
- Nonlinear structural analysis of Mariner spacecraft solar panel, using damper test characteristics 17 p3022 A70-34769
- Black Arrow X3 spacecraft design and experiments, including silicon cells performance electronic assemblies and micrometeoroid fluxes 17 p3178 A70-35256
- Photoelectric conversion efficiency and radiation resistance of Li-doped Si solar cells, showing improved reliability over Li-free cells 17 p3023 A70-35311
- Optimum mounting angles for direct solar radiation flux on solar battery on circular orbit satellite 18 p3215 A70-36176
- Heterogeneous solar cells based on polycrystalline cadmium sulfide and selenide, discussing preparation methods and photoelectric and electric properties 18 p3215 A70-36238
- British X 3 satellite for investigating thermal control surface finishes stability, ultrathin solar cells, electronic systems reliability and micrometeoroid flux measurement 18 p3333 A70-36511
- Antireflection titanium dioxide thin films for aerospace silicon solar cells 19 p3358 A70-38201
- SI and thin film solar cells for satellite power supplies, considering manufacture and space environment 19 p3358 A70-38478
- Si photocells fabrication, reliability and energy conversion efficiency 19 p3358 A70-38479
- Posterior electrode structural modification for reducing silicon photovoltaic cells absorptivity and operating temperature 19 p3358 A70-38492
- Aircraft auxiliary systems and spacecraft power supplies, considering fly-by-wire control actuators, pyrotechnics and stowable solar array 20 p3564 A70-39669
- SERT 2 solar array power system in sun synchronous orbit, considering power conditioning and deployment technique [AIAA PAPER 70-1159] 20 p3567 A70-40202
- Solar panel flexibility effect on attitude control of solar electric spacecraft for deep space mission [AIAA PAPER 70-1140] 20 p3716 A70-40209
- Power loss due to cumulative meteoroid impacts on solar cells during extended planetary missions, investigating hypervelocity particle impacts into glass [AIAA PAPER 70-1139] 20 p3567 A70-40210
- Collection efficiency and spectral response calculations for semiconductor heterojunction solar cells 21 p3861 A70-40623
- Silicon solar cell specifications and cost reduction without output or reliability loss 21 p3756 A70-41008
- Silicon solar cell array interconnector design based on analysis of stresses caused by thermal expansion and vibrational motion 21 p3756 A70-41009
- Solar arrays for Venus-Mercury flyby, evaluating temperature and power performance 21 p3756 A70-41010
- Solar cell/battery systems for spacecraft, discussing power system evaluator, NiCd thermal control, lightweight rigid panels design, etc 21 p3757 A70-41011
- Regulated spacecraft solar array mathematical model for high voltage power supply regulator analysis 21 p3757 A70-41208
- Solid state switches for operating ion thrusters directly from high voltage solar cells, noting satellite weight saving 21 p3798 A70-41215
- Automatic and command multiple sequencer for spacecraft solar cell battery charger, providing switching logic by integrated circuits design 21 p3758 A70-41218
- Buck-boost main bus voltage regulator for solar array battery space power system 21 p3758 A70-41219
- Solar cell array maximum power point in scientific satellites via closed loop conductance matching regulator 21 p3758 A70-41220
- Solar cell array peak power tracker and battery charger for Airlork Vehicle coupling Apollo spacecraft and Saturn IVB stage to form manned orbiting workshop 21 p3759 A70-41221
- Copper disulfide-cadmium sulfide thin film solar cell degradation under simulated low orbit conditions, investigating thermal stress 21 p3759 A70-41313
- High voltage solar arrays, considering plasma power losses dielectric stresses design, fabrication and testing [AIAA PAPER 70-1137] 21 p3759 A70-41780
- High voltage solar array with integral power conditioning, discussing weight factors, panel design and layout, mechanization, performance prediction, etc [AIAA PAPER 70-1158] 21 p3759 A70-41787
- Silicon solar cell design optimization for near solar missions, discussing electrical characteristics and performance obtainable under various solar radiation conditions 22 p3964 A70-42496
- CdS thin film solar cells, describing manufacture for increased degradation resistance 22 p3966 A70-43537
- High voltage solar array operational problems in earth orbit environment, discussing conducting surfaces, power loss, plasma effects, leakage, etc 22 p3967 A70-43544
- Cu and Ni doped n-p and p-n silicon solar cells, examining radiation damage and isochronal annealing properties 24 p4294 A70-45810
- Apollo 11 deployed solar cells, investigating degradation of surface properties and thermal control due to lunar module ascent effects 24 p4295 A70-46262
- SOLAR CHROMOSPHERE**
U CHROMOSPHERE
U SOLAR ATMOSPHERE
SOLAR COLLECTORS
NT SOLAR REFLECTORS
- Direct solar radiation concentration by paraboloid mirrors, analyzing energy transport and distribution functions, based on statistically distributed imperfections of reflecting surfaces 01 p0010 A70-10762
- Absorber positioning inaccuracy influence in concentrating solar unit mirror on unit energy parameters, discussing defocusing 01 p0010 A70-10763
- Solar installations optical properties selectivity increase by light-collecting surfaces mechanical treatment, describing plate grinding with abrasive powders 07 p1196 A70-19625
- Nonsliding rotary electrical connector for conducting current and signals from satellite solar panel [AIAA PAPER 70-458] 11 p2016 A70-25453
- Design requirements for solar cells and arrays as function of illumination, orbit, geometry and type of stabilization, space environment, etc 13 p2349 A70-29554
- Space environment simulators and test facilities for solar cells and arrays, describing solar and magnetic field simulators and universal battery charger 13 p2385 A70-29555
- Flexible antennas and solar panels effect on dynamic behavior and control system response of dual spin spacecraft 21 p3931 A70-41855
- SOLAR CONSTANT**
Solar constant measurement by Eppley normal incidence pyrheliometers on high altitude balloons 08 p1501 A70-21920
- Solar constant dependence on Wolf number and variations in transmission factor from balloon observations of radiation balance vertical distribution 14 p2568 A70-30126
- Atmospheric transmission variability related to solar constant variations 15 p2801 A70-32371
- Engineering standard for solar constant and zero air mass solar spectral irradiance from high altitude measurements 17 p3077 A70-35161
- Solar constant measurements by high altitude balloon sounding, noting anomalous turbidity in upper atmospheric layers due to nuclear explosions and volcanic eruptions 20 p3703 A70-39375
- SOLAR CONVERTERS**
U SOLAR GENERATORS
SOLAR CORONA
Coronal gas pressure boundary conditions on model upper chromosphere, determining temperature and hydrogen density assuming hydrostatic equilibrium 01 p0175 A70-10243
- Solar corona red and green lines during 30 May 1965 total eclipse, discussing indicated radial, turbulent and displacement velocities 01 p0176 A70-10249
- Solar corona magnetic field determination from photospheric magnetic field line-of-sight component observations, describing various mathematical methods 01 p0176 A70-10250
- Coronal electron densities and magnetic fields determined from K-coronameter and type 4 radio burst data 01 p0168 A70-10255
- Photography and photometry of solar corona during 25 February 1952 and 22 September 1968 eclipses, discussing photographic weighting techniques 01 p0181 A70-10576
- Solar corona heating by shock waves, considering chromosphere and solar wind physical properties, heat flow channeling, etc 02 p0361 A70-11750
- Coronal emission lines wide slit photometry systematic error analysis and suggested error elimination by varying observation method 02 p0373 A70-12375
- Aerosol size distribution from data on atmospheric spectral transmittance and solar corona brightness spectral and angular variations 02 p0292 A70-12434
- Dynamic electric field in solar coronal exosphere on basis of kinetic and hydrodynamic theories, giving estimate of solar wind 02 p0359 A70-12609
- Transition probabilities computed for spectral lines due to magnetic quadrupole radiation, discussing deexcitation of excited atoms in solar corona 02 p0359 A70-12706
- Solar corona photographs for isophotes during solar eclipse of 22 September 1968 revealing chromospheric flare and prominences 03 p0569 A70-13362
- Ar X and Ar XIV identification in solar corona and unidentified coronal lines origin, discussing Fe and Ni transitions from metastable levels 03 p0571 A70-13598
- Solar wind acceleration and coronal plasma heating above plage regions from spectra of solar radio echoes, computing temperature rise and energy input 04 p0740 A70-15049

Excitation of ground configuration of Fe XIII for density and temperature range in solar corona, using proton collisions, electron collision strengths, etc
05 p0902 A70-16434

Coronal features rotation rates as function of latitude and height above limb from autocorrelation analyses of K-coronameter observations
05 p0902 A70-16435

Solar radio emission intensity-solar flare index and 5303 A coronal line intensity-proton flare numbers relations
05 p0911 A70-16438

Neutral Ne emission line in visible solar spectrum during bright events in inner corona, noting 1958 outburst of RS Oph
05 p0920 A70-16944

Solar corona at sunspot maximum observed during 22 September 1968 total solar eclipse, noting coronal streams unpredicted by magnetostatic model
06 p1138 A70-17278

Radioheliograph observations at 80 MHz of directive shock wave propagation in solar corona
06 p1144 A70-18007

Steady spherical plasma flow from sun analyzed by equations of solar corona hydrodynamical model
07 p1378 A70-19033

Excitation, ionization and recombination rates for charged ions during collisions with electrons in solar corona assuming Maxwellian electron distribution
07 p1384 A70-19409

Galactic cosmic rays intensity long term modulation, studying roles of solar corona, solar wind and interplanetary electromagnetic field
07 p1369 A70-20075

Kinetic temperature estimate for solar corona based on time profile of type 3 bursts
08 p1565 A70-20565

Solar system origin theory emphasizing brother star approaching nebula for instability of boundary layer
08 p1568 A70-20638

F corona heliocentric dust cloud model to account for temperature variations with particle size and optical properties, computing thermal emission
08 p1571 A70-20907

Stellar gas ejection processes in corona-interplanetary plasma system, proposing hydrodynamic model with frequent collision region having finite radius
08 p1573 A70-21060

Solar corona and interplanetary plasma structure and dynamics, calculating solar wind velocity as function of distance from sun
08 p1576 A70-21397

Solar and stellar convection regions and coronas using photospheric models, taking into account molecule formation
08 p1581 A70-21953

Corona green /5303 A/ and red /6374 A/ lines during minimum solar activity in 1964, discussing N-S and E-W asymmetries and intensities
09 p1750 A70-22100

Allowed and forbidden transitions probability in isoelectron sequences of solar corona, using scale factor method and variational wave functions
09 p1751 A70-22155

Solar chromosphere-corona transition region properties, discussing temperature increase within very thin layer and inferring temperature-density structure from emission line intensities
09 p1752 A70-22246

Solar corona heating, discussing theories of Schwarzschild, Schatzman, Alfven, Osterbrock, Uchida, Whitaker and Kuperus
09 p1757 A70-22686

Solar equatorial XUV limb brightening for resonance lines of Li-like ions from OSO-4 observations interpreted by coronal model
09 p1757 A70-22732

Excitation equilibrium relative populations calculations for Fe, Ni and Ca ions under solar coronal conditions
09 p1757 A70-22735

Solar eclipse coronal polarization and intensity measurements, discussing equipment, calibration, photometric reduction and results
09 p1757 A70-22736

Solar U-burst radiospectrographic observations, investigating disturbing trajectories and longitudinal distribution in combination with model coronal condensation
09 p1758 A70-22737

Solar corona pulsating metric radio emissions, indicating phenomena as type 4 radiation phases
09 p1758 A70-22738

Probability coefficients computation for transitions between energy levels of ion A XIV in solar corona
09 p1761 A70-23060

Outer corona brightness and polarization during total solar eclipse from satellite photographs
10 p1947 A70-24988

Spectroscopy in astrophysical research, discussing solar corona chemical elements, forbidden lines and temperature determination
10 p1948 A70-25181

Solar corona magnetic field estimated from type II bursts correlated with photospheric, chromospheric and geophysical phenomenon
10 p1934 A70-25275

Solar outer corona brightness distribution from rocket observation with scanning devices during solar eclipse, estimating error
11 p2107 A70-25397

Electron and proton excitation of forbidden transition lines in Ca XV ground configuration determined for coronal densities and temperature
11 p2109 A70-25742

Solar corona photographs for isophotes during solar eclipse of 22 September 1968 revealing chromospheric flare and prominences
11 p2118 A70-26727

Solar wind structure as function of corotating coronal inhomogeneities determined using perturbation equations for spherical polar coordinate system
12 p2292 A70-27179

Solar active regions in chromosphere and corona observed by EUV spectroheliometer aboard OSO-4 spacecraft, discussing ion formation and temperatures
12 p2303 A70-27705

Coronal condensation spectra during 4 February 1962 total eclipse, determining abundances, ionization equilibria, electron densities, etc, from Fe and Ca XV lines analysis
12 p2303 A70-27712

Coronal structure prediction for 7 March 1970 solar eclipse, using model for 22 September 1968 eclipse
12 p2304 A70-27718

Solar flares responsible for Faraday rotation events observed in passage of Pioneer 6 radio signal through solar corona
12 p2295 A70-28023

Coronal condensations temperature and electron density measurements at meter wavelengths and in white light
13 p2488 A70-28717

Hydrodynamic equations to obtain transformation coefficient for HF weakly damped waves in magnetoactive plasma, applying to solar corona
13 p2463 A70-29227

Upper atmospheric temperature-gravitational potential relationship for sun, earth and several planets
13 p2495 A70-29765

Solar radar echo characteristics, discussing coronal compressional waves and refraction by plasma clouds and moving plasma irregularities
13 p2370 A70-29852

Electron density, characteristic dimensions and vertical density gradient of coronal enhancements in white light, observing elliptical cross section
13 p2479 A70-30004

Solar catadioptric coronagraph design free from chromatic image defects
15 p2737 A70-32041

Polarization characteristics of solar radio waves reflected from coronal waves in meter wavelength range
15 p2802 A70-32485

Solar coronal streamers, considering disk locations, evolution, classification and morphological model
15 p2804 A70-32621

Solar stray light, determining spread function, limb profile and aureole at various wavelengths
15 p2795 A70-32625

Kinetic temperature estimate for solar corona based on time profile of type 3 bursts
15 p2805 A70-32720

Solar corona predicted and observed structure compared during eclipse of 7 March 1970
16 p2977 A70-33837

Coronal observations from Aerobee 150 rocket after total solar eclipse of 7 March 1970 in Mexico, combining coronagraph flight record with ground photography
16 p2977 A70-33839

Doppler temperature and motion of solar corona from ionized Fe line using Fabry-Perot interferometer
16 p2977 A70-33841

Outer corona during 7 March 1970 eclipse, discussing distance dominance of K corona
16 p2977 A70-33842

Coronal structures relationship to chromospheric features in H alpha and Ca II K
16 p2977 A70-33843

Plasma wave radiation by electron stream in active solar corona, obtaining spectrum and growth rate
16 p2979 A70-34189

Gaseous disk in equatorial plane of solar nebula, determining dimensions from accretional theory for planets formation
17 p3172 A70-35584

Solar wind velocity profile in rapid acceleration of coronal plasma from type I, III and V bursts
17 p3152 A70-35745

Cerenkov plasma waves generation by fast electron streams in solar corona and conversion into EM waves
17 p3173 A70-35768

Slow and fast coronal expansion phenomena associated with solar flares
17 p3152 A70-35869

Ions acceleration and motion in corona and solar wind, discussing equation derivation, He abundance, nonMaxwellian distribution functions, minimum flux estimation, etc
17 p3152 A70-35870

Coronal magnetic bottle at ten solar radii from Faraday rotation measurements of occulted spacecraft radio source
17 p3174 A70-35871

Solar corona structure on 22 September 1968 using radio astronomical and optical eclipse data
18 p3313 A70-36607

Solar wind velocity variations showing relationship with electron density excess and localized region temperature of corona
19 p3512 A70-38693

Solar eclipse microwave spectral observations for coronal condensation sources characteristics of solar radio emission slowly varying component, discussing ionospheric recombination coefficients
19 p3531 A70-38910

Coronal data comparison based on 5303 A line intensities and distribution with respect to position angles
20 p3704 A70-39461

Electric fields influence on emission lines shape of multiply charged ions in coronal plasma, discussing kinetic temperature
20 p3704 A70-39462

Solar outer corona brightness distribution from rocket observation with scanning devices during solar eclipse, estimating error
20 p3710 A70-40089

Upper atmospheric temperature-gravitational potential relationship for sun, earth and several planets
20 p3710 A70-40090

Solar corona current free magnetic field distribution relationship to plasma density structure
20 p3712 A70-40415

Coronal streamers structure and evolution from photographic and K-coronameter data, indicating photospheric bipolar magnetic regions as origin
20 p3712 A70-40416

Solar corona streamer and interstreamer regions, examining geometrical and dynamic structure by energy transport process
20 p3712 A70-40417

Solar X-ray corona during eclipse of 7 March 1970, using Aerobee rocket photographs
20 p3713 A70-40430

Solar radio pulsations, observing modulation of coronal microwave, X ray and type III emission
21 p3880 A70-40965

Taurus A 21 cm radiation anomalous frequency decrease during occultation by sun attributed to particle streams propagating in solar corona
21 p3886 A70-41064

Radio observations of limb darkening and structure of solar corona at 80 MHz
21 p3890 A70-41177

Radioheliograph observations of solar outbursts involving MHD waves propagation along curved paths in corona at 80 MHz
21 p3891 A70-41178

Two dimensional positions of fundamental and harmonic type 2 solar bursts, using coronal streamer plasma and backward refracted radiation model
21 p3891 A70-41179

Position scatter of 80 MHz sources of type 3 solar bursts reflecting outer corona structure
21 p3891 A70-41182

Chromosphere-corona transition region - Conference, Boulder, Colorado, August 1969
21 p3924 A70-42182

Transition region structure between chromosphere and corona, discussing temperature, theoretical models, energy balance and magnetic fields from far UV data
21 p3924 A70-42183

Chromosphere-corona transition region model from limb-disk optically thin line intensities
21 p3924 A70-42184

OSO-4 far UV observations of solar chromosphere and corona active regions
21 p3925 A70-42187

Heating and extension of solar chromosphere and corona via shock waves generated by piston below convection zone surface
21 p3925 A70-42189

Energy deposition in solar corona associated with momentum transfer from heating wave in transition region, discussing wave pressures
21 p3925 A70-42190

Solar coronal and photospheric iron abundances from absorption forbidden lines, discussing discrepancy with permitted lines
21 p3925 A70-42195

Vertical oscillations in solar temperature minimum suggested as acoustic-gravity waves modes dependent on height at chromosphere-corona interface
21 p3926 A70-42196

Transition zone height in corona-chromosphere interface from high resolution disk spectra near limb
21 p3926 A70-42198

One fluid solutions for solar wind with reduced electron heat conduction in agreement with observed characteristics at corona base 22 p4093 A70-42472

Pulsar pulse arrival time fluctuations, examining solar coronal nature by angular broadening, scintillation and turbulence spectrum 22 p4101 A70-42935

Polarization characteristics of solar radio waves reflected from coronal waves in meter wave length range 23 p4240 A70-43909

Coronal shock growth as source of thermal solar X ray bursts associated with optical events 24 p4401 A70-45320

Solar wind two fluid model with boundary conditions describing electron and proton behavior in expanding corona 24 p4397 A70-45770

SOLAR CORPUSCULAR RADIATION

NT SOLAR PROTONS

Secondary corpuscular stream effect on diurnal variations in cosmic ray intensity obtained from statistical analysis 01 p0172 A70-11524

Geomagnetic micropulsations fluctuations during solar activity cycle showing changes in excitation frequency with change in corpuscular fluxes parameters 01 p0083 A70-11539

Corpuscular sources geoeffectiveness related to position on solar disk at maximum flare activity 03 p0569 A70-13359

Solar interior temperature measurement by Cl, Ga and Li isotopic detectors of solar neutrinos, discussing effectiveness and upper temperature bound 05 p0899 A70-15951

Solar neutrino detectors calibration with artificial neutrino sources produced by reactors, electron and proton accelerators 05 p0846 A70-15953

Night lower ionosphere at midlatitudes additional ionization ascribed to solar corpuscular fluxes 06 p1135 A70-17839

Electric field in earth magnetotail via Explorer 33 and 35 satellite observation of solar electrons above 50 keV energy 06 p1058 A70-18528

Solar particles penetration to lower ionospheric heights at low latitudes indicated from proton flux measurements by Explorer 33 satellite and Calcutta station 07 p1366 A70-18849

Solar corpuscular fluxes directional distribution time dependent changes effect on lower ionospheric electron production rates 07 p1373 A70-20344

Geomagnetic storms data compilation /1957-1964/, showing solar activity effect on solar corpuscular stream velocity 07 p1373 A70-20436

Solar cosmic rays development, discussing corpuscular radiation of flare origin, radio noise, geomagnetic activity and intensity measurements 09 p1745 A70-23128

Solar corpuscular streams effect on meteoric particles behavior in circular orbit around sun, determining lifetime on basis of mass loss due to pulverization 09 p1763 A70-23382

Satellite mounted device for detecting and recording 20-110 Mev solar neutrons 10 p1889 A70-24488

Solar corpuscular fluxes angular characteristics, derived from observational data analysis, showing circular or elliptical transverse cross sections 11 p2104 A70-25545

Corpuscular sources geoeffectiveness related to position on solar disk at maximum flare activity 11 p2118 A70-26724

Solar neutrino flux measurement based on neutrino capture by large chlorine mass and subsequent Ar 37 decay in low noise environment 12 p2293 A70-27389

Low energy solar flare electrons scatter-free propagation through interplanetary medium, considering rise, decay and travel times 13 p2477 A70-29194

X ray and proton flux measurement during solar flare of 29 September 1968 by balloon-borne detectors 14 p2633 A70-31310

Solar flare particle flux equilibrium anisotropy and convection in solar wind 15 p2793 A70-31901

Solar neutrino fluxes, calculating capture rates and primordial helium abundance 17 p3151 A70-34847

Electron correlations and solar neutrino counts, correcting frequency independent Thomson cross section 18 p3308 A70-36485

Peripheric umbra photometric analysis during lunar eclipses based on homogeneous observational material, revealing luminescence excited by solar corpuscular radiation 18 p3319 A70-37055

Nitrogen dioxide and molecular oxygen ions densities in lower ionosphere as function of solar corpuscular radiation 19 p3409 A70-37325

Global diurnal variations in F 2 layer seasonal anomaly during high and low solar activity, noting corpuscular radiation role 19 p3491 A70-37326

Solar energetic charged particles interaction with earth bow shock and magnetopause 19 p3494 A70-37482

Solar particle observations over polar caps, considering spatial and angular distribution measurements 19 p3494 A70-37484

Interplanetary magnetic field during solar particle event of 25 February 1969 from Heos 1 measurements 19 p3495 A70-37500

High energy solar electrons observed by HEOS-A1 satellite, discussing semitransparent barrier existence at distance from sun 19 p3497 A70-37521

Ammonium molecules dissociation and ionization in comet atmospheres due to solar corpuscular and photon radiation 19 p3514 A70-37642

Solar wind and flare energetic particles properties and interactions, surveying interplanetary magnetic field, planetary bow shock waves, neutrons, neutrinos, etc 19 p3511 A70-38418

Solar neutrinos flux upper limit determination, describing detection equipment and procedures 19 p3511 A70-38486

Geomagnetic perturbation indices indicating different solar corpuscular streams and heliogeophysical properties 20 p3618 A70-39182

Polar stratospheric winter explosive warmings correlated with solar high energy charged particles injections 20 p3618 A70-39185

Solar B8-Be8 decay neutrinos energy spectrum and absorption cross sections calculation 20 p3698 A70-39307

Solar corpuscular fluxes angular characteristics derived from observational data analysis, showing circular or elliptical transverse cross sections 21 p3882 A70-41295

Solar high energy particles penetration into ionospheric heights at equator, analyzing optical flare and solar proton data from ATS-1 and Explorer 34 23 p4235 A70-43816

High energy solar neutron flux via balloon measurement of flux difference from solar direction and from symmetrical direction about zenith 23 p4236 A70-43881

Helios solar observation satellite equipment design study for solar plasma low energy particles onboard measurements 23 p4262 A70-44844

Solar neutron flux density relation to solar flare of 28 September 1968, using high altitude balloon-borne neutron detector 23 p4238 A70-44925

Solar corpuscular flux and visible solar spot area correlation with geomagnetic planetary index for 27-day intervals, considering relationship to earth satellites motion 24 p4408 A70-45547

SOLAR COSMIC RAYS

Iron group nuclei abundance relative to oxygen determined for solar cosmic ray event of 2 September 1966 01 p0167 A70-10042

Secondary corpuscular stream effect on diurnal variations in cosmic ray intensity obtained from statistical analysis 01 p0172 A70-11524

Solar flare cosmic rays confinement to definite solar magnetic field sectors using Laplace transformation 03 p0560 A70-13977

IMP F solid state detector data on 13 day solar proton event at low energy, considering cosmic rays anisotropy and interplanetary magnetic field 04 p0738 A70-14512

Solar cosmic ray dose rate and total dose magnitude predictions based on Epeak and isotropic diffusion models 04 p0742 A70-15584

Drift, anti-Fermi retardation, convective transfer and diffusion effects on solar cosmic ray energy spectrum in earth orbit proximity 05 p0898 A70-15943

Venus-earth carbon dioxide atomic parameters used to determine ionization and optical emission rates in Venus upper atmosphere resulting from solar cosmic rays 05 p0901 A70-16276

Energy spectrum time dependence of solar cosmic ray event of 28 January 1967 measured in Northern Hemisphere, discussing particle diffusion and magnetic trap 05 p0902 A70-16459

Solar cosmic ray flare /28 January 1967/ observed by neutron monitors, determining emission and particle spectrum at atmosphere boundary 05 p0903 A70-16752

Solar cosmic rays diffusion enclosure in interplanetary space magnetic boundary suggested from balloon, satellite and ground observations of solar flare neutron component 05 p0904 A70-16753

X ray and H alpha emissions associated with solar proton flares, correlating rise time with solar cosmic rays 06 p1137 A70-18547

Solar wind, using data on solar and galactic cosmic rays in interplanetary space 07 p1366 A70-19030

Electron production rate enhancement by solar cosmic rays in lower ionosphere, considering particle distribution and polar cap absorption 07 p1369 A70-20153

Electron production in lower ionosphere by solar cosmic rays, calculating rates by computer as function of nuclear charge number, energy spectrum and height 07 p1373 A70-20348

Solar flare cosmic ray rigidity spectrum determination based on ratio of relative enhancements, assuming isotropic arrival of particles at earth 09 p1744 A70-22489

Solar cosmic rays development, discussing corpuscular radiation of flare origin, radio noise, geomagnetic activity and intensity measurements 09 p1745 A70-23128

Solar cosmic ray ionization of upper atmosphere, calculating electron production rate distribution 10 p1934 A70-25199

Solar cosmic rays interaction with interplanetary shock waves, discussing chromospheric eruptions 13 p2476 A70-28959

Proton cosmic ray flare development and spatial structure, discussing magnetic field annihilation process for particle energy and photon ejection 13 p2476 A70-29046

Solar cosmic rays entry into magnetosphere, showing entrance on smoothly connected field lines 13 p2480 A70-30059

Anisotropic solar cosmic rays in inhomogeneous medium, investigating shell effect on propagation by one dimensional model 15 p2795 A70-32624

Statistical accuracy of standard muon azimuthal semicubic telescope for solar cosmic rays, discussing rms error 18 p3256 A70-36103

Solar cosmic rays satellite observation, considering flare associated, recurrent and storm particle events and active center associated energetic particles 19 p3493 A70-37474

Low energy solar and galactic cosmic rays propagation in interplanetary medium observed by Zond and Venus space probes, discussing shock waves retardation 19 p3493 A70-37475

Solar cosmic ray protons and electrons increase during 23 February-5 March 1969 observed by Venus 5 and 6 space probes, discussing interplanetary medium disturbance 19 p3495 A70-37504

Solar cosmic rays emission spectrum for 23 February 1956 flare, taking into account nucleon diffusion coefficient dependence on particle rigidity and distance to sun 20 p3697 A70-39287

Solar cosmic rays diurnal and semidiurnal variations modulation by noncoincidence between earth rotation axis and normal to ecliptic plane 20 p3697 A70-39289

Supersonic transport radiation hazards to flight crew, passengers and population, discussing dosages, probabilities, solar cosmic ray encounters, warning systems, etc 20 p3700 A70-39923

SOLAR CYCLES

NT SUNSPOT CYCLE

Two layer truncated harmonic model of Rossby wave dynamo for solar cycle, accounting for maintenance and reversal of magnetic fields 01 p0174 A70-10238

Atmospheric density variations during solar maximum and minimum, discussing solar corpuscular stream and EUV radiation 01 p0075 A70-10594

Regular/irregular micropulsations variations during solar cycle, noting possible magnetospheric contraction and solar wind velocity influence 01 p0075 A70-10600

Solar brightness variations observed photometrically, discussing periodicity, sunspot locations, photosphere and subsurface rotations, etc 01 p0186 A70-11273

Geomagnetic micropulsations fluctuations during solar activity cycle showing changes in excitation frequency with change in corpuscular fluxes parameters 01 p0083 A70-11539

Cosmic ray variations concepts with reference to 11, 22 and 80-90 year solar cycles Wolf number variations

03 p0568 A70-13355

Interplanetary magnetic field during solar cycle rise and minimum based on Explorer 33 magnetometer measurements

03 p0575 A70-13999

Eleven year cosmic ray variation and solar activity cycle analysis, showing variation amplitude dependence on both numbers and heliolatitudinal distribution of sunspots

04 p0742 A70-15718

Spectral characteristics of B and S components of solar radio emission from statistical data, investigating dependence on 11-yr cycle and minimum solar activity

07 p1378 A70-19031

East-west dissymmetry in solar activity center births for solar cycles XII-XIX, noting independence of latitude and invariance throughout last eight cycles

08 p1567 A70-20599

Cosmic ray intensity variation correlated with amplitude changes in 27 day variation during solar cycle 18

09 p1745 A70-22740

Cosmic ray diurnal anisotropy, demonstrating two-solar-cycle variations for nucleonic component

09 p1746 A70-23478

Seasonal variation of spread F near magnetic equator, showing relationship with solar cycle at different geographic locations

10 p1881 A70-24818

Cosmic ray variations concepts with reference to 11, 22 and 80-90 year solar cycles Wolf number variations

11 p2118 A70-26720

Ionospheric electron content at temperate latitudes during solar cycle increasing phase by radio beacon satellite, discussing diurnal, seasonal and latitudinal variations

12 p2225 A70-27892

High energy proton flux variations in inner belt during solar cycle and magnetic storm, using satellite and balloon measurements

13 p2483 A70-30091

Morphology of thermal and energetic particles in inner magnetosphere during geomagnetic disturbances and solar cycles

14 p2630 A70-30358

Eleven year cosmic ray variation and solar activity cycle analysis, showing variation amplitude dependence on both numbers and heliolatitudinal distribution of sunspots

14 p2632 A70-30802

Planetary tidal force effect on solar activity cycle, showing amplitude proportionality to solar and gravity center deviation

14 p2649 A70-31199

Residual solar modulation of relativistic cosmic ray nuclei in galaxy over eleven years, observing magnitude at solar activity minima

18 p3309 A70-37009

Solar X ray emissions from quiet and active sun compared with radio flux to investigate production mechanisms

19 p3512 A70-38909

Solar activity effects on Northern Hemisphere atmospheric temperature, mapping gradients for 11 year solar cycle

20 p3662 A70-39188

Twenty two year solar activity cycle effect on earth climate, plotting odd and even 11 year cycle curves for pressure and temperature

20 p3662 A70-39189

Interplanetary magnetic field large scale structure from cosmic ray intensity secular variations during solar activity cycle

20 p3696 A70-39276

Stellar matter density and composition in proton-proton cycle, applying results to real solar model

20 p3698 A70-39308

Spot groups longitude distribution in 11 year solar activity cycle in Northern and Southern Hemispheres based on correlation functions, observing period variation

20 p3704 A70-39466

Supergranular network time and shape changes, examining correlations with solar rotation, activity and cycles

21 p3885 A70-40954

Ionospheric electron content measurement during solar activity cycle, noting temporal and spatial variations

22 p4020 A70-43159

Butterfly diagram for describing latitude distribution of sunspots during solar cycle, considering representation methods

22 p4106 A70-43264

Temporal sequence correlation between surges and associated flares during solar cycle

22 p4095 A70-43265

Soft solar X rays cyclic variation from satellite observation, noting relation to sunspot group magnetic field complexity

22 p4096 A70-43301

Cosmic ray 11-year variation pattern change in 19th and 20th solar activity cycles determined by latitude expeditions spectrum analysis

23 p4237 A70-44071

SOLAR DISK

U SUN

SOLAR ECLIPSES

Chromospheric slitless spectrograms at 1962 eclipse, discussing Balmer-Paschen line intensities, continuum data, reduction and source error

01 p0175 A70-10244

Slitless spectrograms of chromosphere obtained during 1962 eclipse to determine H level populations decrements, self absorption in Balmer lines and chromosphere model

01 p0175 A70-10245

Solar corona red and green lines during 30 May 1965 total eclipse, discussing indicated radial, turbulent and displacement velocities

01 p0176 A70-10249

Photography and photometry of solar corona during 25 February 1952 and 22 September 1968 eclipses, discussing photographic weighting techniques

01 p0181 A70-10576

Near limb solar IR brightness distribution observed during total solar eclipse of 12 November 1966 in Argentina by sounding rocket photometers

01 p0186 A70-11271

Optical and radioastronomical observations of 1966 solar eclipse, discussing data and instruments

01 p0191 A70-11472

Solar and lunar disks instant of contact during solar eclipse determined by chord measurements, comparing three methods for successive time intervals

01 p0191 A70-11473

Heat sources in E region from electron temperature data analysis recorded by rockets during eclipses in July 1963

01 p0082 A70-11491

Solar eclipse effects in equatorial F region electron density, noting data analysis method for reexamining existing measurements

02 p0290 A70-12157

Solar corona photographs for isophotes during solar eclipse of 22 September 1968 revealing chromospheric flare and prominences

03 p0569 A70-13362

D layer radio absorption during solar eclipse of 22 September 1968 attributed to two solar X-ray sources

03 p0559 A70-13602

Solar corona at sunspot maximum observed during 22 September 1968 total solar eclipse, noting coronal streams unpredicted by magnetostatic model

06 p1138 A70-17278

Viking Mars orbiter/lander mission planning, studying sun, earth and star occultations sensitive mission characteristics

[AIAA PAPER 70-62]

06 p1146 A70-18193

Atmospheric ozone content and mass effect on solar radiation flux measured during total solar eclipse of 22 September 1968

07 p1275 A70-20310

Illumination of zenith region of sky before and during solar eclipse of September 1968 measured by luxometer

08 p1573 A70-20950

May 1966 solar eclipse effects on sporadic E layer, including ionizing radiation decrease relation to boundary and blanketing frequencies decrease

08 p1490 A70-21432

Solar eclipse coronal polarization and intensity measurements, discussing equipment, calibration, photometric reduction and results

09 p1757 A70-22736

Vertical incidence /VI/ F layer ionograms, magnetograms and signal amplitude data obtained during annular eclipse of 23 November 1965

09 p1671 A70-23494

Outer corona brightness and polarization during total solar eclipse from satellite photographs

10 p1947 A70-24988

Solar outer corona brightness distribution from rocket observation with scanning devices during solar eclipse, estimating error

11 p2107 A70-25397

Critical review of Meisel paper on solar X ray source identification using D layer ionization behavior during eclipse

11 p2109 A70-25750

Solar corona photographs for isophotes during solar eclipse of 22 September 1968 revealing chromospheric flare and prominences

11 p2118 A70-26272

Coronal condensation spectra during 4 February 1962 total eclipse, determining abundances, ionization equilibria, electron densities, etc. from Fe and Ca XV lines analysis

12 p2303 A70-27712

UV flash spectra of total solar eclipse of 7 March 1970 obtained by Aerobee 150 rocket

12 p2304 A70-27717

Coronal structure prediction for 7 March 1970 solar eclipse, using model for 22 September 1968 eclipse

12 p2304 A70-27718

Two dimensional structure of 20 May 1966 noise storm from solar eclipse data obtained at ground stations

13 p2493 A70-29390

Solar limb integrated brightness distribution in continuous spectrum during 20 May 1966 solar eclipse

13 p2498 A70-30003

Lower ionosphere radio reflection during solar eclipse of 22 September 1968

14 p2571 A70-30237

LF signals phase determination during solar eclipse of 22 September 1968, noting frequency shift magnitude

14 p2547 A70-30238

Solar eclipse of March 1970 observation by sounding rockets, discussing ionospheric and meteorological measurements

14 p2586 A70-30800

F region electron and ion densities, temperatures and plasma velocities computed for eclipse at Wallops Island on 7 March 1970

15 p2726 A70-31866

Electron density measurements by partial reflection and rocket techniques during 20 May 1966 solar eclipse, showing agreement below 82 km height

15 p2726 A70-31869

Moon shadow solar eclipse encounter probability for high altitude satellite in circular earth orbit

15 p2803 A70-32502

Illumination of zenith region of sky before and during solar eclipse of September 1968 measured by luxometer

15 p2806 A70-32762

Equatorial F 2 region response during solar eclipse of 7 March 1970, emphasizing ionization production and loss, transport processes and electron temperature

16 p2897 A70-33826

Solar radiation intensity at Lyman alpha wavelength and X ray spectrum before and during solar eclipse of 7 March 1970

16 p2972 A70-33827

Atmospheric temperature and wind data before, during and after solar eclipse of 7 March 1970, using ARCAS meteorological rockets

16 p2977 A70-33828

F region electron content and recombination times during solar eclipse of 7 March 1970, using Faraday rotation technique

16 p2897 A70-33829

Ionospheric electron content measurement during solar eclipse of 7 March 1970, using VHF radio waves from geostationary satellites

16 p2897 A70-33830

Ionospheric electron density during solar eclipse of 7 March 1970, using Faraday rotation measurements of geostationary satellites VHF transmissions

16 p2898 A70-33831

D region electron density variations during solar eclipse of 7 March 1970, using wave interaction technique

16 p2898 A70-33832

Sky wave amplitudes analysis recorded at D region height by loop and short whip antennas during 7 March 1970 solar eclipse

16 p2898 A70-33833

D region electron energy loss factor during solar eclipse of 7 March 1970, using wave interaction technique

16 p2898 A70-33834

F region integrated electron density response during solar eclipse of 7 March 1970, using Faraday rotation of linearly polarized signals from ATS 3

16 p2898 A70-33835

Gravity wave generation during solar eclipse confirmed by satellite observation on Faraday rotation angle of ionospheric VHF transmissions

16 p2898 A70-33836

Solar corona predicted and observed structure compared during eclipse of 7 March 1970

16 p2977 A70-33837

Solar UV flash spectrum by spectroheliographs flown aboard Aerobee 170 mission during total solar eclipse

16 p2977 A70-33838

Coronal observations from Aerobee 150 rocket after total solar eclipse of 7 March 1970 in Mexico, combining coronagraph flight record with ground photography

16 p2977 A70-33839

Ground based photographic experiments using portable equipment during 7 March 1970 solar eclipse in North Carolina

16 p2977 A70-33840

Outer corona during 7 March 1970 eclipse, discussing distance dominance of K corona

16 p2977 A70-33842

Photospheric magnetic fields by magnetograph during and one week before and after eclipse of 7 March 1970

16 p2977 A70-33844

Solar radio spectrum and history of McMath 607 plage region during eclipse of 7 March 1970, considering residual emission

16 p2977 A70-33845

- Radio observations of chromospheric brightness temperature distribution during solar eclipse of March 1970 16 p2977 A70-33846
- H alpha filtergrams of sun during solar eclipse of 7 March 1970, showing bright plage area 16 p2980 A70-34226
- Shooting star shower and solar eclipse frequencies correlation with long term climatic changes 17 p3168 A70-35310
- Solar corona structure on 22 September 1968 using radio astronomical and optical eclipse data 18 p3315 A70-36607
- Geometric relations for contact moments of solar eclipse, using crescent cord photographic measurements 18 p3315 A70-36610
- Ba II emission lines in solar chromosphere, examining excitation and ionization equilibrium and resonance line intensities by eclipse observations 18 p3317 A70-37010
- Solar eclipse of 7 March 1970 in Mexico, discussing characteristics, research program, equipment and photographs 18 p3318 A70-37046
- E layer electron concentrations, effective recombination coefficient and ionization sources during solar eclipse, noting soft X radiation intensity 19 p3408 A70-37310
- Color film /XRC/ application in Mexico during solar eclipse of 7 March 1970, showing little color and tone distortion 19 p3423 A70-37751
- Solar eclipse of 20 May 1966, analyzing radio observations 19 p3521 A70-38554
- Solar eclipse of 22 September 1968, analyzing radio observations 19 p3521 A70-38555
- Solar radio emission intensity distribution across disk during eclipse, constructing relative RF spectrum of uncovered region 19 p3522 A70-38556
- Solar UV radiation contributing to ionization in higher ionospheric layer over Dushanbe during partial solar eclipse of 20 May 1966 19 p3417 A70-38786
- Solar eclipses and ionosphere - NATO Conference, Lagonissi, Greece, May-June 1969 19 p3417 A70-38901
- Ionospheric effects in solar eclipse compared with full sun conditions at same elevation angle, emphasizing E, F and D regions ion and electron composition 19 p3418 A70-38902
- Solar eclipse effects on E and F layers, discussing photoionization rate, electron density and temperature, plasma diffusion, electric fields, etc 19 p3418 A70-38903
- Earth exospheric plasma distribution, relating solar eclipses effects to geophysical phenomenon 19 p3418 A70-38904
- Ozone concentration variations in upper atmosphere during solar eclipses 19 p3418 A70-38906
- Ionospheric rocket measurements during solar eclipse of 12 November 1966, observing electron and ion density decrease 19 p3418 A70-38907
- Solar spectral intensity distribution and ionizing radiation spatial emission patterns during eclipse, discussing effects on ionosphere 19 p3418 A70-38908
- Solar eclipse microwave spectral observations for coronal condensation sources characteristics of solar radio emission slowly varying component, discussing ionospheric recombination coefficients 19 p3531 A70-38910
- Solar eclipse measurements in 1-30 mm range, examining chromosphere, flares and radio emission 19 p3531 A70-38911
- D region electron density profiles during solar eclipse from X ray rocket and satellite observations 19 p3419 A70-38913
- D region electron densities during 20 May 1966 solar eclipse, using partial reflection and rockets 19 p3419 A70-38914
- Ionospheric electron content measurements during 20 May 1966 solar eclipse by Beacon S-66 satellite 19 p3419 A70-38915
- E and F region electron density response to incident radiation intensity on upper atmosphere during solar eclipses 19 p3419 A70-38916
- Annular solar eclipse of 20 May 1966 effects on ionosphere, discussing regions virtual heights, critical frequency variations, ion production rates, etc 19 p3419 A70-38917
- Ionospheric observations of solar eclipse of 20 May 1960, using panoramic probe 19 p3419 A70-38918
- Ionospheric ionization minimum delay and F region alpha variation during solar eclipse 19 p3419 A70-38919
- Vertical electron concentrations in upper F region during solar eclipses in South Atlantic from satellite observation 19 p3419 A70-38920
- Atmospheric ozone content during May 1966 solar eclipse, noting solar disk darkening effect on measurements 20 p3615 A70-39031
- Solar eclipse effects on equatorial F 2 layer by transient solutions of time dependent continuity equation, calculating electron concentrations 20 p3622 A70-39453
- Solar outer corona brightness distribution from rocket observation with scanning devices during solar eclipse, estimating error 20 p3710 A70-40089
- Solar X-ray corona during eclipse of 7 March 1970, using Aerobee rocket photographs 20 p3713 A70-40430
- Solar active region radio spectrum during 12 November 1966 eclipse, discussing flux, magnetic field effects, temperature and electron density 21 p3886 A70-40961
- Astronomical events observed in 1970 by amateur astronomers, discussing sun and moon eclipses and planets visibility 21 p3886 A70-41074
- Earthshine bright parts relationship to average brilliance of sun during total eclipse 21 p3893 A70-41445
- Solar eclipse calculation and prediction, discussing relationship between possible forms and earth-moon orbital configurations 21 p3924 A70-42173
- Solar radio to optical radius ratio calculated from residual flux measurements during 7 March 1970 solar eclipse 22 p4097 A70-42466
- Solar radio burst observation before 7 March 1970 solar eclipse, tabulating spectrum data 22 p4095 A70-43266
- Lower atmosphere gravity wave motions due to cooling by solar eclipse shadow 23 p4185 A70-43845
- IR observation of chromospheric Ca II K-line during total eclipse of 7 March 1970 24 p4401 A70-45314
- Solar limb photographic, isodensity and isophotal data for eclipse of 7 March 1970 from coronagraph observations, noting coronal green line and prominence activity 24 p4402 A70-45389
- Lower ionosphere radio reflection during solar eclipse of 22 September 1968 24 p4332 A70-46312
- LF signals phase determination during solar eclipse of 22 September 1968, noting frequency shift magnitude 24 p4316 A70-46313
- SOLAR ENERGY**
- Solar energy concentrator with truncated conical mirror and toroidal lens to illuminate cylindrical thermoelectric generators or radiation pumped lasers 01 p0010 A70-10760
- Optical measurements of mirrors reflectance and solar radiation transmittance to solve problems specific to solar energy engineering by standard optical equipment 01 p0010 A70-10765
- Stannic or cobalt oxide film coated glasses optical and energy characteristics determined for potential use in solar energy engineering 01 p0159 A70-10766
- Reflected solar energy measurements by ATS satellites applied to meteorological research, emphasizing high areal resolution and dynamic range of cameras 01 p0094 A70-11297
- Solar energy as spacecraft power source emphasized in operating life comparison with chemical, electrochemical and nuclear energy, discussing silicon solar cells 05 p0799 A70-17023
- Localized high energy flaring of active center monitored with time-associated radio bursts in spot umbrae 08 p1561 A70-20905
- Solar energy exchange with radiator surface recessed within specular axisymmetric cylindrical spinning cavity, using deterministic ray tracing scheme 11 p2150 A70-26353
- Solar, nuclear, chemical and thermal energy sources for short and long duration exploration on moon 14 p2634 A70-30195
- Solar energy direct conversion into electricity, surveying photoelectric, thermoelectric and thermoemissive methods 15 p2677 A70-31598
- Biological conversion of solar energy, discussing photosynthesis and nonphotosynthesis mechanisms 15 p2688 A70-31600
- Solar energy - Conference, Athens, September 1969 15 p2677 A70-32418
- Thermal EM field as function of coherent states, outlining quantum theory for thermal radiation and solar energy 15 p2678 A70-32423
- Passive sun trackers using solar energy activated bimetal helix thermal heliotrope 16 p2846 A70-34131
- Solar atmospheric hydrodynamic response to stationary random forces homogeneous over horizontal planes, discussing common energy argument, various models and photospheric oscillation 19 p3523 A70-38690
- Solar flare parameters, statistical relationships and energy estimates from optical characteristics 20 p3699 A70-39465
- Ratio between mechanical energy flux in nonmagnetic region and magnetic region associated with solar chromospheric mottles 20 p3712 A70-40414
- SOLAR ENERGY ABSORBERS**
- High temperature solar energy converter cavity absorbers geometry, considering absorption parameters of radiation reflected by concentrator 01 p0010 A70-10761
- Absorber positioning inaccuracy influence in concentrating solar unit mirror on unit energy parameters, discussing defocusing 01 p0010 A70-10763
- Solar energy absorbers and thermal storage devices for high temperature energy conversion to electric power by thermionic or thermoelectric method 01 p0010 A70-10764
- Orbital mission solar energy power conversion system, discussing heat transfer processes for storage feasibility 21 p3951 A70-41852
- SOLAR FACULAE**
- U FACULAE**
- SOLAR FLARES**
- Solar X ray flare regions size, structure and localization from Cosmos 166 and 230 heliograph observations 01 p0168 A70-10252
- Radioheliograph observations of position and motion of type 2 and 4 radio sources during flares based on proton model 01 p0168 A70-10256
- Meter wave type 3 solar radio waves associated with solar X ray flares, discussing sudden enhancements of LF field strength due to D layer ionization enhancement 01 p0168 A70-10257
- Sudden cosmic noise absorption /SCNA/ in polar cap during 7 July 1966 solar proton flare, estimating SCNA latitudinal distribution and protons magnetic cut-off boundary 01 p0172 A70-11527
- Hydrodynamic approximation to interplanetary gas motion influenced by solar flare caused perturbations 01 p0192 A70-11586
- Extreme UV spectral line intensity enhancement during class 3 flare related to abundance of radiating element 02 p0358 A70-12205
- Time lag of commencement of PCA effect behind occurrence of Y-shaped phase of solar flares, tabulating data for several flares and particle effects 02 p0358 A70-12373
- Chromospheric flares, loop prominences and filament activation and dissipation attributed to decelerated annihilation of prominence field in upper active region 03 p0557 A70-13218
- Corpuscular sources geoeffectiveness related to position on solar disk at maximum flare activity 03 p0569 A70-13359
- Flare rising from behind solar limb deoculated by simultaneous recording by OSO III X ray detector and photoheliograph 03 p0558 A70-13589
- Visible solar hemisphere circumstances for 28 January 1967 and ground level cosmic rays enhancement not preceded by intense H alpha flares 03 p0558 A70-13590
- Azur satellite launching project by NASA and Germany, describing orbit for investigating earth inner radiation belt, auroral zone and solar flares 03 p0580 A70-13797
- Pressure changes in troposphere and lower stratosphere after strong solar flares analyzed statistically for Northern Hemisphere 03 p0476 A70-13909
- Solar flare cosmic rays confinement to definite solar magnetic field sectors using Laplace transformation 03 p0560 A70-13977
- Magnetic fields neutral lines length as indicator of solar flare productivity 03 p0561 A70-14001
- Fe I line enhancement in flare of 7 August 1958 interpreted as selective excitation effect, discussing similarity to late type dwarf stars observations 04 p0739 A70-14598
- Long range solar flare forecasting noting correlation between planetary conjunctions and proton events [AAS PAPER 69-624] 04 p0740 A70-14658

Solar flare duration effect on propagation and modification of forward-reverse shock pair between sun and 1 AU, using equations of motion for spherically symmetric flow

04 p0740 A70-15104

Solar microwave and soft X ray radiation emission correlation to determine flare peak temperature and solid angle

04 p0741 A70-15126

Tropospheric periodic responses to chromospheric flares, analyzing stations atmospheric pressure power spectra

04 p0742 A70-15524

Solar radio emission intensity-solar flare index and 5303 A coronal line intensity-proton flare numbers relations

05 p0911 A70-16438

Flare radiation influence on high photospheric and low chromospheric lines in H alpha, H and K regions

05 p0902 A70-16439

MM wave outbursts of 1 and 2 November 1968, discussing wavelength dependence of flux density

05 p0912 A70-16441

Lyman alpha flux observed by satellite-borne ion chambers during solar flare of 20 March 1966

05 p0902 A70-16442

High energy solar flare data from neutron monitor stations supplemented by low energy data from interplanetary space probes Pioneer 6 and 7

05 p0902 A70-16443

Solar flare alpha to proton flux ratios on 23 May 1967 observed following interplanetary disturbances, suggesting electric fields as cause of modulations

05 p0902 A70-16444

Cosmic ray intensity preceding Forbush effects as function of chromospheric flares solar longitude and solar wind velocity

05 p0903 A70-16730

Solar cosmic ray flare /28 January 1967/ observed by neutron monitors, determining emission and particle spectrum at atmosphere boundary

05 p0903 A70-16752

Solar cosmic rays diffusion enclosure in interplanetary space magnetic boundary suggested from balloon, satellite and ground observations of solar flare neutron component

05 p0904 A70-16753

Flares and fast processes interrelation with active region stationary filaments, filament field magnetic envelope explosion stimulation of surges, plasma stream ascents, etc

05 p0904 A70-16910

Spectral characteristics of solar proton flare on 2 September 1966 noting light intensity variations

05 p0904 A70-16911

Extreme UV flashes of solar flare observed by sudden ionospheric frequency deviations compared with energetic X rays observations

05 p0905 A70-16981

Solar proton flare dose rates, discussing tissue-equivalent-ionization-chamber (TEIC) data usefulness in analyzing possible dose received by man behind shielding

06 p1134 A70-17265

Solar flare H alpha brightness measurement from photograph taken through birefringent filter, deriving flare morphological changes from isophotes

06 p1135 A70-18004

High energy neutrons searched for during solar flares by balloon flights, giving upper limits for gamma ray and neutron fluxes

06 p1136 A70-18008

Solar flare induced interplanetary shock and helium enriched driver gas observed on 13 February 1967, discussing wind velocity and plasma acceleration

06 p1152 A70-18526

X ray and H alpha emissions associated with solar proton flares, correlating rise time with solar cosmic rays

06 p1137 A70-18547

Kilston comet 1966b brightness correlated with solar flares occurrence

07 p1379 A70-19041

Solar flare protons motion in sun radial magnetic field, considering protons interaction with interplanetary field inhomogeneities

07 p1366 A70-19427

Solar proton flares radiometric measurement on-board Molniya 1 satellite, detecting intensities in outer regions of magnetosphere

07 p1366 A70-19428

Strong explosion model for analyzing shock wave propagation after chromospheric flare allowing for quasi-radial motion of unperturbed solar wind

07 p1367 A70-19489

H alpha brightening areas related to sunspot magnetic fields configuration and solar proton flares

07 p1369 A70-20072

Diurnal variations of cosmic ray neutrons following solar proton flares, proposing anisotropic diffusion model for phase and amplitude

07 p1372 A70-20342

Cosmic rays sudden intensity increases during proton flares of 28 January 1967 and 7 July and 2 September 1966, plotting proton density vs pressure

07 p1374 A70-20445

Particle properties and solar flare radiation hazards for passengers in supersonic flight

08 p1435 A70-20632

Localized high energy flaring of active center monitored with time-associated radio bursts in spot umbrae

08 p1561 A70-20905

Solar microwave bursts with double structure, discussing single frequency observations and flare patrols, time variations of flux density and brightness

08 p1561 A70-21259

Chromospheric flares, loop prominences and filament activation and dissipation attributed to decelerated annihilation of prominence field in upper active region

08 p1562 A70-21651

Solar flare cosmic ray rigidity spectrum determination based on ratio of relative enhancements, assuming isotropical arrival of particles at earth

09 p1744 A70-22489

Solar cosmic rays development, discussing corpuscular radiation of flare origin, radio noise, geomagnetic activity and intensity measurements

09 p1745 A70-23128

Solar x-ray flare of 17 August 1966, describing rocket-borne instruments and measurements

09 p1746 A70-23479

Heliocentric longitude intensity profiles of protons associated with solar flare of 5 February 1965, discussing data from Mariner 4 and IMP 2

09 p1746 A70-23480

Flare star burst energy from radio telescope observations compared with solar flares

10 p1936 A70-23916

Circular polarization time dependent reversals during simultaneous microwave solar bursts at different phases, considering relations to coincident flares

10 p1932 A70-24626

Solar flares period, core and physical nature of areas by measurements at millimeter wavelengths, discussing radio source center

10 p1934 A70-25277

Type 4 solar radio bursts compared with flare observations, geophysical effects and satellite monitors data to detect proton flares spectra

10 p1934 A70-25278

Solar flare videometer for measuring flare area and peak and integrated intensity in real time

11 p2104 A70-25744

Hard X-ray pulse identification with formation of brilliant kernel /11-12 September 1968/ flare by comparison with optical data

11 p2104 A70-25746

Optical and radio homologues of solar flares, studying correlation from astronomical telescope pictures

11 p2105 A70-25747

Onset, mass motion and flash phase in 2b solar flares observed in filtergrams spanning H alpha line

11 p2105 A70-25748

Oblique shock initiated by 7 July 1966 proton flare in solar wind observed by satellite magnetometers outside magnetosphere

11 p2105 A70-26562

Zeeman effect on solar flares metallic lines splitting

11 p2106 A70-26592

Statistical analysis of latitude distribution of magnetically classified sunspot groups and associated flares

11 p2106 A70-26646

Corpuscular sources geoeffectiveness related to position on solar disk at maximum flare activity

11 p2118 A70-26724

Solar flare relation to local magnetic field in active regions, discussing sunspot and weak field measures

12 p2297 A70-26986

VLF and ELF EM wave propagation in earth-ionosphere cavity during solar flares

12 p2183 A70-27189

Microwave solar bursts intensity and polarization measurements at 17 GHz, discussing chromospheric flares and X ray emission

12 p2293 A70-27592

Solar flares of 6 and 8 July 1968 correlation regarding electromagnetic radiation emission, radio flux, corpuscular radiation, etc

12 p2294 A70-27708

Emission asymmetry of solar limb flares, inferring luminescent layer contraction-expansion from spectral qualitative analysis

12 p2294 A70-27859

Solar flares responsible for Faraday rotation events observed in passage of Pioneer 6 radio signal through solar corona

12 p2295 A70-28023

Solar flare proton induced radioactivity in Apollo 11 lunar surface material compared with stony meteorite data, noting cobalt 56 concentration

13 p2489 A70-28910

Spectrograph design and specifications for solar radio flare structure, obtaining constant sum frequency by heterodyne conversion

13 p2406 A70-28948

Proton cosmic ray flare development and spatial structure, discussing magnetic field annihilation process for particle energy and photon ejection

13 p2476 A70-29046

Solar flares number decrease near central meridian noting no sunspot decrease

13 p2477 A70-29047

Visual aurora properties attributed to magnetic storm following solar flare, using multiple channel photometer measurements

13 p2478 A70-29231

Chromospheric flares electron concentration and structure from half widths and Balmer lines numbers

13 p2493 A70-29394

Geoactive ionizing radiation emitted by solar flares having metallic spectral lines of various brightness intensities

14 p2630 A70-30219

X ray and proton flux measurement during solar flare of 29 September 1968 by balloon-borne detectors

14 p2633 A70-31310

Solar proton flare of 2 September 1966, discussing Abastuman observatory photographic observations and radio noise emission changes

15 p2792 A70-31618

Report to COSPAR on Czechoslovakian space research /1969/ covering satellite telemetry and tracking, proton flares, aeronomy, etc

15 p2829 A70-31710

Solar flare particle flux equilibrium anisotropy and convection in solar wind

15 p2793 A70-31901

Intercoms 1 satellite for observing solar UV and X-ray emission in solar flares prediction

15 p2738 A70-32145

Proton Flare Project 1969, reporting synoptic observations of sun and solar terrestrial effects

15 p2794 A70-32291

Solar activity during Proton Flare Project Retrospective Interval 1969, discussing empirical flare forecasting methods

15 p2794 A70-32292

Solar radio burst satellite observation during Proton Flare Project, giving dynamic spectra

15 p2794 A70-32293

Sudden phase anomaly (SPA) in VLF radio wave propagation during Proton Flare Project, noting corresponding solar X-ray flux intensity enhancement

15 p2794 A70-32294

Solar Proton Flare Project 1969, summarizing observations and solar activity-terrestrial event correlation for June retrospective interval

15 p2794 A70-32296

Type 2 and 4 solar radio emission, showing bursts excitation by common shock wave ejected from flare region

15 p2794 A70-32620

Low energy electron emission during solar flares relation to radio and X ray emission

15 p2795 A70-32622

Strong explosion model for analyzing shock wave propagation after chromospheric flare allowing for quasi-radial motion of unperturbed solar wind

15 p2795 A70-32734

Iron line emission at 1.9 A during solar flares observed by OSO-4 proportional counter spectrometer

17 p3150 A70-34836

Solar UV spectrum variations due to flares and solar activity diurnal variations from satellite spectrometry

17 p3161 A70-34894

Solar flare radiation protection requirements, considering bulk and plasma radiation shielding

17 p3040 A70-35647

Slow and fast coronal expansion phenomena associated with solar flares

17 p3152 A70-35869

Proton flares showing enhancement of ionospheric absorption and complex magnetic disturbances

18 p3306 A70-36087

Periodic cosmic ray variations near Southern magnetic pole related to chromospheric flares

18 p3307 A70-36102

Solar flare protons motion in sun radial magnetic field, considering protons interaction with interplanetary field inhomogeneities

18 p3309 A70-36901

Solar proton flares radiometric measurement on-board Molniya 1 satellite, detecting intensities in outer regions of magnetosphere

18 p3309 A70-36902

Solar flares associated interplanetary and terrestrial phenomena by satellite, space probe and rocket observation, investigating solar wind disturbances, geomagnetic storms, ionospheric effects, etc

19 p3493 A70-37472

Flare associated high energy photon and particle fluxes characterized by short rise times and longer lasting decays, discussing plasma emissions

19 p3493 A70-37473

Solar cosmic rays satellite observation, considering flare associated, recurrent and storm particle events and active center associated energetic particles

19 p3493 A70-37474

Solar particle events forecasting based on classification scheme, discussing proton active regions

19 p3493 A70-37476

- Solar flare of 25 February 1969 ground observations comparison to satellite data, measuring magnetic fields, radio emission, sunspots, ionospheric effects, etc 19 p3513 A70-37497
- Solar flare of 25 February 1969 at soft X ray frequencies by ESRO 2 satellite observation 19 p3495 A70-37499
- Interplanetary magnetic field during solar particle event of 25 February 1969 from Heos 1 measurements 19 p3495 A70-37500
- Solar wind discontinuity during solar flare from Heos A measurements, observing shock wave propagation 19 p3495 A70-37502
- Proton spectra and time history in interplanetary space during solar flare by satellite observation, investigating particle flux by shock waves 19 p3495 A70-37503
- Solar protons directional and omnidirectional measurements during particle event of 25 February 1969 by Heos 1 spacecraft, indicating particle diffusion in interplanetary space 19 p3496 A70-37506
- Cosmic ray electron and low energy proton fluxes by satellite-borne detector during solar flare of 25 February 1969 19 p3496 A70-37507
- Solar protons distributions in 1-30 MeV range over northern polar cap during 25 February 1969 solar event by ESRO 1 satellite 19 p3496 A70-37508
- Protons and alpha particles energy spectra during 25 February 1969 solar event from Centaur rocket measurements 19 p3496 A70-37509
- Protons and alpha particles energy spectra following solar flares of 24-25 February 1969 from rocket measurements, estimating proton mean free path 19 p3496 A70-37510
- Electron density measurements by rocket observation during PCA after solar flare of 25 February 1969, deriving effective loss rates in terms of recombination model 19 p3496 A70-37511
- D region positive ion density during solar proton event by Arcas rocket-borne cylindrical electrostatic probe 19 p3411 A70-37512
- Magnetospheric thermal plasma electron density measurement during solar flare byOGO-5 satellite 19 p3411 A70-37513
- Interplanetary shock wave of 26 February 1969, discussing association with solar flares 19 p3513 A70-37517
- Low energy solar protons observation by Esro 1 satellite during solar flare of 25 February 1969 19 p3497 A70-37520
- Syrovtaskii mechanism of high energy particle production near neutral line of magnetic field, noting solar flares occurrence conditions 19 p3478 A70-37581
- Solar flare of 30 October 1968, describing sunspot development 19 p3497 A70-37973
- Solar wind and flare energetic particles properties and interactions, surveying interplanetary magnetic field, planetary bow shock waves, neutrons, neutrinos, etc 19 p3511 A70-38418
- Solar eclipse measurements in 1-30 nm range, examining chromosphere, flares and radio emission 19 p3531 A70-38911
- Solar X ray emission during flares from ionospheric absorption measurements, discussing continuous ionograms method 19 p3512 A70-38912
- Dwarf Me stars flare spectra, examining hydrogen recombination layer and impulse heating of photosphere 20 p3702 A70-39013
- Stratospheric cosmic ray intensity increases unassociated with chromospheric flares 20 p3696 A70-39278
- Solar cosmic rays emission spectrum for 23 February 1956 flare, taking into account nucleon diffusion coefficient dependence on particle rigidity and distance to sun 20 p3697 A70-39287
- Explosive phase of solar flares in nonuniform atmosphere, determining explosion energy and shock wave front shape for various times 20 p3699 A70-39463
- Solar flare parameters, statistical relationships and energy estimates from optical characteristics 20 p3699 A70-39465
- Solar flares catalog with patrol time given on graphs, tabulating principal characteristics 20 p3700 A70-39467
- Solar proton intensity measurement during flare by satellite Proton 3 apparatus 20 p3700 A70-39729
- Solar soft X ray flare spectra of 16 November 1967, examining electron temperatures and emission lines by OSO-4 20 p3700 A70-40419
- Helium-like resonance, intercombination and forbidden transitions of Ca, Si and S lines during 3b solar flare decay 20 p3700 A70-40420
- Correlated microwave bursts between adjacent active regions associated with solar flares 20 p3700 A70-40421
- Umbra flash as magnetoacoustic wave, examining Ca II K line variations formation during adiabatic compression 21 p3885 A70-40958
- Solar flaring on 25 April 1968, examining radio H alpha and X ray emission, magnetic field configuration and temperatures 21 p3879 A70-40959
- Solar flare relation to radio emission at 3.3 mm, discussing sunspots, temperature gradients and magnetic fields 21 p3879 A70-40962
- H alpha flares occurrence in plages with little or no spots 21 p3880 A70-40964
- Soft X-ray enhancement during solar flares due to coronal condensation temperature increase 21 p3880 A70-40969
- Particle acceleration phase in solar flare development, discussing H alpha maximum, hard X ray burst and bremsstrahlung 21 p3880 A70-40971
- Large scale flare associated solar wind disturbances observed by Vela satellites, noting prolonged elevated flow speed after shock 21 p3881 A70-41080
- Nuclear particle tracks in Apollo 11 samples due to galactic cosmic rays and solar flares relationship to dynamic surface processes 21 p3914 A70-41648
- Fe-group cosmic ray exposure tracks in Apollo 11 lunar rock interior, erosion rate and solar flare paleontology 21 p3917 A70-41673
- Shock waves formation and dynamic characteristics in transition region response to infalling material from solar flares 21 p3883 A70-42193
- Temporal sequence correlation between surges and associated flares during solar cycle 22 p4095 A70-43265
- Solar atmosphere three dimensional microstructure observation, considering hypothesis linking flares to magnetic field 22 p4107 A70-43450
- Solar flare effects in ionosphere observed at Lindau, collating with heavy geomagnetic storm 23 p4237 A70-44876
- Solar neutron flux density relation to solar flare of 28 September 1968, using high altitude balloon-borne neutron detector 23 p4238 A70-44925
- Solar flares X ray emission polarization measured by Thomson scattering instrument on Intercosmos-1 satellite 24 p4396 A70-45321
- H alpha solar spray-like prominence ejected in association with bright limb flare, determining knots trajectories and velocities from coronagraph observations 24 p4396 A70-45323
- Solar flare microwave spectra from coherent plasma emission mechanism 24 p4396 A70-45390
- Class 1b solar flare X ray examination, using rocket-borne liquid N cooled solid state detector 24 p4397 A70-45767
- Solar X-ray flare temperature and emission measure profiles usingOGO 5 satellite detector, interpreting energy dispersion of peak times 24 p4397 A70-45768
- Geoactive ionizing radiation emitted by solar flares having metallic spectral lines of various brightness intensities 24 p4398 A70-46294
- SOLAR FLUX**
- Simultaneous filtergrams of velocity and intensity field of central solar disk obtained in blue and red wings of Fraunhofer line 01 p0175 A70-10242
- Stellar X ray sources quanta fluxes estimation based on solar coronal emissions analysis 02 p0360 A70-12793
- Surface roughness effects on radiant heat transfer rate of isolated plane surface with uniform temperature illuminated by collimated solar flux 06 p1172 A70-17178
- Solar radiation flux observation-prediction discrepancies due to Fraunhofer line absorption, studying Balmer continuum as atmospheric model criterion 06 p1148 A70-18451
- Atmospheric ozone content and mass effect on solar radiation flux measured during total solar eclipse of 22 September 1968 07 p1275 A70-20310
- Electric field sense and magnitude determination from lunar particle shadows in solar electron fluxes 13 p2492 A70-29196
- Precision radiometry of electromagnetic energy transfer in atmospheric and space physics emphasizing solar and terrestrial radiative fluxes measurements 13 p2409 A70-29652
- Daily amplitude variability of equatorial electrojet current related to solar extreme ultraviolet radiation /XUV/ influx 15 p2727 A70-31873
- Radiatively interacting adjoin plates in presence of collimated solar flux, considering surface roughness effects on equilibrium temperature distribution [AIAA PAPER 70-817] 16 p3002 A70-33946
- Non-LTE effects on flux and center to limb variation of solar spectrum at 1500-1680 A 17 p3169 A70-35384
- Solar chromosphere model evaluation using sensitivity of flux emission in Lyman continuum 17 p3170 A70-35386
- Solar proton events classification system based on solar flux logarithm 19 p3493 A70-37477
- Solar equatorial limb brightening at quiet sun from solar disk scanning statistical analysis 20 p3712 A70-40418
- Solar radio to optical radius ratio calculated from residual flux measurements during 7 March 1970 solar eclipse 22 p4097 A70-42466
- Phase delay between thermospheric neutral temperature and neutral density, considering frequency dependent time response to solar heat input 23 p4187 A70-43858
- SOLAR FLUX DENSITY**
- NT SOLAR CONSTANT
- Absolute calibration method for daily solar flux density discrepancies measurements at UHF, describing equipment and error analysis 01 p0168 A70-10259
- Nimbus 3 satellite observations of near UV solar flux intensity and variability, describing instrumentation and measurement of radiation producing molecular oxygen photodissociation 02 p0291 A70-12295
- Lyman alpha flux observed by satellite-borne ion chambers during solar flare of 20 March 1966 05 p0902 A70-16442
- Solar radio observations tabulated for radioelectric flux density and behavior for three hour periods, average diurnal results, etc 10 p1940 A70-24414
- Sunspot minimum intensity dependence on area, including correction for blurring or image motion, scattered light and line absorption 13 p2496 A70-29846
- IR balloon observations of absolute solar brightness and stratosphere transparency, discussing BCA and HSRA models 17 p3078 A70-35580
- Solar radio U burst second branch low relative intensity, contradicting previous theory for trajectories 21 p3880 A70-40966
- Near earth solar UV flux measurement by Spades satellite, discussing nonrandom variations and Ca plage regions 21 p3881 A70-41078
- Solar spectral irradiance measurements at different altitudes, using multichannel radiometers 22 p4013 A70-42599
- SOLAR FURNACES**
- High temperature solid-solid reactions and solid-liquid or condensed phase-gas equilibria, using solar furnace 14 p2545 A70-30907
- Solar furnaces in space for treatment of high purity products in space vacuum, discussing design and operational problems 15 p2717 A70-31802
- Temperature measurement of products in solar furnace by IR pyrometers, considering interference filters, reflections parasitic effects, etc 15 p2740 A70-32424
- Parabolic solar furnace for chemical manufacture of impurity sensitive materials in orbiting spacecraft 21 p3804 A70-41001
- High temperature solar furnace for investigating heat resistant protective coatings thermal stability 24 p4350 A70-46331
- SOLAR GENERATORS**
- NT SOLAR CELLS
- GaAs and Si photocell batteries powered by solar radiation, investigating temperature dependence of efficiency I-V characteristics and optimal power 01 p0007 A70-10177
- Soviet papers on semiconductor solar energy converters covering design and tests for thermoelectric, thermionic and photoelectric units, properties, materials, etc 01 p0008 A70-10750
- Semiconductor solar thermoelectric generator allowing thermoelement replacement during service including construction, bridging methods and characteristics 01 p0009 A70-10751

Current-voltage characteristics of cascaded solar thermoelectric generator, determining optimum hot junction temperature as function of radiation concentration

01 p0009 A70-10752

Cascaded thermoelements with high figure of merit for increasing solar thermoelectric generator efficiency, noting high temperature materials effect

01 p0158 A70-10754

Solar energy absorbers and thermal storage devices for high temperature energy conversion to electric power by thermionic or thermoelectric method

01 p0010 A70-10764

Selective glass coatings applications in solar thermoelectric generators working without radiation concentrators

01 p0011 A70-10767

Solar photoelectric power ion propelled probe of asteroid region, describing design and mission planning

[AIAA PAPER 69-1105] 02 p0382 A70-12529

Electric propulsion technology status for auxiliary and solar electric prime propulsion applications

[AIAA PAPER 69-1107] 02 p0356 A70-12530

Solar powered electric propulsion systems for automated missions throughout solar system by extending range of Atlas Centaur-Titan 3-C launch vehicles

[AIAA PAPER 68-1120] 04 p0736 A70-15401

Photoelectric composite multicell solar generator, deriving empirical equation for external I-V characteristic

07 p1196 A70-19623

Solar energy converter with shutter, determining light pulse power from solar light intensity and exposure time

07 p1196 A70-19624

Protective coatings for silicon photosensitive elements to reflect incident energy at wavelengths not participating in conversion into electricity

15 p2677 A70-31599

Solar thermoelectric generator /STEG/ with two stage converter, discussing weight factors and efficiency

15 p2678 A70-32425

Solar electric spacecraft for interplanetary missions including asteroid belt survey, Jupiter flyby and out-of-elliptic survey

[AIAA PAPER 70-645] 16 p2981 A70-33531

High voltage solar arrays for ion engines, discussing spacecraft propulsion, electric generation, insulation integrity, cell degradation and current leakage

[AIAA PAPER 70-1138] 20 p3567 A70-40211

Orbital mission solar energy power conversion system, discussing heat transfer processes for storage feasibility

21 p3951 A70-41852

Semiconductor solar energy converter, deriving conditions for occurrence of photoconductivity quenching

24 p4391 A70-46325

SOLAR GRAVITATION

Jupiter capture of comets with parabolic orbits taking into account solar gravitational influence

05 p0905 A70-15757

Solar oblateness and gravitational quadrupole moment related under assumption of magnetic and velocity fields absence in surface layers, including rotation effects

08 p1570 A70-20902

General relativity equations of gravitation consistent with empirical data, discussing curvature tensor, scalar gravitational waves and solar mass difference

08 p1577 A70-21419

Solar attraction effects on zero-mass body planar motion near triangular earth-moon libration points, obtaining variational equations of motion

09 p1754 A70-22477

Satellite motion in lunar orbit by von Zeipel method, considering perturbations due to nonspherical lunar gravity field and earth and solar attraction

10 p1939 A70-24186

Einstein theory applied to sample modeling of planetary orbits and light beams touching sun in solar gravitational field

10 p1939 A70-24268

Solar charge effects on Mercury perihelion motion, relativistic light deflection and gravitational red shift, using Reissner-Nordstrom solution

11 p2107 A70-25395

Space probe trajectory near second order integration under influence of solar oblateness and gravitation

14 p2635 A70-30288

Radio source 3C279 position during October 1969 occultation by sun, determining SHF deflection in solar gravitational field

16 p2972 A70-33049

Solar potassium resonance line shape and gravitational red shift, using atomic beam technique

17 p3173 A70-35861

Einstein theory applied to sample modeling of planetary orbits and light beams touching sun in solar gravitational field

19 p3520 A70-38393

Solar envelope unstable gravitational mode model, considering spherical harmonics by numerical integration and asymptotic representation

19 p3523 A70-38688

Planetary orbiter parameters long term variations under central body oblateness, solar and atmospheric drag perturbations

[AIAA PAPER 70-1055] 19 p3528 A70-38870

Space-time Riemann metric for scalar-tensor gravitational theories with arbitrary omega parameter

22 p4104 A70-42991

Solar rotation, discussing oblateness, solar wind torque, main sequence stars rotating core, gravitational quadrupole moments and Li and Be depletion

23 p4252 A70-44829

SOLAR HEAT FLOW

U HEAT FLUX

U SOLAR FLUX

SOLAR HEATING

Projector with paraboloid mirror solar radiation condensing lens for studying heat resistant materials mechanical properties at high temperatures

01 p0055 A70-10179

Nonlinear flow conductance and convective terms effects on planetary thermospheres heating diurnal variations, emphasizing solar EUV heating

01 p0178 A70-10413

Solar corona heating by shock waves, considering chromosphere and solar wind physical properties, heat flow channeling, etc

02 p0361 A70-11750

Spacecraft components temperature response predicted in nonstandard solar orientation

04 p0786 A70-15432

Solar heating determination by using transmission factors derived for atmospheric constituents together with spectral irradiance curves outside atmosphere

08 p1573 A70-21032

Solar corona heating, discussing theories of Schwarzschild, Schatzman, Alfvén, Osterbrock, Uchida, Whitaker and Kuperus

09 p1757 A70-22686

Solar radiation heated boilers efficiency and operational temperature range improved by application of coatings, noting surface absorption properties

11 p2148 A70-25930

Criticism of hypothesis regarding solar flash heating mechanism creating glaze within lunar craterlets at Apollo 11 landing site

13 p2489 A70-28912

Optimum overlap design of thin walled tubular extendible spacecraft structures under solar heating in zero-g environment

14 p2657 A70-30762

Total solar radiation calculation for inclined and horizontal surfaces, noting application to solar heating

15 p2774 A70-31803

Heat stress levels in cockpit of AH-1G Hueycobra helicopter parked in sunlight with closed canopy, using sweating copper mannikin

15 p2689 A70-31881

Thin walled spherical shell spacecraft solar heating in planetary surface proximity, considering skin temperature distribution

21 p3944 A70-41019

Temperature distribution in rotating thin cylindrical shell with line conduction discontinuity under solar heating, evaluating tubular elements thermal bending on spinning spacecraft

21 p3951 A70-41875

Transient heating by solar radiation of semitransparent solid medium and adjoining fluid, establishing criteria for maximum fluid temperature

22 p4123 A70-42598

Thermospheric heating by solar radiation in Schumann-Runge continuum, taking height and atmospheric components distribution into account

23 p4188 A70-44060

Chromospheric heating in magnetic field above supergranular cell boundaries, using geometric optics method for energy transport by hydromagnetic shock waves

24 p4400 A70-45304

Uranus and Neptune millimeter wave observations, showing brightness temperatures in excess of black body equilibrium temperatures derived from solar heating

24 p4403 A70-45398

Al alloy sheets with multicolor protective coatings, measuring surface temperature under solar radiation

24 p4428 A70-45434

SOLAR INSTRUMENTS

NT SPECTROHELIOGRAPHS

Solar magnetograph modified to simplify calibration, using polarimeter with special exit slit geometry

11 p2057 A70-26650

OSO 1-6 spacecraft design, payloads and performance for continuous solar observation, discussing instrumentation and Delta launch vehicle characteristics

14 p2638 A70-30691

Photometric calibration changes in EUV solar satellite instruments during orbital operation

15 p2373 A70-32045

Solar spar telescope of Lockheed Solar Observatory with closed tube protection from dust and wind

16 p2911 A70-33794

SOLAR LIMB

Triatomic hydrogen ion role in solar photosphere opacity implied from limb darkening and specific intensity data

11 p2104 A70-25739

Solar limb brightening of XUV lines of carbon, nitrogen, oxygen and silicon ions in chromospheric-coronal transition region

11 p2108 A70-25740

Emission asymmetry of solar limb flares, inferring luminescent layer contraction-expansion from spectral qualitative analysis

12 p2294 A70-27859

Solar limb integrated brightness distribution in continuous spectrum during 20 May 1966 solar eclipse

13 p2498 A70-30003

Solar stray light, determining spread function, limb profile and aureole at various wavelengths

15 p2795 A70-32625

Polar and equatorial limb darkening related to solar rotation and thermal flow, using photospheric models

15 p2807 A70-32812

Solar limb image vibrations, establishing quantitative comparisons between statistical characteristics of fluctuations and weather conditions on propagation path

16 p2979 A70-34179

Solar limb intensity distribution in Lyman alpha line, computing LTE departures

17 p3162 A70-34895

Non-LTE effects on flux and center to limb variation of solar spectrum at 1500-1680 Å

17 p3169 A70-35384

Fe II line behavior in plages near solar limb

17 p3174 A70-35866

Hour-angle and declination center-to-limb profiles of quiet sun 3.3mm brightness temperature distribution

17 p3174 A70-35868

Antenna systems with minimum angular resolving power for solar limb radio sources recording, using data from solar meridian passage

19 p3522 A70-38563

Solar equatorial limb brightening at quiet sun from solar disk scanning statistical analysis

20 p3712 A70-40418

Quantitative measurement of solar limb image motion and blurring, noting role of telescope aperture

20 p3634 A70-40424

Sunspot intensity profiles near solar limb, observing center side penumbra photosphere border

21 p3885 A70-40957

Solar equatorial limb brightening of far UV resonance lines of lithium-like N V, O VI, Ne VIII, Mg X and Si XIII ions, interpreting oso-4 data with coronal model

21 p3924 A70-42185

Solar far UV limb brightening of C III, N III, N IV, O III, O IV and Si IV lines in chromospheric-corona transition region, correcting coronal model for spicule effects

21 p3925 A70-42186

Instrumental and atmospheric observational problems regarding dark mottles, fibrils and H alpha solar limb photographic interpretations

21 p3926 A70-42199

Continuum polarization at solar limb at various wavelengths, using source functions

23 p4246 A70-44754

Solar limb emission spectrum between 300-2803 Å, using Skylark rocket instrumentation

24 p4399 A70-45301

Solar center-limb observations of line brightness and Doppler shift fluctuations for Mg b lines

24 p4399 A70-45302

Solar limb photographic, isodensity and isophotal data for eclipse of 7 March 1970 from coronagraph observations, noting coronal green line and prominence activity

24 p4402 A70-45389

SOLAR MAGNETIC FIELD

Solar structural periodicities in quiescent prominences and filaments, considering plasma instability and supporting magnetic field characteristics

01 p0176 A70-10248

Solar corona magnetic field determination from photospheric magnetic field line-of-sight component observations, describing various mathematical methods

01 p0176 A70-10250

Coronal electron densities and magnetic fields determined from K-coronameter and type 4 radio burst data

01 p0168 A70-10255

Solar magnetic field investigated with parallel beam from coelostat mounting falling on magnetograph slit of solar telescope, noting field polarity change periodicity

01 p0177 A70-10347

Penumbra forms and magnetic polarity distribution relationship in sunspot groups

01 p0184 A70-10955

- Solar mean magnetic field relation to sector structure of interplanetary magnetic field, discussing Explorer 33 and 35 observations 02 p0371 A70-12206
- Radiative energy transport in sunspot region via model computations, obtaining reduced subphotospheric flux estimates for given magnetic field 02 p0372 A70-12254
- Joule dissipation model for sunspot magnetic field, discussing field fine structure and lifetime 02 p0373 A70-12374
- Magnetic structure of type 4 solar outburst from continuous record of 80 MHz image and polarization 03 p0558 A70-13587
- Solar flare cosmic rays confinement to definite solar magnetic field sectors using Laplace transformation 03 p0560 A70-13977
- Magnetic fields neutral lines length as indicator of solar flare productivity 03 p0561 A70-14001
- Solar atmospheric structure near sunspots by spectrophotometry, presenting observational and theoretical sunspot magnetic and velocity field data 04 p0754 A70-15351
- Magnetic vector directions over sunspot near central meridian passage measured, showing axisymmetric arrangement 04 p0758 A70-15697
- Solar magnetic discontinuity fluxes analyzed by studying 27-day cosmic ray and geomagnetic activity variations using linear filtration method 05 p0900 A70-15969
- Mass loss role in early despinning of sun without magnetic field braking effect, considering present surface vs core rotating velocity 05 p0913 A70-16569
- Flares and fast processes interrelation with active region stationary filaments, filament field magnetic envelope explosion stimulation of surges, plasma stream ascents, etc 05 p0904 A70-16910
- Granular and intergranular region solar magnetic field difference detection attempt from line profiles, noting equivalent width increase in ionized Cr line 06 p1142 A70-17989
- Photospheric magnetic flux quantization away from sunspots, studying nonsunspot field strength distribution 06 p1142 A70-17992
- Magnetic and velocity fields in unipolar sunspot, discussing fluctuations associated with penumbral and umbral fine structures 06 p1144 A70-18002
- Solar magnetic field spectroheliographic mapping, discussing detection levels, resolution, applications, etc 06 p1148 A70-18454
- Sunspot magnetic field structure, determining vector field from longitudinal component perspective effect observations 06 p1149 A70-18457
- Electromagnetic acceleration and energy losses of charged chromospheric-coronal plasma electrons and protons in unsteady magnetic fields of sunspots 07 p1384 A70-19417
- Solar flare protons motion in sun radial magnetic field, considering protons interaction with interplanetary field inhomogeneities 07 p1366 A70-19427
- H alpha brightening areas related to sunspot magnetic fields configuration and solar proton flares 07 p1369 A70-20072
- Sunspot group of July 1966, studying umbrae structures relation to magnetic field 08 p1569 A70-20835
- Solar magnetic field strength determination from various absorption lines, considering Rowland intensity, line lower level excitation potential, optical depth, etc 08 p1569 A70-20836
- Faculae and flocculi intensity relationship to orientation of magnetic fields in solar photosphere and magnetosphere 08 p1560 A70-20837
- Longitudinal magnetic field measurement along H alpha line of solar prominence 08 p1560 A70-20838
- Darkening and brightening of disturbed spot on sun surface determined by abnormal stress in seen layers due to magnetic and velocity fields 08 p1570 A70-20903
- Sunspots photospheric layers magnetic field structure, analyzing anomalous Zeeman pi-components in umbra 09 p1757 A70-22685
- Magnetic field and gas thermal conductivity effects in analysis of solar wind as one dimensional, steady and spherically symmetric flow 09 p1745 A70-22687
- Penumbral magnetic field strength on basis of photoelectric spectra of undisturbed photosphere 09 p1757 A70-22730
- Magnetic fields model for quiescent solar prominences with helical structure 09 p1757 A70-22734
- Solar magnetic field measurement emphasizing circular and total polarization characteristics 10 p1939 A70-24275
- Comets ionized shells, studying plasma expansion in corpuscular solar wind magnetic field 10 p1940 A70-24372
- Solar corona magnetic field estimated from type II bursts correlated with photospheric, chromospheric and geophysical phenomenon 10 p1934 A70-25275
- Solar magnetograph modified to simplify calibration, using polarimeter with special exit slit geometry 11 p2057 A70-26650
- Solar flare relation to local magnetic field in active regions, discussing sunspot and weak field measures 12 p2297 A70-26986
- Solar radio types I and III sources spatial distribution of circular polarization and coronal magnetic field configurations in active regions 12 p2294 A70-27710
- Proton cosmic ray flare development and spatial structure, discussing magnetic field annihilation process for particle energy and photon ejection 13 p2476 A70-29046
- Statistical heliographic latitude dependence of dominant polarity of interplanetary magnetic field, using photospheric synoptic chart 13 p2492 A70-29195
- Magnetic field spatial structure in sunspot with photospheric bridge, using photographic observations of solar spectrum lines 13 p2493 A70-29391
- Toroidal solar field emergence to surface forming magnetic field of active region 13 p2493 A70-29392
- Solar magnetic and brightness fields simultaneous measurement by multiimage spectroheliograph 13 p2496 A70-29844
- Photosphere model and magnetic field gradient effects on line contours and magnetographic calibration curves, using nonlinear source function 13 p2496 A70-29845
- Sunspot electric current density accounting for magnetic field abrupt reversal 13 p2496 A70-29848
- Galactic, stellar and solar magnet fields origin, considering fluid motions role 14 p2641 A70-30876
- Sunspot electric current evaluation from analyzing transverse component of magnetic field, discussing difficulties and errors in data reduction 15 p2804 A70-32615
- Line formation in solar magnetic fields with allowance for absorption emission and scattering processes, discussing Hanle effect and atomic level polarization 15 p2804 A70-32617
- Photospheric magnetic fields by magnetograph during and one week before and after eclipse of 7 March 1970 16 p2977 A70-33844
- Magnetic flux measurements in quiescent solar filaments and adjacent photosphere using magnetograph observations 17 p3157 A70-34837
- Chromospheric photoelectric magnetograms with high resolution H alpha pictures for deriving magnetic field directly from filtergrams 17 p3096 A70-35864
- Coronal magnetic bottle at ten solar radii from Faraday rotation measurements of occulted spacecraft radio source 17 p3174 A70-35871
- Solar flare protons motion in sun radial magnetic field, considering protons interaction with interplanetary field inhomogeneities 18 p3309 A70-36901
- Sunspot spectrograms analysis, observing wavelength shift in Zeeman triplet circular components and magnetic splitting inequality under different circular polarizations 18 p3322 A70-37136
- Magnetic field variations and structures in interplanetary space relationship to sun, discussing photospheric field lines random walk transport 19 p3494 A70-37480
- Solar magnetic field origin and behavior, discussing hydromagnetic dynamos, cyclonic convection and generation times 20 p3706 A70-39927
- Sun photographs with violet interference filter, determining photospheric magnetic fields position by cospatial network 20 p3634 A70-40410
- Photospheric pore magnetic field model, investigating pore-sunspot distinctions 20 p3711 A70-40411
- Photoelectric polarimetry of dark unipolar type H sunspot in terms of value and direction of magnetic field vector 20 p3712 A70-40413
- Ratio between mechanical energy flux in nonmagnetic region and magnetic region associated with solar chromospheric mottles 20 p3712 A70-40414
- Solar corona current free magnetic field distribution relationship to plasma density structure 20 p3712 A70-40415
- Coronal streamers structure and evolution from photographic and K-coronameter data, indicating photospheric bipolar magnetic regions as origin 20 p3712 A70-40416
- Photospheric magnetic field differential rotation using synoptic charts for autocorrelation technique 21 p3885 A70-40951
- Solar photosphere vertical velocities and horizontal wave propagation, discussing magnetic fields, phase coherence and behavior and oscillations 21 p3885 A70-40952
- Solar flaring on 25 April 1968, examining radio H alpha and X ray emission, magnetic field configuration and temperatures 21 p3879 A70-40959
- Solar flare relation to radio emission at 3.3 mm, discussing sunspots, temperature gradients and magnetic fields 21 p3879 A70-40962
- Dynamic spectra and two dimensional radioheliograph maps of solar U bursts at 80 MHz consistent with electron streams along loops in coronal magnetic field 21 p3891 A70-41183
- Soft solar X rays cyclic variation from satellite observation, noting relation to sunspot group magnetic field complexity 22 p4096 A70-43301
- Solar atmosphere three dimensional microstructure observation, considering hypothesis linking flares to magnetic field 22 p4107 A70-43450
- Solar activity research, discussing optical facilities, photoelectric magnetographs, magnetic field measurement, solar cycles and flares, etc 23 p4256 A70-45034
- Chromospheric heating in magnetic field above supergranular cell boundaries, using geometric optics method for energy transport by hydromagnetic shock waves 24 p4400 A70-45304
- SOLAR NEBULA**
U SOLAR CORONA
SOLAR NOISE
U SOLAR RADIO EMISSION
SOLAR OBSERVATORIES
NT OSO
NT OSO-B
NT OSO-I
- Sunspot motion statistics for 1965-1967 from observatory data, complementing electron-corona differential rotation and spectroscopic measurements 03 p0571 A70-13597
- High altitude observatory solar magnetograph installation modifications including computer control, improved Zeeman effect observation instrument, etc 04 p0691 A70-15037
- Sacramento Peak Observatory vacuum tower solar telescope and auxiliary instrumentation, providing flexibility in data collection and system adjustment by computer control 04 p0663 A70-15273
- Solar observatory at San Fernando Valley, describing evacuated aperture reflecting telescope function and design, data recording cameras, etc 09 p1688 A70-23772
- Big Bear Solar Observatory, discussing site selection, observatory construction and telescope optical system 12 p2205 A70-26864
- Heliostationary spacecraft for solar observation near libration point between sun and earth, discussing attitude stabilization by solar pressure 17 p3178 A70-35254
- Optical solar observatory for investigation of solar activity and impact on earth environment, discussing site selection and equipment 22 p4005 A70-42349
- Solar optical and radio activity observation in 1968, noting optical-radio data correlation 22 p4095 A70-43259
- SOLAR ORBITS**
NT PERIHELIONS
- Solar motion effects on planetary orbits, discussing preferred coordinate systems of scalar theory of gravitation 01 p0186 A70-11104
- Solar system various natural members examination for suitability to relativistic pericentron motion investigation 02 p0373 A70-12255
- Artificial satellites in short period highly eccentric solar orbits of arbitrary inclination for solar gravitational quadrupole moment measurement to test general relativity 06 p1139 A70-17552
- Heliocentric low thrust spacecraft trajectory analysis using two-variable asymptotic expansion method [AIAA PAPER 70-214] 06 p1145 A70-18064
- Asteroid families and jet streams, searching for regularities and resonances in mean family elements 06 p1151 A70-18491

- Planetary satellites perturbation by sun for elliptical solar orbit, applying Zeipel method to equations of motion 09 p1754 A70-23480
- Solar system planetary mean motions calculation from characteristic equations roots at equilibrium points of restricted three body problem, using Taylor series solution 09 p1760 A70-23915
- Solar corpuscular streams effect on meteoric particles behavior in circular orbit around sun, determining lifetime on basis of mass loss due to pulverization 09 p1763 A70-23382
- Einstein theory applied to sample modeling of planetary orbits and light beams touching sun in solar gravitational field 10 p1939 A70-24268
- Small natural vibrations effect of solar sail-propelled system on heliocentric orbit motion 10 p1950 A70-24319
- Quaternum representation of general relativity applied to geodesic equation and planetary motion, noting difference from Einstein formulation 10 p1944 A70-24859
- Planetary motion zero-rank effects numerical integration, using Hill secular perturbation method and trace of dyadics 14 p2639 A70-30704
- First vector integral of planetary motion different from moment of momentum and Runge-Lenz integrals 15 p2806 A70-32797
- Heliostationary spacecraft at L2 point for solar wind observation, describing mission, instrumentation and spacecraft design 17 p3168 A70-35252
- Heliostationary spacecraft for solar observation near libration point between sun and earth, discussing attitude stabilization by solar pressure 17 p3178 A70-35254
- Perturbative effects of Jupiter moons on spacecraft flyby and postencounter heliocentric trajectories, noting precision targeting [AIAA PAPER 69-932] 18 p3316 A70-36680
- Einstein theory applied to sample modeling of planetary orbits and light beams touching sun in solar gravitational field 19 p3520 A70-38393
- Planetary theory construction to second order of disturbing masses, applying to motions of any set of two or three planets in solar system 19 p3523 A70-38687
- SERT 2 solar array power system in sun synchronous orbit, considering power conditioning and deployment technique [AIAA PAPER 70-1159] 20 p3567 A70-40202
- Titius-Bode law conclusions regarding solar system planetary distances numerical relations, considering planetary evolution 22 p4101 A70-42863
- ### SOLAR PHYSICS
- Solar-terrestrial physics, Terrestrial aspects - IQSY and COSPAR Conference, London, July 1967 01 p0071 A70-10577
- Radiative energy transport in sunspot region via model computations, obtaining reduced subphotospheric flux estimates for given magnetic field 02 p0372 A70-12254
- One dimensional magnetograph scans studying photospheric velocity oscillations and supergranulation, noting downward flows coincident with chromospheric network 03 p0570 A70-13593
- Block diagrams of three stage device for extracting radioactive Ar from perchloroethylene considered for solar nucleus studies 05 p0845 A70-15933
- Time variation of gravitational constant on structure of central solar region and neutrino luminosity 05 p0899 A70-15952
- Gas pressure and pressure stratification in sunspot, using curve of growth analysis 05 p0911 A70-16432
- Limb effect of solar Fraunhofer lines determined by telescope equipped with autocollimated type diffraction spectrograph 05 p0918 A70-16912
- Sunspot magnetic field structure, determining vector field from longitudinal component perspective effect observations 06 p1149 A70-18457
- International data exchange guide for solar terrestrial physics, including listing of stations active during International Years of Active Sun 07 p1377 A70-18937
- Steady state spherically symmetrical ejection of multicomponent plasma from sun determined with hydrogen approximation, considering ion composition 07 p1391 A70-20418
- Solar wind ejection, analyzing regions of heat conducting fluxes and laminar patterns 08 p1561 A70-21059
- Monograph on solar wind covering solar physics, space observation methods, solar system interactions, etc 09 p1745 A70-23475
- Soviet collection of papers on solar and stellar physics covering degenerate gases, variable stars, energy sources, stellar atmospheric and shell models, star clusters, etc 11 p2114 A70-26576
- Book on space physics covering earth radiation belts, atmosphere, ionosphere, and magnetosphere, solar structure and composition, interplanetary space, etc 12 p2309 A70-27973
- Glancing incidence extreme UV telescopes optical design in solar physics applications, employing surfaces of revolution 15 p2736 A70-32029
- Report on ASA meeting in Pasadena February 1969 covering solar observation program, solar temperature inversion, solar spin-down, etc 19 p3518 A70-38014
- Carbon-nitrogen-oxygen isotope bi-cycle function in solar evolution, noting first cycle role in solar energy release and neutrino production 20 p3698 A70-39306
- Astronomy - Conference, Canberra, Australia, December 1969 21 p3890 A70-41176
- Photospheric metallic line profiles numerical experiment, investigating physical processes causing shape and asymmetry change 22 p4101 A70-42866
- ### SOLAR PLASMA (RADIATION)
- #### U SOLAR WIND
- #### SOLAR POSITION
- Solar activity effect on ionospheric total electron content via Explorer 22 observations, discussing relationship to solar elevation angle 02 p0292 A70-12561
- Cosine dependence of F1 critical characteristics on solar zenith angle discriminating alpha neutralization and mixed alpha-beta deionization 06 p1057 A70-17841
- Ionospheric absorption at oblique incidence during IQSY, studying seasonal and diurnal variations as solar zenith angle function 06 p1009 A70-17905
- Solar asymmetries associated with sun motion toward apex related to formation of N-S asymmetries of geomagnetic storms 06 p1144 A70-18011
- Sun-pointing spinning spacecraft attitude control by solar radiation pressure using paddle arrangement without power, sensor and moving parts requirement 11 p2123 A70-26145
- Sky radiation scattering and polarization functions for various solar altitudes at Lomitzer Peak observatory 12 p2294 A70-27674
- Negative sudden phase anomaly (SPA) in VLF radio transmission, noting solar X ray flux intensity and zenith angle effects 15 p2699 A70-32297
- Low latitude boundary of ionospheric absorption during winter anomaly showing enhancement dependence on solar zenith angle 21 p3815 A70-40944
- Position tracking of SOMEX superpressure balloons by solar angle method 24 p4372 A70-45423
- ### SOLAR POWER GENERATION
- #### U SOLAR GENERATORS
- #### SOLAR POWER SOURCES
- #### U SOLAR GENERATORS
- #### SOLAR PROBES
- Flight test results of attitude control device for TACITE rocket probe to explore solar disk and neighborhood [ONERA-TP-762] 03 p0523 A70-13626
- Electrical power system adaptable to intermediate solar probes, discussing thermoelectric, thermionic, photovoltaic systems and battery for energy storage [ASME PAPER 69-WA/SOL-5] 04 p0625 A70-14753
- Surface coating optical and thermal properties investigated in preparation for HELIOS solar probe [DGLR-69-46] 04 p0762 A70-15163
- Tangential thrust, constant acceleration trajectories for close solar probe missions using low thrust electric engines 06 p1137 A70-17177
- Space research in terms of earth environment in space, discussing near-earth spacecraft role in solar, magnetospheric and ionospheric studies 08 p1488 A70-21344
- Spectrometer design for Helios solar probe using semiconductor detectors to identify particles separated by magnetic field 10 p1888 A70-24487
- Solar probe Helios data processing and transmission system, describing block diagram, PCM/PSK/PM telemetry and transmitter 13 p2367 A70-29558
- Space probe trajectory near second order integration under influence of solar oblateness and gravitation 14 p2635 A70-30288
- American-German solar probe HELIOS mission parameters for interplanetary and close proximity solar research, discussing spacecraft building and launching 15 p2801 A70-32281
- German-American HELIOS solar probe for solar wind, interplanetary magnetic field and cosmic rays 16 p2987 A70-34343
- Helios solar probe magnetic field measurements, discussing magnetometer systems, interplanetary magnetic field implications, shock waves, magnetic storms, etc 21 p3923 A70-42172
- Solar probe trajectory optimization, using Venus gravitational field for braking 23 p4243 A70-44506
- Helios solar probe for automated spacecraft exploration of interplanetary space near sun, considering design, mission planning and U.S.-German cooperation 23 p4245 A70-44689
- Helios solar observation satellite equipment design study for solar plasma low energy particles onboard measurements 23 p4262 A70-44844
- Astronomical observations from outside terrestrial atmosphere, discussing vehicles and equipment for solar and stellar research, rocket and balloon data, etc 23 p4257 A70-45043
- ### SOLAR PROMINENCES
- Solar structural periodicities in quiescent prominences and filaments, considering plasma instability and supporting magnetic field characteristics 01 p0176 A70-10248
- Chromospheric flares, loop prominences and filament activation and dissipation attributed to decelerated annihilation of prominence field in upper active region 03 p0557 A70-13218
- Solar protuberance radiation polarization in Ca I 4227 A line, discussing depolarization and electron-and photoexcitation 07 p1384 A70-19416
- Population of P level He excitation in solar prominences in H luminescence regions, noting ionization-recombination mechanism by UV radiation 08 p1564 A70-20555
- Longitudinal magnetic field measurement along H alpha line of solar prominence 08 p1560 A70-20838
- Turbulence in quiescent prominences relationship to shock waves in upper atmosphere 08 p1570 A70-20840
- Sunspots narrow and double K lines probable emission by quiescent type prominences 08 p1575 A70-21372
- Chromospheric flares, loop prominences and filament activation and dissipation attributed to decelerated annihilation of prominence field in upper active region 08 p1562 A70-21651
- Magnetic fields model for quiescent solar prominences with helical structure 09 p1757 A70-22734
- Limb-SD type ascending prominences direction and velocity correlated to flares and solar radio emission 12 p2303 A70-27707
- Sudden disappearance of large quiescent prominence on solar disk with subsequent brightenings, using photospheric and gravitational model 13 p2497 A70-29850
- Solar prominences monochromatic images in He I D3 and He II 4686 lines allowing for contamination in 4686 images 15 p2803 A70-32614
- Solar coronal streamers, considering disk locations, evolution, classification and morphological model 15 p2804 A70-32621
- Population of P level He excitation in solar prominences in H luminescence regions, noting ionization-recombination mechanism by UV radiation 15 p2805 A70-32710
- Magnetic flux measurements in quiescent solar filaments and adjacent photosphere using magnetograph observations 17 p3157 A70-34837
- Solar prominences thermal and dynamical stability in terms of optically thin plasma supported by magnetic field against gravity 17 p3174 A70-35867
- Solar flare of 30 October 1968, describing sunspot development 19 p3497 A70-37973
- Coronal streamers structure and evolution from photographic and K-coronameter data, indicating photospheric bipolar magnetic regions as origin 20 p3712 A70-40416
- Moving type 4 solar burst on 1 March 1969 observed at 80 MHz, discussing plasma cloud associated with prominence 21 p3880 A70-40967
- Coherent motion effects on brightness of clouds moving above photosphere, describing H alpha Doppler brightening and Lyman alpha Doppler dimming in solar prominences 24 p4400 A70-45313

H alpha solar spray-like prominence ejected in association with bright limb flare, determining knots trajectories and velocities from coronagraph observations

24 p4396 A70-45323

SOLAR PROPULSION

Solar electric spacecraft field interaction with space plasma affecting collection and interpretation of scientific data, emphasizing required system configurations and constraints

[AIAA PAPER 69-1106] 01 p0162 A70-10601

Advanced reconnaissance electric planetary spacecraft /AREPS/ concept for repeated coverage of Mars or Venus surface, using solar- photovoltaic system

[AIAA PAPER 69-253] 01 p0196 A70-10837

Electric propulsion technology status for auxiliary and solar electric prime propulsion applications

[AIAA PAPER 69-1107] 02 p0356 A70-12530

Solar electric propulsion /SEP/ for automated planetary missions, discussing system characteristics, capabilities and costs

[AIAA PAPER 69-1103] 02 p0382 A70-12531

Solar powered communications spacecraft weight, electrical power and communication capacity models for optimizing size and launch vehicle fractionation

[AIAA PAPER 69-252] 04 p0763 A70-15412

Spacecraft design, trajectory and mission analyses for multipurpose solar electric propulsion missions, emphasizing modular ion engine and fixed attitude spacecraft designs

[AIAA PAPER 70-212] 06 p1145 A70-18081

Small natural vibrations effect of solar sail-propelled system on heliocentric orbit motion

[AIAA PAPER 70-24319] 10 p1950 A70-24319

Hollow cathode ion thruster and lightweight power conditioner of solar-electric propulsion system for unmanned deep space probes

[AIAA PAPER 70-648] 16 p2966 A70-33546

Solar electric propulsion system performance consisting of thrusters with thrust vector aligning actuators, switching network and flight type power conditioner

[AIAA PAPER 70-1120] 20 p3688 A70-39687

Algorithm for trajectory analysis in closed loop terminal guidance of solar electrically thrusted interplanetary spacecraft

[AIAA PAPER 70-1152] 20 p3670 A70-40203

Optimized trajectories and spacecraft for solar-electric missions to asteroids, using chemical booster for injection

[AIAA PAPER 70-1120] 20 p3710 A70-40223

Solar electric propulsion Mars high data rate orbiter trajectory design and analysis, including landing site selection and spacecraft parameters optimization

[AIAA PAPER 70-1119] 20 p3710 A70-40224

Solar electric propulsion application to out-of-ecliptic mission for interplanetary fields and particles data, comparing performance with chemical systems

[AIAA PAPER 70-1118] 20 p3691 A70-40225

Interplanetary solar electric spacecraft performance improvement by mission mode including earth swing-by maneuver in solar orbit inclined to ecliptic

[AIAA PAPER 70-1117] 20 p3710 A70-40226

Primary solar electric propulsion for automated space transportation propulsion program, considering performance and technology readiness

[AIAA PAPER 70-1115] 20 p3691 A70-40228

Solar electric propulsion systems technology development at JPL, discussing performance data and relationship to spacecraft requirements

[AIAA PAPER 70-1153] 20 p3695 A70-40520

Solar electric propulsion unmanned asteroid belt probe, discussing propulsion system, flux data acquisition, etc

[AIAA PAPER 70-1121] 20 p3717 A70-40525

Three axis attitude ion thrust vector control mechanism for solar electric propulsion spacecraft, discussing gimbal and translation actuators, array and cabling

[AIAA PAPER 70-1156] 21 p3759 A70-41784

Multimission solar electric spacecraft propulsion module design for Asteroid Belt, Jupiter and out-of-ecliptic missions, including thruster failure and power conditioning requirements

[AIAA PAPER 70-1155] 21 p3868 A70-41785

Solar-electric ion propulsion mission analysis and spacecraft designs, discussing thruster, power conditioning, propellant storage and feed, etc

[AIAA PAPER 70-1121] 23 p4234 A70-44631

SOLAR PROTONS

Sudden cosmic noise absorption /SCNA/ in polar cap during 7 July 1966 solar proton flare, estimating SCNA latitudinal distribution and protons magnetic cut-off boundary

[AIAA PAPER 70-1127] 01 p0172 A70-11527

Solar microwave burst of 30 March 1969 associated with behind-limb proton flare, studying burst spectrum

[AFRL-70-0141] 02 p0358 A70-12200

Low energy solar proton flux propagation model in interplanetary medium based on satellite data beyond earth magnetosphere

04 p0737 A70-14434

IMP F solid state detector data on 13 day solar proton event at low energy, considering cosmic rays anisotropy and interplanetary magnetic field

04 p0738 A70-14512

Solar proton latitude profiles relation to outer radiation zone electron measurements by Alouette 2 satellite charged particle detectors during quiet magnetic conditions

04 p0740 A70-15105

VLF phase disturbances and HF absorption during solar proton events of 28 August and 2 September 1966 related to proton intensities, energies and cut-off latitudes

04 p0741 A70-15124

Solar particle events 1966 /August-September/ in McMath region 8461

05 p0901 A70-16426

Solar radio emission intensity-solar flare index and 5303 A coronal line intensity-proton flare numbers relations

05 p0911 A70-16438

Solar flare alpha to proton flux ratios on 23 May 1967 observed following interplanetary disturbances, suggesting electric fields as cause of modulations

05 p0902 A70-16444

Relativistic solar proton propagation fluctuation effects in interplanetary magnetic field during cosmic ray intensity increase

05 p0903 A70-16731

Spectral characteristics of solar proton flare on 2 September 1966 noting light intensity variations

05 p0904 A70-16911

Local time dependence of geomagnetic cut-offs for solar protons in 0.52-4.0 Mev range from satellite observations

06 p1136 A70-18529

X ray and H alpha emissions associated with solar proton flares, correlating rise time with solar cosmic rays

06 p1137 A70-18547

Solar flare protons motion in sun radial magnetic field, considering protons interaction with interplanetary field inhomogeneities

07 p1366 A70-19427

Solar proton flares radiometric measurement on-board Molniya 1 satellite, detecting intensities in outer regions of magnetosphere

07 p1366 A70-19428

H alpha brightening areas related to sunspot magnetic fields configuration and solar proton flares

07 p1369 A70-20072

Solar protons captured in earth dipole trap, discussing conditions for nonadiabatic escape

07 p1374 A70-20442

Solar protons in subpolar stratosphere during solar activity minimum indicated from proton measurements at Tiksi Bay

07 p1374 A70-20444

Cosmic rays sudden intensity increases during proton flares of 28 January 1967 and 7 July and 2 September 1966, plotting proton density vs pressure

07 p1374 A70-20445

Solar proton flux increases associated with sudden commencements observed by geostationary ATS-1 satellite

08 p1562 A70-21378

Heliocentric longitude intensity profiles of protons associated with solar flare of 5 February 1965, discussing data from Mariner 4 and IMP 2

09 p1746 A70-23480

Proton injection into radiation belt, comparing solar neutron decay /SND/ and cosmic ray albedo neutron decay /CRAND/ as proton sources

09 p1746 A70-23489

Radiation hazard to space vehicles by solar flare protons, calculating risk dose by computerized Monte Carlo simulation, applying importance sampling

10 p1934 A70-25190

Type 4 solar radio bursts compared with flare observations, geophysical effects and satellite monitors data to detect proton flares spectra

10 p1934 A70-25278

Oblique shock initiated by 7 July 1966 proton flare in solar wind observed by satellite magnetometers outside magnetosphere

11 p2105 A70-26562

Low energy solar proton flux propagation model in interplanetary medium based on satellite data beyond earth magnetosphere

13 p2475 A70-28459

Proton cosmic ray flare development and spatial structure, discussing magnetic field annihilation process for particle energy and photon ejection

13 p2476 A70-29046

Solar protons and electrons spatial and angular distributions over polar caps by USAF-OAR satellites 1966-70A, 1967-72D and 1968-59A

13 p2482 A70-30073

Low energy charged particle distribution within earth magnetosphere and environs, suggesting solar origin for storm time ring current protons

13 p2483 A70-30089

Solar proton flare of 2 September 1966, discussing Abastuman observatory photographic observations and radio noise emission changes

15 p2792 A70-31618

Solar proton structure across polar cap and anomalous latitude cut-off explained by local pitch angle variations

15 p2792 A70-31672

Proton Flare Project 1969, reporting synoptic observations of sun and solar terrestrial effects

15 p2794 A70-32291

Solar activity during Proton Flare Project Retrospective Interval 1969, discussing empirical flare forecasting methods

15 p2794 A70-32292

Solar radio burst satellite observation during Proton Flare Project, giving dynamic spectra

15 p2794 A70-32293

Sudden phase anomaly /SPA/ in VLF radio wave propagation during Proton Flare Project, noting corresponding solar X-ray flux intensity enhancement

15 p2794 A70-32294

Polar cap disturbance of 7 June 1969 due to small proton enhancement, describing detection by transpolar VLF phase measurement

15 p2794 A70-32295

Solar Proton Flare Project 1969, summarizing observations and solar activity-terrestrial event correlation for June retrospective interval

15 p2794 A70-32296

Tiros solar proton monitor program, describing detector design, operational data processing and early warning network

17 p3180 A70-35304

Solar protons penetration into magnetosphere and magnetotail

18 p3306 A70-36004

Proton flares showing enhancement of ionospheric absorption and complex magnetic disturbances

18 p3306 A70-36087

Solar flare protons motion in sun radial magnetic field, considering protons interaction with interplanetary field inhomogeneities

18 p3309 A70-36901

Solar proton flares radiometric measurement on-board Molniya 1 satellite, detecting intensities in outer regions of magnetosphere

18 p3309 A70-36902

Solar particle events forecasting based on classification scheme, discussing proton active regions

19 p3493 A70-37476

Solar proton events classification system based on solar flux logarithm

19 p3493 A70-37477

Temporal and spectral changes in solar protons and alpha particles access to synchronous altitude in magnetosphere

19 p3494 A70-37485

Low energy solar protons temporal and spatial variations in magnetosphere by data comparison from polar orbiting satellite and Explorers 33 and 34

19 p3494 A70-37486

Polar cap absorption correlation with solar protons flux into magnetosphere, discussing diurnal and spatial variations and magnetic storm effects

19 p3411 A70-37492

Proton spectra and time history in interplanetary space during solar flare by satellite observation, investigating particle flux by shock waves

19 p3495 A70-37503

Solar cosmic ray protons and electrons increase during 25 February-5 March 1969 observed by Venus 5 and 6 space probes, discussing interplanetary medium disturbance

19 p3495 A70-37504

HEOS 1 low energy proton measurements in interplanetary space, discussing particle direction during solar event and anisotropy time history

19 p3495 A70-37505

Solar protons directional and omnidirectional measurements during particle event of 25 February 1969 by Heos 1 spacecraft, indicating particle diffusion in interplanetary space

19 p3496 A70-37506

Solar protons distributions in 1-30 MeV range over northern polar cap during 25 February 1969 solar event by ESRO 1 satellite

19 p3496 A70-37508

Protons and alpha particles energy spectra during 25 February 1969 solar event from Centaur rocket measurements

19 p3496 A70-37509

Protons and alpha particles energy spectra following solar flares of 24-25 February 1969 from rocket measurements, estimating proton mean free path

19 p3496 A70-37510

D region positive ion density during solar proton event by Arcas rocket-borne cylindrical electrostatic probe

19 p3411 A70-37512

- Ionospheric electron density and temperature variation measurements after solar proton event of 25 February 1969, using ESRO 1 satellite
19 p3411 A70-37514
- Energetic storm particle events observation, noting association with solar protons and interplanetary shock waves
19 p3496 A70-37518
- Low energy solar protons observation by Esro 1 satellite during solar flare of 25 February 1969
19 p3497 A70-37520
- Solar proton intensity measurement during flare by satellite Proton 3 apparatus
20 p3700 A70-39729
- Atmospheric neutron flux increase during solar proton event, measuring flux and energy spectrum of particles by balloon sounding
21 p3881 A70-41076
- Low energy solar protons penetration, examining geomagnetic cutoff latitude during magnetically disturbed period
21 p3881 A70-41077
- Solar wind proton properties examined by Vela 3, observing density distribution, flow speed and direction, thermal anisotropy, magnitude and orientation
21 p3881 A70-41081
- Solar wind instability from TEM waves propagating parallel to magnetic field in electron-proton plasma
23 p4235 A70-43826
- Solar proton events indication by 15.8 mm bursts during 1968
24 p4401 A70-45324
- VLF phase disturbances, HF absorption and solar protons in 1967 PCA events, using ionization model
24 p4314 A70-46128
- SOLAR RADAR ECHOES**
Solar radar echo characteristics, discussing coronal compressional waves and refraction by plasma clouds and moving plasma irregularities
13 p2370 A70-29852
- SOLAR RADIATION**
NT SOLAR CORPUSCULAR RADIATION
NT SOLAR COSMIC RAYS
NT SOLAR PROTONS
NT SOLAR RADIO BURSTS
NT SOLAR RADIO EMISSION
NT SOLAR WIND
NT SOLAR X-RAYS
NT SUNLIGHT
NT TYPE 2 BURSTS
NT TYPE 3 BURSTS
NT TYPE 4 BURSTS
NT TYPE 5 BURSTS
Disk-shaped Mo and Nb specimens solar radiation reflection and absorption characteristics observed for temperature effect
01 p0117 A70-10176
- Solar Mg II doublet and XUV images obtained by Fabry-Perot interferometer mounted in Skylark spectrograph
01 p0177 A70-10339
- Solar radiation pressure effects on zodiacal dust particle orbital velocity, computing Doppler shift of H-beta absorption line as function of elongation
01 p0070 A70-10348
- Optical measurements of mirrors reflectance and solar radiation transmittance to solve problems specific to solar energy engineering by standard optical equipment
01 p0010 A70-10765
- Cosmos 149 meteorological satellite telephotometers for measuring reflected solar radiation from earth
01 p0095 A70-11612
- Absorption band observation near 0.43 μ in solar spectra and scattered radiation of sky, determining nontelluric origin
01 p0084 A70-11613
- Solar UV radiation reflected from Echo satellites measured and compared with UV fluxes from Lyrae
01 p0095 A70-11614
- Secular and short period perturbations calculation of satellite orbital elements under action of solar radiation pressure
02 p0362 A70-11763
- Period changes of satellite 1963 53 A due to accelerations from atmospheric drag and solar radiation pressure
02 p0362 A70-11764
- Absorption of EUV sunlight by Jupiter upper atmosphere, discussing photoelectron energy loss, thermal equilibrium and heating efficiencies
02 p0367 A70-11816
- Solar radiation influence on Alouette satellite spin behavior with long flexible antennae, taking into account sunlight/shadow history and solar vector inclination
02 p0380 A70-11852
- Atmospheric penetration of UV and visible solar radiation during twilight, oxygen and ozone absorption, Rayleigh scattering and atmosphere refraction
02 p0357 A70-12155
- Earth climatic control by reflecting satellites producing artificial solar irradiation
03 p0581 A70-13835

- Solar IR light brightness distribution reflected by volcanic covers compared with lunar observation data
04 p0744 A70-14439
- Extraterrestrial solar spectral irradiance at earth mean solar distance within 300 to 2500 nm wavelength region, from NASA CV-990 aircraft research flights
04 p0690 A70-15019
- Excitation of H-alpha and H-beta lines in night sky, calculating solar L radiations variation with altitude
04 p0679 A70-15075
- Solar Lyman-alpha radiation observed by OGO 4 spacecraft showing short term fluctuations superposed with monthly variation
04 p0741 A70-15128
- Solar and sky far IR radiation in upper atmosphere, estimating precipitable water quantities and low absorption regions
04 p0681 A70-15521
- Simulation equipment for extraterrestrial solar radiation for spacecraft components evaluation tests, describing spectral characteristics
04 p0665 A70-15663
- Ionospheric inhomogeneities motion and vertical profile of atomic oxygen concentration associated with solar particle absorption in upper layer
04 p0681 A70-15724
- Solar structure models for neutrino flux prediction compared with solar structure, suggesting modification in solar and stellar evolution calculations
05 p0906 A70-15895
- Solar neutrino spectroscopy using various radiochemical detectors for Be 7, N 13, O 15 and B 8 neutrino fluxes, noting Li 7 suitability for determining CNO cycle
05 p0898 A70-15949
- Deuteron splitting by solar neutrinos for neutrino detection, describing deuterium scintillation detector characteristics
05 p0899 A70-15954
- Gallium trichloride and aqueous solution of lithium chloride as solar neutrino detectors
05 p0899 A70-15956
- Solar neutrinos detection from recording high energy electrons in reactions, using Li 7, Be 9 and B 11 as detectors
05 p0899 A70-15964
- Experimental determination of solar neutrino activity from interaction cross section between neutrinos and target nuclei
05 p0900 A70-15965
- Earth and atmosphere effect on solar radiation balance in Southern Hemisphere
06 p1054 A70-17413
- Radiation scattering during upper cloud altitude determination by satellite
06 p1097 A70-17790
- Instantaneous and integral solar irradiance of earth orbiting satellite surface, noting solar illumination nomogram representation
06 p1155 A70-17893
- Space forecasting system to predict solar radiation bursts and effects on earth
06 p1136 A70-18023
- Light intensity and polarization in twilight sky atmosphere at solar depressions
07 p1263 A70-19047
- Spin decay from telemetered flight data of Explorer 20 compared with calculation based on solar influence theory
07 p1394 A70-19721
- Lepton charge and neutrino astrophysics, discussing oscillations role in solar neutrino detection difficulties
07 p1371 A70-20329
- Interkosmos-1 satellite for studying solar radiation and effects on ionization and molecular dissociation in atmosphere, weather and radio signals reception
08 p1582 A70-20714
- Solar radiation reflection function for plane-parallel atmosphere with isotropic phase function calculated by successive scattering method, noting application to planetary atmospheres
08 p1571 A70-20909
- Center to limb variation of solar brightness measured at 5, 10 and 20 microns, discussing data collection and reduction and previous IR and UV measurements
08 p1562 A70-21396
- Solar meter wave emissions enhancement or emission centers, comparing radio and optical coronal enhancements
08 p1576 A70-21402
- OI 6300 A airglow intensity decrease at dawn ascribed to scattered solar radiation
08 p1492 A70-21720
- Solar radiation variations effect on earth climate, noting atmospheric transparency role in glaciation on thermal regime
08 p1539 A70-21919
- Climate variations and earth orbital elements secular perturbations, noting solar radiation and celestial mechanics roles
09 p1666 A70-22177
- Solar continually changing features (brightenings, darkenings, condensations and groupings) associated

with solar activity, emphasizing sunspot number formulas

- Earth shadow effect on solar radiation pressure induced short periodic perturbations of satellite orbits
09 p1751 A70-22197
- Thermal controls for spacecraft in space and planetary atmospheres, including heat inputs by solar radiation and planetary albedos
09 p1761 A70-23054
- Reflection patterns of solar radiation from cloud, water and land surfaces measured by airborne radiometer, observing anisotropy
09 p1789 A70-23130
- Reflected solar radiation polarization over land, sea and cloud surfaces to determine atmospheric pollution
09 p1747 A70-23603
- Ionospheric photoelectrons resulting from solar UV radiation interaction with atmospheric gases, obtaining escape fluxes using Monte Carlo method
09 p1747 A70-23667
- Solar radiation energy distribution simulated using vacuum monochromator, discussing Ar-Kr-Xe-methane mixture
10 p1931 A70-24317
- Cosmic radiation low energy positrons flux estimation compared with calculation from solar modulation models
10 p1932 A70-24537
- Radiation scattering during upper cloud altitude determination by satellite
10 p1913 A70-25022
- Polarization of solar scattered radiation measured by radio probes for aerosol particle concentration and size distribution as function of altitude
10 p1884 A70-25253
- Solar XUV lines photon flux based on one dimensional model of chromosphere-corona transition region
10 p1949 A70-25271
- Solar simulation laboratory test facility for extraterrestrial solar radiation effects on vehicles beyond earth atmosphere, emphasizing spectral filters
11 p2030 A70-25353
- Atmospheric absorption by ozone of solar radiation measured by balloon-borne spectrometer in 9-10 micron region
11 p2045 A70-25627
- Solar moustaches /transient emissions/ far wing asymmetry studied photometrically
11 p2109 A70-25745
- Global distribution and intensity of solar radiation, determining radiation of satellites and other high altitude devices
11 p2105 A70-26010
- Corrugated skins solar absorbance and IR emittance computed for spacecraft thermal design, analyzing other nondiffusive radiative enclosures
11 p2150 A70-26352
- Ionosphere dynamo region thermal input by Joule heating and solar radiation and coupling to various thermotidal modes, observing semidiurnal and semianual effects
11 p2047 A70-26569
- Solar radiation effects on evaporation of dust with high latent heat of vaporization, considering particles in comets and zodiacal cloud
11 p2117 A70-26648
- Solar radiation transmitted and reflected by earth atmosphere, solving absorption and scattering by computer programs
12 p2262 A70-26951
- Solar light brightness distribution reflected by volcanic covers compared with lunar observation data
13 p2485 A70-28464
- Soviet book on solar short wave radiation effects on ionosphere, covering solar atmosphere and spectra, ionospheric ion concentration vertical distribution, etc
13 p2487 A70-28649
- Solar spectra recording by balloon-borne monochromator, measuring stratospheric IR absorption
13 p2491 A70-29050
- Sun-planet-particle problem, considering solar radiation total pressure, Lagrangian solutions instability and differential equations of motion
13 p2494 A70-29400
- Solar radiation absorption by atmospheric ozone observations by ground stations for meteorological data
13 p2400 A70-29642
- Circumsolar sky radiation effect on pyrheliometric measurements, considering atmospheric scattering and turbidity
13 p2400 A70-29660
- Solar and terrestrial radiation measurements and computations in meteorology, considering diffuse radiation and radiative transfer in atmosphere
13 p2410 A70-29661
- Evaporated multilayer optical bandpass filters in solar radiation technology, discussing design and construction
13 p2411 A70-29665
- Lunar horizontal and inclined surfaces net radiation and components, discussing surface temperature, thermal emission and absorbed solar radiation
14 p2634 A70-30194

- Thermospheric heating and conversion efficiency of short wave radiation as functions of solar radiation spectral flux, atmospheric components concentration and elementary processes cross sections
14 p2569 A70-30212
- Sun glitter on sea surface from space photographs, considering wind and sea conditions effect on shape and brightness of patterns
14 p2572 A70-30345
- Field characteristics of solar radiation reflected and scattered into outer space by earth atmosphere, discussing brightness and angular distribution of outgoing component
14 p2603 A70-30406
- Ionospheric inhomogeneities motion and vertical profile of atomic oxygen concentration associated with solar particle absorption in upper layer
14 p2575 A70-30808
- Angular distribution of diffusely reflected solar rays over spherical shell planetary atmosphere, determining halo brightness
14 p2632 A70-31222
- Earth satellite motion about center of mass, examining effects of random variations in atmospheric density, geomagnetic intensity and solar radiation
15 p2809 A70-31650
- Solar extreme UV radiation measurements over rotation period onboard satellite OSO-3, using atmospheric absorption correction
15 p2792 A70-31666
- Report to COSPAR on Netherlands space research /1969/ including solar and stellar X radiation and UV spectrophotometry, cosmic ray measurements, satellite geodesy, etc
15 p2830 A70-31719
- Total solar radiation calculation for inclined and horizontal surfaces, noting application to solar heating
15 p2774 A70-31803
- Solar radiation and aureole measuring instrument composed of telescope, double monochromator, amplifier and recorder
15 p2735 A70-31807
- Solar simulation systems for uniform collimated intense light, noting high intensity lamp development
15 p2717 A70-32034
- Rocket and satellite data on upper atmospheric neutral/charged particles, short wave solar radiation, temperature and photochemical reactions
15 p2730 A70-32089
- Solar, clear sky and overall radiation characteristics, calculating incidence of light and radiation in room interiors
15 p2732 A70-32461
- Solar stray light, determining spread function, limb profile and aureole at various wavelengths
15 p2795 A70-32625
- UV solar opacity observations, comparing solar model predictions
17 p3160 A70-34884
- Solar corona radiation at 1-100 A for 1-10 million K, using Jordan ionization equilibrium calculations
17 p3151 A70-35582
- Solar and IR radiation distribution in multiple scattering and absorbing ground fog, obtaining intensities, fluxes and vertical divergence
18 p3284 A70-35943
- Latitude profiles made of low energy solar electrons over polar cap, finding latitude knee position
18 p3306 A70-36020
- Laminar heat transfer in circular tube under solar radiation in space
18 p3347 A70-36503
- Human bioclimatology at high altitude, discussing energy balance in terms of net solar and terrestrial radiation balance in mountain area
19 p3367 A70-37369
- Balloon-borne spectrophotometer with diffraction grating for upper atmospheric solar radiation attenuation measurement
19 p3422 A70-37639
- Fine structure of solar radiation-induced electrostatic fields on dielectric surface of comets and meteoroids
19 p3514 A70-37656
- Angular and geometric properties of actinometers, pyrheliometers and photometers, measuring direct and scattered circumsolar radiation
20 p3625 A70-39028
- Correction procedures for measurement errors in actinometers and pyrheliometers caused by circumsolar radiation
20 p3625 A70-39029
- Inverse beta decay thermonuclear reactions induced by neutrinos proposed for neutrino detection from solar interior
20 p3704 A70-39471
- Atomic hydrogen emissions in dayglow, considering excitation by resonance absorption of solar radiation
21 p3812 A70-40728
- D region electron density profiles from high power wave interaction measurements during solar flare, indicating non-X-ray production rate
21 p3879 A70-40942
- Lunar luminescence phenomena, examining gas eruptions from volcanic activity, solar radiation and color
21 p3886 A70-41070
- Apollo 11 lunar fines, investigating solar radiation effects on optical properties by standing and heating
21 p3915 A70-41660
- Silicon solar cell design optimization for near solar missions, discussing electrical characteristics and performance obtainable under various solar radiation conditions
22 p3964 A70-42496
- Global solar radiation climatology of earth including direct and diffusive radiation
22 p4013 A70-42600
- Upper atmosphere electric field nature, considering solar radiation as major source of ionization
22 p4017 A70-42788
- Vertical atmospheric ozone distribution according to direct solar radiation received on ground, using UV and IR observations
22 p4023 A70-43296
- Upper atmosphere photoionization by extreme UV solar radiation compared with ionization by charged particles collisions
22 p4096 A70-43302
- E region winds response to solar radiation variations, including geomagnetism role
23 p4186 A70-43848
- Solar L alpha absorption in upper atmosphere, using rocket-borne ionization chamber
23 p4191 A70-44270
- Solar atmosphere radiation and structure, discussing continuum and line spectra, solar rotation, chromosphere, spicules, etc
23 p4256 A70-45035
- Atmosphere and earth-reflected solar radiation pressure effects on high altitude satellite orbits
24 p4408 A70-45555
- Satellite orbit perturbation due to earth reflected or reradiated solar radiation pressure
24 p4409 A70-45556
- Solar XUV and soft X ray photometry, describing sounding rocket and satellite grazing incidence spectrometers
24 p4339 A70-45822
- D2A satellite optical experiments, examining atmospheric atomic H and solar and extraterrestrial I216 A emission
24 p4339 A70-46094
- Sunlight induced pyrimidine dimers formation in human cells in vitro, relating DNA lesions by 254 nm irradiation
24 p4304 A70-46139
- Optical solar polarization broadband measurement interpretation with depolarization factor due to elastic collisions or additional source
24 p4414 A70-46172
- Mm wavelength radiometer for recording solar activity and radiation attenuation in atmosphere as function of time
24 p4315 A70-46236
- Thermospheric heating and conversion efficiency of short wave radiation as functions of solar radiation spectral flux, atmospheric components concentration and elementary processes cross sections
24 p4331 A70-46287
- SOLAR RADIATION OBSERVATION**
U SOLAR RADIATION
SOLAR RADIATION SHIELDING
Expandable rigidizable solar shields operational, structural and thermal performance tests conducted with spherical models for cryogenically fueled space vehicles
12 p2312 A70-27131
- Thermal testing of inflatable solar shields for cryogenic space vehicles, discussing shield misalignment effects on propellant tank temperatures [AIAA PAPER 70-856]
16 p2982 A70-33901
- Solar flare radiation protection requirements, considering bulk and plasma radiation shielding
17 p3040 A70-35647
- SOLAR RADIO BURSTS**
NT TYPE 2 BURSTS
NT TYPE 3 BURSTS
NT TYPE 4 BURSTS
NT TYPE 5 BURSTS
Polarized and unpolarized impulsive solar centimeter radio bursts spectral peak interpretations
01 p0168 A70-10253
- MHD model for microwave solar circular polarization bursts interpretation, suggesting Alfvén wave disturbances in solar atmosphere
01 p0168 A70-10254
- Absolute calibration method for daily solar flux density discrepancies measurements at UHF, describing equipment and error analysis
01 p0168 A70-10259
- Sudden frequency deviation (SFD) correlation with solar radio bursts at different frequencies following inverse square law of intensity
01 p0171 A70-10871
- Solar microwave burst of 30 March 1969 associated with behind-limb proton flare, studying burst spectrum [AFCRL 70-0141]
02 p0358 A70-12200
- Pencilbeam scanning observations of solar bursts revealing recognizable postincrease phase
03 p0558 A70-13588
- Solar radio bursts time-variable structure at 12 M wavelength recorded on Ediswan pen oscillograph
06 p1144 A70-18005
- Metric type I and decametric type III bursts relationship, suggesting common generation by high energy electron outward streams from photosphere or low chromosphere
06 p1150 A70-18466
- Solar bursts of enhanced intensity at millimeter wavelengths suggested for limb brightening mechanism
06 p1153 A70-18545
- Contraction and expansion in solar region producing synchrotron emission of relativistic electrons to explain solar burst behavior
08 p1560 A70-20841
- Catalog of solar radio bursts recorded at 208 MHz during IGY and IQSY
08 p1570 A70-20843
- Localized high energy flaring of active center monitored with time-associated radio bursts in spot umbrae
08 p1561 A70-20905
- Solar microwave bursts with double structure, discussing single frequency observations and flare patrols, time variations of flux density and brightness
08 p1561 A70-21259
- Solar activity analysis emphasizing sunspots, magnetic disturbances and bursts data
09 p1752 A70-22199
- Solar U-burst radiospectrographic observations, investigating disturbing trajectories and longitudinal distribution in combination with model coronal condensation
09 p1758 A70-22737
- Circular polarization time dependent reversals during simultaneous microwave solar bursts at different plages, considering relations to coincident flares
10 p1932 A70-24626
- SID observed as VLF phase anomalies correlated with solar microwave radio bursts
10 p1933 A70-24816
- Narrow band radiation from longitudinal plasma waves nonlinear interactions during solar bursts, comparing flux intensities for Corona single or double shock wave frequencies
10 p1934 A70-25272
- Solar radio bursts dynamic spectra by magnetic tape recording of digital signal, obtaining frequency and time profiles and intensity layers
10 p1934 A70-25276
- Optical and radio homologues of solar flares, studying correlation from astronomical telescope pictures
11 p2105 A70-25747
- Solar microwave bursts polarization reversal mechanism, considering radiating electrons gyrosynchrotron absorption
11 p2106 A70-26617
- Microwave solar bursts intensity and polarization measurements at 17 GHz, discussing chromospheric flares and X ray emission
12 p2293 A70-27592
- Solar plasma and energy and radiation fading during microwave bursts due to synchrotron radiation losses, determining magnetic field strength
12 p2294 A70-27593
- Gyrosynchrotron emission from nonthermal electrons trapped in magnetic dipole field to interpret center-to-limb spectrum and polarization variations of microwave impulsive bursts
12 p2294 A70-27709
- Solar radio emissions of types I, II, III and IV activity and polarization during 18-26 May 1967 observed by narrow-band timesharing polarimeter
12 p2294 A70-27711
- Spectrograph design and specifications for solar radio flare structure, obtaining constant sum frequency by heterodyne conversion
13 p2406 A70-28948
- Galactic noise spectrum and solar radio bursts in hecto-decametric wave region observed by Alouette 2 satellite
13 p2491 A70-29093
- Circularly polarized emission from types I and 4 bursts and noise storms, considering mode coupling in warm plasma, gyroradiation and Cerenkov radiation
13 p2479 A70-29851
- Type I solar radio burst chains during noise storms, determining lifetime, bandwidth, frequency drift and fine structure
13 p2479 A70-30002
- Solar radio burst satellite observation during Proton Flare Project, giving dynamic spectra
15 p2794 A70-32293
- Type I burst effects on type III and V bursts occurrence, suggesting Langmuir waves excited by suprathermal electrons
17 p3173 A70-35746

- Solar radio bursts recording by spectrographs in 500-1500 MHz band, discussing sensitivity 18 p3307 A70-36109
- Correlated microwave bursts between adjacent active regions associated with solar flares 20 p3700 A70-40421
- Solar radio U burst second branch low relative intensity, contradicting previous theory for trajectories 21 p3880 A70-40966
- Complex burst of 2 September 1966, comparing dynamic radio spectra from Culgoora and Weissenau 21 p3880 A70-40968
- Solar X-ray bursts correlation with H alpha flares and microwave bursts observed by Explorer 34 experiment 21 p3880 A70-40970
- Radioheliograph observations of solar outbursts involving MHD waves propagation along curved paths in corona at 80 MHz 21 p3891 A70-41178
- Dynamic spectra and two dimensional radioheliograph maps of solar U bursts at 80 MHz consistent with electron streams along loops in coronal magnetic field 21 p3891 A70-41183
- Solar radio burst observation before 7 March 1970 solar eclipse, tabulating spectrum data 22 p4095 A70-43266
- Circular polarization time evolution during solar microwave impulsive bursts 24 p4401 A70-45319
- Coronal shock growth as source of thermal solar X ray bursts associated with optical events 24 p4401 A70-45320
- Solar proton events indication by 15.8 mm bursts during 1968 24 p4401 A70-45324

SOLAR RADIO EMISSION

- NT SOLAR RADIO BURSTS
- NT TYPE 2 BURSTS
- NT TYPE 3 BURSTS
- NT TYPE 4 BURSTS
- NT TYPE 5 BURSTS
- Extraterrestrial sources radiation including galactic, solar and magnetospheric radio emissions observed by RAE-1 satellite at long wavelengths [AIAA PAPER 69-1049] 01 p0170 A70-10603
- Correlation between sunspot number index and solar radio noise index relative to ionospheric propagation, noting computer analysis program and hypothesis effect 02 p0289 A70-12107
- Subcritical wavelengths processing of solar radio emission, allowing for antenna radiation pattern distortion due to surface defects 04 p0745 A70-14498
- Solar microwave and soft X ray radiation emission correlation to determine flare peak temperature and solid angle 04 p0741 A70-15126
- Tabulated values of F 2 mean solar noise indexes predicted by fifteenth degree polynomials 05 p0813 A70-16275
- Solar radio emission intensity-solar flare index and 5303 A coronal line intensity-proton flare numbers relations 05 p0911 A70-16438
- Solar activity centers life history in terms of radio emission and Ca plage intensity, noting radio emission decay faster than plage intensity 05 p0911 A70-16440
- Spectral characteristics of B and S components of solar radio emission from statistical data, investigating dependence on 11-yr cycle and minimum solar activity 07 p1378 A70-19031
- Book on solar and planetary radio emission covering solar system physical characteristics, quiet Sun, thermal and nonthermal emission, etc 09 p1752 A70-22201
- Solar corona pulsating metric radio emissions, indicating phenomena as type 4 radiation phases 09 p1758 A70-22738
- Solar radio observations tabulated for radioelectric flux density and behavior for three hour periods, average diurnal results, etc 10 p1940 A70-24414
- Low noise temperature radiometer to study solar radio emission, measuring atmospheric absorption 12 p2184 A70-27235
- Solar radio emission maps at 8.6 mm using parabolic antenna and TV camera for optical control 12 p2293 A70-27591
- Solar flares of 6 and 8 July 1968 correlation regarding electromagnetic radiation emission, radio flux, corpuscular radiation, etc 12 p2294 A70-27708
- Radio sources positions on solar disk by 2800 and 408 MHz high resolution fan beams 13 p2491 A70-29161
- Solar proton flare of 2 September 1966, discussing Abastuman observatory photographic observations and radio noise emission changes 15 p2792 A70-31618

- SHF radio telescope for solar radio wave observation, describing design and performance 15 p2717 A70-31897
- Polarization characteristics of solar radio waves reflected from coronal waves in meter wavelength range 15 p2802 A70-32485
- X ray and microwave emissions relationship to sources on sun, discussing development and structure of sunspot groups 15 p2794 A70-32486
- Low energy electron emission during solar flares relation to radio and X ray emission 15 p2795 A70-32622
- Solar radio spectrum and history of McMath 607 plage region during eclipse of 7 March 1970, considering residual emission 16 p2977 A70-33845
- Solar disk dimensions and RF emission characteristics from eclipse observation and flux recordings, considering brightness temperature distribution and lunar edge diffraction effects 19 p3521 A70-38551
- Solar radio emission slowly varying component, analyzing random aspects, correlation functions and relationship to spot groups 19 p3521 A70-38552
- Solar radio emission and optical features correlation, considering integral RF flux, spot groups, main spots and flocculi areas 19 p3521 A70-38553
- Solar eclipse of 20 May 1966, analyzing radio observations 19 p3521 A70-38554
- Solar eclipse of 22 September 1968, analyzing radio observations 19 p3521 A70-38555
- Solar radio emission intensity distribution across disk during eclipse, constructing relative RF spectrum of uncovered region 19 p3522 A70-38556
- Temperature and radio brightness distributions in active regions and upper chromosphere during minimum activity periods 19 p3522 A70-38557
- Solar radio flux variations prediction for various activity levels based on random functions theory 19 p3522 A70-38558
- Solar radio emission flux as activity index, analyzing permissible deviations from recommended wavelength 19 p3522 A70-38559
- Sun role in radio telescope radiation patterns analysis and adjustment, allowing for solar radio source finite dimensions and nonuniform brightness 19 p3390 A70-38560
- Solar radio radiation effective gravity center shift determination, considering directivity diagram scanning phase for radio transit instrument adjustment 19 p3522 A70-38562
- Antenna systems with minimum angular resolving power for solar limb radio sources recording, using data from solar meridian passage 19 p3522 A70-38563
- Moon as standard radio source for eliminating earth atmosphere influence during solar radio radiation measurements 19 p3522 A70-38564
- Solar X ray emissions from quiet and active sun compared with radio flux to investigate production mechanisms 19 p3512 A70-38909
- Solar eclipse microwave spectral observations for coronal condensation sources characteristics of solar radio emission slowly varying component, discussing ionospheric recombination coefficients 19 p3531 A70-38910
- Solar eclipse measurements in 1-30 mm range, examining chromosphere, flares and radio emission 19 p3531 A70-38911
- Millimeter wave observation of sun, deriving empirical relationships between atmospheric attenuation, emission and water vapor 20 p3623 A70-40304
- Microwave scintillations at sunrise indicating solar point sources at sunspot cycle peak and terrain configuration influence on ionospheric disturbances 20 p3591 A70-40493
- Solar active regions at millimeter wavelengths, discussing brightness temperature, background radiation, electron density, optical thickness, polarization and chromospheric magnetic fields 21 p3886 A70-40960
- Solar active region radio spectrum during 12 November 1966 eclipse, discussing flux, magnetic field effects, temperature and electron density 21 p3886 A70-40961
- Solar flare relation to radio emission at 3.3 mm, discussing sunspots, temperature gradients and magnetic fields 21 p3879 A70-40962
- Solar radio pulsations, observing modulation of coronal microwave, X ray and type III emission 21 p3880 A70-40965

- Radio observations of limb darkening and structure of solar corona at 80 MHz 21 p3890 A70-41177
- Solar radio to optical radius ratio calculated from residual flux measurements during 7 March 1970 solar eclipse 22 p4097 A70-42466
- Nonflaring solar X-ray and microwave radiation flux correlation from satellite data 22 p4104 A70-42995
- Solar optical and radio activity observation in 1968, noting optical-radio data correlation 22 p4095 A70-43259
- Polarization characteristics of solar radio waves reflected from coronal waves in meter wave length range 23 p4240 A70-43909
- X ray and microwave emissions relationship to sources on sun, discussing development and structure of sunspot groups 23 p4236 A70-43910
- Radio astronomy research covering solar radio emission, Milky Way radiation, molecular radio line spectra, etc 23 p4256 A70-45041
- Millimeter wave solar radiation atmospheric absorption examined at sea level with Michelson interferometer 24 p4398 A70-45785
- SOLAR RADIO WAVES
- U SOLAR RADIO EMISSION
- SOLAR REFLECTORS
- Qualitative analysis and comparison of hypothesis versions of Martian point flare observed by Maeda, considering solar ray reflection from ice cloud or vertical surface object 07 p1385 A70-19420
- Film type solar energy reflector peripheral blades for connection to receiver, discussing precession control and despin for rotating concentrators 07 p1196 A70-19501
- Thermal control coatings as solar reflectors for spacecraft heat dissipation 08 p1527 A70-21357
- Film type solar energy reflector peripheral blades for connection to receiver, discussing precession control and despin for rotating concentrators 15 p2678 A70-32746
- Satellite-borne test instrument for determining mirror materials degradation due to long solar exposure 16 p2921 A70-34109
- SOLAR ROTATION
- Angular momentum conservations for solar gas confined by closed field lines or outflowing along open magnetic field lines 01 p0176 A70-10251
- Rapidly rotating solar interior damping by large scale convection analysis via maximum buoyancy force in water cylinder transition 02 p0373 A70-12391
- Coronal features rotation rates as function of latitude and height above limb from autocorrelation analyses of K-coronameter observations 05 p0902 A70-16435
- Mass loss role in early spinning of sun without magnetic field braking effect, considering present surface vs core rotating velocity 05 p0913 A70-16569
- Mathematical model for testing theory of solar differential rotation maintenance by two dimensional turbulence 06 p1144 A70-18009
- Solar differential rotation relation to Rossby waves in upper convection zone based on energy conversion rate estimates 06 p1144 A70-18010
- Solar oblateness and gravitational quadrupole moment related under assumption of magnetic and velocity fields absence in surface layers, including rotation effects 08 p1570 A70-20902
- Type I comet tails orientations dispersion attributed to nonradial plasma waves and discontinuities in interplanetary gas, calculating solar angular momentum loss rate 10 p1947 A70-24987
- Exospheric density from Echo 2 orbit, observing 27 day variations associated with sun rotation and correlation with geomagnetic disturbances 11 p2046 A70-26566
- Sunspots butterfly diagram shape relation to solar differential rotation 13 p2491 A70-29048
- Solar differential rotation measurement by spectral line shift data analysis, noting angular velocity-heliographic latitude relationship 13 p2496 A70-29840
- Solar extreme UV radiation measurements over rotation period onboard satellite OSO-3, using atmospheric absorption correction 15 p2792 A70-31666
- Polar and equatorial limb darkening related to solar rotation and thermal flow, using photospheric models 15 p2807 A70-32812

Solar rotation effects on velocity field in nonspherical solar wind, using axisymmetric wind model
17 p3151 A70-34861

Energy transfer in convective envelope of rotating star and solar differential rotation, using Lucy gravity-darkening law
18 p3313 A70-36214

Solar quadrupole moment effect on secular perturbations of planetary orbital elements
18 p3313 A70-36325

Report on ASA meeting in Pasadena February 1969 covering solar observation program, solar temperature inversion, solar spin-down, etc
19 p3518 A70-38014

Interplanetary magnetic field structure, using solar wind model accounting for solar rotation
20 p3704 A70-39474

Solar internal rotation, examining oblateness, velocity and magnetic fields, wind structure and Li and Be abundances
20 p3707 A70-39936

Differential rotation at solar surface caused by anisotropic turbulent viscosity in hydrogen convection zone, solving via Navier-Stokes equation
20 p3711 A70-40404

Synoptic charts of polar magnetic fields plotted in polar coordinate system for consecutive solar rotations
20 p3711 A70-40408

Photospheric magnetic field differential rotation using synoptic charts for autocorrelation technique
21 p3885 A70-40951

Supergranular network time and shape changes, examining correlations with solar rotation, activity and cycles
21 p3885 A70-40954

Nonaxisymmetric convection of rotating spherical shell in Herring approximation, noting applicability to sun
22 p4104 A70-42994

Solar rotation, discussing oblateness, solar wind torque, main sequence stars rotating core, gravitational quadrupole moments and Li and Be depletion
23 p4252 A70-44829

Equatorial acceleration of sun, considering rotation and turbulent energy transport in convective zone
23 p4252 A70-44830

Spectroscopic differential photosphere and chromosphere rotation with height in solar envelope
23 p4252 A70-44831

Solar spin down procedure simulated via Boussinesq fluid spin down in circular cylinder
23 p4252 A70-44832

Nonspherical stars thermal stability, considering solar rotational models and oblateness problem
23 p4252 A70-44833

Solar interior differential rotation, developing angular velocity distribution equilibrium model
23 p4252 A70-44834

Solar oblateness calculation based on Stoeckly differential rotation law application to polytropes
23 p4253 A70-44835

Zonal spot activity duration dependence on daily angle of solar rotation
24 p4401 A70-45316

SOLAR SAILS

Small natural vibrations effect of solar sail-propelled system on heliocentric orbit motion
10 p1950 A70-24319

SOLAR SENSORS

Fluidic sun sensor design and breadboard test for spacecraft and missile attitude control systems
04 p0716 A70-15415

Gyroless attitude control system for pointing Aerobee sounding rocket payload at sun using solar sensors
13 p2501 A70-28422

Projectiles yawing and rolling over long flight paths, describing onboard solar aspect sensor and telemetry link to ground stations
13 p2406 A70-29005

Stepper motor for pointing Surveyor spacecraft TV transmitting antenna and solar panel at earth and sun
16 p2845 A70-34110

Solar power panel orientation servomechanism using passive elements without power consumption
16 p2846 A70-34130

Passive sun trackers using solar energy activated bimetal helix thermal heliotrope
16 p2846 A70-34131

SOLAR SIMULATION

Solar simulation /SISS/ for evaluating human visual system performance in contrasting space environment
09 p1655 A70-22680

Solar radiation energy distribution simulated using vacuum monochromator, discussing Ar-Kr-Xe-methane mixture
10 p1931 A70-24317

Solar simulation laboratory test facility for extraterrestrial solar radiation effects on vehicles beyond earth atmosphere, emphasizing spectral filters
11 p2030 A70-25353

Spectral irradiances of inert gases and mixtures for laboratory solar simulation
15 p2717 A70-32028

Solar prominences thermal and dynamical stability in terms of optically thin plasma supported by magnetic field against gravity
17 p3174 A70-35867

Solar simulation methods, discussing optical elements and artificial radiation sources suitability for thermal testing
19 p3398 A70-38282

Solar spin down procedure simulated via Boussinesq fluid spin down in circular cylinder
23 p4252 A70-44832

SOLAR SIMULATORS

Explorer 38 critical component equilibrium temperature tests in thermal vacuum chamber using modified solar simulator, noting agreement with model [ALAA PAPER 69-999]
02 p0275 A70-12527

Simulation equipment for extraterrestrial solar radiation for spacecraft components evaluation tests, describing spectral characteristics
04 p0665 A70-15663

Solar plasma wind simulator design and performance, discussing ion source, mass separator, beam mass analyzer and Faraday cup [ALAA PAPER 70-31]
06 p1030 A70-18223

Thermal vacuum simulator for testing manned Lunar Module Test Vehicle, using conformal skin heaters to control heating rates and skin temperature
09 p1656 A70-23241

Solar simulator built into multiwall ultrahigh vacuum chamber, describing simulator and chamber modifications
09 p1657 A70-23264

Xenon high wattage short arc lamps for space/ solar simulators, describing seals, electrodes shapes and cooling, operating characteristics, etc [ALAA PAPER 69-998]
13 p2384 A70-28520

Solar simulation systems for uniform collimated intense light, noting high intensity lamp development
15 p2717 A70-32034

Solar alignment, control, intensity scanner and data collection for large Space Environmental Simulator
17 p3058 A70-35155

Solar simulators using water cooled 30 kw Xe arc lamps
17 p3060 A70-35248

Solar simulator combined with space environment simulation chamber for thermal tests of artificial satellites
19 p3398 A70-38283

SOLAR SPECTRA

Photospheric Fe I abundance variation with excitation potential
01 p0175 A70-10239

Reply to Swings comments on validity of forbidden SI lines in solar spectrum communicated by Swenson
01 p0175 A70-10240

Solar corona red and green lines during 30 May 1965 total eclipse, discussing indicated radial, turbulent and displacement velocities
01 p0176 A70-10249

Solar Mg II doublet and XUV images obtained by Fabry-Perot interferometer mounted in Skylark spectrograph
01 p0177 A70-10339

Solar Lyman alpha line profile and atomic hydrogen vertical distribution measurement method for terrestrial atmosphere in 200-500 km range
01 p0078 A70-11208

Stratospheric water vapor distribution from analyzing IR solar spectrum during sunset observed by balloon-borne spectrometer
01 p0081 A70-11295

Absorption band observation near 0.43 mu in solar spectra and scattered radiation of sky, determining nontelluric origin
01 p0084 A70-11613

Extreme UV spectral line intensity enhancement during class 3 flare related to abundance of radiating element
02 p0358 A70-12205

Coronal emission lines wide slit photometry systematic error analysis and suggested error elimination by varying observation method
02 p0373 A70-12375

Crossed Fabry-Perot etalons and spectrographs for studying atmospheric solar absorption spectra
02 p0299 A70-12438

Rocket-borne spectroheliograph for taking X ray and monochromatic pictures of sun in Mg II line
03 p0570 A70-13594

Ar X and Ar XIV identification in solar corona and unidentified coronal lines origin, discussing Fe and Ni transitions from metastable levels
03 p0571 A70-13598

Absorption line identification in sunspot spectra by calculating Zeeman patterns, using Zeeman splitting for magnetic field measurement
03 p0574 A70-13934

Extraterrestrial solar spectral irradiance at earth mean solar distance within 300 to 2500 nm wavelength region, from NASA CV-990 aircraft research flights
04 p0690 A70-15019

HF molecular vibration rotation band observed in sunspot spectra, carrying out model calculations for spots differing in temperature for fluorine abundance
04 p0751 A70-15048

Solar helium-like ion line intensities, determining electron densities and excitation rate ratios
04 p0758 A70-15696

Drift, anti-Fermi retardation, convective transfer and diffusion effects on solar cosmic ray energy spectrum in earth orbit proximity
05 p0898 A70-15943

Identification of lines in Mohler photometric atlas of IR solar spectrum wavelengths
05 p0910 A70-16427

Diatomic carbon swan band violet line absence from sunspot suggested in accordance with molecular equilibrium predictions
05 p0911 A70-16433

IR solar spectrum including water vapor, carbon dioxide and methane bands
05 p0913 A70-16566

Solar activity study based on solar X ray spectra observation, considering flare mechanism
05 p0903 A70-16719

Spectral characteristics of solar proton flare on 2 September 1966 noting light intensity variations
05 p0904 A70-16911

Periodicities in solar activity variation from correlation spectral analysis, establishing monotonically decreasing component and secular variations in activity
05 p0918 A70-16913

Empirical astrophysical damping constants derived for neutral Fe lines using solar spectra, applying constants to abundances and surface gravity determination
05 p0919 A70-16939

Neutral Ne emission line in visible solar spectrum during bright events in inner corona, noting 1958 outburst of RS Oph
05 p0920 A70-16944

Radiative transfer equations for Zeeman multiplets of electric and magnetic dipoles and quadrupole radiation in solar Fraunhofer spectrum
06 p1142 A70-17991

Ca II 7233 forbidden line in solar Fraunhofer spectrum, estimating center-limb variation of equivalent width of transition
06 p1143 A70-17994

Solar Cd abundance, using spectrograph and synthetic spectral line computer program
06 p1143 A70-17995

SiH molecular absorption lines in solar disk spectrum, determining maximum equivalent widths and oscillator strength
06 p1143 A70-17996

Rocket-borne spectrometer intensity measurements UV region of solar spectrum, noting agreement with IR observations of solar temperature minimum
06 p1143 A70-17998

Solar radiation flux observation-prediction discrepancies due to Fraunhofer line absorption, studying Balmer continuum as atmospheric model criterion
06 p1148 A70-18451

Grating spectrometer with Ge-Cu detector used on balloon flights for studying variations of IR solar spectrum with altitude, emphasizing sunset features
06 p1152 A70-18523

Turbulent velocities of convective motions in active and unperturbed photospheric faculae based on spectral observations
07 p1384 A70-19415

Solar protuberance radiation polarization in Ca I 4227 A line, discussing depolarization and electron-and photoexcitation
07 p1384 A70-19416

Solar soft X ray spectrum analyzed by OSO 4 proportional counter, discussing slowly varying component, corona active regions and impulsive event characteristics
07 p1369 A70-20289

Solar magnetic field strength determination from various absorption lines, considering Rowland intensity, line lower level excitation potential, optical depth, etc
08 p1569 A70-20836

Brightness distribution of spectroheliograms taken in metal lines reflecting velocity field structure in photosphere
08 p1570 A70-20839

Magnesium hydride absorption lines in sunspot spectrograms indicating heavy Mg enhancement in sun relative to earth
08 p1571 A70-20904

Sunspots narrow and double K lines probable emission by quiescent type prominences
08 p1575 A70-21372

Molecular oxygen concentration determined by absorption spectroscopy of solar hydrogen Lyman alpha line
08 p1490 A70-21390

Oscillator strengths of Fe II lines and solar iron abundance measured by arc burning in Ar with iron chloride admixture
08 p1576 A70-21398

Corona green /5303 A/ and red /6374 A/ lines during minimum solar activity in 1964, discussing N-S and E-W asymmetries and intensities
09 p1750 A70-22100

Fabry-Perot interferometer application to photometric analysis of solar line profiles 09 p1756 A70-22652

Solar IR Fraunhofer line damping constants empirical values and variation with optical depth, noting discrepancy with theoretical constants 09 p1757 A70-22726

Solar equatorial XUV limb brightening for resonance lines of Li-like ions from OSO-4 observations interpreted by coronal model 09 p1757 A70-22732

Airborne monochromator and photoelectric filter radiometer for solar spectral irradiance measurements, estimating instrument errors 09 p1683 A70-23515

Far IR airborne spectroscopy for measuring solar brightness temperature, emphasizing scanning Michelson interferometer and radiometric calibration 09 p1683 A70-23525

Resonance, intercombination and forbidden lines observed in solar He isoelectronic sequence of oxygen, Ne, Al, Si and sulfur with Bragg crystal spectrometer 10 p1944 A70-24954

Approximations implicit in Cayrel statistical equilibrium or non-LTE analysis of ionic hydrogen bound free continuum in sun 10 p1947 A70-24989

Gadolinium II solar lines classification from photographic IR observations 10 p1947 A70-24990

Spectroscopy in astrophysical research, discussing solar corona chemical elements, forbidden lines and temperature determination 10 p1948 A70-25181

Solar XUV lines photon flux based on one dimensional model of chromosphere-corona transition region 10 p1949 A70-25271

Solar radio bursts dynamic spectra by magnetic tape recording of digital signal, obtaining frequency and time profiles and intensity layers 10 p1934 A70-25276

Type 4 solar radio bursts compared with flare observations, geophysical effects and satellite monitors data to detect proton flares spectra 10 p1934 A70-25278

Solar boron abundance from BH, BN and BO absorption bands in sunspot spectra, noting no traces in solar atmosphere 11 p2108 A70-25738

Solar limb brightening of XUV lines of carbon, nitrogen, oxygen and silicon ions in chromospheric-coronal transition region 11 p2108 A70-25740

Electron and proton excitation of forbidden transition lines in Ca XV ground configuration determined for coronal densities and temperature 11 p2109 A70-25742

Solar photospheric turbulence from observing Ti I line profiles at different center to limb distances, showing anisotropy 11 p2116 A70-26591

Zeeman effect on solar flares metallic lines splitting 11 p2106 A70-26592

Luminescing materials remote sensing during daylight by Fraunhofer line depth method with sun as excitation source 12 p2221 A70-26958

Absorption at solar H Lyman alpha line by earth hydrogen atmosphere measured as function of altitude from Aerobee flight spectrograms 12 p2222 A70-27182

Molecular line identification in solar spectrum of CN, diatomic carbon, TiO, MgH, CaH, NiH and water vapor 12 p2302 A70-27590

Violet K2 emission in H and K line cores of solar calcium ions using atmospheric model in state of motion 12 p2303 A70-27701

Solar IR triplet of singly ionized Ca, suggesting limb darkening caused by chromospheric inhomogeneities for source function inequality 12 p2303 A70-27703

Solar rotational line positions due to red band in IR continuum region to resolve blue-violet ambiguity 12 p2303 A70-27704

Magnetically sensitive Fe lines usefulness to solar polarimetry, observing absorption coefficient dependence on temperature variations 12 p2303 A70-27706

Gyrosynchrotron emission from nonthermal electrons trapped in magnetic dipole field to interpret center-to-limb spectrum and polarization variations of microwave impulsive bursts 12 p2294 A70-27709

Solar radio emissions of types I, II, III and IV activity and polarization during 18-26 May 1967 observed by narrow-band timesharing polarimeter 12 p2294 A70-27711

CH molecule line formation mechanism for 4300 Å transition in solar photosphere, noting collisions with hydrogen atoms 12 p2311 A70-28309

Dark band in H alpha solar chromosphere above photospheric limb, outlining approaches to obtain spectrally pure observational results 13 p2486 A70-28627

Solar iron-to-hydrogen ratio and oscillator strengths for Fe I lines compared with laboratory measurements of line broadening by neutral atoms 13 p2486 A70-28628

Solar spectra recording by balloon-borne monochromator, measuring stratospheric IR absorption 13 p2491 A70-29050

Magnetic field spatial structure in sunspot with photospheric bridge, using photographic observations of solar spectrum lines 13 p2493 A70-29391

Formation mechanism of molecular CN violet bands in solar photosphere 13 p2493 A70-29393

Solar Ca II H and K lines formation, discussing double reversal, limb darkening, plage and spot lines and anomalous line ratios 13 p2494 A70-29481

Solar far UV continuum photometry illustrating spectral temperature minimum transition, comparing to far IR temperature 13 p2496 A70-29841

Solar spectral line source function frequency dependence 13 p2496 A70-29842

Table of Fraunhofer solar lines without Zeeman splitting 13 p2496 A70-29843

HOH lines existence in sunspot umbral spectrum 13 p2496 A70-29847

Solar limb integrated brightness distribution in continuous spectrum during 20 May 1966 solar eclipse 13 p2498 A70-30003

Solar observations in intermediate IR, measuring continuum intensity of disk center in atmospheric water vapor window 13 p2498 A70-30006

Geoactive ionizing radiation emitted by solar flares having metallic spectral lines of various brightness intensities 14 p2630 A70-30219

Forbidden lines of OI, NI, CI, Fe II, Ni II, Si I, Si and Ca II in solar absorption, investigating effects on element abundance and gaps in thermodynamic equilibrium 14 p2637 A70-30339

Water vapor absorption bands in solar IR spectrum, considering earth curvature and atmospheric inhomogeneity and refraction 14 p2572 A70-30404

Water vapor in sunspots, taking into account red shift between telluric and intrinsic sunspot HOH lines 14 p2641 A70-30790

Ionized iron lines observations under coronal conditions, giving half-widths and kinetic temperatures for forbidden lines Fe X-Fe XV 14 p2651 A70-31377

Sun Lyman alpha emission line monitoring, describing intensity variations correlation with Zurich number 15 p2798 A70-31654

Spectral irradiances of inert gases and mixtures for laboratory solar simulation 15 p2717 A70-32028

Solar disk 10830 Å He absorption line, attributing depression at blue wing to triplet 15 p2802 A70-32488

Solar prominences monochromatic images in He I D3 and He II 4686 lines allowing for contamination in 4686 images 15 p2803 A70-32614

H alpha and Fe I lines, calculating velocity effects on profiles for differentially moving atmosphere 15 p2804 A70-32616

Line formation in solar magnetic fields with allowance for absorption emission and scattering processes, discussing Hanle effect and atomic level polarization 15 p2804 A70-32617

Fine structure in Ca II K line core, determining reduced high dispersion spectra at solar disk center 15 p2804 A70-32618

Orbiting solar telescope design for solar disturbances location and monitoring in H alpha line 16 p2907 A70-33188

Solar UV flash spectrum by spectroheliographs flown aboard Aerobee 170 mission during total solar eclipse 16 p2977 A70-33838

Coronal structures relationship to chromospheric features in H alpha and Ca II K 16 p2977 A70-33843

Solar radio spectrum and history of McMath 607 plage region during eclipse of 7 March 1970, considering residual emission 16 p2977 A70-33845

Telluric lines seasonal variations, discussing oxygen and water vapor photoelectric recordings in solar spectrum 16 p2976 A70-34185

Solar disk center to limb variation of Fraunhofer lines, comparing measurements to predictions by BCA, Elste and Holweger models 16 p2980 A70-34307

Solar X-ray spectrum and intensity and diffuse cosmic flux measurements, using polar orbiting satellite-borne instruments 17 p3149 A70-34534

Resonance and satellite lines of highly ionized iron in solar spectra, discussing spectrum features during chromospheric flares 17 p3154 A70-34541

Solar X-ray flux measurements in selected emission lines, using curved crystal Bragg spectrometers in low altitude sounding rockets 17 p3150 A70-34834

Iron line emission at 1.9 Å during solar flares observed by OSO-4 proportional counter spectrometer 17 p3150 A70-34836

Solar atmosphere structure and chemical composition by UV spectrum analysis 17 p3161 A70-34892

Solar chromosphere resonance lines, observing H and K line profiles of Mg ions 17 p3161 A70-34893

Solar UV spectrum variations due to flares and solar activity diurnal variations from satellite spectrometry 17 p3161 A70-34894

High resolution solar spectrum at 2000-2200 Å from sunpointing Skylark rocket flight, noting detectable absorption lines 17 p3162 A70-34896

Fabry-Perot interferometry of solar Mg II resonance lines 17 p3162 A70-34897

Engineering standard for solar constant and zero air mass solar spectral irradiance from high altitude measurements 17 p3077 A70-35161

Lyman alpha wing resonance broadening opacity effects on solar spectrum in 1500 Å to 8000 Å range 17 p3169 A70-35383

Non-LTE effects on flux and center to limb variation of solar spectrum at 1500-1680 Å 17 p3169 A70-35384

Continuous UV opacity effects on visual spectrum observations and predictions for solar photosphere 17 p3169 A70-35385

Fraunhofer line equivalent widths differences between pole and equator spectra of solar disk 17 p3173 A70-35734

Gamma ray pulse height spectra during active and quiet solar periods from midlatitude balloon flights 17 p3152 A70-35774

Solar potassium resonance line shape and gravitational red shift, using atomic beam technique 17 p3173 A70-35861

Solar C II resonance doublet profiles, discussing possible broadening mechanisms 17 p3174 A70-35862

Fe II line behavior in plages near solar limb 17 p3174 A70-35866

Solar image spectrum magnetic recording for computer, using photomultipliers with coding devices 18 p3256 A70-36107

Solar Ga abundance from spectral synthesis of region around 4172 Å line 18 p3316 A70-36894

Spectrophotometric solar brightness temperature measurements in far IR, discussing collision type spectral variation of absorption coefficient 18 p3319 A70-37056

Solar spectral intensity distribution and ionizing radiation spatial emission patterns during eclipse, discussing effects on ionosphere 19 p3418 A70-38908

Non-LTE line blanketed solar model atmospheres with various temperature distributions 20 p3703 A70-39020

Photographic polarimeter based on Savart and lambda/4 plates combination for linear polarization measurements of coronal and prominence emission lines during solar eclipse 20 p3627 A70-39092

Solar photospheric spectrum Ni II forbidden lines analysis, determining abundance of Ni for comparison with coronal and meteoritic data 20 p3711 A70-40405

Solar search for neutral rhenium lines using low noise, high resolution photometric tracings of Fraunhofer spectrum 20 p3711 A70-40406

Photoelectric spectra of photosphere and sunspot umbra and penumbra ranging from 3900 to 8000 Å 20 p3712 A70-40412

Solar soft X ray flare spectra of 16 November 1967, examining electron temperatures and emission lines by OSO-4 20 p3700 A70-40419

OSO far UV solar spectroheliograms atlas, describing instrumentation, data acquisition, etc 20 p3713 A70-40540

- Solar photosphere absorption line weakened region, examining temperature increase effects on neutral and ionized lines
21 p3885 A70-40953
- Large sunspot umbra continuum intensity, examining visible spectra
21 p3885 A70-40956
- Solar X-ray spectra of active regions, examining emission lines, fluxes electron temperature and density and transitions
21 p3879 A70-40963
- Sunspot umbras and penumbras magnetically nonsplit lines measured photographically by spot contrast discriminator
21 p3887 A70-41115
- Solar iron abundance from forbidden Fe II magnetic dipole transition probabilities
21 p3888 A70-41118
- Dynamic spectra and two dimensional radioheliograph maps of solar U bursts at 80 MHz consistent with electron streams along loops in coronal magnetic field
21 p3891 A70-41183
- Solar equatorial limb brightening of far UV resonance lines of lithium-like N V, O VI, Ne VIII, Mg X and Si XIII ions, interpreting os0-4 data with coronal model
21 p3924 A70-42185
- Solar far UV limb brightening of C III, N III, N IV, O III, O IV and Si IV lines in chromospheric-corona transition region, correcting coronal model for spicule effects
21 p3925 A70-42186
- Solar spectra isodentitraces indicating transition zones between and on sides of spicules in sheaths
21 p3926 A70-42197
- Transition zone height in corona-chromosphere interface from high resolution disk spectra near limb
21 p3926 A70-42198
- Photospheric metallic line profiles numerical experiment, investigating physical processes causing shape and asymmetry change
22 p4101 A70-42866
- EUV solar spectral intensity distribution and cyclic variations
22 p4106 A70-43299
- Solar disk 10830 Å He absorption line, attributing depression at blue wing to triplet
23 p4240 A70-43911
- Solar X ray spectra interpretation by laboratory measurements, using plasma X ray source and potassium acid phthalate spectrometer
23 p4237 A70-44419
- Solar center-limb observations of line brightness and Doppler shift fluctuations for Mg b lines
24 p4399 A70-45302
- MgH molecular lines Zeeman splitting in sunspot spectra confirmed by photoelectric observations
24 p4400 A70-45308
- Solar radio maps compared with H alpha pictures, correlating bright and dark features
24 p4401 A70-45317
- Solar VHF radio spectra indicating type 4 burst activity associated with type 3 formation
24 p4401 A70-45318
- Solar spectrum O I, obtaining high resolution UV line profiles from rocket-borne spectrograms
24 p4410 A70-45766
- Geoeactive ionizing radiation emitted by solar flares having metallic spectral lines of various brightness intensities
24 p4398 A70-46294
- SOLAR SPECTROMETERS**
- Solar atmospheric structure near sunspots by spectrophotometry, presenting observational and theoretical sunspot magnetic and velocity field data
04 p0754 A70-15351
- Grating spectrometer with Ge-Cu detector used on balloon flights for studying variations of IR solar spectrum with altitude, emphasizing sunset features
06 p1152 A70-18523
- Fabry-Perot interferometer application to photometric analysis of solar line profiles
09 p1756 A70-22652
- Spectrometer design for Helios solar probe using semiconductor detectors to identify particles separated by magnetic field
10 p1888 A70-24487
- Atmospheric absorption by ozone of solar radiation measured by balloon-borne spectrometer in 9-10 micron region
11 p2045 A70-25627
- Solar gamma ray lines search with high resolution balloon-borne directional spectrometer based on lithium-drifted germanium detector
12 p2292 A70-27178
- Spectrograph design and specifications for solar radio flare structure, obtaining constant sum frequency by heterodyne conversion
13 p2406 A70-28948
- EUV solar spectrometer in orbiting solar observatory /OSO-1/, describing satellite, optics and detector, data coding, etc
15 p2736 A70-32027
- Scanning mirror system for Apollo telescope mount UV spectroheliometer, describing design, fabrication and testing
17 p3083 A70-34764
- Slit quality and instrument contour of diffraction spectrograph for solar observations
24 p4335 A70-45638
- SOLAR STORMS**
- Solar proton flux increases associated with sudden commencements observed by geostationary ATS-1 satellite
08 p1562 A70-21378
- Type 1 solar radio burst chains during noise storms, determining lifetime, bandwidth, frequency drift and fine structure
13 p2479 A70-30002
- Energetic storm particle events observation, noting association with solar protons and interplanetary shock waves
19 p3496 A70-37518
- SOLAR STREAMS**
- U SOLAR CORPUSCULAR RADIATION**
- SOLAR SYSTEM**
- Three mode galactic age model for nucleosynthesis of solar radioisotopic material produced by r-processes
01 p0182 A70-10720
- White dwarf luminosity functions based on birth rate, white dwarf space density in solar neighborhood and possible red degenerate stars deficiency
01 p0189 A70-11339
- Radar probing of solar system noting contributions to knowledge on planets
01 p0192 A70-11485
- Solar system evolution based on Darwin theory, discussing energy inputs effect on primeval atmospheric molecules
02 p0229 A70-11666
- Solar system various natural members examination for suitability to relativistic pericentrum motion investigation
02 p0373 A70-12255
- Undiscovered satellites of solar system major planets, predicting Jupiter satellites
03 p0569 A70-13360
- Soviet Venus probes Venera 1, 2, 3, 4 and 5 emphasizing aims, implementation means and information yields influence on theory of solar system planets origin and evolution
04 p0757 A70-15672
- Critique of solar system resonant structure hypothesis based on planetary orbital frequencies errors
05 p0910 A70-16394
- Critique of resonant structure of solar system noting chance effects possibility
05 p0910 A70-16395
- Rebuttal of criticisms on resonant structure hypothesis, giving probability value for chance stellar system formation similar to solar system
05 p0910 A70-16396
- Solar system resonant structure probability analyzed by matrix methods
05 p0910 A70-16397
- Solar orbiting planets formation theory agreement with actual planetary system proved in terms of planetary masses and distances
05 p0913 A70-16567
- Cosmic ray triggering of solar system formation by ionizing in solar disk
06 p1135 A70-17539
- Meteors orbital elements distribution in solar system from radio observation data
06 p1141 A70-17737
- Outer solar system exploration, discussing swingby and junction missions, Jovian satellite grand tours, mission energy requirements, etc
06 p1147 A70-18229
- Unmanned exploration program to study magnetic fields and chemical composition of five outer planets in solar system
07 p1375 A70-18871
- Solar system evolution theories to explain planetary orbits, angular momentum and matter distribution, satellite systems and chemical composition
07 p1376 A70-18898
- Solar system cosmic ray time-space variations analysis based on simulation of meteorite nuclear processes
07 p1372 A70-20338
- Historical survey of celestial mechanics including three body problem and solar system dynamic model construction
08 p1565 A70-20561
- Solar system origin theory emphasizing brother star approaching nebula for instability of boundary layer
08 p1568 A70-20638
- Book on solar and planetary radio emission covering solar system physical characteristics, quiet Sun, thermal and nonthermal emission, etc
09 p1752 A70-22201
- Planetary satellites perturbation by sun for elliptical solar orbit, applying Zeipel method to equations of motion
09 p1754 A70-22480
- Solar system planetary mean motions calculation from characteristic equations roots at equilibrium points of restricted three body problem, using Taylor series solution
09 p1760 A70-22915
- Extinct radioactive isotopes of solar system, discussing decay during nuclear synthesis and planetary formation periods
09 p1762 A70-23126
- Monograph on solar wind covering solar physics, space observation methods, solar system interactions, etc
09 p1745 A70-23475
- Bode law development from dynamical relaxation suggested from comparison of Jupiter, Saturn and Uranus inner satellite systems with planetary system
09 p1765 A70-23796
- Collection of papers on analytical chemistry in space covering solar system history, atmospheres, composition, lunar and planetary surface analysis, mass spectroscopy, etc
10 p1941 A70-24608
- Solar system objects /earth, moon, planets, meteorites, etc/ chemical composition data and analysis techniques
10 p1942 A70-24609
- Solar and solar system planetary atmospheres including interplanetary space filled with solar wind
10 p1942 A70-24611
- Mass spectroscopy for solar system exploration, discussing ion sources, mass analyzers and ion detectors meeting mission requirements
10 p1942 A70-24612
- Barnard two planet solar system, dwarf star perturbations, orbital parameters and comparison with Solar system
10 p1943 A70-24758
- Jupiter atmospheric composition, gas and dust cloud formation as clues to origin and evolution of solar system
11 p2108 A70-25654
- Nuclear pulse propulsion system for manned missions to outer planets of solar system, discussing energy and travel time requirements
11 p2082 A70-26059
- Space propulsion systems for public transportation to and from orbit and throughout near solar system, discussing commercial requirements
11 p2102 A70-26060
- Outer solar system exploration, discussing planetary data, interplanetary environment, atmospheric models, data acquisition, etc
11 p2112 A70-26062
- Solar system and interstellar space exploration phases, manned and unmanned missions, meta and microprobes, propulsion systems, etc
11 p2112 A70-26063
- Undiscovered satellites of solar system major planets, predicting Jupiter satellites
11 p2118 A70-26725
- Antimatter motion in solar system and earth atmosphere, discussing vaporization and annihilation energy in collisions with interplanetary gas atoms
11 p2119 A70-26793
- Cosmic electron detection and measurement techniques, considering presence in solar system, interstellar space and metagalaxy and galactic continuum radio emission
12 p2293 A70-27572
- Lunar rocks and dust from Apollo 11 mission investigated for origin and history of moon and solar system
12 p2310 A70-28049
- Nomogram construction for graphical solution of two body problem using radius-vector and velocity components applied to solar system
12 p2311 A70-28310
- Preplanetary matter irradiation by solar particles, noting isotopic abundances for evidence of nucleosynthesis induced by proton and alpha bombardment
13 p2486 A70-28619
- Soviet monograph on minor planets origin and physical nature, considering orbits, investigative techniques, etc
13 p2488 A70-28800
- Interstellar hydrogen density around solar system from calibrated Lyman-alpha intensity measurements of Vela 7
13 p2489 A70-28894
- Cryobiological data for life mechanisms on planets in solar system emphasizing Mars
14 p2536 A70-30344
- Solar wind interaction with earth, moon, planets and comets, using hypersonic fluid analog involving shock wave interactions
14 p2631 A70-30360
- Galactic cosmic ray actions on interstellar medium for origin of Li, Be and boron in stellar atmospheres and solar system
14 p2640 A70-30786
- Atomic hydrogen distribution in upper atmosphere and solar system obtained during spin operation of OGO 5 with Lyman alpha photometer
15 p2798 A70-31655

Trojan Relay system with satellites preceding and following earth in solar orbit ensuring radio communication throughout solar system

15 p2698 A70-32061

Historical survey of celestial mechanics including three body problem and solar system dynamic model construction

15 p2805 A70-32716

Solar system Eotvos experiments for measuring gravitational to inertial mass ratio of celestial bodies

16 p2978 A70-34033

Solar wind interaction with earth, moon, Venus and Mars, reviewing literature on continuum fluid model, spacecraft observations, plasma characteristics, etc

17 p3150 A70-34669

German monograph on heavy space probes for solar system investigation covering systems analysis, mission success, flight programs, Saturn 5 launch vehicle, etc

17 p3168 A70-35378

Local system interstellar medium thermal electron distribution, synchrotron radiation emissivity, cosmic ray electron flux and spectrum

17 p3152 A70-35583

Gaseous disk in equatorial plane of solar nebula, determining dimensions from accretional theory for planets formation

17 p3172 A70-35584

Lunar gravitational field effect on sun-earth exterior libration point location, examining placement on line passing through sun and earth-moon barycenter

18 p3320 A70-37059

Integrated Milky Way spectrum, examining composition and galactic structure in solar neighborhood

18 p3329 A70-37182

Humason 1960e-1959X comet hyperbolic orbit, indicating solar system permanent membership

19 p3516 A70-37934

Galactic cosmic rays temporal and spatial variations in solar system, discussing nuclear active particles and spallation products depth distribution in meteorites

19 p3509 A70-38143

Planetary theory construction to second order of disturbing masses, applying to motions of any set of two or three planets in solar system

19 p3523 A70-38687

Solar system unmanned exploration decision making, discussing resource utilization, sequence optimization, etc

20 p3710 A70-40335

Scientific motivation for outer planets exploration covering solar system clues, atmosphere comparisons with earth, radiation and planetary radii measurement, etc

21 p3920 A70-41794

Titius-Bode law conclusions regarding solar system planetary distances numerical relations, considering planetary evolution

22 p4101 A70-42863

Solar motion apex for neutral hydrogen concentrations at different velocities, suggesting relationship to galaxy

23 p4239 A70-43815

Solar nebula rings and planet formation by sedimentation of solid particles in mechanical equilibrium, including Jupiter and Saturn protoplanets

23 p4239 A70-43867

Planetary exploration for solar system origin and evolution, identifying outer planet mission scientific values

24 p4411 A70-45962

[AIAA PAPER 70-1244] Stellar surface and solar system light element abundances, explaining formation by energetic proton flux nucleosynthetic effect

24 p4398 A70-46163

SOLAR TEMPERATURE

Solar interplanetary temperature measurement by Cl, Ga and Li isotopic detectors of solar neutrinos, discussing effectiveness and upper temperature bound

05 p0899 A70-15951

Far IR measurement of solar minimum temperature with Michelson interferometer carried on NASA research aircraft

06 p1143 A70-17997

Rocket-borne spectrometer intensity measurements UV region of solar spectrum, noting agreement with IR observations of solar temperature minimum

06 p1143 A70-17998

Polar and equatorial limb darkening related to solar rotation and thermal flow, using photospheric models

15 p2807 A70-32812

Doppler temperature and motion of solar corona from ionized Fe line using Fabry-Perot interferometer

16 p2977 A70-33841

Solar photosphere temperature constancy in thin CO layer from equivalent spectral line width determination

18 p3322 A70-37134

Report on ASA meeting in Pasadena February 1969 covering solar observation program, solar temperature inversion, solar spin-down, etc

19 p3518 A70-38014

Temperature and radio brightness distributions in active regions and upper chromosphere during minimum activity periods

19 p3522 A70-38557

Temperature difference between equator and solar poles from spectral line equivalent width variation

20 p3711 A70-40407

Solar photosphere absorption line weakened region, examining temperature increase effects on neutral and ionized lines

21 p3885 A70-40953

Soft X-ray enhancement during solar flares due to coronal condensation temperature increase

21 p3880 A70-40969

Vertical oscillations in solar temperature minimum suggested as acoustic-gravity waves modes dependent on height at chromosphere-corona interface

21 p3926 A70-42196

Solar X-ray flare temperature and emission measure profiles using OGO 5 satellite detector, interpreting energy dispersion of peak times

24 p4397 A70-45768

SOLAR VELOCITY

Simultaneous filtergrams of velocity and intensity field of central solar disk obtained in blue and red wings of Fraunhofer line

01 p0175 A70-10242

SOLAR WIND

Solar wind-induced drag resulting from collisionless plasma shock on sunward-side of large magnetic comet, using similarity with earth magnetosphere

01 p0168 A70-10258

Geomagnetic bays produced by neutral sheet plasma earthward movement resulting from solar wind enlargement of geomagnetic tail

01 p0071 A70-10409

Geomagnetic micropulsations relation to magnetospheric boundary location on sun-earth line, noting influence of solar wind pressure variations

01 p0071 A70-10412

Steady state spherically symmetric model for solar plasma acceleration with distance, showing essential role of viscosity

01 p0172 A70-11519

Electrical phenomena in upper atmosphere and solar wind may control geomagnetic disturbances and aurorae

01 p0082 A70-11523

One dimensional nonlinear model of anisotropic plasma instability with respect to Alfvén waves growth, noting applicability to solar wind processes

01 p0153 A70-11597

Solar/stellar wind solutions asymptotic behavior at large distances from central star for equations including effects of rotation and anisotropy

02 p0358 A70-12253

Dynamic electric field in solar coronal exosphere on basis of kinetic and hydrodynamic theories, giving estimate of solar wind

02 p0359 A70-12609

HEOS-1 satellite development for ESRO to investigate interplanetary magnetic fields, cosmic radiation, solar wind outside magnetosphere and earth shock wave

02 p0382 A70-12646

Linearized steady state hydrodynamic equations describing solar wind meridional motions used for studying zonal pressure perturbations

03 p0558 A70-13599

Solar wind discontinuity surfaces observed by spacecraft magnetometers determined from measured time delays and solar wind speed

03 p0558 A70-13600

Tropospheric circulation transformation from meridional to zonal forms due to macrostructure activity of solar wind, considering magnetospheric perturbations

03 p0559 A70-13757

Astronomical and space research methods probing fundamental questions concerning universe unsolvable by classical astronomy, discussing solar wind and stellar formation and evolution

03 p0571 A70-13790

Interplanetary field influence on auroral radio absorption, considering sector structure of solar wind

03 p0476 A70-13915

Thermal model for Venus ionosphere, considering photoionization and solar wind influx for possible heat sources

03 p0575 A70-13981

Magnetopause shape determination model allowing for solar wind direction obliquely toward geomagnetic dipole axis

03 p0560 A70-13984

Spacecraft surface secondary electron emission effects on electron trap measurements in magnetosphere and solar wind, noting agreement with positive ion densities

03 p0561 A70-13994

Nonthermal heating mechanism in quiet solar wind, tabulating observed and predicted parameters

03 p0561 A70-13998

Magnetospheric magnetic field disturbance due to abrupt solar wind parameters change, using Explorer 26 data

04 p0738 A70-14444

Solar wind-induced torque calculated considering special and general relativistic effects, extending method to pulsar rotational model

04 p0739 A70-14593

Galactic cosmic rays scattering by solar wind magnetic field fluctuations, considering energy and momentum transfer

04 p0739 A70-14596

Solar wind acceleration and coronal plasma heating above plage regions from spectra of solar radio echoes, computing temperature rise and energy input

04 p0740 A70-15049

Dynamic model for Martian ionosphere modification by solar wind, assuming negligible Mars magnetic moment and neutral atmosphere

04 p0753 A70-15103

Cosmic ray flux modulation in earth atmosphere produced by solar wind and geomagnetic variations, considering effects on atmospheric carbon 14 variations

04 p0680 A70-15114

Interplanetary magnetic field fluctuations stimulated by lunar wake, using Explorer 35 satellite measurements

04 p0753 A70-15122

Turbulent-plasma electrons ballistic effects on solar wind magnetic field fluctuations in lunar vicinity

04 p0753 A70-15123

Solar wind as one dimensional flow analogous to Laval nozzle flow, discussing rotation and magnetic field effect on model with heat conduction

04 p0754 A70-15352

Anomalous ionization variations of F 2 layer at northern geomagnetic pole during winter coincident with decrease in solar plasma density

04 p0682 A70-15726

Satellite HEOS-1 S 73 experiment launched during solar maximum to determine flux and energy distribution of solar wind positive component

05 p0900 A70-16077

Al foil exposed to solar wind on moon during Apollo 11 mission examined for helium particles, finding lunar solar wind albedo

05 p0900 A70-16093

Gray and colorless features of moon explained as atomic H imported by solar wind replacing lost H by photolytic decomposition of water vapor

05 p0908 A70-16303

Magnetized solar wind steady state inviscid single fluid model developed using MHD, including heat equation with thermal conduction

05 p0902 A70-16445

Earth bow shock and magnetopause oscillatory motions with respect to positions assumed under quiet solar wind conditions, discussing satellite observations

05 p0840 A70-16586

Tangential solar wind discontinuity observed by Vela 2A satellite, producing ground magnetic disturbances conjunctively with magnetospheric, ground and ionospheric currents

05 p0903 A70-16727

Cosmic ray intensity preceding Forbush effects as function of chromospheric flares solar longitude and solar wind velocity

05 p0903 A70-16730

Solar wind clues, discussing ionization blowoff, Halley comet tail and solar corona

06 p1134 A70-17322

Solar wind temperature, using distribution function for solar wind ions in anisotropic Maxwell distribution form

06 p1135 A70-17895

Spherical cylindrical and toroidal electrostatic analyzers with symmetrical angular characteristics for solar wind investigations

06 p1135 A70-17896

Spatial properties of solar wind during maximum and minimum activity inferred from sodium D-line emissions from cometary nuclei

06 p1136 A70-18012

Large scale artificial plasma cloud experiments for magnetosphere, solar wind and cometary physics, discussing Ba ion and ice clouds released by satellites [AIAA PAPER 70-33]

06 p1145 A70-18183

Kinetics of solar wind interaction with moon and planetary bodies using perturbation scheme to obtain ion density distribution on antisolar side [AIAA PAPER 70-61]

06 p1136 A70-18192

Solar plasma wind simulator design and performance, discussing ion source, mass separator, beam mass analyzer and Faraday cup [AIAA PAPER 70-31]

06 p1030 A70-18223

Solar wind flow different interactions with earth, Venus and moon

06 p1136 A70-18284

Solar wind interaction with moon derived for model and compared with satellite data

06 p1147 A70-18291

Solar flare induced interplanetary shock and helium enriched driver gas observed on 13 February 1967, discussing wind velocity and plasma acceleration

06 p1152 A70-18526

Collisional skewing of electron distribution function associated with heat conduction in solar wind, exciting collisionless ion-acoustic, electrostatic ion cyclotron and magnetoacoustic waves

06 p1136 A70-18527

- Magnetic activity effect on magnetospheric
plasmopause position, measuring ion concentrations
as function of local time from OGO 5 observations
06 p1058 A70-18530
- Lunar interior electrical conductivity estimated
using lunar interaction with solar wind and interplanetary
electric and magnetic fields
06 p1153 A70-18544
- Earth magnetosphere physics, considering solar
plasma flow, ring currents, charged particles during
magnetic storms, solar wind energy transfer, etc
06 p1060 A70-18552
- Magnetic field and plasma variations in lunar wake
using Maxwell equations
06 p1153 A70-18636
- Unipolar induction to calculate moon interior electric
field profiles, noting magnetic back pressure as
limb shock wave and interaction with solar wind
07 p1377 A70-18970
- Solar wind, using data on solar and galactic cosmic
rays in interplanetary space
07 p1366 A70-19030
- Steady spherical plasma flow from sun analyzed by
equations of solar corona hydrodynamical model
07 p1378 A70-19033
- Circumsolar plasma structural inhomogeneity origin
07 p1384 A70-19418
- Solar wind effects on galactic cosmic rays isotropic
diffusion and density distribution in interplanetary
space in presence of azimuthal asymmetry
07 p1366 A70-19429
- Solar wind velocity anisotropy effect on interplanetary
magnetic field inhomogeneity
07 p1366 A70-19443
- Strong explosion model for analyzing shock wave
propagation after chromospheric flare allowing for
quasi-radial motion of unperturbed solar wind
07 p1367 A70-19489
- Hydromagnetic wave interaction with magnetopause
and bow shock, considering solar wind turbulence
and magnetopause tail stability
07 p1270 A70-20070
- Galactic cosmic rays intensity long term modulation,
studying roles of solar corona, solar wind and
interplanetary electromagnetic field
07 p1369 A70-20075
- Cosmic ray microvariations relation to solar wind
structure, particle scattering models, spatial distribution,
time variations, etc
07 p1372 A70-20336
- Solar wind structural characteristics determination
from cosmic ray variations in interplanetary medium,
considering interplanetary magnetic field structure
and spatial orientation
07 p1372 A70-20337
- Solar wind interaction with galactic cosmic radiation
resulting in wind radial motion braking, discussing
possible solar wind focusing
07 p1373 A70-20343
- Steady state spherically symmetrical ejection of
multicomponent plasma from sun determined with
hydrogen approximation, considering ion composition
07 p1391 A70-20418
- Solar wind velocity cycles from fluid MHD viewpoint,
applying Kelvin theorem on circulation stability
in closed fluid system
07 p1373 A70-20441
- Alfvén wave structure mechanism of geomagnetic
micropulsation type in cometary tails, assuming Kelvin-
Helmholtz instability at comet plasma-solar wind
interface
08 p1565 A70-20567
- Hydrogen supply rate by solar wind found comparable
to hydrogen losses from earth by diffusion into
space
08 p1487 A70-20637
- Solar wind ejection, analyzing regions of heat conducting
fluxes and laminar patterns
08 p1561 A70-21059
- Solar wind velocity radioastronomical measurements,
discussing radio wave fluctuations, telescope
antenna designs, radiometers and observations
08 p1474 A70-21070
- Plasma instabilities in solar wind for frequencies
near proton gyrofrequency, driving instabilities by
electron and proton thermal anisotropies
08 p1561 A70-21261
- Initial deceleration of solar wind positive ions
upstream of earth bow shock determined from OGO 5
high time resolution plasma measurements
08 p1562 A70-21377
- Solar corona and interplanetary plasma structure
and dynamics, calculating solar wind velocity as function
of distance from sun
08 p1576 A70-21397
- Interplanetary density distribution of cold interstellar
origin hydrogen dependent on solar EUV flux,
considering interaction with solar wind protons
08 p1562 A70-21401
- Solar wind and Venus topside ionosphere interaction,
discussing charged particle density, temperature
and pressure distribution
08 p1578 A70-21550
- Laboratory irradiation of rock samples for solar
wind flux effects on IR reflectivity of lunar rocks
08 p1579 A70-21565
- Energy distribution of solar wind alpha particles in
magnetosheath observed by Heos A satellite
09 p1744 A70-22305
- Solar wind heating, determining roles of various
energy sources from Explorer 34 observations
09 p1755 A70-22511
- Magnetic field and gas thermal conductivity effects
in analysis of solar wind as one dimensional, steady
and spherically symmetric flow
09 p1745 A70-22687
- Refractive index variation regions and mapping
along propagation path in random medium, noting
application to solar wind electron density structures
measurements
09 p1634 A70-22699
- Solar wind magnitude and variability effects on
geomagnetic activity and cosmic ray intensity modulation
from satellite observations
09 p1745 A70-23272
- Monograph on solar wind covering solar physics,
space observation methods, solar system interactions,
etc
09 p1745 A70-23475
- Solar wind properties and helium abundance determined
from satellite-borne electrostatic analyzers
09 p1746 A70-23482
- Lunar limb weak solar wind shock due to conducting
crust-interplanetary magnetic field interaction
09 p1764 A70-23485
- Magnetic disturbances caused by magnetosphere-solar
wind filamentary inhomogeneity interaction observed
by Pioneer 6
10 p1931 A70-24320
- Comets ionized shells, studying plasma expansion in
corpuscular solar wind magnetic field
10 p1940 A70-24372
- Solar wind model with electrons, protons and alpha
particles coupled by electric field and expanding due
to pressure gradient and solar gravitation
10 p1931 A70-24433
- Magnetopause boundary between shocked streaming
solar plasma and geomagnetic tail observed at
lunar orbit by magnetometer on Explorer 35
10 p1941 A70-24436
- Isotopic ratio anomaly of Re and detection at nanogram
level in solar wind using decay curves of Re
source from lunar specimen
10 p1932 A70-24532
- Solar wind-geomagnetic field interactions, considering
day and night hemispheres, satellite observations,
shock and magnetopause motion, shock structure, etc
10 p1932 A70-24553
- Solar and solar system planetary atmospheres including
interplanetary space filled with solar wind
10 p1942 A70-24611
- Pressure anisotropies contribution to solar wind
corotation, discussing angular momentum and magnetic
field
10 p1935 A70-25285
- Satellite solar wind observations concerning interplanetary
magnetic field direction and strength, proton
distribution, solar wind velocity, density and direction
10 p1935 A70-25286
- Particle acceleration during solar plasma ejection,
disregarding magnetic effects on flux
11 p2107 A70-25526
- F region magnetic disturbances due to low energy
solar plasma penetration during proton bursts
11 p2104 A70-25535
- Polar ionospheric current and interplanetary magnetic
field directions related from mean diurnal values
of solar wind velocity
11 p2044 A70-25551
- Swiss Solar Wind Composition Experiment, analyzing
trapped particles characteristics of Apollo 11 and
12 lunar exposed aluminum foil
11 p2105 A70-25950
- Solar wind correlation with geomagnetic activity,
comparing Vela 3 and 4 observations with Mariner 2
measurements
11 p2105 A70-26075
- Plasma density and velocity required for simulating
solar wind flow over magnetosphere (bow shock/ in
plasma wind tunnel
11 p2032 A70-26372
- Interplanetary medium kinetic equations to limit ion
temperature anisotropies in solar wind, discussing
Coulomb collisions and ion-cyclotron instability effects
11 p2105 A70-26561
- Oblique shock initiated by 7 July 1966 proton flare in
solar wind observed by satellite magnetometers outside
magnetosphere
11 p2105 A70-26562
- Geomagnetic damped type pulsations associated
with storms interpreted as interaction between
hydromagnetic oscillations and magnetospheric motions
caused by solar wind
11 p2047 A70-26567
- Comet Morehouse /1908III/ tail rays waviness interpreted
in terms of fluctuations in solar wind direction
11 p2117 A70-26649
- Solar wind magnetic field power spectra and plasma
velocity, discussing turbulence, viscosity and dissipation
11 p2106 A70-26770
- Solar wind structure as function of corotating
coronal inhomogeneities determined using perturbation
equations for spherical polar coordinate system
12 p2292 A70-27179
- Very low frequency radio noise in ionosphere, magnetosphere
and solar wind, using multiple receivers to measure
mathematical relations between direction magnitude
and polarization characteristics
12 p2184 A70-27574
- Solar plasma and energy and radiation fading during
microwave bursts due to synchrotron radiation losses,
determining magnetic field strength
12 p2294 A70-27593
- Lunar limb shock wave observed by Explorer 35
satellite defined with respect to solar wind flow
direction, discussing formation mechanism
12 p2294 A70-27594
- Magnetospheric magnetic field disturbance due to abrupt
solar wind parameters change, using Explorer 26 data
13 p2475 A70-28469
- Semiannual variation of geomagnetic activity related
to incident solar wind, considering Mariner 2 measurements
13 p2475 A70-28573
- Monograph on polar aurora with emphasis on solar
wind and interplanetary magnetic fields, discussing
substorms, particle acceleration in current sheet, etc
13 p2395 A70-28983
- Two fluid model for solar wind treating constant
temperature electrons hydrodynamically and protons
as collisionless
13 p2477 A70-29178
- Steady state symmetrical model for solar wind near
equatorial plane, investigating effects of magnetic
forces, viscosity and anisotropic pressure on
azimuthal motion
13 p2477 A70-29179
- Solar wind effect on structure of magnetic field in
magnetosphere and interplanetary space, noting
interaction with moon
13 p2498 A70-30051
- Magnetotail plasma sheet temporal variations during
substorms and plasma pressure as related to dynamic
pressure of solar wind from Vela satellites observation
13 p2480 A70-30061
- Radiation belt and auroral primary ions, comparing
origin possibilities of ionosphere and solar wind
13 p2481 A70-30063
- Solar wind parameters time variations influence on
geomagnetic activity from measurements by electrostatic
analyzers on Vela satellites
13 p2481 A70-30065
- Interplanetary shock wave properties in solar wind,
determining propagation velocity, transit times proton
density, proton and electron temperatures
13 p2481 A70-30066
- Hydromagnetic fluid model of solar wind for interpreting
discontinuities in plasma and magnetic field,
interaction with atmosphere, heating mechanism and
chemical composition
13 p2481 A70-30067
- Satellite plasma diagnostics for electric and magnetic
fields and fine structure of collisionless shocks in
solar wind plasma flows and interplanetary shocks
13 p2481 A70-30069
- Plasma wave particle interactions in outer magnetosphere,
magnetosheath and solar wind, noting role of
AC electric fields
13 p2483 A70-30085
- Solar wind interaction with moon, constructing
mathematical model based on MHD equations and Explorer
35 data
14 p2630 A70-30356
- Solar wind energies spherical surface average and
fluctuations from integration of conservation equations
14 p2630 A70-30357
- Solar wind interaction with earth, moon, planets and
comets, using hypersonic fluid analog involving shock
wave interactions
14 p2631 A70-30360
- Mathematical model for interaction of solar wind
with geomagnetic field, predicting magnetosphere
shape
14 p2574 A70-30736
- Anomalous ionization variations of F 2 layer at
northern geomagnetic pole during winter coincident
with decrease in solar plasma density
14 p2575 A70-30810
- Cosmic ray transport in solar wind generalized with
anisotropic diffusion approximation
14 p2632 A70-30887
- Solar wind turbulence, demonstrating radio source
interplanetary scintillation consistent with plasma density
correlation
14 p2642 A70-30888

Solar wind interaction with planetary ionosphere, considering flow behavior across bow MHD shock 14 p2647 A70-31073

Solar flare particle flux equilibrium anisotropy and convection in solar wind 15 p2793 A70-31901

Apollo 11 lunar mission results, discussing surface, seismology, laser ranging retroreflector, solar wind and rock samples 15 p2800 A70-32073

Terrestrial magnetosphere dynamics in magnetosheath disturbances, analyzing solar wind-geomagnetic field interaction and storm development 15 p2729 A70-32080

Magnetosphere survey, including solar wind flow theory, observational techniques, radiation belt theory, magnetic storms, etc 15 p2732 A70-32544

Solar wind models based on exospheric theory assuming collisionless particles 15 p2794 A70-32613

Alfvén wave structure mechanism of geomagnetic micropulsation type in cometary tails, assuming Kelvin-Helmholtz instability at comet plasma-solar wind interface 15 p2805 A70-32722

Strong explosion model for analyzing shock wave propagation after chromospheric flare allowing for quasi-radial motion of unperturbed solar wind 15 p2795 A70-32734

Collisionless shock waves model in solar wind plasma, discussing instability and energy dissipation 15 p2795 A70-32825

Solar wind observations by Pioneer 6, considering particle density, flux and kinetic energy 16 p2972 A70-32949

German-American HELIOS solar probe for solar wind, interplanetary magnetic field and cosmic rays 16 p2987 A70-34343

Solar wind interaction with earth, moon, Venus and Mars, reviewing literature on continuum fluid model, spacecraft observations, plasma characteristics, etc 17 p3150 A70-34669

Periodic comet nature, origin and anomalous behavior with space mission planning implications, assuming solar plasma source and solar-interstellar interaction AAS PAPER 70-029 17 p3155 A70-34795

Solar rotation effects on velocity field in nonspherical solar wind, using axisymmetric fluid model 17 p3151 A70-34861

Heliostationary spacecraft at L2 point for solar wind observation, describing mission, instrumentation and spacecraft design 17 p3168 A70-35252

Lunar atmosphere as source of Ar 40 and other elements in surface materials, discussing implantation by photoionization and subsequent interaction with solar wind fields 17 p3172 A70-35624

Solar wind velocity profile in rapid acceleration of coronal plasma from type I, III and V bursts 17 p3152 A70-35745

Ions acceleration and motion in corona and solar wind, discussing equation derivation, He abundance, nonMaxwellian distribution functions, minimum flux estimation, etc 17 p3152 A70-35870

Radio sources angular broadening by solar wind turbulence used for solar corona probe 18 p3311 A70-36003

OGO 5 observations of quasi-trapped electromagnetic waves in solar wind at 70 kHz 18 p3306 A70-36005

Interplanetary plasma disturbances in Venus proximity from Venera measurements 18 p3312 A70-36172

Temporal and spatial covariation of high latitude geophysical phenomena, using unified mechanism of solar plasma stream interaction with geomagnetic field 18 p3247 A70-36404

Solar wind effects on galactic cosmic rays isotropic diffusion and density distribution in interplanetary space in presence of azimuthal asymmetry 18 p3309 A70-36903

Solar wind velocity anisotropy effect on interplanetary magnetic field inhomogeneity 18 p3309 A70-36917

Elastic energy transfer cross sections calculation of H-H scattering to estimate neutralized solar wind particles thermalization 18 p3309 A70-36951

Mass spectrometric analysis of lunar rocks for rare gases of solar wind, determining relative abundance, isotopic composition, rock age, exposure time, etc 18 p3320 A70-37083

Geomagnetic activity relation to large scale variations in interplanetary magnetic field and solar wind deformation velocity, using satellite and space probe observations 19 p3491 A70-37304

Flare associated high energy photon and particle fluxes characterized by short rise times and longer lasting decays, discussing plasma emissions 19 p3493 A70-37473

Solar wind disturbances associated with solar activity observed by spacecraft probing interplanetary space, considering geomagnetic activity classes 19 p3494 A70-37478

Solar wind fluxes observed onboard Venera 2 and 6 compared with earth electromagnetic field pulsations and short period disturbances 19 p3494 A70-37479

Plasma properties across bow shock and in magnetosheath as function of supersonic solar wind 19 p3494 A70-37481

Trapped particle population changes associated with solar events, discussing solar wind discontinuity effects on magnetosphere 19 p3495 A70-37487

Interplanetary plasma observations by Vela satellites in solar wind and plasma sheet of magnetotail during magnetic storm 19 p3410 A70-37490

Solar wind discontinuity during solar flare from Heos A measurements, observing shock wave propagation 19 p3495 A70-37502

Solar wind and flare energetic particles properties and interactions, surveying interplanetary magnetic field, planetary bow shock waves, neutrons, neutrinos, etc 19 p3511 A70-38418

Geomagnetic field pulsations prior to polar magnetic disturbance onset, discussing solar wind role 19 p3416 A70-38588

Solar wind velocity variations showing relationship with electron density excess and localized region temperature of corona 19 p3512 A70-38693

Plasmapause motion in equatorial plane under sudden dawn-dusk field with constant solar wind-magnetosphere interaction 20 p3620 A70-39341

Maximum to minimum exospheric temperature ratio determination, concluding solar wind dependence of diurnal variation in thermosphere 20 p3621 A70-39345

Interplanetary magnetic field structure, using solar wind model accounting for solar rotation 20 p3704 A70-39474

Solar wind effects on thermal control coatings reflectance and absorbance, noting simulation and thermophysical measurement requirements AIAA PAPER 70-833 20 p3655 A70-39825

Solar internal rotation, examining oblateness, velocity and magnetic fields, wind structure and Li and Be abundances 20 p3707 A70-39936

Solar wind flow behind shock fronts from Mariner 5 and Explorer 34 spacecraft 20 p3701 A70-40422

Interplanetary plasma torque due to temperature and pressure anisotropy, considering solar wind angular velocity and sun angular momentum 20 p3712 A70-40423

Solar wind X ray emission, investigating diffused cosmic ray origin and flow pattern models 21 p3878 A70-40708

Solar wind static and dynamic pressures on earth magnetosphere, using geomagnetic parameters 21 p3878 A70-40845

Flow parameters radial dependence of thin solar wind filament corotating with sun 21 p3881 A70-40972

Solar wind free electron number density measurement by Pioneer 6 spacecraft after solar proton flare, constructing plasma cloud models 21 p3881 A70-41079

Large scale flare associated solar wind disturbances observed by Vela satellites, noting prolonged elevated flow speed after shock 21 p3881 A70-41080

Solar wind proton properties examined by Vela 3, observing density distribution, flow speed and direction, thermal anisotropy, magnitude and orientation 21 p3881 A70-41081

Inner magnetosheath large amplitude hydromagnetic waves, discussing power spectrum, earth bow shock and solar wind 21 p3816 A70-41083

Particle acceleration during solar plasma ejection, disregarding magnetic effects on flux 21 p3892 A70-41276

F region magnetic disturbances due to low energy solar plasma penetration during proton bursts 21 p3882 A70-41285

Polar ionospheric current and interplanetary magnetic field directions related from mean diurnal values of solar wind velocity 21 p3819 A70-41301

Apollo 11 lunar fines trapped noble gas elemental and isotopic abundances, suggesting solar wind origin 21 p3906 A70-41565

Radiogenic and cosmogenic inert gases and isotopic ratios in Tranquility Base fines indicating solar wind saturation 21 p3775 A70-41581

Rare gas distribution in grain surfaces of lunar soil, breccias and rocks originating from solar wind, using microhelium probe 21 p3908 A70-41587

Apollo 11 lunar soil irradiation history from solar wind rare gas abundances and cosmic ray spallation products 21 p3908 A70-41590

Rock particle tracks of primary cosmic rays, spallation recoil nuclei, nuclear fission and solar wind ions, observing time scale multiple soil orientation 21 p3914 A70-41652

Proton and UV excited luminescence of Apollo 11 Tranquility rocks and fines, indicating solar wind impingement 21 p3917 A70-41672

Cosmic ray energy loss in interplanetary medium, discussing solar wind effects on low energy particles 21 p3883 A70-42111

Steady state tangential drag by solar wind on geomagnetic cavity, describing unipolar induction 22 p4013 A70-42469

Solar-magnetospheric neutral sheet reconnection and noise in geomagnetic tail from Explorer 33 Ames magnetometer 22 p4013 A70-42471

One fluid solutions for solar wind with reduced electron heat conduction in agreement with observed characteristics at corona base 22 p4093 A70-42472

Reverse hydromagnetic shock in solar wind as discontinuity of plasma density, proton temperature and magnetic field density, using spacecraft data 22 p4093 A70-42474

Comet Schwassmann-Wachmann I brightness variations due to interplanetary shock waves in solar wind 22 p4097 A70-42475

Solar wind source, nature and propagation, discussing wind-magnetosphere interaction, corpuscular radiation channeling along force lines and effects in space and on planets 22 p4093 A70-42523

Space electric field considered for solar wind plasma drift origin and possible energy source for spacecraft propulsion, estimating intensity on lunar surface 22 p4100 A70-42789

Planetary unipolar electric generator system theoretical model based on polarization charges deposition by solar wind 22 p4100 A70-42790

Weak-scattering limit in thin screen model of interplanetary scintillations of radio sources involving solar wind fluctuations at Fresnel scale 22 p4104 A70-42996

Hydromagnetic theory of solar wind flow past earth extended to nonmagnetic planets Venus and Mars 22 p4095 A70-43106

Worldwide geomagnetic fluctuations during disturbed conditions computed from spectrum analysis, considering long period oscillation caused by solar wind structure changes 22 p4019 A70-43114

Solar wind intensity and direction correlated with intensity of earth surface magnetic disturbances and geomagnetic pi-2 type pulsations 22 p4022 A70-43284

Magnetospheric and magnetic storms correlated to solar wind energy penetration, noting roles of energetic plasma and magnetospheric low energy plasma convection 22 p4022 A70-43287

Solar wind properties correlated with geomagnetic activity, discussing interplanetary discontinuities, shock waves, flare associated disturbances and geomagnetic activity sequences 22 p4022 A70-43288

Solar wind instability from TEM waves propagating parallel to magnetic field in electron-proton plasma 23 p4235 A70-43826

Geomagnetic wake in solar wind at 500 earth radii, correlating Explorer 35 and Pioneer 8 data 23 p4184 A70-43828

Solar wind flux correlation with earth EM field pulsations, noting flare-generated shock front effects on magnetosphere 23 p4236 A70-44051

Solar wind electric field relation to ground magnetic disturbances during magnetic storm from Explorer 28 and ground data 23 p4188 A70-44062

Helios solar observation satellite equipment design study for solar plasma low energy particles onboard measurements 23 p4262 A70-44844

MHD stability of tangential discontinuities in solar wind flow 24 p4396 A70-45325

Discontinuity in solar wind energy and angular distribution from 2 January 1970 ESRO satellite HEOS-1 observation 24 p4396 A70-45326

- Solar wind two fluid model with boundary conditions describing electron and proton behavior in expanding corona
24 p4397 A70-45770
- SOLAR X-RAYS**
Solar X ray flare regions size, structure and localization from Cosmos 166 and 230 heliograph observations
01 p0168 A70-10252
Meter wave type 3 solar radio waves associated with solar X ray flares, discussing sudden enhancements of LF field strength due to D layer ionization enhancement
01 p0168 A70-10257
Intensity distribution determination in spectrum of solar XUV fluxes incident upon upper atmosphere, considering quantitative model construction
01 p0170 A70-10593
Statistical analysis of satellite drag data for characteristic time of thermal fluctuations in upper atmosphere caused by soft solar X-rays
03 p0472 A70-13179
Solar X-ray bursts observations correlation with sudden phase anomalies measured at long VHF propagation paths in lower ionosphere
03 p0558 A70-13601
D layer radio absorption during solar eclipse of 22 September 1968 attributed to two solar X-ray sources
03 p0559 A70-13602
Solar microwave and soft X ray radiation emission correlation to determine flare peak temperature and solid angle
04 p0741 A70-15126
Solar particle events 1966 /August-September/ in McMath region 8461
05 p0901 A70-16426
Solar activity study based on solar X ray spectra observation, considering flare mechanism
05 p0903 A70-16719
Rapid fine structure in hard solar X ray bursts observed by OSO-5, explaining time structure by mechanism based on repetitive production of monoenergetic electrons
05 p0904 A70-16980
Extreme UV flashes of solar flare observed by sudden ionospheric frequency deviations compared with energetic X rays observations
05 p0905 A70-16981
Solar X-ray flux from Explorer 33 and 35 observations, presenting catalog of tabular and graphical data
06 p1135 A70-18006
X ray and H alpha emissions associated with solar proton flares, correlating rise time with solar cosmic rays
06 p1137 A70-18547
Solar soft X ray spectrum analyzed by OSO 4 proportional counter, discussing slowly varying component, corona active regions and impulsive event characteristics
07 p1369 A70-20289
Solar low energy X ray bursts using data from OSO-4 proportional counter spectrometer
09 p1745 A70-22739
Solar X-ray flare of 17 August 1966, describing rocket-borne instruments and measurements
09 p1746 A70-23479
SID effects during recording of long wave transmitter field strength, indicating relation between solar X-ray flares and field anomalies
10 p1932 A70-24485
Hard X-ray pulse identification with formation of brilliant kernel /11-12 September 1968/ flare by comparison with optical data
11 p2104 A70-25746
Critical review of Meisel paper on solar X ray source identification using D layer ionization behavior during eclipse
11 p2109 A70-25750
Solar X rays observation from manned orbiting workshop of Apollo Applications Program, describing telescope/camera assembly and X ray event analyzer
11 p2057 A70-26506
Solar L alpha and X ray emission contribution to lower ionosphere ion production, discussing altitudinal, latitudinal and temporal variations
11 p2106 A70-26789
X ray and proton flux measurement during solar flare of 29 September 1968 by balloon-borne detectors
14 p2633 A70-31310
Solar X-rays measurements with spectroheliograph conducted on rocket flights
14 p2589 A70-31339
X ray bursts rise and fall observed by spectrometer onboard OSO-4
15 p2792 A70-31670
Intercomos 1 satellite for observing solar UV and X-ray emission in solar flares prediction
15 p2738 A70-32145
Sudden phase anomaly /SPA/ in VLF radio wave propagation during Proton Flare Project, noting corresponding solar X-ray flux intensity enhancement
15 p2794 A70-32294
Negative sudden phase anomaly /SPA/ in VLF radio transmission, noting solar X ray flux intensity and zenith angle effects
15 p2699 A70-32297
- X ray and microwave emissions relationship to sources on sun, discussing development and structure of sunspot groups
15 p2794 A70-32486
Low energy electron emission during solar flares relation to radio and X ray emission
15 p2795 A70-32622
Solar radiation intensity at Lyman alpha wavelength and X ray spectrum before and during solar eclipse of 7 March 1970
16 p2972 A70-33827
Solar X-ray spectrum and intensity and diffuse cosmic flux measurements, using polar orbiting satellite-borne instruments
17 p3149 A70-34534
Solar X-ray flux measurements in selected emission lines, using curved crystal Bragg spectrometers in low altitude sounding rockets
17 p3150 A70-34834
Solar X-ray emission localization, examining spatial distribution by rocket-borne collimated proportional counter
17 p3151 A70-34864
Ionospheric E layer formation, investigating role of solar X ray control by electron production rate and density calculations
17 p3151 A70-34943
Solar flare of 25 February 1969 at soft X ray frequencies by ESRO 2 satellite observation
19 p3495 A70-37499
Solar X ray emissions from quiet and active sun compared with radio flux to investigate production mechanisms
19 p3512 A70-38009
Solar X ray emission during flares from ionospheric absorption measurements, discussing continuous ionograms method
19 p3512 A70-38912
Solar soft X ray flare spectra of 16 November 1967, examining electron temperatures and emission lines by OSO-4
20 p3700 A70-40419
Solar X-ray corona during eclipse of 7 March 1970, using Aerobee rocket photographs
20 p3713 A70-40430
Solar X-ray spectra of active regions, examining emission lines, fluxes electron temperature and density and transitions
21 p3879 A70-40963
Soft X-ray enhancement during solar flares due to coronal condensation temperature increase
21 p3880 A70-40969
Solar X-ray bursts correlation with H alpha flares and microwave bursts observed by Explorer 34 experiment
21 p3880 A70-40970
Particle acceleration phase in solar flare development, discussing H alpha maximum, hard X ray burst and bremsstrahlung
21 p3880 A70-40971
Nonflaring solar X-ray and microwave radiation flux correlation from satellite data
22 p4104 A70-42995
Solar X-ray data from rocket and satellites, discussing hot dense plasmas and correlation with H alpha flares, calcium plages and microwave emission
22 p4096 A70-43300
Soft solar X rays cyclic variation from satellite observation, noting relation to sunspot group magnetic field complexity
22 p4096 A70-43301
X ray and microwave emissions relationship to sources on sun, discussing development and structure of sunspot groups
23 p4236 A70-43910
Solar X ray spectra interpretation by laboratory measurements, using plasma X ray source and potassium acid phthalate spectrometer
23 p4237 A70-44419
Coronal shock growth as source of thermal solar X ray bursts associated with optical events
24 p4401 A70-45320
Solar flares X ray emission polarization measured by Thomson scattering instrument on Intercomos-1 satellite
24 p4396 A70-45321
Class 1b solar flare X ray examination, using rocket-borne liquid N cooled solid state detector
24 p4397 A70-45767
Solar X-ray flare temperature and emission measure profiles using OGO 5 satellite detector, interpreting energy dispersion of peak times
24 p4397 A70-45768
Solar XUV and soft X ray photometry, describing sounding rocket and satellite grazing incidence spectrometers
24 p4339 A70-45822
Esro 2 satellite instrument measuring soft solar X-rays
24 p4340 A70-46358
- SOLDERED JOINTS**
Ceramic plasma containers construction by soldered seal technique for ion lasers, noting moly- manganese process
02 p0314 A70-12746
- Silicon solar cell panels, studying roles of solder, interconnector metals and substrate materials in failures under thermal cycling
04 p0628 A70-15333
Brittleness of joints using Ga solders prevention by high temperature annealing noting application to aluminum alloys
05 p0628 A70-15333
Hard wire hermetically sealed two degrees of freedom rotating coupling design for continuous soldered wire connections between spacecraft and oriented solar array
16 p2924 A70-34172
Nondestructive measurement of elastic and plastic deformation in soldered joints and printed circuit boards by holographic interferometry
22 p4047 A70-43521
- SOLDERING**
NT ULTRASONIC SOLDERING
Boron carbide soldering with refractory metals by molybdenum disulfide as solder, analyzing electrical resistance and gas tightness
09 p1707 A70-23123
- SOLDERS**
Molten bridging alloy deposition on p and n type thermoelectric materials, utilizing diffusion process brief duration during contact
01 p0059 A70-10758
Solder mechanical contact strength to CdS insulating crystal platelets tested in liquid N, noting Ag epoxy
02 p0319 A70-12738
- SOLENOIDS**
Spectral line width and shift measured by spectrograph crossed with Fabry-Perot interferometer in pressure chamber, measuring magnetic field in solenoid
12 p2238 A70-28178
- SOLID ARGON**
U SOLIDIFIED GASES
SOLID LUBRICANTS
Low speed Ga lubricated sliding electrical contacts of Be in vacuum, discussing Ga film role in friction and contact resistance
01 p0059 A70-10325
Polybenzimidazole /PBI/ resin-bonded solid film lubricants composed of molybdenum disulfide, antimony trioxide and PBI resins
01 p0101 A70-10390
Bonded solid lubricant films wear life equation for low contact stress conditions, determining optimal film thickness
01 p0102 A70-10397
Load, speed and coating thickness effect on wear life of resin bonded solid lubricant, using oscillating motion and low pressure blocks
01 p0103 A70-10447
Friction and wear tests on solid lubricant graphite fluoride compared with molybdenum disulfide at specific temperatures, considering friction coefficient
02 p0321 A70-12536
Potential lubricants in friction and cup forming tests of stainless steel, Ti- and Ni-base alloys, considering boron nitride, graphitic materials and Mo oxides
02 p0309 A70-12540
Solid lubricant films adhesion to metallic surfaces measured using pivot-twist technique
03 p0485 A70-13485
Particle, resin and inorganic bonding of solid lubricant to surface and dry lubricant film performance
05 p0855 A70-16043
Molybdenum disulfide solid film lubricant with increased wear life developed from in situ conversion of electrodeposited molybdenum trioxide
06 p0191 A70-17339
Solid lubricants friction and wear bench testing under simulated space environment
06 p1075 A70-17340
Solid film lubricants pretreatment and applications in aircraft and aerospace industries
06 p1075 A70-17340
Liquid and solid lubricants, discussing properties, temperature ranges, costs, environmental effects and outlook
07 p1316 A70-18953
Synthetic molybdenum disulfide crystal properties compared to natural crystals, discussing friction coefficient, adherence to metal surfaces, etc
10 p1907 A70-24785
Molybdenum disulfide dry film lubricant wear life as film sintering process dependent on binder, additive or atmosphere chemical effects
11 p2058 A70-25571
Service life and friction coefficient of molybdenum disulfide-silicon lubricating coating as function of load, sliding rate and vacuum level
11 p2090 A70-25943
Solid lubricant crystallographic orientation selection for antifriction cermet material silver- molybdenum disulfide
12 p2254 A70-27286
Solid lubricated contacts performance in Nimbus and OAO spacecraft, discussing slip ring assembly and noise problems in Ag-graphite brushes
16 p2920 A70-33819

Materials test fixture design and fabrication for vacuum testing and evaluation of slip rings and brushes, discussing dry film lubrication 16 p2920 A70-33812

Instrument size ball bearings lubricated with bonded dry or transfer films in simulated interplanetary spacecraft tests 16 p2923 A70-34166

Solid film lubricants deposited by DC and RF sputtering on metal and glass surfaces, determining friction characteristics by electron microscopy 17 p3099 A70-34516

Transition metal disulfides and diselenides as solid lubricants, investigating sliding friction characteristics [ASLE PREPRINT 70AM 6E-1] 19 p3438 A70-38801

Binder wetting relation to solid film lubricant wear life [ASLE PREPRINT 70AM 5A-3] 19 p3439 A70-38810

Molybdenum disulfide abrasiveness on test rings coated with bonded solid lubricant [ASLE PREPRINT 70AM 5A-1] 19 p3439 A70-38811

High temperature organic resin binders and solid lubricant thermal and oxidative behavior examined by thermogravimetric analysis [ASME PAPER 70-HT-30] 22 p4058 A70-42436

SOLID NITROGEN

U SOLIDIFIED GASES

SOLID PHASES

Ni-based superalloys microstructure, describing composition, formation and characteristics of various phases 01 p0124 A70-11448

Quenched Ti-Mn alloy omega transition phase microstructure characteristics by transmission electron microscopy using thin foils 01 p0125 A70-11639

Ti-Al-Co alloys reactions in solid phase in Ti-rich region, using optical microscopy and X ray diffraction analysis 01 p0125 A70-11645

Flame spreading mechanism over surface of igniting condensed phase materials in quiescent gaseous environment with chemically reacting component 02 p0396 A70-12014

Phase content determination in borides and borocarbides mixtures based on compounds different chemical stabilities during hydrolysis and reaction with acids 03 p0514 A70-12984

Shear moduli and lattice parameters effect on screw dislocation equilibrium in bimetallic medium of soft and hard phases 03 p0587 A70-13117

Lattice misfit influence on metastable omega phase morphology and stability in Ti transition metal alloys 03 p0508 A70-13146

Carbide phase in Cr-Mn heat resistant steels at annealing temperatures, isolating gamma phase, chromium carbide and niobium carbide phases 03 p0509 A70-13279

Heat treatment effects on phase components of Cr-Mn-B alloys with W and Nb additions, discussing heat resistance 03 p0510 A70-13280

Phase structure and corrosion resistance of alloys in Ti-V-Cr system, discussing effects in HCl, sulfuric acid, nitric acid, acetic acid and NaCl solution 03 p0510 A70-13282

Extension characteristics of delta and sigma related phases in Mo-Ni ternary systems and evaluation of unit cell dimension variations on alloying 04 p0704 A70-14392

Polymorphic transformation effects on oxygen diffusion rate in alpha and beta phases of Ti, considering temperature effects and activation energy 04 p0707 A70-15211

Peptides removal from Merrifield solid phase by transesterification with anion exchange resin 06 p1003 A70-17154

Thermal control of spacecraft via solid-liquid phase change materials [AIAA PAPER 70-12] 06 p1092 A70-18137

Caloric data determining saturated vapor pressure of nitrogen tetroxide and heat of sublimation for sublimation curve 07 p1358 A70-19206

Forces at boundary surface in solid phase in solids and adhesive film interactions, considering boundary surface energy 08 p1503 A70-20879

Allende meteorite showing presence of Ca-Al-rich glasses associated with other crystalline phases 08 p1579 A70-21562

Creep deformation in single crystals of gamma prime precipitation hardened nickel base alloys at intermediate temperatures 09 p1705 A70-22809

Sigma phase occurrence in transition/nontransition elements alloys, discussing solid solubility limits 09 p1708 A70-23424

Optical properties of beta prime phase CoAl, CoGa and NiGa as functions of composition and photon energy 10 p1919 A70-23986

Solid-gas phase equilibria of binary systems related to cryogenics 12 p2329 A70-27023

Phase lattice constants determination by computer method of debyeogram line indexing 12 p2258 A70-28350

Specific heat measurements on disordered and ordered phases of Cu-Au alloys at low temperatures 14 p2626 A70-30497

Superconductivity in noble metal rich hexagonal close packed phases and fcc solid solutions ascribed to Fermi surface-Brillouin zone interaction 15 p2785 A70-32398

Metastable beta phase decomposition in Ti alloy during mechanothermal treatment and aging, determining correspondence to alpha phase segregations via electron microscopy 16 p2931 A70-33207

Gamma phase particle distribution changes in homogeneous segregation in Co-Ti alloy attributed to elastic interaction during aging temperature changes 16 p2931 A70-33208

Ti alloys systems physical properties and structural phase stability, discussing electronic Fermi state density variation 17 p3114 A70-34376

Titanium base binary systems phase diagrams, describing component activity and compound phases heat of formation 17 p3114 A70-34379

Ti alloys martensitic transformations, metastable beta-phase decomposition and alpha-phase ordering 17 p3118 A70-34403

Metastable Ti alloys beta-omega-alpha decomposition and Ti-8Al alpha-ordered alpha transformation, using automatic measuring apparatus 17 p3118 A70-34409

Omega phase morphology in Ti alloy by electron microscope techniques, noting cubic structure 17 p3118 A70-34410

Omega phase stability in Ti and Zr alloys, interpreting upper temperature limit from critical temperature associated with peritectoid reaction 17 p3119 A70-34411

Heat treatment and composition effect on mechanical properties of alpha Ti-base alloy, discussing creep resistance, tensile strength, etc 17 p3122 A70-34439

Fe-Ni alloy alpha-gamma phase transformation after heating, noting deformation planes and directions in martensite 18 p3275 A70-36204

Titanizing Armco iron and carbon steels, examining diffusion layer structure and phase composition 19 p3451 A70-37460

Solid-solid phase transitions in molecular crystals of organic tetrahedral substances, using differential scanning calorimetry 19 p3373 A70-38193

Phase formation and mass transport during iodine-refined Ti reaction with nitrogen at various elevated temperatures 19 p3452 A70-38364

Solid phase stabilization of zirconium dioxide by combined addition of yttrium and magnesium oxides 19 p3455 A70-38732

Ti alpha alloys subjected to heating in beta region, investigating plate-like precipitates by electron transmission microscopy 20 p3645 A70-39042

Two phase Ti alloy subjected to quenching and annealing studied by diffraction electron microscope, discussing needles complex fine structure 20 p3645 A70-39043

Microstructure and composition of hafnium dioxide stabilized with Ca, Y and Mg oxides using metallographic, X ray and microprobe 20 p3654 A70-39242

Liquid and solid phases of substance, calculating thermodynamic properties and vapor pressure logarithm dependence on temperature 22 p4124 A70-42683

Phase analysis for individual multicomponent alloys, discussing chemical composition in case of invariant equilibria and electron beam microprobe 22 p4053 A70-42734

Ni base superalloys gamma prime phase long range order parameter measured by X ray diffraction 23 p4207 A70-44423

Solid phase energy role in flame spreading over solid fuel bed surface in oxidant-containing environment 23 p4281 A70-44424

Ni-Fe-Cr-Nb alloy, investigating precipitation hardening of Ni3Nb phases by transmission electron microscopy 24 p4357 A70-45226

Al-Mg alloys solid phases free energy, entropies and formation heats determination by electromotive force measurement 24 p4357 A70-45230

Subsolidus state multicomponent eutectics systems temperature range based on number and melting points ratios of individual components 24 p4367 A70-45476

Chemical diffusion kinetics of zirconium silicates formation during sintering under pressure, noting activation energy estimation 24 p4367 A70-45479

Aluminized Armco iron and steel diffusion layers phase composition and microstructure 24 p4350 A70-46337

SOLID PROPELLANT IGNITION

Solid propellant combustion instability advances, discussing combustion flow interactions, response functions, etc 02 p0351 A70-12008

Flame spreading mechanism over surface of igniting condensed phase materials in quiescent gaseous environment with chemically reacting component 02 p0396 A70-12014

Solid propellants ignition response to radiative and conductive heat transfer 03 p0544 A70-13921

Saturn 5 thru-bulkhead initiator for solid propellant rocket motor ignition, discussing transfer design, pressure output and postfire leakage 03 p0546 A70-14105

Flame spreading velocity characteristics over solid fuel surfaces, discussing environmental pressure, chemical reactivity, pyrolysis, forced convection, etc [WSCIPAPER 69-33] 06 p1178 A70-17979

Ignition of single particles of light metal hydrides, considering combustion stages and heat transfer [WSCIPAPER 69-47] 06 p1179 A70-17984

Heterogeneous ignition mechanism of solid fuels, deriving surface temperature history for time and nature of transition from weak to strong combustion mode [AIAA PAPER 70-119] 06 p1128 A70-18041

Light emission and gas phase ignition of homogeneous solid propellants under shock tube conditions [AIAA PAPER 70-120] 06 p1128 A70-18042

Surface thermal factors influencing ignition delay time of composite solid propellants, using double wavelength optical detector [AIAA PAPER 70-121] 06 p1128 A70-18043

Book on fundamental aspects of solid propellant rockets covering nozzle flow, solid propellants performance, ignition, combustion stability, etc [AGARDGRAPH-116] 09 p1743 A70-22635

Composite solid propellant ignition characteristics using arc imaging furnace for radiant energy source, discussing minimum initial pressure determined by binder thermal decomposition 09 p1742 A70-23226

Exothermic bimetallic ignition systems (EBIS)/design for solid propellant rocket motors of tactical missiles to reduce shock loadings 12 p2289 A70-27694

Acoustic conductivity of burning solid propellant surface, discussing critical conditions and variable surface measurement methods 13 p2522 A70-29421

Ignition transients in solid propellant rocket engines, taking into consideration flame temperature changes with pressure and igniter secondary mass addition 14 p2628 A70-30778

Composite solid propellants surface structure and profile characteristics burning with various oxidizers and polyurethane binder by scanning electron microscopy 14 p2628 A70-30948

Ignition delay of uncompressed composite solid or hybrid propellant mixtures in rocket engine igniters 18 p3301 A70-36651

Autoignition, ignition and surface temperatures of M-2 double base propellant at low pressure, correcting thermocouple measurements by theoretical model 18 p3299 A70-36697

Homogeneous opaque reactive solid heating and ignition by constant energy flux, examining physical and chemical parameters at critical conditions 20 p3738 A70-40078

Solid propellant radiant and hypergolic ignition, examining radiation absorption and surface reaction between fuel and gaseous oxidizer 20 p3689 A70-40081

Temperature measurements in gaseous reaction zone near surface of burning composite solid propellant, using modified line reversal pyrometer 20 p3694 A70-40273

Composite solid propellant thermal ignition from hot wire tests and model 21 p3942 A70-40877

Aft-end igniter design and placement for solid propellant rocket motors avoiding overpressurization and nozzle pressure oscillations 21 p3866 A70-40892

Solid phosphorus triamide derivatives as ignition aids in hypergolic propellant systems, testing characteristics in interaction with oxidizers 21 p3865 A70-41404

Solid phase energy role in flame spreading over solid fuel bed surface in oxidant-containing environment 23 p4281 A70-44424

SOLID PROPELLANT ROCKET ENGINES

Chemical engineering application to solid propellant rocket motors optimization for specific operations, discussing fuel properties, formulation and additives, mixing and casting
[AICHE PAPER 28A] 01 p0166 A70-10971

Soviet book on gas thermodynamics of solid propellant rocket engines covering combustion products equilibrium in nozzle and chamber, engine design, etc
02 p0353 A70-11690

Axial mode shock wave oscillations in end-burning solid rocket motor, obtaining periodic solutions for flow properties, solid temperature and burning rate
02 p0353 A70-12010

Sensing device to measure radial stress induced at solid propellant grain-to-case bond interfaces during wide temperature variations, detailing instrumentation and operation
03 p0480 A70-12882

Three dimensional photoelastic case bonded solid propellant motor model, analyzing stress distribution using scattered light photoelasticity
[SESA PAPER 1587] 03 p0583 A70-12885

Mathematical model for burning rates of solid propellant rocket motors during pressure transients, coupling conservation equations with mass balance equation
03 p0543 A70-12912

Case bonded solid propellant rocket motors stresses under transverse body force loading as function of load orientation, case stiffness and support method
[SESA PAPER 1502] 03 p0579 A70-12961

Two dimensional plane stress photoelastic models of star configurations in elastic case bonded solid propellant rocket motors under transverse body force loading
03 p0582 A70-14312

Solid rocket engine components technologies, studying effects of cost consciousness
[SAE PAPER 690702] 05 p0922 A70-15828

Solid propellant motors relative performance as related to intermediate payload missions, considering reusable liquid strap-on stages for post-Saturn payloads
05 p0897 A70-16897

Hazards model for probabilistic prediction of casualties by exploding solid propellant rockets, deriving casualty expectation equation
[AIAA PAPER 69-461] 06 p1154 A70-17169

Solid rocket motor ignition system based on exothermic alloying of bimetallic wire constituents
[AIAA PAPER 69-425] 06 p1128 A70-17179

Soviet book on guided ballistic missiles design and construction employing liquid and solid propellant engines with emphasis on aerodynamic heating
06 p1155 A70-17410

Soviet book on thermodynamic and ballistic fundamentals of designing solid propellant rocket engines
06 p1130 A70-17421

LF nonacoustic instability of solid propellant rocket motors, using combustion model allowing flame temperature oscillations with chamber pressure
[AIAA PAPER 68-179] 07 p1421 A70-19319

Fluid controlled solid rocket motors design for Mars mission with acceleration level as parameter, discussing mission specifications, system design and component considerations
[AIAA PAPER 69-446] 07 p1365 A70-19707

Sterilized solid propellant motors applicability to planetary landing capsule spin stabilization
[AIAA PAPER 69-823] 07 p1365 A70-19716

Saturn ULLAGE solid propellant rocket motor vibration test evaluation
07 p1365 A70-20039

Solid propellant rocket engines design, considering nonlinear longitudinal combustion instability encountered in aluminized propellants
08 p1558 A70-20623

Quality planning for Japanese solid propellant sounding rocket motor production, discussing documentation, design, development and process controls, inspection and tests, etc
09 p1691 A70-22570

Book on fundamental aspects of solid propellant rockets covering nozzle flow, solid propellants performance, ignition, combustion instability, etc
[AGARDGRAPH-116] 09 p1743 A70-22635

Pressure surges originated by tangential instabilities in solid propellant motors, using double base homogeneously compounded cylindrical grains
09 p1743 A70-22661

Structural reliability of missile and aircraft solid propellant engines, estimating effect of loads variance, geometrical dimensions and mechanical strength
10 p1930 A70-24294

Solid rocket motor performance prediction including motor pressure, thrust and propellant parameters, discussing mathematical modeling of flow fields
[AIAA PAPER 69-732] 11 p2102 A70-26117

Interior ballistics for wide temperature throttling of solid propellant rockets by variable-throat-area nozzle, noting composition effect screening
11 p2103 A70-26154

Exothermic bimetallic ignition systems /EBIS/ design for solid propellant rocket motors of tactical missiles to reduce shock loadings
12 p2289 A70-27694

Cost optimal booster stage for European satellite launchers, comparing liquid and solid propellant rockets
13 p2502 A70-28450

Soviet book on dynamics of rockets covering solid and liquid fuel rocket stability, controllability and transfer functions
13 p2505 A70-28799

Stagnation point electrostatic probe for measuring local electrical properties of solid propellant rocket exhausts
[AIAA PAPER 69-573] 13 p2475 A70-29960

Soviet book on rocket engine theory covering liquid and solid propellants, combustion physics, nozzle and thrust chamber geometry, etc
14 p2628 A70-30628

Ignition transients in solid propellant rocket engines, taking into consideration flame temperature changes with pressure and igniter secondary mass addition
14 p2628 A70-30778

Solid rocket motors potential hazards explosive reactions and temperature and blast effects
14 p2629 A70-30782

Spacecraft propulsion development guidelines concerning rocket engines with storable propellants, rotating solid propulsion systems, cryogenic propellants, etc
15 p2790 A70-32256

Spin effect on internal ballistic of radial burning solid propellant rocket motor spun about longitudinal axis
15 p2791 A70-32794

Solid propellant rocket motor combustion control by fluidic vortex valve, considering thrust variation
[AIAA PAPER 70-643] 16 p2965 A70-33535

Optimal water quench of solid rockets using injection normal to propellant surface
[AIAA PAPER 70-640] 16 p2968 A70-33598

Combustion extinguishment of composite solid propellant motors by fluid injection, considering binder, curing agent and burning rate catalyst
[AIAA PAPER 70-641] 16 p2968 A70-33599

Titan 3C solid rocket motor exhaust plumes thermal radiation analysis for designing Stage I engines and components thermal protection
[AIAA PAPER 70-842] 16 p3000 A70-33925

Radiative heat transfer effects on polymeric combustion-inhibiting coatings in solid propellant rocket motors
[AIAA PAPER 70-835] 16 p2971 A70-33930

Solid rocket motors, investigating thrust magnitude and stop-restart control
17 p3148 A70-35207

Solid propellant rocket motor, discussing manufacture, materials and configuration of 156 inch engine
17 p3148 A70-35217

Adhesive debonding in case-bonded solid propellant rocket motors, describing stress analysis and interfacial surface energy measurement
17 p3146 A70-35222

Combustion instability due to narrow cavities in solid propellant engines
17 p3198 A70-35739

Integrated structural analysis for reliability prediction of solid propellant rocket motors
19 p3489 A70-38844

Sensing device to measure radial stress induced at solid propellant grain-to-case bond interfaces during wide temperature variations, detailing instrumentation and operation
20 p3718 A70-39158

Spinning satellites stationkeeping at synchronous altitude, using solid propellant pulsed plasma microthrusters
[AIAA PAPER 70-1148] 20 p3690 A70-40206

Tank collection and spectrophotometric tests in determining aluminum oxide particle size produced by small rocket engine
[AIAA PAPER 69-146] 21 p3867 A70-41727

Solid propellant rocket motors performance, manufacture and hardware, discussing mechanical properties, storage, combustion, nozzle expansion, etc
21 p3869 A70-42040

Otomat surface to surface missile with turbojet engine for extended range subsonic cruise and two solid propellant rocket engines for launch
22 p4110 A70-43211

Gyroscopically stabilized solid propellant apogee motor for experimental satellite of CECLES/ELDO Europa 2 program
23 p4235 A70-45018

High strength low-alloyed steel for solid propellant rocket engine case, discussing high temperature production and test methods
23 p4208 A70-45046

Lockseal /flexible joint/ for solid propellant rocket motor thrust vector control, considering construction, operating characteristics and tradeoffs
[SAE PAPER 700777] 24 p4393 A70-45865

Low cost fabrication for solid rocket nozzles using carbon or graphite reinforcements in throat inserts
[SAE PAPER 700796] 24 p4349 A70-45897

SOLID PROPELLANTS

NT CASE BONDED PROPELLANTS

NT COMPOSITE PROPELLANTS

NT DOUBLE BASE ROCKET PROPELLANTS

NT METAL PROPELLANTS

NT PLASTIC PROPELLANTS

NT SOLID ROCKET PROPELLANTS

Position control of burning solid nonmetalized propellant strand in combustion bomb using closed loop servomechanism
01 p0215 A70-10830

Combustion instability of solid propellants using response to pressure perturbations for T and L burners
02 p0352 A70-12013

Transient response of heterogeneous solid propellant combustion surface determined by step technique regarding pressure buildup and drop conditions
[ONERA-TP-748] 03 p0544 A70-13635

Copper chromite catalyst effects on sublimated ammonium perchlorate dissociation products, noting applications to solid propellants
03 p0544 A70-13923

Fragment fabrication of hybrid propellant solid grain emphasizing spherical shape and diameter uniformity
04 p0737 A70-15673

Combustion model for temperature inhomogeneities effect on stability of solid fuels steady combustion
05 p0958 A70-16960

Solid propellant cool gas generating systems applications to inflating emergency escape slides, rafts, pontoons and flotation bags
06 p0986 A70-17720

Hazards in manufacturing solid propellants evaluated to design tests and suggest process conditions
07 p1361 A70-19915

Solid propellant technology, discussing manufacturing processes, sample testing, inspection, etc
08 p1557 A70-20690

Acoustic conductivity of burning solid propellant surface calculated, showing positive values or possible amplification at LF
09 p1741 A70-22113

Transient regimes of solid fuel diffusion combustion in channel with oxidizer fed in from outside, proposing finite difference scheme for integrating equations
09 p1741 A70-22114

Solid propellants mechanical properties under uniaxial tension
09 p1741 A70-22423

Polybutadiene-ammonium perchlorate solid propellant microscopic failure analysis under uniaxial tension
09 p1741 A70-22424

Polybutadiene-ammonium perchlorate solid propellant BPT-1 mechanical properties viscoelastic analysis under constant strain rate tension
09 p1742 A70-22425

Burning solid ammonium perchlorate composite propellants surface structure observation to assess heterogeneous or subsurface reactions, using scanning electron microscope
09 p1742 A70-23234

Fluidic vortex valve to modulate solid propellant generated hot gas flow
[AIAA PAPER 69-424] 09 p1743 A70-23249

Mandel adhesion and cure shrinkage impact on structural integrity of solid propellant grain
09 p1742 A70-23263

Oxidizer particle size and binder type effects on nonacoustic combustion instability of solid propellants
[AIAA PAPER 69-175] 12 p3332 A70-27804

Solid propellant combustion - Conference, Novosibirsk, November 1965
13 p2519 A70-28576

Solid fuel steady combustion regime stability dependence on heat generation in reaction zones and temperature and velocity fields inhomogeneity
13 p2522 A70-29423

Longitudinal temperature gradients effects on stress analysis in solid propellants, using viscoelastic data
14 p2627 A70-30755

Linear regression rate of spherical solid hybrid fuel grains oxidized in reducing gas flow
15 p2786 A70-32263

Motor design parameters effects on solid propellant extinguishment predicted from mathematical combustion model
16 p2962 A70-33571

Solid propellant extinguishment by rapid depressurization, investigating motor configuration effect, binder, burning rate catalyst, oxidizer, metal loading and exhaust pressure levels
16 p2962 A70-33572

Diaphragm pressure transducer interaction with solid propellant grain, superposing solutions to clamped circular plate and half-space
16 p2992 A70-33987

Solid propellant combustion, observing burning rate in spin acceleration environments
17 p3145 A70-35209

SOLID ROCKET BINDERS

Ammonium perchlorate filler fraction effect on viscoelastic behavior, relaxation modulus and failure mechanisms of solid composite propellants 17 p3145 A70-35216

Nonsteady combustion analysis, using method of flame front penetration through fine metal layer in solid propellant 18 p3300 A70-36704

Turbofan engine aerodynamic interactions, cryogenic space storable propellants, space station attitude control biowaste resistojet and long burning time solid propellants 20 p3688 A70-39667

Solid propellant ingredients and explosives differential thermal analyses, discussing thermogravimetry, isothermal or adiabatic constant volume decomposition, crystallographic phase changes, etc 21 p3865 A70-42263

Solid propellant cool gas generating systems, discussing development history, general capabilities and applications 22 p3962 A70-42297

Quasi-hybrid rocket engines with solid propellant and liquid hydrogen injection, discussing performance in comparison with other propellant systems 22 p4089 A70-42498

Warm gas reaction control thrusts via solid propellant exhaust products for ballistic missiles attitude control [SAE PAPER 700780] 24 p4295 A70-45863

Tempering stress in circular plates and cylinders in casting of solid propellants 24 p4427 A70-46147

SOLID ROCKET BINDERS

Propellants chemistry based on chemically cross-linked binder 07 p1360 A70-19909

Solid propellant binders of saturated aliphatic hydrocarbons, describing microstructure, performance contribution, etc 21 p3865 A70-42143

Saturated hydrocarbon prepolymers for solid propellant elastomeric binders 21 p3865 A70-42144

SOLID ROCKET PROPELLANTS

NT DOUBLE BASE ROCKET PROPELLANTS

NT METAL PROPELLANTS

Abnormal burning surface regression in rocket motor solid propellant detected with flash X ray exposures 01 p0085 A70-10021

Chemical engineering application to solid propellant rocket motors optimization for specific operations, discussing fuel properties, formulation and additives, mixing and casting [AICHE PAPER 28A] 01 p0166 A70-10971

Combustion chamber traveling oscillating shock wave as driving mechanism of high amplitude axial mode solid rocket combustion instability 02 p0353 A70-12009

Pseudo two dimensional photoelastic test method applied to axisymmetric solid propellant rocket grains under pressure and thermal loads [SESA PAPER 1482] 03 p0482 A70-12968

Powder and solid propellant combustion, discussing heterogeneous and homogeneous systems, characteristics of foam, fizz and flame zones, etc 03 p0544 A70-13860

Stress analysis for nonlinear viscoelastic cylinder with ablating moving inner surface used to investigate propellant grain in solid fuel rocket under firing condition [ASME PAPER 69-WA/APM-14] 04 p0771 A70-14914

Dynamic response of solid propellant flame to oscillating pressure field using T-tube rocket motor, discussing entropy waves produced in oscillatory combustion [ALAA PAPER 68-499] 04 p0737 A70-15580

Aluminized solid propellant transient burning rate augmentation during acceleration loads [ALAA PAPER 70-126] 06 p1129 A70-18047

Burning rate for composite solid propellant, using model with specific gas phase combustion distribution 07 p1422 A70-19584

Metal particles additives behavior in solid rocket propellant combustion, using scanning electron microscope 07 p1359 A70-19585

Slurry-cast filled nitrocellulose plastisols as solid propellants, discussing compositions, performance and applicability to beryllium fuel 07 p1360 A70-19907

Polyurethane-based solid rocket propellants, discussing catalyst modification, mix viscosities, moisture embrittlement, etc 07 p1360 A70-19910

Butadiene prepolymers containing carboxyl functional groups used in binder matrix for solid composite propellants 07 p1360 A70-19911

Processing methods for manufacturing composite solid propellants, describing oxidizer, binder and fuel

preparation, propellant mixing and chamber insulation and lining and instrumental analysis 07 p1361 A70-19912

Solid propellant mechanical properties tests, failure and physical deterioration /aging/ 07 p1361 A70-19913

Granular diffusion flame theory application to low pressure burning of composite solid AP propellants 07 p1361 A70-19914

Pressure decay prediction improvement for venting and quenching processes of solid propellants using analytical method 11 p2101 A70-25683

Solid rocket motor performance prediction including motor pressure, thrust and propellant parameters, discussing mathematical modeling of flow fields [ALAA PAPER 69-732] 11 p2102 A70-26117

Styrene-oxygen copolymer preparation methods, discussing burning rates for rocket solid propellants mixtures with ammonium perchlorate 11 p2100 A70-26146

Grain configurations classification for solid propellant rockets by relative web thickness and mean vector direction of burning surface into topological continuum 11 p2100 A70-26288

Reissner variational theorem applied to stress analysis of vertically accelerated end burning solid propellant grain in studying elastic rocket launch failure 12 p2313 A70-27196

Collection of papers on solid propellant technology covering rocket interior ballistics, composite rocket propellants, etc 13 p2472 A70-29602

Incompressible solid propellant rocket charges axisymmetric problems, using Galerkin stress functions 14 p2657 A70-30772

Instantaneous burning rates prediction methods based on flame structure model and steady state burning rate data as pressure and initial temperature functions [ALAA PAPER 70-667] 16 p2971 A70-33949

Secondary combustion products of air augmented boron loaded solid propellant rocket ramjet, measuring properties by spectroscopy 17 p3196 A70-35196

Solid propellant rocket motor, discussing manufacture, materials and configuration of 156 inch engine 17 p3148 A70-35217

Flame propagation in narrow slit and fine hole of solid propellant grain 18 p3300 A70-36698

Wire reinforced solid rocket propellant grains mechanical properties and failure modes 20 p3689 A70-40050

Solid rocket propellants linear and nonlinear pressure coupled combustion instability behavior relationship to exothermic surface processes 20 p3694 A70-40274

Forces acting at thrust termination time with aluminized solid propellant rocket fuel, predicting thrust reversal ratio under vacuum conditions 21 p3869 A70-41869

Solid rocket fuels mechanical properties, using high speed pneumatic test machine and impact tensile tester 22 p4088 A70-42342

Radiant energy flux effect on atmospheric pressure burning rate of composite solid propellant 23 p4232 A70-44552

SOLID ROTATION

U ROTATING BODIES

SOLID SOLUTIONS

Phase equilibria in Mn-S, Mn-Se and MnS-MnSe systems by X ray diffraction after preparation by annealing 02 p0249 A70-11652

Size distribution of Ni-Si particles precipitated from Si solid solution in Ni measured as function of concentration, aging time and temperature 02 p0317 A70-12320

Nb-NbH solid solutions thermodynamic properties at various temperatures described by formulas 02 p0320 A70-12819

Aluminum oxide solid state reaction with Ta at high temperatures using chemical analysis 03 p0511 A70-13487

Raman spectra of lead titanate, sodium tantalate /potassium tantalate and potassium tantalate/ potassium niobate solid solutions at various temperatures 03 p0542 A70-13824

AsSbSI crystal production technology concerning substitution type solid solution structure and photoconducting ferroelectric properties 04 p0729 A70-14409

InAs-GaAs solid solutions microhardness and brittleness, studying chemical composition effects 04 p0730 A70-14464

Ni-V alloys precipitation behavior with 15.4/16.5 wt percent V content, observing tetragonal equilibrium theta phase precipitation 04 p0708 A70-15368

Alpha and beta solid solutions chemical composition in two phase alloys of Ti-Al-Mo and Ti-Al-V determined by electron microprobe analyzer 05 p0864 A70-16549

Solid solution softening in bcc Ta-Re alloy system attributed to substitutional-interstitial interaction 07 p1310 A70-19736

Phase equilibrium and homogeneity regions of solid solutions system Ni-Nb-O at elevated temperature 07 p1315 A70-20313

Mo effect on structure and properties of Ni-Al-Nb system alloys in gamma and gamma prime solid solutions range, discussing high temperature strength 08 p1514 A70-20549

Literature on IV-VI semiconducting Pb compounds PbTe, PbSe, PbS and PbO, discussing PbTe-SnTe and PbSe-SnSe solid solutions 08 p1555 A70-20584

Graphite crystals surface ribbed growth in Ni-C solutions due to B content observed by scanning electron microscope 08 p1520 A70-21552

Phase diagrams of metal systems - U.S.S.R. Conference, Moscow, June 1967 09 p1702 A70-22559

Metallic solutions formation dependence on alloying elements electron structure assumed by atoms in solvent lattice 09 p1702 A70-22560

Magnesium solubility in titanium from X ray analysis of Mg distribution in diffusion zones at high temperature and pressures 09 p1703 A70-22567

Combined solubility of group IVA metals and carbon in solid state molybdenum at various temperatures 09 p1704 A70-22754

Alkali-alkaline earth niobates phase equilibrium study revealing tetragonal tungsten bronze-type solid solutions existence range 09 p1740 A70-22983

Ni alloys with Ir and Rh using X ray diffraction and microscopy, exhibiting continuous solid solutions 09 p1708 A70-23423

Sigma phase occurrence in transition/nontransition elements alloys, discussing solid solubility limits 09 p1708 A70-23424

Phase diagram of rapidly crystallized Al-Cu-Mn alloys, observing ternary solid solutions formation during high cooling rate of melt 09 p1709 A70-23786

Phase diagram of Ti-Ta-V system, determining solubility of sigma Ta and V in alpha and beta Ti in solid solutions 09 p1709 A70-23788

Fiber-reinforced composite alloys prepared by controlled dissociation of Au-Ni and Al-Zn solid solutions 10 p1902 A70-23814

Tantalum solubility in alpha titanium and Ti-Ta system physicochemical properties using metallographic, X ray, hardness and resistance analysis 10 p1903 A70-23864

Fe-Mo-C and Fe-Ti-C alloys microstructure and hardness after rapid cooling from melt, considering phase dispersion and particle size, spacing and shape 11 p2065 A70-25774

Zone and phase aging of aluminum alloys, discussing structural and property characteristics of solid solution decomposition 11 p2066 A70-25912

Ternary phase diagrams and quaternary excess free energy prediction using binary data, applied to Pb-Sn-Zn, Ag-Pd-Cu and Pb-Sn-Cd-Bi systems 12 p2254 A70-27475

Interstitial solid solutions stability in cast molybdenum subjected to heat treatment 12 p2257 A70-28225

Decomposition of supersaturated solid solutions in granulated Al alloys with Mn, Cr, Zr, Ti, V and Mo, studying microhardness and electrical resistivity 12 p2258 A70-28274

Phase equilibria in quasi-ternary alloys by microstructural, thermographic and X ray analyses, showing continuous solid solutions formation in titanium-niobium-titanium aluminide 12 p2258 A70-28275

Residual stresses in cylindrical shell made of two component solid solution under thermal diffusion 12 p2329 A70-28323

Ni alloys hardening by solid solution precipitation and insoluble particles dispersion, emphasizing heat resistant alloys and mechanical properties 13 p2433 A70-28762

Temperature dependence of electrical properties and permittivity of barium titanate solid solutions containing Nb, Ta, Sb and La, using bridge-circuit of resonance techniques 13 p2469 A70-28853

Solid solutions of GaAs with 2B or 6A intermetallic compounds, using metallographic and X ray methods 13 p2469 A70-28856

Ta solid solution hardening by nitrogen and oxygen, noting yield stress variation with interstitial gas concentration 13 p2434 A70-29084

DC plasma arc jet excitation and emission characteristics for solution analysis with economical inert gas flow rates

13 p2362 A70-29107

Interatomic bond strength in solid solutions of Ti-Sn-O with respect to heat resistance at elevated temperatures

14 p2595 A70-30170

V-N and V-O solid solutions magnetic, electrical, crystallographic and mechanical properties as function of gas concentration

14 p2596 A70-30842

Nitrogen solubility in Nb-Mo solid solutions, determining relationship between N partial pressure, temperature and concentration

14 p2598 A70-31285

Magnetically ordered ferroelectric materials properties for various compounds and solid solutions

15 p2785 A70-32749

Yield strength of Nb-O single crystal solid solutions as function of temperature

15 p2763 A70-32808

Hydrogen separation from supersaturated solid solution in Zn-Zr alloy, measuring at room temperature with eudiometer

15 p2764 A70-32856

Composition dependence of optical energy gap and diffuse reflectance in MnSe-CdSe solid solutions

16 p2960 A70-33094

Ti-Cu-Ag phase diagrams and liquidus surface structure, using metallographic, thermal and X ray techniques

16 p2931 A70-33221

Polycrystalline NaCl-KCl solid solution alloy, considering high temperature creep under constant compression stress

16 p2961 A70-33275

Decomposition of unstable beta solid solution of Ti-V alloy, using X ray and microscopic analyses

17 p3125 A70-35336

Aligned composite materials preparation by unidirectional lamellar eutectoid decomposition in Co-Si, Cu-Al, Ni-In and in supersaturated solid solution Sn in Pb

18 p3274 A70-36052

Relaxation peaks associated with interaction clusters of Zr and Nb dissolved in Nb

18 p3274 A70-36056

Internal residual stress relaxation theory in dielectric aging in tetragonal solid solutions of calcium titanate in barium titanate

19 p3486 A70-37776

Yield stress in electron beam-refined Nb-N solid solution at room temperature and specific strain rate range

19 p3454 A70-38813

Nb-Ta and Nb-Mo alloys single crystal solid solution strengthening as function of composition, temperature and strain rate

20 p3646 A70-39105

Duplex eutectic with Ni-Be fibers embedded in Ni-Cr solid solution matrix, discussing solidification conditions, optimum composition, heat treatment, mechanical properties and oxidation

20 p3647 A70-39107

Epitaxial GaAs films growth from solid solutions of InAs-GaAs system deposited on GaAs substrates, noting electron mobility and temperature effect

20 p3686 A70-39629

Ni-Cu-C solid solutions, measuring temperature dependence of graphite solubility by vapor transport method

21 p3841 A70-42149

Grain boundary damping characteristics of Cu-Ni alloys solid solutions, discussing height, temperature and activation energy of solute peak

22 p4053 A70-42729

Temperature stable homogeneous single phase zirconate solid solution ceramics for microwave dielectric resonators and microstrip substrates

22 p3996 A70-42922

Al-Be-Mg alloys under solution treatment, noting aging and prolonged heating effects on mechanical properties from solid solution decomposition diagram

22 p4056 A70-43127

Solid solutions of quasi-binary cross section CdP-CdTe and ZnP-CdTe, using X ray, thermal, microstructural and microhardness analyses

22 p4086 A70-43132

Solid solutions properties in Nb-oxygen system, examining atomic bond nature by elastic modulus measurement

22 p4056 A70-43345

Superconductivity and crystalline structure of laminar solid solutions of niobium-selenide-niobium-telluride single crystals

22 p4088 A70-43464

Rare earth metals-ruthenium Laves phases solid solutions superconducting transition temperature measurement

23 p4231 A70-44885

Solid solution of GaAs with CdSe and CdS compounds, investigating intrinsic absorption edge dependence on temperature

24 p4390 A70-45663

Solubility isotherms of alloying elements in Ge-Al-P semiconductor-acceptor-donor system at high temperatures

24 p4391 A70-46143

Solid solution hardening of single crystal Ta base alloys, measuring critical shear stress at various temperatures

24 p4365 A70-46370

SOLID STATE

Characteristics of dynamic mechanical systems including solid state and hydrodynamic analogs of ideal incompressible fluids, based on statistical theory of turbulence

01 p0068 A70-11594

Wave propagation in solid state plasma with ferroelectric and ferromagnetic properties, deriving matrix equation allowing for nonlinearity of dielectric constant and magnetic permeability

12 p2283 A70-26970

Dispersion relations between wave frequency and vector obtained from matrix equation for wave propagation in solid state plasma with ferroelectric and ferromagnetic properties

12 p2283 A70-26971

Solid state diffusion bonding applied to rocket engine injectors manufacture [ALAA PAPER 70-639]

16 p2968 A70-33597

Deformable Al alloys hardening, emphasizing heat treatment in solid state

18 p3276 A70-36308

SOLID STATE DEVICES

NT AVALANCHE DIODES

NT CRYSTAL RECTIFIERS

NT GALLIUM ARSENIDE LASERS

NT GERMANIUM DIODES

NT JUNCTION DIODES

NT JUNCTION TRANSISTORS

NT METAL OXIDE SEMICONDUCTORS

NT MIS [SEMICONDUCTORS]

NT PARAMETRIC DIODES

NT PHOTODIODES

NT PHOTOTRANSISTORS

NT PHOTOVOLTAIC CELLS

NT RUBY LASERS

NT SEMICONDUCTOR DEVICES

NT SEMICONDUCTOR LASERS

NT SILICON TRANSISTORS

NT SOLID STATE LASERS

NT THERMISTORS

NT THYRISTORS

NT TRANSISTOR AMPLIFIERS

NT TRANSISTORS

NT VARACTOR DIODES

Solid state electronics application in automatic flight control, discussing redundancy, internal failure correction, fault isolation and automatic checkout

02 p0335 A70-12178

Airborne UHF transmitters, discussing data on designs, performance, packaging and limiting factors of solid state devices for RF utilization

02 p0267 A70-12183

Tuneable adjustable solid state bandwidth filter using N path system for low pass to bandpass filter transformation

02 p0270 A70-12666

Josephson effect in superconductors emphasizing Josephson junction electrical properties and applications to devices and measuring techniques

03 p0542 A70-14190

Solid state digital pressure transducer incorporating Si diaphragm with piezoresistive sensing elements for computerized supersonic and subsonic data applications

03 p0496 A70-14194

Microwave low power electron tube oscillators and solid state technology

05 p0823 A70-16882

Solid state microwave acoustic variable delay devices for radar, fuses, repeaters, altimeters, etc, emphasizing magnetoelastic wave method

06 p1018 A70-17356

Solid state VHF omnirange navigation system operation, principle, equipment, applications, advantages, etc

07 p1241 A70-19622

Computer managed display system using CRT and appropriate solid state displays providing flight crew with automatically sequenced time varying information

08 p1498 A70-21677

Solid state IC-compatible display devices optical, electrical, mechanical and thermal characteristics

09 p1642 A70-22018

Current-voltage characteristics and lifetime of thin film diodes on chalcogenide glass substrate with symmetrical and asymmetrical electrodes

09 p1647 A70-22751

Covert solid state imaging system applicability to totally dark laboratory environment

09 p1686 A70-23752

Solid state resonant bandpass electronic filter composed of ferroelectric dielectric capacitors with adaptable voltage gain

09 p1653 A70-23801

Alphanumeric solid state displays with vertically stacked character rows for text format reading, using injection electroluminescence technology

10 p1846 A70-23882

Integrated circuit microwave phased array radar antenna systems for multiple frequency bands and multifunction operations to save cost and space

10 p1851 A70-24878

Microwave devices including gridded tubes, magnetrons, traveling wave tubes, amplifiers, solid state devices for radar and communication applications

10 p1851 A70-24885

Rocket- and projectile-borne microwave miniature solid state transmitters, discussing transistor oscillator-multiplier, hybrid integrated circuits, bulk effect devices, etc

10 p1852 A70-24887

Complex microwave solid state subsystems designs for specialized systems

10 p1852 A70-24889

Book on integrated electronic systems covering integrated circuit design, device and material properties, quality control, applications, etc

10 p1853 A70-25049

Solid state proximity switches, sensors, logic and self test circuits for aircraft electrical applications to improve reliability and maintainability over mechanical switches

[SAE PAPER 700305]

12 p2195 A70-27449

Solid state power controllers for aircraft electrical power systems

[SAE PAPER 700304]

12 p2195 A70-27450

Electronic tuning range of solid state microwave oscillators, deriving equations in terms of tuning device Q factor and available power output

13 p2376 A70-28802

Solid state device inductance by thermal effects, describing characteristics and applications in resonant circuits

15 p2783 A70-31839

Transistor densitometer used for variable star interpretation by amateur photographers

15 p2740 A70-32348

Solid state UHF and microwave device testing by computer automated network analyzers, measuring scatter parameters

15 p2742 A70-32590

Solid state subnanosecond electro-optic light switch for mode locked laser controller or light shutter

15 p2753 A70-32815

Microwave IC methods applied to solid state signal sources design, using varactor tuned transistor oscillators, resistive isolation pads, amplifiers and frequency multipliers

16 p2872 A70-33069

Solid state logarithmic radiometer, measuring radiation within narrow portions of optical spectrum

16 p2905 A70-33160

Solid state electroluminescent phosphor displays for aircraft/spacescraft instrument panels

16 p2906 A70-33178

Solid state dipole antenna array miniaturization by etching microstrip components on alumina substrate having high dielectric constant

16 p2876 A70-33409

Solid state phased array radar employing MIC modules in radiating elements, achieving reliability by redundancy

16 p2877 A70-33411

Thermal noise in space charge limited solid state diodes by Langevin equation, relating spectral intensity for open and short circuit voltage and current

16 p2878 A70-33694

Solid state IR to visible converter, using minority carriers stimulated tunnel injection into wide band gap phosphor

17 p3081 A70-34648

Hybrid solid state image detectors, discussing integration and excitation storage operation modes

17 p3053 A70-35122

Book on design of resonant piezoelectric devices covering linear piezoelectric materials, Green function, variational methods for dimensional motions and modes, etc

17 p3143 A70-35188

Solid state display for on-line information retrieval using light emitting crystals, integrated circuits and hybrid packaging

17 p3063 A70-35514

Subminiature solid state piezoelectric accelerometer using diffused four arm Wheatstone bridge sensor

17 p3094 A70-35522

Solid state switching effect on aerospace electric power conditioning equipment

[SAE PAPER 700306]

18 p3302 A70-36802

Solid state multiplexed electrical power distribution system for future generation military and commercial airplanes

[SAE PAPER 700301]

18 p3216 A70-36803

Thin films for semiconductor integrated circuits and solid state devices

19 p3389 A70-38195

- Superconductor thin films, discussing transition temperature, critical field and current, solid state applications, etc 19 p3488 A70-38198
- Solid state, digital, Resonant Capsule Pressure Transducer based on natural frequency variation of aneroïd capsules by pressure induced curvature changes 19 p3430 A70-38520
- Solid state switching effect on aerospace electric power conditioning equipment 21 p3758 A70-41210
- Solid state switches for operating ion thrusters directly from high voltage solar cells, noting satellite weight saving 21 p3798 A70-41215
- Shot, thermal, induced gate and flicker noise in various solid state devices and lasers 21 p3792 A70-42112
- Thermally induced oscillations and negative resistance in seminsulating oxygen-doped GaAs double injection devices via heating beyond critical temperature 22 p4084 A70-42326
- Liquid crystals as solid state organic material with physical properties of liquid, discussing electro-optical properties and applications 22 p4085 A70-42724
- Solid state batteries based on highly conducting solid electrolyte rubidium silver iodide, testing discharge performance 22 p3966 A70-43543
- Solid state high energy light detector for pulsed ruby and glass lasers in long pulse mode 22 p4052 A70-43614
- Solid state IF or baseband switching elements design for high capacity multichannel microwave systems 23 p4172 A70-44014
- Computer optimization program for solid state components and integrated circuits design with conversational system for man machine dialogues 24 p4317 A70-46321
- ### SOLID STATE LASERS
- #### NT RUBY LASERS
- Solid state ring laser properties as oscillator, waveguide, interferometer and mechanical gyro considered for potential as rate gyro 01 p0108 A70-10417
- Q switching of continuously pumped Nd/YAG using double Fabry-Perot etalons to replace laser resonator output mirror 01 p0112 A70-10903
- Diffraction loss measurement in solid state laser to determine laser material contribution to total cavity loss 01 p0113 A70-10919
- Optical parametric oscillator pumped by continuously repetitively Q switched Nd/YAG laser output 01 p0113 A70-11171
- High output neodymium glass laser with small emission divergence angle using four lamp pumping system 01 p0114 A70-11267
- Luminescence quantum yield in neodymium glass, noting independence to stimulating light frequency 01 p0114 A70-11595
- Soviet book on methods in laser design, Volume 2, covering pumping radiation in active rods, unsteady modes, ruby and Nd glass lasers 02 p0310 A70-11691
- Resonant energy transfer of trivalent Yb into trivalent Eb for optical pumping improvement for fluorophosphate glass lasing 02 p0314 A70-12725
- Quasi-classical theory of solid state lasers generation and amplification, describing radiation by Maxwell equations and atoms in external fields by Schrodinger equation 02 p0315 A70-12832
- Angular dependence of one dimensional first and second index matching for optical parametric mixing of laser and SRS Stokes beams for tunable laser source 03 p0498 A70-13157
- Linearly polarized radiation in Nd-glass laser obtained without energy loss by placing glass plates in resonator at Brewster angle to axis 03 p0499 A70-13257
- Population inversion distribution effect on resonator losses of Nd-glass laser, showing threshold limits 03 p0500 A70-13527
- Pico-nanosecond light pulses from mode-locked Nd glass laser with spectral mode selector, noting correspondence between pulse duration and inverse bandwidth 03 p0503 A70-14210
- Pumping techniques, design and properties of pulsed and CW lasers based on Nd-glass, ruby, barium fluoride and calcium tungstate crystals 05 p0860 A70-16821
- Single mode neodymium laser second harmonic radiation self focusing resulting in filamentary fractures in solid dielectrics 06 p1080 A70-17496
- Spectral power distribution and ultrashort pulses limiting duration of ruby-neodymium laser with passive shutter 06 p1081 A70-17766
- Time characteristics of pulsed calcium fluoride-dysprosium laser in single mode, observing constant emission and peak regime 06 p1082 A70-17808
- Nd glass laser emission spectral width reproducibility as function of flash intervals and pump energy 07 p1297 A70-18869
- Resonator aberrations and active element imperfections effect on formation of spatial and angular structures of solid state laser modes 07 p1299 A70-19854
- Caustic surface of spherical resonator with external mirrors used to calculate light angular divergence and spectral properties 07 p1299 A70-19859
- Solid state laser kinetic regime as function of diffusive and directional motions of active medium excitations 07 p1299 A70-19860
- Solid state lasers thermal resonator buckling time dependence and compensation, graphing results of resonator field analysis 07 p1303 A70-20359
- Raman effect in liquid nitrogen resonator with light from Q modulated Nd laser pumped into resonator at small angle to axis 07 p1303 A70-20366
- Solid state lasers with strongly degenerated modes investigated for induced radiation spectral composition inertial properties 08 p1510 A70-20507
- Polarization anisotropy effect of laser cavity on neodymium glass laser output power 08 p1510 A70-20513
- Uncontrolled and controlled neodymium glass laser outputs, using ultrasonic traveling wave diffraction modulator 08 p1510 A70-20514
- Neodymium laser frequency doubling based on nonlinear functional relation between polarization and electric vector in matter 08 p1512 A70-20677
- Population inversion in neodymium glass impurities in four level laser dependent on electron beam intensity and energy 08 p1512 A70-21205
- Neodymium glass laser stimulated by pinch discharge radiation in He and Kr, increasing power, energy and pulse repetition frequency by improved pumping energy coupling 08 p1512 A70-21213
- Solid state and gas lasers industrial applications in machining and nonmachining areas, discussing limiting factors 09 p1692 A70-22706
- Holographic recording of Q switched neodymium laser beam achieved through lens testing on reconstructed beam 09 p1697 A70-22845
- Pulse train transition in Nd-YAG and He-Ne lasers mode-locked by intracavity phase modulator 09 p1697 A70-22919
- Strontium fluoride crystals containing trivalent neodymium cations investigated for laser action and radiation characteristics by spectroscopy 10 p1899 A70-24253
- Pulsed solid state laser power output stability in terms of kinetic theory noting laser action threshold role 10 p1899 A70-24254
- Neodymium glass laser fundamental frequency spatial structure effects on KDP crystal second harmonic generation efficiency, describing optimal system for laser beam shaping 10 p1899 A70-24262
- Neodymium spectral line widths in various glasses, studying role of inhomogeneous broadening 10 p1900 A70-24266
- CW Nd-doped YAG laser rods, measuring thermal and optical properties before and during pumping with W lamps 10 p1900 A70-24942
- Axial mode selection and frequency stabilization of Nd-YAG laser by optimally designed crystal quartz etalon 10 p1900 A70-24943
- Ultrasonic LF modulation of solid state traveling medium lasers radiation intensity attributed to elastic vibrations of rods 11 p2062 A70-25398
- Monopulse laser operating on ruby and neodymium glass using quarter-wave electro-optical Q switch 11 p2064 A70-26810
- Solid state laser with traveling wave during steady state emission, determining pulse shape, duration and amplitude 12 p2247 A70-27497
- Laser output energy decreased by microscopic fractures masking effect in neodymium glass laser rod during monopulse operation 12 p2250 A70-28152
- Population inversion effect on angular divergence of neodymium glass laser radiation, observing energy independence for refractive index of medium surrounding active rod 12 p2250 A70-28154
- Solid state laser transverse modes maximum dependence on resonator geometrical parameters usable for producing stable kinetic emission mode with narrow spectral line 13 p2428 A70-29410
- Solid state laser optical pumping energy density calculations for case of circular cylindrical image of pumping lamp formed in rod 13 p2429 A70-29476
- Non Q switched Nd laser light intensity correlation function measurement, using optical gate for producing second harmonic light 13 p2430 A70-29706
- Thermo-optical constant of laser neodymium glasses measured with interferometer 13 p2430 A70-29761
- Temporal structure and spectral evolution of Nd laser emission with self locking axial modes, noting gain saturation effects 13 p2430 A70-29776
- Electron beam-pumped ZnO laser emission wavelength at various temperatures 13 p2430 A70-29833
- Nitrous oxide and carbon dioxide laser Q switching by ammonia Stark effect 13 p2431 A70-29835
- Ultrashort pulse generation by solid state Q switched lasers, discussing spontaneous emission effects, atomic polarization and populations variation 14 p2594 A70-30477
- Luminescent line broadening effect on axial mode selectivity in pulsed neodymium lasers with Fabry-Perot resonator at above-threshold pumping power 15 p2749 A70-31554
- Solid state traveling medium laser pulsed emission characteristics and nonlinear intensity distribution 15 p2753 A70-32699
- Ruby and neodymium glass free running lasers output power modulation relationship to excited modes and active rod position in resonator 15 p2753 A70-32822
- Optical resonator thermal deformations during pumping of circular cylindrical interferometer rods in illuminators, measuring thermo-optical constants of neodymium glass 15 p2754 A70-32863
- Mechanically heterogeneous and optically homogeneous solid/liquid mixed laser with active centers contained in Ne bathed in liquid 16 p2926 A70-33109
- Amplitude modulation of ruby and neodymium-doped glass lasers via ultrasonic acoustic wave injection 16 p2926 A70-33162
- Inorganic laser materials containing ionic crystalline structures, including fluorides, oxides, rubies, garnets and oxygen containing complex compounds 16 p2927 A70-33223
- Laser design for production tool applications, noting use of Nd-YAG and carbon dioxide laser [ASME PAPER 70-DE-1] 16 p2917 A70-33418
- Low threshold electron beam pumped CdS lasers with improved Al coated Fabry-Perot mirrors in end-pumped configuration 16 p2928 A70-33642
- Nd-glass laser operation in giant pulse mode with passive or optomechanical shutter, noting applications 16 p2929 A70-34211
- Solid state laser active element lateral surface microprofile effect on heat endurance 16 p2929 A70-34220
- Solid state giant pulse laser with small divergence angle, using polymethyl dye solution in nitrobenzene as Q switch 16 p2929 A70-34221
- High power Nd-glass solid state laser characteristics measured to improve beam properties 17 p3105 A70-35090
- High-power Q switched solid state laser radiation intensity measurement methods for multi and single modes 17 p3105 A70-35094
- Oscillation frequency retuning and stabilization and loss factor determination in solid state lasers by dispersive resonators 17 p3106 A70-35100
- Fluorescence method of determining solid state laser parameters using spontaneous and stimulated emission observations 17 p3106 A70-35101
- Solid state laser polarization mechanism, considering isotropic and anisotropic cavities 17 p3106 A70-35103
- Crystal and glass lasers activated by Nd ions, examining stimulated emission temperature dependence by high temperature spectroscopy 17 p3106 A70-35105
- Picosecond pulses in Q switched neodymium glass and ruby lasers, describing pulse measurement with fluorescence 17 p3108 A70-35623

Spectral emission kinetics from neodymium glass laser with rod in translational motion during laser action 18 p3267 A70-36613

Nd-YAG Q switched laser using feedback loss control to increase switching speed for digital scanning 18 p3270 A70-36744

Nd glass laser ultrashort light impulse optical rectification, presenting lower harmonics angular dependence 19 p3443 A70-37287

Traveling medium solid state lasers radiation intensity modulation by active element motion 19 p3444 A70-37442

Subnanosecond jitter spark gap obtained with YAG-Nd pulsed laser triggered switching at moderate repetition rates 19 p3444 A70-37666

Low jitter multiple high voltage spark gaps switching at 50 pps by Q spoiled YAG laser triggering 19 p3444 A70-37667

Energy levels and spectral broadening of neodymium ions in laser glass from fluorescence and absorption spectra 19 p3445 A70-37760

Solid state laser with transverse mode selection to increase brightness, discussing plano-concave resonator 19 p3447 A70-38508

Protein solutions and cell cultures changes by ruby and Nd lasers radiation, noting threshold energy 20 p3579 A70-39419

Solid state laser glass filters for absorbing UV light emitted by pumping tubes 20 p3641 A70-39739

Pulsed composite laser performance with He-Ne active section and neodymium-glass power gain section 20 p3641 A70-39740

Smooth periodic wavelength retuning in organic dye laser, using neodymium glass laser with YAG for pumping 20 p3642 A70-39742

High radiation intensity neodymium glass laser, describing installation for heating plasmas to high temperatures 20 p3643 A70-39758

Fluctuations in radiation power density of solid state laser near focal plane of convergent lens, using device for selecting and recording individual peaks 20 p3643 A70-40022

Ultrasonic LF modulation of solid state traveling medium lasers radiation intensity attributed to elastic vibrations of rods 20 p3643 A70-40092

Thermally induced stress birefringence effect on linearly polarized CW YAG-Nd laser 21 p3834 A70-40566

YAG-ND laser volume limits condition for high power fundamental mode operation 21 p3836 A70-40808

Nd-YAIG laser design for sleeve stabilization, discussing flicker problem and rod cladding 21 p3836 A70-40822

Thermal and birefringent effects on output of continuous Nd-YAG laser rod, using 6328 A probe 21 p3837 A70-41906

Laser characteristics of Nd doped lithium germanate and silicate glasses, discussing spectroscopic properties 21 p3838 A70-42010

Host materials for increasing optically pumped solid state CW laser fundamental mode output power 22 p4048 A70-42333

Solid state laser optical pumping systems design and evaluation 22 p4049 A70-42514

LF cavity loss modulations of homogeneous four-level CW Nd-YAG laser, including relaxation-oscillation regime 22 p4050 A70-43005

Particle size, shape and absorptivity effects on inclusion damage of Nd-doped barium crown laser glass 22 p4050 A70-43007

Phase locked solid state laser with picosecond pulses applied to high speed cinematography [SMPT PREPRINT 22] 22 p4034 A70-43051

Ruby and Nd glass solid state lasers modes partial self synchronization investigated by spectral time resolution method 22 p4051 A70-43463

Nd-glass mode-locked laser with KDP crystal frequency doubling and pulse selection with Pockels cell 23 p4201 A70-44476

Monopulse laser operating on ruby and neodymium glass using quarter-wave electro-optical Q switch 24 p4351 A70-45182

Single mode ruby and Nd glass lasers axial mode selection by dye filters, noting radiation spectra and spatial coherence 24 p4352 A70-45462

Nd glass laser with smooth emission frequency scanning, giving block diagrams and radiation spectra 24 p4353 A70-45464

Mode locked neodymium-glass pulsed laser stimulated picosecond time resolved light emission observation by cross beam technique 24 p4354 A70-45647

SOLID STATE PHYSICS

Cryogenically cooled superconducting electromagnets design, construction and properties for research in plasma and solid state physics, considering coil systems 01 p0143 A70-10970

Book on thin film transistors microelectronics covering semiconductor physics, fabrication, analysis, applications and comparison with MOS transistors 01 p0052 A70-11329

Cryogenics applications to solid state physics and materials research tabulated for experimental methods and objectives 05 p0892 A70-16398

Bismuth oxide resistivity and structural characteristics at high temperature and during transformation from solid to liquid state 10 p1927 A70-24272

Solid state plasma drift velocity effect on helicon propagation constant assuming isotropic momentum relaxation time and effective mass 10 p1928 A70-24831

Solid state welding processes for space, nuclear and deep submergence technologies, discussing diffusion bonding of Al and stainless steels 13 p2419 A70-29117

Solid state mechanics of deformable media, surveying development trends with emphasis on rheology and dislocation theory 15 p2818 A70-32176

Reliability physics role in kinetic studies of physical and chemical degradation and failure mechanisms in semiconductor devices 15 p2713 A70-32661

Glass switching /Ovshinsky effect/, discussing various theoretical explanations 18 p3298 A70-36956

Soviet papers on physics of semiconductors and semiconductor devices covering kinetic equation, electrical conductivity anisotropy, thermal emf, current carrier recombination, radiation flaws, etc 19 p3482 A70-37292

Kinetic equation in strong electric fields, describing current carrier behavior in semiconductors 19 p3483 A70-37293

Solid state plasmas waves and oscillations in metals, semimetals and semiconductors, noting applications for microwave devices 19 p3479 A70-37944

Thin films physics for microelectronic applications 19 p3389 A70-38194

SOLID SURFACES

NT CRYSTAL SURFACES

Computerized calculations for cylindrical tank bottoms with outlet based on strength analysis, using zero moment theory for surface stability under uniform pressure 05 p0946 A70-16957

Unsteady inverse heat conduction of semibounded body solved by least squares method 06 p1178 A70-17856

Unsteady calorimetric sensor for measurement of heat transfer between gas jets and solid targets 06 p1064 A70-17857

Three dimensional model for high energy scattering of inert gas atoms from solid surfaces, calculating trapping, accommodation and flux and velocity distributions 06 p1110 A70-18261

Solid surface-compressible liquid drop high speed impact damage, discussing contact pressure 06 p1053 A70-18611

Wall boundary condition model modification applied to molecular beam-solid surface scattering, noting qualitative agreement with observed distributions 07 p1342 A70-20118

Solid surface roughness influence on reflection of thermal energy molecular jets, showing shock determined by incidence angle 07 p1343 A70-20121

Gas molecules scattering by solid surface for monoenergetic and Maxwellian beams, discussing model with different values for magnitude and velocity direction 07 p1343 A70-20124

Solid Mo, Ni, Ta and W surface energies determined by multiphase equilibration technique 08 p1522 A70-21749

Three dimensional oblique incidence liquid jet impinging on solid surface, evaluating flow force by applying mass and momentum conservation 13 p2389 A70-29540

Light gas atoms adsorption on solid surfaces, calculating wave function, energy, mobility, sticking coefficient, etc 18 p3225 A70-36186

Nucleation phenomena associated with boiling heat transfer in pure liquids at solid heating surfaces 21 p3948 A70-41205

Acoustic field scattering from multipole point sources by solid spherical surface 22 p4010 A70-42693

Water drop-solid surface collision experiments to study rain impact erosion process, using gas gun projectiles, high speed photography, photomicrography and profilometry techniques 22 p4116 A70-43096

Solid surface interaction between surface with normal molecular beam, generalizing model by energy parameter simulating dissipative forces 23 p4223 A70-44994

SOLID-SOLID INTERFACES

Space charge barriers AC impedance modification at metal/semiconductor contacts due to trapping 01 p0157 A70-10296

Fiber-polymer matrix interfacial tensile and shear strengths evaluation methods, including data correlation from various tests 01 p0087 A70-10478

Antiplane strain deformation problems concerning crack extension along circular interface separating materials with different shear moduli 05 p0931 A70-16091

Thermal resistance of multicontact heat conducting stainless steel plate stacks with different interface purities in vacuum 05 p0957 A70-16293

Temperature of contact surface between two homogeneous isotropic solid bodies determined by calculating plane heat source of steady three dimensional temperature field 05 p0958 A70-17014

Contact resistance measurements used in contaminant removal and metallic adhesion on iron surfaces 07 p1293 A70-18940

Elastic fields in bimaterial plate under uniform compressive and anti-plane shear loadings, finding stress distribution and induced interfacial shear stresses 07 p1412 A70-19957

Orthogonal polynomials in three dimensional contact problems without friction, discussing construction of kernels over finite and semiinfinite intervals 08 p1594 A70-21634

Interfacial thermal conductivity model based on statistical features of two faces in contact, discussing surface roughness and heat flow 11 p2083 A70-25763

Effusion steady state pressures time dependence of carbon monoxide and calcium vapors generated during calcium oxide-graphite interaction 11 p1995 A70-26602

Reaction impulse during steel spheres impacts at lead surface in vacuum dependent on kinetic energy, velocity and spheres material 11 p2146 A70-26794

Interfacial tractions between matrix and fiber in elastic composite materials reinforced with elastic fibers 12 p2322 A70-27230

Stress and strain in matrix of fiber reinforced material within elastic region, calculating interface shear stress for rectangular fiber 12 p2322 A70-27231

Heat resistance of machined stainless steel and molybdenum contact pairs in vacuum, discussing compressive loads and surface defects effects 12 p2243 A70-27290

Silicon and alpha-alumina support interface reactions during nucleation-coalescence and after epitaxial growth, investigating electrical properties 13 p2470 A70-28958

Computerized analysis of shear failure at initial fragment collision during trifragment rotor disk interaction with containment rings 14 p2563 A70-30870

High temperature solid-solid reactions and solid-liquid or condensed phase-gas equilibria, using solar furnace 14 p2545 A70-30907

Double ended dislocation pileups and elastic cracks at bimaterial interface under screw, edge and shear modes 15 p2756 A70-31561

Photoemission of electrons and holes from Al into aluminum oxide, giving approximate energy band diagram of Al-aluminum oxide interface 15 p2783 A70-31759

Reinforced plastics adhesion to hydrophilic mineral surfaces by using silane coupling agents 16 p2937 A70-33374

Radioisotopic and complementary surface chemical analysis of coupling agent films on glass surfaces 16 p2917 A70-33375

Thermal constriction resistance between contacting metallic paraboloids applied to instrument bearings [AIAA PAPER 70-857] 16 p2998 A70-33902

Heat transfer in tungsten-tungsten and Armcro Iron-Armco Iron specimens, confirming Bowden-Tabor model of elastoplastic events during cyclic engagement of surfaces [AIAA PAPER 70-853] 16 p3000 A70-33920

Circular inclusion interface separation in matrix under incident compressive waves interpreted for fiber reinforced composites

17 p3185 A70-34963

Heat resistance of machined stainless steel and molybdenum contact pairs in vacuum, discussing compressive loads and surface defects effects

20 p3638 A70-40340

Interface interaction of colliding plates of different materials, reducing flow problem to differential equation via hodograph transformation

21 p3747 A70-41962

Octahedral solid-solid phase transitions by differential thermal analyzer and scanning calorimeter module, discussing entropy change causes

21 p3784 A70-42264

Rigid circular cylindrical inclusion elastic bedding dynamic loading, calculating stresses in interface

22 p4112 A70-42345

Isothermal kinetic rates of penetration of polymer by spherical indenter, using thermomechanical analyzer

22 p4059 A70-43079

Solid particles interactions during entrainment by viscous incompressible fluid in pipe, calculating interaction force as function of radius, distance and Reynolds number

23 p4181 A70-44310

Thermal constriction resistance due to nonuniform metal surface conditions, considering macroscopic contact resistance for nonuniform interface pressure distribution

24 p4429 A70-46177

SOLIDIFICATION

Effects of solidification conditions and gas content in melt on continuously cast Al ingots as-cast structure

02 p0316 A70-12297

Al solidification in direct chilling molds effect on as-cast structure, analyzing heat removal, casting rate and application of water to outgoing ingot

02 p0316 A70-12298

Filamentary casting technique for nonequilibrium alloy structures to produce continuous specimens by rapid solidification

04 p0698 A70-15135

Heat transfer effects during solidification on mechanical properties of Al alloy castings compared with sand castings

[ASM PAPER W9-7.2]

07 p1293 A70-18998

Mutual thermal influence zone between parts of die casting during solidification established as function of time

08 p1506 A70-21138

Heat exchange during solidification of castings in molds, studying thermal properties effect for achieving constant mold surface temperature

08 p1506 A70-21141

Solidification thermal conditions during Ti casting by melting out patterns in graphite molds, investigating heat accumulation coefficients in molds

08 p1506 A70-21142

Copper alloy composite reinforced by unidirectional solidification of pseudobinary eutectic Cu-ZrCuSi, discussing mechanical properties and electrical conductivity

11 p2066 A70-25775

Eutectic NiAl-Cr structure and high temperature tensile strength as function of solidification rate

15 p2755 A70-31560

Unidirectional-solidification casting of superalloys of refractory metals in turbine blade production

15 p2757 A70-31811

Materials preparation processes and improvements in space weightless environment, considering metals and ceramics melting, solidification, electromagnetic process control, etc

16 p2919 A70-33717

Lunar cratering rates from Apollo flights data on solidification ages for Mare Tranquillitatis

16 p2979 A70-34037

Solidification theory application to Ti alloys, predicting microsegregation in binary alloys

17 p3112 A70-34352

Two dimensional solidification of forced viscous flow over flat plate with constant heat removal

17 p3194 A70-34634

Ti-Si eutectic alloys unidirectional solidification by zone melting

19 p3450 A70-37375

Solidification and composition model of macroscopic freckles in nickel base superalloys single crystals

20 p3646 A70-39101

Cold plate immersed in warm flowing liquid, calculating two dimensional transient and steady state solidification by conformal mapping

21 p3949 A70-41319

Solar nebula rings and planet formation by sedimentation of solid particles in mechanical equilibrium, including Jupiter and Saturn protoplanets

23 p4239 A70-43867

Columnar grain and Ni alloy single crystal gas turbine engine components resistant to high temperatures produced by precision casting, using directional solidification

23 p4207 A70-44857

Ternary Co-Cr-C alloys unidirectional solidification with metal matrix and carbide simultaneous freezing at eutectic liquidus line

24 p4358 A70-45235

Nonequilibrium solidification and metastable-stable phase transformation during heating of Al-Mo and Al-Cr alloys

24 p4360 A70-45829

Al-Cu alloy unidirectional solidification, investigating interfacial transition from plane to cellular structure and segregation pattern

24 p4362 A70-46179

Cellular breakdown in binary Al-Cu alloys in unidirectional solidification, observing small pit stability on solid-liquid interface

24 p4362 A70-46180

Eutectic and hypereutectic Al-Si alloy quench modification by rapid solidification, investigating microstructure and mechanical properties

24 p4362 A70-46183

SOLIDIFIED GASES

Solid hydrogen condensation on interstellar grain surfaces at extremely low temperatures related to H atoms density

01 p0183 A70-10896

Thermal stability of graphite core-solid hydrogen mantle grains determined from temperature and evaporation rates calculated for interstellar space

04 p0743 A70-14398

Molecular and solid hydrogen in dense interstellar clouds suggested from underabundance of neutral atomic hydrogen, discussing grain temperature

04 p0747 A70-14585

Solid carbon dioxide measured for complex index of refraction at IR wavelengths

04 p0719 A70-15036

Fusion reactions generation by high power laser beams focused on solid deuterium target

05 p0857 A70-15992

Mariner 6 and 7 missions IR spectrometric records showing evidence of solid carbon dioxide in Martian upper atmosphere

06 p1137 A70-17194

Spectral reflectance of carbon dioxide and water frosts at 0.8-3.2 microns, growing frosts in cold vacuum chamber from high purity gases

07 p1388 A70-19945

Plasma production by solid hydrogen-giant pulse laser interaction, studying time dependent distributions of plasma density, temperature and velocity

10 p1902 A70-25222

Plasma production by irradiating solid hydrogen foils with intense pulse ruby laser

14 p2622 A70-30659

Capture coefficients and reflected flux measurements for gaseous nitrogen molecular beams impinging on solid nitrogen cryodeposit surface

20 p3675 A70-39390

Solid para hydrogen IR and Raman spectra frequency analysis, examining lattice vibration effects

21 p3853 A70-41721

SOLIDS

NT SOLIDIFIED GASES

Lamb wave techniques using guided ultrasonic waves for solid cylindrical objects nondestructive testing

01 p0098 A70-10019

Solid bodies unsteady thermal conductivity in presence of quasi-steady heat transfer under combined radiant and thermal fluxes, presenting thermodynamic nomograms

01 p0213 A70-10215

Book on nonlinear stress waves propagation in elastic solids covering adiabatic shocks, isentropic plane waves, Lagrange equation, spherical waves, heat conduction effect, etc

01 p0202 A70-10966

Light emission by solids, discussing injection lasers, luminescence semiconductor diodes, group 2 and 6 compounds, etc

01 p0160 A70-11288

Kharlamova solution for solid body motion in Newtonian force field represented as rolling, without slipping, of mobile hodograph of angular velocity vector

01 p0145 A70-11431

Kharlamova motion equations solution for solid body with fixed point in potential force field, assuming fixed center of gravity

01 p0145 A70-11432

Kharlamov motion equations solution for solid body with fixed point subjected to zero-potential forces

01 p0145 A70-11433

Euler-Poisson equations application to motion of heavy solid body about fixed point to determine kinetic momentum vector relative to fixed reference system

01 p0145 A70-11434

Canonic equations of motion of heavy solid body with fixed point

01 p0145 A70-11436

Body motions containing cavity filled with viscous fluid under influence of gravity, formulating motion equations for fluid and body

01 p0068 A70-11576

Variational principle for admissible functions particular solution in elasticity theory involving solid bodies with cracks

01 p0212 A70-11608

Lamb waves behavior applied to defect evaluation in nondestructive tests of solid elongated cylindrical objects

02 p0276 A70-12552

Variational equation describing thermal diffusion in solid body undergoing deformation

03 p0589 A70-13348

Optimal stabilization of free solid body equilibrium state with gyroscope, using solution of three flywheel system stabilization

03 p0484 A70-13364

Extrapolation formulas to calculate temperature gradients and heat fluxes in solid heated by variable heat flux, estimating errors

03 p0606 A70-13521

Nonlinear solid applied mechanics, emphasizing nonlinear constitutive equations and related subjects, cyclic loading effect on solid materials, etc

03 p0610 A70-14230

Creep rupture and fatigue strength in solid body mechanics, considering triaxial stress state and simplified creep rupture theory variant

03 p0599 A70-14249

Deformability calculation of two phase composite solid materials through laminated structural models

03 p0602 A70-14337

Finite element method applied to heat conduction in solids with temperature dependent thermal conductivity, using nonlinear constitutive equation for heat flux [ASME PAPER 69-WA/HT-34]

04 p0782 A70-14806

Effective wave propagation velocities, bulk and shear moduli of elastic heterogeneous solids approximated by self consistent method

04 p0777 A70-15496

Three dimensional analysis of nonhomogeneous elastic solids based on finite element method and equilibrium equations, discussing iterative solution

05 p0926 A70-15915

Propagation and growth equations governing wave propagation in micropolar viscoelastic solids couplings between discontinuities in macroscopic and microscopic fields

05 p0929 A70-16063

Spread criterion and stress distribution near penny shaped crack in elastic solid under axisymmetric body forces distribution

05 p0930 A70-16079

Stress distribution in vicinity of stress-free Griffith crack in elastic solid acted upon by symmetric distribution of body forces

05 p0930 A70-16084

Three dimensional brittle body limiting axisymmetric stability under tensile stresses and weakened by ring shaped cracks, determining critical tensile loads

05 p0945 A70-16855

Incremental stress distribution near circular crack with internal pressure in neo-Hookean solid under deformation due to triaxial compression, illustrating initial stress effect

05 p0956 A70-17108

Inherent stresses in elastic solid assuming inherent strain as stress source, integrating stress functions

06 p1160 A70-17131

Activated carrier mobility confirmed in organic solids

06 p1004 A70-17325

Compatibility conditions of theory of micromorphic elastic solids using Riemann theorem

06 p1164 A70-17530

Limiting stress states analysis in isotropic solids using loading history and replacing nonlinear stress-strain curve by approximating rectilinear polygon

06 p1165 A70-17547

Dual model for describing brittleness and plasticity of solid elastic deformable body, formulating criteria for passage into inelastic state

06 p1166 A70-17656

Shear and linear strain energy criteria for limiting stress state model of solid deformable bodies, considering uniaxial, biaxial and triaxial loading

06 p1166 A70-17657

Temperature distribution law for semifinite and infinite solid bodies under steady heat conduction in presence of concentrated heat source

06 p1178 A70-17872

Uncoupled quasi-static boundary value problem for linear viscoelastic solids undergoing thermal and mechanical deformation solved by computational algorithm

06 p1168 A70-17937

Pyrolysis effect on infinite slab subjected to front heat flux, attributing increased porosity to mass loss [WSCIPAPER 69-27]

06 p1178 A70-17978

Hyperboloids and paraboloids in flow of Reynolds number 22-65000 and Mach number 10, discussing viscous interactions effects on pressure, drag and skin friction

[AIAA PAPER 70-182]

06 p0976 A70-18240

- Faint meteor ablation processes, presenting evidence of solid consistency prior to atmospheric entry, vaporization, wake blending and trails
06 p1151 A70-18481
- Micropolar homogeneous and anisotropic elastic solids linear dynamic theory, deriving reciprocity and variational theorems
06 p1172 A70-18512
- Soviet monograph on theory and calculations of impact systems covering solid body collisions, elasticity, wave mechanics and nonflat rod applications
07 p1400 A70-18732
- Frequency equation for harmonic waves propagating in fluid filled circular cylindrical cavity in infinite isotropic solid medium
07 p1253 A70-18846
- Inelastic behavior of solids strained at high temperature emphasizing hot creep phenomena in aviation materials
07 p1406 A70-19346
- Heavy solid body motion about stationary point at small nutation angle, estimating region of series convergence representing periodic solutions to motion equations
07 p1336 A70-20298
- Aerodynamic characteristics of nonconvex bodies in free molecular flow of monatomic gas
08 p1547 A70-21081
- Aerodynamic coefficients of nonconvex bodies in free molecular flow of monatomic gases based on delta representation of flow velocity distribution function
08 p1432 A70-21084
- Electromagnetic fields interaction with nonconducting neutral elastic solid, formulating relativistic variational principle for balance laws and constitutive equations
08 p1545 A70-21252
- High speed testing - Conference, Boston, March 1969, Volume 7, Rheology of solids
08 p1526 A70-21326
- Strain rate effects on mechanical properties of solids under dynamic loading
08 p1590 A70-21328
- Constitutive inequalities for isotropic elastic solids under finite strain generated by introducing concept of conjugate pairs of stress
08 p1590 A70-21351
- Laser-induced electron emission from metals and insulators in form of evaporated films and single crystals, discussing many-photon photoelectric effects and thermionic emission
08 p1556 A70-21509
- Pressure effects on melting temperature curves of solids, considering Van der Waals solids, metals and ionic compounds
09 p1665 A70-22056
- Laser heating of plasma, motion pattern and shock wave parameters during absorption burst in solid body vapor, using numerical analysis
09 p1695 A70-22181
- Variational theorem for compatibility and plasticity for Mises solids based on stress functions
09 p1771 A70-22397
- Vitreous transparent solids emission after irradiation by Q switched laser, ascribing luminescence to multiphonon and excitonic phenomenon
09 p1710 A70-22836
- Irreversible processes thermodynamics during thermoelastic deformation of solid bodies, deriving thermodynamic potentials, state and coupled heat equations
09 p1777 A70-23077
- Thermal conductivity of arbitrarily inhomogeneous bodies, considering vectorial field isotropy and temperature gradients dispersion
09 p1789 A70-23103
- Equations of motion integration for solid body in potential forces field induced by elastic springs
09 p1728 A70-23386
- Book on solid materials under stress covering mechanical testing, metals and polymers structure, ceramic crystals and creep and composite materials properties
09 p1708 A70-23476
- Solid dielectrics permittivity measurement using beam deflection phenomenon in multislot waveguide antenna
09 p1652 A70-23656
- Two dimensional MHD flow past solid body at large Reynolds numbers, treating boundary layer transition
10 p1922 A70-24011
- Equilibrium equations integration for body in isotropic linear viscoelastic medium with contact-type boundary conditions
10 p1957 A70-24267
- Crack development in solid body, considering condition at crack tip not derivable from equation of motion and strain equation
10 p1960 A70-25007
- Solid body acceleration by ideally conducting gas in constant gravity field under magnetic field, considering rarefaction, reflected waves, motion equation, wall pressure, etc
11 p2082 A70-25389
- Elastodynamics mixed initial and boundary value problems numerical solution method applied to deformation of elastic solid
11 p2140 A70-26485
- Mechanical properties in solids under dynamic incremental shear loading, discussing wave propagation tests on steel, Cu and Al
11 p2143 A70-26669
- Slow electrons interaction with periodic and nonperiodic solid surfaces, investigating elastic scattering
12 p2275 A70-27252
- Analytic expressions for concentration distribution functions in inhomogeneous solids within intermediate stages of homogenization process
12 p2253 A70-27282
- Rigid solid replacement by elastic body in relativistic mechanics
13 p2451 A70-28955
- Elastoplastic continuum under specified rates of body forces, surface tractions and displacements, formulating minimum principle for solving boundary value problem
13 p2513 A70-29154
- Variational principles derivation for inelastically deformable body mixed boundary value problem, considering loading conditions with basic functions free of discontinuities
13 p2516 A70-29524
- Jet collisions solutions for impact of pin at obstacle, solid body impact at surface, cylindrical shells longitudinal impact and jets interactions
13 p2453 A70-29771
- Mechanics of solid structures including shells and beams, considering three dimensional behavior laws in plasticity and creep
14 p2656 A70-30294
- Variational equation describing thermal diffusion in solid body undergoing deformation
14 p2657 A70-30722
- Finite elements for three dimensional compressible and incompressible solid continua based on minimum potential energy and variational principles
14 p2659 A70-31128
- Thermoelasticity of incompressible solids, integrating linearized equations using Helmholtz solution
14 p2660 A70-31224
- Thermocouples performance during fast varying temperature measurements in solids, considering physical parameters effects on accuracy
15 p2734 A70-31646
- Viscoelastic-plastic solid delayed fracture associated with wedge formation of crazed material at crack tip
15 p2816 A70-32010
- Free solid body time optimal rotation about fixed central axis under action of external control moment vector, assuming zero initial and terminal angular velocity
15 p2775 A70-32447
- Stress wave propagation in solid infinite elastic medium and laminated materials
15 p2823 A70-32784
- Equation of state of solids measured by shock wave techniques, considering elastic-plastic flow in plane wave geometry
15 p2824 A70-32789
- Initial thermally stressed state of solid bounded by concentric circular cylinders, applying Cauchy thermoelastic stress theory
16 p2987 A70-32993
- Rigid inclusion effect on stress distribution in isotropic infinite solid with Griffith crack under plane strain
16 p2994 A70-34250
- Stress wave generation in elastic temperature-dependent absorbing solids by impulsive EM radiation
17 p3185 A70-34967
- Shock wave response of metals and nonmetals under high strain rates
17 p3188 A70-35223
- Nonaxisymmetric thermal stress distribution in infinite elastic solid containing external stress-free crack with prescribed heat flux
17 p3196 A70-35437
- Heat conduction from sliding solids, discussing restrictions effect on temperature field near interface
17 p3197 A70-35543
- Equilibrium theory of finite deformation of elastic solids, discussing applications and approximate solution methods
18 p3335 A70-35975
- Thermodynamic application to strained solids, considering paradoxes, irreversible processes and continuum mechanics
18 p3340 A70-36555
- Thermodynamics of solids deformation, tracing macroscopic inelastic behavior to deformation induced internal structural changes governed by atomic and molecular processes
18 p3340 A70-36556
- Hybrid rocket engine with solid oxidizer, noting applications as apogee or perigee motor
18 p3301 A70-36655
- Heat transfer rates in short flow duration facilities /shock tubes/ from surface temperature measurement of solid exposed to flow
18 p3348 A70-36715
- Torsional and longitudinal vibrations of circular cylinders of micropolar elastic solids in terms of Laplace and Helmholtz equations solutions
19 p3537 A70-37789
- Plane waves superposed on solid during steady state isothermal creep deformation subjected to unidirectional constant initial tensile stress
19 p3537 A70-37791
- Infinite linearly elastic solid response with random variations in material elastic properties, obtaining average energy in displacement field by method of moments
19 p3538 A70-37796
- Elastic particulate composite solid with microinclusions, deriving dispersion relations governing plane longitudinal wave propagation modes by analogy with continuum theory
19 p3540 A70-37942
- Fiber reinforced solid material, determining swelling or temperature change induced dilatation by micromechanics and physical chemistry
19 p3540 A70-37943
- Safety factor limit analysis for anisotropic nonhomogeneous solids by variational method, exemplifying by four layer rectangular beam
19 p3547 A70-38355
- Equilibrium equations integration for body in isotropic linear viscoelastic medium with contact-type boundary conditions
19 p3547 A70-38395
- Surface layer heating of solid body by dense gas discharge plasma radiation, comparing vaporization and reversible opacity onset times in quartz
19 p3482 A70-38733
- Variational principles in linear quasi-static theory of inhomogeneous and isotropic viscoelastic solids with microstructure
20 p3718 A70-39229
- Solid body nonelastic deformation in terms of thermodynamic principles of nonequilibrium processes
20 p3718 A70-39246
- Perforated solid body moving in ideal incompressible fluid, deriving equations of motion in Lagrangian form
20 p3610 A70-39732
- Soviet papers on mechanics of solid deformed body covering elasticity and plasticity theories, shell stability, eigenvalue problems, etc
20 p3722 A70-39851
- Fatigue phenomena based on solid body model, establishing breaking stress dependence on time or load cycles number
20 p3740 A70-39854
- Solid bodies statistical creep analysis, assuming macroscopically homogeneous isotropic polycrystallinity
20 p3725 A70-39866
- Book on stability of dynamic systems and solid bodies covering variation equations, Liapunov method and functions, approximations, harmonic balance and applications
21 p3850 A70-41370
- Anisotropic elastic solid body thermal stresses, investigating static plain strain problem in thermoelastic linear theory
21 p3936 A70-41414
- Microelastic solids theory achieved with application of internal constraints from postulate of principal coincidence
21 p3939 A70-42029
- Constitutive equation for homogeneous and isotropic elastic solids
21 p3940 A70-42101
- Temperature distribution measurement inside solid samples by Mossbauer effect, considering application to turbine blades
21 p3830 A70-42165
- Linear coupled thermoelasticity theory for homogeneous isotropic solid with two temperatures
22 p4123 A70-42540
- Crack growth study in viscoelastic solids by linear continuum mechanics, discussing cyclic loads, composite solids mechanical behavior and thermodynamics
22 p4115 A70-42937
- Sound velocity in isotropic nonlinearly elastic continuum with microstructure, showing dispersion coincident with Cosserat constant
22 p4120 A70-43713
- Strong fibrous solids - Conference, London, January 1970
24 p4366 A70-45165
- Electromagnetic waves nonlinear interaction at various threshold powers, inducing propagation in solid body plasma
24 p4388 A70-45201
- Linear viscoelastic solid quasi-static deformation, deducing associated minimum principles under assumption of unique solutions existence for boundary value problems
24 p4420 A70-45264

- Hercules 89 supergiant abnormal IR radiation flux originating in circumstellar shell of solid particles radiating at observed long wavelengths
24 p4410 A70-45772
- Two incompressible isotropic nonlinear elastic solids mixture, investigating entropy production inequality effects
24 p4425 A70-45991
- Plane parallel collision of two solid spherical bodies with mass centers coincident with geometrical centers
24 p4427 A70-46377
- SOLIDUS**
Ternary Ti-Ta-Nb solidus surface determination by simplex lattices and cubic approximation, statistically evaluating equation derived
05 p0864 A70-16547
- Visualized multicomponent systems subsolidus structures, studying physicochemical characteristics
13 p2470 A70-28885
- Subsolidus state multicomponent eutectics systems temperature range based on number and melting points ratios of individual components
24 p4367 A70-45476
- Simplex lattice mathematical models of solidus volume for quaternary Nb-W-Ti-Zr system
24 p4361 A70-45833
- SOLSTICES**
F 2 layer midday ionization equatorial anomaly during summer and winter solstices, using calculated mean critical frequencies
11 p2042 A70-25533
- Solstitial solar quiet currents along magnetic lines of force in magnetosphere, discussing ionospheric wind asymmetry effects
17 p0377 A70-34949
- F 2 layer midday ionization equatorial anomaly during summer and winter solstices, using calculated mean critical frequencies
21 p3819 A70-41283
- SOLUBILITY**
Gas solubilities investigated for gaseous pressurization of propellants
01 p0160 A70-10840
- Ternary chemical element additions (O, Sn, Zr, Cu, Mo, V) effects on solubility range of primary alpha region of Ti-Al base alloys
01 p0122 A70-11239
- Temperature and hemoglobin concentration effect on oxygen solubility in blood, constructing table for Bunsen solubility coefficients
03 p0428 A70-14156
- Solubilities and heats of solutions of Mo, W, V, Ti and Zr in liquid K
04 p0710 A70-15632
- Binary system Mo-C determined in temperature range 1250-2270 C, using microscopic and thermal analyses and microhardness testing
05 p0862 A70-16198
- Metastable tau-phase in Fe-Ni-B melt solidifying into boride, noting lattice constant and solubility
07 p1307 A70-19393
- Waspaloy gamma prime solvus temperature relationships as function of solution treatment and precipitation strengthening additives, discussing microstructure and tensile properties
08 p1520 A70-21555
- Transition metal alloys electronic effect on solubility of interstitials
08 p1521 A70-21695
- Combined solubility of group IVA metals and carbon in solid state molybdenum at various temperatures
09 p1704 A70-22754
- Oxygen solubility in liquid Mo in presence of volatile oxides, determining equilibrium constant of dissolution reaction
09 p1709 A70-23784
- Tantalum solubility in alpha titanium and Ti-Ta system physicochemical properties using metallographic, X ray, hardness and resistance analysis
10 p1903 A70-23864
- Nitrogen solubility in Nb-Mo solid solutions, determining relationship between N partial pressure, temperature and concentration
14 p2598 A70-31285
- Hydrogen solubility in electrically exploded metals
15 p2762 A70-32747
- Impurities solubility in semiconductor indium telluride with stoichiometric vacancies, verifying thermodynamic model by phase diagrams
16 p2960 A70-33224
- Mo, W, V, Ti and Zr solubilities in liquid K
16 p2933 A70-34210
- Nitrogen solubility calculation in transition metals liquid binary systems, using quasi-chemical model
18 p3273 A70-36045
- Ti, Nb and Mo solubility during surface doping in Al melts containing various metals, discussing melt lattice structure effects
18 p3276 A70-36208
- Oxygen solubility in Nb-Hf alloys at elevated temperatures, using isothermal sections for Nb-rich part
19 p3453 A70-38708
- Ni-Cu-C solid solutions, measuring temperature dependence of graphite solubility by vapor transport method
21 p3841 A70-42149

- Solubility isotherms of alloying elements in Ge-Al-P semiconductor-acceptor-donor system at high temperatures
24 p4391 A70-46143
- Fe-Cr and Fe-Cr-V system miscibility gap, using differential thermal analysis and Mossbauer effect measurements
24 p4362 A70-46190
- Fe-Ni-Mn ternary martensitic alloy, discussing metastable miscibility gap island existence in bcc phase
24 p4363 A70-46193
- SOLUTES**
Helical twisting power of steroidal solutes in cholesteric mesophases, discussing nematic temperature shift dependence on ester chain
08 p1455 A70-21524
- Interstitial solutes effect on athermal component of flow stress in alpha titanium
08 p1521 A70-21577
- Organic solutes diffusion in stagnant blood plasma and red cell suspensions, using models from transport theory
15 p2686 A70-32847
- SOLUTIONS**
NT AQUEOUS SOLUTIONS
NT DETONABLE GAS MIXTURES
NT GAS MIXTURES
NT NUCLEAR EMULSIONS
NT PHOTOGRAPHIC EMULSIONS
NT SOLID SOLUTIONS
Turbulent flow theory of dilute linear polymer solutions in smooth and rough tubes based on Reynolds equation
15 p2719 A70-31491
- Molecular interactions, surface pressures and potentials of mixed monolayers of stearic acid and stearyl alcohol with inorganic subsolutions
15 p2695 A70-32547
- SOLVENTS**
Thermodynamics of LiBr in anhydrous dimethyl sulfoxide determined at several temperatures using EMF method
06 p1003 A70-17219
- Lil thermodynamic properties in dimethyl sulfoxide determined by emf method, discussing ionic solution energies
10 p1831 A70-25041
- Propylene carbonate, dimethyl formamide, acetonitrile and methyl formate diffusion coefficients measurement for estimating nonaqueous Li batteries transport limitations
15 p2766 A70-32528
- Free energy and enthalpy of single ion solvation in water and propylene carbonate, using electrostatic model
15 p2695 A70-32829
- SOMMERFELD APPROXIMATION**
Laminar flow stability along flexible boundary on basis of Orr-Sommerfeld equation
05 p0836 A70-16923
- Orr-Sommerfeld equation asymptotic solution corresponding to boundary layer velocity distribution
15 p2721 A70-32357
- Leaky wave antennas, deriving radiation field distribution in terms of power leakage from interior by Sommerfeld integral and Kirchhoff-Huygens integration
17 p3052 A70-35071
- Numerical integration of Orr-Sommerfeld equation for flat plate Blasius boundary layer transition
23 p4179 A70-43973
- Linear stability of fluid flow, proving equivalence of slow and rapid asymptotic solutions of Orr-Sommerfeld equations
23 p4180 A70-43994
- Laminar to turbulent boundary layer flow transition over flat plate, using space amplified numerical solutions of Orr-Sommerfeld equation
23 p4181 A70-44234
- SOMMERFELD WAVES**
Sommerfeld type radiation conditions for linear homogeneous isotropic elastic materials with microstructure, discussing field equations, displacement and rotation vector and scalar conditions
21 p3936 A70-41417
- SONAR**
Radar and sonar data processing for display in command and control systems using digital technique, discussing processor configuration
05 p0828 A70-16189
- Echoes with ion sonar waves in ionized gases, considering ion density disturbances under local excitation
24 p4387 A70-45795
- SONDES**
NT IONOSONDES
NT RADIOSONDES
NT RAWINSONDES
Global meteorological sounding network requirements, restraints and sensors, considering gun launched meteorological probe role
01 p0054 A70-10082
- Drop sondes dynamic and aerodynamic design for lower Venus atmosphere based on solution for free

- fall of body in atmosphere with constant temperature gradient
09 p1766 A70-22935
- SONIC ANEMOMETERS**
Atmospheric wind velocity and temperature oscillations measurement using acoustic anemometer, resistance thermometer and multichannel signal spectrum analyzer
07 p1284 A70-19833
- Acoustic piezoceramic anemometer for steady state measurements of wind turbulence on meteorological tower
07 p1285 A70-19835
- Acoustic piezoceramic anemometer for steady state measurements of wind turbulence on meteorological tower
20 p3634 A70-40342
- SONIC BOOMS**
Sonic boom pressure signatures for uniform and maneuvering flight conditions determined for fighter and SST aircraft
[AIAA PAPER 69-1134] 01 p0005 A70-10606
- Sonic boom wave shapes and amplitudes determination in still stratified atmosphere, comparing U.S. standard atmosphere results to various atmospheric models
03 p0411 A70-12927
- Sonic boom propagation in still atmosphere with vertical temperature gradient, using graphical method of determining rays for aircraft motion
05 p0791 A70-15786
- Sonic boom overpressures generated by aircraft level rectilinear flight at supersonic speed in temperature and wind stratified atmosphere, calculating atmospheric correction factor
05 p0794 A70-16411
- Sonic boom theory of geometric acoustics with nonlinear effects modification, emphasizing horizontally stratified atmospheric propagation, discussing failure near caustic
05 p0796 A70-16794
- Sonic boom research, considering exposure pattern development, propagation in inhomogeneous atmosphere and effects on structural responses
05 p0796 A70-16795
- Sonic bang simulation by linearly distributed explosives, creating blast waves with wide range of shapes and durations
05 p0796 A70-16796
- Aircraft configurations designed for eliminating sonic boom due to lift
05 p0791 A70-16798
- Weak shock thicknesses with turbulent scattering as dissipative mechanism compared with magnitude in sonic boom flight tests and explosions
[AIAA PAPER 70-54] 06 p1042 A70-18190
- Sonic booms propagation in nonhomogeneous atmosphere, outlining effects on intensity and range for transport and military fighter aircraft
07 p1190 A70-18779
- Sonic boom focalization, considering linear propagation for real atmosphere with wind and Jericho experiments
07 p1193 A70-19130
- Book on sonic boom effects covering shock waves generation and propagation, elastic structures response to dynamic loads, structural damage, etc.
09 p1609 A70-22203
- Super sonic booms occurrence and propagation, discussing aircraft operating conditions for prevention of effect on ground
10 p1805 A70-24130
- Shock impedance definition consistent with acoustic limit, considering use of impedance mismatch to reduce sonic boom overpressure
10 p1805 A70-24522
- Coupled panel-cavity vibrations analysis, emphasizing sonic boom excitation of large window-room combinations
11 p2133 A70-25728
- Seismic measurements of sonic boom induced ground vibrations for hazard to structures
12 p2227 A70-28078
- Plane acoustic shock wave vertical propagation in gravity-stratified atmosphere with temperature gradient, using homogeneous perturbation velocity
[DFVLR-SONDDR-35] 12 p2212 A70-28209
- Climatology of safe threshold Mach number and airplane ground speed for boomless supersonic cruise, considering San Francisco-New York route
14 p2530 A70-30606
- Overpressure, rise time and wave period of sonic boom signatures at ground level from unaccelerated supersonic overflights
14 p2530 A70-30608
- Sonic boom incident and ground reflected waves action on exterior wall, calculating arrival time as functions of aircraft speed and altitude and wall slope
14 p2566 A70-30861
- Sonic boom minimization methods involving mass or energy addition
14 p2531 A70-30868
- Sonic boom causes and nature, considering aircraft configuration and attitude and minimizing effects
15 p2673 A70-31852

Sonic boom variation with aircraft geometry, volume, weight, weather and environment conditions, noting effects on structures and people
16 p2840 A70-32947

Sonic boom penetration into water, discussing N wave reflection and refraction, sound fields, etc
16 p2952 A70-34095

Supersonic transport sonic boom theory and effect reduction, discussing Whitham rule, bow shock, overpressure, engine and aircraft design and shock wave control
16 p2843 A70-34263

Annoyance assessment for sonic boom series exposure near airport
16 p2843 A70-34325

Sonic boom minimization through airstream alteration by force or heat fields and aircraft body shaping [AIAA PAPER 70-903]
17 p3019 A70-35817

Supersonic boom intensity calculation on ground, assuming isobaric inhomogeneous atmosphere and weak shock wave
18 p3213 A70-36380

Lower bounds for sonic boom, considering negative overpressure region in configuration tailoring
18 p3241 A70-36456

Liability for damages due to supersonic flight sonic booms, discussing pertinent provisions in Dutch and international law
19 p3553 A70-37561

Intersecting shock waves propagation, deriving equations for aircraft sonic boom intensity
19 p3355 A70-38484

Atmospheric inhomogeneity and temperature gradient effects on sonic booms, discussing displacement, growth rate and shock wave radii refraction
22 p3961 A70-42311

Two dimensional flow about supersonic airfoil, considering trailing Taylor columns behavior like sonic booms
22 p4009 A70-42629

Human disturbance from SST overflight sonic booms, discussing overpressure, rise times and durations
23 p4137 A70-44016

SST configurations minimizing sonic booms obtainable for given length and weight [ICAS PAPER 70-23]
23 p4138 A70-44110

Near field flow effects on sonic boom for incident triangular wing with constant lift distribution [ICAS PAPER 70-20]
23 p4138 A70-44113

Sonic boom effects on building structures, using Concorde measurements and explosion simulation studies
24 p4289 A70-45151

Sonic boom waves diffraction and reflection, developing analytical method for pressure-time history in vicinity of walls and corners
24 p4289 A70-45266

Sonic boom, discussing characteristic flow phenomena, intensity, effects on buildings and animals, human reactions, etc
24 p4289 A70-45786

SST sonic boom noise level reduction by thermal simulation of long body aircraft, considering thermal spike or keel [AIAA PAPER 70-1323]
24 p4291 A70-45942

All-body configuration hypersonic transport aircraft performance by computer synthesis, considering sonic boom constraint, maximum payload ratio and optimal cruise speed [AIAA PAPER 70-1224]
24 p4291 A70-45957

Sonic boom effects on guinea pigs Corti organ, comparing auditory damage in cochlea with hair cell damage
24 p4305 A70-46374

SONIC FLOW

U TRANSONIC FLOW

SONIC NOZZLES

Exhaust plume from underexpanded sonic and supersonic nozzles including boundary mixing analyzed by approximate model to predict Mach disk location [AIAA PAPER 70-229]
06 p0972 A70-18135

Relaxation time influence on mass output calculation errors for gases in small diameter sonic nozzles
09 p1604 A70-22841

Exhaust plume rarefaction from sonic orifice, considering continuum to transitional behavior for perfect gas [AIAA PAPER 69-657]
21 p3745 A70-41742

SONIC SOLDERING

U ULTRASONIC SOLDERING

SONIC SPEED

U ACOUSTIC VELOCITY

SONIC WAVEGUIDES

U ACOUSTIC DELAY LINES

SOOT

Liquid fuel combustion luminous flame monochromatic radiation distribution, considering soot particle clouds effective emission thickness
06 p1172 A70-17142

Jet aircraft air pollutant production and dispersion of nitric oxide and soot, discussing mixing process [AIAA PAPER 70-115]
06 p1131 A70-18070

German monograph on soot formation and separation in turbulent diffusion flame in power plant combustion chamber, noting pyrolysis role
24 p4428 A70-45087

SORBENTS

NT ABSORBENTS

NT ADSORBENTS

SORPTION

NT ADSORPTION

NT CHEMISORPTION

Gases interaction with ablator and components during thermal conductivity, measuring nitrogen, helium, carbon dioxide and water sorption
21 p3951 A70-41873

SORTING

U CLASSIFYING

SOUND

U ACOUSTICS

SOUND ABSORPTION

U SOUND TRANSMISSION

SOUND AMPLIFICATION

Mechanical parametric amplification, improving SNR of acoustic systems in hostile environments
19 p3422 A70-37695

SOUND BARRIER

U ACOUSTIC VELOCITY

SOUND DETECTORS

U SOUND TRANSDUCERS

SOUND FIELDS

Horizontal and vertical sound fields local effects on natural convection from heated horizontal circular cylinder, using shadowgraphy
01 p0219 A70-11198

Mean acoustic force on small spherical and nonspherical inclusions in standing acoustic field, discussing equilibrium orientations of body
04 p0720 A70-15085

Near noise fields of choked axisymmetric air jet, discussing sound pressure levels surrounding jet
05 p0834 A70-16783

Pseudosound field wall pressure correlation obtained to predict response characteristics of aircraft panel mounted along jet wake
05 p0835 A70-16785

Noise field from ground testing of nuclear rocket engines operated at various reactor power levels
06 p1133 A70-18234

Bragg diffraction imaging for sound fields visualization
10 p1893 A70-24170

Sound radiation from rigid flow spoilers correlated with fluctuating forces, measuring jet-pipe drag and lift components with transducers
11 p2085 A70-26699

Pressure fluctuations in acoustic field of boundary layer under slot suction, considering vortex formation and separation on edges
12 p2209 A70-27298

Interference phenomenon observable by ultrasonic fields visualization in 1-10 MHz range, discussing beam stratification
13 p2404 A70-28646

Plane rectangular plate in acoustic field of jet engine exhaust, calculating surface stresses
15 p2819 A70-32186

Sonic boom penetration into water, discussing N wave reflection and refraction, sound fields, etc
16 p2952 A70-34095

Holographic flow and sound visualization, determining three dimensional density distributions in aerodynamic flows
19 p3425 A70-37888

Cylindrical radiator radiation resistance and mass in waveguide with reflecting boundaries, calculating sound field for effect of medium reaction
19 p3472 A70-38656

Sound field produced in uniform moving ideal fluid stream by nonuniform oscillating elastic wall
19 p3353 A70-38657

Noise field from ground testing of nuclear rocket engines operated at various reactor power levels
20 p3689 A70-39688

Sound generation by fluctuating subsonic jet flow, considering field directional characteristics and sound pressure variations with Mach number
21 p3850 A70-41422

Frequency dependent effects of applied acoustic fields on attached jet flows for Reynolds numbers over curved surfaces [ASME PAPER 70-FLCS-1]
22 p4008 A70-42430

Acoustic fields of circular, rectangular and line focused ultrasonic emitters for small defect detection
22 p4048 A70-43618

Lighthill aerodynamic noise theory fundamental equation for acoustic field density distribution, determining flow fields for surfaces in uniform translational motion
24 p4324 A70-45268

Ultrasonic angle probes with circular and rectangular transducers, discussing radiation field characteristics
24 p4336 A70-45686

SOUND GENERATORS

Sound radiation from airfoil in turbulent jet flow, discussing direct correlation of fluctuating lift
01 p0004 A70-11192

Sound generation by multibladed single stage fans operating in free field, deriving model as boundary value problem involving inhomogeneities due to quadrupole distribution
01 p0166 A70-11197

Sound generation in axial-flow subsonic turbomachinery, using two dimensional model [ASME PAPER 69-WA/FE-4]
04 p0733 A70-14785

Discrete noise generation and propagation due to fan engine rotor forcing excitation and interaction with downstream stator
05 p0896 A70-16791

Sound radiated by fluctuating forces on helicopter rotor analyzed, predicting noise output variation as function of helicopter design parameters
05 p0796 A70-16792

Ground reflection effect on plane uniform sound source distribution applicable to compressor and fan noise under far field conditions
09 p1726 A70-22240

Acoustic radiation produced in response to harmonically oscillating circular cylinder rotating in viscous fluid solved within Lighthill-Curle formalism for aerodynamically generated sound
09 p1726 A70-22391

Rigid rectangular box with supported flexible wall analyzed for internal acoustostructural mode coupling factors and corresponding modal average radiation efficiency
09 p1770 A70-22393

Low Mach number aerodynamic sound generation by turbulent flow at sharp edged thin scattering half plane solved with Green function
10 p1802 A70-24521

Sound generation and detection by distributed piezoelectric sources using frequency response and equivalent circuit
11 p2085 A70-26701

Mechanical seals ringing sound relationship with heat transfer and interfacial conditions, noting sliding surfaces temperature effect
13 p2417 A70-28611

Cylindrical radiator radiation resistance and mass in waveguide with reflecting boundaries, calculating sound field for effect of medium reaction
19 p3472 A70-38656

Sound vibrations resonant frequency relation to jet internal structure in gas jet stem radiator
19 p3354 A70-38658

Sound generation by fluctuating subsonic jet flow, considering field directional characteristics and sound pressure variations with Mach number
21 p3850 A70-41422

SOUND INTENSITY

NT ZERO SOUND

Subjective measurement of sound level of impulses and pulses, investigating 1 kHz tone and selection of time length between sound events
05 p0882 A70-16344

Sound levels and frequency spectra of noises measured in AN-24 and IL-18 turboprop aircraft cockpits
05 p0796 A70-16925

Pro- and anticoagulants dynamics in rats blood during early phases of prolonged sound effect
12 p2168 A70-27347

Shock wave radiation from supersonic ducted rotor, determining sound power at blade passing harmonic frequency
19 p3353 A70-38614

Rod surface roughness effect on eddying sound frequency and intensity and on aerodynamic resistance
19 p3353 A70-38654

Sound level vs duration evaluated for noise exposure using different exchange rates [ASA PAPER FF2]
20 p3578 A70-39125

SOUND LOCALIZATION

Directional dependence of broadband artificial ear signal spectrum and correlation functions using dummy head
09 p1624 A70-22761

Frequency function of sound localization in median plane measured psychoacoustically at both ears with narrow band signals
09 p1624 A70-22762

Auditory and cutaneous sound localization acuity
13 p2354 A70-29597

SOUND MEASUREMENT

U ACOUSTIC MEASUREMENTS

SOUND PERCEPTION

U AUDITORY PERCEPTION

SOUND PRESSURE

Acoustical resonators free oscillations and pressure effects on damping, amplification, decay decrement and relaxation time
02 p0304 A70-12772

Spectral response of cylindrical shell due to random acoustic pressure input computed using modal approach
04 p0778 A70-15528

Sound pressure field from stationary and moving jets determined from jet and aircraft trajectory parameters

05 p0834 A70-16781

Microphone output level in airstream relation to sound pressure and pressure fluctuations caused by turbulent flow

07 p1334 A70-19372

Probability theory of stresses during random vibrations of flat panel in acoustic field of jet engine exhaust

18 p3301 A70-36301

Error analysis of Corcos hypothesis concerning cross spectra of pseudoacoustic LF turbulent pressure pulsations on flat plate

18 p3241 A70-36305

Sound generation by fluctuating subsonic jet flow, considering field directional characteristics and sound pressure variations with Mach number

21 p3850 A70-41422

SOUND PROPAGATION

Acoustic and shock waves propagation in multicomponent media, assuming uniform speed for components and complex density dependence of media on pressure

03 p0465 A70-13329

Sound propagation along cylindrical duct of wind tunnel, discussing fluid flow effect on modal cut-off frequencies

04 p0719 A70-15078

Surface inhomogeneities effect on sound radiated by nearby turbulence near flexible boundary, using converted Lighthill wave equation to obtain far field radiation

07 p1256 A70-19262

Two phase supersonic continuum flow of dispersed equal gas-liquid volume ratio in shock tunnel using continuum theory, considering sound propagation

07 p1256 A70-19311

Vertical propagation of short acoustic waves from harmonic source in inhomogeneous atmosphere, calculating shock front width and heating rate

12 p2264 A70-27519

Nonviscous relativistic fluid energy momentum tensor modification to rule out sound wave propagation velocities above speed of light

13 p2454 A70-29900

Acoustic and shock waves propagation in multicomponent media, assuming uniform speed for components and complex density dependence of media on pressure

14 p2566 A70-37079

Sound propagation in atmospheric fog, considering mass, momentum and energy transfer mechanisms between particles and gas

15 p2769 A70-31443

Sonic boom penetration into water, discussing N wave reflection and refraction, sound fields, etc

16 p2952 A70-34095

Perturbation method to obtain analytical expressions for attenuation of plane wave sound propagation in lined ducts

17 p3136 A70-34523

Axial compressor air intake wall design influence on sound propagation

19 p3353 A70-38653

Sound propagation in cylindrical waveguide with impedance walls in presence of flow

19 p3472 A70-38655

Perturbation method for nonlinear wave propagation in inhomogeneous media, considering sound propagation in ducts and hydromagnetic waves across nonuniform magnetic field

20 p3672 A70-39611

Mach number effect on sound propagation in tuning acoustically lined rectangular duct with uniform flow

20 p3673 A70-39709

Vertical propagation of short acoustic waves from harmonic source in inhomogeneous atmosphere, calculating shock front width and heating rate

21 p3818 A70-41167

One dimensional sound propagation in reacting gas mixture near equilibrium, obtaining equilibrium and frozen sound speed

22 p4074 A70-42752

SOUND RANGING

SOFAR /sound fixing and ranging/ systems for location and recovery of reentry vehicles and missile cases and rescue of disabled transoceanic aircraft

13 p2449 A70-29169

Simultaneous equations for motion location, speed and direction in acoustic tracking of supersonic objects, recording shock wave times of arrival with microphone system

13 p2450 A70-29988

SOUND TRANSDUCERS

NT ELECTROACOUSTIC TRANSDUCERS

NT LOUDSPEAKERS

NT MICROPHONES

Impedance, transfer and scattering characteristics for interdigital acoustic surface wave transducers, using linear equivalent circuit model

06 p1062 A70-17478

Acoustic scattering parameters for interdigital transducer as function of electrical loading and frequency using equivalent circuit model

06 p1062 A70-17485

Turbulence measurement by piezoceramic acoustic sensors, considering capacitance

07 p1284 A70-19829

Acoustic emission monitoring methods to detect crack formation and growth in ceramics

10 p1894 A70-24174

Sound generation and detection by distributed piezoelectric sources using frequency response and equivalent circuit

11 p2085 A70-26701

Precision components engineering inspection and sonic transducer surface vibration modes analysis by hologram interferometry

17 p3087 A70-35021

SOUND TRANSMISSION

Brittle composites /including fiber reinforced material/ deformability and plastic deformation effect on tensile strength, discussing pressure induction of sound flow

[ASME PAPER 69-WA/PROD-28]

04 p0705 A70-14834

Theoretical model of fan/compressor noise blade passing frequency generation and transmission, noting duct length and configuration in engine operation

04 p0734 A70-14886

Sound energy transmission and radiation into room by flexible structural panels subjected to acoustic excitation using wave equations

10 p1964 A70-25224

Sound transmission properties in terms of medium excitation by primary and secondary sound sources

11 p2083 A70-25730

Pilot helmets, discussing sound attenuation, noise protection and speech intelligibility

12 p2177 A70-27040

Plane harmonic sound wave reflection and transmission in flowing medium by infinite set of arbitrary spaced and staggered flat plates

16 p2971 A70-34016

Sound passage through rigid screen of arbitrary wave thickness with apertures, using linear algebraic equations

18 p3291 A70-36306

Sound transmission and suppression in turbomachinery fans and compressor ducts, using three dimensional wave equation

18 p3304 A70-36873

Space law aspects of direct broadcasting satellites for TV and sound transmission

20 p3740 A70-39408

Acoustic pulse transmission through plane vortex sheet, examining zone of silence, geometrical acoustics and sound radiation

21 p3849 A70-41243

Ultrasound inductive absorption coefficient of metals in quantized magnetic field

22 p4075 A70-43474

SOUND VELOCITY

U ACOUSTIC VELOCITY

SOUND WAVES

NT AERODYNAMIC NOISE

NT AIRCRAFT NOISE

NT ENGINE NOISE

NT JET AIRCRAFT NOISE

NT LAMB WAVES

NT NOISE [SOUND]

NT ROCKET ENGINE NOISE

NT SONIC BOOMS

NT THERMAL NOISE

Emission from broadband impulsive point source refracted by spherical interface between fluids with different acoustic velocities, showing emitted and inverse waveform disturbances

01 p0046 A70-11190

Short sound waves propagation in moving inhomogeneous medium, studying viscosity and heat conductivity influence

01 p0146 A70-11581

F 2 region acoustic waves over Kansas and Nebraska attributed to local storms in troposphere

02 p0290 A70-12158

Traveling wave velocity in human cochlea determined by equally loud tonal pairs, comparing results to psychophysical and electrophysiological findings

02 p0237 A70-12323

Charged particles motion in isotropic weakly ionized plasma acoustic wave associated with difference in electrons and ions entrainment by neutral particles

03 p0530 A70-13087

LF sound velocity measurement in carbon dioxide near critical point, noting existence of logarithmic divergence

04 p0718 A70-14685

Sound wave propagation in liquid containing gas bubbles allowing for relative motion of bubbles and liquid, deriving steady shock wave structure

04 p0671 A70-14991

Radiation from and panel response to supersonic turbulent boundary layer, emphasizing panel mode coupling to acoustic field

04 p0615 A70-15081

Sound vibrations effect on pulsation characteristics of turbulent gas jet

04 p0618 A70-15248

Auroral radio reflections using two coherent bistatic radio systems, discussing ionoacoustic waves in auroral plasma

05 p0837 A70-16072

Kirchhoff wave scattering geometric optics theory accuracy, using multifrequency acoustic wave backscatter data obtained from rough surfaces

05 p0814 A70-16401

Optical wave front reconstruction principles applied to sonic and seismic wave holography for mapping earth subsurface structure

05 p0850 A70-16685

Acoustic radiation from underexpanded supersonic main jet flow from nozzle impinged upon by annular jet

05 p0835 A70-16784

Experimental and analytical work on structural panels vibratory response and acoustic radiation excited by turbulent boundary pressure fluctuations, evaluating applicability to noise research

05 p0835 A70-16789

Surface acoustic wave components for performing transduction, amplification and coupling functions, considering compatible component configurations

06 p1018 A70-17477

Electrical impedance, conversion loss and bandwidth for piezoelectric film or plate transducers used for generating planar volume-acoustic waves at microwave frequencies

06 p1062 A70-17480

Plane light wave diffraction incident upon isotropic dielectric layer traversed by acoustic microwave using guided microwave theory

06 p1105 A70-17484

Sound wave velocity and damping in liquid N measured along saturated vapor line using thermal Brillouin scattering techniques

06 p1105 A70-17491

Witham radiative acoustics, analyzing nonequilibrium waves propagating in nongray radiating and absorbing gas

06 p1173 A70-17514

Radiatively driven plane acoustic wave in nongray radiating and absorbing gas assuming local molecular equilibrium

06 p1173 A70-17515

Pipe bounding walls effect on sound waves dispersion in rarefied gas, deriving integral equations showing frequency range decrease with container size

06 p1107 A70-18315

Electromagnetic-acoustic probe for remote wind velocity sensing and radar range performance

06 p1071 A70-18509

Frequency calculation and measurement for acoustic waves produced by carbon dioxide Q switched lasers

06 p1084 A70-18620

Optical system with orthogonal standing waves in liquid used for two dimensional scanning of laser beam in ultrasonic field

07 p1296 A70-18765

Plane acoustic wave steady state scattering at circular cylinder in semibounded region

07 p1334 A70-19089

LF ion-acoustic waves in ionosphere, considering electric and magnetic field variations, instability, etc

07 p1347 A70-19187

Sound waves dispersion and attenuation produced in gas flow by relaxation effects of solid particles presence

07 p1258 A70-19567

Dispersion of ion-acoustic waves in quiescent rare gas discharge plasmas, discussing model simulating ion waves generated by finite sine wave bursts

07 p1352 A70-19990

Propagation pattern of surface acoustic wave visualized in piezoelectric and nonpiezoelectric materials by dusting delay line with fine particles

07 p1336 A70-20283

Radial vibrations of hollow elastic sphere in acoustic medium, considering Laplace transform of field equations with respect to time

08 p1587 A70-21076

Acoustic wave propagation in partially ionized gas in external electric field, solving differential equations by Laplace transformation

08 p1552 A70-21503

Nondestructive testing and inspection by acoustic emission from stressed materials, discussing microstructure effect and crack initiation detection

08 p1508 A70-21747

Acoustic radiation produced in response to harmonically oscillating circular cylinder rotating in viscous fluid solved within Lighthill-Curle formalism for aerodynamically generated sound

09 p1726 A70-22391

Rigid rectangular box with supported flexible wall analyzed for internal acoustostructural mode coupling factors and corresponding modal average radiation efficiency 09 p1770 A70-22393

Thermoacoustic waves formation and propagation in metallic rods by light pulses, studying pulse rise time influence on waves shape and amplitude 09 p1778 A70-23090

Ion-acoustic wave oscillations of weak collision plasma in strong electromagnetic field, discussing instability 09 p1736 A70-23198

Acoustic gravity waves horizontal ducting in atmosphere with spatially periodic wind shears 09 p1671 A70-23498

Nonlinear oscillations averaging method applied to resonant interactions of acoustic gravity waves 09 p1729 A70-23666

Vertical liquid jets capillary instability under audio frequency disturbances, measuring disturbance growth rates for various wavelengths and fluid viscosities 09 p1664 A70-23678

Ion acoustic wave propagation near sheath at plasma-wall boundary in low pressure argon plasma measured by electron beam probe 10 p1921 A70-23965

Acoustic wave amplification and generation in piezoelectric semiconductors and semimetals by super-sonic carrier drift currents 10 p1925 A70-25030

Sound energy transmission and radiation into room by flexible structural panels subjected to acoustic excitation using wave equations 10 p1964 A70-25224

Sound transmission properties in terms of medium excitation by primary and secondary sound sources 11 p2083 A70-25730

Crack propagation in tensioned plates subjected to sonically induced vibrations 11 p2133 A70-25731

Microwave amplifiers based on interaction between piezoelectric acoustic waves and collinearly drifting carriers, analyzing gain, frequency response, etc 11 p2018 A70-26164

Acoustic perturbations in stationary weakly ionized pulsed neon plasma 11 p2096 A70-26842

Radiation characteristics of ion acoustic waves from monopole and dipole antennas, observing patterns of longitudinal wave in isotropic plasma 12 p2279 A70-27778

Plane acoustic shock wave vertical propagation in gravity-stratified atmosphere with temperature gradient, using homogeneous perturbation velocity [DFVLR-SONDDR-35] 12 p2212 A70-28209

Oscillating infinite cylinder as acoustic waves source in homogeneous viscous medium, deriving scalar and vector potentials 12 p2274 A70-28240

One dimensional radiatively driven acoustic waves analysis by approximation for radiative heat addition, achieving better accuracy than substitute-kernel method 13 p2520 A70-28633

Textbook reissue on diffraction of electromagnetic and acoustic waves at open end of waveguide, using Wiener-Hopf-Fock factorization method 13 p2363 A70-28724

Atmospheric turbulence effects on acoustic-gravity waves propagation, deriving dispersion relation for phase velocity and propagation constants 14 p2579 A70-31252

Amplitude modulation of ruby and neodymium-doped glass lasers via ultrasonic acoustic wave injection 16 p2926 A70-33162

Acoustic and magnetic surface waves technologies for radar signal processing 16 p2874 A70-33390

Sound wave phase fluctuations from ultrasonic waves traveling through turbulent wakes of circular cylinders and plates, using multichannel pulse height analysis 16 p2839 A70-34086

Plane acoustic wave interaction with elastic spherical shell, discussing effects of membrane, bending, rotatory inertia and shear deformation 16 p2993 A70-34087

Optical system with orthogonal standing waves in liquid used for two dimensional scanning of laser beam in ultrasonic field 18 p3271 A70-37109

Long range infrasound from rockets, showing two wave groups generated by launch and first stage reentry 19 p3531 A70-37694

Sound wave radiation and excitation in plane infinite plate by vortices 19 p3354 A70-38722

High temperature acoustic waves, examining solid and fluid properties, weld integrity nondestructive material tests and nondisruptive process measurement 20 p3628 A70-39170

Nonlinear acoustic absorbers behavior analysis, discussing spectral and temporal computation methods 20 p3672 A70-39237

Perturbation method for nonlinear acoustic wave propagation in steady one dimensional flow through variable cross section duct 20 p3673 A70-39612

Flow rate, momentum and energy perturbations during gas motions through shock wave, discussing acoustic waves impinging from supersonic region 20 p3612 A70-39815

Radio aurora model based on two stream, ion acoustic wave instability, investigating radar backscatter 20 p3623 A70-40465

Collisionless shock wave geometry, determining dispersion relation for ion acoustic waves propagating in plasma 21 p3856 A70-41082

Ion sound system one dimensional hydrodynamic equations, examining formation and interaction of nonlinear ion acoustic shock waves 21 p3857 A70-41384

Continuous pseudoacoustic and ion waves excitation and damping in plasma sheath around grid, taking into account transit time effect on ion acceleration 21 p3858 A70-41710

Collisionless nitrogen plasma drift velocity measurement by ion acoustic wave method 21 p3859 A70-41760

Acoustic surface waves phase velocity on lithium niobate with gold layer for propagation modes, predicting LF cut-off by substrate anisotropy 21 p3863 A70-42001

Acoustic waves in carbon dioxide at 2-25 torr initial pressures induced by heat from incident carbon dioxide laser pulses 21 p3837 A70-42003

Brillouin effect lines shape dependence on analogous acoustical waves temporal and spatial coherence 21 p3839 A70-42100

Acoustic waves generation from decay region of pulsating supersonic jet expelled from nozzle 21 p3748 A70-42211

Radiation patterns and scattering cross sections of plane black disks excited by electromagnetic and acoustic waves 22 p3984 A70-42391

Monochromatic acoustic wave interaction with turbulent jet fluctuating vorticity field, using Fourier analysis to extend spectral relations [ASME PAPER 70-FLCS-6] 22 p4008 A70-42426

Acoustic frequency spectra of transverse vibrations in bracketed bar caused by dry friction, using Lagrange method 22 p4073 A70-42612

Elastic cylindrical shell transient response to plane acoustic shock wave traveling through light fluid medium 22 p4114 A70-42647

Compressional sound waves electromagnetic generation in metals in static magnetic fields, examining acoustic amplitude variations 22 p4074 A70-42968

ELF acoustic gravity wave arrival from Apollo launches recorded by Doppler shift ionospheric sounder channeled near mesopause and lower thermosphere 23 p4187 A70-43859

Far field diffraction spreading of surface acoustic waves on cut Li-niobate in two directions 23 p4230 A70-44199

Fatigue crack growth detection by acoustic emission techniques 23 p4194 A70-44214

Gravitational acoustic wave emission in isothermal stellar atmosphere with mass sources 23 p4242 A70-44267

Sound radiation from unflanged circular waveguide duct with flow, calculating reflection coefficients, directivity pattern and power for comparison with approximate methods 23 p4219 A70-44392

Bunched ion bursts amplitude modulation effects on nonlinear ion acoustic waves in grid plasma system 23 p4229 A70-44989

Ion acoustic wave propagation in collisionless gravity-supported plasma in static magnetic field calculated from linearized Vlasov equation 24 p4382 A70-45109

Acoustic plasma wave excitation by transverse electromagnetic wave beam, calculating LF instabilities and energy losses 24 p4384 A70-45149

Single crystal piezoelectric materials growth characteristics and wave propagation properties for surface acoustic wave applications 24 p4367 A70-45399

Electron plasma oscillations excitation by ion acoustic waves 24 p4386 A70-45607

SOUNDERS
U SOUNDING

SOUNDING
NT BALLOON SOUNDING
NT IONOSPHERIC SOUNDING
NT ROCKET SOUNDING
IR equipment on Tiros and Nimbus 1 and 2 satellites, describing vertical atmospheric sounding 03 p0492 A70-13833

Meteorological guns for synoptic sounding of stratospheric circulation, discussing system characteristics and operations 07 p1250 A70-20280

SOUNDING ROCKETS
NT AEROBEE ROCKET VEHICLE
NT ANTARES ROCKET VEHICLE
NT APACHE ROCKET VEHICLE
NT ARCAS ROCKET VEHICLES
NT SKUA ROCKET VEHICLES
NT SKYLARK ROCKET VEHICLE
Burning program for sounding rocket to reach maximum altitude with given initial and propellant masses, discussing numerical parameter optimization technique 01 p0161 A70-10150

Graphical method for determining sounding rocket attitudes from optical sensor and flux gate magnetometer data 01 p0196 A70-10841

Time optimal attitude control for alignment of spin stabilized sounding rocket, discussing feedback control system 03 p0580 A70-13805

Parachute design for decelerating upper atmosphere rocket probes at high altitudes, using high drag coefficients in Stokes flow regime [AIAA PAPER 68-949] 04 p0624 A70-15410

Sounding rocket Vera 15 design with emphasis on operation safety, discussing payload capacity 04 p0765 A70-15669

Fluidics application in sounding rocket guidance control circuits used in space boosters 05 p0797 A70-15809

Response characteristics of height-based and time-based wind reduction techniques for meteorological rocketsondes 05 p0879 A70-17101

Meteorological Rocket Network for limited synoptic inspection of stratospheric circulation 07 p1273 A70-20252

Meteorological rocket system Meteor 1 firing procedure 07 p1395 A70-20254

PWN-8B meteorological rocket system for synoptic investigation of stratospheric circulation, describing sensor system deployment for descent measurements of wind and temperature 07 p1395 A70-20255

Kookaburra meteorological rocket system for sounding stratospheric circulation, describing instrument payload deployment for descending wind and temperature measurements 07 p1395 A70-20257

Parachute wind sensors used in Arcas and Loki sounding rocket systems for stratospheric sounding, describing position data acquisition via radar tracking 07 p1395 A70-20259

Temperature measurement in stratospheric circulation by meteorological rocketsonde wire sensor, presenting error correction technique 07 p1289 A70-20264

Meteorological rockets fired in Spain, obtaining stratospheric wind and circulation data 07 p1396 A70-20278

Quality planning for Japanese solid propellant sounding rocket motor production, discussing documentation, design, development and process controls, inspection and tests, etc 09 p1691 A70-22570

Nose cone modifications for Meteor-1 meteorological sounding rocket used for wind velocity measurements 09 p1767 A70-23406

Sounding rockets impact dispersion associated with wind measurement errors and thrust misalignments, discussing correction via reduced aerodynamic stability and initial rocket spin 13 p2503 A70-28677

Industry role in sounding rocket program, highlighting activities in various areas 13 p2523 A70-28679

Sounding rocket telemetry systems, discussing use of PCM and thick film techniques 13 p2363 A70-28681

Petrel payloads taking into consideration rocket stability after launch and compartment design 13 p2503 A70-28683

British national and Commonwealth collaborative sounding rocket programs, discussing organization, scope and range facilities 13 p2523 A70-28685

INTA-255 ionospheric sounding rocket, describing vehicle and launcher design, test firings, ground facilities, etc 13 p2504 A70-28686

- Altimeter-telemetry system for small sounding rockets, discussing ground and flight test results
13 p2363 A70-28688
- SR-1 hybrid propellant engine for sounding rockets, describing design and operating characteristics
13 p2474 A70-28689
- ESRange-high altitude sounding rocket range for European space research, discussing location, safety, equipment, instrumentation, staff and programs
13 p2523 A70-28690
- Petrel sounding rocket design and performance
13 p2504 A70-28692
- Petrel sounding rocket performance and facilities, describing rocket firings at Hebrides range
13 p2504 A70-28693
- Balloon flight measurements clarifying Arcasonde sensor bias over radiosonde atmospheric temperature data
14 p2585 A70-30570
- Pitot probe for high altitude atmospheric density measurements integrated with telemetry system mounted on two stage Super Loki sounding rocket
14 p2585 A70-30576
- Parachute altitude wind sensor (PAWS) project for real time wind profile determination, using modified HASPI sounding rocket
14 p2585 A70-30577
- Report to COSPAR on Australian space research /1969/ including tracking stations, sounding rockets, technology utilization, etc
15 p2829 A70-31706
- Report to COSPAR on space research in Pakistan, covering rocket, satellite and ground based investigations, etc
15 p2830 A70-31718
- Meteorological rocket probing, noting 100 and 170 km range probes in U.S.S.R., thermobaric maps and aerological stations for high altitude aviation
15 p2771 A70-32108
- Upper atmosphere sounding vehicle /Bora-Sond/, describing payload section, launch acceleration, apogee time, weight and length, staging, etc
15 p2811 A70-32259
- Sounding rockets safe operation and handling, examining ground and flight factors
16 p2981 A70-32923
- Atmospheric temperature and wind data before, during and after solar eclipse of 7 March 1970, using ARCAS meteorological rockets
16 p2977 A70-33828
- Japanese sounding rockets for space research, discussing missions, launchings, flight tests, etc, of Kappa and MT-135 rockets and M-45 launch vehicle
17 p3177 A70-35205
- UK space program, describing scientific satellites, Black Arrow launch vehicle and sounding rockets
17 p3167 A70-35206
- Bora-Sond atmospheric probe providing two stage minimum cost high altitude sounding for supersonic transport /SST/, discussing hot water propulsion system
17 p3178 A70-35257
- Electrical power supply systems for meteorological sounding rockets under vibration, acceleration and temperature variation conditions during flight
18 p3215 A70-36251
- Mechanical passive cone angle amplifier for spinning sounding rockets for IR sky scanning, solving equations of motion for system
21 p3931 A70-41905
- Sounding rockets dispersion, considering deviations from predicted point of impact due to wind effects, thrust vector errors and manufacturing inaccuracies
23 p4262 A70-44845
- High performance reaction pointing control systems for sounding rockets, using proportional control of differential thrust and adaptive control of thrust magnitude
24 p4415 A70-45861
- British National and Commonwealth collaborative sound rocket programs, discussing organization, scope and range facilities
24 p4431 A70-46124
- SOUTHERN HEMISPHERE**
- NT ANTARCTIC REGIONS**
- Meteor rate data tabulated from controlled parameter radar survey of Southern Hemisphere activity, noting diurnal and annual variations
05 p0907 A70-16001
- Earth and atmosphere effect on solar radiation balance in Southern Hemisphere
06 p1054 A70-17413
- Interhemispheric mass exchange as function of eddy transfer and meridional circulation
08 p1539 A70-21922
- Middle stratospheric circulation in Southern Hemisphere, associating temperature changes and ozone content with planetary wave passage in Antarctic polar vortex
14 p2568 A70-30123
- F 2 layer ionization asymmetry for Northern and Southern Hemispheres during solstice periods due to electron density variations and aeronomic conditions
14 p2569 A70-30206
- Magnetic activity intensity comparison in Northern and Southern hemispheres, noting correlation with solstices and equinoxes
14 p2580 A70-31260
- Exospheric density at opposite hemispheres, showing variations from winter helium bulge
15 p2724 A70-31679
- Upper stratosphere and mesosphere structure and circulation in Southern Hemisphere, using meteorological rockets and radiosonde data
15 p2724 A70-31683
- Comet Bennett 1969 visual observations in Southern Hemisphere, using photometer ocular
18 p3319 A70-37049
- Atmospheric ozone longitudinal variation in lower middle latitudes of Southern Hemisphere
18 p3256 A70-37117
- Meridional mean eddy transport of enthalpy in Southern Hemisphere during IGY, comparing results with Northern Hemisphere
20 p3661 A70-39143
- Southern objective prism plates B stars with strong neutral He I absorption lines
21 p3890 A70-41160
- F 2 layer ionization asymmetry for Northern and Southern Hemispheres during solstice periods due to electron density variations and aeronomic conditions
24 p4330 A70-46281
- SOVEREIGNTY**
- Legal implications of national flags on moon as symbols of national sovereignty, considering spacecraft and lunar colonies legal status by international agreements
07 p1426 A70-18877
- Line of demarcation of national sovereignty between air space and free space
12 p2334 A70-27009
- Human and divine aspects of space law, discussing ownership and sovereignty problems connected with space and celestial body exploration and utilization
16 p3004 A70-34344
- Juridical status and sovereignty of rocket launching and cosmic stations in international law
17 p3202 A70-35786
- SOYUZ SPACECRAFT**
- Radiation level recordings during Soyuz manned orbital flights indicating safety standards maintenance
03 p0580 A70-13704
- Soviet space activities /1969/, discussing Soyuz orbital flights, Venera probes, Zond lunar orbiters and Proton 4 space laboratory scientific results
05 p0917 A70-16862
- Cold pressure welding of space station tested on Soviet Soyuz spacecraft
06 p1078 A70-18503
- Radiation level recordings during Soyuz manned orbital flights indicating safety standards maintenance
11 p2121 A70-25504
- Soyuz 6, 7 and 8 group flight as step in Soviet space program to place manned station in earth orbit
11 p2121 A70-25623
- Twilight sky color visual estimation from Soyuz 5 spacecraft noting cloudiness effects
15 p2723 A70-31597
- Monograph on upper atmosphere and outer space studies in U.S.S.R. /1969/ covering Soiuz 4, 5, 6, 7, 8 and Venera 5, 6 flights
15 p2829 A70-31702
- Soyuz-9 manned space mission, outlining craft occupants personal background and statements
15 p2814 A70-32792
- Twilight colorimetry from horizon spectra obtained by Soyuz 5, computing chromaticity coefficients for purely scattering molecular atmosphere
16 p2896 A70-33260
- Physiological reactions of Soyuz 6, 7 and 8 crew during group flights, noting cardiovascular and respiratory reaction to submaximum stresses after flight
17 p3038 A70-35361
- Arc welding in space under high vacuum weightless conditions, describing equipment design and Soyuz 6 experiments
19 p3436 A70-37803
- Medical monitoring system onboard Soyuz spacecraft, describing equipment design, data acquisition and analysis, telemetric recordings, etc
20 p3581 A70-40193
- Soyuz and Apollo spacecraft on board computers, discussing design, guidance, navigation and requirements
21 p3793 A70-41071
- Astronaut physiological monitoring aboard Soyuz spacecraft
22 p3980 A70-43691
- Spectrophotometry of earth surface from manned Soyuz spacecraft, obtaining transfer function of atmosphere by aircraft flights
23 p4191 A70-44636
- Astronaut work capacity and adaptation during long term flight of space vehicle Soyuz-9
23 p4154 A70-44651
- SPACE**
- Space three dimensionality compared with Huygens principle via quantum mechanics, discussing past and current theories and empirical arguments
24 p4380 A70-45643
- SPACE BASES**
- Artificial gravity simulation effects on human performance in space base
24 p4417 A70-45938
- NERVA Technology Reactor design integrated with Brayton cycle space power conversion systems, considering space bases and shielding analysis
24 p4377 A70-45955
- SPACE BIOLOGY**
- U EXOBIOLOGY**
- SPACE BUSES**
- U FERRY SPACECRAFT**
- SPACE CAPSULES**
- NT ESCAPE CAPSULES**
- NT MERCURY SPACECRAFT**
- Display systems used in space capsule window simulation for flight training, discussing erecting eyepieces, field of view and exit pupils
01 p0058 A70-10814
- Dry heat resistance of bacillus subtilis var. niger spores on selected planetary lander capsule surface materials
04 p0645 A70-15442
- Sterilized solid propellant motors applicability to planetary landing capsule spin stabilization
07 p1365 A70-19716
- Differential thermal analysis-effluent gas analysis /DTA-EGA/ experiment for lightweight Martian landed capsule
11 p2050 A70-25802
- Rough-landing space capsule for omnidirectional touchdown in lunar and Martian missions, tabulating design characteristics and functional capabilities
11 p2123 A70-26053
- Lunik 16 lunar probe recovery technique, using steep angle and high deceleration reentry trajectory for unmanned capsule
23 p4257 A70-44096
- SPACE CHARGE**
- Double injection in semiconductors at high current densities, discussing procedure yielding space charge and field distribution and voltage drop
01 p0154 A70-10123
- Space charge barriers AC impedance modification at metal/semiconductor contacts due to trapping
01 p0157 A70-10296
- Space charge injection-impulse voltage separation technique for nonuniform field breakdown phenomena
01 p0110 A70-10560
- Electron flux interaction with electromagnetic field in comb type waves via linear approximation assuming small space charge
03 p0447 A70-13291
- Atmospheric space charge magnitude and polarity below 50 km based on rocket probes
04 p0675 A70-14437
- Neutron induced defect clusters in high field space charge region of Si p-n junctions, noting rate of volume damage dependence on electric field strength
04 p0730 A70-14728
- Neutron irradiation effect on space charge limited current of electrons in high purity silicon, noting SCLC sensitivity in detecting traps and changes
04 p0731 A70-14730
- Ion implantation for reducing space charge buildup in thermal oxides on silicon exposed to ionizing radiation
04 p0731 A70-14743
- Magnetron electron beam amplifier large signal operation analysis using model with thin beam to calculate space charge
05 p0823 A70-16884
- Optimal electron bunching in two cavity klystron by varying parameters and nonlinear one dimensional approximation
05 p0823 A70-16888
- Convection currents calculation in multicavity klystron allowing for space charge forces influence
05 p0823 A70-16889
- Phase velocities of intrinsic normal waves of electron beam in three frequency parametric amplifier of space charge waves, determining optimal wave interaction conditions
05 p0823 A70-16890
- Convergent ribbon electron beam shaping for vacuum welding with double anode gun, considering space charge effect
06 p1076 A70-17784
- Plasma polarization shift for resonance line of ionized He in shock tube due to negative space charge
07 p1348 A70-19273
- Hydrodynamic stability criterion of isolating incompressible fluids subjected to unipolar space charge injection
09 p1737 A70-23311
- Cylindrical magnetrons steady state characteristics with thick and infinitely thin cathodes for full space charge and inclined magnetic field
09 p1651 A70-23641

Space charge parameters influence on electron wave and traveling wave interactions in TWT
09 p1652 A70-23654

Electrostatic energy converter load current analysis, deriving expression for space charge electric field with axially varying or constant charge distribution
10 p1808 A70-25036

Amplitude and phase constants of interacting waves in three frequency nondegenerate parametric amplifier of fast space charges using coupled wave technique
10 p1853 A70-25133

Space charge sheath electric thruster principles, construction and performance using laboratory test model
[AIAA PAPER 69-282] 11 p2102 A70-26121

Dispersion relation derived for space-charge waves propagating in thick Gunn diode, showing validity limit of one dimensional approach
12 p2194 A70-27164

Read-diode microwave oscillators performance degradation due to space charge and series resistance, discussing RF power optimization
12 p2194 A70-27167

Atmospheric space charge magnitude and polarity below 50 km based on rocket probes
13 p2392 A70-28462

Electrostatic probes response due to thermionic electron emission, considering I-V characteristics and space-charge-limited current
13 p2459 A70-28635

Electric field intensity and extension of space charge sheath for ion extraction from nitrogen plasma
14 p2622 A70-30661

GaAs epitaxial layered wafer natural CW R band oscillations in LSA mode
14 p2550 A70-30688

Coulomb force effect on electron beam spatial charge for optimal three resonator transit type klystron, regarding buncher length
15 p2707 A70-31507

Spectral distribution of GaAs photoconductivity, allowing for coordinate dependence of minority carrier lifetime in surface space charge region
15 p2782 A70-31626

Space charge waves in electron beams with velocity distribution, considering dispersion equation and Landau damping
15 p2708 A70-31831

Electric space charge pulse density measurements near ground in sunny weather related to free convection
15 p2726 A70-31868

Photovoltaic effects in diodes with generation-recombination process in space charge region
15 p2709 A70-32427

Millimeter wave amplification by pumped n-type gallium arsenide oscillating in limited space charge accumulation mode
16 p2875 A70-33399

Thermal noise in space charge limited solid state diodes by Langevin equation, relating spectral intensity for open and short circuit voltage and current
16 p2878 A70-33694

Space charge sign distribution sounding in atmosphere by electrode potential difference measurement
18 p3246 A70-36180

High resistance space charge region formation near crystal cathode in GaAs due to limited contact emissive capacity
18 p3297 A70-36417

Colloid annular thruster performance, using low mass flow rate data and space charge formulas
[AIAA PAPER 70-1113] 20 p3692 A70-40230

Gunn oscillation stabilization in layered semiconductors based on space charge growth reduction via two-stream interaction between GaAs diode and passive bias semiconductor
23 p4230 A70-44196

Ion source emitter plasma column generated by electron beam injection through gas filled chamber, compensating ion space charge with fast discharge electrons
24 p4385 A70-45451

Light reflectance from optically inhomogeneous medium due to space charge near semiconductor surface
24 p4390 A70-45661

Spin waves amplification in ferromagnetic conductor crystals, taking into account arbitrary external electric field and propagation vector orientations and space charge
24 p4392 A70-46363

SPACE COMMUNICATION
NT INTERPLANETARY COMMUNICATION
NT LUNAR COMMUNICATION
NT REENTRY COMMUNICATION
NT SPACECRAFT COMMUNICATION

Laser communication system for outer space, beam guiding and fiber optical guiding systems
04 p0649 A70-15038

Electrical and mechanical characteristics and specifications of second parabolic reflector antenna at Pleumeur-Bodou space communications center
05 p0819 A70-15982

Electrical and hydraulic units controlling second antenna at Pleumeur-Bodou space communication center
05 p0819 A70-15984

Antenna-central building connecting equipment at Pleumeur-Bodou space telecommunication center, discussing frequency compression demodulators
05 p0819 A70-15985

Transmission equipment of Pleumeur-Bodou space communication installation including modulators, converters and amplifiers for telephone and TV carriers
05 p0819 A70-15986

Practical codes in digital space communication systems, reviewing Shannon information theory theorems
15 p2698 A70-31963

Repeater and antennas for space telecommunications onboard ELDO STV-F9 satellite, describing tests and measurements
15 p2811 A70-32282

Deep space optical communications link, fabricating operational prototype of flight hardware for spaceborne terminal
16 p2863 A70-33190

Mars photography from flybys and orbiters, communicating planetary scene information to eye-brain receiver of earth based interpreters
16 p2912 A70-33976

Mechanically despun multifrequency, attitude sensing antenna for spin stabilized spacecraft, deep space probes, tactical communications and community broadcast applications
16 p2986 A70-34159

Book on law relating to activities of man in space covering liability, space communication, international organization, military implications, etc
19 p3553 A70-37676

Optical communications in space, considering multiple access low earth orbit-to-synchronous and synchronous-to-synchronous links
19 p3379 A70-37878

Deep space microwave and optical communications, describing ground tour requirements
21 p3784 A70-40546

Millimeter wave space-to-space and space-to-ground satellite communication links frequency allocation problems
21 p3787 A70-41335

Carbon dioxide laser systems for various space communication links between ground, satellites and Mars probe
21 p3787 A70-41338

Information theory in physics and engineering, considering data processing, error correction codes, space communication, optical data transmission, noise effects and holography
24 p4379 A70-45616

SPACE DEBRIS
Water vapor homogeneous nucleation in simulated spacecraft debris clouds
22 p4110 A70-43115

SPACE DENSITY
White dwarf luminosity functions based on birth rate, white dwarf space density in solar neighborhood and possible red degenerate stars deficiency
01 p0189 A70-11339

Dynamic spectrum of density fluctuations and galaxy clustering in Einstein universe, considering self gravitation of medium
14 p2652 A70-31389

Universe density estimation by galaxy formation theory, discussing spiral galaxies intergalactic gas thermal radiation and soft X rays
21 p3887 A70-41113

SPACE ELECTRIC ROCKET TESTS
Space electric rocket test /SERT/ II thruster system, discussing flight worthiness and mercury bombardment discharges
[AIAA PAPER 67-700] 07 p1364 A70-19701

SERT 2 thruster system performance over expected mission parameters, noting operational lifetime excess over mission requirements
[AIAA PAPER 69-235] 07 p1364 A70-19702

Passive thermal control system design of SERT II nonspinning satellite based on 534-node analytical model calibrated against test data
11 p2127 A70-26358

Mercury bombardment ion thruster life test in space environment onboard space electric rocket test /SERT/ satellite, describing passive satellite thermal control system design
11 p2127 A70-26606

SERT 2 mercury vapor fed hollow cathode operated in bell jar, determining volt-ampere characteristics and flow rates for plasma diagnostics
[AIAA PAPER 69-258] 13 p2473 A70-28515

Emissive probes for measuring plasma potentials over different ion density ranges on SERT spacecraft, detailing calibration and mechanical and electronic configurations
[AIAA PAPER 69-272] 13 p2404 A70-28519

SPACE ENVIRONMENT
U AEROSPACE ENVIRONMENTS
SPACE ENVIRONMENT SIMULATION
NT WEIGHTLESSNESS SIMULATION

Display systems used in space capsule window simulation for flight training, discussing erecting eyepieces, field of view and exit pupils
01 p0058 A70-10814

Human factors research with simulated reduced gravity conditions by parabolic flight technique with aircraft
[AMRL-TR-69-16] 01 p0037 A70-10962

Life support system model using heart rate to monitor man doing physical work in space suits under simulated space environment
02 p0245 A70-12146

Venus probe high level entry deceleration simulation, discussing test program, equipment and results
03 p0463 A70-13541

Space suit meteoroid protection for extravehicular activity, discussing Gemini and lunar surface EVA suits and bumper concept
[AIAA PAPER 69-366] 04 p0645 A70-15402

Distance discrimination experiment in reduced cue setting simulating outer space, confirming Weber power function exponent
04 p0645 A70-15647

Radiation fluxmeters involving black plates and sensor disk respectively for use in space simulation chambers
05 p0849 A70-16636

Mathematical model for investigating satellite thermal behavior in space based on space simulation in vacuum chamber with walls maintained at liquid nitrogen temperature
05 p0924 A70-17022

Solid lubricants friction and wear bench testing under simulated space environment
06 p1075 A70-17340

Thermal efficiency of modified transtage of Titan 3C spacecraft, discussing environmental simulation, heat rejection system and test firing
[AIAA PAPER 70-171] 06 p1156 A70-18027

Laboratory simulation of interactions between ionospheric plasma and diverse spacecraft systems
06 p1029 A70-18067

Interplanetary plasma flow past earth and planets simulation using kinetic equations
06 p1147 A70-18292

Satellite wake in ionosphere simulated in cold ion plasma without magnetic field, observing complex far wake structure and peculiar electrostatic probes response
06 p1147 A70-18297

U.S., U.S.S.R. and European space environment simulation chambers accommodating assembled spacecraft for thermal tests, describing design and characteristics
07 p1249 A70-19659

Solar simulation /SISS/ for evaluating human visual system performance in contrasting space environment
09 p1655 A70-22680

Space environment simulation chamber free from oil molecules contamination
09 p1655 A70-22830

Thermal vacuum simulator for testing manned Lunar Module Test Vehicle, using conformal skin heaters to control heating rates and skin temperature
09 p1656 A70-23241

Simulated degrading environment effect on spacecraft thermal control surfaces subjected to plume heating during apogee firing and solar irradiation
[AIAA PAPER 69-1024] 09 p1657 A70-23259

Solar simulator built into multiwall ultrahigh vacuum chamber, describing simulator and chamber modifications
[AIAA PAPER 69-1001] 09 p1657 A70-23264

Apollo lunar module manned testing in thermal vacuum, emphasizing safety aspects of hardware, procedures and training
10 p1859 A70-24389

Environmental engineering at NASA MSC, surveying Lunar Receiving Laboratory, microbe incinerator, radon adsorption, Apollo Post-Landing Environmental Test Tank and vacuum chamber
10 p1860 A70-24411

Aerospace vehicles structural vibration environments prediction methods emphasizing vibration sensor mounting resonances
[AIAA PAPER 70-402] 10 p1959 A70-24903

Apollo lunar module mechanical acceptance tests evaluation based on reported flight anomalies review
[AIAA PAPER 70-401] 10 p1951 A70-24904

Ar-arc-produced dust of iron, carbon, silicon carbide and silica, investigating shapes, sizes, grouping and optical absorption to simulate interstellar grains
10 p1944 A70-24957

Laboratory simulation for shock waves around earth, moon and Venus based on artificial solar wind and magnetic dipole interaction study
10 p1948 A70-25182

Radiation environmental model of synchronous communication satellite solar cell degradation by particle fluxes
[AIAA PAPER 70-481] 11 p2103 A70-25411

Wakes of cylinder in collision-free plasma wind tunnel simulating ionospheric satellite conditions, noting decaying oscillation

11 p1976 A70-26018

Test model thermal balance in space simulator, measuring effects of solar simulator irradiance reflected from carbon dioxide cryopanel deposits

[AIAA PAPER 69-1012] 11 p2149 A70-26153

Comet tail simulation by using fast acting gas valve to produce gas cloud for interaction with plasma stream

12 p2298 A70-27190

Pressure measurements and gas flow analysis during thermal vacuum tests of manned spacecraft indicating adequate space vacuum simulation

[AIAA PAPER 69-1033] 13 p2384 A70-28518

Stomatologic diseases during prolonged space flights simulation, discussing gingivitis, stomatitis, dental caries, parodontitis and odontogenous inflammations

13 p2352 A70-29338

Space environment simulators and test facilities for solar cells and arrays, describing solar and magnetic field simulators and universal battery charger

13 p2385 A70-29555

Seed germination in simulated planetary atmospheres, considering biological responses of various organisms

14 p2537 A70-30692

Simulated Venusian atmosphere effects on polymeric plastic and rubber materials, comparing with high temperature air and nitrogen exposures

14 p2640 A70-30781

Mission simulation testing in thermal vacuum environment for Apollo Lunar Module, noting conformal skin heaters

[AIAA PAPER 69-991] 15 p2718 A70-32515

U.S., U.S.S.R. and European space environment simulation chambers accommodating assembled spacecraft for thermal test, describing design and characteristics

15 p2718 A70-32696

Apollo telescope mount postmanufacturing checkout under simulated mission environment, ensuring flight readiness

16 p2889 A70-33723

Instrument size ball bearings lubricated with bonded dry or transfer films in simulated interplanetary spacecraft tests

16 p2923 A70-34166

Space molecular sink simulator facility /Molsink/ for extreme high vacuum outer space environment simulation, discussing Mariner Mars 1969 spacecraft components tests

16 p2889 A70-34167

Solar alignment, control, intensity scanner and data collection for large Space Environmental Simulator

17 p3058 A70-35155

Test machine for partial gravity environment simulation for aerospace subsystem testing in vacuum chamber

17 p3060 A70-35181

Cryopumping systems of ultrahigh vacuum space environmental chambers

17 p3060 A70-35247

Adenosine triphosphate and vitamins /amitetraviv/ as prophylactics against radiation injuries in dogs during simulated space flight

17 p3038 A70-35351

Plasma induced radio frequency interferences from DC-DC converter to receiving antenna simulated for REXS satellite in space chamber

17 p3047 A70-35400

Spacecraft simulator using air bearing technique to simulate low friction aspect of environment, considering application to satellite attitude control

18 p3236 A70-36064

Thermal conductivity of particulate basalt as function of density in simulated lunar and Martian environments, noting temperature and pressure effects

18 p3316 A70-36772

Aerospace coldness and vacuum simulation, discussing uses of cryogenic, titanium sublimation, ion and molecular pumps

19 p3396 A70-37462

Space simulation for satellites and space probes - Conference, Aachen, Germany, March 1970

19 p3397 A70-38276

Space environment simulation installations design, discussing aerospace industry requirements

19 p3554 A70-38278

Space environment simulation in terrestrial laboratories, discussing test instruments and procedures

19 p3398 A70-38279

Vacuum pump systems properties for space environment simulation installations

19 p3358 A70-38280

Space cold simulation installations, discussing cold wall design

19 p3398 A70-38281

Solar simulator combined with space environment simulation chamber for thermal tests of artificial satellites

19 p3398 A70-38283

Space corpuscular radiation simulation to obtain data for increased spacecraft life

19 p3511 A70-38284

Space simulation for satellites and space probes - Conference, Aachen, Germany, March 1970

19 p3398 A70-38285

Magnetic perturbations effect neutralization for satellite attitude stabilization by real time simulation of satellite angular motion in magnetic field

19 p3399 A70-38286

Thermal space simulation tests on Azur research satellite relating to temperature control subsystems and qualification and acceptance procedures

19 p3399 A70-38288

Spacecraft test programming at test facilities providing vacuum and thermal space simulation suggested by Azur and Dial satellite development experience

19 p3399 A70-38290

Heos 1 research satellite space simulation tests at ESTEC test facility

19 p3399 A70-38292

German papers on space simulation for satellites and space probes, covering spacecraft structures measurement and magnetic parameters, motion simulators, thermal vacuum tests, etc

19 p3400 A70-38294

Azur satellite magnetic parameters simulation, noting spacecraft structure effect

19 p3400 A70-38295

Space motion simulators for Azur satellite, considering satellite attitude related to sun

19 p3400 A70-38296

Signal measurement and processing in thermal vacuum and space simulation tests of Azur and Dial satellites

19 p3400 A70-38298

Space environment simulation and thermal vacuum tests for satellite thermal balance during development

19 p3401 A70-38300

Thermal error in temperature differences between actual and simulated space environment

19 p3401 A70-38301

Space environment simulator for thermal vacuum performance of artificial satellites and components

19 p3401 A70-38308

Space environment simulation chamber for testing of equipment temperature and satellite thermal model

19 p3402 A70-38897

Systemic bacterial infection resistance in white mice exposed to simulated hypobaric normoxic space cabin environment

20 p3572 A70-39431

Laboratory simulation of interactions between ionospheric plasma and diverse spacecraft systems

[AIAA PAPER 70-169] 20 p3606 A70-39695

Solar wind effects on thermal control coatings reflectance and absorbance, noting simulation and thermophysical measurement requirements

[AIAA PAPER 70-833] 20 p3655 A70-39825

Simulated space flight radiation effects on dogs DNA synthesis and bone marrow cell differentiation

20 p3575 A70-40191

Surface contamination and degradation effect on reflectance of evaporated vacuum UV mirrors and temperature control coatings under simulated space environments

21 p3842 A70-40815

Integrated temperature and humidity control and water recovery subsystem for manned test in space station simulator

21 p3769 A70-40998

Thermal scale modeling of heat pipe in deep space, using material and heat flux preservation techniques

21 p3946 A70-41048

Apollo spacecraft tests in Space Environment Simulation Laboratory, discussing thermal data, astronaut training, extravehicular activity, reaction control system, etc

21 p3805 A70-41271

Copper disulfide-cadmium sulfide thin film solar cell degradation under simulated low orbit conditions, investigating thermal stress

21 p3759 A70-41313

Electron pulse generator for imaging of glass microspheres simulating meteorite flight and impact in evacuated vessel

[SMPT PREPRINT 96] 22 p4036 A70-43059

Water vapor homogeneous nucleation in simulated spacecraft debris clouds

22 p4110 A70-43115

Man-rated chamber facilities at Manned Spacecraft Center /MSC/, discussing safety requirements and criteria, environmental test chamber design and test results

23 p4152 A70-44458

Artificial gravity simulation effects on human performance in space base

[AIAA PAPER 70-1329] 24 p4417 A70-45938

SPACE ENVIRONMENTAL LUBRICATION

U SPACECRAFT LUBRICATION

SPACE ERECTABLE STRUCTURES

NT BEACON SATELLITES

NT EXPLORER 22 SATELLITE

Deployment systems for extending large area lightweight flexible solar arrays in space, tabulating estimated design weights including power-weight ratios

02 p0228 A70-11932

Expandable space hangar with composite wall for orbiting maintenance shelter, providing radiation and meteoroid protection for occupants

02 p0380 A70-11934

Spacecraft boom design and performance, including Russian spacecraft photographs

16 p2985 A70-34137

Thermal and mechanical properties of materials for spacecraft booms design

16 p2986 A70-34138

Storable tubular extendible member /STEM/, discussing advantages of BI-STEM for erecting unfurlable structures in space

16 p2846 A70-34141

Closed tubular extendible boom /Multiple Applications Storable Tube/ design, fabrication and applications, including stress factors and materials

16 p2846 A70-34142

Space erectable boom with interlocked seam, perforations and coatings to provide torsional rigidity and thermal stability

16 p2986 A70-34143

Dynamics of deployable space structures stiffened by centrifugal forces due to spin, discussing LF radio telescope

21 p3931 A70-41854

Rotating cable-connected orbital space stations deployment dynamics, considering cable mass and motion equation

23 p4258 A70-44529

SPACE EXPLORATION

NT VIKING MARS PROGRAM

Solar and nuclear electric propelled spacecraft applications to planetary and interplanetary missions, considering asteroid survey, out-of- ecliptic, Mercury orbiter, comet rendezvous, etc

[AIAA PAPER 69-1108] 01 p0181 A70-10619

Interplanetary space investigation by HEOS 1 satellite during maximum solar activity, discussing orbital apogee, mission and technical requirements

01 p0186 A70-11113

IR systems in military intelligence and space research including aerospace and planetary investigations, discussing IR detection and IR and earth radiation

01 p0144 A70-11255

Slow scan TV systems for planetary exploration, discussing sampled vidicon operation, digital encoding, data storage, signal to noise ratio, future design trends, etc

[SMPT PREPRINT 106-3] 02 p0294 A70-11682

Solar electric propulsion /SEP/ for automated planetary missions, discussing system characteristics, capabilities and costs

[AIAA PAPER 69-1103] 02 p0382 A70-12531

Space exploration, discussing nationalism, technological benefits, etc

02 p4042 A70-12629

HEOS-A2 project development plan for investigating unexplored interplanetary space in eccentric orbit

05 p0923 A70-16588

Electric propulsion system and initial gross weights estimation for manned Mars missions

05 p0924 A70-17093

Low thrust trajectory and performance analysis of solar electric propulsion system for unmanned interplanetary exploration

[AIAA PAPER 70-212] 06 p1145 A70-18081

Outer solar system exploration, discussing swifby and junction missions, Jovian satellite grand tours, mission energy requirements, etc

[AIAA PAPER 70-58] 06 p1147 A70-18229

Unmanned exploration program to study magnetic fields and chemical composition of five outer planets in solar system

07 p1375 A70-18871

International law applicability to national activities regarding exploration and use of space, examining Space Treaty and UN resolutions

07 p1426 A70-18879

Space role in competition between U.S. and U.S.S.R. since August 1957, discussing armament control agreements regarding space

07 p1426 A70-18882

Book on space observatories covering rocket mounted telescopes for atmospheric structure, opaque wall, air diffusion, clouds and refraction, particle bombardment, meteorite melting, etc

07 p1379 A70-19099

UN treaty based on U.S.-U.S.S.R.-UK agreement banning nuclear arms in space and establishing international law covering space exploration

07 p1428 A70-19106

Peaceful uses of outer space, discussing committee reports and recommendations, direct broadcast satellites, administrative and financial implications, etc

07 p1428 A70-19688

Astronomy role in physical science and space exploration

10 p1940 A70-24373

Space engineering, flight instrumentation features and spacecraft subsystems integration problems
10 p1950 A70-24610

Mass spectroscopy for solar system exploration, discussing ion sources, mass analyzers and ion detectors meeting mission requirements
10 p1942 A70-24612

Lunar and planetary surface chemical composition analysis using neutron inelastic scattering as optimum for unmanned missions
10 p1942 A70-24613

High energy neutron activation method for remote extraterrestrial in situ rock surface constituents analysis
10 p1932 A70-24614

Recovered extraterrestrial material, considering analysis, mass spectroscopy, emission spectroscopy, flame photometry, etc
10 p1942 A70-24615

Interstellar flights, discussing human limitations, star systems with habitable planets and possible galactic communities
10 p1943 A70-24759

TRW space program to 1978, discussing lunar optical observatory, orbital radio astronomical observatory, satellite applications, planetary exploration spacecraft, etc
10 p1951 A70-24875

Nuclear propulsion systems types, discussing relative capabilities and future roles in aerospace applications
11 p2082 A70-26055

Unmanned exploration of planetary surfaces in preparation for manned landings, describing Surveyor lunar probes
11 p2112 A70-26056

Mankind role in cosmos as function of self realization developed by science and technology
11 p2153 A70-26057

Nuclear pulse propulsion system for manned missions to outer planets of solar system, discussing energy and travel time requirements
11 p2082 A70-26059

Lunar and planetary exploration costs and technology, discussing role of nuclear propelled passenger vehicles
11 p2082 A70-26061

Outer solar system exploration, discussing planetary data, interplanetary environment, atmospheric models, data acquisition, etc
11 p2112 A70-26062

Solar system and interstellar space exploration phases, manned and unmanned missions, meta and microprobes, propulsion systems, etc
11 p2112 A70-26063

Interstellar exploration mission profiles, considering technical constraints, propulsion modes, environmental hazards, spacecraft communications and control, etc
11 p2112 A70-26065

Spacecraft propulsion systems selection for particular exploration missions including planets, comets and interstellar space
11 p2112 A70-26066

Orbital laboratories role in planetary manned exploration, discussing flyby missions, flyby/lander modes, periodic orbits, etc
12 p2314 A70-27748

Space information systems effectiveness evaluation based on generalized homomorphous model
13 p2372 A70-28377

Unmanned vehicles for planet surface exploration, discussing design and control using self adjusting and logic circuits
13 p2384 A70-28418

Soviet lunar and interplanetary space missions during 1969 including Venera, Cosmos, Luna and Meteor satellite activities
13 p2505 A70-28901

Dual mode algorithm for routing unmanned autonomous roving vehicle around obstacles on planets, using dynamic programming and terrain information [JPL-TR-32-1484]
14 p2655 A70-31183

Monograph on upper atmosphere and outer space studies in U.S.S.R. /1969/ covering Soiuz 4, 5, 6, 7, 8 and Venera 5, flights
15 p2829 A70-31702

Report to COSPAR on East German space research including Intercosmos satellites scientific apparatus preparation, meteorological and ionospheric research, etc
15 p2830 A70-31712

Report to COSPAR on Greek space research /1969/ covering big planets observations, solar activity, ionospheric propagation, airglow measurements, satellite trackings, etc
15 p2830 A70-31714

Report to COSPAR on Japanese space research including satellite, rocket and balloon observations of ionosphere, magnetosphere, interplanetary space, moon, planets, cosmic rays, etc
15 p2830 A70-31720

Report to COSPAR on space exploration research in Poland including satellite tracking, geodesy, meteorology and aerospace medicine
15 p2830 A70-31721

COSPAR report on UK space research /1969/ covering neutral atmosphere, ionosphere, solar radiation, etc
15 p2831 A70-31723

Mars geology, discussing polar caps phenomena, diurnal variations, orbital eccentricity, seasonal meteorology, volcanism, erosion, etc
15 p2800 A70-32059

Reliability factors in design and development staging systems /DDSS/ for military and space exploration programs
15 p2747 A70-32639

Outer space exploration and utilization, analyzing 1967 UN treaty provisions from standpoint of war potential inherent in space stations existence
16 p3003 A70-33100

Human and divine aspects of space law, discussing ownership and sovereignty problems connected with space and celestial body exploration and utilization
16 p3004 A70-34344

Future manned planetary missions with reusable nuclear shuttles, comparing operating modes in terms of propellant requirement, costs, complexity, etc [AAS PAPER 70-040]
17 p3155 A70-34781

Outer planets exploration program using unique planetary alignment in 1977, discussing mission profiles, spacecraft designs, etc [AAS PAPER 70-028]
17 p3155 A70-34797

Unmanned flyby missions to Mercury in 1973-1990, discussing scientific objectives and payloads [AAS PAPER 70-027]
17 p3155 A70-34798

Slow scan TV systems for planetary exploration, discussing sampled vidicon operation, digital encoding, data storage, signal to noise ratio, future design trends, etc [SMPT PREPRINT 106-3]
17 p3095 A70-35634

Treaty on principles governing activities of states in exploration and use of outer space, appraising various provisions
17 p3173 A70-35792

International juridical discipline of space including moon and other celestial bodies, discussing shortcomings and limitations
18 p3349 A70-36653

Mission success model for unmanned space exploration, combining expected data return with computer technique
19 p3527 A70-38838

Solar system unmanned exploration decision making, discussing resource utilization, sequence optimization, etc
20 p3710 A70-40335

Life detection for unmanned planetary exploration from extraterrestrial sample involving growth, gas changes and carbon dioxide fixation
21 p3769 A70-41003

Scientific motivation for outer planets exploration covering solar system clues, atmosphere comparisons with earth, radiation and planetary radii measurement, etc
21 p3920 A70-41794

Polymers in space research - ACS Conference, Pasadena, July 1968
21 p3781 A70-42126

Planetary probes, orbiting space stations and manned spacecraft in interplanetary flights, discussing Mariner, Gemini and Apollo reentry and Venus landing
22 p4109 A70-42313

Manned space program goals, discussing orbiting observatories, lunar bases, biological and earth resources satellites
22 p4128 A70-43627

Geolunar space development with transportation based on shuttle stations, describing communication, orbits, logistics, etc
22 p4108 A70-43628

International cooperation in space exploration, UN role and benefits for nonspace nations
22 p4128 A70-43632

Full-scanning random arrays with high resolution for space exploration, radio astronomy and long range radar
23 p4160 A70-43770

Jupiter Orbiting Vehicle for Exploration system for gathering Jupiter atmosphere, magnetic, radiation, gravitation, temperature, topography and interplanetary data
23 p4264 A70-45010

Space vehicle for interstellar flight, discussing propulsion concepts, mission implications and international cooperation
23 p4254 A70-45011

Automated mission requirements for outer planets, discussing flyby spacecraft, orbiters, atmospheric entry and grand tour missions [AIAA PAPER 70-1246]
24 p4411 A70-45919

Planetary exploration for solar system origin and evolution, identifying outer planet mission scientific values [AIAA PAPER 70-1244]
24 p4411 A70-45962

Space biological exploration for determining life origin on earth, emphasizing extraterrestrial life possibilities on other planets
24 p4301 A70-46000

SPACE FLIGHT

NT APOLLO FLIGHTS
NT APOLLO 7 FLIGHT
NT APOLLO 8 FLIGHT
NT APOLLO 9 FLIGHT
NT APOLLO 10 FLIGHT
NT APOLLO 11 FLIGHT
NT GEMINI FLIGHTS
NT GEMINI 4 FLIGHT
NT GEMINI 6 FLIGHT
NT GEMINI 11 FLIGHT
NT GEMINI 12 FLIGHT
NT HYPERSONIC REENTRY
NT INTERPLANETARY FLIGHT
NT INTERSTELLAR TRAVEL
NT LUNAR FLIGHT
NT MANNED REENTRY
NT MANNED SPACE FLIGHT
NT RETURN TO EARTH SPACE FLIGHT
NT SPACECRAFT REENTRY
NT VIKING MARS PROGRAM

Skeletal status evaluation in space flight, describing instrumentation for bone mineral measurement and acoustic velocity method for bone elasticity
01 p0032 A70-10369

Mission model construction for power limited systems, discussing flight concepts, propulsion mixes and electric propulsion
01 p0183 A70-10848

Automatic IR control and tracking systems for aviation, space flights and military use, discussing sensor elements
01 p0139 A70-11262

Meteoroid collision hazards of space travel, discussing meteor flux, mass and impact measurements
02 p0360 A70-11668

Soviet book on flight vehicle trajectories covering equations of motion, flight mechanics, reference systems, etc, for rockets and spacecraft
03 p0410 A70-12871

Radiation damage recuperation process in living organisms and justified risk dose in prolonged space flights using Blair model
03 p0423 A70-13705

Soviet engineering reference book on space flight technology covering astronomical and geophysical data, flight mechanics, vehicles and systems
04 p0761 A70-14703

Three man space escape system, describing emergency situations, parachute descent, life raft design, rescue operations and engineering tests [AIAA PAPER 68-936]
04 p0763 A70-15403

Soviet monograph on optimal space flight trajectory control, covering vehicle CG trajectory and synthesis of automatic stabilization system using variational calculus
04 p0764 A70-15493

Collection of papers on spaceflight radiological problems experimentation covering satellite data, dosimetry, solar flares, etc
06 p0989 A70-17259

Broad beam Tracking Data Relay Satellite /TDRS/ for manned and automated spacecraft using VHF bands
06 p1006 A70-17345

Legal status of space flights in view of physical effects on atmosphere and near-earth space, discussing international and Polish air traffic statutes
07 p1425 A70-18783

Book on spaceflight propulsion covering jet thrust, energy release, chemical, nuclear and electric propulsion, transportable and environmental systems
09 p1742 A70-22202

Orbital space flight effects on dry barley seeds, noting increased intracellular rearrangements
10 p1811 A70-24324

Spacecraft optimal flight from earth orbit to outer planet orbit with ideally controlled engine using differential motion equations
10 p1941 A70-24512

Time dilation in space travels at light velocity under influence of special theory of relativity
10 p1943 A70-24760

Radiation damage recuperation process in living organisms and justified risk dose in prolonged space flights using Blair model
11 p1985 A70-25505

Space flight thermodynamics and thermophysics - Conference, Palo Alto, California, March 1970
11 p2149 A70-26351

Lunar physics expansion stemming from physical, geophysical and chemical experiments and measurements by manned and unmanned space flight
12 p2302 A70-27583

High intensity noise effects on auditory thresholds, blood pressure and time response to light stimuli, showing permissible levels during space flights
13 p2358 A70-29334

Coriolis illusions amelioration during space flight, noting cross coupling effects minimization by reflex vestibular stabilization of head
13 p2358 A70-29432

Infectious disease hazards on space flight, discussing internal environmental factors including resistance and etiologic agents transmission

14 p2537 A70-30366

Book on space flight simulation systems examining real time and real performance requirements, mathematical models and various simulation programs

14 p2563 A70-30955

Electrostatic analyzer without fringe field effects for measuring low energy particles on spacecraft

15 p2740 A70-32432

Space travel genetic effects, discussing radiation, weightlessness, vibration and acceleration

21 p3761 A70-40842

OP-EX, optimal explicit guidance algorithm for powered flight outside atmosphere

[AIAA PAPER 68-869]

21 p3848 A70-41734

Space flight effects on dogs cardiac activity, brain circulation and systemic-tissue circulation interactions

22 p3972 A70-43635

SPACE FLIGHT FEEDING

Human response in Apollo flights emphasizing astronaut food, water, waste management, physical examination, preventive medicine problems, etc

02 p0239 A70-12669

Sweet potatoes productivity and nutritive value as carbohydrates source in manned space flights

04 p0641 A70-14572

Manned space flight requirements connected with cabin atmosphere, food/water supplies and waste disposal and environmental conditioning

05 p0807 A70-16632

Nutritive value of mycelium of *Cantharellus cibarius* mushroom on rats compared with eggs and fresh and sour milk

05 p0809 A70-17111

Space diets tests for mean DAR of proteins, carbohydrates, fats and water, considering body weight and required energy expenditure

09 p1623 A70-22088

Rehydratable food consumption in zero-gravity environments with spoons and forks, observing interfacial tensions between water and food, containers and utensils

09 p1628 A70-23464

Human response in Apollo flights emphasizing astronaut food, water, waste management, physical examination, preventive medicine problems, etc

13 p2353 A70-29434

Space diets tests for mean DAR of proteins, carbohydrates, fats and water, considering body weight and required energy expenditure

15 p2693 A70-32684

Hydrogenomonas vs *Chlorella* spacecraft life support systems, discussing human requirements and equipment for balanced food supply on long duration space missions

16 p2855 A70-34315

Microwave feeding system for heating and cooking prepackaged meals during extended space missions

19 p3368 A70-37747

Long term space flight crew habitation emphasizing food management, station housekeeping, personal hygiene and waste handling

23 p4154 A70-44622

Space diets with pure nutrition for balanced nutrition obtained through biological and physicochemical synthesis

23 p4157 A70-45027

SPACE FLIGHT STRESS

Interview with Yegorov, discussing ECG, EEG, muscular effort, eyeball movement, blood pressure changes and vision changes during space flight

02 p0230 A70-11675

Biological rhythm disturbances of astronauts during air and space travel, discussing sleeping habits, alertness under weightlessness conditions, etc

02 p0241 A70-12763

Motion sickness causes and prevention during prolonged space flights, discussing vestibular system and characteristics of visual-inertial and canal-otolith incongruities

03 p0421 A70-13542

Spine acceleration tolerance after prolonged human exposure to weightlessness, noting osseous apparatus tissue decalcination

03 p0423 A70-13712

Pharmacology for long term manned space

04 p0629 A70-14566

Biological rhythm perturbations effect on astronauts, emphasizing waking-sleeping rhythm during space flights

04 p0630 A70-14610

Atrophic changes in tortoises during roundtrip to moon on Zond 5 ascribed to hunger and space flight factors

07 p1207 A70-19496

Astronauts visual performance during space flight, studying reduction of visual disturbances from various physiological flight factors

08 p1444 A70-20741

Physiopathological effects of weightlessness, showing desirability of partial gravity for long voyages via spacecraft rotation

09 p1621 A70-23439

Spaceflight effects on dry crepis capillaris seeds in five day orbit, showing chromosome rearrangements and increased mutagenic sensitivity

10 p1811 A70-24323

Spine acceleration tolerance after prolonged human exposure to weightlessness, noting osseous apparatus tissue decalcination

11 p1985 A70-25512

Physiological and psychological human reactions during space flight concerning hypokinesia, space kinetosis, isolation and limited room conditions

11 p1986 A70-25707

Atrophic changes in tortoises during roundtrip to moon on Zond 5 ascribed to hunger and space flight factors

15 p2685 A70-32741

Dynamic spacecraft cabin atmospheres for extended operation, discussing gas composition, weightlessness and various stress factors

22 p3980 A70-43643

Reflex vestibular disturbances and motion sickness prevention in artificial gravity of rotating space base, by incremental adaptation tests and drugs

23 p4154 A70-44625

Astronaut work capacity and adaptation during long term flight of space vehicle Soyuz-9

23 p4154 A70-44651

Space environment husbandry, examining chickens stress response to restraint and parenteral hydration

24 p4296 A70-45337

SPACE FLIGHT TRAINING

Display systems used in space capsule window simulation for flight training, discussing erecting eyepieces, field of view and exit pupils

01 p0058 A70-10814

Astronauts physical training for space flight requirements

04 p0629 A70-14564

Visual spaceflight simulators for spacemen and aircraft pilot training

04 p0663 A70-14691

Water immersion facility training for extravehicular activities and man physical movements in spacecraft, utilizing buoyancy-gravitation balance

21 p3804 A70-41191

SPACE GLIDERS

U LIFTING REENTRY VEHICLES

SPACE LABORATORIES

NT MANNED ORBITAL LABORATORIES

NT MANNED ORBITAL RESEARCH LABORATORIES

Aerospace laboratories organization concepts, discussing dependence on product, size, location and technological trends

03 p0612 A70-14313

Crew requirements influence on systems design and operations criteria for long duration biomedical and behavioral measurement program in earth orbiting space laboratory

[ASME PAPER 69-WA/BHF-17]

04 p0643 A70-14858

Four satellite cluster laboratory in near-earth environment to investigate solar-terrestrial relationships, emphasizing interaction of solar wind and magnetosphere

07 p1387 A70-19711

Manned laboratories in space - Conference, New York, October 1968

12 p2313 A70-27741

Orbital laboratories role in planetary manned exploration, discussing flyby missions, flyby/lander modes, periodic orbits, etc

12 p2314 A70-27748

Orbital laboratories and international cooperation, discussing national and foreign viewpoints

22 p4128 A70-43631

Space treaty obligations concerning orbital laboratories, discussing legal conflicts and establishment of international organization for protection of common interests

23 p4286 A70-44673

International earth orbital space laboratory program, discussing objectives, management, stations, shuttles, tugs, tracking, communication, data distribution network, etc

23 p4262 A70-44687

Iantar 1 automatic ionospheric laboratory flight tests results, investigating Arion engine performance

23 p4264 A70-45009

SPACE LAW

Legal aspects concerning outer space and boundaries, discussing treaty aspects considered by various international congresses

01 p0220 A70-10333

Book on space law covering space exploration and research, air and space sovereignty, legal terminology and principles, etc

01 p0221 A70-11304

UN General Assembly outer space treaties governing international exploration and use and rescue and return of astronauts and objects

02 p0402 A70-12308

Experimental Washington Agreement /1964/ governing international juridical rules and regulations regarding telecommunication satellites

03 p0609 A70-13853

Collection of papers on space law with regional viewpoints on peaceful cooperation in outer space

03 p0610 A70-14255

Space law applicability noting space activity not regulated by Space Treaty of 27 January 1967

03 p0611 A70-14256

International law framework for outer space, resolutions and recommendations by UN and international bodies and Space Treaty of 27 January 1967

03 p0611 A70-14257

International Law Association and development of legal regime of outer space, discussing treaties

03 p0611 A70-14258

Latin American viewpoint on Space Treaty and prior UN Declaration implications, discussing military activity, astronaut legal treatment, liability, information access, etc

03 p0611 A70-14260

Soviet viewpoint of international law regulating space activities, discussing space exploration and exploitation, legal liability, accidents, emergencies, landings, etc

03 p0611 A70-14261

Liability convention requirements for international space law, considering personal injury or property damage caused by space activities of another state

03 p0612 A70-14262

Astronaut rescue and return of objects launched into space, discussing U.S.S.R. and U.S. proposals

03 p0612 A70-14263

Spacecraft registration and legal liability issues, noting UN Treaty assumption of registration

03 p0612 A70-14264

Legal status of space flights in view of physical effects on atmosphere and near-earth space, discussing international and Polish air traffic statutes

07 p1425 A70-18783

Legal implications of national flags on moon as symbols of national sovereignty, considering spacecraft and lunar colonies legal status by international agreements

07 p1426 A70-18877

International law applicability to national activities regarding exploration and use of space, examining Space Treaty and UN resolutions

07 p1426 A70-18879

Space law by analogy with earth legal concepts, considering possible relations with extraterrestrial life

07 p1427 A70-18887

Liability for damage due to space objects, discussing questions before UN juridical subcommittee

12 p2334 A70-26999

Line of demarcation of national sovereignty between air space and free space

12 p2334 A70-27009

International law applications to space, analyzing Space Treaty provisions

12 p2336 A70-27773

Lunar spaceports for military uses from legal viewpoint, considering Space Treaty

12 p2336 A70-27774

Book on aerospace law covering legal status of space and spacecraft use in scientific research and telecommunications, international cooperation, etc

14 p2667 A70-30375

Outer space exploration and utilization, analyzing 1967 UN treaty provisions from standpoint of war potential inherent in space stations existence

16 p3003 A70-33100

Human and divine aspects of space law, discussing ownership and sovereignty problems connected with space and celestial body exploration and utilization

16 p3004 A70-34344

Moon legal status, discussing territorial sovereignty, peaceful uses, UN Resolutions and Space Treaty, rule of occupation, etc

17 p3200 A70-35323

Space law treaties and UN programs

17 p3200 A70-35324

Outer space law - Conference, Mar del Plata, Argentina, October 1969

17 p3200 A70-35776

Legal problems of space telecommunications, discussing world juridical regime, United Nations work and satellite systems broadcasting

17 p3201 A70-35777

Legal questions of satellites telecommunications at Washington Intelsat Conference

17 p3201 A70-35778

UN space committee discussion on rules governing direct TV broadcasting by satellite, taking into account frequency allocation, geostationary orbits, etc

17 p3201 A70-35779

Legal aspects of telecommunications by satellite systems, discussing international organization, Intelsat integration and direct broadcasting

17 p3202 A70-35781

Juridical structure, risks and control of satellite telecommunication ensuring equality of nations

17 p3202 A70-35782

Liability for damages by space objects, taking into account states and international organizations

17 p3202 A70-35783

International organizations participation in convention on liability for damage caused by launching of objects into outer space
17 p3202 A70-35784

Juridical condition of earth orbiting space stations, discussing term definitions in treaty on outer space
17 p3202 A70-35785

Juridical status and sovereignty of rocket launching and cosmic stations in international law
17 p3202 A70-35786

Space object, launching and platform registration
17 p3202 A70-35787

Registration procedure for space exploration objects
17 p3202 A70-35788

Spacecraft launch registration, comparing Soviet and American information furnished to UN
17 p3202 A70-35789

Legal status of ownership rights of lunar soil samples and objects left on moon by astronauts
17 p3203 A70-35790

Legal problems arising from Apollo 11 lunar landing with respect to Space Treaty, discussing lunar soil removal, flag planting, Luna 15 flight, etc
17 p3203 A70-35791

Treaty on principles governing activities of states in exploration and use of outer space, appraising various provisions
17 p3173 A70-35792

Meteorites and celestial products legal status with respect to rights of property
17 p3173 A70-35793

Legal aspects concerning lunar matter and product disposal resulting from human cosmic expansion
17 p3203 A70-35795

Legal status of natural resources of celestial bodies, discussing limitations of Space Treaty of 27 January 1967
17 p3203 A70-35796

Space law foundations, outlining natural scientific bases
17 p3203 A70-35797

Regulations existence and application to exploitation of resources in celestial bodies
17 p3203 A70-35798

Space legal problems involving earth resource survey (ERS) satellites and weather modification
17 p3203 A70-35799

Legal problems in satellite communications, emphasizing copyright, satellite television legality and protection of transmission and broadcasts
17 p3203 A70-35800

Space law teaching and study facilities
17 p3204 A70-35801

International juridical discipline of space including moon and other celestial bodies, discussing shortcomings and limitations
18 p3349 A70-36653

Legal aspects of suborbital space transports based on air transportation concepts
18 p3350 A70-36661

Book on law relating to activities of man in space covering liability, space communication, international organization, military implications, etc
19 p3553 A70-37676

Space law aspects of direct broadcasting satellites for TV and sound transmission
20 p3740 A70-39408

Space treaty obligations concerning orbital laboratories, discussing legal conflicts and establishment of international organization for protection of common interests
23 p4286 A70-44673

SPACE LOGISTICS
Space station operations and logistics scheduling for long duration missions, using activity network model
01 p0179 A70-10487

Space station-logistics vehicle docking and men-material transfer problem
[AIAA PAPER 69-1118] 01 p0193 A70-10612

Extraterrestrial resources for space flight maintenance and human life support in space and on extraterrestrial bodies
14 p2634 A70-30199

Space shuttle logistics transportation for long duration space station with crew rotation and resupply cycle, considering NASA and DOD requirements
16 p2983 A70-34069

Logistic support reusable earth to orbit space shuttle design, noting weight penalties, payloads and development time
[AAS PAPER 70-042] 17 p3175 A70-34782

Space Station long term operations and logistics concerning inventory, configuration and cargo management
[SAE PAPER 700757] 24 p4416 A70-45871

SPACE MAINTENANCE
Equipment reliability data application in analytic techniques to predict human requirements for system, using in-space maintenance as reference frame
01 p0055 A70-10117

Cost reductions achieved by space payload life extension through manned maintenance and increased transportation economies via refueling and improved space propulsion
01 p0196 A70-10844

Expandable space hangar with composite wall for orbiting maintenance shelter, providing radiation and meteoroid protection for occupants
02 p0380 A70-11934

Extraterrestrial resources for space flight maintenance and human life support in space and on extraterrestrial bodies
14 p2634 A70-30199

Ground controlled remote manipulator spacecraft system through wideband radio link for satellite maintenance and repair
15 p2810 A70-31780

Maintenance vs redundancy for manned space station economy, considering costing structure and time increase for maintenance
15 p2713 A70-32666

Magnetomotive tools and power systems for maintenance, repair and assembly in space weightless environment
19 p3436 A70-37949

Space maintenance tools necessity on long duration manned space missions 1972-1980
19 p3442 A70-38836

SPACE MECHANICS
NT ASTRODYNAMICS
NT CELESTIAL MECHANICS
NT KEPLER LAWS
NT ORBITAL MECHANICS

Space mechanics problem of passing from perigee to radial distance in given time determined by fitting conic to radii, using iteration method
09 p1760 A70-22927

SPACE MISSIONS
Space station operations and logistics scheduling for long duration missions, using activity network model
01 p0179 A70-10487

Earth and planetary entry vehicle designs for manned and unmanned space missions, noting thermal protection, environmental control requirements and communication systems
[AIAA PAPER 68-1080] 01 p0195 A70-10826

AMPROD (Automated Mission Profile Design) generating schedules for long duration missions with real cost and time savings
03 p0581 A70-14023

Solar powered electric propulsion systems for automated missions throughout solar system by extending range of Atlas Centaur-Titan 3-C launch vehicles
[AIAA PAPER 68-1120] 04 p0736 A70-15401

Automated parameter search techniques applied to low thrust mission design, stressing trajectories and mission optimization
[AIAA PAPER 69-261] 04 p0736 A70-15404

Spacecraft design, trajectory and mission analyses for multipurpose solar electric propulsion missions, emphasizing modular ion engine and fixed attitude spacecraft designs
[AIAA PAPER 69-252] 04 p0763 A70-15412

Saturn 5 program status to meet mission requirements for manned lunar exploration, space station/base programs and outer planet exploration with unmanned probes
[SAE PAPER 690715] 05 p0922 A70-15852

Electric thrusters for putting communications satellite into synchronous orbit analyzed for mission performance, finding hydrogen resistojets as attractive compromise between payload and transfer time
05 p0897 A70-16899

Manned or unmanned missions to asteroids close to earth as intermediate stage in planets formation
06 p1139 A70-17551

Analytic Trajectory Optimization Model to develop computational techniques for low thrust mission analysis
[AIAA PAPER 70-96] 06 p1159 A70-18230

Instrumental space flight internationalization considering manned flight and military obstacles, suggesting scientific and political steps
07 p1427 A70-19097

Apollo Program mission evaluation and flight anomalies team to identify and understand unforeseen peculiarities and systems problems during spacecraft mission
09 p1768 A70-23708

Operational planning for earth resources surveys using spacecraft
09 p1672 A70-23762

Planetology and space mission planning - Conference, New York, October 1967
11 p2110 A70-26026

Signature theory application to space mission planning and archeological project
11 p2051 A70-26034

Biosatellite environmental control coolant loop system design for 30-day mission program, discussing fuel cell power source, cryogenic subsystem, etc
11 p2127 A70-26360

Small satellites for scientific technological and operational missions, discussing piggyback launching, command, battery storage, telemetry and attitude control systems
15 p2810 A70-31781

International Aeronautical Federation space records, discussing record classification for suborbital, earth orbital and lunar and planetary missions
15 p2831 A70-32245

American-German solar probe HELIOS mission parameters for interplanetary and close proximity solar research, discussing spacecraft building and launching
15 p2801 A70-32281

Periodic comet nature, origin and anomalous behavior with space mission planning implications, assuming solar plasma source and solar-interstellar interaction
[AAS PAPER 70-029] 17 p3155 A70-34795

Japanese sounding rockets for space research, discussing missions, launchings, flight tests, etc, of Kappa and MT-135 rockets and M-45 launch vehicle
17 p3177 A70-35205

Titan 3 launch vehicle for scientific space missions, discussing building blocks, performance and payloads
17 p3178 A70-35260

Low thrust high impulse nuclear and electric space propulsion systems, discussing performance capability for space missions
18 p3290 A70-36566

Future space missions for observing solar events, magnetospheric problems, cosmic rays and low energy plasma, considering use of multiple satellites
19 p3513 A70-37523

Mariner Mars 1971 mission design, discussing objectives, orbit selection, guidance, navigation and sequence analysis
[AIAA PAPER 70-1048] 19 p3527 A70-38863

Solar electric propulsion application to out-of-ecliptic mission for interplanetary fields and particles data, comparing performance with chemical systems
[AIAA PAPER 70-1118] 20 p3691 A70-40225

High impact Ag-Zn cell design for space missions instrument package landing, considering heat sterilization and minimum operational capability
21 p3757 A70-41013

Mission Control Center and Apollo flight controller team, discussing personnel qualifications, equipment and individual evaluation
21 p3805 A70-41197

TOPS /thermoelectric outer planet spacecraft/ project integrating R and D for specific space missions
21 p3920 A70-41793

Thermoelectric outer planet spacecraft (TOPS) data subsystems for 12 year missions compared with Mariner subsystem
21 p3795 A70-41796

Silicon solar cell design optimization for near solar missions, discussing electrical characteristics and performance obtainable under various solar radiation conditions
22 p3964 A70-42496

Lunar orbital science, discussing U.S. and Soviet missions, NASA plans and results concerning remote sensing, force field and particle studies
22 p4105 A70-43144

Apollo project technology for future space missions, discussing space shuttles, management, material procurement, test programs and computer utilization
22 p4128 A70-43513

Automated and manned spacecraft design, discussing mission objectives and present and potential applications
23 p4264 A70-45003

Venus atmosphere exploration by multiple entry probe, describing spacecraft system design, launch and earth-Venus transfer trajectory, approach and entry sequence, etc
[AIAA PAPER 70-1245] 24 p4417 A70-45963

SPACE NAVIGATION
NT INTERPLANETARY NAVIGATION

Orbital charts development for space navigation, discussing cartography and orbital navigation
01 p0138 A70-11251

Optimum estimation equations as simple averaging extension, considering application to Kalman filtering in integrated space navigation system
03 p0522 A70-13608

Launch vehicles design, propulsion, maneuverability and navigation
05 p0923 A70-16565

Apollo translunar and transearth orbit determination and navigation using ground and onboard systems
[AIAA PAPER 70-27] 06 p1103 A70-18124

Ground-based and onboard guidance and navigation systems for outer planet flyby missions concerning direct, Jupiter swingby and Grand Tour trajectories
[AIAA PAPER 70-71] 06 p1104 A70-18194

Space rendezvous navigation and guidance based on optical sightings with hand-held sextant entered into and processed by small digital computer
07 p1331 A70-20061

Apollo space vehicles guidance and navigation using data obtained onboard, discussing inertial platforms, accelerometers and trajectory calculations
08 p1541 A70-21023

Gradient method applied to onboard analysis of astronavigational bearings of spacecraft
09 p1719 A70-22165

- Keplerian integrals analogy to integrals of adjoint equations suggested by optimum space navigation trajectories considerations 12 p2261 A70-27834
- Lunar far side features position from Apollo 8 data, evaluating Apollo navigation system accuracy 12 p2309 A70-27949
- Mariner Mars 1969 navigation, guidance and control systems design, mechanization and flight testing 13 p2446 A70-28393
- Earth orbital parameters estimation in manned flight by manual space navigation sensors and computer 13 p2446 A70-28406
- Space navigation procedures verification considering vehicle trajectory parameters, noting applicability to linear systems with estimable parameters 13 p2447 A70-28412
- Space navigation for Apollo 11 mission, emphasizing ground and onboard systems, interfaces with guidance and use in phases of lunar landing 13 p2447 A70-28547
- Space navigation theory and practice - Conference, Ames Research Center, Moffett Field, California, February 1970 14 p2612 A70-30451
- Saturn 5 launch vehicle navigation system design, discussing configurations, implementation schemes, system tradeoffs and performance 14 p2613 A70-30453
- Apollo 12 navigation for pinpoint lunar landing, correcting errors in downtrack position in guidance computer near powered descent initiation time 14 p2613 A70-30456
- Lunar based radar beacons for nearby spacecraft navigation, noting trajectory determination advantages 14 p2614 A70-30461
- Synchronous navigation satellite system for ships and aircraft applicable to earth orbital and lunar operations 14 p2614 A70-30463
- Operational and environmental factors constraining onboard navigation system design for outer planet flyby missions 14 p2614 A70-30467
- Navigation data from Mariner Mars 1969 TV pictures, estimating spacecraft trajectory to planetary center 14 p2614 A70-30468
- Apollo navigation methods and data analysis covering inertial guidance with gyro-stabilized platforms, acceleration sensors, sextants and telescopes, ergodicity, filtering, etc 15 p2772 A70-31549
- Transstellar space navigation, discussing system concepts, measured observables during flight, instrumentation, etc 15 p2773 A70-32060
- Statistical error analysis of autonomous manned spacecraft navigation in long duration eccentric Mars orbits [AIAA PAPER 69-880] 15 p2773 A70-32503
- Three body numerical solutions to low thrust guidance and navigation for outer planet orbiter with nuclear-electric propulsion [AIAA PAPER 70-1040] 19 p3527 A70-38855
- Guidance and navigation system design for automatic stationkeeping one earth orbiting vehicle with respect to other [AIAA PAPER 70-1005] 20 p3667 A70-39526
- Inertial guidance technology applications for space navigation, considering instrument design tradeoff between accuracy and cost for performance and reliability improvements 21 p3848 A70-41128
- Mariner 6 and 7 navigational accuracies prior to time of planetary encounter 21 p3888 A70-41129
- ### SPACE ORIENTATION
- Space triangulation equations based on simultaneous measurements of satellite topocentric coordinates and distances between tracking station and satellite 02 p0254 A70-11753
- Simultaneity circle for calculating spatial direction of straight line joining satellite observation stations, noting time factor role 06 p1139 A70-17548
- Spatial direction Riga-Cairo determined using simultaneous photographic observations of Pagesa A satellite 06 p1054 A70-17550
- USAF undergraduate pilot trainees responses in prototype spatial orientation trainer 13 p2359 A70-29439
- ### SPACE PERCEPTION
- Motion perception sensitivity measurement in various portions of retina for operation accuracy of photooptical systems of simulation 01 p0036 A70-10820
- Perceived size relation to retinal size under reduced observation conditions compared with size-distance invariance hypothesis for binocular and monocular observations 01 p0025 A70-11051
- Sensory and muscular factors interaction in space perception via empirical test of summative hypothesis derived from sensory tonic field theory 02 p0239 A70-12626
- Visual, motion and auditory stimuli role in enhancing aircraft pilot training simulators realism, considering motion perception research [ASME PAPER 69-WA/BHF-9] 04 p0642 A70-14853
- Distance discrimination experiment in reduced cue setting simulating outer space, confirming Weber power function exponent 04 p0645 A70-15647
- Mathematical models for describing visual perception of distance to ground during VTOL landing and takeoff 05 p0810 A70-17119
- Flight crews spatial vision, estimating absolute distance perception of pilots and navigators with emmetropic refraction 08 p1450 A70-20742
- Convergence role in distance perception during aircraft landing, testing subjects with normal binocular vision, emmetropic refraction and visual acuity 08 p1450 A70-20744
- Horizontal disparity and ratio of perceived egocentric distance related in stereoscopic vision during investigation of three point light sources problem 08 p1447 A70-21725
- Optic chiasm damage effects on human depth perception implying interhemispheric link for binocular integration in central vision 09 p1618 A70-22669
- Corpus callosum damage effects on human depth perception implying interhemispheric link for binocular integration in central vision 09 p1618 A70-22670
- Movement information from spatio-temporal integration in binocular-kinetic space perception of time varying optical inputs 09 p1618 A70-22672
- Solar simulation /SISS/ for evaluating human visual system performance in contrasting space environment 09 p1655 A70-22680
- Psychophysical metric for space perception visual cues measurement, describing applications to distance discrimination 10 p1827 A70-24768
- Stimuli eliciting vergence eye movements and stereopsis, discussing retinal disparity locations and limits due to form, spatial position, luminance, contrast and onset 12 p2171 A70-28034
- Neuron processing of retinal activity in estimating distances and sizes of objects in field of vision 12 p2172 A70-28312
- USAF undergraduate pilot trainees responses in prototype spatial orientation trainer 13 p2359 A70-29439
- Perceptual displacement of hashmark between unequal squares, discussing contour repulsion and perspective interpretation 14 p2537 A70-30899
- Neurophysiological framework for binocular single vision and depth discrimination, concerning construction of horopter for cat 14 p2539 A70-31348
- Book on visual perception space covering biological optics, eye model, monocular vision, etc 14 p2539 A70-31349
- Book on psychophysical analysis of visual size-distance perception and physiological optics 15 p2688 A70-31575
- Visual effects in astronauts and pilots, discussing optical illusions and distance estimation errors due to accelerations, runway factors, lack of oxygen, etc 18 p3225 A70-36777
- Equidistance effects on human size and distance perception in visual alley 19 p3368 A70-37771
- Human spatio-temporal visual evoked response characteristics, showing potential gradient rotation in same period as input stimulus 19 p3360 A70-37845
- Object identification and form of multidimensional discrimination space, using locus stimulus model 19 p3361 A70-38051
- Spatial disorientation of human subjects in centrifuge, examining otolith role in reorientation and eye sensory mechanisms 22 p3976 A70-43707
- Astronaut distance judgement enhancement in space by combining stereoptics effect with apparent movement phenomenon 23 p4150 A70-43965
- ### SPACE PHOTOGRAPHY
- #### U SPACEBORNE PHOTOGRAPHY
- #### SPACE POWER UNIT REACTORS
- #### NT SNAP 8
- Optimal control for thermionic nuclear reactor space power plant utilizing state variable feedback with limited input simplifying computation 03 p0461 A70-14342
- NERVA Technology Reactor design integrated with Brayton cycle space power conversion systems, considering space bases and shielding analysis [AIAA PAPER 70-1226] 24 p4377 A70-45955
- ### SPACE PROBES
- #### NT JUPITER PROBES
- #### NT LUNAR PROBES
- #### NT LUNIK LUNAR PROBES
- #### NT LUNIK 3 LUNAR PROBE
- #### NT LUNIK 12 LUNAR PROBE
- #### NT MARINER SPACE PROBES
- #### NT MARINER SPACECRAFT
- #### NT MARINER 2 SPACE PROBE
- #### NT MARINER 4 SPACE PROBE
- #### NT MARINER 5 SPACE PROBE
- #### NT MARINER-MERCURY 1973
- #### NT MARS PROBES
- #### NT PIONEER SPACE PROBES
- #### NT PIONEER 6 SPACE PROBE
- #### NT PIONEER 8 SPACE PROBE
- #### NT PIONEER 9 SPACE PROBE
- #### NT RANGER LUNAR PROBES
- #### NT SOLAR PROBES
- #### NT SURVEYOR LUNAR PROBES
- #### NT SURVEYOR 5 LUNAR PROBE
- #### NT VENERA SATELLITES
- #### NT VENUS PROBES
- #### NT VIKING MARS PROGRAM
- #### NT ZOND 3 SPACE PROBE
- Jupiter chemical composition and atmosphere, considering space probe experiments 01 p0185 A70-11047
- In-flight compensation for space probe trajectory deviations, discussing attitude determination and control of triaxial and spin stabilized space probes 01 p0186 A70-11265
- Venusian atmospheric model based on Venera 4 measurements, calculating probe distance travel, temperature, density and pressure profiles 01 p0192 A70-11504
- Space probe investigation of comets, discussing feasibility, instrumentation, mission planning, etc 06 p1153 A70-18550
- Grand tour space probe optics for observation of objects on planet, considering atmospheric refraction indices effect 09 p1700 A70-23768
- Ground stationed automatic orbital operations system /AOOSY/ for satellites and space probes, discussing flow diagram and Siemens computer programming 13 p2372 A70-28398
- Parametric amplifier as preamplifier for microwave receivers in space probes, presenting block diagrams and test results 13 p2379 A70-29559
- Hollow cathode ion thruster and lightweight power conditioner of solar-electric propulsion system for unmanned deep space probes [AIAA PAPER 70-648] 16 p2966 A70-33546
- Mechanically despun multifrequency, attitude sensing antenna for spin stabilized spacecraft, deep space probes, tactical communications and community broadcast applications 16 p2986 A70-34159
- Digital simulation of linear filter, investigating noise and rounding errors effects on decoding signals from lunar and interplanetary probes 17 p3049 A70-34612
- Interplanetary probes trajectory optimization for minimum energy expenditures, neglecting solar and terrestrial perturbations within earth sphere of influence 17 p3168 A70-35366
- German monograph on heavy space probes for solar system investigation covering systems analysis, mission success, flight programs, Saturn 5 launch vehicle, etc 17 p3168 A70-35378
- Low energy solar and galactic cosmic rays propagation in interplanetary medium observed by Zond and Venus space probes, discussing shock waves retardation 19 p3493 A70-37475
- Solar wind disturbances associated with solar activity observed by spacecraft probing interplanetary space, considering geomagnetic activity classes 19 p3494 A70-37478
- Electron density irregularities convected past space probe relationship to radio intensity power spectrum scintillations 20 p3703 A70-39023
- Pluto space probe using swingby technique with Jupiter, Saturn and Uranus gravitation fields for acceleration 21 p3886 A70-41073
- Space DC electric field measurement by quadrupole probe, discussing geomagnetic field and contact potential effects 22 p4029 A70-42792
- Astronomical observations from outside terrestrial atmosphere, discussing vehicles and equipment for solar and stellar research, rocket and balloon data, etc 23 p4257 A70-45043

SPACE PROGRAMS

NT APOLLO PROJECT
NT EUROPEAN SPACE PROGRAMS
NT FRENCH SPACE PROGRAMS
NT LUNAR PROGRAMS
NT SURVEYOR PROJECT
NT TEKITE PROJECT
NT U.S.S.R. SPACE PROGRAM

Hazards due to nonohmic materials responsible for electrostatic failures in missile and space programs and ground equipment

01 p0141 A70-10088

Space programs to monitor earth resources from synchronous orbit of 19,400 nautical miles, discussing geostationary systems characteristics related to optics and telemetry

01 p0093 A70-11280

Space law applicability noting space activity not regulated by Space Treaty of 27 January 1967

03 p0611 A70-14256

Experiment selection in orbital program planning based on broad system synthesis, discussing identification and grouping of objectives, critical issues and experimental equipment requirements

[AAS PAPER 69-580] 04 p0749 A70-14652

Space projects quality assurance with allowance for technological trends, discussing product and system oriented organizational requirements, failure potentials, contractor performance, etc

04 p0699 A70-15138

Meghdoot program for satellite network communications technology applications to national goals in India

04 p0757 A70-15670

Reliability engineering related to general and professional levels, discussing space program methods and Concerto program for electronic components

05 p0853 A70-15810

Space programs and future missions assessment based on technical feasibility, considering effects of economic and social factors

06 p1185 A70-17644

Integrated space program with merger of manned and automated activities for coming decade permitting costs comparable to aircraft-based scientific programs

07 p1375 A70-18872

Space shuttle program from technological and budgetary objections viewpoint, evaluating risks against program options

[AIAA PAPER 70-264] 07 p1398 A70-20394

National Space Program relevance to human society, discussing solar system exploration, applications in meteorology, communication, etc

09 p1792 A70-22041

Satellites application to studying and monitoring earth ecology, discussing environmental space research and space program priorities

09 p1794 A70-23333

TRW space program to 1978, discussing lunar optical observatory, orbital radio astronomical observatory, satellite applications, planetary exploration spacecraft, etc

10 p1951 A70-24875

Book on aerospace law covering legal status of space and spacecraft use in scientific research and telecommunications, international cooperation, etc

14 p2667 A70-30375

Scientific satellites history, projects, technology, coordination and international collaboration

14 p2655 A70-31416

Report to COSPAR on Argentine Space Research Commission covering sounding rockets, cameras, launching bases, research, balloon flight, etc

15 p2829 A70-31701

Report to COSPAR on space research in Bulgaria, considering ionospheric physics, cosmic rays, satellite observations, meteorology and space communications

15 p2829 A70-31704

Report to COSPAR on Australian space research /1969/ including tracking stations, sounding rockets, technology utilization, etc

15 p2829 A70-31706

Report to COSPAR on space research in Canada, covering Alouette satellites, ISIS I, international cooperation, etc

15 p2829 A70-31708

Report to COSPAR on space research covering satellite tracking telemetry, Apt, meteorology, cosmic rays, solar activity and international cooperative programs, etc

15 p2829 A70-31709

Report to COSPAR on Indian space research describing organizational structure, facilities, experiments and international cooperation

15 p2830 A70-31715

Report to COSPAR on 1968/1969 Indonesian space research including TV broadcasts through Intelsat 3 satellite, sounding rocket research, atmospheric physics, etc

15 p2830 A70-31716

Report to COSPAR on space research in Pakistan, covering rocket, satellite and ground based investigations, etc

15 p2830 A70-31718

Report to COSPAR on Japanese space research including satellite, rocket and balloon observations of ionosphere, magnetosphere, interplanetary space, moon, planets, cosmic rays, etc

15 p2830 A70-31720

Space research cost effectiveness in weather forecasting, TV broadcasting, space biology and medicine, geodesy, aerial and maritime navigation, earth resources, etc

15 p2811 A70-32283

Space program planning for scientific and application earth satellites, stressing image sensors development

15 p2812 A70-32289

Fluidic technology applications to space and oceanography, discussing control, monitoring, sequencing and signal processing

16 p2845 A70-33714

NASA program for international cooperation in space involving developing and advanced nations, discussing television instruction for India, resource surveys, etc

18 p3349 A70-36514

Cost effectiveness methodology for space program, industry, military sector, etc

19 p3554 A70-38402

Post Apollo space research, discussing Saturn Workshop /Skylab/, Nerva nuclear rocket engine and international cooperation

21 p3956 A70-41496

U.S. and Soviet space program administration and management

21 p3956 A70-41893

Earth orbital experiments synthesis in space programs methodology, discussing examples in astronomy, biology and oceanography research

22 p4097 A70-42500

Earth resources information systems using space, aerial and ground measurements, discussing Apollo 9 IR color photograph of Mississippi Valley and timber inventory applications

23 p4192 A70-44679

International earth orbital space laboratory program, discussing objectives, management, stations, shuttles, tugs, tracking, communication, data distribution network, etc

23 p4262 A70-44687

International Space Research Organization /ISRO/ for space operations, considering political, economic, technical and scientific requirements

23 p4286 A70-44688

Manned space flight programs management, discussing organizational aspects of projects including Apollo, space shuttle and space station

23 p4286 A70-44696

Free-flying modules interface and operation in conjunction with space station for orbital research into manned space program

[AIAA PAPER 70-1300] 24 p4417 A70-45950

SPACE RADIATION

U EXTRATERRESTRIAL RADIATION

SPACE RADIATORS

U SPACECRAFT RADIATORS

SPACE RATIONS

Prototype space foods effects on humans, determining changes in bacterial fecal flora content

17 p3032 A70-35565

Space diets with pure nutrition for balanced nutrition obtained through biological and physicochemical synthesis

23 p4157 A70-45027

SPACE RENDEZVOUS

NT EARTH ORBITAL RENDEZVOUS

NT LUNAR ORBITAL RENDEZVOUS

NT ORBITAL RENDEZVOUS

Minimum propellant rendezvous maneuver of space vehicles in neighboring circular orbits

01 p0193 A70-10555

Manned vehicles rendezvous missions in space and hydrospace, proposing functional structure involving concurrent ship control, navigation, perception, communication and prehension

[AIAA PAPER 69-1102] 01 p0034 A70-10615

Minimum propellant maneuver during docking of elliptical orbit rendezvous between propelled and passive target vehicles, analyzing as variational problems

02 p0380 A70-12784

Analytic guidance and control for minimum fuel expenditure and optimal guidance corrections for low thrust vehicle in Martian orbit

[AIAA PAPER 68-862] 04 p0716 A70-15544

Time optimal rendezvous maneuver between neighboring elliptic orbits, discussing propulsive jet system with variable thrust

07 p1381 A70-19357

Space rendezvous navigation and guidance based on optical sightings with hand-held sextant entered into and processed by small digital computer

07 p1331 A70-20061

Computer program /TACTICS/ for simulating three vehicles simultaneous motion in space, considering interceptor-target guidance and intercept trajectories

07 p1239 A70-20414

Rendezvous problems formulated as optimal control problems in combined state space, considering decomposition in optimality criteria and solution existence

11 p2127 A70-26331

Manual spacecraft rendezvous system based on handheld instruments and manual computations, considering error analysis and simulation

13 p2357 A70-28392

Automatic rendezvous and mooring-coupling of spin stabilized satellites, discussing configuration, guidance and dynamics model

13 p2499 A70-28397

Spacecraft rendezvous control at minimal propellant consumption, deriving algorithm

13 p2499 A70-28400

Automatic-manual space rendezvous control system for Cosmos and Soyuz satellites, considering terminal phase control at specific closing range and velocity

13 p2499 A70-28402

Radio command guidance system for Mars probe ascent from surface to rendezvous with flyby vehicle on escape trajectory

13 p2447 A70-28421

Minimum-fuel multiple impulse orbital fixed time rendezvous in circular orbit vicinity

18 p3289 A70-36682

Future spacecraft mission for short period comets rendezvous, considering trajectory requirements and launch vehicle payload capabilities

[AIAA PAPER 70-1072] 19 p3530 A70-38885

Jupiter swingby trajectory analysis for comet flyby and rendezvous missions, discussing approach velocity and payloads

[AIAA PAPER 70-1074] 19 p3530 A70-38886

SPACE RENDEZVOUS MANEUVERS

U SPACE RENDEZVOUS

U SPACECRAFT MANEUVERS

SPACE SCIENCES

U AEROSPACE SCIENCES

SPACE SELF MANEUVERING UNITS

U SELF MANEUVERING UNITS

SPACE SHUTTLES

Saturn launch vehicle systems in terms of design, operating characteristics and potential applications, showing need for reusable space shuttle systems

[SAE PAPER 690703] 05 p0922 A70-15830

Onboard and ground checkout systems for space station and space shuttle operations

[AIAA PAPER 70-245] 07 p1251 A70-20373

Launch facilities institutionalization for space shuttles launch cost minimization

[AIAA PAPER 70-244] 07 p1251 A70-20374

Low operating cost space shuttle system for cargo and personnel transportation to earth orbiting stations involving reusable winged vehicles

[AIAA PAPER 70-242] 07 p1396 A70-20376

Reusable air breathing launch vehicle for earth orbit shuttle, comparing performance, costs and operation with rocket powered systems

[AIAA PAPER 70-270] 07 p1396 A70-20381

Reusable metallic and nonmetallic thermal protection materials for space shuttle applications

[AIAA PAPER 70-273] 07 p1397 A70-20383

Ground and onboard electronics systems for space shuttle vehicles, discussing role in equipment reliability and maintainability, life cycle costs, management control, etc

[AIAA PAPER 70-261] 07 p1398 A70-20391

Integrated electronics system for space shuttles including propulsion, electrical power, life support and flight control

[AIAA PAPER 70-257] 07 p1398 A70-20392

Space shuttle program from technological and budgetary objections viewpoint, evaluating risks against program options

[AIAA PAPER 70-264] 07 p1398 A70-20394

Unmanned and manned interorbital shuttle systems for satellite placement and repair and planetary spacecraft insertion, emphasizing cost analysis

[AIAA PAPER 70-267] 07 p1398 A70-20396

Orbit-to-orbit shuttle for launch in earth-to-orbit shuttle vehicle, discussing design requirements

[AIAA PAPER 70-268] 07 p1399 A70-20397

Reusable passenger and cargo shuttle system based on integral launch and reentry vehicle /ILRV/, considering propulsion systems, aerodynamic and structural configurations, aerothermal characteristics, etc

08 p1582 A70-20689

NASA earth-orbit shuttle /EOS/ for achieving routine arrival, conventional landing after orbital flight and reentry

09 p1766 A70-22677

NASA future space programs, discussing space shuttle and station, nuclear propulsion, manned Mars landing, unmanned Venus-Mercury probes, etc

09 p1762 A70-23065

Space shuttle program, considering vehicle configurations mission capabilities and cost estimates with emphasis on ground and flight tests

[AIAA PAPER 70-739] 10 p1953 A70-25074

Space shuttle structural dynamic problems, discussing stall flutter due to transition from high angle of attack to normal aircraft flying attitude

[AIAA PAPER 70-740] 12 p2312 A70-27150

Checkout systems for shuttle and orbiting space stations, discussing shift from ground to onboard operation 12 p2208 A70-27691

Low cost orbital space transportation system with shuttle service, discussing booster and configuration selections, weight, costs, etc [AIAA PAPER 70-256] 13 p2506 A70-29615

Space shuttle automatic landing system based on aircraft low visibility landing, considering economy and safety 14 p2614 A70-30466

Atmospheric elements and properties pertinent to design and operations of Space Shuttle 14 p2606 A70-30556

CAT and small scale atmospheric motions in relation to supersonic transport and space shuttle design and operation 14 p2609 A70-30602

Two stage reusable space shuttle consisting of booster and orbiter 15 p2789 A70-32255

Reusable ferry spacecraft program, discussing space shuttles, cost reduction and nuclear propulsion for deep space missions 15 p2791 A70-32300

Reusable nuclear shuttles/RNS/ for interorbital and escape missions, discussing alternate stage configurations, radiation shielding, subsystem options, etc [AIAA PAPER 70-678] 16 p2950 A70-33579

Space shuttle aerodynamic studies including staging, launching, entry and booster cruise 16 p2981 A70-33702

Space shuttle booster configurations, including wing and tail sizes, vehicle balance and engine location 16 p2982 A70-33706

Space shuttle avionics cost effective design approach, discussing guidance, commonality, reliability, communications and autonomy 16 p2982 A70-33802

Meteorological problems associated with space shuttle design and operations, permitting tradeoff analysis on environment effects 16 p2946 A70-33804

Space shuttle logistics transportation for long duration space station with crew rotation and resupply cycle, considering NASA and DOD requirements 16 p2983 A70-34069

Space shuttle systems structural design and thermal protection technology, stressing hardware reliability and reusability 16 p2986 A70-34227

Materials technology for reuse capability of space shuttle, discussing normal and stress corrosion, hydrogen embrittlement and flammability 16 p2987 A70-34228

Reusable nuclear shuttle/RNS/ for space program providing low cost transportation beyond earth orbit [AIAA PAPER 70-679] 17 p3174 A70-34512

Experiment space module combined with space station and serviced by shuttle for low total cost and maximum flexibility in funding and scheduling [AAS PAPER 70-034] 17 p3175 A70-34777

Manned planetary flight systems engineering, discussing feasibility, objectives, propulsion, transplanet injection via geospace shuttle station, energy requirements for various synodic modes [AAS PAPER 70-037] 17 p3155 A70-34778

Future manned planetary missions with reusable nuclear shuttles, comparing operating modes in terms of propellant requirement, costs, complexity, etc [AAS PAPER 70-040] 17 p3155 A70-34781

Logistic support reusable earth to orbit space shuttle design, noting weight penalties, payloads and development time [AAS PAPER 70-042] 17 p3175 A70-34782

Configurational and operational characteristics for space shuttle design, considering economic tradeoffs between expendable and reusable systems [AIAA PAPER 70-045] 17 p3175 A70-34783

Propulsion requirements for reusable space shuttle, discussing engine development program [AAS PAPER 70-044] 17 p3147 A70-34784

Cost reduction in designing space shuttle system using reusable winged vehicles, suggesting airlines operations method [AAS PAPER 70-043] 17 p3175 A70-34785

Space shuttle weight, reliability and reuse cost factors, discussing Phase A ILRV project reducing cost per pound of payload to orbit [AAS PAPER 70-046] 17 p3175 A70-34786

Space shuttle atmospheric maneuvers, examining booster and orbiter entry, flyback and abort [AAS PAPER 70-047] 17 p3175 A70-34787

Space shuttle mission trajectory optimization with steering in atmospheric flight and orbiter maneuvers [AAS PAPER 70-048] 17 p3176 A70-34788

Space shuttle-manned space station integration, discussing design and operation, crew rotation, station resupply, docking, etc [AAS PAPER 70-051] 17 p3176 A70-34789

Space shuttle safety program for low risk passenger transportation, combining large aircraft experience with spacecraft technology [AAS PAPER 70-055] 17 p3176 A70-34793

Low cost earth-moon transportation system based on shuttle station mode concept [AAS PAPER 70-058] 17 p3176 A70-34806

Unmanned and manned interorbital shuttle systems for satellites placement and repair and planetary spacecraft insertion, emphasizing cost analysis [AIAA PAPER 70-267] 17 p3172 A70-35650

Space station with shuttle and tug service, discussing reduced costs, reusability and commonality 18 p3333 A70-36318

Space shuttle development, discussing weight and lateral separation distance 19 p3531 A70-37378

European participation in American space program, considering space station, shuttle and tug 19 p3531 A70-37379

Optimal angle of attack transition trajectories for space shuttle from atmospheric entry to cruising flight for conventional airport landing 20 p3713 A70-39515

Atmospheric ascent optimal trajectories for medium to high lift drag ratio space shuttle type rocket vehicles [AIAA PAPER 70-978] 20 p3714 A70-39551

Nonrolling lifting gliding vehicle hypersonic longitudinal dynamic stability, applying analysis to space shuttles [AIAA PAPER 70-977] 20 p3715 A70-39552

Launch facilities institutionalization for space shuttles launch cost minimization [AIAA PAPER 70-244] 20 p3606 A70-39697

Space shuttle design, considering costs, boosters, payloads and orbits 20 p3716 A70-39795

Reusable rocket engine for space shuttle, discussing propellants, configuration, design, combustion cycle and size 20 p3689 A70-40084

Space shuttle with reusable launch system, discussing payload sensitivities regarding orbiter and booster weight and engine reliability [SAWE PAPER 849] 20 p3716 A70-40377

Two stage reusable shuttle for space transportation, discussing aerodynamic characteristics, thermal protection system, performance requirements, etc 21 p3929 A70-40981

Space transportation system, discussing shuttle costs, aerodynamic and propulsion configurations, management planning, etc 21 p3929 A70-40982

Space shuttle vehicle requirements, discussing configurations aerodynamic characteristics, aerothermodynamics, materials technology, etc 21 p3929 A70-40983

Cost optimal space shuttle systems, discussing booster configurations, weight and performance factors, technology utilization, etc 21 p3929 A70-40984

Reusable space shuttle technology, discussing vehicle configurations, system growth capability, thermal protection, cryogenics, integrated avionics, etc 21 p3929 A70-40985

Boundary layer transition application to space shuttle design, relating aerodynamic noise to turbulent boundary layers 21 p3744 A70-41015

Aerodynamic heating prediction methods for delta body space shuttle orbiter, comparing with wind tunnel test data 21 p3744 A70-41016

Aerodynamic heating constraints on space shuttle design, discussing prediction uncertainties for boundary layer transition, laminar, turbulent heating, etc 21 p3744 A70-41017

Nuclear rocket applications in Nuclear Flight Propulsion Module/NFPM/ and Reusable Nuclear Shuttle/RNS/ 22 p4070 A70-43180

Lubrication technology for space shuttles, discussing vehicles and airbreathing and rocket engines 22 p4047 A70-43325

Space shuttle mission and economics, discussing cost effectiveness, capabilities, satellite transportation payloads and traffic forecasts 22 p4127 A70-43505

European-U.S. cooperation in shuttle and space station program, noting experience in unmanned systems 22 p4127 A70-43508

European participation in small space shuttle development, discussing design, test vehicle program and European applications 22 p4111 A70-43511

Space shuttle structural technology for booster and orbiter, discussing hot and cold structure concepts, reentry bodies, military payloads, radiating protective coatings, refractory materials, etc 22 p4111 A70-43516

Geolunar space development with transportation based on shuttle stations, describing communication, orbits, logistics, etc 22 p4108 A70-43628

Space shuttle configurations, discussing launch, entry and landing characteristics 22 p4111 A70-43629

NASA design objectives for space transportation, discussing space shuttle, airlines-aerospace industry cooperation, computerization, etc 23 p4257 A70-44173

Operational requirements for NASA space shuttle Survival and Flight Equipment, discussing protection during launch and ascent 23 p4258 A70-44484

Hypersonic viscous effects on space shuttle entry trajectory, measuring lift and drag in free flight regime 23 p4258 A70-44526

Space station requirements and design, discussing space shuttles, operational personnel, long term effects, logistical systems, functions, etc 23 p4259 A70-44606

Space shuttle electronics requirements, considering systems in Mercury and Gemini spacecraft and Apollo lunar and command service modules 23 p4259 A70-44612

Reusable earth surface-to-orbit shuttle, discussing cost and performance design considerations 23 p4260 A70-44618

Space rescue operations in orbit during heavy traffic of spacecraft with large passenger loadings, noting role of space shuttles and tugs 23 p4260 A70-44619

Space shuttle transition trajectory optimization for cruising flight entry, considering longitudinal control, pitchup instability and angle of attack 23 p4244 A70-44623

Space transportation, discussing space shuttles, technological, commercial, human and philosophical aspects 23 p4245 A70-44641

Free flight remote controlled teleoperator system applications in manned orbital space station/space shuttle program 23 p4260 A70-44644

Space shuttle economic risk analysis, using computer program as design and management tool 23 p4261 A70-44674

Space shuttle for low cost transportation, discussing reusable vehicles, payload, design, orbital inclination, mission capabilities and international participation 23 p4261 A70-44676

Single stage reusable ballistic space shuttle, featuring minimum payload mass ratios and high propulsive efficiency 23 p4262 A70-44686

Aeroelastic and aerothermoelastic development of winged interorbital space shuttle concerning panel flutter, stability and nonstationary lifting surface theory 23 p4273 A70-44760

Orbital space station program, discussing common module design, support, space shuttles and objectives [SAE PAPER 700755] 24 p4415 A70-45852

Space shuttle structural design concepts and fabrication, tabulating structural and heat shield materials [SAE PAPER 700768] 24 p4415 A70-45867

Economic and design aspects of universal Orbit-to-Orbit Shuttle component of Space Transportation System [SAE PAPER 700763] 24 p4416 A70-45868

Low and high chamber pressure concepts for space shuttle reaction control system [SAE PAPER 700802] 24 p4416 A70-45909

Biotechnological design of shirt-sleeve side-by-side crew station for shuttle vehicle, including pilot vision and landing experience from X-15 program [AIAA PAPER 70-1327] 24 p4416 A70-45923

Orbit-to-orbit space shuttle toroidal propellant tank design, construction and testing for outflow and slosh characteristics [AIAA PAPER 70-1325] 24 p4417 A70-45940

Earth-orbiting manned space station design, describing shuttle support and experimentation in attached and free-flying modules [AIAA PAPER 70-1299] 24 p4417 A70-45951

Integrated electronics for NASA space shuttle program, discussing costs, configurations and technologies application [AIAA PAPER 70-1252] 24 p4418 A70-45966

Earth-to-orbit space shuttle environmental control and life support system [AIAA PAPER 70-1253] 24 p4418 A70-45967

Space shuttle onboard cost effective data management system, discussing checkout, fault isolation, redundant element switching and crew interaction [AIAA PAPER 70-1293] 24 p4418 A70-45975

SPACE SIMULATORS

NT HIGH VACUUM ORBITAL SIMULATOR

Ground based space simulation of arc-type electrothermal propulsion systems, discussing test facilities 01 p0161 A70-10225

Automatic simulator for guidance system installed on cartographic satellite in circular orbit at 600 km, discussing weightlessness and vacuum simulation devices 03 p0464 A70-13834

Space simulation test results compared with analytical methods for thermal data prediction of Azur satellite 04 p0762 A70-15182

French guided satellite space flight simulator developed in search for suitable three axial onboard guidance systems

06 p1028 A70-17933

Thermal testing of planetary lander vehicle in vacuum chamber, modeling electronics modules and experiments using resistance heaters

06 p1157 A70-18128

Xenon high wattage short arc lamps for space/solar simulators, describing seals, electrodes shapes and cooling, operating characteristics, etc

13 p2384 A70-28520

Spacecraft simulator using air bearing technique to simulate low friction aspect of environment, considering application to satellite attitude control

18 p3236 A70-36064

Ames Hypervelocity Free Flight Facility, discussing aerodynamic tunnel, radiation tunnel and light gas gun for reentry simulation

22 p4006 A70-42764

SPACE STATIONS

NT ORBITAL SPACE STATIONS

NT ORBITAL WORKSHOPS

Space station operations and logistics scheduling for long duration missions, using activity network model

01 p0179 A70-10487

Space station-logistics vehicle docking and material transfer problem

01 p0193 A70-10612

Manned space station power systems design and selection problems, discussing requirements based on impacts on space station design and operations

01 p0008 A70-10625

Buoyant Venus station using superpressure balloon, discussing requirements for structural design and station position tracking capability

01 p0195 A70-10633

Mission simulation mathematical modeling technology developed for optimization of experiment program management and operational planning for manned space station missions

01 p0181 A70-10634

Space station flexibility design based on INT-21 payload capability emphasizing volume and weight factors

01 p0195 A70-10635

Spaceborne computer system for manned space station to perform functions in addition to guidance and navigation including processing

04 p0654 A70-14651

Space station damage containment and control, emphasizing safety problems and guidelines

04 p0762 A70-14933

Manned space stations development, objectives, supply, storage and waste disposal, launching and artificial gravity

05 p0923 A70-16042

Resistojet design criteria for performance modeling of ammonia propellant thrusters and manned space stations using biowaste propellants

06 p1131 A70-18026

Cold pressure welding of space station tested on Soviet Soyuz spacecraft

06 p1078 A70-18503

Onboard and ground checkout systems for space station and space shuttle operations

07 p1251 A70-20373

Space stations life support systems for air purification, water reclamation and oxygen recovery

08 p1449 A70-20630

NASA future space programs, discussing space shuttle and station, nuclear propulsion, manned Mars landing, unmanned Venus-Mercury probes, etc

09 p1762 A70-23065

Space station program development requirements, describing ground and flight tests synthesis

10 p1952 A70-24926

Space station design for long duration operation, considering optimum mix of redundancy, maintainability and checkout

12 p2313 A70-27743

Space station experiments, payloads and activity planning

16 p2983 A70-34067

Space shuttle logistics transportation for long duration space station with crew rotation and resupply cycle, considering NASA and DOD requirements

16 p2983 A70-34069

Candidate products for manufacturing on space station, emphasizing liquid solid transformations, bubbles and droplets, polymerization, and cost effectiveness

17 p3041 A70-34791

Manned space station safety, discussing hazards identification and elimination, rescue/escape systems, etc

17 p3016 A70-34792

Subsystem selection integration and technology for space base and planetary mission module /PMM/ of space station program

17 p3023 A70-34801

Habitability factors in space station crew quarter design, discussing hygiene and dining facilities

17 p3036 A70-34803

Low cost earth-moon transportation system based on shuttle station mode concept

17 p3176 A70-34806

Juridical status and sovereignty of rocket launching and cosmic stations in international law

17 p3202 A70-35786

European participation in American space program, considering space station, shuttle and tug

19 p3531 A70-37379

Manned space station design, discussing durations of scientific experiments and crew operation

19 p3532 A70-37752

Optimization model for evaluating information management systems for handling control functions of long duration space station missions

19 p3532 A70-37851

Algorithms for processing of cosmic ray data monitored by space station with multichannels for neutron and meson components recordings

20 p3698 A70-39309

Buoyant Venus station using superpressure balloon, discussing requirements for structural design and station position tracking capability

20 p3715 A70-39677

Waste management for large space stations, discussing removal, venting, utilization, processing techniques, etc

21 p3769 A70-40996

Integrated temperature and humidity control and water recovery subsystem for manned test in space station simulator

21 p3769 A70-40998

European-U.S. cooperation in shuttle and space station program, noting experience in un manned systems

22 p4127 A70-43508

Space station mission and configuration concepts, discussing experimental/operational capability, crew assignments, accommodation and module sizing

22 p4111 A70-43517

Space station development and missions, discussing general design philosophy, successive project lineage and applications programs

22 p4108 A70-43653

Rotating flexible cable-connected space station dynamic scale model, describing suspension system and artificial gravity generation

23 p4258 A70-44528

Space station requirements and design, discussing space shuttles, operational personnel, long term effects, logistical systems, functions, etc

23 p4259 A70-44606

Space station program information management system involving data acquisition and extended manned flight operation with minimum ground support

23 p4164 A70-44637

Space Station long term operations and logistics concerning inventory, configuration and cargo management

[SAE PAPER 700757] 24 p4416 A70-45871

Spacecraft sensor trends from space station research and technology requirements regarding astronomy, biomedicine and biology, earth resources, etc

[AIAA PAPER 70-1291] 24 p4418 A70-45974

International participation in U.S. post-Apollo program involving reusable space transportation system and multipurpose space station

24 p4431 A70-46123

SPACE STORAGE

Thermally induced convective mixing motion in rotating cylindrical cryogen space storage tank model under heat flux, calculating critical Rayleigh number

07 p1257 A70-19320

Payload optimization factors for orbital storage of liquid hydrogen, considering payload cost of agitation, tank pressure, pressurant weight, etc

09 p1767 A70-23262

Supercritical pressure system heat transfer characteristics for cryogenic space oxygen storage and supply

14 p2667 A70-31342

Heat pipe cooled thrust chambers for space storable propellants, discussing design feasibility for radiation and regeneratively cooled concepts

[AIAA PAPER 70-942] 16 p2965 A70-33541

Gelled space-storable oxygen difluoride and diborane analysis, including particle preparation, yield stresses, viscosities and storability

[AIAA PAPER 70-609] 16 p2962 A70-33607

Storable tubular extendible member /STEM/, discussing advantages of BI-STEM for erecting unfurlable structures in space

16 p2846 A70-34141

SPACE SUITS

Simulated zero gravity tests of force application by subjects in Apollo suits, varying worksite geometry, personnel restraints and force type and direction

01 p0038 A70-10964

Life support system model using heart rate to monitor man doing physical work in space suits under simulated space environment

02 p0245 A70-12146

Space suit meteoroid protection for extravehicular activity, discussing Gemini and lunar surface EVA suits and bumper concept

[AIAA PAPER 69-366] 04 p0645 A70-15402

Open loop portable life support system containing light breathing vest within space suit

05 p0806 A70-16123

Computerized mass spectrometer for monitoring atmosphere in astronaut suits and cabin

[AIAA PAPER 69-1016] 07 p1249 A70-19730

Antigravitation suit effects on rheoencephalography changes during Valsalva maneuver and horizontal-passive orthostatism transition in humans

07 p1212 A70-19738

Water cooled space suits automatic control based on physiological changes in astronaut during hard work

09 p1627 A70-23458

Extravehicular activity space suits evolution emphasizing appropriate body temperature control under various conditions and work loads

10 p1824 A70-24412

Minimum ventilation volume requirement for space suit relation to air contaminants and body gas discharge intensities and locations

13 p2358 A70-29333

Space suit thermal insulation properties, wear durability and nonflammability improvements, reflecting techniques in fabricating cryogenic multilayer insulation systems

[AIAA PAPER 70-851] 16 p2939 A70-33918

Human cardiac flow during acceleration as function of time with and without anti-g suit, using electric plethysmograph

17 p3040 A70-35915

Portable contingency transfer life support system for crewman of Apollo missions providing oxygen and cooling

20 p3580 A70-39441

Rapid decompression due to pressure loss in space vehicle or suit, discussing fulminating hypoxia, mechanical trauma and ebullism

22 p3973 A70-43639

Decompression sickness prevention in space flight, discussing suit and capsule pressure, extravehicular activity and alleviation of conditions

22 p3980 A70-43640

SPACE SURVEILLANCE

Aircraft and ship position surveillance by satellites system with independent capability and undelayed voice and digital communication

09 p1723 A70-23043

Radar target optimal detection algorithms in cloud of passive reflectors, noting space surveillance regularities

15 p2696 A70-31516

Satellite based systems for aircraft surveillance, discussing satellite power and bandwidth conservation, pulse techniques and interrogators

18 p3288 A70-36391

SPACE SURVEILLANCE [SPACEBORNE]

Planetary film system /PFS/ camera-processor-scanner for scientific spaceborne applications, detailing design and performance

03 p0490 A70-13664

Satellite surveillance in cloud and weather modification, considering area selection for cloud seeding, atmospheric energy redistribution, etc

[AAS PAPER 69-621] 04 p0677 A70-14645

Air traffic control surveillance and data system using synchronous satellites in inclined elliptical orbits for communications and aircraft position determination

12 p2268 A70-27644

Ground and cockpit initiated collision avoidance commands system based on satellites surveillance of aircraft position and velocity data

19 p3466 A70-38242

SPACE SYSTEMS ENGINEERING

U AEROSPACE ENGINEERING

SPACE TEMPERATURE

Space temperature determination, discussing planet or satellite absorption and radiation rate dependence on surface characteristics, solar radiation, planet albedo and thermal radiation

05 p0914 A70-16629

SPACE TOOLS

Welding of satellite and spacecraft segments in space, discussing arc, electron beam, resistance, vacuum diffusion, cold pressure and brazing techniques

05 p0855 A70-16375

Cold pressure welding of space station tested on Soviet Soyuz spacecraft

06 p1078 A70-18503

Orbital zero and low g environment utilization for space manufacturing processes and related operational and tooling requirements

16 p2919 A70-33718

Systems design and instrumentation for chemical/biochemical space manufacturing at zero g, developing scaling laws for transition to larger production units

16 p2919 A70-33719

SPACE TRANSPORTATION

Magnetomotive tools and power systems for maintenance, repair and assembly in space weightless environment

19 p3436 A70-37949

Space maintenance tools necessity on long duration manned space missions 1972-1980

19 p3442 A70-38836

SPACE TRANSPORTATION

Plasma devices for spacecraft propulsion taking into account electrothermal, electromagnetic and electrostatic systems

05 p0895 A70-15817

Reusable space shuttle employing two stages resembling subsonic aircraft for carrying passengers and cargo between earth surface and orbit

07 p1392 A70-18873

Low operating cost space shuttle system for cargo and personnel transportation to earth orbiting stations involving reusable winged vehicles

[AIAA PAPER 70-242]

07 p1396 A70-20376

Structural composite materials for thermal protection of reusable weight-saving vehicles in space transportation system

[AIAA PAPER 70-272]

07 p1397 A70-20382

Environmental test facilities for space transportation systems, discussing aerodynamic, propulsion and structural problems, operational requirements and existing capabilities

[AIAA PAPER 70-275]

07 p1251 A70-20384

Space transportation system booster and orbiter development ground and flight tests, considering vehicle size and reusability requirements

[AIAA PAPER 70-276]

07 p1397 A70-20385

Space transportation system objectives including design, operations and economics

[AIAA PAPER 70-263]

07 p1398 A70-20393

Reusable space transportation vehicle design evolution, considering staging, aerodynamic shapes, etc

[AIAA PAPER 70-265]

07 p1398 A70-20395

Reusable passenger and cargo shuttle system based on integral launch and reentry vehicle (ILRV), considering propulsion systems, aerodynamic and structural configurations, aerothermal characteristics, etc

08 p1582 A70-20689

NASA earth-orbit shuttle (EOS) for achieving routine arrival, conventional landing after orbital flight and reentry

09 p1766 A70-22677

Low cost orbital space transportation system with shuttle service, discussing booster and configuration selections, weight, costs, etc

[AIAA PAPER 70-256]

13 p2506 A70-29615

Reusable earth-moon and deep space return transportation, assuming extraterrestrial nuclear rocket propellant source

14 p2653 A70-30766

Space shuttle logistics transportation for long duration space station with crew rotation and resupply cycle, considering NASA and DOD requirements

16 p2983 A70-34069

Low cost earth-moon transportation system based on shuttle station mode concept

[AAS PAPER 70-058]

17 p3176 A70-34806

Legal aspects of suborbital space transports based on air transportation concepts

18 p3350 A70-36661

Suborbital space transports problem solution by recoverable jet orbital or jet assisted aircraft, discussing implications of Concorde supersonic flight

18 p3350 A70-36663

Extraterrestrial transport trajectory control by jet assistance

18 p3333 A70-36670

Primary solar electric propulsion for automated space transportation propulsion program, considering performance and technology readiness

[AIAA PAPER 70-1115]

20 p3691 A70-40228

Two stage reusable shuttle for space transportation, discussing aerodynamic characteristics, thermal protection system, performance requirements, etc

21 p3929 A70-40981

Space transportation system, discussing shuttle costs, aerodynamic and propulsion configurations, management planning, etc

21 p3929 A70-40982

Nuclear rockets for interorbit transportation, discussing reuse economics, propulsion system performance, etc

21 p3886 A70-40987

Reusable space transporter predicted applications evolution from earth circling to space bases and space colonies for deep space missions

21 p3930 A70-41495

Operational safety of nuclear rockets in orbit-to-orbit transportation in regard to radiation doses from plume and reactor, including malfunction condition

22 p4070 A70-43183

Space shuttle mission and economics, discussing cost effectiveness, capabilities, satellite transportation payloads and traffic forecasts

22 p4127 A70-43505

Space transportation systems cost comparison, taking into account national program goals and near/far orbit traffic fraction

23 p4285 A70-44511

Space transportation, discussing space shuttles, technological, commercial, human and philosophical aspects

23 p4245 A70-44641

Economic and design aspects of universal Orbit-to-Orbit Shuttle component of Space Transportation System

[SAE PAPER 700763]

24 p4416 A70-45868

Space transportation system concept and operational objectives, discussing configurational aspects, aerodynamic complexity, propulsion systems, payloads, performance and aerothermodynamic constraints, etc

[AIAA PAPER 70-1249]

24 p4418 A70-45965

International participation in U.S. post-Apollo program involving reusable space transportation system and multipurpose space station

24 p4431 A70-46123

SPACE TUGS

Space based reusable manned/unmanned tug, discussing potential missions, system requirements and auxiliary hydrogen oxygen propulsion system

[AIAA PAPER 70-719]

16 p2964 A70-33533

Space station with shuttle and tug service, discussing reduced costs, reusability and commonality

18 p3333 A70-36318

Aerodynamic braking for returning high speed recoverable space tug to low earth orbit

23 p4259 A70-44611

SPACE VEHICLE CHECKOUT PROGRAM

Temperature distribution causes in earth orbiting satellite, outlining thermal control and temperature calculation methods and prelaunch ground tests

05 p0956 A70-15813

Digital computer impact on aerospace sciences and technologies in terms of computerized design, interactive graphics, flight simulation, Apollo systems checkout, etc

09 p1642 A70-23277

Apollo lunar module mechanical acceptance tests evaluation based on reported flight anomalies review

[AIAA PAPER 70-401]

10 p1951 A70-24904

Launch vehicle automatic checkout methods emphasizing guidance and control equipment performance in real time operations

[AIAA PAPER 70-393]

10 p1952 A70-24912

Apollo Spacecraft Certification Test Program at replaceable hardware assembly level noting future manned spacecraft applications

[AIAA PAPER 70-375]

10 p1952 A70-24928

Apollo Lunar Module Test Program Management, discussing test requirements optimization, control, planning, etc

[AIAA PAPER 70-368]

10 p1952 A70-24932

Automatic test and checkout system difficulties in space vehicles

11 p2032 A70-26338

Checkout systems for shuttle and orbiting space stations, discussing shift from ground to onboard operation

12 p2208 A70-27691

Apollo Guidance, Navigation and Control system prelaunch checkout, flight experience and error analysis

[AIAA PAPER 69-891]

14 p2615 A70-30758

Spacecraft onboard computer for prelaunch targeting constants verification through checksum equation and error detection scheme, using generated number sequence

[AIAA PAPER 69-946]

14 p2599 A70-30769

Real time simulation of space vehicle and ground support equipment by digital computer for launch programs checkout

16 p2870 A70-33733

Onboard automatic checkout systems for manned space vehicles, investigating data management development costs for thorough tradeoff studies

16 p2889 A70-33803

Digital data acquisition and control system for acoustic testing of large spacecraft

17 p3062 A70-35506

Computerized automatic ground equipment (CAGE) as intelligence system for checkout and control of launch vehicles and spacecraft

19 p3397 A70-37915

Surveyor spacecraft testing at Environmental Test Laboratory, describing facilities and innovations designed for temperature extremes

19 p3532 A70-37960

Environmental tests and checkout procedures for Azur satellite subsystems and subassemblies integration into flight readiness

19 p3533 A70-38289

Spacecraft test programming at test facilities providing vacuum and thermal space simulation suggested by Azur and Dial satellite development experience

19 p3399 A70-38290

Cost effective spacecraft testing in terms of statistical reliability, program effectiveness and equipment costs

19 p3554 A70-38293

NASA automatic checkout systems for Saturn 5 stages and instrument units

21 p3803 A70-40770

Computer real time Apollo simulation, checkout and training system duplicating actual mission for flight controllers in Mission Control Center

21 p3805 A70-41198

Programming and checkout of computer for ELDO inertial guidance system, including flight simulation and autopilot tests

[AIAA PAPER 69-961]

21 p3795 A70-41862

SPACE VEHICLE CONTROL

U SPACECRAFT CONTROL

SPACE VEHICLES

U SPACECRAFT

SPACE WEAPONS

Future U.S. aerospace power in terms of military technology and defense policies and attitudes

05 p0960 A70-16633

SPACE-TIME CONTINUUM

U RELATIVITY

SPACE-TIME FUNCTIONS

Four dimensional optimal interpolation for maximum wind velocity components, calculating spatiotemporal correlation functions

01 p0135 A70-10205

Gravitational theories scheme combining tetrad field with bimetric theories, including general relativity, space-time dependent Lorentz rotations, red shift and light deflection

01 p0141 A70-10232

Gravitational field equations in flat space, using quaternion representation of general relativity Riemannian space time in terms of spinors

01 p0141 A70-10279

Field equations in particle neighborhood for spherically symmetric metric in conformal gravitation theory, considering particle inertial mass as function of position

01 p0142 A70-10492

Motion equations of material point in general relativity theory found analogous to equations in classical mechanics for metric in introduced physical space

01 p0146 A70-11443

F 2 layer state prediction as function of solar activity by series expansion for describing space-time variations of monthly F 2 medians critical frequencies

01 p0083 A70-11547

Einstein equations for five dimensional spherically symmetric space solved using gravitational constant without singularities on Schwarzschild sphere

05 p0880 A70-15793

Relativistic length contraction, time dilation and classical electrodynamics formulated in terms of special relativity using Galilean transformations

05 p0881 A70-15875

Seasonal variation in ionospheric radiation absorption related to time variation between sunrise and constant angle attainment of sun

05 p0842 A70-16758

Criteria for particle motion with constant acceleration in curved space-time

06 p1104 A70-17186

Back reflection of zero-mass scalar or vector waves in gravitational fields produced by non-Lorentz part of spatial metric components

07 p1387 A70-19923

Solar system cosmic ray time-space variations analysis based on simulation of meteorite nuclear processes

07 p1372 A70-20338

Space-time singularities of gravitational collapse and cosmology indicated by timelike or null geodesic incompleteness

08 p1575 A70-21353

Asymptotic model for stationary radiative stationary transitions using Newman-Penrose spin coefficient approach to gravitational radiation for Riemann space-time

11 p26547 A70-26547

Metric analyticity around each point of C cubed static vacuum space-time for Einstein equations

11 p2084 A70-26553

Neutral-dominated plasma turbulence, discussing space-time plasma probe correlation functions for electron density fluctuations measurements

11 p2095 A70-26757

Turbulent flowing plasma, analyzing wavenumber frequency dependent spectral function and space-time correlation function

11 p2096 A70-26768

Clock synchronization in general relativity theory, investigating temporal and spatial relations in four dimensional continuum using simultaneous hypersurface

12 p2272 A70-27357

General relativity integral conservation laws of system of bodies in curved space-time obtained from symmetrical energy-momentum tensor

12 p2274 A70-28222

Eulerian space-time correlations of velocity and pressure for universal homogeneous turbulence by separating kinematic convection effects of large eddies from velocity assumption

13 p2386 A70-28645

Oscillator perturbed motion of elastic body in general relativity space time, discussing energy tensor, unitary speed vector and density 13 p2451 A70-28954

Kerr-Schild space-time manifolds with electromagnetic field, solving Einstein equations 13 p2451 A70-29166

Pseudoisotropic surfaces in Minkowski space-time with proof of existence, formulating congruencies of normal fiber 13 p2452 A70-29634

Homogeneous isotropic turbulence velocity field space-time variable correlation functions in fluid flow 15 p2719 A70-31487

Pulsar models distinguishing by Huygens principle in flat space-time, describing electromagnetic propagation in Riemann space 17 p3173 A70-35757

Circular orbit stability in stationary axisymmetric space-times dependence on angular momentum per unit mass increases outward from symmetry axis 18 p3317 A70-37004

Ricci curvature tensor perturbations of space-time on Alfvén wave fronts 19 p3472 A70-38935

Midtropospheric frontogenesis, using three hourly rawinsonde data for isentropic trajectories to describe velocity field in space and time 20 p3664 A70-39374

General relativity integral conservation laws of system of bodies in curved space-time obtained from symmetrical energy-momentum tensor 20 p3673 A70-40097

Invariance principle in mechanics of deformable continua connecting three dimensional and relativistic space-time formulation 21 p3940 A70-42097

Chronometrically invariant formulation of Petrov gravitational fields algebraic classification at space-time fixed point in general relativity 21 p3851 A70-42239

Einstein equations solved for steady axisymmetric physical schemes by varying Kerr metric constants, considering electromagnetic field case 22 p4073 A70-42717

Space-time Riemann metric for scalar-tensor gravitational theories with arbitrary omega parameter 22 p4104 A70-42991

Gravitational equations with oscillatory physical singularity, noting Bianchi type IX homogeneous metric 22 p4063 A70-43477

Metric evolution in oscillatory mode of approach to singularity in homogeneous cosmological models in asymptotic region, showing Kasner epoch dependence on perturbation 22 p4075 A70-43478

Clock synchronization in general relativity theory, investigating temporal and spatial relations in four dimensional continuum using simultaneous hypersurface 22 p4075 A70-43598

Optical point characteristics of static spherically symmetric space-times of de Sitter universe, Einstein universe and exterior Schwarzschild field 23 p4239 A70-43821

Einstein-Rosen matter concept given by space-time with isometric domains, discussing hypersurface derivatives 24 p4379 A70-45486

SPACE-TIME METRIC

U SPACE-TIME FUNCTIONS

SPACEBORNE PHOTOGRAPHY

NT SATELLITE-BORNE PHOTOGRAPHY

Mars craters and crater-like objects catalog from Mariner 4 photographs, statistically analyzing diameter-frequency relations 01 p0179 A70-10523

Spacecraft orientation from onboard stellar photographs, calculating absolute and relative elements, accuracy and camera parameters 01 p0198 A70-11512

Rb-75 adapted reconnaissance cameras error sources on basis of processed Echo 2 satellite photographs 02 p0294 A70-11772

Space research photography role in studying earth and moon atmospheres and surfaces, determining spectral bands for contrast 03 p0483 A70-13168

Planetary film system (PFS) camera-processor-scanner for scientific spaceborne applications, detailing design and performance 03 p0490 A70-13664

Meteorological satellite TV cameras development, discussing image sensors and tabulating characteristics 03 p0491 A70-13665

Multispectral scanner technology for earth resources exploration from space 03 p0492 A70-13671

Visual interpretation of moon and Mars surface photographs taken from satellites, analyzing craters and bumps 04 p0686 A70-14266

Cloud cover consequence on earth photographing space missions simulated by Monte Carlo method using worldwide statistics 04 p0676 A70-14636

Apollo 9 space photography of earth surface and use for quantitative analysis of earth resources, including supporting aircraft photography 04 p0687 A70-14650

Multiband photographic system for automatic earth resources aerial sensing and lunar orbital mapping with manual override provisions 04 p0687 A70-14657

Remote sensing aerial and space surveys application to agriculture, forestry and water resources, discussing imaging systems and information acquisition and analysis techniques 05 p0838 A70-16164

Earth resources remote sensing investigations from spacecraft and aircraft, noting Gemini and Apollo photography, hydrological surveys and radar techniques 05 p0849 A70-16450

Modern astronautics, discussing postwar rocket motors and ballistic missiles construction, ELDO program, moon and planetary photographs and space walk, etc 05 p0960 A70-16627

Spatial resolution and repetition intervals for optimum utilization of space-derived remotely sensed data of ocean surface features 06 p1060 A70-18593

Lunar photography interpretation, discussing topographic maps obtained by spacecraft 07 p1284 A70-19779

Geology from air covering aerial and space photography, nonvisible spectrum utilization, photograph transmission from Mars and moon, balloon flights, etc 07 p1272 A70-20225

Lunar Orientale region structure geological interpretation based on Lunar Orbiter 4 photographs 09 p1751 A70-22196

Automated crop surveys from integrating observations made at different times/time dimensioning/ during growing season, noting earth resources satellites role 09 p1666 A70-22263

Multiband high resolution spaceborne imagery telemetry with optical mechanical scanners from earth orbiting satellites in earth resource applications 09 p1677 A70-22873

EROS program earth imaging models characteristics, describing airborne and spaceborne film return and global and geosynchronous space data transmission 09 p1678 A70-22889

Mars primitive atmosphere analyzed from statistics of craters quantity as function of diameter, using Mariner 6 and 7 probe photographs 09 p1763 A70-23318

Crop species and soil conditions identification from space by comparison of multivase and multiemulsion photography, assigning standard signature to optical fields 10 p1879 A70-24745

Gemini 12 photographs examined for urban and transportation data content 12 p2228 A70-26909

Spaceborne photography for detecting and identifying road networks, using color separation plates and photograph enlargement 12 p2216 A70-26910

Aerial oceanographic photographic image enhancement by including blue spectral region, presenting Apollo 9 space photographs 12 p2217 A70-26917

Multistage sampling of space and aircraft remote sensor imagery for forest inventory 12 p2228 A70-26921

Photography for geological interpretation, comparing color, color IR, and black-and-white photographs from spacecraft and aircraft 12 p2221 A70-26956

Relative control data incorporation into sequential or simultaneous analytical triangulation systems, considering extraterrestrial photographs reduction 12 p3088 A70-27875

Photographic apparatus for lunar orbiters and Apollo spacecraft, describing lunar surface closeup camera for astronauts, launch photography, etc 13 p2406 A70-28926

Lunar surface terrain types and chemical composition based on Surveyor pictures 14 p2634 A70-30193

Apollo 9 scientific multispectral photography mission, discussing meteorological support aspect of real time planning 14 p2610 A70-30614

Nimbus weather satellite as laboratory for sensors collecting data for global weather system, describing launching, attitude control systems and cameras 14 p2654 A70-31149

Cloud cover stationary pictures by spin-scan camera in synchronous orbit over Pacific converted into motion pictures showing cloud pattern changes and storm development 14 p2587 A70-31150

Light sources design with variable uniform luminance for space exploration cameras calibration [JPL-TR-32-1470] 15 p2737 A70-32037

Oceanographic phenomena inference from satellite cloud photographs, developing seasonal cloud climatology for Peru Current area 16 p2897 A70-33713

Mars photography from flybys and orbiters, communicating planetary scene information to eye-brain receiver of earth based interpreters 16 p2912 A70-33976

Combination shutter and filter-changing mechanism for spacecraft vidicon cameras 16 p2914 A70-34150

Mariner 6 and 7 TV camera pictures of Mars during approach and encounter, discussing IR spectroscopy, celestial mechanics experiment and Martian terrain 17 p3158 A70-34875

Gemini spacecraft photograph patterns revealing relationship between cloud formation and topography 18 p3258 A70-36298

Lunar regolith depth measurement by Lunar Orbiters 4 and 5 high resolution photographs, discussing thickness relation with sinuous rilles in marial regions 18 p3319 A70-37054

Mariners 6 and 7 orbits determination by weighted least squares estimation based on common surface features in overlapping TV pictures [ALAA PAPER 70-1066] 19 p3529 A70-38879

Earth resources data from man operated airborne/spaceborne sensors and data handling systems, examining Apollo Applications Program 20 p3616 A70-39056

Geological and cartographical data acquisition and processing, considering aircraft and satellite-borne photography of earth surface 20 p3616 A70-39061

Orbital photography interpretation from test rockets and Apollo-Gemini spacecraft, considering environmental applications 20 p3634 A70-40321

EROS program earth imaging models characteristics, describing airborne and spaceborne film return and global and geosynchronous space data transmission 21 p3829 A70-41871

Mapping from satellite-collected earth surface images, emphasizing optical/mechanical scanner images 22 p4037 A70-43089

Meteorological TV imaging systems development in last decade, including low and synchronous altitude camera, sensors, orthicons, etc 23 p4193 A70-43963

Apollo and Skylab photographic systems, describing equipment and missions 24 p4333 A70-45360

Earth Resources Technology Satellites (ERTS) providing high resolution image data regarding agriculture, geology, hydrology, geography, etc [SAE PAPER 700761] 24 p4416 A70-45869

SPACECRAFT

Registration procedure for space exploration objects 17 p3202 A70-35788

Computerized assembly of production space vehicle with controlled mass properties, discussing automated system of data collection, storage and retrieval [SAWE PAPER 851] 20 p3639 A70-40375

Astronautics - IAF Conference, New York, October 1968, Volume 1, Spacecraft systems 23 p4262 A70-45001

SPACECRAFT ANTENNAS

Radiation enhancement from spherical antenna by overdense plasma coating, noting use for reentry vehicle blackout prevention 02 p0262 A70-12601

High gain antenna for 1973 Mars Soft Lander data transmission using sensors and digital computer to achieve autonomous precision pointing to earth [AAS PAPER 69-578] 04 p0716 A70-14653

Oil vapor lubricated bearing for compensated antenna of spin stabilized spacecraft, discussing service life, power and storage in sintered porous material [DGLR-69-062] 07 p1391 A70-18775

Spacecraft phased array antenna techniques, discussing tape helix radiators design for applications in navigation, TV broadcasting and data relay systems [ALAA PAPER 70-425] 11 p2015 A70-25452

Spacecraft high efficiency phased arrays with deployable helix radiating elements, considering gain and weight factors 12 p2197 A70-27930

Oil-vapor lubricated ball bearing system for deployable spin-free antenna of spin stabilized spacecraft 13 p2349 A70-28843

Magnetospheric plasma density effects on impedance of VLF electric field spacecraft antenna 13 p2397 A70-29186

High gain helix radiators for spacecraft phased arrays, measuring performance vs design parameters 15 p2678 A70-32600

Lunar Module landing radar system design, discussing antenna and electronics assembly 16 p2865 A70-33681

- Stepper motor for pointing Surveyor spacecraft TV transmitting antenna and solar panel at earth and sun
16 p2845 A70-34110
- Mechanically despun multifrequency, attitude sensing antenna for spin stabilized spacecraft, deep space probes, tactical communications and community broadcast applications
16 p2986 A70-34159
- Flush mounted lightweight antennas for rockets, discussing construction radiation patterns, input impedance, etc
17 p3053 A70-35273
- Thermoelectric outer planets spacecraft /TOPS/ attitude control subsystem providing accurate antenna pointing and trajectory correction engine thrust vector orientation
21 p3930 A70-41801
- Thermoelectric outer planet spacecraft /TOPS/ structural problems associated with high gain antenna and electronic equipment
21 p3930 A70-41803
- Flexible antennas and solar panels effect on dynamic behavior and control system response of dual spin spacecraft
21 p3931 A70-41855
- Sheaths effect on capacitance of plane grid capacitor in plasma, discussing satellite aerials admittance
21 p3792 A70-42046
- SPACECRAFT CABIN ATMOSPHERES**
- Volatile contaminants emitted from space cabin construction materials tested under simulated space conditions
01 p0031 A70-10237
- Apollo space cabin atmospheres, evaluating diluent N effect on decompression sickness in intermittently exercising men
01 p0032 A70-10368
- Molecular sieve mixed gas adsorption and vacuum desorption of carbon dioxide in Apollo spacecraft cabin
01 p0040 A70-11450
- Physiological effects on men of 10 hr exposure to nitrogen-oxygen mixture followed by pure oxygen 4 hr exposure, simulating conditions during EVA
03 p0436 A70-13899
- Space cabin atmosphere effects on primary and secondary immunological responses in mice relative to spleen weight and antibody titers following antigenic stimulation
03 p0437 A70-14062
- Spacecraft cabin atmosphere effects on mice primary and secondary immunological responses relative to spleen histochemical and biochemical changes in enzyme activity
03 p0437 A70-14063
- Ground level denitrogenation duration effects on decompression sickness occurrence in space cabin atmospheres
06 p0999 A70-17289
- Physiological and hygienic data on oxygen partial pressure in space cabin atmosphere analyzed for manned space flights
07 p1220 A70-19502
- Human exhaled air contaminants analysis role in disease diagnosis, metabolism study and spacecraft cabin atmosphere changes
07 p1220 A70-19514
- Computerized mass spectrometer for monitoring atmosphere in astronaut suits and cabin
[ALAA PAPER 69-1016] 07 p1249 A70-19730
- Soviet monograph on toxicology of active human life gaseous products, noting implications for artificial atmosphere formation in pressurized compartments
09 p1624 A70-22549
- Physiological and hygienic data on oxygen partial pressure in space cabin atmosphere analyzed for manned space flights
11 p1991 A70-26101
- Human exhaled air contaminants analysis role in disease diagnosis, metabolism study and spacecraft cabin atmosphere changes
11 p1991 A70-26113
- Combustion efficiency and rate in oxygen enriched spacecraft atmosphere
17 p3177 A70-35210
- Hypoxia warning systems using polarographic sensor and miniaturized electronics for face-mask and cabin installation for aircraft and spacecraft
20 p3579 A70-39429
- Systemic bacterial infection resistance in white mice exposed to simulated hypobaric normoxic space cabin environment
20 p3572 A70-39431
- Prototype electrolyzer for generating oxygen from water vapor under various atmospheric conditions, noting spacecraft cabin application
20 p3564 A70-39696
- NASA aircrew oxygen system, describing carbon dioxide control and oxygen generation subsystems
21 p3768 A70-40990
- Oxygen-nitrogen generation for long manned space flight based on liquid center dual matrix electrolysis cell
21 p3768 A70-40992

- Corona and voltage breakdown for spacecraft electrical components in low pressure helium-oxygen atmospheres, measuring between parallel plates
21 p3851 A70-42124
- Dynamic spacecraft cabin atmospheres for extended operation, discussing gas composition, weightlessness and various stress factors
22 p3980 A70-43643
- Alpine 11,500 ft air atmosphere for manned orbiting laboratory, noting reduced risk of dysbarism during space suit operations
22 p3980 A70-43645
- Space cabin atmosphere regeneration by unicellular algae photosynthesis, discussing Chlorella cultivation procedures and additional functions in life support systems
23 p4154 A70-44655
- SPACECRAFT CABIN SIMULATORS**
- Crew locomotion effect on spacecraft attitude control using space cabin simulator tests
01 p0036 A70-10853
- Apollo mission simulation, discussing Command Module Simulator /CMS/, onboard computer system and dynamic visual presentation via infinity-optics display
[SMPT PAPER 105-74] 09 p1655 A70-22226
- Command module simulators for Apollo astronaut training in moon landing, using computer, exterior visual scenes and spacecraft interior replica
21 p3804 A70-41195
- Lunar module simulator for Apollo flight training using computers, digital conversion, cockpit replica, infinity-optics display and instructor control
21 p3805 A70-41196
- Trace contaminants associated with habitation by man in space cabin simulator by gas chromatography and IR and mass spectroscopy
21 p3770 A70-41482

SPACECRAFT CABINS

- Artificial gravitation parameters for manned compartments of spacecraft, analyzing permissible angular velocity and rotation radius regarding vestibular-vegetative disorders
04 p0760 A70-14446
- Spacecraft cabins illumination conditions selection based on cosmonaut visual perception of luminous objects
07 p1221 A70-19515
- Spacecraft cabins illumination conditions selection based on cosmonaut visual perception of luminous objects
11 p1991 A70-26114
- Environmental control of confined spaces and life support systems by Pontryagin maximum principle of optimal control theory, discussing cabins, heat exchanger, etc
11 p1991 A70-26363
- Artificial gravitation parameters for manned compartments of spacecraft, analyzing permissible angular velocity and rotation radius regarding vestibular-vegetative disorders
13 p2503 A70-28471
- Closed compartment fire mathematical model to analyze combustion parameter effects, atmosphere pressure and temperature during fire
17 p3198 A70-35646
- Flame resistant nonmetallic materials for manned spacecraft and aircraft interiors, considering fibers, polymers, paper and composites
22 p4058 A70-42295
- Decompression sickness prevention in space flight, discussing suit and capsule pressure, extravehicular activity and alleviation of conditions
22 p3980 A70-43640

SPACECRAFT COMMUNICATION

- NT REENTRY COMMUNICATION**
- Communications subsystem configuration for orbital manned space station, describing data rates and processing, multiplexing and associated modulation methods
[ALAA PAPER 69-1079] 01 p0043 A70-10627
- HEOS 1 satellite for interplanetary space exploration, describing eccentric orbit, structure, power supply, attitude measurement and control, spin rate control, telemetry and telecommand systems
01 p0196 A70-11114
- HEOS 1 satellite telemetry, telecommand and tracking systems, noting data transmission degradation due to high solar activity
01 p0045 A70-11115
- Multipath spectral and statistical characteristics in VHF satellite-aircraft link, discussing geometric considerations and reflection from Gaussian surfaces
02 p0259 A70-12565
- Solar phenomena effect on VHF communications between synchronous satellite relay and earth ground stations
02 p0259 A70-12566
- UHF shallow-cavity crossed-slot aircraft antenna for satellite to air communications
02 p0269 A70-12585
- Apollo 11 electronics, discussing inertial measurement unit, optical navigation system, command

module computer, communication network, TV and experimental packages

- 02 p0270 A70-12633
- Intelsat satellites telemetry and telecontrol /ITTC/, describing Fucino plant design and operation
02 p0263 A70-12647
- Phase lock loop circuit for spacecraft communication noise filtration, describing linear study of first-four-order loops
03 p0448 A70-13537
- Troposphere effects on low incident Explorer 22 satellite signal amplitude, noting role of diffraction
03 p0449 A70-13611
- Bandwidth reduction for interlacing two voice and three additional teletype subchannels in standard phone frequency range for use in VHF/UHF satellite link
03 p0450 A70-13623
- Mission design, spacecraft characteristics, communications and experimental approaches for Viking 1973 Mars Project
03 p0576 A70-14020
- High gain antenna for 1973 Mars Soft Lander data transmission using sensors and digital computer to achieve autonomous precision pointing to earth
[AAS PAPER 69-578] 04 p0716 A70-14653
- Linear phase detection using FM demodulation for Apollo S band communication system eliminating baseband voice interference with telemetry
[AAS PAPER 69-610] 04 p0648 A70-14659
- Phase feedback demodulation technique to analyze telemetry performance degradation caused by voice interference in modes of Apollo communication system, providing linear detection scheme
[AAS PAPER 69-609] 04 p0648 A70-14660
- Ground station location, equipment and function for radio communication with German research satellites, noting NASA and ESRO cooperation
04 p0664 A70-15304
- Meghdoot program for satellite network communications technology applications to national goals in India
04 p0757 A70-15670
- Satellite communications influence on ground stations design, describing steerable antenna and receive and transmit configurations for domestic station
05 p0811 A70-16095
- Spacecraft telecommunication and tracking systems in Gemini, Mercury and Apollo programs, emphasizing Apollo command and lunar modules equipment and mission ground stations
05 p0813 A70-16326
- Aerodynamic damping measured for parabolic satellite communication antenna with pronounced flexibility in azimuth drive, simulating by scaled wind tunnel models
05 p0938 A70-16455
- Assignment problem for finite set elements pairing, discussing probabilistic formulations and applications to satellite communications problems
05 p0815 A70-16716
- PCM time division satellite multiple access communication system to increase time slot utility, considering individual earth station control and common signaling circuit features
06 p1011 A70-18409
- Acquisition system design and experimental results for time division multiple access satellite communication system
06 p1011 A70-18410
- Clock synchronization system design and test results for PCM time division multiple access satellite communication system
06 p1011 A70-18411
- L band transponder design for aeronautical satellite, giving block diagrams
07 p1234 A70-19292
- Radio wave refraction and field strength in model Venus atmosphere for various spacecraft trajectories
07 p1235 A70-19492
- Communication satellite transponders design, cost, reliability, manufacturing, testing and future developments
07 p1241 A70-19620
- Deep space network /DSN/ functions and characteristics, discussing spacecraft control, data acquisition, orbit determination, data processing, etc
08 p1481 A70-20614
- Laser and quasi-laser systems modulation for wide spectrum communications, discussing global potentials and application as low cost satellite links
08 p1459 A70-20802
- UHF satellite receiver for binary FSK data collection system using matched integrate and dump filter detectors
08 p1459 A70-20804
- Optimal satellite communication system design concerning station spectrum and interference limits
08 p1459 A70-20805
- Low noise tunable parametric amplifier for tactical satellite communications, discussing characteristics and varactor diode mount
08 p1471 A70-20806

- Modern selection for satellite communications system, considering bandwidth and power constraints, propagation characteristics, point-to-multipoint operation, etc 08 p1459 A70-20807
- German satellite ground station system central station design, discussing cooperation between aerospace institute and electronic company 08 p1481 A70-21368
- Atmospheric turbulence regarding refractive index fluctuations over UK measured by radio telescope, discussing effects on satellite communication 09 p1667 A70-22384
- ARCOM earth terminal for Domestic Satellite Communication System bringing telephone, TV and data service to northern Canada 09 p1656 A70-22945
- Optical transmission technology for aerospace launch operations investigated on wideband communication systems projects involving use of gallium arsenide lasers and diodes 09 p1640 A70-23776
- Independent burst and burst coherent TDMA methods compared for ground station-satellite communication 10 p1836 A70-24340
- Error probability degradation for digital satellite communication systems, employing multiphase signal sets distorted by bandlimited filtering 10 p1836 A70-24342
- Adaptive multiple access satellite communication system at millimeter wavelengths in time- and frequency-division modes, compensating rainfall attenuation 10 p1838 A70-24358
- Multiple access technique for millimeter wave satellite communications, noting weight and size of on-board equipment 10 p1838 A70-24359
- Demand assignment economics relative to ground stations in satellite telecommunication systems 10 p1838 A70-24360
- TDMA demand-assigned satellite communication system developed for INTELSAT, discussing PCM, voice signals and channels, etc 10 p1839 A70-24362
- Review of 1969 London International Conference on Digital Satellite Communication session covering modulation, synchronization and coding [AIAA PAPER 70-464] 11 p1997 A70-25409
- Communications and attitude control on Phase 2 satellite for Defense Satellite Communication System [AIAA PAPER 70-493] 11 p1998 A70-25427
- Satellite communications subsystem performance testing from initial integration through launch under all environmental exposure 11 p2030 A70-25445
- Microwave tubes for high power transmission from space to ground and in deep space communications, discussing klystrons, TWT and crossed field amplifiers [AIAA PAPER 70-435] 11 p2016 A70-25456
- Satellite Integrated Communications, Navigation and Identification System for implementing worldwide command-control system and equipment and signal integration [AIAA PAPER 70-503] 11 p2000 A70-25466
- Navigational satellite communication experimental design emphasizing mobile, ship or aircraft station technical characteristics [AIAA PAPER 70-407] 11 p2001 A70-25469
- S band communications repeater using retrodirective phased array on synchronous altitude data relay satellite /DRS/ for intersatellite and ground links [AIAA PAPER 70-424] 11 p2001 A70-25472
- LES 5 and 6 feasibility demonstration of satellite communications at VHF/UHF to mobile terminals and as test beds, emphasizing stationkeeping and attitude control [AIAA PAPER 70-494] 11 p2121 A70-25474
- Low noise wideband uncooled preamplifier for small unattended satellite communication terminals, discussing theory, design and performance [AIAA PAPER 70-419] 11 p2016 A70-25485
- Report on Spectrum Utilization and System Constraints session of Intelsat/IEEE International Conference on Digital Satellite Communication, London, November 1969 11 p2002 A70-25486
- Digital satellite communications systems, discussing time division multiplexing, steerable beam antennas and satellite-to-satellite transmission [AIAA PAPER 70-491] 11 p2003 A70-25492
- Telemetry tracking and command antenna array of Central German Ground Station for satellite communication [DFVLR-SONDDR-52] 11 p2017 A70-25800
- Laser systems for deep space communications, considering high data rates, laser types, systems operation, earth atmosphere effects, hardware reliability, etc 11 p2005 A70-26036
- Cassegrain antenna feed system for satellite communication earth stations, noting low noise characteristics 11 p2011 A70-26716
- Satellite signal scintillation spectrum analysis by digital filtering of magnetic tape recording 11 p2012 A70-26718
- Modulation-demodulation system for multiple access tactical satellite communication 12 p2187 A70-27915
- TDMA applicability to military satellites, describing synchronization process 12 p2187 A70-27916
- RF EMI propagation between manned spaceflight network and Apollo 10 launch vehicle in trans lunar mission, considering cochannel interference possibilities 12 p2189 A70-28137
- Atmospheric water effect on satellite communications in UHF region and above, discussing signal attenuation 13 p2364 A70-28782
- Space-surface path loss due to atmospheric gases, rain and clouds, considering military ground site location for space communication 14 p2608 A70-30596
- Satellite laser communication system using dual scan acquisition technique 14 p2552 A70-31197
- S band telemetric signals reception transmitted by Apollo 12 during occultation behind lunar disk, discussing lunar surface reflectivity 15 p2699 A70-32290
- Radio wave refraction and field strength in model Venus atmosphere for various spacecraft trajectories 15 p2705 A70-32737
- Optical spacecraft communication system, discussing size, weight, power, etc 16 p2864 A70-33484
- Range and velocity components for ray paths between tracking and data relay satellite and user communication satellite 16 p2866 A70-34073
- High power TWT for satellite communications ground stations, including Intelsat experience 17 p3054 A70-35282
- Space vehicle and mission control center telecommunications networks for Apollo lunar landing program, considering NASCOM relay system 17 p3047 A70-35585
- Legal problems in satellite communications, emphasizing copyright, satellite television legality and protection of transmission and broadcasts 17 p3203 A70-35800
- Apollo digital Range Safety Command System for signal-crowded communications channels 20 p3605 A70-39497
- Transmission power formula for satellite to ground station and slant ranges calculations 21 p3785 A70-40755
- Satellite communications performance improvement by use of multipath signal for channel models including noncoherent FSK 21 p3787 A70-41329
- Wideband millimeter wave communications experiments for satellite applications, considering ATS-5, radiometry and future lunar base 21 p3787 A70-41337
- Fences and pits effectiveness for shielding satellite earth stations from local terrestrial facilities interference 21 p3789 A70-41342
- Transportable earth station for satellite communications system, describing antenna design and transportation modes 21 p3798 A70-41344
- Ground station requirements for transition to multitransponder INTELSAT 4 satellite, discussing interference filtering, group delay distortion, etc 21 p3789 A70-41346
- Multiple beam earth station torus microwave antenna for satellite communication with nonplanar field of view over geostationary arc 21 p3798 A70-41357
- Synchronous satellites VHF signal fading attributed to high latitude scintillations, noting intensity at night and during magnetic storms 21 p3790 A70-41362
- ATS-5 spacecraft L band propagation performance, describing up and downlink test methods 21 p3790 A70-41363
- Spacecraft data transmission efficiency improvement by budgeting onboard electric energy consumption among data types 21 p3790 A70-41364
- Single channel per carrier PCM FDMA demand assignment satellite communication system, discussing digital encoding, quadrature PSK modulation, etc 21 p3791 A70-41367
- RF requirements of deep space-outer planet spacecraft communications for Jupiter, Saturn, Uranus and Neptune flyby missions 21 p3791 A70-41369
- Mariner 1969 communication system modified for thermoelectric outer planet spacecraft /TOPS/, noting X band addition to S band and associated problems 21 p3791 A70-41797
- Interference coupling between satellite ground station and radio relay station due to rain scattering at SHF 22 p3990 A70-43201
- Satellite technology application to aeronautics, predicting synchronous satellites communication for transoceanic and overland ATC 22 p4111 A70-43512
- Rescue waiting time relation to number of communication and return sites for emergency astronaut return, considering day vs day/night recovery 23 p4245 A70-44639
- ### SPACECRAFT COMPONENTS
- #### NT LANDING MODULES
- #### NT LUNAR LANDING MODULES
- #### NT LUNAR MODULE
- #### NT MARS EXCURSION MODULE
- #### NT SPACECRAFT CABINS
- #### NT SPACECRAFT MODULES
- Machined surface evaluation of fabricated components by electron microscopy to identify defects 01 p0097 A70-10012
- Cost-effective look at vacuum testing of spacecraft components, noting sensitivity prediction and thermal cycle test 01 p0055 A70-10113
- Magnetic components design, manufacturing and handling for use in space communication satellites, noting design group role in parts construction and quality control 02 p0267 A70-12057
- Explorer 38 critical component equilibrium temperature tests in thermal vacuum chamber using modified solar simulator, noting agreement with model [AIAA PAPER 69-999] 02 p0275 A70-12527
- Logic methods of efficient organization of satellite integration, considering project, physical components and program elements 03 p0609 A70-13842
- Spacecraft components temperature response predicted in nonstandard solar orientation 04 p0786 A70-15432
- Simulation equipment for extraterrestrial solar radiation for spacecraft components evaluation tests, describing spectral characteristics 04 p0665 A70-15663
- Soviet unmanned spacecraft and components displayed at Le Bourget show, including Molniya 1, Proton 4 satellites, Venus 4 station, vertical cosmic probe, etc 05 p0921 A70-15814
- Spacecraft contamination control teamwork operation, examining procedures and processes to ensure components cleanliness 05 p0809 A70-16713
- Laboratory simulation of interactions between ionospheric plasma and diverse spacecraft systems 06 p1029 A70-18067
- Space engineering, flight instrumentation features and spacecraft subsystems integration problems 10 p1950 A70-24610
- Biosatellite Primate Mission Program for component qualification levels validated by flight tests data, performing vibration tests on prime structure spacecraft [AIAA PAPER 70-403] 10 p1951 A70-24902
- Microwave tubes for high power transmission from space to ground and in deep space communications, discussing klystrons, TWT and crossed field amplifiers [AIAA PAPER 70-435] 11 p2016 A70-25456
- Syncom and Early Bird systems development, launch procedure and operation, discussing common components 14 p2654 A70-31144
- Redundancy for spacecraft elements, describing various factors for priority establishment 15 p2712 A70-32643
- Reliability life tests preventing sliding electrical contacts failure in space vehicles, discussing data dissemination 16 p2920 A70-33806
- Literature review of sliding electrical contacts in space vehicles, covering heavy aromatic hydrocarbons, molybdenum disulfide and other lubrication materials 16 p2920 A70-33811
- Explosively actuated /pyromechanical/, devices for spacecraft, discussing guidelines for design, testing, application and cost efficiency 16 p2963 A70-34125
- Flow control valve without moving parts used in ATS A and D, describing design, operation and theoretical performance 16 p2846 A70-34132

Space molecular sink simulator facility /Molsink/ for extreme high vacuum outer space environment simulation, discussing Mariner Mars 1969 spacecraft components tests 16 p2889 A70-34167

Torsion, filar, flexure and coil type mechanical suspensions for space applications, considering instability due to temperature changes and magnetic, electric and force fields 16 p2924 A70-34169

Spacecraft waste management system zero-gravity flight tests, describing components and functions 17 p3036 A70-34751

Apollo spacecraft parts environmental simulation and testing, using real time computer generated graphic display 19 p3532 A70-37918

Electrical tests on satellites and space probes applied to spaceborne subassemblies, subsystems and electronic systems EM compatibility 19 p3532 A70-38287

Laboratory simulation of interactions between ionospheric plasma and diverse spacecraft systems [AIAA PAPER 70-169] 20 p3606 A70-39695

SPACECRAFT CONFIGURATIONS

NT APOLLO TELESCOPE MOUNT

NT SATELLITE CONFIGURATIONS

Air force booster growth inventory, noting combination with space-configured upper stages and strap-on solid motors [SAE PAPER 690713] 05 p0922 A70-15831

Dosimetry data and personal radiation sensors from Apollo and Gemini flights, noting spacecraft geometry shielding effects 06 p1134 A70-17268

Reusable space shuttle employing two stages resembling subsonic aircraft for carrying passengers and cargo between earth surface and orbit 07 p1392 A70-18873

Space transportation system booster and orbiter development ground and flight tests, considering vehicle size and reusability requirements [AIAA PAPER 70-276] 07 p1397 A70-20385

Modular earth orbiting space station design, configuration and operation 08 p1568 A70-20688

Space shuttle program, considering vehicle configurations mission capabilities and cost estimates with emphasis on ground and flight tests [AIAA PAPER 70-739] 10 p1953 A70-25074

Low cost orbital space transportation system with shuttle service, discussing booster and configuration selections, weight, costs, etc [AIAA PAPER 70-256] 13 p2506 A70-29615

Aerodynamic and structural configuration effects on spacecraft inflight wind load calculations, showing Apollo interface lateral bending 14 p2653 A70-30585

Europa 3 configurations for launching payloads into geostationary orbit using various rocket stage combinations 15 p2789 A70-32254

Nuclear orbital launch stages for interplanetary departure, comparing parallel and tandem spacecraft configurations [AIAA PAPER 70-680] 16 p2950 A70-33580

Configurational and operational characteristics for space shuttle design, considering economic tradeoffs between expendable and reusable systems [AIAA PAPER 70-045] 17 p3175 A70-34783

Spacecraft shape and thermal coating pattern optimization by computer program 17 p3178 A70-35251

Structurally similar models, investigating space vehicles dynamic characteristics 18 p3332 A70-36161

Space vehicles dimensions effects on working fluid mass and power required for orientation 21 p3927 A70-40826

Thin walled spherical shell spacecraft solar heating in planetary surface proximity, considering skin temperature distribution 21 p3944 A70-41019

Structural configurations effect on momentum imparted to spacecraft by hypervelocity meteoroid impact 21 p3938 A70-41879

Space station mission and configuration concepts, discussing experimental/operational capability, crew assignments, accommodation and module sizing 22 p4111 A70-43517

Space shuttle configurations, discussing launch, entry and landing characteristics 22 p4111 A70-43629

Pressure distribution, force and heat transfer measurements on varied-configurations of lifting reentry vehicles in hypersonic flow [ICAS PAPER 70-03] 23 p4132 A70-44117

Venus atmosphere flight vehicle configuration, discussing payload capacity, range, velocity, flight altitude and aerostatic aerodynamic, ground effect and underwater capabilities 23 p4260 A70-44627

Skylab mission in 1972, describing orbital workshop configuration and three man crew integration for operational experiments [AIAA PAPER 70-1328] 24 p4417 A70-45939

Space transportation system concept and operational objectives, discussing configurational aspects, aerodynamic complexity, propulsion systems, payloads, performance and aerothermodynamic constraints, etc [AIAA PAPER 70-1249] 24 p4418 A70-45965

SPACECRAFT CONSTRUCTION MATERIALS

Volatile contaminants emitted from space cabin construction materials tested under simulated space conditions 01 p0031 A70-10237

Optical and mechanical techniques for space experiment structures and metals satisfying space requirements 03 p0492 A70-13848

Nonflammable material development program for Apollo spacecraft, noting requirements imposed by high oxygen environments, toxic offgassing and temperature range 03 p0436 A70-14055

Materials selection and Apollo command module atmosphere design considerations, discussing fire extinguisher system, equipment design changes, etc 03 p0437 A70-14058

Apparatus and techniques for investigating spacecraft materials mechanical and thermal properties, using vacuum effect to simulate space environment [ASME PAPER 69-WA/PID-22] 04 p0663 A70-14752

Ti alloys, high strength steels and plastics for aircraft and spacecraft constructions, including aging behavior of lap joints and prepreg laminates in vacuum [DGLR-69-58] 04 p0699 A70-15162

Micro and macromechanics for design and mechanical properties prediction of laminated fibrous composites for airframes and space structures 05 p0941 A70-16619

Structural material selection for thermal shock conditions, deriving index from parameters governing solutions in thermoelasticity 07 p1413 A70-20002

Reusable metallic and nonmetallic thermal protection materials for space shuttle applications [AIAA PAPER 70-273] 07 p1397 A70-20383

Boride composites with high strength and thermal resistance suitable as nose cap and leading edge materials for reusable lifting reentry systems [AIAA PAPER 70-278] 07 p1315 A70-20387

Apollo command and service modules from metallurgical viewpoint 09 p1766 A70-22792

Silicone products with low outgassing characteristics for spacecraft applications, discussing fluids, compounds and elastomers 10 p1906 A70-23914

Hemispherical emissivity measurement in vacuum chamber for thermal testing of space satellite structural materials 12 p2332 A70-27984

Sliding electrical contacts for unmanned scientific satellites, discussing Nimbus AVCS camera iris motors 16 p2920 A70-33809

Thermal and mechanical properties of materials for spacecraft booms design 16 p2986 A70-34138

Space vehicle optimal design based on reliability analysis, taking into account cost of materials strength tests [JPL-TR-32-1496] 17 p3188 A70-35224

Cs and Hg electrostatic thruster effluents effects on spacecraft materials, describing chemical, metallurgical and thermophysical experiments [AIAA PAPER 70-1144] 20 p3652 A70-40519

Materials problems in space and spacecraft environments, discussing particle density, composition and UV radiation, spacecraft structure, payloads, vibration, etc 23 p4209 A70-44328

Fibrous, cellulosic, elastomeric and plastic materials with improved flame resistant properties for space applications 23 p4152 A70-44461

Manned spacecraft nonmetallic construction materials selection criteria, testing and configuration control, considering flammability hazard 23 p4152 A70-44462

Fireproof nonmetallic materials for spacecraft and aircraft, discussing functional utility, durability and aesthetic requirements relative to environmental conditions 23 p4210 A70-44610

Space shuttle structural design concepts and fabrication, tabulating structural and heat shield materials [SAE PAPER 700768] 24 p4415 A70-45867

SPACECRAFT CONTAMINATION

Apollo spacecraft contamination control program, considering NASA role in management, contractor controls, criteria establishment and enforcement, etc 01 p0220 A70-11076

Apollo spacecraft contamination control, discussing Boeing responsibility for engineering, facilities, materials, etc, for Saturn rocket 01 p0058 A70-11077

Apollo spacecraft contamination control, describing Rocketdyne programs for rocket engines 01 p0059 A70-11078

Apollo spacecraft contamination control, describing McDonnell Douglas role in S-4B stage production 01 p0059 A70-11079

Apollo spacecraft contamination control, describing organization and operation of Grumman Contamination Control Committee 01 p0059 A70-11080

Contamination control of spacecraft for planetary exploration missions emphasizing monitoring equipment and cleaning procedures 05 p0808 A70-16702

Microbial contamination levels and types detected on Apollo 9 spacecraft and related effects of various test and assembly environments 05 p0809 A70-16711

Spacecraft contamination control teamwork operation, examining procedures and processes to ensure components cleanliness 05 p0809 A70-16713

Spacecraft window cleaning with methyl alcohol and low pressure nitrogen providing filming control for Apollo optical experiments 11 p2051 A70-26143

Infectious disease hazards on space flight, discussing internal environmental factors including resistance and etiologic agents transmission 14 p2537 A70-30366

Microbial release from solid spacecraft materials after hard landings, testing survival during decontamination or terminal sterilization 15 p2688 A70-31664

Microbial contamination levels on Apollo 6 spacecraft, discussing intramural environments for assembly and testing 16 p2849 A70-33995

Thruster exhaust effluent characteristics relating to spacecraft contamination [AIAA PAPER 70-1143] 20 p3690 A70-40208

SERT 2 spacecraft surface contamination by Hg ion thruster effluents, using solar cell sensors [AIAA PAPER 70-1128] 20 p3690 A70-40217

Scientific payloads integration with multimission electric propulsion interplanetary spacecraft, discussing possible contamination effects due to solar electric propulsion system [AIAA PAPER 70-1141] 21 p3930 A70-41781

SPACECRAFT CONTROL

NT SATELLITE ATTITUDE CONTROL

NT SATELLITE CONTROL

Manned space station system analysis for identifying control subsystem functions /weight penalties/ and system characteristics to minimize penalties [AIAA PAPER 69-1078] 01 p0194 A70-10628

Roll control method using recirculating base flow reaction against oriented blades or fins attached to reentry vehicle base to produce rolling moments 01 p0003 A70-10847

Crew locomotion effect on spacecraft attitude control using space cabin simulator tests 01 p0036 A70-10853

Rotational motion of self excited symmetric gyroscopes applied to attitude control and nutation damping of space vehicles 01 p0143 A70-10929

Spacecraft longitudinal control during reentry of Lunar Orbiter into atmosphere, analyzing final range prediction, trajectory tracking and accelerometers performance 01 p0197 A70-11497

Spacecraft range control algorithm during reentry at parabolic velocity into atmosphere with varying parameter distributions 01 p0197 A70-11498

Optimal control algorithm for spacecraft descent in atmosphere based on nominal trajectory and acceleration measurements 01 p0197 A70-11499

Optimal motion control of spacecraft refueling during flight by liquefying atmospheric gas along prescribed trajectory under constant thrust 01 p0197 A70-11502

Man machine system consisting of manned station controlling distant spacecraft via wideband radio link 02 p0229 A70-12145

Optimum angle of attack control for multistage rocket as function of phase coordinates and time by solving functional equation with finite difference method 02 p0381 A70-12407

Optimum power and operation mode of space vehicle engine with control error allowance as function of mass and velocity 04 p0760 A70-14433

Fluidic sun sensor design and breadboard test for spacecraft and missile attitude control systems 04 p0716 A70-15415

Free gas formation in propellant systems and effects on attitude control systems [AIAA PAPER 69-434] 04 p0763 A70-15418

Mariner 4 guidance and control system performance from mission nominal end to final termination time
04 p0765 A70-15664

Display/control system and key technical decisions at Manned Space Mission Control Center, discussing command consoles
05 p0829 A70-16194

Biological model describing spacecraft operator sensorimotor activity in response to various spacecraft control stimuli, outlining computer algorithm
05 p0810 A70-17118

Launch vehicle control system synthesis based on mode control theory state variable formulations
06 p1156 A70-17958

Thermal control of spacecraft via solid-liquid phase change materials
[AIAA PAPER 70-12]
06 p1092 A70-18137

Screening devices to control heat supplied to spacecraft, discussing mathematical model to determine effective emission
[DGLR-69-060]
07 p1392 A70-18816

Space vehicle digital control system attitude computations using quaternion matrix algebra to simplify control equations
[AIAA PAPER 68-825]
07 p1393 A70-19302

Range safety philosophy and practice concerning malfunctioning missile and space vehicle launch and flight
[AIAA PAPER 70-249]
07 p1250 A70-20369

Deep space network /DSN/ functions and characteristics, discussing spacecraft control, data acquisition, orbit determination, data processing, etc
08 p1481 A70-20614

Queue control techniques in generating predicted trajectory, discussing queue control logic requiring minimum storage
08 p1467 A70-21049

Control display requirements for manned spacecraft, integrating human operator with vehicle control system and determining man machine relations in stabilization, control and guidance
08 p1498 A70-21678

Active and passive geomagnetic rate dampers for attitude control systems of geomagnetically, gravitationally or spin stabilized spacecraft
09 p1766 A70-22936

Space vehicle attitude stabilization by passive control moment gyros, discussing viscous and Coulomb friction effects
10 p1950 A70-24054

Coupled control of space vehicle orientation with reference to three celestial bodies, reducing plane vibrations to dynamic third order system
10 p1914 A70-24307

Soviet book on rendezvous in orbit, flight dynamics and control of spacecraft covering trajectory synthesis, optimization and control for approach stage
10 p1950 A70-24656

Large angle suboptimal attitude control of rigid spinning spacecraft
10 p1856 A70-25236

Fuel suboptimal attitude control of spin stabilized axisymmetric spacecraft
10 p1953 A70-25237

ATS-3 hydrazine orbit control system efficiency evaluation statistical method, considering stationkeeping maneuvers
[AIAA PAPER 70-460]
11 p2121 A70-25464

Control theory, Volume 2, Analysis and design of space vehicle flight control systems
11 p2122 A70-25772

Three axis motion simulator for in-orbit spacecraft attitude control evaluation using earth, sun and star sensor references
[AIAA PAPER 69-1029]
11 p2031 A70-26147

Initial parameter conditions influence on sustained unstable oscillations of attitude control system for large space vehicle, calculating stable region by nonlinear method
11 p2124 A70-26149

Radar signal quick indication and extrapolation for terminal guidance control of Mars soft lander, reducing radar lock on loss sensitivity and engine spurious noise throttling
11 p2080 A70-26210

Space vehicle velocity-attitude optimal control for on-line trajectory control schemes
11 p2025 A70-26216

Spacecraft stochastic optimal control, discussing design of least upper bound fuel optimal system with measurement uncertainty
11 p2025 A70-26222

Digital guidance computer compatibility with analog attitude control loop in Digital Inertial Guidance System used in ELDO launch vehicle
11 p2080 A70-26280

Mercury bombardment ion thruster life test in space environment onboard space electric rocket test /SERT/ satellite, describing passive satellite thermal control system design
11 p2127 A70-26606

Apollo Command Module inverter experience for post-Apollo spacecraft applications, discussing phase loads and control logic circuits
12 p2165 A70-27693

Spacecraft autonomous control algorithm to ensure geographically specified landing accuracy without considering atmospheric density distribution
12 p2270 A70-28251

Reentry control algorithm for prescribed landing point of space vehicle entering earth atmosphere at parabolic velocity, discussing double-dip reentry and digital simulation
13 p2499 A70-28376

Apollo man-machine control design, discussing communication, integration, lunar landing, attitude control, CMC and LGC programs
13 p2357 A70-28379

Man machine function distribution optimization in spacecraft closed-loop automatic control system
13 p2380 A70-28381

Manual spacecraft rendezvous system based on handheld instruments and manual computations, considering error analysis and simulation
13 p2357 A70-28392

Mariner Mars 1969 navigation, guidance and control systems design, mechanization and flight testing
13 p2446 A70-28393

Spacecraft rendezvous control at minimal propellant consumption, deriving algorithm
13 p2499 A70-28400

Self contained optimal control synthesis for spacecraft entering atmosphere at first cosmic speed, considering landing spots dispersion component decrease
13 p2500 A70-28407

Booster control system reducing maximal wind-induced bending torques, examining booster response to aerodynamic forces
13 p2500 A70-28413

Spacecraft orientation control system optimization by plotting controlled motion kinematic models
13 p2501 A70-28417

Prelaunch dynamic response test parameter selection for control systems for space complexes with form of Nyquist locus
13 p2381 A70-28423

Optimum power and operation mode of space vehicle engine with control error allowance as function of mass and velocity
13 p2503 A70-28458

Wind effects on rigid launch vehicle guidance and control system design, using model incorporating structural bending and fuel sloshing
[AGARDGRAPH-115]
13 p2448 A70-28755

Shutter thermal control for Helios solar observation satellite, considering closed and open conditions
13 p2505 A70-28769

Nonlinear control systems optimization applied to asymmetrical spacecraft
13 p2382 A70-29071

Performance cost functions for reaction-jet controlled spacecraft during on-off-on limit cycle
13 p2382 A70-29072

Ground support real time operating system 360 for manned spaceflight, discussing system features and performance
13 p2375 A70-29937

Lunar Orbiter Spacecraft Guidance and Control, discussing design and flight results
14 p2613 A70-30455

First pulse vacuum startup measurements of monopropellant hydrazine thrust reactors with spontaneous catalyst, simulating spacecraft control dynamics
14 p2628 A70-30753

Digital guidance and control system, discussing communication device providing data transfer between airborne digital computer and control device
[AIAA PAPER 69-988]
14 p2615 A70-30771

Parameter plane method of stability analysis applied to spacecraft attitude control system with two nonlinearities related by nonlinear differential equation
16 p2881 A70-33032

Digital computer generation of system stability Liapunov functions for ninth order spacecraft attitude control
16 p2867 A70-33043

Optimal desaturation of angular momentum exchange controllers in spacecraft attitude control systems, using natural environmental torques
16 p2947 A70-33345

Speed convergence of hybrid vs digital computer synthesis of optimal boost vehicle controller, considering fuel consumption and pitch dynamics
16 p2981 A70-33442

Waste hydrogen utilization in microthrusters for spacecraft attitude control involving mass expulsion of cold gas
[AIAA PAPER 70-613]
16 p2969 A70-33609

Spacecraft attitude control microthrusters utilizing catalytically reactive gas mixtures during pulse mode and steady state operation
[AIAA PAPER 70-614]
16 p2969 A70-33611

Optimum guidance and control law for lifting reentry bodies, investigating plane descent trajectories for minimum structural heating
16 p2982 A70-33774

Lightweight spiral wound bimetallic actuators for active spacecraft thermal control systems
17 p3022 A70-34755

Mariner Mars 1971 gimbal actuator design and life test for autopilot system using hypergolic bipropellant rocket engine
17 p3022 A70-34758

Flexible space vehicles dynamics and control covering free vibration analysis, thermal flutter and structural deflection effect on attitude control
17 p3177 A70-35233

R-4D multiapplication rocket engine for Apollo spacecraft reaction control, discussing design, performance, quality assurance and tests
17 p3178 A70-35259

Apollo lunar landing guidance, navigation and control, discussing inertial and optical measurements, computer, digital autopilots, rendezvous and mid-course navigation
17 p3134 A70-35288

Continuous time nonlinear filter for space vehicle attitude determination, using estimation theory
17 p3130 A70-35291

Multistage rockets terminal control synthesis based on linear functionals
18 p3333 A70-36163

Optimization model for evaluating information management systems for handling control functions of long duration space station missions
19 p3532 A70-37851

Computerized automatic ground equipment /CAGE/ as intelligence system for checkout and control of launch vehicles and spacecraft
19 p3397 A70-37915

Control moment gyro /CMG/ for spacecraft attitude control, determining optimal gimbal angle rate for desired torque
[AIAA PAPER 70-1042]
19 p3433 A70-38857

Spacecraft fuel optimal controls for out-of-plane motion about translunar libration point based on phase plane methods
[AIAA PAPER 70-1079]
19 p3530 A70-38890

Lunar module digital autopilot design, considering attitude state estimator, reaction control system and thrust vector control
[AIAA PAPER 70-991]
20 p3668 A70-39539

Spacecraft pulse width modulated attitude control system stability, using state space method
[AIAA PAPER 70-984]
20 p3714 A70-39545

Control moment gyro /CMG/ spacecraft attitude control systems, discussing selection and design criteria
[AIAA PAPER 70-976]
20 p3668 A70-39553

Magnetic three degree of freedom attitude control system for axisymmetric spinning spacecraft, using Kalman filter
[AIAA PAPER 70-974]
20 p3668 A70-39555

Direction cosine attitude control logic for spin stabilized axisymmetric spacecraft, using control torques generated by reaction jet system
20 p3669 A70-39679

Nonlinear adaptive reaction jet attitude control for long life space vehicles, providing optimal performance over bias acceleration disturbances
[AIAA PAPER 69-945]
20 p3716 A70-39680

Trajectory correction propulsion subsystem /TCPS/, attitude propulsion subsystem /APS/ and pyrotechnic subsystem of thermoelectric outer planet spacecraft /TOPS/
21 p3868 A70-41800

Thermoelectric outer planets spacecraft /TOPS/ attitude control subsystem providing accurate antenna pointing and trajectory correction engine thrust vector orientation
21 p3930 A70-41801

Flexible antennas and solar panels effect on dynamic behavior and control system response of dual spin spacecraft
21 p3931 A70-41855

Algorithm for spacecraft rotational maneuver control based on single turn around specific axis, using onboard computer
21 p3849 A70-42236

Space vehicle self oscillatory pulsed relay attitude control system with jet nozzles, determining angular motion
22 p4001 A70-42838

Lunik 16 lunar soft landing technique, discussing automatic and ground controlled mission phases
22 p4110 A70-43210

Space vehicle attitude control by cold gas jets, examining principles of operation, optimal conditions for gas consumption and gravitational and gyroscopic effects
[MBB-UR-37-70-0]
23 p4261 A70-44662

Spacecraft trajectory control rockets design and operational characteristics, discussing various propellant types, control valve designs, etc
24 p4393 A70-45640

Manned spacecraft abort guidance and control problems, discussing various modes and emergency conditions
24 p4374 A70-46210

SPACECRAFT DESIGN

NT SATELLITE DESIGN

Systems design experience derived from Mercury, Gemini and Apollo projects, discussing thermal protection, launch propulsion, life support, etc
[AIAA PAPER 69-1077]
01 p0193 A70-10604

Saturn 5 launch vehicle design, role in exploration and anomalous structural vibration and oscillation [AIAA PAPER 69-1094] 01 p0194 A70-10620

Space station flexibility design based on INT-21 payload capability emphasizing volume and weight factors [AIAA PAPER 69-1064] 01 p0195 A70-10635

Orbital space station operations requirements and interactions, considering experimentation, support vehicles, ground support and follow-on growth [AIAA PAPER 69-1062] 01 p0195 A70-10636

Earth and planetary entry vehicle designs for manned and unmanned space missions, noting thermal protection, environmental control requirements and communication systems 01 p0195 A70-10826 [AIAA PAPER 68-1080]

Propellant condensation on surfaces near electric rocket exhaust, calculating particle arrival rates, backflow and desorption energies 01 p0166 A70-10836 [AIAA PAPER 69-270]

Mercury atmospheric models for preliminary environmental criteria to be used in spacecraft design and engineering tradeoff studies 01 p0183 A70-10838 [AIAA PAPER 69-54]

Minimum fuel consumption criteria applied to design of manned spacecraft attitude control system, using reaction jets for lateral and directional controls 01 p0196 A70-10950

HEOS 1 satellite for interplanetary space exploration, describing eccentric orbit, structure, power supply, attitude measurement and control, spin rate control, telemetry and telecommand systems 01 p0196 A70-11114

Soviet book on physicochemical basis of space research covering near earth and interplanetary environmental factors and effects on spacecraft designs and materials 02 p0360 A70-11693

Thermal protection systems (TPS) design criteria for maneuverable reentry spacecraft, comparing weight and cost for various alloy systems 02 p0392 A70-11940

Solar photoelectric power ion propelled probe of asteroid region, describing design and mission planning [AIAA PAPER 69-1105] 02 p0382 A70-12529

Intelsat 4 communications satellite design and manufacture, discussing European participation with emphasis on British involvement 02 p0383 A70-12649

Mission design, spacecraft characteristics, communications and experimental approaches for Viking 1973 Mars Project 03 p0576 A70-14020

Reentry body aerodynamic heating and thermal insulation system design, discussing analytical procedure taking into account complex geometrical configurations 04 p0616 A70-15186

Development models for post-Apollo lunar cargo delivery system utilizing Saturn 1B and Centaur stages [DGLR 69-9] 04 p0763 A70-15187

Spacecraft design, trajectory and mission analyses for multipurpose solar electric propulsion missions, emphasizing modular ion engine and fixed attitude spacecraft designs [AIAA PAPER 69-252] 04 p0763 A70-15412

Parametric performance and cost comparison of separate and integral vehicle concepts for manned space activity using payload criterion 04 p0763 A70-15420

Saturn launch vehicle systems in terms of design, operating characteristics and potential applications, showing need for reusable space shuttle systems [SAE PAPER 690703] 05 p0922 A70-15830

Manned space stations development, objectives, supply, storage and waste disposal, launching and artificial gravity 05 p0923 A70-16042

Launch vehicles design, propulsion, maneuverability and navigation 05 p0923 A70-16565

Optimum second stage sizes for Blue Streak first stage for maximum payload injection into various orbits, tabulating sizes and payloads 05 p0924 A70-16589

Spacecraft design for manned interplanetary missions, considering structural materials and weights, cryogenic insulation, meteoroid protection, landing gear, etc 05 p0924 A70-16720

Radio astronomy spacecraft (RAS) engineering design, technology and flight results 06 p1153 A70-17151

Attitude performance of GEOS 2 gravity gradient spacecraft, discussing prelaunch design and post-launch analyses 06 p1154 A70-17162

Systems engineering aspects of Apollo Telescope Mount spacecraft, considering design and manned space flight role 06 p1061 A70-17312

Multilayer insulation blankets with slits normal to energy transfer direction for thermal control of spacecraft and cryogenic tankage [AIAA PAPER 70-15] 06 p1156 A70-18076

Trajectory, guidance and environmental parameters and uncertainties effect on design optimization of out-of-orbit Viking soft lander 06 p1157 A70-18134 [AIAA PAPER 70-99]

Hybrid coordinate formulation for flexible space vehicle attitude control system design 06 p1158 A70-18180 [AIAA PAPER 70-20]

Compact reentry flight test body construction featuring extended permissible entry corridor by means of generated lift [DGLR-69-035] 07 p1392 A70-18987

NASA three meter orbital telescope discussing configuration, optical geometry, launching, power supply, etc 07 p1280 A70-19150

Streamlining design for high altitude hypersonic flight vehicles based on drag minimization at flight condition 07 p1189 A70-19717

Low operating cost space shuttle system for cargo and personnel transportation to earth orbiting stations involving reusable winged vehicles [AIAA PAPER 70-242] 07 p1396 A70-20376

Launch vehicle minimum cost design emphasizing flight vehicle evolution stages via effect on costs [AIAA PAPER 70-240] 07 p1396 A70-20378

Reusable space transportation vehicle design evolution, considering staging, aerodynamic shapes, etc [AIAA PAPER 70-265] 07 p1398 A70-20395

Orbit-to-orbit shuttle for launch in earth-to-orbit shuttle vehicle, discussing design requirements [AIAA PAPER 70-268] 07 p1399 A70-20397

Modular earth orbiting space station design, configuration and operation 08 p1568 A70-20688

Mars lander atmospheric entry digital simulation for deceleration system design, discussing ballistic coefficient, aeroshell diameter, parachute size and deployment altitude, etc 08 p1582 A70-20932

Test-aided aerospace design, noting design engineer attitude and software problems 09 p1766 A70-22678

Manned Spacecraft Center spacecraft development, mission design and planning, flight crew operations for Apollo, discussing spacecraft design principles 09 p1767 A70-23703

Apollo project hardware design and evaluation principles coupling simple design practice with stringent technical and administrative discipline 09 p1768 A70-23704

Materials and processing technology roles in NASA programs involving manned space stations, service spacecraft and unmanned space exploration 10 p1902 A70-23855

Spacecraft and boosters for earth resources surveys, discussing design, payloads, orbits, etc 10 p1902 A70-24641

Ground based simulation for hypersonic reusable lifting reentry vehicle design with pilot-in-loop, discussing six degree of freedom simulation [AIAA PAPER 70-385] 10 p1861 A70-24920

Apollo Applications Program command and service module test requirements to achieve reliable hardware for extended missions [AIAA PAPER 70-378] 10 p1952 A70-24925

Electric propulsion system selection for Lockheed Communications Satellite (LCS) based on weight, development status and complexity considerations, discussing optimization procedure [AIAA PAPER 70-478] 11 p2101 A70-25470

Rough-landing space capsule for omnidirectional touchdown in lunar and Martian missions, tabulating design characteristics and functional capabilities 11 p2123 A70-26053

Interstellar transport vehicles design around thermonuclear propulsion plants, discussing weight, mission velocity, acceleration time and fuel costs 11 p2123 A70-26054

Evaluation technique for astronautics subsystems in automated spacecraft designed for interplanetary missions, considering operation times, navigation updating and midcourse correction [AIAA PAPER 69-882] 11 p2079 A70-26118

Martian atmospheric models for lander and simulator design, obtaining effective sky temperatures, surface pressures and temperatures, atmospheric compositions, etc 11 p2112 A70-26141

Subsystem weight trade-offs for design optimization of out-of-orbit Mars soft lander, using atmosphere and surface environmental Monte Carlo model 11 p2124 A70-26215

Computerized tradeoff analysis for planetary landing vehicle entry capsule and lander design optimization, emphasizing weight allocation for Mars 1973 missions 11 p2126 A70-26320

Corrugated skins solar absorbance and IR emittance computed for spacecraft thermal design, analyzing other nondiffusive radiative enclosures 11 p2150 A70-26352

Bidirectional reflectance of three dimensional surfaces described by diffuse triangular subareas network

for spacecraft thermal design, giving numerical technique 11 p2084 A70-26354

Embossed/crinkled aluminized film multilayer insulation blankets with joints performance variation with temperature predicted by radiation heat transfer correlation 11 p2150 A70-26365

Manned space stations size, crew, orbit, lifetime, resupply requirements, etc 12 p2313 A70-27742

Space station design for long duration operation, considering optimum mix of redundancy, maintainability and checkout 12 p2313 A70-27743

Europa 3 satellite carrier system configurations, discussing rocket design, propellant composition, etc 13 p2502 A70-28445

Pioneer 6-9 low magnetism spacecraft for interplanetary magnetic field observation 13 p2507 A70-30046

Space design, considering problems due to weightlessness, vacuum, thermal effects, micrometeorite, cosmic forces, etc 14 p2656 A70-30301

Spacecraft design requirements for scientific zero G cloud physics experiments concerning colloidal modification processes 14 p2584 A70-30552

Aerospace environment models developed by NASA for engineering use in Space Vehicle Design Criteria program 14 p2637 A70-30554

Atmospheric elements and properties pertinent to design and operations of Space Shuttle 14 p2606 A70-30556

Martian atmosphere modeling for obtaining Viking lander spacecraft design margins by Monte Carlo method 14 p2637 A70-30564

Wind gust data analysis for spacecraft design using power spectrum approach 14 p2607 A70-30580

Launch vehicle design, considering tradeoffs between wind effects and analysis time 14 p2653 A70-30589

OSO 1-6 spacecraft design, payloads and performance for continuous solar observation, discussing instrumentation and Delta launch vehicle characteristics 14 p2638 A70-30691

Spacecraft meteoroid protective shield thickness sensitivity relationship to luminous efficiency 15 p2813 A70-32518

Hypervelocity impact damage on complex targets, considering spacecraft and missile design 15 p2824 A70-32791

Lunar surface exploration vehicle (Lunar Rover) design, analyzing stowage aspects in Lunar Module 16 p2888 A70-33680

Space shuttle avionics cost effective design approach, discussing guidance, commonality, reliability, communications and autonomy 16 p2982 A70-33802

Meteorological problems associated with space shuttle design and operations, permitting tradeoff analysis on environment effects 16 p2946 A70-33804

Book on tubular spacecraft booms covering design and flight experiences, system performance, evaluation, etc 16 p2983 A70-33961

Aerospace mechanisms design attitudes effects on cost and success of space mission 16 p2985 A70-34102

Aerospace mechanism design from test laboratory viewpoint, balancing technical, cost and schedule factors with mission objective 16 p2921 A70-34103

Light weight integrated spin-up launch mechanism for rocket propelled payload 16 p2845 A70-34113

Ball-bolt-bolt separation mechanism for spacecraft applications requiring low shock, controlled release, nonfragmenting fastener 16 p2922 A70-34119

Ruggedized spacecraft mechanisms for severe shock environments 16 p2922 A70-34121

Apollo lunar module alightment system, discussing design, performance and reliability 16 p2985 A70-34122

Surveyor spacecraft landing shock absorbers design and performance assessment by digital computer simulation 16 p2922 A70-34123

Explosively actuated (pyromechanical), devices for spacecraft, discussing guidelines for design, testing, application and cost efficiency 16 p2963 A70-34125

Agenda D vehicle self destruct charge ordnance component, discussing design, performance and tests 16 p2963 A70-34126

- Fluid thermal actuator for temperature control of ITOS /Improved Tiros Operational System/ meteorological satellite, discussing design and performance 16 p2846 A70-34129
- Solar power panel orientation servomechanism using passive elements without power consumption 16 p2846 A70-34130
- Aerospace thermophysics considerations in spacecraft and hypervelocity vehicles systems thermal design, discussing thermal control and control coatings optical and radiative properties [AIAA PAPER 70-812] 17 p3194 A70-34509
- Composite materials in aerospace vehicle design, discussing mechanical behavior, applications and characteristics 17 p3127 A70-34674
- Spacecraft separation mechanisms selection, design and use, discussing multiple device point and linear systems 17 p3175 A70-34767
- Logistic support reusable earth to orbit space shuttle design, noting weight penalties, payloads and development time [AAS PAPER 70-042] 17 p3175 A70-34782
- Configurational and operational characteristics for space shuttle design, considering economic tradeoffs between expendable and reusable systems [AIAA PAPER 70-045] 17 p3175 A70-34783
- Space shuttle-manned space station integration, discussing design and operation, crew rotation, station resupply, docking, etc [AAS PAPER 70-051] 17 p3176 A70-34789
- Habitability factors in space station crew quarter design, discussing hygiene and dining facilities 17 p3036 A70-34803
- Expandable and modular structures technology for manned and unmanned space missions, discussing expandable air lock experiment 17 p3177 A70-35230
- Black Arrow X3 spacecraft design and experiments, including silicon cells performance electronic assemblies and micrometeoroid fluxes 17 p3178 A70-35256
- Delta launch vehicle design modifications for increased payload and space research programs 17 p3179 A70-35261
- Apollo docking system design considerations and preliminary models evaluation for best choice to meet requirements 17 p3179 A70-35262
- Systems design experience derived from Mercury Gemini and Apollo projects, discussing thermal protection, launch propulsion, life support, etc [AIAA PAPER 69-1077] 17 p3180 A70-35644
- ELDO launch vehicle design, describing high energy upper stages 18 p3333 A70-36300
- Kinetic heating of spacecraft surfaces, emphasizing materials and fluid circulation cooling devices 18 p3333 A70-36654
- Space shuttle development, discussing weight and lateral separation distance 19 p3531 A70-37378
- Manned space station design, discussing durations of scientific experiments and crew operation 19 p3532 A70-37752
- Papers on thermophysics for spacecraft thermal design 19 p3551 A70-37781
- Axisymmetric dual spin spacecraft consisting of nonconcentric frictionlessly mounted cylinders equipped with viscous damping mechanisms, evaluating stability criteria by energy method [AIAA PAPER 70-973] 20 p3715 A70-39556
- Soviet book on flight vehicle optimal design algorithms, covering mathematical theory of variational method, multistage spacecraft, etc 20 p3716 A70-39898
- Optimized trajectories and spacecraft for solar-electric missions to asteroids, using chemical booster for injection [AIAA PAPER 70-1120] 20 p3710 A70-40223
- Lunar module systems design, describing R and D program and landing mission 21 p3928 A70-40977
- Space shuttle vehicle requirements, discussing configurations aerodynamic characteristics, aerothermodynamics, materials technology, etc 21 p3929 A70-40983
- Cost optimal space shuttle systems, discussing booster configurations, weight and performance factors, technology utilization, etc 21 p3929 A70-40984
- Boundary layer transition application to space shuttle design, relating aerodynamic noise to turbulent boundary layers 21 p3744 A70-41015
- Aerodynamic heating constraints on space shuttle design, discussing prediction uncertainties for boundary layer transition, laminar, turbulent heating, etc 21 p3744 A70-41017
- Thermoelectric outer planet spacecraft /TOPS/ flight environment, systems design and Titan 3D/Centaur launch vehicle with Burner II upper stage 21 p3930 A70-41795
- Small scientific satellite design objectives, structural and electrical requirements, components integration, instrumentation, antennas, spin rates, vibrations, sealing, reliability, etc 22 p4110 A70-42497
- European participation in small space shuttle development, discussing design, test vehicle program and European applications 22 p4111 A70-43511
- Space station development and missions, discussing general design philosophy, successive project lineage and applications programs 22 p4108 A70-43653
- Spacecraft design to overcome space and launch environment, including environmental protection 23 p4257 A70-44327
- Reusable earth surface-to-orbit shuttle, discussing cost and performance design considerations 23 p4260 A70-44618
- Solar-electric ion propulsion mission analysis and spacecraft designs, discussing thruster, power conditioning, propellant storage and feed, etc 23 p4234 A70-44631
- Apollo spacecraft program evolution, discussing Apollo 13 accident, command and service module modifications, oxygen tank design, mission objectives, etc 23 p4245 A70-44640
- Industry-university interaction in competitive teaching of spacecraft design 23 p4285 A70-44643
- Space shuttle economic risk analysis, using computer program as design and management tool 23 p4261 A70-44674
- Space shuttle for low cost transportation, discussing reusable vehicles, payload, design, orbital inclination, mission capabilities and international participation 23 p4261 A70-44676
- Helios solar probe for automated spacecraft exploration of interplanetary space near sun, considering design, mission planning and U.S.-German cooperation 23 p4245 A70-44689
- Automated and manned spacecraft design, discussing mission objectives and present and potential applications 23 p4264 A70-45003
- Spacecraft fluid mechanical system design, considering environments, materials, lubrication, zero gravity and inflight maintenance [SAE PAPER 700781] 24 p4295 A70-45862
- Economic and design aspects of universal Orbit-to-Orbit Shuttle component of Space Transportation System [SAE PAPER 700763] 24 p4416 A70-45868
- Space station design, discussing existing technology base for earth orbital operations program implementation [SAE PAPER 700756] 24 p4416 A70-45872
- Biotechnological design of shirt-sleeve side-by-side crew station for shuttle vehicle, including pilot vision and landing experience from X-15 program [AIAA PAPER 70-1327] 24 p4416 A70-45923
- Orbit-to-orbit space shuttle toroidal propellant tank design, construction and testing for outflow and slosh characteristics [AIAA PAPER 70-1325] 24 p4417 A70-45940
- Earth-orbiting manned space station design, describing shuttle support and experimentation in attached and free-flying modules [AIAA PAPER 70-1299] 24 p4417 A70-45951
- Systems and design requirements for NASA Manned Space Station, discussing projected experiment program for applications and science [AIAA PAPER 70-1298] 24 p4417 A70-45952
- Venus atmosphere exploration by multiple entry probe, describing spacecraft system design, launch and earth-Venus transfer trajectory, approach and entry sequence, etc [AIAA PAPER 70-1245] 24 p4417 A70-45963
- Long life spacecraft design and reliability based on marine practices and advanced system technology project, considering grand tour outer planets mission [AIAA PAPER 70-1247] 24 p4412 A70-45964
- SPACECRAFT DOCKING**
- Space station-logistics vehicle docking and men-material transfer problem [AIAA PAPER 69-1118] 01 p0193 A70-10612
- Minimum propellant maneuver during docking of elliptical orbit rendezvous between propelled and passive target vehicles, analyzing as variational problems 02 p0380 A70-12784
- Three dimensional latching dynamics and loads induced during Apollo spacecraft docking, using linear stiffness or flexibility matrices for structural elasticity [AIAA PAPER 70-21] 06 p1158 A70-18181
- Transposition and lunar docking simulation tests for Apollo 9 and subsequent missions using test vehicles equipped with flight type hardware 06 p1030 A70-18209
- Automatically controlled rendezvous and docking for orbital assembly of spacecraft, deriving motion equations for mass centers 07 p1393 A70-19481
- Optimal control frequency signals for automatic spacecraft docking 08 p1582 A70-21180
- Automatic rendezvous and mooring-coupling of spin stabilized satellites, discussing configuration, guidance and dynamics model 13 p2499 A70-28397
- Automatic-manual space rendezvous control system for Cosmos and Soyuz satellites, considering terminal phase control at specific closing range and velocity 13 p2499 A70-28402
- Automatically controlled rendezvous and docking for orbital assembly of spacecraft, deriving motion equations for mass centers 15 p2813 A70-32726
- Gemini/Agna docking mechanism design and function, describing latch and rigidizing devices 16 p2986 A70-34151
- Apollo docking system for CSM-LM connection and disconnection during lunar landing mission, discussing flight hardware 17 p3175 A70-34768
- Apollo docking system design considerations and preliminary models evaluation for best choice to meet requirements 17 p3179 A70-35262
- Transposition and lunar docking simulation tests for Apollo 9 and subsequent missions using test vehicles equipped with flight type hardware 20 p3606 A70-39685
- Translation and docking simulator for Gemini support modified for Apollo LM active lunar orbital docking with CSM 21 p3804 A70-41194
- Solar cell array peak power tracker and battery charger for Airlark Vehicle coupling Apollo spacecraft and Saturn IVB stage to form manned orbiting workshop 21 p3759 A70-41221
- Automatic control of Cosmos spacecraft docking maneuvers in two successive encounter phases 23 p464 A70-45016
- SPACECRAFT ELECTRONIC EQUIPMENT**
- NT AIRBORNE/SPACEBORNE COMPUTERS**
- Cosmos 149 meteorological satellite telephotometer, radiometer and other electronic equipment for measuring atmosphere and underlying surfaces physical parameters 01 p0095 A70-11611
- Electronic integration assembly/EIA/ incorporating modular electronic packaging design techniques to provide reliable mechanical configuration for spacecraft equipment 02 p0268 A70-12579
- Apollo 11 electronics, discussing inertial measurement unit, optical navigation system, command module computer, communication network, TV and experimental packages 02 p0270 A70-12633
- MOSFET uses in spacecraft electronic subsystems, describing digital control unit and typical logic circuitry 03 p0456 A70-13534
- Spacecraft electronics packaging methods, discussing mechanical engineering aspect of high density component packing in single housing 06 p1017 A70-17337
- Avionic and space electronic equipment converging design, considering chip computer 06 p1017 A70-17354
- Ground and onboard electronics systems for space shuttle vehicles, discussing role in equipment reliability and maintainability, life cycle costs, management control, etc [AIAA PAPER 70-261] 07 p1398 A70-20391
- Integrated electronics system for space shuttles including propulsion, electrical power, life support and flight control [AIAA PAPER 70-257] 07 p1398 A70-20392
- Prototype Onboard Processor /OBP/ designed for high reliability, low power dissipation, small size and low weight, discussing attitude control signal processing 08 p1464 A70-20609
- Maintainable electronic equipment requirements for long duration manned space missions 10 p1852 A70-24895
- Spacecraft S band power amplifier TWT electrical, environmental and life tests under saturated conditions [AIAA PAPER 70-506] 11 p2016 A70-25468
- TWT, obtaining life performance data from spacecraft, discussing distortion characteristics [AIAA PAPER 70-505] 11 p2017 A70-25494
- Alouette satellite antennas and receivers for detecting plasma resonances and VLF signals, noting ground station telemetry link 13 p2380 A70-29902
- MOSFET integrated circuits radiation resistance measurements under electron irradiation, determining

changes in threshold voltage, transconductance and on-resistance for applications in spacecraft
14 p2559 A70-31372

Wire wrapped, soldered, welded and crimped joints and plug/socket connections in electronic packaging for spacecraft
16 p2879 A70-33958

Manufacturing and technology of hybrid microelectronics packaging in Black Arrow X-3 satellite equipment
16 p2879 A70-33959

Satellite electronics production, discussing dielectric film capacitor, solar probe magnetic oxide memory core and thin film assemblies
17 p3053 A70-35268

LSI circuits in space electronics, discussing packaging, reliability, applications, etc
17 p3053 A70-35274

Wideband microwave IC tunnel diode amplifier /TDA/ for artificial satellites, discussing noise, size and weight reduction
17 p3053 A70-35277

LM-Apollo rendezvous radar and transponder electronic assemblies packaging and mechanical design
18 p3332 A70-36762

Soviet book on space electronics fundamentals covering equipment problems, energy requirements, communication, features, radio remote control and correction, radio astronomy, etc
19 p3375 A70-37400

Aerospace electronics covering fly-by-wire aircraft flight control, ATC, star trackers for spacecraft attitude control, etc
20 p3669 A70-39668

Pin fin coldplate heat exchanger for cooling Apollo spacecraft electronic equipment, calculating forced convection heat transfer and fluid pressure drop
21 p3797 A70-41025

Electronic parts testing for long duration Mariner spacecraft missions
21 p3799 A70-41798

Thermoelectric outer planet spacecraft /TOPS/ structural problems associated with high gain antenna and electronic equipment
21 p3930 A70-41803

Space shuttle electronics requirements, considering systems in Mercury and Gemini spacecraft and Apollo lunar and command service modules
23 p4259 A70-44612

Helios solar observation satellite equipment design study for solar plasma low energy particles onboard measurements
23 p4262 A70-44844

Integrated electronics for NASA space shuttle program, discussing costs, configurations and technology application
24 p4418 A70-45966

Miniwire method of packaging high density electronic equipment shown in photographs, including OAO applications
24 p4320 A70-46247

SPACECRAFT ENVIRONMENTS

Simulated zero gravity tests of force application by subjects in Apollo suits, varying worksite geometry, personnel restraints and force type and direction
01 p0038 A70-10964

Plume-induced flow separation effect on thermal environment using Saturn 5 film and instrument data, attributing heating rate increase to recirculated exhaust gases
04 p0761 A70-14815

Mathematical model for investigating satellite thermal behavior in space based on space simulation in vacuum chamber with walls maintained at liquid nitrogen temperature
05 p0924 A70-17022

Space radiation environment, discussing characteristics and measurement techniques of various radiation types and sources
06 p1134 A70-17260

Dose calculation by space radiation dose evaluation codes /SPARDEC/ for various space radiation environments
06 p0990 A70-17261

Space environment radiation dose monitoring systems requirements and implementation, discussing material distribution, dose equivalence, parameters accuracy, etc
06 p0990 A70-17262

Spacecraft radiation environment, dosage and shielding problems, discussing high energy protons and electrons exposure hazards for astronauts and mission planning computer codes
06 p0991 A70-17273

Space environment simulation chamber free from oil molecules contamination
09 p1655 A70-22830

Spacecraft conditions influencing remote imaging sensor performance, discussing altitude, temperature and moisture at sensor, air turbulence, vehicle motion, etc
09 p1677 A70-22853

Solar simulation laboratory test facility for extraterrestrial solar radiation effects on vehicles beyond earth atmosphere, emphasizing spectral filters
11 p2030 A70-25353

Thermal control pressure sensitive adhesive tapes for spacecraft applications, discussing properties degradation due to simulated terrestrial and space environments
11 p2067 A70-26366

Apollo command and service modules environmental control system, discussing redesign of faulty hardware
12 p2167 A70-27948

Computerized thermal modeling of spacecraft environmental control systems /ECS/
15 p2705 A70-32523

Hydrogenomonas vs Chlorella spacecraft life support systems, discussing human requirements and equipment for balanced food supply on long duration space missions
16 p2855 A70-34315

Bioastronautics and earth ecology, discussing environmental pollution, nutritional, microbiological and psychological problems
18 p3350 A70-36757

Thermal error in temperature differences between actual and simulated space environment
19 p3401 A70-38301

Space environment simulator for thermal vacuum performance of artificial satellites and components
19 p3401 A70-38308

Satellite radiation dosage in space proton and electron environment
19 p3511 A70-38490

Soviet monograph on automated physiological measurements with onboard computers, covering EKG, EEG, electromyogram, respiration, muscular activity, etc
19 p3372 A70-38797

Artificial rain erosion effects on missile and spacecraft recorded via high speed photography
20 p3635 A70-40531

Steady one dimensional temperature field of cylindrical shell spacecraft, allowing for heat conduction and convective and radiative heat transfer within shell
21 p3942 A70-40841

Chicken lymphopenia and body mass loss resulting in death from chronic restraint, developing physiologically unstressful restraint for space environmental testing
21 p3765 A70-41488

Mass spectrometer and high voltage converter powering electrostatic plasma and solar wind analyzer for cosmic space studies on Sputnik 3 and Heos A satellites
22 p4025 A70-42312

Stepwise linear regressions method for estimating black body surface radiances from model atmospheres and corresponding simulated Nimbus 2 window-channel radiances
22 p4013 A70-42617

Electrofluid dynamic cooling system for spacecraft environmental control, describing design and operating principles
22 p3965 A70-43142

High voltage solar array operational problems in earth orbit environment, discussing conducting surfaces, power loss, plasma effects, leakage, etc
22 p3967 A70-43544

Manned orbiting laboratory microclimate including atmosphere composition, temperature, humidity and weightlessness effects, radiation and noise protection, etc
22 p3980 A70-43636

Blood-brain and blood-cerebrospinal fluid barriers alterations under various physical environments in manned orbital laboratory
22 p3973 A70-43647

Materials problems in space and spacecraft environments, discussing particle density, composition and UV radiation, spacecraft structure, payloads, vibration, etc
23 p4209 A70-44328

Long term space flight crew habitation emphasizing food management, station housekeeping, personal hygiene and waste handling
23 p4154 A70-44622

SPACECRAFT GUIDANCE

NT SATELLITE GUIDANCE

Two axis spherical gas bearing gyro for accurate measurements of space vehicle position and attitude rates while maintaining compatibility with exotic environments
01 p0086 A70-10308

Strapdown inertial guidance systems performance and applications
02 p0336 A70-12264

Apollo 11 electronics, discussing inertial measurement unit, optical navigation system, command module computer, communication network, TV and experimental packages
02 p0270 A70-12633

Optimal strategies for controlled plant guidance into convex space assuming linear differential equations of motion
03 p0459 A70-13339

Shooting method for real time optimization of multiple burn rocket flights, presenting analysis, algorithm and test results
04 p0761 A70-14932

Analytic guidance and control for minimum fuel expenditure and optimal guidance corrections for low thrust vehicle in Martian orbit
04 p0716 A70-15544

Mariner 4 guidance and control system performance from mission nominal end to final termination time
04 p0765 A70-15664

Onboard computer requirements for inertial navigation of spinning and maneuvering vehicle, determining design parameters
06 p1013 A70-17161

Trajectory, guidance and environmental parameters and uncertainties effect on design optimization of out-of-orbit Viking soft lander
06 p1157 A70-18134

Ground-based and onboard guidance and navigation systems for outer planet flyby missions concerning direct, Jupiter swingby and Grand Tour trajectories
06 p1104 A70-18194

Optimal control program using multiple maxima method for maneuvering spacecraft in earth atmosphere with aim of changing orbital plane
07 p1331 A70-19483

Apollo space vehicles guidance and navigation using data obtained onboard, discussing inertial platforms, accelerometers and trajectory calculations
08 p1541 A70-21023

Apollo crew procedures, simulation and flight planning, discussing navigation, guidance and control procedures
09 p1657 A70-23706

Linearized theory for minimum fuel guidance in neighborhood of minimum fuel space trajectory, unrestricted thrust magnitude and allowances for mid-course impulses
11 p2079 A70-25957

Minimum fuel control for discrete time Gaussian processes, applying results to spacecraft midcourse guidance for earth-Mars mission
11 p2079 A70-25958

Guidance boundary value problem estimation by continuous least mean square /CLMS/ method, describing application to generation of velocity required coefficients
11 p2081 A70-26322

Gimbal influence on three axis gyro stabilized platform in spacecraft guidance during maneuvers
13 p2446 A70-28388

Apollo Guidance Computer operations and functions during lunar orbit rendezvous
13 p2446 A70-28390

Mariner Mars 1969 navigation, guidance and control systems design, mechanization and flight testing
13 p2446 A70-28393

Trajectory predictive lunar return atmospheric reentry guidance of roll-controlled Apollo-type vehicle, using variable integration steps
13 p2446 A70-28396

Optimum filtering techniques for radio guidance of third stage of Europa 1 booster compared for effectiveness
13 p2381 A70-28437

Laser tracking system for space guidance, describing equipment and operations
13 p2447 A70-28529

Onboard navigational requirements for future planetary missions, discussing major subsystems
13 p2448 A70-28701

Wind effects on rigid launch vehicle guidance and control system design, using model incorporating structural bending and fuel sloshing
13 p2448 A70-28755

Centaur space guidance equipment design, development, parts control and reliability
14 p2612 A70-30452

Lunar Orbiter Spacecraft Guidance and Control, discussing design and flight results
14 p2613 A70-30455

Navigation for lunar parking orbit with time varying osculating orbital elements, using Apollo 11 Doppler tracking data
14 p2613 A70-30457

Guidance system cost and reliability by Monte Carlo analysis of failure statistics
14 p2614 A70-30462

Temperature rate flight control system /TRFCS/ for lifting reentry vehicles control and guidance
14 p2614 A70-30464

Onboard moon-to-earth trajectory approach guidance with or without midcourse guidance using optical angular measurements
14 p2615 A70-30470

Apollo Guidance, Navigation and Control system prelaunch checkup, flight experience and error analysis
14 p2615 A70-30758

Restricted three body interplanetary guidance scheme using midcourse fixed time of arrival velocity correction

14 p2615 A70-30760

Apollo navigation methods and data analysis covering inertial guidance with gyro-stabilized platforms, acceleration sensors, sextants and telescopes, ergodicity, filtering, etc

15 p2772 A70-31549

Planetary atmospheres parameters use in spacecraft guidance

15 p2773 A70-32267

Variational equation of ballistic trajectory applied to two point boundary value guidance problems

15 p2812 A70-32504

Optimal control program using multiple maxima method for maneuvering spacecraft in earth atmosphere with aim of changing orbital plane

15 p2813 A70-32728

Star tracker rigidly connected to spacecraft frame for attitude determination by star field correlation

16 p2946 A70-33157

Cross product steering for space vehicles and ballistic missiles guidance during powered vacuum flight, pointing thrust acceleration vector to null velocity at termination

16 p2947 A70-33440

Velocity vector for boost vehicles guidance, comparing implicit and explicit computation

16 p2947 A70-33441

Terminal guidance for Mars softlander utilizing Doppler and range radar for steering and propulsive control

17 p3133 A70-35286

Apollo lunar landing guidance, navigation and control, discussing inertial and optical measurements, computer, digital autopilots, rendezvous and mid-course navigation

17 p3134 A70-35288

Optimal explicit guidance equation using maximum principle for two stage vehicle injecting satellite into parking orbit

17 p3134 A70-35289

Apollo lunar landing flight control functions, organization, disciplines and activities at Mission Control Center

17 p3134 A70-35292

ELDO launch vehicle FE /flat earth/ guidance, discussing perturbations, trajectory optimization, inertial navigation system, onboard computer, etc

18 p3288 A70-36299

Comet de Arrest 1976 opportunity mission analysis, considering flyby and rendezvous trajectories and guidance problems

[AIAA PAPER 70-1073]

19 p3513 A70-37426

Saturn 5 suboptimal continuous guidance design, eliminating discontinuous control encountered in SA-502 flight

[AIAA PAPER 70-965]

20 p3600 A70-39564

Booster parameterized guidance algorithms investigated on basis of steering forms validity, discussing exoatmospheric ascent applications

[AIAA PAPER 70-1006]

20 p3669 A70-39584

Preflight error statistics of earth based Doppler tracking for Mariner navigation concerning Mars 1971 and Venus-Mercury 1973 missions

[AIAA PAPER 70-1077]

20 p3670 A70-40023

OP-EX, optimal explicit guidance algorithm for powered flight outside atmosphere

[AIAA PAPER 68-869]

21 p3848 A70-41734

Manned spacecraft abort guidance and control problems, discussing various modes and emergency conditions

24 p4374 A70-46210

Satellite launch vehicle guidance equations for programmed optimization applied to Eldo inertial guidance system

24 p4375 A70-46359

SPACECRAFT INSTRUMENTS

NT LASER ALTIMETERS

NT SATELLITE INSTRUMENTS

NT SPACECRAFT POSITION INDICATORS

Floated single degree of freedom gyroscope and pendulous integrating gyroscope accelerometer, discussing design features as inertial sensors for future space missions

01 p0086 A70-10313

Cryogenic temperature sensor calibration with automated data readout for spacecraft accuracy requirements, describing potentiometric system

03 p0486 A70-13561

Spacecraft surface secondary electron emission effects on electron trap measurements in magnetosphere and solar wind, noting agreement with positive ion densities

03 p0561 A70-13994

Meteor particles spatial density and energy characteristics on space vehicles, using luminescent sensors coupled with photomultiplier

04 p0744 A70-14445

Apollo lunar mission optics concerning liftoff alignment theodolites, spacecraft atmosphere electro-optical sensor, helmet optical coating and laser experiment

04 p0688 A70-14693

Si fluid thermal actuator as temperature sensor and prime mover for active thermal controller in spacecraft

05 p0806 A70-16124

Scientific equipment on Cosmos 237 satellite for recording extraterrestrial radiation data, discussing specifications, operation and mission purpose

05 p0851 A70-16733

Distance of spacecraft descending on parachute through planetary atmosphere measured from center of planetary mass using onboard instrument data

06 p1155 A70-17897

Electron gun onboard reentering spacecraft to measure densities and temperatures in flowing gases

06 p1066 A70-18286

Visual display media requirements of future high performance vehicles, considering spacecraft and aircraft

08 p1499 A70-21691

Spacecraft conditions influencing remote imaging sensor performance, discussing altitude, temperature and moisture at sensor, air turbulence, vehicle motion, etc

[AIAA PAPER 70-291]

09 p1677 A70-22853

Earth resources sensor integration into satellite or aircraft, discussing cost effectiveness

[AIAA PAPER 70-316]

09 p1677 A70-22871

TV instruments for Mariners 6 and 7 providing analog and digital data, comparing resolutions and accuracies to earth based telescopes and Mariner 4 photographs

09 p1682 A70-23506

Michelson interferometer usable in space for stellar spectroscopy, noting compactness achieved through mirror area reduction

[ONERA-TP-799]

10 p1887 A70-24032

Space engineering, flight instrumentation features and spacecraft subsystems integration problems

10 p1950 A70-24610

Mass spectroscopy for solar system exploration, discussing ion sources, mass analyzers and ion detectors meeting mission requirements

10 p1942 A70-24612

Test program effectiveness for Saturn Instrument Unit (IU), summarizing objectives, costs and results

[AIAA PAPER 70-379]

10 p1891 A70-24924

LiF prism spectrometer for space applications, discussing vacuum UV transmission and mechanical properties

11 p2049 A70-25629

Digital closed-loop inflight calibration system for spaceborne particle spectrometers, utilizing cesium iodide crystal and programmable photomultiplier dynode supply

12 p2232 A70-27405

Optical instruments for space measurements, discussing photoelectric spectroscopic devices, Michelson interferometer, etc

12 p2234 A70-27597

Rocket-borne flight testing of sensitive accelerometer developed to measure small forces applied to satellite or space probe surface

13 p2403 A70-28433

Meteor particles spatial density and energy characteristics on space vehicles, using luminescent sensors coupled with photomultiplier

13 p2485 A70-28470

Spaceborne logarithmic variable prescaling counters for automatic compression of particle measurement data, discussing statistical error

13 p2406 A70-28931

Surface type airborne electrostatic probes in ambipolar diffusion flux measuring ion saturation current, discussing electrode contamination and temperature and ablation tests

[AIAA PAPER 69-700]

13 p2412 A70-29967

Fluxgate and Ru vapor magnetometers for space measurements over wide field intensities, reducing electronic phase shift and experiment weight

13 p2415 A70-30045

Viking Mars mission meteorological instruments for measurements of water vapor content, wind speed/direction, temperature and pressure

14 p2584 A70-30553

Nimbus weather satellite as laboratory for sensors collecting data for global weather system, describing launching, attitude control systems and cameras

14 p2654 A70-31149

Apollo navigation methods and data analysis covering inertial guidance with gyro-stabilized platforms, acceleration sensors, sextants and telescopes, ergodicity, filtering, etc

15 p2772 A70-31549

Low altitude atmospheric effects on IR beam horizon sensors in carbon dioxide band, noting corrections for spacecraft attitude measurement

15 p2735 A70-31792

Mariner spacecraft electro-optically controlled star sensors design and performance, discussing star simulation and stray light test techniques

15 p2736 A70-32033

Atomic clock for climatic and mechanical conditions of aerospace environment, using optically pumped rubidium cell

15 p2740 A70-32366

Solid state electroluminescent phosphor displays for aircraft/spacecraft instrument panels

16 p2906 A70-33178

Automatic active optic control of alignment and figure of primary mirror of spacecraft-borne telescope with response time stability

16 p2907 A70-33189

Spacecraft hydraulic timers design and qualifications testing, discussing oil selection and temperature dependence

16 p2914 A70-34112

Nonmagnetic explosive actuated indexing device permitting precise 180 deg rotation of magnetometer sensor on Pioneer 6 spacecraft

16 p2914 A70-34124

Nonmagnetic lightweight oscillating actuator for multiple indexing of spacecraft magnetometer

16 p2845 A70-34128

Thermal response of passive heliotope solar array orientation device using rotating bimetallic helix, performing energy balance analysis for helix temperature distribution

17 p3082 A70-34761

Astronaut scientific observation capabilities, discussing flexibility and instrumental design

[AAS PAPER 70-035]

Active RC bandpass filter for space fluxgate magnetometer, using state variable synthesis

17 p3054 A70-35526

Spaceborne lightweight mirror blanks made from ceramics fabricated from glass crystallization

18 p3263 A70-36559

Aerospace instrumentation - Conference, Cranfield Institute of Technology, England, March 1970

19 p3428 A70-38514

Launch and reentry vehicles pressure transducers, measuring propellant quantity, water systems, fuel, oxidizer, battery compartment and ascent engines, etc

19 p3430 A70-38519

Spacecraft-based navigation instruments for outer planet missions using celestial directions to outer planet natural satellites

[AIAA PAPER 69-902]

20 p3669 A70-39681

NASA automatic checkout systems for Saturn 5 stages and instrument units

21 p3803 A70-40770

Integrated Cryogenic Isotope Cooling Engine system (ICICE) for spacecraft sensors refrigeration requirements

21 p3947 A70-41053

Spacecraft sheath structure, potential and velocity effects on ion current measurements by traps and mass spectrometers

21 p3816 A70-41087

Transistorized DC to AC converter providing sinusoidal output to power automatic spacecraft control devices via pulse width modulation

22 p3994 A70-42309

Mass spectrometer and high voltage converter powering electrostatic plasma and solar wind analyzer for cosmic space studies on Sputnik 3 and Heos A satellites

22 p4025 A70-42312

Astronaut physiological monitoring aboard Soyuz spacecraft

22 p3980 A70-43691

Soft X ray astronomical instrumentation for space experiments, discussing Geiger tubes, gas counters, modulation collimators, telescopes, etc

23 p4196 A70-44416

Apollo command service module nondispersive X ray detection system for lunar composition map compilation, discussing design and performance

23 p4196 A70-44417

Spacecraft astronomical instrument structural design, examining aging, vibration and temperature distribution deformations and optical surface contamination

24 p4339 A70-45823

Spacecraft sensor trends from space station research and technology requirements regarding astronomy, biomedicine and biology, earth resources, etc

[AIAA PAPER 70-1291]

24 p4418 A70-45974

SPACECRAFT LANDING

NT LUNAR LANDING

NT PLANETARY LANDING

Optimal space vehicle reentry control ensuring minimum scattering of landing points based on accelerometer and free pitch-angle gyroscope data

04 p0760 A70-14431

Chemical heat source combined with metals ignition properties considered for spacecraft heating during Mars nighttime landing

04 p0628 A70-15426

High speed instrumentation camera system for recording rapid motions during Apollo landing impact

09 p1688 A70-23770

Sterile lander recontamination prevention from microorganisms during in-flight transfer from unsterilized carrier vehicle

11 p1991 A70-26049

Mars landing analysis and simulation for unmanned lander prototype, discussing digital simulation by Monte Carlo techniques and physical tests

11 p2032 A70-26291

On-line parameter updating for relationship between Martian atmospheric density and height above surface during spacecraft descent based on least squares approach 11 p2113 A70-26318

Spacecraft autonomous control algorithm to ensure geographically specified landing accuracy without considering atmospheric density distribution 12 p2270 A70-28251

Reentry control algorithm for prescribed landing point of space vehicle entering earth atmosphere at parabolic velocity, discussing double-dip reentry and digital simulation 13 p2499 A70-28376

Manual control systems for spacecraft stabilization involved in rendezvous, midcourse correction, landing, etc 13 p2357 A70-28394

Optimal space vehicle reentry control ensuring minimum scattering points based on accelerometer and free pitch-angle gyroscope data 13 p2503 A70-28456

Microbial release from solid spacecraft materials after hard landings, testing survival during decontamination or terminal sterilization 15 p2688 A70-31664

All-flexible parawing as primary descent system for large spacecraft landing, discussing configuration, structural arrangement, multistage reefing and L/D performance tests [AIAA PAPER 70-1187] 21 p3754 A70-41828

Point accelerations on semirigid body spacecraft from accelerometer data with structural vibration noise at landing 23 p4200 A70-44387

Spacecraft landing gear shock attenuation systems using crushable honeycomb, draw-die tubes and retrorocket skirt jet 23 p4262 A70-44695

SPACECRAFT LAUNCHING

HEOS 1 launch operations, discussing test and checkout phase, mating with Thor Delta launch vehicle, countdown phase and launch 01 p0196 A70-11116

Postlaunching operations putting HEOS 1 satellite into orbit, verifying subsystem functions, starting experiments and tracking for data recovery 01 p0197 A70-11117

European Space Operations Center activities in observing HEOS 1 satellite, discussing launch, data processing and S-11 experiment involving ionized Ba cloud creation 01 p0197 A70-11118

NASA network and Thor Delta type booster to launch Italian satellite to geostationary orbit, evaluating feasibility 03 p0451 A70-13841

Italian space satellite booster programs for launching satellite payloads into low orbit 03 p0609 A70-13846

Orbit determination program for launching and stationkeeping of 24 hr geostationary satellites, using azimuth and elevation of single autotrack antenna 03 p0578 A70-14339

Simple harmonic oscillator vibrations due to local random processes in spacecraft launching, calculating oscillator displacement variance 04 p0774 A70-15102

High energy propulsion module utilizing F/H fuels for planet flyby, orbiter mission and injection of 24-hr satellites, discussing design and equipment [DGLR-69-18] 04 p0736 A70-15176

Orbital rendezvous for inspection, rescue, etc, discussing launch bases number, warning time and alert status effect on reaction time 06 p1027 A70-17173

Satellite launch vehicle attitude control stability study including fuel sloshing and body bending effects 06 p1155 A70-17320

Launch facilities institutionalization for space shuttles launch cost minimization [AIAA PAPER 70-244] 07 p1251 A70-20374

Launch vehicle minimum cost design emphasizing flight vehicle evolution stages via effect on costs [AIAA PAPER 70-240] 07 p1396 A70-20378

Orbit-to-orbit shuttle for launch in earth-to-orbit shuttle vehicle, discussing design requirements [AIAA PAPER 70-268] 07 p1399 A70-20397

Longitudinal structural vibration and lateral bending response mass and spring coupling in Saturn AS-502 during boost with longitudinal excitation by pogo effect 09 p1766 A70-23239

Optical transmission technology for aerospace launch operations investigated on wideband communication systems projects involving use of gallium arsenide lasers and diodes 09 p1640 A70-23776

Spacecraft launch computerized simulator, discussing operational characteristics applicable to on-line real time process control 11 p2013 A70-26217

Atlas/Centaur and Titan/Centaur launching of Intelsat 4 communication satellites, discussing booster, stage characteristics and payload [AIAA PAPER 70-483] 11 p2127 A70-26605

Diamant B satellite launcher testing and construction, discussing DIAL/WIKA scientific satellite launch 12 p2314 A70-28299

Turbopump-fed rocket engine for satellite launchers, discussing gas cooling, fuel tank pressurization, etc 13 p2474 A70-29138

Space vehicle response to in-flight wind turbulence, describing operational procedure for launch advisability determination 14 p2653 A70-30587

Atmospheric wind profiles and boundary layer turbulence power spectra for calculation of wind loads on space vehicles during prelaunch and launch 14 p2653 A70-30600

Syncom and Early Bird systems development, launch procedure and operation, discussing common components 14 p2654 A70-31144

Nimbus weather satellite as laboratory for sensors collecting data for global weather system, describing launching, attitude control systems and cameras 14 p2654 A70-31149

Modular launch vehicle system for European commercial satellites using Eldo-A/I Astris and French rocket stages 16 p2987 A70-34342

Satellite launching rocket guidance and control based on implicit measurement 17 p3133 A70-35283

Optimal explicit guidance equation using maximum principle for two stage vehicle injecting satellite into parking orbit 17 p3134 A70-35289

International organizations participation in convention on liability for damage caused by launching of objects into outer space 17 p3202 A70-35784

Space object, launching and platform registration 17 p3202 A70-35787

Spacecraft launch registration, comparing Soviet and American information furnished to UN 17 p3202 A70-35789

Optimum launch trajectories for ATS-E mission with noncircular parking orbits, considering apogee motor size, perigee radius and duration constraints [AIAA PAPER 70-1051] 19 p3528 A70-38866

Launch facilities institutionalization for space shuttles launch cost minimization [AIAA PAPER 70-244] 20 p3606 A70-39697

ELF acoustic gravity wave arrival from Apollo launchers recorded by Doppler shift ionospheric sounder channelled near mesopause and lower thermosphere 23 p4187 A70-43859

Launch optimization of artificial satellites for minimizing thermal radiative heat input during low altitude orbit 23 p4264 A70-45047

SPACECRAFT LUBRICATION

Vacuum evaluation of lubricants and techniques applicable to miniature ball bearings and instrument gearing for space systems [ASME PAPER 69-LUB-30] 01 p0100 A70-10379

Solid lubricants friction and wear bench testing under simulated space environment 06 p1075 A70-17340

Applied space research covering photovoltaic cells, electric propulsion, onboard data storage, vacuum lubrication and NASA-European organizations budgets 06 p1141 A70-17780

Vacuum evaluation of lubricants and techniques applicable to miniature ball bearings and instrument ball bearings and instrument gearing for space systems 13 p2419 A70-29120

Solid lubricated contacts performance in Nimbus and OAO spacecraft, discussing slip ring assembly and noise problems in Ag-graphite brushes 16 p2920 A70-33810

Slip ring assemblies for spacecraft devices, evaluating sliding electrical contact industry technological capabilities 16 p2920 A70-33811

Lubrication role in aerospace engineering, discussing lubricant and component selection, environmental factors, etc 16 p2923 A70-34155

Lubrication system flight performance and laboratory test data for space applications, considering torque motors, slip rings, bearings and gears 16 p2923 A70-34157

Controlled leakage sealing of hydrodynamic bearing lubrication systems for space vehicles in synchronous orbit 16 p2923 A70-34158

Instrument size ball bearings lubricated with bonded dry or transfer films in simulated interplanetary spacecraft tests 16 p2923 A70-34166

Lubrication technology for space shuttles, discussing vehicles and airbreathing and rocket engines 22 p4047 A70-43325

SPACECRAFT MANEUVERS

Minimum propellant rendezvous maneuver of space vehicles in neighboring circular orbits 01 p0193 A70-10555

Minor circle maneuver solution to equations of motion of vehicle in spherical planet atmosphere for gliding and cruising, discussing cylindrical planar case 01 p0184 A70-10949

Spacecraft horizontal maneuvers in homogeneous gravitational field to achieve soft landing on planetary surface, including optimal liftoff and orbital transfer 01 p0197 A70-11501

Dynamic characteristics of model of spacecraft-astronaut-tether system during approach, deriving kinetic potential 01 p0192 A70-11587

Geostationary satellite payload-optimal injection trajectory from nonequatorial firing range, describing dog-legging maneuvers 03 p0573 A70-13845

Optimal descent maneuver from planetary orbit for fixed atmospheric reentry angle, considering minimum impulse/fuel consumption/ 04 p0745 A70-14496

Launch vehicles design, propulsion, maneuverability and navigation 05 p0923 A70-16565

Orbital rendezvous for inspection, rescue, etc, discussing launch bases number, warning time and alert status effect on reaction time 06 p1027 A70-17173

Satellite electric propulsion system and configuration for orbital transfer maneuvers, describing ELDO launcher, Black Arrow, orbital dynamics, sensor system, etc 06 p1130 A70-17468

Interplanetary swingby trajectory correcting maneuvers for space vehicles return to earth after planar orbiting, with emphasis on singular points 06 p1142 A70-17877

Lunar module motion during optimal ascent from moon surface into circular orbit of command module, noting descent maneuver similarity 06 p1155 A70-17881

Time optimal rendezvous maneuver between neighboring elliptic orbits, discussing propulsive jet system with variable thrust 07 p1381 A70-19357

Optimal control program using multiple maxima method for maneuvering spacecraft in earth atmosphere with aim of changing orbital plane 07 p1331 A70-19483

Flight maneuver for roll modulated lifting reentry vehicle to reduce deployment dynamic pressure 07 p1394 A70-19724

Abort and staging separation maneuvers of two equal size reusable lifting entry vehicles in wind tunnel tests [AIAA PAPER 70-260] 07 p1397 A70-20389

Optimal maneuver decision strategy for space vehicle midcourse trajectory corrections 09 p1760 A70-22928

Capillary barriers to provide propellant positioning, expulsion capability and slosh dampening for spacecraft propulsion systems during rotational maneuvers [AIAA PAPER 69-529] 11 p2123 A70-26119

Space vehicle on-line tracking with impulsive thrust maneuver by sequential estimation scheme, reducing radius measurement error 11 p2008 A70-26237

Spin stabilized satellite attitude and orbital maneuvers computation, considering required accuracy and computer time in numerical integration procedures 11 p2125 A70-26278

Gimbal influence on three axis gyro stabilized platform in spacecraft guidance during maneuvers 13 p2446 A70-28388

Synergetic plane change maneuver optimal control, combining aerodynamic and propulsive flight phases for efficiency 15 p2715 A70-31874

Optimal control program using multiple maxima method for maneuvering spacecraft in earth atmosphere with aim of changing orbital plane 15 p2813 A70-32728

Space shuttle mission trajectory optimization with steering in atmospheric flight and orbiter maneuvers [AAS PAPER 70-048] 17 p3176 A70-34788

Parking orbit optimal orientation for minimal impulsive maneuvers total velocity increment in three dimensional capture-escape mission [AIAA PAPER 69-918] 17 p3172 A70-35649

Covariance matrices estimates for trajectory parameter tracking of thrust-maneuvering spacecraft [AIAA PAPER 70-1017] 20 p3666 A70-39516

German monograph on satellite orbit synergetic plane change maneuver optimal control by entry into denser atmosphere 20 p3705 A70-39924

Large earth orbiting spacecraft minimum time attitude maneuvers with control moment gyroscopes, discussing torque calculation and gimbal angle rates 20 p3670 A70-40284

- Optimal low thrust power plant for spacecraft payload-maneuver tradeoff 21 p3866 A70-40832
- Algorithm for spacecraft rotational maneuver control based on single turn around specific axis, using onboard computer 21 p3849 A70-42236
- Rocket nose cone optimal turn into horizontal ballistic trajectory after separation from booster, using dynamic programming 22 p3962 A70-43351
- Satellite dynamics - Conference, Prague, May 1969 24 p4405 A70-45526

SPACECRAFT MODELS

- Mission model construction for power limited systems, discussing flight concepts, propulsion mixes and electric propulsion 01 p0183 A70-10848
- Dynamic characteristics of model of spacecraft- astronaut-tether system during approach, deriving kinetic potential 01 p0192 A70-11587
- Mathematical model for investigating satellite thermal behavior in space based on space simulation in vacuum chamber with walls maintained at liquid nitrogen temperature 05 p0924 A70-17022
- Passive thermal control system design of SERT II nonspinning satellite based on 534-node analytical model calibrated against test data 11 p2127 A70-26358
- Wind effects on rigid launch vehicle guidance and control system design, using model incorporating structural bending and fuel sloshing [ACARDOGRAPH-115] 13 p2448 A70-28755
- Spacecraft thermal mathematical model adjustment to fit measured temperatures, using iteration method 15 p2812 A70-32513
- Rotating flexible cable-connected space station dynamic scale model, describing suspension system and artificial gravity generation 23 p4258 A70-44528

SPACECRAFT MODULES

- NT LANDING MODULES
- NT LUNAR LANDING MODULES
- NT LUNAR MODULE
- NT MARS EXCURSION MODULE
- High energy propulsion module utilizing F/H fuels for planet flyby, orbiter mission and injection of 24-hr satellites, discussing design and equipment [DGLR-69-18] 04 p0736 A70-15176
- Experiment space module combined with space station and serviced by shuttle for low total cost and maximum flexibility in funding and scheduling [AAS PAPER 70-034] 17 p3175 A70-34777
- Subsystem selection integration and technology for space base and planetary mission module /PMM/ of space station program [AAS PAPER 70-021] 17 p3023 A70-34801
- Nuclear rocket applications in Nuclear Flight Propulsion Module /NFPM/ and Reusable Nuclear Shuttle /RNS/ 22 p4070 A70-43180
- Orbital space station program, discussing common module design, support, space shuttles and objectives [SAE PAPER 700755] 24 p4415 A70-45852
- Free-flying modules interface and operation in conjunction with space station for orbital research into manned space program [AIAA PAPER 70-1300] 24 p4417 A70-45950
- Earth-orbiting manned space station design, describing shuttle support and experimentation in attached and free-flying modules [AIAA PAPER 70-1299] 24 p4417 A70-45951

SPACECRAFT MOTION

- U SPACECRAFT TRAJECTORIES
- Mathematical relations and procedures for automatic satellite tracking by four axis Zeiss camera, discussing motion along small circle approximation and punch tape criteria 02 p0255 A70-11770
- Satellite motion in earth gravitational field under additional forces using Stockel theorem 04 p0760 A70-14432
- Ion and electron concentrations far field disturbances caused by satellite motion in ionosphere and lower exosphere, deriving plasma drag 04 p0762 A70-14935
- Meteoroids average velocity relative to spacecraft determined using sporadic meteors orbital elements data in interplanetary space 04 p0757 A70-15550
- Kalman-Bucy filtering for estimating initial conditions and smoothing problems in linear dynamic systems, applicable to rectilinear motion of randomly accelerated spacecraft 12 p2186 A70-27905
- Satellite stationary motions stabilization using rotors with axes fixed inside spacecraft 13 p2499 A70-28389
- Satellite motion in earth gravitational field under additional forces using Stockel theorem 13 p2503 A70-28457

- Reentry vehicles dynamic stability analysis involving pitch, yaw and roll motions modes coupled by asymmetries 13 p2341 A70-29027
- [AIAA PAPER 70-561] 13 p2341 A70-29027
- Ionospheric plasma disturbances due to moving space vehicle, investigating by electron density measurements in rarefied wake regions using gyro-plasma probe 17 p3142 A70-35763
- Motion perturbation equations for guided space vehicles, allowing for sloshing liquid propellant viscosity effects 18 p3332 A70-36160
- Intermediate orbit calculation, allowing for spacecraft large gravitational perturbation during motion near planetary sphere of influence 18 p3312 A70-36166
- Satellite translational motion in circular problem of three bodies, discussing existence of equations in integral 18 p3324 A70-37150
- Space motion simulators for Azur satellite, considering satellite attitude related to sun 19 p3400 A70-38296
- Apollo service module retrograde motion due to propellants reorientation after reentry jetison predicted by digital simulation 19 p3534 A70-38862
- [AIAA PAPER 70-1047] 19 p3534 A70-38862
- Motion and stability of rotating connected two body space station satellite system, developing Lagrangian equations of motion and optimizing damping system parameters 20 p3716 A70-39678
- [AIAA PAPER 69-919] 20 p3716 A70-39678
- Elastic deformable satellite motion stability in central Newtonian force field 21 p3927 A70-40827
- Spacecraft sheath structure, potential and velocity effects on ion current measurements by traps and mass spectrometers 21 p3816 A70-41087
- Lifting reentry vehicle two dimensional motion optimization with inequality constraints explicitly containing control by perturbation method 21 p3845 A70-41265
- Space vehicle self oscillatory pulsed relay attitude control system with jet nozzles, determining angular motion 22 p4001 A70-42838
- Artificial satellite motion theory, discussing gravitational and nongravitational force effects 24 p4406 A70-45527
- Solar corpuscular flux and visible solar spot area correlation with geomagnetic planetary index for 27-day intervals, considering relationship to earth satellites motion 24 p4408 A70-45547
- SPACECRAFT ORBITAL ASSEMBLY
- U ORBITAL ASSEMBLY
- SPACECRAFT ORBITS
- NT INTERPLANETARY TRANSFER ORBITS
- NT PARKING ORBITS
- NT POLAR ORBITS
- NT SATELLITE ORBITS
- NT STATIONARY ORBITS
- NT TRANSFER ORBITS
- NT TROJAN ORBITS
- NT TWENTY-FOUR HOUR ORBITS
- Orbital spacecraft/sensor systems for earth resource surveys and measurement, considering agriculture, forestry, geology, mineralogy, hydrology, etc [AAS PAPER 69-584] 04 p0761 A70-14643
- Large spacecraft in circular earth orbit calculated for internal gravitational field 05 p0924 A70-16637
- Solar, albedo and earth thermal radiations absorbed by partially obscured spacecraft calculated on digital computer for various orbital positions 06 p1173 A70-17556
- Lunar mascon effects on Apollo type spacecraft orbits calculated for minimizing orbital instabilities 07 p1387 A70-19715
- Analytical solutions to optimum orbit modifications including atmospheric maneuver 14 p2649 A70-31171
- Statistical error analysis of autonomous manned spacecraft navigation in long duration eccentric Mars orbits [AIAA PAPER 69-880] 15 p2773 A70-32503
- Orbiting spacecraft angular velocities via inertial sensing platform consisting of linear accelerometers 24 p4372 A70-45475
- SPACECRAFT PERFORMANCE
- Weather satellites performance emphasizing designs for geostationary altitude and hydrological, oceanographic and earth science applications 01 p0135 A70-10648
- [AIAA PAPER 69-1082] 01 p0135 A70-10648
- Parametric performance and cost comparison of separate and integral vehicle concepts for manned space activity using payload criterion 04 p0763 A70-15420
- Mariner 4 guidance and control system performance from mission nominal end to final termination time 04 p0765 A70-15664

- Jet engine risetime effect on spacecraft orientation control system performance, assuming monotonic or extremal thrust mode 06 p1103 A70-17883
- Reusable air breathing launch vehicle for earth orbit shuttle, comparing performance, costs and operation with rocket powered systems [AIAA PAPER 70-270] 07 p1396 A70-20381
- Saturn IB Orbital Workshop solar array thermal and performance analysis for various vehicle orientations and orbital conditions, emphasizing modeling and data handling 11 p2127 A70-26357
- Space environment effects on spacecraft payload materials and performance, discussing atmospheric pressure, outgassing, radiation and meteoroid collision 13 p2485 A70-28434
- Meteorological problems associated with space shuttle design and operations, permitting tradeoff analysis on environment effects 16 p2946 A70-33804
- Titan 3 launch vehicle for scientific space missions, discussing building blocks, performance and payloads 17 p3178 A70-35260
- Orbiting Astronomical Observatory II systems performance 21 p3928 A70-40980
- Mariner 6 and 7 navigational accuracies prior to time of planetary encounter 21 p3888 A70-41129
- SPACECRAFT POSITION INDICATORS
- Instrument error analysis for spacecraft orientation and positioning near planet from planet disk observations 01 p0094 A70-11511
- Spacecraft orientation from onboard stellar photographs, calculating absolute and relative elements, accuracy and camera parameters 01 p0198 A70-11512
- Star field pattern recognition methods for spacecraft attitude determination without a priori knowledge of star position-vehicle attitude relationship 09 p1725 A70-23516
- Coupled control of space vehicle orientation with reference to three celestial bodies, reducing plane vibrations to dynamic third order system 10 p1914 A70-24307
- SIRIO mission algorithm and computer program, determining spacecraft position, ground trace and tracking station visibility 15 p2811 A70-32286
- Spacecraft position determination by holographic approach involving single star formation 20 p3665 A70-39422
- SPACECRAFT POWER SUPPLIES
- Electric power generators performance based on kinetic energy conversion of radioactive isotope decay products, noting space applications 01 p0140 A70-10217
- Manned space station power systems design and selection problems, discussing requirements based on impacts on space station design and operations [AIAA PAPER 69-1081] 01 p0008 A70-10625
- Guidebook on application of space nuclear power systems covering radioisotope and reactor systems, static and dynamic systems, power system suppliers and users, etc 01 p0140 A70-10942
- Si solar cells for powering artificial satellites on-board equipment, discussing fabrication and substitute materials 01 p0011 A70-11253
- Deployment systems for extending large area lightweight flexible solar arrays in space, tabulating estimated design weights including power-weight ratios 02 p0228 A70-11932
- Structural design experience in developing large area Be solar array for Mars flyby mission, describing configurations, requirements, material and manufacturing 02 p0228 A70-11935
- Solar power system of ELDO F-9 satellite boosted into polar orbit by EUROPA 1, discussing cell placement 03 p0573 A70-13847
- German developments in electric propulsion and energy supply systems for commercial satellites in geostationary orbits [DGLR-69-20] 04 p0735 A70-15169
- Computer program for electrical and transient thermal analysis of satellite electric power subsystem consisting of solar array, battery and power controls 04 p0628 A70-15332
- Gas core nuclear reactors feasibility based on gas core hydrodynamics, heat transfer and neutronics development, noting spacecraft weight and trip time reduction potential 04 p0717 A70-15639
- Liquid metal pump design and performance in SNAP 8 Mercury Rankine and Advanced Rankine fluid power systems, including containment materials and corrosion effects 04 p0718 A70-15641

Sealed Ni-Cd aerospace battery design, discussing recombination of gases produced during prolonged overcharging at low temperature, separator material, plate balance, etc

05 p0798 A70-16096

Solar energy as spacecraft power source examined in operating life comparison with chemical, electrochemical and nuclear energy, discussing silicon solar cells

05 p0799 A70-17023

Lewis Research Center applications of optics to research in flight propulsion and space power generation, discussing gas density visualization, radiative heat transfer, etc

09 p1657 A70-23522

Oriented flexible rolled-up solar array (FRUSA) for spacecraft electric power generation, describing orientation and deployment mechanisms, solar panel, system operation, etc

[AIAA PAPER 70-738] 11 p2119 A70-25434

Nonislanding rotary electrical connector for conducting current and signals from satellite solar panel

[AIAA PAPER 70-458] 11 p2016 A70-25453

Rankine 10 MWe nuclear electric space power system design, discussing reactor power, fuel, coolant, structural material, control system, shield, etc

11 p2082 A70-26123

Electrostatic rocket exhaust condensation on spacecraft solar electric panels cover glasses, noting deleterious effects

[AIAA PAPER 69-271] 11 p2103 A70-26131

Weights, sizes and costs of nuclear and nonnuclear spacecraft power systems with reference to mission duration

11 p2082 A70-26260

Hybrid Cockcroft Walton multinode photomultiplier supply for space applications, using miniature components and thick film technology

12 p2233 A70-27406

Optimal control of nuclear propulsion and energetic plants of space vehicle, considering thermionic generator

13 p2450 A70-28436

Brayton, Hg, organic-Rankine and potassium-Rankine dynamic space power systems for use with nuclear energy sources

13 p2450 A70-29492

Nuclear power systems for manned orbiting space stations, noting Brayton aggregate and NASA objectives

13 p2450 A70-29493

Azur satellite p- and n-type Si solar cell system providing both power supply and storage battery charging

13 p2506 A70-29553

Solar cell power supplies for weather balloon and satellite systems

14 p2535 A70-31146

Spacecraft electric power supplied by isotope nuclear sources, discussing heat sources, energy converters and heat rejection systems

14 p2616 A70-31147

OGO spacecraft structures, thermal control systems, attitude control, weight and power supplies

15 p2810 A70-31782

Ion thrusters and sources in space propulsion, discussing power supply level, efficiency and service lifetime

[ONERA-TP-739] 15 p2787 A70-31808

Ripple filters for DC power supplies using reliable small capacitance capacitors suitable for spacecraft applications

15 p2714 A70-32806

Large capacity sealed nickel cadmium battery for spacecraft, describing mechanical and electrical characteristics

16 p2844 A70-33473

Space collector ring systems surface physics, discussing dry thin film lubricants, smoothness, service life, etc

16 p2917 A70-33485

Solar electric spacecraft for interplanetary missions including asteroid belt survey, Jupiter flyby and out-of-elliptic survey

[AIAA PAPER 70-645] 16 p2981 A70-33531

Power conditioning and control system prototype for Mercury spacecraft ion thruster, describing supply subsystems, circuit design, component selection and reliability

[AIAA PAPER 70-649] 16 p2970 A70-33615

MHD electric power generators characterized by high power level and duration for future application in space

16 p2844 A70-33711

Rotary relay for solar array space power transfer using clutch of low moment of inertia capable of recycling once each orbit

17 p3101 A70-34765

Deep space spacecraft radioisotope thermoelectric generators, discussing testing and evaluating for future missions

18 p3215 A70-36229

Electrical power supply systems for meteorological sounding rockets under vibration, acceleration and temperature variation conditions during flight

18 p3215 A70-36251

Radiant gas heater for Brayton cycle space power system

[ASME PAPER 70-GT-36] 18 p3303 A70-36834

SI and thin film solar cells for satellite power supplies, considering manufacture and space environment

19 p3358 A70-38478

Aircraft auxiliary systems and spacecraft power supplies, considering fly-by-wire control actuators, pyrotechnics and stowable solar array

20 p3564 A70-39669

SERT 2 solar array power system in sun synchronous orbit, considering power conditioning and deployment technique

[AIAA PAPER 70-1159] 20 p3567 A70-40202

Nuclear space power three stage potassium turbine erosion testing in stainless steel loop with various contamination levels

21 p3756 A70-41005

Regenerative hydrogen-oxygen secondary fuel cells as rechargeable battery for communication satellites

21 p3756 A70-41007

Solar arrays for Venus-Mercury flyby, evaluating temperature and power performance

21 p3756 A70-41010

Solar cell/battery systems for spacecraft, discussing power system evaluator, NiCd thermal control, lightweight rigid panels design, etc

21 p3757 A70-41011

Ni-Co aerospace batteries thermal and mechanical design for orbiting space vehicles

21 p3757 A70-41012

Power conditioning systems for INTELSAT satellites, describing methods for battery charging, charge control, voltage regulation and power management

21 p3757 A70-41207

Regulated spacecraft solar array mathematical model for high voltage power supply regulator analysis

21 p3757 A70-41208

Solid state switching effect on aerospace electric power conditioning equipment

21 p3758 A70-41210

Integrated circuit requirements for space power conditioning equipment for ion thrusters

21 p3797 A70-41211

Modular Dc to Dc switching mode converter for space power system

21 p3758 A70-41217

Automatic and command multiple sequencer for spacecraft solar cell battery charger, providing switching logic by integrated circuits design

21 p3758 A70-41218

Buck-boost main bus voltage regulator for solar array battery space power system

21 p3758 A70-41219

Solar cell array peak power tracker and battery charger for Airlock Vehicle coupling Apollo spacecraft and Saturn IVB stage to form manned orbiting workshop

21 p3759 A70-41221

Electrical design of ferrite configuration high power rotary transformer for satellite slip ring replacement, minimizing transistor turn-off losses

21 p3759 A70-41222

Spacecraft data transmission efficiency improvement by budgeting onboard electric energy consumption among data types

21 p3790 A70-41364

High voltage solar arrays, considering plasma power losses dielectric stresses design, fabrication and testing

[AIAA PAPER 70-1137] 21 p3759 A70-41780

High voltage solar array with integral power conditioning, discussing weight factors, panel design and layout, mechanization, performance prediction, etc

[AIAA PAPER 70-1158] 21 p3759 A70-41787

Thermoelectric outer planet spacecraft (TOPS)/solar-independent power subsystem

21 p3760 A70-41802

Orbital mission solar energy power conversion system, discussing heat transfer processes for storage feasibility

21 p3951 A70-41852

Transistorized DC to AC converter providing sinusoidal output to power automatic spacecraft control devices via pulse width modulation

22 p3994 A70-42309

Finned tube-sheet spacecraft radiator transient response for perturbations caused by power supply and heat sink temperature changes

22 p4123 A70-42519

Space electric field considered for solar wind plasma drift origin and possible energy source for spacecraft propulsion, estimating intensity on lunar surface

22 p4100 A70-42789

Brayton, Hg, organic-Rankine and potassium-Rankine dynamic space power systems for use with nuclear energy sources

22 p4071 A70-43189

ZrH reactor program and multikilowatt space oriented thermoelectric power conversion systems

22 p4071 A70-43190

Space nuclear power system design and operation related to safety, discussing SNAP flights

22 p4071 A70-43192

Nuclear power systems for manned orbiting space stations, noting Brayton aggregate and NASA objectives

22 p4071 A70-43193

Earth orbital space station electrical power systems, discussing power sources, effect on structural configuration, environmental control and launch and resupply operations

[MDAC-WD-1461] 23 p4143 A70-44605

Spacecraft radioisotope thermoelectric generator interference in onboard instrument operation, using analytical models to determine necessary shielding

24 p4375 A70-45175

SPACECRAFT PRELAUNCH TESTS

U SPACE VEHICLE CHECKOUT PROGRAM

SPACECRAFT PROPULSION

NT ELECTROMAGNETIC PROPULSION

NT ELECTROSTATIC PROPULSION

NT ION PROPULSION

NT PHOTONIC PROPULSION

NT PLASMA PROPULSION

NT SOLAR PROPULSION

Minimum propellant rendezvous maneuver of space vehicles in neighboring circular orbits

01 p0193 A70-10555

Solar and nuclear electric propelled spacecraft applications to planetary and interplanetary missions, considering asteroid survey, out-of-elliptic, Mercury orbiter, comet rendezvous, etc

[AIAA PAPER 69-1108] 01 p0181 A70-10619

Simulator for testing colloid microthruster, discussing spacecraft interfaces and time of flight thrust data

[AIAA PAPER 69-314] 01 p0058 A70-10834

Performance boundaries of space propulsion systems containing nuclear electric stages

[AIAA PAPER 69-249] 01 p0196 A70-10839

Cost reductions achieved by space payload life extension through manned maintenance and increased transportation economies via refueling and improved space propulsion

01 p0196 A70-10844

Chemical engineering application to solid propellant rocket motors optimization for specific operations, discussing fuel properties, formulation and additives, mixing and casting

[AICHE PAPER 28A] 01 p0166 A70-10971

Propulsion efficiency in air and in space measured according to relativity concepts, including electric field inertia explanation

02 p0355 A70-12364

Solar electric propulsion (SEP) for automated planetary missions, discussing system characteristics, capabilities and costs

[AIAA PAPER 69-1103] 02 p0382 A70-12531

Optimum power and operation mode of space vehicle engine with control error allowance as function of mass and velocity

04 p0760 A70-14433

Solar or nuclear energy powered electric propulsion systems for transferring satellite from low to geostationary orbit, discussing feasibility and costs of various designs

04 p0735 A70-15174

Apollo spacecraft propulsion systems design and operational requirements, emphasizing use of redundant components and system backups to achieve reliability

[SAE PAPER 690704] 05 p0923 A70-15858

Launch vehicles design, propulsion, maneuverability and navigation

05 p0923 A70-16565

SERT 2 thruster hollow cathode durability tested in bell jar

[AIAA PAPER 69-304] 07 p1364 A70-19703

Book on spaceflight propulsion covering jet thrust, energy release, chemical, nuclear and electric propulsion, transportable and environmental systems

09 p1742 A70-22202

Lewis Research Center applications of optics to research in flight propulsion and space power generation, discussing gas density visualization, radiative heat transfer, etc

09 p1657 A70-23522

Spacecraft optimal flight from earth orbit to outer planet orbit with ideally controlled engine using differential motion equations

10 p1941 A70-24512

Nuclear propulsion systems types, discussing relative capabilities and future roles in aerospace applications

11 p2082 A70-26055

Space propulsion systems for public transportation to and from orbit and throughout near solar system, discussing commercial requirements

11 p2102 A70-26060

Spacecraft propulsion systems selection for particular exploration missions including planets, comets and interstellar space

11 p2112 A70-26066

Background pressure and magnetic field shape effect on MPD thruster performance, testing radiation cooled thrusters

[AIAA PAPER 69-243] 11 p2102 A70-26122

Optimum power and operation mode of space vehicle engine with control error allowance as function of mass and velocity

13 p2503 A70-28458

Pulsed plasma microthruster propulsion system for synchronous orbit LES 6 satellite [AIAA PAPER 69-298]

13 p2473 A70-28504

Hollow cathode mercury electron bombardment thruster design, emphasizing low specific impulse operation and discharge chamber improvements

13 p2473 A70-28505

Ion thrusters and sources in space propulsion, discussing power supply level, efficiency and service lifetime [ONERA-TP-739]

15 p2787 A70-31808

Space propulsion evolution in 1970s - Conference, Rome, March 1970

15 p2788 A70-32251

Space propulsion research with emphasis on tripropellant mixtures, discussing increased combustion pressure, nozzle design, reusable orbital transporter, etc

15 p2789 A70-32252

Spacecraft propulsion development guidelines concerning rocket engines with storable propellants, rotating solid propulsion systems, cryogenic propellants, etc

15 p2790 A70-32256

Space vehicles chemical propulsion limitations and potential applications

15 p2786 A70-32268

Reusable ferry spacecraft program, discussing space shuttles, cost reduction and nuclear propulsion for deep space missions

15 p2791 A70-32300

Rocket engine prototype for Mariner Mars 71 spacecraft, describing performance test results and response, thermal and throttling characteristics [AIAA PAPER 70-716]

16 p2966 A70-33545

Spacecraft propellant expulsion systems, comparing capillary with conventional techniques [AIAA PAPER 70-685]

16 p2962 A70-33584

Manned planetary flight systems engineering, discussing feasibility, objectives, propulsion, transplanet injection via geospace shuttle station, energy requirements for various synodic modes [AAS PAPER 70-037]

17 p3155 A70-34778

Propulsion requirements for reusable space shuttle, discussing engine development program [AAS PAPER 70-044]

17 p3147 A70-34784

Quantum electronic space vehicle, discussing time reversing motor or inverse /anti-/ atomic engine

17 p3148 A70-35213

Electromagnetic, mechanical and chemical methods for automatic checkout of nonelectronic aerospace propulsion systems

17 p3095 A70-35525

Unmanned nuclear electric propelled spacecraft using reactor with liquid metal MHD power conversion system

20 p3566 A70-40016

One millipound cesium ion thruster for synchronous ATS-F satellite, describing power conditioning and control logic subsystems [AIAA PAPER 70-1149]

20 p3690 A70-40205

Electric propulsion systems integration into SERT 2 spacecraft, discussing launch imposed environment, thrust vector control, thruster breakdown, power conditioning, etc [AIAA PAPER 70-1123]

20 p3691 A70-40222

Primary solar electric propulsion for automated space transportation propulsion program, considering performance and technology readiness [AIAA PAPER 70-1115]

20 p3691 A70-40228

Micropond extended range thrust stand /MERTS/ for testing electric thrusters for spacecraft auxiliary propulsion, providing three thrust measurement ranges and data telemetry system

20 p3607 A70-40232

Kaufman ion thruster providing electric propulsion for satellite spiraling from parking to synchronous orbit [AIAA PAPER 70-1101]

20 p3692 A70-40237

Third stage engine performance from mass properties data for space vehicles with side-by-side tanks [SAWE PAPER 846]

20 p3717 A70-40378

Solar electric propulsion systems technology development at JPL, discussing performance data and relationship to spacecraft requirements [AIAA PAPER 70-1153]

20 p3695 A70-40520

Concentric tube resistojet life tested on hydrogen and ammonia propellants for use with biowaste propellants [AIAA PAPER 70-1133]

20 p3568 A70-40521

Drag-free satellite design and propulsion requirements, noting orbit perturbation mechanisms [AIAA PAPER 70-1145]

20 p3717 A70-40523

Thermionic reactor electric propulsion for unmanned outer planets exploration, discussing spacecraft design, launch vehicle, weight factors, etc [AIAA PAPER 70-1122]

20 p3717 A70-40524

Optimal control of composite spacecraft propulsion system incorporating high thrust-weight ratio chemical engine and low thrust ion engine

21 p3865 A70-40831

Vapor biowaste electric spacecraft propulsion system, discussing recovery cycles and subsystem tradeoffs, specific impulse, chamber heating, power input and reaction products

21 p3866 A70-40869

Secondary propulsion subsystem earth synchronous orbital mission requirements, discussing thrust vector alignment and control, colloidal propellants and pulsing [ASME PAPER 70-AV/SPT-31]

21 p3866 A70-40870

Resistojet thrusters for spacecraft propulsion and control, discussing systems configurations, performance, weight, etc

21 p3866 A70-40986

Space compatible flight prototype ion engine power conditioning system design for Hg thruster using oxide cathode

21 p3867 A70-41006

Power conditioning requirements and specifications for spacecraft electric propulsion ion thruster

21 p3758 A70-41209

Nuclear fusion reactor spacecraft propulsion system using ion rocket with charged deuterium nuclei fuel, emphasizing nuclear plasma confinement problem

21 p3867 A70-41498

Pulsed plasma and low pressure detonator thrusters for long life secondary spacecraft propulsion, considering satellite stationkeeping and attitude control [AIAA PAPER 70-1147]

21 p3868 A70-41782

Mars and Venus orbiter spacecraft electric propulsion system, discussing Hg electron bombardment ion engine [AIAA PAPER 70-1154]

21 p3868 A70-41786

Rocket motion and space propulsion systems, discussing exhaust velocity effect on payload

21 p3869 A70-42039

Spacecraft electric propulsion system performance, discussing exhaust velocity optimization

21 p3869 A70-42043

Radioisotope thrusters for space propulsion, considering thermal heating methods and direct recoil

22 p4070 A70-43185

Nuclear electric space propulsion, emphasizing systems uncertainties and cost aspects

22 p4070 A70-43187

Thermionic reactors for spacecraft auxiliary power and electric propulsion, discussing in-core conversion system and diodes

22 p4071 A70-43191

Space vehicle for interstellar flight, discussing propulsion concepts, mission implications and international cooperation

23 p4254 A70-45011

Astronautics - IAF Conference, New York, October 1968, Volume 3, Propulsion reentry physics

23 p4234 A70-45017

Hydrogen oxygen engine designs for space vehicle auxiliary propulsion systems, considering long life thrust chamber performance with compatible heat transfer characteristics [SAE PAPER 700803]

24 p4395 A70-45908

Thermonuclear spacecraft propulsion, comparing X ray pumped gas laser and ion drive systems

24 p4377 A70-46211

SPACECRAFT RADIATORS

Radiator selection for manned spacecraft, considering thermal coating degradation, structural design, micrometeorite protection, plume impingement, reliability and fabrication

01 p0215 A70-10631

Optimal steady state thermal design for fin-tube single and double surface space radiators, including meteoroid protection and pumping power weight penalties

01 p0215 A70-10829

Circumferential wall temperature gradients in spacecraft radiator tubes as function of tube wall fins

09 p1789 A70-23261

Transient response of fin-tube space radiators sudden steady state operation halting and system cooling

09 p1790 A70-23564

Increased heat transfer for thermal coupling by interleaving fins in space applications

13 p2519 A70-28522

Passive radiative coolers role in utilizing IR detector systems for low temperature spacecraft applications, describing staged radiator design, optimization and tests [AIAA PAPER 70-854]

16 p2983 A70-33921

Thin plates radiant cooling with mutual irradiation in spacecraft radiators

22 p4122 A70-42518

Finned tube-sheet spacecraft radiator transient response for perturbations caused by power supply and heat sink temperature changes

22 p4123 A70-42519

Space vehicles with shielding for protection against meteor impacts, discussing tubular radiator design for heat removal

23 p4284 A70-45008

SPACECRAFT RECOVERY

Space rescue techniques and equipment in NASA recovery programs, considering low earth orbit and water landing

01 p0035 A70-10717

Space rescue requirements for earth-returning astronauts recovery under emergency conditions, discussing recovery zones determination by space flight mission control

04 p0761 A70-14929

Command and control functions of DOD Manager for Manned Space Flight Support Operations in spacecraft recovery

05 p0827 A70-16180

SOFAR /sound fixing and ranging/ systems for location and recovery of reentry vehicles and missile cases and rescue of disabled transoceanic aircraft

13 p2449 A70-29169

Space rescue probabilities, considering spacecraft emergency returns from orbit to earth surface and time sequences

14 p2654 A70-30780

Spacecraft or escape capsule rescue, discussing design, recovery planning, forces and sites

17 p3180 A70-35301

Reentry vehicle recovery deployment initiation, comparing performances of conical wake drogue and body attached spoilers hypersonic deceleration devices [AIAA PAPER 70-1207]

21 p3752 A70-41811

Lunik 16 lunar probe recovery technique, using steep angle and high deceleration reentry trajectory for unmanned capsule

23 p4257 A70-44096

Space rescue operations in orbit during heavy traffic of spacecraft with large passenger loadings, noting role of space shuttles and tugs

23 p4260 A70-44619

Space vehicle personnel escape/rescue/ survivability capabilities, considering on board, prepositioned aid and earth launched concepts

23 p4260 A70-44620

Rescue waiting time relation to number of communication and return sites for emergency astronaut return, considering day vs day/night recovery

23 p4245 A70-44639

SPACECRAFT REENTRY

Spacecraft reentry trajectory optimization, considering minimum coolant weight requirement in internal cooling system

02 p0381 A70-12416

Spacecraft thermal control during reentry, considering heat absorption, cooling by gas injection, radiant heat removal and shielding

04 p0780 A70-14407

Optimal space vehicle reentry control ensuring minimum scattering of landing points based on accelerometer and free pitch-angle gyroscope data

04 p0760 A70-14431

Electron gun onboard reentering spacecraft to measure densities and temperatures in flowing gases

06 p1066 A70-18286

Optimum impulsive velocity calculation for three dimensional deorbit from elliptical orbits to achieve specified reentry angle

06 p1152 A70-18496

Control algorithm for vehicle descent after reentry based on descent range prediction by integrating motion equations allowing for motion three dimensionality

07 p1393 A70-19482

Reentry into earth atmosphere of heavy ballistic missiles with variable and constant geometry compared with light missile

08 p1433 A70-21766

Mathematical model for determining optimal control of spacecraft reentry into atmosphere

10 p1940 A70-24318

Spacecraft optimal impulsive braking by onboard engine to ensure maximum angle of atmospheric reentry

12 p2310 A70-28253

Spacecraft reentry trajectory reconstruction using accelerometer and onboard navigation data from Apollo flights

13 p2485 A70-28378

Stochastic optimal trajectory control for spacecraft reentry at supercircular velocity, deriving computer algorithm

13 p2499 A70-28382

Optimal space vehicle reentry control ensuring minimum scattering points based on accelerometer and free pitch-angle gyroscope data

13 p2503 A70-28456

Radiation from electric dipole oriented normal to magnetostatic field in plasma column improving antenna transmission characteristic during reentry

13 p2467 A70-29913

Heating and g forces on rockets and space vehicles in descent trajectories as function of reentry velocity, achieving control by attack angle variation

15 p2812 A70-32361

Apollo thermal protection system noting low density ablation, flight and ground tests [AIAA PAPER 68-1142]

15 p2813 A70-32514

Control algorithm for vehicle descent after reentry based on descent range prediction by integrating motion equations allowing for motion three dimensionality

15 p2813 A70-32727

Optimal open loop controller and suboptimal feedback law to minimize terminal error of entry vehicle

16 p2947 A70-33439

Automated orbiting biosatellite program with reentry system, studying long term weightlessness and radiation effects

17 p3178 A70-35258

Space vehicle reentry hypersonic boundary layer characteristics, considering air components chemical reactions due to excessive heat

18 p3346 A70-36384

Planetary probes, orbiting space stations and manned spacecraft in interplanetary flights, discussing Mariner, Gemini and Apollo reentry and Venus landing

22 p4109 A70-42313

SPACECRAFT RELIABILITY

Apollo spacecraft hardware, command, service and lunar modules, discussing design factors and tests contributing to spacecraft reliability

[ALAA PAPER 69-1095] 01 p0194 A70-10618

Structural qualification testing of experimental tactical communication satellite (TAC COM SAT)

02 p0274 A70-13936

Space station damage containment and control, emphasizing safety problems and guidelines

04 p0762 A70-14933

German Space Research Association reliability and testing function, using failure analysis for space projects components and structures

[DGLR-69-30] 04 p0698 A70-15137

Inertial navigation system reliability indices and improvement, discussing mission success, mean time between failure and automatic monitoring

04 p0716 A70-15166

NASA aerospace system safety program implementation and supporting organization with emphasis on background, concepts, constraints, methods and results

[SAE PAPER 690710] 05 p0792 A70-15856

Apollo spacecraft propulsion systems design and operational requirements, emphasizing use of redundant components and system backups to achieve reliability

[SAE PAPER 690704] 05 p0923 A70-15858

Apollo reliability and quality requirements, reviewing changes due to cost reductions in space program

06 p1065 A70-17988

Thermal testing of planetary lander vehicle in vacuum chamber, modeling electronics modules and experiments using resistance heaters

[ALAA PAPER 70-222] 06 p1157 A70-18128

Aerospace vehicles testing cost and technical analysis, discussing component failure, motivation effects, test design optimization, flight simulation, etc

[ALAA PAPER 70-239] 07 p1396 A70-20379

Weapon Systems Level testing methods and machines application to missiles, manned space flight vehicles and Safeguard System

[ALAA PAPER 70-380] 10 p1862 A70-24923

Systems engineering approach to test planning with emphasis on risk reduction for spacecraft

[ALAA PAPER 70-367] 10 p1952 A70-24933

Launch load simulation on scaled vibration model concerning Saturn 5 structural integrity and flight failure

10 p1953 A70-25072

Thermoelectric outer planet spacecraft (TOPS) project incorporating adaptable data handling system and self testing and repairing computer with triple redundancy subsystems

11 p1996 A70-25368

Interplanetary space systems, analyzing failure factors to assure reliability

11 p2112 A70-26051

Quality assurance R and D for product design and operational integrity in manned space flight, noting space developments application to aircraft safety

15 p2676 A70-32231

Redundancy for spacecraft elements, describing various factors for priority establishment

15 p2712 A70-32643

Satellite reliability, discussing quality control, contractual matters, mathematical models, project management, failure modes, etc

15 p2813 A70-32826

Apollo lunar module rendezvous radar redundant gyro system for reliability enhancement, discussing principles and logic

16 p2983 A70-34066

Surveyor thermal switch for temperature control to assure spacecraft components performance during temperature extremes on lunar surface

16 p2845 A70-34127

Cost effective reliability apportionment in spacecraft subsystems, allocating failure-risk goals by mathematical model

17 p3101 A70-35160

Spacecraft flight systems voltage breakdown due to DC gas discharge, discussing occurrence and preventive techniques

17 p3053 A70-35164

Real time data processing and display for spacecraft thermal vacuum testing, using hybrid computer

17 p3059 A70-35176

Space corpuscular radiation simulation to obtain data for increased spacecraft life

19 p3511 A70-38284

Cost effective spacecraft testing in terms of statistical reliability, program effectiveness and equipment costs

19 p3554 A70-38293

Mariner 1969 test and operations program evaluated by ground tests and flight results, giving flight acceptable spacecraft recommendations

19 p3533 A70-38819

Mariner 7 preencounter anomaly in radio tracking data and trajectory investigated by computerized simulation

[ALAA PAPER 70-1065] 19 p3534 A70-38878

SERT 2 for testing ion thruster reliability and operational characteristics, discussing design and mission objectives

[ALAA PAPER 70-124] 20 p3716 A70-40221

Aerospace vehicles testing cost and technical analysis, discussing component failure, motivation effects, test design optimization, flight simulation, etc

[ALAA PAPER 70-239] 21 p3931 A70-41876

Lunar launch vehicles quality control and reliability, describing management procedures for test facilities, preproduction and purchased materials quality

22 p4126 A70-42384

Operational safety of nuclear rockets in orbit-to-orbit transportation in regard to radiation doses from plume and reactor, including malfunction condition

22 p4070 A70-43183

Long life spacecraft design and reliability based on marine practices and advanced system technology project, considering grand tour outer planets mission

[ALAA PAPER 70-1247] 24 p4412 A70-45964

SPACECRAFT RENDEZVOUS

U SPACE RENDEZVOUS

SPACECRAFT SENSORS

U SPACECRAFT INSTRUMENTS

SPACECRAFT SHIELDING

Radiation dosimetry and shielding onboard Cosmos 110 artificial satellite, noting earth belt proton radiation

01 p0198 A70-15158

Penetration criterion for double walled structures subject to hypervelocity meteoroid impact providing choice of protective material properties

[ALAA PAPER 68-1058] 03 p0584 A70-12921

Shield mass optimization of low thrust nuclear powered space vehicle for occupant shielding against reactor radiation

03 p0523 A70-13575

Spacecraft thermal control during reentry, considering heat absorption, cooling by gas injection, radiant heat removal and shielding

04 p0780 A70-14407

Meteoroid hazard to spacecraft, discussing penetration and protection information reliability obtained from terrestrial and satellite observations

05 p0914 A70-16631

Computer optimization of spacecraft optical coatings for temperature control, using finite element analysis and matrix inversion

[ALAA PAPER 69-979] 06 p1172 A70-17180

Satellite radiation dose rate experiment with simultaneous trapped particle and absorbed dose rate measurements, discussing proton spectra, material distribution, shielding effects, etc

06 p1061 A70-17263

Dosimetry data and personal radiation sensors from Apollo and Gemini flights, noting spacecraft geometry shielding effects

06 p1134 A70-17268

Gemini spacecraft shielding configuration and radiation detectors, describing cabin radiation distributions

06 p0990 A70-17269

Lightweight double walled meteoroid shield for Mariner Mars 1971, considering Teflon impregnated glass fabric outer sheet and multilayer thermal insulation

[ALAA PAPER 69-377] 07 p1394 A70-19712

Refurbishable ablative thermal protection for reusable lifting reentry vehicles

[ALAA PAPER 70-277] 07 p1397 A70-20386

Thermal control coatings as solar reflectors for spacecraft heat dissipation

08 p1527 A70-21357

Nondestructive tests for diffusion-formed refractory alloy coatings used as oxidation protection for hypervelocity spacecraft and reusable systems

09 p1692 A70-22679

Silicon oxide films coated satellite aluminum surfaces solar absorptivity and thermal emissivity, noting suitability as temperature control coatings

09 p1613 A70-23514

Insulation foils and surface coatings thermal properties effect on radiation properties for spacecraft thermal control systems

10 p1951 A70-24863

Radiation hazard to space vehicles by solar flare protons, calculating risk dose by computerized Monte Carlo simulation, applying importance sampling

10 p1934 A70-25190

Two plate meteoroid shields effectiveness determined by analyzing debris cloud ejected behind front plate after hypervelocity impact

[ALAA PAPER 69-380] 11 p2138 A70-26132

Spacecraft temperature prediction and heat conduction problems with nonlinear radiation boundary conditions by perturbation theory, applying to heat shield analysis

11 p2150 A70-26355

Expandable rigidizable solar shields operational, structural and thermal performance tests conducted with spherical models for cryogenically fueled space vehicles

12 p2312 A70-27131

Spacecraft meteoroid protective shield thickness sensitivity relationship to luminous efficiency

15 p2813 A70-32518

Damage mechanisms of hypervelocity projectile impact on thin targets and spacecraft shields

15 p2823 A70-32786

Thermal testing of inflatable solar shields for cryogenic space vehicles, discussing shield misalignment effects on propellant tank temperatures

[ALAA PAPER 70-856] 16 p2982 A70-33901

ZnO coating pigment for spacecraft thermal control, examining UV irradiation effects on electrical properties

16 p2961 A70-34056

Spacecraft shape and thermal coating pattern optimization by computer program

17 p3178 A70-35251

Solar flare radiation protection requirements, considering bulk and plasma radiation shielding

17 p3040 A70-35647

Earth intrinsic radiation flux incident angular coefficient, examining effect on partially screened flat spacecraft elements

21 p3942 A70-40847

Spacecraft thermal control coatings scale models, discussing temperature errors due to energy transport along surfaces

21 p3951 A70-41874

Spacecraft magnetic radiation shield optimization based on thickness criterion and system mass consideration

22 p3979 A70-43390

Deployable meteoroid shield for Saturn 1 workshop, describing design and hardware kinematics

23 p4257 A70-44386

Temperature measurement on thin steel shield subjected to hydrogen peroxide motor exhaust heating at cryogenic temperatures in space

23 p4280 A70-44389

Space vehicles with shielding for protection against meteor impacts, discussing tubular radiator design for heat removal

23 p4284 A70-45008

Environmental heat shielding for various sized Jupiter atmospheric entry probes

[ALAA PAPER 70-1324] 24 p4429 A70-45941

SPACECRAFT STABILITY

Time history of spin and forward motion accuracy of rocket launched from smoothbore, using analytical model and motion coupling through dynamic friction coefficient

03 p0582 A70-14311

Deployable STEM /storable tubular extendible member/ booms for aerospace gravity gradient stabilization, noting interlocked BI-STEM

04 p0761 A70-14725

Optimal iterative weighted least squares estimation of rotation-coupled flexural oscillations of boom stabilized satellites in earth orbits

04 p0763 A70-15413

Soviet monograph on optimal space flight trajectory control, covering vehicle CG trajectory and synthesis of automatic stabilization system using variational calculus

04 p0764 A70-15493

Liquid filled dampers for nutation damping of spacecraft with momentum wheel for attitude stabilization

06 p1154 A70-17163

Installed thrust vector for scarfed attitude control nozzles flush mounted with spacecraft cylindrical surface, predicting pressure distributions for internal thrust

06 p1154 A70-17167

Capture and gravity gradient stabilization of LIDOS satellite in eccentric orbit

[ALAA PAPER 69-921] 06 p1154 A70-17175

Spacecraft level vibrations and gravity effects on blue-green algae Plectonema Boryanum proposed as gas exchange medium

06 p0999 A70-17292

- Satellite launch vehicle attitude control stability study including fuel sloshing and body bending effects 06 p1155 A70-17320
- Suboptimal stabilization of axially symmetric satellite angular velocity, using ionic propulsion system as control torque 06 p1155 A70-17554
- Stochastic Liapunov stability of satellite motion influenced by aerodynamic and gravity gradient torques, considering atmospheric density uncertainty [AIAA PAPER 70-37] 06 p1159 A70-18185
- DODGE satellite launched into near-synchronous orbit to demonstrate gravity-gradient stabilization at high altitude and to experiment with damping techniques [AIAA PAPER 70-69] 06 p1159 A70-18218
- Flywheel stabilization for communication satellites, considering stabilization by reaction wheels, gyros, gas jets, etc [DGLR-69-058] 07 p1392 A70-18817
- Discures project satellites design, considering use of rotation stabilization 07 p1392 A70-18989
- Lunar mascon effects on Apollo type spacecraft orbits calculated for minimizing orbital instabilities 07 p1387 A70-19715
- Ammonia micropropulsion for geostationary satellites stabilization, discussing principle and working mode of thrusters 09 p1743 A70-22660
- Tethered orbiting interferometer configurations for future Radio Astronomy Explorer satellites, discussing gravitational stabilization and delta launching into orbit as single payload [AAS PAPER 69-255] 09 p1766 A70-22930
- Nonspinning satellite orbit eccentricity effect on attitude stability 09 p1766 A70-23229
- Small plane perturbations stability losses in uniform rectilinear motion of nonrigid deformable rocket, using slender bodies pressure theory 10 p1950 A70-24528
- Orbital stability of geostationary vehicle at arbitrary latitude, considering nonlinear equations and deducing stability conditions by Liapunov method 10 p1950 A70-24783
- Delayed feedback for LF periodic conditions /auto-oscillations/ in relay systems of cosmic flying apparatus stabilization 11 p2119 A70-25342
- Motion stability of rapidly spinning satellite, discussing elastic booms effect 11 p2128 A70-26784
- Equations of motion for dynamic stability of flexible freely spinning Alouette-type satellite with crossed dipole configuration 12 p2312 A70-27194
- Dual spin satellite stability with four mass nutation damper 12 p2314 A70-27842
- Satellite stationary motions stabilization using rotors with axes fixed inside spacecraft 13 p2499 A70-28389
- Dynamics of gravity stabilized satellite having maximum damping rate 13 p2499 A70-28391
- Manual control systems for spacecraft stabilization involved in rendezvous, midcourse correction, landing, etc 13 p2357 A70-28394
- Satellite stabilization one-axis control system using earth magnetic torquer 13 p2500 A70-28405
- Admissible controls synthesis for closed loop system /satellite/ stability 13 p2500 A70-28410
- Circular orbit gravitationally stabilized satellite oscillation damping by changes of moments of inertia 13 p2501 A70-28420
- Attitude-translation motion coupling effect on stability of gravity-stabilized drag-free satellites 13 p2501 A70-28424
- DODGE satellite gravity gradient stabilization at synchronous altitude by flywheel and magnetic sample-and-hold damping, noting boom bending 13 p2501 A70-28425
- Symphonic communication satellite orbit and attitude stabilization systems components, operation and accuracy requirements 13 p2502 A70-28432
- Petrel payloads taking into consideration rocket stability after launch and compartment design 13 p2503 A70-28683
- Stability and wind response determining spacecraft structure forces and bending moments [AGARDOGRAPH-115] 13 p2504 A70-28754
- Spacecraft parameters role in response to atmospheric disturbances, considering model design and control systems effects [AGARDOGRAPH-115] 13 p2504 A70-28757
- Numerical solution of satellite rotational damping by onboard motors using Euler equations, local variations and finite control time 13 p2505 A70-28963
- Gravity gradient stabilization systems for earth-pointing satellites, noting long term reliability and accuracy 13 p2507 A70-29828
- Nonspin stabilized satellite attitude reconstruction using least squares estimate 14 p2654 A70-30775
- Equilibrium configurations, considering aerodynamic forces for axisymmetric satellites attitude stability using infinitesimal analysis and Liapunov method 15 p2809 A70-31779
- Gravity stabilized gyrostabilized satellites internal angular momentum effect on nonlinear resonant attitude motions 15 p2810 A70-31785
- Scanning celestial attitude determination system /SCADS/, providing triaxial information for earth stabilized satellites 16 p2946 A70-33159
- Manned and unmanned orbital space facilities pointing and stability requirements, noting application to stellar and solar astronomy, earth observations, etc 16 p2979 A70-34068
- Bearing assembly energy dissipation effects on dual spin spacecraft attitude stability, explaining satellite motion anomalies 17 p3100 A70-34756
- Dual spin satellites considered as deformable flexible gyrostats, obtaining stability criteria 17 p3177 A70-35234
- Stable equilibrium positions for satellite consisting of many rigid bodies in circular orbit about center of gravity, using numerical method 18 p3332 A70-35963
- Satellite vibration tests simulation installations, describing measurement and control devices for lateral motion and test object safety 19 p3401 A70-38299
- Nonspinning symmetrical satellite in circular orbit, analyzing laterally oriented rotor effect on attitude stability 19 p3533 A70-38340
- Dual spin spacecraft bearing assembly flexibility effects on attitude stability [AIAA PAPER 70-1043] 19 p3533 A70-38858
- Dual spin spacecraft, considering nonlinear damping effect on attitude stability [AIAA PAPER 70-1044] 19 p3533 A70-38859
- Torque free spinning satellite with flexible appendages, investigating design parameters effects on nutational stability [AIAA PAPER 70-1046] 19 p3534 A70-38861
- Nutational stability and closed loop position control of dual spin spacecraft with despun platform [AIAA PAPER 70-975] 20 p3715 A70-39554
- Axisymmetric dual spin spacecraft consisting of nonconcentric frictionlessly mounted cylinders equipped with viscous damping mechanisms, evaluating stability criteria by energy method [AIAA PAPER 70-973] 20 p3715 A70-39556
- Motion and stability of rotating connected two body space station satellite system, developing Lagrangian equations of motion and optimizing damping system parameters [AIAA PAPER 69-919] 20 p3716 A70-39678
- Adaptive tracking filter for bending mode stabilization of large flexible boosters [AIAA PAPER 69-874] 20 p3716 A70-39682
- Multiplane balancing method for minimizing weight required for spacecraft stability [SAWE PAPER 848] 20 p3595 A70-40362
- Air navigation Discourses project satellites, discussing spin or three axis stabilization, system replenishment strategies and subsystem reliability 21 p3929 A70-41259
- Magnetic desaturation of inertia flywheels of satellite in equatorial or slightly inclined orbit, discussing satellite stabilization 22 p4110 A70-42488
- Radiation forces on flat plate in ecliptic earth orbit applicable to satellite attitude dynamics during pitching libration 22 p4125 A70-43437
- Comparative stability of freely spinning satellites for arbitrary number of flexible booms in rotation plane 22 p4111 A70-43440
- Aerodynamic and gravitational torque effects on orbiting satellites attitude stability, applying Liapunov direct method in case of conservative aerodynamic torque [AIAA PAPER 69-832] 23 p4258 A70-44559
- Space shuttle transition trajectory optimization for cruising flight entry, considering longitudinal control, pitchup instability and angle of attack 23 p4244 A70-44623
- Optimal moments of inertia of rigid satellite in circular orbit by generalization of Beletskij concept, discussing libration boundaries 23 p4261 A70-44677
- Satellites with many flexibly coupled rigid bodies, calculating libration upper bounds for predicting perturbation and stability 23 p4262 A70-44682
- Magnetically stabilized satellites passive roll control, discussing resonance solutions by variational approach 23 p4262 A70-44690
- Parameter optimization of gravity gradient stabilized satellite in circular orbit, considering minimum transition time and eccentricity oscillation 23 p4264 A70-45014

SPACECRAFT STERILIZATION

Collection of papers on planetary quarantine and spacecraft sterilization covering microbiology, spacecraft components, launching and environments, planetary landing, etc 03 p0433 A70-12996

Electro-pyrotechnic initiators for space applications subjected to dry heat sterilization cycles and to post-sterilization mechanical and electrical environments 03 p0495 A70-14131

Microbiological assay procedures for spacecraft sterilization and tabulation of microorganisms found on Surveyor 7 05 p0808 A70-16705

Sterile access system using pilot assembly sterilizer system /PASS/ for NASA Planetary Quarantine Program 05 p0808 A70-16708

Spacecraft contamination control teamwork operation, examining procedures and processes to ensure components cleanliness 05 p0809 A70-16713

Sterilized solid propellant motors applicability to planetary landing capsule spin stabilization [AIAA PAPER 69-823] 07 p1365 A70-19716

Sterile lander recontamination prevention from microorganisms during in-flight transfer from unsterilized carrier vehicle 11 p1991 A70-26049

SPACECRAFT STRUCTURES

Al-B composite missile adapter design for aerospace structures 02 p0306 A70-11951

Optical and mechanical techniques for space experiment structures and metals satisfying space requirements 03 p0492 A70-13848

Hypervelocity projectile size and density effect on ballistic limit of dual sheet spacecraft meteoroid protection structures, considering penetration of low and high density particles [AIAA PAPER 69-376] 04 p0776 A70-15422

Welding of satellite and spacecraft segments in space, discussing arc, electron beam, resistance, vacuum diffusion, cold pressure and brazing techniques 05 p0855 A70-16375

Atmospheric turbulence characteristics related to drag loads of tall spacecraft structures by boundary layer wind model 06 p1160 A70-17165

Flexible spacecraft equations of motion derived by modeling as rigid central body with arbitrary subsidiary flexible bodies [AIAA PAPER 70-19] 06 p1157 A70-18116

Lightweight double walled meteoroid shield for Mariner Mars 1971, considering Teflon impregnated glass fabric outer sheet and multilayer thermal insulation [AIAA PAPER 69-377] 07 p1394 A70-19712

Structural analysis of boron filament-epoxy composite laminate tubes for use as spacecraft long column members 08 p1595 A70-21911

Space engineering, flight instrumentation features and spacecraft subsystems integration problems 10 p1950 A70-24610

Tiros M requirements for earth resources sensor systems, discussing spacecraft structure, dynamics, power, command and communications subsystems 10 p1950 A70-24638

Aerospace vehicles structural vibration environments prediction methods emphasizing vibration sensor mounting resonances [AIAA PAPER 70-402] 10 p1959 A70-24903

Vibration behavior theory for elastomechanical systems applied to aircraft and space constructions 10 p1961 A70-25054

Space vehicle residual thrust oscillation and dynamic response using power spectral density functions from flight data 10 p1953 A70-25068

Corrugated skins solar absorptance and IR emittance computed for spacecraft thermal design, analyzing other nondiffusive radiative enclosures 11 p2150 A70-26352

Radiation stable refractory oxides in white spacecraft thermal control coatings, discussing photocatalysis application to degradation analysis 11 p2067 A70-26364

Solid state diffusion bonding techniques for aerospace Ti structural components 12 p2242 A70-27093

Penetration mechanics of multishield structures based on discrete particle modeling of impact debris [AIAA PAPER 69-371] 13 p2509 A70-28521

Stability and wind response determining spacecraft structure forces and bending moments
[AGARDGRAPH-115] 13 p2504 A70-28754

Aerodynamic and structural configuration effects on spacecraft inflight wind load calculations, showing Apollo interface lateral bending 14 p2653 A70-30585

Optimum overlap design of thin walled tubular extendible spacecraft structures under solar heating in zero-g environment 14 p2657 A70-30762

OGO spacecraft structures, thermal control systems, attitude control, weight and power supplies 15 p2810 A70-31782

Book on tubular spacecraft booms covering design and flight experiences, system performance, evaluation, etc 16 p2983 A70-33961

Compression spring mechanisms for separation of spacecraft and shrouds, summarizing design characteristics 16 p2921 A70-34116

Mariner 4 spacecraft structural dampers construction and performance 16 p2922 A70-34120

Ruggedized spacecraft mechanisms for severe shock environments 16 p2922 A70-34121

Spacecraft boom design and performance, including Russian spacecraft photographs 16 p2985 A70-34137

Spacecraft boom selection, discussing parameters, intended use, environment and effect on vehicle 16 p2986 A70-34140

High intensity noise enveloping space vehicle as distributed excitation, examining correlation effects on structural response 17 p3059 A70-35170

Space vehicle optimal design based on reliability analysis, taking into account cost of materials strength tests [JPL-TR-32-1496] 17 p3188 A70-35224

High intensity noise testing of missile and spacecraft structures, simulating acoustically induced vibrations due to aerodynamic turbulence 19 p3531 A70-37697

Azur satellite magnetic parameters simulation, noting spacecraft structure effect 19 p3400 A70-38295

Spacecraft thermal vacuum test installations design and operations for locating spacecraft structural weak points 19 p3400 A70-38297

Filamentary composite materials for space vehicles structural design, noting mass reduction, strength, foldability, formability, etc 20 p3656 A70-40030

Aircraft, rocket or other rigid or flexible structure, computing inertial constants based on measurements of generalized masses of natural modes 21 p3935 A70-41408

Thermoelectric outer planet spacecraft (TOPS)/structural problems associated with high gain antenna and electronic equipment 21 p3930 A70-41803

All-flexible parawing as primary descent system for large spacecraft landing, discussing configuration, structural arrangement, multistage reefing and L/D performance tests [AIAA PAPER 70-1187] 21 p3754 A70-41828

Dynamics of deployable space structures stiffened by centrifugal forces due to spin, discussing LF radio telescope 21 p3931 A70-41854

Small scientific satellite design objectives, structural and electrical requirements, components integration, instrumentation, antennas, spin rates, vibrations, sealing, reliability, etc 22 p4110 A70-42497

Earth orbital space station electrical power systems, discussing power sources, effect on structural configuration, environmental control and launch and resupply operations [MDAC-WD-1461] 23 p4143 A70-44605

SPACECRAFT TELEVISION

NT SATELLITE TELEVISION

Slow scan TV systems for planetary exploration, discussing sampled vidicon operation, digital encoding, data storage, signal to noise ratio, future design trends, etc [SMPT PREPRINT 106-3] 02 p0294 A70-11682

Secondary electron conduction TV camera tube with three color filter wheel for Apollo missions 03 p0493 A70-14025

Black and white and color Apollo 11 secondary electron conduction TV cameras, discussing characteristics and mission requirements 04 p0688 A70-14692

Lunar regolith and polarized component of earthlight observations by Surveyor 7 TV camera 04 p0752 A70-15061

Prelaunch photometric calibration of Surveyor TV system for reconstruction of lunar terrain televised

pictures permitting system lunar performance prediction [AIAA PAPER 68-1138] 04 p0692 A70-15405

Apollo 7 and 8 command modules TV camera systems design, considering additional function of public information 07 p1280 A70-19229

Visual imaging systems for Mars orbiter compared for performance and interactions with mission and spacecraft design 07 p1280 A70-19230

TV test chart for evaluating Surveyor lunar spacecraft TV system covering resolution, photometric and colorimetric response and sun angular position [SMPT PAPER 105-71] 10 p1890 A70-24601

Geometric distortions in ESSA 7, Surveyor 7 and Mariner 4 TV systems caused by scale distortion, discussing stability of systematic component in magnitude and shape 10 p1890 A70-24727

Satellite video-telephone systems promoting economic growth in developing nations through linkage with developed nations advanced centers [AIAA PAPER 70-474] 11 p2000 A70-25455

Crosstalk effects on data transmission in multiplex TV systems for aerospace communications analyzed by signal and noise models 13 p2363 A70-28384

Navigation data from Mariner Mars 1969 TV pictures, estimating spacecraft trajectory to planetary center 14 p2614 A70-30468

ESSA 7, Surveyor 7 and Mariner 4 space TV systems geometric distortions analysis and potentials in analytic photogrammetry and topographical mapping 14 p2586 A70-30982

Low light level TV /LLLTV/ tube, camera and sensor development for military and space applications 16 p2903 A70-33129

Apollo 10 color TV camera for real time scenes, describing configuration performance and total system operation 16 p2907 A70-33187

TV experiment for Mariner Mars 1971 Project, providing fixed and variable feature imaging data 16 p2978 A70-34027

Surveyor TV mechanisms, discussing camera, mirror, zoom lens, filter wheel, focal plane shutter and lubrication 16 p2914 A70-34147

Spaceborne narrow band TV system with image memory tube and electronic shutter, noting variable exposure time, motion compensation and multimode scanning 17 p3089 A70-35267

Slow scan TV systems for planetary exploration, discussing sampled vidicon operation, digital encoding, data storage, signal to noise ratio, future design trends, etc [SMPT PREPRINT 106-3] 17 p3095 A70-35634

Surveyor 7 TV system in photon integration mode, analyzing slow scan vidicon storage characteristics and dark current limitations 17 p3095 A70-35635

Apollo black and white TV scan converter design and operation 17 p3095 A70-35636

Mariners 6 and 7 orbits determination by weighted least squares estimation based on common surface features in overlapping TV pictures [AIAA PAPER 70-1066] 19 p3529 A70-38879

Grand tours navigation system consisting of deep space network radio and onboard TV for future TOPS /Thermoelectric Outer Planet Spacecraft/ applications 21 p3849 A70-41799

Meteorological TV imaging systems development in last decade, including low and synchronous altitude camera, sensors, orthicons, etc 23 p4193 A70-43963

Integrated data processor-operation controller for stellar TV photometer systems in spaceborne observatory, considering limited channel transmission capacity 23 p4167 A70-44649

SPACECRAFT TRACKING

NT SATELLITE TRACKING

Two axis spherical gage bearing gyro for accurate measurements of space vehicle position and attitude rates while maintaining compatibility with exotic environments 01 p0086 A70-10308

HEOS 1 satellite telemetry, telecommand and tracking systems, noting data transmission degradation due to high solar activity 01 p0045 A70-11115

Lunar gravitational field determination from analysis of Lunar Orbiter spacecraft tracking data 03 p0562 A70-12915

Artemis I and II telemetering antennas at Guiana Space Center for spacecraft tracking 05 p0819 A70-15987

Spacecraft telecommunication and tracking systems in Gemini, Mercury and Apollo programs, emphasizing

ing Apollo command and lunar modules equipment and mission ground stations 05 p0813 A70-16326

Apollo onboard computers tracking data state-vector corrections covariance matrix, considering initial estimate, noise and tracking geometry errors [AIAA PAPER 70-162] 06 p1015 A70-18072

Navigation accuracy of two way Doppler tracking of interplanetary spacecraft during heliocentric and planetary encounter trajectory phases [AIAA PAPER 69-899] 07 p1331 A70-19727

Linear FM pulse compression radar system operating at 94 GHz, obtaining echoes from orbiting objects for identification 08 p1462 A70-21290

ELDO rocket tracking error, considering guidance antenna angular precision and UHF circuit performance in signal comparison 09 p1720 A70-22649

Step-Track automatic angle tracking technique for communication satellites, seeking peak of antenna single beam [AIAA PAPER 70-416] 11 p1999 A70-25454

Space vehicle on-line tracking with impulsive thrust maneuver by sequential estimation scheme, reducing radius measurement error 11 p2008 A70-26237

Binary-coded sequential acquisition spacecraft ranging system operating at weak signals using HF digital logic 11 p2009 A70-26252

Optimal linear estimation and control theory application to high precision optical spacecraft tracking systems design 11 p2028 A70-26302

Telescope servocontrol system with low pointing error and drift rate, permitting extended time exposure photography of star or deep space probe 12 p2202 A70-26869

Lunar gravity correlation with large craters indicated from negative accelerations recorded in Apollo 12 lunar module Doppler radio tracking data 12 p2298 A70-27270

Deep Space Network /DSN/ data accuracy limitations relation with ability to determine orbit of probe, examining improvements after Mariner 2 and trends 13 p2448 A70-28702

Spacecraft tracking methods applied to solid earth and ocean physics 15 p2809 A70-31685

Recursive estimation and Kalman filtering for space vehicle trajectory tracking, using Doppler shift measurements 16 p2866 A70-34071

Digital computer controlled positioning of telemetry antennas for tracking spacecraft 17 p3062 A70-35508

Search optimization for object drifting in outer space, considering approximate location and speed 17 p3172 A70-35668

Covariance matrices estimates for trajectory parameter tracking of thrust-maneuvering spacecraft [AIAA PAPER 70-1017] 20 p3666 A70-39516

Gravitational relativistic theory tests using tracking data from interplanetary spacecraft, orbiters and landers [AIAA PAPER 70-1317] 24 p4414 A70-46326

SPACECRAFT TRAJECTORIES

NT CIRCUMLUNAR TRAJECTORIES

NT EARTH-MARS TRAJECTORIES

NT EARTH-MOON TRAJECTORIES

NT EARTH-VENUS TRAJECTORIES

NT INTERPLANETARY TRAJECTORIES

NT LUNAR TRAJECTORIES

NT MOON-EARTH TRAJECTORIES

In-flight compensation for space probe trajectory deviations, discussing attitude determination and control of triaxial and spin stabilized space probes 01 p0186 A70-11265

Spacecraft trajectory optimal determination without knowing measurements error distribution function, examining computer solution properties of linear programming 01 p0192 A70-11477

Minimum time turns for spacecraft about fixed axis lying beyond plane of vehicle forces 01 p0197 A70-11480

Spacecraft motion parameters and physical characteristics of space determined from statistical analysis of measurement data 01 p0094 A70-11484

Optimal motion control of spacecraft refueling during flight by liquefying atmospheric gas along prescribed trajectory under constant thrust 01 p0197 A70-11502

Osculating transfers between two prescribed trajectories without considering optimization problem, obtaining in-space launching point of artificial cosmic bodies 03 p0575 A70-13972

Optimal control of thrust limited minimum-propellant rocket-powered vehicle using expansion about optimal trajectory 04 p0750 A70-14928

- Patch-conic method accuracy and limitations in determining space trajectories as function of planetary zones of influence 04 p0750 A70-14941
- Soviet monograph on optimal space flight trajectory control, covering vehicle CG trajectory and synthesis of automatic stabilization system using variational calculus 04 p0764 A70-15493
- Tangential thrust, constant acceleration trajectories for close solar probe missions using low thrust electric engines 06 p1137 A70-17177
- Satellites and space probes orbital parameters calculation, considering circular and elliptical trajectories and rendezvous maneuver example 06 p1140 A70-17583
- Optimal landing of spacecraft on moon surface from low circular orbit, analyzing rocket thrust, altitude and landing site distance effect on spacecraft mass 06 p1155 A70-17880
- Optimal information selection for determining spacecraft trajectory, considering atmosphere, light speed and series expansion coefficients of planetary gravitational potentials 06 p1142 A70-17891
- Manual onboard orbit determination assuming electronic equipment failure, discussing geometric in-plane orbital parameters and safe orbit check [AIAA PAPER 70-159] 06 p1144 A70-18033
- Heliocentric low thrust spacecraft trajectory analysis using two-variable asymptotic expansion method [AIAA PAPER 70-214] 06 p1145 A70-18064
- Trajectory, guidance and environmental parameters and uncertainties effect on design optimization of out-of-orbit Viking soft lander [AIAA PAPER 70-99] 06 p1157 A70-18134
- Computation methods for optimal rocket trajectories closely approaching gravitating celestial bodies, alleviating computational difficulties with regularizing techniques [AIAA PAPER 70-95] 06 p1146 A70-18202
- Hybrid patched conic technique as iterative procedure for generating translunar and transearth trajectories emphasizing computing time saving 06 p1152 A70-18495
- Lawden primer vector theory applied to matched conic spacecraft trajectories optimization 07 p1381 A70-19325
- Soviet book on motion of guided rockets in space covering aerodynamic and structural aspects, stabilized and disturbed rocket motion, etc 08 p1582 A70-20756
- Queue control techniques in generating predicted trajectory, discussing queue control logic requiring minimum storage 08 p1467 A70-21049
- Spacecraft mission planning for trajectory control after establishing mission objectives, trajectory plan and crew timeline for Apollo flights 09 p1725 A70-23709
- Selection of uncorrelated measurement composition ensuring optimal accuracy of space vehicle trajectory 10 p1939 A70-24301
- Free fall vehicle dynamics for wind tunnel measurements of research shapes used in computer simulation of vehicle trajectories [AIAA PAPER 69-229] 12 p2157 A70-28081
- Satellite rendezvous programmed control with allowance for thrust limitation by free trajectories method, determining impulse duration, magnitude and time 12 p2314 A70-28257
- Adaptive variable-parameter spacecraft trajectory control, discussing loop synthesis and model reference system stability and dynamic accuracy 13 p2380 A70-28383
- Space navigation procedures verification considering vehicle trajectory parameters, noting applicability to linear systems with estimable parameters 13 p2447 A70-28412
- Space probe trajectory near second order integration under influence of solar oblateness and gravitation 14 p2635 A70-30288
- Lunar based radar beacons for nearby spacecraft navigation, noting trajectory determination advantages 14 p2614 A70-30461
- Navigation data from Mariner Mars 1969 TV pictures, estimating spacecraft trajectory to planetary center 14 p2614 A70-30468
- Jet assisted orbital spacecraft trajectories equations derivation, considering Kepler trajectories and orbital velocities 15 p2800 A70-32260
- Semiwideband and adaptive noise variance recursive estimation techniques applicable to spacecraft trajectory analysis 15 p2803 A70-32586
- Branched trajectory optimization for split rocket vehicles using projected gradient or steepest descent method 16 p2977 A70-33871
- Recursive estimation and Kalman filtering for space vehicle trajectory tracking, using Doppler shift measurements 16 p2866 A70-34071
- Interstellar drag resulting from relativistic rocket elastic collisions with interstellar matter, discussing effects on minimum time acceleration limited relativistic trajectories 17 p3155 A70-34752
- Computation methods for optimal rocket trajectories closely approaching gravitating celestial bodies, alleviating computational difficulties with regularizing techniques 17 p3172 A70-35666
- Space vehicle trajectories, discussing programming method to control motion for prescribed boundary conditions 17 p3173 A70-35700
- Extraterrestrial transport trajectory control by jet assistance 18 p3333 A70-36670
- Perturbative effects of Jupiter moons on spacecraft flyby and postencounter heliocentric trajectories, noting precision targeting [AIAA PAPER 69-932] 18 p3316 A70-36680
- Closed form solution for minimum fuel constant thrust trajectories for vehicle transfer in vacuum between arbitrary boundary conditions 18 p3316 A70-36683
- Pioneer-F Jupiter flyby mission planning, considering use of optimum broken plane trajectories to increase launch opportunity and/or payload capability [AIAA PAPER 70-1050] 19 p3528 A70-38865
- Closed form approximate solution for restricted three body motion of lunar or interplanetary spacecraft, demonstrating accuracy and flexibility in lunar mission trajectory calculations [AIAA PAPER 70-1061] 19 p3529 A70-38875
- Multiconic method space flight trajectories analysis, discussing computation time and circumlunar flight altitude and velocity errors [AIAA PAPER 70-1062] 19 p3529 A70-38876
- Mariner 7 preencounter anomaly in radio tracking data and trajectory investigated by computerized simulation [AIAA PAPER 70-1065] 19 p3534 A70-38878
- Future spacecraft mission for short period comets rendezvous, considering trajectory requirements and launch vehicle payload capabilities [AIAA PAPER 70-1072] 19 p3530 A70-38885
- Spacecraft trajectory initial conditions expressions as parameters dependent functions, applying results to Mars lander mission [AIAA PAPER 70-1016] 20 p3666 A70-39517
- Closed form expressions for linear and higher order corrections to multipulse approximations of space flight trajectory optimization solutions, using bang-bang thrust control [AIAA PAPER 70-1014] 20 p3667 A70-39519
- Space vehicle trajectories power-optimal single parameter nonlinear correction, assuming ideal impulse performance 21 p3883 A70-40829
- Midlatitude stratosphere and lower ionosphere density model, discussing vertical, diurnal and seasonal variations effects on spacecraft trajectories 21 p3813 A70-40830
- Low thrust trajectory transfer from low to synchronous orbit, examining hydrogen resistance jet and mercury bombardment ion thruster 22 p4089 A70-42487
- Analytic approximation for initial adjoint vector for optimal/minimum propellant/ space trajectories [AIAA PAPER 69-916] 23 p4243 A70-44509
- Algorithm for space trajectories optimization with delta velocity constraints 23 p4245 A70-44683
- SPACECREWS**
- Crew locomotion effect on spacecraft attitude control using space cabin simulator tests 01 p0036 A70-10853
- Crew requirements influence on systems design and operations criteria for long duration biomedical and behavioral measurement program in earth orbiting space laboratory [ASME PAPER 69-WA/BHF-17] 04 p0643 A70-14858
- Space flight emergencies causes and consequences, underlying life threats and crew survival times, considering equipment failures, personnel errors, etc 04 p0761 A70-14926
- Physiological and physiopathological effects of transverse accelerations on spacecraft crews, discussing cardiovascular and respiratory systems 05 p0799 A70-15763
- Wake-sleep rhythm of spacecrews for operational capacity to maintain constant watch of spacecraft, suggesting recreation of terrestrial time cycle in space 05 p0799 A70-15766
- Regenerative life support system development for multiman crews on extended space missions, considering maintainability, reliability and automation [SAE PAPER 690637] 05 p0804 A70-15845
- Spacecraft incorporated emergency rescue systems, discussing design of nonseparable crew escape compartment and separable capsule 07 p218 A70-19010
- Crew visibility requirements for rendezvous, docking and earth landing of reusable reentry vehicles [AIAA PAPER 70-262] 07 p1399 A70-20398
- Spacecrew candidates leisure time preferences, discussing off-duty concepts for long space missions 16 p2853 A70-33709
- NASA ten year space station operational concepts, discussing mission planning, crew scheduling and management [AAS PAPER 70-031] 17 p3176 A70-34804
- Physiological reactions of Soyuz 6, 7 and 8 crew during group flights, noting cardiovascular and respiratory reaction to submaximum stresses after flight 17 p3038 A70-35361
- Medicobiological approach to living conditions for sustained residence and human activity during prolonged space flights, describing sealed chamber experiment 19 p3367 A70-37525
- Manned space station design, discussing durations of scientific experiments and crew operation 19 p3532 A70-37752
- SkyLab mission in 1972, describing orbital workshop configuration and three man crew integration for operational experiments [AIAA PAPER 70-1328] 24 p4417 A70-45939
- SPACERS**
- Spaced damping reducing structural response to vibration, discussing efficiency, design flexibility and weight addition 08 p1507 A70-21269
- Lateral heat transfer along parallel conducting and radiating plates spaced by absorbing and isotropically scattering dielectric [AIAA PAPER 70-849] 16 p2939 A70-33916
- SPACING**
- NT AIRCRAFT APPROACH SPACING**
- Electromagnetic energy transmission factors for metal-dielectric-metal system, calculating net energy flux, noting effects of metal spacing, time, temperature level, etc [ASME PAPER 69-WA/HT-8] 04 p0784 A70-14822
- Close-spaced nozzles twin jet configuration, achieving low nozzle and total afterbody drag [AIAA PAPER 70-934] 17 p3149 A70-35844
- Dolph-Pritchard technique limitations for transformation of array factor into Chebyshev polynomial as related to element spacing for single lobe endfire arrays 20 p3599 A70-40315
- SPAIN**
- Meteorological rockets fired in Spain, obtaining stratospheric wind and circulation data 07 p1396 A70-20278
- INTA-255 ionospheric sounding rocket, describing vehicle and launcher design, test firings, ground facilities, etc 13 p2504 A70-28686
- SPALLATION**
- Cross sections of fragments emitted in spallation reactions of carbon and nitrogen nuclei emulsion with alpha particles 09 p1733 A70-23549
- Radionuclides production rates in stratosphere from spallation reactions of cosmic rays with Ar 17 p3152 A70-35759
- Cosmic ray track sources in meteoritic minerals, considering heavy primaries, secondary spallation and fission products 19 p3508 A70-38142
- High energy alpha particle beam exposed to plastic scintillators, determining spallation cross section for C12/alpha, alpha n/C11 21 p3852 A70-41138
- Apollo 11 lunar dust examination by neutron activation analysis, determining spallogenic manganese 53 21 p3908 A70-41579
- Rock particle tracks of primary cosmic rays, spallation recoil nuclei, nuclear fission and solar wind ions, observing time scale multiple soil orientation 21 p3914 A70-41652
- Spallation limits on low energy cosmic and nuclear gamma rays interstellar fluxes, evaluating fast particle effects on interstellar medium 24 p4397 A70-45758
- SPALLING**
- Stress gradient theory interpreted in terms of time dependent failure criterion to study critical stress vs impulse theory of spall fracture 05 p0938 A70-16481
- High purity beryllium dynamic tests determining Hugoniot equation of state, shock profile and spall threshold /onset of microcracking/ for elastic pulses [AIAA PAPER 69-360] 11 p2066 A70-25964
- Fractography of spall cavities and crack growth in ball rolling contact fatigue, using scanning electron microscope 15 p2745 A70-32444

SPARE PARTS

Spall nucleating mechanism for Al, noting microcracks in embedded particles 16 p2991 A70-33894

SPARE PARTS

Integrated materiel management for systems or product costs reduction applied to high cost spares management 02 p0401 A70-11671

Spares management of large aircraft contract in relationship to total integrated logistics support systems management 02 p0401 A70-11672

Optimal spare parts inventory determined for stochastically failing components using mathematical model 08 p1501 A70-20603

Computerized control of aircraft spare parts inventories, using optimization method maximizing aircraft availability and minimizing handling costs 13 p2524 A70-28836

Cost effective spares provisioning models for airline operations, minimizing availability-cost ratio for line replaceable unit and total fleet 13 p2525 A70-29571

Availability assurance using computerized spare allocation model for optimal selection of sufficient spares to achieve required protection against system failures 14 p2592 A70-31114

Comparative demand forecasting for military helicopter spare parts, stressing exponential smoothing model 20 p3740 A70-39643

SPARK CHAMBERS

Monograph on balloon and satellite borne spark chambers for cosmic gamma radiation energy and direction determination, discussing relativistic electrons multiple scattering 07 p1368 A70-19617

Primary cosmic ray particles location in photographic emulsions exposed to balloon elevations by spark chambers, noting stack alignment 09 p1679 A70-22990

Pulsed gamma ray emission from Crab Nebula pulsar NP 0532 investigated by balloon-borne spark chamber detector 13 p2492 A70-29271

Astronomical gamma ray emission measurement by balloon-borne spark chamber, presenting results for discrete and diffuse sources and albedo intensities 19 p3501 A70-38088

SPARK DISCHARGES

U ELECTRIC SPARKS

SPARK GAPS

Space charge injection-impulse voltage separation technique for nonuniform field breakdown phenomena 01 p0110 A70-10560

Fixed gap electrostatic spark discharge apparatus for booster type explosive sensitivity tests, discussing construction of two models, safety features and results 03 p0548 A70-14120

Laser induced ion emission triggering of spark gaps, distinguishing channels due to electrons and ions by high speed shadowgraph technique 13 p2426 A70-28797

Laser triggered spark gap /LTSG/ with subnanosecond rise time, describing construction and operating characteristics 18 p2371 A70-37092

Subnanosecond jitter spark gap obtained with YAG-Nd pulsed laser triggered switching at moderate repetition rates 19 p3444 A70-37666

Low jitter multiple high voltage spark gaps switching at 50 pps by Q spoiled YAG laser triggering 19 p3444 A70-37667

Breakdown mechanism in Q switched ruby laser triggered spark gap, noting pulse duration and power peak 22 p4049 A70-42352

Air spark gap to switch stored charge in LC circuit, using auxiliary triggering circuit to clamp magnetic flux 23 p4177 A70-44471

Spark gap triggering with Q switched laser, comparing performance with electrical method 24 p4353 A70-45560

SPARK IGNITION

Arc ignition and cathode spot movement dynamics of thermionically emitting cathode surfaces in heat feedback plasma 21 p3859 A70-41903

Spark gap triggering with Q switched laser, comparing performance with electrical method 24 p4353 A70-45560

SPARK MACHINING

Electrical discharge machining showing close tolerance sizing capability on honeycomb panels 02 p0310 A70-12665

Electrical discharge machining using electrical spark eroding action for machining tough metals in burr-free

intricate configurations, including narrow slots and blind holes 03 p0497 A70-13564

Current density distribution during electroerosive machining, discussing current diagram construction and tool profile 11 p2060 A70-25935

Electric discharge machining technology, discussing quality control factors 12 p2239 A70-26990

Cobalt surface X ray analysis after spark erosion treatment, revealing phase with high temperature stability 14 p2596 A70-30840

Spark erosion milling machines adaptable to piece and mass production 15 p2744 A70-31899

SPARK SHADOWGRAPH PHOTOGRAPHY

U SHADOWGRAPH PHOTOGRAPHY

SPARKS

NT ELECTRIC SPARKS

Light spark and rapid nonlinear effects in focusing powerful light by longitudinal beam 04 p0718 A70-14405

Energy distribution of laser spark spectrum in air, He and Ar, determining transmission coefficients of spark plasmas by self absorption method 18 p3265 A70-36151

Spark tracing in gaseous flows in flames, wind tunnels, nozzles and pneumatic valves, using pulse transformer [SMPTE PREPRINT 41] 22 p4033 A70-43041

SPATIAL DEPENDENCIES

Random fields entropy estimation technique taking into account higher than immediately adjacent spatial dependencies 12 p2192 A70-27771

Free generation regime of ruby laser studied by electro-optical method of smoothing spatial inversion inhomogeneities 16 p2927 A70-33192

Doppler shifted radiation production, using time and space dependent radiant energy sources 16 p2952 A70-34255

Spatial summation of retinal neurons receptive field centers excitation from single optic tract fibers action potential in light-adapted cats 22 p3971 A70-43403

SPATIAL DISTRIBUTION

NT STAR DISTRIBUTION

Quasars variability, distribution, absorption line characteristics, red shift peaks, physical models, cosmological problems, etc 01 p0177 A70-10341

Spatial characteristics of magnetosheath magnetic field observed simultaneously by Explorer satellites, showing zero order agreement with prediction of MGD theory 01 p0071 A70-10410

Optical scintillation measurements applied to turbulence diagnostics, inferring spatial spectrum of turbulent scatterers, using Monte Carlo numerical procedure 02 p0296 A70-11892

Spatial distribution of Pi 2 micropulsations over specific distances and geomagnetic latitudes, noting coastline and geological effects 02 p0290 A70-12154

Propagation velocity relation with time delay in human visual system, using various sets of line stimuli having different spatial distance 02 p0237 A70-12457

Threshold visibility of uniformly moving colored gratings, noting chromaticity discrimination dependence on spatial and temporal frequencies 02 p0237 A70-12460

Spatial distribution function calculation for muons in extensive air shower model and secondary particles mean transverse momentum estimation 03 p0556 A70-13039

Scintillation counters hodoscopic system for studying spatial distribution of muon and muon-number fluctuations in extensive air showers 03 p0482 A70-13042

Spatial distribution of cascade shower particles in atmosphere described by integrodifferential equations system, considering medium ionization 03 p0557 A70-13049

Electron and photon spatial distributions in cascade air shower, applying moment method to space/angle problem solution 03 p0557 A70-13050

Electromagnetic field spectrum and spatial distribution in ring laser, considering transverse modes influence 03 p0500 A70-13462

Large amplitude wave trains in cosmic ray neutron intensity compared with diurnal variations, determining interplanetary space directional distribution from monitor data 03 p0559 A70-13912

Cosmic ray increases during Forbush decrease onset stage in terms of transient spatial anisotropy 03 p0559 A70-13914

Correlation function for spatial distribution of galaxies determined as function of inverse distance between galaxies 04 p0744 A70-14470

Stress-strain spatial distribution in notched plate fatigue specimen of mild steel determined by finite element method, noting cyclic strain softening effect [ASME PAPER 69-MET-C] 04 p0770 A70-14876

Plasma camera photographs of K plasma spatial distribution with electric fields and density gradients perpendicular to magnetic field, observing rotating irregularities around edge 04 p0728 A70-15005

Resonant compression waves in geomagnetic tail estimated for frequency and spatial distribution by single layered two dimensional model 04 p0680 A70-15127

Spatial distribution of field intensities of resonators, using diffraction gratings and prisms 04 p0651 A70-15289

Spatial resonance capture rates for U-238 thick slabs to correct gamma ray attenuation errors in broad group shielding calculations 05 p0884 A70-16169

Spatial and temporal relations between auroral emission at green line 5577 and cosmic noise absorption studied to determine energy spectra and particles distribution 05 p0907 A70-16281

Size and spatial distribution of meteoritic showers, establishing fragment distribution pattern relationship to sorting factor 05 p0912 A70-16464

Spatially homogeneous distribution function describing uniform gas motion derived to permit computer calculations in obtaining numerical solutions to kinetic equation 06 p1036 A70-17753

Kinetic Boltzmann equations for spatially uniform two component gas mixture solved with allowance for relaxation processes, assuming differing temperatures 06 p1109 A70-17754

Molecule spatial and velocity distributions of supersonic molecular beams, measuring scattering cross sections of He and Ar on noncondensable gases 06 p1043 A70-18252

Species spatial distribution measured for He-Ar gas mixtures expanding in supersonic jets, compared to measurements with skimmer-nozzle arrangement 06 p1066 A70-18256

Particle, momentum and energy flux spatial distributions of molecules scattered in collisions of low energy Ar atoms with mica and Ag surfaces 06 p1111 A70-18268

Transverse mode locking for carbon dioxide laser achieved with nonlinear boron chloride absorber, observing emission spatial buildup 06 p1083 A70-18425

Propagation in perturbed magnetically focused electron beams, noting influence of spatially varying drift velocity and damping effect 07 p1239 A70-18867

Three dimensional unsteady and steady sediment distribution obtained by Monte Carlo simulation method, using stochastic hydrodynamics model for transport 07 p1255 A70-19103

Horizontal ionospheric drift over Northern Hemisphere during low solar activity, studying spatiotemporal distribution patterns of drift parameters 07 p1266 A70-19438

Sporadic E layer parameters spatial distribution, describing analytic planetary coordinate system 07 p1267 A70-19453

Geomagnetic micropulsation amplitudes and polarization along meridional profile analyzed from simultaneous ground station recording 07 p1268 A70-19463

Charged particles and He nuclei spatial distribution from recordings in cosmic ray equator region by Cerenkov counter mounted on Proton 2 satellite 07 p1367 A70-19490

Kinetic theory of laser emission on band impurity transitions, noting spatial homogeneity effect on laser mode 07 p1299 A70-19852

Resonator aberrations and active element imperfections effect on formation of spatial and angular structures of solid state laser modes 07 p1299 A70-19854

Cosmic ray microvariations relation to solar wind structure, particle scattering models, spatial distribution, time variations, etc 07 p1372 A70-20336

Spatial and temporal cosmic plasma variations over various energy and wavelength ranges using cosmophysical and aeronautical facility 07 p1372 A70-20339

Lower ionosphere geomagnetic field local gradients determination by partial reflection method 07 p1277 A70-20455

Mathematical model of extensive air showers, calculating lateral distribution of photoelectronic component at all altitudes 08 p1560 A70-20598

Spatially inhomogeneous semiconductor structures dynamic characteristics, obtaining equations
08 p1474 A70-21207

Stress and strain spatial distribution in notched steel plate under cyclic loading determined by finite element method
08 p1590 A70-21315

Auroral zone electrojets spatial structure and dynamic behavior based on IGY and IQSY geomagnetic data
08 p1491 A70-21717

Auroral zone electrojet return current spatial distribution using idealized models for stationary state
08 p1491 A70-21718

Auroral electrons and photoelectrons spatial, energy and angular distributions measurements using low energy electron spectrometer onboard satellite Cosmos-261
08 p1500 A70-21797

Umkehr observation days selectivity effects on calculated mean ozone distributions in layers 2 and 3
08 p1492 A70-21970

Perseids time distribution, based on observations during meteor showers, contradicting appearance of homogeneous Poisson process
09 p1750 A70-22099

Quasar sky distribution as function of apparent magnitude for identification with galaxies of origin
09 p1759 A70-22909

Fast electrons spatial distribution for multiple scattering in nitrogen and argon, noting target thickness and incident energy
09 p1735 A70-23179

Compact galaxies, discussing distribution, integral photometry and isophotometry, brightness outbursts, etc
09 p1763 A70-23373

Low energy protons omnidirectional intensity contours in outer radiation zone at magnetic equator
09 p1747 A70-23491

Optimal control of distributed parameter systems, discussing necessary and sufficient optimality conditions based on functional analysis with emphasis on thermal processes
09 p1654 A70-23542

Neodymium glass laser fundamental frequency spatial structure effects on KDP crystal second harmonic generation efficiency, describing optimal system for laser beam shaping
10 p1899 A70-24262

Spatial frequency spectra of three dimensional phase object and three dimensional hologram, discussing interaction characteristic for monochromatic illumination
10 p1888 A70-24263

Stationary low pressure plasma enclosed in emitting surfaces calculated for spatial charge density distribution
10 p1923 A70-24539

Coherent photon responses production in liquids and glasses by superposing trains of giant laser pulses, achieving spatial separation of responses by combining pulse trains
10 p1900 A70-24564

Explosion aerial blast wave for producing impulsive structural forced response, discussing spatial distribution method for increased wave duration
11 p2133 A70-25729

Integral relay operations effectiveness based on random spatial distribution of aircraft under control of Army flight operations center
11 p2080 A70-26265

Elastic wedge under spatially uniform but time dependent shear tractions, studying shear stress and transient wave propagation
11 p2142 A70-26629

Cosmic X ray sources searched for by Aerobee rockets, noting locations and distribution correlation with galactic novae
12 p2292 A70-27385

Brightness distribution in hologram generated image modulated by square of temporal-spatial coherence modulus of laser emitting longitudinal and transverse modes
12 p2233 A70-27503

Spatial-temporal distribution of meteorological elements allowing for effects of underlying surface
12 p2263 A70-27511

Spatial-temporal distribution of wind swell HF components measured by two dimensional antenna array fed by DC signals
12 p2263 A70-27516

Growth rate and spatial distribution of solid deposit freezing onto vertical surface in presence of convective heat transfer at moving phase interface
12 p2331 A70-27696

Solar radio types I and III sources spatial distribution of circular polarization and coronal magnetic field configurations in active regions
12 p2294 A70-27710

Wave propagation in spatially homogeneous time varying dispersive media, emphasizing excitation and source dependent phenomenon
12 p2188 A70-27961

One dimensional perfect gas motion under spatial pressure distribution, investigating self similar solutions
12 p2212 A70-28189

Einstein equations derivation in comoving reference frame for spatially homogeneous gravitational fields
12 p2310 A70-28221

Soft electron fluxes spatial distribution and temporal variations in magnetosphere based on Elektron 2 charged particle trap data
12 p2295 A70-28259

Transverse laser modes interaction in traveling and standing wave generators allowing for spatial distribution
13 p2424 A70-28597

Solar flares number decrease near central meridian noting no sunspot decrease
13 p2477 A70-29047

Interferometric measurement of spatial correlation function of optical radiation fields propagating through turbulent atmosphere
13 p2454 A70-29825

Spatial distribution and directional anisotropies of tail plasma sheet energetic electrons from measurements by electrostatic analyzer and energetic particle experiments on Vela 4
13 p2482 A70-30071

Solar protons and electrons spatial and angular distributions over polar caps by USAF-OAR satellites 1966-70A, 1967-72D and 1968-59A
13 p2482 A70-30073

Standard pattern recognition with spatial discretization, concerning discrete cell or segment viewing
14 p2553 A70-30422

Optimal spatial discretization and brightness quantization of graphical symbols for pattern recognition, considering illumination and reflection coefficient
14 p2553 A70-30423

Statistical mesosphere temperature, density and wind profiles models based on rocket soundings
14 p2608 A70-30593

Coherent or spatially incoherent light recordings of Fourier transform holograms, investigating resolution cells film grain and signal to noise ratio
14 p2588 A70-31207

Night airglow space and time variations from jet aircraft observations, measuring conjugate enhancements
14 p2580 A70-31266

Atomic hydrogen distribution in upper atmosphere and solar system obtained during spin operation of OGO 5 with Lyman alpha photometer
15 p2798 A70-31655

Ionospheric currents time-space distribution noting rocket data, induction mechanism and geophysical effects
15 p2730 A70-32087

Geomagnetic disturbances temporal behavior and spatial scales
15 p2732 A70-32543

Charged particles and He nuclei spatial distribution from recordings in cosmic ray equator region by Cerenkov counter mounted on Proton 2 satellite
15 p2795 A70-32735

Ruby laser spatial and temporal characteristics improvement with bleachable dye filter, using local negative feedback
15 p2754 A70-32865

LF oscillations of bounded low pressure plasma under magnetic field in discharge chamber, determining spatial distribution by Langmuir sliding probes
16 p2958 A70-33254

Meteoroids origin and distribution, examining collisional and radiative processes effects
16 p2974 A70-33650

Solar X-ray emission localization, examining spatial distribution by rocket-borne collimated proportional counter
17 p3151 A70-34864

Orowan stress calculation, discussing line tension, screw or edge character, spatial distribution and yield strength
17 p3191 A70-35457

Optimal temporal and spatial-temporal resolution for unknown parameter of interfering signal on white noise background
17 p3048 A70-35680

Pulsars spatial distribution, comparing actual distribution to Monte Carlo computations
17 p3173 A70-35755

Spatial-temporal distribution of laser spark plasma electron density and temperature based on holographic interferometry
18 p3265 A70-36152

Pulsars period galactic equator concentration correlation, discussing period-radio luminosity relation and spatial distribution
18 p3314 A70-36335

Spatial signal transmission through open resonator determination based on resonator integral equation, extending to dielectric lens with finite Fresnel diffraction number
18 p3259 A70-36480

Brightness field spatial structure of solar radiation reflected from earth by Cosmos 149 satellite, discussing homogeneity and isotropy
18 p3247 A70-36629

Horizontal ionospheric drift over Northern Hemisphere during low solar activity, studying spatiotemporal distribution patterns of drift parameters
18 p3249 A70-36912

Sporadic E layer parameters spatial distribution, describing analytic planetary coordinate system
18 p3249 A70-36927

Geomagnetic micropulsation amplitudes and polarization along meridional profile analyzed from simultaneous ground station recording
18 p3250 A70-36937

Pulsar galactic longitudinal distribution, discussing observability impaired by high electron density in spiral
18 p3328 A70-37173

Interstellar dust spatial distribution, indicating galactic spiral structure
18 p3329 A70-37183

Solar particle observations over polar caps, considering spatial and angular distribution measurements
19 p3494 A70-37484

Polar cap absorption correlation with solar protons flux into magnetosphere, discussing diurnal and spatial variations and magnetic storm effects
19 p3411 A70-37492

Diurnal variations of thermospheric atomic hydrogen, investigating lateral flow effects on global distribution
19 p3415 A70-38419

Spatial gain variations transverse to discharge in axially flowing carbon dioxide laser amplifier, noting relationship to flow velocity
20 p3640 A70-39391

Einstein equations derivation in comoving reference frame for spatially homogeneous gravitational fields
20 p3710 A70-40096

Diurnal variations and spatial distribution of total electron content in equatorial ionosphere
20 p3623 A70-40477

Extended extragalactic bright radio sources with complex structure, comparing radio to optical field
21 p3892 A70-41189

CW gas laser improvement, discussing optimum efficiency and photon beam spatial distribution
21 p3836 A70-41419

Electron beam instability in cylindrical magnetically confined plasma column, calculating quasi-static spatial growth increments
22 p4080 A70-42403

Ionospheric electron content measurement during solar activity cycle, noting temporal and spatial variations
22 p4020 A70-43159

Butterfly diagram for describing latitude distribution of sunspots during solar cycle, considering representation methods
22 p4106 A70-43264

One dimensional perfect gas motion under spatial pressure distribution, investigating self similar solutions
22 p4012 A70-43314

Globular cluster relaxation time using non-Maxwellian velocity distribution and polytropic spatial distribution
22 p4109 A70-43744

Secondary source distribution of EM field induced on ground-air interface by antenna
23 p4161 A70-43773

LF oscillations of bounded low pressure plasma under magnetic field in discharge chamber, determining spatial distribution by Langmuir sliding probes
23 p4226 A70-44283

Auroral electrojet return current spatial extent from model ionospheric current distribution and geomagnetic variations
23 p4192 A70-44922

Rumanian book on spatial problems in elasticity theory covering deformation geometry, temperature effects, elastic parallelepipeds, etc
23 p4275 A70-44999

Spatial potential measurements in magnetized non-Maxwellian hydrogen plasma, using Zaitsev-Mnev method
24 p4385 A70-45464

SPATIAL FILTERING

Optical spatial amplitude filtering techniques application to moire fringe patterns processing
01 p0058 A70-11060

Image formation from wave front sampling in holography by spatial filtering, comparing Monte Carlo sampling to spaced sampling
04 p0692 A70-15365

Photographic film imagery, degraded by long term artificial atmospheric turbulence, restored by spatial filters placed in Fourier transform plane
07 p1336 A70-20090

Optical data processing systems with spatial filters for two dimensional signals detection, using film nonlinearities to record Fourier transform hologram
07 p1287 A70-20094

- Hologram data efficiency improvement by spatial offset removal, analyzing plane and spherical reference waves and plane and solid objects
08 p1500 A70-21787
- Hologram spatial bandwidth reduction by space-time multiplexing
09 p1673 A70-22074
- Optical signal processing using circular array and spatial frequency filtering to yield azimuthal distribution of sources
09 p1678 A70-22969
- Optical processing of signals from circular aerial arrays involving use of spatial filter
09 p1678 A70-22970
- Parametric image transformation during sum frequency generation
09 p1636 A70-23134
- Deformed grating frequency multiplication by filtering in Fourier plane of lens, forming moire pattern in image plane by mechanical interference
10 p1890 A70-24592
- Laser-light spatial-domain scanning function for deconvolution of blurred photographs using point-spread and holographic Fourier transform division filter
11 p2050 A70-25832
- Spatial domain deconvolution by laser scanning of blurred photographs, using holographic Fourier transform division filter and photoelectric integration
12 p2230 A70-26979
- Spatial filters for ratio W/H measurement in aerial mapping
14 p2581 A70-30144
- Book on holography covering principles, applications, spatial and temporal coherence, interference and diffraction theory and optical filtering
16 p2908 A70-33266
- Automatic speech recognition using spatial filtering and Fourier transforms
16 p2869 A70-33462
- Spatial filter properties of antennas, discussing system performance optimization and incoherent source transfer functions
17 p3045 A70-35077
- Hologram line scattering function dependence on light source spatial coherence, presenting quantitative evaluation, theoretical and experimental data
20 p3633 A70-39760
- Arbitrary mode launching on fiber-optical dielectric waveguides by spatial filtering technique
21 p3829 A70-41930
- Microwave antenna array irregularity location from hologram by optical signal processing, using far field spatial filter
21 p3792 A70-42048
- One, two and three dimensional array receiving systems, determining signal detectability characteristics by spatial filtering variation
22 p3986 A70-42527
- Seeding particles motion recording in fluid flow by holographic velocimetry, using optical matched spatial filtering to determine particle location
24 p4340 A70-46350

SPATIAL ISOTROPY

U ISOTROPY

U SPATIAL DISTRIBUTION

SPATIAL ORIENTATION

U ATTITUDE [INCLINATION]

SPECIES DIFFUSION

- Diffusive separation of Ar 36 and 40 and He in axisymmetric supersonic jet taking into account pressure diffusion
08 p1431 A70-21027

- Ultrasonic irradiation effects on steel hardenability and carbon diffusion rate during annealing, noting microstructure
18 p3273 A70-36049

- Molybdenum trisilicide-tantalum trisilicide and molybdenum trisilicide-tungsten trisilicide interdiffusion for molybdenum disilicide protective coating on Ta and W surfaces
21 p3840 A70-42056

SPECIFIC HEAT

NT HEAT OF SOLUTION

- Boundary conditions of heat conduction in systems of vessels connected by rods with given heat capacity and unknown temperature
02 p0400 A70-12674

- Three dimensional elasticity theory of generalized continua developed from atomic lattice theory model, discussing frequency spectra, specific heat and applications to crystal defects
03 p0525 A70-14232

- Specific heat, electrical resistivity and thermal conductivity changes in materials properties at cryogenic temperatures, noting parasitic phenomena, mechanical and dielectric properties
03 p0525 A70-14269

- Hypersonic flow over blunt bodies, discussing Mach number, specific heat and blast wave limits
04 p0613 A70-14454

- Two phase liquid-vapor system specific heat increase at temperatures approaching critical point,

- using nonanalytic vapor pressure equation with data for nitrogen and oxygen
04 p0780 A70-14584

- Specific heat and thermal EMF increase due to radiation damage in lattice of fast neutron bombarded Cu, Mo and W specimens
05 p0863 A70-16292

- Steady and frictionless supersonic flow of ideal gas of constant heat capacity around slightly deformed cone, calculating force exerted by gas
06 p0964 A70-17240

- Specific radiant heat flow and spectral blackness degree of tungsten with different surface finish
07 p1309 A70-19662

- Silicates thermal conductivity-Debye temperature relationship from thermal conductivity and acoustic data, applying to earth conductivity measurements
09 p1665 A70-22054

- Composite materials macroscopic thermoelastic properties relationships to constituents properties, discussing effective thermal expansion coefficients and specific heats
09 p1703 A70-22682

- Molybdenum heat capacity, electrical resistivity and thermal radiation measurements at high temperatures with millisecond resolution
09 p1706 A70-22955

- Specific heat ratio and configuration effects on flow in subsonic, transonic and supersonic sections of Laval nozzle
12 p2159 A70-28233

- Linear high polymers heat capacity measurements theory emphasizing simple mechanical systems and contribution of lattice vibrations
13 p2438 A70-28997

- Calorimetric measurements for Re specific heat in normal and superconducting states, comparing to theoretical calculation
14 p2626 A70-30478

- Temperature dependence of short wavelength magnon energies correlated with heat capacity
14 p2619 A70-30487

- Specific heat measurements on disordered and ordered phases of Cu-Au alloys at low temperatures
14 p2626 A70-30497

- Specific heat, thermal pressure and molar volume of liquid krypton measured with adiabatic calorimeter, discussing thermal expansion coefficients
14 p2617 A70-31016

- Electrical conductors specific heat measurement at high temperatures, using optical techniques and digital systems
15 p2826 A70-31942

- Specific heat and enthalpy of body centered cubic refractory metals at high temperatures
15 p2757 A70-31943

- Sound velocity relation with specific heat at constant volume at liquid-gas equilibrium critical point
15 p2826 A70-32022

- Graphite surface Debye temperature calculation based on crystal lattice dynamics
15 p2765 A70-32024

- Weak steady shock waves formation in relaxing binary gas mixture, discussing vibrational specific heat temperature dependence
20 p3614 A70-40350

- Apollo 11 rocks IR absorption properties, specific heat and thermal conductivity, discussing heat flow in surface layer
21 p3913 A70-41642

- Apollo 11 sample specific heats at 90-350 K, using adiabatic calorimeter
21 p3917 A70-41674

- Surface pressure coefficient dependence on specific heat ratio for yawed conical lifting bodies in supersonic streams
21 p3747 A70-41877

- Amorphous and partly crystalline polymers low temperature thermal conductivity and heat capacity
21 p3844 A70-42136

- Linear aliphatic polyesters melting point, fusion heat and entropy correlations to molecular parameters
22 p3982 A70-42502

- Specific heat and thermodynamic functions of endo- and exo-isomers of 2-methylbicyclo heptane in 12-310 K temperature range
22 p3982 A70-42681

- Fluorine specific heat derived from measurements on two phase liquid vapor system at constant volume by PVT properties at coexistence
23 p4157 A70-44001

- High temperature specific heat terms for refractory metals and ceramics from room temperature to near-melting point
23 p4207 A70-44440

- High speed photoelectric pyrometry of Ta heat capacity at high temperatures induced by pulse heating
23 p4207 A70-44441

- Al and W specific heat and Al heat of fusion by quasi-adiabatic calorimetry, estimating anharmonic lattice vibrations role via atomic thermodynamic analysis
23 p4208 A70-44931

- Specific heat of amorphous polymethyl methacrylate and polystyrene by pulse method below 4 K, comparing Debye and acoustic values
24 p4367 A70-45598

SPECIFIC IMPULSE

- Agna propulsion system performance model for predicting propellant flow rate, mixture ratio, thrust time and specific impulse
14 p2629 A70-30754

- Electrothermal thruster with liquid propellant, describing energy dissipation and high specific impulse
15 p2791 A70-32280

- Engine weight estimation for showing effect on thrust, specific impulse and uranium loss rate for open cycle gas fueled nuclear rocket engine
16 p2949 A70-33553

- Low, medium and high specific impulse microthrusters development in France, using cold gases, subliming solids, hydrazine, ammonia and cesium ions
16 p2969 A70-33613

- NERVA XE-Prime test series, discussing computer simulation, full power and high specific impulse operation and startup under varying initial conditions
16 p2951 A70-33950

- Thrust measurements on pulsed vacuum-arc thruster, comparing specific impulse and efficiency with exhaust velocity measurements by ion collecting double probes
20 p3567 A70-40207

- Nonuniform flow parameters for maximum thrust in nozzle, discussing specific impulse determination
22 p3960 A70-43366

SPECIFICATIONS

NT AIRCRAFT SPECIFICATIONS

NT EQUIPMENT SPECIFICATIONS

- Process specifications to control manufacturing operations, describing contents, purposes and preparation, emphasizing three levels of control
06 p1184 A70-17601

- Monograph on adhesive materials covering selection criteria tables, mechanical properties, specifications, surface preparation and joint strength
10 p1908 A70-25225

- Inter-Range Instrumentation Group /IRIG/ document regarding meteorological data reliability, defining measuring process accuracy and errors
14 p2606 A70-30567

- F-111A reliability levels achieved via high reliable hardware and redundancy and alternate mode capability requirements in contract
15 p2676 A70-32638

SPECIMENS

- Welded flat plate specimen to evaluate low cycle crack initiation and propagation of butt welds under compressive loading, discussing design, fabrication and testing
01 p0199 A70-10452

- Specimen design of laminated angle-ply composite materials for straight-sided axial coupon and long beam flexure tension testing
08 p1530 A70-21885

- Specimen size and mechanical factors in plane strain fracture toughness testing of metallic materials
23 p4206 A70-44195

SPECTRA

NT ABSORPTION SPECTRA

NT ATOMIC SPECTRA

NT BALMER SERIES

NT D LINES

NT ELECTROMAGNETIC SPECTRA

NT ELECTRONIC SPECTRA

NT EMISSION SPECTRA

NT ENERGY SPECTRA

NT FRAUNHOFER LINES

NT H ALPHA LINE

NT H BETA LINE

NT H GAMMA LINE

NT H LINES

NT HERZBERG BANDS

NT INFRARED SPECTRA

NT K LINES

NT LINE SPECTRA

NT LYMAN SPECTRA

NT MASS SPECTRA

NT MICROWAVE SPECTRA

NT MOLECULAR SPECTRA

NT NEUTRON SPECTRA

NT NOISE SPECTRA

NT OXYGEN SPECTRA

NT PASCHEN SERIES

NT PLASMA SPECTRA

NT POWER SPECTRA

NT RADIATION SPECTRA

NT RADIO SPECTRA

NT RAMAN SPECTRA

NT RYDBERG SERIES

NT SCHUMANN-RUNGE BANDS

NT SHOCK SPECTRA

NT SOLAR SPECTRA

NT SPECTRAL BANDS

NT STELLAR SPECTRA

NT SWAN BANDS

NT TELLURIC LINES

NT ULTRAVIOLET SPECTRA
NT VEGARD-KAPLAN BANDS
NT VIBRATIONAL SPECTRA

Spectral efficiency of coaxial flash lamp pumping gas laser, noting dependence on geometrical and physical parameters of source and active body
01 p0106 A70-10061
Solid state logarithmic radiometer, measuring radiation within narrow portions of optical spectrum
16 p2905 A70-33160

SPECTRAL ABSORPTION

U ABSORPTION SPECTRA

SPECTRAL ANALYSIS

U SPECTRUM ANALYSIS

SPECTRAL BANDS

NT ABSORPTION SPECTRA
NT FRAUNHOFER LINES
NT HERZBERG BANDS
NT SCHUMANN-RUNGE BANDS
NT SWAN BANDS
NT TELLURIC LINES
NT VEGARD-KAPLAN BANDS

Martian carbon dioxide band observations using multislit spectrophotometer, indicating surface height variations near Syrtis Major

01 p0182 A70-10723
Venus upper atmosphere average rotational temperature determined from high dispersion spectroscopic observations of 7883 A carbon dioxide band
01 p0184 A70-10912
Carbon dioxide laser with incorporated grating for measuring line strength to width ratio for various rotational lines

01 p0112 A70-10916
Ammonia red and green bands measured line positions, strengths and half widths applied to Jupiter atmospheric pressure determination

02 p0368 A70-11821
Collision-narrowed growth curves for interpreting hydrogen quadrupole lines applied to photoelectric observations of Jupiter vibration-rotation bands

02 p0368 A70-11824
IR spectra of four carbon stars and Sirius obtained with Michelson interferometer, indicating diatomic carbon and CO bands

02 p0372 A70-12252
Ammonia absorption band at 6450 A in Jovian atmosphere, clarifying controversial absorption time variations

02 p0375 A70-12428
NH bands in stellar spectra by visual inspection of spectrograms, noting abundance of N in normal and strong CN stars

02 p0379 A70-12708
Rotational lines in iodine B-X system vibrational bands, calculating Doppler, natural and collisional widths

03 p0527 A70-13298
Spectral index for diffuse X ray sky background within specific band determined from rocket observations with wide angle telescope

03 p0479 A70-14223
Integrated intensity measurements of carbon dioxide bands in micron regions, using self-broadening method

04 p0690 A70-15025
HF molecular vibration rotation band observed in sunspot spectra, carrying out model calculations for spots differing in temperature for fluorine abundance

04 p0751 A70-15048
Line transfer with scattering described by redistribution function numerically solved, using discrete ordinate method

04 p0720 A70-15701
High resolution Venus spectra, obtaining band spectra growth curve of C13O16O18 isotope of carbon dioxide, comparing data reduction methods

05 p0910 A70-16392
IR solar spectrum including water vapor, carbon dioxide and methane bands

05 p0913 A70-16566
Electrically discharged O effect on N first positive band emission in surface catalyzed excitation

06 p1109 A70-17489
Methylamine crystals lattice vibrations IR spectra recordings, making spectral band assignments according to translational and librational motions

07 p1356 A70-18958
Spectral band transmission functions of atmospheric water vapor, nitrogen, ozone, nitrous oxide and methane in IR region

07 p1330 A70-20306
Emission and absorption by nonhomogeneous gases with vibration-rotation bands determined by scaling approximation

10 p1968 A70-24474
Translational spectral bands of compressed rare gas binary mixtures, considering mass and temperature effects

12 p2275 A70-27172
Auroral enhancement of IR oxygen band at 1.27 micron compared with molecular nitrogen band intensity

12 p2222 A70-27185

IR absorption in ozone band, including atmospheric inhomogeneity effects on accuracy of transmittance calculations

12 p2223 A70-27515
Experimental IR earth horizon profiles measured by satellite in F region, discussing spectral channels and attitude control

12 p2225 A70-27751
Elsasser and statistical band models in single parameter functions representing mean absorption in given spectral range

12 p2191 A70-28295
Dark band in H alpha solar chromosphere above photospheric limb, outlining approaches to obtain spectrally pure observational results

13 p2486 A70-28627
Reflecting surface nonplane parallelism effects on Fabry-Perot interferometers superposition bands contrast and multiplied length measurement accuracy

13 p2408 A70-29366
Formation mechanism of molecular CN violet bands in solar photosphere

13 p2493 A70-29393
Temperature dependence of laser emission line self broadened half widths in spectral band of carbon dioxide at constant pressure

15 p2752 A70-32056
Pressure broadened line widths in electric field induced fundamental hydrogen spectral band, noting linear variation with density

16 p2954 A70-33276
Diatomic nitrogen ions branch overlapping, discussing rotational line structure in first negative system vibrational bands

16 p2956 A70-34254
Delta Scuti stars, determining consistent absolute magnitudes by Stromgren intermediate band colors and Crawford photoelectric H beta indices

17 p3171 A70-35443
Spectrophotometric airglow intensity measurements of OH, O I 6300, hydrogen H alpha and oxygen Herzberg I bands by airborne laboratory

17 p3080 A70-35769
Close-confinement LPE AlGaAs junction laser properties, examining range of alloy direct bandgap transition

18 p3268 A70-36727
Atmospheric water vapor distribution by intensity measurements of outgoing radiation from satellites in carbon dioxide and water vapor spectral bands

18 p3287 A70-36971
Arcturus Co bands, examining equivalent widths, rotational lines and 12C/13C ratio

18 p3318 A70-37015
High altitude humidity from millimeter-band water vapor lines, using EHF atmospheric spectral transparency calculation

19 p3461 A70-37633
Evening twilight airglow oxygen IR band ground based observation by two-channel photometric technique

19 p3415 A70-38385
Solar eclipse measurements in 1-30 mm range, examining chromosphere, flares and radio emission

19 p3531 A70-38911
Oscillator strengths for aluminum oxide molecular electronic sigma band system from intensity measurements in cyanogen-oxygen flame system

20 p3676 A70-40474
Nitrogen photoelectron excitation in dayglow, examining 3371 A band intensity, energy spectrum and flux in ionosphere

21 p3882 A70-41093
Hydrogen chloride self broadened fundamental vibration rotation band intensity variation with pressure investigated by absorption spectroscopy analysis

22 p3983 A70-42945
Water vapor emission computation from statistical band model, investigating accuracy limitations

22 p4065 A70-43169
Auroral molecular nitrogen bands tentative identification based on rocket-borne spectrometer results

23 p4186 A70-43856
IR absorption bands absolute intensities determination method, giving special consideration to absorption band wings and precision

23 p4217 A70-44203
Molecular oxygen ions 1Ng band and molecular nitrogen 1Pg band relative intensities in normal and type B auroras

23 p4191 A70-44408
Low temperature stars SiO IR spectral band identification based on rotation-vibration spectrum calculation

24 p4411 A70-45777
SPECTRAL CORRELATION
Complex burst of 2 September 1966, comparing dynamic radio spectra from Culgoora and Weissenau

21 p3880 A70-40968
Nonflaring solar X-ray and microwave radiation flux correlation from satellite data

22 p4104 A70-42995

SPECTRAL EMISSION

Far IR night sky emission above 120 km over millimeter range, using rocket-borne telescope

01 p0069 A70-10040
Thermodynamic aspects of ray invariance of spectral brightness ratio to square of local index of refraction compared to black body power radiation

01 p0144 A70-11293
Helium-neon laser wavelength calculations from spectral observations by Fabry-Perot etalon, proposing formulas to enhance accuracy

02 p0299 A70-12439
Peculiar emission object with emissions narrower and with lower ionization lines than cool Wolf-Rayet stars

03 p0574 A70-13933
Ablation chars, carbon and graphite spectral emittance and reflectance as function of wavelength and temperature, noting applications to atmospheric entry heat shielding

04 p0787 A70-15590
Antarctic twilight Na emission abundance and concentration in lower E region, discussing meteor ablation models

05 p0836 A70-15819
Sco X-1 line spectra search in X ray spectrum by rocket-borne proportional counters, noting iron line emission

05 p0904 A70-16979
IR region spectral hemispherical emittance of surfaces measured by bihemispherical reflectometer

06 p1107 A70-18205
[AIAA PAPER 70-65]
Hydrogen 109 alpha recombination line emission in galactic H II regions surveyed at National Radio Astronomy Observatory

10 p1936 A70-23942
Stellar atmosphere model for multilevel spectral line emission, assuming semiinfinite hydrogen atmosphere with sequence of plane parallel zones

12 p2306 A70-27856
Low pressure nitrogen and air spectra excitation by low energy proton bombardment, using spectroscopic, photometric and microphotometric analyses

14 p2619 A70-30653
Spectral line formation, assuming frequency redistribution for plane parallel stellar atmosphere containing nonuniform distribution of internal emission sources

14 p2651 A70-31289
Spectral emission in trivalent Ho doped Yb-Al garnet single crystals grown by optical zone melting

15 p2784 A70-32198
Reflectance measurements of directional spectral emittance of black body cavities with specific geometries, using laser source and integrating hemi-ellipsoid

20 p3627 A70-39091
Organic laser spectral and energy characteristics, discussing practical operation principles, low generation threshold and harmonic energy

20 p3642 A70-39754
Time varying flow properties effects on hypersonic wind tunnel spectroscopic measurements, considering direct emission and electron beam techniques

20 p3607 A70-40271
Shock tube measurements of bimolecular reaction rates in branched chain hydrogen-carbon monoxide-oxygen system, monitoring flame band emission

21 p3773 A70-41314
Stellar population of young clusters containing red supergiants, determining spectral types and luminosity classes

22 p4102 A70-42979
Spectral radiation extinction at atmospheric aerosol particles, discussing particles complex refractive indices and size distributions

22 p4065 A70-43171
Ti phase transformation effects on thermal conductivity, electrical resistivity and spectral and total emittances at 1100-1500 K

22 p4056 A70-43222
Spectral brightness temperature, directional emissivity and surface temperature of earth from remote radiance observations by balloon-borne multidetector grating spectrometer

23 p4194 A70-44035
Ta spectral emissivity, using ratio of specimen surface and black body spectral radiant intensities

23 p4207 A70-44447
Spectral and threshold emission from optically pumped semiconductor lasers as function of carrier type and concentration in GaAs single crystals

23 p4203 A70-45069

SPECTRAL ENERGY DISTRIBUTION

X ray line emission from Sco X-1 using Monte Carlo estimates of spectral distribution of scattered photons in terms of Fe line and cosmic abundance

01 p0169 A70-10338
Intensity distribution determination in spectrum of solar XUV fluxes incident upon upper atmosphere, considering quantitative model construction

01 p0170 A70-10593

Spectral distribution of X ray atmospheric absorption to determine high energy photoelectrons spectrum

01 p0172 A70-11494

Directional and spectral characteristics of bremsstrahlung X rays from auroral arc in low energy range during cosmic rays sounding rocket measurements

02 p0357 A70-12069

Jupiter Red Spot continuous spectrum intensity distribution and methane/ammonia absorption between 3300-6500 Å

02 p0374 A70-12427

Double exposure holograms in diffuse radiation used to reconstruct in white light interferogram images localized in hologram plane

03 p0483 A70-13259

Solar IR light brightness distribution reflected by volcanic covers compared with lunar observation data

04 p0744 A70-14439

Statistical model of ozone absorption bands for calculating intensity, rotational line position and transmission functions of complex spectral regions

04 p0680 A70-15252

Simulation equipment for extraterrestrial solar radiation for spacecraft components evaluation tests, describing spectral characteristics

04 p0665 A70-15663

Wall effect on differential spectral distortions in cylindrical ionization chamber and proportional counter type detectors

05 p0900 A70-15971

Visible light emission from nonequilibrium Cs plasma measured for spectral intensity distribution, suggesting excitation mechanism in terms of collision-radiation model

05 p0887 A70-16109

Power spectra, modulation indices, frequency distributions and decorrelation frequencies of intensity fluctuations of pulsar radiation consistent with interstellar scintillation theory

05 p0908 A70-16302

Spectral power distribution and ultrashort pulses limiting duration of ruby-neodymium laser with passive shutter

06 p1081 A70-17766

Tropospheric and stratospheric turbulent horizontal heat and momentum transfer spectral density profiles calculations from radio launchings data

07 p1269 A70-19646

Spectral line intensities in hydrogen plasma, calculating relative intensities and Balmer line width for various electron temperatures and optical thicknesses in H alpha line

07 p1389 A70-20205

Spectral intensity distribution of night airglow noting visual spectra distribution difference from G2 stars

07 p1277 A70-20457

FM spectral density model with applications to radio transmitter bandwidth estimation and interference analysis

08 p1456 A70-20473

Quasi-stellar objects absolute spectral energy distribution, considering electron temperature and photon density

08 p1572 A70-20916

Meteors spectral intensity variations along flight path noting color dependence on brightness

08 p1572 A70-20946

Spectral densities of phase coordinates of nonlinear automatic systems in steady states at random disturbances determined by statistic linearization

08 p1480 A70-21016

Modified diffusion approximation for spectral transfer of isotropic turbulent pulsation energy for temperatures with low Prandtl number

08 p1538 A70-21429

Surface roughness effects on measured cross spectral density of wall pressure fluctuations beneath turbulent boundary layer

08 p1486 A70-21859

Anisotropic turbulent energy spectral distribution approximated assuming homogeneous and axisymmetric turbulence with vertical axis of symmetry

09 p1717 A70-22374

Book on rotational structure of diatomic molecules spectra covering multiplets, intensity distributions and perturbations

12 p2274 A70-27094

Calcium H and K lines core residual intensities in stars with quiet and active chromosphere, suggesting activity due to thermal gradient

12 p2303 A70-27702

Energy distribution in dark and light details on Venus spectrograms, considering relation to clouds in upper atmosphere

12 p2311 A70-28304

Solar light brightness distribution reflected by volcanic covers compared with lunar observation data

13 p2485 A70-28464

Tungsten strip lamps spectral radiance calibration, discussing accuracy requirements for radiation constants, wavelength and black body temperature

13 p2410 A70-29655

Temporal structure and spectral evolution of Nd laser emission with self locking axial modes, noting gain saturation effects

13 p2430 A70-29776

Metastable He ion two photon decay, observing photon coincidence angular correlation in spectral distribution

13 p2456 A70-29811

Solar far UV continuum photometry illustrating spectral temperature minimum transition, comparing to far IR temperature

13 p2496 A70-29841

Si solar cell power output and spectral response as function of angle illumination, eliminating atmospheric influence

14 p2533 A70-30337

Heterochromatic spectrophotometry, discussing maxima and integral techniques for line measurement, photoemulsion properties and Eberhard effect

14 p2585 A70-30784

Comet Bennett 1969i photometric observations, showing blackbody-like continuum at short wavelengths with sharp peak due to silicate grains

14 p2642 A70-30895

Spectral line formation, assuming frequency redistribution for plane parallel stellar atmosphere containing nonuniform distribution of internal emission sources

14 p2651 A70-31289

Nitrogen K-LL Auger spectrum high energy lines measurement by high resolution electron spectrometer

14 p2620 A70-31301

Cosmic X ray and gamma ray spectral energy distribution slope change explained by measurement process involving photon spectrum

15 p2792 A70-31431

Spectral distribution of GaAs photoconductivity, allowing for coordinate dependence of minority carrier lifetime in surface space charge region

15 p2782 A70-31626

Clutter signals in radar receiver antenna, determining autocorrelation function and spectral power density

15 p2701 A70-32466

Atmospheric temperature fluctuation spectrum determination by energy budget solution, considering spectral density dependence on Richardson number

15 p2732 A70-32542

Meteors spectral intensity variations along flight path noting color dependence on brightness

15 p2806 A70-32758

Energy distribution in continuous spectrum of star MWC 334 from spectrophotometric observations

15 p2808 A70-32888

Quantum theory for spontaneous parametric light scattering, determining photon spectral distribution

16 p2951 A70-33196

Spectral densities of intensity and frequency fluctuations of single frequency He-Ne laser radiation

17 p3105 A70-35092

Spectral radiation and polar distribution from high power Ar, Kr and Xe arcs

17 p3023 A70-35156

Hour-angle and declination center-to-limb profiles of quiet sun 3.3mm brightness temperature distribution

17 p3174 A70-35868

Spectral densities of input and output signals of discretely continuous systems as function of comparison moment

18 p3233 A70-36069

Optimum spectral control of nonlinear plant, using Newton iteration and linear programming

18 p3234 A70-36075

Star AG Draconis spectrum in visible range by meniscus prismatic camera, deriving energy distribution

18 p3315 A70-36575

Quasar 4C 05.34 absolute spectral energy distribution by multichannel photoelectric spectrometry

18 p3318 A70-37019

Galactic spiral structure from atomic hydrogen line intensity longitudinal distribution

18 p3328 A70-37168

Spectral radiative capacity of lower level clouds in specific transmittance window, using airborne diffraction spectrometer measurements

19 p3461 A70-37424

Spectral intensity distribution of extragalactic radio sources, comparing spectral deviations from simple power law to radio emission from relativistic electrons in magnetic field

19 p3524 A70-38749

Spectral energy distribution of meteor trail in Leonid meteor shower from photographic analysis

19 p3526 A70-38779

Spectral energy distribution curves and color indices of specific meteor trails observed on 12 August 1959 and 25 July 1963

19 p3526 A70-38780

Solar spectral intensity distribution and ionizing radiation spatial emission patterns during eclipse, discussing effects on ionosphere

19 p3418 A70-38908

Nebula K3-50 IR radiation source observation, noting energy distribution resembling NGC 7027 and W51-IRS 2

20 p3701 A70-39003

Carbon monoxide laser efficiency increase through addition of Xe, noting change in laser output spectral intensity distribution

21 p3835 A70-40572

Omnidirectional cosmic gamma ray flux near one MeV observed by ERS-18 satellite, plotting spectral energy distribution

21 p3876 A70-40697

Magnesium-sodium nitrate porotechnic flare spectral radiant energy comparison with radiative transfer theory data, considering Na resonance continuum formation

21 p3850 A70-41937

Semiconductor junction diode spontaneous emission sources, considering frequency-energy characteristics relationship

22 p4085 A70-42504

Solar spectral irradiance measurements at different altitudes, using multichannel radiometers

22 p4013 A70-42599

Exploding wire light source modification by immersing in transparent fluid to increase intensity, measuring spectral characteristics

22 p4032 A70-43037

EUV solar spectral intensity distribution and cyclic variations

22 p4106 A70-43299

SPECTRAL LINE WIDTH

Velocity distribution and optical depth of line formation in solar atmosphere using blue and red wing filtergram and numerical experiment

01 p0175 A70-10241

Critique of double resonance theory in gaseous lasers, including correction regarding saturation parameter for small RF perturbations and line width dependence

01 p0109 A70-10432

Carbon dioxide laser with incorporated grating for measuring line strength to width ratio for various rotational lines

01 p0112 A70-10916

Oscillation and doubling of 0.946 micron line in Nd ion doped YAG, calculating optimum nonlinear coupling to internal Q switched laser

01 p0113 A70-11169

Pressure and line width estimate from high resolution image tube spectra of Jupiter at 11,000 Å

02 p0366 A70-11808

Rotational temperatures and methane abundances in Jovian atmosphere calculated for various Lorentz half widths

02 p0366 A70-11809

Two layer model of Jovian clouds including clear space, showing computed and measured equivalent widths of H quadrupole lines

02 p0367 A70-11813

Pioneer 6 radio signal spectrograms during solar occultation, noting solar event effects on bandwidth

02 p0369 A70-12060

Microwave dispersion caused by atmospheric gases at water vapor line, using microwave spectrometer based on dispersion detection in refraction spectrum

02 p0260 A70-12571

Atmospheric oxygen A band individual rotational lines intensities and half widths measurements

02 p0344 A70-12656

Demodulation of signals modulated with respect to wave period, deriving spectral width of pulsed period modulation

03 p0446 A70-13200

Rotational lines in iodine B-X system vibrational bands, calculating Doppler, natural and collisional widths

03 p0527 A70-13298

Spectral line widths in MPD arc jet measured to determine plasma electron density and heavy particle temperature

03 p0536 A70-14371

Classical path methods for treating Stark spectral line broadening in plasmas illustrated by Lyman alpha line of hydrogen calculations

04 p0726 A70-14670

Hydrogen atoms van der Waal dispersion interaction effects on H lines broadening in neutral medium, taking into account resonance interaction

04 p0723 A70-15714

Charged particle concentration emitted by inhomogeneous plasma determinable from emission spectral lines broadening, suggesting error correction procedure

05 p0889 A70-16541

Methane abundance in Jovian atmosphere deduced from line equivalent widths, obtaining line intensity for J manifolds

05 p0919 A70-16940

Self broadened semihalf widths measurement in pure rotational spectrum of carbon monoxide compared with vibration-rotation calculation

05 p0886 A70-17086

Photon number per mode for laser with nonresonant feedback for homogeneous and inhomogeneous atomic line broadening

06 p1081 A70-17746

SiH molecular absorption lines in solar disk spectrum, determining maximum equivalent widths and oscillator strength

06 p1143 A70-17996

Excitation emission of diatomic nitrogen molecule for first negative band broadening, considering high energy primary beam with secondary electrons

06 p1124 A70-18305

Calcium neutral and ionic lines broadening and shift by microfields measured by plasma flame observations

06 p1148 A70-18453

Spectral broadening mechanisms for trivalent Eu ions in glass, considering fluorescence and absorption spectra measurements

06 p1127 A70-18640

Nd glass laser emission spectral width reproducibility as function of flash intervals and pump energy

07 p1297 A70-18869

Hydrogen fluoride fundamental vibration rotation band spectral line shift and broadening due to carbon dioxide

07 p1337 A70-19365

Pressure-narrowing theory applied to calculating equivalent widths of lines in quadrupole rotation-vibration spectrum of molecular hydrogen

07 p1338 A70-19366

Axicon systems for spectroscopy of light emitted by foil-excited accelerator beams, discussing scattering contribution to spectral line widths

07 p1287 A70-20083

Spectral line intensities in hydrogen plasma, calculating relative intensities and Balmer line width for various electron temperatures and optical thicknesses in H alpha line

07 p1389 A70-20205

Resonant and foreign gas broadening using Schrodinger equations for collision problems

07 p1346 A70-20244

Spectral line shapes determination for radiating atoms immersed in plasma developed without neglecting ion-electron interaction and static-ion assumption

07 p1346 A70-20247

Equivalent line widths of anomalously fast stars of early spectral classes and reference stars, discussing binary nature and radial velocities of OB stars

08 p1569 A70-20828

Absorption lines in hazy planetary atmosphere with isotropic scattering, examining phase variations of equivalent width

08 p1571 A70-20910

O and B type stars neutral He lines, studying UV line blanketing effects on predicted departures from LTE

08 p1571 A70-20912

Iron ions EPR lines widening in corundum crystals due to lattice defects, estimating mosaic blocks disorientation parameter and point defects density

08 p1556 A70-21122

Plasma electron density determination by number of extreme resolved line, considering broadening action by Doppler effect for Balmer, Lyman and Paschen series

09 p1734 A70-22731

Stark broadening of singly ionized nitrogen lines measured in dense high temperature plasma behind reflected shock wave in T tube

09 p1731 A70-22776

Singly ionized Mg resonance lines electron impact broadening quantum mechanical calculation

09 p1732 A70-22827

Wave number, intensity and half width of vibrational-rotational lines pertaining to transition of carbon monoxide perturbed by argon

09 p1733 A70-23316

Line profiles and equivalent widths from Si II, Mg II, Ni II and Fe II spectra of shell star zeta Tauri

10 p1936 A70-23941

Equivalent widths for rotational lines to detect interstellar hydrogen gas, discussing absorption line

10 p1937 A70-23947

Pulsars dynamic spectra in 110-420 MHz range, observing emission bandwidths to formulate power law

10 p1938 A70-24099

Neodymium spectral line widths in various glasses, studying role of inhomogeneous broadening

10 p1900 A70-24266

Absorption strengths of j-manifolds in R branch of Jupiter atmosphere methane band, discussing fine structure blending

10 p1919 A70-24473

EPR line width angle and temperature dependences assuming line widening due to electric field of lattice defects, dipole-dipole interactions and spin-lattice relaxation

11 p2097 A70-25382

Optical heterodyning of Doppler shifted signal with minimal instrumental spectral broadening and high SNR, applying to turbulence structure measurement by CW laser

11 p2062 A70-25630

Neutral helium line profiles for line-blanketed model atmospheres grid

11 p2117 A70-26660

Ruby laser with electro-optical Q switching, using polarization element for emission spectrum narrowing to single longitudinal mode

12 p2245 A70-27303

Inhomogeneous interatomic magnetic field effects on spectral line widening and shifts of emitting atoms in low temperature plasma

12 p2278 A70-27318

Spectral line width and shift measured by spectrograph crossed with Fabry-Perot interferometer in pressure chamber, measuring magnetic field in solenoid

12 p2238 A70-28178

Solar iron-to-hydrogen ratio and oscillator strengths for FeI lines compared with laboratory measurements of line broadening by neutral atoms

13 p2486 A70-28628

Cs atomic spectral line broadening under simultaneous electric and magnetic fields, observing Zeeman and Stark splitting

13 p2460 A70-28711

HCN laser 890 GHz line phase locked to multiplied standard frequency with wide bandwidth loop, narrowing line widths

13 p2426 A70-28798

Stark-broadened neutral atomic line widths and shifts, determining electron densities from H beta profiles and pressure-temperature data

13 p2455 A70-29220

Stark broadening of neutral helium line in plasmas for electron densities measurements accuracy, comparing to H beta determined densities

13 p2456 A70-29225

Homogeneous absorption line and peak power widths relationship in high resolution gas laser with internal absorbing cell

13 p2428 A70-29365

Solid state laser transverse modes maximum dependence on resonator geometrical parameters usable for producing stable kinetic emission mode with narrow spectral line

13 p2428 A70-29410

Ca atom-graphite grain model for interstellar absorption at 4430 A, calculating resonant line shift and width as functions of atom-surface distance

14 p2639 A70-30729

Non-LTE and LTE line profiles and equivalent widths for transitions in singlet and triplet systems of neutral He in hot stars, explaining anomaly

14 p2641 A70-30884

Nightglow OI lambda 6300 line width measurements during magnetic storm, discussing temperatures and intensity variations

14 p2579 A70-31250

Stark broadening calculations of H alpha and H gamma hydrogen lineshapes

14 p2620 A70-31303

Ion line Stark broadening, considering electron-ion quadrupole excitation and electron resonant scattering

14 p2620 A70-31376

Opposing mode interaction effect on ring laser unidirectional emission instability, discussing homogeneous and inhomogeneous line broadening

15 p2749 A70-31552

Diagram extracting Lorentzian line widths from Fabry-Perot interferometer profiles

15 p2737 A70-32050

Temperature dependence of laser emission line self broadened half widths in spectral band of carbon dioxide at constant pressure

15 p2752 A70-32056

Cygnus loop nebula H alpha line halfwidths and radial velocities

15 p2802 A70-32482

H alpha and H beta lines electrodynamic broadening with linear Stark effect, calculating relative intensity

15 p2777 A70-32490

Optical quantum amplifier frequency characteristics dependence on broad spectral composition amplified signal intensity and resonator parameters

15 p2754 A70-32862

Digital logic control of chromatographic system for measuring instrumental contributions to band broadening

16 p2855 A70-33120

Book on stellar spectra theory covering line absorption coefficient expressions, radiative transfer, line source function, line broadening, etc

16 p2974 A70-33270

Pressure broadened line widths in electric field induced fundamental hydrogen spectral band, noting linear variation with density

16 p2954 A70-33276

Spectral line formation in Mars and Venus atmospheres, discussing Lorentz and Doppler broadening

16 p2976 A70-33793

He-Ne CW laser emission line width measurement, describing apparatus and technique

17 p3106 A70-35108

Lyman alpha wing resonance broadening opacity effects on solar spectrum in 1500 A to 8000 A range

17 p3169 A70-35383

Fraunhofer line equivalent widths differences between pole and equator spectra of solar disk

17 p3173 A70-35734

Solar C II resonance doublet profiles, discussing possible broadening mechanisms

17 p3174 A70-35862

Upper atmospheric ions kinetic temperatures based on chromatic broadening of mass spectral lines

18 p3252 A70-36985

Na I 5889 A pressure broadening by high temperature neutral He, allowing damping constant direct measurements

18 p3318 A70-37013

Arcturus Co bands, examining equivalent widths, rotational lines and 12C/13C ratio

18 p3318 A70-37015

Solar photosphere temperature constancy in thin CO layer from equivalent spectral line width determination

18 p3322 A70-37134

Near collisions approximation in Stark broadening of hydrogen Lyman alpha line

18 p3296 A70-37227

Energy levels and spectral broadening of neodymium ions in laser glass from fluorescence and absorption spectra

19 p3445 A70-37760

Real time narrow band vibration spectrum analysis techniques, discussing application to failure prediction and flight and wind tunnel tests

19 p3430 A70-38528

Helium II line broadening in high temperature plasma, measuring profile for comparison with theoretical prediction

20 p3677 A70-39115

Wave particle resonances broadening by particles random motion in turbulent electric field, determining cyclotron instabilities saturation level from vanishing nonlinear growth rate

20 p3679 A70-39661

Pulsed ruby free emission mode laser spectrum narrowing, using diffraction lattice adjusted in resonator transversely to beam axis

20 p3643 A70-39757

Temperature difference between equator and solar poles from spectral line equivalent width variation

20 p3711 A70-40407

Coupling constant and binary collision expansions for ion motion in plasma line broadening

21 p3855 A70-40722

Inhomogeneous interatomic magnetic field effects on spectral line widening and shifts of emitting atoms in low temperature plasma

21 p3860 A70-42059

Radiative transfer equations quantum theoretical deduction in spectral line regime, considering Planck law, Einstein coefficients and kinetic equations

22 p4072 A70-42339

T tauri star mass loss, observing variations in spectral emission line widths

22 p4101 A70-42858

Silicon line collisional broadening by electrons and hydrogen atoms, discussing Stark effect and van der Waal interactions

22 p4076 A70-42861

Be stars hydrogen emission lines widths measurement

22 p4101 A70-42867

H alpha and H beta lines electrodynamic broadening with linear Stark effect, calculating relative intensity

23 p4221 A70-43912

CA II chromospheric emission lines for deriving Mn in stellar luminosity, discussing calibration

23 p4242 A70-44293

Stellar abundance determination, considering rapid uniform rotation effects on equivalent spectral line widths

23 p4250 A70-44811

Early type Ia and Iab supergiant stars macroturbulence and rotation, investigating spectral line broadening, mass loss and angular momentum

23 p4250 A70-44813

Spectral line width distributions in main sequence stars, emphasizing B2 to A2 range rotational velocities with Maxwellian distribution

23 p4251 A70-44821

UV Cet type flare star rotational velocity upper limits from H alpha emission line width in chromospheres

23 p4251 A70-44824

Deutsch period vs line width relation for periodic Ap stars, determining rotational velocities with rigid rotator model

23 p4251 A70-44825

Nd laser single picosecond pulse energy, duration and frequency width

24 p4354 A70-45664

ESR intensities and line widths at X and Q bands of Cr and Fe molecular ions in water/glycerol mixtures

24 p4310 A70-46045

SPECTRAL LINES

U LINE SPECTRA

SPECTRAL NOISE

U WHITE NOISE

SPECTRAL RECONNAISSANCE

Wheat fields recognition, mapping and acreage measurement by multispectral scanning with real time analog data processing, considering seasonal and observation altitude effects

12 p2219 A70-26930

Spectral discrimination technique for crops remote sensing, comparing statistical irradiance model with airborne multispectral scanner data

12 p2219 A70-26931

Engineering soils mapping by multispectral techniques, describing image interpretation by visual means, densitometric measurements and automatic spectral response classification

12 p2220 A70-26932

Collapse prone land detected by multispectral scanning and photography with analog data processing

12 p2220 A70-26933

Hydrobiological features mapping in Everglades by multispectral scanning and analog data processing

12 p2220 A70-26934

Multispectral color aerial photography, describing instrumentation, oceanographic and agricultural applications, atmospheric effects on images, etc

12 p2220 A70-26937

UV flash spectra of total solar eclipse of 7 March 1970 obtained by Aerobee 150 rocket

12 p2304 A70-27717

Terrain spectral imagery from satellites for natural resources investigations

12 p2235 A70-27745

SPECTRAL REFLECTANCE

Venusian atmosphere low reflectivity reinterpretation based on spectrophotometric data indicating constituents of yellow and upper UV haze layers

02 p0377 A70-12555

Mars multicolor filter photometry showing variation in whole-disk reflectivity

02 p0378 A70-12560

GaAs n-type single crystals thermorefectance spectra at various energies

03 p0541 A70-13721

Mars surface reddish color due to carbon suboxide suggested based on spectral reflectivity measurements and matching in laboratory

04 p0743 A70-14423

Relative reflectivity of lunar landing site Apollo 7 compared to site Apollo 2, showing compositional and mineralogical differences

04 p0751 A70-15059

Ablation chars, carbon and graphite spectral emittance and reflectance as function of wavelength and temperature, noting applications to atmospheric entry heat shielding

04 p0787 A70-15590

Reflectance spectra obtained for igneous rocks and minerals, establishing correlation between reflectance and energy wavelength, composition and sample particle size

05 p0839 A70-16390

Near IR reflectance spectrometer integrated into environmental chamber to study frost spectral properties

06 p1072 A70-18522

Spectral reflectance of carbon dioxide and water frosts at 0.8-3.2 microns, growing frosts in cold vacuum chamber from high purity gases

07 p1388 A70-19945

Martian polar cap spectra interpreted with laboratory measurements of water-carbon dioxide frost spectral reflectance

07 p1388 A70-19946

Jupiter and Saturn IR reflection spectra observed with Michelson interferometer-spectrometer, eliminating effects of terrestrial atmospheric absorption, solar spectral lines, etc

08 p1570 A70-20895

Microphotometric spectral reflectivity correlation to static Young moduli of carbon and graphite yarn filaments as optical testing method

08 p1497 A70-21350

Fluorel spectral reflectance, transmittance and absorbance under monochromatic irradiation, considering thermal analysis and surface finish

09 p1710 A70-22794

Gallium arsenide phosphide epitaxial films electroluminescence spectra noting composition effect

10 p1928 A70-24833

Plant leaves discrimination by multispectral reflectance indicated in transmittance measurements via remote sensing from aircraft and spacecraft

12 p2218 A70-26920

Absorption bands in reflection spectra of various asteroids, comparing Vesta composition to meteorites and Apollo 11 samples

16 p2972 A70-32987

Model relating spectral reflectance to thermal control materials properties and environment induced changes

16 p2940 A70-33934

Rough surface radiative properties, determining electromagnetic wave scattering by Maxwell equation solution

17 p1315 A70-34508

Ecological potentials in spectral signature analysis, using laboratory leaf and soil spectral reflectance data

17 p3078 A70-35612

False color aerial photography with IR film for distinguishing vegetation types and assessing plant vigor based on leaf reflectance

17 p3078 A70-35613

Mars UV reflectivity, examining spectrum, absorption features, planet albedo and ozone content by rocket-borne instruments and atmospheric models

18 p3317 A70-37011

Mercury photometric measurement, examining surface brightness for photometric function

18 p3319 A70-37052

Lunar surface spectral reflectivity measured with ground based telescopes for remote mineralogical analysis

20 p3709 A70-39977

Directional, spectral and total reflectance for Apollo 11 fines and rock chips, observing dependence on illumination angle

21 p3913 A70-41643

Apollo 11 rocks spectral reflectance and albedo before/after proton irradiation and vitrification, investigating color differences for lunar surface dark and bright areas

21 p3913 A70-41645

Spectral bidirectional reflectance measurements of rough metallic surfaces for reflected energy spatial distribution determination in radiative heat transfer problems

23 p4281 A70-44446

Highly alloyed indium arsenide reflection spectra and band structural characteristics

24 p4389 A70-45482

SPECTRAL RESOLUTION

Spectrometer scanning, 20-15 microns in 3 sec, measuring absorption and emission spectra of hot samples alternately, discussing resolutions at various bands

01 p0091 A70-10914

Jovian surface elements spectral and color contrasts from spectrograms obtained between 3200- 4900 A wavelengths

02 p0375 A70-12429

Spectrophotometric facility for measuring spectral characteristics of color filters, photomultipliers and photographic plates as function of temperature

02 p0301 A70-12494

Image intensifiers to improve telescope system sensitivity and spectral resolution in radiometric measurements of reentry vehicles

03 p0489 A70-13654

Low resolution spectra of IR stars NML Tau, CIT 3, 6 and 13 considered inadequate for molecular band identification

04 p0748 A70-14591

Spectrally and spatially resolved measurements on arc heated Ar plasma radiation for eliminating discrepancies in transition probabilities

06 p1122 A70-18187

High resolution mass spectrography using AgBr photographic plates as ion detectors for organic chemical problems

07 p1224 A70-18894

Time variations in human spectral response, considering sequential gain and phase estimates formation by Gabor elementary signals theory

10 p1823 A70-23895

Grate spectrometer with high resolution for 20-45 micron range, describing water vapor transmission spectrum

10 p1886 A70-23912

Precise sweep calibrations and simultaneous spectrum recording for high resolution nuclear magnetic resonance spectroscopy

11 p2052 A70-26375

Monochromators dispersion and resolution increased by multiple passage of light through singly dispersive element, comparing optical schemes

12 p2237 A70-28160

Dynamic spectra of type 3 solar bursts from OGO-3 antenna/radiometer observations

17 p3150 A70-34835

Photographic materials for holography, discussing spectral sensitivity, grain size, resolution, transfer functions, diffraction efficiency, etc

17 p3084 A70-35003

Error analysis of Corcos hypothesis concerning cross spectra of pseudoacoustic LF turbulent pressure pulsations on flat plate

18 p3241 A70-36305

Ruby and Nd glass solid state lasers modes partial self synchronization investigated by spectral time resolution method

22 p4051 A70-43463

Reflection echelon and Fabry-Perot interferometer with surface imperfections, comparing spectral resolution limit with Rayleigh limit

22 p4040 A70-43612

SPECTRAL SIGNATURES

ERTS multispectral scanner with optimal sensitivity and resolution for agricultural scenes signature analysis

12 p2229 A70-26941

Spectral signature recognition for automatic interpretation of earth resources multispectral data

22 p4037 A70-43088

SPECTRAL THEORY

Pressure-narrowing theory applied to calculating equivalent widths of lines in quadrupole rotation-vibration spectrum of molecular hydrogen

07 p1338 A70-19366

Cosmic X ray source spectra possibly due to plasma bremsstrahlung

07 p1368 A70-19700

Comet model atmospheres for head theoretical spectra computation, considering collisional effects through total gas density distribution

11 p2116 A70-26647

Plasma turbulence spectral theory, considering cascade processes in collisional and collisionless dissipation

11 p2095 A70-26756

Radar spectrum control based on two pulse shaping techniques using klystron transmitter

12 p2188 A70-27941

Turbulent shear flow energy spectrum theory for unstratified fluid with arbitrary eddies-mean velocity gradient interaction

12 p2214 A70-28364

Linear distributed system with periodic parameters spectral characteristics based on multidimensional Fourier transforms with drift

13 p2383 A70-29718

Spectral transmittance coefficients at Naugazan astronomical station, using Bouguer method

15 p2809 A70-32909

Stellar UV spectral line profiles interpretation, using atmospheric models and line formation theory

17 p3161 A70-34890

Acoustic turbulence spectrum in compressible fluid with potential motion, using complex traveling wave amplitudes in hydrodynamic equations

18 p3242 A70-36637

SPECTROGRAMS

Atlas of near IR spectra of Venus, Mars, Jupiter and Saturn obtained by Fourier spectroscopy, discussing observational procedures, data recording and processing

01 p0173 A70-10078

Jovian surface elements spectral and color contrasts from spectrograms obtained between 3200- 4900 A wavelengths

02 p0375 A70-12429

SPECTROGRAPHS

U SPECTROMETERS

SPECTROHELIOGRAPHS

Simultaneous filtergrams of velocity and intensity field of central solar disk obtained in blue and red wings of Fraunhofer line

01 p0175 A70-10242

Chromospheric slitless spectrograms at 1962 eclipse, discussing Balmer-Paschen line intensities, continuum data, reduction and source error

01 p0175 A70-10244

Chromospheric structural parameters determined from XUV spectroheliograms, discussing He 2 emission, O 4 and O 5 emission distribution, etc

01 p0175 A70-10246

Rocket-borne spectroheliograph for taking X ray and monochromatic pictures of sun in Mg II line

03 p0570 A70-13594

Multichannel magnetograph display for pattern recognition of solar feature morphology compared with spectroheliograms

06 p1142 A70-17993

Radioheliograph observations at 80 MHz of directive shock wave propagation in solar corona

06 p1144 A70-18007

Solar magnetic field spectroheliographic mapping, discussing detection levels, resolution, applications, etc

06 p1148 A70-18454

Brightness distribution of spectroheliograms taken in metal lines reflecting velocity field structure in photosphere

08 p1570 A70-20839

Atomic frequency standards for phase calibration of large aerial arrays applied to radioheliograph

11 p2019 A70-26300

Statistical heliographic latitude dependence of dominant polarity of interplanetary magnetic field, using photospheric synoptic chart

13 p2492 A70-29195

Solar X-rays measurements with spectroheliograph conducted on rocket flights

14 p2589 A70-31339

SHF radioheliograph with T shaped dish antenna array, noting high resolution and special applications

17 p3061 A70-35397

Solar radio bursts recording by spectrographs in 500-1500 MHz band, discussing sensitivity

18 p3307 A70-36109

Laser aided frequency and amplitude analysis of vacuum test chamber vibration during alignment of orbiting UV spectroheliograph

19 p3396 A70-37877

Spectroscopic differential photosphere and chromosphere rotation with height in solar envelope
23 p2452 A70-44831

SPECTROHELIOSCOPES
U SPECTROHELIOGRAPHS
SPECTROMETERS
NT FABRY-PEROT SPECTROMETERS
NT INFRARED SPECTROMETERS
NT MASS SPECTROMETERS
NT NEUTRON SPECTROMETERS
NT SOLAR SPECTROMETERS
NT SPECTROHELIOGRAPHS
NT TIME OF FLIGHT SPECTROMETERS
NT ULTRAVIOLET SPECTROMETERS
Holographic spectroscopy design and development, discussing components and recording yellow Na doublet
01 p0087 A70-10659
Spectrometer scanning .20-15 microns in 3 sec, measuring absorption and emission spectra of hot samples alternately, discussing resolutions at various bands
01 p0091 A70-10914
X ray spectrometer for space science and laboratory research, presenting CrK spectrum and fine structure
01 p0092 A70-11172
X band electron paramagnetic resonance spectrometer with ruby maser preamplifier, correcting misinterpretation and noise figure analysis
01 p0114 A70-11196
Nutational NMR nonuniform magnetic field stabilizer for beta spectrometer, structural details and circuit schematic
03 p0485 A70-13467
Electron spectrometer for nitrogen energy loss spectrum in 12-14 eV region, detailing relative intensities of transition bands
03 p0528 A70-13577
Multichannel spectrometer electronic circuitry for ionization colorimeter providing data on low energy particle interactions, emphasizing reliability and accuracy
05 p0846 A70-15948
Scintillation spectrometer design for mass and energy spectra of elementary particles, discussing block diagram
05 p0846 A70-15962
On-line system transmitting experimental data from optical spectrometer to central computing facility for magnetic tape recording
05 p0818 A70-16846
Binary cyclic coding schemes for multiplex spectrometry in terms of linear least mean square unbiased estimate
06 p1013 A70-17217
Pulsed grid modulation for ion cyclotron resonance spectrometer
07 p1286 A70-19974
Anamorphic optics to focus luminous wakes of hypervelocity projectiles onto focal plane of slitless spectrograph in free flight ballistic range launching
07 p1287 A70-20082
Rapid scanning high resolution photoelectric spectrometer for sunspot spectra study
07 p1289 A70-20291
Sea level testing of magnetic spectrograph and calorimeter apparatus for studying cosmic ray spectra at different atmospheric depths
08 p1560 A70-20474
Emission flame spectrometer based on double diffraction monochromator, describing design features and operating characteristics
08 p1493 A70-20545
Longitudinal nuclear-electromagnetic cascade in ionization spectrometer simulated by Monte Carlo method, noting energy relationship to particle sum recording
08 p1500 A70-21743
Low energy ion spectrum and spatial distribution measurements in auroral zones by Cosmos-261 satellite spectrometer
08 p1492 A70-21798
Cosmos-261 satellite-borne scintillation electron proton spectrometers and lead shielded Geiger counter, measuring electron and proton energy spectra, pitch distributions, etc
08 p1501 A70-21799
LEPR spectrometer with sample cavity as part of HCN laser for experiments with gases, noting improved sensitivity
09 p1698 A70-22991
Kerr cell-shuttered high speed stigmatic spectrograph for shock tube electron density distribution measurement
09 p1682 A70-23503
Spectroscopic instruments for atmospheric temperature measurements classified in terms of filtering, modulating and multiplexing systems
10 p1873 A70-23828
Satellite-borne spectrometer for low energy electrons measurement, describing virgin photoelectrons equilibrium energy spectrum for different latitudes and pitch angles
10 p1874 A70-24313

Satellite-borne spectrometer for low energy ion measurement
10 p1874 A70-24314
Satellite-borne scintillation spectrometers for medium and high energy electron and proton measurements
10 p1931 A70-24315
Rocket-borne spectrometer for measuring 1-13 keV electron fluxes in auroral zone, describing design, operation and calibration
10 p1889 A70-24493
High sensitivity particle spectrometer for onboard OV-1-18 satellite measurements of precipitating protons, electrons and alpha particles during PCA events
12 p2232 A70-27402
Particle spectrometer for Apollo measurements of trapped protons and electrons, using directional telescope composed of solid state and scintillation counters
12 p2232 A70-27404
Digital closed-loop inflight calibration system for spaceborne particle spectrometers, utilizing cesium iodide crystal and programmable photomultiplier dynode supply
12 p2232 A70-27405
Spectral line width and shift measured by spectrograph crossed with Fabry-Perot interferometer in pressure chamber, measuring magnetic field in sodium
12 p2238 A70-28178
Spectrometer model for short wave radiation in atmosphere, measuring sky brightness, polarization and total solar flux
14 p2583 A70-30413
Spectropolarimeter for measurements of polarization characteristics of atmospheric radiation in nanometer range
14 p2583 A70-30414
Carrier distillation DC arc emission spectrography, determining lead, bismuth and tin traces in nickel base alloys after conversion to oxides
14 p2546 A70-30957
NaI scintillation spectrometer response function matrices semiautomatic generation, using standard source spectra to obtain normalized Compton continua
14 p2587 A70-31006
Automatic audio frequency spectrometer for ELF and VLF amplitude spectrum of atmospherics, discussing attenuation band near 3 kHz
15 p2725 A70-31856
IR reflectometer system using Fourier transform spectrometer and ellipsoidal mirror, describing design, construction and performance
16 p2905 A70-33171
Low energy electron impact spectrometry, discussing apparatus, procedures, electronic excitation of gas molecules, etc
16 p2857 A70-33797
Digital spectrophotometer with automatic continuous wavelength selection, sample feed, measurement and printout
16 p2914 A70-34098
Aircraft engine failures advanced detection by spectrometric lubricating oil analysis
17 p3061 A70-35481
Image intensifier apparatus photographing nuclear electromagnetic cascades in ionization spectrometer
18 p3261 A70-37091
Inlet optics modification in Raman laser spectrometer, discussing high pressure gas storage and support plate enlargement
19 p3443 A70-37361
Spectrosensitometer for standardizing meteor spectrograms
19 p3514 A70-37643
X rays measurement by spectrometer on satellite Cosmos 207
19 p3506 A70-38122
Photoelectron spectra of methane, silane, germane, methyl fluoride, difluoromethane and trifluoromethane, describing electron spectrometer with double focusing electrostatic plates
19 p3374 A70-38269
Correlation spectrometry for earth resources, considering sulfur dioxide, nitrogen oxide and iodine pollution
20 p3626 A70-39055
Primary cosmic rays spectrographic measurement, using hard muon component intensity variations data
20 p3629 A70-39320
Event-triggered high speed spectrograph shutter, studying shock tube plasmas
20 p3630 A70-39484
Air polluting sulfur dioxide and nitrogen dioxide remote sensing based on radiation molecular absorption using long line correlation spectrometer
20 p3633 A70-39793
Ionization spectrometer for hadron energy measurement, analyzing instrument accuracy by Monte Carlo model for nuclear-EM cascade in iron absorber
20 p3635 A70-40456

Dispersive spectrometer multiplexing light in entrance and exit slit positions compared with Michelson interferometric spectrometers
21 p3823 A70-40848
Interplanetary medium energetic electrons and isotopes measurement, discussing spectrometer electronics of IMP H and J
21 p3825 A70-41000
Photoelectron production and escape flux at midlatitudes, using spectrometric measurements from ISIS-1 satellite
21 p3818 A70-41102
Microwave frequency marginal oscillator for electron spin resonance spectrometer, using Gunn diode in sample cavity
21 p3827 A70-41460
Wide frequency range dielectric spectrometer for insulating materials permittivity and loss factor measurement and display
21 p3830 A70-41950
Three dimensional hologram diffractive efficiency measurement by spectrographic attachment
22 p4026 A70-42508
High dispersion stellar spectroscopy with echelle grating, discussing instrument design, operation and performance
22 p4040 A70-43613
Superheterodyne EPR spectrometer microwave bridge using single X band klystron
23 p4170 A70-43798
Soft X ray slitless spectrometer with gold-shadowed transmission gratings for rapid astronomical spectral surveys
23 p4196 A70-44418
Soft particle spectrometer in Isis-1 satellite using electrostatic deflection for differential energy spectra measurements for electrons and protons
23 p4197 A70-44468
Varian HA-100 spectrometer eliminating phase change by compensation network in synchronous audio detector reference signals
23 p4199 A70-44949

SPECTROMETRY
U SPECTROMETERS
SPECTROPHOTOGRAPHY
Photographic films for astronomy and spectroscopy, discussing resolving power, light sensitivity, antihalo lacquer and emulsions
10 p1892 A70-25129
Chilled emulsion photography for astronomy and spectrography, reducing long exposures with chilled plates
14 p2585 A70-30649
SFR high speed photochronograph for visible and UV raster, stereoscopic and spectral photography
24 p4335 A70-45652

SPECTROPHOTOMETERS
NT INFRARED SPECTROPHOTOMETERS
NT ULTRAVIOLET SPECTROPHOTOMETERS
Monk-Gilleson convergent beam dispersion method applied to rocket-borne photoelectric spectrophotometer for far UV stellar spectra observation
01 p0090 A70-10904
Remote sensors for measurement and mapping of ocean color variations, discussing Widerange Image Spectrophotometer and Water Color Spectrometer
06 p1073 A70-18592
Multichannel IR spectrophotometer to obtain albedo curves of Martian surface
12 p2229 A70-26927
Manual spectrograph for distant objects spectrophotometry under natural conditions and solar illumination
14 p2583 A70-30415
Concentric polarization Fabry-Perot duochromator for spectral line displacement measurements applied to ion drifts in hollow cathode plasma
15 p2737 A70-32042
Atmosphere spectral transparency and stability spectrophotometric studies based on measuring solar aureole brightness
16 p2899 A70-34183
Balloon-borne spectrophotometer with diffraction grating for upper atmospheric solar radiation attenuation measurement
19 p3422 A70-37639
Pulse counting and encoding system on rocket-borne spectrophotometer for starlight collected by primary telescope mirror
22 p4038 A70-43174
Phosphor-output image intensifier response to single photon inputs in multichannel spectrophotometer for faint optical sources
23 p4195 A70-44291

SPECTROPHOTOMETRY
NT STELLAR SPECTROPHOTOMETRY
Spectrophotometric facility for measuring spectral characteristics of color filters, photomultipliers and photographic plates as function of temperature
02 p0301 A70-12494
Venusian atmosphere low reflectivity reinterpretation based on spectrophotometric data indicating constituents of yellow and upper UV haze layers
02 p0377 A70-12555

Satellite multispectral photometry data in airglow bands correlated with cloud characteristics and surface albedo variations

04 p0715 A70-15522

Spectral, angular and spatial evolution of earth twilight aureole brightness pattern from visual observation and spectrophotometry on Soyuz 5 spacecraft

10 p1873 A70-24270

Heterochromatic spectrophotometry, discussing maxima and integral techniques for line measurement, photoemulsion properties and Eberhard effect

14 p2585 A70-30784

Aerospectrometric camera facilitating spectral brightness coefficients determination for object identification

16 p2908 A70-33227

Supergiant alpha Car UV spectrophotometry from Gemini 11, comparing with model atmosphere

17 p3161 A70-34888

Upper atmospheric gas components vertical distribution by airborne photometric absorption and attenuation measurements in UV spectrum

18 p3248 A70-36633

Optical density of valence and conduction states by UV photoelectric spectroscopy, outlining experimental techniques and inelastic scattering effects

19 p3471 A70-37711

Evening twilight airglow oxygen IR band ground based observation by two-channel photometric technique

19 p3415 A70-38385

Ikeya-Seki /1967n/, Thomas /1968b/ and Honda /1968c/ comet photoelectric spectrum, examining swan bands, continuum and reflected scattered light

20 p3703 A70-39024

Plate illumination relation to opacity in photometry and spectrophotometry, using digital techniques

20 p3630 A70-39475

High temperature combined differential thermal analysis and spectrophotometric cell for phase transformation monitoring of evaporated thin film and bulk phthalocyanine

21 p3827 A70-41459

Spectrophotometry of earth surface from manned Soyuz spacecraft, obtaining transfer function of atmosphere by aircraft flights

23 p4191 A70-44636

SPECTORADIOMETERS

Optical telescope spectrograph to obtain radiometric and spectrographic data on vehicles reentering atmosphere, discussing performance criteria and tests

03 p0489 A70-13653

Extraterrestrial solar spectral irradiance at earth mean solar distance within 300 to 2500 nm wavelength region, from NASA CV-990 aircraft research flights

04 p0690 A70-15019

Spectral radiometer for observing excited hydrogen radio frequency lines using paramagnetic traveling wave quantum amplifier

08 p1495 A70-21052

Radiometers sensitivity increaseable by combining quasi-zero method with compensation circuits

08 p1495 A70-21053

Spectroradiometer with paramagnetic traveling wave quantum amplifier applied to radio telescope, studying noise, temperature and fluctuation sensitivity at given time constant

08 p1495 A70-21054

Zero radiospectrometer for spectral observations of radio emission of excited galactic hydrogen at centimeter wavelength, noting Omega nebula detection

08 p1495 A70-21063

Parametric amplifier for spectral radiometer of U.S.S.R. astronomical telescope, showing improved sensitivity observations of neutral H emission

08 p1473 A70-21066

Modulation lanes in fine structure of dynamic spectra of Jovian L bursts possibly due to ionosphere or magnetosphere

08 p1576 A70-21394

Solar U-burst radiospectrographic observations, investigating disturbing trajectories and longitudinal distribution in combination with model coronal condensation

09 p1758 A70-22737

Airborne monochromator and photoelectric filter radiometer for solar spectral irradiance measurements, estimating instrument errors

09 p1683 A70-23515

Color TV tubes white field balancing by spectroradiometer, colorimeter and colorgram meter

12 p2195 A70-23732

Remote sensing of plankton and matter in sea by determining spectral changes in scattered light measured with radiometer

17 p3079 A70-35619

SPECTROSCOPES

U SPECTROMETERS

SPECTROSCOPIC ANALYSIS

Spectroscopically active compounds observability in Jupiter atmosphere using solar composition adiabatic equilibrium model

01 p0180 A70-10530

Spectroscopic quantitative diagnostics of high density plasma sources encountered in aerospace applications and chemistry

06 p1063 A70-17729

Axicon systems for spectroscopy of light emitted by foil-excited accelerator beams, discussing scattering contribution to spectral line widths

07 p1287 A70-20083

Consumable protective coat /silasene/ application to reentry models to eliminate metallic pollution in hotshot wind tunnels for spectroscopic analysis

10 p1825 A70-24548

Wall stabilized arc source for spectroscopic measurements of isothermal plasma at various pressures

14 p2584 A70-30505

Book on interpretation of spectra and atmospheric structure of cool stars covering line identification, dissociative equilibrium, opacity, chemical composition, carbon stars, etc

16 p2978 A70-33962

Time varying flow properties effects on hypersonic wind tunnel spectroscopic measurements, considering direct emission and electron beam techniques

20 p3607 A70-40271

Mossbauer effect spectrometry application to Apollo 11 lunar rocks composition, using nuclear gamma resonance measurements for nuclide Fe 57

21 p3916 A70-41662

Venus spectrum from high resolution Michelson interferometers with Fourier transform and digital computation, discussing Venus atmospheric models

22 p4099 A70-42721

Shock wave propagation studies by grating spectrograph with high speed camera, computing equilibrium detonation gases temperature from emitted light [SMPTE PREPRINT 98]

22 p4035 A70-43057

Ion cyclotron resonance spectroscopy for detecting trapped gaseous ions in analyzer cell, observing ion-molecule reactions

23 p4196 A70-44390

Spectroscopic features of mercury laser associated with electron energy levels and spontaneous emission line structure, giving excitation and disruption mechanisms

23 p4202 A70-45054

SPECTROSCOPIC TELESCOPES

Rocket telescope spectrometer precision pointing achieved by servocontrolling secondary mirror, discussing use for planetary atmospheres far UV spectrum studies

02 p0296 A70-11916

Optical telescope spectrograph to obtain radiometric and spectrographic data on vehicles reentering atmosphere, discussing performance criteria and tests

03 p0489 A70-13653

Image intensifiers to improve telescope system sensitivity and spectral resolution in radiometric measurements of reentry vehicles

03 p0489 A70-13654

Optical systems for coude focus spectroscopic telescopes, discussing advantages over Newtonian and Cassegrain foci

04 p0685 A70-14522

Speckle patterns Fourier transform analysis for diffraction limited resolution attainment in large telescopes

14 p2589 A70-31382

Astronomical Fourier spectroscopy, discussing techniques, improvements, advantages and mode of use

20 p3706 A70-39933

OAO 2 for UV telescope sky mapping and spectrophotometric measurements of celestial bodies

23 p4261 A70-44666

SPECTROSCOPY

NT ABSORPTION SPECTROSCOPY

NT ASTRONOMICAL SPECTROSCOPY

NT AURORAL SPECTROSCOPY

NT GAS SPECTROSCOPY

NT INFRARED SPECTROSCOPY

NT MAGNETIC SPECTROSCOPY

NT MASS SPECTROSCOPY

NT MOLECULAR SPECTROSCOPY

NT OPTICAL EMISSION SPECTROSCOPY

NT RADIO SPECTROSCOPY

NT RAMAN SPECTROSCOPY

NT SPECTROPHOTOGRAPHY

NT SPECTROPHOTOMETRY

NT SPECTROSCOPIC ANALYSIS

NT STELLAR SPECTROPHOTOMETRY

NT ULTRAVIOLET SPECTROSCOPY

NT X RAY SPECTROSCOPY

Laser optoelectronic and spectroscopic methods using fixed gap spherical mirror confocal Fabry-Perot interferometer and multiple beam image tube framing camera

01 p0112 A70-10901

Far IR airborne spectroscopy for measuring solar brightness temperature, emphasizing scanning Michelson interferometer and radiometric calibration

09 p1683 A70-23525

Spectroscopy applied to spontaneous combination scattering of light

10 p1892 A70-25026

Heavy particle spectroscopy, deducing collision parameters from empirical observations

13 p2456 A70-29810

Efficiency of holographic gratings in instrumental spectroscopy

19 p3421 A70-37360

Integrating cavity spectroscopy for measuring absorption coefficient of material

21 p3822 A70-40817

Multichannel monitor for repetitive short scan Auger electron spectroscopy for surface composition changes, using low energy electron diffraction

21 p3827 A70-41467

Carbon monoxide-nitrogen laser luminescent phenomena by electronic spectroscopy

21 p3837 A70-41717

Ultrasonic spectroscopy in nondestructive materials tests, discussing electronic equipment design, FM, pulse and pulsed FM methods

22 p4027 A70-42583

Image orthicon detection and recording system adapted for spectroscopic measurements in shock tube emission studies

23 p4197 A70-44469

SPECTRUM ANALYSIS

Slitless spectrograms of chromosphere obtained during 1962 eclipse to determine H level populations decrements, self absorption in Balmer lines and chromosphere model

01 p0175 A70-10245

Pulse width and spectrum generated by ring laser mode locked by synchronously modulated absorber as function of modulator waveform curvature and active medium

01 p0109 A70-10430

Interferometer for compressing linearly FM light pulses and analyzing spectra of picosecond pulses

01 p0111 A70-10670

Galactic water vapor line emission observations indicating short term variability in spectra of several sources

01 p0182 A70-10722

Electromagnetic procedures and camera-spectrometer system for studying detonation processes, measuring mass flow rates and explosives spectra

01 p0090 A70-10887

Spectrometer scanning .20-15 microns in 3 sec, measuring absorption and emission spectra of hot samples alternately, discussing resolutions at various bands

01 p0091 A70-10914

CW laser ranging systems power and signal to power ratio characteristics, finding possible advantages over pulsed systems

01 p0114 A70-11321

Real configuration effect of magnetic field in moderately perturbed magnetosphere on whistlers dynamic spectra, stressing geomagnetic perturbation detection

01 p0082 A70-11486

Pressure and line width estimate from high resolution image tube spectra of Jupiter at 11,000 A

02 p0366 A70-11808

Ammonia spectral lines positions, intensities and half widths under Jovian conditions calculated, including ground state rotation and rotation inversion bands

02 p0368 A70-11820

Collision-narrowed growth curves for interpreting hydrogen quadrupole lines applied to photoelectric observations of Jupiter vibration-rotation bands

02 p0368 A70-11824

Stellar spectral lines fine analysis methods compared for curves of growth, line profiles and related contribution curves in model atmospheres for Procyon and sun

02 p0343 A70-11906

Molecular rotations and kinetics from spectral features of molecular Raman spectra, using light scattering spectroscopy

02 p0343 A70-12077

VLF observations of auroral beams for auroral V-emissions source and characteristics, explaining spectral shape

02 p0291 A70-12204

Cape Kennedy vertical wind speed profiles measured by spectral analysis using fast Fourier transform method

02 p0325 A70-12285

Correlation characteristics and dimensionality of speech spectra from statistical properties derived from continuous speech and summarized by covariance-matrix eigenvectors

02 p0237 A70-12324

IR spectrum of Jupiter with calibrations from laboratory studies of methane and ammonia bands

02 p0378 A70-12559

Satellite lines of forbidden transition in laser-produced He plasma attributed to longitudinal plasma oscillations

02 p0379 A70-12717

Optical transmission spectra of polypeptide films showing exciton structure near 1600 A for alpha and polyproline II helices

02 p0345 A70-12723

Scattering functions from sky light spectra measurements on high mountain for various sun altitudes, obtaining color value functions

02 p0359 A70-12776

Ionized matter complex at galactic periphery deduced from neutral hydrogen line and continuous spectrum observations

03 p0564 A70-13222

Spectral polarization characteristics phase variations used for classifying lunar surface features

03 p0565 A70-13234

Late stars spectral characteristics, verifying criteria for spectral classification and anomalous spectra determination

03 p0569 A70-13424

Electromagnetic field spectrum and spatial distribution in ring laser, considering transverse modes influence

03 p0500 A70-13462

Spectrum parameters analysis of signal in form of radio pulses sequence with harmonic angular modulation

03 p0448 A70-13511

Sampled signal and associated sequence with identical Fourier transforms, noting applications to digital spectral analysis onboard spacecraft

03 p0449 A70-13538

Airborne multispectral sensing based on modified AN/AAS-5/XE-2/ scanners mounted in C47 aircraft, discussing applications

03 p0491 A70-13669

Periodic clustering of red shift values in quasi-stellar and unusual objects spectra, using power spectra

03 p0577 A70-14217

Analog techniques for pulse integration based on sonograph audio spectrum analyzer for pulsar observation by radio telescopes near Hobart, Tasmania

04 p0655 A70-14520

Slitless system using interference filter, fixed Fabry-Perot etalon and automatically controlled etalon for recording spectral information for efficient light detection

04 p0685 A70-14523

Decaying isotropic turbulence spectrum evolution model, verifying numerical integration of differential equations

04 p0673 A70-15249

Shear-dependent nearly isotropic turbulence energy spectrum theory, considering effects of viscous loss, shear production and inertial and velocity gradient transfer

04 p0674 A70-15520

Line transfer with scattering described by redistribution function numerically solved, using discrete ordinate method

04 p0720 A70-15701

Surface wave spectrum and propagation in non-homogeneous bounded elastic solid, considering existence and eigenvalues approximation

05 p0925 A70-15789

Spectral and lasing characteristics of microwave frequency modulated He-Ne laser operating at 0.63 micron wavelength

05 p0858 A70-16257

Reflectance spectra obtained for igneous rocks and minerals, establishing correlation between reflectance and energy wavelength, composition and sample particle size

05 p0839 A70-16390

High resolution Venus spectra, obtaining band spectra growth curve of C13O16O18 isotope of carbon dioxide, comparing data reduction methods

05 p0910 A70-16392

Periodicities in solar activity variation from correlation spectral analysis, establishing monotonically decreasing component and secular variations in activity

05 p0918 A70-16913

C V lines measured near 1s-2p line of C VI, identifying lines belonging to various transitions

05 p0921 A70-16982

Cosmic ray electron spectrum above 200 Gev based on pure nuclear emulsion stack using horizontal sandwich assembly

06 p1135 A70-17473

Discrete spectrum of fourth order differential operator estimating number of eigenvalues in bounded interval of real line

06 p1094 A70-17740

Spectral transparency inversion of aerosol-containing atmosphere

06 p1098 A70-17832

Granular and intergranular region solar magnetic field difference detection attempt from line profiles, noting equivalent width increase in ionized Cr line

06 p1142 A70-17989

Solar Cd abundance, using spectrograph and synthetic spectral line computer program

06 p1143 A70-17995

Optical spectra of discharge chambers of electron bombardment mercury ion thrusters with hollow and oxide cathodes

06 p1132 A70-18157

[ALAA PAPER 70-176]

Spectral characteristics of B and S components of solar radio emission from statistical data, investigating dependence on 11-yr cycle and minimum solar activity

07 p1378 A70-19031

Absorption lines in quasars spectra indicating line formation close to quasar nucleus

07 p1383 A70-19402

Spectral functions of airflow velocity pulsations in circular pipe at various Reynolds numbers, considering laminar, transition and turbulent regimes

07 p1259 A70-19826

Holographic system to obtain time-bandwidth product improvement in spectral analysis without sacrificing multichannel processing capability

07 p1288 A70-20098

Optical hardness effect on dispersed particles spectrum determination accuracy by spectral transmittance

07 p1330 A70-20309

Solid state lasers with strongly degenerated modes investigated for induced radiation spectral composition inertial properties

08 p1510 A70-20507

Soviet book on celestial bodies radiation transfer and spectra covering light scattering, radiation fields, absorption, etc

08 p1568 A70-20768

Free radical formation in irradiated pyrimidines from ESR spectrum analysis of gamma irradiated single crystals of alloxantin, confirming radical stability

08 p1455 A70-20774

Binary star spectrum analysis establishing seasonal and season-to-season variations in He II emission band intensity and shift toward long wave region

08 p1569 A70-20827

Equivalent line widths of anomalously fast stars of early spectral classes and reference stars, discussing binary nature and radial velocities of OB stars

08 p1569 A70-20828

Celestial emission bodies forbidden line analysis for physical conditions determination using formulas and graphs

08 p1569 A70-20831

Jupiter atmospheric properties on basis of spectrograms analysis

08 p1569 A70-20833

Venus clouds absorption spectra correlation with carbon suboxide first reflection spectra, suggesting absence of carbon suboxide in atmosphere

08 p1571 A70-20911

Von Zeipel 1128 O star spectrum analysis, discussing mass, He/H ratio, metal abundances, etc

08 p1571 A70-20913

Spectral radiometer for observing excited hydrogen radio frequency lines using paramagnetic traveling wave quantum amplifier

08 p1495 A70-21052

Nitrogen dioxide presence in solar atmosphere from balloon-borne spectrometer observations, presenting graph of sunset solar spectrum

08 p1575 A70-21262

Ionized matter complex at galactic periphery deduced from neutral hydrogen line and continuous spectrum observations

08 p1580 A70-21655

Spectral polarization characteristics phase variations used for classifying lunar surface features

08 p1580 A70-21667

IR absorption spectral curve interpretation using computer program for iterative solution

09 p1726 A70-22138

Solar chromosphere-corona transition region properties, discussing temperature increase within very thin layer and inferring temperature-density structure from emission line intensities

09 p1752 A70-22246

Backscattered sun and skylight spectra from sea obtained from low flying aircraft as measure of chlorophyll concentration

09 p1666 A70-22250

Spectra of meteorological variables - Conference, Stockholm, June 1969

09 p1713 A70-22351

Turbulence and internal waves in stably stratified atmosphere and ocean, proposing velocity and temperature spectral behavior model

09 p1716 A70-22370

Dynamics dominant on different scales in atmosphere by spectral analysis, showing marked gap under most synoptic conditions

09 p1717 A70-22376

Pulsed microwave spectrum analyzer using holography and Fourier spectroscopy compared with frequency methods

09 p1675 A70-22485

Europium isotope ratio in solar atmosphere equal to terrestrial using spectral line profiles analysis

09 p1757 A70-22727

Automatic spectral data reduction and analysis system consisting of densitometer, analog-digital converter and IBM 1800 process computer with magnetic disk memory

09 p1629 A70-22765

Critical review of paper on molecular oxygen microwave spectrum analysis

09 p1732 A70-22829

Scanning spherical mirror interferometer for carbon dioxide lasers radiation spectrum analysis, discussing instrument errors in mode and wavenumber studies

09 p1683 A70-23519

Fourier spectrum of chopped bivariate normal intensity distribution with coefficients calculated numerically by computer, verifying by chopped laser beam signal analysis

09 p1729 A70-23520

Galactic sources H109 alpha line and continuum surveys, showing thermal continuum spectrum for sources with radio recombination lines

10 p1936 A70-23903

Exploding tungsten wires in air and vacuum, describing visible and X-ray spectrum characteristics

10 p1915 A70-23994

Spectrum analysis of unsteady duct flow caused by pressure loss induced instability

10 p1863 A70-24026

Mariner 6 spectra establishing Fox-Duffendack-Barker bands and ionized carbon dioxide UV doublet bands as important components of Martian dayglow

10 p1938 A70-24073

Intensity vs voltage curves for LEED beams from clean Ni surface, calculating Bragg spectrum with energy diagram method

10 p1927 A70-24077

Excited gas kinetic state determination from observed spectral profiles during interaction with radiation

10 p1919 A70-24147

Oscillator strengths relative values determined from flame atom absorption line sensitivity measurements

10 p1828 A70-24259

Spatial frequency spectra of three dimensional phase object and three dimensional hologram, discussing interaction characteristic for monochromatic illumination

10 p1888 A70-24263

Plasma magnetic field measurement by scattered light, analyzing electron spectrum modulation with gyration frequency

10 p1916 A70-24401

Ultrasonic pulse frequency spectrum analyzer, describing electronic components, transducer type and positioning, beam collimation, applications in testing, etc

10 p1895 A70-24830

Resonance, intercombination and forbidden lines observed in solar He isoelectronic sequence of oxygen, Ne, Al, Si and sulfur with Bragg crystal spectrometer

10 p1944 A70-24954

H II region properties from non-LTE analysis of alpha, beta, gamma, delta and epsilon radio recombination line data, determining electron temperature and concentrations

10 p1945 A70-24959

Quasar spectra searched for intergalactic absorption lines, discussing red shift

10 p1947 A70-24998

Radio wave reflection spectra from plane surfaces, determining physical properties and composition

10 p1843 A70-25154

Sulfur beam foil spectrum in 600-4000 A range, identifying transitions in S I-S VI

11 p1994 A70-25362

Raman and IR spectrum analysis of polywater indicating impurities role in anomalous properties

11 p1994 A70-25655

Solar moustaches /transient emissions/ far wing asymmetry studied photometrically

11 p2109 A70-25745

Turbulent ionized wakes Doppler radar scattering spectrum parameters in terms of wake characteristics using double convolution integral

11 p2010 A70-26271

Excess color method for photometric and spectral studies of interstellar absorption in cluster NGC 6913

11 p2116 A70-26585

Excess color method for studying interstellar absorption around cluster NGC 6823

11 p2116 A70-26586

Spectral classification of stars from unbroadened spectra recordings possible when comparing optical depths of lines

11 p2116 A70-26589

Satellite signal scintillation spectrum analysis by digital filtering of magnetic tape recording

11 p2012 A70-26718

Spectroscopic diagnostics of erosion plasma jets from cylindrical pulsed plasma generator operating in vacuum

11 p2093 A70-26745

Turbulent flowing plasma, analyzing wavenumber frequency dependent spectral function and space-time correlation function

11 p2096 A70-26768

Cosmos 137 proton spectra data obtained in inner radiation belt agreeing with Relay 1 data

11 p2106 A70-26786

Single mode TW ruby laser with ring resonator, analyzing emission spectral characteristics by Fabry-Perot etalon 12 p2246 A70-27356

Alias-free randomly timed sampling of stochastic processes, considering spectrum recovery by linear operation 12 p2204 A70-27419

Primary cosmic ray proton and alpha particle spectral measurements by balloon flights 12 p2293 A70-27586

Molecular line identification in sunspot spectrum of CN, diatomic carbon, TiO, MgH, CaH, NiH and water vapor 12 p2302 A70-27590

Computer programs for calculating spectral lines oscillator strength in Coulomb approximation, proposing Fortran program 12 p2192 A70-27595

Coronal condensation spectra during 4 February 1962 total eclipse, determining abundances, ionization equilibria, electron densities, etc, from Fe and Ca XV lines analysis 12 p2303 A70-27712

Emission asymmetry of solar limb flares, inferring luminescent layer contraction-expansion from spectral qualitative analysis 12 p2294 A70-27859

Merope /IC 349/ nebula, noting luminescence and continuous spectrum fine structure 12 p2307 A70-27867

Integral color indices relation to spectral type on NGC 3077 and M82 galaxies 12 p2308 A70-27871

Primordial radiation spectrum, discussing possible distortions due to energy injection before and after recombination 12 p2308 A70-27886

Absolute sky brightness temperatures measured with horn antennas and Dicke receivers, indicating spectrum change due to galactic nonthermal radiation 12 p2309 A70-27893

Pipeline fast Fourier transform signal processor for digital spectrum analysis of wideband radars 12 p2186 A70-27904

Microwave signals covariance and spectra calculation for amplitude and phase fluctuations propagated over line-of-sight path through turbulent atmosphere 12 p2189 A70-27963

Closed product form and simplified algorithm for efficient operation of generalized Kronecker matrices, considering role in spectral analysis 12 p2193 A70-28029

Mathematical models for radar transmitters emission spectra envelopes calculation, considering effects of pulse width, rise and fall times, corner smoothing and frequency modulation 12 p2189 A70-28136

Maximum mode selection tuning of scanning interferometer with spherical mirrors applied to He-Ne laser spectrum analysis 12 p2250 A70-28182

Output signal spectrum analysis for nonlinear active element in presence of distorted modulating voltage 12 p2191 A70-28342

Anisotropic two phase plates gas laser resonator spectrum, analyzing zero or 90 degree angles between plates 13 p2424 A70-28594

Three mirror resonator He-Ne laser output spectra, studying frequencies and intensities of generated modes 13 p2424 A70-28595

Spectral analysis of LF pulses from defects obtained by modulation method of monitoring using eddy currents with superposed converter 12 p2404 A70-28660

Star eta Arietis spectra analyzed for Fe and V abundance 13 p2487 A70-28715

Laser field structure effect on spectrum of Q switched laser nonmonochromatic emission after amplitude modulation 13 p2426 A70-28872

Nonoriented cadmium silicon arsenide single crystals optical properties, determining spectral distribution of IR absorptivity for various photon energies 13 p2470 A70-28883

Strontium chloride lanthanum ion system with dynamic Jahn-Teller effect, indicating isotropic EPM spectrum resulting from averaging by relaxation 13 p2470 A70-29109

Fast time-resolved spectra of earth bow shock electrostatic turbulence based on broadband analog electric data fromOGO-5 13 p2396 A70-29111

Kinetic changes in spectral lines and bands intensity of individual molecular gases and mixtures for carbon dioxide lasers 13 p2428 A70-29361

Pulsed Ne laser superradiation spectrum fine structure, using Fabry-Perot interferometer 13 p2428 A70-29362

Lunar crater Aristarchus red spot spectrum analysis, determining emission bands 13 p2494 A70-29398

Oscillators frequency instability and spectral purity relations [ONERA-TP-829] 13 p2383 A70-29637

Two body system with Newtonian force interaction, calculating gravitational wave energy losses and spectral decomposition 13 p2453 A70-29668

Real time signal processor for correlation and spectrum analysis, displaying results on cathode ray oscilloscope 13 p2370 A70-29817

Solar differential rotation measurement by spectral line shift data analysis, noting angular velocity-heliographic latitude relationship 13 p2496 A70-29840

Solar observations in intermediate IR, measuring continuum intensity of disk center in atmospheric water vapor window 13 p2498 A70-30006

Fog droplet size growth time dependence and spectral variations during simulated cloud formation by water vapor condensation in chamber 14 p2601 A70-30128

Model for droplet size spectrum in cloud with spatial inhomogeneity of nuclei concentration, determining characteristic size dependence on altitude 14 p2601 A70-30129

Entire functions for analysis and representation of distant atmospherics, using concentrated spectrum and zero coordinate readings 14 p2569 A70-30210

Bright IR stars observed using photometry and spectroscopy, suggesting protostars presence 14 p2641 A70-30880

Venus carbon dioxide absorption bands determining atmospheric scattering model suitability for all data 14 p2642 A70-30889

Water vapor abundance in Mars atmosphere from high resolution spectroscopy 14 p2649 A70-31211

Galactic abundances and cosmic ray spectra by IMP-4 satellite, obtaining He ratio 15 p2793 A70-31794

Continuous differential energy pulse height spectra reduction to photon upper atmospheric spectra 15 p2694 A70-31800

Generalized spectral analysis method implementing orthogonal transformations through Kronecker product representation and matrix factorization 15 p2767 A70-32099

Rocket engine propellants flame temperature measurement by spectral line intensity comparison method 15 p2786 A70-32270

Turbulence spectrum functions time variations, examining electron density fluctuations in ionized gas 16 p2894 A70-33886

Equipment shock test model, using impedance method for spectrum analysis 16 p2992 A70-33988

Venus upper atmosphere carbon atoms detection based on low resolution spectra analysis of solar illuminated atmosphere 16 p2979 A70-34036

Automatic spectrophotometer for measuring sky spectrum brightness at 6910-4040 A, determining point of minimum brightness 16 p2899 A70-34182

Atmosphere spectral transparency and stability spectrophotometric studies based on measuring solar aureole brightness 16 p2899 A70-34183

X ray spectrum analysis for Crab, Cas A and SN 1572 supernova remnants 17 p3156 A70-34830

Mercury disk temperature from microwave spectrum analysis, proposing subsurface greenhouse effect 17 p3157 A70-34838

Hypersonic velocity and turbulence measurements in wind tunnels, using spectral analysis of Doppler shifted laser light 17 p3103 A70-34849

Discrete Fourier transform method for factoring spectral density functions, calculating absolute error 17 p3129 A70-34855

Early-type star spectral scan analysis from OAO observation, comparing model atmosphere calculations 17 p3161 A70-34887

Solar atmosphere structure and chemical composition by UV spectrum analysis 17 p3161 A70-34892

Nonhydrogen spectral lines in interstellar gas, discussing Ca/Na abundance anomaly 17 p3162 A70-34900

Real time swept sine wave spectrum analyzer using time compression to change filter bandwidth as function of control signal 17 p3059 A70-35166

Sine wave discrete components detection from complex spectrum with random noise, evaluating errors 17 p3059 A70-35168

Automatic shock spectrum synthesizer/analyzer for shock testing of field environments 17 p3059 A70-35175

Ecological potentials in spectral signature analysis, using laboratory leaf and soil spectral reflectance data 17 p3078 A70-35612

Fine structure of hydromagnetic ULF emissions on spectrograms of whistlers, periodic emissions, choruses and sweepers 17 p3047 A70-35640

Crab Nebula X ray flux pulsations, analyzing spectra 17 p3152 A70-35756

Water vapor pure rotational absorption spectrum compared with calculated far and near IR spectra 18 p3244 A70-35949

Solar image spectrum magnetic recording for computer, using photomultipliers with coding devices 18 p3256 A70-36107

Energy distribution of laser spark spectrum in air, He and Ar, determining transmission coefficients of spark plasmas by self absorption method 18 p3265 A70-36151

Quasar 4C 05.34 absolute spectral energy distribution by multichannel photoelectric spectrometry 18 p3318 A70-37019

P Cygni line profiles emission and absorption components rectification procedure, considering errors 18 p3321 A70-37123

Relativistic electron spectra of cosmic rays accelerated by plasma turbulence, examining singularity in solution 18 p3322 A70-37127

Integrated Milky Way spectrum, examining composition and galactic structure in solar neighborhood 18 p3329 A70-37182

Atmospheric turbulence vertical component spectral density observation by aircraft in steady flight, considering transfer function computation methods 19 p3351 A70-37646

RMS spectrum analysis system for wideband acoustic data processing, using analog method with digital output 19 p3397 A70-37910

Spectra and cross-spectra estimation by fast Fourier transform algorithm 19 p3384 A70-38040

Ballistocardiogram autocorrelation function and spectrum by scanning graph decoder and computer, determining total power, harmonics periodicity and energy concentration 19 p3370 A70-38211

Real time narrow band vibration spectrum analysis techniques, discussing application to failure prediction and flight and wind tunnel tests 19 p3430 A70-38528

Solar radio emission intensity distribution across disk during eclipse, constructing relative RF spectrum of uncovered region 19 p3522 A70-38556

Power spectrum analysis of division errors of graduated circles associated with meridian astronomy 19 p3523 A70-38686

Spectrum analysis of P Cygni star AG Carinae and derivation of mean radial velocities for different epochs 19 p3523 A70-38694

Spectral energy distribution of meteor trail in Leonid meteor shower from photographic analysis 19 p3526 A70-38779

Cardiac contraction rhythm autocorrelation and spectral analysis in healthy subjects and patients with disturbed sinus node functional states 20 p3578 A70-38963

Quasars PHL 5200 and RS 23 spectra absorption lines, examining resonance line transfer of radiation through differentially expanding atmosphere 20 p3701 A70-39006

Laser beam method sensitivity for spectral emission analysis of nonconducting materials 20 p3642 A70-39743

Amplitude-phase data from gathering receiving antenna array, obtaining Doppler frequency spectrum as arrival angle function 20 p3599 A70-40319

Diatomic Cs 7667 A band vibrational spectrum analysis 20 p3676 A70-40349

Solar photospheric spectrum Ni II forbidden lines analysis, determining abundance of Ni for comparison with coronal and meteoritic data 20 p3711 A70-40405

Human body radioactive nuclides in vivo quantitative analysis by gamma ray spectra, considering matrix method accuracy 20 p3582 A70-40449

Current driven ion wave plasma turbulence in collisionless shock, measuring frequency and wave number spectra by shock front light scattering 20 p3685 A70-40497

Cosmic hard X ray sources spectra and time variations by balloons and OSO-3 satellite observations of Crab Nebula 21 p3872 A70-40657

Hyades giant stars epsilon and gamma Tau strong line profile analysis, obtaining effective temperatures 21 p3885 A70-40931

Apollo 11 lunar samples spectral analysis, discussing Fe and Mn electron paramagnetic resonance and Al 27 nuclear magnetic resonance spectra 21 p3919 A70-41683

Solid para hydrogen IR and Raman spectra frequency analysis, examining lattice vibration effects 21 p3853 A70-41721

Autoionization spectral lines growth curves analysis, applying to 3s-4p transition in Ar at 466 A with specified absorption cross section 21 p3781 A70-41931

Acoustoelectric domain spectra in n-GaAs by microwave emission, comparing results with parametric conversions theory 21 p3863 A70-42002

Accurate tuning methods for laser mode locking device, using diffracted light measurement and photodiode with LF spectrum analyzer 21 p3838 A70-42047

Cadmium sulfide pulsed laser spectrum analysis, discussing laser output stabilization by mode selection and electron beam scanning 22 p4049 A70-42405

Ultrasonic transducer diffraction fields in highly anisotropic crystals obtained by plane waves angular spectrum 22 p4029 A70-42643

Worldwide geomagnetic fluctuations during disturbed conditions computed from spectrum analysis, considering long period oscillation caused by solar wind structure changes 22 p4019 A70-43114

Pc-1 and IPPD pulsations propagation characteristics from ground based measurements, discussing spectral structure, waveforms, polarization, time delay between different observation stations, etc 22 p4021 A70-43277

Laser light pulse interaction with solid targets, observing second harmonic generation in induced plasma from time resolved spectra 22 p4084 A70-43673

F region night airglow in equatorial and midlatitudes, discussing red and blue emission origins 23 p4185 A70-43839

Global geomagnetic field fluctuations of internal and external origins, analyzing HF spectrum based on monthly mean plots 23 p4187 A70-43861

Cosmic ray 11-year variation pattern change in 19th and 20th solar activity cycles determined by latitude expeditions spectrum analysis 23 p4237 A70-44071

Wind generated water waves spectral characteristics at low momentum levels 23 p4215 A70-44273

Solar X ray spectra interpretation by laboratory measurements, using plasma X ray source and potassium acid phthalate spectrometer 23 p4237 A70-44419

Auger spectra characteristics obtained with X rays and electrons from radioactive alpha sources 23 p4222 A70-44421

Mars topography from Mariner 6 and 7 IR spectra, discussing geographical resolution, surface carbon dioxide pressure, depressions, ridges and valleys 24 p4399 A70-45128

Sunspot penumbra velocity field spatial structure by filament spectrum analysis, plotting radial velocities relative to undisturbed photosphere 24 p4400 A70-45310

Multiply ionized Fe valence and inner shell transitions from spectrum analysis, noting similarities to solar flares 24 p4401 A70-45315

Entire functions for analysis and representation of distant atmospheres, using concentrated spectrum and zero coordinate readings 24 p4330 A70-46285

SPECULAR REFLECTION

Speckle pattern in image plane of laser illuminated diffuse object, calculating pattern intensity and contrast 02 p0312 A70-12106

Specular reflections influence on bistatic tropospheric radio scatter from turbulent perturbations in refractivity 02 p0326 A70-12289

Monte Carlo simulation for shock wave formation by specularly reflecting piston, discussing reflection from specularly reflecting wall 06 p1049 A70-18334

Hologram interference fringes formation and location using grating model of diffusely reflecting surface 07 p1280 A70-19144

Specular reflectivity measurement method for optical thin film coating in 10.6 micron IR region using carbon dioxide laser source 07 p1302 A70-20084

Passive radiant cooler design involving patch cone radiative coupling calculation based on specular image technique 07 p1425 A70-20091

Argon ion laser output powers dependence on discharge tube design and mirror reflection coefficient in emission line 08 p1511 A70-20541

Monochromatic plane electromagnetic wave incident from vacuum on plane boundary of plasma half space, discussing specular reflection and diffuse scattering boundary conditions 08 p1553 A70-21611

Laser radiation diffuse reflection from rough surfaces, considering surface specularity and reflected waves polarization and spatial structure 09 p1696 A70-22630

Aluminized epoxy integrating hemiellipsoidal reflector, discussing fabrication, focusing properties and selection of detector size 09 p1683 A70-23530

Radiant heat transfer predictions between isothermal plates based on diffuse plus specular directional property model [AIAA PAPER 69-624] 11 p2149 A70-26157

Transition radiation in plasma sheet in vacuum assuming specular reflection of electrons at vacuum boundary 13 p2464 A70-29512

Speckle patterns Fourier transform analysis for diffraction limited resolution attainment in large telescopes 14 p2589 A70-31382

Diffuse specular rough surface measure for imperfect reflections in thermal radiation transfer through slot passages 16 p2999 A70-33905

Super and sub specular maxima in angular distribution of polarized radiation reflected from roughened dielectric surfaces 16 p2999 A70-33906

Diffuse-specular models for radiant heat interchange prediction for isothermal-adiabatic surface enclosure tested for steel and gold 16 p3003 A70-34197

Spectral and temporal characteristics of ruby laser operating with dielectric coated mirror scatterer 17 p3108 A70-35673

Thick plane fog layers reflection and transmission properties, using emerging light angular distribution for Milne problem 18 p3284 A70-35944

Integrating sphere theory with wall mounted specular sample in reflectance and transmittance measurements 18 p3284 A70-36776

Monochromatic radiant flux angular distribution reflected from water and carbon dioxide cryodeposits, discussing incidence, deposit thickness and wavelengths [ASME PAPER 70-HT-34] 22 p4122 A70-42433

Turbomolecular pumps efficiency calculation by Maxwell transport equation, assuming gas molecules perfect specular reflection from blade surface 22 p4009 A70-42607

Cotton leaves ammonia induced discoloration spectrophotometric examination, discussing light reflectance, transmittance and absorbance 22 p4014 A70-42771

Light beam direction variation by crystal deflectors, examining changing internal reflection angle by applied electric field or mechanical stress 23 p4196 A70-44411

Narrow capillary supermolecular flow density relation to vapor molecule specular reflection, considering Knudsen flow conditions 24 p4381 A70-45491

SPEECH

NT ARTICULATION

NT WORDS [LANGUAGE]

Correlation characteristics and dimensionality of speech spectra from statistical properties derived from continuous speech and summarized by covariance-matrix eigenvectors 02 p0237 A70-12324

Soviet monograph on secondary signaling system role in development of speech, thought, conditioned and unconditioned reflexes, human will and hypnosis, noting salivary gland function 19 p3359 A70-37407

SPEECH DISCRIMINATION

U SPEECH RECOGNITION

SPEECH RECOGNITION

Speech intelligibility tested using Modified Rhyme Test and air traffic control and civil disaster vocabularies, noting Articulation Index for signal-noise conditions 02 p0246 A70-12150

Automatic formant-frequency extraction using vowel-type spectrum, inverse filtering, moment calculation and evaluation by synthesized speech 06 p1009 A70-17909

Analysis method permitting English speech sound recognition by computer for different speakers 08 p1460 A70-20815

Algorithms based on continuous-group pattern recognition, distinguishing human faces, speech and handwritten characters 09 p1640 A70-22143

Commercial aircraft peak cockpit noise level during cruise and high speed descent, discussing damage risk criteria and interpolator speech interference 11 p1991 A70-26275

Transmission delay and echo effects in long distance satellite relay telephony links, describing echo suppression and speech quality 12 p2183 A70-27004

Pilot helmets, discussing sound attenuation, noise protection and speech intelligibility 12 p2177 A70-27040

Real time sonic information input/output computer system for acoustic signals and speech synthesis, concerning man machine communication 14 p2553 A70-30425

Speech signals reflection in nervous system, constructing functional perception model for signals conversion into phonetic patterns 15 p2687 A70-32870

Automatic speech recognition using spatial filtering and Fourier transforms 16 p2869 A70-33462

Automatic speech recognition and tracking techniques of moving objects, considering applicability to processing data from earth resources satellites 16 p2871 A70-34313

Loudspeaker optimal arrangement for speech intelligibility in aircraft crew compartments, discussing apparent SNR improvement 17 p3039 A70-35564

Attention direction role in auditory recognition, testing unwanted inputs attenuation hypothesis 19 p3362 A70-38317

SPEED

U VELOCITY

SPEED BRAKES

U BRAKES [FOR ARRESTING MOTION]

SPEED CONTROL

Brushless DC motors speed regulation with electronic commutators, discussing photoelectric, magnetic sensing and magnetic coil commutation 02 p0229 A70-12616

Thrust control unit in Lufthansa Boeing 707 aircraft designed to maintain landing approach speed by adjusting throttle setting and landing flap position 05 p0845 A70-15903

Pre-set Mach number control in supersonic wind tunnel, evaluating effects of nozzle installation, stagnation temperature drop and pressure errors 06 p1028 A70-17912

Closed loop automatic speed control system for working shaft of two stage alternating current electric servomotor, using invariance principle 20 p3564 A70-39849

SPEED INDICATORS

NT ANEMOMETERS

NT HOT-WIRE ANEMOMETERS

NT SONIC ANEMOMETERS

NT TACHOMETERS

Laser Doppler velocimeter optics, noting minimal heterodyne alignment needs and stress and vibration stability 10 p1889 A70-24556

Carbon dioxide CW laser-Doppler velocimeter for detecting aircraft wing tip trailing vortices by measuring atmospheric aerosols backscatter 12 p2249 A70-27630

Air-damped capacitance accelerometers and velocimeters in data acquisition systems using signal processing 13 p2405 A70-28813

Air velocities measurement with heated thermistors probe, discussing calibration and reliability dependence on flow velocity range 13 p2405 A70-28841

Graphical plotting of critical Preston tube diameter, allowing for Mach and Reynolds numbers effects and introducing limiting line 14 p2586 A70-30871

SPEED REGULATION

U SPEED CONTROL

SPEED REGULATORS

Helicopter gas turbine governor systems for engine and rotor speed control, minimizing pilot activity [ASME PAPER 70-GT-37] 18 p3214 A70-36835

Hydraulic synchronizers for motors and actuators speed equalization, describing operation and technical specifications 21 p3756 A70-40800

SPEEDOMETERS

U SPEED INDICATORS

SERMATOGENESIS

Pre-sage flight tests effects on Macaca nemestrina monkeys spermatogenesis, considering immobilization and exposure time effects 06 p0991 A70-17287

SPHERES

NT CELESTIAL SPHERE

NT POINCARE SPHERES

NT ROTATING SPHERES

Solid glass sphere reinforced nylon resins properties, processing and applications, noting tensile and impact strength and heat distortion

01 p0128 A70-10772

Time dependence of contact zone radius of rigid sphere pressed against viscoelastic half space by normal force

02 p0384 A70-11738

Geodesic motion of massless particles inside static sphere of small volume, analyzing relativistic effect of energy accumulation and release

02 p0339 A70-12117

Spherical conducting body effect on induction coil impedance and EMF in nondestructive testing using eddy current probes

02 p0300 A70-12478

Geometrical optics method for obtaining radar cross section of perfectly conducting sphere with inhomogeneous dielectric coating

02 p0262 A70-12599

Radiative energy transfer from single small sphere to quiescent nonconducting gas with constant volumetric absorption coefficient, using method of matched asymptotic expansions

02 p0400 A70-12861

Two spheres moving in ideal incompressible fluid, studying velocity field, hydrodynamic forces, kinetic energy, etc

03 p0465 A70-13335

Equilibrium temperature and heat transfer of sphere in supersonic flow of rarefied air

03 p0409 A70-13874

Magnetic boundary layer equations applied to flow past stationary circular cylinder and sphere, showing graphical variation of slip velocity with angle

03 p0471 A70-14334

Mass and radius relations for zero temperature spheres of chemical elements, using equation of state and numerical integration

04 p0749 A70-14599

Ideal fluid flow past sphere in rectangular duct and slot solved in series form in spherical functions

04 p0666 A70-14605

Viscous ideal gas supersonic flow past spheres, using integral relations based on Navier-Stokes equations

04 p0613 A70-14606

Electron heat transfer to spherical body in nonequilibrium quiescent plasma by asymptotic solution

[ASME PAPER 69-WA/HT-56] 04 p0727 A70-14793

Configuration factors independence on Lambert law in radiation from spheres and infinitely long cylinders

[ASME PAPER 69-HT-J] 04 p0784 A70-14870

Aligned electric current effect on drag of sphere with arbitrary conductivity moving in current carrying fluid

04 p0671 A70-14993

Temperature distribution around radiating sphere in homogeneous gas medium with molecular heat transfer, solving energy transport equation

04 p0785 A70-15012

Ideal fluid motion characteristics near variable volume spheres with radial mass transfer through surfaces

04 p0672 A70-15198

Penetration depth calculation of high speed nondeformable sphere into massive body, approximating force on sphere by ideal incompressible fluid cavitating flow

04 p0776 A70-15269

Motion generated by spherical body moving along axis of uniformly rotating fluid, measuring particle velocities ahead of and behind body

05 p0789 A70-16013

Hydrodynamic fields of revolution around sphere in unbounded fluid governed by Oseen equation, emphasizing streamlines and attached vortex

05 p0832 A70-16157

Stress distribution in restrained hyperelastic sphere based on elastomer reinforcement theory by carbon black

05 p0940 A70-16510

Forward angle microwave scattering by plasma covered magnetized metallic sphere, calculating radial electron density distribution

06 p1008 A70-17576

Homogeneous gravitating sphere deformation by internal dislocations determined using Green dyad

06 p1055 A70-17605

Sphere drag measurements in low density hypersonic transition and near free molecular flow

06 p1124 A70-18373

Dynamic simulation parameters for sphere drag coefficient data correlation in near free molecular flow

06 p0983 A70-18374

Free molecular heat transfer from sphere at rest in rarefied monatomic gas solved for Krook model of Boltzmann equation

06 p1183 A70-18375

Sphere drag in near free supersonic molecular flow

06 p0983 A70-18377

First collision Monte Carlo method for calculating aerodynamic drag on hard sphere and Maxwell molecular models in near-free molecular flow

06 p0983 A70-18379

Drag and heat transfer predicted by kinetic theory for rarefied gas flow over sphere at low Mach numbers, analyzing flow field

06 p0984 A70-18381

Hypersonic rarefied gas flow near stagnation point investigated to predict drag on sphere in high speed gas stream with densities in transition regime

06 p0984 A70-18382

Sphere and sharp slender cone drag coefficients in hypersonic transitional flow measured by flow modulation technique

06 p0984 A70-18389

Rarefied gas flow past sphere, using integral iteration method for Krook equation

07 p1187 A70-18675

Quasi-steady radially symmetric theory of liquid drop vaporization and homogeneous combustion extended to burning of solid carbon spheres gasified by chemical attack

07 p1419 A70-18915

Gaseous spheres gravitational stability in proper field, considering convection and radial perturbations effects

07 p1383 A70-19408

Unsteady heat conduction in plate, solid or hollow infinite cylinder and sphere with internal heat source and radiative heat transfer on surface

07 p1423 A70-19818

Temperature stress distribution in cylinder or sphere with variable surface temperature and heated by external sources

07 p1411 A70-19819

Viscous hypersonic flow past sphere in presence of strong injection through front surface at large Reynolds numbers using asymptotic method

07 p1189 A70-20146

Gravitating particles systems equilibrium states, solving kinetic equations for sphere and cylinder in isotropic and anisotropic cases

07 p1389 A70-20207

Particle flux densities in electric field near spherical body moving in rarefied plasma

07 p1355 A70-20368

Density profiles of sphere wake in rarefied hypersonic flow compared to free molecular flow calculations

08 p1431 A70-20591

Quadrature solution for elastic sphere deformation by axisymmetric normal loads, writing Green function of boundary value problem in finite form

08 p1585 A70-20956

Potential distribution outside ideally reflecting charged sphere immersed in resting plasma described by nonlinear integral equation, allowing for polarization

08 p1432 A70-21090

Flow characteristics behind sphere suspended in vertical axisymmetric jet dependent on ratio of specific parameter

09 p1658 A70-22118

Electromagnetic wave diffraction by sphere and spheroid at resonance frequencies with incident wavelength comparable to bodies dimensions

09 p1632 A70-22402

Refractive index chart for scattered electromagnetic fields from sphere, evaluating modal coefficient for lossy materials

09 p1633 A70-22697

Stokes flow around sphere moving along axis of cylinder with near-unity diameters relationship

09 p1661 A70-22839

Drag coefficients for spheres and sharp cones in rarefied hypersonic air flow obtained in shock tunnel using free flight technique

[AIAA PAPER 69-140] 09 p1605 A70-23221

Three dimensional flow field codes for spheres: cones at nonzero angles of attack, comparing numerical and experimental results

09 p1606 A70-23254

Sphere motion in laminar flow, postulating absolute velocity as resultant of entrainment and fall velocities and stable position in tube with ascending flow

09 p1663 A70-23309

Static gravitation field of spherical mass immersed in cosmological gas, using combined model of Einstein and de Sitter static universes and Schwarzschild solutions

09 p1763 A70-23312

Solid radiating sphere cooling in space, determining transient temperature distribution by finite difference computing techniques

09 p1790 A70-23562

Flow field around and drag on sphere rising axially through rotating viscous fluid

09 p1663 A70-23676

Shear flow of inviscid incompressible fluid past sphere, calculating secondary vorticity and upstream velocity distribution

09 p1664 A70-23680

Combustible gas /hydrogen-air/ subsonic and transonic flow past sphere, approximating combustion zone structure by model

10 p1801 A70-24142

Nusselt numbers of nonstationary and stationary heat transfer between metal spheres and liquid flow, showing bulk heat and geometry dependence

12 p2330 A70-27288

Gravitational collapse of slightly spherical body with axial symmetry characteristics, taking linear approximation of equation for additions to metric in empty space

12 p2310 A70-28223

Sphere supersonic motion in combustible gas mixture of given temperature and pressure, discussing constant density two front detonation wave model

12 p2334 A70-28242

Hard sphere model for reactive molecular collisions based on energy and momentum of reactants and products

13 p2361 A70-28497

Thermal stresses in solid nonhomogeneous sphere in high periodic temperature field, assuming temperature dependent Young modulus and linear thermal expansion coefficient

13 p2512 A70-28979

Radiative heat transfer through gray gas in equilibrium between concentric spheres, using variational method

13 p2521 A70-29137

Double sphere dipole antenna detecting VLF electrostatic plasma waves, discussing induced and contact potentials

13 p2372 A70-29927

Electric current direction effect on wake of copper sphere moving in electrolyte

13 p2391 A70-29968

Thermoelastic stresses in sphere with cylindrical cut under axisymmetric temperature field and constant surface temperature

14 p2655 A70-30135

Radiative heat transfer in optically thick gas between concentric spheres treated by matched asymptotic expansions, comparing results with Roseland approximation and numerical solution

14 p2663 A70-30266

Plane wave ray optical scattering by two spheres for arbitrary angle of incidence and observation, noting importance of first order interaction terms

14 p2551 A70-31157

Rarefied gas flow past sphere, using integral iteration method for Krook equation

15 p2671 A70-31467

Conducting incompressible fluid flow past sphere, examining effect on magnetic field for small magnetic Reynolds number

15 p2778 A70-31913

Wave scattering by acoustically soft, hard and perfectly conducting spheres

15 p2700 A70-32410

Aerodynamic wake structure of cylinders and spheres in hypersonic rarefied gas flow as function of Mach and Knudsen numbers

16 p2836 A70-33756

Hypervelocity impact of spheres on thin targets using numerical solutions utilizing STEEP code two dimensional technique based on hydrodynamic elastoplastic model

16 p2991 A70-33853

Sphere slow motion in viscous fluid with solid particle suspension, considering Stokes flow pattern small relaxation time perturbation

16 p2896 A70-34272

Critical Levitation Loci for floating spheres on cryogenic fluids

17 p3136 A70-34743

German monograph on shock wave diffraction at spheres and cylinders

17 p3071 A70-35377

Al spheres hypervelocity impact against dry quartz sand targets in light gas gun facility, discussing energy partitioning

18 p3344 A70-36769

Integrating sphere theory with wall mounted specular sample in reflectance and transmittance measurements

18 p3284 A70-36776

Projection of integrating photometric spheres, discussing angular dependence on wall thickness, radiation losses and aperture dimensions

18 p3260 A70-36974

Magnetic field and permeability effects on drag in steady axisymmetric MHD flow of incompressible fluid around full and hollow spheres

19 p3477 A70-37577

Lift forces acting on spheres in cylindrical tube laminar flow

19 p3352 A70-37647

Interference wave functions for diffraction on cylinder and sphere, including noninterfering waves of geometric optics

19 p3380 A70-38398

Quadrature solution for elastic sphere deformation by axisymmetric normal loads, writing Green function of boundary value problem in finite form
20 p3719 A70-39379

Gravitational collapse of slightly spherical body with axial symmetry characteristics, taking linear approximation of equation for additions to metric in empty space
20 p3710 A70-40098

Viscous conducting fluid slow motion past sphere in presence of toroidal magnetic field, calculating Stokes flow perturbations
20 p3682 A70-40113

Hypersonic sphere turbulent wake velocity measurement by spark technique, determining distribution from least mean squares fits of Gaussian curves
20 p3559 A70-40283

Radiative heat transfer between concentric spheres separated by absorbing-emitting medium with heat sources, deriving approximate solution
20 p3739 A70-40294

Dynamic external boundary value problems for elastic body bounded by spherical surfaces
20 p3734 A70-40433

Pool film boiling heat transfer data from small spheres, noting curvature effects and similarities of flat plate, cylinder and sphere theoretical analyses
21 p3949 A70-41310

Turbulent energy balance and spectra of axisymmetric wake behind sphere in incompressible fluid, measuring flow velocity
21 p3745 A70-41376

Free stream turbulence effect on heat transfer to stagnation point of sphere
21 p3953 A70-42095

Sphere and axisymmetric body with spherical blunting in low density gas flow, measuring local heat transfer flux
21 p3748 A70-42218

Micropolar incompressible fluid slow stationary flow past sphere
21 p3812 A70-42252

Spherical cavity nonuniform expansion in compressible elastic plastic solid, calculating velocity field and pressure by approximate similarity solution
22 p4114 A70-42635

Spatial problem of elastic spherical transversal isotropic medium solved by reducing Lamé equations
22 p4118 A70-43481

EM wave multiple scattering by spheres, attributing cross-polarization absence in backscattered field to spherical symmetry
23 p4160 A70-43767

Mass transfer between sphere and liquid flow at small Reynolds numbers
23 p4276 A70-44219

Chemical reaction product fluctuations in reacting and nonreacting turbulent wake of sphere in water tunnel detected by injected salts conductimetric titration [AIAA PAPER 68-686]
23 p4134 A70-44570

EM wave backscattering from lossless dielectric sphere, examining diffracted field surface waves role
23 p4165 A70-44960

Two monopole antennas on perfectly conducting sphere, calculating radiation pattern by numerical technique
23 p4165 A70-44968

Porous media MHD equations for general case, considering magnetized sphere surrounded by homogeneous envelope
24 p4384 A70-45367

Beltrami flows on spherical surfaces, using scalar equations from kinematic conditions
24 p4326 A70-45990

Spherical shape gas or liquid drop steady motion at large Reynolds numbers, examining buoyancy forces and velocity gradients
24 p4326 A70-45996

Inertia effects and suspension rheology for incompressible Newtonian fluid shear flow around neutrally buoyant rigid sphere
24 p4327 A70-46243

Plane parallel collision of two solid spherical bodies with mass centers coincident with geometrical centers
24 p4427 A70-46377

SHERICAL CAPS

Torospherical heads attached to cylinders and under internal pressure as elastic and/or elastic-plastic shells, using finite element
[AIAA PAPER 69-WA/PVP-7] 04 p0769 A70-14792

Spherical caps axisymmetric static and dynamic buckling under load, using axisymmetric nonlinear elastic shell theory approximation and finite difference equations
[AIAA PAPER 69-89] 04 p0778 A70-15587

Torospherical heads design pressures compared from results of elastic-plastic and elastic-stress analyses to examine use of limiting stress criteria
05 p0944 A70-16816

Continuum mechanics equations for calculating strain energy in spherical bottoms production as function of radius and angle
06 p1077 A70-17870

Shallow spherical caps elastic buckling under uniform pressure, considering symmetric and asymmetric deformation modes
07 p1405 A70-19252

Partially loaded clamped plastic shallow spherical caps collapse loads and stress and velocity distributions
09 p1781 A70-23230

Clamped shallow spherical cap elastic buckling and initial postbuckling behavior under uniformly distributed load over circular region centered at apex
12 p2326 A70-27814

Boundary value problems in potential theory for electrical disk and spherical cap reduced to problems for two dimensional Laplace equation
20 p3657 A70-39446

SHERICAL HARMONICS

Atmospheric dynamics nonlinear equations reduction to spectral form using generalized spherical functions series
01 p0135 A70-10203

Geomagnetic field representation in terms of spherical harmonics, analyzing data for spherical and oblate models of earth
03 p0476 A70-13906

Earth external gravitational potential expressed as infinite series of spherical harmonics, using transformation property on coefficients
03 p0478 A70-14178

Coordinates computation method using spherical harmonic expansion of geomagnetic field, discussing direct computations by perturbation method
05 p0837 A70-15926

Spherical harmonics expansion for earth surface and outer space geopotential by mapping earth surface onto sphere
05 p0837 A70-15926

Geomagnetic normal fields determination using spherical harmonic analysis, including extension to local fields
05 p0842 A70-16749

Geomagnetic field lines coordinates calculation based on coefficients obtained in spherical harmonic analysis
07 p1278 A70-20460

Paired integral equations of elasticity with kernels containing Legendre spherical harmonics, admitting exact solution in quadratures
08 p1544 A70-20960

Geometric and predictive methods for developing bounds on epsilon-entropy for infinity error norm constraint
11 p2014 A70-26306

Spherical harmonic coefficients of eccentric dipole potential and coinciding magnetic and mass center, noting geophysical prospecting applicability
11 p2047 A70-26571

Explorer 4 magnetic coordinates recalculation using spherical harmonic representation and modified B-L package
12 p2222 A70-27191

Cross coupling relations in Boltzmann equations solution for inhomogeneous plasmas, using spherical harmonics expansion and Laguerre-Sonine polynomials
13 p2464 A70-29539

Numerical solution to Laplace equation in spherical coordinates with axial symmetry, using Dirichlet method to obtain difference equations
15 p2767 A70-31751

Spherical harmonic analysis of geomagnetic secular variation, applying to regional effects
15 p2799 A70-31992

Artificial satellite orbital motion numerical integration, computing spherical harmonic terms for earth gravitational potential
18 p3334 A70-37063

Spherical harmonic analysis of geomagnetic field strength for global magnetic anomaly charts
19 p3408 A70-37317

Solar envelope unstable gravitational mode model, considering spherical harmonics by numerical integration and asymptotic representation
19 p3523 A70-38688

Computer program transforming spherical harmonic coefficients into arbitrarily tilted coordinate systems, tabulating coefficients of International Geomagnetic Reference Field 1965 in dipole coordinate system
20 p3621 A70-39353

Paired integral equations of elasticity with kernels containing Legendre spherical harmonics, admitting exact solution in quadratures
20 p3672 A70-39382

Microwave antenna near field patterns analysis by spherical harmonic expansion, discussing validity conditions and convergence
21 p3796 A70-40556

Spherical harmonic analysis of declination and secular geomagnetic variation
21 p3820 A70-41884

Magnetic declination data, using spherical harmonics to examine global and secular geomagnetic field variations
23 p4189 A70-44067

Gravitational field fine structure representation near earth surface as sum of global model in spherical harmonics and local model in harmonic B functions
24 p4328 A70-45287

Geopotential zonal spherical harmonics coefficients revised values determined from reduced Baker-Nunn observations for satellites
24 p4407 A70-45537

SHERICAL SHELLS

NT SHERICAL CAPS

Interior shell equations compared with classical shell theory, considering helicoidal, spherical and circular cylindrical geometry
01 p0200 A70-10542

Pressure waves in accelerated sphere filled with compressible liquid, using convolution integral for pressure distribution on inner surface
01 p0067 A70-11186

Thick walled incompressible hyperelastic dielectric sphere periodic oscillations, noting dielectric properties influence on amplitude and period
01 p0209 A70-11386

Electromagnetic field structure and interaction inside and outside of spherical shell of arbitrary linear media excited by monochromatic plane wave
03 p0443 A70-13151

Spherical shell elasticity having circular hole at apex using asymptotic method, calculating stress concentration at hole
03 p0590 A70-13381

Unsteady temperature field induced stresses and strains in hollow viscoelastic sphere calculated by solving integrodifferential equation having right hand side dependent on time function
03 p0590 A70-13398

Stress-strain state equations of shallow spherical shells in rectangular and polar coordinates, discussing reduction to plate and Cauchy-Riemann equations
03 p0591 A70-13427

Stress-strain state under bending of shallow spherical shell having form of circular rectangle with clamped edges
04 p0767 A70-14486

Elastic spherical shell excited by point force, analyzing HF response in terms of near field and flexural wave field [ASME PAPER 69-WA/APM-18]
04 p0771 A70-14912

Spherical shells axisymmetric equilibrium properties under uniformly distributed external compression
04 p0773 A70-15008

Clamped and simply supported shallow spherical shells buckling using computer programs
04 p0778 A70-15555

Polooidal magnetic field influence on compressible fluid convection in spherical shells, using variational method to obtain stability criteria
04 p0758 A70-15695

Stress concentration of spherical hoop with discretely spaced meridional ribs under uniform pressure
05 p0935 A70-16229

Stressed state of shallow spherical shells of revolution undergoing large displacements reduced to Karman equation, solved by small parameter method
05 p0935 A70-16235

Shallow spherical shells stability under combined loading, hinging and edge clamping conditions, deriving strain energy expressions
05 p0936 A70-16238

Shallow spherical shell subjected to arbitrarily located concentrated normal force, discussing boundary effects on resulting stress distribution
05 p0945 A70-16817

Thermal stresses in shell with spherical and circular cylindrical sections, using thin shell approximations and shallow shell theory
05 p0945 A70-16818

Thin shell buckling stressing maximum applied loads analysis for circular cylindrical shells with imperfect walls under axial compression
06 p1165 A70-17647

Velocity, magnetic field and drag equations for steady incompressible viscous conducting fluid flow around spherical hollow shell
06 p1122 A70-17917

Nonlinear postbuckling equilibrium of thin cylindrical shell and axisymmetric buckling pressure of imperfect spherical shell calculated by Rayleigh-Ritz method
[AIAA PAPER 70-102] 06 p1169 A70-18036

Interface stresses in ceramic/metallic spherical shells for deep submergence structures using hydrostatic testing and photoelastic analysis
[AIAA PAPER 70-135] 06 p1170 A70-18089

Shallow spherical sandwich shells under concentrated forces, obtaining inhomogeneous equations solution by integral Hankel transforms
07 p1402 A70-19053

Human head model for craniocerebral trauma analysis, studying fluid filled spherical shell free vibrations axisymmetric response
07 p1219 A70-19243

Nonlinear spinning shallow spherical shell equations solved for equilibrium stress and displacement distributions, discussing inertia loading
07 p1406 A70-19342

Radial vibrations of hollow elastic sphere in acoustic medium, considering Laplace transform of field equations with respect to time
08 p1587 A70-21076

Rheological factors effect on deformation behavior of thin walled spherical shell made of strongly extensible elastically hereditary material and subjected to internal pressure
08 p1587 A70-21168

Spherical and cylindrical cavities dynamic plastic expansion analysis by finite element method allowing for inertia forces
09 p1777 A70-22724

Asymmetric deformation of spherical shell by solving homogeneous differential equation in spherical functions, assessing approximation error
09 p1786 A70-23719

Spherical isotropic shells motion equations solved in terms of associated Legendre functions, considering surface loads and body forces
10 p1953 A70-23876

Membrane deformations in second order rotating surfaces with positive Gaussian curvature investigated for external couple loaded spherical shells
10 p1958 A70-24515

Tapered spherical shell under constant initial pressure calculated for strength, stiffness and durability on digital computer using numerical algorithm
11 p2134 A70-25846

Creep deflections and collapse times for supported thin shallow spherical shells under uniform pressure predicted using variational theorem
11 p2135 A70-25963

Elastic properties determined for reinforced composite material with hollow spherical inclusions embedded in matrix
11 p2136 A70-26083

Stresses and displacements determinations in spherical shells under concentrated loads, considering transverse shear deformation effect
11 p2139 A70-26347

Blunted spherical shells stability under hydrostatic pressure by reducing equilibrium equations to differential
12 p2322 A70-27333

Shallow spherical shells stress-strain state in multiply connected regions resting on Winklerian base
12 p2323 A70-27334

Composite spherically aeolotropic sphere with isotropic core, analyzing stress concentration during twisting
12 p2327 A70-27836

Three-nodes analysis for thermal design of spinning spherical satellite using heat transfer equations in mathematical model
12 p2332 A70-28061

Transversely isotropic hollow spherical shell with elastic filler, analyzing stability
12 p2328 A70-28281

Thermal stability of simply supported bimetallic shallow spherical shell, considering rotationally symmetric deflection modes
14 p2657 A70-30845

Thin spherical shell postbuckling behavior with constrained rigid boundary under edge load, using deep and shallow shell theory
14 p2658 A70-30848

Angular distribution of diffusely reflected solar rays over spherical shell planetary atmosphere, determining halo brightness
14 p2632 A70-31222

Shell homogeneity theory, considering uniform states, spheres and circular cylinders
14 p2600 A70-31280

Convective heat transfer in Cu spherical shell and plate in supersonic rarefied gas flow at zero angle of attack from wind tunnel experiments
15 p2824 A70-31497

Strength and critical load determination for spherical shells with reinforced hole under internal pressure based on stress-strain state analysis during deformations
15 p2814 A70-31543

Stress-strain state of catenoid, cylindrical and spherical shells of revolution, emphasizing catenoid shell bending problem
15 p2815 A70-31648

Closed spherical shell, demonstrating effects of concentrated forces at poles
15 p2818 A70-32170

Gravitational instability and collapse of thin spherical shell of charged fluid, using energy conservation law
16 p2952 A70-33787

Plane acoustic wave interaction with elastic spherical shell, discussing effects of membrane, bending, rotatory inertia and shear deformation
16 p2993 A70-34087

Displacements and stresses in freely vibrating aeolotropic deep spherical shells, including effects of

shear deformation, rotatory inertia and transverse normal strain
16 p2993 A70-34091

Radial vibration frequency variation with wall thickness in hollow spherical shells, tabulating and plotting results
17 p3186 A70-34978

Nonlinear three nodes analysis for thermal design of spinning spherical satellite
17 p3177 A70-35249

Spherical shell of variable thickness, calculating stress-strain state around reinforced circular hole during elastoplastic deformation
18 p3336 A70-36138

Shallow spherical shell dynamics nonlinear problems solution with algorithm permitting use of straight lines method
18 p3341 A70-36590

Transient thermal stresses in spherical shell with distributed source and general Sturm-Liouville boundary conditions
19 p3539 A70-37800

Complete elastic spherical shell asymmetric buckling mode under pressure
19 p3539 A70-37801

Forced torsional vibrations of thin elastic spherical and hemispherical shells with free or restrained edge, using Gegenbauer transform
19 p3541 A70-38037

Boundary value problems for elastic sphere, extending Kelvin general solution of Cauchy equations
19 p3545 A70-38333

Clamped spherical shells under concentrated, distributed and ring loadings, analyzing large axisymmetric deflections for prebuckled and postbuckled states
19 p3545 A70-38336

Solid and hollow spheres gravitational and surface load stresses determination by freezing method of photoelasticity and mercury immersion
20 p3717 A70-38998

Spherical shell under nonuniform temperature field, calculating stress-strain state around round hole
20 p3719 A70-39247

Radial and shearing stresses in hollow composite sphere due to thermoelastic strain nucleus
20 p3719 A70-39602

Spherical shell equilibrium states dynamic calculation method applied to thin plates nonlinear theory statistical problems
20 p3725 A70-39871

Statistically nonhomogeneous fields by variational principles of elasticity, obtaining bounds of average displacement for hollow sphere under pressure
20 p3732 A70-40112

Thin walled spherical shell spacecraft solar heating in planetary surface proximity, considering skin temperature distribution
21 p3944 A70-41019

Uniformly loaded thin elastoplastic spherical shells, calculating strain hardening and strain rate effects on transient response
21 p3935 A70-41255

Cyclic thermal loading in viscoelastic spherical and cylindrical pressure vessels, investigating thermal frequency effect
21 p3937 A70-41430

Fluid filled elastic spherical shell, calculating free vibration axisymmetric response and fundamental mode
21 p3940 A70-42053

Hollow spheres and hemispheres nonlinear axisymmetric deformation, using shell theory reduced to two point boundary value problem for differential equations
22 p4112 A70-42288

Electron beam welded hollow balls for high speed ball bearings, comparing fatigue life with solid balls [ASME PAPER 70-LUBS-17]
22 p4044 A70-42444

Nonaxisymmetric convection of rotating spherical shell in Herring approximation, noting applicability to sun
22 p4104 A70-42994

Stress-strain of thin multilayer isotropic spherical shell under radial load employing shallow shell theory
22 p4120 A70-43716

Limiting pressure for isotropic plastic plates and spherical shells with stress dependent yield, using flow theory
22 p4120 A70-43717

Spherical multilayer shell unsteady temperature fields, assuming mixed convective and radiative transfer at inner surface due to hot gas flow
23 p4276 A70-44165

Spherical shell nonaxisymmetric deformation under varying loads, relating parameters, Poisson coefficient and complex function
23 p4267 A70-44168

Stability of elastic stretched ring on thin spherical shell under critical loads
23 p4268 A70-44318

Plastic postbuckling and imperfection sensitivity of spherical shells under axisymmetric bifurcation
23 p4272 A70-44714

Rotating spherical shell equations as initial value problem, noting maximum convective heat transport at equator
23 p4249 A70-44805

Radar cross section for thin dielectric plate and spherical and conical shells
23 p4166 A70-44975

Perturbation of steady MHD Stokes flow past hollow sphere assuming small Hartmann and Reynolds numbers
24 p4384 A70-45262

Axisymmetrically imperfect spherical thin shell stability analysis, comparing results with theory of initial postbuckling behavior
24 p4421 A70-45282

Truncated spherical shells nonlinear asymmetric buckling calculation from equilibrium equations
24 p4421 A70-45284

SPHERICAL TANKS

Spherical pressure vessel fracture initiation and propagation from long flaws considered from theoretical and experimental approaches
01 p0199 A70-10264

Ideal fluid in lightly filled spherical vessel under gravitational force investigated for surface tension effect on vibration frequencies
08 p1482 A70-20853

Simulated low gravity propellant sloshing in spherical, ellipsoidal and cylindrical tanks, discussing Bond number simulation and tank geometry effects [AIAA PAPER 69-1004]
09 p1657 A70-23255

SPHERICAL WAVES

Spherical detonation waves propagation initiated by laser-induced spark in gaseous explosives, discussing propagation energy regimes
02 p0278 A70-12029

Propagation equations for spherical waves in elastoplastic work hardening materials
03 p0585 A70-12972

Holographic technique for transferring phase perturbation of subject waves onto spherical waves focusable through aperture and examinable by interferometric and schlieren methods
04 p0691 A70-15034

Small amplitude spherical elastic-plastic waves initial behavior studied for critical and supercritical loading
05 p0945 A70-16819

Eigenvalues of spheroidal wave functions calculations dependent on complex propagation constants, discussing branch point values in tabular form
06 p1009 A70-17907

Isentropic model for time behavior of steady spherical source expanding into arbitrary ambient gas [AIAA PAPER 70-232]
06 p1042 A70-18215

Pressure-time history in spherical shock waves flow field at low ambient pressures recorded with piezoelectric transducers, showing shock strength decrease
06 p1052 A70-18385

Radio wave sphericity influence on scattering at moving body wake in ionosphere, determining scattering cross section principal maximum
07 p1237 A70-20424

Amplitude and phase correlations of spherical waves propagating in turbulent atmosphere using smooth perturbation method
09 p1636 A70-23139

Diffraction of plane cylindrical and spherical waves in wedge-shaped regions with reflecting edge, using asymptotic expansions
10 p1911 A70-25186

Spherical electroacoustic waves in drifting thermal plasma, describing ion acoustic perturbations
12 p2279 A70-27779

Plane cylindrical and spherical explosion waves propagation in detonating gas mixtures with counter-pressure, calculating perturbed flow parameters by numerical method of integral relations
13 p2388 A70-29308

Radial displacements in cylindrical circular shell by impinging spherical waves propagating in acoustic medium, deriving equations by Fourier and Laplace transforms
13 p2515 A70-29318

Obliquely incident spherical wave amplitude and phase fluctuations, deriving formulae to compare variances behavior for refractive index fluctuation autocorrelation functions
14 p2574 A70-30750

Holography without reference waves, describing image characteristics of spherical waves from point source
15 p2743 A70-32893

Atmospheric optical inhomogeneity effect on image quality, investigating deflection angles for spherical light wave passage at various altitudes
16 p2915 A70-34215

Convergent spherical rarefaction wave asymptotic behavior
17 p3075 A70-35892

Electromagnetic wave Poynting vector trajectories in absorbing inhomogeneous media, discussing rever-

- stability and energy propagation of spherical and plane structures
18 p3293 A70-36144
- Holographic velocity data recording /velocimetry/, discussing axial resolution enhancement by spherical wave illumination
19 p3423 A70-37859
- Electromagnetic wave propagation in spherical impedance waveguide, determining eigenvalues with negligible refraction
19 p3381 A70-38565
- Spherical radiation drive shock wave similarity solution, discussing time function, velocity, radial dependence and density
21 p3948 A70-41245
- One-dimensional propagation of elastic spherical waves in inhomogeneous unbounded medium under normal stress on cavity surface
24 p4424 A70-45631
- Spheroidal wave function theory, calculating eigenvalues with branch points for propagation constants complex values
24 p4315 A70-46134
- ## SPHEROIDS
- ### NT OBLATE SPHEROIDS
- ### NT PROLATE SPHEROIDS
- Relative motion of two spheroidal homogeneous rigid bodies of isolated binary system, obtaining potential energy
05 p0880 A70-15760
- Steady motions and stability of gravitating gyrostat and spheroid, considering dynamically asymmetrical and symmetrical conditions
08 p1544 A70-20965
- Electromagnetic wave diffraction by sphere and spheroid at resonance frequencies with incident wavelength comparable to bodies dimensions
09 p1632 A70-22402
- Dynamic stability of Jeans spheroid and Roches ellipsoid using small perturbations method
09 p1759 A70-22749
- Refractory oxide submillimeter spherical particle preparation by focused emission from carbon dioxide laser
09 p1697 A70-22984
- Rigid body mode of viscous incompressible fluid flow response to small perturbations of rotating spheroidal container, applying torque interaction
10 p1868 A70-24196
- Elongated rotating configuration evolution by gravitational radiation and secular instability using homogeneous figures of Maclaurin and Jacobi
10 p1916 A70-24404
- Steady motions and stability of gravitating gyrostat and spheroid, considering dynamically asymmetrical and symmetrical conditions
20 p3672 A70-39387
- Spheroidal wave function theory, calculating eigenvalues with branch points for propagation constants complex values
24 p4315 A70-46134
- ## SPHERULES
- Fluid flow visualization in closed channels, using spherules of pulverized fusible materials prepared in swirl injector
03 p0485 A70-13473
- Fragment fabrication of hybrid propellant solid grain emphasizing spherical shape and diameter uniformity
04 p0737 A70-15673
- Free flight ballistic range method for measuring average drag coefficients for microscopic spherical iron particles in free molecular flow
06 p0983 A70-18378
- Magnetic spherules extracted from manganese nodules classified by X ray diffraction and electron microprobe data, suggesting volcanic, stony and iron meteoritic origins
08 p1578 A70-21560
- Microscopic meteoritic spherules in soil surrounding terrestrial impact craters
09 p1758 A70-22745
- Pelagic sediment natural spherules identification based on formation process and manganese nodules abundance
13 p2400 A70-29859
- Extraterrestrial magnetic spherules concentration in relation to meteor shower activity and rainfall probability
14 p2640 A70-30740
- Compositions of lunar fines, crystalline rock and glass spherules, showing high normative anorthite
21 p3899 A70-41531
- Glass spherule lunar particles and breccia from Apollo 11 site, showing passage through impact generated cloud of hot fragmental material
21 p3901 A70-41541
- Microprobe analysis of glass spherules from Apollo 11 lunar regolith, discussing zoning, composition and hypervelocity impact formation
21 p3903 A70-41558
- Apollo 11 lunar fines glass spherules magnetic properties, considering soft and hard ferromagnetic components
21 p3918 A70-41681
- Apollo 11 lunar dust small glassy spherules and cylinders examination by interferometry, discussing specular reflection, microcracking, chipping and origin
21 p3919 A70-41682
- ## SPHYGMOGRAPHY
- Human body elastic properties effects on arterial pressure measurement by sphygmomanometer
20 p3581 A70-39879
- Differential sphygmogram of young men, determining lean body mass on basis of anthropometrical data
21 p3763 A70-41229
- ## SPICULES
- High resolution observations of low chromosphere beyond limb at H-alpha line center revealing fine structures, identifying chromospheric spicules with dark mottles
05 p0910 A70-16429
- Monte Carlo radiative transfer techniques applied to develop height dependent spicule model, computing contrast curves of model against chromospheric background
05 p0911 A70-16431
- Solar chromosphere dark and bright mottles mean lifetime from photographs, identifying with spicules
09 p1757 A70-22733
- Chromospheric spicules fine structure recorded on H alpha spectrograms and filtergrams from high altitude coronagraph
17 p3174 A70-35863
- Supergranular network time and shape changes, examining correlations with solar rotation, activity and cycles
21 p3885 A70-40954
- Spinning cylindrical spicule model with radial and axial gradients in electron number and temperature forming Ca II K line
21 p3879 A70-40955
- Solar far UV limb brightening of C III, N III, N IV, O III, O IV and Si IV lines in chromosphere-corona transition region, correcting coronal model for spicule effects
21 p3925 A70-42186
- Solar chromosphere spicules acceleration via supersonic jet formed by magnetic field under gravity and Melon seed effect
21 p3925 A70-42192
- Solar spectra isodentitraces indicating transition zones between and on sides of spicules in sheaths
21 p3926 A70-42197
- ## SPIKE ANTENNAS
- ### U MONOPOLE ANTENNAS
- ## SPIKE POTENTIALS
- Alouette spikes decrease with time equivalent to antenna transient response during hot plasma immersion
13 p2371 A70-29921
- ## SPIKES
- Floating resonance spike on Alouette 2 ionograms after sounder pulse transmission at half upper hybrid frequency, noting harmonic excitation role
13 p2370 A70-29905
- ## SPIKES (AERODYNAMIC CONFIGURATIONS)
- Spike effect on nose drag and static stability of blunt bodies, estimating optimum length for drag reduction at zero angle of attack
20 p3558 A70-39702
- ## SPIKING
- Ammonia maser transient spiking effects under periodic oscillation condition modulation, noting frequency sweep width role
07 p1299 A70-19685
- Spiking in deep partial penetration electron beam weld in U dependence on machine parameters
18 p3264 A70-37116
- ## SPILLING
- Spilled Hg removal from metal surfaces, describing brush technique based on capillary action
15 p2748 A70-32775
- Liquid or solid Leidenfrost film boiling on saturated cryogenic liquid surface, discussing hydrodynamic model similar to propellant spillage accidents
17 p3194 A70-34744
- ## SPIN
- ### NT ELECTRON CAPTURE
- ### NT ELECTRON SPIN
- ### NT HYDROSPINNING
- ### NT NUCLEAR SPIN
- ### NT SPIN-ORBIT INTERACTIONS
- ### NT SPIN-SPIN COUPLING
- Infinite-dimensional relativistic wave equations for mass spin dependence
07 p1333 A70-18959
- Aerodynamic causes for aircraft spinning, discussing initiation and termination
16 p2842 A70-34173
- ## SPIN DYNAMICS
- Spinning top motion stability in homogeneous incompressible ideal resting fluid, using stability derivative for body of revolution
01 p0145 A70-11438
- Cross section calculation for spin change in H atoms pair collision, discussing wave number and temperature effects
02 p0341 A70-11796
- Solar radiation influence on Alouette satellite spin behavior with long flexible antennae, taking into account sunlight/shadow history and solar vector inclination
02 p0380 A70-11852
- Time history of spin and forward motion accuracy of rocket launched from smoothbore, using analytical model and motion coupling through dynamic friction coefficient
03 p0582 A70-14311
- Anomalous roll behavior of spinning ballistic reentry vehicles with compound aerodynamic asymmetry consisting of lateral offset combined with trim angle of attack
04 p0763 A70-15411
- Spin-up of electrically conducting fluid between infinite flat plates under axial magnetic field, considering Ekman-Hartmann boundary layer on single plate
05 p0832 A70-16017
- Magnetoelastic spin Hamiltonians applied to magnetostriiction of Yb in YIG
06 p1128 A70-18642
- Spin decay from telemetered flight data of Explorer 20 compared with calculation based on solar influence theory
07 p1394 A70-19721
- Spin angular momentum of planets based on particle accretion, discussing particles cloud condensation
08 p1576 A70-21400
- Spin axis motion of n-body coaxially mounted cluster of differentially spinning bodies, considering combined precession and nutation
11 p2123 A70-26128
- Venus obliquity dynamic implications, developing equations for independent parameter set to define spin vector
13 p2489 A70-28907
- Wind tunnel tests, analytical methods and fixed base simulation for predicting fighter aircraft spin characteristics
13 p2346 A70-29030
- Galactic formation by spinning core theory, determining core properties by mass, energy and spin fluctuation parameters
14 p2640 A70-30734
- Attitude dynamics of slowly spinning axisymmetric satellites under influence of gravity gradient torques, using analytical and numerical techniques
15 p2809 A70-31778
- Small reentry vehicles roll motions and impact point dispersion due to spin reversal
15 p2813 A70-32522
- Spinning symmetric satellite attitude stability in hyperbolic orbit on flyby mission, examining by numerical integrations of equations of motion
17 p3181 A70-35753
- Spinning body with rigid and elastic parts, using Liapunov direct method for attitude stability analysis
18 p2922 A70-36677
- Full scale aircraft spinning motion, computing static, damping, cross and acceleration aerodynamic characteristics for antispin devices
20 p3561 A70-39581
- Dynamics of deployable space structures stiffened by centrifugal forces due to spin, discussing LF radio telescope
21 p3931 A70-41854
- Flexible antennae and solar panels effect on dynamic behavior and control system response of dual spin spacecraft
21 p3931 A70-41855
- Single crystal and pyrolytic graphite, examining spin split Landau levels, Fermi energy changes and anomalous g shifts
21 p3854 A70-42110
- Atomic and molecular spin in cosmic medium
22 p4107 A70-43460
- Rigid body with external torque acting along one principal axis, deriving Euler equations of motion
23 p4221 A70-44572
- Dynamics of spin-stabilized flexible satellites of long crossed dipoles or slender beams, noting Alouette and ISIS-1 spacecraft
24 p4415 A70-45549
- ## SPIN REDUCTION
- Aircraft optimal spin recovery by aileron, elevator and rudder control calculated using Pontryagin principle to minimize altitude loss
01 p0006 A70-10924
- Mass loss role in early despinning of sun without magnetic field braking effect, considering present surface vs core rotating velocity
05 p0913 A70-16569
- Despin ball bearing assemblies performance data for TACSAT and Intelsat 4, discussing technology needed for accelerated testing, higher precision, failure detection and lubricants
11 p2058 A70-25471
- X band mechanically despun antenna system with RF and motor drive assembly developed for earth coverage communications satellite
11 p2001 A70-25481

Rigid and stretch yo-yo device equations of motion for despinning rotating rigid body derived for two and three dimensional model

12 p2271 A70-27228

Single stage /rigid/, two stage and stretch yo-yo despin mechanisms, discussing advantages, disadvantages and flight tests

16 p2985 A70-34114

Two stage yo-yo with nutation damper for despinning ATS synchronous satellites, describing mechanical and thermal design, lubrication, assembly, testing, etc

16 p2985 A70-34115

Torque motor driven despin bearing assembly design with integral slip ring for tactical communications satellite [TACOMSAT]

16 p2986 A70-34160

Brushless despin mechanical drive and control system design and performance for orientation of high gain communications antenna from spin stabilized satellite

16 p2986 A70-34161

Luneberg lens application to construct multiple beam mechanically despun antenna for spin stabilized satellites, discussing temperature problems

17 p3055 A70-35663

Fighter aircraft design for spin resistance and recovery using analytical approach, wind tunnel and flight tests

17 p3020 A70-35838

Spacecraft thin walled tubular booms thermal curvature time constants in relation to solar induced despin of satellites

23 p4258 A70-44521

SPIN RESONANCE

Mercury shape estimated with isostatic form of equilibrium controlled by situation near perihelion passage at 3-2 resonance spin rate, discussing solidification thermal effects

05 p0908 A70-16332

Venus spin-orbit resonance resulting in consistent inferior conjunction with earth, suggesting solar atmosphere tidal influence

14 p2650 A70-31216

Microwave oscillator by transposing principle of spin oscillator at low frequencies in nuclear magnetic resonance in X band

16 p2877 A70-33413

SPIN STABILIZATION

Satellite attitude control, discussing passive, active and hybrid stabilization methods including spin, gravity gradient and magnetic stabilization

01 p0197 A70-11264

Time optimal attitude control for alignment of spin stabilized sounding rocket, discussing feedback control system

03 p0580 A70-13805

ASTRID two axis stabilization system for rocket payloads, aligning optical axis of experiment with star [DGLR-69-42]

04 p0762 A70-15161

Dodge satellite postlaunch attitude stabilization and flight data comparison with digital simulation, underlying simulation use in design analyses

04 p0765 A70-15674

Optimal stabilization of spinning body motion about dynamic symmetry axis by controllable gyroscope

05 p0923 A70-16221

Onboard computer requirements for inertial navigation of spinning and maneuvering vehicle, determining design parameters

[AIAA PAPER 68-839]

06 p1013 A70-17161

Spread fin design as antisuperstall and antispin auxiliary device, discussing wind tunnel and simulation tests

06 p0967 A70-17258

Suboptimal stabilization of axially symmetric satellite angular velocity, using ionic propulsion system as control torque

06 p1155 A70-17554

Oil vapor lubricated bearing for compensated antenna of spin stabilized spacecraft, discussing service life, power and storage in sintered porous material [DGLR-69-062]

07 p1391 A70-18775

Sterilized solid propellant motors applicability to planetary landing capsule spin stabilization

[AIAA PAPER 69-823]

07 p1365 A70-19716

Earth horizon signal sensors on spin stabilized satellites using micron filters for cloud signal rejection

09 p1686 A70-23757

Large angle suboptimal attitude control of rigid spinning spacecraft

10 p1856 A70-25236

Fuel suboptimal attitude control of spin stabilized axisymmetric spacecraft

10 p1953 A70-25237

Nutation damping in gyrostat stabilization for multispin satellites in terms of energy momentum and damping torque arguments

11 p2119 A70-25357

Linearized equations of motion solved for stability of dual spin satellite with two dampers, comparing to Floquet analysis

[AIAA PAPER 70-431]

11 p2120 A70-25440

TACSAT 1 communication satellite design, dual-spin stabilization principles and dynamic characteristics, noting nutation behavior

[AIAA PAPER 70-455]

11 p2120 A70-25447

Sun-pointing spinning spacecraft attitude control by solar radiation pressure using paddle arrangement without power, sensor and moving parts requirement

11 p2123 A70-26145

Spin stabilized satellite attitude and orbital maneuvers computation, considering required accuracy and computer time in numerical integration procedures

11 p2125 A70-26278

Kalman filter modifications for spinning satellite attitude determination in elliptical orbit prior to apogee maneuver, using sun and IR earth sensors

11 p2028 A70-26304

Equations of motion for dynamic stability of flexible freely spinning Alouette-type satellite with crossed dipole configuration

12 p2312 A70-27194

Spin requirement to limit projectile yawing oscillations in hyperballistic range

12 p2157 A70-27835

Dual spin satellite stability with four mass nutation damper

12 p2314 A70-27842

Spin stabilized nonrigid satellite dynamics, considering liquid propellant behavior effect

13 p2499 A70-28401

Electromagnetic control system for spin rate and axis orientation of ISIS ionospheric research satellites, describing design parameters

13 p2501 A70-28414

Spin-stabilized rockets stage separation dynamics, considering guide shoe-guide rail lateral motion constraint system

13 p2503 A70-28508

Attitude control system of three axis stabilized payload for spectral survey of comet head light

13 p2505 A70-28770

Oil-vapor lubricated ball bearing system for deployable spin-free antenna of spin stabilized spacecraft

13 p2349 A70-28843

Subcaliber cylindrical boom at base of spin stabilized projectile shown to produce aerodynamic changes in static and Magnus moments

[AIAA PAPER 70-558]

13 p2340 A70-29023

Freely spinning finned stabilizer static wind tunnel tests on free fall research store, determining Magnus effect, body flow interference and static stability

[AIAA PAPER 70-559]

13 p2340 A70-29024

Satellite spin stabilization by Cs contact ion microthrusters with beam deflection, investigating performance obtained by optimal and suboptimal laws

13 p2506 A70-29143

Satellite orientation control and stabilization by gyro with statically and dynamically balanced rotors, showing steady motions and stability region augmentation

13 p2507 A70-29769

Gravity gradient ATS program experiments including spin scan cloud cover and stabilization research

14 p2654 A70-31145

Nutation damper for dual-spin spacecraft, considering various two degree of freedom systems with two natural frequencies

14 p2655 A70-31367

Spin stabilized Project Scanner spacecraft attitude determination by star mapping technique, describing optics, photomultiplier, reticle, electronics and sun shield

15 p2772 A70-31791

Damping by hemispheric torquing to control spin axis in gyroscope rotor while remaining unchanged with respect to case fixed reference

15 p2741 A70-32505

Motion and stability characteristics of dual spin satellite system with pendulous type nutation dampers, noting mass unbalance effect

[AIAA PAPER 69-857]

15 p2812 A70-32508

Optimal orientation of axisymmetric spin stabilized rigid bodies as function of moments of inertia ratios, using single jet for alignment

[DFVLR-SONDDR-50]

16 p2976 A70-33773

Single stage /rigid/, two stage and stretch yo-yo despin mechanisms, discussing advantages, disadvantages and flight tests

16 p2985 A70-34114

Mechanically despun multifrequency, attitude sensing antenna for spin stabilized spacecraft, deep space probes, tactical communications and community broadcast applications

16 p2986 A70-34159

Solid propellant combustion, observing burning rate in spin acceleration environments

17 p3145 A70-35209

Electronically despun antenna for spin stabilized medium altitude satellites

17 p3179 A70-35270

Spin stabilized satellite reorientation, using magnetic dipole interaction with geomagnetic field

17 p3179 A70-35287

Control moment gyros for spinning satellite stabilization and attitude control

18 p3289 A70-36714

Dual spin spacecraft bearing assembly flexibility effects on attitude stability

[AIAA PAPER 70-1043]

19 p3533 A70-38858

Dual spin spacecraft, considering nonlinear damping effect on attitude stability

[AIAA PAPER 70-1044]

19 p3533 A70-38859

Liapunov stability analysis of dynamic systems described by simultaneous ordinary and partial differential equations of motion, applying to satellite spin stabilization

[AIAA PAPER 70-1045]

19 p3472 A70-38860

Torque free spinning satellite with flexible appendages, investigating design parameters effects on nutational stability

[AIAA PAPER 70-1046]

19 p3534 A70-38861

Freely spinning satellites gimbal and momentum wheel system, determining static equilibrium states by analog computer simulations

[AIAA PAPER 70-982]

20 p3714 A70-39547

Nutational stability and closed loop position control of dual spin spacecraft with despun platform

[AIAA PAPER 70-975]

20 p3715 A70-39554

Magnetic three degree of freedom attitude control system for axisymmetric spinning spacecraft, using Kalman filter

[AIAA PAPER 70-974]

20 p3668 A70-39555

Axisymmetric dual spin spacecraft consisting of nonconcentric frictionlessly mounted cylinders equipped with viscous damping mechanisms, evaluating stability criteria by energy method

[AIAA PAPER 70-973]

20 p3715 A70-39556

Direction cosine attitude control logic for spin stabilized axisymmetric spacecraft, using control torques generated by reaction jet system

20 p3669 A70-39679

Air navigation Dioscures project satellites, discussing spin or three axis stabilization, system replenishment strategies and subsystem reliability

21 p3929 A70-41259

Dual spin bodies stability, controlling nutation by passive damper fitted to despun platform

22 p4110 A70-42486

Earth gravity deforming effect on flexible crossed-dipole satellite configuration, considering dynamic stability and spin stabilization

22 p4110 A70-43434

Earth gravity effect on spin vector attitude stability of flexible crossed dipole satellite configuration

22 p4110 A70-43435

Comparative stability of freely spinning satellites for arbitrary number of flexible booms in rotation plane

22 p4111 A70-43440

Dynamics of spin-stabilized flexible satellites of long crossed dipoles or slender beams, noting Alouette and ISIS-1 spacecraft

24 p4415 A70-45549

SPIN TESTS

Helical engraving influence on aerodynamic stability of bullets at long range, discussing wind tunnel tests

[AIAA PAPER 70-557]

13 p2340 A70-29022

Spin effect on internal ballistic of radial burning solid propellant rocket motor spun about longitudinal axis

15 p2791 A70-32794

SPIN WAVES

U MAGNONS

SPIN-LATTICE RELAXATION

Spin-lattice NMR and EPR relaxation time measurements, using train signals and free induction decays

09 p1679 A70-22995

Ag species paramagnetic relaxation in gamma-irradiated frozen aqueous solutions and in frozen methanol, relating spin-lattice relaxation to isotropic coupling

14 p2544 A70-30117

SPIN-ORBIT INTERACTIONS

NT ELECTRON CAPTURE

Ruby green [U] absorption band magnetic circular dichroism calculations in linear approximation, considering spin-orbital interaction constant and magnetic field strength

01 p0156 A70-10188

Venus obliquity dynamic implications, developing equations for independent parameter set to define spin vector

13 p2489 A70-28907

Ferromagnetic Ni band structure and Fermi surface including spin-orbit and exchange interactions obtained by Mueller interpolation scheme

14 p2626 A70-30479

Bilinear scalar spin Hamiltonian inadequacy to describe electron exchange in systems containing orbitally degenerate ions, considering cobalt magnon spectra

15 p2777 A70-32399

Differential elastic cross sections of 42 MeV alpha particles scattering from He 3, using optical model with spin-orbit potential

22 p4076 A70-42722

Spin waves amplification in ferromagnetic conductor crystals, taking into account arbitrary external electric field and propagation vector orientations and space charge

24 p4392 A70-46363

SPIN-SPIN COUPLING

Gravitational wave propagation velocity determined by laboratory measurement of spin-spin coupling of two rotating masses 04 p0718 A70-14397

Ferromagnetic crystal weakly coupled spin Green and correlation functions calculated for wide temperature range 09 p1740 A70-23193

Atomic Russell-Saunders coupling states classification from equivalent electrons configurations, using Young diagrams method 14 p2618 A70-30450

Spin-spin correlation in Heisenberg magnet linear chain at infinite temperature, discussing non-monotonic frequency dependence 14 p2619 A70-30486

NMR spin-spin coupling constants between vinyl protons in cyclopentadiene, 1,3-cyclohexadiene and 1-3-cyclooctadiene from spectrum analysis 21 p3780 A70-41704

Binary star axial rotational correlation, determining coupling between components spin angular momenta 23 p4250 A70-44817

SPINACH

Electron paramagnetic property in chlorophyll molecules of spinach subchloroplast determined using pulsed ruby laser 03 p0421 A70-13551

SPIRAL CORD

NT SPINE

Vasomotor activity of neurons located in spinal cord lateral crescent in curarized decerebrated and intact cats 01 p0030 A70-11471

Spinal cord blood flow response to carbon dioxide partial pressure in anesthetized goats 02 p0232 A70-11713

Spinal cord and skin temperature effects on tension-extension diagrams in cats red and pale muscles 02 p0236 A70-12092

Spinal cord overstretching and circumscribed pathological tension mechanism, considering histological and radiological findings 07 p1204 A70-19242

Connection character of rubrospinal tract fibers with various neuron groups of spinal cord on basis of electrophysiological and morphological investigations 07 p1206 A70-19468

Dogs spinal cord bioelectric activity monitoring by implanted electrodes, noting interelectrode resistances after prolonged operation 09 p1615 A70-22091

Neurological differences in spinal projections of animals subjected to cordotomies compared with human material, using selective silver impregnation technique 13 p2350 A70-28998

Evoked cerebellar potentials time characteristics during spinal cord stimulation in cats, investigating cerebellar intercentral connections effect 13 p2353 A70-29357

Fatigue phenomena at spinal motor synapses, investigating role of accompanying vegetative phenomena as source of fatigue 15 p2680 A70-31740

Dogs spinal cord bioelectric activity monitoring by implanted electrodes, noting interelectrode resistances after prolonged operation 15 p2685 A70-32687

Spinal reflex activity in normal and altitude exposed cats before, during and after acute hypoxia 17 p3031 A70-35430

Posterior ventral thalamic nucleus neuron reactions converging lemniscus and spinothalamic signals in cats 18 p3221 A70-36639

Localization and functional topology of thermosensitive central nervous structures in rats cervical spinal cord, discussing role in generating heat to avert coldness 22 p3967 A70-42316

Blood flow antagonistic changes in various vascular beds following spinal cord central thermal stimulation attributed to sympathetic vasoconstrictor activity 22 p3971 A70-43405

Spinal cord thermal stimulation effects on regional sympathetic activity in rabbits and cats determined from integrated sympathetic efferents discharges 22 p3971 A70-43406

SPINE

Spine acceleration tolerance after prolonged human exposure to weightlessness, noting osseous apparatus tissue decalcination 03 p0423 A70-13712

Radiography of spine in seated position, discussing aircraft seats, aeronautical ergonomics, etc 05 p0804 A70-15765

Spine acceleration tolerance after prolonged human exposure to weightlessness, noting osseous apparatus tissue decalcination 11 p1985 A70-25512

Radiological studies of young adult spines for selecting aircrew personnel and collecting data to compile reference dossiers in case of accidents 12 p2171 A70-28039

Intentional scolioses effect on intrapulmonary blood circulation, using photoelectrical cinedensigraphic technique 14 p2537 A70-30384

Spinal injury prediction during emergency ejection and crash impact protection research 23 p4153 A70-44489

SPINEL

Oxide spinel formation kinetics and reaction mechanisms with emphasis on Ni and Co chromites, discussing cation diffusion 09 p1739 A70-22307

Elastic constants pressure dependence of cubic crystals in NaCl and spinel structures using homogeneous static deformation method 13 p2396 A70-29172

Magnetite and ferrite spinels Hall effect, magnetoresistance and electrical conductivity over wide temperature range 19 p3485 A70-37627

Titanium and aluminian chromites and chromian ulvospinel in Apollo 11 fines, microbreccias and basaltic type igneous rocks 21 p3895 A70-41505

SPIROR GROUPS

Five dimensional rotations and representation of isomorphic spinor groups by boson operators calculus, expanding Gelfand states in Weyl patterns 01 p0147 A70-10521

Explicit spinor basis states for irreducible unitary representations of spinor covering group of deSitter group SO(4,1) 02 p0344 A70-12282

Electromagnetic and gravitational fields classification methods using spinor techniques, introducing five dimensional complex linear space with Weyl tensors elements 07 p1337 A70-20302

SPIRAL ANTENNAS

Ionosonde spiral antenna for HF polarization studies 02 p0269 A70-12584

Active AM scatterer/spiral antenna/used as transponder in elementary CW radar system 04 p0652 A70-15346

Dual mode log periodic spiral DF antenna system, using monopulse to provide azimuth and bearing elevation data 16 p2863 A70-33450

Unidirectional tear drop radiation Archimedean spiral broad band frequency independent antenna using printed circuit with cavity 21 p3801 A70-42246

N-arm spiral or conical antennas radiation patterns calculation for sigma and delta excitations, using bicomplex functions 23 p4176 A70-44965

SPIRAL GALAXIES

NT MILKY WAY GALAXY

Two armed spiral galactic shock waves as triggering mechanism for gravitational collapse leading to star formation, considering gaseous disk motion using Schmidt model 02 p0363 A70-11781

Gravitational theory for disk galaxies, considering radial velocity variations, spiral structure, heat equation verification, etc 02 p0378 A70-12688

Energy analysis of unstable gravitational oscillations in galaxies, using two component model for normal spiral galaxies 03 p0570 A70-13532

Companion galaxies on spiral arms endings, discussing age, expansion and ejection and stopping mechanism 04 p0759 A70-15710

Nonlinear effects in spiral galaxies with emphasis on solar neighborhood region, discussing radial motion, stationary state with excited waves and vertex deviation 05 p0917 A70-16905

Barred galaxies colorimetric data to study relative intensities and mean surface brightnesses as function of color 07 p1376 A70-18905

Interstellar gas ionization and heating by background X radiation, studying neutral hydrogen density distribution between spiral arms and at galactic peripheries 07 p1383 A70-19401

Galaxies and stars interactions, explaining observe peculiarities by electrostatic and electromagnetic forces 09 p1750 A70-22097

Uniformly rotating gas disk large scale spiral structure analysis, studying density waves due to gravitational disturbance by supersonic particle 09 p1755 A70-22503

Nonaxisymmetric free oscillations of self gravitating disk reduced to eigenvalue problem to investigate galactic spiral structures 10 p1917 A70-25207

Observational data for distributions of physical and optical companions to spiral galactic systems and number of satellites as function of central galaxy size 10 p1948 A70-25247

Spiral structure of disk galaxies as nonaxisymmetric perturbations in density, using pressure free hydrodynamical equations 14 p2639 A70-30731

Galactic spiral structure effects on residual stellar velocities local distributions 14 p2652 A70-31380

Absolute photovisual magnitude and classification of supernova in NGC 3389 spiral galaxy, using UVB measurements and comparison stars 15 p2797 A70-31611

Normal logarithmic spiral model of radius vector-tangent characteristic angles for multiarm galaxies 15 p2797 A70-31617

Galactic spiral structure model, examining nonlinear stellar density waves in plasma cylinder 18 p3322 A70-37131

Milky Way spiral structure - Conference, Basel, August-September 1969 18 p3324 A70-37151

Spiral galaxies structure, considering maintenance problem and effect of possible gas inflow from intergalactic space 18 p3326 A70-37152

Spiral structure definition in external galaxies, discussing optical form types, Messier 33 outer and inner parts and differences in arms 18 p3326 A70-37153

Milky Way and other galaxies spiral arms configuration, comparing to Andromeda 18 p3326 A70-37154

Spiral galaxies pattern statistics, examining morphological type of Milky Way galaxy 18 p3326 A70-37155

H 2 regions in Sc galaxies NGC 628, 4254 and 5194 18 p3327 A70-37159

Spiral galaxy NGC 6946 structure and stellar associations distribution, indicating no relation between color and magnitude and distance from center 18 p3327 A70-37160

Galactic spiral structure from atomic hydrogen line intensity longitudinal distribution 18 p3328 A70-37168

Galactic spiral structure from optical radial velocities of H II regions 18 p3329 A70-37179

Milky Way appearance and galactic spiral structure, using models with variable and different absorption values of arms 18 p3329 A70-37181

Young cepheids galactic distribution determined by photometric method, showing correlation with spiral arms 18 p3330 A70-37184

Tightly wound spiral nonlinear density waves in pressureless self gravitating disk with external gravitational field, examining solid body and differential rotation 18 p3331 A70-37192

Plane galactic orbits near spiral field particle resonance, calculating numerically for ring orbits librating near maxima at Lagrangian points 18 p3331 A70-37193

Dynat-type barred spiral galaxies structure and dynamics with asymmetric mass distribution, using model consisting of small prolate spheroid displaced from disk center 18 p3331 A70-37194

Stellar isolated disks spiral structure, examining large numbers of point masses self consistent motion in galactic plane 18 p3331 A70-37195

Large scale spiral galaxy structure interpretation, examining density wave theory, Milky Way System and spiral form origin 18 p3331 A70-37196

Disk shaped galaxy stationary spiral shock pattern, examining gas cloud gravitational collapse for star formation 18 p3331 A70-37198

Galactic spiral structure, discussing gravitational theory, pattern origin, radio and optical structure and magnetic field effects 18 p3332 A70-37201

Sbc galaxy NGC 7320 radio emission and neutral H observations, showing improbability of physical association with Stephan Quintet by distance measurement 19 p3524 A70-38699

Spiral galaxy NGC 4319 arms high red shift Seyfert nucleus, discussing UV continua of Markarian 205 20 p3701 A70-39005

Universe density estimation by galaxy formation theory, discussing spiral galaxies intergalactic gas thermal radiation and soft X rays 21 p3887 A70-41113

Computer model of self gravitating gas-stars system with spiral structure surviving galactic rotations 22 p4103 A70-42982

Supernovae frequency in Sb and Sc spiral galaxies, considering luminosity class, absolute magnitude and mass of parent galaxy 24 p4413 A70-46164

SPIRALS

SPIRALS

Varianular wind spirals for vertical wind and shear profile estimation in atmospheric boundary layer
14 p2602 A70-30370

Neutral H spiral structure in Milky Way galaxy, discussing map derivation, pattern interpretation, arm characteristics and kinematics
18 p3327 A70-37161

H 2 region and neutral gas spiral structure and radial distribution, using optical observations and radio continuum surveys
18 p3327 A70-37162

Milky Way galaxy spiral structure analysis, using neutral H Hat Creek survey with southern observations
18 p3327 A70-37164

Interstellar dust spatial distribution, indicating galactic spiral structure
18 p3329 A70-37183

Spiral structure gravitational theory, discussing separation between linear and nonlinear effects
18 p3330 A70-37189

Large scale spiral galaxy structure interpretation, examining density wave theory, Milky Way System and spiral form origin
18 p3331 A70-37196

Organic spiropolymers synthesis for thermal stability by condensation of aliphatic spirotetraamines and aromatic dianhydrides
21 p3782 A70-42128

German monograph on Milky Way spiral structure, describing elliptic orbit model
24 p4399 A70-45100

SPIROMETERS

Spirometers for ventilation measurement of separate lungs, recording impedance changes during respiratory cycle
14 p2541 A70-30378

Human respiration activity measurement in pressure chamber with different pressures and mixture compositions by spiograph equipment
20 p3581 A70-40175

SPLASH POINTS

U RECOVERY ZONES

U WATER LANDING

SPLEEN

High speed fluorescent cell sorting system for sorting mouse spleen cells from Chinese hamster ovarian tumor cells
02 p0240 A70-12695

Space cabin atmosphere effects on primary and secondary immunological responses in mice relative to spleen weight and antibody titers following antigenic stimulation
03 p0437 A70-14062

Spacecraft cabin atmosphere effects on mice primary and secondary immunological responses relative to spleen histochemical and biochemical changes in enzyme activity
03 p0437 A70-14063

Acid soluble nucleotides content in normal and gamma irradiated rat spleens, presenting table
06 p0995 A70-17799

SPLICING

Al alloys missile splice rings fabrication, discussing extrusion, draw forming, flash butt welding and stretch sizing
18 p3264 A70-37112

SPLINE FUNCTIONS

Spline data techniques for error elimination in trajectory optimization to offer improvement over linear interpolation scheme
07 p1325 A70-19340

Quadrature formulas with minimum remainder estimate for differentiable functions classes, considering piecewise polynomial /spline/ functions characteristic properties
09 p1711 A70-22147

Quasi-linearization for VTOL aircraft equations of motion, using spline functions for unknown parameters initial estimation
16 p2942 A70-33328

Periodic boundary value problems with cyclic totally positive Green functions, considering applications in vibrating physical systems and spline theory
23 p4213 A70-44899

Approximations by spline functions and polynomials, discussing modulus of continuity
24 p4369 A70-45126

SPLITTING

Splitting procedures application to steady and unsteady problems of mathematical physics and predictor-corrector method application to unsteady problems
04 p0719 A70-14959

Sunspot spectrograms analysis, observing wavelength shift in Zeeman triplet circular components and magnetic splitting inequality under different circular polarizations
18 p3322 A70-37136

SPOILERS

Flow field of jet spoilers downstream from nozzle, accounting for main stream and secondary jet mixing

and fuel injection problems during supersonic combustion
03 p0608 A70-14098

Tail screens and spoiler rings aerodynamic braking effect in hypersonic range, discussing separated boundary layer periodic unsteady flow
06 p0965 A70-17247

Sound radiation from rigid flow spoilers correlated with fluctuating forces, measuring jet-pipe drag and lift components with transducers
11 p2085 A70-26699

Pressure distribution in two dimensional incompressible potential flow on Joukowski airfoils with normal upper surface spoilers, emphasizing potential flow theory
12 p2155 A70-27193

Supersonic jet spoilers flow fields with various nozzle shapes to determine secondary jets penetration depth and mixing in wake
13 p2338 A70-28480

Reentry vehicle recovery deployment initiation, comparing performances of conical wake drogue and body attached spoilers hypersonic deceleration devices
21 p3752 A70-41811

Spoiler theory based on mathematical model, using two dimensional potential theory in conjunction with experimental data on wake phenomena
22 p3957 A70-42273

SPONGES [MATERIALS]

Titanium sponge secondary structure obtained by magnesiothermal reduction of concentrated Ti-containing chloride melts, discussing temperature effect on porosity
09 p1709 A70-23783

SPONTANEOUS COMBUSTION

Liquid sodium droplets spontaneous ignition and combustion in controlled oxidizing atmosphere, discussing vapor phase diffusion flame, burning rates and evaporation constants
02 p0396 A70-12005

Gas detonation dynamics associated with shock tube self ignition kinetics, noting chemokinetic factors role
02 p0397 A70-12024

Limits of self ignition in reaction of F with H detected photoelectrically
05 p0956 A70-16156

Spontaneous ignition temperature as function of surface-to-volume ratio in static systems for fuels
11 p2151 A70-26384

Spontaneous ignition dependence on transient temperature variations accompanying gas entry to evacuated vessel
12 p2330 A70-27222

Thermal testing of decomposition and spontaneous ignition of diethyl peroxide before explosion
12 p2330 A70-27224

Combustion rates and self ignition vs pressure and activity in ammonium perchlorate mixtures with Al and Mg powders compressed to maximum densities
18 p3299 A70-36249

Self flammability temperature of binary alloy Al-Si powders in aerosol state as function of chemical and phase compositions
23 p4205 A70-44046

SPONTANEOUS EMISSION

Ar ion laser with high discharge current density observed for working level populations by simultaneously measuring power gain and spontaneous emission lines intensity
01 p0106 A70-10063

GaAs - Conference, Dallas, October 1968
01 p0157 A70-10515

Phase lock technique study of 10.6 micron radiation effect in carbon dioxide laser plasmas on 2.4 micron spontaneous emissions and plasma impedance
05 p0857 A70-16071

Emission saturation in Ar CW laser at high discharge current densities under different pressures and tube channel parameters
08 p1511 A70-20542

Quantization of Wheeler-Feynman electrodynamics, discussing spontaneous emission and connection between quantum and classical interparticle action theories
11 p2108 A70-25700

Amplitude and phase fluctuations in laser with nonlinear absorption due to spontaneous emission, studying lasing instability near hysteresis threshold
12 p2248 A70-27548

Hanle effect in single mode He-Ne laser, observing spontaneous emission on different spectral lines and estimating lifetimes of Ne excited states
13 p2424 A70-28598

Spontaneous emission modulation, interference beat and level crossings observable in gas laser operating at two output frequencies
13 p2425 A70-28599

P-type GaAs laser diodes spontaneous emission power temperature dependence, considering radiative recombination mechanism
13 p2378 A70-29545

Ultrashort pulse generation by solid state Q switched lasers, discussing spontaneous emission effects, atomic polarization and populations variation
14 p2594 A70-30477

Fluorescence method of determining solid state laser parameters using spontaneous and stimulated emission observations
17 p3106 A70-35101

Spontaneous megawatt pulsing in ruby laser with output beam reflected back into cavity
17 p3108 A70-35909

Spontaneous emission spectra and band tailing from GaAs laser diodes fabricated by vapor phase epitaxy with compensation in p-type side of junction
18 p3268 A70-36730

Excitation transfer by spontaneous emission in atomic gas, investigating static magnetic field effect on radioactive cascade
19 p3443 A70-37363

Spontaneous and induced Cerenkov emission by charged particle in turbulent medium, discussing random fluctuations effect on radiation spectra
21 p3879 A70-40928

Semiconductor junction diode spontaneous emission sources, considering frequency-energy characteristics relationship
22 p4085 A70-42504

Magnetic flux dependent interference beats in spontaneous emission of gas discharge of He-Ne laser, estimating Hertzian coherence duration
23 p4202 A70-45052

Spectroscopic features of mercury laser associated with electron energy levels and spontaneous emission line structure, giving excitation and disruption mechanisms
23 p4202 A70-45054

Pb-Sn-Te junction diodes prepared by Sb diffusion, investigating spontaneous and laserlike emission
24 p4355 A70-46086

SPONTANEOUS IGNITION TEMPERATURE

U IGNITION TEMPERATURE

U SPONTANEOUS COMBUSTION

SPOOLS

Three spool turbopump engine design regarding maintainability, noting on-condition module removal and overhaul
11 p2101 A70-25877

SPORADIC E LAYER

Diurnal variations in sporadic E layer and wind in ionosphere during equinox and solstice periods, noting wind shear mechanisms and ambient electron density
01 p0084 A70-11552

Vertical probe observations of short radio waves propagation through sporadic E at various frequencies and path lengths
01 p0084 A70-11553

Auroral breakup effects on sporadic E via comparison between sequential ionograms and riometer absorption data indicating transient effect in D/E regions
02 p0288 A70-11744

Seasonal variations of sporadic E virtual height at middle latitudes attributed to hemispheric expansion depending on ozone amount
03 p0476 A70-13907

Statistical ionospheric model of sporadic E layer frequency characteristics dependence on equipment parameters, determining permissible variation of transmitter power and receiver gain
04 p0682 A70-15727

Vertical motion of ionized formations in ionospheric F region related to sporadic E layer
05 p0842 A70-16760

Temporal and spatial variations and patch velocity of sporadic E layer obtained at Japan ionospheric stations
06 p1057 A70-17906

Ionization irregularities and drift in sporadic E layer determined using Mitra method for ground based radio reflection
06 p1012 A70-18543

Sporadic E layer parameters spatial distribution, describing analytic planetary coordinate system
07 p1267 A70-19453

Sporadic E layer formation by vertical winds, discussing effect on ionospheric electron concentration distribution
07 p1267 A70-19454

Sporadic E layers structure and dynamic characteristics during polar aurorae, determining critical frequencies
07 p1267 A70-19455

Simultaneous riometer and ionosonde measurements at high latitude suggesting absorption events due to cosmic noise scattering by auroral sporadic E
07 p1271 A70-20165

May 1966 solar eclipse effects on sporadic E layer, including ionizing radiation decrease relation to boundary and blanketing frequencies decrease
08 p1490 A70-21432

Blanketing type sporadic E layer associated with equatorial electrojet as thin layer of enhanced ionization
10 p1880 A70-24801

- Midlatitude sporadic E layer critical frequencies dependence on solar activity using vertical ionospheric sounding data, observing ionization correlation
10 p1882 A70-25197
- Sporadic E formation correlation to geomagnetic activity from ionospheric radio absorption observed at midlatitude and polar zone stations
11 p2044 A70-25554
- Diurnal and seasonal variations of sporadic E layer observed at ionospheric station
14 p2568 A70-30134
- Sporadic E layer space diversity reception data from stations 20 km apart, noting horizontal ionization gradient effect
14 p2571 A70-30234
- Lower ionosphere influence on radio reflection from sporadic E layer, determining diurnal variations of D region absorption for various frequencies
14 p2547 A70-30235
- Geomagnetism-sporadic E layer relationship, discussing critical frequencies and H component variations
14 p2571 A70-30236
- Statistical ionospheric model of sporadic E layer frequency characteristics dependence on equipment parameters, determining permissible variation of transmitter power and receiver gain
14 p2575 A70-30811
- Lunar tidal diurnal and semi-diurnal variations in equatorial sporadic E layer related to H geomagnetic field and sunspot period
15 p2726 A70-31862
- Synchronous measurements of reflection coefficient and frequency characteristics of sporadic E layer by ionospheric sounding
18 p3247 A70-36293
- Sporadic E layer parameters spatial distribution, describing analytic planetary coordinate system
18 p3249 A70-36927
- Sporadic E layer formation by vortical winds, discussing effect on ionospheric electron concentration distribution
18 p3249 A70-36928
- Sporadic E layers structure and dynamic characteristics during polar aurorae, determining critical frequencies
18 p3250 A70-36929
- Sporadic ionization occurrences nighttime observation in auroral E region, describing vertical electron concentration profile
19 p3410 A70-37331
- Temperate equatorial and auroral zones sporadic E observations and formation theories survey for prediction
19 p3416 A70-38441
- Sporadic E layer occurrence probability over Dushanbe from ionospheric station data, discussing curves for diurnal and annual PE variations
19 p3417 A70-38785
- High scintillation indices associated with vertical spreading of sporadic E layer from minute-by-minute ionograms and signal amplitude recordings from Explorer 22 satellite
20 p3624 A70-40489
- Sporadic E layer ionization correlated with geomagnetic disturbances in northern auroral and polar regions
21 p3812 A70-40592
- Sporadic E formation correlation to geomagnetic activity from ionospheric radio absorption observed at midlatitude and polar zone stations
21 p3819 A70-41304
- Day and nighttime E and sporadic E layer drifts over low latitude station recorded by spaced receiver technique
22 p4020 A70-43166
- Sporadic E layer characteristics from spaced ionogram analysis, discussing layers formation and dispersion and ionization irregularities motions
24 p4328 A70-45352
- Sporadic E layer space diversity reception data from stations 20 km apart, noting horizontal ionization gradient effect
24 p4331 A70-46309
- Lower ionosphere influence on radio reflection from sporadic E layer, determining diurnal variations of D region absorption for various frequencies
24 p4316 A70-46310
- Geomagnetism-sporadic E layer relationship, discussing critical frequencies and H component variations
24 p4332 A70-46311
- SPORES**
Spore and vegetative cell adenylate kinases of *Bacillus subtilis* proved indistinguishable by polyacrylamide gel electrophoresis DEAE cellulose chromatography
01 p0021 A70-10789
- Dry heat resistance of *Bacillus subtilis* var. niger spores on selected planetary lander capsule surface materials
04 p0645 A70-15442
- SPOT WELDS**
Solar cell array fabrication methods extending operating temperature by pulsed spot welding techniques and deletion of adhesives
02 p0228 A70-12080
- Strain gage high temperature performance in rocket engines tested by spot welding to turbine manifold, noting installation and position influence
06 p1069 A70-18440
- Nondestructive process control analyzer for spot welds in aircraft structural components, monitoring expansion, current and spotweld properties
08 p1507 A70-21486
- High fatigue life resulting from titanium spot welding realized by preweld and postweld treatment
11 p2059 A70-25662
- Metal matrix composite resistance spot welding, discussing value of nondestructive tests
17 p3100 A70-34636
- Microwelding by pulsed ruby laser radiation, discussing characteristics and advantages
20 p3638 A70-40149
- Stainless steel gas tungsten arc welding, considering anode spot size variation and current density
22 p4042 A70-42377
- SPRAY CHARACTERISTICS**
Electronic spray analyzers and conductance and capacitance probes for two phase flow studies, describing operation, characteristics and types of data obtainable
02 p0305 A70-12837
- Parameters effect on radius of dispersion during plasma and detonation spray coating process of niobium and zirconium carbides
06 p1076 A70-17849
- Liquid propellant spray injection into high pressure gaseous environment noting geometric, dynamic and thermal characteristics
06 p1182 A70-18211
- Propellant sprays behavior in high pressure combustors, calculating jet breakup or atomization length
07 p1257 A70-19331
- SPRAYED COATINGS**
Parameters effect on radius of dispersion during plasma and detonation spray coating process of niobium and zirconium carbides
06 p1076 A70-17849
- Abradable and abrasive types thermal spray coatings application to jet engine parts
10 p1893 A70-23856
- Thermal conductivity and shock resistance of flame and plasma sprayed zirconia coatings on Ni-Mo-C metal
15 p2762 A70-32527
- Fatigue properties of solution treated and age hardened hot rolled Ti alloy bars, discussing sprayed tungsten carbide coatings effects on bearing properties
17 p3121 A70-34432
- SPRAYED PROTECTIVE COATINGS**
U PROTECTIVE COATINGS
U SPRAYED COATINGS
- SPRAYERS**
Temperature limit of efficiency threshold for ground based liquid propane sprayer for supercooled fog dispersal at Orly airport
02 p0324 A70-11872
- SPRAYING**
NT ARC SPRAYING
NT METAL SPRAYING
NT PLASMA SPRAYING
- Reflection of single leaves and field plots of cotton, determining Cycocel treatment effects on aerial IR photography
14 p2577 A70-31233
- SPRAYING APPARATUS**
U SPRAYERS
- SPRAYS**
U SPRAYERS
- SPREAD F**
Spread F echoes occurrence variations over solar cycle, observing range and frequency splitting type during maximum and minimum sunspot years
01 p0080 A70-11222
- Electrostatic drift-dissipative plasma instability and nocturnal equatorial spread F irregularities, discussing amplification in collision dominated medium
03 p0477 A70-13990
- Spread F echoes due to total reflection from large tilted ionized surfaces, using ionograms and airglow observations to study surface geometry
07 p1271 A70-20158
- Seasonal variation of spread F near magnetic equator, showing relationship with solar cycle at different geographic locations
10 p1881 A70-24818
- Low latitude scintillations from satellite transmission scintillations correlation with solar activity spread F, electron content and ionospheric irregularities
13 p2397 A70-29189
- Low latitude observations of spread F echoes and stationary satellite scintillations, correlating with ionospheric disturbances and geomagnetic activity
21 p3818 A70-41097
- SPREAD REFLECTION**
U DIFFUSE RADIATION
- U REFLECTION**
- SPRINGS [ELASTIC]**
Cessna single engine aircraft tubular and flat steel landing gear springs, describing quality control through nondestructive testing
01 p0098 A70-10018
- Motion equations for vibratory two degrees of freedom spring mass system subjected to rotation, discussing use for small rates of turn measurement
01 p0199 A70-10266
- Dynamic response to step transverse loads of viscoelastic annulus of constant Poisson ratio in plane strain, analyzing work and spring-dashpot model [ASME PAPER 69-LUB-23]
01 p0101 A70-10384
- Cylindrical compression spring relaxation at high temperatures, presenting design data for time-temperature initial stress relationships [ASME PAPER 69-WA/MET-10]
04 p0697 A70-14758
- Dynamic torsion of anisotropic circular cantilever beams and small pitch diameter springs under linear time dependent moment calculated by Saint Venant method
06 p1037 A70-17862
- Static deflection effect on harmonic vibration of system with restoring forces of hardening nonlinear spring, considering gravity effect
08 p1586 A70-21035
- Popping pressure of relief valve with helical spring under dynamic load noting frequency dependence [ASME PAPER 69-VIBR-48]
08 p1441 A70-21479
- Equations of motion integration for solid body in potential forces field induced by elastic springs
09 p1728 A70-23386
- Cylindrical coil springs cold winding loading processes, considering initial tension or compression of wire and combined stresses
10 p1894 A70-24297
- Euler-Bernoulli and Timoshenko beam impact models compared for case of finite beam resting on spring supports
12 p2327 A70-27843
- Age hardenable monolithic spring material composed of Ag-Pd-Cu alloys for make-break electrical contact
13 p2376 A70-28839
- Ultrahigh strength stainless steel for light gage springs and satellite antennas
13 p2420 A70-29248
- Compression spring mechanisms for separation of spacecraft and shrouds, summarizing design characteristics
16 p2921 A70-34116
- Minimum weight springs design, discussing load deflection curves, materials resilience, etc
16 p2924 A70-34171
- Harmonic oscillator with exponentially decreasing spring constant, obtaining closed form solution for equation of motion
17 p3137 A70-35602
- Dynamic response to step transverse loads of viscoelastic annulus of constant Poisson ratio in plane strain, analyzing work and spring-dash model [ASME PAPER 69-LUB-23]
19 p3435 A70-37607
- Undamped forced two degree of freedom system with one linear and one nonlinear spring, analyzing subharmonic vibrations by Ritz averaging method
19 p3544 A70-38329
- Static and dynamic spring constants of peripheral jet air cushion vehicle in heaving motion, obtaining sinusoidal input response characteristics
22 p3960 A70-42279
- Periodic motions of arbitrarily long periods for idealized nonlinear spring-mass systems with two or more degrees of freedom
22 p4073 A70-42699
- SPUR [REACTORS]**
U SPACE POWER UNIT REACTORS
- SPUTTERING**
Sputtering yield of amorphous and polycrystalline targets bombarded by energetic ions or recoil atoms calculated by integrodifferential equations derived from Boltzmann transport equation
02 p0343 A70-11885
- Temperature dependence of sputtering coefficient of quartz and chondrites at 2000 K and mass decrease prior to evaporation
03 p0569 A70-13357
- Sputter machining thickness reduction methods for VHF resonant piezoelectric transducers
03 p0496 A70-14207
- Sputtering method used for applying metallizing layer to ceramics in producing ceramic to metal seals
10 p1895 A70-24555
- Temperature dependence of sputtering coefficient of quartz and chondrites at 2000 K and mass decrease prior to evaporation
11 p2118 A70-26722
- Superconducting thin films of beta-tungsten structure Nb-Al-Ge compound, discussing high purity sputtering preparation techniques and properties in magnetic fields
12 p2285 A70-27259
- RF-sputtered CdS thin films structural and electrical characteristics from X ray diffractometer tracings,

reflection electron diffraction and X ray double crystal spectrometry

13 p2470 A70-29201

Solid film lubricants deposited by DC and RF sputtering on metal and glass surfaces, determining friction characteristics by electron microscopy

17 p3099 A70-34516

Adherent Ta films deposition onto Teflon disks by sputtering

18 p3264 A70-37098

Optical multilayer metal coatings vacuum deposition by cathode sputtering, using automatic apparatus

22 p4045 A70-42510

Semiconductor junctions passivation by silicon nitride insulation layers, discussing pyrolysis and cathode sputtering fabrication methods

22 p4087 A70-43444

SQUALLS

Stratospheric clear air turbulence over squall line, discussing turbulence over thunderstorms

06 p1102 A70-18588

Heavy squalls observations by satellite TV and radar, considering wave disturbances at cold front

13 p2444 A70-28585

SQUARE WAVES

Reactive filter synthesis for step-voltage output inverter smoothing, using network theory

14 p2559 A70-30373

High power short rise time square wave inverter using power transistors

22 p3965 A70-43336

SQUEEZING

U COMPRESSING

ST VENANT FLEXURE PROBLEM

U SAINT VENANT PRINCIPLE

STABILITY

NT ACOUSTIC INSTABILITY

NT AERODYNAMIC STABILITY

NT AIRCRAFT STABILITY

NT ATTITUDE STABILITY

NT BOUNDARY LAYER STABILITY

NT COMBUSTION STABILITY

NT CONTROL STABILITY

NT DIMENSIONAL STABILITY

NT DIRECTIONAL STABILITY

NT DYNAMIC STABILITY

NT FLAME STABILITY

NT FLOW STABILITY

NT FREQUENCY STABILITY

NT GYROSCOPIC STABILITY

NT HOVERING STABILITY

NT LATERAL STABILITY

NT LONGITUDINAL STABILITY

NT LOW SPEED STABILITY

NT MAGNETOHYDRODYNAMIC STABILITY

NT MAGNETOSPHERIC INSTABILITY

NT MOTION STABILITY

NT ROTARY STABILITY

NT SHELL STABILITY

NT SPACECRAFT STABILITY

NT STATIC STABILITY

NT STORAGE STABILITY

NT STRUCTURAL STABILITY

NT SURFACE STABILITY

NT SYSTEMS STABILITY

NT THERMAL STABILITY

Dissipativity and asymptotic stability criteria derived for systems of ordinary differential equations, considering application to automatic control problem

03 p0518 A70-13469

Existence and uniqueness, stability and asymptotic stability of nonlinear operator differential equation

05 p0878 A70-17098

Existence and stability problems of nonlinear operator differential equations containing linear operator with domain and range contained in real Hilbert space

05 p0878 A70-17099

Stability and limiting frequency of analog computer solutions of differential equations with root shifts caused by resolver imperfection

07 p1321 A70-18689

Nonlinear computational stability of partial difference approximations to meteorological equations

08 p1534 A70-21024

Stability of solutions to linear differential equations pair, determining bound conditions having S-property

08 p1534 A70-21100

Interval of values with stability and convergence for correctors for differential equations

09 p1641 A70-22286

Liapunov stability conditions for critical point of ordinary differential equation, determining optimal criterion

09 p1727 A70-22664

Triangular Lagrangian equilibrium points stability in planar restricted problem of three bodies at order two mass ratio using two variable expansion method

10 p1939 A70-24184

Distance separating shock wave front of contact surface between motor and target gases in electromagnetic shock tube, discussing surface instabilities

11 p1977 A70-26467

Linear periodic coefficient differential equations stability analysis by infinite determinate method, con-

sidering applications to damped mechanical systems motion and dual spin satellite

12 p2261 A70-27813

Algorithm for integrating ordinary differential equations system determined for stability condition by trial-and-error procedure programmed on computer

12 p2262 A70-28030

Variable mesh multistep predictor-corrector method for iterative solution of ordinary differential equations, considering numerical stability and algorithm efficiency

13 p2440 A70-29087

Banach space stability in presence of constantly acting perturbations bounded in mean, investigating differential operator equation

13 p2452 A70-29309

Stability requirements for precision magnetic field measurements on ground and in space, discussing magnetic balances and fluxgate magnetometers for geomagnetic variations and spacecraft attitude

13 p2415 A70-30050

Algorithm for fourth order stability equation

16 p2867 A70-32925

Shock wave stability in plane steady flow at uniform entropy and limiting velocity

16 p2890 A70-33101

Ti alloy stability after long term creep exposure at various temperatures

17 p3120 A70-34421

Triangular libration points stability in elliptic restricted three body problem, determining parametric resonance region

17 p3137 A70-35690

Stability criteria for differential equations with complex variables, considering boundary value requirements and sufficient conditions theorems

18 p3281 A70-36352

Schwarzschild exterior metric stability against perturbations from asymptotic behavior of Einstein field equations solution in Kruskal coordinates

18 p3291 A70-36650

Real matrix stability determination by right half plane eigenvalues, using symmetric solution of Liapunov equation

24 p4370 A70-46098

STABILITY AUGMENTATION

U FEEDBACK CONTROL

U STABILIZATION

STABILITY DERIVATIVES

NT PITCHING MOMENTS

NT ROLLING MOMENTS

NT YAWING MOMENTS

Stability and asymptotic stability criteria for attraction sets in dispersed dynamic systems obtained in terms of Liapunov function

01 p0141 A70-10152

Spinning top motion stability in homogeneous incompressible ideal resting fluid, using stability derivative for body of revolution

01 p0145 A70-11438

Aerodynamic derivatives in equations of motion governing aircraft longitudinal short period motion estimated using least squares methods

02 p0224 A70-11866

Internal stability of turbulent combustion, developing analysis for one dimensional model and deriving sufficient instability criterion

03 p0607 A70-13862

Stability characteristics from flight test results using regression analysis

04 p0623 A70-15155

Longitudinal stability derivatives prediction for rigid and elastic airplanes, using influence coefficient method

[AIAA PAPER 69-131]

04 p0624 A70-15383

Roll acceleration influence on angle of attack convergence and windward meridian rotation rate of rolling reentry vehicles

[AIAA PAPER 69-100]

04 p0764 A70-15546

Einstein field equations based on variational principle applied to stability of general self gravitating relativistic gaseous mass obeying specific equation of state

06 p1138 A70-17304

Gyrostatt satellite equilibrium positions in circular equatorial orbit under action of gravitational magnetic and aerodynamic moments based on gyrostatic satellite equations of motion

06 p1155 A70-17884

Nonlinear aerodynamic moments for arbitrary motions of bodies of revolution in free flight

[AIAA PAPER 70-205]

06 p0971 A70-18102

Stability derivatives for bodies of revolution at subsonic and transonic speeds

[AIAA PAPER 70-190]

06 p0976 A70-18239

Stability derivatives from flight data of fixed-wing aircraft determined by modified Newton-Raphson method

07 p1194 A70-19272

Satellite orbit using analytic partial derivatives of perturbed motion based on state transition matrices

07 p1381 A70-19301

Laminar boundary layer critical height determination using Rouse stability parameter

07 p1257 A70-19336

Aerodynamic drag coefficients and moments for axisymmetric bodies of revolution in rarefied plasma derived for limiting case of delta flux

08 p1432 A70-21088

Aerodynamic forces and moments effect of VTOL aircraft lift fan configurations on flow past wing

10 p1798 A70-24047

Finite difference methods stability for time dependent Navier-Stokes equations coupled to energy equation with quadratic terms in velocity gradients

10 p1866 A70-24106

Triangular system of linear differential equations reducible to block form by Liapunov transformation, deriving indices stability conditions

10 p1911 A70-25303

Aerodynamic moment on satellite with asymmetrically positioned solar cell platforms, analyzing motion around center of mass for diffuse scattering flow

12 p2314 A70-28254

Nondimensional aerodynamic forces and moments coefficients independent of air density and acting on satellites in low orbits

13 p2500 A70-28403

Dimensional stability derivatives from XV-4B aircraft simulator varied in computer program for extracting roots of lateral-directional characteristic equation

[AIAA PAPER 70-551]

13 p2346 A70-29016

Atmospheric density variations and functional dependence of aerodynamic moment coefficient on incident angle from Saturn Workshop flight experiment

14 p2528 A70-30559

Dynamic stability derivatives calculation using steady and oscillatory lifting surface theory with allowance for Bryan limitations

14 p2529 A70-30864

Wind velocity derivative statistical characteristics in atmospheric surface layer, using thermoanemometer, functional converter, differentiating circuit and loop oscillograph

16 p2945 A70-33219

Blade flexibility effects on static stability derivatives of prop/rotors in propeller flight mode

17 p3013 A70-34701

Parameter model of VTOL airplane in transition, considering aerodynamic forces and moments and digital simulation

17 p3015 A70-34724

Flight test instrumentation for V/STOL stability derivatives extraction, noting instrument errors and required compensation

17 p3094 A70-35502

Wind velocity derivative statistical characteristics in atmospheric surface layer, using thermoanemometer, functional converter, differentiating circuit and loop oscillograph

24 p4371 A70-45194

Gyro system determining aerodynamic moment integral vector in wind measurements

24 p4340 A70-46402

STABILITY TESTS

NT FLIGHT STABILITY TESTS

NT WIND TUNNEL STABILITY TESTS

Dimensional stability of nickel maraging steel at ambient temperature measured for applications as gage block materials

01 p0102 A70-10742

Structural qualification testing of experimental tactical communication satellite /TAC COM SAT/

02 p0274 A70-11936

Transverse g-force tolerance and stability after prolonged hypodinaemia in bed rest, noting effects of pharmaceuticals, physical exercise and prophylactic measures

10 p1817 A70-24695

Powered nacelles simulating exhaust flow for propulsion and airframe problems in subsonic flow

[AIAA PAPER 70-636]

16 p2888 A70-33594

Modeling techniques based on Froude scaling laws for helicopter ditching and flotation stability characteristics

17 p3016 A70-34738

Helicopter dynamic tests for aeroelastic and mechanical instabilities and forced vibration problems

21 p3749 A70-40583

STABILIZATION

NT SIGNAL STABILIZATION

NT SPIN STABILIZATION

Algebraic criteria for absolute stability and equilibrium position in nonlinear continuous automatic control systems, using complex gain amplifier substitution

01 p0053 A70-11041

Nutational NMR nonuniform magnetic field stabilizer for beta spectrometer, structural details and circuit schematic

03 p0485 A70-13467

Splitting procedures application to steady and unsteady problems of mathematical physics and predictor-corrector method application to unsteady problems

04 p0719 A70-14959

Variational problems of stationarization under constraints, using imbedding integrodifferential equations

05 p0882 A70-16085

Monograph on conditions for stabilization of oscillatory systems with random parametric excitations covering approximate calculations, stability concept definition, etc
11 p2129 A70-25496

Amplitude stabilization transient processes at output of four terminal network with arbitrary phase and amplitude characteristics by representing pulse transfer function in series
12 p2184 A70-27537

Satellite orientation control and stabilization by gyro with statically and dynamically balanced rotors, showing steady motions and stability region augmentation
13 p2507 A70-29769

VTOL aircraft stability augmentation system design based on control theory state variable methods, using minimum power levels
14 p2531 A70-30856

Relay stabilization system for flight vehicle motion about center of mass, using point transformations method and bifurcations theory
15 p2674 A70-32151

Optimal control in nonlinear systems, discussing conditions for analytical solutions for Hamilton-Jacobi equations
16 p2886 A70-33335

Aircraft stability augmentation systems design by parameter optimization techniques and feedback selection
16 p2840 A70-33342

Automatic stabilization and control of computerized nonlinear processes, proposing algorithm for stability criteria
17 p3049 A70-34640

Satellite optimal guidance, discussing gyroscope application for stabilization and orientation control
17 p3181 A70-35691

Solid phase stabilization of zirconium dioxide by combined addition of yttrium and magnesium oxides
19 p3455 A70-38732

Nd-YAIG laser design for sleeve stabilization, discussing flicker problem and rod cladding
21 p3836 A70-40822

Stability augmentation in aircraft design for handling and operation benefits, discussing control techniques, autopilot modes and load limitations [ICAS PAPER 70-24]
23 p4138 A70-44109

Hybrid fluidic damper control for yaw axis stability augmentation of commercial jet aircraft [SAE PAPER 700794]
24 p4294 A70-45853

Hydrofluidics flight controls for aircraft stability augmentation systems, noting component performance, transfer functions and operation [SAE PAPER 700793]
24 p4294 A70-45854

STABILIZED PLATFORMS
Project ABLE stabilized platform, discussing logistics support requirement effects on system design and acquisition, reliability, maintainability and costs
02 p0401 A70-11670

Gyroplatform angular position with respect to reference stars from solving nonlinear differential equations, applying Liapunov method
03 p0524 A70-13366

Gyrostabilized attitude reference platform for high altitude rotating research rocket payload alignment with preselected star
03 p0579 A70-13606

Semiactive gravity gradient attitude stabilization system /SAGS/ providing active pitch control and semipassive roll/yaw control, discussing design, development and testing [SAE PAPER 690691]
05 p0923 A70-15863

Closed form variational synthesis of optimally fast acting stabilization systems for rigid single axis gyroscopic platforms using integrating nonanalytic equations
06 p1103 A70-17860

Flywheel stabilization for communication satellites, considering stabilization by reaction wheels, gyros, gas jets, etc [DGLR-69-058]
07 p1392 A70-18817

Kinematic drifts of three axis gyrostabilizer platform associated with angular oscillations using theory of finite rotations
07 p1282 A70-19531

Gyrocompass with sensitive element mounted on horizontally stabilized platform and aligned with meridian by applied correcting moments, deriving equations of motion
07 p1282 A70-19532

Stability of three axis indicator gyrostabilizer system consisting of stabilized platform mounted in three degree of freedom Cardan suspension
07 p1288 A70-20179

Stable moored ocean platforms providing reliable VHF communications and secondary surveillance radar facilities for civil aviation operations over North Atlantic
09 p1723 A70-23035

North-finding gyroscope applicability for directional gyros and stabilized platforms
10 p1891 A70-24865

Gyroscopic platform stabilizers /GPS/ dynamic properties improved by compensation of perturbing torques
12 p2237 A70-28155

Gimbal influence on three axis gyrostabilized platform in spacecraft guidance during maneuvers
13 p2446 A70-28388

Dynamics of gravity stabilized satellite having maximum damping rate
13 p2499 A70-28391

Gyrostabilized platforms for astronomical observations, minimizing position errors
13 p2403 A70-28441

Drift of two platform gyroazimuth with stabilized base under harmonic or random vibrations
15 p2734 A70-31622

Stabilized platform stellar detector for French probe balloons, using semicircular light modulator
15 p2738 A70-32249

Gyroplatform for controlling rocket motion during rotation about longitudinal axis
19 p3420 A70-37258

Instruments for platforms stability determination, considering azimuth, tilt rotation and translational motion [AIAA PAPER 70-961]
20 p3605 A70-39568

STABILIZERS
Wing and empennage structures automated fully stressed design procedures, discussing application to supersonic aircraft stabilizer
12 p2319 A70-27136

Aircraft all-movable stabilator computer aided design for optimized structural weight and performance
12 p2319 A70-27137

Flameout and ignition correlation for diffusion fuel burnup behind angled stabilizers in annular turbine combustion chamber
18 p3300 A70-36127

STABILIZERS [AGENTS]
Gas saturation and inhomogeneity in surface layer of Ti alloys with alpha and beta stabilizers after high temperature heating
09 p1700 A70-22078

STABILIZERS [FLUID DYNAMICS]
NT HORIZONTAL TAIL SURFACES
Wind tunnel investigated flow stabilization at horizontal control surfaces by vortex BCL technique, considering angles of attack, elevator deflection and shape
06 p0968 A70-17853

Lifting reentry dynamic stability of flare stabilizers and flap controls
09 p1766 A70-23242

STABLE OSCILLATIONS
Stable geomagnetic pulsations related to plasma density shock position in magnetosphere and to magnitude of diurnal variations
01 p0082 A70-11508

Pressure and temperature sensitivity tests of fluoric oscillator for timer application, testing fluid relaxation oscillators using R-C-R feedback loops [ASME PAPER 69-WA/FLCS-9]
04 p0626 A70-14844

Oscillations stability along symmetrical axis in galaxies analyzed by Jacobi and Lagrange equations, obtaining cylindrical coordinates upper and lower limits
09 p1761 A70-23052

Steady harmonic oscillations of half space with circular holes, deriving algebraic equations for boundary value problems
09 p1782 A70-23296

Flat rectangular elastic body stable oscillations with clamped base under compression loads, deriving difference scheme for approximation
09 p1782 A70-23297

Unsteady plasma oscillation stabilization by envelope controller with spatial and temporal dispersion
11 p2087 A70-25604

Forced oscillations of oscillator matched to transistor as active element, obtaining stability conditions by Liapunov first method
11 p2018 A70-25945

High stability oscillators frequency check, using meteor trails and combined least squares and moving averages methods
14 p2583 A70-30320

Oscillation frequency retuning and stabilization and loss factor determination in solid state lasers by dispersive resonators
17 p3106 A70-35100

Unmodulated microwave oscillations power stabilizer with semiconductor attenuator
21 p3796 A70-40635

Oscillation stability of stars moving along axis of symmetry in galaxy, discussing first order orbit perturbations in general resonance case
21 p3884 A70-40873

Oscillatory stability of selective RF transistor amplifiers, using stage dimensioning and gain graphs
22 p3996 A70-42818

Gunn oscillation stabilization in layered semiconductors based on space charge growth reduction via

two-stream interaction between GaAs diode and passive bias semiconductor
23 p4230 A70-44196

Single-frequency oscillations mode in nonlinear catenary systems, considering factors promoting stabilization and uniformity
23 p4218 A70-44344

Pendulum dynamic stability under parametric excitation, presenting transient and steady state solutions by linear and nonlinear theory applications
24 p4379 A70-45587

STACKING FAULT ENERGY
Transmission electron microscopy observation of thermal annihilation of stacking faults in epitaxial layers of GaAs grown from liquid phase
21 p3863 A70-42004

Alloys stacking faults thermodynamics based on Gibbs treatment of interfacial free energy
22 p4124 A70-42726

Stacking fault energy determination, discussing impurities influence in equilibrium dimensions distortion of extended nodes in titanium carbide
22 p4053 A70-42727

Stacking faults in gamma prime precipitation hardened high temperature Ni base alloys, relating fault energy to strength
22 p4053 A70-42728

STACKING FAULTS
U CRYSTAL DEFECTS
STAGE SEPARATION
ELDO booster rocket third stage design and construction, including pictures of parts and devices
03 p0580 A70-13795

Linear separation systems for aerospace applications covering mild detonating fuse and cord flexible linear shaped charge, SUPER ZIP concepts, etc
03 p0546 A70-14103

Scout missile destruct charge system premature operational response to high temperature environment caused by combustion gas leak during stage separation
03 p0550 A70-14140

Design and qualification test criteria for components derived by enveloping peaks of shock response spectra in ground tests of missile stages explosive separation [SAE PAPER 690616]
05 p0922 A70-15849

Abort and staging separation maneuvers of two equal size reusable lifting entry vehicles in wind tunnel tests [AIAA PAPER 70-260]
07 p1397 A70-20389

Staging along reentry trajectory in atmosphere, discussing parent body and separation point influence on aerodynamic loading and heating of ejected body
11 p2124 A70-26151

Spin-stabilized rockets stage separation dynamics, considering guide shoe-guide rail lateral motion constraint system
13 p2503 A70-28508

Delta launch vehicle for scientific and application satellites, describing three stage liquid and solid propulsion systems
15 p2810 A70-31783

Flight behavior of pyrotechnic circuits in ELDO-EUROPA 1 booster for separating stages and autodestruction
15 p2709 A70-32288

Multibody lifting entry vehicle clusters separation dynamics, describing digital simulation, wind tunnel tests, separation mechanisms, etc
16 p2981 A70-33704

Reliable latch diaphragm release mechanism for separation of payload from spacecraft, discussing design, operation and tests
16 p2921 A70-34117

Reliable collet release mechanism design for separation and ejection of reentry vehicle payload from booster
16 p2922 A70-34118

Spacecraft separation mechanisms selection, design and use, discussing multiple device point and linear systems
17 p3175 A70-34767

Dynamic force and pressure measurement on rocket nozzle during simulated stage separation, describing instrumentation and control system
17 p3061 A70-35478

Optimal separation height of instrument container in atmospheric gas composition mass spectrometric studies
18 p3260 A70-36996

Europa 2 launcher fourth /perigee/ stage, describing trajectories, propulsion system design and performance, separation systems, etc
19 p3532 A70-37871

Rocket nose cone optimal turn into horizontal ballistic trajectory after separation from booster, using dynamic programming
22 p3962 A70-43351

STAGING [ROCKETS]
U STAGE SEPARATION
STAGNATION
U STAGNATION POINT

STAGNATION FLOW

Hydrodynamic model of blood coagulation in stagnation point flow, analyzing platelet diffusion, white cell bonding stress and thrombus formation [AIAA PAPER 70-143] 06 p1003 A70-18123

Plasma arc tests to simulate stagnation reentry heating on spherical subized models of nuclear heat source to investigate heat shield materials ablation characteristics [AIAA PAPER 70-200] 06 p0974 A70-18172

Navier-Stokes equations solved for unsteady incompressible three dimensional stagnation point flow, noting reduction to two dimensional and axisymmetric cases 07 p1188 A70-19343

Pressure recovery for stagnation of underexpanded sonic air jet in chamber having transparent walls and containing nozzle and diffuser in coaxial positions 07 p1189 A70-19811

Radiation effects on viscous hypersonic low density stagnation flow using two layer model, calculating flow field and heat transfer coefficient 12 p2158 A70-28204

Gas phase chemical reactions effect on heat transfer to charring ablator, deriving numerical solution for multicomponent stagnation point flow [AIAA PAPER 70-869] 16 p2999 A70-33912

Falkner-Skan type boundary value problem of three dimensional flow near stagnation point 20 p3658 A70-40103

STAGNATION POINT

Transient heat transfer near two dimensional stagnation point in viscous incompressible fluid steady flow 01 p0002 A70-10457

Flow about blunted wedge with laminar boundary layer at stagnation point and approaching Falkner-Skan flow at infinity, discussing asymptotic behavior 01 p0061 A70-10540

MHD boundary layers in transverse magnetic field with low Reynolds number, investigating suppression of separation with emphasis on behavior near rear stagnation point 01 p0152 A70-11095

Boundary layer and singular inviscid stagnation point reacting flow matching, corrections structure and decay and ranking comparison with second order effects in fluid mechanics 01 p0065 A70-11096

Laminar counterflow diffusion flame chemical structure and blow-off mechanism established in forward stagnation region of porous cylinder at atmospheric pressure 02 p0398 A70-12032

Stagnation point velocity gradients for spherical segment models with bluntness ranging from hemisphere to flatnose cylinder in hypersonic flow 03 p0406 A70-12947

Approximate solution for hypersonic inviscid flow around spherically blunted bodies at small angle of attack, noting stagnation problems 03 p0407 A70-13547

MHD boundary layer separation near rear stagnation point with magnetic field normal to wall solved by series expansion, calculating skin friction by numerical quadratures 03 p0469 A70-14182

Free stream turbulence effect on heat transfer in circular cylinder stagnation region 03 p0469 A70-14216

Heat transfer rates to stagnation point of hemisphere in supersonic high enthalpy low density nitrogen plasma flow [ASME PAPER 69-WA/HT-49] 04 p0614 A70-14799

Thermal recovery factors at hemispheric probe stagnation point in low density supersonic jets of He-Ar and H-N mixtures [ASME PAPER 69-WA/HT-27] 04 p0782 A70-14810

Viscous shock layer at hypersonic blunt body stagnation point, applying finite difference and nonlinear overrelaxation methods to seven species air model 04 p0620 A70-15539

Surface recession of low density phenolic nylon in arc heated air using stagnation point models, noting char removal processes 04 p0787 A70-15602

Self similar problems of anisotropic fluid boundary layer involving infinite disk rotation and fluid flow near stagnation point 05 p0835 A70-16857

Inviscid hypersonic blunt body flow of hydrogen-oxygen mixtures in shock layer stagnation region 06 p0968 A70-17555

Heat and mass transfer across laminar boundary layer around stagnation line of cylinder in crossflow affected by free stream turbulence intensity 06 p1176 A70-17693

Massive blowing effect on stagnation point radiative energy transfer of ablative heat shield during planetary entry at hypersonic velocities 06 p0971 A70-18101

Hypersonic rarefied gas flow near stagnation point investigated to predict drag on sphere in high speed gas stream with densities in transition regime 06 p0984 A70-18382

Stagnation point heating in hypersonic gas flow past blunt bodies, considering radiative transfer effects on shock wave temperature and density distribution, wave separation, etc 06 p0985 A70-18557

Asymptotic behavior of inviscid radiating gas flow near stagnation point of blunt body 07 p1188 A70-19315

Unsteady MHD flow at forward stagnation point analyzed for magnetic field effect on transient phenomena, using difference-differential numerical method 07 p1354 A70-20235

Incompressible conducting fluid MHD flow at infinite plane wall forward stagnation point, considering suction or injection effects 07 p1354 A70-20237

Heat exchange at stagnation point of subsonic and supersonic axisymmetric jets interacting with perpendicular plane partition, allowing for turbulence 08 p1482 A70-20919

Monograph on convective heat flow in stagnation points of turbulent partly premixed free jet flames at cooled plates 08 p1598 A70-21343

Shock layer thickness in supersonic inviscid gas flow past blunt bodies, calculating boundary layer near stagnation point 09 p1603 A70-22442

Supersonic flow behind cone, studying subsonic pressure and stagnation zone dependence on incident flow parameters and static pressure distribution 09 p1663 A70-23623

Plane shock wave interaction with supersonic blunt body, considering pressure-time studies for stagnation point of flow 10 p1801 A70-24145

Laminar boundary layer and heat flux at forward stagnation point of indestructible body in partially ionized air flow calculated as function of enthalpy 12 p2156 A70-27287

Solid particle motions in dusty gas in inviscid hypersonic shock layers of slender wedges and cones and stagnation regions of cylinders and spheres 12 p2156 A70-27827

Stagnation point position as function of gas thermodynamic state behind detached shock for spherical segment at incidence in three dimensional hypersonic flow 12 p2159 A70-28247

Stagnation point position and entropy at surfaces of supersonic paraboloids in perfect gas 12 p2160 A70-28250

Heat transfer increase near stagnation point for turbulent jet impinging on paraffin coated plates used for flow visualization 13 p2521 A70-28866

Stagnation point electrostatic probe for measuring local electrical properties of solid propellant rocket exhausts [AIAA PAPER 69-573] 13 p2475 A70-29960

Shock slip analysis of merged layer stagnation point air ionization, clarifying effects of reaction rates, species diffusion, etc 13 p2343 A70-29987

Chemically reacting stagnation point boundary layers with wall injection of gas, comparing multicomponent solution with binary approximation and chemical simplifications 14 p2565 A70-30265

Three dimensional boundary layer along semi-infinite swept stagnation line, assessing counteracting effects of cross flow and mass transfer 14 p2565 A70-30278

Viscous absorbing emitting shock layer in blunt body stagnation region, calculating skin friction and radiative heat transfer [AIAA PAPER 70-868] 16 p2999 A70-33911

Continuum radiative flux from nonisothermal stagnation shock layer of nongray atomic gases, employing ionization edges and bound free spectral forms [AIAA PAPER 70-837] 16 p3001 A70-33932

Equilibrium air boundary layer flows at three dimensional stagnation points, discussing flow characteristics and real gas heat transfer parameters [AIAA PAPER 70-806] 17 p3005 A70-34455

Thrombus formation on foreign surface in fresh blood stagnation point flow, applying fluid mechanical and mass transfer models 17 p3035 A70-34470

Laminar gas flow enthalpy determination in stagnation regions based on energy balance equation across separation streamline 18 p3240 A70-36266

Nonuniform external flow near blunt body stagnation point in diverging hypersonic thin shock layer 18 p3206 A70-36267

Nonequilibrium processes and body geometry as stagnation point conditions in blunt body inviscid flow 20 p3557 A70-39355

Stagnation point heat transfer coefficient to elliptical model taking into account pressure, model blunting and diameter, Mach number, etc 20 p3737 A70-39699

Stagnation point heat transfer of spherical cylinder in argon and air, developing electrically insulated calorimeter gage theory 21 p3941 A70-40774

Reentry vehicle with multicomponent gas mixture injection, calculating heat and mass transfer correlations for stagnation point flow 21 p3945 A70-41033

Freezing and melting of warm water flow at stagnation point over cooled plate for convective condition at solid-liquid interface 21 p3949 A70-41311

Free stream turbulence effect on heat transfer to stagnation point of sphere 21 p3953 A70-42095

Three dimensional laminar boundary layer equations for film condensation on curved surface in quiescent vapor, investigating flow at stagnation point 21 p3954 A70-42168

Thermal boundary layer near stagnation point in three dimensional fluctuating incompressible flow, using Lighthill method 22 p4124 A70-42685

Time-mean velocity and skin friction of laminar boundary layer near two dimensional stagnation point with oscillating oncoming flow 22 p4010 A70-42686

Nonequilibrium radiation from stagnation region of high velocity spherical gas cap traveling through air 22 p4124 A70-42758

Radiative transfer upstream absorption effect on inviscid stagnation region shock layer radiation 23 p4133 A70-44551

Three dimensional laminar boundary layer separation at infinite swept stagnation line with high mass injection rates 23 p4182 A70-44568

Inviscid rotational supersonic flow near three dimensional stagnation point, examining solutions for compatibility with vortical shock layer boundary conditions 23 p4183 A70-44692

STAGNATION PRESSURE

Stagnation pressure losses in radial vaneless diffusers to estimate compressor performance, noting one dimensional analysis 11 p1974 A70-25782

Large MHD generator channel aerodynamics, discussing pressure distributions to stall and stagnation pressure loss 20 p3612 A70-40002

STAGNATION REGION

U STAGNATION POINT

STAGNATION TEMPERATURE

Heat transfer boundary conditions determination in studying heat protective coatings effectiveness, discussing measurement methods for stagnation temperatures and heat fluxes from exhaust gases 06 p1173 A70-17662

Injectant stagnation temperature and molecular weight variation effect on flow field generated from secondary gas injection into supersonic stream [AIAA PAPER 69-1] 09 p1733 A70-23217

Injectant stagnation temperature and molecular weight effects in jet interaction flowfield 11 p2036 A70-25989

Stagnation temperature of two phase nozzle gas jet containing solid particles on particle density and velocity 21 p3748 A70-42220

STAINLESS STEELS

NT AUSTENITIC STAINLESS STEELS

NT MARTENSITIC STAINLESS STEELS

Ferritic stainless steel embrittlement caused by He injected into tensile samples by alpha particle cyclotron irradiation tested at elevated temperatures 01 p0122 A70-11235

High temperature ductility improvement in stainless steels containing He, analyzing lattice damage and interphase cavities after fast neutron irradiation 01 p0123 A70-11246

Potential lubricants in friction and cup forming tests of stainless steel, Ti- and Ni-base alloys, considering boron nitride, graphitic materials and Mo oxides 02 p0309 A70-12540

Structure and segregation effects in Type 304L stainless steel weldments using transmission electron microscopy, optical microscopy and electron microprobe, comparing weld types 02 p0319 A70-12754

Reversed bending fatigue tests on stainless steel fibermetal with porous structure to investigate effects of density, thickness, wire diameter, screen stiffening, etc 03 p0481 A70-12957

Intergranular corrosion mechanisms in ferritic stainless steels observed by electronmicroscopic examination on Cr Fe-base alloys vacuum-melt with C and N 03 p0506 A70-13131

Surface treatment effects on stainless steels corrosion resistance, relating resistance changes to surface composition, integrity, stability and roughness 03 p0507 A70-13136

Heat transfer effects on corrosion behavior of stainless steel in boiling water, noting stress corrosion cracking increase with chloride ion contamination

03 p0507 A70-13137

Mechanical responses and residual defect structures in brass and stainless steel following explosive shock loading and cold reduction by rolling

03 p0507 A70-13139

Stainless steel stress corrosion cracking test in magnesium chloride solution, emphasizing crack crystallographic orientation observation

03 p0513 A70-14299

Press load prediction for deep drawing Ti-Al-V alloy, stainless steel and Inconel X under various lubrication conditions at room temperature
[ASME PAPER 69-WA/PROD-15]

04 p0698 A70-14835

Thermal resistance of multicontact heat conducting stainless steel plate stacks with different interface purities in vacuum

05 p0957 A70-16293

Chromium stainless steels nitrided cases formation and phase composition, studying temperature effects

07 p1304 A70-18744

Stainless steels case hardening in hydrogen, nitrogen, propane and butane mixture, showing temperature and process duration effects

07 p1291 A70-18831

High chromium stainless steels nitriding and carburizing processes stabilized by nickel galvanic coating, enhancing nitrogen or carbon diffusion into steel

07 p1291 A70-18832

Reverse-bend and tension-tension fatigue properties of high strength Cr-Mn-N stainless steel sheet in notched and unnotched conditions

07 p1305 A70-18993

Dynamic creep rupture of stainless steel tested at high stress levels and temperatures

08 p1518 A70-21333

High temperature thermomechanical treatment effects on stainless steels and Ti alloys microheterogeneity, noting corrosion resistance improvement

08 p1519 A70-21444

Automatic cladding method for submerged arc stainless steel welding, discussing delta ferrite to sigma phase transformation for surfacing with low ferrite stainless steel

08 p1508 A70-21489

Stainless steel wire-reinforced Al alloy diffusion bonded scarf joints, considering aluminum oxide coating and bonding times effects

08 p1509 A70-21906

Passive film on stainless steels in boiling nitric medium studied by recording constant potential on sample subjected to polarizations

09 p1700 A70-22010

Internal stresses and substructures dependence on thermomechanical histories of stainless steel during creep, noting subgrain orientation

09 p1705 A70-22805

Particle fracture in oxide dispersed stainless steels during plastic deformation at room temperature

09 p1706 A70-22813

Zr and stainless steel pitting in acidic and near neutral chloride media, comparing controlled potential and conventional chemical corrosion tests results

09 p1706 A70-22939

Stainless steel corrosion rates in flowing liquid Na from mechanism based on thermodynamic partitioning of oxygen

09 p1706 A70-22942

Fatigue properties of electron beam welded precipitation hardening stainless steels

11 p2059 A70-25664

Low cycle fatigue tests on stainless steel, discussing crack behavior dependence on temperature and plastic strain range

11 p2139 A70-26405

Regeneratively cooled stainless steel thrust chamber failure related to internal carburization by fuel decomposition and propellant combustion

12 p2290 A70-27111

Annealed stainless steel low cycle fatigue data analysis leading to method of characteristic slopes approach for correlating plastic strain range to fracture time

12 p2255 A70-27604

Ductile fracture in Al matrix composite reinforced with unidirectional stainless steel fibers described by critical crack tip displacement and fracture strain criteria

13 p2512 A70-28917

Solid state welding processes for space, nuclear and deep submergence technologies, discussing diffusion bonding of Al and stainless steels

13 p2419 A70-29117

Ultrahigh strength stainless steel for light gage springs and satellite antennas

13 p2420 A70-29248

Stainless steel fiber reinforced Sn-Pb eutectic alloy composite mechanical properties, noting tensile strength and rupture behavior

13 p2436 A70-29625

Uniaxial yielding correlation with substructure in Al-stainless steel metal matrix composites, using compressive loading test

15 p2756 A70-31565

High temperature oxidation of Ni-Cr alloys and stainless steels in molten salt, observing grain boundary corrosion with electron probe

15 p2757 A70-31875

Thermal-mechanically treated stainless steels structure and properties, discussing stress relief aging effects

15 p2761 A70-32380

Stainless steels creep behavior under long term tensile loads at high temperature

15 p2764 A70-32898

Molten contaminated Li effects on microstructure, tensile strength and stress corrosion of stainless steels and refractory metals

16 p2933 A70-34206

Iron, Ni, Cr and Co corrosion and mass transfer in high temperature Na, examining properties of stainless steels and cobalt base alloys

16 p2933 A70-34209

Cr-Ni stainless steels room temperature yield and tensile strengths improvement by nitrogen addition

17 p3122 A70-34553

Low cycle fatigue and short term tensile behavior correlation for irradiated and unirradiated stainless steels

17 p3123 A70-34627

Precipitation hardening Co-Cu-Mo stainless steels, determining martensitic structures free from delta ferrite and residual austenite

18 p3262 A70-35965

Two phase stainless steels with microduplex structures, taking into account martensite and ferrite effects on mechanical properties

18 p3272 A70-36038

Oxygen pressure effect on stainless steel cyclic hardening during vibration tests at resonant frequency

18 p3273 A70-36042

Stainless steel load-strain characteristics and cumulative damage in cyclic fatigue life

18 p3273 A70-36048

Carbide precipitation and grain boundary migration in solution annealed duplex stainless steel as function of aging time

18 p3274 A70-36050

Physiosorption isotherms for nitrogen on stainless steel at various temperatures and very low pressures

18 p3226 A70-36322

Concorde engine bay thermal insulation combining stainless steel foil and polytetrafluorethylene film, considering noise level, engine fire conditions and molten Ti globules penetration

18 p3346 A70-36345

Al alloy matrix-boron fiber-stainless steel wire composites fabrication into various shapes with desired mechanical properties for aerospace structural components applications

18 p3263 A70-36837

Fluxless paste for thermomodification coloring stainless and heat resistant steels and alloys

19 p3434 A70-37459

Steady state and transient fatigue behavior of stainless steel wire-Al alloy composite subjected to push-pull and pull-release frequency tests

20 p3649 A70-39946

Stainless maraging steel bolts tensile, shear and fatigue strengths and stress corrosion resistance at room and high temperatures

20 p3650 A70-39964

Al alloys and stainless steels tensile properties and application in lightweight cryogenic propellant tank structures, discussing Ti alloys and reinforced composite materials tests

20 p3651 A70-40123

One-step closure sealing of pressurized stainless steel capillary tubes by resistance pinch welding

21 p3832 A70-40789

Stainless steel sheet-to-plate tee joint resistance welded by Magnetic Force Upset Welding process, testing performance

21 p3832 A70-40792

Accelerated failure tests of ammonia-Al-stainless steel heat pipes for fluid loss or energy transport degradation

21 p3947 A70-41049

Stainless steel gas tungsten arc welding, considering anode spot size variation and current density

22 p4042 A70-42377

Fatigue of turbine blade stainless steels and nickel alloys as function of temperature, stress and surface layers

23 p4205 A70-44135

Aluminum, duraluminum and stainless steel tensile strength tests at cryogenic temperatures

23 p4206 A70-44353

18-8 stainless steels pitting corrosion, examining grain boundaries influence

24 p4362 A70-46184

Stainless steel oxide films structures and chemical compositions, examining oxidation time, polishing conditions, vapor humidity and temperature effects

24 p4362 A70-46191

STALL

U BOUNDARY LAYER SEPARATION

STAMPING

Facility for studying energy characteristics of electrohydraulic stamping, discussing copper wire exploding in water

06 p1077 A70-17869

STANDARD ATMOSPHERES

U REFERENCE ATMOSPHERES

STANDARD DEVIATION

Reconnaissance uncertainty effect on precision of return to fixed point applied to circular error probable, drms calculations and Loran

04 p0652 A70-15345

Arithmetic mean, least squares method and standard deviation concepts in random error analysis of measurement data

11 p2117 A70-26674

STANDARDIZATION

Human factors data standardization in NASA Apollo Applications Program for computer data processing

09 p1623 A70-22295

Absolute radiometric reference scale, noting International Pyrheliometric Scale 1956 materialization by standard instruments

15 p2735 A70-31805

Parts standardization in military electronics industry for cost reduction and reliability, discussing design transform from software to hardware

15 p2831 A70-32632

Fastener standardization for airline maintenance requirements

17 p3102 A70-35811

Spectrosensitometer for standardizing meteor spectrograms

19 p3514 A70-37643

Flight data acquisition methods standardization, discussing digital recording modes and formats and hardware rationalization

19 p3429 A70-38515

STANDARDS

NT FREQUENCY STANDARDS

NT REFERENCE ATMOSPHERES

Earth satellites magnetic survey contributions to World Magnetic Survey project (WMS), discussing international reference standards and magnetic mapping

01 p0075 A70-10595

Recommended design practices to assure good brake system performance with compatibility for skid control equipped aircraft

01 p0007 A70-11457

Aircraft/aerospace fluid systems flexible hose and rigid tube assemblies fire resistance and test requirements

01 p0011 A70-11459

Quick-disconnect couplings selection guide for aerospace fluid systems, emphasizing functional and weight considerations

01 p0197 A70-11461

Helicopter turbine engine bleed air requirements obtained by compressor extraction for engine designers

01 p0167 A70-11462

Photoelectric UVB photometry of stars in Carina, Vela and Centaurus, giving standard connection sequences for continued photometry

02 p0370 A70-12074

FAA engineering approach to SST certification involving airworthiness standards development and coordination with industry and foreign governments

03 p0437 A70-14060

Allowable leakage guidelines for in-service aircraft hydraulic components, discussing causes and measurements, tabulating rates for static and dynamic seals

05 p0797 A70-15776

Systems engineering management process for satisfying MIL-STD-499 requirements, detailing functional analysis, tradeoffs and resulting design analysis data

05 p0959 A70-16462

Selection criteria for nonturbobcharged air or liquid cooled reciprocating type prime movers used in aircraft ground support equipment

07 p1248 A70-18801

Back-up rings and special sealing devices performance qualification testing specifications

07 p1290 A70-18802

Liquids particulate contamination sizing and counting by membrane filtration, specifying procedures and apparatus used

07 p1195 A70-18804

Propellant transfer unit for weapon or space vehicle systems, specifying aerospace ground equipment criteria

07 p1248 A70-18806

Fluids for aerospace power technology, tabulating properties of hydraulic, damper and heat transfer fluids, fuels, oils, etc

07 p1316 A70-18807

Specification of minimum performance standards and test procedures for automatic pressure altitude digitizer equipment

07 p1279 A70-18901

Air-land demountable cargo containers specifications, establishing dimensional, structural and environmental requirements
[SAE-AS-832] 07 p1249 A70-19599

Test standards for boron epoxy flat laminates, proposing specimen geometries and testing methods
08 p1530 A70-21887

Sailplane design standards concerning retractable undercarriage and trailing-edge flaps revised to achieve better performance
09 p1612 A70-23575

Abbot pyranometer as reference standard for calibration, reporting performance tests of time constant, cosine response and attitude
10 p1886 A70-23933

FAA recommendations on general aviation airports and heliport design standards, explaining standards establishment or modification procedures
[SAE PAPER 700231] 11 p2031 A70-25900

Bonded resistance strain gages technical characteristics noting need for uniform standards
11 p2053 A70-26427

International safety standards for SST airworthiness
12 p2161 A70-27599

Minimum performance standards established by Radio Technical Commission for Aeronautics for airborne radio marker receiving equipment operating on 75 MHz
13 p2364 A70-28999

Minimum performance standards for airborne radio receiving and direction finding equipment covering normal and environmental test procedures
13 p2365 A70-29000

Black bodies radiation properties and design for applications as absolute radiation standards
13 p2410 A70-29657

Standard pattern recognition with spatial discretization, concerning discrete cell or segment viewing
14 p2553 A70-30422

Radiometers calibration equipment maintaining radiation standards, investigating long and short waves by digital voltmeter coupled to paper tape punch
15 p2735 A70-31806

Airport safety standards for overall system including aircraft, ATC, navigation, runways, etc
15 p2717 A70-32229

Computer system maintainability demonstration test in accordance with MIL-STD-471, discussing techniques for failure indication and repair crew qualifications and training
15 p2706 A70-32657

Air safety R and D and future safety standards
16 p2842 A70-33816

Engineering standard for solar constant and zero air mass solar spectral irradiance from high altitude measurements
17 p3077 A70-35161

Piezoelectric controlled device as standard for holographic interferometry, providing continuously variable subject plate displacement and/or rotation
19 p3425 A70-37890

Defect grouping role in MIL-STD-105D inspection techniques, discussing costs and acceptance probabilities
22 p4048 A70-43727

MIL-STD-882 systems and subsystems and equipment safety requirements related to program management activities
22 p4048 A70-43730

Information handling for safety design concerning standards, criteria and requirements
23 p4153 A70-44493

STOL aircraft FAA airworthiness standards and certification rules, examining noise, control systems, all weather operation, fire protection, handling qualities and performance
[AIAA PAPER 70-1331] 24 p4291 A70-45937

STANDING WAVE RATIOS

Standing wave ratio of ultrasonic field determined by holographic method, using acoustic transmission lines with termination impedances
05 p0848 A70-16403

Rectangular-slot antenna pair self and mutual admittances in inhomogeneous plasma layer on slender conical body, calculating VSWR and isolation
06 p1020 A70-17565

Standing wave ratio frequency dependence in miniature stripline power dividers and ring structure hybrid junction
09 p1652 A70-23653

Thin window for circularly polarizing antennas, measuring circularity and VSWR performance on S and X band test sections
16 p2877 A70-33410

STANDING WAVES

Vertical wind observations during lower ionosphere wind measurements by Na release method, discussing gravity effects and standing waves
01 p0078 A70-11213

Resonance amplification theory of standing interfacial gravity waves in viscous fluids applied to obtain wavelengths prediction of atmospheric bow waves
01 p0081 A70-11299

Standing bow shock in plasma flow into dipole magnetic field, measuring particle density, electron temperature, magnetic field flux and oscillations
03 p0530 A70-13158

T and L spiral waves existence in disk galaxies, noting helical and ring structures formation near center from standing waves onset
03 p0564 A70-13223

Mean acoustic force on small spherical and nonspherical inclusions in standing acoustic field, discussing equilibrium orientations of body
04 p0720 A70-15085

Optical system with orthogonal standing waves in liquid used for two dimensional scanning of laser beam in ultrasonic field
07 p1296 A70-18765

T and L spiral waves existence in disk galaxies, noting helical and ring structures formation near center from standing waves onset
08 p1580 A70-21656

Standing wave measurements on radiating traveling wave dipole arrays with glide symmetric excitation, showing multimode propagation and effect on log periodic balancing
09 p1633 A70-22688

Stationary collisionless shock waves in hot initial plasma produced by theta pinch discharge, discussing magnetic field, density and electron temperature profiles
10 p1924 A70-24697

Transverse laser modes interaction in traveling and standing wave generators allowing for spatial distribution
13 p2424 A70-28597

Optical system with orthogonal standing waves in liquid used for two dimensional scanning of laser beam in ultrasonic field
18 p3271 A70-37109

STANDS

U SUPPORTS

STAR CLUSTERS

NT VIRGO STAR CLUSTER

Stellar systems models numerical construction, using data on star cluster density distribution, centroid velocity, potential distribution, etc
01 p0174 A70-10200

Computer model for evolution investigation of disks of stars, discussing methods to obtain gravitational potential
01 p0185 A70-11065

Soviet collection of articles on structure and dynamics of stellar systems, Part 2
02 p0375 A70-12442

Stellar clusters equilibrium state in gravitational field, discussing dispersed clusters formation by gravitational instability in gas containing stars of various ages
02 p0376 A70-12446

Anomalous fast OB stars separation method based on spatial kinematic characteristics measurements, noting accuracy
03 p0565 A70-13230

Lagrangian stability of stellar systems of Trapezium in Orion type situated within large stellar cluster or cosmic cloud
03 p0565 A70-13235

Envelope stars evaporation effects on star cluster contraction, discussing energy inflow from envelope to nucleus
04 p0745 A70-14475

Stars distribution in depleted globular clusters determined by integral equations describing distribution as function of cluster parameters
04 p0754 A70-15256

Horizontal branch and red giant stars ratio estimated in globular clusters for He abundance
05 p0906 A70-15894

Pulsed gravitational radiation emitted by dense star clusters
05 p0921 A70-16977

Neutrino emission, mass loss and giant branch termination in young clusters with giants originating from intermediate mass main sequence stars
06 p1138 A70-17277

Globular clusters in M31, discussing metallicity and heavy element enrichment in Andromeda
06 p1138 A70-17306

Mean magnitudes, colors and amplitudes for RR Lyrae variables in omega Centauri cluster obtained from photometric observations
06 p1148 A70-18455

Stellar velocity distribution function for small mass stars in nonrotating systems
07 p1389 A70-20208

Double and multiple stars components magnitude differences tabulated based on visual and photometric observations
08 p1574 A70-21163

Pulsar clusters and associations within 1 kpc of sun and hot O-stars and supergiants, calculating radius of surrounding H II regions
08 p1577 A70-21493

Anomalous fast OB stars separation method based on spatial kinematic characteristics measurements, noting accuracy
08 p1580 A70-21663

Lagrangian stability of stellar systems of Trapezium in Orion type situated within large stellar cluster or cosmic cloud
08 p1580 A70-21668

Hydrogen 21 cm emission line in Perseus region observed for motion of neutral hydrogen connected with II Per, discussing stellar radial velocity
10 p1937 A70-23944

Excess color method for photometric and spectral studies of interstellar absorption in cluster NGC 6913
11 p2116 A70-26585

Excess color method for studying interstellar absorption around cluster NGC 6823
11 p2116 A70-26586

Densities and extents of absorbing clouds in open cluster NGC 7086 determined from photometry and spectral classifications of stars
11 p2116 A70-26587

Young stars evolution rates in expanding and disintegrating stellar associations, giving age estimates
12 p2306 A70-27862

Red dwarfs and supernovae determination in stellar clusters, outlining statistical probability technique for total number of flare stars
12 p2308 A70-27872

Self gravitating three dimensional particles system evolution using water bag model
13 p2498 A70-30012

Galactic structure of Milky Way towards Taurus based on two dimensional classification and three color photography of star group
15 p2797 A70-31621

Stellar associations formation theory including effects of radiation, Rayleigh-Taylor instability and interstellar gas cold regions
15 p2801 A70-32478

Flare stars distribution in Pleiades, discussing flare visual magnitude and frequency
15 p2807 A70-32876

Quasars as protoclusters of galaxies, discussing hypothesis of dense matter cascading fragmentation with subsequent scattering in form dispersing stellar systems
15 p2808 A70-32881

Stellar evolution in globular clusters, considering H-R diagrams of age, He abundance and thermal instability
16 p2973 A70-33076

Globular cluster stars, discussing cosmological importance, stellar development models, main sequence stars, red giant models, He content, age computation, etc
17 p3171 A70-35447

Galaxies and globular clusters, obtaining data by measurements with intermediate bandpass photometry
18 p3321 A70-37121

Dispersed stellar clusters color excesses and distance moduli from color-magnitude diagram, considering evolutionary deviation from main sequence
18 p3323 A70-37138

Peculiar velocities nonisotropic distribution in stationary differentially rotating stellar system based on Boltzmann equation solution
18 p3324 A70-37149

Spiral galaxy NGC 6946 structure and stellar associations distribution, indicating no relation between color and magnitude and distance from center
18 p3327 A70-37160

O type stellar clusters hydrogen line observation revealing associated gas clouds
18 p3328 A70-37172

Galactic spiral structure relation to local stellar distribution, discussing OB associations, galactic cluster, WR stars, cepheids, and common stars in sun neighborhood
18 p3329 A70-37176

H 2 region galactic clusters and exciting stars, reevaluating distances by color magnitude diagrams
18 p3329 A70-37178

Association Carina OB 2 photometric investigation of mean distances
18 p3330 A70-37186

Rotating stellar systems cooperative phenomena, estimating star-star collisions effect on perturbation rate and damping
19 p3525 A70-38772

Relativistic gas spheres and collisionless star cluster models with large red shifts, showing radial perturbation stability
20 p3703 A70-39175

Globular cluster color-magnitude diagram parameters, examining giant branch and metal content
21 p3889 A70-41153

Color-color diagram of M92, computing synthetic stellar spectra for line absorption effect
21 p3892 A70-41249

Open star h and chi Persei cluster four color and H beta photoelectric photometry, discussing interstellar reddening, ages and distances
21 p3922 A70-41982

Color-magnitude diagram of star cluster Kron 3 in Small Magellanic Cloud, using electronographic photometry
22 p4102 A70-42978

Stellar population of young clusters containing red supergiants, determining spectral types and luminosity classes 22 p4102 A70-42979

Time constant loci and theoretical luminosity functions for various compositions and ages of metal poor globular clusters 22 p4108 A70-43735

Globular cluster relaxation time using nonMaxwellian velocity distribution and polytropic spatial distribution 22 p4109 A70-43744

Globular cluster M5 giant, asymptotic and horizontal branches, determining color-magnitude diagram and luminosity 22 p4109 A70-43745

Stellar associations formation theory including effects of radiation, Rayleigh-Taylor instability and interstellar gas cold regions 23 p4239 A70-43903

Stellar spectra above horizontal branch in globular clusters, discussing stellar evolution, composition and structure 23 p4246 A70-44755

Stellar rotational velocities in open star clusters, noting evolutionary expansion, tidal coupling in binaries and Ap stars magnetic braking 23 p4251 A70-44820

Cluster evolution model for stars with equal masses, calculating density and velocity distribution for various cluster types 24 p4404 A70-45417

Old open clusters red giant observations comparison with stellar evolution calculations, discussing proper motions, magnitudes, data acquisition and analysis, etc 24 p4404 A70-45418

STAR DISTRIBUTION

Duplication characteristics of low luminosity stars, considering nearby M dwarfs, white dwarfs and high velocity subdwarfs 01 p0188 A70-11334

PreHayashi phase of stellar evolution, discussing protostellar disks /stellisks/ formation from flattened fragments of collapsed interstellar cloud under turbulent viscosity 01 p0190 A70-11346

Spacecraft orientation from onboard stellar photographs, calculating absolute and relative elements, accuracy and camera parameters 01 p0198 A70-11512

MK stellar spectral types in Monoceros, analyzing spatial distribution and interstellar absorption using slit spectograms 02 p0369 A70-12063

Radio sources emission separations statistical analysis, establishing little physical association in pairs of sources 02 p0370 A70-12112

Pulsar distance and distribution estimation, considering galactic spiral structure and nature of interstellar medium 02 p0371 A70-12201

Anomalous fast OB stars separation method based on spatial kinematic characteristics measurements, noting accuracy 03 p0565 A70-13230

Young flare stars in solar vicinity, considering spatial density, kinematic properties and luminosities 03 p0567 A70-13318

Smithsonian Astrophysical Observatory (SAO) Star Atlas of reference stars and nonstellar objects 04 p0749 A70-14676

Stars distribution in depleted globular clusters determined by integral equations describing distribution as function of cluster parameters 04 p0754 A70-15256

Time determination at astronomical observatories using transit instrument observations concerning stellar distributions and magnitudes 04 p0756 A70-15486

Elliptical cosmology, discussing evolutionary geometry, Synge distribution, galactic age and distance from earth, Friedman equations and independence of constants 05 p0905 A70-15794

Horizontal branch and red giant stars ratio estimated in globular clusters for He abundance 05 p0906 A70-15894

Diffuse far UV radiation analysis in connection with stars and dust grains distribution and grains optical properties 05 p0903 A70-16571

Binary star frequency and orbital axes distribution, discussing visual orbits, mass ratios, photometrical detection, etc 06 p1138 A70-17308

Milky way and interstellar clouds brightness fluctuations statistical analysis by surface photometry, studying dust distribution, cloud absorption and dimensions, star distribution, etc 06 p1149 A70-18463

Neutron stars equation of state derived, suggesting three body forces inclusion at high densities 07 p1388 A70-19924

Anomalous fast OB stars separation method based on spatial kinematic characteristics measurements, noting accuracy 08 p1580 A70-21663

Galaxies and stars interactions, explaining observed peculiarities by electrostatic and electromagnetic forces 09 p1750 A70-22097

Nonlinear stellar density waves in galaxy using gas dynamic equations, assuming one dimensional and steady waves 09 p1762 A70-23073

Star field pattern recognition methods for spacecraft attitude determination without a priori knowledge of star position-vehicle attitude relationship 09 p1725 A70-23516

Multiplicity recorder for cosmic rays neutron component studies, reducing star redistribution errors by coincidence effect compensation 11 p2103 A70-25527

Stars identification on photographic plates and position computation in FORTRAN, using CONTROL DATA 6600 and IBM 1130 computers 11 p2113 A70-26183

Diffuse matter distribution in northern region of Milky Way, examining relation with O-BO stars distribution 11 p2116 A70-26588

Latitude determination from observations of pairs of bright stars at equal altitudes, using computer ephemeris calculations 14 p2633 A70-30142

Spiral structure of disk galaxies as nonaxisymmetric perturbations in density, using pressure free hydrodynamical equations 14 p2639 A70-30731

Near Galactic plane condensations of spectral A stars in HD catalog, investigating by Monte Carlo method and Poisson formula 15 p2797 A70-31616

Galactic structure of Milky Way towards Taurus based on two dimensional classification and three color photography of star group 15 p2797 A70-31621

Holographic device for satellite attitude determination, providing three axis reference information in analog or digital form from single star field sampling 16 p2946 A70-33158

G and K stars spectral classification using narrow band photometry 17 p3169 A70-35380

Soviet book on declination observation of bright and faint stars in one system 18 p3314 A70-36402

Galactic spiral structure model, examining nonlinear stellar density waves in plasma cylinder 18 p3322 A70-37131

Dispersed stellar clusters color excesses and distance moduli from color-magnitude diagram, considering evolutionary deviation from main sequence 18 p3323 A70-37138

Clock corrections determinations by stars pairs situated symmetrically around zenith, obtaining formulas by various methods 18 p3324 A70-37146

Spiral structure definition in external galaxies, discussing optical form types, Messier 33 outer and inner parts and differences in arms 18 p3326 A70-37153

Milky Way and other galaxies spiral arms configuration, comparing to Andromeda 18 p3326 A70-37154

M-31 galaxy OB /outermost border/ stars 18 p3326 A70-37156

Spiral galaxy NGC 6946 structure and stellar associations distribution, indicating no relation between color and magnitude and distance from center 18 p3327 A70-37160

Pulsar galactic longitudinal distribution, discussing observability impaired by high electron density in spiral 18 p3328 A70-37173

Galactic spiral structure relation to local stellar distribution, discussing OB associations, galactic cluster, WR stars, cepheids, and common stars in sun neighborhood 18 p3329 A70-37176

Orion arm local structure and kinematics, discussing outward or inward motion to galactic center and component direction 18 p3329 A70-37177

Local spiral arm H 2 regions distribution in Cygnus direction, discussing symmetry due to magnetic field 18 p3329 A70-37180

Young cepheids galactic distribution determined by photometric method, showing correlation with spiral arms 18 p3330 A70-37184

Association Carina OB 2 photometric investigation of mean distances 18 p3330 A70-37186

Stellar rings and galactic structure, examining protol elliptoidal star aggregate diameter constancy 18 p3330 A70-37187

O-B5 stars mean ages estimation by hyperbolic approximation based on distribution in stellar associations 19 p3524 A70-38762

Stellar ring 373, comparing color-magnitude and color-color diagrams to adjacent star fields 21 p3888 A70-41121

Photographic determination of star positions at closed block plate adjustment, considering accuracy expectancy 21 p3889 A70-41146

Intermediate band photometry of companions to RR Lyrae variables, identifying AP Ser K line excess subdwarf 21 p3892 A70-41187

Galactic distribution of supernova remnants and association with pulsars and X ray sources 21 p3892 A70-41188

Multiplicity recorder for cosmic rays neutron component studies, reducing star redistribution errors by coincidence effect compensation 21 p3882 A70-41277

Sirius components relative photographic positions and magnitude difference, discussing color effect, grating image separations and emulsion contraction 21 p3922 A70-41984

Star content in Small Magellanic Cloud wing counted to determine detachability from tidal arm and main body 22 p4099 A70-42628

OB star distribution statistical analysis in Southern Milky Way, discussing concentrations, relations and systematic deviations 22 p4100 A70-42854

Stellar ring 274 reality confirmed by photometric measurements of OB member stars, determining variable shell star P Cygni location 22 p4101 A70-42868

Computer model of self gravitating gas-stars system with spiral structure surviving galactic rotations 22 p4103 A70-42982

Cosmic rays galactic propagation and confinement, discussing matter and star distributions, magnetic fields, positron flux and energy spectrum, etc 22 p4096 A70-43396

Photometric search for metal deficient stars, using objective prism plates and four color Stromgren technique 22 p4109 A70-43736

Radial velocity-light amplitude ratios of grouped variable stars in continuous sequence, comparing pulsation prediction 23 p4247 A70-44793

Pulsars correlation with stellar evolution using model, discussing distribution and formation rate in Milky Way galaxy 24 p4412 A70-45981

STAR FIELDS

U STAR DISTRIBUTION

STAR TRACKERS

Statistical decision problem of Brownian motion with moving boundaries in automatic daylight star tracker design for aircraft navigation solved by image method 01 p0139 A70-11635

Gyrostabilized attitude reference platform for high altitude rotating research rocket payload alignment with preselected star 03 p0579 A70-13606

Delay characteristics of narrow band double bridge amplifier used as inertial component of photoelectric star transit recorder 04 p0693 A70-15489

Transistorized photoelectric star transit recorder operable in ambient media with large temperature variations ensuring low zero point drift 04 p0694 A70-15490

Electronic recorder design and operation for mean moments of star transit times 04 p0694 A70-15491

Danjon astrolabe for star position and aberration constant determination with improved accuracy, discussing Mars observation 05 p0912 A70-16453

Stars photographic position determination errors with NAFA-3C/25 camera, comparing films and plates 09 p1673 A70-22164

Wide angle electronic camera for astronomical photometry designed to seek photometric standard stars remote from nebular regions 09 p1681 A70-23313

Star field pattern recognition methods for spacecraft attitude determination without a priori knowledge of star position-vehicle attitude relationship 09 p1725 A70-23516

Star tracker linear and nonlinear model selection influence on satellite attitude stability 10 p1953 A70-25231

Three axis star pointing attitude control system for stabilized Skylark sounding rocket program 13 p2447 A70-28687

Stellar sensors and deviation measurement procedures, discussing photosensitive elements, astrophysical data, etc

13 p2407 A70-29140

Spin stabilized Project Scanner spacecraft attitude determination by star mapping technique, describing optics, photomultiplier, reticle, electronics and sun shield

15 p2772 A70-31791

Mariner spacecraft electro-optically controlled star sensors design and performance, discussing star simulation and stray light test techniques

15 p2736 A70-32033

Stabilized platform stellar detector for French probe balloons, using semicircular light modulator

15 p2738 A70-32249

Attitude sensing and target pointing instrumentation in earth orbiting stellar telescopes in inertial space

16 p2905 A70-33155

Shipborne day/night star tracker assisting Missile Guidance System monitoring in Atlantic and Pacific Missile Ranges

16 p2905 A70-33156

Star tracker rigidly connected to spacecraft frame for attitude determination by star field correlation

16 p2946 A70-33157

Surveyor Canopus sensor and Project Scanner dual IR radiometer mechanical design

16 p2914 A70-34107

Balloon-borne X ray telescope star sensor with one arc minute accuracy, discussing design and Cyg X-1 location measurement

17 p3090 A70-35312

Mariner spacecraft roll control star sensors and trackers design and flight performance

20 p3665 A70-39239

Spacecraft position determination by holographic approach involving single star formation

20 p3665 A70-39422

Navigation instrument geometrical calibration by natural satellites and reference stars during interplanetary flight

[AIAA PAPER 70-1023] 20 p3669 A70-39586

Aerospace electronics covering fly-by-wire aircraft flight control, ATC, star trackers for spacecraft attitude control, etc

20 p3669 A70-39668

Guidance and navigation systems precision azimuth measurement by star sighting and gyrocompass techniques

22 p4067 A70-42663

STAR TRACKING

U STAR TRACKERS

STARFIGHTER AIRCRAFT

U F-104 AIRCRAFT

STARK EFFECT

Classical path methods for treating Stark spectral line broadening in plasmas illustrated by Lyman alpha line of hydrogen calculations

04 p0726 A70-14670

Stark broadening of ionized helium lines by collective electric fields in theta pinch

04 p0722 A70-14684

Transition probability and Stark profile of H alpha standards for absolute intensity calibration of spectroscopic data from thermal shock tube plasma

05 p0853 A70-17083

Carbon dioxide laser beam modulation by molecular Stark effect

06 p1080 A70-17448

Numerical calculation of S matrices for Stark broadening of Lyman-alpha line based on straight line classical path model

09 p1730 A70-22228

Stark broadening of singly ionized nitrogen lines measured in dense high temperature plasma behind reflected shock wave in T tube

09 p1731 A70-22776

Stark effect He II and H beta on lines observed for transverse and longitudinal fields, using beam-foil light source

09 p1731 A70-22779

Measured and theoretical Stark-broadened line profiles and asymptotic wing approximation of hydrogen Balmer lines at specific electron density and temperature

09 p1732 A70-22782

Quadratic Stark shifts of absorption lines hyperfine components in cesium atom beam measured using optical spectroscopy

10 p1887 A70-24033

Stark cell with high electric fields for studying inactive IR spectrum of homonuclear diatomic gas molecules

13 p2450 A70-28499

Stark-broadened neutral atomic line widths and shifts, determining electron densities from H beta profiles and pressure-temperature data

13 p2455 A70-29220

Stark broadening of neutral helium line in plasmas for electron densities measurements accuracy, comparing to H beta determined densities

13 p2456 A70-29225

Nitrous oxide and carbon dioxide laser Q switching by ammonia Stark effect

13 p2431 A70-29835

Stark broadening calculations of H alpha and H gamma hydrogen lineshapes

14 p2620 A70-31303

Ion line Stark broadening, considering electron-ion quadrupole excitation and electron resonant scattering

14 p2620 A70-31376

H alpha and H beta lines electrodynamic broadening with linear Stark effect, calculating relative intensity

15 p2777 A70-32490

Near collisions approximation in Stark broadening of hydrogen Lyman alpha line

18 p3296 A70-37227

H alpha and H beta lines electrodynamic broadening with linear Stark effect, calculating relative intensity

23 p4221 A70-43912

Stark effect in hydrogen atoms for nonuniform electric fields, considering correction of energy eigenvalues of Schrodinger equation by WKB method

23 p4221 A70-44401

Hydrogen cluster beam discharges, determining transient plasma ion density from Stark broadening measurements of H beta line

23 p4228 A70-44939

STARLIFTER AIRCRAFT

U C-141 AIRCRAFT

STARS

NT A STARS

NT B STARS

NT BINARY STARS

NT CEPHEID VARIABLES

NT DWARF STARS

NT EARLY STARS

NT ECLIPSING BINARY STARS

NT GIANT STARS

NT HERCULES NOVA

NT HOT STARS

NT MAGNETIC STARS

NT MAIN SEQUENCE STARS

NT NEUTRON STARS

NT NOVAE

NT O STARS

NT OMICRON CETI STAR

NT PROTOSTARS

NT PULSARS

NT RADIO STARS

NT SUN

NT SUPERGIANT STARS

NT SUPERNOVAE

NT T TAURI STARS

NT VARIABLE STARS

NT WHITE DWARF STARS

Stellar objects position accuracy with respect to reference stars improved by applying differential corrections methods to optical center coordinates of stellar photographs

02 p0362 A70-11759

Selenodetic control systems orientation based on lunar features correlation with reference stars, considering ephemeris times corrections

08 p1572 A70-20941

Stars of galactic nebulae - Conference, Buirakan, Armenian SSR, September 1968

12 p2304 A70-27851

Selenodetic control systems orientation based on lunar features correlation with reference stars, considering ephemeris times corrections

15 p2806 A70-32753

Diffraction by star bounded by closed contour scalar field created by surrounding medium, reducing solution to boundary value problem via algorithm

19 p3470 A70-37431

STARTERS

NT ENGINE STARTERS

STARTING

Combined gyromotors optimal starting and operating conditions, considering size and weight characteristics

09 p1680 A70-23146

Nickel cadmium battery for aircraft jet engine starting, discussing selection for optimum service life and reliability under maintenance and environmental conditions

[SAE PAPER 700211] 11 p1980 A70-25883

Low drag supersonic compressors for aircraft engines, calculating start and cruise conditions of quasi-isentropic flow cascades

21 p3745 A70-41405

Gas turbine engine combustion chamber starting, discussing effects of temperature, nozzle characteristics and fuel physicochemical properties

22 p4092 A70-43356

Start-up characteristics for three-phase synchronous reactive motors with various starting unit designs

24 p4293 A70-45471

STATE EQUATIONS

U EQUATIONS OF STATE

STATE VECTORS

State variable diagram for transfer function of single output/input linear stationary system obtained by parallel, direct and iterative methods

05 p0928 A70-16027

Liapunov functions generation by matrix transformation of state-space system vector applicable to linear and nonlinear systems

06 p1023 A70-17544

Apollo onboard computers tracking data state-vector corrections covariance matrix, considering initial estimate, noise and tracking geometry errors

[AIAA PAPER 70-162] 06 p1015 A70-18072

State transition matrix computation method with efficient algorithm for orbit prediction in n-body gravitational field

06 p1095 A70-18497

Final state vector norm minimizing in linear optimal control, using successive approximation and quadratic programming

10 p1856 A70-25188

State space models of remote manipulation problem applied to human supervised or autonomous computer manipulators

10 p1828 A70-25230

Transition matrix of Markov chain with finite states from noisy measurements of state, discussing algorithms convergence rates and computations

12 p2261 A70-27421

State-space synthesis of multipoint passive reciprocal networks with minimum number of resistors, using Gauss factorization procedure

14 p2556 A70-30516

State transitions and couplings in reliability of complex systems, using logic algebra suitable for computer

15 p2709 A70-32132

Augmented state variable method of nonlinear discrete system identification with noise corrupted input observations

15 p2704 A70-32592

Decoupling by dynamic compensation using algebraic machinery, considering state space extension role in pole assignment

16 p2886 A70-33333

Systems consisting of redundant and different modules, deriving vector and matrix expressions for effectiveness

17 p3099 A70-34581

Constraint optimization in state coordinates by variable structure system flexibility, using mathematical model

18 p3281 A70-36353

Kalman filter set for state vector and observation error variance estimation in discrete-time linear system, using empirical Bayes techniques

[AIAA PAPER 70-1058] 19 p3395 A70-38873

Dynamic plants optimal control, deriving algorithm for determining a posteriori probability density of generalized state vector

20 p3604 A70-39907

General linear /Kalman/ sequential filter to account for finite correlated white noise without state vector augmentation or measurement differentiation

21 p3828 A70-41735

Stochastic optimal control for nonlinear dynamical systems under noisy observations, designing suboptimal state estimates and feedback controls

22 p4063 A70-43429

State-space method of parameter tracking for adaptive control, using Riccati equation and Kalman filtering

23 p4177 A70-44675

Controllable states with prescribed heat flux for incompressible isotropic thermoelastic bodies with temperature dependent response functions

24 p4426 A70-46041

STATIC AERODYNAMIC CHARACTERISTICS

Pitch damping derivatives computation for missile configurations undergoing small amplitude oscillations at subsonic speeds, using static aerodynamic data

[AIAA PAPER 70-537] 13 p2339 A70-29004

Static longitudinal aerodynamic characteristics predictions for missile configurations at various angles of attack, using digital computer

[AIAA PAPER 70-981] 20 p3558 A70-39548

Full scale aircraft spinning motion, computing static, damping, cross and acceleration aerodynamic characteristics for antispin devices

[AIAA PAPER 70-946] 20 p3561 A70-39581

STATIC DEFORMATION

Static deformation of radially polarized inhomogeneous rotating cylindrical shaft of barium titanate using elasticity, electric field and constitutive equations for piezoelectric materials

01 p0118 A70-10549

Triangular conforming plate bending element applied to static and dynamic problems, investigating convergence rates of finite element approximations

03 p0584 A70-12924

Static and shock kink bands in biotite deformed by metamorphism, meteorite impact, nuclear explosion and laboratory experiments

09 p1665 A70-22053

Elastic constants pressure dependence of cubic crystals in NaCl and spinel structures using homogeneous static deformation method

13 p2396 A70-29172

Lunar crystalline rock static and dynamic deformation, examining regolith and silicates textures and structures

21 p3897 A70-41515

STATIC DISCHARGERS

Static electricity generation and discharge in human beings due to clothing layers, analyzing body capacitance, resistance and inductance for ordnance and fuels safety

- 03 p0439 A70-14133
- Wire dischargers at helicopter propeller blade tips reducing electrostatic RF interference, substituting stainless steel wire tufts for nichrome wire
- 05 p0848 A70-16320
- Static charge reducer for aircraft fuels handling safety, discussing performance factors
- [SAE PAPER 700277]
- 18 p3263 A70-36808

STATIC ELECTRICITY

Integrated static discharge frequencies of cat lingual cold receptors measured as function of constant temperature

- 01 p0017 A70-10472
- Static breakdown voltage of air and nitrogen measured under uniform field conditions for specific gas number densities, comparing results with Paschen law
- 03 p0528 A70-14086
- Static electricity generation and discharge in human beings due to clothing layers, analyzing body capacitance, resistance and inductance for ordnance and fuels safety
- 03 p0439 A70-14133

Static electricity suppression for textile materials by blending conducting metal fibers into yarn

- 05 p0870 A70-16299
- Static electricity hazards and problems in electronics and aerospace industries
- 07 p1333 A70-18930

Avalanche diodes properties, establishing equivalent circuit accounting for static electricity, carriers transit time and thermal effects

- 10 p1850 A70-24625
- Electrostatic discharge at magnetopause by idealized circuit analog, discussing transmission lines and terminal impedances
- 14 p2579 A70-31247

Slow tail atmospheric and VLF pulse measurements at close-to-thunderstorm fields, indicating return stroke origin

- 17 p3046 A70-35395
- Soviet book on aircraft electrification in clouds and precipitation during subsonic flight covering atmospheric electrical properties, flight dynamics modification, communications interference, etc
- 19 p3356 A70-38800

STATIC FIRING

Pressure peaks control in hydrazine propulsion system during static tests by controlling initial hydrazine injection

- 11 p2101 A70-25691

STATIC FRICTION

Elastoplastic strains in machine element surface layers under static friction force using polarization-optical techniques

- 04 p0696 A70-14410
- Radial clearance, pressure and piston length and diameter dependence of friction force at rest in piston type hydraulic devices
- 14 p2534 A70-30872

Ball in tube nutation damper for spinning satellite, describing design, testing and fabrication techniques for achieving low friction level

- 16 p2985 A70-34136

STATIC INVERTERS

Operation mode for full-bridge programmed waveform static inverter permitting saturation of power transistors in DC power conversion

- 08 p1439 A70-20707

STATIC LOADS

Computer calculation in elastoplastic range of statically indeterminate structure of bars, considering collapse load, stress and hinge rotation

- 01 p0200 A70-10524
- Finite element bending stiffness matrices for deflections analysis of pretwisted cantilever plate subjected to static loads
- 02 p0384 A70-11858

Static and cyclic stress distributions in buckling shear panel comprising flat plate of clad Cu-Al alloy

- 02 p0388 A70-12497
- Correlation between sustained-load and fatigue crack growth in high strength steels for aggressive environment effects
- 02 p0318 A70-12544

Stress concentration in optically active fiberglass reinforced plastics during static loading determined by optical polarization method

- 02 p0390 A70-12812
- Support moment of beam with ends embedded in elastic medium subject to creep, noting dependence on load
- 05 p0947 A70-17010

Friction on fuselage surface layer under static and instantaneous loads without allowance for oscillation

- 05 p0856 A70-17015
- E1617 alloy breakdown resistance tests under multiple alternating static tension-compression and vibrational loads at 800 C
- 05 p0867 A70-17044

Complex load strength criterion containing stress and strain invariants applied to simple static loads and cyclic symmetric deformation

- 06 p1162 A70-17389
- Damage accumulation and failure of low carbon and low alloy steels subjected to repeated static loading, varying cyclic load frequency
- 06 p1085 A70-17400

Metal adhesive joints behavior under prolonged static stresses, showing time dependence of tensile strength

- 08 p1504 A70-20887
- Static loading effect at high temperatures in argon and liquid lithium on mechanical properties stability of steel
- 08 p1515 A70-20920

Toroidal metallic shells stability under static loads, determining snap-through pressures in pressure chamber with nitrogen working gas

- 08 p1588 A70-21195
- Turbine components thermal stress calculations for static and variable loads, considering plastic strain, creep and temperature effects
- 09 p1775 A70-22592

Fatigue strength tests of alloy during static and programmed loading at high temperatures from statistical standpoint

- 09 p1703 A70-22620
- Gages for static strain measurements at high temperatures, discussing resistivity temperature coefficient compensation
- 09 p1680 A70-23109

Airframe critical part structural reliability on basis of ultimate static strength test data and extreme gust spectrum and maneuver loads

- 14 p2658 A70-30852
- Dynamic and static stress effects on martensite formation temperature in Fe-Ni-C alloys
- 19 p3451 A70-37569

Complementary energy bounding theorem for statically loaded bodies composed of time independent plastic material

- 19 p3546 A70-38353
- Cosserrat spectrum elastic theory, considering static problems
- 20 p3726 A70-39876

Skeletal muscles static tension influence on dog respiratory center functional properties, showing increased frequency volume and sensitivity under stimulation

- 20 p3574 A70-40174
- Hypokinesia and reduced diet effects on human tolerance to static loads, discussing acceleration tolerance prediction
- 20 p3576 A70-40198

Dynamic stability of cylindrical shell with small curvature under static or periodically variable axial pressure loads

- 21 p3932 A70-40554
- Pure Ni plastic flow threshold measurement under combined ultrasonic and static loadings, noting annealing
- 22 p4053 A70-42644

Optimal design of minimum weight bar and beam structures under static loads, comparing computer time with nonlinear programming methods

- 23 p4271 A70-44702

STATIC PRESSURE

NT HYDROSTATIC PRESSURE

Static pressure distributions and velocity profiles for Hg flow through circular pipes in transverse magnetic field, studying laminar and turbulent flows

- 04 p0728 A70-15001
- Static pressure, temperature profiles, heat transfer and optical data for turbulent boundary layer-shock interaction with/without injection
- [AIAA PAPER 70-91]
- 06 p1042 A70-18210

Premixed compression initiated supersonic combustion, noting sensitivity to small perturbations in inlet flow variables

- [AIAA PAPER 68-995]
- 07 p1421 A70-19318
- Radial static pressure distribution of turbulent jet flow over rotating cylinder with constant curvature
- 14 p2567 A70-31399

Error measurements of sharpened edged circular static pressure hole normal to moving fluid boundary using flush transducers

- 15 p2722 A70-32374
- Static pressure probes selection for measuring three dimensional flow at high velocities, considering sensitivity and errors
- 20 p3628 A70-39262

Solar wind static and dynamic pressures on earth magnetosphere, using geomagnetic parameters

- 21 p3878 A70-40845
- Nitrogen plasma viscosity measurements as function of velocity and axial static pressure gradient
- 23 p4226 A70-44439

Static pressure effects on heat flux critical density for free convection and forced flow in circular pipes

- 23 p4282 A70-44726

STATIC STABILITY

NT DIMENSIONAL STABILITY

NT SHELL STABILITY

NT STRUCTURAL STABILITY

Spherical caps axisymmetric static and dynamic buckling under load, using axisymmetric nonlinear elastic shell theory approximation and finite difference equations

- [AIAA PAPER 69-89]
- 04 p0778 A70-15587
- Static stability criterion applicable to elastoplastics problems with/without nontrivial equilibrium states, noting effect on buckling loads
- 06 p1167 A70-17900

Equilibrium equations solved for statics of double row radial thrust ball bearing, neglecting load angle changes caused by deformations of races and ball bearings

- 06 p1077 A70-17929
- Rotating parabolic mirror /antenna/ on multisupported suspension analyzed for static rigidity, determining elastic deformation under mirror weight
- 08 p1586 A70-21055

Dynamic tensile properties of monolithic and pyrolytic graphite compared with static tensile strength

- 08 p1527 A70-21334
- Soviet book on servo systems for radar automatic tracking and control stations covering static, dynamic and frequency characteristics, amplifiers and correction devices
- 09 p1654 A70-22597

Free flight static, dynamic stability and drag data for 10 degree semiangle cone obtained at 8-16 Mach numbers

- [AIAA PAPER 69-133]
- 09 p1605 A70-23218
- Long time static strength, durability and thermal stability relations determined for heat resistant alloys at operational temperatures
- 10 p1903 A70-24238

Static longitudinal stick free and stick fixed aircraft stability equations for several configurations and power effects

- [SAE PAPER 700238]
- 11 p1981 A70-25907
- Three dimensional variational dynamic and static large deformation equations solutions for stability and natural frequencies and wave propagation in bodies under initial strains
- 12 p2322 A70-27331

Transonic static and dynamic stability of large angle spherically blunted high-drag cones

- [AIAA PAPER 70-564]
- 13 p2341 A70-29029
- Static and dynamic stability of wind tunnel models with flexible support, considering binary rigid body freedoms
- 14 p2564 A70-31398

Static stability requirements relaxation and wing control devices additions for alleviating wing root bending moments in controls configured vehicle /CCV/ design concepts

- 19 p3355 A70-37395
- Asymmetric boundary layer transition effects on slender reentry vehicle motion by changing static stability characteristics
- [AIAA PAPER 70-987]
- 20 p3557 A70-39542

Spike effect on nose drag and static stability of blunt bodies, estimating optimum length for drag reduction at zero angle of attack

- 20 p3558 A70-39702
- Elastic bodies static stability theory variational principles, introducing equilibrium equations and boundary conditions of initial state by Lagrange multipliers
- 20 p3724 A70-39857

Static and dynamic longitudinal stability of semirigid parafoil gliding descent system in pitching motion

- [AIAA PAPER 70-1191]
- 21 p3753 A70-41825

STATIC TESTS

NT STATIC FIRING

Photogrammetric deformation measurement of thin steel sheets during static bending tests

- 02 p0302 A70-12653
- Metal particle and wire combustion using static and flow methods, obtaining experimental results for Al, Be, Mg and B
- [ONERA-TP-735]
- 03 p0543 A70-13633

Analytical structural design reliability, discussing static test failures of wings, fuselage, horizontal and vertical stabilizer and landing gear

- 07 p1417 A70-20400
- Flowfields in lifting-line approximation for finite bladed, lightly loaded propellers in axial cruise and heavily loaded propellers in static operation
- 07 p1190 A70-20411

Metal adhesive joints peeling and stripping strength determinations, describing static and dynamic tests

- 08 p1503 A70-20884
- Start-stop dynamics as cost effective method for computerized testing of digital modules and subassemblies, providing static and dynamic capability
- 17 p3062 A70-35504

Strapdown inertial attitude indication, describing static and dynamic tests, error propagation profiles, performance prediction, etc

- 22 p4068 A70-42668

STATIC THRUST

Thrust static characteristics of poppet valves with specific angle range indicating validity of momentum theory for thrust estimation

- 06 p1075 A70-17139

STATICS

NT ELECTROSTATICS
NT HYDROSTATICS

Spherical gas bearings static characteristics and performance, discussing materials selection, optimum clearances and surface hardness

07 p1294 A70-19122

People as conservative processors of fallible information, treating stationary data generating process as nonstationary

14 p2537 A70-30898

Linear stationary systems observability with stochastic inputs for linearly independent row vectors, determining state vector components mean values

15 p2716 A70-32346

Transversely isotropic Timoshenko beam statics and dynamics under initial stress and transverse loading

17 p3182 A70-34561

Relativistic three force transformation showing no contraction in static conditions

17 p3136 A70-34823

Quasi-equilibration of static or dynamic universal solutions of compressible or incompressible simple bodies, investigating homogeneity of symmetry and objectivity conditions

18 p3336 A70-36221

STATIONARY ORBITS

NASA network and Thor Delta type booster to launch Italian satellite to geostationary orbit, evaluating feasibility

03 p0451 A70-13841

Solar or nuclear energy powered electric propulsion systems for transferring satellite from low to geostationary orbit, discussing feasibility and costs of various designs

04 p0735 A70-15174

Geostationary mode application to earth sensing, examining resolution requirements for earth scanning tracking telescope

06 p1154 A70-17152

Stationary satellite perturbed motion calculations, assuming small initial orbital eccentricity and inclination and revolution period close to that of earth

07 p1386 A70-19485

European launcher for geostationary orbit (ELGO) program, describing Europa 3 payload, propulsion unit, propellant transfer, etc

13 p2502 A70-28449

Ion electric propulsion system coupled with small booster for geostationary orbit realization

15 p2790 A70-32276

Stationary satellite perturbed motion calculations, assuming small initial orbital eccentricity and inclination and revolution period close to that of earth

15 p2805 A70-32730

Synchronous satellites characteristics and applications to radio connection, light signals, positioning, telecommunications, manned space stations and space shuttles

22 p4109 A70-42467

Low thrust trajectory transfer from low to synchronous orbit, examining hydrogen resistance jet and mercury bombardment ion thruster

22 p4089 A70-42487

Geostationary satellites for magnetosphere and ionosphere sounding, discussing specific observational capabilities

22 p4024 A70-43397

Ion micropulsion for geostationary satellites time optimal attitude control

23 p4261 A70-44669

Europa III SLV payload for geostationary equatorial orbit, describing engine thrust and propellant capacity for high energy second stage

24 p4414 A70-46357

STATIONKEEPING

Orbit determination program for launching and stationkeeping of 24 hr geostationary satellites, using azimuth and elevation of single autotrack antenna

03 p0578 A70-14339

Satellite stationkeeping by ground command, self contained or combined methods compared for networks of synchronous satellites

[AIAA PAPER 70-479]

11 p2121 A70-25463

ATS-3 hydrazine orbit control system efficiency evaluation statistical method, considering stationkeeping maneuvers

[AIAA PAPER 70-460]

11 p2121 A70-25464

LES 5 and 6 feasibility demonstration of satellite communications at VHF/UHF to mobile terminals and as test beds, emphasizing stationkeeping and attitude control

[AIAA PAPER 70-494]

11 p2121 A70-25474

Roll and pitch attitude control for long range stationkeeping mission of synchronous flywheel stabilized communication satellite, discussing constraints on on-board equipment and technology

11 p2126 A70-26279

Low thrust station keeping guidance scheme for gravity gradient stabilized 24-hour satellite, solving equations of motion for near circular equatorial orbit

18 p3289 A70-36676

Guidance and navigation system design for automatic stationkeeping one earth orbiting vehicle with respect to other

[AIAA PAPER 70-1005]

20 p3667 A70-39526

Spinning satellites stationkeeping at synchronous altitude, using solid propellant pulsed plasma microthrusters

[AIAA PAPER 70-1148]

20 p3690 A70-40206

Parameterized design data and selection criteria of biowaste resistojet system for orbit keeping and control moment gyro desaturation of manned space station

[AIAA PAPER 70-1132]

20 p3567 A70-40213

Ion thrust vectoring systems for satellite attitude control and stationkeeping, discussing deflection techniques

[AIAA PAPER 70-1150]

21 p3868 A70-41783

Attitude and orbit control electric propulsion systems for long term space stations, discussing resistojets and electron bombardment and contact ionization ion thrusters

22 p4092 A70-43654

Formation flight stability in dynamic environment, using stationkeeping geometry simulation

[AIAA PAPER 70-1337]

24 p4373 A70-45931

STATIONS

NT DEEP SPACE INSTRUMENTATION

FACILITY

NT EOSS

NT GROUND STATIONS

NT INTEGRATED MISSION CONTROL

CENTER

NT ORBITAL SPACE STATIONS

NT ORBITAL WORKSHOPS

NT SPACE STATIONS

NT TRACKING STATIONS

NT WEATHER STATIONS

STATISTICAL ANALYSIS

NT AMPLITUDE DISTRIBUTION ANALYSIS

NT BIVARIATE ANALYSIS

NT CORRELATION COEFFICIENTS

NT FACTOR ANALYSIS

NT MAXWELL-BOLTZMANN DENSITY

FUNCTION

NT MULTIVARIATE STATISTICAL ANALY-

SIS

NT NONPARAMETRIC STATISTICS

NT NORMAL DENSITY FUNCTIONS

NT POISSON DENSITY FUNCTIONS

NT PROBABILITY DENSITY FUNCTIONS

NT PROBABILITY DISTRIBUTION FUNC-

TIONS

NT RANK TESTS

NT RAYLEIGH DISTRIBUTION

NT REGRESSION ANALYSIS

NT REGRESSION COEFFICIENTS

NT SEQUENTIAL ANALYSIS

NT STANDARD DEVIATION

NT STATISTICAL CORRELATION

NT STATISTICAL DECISION THEORY

NT STATISTICAL TESTS

NT VARIANCE [STATISTICS]

NT WEIBULL DENSITY FUNCTIONS

Life-test sampling plan for electron tubes based on

exponential failure distribution for reliability demand

of military specifications

01 p0099 A70-10112

Missile miss distance evaluation model with emphasis on statistical nature, noting application to systems analysis

01 p0193 A70-10118

Probability selection of useful plants based on distribution of resolving statistics

01 p0053 A70-11023

Mathematical theory of time domain statistical description of random signals in terms of probability theory

01 p0044 A70-11042

Nonlinear system under random excitation, discussing analytic solution method and statistical properties

01 p0206 A70-11149

Book on mathematical methods of reliability theory covering probability theory, statistics, Laplace transformation, set theory, testing, quality control, mass production, sampling, etc

01 p0133 A70-11308

Gas turbine engines vibration characteristics, discussing statistical analysis obtained through condensed vibration overload control program

01 p0166 A70-11420

Materials strength characteristics with respect to breakdown probability parameter by statistical fatigue stability analysis under unsteady loads and various distribution laws

01 p0211 A70-11424

Spacecraft motion parameters and physical characteristics of space determined from statistical analysis of measurement data

01 p0094 A70-11484

Secondary corpuscular stream effect on diurnal variations in cosmic ray intensity obtained from statistical analysis

01 p0172 A70-11524

Ionized meteor trails initial radii statistical characteristics determined for two models

01 p0192 A70-11537

Characteristics of dynamic mechanical systems including solid state and hydrodynamic analogs of ideal incompressible fluids, based on statistical theory of turbulence

01 p0068 A70-11594

Shock wave structure determination in simple monatomic gas, using statistical counting and successive approximation algorithm

01 p0068 A70-11601

Radio sources emission separations statistical analysis, establishing little physical association in pairs of sources

02 p0370 A70-12112

Expected values optimal measurement, given auxiliary conditions between measured value number and quantization

02 p0299 A70-12400

Discrete statistical stellar system relation existence with continuous model proved by introducing unique volume concept for discrete systems

02 p0376 A70-12443

Stationary Gaussian stochastic processes sample functions properties and local times

02 p0324 A70-12504

Statistical measurements of deformation structures and refractive indices in experimentally shock loaded quartz specimens with different crystallographic orientations

02 p0292 A70-12509

Geomagnetic activity effect on ionospheric electron content from statistical analysis of data obtained during three year period

02 p0293 A70-12576

Statistical model of turbulent chemically reacting shear flows, analyzing wave number fluctuations effect and Couette flow

03 p0464 A70-12928

Single dispersion statistical analysis by simultaneous parameters tolerances application

03 p0518 A70-12937

Human blood platelets volume measured in Coulter counter, noting relation to temperature

03 p0416 A70-13008

Statistical analysis of satellite drag data for characteristic time of thermal fluctuations in upper atmosphere caused by soft solar X-rays

03 p0472 A70-13179

Nonperiodic phenomena in variable stars by statistical and physical analysis, noting role of magnetic fields

03 p0566 A70-13313

Statistical equation of motion of blood by averaging motion of individual blood elements over small volume, finding constitutive equations

03 p0434 A70-13572

Sunspot motion statistics for 1965-1967 from observational data, complementing electron-corona differential rotation and spectroscopic measurements

03 p0571 A70-13597

Meteor flakes nature and statistics obtained from meteors characterized by irregular brightness curve

03 p0574 A70-13883

Pressure changes in troposphere and lower stratosphere after strong solar flares analyzed statistically for Northern Hemisphere

03 p0476 A70-13909

Statistical data to demonstrate atherosclerotic diseases affected by cholesterol and saturated fatty acids in foods

03 p0430 A70-14277

Statistical model equations to predict discharge coefficients for concentric orifice plates as function of line size, diameter ratio and Reynolds number

[ASME PAPER 69-WA/FM-6]

04 p0667 A70-14837

HF propagation losses from statistical measurement over north-south path found dependent on mode, day and night and high and low ray

04 p0649 A70-14968

Statistical model of ozone absorption bands for calculating intensity, rotational line position and transmission functions of complex spectral regions

04 p0680 A70-15252

Public health services problems analyzed by statistical simulation method, using Markov process

04 p0644 A70-15356

Statistical stress distribution of breakdown during scaling of wound fiberglass reinforced plastics, noting relation between critical stress and defects

05 p0870 A70-16214

Statistical characteristics of field of linear antenna with square phase characteristics, deriving formulas for presence of amplitude phase errors

05 p0820 A70-16255

Computerized statistical analysis of digital filters used to eliminate digital radar interference

05 p0822 A70-16530

Ternary Ti-Ta-Nb solidus surface determination by simplex lattices and cubic approximation, statistically evaluating equation derived

05 p0864 A70-16547

Statistical analysis for personal variations contribution to total mean square error in time determinations
05 p0914 A70-16649

Statistical analysis of Zwicky catalog of galaxies and clusters of galaxies, interpreting very distant clusters in terms of intergalactic extinction
05 p0915 A70-16697

Statistical description of geomagnetic field as random vector field, presenting correlation functions from empirical estimates from geomagnetic charts
05 p0842 A70-16748

Dispersion and correlation function for atmospheric transparency due to water vapor, from statistical model of absorption bands and effective mass
06 p1053 A70-17204

Electromagnetic wave scattering from finite plasma, discussing statistical measurement errors in degrees of freedom studies
06 p1007 A70-17464

Classification analysis methods application to plant identification for case with incomplete initial statistical information
06 p1014 A70-17632

Ionosphere disturbances due to high altitude thermonuclear explosions, discussing experimental proof by cosmo satellites short wave transmitter radio signal scintillation statistical evaluation
06 p1057 A70-17888

Statistical orbit and position determination for Mars orbiters and landers based on Viking 1973 mission requirements, discussing tracking problems
[AIAA PAPER 70-160] 06 p1158 A70-18177

Statistical model based on kinetic and probability theories to determine drag coefficient of orbiting satellites
06 p1159 A70-18289

Statistical models in kinetic theory for describing gases ranging from gas with no internal degrees of freedom to multicomponent reacting mixtures
06 p1047 A70-18312

Statistical analysis of dynamic plant based on steady signal, showing numerical determination of operator by least squares method
07 p1226 A70-18726

Metal particle size relation to combustion time using statistical method applied to polydisperse Mg powder
07 p1419 A70-18756

Statistical analysis of pulmonary ventilation and gas exchange indices during orthostatic tests before and after water immersion
07 p1209 A70-19517

Static tensibility and vital capacity of lungs statistically analyzed in relation to sex and age
07 p1210 A70-19524

Statistical methods for characterizing interval sequences of ECG, treating interval distribution and joint probability density function of adjacent interval pairs
07 p1211 A70-19593

Ergodic steady random functions measurement and analysis in terms of statistical properties
[ONERA-TP-720] 07 p1411 A70-19825

Book on statistical methods in structural mechanics covering design, fracture, stability, random loads, damage accumulation, reliability, etc
07 p1411 A70-19849

Extremal statistics for signal and noise error probabilities estimation and computer simulation of digital feedback communication systems
08 p1459 A70-20800

Error statistics recording for digital communications channel performance by extreme value technique
08 p1459 A70-20801

Statistical analysis of rotation and macroturbulence in early type Ia and IaB supergiants, discussing evolutionary effects
08 p1571 A70-20908

Statistical characteristics of random wind effects on radio telescopes tracking cosmic object
08 p1586 A70-21062

Meteor flare photographs statistical analysis, noting duration and weight distribution dependence on meteor velocity
08 p1574 A70-21214

Statistics and coincidences of Argonne-Maryland gravitational radiation detector array with and without time delays
08 p1545 A70-21271

Partial statistical description of turbulent flame interior and turbulent flame speed determination for effects of turbulence on flame propagation
08 p1485 A70-21607

Reliability engineering for complex systems of multiple repairable parts based on analysis involving signal flow graphs and Markov renewal processes
09 p1691 A70-22574

Soviet collection of papers on mechanical fatigue from statistical standpoint
09 p1775 A70-22614

Stress concentration effect, surface states and similarity conditions in fatigue ruptures in machine construction, considering statistical analysis
09 p1776 A70-22615

Fatigue life cyclic sensitivity threshold with random nature statistically estimated on basis of maximum likelihood principle
09 p1776 A70-22618

Remote sensing data applications to agricultural statistics, discussing policy and standards for aggregate data release, confidentiality, error analysis, etc
[AIAA PAPER 70-312] 09 p1793 A70-22868

Statistical linearization technique for nonlinear control systems with feedback and zero memory under random input excitation evaluated for output signal characteristics
09 p1654 A70-22960

Mars primitive atmosphere analyzed from statistics of craters quantity as function of diameter, using Mariner 6 and 7 probe photographs
09 p1763 A70-23318

Soviet book on solar activity influence on earth natural processes covering atmospheric circulation and pressure, air temperature, precipitations and hydrological changes
09 p1719 A70-23471

Molecular-statistical theory of second-harmonic light generation by isotropic bodies immersed in external AC or DC electric field
10 p1916 A70-24379

Statistical chance characteristics of velocity profiles and friction for flow along infinite plane wall with constant suction
10 p1869 A70-24519

Probability of given configuration and statistical distribution of peaks between mean crossings of broad-band locally stationary and Gaussian processes
[ONERA-TP-806] 10 p1805 A70-24546

Statistical methods for flying quality research concerning sailplane dynamic stability, maneuverability, sensitivity, rolling and pilot induced oscillations
10 p1805 A70-24582

Statistical estimation of aeromagnetic survey data errors due to diurnal variations, navigational inaccuracies and instrument drift
10 p1914 A70-24646

Approximations implicit in Cayrel statistical equilibrium or non-LTE analysis of ionic hydrogen bound free continuum in sun
10 p1947 A70-24989

Stress, strain and acceleration spatial variation in plate structures under broad frequency band excitation using statistical energy method
10 p1962 A70-25065

VLF radio noise statistical parameters observed as functions of azimuth, considering atmospheric distribution and parameters correlations
10 p1884 A70-25259

Statistical analysis of aurora backscatter VHF measurements, discussing related stream plasma instability theory and diurnal variation
10 p1885 A70-25263

Statistical energy concepts application to Mariner Mars 1969 spacecraft, estimating coupling of damping factors to analyze structural vibration
[SAE PAPER 700171] 11 p2128 A70-25374

Interfacial thermal conductivity model based on statistical features of two faces in contact, discussing surface roughness and heat flow
11 p2083 A70-25763

Statistical analysis of pulmonary ventilation and gas exchange indices during orthostatic tests before and after water immersion
11 p1988 A70-26116

Additive pseudorandom number generator with semiinfinite sequence length, proposing statistical tests for randomness
11 p2074 A70-26325

Book on statistical processing of geophysical and meteorological data covering independent and autocorrelated data, random processes, check tests, stochastic functions, filtering, etc
11 p2046 A70-26425

Statistical classifier for analyzing tape recorded transients
11 p2056 A70-26457

Time-convergent approximations to statistical turbulence functions constructed starting with functions expansion as Taylor series in time
11 p2074 A70-26534

Statistical analysis of latitude distribution of magnetically classified sunspot groups and associated flares
11 p2106 A70-26646

Asymptotics of linear diffusion processes altered by weak nonlinear effects, discussing deterministic and statistical initial value problems
11 p2074 A70-26686

Atmospheric turbulence effects on line-of-sight electromagnetic wave propagation, deriving signal statistics for nonvalid weak scattering solutions case
11 p2012 A70-26764

Statistical properties of random intensity field during coherent laser radiation scattering by moving diffuse surface
11 p2064 A70-26812

Superlayer structure in turbulent boundary layer on flat plate obtained by statistical processing of signals from hot-wire probes
12 p2209 A70-27226

Transient process statistical characteristics in He-Ne laser operating near excitation threshold with pronounced rise time oscillations of light wave field
12 p2247 A70-27507

Phase modulated laser light beam statistical analysis, using Michelson interferometer with piezoelectric crystal driven mirror connected to Gaussian random noise generator
12 p2249 A70-27877

Statistical analysis of control system with nonlinear zero-memory element evaluated for error using Fokker-Planck equation
12 p2204 A70-27985

Statistical design of density tapered planar circular and elliptical arrays for radiation patterns with good sidelobe behavior
12 p2199 A70-27987

Cosmic rays components fluxes, interactions, lifetimes and anisotropy in statistical discrete source model, tabulating and graphing results
12 p2295 A70-27996

Statistical analysis of atmospheric wind and temperature variables relationships to high altitude clear air turbulence observed by U-2 flights
12 p2264 A70-28092

Nonlinear rotating systems optimal control problems approximation by modified Krylov-Bogoliubov averaging technique
12 p2273 A70-28192

Elsasser and statistical band models in single parameter functions representing mean absorption in given spectral range
12 p2191 A70-28295

Meteorological situations and fields quantitative classification and regional grouping by statistical main components application
12 p2265 A70-28333

Wind field statistical properties using model incorporating quasi-steady state speed, shear, gusts and small scale motions
[AGARDGRAPH-115] 13 p2444 A70-28752

Cratered planetary surface distribution and covariance functions of elevations using statistical model
13 p2488 A70-28763

Atmospheric turbulence and irregularities, examining classical exchange coefficient and statistical theories
13 p2445 A70-28788

Burger turbulence model late decay statistical analysis using kernels of Cameron-Martin-Wiener expansion of random velocity field
13 p2386 A70-28820

Statistical characteristics and energy spectra of pulse code signals in data transmission estimated by matrix methods
13 p2364 A70-28871

Random-input describing function as linear approximation to instantaneous nonlinearity in terms of minimum mean-squared error
13 p2382 A70-29070

Plane multielement antenna field statistics as function of correlated phase-amplitude aperture errors
13 p2378 A70-29306

Galaxies rotation, applying optical and radio data to statistical analysis of angular velocities and periods
13 p2492 A70-29386

Extratropical planetary high altitude frontal zones statistical analysis and position forecasting by eigenfunction expansion
13 p2445 A70-29673

Geopotential fields seasonal statistical analysis over first natural synoptic region, using expansion into orthogonal eigenfunctions
13 p2446 A70-29674

Statistical estimation of resolvability of incoherently radiating object sampled at aperture field of observing optical instrument, using Cramer-Rao inequality
13 p2453 A70-29823

Random data analysis application to aircraft inlet diagnostics
[AIAA PAPER 70-597] 13 p2375 A70-29878

Parameters optimization of nonlinear electric servo actuator on basis of statistical criteria
14 p2559 A70-30157

Computer-controlled single-server queueing system with constant access cycle and general service times, calculating mean size and waiting time at statistical equilibrium
14 p2553 A70-30518

Surface wind speed durations statistics analysis, discussing meteorological, orographic and physiographic features
14 p2607 A70-30582

Cloud size clear area spacing statistics development for satellite mission and simulation analyses
14 p2609 A70-30598

SCAMP I DC statistical circuit analysis program for linear and nonlinear circuits, describing program structure
14 p2560 A70-30664

SCAMP 2 program for statistical analysis of electronic circuit sensitivity to variations in parameters and DC input values

14 p2560 A70-30665

SCAMP 4 program for electronic circuits statistical analysis in frequency domain, obtaining mathematical models and transfer functions

14 p2561 A70-30667

Weibull distribution as statistical method for interpreting fatigue test data

14 p2656 A70-30700

Cloud cover statistical data applied to planning remote satellite-borne sensing missions, using Monte Carlo method

14 p2611 A70-31232

Radar imagery for crop discrimination, discussing sensor and data requirements and statistical analysis methods

14 p2578 A70-31237

Statistical analysis of photogrammetrically surveyed three dimensional space points sets for aerospace vehicles and projectiles position location

15 p2733 A70-31550

Computerized statistical analysis programs finding plastic stress and acoustic emission as predictors of annealed steel fatigue life

15 p2760 A70-32326

Statistical test of Melchior laws governing Chandlerian motion of earth pole based on polar coordinates

15 p2732 A70-32497

Statistical error analysis of autonomous manned spacecraft navigation in long duration eccentric Mars orbits

15 p2773 A70-32503

Vector valued Gaussian random processes with Gaussian measurement noise, estimating phase and time delay parameters by maximum likelihood theory

15 p2704 A70-32593

Plane wave random signals arrival angle maximum likelihood estimation for multiple antenna systems

15 p2704 A70-32594

Statistical theory of material strength applied to composite materials reinforced with whiskers and noncontinuous fibers

15 p2763 A70-32833

Diffusion flame development in homologous turbulent shear flow, investigating flame structure and chemical reaction by statistical theory

16 p2997 A70-33499

Corporate aircraft accident statistics, causes and prevention, noting pilot errors, mechanical failures, etc

16 p2842 A70-33814

Mechanical system random excitation, evaluating parameters to satisfy conditions for statistical characteristics of steady state output processes

16 p2953 A70-34296

Helicopter structural weight statistical prediction and evaluation, discussing comparable fixed wing experience

17 p3015 A70-34728

Antenna arrays with nonuniform spacings, synthesizing radiation patterns by deterministic and statistical density taper methods

17 p3044 A70-35056

IR heterodyne signal statistics, discussing receiver characteristics and design

17 p3105 A70-35096

Atmospheric noise statistical parameters analysis on digital computer designed to measure short duration atmospheric radio noise

17 p3170 A70-35396

Statistical theory of irreversible transport processes in fluids, considering deviation from equilibrium as stochastic process

17 p3131 A70-35532

Statistical directivity, radiation pattern, drift and dispersion of segmented traveling wave antennas

17 p3055 A70-35687

Statistical properties of subtropical jet stream maxima over U.S. from Nimbus II IR radiometry

17 p3133 A70-35931

German Air Force aircraft bird strikes statistics

18 p3211 A70-35979

Statistical measurement of bird hazards to aircraft in terms of strike rates at airports, considering international strike rate standard

18 p3211 A70-35981

Statistical characteristics of steady random signal of pulse frequency modulator, obtaining moments of output signal

18 p3234 A70-36072

Statistical analysis of cosmic radiation neutron component monitor error, taking into account generation multiplicity

18 p3307 A70-36097

Statistical properties of civil ATC system based on central processor, discussing system informational congestion

18 p3288 A70-36394

Partially polarized wave with log-normal distribution law of component envelopes, investigating statistical characteristics of polarization parameters

18 p3228 A70-36624

Vertical deflections errors statistical analysis by gravity anomaly measurements, determining autocorrelation functions

18 p3248 A70-36771

Soviet book on statistical calculation methods for linear and nonlinear automatic aircraft control systems design, using correlation theory of stochastic processes

19 p3463 A70-37403

Daylight sky brightness at different wavelengths by airborne photometer, investigating statistical characteristics

19 p3460 A70-37419

Forecasted algorithms to predict random processes, using mathematical statistics

19 p3382 A70-37450

Statistical analysis of short periodic time series in biological rhythms including cosinor, periodic regression, harmonic and synchronization analyses

19 p3365 A70-38412

Random values statistical characteristics by digital methods, deriving errors as function of quantization parameters

19 p3432 A70-38705

Satellite TV cloud picture digital representation, deriving algorithms for statistical analysis of geometrical features

19 p3463 A70-38755

Soviet book on statistical algorithms for reliability covering repairable and first failure systems with ideal and imperfect switching

19 p3395 A70-38798

Pulsar 1919 plus 21, discussing pulse intensity vs phase and number by statistical analysis of two dimensional data array

20 p3705 A70-39489

Missile systems accuracy determination, analyzing pertinent errors statistical properties

20 p3657 A70-39525

Automatic control system stability error analysis, discussing sensitivity and statistical dispersion analysis

20 p3668 A70-39544

Discrete Kalman-Bucy linear filtering with inaccurate noise covariances, considering optimal and sub-optimal systems, error analysis, probability theory, etc

20 p3601 A70-39573

Failure probability from finite sampling characteristics, emphasizing statistical safety factors to characterize structures strength reliability

20 p3724 A70-39856

Solid bodies statistical creep analysis, assuming macroscopically homogeneous isotropic polycrystallinity

20 p3725 A70-39866

Soviet book on brightness of irregular and semiregular variable stars by statistical methods

20 p3705 A70-39899

Statistical problems in technical automation - Conference, Moscow, February 1967

20 p3592 A70-39901

Complex plants process control by experimental statistical methods, considering curves plotting, computer requirements, optimum method selection, etc

20 p3592 A70-39902

Computer calculations automation in mathematical models construction by statistical methods, discussing programs for distributed parameter systems, stochastic approximation, etc

20 p3592 A70-39903

Controlled systems characteristics multistep statistical evaluation by extrapolation, analyzing prediction errors

20 p3593 A70-39904

Extremal dynamic controlled plant with random input signals, identifying components weighting functions by statistical approximation

20 p3604 A70-39908

Statistical analyzer for complex plants dynamic characteristics

20 p3604 A70-39912

Small hybrid computer design, describing algorithms and subsystems for statistical studies

20 p3593 A70-39914

Statistical information processing equipment, describing correlators and digital coding devices design for graphic form information transformation into binary code

20 p3594 A70-39919

Multichannel computer for statistical investigations of complex nonlinear controlled plants based on recordings of input, output and internal state variables

20 p3594 A70-39921

Heterogeneous materials statistical theory, evaluating bounds for effective elastic constants by cell model using variational principles and perturbation solution

20 p3729 A70-40033

Differential game theory, discussing two player zero sum situation

20 p3659 A70-40108

Nonlinear dynamic systems phase coordinate variations statistical characteristics, describing data reduction method

20 p3674 A70-40183

Statistical analysis of random oscillations excited in electron beam-plasma system based on signal recording data

21 p3855 A70-40631

Statistical data for optimum fatigue reliability design for dynamic and rotary machinery, considering static strength, cycle-to-failure and stress-to-failure distributions

21 p3833 A70-41004

Pc 1 geomagnetic micropulsation statistics for middle latitudes, discussing solar cycle and annual variations in occurrence rates

21 p3817 A70-41088

Turbulent density fluctuations statistical properties analysis by cross correlation technique with schlieren instruments

21 p3807 A70-41242

Statistical pattern recognition and threshold learning in signal detection of noisy binary pulses

21 p3794 A70-41332

Plasma turbulence statistical theory in magnetic field based on averaging operators, deriving nonlinear dispersion relation

21 p3857 A70-41386

Statistical data on waivers granted to airline flight crew members by French Civil Aviation Medical Board based on ICAO medical standards

21 p3771 A70-41491

Statistical orbit and position determination for Mars orbiters and landers based on Viking 1973 mission requirements, discussing tracking problems

21 p3931 A70-41861

Natural language a priori description and linguistic algorithms construction, using statistical phrase contraction with Hoffman codes

22 p3993 A70-42492

Meteor impact probability on spacecraft from statistical evidence from Pegasus, Explorer and Gemini spacecraft, discussing damage prevention methods

22 p4097 A70-42524

Soviet papers on statistical methods in nonlinear automatic control systems design

22 p4002 A70-42881

Statistical methods for nonlinear automatic control systems, including Monte Carlo method, equivalent perturbations, linearization and analytical techniques

22 p4002 A70-42882

Quantitative reduction of statistical nodes for nonlinear automatic control system with random noise, using minimal approximating polynomials

22 p4003 A70-42887

Digital statistical modeling of nonlinear automatic control systems including accuracy analysis, generation of random perturbations and parameter optimization

22 p4004 A70-42892

Water vapor emission computation from statistical band model, investigating accuracy limitations

22 p4065 A70-43169

Nonlinear rotating systems optimal control problems approximation by modified Krylov-Bogoliubov averaging technique

22 p4004 A70-43317

Brittle fracture stress statistics for Weibull distribution function parameter determination, comparing linearizing, least squares curve fitting and maximum likelihood techniques

22 p4117 A70-43414

Statistical test of Melchior laws governing Chandlerian motion of earth pole based on polar coordinates

23 p4187 A70-43918

Statistical analysis of durability data of heat resistant alloys for gas turbine engines, using long term strength tests of melts in mass production

23 p4204 A70-43940

Strong coupled rotational excitation problem in atom-diatom molecule scattering system, discussing transition probability matrices statistical analysis

23 p4212 A70-44600

Statistical estimates of precessional corrections, solar motion and galactic rotation from proper motions

23 p4246 A70-44752

Stellar axial rotational velocity statistical analysis to break-up limit, obtaining velocity distribution approximation from observed histogram

23 p4251 A70-44823

Statistical properties of random intensity field during coherent laser radiation scattering by moving diffuse surface

24 p4351 A70-45184

Turbulent flow mechanics heuristic exposition, discussing random processes, instability, nonlinear interactions, energy exchange, intermittency dependence on Reynolds number, fluid properties and boundary conditions effects, etc

24 p4326 A70-45948

Perfect gas statistical relations by perturbation form of state equation for atmosphere

24 p4372 A70-46071

Time evolution of instantaneous light intensity mean and variance for Q switched single mode laser near oscillation threshold
24 p4355 A70-46090

Aircraft maintenance cost statistical analysis recursive regression model for aircraft failure and manhour cost data
24 p4292 A70-46125

Statistical characteristics of stability of single phase one component system under external force
24 p4381 A70-46144

STATISTICAL COMMUNICATION THEORY
U COMMUNICATION THEORY

STATISTICAL CORRELATION

Correlation characteristics and dimensionality of speech spectra from statistical properties derived from continuous speech and summarized by covariance-matrix eigenvectors
02 p0237 A70-12324

Correlations between organizational factors and individual engineer performance, analyzing stability of relationships and time lags in measurement
02 p0246 A70-12378

Temporal and statistical characteristics of HF oscillations from electron beam interaction with plasma in magnetic field
03 p0532 A70-13524

Reflectance spectra obtained for igneous rocks and minerals, establishing correlation between reflectance and energy wavelength, composition and sample particle size
05 p0839 A70-16390

Meteorite falls statistics correlations for fragmentation relationships with mass, time of fall and class
05 p0912 A70-16447

Surface and underwater swimming tests for statistical correlation to linear maximum accelerations effects
07 p1201 A70-18788

Cosmic ray intensity increase preceding Forbush effect using statistical correlation method
07 p1367 A70-19444

Statistical correlation between polar magnetic disturbances and magnetospheric energetic electron flux increase from IMP-1 satellite observations
08 p1491 A70-21714

Random processes correlation functions determined by stochastic differential equations applied to lunar surface statistical characteristics determination
11 p2118 A70-26785

Aircraft turbojet and turbofan engines cost correlation to performance statistically analyzed in terms of various parameters
12 p2335 A70-27437

Midair collisions incidence correlated with traffic factor proportional to square of number of operations
12 p2269 A70-27912

Sufficient statistics for optimal correlation function in classifying optical images in pattern recognition, using permissible transformations
14 p2553 A70-30421

Human and machine pattern discrimination correlated by statistical correlation method from pattern recognition task involving computer simulation and humans
16 p2852 A70-33461

Cosmic ray intensity increase preceding Forbush effect using statistical correlation method
18 p3309 A70-36918

Spiral galaxies pattern statistics, examining morphological type of Milky Way galaxy
18 p3326 A70-37155

Bounded electromagnetic wave propagation in randomly inhomogeneous medium, calculating correlation in amplitude and phase fluctuations
19 p3375 A70-37282

Turbulent velocity correlation function computation in Burger fluid model, using functional integral expression
19 p3403 A70-37530

Gaussian gravity field structure, calculating gravity correlation function using differential equation from density correlation function
20 p3617 A70-39075

Radar angels activity seasonal variation and height distribution statistical relationship to meteorological parameters
20 p3661 A70-39169

Cardiovascular blood circulation system dynamic characteristics analysis by linear statistical correlation methods, describing test for determining weighting function
20 p3581 A70-39905

Photon flow delay regarding fluctuating source field in two points, applying correlation statistics by Pearson method of moments
22 p3988 A70-42564

Galactic noncircular velocity fields, discussing statistical correlation with radio luminosity, nuclear brightness and total mass
22 p4100 A70-42844

Nighttime and daytime midlatitude magnetic bays statistical correlations with riometer-auroral absorption, suggesting precipitating particles role
22 p4018 A70-43107

Ionospheric electron trough and magnetospheric plasmapause movements from satellite observations, showing statistical correlation with geomagnetic field
23 p4186 A70-43854

STATISTICAL DECISION THEORY

Statistical decision problem of Brownian motion with moving boundaries in automatic daylight star tracker design for aircraft navigation solved by image method
01 p0139 A70-11635

Quantum statistical decision theory for detection and estimation of signals in random noise
07 p1333 A70-18919

Statistical methods for feature selection and ordering, mode estimation and pattern classification in pattern recognition, describing sequential decision model
13 p2374 A70-29578

Error correcting algorithms for pattern classification, finding optimal approximation to unknown optimal decision function
13 p2374 A70-29579

Decision directed receiver with unknown a priori probabilities, obtaining tight bound on runaway for binary and multiple signal detection
14 p2554 A70-31117

Decision making role in management contribution towards success of research and development based on statistical decision theory
15 p2828 A70-31573

Optimum decision rule /likelihood ratio/ algorithm for random signals detection in Gaussian noise, using pseudo Bayes approach
15 p2703 A70-32560

STATISTICAL DISTRIBUTIONS

NT PROBABILITY DISTRIBUTION FUNCTIONS

NT RAYLEIGH DISTRIBUTION

Materials strength characteristics with respect to breakdown probability parameter by statistical fatigue stability analysis under unsteady loads and various distribution laws
01 p0211 A70-11424

Elasticity theory equilibrium equations derivation using distribution theory
02 p0388 A70-12270

Electromagnetic scattering from randomly rough surface with finite conductivity, using Kirchhoff approximation
02 p0261 A70-12587

Statistical electron density distributions and Thomas-Fermi-Dirac screening functions for positive ions with various ionization degrees
04 p0721 A70-14666

Subjects sensitivity to differences in statistical distributions of locally defined element density and shape, using stochastically textured visual patterns
06 p0998 A70-17223

Grouping method estimation of statistical data during hydrometeorological information processing to calculate essential data for distribution curve judgement
06 p1096 A70-17786

Statistical distribution of quasi-stellar objects with known red shifts over celestial sphere, observing symmetry over galactic equator
07 p1374 A70-18706

Galaxies statistical distribution studied to determine superclusters existence, correlating results with random distribution expectations
07 p1375 A70-18868

Convolution formulas for Cauchy and standard normal random variable distributions derived from geometry of circular symmetric distribution on plane
07 p1323 A70-18946

Distributional results pertaining to complex Wishart processes and time varying spectral estimators on null hypothesis of stationary Gaussian time series
07 p1323 A70-19028

Statistical characteristics of Q switched He-Ne laser emission gain during transient process from subthreshold to superthreshold value
08 p1514 A70-21814

Optical coherence and light fluctuations, determining statistical distributions of light from photoelectric counting experiments
09 p1728 A70-23372

Transient process statistical calculation in discrete elastic mechanical system possessing energy dissipation under time dependent cross correlated random forces
09 p1729 A70-23595

Intercensus population estimate by air photos, topographic maps and local and state census of population and housing
10 p1878 A70-24737

Atmospheric turbulent boundary layer velocity signals correlation with lognormal distribution
11 p2076 A70-26531

Wave scattering by statistical distributions of discrete obstacles, deriving various functions for diagnostic applications
11 p2086 A70-26762

Materials fatigue life dependence on statistical characteristics of random loads obtained from energy balance equation solution
12 p2323 A70-27339

Electromagnetic wave scattering on passively reflecting statistical clusters of inhomogeneities
12 p2184 A70-27498

Intensity and photocounts statistical distribution of harmonic generated in nonlinear crystal by laser and thermal radiation
12 p2248 A70-27547

Random reversible failures effect on linear automatic control systems precision treated as randomly varying structure, proposing statistical characteristics calculation
13 p2382 A70-29279

Statistical variation of number of VLF atmospherics per unit time above given vertical electric field strength threshold
14 p2550 A70-30515

SCAMP 3 program for calculation of electronic circuit DC performances statistical distribution as function of component parameters variation
14 p2560 A70-30666

Wind velocity derivative statistical characteristics in atmospheric surface layer, using thermoanemometer, functional converter, differentiating circuit and loop oscillograph
16 p2945 A70-33219

Alloy hardening statistical theory, applying flow stress to second phase randomly dispersed particles
17 p3191 A70-35458

Warm fog clearing effectiveness by seeding with hygroscopic nuclei as function of fog droplet and seeding nuclei distribution
17 p3132 A70-35928

Brittle fibers strand strength as function of statistical distribution of limiting stresses
18 p3342 A70-36648

Density and distribution functions for quotient of ellipsoids of variance volumes, yielding probabilities and fractiles in three dimensional sets of points
19 p3382 A70-37835

Plane symmetrical and axisymmetrical laminar and turbulent free jets, interpreting statistical character of boundary layer profiles
19 p3407 A70-38684

Prior distributions computer aided selection for generating Monte Carlo confidence bounds on system reliability
20 p3658 A70-39641

Inclined electromagnetic wave incidence on randomly inhomogeneous medium with changing mean dielectric permittivity, calculating reflected and scattered fields
20 p3587 A70-39726

Statistically nonhomogeneous fields by variational principles of elasticity, obtaining bounds of average displacement for hollow sphere under pressure
20 p3732 A70-40112

Computerized mathematical modeling of transistors statistical and dynamic characteristics as functions of structural parameters
23 p4171 A70-43954

Wind velocity derivative statistical characteristics in atmospheric surface layer, using thermoanemometer, functional converter, differentiating circuit and loop oscillograph
24 p4371 A70-45194

STATISTICAL MECHANICS

Soviet monograph on transfer processes theory in statistical mechanical systems based on probabilistic approach to random particle walk
01 p0215 A70-10650

Statistical mechanical method deriving ionization equilibrium and equations of state for low mass stars, considering Coulombic interactions, nonideal effects, etc
01 p0188 A70-11336

Multiple particle production at high energy levels and associated peripheral interaction and statistical theories
03 p0555 A70-13035

Euler-Lagrange linear operators in variational embedding with one dependent function
05 p0881 A70-16058

Stationarization problems involving nonlocal and null class Euler-Lagrange operators, considering vector spaces of function spaces
05 p0881 A70-16059

Analytical mechanics of discrete and continuous systems covering systems with limited degrees of freedom, statistical and continuum mechanics
08 p1543 A70-20526

Soviet monograph on accelerated convergence method in nonlinear mechanics, discussing quasiperiodic differential equations solutions, smoothing techniques, etc
09 p1729 A70-23726

Information theory as basis for statistical thermodynamics, discussing maximum entropy principle and probability as frequency in Gibbs ensemble
11 p2083 A70-25694

Thermodynamics and statistical mechanics taking into account irreversibility, arrow of time and astrophysical schemes

11 p2146 A70-25695

BBGKY hierarchy state functional formalism in nonequilibrium statistical mechanics for many particle system using Fourier transformation

11 p2087 A70-26548

Statistical mechanics of partially ionized hydrogen plasma, deriving Saha equation to calculate ionization degree and potential for various electron densities and temperature

12 p2281 A70-27882

Incompressible fluid turbulent motion statistical equations, considering Lagrangian distributions of fluid particles coordinates and velocities

12 p2212 A70-28190

First order statistical model for temperature dependence of carbon activity in austenite

13 p2436 A70-29605

Galactic cosmic rays origin in terms of statistical mechanical model of supernova explosions

15 p2799 A70-31793

Polyatomic molecules radiationless transition rate statistical analysis, suggesting role of Franck-Condon principle in determination of nonradiative decay rates

16 p2858 A70-34014

Coherent behavior associated with thermodynamic description projected from dynamical behavior of many body system, using relation between asymptotic operators

22 p4062 A70-42547

Stellar system statistical mechanics, discussing collisionless gas in gravitational field, galaxy formation, stellar dynamics, double stars and bounded isothermal spheres

22 p4098 A70-42577

Incompressible fluid turbulent motion statistical equations, considering Lagrangian distributions of fluid particles coordinates and velocities

22 p4012 A70-43315

Thermodynamics and statistical physics of dense plasma with particle interaction energy exceeding kinetic energy, discussing three-component model phase equilibrium

23 p4229 A70-45073

STATISTICAL MOMENTS

U DISTRIBUTION MOMENTS

STATISTICAL PROBABILITY

U PROBABILITY THEORY

STATISTICAL TESTS

NT RANK TESTS

Turbine blades durability and fatigue characteristics, plotting fatigue diagram from statistical tests

01 p0105 A70-11418

Protruding, stepped and conical end fittings for confined detonating fuse, discussing assembly procedures effect on characteristics based on statistical scanning test

03 p0547 A70-14115

Statistical control charts for evaluating instrumentation performance during ordnance devices testing, discussing evolution, interpretation and application

03 p0494 A70-14126

Chain pooling tests for two level factorial replication-free experiments using Monte Carlo methods

06 p1093 A70-17305

Dependence effects on nonparametric mixed statistical tests

06 p1095 A70-18622

Statistical testing role in synoptic meteorological analysis, discussing pressure and temperature patterns, front identification, computer applications, etc

07 p1329 A70-19574

Destructive and nondestructive tests optimum procedure for quality control based on information theory, decision statistics and cost optimization

09 p1691 A70-22573

Variables control charts based on sample means for determining in-control probability properties

09 p1691 A70-22575

Cramer-Rao efficiencies of best linear invariant estimators, using Weibull distribution in model for survival populations connected with life testing

10 p1910 A70-24604

Nonlinear regression techniques for statistical simultaneous measurement of thermal properties including convergence criterion

16 p2998 A70-33859

Parallelism of two regression lines, suggesting distribution free signed rank test

22 p4064 A70-43526

Critical values tables for Wilcoxon rank sum test in randomized blocks

22 p4064 A70-43729

STATISTICAL WEATHER FORECASTING

Linear statistical forecast accuracy and optimal predictor dimensionality based on multiple regression equation

04 p0715 A70-15251

Statistical testing role in synoptic meteorological analysis, discussing pressure and temperature patterns, front identification, computer applications, etc

07 p1329 A70-19574

Combined statistical synoptic methods for mesometeorological forecasts

10 p1913 A70-24947

Soviet book on statistical analysis of meteorological elements based on expanding natural orthogonal functions covering horizontal, vertical and time distributions including applications

15 p2772 A70-32842

Synoptic meteorological prediction by statistical and dynamical theory based on statistical mechanics

17 p3131 A70-35926

Sea surface temperature determination from satellite high resolution IR window radiation measurements by statistical histogram inference method

21 p3820 A70-42122

Airport fog layers repetition frequency after low visibility periods

22 p4065 A70-43246

Weather regimes in statistical meteorology constructed in stochastic models representing randomly transformed Markov chain

24 p4371 A70-46035

STATISTICS

Climatological cloud type statistics for simulating earth sensing mission data output as function of sensor field of view and spatial resolution

06 p1065 A70-18098

STATOR BLADES

Axial flow turbine stator and impeller blade twist calculated from gas flow stage area diameter using continuity and vorticity equations

01 p0001 A70-10175

Nickel base alloy, WAZ-20 with improved strength in 2000-2200 F range for application to gas turbine engine stator vanes

04 p0706 A70-15097

Discrete noise generation and propagation due to fan engine rotor forcing excitation and interaction with downstream stator

05 p0896 A70-16791

Rotor wakes intrastator transport effects on high Mach number axial flow compressors performance, considering stagnation temperature profile and rotor blade loss factor

18 p3209 A70-36869

Transonic high turning low aspect ratio stator cascades flow field performance prediction, reducing secondary flows by partial slots

18 p3209 A70-36875

STATORS

Brushless DC motor consisting of permanent magnet rotor, wound stator and optical rotor position sensing

16 p2843 A70-33000

Monograph on radial flow between air cooled gas turbine rotating and stationary disk near stator covering turbulent boundary layer, velocity distribution, etc

19 p3404 A70-38007

STEADY FLOW

NT COUETTE FLOW

NT HARTMANN FLOW

Hall current effect on steady boundary layer flow of incompressible viscous electrically conducting fluid past semiinfinite flat plate in transverse magnetic field

03 p0469 A70-14183

Martin method for reducing determination of steady plane MHD flow to Bernoulli and direct functions satisfying quasi-linear partial differential equations

03 p0533 A70-14200

Boundary value problems for partial differential equations representing steady gas flow hydrodynamic problems

03 p0469 A70-14228

Heat transfer in steady state flow of electrically conducting incompressible viscous fluid in annular channel between coaxial circular cylinders under magnetic field

03 p0608 A70-14335

Method of integral relations, finite differences and method of characteristics applied to numerical solution of steady state problems of gas dynamics

04 p0670 A70-14961

One dimensional steady adiabatic source nonisentropic flow of thermally and calorically perfect gas in conical nozzle, considering exit divergence and nonuniform flow effects

04 p0619 A70-15427

Steady state boundary layer of anisotropic Erickson fluid incident obliquely on infinite cylinder, obtaining differential equations for dynamic behavior

05 p0835 A70-16860

Steady laminar flow with frictionless central core surrounded by boundary layer in circular curved pipe, discussing friction factor and flowmeter discharge coefficient

05 p0836 A70-17107

Laminar steady radial flow of simple fluid of short memory between two parallel disks, demonstrating relation to Newtonian fluid

06 p1037 A70-17915

Far and near field solutions of plane steady transonic flow past thin airfoil including imbedded shock waves using small disturbance theory

06 p0969 A70-18056

Steady supercritical planar inviscid transonic flows over lifting airfoils, generating unsteady flow by impulsively imposing airfoil boundary condition

[AIAA PAPER 70-47] 06 p0972 A70-18130

Asymptotic behavior /for small mean free path/ of rarefied gas steady flow over smooth solid boundary

06 p1048 A70-18328

Free steady convective flow stability relative to three dimensional disturbances between parallel planes reduced to equivalent plane disturbances problem

07 p1252 A70-18669

Steady viscoplastic boundary layer near hard wall with power law velocity distribution along outer boundary, deriving self similar solution

07 p1252 A70-18670

Steady and unsteady flow through Napier turboblower axial flow turbine for full and partial admission, estimating mass flow and power output

07 p1189 A70-20294

Steady pressure driven flow of conducting fluid through insulating circular pipe in transverse magnetic field

08 p1549 A70-20502

Navier-Stokes equations exact solutions for two dimensional steady flow of compressible viscous heat conducting perfect gas

08 p1485 A70-21638

Viscoelastic fluid steady flow in porous walled channel, examining mass flow solution continuity

08 p1485 A70-21639

Steady laminar gas flow on duct wall boundary layer considering external swirling flow and wall heat transfer

09 p1659 A70-22428

Steady turbulent perfect compressible gas flow in axisymmetrical or plane channel, using equations governing channel height and static pressure variations

09 p1659 A70-22429

Self similar and steady state flows near singularities, studying flow stability by partial differential equations

10 p1863 A70-24071

Plane steady flows characteristics of incompressible viscous fluids in rigid walled rectangular channels found asymptotic to Poiseuille and Couette flows

10 p1866 A70-24112

Steady two dimensional cavity flow past sharp-edged airfoil and blunt nosed obstacle, using linearization hypothesis

10 p1801 A70-24193

Analog computation in supersonic steady flow and digital technique for wing-fuselage and wing-tail interactions

10 p1802 A70-24544

Monograph on Beltrami steady state, frictionless flow of incompressible medium past spherical surfaces, assuming vortex and stream lines agreement

11 p2034 A70-25498

Three dimensional hypersonic steady flow around blunt and pointed cones at nonzero angles of attack calculated by method of characteristics

11 p1975 A70-25969

Linear viscous theory of steady rotating fluid flows with nonlinear modification of boundary layers, considering inertial modifications

11 p2036 A70-26011

Perturbation theory of supersonic steady anisotropic flow with radiative heat transfer using hyperbolic characteristic coordinates

12 p2334 A70-28203

Liquid film steady motion on ablating body surface allowing for radiative heat transfer from interior

12 p2334 A70-28244

Steady expansion flows at three dimensional supersonic edges with small corner angles using analytical method of characteristics

13 p2338 A70-28491

One dimensional steady state flows and discontinuities in radiation gas dynamics, neglecting radiation pressure, viscosity and heat conduction

13 p2387 A70-28937

Basic flow convergence or divergence effect on steady flow pattern around circular cylinder using fluid motion visualization

13 p2387 A70-29058

Steady diabatic complex lamellar gas flow, obtaining parameters by extending geometric theory of surfaces and curves in fluid flow theory

13 p2387 A70-29122

Two dimensional incompressible steady turbulent flows based on Prandtl hypothesis relating eddy viscosity to kinetic energy and scale

14 p2564 A70-30259

Steady plane relativistic flow small irrotational perturbation theory determining subsonic, transonic and supersonic approximation

14 p2566 A70-30472

Boundary value problem for Navier-Stokes equations to obtain stationary flows as limits of nonstationary solutions

14 p2600 A70-31347

Laminar velocity distribution from temperature profiles developed under steady flow through tube, constructing numerical temperature grid
15 p2718 A70-31449

Free steady convective flow stability relative to three dimensional disturbances between parallel planes reduced to equivalent plane disturbances problem
15 p2718 A70-31461

Steady viscoplastic boundary layer near hard wall with power law velocity distribution along outer boundary, deriving self similar solution
15 p2718 A70-31462

Finite difference algorithm for supersonic three dimensional steady flow past blunt bodies with generating line bends, allowing for gas equilibrium and frozen states
15 p2671 A70-31495

Incompressible viscous fluid steady flow admission into bounded space from cylindrical tube, demonstrating solvability of plane and three dimensional versions
15 p2720 A70-31642

Steady and nonsteady engine/inlet flow field simulation for engine/compressor testing, determining feasibility of variable ramp aerodynamic device
[AIAA PAPER 70-591] 15 p2672 A70-31788

Axial wall conduction effects on steady state laminar flow heat transfer
15 p2825 A70-31815

Steady flow of incompressible fluid through converging-diverging tube, considering implications in occlusive vascular disease
15 p2691 A70-31936

Baecklund transformations applications to hodograph equations for steady two dimensional nondissipative MGD flows with aligned velocity and magnetic fields
15 p2781 A70-32453

Shock wave stability in plane steady flow at uniform entropy and limiting velocity
16 p2890 A70-33101

Steady isentropic weakly perturbed supersonic flows past arbitrary slender tapered wings with subsonic leading edges
16 p2838 A70-33971

Steady two dimensional MHD boundary layer flow with uniform suction or injection past semiinfinite flat plate in cross fields
17 p3067 A70-34618

Steady and unsteady gas dynamics analogies with two dimensional water flow, taking into account energy and continuity equations
17 p3069 A70-35032

Steady supersonic flow past conical bodies at yaw, adapting Telenin numerical method
17 p3012 A70-35889

Steady incompressible flow past circular cylinder at Reynolds numbers up to 100, using finite difference solutions of motion equations
18 p3238 A70-36191

One dimensional steady gas flow, deriving algorithm for iterative solution of Boltzmann kinetic equation by statistical approach
18 p3241 A70-36285

Compression and expansion characteristics of steady supersonic flow passing along yawing slender body of rotation, linearizing differential equations
18 p3207 A70-36382

Temperature profile along hot-wire anemometer attached to wall and normal to subsonic velocity steady flow field, using singular perturbation techniques
18 p3242 A70-36488

Velocity profiles in steady and unsteady rotating flows for impulsive slow down and acceleration in cylindrical chamber
19 p3403 A70-37527

Steady symmetric flow model for Jupiter cloud banded structure, representing variable concentration of condensing constituents with latitude
19 p3519 A70-38254

Steady two dimensional incompressible shear flow, correlating velocity profiles with resistance distribution
19 p3406 A70-38350

Viscous incompressible electrically conducting fluid steady flow between parallel coaxial rotating disks with transverse magnetic field
19 p3481 A70-38446

Hodograph equations for relativistic irrotational steady plane flows, investigating transformation to physical plane
19 p3406 A70-38664

Two dimensional steady inviscid incompressible flow past profiles in parallel flow with noniform velocity distribution
19 p3354 A70-38676

Steady compressible supersonic planar flow of viscous heat conducting fluid under linearization freestream conditions, describing slip flow past finite flat plate
20 p3557 A70-39228

Weak stratification and geometry effect on steady mechanically driven motion of contained rotating viscous fluid
20 p3608 A70-39357

Perturbation method for nonlinear acoustic wave propagation in steady one dimensional flow through variable cross section duct
20 p3673 A70-39612

Steady sub and supersonic flow calculations behind receding shock wave, using finite difference scheme
20 p3611 A70-39803

Compressible viscous fluid steady plane flow in laminar boundary layer on impermeable isothermal surface, describing parametric method of integrating flow equations
20 p3611 A70-39806

Steady turbulent flow heat exchange in near wall region at large Prandtl numbers, plotting temperature distribution curves
20 p3612 A70-39811

Aerodynamics of steady, inviscid transonic flows around slender bodies and wing-body combinations at free stream Mach number one
[AIAA PAPER 70-798] 20 p3559 A70-39900

Stellar wind theory and related steady radial flows, discussing gravitating point mass, heat conduction, shocks, viscosity, outflows and inflows
20 p3706 A70-39928

Shock wave extinction point within plane steady upstream flow with uniform entropy and limit velocity
21 p3808 A70-41441

Aerodynamic parameters of ionized Ar supersonic steady one dimensional nonviscous flow in thermodynamic equilibrium and subjected to Laplace accelerating forces
21 p3858 A70-41444

Steady viscous flow past oblique flat plate at high Reynolds number, using Oseen linearized approximation
21 p3809 A70-41714

Two dimensional steady flow around slender profiles at free transonic stream with curved compression shocks, approximating by hodographic method
23 p4131 A70-44023

Rotational two dimensional steady shear flows of perfect incompressible fluid, considering channel flow characteristics for various wave modes
23 p4181 A70-44202

MHD equations for one dimensional plane steady flow, considering conservative difference schemes for approximation
23 p4226 A70-44307

Pressure distribution on thin nonlifting airfoils in steady two dimensional flow with freestream Mach number at or near unity
23 p4134 A70-44583

Collisionless plasma, calculating effects of energy dissipation due to weak firehose instability on steady planar flow, based on quasi-linear fluid equations
24 p4382 A70-45110

Perturbation of steady MHD Stokes flow past hollow sphere assuming small Hartmann and Reynolds numbers
24 p4384 A70-45262

Spherical shape gas or liquid drop steady motion at large Reynolds numbers, examining buoyancy forces and velocity gradients
24 p4326 A70-45996

Simple wave functions solutions in multidimensional nonviscous polytropic gas unsteady and steady flow
24 p4327 A70-46030

Inviscid conducting incompressible fluid steady motion past thin airfoils, presenting crossed and aligned fields and Alfvén motion with Hall effect
24 p4289 A70-46033

Diabatic steady gas flow vorticity, examining various kinematic and kinetic properties
24 p4328 A70-46365

STEADY STATE
System with recovery consisting of n elements, discussing reliability and solution to steady state problem
10 p1855 A70-24798

Steady state symmetrical model for solar wind near equatorial plane, investigating effects of magnetic forces, viscosity and anisotropic pressure on azimuthal motion
13 p2477 A70-29179

Steady state heat conduction in wedge shaped bodies with boundary conditions of third kind
13 p2522 A70-29515

Gravity effects on impact damper performance, investigating dynamic stability and kinematic viability of various steady state motion solutions
20 p3717 A70-38974

Steady state magnetic and electric fields in magnetosheath by linear superposition of field vectors, using axisymmetric velocity function from gas dynamics
21 p3815 A70-41063

Pulse-time multistable state elements for automatic and remote control constructed from pulse sequence interactions with multiple frequency relations
22 p4005 A70-43567

Glauber equations applied to trailing wire shape for steady state aerodynamic forces on aircraft and trailing antennas, discussing computer solutions
23 p4131 A70-43893

Gyroscope system steady states, showing dynamic couplings centering in finite angular precession rate case
24 p4335 A70-45630

STEADY STATE CREEP
Polycrystalline Ni steady state creep characteristics measurement emphasizing temperature dependence of creep rate
03 p0504 A70-13022

Thin walled tubular aluminum specimens hardening by temporary reduction of temperature during creep under torsion
06 p1089 A70-17795

Steady creep process microscopic mechanisms, discussing creep due to glide of jogged screw dislocations, climbing of edge dislocations and stress directed vacancy diffusion
08 p1593 A70-21519

Stress concentrations in turbine disks with eccentric holes under steady creep
09 p1780 A70-23200

Steady state creep of composite material with short fibers, discussing effects of fiber/aspect ratio, fiber volume fraction and distribution
11 p2144 A70-26671

Al-aluminum oxide composite steady state creep due to grain boundary sliding, accounting for activation energy level
12 p2258 A70-28348

Steady state high temperature creep theory, including internal back stress and temperature dependencies
15 p2765 A70-32810

Tubular Al creep resistance increase by temperature jumps during steady phase of creep
22 p4056 A70-43344

Steady state creep behavior during multiple deformation process, developing grain boundary sliding relation to grain size
23 p4207 A70-44759

STEADY STATE FLOW
U EQUILIBRIUM FLOW
STEAM
Charge exchange and electron loss measurements in steam target exposed to high energy hydrogen ions beam, using equilibrium fractions method
07 p1345 A70-20142

Subsonic flow visualization, using steam and cold nitrogen gas mixture and normal tunnel lighting
18 p3237 A70-36460

STEAM FLOW
High velocity isothermal viscous compressible steam flow in circular tubes, measuring pressure drops
22 p4011 A70-42845

STEAM GENERATORS
U BOILERS
STEAM TURBINES
Fatigue strength of T-shaped blade roots of steam turbine regulating stages subjected to combined static tension and cyclic bending
05 p0954 A70-17060

Thermal gradients and associated strains measurement in steam turbogenerator casings, considering strain gage placement and heat transfer calculations
09 p1774 A70-22590

STEEL STRUCTURES
Steel objects microstructure and hardness tested by continuous magnetic technique, describing experimental apparatus model
02 p0300 A70-12479

Ductile-brittle fracture transition in steel pressure vessels suppressed by utilizing thin laminations
03 p0583 A70-12903

Flight type pressure vessels fabricated with quenched and tempered Ni-Cr-Mo-V structural steel, discussing fracture toughness, design, fabrication techniques
[SAE PAPER 690680] 05 p0853 A70-15866

Steel tube deformation under constant internal pressure and cyclic heating, plotting tangential and axial strain curves as function of cyclic loading
06 p1163 A70-17399

Hydrogen embrittlement of landing gear steels, discussing plating bath program additions for optimum safety conditions
07 p1294 A70-19349

Steel conical disks two dimensional stressed state determined with deformations at elastic and elastoplastic strains using digital computers
10 p1956 A70-24242

Fracture toughness and cyclic crack propagation of surface cracked high strength aircraft structure steels
12 p2254 A70-27467

Dislocation structure during fretting corrosion in steel plates, analyzing via electron microscopy
12 p2258 A70-28318

Steel plates with penetration of oblique circular cylindrical aperture tested for effects on stress concentration
13 p2510 A70-28728

Instrumented Charpy impact test evaluating strain rate, alloying and irradiation effects on ductile-brittle transition temperature and fracture of pressure vessel steels
15 p2820 A70-32239

STEELS

- F-111 high strength steel design experience concerning wing, fuselage and empennage support structure [AIAA PAPER 70-884] 17 p3018 A70-35803
- Longitudinal and transverse tensile strengths of Al sheet reinforced with continuous oriented steel wire of various cross sectional shapes 19 p3541 A70-38047
- Perforated steel strip axial tension load limit, considering various hole diameters and numbers 21 p3936 A70-41415
- Nonweldable internal flaws detection containing oxides in steel slabs by neutron activation analysis 24 p4376 A70-45750

STEELS

- NT AUSTENITIC STAINLESS STEELS
- NT BAINITIC STEEL
- NT CARBON STEELS
- NT CHROMIUM STEELS
- NT HIGH STRENGTH STEELS
- NT MARAGING STEELS
- NT MARTENSITIC STAINLESS STEELS
- NT NICKEL STEELS
- NT STAINLESS STEELS
- Transformation induced plasticity steels tensile properties measurement indicating loss of ductility due to H embrittlement 01 p0118 A70-10729
- Martensite start depressed temperatures vs pressure for steels, discussing hardness effects and microstructure 01 p0120 A70-10740
- Crack propagation mode in laminated steel-Ni composites, analyzing softer layer effect using impact tests and C replica fractographs 01 p0120 A70-10743
- Steels tested to evaluate proposed incremental strain theories predicting loads on thin walled cylinders subjected to nonproportionate loading, discussing stress-strain diagram 01 p0202 A70-11057
- Fretting corrosion effect on structural steel fatigue strength under asymmetric load cycles 01 p0207 A70-11155
- Carrying capacity of heat resistant steel turbomachine elements, discussing plastic deformation and cyclic load effects, breakdown load determination, stress analysis, etc 02 p0352 A70-11659
- Mechanical strength and breakdown metallography of plate shaped structural steel and Al alloy specimen under various HF elastic vibrations 02 p0318 A70-12398
- Low alloy and stainless steels durability in various natural atmospheres, discussing corrosivity dependence on atmosphere pollutants, temperature and humidity 02 p0318 A70-12476
- Sheath-enclosed steel cable inspection using induction coil transducer in conical sleeve 02 p0301 A70-12490
- Sliding steel specimens anomalous friction behavior in vacuum, noting friction-time plot dependence on oxide film rupture, load, environmental pressure, etc 02 p0321 A70-12534
- Photogrammetric deformation measurement of thin steel sheets during static bending tests 02 p0302 A70-12653
- Cr diffusion coating influence on fatigue life of Fe and steel, discussing residual stress measurement technique 02 p0320 A70-12848
- Failure and defect formation in gas turbine engine disks made of steel alloys, stressing fabrication methods effect on reliability 03 p0588 A70-13251
- Al alloy and structural steel fatigue strength under superelastic cyclic axial stresses, describing observed plastic deformation patterns 03 p0509 A70-13271
- Case hardened steels structure and properties, intermetallic phases, hardness variation with depth and hardening techniques by Be and B 03 p0510 A70-13351
- Steel crystal lattice fine structure and mechanical properties during annealing using X rays as function of temperature 03 p0511 A70-13422
- Rolling, pickling and annealing influence on composition of steel sheet surface 03 p0497 A70-13775
- Sound attenuation rate of rectangular flat steel plates contact and branch point relation to velocity difference and absorption length 03 p0526 A70-14353
- Stress-strain spatial distribution in notched plate fatigue specimen of mild steel determined by finite element method, noting cyclic strain softening effect [ASME PAPER 69-MET-C] 04 p0770 A70-14876
- Steel welding processes in thicknesses useful to future booster production 04 p0700 A70-15652
- Dilatometric diagrams of phase transformations at low temperatures in Re steels, studying dilatation coefficient behavior 05 p0862 A70-16201

Internal friction method for studying dislocation, stacking points and strengthening processes in steels and heat resisting austenitic steel behavior at high temperatures 05 p0864 A70-16870

Low cycle fatigue of alloy and steel materials under bending and cyclic heating, relating strains and number of cycles to failure 05 p0866 A70-17036

Optimal thermomechanical treatment for austenitic steel stability to resist propagation and unloading of dislocations in cyclic loading process 05 p0867 A70-17041

Heat resistant steel and nickel alloys stress rupture strength at operating temperatures, discussing endurance diagrams under cyclic bending loads 05 p0868 A70-17047

Vibration damping properties of steels and Ti- and Al-based alloys at various temperatures under tensile and compression loads 05 p0868 A70-17048

Heat resistant enamel coatings effect on vibration damping of cast steels for turbine blades 05 p0868 A70-17050

Heating influence on circular bending fatigue strength of refractory steel and alloys, using radiative and HF inductive heating 05 p0868 A70-17059

Cyclic creep curves plotted from expansion diagrams for steel, copper and brass under small numbers of cyclic compression tension loads 06 p1162 A70-17388

Steel elements failure during nonstationary thermal fatigue with varying strain and temperature, discussing linear damage accumulation theory 06 p1163 A70-17397

Damage accumulation and failure of low carbon and low alloy steels subjected to repeated static loading, varying cyclic load frequency 06 p1085 A70-17400

Steels crack propagation direction dependence on load magnitude in low cycle fatigue, noting groove width effects on resistance to static loading 06 p1163 A70-17401

Surface work hardening effects on steels resistance to low cycle fatigue with stress concentration, applying results to aircraft parts 06 p1085 A70-17403

Normalized steel low cycle fatigue strength under bending and torsional rotation, testing linear damage accumulation theory 06 p1163 A70-17404

Energy dissipation patterns of metal fatigue failure during static and cyclic loading applied to untreated and heat treated steel samples 06 p1166 A70-17651

Mean cyclic stress effect on stress concentration and fatigue strength of smooth and notched steel specimens at normal and high temperatures with superimposed bending 06 p1088 A70-17653

Critical brittleness temperatures of low C steels determined to distinguish main failure types 06 p1166 A70-17655

Steels microstructural plastic deformation under pulsed laser irradiation 07 p1303 A70-18712

Steels fatigue strength under biaxial tension, considering complex stress-strain state 07 p1304 A70-18823

Selenium additions effect on structural steels transverse mechanical properties, emphasizing plasticity, shock resistance and machinability 07 p1310 A70-19750

Dynamic pearlite-austenite transformation and melt temperatures measured in laser-irradiated steel, discussing thermal response as function of heating rate 07 p1301 A70-19897

Soviet book on mechanical properties of heat resistant steels and alloys at room and elevated temperatures 08 p1515 A70-20691

Static loading effect at high temperatures in argon and liquid lithium on mechanical properties stability of steel 08 p1515 A70-20920

Quenched and tempered steels ductile fracture with respect to plasticity, structure and crack development conditions using microfractography 08 p1515 A70-20922

Hydrogen penetrability in heat resistant steels subjected to high temperature creep, observing activation energy decrease with increased stress 08 p1515 A70-20923

Ti additions influence on steel work hardening, specific weight, magnetic properties and structure 08 p1515 A70-20924

Steel strength under prolonged preliminary loading at elevated temperatures 08 p1515 A70-20934

Steel structure and mechanical properties under preliminary loading at elevated temperature and liquid Li at various exposure times 08 p1515 A70-20935

Epoxy-phenolic coatings effect on fatigue durability of bent steel samples 08 p1587 A70-21075

Stress and strain spatial distribution in notched steel plate under cyclic loading determined by finite element method 08 p1590 A70-21315

Static and dynamic low temperature crack toughness behavior of steels, determining strain rate effect 08 p1518 A70-21317

Nonmetallic inclusions effect on steels cyclic strength dependence on inclusion composition and metallic matrix properties derived from fatigue tests 08 p1590 A70-21413

Carburization resistance of refractory steels, emphasizing chemical composition effect on corrosion rate 08 p1519 A70-21434

Aluminum nitride morphology in structural Cr-Ni-Mo steel, discussing dependence on austenitization temperature and cooling conditions 08 p1519 A70-21435

Simultaneous titration of gases, metalloids and metals in steels and refractory alloys by far UV vacuum spectrometry [ONERA-TP-765] 08 p1455 A70-21842

Brittle failure mechanics application to steels sensitivity to rupture at low temperatures, discussing crack propagation resistance and heat treatment effect on impact toughness 09 p1768 A70-22076

Strain rate and hold time effects on steels low cycle fatigue behavior, graphing various correlations among stress amplitude, time to fracture, etc 09 p1774 A70-22589

Heat treatment effects on hardened steels acoustic constants, calculating sound velocity in liquid metals 09 p1692 A70-22643

Kinematic viscosity of molten steel containing corundum inclusions as function of temperature 10 p1904 A70-24271

Microstructure and ductility of air- and vacuum-melted heats of corrosion resistant steels, investigating tensile and yield strengths for all grain directions 10 p1905 A70-25170

Prestrain and mean stress effects on fatigue life using cumulative damage procedure based on Al alloy and aircraft quality steel tests 11 p2137 A70-26092

Low temperature tempering effects on steel transformations and axial rigidity of radial thrust ball bearings in aircraft 12 p2243 A70-27568

Plastic strain state effect on ductility and toughness of structural steels 13 p2432 A70-28675

Large deflections in impulsively loaded clamped circular Al alloy and steel viscoplastic plates 13 p2511 A70-28736

Diffuse coatings effect on strength characteristics and corrosion resistance of steels, analyzing structure, thickness and purity of surface layers 13 p2433 A70-28888

Oxygen motion velocity effect at various pressures on heatproof and heat resistant steels and alloys ignition, noting minimum ignition temperature 13 p2434 A70-29168

Transformations on surfaces of molybdenum disulfide-steel system during friction in air, noting Mo oxides formation and friction coefficient increase 13 p2421 A70-29427

Total nitrogen content determination in silicate samples of rocks, synthetic silicate standards, NBS steels and meteorites using inert carrier-gas extraction-gas chromatography 13 p2362 A70-29497

Titanium effect on iron and steels nitriding at high temperature, obtaining high surface hardness 13 p2423 A70-29773

Fine grained structure effect on steels and Ni alloys short term heat resistance at high temperatures 14 p1594 A70-30168

Austenitization temperature, cooling rate and tempering conditions effect on steel castings structure, strength and impact properties 14 p2596 A70-30875

Fast brittle crack slowing by mechanical twins in transformer steel and by slip bands in LiF and NaCl crystals 15 p2755 A70-31526

Plastic deformation and aging effects on fatigue characteristics of steels until rupture under cyclic loads 15 p2755 A70-31540

Transient overloads effect on long term fatigue strength of notched and smooth steel samples, emphasizing heat treatment effect on notch sensitivity at high temperatures 15 p2814 A70-31546

Oxygen interlayer diffusion effects on wear change during gliding friction of normalized steel samples 15 p2743 A70-31636

Molybdenum disulfide and phenol formaldehyde resin lubricants for hydroextrusion of steel 15 p2743 A70-31639

Ultrasonics for steel cleanliness rating, considering advantages and fatigue life 15 p2743 A70-31768

Alloying elements and austenization conditions effects on hardenability of steels, investigating critical cooling rates based on TTT diagrams 15 p2744 A70-31929

Niobium carbides formation in Nb containing steels during gamma-alpha transformation, establishing relationship between brittleness and carbide distribution characteristics 15 p2758 A70-32123

Dynamic fracture toughness measurement of low strength steels via instrumented Charpy impact test with correction factor for inertia loading effects 15 p2820 A70-32237

Impact test machines, specimen design and energy measurement in dynamic tear test method for steel fracture strength 15 p2759 A70-32242

Dynamic fracture toughness test on heat treated precracked steel specimens under dynamic loading 15 p2759 A70-32243

Steel and copper alloys torsion-tension members under nonproportionate loads, predicting creep behavior [SESA PAPER 1615] 15 p2759 A70-32316

Computerized statistical analysis programs finding plastic stress and acoustic emission as predictors of annealed steel fatigue life 15 p2760 A70-32326

Size effects on impact energy disposition in plastically deformed thick steel specimens at shelf temperature, using similitude laws 15 p2760 A70-32332

Austenite strength effect on austenite-martensite transformation in alloy steels, measuring resistance to plastic deformation 15 p2760 A70-32376

Fracture of failed tensile impact and compression test pieces of hardened SAE 52100 steel, using scanning electron microscope 15 p2745 A70-32443

Pyrolyzed tetraethoxysilane for carburizing steels and Ti alloys at 850-1050 C 17 p3102 A70-35409

Cyclic strain effects on creep for steel at elevated temperatures, discussing overload frequency effects on plastic strain buildup 17 p3127 A70-35719

Steel and cast iron early stage fatigue failure, using photoelastic coatings 17 p3192 A70-35741

Ultrasonic irradiation effects on steel hardenability and carbon diffusion rate during annealing, noting microstructure 18 p3273 A70-36049

Automatic dilatometers for volume variations in steel and Co-W alloy during aging and heat treatment, noting microstructural changes 18 p3257 A70-36202

Quantitative analysis of nonmetallic inclusions in steels containing Ti after electrochemical anodic dissolution 18 p3277 A70-36464

Photometric determination of Ti with diantipyril-methane in steels containing Se 18 p3277 A70-36465

Carrying capacity of heat resistant steel turbomachine elements, discussing plastic deformation and cyclic load effects, breakdown load determination, stress analysis, etc 19 p3547 A70-38432

Failure and defect formation in gas turbine engine disks made of steel alloys, stressing fabrication methods effect on reliability 19 p3548 A70-38469

Nb effects on steel susceptibility to brittle fracture at various temperatures, discussing impact strength and nucleation energy of crack formation 19 p3453 A70-38709

Soviet papers on heat resistant alloys and steels structure by electron microscopes 20 p3644 A70-39036

Fretting corrosion zone steel, measuring transient temperature distribution during contact friction 20 p3647 A70-39243

Steels thermal fatigue in testing machine, investigating strains and stresses due to nonuniform temperature distribution during thermal cycle 21 p3840 A70-41433

Polyvinyl chloride sheet steel manufacture, properties and welding methods 22 p4045 A70-42479

Fracture behavior and tempered martensite embrittlement relationship in steel, using V- notched and fatigue precracked Charpy specimens 22 p4054 A70-42736

Succession of passes in rolling and hot shaping of thin walled angle steel 22 p4045 A70-42813

Low cycle notch fatigue tests on Inconel and low alloy steel, giving fatigue strength reduction factors for design 22 p4055 A70-43103

Pulsed spray welding electrode melting rates for Al alloy, mild steel and stainless steel electrodes over range of pulse current levels 22 p4046 A70-43147

German monograph on notched structural steels fatigue properties and crack propagation under tensile-compressive alternating loads 24 p4356 A70-45086

Steel and duralumin strips with circular holes tested under axial tension, determining relationship between strength weakening and ultimate stress 24 p4420 A70-45272

Crack detection in cyclic strained steel and Al alloys, using ultrasonic Rayleigh and longitudinal waves 24 p4424 A70-45718

Brittle fracture of welded notched steels with different stress concentrations, using subzero tensile tests 24 p4347 A70-45732

High purity Cr-Ni heat resisting steels, investigating phase transformations with microhardness measurements magnetic analysis, X ray diffraction and microstructure examination 24 p4362 A70-46181

Steel surface diffusive saturation with elements of chlorides, noting role of iron chloride phase in promoting coating uniformity 24 p4350 A70-46332

Aluminized Armco iron and steel diffusion layers phase composition and microstructure 24 p4350 A70-46337

STEEP GRADIENT AIRCRAFT

U V/STOL AIRCRAFT

STEEPEST ASCENT METHOD

U STEEPEST DESCENT METHOD

STEEPEST DESCENT METHOD

Closed loop frequency response analyzer with steepest descent computing procedure to obtain in-phase and quadrature signal components in linear or nonlinear systems [ASME PAPER 69-WA/AUT-3] 04 p0688 A70-14830

Radar signals synthesis using steepest descent for minimizing Hermitian form 05 p0812 A70-16247

Asymptotic expansion of contour integrals involving analytic functions of complex variable, using steepest descent method 15 p2767 A70-31696

Branched trajectory optimization for split rocket vehicles using projected gradient or steepest descent method 16 p2977 A70-33871

Tangential descent direction determination for optimum control problems based on problem of moments 18 p3235 A70-36574

Stochastic approximation iterative algorithms for multivariable plants mathematical models, including steepest descent method 20 p3593 A70-39910

Steepest descent method for determining lowest ground state eigenvectors for molecular wave configurations 22 p4062 A70-42747

STEEPNESS

U SLOPES

STEERABLE ANTENNAS

Design methods for self steerable antenna arrays in unidirectional and two directional radio links 03 p0456 A70-13196

Satellite communications influence on ground stations design, describing steerable antenna and receive and transmit configurations for domestic station 05 p0811 A70-16095

Cross type radio telescope beam forming and steering system, describing switched delay lines and phasing circuits 08 p1477 A70-21823

Elevation patterns of vertically polarized elements above circular finite ground screens directly on soil, discussing steering illumination 09 p1634 A70-22700

Vertical tilt and horizontal position of antenna rotating device in radio astronomy and radar observations using photogrammetric methods 12 p2195 A70-27478

Radiation patterns of phased array scanning antenna using digital phase shifter, reducing peak sidelobe level 13 p2380 A70-29785

Steerable microwave circular array to provide 360 deg electronic beam steering with computerized adaptive amplitude and phase control 16 p2874 A70-33392

C band radar antenna with pencil beam steered in plane by ferrite phase shifters 16 p2875 A70-33394

Steerable C band waveguide arrays design for forming monopulse cluster of sum and difference beams 16 p2875 A70-33395

Steerable 100 meter radio telescope, discussing foundations, azimuth towers, reflector, assembly, electric motors, steering and receivers 16 p2888 A70-33656

X band aircraft antennas selection and design for defense communications satellite systems, emphasizing steerable phased array 16 p2865 A70-33712

Artificial pilot phased array /APPA/ for use as multiple narrow beam communication satellite, obtaining beam steering from phase shifter setting 16 p2983 A70-34070

STEERING

Hydrostatic synchronized steering of tow tractor for Boeing 747 and wide body jets compared to mechanical system 05 p0829 A70-16421

Minimum fuel continuous thrust elliptical orbit transfer problem, obtaining optimal steering function for departure and arrival points 11 p2124 A70-26214

Lunar vehicle design, discussing dual power steering, switching and joystick control handle 12 p2208 A70-27944

Lunar roving vehicle stability and agility design approach by Grumman, using articulated steering and conical wheels 12 p2208 A70-27946

Chrysler lunar vehicle design featuring flexible metal wheels and Ackerman front wheel steering, noting back-to-back seating and centrally mounted control display panel 12 p2208 A70-27947

Visual feedback delay effects on steering and tracking performance 12 p2179 A70-28147

Steerable landing gear system consisting of freely castoring corotating wheel nose gear, tiltable axle and main gear skids for lifting body spacecraft [AIAA PAPER 69-790] 13 p2344 A70-28514

Cross product steering for space vehicles and ballistic missiles guidance during powered vacuum flight, pointing thrust acceleration vector to null velocity at termination 16 p2947 A70-33440

Feedback analysis of learning and performance in hand-yoked, steering and stimulus tracking control of breath-produced visual target 16 p2852 A70-33660

Feedback delay effects on eye-hand synchronism in stimulus tracking and steering using self generated body movements 16 p2852 A70-33662

Thor launch vehicles steering filters design using automated method of optimizing large order linear stochastic systems control 20 p3600 A70-39543

Booster parameterized guidance algorithms investigated on basis of steering forms validity, discussing exoatmospheric ascent applications [AIAA PAPER 70-1066] 20 p3669 A70-39584

Steering behavior during learning as function of self generated stimuli by movement compared with stimulus tracking 20 p3580 A70-39674

STEERING ROCKETS

U CONTROL ROCKETS

STEFAN-BOLTZMANN LAW

Stefan heat conduction problem with time dependent first kind boundary conditions approximate solution, taking into account unsteady temperature field of solidifying liquid 03 p0604 A70-13210

Positive time-periodic solutions to parabolic problems with Stefan-Boltzmann boundary conditions using straight lines method 07 p1333 A70-18748

Nonlinear difference approximating scheme and iterative method for Stefan problem with several unknown fronts 08 p1534 A70-20851

Stefan-Boltzmann formula validity for flames and combustion products radiation affected by time dependence of emissivity coefficient, place and wavelength 14 p2662 A70-30179

STELLAR ATMOSPHERES

NT CHROMOSPHERE

NT SOLAR ATMOSPHERE

White dwarf spectra interpretation based on model atmosphere method, discussing chemical composition, low luminosity high pressure atmospheres, electron density, etc 01 p0189 A70-11340

Cool dwarf stars atmospheric models including IR opacity due to water vapor and pressure induced dipole of molecular hydrogen 01 p0190 A70-11347

M dwarf stars model atmosphere construction taking into account molecular opacities in cool stellar atmospheres 01 p0190 A70-11348

High temperature atmospheric models for red dwarf stars and sun to determine convection effect on atmospheric surface layers and emitted flux
01 p0190 A70-11349

Nongray and constant radiative flux model atmosphere for K dwarf stars with 4000 K effective temperature and 4.5 log surface gravity
01 p0191 A70-11350

Electron pressure and negative H ion population in late type dwarfs atmospheres by Ca I resonance line observation, noting non-LTE mechanism
01 p0191 A70-11351

Stellar spectral lines fine analysis methods compared for curves of growth, line profiles and related contribution curves in model atmospheres for Procyon and sun
02 p0343 A70-11906

Neutron star atmospheric composition as function of time, including effects of diffusion, cooling and nucleosynthesis
02 p0378 A70-12698

Hyperon and resonance particle effects on neutron star vibration, discussing vibrational energy storage and atmospheric electromagnetic generation
02 p0379 A70-12699

Stellar model surface convective zone using diffusion equation taking into account transport due to gravitational separation, noting role of turbulent diffusion
03 p0574 A70-13932

Convective nongray stellar atmospheres construction for stellar stability studies, accounting for convective flow nonlocality and nongray radiative transfer
04 p0745 A70-14472

Stellar atmosphere high dispersion spectroscopy, discussing limitations for stars over 17,000 K
04 p0746 A70-14508

Rayleigh scattering cross sections of stellar He C, N and O computed by quantum defect method, discussing effects of wavelength dependent polarizabilities
04 p0723 A70-15692

Stellar atmospheric models thermal conductivity coefficient computation for various temperatures and pressures neglecting magnetic field
06 p1150 A70-18464

Carbon particles formation and growth model for cool variable carbon star atmosphere with sinusoidal carbon star atmosphere with sinusoidal temperature variations
07 p1380 A70-19260

Carbon particles formation and growth in Mira variables atmospheres, considering extinction effects on stellar structure and appearance
07 p1380 A70-19261

Line profiles in expanding and rotating atmospheres via Monte Carlo techniques, considering noncoherent scattering, atomic levels and atmospheric characteristics
07 p1339 A70-20057

Von Zeipel 1128 O star spectrum analysis, discussing mass, He/H ratio, metal abundances, etc
08 p1571 A70-20913

Sigma Orionis E hydrogen-deficient atmosphere, using grid of constant-flux model atmospheres to determine abundances of five elements
09 p1755 A70-22504

Book on stellar spectroscopy, covering stellar atmospheric models, rotation, evolution, etc
09 p1756 A70-22640

Stellar wind theory based on spherically symmetric isothermal and stationary stellar atmosphere with non-negligible gravitational potential
09 p1747 A70-23605

Model for FU Orion irregular variable to determine turbulent convection characteristics in atmosphere at optical transparency level
11 p2115 A70-26580

Stellar atmosphere and shell models in spectral range AO-G5 for studying stellar structures dependence on chemical composition
11 p2115 A70-26582

OB supergiants atmospheric expansion indicated by medium-dispersion spectra, noting mass loss rate increase with luminosity and effective temperature
11 p2117 A70-26657

Nonlinear integral equations of radiation transfer of stellar and planetary atmospheres
12 p2305 A70-27852

Stellar atmosphere model for multilevel spectral line emission, assuming semiinfinite hydrogen atmosphere with sequence of plane parallel zones
12 p2306 A70-27856

Thermal shock waves structure and effective temperature in stellar atmospheres taking into account absorption effects and possible isothermicity
12 p2306 A70-27861

Stellar upper atmospheric shock wave motion, discussing emission spectra interpretation and temperature gradients
13 p2493 A70-29395

Stellar observations in near UV by camera having two color photometric slides, discussing atmospheric models
13 p2498 A70-30013

Arcturus atmosphere Mg abundances from rotational lines noting terrestrial proportions
14 p2637 A70-30540

Narrow band photometry calibration, using model stellar atmospheres and laboratory data for high resolution synthetic spectra of G and K giant stars
14 p2639 A70-30728

Galactic cosmic ray actions on interstellar medium for origin of Li, Be and boron in stellar atmospheres and solar system
14 p2640 A70-30786

Non-LTE and LTE line profiles and equivalent widths for transitions in singlet and triplet systems of neutral He in hot stars, explaining anomaly
14 p2641 A70-30884

A-type supergiants microturbulence, determining atmospheric small scale velocity fields
14 p2641 A70-30885

Spectral line formation, assuming frequency redistribution for plane parallel stellar atmosphere containing nonuniform distribution of internal emission sources
14 p2651 A70-31289

Ap star kappa Cancr model atmosphere analysis based on observed energy distribution and hydrogen line profiles
14 p2652 A70-31381

B3V stars atmospheres by LTE model and spectroscopic techniques
14 p2652 A70-31384

CH Cygni irregular light variations and spectrum peculiarities, considering upper atmosphere perturbation by variable hot satellite
15 p2809 A70-32904

Radiative transfer in spherical stellar atmosphere, considering free electrons density gradient and thermal motions, atmospheric layer curvature, optical thickness, etc
15 p2732 A70-32905

Book on interpretation of spectra and atmospheric structure of cool stars covering line identification, dissociative equilibrium, opacity, chemical composition, carbon stars, etc
16 p2978 A70-33962

Shock wave propagation through giant star atmosphere, using approximate analytical method
16 p2980 A70-34305

Spectrum of bright IR object VY Canis Majoris, noting absorption feature attributed to SiO molecules in stellar atmosphere
17 p3154 A70-34540

Stellar UV and visual continuum observations, discussing recalibration of absolute energy distribution of alpha Lyr to improve model atmospheres
17 p3160 A70-34881

Early-type star spectral scan analysis from OAO observation, comparing model atmosphere calculations
17 p3161 A70-34887

Supergiant alpha Car UV spectrophotometry from Gemini 11, comparing with model atmosphere
17 p3161 A70-34888

Normal stellar atmospheres - Conference, Cambridge, Mass., April 1968
17 p3168 A70-35379

Observational evidence concerning validity of Saha and Boltzmann laws in O, B and A stellar atmospheres
17 p3170 A70-35387

Meridional circulation velocities in Roche envelope of uniformly rotating star, using nonlocal equation for radiative heat transfer
17 p3171 A70-35560

Energy transfer in convective envelope of rotating star and solar differential rotation, using Lucy gravity-darkening law
18 p3313 A70-36214

Stellar atmosphere radiation field quantity vs quality, deriving electron temperature as function of tau
18 p3309 A70-37007

Ionization degree in moving stellar envelopes with large optical thickness
19 p3525 A70-38763

Dwarf Me stars flare spectra, examining hydrogen recombination layer and impulse heating of photosphere
20 p3702 A70-39013

K and M star molecular constituent density calculations using model atmospheres and observations
20 p3702 A70-39015

Neutron stars, discussing equations of state and stellar interiors, models, atmosphere, cooling, vibration, rotation and magnetic fields
20 p3706 A70-39932

Stellar coronas X ray fluxes from models of convection zones and corresponding mechanical energy fluxes
21 p3875 A70-40681

Schroedinger equation for hydrogen solved for high pressure behavior of materials, applying to stellar atmospheres and laboratory plasmas
21 p3849 A70-40933

Be star HD 37202 zeta Tauri II envelope instability, discussing radial velocities, profiles, line width and electron density in layers
21 p3888 A70-41119

Radiation line transfer in Wolf-Rayet envelopes with rapid radial expansion by escape probability method, including radiation effect from stellar core
21 p3892 A70-41248

Book on astrophysics and stellar structure covering physical characteristics, atmospheres, interiors and evolution
21 p3919 A70-41792

Stellar envelope physical structure studied to solve equilibrium equation, applying results to stellar model
22 p4097 A70-42545

Gravitational acoustic wave emission in isothermal stellar atmosphere with mass sources
23 p4242 A70-44267

Stellar rotation effects on atmospheres of early type main sequence stars, using models for surface gravity and temperature variations
23 p4249 A70-44810

Rotating stellar atmospheric models for middle and late A star masses, emphasizing Altair observed and predicted energy distribution
23 p4250 A70-44812

Effective temperature of star zeta Puppis from combined angular diameter measurement and model atmospheres, comparing hot stars
24 p4404 A70-45414

Cool star atmospheric structure, discussing models with and without graphite particle inclusion opacity
24 p4410 A70-45765

Stellar structure in advanced phases of evolution, considering mixing between hydrogen-rich envelope and core through surface convection zone
24 p4412 A70-46102

Main sequence and giant stars atmospheric structure models, noting metal deficiency effects
24 p4413 A70-46159

Novae and supernovae envelope properties, observing optical polarization and magnetic field for Crab Nebula
24 p4413 A70-46169

Atmospheric composition of cool stars in relation to nucleosynthesis and galactic evolution
24 p4414 A70-46227

STELLAR DOPPLER SHIFT
U DOPPLER EFFECT
U EXTRATERRESTRIAL RADIATION

STELLAR EVOLUTION
White dwarf luminosity functions based on birth rate, white dwarf space density in solar neighborhood and possible red degenerate stars deficiency
01 p0189 A70-11339

Cooling time estimation for white dwarf stars with ion component undergoing condensation, based on plasma thermodynamic properties
01 p0189 A70-11341

High luminosity white dwarfs possible evolution from planetary nebulae, discussing plasma neutrino processes
01 p0189 A70-11342

White dwarfs formation in close binary systems ascribed to mass exchange between components, describing evolutionary followup of primary from main sequence by model
01 p0189 A70-11343

Protostars rapid contraction and flare up evolutionary phases, solving hydrodynamic equations of motion
01 p0190 A70-11344

Low mass protostar evolution in dynamic collapse, investigating opacity laws
01 p0190 A70-11345

PreHayashi phase of stellar evolution, discussing protostellar disks/stellisks/formation from flattened fragments of collapsed interstellar cloud under turbulent viscosity
01 p0190 A70-11346

Two armed spiral galactic shock waves as triggering mechanism for gravitational collapse leading to star formation, considering gaseous disk motion using Schmidt model
02 p0363 A70-11781

Final state of matter resulting from star contraction, white dwarfs development and neutron stars problem, explaining hydrostatic equilibrium
02 p0370 A70-12085

Thermal energies and angular momenta of Hubble galactic sequence using differential rotation and decreasing density stellar system model to test stellar evolution theories
02 p0376 A70-12447

Relativistic phase of stellar system evolution caused by inelastic stellar collisions, discussing thermal relaxation rate, obtaining distribution function
03 p0564 A70-13226

Late stars spectral characteristics, verifying criteria for spectral classification and anomalous spectra determination
03 p0569 A70-13424

Astronomical and space research methods probing fundamental questions concerning universe unsolvable by classical astronomy, discussing solar wind and stellar formation and evolution
03 p0571 A70-13790

Neutron star electrical conductivity, discussing stellar flux and magnetic field decay times
03 p0578 A70-14220

- Binary star formation using singular solution of Kepler problem in general theory of relativity
04 p0755 A70-15355
- S Doradus spectroscopic behavior study during minimum and maximum phases suggesting ejected-shell mechanism and premain sequence star classification
04 p0759 A70-15712
- Time variation of gravitational constant on structure of central solar region and neutrino luminosity
05 p0899 A70-15952
- Thermal and dynamical evolution of gas clouds in transparent and opaque stages by comparing rates of cooling, heating, contraction and expansion
05 p0907 A70-16041
- Models constructed for advanced evolution phases in massive convective red supergiants, considering carbon, Ne and oxygen burning in stellar core
05 p0919 A70-16935
- Metal content effects on evolution tracks of five solar mass stars with different chemical composition, discussing Magellanic Clouds composition
05 p0919 A70-16936
- LTE departures in late B stars from measurements of Balmer and Paschen discontinuities
05 p0919 A70-16937
- Red giants age and mass estimation based on K-line luminosities, noting role of metal abundance
06 p1139 A70-17416
- Cosmological theories taking into consideration gravitational collapse, discussing pulsars, quasars and X ray stars evolution
06 p1140 A70-17584
- Age mixtures and physical heterogeneity of G-M cold stars emphasized in study of galactic fine structure and evolution
06 p1140 A70-17640
- Solar system evolution theories to explain planetary orbits, angular momentum and matter distribution, satellite systems and chemical composition
07 p1376 A70-18898
- Interstellar cloud models to investigate heating, cooling and density distribution effects on collapse and to suggest theory of stellar evolution
07 p1390 A70-20292
- Earth observations of collapsing star neutrinos and neutrino oscillations in Milky Way galaxy
07 p1371 A70-20331
- Age dating of earth and universe emphasizing methods based on radioactivity, discussing stellar evolution, galactic age and assessment of cosmic time
08 p1568 A70-20633
- Solar system origin theory emphasizing brother star approaching nebula for instability of boundary layer
08 p1568 A70-20638
- Statistical analysis of rotation and macro turbulence in early type Ia and IaB supergiants, discussing evolutionary effects
08 p1571 A70-20908
- Magnetothermal instability and radiative effects on incipient fragmentation of rotating gravitating interstellar fluid forming condensations
08 p1578 A70-21545
- Stellar formation and explosions in compact gas clouds to explain quasar phenomenon, discussing temporary star concept
08 p1578 A70-21548
- Relativistic phase of stellar system evolution caused by inelastic stellar collisions, discussing thermal relaxation rate, obtaining distribution function
08 p1580 A70-21659
- Supernovae remnants evolution, properties and galactic distribution, discussing criteria for catalog listing and remnants as X ray sources
09 p1749 A70-21990
- Relativistic gravitational stellar collapse calculations for stars exceeding neutron star limit, discussing results in terms of supernovae or neutrinos
09 p1749 A70-21991
- Late stage stellar evolution association with supernovae in terms of gravitational collapse and exploding light emission using evolutionary model
09 p1749 A70-21993
- Quasar-associated evolutionary effects, considering uniform distribution, constant optical luminosity and evolving radio luminosity
09 p1753 A70-22455
- Metal-poor stars evolution during hydrogen and helium burning from main sequence to giant branch, estimating relative cluster ages
09 p1755 A70-22507
- Stellar evolution computations numerical instability due to coupling between hydrostatic equilibrium and thermal processes
09 p1755 A70-22508
- Book on stellar spectroscopy, covering stellar atmospheric models, rotation, evolution, etc
09 p1756 A70-22640
- Galactic halo origin and evolution postulated from chemical evolution assuming stellar evolution details
09 p1758 A70-22742
- Twelffold solar mass star evolution computed using chemically homogeneous model showing faster evolution rate
09 p1758 A70-22746
- Stellar rotation theory applied to evolution of nine solar mass star from main sequence to helium exhaustion
10 p1946 A70-24969
- Low mass star evolution from helium burning to white dwarf, describing red giant and mass loss stages in model
10 p1946 A70-24982
- WZ Sagittae ultrashort period binary evolution, considering mass-radius relation, initial separation and present position
11 p2108 A70-25696
- Evolution of very low mass stars with low mass companions in solar neighborhood
11 p2111 A70-26033
- Pulsars nature based on hypothesis for main energy of novae and supernovae bursts equaling gravitational energy of collapse
11 p2117 A70-26708
- Stellar plasma neutrino pair emission, comparing photon neutrino coupling with current current coupling theory and white dwarf evolution
12 p2297 A70-26976
- Gravitational collapse of star and general relativity role, considering Schwarzschild solution to Einstein vacuum equations
12 p2298 A70-27058
- Vibrationally unstable high mass main sequence star, reinvestigating destruction by radial oscillations
12 p2302 A70-27587
- Young stars evolution rates in expanding and disintegrating stellar associations, giving age estimates
12 p2306 A70-27862
- Vlasov equation approximate solution by minimum energy principle, deriving equilibrium equation for stellar gas
13 p2457 A70-28552
- Density wave theory and spiral gravitational field effects in migrating stars orbits and origins in Milky Way spiral arm, using Schmidt model
13 p2495 A70-29801
- Stellar evolution numerical model for point masses constant with time in absence of external field
13 p2498 A70-30011
- Self gravitating three dimensional particles system evolution using water bag model
13 p2498 A70-30012
- Red giant model, investigating inclusion of semirelativistic partially degenerate gas characteristics by perturbatory technique
14 p2651 A70-31290
- Overstable convection formation of semiconvective zones in massive stars, noting Schwarzschild and Harm models
14 p2652 A70-31386
- O-Of stellar evolution yielding Wolf-Rayet type, considering spectral evidence and H-He interaction
15 p2800 A70-32202
- Massive hydrogen burning stars evolution with pulsational mass loss based on minimizing pulsational instability degree to specify mass loss rate
15 p2803 A70-32612
- Pulsar formation mechanism, showing core collapse to neutron star state
15 p2806 A70-32773
- Hot small mass neutron stars cooling time and internal characteristics, discussing evolution based on H-R diagram
15 p2808 A70-32886
- Stellar evolution in globular clusters, considering H-R diagrams of age, He abundance and thermal instability
16 p2973 A70-33076
- Cosmic time varying gravitational constant effects on stellar age determination
16 p2978 A70-33966
- Pulsar observations based on magnetic dipole model, discussing turnover time, emission characteristics, birth rate and scale height
17 p3153 A70-34531
- Globular cluster stars, discussing cosmological importance, stellar development models, main sequence stars, red giant models, He content, age computation, etc
17 p3171 A70-35447
- Stellar thermal and vibrational energy losses due to URCA shells in interiors
18 p3310 A70-35935
- Asteroidal parent bodies heating by electrical induction during early solar evolution
18 p3310 A70-35938
- Helium abundance in unevolved main sequence eclipsing binaries by comparing to homogeneous models in mass luminosity plane
18 p3318 A70-37023
- Dispersed stellar clusters color excesses and distance moduli from color-magnitude diagram, considering evolutionary deviation from main sequence
18 p3323 A70-37138
- Disk shaped galaxy stationary spiral shock pattern, examining gas cloud gravitational collapse for star formation
18 p3331 A70-37198
- Young star velocity ellipse vertex deviation, discussing formation at right angles to galactic center direction
18 p3331 A70-37199
- Soviet book on variable stars covering properties, evolution, structure, methods of investigation, etc
19 p3520 A70-38397
- Stellar evolution covering formation, structure and time-varying properties of single spherical, nonspherical, magnetic and binary stars
19 p3531 A70-38950
- Horizontal branch stars evolution based on mass distributions from comparison with giant branch, investigating evolutionary track characteristics during core helium burning
20 p3702 A70-39019
- Carbon-nitrogen-oxygen isotope bi-cycle function in solar evolution, noting first cycle role in solar energy release and neutrino production
20 p3698 A70-39306
- Explosive nucleosynthesis as heavy nuclei source for stars
20 p3712 A70-40426
- Close binary stars evolution, discussing initial parameters effects on mass exchange and orbital period model
21 p3884 A70-40872
- Pulsar research review, discussing characteristics, neutron star theory and galactic origin
21 p3886 A70-41072
- Stable hyperon star existence in general relativity, discussing state equations for baryon matter, radial pulsation and superlumina and ultrablastic conditions
21 p3888 A70-41116
- Beta Cephei star discovery criteria, examining mu-mechanism theory by He and N overabundances, far UV flux, spectral line width and binary character
21 p3890 A70-41159
- Book on astrophysics and stellar structure covering physical characteristics, atmospheres, interiors and evolution
21 p3919 A70-41792
- Rotating magnetic star thermal behavior, discussing central nuclear burning stability, homologous changes, cooling, degeneracy and helium flash
22 p4100 A70-42855
- Stellar evolution, rotation and atmospheric motion, discussing gravity darkening, spectral lines, angular momentum, braking mechanisms and late stars
22 p4102 A70-42970
- Electron capture involving iron nuclei in contracting iron stars treated as endothermic nuclear reaction
22 p4104 A70-42992
- Polytropic premain-sequence evolutionary tracks and main sequence models of solar composition low mass stars
22 p4104 A70-42993
- Interstellar molecules from stellar and galactic evolution viewpoint, emphasizing OH emission spectrum characteristics
23 p4238 A70-43801
- Stellar spectra above horizontal branch in globular clusters, discussing stellar evolution, composition and structure
23 p4246 A70-44755
- Be stars rotation, considering emission properties and evolutionary state of main sequence
23 p4249 A70-44807
- Rapidly rotating B and Be stars interior evolution models, considering mass and radiation pressure
23 p4249 A70-44808
- Stellar rotation angular momentum loss in premain sequence convective phase, discussing polytropic structure, formation time and velocity changes
23 p4249 A70-44809
- Upper main sequence and close early type binaries evolution by fission of rapidly rotating protostars
23 p4250 A70-44815
- Stellar rotational velocities in open star clusters, noting evolutionary expansion, tidal coupling in binaries and Ap stars magnetic braking
23 p4251 A70-44820
- Cluster evolution model for stars with equal masses, calculating density and velocity distribution for various cluster types
24 p4404 A70-45417
- Old open clusters red giant observations comparison with stellar evolution calculations, discussing proper motions, magnitudes, data acquisition and analysis, etc
24 p4404 A70-45418
- Massive star pulsational stability in He burning phase, investigating opacity variation effects on flux dissipation in outer layers
24 p4405 A70-45419
- Heavy elements diffusive separation as explanation of metallic and magnetic A stars abundance anomalies at outer convective envelope bases
24 p4410 A70-45775
- Pulsars correlation with stellar evolution using model, discussing distribution and formation rate in Milky Way galaxy
24 p4412 A70-45981

Pulsars radio evolution mechanism by phenomenological analysis, deriving time dependences of period, luminosity and emitting region size
24 p4412 A70-46101

Stellar structure in advanced phases of evolution, considering mixing between hydrogen-rich envelope and core through surface convection zone
24 p4412 A70-46102

Pulsar distributions without magnetic decay, concerning age dependence of surface field and radio luminosity of neutron stars
24 p4413 A70-46138

STELLAR FIELDS

U STAR DISTRIBUTION

STELLAR INERTIAL NAVIGATION

U CELESTIAL NAVIGATION

U INERTIAL NAVIGATION

STELLAR LUMINOSITY

Solar brightness variations observed photometrically, discussing periodicity, sunspot locations, photosphere and subsurface rotations, etc
01 p1886 A70-11273

Low luminosity stars - Conference, Charlottesville, March 1968
01 p1887 A70-11330

Photometric data for white dwarf low luminosity stars listed in color classes and proper motion fields
01 p1887 A70-11331

Lowell Observatory Northern Hemisphere proper motion survey, analyzing preliminary data for low luminosity stars
01 p1887 A70-11332

Duplicity characteristics of low luminosity stars, considering nearby M dwarfs, white dwarfs and high velocity subdwarfs
01 p1888 A70-11334

Faint, metal poor, subluminescent and red degenerate stars occurrence and properties, considering spectra of candidate degenerates
01 p1888 A70-11338

White dwarf luminosity functions based on birth rate, white dwarf space density in solar neighborhood and possible red degenerate stars deficiency
01 p1889 A70-11339

High luminosity white dwarfs possible evolution from planetary nebulae, discussing plasma neutrino processes
01 p1889 A70-11342

Protostars rapid contraction and flare up evolutionary phases, solving hydrodynamic equations of motion
01 p1890 A70-11344

Catalog of faint Ob stars between Carina and Centaurus
02 p0370 A70-12075

Beta Lyr spectral and brightness characteristics long period variations related to orbital motion perturbations
03 p0564 A70-13229

Young flare stars in solar vicinity, considering spatial density, kinematic properties and luminosities
03 p0567 A70-13318

Light variation curves for distorted white dwarf hypothetical secondaries in close binary systems calculated by integrating monochromatic fluxes
03 p0567 A70-13323

Beta lyrae light curve changes by comparing international program observations with 1958 Lick Observatory results, discussing period, brightness, spectra, etc
03 p0568 A70-13327

Psi Orionis light variations, using photoelectric photometry, indicating ellipsoidal variability
03 p0570 A70-13552

Time determination at astronomical observatories using transit instrument observations concerning stellar distributions and magnitudes
04 p0756 A70-15486

Hot star photogravitational acceleration determined from difference between apex and antipex brightness, noting constant magnitude and direction of principal component of apex force
05 p0918 A70-16914

Red giants age and mass estimation based on K- line luminosities, noting role of metal abundance
06 p1139 A70-17416

Mean magnitudes, colors and amplitudes for RR Lyrae variables in omega Centauri cluster obtained from photometric observations
06 p1148 A70-18455

HR diagram calibration based on proper motions and radial velocities, deriving absolute magnitudes and statistical parallaxes
06 p1149 A70-18456

Milky way and interstellar clouds brightness fluctuations statistical analysis by surface photometry, studying dust distribution, cloud absorption and dimensions, star distribution, etc
06 p1149 A70-18463

Optical density vs illumination amount characteristic curve determined for photometric calibration of astronomical photographs of celestial bodies
07 p1279 A70-19046

Effective, brilliance, color and gradient temperature measurements in astrophysics, considering observer bond and thermodynamic nonequilibrium of stars
07 p1386 A70-19597

Supernova remnant luminosity dependence on central star rotation period, deriving parameters for pulsars in Cas A
08 p1570 A70-20897

Quasi-stellar objects absolute spectral energy distribution, considering electron temperature and photon density
08 p1572 A70-20916

Double and multiple stars components magnitude differences tabulated based on visual and photometric observations
08 p1574 A70-21163

Cosmic rays induced Cerenkov light pulses effect on stellar intensity interferometer from measuring correlated pulses
08 p1497 A70-21492

Beta Lyr spectral and brightness characteristics long period variations related to orbital motion perturbations
08 p1580 A70-21662

Secondary minimums role in studying eclipsing variable stars, correlating observability with detection of line of apsides motion
08 p1581 A70-21759

Supernovae and remnants, data concerning radio brightness distribution of Tycho supernova remnant and Cassiopeia and Crab Nebula origin
09 p1748 A70-21989

Stellar scintillation saturation at large zenith angles interpreted in terms of combined dispersion and aperture filtering
09 p1726 A70-22073

Bright star weak longitudinal magnetic fields from telescope spectrograph
09 p1755 A70-22515

Electron-neutrino weak interaction and beat decay coupling constants found nearly equal, describing astrophysical tests based on white dwarf stars luminosity intervals
09 p1733 A70-23451

Cepheid type variable stars nuclear reaction and opacity pulsation excitation mechanisms
10 p1940 A70-24409

Zero-point of period-luminosity-relation of Cepheids based on proper motions, radial velocities and photometric data, applying secular parallax method
10 p1945 A70-24964

Coefficients for linear and nonlinear limb darkening in early type stars
11 p2113 A70-26469

VX Cas brightness determination from color plates, giving values in tabular form
11 p2115 A70-26583

Coordinates and brightness characteristics of variable observed during photographic studies of VX Cas
11 p2116 A70-26584

Densities and extents of absorbing clouds in open cluster NGC 7086 determined from photometry and spectral classifications of stars
11 p2116 A70-26587

Spectra, luminescence and gas dynamic effects in variable stars, discussing nonthermal theory to explain continuous emission
12 p2306 A70-27857

Nova Delphini brightness variations, observing absorption lines shift toward violet
12 p2306 A70-27860

Comet-like nebulae, describing brightness and spectral characteristics of variable stars in nebulae
12 p2307 A70-27863

Sudden disappearance of large quiescent prominence on solar disk with subsequent brightenings, using photospheric and gravitational model
13 p2497 A70-29850

Bright southern Cepheids UVB observations, discussing blue companion effect on two color plot
14 p2639 A70-30726

Stellar intensity interferometer for close binaries and emission line stars, investigating gamma-two Velorum
14 p2640 A70-30733

A-type supergiants microturbulence, determining atmospheric small scale velocity fields
14 p2641 A70-30885

Cepheids distance scale from proper motions data, using maximum likelihood method for period-luminosity relation
14 p2652 A70-31387

Binary AX Monocerotis brightness variations in UV from photoelectric UVB observations
15 p2796 A70-31610

Absolute photovisual magnitude and classification of supernova in NGC 3389 spiral galaxy, using UVB measurements and comparison stars
15 p2797 A70-31611

Spectral classification of relatively bright stars in near UV based on moderate and low dispersion spectra including F, G and K stars
15 p2797 A70-31614

Cepheids nonequilibrium continuous emission at maximum brightness, considering phase shift between radiation intensity and stellar contraction
15 p2802 A70-32483

Luminosity criteria in O stars via narrow band photoelectric photometry suggesting VI Cygni proximity
15 p2807 A70-32804

Flare stars distribution in Pleiades, discussing flare visual magnitude and frequency
15 p2807 A70-32876

RW Aur type variable stars percentage with photographically observable flares
15 p2807 A70-32877

AG Peg brightness variations by three color photoelectric photometry, discussing orbital motion of cold component
15 p2807 A70-32878

Long period variable stars light polarization as function of brightness and wavelength, discussing molecular scattering and nonthermal emission
15 p2808 A70-32879

CH Cygni irregular light variations and spectrum peculiarities, considering upper atmosphere perturbation by variable hot satellite
15 p2809 A70-32904

Hyades stars between F4 and K5, measuring chromospheric H and K emission lines dependence on bolometric luminosity
17 p3157 A70-34832

Stellar UV photometry using telescope experiment in OAO
17 p3160 A70-34883

Luminosity effects in Balmer lines of early type stars, noting H alpha equivalent width decrease
17 p3170 A70-35388

Hydrogen abundance in white dwarfs, discussing inconsistencies in mass and bolometric magnitude models for Sirius and Eri B
17 p3170 A70-35389

Delta Scuti stars, determining consistent absolute magnitudes by Stromgren intermediate band colors and Crawford photoelectric H beta indices
17 p3171 A70-35443

Central pulsars effects on supernova envelopes, examining luminosity, energy input, shape and light curve
18 p3314 A70-36333

Pulsars period galactic equator concentration correlation, discussing period-radio luminosity relation and spatial distribution
18 p3314 A70-36335

Soviet book on declination observation of bright and faint stars in one system
18 p3314 A70-36402

Initial horizontal branch metal poor star models, examining opacities, luminosity and cluster ages of RR Lyrae stars
18 p3317 A70-37006

Stellar magnitude equation from corrected catalog data to determine absolute proper motions relative to galaxies
18 p3323 A70-37145

Spiral galaxy NGC 6946 structure and stellar associations distribution, indicating no relation between color and magnitude and distance from center
18 p3327 A70-37160

Soviet book on variable stars covering properties, evolution, structure, methods of investigation, etc
19 p3520 A70-38397

Light curves bumps properties of Population I cepheids in Magellanic Clouds, Milky Way galaxy and M 31 as function of period
19 p3523 A70-38691

Binary stars dynamical parallaxes, masses, absolute magnitudes and provisional orbits, fitting deduced masses into empirical visual mass-luminosity relations
19 p3531 A70-38896

Nova Ser 1970 and Aql 1970 luminous IR emission, discussing stellar brightness, grain formation and optical decay
20 p3701 A70-39004

Main sequence stars faint end IR observations for luminosities and temperatures
20 p3702 A70-39014

Soviet book on brightness of irregular and semiregular variable stars by statistical methods
20 p3705 A70-39899

OPL astrolabe catalog corrections, discussing Danjon prototype, color-magnitude effect, time and latitude values
21 p3887 A70-41111

Reflection nebulae dust density, noting lower limit dependence on absolute magnitude of illuminating star
21 p3889 A70-41149

Total energies of stars with velocities perpendicular to galactic plane, examining absolute luminosities, galaxy size and local gravitational potential
21 p3890 A70-41162

Sirius components relative photographic positions and magnitude difference, discussing color effect, grating image separations and emulsion contraction
21 p3922 A70-41984

- Blue stellar objects emission at 9.5 and 3.5 mm, suggesting quasi-stellar objects with small intrinsic radio luminosity 21 p3922 A70-41993
- Emission and escape of light from inside spherically symmetric gravitational mass, examining escape cone 21 p3923 A70-42106
- Solar equatorial limb brightening of far UV resonance lines of lithium-like N V, O VI, Ne VIII, Mg X and Si XIII ions, interpreting os0-4 data with coronal model 21 p3924 A70-42185
- Star flare HD 160202 in M6, discussing luminosity, time duration, magnitude and temperature 22 p4102 A70-42971
- Color-magnitude diagram of star cluster Kron 3 in Small Magellanic Cloud, using electronographic photometry 22 p4102 A70-42978
- Stellar population of young clusters containing red supergiants, determining spectral types and luminosity classes 22 p4102 A70-42979
- Light curve for eclipsing stars with scattering envelopes applied to V444 Cygni binary system 22 p4103 A70-42989
- Time constant loci and theoretical luminosity functions for various compositions and ages of metal poor globular clusters 22 p4108 A70-43735
- Globular cluster M5 giant, asymptotic and horizontal branches, determining color-magnitude diagram and luminosity 22 p4109 A70-43745
- Cepheids nonequilibrium continuous emission at maximum brightness, considering phase shift between radiation intensity and stellar contraction 23 p4240 A70-43907
- Orbital eccentricity effects on solutions of eclipsing binary light curves, comparing circular orbits solutions 23 p4242 A70-44290
- CA II chromospheric emission lines for deriving Mnu in stellar luminosity, discussing calibration 23 p4242 A70-44293
- Eclipsing binary stars minima variations related to orbit perturbations and rotational angular momentum of component interiors 23 p4251 A70-44819
- Neutron star or defunct pulsar accretion of interstellar matter, discussing effects on total luminosity and radiation spectrum 24 p4403 A70-45397
- Southern early stars away from galactic plane, reporting magnitudes and colors on UVB system and MK spectral classifications 24 p4404 A70-45412
- Gamma Cas star time and spectra observations, examining emission line profile variations and envelope and stellar model 24 p4404 A70-45415
- Pulsar intensity variations, showing fine frequency structure by interstellar scintillation model 24 p4404 A70-45416
- Light velocity frequency dependence in variable stars gravitational fields suggested from yellow and UV NP 0532 observations 24 p4405 A70-45488
- Sc0 XR-1 optical intensity power spectra oscillations searched for in pulsar frequencies and fundamental radial mode vibrations in white dwarfs and neutron stars 24 p4410 A70-45762
- High luminosity M type star photometry, determining supergiant intrinsic properties, interstellar extinction mean law and galactic evolution 24 p4410 A70-45764
- Pulsars radio evolution mechanism by phenomenological analysis, deriving time dependences of period, luminosity and emitting region size 24 p4412 A70-46101
- STELLAR MAGNETIC FIELDS**
- NT SOLAR MAGNETIC FIELD**
- Dynamo theory of stellar and planetary magnetic fields, discussing mathematical analysis and electronic computation of eigenvalue problems and field parameters 01 p0185 A70-10957
- Neutron star X synchrotron radiation from gas accretion producing strong magnetic field with high electron temperature 03 p0557 A70-13220
- Nonperiodic phenomena in variable stars by statistical and physical analysis, noting role of magnetic fields 03 p0566 A70-13313
- Neutron star electrical conductivity, discussing stellar flux and magnetic field decay times 03 p0578 A70-14220
- Prescribed circulations within conducting spheres effect on initially prescribed magnetic fields, discussing magnetic field structure in uniformly rotating stars 04 p0758 A70-15694
- Landau Orbital Ferromagnetism in electron gas as magnetic field source for neutron stars 07 p1380 A70-19279
- Compton scattering of synchrotron radiation from parent electrons in pulsars, calculating Compton-synchrotron radiation from NP 0532 leads to lower limit for magnetic field 07 p1369 A70-20221
- Pulsar magnetorelativistic model assuming neutron star with magnetic field 08 p1563 A70-20478
- Neutron star X synchrotron radiation from gas accretion producing strong magnetic field with high electron temperature 08 p1563 A70-21653
- Magnetic moment associated with Landau levels in magnetic induction in electron gas and magnetic fields of white dwarfs and neutron stars 09 p1752 A70-22306
- Bright star weak longitudinal magnetic fields from telescope spectrograph 09 p1755 A70-22515
- Pulsars period distribution not related to decay of magnetic field in rotating neutron star 09 p1756 A70-22518
- Poloidal magnetic field effects on main sequence stars core convection 11 p2117 A70-26654
- Stellar and nebular magnetic fields formation, considering role of high temperature plasma random charge and current fluctuations 12 p2307 A70-27864
- Galactic, stellar and solar magnet fields origin, considering fluid motions role 14 p2641 A70-30876
- Magnetic fields of DA dwarfs observed with photoelectric polarimeter, noting no fields observable 17 p3154 A70-34537
- Pulsars theories review, discussing geometrical model picturing pulsar as rotating neutron star with high magnetic field 17 p3164 A70-35117
- Pulsars electrodynamics concerning EM emissions, discussing roles of rotation and magnetic field 17 p3172 A70-35591
- Pulsar radiation mechanisms, discussing magnetic field topology and current distribution estimation 19 p3518 A70-38022
- White dwarf star circular polarized light, indicating strong magnetic field 20 p3701 A70-39001
- Pulsars subpulse intensities and shapes in magnetic field, noting drift speed sawtooth patterns 20 p3713 A70-40428
- Sc0 X-1 extar high energy radiation production, discussing relativistic electron synchrotron emission and magnetic fluctuations spectrum 21 p3878 A70-40709
- Corotating magnetic field model of pulsar, using electromagnetic field equations of dipole radiation in low density plasma 24 p4413 A70-46137
- Pulsar distributions without magnetic decay, concerning age dependence of surface field and radio luminosity of neutron stars 24 p4413 A70-46138
- Novae and supernovae envelope properties, observing optical polarization and magnetic field for Crab Nebula 24 p4413 A70-46169
- STELLAR MASS**
- White dwarf mass changes during cooling, describing white dwarf collapse-type I supernova outbursts relationship 01 p0174 A70-10197
- Statistical mechanical method deriving ionization equilibrium and equations of state for low mass stars, considering Coulombic interactions, nonideal effects, etc 01 p0188 A70-11336
- Low mass protostar evolution in dynamic collapse, investigating opacity laws 01 p0190 A70-11345
- Upper mass limit of quasar in galactic cluster from velocity dispersion of galaxies using generalized form of virial theorem, determining B264 mass 02 p0372 A70-12245
- Physical conditions of stars in presupernova stage for type II supernovae with outburst expected due to Fe-He transition in core, confirming lower mass limit 03 p0566 A70-13314
- Superfluid states of matter in interior of neutron stars, discussing strong interaction forces role 03 p0578 A70-14219
- Galactic expansion due to mass energy loss by gravitational radiation 05 p0913 A70-16557
- Metal content effects on evolution tracks of five solar mass stars with different chemical composition, discussing Magellanic Clouds composition 05 p0919 A70-16936
- Red giants age and mass estimation based on K-line luminosities, noting role of metal abundance 06 p1139 A70-17416
- Stellar velocity distribution function for small mass stars in nonrotating systems 07 p1389 A70-20208
- O star red shift considering gravitation interpretation effects on stellar masses 07 p1391 A70-20465
- Von Zeipel 1128 O star spectrum analysis, discussing mass, He/H ratio, metal abundances, etc 08 p1571 A70-20913
- General relativity equations of gravitation consistent with empirical data, discussing curvature tensor, scalar gravitational waves and solar mass difference 08 p1577 A70-21419
- Neutron stars properties, using static cold stellar model to examine relation between central density and mass, and cool hyperonic matter composition 09 p1749 A70-21995
- Twelvefold solar mass star evolution computed using chemically homogeneous model showing faster evolution rate 09 p1758 A70-22746
- Zero age intermediate and low mass stellar models and evaluation of physical parameters for population I and II chemical compositions 10 p1944 A70-24955
- Stellar rotation theory applied to evolution of nine solar mass star from main sequence to helium exhaustion 10 p1946 A70-24969
- WZ Sagittae ultrashort period binary evolution, considering mass-radius relation, initial separation and present position 11 p2108 A70-25696
- Evolution of very low mass stars with low mass companions in solar neighborhood 11 p2111 A70-26033
- Vibrationally unstable high mass main sequence star, reinvestigating destruction by radial oscillations 12 p2302 A70-27587
- Mass transfer in close binary stars and in highly variable stars 12 p2306 A70-27858
- Stellar evolution numerical model for point masses constant with time in absence of external field 13 p2498 A70-30011
- Hot small mass neutron stars cooling time and internal characteristics, discussing evolution based on H-R diagram 15 p2808 A70-32886
- Massive homogeneous star pulsation stability, determining maximum mass by opacity formula 17 p3154 A70-34533
- Stellar mass loss, considering radiation field momentum transfer or coronal heating as mechanisms 17 p3157 A70-34841
- Hydrogen abundance in white dwarfs, discussing inconsistencies in mass and bolometric magnitude models for Sirius and Eri B 17 p3170 A70-35389
- Binary stars dynamical parallaxes, masses, absolute magnitudes and provisional orbits, fitting deduced masses into empirical visual mass-luminosity relations 19 p3531 A70-38896
- Horizontal branch stars evolution based on mass distributions from comparison with giant branch, investigating evolutionary track characteristics during core helium burning 20 p3702 A70-39019
- Emission and escape of light from inside spherically symmetric gravitational mass, examining escape cone 21 p3923 A70-42106
- Pulsars and neutron stars origin and properties, discussing superdense star angular velocity, blackholes, supernovae remnants, rotation, etc 21 p3923 A70-42171
- Polytropic premain-sequence evolutionary tracks and main sequence models of solar composition low mass stars 22 p4104 A70-42993
- Stability conditions for relativistic stars, discussing mass-energy density distribution, Taylor instability, Schwarzschild criterion, Newtonian stellar model, gravitational red shift, etc 22 p4104 A70-42999
- STELLAR MASS EJECTION**
- S Doradus spectroscopic behavior study during minimum and maximum phases suggesting ejected-shell mechanism and premain sequence star classification 04 p0759 A70-15712
- Mass loss role in early spinning of sun without magnetic field braking effect, considering present surface vs core rotating velocity 05 p0913 A70-16569
- Stellar mass loss in gravitational contraction and variation of rotation law during transition to main sequence 05 p0917 A70-16909
- Steady state spherically symmetrical ejection of multicomponent plasma from sun determined with hydrogen approximation, considering ion composition 07 p1391 A70-20418

Solar wind ejection, analyzing regions of heat conducting fluxes and laminar patterns
08 p1561 A70-21059

Stellar gas ejection processes in corona-interplanetary plasma system, proposing hydrodynamic model with frequent collision region having finite radius
08 p1573 A70-21060

Hydrogen rich material forming planetary nebula ejected from contracted core of evolved star with 20,000 times solar luminosity
10 p1936 A70-23906

Potential flow pertaining to motion of gas surrounding close binary systems generated by orbital motion of stars and matter outflow from stars
10 p1946 A70-24968

Luminous hot stars mass loss attributed to negative effective gravities in outer parts of reversing layers from ionic UV resonance lines
10 p1946 A70-24981

Low mass star evolution from helium burning to white dwarf, describing red giant and mass loss stages in model
10 p1946 A70-24982

Particle acceleration during solar plasma ejection, disregarding magnetic effects on flux
11 p2107 A70-25526

OB supergiants atmospheric expansion indicated by medium-dispersion spectra, noting mass loss rate increase with luminosity and effective temperature
11 p2117 A70-26657

Massive hydrogen burning stars evolution with pulsational mass loss based on minimizing pulsational instability degree to specify mass loss rate
15 p2803 A70-32612

Stellar wind effect on accretion, showing critical intensity of particle ejection replacement
18 p3324 A70-37148

Cosmic rays shock from small mass supernovae explosions
19 p3507 A70-38128

Close binary stars evolution, discussing initial parameters effects on mass exchange and orbital period model
21 p3884 A70-40872

Particle acceleration during solar plasma ejection, disregarding magnetic effects on flux
21 p3892 A70-41276

T tauri star mass loss, observing variations in spectral emission line widths
22 p4101 A70-42858

Red supergiants location in H-R diagram, discussing significance of mass loss, rotational mixing and neutrino emission as stellar model mechanisms
24 p4403 A70-45393

STELLAR MOTIONS

Elliptic integrals for plane motion of stars, assuming stationary gravitational potential of stellar system
01 p0174 A70-10138

Velocity field measurements in NGC 5128 galaxy, discussing relative motion between gas and stars and correspondence of emission and absorption lines
01 p0184 A70-10898

Solar motion effects on planetary orbits, discussing preferred coordinate systems of scalar theory of gravitation
01 p0186 A70-11104

Photometric data for white dwarf low luminosity stars listed in color classes and proper motion fields
01 p0187 A70-11331

Lowell Observatory Northern Hemisphere proper motion survey, analyzing preliminary data for low luminosity stars
01 p0187 A70-11332

Radial velocities determined from prism spectrograms for O and B stars in Milky Way field in Scorpius
02 p0369 A70-12062

X ray source Sco XR-1 proper motion using photometry, suggesting association with Scorpius-Centaurus complex of young disk stars
02 p0372 A70-12248

Kinetic equation describing variation of distribution function of stellar residual velocities under action of gravitational field, discussing stellar diffusion in velocity field
03 p0564 A70-13227

Lagrangian stability of stellar systems of Trapezium in Orion type situated within large stellar cluster or cosmic cloud
03 p0565 A70-13235

Young flare stars in solar vicinity, considering spatial density, kinematic properties and luminosities
03 p0567 A70-13318

Double galaxy systems hypothesis with tidal interaction, presenting data from galaxy internal motion studies
04 p0747 A70-14519

Models of partially relaxed stellar disks in galaxies, discussing gravitational instability and stellar velocities
04 p0748 A70-14588

Stellar systems dynamics, discussing dynamic interactions of point masses, forces in gravitational field, galactic model construction, etc
04 p0754 A70-15353

Semidiurnal lunar tidal wave influence on clock corrections obtained by observations of stellar meridian passages at four localities
04 p0756 A70-15479

Tsl catalog of right ascensions of stars based on photoelectric observations, including clock corrections
04 p0756 A70-15480

Catalog of right ascensions of stars obtained from photoelectric observations, comparing equatorial and zenith region with F6 catalog
04 p0756 A70-15481

Electronic recorder design and operation for mean moments of star transit times
04 p0694 A70-15491

Von Zeipel method applied to stellar three body problem, eliminating short period terms and establishing two integrals of motion
05 p0909 A70-16337

NonJeans gravitational instability of stars and interstellar gas in Galaxy due to wave interaction with stars having velocity near wave phase velocity
05 p0917 A70-16906

Hot star photogravitational acceleration determined from difference between apex and antipex brightness, noting constant magnitude and direction of principal component of apex force
05 p0918 A70-16914

Galaxy mass loss on billion year time scale, discussing possibility on basis of bound stellar orbits
06 p1139 A70-17472

Stellar velocity distribution function for small mass stars in nonrotating systems
07 p1389 A70-20208

Equivalent line widths of anomalously fast stars of early spectral classes and reference stars, discussing binary nature and radial velocities of OB stars
08 p1569 A70-20828

Instantaneous latitudes observations during stellar transit at Poltava, describing error correction procedure
08 p1488 A70-21153

Latitude observations at Pulkovo, considering star declinations and proper motions
08 p1574 A70-21162

Kinetic equation describing variation of distribution function of stellar residual velocities under action of gravitational field, discussing stellar diffusion in velocity field
08 p1580 A70-21660

Lagrangian stability of stellar systems of Trapezium in Orion type situated within large stellar cluster or cosmic cloud
08 p1580 A70-21668

Nonlinear stellar density waves in galaxy using gas dynamic equations, assuming one dimensional and steady waves
09 p1762 A70-23073

Positional contact micrometer used to eliminate stars apparent oblique motion in astronomical universal instruments
09 p1681 A70-23342

Radial velocities tabulated for late B-type north and south of equator listed in Catalog of Bright Stars
09 p1763 A70-23452

Magnetic funneling model proposed for accretion of matter onto neutron star to study X ray production during motion through interstellar cloud
10 p1931 A70-23902

Hydrogen 21 cm emission line in Perseus region observed for motion of neutral hydrogen connected with II Per, discussing stellar radial velocity
10 p1937 A70-23944

Zero-point of period-luminosity-relation of Cepheids based on proper motions, radial velocities and photometric data, applying secular parallax method
10 p1945 A70-24964

Dynamic orbital mixing in self gravitating spherical stellar system using water bag model
10 p1945 A70-24965

Potential flow pertaining to motion of gas surrounding close binary systems generated by orbital motion of stars and matter outflow from stars
10 p1946 A70-24968

Radial velocities of supergiant distant stars in southern Milky Way regions of I Sco Association
11 p2113 A70-26465

Stellar hydrodynamic equations for thin disk galaxy derived from collisionless Boltzmann equation moments
11 p2117 A70-26688

Pulsars starquakes frequency relationship to solid crust shear strength based on Ruderman model, considering Crab Nebula
12 p2310 A70-27998

Density wave theory and spiral gravitational field effects in migrating stars orbits and origins in Milky Way spiral arm, using Schmidt model
13 p2495 A70-29801

F-type close stars residual spatial motions and rotational velocity relationship, discussing angular momentum loss
13 p2498 A70-30015

Runaway stars and pulsars near Crab Nebula, discussing binary system explosion and remnant motion
14 p2642 A70-30894

Third integral of stellar dynamics, considering Contopoulos galactic system model separability
14 p2651 A70-31288

Galactic spiral structure effects on residual stellar velocities local distributions
14 p2652 A70-31380

Cepheids distance scale from proper motions data, using maximum likelihood method for period-luminosity relation
14 p2652 A70-31387

Orbit and component velocities of double line spectroscopic binary HR4072 on high dispersion spectrograms, noting mass ratio close to Guthrie relation
16 p2976 A70-33786

Galaxies pairs motions, considering disintegrating, rotational and oscillatory types for comparison with observational data
18 p3322 A70-37133

Stellar magnitude equation from corrected catalog data to determine absolute proper motions relative to galaxies
18 p3323 A70-37145

Peculiar velocities nonisotropic distribution in stationary differentially rotating stellar system based on Boltzmann equation solution
18 p3324 A70-37149

Stellar velocity field in M 51 from image tube spectra
18 p3327 A70-37158

Orion arm local structure and kinematics, discussing outward or inward motion to galactic center and component direction
18 p3329 A70-37177

O and B stars velocity dispersion, considering Oort terms and average residual radial velocity
18 p3330 A70-37188

Stellar isolated disks spiral structure, examining large numbers of point masses self consistent motion in galactic plane
18 p3331 A70-37195

Young star velocity ellipse vertex deviation, discussing formation at right angles to galactic center direction
18 p3331 A70-37199

Stars and stellar gas motions interaction equations, analyzing plasma and gravitation problems
19 p3525 A70-38771

Rotating stellar systems cooperative phenomena, estimating star-star collisions effect on perturbation rate and damping
19 p3525 A70-38772

B stars kinematic parameters determination from radial and tangential velocities
19 p3525 A70-38775

Black hole objects in elliptical galaxies, using stellar light and velocity dispersion distribution in nuclear regions for mass limits
20 p3702 A70-39010

Proper motion evidence for existence of X ray stars associated with Sco X-1 and Cen X-2, indicating formation by neutron stars
21 p3873 A70-40673

Oscillation stability of stars moving along axis of symmetry in galaxy, discussing first order orbit perturbations in general resonance case
21 p3884 A70-40873

Total energies of stars with velocities perpendicular to galactic plane, examining absolute luminosities, galaxy size and local gravitational potential
21 p3890 A70-41162

Stellar system statistical mechanics, discussing collisionless gas in gravitational field, galaxy formation, stellar dynamics, double stars and bounded isothermal spheres
22 p4098 A70-42577

High velocity stars in Large Magellanic Cloud from spectroscopic observations, including A dwarfs and G-K giants
23 p4240 A70-44212

Statistical estimates of precessional corrections, solar motion and galactic rotation from proper motions
23 p4246 A70-44752

STELLAR OCCULTATION

Venusian cloud layer radius, discussing error in determination of occultation level height of regulus by venus
03 p0574 A70-13881

Viking Mars orbiter/lander mission planning, studying sun, earth and star occultations sensitive mission characteristics
06 p1146 A70-18193

Meridian circle observations before and after occultation of ZC 2232 by Neptune on 7 April 1968, correcting ephemeris for star and Neptune
06 p1151 A70-18489

Neptune data from photoelectric observations of 7 April 1968 occultation of BD-17 deg 4388, determining hydrogen dominance and molecular density
14 p2642 A70-30890

Lunar occultation photoelectric measurements, investigating irregularities of occulted stars
17 p3171 A70-35442

Lunar limb tabular position angles accuracy, discussing Watt charts used for star occultation examination
18 p3321 A70-37124

Neptune position errors by meridian observations compared with photoelectric observation of stellar occultation
19 p3518 A70-38008

Watts lunar limb correction charts parameters solution, using grazing and total stellar occultations by moon
20 p3705 A70-39478

Pulse counting photoelectric photometer for lunar occultation recording of stars, discussing design, associated equipment and operation principles
22 p4030 A70-42860

STELLAR RADIATION

NT STELLAR WINDS

IR emission from planetary nebulae, W-R, Of and symbiotic stars, discussing dust hypothesis for IR excess
01 p0173 A70-10039

Light curve and relative dimensions of eclipsing system V338 Herculis, from photoelectric measurements, discussing component stars
01 p0184 A70-10951

Light curves of Algol eclipsing variable AD Herculis and semidetached system relative dimensions from BV photoelectric observations
01 p0184 A70-10952

Polarization of nonspherical plasma emission region in thermal X ray stars
02 p0357 A70-11787

Stellar X ray sources quanta fluxes estimation based on solar coronal emissions analysis
02 p0360 A70-12793

Eta Carinae IR region emission and absorption spectra characteristics in tabular form
03 p0565 A70-13269

Free-bound and free-free continuous emission of hydrogen near Balmer jump in T Tauri star AS209
03 p0566 A70-13315

UV Ceti type flare stars observational and theoretical results related to nebular or chromospheric flare models
03 p0566 A70-13316

Nonperiodic changes in radiation connected with orbital period in eclipsing conventional binaries observed in R Canis Majoris
03 p0568 A70-13326

Stellar X ray effect on nighttime lower ionosphere wave reflection suggested from VLF propagation data
03 p0562 A70-14224

Low resolution spectra of IR stars NML Tau, CIT 3, 6 and 13 considered inadequate for molecular band identification
04 p0748 A70-14591

Stratospheric balloon measurement of near UV from early type stars, discussing gondola, observation method, telescope and photographic recordings analysis
04 p0750 A70-14704

Radiative excitation in planetary and Orion nebulae by solving transfer equations for Lyman line and continuum radiation, using normalized on-the-spot/NOS/approximation
04 p0758 A70-15700

Cepheid variable 1 Carinae light curve from photoelectric observations, calculating periodicities from best fitting Fourier series
04 p0759 A70-15708

Experimental observations of neutrino in collapsing stars in Galaxy, showing detector capability of recording positrons or electrons from antineutrino-neutrino flux induced reactions
05 p0900 A70-15966

Bolometric albedo of main sequence stars with deep convective envelopes in close binary systems derived as function of photometric proximity using entropy invariance
05 p0914 A70-16694

Cameras photogrammetric parameters determined from stellar photographs, considering distortion components, reference points, etc
05 p0852 A70-16921

Pulsed gravitational radiation emitted by dense star clusters
05 p0921 A70-16977

Color difference method for interstellar extinction laws applied to O stars study
06 p1140 A70-17641

Stellar light absorption in optically dense cometary atmospheres
06 p1141 A70-17738

Proton satellites measurements reconciliation with diurnal stellar variation data and cosmic rays origin models
06 p1135 A70-17885

Dynamic effect of radiation from massive protostar showing formation of transparent zone free of dust

about star and gas density decrease until pressure equalization
06 p1148 A70-18400

Effective, brilliance, color and gradient temperature measurements in astrophysics, considering observer bond and thermodynamic nonequilibrium of stars
07 p1386 A70-19597

Earth observations of collapsing star neutrinos and neutrino oscillations in Milky Way galaxy
07 p1371 A70-20331

Stellar interferometer with superposed beams designed for measurements of close binaries, showing point light modulation convenient for photoelectric recording
08 p1493 A70-20564

Red giants and supergiants intrinsic radiation polarization characteristics
08 p1569 A70-20826

Binary star spectrum analysis establishing seasonal and season-to-season variations in He II emission band intensity and shift toward long wave region
08 p1569 A70-20827

Optical to IR conversion in circumstellar dust envelope with spherical symmetry based on optical radiation scattering and absorption by dust
08 p1573 A70-21047

Nonthermal mechanism for high energy radiation and particle emission from X-stars and pulsars
08 p1575 A70-21364

Solar and stellar convection regions and coronas using photospheric models, taking into account molecule formation
08 p1581 A70-21953

Supernovae remnants X ray emission associated with explosion process generating relativistic particles, indicating Crab Nebula as X ray object
09 p1749 A70-21998

Phase variations in polarization parameters of eclipsing binary Z Vul during polarimetric studies for interstellar polarization component
09 p1751 A70-22156

Pulsar mathematical model accounting for pulse width, polarization and spectrum of emitted radiation
09 p1753 A70-22383

Free-free opacity of stellar interiors by ion correlations applied to red giant degenerate cores
09 p1755 A70-22510

Stellar optical spectral power measurement by electronic spectroscopic technique using lasers
09 p1696 A70-22785

Flare star burst energy from radio telescope observations compared with solar flares
10 p1936 A70-23916

Thermal imbalance effect on stellar pulsational stability using linear quasi-adiabatic pulsation theory
10 p1946 A70-24980

Stellar plasma neutrino pair emission, comparing photon neutrino coupling with current current coupling theory and white dwarf evolution
12 p2297 A70-26976

Cold variable stars intrinsic polarization model proposing light scattering in circumstellar dust shells
12 p2307 A70-27865

Diffuse galactic radiation and absorbing clouds luminance illuminated by integral stellar radiation in Milky Way
12 p2307 A70-27866

Extragalactic objects polarization due to synchrotron radiation superimposed on stellar radiation, discussing Seyfert galaxies nuclei
12 p2307 A70-27869

Blue-violet and blue minus violet curves for beta Lyrae derived from analyzing photometric materials
12 p2309 A70-27900

Astronomical Netherlands Satellite /ANS/ for carrying out stellar UV and X ray emission experiments
13 p2506 A70-28989

Stellar light pressure and gravitational force ratios for spherical water, quartz and graphite particles in interstellar space, considering refractive dependence on wavelength
13 p2493 A70-29396

Galactic X ray stars and X ray sources positions, appearance frequency and intensities
13 p2495 A70-29818

Emission resonances at harmonics of electron cyclotron frequency in laboratory plasmas, considering stellar optical radiation
13 p2467 A70-29915

Bright IR stars observed using photometry and spectroscopy, suggesting protostars presence
14 p2641 A70-30880

Cosmic IR radiation sources, discussing galactic and stellar masses
14 p2632 A70-30882

Shilts method applicability to electronic camera for stellar magnitude photometry, studying instrument limitations and errors
14 p2589 A70-31379

Stellar interferometer with superposed beams designed for measurements of close binaries, showing point light modulation convenient for photoelectric recording
15 p2742 A70-32719

Flare stars distribution in Pleiades, discussing flare visual magnitude and frequency
15 p2807 A70-32876

Neutron stars gamma and radio emission in gas accretion state, determining surface gravitational potential
15 p2808 A70-32883

Massive homogeneous star pulsation stability, determining maximum mass by opacity formula
17 p3154 A70-34533

Stellar mass loss, considering radiation field momentum transfer or coronal heating as mechanisms
17 p3157 A70-34841

UV interstellar extinction from comparison of epsilon and zeta Persei, noting graphite features
17 p3159 A70-34877

UV interstellar extinction, examining reddened and unreddened early stars with OAO satellite spectrophotometric scans
17 p3159 A70-34878

Stellar UV and visual continuum observations, discussing recalibration of absolute energy distribution of alpha Lyr to improve model atmospheres
17 p3160 A70-34881

Soft X ray extended source in Cygnus Loop, indicating supernova remnant
18 p3310 A70-37022

Guiding center theory for relativistic plasma embedded in strong magnetic field, discussing connection with pulsars emission dynamics
19 p3479 A70-37596

Pulsar radiation mechanisms, discussing magnetic field topology and current distribution estimation
19 p3518 A70-38022

Astronomical gamma ray emission measurement by balloon-borne spark chamber, presenting results for discrete and diffuse sources and albedo intensities
19 p3501 A70-38088

Cosmic gamma ray sources detection in 100-1000 GeV range by atmospheric Cerenkov radiation from energetic particle showers
19 p3501 A70-38091

White dwarf star circular polarized light, indicating strong magnetic field
20 p3701 A70-39001

X ray star effects on ionospheric LF radio wave field strength, examining absorption and ionization in D region
21 p3873 A70-40668

Sco X-1 extar high energy radiation production, discussing relativistic electron synchrotron emission and magnetic fluctuations spectrum
21 p3878 A70-40709

Hyades giant stars epsilon and gamma Tau strong line profile analysis, obtaining effective temperatures
21 p3885 A70-40931

Stellar polarization measurements in Magellanic Clouds, tabulating position, magnitude, spectral type, percentage polarization and electric vector position angle
21 p3922 A70-41979

Ic class variables long wavelength anomalous radiation, discussing emission from circumstellar dust shell
22 p4094 A70-42934

Intrinsic polarization from Thomson scattering in binary systems with tidal distortions, taking into account gray atmosphere, axial rotation, gravitational interaction and radiative interaction
22 p4103 A70-42988

Diffuse X ray background attributed to X ray emission during supernova early phases
22 p4095 A70-42998

Pulsar emission mechanisms, discussing possible magnetospheric physics role and optical pulse generation
22 p4105 A70-43217

Narrow band IR photometry of star alpha Orion, testing hypothetical correlation of emission peak with starlight-reflecting silicate dust
22 p4105 A70-43229

Model fitting procedure applied to lunar occultation data and models analysis for point sources, close binaries and resolvable stars
24 p4399 A70-45130

Optical quasi-stellar objects radio emission observation for identification with radio sources
24 p4413 A70-46167

STELLAR REFRACTION

U ATMOSPHERIC REFRACTION

U STELLAR RADIATION

STELLAR ROTATION

NT SOLAR ROTATION

Solar /stellar/ wind solutions asymptotic behavior at large distances from central star for equations including effects of rotation and anisotropy
02 p0358 A70-12253

Thermal energies and angular momenta of Hubble galactic sequence using differential rotation and decreasing density stellar system model to test stellar evolution theories
02 p0376 A70-12447

Electric fields in rotating magnetic relativistic neutron stars, analyzing static fields in corotating frame and pulsar emission
02 p0379 A70-12726

Star rotation and meridional circulation hydrodynamic theory, considering magnetic fields and internal friction

03 p0564 A70-13228

Rotational properties of neutron star models for Crab Nebula energy source, using expressions for angular momentum and rotational kinetic energy

03 p0571 A70-13817

Pulsars observed properties and interpretation based on oblique rotator model for neutron stars

03 p0577 A70-14099

Prescribed circulations within conducting spheres effect on initially prescribed magnetic fields, discussing magnetic field structure in uniformly rotating stars

04 p0758 A70-15694

Hydrostatic equilibrium in self gravitating core of rotating relativistic star, considering Newton and Einstein gravitation theories

05 p0914 A70-16648

Stellar mass loss in gravitational contraction and variation of rotation law during transition to main sequence

05 p0917 A70-16909

Angular velocities and equilibrium of rotating neutron stars compared with white dwarfs

07 p1376 A70-18911

Supernova remnant luminosity dependence on central star rotation period, deriving parameters for pulsars in Cas A

08 p1570 A70-20897

Statistical analysis of rotation and macroturbulence in early type Ia and Iab supergiants, discussing evolutionary effects

08 p1571 A70-20908

Star rotation and meridional circulation hydrodynamic theory, considering magnetic fields and internal friction

08 p1580 A70-21661

Book on stellar spectroscopy, covering stellar atmospheric models, rotation, evolution, etc

09 p1756 A70-22640

General relativistic expressions for angular momentum and rotational kinetic energy of slowly rotating stars

09 p1764 A70-23608

Stellar rotation theory applied to evolution of nine solar mass star from main sequence to helium exhaustion

10 p1946 A70-24969

Pulsar properties association with neutron star rotation energy, discussing alternate pulsar theories

12 p2301 A70-27579

Rotating stellar configurations structure consisting of degenerate matter or density dependent temperature describing boundary value problem reduction for Cauchy problem

13 p2494 A70-29518

F-type close stars residual spatial motions and rotational velocity relationship, discussing angular momentum loss

13 p2498 A70-30015

Pulsars theories review, discussing geometrical model picturing pulsar as rotating neutron star with high magnetic field

17 p3164 A70-35117

Meridional circulation velocities in Roche envelope of uniformly rotating star, using nonlocal equation for radiative heat transfer

17 p3171 A70-35560

Pulsars electrodynamics concerning EM emissions, discussing roles of rotation and magnetic field

17 p3172 A70-35591

Energy transfer in convective envelope of rotating star and solar differential rotation, using Lucy gravity-darkening law

18 p3313 A70-36214

Pulsars pulsation mechanism, using neutron star model with oblique rotation axis

18 p3319 A70-37048

Rotating neutron stars, pulsars and cosmic X ray sources relationship, discussing stellar model with mass loss in presence of magnetic field

21 p3874 A70-40678

Pulsars and neutron stars origin and properties, discussing superdense star angular velocity, blackholes, supernovae remnants, rotation, etc

21 p3923 A70-42171

Rotating magnetic star thermal behavior, discussing central nuclear burning stability, homologous changes, cooling, degeneracy and helium flash

22 p4100 A70-42855

Main sequence II stars rapid uniform rotation effect on structure

22 p4101 A70-42859

Stellar evolution, rotation and atmospheric motion, discussing gravity darkening, spectral lines, angular momentum, braking mechanisms and late stars

22 p4102 A70-42970

Stellar rotation - Conference, Ohio State University, Columbus, September 1969

23 p4248 A70-44801

Single normal main sequence stars rotational velocities compared with giant, supergiant, Be, A and metallic line stars and Population II objects

23 p4248 A70-44802

Stellar rotation effect on internal structures, discussing angular momentum steady state distribution for main sequence stars

23 p4249 A70-44803

Nonspherical stellar internal structure, developing method for models with rotational and tidal distortion

23 p4249 A70-44804

Rotational velocities for main sequence stars from spectral type A5 to F9, supporting solid body rotation hypothesis

23 p4249 A70-44806

Be stars rotation, considering emission properties and evolutionary state of main sequence

23 p4249 A70-44807

Rapidly rotating B and Be stars interior evolution models, considering mass and radiation pressure

23 p4249 A70-44808

Stellar rotation angular momentum loss in premain sequence convective phase, discussing polytropic structure, formation time and velocity changes

23 p4249 A70-44809

Stellar rotation effects on atmospheres of early type main sequence stars, using models for surface gravity and temperature variations

23 p4249 A70-44810

Stellar abundance determination, considering rapid uniform rotation effects on equivalent spectral line widths

23 p4250 A70-44811

Rotating stellar atmospheric models for middle and late A star masses, emphasizing Altair observed and predicted energy distribution

23 p4250 A70-44812

Early type Ia and Iab supergiant stars macroturbulence and rotation, investigating spectral line broadening, mass loss and angular momentum

23 p4250 A70-44813

Close binary star components axial rotation, considering synchronism, angular velocity and mass exchange

23 p4250 A70-44814

Upper main sequence and close early type binaries evolution by fission of rapidly rotating protostars

23 p4250 A70-44815

Synchronous close binary stars primary component structure, using rapidly rotating polytropic method

23 p4250 A70-44816

Binary star axial rotational correlation, determining coupling between components spin angular momenta

23 p4250 A70-44817

Algol type semidetached eclipsing binaries main sequence components rotational velocities, determining deviations from synchronism

23 p4251 A70-44818

Eclipsing binary stars minima variations related to orbit perturbations and rotational angular momentum of component interiors

23 p4251 A70-44819

Stellar rotational velocities in open star clusters, noting evolutionary expansion, tidal coupling in binaries and Ap stars magnetic braking

23 p4251 A70-44820

Spectral line width distributions in main sequence stars, emphasizing B2 to A2 range rotational velocities with Maxwellian distribution

23 p4251 A70-44821

A type stars rotation, examining UVB color and rotational velocity relationship, spectral classification and spectroscopic binaries

23 p4251 A70-44822

Stellar axial rotational velocity statistical analysis to break-up limit, obtaining velocity distribution approximation from observed histogram

23 p4251 A70-44823

UV Cet type flare star rotational velocity upper limits from H alpha emission line width in chromospheres

23 p4251 A70-44824

Deutsch period vs line width relation for periodic Ap stars, determining rotational velocities with rigid rotator model

23 p4251 A70-44825

Surface field model of rotating magnetic stars involving uniformity and Eddington-Sweet circulation suppression

23 p4251 A70-44826

Rotating magnetic star dynamic evolution, discussing magnetic and rotation axes inclinations for oblique rotator model

23 p4252 A70-44827

Be star rotation dynamics phenomenon, discussing time variations on main sequence scale

23 p4252 A70-44828

Pulsar radiation polarization, examining mean pulse profiles, frequency, position angle and rotational effects

24 p4403 A70-45404

Corotating magnetic field model of pulsar, using electromagnetic field equations of dipole radiation in low density plasma

24 p4413 A70-46137

Differentially rotating stellar interiors nonaxisymmetric perturbation stability in toroidal and poloidal magnetic fields

24 p4413 A70-46165

STELLAR SPECTRA

NT SOLAR SPECTRA

Stellar emission line spectra from comet-like nebulae, discussing stellar position instability and shell movements

01 p0174 A70-10198

Nova Delphini 1967 emission line spectrum at 8400-9600 A, using diffraction spectrograph attached to astronomical telescope

01 p0182 A70-10675

Red subluminescent stars and high UV excess stars in region between main sequence and white dwarfs, tabulating observations of stellar color and magnitude

01 p0182 A70-10795

Monk-Gillieson convergent beam dispersion method applied to rocket-borne photoelectric spectrophotometer for far UV stellar spectra observation

01 p0900 A70-10904

M dwarf stars spectroscopic, spectral and photometric parallaxes calibration based on trigonometric measurements

01 p0188 A70-11333

Faint, metal poor, subluminescent and red degenerate stars occurrence and properties, considering spectra of candidate degenerates

01 p0188 A70-11338

White dwarf spectra interpretation based on model atmosphere method, discussing chemical composition, low luminosity high pressure atmospheres, electron density, etc

01 p0189 A70-11340

Stellar spectral lines fine analysis methods compared for curves of growth, line profiles and related contribution curves in model atmospheres for Procyon and sun

02 p0343 A70-11906

MK stellar spectral types in Monoceros, analyzing spatial distribution and interstellar absorption using slit spectrograms

02 p0369 A70-12063

Galactic interstellar absorption lower limit in selected Area 19 determined from Stellar spectra densities, using Schmidt camera

02 p0370 A70-12073

IR spectra of four carbon stars and Sirius obtained with Michelson interferometer, indicating diatomic carbon and CO bands

02 p0372 A70-12252

NH bands in stellar spectra by visual inspection of spectrograms, noting abundance of N in normal and strong CN stars

02 p0379 A70-12708

Beta Lyr spectral and brightness characteristics long period variations related to orbital motion perturbations

03 p0564 A70-13229

Orbits computation from double line spectra of eclipsing binaries 31 Men and 9 Cha, emphasizing systemic velocity and mass ratio derivation method

03 p0565 A70-13268

Multicolor photometry of Orion flare stars in U, B, V and R, constructing diagrams confirming flare stars scattering about main sequence

03 p0567 A70-13317

U Geminorum type variables properties, orbital period changes in close binaries and origin of outbursts

03 p0567 A70-13322

Late stars spectral characteristics, verifying criteria for spectral classification and anomalous spectra determination

03 p0569 A70-13424

Peculiar emission object with emissions narrower and with lower ionization lines than cool Wolf-Rayet stars

03 p0574 A70-13933

Periodic clustering of red shift values in quasi-stellar and unusual objects spectra, using power spectra

03 p0577 A70-14217

Stellar atmosphere high dispersion spectroscopy, discussing limitations for stars over 17,000 K

04 p0746 A70-14508

IR spectra of M stars and alpha Tau obtained with Michelson interferometer, observing molecular features and water vapor absorption

04 p0747 A70-14548

L-alpha absorption equivalent width measurements in UV spectra of beta-one, delta and pi Scorpii for interstellar hydrogen densities

04 p0748 A70-14586

IR colors and optical and IR spectra of irregular M variable star and bright OH source VY CMa indicating supergiant classification

04 p0749 A70-14592

Variable object BL Lacertae flux measurements using Schmidt telescope photography and radio study, comparing results with quasar

04 p0759 A70-15711

S Doradus spectroscopic behavior study during minimum and maximum phases suggesting ejected-shell mechanism and premain sequence star classification

04 p0759 A70-15712

SS Cygni outburst origin in G type star indicated from radial velocity variations of hydrogen absorption lines during rising light

05 p0915 A70-16695

Color difference method for interstellar extinction laws applied to O stars study

06 p1140 A70-17641

Equivalent line widths of anomalously fast stars of early spectral classes and reference stars, discussing binary nature and radial velocities of OB stars

08 p1569 A70-20828

Titanium monoxide absorption bands in class M stars spectra, estimating band head intensities

08 p1569 A70-20829

Cygnus and Perseus symbiotic stars as binaries, studying radial velocities, relative emission line intensities and energy distribution

08 p1569 A70-20830

Von Zeipel 1128 O star spectrum analysis, discussing mass, He/H ratio, metal abundances, etc

08 p1571 A70-20913

Beta Lyr spectral and brightness characteristics long period variations related to orbital motion perturbations

08 p1580 A70-21662

Supernovae remnants evolution, properties and galactic distribution, discussing criteria for catalog listing and remnants as X ray sources

09 p1749 A70-21990

Water vapor emission detection from IR stars, discussing radial velocities of microwave lines

09 p1756 A70-22523

Book on stellar spectroscopy, covering stellar atmospheric models, rotation, evolution, etc

09 p1756 A70-22640

Planetary faint nebulae containing northern Milky Way portion in direction of galactic anticenter observed with spectral Schmidt camera, noting stellar appearance

09 p1761 A70-23051

Cosmic radio waves discrete sources spectra measured in decametric wavelength range, discussing wave generation and absorption

09 p1762 A70-23189

Line profiles and equivalent widths from Si II, Mg II, Ni II and Fe II spectra of shell star zeta Tauri

10 p1936 A70-23941

G and K stars classification /spectral type and luminosity class/ by narrow band photometry

10 p1937 A70-23945

Star 15 Vulpeculae metal lines analyzed by growth curve differential method

11 p2113 A70-26464

Stellar and planetary IR spectra from spectrometer with rotating circular variable thickness interference filter

11 p2113 A70-26468

Stellar atmosphere and shell models in spectral range AO-G5 for studying stellar structures dependence on chemical composition

11 p2115 A70-26582

Densities and extents of absorbing clouds in open cluster NGC 7086 determined from photometry and spectral classifications of stars

11 p2116 A70-26587

Spectral classification of stars from unbroadened spectra recordings possible when comparing optical depths of lines

11 p2116 A70-26589

Calcium H and K lines core residual intensities in stars with quiet and active chromosphere, suggesting activity due to thermal gradient

12 p2303 A70-27702

Spectra, luminescence and gas dynamic effects in variable stars, discussing nonthermal theory to explain continuous emission

12 p2306 A70-27857

Comet-like nebulae, describing brightness and spectral characteristics of variable stars in nebulae

12 p2307 A70-27863

Star eta Arietis spectra analyzed for Fe and V abundance

13 p2487 A70-28715

Star HBV 475 emission spectra in near IR due to H, He I, O and Ca II, confirming symbiotic character

13 p2495 A70-29641

Rossland stellar opacity calculation allowing for photon absorption in spectral lines using non-relativistic dipole approximation

13 p2495 A70-29752

Stellar intensity interferometer for close binaries and emission line stars, investigating gamma-two Velorum

14 p2640 A70-30733

H II region stellar color anomaly attributed to interstellar extinction

14 p2641 A70-30879

OH radio emission from IR stars, discussing spectra, polarization properties and red giant star model with expanding atmosphere

14 p2641 A70-30881

Rocket spectroscopy of zeta puppis, identifying multiplets of stellar and interstellar origin included in atmospheric models

14 p2641 A70-30883

Ap star kappa Cancr model atmosphere analysis based on observed energy distribution and hydrogen line profiles

14 p2652 A70-31381

Metal to hydrogen ratio for sun, Hyades and F-G stars based on photoelectric measurements of weak metal lines

14 p2652 A70-31388

Papers on spectroscopic astrophysics covering stellar spectral classification, growth curves, hydrogen lines, stellar spectra, interstellar space, stellar rotation, binary stars, etc

15 p2796 A70-31499

Two dimensional quantitative spectral classification of F-G5 stars, using meniscus telescope with preobjective prism at Abastuman observatory

15 p2797 A70-31613

Spectral classification of relatively bright stars in near UV based on moderate and low dispersion spectra including F, G and K stars

15 p2797 A70-31614

Spectral classification and continuous spectrum photometry of weak late stars in visual and near UV regions, noting anomalous C star in CH Cyg

15 p2797 A70-31615

Near Galactic plane condensations of spectral A stars in HD catalog, investigating by Monte Carlo method and Poisson formula

15 p2797 A70-31616

Energy distribution in continuous spectrum of star MWC 334 from spectrophotometric observations

15 p2808 A70-32888

CH Cygni irregular light variations and spectrum peculiarities, considering upper atmosphere perturbation by variable hot satellite

15 p2809 A70-32904

Book on stellar spectra theory covering line absorption coefficient expressions, radiative transfer, line source function, line broadening, etc

16 p2974 A70-33270

Orbit and component velocities of double line spectroscopic binary HR4072 on high dispersion spectrograms, noting mass ratio close to Guthrie relation

16 p2976 A70-33786

Spectrum of bright IR object VV Canis Majoris, noting absorption feature attributed to SiO molecules in stellar atmosphere

17 p3154 A70-34540

Hyades stars between F4 and K5, measuring chromospheric H and K emission lines dependence on bolometric luminosity

17 p3157 A70-34832

UV stellar spectra and related ground based observations - Conference, Luntenen, Netherlands, June 1969

17 p3158 A70-34876

UV stellar spectra absorption, considering silicon and carbon opacity effect on Balmer discontinuity and Paschen continuum

17 p3159 A70-34880

Orion stars far UV intensities, considering photometric data and electronographic spectra from rocket sounding

17 p3160 A70-34882

Stellar UV spectra observation methods, discussing objective spectrograph, scanning spectrometer system with telescope and grating cameras

17 p3160 A70-34885

Rocket spectroscopy of zeta Puppis below 1100 A

17 p3160 A70-34886

Early-type star spectral scan analysis from OAO observation, comparing model atmosphere calculations

17 p3161 A70-34887

Red giant star chromospheric activity, discussing Balmer absorption lines and emission lines

17 p3161 A70-34889

Stellar UV spectral line profiles interpretation, using atmospheric models and line formation theory

17 p3161 A70-34890

Symbiotic stars UV spectrum, discussing molecular fluorescence phenomena

17 p3161 A70-34891

Lyman alpha absorption by interstellar neutral hydrogen observed in O and B stars UV spectra

17 p3162 A70-34898

G and K stars spectral classification using narrow band photometry

17 p3169 A70-35380

H-R diagram stellar spectra interpretation using model atmospheres describing temperature, gravity and chemical composition

17 p3169 A70-35381

Star AG Draconis spectrum in visible range by meniscus prismatic camera, deriving energy distribution

18 p3315 A70-36575

Arcturus Co bands, examining equivalent widths, rotational lines and 12C/13C ratio

18 p3318 A70-37015

P Cygni line profiles emission and absorption components rectification procedure, considering errors

18 p3321 A70-37123

Spiral galaxy NGC 6946 structure and stellar associations distribution, indicating no relation between color and magnitude and distance from center

18 p3327 A70-37160

O type stellar clusters hydrogen line observation revealing associated gas clouds

18 p3328 A70-37172

Galactic spiral structure relation to local stellar distribution, discussing OB associations, galactic cluster, WR stars, cepheids, and common stars in sun neighborhood

18 p3329 A70-37176

Water vapor and OH spectra overlap, investigating association of galactic OH masers and water emission sources with IR stars

19 p3444 A70-37571

Am and Ap stars metallic absorption lines, determining photometrical indices correction

19 p3523 A70-38689

Light curves bumps properties of Population I cepheids in Magellanic Clouds, Milky Way galaxy and M 31 as function of period

19 p3523 A70-38691

Spectrum analysis of P Cygni star AG Carinae and derivation of mean radial velocities for different epochs

19 p3523 A70-38694

Dwarf Me stars flare spectra, examining hydrogen recombination layer and impulse heating of photosphere

20 p3702 A70-39013

X ray sources spectra, discussing distribution, supernova remnants, pulsars nebulae, optical spectra and general characteristics

21 p3873 A70-40670

OPL astrolabe catalog corrections, discussing Dannon prototype, color-magnitude effect, time and latitude values

21 p3887 A70-41111

Gravity darkening of tidally and nonuniformly rotating Roche components of close binary systems, calculating surface temperature and spectral distributions

21 p3888 A70-41120

Nova Vulpeculae 1968 Number 1 medium dispersion spectra, using radial velocity line identification and line profile reductions

21 p3889 A70-41152

Nova HR Delphini 1967 UVB photoelectric photometry, examining absolute magnitude, distance, response curves and spectra

21 p3889 A70-41154

Southern objective prism plates B stars with strong neutral He I absorption lines

21 p3890 A70-41160

BM Orionis eclipsing binary spectra, determining radial velocity curve

21 p3890 A70-41161

Radiation line transfer in Wolf-Rayet envelopes with rapid radial expansion by escape probability method, including radiation effect from stellar core

21 p3892 A70-41248

Color-color diagram of M92, computing synthetic stellar spectra for line absorption effect

21 p3892 A70-41249

Quark in stars, discussing electronic transitions and UV spectral lines

21 p3921 A70-41975

Stellar IR spectra for types A0 to M7, using Mertz type Michelson interferometer as Fourier transform spectrometer

21 p3922 A70-41980

Blue stellar objects emission at 9.5 and 3.5 mm, suggesting quasi-stellar objects with small intrinsic radio luminosity

21 p3922 A70-41993

Rossland stellar opacity calculation allowing for photon absorption in spectral lines using non-relativistic dipole approximation

21 p3923 A70-42072

Abundance ratios of metallic line star 15 UMa, using absorption spectrophotometric observations

21 p3926 A70-42270

Beta CMa variable star HD 43818 spectral observations, discussing line profiles and radial velocities

22 p4100 A70-42853

T tauri star mass loss, observing variations in spectral emission line widths

22 p4101 A70-42858

Computer synthesis of completely eclipsing binary light curves including limb darkening and simulated observational errors

22 p4103 A70-42990

Circumstellar dust cloud model of spectral distribution and anomalous excess emissions in IR T Tauri and red giant stars coincident with photometric measurements

23 p4239 A70-43868

Stellar spectra above horizontal branch in globular clusters, discussing stellar evolution, composition and structure

23 p4246 A70-44755

Rotational velocities for main sequence stars from spectral type A5 to F9, supporting solid body rotation hypothesis

23 p4249 A70-44806

Stellar abundance determination, considering rapid uniform rotation effects on equivalent spectral line widths

23 p4250 A70-44811

Early type Ia and Ia^b supergiant stars macroturbulence and rotation, investigating spectral line broadening, mass loss and angular momentum

23 p4250 A70-44813

Spectral line width distributions in main sequence stars, emphasizing B2 to A2 range rotational velocities with Maxwellian distribution

23 p4251 A70-44821

A type stars rotation, examining UVB color and rotational velocity relationship, spectral classification and spectroscopic binaries

23 p4251 A70-44822

Neutron star or defunct pulsar accretion of interstellar matter, discussing effects on total luminosity and radiation spectrum

24 p4403 A70-45397

Nitrogen abundance of subgiant nu Indi from observed and computed stellar spectra of CN violet bands

24 p4404 A70-45411

Southern early stars away from galactic plane, reporting magnitudes and colors on UBV system and MK spectral classifications

24 p4404 A70-45412

Gamma Cas star time and spectra observations, examining emission line profile variations and envelope and stellar model

24 p4404 A70-45415

White dwarf stars continuum circular polarization as function of time and wavelength, emphasizing magnetic star search

24 p4410 A70-45776

Low temperature stars SiO IR spectral band identification based on rotation-vibration spectrum calculation

24 p4411 A70-45777

G8, IV subdwarf 31 Aql spectrum at 4000-6600 Å, discussing Ba II 4554 Å, G and CN bands and spectral lines

24 p4414 A70-46329

STELLAR SPECTROPHOTOMETRY

Photometric data for white dwarf low luminosity stars listed in color classes and proper motion fields

01 p0187 A70-11331

M dwarf stars spectroscopic, spectral and photometric parallaxes calibration based on trigonometric measurements

01 p0188 A70-11333

Intermediate band four color photometry of white dwarfs, considering hydrogen line blocking and H delta line

01 p0188 A70-11335

Lund astronomical observatory, describing Cassegrain-Nasmyth reflector and attached electrophotometer for stellar measurements

02 p0275 A70-12061

Photoelectric UVB photometry of stars in Carina, Vela and Centaurus, giving standard connection sequences for continued photometry

02 p0370 A70-12074

UV photometry of stars and galaxies from OAO-2, discussing instruments and observational results

02 p0378 A70-12580

Multicolor photometry of Orion flare stars in U, B, V and R, constructing diagrams confirming flare stars scattering about main sequence

03 p0567 A70-13317

Color photoelectric study of eclipsing binary RY Gemini for determining orbital elements and structure

04 p0754 A70-15217

Identification of lines in Mohler photometric atlas of IR solar spectrum wavelengths

05 p0910 A70-16427

Delay in photoelectric recording of transit of stars, considering stellar image brightness distribution and temperature

05 p0918 A70-16920

Stellar systems observations using photometers with long narrow slits in identical telescopes

05 p0852 A70-16922

Magellanic Cloud cepheids two color light curves obtained by photoelectric photometry, discussing reddening

07 p1380 A70-19259

Double and multiple stars components magnitude differences tabulated based on visual and photometric observations

08 p1574 A70-21163

Hypersensitization of IR films for use in stellar photometry, discussing laboratory and astronomical tests

09 p1673 A70-22158

Stellar spectrophotometry by rocket-borne equipment, describing instrumentation, rocket assembly, calibration and spectra obtained

09 p1755 A70-22505

Stellar optical spectral power measurement by electronic spectroscopic technique using lasers

09 p1696 A70-22785

Wide field stellar astronomical ESO project, reviewing application of earth orbiting spin stabilized satellites and OAO

09 p1767 A70-23435

G and K stars classification /spectral type and luminosity class/ by narrow band photometry

10 p1937 A70-23945

Michelson interferometer usable in space for stellar spectroscopy, noting compactness achieved through mirror area reduction

10 p1887 A70-24032

Eclipsing binary beta Aurigae effective temperature and surface gravity determination from photoelectric spectrum and abundance analyses

10 p1938 A70-24100

Algol variable RV Ophiuchi photoelectric observation in B and V, representing light curve characteristics by gas stream model

10 p1945 A70-24967

Blue-violet and blue minus violet curves for beta Lyrae derived from analyzing photometric materials

12 p2309 A70-27900

Stellar observations in near UV by camera having two color photometric slides, discussing atmospheric models

13 p2498 A70-30013

Bend /near 4300 Å/ in Nandy interstellar extinction rules effect on Geneva Observatory photometric index in seven colors

13 p2498 A70-30014

Bright southern Cepheids UVB observations, discussing blue companion effect on two color plot

14 p2639 A70-30726

Narrow band photometry calibration, using model stellar atmospheres and laboratory data for high resolution synthetic spectra of G and K giant stars

14 p2639 A70-30728

Three color photometry of RW Auriga stars, discussing UVB curves, H-R diagram and UV emission excess

15 p2797 A70-31612

Spectral classification and continuous spectrum photometry of weak late stars in visual and near UV regions, noting anomalous C star in CH Cyg

15 p2797 A70-31615

Report to COSPAR on Netherlands space research /1969/ including solar and stellar X radiation and UV spectrophotometry, cosmic ray measurements, satellite geodesy, etc

15 p2830 A70-31719

Luminosity criteria in O stars via narrow band photoelectric photometry suggesting VI Cygni proximity

15 p2807 A70-32804

AG Peg brightness variations by three color photoelectric photometry, discussing orbital motion of cold component

15 p2807 A70-32878

Long period variable stars light polarization as function of brightness and wavelength, discussing molecular scattering and nonthermal emission

15 p2808 A70-32879

Energy distribution in continuous spectrum of star MWC 354 from spectrophotometric observations

15 p2808 A70-32888

Optical heterodyne interferometer for stellar diameter measurements

16 p2925 A70-33025

Book on stellar spectra theory covering line absorption coefficient expressions, radiative transfer, line source function, line broadening, etc

16 p2974 A70-33270

Stellar UV photometry using telescope experiment in OAO

17 p3160 A70-34883

Stellar UV spectra observation methods, discussing objective spectrograph, scanning spectrometer system with telescope and grating cameras

17 p3160 A70-34885

Rocket spectroscopy of zeta Puppis below 1100 Å

17 p3160 A70-34886

G and K stars spectral classification using narrow band photometry

17 p3169 A70-35380

Spectrophotometric solar brightness temperature measurements in far IR, discussing collision type spectral variation of absorption coefficient

18 p3319 A70-37056

Satellite-borne UV TV system for photometric investigations of UV stars

19 p3428 A70-38456

Intermediate band photometry of companions to RR Lyrae variables, identifying AP Ser K line excess subdwarf

21 p3892 A70-41187

Early B stars photometric examination of variable spectral lines, discussing beta Cephei stars possibility

21 p3922 A70-41981

Open star h and chi Persei cluster four color and H beta photoelectric photometry, discussing interstellar reddening, ages and distances

21 p3922 A70-41982

Be stars hydrogen emission lines widths measurement

22 p4101 A70-42867

Stellar ring 274 reality confirmed by photometric measurements of OB member stars, determining variable shell star P Cygni location

22 p4101 A70-42868

Narrow band IR photometry of star alpha Orion, testing hypothetical correlation of emission peak with starlight-reflecting silicate dust

22 p4105 A70-43229

High dispersion stellar spectroscopy with echelle grating, discussing instrument design, operation and performance

22 p4040 A70-43613

Photometric search for metal deficient stars, using objective prism plates and four color Stromgren technique

22 p4109 A70-43736

High velocity stars in Large Magellanic Cloud from spectroscopic observations, including A dwarfs and G-K giants

23 p4240 A70-44212

Omicron Ceti /Mira/ spectrophotometry before, during and after 1969 maximum, noting TiO bandwidth variations

23 p4242 A70-44294

Integrated data processor-operation controller for stellar TV photometer systems in spaceborne observatory, considering limited channel transmission capacity

23 p4167 A70-44649

Astronomical observations from outside terrestrial atmosphere, discussing vehicles and equipment for solar and stellar research, rocket and balloon data, etc

23 p4257 A70-45043

Of stars mean spectrophotometric gradients and Balmer jump data with corrections for interstellar absorption

24 p4409 A70-45632

Hercules 89 supergiant abnormal IR radiation flux originating in circumstellar shell of solid particles radiating at observed long wavelengths

24 p4410 A70-45772

STELLAR STRUCTURE

Convective red dwarfs Kr 60 A and 60 B structure and stability taking into account electrostatic interactions between gas particles

01 p0188 A70-11337

White dwarf spectra interpretation based on model atmosphere method, discussing chemical composition, low luminosity high pressure atmospheres, electron density, etc

01 p0189 A70-11340

Collective interactions effect on electron scattering opacity in stellar interiors, using Debye-Huckel radial distribution function and neglecting collisions

02 p0364 A70-11789

Isophote flattening functions of elliptical galaxies including identification of giant and dwarf galaxies

02 p0377 A70-12449

Physical conditions of stars in presupernova stage for type II supernovae with outburst expected due to Fe-He transition in core, confirming lower mass limit

03 p0566 A70-13314

Binary system Nova WZ Sge model with nonnegligible secondary component contribution to total light explaining W UMa type light curve

03 p0568 A70-13324

Hypotheses for symbiotic stars nature, emphasizing binary with late type giant and hot small star components

03 p0568 A70-13325

Color photoelectric study of eclipsing binary RY Gemini for determining orbital elements and structure

04 p0754 A70-15217

Solar structure models for neutrino flux prediction compared with solar structure, suggesting modification in solar and stellar evolution calculations

05 p0906 A70-15895

Time variation of gravitational constant on structure of central solar region and neutrino luminosity

05 p0899 A70-15952

Proton-proton cycle in star interior, calculating isotope concentrations, reaction duration and energy release as function of temperature and chemical composition

05 p0900 A70-15972

Relativistic stellar structure equations for spherically symmetric configurations in slow motion, using Einstein gravitational field and conservation equations

05 p0912 A70-16454

Variable stars, discussing equation of motion for envelope structure properties and determining oscillation energy change rate from linear theory

06 p1138 A70-17309

Hydrostatic equilibrium solutions of internal structure of neutron stars using Brueckner equation

06 p1139 A70-17541

Granular and intergranular region solar magnetic field difference detection attempt from line profiles, noting equivalent width increase in ionized Cr line

06 p1142 A70-17989

Dense pulsating stellar core structure model for pulsars, discussing catastrophic collapse mechanism

07 p1380 A70-19278

Book on physics of stellar interiors covering radiant energy, mechanical equilibrium, mass density distribution, nuclear reactions, etc

08 p1568 A70-20758

Stellar atmosphere and shell models in spectral range AO-G5 for studying stellar structures dependence on chemical composition

11 p2115 A70-26582

Linearized perturbation theory for quasi-static equilibrium stellar interior models, obtaining correction through bidirectional quadrature

11 p2118 A70-26709

Neutrino astronomy for processes in stellar interiors, emphasizing thermonuclear reactions in sun and main sequence stars

13 p2490 A70-28947

Rotating stellar configurations structure consisting of degenerate matter or density dependent temperature describing boundary value problem reduction for Cauchy problem

13 p2494 A70-29518

Pulsars crust plastic deformation leading to rotation damping, higher magnetic moments and rarer starquakes

14 p2638 A70-30672

Rocket spectroscopy of zeta puppis, identifying multiplets of stellar and interstellar origin included in atmospheric models

14 p2641 A70-30883

Overstable convection formation of semiconvective zones in massive stars, noting Schwarzschild and Harm models

14 p2652 A70-31386

Shock wave front propagation instability in decreasing density medium, applying to stellar structure

16 p2890 A70-33200

Outer corona during 7 March 1970 eclipse, discussing distance dominance of K corona

16 p2977 A70-33842

Book on interpretation of spectra and atmospheric structure of cool stars covering line identification, dissociative equilibrium, opacity, chemical composition, carbon stars, etc

16 p2978 A70-33962

Stellar thermal and vibrational energy losses due to URCA shells in interiors

18 p3310 A70-35935

Solar corona structure on 22 September 1968 using radio astronomical and optical eclipse data

18 p3315 A70-36607

Solar core opacity, investigating individual heavy elements influence and effect of changes in abundances

18 p3317 A70-37005

Soviet book on variable stars covering properties, evolution, structure, methods of investigation, etc

19 p3520 A70-38397

Stellar interiors and cosmic He abundance observations, discussing B stars, sun galactic and globular clusters, planetary nebulae, interstellar medium, novae, etc

20 p3706 A70-39931

Neutron stars, discussing equations of state and stellar interiors, models, atmosphere, cooling, vibration, rotation and magnetic fields

20 p3706 A70-39932

Sodium behavior in young and old late type stars, examining relation to iron abundance in F, G and K dwarf and giant stars

21 p3887 A70-41114

Beta Cephei star discovery criteria, examining mu-mechanism theory by He and N overabundances, far UV flux, spectral line width and binary character

21 p3890 A70-41159

Radio observations of limb darkening and structure of solar corona at 80 MHz

21 p3890 A70-41177

Position scatter of 80 MHz sources of type 3 solar bursts reflecting outer corona structure

21 p3891 A70-41182

Book on astrophysics and stellar structure covering physical characteristics, atmospheres, interiors and evolution

21 p3919 A70-41792

Stellar envelope physical structure studied to solve equilibrium equation, applying results to stellar model

22 p4097 A70-42545

Main sequence II stars rapid uniform rotation effect on structure

22 p4101 A70-42859

Thermodynamic parameters of stellar matter in electronic degeneration conditions, discussing energy balances discrepancies

22 p4106 A70-43260

Stellar rotation effect on internal structures, discussing angular momentum steady state distribution for main sequence stars

23 p4249 A70-44803

Nonspherical stellar internal structure, developing method for models with rotational and tidal distortion

23 p4249 A70-44804

Synchronous close binary stars primary component structure, using rapidly rotating polytrope method

23 p4250 A70-44816

Nonspherical stars thermal stability, considering solar rotational models and oblateness problem

23 p4252 A70-44833

Solar interior differential rotation, developing angular velocity distribution equilibrium model

23 p4252 A70-44834

Giant cell regular structures in solar atmosphere, using magnetic synoptic charts of solar activity

24 p4400 A70-45305

Neutron star crust conductivity, obtaining electrical conductivity formula for outer kilometer

24 p4403 A70-45394

Cool star atmospheric structure, discussing models with and without graphite particle inclusion opacity

24 p4410 A70-45765

Stellar structure in advanced phases of evolution, considering mixing between hydrogen-rich envelope and core through surface convection zone

24 p4412 A70-46102

Main sequence and giant stars atmospheric structure models, noting metal deficiency effects

24 p4413 A70-46159

Stellar surface and solar system light element abundances, explaining formation by energetic proton flux nucleosynthetic effect

24 p4398 A70-46163

Differentially rotating stellar interiors nonaxisymmetric perturbation stability in toroidal and poloidal magnetic fields

24 p4413 A70-46165

STELLAR WINDS

Solar/stellar/ wind solutions asymptotic behavior at large distances from central star for equations including effects of rotation and anisotropy

02 p0358 A70-12253

Solar wind-induced torque calculated considering special and general relativistic effects, extending method to pulsar rotational model

04 p0739 A70-14593

Stellar wind theory based on spherically symmetric isothermal and stationary stellar atmosphere with non-negligible gravitational potential

09 p1747 A70-23605

Relativistic solutions to model stellar wind, discussing equation of radial momentum

17 p3153 A70-34530

Stellar wind effect on accretion, showing critical intensity of particle ejection replacement

18 p3324 A70-37148

Stellar wind theory and related steady radial flows, discussing gravitating point mass, heat conduction, shocks, viscosity, outflows and inflows

20 p3706 A70-39928

STELLARATORS

Trapped particle vibrations stability during quasi-neutral plasma disturbance due to centrifugal drift in stellarator electric field

08 p1555 A70-21982

Plasma stabilizing effect of shear and magnetic flux minimum in asymmetric conductors and currents in helical stellarator winding

11 p2088 A70-25711

Plasma equilibrium in stellarator type magnetic trap /vintotron/ with magnetic configuration created by strong longitudinal field

12 p2277 A70-27313

Plasma source design using stellarator type magnetic field, eliminating electron beam and electrode produced impurities

21 p3858 A70-41713

Stochastic heating of plasma in toroidal trap /stellarator/, showing discharge ignition potential dependence on microwave oscillator frequency

22 p4084 A70-43394

Inertia effect on low density plasma losses in toroidal MHD equilibrium in model stellarator field

24 p4383 A70-45115

Plasma jet motion stability in axial magnetic field of stellarator diverter and solenoid

24 p4386 A70-45660

STENCIL PROCESSES

Printing, electro etching and vacuum deposition stencil methods for preparing moire grids

19 p3432 A70-38721

STEP FUNCTIONS

Uniaxial strain pulse propagation through various materials loaded uniformly with step function pressure by gas dynamic shock wave reflection

09 p1783 A70-23449

Piezoelectric annular disk transducer mechanical response to step voltage input with prescribed temperature field

14 p2588 A70-31228

Pulse characteristics received by loop antenna in field of second antenna excited with step functions, calculating radiation characteristics

16 p2871 A70-32961

Electric and magnetic field components of step function excited electric dipole immersed in dissipative homogeneous medium with specified conductivity and dielectric constant

20 p3589 A70-40464

Step and ramp input functions and pursuit and compensatory display modes effects on tracking performance

21 p3767 A70-40753

Dual mode suboptimum minimum time control of high order systems with negative roots and step displacement inputs, using simplified computer switching

21 p3801 A70-40756

STEPS

Incompressible turbulent boundary layer and separation flow into forward facing normal step, considering step heights and boundary layer thickness

01 p0066 A70-11133

Step tracking in normal human subjects, studying muscle system around ankle joint

10 p1824 A70-23898

Backward facing separated step boundary layer flow at Mach 2.25 investigated by diffraction grating interferometer and color schlieren technique

13 p2343 A70-29898

STEREOCHEMISTRY

Isomeric 1-phenylheptenes mass spectra, investigating electron impact induced rearrangements of double bond

09 p1631 A70-23401

Stereospecificity and reaction rate of enzymatic hydrolysis of racemic substrate by pepsin determined by nuclear magnetic resonance spectroscopy

12 p2181 A70-27472

Sterically hindered aryldiazonium salts absorption spectra and quantum yield data interpretation, considering photochemical properties

12 p2182 A70-28300

Electron impact promoted phenyl migration of trans phenylcyclohexane, considering mass spectrometry and stereochemistry

14 p2544 A70-30189

Optically active amino acids synthesis by reduction of Schiff bases with sodium borohydride

17 p3041 A70-34748

Stereochemical course of sterically controlled syntheses of dipeptides, using optically active amino acids

22 p3983 A70-43095

STEREOGRAPHY

U STEREOGRAPHY

STEREOGRAPHY

U STEREOGRAPHY

STEREOGRAPHY

Lunar surface far side stereoscopic photography by Apollo 8 mission considered for lunar control

04 p0686 A70-14618

Scaling and angular resolution for sequential type holographic stereogram, comparing results with conventional hologram

04 p0695 A70-15574

Stereophotogrammetric measurement for dynamic deformation of circular membrane subjected to underwater detonation

05 p0927 A70-16009

Aircraft range-only radar trial applications in stereotopographic surveys of difficult-access areas, discussing organizational problems

07 p1282 A70-19632

Light beam deflection for three dimensional fixed and time varying visual displays, discussing mechanical, acousto-optic, electro-optic, digital and holographic techniques

08 p1449 A70-20673

Holographic recording of three dimensional rapid events, using Q switched laser pulses with sufficient coherence length for illumination

09 p1676 A70-22786

Stereo photographs conjugate image area matching, comparing automatic optical and electronic correlation techniques

09 p1680 A70-23067

Errors in aerial stereo photogrammetry, deriving equation to account for lens distortion and internal orientation

09 p1682 A70-23394

Radar flight configuration parameters effect on visual stereo model, expressing equivalent camera locations in terms of radar beams depression angles

10 p1841 A70-24752

Modified holographic technique for three dimensional display of X ray pictures

11 p2050 A70-25644

Cloud formation and structure determination using aircraft-borne IR stereo imagery

15 p2769 A70-31687

Holographic stereo model, comparing stereoscopic perception of phase and amplitude to model consisting of overlapping photos

16 p2908 A70-33228

Stereo synchroballistic shadowgraph system for explosively projected shock wave, using streak camera [SMPT PREPRINT 114]

22 p4031 A70-43027

Stereo laser framing camera for miniature surface cracks and perturbations produced in materials by explosively induced shock waves

22 p4035 A70-43052

SFR high speed photochronograph for visible and UV raster, stereoscopic and spectral photography

24 p4335 A70-45652

STEREOSCOPIC PHOTOGRAPHY

U STEREOGRAPHY

STEREOSCOPIC VISION

Autostereoscopic display using vibrating varifocal mirrors, including laboratory computer generated real time image and movie projection systems

02 p0302 A70-12631

Macaque monkey stereoscopic vision, obtaining behavioral evidence by random dot stereoscopic patterns and finding cells sensitive to binocular depth in cortex

07 p1205 A70-19276

Macaque monkey stereoscopic vision demonstrated behaviorally by combining random dot patterns with standard operant conditioning

07 p1205 A70-19277

Horizontal disparity and ratio of perceived egocentric distance related in stereoscopic vision during investigation of three point light sources problem

08 p1447 A70-21725

Stimuli eliciting vergence eye movements and stereopsis, discussing retinal disparity locations and limits due to form, spatial position, luminance, contrast and onset

12 p2171 A70-28034

Distorting and distorted components during geometrical illusions stereoscopic registration

19 p3366 A70-38926

Hypoxia effects on aviators visual accommodation, convergence and stereoacuity, noting myopia increase with altitude

20 p3569 A70-38996

Astronaut distance judgement enhancement in space by combining stereopsis effect with apparent movement phenomenon

23 p4150 A70-43965

Stroboscopic stereophenomenon, investigating depth shift of oscillating target motion binocularly viewed for interocular luminance differences

23 p4147 A70-44781

STEREOSCOPY

Stereoscopic device for photogrammetric points selection and marking on aerial photographs

03 p0482 A70-13109

STEREOTELEVISION

Roving vehicle self contained automatic control systems, discussing terrain scanning technique, stereo TV and electronic coordinate measuring and data processing equipment

23 p4260 A70-44628

STERILIZATION

NT CHEMICAL STERILIZATION

NT SPACECRAFT STERILIZATION

STERNS

U AFTERBODIES

STEROIDS

NT ALDOSTERONE

NT CHOLESTEROL

NT CORTICOSTEROIDS

NT CORTISONE

NT STREPTOMYCIN

Synthesis of alpha-dichloro-seco-A-norcholestone from diol monoacetate reaction with triphenylphosphine followed by hydrolysis and repeated chlorination

06 p1005 A70-17975

Electron impact induced fragmentation of androstane using deuterium labeling

08 p1454 A70-20524

Helical twisting power of steroidal solutes in cholesteric mesophases, discussing nematic temperature shift dependence on ester chain

08 p1455 A70-21524

Chlorella species found to contain ergosterol as major sterol

09 p1616 A70-22330

Circadian variation of pituitary-adrenal steroid levels, noting light role

14 p2540 A70-31430

STIELTJES INTEGRAL

Mathematical programming and conditional extremum problems solution in analytic functions based on Chebyshev function systems and Stieltjes moments

08 p1534 A70-21451

Relaxation function of linear viscoelastic body, defining mechanical deformation process using Stieltjes integral

12 p2327 A70-28046

STIFF STRUCTURES

U RIGID STRUCTURES

STIFFENING

Stiffeners reinforced rectangular plates parametric stability under dynamic load, deriving equilibrium equations and boundary conditions by averaging stiffener effects

01 p0205 A70-11146

Stiffener inclination effect on pressurized cylinder instability under pure bending

04 p0769 A70-14868

Stiffeners inclination effects on instability of pressurized cylinder under bending by Ritz method, considering finite deflection and initial imperfections in strain-displacement relations

08 p1591 A70-21464

Minimum weight design for symmetrically stiffened cylindrical shells under compression based on linear orthotropic stability theory

10 p1958 A70-24560

Integrally stiffened structures made by hot isostatic pressing of metal powders followed by conventional rolling

12 p2242 A70-27109

Waffle plate structures least weight design under uniaxial, biaxial and multiple combined loading with various stiffening patterns, investigating pyramiding concept

12 p2318 A70-27133

Postbuckled integrally stiffened wide column weight optimization, developing stress equation

18 p3339 A70-36447

Disk equations to determine tensions around arbitrary hole or stiffening contours

20 p3720 A70-39623

STIFFNESS

Helical journal bearings analysis operated in turbulent regime with incompressible lubricant, determining optimum groove parameters for maximum radial stiffness

01 p0100 A70-10381

Stiffness values of externally pressurized incompressible fluid-film thrust bearings under turbulent Couette flow, discussing Reynolds number effects

[ASME PAPER 69-LUB-25] 01 p0100 A70-10383

Elastic bending of pretwisted elliptical bars, showing stiffness response

02 p0387 A70-12216

Stiffness matrix derivation for curved beam emphasizing uncoupled normal to plane loads

03 p0584 A70-12949

Laminate approximation model of randomly oriented fibrous composites estimating stiffness and thermal and expansional strains

03 p0587 A70-13126

Stiffness and expansion properties of oriented short fiber composites, discussing longitudinal modulus and expansion strain dependence on aspect ratio

03 p0587 A70-13129

Natural frequency calculation accuracy for coupled beam bending vibrations shown dependent on connection stiffness determination

03 p0595 A70-13929

Adiabatic elastic stiffness constants of single crystal forsterite measured as function of hydrostatic pressure and temperature, using pulse superposition technique

04 p0678 A70-15055

Composite strength and stiffness prediction from fiber and matrix properties using computer

05 p0870 A70-16579

Minimum weight design of elastic sandwich beams with deflection constraints using n-dimensional space of discretized bending stiffness

07 p1407 A70-19358

Dissipative heating effects on loss factor of viscoelastically damped beam, discussing stiffness effects

[ASME PAPER 69-VIBR-37] 08 p1592 A70-21478

Panel sound absorber acoustic impedance variation with frequency predicted taking into account panel mass, stiffness and internal damping

09 p1770 A70-22390

Adiabatic elastic stiffness of single crystals of Ni-Co alloys, determining bulk modulus dependence on chemical composition

10 p1904 A70-24699

Finite element matrix structural analysis by direct stiffness method and use of computers, considering thin wall box beams

[SAE PAPER 700218] 11 p2134 A70-25890

Finite element bending stress analysis of thin rectangular and skew plates, discussing computational procedure generating stiffness matrices

11 p2143 A70-26641

Nonuniform beam element stiffness matrices for dynamic and elastic instability analysis, determining frequencies, mode shapes and critical loads

11 p2143 A70-26643

Elastic stiffness of unidirectional glass reinforced epoxy fiber composite determined from ultrasonic velocity measurements

11 p2071 A70-26692

Optimum damping and stiffness in nonlinear single degree of freedom systems, discussing protection from ground and velocity shock during landing impact

11 p2145 A70-26695

Stiffness matrices of three dimensional finite elements, considering tetrahedron, hexahedron and nodal configurations

14 p2659 A70-31127

Thin shells stiffness matrix and shear by finite curved triangular elements based on discrete Kirchhoff hypothesis

14 p2659 A70-31129

Curved finite element for shells of revolution based on minimum potential energy principle, discussing stiffness and equilibrium of domed and branched shells

14 p2659 A70-31130

Dynamic stiffness, natural frequencies and mode shapes of prismatic and thin walled open grids, including warping and shear flange deformation

14 p2659 A70-31132

Stress concentration in flat rectangular and skew panels with circular holes from photoelastic verification of direct stiffness method

[SESA PAPER 1633] 15 p2820 A70-32303

Stiffness of multipad externally pressurized journal bearings with incompressible fluid feeding, comparing hydrodynamic and rolling bearings

15 p2745 A70-32445

Flight vehicle dynamic response prediction from elastic fluid stiffness contained between rigid sphere and ellipsoidal shell

16 p2991 A70-33878

Twisted uniform beam element flexibility and stiffness matrices, using continuous bending theory

16 p2894 A70-33887

Stiffness matrix correction for curved element deficient in rigid body motion

18 p3342 A70-36687

Stiffness values of externally pressurized incompressible fluid-film thrust bearings under turbulent Couette flow, discussing Reynolds number effects

[ASME PAPER 69-LUB-25] 19 p3435 A70-37611

Aerostatic journal bearings with double plane admission feeder holes, determining maximum load and stiffness by numerical method

19 p3443 A70-38898

Finite element stiffness matrix technique for composite structures, discussing airplane component design program

20 p3730 A70-40040

Optimum automatic selection of redundancies, discussing weighting and pivot choice and rigid element incorporation

20 p3732 A70-40264

Externally pressurized air lubricated journal bearing with multiple supply holes, predicting load carrying capacity, flow requirement and stiffness

20 p3639 A70-40505

Parachute flexibility as performance parameter, discussing stiffness-weight index, inflation process, squidding, etc

[AIAA PAPER 70-1166] 21 p3755 A70-41845

Directional dependence of elastic shear stiffness on cubic axes for Si, Cu and Mo, making polar plots of shear stiffness coefficients

21 p3850 A70-41909

High thermal stability glass fibers alternatives improving stiffness-to-weight ratio of resin and Al-based composites used in F-111 boron epoxy wings

22 p4058 A70-42480

Boron-epoxy composites rectangular reinforcing arrays spacing aspect ratios, considering matrix stress concentrations and stiffness estimates

22 p4119 A70-43688

Finite beam element in bending, deriving shear deflection terms in stiffness matrix based on stress assumption

23 p4274 A70-44909

Large element method for stiffness matrix order reduction in two-dimensional continua problems

23 p4275 A70-44940

Rope transverse oscillations due to impact taking bending rigidity into account

24 p4424 A70-45627

STILBENE

Dicyanostilbene formation from phenylethynyl azide and isocyanate

05 p0811 A70-16054

Anthracene, polystyrene and stilbene for scintillation counters measuring cosmic ray protons, analyzing dosimetric properties

17 p3151 A70-35352

STIMULANT

NT ATROPINE

NT CAFFEINE

NT CENTRAL NERVOUS SYSTEM STIMULANTS

NT NORADRENALINE

NT NOREPINEPHRINE

Propranolol effects on human cardiac conduction and intraventricular conduction in dogs studied by recording His bundle electrograms, noting P-H interval prolongation

05 p0800 A70-16102

Electrocardiographic changes during positive headward acceleration of normal human subjects after oxygen breathing and propranolol administration

05 p0808 A70-16675

Vascular smooth muscle contraction regulation, discussing contractile protein, energy metabolism, excitation-contraction coupling, spontaneous rhythmicity, response to stimulants, etc

24 p4299 A70-45807

STIMULATED EMISSION

GaAs - Conference, Dallas, October 1968

01 p0157 A70-10515

Stimulated emission of RF recombination lines from ionized atoms in H I regions

02 p0372 A70-12251

- Maser-like stimulated OH emission regions observed in interstellar rarefied gas 06 p1148 A70-18391
- Doped semiconductor unsteady stimulated emission, solving kinetic reactions in multimodal approximation 07 p1357 A70-19862
- Laser emission from organic molecules under neodymium laser harmonics excitation, describing absorption and photochemical inversions effects and emission spectra characteristics 07 p1300 A70-19866
- Solid state lasers with strongly degenerated modes investigated for induced radiation spectral composition inertial properties 08 p1510 A70-20507
- Stokes components generation in presence of stimulated combination radiation in optical cavity, considering interaction between components and effect of material dispersion on interaction 08 p1510 A70-20511
- Stokes components simultaneous generation in presence of stimulated combination radiation in optical cavity, noting effects of incident monochromatic beam intensity 08 p1511 A70-20520
- Anisotropic angular distribution of electrons and ions emitted from W targets irradiated by ruby laser pulses 08 p1512 A70-21211
- Output energies of Stokes components of stimulated combination scattering excited by pulsed laser 09 p1696 A70-22482
- Transient stimulated rotational and vibrational Raman scattering in gases using mode locked ruby laser 09 p1700 A70-23568
- Strontium fluoride crystals containing trivalent neodymium cations investigated for laser action and radiation characteristics by spectroscopy 10 p1899 A70-24253
- Second harmonic emission from GaAs injection laser and from stimulated KDP crystal at room temperature 12 p2245 A70-27306
- Giant Stokes radiation pulse generation during stimulated combination scattering, emphasizing pulses traveling counter to pumping wave 12 p2250 A70-28288
- Thermospectrometric investigation of stimulated Raman lines in benzene to identify generation modes, observing optical sideband effect at 8050 A 13 p2425 A70-28712
- Flashlamp-excited organic liquid UV lasers 13 p2427 A70-29141
- Stimulated emission cut-off characteristics of laser based on crystals with Nd ions under UV irradiation 13 p2429 A70-29505
- Whistler mode VLF emissions stimulation mechanism 13 p2401 A70-29930
- Fluorescence method of determining solid state laser parameters using spontaneous and stimulated emission observations 17 p3106 A70-35101
- Crystal and glass lasers activated by Nd ions, examining stimulated emission temperature dependence by high temperature spectroscopy 17 p3106 A70-35105
- CdS crystals luminescence spectrum excitation by UV light of ruby laser, noting excitons and phonons recombination 19 p3444 A70-37368
- Vacuum UV laser action in molecular hydrogen Lyman bands, examining stimulated emission in P branch lines and light pulse duration 20 p3643 A70-40496
- Semiconductor platelet laser stimulated emission visual observation in unwanted reflected modes 21 p3838 A70-42022
- Excited state complexes laser action in coumarin dyes indicated from stimulated fluorescence time dependence 22 p4048 A70-42328
- Mode locked neodymium-glass pulsed laser stimulated picosecond time resolved light emission observation by cross beam technique 24 p4354 A70-45647
- STIMULATED EMISSION DEVICES**
- NT ARGON LASERS
- NT CARBON DIOXIDE LASERS
- NT CHEMICAL LASERS
- NT GALLIUM ARSENIDE LASERS
- NT GAS LASERS
- NT GAS MASERS
- NT INFRARED LASERS
- NT INJECTION LASERS
- NT LASERS
- NT LIQUID LASERS
- NT MASERS
- NT ORGANIC LASERS
- NT PULSED LASERS
- NT Q SWITCHED LASERS
- NT RING LASERS
- NT RUBY LASERS
- NT SEMICONDUCTOR LASERS
- NT SOLID STATE LASERS
- NT TRAVELING WAVE MASERS
- Ruby laser giant pulses time stretching and shaping using stimulated Raman scattering in liquid nitrogen cell inserted in laser resonator 05 p0857 A70-16076
- Multilevel quantum systems interaction with electromagnetic fields at frequencies near quantum transitions using small signal analysis 09 p1695 A70-22256
- STIMULATION**
- NT AUDITORY STIMULI
- NT SENSORY STIMULATION
- Non-specific influences on rabbits neurons reaction to nonvisual stimuli in central visual pathway using microelectrodes implantation in visual cortex 05 p0802 A70-16624
- STIMULI**
- Attention and cue-producing responses in response-mediated stimulus generalization 09 p1617 A70-22342
- Interindividual differences in judging stimulus similarities, explaining unsatisfactory results obtained by average scalings 19 p3366 A70-38506
- Selective stimulus encoding and overlearning in paired associate learning 22 p3971 A70-43401
- STIRLING CYCLE**
- Stirling free piston engine operating principles, performance limitations, heat transfer problems, fluid flow, mechanical design, test results and applications [ASME PAPER 69-WA/ENER-15] 04 p0627 A70-14895
- Equilibrium performance of closed Stirling cycle with chemically reactive gas as working fluid, discussing power density and thermal efficiency 22 p3982 A70-42756
- Effective pressure ratio nomographs for mechanical energy conversion and heat transfer of closed regenerative Stirling engines, using isothermal theory 22 p4091 A70-42757
- STOCHASTIC PROCESSES**
- NT MARKOV CHAINS
- NT MARKOV PROCESSES
- NT RANDOM PROCESSES
- Algorithm for L-shaped linear programs in optimal control problems and stochastic programming, outlining cutting hyperplane 01 p0047 A70-11069
- Stochastic processes providing exposition of differential-integral calculus for Brownian motion paths, with applications to diffusion processes and related parabolic partial differential equations 01 p0133 A70-11322
- Monograph on stochastic theory and cascade processes, discussing branching phenomena, point processes, electromagnetic cascades, extensive air showers, polarization, population growth, etc 01 p0134 A70-11327
- Optimal control algorithm for spacecraft descent in atmosphere based on nominal trajectory and acceleration measurements 01 p0197 A70-11499
- Stationary Gaussian stochastic processes sample functions properties and local times 02 p0324 A70-12504
- Nonlinear stochastic differential equations formulated during random loading processes generation, designing testing devices with stable performance parameters 03 p0598 A70-14236
- Optical position estimation model based on defining photon density profile center of gravity in noise, using photon Poisson process theory 04 p0652 A70-15337
- Structure safety in cumulative damage, considering loading as time dependent stochastic process 05 p0937 A70-16369
- Random vibrations of linear system with viscous damping excited by stochastically acting force with monotonically varying frequency, using correlation method 05 p0882 A70-16372
- Arterial pressure and suprarenal blood flow in dogs under basal conditions and nerve stimulation by stochastic method using analog correlator 05 p0806 A70-16400
- Diffusion processes governed by stochastic equations 06 p1093 A70-17581
- Monograph on computation of density functions of parameters in stochastic systems, giving algorithms involving only matrix computations of fixed dimensionality 06 p1093 A70-17730
- Stochastic differential games with constrained state estimators, involving linear system, quadratic cost functional and white Gaussian noises corrupting output measurements 06 p1024 A70-17954
- Linear-quadratic pursuit-evasion game with dynamics perturbed by additive white Gaussian noise, obtaining linear minimax solutions 06 p1025 A70-17957
- M measurement optimal feedback control algorithm for stochastic discrete time systems, considering nonlinear plant, constrained controls, nonquadratic cost and simulations 06 p1025 A70-17962
- Separation theorem for nonlinear measurements, discrete-time linear systems and quadratic cost to achieve stochastic control without dynamic programming 06 p1026 A70-17967
- Nonlinear control systems stability with stochastic coefficients, applying Liapunov function 06 p1026 A70-17971
- Linear optimal stochastic control systems described by covariance matrix correlating errors and estimates of state variables, analyzing instability under parameter variations 06 p1095 A70-18054
- Stochastic model of information handling centers as typified by document storage and retrieval derived from integral equation to determine expected primary store size 06 p1016 A70-18450
- Superposition of dressed particles in plasma kinetic theory proved by using generalized stochastic equation for conditional probability density for one particle 06 p1124 A70-18500
- Stochastic automata for parameter self optimization with multimodal performance criteria 07 p1244 A70-18861
- Kolmogoroff partial differential equations for non-Markovian stochastic processes, noting applications to reliability theory 07 p1323 A70-18938
- Distributional results pertaining to complex Wishart processes and time varying spectral estimators on null hypothesis of stationary Gaussian time series 07 p1323 A70-19028
- Multidimensional stochastic approximation theorems useful for infinite-dimensional Hilbert space or Banach space 07 p1324 A70-19029
- Stochastic differential equations for approximate continuous nonlinear minimal variance filtering, discussing existence and uniqueness conditions 07 p1245 A70-19092
- Multidimensional Kiefer-Wolfowitz stochastic approximation algorithm modified to locate regression function minimum 07 p1247 A70-20028
- Stability criteria for systems of nonlinear stochastic differential equations on finite time interval, considering stable motion of physical processes 08 p1533 A70-20488
- Deterministic and stochastic simulation models for obtaining optimal solution in operations research by trial and error 08 p1464 A70-20579
- Optimal spare parts inventory determined for stochastically failing components using mathematical model 08 p1501 A70-20603
- Stochastic programming models for flight scheduling within airlift system accounting for cargo uncertainties, using convex programming, linear programming codes, etc 08 p1600 A70-20605
- SOAR (Simulation of Airlift Resources) model for stochastic productivity variations of strategic airlift systems 08 p1466 A70-20930
- Existence theorem for linear stochastic systems optimal control described by differential equation with random coefficients, providing rms stabilization 08 p1480 A70-21637
- Optimal control mathematical modeling for dynamic systems under statistically indeterminate disturbances based on game theory and pattern recognition 09 p1653 A70-22141
- One dimensional Poisson production process under costly surveillance, considering maximum attainable income rate approximation 09 p1653 A70-22347
- Stochastic predictor model for process control, discussing multivariable search techniques and effect of forcing function and noise 10 p1856 A70-24872
- Hardware and system testing mathematical model assuming stochastic design and manufacturing defects detection and nondetection probability equations analogous to reliability function 10 p1896 A70-24915
- Nonlinear system with piecewise linear spring characteristic response to stochastic excitation of white noise type process, discussing technical stability 10 p1918 A70-25323
- Control theory, Volume 1, covering linear, nonlinear, stochastic, optimal, adaptive and learning systems, sensitivity analysis, etc 11 p2023 A70-25771
- Error analysis algorithms for reducing computational load in stochastic estimation and control problems in hybrid navigation systems 11 p2025 A70-26208

Spacecraft stochastic optimal control, discussing design of least upper bound fuel optimal system with measurement uncertainty

11 p2025 A70-26222

Feedback controller specific suboptimal estimation and control parameters determination using stochastic approximation algorithms

11 p2026 A70-26236

Stochastic control system design methodology noting applications to ASW, law enforcement, document retrieval and autopilots

11 p2029 A70-26336

Gain determination from dynamic /on line/ solutions to Riccati equation for model reference adaptive control applicable to multiple input/ output or stochastic systems

11 p2029 A70-26339

Stochastic dynamic prediction assuming deterministic laws for atmospheric behavior while seeking solutions corresponding to probabilistic statements of initial conditions

11 p2076 A70-26497

Stochastic differential equations objectives, limitations and restrictive assumptions in physical problems, discussing electromagnetic wave propagation in random continuum or random d'Alembertian operator

11 p2074 A70-26550

Plasma turbulence stochastic processes, considering radiation, transport and acceleration mechanisms and relationships to fluid turbulence

11 p2094 A70-26752

Plasma turbulence theory, discussing particles stochastic acceleration in strong electric field

11 p2094 A70-26753

Transfer matrix spectrum for lattice gas models with finite interaction, constructing stochastic operator as stochastic matrices limit

12 p2272 A70-27343

Poisson shot noise process relationship with continuous stochastic intensity as sample function

12 p2203 A70-27418

Alias-free randomly timed sampling of stochastic processes, considering spectrum recovery by linear operation

12 p2204 A70-27419

Linear time dependent stochastic optimal control with nonquadratic performance indices using function space approach

12 p2204 A70-27668

Wideband stochastic signals for radar range and velocity measurements using polarity coincidence correlation technique

12 p2188 A70-27942

Diffusion processes on multidimensional cylindrical phase space for studying stochastic processes for physical systems with angular measurements, developing model for satellite under torque

12 p2273 A70-28067

Nonlinear discrete time sampled systems optimal control by dynamic programming, with application to stochastic systems

12 p2204 A70-28068

Stochastic optimal trajectory control for spacecraft reentry at supercircular velocity, deriving computer algorithm

13 p2499 A70-28382

Stochastic processes optimal control theory application to launcher attitude control under wind disturbance

13 p2501 A70-28428

Newton-Raphson method analog accelerating convergence of multidimensional stochastic approximation algorithm to local minimum for attitude controller design

13 p2382 A70-29069

Stochastic adaptation process, investigating asymptotic properties based on concept of random system with complete connections

13 p2383 A70-29490

Book on stochastic processes and filtering theory covering probability theory, Markov processes, linear and nonlinear filters, etc

13 p2442 A70-29575

Stochastic reinforcement learning model synthesizing control and pattern recognition systems with learning attributes

13 p2374 A70-29584

Stochastic analog approximation method minimizing criterion functions and for recovering functions from noisy measurements of values in learning systems

13 p2442 A70-29585

Stochastic approximation methods applied to pattern classification, estimation and control

13 p2442 A70-29586

Stochastic automata as learning system models in random environments with penalty-nonpenalty expectations, demonstrating convergence

13 p2374 A70-29587

Stochastic particle acceleration by VLF in weakly turbulent plasma in magnetic field, considering nonlinear cyclotron damping

13 p2468 A70-29935

Book on differential dynamic programming covering algorithms for continuous time control, bang-bang, discrete time and stochastic systems

14 p2560 A70-30631

Stochastic terminal optimal control for nonlinear dynamical systems with state independent noise

14 p2600 A70-31420

Stochastic processes for physiological analysis of cardiac rhythm dynamics during work

15 p2680 A70-31609

Stochastic linearized state estimator for nonlinear dynamic systems with Markovian noise, using digital simulation

15 p2715 A70-31975

Linear stationary systems observability with stochastic inputs for linearly independent row vectors, determining state vector components mean values

15 p2716 A70-32346

Optimal control stochastic problem with initial conditions treated as random variables, using matrix minimum principle

15 p2716 A70-32563

System maintainability stochastic modeling using probability density functions

15 p2748 A70-32670

Discrete stochastic optimal control model of human operator for single loop compensatory/pursuit tracking

16 p2851 A70-33340

Linear systems simultaneous optimal stochastic control and observation strategies, assuming quadratic observation cost

16 p2886 A70-33346

Discrete stochastic optimal control model of human operator for single loop compensatory/pursuit tracking situation, considering application to manual control system design

16 p2852 A70-33463

Limit theorems for sums of multidimensional stochastic step processes, giving necessary and sufficient conditions for convergence to Poisson measures

16 p2942 A70-33700

Kinetic theory of fatigue crack propagation, discussing stochastic nucleation process and power exponent relation

16 p2992 A70-33968

Thermorheologically simple model for viscoelastic materials stochastic behavior in random temperature fields, introducing reduced time scale

16 p3003 A70-34238

Stochastic systems technical stability problem solution by Fokker-Planck equation

16 p2944 A70-34294

Systems subject to failure and repair cycles, describing performance and reliability by stochastic processes in terms of excess time

17 p3099 A70-34580

Book on stochastic tools in turbulence covering generalized functions, probability, moments, characteristic functions, Gaussian distribution, random functions and multidimensional fields

17 p3128 A70-34601

Convolutional code decoder modeled as autonomous stochastic sequential machine, considering finite Markov chain theory for error probability

17 p3049 A70-34854

Stochastic linearization approximation to solve nonlinear dynamical systems filtering problems in Markovian framework

17 p3056 A70-34953

Sufficient condition for asymptotic stability of ergodic coefficient linear stochastic systems

17 p3129 A70-34982

Statistical theory of irreversible transport processes in fluids, considering deviation from equilibrium as stochastic process

17 p3131 A70-35532

Stochastic approximation for identification of distributed parameter system solutions described by linear partial differential equations

17 p3131 A70-35557

Stochastic processes with linear dynamics and quadratic control cost, considering application to aircraft landing approach path optimization

18 p3279 A70-35973

Noisy stochastic pattern recognition system, determining optimal measurement sequence by discrete Pontryagin maximum principle

18 p3234 A70-36337

Nonlinear stochastic discrete time processes prediction and filtering by Monte Carlo techniques

18 p3234 A70-36338

Nontrivial eigenvalues of stochastic matrices

19 p3456 A70-37414

Linear stochastic continuous feedback system with white noise and control input, investigating combined problem of filtering and optimal control

19 p3393 A70-37850

Satellite-based air traffic control system for North Atlantic, applying stochastic optimal control theory [AIAA PAPER 70-966]

20 p3669 A70-39563

Computer calculations automation in mathematical models construction by statistical methods, discussing

programs for distributed parameter systems, stochastic approximation, etc

20 p3592 A70-39903

Stochastic approximation iterative algorithms for multivariable plants mathematical models, including steepest descent method

20 p3593 A70-39910

Discrete parameter stochastic optimization problems necessary conditions, deriving maximum principle

20 p3659 A70-40107

Skeletal muscle force generation stochastic model based on motor unit, discussing Poisson distribution and dynamic force response

21 p3769 A70-41199

Control processes and optimization problems solutions by stochastic differential equations, discussing dynamic models and programming, linear filtering and optimal feedback

21 p3802 A70-41275

Thermoviscoelasticity stochastic problems for bar with temperature independent viscosity, discussing Fokker-Planck equation for two temperature processes

21 p3937 A70-41435

Stochastic kinetic theory for plasma turbulent heating by random fields, predicting acceleration effects

21 p3859 A70-41899

Stochastic processes control optimization, selecting elastic aircraft stabilizer planform

22 p4004 A70-43352

Stochastic heating of plasma in toroidal trap /stellarator/, showing discharge ignition potential dependence on microwave oscillator frequency

22 p4084 A70-43394

Stochastic optimal control for nonlinear dynamical systems under noisy observations, designing suboptimal state estimates and feedback controls

22 p4063 A70-43429

Stochastic control optimization, examining self organizing approach for performance adaptive controller with asymptotic optimal properties

22 p4005 A70-43733

Iterative linear prediction method for stochastic process with zero mean value and known covariance function

23 p4211 A70-44026

Deterministic vs stochastic signals for equipment and installations short cycle reliability tests over service life during changing environments

23 p4166 A70-44332

Weak compactness of set of measures in functional space corresponding to stochastic differential equations solutions for n-dimensional Euclidean space

23 p4212 A70-44341

Nonlinear filtering for linear parabolic distributed parameter systems with white noise, considering stochastic boundary value problem

23 p4177 A70-44905

Stochastic behavior of failed standby redundant electronic equipment with imperfect switching and opportunistic repairs

24 p4319 A70-46016

Stochastic boundary value problem involving differential equation with random forcing function, proving monotone property of solution covariance variation

24 p4426 A70-46039

STOICHIOMETRY

Color-electric voltage calculation for stoichiometric flame burning in air introducing allowance for charged particle densities

04 p0780 A70-14706

Stoichiometric compositions of niobium dioxide to pentoxide range, investigating X ray characteristics and thermal stability

07 p3135 A70-20312

Open cycle MHD generator operation, comparing below stoichiometric air-fuel ratios to excess air level

14 p2533 A70-30534

Impurities solubility in semiconducting indium telluride with stoichiometric vacancies, verifying thermodynamic model by phase diagrams

16 p2960 A70-33224

STOKES FLOW

MHD Stokes flow for magnetized bodies of revolution, rotating with steady motion in viscous conducting fluid at rest at infinity

04 p0726 A70-14615

Parachute design for decelerating upper atmosphere rocket probes at high altitudes, using high drag coefficients in Stokes flow regime

04 p0624 A70-15410

Stokes flow around sphere moving along axis of cylinder with near-unity diameters relationship

09 p1661 A70-22839

Homogeneous viscous fluid steady state parallel Stokes flow in annular region between concentric cylinders at low Reynolds numbers

11 p2038 A70-26478

Suspended Stokes particle-single wave interaction effect on energy dissipation and vorticity of random turbulent incompressible fluid approximated by Fourier-Stieltjes integral

12 p2213 A70-28236

Sphere slow motion in viscous fluid with solid particle suspension, considering Stokes flow pattern small relaxation time perturbation

16 p2896 A70-34272

Compressible and incompressible Stokesian fluids motion described by finite element analog of Navier-Stokes equation

20 p3607 A70-38999

Viscous conducting fluid slow motion past sphere in presence of toroidal magnetic field, calculating Stokes flow perturbations

20 p3682 A70-40113

Low Reynolds number gas flow past heated circular cylinder, considering Stokes region transport properties

23 p4284 A70-44978

Perturbation of steady MHD Stokes flow past hollow sphere assuming small Hartmann and Reynolds numbers

24 p4384 A70-45262

STOKES LAW

Stokes components generation in presence of stimulated combination radiation in optical cavity, considering interaction between components and effect of material dispersion on interaction

08 p1510 A70-20511

Stokes components simultaneous generation in presence of stimulated combination radiation in optical cavity, noting effects of incident monochromatic beam intensity

08 p1511 A70-20520

Output energies of Stokes components of stimulated combination scattering excited by pulsed laser

09 p1696 A70-22482

Giant Stokes radiation pulse generation during stimulated combination scattering, emphasizing pulses traveling counter to pumping wave

12 p2250 A70-28288

Uniform asymptotic solutions of second order linear differential equations with arbitrarily many turning points or Stokes lines

19 p3457 A70-37681

Stokes earth constants from gravity anomalies

20 p3617 A70-39070

STOKES LAW (FLUID MECHANICS)

Erythrocyte sedimentation rate in chicken blood predictable by Stokes equation

02 p0238 A70-12547

Viscous incompressible fluid secondary steady state flow due to rotating spheroid, considering acceleration terms in Stokes linear equation solution

11 p2034 A70-25390

STOKES THEOREM (VECTOR CALCULUS)

Radiation view factor from differential area to conical surface determined using Stokes theorem and contour integration

04 p0787 A70-15598

STOMACH

Pesinogens A, C and D from stomach mucosae of smooth dogfish separated by chromatography on DEAE cellulose

11 p1987 A70-26007

STONES (ROCKS)

U ROCKS

STONY METEORITES

NT ACHONDrites

NT AUSTRALITES

NT CARBONACEOUS METEORITES

NT CHONDRITES

NT KAPOETA ACHONDRITE

NT NORTON COUNTY ACHONDRITE

NT ORGUEIL METEORITE

NT TEKITES

NT TUNGUSK METEORITE

Stony meteorite trace elements groups neutron activation analysis with computer reduction of Ge/Li spectra

02 p0249 A70-11680

Dating method for stony meteorites feldspar phase based on time interval between solar nebula Al 26 production and decay into Mg 26

06 p1150 A70-18479

Stony meteorites age determination from decay of cosmic ray produced Kr 81 and 78, comparing production rate to He 3 ages

08 p1563 A70-20499

Magnetic spherules extracted from manganese nodules classified by X ray diffraction and electron microprobe data, suggesting volcanic, stony and iron meteoritic origins

08 p1578 A70-21560

Angra dos Reis stone meteorite containing cosmogenic and fissiogenic xenon

10 p1935 A70-23850

Ureilite structures and relationship to carbonaceous chondrites, considering chemical composition, diamond content, age, size, etc

10 p1941 A70-24552

Ar 37 and Ar 39 isotopes in recently fallen iron-ataxite and stony meteorites, discussing relevance to cosmic ray variations in space

12 p2309 A70-27950

Solar flare proton induced radioactivity in Apollo 11 lunar surface material compared with stony meteorite data, noting cobalt 56 concentration

13 p2489 A70-28910

Iron and stony iron meteorite cooling rates and thermal models, showing melting, radioactive heat source redistribution and surface heating effects

13 p2497 A70-29861

Gold and iridium distribution in stony meteorites, discussing metal silicate fractionation process during chondrite formation

13 p2497 A70-29862

Stony meteorites radionuclides gamma emission measurement, determining specific activity ratios

20 p3703 A70-39322

Dosso stony meteorite gamma emitters radioactivity by nondestructive spectroscopy, obtaining quantitative analysis by least squares method

21 p3893 A70-41446

Apollo 11 samples compared to stony meteorites and terrestrial basalt, discussing lunar rock formation processes

21 p3900 A70-41540

Sequential instrumental activation analysis for trace elements in rocks and stony meteorites, comparing with silicate method

24 p4310 A70-46407

STOPPING

NT THRUST TERMINATION

STORABLE PROPELLANTS

Earth storable liquid propellants combustion products simulation by combustion of gaseous fuel and oxidizer combination, discussing elemental composition and thermodynamic considerations

08 p1557 A70-21622

Gelled space-storable oxygen difluoride and diborane analysis, including particle preparation, yield stresses, viscosities and storability

16 p2962 A70-33607

STORAGE

Stochastic model of information handling centers as typified by document storage and retrieval derived from integral equation to determine expected primary store size

06 p1016 A70-18450

Light storage by Venus machine using refractive properties of gas and involving fluid mechanical optics

11 p2114 A70-26575

Lunar surface exploration vehicle (Lunar Rover)/design, analyzing stowage aspects in Lunar Module

16 p2888 A70-33680

STORAGE BATTERIES

NT NICKEL CADMIUM BATTERIES

NT NICKEL ZINC BATTERIES

NT SILVER ZINC BATTERIES

Book on alkaline storage batteries, design, manufacture, performance characteristics, charging and maintenance, electrochemical and thermodynamical background of alkaline systems, electrode kinetics, etc

09 p1612 A70-22638

Regenerative hydrogen-oxygen secondary fuel cells as rechargeable battery for communication satellites

21 p3756 A70-41007

Gas tight lead storage battery with negative plates for oxygen absorption

24 p4295 A70-46352

STORAGE STABILITY

Long term storage effects on noise, leakage current and thickness of Li drifted Si surface barrier detectors

03 p0482 A70-13023

Long term storage effects on systems reliability, emphasizing tradeoffs regarding availability, reliability and costs

15 p2712 A70-32637

Test data interpretation by design margin techniques in poststorage reliability of high quality gyro assemblies

19 p3441 A70-38822

Technical methods defining, monitoring and controlling life limited aerospace components during storage

19 p3441 A70-38831

Hydrogen slush characteristics, discussing advantages of liquid-solid mixture over liquid hydrogen, production methods, aging effects, transfer and pumping losses, storage, instrumentation, etc

23 p4232 A70-45075

Long term storage effects on recalibrated thermistors performance stability, comparing measurements with first calibration data

24 p4333 A70-45136

STORAGE TANKS

Fire performance of spray applied rigid urethane foam applied as storage vessel insulation, noting continued functioning until destruction

09 p1710 A70-23345

STORMS

NT CYCLONES

NT HURRICANES

NT IONOSPHERIC STORMS

NT MAGNETIC STORMS

NT NOISE STORMS

NT SOLAR STORMS

NT STORMS (METEOROLOGY)

NT SUDDEN IONOSPHERIC DISTURBANCES

NT THUNDERSTORMS

NT TORNADOES

NT TROPICAL STORMS

STORMS (METEOROLOGY)

NT HURRICANES

NT THUNDERSTORMS

NT TORNADOES

NT TROPICAL STORMS

Forward sounding sensors /weather radar/ development for aiding human eye in detecting flight hazards /storms and CAT/

02 p0297 A70-11989

F 2 region acoustic waves over Kansas and Nebraska attributed to local storms in troposphere

02 p0290 A70-12158

Ball lightning mechanism proposal based on mathematical model for electric discharge current in parabolic plasma shell forming vortex-type storm front

05 p0879 A70-17021

Deflecting forces on nonrotating convecting systems due to environmental shear, comparing magnitude to rotation forces

06 p1100 A70-18571

Pacific ocean equatorial trough zone disturbances structure, discussing organized convective downdrafts role in rapid structural decay

06 p1101 A70-18578

Objective quasi-Lagrangian index for forecasting convective weather outbreaks based on outbreak occurrence likelihood in convective instability areas

06 p1101 A70-18579

Satellite observed characteristics of severe local storms in central and eastern U.S., noting potential use for storm forecasting

06 p1102 A70-18584

Severe storm research importance to aircraft design and operating efficiencies improvement by identifying meteorological alternatives for operations in and near adverse environments

06 p1102 A70-18587

Hot-film anemometers for measuring storm turbulence in presence of heavy rain

10 p1887 A70-23940

Radar meteorology in electromagnetic communications to provide storm systems data, noting clear air radar echoes

13 p2445 A70-28791

STRAIGHT WINGS

U RECTANGULAR WINGS

STRAIN AGING

U PRECIPITATION HARDENING

STRAIN DISTRIBUTION

U STRESS CONCENTRATION

STRAIN ENERGY METHODS

Strain energy function for swollen crosslinked elastomers, extending application range by including third invariant

05 p0927 A70-15980

Strain energy release rate in terms of propagating crack surface displacements applied to infinite solid loaded in tension

05 p0938 A70-16480

Shear and linear strain energy criteria for limiting stress state model of solid deformable bodies, considering uniaxial, biaxial and triaxial loading

06 p1166 A70-17657

Continuum mechanics equations for calculating strain energy in spherical bottoms production as function of radius and angle

06 p1077 A70-17870

Strain energy method applied to stability analysis of short longitudinally reinforced cylindrical shells under axial compression

08 p1584 A70-20536

Critical radii of curvature in elastoplastic bending of rib-reinforced aircraft components from wafer panels determined using strain energy method

08 p1506 A70-21183

Flexural stress relaxation properties of thermoplastics and composite materials, assessing strain energy by ballistic pendulum

11 p2070 A70-26342

Cyclic strain energy method determining oxygen consumption rate of intact working human left ventricle by closed chest measurements

12 p2167 A70-27018

Shells of revolution nonlinear finite element analysis by matrix displacement method, including higher order strain energy terms

16 p2991 A70-33885

Strain compatibility equations for continuous shells from physical and mathematical considerations

16 p2991 A70-33893

Low aspect ratio wings under conditions of creep, calculating stress by method of strains

19 p3534 A70-37244

Strain gradient theory for random media, considering equations for response to forcing field

19 p3456 A70-37382

Isotropic finite strain expressions for compressional and shear velocities, noting no discrepancy with ultrasonic and seismic data

20 p3619 A70-39218

STRAIN FATIGUE

U FATIGUE (MATERIALS)

STRAIN GAGE ACCELEROMETERS

Simple harmonic scotch yoke mechanical oscillator for strain gage accelerometer calibration in VLF range

16 p2900 A70-32995

Subminiature three directional cantilever beam accelerometer using semiconductor strain gages

21 p3824 A70-40861

STRAIN GAGES

S/N fatigue life gage for nondestructive evaluation of cumulative damage, discussing calibration and two step, block and random tests

01 p0053 A70-10009

Silicon strain gage transducer for measurement of pressure between tongue and teeth, developing two types of temperature compensated strain gages

02 p0242 A70-12054

Resistance strain gage performance prediction, investigating response during temperature change for preattachment matching

02 p0302 A70-12498

Strain gage data obtainable on rosettes used for measuring test component stresses at 550 F in inert atmosphere

03 p0482 A70-12965

Time sharing computer systems for data reduction from semiconductor strain gauges applied to FORTRAN IV programs

03 p0453 A70-12969

Twin wave interferometer and strain gage mechanism for press-fit measurements of contact deformation on metallic and polymer samples

03 p0484 A70-13426

Inductive eddy current strain gage for repeated strains measurement in magnetic and nonmagnetic sheets offering direct readout and remote recording

03 p0485 A70-13475

Micrometeorite detection involving impact stress wave monitoring by strain gages embedded in viscoelastic plastic

03 p0487 A70-13573

P-n heterojunction diode strain sensor fabricated by vacuum evaporation onto substrate, investigating mechanical input and output impedance characteristics

03 p0495 A70-14192

Variable strain bending form design for determining environmental craze resistance of polymers

04 p0713 A70-15375

Dynamic strain measurement by solid state direct coupled amplifier with flat frequency response

05 p0936 A70-16322

Resistance strain gage load cell for measuring compressive loads under high hydrostatic pressure, discussing gage bonding

05 p0848 A70-16377

Miniature temperature and strain telemetry transmitters developed for measurements in areas inaccessible to direct wire connections

06 p1069 A70-18433

Subminiature sensor element integrated with silicon semiconductor strain gages for simultaneous three dimensional measurement of acceleration components

06 p1069 A70-18434

Magnetic, electrostatic and RF fields noise reduced for strain gage data acquisition

06 p1069 A70-18435

Strain gage high temperature performance in rocket engines tested by spot welding to turbine manifold, noting installation and position influence

06 p1069 A70-18440

Silicon semiconductor irradiated strain gages for precision measurement of low level strain

06 p1069 A70-18441

Electron irradiation for reducing thermal coefficient of resistance of Si strain gages, noting crystal orientation dependence of gage factor

06 p1070 A70-18442

Miniature resistance strain gage performance in low cycle fatigue, discussing zero drift and gage sensitivity changes

07 p1281 A70-19241

Active and compensating sensors resistances, strain sensitivities, temperature gradients and lead resistances differences effect on accuracy of resistance strain gage measurements

07 p1283 A70-19747

High precision strain gage installation, discussing specifications and errors caused by oblique load action, natural frequency and deformation

08 p1493 A70-20585

Strain gages design and development for small loads

08 p1493 A70-20586

Vinoflex glue for constantan strain gauges in low temperature tensometry, showing satisfactory recording at single and multiple loadings

08 p1495 A70-20984

Thermal strain measurement in operational and experimental components of high temperature plant, discussing full-bridge weldable type strain gage for transient strains

09 p1675 A70-22582

Thermal gradients and associated strains measurement in steam turbogenerator casings, considering strain gage placement and heat transfer calculations

09 p1774 A70-22590

Strain gages for static deformation measurement of fiberglass reinforced plastics at room and higher temperatures, discussing error sources and gage-specimen adhesive bonding

09 p1780 A70-23107

Gages for static strain measurements at high temperatures, discussing resistivity temperature coefficient compensation

09 p1680 A70-23109

Strain gage for measuring strain waves amplitude on surface of fused quartz to study electromagnetic waves interaction in Permalloy films

09 p1681 A70-23349

Transient and steady state thermal stress distribution measured by strain gages embedded in epoxy models

11 p2130 A70-25585

Strain gages moisture protection, deriving formula for calculating acceptable protection time of insulator

11 p2049 A70-25586

Slip-ringless propeller blade mounted measurement system for steady state and vibratory stresses from multiple strain-gage locations during flight and ground tests

[SAE PAPER 700223] 11 p2051 A70-25891

Bonded resistance strain gages technical characteristics noting need for uniform standards

11 p2053 A70-26427

Foil type resistance strain gages /tensometers/, studying measurement current effects on readings

11 p2053 A70-26428

Semiconductor strain gages /tensometers/ materials, fabrication and properties

11 p2054 A70-26429

Hermetically sealed miniature strain gages /tensometers/ design and testing, noting insensitivity to effects of fuels and oils

11 p2054 A70-26430

Resistance strain gages /tensometers/ for force and moment measurement in aerodynamic research, giving design and structural recommendations

11 p2054 A70-26431

Lead resistance effects on resistance strain gage measurements as function of utilized measurement system and procedure

11 p2054 A70-26432

Unbalanced Wheatstone bridge network operation for resistance strain gage measurements, determining dynamic transients variable extremes

11 p2054 A70-26434

Multichannel tensometric AC bridge network for static and dynamic measurements of mechanical quantities in structural elements

11 p2054 A70-26436

Transistorized system for static and dynamic strain measurements of mechanical quantities

11 p2055 A70-26437

Brush collector for strain measurement in jet engine compressor and turbine elements at high RPM

11 p1983 A70-26439

Cross sensitivity errors effect on stress determination by free-filament wire strain gages used at high temperature

11 p2058 A70-26838

Instrument for measuring and recording strains and birefringence in glasses and crystal under compressive, tensile or bending loads at low/high temperatures and in vacuum

12 p2237 A70-28161

Electric resistance type strain gages, eliminating errors due to device length

14 p2582 A70-30174

Thermally induced strain measurement using four gage rosettes without temperature gradient limitations

14 p2585 A70-30684

Heating rate effect on parameters of resistance wire strain gages subjected to temperature gradients

15 p2733 A70-31536

Measuring apparatus for cyclic plastic strains at high temperatures, discussing data processing techniques

15 p2733 A70-31538

Miniature wireless strain and temperature radio telemetry transmitters for measurements in areas inaccessible to direct wire connections

15 p2738 A70-32301

Strain gage maximum rise time estimation for longitudinally sweeping strain pulse, reducing gage length/pulse velocity ratio effects

[SESA PAPER 1620] 15 p2739 A70-32302

Electromechanical transducer to sense and record strain cycles, describing motion magnification principle, system and prototype evaluation

15 p2739 A70-32310

Piezoelectric field effect strain gage with semiconducting film for extremely small strains in electrically noisy background

[SESA PAPER 1676] 15 p2739 A70-32317

Glass bonding techniques for semiconductor strain gages, discussing outgassing minimization, hysteresis and repeatability and operational temperature range extension

15 p2739 A70-32325

Open faced polyimide-backed strain gage for transducer and/or long term applications, considering drift and zero shifts

15 p2739 A70-32329

Displacement and velocity measurements using strain gauges, linear potentiometers and seismic transducers

15 p2743 A70-32799

Servocontrolled laser strainmeter based on Michelson-Morley interferometer, determining dynamic characteristics dependence on feedback loop filter type

16 p2925 A70-33022

Laser interferometry strain gage for measuring earth strain, taking into account wavelength stabilization

16 p2925 A70-33023

Vacuum interferometer strain gage for absolute earth strain measurement via length change comparison with wavelength standard

16 p2925 A70-33024

Omnidirectional dynamic stress gage as embedded elastic inclusion, discussing transient response to ground shock compression wave pressure

19 p3422 A70-37699

Welded joint strain measurement by grating etching and moire fringe technique

19 p3428 A70-38513

Strain measurement on filament-wound structural members, incorporating electric resistance wire as strain gage within windings

19 p3550 A70-38719

Strain multiplier for fatigue sensor in moderate amplitude cyclic strain applications

20 p3628 A70-39159

Strain measuring apparatus for multiple samples simultaneous compression tests at near absolute zero temperatures

20 p3632 A70-39628

Tensile test device for continuous recording of sample load and strain

20 p3728 A70-40000

Strain gages for structural stress analysis in cryogenic environments, discussing correction factors for temperature dependent characteristics

21 p3932 A70-40545

Crystal orientation dependence of thermal resistance and gage factor in electron irradiated n-type silicon strain gages

21 p3824 A70-40862

Resistance strain foil gage response to dynamic plastic strain

22 p4039 A70-43451

Strain gage stress measurement under elastic-plastic strain conditions at high temperature

22 p4117 A70-43454

Aircraft structure fatigue load monitoring, discussing strain gage installation in critical areas [ICAS PAPER 70-31]

23 p4267 A70-44102

STRAIN HARDENING

Dislocation climb theories of creep and superplasticity derived, postulating strain hardening and recovery processes with independently determined rates

02 p0317 A70-12315

Strain hardening on single crystals of aging Ni-based alloys with ordered separated phase

03 p0505 A70-13104

Ni-Nb intermetallic compound precipitation effect on various phase formations in strained samples of Alloy 718 /wrought Ni base alloy/

03 p0511 A70-13568

Transient creep analysis of simply supported circular cylindrical shells subjected to internal pressure based on strain and time hardening theories

03 p0595 A70-13813

Elastoplastic analysis of strain hardening materials under multiaxial states of stress based on von Mises yield condition and stress-strain relationship

03 p0596 A70-14012

Strain hardening equation for anisotropic medium under creep

05 p0952 A70-17035

Mechanical and electrochemical polishing effect on turbine blade alloy fatigue strength, discussing surface strain hardening as function of temperature in mechanical polishing

07 p1304 A70-18838

Stress corrosion testing of vanadium alloys using precracked specimens in cantilever beam apparatus, discussing strain hardening exponent role and propagation rates

07 p1306 A70-19299

Dynamic strain aging effect on Mo-Ti-C alloy creep, relating carbides precipitation during plastic deformation to mobile dislocations density

08 p1524 A70-21954

Cold rolling characteristics of unidirectionally reinforced Al-B fiber composites, measuring hardness and tensile properties

08 p1524 A70-21957

Metals yield locus in strain hardening range in sigma-tau plane determined using slip theory, considering Bauschinger effects

09 p1771 A70-22395

Temperature and strain dependence of strain anisotropy in Ti tested on longitudinal and transverse tensile specimens

09 p1705 A70-22807

Thermal cyclic loads effects on heat resistant materials strength during strain hardening, considering role of time factors in durability

09 p1779 A70-23104

Total Poisson ratio derivation from stress-strain relationship with known variations of elastic and plastic Poisson ratios for particular strain-hardening case

10 p1956 A70-24096

Power-law stress-strain relation in plastic complex stressed state, showing identical strain hardening curves for shear and tension

10 p1957 A70-24280

Plastic strains buildup during thermal cycling, establishing relation between strain interval and cycles number to failure for strain hardening materials

10 p1965 A70-25293

Tensile strain rate and oxygen concentration effects on peaks of niobium hardening zones involving interstitial atoms

12 p2252 A70-27001

Airframe structures fatigue crack propagation with and without strain hardening during variable amplitude loading

12 p2315 A70-27014

Kinetic theory for fatigue crack propagation using cyclic stress-strain relation in connection with strain hardening characteristics

12 p2322 A70-27208

Structural Al-Zn-Mg alloys strain hardening effect on mechanical and corrosion properties, noting relationship between stress corrosion cracking and shear cracks

13 p2434 A70-29155

Finite element displacement method for elastoplastic bilinear strain hardening orthotropic plates and shells, comparing initial and tangent stiffness

14 p2660 A70-31136

Al-Mg alloy nonpropagating fatigue cracks at roots of sharp notches, discussing cyclic strain hardening

14 p2598 A70-31299

Unloading shock waves propagation in elastoplastic medium, investigating strain hardening effect on shock strength decay, residual strains and radial stresses

15 p2815 A70-32002

Beta phase decomposition kinetics and strain hardening inhibitions in Ti-base Mo alloys, using metallographic, dilatometric and X ray analyses

15 p2764 A70-32855

Hysteresis loop behavior under tension-compression cycle fatigue related to Meyer strain hardness values of cyclically strained metals

16 p2934 A70-34334

Unalloyed alpha titanium mechanical properties, emphasizing grain size and interstitial content effects on strain hardening and deformation dynamics

17 p3116 A70-34391

Rate-sensitive perfectly plastic linear strain hardened rings and tubes, calculating response to impulsive loads

17 p3184 A70-34907

Fiber reinforced composite with ductile matrix, discussing fatigue life prediction from strain hardening characteristics

17 p3128 A70-35465

Elastoplastic deformations during explosive extrusion of pipes of different materials with linear strain hardening law

18 p3335 A70-36132

Strain hardening directionality during creep tests of tubular samples under combined tensile stresses and bending moments

18 p3341 A70-36588

Plasticity and strain hardening in sintered metals, considering pressure at pores and elastoplastic limit under small plastic deformation

20 p3644 A70-38962

Structural Ti, investigating effect of surface strain hardening by cold rolling on fatigue strength

20 p3648 A70-39250

Uniformly loaded thin elastoplastic spherical shells, calculating strain hardening and strain rate effects on transient response

21 p3935 A70-41255

Mo alloys strengthening by hydrostatic extrusion, combining dynamic strain aging with low temperature strain hardening

24 p4341 A70-45251

Solid solution hardening of single crystal Ta base alloys, measuring critical shear stress at various temperatures

24 p4365 A70-46370

STRAIN RATE

Strain rate, temperature and alloy content effects on plastic flow in binary substitutional alloys of bcc iron

01 p0119 A70-10735

Test fixture for determining mechanical properties of metals and steels at moderate strain rates, detailing design and instrumentation

03 p0462 A70-12883

Polycrystalline material tensile failure at high temperature, discussing intergranular cracking, shearing, etc

03 p0508 A70-13155

Polycrystalline Co strength and plastic properties tested at various temperatures and strain rates

03 p0510 A70-13352

Tensile tests on alpha Ti containing oxygen and hydrogen at various temperatures and strain rates to determine deformation and fracture

04 p0706 A70-15133

Plastic-viscoplastic bar wave propagation due to longitudinal impact, analyzing stress profiles to determine effect of strain rate

05 p0926 A70-15913

Adverse effects of temperature and strain rate on low cycle fatigue resistance of austenitic stainless steels at elevated temperatures compared with tension tests

06 p1086 A70-17452

Strain rate tensor coincidence in Lagrangian and Eulerian descriptions of turbulence demonstrated for homogeneous flow of incompressible fluid

07 p1252 A70-18672

Dislocation velocity-stress exponent for Nb single crystals calculated from strain rate sensitivity measurements of effective flow stress

07 p1314 A70-20011

Polycarbonate ductile fracture measured for strain energy release rates and plastic zone size and shapes to correlate with existing theories and experimental data

07 p1321 A70-20041

Electrically conductive ablative materials rapidly heated to 7000 F in test facility, discussing heating method and high strain rate testing

07 p1250 A70-20042

Viscoelastic perfectly plastic ring failure under uniform external pressure characterized by infinite strain rate occurring at finite value of ring deflection

07 p1416 A70-20300

Loading frequency effect on carbon steel energy dissipation at large stress amplitudes, deriving strain rate relations

08 p1516 A70-20980

Static and dynamic low temperature crack toughness behavior of steels, determining strain rate effect

08 p1518 A70-21317

Strain rate effects in cold metal working processes involving rolling and drawing

08 p1590 A70-21327

Strain rate effects on mechanical properties of solids under dynamic loading

08 p1590 A70-21328

Dynamic compressive properties of polypropylene, polystyrene bead and extruded polystyrene foams tested at given strain rate under room temperature

08 p1527 A70-21329

Tensile properties of yarns at high strain rates and subambient temperatures determined for nylon, Dacron, Nomex, Beta Fiberglass and Karma metal

08 p1527 A70-21330

Stress-strain behavior of Al and Ti alloys, beryllium and nonmetallic structural materials based on constitutive equations describing strain rate and temperature effects

08 p1518 A70-21331

Elastic-plastic work hardening sandwich arch under given loading rate analyzed for stress rates using integral equation [ASME PAPER 69-APM-21]

08 p1593 A70-21616

Temperature, transformation and strain rate effects on tensile ductility properties of stable and metastable compositions of austenitic stainless steels

08 p1524 A70-21956

Potential function of creep strain rates for incompressible nonstrengthening materials exhibiting different creep characteristics in tension and compression

09 p1769 A70-22122

Strain rate and hold time effects on steels low cycle fatigue behavior, graphing various correlations among stress amplitude, time to fracture, etc

09 p1774 A70-22589

Metals and plastics tensile strain rate sensitivity tested by drop weight tests, obtaining dynamic and static stress-strain curves

09 p1704 A70-22725

Chromium structural dislocation and cell formation during deformation as function of temperature, impurities and strain rate

10 p1902 A70-23861

Aluminum and aluminum-copper alloys dislocation damping at high strain rates using impact shear tests

10 p1903 A70-23983

Flow rule for viscoplastic symmetric cylindrical shells, using constitutive equations for strain rate sensitive materials based on Huber-Mises yield condition

10 p1954 A70-24020

Tantalum mechanical properties dependence during deformation on temperature and strain rate irregularities, discussing serrated yielding

10 p1904 A70-24386

Glass-epoxy composites failure mode dependence on matrix characteristics and fiber orientation, observing flexural strength increase with strain rate

10 p1908 A70-25174

Filament reinforced composites tested under dynamic compression loads for determining relations among strain rate, constituent properties, stress-strain behavior, fracture energy and mode

12 p2253 A70-27119

Stress relaxation in alpha titanium during plastic strain, measuring temperature and strain rate dependence

12 p2255 A70-27608

High temperature dislocation model based on dislocation dynamics, rate theory and varying back stress ratio

13 p2436 A70-29563

S glass fibers strength characteristics at quasi-static strain rates, considering temperature effects on elastic modulus

13 p2439 A70-29707

Cr-Ni cold worked austenitic steel dislocation structure in tensile tests at different strains

14 p2596 A70-30874

Tensile properties of fibrous materials at high rates of strain and subambient temperatures, considering nylon, Dacron, Nomex, Beta Fiberglass and Karma metal yarns

14 p2598 A70-30928

Strain rate tensor coincidence in Lagrangian and Eulerian descriptions of turbulence demonstrated for homogeneous flow of incompressible fluid

15 p2718 A70-31464

Iron sample shape determination for studying relationship between tensile strength and rate from stress wave propagation during high speed tensile tests

15 p2814 A70-31547

Nonlinearly elastic bodies under subcritical strain, analyzing boundary value problems for three dimensional stability

15 p2818 A70-32179

Plane deformation of anisotropic plastic nonstrain-hardenable material, analyzing state equations for stresses and strain rates

15 p2818 A70-32184

Precrack Charpy slow rate straining sensitivity of high strength steel at increased temperatures, comparing fracture energy of impact tests

15 p2758 A70-32238

Tapered cantilever Al plate load characteristics, determining elastic and plastic strain due to regular, reverse and second regular deflection sequence

15 p2821 A70-32307

Human skull porous dipole layer shear and compressive properties, measuring static and dynamic strain rates

15 p2683 A70-32308

Heat treatment effect on maraging steel fracture toughness and subcritical crack growth loaded at slow strain rate in laboratory air

15 p2760 A70-32377

Inconel 600 high temperature high strain rate fracture process by hot torsion tester, noting temperature effects

15 p2762 A70-32389

Metal property effects on deformation and strain energy distribution during hypervelocity projectile cratering

15 p2824 A70-32790

Materials testing machine for tension, compression and flexure at constant strain rate and for fatigue

16 p2900 A70-33067

Hot plasticity elongation of cast and wrought Ti-Al-V alloy as function of temperature and strain rate

17 p3117 A70-34401

Temperature and strain rate effects on polycrystalline Al strength

17 p3124 A70-34655

Rate-sensitive perfectly plastic linear strain hardened rings and tubes, calculating response to impulsive loads

17 p3184 A70-34907

Strain rate effect on cyclic behavior of materials with hardening and softening characteristics

17 p3187 A70-34988

Shock wave response of metals and nonmetals under high strain rates

17 p3188 A70-35223

Work hardening maxima of alpha-Ti as function of strain rate and temperature

19 p3451 A70-37568

Linear relations between stress state and Euler strain rate in isotropic elastic bodies during superposition of small deformation on finite strain

20 p3728 A70-39893

- Strain component determination for grain boundary sliding influence in creep of alpha iron
20 p3735 A70-40446
- Stress-strain characteristics at high strain rates, obtaining materials dynamic plastic properties by thin wafer technique
21 p3932 A70-40543
- Uniformly loaded thin elastoplastic spherical shells, calculating strain hardening and strain rate effects on transient response
21 p3935 A70-41255
- Deformations with constant strain invariants for elastic bodies under surface traction
22 p4113 A70-42543
- Strain rate change effect on stress-strain diagram shape of polycrystalline alpha-Ti during tensile tests over temperature range
22 p4054 A70-42737
- Ti embrittlement by liquid Cd, discussing ductile-brittle transition temperature dependence on strain rate
22 p4054 A70-42738
- Strained state of Ti and steel sheets during unsymmetric rolling, constructing deformed metal particles displacements rates field based on ideal fluid motion equations
22 p4045 A70-42814
- Strain rate sensitivity and stress waves effects on dynamic response and adhesion failures of rain erosion resistant coatings
22 p4059 A70-43102
- Strain rate sensitive materials tensile tests using machine with external variable speed motor
24 p4422 A70-45517
- Zn-Al alloy high velocity deformation characteristics, examining ductility and aging at various temperatures and heat treatments
24 p4363 A70-46194
- Superplasticity, discussing strain rate-flow stress relationship and grain boundary sliding
24 p4363 A70-46218

STRAIN SOFTENING

U PLASTIC DEFORMATION

STRANDS

- Brittle fibers strand strength as function of statistical distribution of limiting stresses
18 p3342 A70-36648

STRAPDOWN INERTIAL GUIDANCE

- Strapdown inertial guidance systems performance and applications
02 p0336 A70-12264
- Onboard modular computer research in strapdown guidance technology for computational ability and long term reliability of unmanned missions
07 p1238 A70-20062
- Nonlinear filtering methods for attitude computation in strapdown inertial navigation system
13 p2382 A70-29067
- Stable, soupcan size, field replaceable, plug in/out gyro unit strapped to vehicle body without gimbals
13 p2409 A70-29480
- Gyro test package, dynamic test facility and real time attitude algorithm to investigate operational capabilities of strapdown inertial attitude package
17 p3134 A70-35652
- Commercial aircraft strapdown inertial navigation systems, examining initial self alignment techniques
18 p3289 A70-36442
- Strapdown inertial guidance systems critical dynamic errors mathematical modeling and verification
[AIAA PAPER 70-1029] 20 p3666 A70-39508
- Apollo Lunar Module strapdown Abort Guidance system, correlating performance prediction with flight test results
[AIAA PAPER 70-1028] 20 p3666 A70-39509
- Ring laser gyro angular rate sensor for strapdown inertial systems
[AIAA PAPER 70-1025] 20 p3631 A70-39510
- Strapdown redundant experimental sensor inertial navigation package containing gyros and accelerometers, discussing signal real time processing by digital computer
[AIAA PAPER 69-851] 21 p3849 A70-41858
- Single degree of freedom gyroscope design factors applicable to strapdown guidance system, discussing torque-to-balance loop, multiple pulse bursting and error sources
[AIAA PAPER 69-848] 21 p3849 A70-41859
- Strapdown inertial system mechanization and modularized instrument packaging with self contained failure isolation, temperature control and redundant components
[AIAA PAPER 70-1027] 22 p4066 A70-42315
- Strapdown inertial attitude indication, describing static and dynamic tests, error propagation profiles, performance prediction, etc
22 p4068 A70-42668
- Gyro misalignment and encoder quantization effects for strapdown attitude error sources
22 p4040 A70-43588

STRATA
NT SUBSTRATES

- Sonic boom wave shapes and amplitudes determination in still stratified atmosphere, comparing U.S.

standard atmosphere results to various atmospheric models
03 p0411 A70-12927

Radio wave propagation in stratified media consisting of periodically stacked dielectric slabs solved for boundary condition by reducing Maxwell equations to Hill equation
06 p1007 A70-17463

Dynamic shear modulus and depth of dominant layer of vibrating elastic medium, assuming foundation as isotropic stratum on rigid bed
10 p1957 A70-24481

STRATEGY

- Optimal strategy for searching for object hidden in box involving use of optimal return function
05 p0877 A70-16715
- Sufficient conditions of optimality for strategic couple in theory of quantitative differential games
07 p1245 A70-19379
- Fault finding strategy optimization in systems with single defective element
09 p1693 A70-22974
- Optimal strategies for game with nature and two-automata zero sum game under finite memory constraints
11 p2073 A70-26241
- Continuous and discrete minimum time problems relationships and state space portraits during application of optimal strategies to system
11 p2029 A70-26749
- Extremal strategy to assure successful termination of pursuit at definite time, investigating sufficient conditions theorem
13 p2443 A70-29754
- Linear systems simultaneous optimal stochastic control and observation strategies, assuming quadratic observation cost
16 p2886 A70-33346

STRATIFICATION

NT ATMOSPHERIC STRATIFICATION

- Electromagnetic wave propagation through stratified positive plasma column in waveguide, noting stratification travel effects on wave amplitude and phase shift
03 p0443 A70-13096
- Refractive index profile analysis for hypergeometric functions solutions for vertically polarized electromagnetic waves propagating in horizontally stratified isotropic media
04 p0647 A70-14616
- Automatic control for filling tanks with stably stratified liquids using analog mixture valve and digital metering pump methods
06 p1062 A70-17617
- HF cylindrical waves propagation by line source in stratified medium, investigating refraction and diffraction at plane boundary using mathematical and ray methods
07 p1335 A70-19683

STRATIFIED FLOW

- Stratified air flow above relief in baroclinic atmosphere, considering plane nonlinear and three dimensional linearized flow models
03 p0521 A70-13270
- Wave drag in stratified flow lee waves without upstream influence calculated for cylindrical and three dimensional obstacles
03 p0479 A70-14229
- Forced vertical oscillations in viscous stratified fluid, showing phase angle dependence on amplitude and relation to Brunt-Vaisala frequency
04 p0666 A70-14611
- Natural convection heat transfer from vertical plate immersed in thermally stratified fluid
06 p1175 A70-17685
- Instability of plane Couette flow of three superposed layers of fluids of different viscosity between two horizontal planes
07 p1260 A70-19978
- Turbulent energy spectra in stably stratified atmospheric boundary layer flow
09 p1715 A70-22360
- Stably stratified atmospheric turbulent shear flow governing spectral equations asymptotic solutions for buoyancy subrange
09 p1659 A70-22372
- Elasticity stratification stabilization effect on two layer flows down inclined plane found dependent on time response difference between layers
10 p1863 A70-24009
- Waves and mean currents excitation in stratified fluid due to moving heat source, studying effect on mean motion
11 p2036 A70-26167
- Interfacial and free surface mode instabilities of time periodic flows of viscosity and density stratified fluids at various Froude numbers
14 p2566 A70-31026
- Turbulent flow in stratified fluids over flat plate, relating density profile curvature and heat transfer
16 p2895 A70-34242
- Shear flow perturbations in inviscid incompressible stratified fluid of given density, comparing stability characteristics with jet flow
16 p2895 A70-34243

Stratified-rotating fluids mathematical analogy, examining flow constraints, parameters and variables
17 p3068 A70-34664

Horizontal boundary layers development on flat plate in nondiffusive stratified flow characterized by Reynolds and Russell numbers
18 p3239 A70-36192

Density diffusion and buoyancy effects on horizontal boundary layers in stratified flow
18 p3239 A70-36193

Viscoelastic fluids stratified flow down inclined plane, examining liquids elasticity role in stability
19 p3403 A70-37531

Stability of thermal and inertial perturbations superimposed on unstably stratified plane parallel flow with variable vertical shear
19 p3462 A70-37753

Weak stratification and geometry effect on steady mechanically driven motion of contained rotating viscous fluid
20 p3608 A70-39357

Small viscosity and heat conductivity in solutions to critical layer in stratified shear flow
20 p3608 A70-39447

Two dimensional body slow motion through stratified fluid bounded by parallel vertical walls, examining flow at different Peclet numbers
21 p3744 A70-41246

Miles-Howard theorem extension to gravitationally stratified compressible fluid containing parallel shear flow, considering stability against adiabatic perturbations
23 p4179 A70-43976

Two dimensional stratified flow over extended obstacles with source disturbances, indicating topographical effect on vertical wind shear in troposphere
23 p4214 A70-44031

STRATIFIED LAYERS

U STRATA

STRATIGRAPHY

- Continental migration role in lunar maria formation, suggesting similarity with geological formation of earth ocean floor
09 p1765 A70-23797
- Book on stratigraphic view of lunar geology covering lunar craters and terrestrial analogs, remote sensing, material ages, surface interpretations and Apollo mission results
13 p2491 A70-29060

STRATOCUMULUS CLOUDS

- Upper surface roughness of internal st-sc clouds as function of vertical temperature and moisture in overlying inversion layers
08 p1537 A70-21106
- Cloud layer vertical displacement effects on upper boundary and temperature changes in st-sc using aircraft sounding data
08 p1537 A70-21107

STRATOFORTRESS AIRCRAFT

U B-52 AIRCRAFT

STRATOPAUSE

- Molecular hydrogen, methane, water vapor and tritium concentrations near stratopause from air samples collected on Aerobee flight with liquid hydrogen cooled cryocondenser
15 p2728 A70-31995
- Zero pressure balloon as base for stratopause pressure and temperature measurements, analyzing winds and balloon trajectory and dynamics
17 p3075 A70-34608

STRATOSPHERE

- Stratospheric circulation and temperature variations periodicity, discussing midwinter warmings, polar vortex breakdown and relations to D region anomalies and solar events
01 p0072 A70-10580
- Stratospheric temperature changes connection with winter D region absorption changes
01 p0073 A70-10583
- Wind oscillations in stratosphere, lower mesosphere and meteor heights noting periodicities
01 p0074 A70-10591
- Stratospheric water vapor distribution from analyzing IR solar spectrum during sunset observed by balloon-borne spectrometer
01 p0081 A70-11295
- Ionospheric absorption associated with sudden stratospheric warmings following geomagnetic disturbances in 1958 and 1963
02 p0290 A70-12159
- Stratospheric circulation model developed from radioactive element measurements, discussing large scale processes, seasonal variations, etc
02 p0291 A70-12291
- Vertical ion concentration profile in troposphere and stratosphere from ozone distribution satellite measurements using aeronomical reactions
02 p0291 A70-12389
- Stratospheric air intrusion into troposphere calculated for speed and frequency of occurrence, considering mass and energy transfer
02 p0329 A70-12690
- Superpressure balloon flight trajectories for dynamics of tropical stratosphere, revealing distinctive circulation features
02 p0228 A70-12694

Vertical concentration and size distribution determinations for aerosols in stratosphere, suggesting volcanic origin

02 p0294 A70-12842

Rocket-borne cryogenic sampler for stratospheric composition measurement by mass spectrometer analysis for computing radiation balance in stratosphere [AAS-PAPER 69-569]

04 p0687 A70-14661

Daily variations of winter stratospheric zonal wind and planetary waves based on synoptic charts from balloon observation

05 p0878 A70-16148

Meteorological conditions effects on SST aircraft flight safety and economics, emphasizing stratospheric information for forecasting

06 p1095 A70-17193

Stratospheric clear air turbulence over squall line, discussing turbulence over thunderstorms

06 p1102 A70-18588

Soviet book on nonperiodic processes in Northern Hemisphere stratosphere, discussing seasonal temperature fields, geopotential and circulation formation

07 p1261 A70-18733

Tropospheric and stratospheric turbulent horizontal heat and momentum transfer spectral density profiles calculations from radio launchings data

07 p1269 A70-19646

Collection of papers on stratospheric circulation covering rocket sounding, upper atmospheric clouds, climatology, etc

07 p1272 A70-20251

Meteorological Rocket Network for limited synoptic inspection of stratospheric circulation

07 p1273 A70-20252

Skua meteorological rocket system for synoptic stratospheric sounding, describing system, launch preparation, firing and flight characteristics

07 p1395 A70-20253

PWN-8B meteorological rocket system for synoptic investigation of stratospheric circulation, describing sensor system deployment for descent measurements of wind and temperature

07 p1395 A70-20255

Kookaburra meteorological rocket system for sounding stratospheric circulation, describing instrument payload deployment for descending wind and temperature measurements

07 p1395 A70-20257

Parachute wind sensors used in Arcas and Loki sounding rocket systems for stratospheric sounding, describing position data acquisition via radar tracking

07 p1395 A70-20259

Temperature measurement in stratospheric circulation by meteorological rocketed-on wire sensor, presenting error correction technique

07 p1289 A70-20264

Stratosphere-ionosphere coupling, dynamo theory on geomagnetic Sq variation and ionosphere radio wave absorption and reflection

07 p1274 A70-20271

Planetary scale disturbances in winter stratospheric circulation during sudden warming using rocket observations

07 p1274 A70-20272

Stratospheric and mesospheric circulation during winter, investigating wind fluctuations using meteorological rocket observations

07 p1274 A70-20274

Spatial variations in zonal and meridional components of stratospheric and mesospheric winds traced over horizontal distances by Arcas ROBIN rockets

07 p1274 A70-20275

Atmospheric gravity wave generation, propagation and dissipation, considering stratospheric tides

07 p1275 A70-20276

Synoptic changes associated with midwinter 1967-1968 major stratospheric warming, including pressure and wind distributions and temperature maps

07 p1275 A70-20277

Meteorological rockets fired in Spain, obtaining stratospheric wind and circulation data

07 p1396 A70-20278

Meteorological guns for synoptic sounding of stratospheric circulation, discussing system characteristics and operations

07 p1250 A70-20280

Seasonal variation of vertical profiles of atmospheric radioactivity concentration between stratosphere and troposphere due to meridional zonal wind distribution caused by eddy diffusion

08 p1539 A70-21923

Troposphere-stratosphere kinetic energy transfer during 1967-1968 midwinter warming, comparing calculation by pressure interaction term with direct calculation of vertical velocity fields

08 p1540 A70-21969

Lee wave theory for two dimensional stratified atmospheric models, noting local intense vertical beam into high stratosphere

08 p1540 A70-21972

Linear nonstationary quasi-geostrophic model with external and internal heating and forcing for dynamics of ultralong waves in troposphere and lower stratosphere

09 p1713 A70-22304

Stratospheric CAT layer energy budget analysis, considering energy shear feeding, buoyant extraction and frictional dissipation

09 p1715 A70-22357

Stratosphere-mesosphere coupling phenomena during sudden stratospheric warmings, considering ozone and ionospheric drift measurements

10 p1913 A70-24948

Stratospheric equatorial wind period phases correlation with central European westerlies frequency, intensity and persistency, noting seasonal differences

10 p1913 A70-24950

Tropical and midlatitude stratospheric dust by twilight photometry, considering possible causes of anomalous turbidity levels

11 p2046 A70-26388

Water vapor pollution of stratosphere by supersonic transports, considering effects on temperature, cloudiness, albedo, etc

11 p2077 A70-26618

Stratospheric water vapor measurement by submillimeter wave sounding, considering signal fluctuations due to scattering by high cirrus clouds

11 p2077 A70-26619

Stratospheric clear air turbulence (CAT) vertical extent above thunderstorm graphically represented

12 p2265 A70-28095

Solar spectra recording by balloon-borne monochromator, measuring stratospheric Ir absorption

13 p2491 A70-29050

Lower stratosphere ozone formation, suggesting origin in cosmic rays absorption

13 p2400 A70-29472

Vertical momentum flux correction for planetary scale gravity waves in equatorial lower stratosphere

13 p2445 A70-29623

Middle stratospheric circulation in Southern Hemisphere, associating temperature changes and ozone content with planetary wave passage in Antarctic polar vortex

14 p2568 A70-30123

Lower stratosphere temperature and wind periodic variations associated with shear flow gravity waves

14 p2601 A70-30124

NO and nitrogen dioxide influence on ozone concentration and production rate in stratosphere

14 p2568 A70-30125

Mesoscale stratospheric turbulence recording using even activated memory recorder

14 p2573 A70-30578

Upper stratosphere-mesosphere monthly-mean charts from reentry heating and atmospheric model based on hydrodynamics

14 p2608 A70-30590

Stratospheric warmings effect on atmospheric density field variations

14 p2608 A70-30592

Strong wind and vertical wind shear in upper stratosphere and mesosphere

14 p2608 A70-30594

Stratospheric CAT-internal wave relationship, using aircraft and radiosonde HICAT measurements

14 p2609 A70-30603

Stratospheric and mesospheric ozone diurnal variation by rocket-borne ozonesonde in January 1968

14 p2577 A70-31170

Stabilized balloon flights during weak winds in stratosphere, discussing pressure vs time curves

14 p2531 A70-31311

Troposphere-stratosphere kinetic energy transfer (1964-1968), annual variations and vertical flux correlation to circulation pattern

15 p2722 A70-31441

Solar Monitoring Experiment program, observing solar activity relation to large enhancements of lower stratosphere secondary radiation

15 p2792 A70-31656

Vertical temperature profiles and global circulation patterns in stratosphere and mesosphere, discussing Northern Hemispheric seasonal, latitudinal and longitudinal variations

15 p2724 A70-31665

Upper stratosphere and mesosphere structure and circulation in Southern Hemisphere, using meteorological rockets and radiosonde data

15 p2724 A70-31683

Troposphere and lower stratosphere trace element concentration measurements, establishing origin, history and movement of various air masses

15 p2728 A70-31996

Kelvin wave propagation numerical model, showing influence of mean zonal wind vertical and horizontal shear in lower stratosphere

15 p2771 A70-32370

Lidar probing of stratosphere and mesosphere using automatic data acquisition system

16 p2862 A70-33016

Winter stratospheric circulation quasi-geostrophic model based on joint radiative-photochemical equilibrium, investigating ozone cycle and warming

16 p2945 A70-33250

Constant altitude helium filled zero pressure polyethylene balloon for stratospheric meteorological data and atmospheric tides studies

17 p3075 A70-34607

IR balloon observations of absolute solar brightness and stratosphere transparency, discussing BCA and HSRA models

17 p3078 A70-35580

Radionuclides production rates in stratosphere from spallation reactions of cosmic rays with Ar

17 p3152 A70-35759

Weak ion concentration in stratosphere and mesosphere measured using accumulated capacity amplifier

18 p3257 A70-36179

Charged particle balance equations for stratosphere and mesosphere, noting particle composition investigation and formation and annihilation processes

19 p3491 A70-37311

Ozone effect on stratospheric electricity based on numerical calculations of ion densities

19 p3413 A70-38005

Annual temperature variation in low stratosphere based on harmonic analyses at 100 mb

19 p3462 A70-38263

Stratospheric perturbation sources from atmospheric circulation as function of season, geographic latitude and altitude, suggesting high energy protons in atmosphere

20 p3618 A70-39183

Explosive and diffuse stratospheric warmings over Arctic attributed to solar activity and stratospheric circulation

20 p3618 A70-39184

Polar stratospheric winter explosive warmings correlated with solar high energy charged particles injections

20 p3618 A70-39185

Synoptic processes in Arctic tropospheric and lower stratospheric warming correlated with atmospheric circulation transformations

20 p3619 A70-39186

Synoptic processes in troposphere and stratosphere with large air temperature anomalies during early summer in U.S.S.R.

20 p3663 A70-39272

Troposphere and lower stratosphere circulation during natural synoptic autumn seasons in Northern Hemisphere, noting temperature role

20 p3663 A70-39273

Trace constituent changes effects on stratospheric properties after volcanic eruption, showing prolonged atmospheric temperature increase

20 p3622 A70-39490

Book on molecular and aerosol backscatter measurement from stratosphere by means of ground based laser beams

20 p3623 A70-39925

Midlatitude stratosphere and lower ionosphere density model, discussing vertical, diurnal and seasonal variations effects on spacecraft trajectories

21 p3813 A70-40830

Midwinter warming period upper stratospheric vertical motion fields, obtaining 2-mb charts

21 p3847 A70-42123

Temperature and height data for synoptic stratospheric evaluation, using Nimbus 3 satellite IR spectrometer

22 p4064 A70-42618

Stratospheric clear air turbulence probability based on vertical temperature gradients and rawinsonde ascensional rates

22 p4064 A70-42619

Air-earth current density time variation in stratosphere by high altitude balloon, comparing with potential gradient diurnal variation over ocean

22 p4017 A70-42798

Stratospheric electric field and conductivity measurements using balloon-borne electrometer tube circuit

22 p4018 A70-42799

Stratosphere annual temperature cycle amplitude, using biannual daily temperatures over Northern Hemisphere from IQSY data

22 p4018 A70-42913

Thermosphere, stratosphere and mesosphere reactions involving water, hydrogen, methane, ozone, nitric oxide and nitrogen peroxide

22 p4023 A70-43298

Air circulation spring restructuring in Northern Hemisphere upper stratosphere, investigating summer stratospheric anticyclone evolution

22 p4066 A70-43378

Stationary disturbances in winter Northern Hemisphere stratosphere considered as upward propagating Rossby waves, assuming zonal winds profile

23 p4213 A70-44030

STRATOSPHERE RADIATION

Solar protons in subpolar stratosphere during solar activity minimum indicated from proton measurements at Tiksi Bay

07 p1374 A70-20444

Stratosphere radiation measurements by Nimbus 3 infrared spectrometer for 15 micron frequency, considering temperature variations

24 p4330 A70-46074

STRATOTANKER AIRCRAFT

U C-135 AIRCRAFT

STRATUS CLOUDS

Time dependent height of lower boundary of subinversion stratus clouds using atmospheric moisture and heat transport equations

08 p1537 A70-21102

Vertical motions and turbulent exchange influence on height variation of stratus clouds based on atmospheric moisture and heat transport equations

08 p1537 A70-21103

Short wave radiation model of single layer stratus and stratocumulus cloud based on actinometric soundings of lower troposphere

08 p1537 A70-21104

Upper surface roughness of internal st-sc clouds as function of vertical temperature and moisture in overlying inversion layers

08 p1537 A70-21106

Cloud layer vertical displacement effects on upper boundary and temperature changes in st-sc using aircraft sounding data

08 p1537 A70-21107

Artificial crystallization theory for supercooled dry-ice seeded stratus clouds, taking into account condensation growth and turbulent diffusion of crystals

08 p1538 A70-21108

Vertical and horizontal expansion rate of crystallization of dry-ice seeded internal stratus clouds

08 p1538 A70-21109

IR reflectance of cirrostratus and cirrus clouds and jet contrail measured by spectrometer on high altitude aircraft

11 p2045 A70-25626

Vertical profiles of daytime and nighttime long wave radiation fluxes in atmosphere under stratus cloud conditions

12 p2264 A70-27521

Stratus cloud dissipation process in descending vertical currents, using thermohydrodynamic and kinetic equations for cloud droplet distribution function

22 p4066 A70-43377

STREAM FUNCTIONS [FLUIDS]

Ideal fluid planar potential flow, approximating stream function and velocity potential by matrix method

07 p1253 A70-18925

Nonlinear stability of plane Couette flow, computing stream function, vorticity distribution and Reynolds stresses

07 p1255 A70-19211

Two-stream and cross-stream effects on nonlinear wave stability with shock in collisionless plasma

10 p1921 A70-23967

Monograph on Beltrami steady state, frictionless flow of incompressible medium past spherical surfaces, assuming vortex and stream lines agreement

11 p2034 A70-25498

Regularity domain and singularity location of stream function of transonic two dimensional compressible fluid flow, using integral operators

12 p2260 A70-26972

Shear stress and velocity profiles in three dimensional mixing layer between grazing perpendicular streams

20 p3608 A70-39356

Coriolis parameter effects on stream and pressure functions in geostrophic wind equation

22 p4065 A70-43167

Momentum source interaction with viscous uniform stream, constructing perturbation solutions from nonlinear equations

24 p4327 A70-46040

STREAMLINE FLOW

U LAMINAR FLOW

STREAMLINED BODIES

Flow and pressure distribution for large normal injection along surface in supersonic stream solved numerically for two dimensional or axisymmetric body and wedge

01 p0001 A70-10336

Transonic flow theory for two and three dimensional streamlined bodies in steady irrotational flow of inviscid perfect gas

12 p2158 A70-28201

Flow past streamlined obstacles under nonNewtonian fluid injection into hydrodynamic laminar and turbulent boundary layer

21 p3812 A70-42266

STREAMLINING

Streamlining design for high altitude hypersonic flight vehicles based on drag minimization at flight condition

07 p1189 A70-19717

STREAMS

NT GAS STREAMS

NT RIVERS

Lunar sinuous rilles and Mojave desert stream channels similarities, discussing presence of terraces

11 p2108 A70-25701

STRENGTH OF MATERIALS

U MECHANICAL PROPERTIES

STREPTOMYCIN

Streptomycin effects on euglena gracilis chloroplasts, comparing effects on chloroplast ribosomal system to cytoplasmic ribosomal system

09 p1616 A70-22302

STRESS [BIOLOGY]

Penicillium mutant chemical stress tolerance in boric acid and potassium chloride selective media, studying carbohydrate and inosine-5-phosphate effects on growth rate

10 p1811 A70-24325

Force input and thoraco-abdominal strain due to sinusoidal motion of electrohydraulic shake table over 2-14 Hz range imposed on human body

13 p2359 A70-29438

Day/night thermal IR imagery detection of moisture stress of girdled trees in upland forest

16 p2898 A70-34047

STRESS [PHYSIOLOGY]

NT ACCELERATION STRESSES (PHYSIOLOGY)

NT CENTRIFUGING STRESS

Human EEG relationship to verbal behavior, discussing separation of stressful from nonstressful verbal stimuli, semantics and question-answer sequences

02 p0236 A70-12119

Prolonged hypokinesia effect on human resistance to physical stress, noting prophylactic influence of physical exercises

03 p0425 A70-13898

Mechanical vibrations effect on man including motor vehicle dynamic vibrations

03 p0439 A70-14097

Physiological limitations of air traffic controllers, considering stress factors connected with workload

04 p0716 A70-15314

Coronary atheroma in hyperlipemic dog occurring in arterial tree at most intense physical stress exposure point, discussing interfacial tissue permeation

04 p0635 A70-15460

Glutethimide and aminoglutethimide reversible inhibitory effect on rat pituitary adrenal system in response to stress

07 p1203 A70-18902

Physiology of high altitude, studying animal and man adaptation and changes in body processes due to life stresses and hypoxia

08 p1441 A70-20469

Beta-adrenergic blockade effect on abnormal R-ST segment and T-wave changes, showing propranolol use in stress catecholamine and organic cardiovascular diagnosis

08 p1449 A70-21945

Heart frequency profiles of persons during parachute jumps measured by electrocardiograms recorded directly and telemetrically to investigate psychical and physical stresses

09 p1626 A70-23010

Biological performance studies under extreme environmental stresses for gaining insight into potential of earth-type life here and in universe

09 p1623 A70-23699

Prolonged hypodynamia effect on human external respiration, arterial blood oxygenation, circulation rate and gas exchange under various physical stress conditions

10 p1814 A70-24674

Ischemic heart disease /IHD/ prognosis using abnormal electrocardiographic stress test

10 p1820 A70-24940

Thermal stress /high ambient and body temperatures/ effect on human performance in high mental and low physical activities

12 p2177 A70-27043

Civilian pilot trainee stress level dependence on individual flying instructors, detecting psychophysiological variables by inflight recording

12 p2178 A70-27044

Physiological indices criteria for human thermal stress tolerance, discussing rectal temperature, body surface condition, body temperature and local cooling effects

13 p2351 A70-29332

Stress distribution and pressure distending air spaces in lungs, using mechanical pulmonary elasticity model

13 p2356 A70-29945

Human femur junctions load actions and stresses during walking calculated from measurements

15 p2692 A70-32327

Nonlinear wave equations model for human torso under impulsive stress, obtaining asymptotic solution

16 p2854 A70-34247

Environmental heat stress indices of human subjects in bicycle ergometer experiment

18 p3224 A70-36226

Heat stress effects on serial reaction time in subjects performing visual tasks

19 p3361 A70-38053

Cardiovascular stress testing using posterior bipolar lead for radiotelemetry monitoring

20 p3578 A70-39199

Sinusoidal vibrations effects on rats at different air pressures, discussing human vibration tolerances and resonant frequencies of thoraco-abdominal system

20 p3572 A70-39434

Book on environment and human efficiency covering stress mechanisms, experimentation, exposure to chemicals, radiation, noise, heat, cold, machines, etc

22 p3967 A70-42457

Epidemiological investigations of coronary disease in Finland, relating customary loads and working capacity

22 p3969 A70-42903

Sympathetic transmission model, discussing transmitter liberation capacity under various stresses by mobilization of stores, acceleration of synthesis, etc

24 p4299 A70-45804

Brain cortex protein metabolism alterations induced by anticipation stress and ACTH in rats

24 p4301 A70-45999

STRESS [PSYCHOLOGY]

Nervous stress effect on coronary thrombosis, deriving mathematical theory based on biophysical and biochemical approaches

01 p0028 A70-11369

Human EEG relationship to verbal behavior, discussing separation of stressful from nonstressful verbal stimuli, semantics and question-answer sequences

02 p0236 A70-12119

Management role in air traffic controllers stress reduction, considering human factors affecting ATC system capacity

03 p0439 A70-14316

Exercise habits and environmental emotional stresses role in origin and prevention of degenerative heart disease

07 p1212 A70-19692

Aircraft pilots psychic and flight stress admissible degree not resulting in hazardous consequences, suggesting measures to increase resistance

09 p1625 A70-23006

Heart frequency profiles of persons during parachute jumps measured by electrocardiograms recorded directly and telemetrically to investigate psychical and physical stresses

09 p1626 A70-23010

Psychic stress causing factors and reactions in aircraft pilots on duty, analyzing harmful effects on organism

09 p1620 A70-23012

Aircraft pilots physical exercise program to maintain optimal state of fitness, discussing harmful effects caused by nervous and psychic strains

09 p1626 A70-23014

Soviet book on nervous stress and cardiac activity covering hypothalamus and cardiovascular reactions and cardiac component of complex conditioned reflexes and emotional reactions

10 p1809 A70-23873

Mental blocking /incidental long reaction times/ during continuous serial performance using perceptual-selection and response theories

12 p2178 A70-27045

Human tracking performance in position, rate and acceleration control systems under short term psychological stress induced by electric shocks

16 p2853 A70-33689

Rheoencephalographic recording of healthy persons during rest and mental tension in expectation of stimulus

18 p3222 A70-37219

Air traffic controller stress reduction, discussing work-rest intervals and various management and human factors

19 p3371 A70-38647

Human mental stress evaluation through chemical analysis of 17-hydrocorticosteroid level in parotid fluid

24 p4308 A70-45509

Psychological training and selection of airline pilots for stress resistance [DEVL-SONDDR-53]

24 p4310 A70-46413

STRESS ANALYSIS

NT PHOTOGRAPHIC MEASUREMENT

NT SCHWARTZ METHOD

NT X RAY STRESS ANALYSIS

Holographic interferometry as stress analysis technique for crack propagation studies, discussing advantages over classic interferometric and conventional photoelastic methods

01 p0198 A70-10002

Stress criterion for unstable crack propagation from Al alloy sheet tests, examining fracture data for vessels of various geometries and materials [ASME PAPER 69-SESA-2]

01 p0117 A70-10451

Thermal stresses in infinite layer of transversely isotropic material due to crack with prescribed normal displacement, deriving temperature distribution

01 p0200 A70-10552

Nonlinear stress relation in elastic media incompatible deformations, eliminating elastic distortions for known temperature distribution and thermal distortion

01 p0201 A70-10890

Out-of-plane displacement restraint at thin photoelastic plates bonded to rigid boundaries of inclusions inducing transverse stress components causing plane stress solution deviation

01 p0202 A70-11059

Numerical solution of bending stresses in internally pressurized elliptical tubular or ring specimens for testing uniaxial and multiaxial fracture strength

01 p0203 A70-11061

- Stresses in plane elastic bodies analyzed by generalizing biharmonic stress function equation in polar coordinates, assuming constant Poisson ratio and nonhomogeneity 01 p0206 A70-11152
- Transient thermal stress concentration at small thickness change of plate obtained by photoelastic studies 01 p0207 A70-11157
- Residual stress determination in elastoplastic body with known plastic strains, using Hilbert space for symmetric tensor fields 01 p0209 A70-11399
- Sandwich panel equations derived from elasticity theory equations applicable to stress analysis in internal zone and edge effects analysis 01 p0210 A70-11409
- Stressed state of circular notched plane in tension under creep conditions 01 p0210 A70-11410
- Construction of formulas relating stresses and plastic deformations describing inelastic bodies behavior under complex loads 01 p0210 A70-11411
- Stress analysis of eyebolts in turbine blades hinged loads based on perforated plate theory with concentrated force, discussing stress distributions 01 p0210 A70-11416
- Automated structural design program to treat stress, displacement, gauge and cross sectional constraints, discussing applications to aircraft structures 02 p0386 A70-11944
- Linear theory of second grade elastic materials for small deformations, discussing special case of couple stress 02 p0387 A70-11995
- Photoelastic stress analysis of shouldered shafts with keyways in shanks under direct loading and torsion, including keyway and shoulder fillet stresses 02 p0388 A70-12496
- Stress-strain analysis of rectangular plates under concentrated load, noting sealed liquid compressibility effect on deflections and bending moments 02 p0388 A70-12499
- Piezoelectric transducer for photoelastic analysis of HF stress waves in thick ring subjected to transient loads 02 p0389 A70-12500
- Elastic deformation of plates with circular holes, determining stress concentration factors for compressible and incompressible materials on digital computer 02 p0390 A70-12810
- Bending strength analysis for high strength beam with thin and long fibers embedded in matrix of viscoelastic material noting maximum stress 03 p0584 A70-12934
- Out-of-plane restraint effect on plane-stress solutions near straight boundaries, predicting deviation of two dimensional photoelastic results 03 p0584 A70-12951
- Frozen stress techniques for photoelastic analysis of orthotropic plate on nonlinear foundation, providing results to compare with future finite element analysis 03 p0480 A70-12952
- Incremental strain theories for nonproportionate loading of thin walled cylinders, discussing Tresca flow, von Mises theory and Prandtl-Reuss relations 03 p0480 A70-12953
- Stress-optic law for orthotropic composites photoelastic stress analysis, investigating use of transparent filament-resin composites 03 p0481 A70-12956
- Case bonded solid propellant rocket motors stresses under transverse body force loading as function of load orientation, case stiffness and support method [SESA PAPER 1502] 03 p0579 A70-12961
- Servo systems for analog automatic reduction of time dependent photomechanical model materials fringe data in stress analysis 03 p0482 A70-12967
- Pseudo two dimensional photoelastic test method applied to axisymmetric solid propellant rocket grains under pressure and thermal loads 03 p0482 A70-12968
- Axisymmetric elasticity theory problem of stressed state of space weakened by concentric circular cracks solved using p-analytic functions to generate boundary value problems 03 p0586 A70-13077
- Plane elasticity solution for differential expansion stresses on interface of laminated elastic rectangular strip 03 p0586 A70-13114
- Stress-strain state of material computed from strain measurements using strain gages and strain circle 03 p0588 A70-13272
- Monograph on elevated temperature strength data for wrought austenitic stainless steels, considering yield, tensile, creep and rupture strengths for allowable stresses 03 p0510 A70-13300
- Stress distribution in half space of inhomogeneous media, studying scale and edge effects relation for elastic and ideally plastic media 03 p0590 A70-13376
- Spherical shell elasticity having circular hole at apex using asymptotic method, calculating stress concentration at hole 03 p0590 A70-13381
- Unsteady temperature field induced stresses and strains in hollow viscoelastic sphere calculated by solving integrodifferential equation having right hand side dependent on time function 03 p0590 A70-13398
- Stress-strain state of body of revolution having transversely isotropic elastic properties, using perturbation technique 03 p0591 A70-13441
- Thin shells stressed state calculations by iteration, considering suitability for computer adaptation 03 p0592 A70-13442
- Plane-strain equations for deformation of weakly plastic anisotropic body analyzed by small parameter method 03 p0592 A70-13446
- Rectangular anisotropic beam torsion using Green function combined with wide step network method 03 p0593 A70-13471
- Stress differential equations of equilibrium for thick prolate spheroid /left ventricle/, yielding practical values for mean stresses in thick walled ventricles 03 p0434 A70-13571
- Scattered light photoelastic stress analysis using doubly refracting materials and lasers 03 p0594 A70-13657
- Variational stress solutions for static case of bounded bodies in Cosserat continuum theory, assuming anisotropic inhomogeneous material and defining boundary value problem solution 03 p0596 A70-13973
- Variational principles in linear elasticity theory with couple stresses, solving boundary value problems in Mindlin theory with microstructure and first strain gradient theory 03 p0596 A70-13974
- Elastoplastic analysis of strain hardening materials under multiaxial states of stress based on von Mises yield condition and stress-strain relationship 03 p0596 A70-14012
- Shadow optical raster method for quantitative investigation of dynamic stress states in two dimensional transparent or reflecting bodies 03 p0496 A70-14215
- Polyurethane rubber time- and temperature- dependent visco- and photoviscoelastic coefficients using two dimensional strain and stress wave propagation photoviscoelastic analysis 03 p0599 A70-14243
- Book on stress analysis for designers covering stress types and calculation, specimen geometry, structural fatigue and stability, etc 03 p0600 A70-14307
- Transient thermal stresses in photoelastic models of various shapes under various steady state or transient temperature conditions, describing instrumentation and experimental methods 03 p0600 A70-14308
- Long thin cylindrical tube with circumferential restraint analyzed for thermal expansions, obtaining maximum strains, bending moments, shear forces and plastic zone extent [ASME PAPER 69-WA/NE-7] 04 p0768 A70-14756
- Pressure vessel deformation and stress analysis by matrix displacement method, considering solids and membrane shells under axisymmetric and asymmetric loading [ASME PAPER 69-WA/PVP-3] 04 p0768 A70-14790
- Astatic equilibrium loadings in Saint Venant principle for linear elasticity, analyzing physical distinction from self equilibrated loadings to explain smaller long range stresses [ASME PAPER 69-APM-L] 04 p0769 A70-14860
- Solid viscoelastic cylinder bonded to thin elastic casing, analyzing normal and tangential stresses for stress and displacement frequency responses in forced transverse vibration [ASME PAPER 69-WA/APM-20] 04 p0771 A70-14911
- Stress analysis for nonlinear viscoelastic cylinder with ablating moving inner surface used to investigate propellant grain in solid fuel rocket under firing condition [ASME PAPER 69-WA/APM-14] 04 p0771 A70-14914
- Stress analysis of shell loaded at free edge by concentrated forces and moments 04 p0772 A70-14920
- Disk stress concentrations calculation beyond elastic limits taking into account effect on bearing capacity 04 p0775 A70-15261
- Stress analysis split method for determining residual strength and fatigue crack life of damaged or initially cracked VTOL structures [AIAA PAPER 69-214] 04 p0624 A70-15395
- Stress factor-displacement relation in cruciform line crack deformation in elastic medium under arbitrary internal pressure 05 p0926 A70-15976
- Stress concentration effects around spherical cavity under uniaxial tension calculated by constitutive equations of micropolar elasticity 05 p0927 A70-15994
- Torsion tests on cylindrical plastic metals, considering shear stresses calculation as function of torsion angle and changes determination as function of increasing cold work 05 p0927 A70-15996
- Photoelastic and photorheological analysis of time-dependent variation of stress distribution in long strip compressed oppositely with elastic flat punches 05 p0928 A70-16012
- Materials in spatial motion criteria of stress power positiveness 05 p0929 A70-16069
- Axial point force stresses in infinite elastic cylinder determined by superposition of Love solution and normal and shearing tractions 05 p0930 A70-16081
- Axisymmetrical stress-strain analysis of viscoelastic cylinder enclosed in elastic shell under internal pressure using singular kernels 05 p0933 A70-16207
- Linear isothermal quasi-static theory for homogeneous and isotropic viscoelastic bodies with couple stresses 05 p0938 A70-16425
- Stress gradient theory interpreted in terms of time dependent failure criterion to study critical stress vs impulse theory of spall fracture 05 p0938 A70-16481
- Elastoplastic thick layer with disk-shaped crack analyzed for stress and strain, determining width of plastic zone 05 p0939 A70-16482
- Stress analysis of curved tubes capable of accounting for all end effects based on shell theory equations 05 p0944 A70-16811
- Torospherical heads design pressures compared from results of elastic-plastic and elastic-stress analyses to examine use of limiting stress criteria 05 p0944 A70-16816
- Effective stress evaluation under cyclic trapezoidal loading and creep noting use in stationary test data conversion 05 p0951 A70-17031
- Analog to Burger model applied to rotating disk creep problem solution and stress-strain state of plane sample with hyperbolic groove 05 p0952 A70-17038
- Turbine blades root joints endurance limit concerning tensile stress determination at stress raiser contour for elastoplastic deformation and creep 05 p0954 A70-17062
- Shell shear strain determined by expanding displacement vectors into covariant power series of distance from middle surface [DFVLR-SONDDR-23] 05 p0955 A70-17078
- Three dimensional stress-strain analysis of rotating finite hollow cylinder, emphasizing wall thickness effect on stress and strain distribution 06 p1160 A70-17130
- Inherent stresses in elastic solid assuming inherent strain as stress source, integrating stress functions 06 p1160 A70-17131
- Fractography utility to stress analyst, discussing fracture causes 06 p1085 A70-17438
- Finite element method applied to potential distribution and stress analysis in earth sciences, determining elastic response of rock layer using structural matrix analysis 06 p1055 A70-17606
- Shear and linear strain energy criteria for limiting stress state model of solid deformable bodies, considering uniaxial, biaxial and triaxial loading 06 p1166 A70-17657
- Uncoupled quasi-static boundary value problem for linear viscoelastic solids undergoing thermal and mechanical deformation solved by computational algorithm 06 p1168 A70-17937
- Liquid propellant rocket nozzle configurations maximum stress and stability limits using computer program for composite ring-stiffened shells of revolution [AIAA PAPER 70-138] 06 p1014 A70-18053
- Contact stresses between elastic half planes and elastic cover plates determined by integrodifferential equation with Hilbert kernel 07 p1400 A70-18667
- Plane elasticity problem for Cosserat medium rectangular region with parallel boundaries free of force and moment stresses solved by Airy and Mindlin stress functions 07 p1400 A70-18668
- Critical stresses for plate with circular hole and cracks assuming symmetrical load 07 p1402 A70-19054

Isotropic shells with shear deformations, investigating stress-strain relations in Cosserat continuum applied to plates [DFVLR-SONDDR-23] 07 p1404 A70-19233

Basic equations governing optical properties of telecentric lens systems for moire analysis, discussing suitability for stress analysis 07 p1248 A70-19238

Stress rate boundary value problem formulation for elastoplastic body by singular integral equations 07 p1405 A70-19258

Optimal localized heat treatment of welded products, analyzing temperature fields and stresses during heating and cooling of ferromagnetic materials 07 p1294 A70-19477

Stress concentrations calculation at holes in plates and shells of positive Gaussian curvature applicable to hyperbolic shells 07 p1408 A70-19548

Lens effects applied to measurement of stresses on plane transparent models in photoelastic analyses, visualizing stresses from moire fringes 07 p1409 A70-19746

Stress analysis of multiaxially loaded tubes of fiberglass reinforced composite wound in three directions 07 p1318 A70-19755

Buckling stress calculation and measurement in cylindrical fiberglass reinforced composite shells under axial pressure 07 p1409 A70-19756

Plane anisotropic elastic bodies stress determination using Somigliana type integral formula to relate elastic displacement field to boundary traction and displacement vectors 07 p1412 A70-19953

Photoelastic stress analysis of composite structures subjected to gravitational forces using immersion analogy, considering constant acceleration stresses 07 p1413 A70-20038

Servo systems for analog automatic reduction of time dependent photomechanical model materials fringe data in stress analysis 07 p1286 A70-20040

Thick walled orthotropic cylinder subjected to internal pressure analyzed for stress distribution and creep rates, using constitutive equations and Norton law 07 p1416 A70-20234

Infinite strip with longitudinal crack and under loading, analyzing stress-strain state 08 p1585 A70-20938

Membrane stress in thin circular viscoelastic ring under impulsive loads and internal heat, using stress-strain relation for linear Maxwell material model 08 p1589 A70-21311

Elastically symmetric thin plate stress-strain state under uniformly distributed load applied to edges 08 p1591 A70-21415

Temperature dependence of microplastic yield and flow stress and transient creep responses of gamma prime phase 08 p1522 A70-21709

Stress analysis of composite materials reinforced with glass ribbons embedded in epoxy matrix by photoelastic technique, discussing perturbation effect 08 p1594 A70-21862

Temperature fields and thermoelastic stresses in doubly connected structural elements solved in curvilinear coordinates system corresponding to conformal mapping of annulus 09 p1777 A70-23080

Thermal stress state of nonuniformly heated elastic body with bounding surfaces formed by parts of coordinate surfaces 09 p1778 A70-23087

Axisymmetric thermal stress state in bodies of revolution studied by successive approximation algorithm for digital computer 09 p1778 A70-23088

Elastoplastic stressed state of variable thickness disk under combined effects of nonuniform heating, repeated centrifugal and surface tensile loads 09 p1778 A70-23091

Elastoplastic stressed state of thin walled shells of revolution under repeated loads, assuming isotropic incompressible material 09 p1779 A70-23092

Elastoplastic stress state of variable thickness disk under combined effect of nonuniform heating and centrifugal forces, applying flow theory to stress component determination 09 p1779 A70-23095

Nonisothermal loading model of polycrystalline material, investigating tangential stresses in slip direction and plastic deformation using linear strengthening law 09 p1779 A70-23102

Kantorovich variational method extended to thermoelastic plane stress problem of rectangular plates 09 p1781 A70-23278

Stress analysis for cylindrical shells with reinforced circular holes by collocation method 09 p1781 A70-23280

Magnetophotoelastic model applied to plates bending stress analysis, deriving polarized light propagation equations 09 p1728 A70-23447

Stress concentration analysis using Chebyshev polynomial curve fitting 09 p1784 A70-23450

Book on solid materials under stress covering mechanical testing, metals and polymers structure, ceramic crystals and creep and composite materials properties 09 p1708 A70-23476

Thermal stresses determination in turbine blades by making analogy between actual and electrical model, using EGDA integrator 09 p1785 A70-23598

Fracture mechanics applications in stress analysis and structural design, considering rocket motor case failure 09 p1786 A70-23799

Stress distribution in infinite strip of finite thickness under symmetric edge loading analyzed by linear couple stress theory using Fourier transforms 10 p1954 A70-24017

Stress-strain state analysis of prestrained thin circular cylindrical shell using Vlasov general shell theory 10 p1955 A70-24021

Thick-walled toroidal shell under various load distributions, analyzing stress-strain state by networks method using computer program 10 p1957 A70-24250

Adhesive bond stress of aircraft structural joints between metal plates of variable cross section designed for shear 10 p1957 A70-24296

Crack development in solid body, considering condition at crack tip not derivable from equation of motion and strain equation 10 p1960 A70-25007

Shrouded aircraft engine turbine blades vibration stresses found minimum by setting up paired blades with fixed tension along shroud 10 p1964 A70-25288

Electronic stress wave analysis technique /SWAT/ for delayed weld cracking data acquisition 10 p1897 A70-25312

Contact stresses in elastic half plane with boundary connected to rod and moment applied at arbitrary point 10 p1965 A70-25324

Thin cylindrical shell stresses and displacements enclosed in elastic casing under pressure band using classical theory of Flugge and Love functions 11 p2128 A70-25336

Experimental stress analysis and influence on design - Conference, Cambridge, England, April 1970 11 p2130 A70-25584

Profile plane state of stress in wedge with and without external notch using combined photoelastic analysis and moire method 11 p2131 A70-25591

Stress distributions in thin walled pressure vessels analyzed by scattered light photoelasticity technique compared to strain gage analysis 11 p2131 A70-25593

Photoelasticity stress analysis, determining principal stress differences and orientation, using holographic interferometry to obtain sum and separation 11 p2049 A70-25596

Macroscopic internal stresses in plastics surfaces, discussing stress effect on plastic moulding service life, Knoop hardness test and charts 11 p2132 A70-25597

Components life determination from calculating cumulative damage using empirical stress amplitude distributions 11 p2133 A70-25844

Interlaminar shear stresses analysis for laminated composites under generalized plane stress 11 p2136 A70-26080

Prestrain and mean stress effects on fatigue life using cumulative damage procedure based on Al alloy and aircraft quality steel tests 11 p2137 A70-26092

Temperature, stresses and deformations in melting plates of elastic perfectly plastic material, using penetration depth concept with heat balance approach 11 p2138 A70-26134

Stresses and displacements determinations in spherical shells under concentrated loads, considering transverse shear deformation effect 11 p2139 A70-26347

Moire-holographic technique for deformed plane spatial displacements determination, describing diffraction patterns generation and stress analysis 11 p2140 A70-26487

Solid and foam polyurethane creep stress, using multiplier for foam stress for comparison 11 p2141 A70-26601

Finite element bending stress analysis of thin rectangular and skew plates, discussing computational procedure generating stiffness matrices 11 p2143 A70-26641

Conforming plate bending solution with third degree polynomial deflection functions in triangular finite elements, using Lagrange multipliers as stress parameters 11 p2143 A70-26642

Finite element computer code /AXICRP/ for creep analysis of plane stress, plane strain and axisymmetric bodies of revolution 11 p2015 A70-26682

Elastic conical shells of revolution linear theory, calculating stress resultants and couples 11 p2145 A70-26689

Computer analysis of degree of constraint against butt joint transverse shrinkage, using finite element method for stress analysis 12 p2239 A70-26854

Stresses in dynamically loaded struts with one or three holes by photoelasticity, using Fastax camera 12 p2315 A70-26878

Stress analysis of plane, shell and three dimensional structures using finite element method 12 p2315 A70-26886

Stress analysis experimental techniques in aerospace engineering including strain gages, deformation methods, photoelasticity, etc 12 p2205 A70-27127

Experimental stress analyses for aircraft design enhancing structural fatigue strength, using S-N diagrams and photoelastic models 12 p2318 A70-27128

Wing and empennage structures automated fully stressed design procedures, discussing application to supersonic aircraft stabilizer 12 p2319 A70-27136

Shells of revolution under combined thermal and mechanical loading, presenting analytical basis of BOSOR 3 digital stress analysis program 12 p2320 A70-27144

Plates elastic-plastic behavior under combined stretching and bending by finite element method 12 p2320 A70-27146

Two dimensional structures large strain elastoplastic analysis by finite element method, using variational principles to derive equilibrium equations 12 p2320 A70-27148

Reissner variational theorem applied to stress analysis of vertically accelerated end burning solid propellant grain in studying elastic rocket launch failure 12 p2313 A70-27196

Stress and strain in matrix of fiber reinforced material within elastic region, calculating interface shear stress for rectangular fiber 12 p2322 A70-27231

Stress analysis using transmitted light polariscope and Mach-Zehnder interferometer for frozen-stress slice 12 p2325 A70-27620

Interferometric stress analysis in three dimensional photoelasticity, including practical measurements and analysis in terms of refractive index 12 p2326 A70-27621

Elastic-plastic plane stress analysis of two dimensional structures based on Tresca yield criterion, using finite element technique 12 p2326 A70-27795

Residual stresses in cylindrical shell made of two component solid solution under thermal diffusion 12 p2329 A70-28323

Stress analysis of infinite elastic plate containing elastic rectangular inclusion subjected to uniform stress field 13 p2508 A70-28486

Circular cylinders torsion and plain strain analysis, completing statics by asymmetric shear and moment stresses according to Cosserat theory for plastic flow 13 p2508 A70-28492

Configurations stress stability liquid propellant rocket nozzle analysis by BOSOR 3 digital program, describing mathematical model construction 13 p2508 A70-28509

Tensile prestrain effect on yield locus of thin walled Al tubes from stress tests in torsion-tension space 13 p2431 A70-28536

Elastoplastic thermal stress analysis using finite element matrix method exemplified by cylindrical bar induction quenching 13 p2513 A70-28992

Isotropic elastic three dimensional body steady stressed state under large subcritical triaxial strains described by solving linearized equations 13 p2515 A70-29316

Irreversible yield stress component of aluminum, Armco iron and tantalum with fcc lattice, showing temperature dependence 13 p2436 A70-29500

Contact stresses and radial displacements in circular rings with loaded inner and outer boundaries 13 p2515 A70-29506

Stress concentration coefficient around hole in isotropic nonlinear plate under shear, reducing solution to integrating fourth order differential equation 13 p2516 A70-29510

Composite cylindrical laser rods end region stress and optical pathlength change with thermal expansion or contraction between core and cladding 13 p2429 A70-29703

- Brittle rupture cracks theory, discussing unstable /Griffith/ crack, stress intensity coefficient, propagation criterion, etc 13 p2517 A70-29715
- Longitudinal temperature gradients effects on stress analysis in solid propellants, using viscoelastic data 14 p2627 A70-30755
- Flat circular parachute stress analysis in steady vertical descent, using computer program for design change effects on shape, drag and stress 14 p2531 A70-30863
- Plane waves propagation in elastic layer using Cauchy theory of initial stress 14 p2658 A70-30998
- Axisymmetric postyielded tongue and groove cylindrical joint stress analysis using finite element method 14 p2627 A70-31131
- Stress and deflection of nonisotropic assembled bar and plate composite structures, using computerized matrix displacement method 14 p2660 A70-31133
- Stresses in plate containing circular hole with notch under uniaxial tension, determining parametric coefficients by Fourier transforms 14 p2661 A70-31326
- Fracture mechanics and stress analyses comparison for fatigue cracked steel cantilever beam stress corrosion specimens 15 p2755 A70-31473
- Creep rate intensity approximate solution as invariant function of stress intensity, determining equivalent stresses under creep 15 p2814 A70-31542
- Shells of revolution zero moment stressed state calculation by analytical functions, solving boundary value problem for edge loading 15 p2814 A70-31587
- Photoelastic stress analysis, discussing holographic interferometry for main stresses separation and polyester resins application to birefringence pattern superposition elimination 15 p2815 A70-31809
- Elastic half plane with crack perpendicular to free surface and under arbitrary pressure distribution, obtaining exact solution for stress and displacement fields 15 p2767 A70-31854
- Saint Venant principle treating Neumann problem with nonthin two dimensional domain 15 p2767 A70-31855
- Elastic shells of revolution stability and critical loads, discussing moment stress state and edge effect 15 p2816 A70-32158
- Stress analysis of polystyrene plate weakened by doubly periodic system of equal circular holes 15 p2817 A70-32166
- Plane deformation of anisotropic plastic nonstrain-hardenable material, analyzing static equations for stresses and strain rates 15 p2818 A70-32184
- Plane rectangular plate in acoustic field of jet engine exhaust, calculating surface stresses 15 p2819 A70-32186
- Addition theorems for cylindrical functions, discussing applications to shell stress analysis and three dimensional elasticity theory 15 p2819 A70-32187
- Circular cylindrical cavity in elastic space, calculating stresses due to incident plane harmonic compression wave 15 p2819 A70-32204
- Stress analysis for plate with large displacements by multicamera photogrammetry, comparing results with numerical solution by finite differences 15 p2821 A70-32313
- Elastic and optical properties of polyurethane rubber under large deformation using natural stress concept derived from stress-strain linear relationship [SESA PAPER 1608] 15 p2821 A70-32319
- Scattered light rosette using three polarized light beams intersecting at surface point to evaluate photoelastic stress data 15 p2739 A70-32320
- Computerized statistical analysis programs finding plastic stress and acoustic emission as predictors of annealed steel fatigue life 15 p2760 A70-32326
- Semiclamped strut supported rectangular plate deflection determined holographically, mechanically and analytically 15 p2740 A70-32331
- Dangerous plane stressed state surfaces for fiberglass reinforced plastic pipes, using fourth degree polynomial 15 p2766 A70-32852
- Reference stress evaluated by numerical analysis techniques, discussing rectangular beam in pure bending 16 p2987 A70-32921
- Small displacements in noncircular cylindrical shells under various loads 16 p2987 A70-32992
- Holographic interferometry for moire strain analysis, discussing theory and applications 16 p2904 A70-33149
- Stress and vibration analysis of rocket engine turboprop inducer blades, using finite element method [AIAA PAPER 70-630] 16 p2964 A70-33529
- Membrane stresses on nonspherical domes with axisymmetric loads 16 p2990 A70-33743
- German monograph on stress calculation for rotating elliptical rimmed and notched turbine disks using Weinel integral equations and cascade computer procedure 16 p2993 A70-34079
- Displacements and stresses in freely vibrating aeolotropic deep spherical shells, including effects of shear deformation, rotary inertia and transverse normal strain 16 p2993 A70-34091
- Book on elasticity theory covering end effects, Saint Venant principle, edge and screw dislocations, moire method, thermoelasticity, cavity and inclusion effects, Muskhelishvili methods, etc 17 p3183 A70-34603
- Elastic thin walled toroidal shell under internal pressure, investigating large deformation and stress behavior 17 p3184 A70-34910
- One dimensional analysis of stress and strain concentration resulting from longitudinal impact of viscoelastic rods 17 p3185 A70-34965
- Membrane and bending stresses at crack tip in cylindrical shell weakened by elliptic hole with major axis perpendicular to shell axis 17 p3186 A70-34981
- Stress intensity analysis method for plates with random cracks array under plane stress 17 p3187 A70-34997
- Dynamical stresses in members and structures under impulsive loads, taking into account solid viscosities and frequencies effects 17 p3187 A70-34998
- German monograph on stress and displacement in plane elastic circular rings, disk strips and wedges, considering single load distributions 17 p3189 A70-35370
- German monograph on thermal stresses due to thermal shocks on front surface of infinitely long circular solid cylinder 17 p3189 A70-35371
- German monograph on form factors and torsion at shafts with longitudinal keyways under pure torsion 17 p3189 A70-35374
- Orowan stress calculation, discussing line tension, screw or edge character, spatial distribution and yield strength 17 p3191 A70-35457
- Alloy hardening statistical theory, applying flow stress to second phase randomly dispersed particles 17 p3191 A70-35458
- Unsymmetric vibrations of cylindrical shells, analyzing stress states by asymptotic method 18 p3335 A70-36059
- Singular integral equations of elasticity theory, formulating boundary value problem for discontinuous plane stresses 18 p3337 A70-36370
- Pressurized shells of revolution loaded axisymmetrically, formulating equations for calculation of displacements, forces and stresses 18 p3338 A70-36406
- Postbuckled integrally stiffened wide column weight optimization, developing stress equation 18 p3339 A70-36447
- Axisymmetric structure with elastic contact, analyzing stresses by finite element method with differential displacements 18 p3339 A70-36496
- Discrete element stress and displacement analysis of elastoplastic plates 18 p3342 A70-36686
- Holographic interferometry applications in stress analysis of photoelastic resins, describing holographic interferometry assembly 18 p3262 A70-37209
- Low aspect ratio wings under conditions of creep, calculating stress by method of strains 19 p3534 A70-37244
- Shallow circular cylindrical shell with rigid collar on lateral surface, calculating stress under axial tension and internal pressure loading 19 p3534 A70-37245
- Mechanical stresses effect on Vicalloy rotor packets magnetic properties 19 p3357 A70-37265
- Fiber reinforced materials with oriented armoring, calculating stress strain state under transverse shear 19 p3454 A70-37348
- Stress and displacement within internally pressurized composite cylinders having continuous fiber reinforcement in circumferential direction, using finite element method 19 p3538 A70-37797
- Physically nonlinear elastic solid three dimensional and generalized plane strain problem, discussing application to composite materials 19 p3538 A70-37798
- Composite bodies under plane deformations, determining stress dependence on elastic constants 19 p3455 A70-37952
- Micropolar mechanics application to stress and displacement within separate components of fibrous composite material 19 p3541 A70-37961
- Nonlinear stress-strain model of unloading in symmetric longitudinal impact of two elastic-plastic bars, using numerical method 19 p3541 A70-38046
- Elastic boundary layers analysis based on strain gradient theory of linear elasticity 19 p3544 A70-38331
- Composite body with free surface under plane deformation, analyzing residual, thermal and dislocation stresses dependence on elastic constants 19 p3544 A70-38332
- Clamped spherical shells under concentrated, distributed and ring loadings, analyzing large axisymmetric deflections for prebuckled and postbuckled states 19 p3545 A70-38336
- Anisotropic axisymmetric elastic shell theory including transverse stress effects, with application to orthotropic cylinder 19 p3545 A70-38337
- Long orthotropic pressurized cylindrical shell under radial line loads along equally spaced generators, analyzing stresses and deflections by linearization 19 p3545 A70-38338
- Open and multiply connected closed sections of varying thicknesses, solving for unrestrained torsion 19 p3545 A70-38339
- Sandwich panels geometrically and physically nonlinear theory, obtaining equations of motion and boundary conditions consistent with strain displacement relations 19 p3547 A70-38360
- Crack tip stress intensity factor in sheet structures, applying complex stress potentials and perturbation techniques in numerical calculations 19 p3549 A70-38627
- Stress differential equations of micropolar elasticity, considering mass forces and moments of inertia 19 p3549 A70-38672
- Solid and hollow spheres gravitational and surface load stresses determination by freezing method of photoelasticity and mercury immersion 20 p3717 A70-38998
- Spherical shell under nonuniform temperature field, calculating stress-strain state around round hole 20 p3719 A70-39247
- Transparent polymers stress-strain state induced by elastic waves, using model with space and time dependence of laser beam 20 p3654 A70-39248
- Radial and shearing stresses in hollow composite sphere due to thermoelastic strain nucleus 20 p3719 A70-39602
- Cylindrical shells subjected by sectors to constant radial pressure, investigating stress state and deformation 20 p3719 A70-39620
- Infinite elastic plate with pair of insulated unequal circular holes, calculating thermal stresses 20 p3720 A70-39672
- Long hollow nonlinearly viscoelastic cylinder in elastic shell, calculating stress and strain under internal pressure 20 p3720 A70-39731
- Axisymmetric contact problem of hollow semi-infinite elastic cylinder subjected to stresses on lower end face, solving by Fourier integral transform 20 p3720 A70-39734
- Microstresses in plasticity theory, considering continuous elastic body model of crystal with dislocations 20 p3724 A70-39859
- Brittle bodies with sharp pointed defects, constructing limiting equilibrium diagrams by stress concentration factor representations 20 p3733 A70-40393
- Strain gages for structural stress analysis in cryogenic environments, discussing correction factors for temperature dependent characteristics 21 p3932 A70-40545
- Brittle elastic material with wedge shaped void, calculating shear stresses during crack propagation generated by horizontally polarized shear wave 21 p3932 A70-40547
- Silicon solar cell array interconnector design based on analysis of stresses caused by thermal expansion and vibrational motion 21 p3756 A70-41009
- Cantilever bending under gradual contact with cylindrical supporting surface compared with solution by elasticity theory 21 p3934 A70-41251
- Bond stresses between fiber and matrix of fiber reinforced composite materials determined by numerical method based on superposition 21 p3934 A70-41252
- Swing tail cargo aircraft fuselage section stress analysis by finite element method, discussing displacement models, deformation modes and economics 21 p3935 A70-41260

Steels thermal fatigue in testing machine, investigating strains and stresses due to nonuniform temperature distribution during thermal cycle

21 p3840 A70-41433

Spacecraft parachute stress analysis, using finite elements with nonlinear elastic properties to obtain shape and load distribution

[AIAA PAPER 70-1195] 21 p3753 A70-41821

Half plane with stress-free surface deformed by protrusions or notches, deriving edge force or screw dislocation by linear elastic analysis

21 p3939 A70-42028

Cosserat elasticity constitutive equations, coupling rotation vectors to eliminate stress indeterminacies

21 p3941 A70-42251

Third isotropic point in rectangular beam under bending stresses by Hertzian load, using Stokes-Wilson method and photoelastic comparison

21 p3941 A70-42265

Filamentary composites stress wave amplitude distribution calculation and plotting

22 p4114 A70-42645

Elastoplastic flexure and critical loading of isotropic rectangular plates of constant and variable thickness, using Lagrange principle with numerical integration

22 p4115 A70-42810

Bounds to direct influence coefficient derived by hybrid stress finite element method

22 p4116 A70-43203

Brittle fracture stress statistics for Weibull distribution function parameter determination, comparing linearizing, least squares curve fitting and maximum likelihood techniques

22 p4117 A70-43414

Composite laminates under uniform axial strain, determining interlaminar stresses and displacements by finite difference techniques

22 p4060 A70-43684

Stress analysis of anisotropic circular ring with pressed-in solid disk, using sectionally holomorphic functions

22 p4119 A70-43686

Stress-strain of thin multilayer isotropic spherical shell under radial load employing shallow shell theory

22 p4120 A70-43716

Three dimensional elasticity for figures close to ellipsoid of revolution with displacements on boundary

23 p4266 A70-43988

Centrally cracked sheet, calculating riveted and uniformly spaced stringers effect on stress intensity factor

23 p4270 A70-44549

Incremental complementary energy method of stress analysis of orthotropic nonlinear materials having different behavior in tension and compression

[AIAA PAPER 69-119] 23 p4270 A70-44563

Stress, buckling and vibration analysis of shells of revolution by numerical integration and finite difference methods, summarizing computer programs

23 p4273 A70-44725

Fiber-reinforced narrow rectangular beam flexural strain analysis by birefringent coating technique, deriving isochromatic and isoclinic patterns

23 p4275 A70-44915

German monograph on stress-strain state in prestressed, rigidly supported flexible plates subjected to large deflections, using extended Wolmir solution

24 p4418 A70-45083

Shell of revolution /pressure vessel/ with meridional slope discontinuity, calculating pressurization effect on stresses by computer program

24 p4420 A70-45277

Bending vibrations of propeller blades calculated by successive approximation

24 p4422 A70-45300

Polar elastic materials constitutive relations for thermoelastic couple stresses by general theory of incompatible strains, obtaining linearization for isotropic materials

24 p4428 A70-45578

Inhomogeneous anisotropic elastic plates large deflection, using asymptotic integration of nonlinear elasticity equations to obtain successive field equations systems

24 p4423 A70-45580

STRESS CALCULATIONS

U STRESS ANALYSIS STRESS CONCENTRATION

Bonded solid lubricant films wear life equation for low contact stress conditions, determining optimal film thickness

[ASME PAPER 69-LUB-5] 01 p0102 A70-10397

Transient temperature profiles and thermal stress distribution in circular plates and cylinders with eccentric hole determined by conformal mapping

01 p0207 A70-11153

Transient thermal stress concentration at small thickness change of plate obtained by photoelastic studies

01 p0207 A70-11157

Strain field association with random TaC precipitate particles in austenitic stainless steel shown by electron microscope

01 p0123 A70-11242

Stressed state of circular notched plane in tension under creep conditions

01 p0210 A70-11410

Elastoplastic stress concentrations calculations in notched strips and shafts under tension, bending and torsion, using approximate method

01 p0211 A70-11425

Stressed state of isotropic nonlinear multiply connected media with large deformations, using nonlinear elasticity theory

01 p0212 A70-11446

Curvature and hole spacing effects on stress concentration of isotropic plate weakened by two curvilinear holes, applying small parameter method

01 p0212 A70-11447

Two asymptotic dimensional moment theory of elasticity, analyzing stress concentration at curvilinear holes and fluctuating boundary loads

01 p0212 A70-11563

Error estimates of stress concentration at free hole determined by two dimensional elasticity theory of thick plates

01 p0212 A70-11564

Green function type solutions of shell equations by small parameter technique for case of free terms consisting of Dirac delta function

01 p0212 A70-11565

Stress concentrations and load cycle asymmetry effect on materials stress and breakdown behavior under various load cycles

02 p0383 A70-11656

Extended mixing length method for computing turbulent shear stress distribution required in calculating two dimensional incompressible turbulent boundary layer

02 p0282 A70-12333

Dynamic stress concentration factor in strut containing symmetrically located elliptical discontinuity, using photoelastic technique with modulated ruby laser light source

02 p0388 A70-12495

Static and cyclic stress distributions in buckling shear panel comprising flat plate of clad Cu-Al alloy

02 p0388 A70-12497

Reinforced plastics models for determining internal stress, temperature and electromagnetic fields of multicomponent reinforced plastics

02 p0323 A70-12806

Elastic deformation of plates with circular holes, determining stress concentration factors for compressible and incompressible materials on digital computer

02 p0390 A70-12810

Stress concentration in optically active fiberglass reinforced plastics during static loading determined by optical polarization method

02 p0390 A70-12812

Photoelasticity extension to plane elastic problems with stress state depending on Poisson ratio, discussing multiple connected body with nonzero surface tractions on internal boundaries

[SESA PAPER 1570] 03 p0583 A70-12884

Three dimensional photoelastic case bonded solid propellant motor model, analyzing stress distribution using scattered light photoelasticity

[SESA PAPER 1587] 03 p0583 A70-12885

Out-of-plane restraint effect on plane-stress solutions near straight boundaries, predicting deviation of two dimensional photoelastic results

03 p0584 A70-12951

Stress distribution along stud hole threads in Al case, investigating stud design effect using strain gauge on models

03 p0585 A70-12962

Hologram interferometry to study stresses in fixed two dimensional photoelastic models and three dimensional slice qualitative analysis

[SESA PAPER 1530] 03 p0482 A70-12964

Complex stress functions and stress intensity factors at tips of star-shaped contour hole in infinite tensile sheet, including crack forking with arbitrary angle

03 p0585 A70-12974

Honeycomb structure fracture initiation flow detection method using liquid crystal determination of stress concentration sites, noting absence of external heat source

03 p0515 A70-13121

Constitutive equations for orthotropic bilinear elastic materials in plane stress case, discussing unidirectional composites

03 p0587 A70-13127

Stress state of brittle alloy turbine disks with eccentric hole distributions, studying stress concentrations, hole number effects, etc

03 p0588 A70-13243

Inhomogeneous deformation measurements in stress concentration zones using differential rasters in direction of distance between moire bands

03 p0588 A70-13248

Stress-strain state of material computed from strain measurements using strain gages and strain circle

03 p0588 A70-13272

Plane longitudinal elastic monochromatic wave diffraction on stress free circular holes in infinite plate, calculating stresses between holes

03 p0589 A70-13375

Stress distribution in half space of inhomogeneous media, studying scale and edge effects relation for elastic and ideally plastic media

03 p0590 A70-13376

Hole reinforcement providing stressed state beyond hole equivalent to plate stress without hole, reducing problem to annulus region mapping

03 p0590 A70-13378

Spherical shell elasticity having circular hole at apex using asymptotic method, calculating stress concentration at hole

03 p0590 A70-13381

Stress-strain state equations of shallow spherical shells in rectangular and polar coordinates, discussing reduction to plate and Cauchy-Riemann equations

03 p0591 A70-13427

Approximate method of boundary perturbation to solve elasticity and viscoelasticity problems for non-canonical bodies of revolution applied to stress concentration at ellipsoidal cavity

03 p0591 A70-13439

Thin shells stressed state calculations by iteration, considering suitability for computer adaptation

03 p0592 A70-13442

Nonuniformity of dislocation structure and stress distribution in deformation of Cr samples longitudinal sections subjected to upsetting

03 p0511 A70-13488

Circular cylindrical shell stressed state with rectangular opening under compressed torsion, noting opening effect on loads nonuniform distribution

03 p0593 A70-13501

Steady thermoelastic state of inhomogeneous plane with circular discontinuity on perimeter, studying stress concentration at thermally insulated crack

03 p0595 A70-13738

Strain distribution measurement in plastically deformed region around crack tip in metals using moire grid and optical interference

03 p0513 A70-14019

Stress distribution of thin walled structure of open section, considering warping and torsional bending, using calculus of variations

03 p0596 A70-14030

Residual stress distribution in butt joints during welding of sheet Nb measured by extensometer, noting annealing temperature effect on stress relieving

03 p0513 A70-14072

Creep rupture and fatigue strength in solid body mechanics, considering triaxial stress state and simplified creep rupture theory variant

03 p0599 A70-14249

Thermal stress concentration produced by cracks, notches and fillets in plates free from external loads measured photoelastically

03 p0600 A70-14310

Donnell shallow circular cylindrical shell equation, obtaining approximate solution for stresses in infinitely long circular cylindrical shell with circular hole subjected to edge loading

03 p0601 A70-14320

Stress distribution in anisotropic half plane with reinforced circular hole under external loads applied at plane infinity and ring edge

04 p0765 A70-14417

Linear nonaxisymmetric bending of infinite plate coupled to elastic half space under concentrated loads using double Fourier transforms

04 p0766 A70-14480

Bending analysis of cracked plate with arbitrary stress distribution across thickness

[ASME PAPER 69-WA/PVP-2] 04 p0768 A70-14791

Stress intensity and strain energy release rate in elastic fiber-reinforced composites with different thermomechanical properties and imperfect bonding

[ASME PAPER 69-WA/APM-15] 04 p0771 A70-14913

Linear stress distribution insertion into equations of motion for turbulent boundary layer, considering velocity profile in wall region

04 p0670 A70-14987

Disk stress concentrations calculation beyond elastic limits taking into account effect on bearing capacity

04 p0775 A70-15261

Surface work hardening and stress concentrations effects on fatigue strength of alloy under asymmetric tension and compression load cycles at high temperatures

04 p0707 A70-15270

Radial bond stresses in case/liner bond line of full-scale rocket motor measured, describing instrumentation, motor design and thermal cycling test sequence

[AIAA PAPER 68-510] 04 p0736 A70-15407

One dimensional stress waves propagation in elastoplastic medium, determining stress and velocity fields due to heat sources motion by characteristics method

04 p0776 A70-15447

Internal pressure deformed cruciform crack energy and stress intensity factor determined by linear equations 04 p0777 A70-15499

Plan hybrid element generalized to arbitrary quadrilateral form, considering hybrids having constant and linear stress distributions 04 p0779 A70-15614

Plastic-viscoplastic bar wave propagation due to longitudinal impact, analyzing stress profiles to determine effect of strain rate 05 p0926 A70-15913

Stress concentration effects around spherical cavity under uniaxial tension calculated by constitutive equations of micropolar elasticity 05 p0927 A70-15994

Photoelastic and photorheological analysis of time-dependent variation of stress distribution in long strip compressed oppositely with elastic flat punches 05 p0928 A70-16012

Stress distribution in long beams with circular annular inclusion under concentrated load solved in series form 05 p0928 A70-16024

Stress distributions in infinite elastic solids for shear loadings prescribed over coplanar circular regions, solving integral equations iteratively for coplanar penny-shaped cracks 05 p0928 A70-16057

Spread criterion and stress distribution near penny shaped crack in elastic solid under axisymmetric body forces distribution 05 p0930 A70-16079

Stress distribution in vicinity of stress-free Griffith crack in elastic solid acted upon by symmetric distribution of body forces 05 p0930 A70-16084

Surface stress distribution to maintain Griffith crack in prescribed shape, using theories of Fourier transforms and dual integral equations 05 p0930 A70-16086

Planar dislocation array in displacement dependent stress field, investigating tip stress intensification regarding crack nucleation 05 p0932 A70-16170

Linear and nonlinear inelastic spherical inclusion in elastic and viscoelastic isotropic matrix with constant strain or stress fields at infinity 05 p0932 A70-16171

Mixed boundary value problems of plane elasticity, solving stress field of central Griffith crack in wedge using singular integral equations 05 p0932 A70-16173

Statistical stress distribution of breakdown during scaling of wound fiberglass reinforced plastics, noting relation between critical stress and defects 05 p0870 A70-16214

Stress-strain state of circular orthotropic shells under bending, considering distributed loads applied to shell center 05 p0934 A70-16217

Stress concentration of spherical hoop with discretely spaced meridional ribs under uniform pressure 05 p0935 A70-16229

Steady temperature field and stressed state of elastic plane containing heat resistant arc shaped cracks produced by uniform thermal flux 05 p0935 A70-16231

Stressed state of shallow spherical shells of revolution undergoing large displacements reduced to Kármán equation, solved by small parameter method 05 p0935 A70-16235

Stress gradient theory interpreted in terms of time dependent failure criterion to study critical stress vs impulse theory of spall fracture 05 p0938 A70-16481

Stress distribution around crack tip of initially curved sheets 05 p0939 A70-16484

Stress concentration in long thick cylindrical tube under diametrically opposite normal loads using elasticity theory 05 p0939 A70-16505

Stress distribution in restrained hyperelastic sphere based on elastomer reinforcement theory by carbon black 05 p0940 A70-16510

Displacements and stresses obtained for elastic half plane with variable Poisson ratio under certain traction boundary conditions, using Fourier transform method 05 p0940 A70-16512

Membrane stress concentration near circular cutouts in uniaxially stressed sheets reduced by predeforming immediate surroundings of hole 05 p0940 A70-16515

Shallow spherical shell subjected to arbitrarily located concentrated normal force, discussing boundary effects on resulting stress distribution 05 p0945 A70-16817

Stress-strain state of plates weakened by reinforced hole and under tensile and bending loads, including boundary conditions 05 p0945 A70-16856

Stress concentration effect on mechanical properties of Ti-Ta alloys at low temperatures, showing insensitivity to notch and suitability for cryogenics 05 p0864 A70-16869

Stress concentration of circular cylindrical shell weakened by elliptic hole under torsion 05 p0947 A70-16965

Heat resistant materials damping properties at high temperatures under distributed stresses measured in thin walled tubular specimens with vibrogram 05 p0952 A70-17049

Residual strains determination in rotating disks from photoelastic coatings interference 05 p0955 A70-17063

External hydrostatic pressure effect on fiberglass-reinforced plastics strength under unilateral heating, analyzing stress distribution 05 p0875 A70-17067

Facility for testing thin walled tubular specimens in stressed state at low temperatures by keeping stresses constant with helical gear 05 p0830 A70-17075

Incremental stress distribution near circular crack with internal pressure in neo-Hookean solid under deformation due to triaxial compression, illustrating initial stress effect 05 p0956 A70-17108

Three dimensional stress-strain analysis of rotating finite hollow cylinder, emphasizing wall thickness effect on stress and strain distribution 06 p1160 A70-17130

Plastic bodies stress-strain state under variable loads generalized to cases of cyclic loads and plasticity 06 p1162 A70-17384

Complex load strength criterion containing stress and strain invariants applied to simple static loads and cyclic symmetric deformation 06 p1162 A70-17389

Fatigue breakdown criteria for elastoplastic materials under cyclic loads, deriving equations as functions of stress-strain states kinetic behavior 06 p1162 A70-17390

Normalized steel low cycle fatigue strength under bending and torsional rotation, testing linear damage accumulation theory 06 p1163 A70-17404

Limiting stress states analysis in isotropic solids using loading history and replacing nonlinear stress-strain curve by approximating rectilinear polygon 06 p1165 A70-17547

Mean cyclic stress effect on stress concentration and fatigue strength of smooth and notched steel specimens at normal and high temperatures with superimposed bending 06 p1088 A70-17653

Stress field equations of material in maximum deformation region during inversion of tubular products 06 p1077 A70-17871

Bending stress concentrations in elastic square plate with central hole under uniform load, using finite element solutions of modified Rayleigh-Ritz method 06 p1168 A70-17940

Interface stresses in ceramic/metallic spherical shells for deep submergence structures using hydrostatic testing and photoelastic analysis 06 p1170 A70-18089

Stress-strain state equations for axisymmetrically loaded shells of revolution made of materials with variable moduli 07 p1399 A70-18660

Stress-strain state of curved rod made of anisotropic material under bending loads applied to end face cross sections 07 p1399 A70-18661

Contact stresses between elastic half planes and elastic cover plates determined by integrodifferential equation with Hilbert kernel 07 p1400 A70-18667

Elastic and plastic deformation zones stress-strain state under complex stresses, obtaining relation for stress and strain components 07 p1401 A70-18834

Uniform thickness thin helicoidal shell stress-strain state with middle surface in asymptotic lines, assuming parameters governed by one dimensional law 07 p1402 A70-19055

Rotating disk stability relation with stress distribution in plastic deformation of material 07 p1402 A70-19056

Centrifugal force induced stressed state in gas turbine blades using photoelastic analysis, emphasizing stress distribution at shroud holes 07 p1403 A70-19118

Stress distribution in vicinity of arbitrarily shaped slender notches as function of notch symmetry using photoelastic analysis 07 p1404 A70-19240

Buckling of clamped skew plates under uniform system of applied stress using Galerkin method 07 p1406 A70-19339

Nonlinear spinning shallow spherical shell equations solved for equilibrium stress and displacement distributions, discussing inertia loading 07 p1406 A70-19342

Inelastic behavior of solids strained at high temperature emphasizing hot creep phenomena in aviation materials 07 p1406 A70-19346

Effect of uniformly distributed circular holes infinite double row on stress distribution in transversely bent strip, based on Kirchhoff bending theory 07 p1407 A70-19385

Stressed state of plate with reinforced circular hole under tension and bending using Airy stress functions 07 p1407 A70-19540

Isotropic plate stress-strain state weakened by doubly periodic curvilinear holes using nonlinear theory 07 p1408 A70-19544

Stress concentrations calculation at holes in plates and shells of positive Gaussian curvature applicable to hyperbolic shells 07 p1408 A70-19548

Three dimensional electrostriction theory for stress and displacement on penny-shaped crack in elastic dielectric with conducting oblate spheroidal inclusion 07 p1409 A70-19569

Singular part of half plane stress field solution using Cosserat elasticity theory 07 p1409 A70-19570

Temperature stress distribution in cylinder or sphere with variable surface temperature and heated by external sources 07 p1411 A70-19819

Elastic fields in bimaterial plate under uniform compressive and anti-plane shear loadings, finding stress distribution and induced interfacial shear stresses 07 p1412 A70-19957

Isothermal steady state creep extension and flexure of laminated beams with alternating layers, indicating nonlinear stress distribution 07 p1412 A70-19964

Viscoelasticity in shearing and accelerative flows by integral theory, discussing stress distribution and pressure drop 07 p1412 A70-20000

Horizontally curved I beams flanges elastic buckling, determining prebuckling flange stresses in longitudinal and radial directions 07 p1413 A70-20001

Hole reinforcement in flat plate under uniaxial load with high stress region at boundary, resulting in weight savings 07 p1414 A70-20174

Quasi-steady propagation of Prandtl crack in viscoelastic body, noting stress distribution identity for viscoelastic and elastic cases 07 p1414 A70-20181

Elastoplastic torsion of combined prismatic bars with transverse distribution of constant properties solved by computer 07 p1415 A70-20189

Thick walled orthotropic cylinder subjected to internal pressure analyzed for stress distribution and creep rates, using constitutive equations and Norton law 07 p1416 A70-20234

Two dimensional wave front shapes induced in finitely strained elastic body by impulsive point body force, discussing normal and double inflection points 08 p1584 A70-20581

Metal adhesive joints under cyclic stresses, studying stress distribution and fracture occurrence by high speed cameras 08 p1504 A70-20889

Shear stress distribution in metal adhesive joints, discussing methods for calculating 08 p1504 A70-20892

Darkening and brightening of disturbed spot on sun surface determined by abnormal stress in seen layers due to magnetic and velocity fields 08 p1570 A70-20903

Transparent polymethylene methacrylate and polystyrene stressed state effect on failure characteristics under laser beam irradiation 08 p1526 A70-20936

Interaction between boundary layer and internal stressed state of thin elastic shell by formulating two dimensional linear theory 08 p1585 A70-20955

Strain and stress compatibility from extension of Saint Venant and Beltrami-Mitchell equations for physically and geometrically linear to nonlinear media 08 p1585 A70-20962

Stress concentration on isotropic elastic circular cylindrical shallow shell using plane waves and spherical means method, obtaining periodic solutions convergence 08 p1585 A70-20963

Low temperature effects on deformability of middle C steel under complex stress state, showing invalid stress-strain relation and deviator similarity 08 p1516 A70-20983

Steady temperature field and stresses produced by thermal sources in infinite elastic plane containing insulated rectilinear crack, determining thermoelastic state of half plane 08 p1587 A70-21172

Dynamic creep rupture of stainless steel tested at high stress levels and temperatures 08 p1518 A70-21333

Green function for stress intensity factors of rectangular plate edge cracks, noting application to thermal stresses
[ASME PAPER 68-WA/MET-19]

08 p1591 A70-21457

Astatic equilibrium in Saint Venant principle applied to surface of linear elastic body, discussing stress field produced by boundary loading

08 p1591 A70-21463

Multiple scattering of plane time harmonic compressional elastic wave impinging on parallel circular cylindrical inclusions in finite domain, analyzing stress field

08 p1592 A70-21469

Elastic-plastic plane strain solutions in infinitesimal plastic flow theory with separable stress fields

[ASME PAPER 69-APMW-13] 08 p1592 A70-21470

Hertzian contact stress deformation coefficients defined in transcendental equation with elliptic integrals noting errors

08 p1593 A70-21617

Stresses and displacements in largely deflected cantilever beams subjected to gravity using photoelasticity

08 p1593 A70-21619

Stress concentration in elastic plate reinforced at edge by straight rib analyzed in finite form by Cauchy integrals and Fourier transforms

08 p1594 A70-21635

Nondestructive testing and inspection by acoustic emission from stressed materials, discussing microstructure effect and crack initiation detection

08 p1508 A70-21747

Creep and rupture of graphite-epoxy composites under unidirectional state of stress and controlled temperature environment, extrapolating long term loading behavior

08 p1531 A70-21897

Microstructure of wrought arc-cast polycrystalline W sheet after high temperature creep deformation at various stress levels

08 p1525 A70-21962

Theorem for highest statically admissible multiplier for plates and shells, noting association with stress field satisfying yield equality at all cross sections

08 p1595 A70-21977

High speed rotating disks design and stress analysis [ASME PAPER 69-DE-1]

09 p1770 A70-22268

Stressed state in region of strain raisers /round holes/ in plate subjected to two axial tension associated with plastic yield

09 p1771 A70-22464

Alloy equivalent susceptibility to damage at intermediary service periods and different stress levels under creep conditions at 750 C

09 p1701 A70-22470

Turbines rotary shafts and stationary components thermal fatigue analysis, considering cycle numbers and stress concentrations under start-up, continuous operation and shut-down

09 p1775 A70-22593

Stress and displacement distribution formulas for two and three dimensional crack extension problems in linear viscoelastic body

09 p1775 A70-22611

Stress concentration effect, surface states and similarity conditions in fatigue ruptures in machine construction, considering statistical analysis

09 p1776 A70-22615

Fatigue limits distribution functions of full-scale machine parts estimated by rupture similarity criterion, discussing stress concentration and scale factor effects

09 p1776 A70-22616

Stress concentration effect on fatigue strength of Al- and Mg-base structural alloy specimens of different sizes analyzed statistically

09 p1703 A70-22617

Fatigue limit and rupture stress distribution patterns of Al- and Mg-base structural alloys using accelerated Prot and Enomoto methods

09 p1703 A70-22621

Stress concentrations and load transfer around cutouts in fiber reinforced laminates, discussing boron epoxy plates with circular holes

09 p1710 A70-22793

Temperature and stress fields in orthotropic plate with partial surface insulation, examining boundary conditions

09 p1777 A70-23078

Temperature fields and stress-strain state in elastic bodies with thin walled cylindrical shell inclusions during uniform heat flow at infinity

09 p1778 A70-23083

Thermal stress concentrations at arbitrary holes for nonlinearly elastic materials, developing small deformation theory for two dimensional problem

09 p1779 A70-23093

Stress concentrations in turbine disks with eccentric holes under steady creep

09 p1780 A70-23200

Partially loaded clamped plastic shallow spherical caps collapse loads and stress and velocity distributions

09 p1781 A70-23230

Strain and temperature fields interrelation effect on longitudinal wave propagation in viscoelastic cylinder, determining phase velocities and attenuation coefficients

09 p1781 A70-23285

Stress distribution in shells of revolution with variable elastic moduli, considering material rigidity and strain state

09 p1781 A70-23286

Stress concentration at circular hole in plate, considering material creep and aging effects

09 p1782 A70-23290

Stress-strain state analysis of transversely isotropic plates with inclusions under bending loads

09 p1782 A70-23298

Stress concentration at elliptical hole of arbitrary eccentricity in shallow sandwich shells with hard and soft fillers

09 p1783 A70-23385

Cylindrical shell critical load boundaries under uniform external stress and small torsion

09 p1783 A70-23389

Dynamic photoelastic analysis of fracturing plastic plates, studying elastic and stress fields around propagating cracks

09 p1783 A70-23448

Stress concentration analysis using Chebyshev polynomial curve fitting

09 p1784 A70-23450

Elastic ribs reinforced thin cylindrical shells stress-strain state under arbitrary load distribution allowing for rib spacing discreteness

09 p1784 A70-23590

Stress concentration in plate with hole reinforced by elastic cylinder described by equations of three dimensional elasticity theory

09 p1784 A70-23592

Crack widening in infinite plane field with wedge in absence of slip, based on elasticity theory, plotting contact forces and stresses on crack boundary

09 p1785 A70-23624

Stress distribution in rib reinforced cylindrical shells under concentrated forces calculated using finite difference scheme

09 p1791 A70-23718

Transition of stress distribution on collision surface of semiinfinite elastic plane with rigid beam, using Fredholm integral equation

10 p1954 A70-23950

Stress distribution in infinite strip of finite thickness under symmetric edge loading analyzed by linear couple stress theory using Fourier transforms

10 p1954 A70-24017

Stress distribution in strip with asymmetrically positioned infinite row of equal and equally spaced circular holes subjected to longitudinal tension or transverse bending

10 p1955 A70-24082

Stress distribution in anisotropic disk shaped into wedge loaded at vertex by concentrated moment determined by complex potentials method

10 p1956 A70-24084

Stress intensity and strain energy of pressurized line crack in cross form in thin elastic plate solved by Wiener-Hopf technique

10 p1956 A70-24192

Steel conical disks two dimensional stressed state determined with deformations at elastic and elastoplastic strains using digital computers

10 p1956 A70-24242

Aluminum alloy deformations and rupture strength under complex stress at low temperatures, observing anisotropy decrease with temperature

10 p1903 A70-24243

Stress, strain and acceleration spatial variation in plate structures under broad frequency band excitation using statistical energy method

10 p1962 A70-25065

Rigid/plastic or rigid/perfectly plastic anisotropic plate under uniform bending, analyzing stress distribution

10 p1964 A70-25092

Design mean stress and ground-air cycles minimum stress effect on fatigue behavior of titanium alloy in supersonic transport operating environment [SAE PAPER 700033]

11 p2128 A70-25370

Stress concentration near ellipsoidal cavity in transversely isotropic body using solutions for transversely isotropic ellipsoid of revolution

11 p2129 A70-25564

Transient and steady state thermal stress distribution measured by strain gages embedded in epoxy models

11 p2130 A70-25585

Stress distributions in thin walled pressure vessels analyzed by scattered light photoelasticity technique compared to strain gage analysis

11 p2131 A70-25593

Nonuniform stress distribution along side fillet welds and in welded plates of lap joint, discussing tangential stresses and plate width

11 p2058 A70-25598

Wall shear stress distribution in rectangular ducts, discussing secondary currents and main flow prediction

11 p2035 A70-25779

Stress concentration in elastoplastic and creep deformations determined by approximate solution

11 p2134 A70-25845

Geometrically exact finite element for thin shells of revolution, using approximation to predict boundary layer stress distribution during vibration

[AIAA PAPER 69-56] 11 p2135 A70-25962

Interlaminar shear stresses analysis for laminated composites under generalized plane stress

11 p2136 A70-26080

Stress peak distribution effects on fatigue life of test specimen excited to bending by Gaussian random vibrations

11 p2137 A70-26093

Stress level, block size and constant and variable loading sequence effect on fatigue life of Al alloy box beams

11 p2138 A70-26094

Piezo-rotatory coefficients $R_{11}/$ and $R_{12}/$ of isotropic non-enantiomorphic optically active crystals from fourth rank axial tensor, discussing stress effects

11 p2098 A70-26298

Semiinfinite elastic body with instantaneous heat source on surface, analyzing temperature and thermal stress distributions

11 p2139 A70-26406

Stress concentration around elastic spheroidal inclusions in isotropic elastic body under shear

11 p2140 A70-26483

Crack model analysis taking into account nonlinear force-deformation ahead of crack tip

11 p2143 A70-26667

Finite element methods applications to linear fracture mechanics and crack propagation theory, computing stress intensity

11 p2144 A70-26685

Extensional waves asymptotic nature and stress distributions in infinite elastic plate of finite thickness under axisymmetric and in-plate disturbances using perturbation

11 p2145 A70-26696

Flexural vibrations of homogeneous elastic circular cylinder supported at both ends, imposing zero stress conditions on skirt

12 p2321 A70-27154

Wall shear stress distribution in noncircular ducts with steady incompressible fluid flow

12 p2209 A70-27217

Stress-strain state of thin revolving shells composed of multiple variable thickness layers, assuming layers deformation free of slipping and separation

12 p2322 A70-27332

Shallow spherical shells stress-strain state in multiply connected regions resting on Winklerian base

12 p2323 A70-27334

Stress concentration coefficients in multiply connected plates and bulky elements made of nonlinearly elastic materials

12 p2323 A70-27336

Thermal stress concentration in constant thickness orthotropic plate with rounded square hole

12 p2323 A70-27338

Stress-strain state of epoxy resin cylinder situated in centrifugal force field using three dimensional photoelastic method

12 p2323 A70-27340

Orthotropic plates bending with shallow and sharp fillets, determining normal stresses

12 p2325 A70-27533

Residual stresses levels in glass fiber reinforced plastic components after production by compression or winding

12 p2325 A70-27534

Composite spherically aeolotropic sphere with isotropic core, analyzing stress concentration during twisting

12 p2327 A70-27836

Stress concentration in fiberglass reinforced plastic composite cantilever cylindrical shell in round hole region subjected to concentrated load on free supported end

12 p2328 A70-28286

Anisotropy effect on stress distribution at crack apex in elastic plate

12 p2329 A70-28322

Thermoelastic stresses distribution in transmitting dielectric under short nonfocused laser pulses

12 p2251 A70-28327

Pressure buckling values of rod and plate profiles with thicknesses graduated across pressure direction in presence of uniform and nonuniform stress distributions

13 p2507 A70-28477

Stress analysis of infinite elastic plate containing elastic rectangular inclusion subjected to uniform stress field

13 p2508 A70-28486

Stresses in cylindrical pressure vessels with heads formed by internal fluid pressure

13 p2509 A70-28532

Stress concentration in fiber reinforced materials resulting from thermal self straining, using finite element method and photoelastic analysis
13 p2509 A70-28533

Stress concentration factors determined for u-shaped and semielliptical edge notches in semiinfinite sheet under uniaxial tension parallel to edge
13 p2509 A70-28535

Width corrections in calculation of stress intensity factor for sheet with central crack in uniform uniaxial tension
13 p2510 A70-28608

Steel plates with penetration of oblique circular cylindrical aperture tested for effects on stress concentration
13 p2510 A70-28728

Stress concentrations and optimum shape minimum-weight reinforcement of circular holes in plates determined by polarization-optical technique
13 p2512 A70-28864

Vibrocreep effect on Al-Mg-Si alloy vibration frequency and mean and maximum stress at constant temperature
13 p2512 A70-28980

Stress distribution in isotropic plates weakened by elliptical holes under bending based on elastic shallow shell theory and small parameter technique
13 p2514 A70-29291

Stressed state of infinite plate with circular hole induced by displacement discontinuity in form of cracks
13 p2514 A70-29292

Stress-strain state of infinite isotropic plate weakened by curvilinear slit
13 p2514 A70-29293

Elastic isotropic circular perforated plate stress-strain state, proving quasi-regularity of infinite linear algebraic equations
13 p2515 A70-29317

Critical equilibrium of plate under omnidirectional tension with radial rectilinear cracks
13 p2515 A70-29429

Stress concentration coefficient around hole in isotropic nonlinear plate under shear, reducing solution to integrating fourth order differential equation
13 p2516 A70-29510

Tensile test on perforated Al-filled rectangular plate of photoelastic material, obtaining stress concentration at hole by photoelastic visualization
13 p2516 A70-29628

Contour notch position effects on stress concentration in taper section of dumbbell shafts, using photoelastic shaft models and cyclic tests
13 p2517 A70-29750

Nonlinear wave propagation in continuous media involving stress-strain state of half space under pressure or load expanding over boundary
13 p2517 A70-29770

Polycrystalline Al microstrain distribution nonuniformity under creep and static tension
14 p2595 A70-30173

Stress distributions in elastomers under different loads, proposing appropriate measuring technique
14 p2655 A70-30178

Soviet monograph on thermal conductivity of plates and bodies of revolution covering temperature and stress distributions, multilayer shells, etc
14 p2666 A70-30952

Stress distribution in aeolotropic cylindrical shell due to shearing force varying linearly and quadratically with depth on inner boundary
14 p2658 A70-30994

Stress, strain, temperature, electric and magnetic field distributions resulting from magneto-thermoelastic interactions in infinite elastic solid subjected to transient heat source
14 p2661 A70-31229

Stress distribution in spirally corrugated shell under torsional deformation, calculating twisting moment for stiffness
14 p2661 A70-31327

Stress and deformations three dimensional solution in semiinfinite elastic body with spherical cavity based on Boussinesq stress function
14 p2661 A70-31328

Thermoplastics fatigue strength, considering stress variations with time in constant strain tests
14 p2598 A70-31425

Materials durability in presence of stress concentration under biharmonic loading
15 p2813 A70-31527

Two dimensional stress-strain fields under elastic and elastic-plastic strains and steady state creep, calculating stress distribution around hole in cylindrical shell
15 p2813 A70-31533

Creep rate intensity approximate solution as invariant function of stress intensity, determining equivalent stresses under creep
15 p2814 A70-31542

Yield criteria for plastic deformation on glassy high polymers induced by stress field, noting crazing and shear yielding dependence on first stress invariant
15 p2764 A70-31787

Elastic half plane with crack perpendicular to free surface and under arbitrary pressure distribution, obtaining exact solution for stress and displacement fields
15 p2767 A70-31854

Structural components strength calculation with design required functional notches, noting stress limit for ductile materials under static loads
15 p2815 A70-31874

Lamellae stresses and magnetostrictive effects on magnetic properties of titanomagnetite and ilmenohematite series minerals
15 p2728 A70-31993

Positive/negative curvature shells local stresses due to concentrated loads and heat sources, deriving approximate solutions
15 p2817 A70-32161

Influence function for the thin toroidal shell under uniformly distributed axisymmetric load, determining stresses and displacements in various cross sections
15 p2817 A70-32163

Stress distribution in fiberglass unidirectionally reinforced composite material under uniaxial tension
15 p2765 A70-32180

Point heat source generation of thermal stresses in elliptical plate with circular hole, using functions of complex variable for stress field determination
15 p2818 A70-32182

Stress concentration problems for partially strengthened circular hole in plate under uniaxial tension
15 p2819 A70-32185

Plane strain stress intensity factor-Charpy V notch impact test correlations in transition temperature range under slow bend and dynamic loading
15 p2759 A70-32244

Stress concentration in flat rectangular and skew panels with circular holes from photoelastic verification of direct stiffness method
15 p2820 A70-32303

[SESA PAPER 1633] Stress distribution around oblique holes in uniaxially loaded plate using three dimensional photoelastic analysis
15 p2820 A70-32305

[SESA PAPER 1618] Stress concentration around oblique circular cylindrical apertures in steel plates
15 p2820 A70-32306

[SESA PAPER 1533] Axial stress at notch root of shafts under axially symmetric loading, utilizing integrated birefringent patterns in transmitted light at room temperature
15 p2821 A70-32315

[SESA PAPER 1970] Radial and tangential stress distribution through annulus fibrosus dependence on material inhomogeneity for human intervertebral disk
15 p2692 A70-32328

Cumulative creep strain and damage based on stress amplitude coefficients, considering continuous single step system of loads
15 p2821 A70-32339

Boundary value problem of elastic isotropic material, obtaining pointwise bounds of Cosserat continuum, considering couple stresses and constrained rotation of particles
15 p2821 A70-32340

Monograph on temperature dependent material properties effect on elastic stress distribution in thin rotating disks of arbitrary profile
15 p2823 A70-32700

Maximum stress distribution in laminar composites, considering loads on boundary of reinforcing layers
15 p2766 A70-32854

Shear stress distribution in axially nonuniform circular shaft subjected to torsion, using finite difference approximations
16 p2988 A70-33001

Flow stress and dislocation density dependence on temperature in polycrystalline molybdenum
16 p2930 A70-33085

Elastoplastic bending of thin plate under increasing and uniformly distributed loads, defining statically admissible stresses
16 p2988 A70-33107

Stress distributions in tapered bolt assemblies due to interference and uniaxial tension
16 p2992 A70-33989

Stress, strain and acceleration spatial variation in structures subject to broad frequency band vibration excitation, considering simply supported flat plate
16 p2992 A70-34017

German monograph on calculation and measurement of stress distribution in turbine rotors with radial flow, discussing differential equations for rotating disks
16 p2993 A70-34076

Rigid inclusion effect on stress distribution in isotropic infinite solid with Griffith crack under plane strain
16 p2994 A70-34250

Polymeric materials fatigue tests, investigating correlation between crack propagation and stress intensity factor
17 p3127 A70-34624

Stress concentration around small elastic spherical inhomogeneous inclusion on circular cylinder in torsion
17 p3183 A70-34631

Residual stress concentration at fatigue crack tip, using oscillating crystal X ray microbeam diffraction photographic method
17 p3183 A70-34652

Composite orthotropic cylindrical shells linear thermoelastic equations solution for fixed end boundary conditions, noting heterogeneity effects on stress distribution
17 p3184 A70-34909

Bond stress distribution in elastic solid with axisymmetrical inclusions under uniform tension, using three function and point matching techniques
17 p3184 A70-34911

Anisotropy and variable thickness effects on elastic stress distribution in rotating disks, discussing limiting cases
17 p3185 A70-34912

One dimensional analysis of stress and strain concentration resulting from longitudinal impact of viscoelastic rods
17 p3185 A70-34965

Singular solutions to concentrated loads on shallow shell equations with quadratic middle surface
17 p3186 A70-34968

Fatigue life prediction under irregular stress conditions, considering material characteristics determination by standard tests
17 p3187 A70-34990

Plastic flow and failure of elastic fiber reinforced composite materials with noninteracting and interacting discontinuities, obtaining stress distribution for various work hardening degrees
17 p3187 A70-34991

Viscoelastic materials cut growth, discussing strain, fracture and modulus of elasticity dependence on temperature variations
17 p3146 A70-35220

Nonstationary temperature fields and stresses in wedge shaped strip and thin plates with heat transfer for discontinuous boundary conditions
17 p3189 A70-35342

Nonaxisymmetric thermal stress distribution in infinite elastic solid containing external stress-free crack with prescribed heat flux
17 p3196 A70-35437

Elastic properties of complex screw dislocation arrays from equations for stress fields of dislocation segments
17 p3190 A70-35455

Thin elastic shells linear theory, examining three dimensional stress distribution and displacement field
17 p3191 A70-35608

Shallow shell theory boundary value problems, calculating stress concentration for domes and shells with holes
17 p3192 A70-35694

Elastic layer with circular cylindrical cavity under axial tension /Kirsch problem/, determining stress concentration from boundary value problem
18 p3335 A70-36130

Circular cylindrical shell with round holes along generatrix subjected to internal pressure, determining stress concentration with aid of computer
18 p3335 A70-36131

Stress concentration near holes in plate in plane problem of thermoelasticity, taking into account physical and geometrical nonlinearities
18 p3336 A70-36133

Nonlinearly elastic plate with hole of general shape, determining stress concentration
18 p3336 A70-36139

Probability theory of stresses during random vibrations of flat panel in acoustic field of jet engine exhaust
18 p3301 A70-36301

Stress concentration on axisymmetric annular rings calculated using method of singularities
18 p3207 A70-36377

Stress concentration in notched flat samples under plane plastic deformation
18 p3340 A70-36570

Plane cross section hypothesis applied to fully developed creep in thin walled tube subjected to internal pressure and bending moments, calculating stress concentration
18 p3340 A70-36571

Brittle fibers strand strength as function of statistical distribution of limiting stresses
18 p3342 A70-36648

Plates and rods tendency to warp and form nonsymmetrical stress systems during heat treatment
19 p3433 A70-37272

Power and exponential time dependences of long term creep strength for wide stress range, assuming linear heat resistance
19 p3449 A70-37340

Stress concentrations in edge-bonded elastic quarter planes with normal and shear loading at boundary
19 p3535 A70-37384

Holographic registration of isochromatic and isopachous diffraction patterns of photoelastic birefringent objects, showing stress concentrations 19 p3422 A70-37649

Granular medium particles contact forces distribution measurement by absolute retardation method using photoelastic techniques 19 p3427 A70-38344

Stress concentrations and load cycle asymmetry effect on materials stress and breakdown behavior under various load cycles 19 p3547 A70-38429

Stress state of brittle alloy turbine disks with eccentric hole distributions, studying stress concentrations, hole number effects, etc 19 p3548 A70-38461

Inhomogeneous deformation measurements in stress concentration zones using differential rasters in direction of distance between moiré bands 19 p3548 A70-38466

Blade root design for axial flow compressors and turbines, avoiding tensile stress concentration 19 p3490 A70-38616

Finite element method with first order displacement functions to compute crack tip stress intensity factor in various shapes under different loading conditions 19 p3548 A70-38623

Fatigue crack closure in flat sheet specimens under zero-to-peak tension cyclic loading, analyzing stress distribution from fractographic striation patterns 19 p3549 A70-38625

Pop-in fractures analyzed by semiquantitative model, establishing relationship between pop-in length, stress intensity factor and crack-front plastic deformation 19 p3549 A70-38626

Crack tip stress intensity factor in sheet structures, applying complex stress potentials and perturbation techniques in numerical calculations 19 p3549 A70-38627

Interaction between boundary layer and internal stressed state of thin elastic shell by formulating two dimensional linear theory 20 p3719 A70-39378

Strain and stress compatibility from extension of Saint Venant and Beltrami-Mitchell equations for physically and geometrically linear to nonlinear media 20 p3719 A70-39384

Stress concentration on isotropic elastic circular cylindrical shallow shell using plane waves and spherical means method, obtaining periodic solution convergence 20 p3719 A70-39385

Plate temperature field and stress distribution under thermal pulses, evaluating critical heat load for damage 20 p3737 A70-39635

Stressed state in thermoelasticity plane steady state problem of thin plate under bending based on dislocations and temperature stresses relationship 20 p3721 A70-39780

Fatigue phenomena based on solid body model, establishing breaking stress dependence on time or load cycles number 20 p3724 A70-39854

Low cycle metal fatigue under stress concentration, examining complex loading, cyclic strain, stress-strain state and plastic deformation 20 p3727 A70-39885

Thermoelasticity of fiber reinforced materials, considering stress concentration in beams and reinforcing fibers buckling under thermal loading 20 p3730 A70-40037

Stress concentrations due to cylindrical inclusions in homogeneous matrix, using stress function methods 20 p3656 A70-40045

Brittle bodies with sharp pointed defects, constructing limiting equilibrium diagrams by stress concentration factor representations 20 p3733 A70-40393

Longitudinal shear crack propagation in random internal stress field, examining quasi-brittle rupture theory and cyclic loading 20 p3733 A70-40396

Stress distribution at hole in orthotropic cylindrical sandwich shell under internal pressure 20 p3734 A70-40440

Cross shaped plates with circular hole, determining stress concentrations under uniaxial and biaxial tension 20 p3734 A70-40443

Strain component determination for grain boundary sliding influence in creep of alpha iron 20 p3735 A70-40446

Perforated cantilever beams and plates vibration damping capacity improvement by stress concentration introduction 21 p3933 A70-40729

Stresses around circular hole in shallow conical shell under torsional load, using perturbations in parameters for curvature and cone angle 21 p3934 A70-40779

Notched polycrystalline Al-Mg alloy dislocation structure near propagating fatigue crack at various stress levels 21 p3839 A70-40925

Slip band formation dislocation-diffusion mechanism for single crystal and polycrystalline metals, considering stress intensity and load cycles effects 21 p3936 A70-41416

Bending stress at clamped support of impulsively loaded semiinfinite conical shell, obtaining formulas from perturbation theory 21 p3938 A70-41759

Stress distribution and shape in arbitrarily shaped gore parachute under unsteady pressure distribution during inflation and descent 21 p3752 A70-41819

Finite element analysis of critical stress distribution in canopy of deployed twin keel parawing, predicting failure stress levels 21 p3753 A70-41820

Stress concentration effect on perforated Al alloy panel fatigue, using theory for material critical thickness near notch 21 p3938 A70-41955

Boundary value problem solution for elliptical crack subjected to impulsive load by method of characteristics and discontinuity relations, calculating stress distribution 21 p3938 A70-41960

Butt joined epoxy Al plates tensile strength, observing fracture strength dependence on stress concentration at bond edges below characteristic crack length 21 p3939 A70-42032

Stress intensity factors for complicated crack configurations in finite plates, using finite element method with cracked elements 21 p3940 A70-42034

Cracks stress intensity factors in plane problems by combined conformal mapping and boundary collocation technique 21 p3940 A70-42036

Circular cylindrical hole in uniaxial tension field of elastic media, solving plane strain problem for stress concentration factors 21 p3941 A70-42107

Flow structure in plane submerged turbulent jet, determining velocity, friction stress and correlation coefficients distributions 21 p3749 A70-42221

Filamentary composites stress wave amplitude distribution calculation and plotting 22 p4114 A70-42645

Stresses and strains concentration around elliptic hole in finite plates subjected to uniform load, using photoelasticity, moiré effect and grids 22 p4114 A70-42697

Stress distribution around moving cracks in finite width strip, obtaining solutions for boundary conditions by Schwarz-Christoffel transformation and complex functions theory 22 p4116 A70-43025

Inconel short term creep properties measured for various temperature and stress levels, presenting results in polynomial and graph form 22 p4055 A70-43098

Elastic plane equilibrium with thin walled flexible rectangular finite inclusion under symmetrical concentrated load, including computer calculated tangential stresses 22 p4118 A70-43569

Boron-epoxy composites rectangular reinforcing arrays spacing aspect ratios, considering matrix stress concentrations and stiffness estimates 22 p4119 A70-43688

Isotropic nonlinear elasticity problems of stress concentration near spherical cavity in field of triaxial tension, using small parameter method 22 p4120 A70-43714

Mg high temperature creep mechanism in high and low stress regions, using isothermal tensile creep tests 23 p4204 A70-43885

Free and supported curvilinear holes with random roughness, investigating stress concentration by conformal mapping 23 p4265 A70-43984

Anisotropic media weakened by elliptical holes, using doubly periodic solution for stress concentration 23 p4266 A70-43986

Stress concentration near holes in nonlinear viscoelastic plate, using elastic theory 23 p4266 A70-43989

Notch stress intensity factor representation as boundary traction weighted average, deriving weight functions from stress field boundary displacements 23 p4266 A70-44021

Stress fields of screw and edge dislocations in linearly elastic isotropic Cosserat continuum using stress functions 23 p4266 A70-44022

Plane strain fracture toughness testing of high strength Al alloys and steels, using fatigue cracked bend specimens 23 p4206 A70-44191

Specimen size and mechanical factors in plane strain fracture toughness testing of metallic materials 23 p4206 A70-44195

Turbulent boundary layer velocity profiles and shear stress distributions computation based on mixing length approach 23 p4182 A70-44574

Wrought Nimonic alloy, measuring stress redistribution due to creep under variable load and temperature 23 p4274 A70-44911

German monograph on stress concentration around doubly symmetrical cut-out in cylindrical shells subjected to symmetrical load, using elliptical cut-out theory 24 p4418 A70-45092

Fibrous composite interface effects and fracture work, discussing tip stresses of crack normal to fiber, energy dissipation by pullout and debonding in brittle fiber composites, etc 24 p4419 A70-45171

Unimodal and bimodal distribution of fiber composite properties at different stress levels using quantitative metallography 24 p4359 A70-45250

Semiinfinite elastic medium under variable dynamic pressure on boundary, investigating couple stresses effect on stress distribution 24 p4426 A70-46006

Crystal elastic dislocations general solution, deriving stress function for stress and displacement fields in bipolar coordinates 24 p4426 A70-46018

Plane flow of incompressible elastic perfectly plastic solid, deriving hyperbolic stress and velocity equations 24 p4427 A70-46043

STRESS CORROSION

Stress corrosion cracking in Cu-Al alloys shown dependent on alloy and Cu ion content, solution pH and stress level, discussing tarnish film formation role 01 p0119 A70-10734

Ternary Al-Zn-Mg alloys stress corrosion cracking properties, showing effects of aging temperature and prestrain 01 p0123 A70-11387

Al alloy rectangular beam stress corrosion crack initiation and propagation measurement using ultrasonic techniques, showing relationship between crack velocity and initial stress 03 p0481 A70-12958

Heat transfer effects on corrosion behavior of stainless steel in boiling water, noting stress corrosion cracking increase with chloride ion contamination 03 p0507 A70-13137

Stainless steel stress corrosion cracking test in magnesium chloride solution, emphasizing crack crystallographic orientation observation 03 p0513 A70-14299

Silicon effect on stress corrosion resistance of low alloy high strength steels in NaCl solution for different tensile strength ranges 04 p0707 A70-15272

Heat treatment produced semicoherent and incoherent precipitations diminished susceptibility to stress corrosion cracking of aluminum binary and ternary alloys 04 p0708 A70-15370

Stress corrosion testing method to separate corrosion and stress effects applied to Al and Ti alloys 04 p0708 A70-15374

Stress corrosion of martensitic and austenitic steels, discussing hydrogen embrittlement, mechanical strains, etc 04 p0710 A70-15676

Delayed failure due to hydrogen embrittlement of structural high strength steels, discussing stress corrosion 04 p0710 A70-15678

Aircraft Ti alloys failure due to stress-induced pseudocorrosion caused by trichloroethylene and Freon noting microstructure, heat treatment and welding effects 04 p0710 A70-15679

Aluminum alloys intergranular and stress corrosion, noting electron microscopy application for alloys performance improvement 04 p0710 A70-15680

Martensitic steels microstructure and ductility influence on stress corrosion resistance in magnesium chloride salt chamber 04 p0711 A70-15681

Stress corrosion testing of vanadium alloys using precracked specimens in cantilever beam apparatus, discussing strain hardening exponent role and propagation rates 07 p1306 A70-19299

Stress and intercrystalline corrosion causes and sensitivity in supersaturated Al alloys 07 p1307 A70-19391

Corrosion cracking mechanism for notched metal surface in aqueous environment under tensile stress, discussing electron distribution and H ion concentration 07 p1310 A70-19737

Maraging steels stress corrosion sensitivity in marine environment tested in humid atmosphere, salt fog, natural seawater and salt solutions
07 p1310 A70-19749

Stress corrosion-fatigue crack propagation in high strength structural steels, relating growth rates to crack tip stress intensity factor
[ASME PAPER 69-MET-5] 08 p1519 A70-21452

Ti alloys failure-safe design developing procedures for incorporation of stress-corrosion cracking characterizations into ratio analysis diagram system
08 p1519 A70-21456

High strength stress corrosion resistant aluminum alloy die forgings, evaluating tensile, tensile fatigue and fracture toughness properties
09 p1702 A70-22556

Transcrystalline stress corrosion crack initiation in austenitic stainless steel tested in boiling magnesium chloride solution
09 p1706 A70-22940

Fracture mechanics model for stress corrosion cracking of Al alloys, discussing bond strength lessening by adsorption of damaging species
09 p1706 A70-22941

Polyamides /nylons/ stress cracking by metal halides and halide-like salts, investigating effects of nylon temperature, moisture content, concentration, etc
10 p1907 A70-24224

Polyamide and secondary amide mode compounds stress cracking by metal halides using IR and nuclear magnetic resonance techniques
10 p1907 A70-24299

Li and Cr additives effects on Al-Zn-Mg stress corrosion resistance, considering cracking, precipitation hardening and intercrystalline corrosion
13 p2433 A70-28844

Structural Al-Zn-Mg alloys strain hardening effect on mechanical and corrosion properties, noting relationship between stress corrosion cracking and shear cracks
13 p2434 A70-29155

PH variation effect on sea water on stress corrosion cracking behavior of Ti alloys
13 p2435 A70-29174

Quality control technique for predicting exfoliation and stress corrosion resistance of Al alloy sheet and plate
13 p2435 A70-29175

Work hardening and tempering effects on Al-Mg alloy stress corrosion and mechanical properties
14 p2597 A70-30963

Fracture mechanics and stress analyses comparison for fatigue cracked steel cantilever beam stress corrosion specimens
15 p2755 A70-31473

Electrochemical processes associated with stress corrosion cracking of Ti-Al-Mo-V alloy in aqueous environments
15 p2755 A70-31474

Stress corrosion cracking of Ti and Ti-Al-V alloy in liquid nitrogen tetroxide
15 p2755 A70-31475

Plain strain fracture toughness index measurement, discussing application to metal fatigue and stress corrosion
15 p2757 A70-31927

Ti alloy suitability for fastener applications noting cold workability, high strength and stress corrosion resistance
[ASM PAPER W70-17.3] 15 p2760 A70-32338

High temperature scaling of Ni, investigating role of oxide microstructure and growth stresses
15 p2762 A70-32388

Stress corrosion cracking of high strength structural, tool and marring steels due to hydride, diffusion controlled and mixed embrittlement
16 p2934 A70-34301

Electrochemical mechanism in Ti alloys stress corrosion cracking, formulating mass transport kinetics model
17 p3113 A70-34368

Stress corrosion cracking of alpha-Ti alloys at room temperature, suggesting cathodic polarization promotion of film buildup
17 p3113 A70-34369

Aqueous stress corrosion dependence on microstructural features of Ti alloys, using optical and electron microscopy and X ray diffraction
17 p3113 A70-34370

Ti-Al-Mo-V alloy stress corrosion cracking, investigating correlation between dislocation substructure and ambient temperature corrosion susceptibility
17 p3113 A70-34371

Stress corrosion cracking in Ti and alloys, discussing metallurgical and environmental factors emphasizing exposure to hot salt, methanol, seawater, etc
17 p3114 A70-34372

Stress corrosion cracking in Ti-Al-V alloy exposed to Freon environments
17 p3114 A70-34373

Ti alloys crack formation during oxidation under stress, considering annealing and recrystallizing effects
17 p3114 A70-34374

Ti alloys crack initiation and propagation during hot salt stress corrosion
17 p3114 A70-34375

Titanium hydride deformation assisted nucleation in alpha-beta titanium alloy, showing low strain rate embrittlement and stress corrosion crack propagation in aqueous environments
17 p3116 A70-34395

Stress corrosion cracking of Ti alloys in nitrogen tetroxide and methyl alcohol environments in Apollo spacecraft pressure vessels
17 p3199 A70-34453

High strength ferrous alloys susceptibility to stress corrosion in seawater environment, tension loading single edge notched and fatigue cracked specimens in NaCl solution
17 p3123 A70-34554

Neutron irradiation effects on stress corrosion susceptibility of Al alloy
17 p3124 A70-34822

Corrosion and stress corrosion behavior comparison of aged Al-Zn-Mg alloy in aqueous chloride solution, discussing pH variation effect
18 p3271 A70-36028

Precorrosion effects on strained Al alloy electrochemical response, examining strain test results graphically
19 p3451 A70-37780

High strength and stress corrosion resistant materials, considering Ti, Ni, Al alloys, metal-matrix composites and polymers
20 p3655 A70-39666

Al alloy stress corrosion susceptibility, examining grain size and anisotropy role
20 p3651 A70-40070

Two stage aging effects on stress corrosion cracking of Al-Zn-Mg alloys, discussing precipitated particles size, surface roughness change and temperature effects
22 p4052 A70-42306

Atmospheric environment effect on residual shear stress corrosion cracking of commercial Al-Zn-Mg alloys subjected to heat treatment regimes
22 p4052 A70-42307

High strength martensitic stainless steel stress corrosion resistance and fatigue crack growth rate, considering austenite content, strain aging and tempering temperatures
24 p4359 A70-45245

Nondestructive inspection methods for welded structures affected by stress corrosion
24 p4347 A70-45730

Cold reduction, refrigeration and annealing effects on stress corrosion cracking of austenitic stainless steels
24 p4365 A70-46389

STRESS CYCLES

Ultrasonic detection system for crack initiation and propagation in notched low cycle axial fatigue testing using surface and longitudinal waves
01 p0096 A70-10004

Metal fatigue in Al alloys subjected to stress cycles, determining macrocracks propagation stages
01 p0212 A70-11607

Static and cyclic stress distributions in buckling shear panel comprising flat plate of clad Cu-Al alloy
02 p0388 A70-12497

Periodic biharmonic stress cycling determination of load influence of fatigue failure used for random load serviceability tests
02 p0391 A70-12855

Out-of-phase or nonsynchronous biaxial straining effects on low cycle fatigue observed on Al specimen by cycling tension-compression and cyclic torsion
03 p0481 A70-12955

Stress cycle asymmetry effects on energy dissipation in rods under torsional vibration
03 p0588 A70-13249

Al alloy and structural steel fatigue strength under superelastic cyclic axial stresses, describing observed plastic deformation patterns
03 p0509 A70-13271

Equipment for cyclic biaxial testing, producing five biaxial stress states by simultaneous direct pressurization and axial loading of thin walled cylindrical specimen
03 p0464 A70-14309

Thermoelastic stresses in solid cylinder under cyclic temperature variation, calculating amplitude for Biot numbers
04 p0766 A70-14477

Cyclic bending stress in disk type gyroscope rotor under steady precession, discussing solutions for modal functions and resonant frequencies
[ASME PAPER 69-DE-A] 04 p0689 A70-14873

Overstress cycles sensitivity for welded specimens on basis of French fatigue damage line and Wohler S-N line
05 p0941 A70-16520

Low cycle fatigue of alloy and steel materials under bending and cyclic heating, relating strains and number of cycles to failure
05 p0866 A70-17036

Stress kinetics and breakdown time of hardening Al alloys and steels under cyclic loads, noting dependence on plastic deformation
06 p1162 A70-17391

Rotation of circular cross sectioned continuous rod with constant bending moment, assuming linear strengthening with fixed cyclic strain diagram
06 p1163 A70-17396

Mean cyclic stress effect on stress concentration and fatigue strength of smooth and notched steel specimens at normal and high temperatures with superimposed bending
06 p1088 A70-17653

Spiral gears bearing disks contact fatigue endurance process, deriving critical points cyclic stability from stress distribution considerations
07 p1291 A70-18819

Cylindrical Mo single crystals during cyclic heating, studying characteristic dislocation changes at various stages of thermal fatigue
07 p1308 A70-19609

Tensile and compressive stress cycles effect on short term strength of glass fiber plastic laminates
07 p1411 A70-19769

Stability criterion applied to asymmetric rigid cyclic strains and plastic cyclic strains, considering failure of metals
07 p1315 A70-20182

Adhesive bonds strength in metal joints under stress cycling, examining effects of temperature and cycles frequency
08 p1504 A70-20888

Metal adhesive joints under cyclic stresses, studying stress distribution and fracture occurrence by high speed cameras
08 p1504 A70-20889

Cyclic bending stresses in web of precessing disk-type gyroscope rotor, considering fatigue failure and forced vibration response
09 p1770 A70-22270

Thermal and high strain fatigue covering cyclic tests, crack initiation and propagation, stress-strain behavior, structural design, frequency and temperature effects, etc
09 p1773 A70-22576

Damage model for materials failure prediction under cyclic loading developed for strain controlled cycle with hold time
09 p1774 A70-22588

Mean stress effect on low cycle fatigue strength, deriving expression for completely reversed stress cycling
10 p1964 A70-25091

Plastic strains buildup during thermal cycling, establishing relation between strain interval and cycles number to failure for strain hardening materials
10 p1965 A70-25293

Programmed and randomized loading flight-by-flight tests for fatigue life, noting stress cycles
11 p2138 A70-26096

Collection of papers on low cycle fatigue testing covering mechanical properties and test facilities
11 p2033 A70-26608

Metals low cycle fatigue resistance, discussing repeated plastic straining effect on mechanical properties
11 p2141 A70-26609

Low cycle fatigue testing facility and methods used at NASA Lewis Research Center
11 p2033 A70-26610

Low cycle fatigue tests advantages by reversed bending ascribed to simplicity, specimen stability at high strain levels and minimum equipment costs
11 p2034 A70-26614

Uniaxial low cycle thermal fatigue test procedure for ductile metals, describing strain measuring system allowing direct recording of load vs mechanical deformation
11 p2034 A70-26615

Metallic materials under cyclic stress conditions, investigating creep rate dependence on cycling frequency and impurities during static-to-dynamic transition
13 p2513 A70-28993

Automatic Failure Rate Assessment Machine /FRAM/ for subjecting guided weapons electronic modules to cyclic stresses inducing failure of inherent weakness
13 p2379 A70-29686

Fibre reinforced polymers fatigue life under cyclic stresses, obtaining data from rotary cantilever tests
15 p2764 A70-31933

Electromechanical transducer to sense and record strain cycles, describing motion magnification principle, system and prototype evaluation
15 p2739 A70-32310

Alternating stress required for edge crack propagation in metal plates under tensile loading cycles
15 p2762 A70-32464

Unalloyed polycrystalline Ti fatigue tests, observing cyclic stresses effect on twinning
17 p3116 A70-34393

Strain rate effect on cyclic behavior of materials with hardening and softening characteristics
17 p3187 A70-34988

- Combined mechanical and cyclic thermal stresses effect on plastic deformation buildup in E1435 alloy preceding breakdown 19 p3449 A70-37349
- Stress cycle asymmetry effects on energy dissipation in rods under torsional vibration 19 p3548 A70-38467
- Fatigue crack propagation under programmed loads, correlating crack growth rates and tip opening displacements 19 p3549 A70-38628
- Statistical data for optimum fatigue reliability design for dynamic and rotary machinery, considering static strength, cycle-to-failure and stress-to-failure distributions 21 p3833 A70-41004
- Low cycle notch fatigue tests on Inconel and low alloy steel, giving fatigue strength reduction factors for design 22 p4055 A70-43103
- Step-amplitude stress cycle program effects on durability of heat resistant alloy for turbine blades under cyclic loading 23 p4204 A70-43934
- ### STRESS DISTRIBUTION
- #### U STRESS CONCENTRATION
- #### STRESS FUNCTIONS
- Moments and shear forces in plate flexure represented by single valued stress functions of position, stating variational principle for compatibility 01 p0201 A70-10931
- Stresses in plane elastic bodies analyzed by generalizing biharmonic stress function equation in polar coordinates, assuming constant Poisson ratio and nonhomogeneity 01 p0206 A70-11152
- Complex stress functions and stress intensity factors at tips of star-shaped contour hole in infinite tensile sheet, including crack forking with arbitrary angle 03 p0585 A70-12974
- Axisymmetric problem analysis for cylindrically anisotropic elastic bodies with restricted orthotropy based on Love-Lekhnitsky stress function generalization 03 p0601 A70-14327
- Strain energy function for swollen crosslinked elastomers, extending application range by including third invariant 05 p0927 A70-15980
- Dynamics theory of displacement on basis of equations of motion solution by stress functions 05 p0931 A70-16133
- Stress functions in three dimensional nonaxisymmetric elastostatics problems in circular cylindrical coordinates, proving representation completeness for cylindrical bodies 05 p0932 A70-16172
- Inherent stresses in elastic solid assuming inherent strain as stress source, integrating stress functions 06 p1160 A70-17131
- Variational theorem for compatibility and plasticity for Mises solids based on stress functions 09 p1771 A70-22397
- Boundary point least squares technique extended to thermal and thermal stress problems in similar regions, deriving temperature and stress functions 09 p1774 A70-22580
- Axisymmetric elasticity theory problem solution for hollow finite cylinder with symmetrical end loading, employing stress function 11 p2128 A70-25388
- Equilibrium displacement equations for linear infinitesimal isotropic Cosserat elasticity solved in terms of stress functions 11 p2142 A70-26630
- Complex potentials used in semicomplex variable method for plane-strain problems in two dimensional linearized elasticity with couple stresses 13 p2508 A70-28494
- Plane stress state equations for micropolar elastic plates using complex potentials 13 p2517 A70-29629
- Incompressible solid propellant rocket charges axisymmetric problems, using Galerkin stress functions 14 p2657 A70-30772
- Stress and deformations three dimensional solution in semiinfinite elastic body with spherical cavity based on Boussinesq stress function 14 p2661 A70-31328
- German monograph on stress-strain state determination for rotors of turbomachines covering strain equations, partial differential equations, boundary conditions, etc 16 p2971 A70-34078
- Double curved shell membrane stress calculation under arbitrary load, using stress functions 18 p3338 A70-36373
- Two dimensional piezoelectric problems of electroelasticity, formulating general solutions in terms of stress and electric potentials using complex variables 19 p3487 A70-37946
- Stress concentrations due to cylindrical inclusions in homogeneous matrix, using stress function methods 20 p3656 A70-40045
- Membrane theory of shells, reducing equilibrium equations to single second order partial differential equation through transformation in terms of stress function derivatives 21 p3939 A70-42031
- Numerical solution of first boundary value problem of elasticity theory involving biharmonic stress function relating to rim loads 23 p4275 A70-44942
- Crystal elastic dislocations general solution, deriving stress function for stress and displacement fields in bipolar coordinates 24 p4426 A70-46018
- ### STRESS MEASUREMENT
- #### NT X RAY STRESS MEASUREMENT
- Sensing device to measure radial stress induced at solid propellant grain-to-case bond interfaces during wide temperature variations, detailing instrumentation and operation 03 p0480 A70-12882
- Strain gauge data obtainable on rosettes used for measuring stress component stresses at 550 F in inert atmosphere 03 p0482 A70-12965
- Equipment for cyclic biaxial stress states testing by simultaneous direct pressurization and axial loading of thin walled cylindrical specimens 03 p0462 A70-12966
- Inhomogeneous deformation measurements in stress concentration zones using differential rasters in direction of distance between moire bands 03 p0588 A70-13248
- Stress-strain state of material computed from strain measurements using strain gages and strain circle 03 p0588 A70-13272
- Inductive eddy current strain gage for repeated strains measurement in magnetic and nonmagnetic sheets offering direct readout and remote recording 03 p0485 A70-13475
- Elastoplastic strains in machine element surface layers under static friction force using polarization-optical techniques 04 p0696 A70-14410
- Turbulent flow velocity and stress components simultaneous measurement by single hot wire, discussing equations and computer program 04 p0685 A70-14447
- Stress analysis based on observing birefringence effects in photoelastic surface coating 04 p0689 A70-14922
- Diodes on cordwood module measured for stress during soldering, foaming and operation, describing methods for mounting semiconductor strain gages 05 p0854 A70-16036
- Laser interferometer for earth strain study, measuring Michelson arm length changes by counting fringes in interference pattern 05 p0861 A70-16843
- Stress and buckling measurement of shallow cylindrical steel shells linked to thin plate using resistant strain gauges and high precision indicators 06 p1167 A70-17866
- Calibrating rods design for vibrating components stress measurement gauges 07 p1400 A70-18822
- Semiconducting components reliability test involving electrical parameters measurement following thermomechanical stresses 09 p1689 A70-22002
- Thermomechanical tests effectiveness and determination of stress level defining boundary between destructive and nondestructive testing 09 p1689 A70-22004
- Sensors design for studying temperature fields and stressed state of structures 09 p1680 A70-23106
- Polarization-optical kinematographic method for study of mechanical stresses during dynamic loading 09 p1680 A70-23174
- Amplitude dependence of Young modulus defect in metals during large stress HF oscillations 10 p1956 A70-24247
- Tensile and compressive strain measurements close to weld deposits, using moire fringe technique and mismatch grating 10 p1890 A70-24591
- Nomograms for thermoelastic stress in plate determined as function of dimensions and heat transfer 10 p1965 A70-25300
- Plane tension in elastic infinite strip covered by elastic plate, considering applicability to strain measurement errors calculation 11 p2129 A70-25565
- Transient and steady state thermal stress distribution measured by strain gages embedded in epoxy models 11 p2130 A70-25585
- Stress measurement in discontinuous layered medium subjected to perpendicular load under sliding friction, using photoelastic interferometric models 11 p2131 A70-25587
- Transient and steady state thermal stresses measured by holographic extension of photoelastic analysis 11 p2049 A70-25592
- Slip-ringless propeller blade mounted measurement system for steady state and vibratory stresses from multiple strain-gage locations during flight and ground tests [SAE PAPER 700223] 11 p2051 A70-25891
- Moire theory applied to direct strain measurement methods based on light diffraction 11 p2058 A70-26835
- Strain measurement over large steel plate surface ground to reasonable flatness and in welded joints by applying moire method 11 p2061 A70-26836
- Cross sensitivity errors effect on stress determination by free-filament wire strain gages used at high temperature 11 p2058 A70-26838
- Residual macrostress measurement by X ray diffractometer methods 11 p2058 A70-26839
- High temperature compressive creep tests at constant stress, describing strain measurement techniques and servocontrolled compressive equipment 12 p2206 A70-27214
- Stress relaxation in alpha titanium during plastic strain, measuring temperature and strain rate dependence 12 p2255 A70-27608
- Athermal component of plastic flow stress in alpha titanium at room temperature using incremental unloading technique 12 p2257 A70-28100
- Spherically cut space elastic properties, determining normal and tangential stresses for uniform axisymmetric edge loading 12 p2328 A70-28200
- Steel plates with penetration of oblique circular cylindrical aperture tested for effects on stress concentration 13 p2510 A70-28728
- Thermocompensated wire loop microtensensors for machine part stress concentration measurements, including parameter selection nomograms 13 p2409 A70-29519
- Inertial load-time effects in instrumented impact tests, showing corrections for bending stress and dynamic fracture toughness measurements 15 p2820 A70-32240
- Pure iron and low carbon steel macroscopic stress measurements, determining correlation between residual stress, fatigue damage and fatigue life 15 p2759 A70-32322
- FM/FM radio telemetry system for transmitting strain and temperature data from rotating parts 15 p2739 A70-32330
- Stress intensity analysis method for plates with random cracks array under plane stress 17 p3187 A70-34997
- Combined lens-hologram system for strain measurements by moire technique 17 p3087 A70-35024
- Stress decay rates in Saint Venant boundary region in truncated semiinfinite elastic cone, using Papkovitch-Neuber functions for eigenfunctions formulation 18 p3339 A70-36489
- Polarization optical determination of plane stress plastic region, using celluloid model 18 p3343 A70-36723
- Stress measurements in rotating plane disks with notched disturbed symmetry, using stroboscopic photoelasticity and numerical methods [ASME PAPER 70-GT-26] 18 p3344 A70-36867
- Omnidirectional dynamic stress gage as embedded elastic inclusion, discussing transient response to ground shock compression wave pressure 19 p3422 A70-37699
- Precorrosion effects on strained Al alloy electrochemical response, examining strain test results graphically 19 p3451 A70-37780
- Stress and vibration effects measurement by holographic interferometry, comparing results with direct measurements 19 p3427 A70-38450
- Inhomogeneous deformation measurements in stress concentration zones using differential rasters in direction of distance between moire bands 19 p3548 A70-38466
- Sensing device to measure radial stress induced at solid propellant grain-to-case bond interfaces during wide temperature variations, detailing instrumentation and operation 20 p3718 A70-39158
- Asymmetric micropolar thermoelasticity, deriving integral expressions for strains, rotations and temperatures in finite body 20 p3726 A70-39878
- Contact shaped fiberglass-reinforced plastic tensile creep tests, showing strain property linearity dependence on direction 21 p3841 A70-40642
- Photoelastic stress measurement of metal powder particles during sintering, using two dimensional models 21 p3935 A70-41410

Compressive and rarefaction shock wave propagation in polymethyl methacrylate, fused silica and sapphire, using laser interferometer measurements
22 p4031 A70-43020

Spherically cut space elastic properties, determining normal and tangential stresses for uniform axisymmetric edge loading
22 p4117 A70-43324

Strain gage stress measurement under elastic-plastic strain conditions at high temperature
22 p4117 A70-43454

Reynolds stress measurement, using laser flowmeter with cylindrical lenses and square aperture mask
23 p4202 A70-44945

Nondestructive testing - Conference, Hanover, June 1970, Materials properties determination, Stress measurements
24 p4347 A70-45728

Residual stress measurement using programmed horizontal X ray diffractometer
24 p4425 A70-45729

STRESS PROPAGATION

Cracks development in hydrogenated silicon iron, investigating plastic strain relation and brittle rupture propagation
06 p1165 A70-17580

Stress wave propagation in particulate loaded carbonaceous materials induced by homogeneous laser beam
07 p1302 A70-20097

Plane and cylindrical stress wave propagation in elastoplastic medium, studying stress interrelations
09 p1775 A70-22610

Uniaxial strain pulse propagation through various materials loaded uniformly with step function pressure by gas dynamic shock wave reflection
09 p1783 A70-23449

Compression stress wave generated by longitudinal impact of two cylindrical elastic rods, measuring propagation along rod by strain gage stations
12 p2325 A70-27617

Longitudinal stress waves propagation in polymeric optically active plastic bars using photoelasticity method
12 p2328 A70-28277

Stress wave generation in elastic temperature-dependent absorbing solids by impulsive EM radiation
17 p3185 A70-34967

Stability conditions in straight bar, taking into account stress direction changes caused by deformation
18 p3337 A70-36372

Stress wave propagation based on elasticity theory for reentry heat shield composites reinforced with unidirectional high strength high modulus fibers
19 p3537 A70-37788

Unidirectional composites subjected to free vibration and axial end loading, considering longitudinal stress wave propagation in fiber direction
19 p3540 A70-37954

Circular cylindrical shell with annular orthotropic elastic core, analyzing stress wave propagation under pressure pulse
21 p3938 A70-41740

STRESS RATIO

Stress ratio effects on Al alloy during crack propagation and fatigue, introducing notch stress and strain approximations
11 p2066 A70-26089

STRESS RELAXATION

Relieving microstrains in Ni powders by cold compaction at room temperature using X ray analysis, discussing polygonization process
01 p0117 A70-10161

Annular metal specimens protection against oxidation during high temperature relaxation testing by covering specimens with Al powder thinned with alcohol
01 p0121 A70-11109

Dislocation climb theories of creep and superplasticity derived, postulating strain hardening and recovery processes with independently determined rates
02 p0317 A70-12315

Short term creep and stress-relaxation curves analytic extrapolation for metals and alloys with lifetimes exceeding test duration
03 p0588 A70-13246

Cylindrical compression spring relaxation at high temperatures, presenting design data for time-temperature initial stress relationships
[ASME PAPER 69-WA/MET-10]
04 p0697 A70-14758

Structural metals hysteresis properties under cyclic plastic loading at room temperature, considering cycle dependent creep and stress relaxation
[ASME PAPER 69-WA/MET-4]
04 p0705 A70-14763

Polystyrene and polyamide stress relaxation graphs, considering tensile stresses and temperature effects
04 p0712 A70-15101

Activation energy measurement using stress relaxation for plastic flow in commercially pure Al compared with creep and tensile method
04 p0777 A70-15495

Plastic deformation of refractory alloys during stress relaxation tests under vibrations, showing enhanced stability
05 p0866 A70-17033

Stress rupture strength and relaxation and time to failure of AMG-6M sheet under creep using energy dissipation method
05 p0952 A70-17034

Test facilities for studying materials thermophysical properties and stress relaxation, including dynamic hardness measurement and torsion tests up to 2500 K
05 p0830 A70-17074

Alloy specimen shortening due to aging during stress relaxation under vibration
07 p1304 A70-18820

Creep and stress relaxation tests to investigate time dependent fracture strength of unidirectional glass fiber reinforced epoxy composites
07 p1321 A70-19962

Stress relaxation in polytetrafluoroethylene (PTFE) at various compression deformations and temperatures, considering residual stresses degree
07 p1321 A70-20228

Cyclic creep and relaxation of heat resistant alloys at high temperatures, showing inapplicability of static load conditions
08 p1516 A70-20982

Thermal and athermal components of flow stress and deformation dynamics in Ti-Al alloy
08 p1521 A70-21578

Energy storage in creep deformed graphite from stress reduction tests, discussing negative creep, test procedures and results
09 p1709 A70-22386

Austenitic steels and alloys high temperature softening under conditions of stress relaxation and creep, noting hardening action of plastic deformation
09 p1709 A70-23785

VTOL aircraft metal fatigue examination by photoelasticity emphasizing stress reduction
11 p2132 A70-25622

Flexural stress relaxation properties of thermoplastics and composite materials, assessing strain energy by ballistic pendulum
11 p2070 A70-26342

Stress relaxation in combined torsion-tension, developing expressions for torque and axial force
11 p2140 A70-26482

Stress relaxation in alpha titanium during plastic strain, measuring temperature and strain rate dependence
12 p2255 A70-27608

Stress relaxation of Mo under plastic deformation controlled by diffusion of interstitial atoms and dislocations, determining activation energy
15 p2758 A70-32124

Holographic interferometry measurements, including low frequency quartz vibration and relaxation effects in materials following strain or impacts
17 p3085 A70-35005

Ring and cylindrical structures comparative stress relaxation at room temperature
19 p3535 A70-37341

Stress relaxation in rings and rods, discussing errors possible in data correlation
19 p3535 A70-37342

Internal residual stress relaxation theory in dielectric aging in tetragonal solid solutions of calcium titanate in barium titanate
19 p3486 A70-37776

Stress relaxation interpretation at wave fronts in one dimensional media by nonlinear viscoelastic models, giving constitutive equations
19 p3542 A70-38057

Short term creep and stress-relaxation curves analytic extrapolation for metals and alloys with lifetimes exceeding test duration
19 p3548 A70-38464

Bcc metals and alloys stress relaxation, internal stress and work hardening, discussing temperature dependence and dislocation motion
20 p3647 A70-39108

Ti alloy tension creep tests at room temperature, determining strength for correlation with stress relaxation
22 p4055 A70-43097

Equations of state in quadratic viscoelasticity for orthotropic media, deriving tensors of creep and relaxation centers
22 p4119 A70-43711

Limiting pressure for isotropic plastic plates and spherical shells with stress dependent yield, using flow theory
22 p4120 A70-43717

Fiberglass reinforced plastic strength and deformation properties under creep and stress relaxation, investigating temperature effects and load duration
23 p4209 A70-43980

STRESS RELIEVING

Fiber composite cylinder tensile performance improvement through mechanical residual stress relief by axial straining
01 p0120 A70-10737

Residual stresses in cylindrical shells eliminated by local heat treatment, determining temperature field in elastic strain regions
03 p0497 A70-13739

Commercial Ni-Co gas tungsten arc filler metal with mechanical properties stable following stress relief
04 p0710 A70-15653

Membrane stress concentration near circular cutouts in uniaxially stressed sheets reduced by predeforming immediate surroundings of hole
05 p0940 A70-16515

Phenomenological properties of stress relief embrittlement in nickel steel, noting toughness recovery via retempering
11 p2059 A70-25665

Residual stresses near weld in spherical rocket motor casing constructed from maraging steel sheet, discussing moire measurement and reduction treatments
15 p2744 A70-31926

STRESS RUPTURE STRENGTH

U CREEP RUPTURE STRENGTH

STRESS TENSORS

Einstein equations for Bianchi type IX universe model suitable for numerical solution and application to cosmology with pure fluid stress tensor
01 p0142 A70-10522

Discontinuity surfaces /cracks/ propagation in continuous medium having energy and stresses as functions of strain tensor gradient, using variational principle
03 p0589 A70-13330

Difference equations and axial stress tensor component for turbomachinery in curvilinear coordinates systems
04 p0776 A70-15268

Time dependent transport equations for full Reynolds stress tensor and turbulence decay function using flux approximations and relaxation model
[AIAA PAPER 70-7]
06 p1038 A70-18080

Stress tensor for relativistic weakly ionized plasma in HF electromagnetic field taking into account collisions
07 p1348 A70-19197

Green and Cauchy deformation tensors determined from moire fringe pitch and angle measurements, deriving equations by specimen and master grid geometries indicial representation
[ASME PAPER 69-APMW-21]
08 p1591 A70-21462

Natural bending vibrations of circular plates with allowance for stress tensor asymmetry, deriving transcendental frequency equation
09 p1782 A70-23292

Stress tensors in initial value problem for incompressible flow with nonlinear viscosity
09 p1663 A70-23570

Stress tensor and displacement vector in thin elastic shells/plates derived from three dimensional nonlinear equations using asymptotic integration
11 p2142 A70-26634

Axisymmetrical stress tensor singularity convergence of rigidly clamped circular plate, showing identity of plane stressed state transcendental equations
12 p2325 A70-27558

Normalized Reynolds stress tensor in upstream region of fully developed turbulent shear flow as function of position, using inviscid linear model
[ASME PAPER 70-FE-2]
16 p2891 A70-33626

Stationarity of complementary energy in nonlinear elasticity theory, using Piola stress tensor representation for isotropic elastic media
17 p3192 A70-35692

Stress energy tensor equal time commutation, observing metric dependence inability to satisfy relations for linearized gravitational fields
19 p3536 A70-37550

STRESS WAVES

Book on nonlinear stress waves propagation in elastic solids covering adiabatic shocks, isentropic plane waves, Lagrange equation, spherical waves, heat conduction effect, etc
01 p0202 A70-10966

Micrometeorite detection involving impact stress wave monitoring by strain gages embedded in viscoelastic plastic
03 p0487 A70-13573

Stress wave propagation tests in thin walled tubes under combined tension and torsion, discussing predicted and observed strain-time profiles discrepancies
03 p0599 A70-14245

Transient processes of strain wave propagation in elastic shells and plates under time varying loads
04 p0773 A70-15010

One dimensional stress waves propagation in elastoplastic medium, determining stress and velocity fields due to heat sources motion by characteristics method
04 p0776 A70-15447

Transient stress waves generated by spatially uniform distribution of transverse forces in laminated medium, using modal analysis
05 p0938 A70-16409

- Radially nonsymmetric stress wave propagation from tip of moving crack in infinite plates, deriving minimal group velocity 05 p0941 A70-16516
- Double giant pulse ruby laser with 1.5 m coherence length for producing double exposure holograms of stress wave propagation in solids 05 p0861 A70-16850
- Stress wave propagation in particulate loaded carbonaceous materials induced by homogeneous laser beam 07 p1302 A70-20097
- Curved thin rods torsional and flexural waves propagation equations, considering geometry and shear and Young moduli 08 p1588 A70-21201
- Dynamic stresses during abrupt temperature changes of medium, showing internal stress waves amplitude increasability by suitable internal stress source selection 09 p1778 A70-23089
- Strain gage for measuring strain waves amplitude on surface of fused quartz to study electromagnetic waves interaction in Permalloy films 09 p1681 A70-23349
- Electronic stress wave analysis technique /SWAT/ for delayed weld cracking data acquisition 10 p1897 A70-25312
- Gas passing through shock wave, investigating constitutive relations for stress and heat flux using Maxwell moment method 11 p2036 A70-26015
- Transient analysis of stress waves around cracks under antplane strain with time dependent loadings based on integral transforms 11 p2145 A70-26698
- Compression stress wave generated by longitudinal impact of two cylindrical elastic rods, measuring propagation along rod by strain gage stations 12 p2325 A70-27617
- Iron sample shape determination for studying relationship between tensile strength and rate from stress wave propagation during high speed tensile tests 15 p2814 A70-31547
- Stress wave propagation in solid infinite elastic medium and laminated materials 15 p2823 A70-32784
- Three dimensional dynamic analysis of small harmonic stress wave propagation in elastic-plastic and viscoplastic materials, using finite differences 18 p3344 A70-36724
- Lumped parameter model for multidimensional solid mechanics problems with inelasticity, discussing stress wave interaction in cylindrical cavity 19 p3458 A70-38357
- Filamentary composites stress wave amplitude distribution calculation and plotting 22 p4114 A70-42645
- Finite difference method for stress wave propagation and multiple reflection in elastic bar with discontinuities 22 p4115 A70-42744
- Strain rate sensitivity and stress waves effects on dynamic response and adhesion failures of rain erosion resistant coatings 22 p4059 A70-43102
- Perturbation effects on nonlinear first order wave equations discontinuous solutions decay, discussing boundary value problem for stress wave propagation in rod with viscous damping 24 p4426 A70-46026
- STRESS-STRAIN DIAGRAMS**
- Nonlinear stress-strain equations for incompressible hyperelastic media developed for undeformed and deformed continuum states 01 p0201 A70-10892
- Digital computer for data recording in stress-strain curves and data points for mechanical tests 01 p0058 A70-11062
- Stress-strain effect on dislocation densities of cylindrical Mg single crystals deformed by torsion basal slip compared to tension test 01 p0122 A70-11236
- Metal and alloys micro and macro stress-strain behavior data correlated for linear differential transformers, strain gages, longitudinal resonance waves and X ray diffraction 01 p0092 A70-11248
- Volterra equations for stresses, strains and displacements of viscoelastic tube with variable radius enclosed in shell under pressure and unsteady temperature field 02 p0384 A70-11663
- Stress-strain state of epoxy resin plates with single or paired wire reinforcement, using polarization-optical method 02 p0384 A70-11664
- Axisymmetrical stress-strain state of body of revolution with complex cross sectional geometry under surface loads, deriving computer algorithm for numerical analysis 02 p0384 A70-11665

- Temperature effects on tensile deformation mechanism of Mo single crystals, investigating stress-strain characteristics and slip geometry 02 p0316 A70-11699
- Left ventricle wall forces and dimensional measurements during cardiac cycle based on stress-strain terms, including results for mitral, aortic and myocardial disease 02 p0238 A70-12512
- Strain rates and stresses relations in plasticity theory for consolidatable orthotropic bodies having three elastic planes of symmetry 02 p0389 A70-12686
- Load and strain trajectory vectors components determined for tension followed by transverse compression in five dimensional space 02 p0390 A70-12803
- Quasi-linear stress-strain deviators relations in viscoelastic theory, indicating kernels and functions determinable from creep relaxation loading and deformation tests 02 p0390 A70-12804
- Stress-strain state of material computed from strain measurements using strain gages and strain circle 03 p0588 A70-13272
- Stress-strain state of perforated shallow shells with arbitrary curvature using Green matrices 03 p0591 A70-13416
- Integral equations for antisymmetric shallow shell stress-strain state with crack, obtaining asymptotic solution in form of power series 03 p0591 A70-13420
- Stress-strain state of body of revolution having transversely isotropic elastic properties, using perturbation technique 03 p0591 A70-13441
- Stress-strain state of infinite isotropic perforated plate under cyclic symmetry, assuming finite strains and nonlinear material 03 p0592 A70-13445
- Stress-strain relations for rigidly sealed orthotropic planes with finite number of slits 03 p0592 A70-13447
- Stress-strain state of arbitrarily cracked cylindrical shell under symmetric and asymmetric loading 03 p0594 A70-13736
- Elastoplastic analysis of strain hardening materials under multiaxial states of stress based on von Mises yield condition and stress-strain relationship 03 p0596 A70-14012
- Stress-strain state under bending of shallow spherical shell having form of circular rectangle with clamped edges 04 p0767 A70-14486
- Cyclic hysteresis-loop stress-strain behavior of 1100 aluminum, deriving power function [ASME PAPER 69-WA/MET-1] 04 p0705 A70-14764
- Stress-strain spatial distribution in notched plate fatigue specimen of mild steel determined by finite element method, noting cyclic strain softening effect [ASME PAPER 69-MET-C] 04 p0770 A70-14876
- Nonlinear stress-strain laws and yield conditions derived for anisotropic materials on basis of one, two and three invariants 05 p0926 A70-15914
- Integral constitutive relation representing incompressible viscoelastic materials and plane stress and strain conditions 05 p0930 A70-16087
- Stress-strain relations for elastic anisotropic crystal lattice systems derived in terms of orientation vectors and scalar moduli 05 p0932 A70-16135
- Stress-strain state of circular orthotropic shells under bending, considering distributed loads applied to shell center 05 p0934 A70-16217
- Book on analysis of laminated composite structures covering orthotropic materials stress-strain relations, laminated composite shells, plates, beams and columns 05 p0938 A70-16467
- Load distribution in Christmas tree turbine attachments due to centrifugal force on blades, showing strain diagrams 05 p0939 A70-16488
- Hydrodynamic theory of elastic-viscous liquid lubrication for journal bearings, assuming stress-strain relationship with unequal cross stresses 05 p0855 A70-16509
- Creep rupture effect on fatigue damage of structural material, constructing nondimensional stress range diagrams 05 p0943 A70-16806
- Stress-strain state of plates weakened by reinforced hole and under tensile and bending loads, including boundary conditions 05 p0945 A70-16856
- Small elastoplastic deformation effects on stress-strain state of rib-reinforced cylindrical shells 05 p0946 A70-16955
- Stress-strain state of drawn and bent circular plate made of rigid viscoplastic work hardened material 05 p0946 A70-16958

- Uniform cross section rings creep characteristics testing method, proposing relations for calculating stresses and strains 05 p0952 A70-17037
- Analog to Burger model applied to rotating disk creep problem solution and stress-strain state of plane sample with hyperbolic groove 05 p0952 A70-17038
- Three dimensional stress-strain analysis of rotating finite hollow cylinder, emphasizing wall thickness effect on stress and strain distribution 06 p1160 A70-17130
- Modulus of rigidity and stress-strain state measured in square plate during shear produced by twisting 06 p1060 A70-17132
- Carrying capacity of machine parts under small numbers of cyclic plastic deformation, reviewing breakdown criteria relation to kinetics of stress-strain states 06 p1161 A70-17383
- Copper specimens stress-strain diagrams under cyclic loads of various amplitudes, noting three stage process plastic deformation 06 p1162 A70-17386
- Rotation of circular cross sectioned continuous rod with constant bending moment, assuming linear strengthening with fixed cyclic strain diagram 06 p1163 A70-17396
- Limiting stress states analysis in isotropic solids using loading history and replacing nonlinear stress-strain curve by approximating rectilinear polygon 06 p1165 A70-17547
- Longitudinal vibration equations of beams for non-linear stress-strain relation reduced to equivalent linear partial differential equations 06 p1106 A70-17863
- Stress-strain state equations for axisymmetrically loaded shells of revolution made of materials with variable moduli 07 p1399 A70-18660
- Stress-strain state of curved rod made of anisotropic material under bending loads applied to end face cross sections 07 p1399 A70-18661
- Steels fatigue strength under biaxial tension, considering complex stress-strain state 07 p1304 A70-18823
- Elastic and plastic deformation zones stress-strain state under complex stresses, obtaining relation for stress and strain components 07 p1401 A70-18834
- Cylindrical shell of revolution stress-strain state calculated during shaping in stamp with unclamping dies 07 p1292 A70-18836
- Stress-strain distributions in linear viscoelastic cylinder, reducing problem of hollow cylinder with moving inner boundary to Volterra integral equation 07 p1406 A70-19303
- Piecewise linear elastic material with jump-like non-homogeneity, analyzing stress-strain relation 07 p1407 A70-19384
- Critical stress-strain diagrams for brittle plate possessing notch-type stress raisers under biaxial tension 07 p1408 A70-19547
- Rib-reinforced cylindrical shells stability under longitudinal compressive loading, studying stress-strain state using network method 08 p1583 A70-20528
- Stress-strain state of flexible circular plates as function of thickness distribution using finite difference theory 08 p1583 A70-20529
- Matrix method for converting time variable stress vector into strain vector allowing for linear creep and aging 08 p1583 A70-20531
- Infinite strip with longitudinal crack and under loading, analyzing stress-strain state 08 p1585 A70-20938
- Electronic recording of cyclic strain diagrams of metals in wide loading frequency range using dynamic hysteresis method 08 p1585 A70-20987
- Stress-strain state of shells with positive Gaussian curvature under concentrated tangential loads, basing fundamental solution on two dimensional Fourier transform 08 p1587 A70-21169
- Stress-strain analysis for rod-shaped structural elements under combined tensile and bending loads 08 p1588 A70-21191
- Stress and strain spatial distribution in notched steel plate under cyclic loading determined by finite element method 08 p1590 A70-21315
- Stress-strain behavior of Al and Ti alloys, beryllium and nonmetallic structural materials based on constitutive equations describing strain rate and temperature effects 08 p1518 A70-21331
- Elastically symmetric thin plate stress-strain state under uniformly distributed load applied to edges 08 p1591 A70-21415

Stress, strain and strain rate relations determined from dynamic flexural beam tests with bending moment in terms of curvature

08 p1592 A70-21475

Residual stresses in continuous fiber reinforced composites with unknown strain history determined by empirical methods

08 p1520 A70-21498

Inplane shear stress-strain response determined for unidirectional composites, using uniaxial test method for laminated plates

08 p1530 A70-21884

Composite materials fatigue determinations providing curves of stress-strain magnitude vs usable life or time to failure, considering environmental effects in service for design criteria

08 p1531 A70-21895

Microstrain characteristics of continuously reinforced W-Cu composites as function of volume fraction of fibers and prestrain, discussing dislocation friction stress

08 p1524 A70-21917

Metastable austenitic steel mechanical properties after thermomechanical treatment with deformation, discussing stress-strain curves to exhibit yield point

08 p1525 A70-21963

Stress-strain characteristics of reinforced elastoplastic layer using mathematical model

09 p1769 A70-22183

Creep behavior transition analysis, considering activation energies and creep rate dependence on temperature, stress and grain size

09 p1704 A70-22720

Metals and plastics tensile strain rate sensitivity tested by drop weight tests, obtaining dynamic and static stress-strain curves

09 p1704 A70-22725

Algorithm for stress-strain state calculation of nonuniformly heated cylinder weakened by star-shaped cavity

09 p1779 A70-23094

Rotating cylinder stress-strain state under steady and unsteady creep, using Lagrange variational principle for differential equations

09 p1779 A70-23100

Reinforced cylindrical shells stress-strain state under concentrated longitudinal loads, considering ribs of variable rigidity

09 p1782 A70-23289

Nb-W single crystal low temperature thermally activated deformation, observing slope change in temperature dependence curves of flow stress and strain rate sensitivity

09 p1708 A70-23572

Elastic ribs reinforced thin cylindrical shells stress-strain state under arbitrary load distribution allowing for rib spacing discreteness

09 p1784 A70-23590

Annealing effect on stress-strain curves of overaged and cold-rolled Al-Li alloy, observing yield drop

09 p1708 A70-23727

Stress-strain state analysis of prestrained thin circular cylindrical shell using Vlasov general shell theory

10 p1955 A70-24021

Total Poisson ratio derivation from stress-strain relationship with known variations of elastic and plastic Poisson ratios for particular strain-hardening case

10 p1956 A70-24096

Thick-walled toroidal shell under various load distributions, analyzing stress-strain state by networks method using computer program

10 p1957 A70-24250

Power-law stress-strain relation in plastic complex stressed state, showing identical strain hardening curves for shear and tension

10 p1957 A70-24280

Stress-strain determination in nonuniformly heated thin walled cylindrical beams with nonlinear stringers and skin

10 p1957 A70-24281

Elastic stress-strain states in spherical reservoir and thick walled tube during nuclear radiation induced phase transformations

10 p1894 A70-24513

Macrolon elastic-plastic strain model, studying stress-strain relationship and optico-mechanical properties

11 p2128 A70-25385

Monograph on integral calculation method for disk problems with mixed boundary conditions covering two dimensional stress-strain state, extrapolation methods, etc

11 p2140 A70-26474

Filament reinforced composites tested under dynamic compression loads for determining relations among strain rate, constituent properties, stress-strain behavior, fracture energy and mode

12 p2253 A70-27119

Kinetic theory for fatigue crack propagation using cyclic stress-strain relation in connection with strain hardening characteristics

12 p2322 A70-27208

Shallow spherical shells stress-strain state in multiply connected regions resting on Winklerian base

12 p2323 A70-27334

Stress-strain state effects on Cu and Ni tubular samples plasticity and strength using polarization-optical technique

12 p2323 A70-27341

Longitudinal waves propagation in polyethylene bar using Boltzmann-Volterra equation, constructing dynamical stress-strain diagrams by viscous-elastic standard body model

12 p2328 A70-28276

Stress-strain relationships model for nonlinear restrained cylinders, using compression tests and finite element method

14 p2660 A70-31135

Alloy high temperature creep and long term strength, determining exponential relations between stress, strain rate and durability

15 p2755 A70-31529

Two dimensional stress-strain fields under elastic and elastic-plastic strains and steady state creep, calculating stress distribution around hole in cylindrical shell

15 p2813 A70-31533

Low temperature tensometry application to stress-strain state of turbine disks

15 p2733 A70-31537

Stress-strain state of catenoid, cylindrical and spherical shells of revolution, emphasizing catenoid shell bending problem

15 p2815 A70-31648

Sinusoidal stress and strain in elastic shells of revolution, reducing linear theory to simultaneous second order differential equations

15 p2816 A70-32008

Internal pressure deformation of thin cylindrical shells of materials with nonlinear stress-strain relations, considering Al alloy shell and axial strain

15 p2816 A70-32009

Torsional vibrations amplitude effect on polycrystalline Al stress-strain curve during uniaxial tensile test

15 p2758 A70-32125

Stress-strain vector for straight bar of constant or stepwise cross section, using initial parameter matrix method

15 p2822 A70-32363

Monograph on elastic stability covering eigenvalues of matrix series, stress-strain state calculation, critical ratio derivation, etc

15 p2823 A70-32550

Nonlinear elasticity equations in displacements by Green and Hencky deformation tensors, discussing stress-strain of body with spherical cavity

16 p2988 A70-33251

Structural fatigue failure analysis and design, applying local stress-strain approach

16 p2989 A70-33424

German monograph on stress-strain state determination for rotors of turbomachines covering strain equations, partial differential equations, boundary conditions, etc

16 p2971 A70-34078

Structural hardening of nickel maraging steels related to Portevin-Le Chatelier effect in necking zone of stress-strain curves

17 p3124 A70-35141

German monograph on two dimensional stress-strain state for material subjected to creep, using differential equations derived from equilibrium conditions

17 p3189 A70-35376

Structural stability in tension and strength tests of thin walled tubes at various stress and strain intensities, noting dependence on stress-strain state type

17 p3192 A70-35713

Deformation behavior of continuous W and B fibers reinforced Al alloy matrix composites, monitoring stress-strain characteristics by X ray diffraction

18 p3272 A70-36036

Spherical shell of variable thickness, calculating stress-strain state around reinforced circular hole during elastoplastic deformation

18 p3336 A70-36138

Plane strain and stress produced in elastic micropolar medium by action of temperature

18 p3338 A70-36429

Stress-strain equilibrium of thin isotropic elastic shells of revolution loaded along meridian

18 p3340 A70-36577

Zero moment theory for stress-strain state of thin walled anisotropic shells with nonuniform moduli under simultaneous torsion and tension

18 p3340 A70-36578

Barium fluorides single crystals compression, investigating stress-strain behavior and dislocation mobility

19 p3483 A70-37339

Fiber reinforced materials with oriented armoring, calculating stress strain state under transverse shear

19 p3454 A70-37348

Volterra equations for stresses, strains and displacements of viscoelastic tube with variable radius en-

cased in shell under pressure and unsteady temperature field

19 p3547 A70-38437

Stress-strain state of epoxy resin plates with single or paired wire reinforcement, using polarization-optical method

19 p3547 A70-38438

Axisymmetrical stress-strain state of body of revolution with complex cross sectional geometry under surface loads, deriving computer algorithm for numerical analysis

19 p3547 A70-38439

Reciprocity theorem for stresses and strains in medium under creep and temperature field

19 p3548 A70-38582

Large deflection of simply supported aluminum alloy annular plate with nonlinear stress-strain curve, considering compressibility effects and membrane force

20 p3718 A70-39138

Polyurethane swelling in liquid media, measuring surface orientation effects during chemical machining on stress strain state

20 p3654 A70-39249

Three dimensional photoelastic analysis of stresses and strains in hollow circular cylinders with conical ends bonded to shell and shrunk

20 p3720 A70-39686

Long hollow nonlinearly viscoelastic cylinder in elastic shell, calculating stress and strain under internal pressure

20 p3720 A70-39731

Elastoplastic deformation in strip with symmetrical semicircular notches simulating stress strain state on celluloid models by polarization-optical method

20 p3720 A70-39735

Stress-strain zero moment state of thin walled helical shell under uniformly distributed tensile loads

20 p3721 A70-39778

Thin shell theory elastic coupling conditions, discussing stress-strain and edge effect states

20 p3726 A70-39875

Hollow shell theory equations for complex stress-strain states, using complex transform method

20 p3726 A70-39880

Low cycle metal fatigue under stress concentration, examining complex loading, cyclic strain, stress-strain state and plastic deformation

20 p3727 A70-39885

Linear relations between stress state and Euler strain rate in isotropic elastic bodies during superposition of small deformation on finite strain

20 p3728 A70-39893

Thin elastic shells displacement vector and strain boundary conditions determination from stress-strain relations

20 p3728 A70-39896

Fiber reinforced composite shell structures stress-strain relations, noting membrane and flexural variables coupling in constitutive relations

20 p3729 A70-40034

Strains and stresses along interfaces and near fiber ends in composite structures made of reinforced matrix, using photoelastic methods

20 p3730 A70-40035

Perturbation method for stress-strain state of circular cylindrical shell with large curvilinear hole

20 p3734 A70-40442

Stress-strain characteristics at high strain rates, obtaining materials dynamic plastic properties by thin wafer technique

21 p3932 A70-40543

Stress-strain state of finite length elastic beam free of bending moments and coupled to semifinite plate

21 p3933 A70-40603

Orthotropic fiberglass-reinforced plastic cylindrical shell with allowance for material creep, calculating stress-strain state during bending under external pressure

21 p3842 A70-40649

Epoxy and polyurethane adhesives stress-strain behavior in lap joints, examining bond thickness and cryogenic temperature effects

21 p3844 A70-42139

Stresses and strains concentration around elliptic hole in finite plates subjected to uniform load, using photoelasticity, moire effect and grids

22 p4114 A70-42697

Strain rate change effect on stress-strain diagram shape of polycrystalline alpha-Ti during tensile tests over temperature range

22 p4054 A70-42737

Strained state of Ti and steel sheets during unsymmetric rolling, constructing deformed metal particles displacements rates field based on ideal fluid motion equations

22 p4045 A70-42814

Transient stresses and strains in plane wedge under dynamic load, using photoelastic, high speed photographic and strain gage studies

22 p4036 A70-43062

Stress-strain diagrams for oriented fiberglass-reinforced plastic under tension taking into account temperature and anisotropy effects

23 p4209 A70-43938

Nonlinear elasticity equations in displacements by Green and Hencky deformation tensors, discussing stress-strain of body with spherical cavity
23 p4268 A70-44287

Simplified Sanders-Koiter linear thin shell equations with uncoupled stress-strain relations for arbitrary, nonzero Gaussian curvature, catenoidal and helicoidal midsurface geometries
23 p4269 A70-44399

Servohydraulic testing machine for measuring cyclic stress-strain behavior of materials subjected to fatigue and creep at elevated temperature
23 p4178 A70-44912

German monograph on stress-strain state in prestressed, rigidly supported flexible plates subjected to large deflections, using extended Wolmir solution
24 p4418 A70-45083

Stress-strain curves of polycrystalline metals and composites using single crystal elastoplastic model
24 p4425 A70-45779

Al-Zn-Mg alloy prolonged aging behavior, examining Gp and intermediate zones, equilibrium phases, maximum strength and serrated stress strain curve
24 p4362 A70-46189

STRESS-STRAIN DISTRIBUTION

U STRESS CONCENTRATION

STRESS-STRAIN RELATIONSHIPS

U STRESS-STRAIN DIAGRAMS

STRESS-STRAIN-TIME RELATIONS

Creep propagation determination in pure Al for microscopic and macroscopic continuum points used for determining stiffness and strain time history
01 p0121 A70-11156

Left ventricular muscle time varying elastic properties, using dynamic model and Fourier series representations
01 p0040 A70-11371

Temperature-time-variable stress-strain state of polymer structures, solving creep equation by linear model with rheological properties
01 p0211 A70-11426

Short term creep and stress-relaxation curves analytic extrapolation for metals and alloys with lifetimes exceeding test duration
03 p0588 A70-13246

Cylindrical compression spring relaxation at high temperatures, presenting design data for time-temperature initial stress relationships
[ASME PAPER 69-WA/MET-10]
04 p0697 A70-14758

Life fraction hypothesis equation in creep testing derived on basis of chemical reaction rate theory
[ASME PAPER 69-MET-A]
04 p0705 A70-14875

Time-to-rupture dependence on temperature and stress related to chemical reaction rate equation in creep testing
[ASME PAPER 69-MET-B]
04 p0770 A70-14877

Time dependent creep and elastic strain interaction in plates and pressure vessels of cylindrical and spherical geometry
05 p0942 A70-16804

Stress, strain and strain rate relations determined from dynamic flexural beam tests with bending moment in terms of curvature
08 p1592 A70-21475

Stresses and strains in multilayer systems of viscoelastic materials showing aging solved by quadratures and Volterra equations, noting dependence on time
08 p1594 A70-21672

Dynamic postbuckling response of thin elastic circular plates under axisymmetric time dependent radial thrust, discussing response to step loading
10 p1964 A70-25206

Versamid cured epoxies time-dependent mechanical properties, determining loading mode, strain level and reinforcing agent effects on time-temperature shift factors
13 p2438 A70-29205

Short term creep and stress-relaxation curves analytic extrapolation for metals and alloys with lifetimes exceeding test duration
19 p3548 A70-38464

Conducting viscoelastic fluid flow near harmonically oscillating nonconducting flat plate under uniform transverse magnetic field, considering stress-strain rate relationship
23 p4226 A70-44375

STRESSED-SKIN STRUCTURES

Crack tip stress intensity factor in sheet structures, applying complex stress potentials and perturbation techniques in numerical calculations
19 p3549 A70-38627

STRESSES

NT AXIAL STRESS
NT COMBINED STRESS
NT CRITICAL LOADING
NT RESIDUAL STRESS
NT SHEAR STRESS
NT TENSILE STRESS
NT THERMAL STRESSES
NT TORSIONAL STRESS
NT TRIAXIAL STRESSES
NT VIBRATIONAL STRESS

STRETCHING

Incompressible elastomer viscoelastic response to exponential extension ratio history in simple tension based on constitutive equations
01 p0201 A70-10893

Static deformation fields producible in isotropic homogeneous incompressible elastic body with uniform transverse stretch
05 p0931 A70-16134

Spinal cord overstretching and circumscribed pathological tension mechanism, considering histological and radiological findings
07 p1204 A70-19242

Orthotropic fiberglass reinforced plastic deformation during stretching with allowance for binder breakdown in transverse layer
12 p2259 A70-28283

Elastoplastic material mechanical theory, considering constitutive equations with plastic deformations and decompositions of total velocity-strain/stretching/
14 p2661 A70-31281

Fiber reinforced solid material, determining swelling or temperature change induced dilatation by micromechanics and physical chemistry
19 p3540 A70-37943

Structural mechanics of continuous fiber reinforced composites, discussing bending and stretching of cylinders, pressure vessels, plates and beams
20 p3730 A70-40039

Snatch force during lines-first deployment of aerodynamic decelerator, including effects of canopy skirt acceleration and suspension wave propagation characteristics
[AIAA PAPER 70-1171]
21 p3754 A70-41842

Stretch fabric materials for personnel high speed escape parachute systems
23 p4141 A70-44482

Metal and alloy sheets, investigating deformation and failure under biaxial stretching tensile tests
24 p4358 A70-45240

STRIATION

Fatigue crack growth rate for high strength steels from crack length during cyclic loading and striation spacings after fracture
01 p0119 A70-10732

Polycarbonate fatigue fracture surfaces and striation feature
12 p2259 A70-27168

He-Ne laser noise caused by discharge current fluctuation and moving striation in long capillary tubes
12 p2245 A70-27272

Barium ion clouds striation formation above E layer ascribed to LF gradient drift instability
15 p2727 A70-31908

Ion density and electron temperature variations as function of maximum electric field density in independently excited plasma column striations
19 p3475 A70-37552

Microwave diagnostics of electron density, temperature and light emission in self excited moving striations in hydrogen plasma
19 p3475 A70-37553

Striation formation in artificial ion clouds aligned with local geomagnetic fields, considering visual indication of ionospheric electric field transferal along magnetic field
19 p3415 A70-38387

Striations due to mechanical oscillations in fast wire explosions, using dispersion for elastic waves in solid cylinders
22 p4074 A70-43002

STRINGERS

Natural oscillation frequencies of closed circular orthotropic cylindrical shells having freely supported end faces, particularly with stringers
01 p0210 A70-11413

Centrally cracked sheet, calculating riveted and uniformly spaced stringers effect on stress intensity factor
23 p4270 A70-44549

STRINGS

Gas effect on natural frequency of electrostatically excited string vibrating between flat electrodes at medium pressures
11 p2048 A70-25582

Self excited systems limiting states with traveling wave, analyzing oscillator moving along string under tension
16 p2990 A70-33781

STRIP

Thin walled strip stability, calculating critical force and rotation angles assuming small subcritical strains
07 p1415 A70-20188

Infinite strip with longitudinal crack and under loading, analyzing stress-strain state
08 p1585 A70-20938

Stripline elements centimeter wavelength emission level determination by comparison with reference antenna radiation patterns
09 p1652 A70-23650

Diffraction on strip, investigating for Dirichlet boundary conditions, deriving excited current density and scattered pattern
15 p2696 A70-31515

Viscoelastic strip in gas flow, analyzing stability conditions
22 p4117 A70-43353

Symmetrical bending of isotropic elastic half-strip with free longitudinal edges and end displacements, indicating use for plate and shell theory
22 p4118 A70-43568

STRIP TRANSMISSION LINES

Microwave conductivity of thick film screen-printed microstrip circuits, measuring closed resonators SHF Q factors
19 p3388 A70-37964

Correction to Wu theory of microstrip leading to exponentially increasing fields
21 p3784 A70-40558

GaAs stripline domains and guided EM waves, discussing velocity, conductivity, drift and transmission amplification gain
22 p3996 A70-42917

Integrated 7 GHz small signal microwave balanced mixer, using microstrip transmission lines
23 p4168 A70-43777

Stripline and microstrip junction circulators analysis for microwave integrated circuits, based on clockwise and counterclockwise rotation modes
23 p4169 A70-43787

Ferrite junction microwave circulator bibliography /1956-1969/ covering stripline and waveguide versions theory, designs, constructions and applications
24 p3318 A70-45210

Variable microwave attenuator using p-i-n diodes and three-port hybrids built in stripline technique
24 p3318 A70-45222

STROBOSCOPES

Stroboscope lighting system for microstructural examination of fatigue test sample failure
05 p0845 A70-15882

Inexpensive live stroboscopic holographic interferometry, discussing time averaged and stroboscopic methods
09 p1676 A70-22787

Electronically modified stroboscope as light source for multiframe photography of transient events, noting mechanical switches elimination
18 p3262 A70-37095

High speed stroboscopic photography, discussing multiple flash and motion picture photography and TV operated strobe light
[SMPT PREPRINT 42]
22 p4033 A70-43040

Stroboscopic stereophenomenon, investigating depth shift of oscillating target motion binocularly viewed for interocular luminance differences
23 p4147 A70-44781

STRONTIUM

NT STRONTIUM ISOTOPES

Submarine basalt sea water alteration effects, examining Sr and rare earth concentrations, Ba enrichments or depletions and trace element data
19 p3413 A70-38015

Luminous intensity profile of optically thick Sr artificial clouds in upper atmosphere, using Monte Carlo calculations
19 p3415 A70-38388

STRONTIUM COMPOUNDS

NT STRONTIUM FLUORIDES

NT STRONTIUM TITANATES

NT STRONTIUM TRICONATES

Strontium chloride lanthanum ion system with dynamic Jahn-Teller effect, indicating isotropic EPM spectrum resulting from averaging by relaxation
13 p2470 A70-29109

Strontium nitride hydrolysis, investigating hydrazine presence among products
23 p4158 A70-44598

Phase transitions in FeW doped strontium and barium oxides, using X ray diffraction and Mossbauer effect for transition temperature
24 p4390 A70-45605

STRONTIUM FLUORIDES

Strontium fluoride crystals containing trivalent neodymium cations investigated for laser action and radiation characteristics by spectroscopy
10 p1899 A70-24253

STRONTIUM ISOTOPES

Age and initial strontium for Guarena chondrite, determining differential evolution of Rb/Sr systems involving simple metamorphism of closed systems or multistage processes
03 p0576 A70-14088

Rb-Sr internal isochron ages from Ocean of Storms, discussing analytical results of two texturally and mineralogically distinct crystalline rocks from Apollo 12
16 p2975 A70-33659

Sr 83, 85 and 87 level structure and mass defect, using stripping and pickup reactions
17 p3138 A70-34625

Middle Devonian Tioga Bentonite age from Rb, Sr and Sr isotopes in weathered whole rock samples
20 p3615 A70-38989

Apollo 11 lunar rock Rb-Sr isotopic age relationships, discussing magmatic fractionation of Rb relative to Sr in moon primordial material
21 p3908 A70-41585

STRONTIUM TITANATES

- Hologram storage and retrieval in photochromic SrTiO crystals at ruby laser wavelengths 06 p1072 A70-18519
- Alkoxy-derived strontium zirconate and titanate preparation and characterization, considering purity control, crystallite size and ceramics synthesis 09 p1740 A70-22981
- Temperature dependence of electrical conductivity and optical properties of strontium titanate semiconductor single crystals doped with Ce and Nb 12 p2288 A70-28328
- Strontium titanates ceramics containing various trivalent rare earth ions, observing dielectric relaxation 19 p3486 A70-37755
- Inorganic photochromic and cathodochromic recording materials, examining transition metal doped strontium titanates, rare earth doped calcium fluorides and Fe or S doped sodalite 22 p4088 A70-43601

STRONTIUM ZIRCONATES

- Alkoxy-derived strontium zirconate and titanate preparation and characterization, considering purity control, crystallite size and ceramics synthesis 09 p1740 A70-22981

STROUHAL NUMBER

- Vibrational response of thin walled pipes to internal turbulent water flow as function of Strouhal number 21 p3940 A70-42052
- Round pulsed jet diffusion rate from velocity measurements, considering Strouhal number and pulse amplitude 24 p4327 A70-46205

STRUCTURAL ANALYSIS

- NT DYNAMIC STRUCTURAL ANALYSIS
- NT ENERGY METHODS
- NT EQUILIBRIUM METHODS
- NT FLUTTER ANALYSIS
- NT MATRIX METHODS
- NT STRAIN ENERGY METHODS
- Acoustic emission to monitor metal structures, pipes, pressure vessels and graphite shapes to detect structural deterioration before failure, emphasizing nuclear reactor pressure systems 01 p0054 A70-10015
- Cantilevered and doubly supported structures calculated for critical aeroelastic divergence speed resulting from lift and drag 01 p0200 A70-10551
- Ultrasonic imaging of internal structure by Bragg diffraction, noting reflection and dark field extension and use for flaw detection and medical diagnostics 01 p0111 A70-10570
- Semiautomatic mass condensation transformation for reducing structural vibration calculations, including computer program and mode shape plotting 01 p0200 A70-10868
- Equilibrium of thin curved cylindrical panels subjected to thermal expansion and pressure numerically analyzed by Ritz method 01 p0201 A70-10945
- Clamped skew plates of orthotropic material under transverse load analyzed by stationary potential energy method and compared with isotropic case 01 p0205 A70-11140
- Linear structures response to pressure fields of deterministic excitation with input function spectra as meromorphic functions of wave number and frequency 01 p0208 A70-11191
- Temperature-time-variable stress-strain state of polymer structures, solving creep equation by linear model with rheological properties 01 p0211 A70-11426
- Semidiscrete approximation of equation for free vibrations of beam with nonuniform cross section, using method of straight lines 01 p0213 A70-11636
- Aerodynamic load distribution due to wind action on elastic structures, calculating various ratios between wind and critical divergence velocity 02 p0385 A70-11913
- Digital computer program /LANDIT/ for predicting structural impact response of axisymmetric landing vehicles consisting of rigid payload and crushable impact limiter system 02 p0380 A70-11945
- Bolted and bonded joints design in composite materials loaded in tension, presenting methods for strength prediction, testing and analysis 02 p0306 A70-11952
- Harmonic vibration testing of aircraft structural nonlinearities caused by dry friction, describing pitch control system 02 p0387 A70-12215
- Two dimensional structural analysis of engineering systems by computer graphics, outlining discrete element representation 02 p0388 A70-12477
- Three dimensional photoelastic case bonded solid propellant motor model, analyzing stress distribution using scattered light photoelasticity [SESA PAPER 1587] 03 p0583 A70-12885

- Finite element method for postbuckling analysis of thin elastic plates, using iterative method to obtain equilibrium configurations 03 p0583 A70-12917
- Snap-through dynamic instability of clamped shallow arches subjected to timewise step loads, establishing stability and instability conditions 03 p0583 A70-12919
- Elastoplastic bodies stability under compression, using theory of small elastoplastic deformations and linearized equations of nonlinear elasticity theory 03 p0591 A70-13440
- Three dimensional structure determination for weakly scattering semitransparent objects from holographic data, discussing inverse scattering problem and refractive index calculation 03 p0487 A70-13647
- Load analysis for aircraft landing gear during touchdown and braking operations 03 p0596 A70-14093
- Wide strut analysis for determining weight minimizing cross sectional dimensions of panels having unflanged integral stiffeners 03 p0596 A70-14145
- Structure theorem for time invariant multivariable linear systems proof and formulation for use in controller design and synthesis 03 p0461 A70-14166
- Buckling in one dimensional elastic media, discussing pendulum equations for Jacobi elliptic functions, critical loads determination, Timoshenko energy method, etc 03 p0597 A70-14227
- Far nonlinear postbuckling behavior of noncircular cylindrical shell under axial compression 03 p0598 A70-14241
- Thermal stress concentration produced by cracks, notches and fillets in plates free from external loads measured photoelastically 03 p0600 A70-14310
- Thermal stresses of semiinfinite plate with circular hole filled with elastic inclusion and subjected to uniform heat flow 03 p0601 A70-14317
- Structural analysis of rectangular plates simply supported on two edges subjected to free edge uniform moments 03 p0602 A70-14332
- Deformability calculation of two phase composite solid materials through laminated structural models 03 p0602 A70-14337
- Kamchatka regions volcanic deposits structural and mechanical characteristics compared with lunar soil characteristics 04 p0744 A70-14440
- Nonlinearity sources in elastic structures under large displacements, developing general matrix formulation 04 p0768 A70-14748
- Computer programs for numerical analysis of shell structures, considering series expansion, numerical integration, finite differences and finite elements 04 p0768 A70-14787
- Elastic postbuckling behavior of axially stiffened and barreled cylindrical shells [ASME PAPER 69-APM-U] 04 p0769 A70-14866
- Governing equations of plane elasticity to define suitable approximate theories for structural analysis [ASME PAPER 69-WA/APM-22] 04 p0771 A70-14909
- Thin walled plate simply supported on three edges, studying behavior following local stability loss 04 p0772 A70-14923
- Matrix algorithm from parallel element method derived for reducing computer time required in structural modification analysis 04 p0779 A70-15589
- Plan hybrid element generalized to arbitrary quadrilateral form, considering hybrids having constant and linear stress distributions 04 p0779 A70-15614
- Optical, electrical and structural properties of transition metal dichalcogenides 05 p0890 A70-15755
- NASTRAN digital computer program for static and dynamic structural analysis using finite element method [SAE PAPER 690612] 05 p0816 A70-15851
- Three dimensional analysis of nonhomogeneous elastic solids based on finite element method and equilibrium equations, discussing iterative solution 05 p0926 A70-15915
- Three dimensional photoelastic model for structural analysis of aircraft bulkhead to improve fatigue life 05 p0937 A70-16376
- Book on analysis of laminated composite structures covering orthotropic materials stress-strain relations, laminated composite shells, plates, beams and columns 05 p0938 A70-16467
- Finite element analysis of elastic thin shells, approximating shell surface by network of triangular plate elements 05 p0944 A70-16813

- Structural elements elastoplastic deformation regularities under repeated loadings, using adaptability theory 06 p1163 A70-17394
- Finite element method applied to potential distribution and stress analysis in earth sciences, determining elastic response of rock layer using structural matrix analysis 06 p1055 A70-17606
- Hybrid finite element analysis for combination of axisymmetric shell and linear displacement triangular ring elements [AIAA PAPER 70-137] 06 p1169 A70-18052
- Triangular plate bending elements with enforced compatibility, using cubic interpolation polynomial to describe element displacement [AIAA PAPER 70-136] 06 p1171 A70-18169
- Structural element for discrete element idealization missile and liquid propellant as one composite structure [AIAA PAPER 70-123] 06 p1042 A70-18182
- Airframes dynamic response during simulated launchings of externally carried missile measured in laboratory, describing dynamic load simulation and structural analysis 06 p1159 A70-18439
- Structural analysis of thin walled cylinder material using normal ultrasonic wave to achieve high resolution determination of components 06 p1172 A70-18630
- Rectangular plates with symmetrical cracks, studying bending under various crack distributions 07 p1399 A70-18662
- Minimum weight beams and frames calculation for random loads taking into account material carrying capacity 07 p1400 A70-18821
- Integration by orthogonalizations of envelopes of revolution loaded asymmetrically, introducing boundary conditions and structure discontinuities 07 p1404 A70-19128
- Optimal linear viscoelastic synthetic sandwich structures, investigating test/calculation agreement for simply supported beams and embedded plates [ONERA-TP-702] 07 p1404 A70-19137
- Governing equations solution for simply supported laminated anisotropic rectangular plate using Fourier series method 07 p1406 A70-19305
- Buckling of clamped skew plates under uniform system of applied stress using Galerkin method 07 p1406 A70-19339
- Inextensional nonlinear theory of arches applied to analysis of hinged-hinged circular arches subjected to downward point load, calculating critical load value 07 p1408 A70-19561
- Book on statistical methods in structural mechanics covering design, fracture, stability, random loads, damage accumulation, reliability, etc 07 p1411 A70-19849
- Digital computer applications to structural analysis, discussing interactive graphics and engineering design 07 p1239 A70-20360
- Structural design analysis techniques for one, two and three dimensional continua, discussing various problem solving methods 07 p1417 A70-20361
- Automatic system of kinematic analysis /ASKA/, based on matrix displacement finite element method, applied to structural strains calculations 07 p1417 A70-20362
- Mo effect on structure and properties of Ni-Al-Nb system alloys in gamma and gamma prime solid solutions range, discussing high temperature strength 08 p1514 A70-20549
- Deformable bodies subjected to given load using method of equivalences 08 p1584 A70-20589
- Soviet book on motion of guided rockets in space covering aerodynamic and structural aspects, stabilized and disturbed rocket motion, etc 08 p1582 A70-20756
- Asymptotic analysis for axisymmetric buckling of axially compressed short cylindrical shells with free edges, using Batterman method 08 p1593 A70-21620
- Semiinfinite elastic strip supporting thin heavy beam using Airy stress function and Laplace transform, with boundary conditions expressed as Fourier series 08 p1594 A70-21768
- Structural analysis of Titan 3 Stage 2 ablative nozzle extension made of composite material 08 p1595 A70-21910
- Structural analysis of boron filament-epoxy composite laminate tubes for use as spacecraft long column members 08 p1595 A70-21911
- Matrix decomposition and full release methods for substructure analysis 09 p1770 A70-22258
- Microhardness method for property changes in structural materials during sequential cyclic loading,

discussing material identification, statistical fatigue theory, fine structure effects, etc

09 p1701 A70-22299

Multispan horizontally curved beams natural frequencies determination illustrated by developing frequency equation

09 p1770 A70-22388

Rigid rectangular box with supported flexible wall analyzed for internal acoustostructural mode coupling factors and corresponding modal average radiation efficiency

09 p1770 A70-22393

Soviet collection of papers on control mechanics and processes, computational mathematics

09 p1772 A70-22532

Axisymmetric thermal stress state in bodies of revolution studied by successive approximation algorithm for digital computer

09 p1778 A70-23088

Dynamic stresses during abrupt temperature changes of medium, showing internal stress waves amplitude increasability by suitable internal stress source selection

09 p1778 A70-23089

Additive elements effect on structure and properties of sintered powder Al-Cr and Al-Fe alloys obtained by atomization method, analyzing homogeneity

09 p1707 A70-23124

Soviet book on creep of structural elements at high temperature noting metals, concrete and polymer materials, buckling, variety of structural elements and creep resistance

09 p1781 A70-23266

Elasticity theory two dimensional problem solution for circular segment in polar coordinates, applying Love symbolic notation and Prokopov minimum potential energy principle

09 p1782 A70-23291

Titanium sponge secondary structure obtained by magnesiothermal reduction of concentrated Ti-containing chloride melts, discussing temperature effect on porosity

09 p1709 A70-23783

Acoustic impact technique (AIT) for aerospace structures nondestructive testing, describing theory, instrumentation and applications

10 p1894 A70-24175

Concorde SST aerodynamic, structural and thermal analysis and simulation using computers

10 p1849 A70-24382

Plate bending triangular finite element for shell structure analysis, considering displacement functions, stiffness matrix and load vector

10 p1957 A70-24482

Membrane deformations in second order rotating surfaces with positive Gaussian curvature investigated for external couple loaded spherical shells

10 p1958 A70-24515

Photogrammetry methods for experimental structural mechanics, describing Balplex 525 Plotter camera system, image measurement and displacement vector computation

10 p1827 A70-24736

Dynamic characteristics of structures measured, using digital computer to analyze transient data from frequency sweep tests

10 p1961 A70-25059

Structural detail in transparent object through holographic measurement of scattered monochromatic light, noting similarity to crystal structure reconstruction in X ray diffraction experiments

11 p2048 A70-25360

Optical filtering applied to moire method for measuring small structural strains

11 p2131 A70-25595

Aircraft design structural development and substantiation utilizing computer analysis and testing [SAE PAPER 700216]

11 p2134 A70-25888

Complex redundant structures matrix analysis by substructure approach, obtaining elastic properties of system by subdivision and synthesis [SAE PAPER 700217]

11 p2134 A70-25889

Finite element matrix structural analysis by direct stiffness method and use of computers, considering thin wall box beams [SAE PAPER 700218]

11 p2134 A70-25890

Elastic properties determined for reinforced composite material with hollow spherical inclusions embedded in matrix

11 p2136 A70-26083

Membrane theory for thin single layer orthotropic cylindrical shells experiencing harmonic axisymmetric motion

11 p2136 A70-26084

Continually changing residual stress patterns effect defined for predicting cumulative damage in structural fatigue

11 p2137 A70-26090

Energy principle providing upper bounds on plastic deformation in elastoplastic structures subjected to blast loading

11 p2144 A70-26670

Materials fatigue lifetime estimation under irregular loads by simultaneous use of random programming for testing machines and computing equipment

12 p2315 A70-26873

Lumped linear model parameters determined from dynamic test data on mode shapes and frequencies for approximating distributed elastic structure

12 p2317 A70-27122

Structures, structural mechanics and materials - AIAA-ASME Conference, Denver, April 1970

12 p2317 A70-27126

Two dimensional structures large strain elastoplastic analysis by finite element method, using variational principles to derive equilibrium equations

12 p2320 A70-27148

Tension rays and load transfer from compact member via wrinkled membrane determined by variational technique using maximum strain energy

12 p2322 A70-27225

Supersonic flutter solutions using finite elements, analyzing rectangular plate bending elements, square simply supported and clamped panels, low aspect ratio configurations, etc

12 p2327 A70-27823

Composite spherically aeolotropic sphere with isotropic core, analyzing stress concentration during twisting

12 p2327 A70-27836

Circular arch finite element solutions compared for convergence rates

12 p2327 A70-27838

Fiber diameter effects on metal matrix composites strength from proposed model

12 p2329 A70-28370

Rotating shaft model with slight curvature for estimating maximum bending moment through Fourier series analysis

13 p2416 A70-28372

Kamchatka regions volcanic deposits structural and mechanical characteristics compared with lunar soil characteristics

13 p2485 A70-28465

Viscoelastic plate crack growth analysis within continuum mechanics framework as analog to Griffith problem

13 p2510 A70-28671

Secondary crack growth direction from preexisting crack under longitudinal shear loading

13 p2510 A70-28674

Buckling, postbuckling and limit analysis of symmetric elastic structure subjected to increasing loads

13 p2511 A70-28737

Saint Venant principle in linear isotropic viscoelasticity of Toupin estimates for body of arbitrary shape to allow integration by parts

13 p2513 A70-28990

Eccentrically stiffened orthotropic cylinders with intermittently attached stiffeners under bending and axial load, analyzing instability and buckling

13 p2518 A70-29966

Arbitrary planform plates with edge clamping and elastic beam spanwise support using Green function

14 p2655 A70-30182

Mechanics of solid structures including shells and beams, considering three dimensional behavior laws in plasticity and creep

14 p2656 A70-30294

Unstable Ekman boundary layer vortex structure analysis by generating similar flow in liquid filled rotating cylinder

14 p2604 A70-30545

Turbulent boundary layer loading function for use with finite element structural analysis system applied to elastic aircraft structures random vibration [AIAA PAPER 69-20]

14 p2658 A70-30853

Stiffness matrices of three dimensional finite elements, considering tetrahedron, hexahedron and nodal configurations

14 p2659 A70-31127

Stress and deflection of nonisotropic assembled bar and plate composite structures, using computerized matrix displacement method

14 p2660 A70-31133

Finite element method applications to structural analysis problems involving geometric and material nonlinearities

14 p2660 A70-31134

Stress concentration in flat rectangular and skew panels with circular holes from photoelastic verification of direct stiffness method [SESA PAPER 1633]

15 p2820 A70-32303

Stress-strain vector for straight bar of constant or stepwise cross section, using initial parameter matrix method

15 p2822 A70-32363

Monograph on elastic stability covering eigenvalues of matrix series, stress-strain state calculation, critical ratio derivation, etc

15 p2823 A70-32550

Book on structural mechanics with introduction to elasticity and plasticity

16 p2987 A70-32915

One dimensional controlled plants structure identification with mathematical model composed of

aperiodic nonlinear and delay components connected in series

16 p2883 A70-33235

Arbitrary shaped shell structures analysis by finite element method, using curved shell elements approach

16 p2988 A70-33289

Glass fiber reinforced resin structures evaluation by photographic analysis using visual, macrographic, stereomicroscopic, and scanning electron microscope methods

16 p2908 A70-33361

Composite beam testing concepts and interpretation under three and four point loading, noting shear deformation effect

16 p2989 A70-33385

Closed form difference equations for finite element models in structural mechanics, noting plate and grid applications

16 p2990 A70-33672

Nonlinear structural analysis of Mariner spacecraft solar panel, using damper test characteristics

17 p3022 A70-34769

Finite element formulation for large strain and displacement problems with emphasis on elastic-plastic behavior in metals

17 p3184 A70-34905

Nonlinear vibrations of beam harmonically excited by periodic motion of supporting base, using Galerkin method

17 p3185 A70-34962

Linear compressibility assumption incorporated into third order multiple integral representation of nonlinear creep of polyurethane, reducing time independent kernel functions

17 p3186 A70-34972

Holographic measurement of transient behavior of structures under unsteady or impulsive loading, using pulsed lasers

17 p3085 A70-35008

Shakedown theory of elastic-plastic structures under time dependent loadings

17 p3188 A70-35191

German monograph on stress and displacement in plane elastic circular rings, disk strips and wedges, considering single load distributions

17 p3189 A70-35370

Structural fatigue testing by computer control of random force cycles

17 p3062 A70-35505

High temperature radial turbine design for small gas turbine engines, discussing aerodynamic, structure and thermal analyses

18 p3301 A70-36450

Buckling problem numerical analysis by nonlinear programming and minimum energy formulation

18 p3339 A70-36495

Discrete element stress and displacement analysis of elastoplastic plates

18 p3342 A70-36686

Late-type barred spiral galaxies structure and dynamics with asymmetric mass distribution, using model consisting of small prolate spheroid displaced from disk center

18 p3331 A70-37194

Stress relaxation in rings and rods, discussing errors possible in data correlation

19 p3535 A70-37342

Bent plates strain analysis using in-plane moire method for small and large deflections

19 p3535 A70-37383

Damped linearly tapered cantilever beam elastically restrained against rotation at wall, analyzing displacement under general initial and distributed load conditions

19 p3539 A70-37802

Book on extremum principles covering energy methods of static and dynamic structural analysis

19 p3541 A70-37976

Boundary value problems for elastic sphere, extending Kelvin general solution of Cauchy equations

19 p3545 A70-38333

Book on structural analysis by finite difference calculus covering elastic and elastoplastic states, vibration and buckling of beams, gridworks, plates and shells

19 p3548 A70-38599

Integrated structural analysis for reliability prediction of solid propellant rocket motors

19 p3489 A70-38844

Soviet book on matrix theory application to problem solutions in structural mechanics covering computer techniques, internal forces, initial parameter method, displacements, etc

20 p3719 A70-39600

Soviet papers on mechanics of solid deformed body covering elasticity and plasticity theories, shell stability, eigenvalue problems, etc

20 p3722 A70-39851

Thin plane bars elasticity theory, constructing integrals of equations by asymptotic series expansion

20 p3726 A70-39881

Finite element stiffness matrix technique for composite structures, discussing airplane component design program

20 p3730 A70-40040

Composites potential structural performance, determining mechanical properties for fiber and matrix materials and unidirectional and isotropic composites in cylinders and box beams

20 p3651 A70-40042

Optimum automatic selection of redundancies, discussing weighting and pivot choice and rigid element incorporation

20 p3732 A70-40264

Finite deflection discrete element analysis of sandwich plates and cylindrical shells with unbalanced laminated faces

20 p3732 A70-40268

Plate structural analysis by finite element method, obtaining geometric continuity by additional displacements and forces at corner nodes

21 p3932 A70-40553

Structural stability analysis by matrix decomposition and iteration, extending to structures with nearly equal critical loads

21 p3934 A70-40888

Decelerator fabric elastic constants for structural analyses using generalized Hooke's law [AIAA PAPER 70-1179]

21 p3843 A70-41834

Structural and environmental design criteria for acoustical duct-lining materials in turbofan noise suppression

22 p4089 A70-42531

Nonlinear heat transport in structural elements due to radiative transfer, analyzing temperature field dynamics

22 p4125 A70-43360

Boundary value problems of elasticity for layer and strip with arbitrary inhomogeneity along thickness

22 p4120 A70-43712

Minimum weight structural design within given stress limits due to different loads or natural frequency vibrations, using finite element method for structural analysis

23 p4268 A70-44226

Aircraft structures acoustic fatigue testing, discussing test facilities, environment simulation, etc

23 p4269 A70-44329

Digital computer codes for production finite element structural analysis, discussing input, output and engineering details

23 p4270 A70-44701

Asymptotic and computer methods interaction in thin walled shells structural analysis and design, considering pressure vessels, cone vibration and dynamic loads

23 p4271 A70-44703

Thin walled shells structural vibration, buckling and stress analysis by computer methods, discussing shell theory and design

23 p4271 A70-44704

Elastic continua structural optimization analysis decisions for maximizing calculation accuracy, insuring efficient complex numerical analyses

23 p4271 A70-44706

General purpose computer programs for shell structural analysis, using finite element modeling and displacement methods

23 p4271 A70-44707

Rectangular and triangular grids with variably sized mesh elements for finite difference analysis of shell structures

23 p4272 A70-44709

Thin shell structural analysis by doubly curved arbitrary quadrilateral finite element, using Kirchhoff theory and cubic polynomial for membrane displacements

23 p4272 A70-44711

Mixed formulations for finite element shell analysis based on flat and curved elements

23 p4272 A70-44713

Shell analysis based on discretization into one, two and three dimensional configurations, comparing finite difference, numerical integration and finite element methods

23 p4272 A70-44715

Finite element structural analysis /FESTRAN/ computer program predicting static structural response of plate and shell structures

23 p4273 A70-44717

Nonlinear material and geometric behavior of shell structures studied by Eulerian and Lagrangian approaches

23 p4273 A70-44718

Integration operators for transient structural response in qualification tests for internal components of dynamically loaded structures

23 p4273 A70-44719

Second approximation for limit loads due to imperfection sensitivity of axisymmetric elastic shell structures with unique harmonic buckling modes

23 p4273 A70-44720

Computer program for geometrical nonlinear static and dynamic structural analysis of arbitrarily loaded shells of revolution

23 p4273 A70-44724

Approximation method for large deflection analysis of impulsively loaded rigid plastic circular plates and symmetric shells

23 p4275 A70-44943

Gradient iterative solution of large algebraic systems arising from finite element discretization, using computer methods

24 p4419 A70-45153

Numerical solutions of three dimensional static elasticity, using physical analogies

24 p4419 A70-45195

Numerical integration of equations of motion from finite element analysis in structural mechanics, using computer program

24 p4420 A70-45278

Bending vibrations of propeller blades calculated by successive approximation

24 p4422 A70-45300

Polyvinyl chloride /Novodur/ mechanical properties application to structural model testing

24 p4367 A70-45445

Al alloys structural analysis using electron diffraction pattern techniques

24 p4360 A70-45737

Rheology and structure formation in three dimensional and two dimensional bulk phase and pigmented systems in surface layers and films, including paints and varnishes

24 p4368 A70-46141

STRUCTURAL BEAMS

U BEAMS [SUPPORTS]

STRUCTURAL DESIGN

NT PRESSURE VESSEL DESIGN

60 cm intermittent blowdown type trisomic wind tunnel, discussing main parts basic dimensions and characteristics determination method, detailing design and construction

01 p0055 A70-10148

Concorde aircraft structural acoustics and design problems, discussing noise, fatigue and testing techniques and facilities

01 p0199 A70-10288

Radiator selection for manned spacecraft, considering thermal coating degradation, structural design, micrometeorite protection, plume impingement, reliability and fabrication [AIAA PAPER 69-1070]

01 p0215 A70-10631

Buoyant Venus station using superpressure balloon, discussing requirements for structural design and station position tracking capability [AIAA PAPER 69-1068]

01 p0195 A70-10633

Optimal structural design including service requirements on strength, buckling and natural frequency stated as optimal control problem

01 p0207 A70-11158

Book on vibrational motions of straight and curved shafts, covering dynamic analysis for noncircular cross sections, applications to machine tools and vehicles design, etc

01 p0209 A70-11378

Aerospace structures design - Conference, Seattle, Washington, August 1969

02 p0385 A70-11931

Structural design experience in developing large area Be solar array for Mars flyby mission, describing configurations, requirements, material and manufacturing

02 p0228 A70-11935

F-8 wing service life extension design techniques, emphasizing fatigue design curves and procedures

02 p0386 A70-11939

Structural design and fabrication of load bearing Ta alloy radiation cooled elevon control surface for high L/D hypersonic flight vehicle

02 p0306 A70-11941

Structural support strut design for cryogenic propellant tanks to optimize load carrying capability and heat transfer characteristics

02 p0306 A70-11942

Automated structural design program to treat stress, displacement, gauge and cross sectional constraints, discussing applications to aircraft structures

02 p0386 A70-11944

Beaded-doubler reinforced skin design concept for Improved HAWK Missile wing, considering compression stress, weight, cost and field service characteristics

02 p0380 A70-11946

Attachment loads and beam bending moments design curves for linear and right angle fittings on honeycomb inserts to determine internal loading

02 p0386 A70-11949

Boron-polyimide composite reinforced Ti fuselage stringers design and test program for SST

02 p0387 A70-11950

Design allowable curves based on laminate test data for high modulus graphite fiber and resin systems, considering Wagner cantilever beam specimens

02 p0387 A70-11954

Safe-life and fail-safe structural design philosophies in fatigue damage and operating lifetime control

02 p0389 A70-12615

Stress distribution along stud hole threads in Al case, investigating stud design effect using strain gauge on models

03 p0585 A70-12962

Momentless design of composite plate and shell structures with variable elastic constants based on loading and shape requirements

03 p0586 A70-13112

Rigid and flexible pavements response to jumbo jets load using elastic theory

03 p0462 A70-13175

Rational design of structurally anisotropic plane multilayer plates with weak binder, suggesting strengthening fibers orientation in internal stresses direction

03 p0516 A70-13379

Two seater hovercraft development, considering lift system, fan, transmission and structural designs and construction steps to keep within automobile cost range

03 p0414 A70-14148

Book on stress analysis for designers covering stress types and calculation, specimen geometry, structural fatigue and stability, etc

03 p0600 A70-14307

Al fasteners design guidelines including material forming capabilities, cost consideration, applications, etc

04 p0697 A70-14722

Pontyagin principle applied to minimum structural weight design problem in optimal control theory with state and control inequality constraints [ASME PAPER 69-WA/AUT-1]

04 p0769 A70-14832

Rectangular waffle plates minimum-weight design efficiency with multiple rib sizes in stiffening direction compared to honeycomb core sandwich construction

04 p0777 A70-15526

Structural design of boron/epoxy front housing for T-56 turboprop reduction gear case achieving reduced weight and increased stiffness

05 p0853 A70-15837

Honeycomb and sandwich construction design, discussing optimal material selection, filament wound technology, panels fabrication, destructive and non-destructive test methods, etc

05 p0941 A70-16616

Clean room design problems concerning dampers, high pressure blowers, humidifiers, filters, etc

05 p0808 A70-16709

Tensile tests facility design for wide temperature ranges with loading system to maintain constant strain rate up to failure

05 p0830 A70-17072

Galerkin method to formulate buckling problem of homogeneous and fiber reinforced anisotropic plates simply supported under uniform membrane loads

06 p1160 A70-17313

Buckling-critical composite shell structures, describing pseudo T-rib stiffening and integrated composite design concepts [AIAA PAPER 70-101]

06 p1171 A70-18235

Design concept, materials application and performance characteristics of high temperature fasteners [AIME PAPER F-69-6]

07 p1290 A70-18811

Ring seal elements structural parameters influence on fluid leakage at various shaft speeds and fluid pressures

07 p1294 A70-19123

Minimum weight design of elastic sandwich beams with deflection constraints using n-dimensional space of discretized bending stiffness

07 p1407 A70-19358

Soviet book on structures design for stability at high temperatures with large gradients, discussing thermoelasticity, thermoplasticity and creep equations for shells, plates, etc

07 p1409 A70-19601

Sizing and design of large vessels of fiberglass reinforced composites based on minimum cost

07 p1409 A70-19757

Fiberglass plastics structure safety design using time dependent limiting states with wear allowance

07 p1410 A70-19761

Reinforced plastics underframe design based on hooks law, noting middle layer loaded laminates and shell advantages

07 p1410 A70-19762

Structural material selection for thermal shock conditions, deriving index from parameters governing solutions in thermoelasticity

07 p1413 A70-20002

Analytical structural design reliability, discussing static test failures of wings, fuselage, horizontal and vertical stabilizer and landing gear

07 p1417 A70-20400

Hawker Siddeley Harrier structural design, power plant, rear fuselage, wing tail unit structures, undercarriage features, weight control, fatigue testing, etc

08 p1435 A70-20620

Metal adhesive joints strength and suitable dimensions determination, presenting parameter relations for design

08 p1584 A70-20893

Spaced damping reducing structural response to vibration, discussing efficiency, design flexibility and weight addition

08 p1507 A70-21269

Ti alloys failure-safe design developing procedures for incorporation of stress-corrosion cracking characterizations into ratio analysis diagram system 08 p1519 A70-21456

Fibrous reinforced composites influence in aircraft structural design based on DOD industry development programs, investigating interlaminar shear 08 p1595 A70-21899

Design allowables and factors of safety for filamentary composite materials, discussing reliability 08 p1595 A70-21900

Seadrome advantages and structural design concepts, describing floating runways, breakwaters, noise reduction, building costs, etc 09 p1655 A70-22243

Minimum weight design for two dimensional bodies with given load system determined by variational method 09 p1771 A70-22400

Soviet book on rocket structure mechanics covering acting loads and selection of tanks, stage segments, nose section and propulsion units 09 p1772 A70-22527

Limit and shakedown loads in creep range investigated on sheet rolled aluminum at room temperature for structural design applications 09 p1775 A70-22591

Aeroelasticity problems, discussing unrestrained flexible structures design, nonconservative systems stability, biomechanics, etc 09 p1777 A70-22972

Prestressing in minimum weight design of statically indeterminate structures 09 p1781 A70-23231

Ribs reinforced shells of revolution designs calculations by approximate numerical method, considering surface geometry and cyclic temperature loads effect 09 p1784 A70-23589

Fracture mechanics applications in stress analysis and structural design, considering rocket motor case failure 09 p1786 A70-23799

Optimal trusses design, considering minimal volume/weight/ and elastoplastic stability in compressed and stretched bars 10 p1958 A70-24514

Minimum weight design for symmetrically stiffened cylindrical shells under compression based on linear orthotropic stability theory 10 p1958 A70-24560

Iterative numerical method for determining optimal mass distribution in complex frameworks, maintaining dynamic response level 10 p1960 A70-25053

Experimental stress analysis and influence on design - Conference, Cambridge, England, April 1970 11 p2130 A70-25584

Compressive stress critical moment induced instability and weakening incorporated in thin walled beam design 11 p2131 A70-25590

Missile radome design optimization, considering compromise between conflicting aerodynamic, thermal and structural aspects 11 p2134 A70-25862

Nonsteady flow past duct junctures, investigating ventilation system of underground bomb shelter for blast wave passage prevention 11 p2036 A70-26139

Thin shell design for minimum bending stresses and transverse shear for composite materials with low interlaminar shear strength 11 p2141 A70-26490

Structural design for allowable plastic deformation under dynamic loads, deriving finite element representation of elastic-plastic plane frame beam 12 p2317 A70-27117

Supersonic aerial target wing synthesis using sandwich construction with graphite-epoxy laminate skins bonded to Al honeycomb, achieving significant weight reduction 12 p2160 A70-27118

Experimental stress analyses for aircraft design enhancing structural fatigue strength, using S-N diagrams and photoelastic models 12 p2318 A70-27128

Waffle plate structures least weight design under uniaxial, biaxial and multiple combined loading with various stiffening patterns, investigating pyramiding concept 12 p2318 A70-27133

Wing and empennage structures automated fully stressed design procedures, discussing application to supersonic aircraft stabilizer 12 p2319 A70-27136

Automated optimum structural design by variable step direct search algorithm, noting application to stiffened cylindrical shells 12 p2319 A70-27138

Stiffened fiber composite cylindrical shells minimum weight design, discussing configuration and material parameters 12 p2319 A70-27139

Cylindrical shells design under axially compressed loads by elastic stability analysis, predicting critical loads 12 p2320 A70-27142

Complex airframe design for economic and safe operation and long life using fatigue and fracture mechanics [AIAA PAPER 70-512] 12 p2324 A70-27466

Radio telescope construction, discussing early planning decisions, site selection, structural compensation for built-in elastic deformation, foundation, telescope mount, etc 12 p2207 A70-27578

Design parameters for optimum heavily loaded single rotation ducted fan characterized by ultimate wake vortex system [AIAA PAPER 69-222] 12 p2157 A70-28083

Elastomeric liner material for missile launch system design, developing bowed-knotted strut for compression-deflection characteristics 13 p2513 A70-29256

Minimum weight structural member size and configuration simultaneous optimization using computer program 13 p2516 A70-29550

Minimum weight design for complex structures subject to frequency constraint using finite element method and computer program 13 p2517 A70-29965

Preliminary aircraft wing design for gusts or landing impacts inducing vibrations, inertia effects and dynamic overloads 14 p2655 A70-30177

Space design, considering problems due to weightlessness, vacuum, thermal effects, micrometeorite, cosmic forces, etc 14 p2656 A70-30301

Optimum overlap design of thin walled tubular extendible spacecraft structures under solar heating in zero-g environment 14 p2657 A70-30762

Structural components strength calculation with design required functional notches, noting stress limit for ductile materials under static loads 15 p2815 A70-31874

Optimal design for composite material structure, considering internal and external reinforcement 15 p2816 A70-32005

Structural fatigue failure analysis and design, applying local stress-strain approach [ASME PAPER 70-DE-24] 16 p2989 A70-33424

Dynamic structures design optimization subject to shock spectrum, describing conversational type computer program [ASME PAPER 70-DE-28] 16 p2989 A70-33501

Reinforced polymer composites design for aircraft structures [ASME PAPER 70-DE-67] 16 p2939 A70-33518

Metallic diaphragms design, fabrication and testing for cryogenic fluid and positive expulsion systems [AIAA PAPER 70-683] 16 p2918 A70-33582

Optimal design of structures with constraints on strength and natural frequency, developing steepest descent boundary value method 16 p2991 A70-33854

Compression spring mechanisms for separation of spacecraft and shrouds, summarizing design characteristics 16 p2921 A70-34116

Mariner 4 spacecraft structural dampers construction and performance 16 p2922 A70-34120

Solar power panel orientation servomechanism using passive elements without power consumption 16 p2846 A70-34130

Flow control valve without moving parts used in ATS A and D, describing design, operation and theoretical performance 16 p2846 A70-34132

Spacecraft boom design and performance, including Russian spacecraft photographs 16 p2985 A70-34137

Space shuttle systems structural design and thermal protection technology, stressing hardware reliability and reusability 16 p2986 A70-34227

Mathematical techniques for optimal design of single purpose structures under dynamic deflection 17 p3182 A70-34544

Anisotropic and laminated cylindrical shells geometric design for reduction of elastic stress gradients to predetermined limit 17 p3182 A70-34559

Aerodynamic and structural considerations in prop/rotor design for tilt-rotor aircraft, discussing blade twist effect on cruise efficiency and figure of merit 17 p3014 A70-34719

Space vehicle optimal design based on reliability analysis, taking into account cost of materials strength tests [JPL-TR-32-1496] 17 p3188 A70-35224

Wide body commercial jet transport structural design considerations applied to DC 10 aircraft [AIAA PAPER 70-895] 17 p3193 A70-35812

Extensible wing flap system for cargo aircraft, discussing structural design details and advantages [AIAA PAPER 70-911] 17 p3020 A70-35823

Optimal design of elastic sandwich, solid beam and plate structures under dynamic harmonically varying loads 18 p3336 A70-36220

Flutter design charts for isotropic panels stressed to verge of buckling for tropical values of structural damping 18 p3338 A70-36446

Soviet book on wing structures analytical design methods covering thin supersonic wings, mass distribution, aerodynamic characteristics, etc 18 p3344 A70-37025

Minimum weight design for structures with stability constraint by nonlinear programming 18 p3344 A70-37068

Optimal rectangular plates with adaptability, using convex programming 19 p3535 A70-37344

Pivoted plane pad bearings, calculating design variables from inner products of two vectors and Rayleigh-Ritz matrix function [ASME PAPER 69-LUB-1] 19 p3435 A70-37612

Minimum weight design of sandwich beams with elementwise constant cross section for prescribed compliances under alternative loads 19 p3543 A70-38303

Classical reliability concept generalization for subjective and objective factors in structural engineering design, obtaining risk of failure 19 p3443 A70-38849

Structural design load factors statistical evaluation for element optimal reliability 19 p3550 A70-38850

Papers on design and materials, discussing alloys for aircraft structures, stress-rupture life of Ni base alloy, single crystal structures, etc 20 p3648 A70-39412

Structural fatigue design loads computation for fighter aircraft using multivariable load environment model from oscillograph recorded multichannel aircraft response data [AIAA PAPER 70-948] 20 p3719 A70-39579

Buoyant Venus station using superpressure balloon, discussing requirements for structural design and station position tracking capability 20 p3715 A70-39677

Filamentary composite materials for space vehicles structural design, noting mass reduction, strength, foldability, formability, etc 20 p3656 A70-40030

Cylindrical or tapered composite shell structures optimal design with closed circular or elliptical cross section under combined bending and torsional loads 20 p3730 A70-40043

Structural synthesis concept in optimal design of composite material structural systems, considering failure modes of rectangular fiber composite plate 20 p3731 A70-40044

Thin cylindrical shells optimum design with symmetrically paired spiral type stiffeners under uniform axial compressible load and lateral pressure 20 p3732 A70-40287

Design management by critical element objectives, correlating various engineering functions in production process [SAWE PAPER 868] 20 p3741 A70-40352

Shape factors for weight prediction and design optimization of structural members requiring given area moment of inertia [SAWE PAPER 828] 20 p3732 A70-40354

Structural weight design optimization by computer aided geometrical programming technique [SAWE PAPER 822] 20 p3733 A70-40357

Helicopter mechanical power transmission design, describing gearing, shaft bending, bearings, lubrication, weight factors, etc [SAWE PAPER 844] 20 p3563 A70-40367

Mathematical techniques for optimal design of single purpose structures under dynamic deflection 20 p3733 A70-40381

Elastic beams optimal design for multipurpose loading, considering compliance and minimum cross section constraints 20 p3733 A70-40382

Thermoelectric outer planet spacecraft /TOPS/ structural problems associated with high gain antenna and electronic equipment 21 p3930 A70-41803

Design component size index as function of various system demands, using Monte Carlo method 21 p3846 A70-41870

Weight-optimal sandwich beam design for given static deflection, using energy approach 22 p4113 A70-42535

Canadair CL-84 V/STOL aircraft flight characteristics and structural design 23 p4137 A70-44017

V/STOL aircraft landing performance, discussing relationships between approach speeds, rates of descent, structural criteria and weight penalties [ICAS PAPER 70-53] 23 p4139 A70-44149

Structural optimization of designs with requirements including restrictions on structure dynamic response and characteristics 23 p4270 A70-44562

Optimal design of minimum weight bar and beam structures under static loads, comparing computer time with nonlinear programming methods 23 p4271 A70-44702

Asymptotic and computer methods interaction in thin walled shells structural analysis and design, considering pressure vessels, cone vibration and dynamic loads 23 p4271 A70-44703

Thin walled shells structural vibration, buckling and stress analysis by computer methods, discussing shell theory and design 23 p4271 A70-44704

Elastic circular sandwich beams optimal design for minimum compliance and given weight, considering rings and semicircular arches 24 p4420 A70-45276

Spacecraft astronomical instrument structural design, examining aging, vibration and temperature distribution deformations and optical surface contamination 24 p4339 A70-45823

Space shuttle structural design concepts and fabrication, tabulating structural and heat shield materials [SAE PAPER 700768] 24 p4415 A70-45867

Bonded honeycomb sandwich structure fastening techniques in aerospace design, noting application to aircraft and spacecraft structures [SAE PAPER 700850] 24 p4425 A70-45882

STRUCTURAL DYNAMICS

U DYNAMIC STRUCTURAL ANALYSIS

STRUCTURAL ENGINEERING

Commercial aircraft design, considering structural allowances effect on economics, using shear web analysis program as example 02 p0225 A70-11947

Two dimensional structural analysis of engineering systems by computer graphics, outlining discrete element representation 02 p0388 A70-12477

Structural reinforcement for existing airport pavements, discussing construction procedures 03 p0462 A70-13174

Structural material selection for thermal shock conditions, deriving index from parameters governing solutions in thermoelasticity 07 p1413 A70-20002

Structural synthesis of functional control systems represented by first order differential equations, determining hypersurface 08 p1479 A70-20871

Computers impact on engineering science and design, detailing digital computers use in aerodynamics, structures and aeroelasticity 08 p1466 A70-21030

Civil engineering research needs in air transportation, discussing information sources and processing and industry estimates of manpower, facilities and funding 08 p1481 A70-21305

Book on torsion emphasizing beam stressed state calculation and civil engineering problems 13 p2512 A70-28850

Engineering properties and structure of plastics - Conference, New York, May 1970 13 p2438 A70-29251

Size and cost of Al mirror IR photometric telescopes optimized for scientific information acquisition 14 p2586 A70-30896

Finite element methods application in civil engineering - Conference, Vanderbilt University, November 1969 14 p2658 A70-31126

Book on engineering properties of thermoplastics covering strength characteristics, plastic components design, etc 15 p2766 A70-32843

Macaulay method extended for slope and deflection of statically indeterminate beams, rewriting design equations into index notation for computer programming [ASME PAPER 70-DE-2] 16 p2989 A70-33419

Flexural pivots for space structures, describing design, fabrication and applications 16 p2924 A70-34170

Fiberglass reinforced plastics fatigue life, analyzing structural factors role 20 p3655 A70-39891

Composite material engineering problems, discussing tensile, compressive and shear strengths, design approaches, unidirectional properties and substance characterizations 20 p3651 A70-40027

Beryllium use in inertial navigation as stable platform structure and control gyro, discussing physical properties, design concept, fabrication, service, cost and tradeoffs 20 p3639 A70-40451

Space shuttle structural technology for booster and orbiter, discussing hot and cold structure concepts, reentry bodies, military payloads, radiating protective coatings, refractory materials, etc 22 p4111 A70-43516

Materials design and development for engineering applications, discussing relationships and importance of strength, stiffness, weight, toughness and work of fracture 24 p4419 A70-45174

STRUCTURAL FAILURE

Stress criterion for unstable crack propagation from Al alloy sheet tests, examining fracture data for vessels of various geometries and materials [ASME PAPER 69-SESA-2] 01 p0117 A70-10451

Fracture predictions in engineering structures based on small scale tests, materials microstructure, crack initiation and propagation 01 p0121 A70-11159

Polymethylmethacrylate block breakdown under focused pulsed laser radiation in free emission regime, noting light absorption during crack development 02 p0314 A70-12813

Polycrystalline material tensile failure at high temperature, discussing intergranular cracking, shearing, etc 03 p0508 A70-13155

Local buckling and failure of thin walled compression column with supported flanges, analyzing strength reduction by eccentricity 03 p0600 A70-14254

Compression failure of unidirectional fiberglass reinforced plastics 04 p0712 A70-14487

Plastic flow failure of matrix of fiber reinforced composite sheet, discussing plane stress and simple tension [ASME PAPER 69-APM-Z] 04 p0770 A70-14869

Fiberglass reinforced plastics energy dissipation during fatigue failure phases, studying mechanical-to-thermal energy transformation under cyclic strain 04 p0713 A70-15263

Fatigue tests results parametric representation for nickel base alloys tested at various temperatures and times to failure 04 p0707 A70-15264

Stress analysis split method for determining residual strength and fatigue crack life of damaged or initially cracked VTOL structures [AIAA PAPER 69-214] 04 p0624 A70-15395

Delayed failure due to hydrogen embrittlement of structural high strength steels, discussing stress corrosion 04 p0710 A70-15678

Aircraft Ti alloys failure due to stress-induced pseudocorrosion caused by trichloroethylene and Freon noting microstructure, heat treatment and welding effects 04 p0710 A70-15679

Stroboscope lighting system for microstructural examination of fatigue test sample failure 05 p0845 A70-15882

Failure prediction for arbitrary shape flawed pressurized vessels using structural geometry, crack length, ultimate and yield stresses and fracture toughness 05 p0942 A70-16803

Reinforced openings effect on burst strength of ductile circular plates subjected to pressure loads 05 p0943 A70-16810

Unsteady cyclic creep effect on stressed state and margin safety of elements, noting discrepancy of experimental and theoretical characteristics 05 p0866 A70-17030

Bursting speed and mode of high speed rotating disk with rim, boss and blades, noting influence of boss thickness 06 p1129 A70-17129

Fatigue breakdown criteria for elastoplastic materials under cyclic loads, deriving equations as functions of stress-strain states kinetic behavior 06 p1162 A70-17390

Elastoplastic rod systems under repeated variable loads, calculating carrying capacity from plastic failure considerations 06 p1163 A70-17395

Steel elements failure during nonstationary thermal fatigue with varying strain and temperature, discussing linear damage accumulation theory 06 p1163 A70-17397

Damage accumulation and failure of low carbon and low alloy steels subjected to repeated static loading, varying cyclic load frequency 06 p1085 A70-17400

Creep effects on structural failure under low cycle fatigue at high temperatures, noting role of plastic deformation 06 p1164 A70-17409

Energy dissipation patterns of metal fatigue failure during static and cyclic loading applied to untreated and heat treated steel samples 06 p1166 A70-17651

Critical brittleness temperatures of low C steels determined to distinguish main failure types 06 p1166 A70-17655

Gas turbine compensating bellows structural strength, discussing low cycle fatigue test under static loads 06 p1167 A70-17664

Materials fatigue failure ultrasonic early detection by continuous surface wave irradiation 06 p1077 A70-17920

Solid propellant mechanical properties tests, failure and physical deterioration/aging/ 07 p1361 A70-19913

Viscoelastic perfectly plastic ring failure under uniform external pressure characterized by infinite strain rate occurring at finite value of ring deflection 07 p1416 A70-20300

Analytical structural design reliability, discussing static test failures of wings, fuselage, horizontal and vertical stabilizer and landing gear 07 p1417 A70-20400

Ductile flexure location in bent beams and systems with variable cross sections to determine critical load using plasticity theory 08 p1587 A70-21072

Fiber-reinforced composite sheet matrix failure by plastic flow, investigating two ply laminate in simple tension 08 p1592 A70-21471

Compression test data of Al-B composites used for predicting structural element failure 08 p1523 A70-21886

Composite materials fatigue determinations providing curves of stress-strain magnitude vs usable life or time to failure, considering environmental effects in service for design criteria 08 p1531 A70-21895

Brittle failure mechanics application to steels sensitivity to rupture at low temperatures, discussing crack propagation resistance and heat treatment effect on impact toughness 09 p1768 A70-22076

Cyclic heating and thermal stresses effect on fatigue strength and durability of turbine blade alloys and structural elements 09 p1771 A70-22463

Variational principle application to stability in failure mechanics of arbitrary linearly elastic bodies, discussing inertia effect on steady state vibrations of cracked bodies 09 p1771 A70-22465

Shallow rectangular shell panels nonsymmetric nonlinear deflection states computed by finite difference equations iteration, discussing snap-through buckling loads 09 p1780 A70-23209

Failure compression tests of flat rectangular Al alloy panels presented in unitary form, adopting structural load index for solution from weight standpoint 09 p1782 A70-23376

Fracture mechanics applications in stress analysis and structural design, considering rocket motor case failure 09 p1786 A70-23799

Subcritical cracking rate behavior estimation in metallic service structures by linear elastic fracture mechanics 10 p1960 A70-24977

Glass-epoxy composites failure mode dependence on matrix characteristics and fiber orientation, observing flexural strength increase with strain rate 10 p1908 A70-25174

First excursion failure survival probability of randomly excited structures, considering single degree of freedom linear oscillator under Gaussian white noise 12 p2327 A70-27819

Seismic measurements of sonic boom induced ground vibrations for hazard to structures 12 p2227 A70-28078

Rotating disk service life and structural failure under creep, using Tresca yield and maximum stress criterion 13 p2514 A70-29290

Crack initiation and breakdown under thermal stresses of boron nitride containing aluminosilicate 15 p2764 A70-31532

Metallic materials damage accumulation and structural failures due to fatigue, considering surface changes, crack initiation and dislocation pattern 15 p2757 A70-31928

Cylindrical shells with longitudinal rib reinforcements, deriving yield surface from strain mapping and collapse under pressure 15 p2816 A70-32006

Moisture induced failure of glass-resin composites at interface, discussing water adsorption, crack propagation, wet strength and nonsilicate reinforcements 16 p2937 A70-33373

Structural fatigue failure analysis and design, applying local stress-strain approach [ASME PAPER 70-DE-24] 16 p2989 A70-33424

Single phase alpha Ti alloy welds breaking strength, discussing delayed failure and cold cracking with various oxygen and hydrogen contents 17 p3117 A70-34399

Inelastic analysis of unidirectional composite subjected to transverse normal loading, discussing linear

response up to elastic limit and subsequent crack propagation and failure 17 p3182 A70-34557

Linear stress based cumulative damage law for structural component failures 17 p3186 A70-34987

Plastic flow and failure of elastic fiber reinforced composite materials with noninteracting and interacting discontinuities, obtaining stress distribution for various work hardening degrees 17 p3187 A70-34991

Failure prediction for interlaminar shear stress in filament wound rectangular plate 17 p3188 A70-35228

Creep and failure tests for Ti alloys at 500 C, discussing work dissipation during creep process 17 p3126 A70-35714

Steel and cast iron early stage fatigue failure, using photoelastic coatings 17 p3192 A70-35741

Cyclic plastic breakdown of thin cylindrical shell under ring shaped load in temperature field, using linear programming method 18 p3341 A70-36585

Failure of materials under multicycle fatigue, deriving general theory of defects 18 p3341 A70-36586

Carrying capacity of nonshallow rectangular shells, showing corner dependent collapse 19 p3535 A70-37345

Nonuniqueness of collapse load for isotropic frictional material with or without cohesion 19 p3433 A70-37385

Circular sandwich arc subject to central concentrated load and symmetrically applied edge couple, obtaining shakedown interaction curve 19 p3546 A70-38354

Notched sheet failure prediction based on Dugdale crack model, including work hardening and finite width effects, strain fracture criterion and yield failure mechanism 19 p3548 A70-38624

Asymmetric snap-through buckling in cantilevered column restrained at tip by stiff wire, discussing ratio of flexural rigidity to extensional stiffness 19 p3549 A70-38670

Creep and breakdown of thin walled cylindrical shells with circular holes subjected to internal loads at high temperature, discussing time to failure 20 p3721 A70-39777

Structural synthesis concept in optimal design of composite material structural systems, considering failure modes of rectangular fiber composite plate 20 p3731 A70-40044

Aircraft wing box beams bending tests to failure loads, considering crushing pressure, bulkhead flexural deformations, structure initial imperfections and instability phenomena [ICAS PAPER 70-33] 23 p4267 A70-44103

Cylindrical shell stability under off-center compression loads applied to end faces, determining collapse conditions 23 p4268 A70-44169

Plastic postbuckling and imperfection sensitivity of spherical shells under axisymmetric bifurcation 23 p4272 A70-44714

Metal and alloy sheets, investigating deformation and failure under biaxial stretching tensile tests 24 p4358 A70-45240

Aircraft design for low weight, discussing structural failures [AIAA PAPER 70-1232] 24 p4425 A70-45917

Miner rule for cumulative fatigue damage, obtaining upper and lower bounds on load cycle number to failure 24 p4426 A70-46024

STRUCTURAL FATIGUE

U FATIGUE (MATERIALS)

STRUCTURAL FOUNDATIONS

U FOUNDATIONS

STRUCTURAL INFLUENCE COEFFICIENTS

Influence function for thin toroidal shell under uniformly distributed axisymmetric load, determining stresses and displacements in various cross sections 15 p2817 A70-32163

Clamped skew plates influence coefficients, natural vibration frequencies and nodal patterns measurement, comparing to Galerkin method results 16 p2988 A70-33124

Environmental factors effect on composite materials structural performance, using rate theory 20 p3656 A70-40053

STRUCTURAL MATERIALS

U CONSTRUCTION MATERIALS

STRUCTURAL MEMBERS

NT ANISOTROPIC PLATES

NT ANNULAR PLATES

NT BEAMS (SUPPORTS)

NT BOX BEAMS

NT CANTILEVER BEAMS

NT CANTILEVER PLATES

NT CIRCULAR PLATES

NT COLUMNS (SUPPORTS)

NT CORRUGATED PLATES

NT CURVED BEAMS

NT ELASTIC PLATES

NT END PLATES

NT FLAT PLATES

NT GIRDER WEBS

NT I BEAMS

NT LONGERONS

NT MEMBRANE STRUCTURES

NT ORTHOTROPIC PLATES

NT PERFORATED PLATES

NT PLATES (STRUCTURAL MEMBERS)

NT POROUS PLATES

NT RECTANGULAR BEAMS

NT REINFORCED PLATES

NT SKIN (STRUCTURAL MEMBER)

NT STRINGERS

NT STRUTS

NT TAPERED COLUMNS

NT TRUSSES

NT WING PANELS

Scale factor effect on crack development in blanks and structure elements undergoing linear and complex stressed states under cyclic thermal loads 05 p0867 A70-17045

Refractory metal structural elements stress rupture strength in vacuum and inert gas tested up to 2000 K 05 p0829 A70-17071

Boundary conditions effect on natural vibration frequencies of unloaded components and components loaded with concentrated masses, obtaining frequency equations 08 p1584 A70-20698

Adhesive joints design, considering layer type, pipe connections and honeycomb structures for application in aircraft and automotive industries 08 p1585 A70-20894

Composite materials application to structural members, considering bond or adhesive shear strength 08 p1594 A70-21855

Diffusion and electron beam welding combined with forging for cost reduction and production enhancement of titanium structural components [SME PAPER AD-70-735] 12 p2241 A70-27087

Titanium structural element allowable requirements and test programs for SST design 12 p2318 A70-27132

Creep properties of torsion-tension metal members subjected to nonproportionate loading at high temperatures 14 p2656 A70-30637

Steel and copper alloys torsion-tension members under nonproportionate loads, predicting creep behavior [SESA PAPER 1615] 15 p2759 A70-32316

Structural members of isotropic and anisotropic polymers, investigating creep behavior under simple stressed state 17 p3192 A70-35740

Magnetomotive loading of cantilevers, beams and frames, studying dynamic loading of structures 19 p3541 A70-38045

Long structural shape production for titanium and super alloys, discussing rolling, extrusion, drawing, frictionless forming and filler techniques 19 p3437 A70-38420

Strain measurement on filament-wound structural members, incorporating electric resistance wire as strain gage within windings 19 p3550 A70-38719

DC potentiometer for nondestructive tests of structural components, obtaining crack detection, depths and angles and wall thicknesses 24 p4338 A70-45740

STRUCTURAL RELIABILITY

Reliability analysis formulation for statically indeterminate structures, using modified transition probabilities and computer program for systematic failure paths counting 04 p0768 A70-14747

Structure safety in cumulative damage, considering loading as time dependent stochastic process 05 p0937 A70-16369

Minimum weight reliable beams and frames calculation for random loads, using one degree of freedom system to obtain closed form solution 07 p1401 A70-18825

Damage tolerance as design consideration for aircraft safety and reliability, discussing application of failed single principal member concept to airframe construction [AIAA PAPER 69-212] 07 p1417 A70-20401

Structural elements reliability determination simulated by microinhomogeneous polycrystalline medium under thermal stresses and in stationary nonuniform temperature fields 09 p1778 A70-23085

Structural reliability of missile and aircraft solid propellant engines, estimating effect of loads variance, geometrical dimensions and mechanical strength 10 p1930 A70-24294

Fatigue behavior prediction for complex parts and structures using laboratory tests of small specimens 11 p2137 A70-26091

Airframe structural tests in elevated temperature environment by applied load ratios and room temperature static results 12 p2205 A70-27134

Complex airframe design for economic and safe operation and long life using fatigue and fracture mechanics [AIAA PAPER 70-512] 12 p2324 A70-27466

Plastic encapsulated semiconductors reliability test programs with emphasis on accelerated humidity-temperature method 13 p2377 A70-29259

Airframe critical part structural reliability on basis of ultimate static strength test data and extreme gust spectrum and maneuver loads 14 p2658 A70-30852

Safety, microdamages and lifetime of elastic structures under random Poisson pulsed loads 16 p2996 A70-34328

Linear stress based cumulative damage law for structural component failures 17 p3186 A70-34987

Structural reliability testing methods and loads prediction for rotary wing vehicle components, considering AH-56A compound helicopter 19 p3356 A70-38612

Classical reliability concept generalization for subjective and objective factors in structural engineering design, obtaining risk of failure 19 p3443 A70-38849

Failure probability from finite sampling characteristics, emphasizing statistical safety factors to characterize structures strength reliability 20 p3724 A70-39856

Laminated composites time dependent static strength and reliability under uniaxial tension 22 p4119 A70-43678

STRUCTURAL RIGIDITY

U STRUCTURAL STABILITY

STRUCTURAL STABILITY

NT SHELL STABILITY

Structural efficiency of composite tube columns with zero axial coefficient of thermal expansion, discussing three dimensional and planar fiber arrays 01 p0126 A70-10120

Elastic properties of thin curved cylindrical panels with constant mechanical properties subjected to thermal expansion and single face pressure 01 p0201 A70-10943

Liquid metals contact effect on mechanical strength of T shaped graphite specimens at high temperatures in argon atmosphere 01 p0129 A70-11038

Sandwich plates plastic buckling stability under uniaxial compressive loads from compressible theory viewpoint 01 p0204 A70-11137

Stiffeners reinforced rectangular plates parametric stability under dynamic load, deriving equilibrium equations and boundary conditions by averaging stiffener effects 01 p0205 A70-11146

Optimal structural design including service requirements on strength, buckling and natural frequency stated as optimal control problem 01 p0207 A70-11158

Elastic ring reinforced annular plate of uniform thickness, heated nonuniformly along radius, discussing axisymmetric and asymmetric stability losses 01 p0210 A70-11415

Impeller elastic and elastoplastic strength of centrifugal supercharger with curved disks and radial blades, using variational method 01 p0211 A70-11417

Chemical composition of cermet material for radial sealing of high temperature gas turbines, ensuring structural stability and oxidation resistance 01 p0124 A70-11621

Structural qualification testing of experimental tactical communication satellite /TACOM SAT/ 02 p0274 A70-11936

Mathematical model for local postbuckling strength of flat truss core sandwich panels loaded in compression, considering application to Ti structures 02 p0386 A70-11948

Ductile-brittle fracture transition in steel pressure vessels suppressed by utilizing thin laminations 03 p0583 A70-12903

Soviet book on experimental investigation of thin walled structures elastoplastic work with complex reinforcement, outlining test procedures 03 p0585 A70-12985

Monograph on buckling and postbuckling behavior of plates tapered in planform, comparing stability of tapered and rectangular plates 03 p0586 A70-13002

Stability analysis of orthotropically symmetric strip under uniformly distributed compressive forces applied to shorter ends, deriving critical load formula 03 p0590 A70-13402

Infinitesimal deflections of piecewise-regular unfolding scanning surfaces fixed along edge with respect to one point, discussing rigidity 03 p0591 A70-13414

Equivalent rigidity of doubly periodic symmetrically perforated infinite plate strengthened by elastic ring under isotropic tension 03 p0595 A70-13754

Elastoplastic bar stability compressed by tangential force, showing ductility effect on critical parameters, perturbed motion and stability loss process
04 p0767 A70-14484

Stiffener inclination effect on pressurized cylinder instability under pure bending
[ASME PAPER 69-APM-X]
04 p0769 A70-14868

Structural strength under impact loading with allowance for shock waves, comparing various strength calculation methods
04 p0774 A70-15098

Thin walled uniform open bar stability under arbitrary boundary conditions, using Vlasov assumptions and matrix methods
04 p0774 A70-15099

Turbine blade materials resonant vibration resistance criterion dependence on temperature and cyclic and static stresses amplitude
04 p0776 A70-15262

Thin cylindrical circular shell and three layered plate, analyzing vibration and stability due to loads and temperature
05 p0926 A70-15916

Computational procedures for matrix analysis of stability and vibration of thin flat rectangular plates in longitudinal compression
05 p0927 A70-16010

Energy method for analyzing rectangular panels buckling under nonuniform in-plane loading, considering stability under uniform compression
05 p0931 A70-16117

Stability and critical loads of transversally isotropic reinforced plastic annular plates with weak shear resistance under axisymmetrical buckling
05 p0933 A70-16213

Three layer plate of elastic fiber glass reinforced plastic outer layers and metallic plastic filler, studying elastoplastic stability
05 p0934 A70-16218

Three dimensional brittle body limiting axisymmetric stability under tensile stresses and weakened by ring shaped cracks, determining critical tensile loads
05 p0945 A70-16855

Computerized calculations for cylindrical tank bottoms with outlet based on strength analysis, using zero moment theory for surface stability under uniform pressure
05 p0946 A70-16957

Thermal stability of materials and structural elements - Conference, Kiev, Ukrainian SSR, December 1967
05 p0947 A70-17026

Heat resistant plastics stability subject to unilateral heating with allowance for mass removal, obtaining dimensionless stability characteristics for structures design
05 p0874 A70-17066

Fiberglass reinforced plastics load carrying capacity under unsteady unilateral heating described by thermal similarity criteria
05 p0955 A70-17070

Modulus of rigidity and stress-strain state measured in square plate during shear produced by twisting
06 p1060 A70-17132

Prismatic pendularly supported beam load-forced vertical vibrations, critical load amplitude and force pulsation in case of stability loss
06 p1165 A70-17586

Rectangular and nonrectangular anisotropic plate bending and stability analysis by difference- differential technique, allowing for combined freely supported and clamped end conditions
06 p1167 A70-17864

Thin walled glass fiber reinforced plastics beams strength analysis combined with results from elasticity theory of anisotropic bodies
06 p1167 A70-17913

Equilibrium cracks in elastic bodies on basis of atomic interaction law, using Griffith problem to estimate bearing capacity
07 p1400 A70-18666

Precision tungsten alloy tubing manufacture and properties, discussing direct conversion of metal powder to finished tubing with high temperature structural stability
07 p1292 A70-18928

Rotating disk stability relation with stress distribution in plastic deformation of material
07 p1402 A70-19056

Critical slope load calculation for circular elastic embedded and supported arcs under radial and variable force
07 p1404 A70-19136

Finite structural rigidity of statically unbalanced three degree of freedom gyroscope influence on operation, discussing instrument error
07 p1282 A70-19535

Three dimensional nonlinear viscoelastic body stability under triaxial compression, extending results obtained for elastic body
07 p1408 A70-19542

Elastic stability theory applied to equilibrium and stability of discrete continuous structural systems, detailing discrete critical points
07 p1408 A70-19560

Soviet book on structures design for stability at high temperatures with large gradients, discussing thermoelasticity, thermoplasticity and creep equations for shells, plates, etc
07 p1409 A70-19601

Creep rupture and residual tensile strength tests to evaluate long time properties and structural stability of Inconel 718 alloy, performing phase analysis
07 p1310 A70-19731

Boron fiber reinforced composites structure and loading capacity, describing network-like fiber winding technique for light reinforced structures
07 p1318 A70-19771

Stability criterion applied to asymmetric rigid cyclic strains and plastic cyclic strains, considering failure of metals
07 p1315 A70-20182

Stability equations of three layer panels with allowance for rigid filler transverse deformations
07 p1415 A70-20186

Thin walled strip stability, calculating critical force and rotation angles assuming small subcritical strains
07 p1415 A70-20188

Limiting equilibrium of rigid-plastic cylinder subjected to compression by concave stamps
08 p1583 A70-20533

Statistical analysis of model parabolic mirror rigidity on multisupported suspension under symmetrically distributed load represented by mirror weight
08 p1586 A70-21057

Multisupported radially symmetrical suspension systems designs for parabolic antennas, assessing performance in terms of maximum rigidities
08 p1586 A70-21058

Nickel alloy based metal fiber reinforced composites long-time structural stability at high temperatures
08 p1517 A70-21150

Lateral buckling of simply supported uniform diaphragm using slope-deflection equations for orthogonally intersecting beams, prescribing boundary conditions
08 p1589 A70-21244

Optimal inextensional buckling of uniformly loaded simply supported arches with large opening angle
08 p1589 A70-21310

Elastic post stability under longitudinal impact on rigid support, considering loading/unloading phases for calculating shock half wave length and critical rate
08 p1591 A70-21443

Cr-Mo steel strength and structural stability during tubular stress-rupture testing with high pressure hydrogen, discussing welding effect on strengths
08 p1519 A70-21455

Stiffeners inclination effects on instability of pressurized cylinder under bending by Ritz method, considering finite deflection and initial imperfections in strain-displacement relations
08 p1591 A70-21464

Laminated anisotropic rectangular plates of boron-epoxy composite material, studying shear stability by potential energy and Ritz method
08 p1595 A70-21903

Theorem for highest statically admissible multiplier for plates and shells, noting association with stress field satisfying yield equality at all cross sections
08 p1595 A70-21977

Limiting equilibrium of unbounded cracked elastic plate with circular hole, studying crack propagation under compression
09 p1769 A70-22121

Book on sonic boom effects covering shock waves generation and propagation, elastic structures response to dynamic loads, structural damage, etc
09 p1609 A70-22203

Aircraft turbine engines strength and gas dynamic characteristics improved by vibration decrease using elastic elements
09 p1742 A70-22471

Elastic body equilibrium forms bifurcation solution for uniform strain applied to cylindrical rod and shell under compressive strain
09 p1773 A70-22539

Creep and stability of perforated and unperforated turbine disks under operating conditions
09 p1779 A70-23097

Elastic beam stability, natural frequencies and critical forces under longitudinal impact with nonuniform compressing force
09 p1780 A70-23116

Mandrel adhesion and cure shrinkage impact on structural integrity of solid propellant grain
09 p1742 A70-23263

Sandwich plates stability in conducting compressible fluid flow under magnetic field
09 p1785 A70-23621

Flexural rigidity of thin walled beams, analyzing relationship between loads and displacements taking into account Saint Venant torsional resistance
10 p1955 A70-24052

Buckling stability of slender knife-edge suspended rods subjected to compression end loads
10 p1955 A70-24053

Rigid fire-retardant polyurethane foams obtained from phosphonopropionate polyols, discussing physical properties and shelf stability tests
10 p1907 A70-24063

Optimal trusses design, considering minimal volume /weight/ and elastoplastic stability in compressed and stretched bars
10 p1958 A70-24514

Beams stability under flexural stress with periodic intensity variations, deriving differential equation of motion
10 p1960 A70-24973

Equivalent rigidity of doubly periodic symmetrically perforated infinite plate strengthened by elastic ring under isotropic tension
10 p1960 A70-25009

Stability conditions in metal specimens tension tests, considering fcc and bcc metals strain hardening, rate and gradients and temperature dependence
10 p1966 A70-25326

Rectangular sandwich plates stability under combined loads, deriving equations for determining critical loads
11 p2129 A70-25563

Panel flutter theory applied to aeroelastic stability of flat unloaded plates and cylindrical shells
11 p2134 A70-25951

Elastic stability of discrete conservative structures under combined loads
11 p2142 A70-26636

Apollo lunar module structural integrity for lunar landing verified by Monte Carlo dynamic analysis
12 p2312 A70-27114

Sandwich beams elastoplastic stability, determining critical load
12 p2323 A70-27342

Synthetic pyroxenoid stability and crystallography, noting pyroxmangite structure similar to yellow lunar mineral from Mare Tranquillitatis
12 p2226 A70-28022

Fiberglass plastic reinforced high pressure balloons design and fabrication with oblated ellipsoid of revolution, discussing deformability, strength and cyclic loadings resistance
12 p2328 A70-28285

Structural stability of friction welded joint between high temperature low alloy weld metal from CrMoV electrode and high temperature Cr steel
12 p2244 A70-28349

Cantilevered column stability under constant follower load in presence of external damping
13 p2510 A70-28733

Elastic stability of structural systems with generalized coordinates and independent loading parameters associated with critical point
13 p2511 A70-28739

Lateral motions of vertical uniform tubular cantilever conveying fluid, considering oscillatory instability at high flow velocities
13 p2511 A70-28741

Dynamic instability of multirecess hydrostatic journal bearings at critical shaft rotation velocity
13 p2418 A70-28745

Fixed end nonprismatic bar stability in fluid flow, studying form influence on critical flow velocity
13 p2512 A70-28982

Critical equilibrium of plate under omnidirectional tension with radial rectilinear cracks
13 p2515 A70-29429

Contact stresses and radial displacements in circular rings with loaded inner and outer boundaries
13 p2515 A70-29506

Eccentrically stiffened orthotropic cylinders with intermittently attached stiffeners under bending and axial load, analyzing instability and buckling
13 p2518 A70-29966

Structural components strength calculation with design required functional notches, noting stress limit for ductile materials under static loads
15 p2815 A70-31874

Boron-epoxy stiffener reinforced metal wings, examining structural efficiency of multiweb beam aluminum cover skins and S stiffened panels
16 p2994 A70-34230

Ti alloys systems physical properties and structural phase stability, discussing electronic Fermi state density variation
17 p3114 A70-34376

Creep resistant Ti alloys with high temperature strength and stability, comparing tensile data for room temperature and 900 F
17 p3122 A70-34440

Optimum filament orientation for maximum strength in composite with combined normal and shear stresses
17 p3183 A70-34563

Displacement bounding principle for finitely deforming rigid plastic structures exhibiting geometric stability, with application to cylindrical shell
17 p3184 A70-34906

Structural stability in tension and strength tests of thin walled tubes at various stress and strain intensities, noting dependence on stress-strain state type
17 p3192 A70-35713

Kinetic instability of elastic cantilever beam under excitation by rotating masses, relating bending and torsional vibrations to masses angular velocity
18 p3334 A70-35960

Mass distribution role in stability theory of rods under nonconservative buckling load
18 p3335 A70-35961

Elastic continuum conducting heat under general loads, investigating stability thermodynamics- Liapunov criterion relations
18 p3337 A70-36336

Critical stresses and stability of thin Maxwell plates under random temperature fields
18 p3337 A70-36368

Stability conditions in straight bar, taking into account stress direction changes caused by deformation
18 p3337 A70-36372

Large wheel and tire imperfection effects on nosegear parametric shimmy instability, using Mathieu equation
18 p3213 A70-36455

Infinite Bernoulli-Euler beam transient and steady state response, considering damping, elastic foundation and constant axial load effects
18 p3339 A70-36490

Structure of flexural members, analyzing torsional and lateral stability by finite element method and matrix formulation
18 p3339 A70-36494

Minimum weight design for structures with stability constraint by nonlinear programming
18 p3344 A70-37068

Soviet book on theory of shell and plate type thin walled structural elements stability covering strength, boundary value problems, oscillations, design, etc
19 p3535 A70-37401

Covariance matrix of mean square response in structural systems under white noise
19 p3536 A70-37702

Spacecraft thermal vacuum test installations design and operations for locating spacecraft structural weak points
19 p3400 A70-38297

Continuous one dimensional nonconservative elastic systems under complex forces, examining stability theory
19 p3546 A70-38341

Complementary energy bounding theorem for statically loaded bodies composed of time independent plastic material
19 p3546 A70-38353

Structural fatigue strength model tests for turbine blade root connections, using asymmetric load cycle and working temperature
19 p3547 A70-38433

Elastic-plastic equilibrium bifurcation in geometrically simple frame model with symmetrically loaded beam, comparing characteristics with Shanley uniformly stressed column model
19 p3549 A70-38671

Oxide dispersed Cu alloys preparation by surface oxidation of powders, considering structural stability and stress rupture properties
20 p3646 A70-39103

Anticlastic bending analysis of long narrow plates oscillations and stability based on elastic plates nonlinear theory
20 p3721 A70-39779

Elastic bodies stability criteria, investigating loss under nonconservative forces influence
20 p3722 A70-39785

Compressive force on elastic plate of arbitrary shape related to number of equilibrium forms, using Karman equations
20 p3724 A70-39861

Harmonic forced transverse vibrations effects on rectangular plates with cross braces, deriving motion stability equations
20 p3725 A70-39867

Prestrained laminated media stability, discussing column buckling, standing waves, natural frequencies, wave propagation, stress-strain relations, motion equations and elastic moduli
20 p3731 A70-40049

Clamped circular shallow Al arches stability under impulsive loading, obtaining deflection time history by high speed photography and computerized data reduction
20 p3732 A70-40265

Limit surface behavior equations for structural membrane elements in terms of number, orientation and limit load of constituent fibers by limit theorems
21 p3934 A70-40778

Structural stability analysis by matrix decomposition and iteration, extending to structures with nearly equal critical loads
21 p3934 A70-40888

Book on stability of dynamic systems and solid bodies covering variation equations, Liapunov method and functions, approximations, harmonic balance and applications
21 p3850 A70-41370

Creep and stability of microstructural Al elements under varying temperatures, noting grain boundary migration
21 p3839 A70-41429

Viscous fluid cylinders electromagnetodynamic stability, discussing viscous forces effects
21 p3858 A70-41699

High strength glass for aircraft structures, discussing applications to passenger cabin windows
21 p3843 A70-41891

Earth upper mantle phase change instability, discussing temperature gradient, transformation influence on fluid, olivine-spinel phase flow patterns and tectonics
21 p3820 A70-41895

Elastic stability theory Cosserat surface subjected to conservative nongravitational surface and edge loading
21 p3939 A70-42027

Metastable beta Ti alloy as-quenched microstructure stability with respect to thin foils transformation during electrolytic polishing and bulk specimens during cold rolling
21 p3841 A70-42150

Acoustic emissions method for monitoring structural stability of solid materials assemblies via crack formation and movement detection
22 p4027 A70-42582

Hyperelastic bodies stability subject to conservative configuration dependent forces, formulating surface potential for hydrostatic loading
22 p4114 A70-42695

Cantilever beam optimal stability under concentrated and uniformly distributed bending loads
23 p4268 A70-44171

Stability of elastic stretched ring on thin spherical shell under critical loads
23 p4268 A70-44318

Survival probability of randomly excited structures, using maximum entropy principle
23 p4270 A70-44582

Elastic structure equilibrium state stability, discussing damping and stiffening effects
23 p4275 A70-44941

Dynamic structural stability analysis, describing integral equation matrix technique
24 p4419 A70-45156

Continuous structural systems stability under random load excitation from linear partial differential equations of motion
24 p4421 A70-45281

Infinite plates and shallow shells stability under doubly periodic surface loadings, using nonlinear analysis
24 p4421 A70-45283

Undamped elastic cantilever column with concentrated masses, considering transition from stability to divergence under nonconservative forces
24 p4421 A70-45286

Shallow arch clamped at ends and subjected to uniform lateral load, deriving nonunique equilibrium stability states
24 p4426 A70-46038

STRUCTURAL STRAIN

Thin elastic shells parallel surface nonlinear tangential strains derived in terms of midsurface tangential and bending strain components
01 p0205 A70-11143

Transient thermal stress concentration at small thickness change of plate obtained by photoelastic studies
01 p0207 A70-11157

Construction of formulas relating stresses and plastic deformations describing inelastic bodies behavior under complex loads
01 p0210 A70-11411

Crack propagation in pure alpha-Ti at room temperature using optical and electron microscopy, considering propagation rate relation to strain amplitude
01 p0125 A70-11643

Stress-strain analysis of rectangular plates under concentrated load, noting sealed liquid compressibility effect on deflections and bending moments
02 p0388 A70-12499

Load and strain trajectory vectors components determined for tension followed by transverse compression in five dimensional space
02 p0390 A70-12803

Cauchy integrals extension to axisymmetric elasticity problems, obtaining numerical results for stressed circularly symmetrical state of hollow cylinder under uniform load
03 p0586 A70-13080

Discontinuity surfaces /cracks/ propagation in continuous medium having energy and stresses as functions of strain tensor gradient, using variational principle
03 p0589 A70-13330

Thin shells stressed state calculations by iteration, considering suitability for computer adaptation
03 p0592 A70-13442

Nonlinear theory for thin elastic shells with small strains and rotations, analyzing nonzero Gaussian curvature
03 p0594 A70-13622

Stress distribution of thin walled structure of open section, considering warping and torsional bending, using calculus of variations
03 p0596 A70-14030

Finite strain in bending rectangular block into right circular cylindrical shell for transversely isotropic medium along radius vector, using Saint Venant stress-strain relations
03 p0602 A70-14329

Nonlinear thin shell theory kinematics generalized in terms of physical strain and surface deformation and geometry
04 p0766 A70-14450

Supercritical strains and buckling in rib-reinforced cylindrical shells under axial compression using strain-energy method
04 p0766 A70-14478

Axisymmetric structures under load and temperature distribution analyzed by matrix displacement method
04 p0774 A70-15167

Divergences in tension textures and values of anisotropy coefficients ascribed to imperfections in cubic texture of aluminum sheet deformed by straining
05 p0927 A70-15995

Plasticity theory of single crystals based on dislocations behavior, considering only plane and elastic strains
05 p0928 A70-16061

Strain parameters and equilibrium equation of rib-reinforced thin shells, analyzing length, curvature and torsion variations using smooth shell analogy
05 p0935 A70-16230

Strain energy release rate in terms of propagating crack surface displacements applied to infinite solid loaded in tension
05 p0938 A70-16480

Inherent stresses in elastic solid assuming inherent strain as stress source, integrating stress functions
06 p1160 A70-17131

Complex load strength criterion containing stress and strain invariants applied to simple static loads and cyclic symmetric deformation
06 p1162 A70-17389

Elastic and plastic deformation zones stress-strain state under complex stresses, obtaining relation for stress and strain components
07 p1401 A70-18834

Cylindrical shell of revolution stress-strain state calculated during shaping in stamp with unclamping dies
07 p1292 A70-18836

Uniform thickness thin helicoidal shell stress-strain state with middle surface in asymptotic lines, assuming parameters governed by one dimensional law
07 p1402 A70-19055

Isotropic plate stress-strain state weakened by doubly periodic curvilinear holes using nonlinear theory
07 p1408 A70-19544

Transverse stress failure analysis of reinforced extruded plastic laminates taking into account cohesive and adhesive failure
07 p1410 A70-19768

Strain and stress compatibility from extension of Saint Venant and Beltrami-Mitchell equations for physically and geometrically linear to nonlinear media
08 p1585 A70-20962

Elastic-plastic plane strain solutions in infinitesimal plastic flow theory with separable stress fields
08 p1592 A70-21470

Stresses and strains in multilayer systems of viscoelastic materials showing aging solved by quadratures and Volterra equations, noting dependence on time
08 p1594 A70-21672

Microstrain characteristics of continuously reinforced W-Cu composites as function of volume fraction of fibers and prestrain, discussing dislocation friction stress
08 p1524 A70-21917

Variable modular elasticity theory demonstrated for anisotropic body subjected to plane stressed state, deriving expression for potential energy of deformation
09 p1779 A70-22547

Beams torsion problems solution by variational method of variables separation, obtaining values for torsional rigidity and stress function
09 p1777 A70-23080

Temperature fields and thermoelastic stresses in doubly connected structural elements solved in curvilinear coordinates system corresponding to conformal mapping of annulus
09 p1781 A70-23233

Stress-strain state analysis of transversely isotropic plates with inclusions under bending loads
09 p1782 A70-23298

Chromium structural dislocation and cell formation during deformation as function of temperature, impurities and strain rate
10 p1902 A70-23861

Stress-strain state analysis of prestrained thin circular cylindrical shell using Vlasov general shell theory 10 p1955 A70-24021

Stress intensity and strain energy of pressurized line crack in cross form in thin elastic plate solved by Wiener-Hopf technique 10 p1956 A70-24192

Steel conical disks two dimensional stressed state determined with deformations at elastic and elastoplastic strains using digital computers 10 p1956 A70-24242

Tensile and compressive strain measurements close to weld deposits, using moire fringe technique and mismatch grating 10 p1890 A70-24591

Plastic strains buildup during thermal cycling, establishing relation between strain interval and cycles number to failure for strain hardening materials 10 p1965 A70-25293

Gasdynamic test stand analyzing elastoplastic strains in aircraft gas turbine disks and liquid-propellant rocket engines turbopumps under alternating nonisothermal loads 10 p1862 A70-25298

Aluminum alloys hot cracking during welding, ascribing failure to combination of strain and susceptible microstructure 10 p1897 A70-25313

Optical filtering applied to moire method for measuring small structural strains 11 p2131 A70-25595

Stress concentration in elastoplastic and creep deformations determined by approximate solution 11 p2134 A70-25845

Brush current collectors for strain measurements in rotating machine parts, discussing acceptance testing 11 p1983 A70-26438

Deformation theory for small elastic-plastic strains in orthotropic material and discretization and iterative solution techniques 11 p2144 A70-26684

Transient analysis of stress waves around cracks under antiplane strain with time dependent loadings based on integral transforms 11 p2145 A70-26698

Stress-strain state of thin revolving shells composed of multiple variable thickness layers, assuming layers deformation free of slipping and separation 12 p2322 A70-27332

Shallow spherical shells stress-strain state in multiply connected regions resting on Winklerian base 12 p2323 A70-27334

Stress-strain state of epoxy resin cylinder situated in centrifugal force field using three dimensional photoelastic method 12 p2323 A70-27340

Strain induced in laminated orthotropic fiberglass plastic cylindrical shell by normal concentrated load, using equations free from rectilinear normals hypothesis 12 p2328 A70-28279

Circular cylinders torsion and plain strain analysis, completing statics by asymmetric shear and moment stresses according to Cosserat theory for plastic flow 13 p2508 A70-28492

Elastic isotropic circular perforated plate stress-strain state, proving quasi-regularity of infinite linear algebraic equations 13 p2515 A70-29317

Nonlinear wave propagation in continuous media involving stress-strain state of half space under pressure or load expanding over boundary 13 p2517 A70-29770

Plain strain fracture toughness index measurement, discussing application to metal fatigue and stress corrosion 15 p2757 A70-31927

Induced strain plane state in elastic micropolar medium by temperature effect, discussing thermoelastic problem stress functions 15 p2821 A70-32341

Materials real time strain measurements by optical correlation techniques, noting sensitivity 16 p2913 A70-33980

Stress, strain and acceleration spatial variation in structures subject to broad frequency band vibration excitation, considering simply supported flat plate 16 p2992 A70-34017

Plane strain vibrations of two layered elastic cylinders, analyzing results for lobar mode numbers 2, 3 and 4 16 p2994 A70-34096

Oxidized alpha Ti crystals strain analysis based on X ray divergent beam, discussing hardening effects 17 p3115 A70-34387

Hologram interferometry for measuring surface deformation under force and anisotropy in transparent objects 17 p3085 A70-35009

Strain transducer/optical diffraction grating/for plastic wave propagation measurement along specimens subjected to impact 19 p3425 A70-37884

Continuum bodies strain subjected to shearing stresses in incremental form based on slip theory of metals plasticity 19 p3549 A70-38668

Strain and stress compatibility from extension of Saint Venant and Beltrami-Mitchell equations for physically and geometrically linear to nonlinear media 20 p3719 A70-39384

Thin circular plate clamped along edge, calculating large displacements and elastoplastic strains for comparison with measurement 21 p3935 A70-41406

Thermomechanical disturbances propagation in viscoelastic solids, investigating effects of viscous flow, second order strains and temperature dependent material properties 21 p3937 A70-41427

Elastic-plastic deformation analysis at finite strain by two component thermodynamic model 21 p3937 A70-41431

Steels thermal fatigue in testing machine, investigating strains and stresses due to nonuniform temperature distribution during thermal cycle 21 p3840 A70-41433

Thin epitaxial Ag films on mica, measuring electrical resistivity strain dependence 24 p4391 A70-46266

STRUCTURAL VIBRATION

NT BENDING VIBRATION

NT FLUTTER

NT LINEAR VIBRATION

NT MISSILE VIBRATION

NT PANEL FLUTTER

NT SELF INDUCED VIBRATION

NT SUBSONIC FLUTTER

NT SUPERSONIC FLUTTER

NT TORSIONAL VIBRATION

NT TRANSONIC FLUTTER

Vibrating system response to damping insert introduced between two distinct coordinates, discussing Butyl rubber and vibration amplitude reduction 01 p0199 A70-10265

Semiautomatic mass condensation transformation for reducing structural vibration calculations, including computer program and mode shape plotting 01 p0200 A70-10868

Book on vibrational motions of straight and curved shafts, covering dynamic analysis for noncircular cross sections, applications to machine tools and vehicles design, etc 01 p0209 A70-11378

Human vibration test program for airline passenger reaction to vibration environments of large commercial aircraft 02 p0244 A70-12132

Flight vehicles intrinsic vibration frequency spectra for controllable flight determined by graph-analytical method 02 p0227 A70-12415

Normal and tangential displacements distribution at surface and along cross section of bar with free boundaries computed for symmetric and antisymmetric oscillations 02 p0301 A70-12484

Elastic stability of Coriolis-coupled oscillations of thin rotating disk under influence of centrifugal forces 02 p0389 A70-12650

Helicopter vibrations recording on magnetic tape for subsequent frequency analysis, describing frequency spectrogram 02 p0304 A70-12761

Vibrational response of simply supported and clamped circular plates subjected to gyroscopically induced inertia loads, using equations of motion 03 p0583 A70-12920

First and second boundary value problems of steady vibrations of viscoelastic bodies reduced to algebraic equations 03 p0589 A70-13345

Eigenfunctions of oscillating infinite perforated membranes for various boundary conditions at holes 03 p0591 A70-13415

Bubnov-Galerkin approximations convergence in problem of thin plate nonlinear vibrations, allowing for inertial forces due to rotation 03 p0593 A70-13470

Nonlinear flexural vibration properties of thin circular cylindrical shells with simply supported ends assuming deflection mode 03 p0594 A70-13549

Elastokinetic three dimensional boundary value vibration problem, involving rectangular area on surface of elastic half space under periodic normal stress 03 p0601 A70-14319

Thin elastic plate oscillations plane two dimensional steady state problem assuming constant thickness, finite dimension and moving load 04 p0766 A70-14420

Natural circular frequencies of small axisymmetric vibrations of shells of revolution of arbitrary shape, using Rutishauser algorithm for eigenvalues 04 p0767 A70-14525

Soviet monograph on numerical determination of dynamic characteristics of plates and shells by method

of summary representations, covering oscillation and stability problems 04 p0773 A70-14954

Spectral response of cylindrical shell due to random acoustic pressure input computed using modal approach 04 p0778 A70-15528

Stiffness and mass matrices of free-free vibration structure reduced to eliminate zero frequencies 04 p0778 A70-15553

Circular sandwich plates fundamental natural frequencies, considering face members membrane characteristics and thickness, face and core isotropy, etc 04 p0778 A70-15559

Kacner method applied to longitudinal vibrations study of nonhomogeneous nonuniform bars, noting applicability to geometrical and elastic properties variations 04 p0779 A70-15702

Ultraharmonic resonance excited by centrifugal force in system with Duffing restoring force characteristic using Ritz method 05 p0925 A70-15886

Thin cylindrical circular shell and three layered plate, analyzing vibration and stability due to loads and temperature 05 p0926 A70-15916

Computational procedures for matrix analysis of stability and vibration of thin flat rectangular plates in longitudinal compression 05 p0927 A70-16010

Parametric oscillations of unclamped rod under variable longitudinal force applied to end, approximating resonance boundaries and instability regions 05 p0934 A70-16226

Natural vibrational frequencies of trapezoidal, triangular, circular and elliptical isotropic flat plates with different edge conditions tabulated 05 p0936 A70-16319

Natural frequencies upper and lower bounds of elastic clamped vibrating curved beams/arcs/ determined on basis of differential operator theory 05 p0937 A70-16405

Displacement determination by orthogonality relationship for dynamic vibrations and stresses in composite elastic plates 05 p0937 A70-16406

Transverse vibrations of isotropic truncated-cone beam fixed at ends compared with cylindrical beam 05 p0942 A70-16666

Experimental and analytical work on structural panels vibratory response and acoustic radiation excited by turbulent boundary pressure fluctuations, evaluating applicability to noise research 05 p0835 A70-16789

Sonic boom research, considering exposure pattern development, propagation in inhomogeneous atmosphere and effects on structural responses 05 p0796 A70-16795

Cylindrical shell walls vibrations under impact loads, calculating damping factor in differential equation of motion of wall element 05 p0947 A70-17008

Longitudinal vibration equations of beams for nonlinear stress-strain relation reduced to equivalent linear partial differential equations 06 p1106 A70-17863

Rectilinear oblique harmonic vibration effect on gyrocompass with torsional suspension 07 p1278 A70-18737

Linear vibrations in gimbal suspension rotor and base, estimating gyroscope drift during base and rotor vibrational coincidence 07 p1279 A70-18738

Forced and free vibrations of shaft carrying unsymmetrical rotor, studying effects of distributed shaft mass and nonlinear shaft stiffness 07 p1401 A70-18976

Unstable vibrations in rotating flat shaft with unsymmetrical flexibility carrying unsymmetrical rotor in four degrees of freedom 07 p1402 A70-18978

Soviet papers on vibrations, strength and structure of aircraft engine elements 07 p1363 A70-19109

Segmented elastic shells of revolution supported by rings, studying buckling and vibration by matrix method 07 p1405 A70-19257

Mechanical vibration of beams analyzed by partial differential equations of beam vibration involving mass concentration and flexibility 07 p1411 A70-19786

Bernoulli-Euler beam equation describing natural frequencies and mode shapes for vibrating beam immersed in fluid 07 p1413 A70-20043

Complex modulus measurement for rigid linear viscoelastic materials over audio frequency spectrum by harmonic end displacement ratio method 07 p1413 A70-20044

Dynamic calculation of oscillating liquid filled elastic cavity on elastic kinematic system under random load, using random signals transmission theory
07 p1416 A70-20194

Von Karman equations for rectilinear plate vibrations used for triangular plates, discussing amplitude/thickness effect and multimodal frequency formula
07 p1416 A70-20211

Single frequency oscillations of variable cross section rods with random perturbations using asymptotic methods of nonlinear mechanics, discussing wedge oscillations
08 p1583 A70-20487

Rotating shaft vibrations on assembly designed to balance rotor in magnetic field, eliminating bearings effect on shaft to determine internal friction
08 p1584 A70-20697

Soviet book on free, forced and parametric vibrations of thin walled shells containing liquid, gas and continuous elastic medium
08 p1584 A70-20762

Elastic systems vibrations calculated with allowance for amplitude and frequency dependent energy dissipation using hysteresis loop contour expression
08 p1585 A70-20978

Vibration insulation of rib estimated with respect to diffuse flexural wave field in reinforced plate
08 p1586 A70-21010

Static deflection effect on harmonic vibration of system with restoring forces of hardening nonlinear spring, considering gravity effect
08 p1586 A70-21035

Computer graphics applications to three dimensional vibration analysis, changing mass, stiffness, exciting load or load frequency at any point with light pen
08 p1467 A70-21050

Radial vibrations of hollow elastic sphere in acoustic medium, considering Laplace transform of field equations with respect to time
08 p1587 A70-21076

Rectangular planform shallow cylindrical shell parametric vibrations using method applied to large bending vibrations of plates
08 p1588 A70-21212

Spaced damping reducing structural response to vibration, discussing efficiency, design flexibility and weight addition
08 p1507 A70-21269

Rigid rotating cylindrical shaft vibrations along diameter in viscous fluid using inner and outer expansions method
08 p1589 A70-21307

Tuned resonant test for measuring damping characteristics of lead and asbestos filled epoxy- polysulfide copolymer
08 p1527 A70-21336

Eigenfrequencies of thin barrel shaped shells on simple supports, noting correspondence of ratio of radius to shell wall thickness
08 p1592 A70-21474

Transverse oscillation periods of cylinder containing flowing fluid obtained by solving nonlinear partial differential equations describing transverse and longitudinal motion
08 p1592 A70-21480

Structural vibration of ring stiffened and mass- attached hemispherical shells
08 p1593 A70-21618

Frequency change for coupled vibrations of slender rotating beam due to hub radius change determined in centrifugal force field by perturbation method
08 p1594 A70-21772

Simply supported rectangular plate investigated for effect of thermal gradient on transverse vibrational frequencies
08 p1595 A70-21976

Cylindrical shell vibration modal characteristics finite element solutions accuracy compared with exact solutions
08 p1596 A70-21979

Book on sonic boom effects covering shock waves generation and propagation, elastic structures response to dynamic loads, structural damage, etc.
09 p1609 A70-22203

Rotatory inertia and shear deformation effects on structural vibrations of Timoshenko beams and frameworks using matrix formulation
09 p1770 A70-22257

Four point supported square plate fundamental frequency by finite difference and energy methods
09 p1770 A70-22389

Self excited vibrations in balanced vertical shaft running on plain lubricated bearings, making numerical analysis of small perturbation transition to fully developed swirl
09 p1690 A70-22399

Vibration of thin bodies subjected to large angle attack in hypersonic flow, discussing curved bodies method to reduce problem to steady state flows
09 p1771 A70-22445

Longitudinal vibrations propagation in nonlinear elastic beam under harmonic kinematic disturbance solved by harmonic linearization method
09 p1773 A70-22541

Truss vibrations calculations by method of dynamic rigidities, describing numerical methods for solving frequency equation to save computer storage capacity
09 p1773 A70-22546

Longitudinal vibration of finite viscoelastic rod with changing boundaries under time-variant force, analyzing impulse response by transform calculus
09 p1777 A70-22833

Stetson-Powell time fringe hologram technique of vibration analysis applied to nodal patterns in compressor blade and turbine disks
09 p1679 A70-22979

Turbine blade vibration measurement by contactless discrete-phase method, discussing sensor positioning for displacement amplitudes and flutter speeds determination
09 p1681 A70-23199

Longitudinal structural vibration and lateral bending response mass and spring coupling in Saturn AS-502 during boost with longitudinal excitation by pogo effect
09 p1766 A70-23239

Rotating cantilever beams mounted on disk periphery, analyzing forced and free vibrations characteristics
09 p1781 A70-23283

Flat rectangular elastic body stable oscillations with clamped base under compression loads, deriving difference scheme for approximation
09 p1782 A70-23297

Torsional vibrations frequency calculations for multibeam system exhibiting linear rigidity and viscous damping, constructing algorithm for digital computer
09 p1783 A70-23409

Centrifugal forces and nonuniform heating effect on natural vibration frequencies of circular plates using lumped parameter method
09 p1784 A70-23588

Elastic chain systems stability and natural vibrations using parameter coupling method permitting integral equation construction
09 p1784 A70-23596

Beam vibration eigenfunctions with allowance for shear compliance used to determine beams dynamic stability under pulsating axial load
09 p1785 A70-23600

Nonlinear many degrees of freedom systems steady state forced vibrations analysis, expressing response in nonlinear normal coordinates
10 p1954 A70-24010

Nonautonomous boundary value problems for plates in plane and three dimensional supersonic flows, obtaining eigenfunctions of vibration by Laplace transform
10 p1956 A70-24118

Energy dissipation-fatigue strength relationships during vibrations for prestained metals and alloys
10 p1956 A70-24244

Amplitude dependence of Young modulus defect in metals during large stress HF oscillations
10 p1956 A70-24247

Large amplitude free vibration of heated circular plates, analyzing energy equations by successive approximation method and elliptic integrals
10 p1957 A70-24480

Linearization of elastic forces in vibration system with percussion
10 p1958 A70-24516

Numerical analysis of forced parametrically excited plate vibration in plane supersonic flow, using digital computer
10 p1958 A70-24527

Synchronous harmonics generation of sinusoidal signal with given frequency for vibration analysis of linear and nonlinear structures
10 p1860 A70-24550

Uniform beams flexural vibration natural frequencies approximate calculation showing effect of shear flexibility and rotatory inertia
10 p1959 A70-24562

Transverse vibrations of rods, plates and shells based on hyperbolic, circular and Bessel functions
10 p1959 A70-24586

Soviet book on vibrations of complex oscillatory systems with mechanical, pneumatic and electromagnetic couplings
10 p1959 A70-24650

Aerospace vehicles structural vibration environments prediction methods emphasizing vibration sensor mounting resonances
10 p1959 A70-24903

Beams stability under flexural stress with periodic intensity variations, deriving differential equation of motion
10 p1960 A70-24973

Free vibration analysis of elastic structures using Rayleigh-Ritz method and finite element methods
10 p1961 A70-25055

Hysteretic linear damping theory applied to representation of structural damping under harmonic excitation
10 p1961 A70-25060

Forced vibrations of cylindrically curved multispan shell structures, using transfer matrix methods
10 p1962 A70-25062

Space vehicle residual thrust oscillation and dynamic response using power spectral density functions from flight data
10 p1953 A70-25068

Launch load simulation on scaled vibration model concerning Saturn 5 structural integrity and flight failure
10 p1953 A70-25072

Two-disk flexible rotor balancing method based on shaft vibration and bearing forces analysis
10 p1896 A70-25093

Truncated, structurally orthotropic and round conical shell oscillations taking into account reinforcing ribs eccentricity
10 p1964 A70-25195

Support vibration effect on zero shift of damped vertical pendulum, using equivalent linearization with perturbation scheme
10 p1917 A70-25205

Multilayer plate vibrations calculated with allowance for energy dissipation in material, deriving equations of motion
10 p1965 A70-25297

Statistical energy concepts application to Mariner Mars 1969 spacecraft, estimating coupling of damping factors to analyze structural vibration
11 p1218 A70-25374

Monograph on conditions for stabilization of oscillatory systems with random parametric excitations covering approximate calculations, stability concept definition, etc
11 p1219 A70-25496

Three degrees of freedom astatic gyroscope drift due to base vibrations according to harmonic law
11 p2048 A70-25579

Natural vibrations of truss systems of four circular cylinders hinged along walls, using linear group representation
11 p1232 A70-25605

ARAVA aircraft free-free vibrational characteristics evaluation by integral-aircraft lumped mass analytical method verified by ground resonance test
11 p1979 A70-25688

Crack propagation in tensioned plates subjected to sonically induced vibrations
11 p1233 A70-25731

Boundary conditions effect on bending, vibrations and buckling of unsymmetrically laminated rectangular plates
11 p1236 A70-26079

Vibration of thin elastic plates under random driving forces simulated digitally, using power residue method for pseudorandom number generation
11 p1239 A70-26277

Multidegree of freedom linear vibrating system analysis by dividing differential equation method
11 p1239 A70-26414

Vibrations of combination of cylindrical shells and circular plates, giving bending moment distribution
11 p1239 A70-26415

Random vibration isolation for two degrees of freedom model system investigated statistically, assuming wide band white noise
11 p1239 A70-26416

Vibration equations for closed and open sandwich cylindrical shell with thickness-shear deformation in core and face layers compared with membrane theory
11 p1245 A70-26697

Metal plates vibration under viscoelastic damping layers using electromagnetic transducer and impact excitation
11 p1245 A70-26702

Lunar Orbiter spacecraft vibration responses based on mathematical models, comparing results with experiment
12 p2315 A70-27098

Limited frequency range analytical model for predicting mass and stiffness changes effect on natural frequencies and normal modes
12 p2317 A70-27121

Complex structures vibration using component vibration modes, considering dynamic behavior from interface reactions effects
12 p2317 A70-27123

Subdivisional method for linear systems vibration and buckling problems, reducing governing equation to ordinary differential equation with variable coefficients
12 p2320 A70-27145

Longitudinal vibrations of circular elastic homogeneous cylinders with end restraints
12 p2321 A70-27152

Three dimensional variational dynamic and static large deformation equations solutions for stability and natural frequencies and wave propagation in bodies under initial strains
12 p2322 A70-27331

- Vibrating thin beam cross sectional displacement-force equations coefficients included in coefficient matrix, considering shear deformation and rotary inertia effects on vibration modes 12 p2324 A70-27397
- Elastic beam vibration under constant amplitude and varying frequency periodic forces during passage through resonance 12 p2326 A70-27798
- VTOL and STOL design and operation, discussing noise and vibration reduction 13 p2344 A70-28544
- Rotorcraft design and aerodynamics, discussing structural vibrations and all-weather operation 13 p2344 A70-28545
- Vibrocreeper effect on Al-Mg-Si alloy vibration frequency and mean and maximum stress at constant temperature 13 p2512 A70-28980
- Pitch damping derivatives computation for missile configurations undergoing small amplitude oscillations at subsonic speeds, using static aerodynamic data [AIAA PAPER 70-537] 13 p2339 A70-29004
- Eigenvalue and eigenvector derivatives in dynamic system designs involving vibrations and oscillations, discussing applications in modeling 13 p2518 A70-29971
- Gutenberg-Bullen interior model applied to fading of earth spheroidal oscillations 14 p2568 A70-30153
- First and second boundary value problems of steady vibrations of viscoelastic bodies reduced to algebraic equations 14 p2657 A70-30720
- Turbulent boundary layer loading function for use with finite element structural analysis system applied to elastic aircraft structures random vibration [AIAA PAPER 69-20] 14 p2658 A70-30853
- Plane frames with and without shear walls, determining dynamic response under vibration by finite element method 14 p2660 A70-31137
- Pontryagin principle for thin vibrating plates under mixed boundary conditions, examining optimal control 14 p2660 A70-31205
- Differential equations for coupled bending and torsional vibrations of slender beam in centrifugal force field 14 p2661 A70-31226
- Cylindrical shell nonaxisymmetric vibration frequencies and boundary values relation, using Lagrangian 14 p2661 A70-31273
- Natural oscillation frequencies in rectangular shallow shells weakened by cuts, using summary representations method for eigenvalues determination 15 p2814 A70-31585
- Differential equation for longitudinal vibrations of rod at high temperature, giving asymptotic solution 15 p2814 A70-31589
- Natural oscillation frequencies of shallow shells with mixed boundary conditions on clamped edges, using summary representations method 15 p2814 A70-31590
- Rarefaction wave analytical construction by successive approximation, solving hyperbolic equations for longitudinal vibrations of rods 15 p2815 A70-31644
- Transverse vibration of thin circular elastic turbine disk of variable thickness rotating axially at constant angular velocity 16 p2916 A70-32994
- Clamped skew plates influence coefficients, natural vibration frequencies and nodal patterns measurement, comparing to Galerkin method results 16 p2988 A70-33124
- Constrained and constant coefficient optimal controls compared in optimizing performance criteria of vibrating beams 16 p2886 A70-33332
- Linear continuous vibratory system unknown parameters identification from frequency response data 16 p2988 A70-33337
- Saturn 5 S-2 stage propellant feedlines and J-2 engines simulating structural longitudinal oscillation by analog computer 16 p2968 A70-33591
- Annular fluids hydrodynamic mass and damping effects on long rotating cylinders vibrations, discussing theory of fluid friction and forces, vortex and turbulent flows, etc [ASME PAPER 70-FE-30] 16 p2892 A70-33636
- Annular fluids hydrodynamic mass and damping effects on long rotating cylinders vibrations, analyzing test results [ASME PAPER 70-FE-31] 16 p2892 A70-33637
- Optimal design of structures with constraints on strength and natural frequency, developing steepest descent boundary value method 16 p2991 A70-33854
- Stress, strain and acceleration spatial variation in structures subject to broad frequency band vibration excitation, considering simply supported flat plate 16 p2992 A70-34017
- Vibrations of shells, plates and membranes carrying dynamic systems at discrete points on surface, obtaining eigenfunction and eigenvalue equations 16 p2993 A70-34090
- Plane strain vibrations of two layered elastic cylinders, analyzing results for lobar mode numbers 2, 3 and 4 16 p2994 A70-34096
- Transversely isotropic elastic plates vibrations without initial specification of field variables spatial dependence on thickness coordinate by two dimensional asymptotic theory 16 p2994 A70-34232
- Free oscillations of Euler-Bernoulli and Timoshenko cantilever beams of variable cross section, obtaining approximate modes and natural frequencies bounds 16 p2994 A70-34234
- Statistically indeterminate Timoshenko beams oscillations natural frequencies and modes by lumping properties of linear and rotary inertia at discrete points 16 p2994 A70-34235
- Free and forced vibrations of linear systems, dissipative systems with nonlinear friction, aeroelastic vibrations, rotor vibrations, mode locking, random vibrations, etc 16 p3004 A70-34277
- Neutral type differential equations transformation to time lag system making periodic vibrations existence and stability theorems applicable 16 p2944 A70-34282
- Mechanical vibrations models and analysis techniques, emphasizing problem of weak couplings in discrete systems 16 p2996 A70-34290
- Frequency analysis of cylindrically curved panel with clamped and elastic boundaries, using mathematical and panel models 17 p3181 A70-34524
- Hingeless rotor helicopter airborne and ground resonance characteristics, noting feedback stability control interference with rotors aerodynamic damping 17 p3015 A70-34733
- Helicopter vibration reduction techniques, considering antivibration devices design and comfort crossover speed increase 17 p3015 A70-34735
- Time-average holographic interferometry applied to HF transverse vibrations of uniform cantilever beam, noting correlation with Timoshenko beam theory 17 p3083 A70-34961
- Nonlinear vibrations of beam harmonically excited by periodic motion of supporting base, using Galerkin method 17 p3185 A70-34962
- Radial vibration frequency variation with wall thickness in hollow spherical shells, tabulating and plotting results 17 p3186 A70-34978
- Turbine blades vibrations based on thick curved shell theory, deriving element from isoparametric solid 17 p3187 A70-34989
- Engineering components vibration mode studies by time averaged holographic interferometry 17 p3087 A70-35019
- Vibrating structure mathematical model for predicting radiated noise level 17 p3187 A70-35169
- High intensity noise enveloping space vehicle as distributed excitation, examining correlation effects on structural response 17 p3059 A70-35170
- Matricial group representation theory for constructing elastic vibration equations of symmetric flexible mobile controlled members 17 p3180 A70-35293
- Natural vibrations of complex plates for combined free and clamped conditions 17 p3189 A70-35343
- Structural vibration test system, using hybrid computer for automatic control and data acquisition and reduction 17 p3061 A70-35488
- Unsymmetric vibrations of cylindrical shells, analyzing stress states by asymptotic method 18 p3335 A70-36059
- Incompressible fluid flow past array of arbitrary profiles vibrating with arbitrary phase shift, taking into account blade displacement and vortex wake effect 18 p3206 A70-36277
- Longitudinal wave absorbers attenuating resonance vibrations in rods and plates 18 p3337 A70-36304
- Automatic matrix method for vibration modes of large structures with multiple degrees of freedom 18 p3342 A70-36684
- Vibration characteristics of low aspect ratio compressor blades, using thin shell theory and Rayleigh-Ritz method 18 p3305 A70-36876
- Soviet book on vibration and balancing of aircraft engine rotors covering structural deformation and dynamics of turbine engines and compressors 19 p3489 A70-37237
- Nonhomogeneous Helmholtz vibration equation for sectorial-annular membranes and plates under arbitrary load, using Fourier method 19 p3535 A70-37343
- Energy dissipation in material under complex vibrations, noting role of summary shear stress 19 p3535 A70-37347
- Rib stiffened elliptical and circular plate vibrations, determining fundamental frequencies by variational techniques 19 p3536 A70-37693
- Constrained viscoelastic layer optimal length for vibration damping of metallic structures 19 p3536 A70-37696
- High intensity noise testing of missile and spacecraft structures, simulating acoustically induced vibrations due to aerodynamic turbulence 19 p3531 A70-37697
- WKB or eikonal approximation for waves and vibrations in inhomogeneous Euler-Bernoulli beams and plates and Timoshenko beams 19 p3536 A70-37700
- Satellite structural vibration damping material and methods, discussing high polymer synthetics and viscoelastic laminae and damping systems data 19 p3533 A70-38291
- Anticlastic bending analysis of long narrow plates oscillations and stability based on elastic plates nonlinear theory 20 p3721 A70-39779
- Vibrating plate thickness function, applying eigenvalue problem 20 p3726 A70-39877
- Structural vibration tests, analyzing errors due to couplings and dampers addition 20 p3734 A70-40439
- Natural flexural vibration frequencies of bars with periodic thickness variations, comparing Hamilton principle, matrix approach and experimental investigations 20 p3735 A70-40536
- Dynamic response of simply supported nonhomogeneous beam and triangular pulse loads 21 p3933 A70-40584
- Rotating shaft system consisting of variable cross sections, disks and journal bearings, calculating unbalance vibration by numerical method 21 p3832 A70-40898
- Linearly elastic skeletal structures, calculating natural frequencies of undamped vibration by computer program 21 p3935 A70-41254
- Solid and sandwich beams lateral vibrations under transverse shear, rotary inertia and variable midplane stretching 21 p3938 A70-41761
- Quasi-harmonic friction induced near sinusoidal form vibration, calculating amplitude dependence on sliding velocity [ASME PAPER 70-LUBS-16] 22 p4044 A70-42445
- Steady vibrations of mechanical system with asymmetrical restoring force, reviewing formulas for mean angular frequency and Fourier expansion coefficients 22 p4113 A70-42544
- Acoustic frequency spectra of transverse vibrations in bracketed bar caused by dry friction, using Lagrange method 22 p4073 A70-42612
- Circular plates dynamic stability under variable periodic loads, using differential equations of vibrational motion for median surface 22 p4114 A70-42613
- Axisymmetric vibrations of cylindrical shell with concentric circular plates at each end, obtaining Lagrangian of combined system 22 p4115 A70-42843
- Linear elastomechanical systems natural vibration parameters by harmonic excitation method 22 p4116 A70-43200
- Elastic bending, vibration and buckling of simply supported thick orthotropic rectangular plates and laminates 22 p4116 A70-43205
- Equations solution for turbine blade flexural vibration, considering internal friction 22 p4117 A70-43363
- Vortex induced vibration problems, deriving mathematical model for periodic lift on circular cylinder 22 p3960 A70-43546
- Data acquisition and processing in structural model characteristics analysis during ground resonance tests [ICAS PAPER 70-36] 23 p4267 A70-44133
- Rigid and elastic rectangular plates vibration under uniformly distributed dynamic load, investigating bending behavior by Galerkin method 23 p4268 A70-44170

- Minimum weight structural design within given stress limits due to different loads or natural frequency vibrations, using finite element method for structural analysis 23 p4268 A70-44226
- Mechanical structure dynamic response to vibration environment, using mobility method analysis 23 p4269 A70-44334
- Point accelerations on semirigid body spacecraft from accelerometer data with structural vibration noise at landing 23 p4200 A70-44387
- Axisymmetric vibration modal properties/frequencies and mode shapes/ of thin conical shell frustums, considering dimensional and boundary condition influences 23 p4270 A70-44501
- Gradient minimization and higher order discrete elements application to shell buckling and vibration eigenproblems, using 48 degree of freedom Bogner cylindrical panel element 23 p4271 A70-44705
- Structural eigenvalue problems solved by sparsely populated matrices for structural vibrations and critical buckling, using finite element method 23 p4271 A70-44708
- Stress, buckling and vibration analysis of shells of revolution by numerical integration and finite difference methods, summarizing computer programs 23 p4273 A70-44725
- Heat exchange during flat plate transverse vibrations in water, discussing frequency and amplitude effects and natural convection role 23 p4282 A70-44728
- Orthogonality of eigenmodes of aircraft vibrations based on F-104G ground measurements 23 p4274 A70-44766
- Oscillating vane and rotating disk pressure gage theory, considering gas damping and density variations 23 p4198 A70-44948
- Rectangular cable networks covered by or embedded in membrane matrix, calculating vibration response under load by Galerkin method 24 p4421 A70-45279
- Coriolis acceleration effect on inplane vibration resonant frequencies of rotating disks 24 p4425 A70-45780
- Saturn 5 Apollo booster stages oscillations induced by coupling between vehicle structure and engine thrust corrected within existing systems [AIAA PAPER 70-1236] 24 p4417 A70-45954
- STRUCTURAL WEIGHT**
- Economic tradeoffs in airport and commercial aircraft design, considering traffic growth, increased weight impact minimization and costs [AIAA PAPER 69-1087] 01 p0056 A70-10623
- Bird impact damage effect on aircraft structural design, considering forward facing areas and minimum weight 01 p0200 A70-10687
- Minimum weight sandwich plates complying with von Mises criterion, providing constant dissipated energy density 01 p0202 A70-10947
- Quick-disconnect couplings selection guide for aerospace fluid systems, emphasizing functional and weight considerations [SAE-AIR-1047A] 01 p0197 A70-11461
- Deployment systems for extending large area lightweight flexible solar arrays in space, tabulating estimated design weights including power-weight ratios 02 p0228 A70-11932
- Functionally integrated superheterodyne receivers design by applying microwave IC technology, providing weight reduction, interconnecting cables elimination and circuit interface problems minimization 02 p0267 A70-12055
- Wide strut analysis for determining weight minimizing cross sectional dimensions of panels having unflanged integral stiffeners 03 p0596 A70-14145
- Aircraft structural weight optimization for given fundamental vibration frequency obtained by aeroelastic constraints 03 p0598 A70-14231
- Pontryagin principle applied to minimum structural weight design problem in optimal control theory with state and control inequality constraints [ASME PAPER 69-WA/AUT-1] 04 p0769 A70-14832
- Performance characteristics analysis of large area roll-up solar arrays based on support structure size and weight [ASME PAPER 69-WA/ENER-11] 04 p0770 A70-14898
- V/STOL power drive systems structural efficiency, comparing mechanical and pneumatic components from weight-optimal viewpoint [ASME PAPER 69-WA/AV-7] 04 p0622 A70-14901
- Rectangular waffle plates minimum-weight design efficiency with multiple rib sizes in stiffening direction compared to honeycomb core sandwich construction 04 p0777 A70-15526
- Airframe production factors involving choice of materials and fabrication methods, emphasizing weight reduction to increase payload 05 p0854 A70-15925
- Minimum weight beams and frames calculation for random loads taking into account material carrying capacity 07 p1400 A70-18821
- Minimum weight reliable beams and frames calculation for random loads, using one degree of freedom system to obtain closed form solution 07 p1401 A70-18825
- Minimum weight design of elastic sandwich beams with deflection constraints using n-dimensional space of discretized bending stiffness 07 p1407 A70-19358
- Hole reinforcement in flat plate under uniaxial load with high stress region at boundary, resulting in weight savings 07 p1414 A70-20174
- Structural composite materials for thermal protection of reusable weight-saving vehicles in space transportation system 07 p1397 A70-20382
- Statistical analysis of model parabolic mirror rigidity on multisupported suspension under symmetrically distributed load represented by mirror weight 08 p1586 A70-21057
- Minimum weight design for two dimensional bodies with given load system determined by variational method 09 p1771 A70-22400
- Weight function minimization of multiweb box beam in pure bending 09 p1777 A70-22769
- Lightweight mirror blanks of titanium silicate for OAO-4 providing thermal and dimensional stability 09 p1678 A70-22952
- Prestressing in minimum weight design of statically indeterminate structures 09 p1781 A70-23231
- Electric propulsion design, considering effects of weight, impedance matching, beam voltage regulation and operating point variations in formulating system mass and reliability 09 p1743 A70-23248
- Minimum weight design for symmetrically stiffened cylindrical shells under compression based on linear orthotropic stability theory 10 p1958 A70-24560
- Optimal traction drive system design for lunar roving vehicle, considering weight, energy consumption, operational flexibility, power supply, motor and power train 11 p2030 A70-25375
- Working pressure effects on size and weight of aircraft hydraulic systems components, allowing for fluid properties change 11 p1982 A70-25865
- Low cost lightweight flight control systems for business aircraft providing equivalent performance to larger equipment [SAE PAPER 700213] 11 p2079 A70-25886
- Computerized tradeoff analysis for planetary landing vehicle entry capsule and lander design optimization, emphasizing weight allocation for Mars 1973 missions 11 p2126 A70-26320
- Limited frequency range analytical model for predicting mass and stiffness changes effect on natural frequencies and normal modes 12 p2317 A70-27121
- Waffle plate structures least weight design under uniaxial, biaxial and multiple combined loading with various stiffening patterns, investigating pyramiding concept 12 p2318 A70-27133
- Aircraft all-movable stabilator computer aided design for optimized structural weight and performance 12 p2319 A70-27137
- Stiffened fiber composite cylindrical shells minimum weight design, discussing configuration and material parameters 12 p2319 A70-27139
- Aerojet engine minimum weight design, suggesting use of welding and brazing instead of nut-and-bolt joints in component fabrication [SAE PAPER 700319] 12 p2243 A70-27457
- Bendix design approach for lunar vehicle using operating mockup, noting trend towards lighter machines 12 p2208 A70-27945
- Aluminum-boron composite material applications to structural components of F-106 aircraft, noting weight saving and mechanical properties [AIAA PAPER 68-975] 12 p2257 A70-28082
- Radioisotope fueled organic Rankine power system with weight dependence on operations depth [AIAA PAPER 70-520] 13 p2349 A70-29037
- Minimum weight design for complex structures subject to frequency constraint using finite element method and computer program 13 p2517 A70-29965
- Short haul Mercure airliner weight saving design and manufacture 14 p2593 A70-31371
- Mercure passenger aircraft development schedule, cost, delivery and features, emphasizing weight balance and convenience 15 p2676 A70-32365
- Solar thermoelectric generator /STEG/ with two stage converter, discussing weight factors and efficiency 15 p2678 A70-32425
- Multistage rocket weight optimization for payload and velocity at burnout, considering specific impulse, drag, etc 15 p2813 A70-32519
- Homopolar Inductor Alternators of minimum weight and maximum efficiency for aerospace power supplies 15 p2710 A70-32587
- Joint design for fiberglass reinforced plastic aircraft composites regarding minimum weight and reliability [ASME PAPER 70-DE-56] 16 p2989 A70-33516
- Unmanned electric propulsion spacecraft with external fuel and flashlight thermionic reactors, discussing thruster arrays, weight and performance for reference Jupiter orbiter mission [AIAA PAPER 70-644] 16 p2966 A70-33547
- Throttleable thruster system for Mars soft landing, selecting catalytic decomposition engine from system weight and performance studies [AIAA PAPER 70-652] 16 p2966 A70-33549
- Weight-dimensions correlation for gas turbine engine/airplane optimization analyses, determining tradeoffs among performance, noise, drag characteristics, etc [AIAA PAPER 70-669] 16 p2967 A70-33575
- Minimum weight springs design, discussing load deflection curves, materials resilience, etc 16 p2924 A70-34171
- Ti alloy forgings for aircraft industry, utilizing high strength/weight ratio 17 p3097 A70-34357
- Ti alloys use in Olympus 593 engine for Concorde SST, discussing weight saving, mechanical properties and manipulation characteristics 17 p3146 A70-34449
- Optimum fiber orientation for minimum weight boron/epoxy shear panel design 17 p3182 A70-34562
- Helicopter structural weight statistical prediction and evaluation, discussing comparable fixed wing experience 17 p3015 A70-34728
- Packable near weightless nylon cloth wings without rigid members for improved aeronautical efficiency in cargo delivery, powered flight and rocket and spacecraft recovery [AIAA PAPER 70-880] 17 p3017 A70-34815
- Structural weight reduction and increased aerodynamic efficiency in aircraft design by including flight control technology early in configuration development phase [AIAA PAPER 70-874] 17 p3017 A70-34817
- Static weight tare compensation for V/STOL wind tunnel models, using accelerometer outputs 17 p3062 A70-35500
- Subsonic aircraft size effect in conventional design, discussing increased weight increments and economic gain rate [AIAA PAPER 70-940] 17 p3021 A70-35849
- Postbuckled integrally stiffened wide column weight optimization, developing stress equation 18 p3339 A70-36447
- Minimum weight design for structures with stability constraint by nonlinear programming 18 p3344 A70-37068
- Space shuttle development, discussing weight and lateral separation distance 19 p3531 A70-37378
- Minimum weight thermoelastic design of sandwich beam for given deflection, using potential energy principle 19 p3541 A70-38044
- Composite technology effects on engineering design, emphasizing carbon-carbon materials for aircraft structural weight reduction, performance improvement and high temperature applications 20 p3653 A70-39202
- RF plasma thrusters for synchronous satellites, estimating weights and efficiencies of various types 20 p3689 A70-40124
- Shape factors for weight prediction and design optimization of structural members requiring given area moment of inertia [SAWE PAPER 828] 20 p3732 A70-40354
- Structural weight design optimization by computer aided geometrical programming technique [SAWE PAPER 822] 20 p3733 A70-40357
- Material thickness tolerances control for weight minimization of aerospace vehicles by abrasive metal grinding, improving surface quality [SAWE PAPER 827] 20 p3638 A70-40358

- Landing gear weight analytical estimation, discussing ground loads, member cross sectional area, parametric variations, etc
[SAWE PAPER 829] 20 p3563 A70-40366
- Fuselage frames minimum weight analysis by automatic iterative method
[SAWE PAPER 826] 20 p3733 A70-40370
- Structural mass properties solution using programmable printing desk computer for fast data point plotting
[SAWE PAPER 856] 20 p3595 A70-40372
- Computerized assembly of production space vehicle with controlled mass properties, discussing automated system of data collection, storage and retrieval
[SAWE PAPER 851] 20 p3639 A70-40375
- Space shuttle with reusable launch system, discussing payload sensitivities regarding orbiter and booster weight and engine reliability
[SAWE PAPER 849] 20 p3716 A70-40377
- Fighter aircraft configuration design balancing, comparing weight penalties
[SAWE PAPER 840] 20 p3563 A70-40380
- Parachute flexibility as performance parameter, discussing stiffness-weight index, inflation process, squidding, etc
[AIAA PAPER 70-1166] 21 p3755 A70-41845
- Optimal weight design of axisymmetric rotating elastic disks for specific edge radial displacement
22 p4112 A70-42463
- Weight-optimal sandwich beam design for given static deflection, using energy approach
22 p4113 A70-42535
- Concorde downstream thrust reversal nozzle, noting weight saving by use of welded stainless steel honeycomb construction
22 p4092 A70-43213
- V/STOL aircraft landing performance, discussing relationships between approach speeds, rates of descent, structural criteria and weight penalties
[ICAS PAPER 70-53] 23 p4139 A70-44149
- Minimum weight structural design within given stress limits due to different loads or natural frequency vibrations, using finite element method for structural analysis
23 p4268 A70-44226
- Optimal design of minimum weight bar and beam structures under static loads, comparing computer time with nonlinear programming methods
23 p4271 A70-44702
- Materials design and development for engineering applications, discussing relationships and importance of strength, stiffness, weight, toughness and work of fracture
24 p4419 A70-45174
- Elastic circular sandwich beams optimal design for minimum compliance and given weight, considering rings and semicircular arches
24 p4420 A70-45276
- Aircraft design for low weight, discussing structural failures
[AIAA PAPER 70-1232] 24 p4425 A70-45917
- STRUTS**
- Structural support strut design for cryogenic propellant tanks to optimize load carrying capability and heat transfer characteristics
02 p0306 A70-11942
- Dynamic stress concentration factor in strut containing symmetrically located elliptical discontinuity, using photoelastic technique with modulated ruby laser light source
02 p0388 A70-12495
- Wide strut analysis for determining weight minimizing cross sectional dimensions of panels having unflanged integral stiffeners
03 p0596 A70-14145
- Differential equations solution in terms of elementary functions applied to evaluate critical buckling loads for struts of variable cross sections
03 p0602 A70-14328
- Stresses in dynamically loaded struts with one or three holes by photoelasticity, using Fastax camera
12 p2315 A70-26878
- Semiclamped strut supported rectangular plate deflection determined holographically, mechanically and analytically
[SESA PAPER 1650] 15 p2740 A70-32331
- STUDS [STRUCTURAL MEMBERS]**
- Stress distribution along stud hole threads in Al case, investigating stud design effect using strain gauge on models
03 p0585 A70-12962
- Mechanical methods locking studs, discussing chemical locking based on hardening of resins by polymerization
06 p1076 A70-17437
- STURM-LIOUVILLE OPERATOR**
- U STURM-LIOUVILLE THEORY**
- STURM-LIOUVILLE THEORY**
- Linear physical chains with Sturm-Liouville characteristic polynomials used for natural frequency determination of coupled harmonic oscillators or electrical analog
01 p0142 A70-10520
- Sturm-Liouville problem associated with Falkner-Skan equation, obtaining asymptotic solutions
03 p0520 A70-14080
- Book on some methods of solving boundary value problems of mathematical physics covering linear operators, boundary conditions, perturbation and Monte Carlo methods
07 p1326 A70-19696
- Transient thermal stresses in spherical shell with distributed source and general Sturm-Liouville boundary conditions
19 p3539 A70-37800
- Whole operator with infinite defective numbers for Sturm-Liouville differential equation, describing spectral functions
23 p4210 A70-43977
- STYRENES**
- NT POLYSTYRENE**
- Flame-resistant trichloromethyl-containing polyester-styrene system, describing curing characteristics at room and higher temperatures
10 p1907 A70-24066
- Styrene-oxygen copolymer preparation methods, discussing burning rates for rocket solid propellants mixtures with ammonium perchlorate
11 p2100 A70-26146
- SUBCARRIER WAVES**
- U CARRIER WAVES**
- SUBCIRCUITS**
- U CIRCUITS**
- SUBCOOLING**
- U SUPERCOOLING**
- SUBCRITICAL FLOW**
- Dynamic behavior of subcritical fluid flow past airfoils, expanding flow potential to obtain formulas for velocities, local Mach numbers and pressure
08 p1433 A70-21173
- Plane diffuser grid profiles for subcritical velocities of oncoming flow, using wind tunnel test data
18 p3205 A70-36129
- Subcritical and supercritical boundary layer problems, reviewing various momentum integral solution methods
18 p3242 A70-36705
- Subcritical viscous flow around arbitrary airfoils, calculating boundary layer effect on pressure distribution from inviscid flow approximation
21 p3744 A70-40924
- Stationary elliptic cylinders in subcritical flow, determining Strouhal number, pressure fluctuations and wake geometry as functions of angle of attack
[AIAA PAPER 69-745] 23 p4134 A70-44564
- SUBDIVISIONS**
- Subdivisional method for linear systems vibration and buckling problems, reducing governing equation to ordinary differential equation with variable coefficients
12 p2320 A70-27145
- SUBGRAVITY**
- U REDUCED GRAVITY**
- SUBHARMONIC GENERATORS**
- Tunnel diode parametric phase locked oscillators as memory elements, considering optimum subharmonic pumping frequencies determination
08 p1477 A70-21642
- SUBLATTICES**
- U LATTICES [MATHEMATICS]**
- SUBLAYERS**
- U SUBSTRATES**
- SUBLIMATION**
- Equilibrium existing at gaseous-condensed phases interface inferred as mechanism for dissociative sublimation of ammonium perchlorate
05 p0894 A70-17079
- Caloric data determining saturated vapor pressure of nitrogen tetroxide and heat of sublimation for sublimation curve
07 p1358 A70-19206
- Ammonium perchlorate decomposition, deflagration, sublimation, crystal growth and surface properties, using scanning electron microscope
07 p1358 A70-19576
- Surface erosion of sublimating graphite and naphthalene due to nonequilibrium mass transfer in gas flows
13 p2437 A70-28580
- Vaporization characteristics of solids for relationship between chemical bonding and sublimation mechanism emphasizing NaCl, CdS and GaAs
14 p2545 A70-30906
- Teflon and polymethyl methacrylate sublimation breakdown in plasma jets, using electric arc heated argon, nitrogen, air and oxygen
15 p2765 A70-32103
- Martian soil thermal conditions at south pole, considering solar cap annual variations and carbon dioxide sublimation
15 p2802 A70-32492
- Radiative energy loss and wall sublimation effects on gas flow parameters behind reflected strong plane shock wave, taking into account small disturbances
18 p3348 A70-36673
- Plane wall surface sublimation under radiation from shock wave heated gas
18 p3348 A70-36721
- Aerospace coldness and vacuum simulation, discussing uses of cryogenic, titanium sublimation, ion and molecular pumps
19 p3396 A70-37462
- Porous matrix explosions during sublimation of dusty ice with nonvolatile particles
19 p3471 A70-37659
- Knudsen effusion measurements of stoichiometric MnTe sublimation at high temperature and low pressure
21 p3773 A70-41273
- Surface ablation patterns in sublimating materials tested in high temperature structures tunnel
21 p3951 A70-41755
- Martian soil thermal conditions, considering polar cap annual variations and carbon dioxide sublimation
23 p4240 A70-43914
- SUBMARINE CABLES**
- Wideband transmission media for global communication networks, comparing submarine cables and satellites based on economic tradeoff in terms of circuit density and distance
[AIAA PAPER 70-444] 11 p2001 A70-25475
- SUBMARINES**
- Aerospace technology contributions to oceanography, discussing lightweight structures, electronics, automatic systems and submarine laboratory application
07 p1263 A70-19135
- Ben Franklin submarine life support systems tested during Gulf Stream Drift Mission, discussing atmosphere control, water, waste and food management
[ASME PAPER 70-DE-60] 16 p2852 A70-33515
- SUBMERGED BODIES**
- NT DIVING [UNDERWATER]**
- Spatial correlation effect of unsteady sectional loads in axial direction on average or apparent loads over finite region of circular cylinder immersed in moving fluid
11 p2036 A70-26148
- Heat exchange during flat plate transverse vibrations in water, discussing frequency and amplitude effects and natural convection role
23 p4282 A70-44728
- SUBMERGING**
- Water immersion for weightlessness simulation, presenting annotated bibliography covering physiological responses, human performance and simulation techniques and facilities
01 p0038 A70-10965
- Control measurements to determine changes in lung volumes, intrapulmonary and intragastric pressure and breathing during submersion in water up to xiphoid process level
01 p0038 A70-10980
- Effect of immersion in thermoindifferent water on circulatory control and work capacity in trained and untrained subjects
02 p0241 A70-12770
- Magnetic field self induction in static fluid-submerged intersecting jet system, calculating required magnetic Reynolds numbers
04 p0726 A70-14541
- Statistical analysis of pulmonary ventilation and gas exchange indices during orthostatic tests before and after water immersion
07 p1209 A70-19517
- Human peripheral blood circulation during prolonged underwater activity, showing compensation for high humidity, noise levels, low water temperatures, isolation and confinement
10 p1822 A70-25178
- Statistical analysis of pulmonary ventilation and gas exchange indices during orthostatic tests before and after water immersion
11 p1988 A70-26116
- Nonself similar problem of plane submerged fluid jet expelled from annular nozzle, obtaining asymptotic expansion for stream function
15 p2719 A70-31485
- Book on survival in cold water covering physiology and treatment of immersion hypothermia and drowning, thermoregulation, etc
19 p3360 A70-37977
- Preliminary physical training for human water immersion resistance improvement
20 p3576 A70-40196
- High speed radiographic observation of electric arc movement and metal transfer during submerged arc welding
24 p4322 A70-45724
- SUBMILLIMETER WAVES**
- Astronomical studies at millimeter wavelengths, describing radiometer and Fabry-Perot interferometer design for submillimeter range
01 p0185 A70-10975
- Extra-atmospheric submillimeter astronomy, discussing emission observations between IR and RF region and astrophysical-cosmological applications
07 p1387 A70-19643
- Submillimeter wave applications in measurement and communication, developing submillimeter gas maser sources
09 p1676 A70-22784

- Frequency measurement in millimeter and submillimeter ranges, using high quality Fabry-Perot resonator
09 p1680 A70-23141
- Digital wavemeter description using interferometer with parallel plates and automatic frequency readout for submillimeter band
09 p1652 A70-23658
- Cyanide gas lasers design for submillimeter region of electromagnetic spectra
11 p2062 A70-25735
- Germanium, silicon and gallium arsenide point contact and Schottky barrier diodes as submillimeter wavelength detectors and mixers
11 p2017 A70-25736
- Brightness temperature of earth atmospheric emission in submillimeter band at 35 km, describing airborne radiometer
12 p2265 A70-28171
- Submillimeter range HCN gas laser design and characteristics, noting single mode, linear polarization and output power
12 p2250 A70-28180
- Submillimeter astronomy, discussing atmospheric absorption difficulties and principal areas of application
12 p2311 A70-28271
- Millimeter and submillimeter radio waves propagation, outlining molecular and aerosol attenuation in real atmosphere together with transmitters and receivers
13 p2366 A70-29401
- Book on millimeter and submillimeter waves covering generation, transmission, components and detection
14 p2548 A70-30426
- Millimeter and submillimeter waves applications, discussing klystron oscillators for spectral purity and coherence
14 p2548 A70-30427
- Megavolt prebunched electron beam systems for electronic sources in millimeter and submillimeter region, describing microwave accelerators and bunchers
14 p2555 A70-30431
- Submillimeter wave devices with prebunched megavolt electron beams in coupling structures, describing electromagnetic beam couplers
14 p2555 A70-30432
- Pulsed molecular and atomic gas laser sources design for submillimeter region
14 p2593 A70-30433
- Millimeter and submillimeter waves generation as difference frequencies of mixed laser beams
14 p2593 A70-30434
- Millimeter and submillimeter wave receivers, describing detectors, mixers, low noise amplifiers and radiometers
14 p2549 A70-30448
- Submillimeter lasers radiation measurement with n-InSb detectors at liquid He temperature
17 p3107 A70-35109
- Submillimeter wavelength night sky radiation background, observing effects on various cosmic ray phenomena
18 p3308 A70-36330
- Communication network approach to submillimeter wave applications in nondestructive testing, deriving transport equations for EM wave propagation
22 p4028 A70-42591
- ### SUBMINIATURIZATION
- Subminiature three directional cantilever beam accelerometer using semiconductor strain gages
21 p3824 A70-40861
- Subminiature transistor photosensor for direct measurements of capillary blood cell motion
24 p4309 A70-46119
- ### SUBORBITAL FLIGHT
- Legal aspects of suborbital space transports based on air transportation concepts
18 p3350 A70-36661
- Suborbital space transports problem solution by recoverable jet orbital or jet assisted aircraft, discussing implications of Concorde supersonic flight
18 p3350 A70-36663
- ### SUBREFLECTORS
- Shaped-reflector Cassegrainian antenna characteristics calculation, using current distribution method to derive subreflector radiation pattern
02 p0270 A70-12617
- Phase center position of field scattered from hyperboloid subreflector in asymmetric Cassegrain antenna feed system
06 p1019 A70-17557
- Spherical reflector antenna with Gregorian correctors, calculating gain, far field radiation pattern and efficiency as functions of subreflector and feed positions
12 p2200 A70-28052
- ### SUBROUTINES
- Fourth generation systems architecture in microprogramming in terms of control logic, describing inner computer as subroutine processor for controlling interstation communication
08 p1465 A70-20816
- Microstrip circuit design, obtaining dimensions by computer programs incorporating subroutine sets
14 p2561 A70-30922
- NTWO Fortran IV family of subroutines for thermodynamic and transport properties of nitrogen
17 p3195 A70-34746
- ### SUBSETS (MATHEMATICS)
- #### U SET THEORY
- #### SUBSIDENCE
- CAT at subsidence inversion in presence of strong wind shear, noting radar echo pattern as Kelvin-Helmholtz instability indicator
17 p3133 A70-35933
- ### SUBSONIC AIRCRAFT
- Man-computer graphic systems utilization for wing/body aerodynamic design and analysis concept for subsonic vehicles
[AIAA PAPER 69-1130] 01 p0002 A70-10610
- Atmospheric turbulence effects on accelerations experienced by passengers in supersonic and subsonic transport aircraft compared
02 p0325 A70-12219
- Rigid wing subsonic and supersonic civil and military aircraft utilizing aerodynamic lift at takeoff and landing
13 p2344 A70-28543
- Aircraft turbulence penetration performance numerical rating, applying concept to large subsonic jet transports
[AIAA PAPER 70-543] 13 p2347 A70-29074
- Subsonic and supersonic aircraft dynamic loads under conditions of variable atmospheric density
17 p3013 A70-34685
- Subsonic aircraft size effect in conventional design, discussing increased weight increments and economic gain rate
[AIAA PAPER 70-940] 17 p3021 A70-35849
- Subsonic and supersonic transport aircraft design, discussing supercritical wing concept, fuel consumption reduction, composite aircraft structures, short haul transports, etc
17 p3022 A70-35854
- Noise reduction regulations effects on subsonic transport design and configuration
[SAE PAPER 700806] 24 p4290 A70-45876
- ### SUBSONIC FLOW
- Sound generation in axial-flow subsonic turbomachinery, using two dimensional model
[ASME PAPER 69-WA/FE-4] 04 p0735 A70-14785
- Unsteady pressure distributions on elastic swept wing upper and lower sides at high subsonic to transonic flow, investigating torsional and bending vibrations
[DGLR-69-31] 04 p0615 A70-15151
- Inviscid flow problems solution by partial differential equations, considering propagation processes, stratified media, potential, subsonic and three dimensional flows
[DGLR-69-2] 04 p0672 A70-15170
- Fundamental matrix asymptotic forms obtained for supersonic and subsonic three dimensional steady flows past body in uniform stream of viscous thermally conducting fluid
04 p0673 A70-15320
- Subsonic lifting surface theory including leading edge, discussing singularities in solution of integral equation for determination of aerodynamic properties
[AIAA PAPER 69-37] 04 p0619 A70-15387
- IR crossed beam system for direct density turbulence measurements in mixing region of subsonic air jet
[AIAA PAPER 70-235] 06 p1065 A70-18091
- Lifting surface theory for calculation of steady subsonic and supersonic flow over various wing and airplane configurations, emphasizing finite element load prediction method
[AIAA PAPER 70-192] 06 p0971 A70-18114
- Roshko model cavity solution based on Falkovich method application to two dimensional permanent irrotational flow of subsonic gas jet
07 p1258 A70-19571
- Interference kernel discontinuities in integral equations relating amplitude of angle of attack and pressure distribution on T tail harmonically oscillating in subsonic flow
07 p1416 A70-20210
- Pressure distribution on flat plate resulting from potential incompressible flow interaction between secondary jet and subsonic mainstream
07 p1190 A70-20415
- Aerodynamic characteristics of rotating transverse cylinder in subsonic normal flow from analysis of cylinder vortex system, discussing friction drag coefficient
08 p1431 A70-20720
- Mean flow and turbulent velocity over noise-producing regions of subsonic jet nozzle with and without delta wings
09 p1610 A70-22239
- Axisymmetric nozzles flow regimes with subsonic ejection velocities analyzed by stabilization method, noting role of pressure in nozzle exit section
09 p1660 A70-22440
- Subsonic compressible or incompressible inviscid flow field through turbomachine blade row determined by matrix and streamline curvature methods
09 p1608 A70-23745
- Combustible gas /hydrogen-air/ subsonic and transonic flow past sphere, approximating combustion zone structure by model
10 p1801 A70-24142
- Chaplygin function approximation in subsonic steady gas flow analysis
10 p1909 A70-24293
- NASA-Lewis closed loop MHD low temperature power generator, describing systems performances during subsonic tests
11 p1982 A70-25614
- Annulus wall boundary layer effect on spatial flow in subsonic axial compressors by shearing stresses concept between stream surfaces
11 p1974 A70-25777
- Secondary peripheral air injection effects on subsonic airflow through slotted tube, discussing primary flow, flow separation, static and stagnation pressures and temperature changes
11 p2036 A70-26140
- Plasmapause form in equatorial plane in presence of magnetospheric tail subsonic potential convective flow
11 p2047 A70-26796
- Aerodynamic loadings on planar wings in oscillatory subsonic flow determined by collocation for performing Gaussian quadrature integration of pressure and kernel functions
12 p2155 A70-27102
- Subsonic, transonic and supersonic laminar boundary layers acceleration and cooling effects, discussing heat transfer and gas enthalpy
12 p2211 A70-27830
- Specific heat ratio and configuration effects on flow in subsonic, transonic and supersonic sections of Laval nozzle
12 p2159 A70-28233
- Plane, steady, irrotational flow of gaseous subsonic stream bounded by two infinite parallel walls, discussing application to incompressible fluids
13 p2389 A70-29631
- Pressure field due to control surface oscillation in subsonic flow, presenting numerical results for rectangular wing
14 p2528 A70-30295
- Subsonic and transonic gas flow in wake behind finite thickness plate based on Navier-Stokes equations
15 p2719 A70-31484
- Deformable and rigid wings aerodynamic characteristics with subsonic leading and trailing edges, calculating action of gust
15 p2671 A70-31486
- Aerothermopressor experiment in subsonic and supersonic gas flow compared with numerical solutions of equations
15 p2720 A70-31900
- Laminar to turbulent transitions determination in sub-/supersonic flows, reviewing methods based on hot-wire anemometer output signal
[ONERA-TP-841] 15 p2720 A70-31918
- Aerodynamic forces exerted by compressible fluid on airfoil cascade in subsonic potential flow
16 p2833 A70-33075
- Integral model for combustion of metal particle laden jet mixing with subsonic secondary stream in duct, considering air breathing engine design
[AIAA PAPER 70-736] 16 p2964 A70-33490
- Subsonic turbulent boundary layer with mass addition and combustion for combustion effects on velocity profiles in constant pressure and accelerating flows
[AIAA PAPER 70-724] 16 p2997 A70-33498
- Forces on two dimensional oscillating airfoil in subsonic compressible wind tunnel flow, solving partial differential equation for pressure potential by integral transform technique
16 p2839 A70-34248
- Aerodynamic and acoustic characteristics of subsonic and supersonic jets from convergent nozzles with room temperature air supply
17 p3005 A70-34460
- Blunt based right circular cylindrical body at subsonic speed, investigating turbulent near wake in wind tunnel
17 p3006 A70-34463
- Convective heat transfer at solid boundaries in separated and reattached subsonic and supersonic flows, considering booster base heating
17 p3007 A70-34484
- Velocity pulsation spectra in subsonic wakes behind circular disks and sphere, using thermoanemometer with constant filament temperature
18 p3207 A70-36279
- Subsonic flow visualization, using steam and cold nitrogen gas mixture and normal tunnel lighting
18 p3237 A70-36460
- Steady sub and supersonic flow calculations behind receding shock wave, using finite difference scheme
20 p3611 A70-39803

Subsonic air flow around airfoil in wind tunnel, detecting density gradients by pulsed ruby laser holographic visualization

21 p3822 A70-40809

Subsonic channel incompressible gas flow past semiinfinite flat plate base, using flow pattern for cavitation flow

21 p3748 A70-42213

Perfect gas acyclic and cyclic, steady and irrotational motions in subsonic regime around convex profile with constant curvature variation by Chaplygin method

21 p3846 A70-42259

Perfect gas circular subsonic flow around convex obstacle, using hodographic method for boundary problem

22 p3958 A70-42608

Harmonically oscillating wing linearized motion in subsonic flow, calculating generalized aerodynamic forces

22 p4105 A70-43118

Subsonic jet engine intake duct radar cross section calculation using waveguide model

22 p3992 A70-43584

Similarity rules for sinusoidal gust loads on thin two dimensional wing in nonstationary subsonic flows

23 p4131 A70-43970

Aerodynamic problems due to mixed subsonic and supersonic/ transonic flows on swept wings, nacelle lips and helicopter rotor blades [ICAS PAPER 70-14]

23 p4132 A70-44125

Subsonic Ludwig/simple expansion/tube as shock tube for aerodynamic testing, examining flow characteristics

23 p4182 A70-44578

High subsonic and transonic effects on pressure distributions for swept wing with oscillating control surface

23 p4274 A70-44763

Aerodynamic interferences of lifting surfaces harmonically vibrating in subsonic flow

23 p4136 A70-44765

Ducted propeller subsonic rotational flow with free boundaries, presenting second-order partial differential equation solution without linearizing assumptions

24 p4287 A70-45269

Stationary aeroelastic cases studied in subsonic flow range, providing criteria for aircraft design with required flight characteristics

24 p4422 A70-45443

Subsonic flow around bodies of revolution in axial direction, using ALGOL program for numerical calculations

24 p4289 A70-46237

SUBSONIC FLUTTER

Parallel isotropic flat plates vibration and flutter in supersonic/subsonic flow over one surface, observing plane loadings and elastic medium stiffness effects

12 p2316 A70-27104

Low aspect ratio plates flutter analysis for subsonic and supersonic models

16 p2991 A70-33888

SUBSONIC SPEED

Numerical method for calculating gust effect on wing of complex planform at subsonic speeds by converting continuous to discrete processes

04 p0618 A70-15242

Subsonic circular jet noise radiation intensity and directional distribution, based on effects of refraction and Lighthill quadrupole model for aerodynamic noise

05 p0834 A70-16780

Aerodynamic flight characteristics of lifting reentry bodies in subsonic to hypersonic range in wind tunnel tests

06 p1154 A70-17249

Stability derivatives for bodies of revolution at subsonic and transonic speeds [AIAA PAPER 70-190]

06 p0976 A70-18239

Strap-on ferry package for reusable spacecraft and launch vehicles subsonic lift/drag increase

07 p1397 A70-20390

Air compressibility effects on aerodynamic characteristics of slender rectangular wings moving at subsonic speed near earth surface approximated by lifting surface theory

10 p1801 A70-24276

Lift and drag characteristics of flexible parawings at subsonic speeds, predicting angle of attack for trailing edge flutter commencement

12 p2157 A70-28079

Subsonic kernel function applicability limited to surfaces with small inclinations to freestream, considering wing with deflected control surface

12 p2212 A70-28089

Vortex- and Doublet-Lattice methods for calculating aerodynamic lift distributions on surfaces in steady and oscillatory motion at subsonic speeds

13 p2339 A70-29006

Slender wings leading edge vortex flow effect on roll damping at subsonic speeds [AIAA PAPER 70-540]

13 p2339 A70-29007

Intermittent blowdown supersonic wind tunnel as economic test facility covering subsonic test velocity range, discussing data quality [AIAA PAPER 70-581]

13 p2342 A70-29889

Single and twin jet afterbody configuration models, describing drag and interference characteristics at subsonic speeds

14 p2528 A70-30862

Exhaust nozzle model tests at high subsonic Mach numbers, investigating differences in nozzle drag in contrast to engine conditions [AIAA PAPER 70-668]

16 p2967 A70-33573

Subsonic wing theory calculation method, obtaining close solutions for integral expression constants for downward air currents

19 p3352 A70-38164

Reentry bodies of revolution subsonic and supersonic aerodynamic characteristics

20 p3558 A70-39704

Streamers /drag devices/ tests at subsonic speeds, measuring drag dependence on size, weight, shape and velocity

20 p3559 A70-40282

Strap-on ferry package for reusable spacecraft and launch vehicles subsonic lift/drag increase [AIAA PAPER 70-259]

21 p3931 A70-41867

Subsonic high lift cruise wing optimal design using kernel function method of planar lifting surface theory

22 p3959 A70-42709

Downwash angle behind straight wing for unsteady aperiodic flight at subsonic speeds, using vorticity model

22 p3959 A70-42802

Drag estimation for circular cylinders at subcritical Reynolds numbers and subsonic speeds, using Kármán vortex street theory for wake

23 p4131 A70-43894

SUBSONIC WIND TUNNELS

60 cm intermittent blowdown type trisonic wind tunnel, discussing main parts basic dimensions and characteristics determination method, detailing design and construction

01 p0055 A70-10148

Heat transfer in turbulent boundary layer of airflow injected on smooth plate from nozzle in subsonic stepwise heated wind tunnel

01 p0216 A70-11001

Airfoil research in S-10 French wind tunnel for two dimensional flow, noting Reynolds and Mach number ranges [ONERA-TP-766]

08 p1433 A70-21843

Aerodynamic subsonic and supersonic wind tunnels parameter measurement methods including static and total pressure, current direction, velocity, density, etc

09 p1674 A70-22314

Missile aerodynamic characteristics investigation in subsonic low turbulence wind tunnel with three degrees of freedom angular motions [AIAA PAPER 70-578]

13 p2342 A70-29891

Subsonic boundary lift interference in wind tunnels with perforated walls, using point matching method

14 p2563 A70-30869

SUBSTRATES

Thickness measurement of nonmagnetic coatings on magnetic substrates taking into account surface roughness effect

02 p0302 A70-12672

Beam-lead substrate package for six stage TTL shift register, discussing metallization systems for interconnections and beams

02 p0271 A70-12846

Organic substrates effects on Hydrogenomonas eutropha autotrophic and heterotrophic metabolism

10 p1817 A70-24700

Adhesive bonds strength parameters, discussing substrate type, surface preparation, etc [ASME PAPER 70-DE-33]

16 p2939 A70-33504

MIS structures with silicon nitride film deposited by RF glow discharge, observing doping increase in epitaxial substrate

17 p3055 A70-35873

Ni base alloys sulfidation kinetics, examining roles of sodium/sulfur compounds-substrate interactions in accelerated oxidation

20 p3651 A70-40072

Acoustic surface waves phase velocity on lithium niobate with gold layer for propagation modes, predicting LF cut-off by substrate anisotropy

21 p3863 A70-42001

Nb-Zr thin films superconducting properties dependence on deposition temperature and rate and substrate material

22 p4085 A70-42623

SUBSTRUCTURES

Matrix decomposition and full release methods for substructure analysis

09 p1770 A70-22258

Complex redundant structures matrix analysis by substructure approach, obtaining elastic properties of system by subdivision and synthesis [SAE PAPER 700217]

11 p2134 A70-25889

Apollo 11 lunar rock clinopyroxene, plagioclase and ilmenite internal substructure, using high voltage transmission electron microscopy

21 p3901 A70-41544

SUBTRACTION

Small digital computer arithmetic unit design, discussing number representation, addition and subtraction methods for performance and cost

21 p3793 A70-40757

SUBTROPICAL REGIONS

U TEMPERATE REGIONS

U TROPICAL REGIONS

SUCTION

Boundary layer processes under unsteady suction allowing for compressibility, relating suction value to external velocity and wall temperature

03 p0465 A70-13275

Asymptotic expansion method to analyze laminar boundary layers with zero wall shear, large suction and adverse pressure gradients

04 p0674 A70-15563

Suction influence on skin friction fluctuations of MHD flow along infinite flat wall using Navier-Stokes equations

05 p0886 A70-15787

Axial flow pump impellers suction performance and cavitation conditions

06 p1075 A70-17137

Upper surface suction effect on thin plate aerodynamic characteristics, considering relations for lift and pitching moment coefficients

06 p0968 A70-17851

Unsteady boundary layer flow with suction, deriving equations for circular cylinder impulsive motion

07 p1253 A70-18862

Steady turbulent boundary layer of compressible perfect gas on heat insulated surface with suction and longitudinal pressure gradient

07 p1254 A70-19081

Turbulent incompressible boundary layer on porous heat insulated plate with uniform suction, calculating ratio of friction drag coefficients

07 p1254 A70-19082

Boundary layers calculation for nonporous surface extended to porous with suction by replacing velocity distribution with longitudinal pressure gradient

07 p1254 A70-19083

Flow properties and heat transfer of wall jet spreading over permeable surface with suction and blowing

07 p1258 A70-19720

Incompressible conducting fluid MHD flow at infinite plane wall forward stagnation point, considering suction or injection effects

07 p1354 A70-20237

Suction effect on thin film laminar flow past vertical wall, obtaining approximate solution for small porosity in accelerated region

08 p1484 A70-21309

MHD flow between two parallel plates, noting pressure gradient and skin friction coefficient

08 p1554 A70-21774

Laminar boundary layer separation noting effect of mass slot suction

09 p1662 A70-23236

Turbulent pipe flow with wall suction, calculating friction factor, pressure gradient, heat and mass transfer coefficients, velocity and temperature profiles [ASME PAPER 69-HT-4]

09 p1790 A70-23558

Motion and continuity equations for unsteady two dimensional flow of incompressible viscous fluid along infinite flat plate with time dependent suction

10 p1862 A70-23877

Suction force increase resulting from turbulent jet interaction with transverse flow

10 p1868 A70-24166

Casing and suction cone effects on fans with cambered forward curved blading

11 p1975 A70-25796

Pressure recovery and energy loss efficiencies of two dimensional diffusers with suction at entrance

11 p1977 A70-26418

Pressure fluctuations in acoustic field of boundary layer under slot suction, considering vortex formation and separation on edges

12 p2209 A70-27298

Wing tip trailing vortices hazard reduction on closely spaced parallel runways by suction application, discussing power requirements

12 p2207 A70-27631

Oscillatory flow in porous channel with suction and injection, using Laplace transform technique

13 p2389 A70-29538

Inflow and pressure difference for mean flow in straight suction duct with porous walls, using elementary momentum analysis

13 p2392 A70-30020

Inducer tip clearance effect on centrifugal pump suction performance with velocity and total head distributions at outlet

14 p2592 A70-31332

Boundary layer retarded flow past porous surface with suction, using Runge-Kutta computerized integration of Falkner-Scan equation

15 p2720 A70-31586

Liquid hydrogen axial flow pump inducer, describing suction pressure measurements, fluid conditions and flow rate [AIAA PAPER 70-627]

16 p2919 A70-33592

SUD AVIATION AIRCRAFT

Conical shock wave-turbulent boundary layer interaction data obtained for adiabatic wall conditions at supersonic free stream Mach numbers, including suction effects

18 p3241 A70-36448

Suction velocity effects on Rayleigh problem in MHD of flat nonmagnetic nonconducting plate, solving for velocity distribution and skin friction

19 p3481 A70-38448

Two dimensional MHD couette flow in slip regime, considering constant suction on stationary plate to determine transverse magnetic effects

20 p3677 A70-39047

Divergent channel with porous walls, calculating effect of suction on laminar incompressible boundary layer by Runge-Kutta method

20 p3609 A70-39671

Unsteady incompressible flow in laminar boundary layer with homogeneous suction during longitudinal flow past flat plates, investigating boundary layer stability

20 p3614 A70-40391

Flat plate boundary layer flow with surface blowing and suction /mass transfer/, investigating stability by numerical techniques

20 p3615 A70-40507

Two dimensional incompressible flow, calculating strong suction effects on laminar boundary layer separation by linear model

22 p4010 A70-42630

Steady incompressible turbulent boundary layer form on permeable curvilinear surface with uniform suction, assuming small pressure gradients

22 p4011 A70-42803

Turbulent boundary layer control by uniform fluid injection and suction, discussing velocity profiles, wall and wake laws, skin friction and shear stress transport equation [ICAS PAPER 70-10]

23 p4180 A70-44121

Two dimensional boundary layer growth with suction for oscillating circular cylinder, considering stream functions and phase angles

24 p4326 A70-46002

SUD AVIATION AIRCRAFT

NT CONCORDE AIRCRAFT

NT SA-330 HELICOPTER

SUD AVIATION SA-330 HELICOPTER

U SA-330 HELICOPTER

SUDDEN ENHANCEMENT OF ATMOSPHERICS

Diurnal variations of sudden enhancements and decreases of ELF atmospherics, using mode theory

21 p3814 A70-40939

SUDDEN IONOSPHERIC DISTURBANCES

Meter wave type 3 solar radio waves associated with solar X ray flares, discussing sudden enhancements of L.F. field strength due to D layer ionization enhancement

01 p0168 A70-10257

Solar X-ray bursts observations correlation with sudden phase anomalies measured at long VHF propagation paths in lower ionosphere

03 p0558 A70-13601

Ionospheric effect sudden commencement parameters of magnetic storm related to distance from origin in polar regions

05 p0841 A70-16737

Extreme UV flashes of solar flare observed by sudden ionospheric frequency deviations compared with energetic X rays observations

05 p0905 A70-16981

SID effects during recording of long wave transmitter field strength, indicating relation between solar X-ray flares and field anomalies

10 p1932 A70-24485

Blanketing type sporadic E layer associated with equatorial electrojet as thin layer of enhanced ionization

10 p1880 A70-24801

SID observed as VLF phase anomalies correlated with solar microwave radio bursts

10 p1933 A70-24816

Scintillation sudden inception in Faraday rotation in Sodankyl and Oulu, noting diurnal north-south frontier movements in polar ionosphere

10 p1884 A70-25262

Sudden phase anomaly /SPA/ in VLF radio wave propagation during Proton Flare Project, noting corresponding solar X-ray flux intensity enhancement

15 p2794 A70-32294

Negative sudden phase anomaly /SPA/ in VLF radio transmission, noting solar X ray flux intensity and zenith angle effects

15 p2699 A70-32297

Whistler VLF radio observations of sudden magnetic impulses in plasmasphere during storms, using ground based magnetometers

20 p3620 A70-39330

Electron precipitation at geomagnetic storm sudden commencement in auroral zone from X ray balloon observations

21 p3814 A70-40937

SUGARS

NT GALACTOSE

NT GLUCOSE

NT LACTOSE

NT MONOSACCHARIDES

Fructose metabolism in liver and extrahepatic tissues of sea level and high altitude natives, noting lactate and pyruvate accumulation in blood

02 p0233 A70-11722

Formose sugars production from formaldehyde, discussing economic conversion by catalytic reactions

16 p2855 A70-33063

3-O-methyl-mannose neutral sugar identification as constituent of fungal polysaccharide

20 p3572 A70-39625

SUITS

NT PRESSURE SUITS

NT SPACE SUITS

SULFATES

Beryllium sulfate effect on rabbits vascular plasma volumes, using albumin method for blood groups

15 p2681 A70-31884

Thermal decomposition of fine-dispersion iron sulfate powders under continuous heating during ferites manufacture

23 p4205 A70-44041

Microgram 2-nitro-1-butyl pyridinium sulfate /NBPS/ inhibition of growth of *Bacillus subtilis* by blocking thymidylate synthetase

23 p4158 A70-44998

SULFATION

Oxidation and sulfidation resistant diffusion coatings for superalloys, discussing processing methods, composition, properties and application [SAE PAPER 690479]

03 p0509 A70-13266

SULFIDES

NT CADMIUM SULFIDES

NT CARBON DISULFIDE

NT COPPER SULFIDES

NT DISULFIDES

NT HYDROGEN SULFIDE

NT MOLYBDENUM DISULFIDES

NT MOLYBDENUM SULFIDES

NT POLYSULFIDES

NT PYRRHOTITE

NT TROILITE

NT ZINC SULFIDES

Alloying elements preventing hot cracking in weld metal by converting iron sulfides into higher melting point sulfides

07 p1293 A70-18979

Ferromagnetic cubic sulfide of Fe easy axis by electron diffraction pattern, aligning sulfide particles along magnetic field

13 p2472 A70-29712

Sulfidation kinetics and scale morphology of Cr and Cr-Mo alloys at high temperatures in hydrogen/hydrogen sulfide atmosphere

19 p3452 A70-37827

SULFONES

Aromatic polysulfone thermomechanical behavior by torsional braid analysis, discussing structure, synthesis, thermal stability, radiation effects, etc

21 p3783 A70-42134

SULFUR

Reply to Swings comments on validity of forbidden S I lines in solar spectrum communicated by Swenson

01 p0175 A70-10240

Hot corrosion reactions in Ni, Co and NiAl-base alloys exposed to salt-sulfur containing simulated gas turbine combustion atmospheres

01 p0118 A70-10728

Manganese and sulfur content effects on martensitic stainless steels machinability, describing effects on mechanical properties, cold formability and corrosion resistance

03 p0507 A70-13135

Earth oxygen atmosphere age estimated from sulfur isotope composition of geological phlogopite and lazurite deposits from South Baikal region

06 p1056 A70-17798

Sulfur beam foil spectrum in 600-4000 Å range, identifying transitions in S I-S VI

11 p1994 A70-25362

Carbon and sulfur reactions with solar hydrogen atoms in Apollo 11 lunar samples accounting for isotopic composition of fine-grained basaltic rocks

14 p2545 A70-30791

Inverted coexistence possibility of spherical and deformed states in Si 28 and S 32 nuclei

17 p3137 A70-34518

Ni-S melts thermodynamic properties in 700-1100 C range by continuous thermal balance method, calculating S vapor pressure

18 p3271 A70-36029

Sulphur in earth core composition, considering volatile element abundances and iron melt in thermal models

18 p3256 A70-37078

Helium-like resonance, intercombination and forbidden transitions of Ca, Si and S lines during 3b solar flare decay

20 p3700 A70-40420

Clean iron /011/ surfaces, determining sulfur, oxygen and hydrogen sulfide films effects on adhesion behavior

21 p3831 A70-40748

Carbon and sulfur concentration and isotopic variations in Apollo 11 fines, breccias and fine-grained basalts

21 p3775 A70-41586

Phase relations in system Ag-Fe-S in 700-1200 C range at various vapor pressures by quenching and differential thermal analysis, observing liquid-immiscibility fields

22 p4053 A70-42732

SULFUR CHLORIDES

Sulfur trichloride-Al tetrachloride complex ionic structure from Raman spectra and nuclear quadrupole resonance data

21 p3772 A70-40912

SULFUR COMPOUNDS

NT CADMIUM SULFIDES

NT CARBON DISULFIDE

NT COPPER SULFIDES

NT CYSTEINE

NT DISULFIDES

NT HYDROGEN SULFIDE

NT MOLYBDENUM DISULFIDES

NT MOLYBDENUM SULFIDES

NT ORGANIC SULFUR COMPOUNDS

NT POLYSULFIDES

NT PYRRHOTITE

NT SULFATES

NT SULFIDES

NT SULFONES

NT SULFUR CHLORIDES

NT SULFUR FLUORIDES

NT SULFUR OXIDES

NT SULFURIC ACID

NT THIOLS

NT TROILITE

NT ZINC SULFIDES

Sulfur compound effects on carbon monoxide-nitrogen laser emission stability, obtaining continuous operation independently of tube quality

01 p0111 A70-10660

Phase equilibria in Mn-S, Mn-Se and MnS-MnSe systems by X ray diffraction after preparation by annealing

02 p0249 A70-11652

Ni base alloys sulfidation kinetics, examining roles of sodium/sulfur compounds-substrate interactions in accelerated oxidation

20 p3651 A70-40072

Thermally stable arylsulfimide polymers incorporating 1, 2-disulfonimide group

21 p3782 A70-42130

SULFUR FLUORIDES

Tunable diode laser for high resolution IR spectroscopy of sulfur hexafluoride absorption near carbon dioxide laser lines

13 p2430 A70-29832

Electron attachment rate to sulfur hexafluoride in He buffered flowing afterglow

21 p3853 A70-41394

Supersonic convective electric arcs with magnetic stabilization in sulfur hexafluoride, examining aerodynamic drag and plasma column slanting

23 p4227 A70-44554

SULFUR OXIDES

Satellite monitoring of air pollution, discussing sulfur dioxide measurement in UV, optical correlation techniques, IR and visible spectra, stratospheric balloon tests, etc

09 p1668 A70-22875

Dual photon emission from chemiluminescent SO-O reaction, proposing two step emission mechanism

09 p1630 A70-23001

Methyl methacrylate and other vinyl monomers polymerization activation by low sulfur dioxide concentrations, noting inert solvents effect

14 p2544 A70-30246

Spectroscopic detection of sulfur dioxide and carbon dioxide molecules and concentrations in polluted atmosphere by laser-Raman radar technique

20 p3640 A70-39389

Air polluting sulfur dioxide and nitrogen dioxide remote sensing based on radiation molecular absorption using long line correlation spectrometer

20 p3633 A70-39793

SULFURIC ACID

Alpha- and beta-styryl azides catalyzed reactions in ethanolic sulfuric acid

05 p0810 A70-16053

Radiation effects on dihydrothymine in frozen sulfuric acid solutions, detecting thymine after melting via low temperature UV absorption measurements

20 p3583 A70-40454

Ni/sulfuric acid AC voltage polarization curves for anodic dissolution region

24 p4364 A70-46220

SUM RULES

Limiting theorems for sums of random variables linked in Markovian chain, applying probabilistic and analytical methods

19 p3456 A70-37235

SUMMARIES

NT ABSTRACTS

SUMMER

Cosmic ray latitude survey in North America in summer using neutron and muon monitors operating near sea level and on mountains

01 p0167 A70-10226

Summertime midnight airglow enhancement of 6300 Å line by sensitive continuum compensating photometer, suggesting F 2 region electron density increase for emission

12 p2225 A70-27895

F 1 region unsteady model, examining vertical distribution profile of electron concentration on summer day

19 p3409 A70-37323

Synoptic processes in troposphere and stratosphere with large air temperature anomalies during early summer in U.S.S.R.

20 p3663 A70-39272

SUMS

Generalized Watson sums evaluation without series expansions or extensive computer summations, calculating magnetization of anisotropic Heisenberg ferromagnet for cubic, bcc and fcc lattices

04 p0730 A70-14689

Bessel generalized polynomial series convergence and summability on contour of convergence region

11 p2071 A70-25521

Cyclic codes for error correction noting connection with exponential sum theorems

11 p2074 A70-26312

Markov renewal processes sums convergence to multidimensional Poisson process, discussing convergence conditions

12 p2260 A70-26884

ALGOL algorithms for solving sum and bottleneck assignment problems

12 p2192 A70-27767

Cesaro Fourier series summation method for boundary value problems in electrostatics

14 p2600 A70-31419

Limit theorems for sums of multidimensional stochastic step processes, giving necessary and sufficient conditions for convergence to Poisson measures

16 p2942 A70-33700

Kaban Babuska summation method variant in Triplex-ALGOL 60 for reducing roundoff errors in finite series calculation

19 p3385 A70-38678

SUN

Simultaneous filtergrams of velocity and intensity field of central solar disk obtained in blue and red wings of Fraunhofer line

01 p0175 A70-10242

Sun-planet systems capture and catapult capacity for interstellar bodies under close flyby conditions

04 p0753 A70-15144

Solar structure models for neutrino flux prediction compared with solar structure, suggesting modification in solar and stellar evolution calculations

05 p0906 A70-15895

Nonlinear effects in spiral galaxies with emphasis on solar neighborhood region, discussing radial motion, stationary state with excited waves and vertex deviation

05 p0917 A70-16905

Solar photographs taken with motion picture cameras in integral light

05 p0920 A70-16974

Resonance in restricted three body problem applied to asteroidal motion in asteroid-Jupiter-sun system

06 p1152 A70-18492

Plasmas role in emission mechanisms active in celestial sources of radiation, discussing sun and quasars

10 p1948 A70-25027

Thermonuclear reactions in interior of sun, discussing models for He isotope concentration and flow to interpret solar neutrino generation

13 p2494 A70-29573

Sudden disappearance of large quiescent prominence on solar disk with subsequent brightenings, using photospheric and gravitational model

13 p2497 A70-29850

Metal to hydrogen ratio for sun, Hyades and F-G stars based on photoelectric measurements of weak metal lines

14 p2652 A70-31388

Solar Ga abundance from spectral synthesis of region around 4172 Å line

18 p3316 A70-36894

Solar core opacity, investigating individual heavy elements influence and effect of changes in abundances

18 p3317 A70-37005

Mercury transit across sun on 9 May 1970, discussing observation, equipment and photographs

18 p3319 A70-37050

Galactic spiral structure relation to local stellar distribution, discussing OB associations, galactic cluster, WR stars, cepheids, and common stars in sun neighborhood

18 p3329 A70-37176

Solar disk dimensions and RF emission characteristics from eclipse observation and flux recordings, considering brightness temperature distribution and lunar edge diffraction effects

19 p3521 A70-38551

Sun photographs with violet interference filter, determining photospheric magnetic fields position by copatial network

20 p3634 A70-40410

Statistical estimates of precessional corrections, solar motion and galactic rotation from proper motions

23 p4246 A70-44752

SUN SENSORS

U SCLAR SENSORS

SUNLIGHT

Solar brightness variations observed photometrically, discussing periodicity, sunspot locations, photosphere and subsurface rotations, etc

01 p0186 A70-11273

Scattering functions from sky light spectra measurements on high mountain for various sun altitudes, obtaining color value functions

02 p0359 A70-12776

Atmospheric absorption anomalies of UV sunlight near 50 km altitude in rocket-borne radiometer determination of ozone distribution

03 p0478 A70-14197

Electron temperature anisotropy in ionospheric plasma for case of ionizing sunlight propagating along geomagnetic field

03 p0479 A70-14376

Sea surface sunglint pattern irregularities in earth orbiting satellite photographs, observing dark patches

05 p0838 A70-16152

Mercury arc injection lamp as radiation source for testing sunlight biological effects

10 p1888 A70-24388

Ozone measurement from satellite by direct beam and scattered light methods employing UV sunlight attenuation

10 p1890 A70-24639

Manual spectrograph for distant objects spectrophotometry under natural conditions and solar illumination

14 p2583 A70-30415

Night airglow space and time variations from jet aircraft observations, measuring conjugate enhancements

14 p2580 A70-31266

Electric space charge pulse density measurements near ground in sunny weather related to free convection

15 p2726 A70-31868

Anomalous dark areas in sunglint patterns from ATS photographs, considering water temperature effect on ocean surface conditions

16 p2897 A70-33725

Directional solar thermal field /sunglint/ effect on coupled nonplanar transverse and torsional vibrations of satellite cylindrical antennas in orbit

20 p3720 A70-39676

Solar optical and radio activity observation in 1968, noting optical-radio data correlation

22 p4095 A70-43259

Linear polarization of sunlight scattered by Venus atmosphere, giving data for integrated disk and equatorial region

23 p4246 A70-44756

Ashen light origin, considering atmospheric refraction of sunlight illuminating dark side of planet

24 p4399 A70-45113

SUNRISE

VLF wave propagation across sunrise line analysis based on idealized model for earth-ionosphere waveguide

01 p0042 A70-10048

Predawn O I 6300 Å airglow enhancement, observing time variations and suggesting mechanism

02 p0289 A70-12120

Transequatorial multisite VLF records establishing solar zenith angle for midpoint of sunrise ionospheric height discontinuity, recomputing magnetic latitude dependent parameters

06 p1054 A70-17590

Sunrise effects in lower ionosphere at midlatitude, discussing long wave absorption measurements, summer electron concentration profile and consistency of aeronomic model

07 p1235 A70-19436

Seasonal measurements of ionospheric absorption during sunrise in D region at medium sunspot numbers, noting disagreement with rocket observation

13 p2392 A70-28574

Ozone content effect on presunrise fall in LF radio waves amplitude from Radio Tashkent to Delhi, noting UV light role

17 p3077 A70-34947

Sunrise effects in lower ionosphere at midlatitude, discussing long wave absorption measurements, summer electron concentration profile and consistency of aeronomic model

18 p3249 A70-36910

SUNSET

Grating spectrometer with Ge-Cu detector used on balloon flights for studying variations of IR solar spectrum with altitude, emphasizing sunspot features

06 p1152 A70-18523

Lunar postsunset horizon afterglow observed by Surveyor 7, discussing small particle diffraction on surface

20 p3708 A70-39960

SUNSPOT CYCLE

Spread F echoes occurrence variations over solar cycle, observing range and frequency splitting type during maximum and minimum sunspot years

01 p0080 A70-11222

Solar corona at sunspot maximum observed during 22 September 1968 total solar eclipse, noting coronal streams unpredicted by magnetostatic model

06 p1138 A70-12728

F 2 field-aligned ion velocity measurement compared with theoretical results, discussing difference at sunspot minimum and daytime ion velocity-plasma loss relation

10 p1881 A70-24815

Sunspot cycle and ionospheric D and E layers daily radio wave absorption correlation, observing seasonal variation effect

10 p1885 A70-25267

Solar activity forecasting using normalized sunspot curves deduced from 200 years of observations, discussing parameters of running 11 year cycle

10 p1949 A70-25287

Wolf numbers monthly fluctuations, giving histogram of fluctuation amplitude distribution

18 p3323 A70-37137

Sunspot number prediction from solar cycles statistical analysis

23 p4254 A70-44902

SUNSPOTS

Chromospheric average velocity field near sunspots determined from M alpha line absorption elements wavelength shifts

01 p0176 A70-10247

Penumbra forms and magnetic polarity distribution relationship in sunspot groups

01 p0184 A70-10955

Correlation between sunspot number index and solar radio noise index relative to ionospheric propagation, noting computer analysis program and hysteresis effect

02 p0289 A70-12107

Radiative energy transport in sunspot region via model computations, obtaining reduced subphotospheric flux estimates for given magnetic field

02 p0372 A70-12254

Joule dissipation model for sunspot magnetic field, discussing field fine structure and lifetime

02 p0373 A70-12374

Magnetic flux trapping experiment with Al conductor, showing decay time constant connection with sunspot theory

02 p0299 A70-12393

Hydrostatic models of sunspot penumbra and umbra, analyzing spot transparency influence on Wilson effect

03 p0571 A70-13596

Sunspot motion statistics for 1965-1967 from observational data, complementing electron-corona differential rotation and spectroscopic measurements

03 p0571 A70-13597

Absorption line identification in sunspot spectra by calculating Zeeman patterns, using Zeeman splitting for magnetic field measurement

03 p0574 A70-13934

Secular variation in F region ionization response to sunspot number, noting dominant component as cosine term equal to four sunspot cycles

04 p0678 A70-14972

HF molecular vibration rotation band observed in sunspot spectra, carrying out model calculations for spots differing in temperature for fluorine abundance

04 p0751 A70-15048

Solar atmospheric structure near sunspots by spectrophotometry, presenting observational and theoretical sunspot magnetic and velocity field data

04 p0754 A70-15351

Magnetic vector directions over sunspot near central meridian passage measured, showing axisymmetric arrangement

04 p0758 A70-15697

Eleven year cosmic ray variation and solar activity cycle analysis, showing variation amplitude dependence on both numbers and heliolatitudinal distribution of sunspots

04 p0742 A70-15718

Gas pressure and pressure stratification in sunspot, using curve of growth analysis

05 p0911 A70-16432

Diatomic carbon swan band violet line absence from sunspot suggested in accordance with molecular equilibrium predictions

05 p0911 A70-16433

Photospheric magnetic flux quantization away from sunspots, studying nonsunspot field strength distribution

06 p1142 A70-17992

Sunspot temperature and pressure gradients from blue, red and IR photographs, deriving umbral depression and density scale height 06 p1143 A70-18000

Wilson effect in sunspot structure as penumbra foreshortening and disappearance or penumbra occultation by photosphere, analyzing intensity profiles on disk passage photographs 06 p1143 A70-18001

Magnetic and velocity fields in unipolar sunspot, discussing fluctuations associated with penumbral and umbral fine structures 06 p1144 A70-18002

Sunspot umbral dot models characteristics based on three dimensional radiative transfer analysis 06 p1144 A70-18003

Sunspot magnetic field structure, determining vector field from longitudinal component perspective effect observations 06 p1149 A70-18457

LOF observations of long distance transequatorial step frequency radio circuits in Pacific Area during sunspot minimum period 07 p1232 A70-19174

Effective LUF fade-out and fade-in times seasonal and diurnal variations for oblique ionospheric propagation paths, noting sunspot number effects 07 p1233 A70-19180

Electromagnetic acceleration and energy losses of charged chromospheric-coronal plasma electrons and protons in unsteady magnetic fields of sunspots 07 p1384 A70-19417

H alpha brightening areas related to sunspot magnetic fields configuration and solar proton flares 07 p1369 A70-20072

Rapid scanning high resolution photoelectric spectrometer for sunspot spectra study 07 p1289 A70-20291

Sunspot group of July 1966, studying umbrae structures relation to magnetic field 08 p1569 A70-20835

Darkening and brightening of disturbed spot on sun surface determined by abnormal stress in seen layers due to magnetic and velocity fields 08 p1570 A70-20903

Magnesium hydride absorption lines in sunspot spectrograms indicating heavy Mg enhancement in sun relative to earth 08 p1571 A70-20904

Localized high energy flaring of active center monitored with time-associated radio bursts in spot umbrae 08 p1561 A70-20905

Sunspots narrow and double K lines probable emission by quiescent type prominences 08 p1575 A70-21372

Critical sunspot dependence of F 2 region noon bite-out phenomenon at various equatorial latitudes, observing magnetic dip 08 p1492 A70-21837

Solar continually changing features /brightenings, darkenings, condensations and groupings/ associated with solar activity, emphasizing sunspot number formulas 09 p1751 A70-22197

Solar activity analysis emphasizing sunspots, magnetic disturbances and bursts data 09 p1752 A70-22199

Sunspots photospheric layers magnetic field structure, analyzing anomalous Zeeman pi- components in umbra 09 p1757 A70-22685

Solar activity /1967/ catalog containing tabulated spot area, Wolf numbers, 1966 spot groups, etc 10 p1935 A70-23838

Solar boron abundance from BH, BN and BO absorption bands in sunspot spectra, noting no traces in solar atmosphere 11 p2108 A70-25738

Solar active centers interaction effects on spot growth and proper motion 11 p2109 A70-25743

Statistical analysis of latitude distribution of magnetically classified sunspot groups and associated flares 11 p2106 A70-26646

Solar flare relation to local magnetic field in active regions, discussing sunspot and weak field measures 12 p2297 A70-26986

Molecular line identification in sunspot spectrum of CN, diatomic carbon, TiO, MgH, CaH, NiH and water vapor 12 p2302 A70-27590

Seasonal measurements of ionospheric absorption during sunrise in D region at medium sunspot numbers, noting disagreement with rocket observation 13 p2392 A70-28574

Solar flares number decrease near central meridian noting no sunspot decrease 13 p2477 A70-29047

Sunspots butterfly diagram shape relation to solar differential rotation 13 p2491 A70-29048

Low latitude scintillations from satellite transmission scintillations correlation with solar activity spread F, electron content and ionospheric irregularities 13 p2397 A70-29189

Magnetic field spatial structure in sunspot with photospheric bridge, using photographic observations of solar spectrum lines 13 p2493 A70-29391

Sunspot minimum intensity dependence on area, including correction for blurring or image motion, scattered light and line absorption 13 p2496 A70-29846

HOH lines existence in sunspot umbral spectrum 13 p2496 A70-29847

Sunspot electric current density accounting for magnetic field abrupt reversal 13 p2496 A70-29848

Lunar tide in ionospheric D region absorption near magnetic equator, noting annual variation relationship to sunspots 14 p2574 A70-30747

Water vapor in sunspots, taking into account red shift between telluric and intrinsic sunspot HOH lines 14 p2641 A70-30790

Eleven year cosmic ray variation and solar activity cycle analysis, showing variation amplitude dependence on both numbers and heliolatitudinal distribution of sunspots 14 p2632 A70-30802

Electron and ion temperature and electron density relationship in F region during sunspot maximum, using incoherent scatter experiment 14 p2581 A70-31271

Sun Lyman alpha emission line monitoring, describing intensity variations correlation with Zurich number 15 p2798 A70-31654

Lunar tidal diurnal and semidiurnal variations in equatorial sporadic E layer related to H geomagnetic field and sunspot period 15 p2726 A70-31862

Daytime seasonal anomaly in electron density of topside F 2 region near sunspot minimum, using Alouette 1 data 15 p2726 A70-31863

X ray and microwave emissions relationship to sources on sun, discussing development and structure of sunspot groups 15 p2794 A70-32486

LF oscillatory convection characteristics in polytropic atmosphere in strong magnetic field based on sunspot theory 15 p2802 A70-32487

Wolf numbers Zurich time series monthly values, evaluating mathematical expectation with probability smoothing by Whittaker operator 15 p2802 A70-32489

Sunspot electric current evaluation from analyzing transverse component of magnetic field, discussing difficulties and errors in data reduction 15 p2804 A70-32615

Overlapping sunspots on photographs from Manila observatory during 10-12 December 1968 16 p2973 A70-33114

F 1 layer occurrence probability as function of mean monthly Wolf numbers at midlatitudes, noting solar activity effect 18 p3254 A70-37032

Sunspots surface layers azimuthal electric current density, assuming specific magnetic force distribution 18 p3322 A70-37135

Sunspot spectrograms analysis, observing wavelength shift in Zeeman triplet circular components and magnetic splitting inequality under different circular polarizations 18 p3322 A70-37136

Solar flare of 30 October 1968, describing sunspot development 19 p3497 A70-37973

Primary cosmic rays energy spectra in interstellar space in relation to sunspot group number 19 p3506 A70-38121

Solar radio emission slowly varying component, analyzing random aspects, correlation functions and relationship to spot groups 19 p3521 A70-38552

Solar radio emission and optical features correlation, considering integral RF flux, spot groups, main spots and flocculi areas 19 p3521 A70-38553

Primary cosmic ray intensity variation during solar activity half cycle, expressing diffusion coefficient as function of sunspot group number 20 p3696 A70-39279

Modified McNish-Lincoln method for Zurich sunspot numbers prediction, adapting for computer operation 20 p3704 A70-39410

Spot groups longitude distribution in 11 year solar activity cycle in Northern and Southern Hemispheres based on correlation functions, observing period variation 20 p3704 A70-39466

Butterfly diagram showing time dependent distribution of sunspots across heliographic latitudes 20 p3704 A70-39473

Auroral physics, discussing visibility, relations to geomagnetism and sunspots spectrum, morphology, optical emissions and particles in magnetosphere 20 p3623 A70-39929

Photospheric pore magnetic field model, investigating pore-sunspot distinctions 20 p3711 A70-40411

Photoelectric spectra of photosphere and sunspot umbra and penumbra ranging from 3900 to 8000 A 20 p3712 A70-40412

Photoelectric polarimetry of dark unipolar type H sunspot in terms of value and direction of magnetic field vector 20 p3712 A70-40413

Large sunspot umbra continuum intensity, examining visible spectra 21 p3885 A70-40956

Sunspot intensity profiles near solar limb, observing center side penumbra photosphere border 21 p3885 A70-40957

Solar flare relation to radio emission at 3.3 mm, discussing sunspots, temperature gradients and magnetic fields 21 p3879 A70-40962

H alpha flares occurrence in plages with little or no spots 21 p3880 A70-40964

Sunspot umbras and penumbras magnetically nonsplit lines measured photographically by spot contrast discriminator 21 p3887 A70-41115

Butterfly diagram for describing latitude distribution of sunspots during solar cycle, considering representation methods 22 p4106 A70-43264

Soft solar X rays cyclic variation from satellite observation, noting relation to sunspot group magnetic field complexity 22 p4096 A70-43301

X ray and microwave emissions relationship to sources on sun, discussing development and structure of sunspot groups 23 p4236 A70-43910

High resolution upper photosphere images obtained by slow raster scanning device and germanium bolometer, noting points around sunspots 24 p4400 A70-45307

MgH molecular lines Zeeman splitting in sunspot spectra confirmed by photoelectric observations 24 p4400 A70-45308

Li doublet in 21 March 1969 sunspot, examining fine structure caused by self reversal in line core 24 p4400 A70-45309

Sunspot penumbra velocity field spatial structure by filament spectrum analysis, plotting radial velocities relative to undisturbed photosphere 24 p4400 A70-45310

Electrical conductivity in inhomogeneous photosphere and sunspots, suggesting sunspot plasma instabilities 24 p4400 A70-45311

Zonal spot activity duration dependence on daily angle of solar rotation 24 p4401 A70-45316

SUPERALLOYS

U HEAT RESISTANT ALLOYS

SUPERCAVITATING FLOW

Plane supercavitating flow past symmetric wedge via open cavity model and application of conformal mapping theory and Riemann-Hilbert techniques 01 p0002 A70-10544

Inverse boundary value problems for supercavitating bodies, deriving singular integral equations using Prandtl acceleration potential method 07 p1254 A70-19076

Direct boundary value problem for supercavitating profile with finite cavity, deriving singular integral equations by Prandtl acceleration potential method 07 p1254 A70-19077

Unsteady hydrodynamic coefficients of supercavitating hydrofoil in harmonic oscillation in Helmholtz flow with free surface, investigating frequency, angle of attack and submergence depth 07 p1255 A70-19134

Direct and inverse problems of hydrodynamics of supercavitating lattices with leading and trailing edge cavities extending over upper surface of profile 08 p1482 A70-20534

Aerodynamic characteristics of supercavitating airfoil, investigating effect of free surface of unsteady fluid flow with stream separation, solving boundary value problem 13 p2391 A70-29650

Off-design performance characteristics of supercavitating hydrofoils in cascade for various arrangements, flap angles and flap chord ratios [ASME PAPER 70-FE-24] 16 p2892 A70-33633

SUPERCAVITATING FLOW

U SUPERCHARGERS

Impeller elastic and elastoplastic strength of centrifugal supercharger with curved disks and radial blades, using variational method 01 p0211 A70-11417

Machine-plotted pseudo three dimensional turbocharger rotor whirl display, discussing amplitude and frequency 08 p1496 A70-21300

Optimum manifold and injector hole area of pulsed exhaust systems of two cycle engine with turbocharger
22 p4091 A70-42809

SUPERCHARGING

U SUPERCHARGERS

SUPERCONDUCTING MAGNETS

Cryogenically cooled superconducting electromagnets design, construction and properties for research in plasma and solid state physics, considering coil systems
01 p0143 A70-10970

Superconducting magnetic system in magnetic analyzer of positrons and electrons in primary cosmic radiation tested on board Cosmos 213
04 p0685 A70-14443

Helium properties and utilization in NASA projects, discussing pressurization of fuel tanks cooling of superconducting magnets
04 p0720 A70-15633

Magnetic suspension and guidance of high speed vehicles realized via magnetic field interaction of vehicle-mounted superconducting magnets with eddy currents
08 p1543 A70-20576

Multiple maser-magnet units packaging in single cryostat for maximum tunability
08 p1513 A70-21599

Strong magnetic field effects on squirrel monkeys electrical and mechanical cardiac functions determined from vectorcardiogram and aortic blood flow characteristics
09 p1617 A70-22524

Three channel traveling wave maser with cryogenic superconducting magnet for C-band monopause radar system, describing construction and electrical characteristics
10 p1900 A70-24894

Superconductive materials and magnet design, discussing stabilization methods
11 p2097 A70-25613

Superconducting magnetic system in magnetic analyzer of positrons and electrons in primary cosmic radiation tested on board Cosmos 213
13 p2403 A70-28468

Cryogenics and nuclear physics, discussing particle beam handling magnets, superconducting accelerators, detectors, moderators, low temperature irradiation facilities, etc
14 p2616 A70-31014

Superconducting resistive critical field H_c of bcc region of Ti-Nb-V ternary system
15 p2782 A70-31754

Doubly pumped ruby maser operating in conjunction with superconducting magnet
18 p3265 A70-35953

Superconducting magnet system design, operation and module tests, noting large and small coil systems performance data relationship
23 p4218 A70-44354

Superconductive magnets with different windings and modular construction for magnetic mirror apparatus, discussing performance tests
23 p4218 A70-44355

Force-reduced superconducting toroidal magnet coils built with Cu plated Nb-Zr wire, investigating current enhancement characteristics
23 p4230 A70-44356

SUPERCONDUCTIVITY

Airborne aeromagnetic gradiometer theory and design, using superconducting thin film tunneling junctions
01 p0085 A70-10289

Superconducting transition temperature variation in bcc region of Ti-Nb-V ternary alloys measured as function of valence electrons and composition
03 p0538 A70-13154

Superfluid states of matter in interior of neutron stars, discussing strong interaction forces role
03 p0578 A70-14219

Quarkian substance properties noting possibility of superconducting state at high densities
04 p0753 A70-15074

Plastic deformation effects on superconductivity of wire specimens of high purity Pb, In and Tl cold worked at liquid He and annealed
06 p1127 A70-18614

Possible pairing without superconductivity at low carrier concentrations in bulk and thin film superconducting semiconductors
06 p1127 A70-18641

Transverse and longitudinal resistive critical fields of Nb wires, discussing superconductivity in dislocation cell walls created by drawing or swaging
09 p1704 A70-22802

GeTe, SnTe and strontium titanate transition into superconducting state including induced superconductivity
10 p1928 A70-25028

Superconducting ellipsoid of revolution in alternating magnetic field, computing disturbed field components using boundary value problem
10 p1917 A70-25201

Superconducting thin films of beta-tungsten structure Nb-Al-Ge compound, discussing high purity sputtering preparation techniques and properties in magnetic fields
12 p2285 A70-27259

Upper critical field dependence on s- and p-wave scattering of Frenkel effects in electron irradiated niobium
13 p2471 A70-29535

Superconducting bolometer operating temperature stabilization
13 p2412 A70-29868

Superconducting lead shell shielding properties in small ambient magnetic fields
13 p2454 A70-30030

Calorimetric measurements for Re specific heat in normal and superconducting states, comparing to theoretical calculation
14 p2626 A70-30478

Current stability and coil tests of force cooled superconducting systems
14 p2617 A70-31017

Superfluidity and superconductivity under cosmic conditions, discussing Bose-Einstein condensation, neutron stars, white dwarfs, etc
15 p2795 A70-31454

Superconductivity in noble metal rich hexagonal close packed phases and fcc solid solutions ascribed to Fermi surface-Brillouin zone interaction
15 p2785 A70-32398

Anisotropic superconducting energy gap of pure Zn from microwave absorption measurements
16 p2961 A70-33776

Teflon bucket and Be-Cu cap seal against hydrostatic pressure, discussing applications for high pressure superconductivity measurements
18 p3262 A70-37097

Substrate and thickness dependence of electrical and superconductivity properties of rhenium and molybdenum films prepared by electron beam evaporation
19 p3485 A70-37684

RF communication signal to noise improvement by time variant tracking filter with high Q superconductive resonant cavity
19 p3391 A70-38892

Nb-Zr thin films superconducting properties dependence on deposition temperature and rate and substrate material
22 p4085 A70-42623

Superconductivity and crystalline structure of laminar solid solutions of niobium-selenide- niobium-telluride single crystals
22 p4088 A70-43464

Current and vector potential in thin superconducting film in HF field, considering high and low temperatures
22 p4088 A70-43467

Rare earth metals-ruthenium Laves phases solid solutions superconducting transition temperature measurement
23 p4231 A70-44885

Superconductive memory type chalcogenide tellurium germanium arsenide, measuring AC magnetic susceptibility and DC electrical resistivity
23 p4231 A70-44892

Vanadium carbide single crystals superconductivity from upper limit on electron phonon interactions at 30 mK
24 p4391 A70-46252

Radiation detectors with superconducting weak links response to single photons, considering Mercereau ring interferometer
24 p4391 A70-46256

SUPERCONDUCTORS

Superconducting properties of polycrystalline disordered cold worked Nb-Ti-V alloys showing unexpected sensitivity to fast neutron irradiation
03 p0508 A70-13144

Thin superconducting films nonlinear microwave properties including impedance-amplitude relation, superconducting current threshold decrease, mode production, frequency mixing, etc
03 p0539 A70-13409

Josephson effect in superconductors emphasizing Josephson junction electrical properties and applications to devices and measuring techniques
03 p0542 A70-14190

Superconducting properties of Nb-Ti-N thin films prepared by reactive sputtering process, obtaining transition temperature maximums
04 p0732 A70-15689

Composite conductors involving conventional conductors and superconductors to obtain satisfactory electrical performance for application to electromagnets
05 p0870 A70-16582

Surface nucleation critical field for pure superconductors at temperatures outside Landau- Ginzburg region
06 p1125 A70-17218

Superconductor tubes experiment, observing flux jump initiation and propagation characteristics
09 p1738 A70-22293

Far IR radiation transmission through bismuth and gallium normal and superconducting thin films, considering transition temperature role
09 p1739 A70-22323

Electromagnetic single-coil suspension for cryogenic gyroscope with superconducting sphere rotor, calculating suspension force characteristics
12 p234 A70-27565

Tantalum RF sputtered superconducting films structure and properties at various substrate temperatures, observing bcc, fcc and amorphous phases by electron microscopy
12 p2288 A70-27876

Liquid He temperature fluctuation effects on cryogenic superconducting bolometer noise spectrum, deriving transfer functions
12 p2237 A70-28156

Light absorption coefficient of two band superconductor with nonmagnetic impurity, observing electron pairs removal from condensate and transition into excited states
13 p2472 A70-29723

Superconducting magnetometers and cryogenic refrigeration techniques, discussing liquid helium refill systems, Joule-Thompson expansion, etc
13 p2414 A70-30027

Superconducting analog and digital magnetometers, discussing instrument principles and operational limitations
13 p2414 A70-30028

Magnetometers based on flux entry into superconducting rings, discussing sensitivity and noise sources
13 p2414 A70-30029

Book on materials for conductive and resistive functions covering superconductive and contacting functions and applications
14 p2557 A70-30951

Nonlinear effects in microwave resonators containing thin superconducting films and low values of microwave power
15 p2782 A70-31525

Superconducting magnetic flux detector magnetic susceptibilities or field measurements
15 p2740 A70-32431

Anisotropic energy gap model in superconducting Zn to describe microwave absorption measurements
16 p2961 A70-33777

Superconducting Nb-Ti-Zr alloy, investigating structure and decomposition at high temperatures by X ray and electron microscopy
18 p3276 A70-36310

Nb-Sn superconductors multiphase structure with three intermetallic phase, constructing diagram based on phase stability and composition
18 p3299 A70-37221

High magnetic fields applications, emphasizing metal forming and superconducting rings levitation
19 p3471 A70-37948

Superconductor thin films, discussing transition temperature, critical field and current, solid state applications, etc
19 p3488 A70-38198

Energy release during flux jump in Nb-Ti single core wires and multifilament composite superconductors
21 p3863 A70-42011

Superconducting Sn bolometer under isothermal and nonisothermal conditions, measuring noise spectra dependence on displacement current and resistance
22 p4026 A70-42397

Thin film granular aluminum superconductors as sensitive thermometers
22 p4031 A70-43009

Ti and Zr based superconducting alloys with Nb content, measuring longitudinal critical currents in wire and ribbon samples
22 p4087 A70-43462

Superconductors resonance and oscillation phenomena, discussing particle motion, energy spectrum, magnetic and temperature effects, etc
22 p4088 A70-43476

Electromagnetic-surface elastic waves conversion in superconductors, considering thin plate forced vibrations and standing waves excitation
24 p4389 A70-45205

Current-phase relationship in short superconducting weak links, using one dimensional model
24 p4389 A70-45224

SUPERCOOLING

Real plasma isotherms using three component atoms, electrons, positive ions/ model in search for supercooled dense plasma
07 p1349 A70-19651

Artificial crystallization theory for supercooled dry ice seeded stratus clouds, taking into account condensation growth and turbulent diffusion of crystals
08 p1538 A70-21108

Vapor bubble separation diameter and flow in channel boiling applied to supercooled boiling zone determination
09 p1789 A70-23379

Undried atmospheric air humidity effect on pressure and water vapor supercooling in supersonic wind tunnel nozzles
09 p1606 A70-23613

Pressure, subcooling and diameter effects on liquid nitrogen film boiling on thin horizontal wires, using high speed movies

17 p3194 A70-34742

Contoured nozzle shock tunnel condensation point, determining flow supercooling over specified pressure range

23 p4182 A70-44588

SUPERCRITICAL FLOW

Torque and flow patterns in supercritical Taylor instability regime of circular Couette flow

03 p0470 A70-14235

Steady supercritical planar inviscid transonic flows over lifting airfoils, generating unsteady flow by impulsively imposing airfoil boundary condition [AIAA PAPER 70-47]

06 p0972 A70-18130

Subcritical and supercritical boundary layer problems, reviewing various momentum integral solution methods

18 p3242 A70-36705

Lifting quasi-elliptical airfoils with supercritical shock free flow, discussing Nieuwland hodograph theory to compute profile number [ICAS PAPER 70-15]

23 p4132 A70-44126

SUPERCRITICAL PRESSURES

N-heptane and Freon-13 droplets vaporizing size and temperature at supercritical pressures in heated air stream

06 p1182 A70-18204

Supercritical pressure system heat transfer characteristics for cryogenic space oxygen storage and supply

14 p2667 A70-31342

Metal vapors electrical conductivity and density measurement at high temperatures and supercritical pressures

20 p3648 A70-39637

Free and forced convection of supercritical carbon dioxide normal to heated cylinder at constant temperature, measuring heat transfer rates

21 p3945 A70-41034

SUPERFLUID FLOW

U SUPERFLUIDITY

SUPERFLUIDITY

Superfluid states of matter in interior of neutron stars, discussing strong interaction forces role

03 p0578 A70-14219

Thermodynamic equilibrium of rotating liquid He II on basis of Landau theory, noting stability and dissipative effects

04 p0785 A70-14986

Hartree model to study superfluid He film bound to uniform substrate

05 p0883 A70-16469

Heat transport by internal convection through He 2 in two fluid hydrodynamics model noting roles of thermal flux, superfluid component vorticity, normal component turbulence, etc

12 p2329 A70-27022

Superfluidity and superconductivity under cosmic conditions, discussing Bose-Einstein condensation, neutron stars, white dwarfs, etc

15 p2795 A70-31454

Energy flow between two superfluid helium baths at different temperatures and separated by thin plate

19 p3471 A70-37648

Critique of Ruderman theory of Crab pulsar LF wobble as long wavelength oscillation of superfluid vortex lattice

19 p3522 A70-38604

Neutron star superfluid turbulent state, applying dynamic model to conditions in pulsars

20 p3713 A70-40429

SUPERGIANT STARS

IR colors and optical and IR spectra of irregular M variable star and bright OH source VY CMa indicating supergiant classification

04 p0749 A70-14592

Models constructed for advanced evolution phases in massive convective red supergiants, considering carbon, Ne and oxygen burning in stellar core

05 p0919 A70-16935

Red giants and supergiants intrinsic radiation polarization characteristics

08 p1569 A70-20826

Statistical analysis of rotation and macroturbulence in early type Ia and Iab supergiants, discussing evolutionary effects

08 p1571 A70-20908

Canopus energy curve derived from UV spectrophotometry on Gemini 11 flight, noting agreement with model atmosphere

10 p1946 A70-24983

Radial velocities of supergiant distant stars in southern Milky Way regions of I Sco Association

11 p2113 A70-26465

OB supergiants atmospheric expansion indicated by medium-dispersion spectra, noting mass loss rate increase with luminosity and effective temperature

11 p2117 A70-26657

Quasar model based on supermassive stars relaxation oscillations, considering energy requirements

12 p2300 A70-27380

A-type supergiants microturbulence, determining atmospheric small scale velocity fields

14 p2641 A70-30885

H gamma profiles of B type supergiants, discussing electron density levels, Stark effect, Balmer and Paschen series breaks, etc

14 p2652 A70-31385

Massive hydrogen burning stars evolution with pulsational mass loss based on minimizing pulsational instability degree to specify mass loss rate

15 p2803 A70-32612

Supergiant alpha Car UV spectrophotometry from Gemini 11, comparing with model atmosphere

17 p3161 A70-34888

IR star types T-Tauri, B-emission and M supergiants observations using UVBRI photometry

21 p3890 A70-41163

Stellar population of young clusters containing red supergiants, determining spectral types and luminosity classes

22 p4102 A70-42979

Single normal main sequence stars rotational velocities compared with giant, supergiant, Be, A and metallic line stars and Population II objects

23 p4248 A70-44802

Early type Ia and Iab supergiant stars macroturbulence and rotation, investigating spectral line broadening, mass loss and angular momentum

23 p4250 A70-44813

Red supergiants location in H-R diagram, discussing significance of mass loss, rotational mixing and neutrino emission as stellar model mechanisms

24 p4403 A70-45393

High luminosity M type star photometry, determining supergiant intrinsic properties, interstellar extinction mean law and galactic evolution

24 p4410 A70-45764

Hercules 89 supergiant abnormal IR radiation flux originating in circumstellar shell of solid particles radiating at observed long wavelengths

24 p4410 A70-45772

SUPERHARMONICS

Steady state ultraharmonic oscillations of first and third order in yielding systems with linear work hardening law

19 p3542 A70-38059

SUPERHEATING

Extended chain crystals of hexagonal Se temporary superheating before final melting, presenting melting equation

01 p0126 A70-10222

Entropy fall in superheated liquid related to vapor bubble growth from finite so-called zero radius to critical radius, noting pressure effects

07 p1418 A70-18645

Phase growth of free vapor bubbles in water, ethanol and isopropanol at uniform superheats under normal and zero gravity

07 p1418 A70-18646

Extended chain polymer crystals temporary superheating before final melting, discussing hexagonal selenium crystals data

11 p2069 A70-25803

Metallic shell with passive thermal protection coating, solving boundary value problem for high temperature heating with simplified mathematical model

20 p3739 A70-40296

SUPERHETERODYNE RECEIVERS

Functionally integrated superheterodyne receivers design by applying microwave IC technology, providing weight reduction, interconnecting cables elimination and circuit interface problems minimization

02 p0267 A70-12055

Laser transmitter and optical superheterodyne receiver performance tests at 6328 A, demonstrating aperture size effect and noncoherent operation superiority

03 p0450 A70-13675

Integrated X band superheterodyne receiver design using planar transmission lines as components

16 p2874 A70-33388

Radio wave holography with unequal reference to signal frequency, recording linear object with superheterodyne receiver

19 p3420 A70-37290

Amplitude modulated optical band signal detection, comparing optimal direct photodetection and superheterodyne receivers sensitivities

21 p3785 A70-40633

Dynamic noise performance equivalence of phase locked or double superheterodyne tracking loops, using noise free external generator

21 p3793 A70-42180

SUPERHIGH FREQUENCIES

Airborne SHF communication system for operation with passive satellites installed in C-121 aircraft

01 p0045 A70-11122

X band electron paramagnetic resonance spectrometer with ruby maser preamplifier, correcting misinterpretation and noise figure analysis

01 p0114 A70-11196

Transient Faraday rotation of S-band telemetry carrier observed during Pioneer 6 occultation by solar corona, correlating with decametric solar radio bursts

02 p0369 A70-12059

X band radar with horizontally and vertically polarized antennas to compare sea clutter suppression by decorrelation and constant alarm rate receivers

03 p0451 A70-13935

Low loss low sidelobe N-way microwave optical power divider for single plane electronically steerable Ku band phased array antenna

04 p0655 A70-14624

S-band omnidirectional antenna patterns measurement procedure and results for Apollo spacecraft configurations, tabulating measure gains

06 p1019 A70-17507

Radiometers with low noise parametric amplifiers at centimeter wavelengths for radio telescope, discussing design, performance and Venus observations

08 p1495 A70-21065

Gunn diode parallel combinations fabricated for X band with n-type GaAs crystals, discussing output power at CW operation

08 p1477 A70-21296

Radio sources linear polarization measurements at 6 cm wavelength, noting intensity changes with polarized flux and position angle

08 p1578 A70-21535

SHF avalanche transit time oscillator with FM noise reduction by injection phase locking

08 p1462 A70-21594

X band Gunn oscillators amplitude modulation by pulse signals from another Gunn diode

09 p1646 A70-22707

Solid state multistage high power avalanche amplifier at X band

10 p1847 A70-23890

Italian SIRIO SHF experiment for study of atmospheric effects on satellite link, discussing system design and performance [AIAA PAPER 70-502]

11 p1999 A70-25442

X band mechanically despun antenna system with RF and motor drive assembly developed for earth coverage communications satellite [AIAA PAPER 70-422]

11 p2001 A70-25481

Microwave acoustic delay lines design and fabrication for UHF to X band frequency ranges

11 p2005 A70-26163

SHF tactical satellite communications ground terminals, discussing system concepts, relationship to satellites and design problems

11 p2031 A70-26259

Italian Sirio project, describing SHF propagation and communication, cosmic ray and confined plasma experiments

11 p2011 A70-26604

Power ferrite modulator and switch for SHF band based on Faraday rotation principle

12 p2199 A70-28000

X band Gunn oscillators for binary FSK regenerator operation employing signal injection triggering

12 p2199 A70-28015

High speed linear phase and amplitude modulation of X band Gunn oscillators

12 p2199 A70-28016

High power L- and S-band transferred-electron oscillators from epitaxial GaAs

13 p2377 A70-28978

Galactic continuum surveys at 8000 MHz by radio telescope, noting North American nebula and Cyg X region

13 p2491 A70-29096

Fabry resonator X band model with step or slope rimmed mirrors, noting periodical trend of power losses

14 p2558 A70-31320

S band transmitters frequency deviations optimization enabling designer to determine optimum value within constraints of associated receiving equipment

14 p2559 A70-31373

SHF radio telescope for solar radio wave observation, describing design and performance

15 p2717 A70-31897

Atmospheric humidity determination from satellite radio emission measurements at SHF

15 p2771 A70-32071

S band telemetric signals reception transmitted by Apollo 12 during occultation behind lunar disk, discussing lunar surface reflectivity

15 p2699 A70-32290

Point to point and radar return attenuation measurements at SHF through clear air and rain

16 p2858 A70-32928

Radio source 3C279 position during October 1969 occultation by sun, determining SHF deflection in solar gravitational field

16 p2972 A70-33049

Integrated X band superheterodyne receiver design using planar transmission lines as components

16 p2874 A70-33388

X band acoustic delay lines using thin film piezoelectric transducers

16 p2874 A70-33391

High power microwave pulse generation in SHF region, discussing use of boat-grown and epitaxial GaAs diodes

16 p2875 A70-33396

Microwave oscillator by transposing principle of spin oscillator at low frequencies in nuclear magnetic resonance in X band

16 p2877 A70-33413

S band GaAs FET fabrication technology and frequency response

16 p2877 A70-33414

- Terminal negative resistance of X band Gunn diodes, discussing frequency conditions for modulation and parametric amplification 16 p2877 A70-33417
- RFI measurements at X band on LES-7 prototype pulsed plasma thruster 17 p3149 A70-35669
- External SHF signal effects on multifrequency spectrum of reflex klystron coupled with long waveguide 17 p3055 A70-35682
- Transmit only solid state radar module built with microstrip techniques for phased array systems operating at L and S dual bands 17 p3056 A70-35899
- Radiation polarization measurements of natural underlying surfaces in centimeter range, noting dependence on sighting angle 18 p3250 A70-36967
- Electro-optical SHF modulator characteristics calculation from light wave interaction with traveling wave 19 p3443 A70-37291
- Magnetization oscillation in single crystal yttrium-iron garnet under fluctuating SHF magnetic field 19 p3484 A70-37625
- Breakdown electric field strength in S band microwave cavity for dry air, water vapor and mixture 19 p3423 A70-37757
- S band telemetry antenna with electronic tracking and polarity diversity for remote location missile testing 19 p3388 A70-37901
- InSb semiconductor, measuring small signal microwave conductivity for hot electron region at 9.4 GHz in high electric DC fields 19 p3488 A70-38747
- Centimeter wave transmitting and receiving equipment for studying nanosecond pulse propagation 20 p3632 A70-39627
- Multifrequency oscillator system with reflex klystron loaded by waveguide line, confirming spectrum conversion under action of SHF signal 20 p3598 A70-40299
- SHF and EHF waves simultaneous propagation over slant line-of-sight overwater path, comparing phase variations and fading for signal coherence 20 p3588 A70-40301
- Rainfall effects on EM wave propagation at centimeter and millimeter wavelengths 20 p3588 A70-40310
- X band electromagnet horn antennas, measuring triangular shape dielectrics effects on radiation pattern 20 p3599 A70-40312
- SHF-EHF region uses, discussing microwave radiometry and applications to radio astronomy and meteorology 21 p3799 A70-41421
- CW silicon SHF TRAPATT diode oscillator, discussing double sided design and fabrication 21 p3800 A70-42118
- Italian Sirio satellite with local and foreign ground stations network measuring SHF wave propagation variables 23 p4158 A70-43753
- Optimum junction area for maximum microwave output power of silicon IMPATT diodes for X band operation 23 p4167 A70-43775
- X band horn antennas precision phase center measurement technique for high resolution system applications 23 p4176 A70-44966
- P-n junction conductance at superhigh frequencies in breakdown region with simultaneous tunneling and impact ionization 23 p4232 A70-45064
- SUPERIMPOSITION [MATHEMATICS]**
- U SUPERPOSITION [MATHEMATICS]**
- SUPERMAGNETS**
- U HIGH FIELD MAGNETS**
- SUPERNOVAE**
- White dwarf mass changes during cooling, describing white dwarf collapse-type I supernova outbursts relationship 01 p0174 A70-10197
- Heavy nuclei survival in cosmic rays Colgate supernova acceleration model, assuming plasma wave instability in shock wave 02 p0357 A70-11788
- Interstellar media under action of supernova or nova, solving Navier-Stokes equations of hydrogen plasma for motion during shock wave formation 03 p0564 A70-13221
- Physical conditions of stars in presupernova stage for type II supernovae with outburst expected due to Fe-He transition in core, confirming lower mass limit 03 p0566 A70-13314
- Supernova light emitted from surrounding gas layer, describing gas density role in type I and type II events 04 p0748 A70-14590
- Pulsars pulse duration and shape as key to neutron stars linkage with supernova explosions 04 p0750 A70-14749
- Radio emission distribution from supernova remnants and galactic magnetic field 06 p1139 A70-17323
- Polarized and unpolarized emission measurements of W 44 supernova remnant with radio telescope, showing results for eastern portion of source 07 p1383 A70-19405
- Supernova pulsars parameters prediction based on Crab and Vela observations, discussing dispersion, period, flux density, etc 07 p1389 A70-20218
- Cosmic rays origin, discussing galactic theory of supernovae and formation mechanisms for energy spectra and composition of sources 07 p1371 A70-20327
- Relativistic particles formation associated with supernovae outbursts estimated to determine relativistic electrons mechanism in Crab Nebula 08 p1564 A70-20552
- Supernova remnant luminosity dependence on central star rotation period, deriving parameters for pulsars in Cas A 08 p1570 A70-20897
- Interstellar media under action of supernova or nova, solving Navier-Stokes equations of hydrogen plasma for motion during shock wave formation 08 p1580 A70-21654
- Supernovae and remnants - Conference, New York, November 1967 09 p1748 A70-21987
- International search for supernovae, considering future projects 09 p1748 A70-21988
- Supernovae and remnants, data concerning radio brightness distribution of Tycho supernova remnant and Cassiopeia and Crab Nebula origin 09 p1748 A70-21989
- Supernovae remnants evolution, properties and galactic distribution, discussing criteria for catalog listing and remnants as X ray sources 09 p1749 A70-21990
- Relativistic gravitational stellar collapse calculations for stars exceeding neutron star limit, discussing results in terms of supernovae or neutrinos 09 p1749 A70-21991
- Supernovae hydrodynamics, discussing early light curves energy requirements and shock wave dynamics in terms of neutrino diffusion 09 p1749 A70-21992
- Late stage stellar evolution association with supernovae in terms of gravitational collapse and exploding light emission using evolutionary model 09 p1749 A70-21993
- Iron peak nuclei synthesis by charged particles under supernova mechanism conditions predicted by hydrodynamic conditions 09 p1749 A70-21994
- Gravitational radiation detection from pulsating neutron star, considering asymmetries in gravitational collapse of massive stars as origin 09 p1749 A70-21996
- Supernova fluorescent light excited by radiation impingement on material surrounding explosion site, assuming explosion time and UV energy 09 p1749 A70-21997
- Supernovae remnants X ray emission associated with explosion process generating relativistic particles, indicating Crab Nebula as X ray object 09 p1749 A70-21998
- Crab Nebula continuing energetic activity study indicating origin in nebula center and association with supernova remnant 09 p1750 A70-22000
- Neutrino emission effect on collapse of supermassive stars, estimating energy radiated, discussing envelope explosion 10 p1938 A70-24022
- Pulsars in supernova remnants emitting X rays 10 p1933 A70-24627
- Pulsars nature based on hypothesis for main energy of novae and supernovae bursts equaling gravitational energy of collapse 11 p2117 A70-26708
- State equations of matter at high density and zero temperature, considering neutron stars relationship to supernova explosions and collapse 12 p2298 A70-27059
- Gravitational forces accompanying radiation bursts of metric outside collapsing supernova core 12 p2300 A70-27393
- Red dwarfs and supernovae determination in stellar clusters, outlining statistical probability technique for total number of flare stars 12 p2308 A70-27872
- Polarization of extragalactic radio sources and supernova remnants emphasizing instrumental effects 12 p2309 A70-27894
- Planetary orbit after central star supernova explosion, discussing effect on pulsar period 14 p2640 A70-30787
- Runaway stars and pulsars near Crab Nebula, discussing binary system explosion and remnant motion 14 p2642 A70-30894
- Absolute photovisual magnitude and classification of supernova in NGC 3389 spiral galaxy, using UVB measurements and comparison stars 15 p2797 A70-31611
- Galactic cosmic rays origin in terms of statistical mechanical model of supernova explosions 15 p2799 A70-31793
- Relativistic particles formation associated with supernovae outbursts estimated to determine relativistic electrons mechanism in Crab Nebula 15 p2805 A70-32707
- Sounding rocket X ray survey of Cassiopeia region for supernova remnants and galactic source distribution 17 p3153 A70-34528
- Nucleosynthesis in supernova models based on neutrino energy transport 17 p3153 A70-34529
- X ray spectrum analysis for Crab, Cas A and SN 1572 supernova remnants 17 p3156 A70-34830
- Central pulsars effects on supernova envelopes, examining luminosity, energy input, shape and light curve 18 p3314 A70-36333
- Soft X ray extended source in Cygnus Loop, indicating supernova remnant 18 p3310 A70-37022
- Atmospheric fluorescence observation of supernova energetic photon short pulse burst, using photomultiplier 19 p3500 A70-38079
- Cosmic rays shock from small mass supernovae explosions 19 p3507 A70-38128
- Pulsars postulated as supernova remnants sources of local cosmic rays 19 p3511 A70-38159
- Supernova remnants catalog based on radio surface brightness, deriving galactic distribution and testing theories for nonthermal radio sources evolution 20 p3709 A70-40077
- X ray sources location, distribution and spectral characteristics, investigating emission from supernova remnants 21 p3872 A70-40662
- Cas A and SN 1572 supernova remnant radio sources X ray spectra, investigating absorption by interstellar medium 21 p3873 A70-40666
- Low energy cosmic ray positrons arising from Co decay in Ni 56-Co 56-Fe 56 reaction chain in supernova Si burning shells 21 p3879 A70-40927
- Galactic distribution of supernova remnants and association with pulsars and X ray sources 21 p3892 A70-41188
- Diffuse X ray background attributed to X ray emission during supernova early phases 22 p4095 A70-42998
- Supernovae frequency in Sb and Sc spiral galaxies, considering luminosity class, absolute magnitude and mass of parent galaxy 24 p4413 A70-46164
- Novae and supernovae envelope properties, observing optical polarization and magnetic field for Crab Nebula 24 p4413 A70-46169
- SUPEROXIDES**
- U INORGANIC PEROXIDES**
- SUPERPOSITION [MATHEMATICS]**
- Mathematical pattern recognition, using potential functions superposition methods for reconstructing probability density from samples 14 p2554 A70-30926
- Localized states reconstructed as superposition of canonical states, using hyperplane generalization 15 p2766 A70-31437
- Bond stresses between fiber and matrix of fiber reinforced composite materials determined by numerical method based on superposition 21 p3934 A70-41252
- SUPERSATURATION**
- Gas bubble formation and equilibrium conditions in air supersaturated fuel stored under atmospheric pressure after injection into evacuated tank 03 p0605 A70-13394
- Supersaturated Al alloy with Zr addition at high temperatures, showing tetragonal equilibrium phase and intermediate phase with cubic structure 04 p0708 A70-15369
- Supersaturation during droplet-liquid phase formation in clouds estimated from trough formed on curve of distribution function 06 p1097 A70-17796
- Stress and intercrystalline corrosion causes and sensitivity in supersaturated Al alloys 07 p1307 A70-19391
- Initial cloud formation model, computing drop concentration and supersaturation 11 p2075 A70-25917
- Decomposition of supersaturated solid solutions in granulated Al alloys with Mn, Cr, Zr, Ti, V and Mo, studying microhardness and electrical resistivity 12 p2258 A70-28274

Hydrogen separation from supersaturated solid solution in Zn-Zr alloy, measuring at room temperature with eudiometer 15 p2764 A70-32856

Critical supersaturation vs phase equilibration of tissue in computing decompression schedules from depth and exposure time 24 p4301 A70-45983

SUPERSONIC AIRCRAFT

NT B-70 AIRCRAFT
NT BOEING 2707 AIRCRAFT
NT CONCORDE AIRCRAFT
NT F-4 AIRCRAFT
NT F-5 AIRCRAFT
NT F-8 AIRCRAFT
NT F-104 AIRCRAFT
NT F-106 AIRCRAFT
NT F-111 AIRCRAFT
NT JAGUAR AIRCRAFT
NT SAAB 37 AIRCRAFT
NT SUPERSONIC TRANSPORTS
NT X-15 AIRCRAFT

Linearized potential theory application in aerodynamic design and analysis of supersonic aircraft emphasizing far field viewpoint [AIAA PAPER 69-1132] 01 p0002 A70-10608
Fuel requirements for supersonic aircraft, discussing operational conditions and fuel quality problems 03 p0544 A70-14032

Energy state approximation for supersonic aircraft performance optimization with extension to maximum range problems, noting comparison with complex dynamic models [AIAA PAPER 68-877] 04 p0623 A70-13376

Aerodynamic characteristics, stability and controllability of swept wing and delta wing supersonic aircraft at subsonic velocities 05 p0796 A70-16966

Supersonic aircraft control and stability at low speeds, discussing sweepback angle, low aspect ratio, lift, etc 05 p0797 A70-17088

Acoustic power output from supersonic jets, considering aerodynamic and acoustic characteristics for supersonic exhaust velocities [AIAA PAPER 70-237] 06 p1132 A70-18115

Supersonic aircraft aerodynamic properties and control systems performance, considering piloting of delta wing fighters 07 p1194 A70-19640

Concorde aerodynamic design compromise between high and low speed requirements, kinetic heat problems and materials selection [AIAA PAPER 69-759] 07 p1195 A70-20399

Trisonic high pressure wind tunnel simulating flow conditions on large transonic aircraft, noting high Reynolds number capability 09 p1655 A70-22023

Pathogenic mechanisms of fatal injuries during supersonic ejection determinable by radiography 09 p1627 A70-23114

Swept and delta wing supersonic military aircraft stability and controllability, discussing variation in maximum lift coefficient as function of Mach number 09 p1611 A70-23129

Supersonic booms occurrence and propagation, discussing aircraft operating conditions for prevention of effect on ground 10 p0000 A70-24130

Clear air turbulence effect on supersonic aircraft safety and comfort, noting shallow zones and effects of topography and thunderstorms 10 p1912 A70-24506

Rigid wing subsonic and supersonic civil and military aircraft utilizing aerodynamic lift at takeoff and landing 13 p2344 A70-28543

Transonic aircraft testing capabilities and limitations, considering tunnel wall interference and Reynolds number effects [AIAA PAPER 70-580] 13 p2348 A70-29876

Rocket and supersonic aircraft weapon systems, discussing missile delivery and interception 13 p2507 A70-30000

Supersonic aircraft lateral stability and controllability design, discussing directional and weathercock stabilities 15 p2673 A70-31625

Supersonic aircraft stability and controllability during turns about longitudinal and vertical axes 16 p2840 A70-33204

SST inlet steady state pressure defects and random pressure fluctuations determining TF30 engine/inlet compatibility [AIAA PAPER 70-632] 16 p2834 A70-33530

Subsonic and supersonic aircraft dynamic loads under conditions of variable atmospheric density 17 p3013 A70-34685

Airframe-inlet integration for supersonic tactical fighters, testing wind tunnel models [AIAA PAPER 70-933] 17 p3149 A70-35843

Subsonic and supersonic transport aircraft design, discussing supercritical wing concept, fuel consumption reduction, composite aircraft structures, short haul transports, etc 17 p3022 A70-35854

Unsteady aerodynamics prediction of supersonic elastic aircraft, discussing aerodynamics influence coefficients/AIC/ method refinement [AIAA PAPER 70-944] 20 p3558 A70-39583

Supersonic aerodynamic design tools, discussing technological application of high speed computer and limitations [AIAA PAPER 68-1018] 22 p3958 A70-42701

Exhaust nozzle/airframe interference test evaluation for twin engine supersonic fighter [AIAA PAPER 69-430] 22 p3958 A70-42702

Two stream ejector type propelling nozzles for supersonic aircraft, investigating various configuration effects over range of secondary/primary air flow ratios [ICAS PAPER 70-48] 23 p4133 A70-44145

SUPERSONIC AIRFOILS

Quasi-conical supersonic wings with curved subsonic leading edges, discussing perturbation potential, boundary conditions, homogeneous flow and gothic and ogee planforms 21 p3747 A70-42108

Two dimensional flow about supersonic airfoil, considering trailing Taylor columns behavior like sonic booms 22 p4009 A70-42629

SUPERSONIC BOUNDARY LAYERS

Radiation from and panel response to supersonic turbulent boundary layer, emphasizing panel mode coupling to acoustic field 04 p0615 A70-15081

Analytical model for jet interaction induced separation of supersonic turbulent boundary layers, conducting flat plate tests at Mach 4 [AIAA PAPER 70-765] 17 p3007 A70-34486

Temperature and Mach number distributions measurements on supersonic turbulent boundary layers for reanalyzing heat transport [AIAA PAPER 70-744] 17 p3066 A70-34499

Probstein-Gold model for ablated materials crosshatching patterns, using interaction between inelastic deformable surface and supersonic turbulent boundary layer [AIAA PAPER 70-768] 17 p3009 A70-34504

Roughness effects on heat transfer to surfaces in supersonic compressible turbulent boundary layer [AIAA PAPER 70-742] 17 p3066 A70-34505

Acoustic measurement of surface pressure fluctuations in supersonic transitional boundary layers 17 p3092 A70-35482

Supersonic boundary layer interaction with shock wave produced by wedge slope 20 p3557 A70-39139

SUPERSONIC COMBUSTION

Compression wave mechanism of supersonic combustion controlled by mixing, discussing multiple injector design, thermal compression and geometry effect 02 p0399 A70-12041

Supersonic diffusion flames produced by subsonic and supersonic free jet injection of hydrogen into high enthalpy airstream 02 p0399 A70-12042

Combustor geometry and heat release effects on supersonic combustor thrust efficiency, considering shock-free, normal and oblique shock situations 02 p0354 A70-12043

Turbulent mixing and supersonic combustion theories applied to internal flow, comparing various mixers and relating mixing intensity to kinetic energy of turbulence 02 p0399 A70-12045

Optimum performance for Mach 3 to 7 fixed geometry ramjet with successive subsonic and supersonic combustion, noting lifting wing conjunction 02 p0355 A70-12365

Flow field of jet spoilers downstream from nozzle, accounting for main stream and secondary jet mixing and fuel injection problems during supersonic combustion 03 p0608 A70-14098

Energy supply for supersonic flight air suction propellant systems using external supersonic combustion, discussing Caret wing and pressure effect 04 p0785 A70-15160

Combustion and flow characteristics associated with direct injection of liquid hydrocarbons into high speed air stream [AIAA PAPER 70-88] 06 p1182 A70-18198

Combustion kinetics in supersonic gas flows past various bodies, assuming exothermal and inverse recombination reactions behind adiabatic shock wave after induction period 08 p1596 A70-20855

Supersonic turbojet propulsion systems and components - NATO/AGARD Conference, Varenna, Italy, May 1967 [AGARDOGRAPH-120] 08 p1559 A70-21926

Hydrogen-air reaction by singular perturbation methods for temperature and pressure values of supersonic combustion, changing reaction velocity by initial stoichiometry 11 p1995 A70-26624

Large scale hydrogen fueled supersonic combustor test at simulated Mach 8 flight, describing fuel injector design [AIAA PAPER 70-715] 16 p2965 A70-33539

SUPERSONIC COMBUSTION RAMJET ENGINES
Fuel injection and mixing and piloted ignition in supersonic flow design principles for scramjet engine, evaluating eddy viscosity model for parallel injection 02 p0354 A70-12047

Premixed compression initiated supersonic combustion, noting sensitivity to small perturbations in inlet flow variables [AIAA PAPER 68-995] 07 p1421 A70-19318

Supersonic burning ramjet /scramjet/ performances, discussing vehicle engine integration, superiority to ordinary ramjets at hypersonic speeds, combustion process-flow field interaction, etc [AGARDOGRAPH-120] 08 p1600 A70-21930

Scramjets for recoverable booster transporting payloads into earth orbits 15 p2811 A70-32258

Integrated double oblique shock scramjet for supersonic combustion tests and instrumentation development, discussing fuel injection through sonic orifices, combustion data, etc [AIAA PAPER 69-827] 21 p3867 A70-41752

SUPERSONIC COMBUSTION RAMJET MISSILE U RAMJET MISSILES U SUPERSONIC COMBUSTION RAMJET ENGINES

SUPERSONIC COMMERCIAL AIR TRANSPORT NT BOEING 2707 AIRCRAFT

SUPERSONIC COMPRESSORS
Supersonic compressor applications for airborne vehicles propulsion systems, discussing axial flow compressors, three dimensional design methods, supersonic radial machines, etc [AGARDOGRAPH-120] 08 p1434 A70-21929

Supersonic axial flow compressors, studying shocks shared by rotor and stator to obtain high efficiency 11 p2101 A70-25819

Rotor wakes intrastator transport effects on high Mach number axial flow compressors performance, considering stagnation temperature profile and rotor blade loss factor [ASME PAPER 70-GT-39] 18 p3209 A70-36869

Cascade tunnel testing role in designing supersonic compressor rotor blading for lower jet engine weight and fuel consumption [ASME PAPER 70-GT-79] 18 p3305 A70-36885

Low drag supersonic compressors for aircraft engines, calculating start and cruise conditions of quasi-isentropic flow cascades 21 p3745 A70-41405

SUPERSONIC DIFFUSERS
Reattachment of supersonic jet with turbulent shear boundary layer abruptly expanding into axisymmetric parallel diffuser, using surface flow technique 04 p0619 A70-15323

Isentropic inlet diffusers of short design length at supersonic velocities 06 p0963 A70-17233

Flow distribution for short isentropic supersonic inlet diffusers, using method of characteristics and Oswatich and Connors procedures 06 p0963 A70-17234

Circular blade cascade design for supersonic vane diffuser of radial flow centrifugal compressor 16 p2837 A70-33764

SUPERSONIC DRAG
Slender bodies optimum aerodynamic shape for supersonic velocities, discussing minimum wave drag and total drag two step analysis using calculus of variations 03 p0408 A70-13801

Slender wings and fuselages resistance at zero lift in supersonic flow, using Karman and Moore linear theory [DGLR-69-28] 04 p0616 A70-15154

Drag coefficients for spheres and sharp cones in rarefied hypersonic air flow obtained in shock tunnel using free flight technique [AIAA PAPER 69-140] 09 p1605 A70-23221

Maximum thrust and drag reduction for supersonic missiles by base burning, showing dependence on chemical reaction and Mach number 12 p2158 A70-28208

Supersonic skin friction measurements in grit type boundary layer transition trips with zero heat transfer 13 p2343 A70-29969

Blunt nose effects on drag of flared conical body in supersonic flow, considering pressure loss through shock wave and vorticity 17 p3196 A70-35237

Drag prediction for Ballute and parachute trailing decelerators at supersonic speed and zero angle of attack, using flow field computations [AIAA PAPER 70-1177] 21 p3746 A70-41836

Cylindrical afterbodies base pressure drag under powered supersonic flight, modifying Korst flow model recompression criterion 22 p3959 A70-42713

Minimum-drag boattail configurations optimization for supersonic flow, determining wave drag coefficients

22 p3961 A70-42714

Vane type vortex generators to prevent turbulent compressible boundary layer separation, measuring drag in supersonic flow

23 p4133 A70-44527

Supersonic convective electric arcs with magnetic stabilization in sulfur hexafluoride, examining aerodynamic drag and plasma column slanting

23 p4227 A70-44554

SUPERSONIC FLIGHT

Combustion effects on base pressure of two dimensional body in supersonic flight, considering air-fuel ratio, combustion length and free stream Mach number

02 p0354 A70-12046

Dynamic stability of flexible aircraft fuselage in controlled supersonic flight at zero angle of attack, basing analysis on elastic oscillation equations

03 p0579 A70-13418

Sonic boom overpressures generated by aircraft level rectilinear flight at supersonic speed in temperature and wind stratified atmosphere, calculating atmospheric correction factor

05 p0794 A70-16411

Second order wave structure theory for shock wave system from body in supersonic flight analyzed for planar flows

05 p0790 A70-16797

Normal force component distribution and aerodynamic pressure position on rocket bodies at supersonic and hypersonic velocities

06 p0964 A70-17238

Opening distance and inflation time prediction for parachutes deployed supersonically based on subsonic performance

07 p1394 A70-19725

Supersonic flight vehicle plasma sheath effect on effective range of onboard radar installation, discussing SNR

08 p1461 A70-20869

Flow past yawed delta wing at supersonic flight velocities, obtaining real velocity near singular surface and replacing Mach number by perturbed parameter

10 p1799 A70-24126

Supersonic aerial target wing synthesis using sandwich construction with graphite-epoxy laminate skins bonded to Al honeycomb, achieving significant weight reduction

12 p2160 A70-27118

Supersonic flight simulation in hypersonic wind tunnels for developing hypersonic air breathing propulsion, describing ceramic storage heaters

13 p2384 A70-28666

Climatology of safe threshold Mach number and air-plane ground speed for boomless supersonic cruise, considering San Francisco-New York route

14 p2530 A70-30606

Overpressure, rise time and wave period of sonic boom signatures at ground level from unaccelerated supersonic overflights

14 p2530 A70-30608

Sonic boom causes and nature, considering aircraft configuration and attitude and minimizing effects

15 p2673 A70-31852

Sympathoadrenals activity in pilots during supersonic flight, investigating urinary catecholamine output

15 p2690 A70-31891

Suborbital space transports problem solution by recoverable jet orbital or jet assisted aircraft, discussing implications of Concorde supersonic flight

18 p3350 A70-36663

Liability for damages due to supersonic flight sonic booms, discussing pertinent provisions in Dutch and international law

19 p3553 A70-37561

Reentry bodies of revolution subsonic and supersonic aerodynamic characteristics

20 p3558 A70-39704

Aerodynamic forces on flexible launch vehicles and missiles in supersonic flight based on first order method, solving boundary value problem for surface velocities

21 p3746 A70-41853

Supersonic flight altitude stability, studying effects of velocity, lift-drag ratio, thrust law, wind direction, engine unstarts, etc

22 p3961 A70-42712

Airframe installation effects at transonic speeds on underwing supersonic cruise exhaust nozzles, using flight and wind tunnel tests

22 p3960 A70-43274

Elastic fuselage flight vehicle dynamic stability at supersonic speeds, using automatic pilot stabilization

23 p4139 A70-44157

SUPERSONIC FLOW

Flow and pressure distribution for large normal injection along surface in supersonic stream solved numerically for two dimensional or axisymmetric body and wedge

01 p0001 A70-10336

Supersonic flow around thin warped delta wing, taking into account current separation at subsonic leading edges for pressure distribution and aerodynamic characteristics

01 p0002 A70-10546

Two velocity hydrodynamic scheme for describing dynamic behavior of two phase supersonic flow past slender body

01 p0003 A70-10995

Characteristics method for calculating steady supersonic flow of burning gas mixture past wedge and rotating cones

01 p0218 A70-11018

Topological properties of plane flow in subsonic region behind smooth shock wave in uniform supersonic flow, discussing shock wave convexity

01 p0608 A70-11580

Fuel injections into supersonic air stream through isolated normal ports and porous wall, using interferometry, schlieren and high speed photography

02 p0354 A70-12044

Fuel injection and mixing and piloted ignition in supersonic flow design principles for scramjet engine, evaluating eddy viscosity model for parallel injection

02 p0354 A70-12047

Water vapor condensation by homogeneous nucleation measured for cluster number using laser light scattering compared with theory in condensing supersonic flow

02 p0279 A70-12048

Wing design optimization for steady and unsteady supersonic flow through computerized simulation and study of leading and trailing edge shape

02 p0223 A70-12208

Magnetically balanced arcs in supersonic external flows, indicating central core with differential Lorentz forces analogous to Grashof number in free convection phenomena

02 p0347 A70-12233

Supersonic flow separation at antisymmetrical delta wing edges, noting eddy layer and vertical velocity fields effects on aerodynamic characteristics

02 p0224 A70-12625

Supersonic plasma jets studied spectroscopically, determining atomic levels populations, population inversion conditions, electron temperature and concentration distributions, etc

03 p0531 A70-13254

Supersonic flow in dihedral angle between intersecting wings and in space between parallel wings, using integrating wave equation by Volterra method

03 p0407 A70-13492

Boundary layer separation in divergent portion of conical ducts in overrelaxed supersonic regime in air and water, showing influence of medium, pressure and thrust

03 p0467 A70-13682

Carbon dioxide supersonic flows, describing numerical integration procedure for chemical and vibrational relaxation

03 p0440 A70-13743

Two dimensional and axisymmetric bodies shapes providing minimum wave drag to supersonic flow of perfect gas, considering bodies around which flow causes bound shock waves

03 p0409 A70-13863

Supersonic unsteady state three dimensional flow around blunt bodies with detached shock wave

03 p0409 A70-13864

Supersonic unsteady gas flow around bodies at low Strouhal numbers, noting angle of attack amplitude and leading edge shock wave

03 p0409 A70-13865

Viscous supersonic flow near wall with large local curvature, using asymptotic solutions to Navier-Stokes equations

03 p0468 A70-13867

Equilibrium temperature and heat transfer of sphere in supersonic flow of rarefied air

03 p0409 A70-13874

Reaction of three dimensional shock wave with turbulent boundary layer in supersonic flow around plate

03 p0409 A70-13876

Integral method for studying wall heat transfer influence on compressible boundary layer on cone at angle of attack in supersonic flow

03 p0409 A70-13953

Similarity properties of laminar or turbulent boundary layer separation in uniform supersonic flow, discussing wall cooling, pressure evolution, etc

03 p0469 A70-14234

Numerical analysis of near equilibrium flow regions in chemically relaxing gas mixtures past blunt bodies at supersonic speeds

04 p0666 A70-14603

Viscous ideal gas supersonic flow past spheres, using integral relations based on Navier-Stokes equations

04 p0613 A70-14606

Supersonic fluid amplifier performance and design for use as power amplifier and high outlet leg differentials in vacuum environments

04 p0626 A70-14846

Difference methods application to supersonic gas flow past blunt body and unsteady axisymmetric flow past body of unspecified configuration, analyzing stability

04 p0670 A70-14957

Schlieren system converted into Kraushaar diffraction grating interferometer with isolated optical platform, considering applications to supersonic flow over airfoil shapes

04 p0689 A70-15016

Monograph on weak interactions on cones in supersonic and hypersonic flows, discussing flow divergence, measurement errors and data reliability

04 p0615 A70-15141

Piston theory application to plates and shells stability in supersonic gas flows, considering critical velocities determination for asymmetric flows and oscillations

04 p0617 A70-15196

Supersonic nonequilibrium two phase flow in Laval nozzle from numerical solution of quasi-linear hyperbolic equations

04 p0617 A70-15229

Heat fluxes, shear stresses and pressures distribution at spike on body in supersonic flow from asymptotic solutions of Navier-Stokes equations

04 p0673 A70-15232

Structural characteristics of supersonic twisting underexpanded air jet, using filming and schlieren photography

04 p0618 A70-15246

Fundamental matrix asymptotic forms obtained for supersonic and subsonic three dimensional steady flows past body in uniform stream of viscous thermally conducting fluid

04 p0673 A70-15320

Fluid mechanical problems with pressure distribution determined by interaction between external supersonic inviscid flow and inner laminar viscous layer

04 p0674 A70-15529

Supersonic wake flow visualization, obtaining direct photographs of various smoke streamlines

04 p0621 A70-15595

Ideal equivalent gas method for studying thermodynamic properties in supersonic gas flows behind shock wave

05 p0831 A70-15872

Supersonic flow past elliptic cone of small eccentricity treated as axisymmetric conical flow perturbation

05 p0790 A70-16506

Inviscid gas injection through flat plate in supersonic flow, obtaining self similar solution by integrating differential equation for stream function

05 p0791 A70-16963

Steady and frictionless supersonic flow of ideal gas of constant heat capacity around slightly deformed cone, calculating force exerted by gas

06 p0964 A70-17240

Three dimensional supersonic flow around delta wings, considering lifting and thickness problems, leading edge characteristics, separated and non-separated shock waves, etc

06 p0964 A70-17241

Supersonic mixing CU chemical lasers, discussing lasing action time duration

06 p1083 A70-17945

Isoenergetic mixing and reattachment processes of two dimensional supersonic turbulent separated flow, modeling mixing process by constant pressure theory

06 p1037 A70-18039

Residence time of foreign gas injected into recirculation region of wake behind slender body in axisymmetric supersonic flow

06 p0968 A70-18040

Cold ducted supersonic flow of premixed ethylene and air ignition by hot turbulent jet

06 p1131 A70-18057

Transpiration and film cooling systems comparison for high speed flows with foreign gas injection effects

06 p1179 A70-18073

Liquid sheet and jet breakup in supersonic gas stream, characterizing breakup mechanism by gross jet fracture

06 p1039 A70-18109

Integral moment method for interactions between laminar boundary layer and external supersonic flow applied to hypersonic laminar boundary layer near sharp expansion corner

06 p1039 A70-18111

Lifting surface theory for calculation of steady subsonic and supersonic flow over various wing and airplane configurations, emphasizing finite element load prediction method

06 p0971 A70-18114

Explosive blast wave effects on flight vehicle in supersonic flow, using conical blast generator and short duration supersonic wind tunnel

06 p0972 A70-18127

Supersonic flow separation over rearward facing step, measuring upstream boundary layer, lip shock and shear layer formation by pitot probe and surface pressure survey

06 p0973 A70-18153

Laminar boundary layer on cone at incidence in supersonic flow evaluated by pressure distribution technique, comparing heat transfer, pitot probe measurements, etc [AIAA PAPER 70-48] 06 p0974 A70-18189

Water droplets and air supersonic mixing, determining droplets size and optical properties [AIAA PAPER 70-90] 06 p0975 A70-18199

Unified model for transverse gaseous jet penetration into supersonic stream agreeing with measured flow field properties [AIAA PAPER 70-93] 06 p0976 A70-18201

Time of flight spectroscopic measurements in arc heated supersonic molecular beam using algebraic relations, sensing modulated beam by Orbitron type detector 06 p1111 A70-18266

Kinetic theory of rarefied supersonic flow over finite plate, calculating molecular velocity distribution functions for flowfield 06 p0981 A70-18356

Drag coefficients of sharp and blunt cones in rarefied supersonic flow for bluntness ratios and angles of attack 06 p0981 A70-18360

Sphere drag in near free supersonic molecular flow 06 p0983 A70-18377

Nonequilibrium processes behind shock wave in shock tube supersonic air and nitrogen flow, using photoelectrical shadow method 06 p1053 A70-18562

Uniform supersonic flow with receding shock wave past smooth profile 07 p1187 A70-18674

Two phase supersonic continuum flow of dispersed equal gas-liquid volume ratio in shock tunnel using continuum theory, considering sound propagation 07 p1256 A70-19311

Infinitely wide plate bending at small angle of attack in supersonic gas flow, obtaining critical flow rate equal to divergence rate 08 p1588 A70-21175

Relaxational oscillations produced by interaction between rarefaction wave in external two dimensional supersonic flow and turbulent near wake 09 p1603 A70-22426

Shock layer thickness in supersonic inviscid gas flow past blunt bodies, calculating boundary layer near stagnation point 09 p1603 A70-22442

Shock wavefront configurations before inclined obstacles in supersonic flow, studying inclination angle role 09 p1604 A70-22443

Massive blowing from porous cone with embedded shock wave in supersonic flow, assuming inviscid and conical injected flow field 09 p1662 A70-23216

Injectant stagnation temperature and molecular weight variation effect on flow field generated from secondary gas injection into supersonic stream [AIAA PAPER 69-1] 09 p1733 A70-23217

Cross hatching on surface of ablating bodies exposed to supersonic turbulent boundary layer flow using mathematical model 09 p1605 A70-23232

Interaction shock shape prediction for gaseous and liquid injection in supersonic flow, using solid body and complementary models 09 p1662 A70-23244

Friction drag on thin pyramidal lobed bodies in supersonic flow, analyzing detached shock region and body geometry function 09 p1606 A70-23612

Supersonic flow behind cone, studying bottom pressure and stagnation zone dependence on incident flow parameters and static pressure distribution 09 p1663 A70-23623

Supersonic leading edge problem solved by ellipsoidal model using discrete ordinate method compared with BGK model solution 10 p1797 A70-23957

Hodograph or Riemann invariants method generalization for nonelliptic systems, discussing three dimensional potential supersonic flows 10 p1863 A70-24087

Perturbed equations solutions for plane supersonic steady and nonsteady gas flows, considering propagation of perturbations in initially nonstationary main flow 10 p1866 A70-24107

Three dimensional supersonic gas flow solution by numerical method of characteristics, discussing direct and inverse tetrahedral and semicharacteristic schemes 10 p1798 A70-24117

Nonautonomous boundary value problems for plates in plane and three dimensional supersonic flows, obtaining eigenfunctions of vibration by Laplace transform 10 p1956 A70-24118

Wing in supersonic flow analyzed for surface pressure taking into account nonlinear effects of vibrations 10 p1798 A70-24119

Supersonic flows over flaps and backward facing steps, using steady state heat transfer measurement technique involving uniform heat flux dissipation at model surface 10 p1798 A70-24120

Triangular conical wing with supersonic leading edges analyzed for aerodynamic forces in supersonic flow 10 p1798 A70-24121

Heat sources effect on pressure and velocity of supersonic flow, discussing iteration procedure and asymptotic expansion 10 p1799 A70-24125

Wind tunnel study of entropy extremum upon critical streamline in supersonic three dimensional flow past blunt bodies at zero angle of attack 10 p1800 A70-24131

Vibrational and dissociation relaxation effects on plane shock wave structure and supersonic flow around blunt bodies 10 p1801 A70-24150

Supersonic gas flow past sphere investigated for characteristics using Fabry-Perot etalon 10 p1888 A70-24258

External supersonic potential flow effects on turbojet engine ring and needle nozzle performance, considering gas overexpansion operation 10 p1930 A70-24286

Numerical analysis of forced parametrically excited plate vibration in plane supersonic flow, using digital computer 10 p1958 A70-24527

Analog computation in supersonic steady flow and digital technique for wing-fuselage and wing-tail interactions [ONERA-TP-804] 10 p1802 A70-24544

Model testing gas flow calculation in system emitting electron beam into atmosphere through supersonic gas seal 10 p1895 A70-24590

Polygonal wings oscillatory motions in unsteady supersonic flow 10 p1803 A70-24778

Head wave distance from body determined for slender pointed profile in subsonic region of transonic flow 10 p1803 A70-24780

Unsteady supersonic flow past tail-body system with harmonic oscillatory motions 10 p1803 A70-24789

Supersonic flow around slender polygonal wings with nonsymmetrically distributed incidence using method for conical flow around angular wings 10 p1805 A70-24797

Nonuniform partitioning of flowfield in three dimensional laminar boundary layer in supersonic conical flow at zero angle of attack, using numerical integration 10 p1804 A70-25192

Gasdynamic functions of supersonic flow past spherically and ellipsoidally blunted inverted cones 11 p1973 A70-25522

Boundary layer transition detection at supersonic speeds using thin film gages to infer local laminar and turbulent supersonic skin friction 11 p2035 A70-25970

CW chemical laser performance using molecular hydrogen diffused into supersonic fluorine atoms streams 11 p2063 A70-26067

Lambda type pseudoshock /shock during supersonic flow deceleration to subsonic in duct/, investigating mechanism by schlieren photography 11 p2037 A70-26408

Monograph on axially symmetric tandem grids for supersonic flow deceleration to subsonic speeds, using schlieren optical tests and pressure measurements 11 p1977 A70-26525

Computer applications in aerospace research involving flutter, supersonic flow, unsteady wing flow, etc 12 p2191 A70-27025

Insulator wall temperature effect on supersonic two temperature MHD generator channel flow at open and short circuit conditions 12 p2163 A70-27067

Numerical solution for steady supersonic inviscid flow around smooth conical bodies by solving elliptic partial differential equations for conical flow 12 p2155 A70-27202

Hall MHD generator with supersonic flow instability to magnetoacoustic waves propagating antiparallel to steady electric current in dense weakly ionized gas 12 p2281 A70-27805

Interaction of laminar hypersonic boundary layer and supersonic corner expansion wave, discussing upstream influence, transverse pressure gradients and external flow [AIAA PAPER 69-137] 12 p2211 A70-27826

Subsonic, transonic and supersonic laminar boundary layers acceleration and cooling effects, discussing heat transfer and gas enthalpy 12 p2211 A70-27830

Perfect gas supersonic flow with constant velocity, pressure and density around finite nonaxisymmetric body at small angles of attack 12 p2158 A70-28197

Three dimensional laminar boundary layer equations for body of revolution at angle of attack in supersonic gas flow derived for equations 12 p2158 A70-28198

Perturbation theory of supersonic steady anisotropic flow with radiative heat transfer using hyperbolic characteristic coordinates 12 p2334 A70-28203

Supersonic flow in inner and outer regions of annular flow by method of singularities, obtaining Abel type integral equations for every step [DFVLR-SONDDER-37] 12 p2158 A70-28207

Supersonic and hypersonic motion past circular cone at angle of attack, analyzing for velocity and pressure distributions by linearizing conical motion equations 12 p2158 A70-28213

Turbulent boundary layer and base pressure profiles of supersonic flow past conical models in wind tunnel 12 p2159 A70-28229

Vortex layer and entropy of supersonic gas flow past circular cones at incidence using surface velocity corrections 12 p2159 A70-28230

Vibrational relaxation effect on supersonic flow past nose section of blunted body 12 p2159 A70-28231

Specific heat ratio and configuration effects on flow in subsonic, transonic and supersonic sections of Laval nozzle 12 p2159 A70-28233

Monge equation in small perturbation method of characteristics applied to propagation phenomena in three dimensional supersonic gas flow 13 p2386 A70-28490

Steady expansion flows at three dimensional supersonic edges with small corner angles using analytical method of characteristics 13 p2338 A70-28491

Pressure distributions and heat transfer at wall calculated to investigate supersonic laminar reattachment 13 p2338 A70-28953

Gaseous injection into supersonic flow, investigating secondary Mach number and injection angle effects on flowfield in supersonic wind tunnel [AIAA PAPER 70-552] 13 p2339 A70-29017

Turbulent base pressure on conical afterbodies in supersonic axisymmetric flow, including initial direction effect [AIAA PAPER 70-555] 13 p2340 A70-29020

Sting diameter and cylindrical protuberance length effects on axisymmetric body base pressure in turbulent supersonic flow [AIAA PAPER 70-585] 13 p2342 A70-29885

Supersonic rarefied flow over sharp flat plate with merged shock layer and free molecular-continuum transition, using electron beam fluorescence 14 p2529 A70-31028

Uniform supersonic flow with receding shock wave past smooth profile 15 p2671 A70-31466

Supersonic nonequilibrium gas mixture flow past segmental bodies nose areas to simulate Venusian atmosphere, determining temperature, pressure and concentration distributions 15 p2796 A70-31483

Finite difference algorithm for supersonic three dimensional steady flow past blunt bodies with generating line bends, allowing for gas equilibrium and frozen states 15 p2671 A70-31495

Nonequilibrium dissociation effect on supersonic oxygen flow past inverted blunted cones at angle of attack, considering thermal fluxes and aerodynamic forces 15 p2671 A70-31496

Convective heat transfer in Cu spherical shell and plate in supersonic rarefied gas flow at zero angle of attack from wind tunnel experiments 15 p2824 A70-31497

Aerothermopressor experiment in subsonic and supersonic gas flow compared with numerical solutions of equations 15 p2720 A70-31900

Thin cylindrical shells flutter analysis in supersonic flow, using linearized potential theory 15 p2815 A70-31916

Laminar to turbulent transitions determination in sub/supersonic flows, reviewing methods based on hot-wire anemometer output signal [ONERA-TP-841] 15 p2720 A70-31918

Linear model of edge effect in supersonic gas flow past dihedral angle of intersecting wings, using Abel equations 15 p2672 A70-32127

Microwave probe for measuring electron density profile in supersonic arc jet plasma 15 p2741 A70-32433

Schlieren optical method for measuring He jet penetration into supersonic flow 15 p2741 A70-32520

High temperature combustion wind tunnels for investigating gas and liquid fuel combustion stabilized by shock waves in supersonic flow

16 p2996 A70-32991

Supersonic and hypersonic gas flow past blunt bodies, using finite difference and integral relation methods

16 p2890 A70-33244

Supersonic flows past two dimensional blunt bodies, using method of ascertainment

16 p2833 A70-33248

Ignition and combustion in ducted turbulent supersonic flow, discussing premixed and unpremixed ethylene

[AIAA PAPER 70-720]

16 p2997 A70-33488

Boron particles ignition and combustion in supersonic air stream, emphasizing axial and lateral two phase flow injection

[AIAA PAPER 70-737]

16 p2856 A70-33496

Two dimensional sonic secondary fluid jet interaction with uniform primary supersonic stream in wind tunnel

[ASME PAPER 70-FE-33]

16 p2835 A70-33638

Blockage ratio effect on supersonic zone with shock layer interaction on nonlifting circular arc airfoils at transonic speeds in wind tunnels

16 p2835 A70-33674

Equations of supersonic and hypersonic motion past circular cone by linearized method based on small perturbations with respect to nearly incompressible flow

16 p2835 A70-33746

Ackeret theory for infinite aspect ratio, rectangular and trapezoidal constant cord wings with arbitrary spanwise variation of profile in supersonic flow

16 p2836 A70-33748

Combined internal pressure and axial loading influence on aeroelastic stability of thin walled cylindrical shell in supersonic flow field

16 p2991 A70-33851

Supersonic plasma flows charge density levels and spatial and temporal variation, discussing theory and use of electrostatic probes

16 p2912 A70-33862

Reaction jets for control force generation in supersonic environment, analyzing downstream pressure distributions for two dimensional jet interactions

16 p2838 A70-33890

Steady isentropic weakly perturbed supersonic flows past arbitrary slender tapered wings with subsonic leading edges

16 p2838 A70-33971

German monograph on supersonic flows calculation past slender bodies of revolution using perturbation approach based on Poincare-Lighthill-Kuo method

16 p2839 A70-34082

Interface stability of thin liquid film adjacent to supersonic air flow, using sphere-cone and blunt wedge test configurations

[AIAA PAPER 70-801]

17 p3005 A70-34461

Convective heat transfer at solid boundaries in separated and reattached subsonic and supersonic flows, considering booster base heating

17 p3007 A70-34484

Supersonic air flow control by electrostatic discharges tested by Mach 3 wind tunnels, using schlieren system for bow shock wave

[AIAA PAPER 70-759]

17 p3008 A70-34492

Atmospheric reentry nosetip shape changes supersonic flow, considering rough surface effects on heat transfer

[AIAA PAPER 70-827]

17 p3196 A70-35193

Supersonic electrically conducting gas flow in flat channel with dielectric walls in inhomogeneous magnetic field

17 p3141 A70-35334

Supersonic axisymmetric flows past bell-shaped bodies of varying bluntness, using Godunov finite difference method

17 p3012 A70-35887

Steady supersonic flow past conical bodies at yaw, adapting Telenin numerical method

17 p3012 A70-35889

Shock layer and combustion in supersonic flows about conical bodies at various angles of attack

17 p3012 A70-35894

Plane nonconducting elastic plate with one side impinged upon by supersonic conducting gas flow, determining magnetic field effect on flutter vibrations

18 p3336 A70-36135

Supersonic conductive gas recombination fronts for arbitrarily oriented magnetic field, allowing for dissipative coefficients

18 p3294 A70-36255

Plane stationary supersonic flows with laminar separation zones at large subcritical Reynolds numbers

18 p3206 A70-36257

Drag optimal stern section of plane body at supersonic flow, allowing for friction forces

18 p3206 A70-36261

Flow velocity and pressure on thin wing of small span width near sonic speed, using parabolic type linear equation

18 p3207 A70-36374

Compression and expansion characteristics of steady supersonic flow passing along yawing slender body of rotation, linearizing differential equations

18 p3207 A70-36382

Pressure distribution shock pattern and impact wave resistance in frictionless plane parallel and source shaped supersonic flow

18 p3207 A70-36385

Equivalent bodies of revolution method extension for use in semicircular approximation technique, calculating pressure distribution of nonaxisymmetric blunt bodies

18 p3208 A70-36569

Viscous supersonic flow near sharp convex corner, discussing visual observation and quantitative surveys of velocity and pressure profiles

18 p3208 A70-36659

Finite plate length effect on two dimensional supersonic turbulent boundary layer with large distributed surface injection

18 p3242 A70-36688

Favorable pressure gradient effect on compressible two dimensional supersonic turbulent boundary, using temperature and pressure probes and shear balance

18 p3242 A70-36690

Skin friction measurement in supersonic flows by thin film heated element method, describing thermal boundary layer properties

18 p3243 A70-36710

Quasi-two dimensional supersonic cascade flow, taking into account transverse stream contraction effect

18 p3210 A70-37206

Method of characteristics for two dimensional steady supersonic gas flows with foreign particles in plane and axisymmetric nozzles

18 p3210 A70-37228

Perfect and dissociating gas nonstationary supersonic flow around sharp profile of finite thickness analyzed by linearization and method of characteristics

19 p3351 A70-37242

Supersonic flow of rarefied plasma around plane bodies, allowing for electric field effect on ion motion

19 p3351 A70-37302

Ionized argon supersonic flow velocity and local electron density by optical methods

19 p3480 A70-38173

Shock wave radiation from supersonic ducted rotor, determining sound power at blade passing harmonic frequency

19 p3353 A70-38614

Steady compressible supersonic planar flow of viscous heat conducting fluid under linearization freestream conditions, describing slip flow past finite flat plate

20 p3557 A70-39228

Combustion of decomposition products of Mg based pyrotechnic fuel in supersonic flow, obtaining heating device characteristics

20 p3736 A70-39266

Two phase flows and atomization jet during fluid injection into supersonic flow, determining vaporization range

20 p3736 A70-39268

Three dimensional supersonic and hypersonic gas flow by Oseen equations, obtaining asymptotic flow field

20 p3609 A70-39656

Supersonic flow past slender bodies in presence of strong blowing, extending solution by expansion at leading edge of thin plate

20 p3559 A70-39771

Steady sub and supersonic flow calculations behind receding shock wave, using finite difference scheme

20 p3611 A70-39803

Turbulent boundary layer on cone in supersonic flow in presence of inflowing foreign substance, considering local surface friction coefficient

20 p3559 A70-39814

Wedge angle large amplitude slow oscillations in hypersonic and supersonic flows, examining attached bow shock

20 p3559 A70-40288

Transport model for flow field and convective heat transport in planar turbulent supersonic base flow

21 p3744 A70-41030

Flow field, heat transfer rates and reattachment surface wall temperature of planar supersonic turbulent flow

21 p3744 A70-41036

Supersonic flows with imbedded separated regions, emphasizing cavities with recompression against solid boundary layer

21 p3745 A70-41372

Aerodynamic parameters of ionized Ar supersonic steady one dimensional nonviscous flow in thermodynamic equilibrium and subjected to Laplace accelerating forces

21 p3858 A70-41444

Nonuniform free stream supersonic flow past aerodynamic decelerators, calculating inviscid flow fields by method of characteristics

21 p3746 A70-41837

Surface pressure coefficient dependence on specific heat ratio for yawed conical lifting bodies in supersonic streams

21 p3747 A70-41877

Upstream mass injection effects on downstream heat transfer of supersonic reacting boundary layer

21 p3952 A70-42079

Decelerated channel flow dynamics of ideal gas with supersonic velocity closed by compression shock, using finite difference method

21 p3747 A70-42203

Supersonic air flow interaction with transverse gas jet from plate orifice

21 p3749 A70-42222

One dimensional supersonic flow of ideal conducting gas in linear channel under transverse magnetic field

21 p3861 A70-42228

Unsteady supersonic flow around oscillating cross-shaped wing-fuselage system, determining perturbation velocities and pressure distributions

22 p3958 A70-42609

Two dimensional flow about supersonic airfoil, considering trailing Taylor columns behavior like sonic booms

22 p4009 A70-42629

Conducting fluid supersonic flow past slender body of revolution in circular wind tunnel under inclined magnetic field, investigating MHD interference problem

22 p3958 A70-42669

Liquid jet breakup in supersonic airstream, using high speed photographic techniques

[SMPT PREPRINT 90]

22 p4036 A70-43063

Heat transfer in heated wire in supersonic flow near molecular transition zone, estimating anemometer sensitivity to motion fluctuations

22 p3959 A70-43240

Perfect gas supersonic flow with constant velocity, pressure and density around finite nonaxisymmetric body at small angles of attack

22 p3960 A70-43322

Three dimensional laminar boundary layer equations for body of revolution at angle of attack in supersonic gas flow derived for equations

22 p3960 A70-43323

Nickel surface layer fine structure changes in supersonic air flows at various temperatures and times

22 p4056 A70-43341

Potential flow around oscillating shell-plate structure subjected to supersonic gas flow at zero angle of attack, solving nonlinear aerodynamicity problem

22 p4117 A70-43362

Curved shock waves regular and Mach reflection in steady supersonic flow at plane wall

[ICAS PAPER 70-11]

23 p4180 A70-44122

Aerodynamic problems due to mixed subsonic and supersonic/transonic flows on swept wings, nacelle lips and helicopter rotor blades

[ICAS PAPER 70-14]

23 p4132 A70-44125

Steady irrotational gas flow characteristics calculation from finite difference scheme for three dimensional method of characteristics, considering supersonic nozzle flow

23 p4133 A70-44308

Heat transfer from turbulent boundary layer interacting with shock and expansion waves in supersonic flow

23 p4134 A70-44573

Reacting gas supersonic flow over two dimensional base, examining reaction rate effects on base pressure

23 p4135 A70-44626

Inviscid rotational supersonic flow near three dimensional stagnation point, examining solutions for compatibility with vortical shock layer boundary conditions

23 p4183 A70-44692

Two dimensional laminar near wake of slender body in supersonic flow at high Reynolds number

23 p4135 A70-44693

Thin liquid film/melt layer on body in supersonic flow, examining crosshatched wave patterns stability

23 p4183 A70-44979

Pointed ogival body of revolution in supersonic flow field, investigating local pressure distributed by variational methods

23 p4136 A70-44992

German monograph on supersonic strongly deflecting retardation cascades covering flow geometry and application to axial flow compressor stage

24 p4287 A70-45095

Kinematically unsteady aerodynamic coefficients consistent with stiffness and inertia properties of lifting surface in supersonic flow by finite element method

24 p4287 A70-45154

Thin cylindrical shell flutter in linearized supersonic potential theory, considering Mach number, aspect ratio and pressure effects on critical wave number

24 p4420 A70-45263

Numerical analysis of fuel combustion in supersonic stationary flows of hydrogen air mixture past bodies by two-component reaction kinetics model

24 p4428 A70-45500

Oscillatory motion of triangular wing with conical body of arbitrary cross section in supersonic flow, considering wing-body interference effects
24 p4288 A70-45592

SUPERSONIC FLOW INLETS

U SUPERSONIC INLETS

SUPERSONIC FLUTTER

Natural oscillations and flutter of three layer cylindrical shell in supersonic gas flow analyzed by semimomentless theory, discussing boundary value problems, damping effects, etc
03 p0600 A70-14301

Liapunov second method extension to dynamical systems stability, illustrating wing torsional divergence and panel supersonic flutter
05 p0941 A70-16564

Nonlinear flutter of three dimensional simply supported curved plates, employing quasi-steady supersonic aerodynamic theory
09 p1780 A70-23212

Flutter suppression in elastic finned beams in supersonic flow controlled automatically by rudder deflection according to flexural strain
09 p1785 A70-23615

Cylindrical shell segments supersonic flutter boundaries engineering estimates related to Saturn 5 booster, obtaining thickness requirement as function of panel geometry
[AIAA PAPER 68-284] 11 p2134 A70-25959

Wind tunnel interference effect on fluttering airfoils and panels supersonic speeds, studying pressure distributions for various tunnel aspect ratios and roof conditions
12 p2155 A70-27103

Parallel isotropic flat plates vibration and flutter in supersonic/subsonic flow over one surface, observing plane loadings and elastic medium stiffness effects
12 p2316 A70-27104

Supersonic flutter solutions using finite elements, analyzing rectangular plate bending elements, square simply supported and clamped panels, low aspect ratio configurations, etc
12 p2327 A70-27823

Low aspect ratio plates flutter analysis for subsonic and supersonic models
16 p2991 A70-33888

Circular cylindrical shells with clamped ends, investigating supersonic panel flutter by two mode approach and Galerkin method
17 p3184 A70-34695

Supersonic panel flutter of circular cylindrical shells at critical dynamic pressure
17 p3188 A70-35227

Plane nonconducting elastic plate with one side impinged upon by supersonic conducting gas flow, determining magnetic field effect on flutter vibrations
18 p3336 A70-36135

Homogeneous orthotropic cantilevered rectangular plate with reinforcing ribs, calculating flutter in supersonic gas flow
18 p3336 A70-36140

Skew panels supersonic flutter and vibration calculated by matrix displacement method
21 p3933 A70-40586

Circular cylindrical shell supersonic panel flutter nonlinear analysis, using averaging and numerical integration methods
22 p4112 A70-42275

Low aspect ratio cantilever plate wings supersonic bending torsion flutter speed calculation, using spanwise and chordwise variables and potential energy principle
22 p4112 A70-42276

Thin circular cylindrical panels in supersonic gas current parallel to generatrices, calculating heterogeneity effect on flutter
22 p4113 A70-42603

Laminar circular cylindrical shells supersonic flutter characteristics determination by dynamic equilibrium boundary value problem eigenvalues analysis, obtaining critical flutter speeds
24 p4424 A70-45588

SUPERSONIC HEAT TRANSFER

Combustor geometry and heat release effects on supersonic combustor thrust efficiency, considering shock-free, normal and oblique shock situations
02 p0354 A70-12043

Performance analysis for electrothermal thruster using lithium propellant with supersonic heat addition
[AIAA PAPER 69-286] 06 p1129 A70-17159

Heat transfer on supersonic sweptback wing for case of laminar boundary layer with vortex distribution
07 p1187 A70-18921

Blunt base heat transfer in axisymmetric supersonic separated flow in axisymmetric near wake tunnel, comparing to previous data
13 p2523 A70-29989

Roughness effects on heat transfer to surfaces in supersonic compressible turbulent boundary layer
[AIAA PAPER 70-742] 17 p3066 A70-34505

SUPERSONIC INLETS

Diffused diaphragm pressure sensors in impact probes used in wind tunnel tests of dynamic response of supersonic air induction systems
06 p1074 A70-18605

Supersonic inlet role and nature in air breathing propulsion system, discussing inlet-engine matching by variable geometry
[AGARDOGRAPH-120] 08 p1434 A70-21928

Stable operating range of supersonic mixed compression inlet increase by air flow removal via throat bleed system
[AIAA PAPER 70-686] 16 p2967 A70-33585

Supersonic air intake unsteady buzz phenomenon, examining shear layer under cowl and boundary layer detachment at shock wave base for design improvement
21 p3744 A70-41262

M 3.5 two dimensional mixed compression inlet system with self restart using flexible variable ramp system
[AIAA PAPER 69-447] 22 p3959 A70-42707

SUPERSONIC JET FLOW

Particle velocity distributions in low density supersonic jets measured by molecular beam sampling technique and multidisk velocity analyzer
02 p0276 A70-11849

Turbulent reattachment of supersonic axisymmetric jet on cylindrical wall in air, investigating wall temperature effect on cavity pressure and heat flux
[ONERA-TP-758] 03 p0467 A70-13643

Thermal recovery factors at hemispheric probe stagnation point in low density supersonic jets of He-Ar and H-N mixtures
[ASME PAPER 69-WA/HT-27] 04 p0782 A70-14810

Supersonic jet flow from diverging nozzle into space with given pressure or into supersonic slipstream, noting barrel shock formation inside jet
04 p0617 A70-15235

Discrete components in noise spectrum of heated and unheated supersonic air jets, using axisymmetric and conical nozzles
04 p0618 A70-15247

Reattachment of supersonic jet with turbulent shear boundary layer abruptly expanding into axisymmetric parallel diffuser, using surface flow technique
04 p0619 A70-15323

Vorticity effects on drag friction and heat transfer near stagnation point of supersonic jet impinging on obstacle
05 p0833 A70-16290

Acoustic radiation from underexpanded supersonic main jet flow from nozzle impinged upon by annular jet
05 p0835 A70-16784

Interacting coaxial supersonic jet flows noise reduction based on noise distribution characteristics measurement in anechoic chamber
[AIAA PAPER 70-236] 06 p1040 A70-18112

Supersonic exhaust plume/boundary layer interactions, developing integral method and extending to turbulent interactions
[AIAA PAPER 70-230] 06 p1040 A70-18117

Helium injection Mach number effect on supersonic jet penetration into Mach 2 air stream from flat plate determined from concentration measurements
[AIAA PAPER 70-92] 06 p0975 A70-18200

Species spatial distribution measured for He-Ar gas mixtures expanding in supersonic jets, compared to measurements with skimmer-nozzle arrangement
06 p1066 A70-18256

Translational relaxation in low density axisymmetric hypersonic free gas jet, describing transition from isentropic to free molecular flow
06 p1043 A70-18277

Supersonic free jets condensation, examining kinetics of reactions in mono- or diatomic gases
06 p1044 A70-18282

Supersonic molecular free jets using electron diffraction technique, discussing vibrational and condensation states
06 p1044 A70-18301

Stable flow distribution of sonic jet exhausting counter to low density supersonic airstream
07 p1189 A70-19982

Supersonic molecular beam source operation, discussing dominant degradation factors and nozzle beam generation intensities and energies improvement
07 p1341 A70-20104

Helium and argon atoms number densities radial profiles in supersonic free jets of binary gas mixtures by molecular beam sampling
07 p1341 A70-20105

Radicals in low pressure supersonic free jets, investigating production by flash photolysis
07 p1343 A70-20126

Supersonic gas jets applicability as vacuum locks for molecular fluxes at thermal velocity in magnetic trap
08 p1549 A70-20509

Heat exchange at stagnation point of subsonic and supersonic axisymmetric jets interacting with perpendicular plane partition, allowing for turbulence
08 p1482 A70-20919

Diffusive separation of Ar 36 and 40 and He in axisymmetric supersonic jet taking into account pressure diffusion
08 p1431 A70-21027

Supersonic air jet structure in central shock wave region affected by both Mach number and flow rarefaction
09 p1734 A70-22185

Supersonic jet force acting on target investigated for air and argon using dimensional analysis
10 p1804 A70-25122

Tapered resonance tubes matching supersonic air jet geometries considered for explosion hazards created by pneumatic system seals failure
11 p2035 A70-25981

Supersonic jet spoilers flow fields with various nozzle shapes to determine secondary jets penetration depth and mixing in wake
13 p2338 A70-28480

Apparent mass measurements of supersonic jet in incalculable flow regimes, determining dependence on Mach number at nozzle and on distance from exit
13 p2387 A70-28859

Combustion effects on mixing of axisymmetric supersonic and turbulent free jets to obtain species concentrations, pitot pressures and temperatures
16 p2998 A70-33860

Nonequilibrium vibrational energy and relaxation equation for carbon dioxide-nitrogen molecular gas mixtures in supersonic free jet exhausting into vacuum
[AIAA PAPER 70-867] 16 p2895 A70-33910

Aerodynamic and acoustic characteristics of subsonic and supersonic jets from convergent nozzles with room temperature air supply
17 p3005 A70-34460

Mach disk structure in free low density expanding supersonic jet from static pressure probe measurements
17 p3068 A70-34696

Turbulent mixing of axisymmetrical supersonic air jet into hot air, investigating Mach number and temperature difference effects on axial decay of velocity
17 p3072 A70-35546

Base flow component of total drag for axisymmetric supersonic afterbody with single exhaust jet, considering turbulent mixing
17 p3011 A70-35656

Retrorocket jet size and structure for scientific instruments soft Mars landing, estimating off-optimum supersonic jet interaction with quiescent atmosphere
17 p3011 A70-35660

Viscosity effect on turbulent supersonic underexpanded jet flow into submerged region
18 p3206 A70-36262

Knudsen effusion in free molecular flows in supersonic jet during expansion through circular orifice, discussing power and heat transmission
18 p3346 A70-36379

Low temperature underexpanded supersonic gas plasma jets behind shock wave, analyzing rarefaction and viscosity effects on parameters distribution
19 p3352 A70-38185

Supersonic air jet noise spectrum analysis at various pressures
19 p3354 A70-38659

Supersonic jets noise spectra, using linear equations of moving medium acoustics
19 p3354 A70-38660

Discrete components of noise frequency spectrum of free supersonic jet
19 p3354 A70-38661

Multilayered and multiple supersonic jets, deriving dispersion equations for boundaries stability
19 p3354 A70-38663

Helium injection Mach number effect on supersonic jet penetration into Mach 2 air stream from flat plate determined from concentration measurements
20 p3558 A70-39690

Supersonic weakly ionized plasma jet in argon, investigating axial and radial temperature profiles by electrical probe techniques and spectroscopic and photographic methods
20 p3685 A70-40463

Supersonic jet force acting on target investigated for air and argon using dimensional analysis
20 p3560 A70-40515

Solar chromosphere spicules acceleration via supersonic jet formed by magnetic field under gravity and Melon seed effect
21 p3925 A70-42192

Acoustic waves generation from decay region of pulsating supersonic jet expelled from nozzle
21 p3748 A70-42211

High speed plasma jet propagation, obtaining time of arrival measurements, brightness temperature, pressure and impact data
22 p4012 A70-43014

SUPERSONIC NOZZLES

Nonequilibrium effect of expanding water vapor condensation on supersonic nozzle flows with or without inert carrier gas
01 p0063 A70-10806

- Air flow density measurements with interferometer in supersonic square Laval nozzle, showing flow core motion and wave structure 01 p0064 A70-11000
- Supersaturated vapor condensation in supersonic nozzles, obtaining flow and droplet growth equations for local equilibrium condition 02 p0279 A70-12049
- Analytical method for design of supersonic flow and maximum thrust nozzles for chemically reacting gases, noting surface geometry [AIAA PAPER 70-129] 06 p0971 A70-18108
- Exhaust plume from underexpanded sonic and supersonic nozzles including boundary mixing analyzed by approximate model to predict Mach disk location [AIAA PAPER 70-229] 06 p0972 A70-18135
- Electronic-vibrational coupling in nonequilibrium MHD generator with molecular gas to suppress electrode layer shorting and recombination in supersonic nozzles [AIAA PAPER 70-41] 06 p0988 A70-18222
- Three dimensional supersonic nozzle geometry optimization using Lagrange multipliers and iteration for solving variational problem 10 p1798 A70-24115
- Adiabatic flow coefficient in supersonic nozzle with choked flow conducted over throat Reynolds number range 11 p1976 A70-25999
- Central shock and target displacement of underexpanded supersonic jets with obstacle at nozzle exit, using Toepler schlieren photographs 12 p2156 A70-27293
- Carrier gas effect on homogeneous condensation in supersonic nozzle using liquid drop theory 12 p2211 A70-27829
- Numerical method of characteristics for three dimensional supersonic nozzle flow field calculations 13 p2338 A70-28512
- Laminar boundary layers in low density supersonic and hypersonic conical and axisymmetric nozzles, treating displacement, transverse curvature, velocity slip and temperature jump [AIAA PAPER 69-653] 13 p2386 A70-28513
- Flow disturbances and side forces in supersonic rocket nozzle due to gaseous secondary injection analyzed by semiempirical models 14 p2629 A70-30756
- Auxiliary inlet ejector and plug nozzle flight performance, describing design variation effects for high supersonic speeds [AIAA PAPER 70-701] 16 p2841 A70-33563
- Supersonic cylindrical ejectors without induced flow for rocket engine studies 16 p2837 A70-33763
- Shock waves in supersonic conical nozzle flow due to secondary gas injection, using conical lens for flow visualization 17 p3011 A70-35236
- Nonequilibrium recombination in supersonic nozzle of dissociated combustion products of hydrogen in air, investigating initial system and rate constants effect 20 p3582 A70-39269
- Supersonic nozzle damping, replacing parameters discontinuities across shocks by continuous variations 21 p3745 A70-41442
- Two layer gas flows in supersonic axisymmetric nozzles, using method of characteristics 21 p3748 A70-42210
- SUPERSONIC PRESSURE DISTRIBUTION**
U PRESSURE DISTRIBUTION
U SUPERSONIC FLOW
- SUPERSONIC SPEEDS**
 Surface shape determination for thin delta wing with variable geometry to minimize drag for given open and closed configurations and cruising supersonic speeds 01 p0002 A70-10547
- Shock wave diffraction at wedge moving at supersonic velocity, solving Hilbert space formulated for constant parameter flow 03 p0406 A70-13333
- Magnus effects on Apache sounding rocket at supersonic speeds, discussing spinning model and static tests [AIAA PAPER 70-207] 06 p1157 A70-18103
- Molecule spatial and velocity distributions of supersonic molecular beams, measuring scattering cross sections of He and Ar on noncondensable gases 06 p1043 A70-18252
- Generatrix shape determined for body of revolution moving at supersonic speed with minimum wave drag 09 p1603 A70-22434
- Initial blast wave axisymmetric shock-on-shock interaction for blunt bodies moving supersonically at zero angle of attack solved in Taylor series 10 p1797 A70-23954
- Gas stream velocity field produced by shock wave impinging against wing moving at supersonic speed 10 p1799 A70-24124
- Plane shock wave interaction with supersonic blunt body, considering pressure-time studies for stagnation point of flow 10 p1801 A70-24145
- Sphere supersonic motion in combustible gas mixture of given temperature and pressure, discussing constant density two front detonation wave model 12 p2334 A70-28242
- Stagnation point position and entropy at surfaces of supersonic paraboloids in perfect gas 12 p2160 A70-28250
- Correction to Smyrl results for perturbation pressure in interaction field behind plane shock diffracted by supersonically moving thin yawed wedge 13 p2338 A70-28822
- Infrasonic waves generation by supersonic translation of auroral electrojet currents 13 p2399 A70-29237
- Supersonic rigid cone motion in elastic medium, obtaining partial solutions to motion equation yielding boundary problem solution 13 p2341 A70-29508
- Simultaneous equations for motion location, speed and direction in acoustic tracking of supersonic objects, recording shock wave times of arrival with microphone system 13 p2450 A70-29988
- Shock wave diffraction at wedge moving at supersonic velocity, solving Hilbert space formulated for constant parameter flow 14 p2528 A70-30712
- Aerodynamic characteristics of transonic and supersonic blunt vehicles, reviewing numerical methods 17 p3012 A70-35895
- Supersonic boom intensity calculation on ground, assuming isobaric inhomogeneous atmosphere and weak shock wave 18 p3213 A70-36380
- Continuous surface of revolution parachute for supersonic/hypersonic speeds, performing wind tunnel tests [AIAA PAPER 70-1173] 21 p3754 A70-41840
- Crack propagation at supersonic velocities in K Cl crystals, noting plasma induction within specimen by laser pulse 21 p3940 A70-42033
- Accelerated supersonic motion of plate with attached shock wave at finite angle of attack in ideal gas, using perturbed nonstationary motion equations 21 p3748 A70-42209
- Aerodynamic lift, drag and momentum coefficients in supersonic regime for rectangular and trapezoidal wings with spanwise variable profile 22 p3958 A70-42615
- Wave-riders aerodynamics and heat transfer, investigating lift to drag ratios for supersonic and hypersonic vehicles [ICAS PAPER 70-18] 23 p4276 A70-44129
- SUPERSONIC STRIKE AIRCRAFT**
U ATTACK AIRCRAFT
U SUPERSONIC AIRCRAFT
SUPERSONIC TEST APPARATUS
 Wall thickness measurement by supersonic testing method based on resonance 24 p4336 A70-45681
- SUPERSONIC TRANSPORTS**
NT CONCORDE AIRCRAFT
 Sonic boom pressure signatures for uniform and maneuvering flight conditions determined for fighter and SST aircraft [AIAA PAPER 69-1134] 01 p0005 A70-10606
- SST Ti body frame optimum design for high temperature environment and economical and fatigue resistance requirements 02 p0386 A70-11937
- Atmospheric effects on SST, discussing turbulence, temperature, wind, cloud cover, hail, toxic gases, etc 02 p0325 A70-12218
- Atmospheric turbulence effects on accelerations experienced by passengers in supersonic and subsonic transport aircraft compared 02 p0325 A70-12219
- Atmospheric environment features bearing on supersonic transport aircraft operations and forecasting, discussing wind and temperature effects 02 p0325 A70-12220
- Meteorological data provision for supersonic civil transport operations, considering various flight phases 02 p0325 A70-12221
- Liquefied natural gas or liquefied methane as burning propulsion system for SST, examining storage volume, fuel-tank insulation and implosion danger 03 p0543 A70-12998
- Modified tailed delta configuration selection for U.S. SST, discussing power plant installation choice [RAES PAPER 17] 03 p0411 A70-13544
- FAA engineering approach to SST certification involving airworthiness standards development and coordination with industry and foreign governments 03 p0437 A70-14060
- Methane fuel systems for high Mach number supersonic transport aircraft on basis of minimum weight [SAE PAPER 69068] 05 p0894 A70-15835
- Aircraft configurations designed for eliminating sonic boom due to lift 05 p0791 A70-16798
- Orbit-shuttle and SST craft hypersonic flight vehicles design, discussing aerodynamic heating, shock stresses and propulsion system requirements 05 p0797 A70-17087
- Meteorological conditions effects on SST aircraft flight safety and economics, emphasizing stratospheric information for forecasting 06 p1095 A70-17193
- Aeronautical satellites application to supersonic air transportation economy, discussing navigational information relay between aircraft and control center 07 p1191 A70-18988
- Particle properties and solar flare radiation hazards for passengers in supersonic flight 08 p1435 A70-20632
- Air breathing engines for long range Mach 4 transport, discussing airplane mission profile- engine configuration interface [AGARDOGRAPH-120] 08 p1560 A70-21934
- ATC and SST operations in terminal area simulation study involving airline crews and controllers in real time traffic situation 09 p1721 A70-22946
- Aircraft certification of supersonic and jumbo jet transports assuring acceptable safety level 09 p1610 A70-22948
- Certification process for supersonic transports taking into account safety and economic considerations 09 p1610 A70-22949
- Primary long range navigation system for SST, considering operational goals, Doppler radar systems, navigation aids, inertial systems, etc 09 p1722 A70-23029
- Supersonic transports bow and rear shock pressure jump lower bounds for various physical constraints 10 p1805 A70-24558
- Design mean stress and ground-air cycles minimum stress effect on fatigue behavior of titanium alloy in supersonic transport operating environment [SAE PAPER 700033] 11 p2128 A70-25370
- Supersonic transport airworthiness criteria tentatively applied to road characteristics of automobiles 11 p1979 A70-25816
- Water vapor pollution of stratosphere by supersonic transports, considering effects on temperature, cloudiness, albedo, etc 11 p2077 A70-26618
- Air transport and European cooperation involving supersonic transports, jumbo jets and STOL aircraft 12 p2334 A70-26966
- Titanium structural element allowances requirements and test programs for SST design 12 p2318 A70-27132
- International safety standards for SST airworthiness 12 p2161 A70-27599
- SST feasibility for U.S., considering program costs, financing, investment return and airport and community noise aspects 12 p2162 A70-27991
- Temperature prediction accuracy over 24-hr period for supersonic transport flight operations 13 p2443 A70-28549
- Elastomeric seals and sealants selection for SST, describing tests in air, fuel vapors and hydraulic fluids at elevated temperatures 13 p2418 A70-28668
- Weather forecasting for SST operations, discussing wind, temperature, turbulence, clouds, etc 13 p2445 A70-29494
- SST aircraft fuels and lubricants, discussing fire hazard and pollution minimization 13 p2473 A70-29999
- CAT and small scale atmospheric motions in relation to supersonic transport and space shuttle design and operation 14 p2609 A70-30602
- Mesoscale slope limits in constant pressure surfaces relation to g-forces on aircraft at SST altitude, using radiosonde measurements 14 p2530 A70-30607
- Northern Hemisphere temperature atlas for SST cruise altitudes, estimating probabilities of enroute temperatures and risk increase 14 p2609 A70-30609
- Meteorological effects on air and noise pollution at U.S. airports 14 p2530 A70-30610
- SST system safety program, discussing federal office structure, planning and control, design support, integration and evaluation, requirement analysis and failure recurrence control 15 p2675 A70-32214
- Aircraft accidents during descent, approach and landing, discussing B 747, CSA and SST 15 p2675 A70-32216
- Bypass door control system for SST axisymmetric intake operation in external compression mode, obtaining dynamic performance [AIAA PAPER 70-695] 16 p2966 A70-33558
- Supersonic transport sonic boom theory and effect reduction, discussing Whitham rule, bow shock, overpressure, engine and aircraft design and shock wave control 16 p2843 A70-34263

Alloy applications to Boeing supersonic transport airframe and components, discussing materials characteristics and manufacturing processes 17 p3099 A70-34451

SST flight efficiency trends, discussing breakthrough and development method and Concorde aerodynamic, propulsion and structural history [AIAA PAPER 70-871] 17 p3016 A70-34811

Bora-Sond atmospheric probe providing two stage minimum cost high altitude sounding for supersonic transport /SST/, discussing hot water propulsion system 17 p3178 A70-35257

SST electrohydraulic primary and standby brake control systems, discussing design and advantages [AIAA PAPER 70-913] 17 p3024 A70-35825

Boeing 2707 SST horizontal tail multiple channel actuation system features 17 p3020 A70-35827

Jet A kerosene deposit accumulation problem and proposed SST fuel tank design [SAE PAPER 700256] 18 p3214 A70-36825

Electronic attitude director indicator /EADI/ for supersonic transport, employing CRT display, head down TV and microvision sensors 19 p3463 A70-37911

ATC integration of SST, discussing en route and terminal projects of national airspace system, modular automation, instrument flight rules, etc 19 p3467 A70-38633

Supersonic transport radiation hazards to flight crew, passengers and population, discussing dosages, probabilities, solar cosmic ray encounters, warning systems, etc 20 p3700 A70-39923

Human disturbance from SST overflight sonic booms, discussing overpressure, rise times and durations 23 p4137 A70-44016

SST configurations minimizing sonic booms obtainable for given length and weight [ICAS PAPER 70-23] 23 p4138 A70-44110

U.S. SST flight deck instrumentation and cockpit displays during flight, discussing economic analysis of operations [ICAS PAPER 70-59] 23 p4139 A70-44155

Boeing 2707 SST design for low community noise, discussing engine-airframe matching effect [SAE PAPER 700808] 24 p4290 A70-45906

Atmospheric pressure surface sharp slopes at SST altitudes producing vertical acceleration based on temperature gradients inspection 24 p4372 A70-46050

Automatic control system for Boeing SST engine air intakes, optimizing engine performance and controlling noise propagation 24 p4396 A70-46214

SUPERSONIC TURBINES

Supersonic fluid turbomachine components and systems innovations and performance trends [AGARDOGRAPH-120] 08 p1434 A70-21927

Supersonic turbine blade rows design, discussing boundary layer interaction around leading edges and flow around trailing edges 19 p3490 A70-38223

SUPERSONIC WAKES

Nonisothermal plasma perturbed by supersonic body, studying plasma rarefaction and condensation cones, particle density, etc, in wake 03 p0407 A70-13413

Supersonic missile drag reduction through wake heating assuming conical shaped missile tail and flow nonseparation [DFVLR-SONDDR-36] 04 p0616 A70-15165

Flowfield and chemical kinetics model to calculate nitrogen dioxide chemiluminescence wake emission [AIAA PAPER 68-702] 04 p0620 A70-15335

Supersonic wake flow visualization, obtaining direct photographs of various smoke streamlines [AIAA PAPER 69-346] 04 p0621 A70-15395

Free recirculation areas in wake of flame holders used for flame stabilization at bluff bodies in supersonic flow 06 p0965 A70-17244

Residence time of foreign gas injected into recirculation region of wake behind slender body in axisymmetric supersonic flow [AIAA PAPER 70-111] 06 p0968 A70-18040

Base mass injection effects of various gases on slender body supersonic near wake stability, diffusion and cooling [AIAA PAPER 70-110] 06 p0970 A70-18075

Two dimensional supersonic turbulent near wake saddle point singularity during recompression analyzed by including transverse momentum integral equation [AIAA PAPER 70-228] 06 p1039 A70-18106

Two dimensional supersonic wake transition characteristics noting effect of heat transfer from vehicle or model body 09 p1605 A70-23184

Pulsed laser holographic interferometry of density field created by high speed projectile motion in air [AIAA PAPER 69-347] 11 p2051 A70-25987

Blunt base heat transfer in axisymmetric supersonic separated flow in axisymmetric near wake tunnel, comparing to previous data 13 p2523 A70-29989

Wedge and cylinder high supersonic wakes stability and transition at various Reynolds numbers 17 p3006 A70-34465

Two dimensional supersonic wake behind heated slender flat plate, considering flow properties in transition zone 17 p3006 A70-34466

Steady state laminar flow model for near wake of slender body in supersonic flow 17 p3006 A70-34467

Turbulence in supersonic wake behind flat plate at zero incidence and heat transfer rate, using hot-wire anemometer 19 p3403 A70-37528

Turbulent mixing in supersonic cone near wake, using laser planogram technique for flow visualization 19 p3351 A70-37529

Base pressure behind supersonic vehicle, examining Crocco-Lees mixing theory critical point in laminar near wake 21 p3747 A70-42109

Low pressure supersonic wake measurement by differential interferometer in double pass polarized light [SMPTE PREPRINT 95] 22 p4036 A70-43060

Supersonic wakes visualization and photographic measurement by schlieren techniques, using amplitude subtraction and He-Ne laser [SMPTE PREPRINT 94] 22 p4036 A70-43061

SUPERSONIC WIND TUNNELS

60 cm intermittent blowdown type trisonic wind tunnel, discussing main parts basic dimensions and characteristics determination method, detailing design and construction 01 p0055 A70-10148

Holographic interferometry with pulsed ruby laser holocamera for examining flow distribution in supersonic free jet wind tunnel 03 p0480 A70-12948

Thermal protective device for models exposed to flow buildup in intermittent wind tunnel, offering straightforward design, easy applicability, low cost and favorable experimental conditions [ONERA-TP-755] 03 p0463 A70-13627

Pre-set Mach number control in supersonic wind tunnel, evaluating effects of nozzle installation, stagnation temperature drop and pressure errors 06 p1028 A70-17912

Explosive blast wave effects on flight vehicle in supersonic flow, using conical blast generator and short duration supersonic wind tunnel [AIAA PAPER 70-221] 06 p0972 A70-18127

Supersonic wind tunnel flow discontinuities effect on oscillatory pressures 07 p1257 A70-19338

Aerodynamic subsonic and supersonic wind tunnels parameter measurement methods including static and total pressure, current direction, velocity, density, etc 09 p1674 A70-22314

Undried atmospheric air humidity effect on pressure and water vapor supercooling in supersonic wind tunnel nozzles 09 p1606 A70-23613

Condensation start dependence on air humidity at inlet and nozzle geometry applied to supersonic wind tunnel using undried atmospheric air 09 p1606 A70-23614

C-4 supersonic free jet test cell, discussing Concorde development contribution and model tests on full scale cell nozzle 11 p2031 A70-25853

Free jet test facility for supersonic engine/ intake combination testing, discussing benefits to aircraft flying hours, development costs and safety 11 p2101 A70-25854

Wind tunnel interference effect on fluttering airfoils and panels supersonic speeds, studying pressure distributions for various tunnel aspect ratios and roof conditions 12 p2155 A70-27103

Vacuum supersonic wind tunnel air continuous dehumidification by using multistage centrifugal blower with/without heat exchanger 12 p2206 A70-27153

Boundary layer transition at high Mach numbers on adiabatic wall, showing effects of wind tunnel size, surface roughness and freestream disturbances [AIAA PAPER 70-586] 13 p2342 A70-29884

Intermittent blowdown supersonic wind tunnel as economic test facility covering subsonic test velocity range, discussing data quality [AIAA PAPER 70-581] 13 p2342 A70-29889

Laminar boundary layer transition on sharp cone at zero yaw in supersonic wind tunnels, correlating aerodynamic noise disturbances with transition Reynolds numbers [AIAA PAPER 70-799] 17 p3006 A70-34462

Supersonic air flow control by electrostatic discharges tested by Mach 3 wind tunnels, using schlieren system for bow shock wave [AIAA PAPER 70-759] 17 p3008 A70-34492

Supersonic cascade wind tunnel performance evaluation, using compressor blades of simple geometric shapes [ASME PAPER 70-GT-110] 18 p3238 A70-36848

Short duration tube wind tunnel supersonic testing, noting Saturn S-IC base heating and solid propellant rocket base burning tests 20 p3606 A70-39698

SUPINE POSITION

Human nostril airflow resistance during supported sitting and lateral recumbency and crutch pressure, discussing ipsilateral nasal congestion mechanisms 08 p1448 A70-21874

Blood flow redistribution during sustained high skin temperatures of men in supine position 12 p2169 A70-27654

Energy consumption in male subjects during walking and running in erect and supine position under simulated gravity 13 p2351 A70-29335

Human acceleration resistance and psychomotor behavior under emergency flight conditions, including high temperature exposure and remaining in clinostatic position 17 p3037 A70-35135

Body position effect on oxygen saturation of regional pulmonary venous blood and arterial-venous shunts in intact dogs 21 p3766 A70-42153

Age determined hemodynamic reactions in men and women performing walking motions in lying position 22 p3970 A70-42908

SUPPORT SYSTEMS

NT GROUND OPERATIONAL SUPPORT SYSTEM

NT GROUND SUPPORT SYSTEMS
Performance characteristics analysis of large area roll-up solar arrays based on support structure size and weight [ASME PAPER 69-WA/ENER-11] 04 p0770 A70-14898

Integrated logistic support economics considered in selecting support system for generating quantitative data for cost optimization [SAE PAPER 690632] 05 p0959 A70-15846

Support facilities requirements and goals for manned and unmanned solar and stellar orbital astronomy [MDAC-WD-1258] 05 p0847 A70-16074

Automatic support systems for advanced maintainability - IEEE Conference, St. Louis, November 1969 08 p1468 A70-20651

Computer controlled automatic test system /NARF 5500/ for naval avionics systems support, discussing system hardware and applications and programming cost reductions 08 p1469 A70-20652

General purpose support system /GPSS/ simulation for carrier operations and avionics maintenance, considering attack aircraft operations, spare parts, personnel requirements, etc 08 p1470 A70-20661

Versatile avionics shop test /VAST/ Implementation Study recommendations on project management for automatic test equipment support system aboard attack aircraft carriers 08 p1601 A70-20663

Deterministic model for cost effectiveness of avionics support programs based on subsystems support ability, test philosophy and test equipment design and manufacture [AIAA PAPER 69-305] 14 p2563 A70-30857

SUPPORTS

Apollo/Saturn 5 space vehicle supporting and restraining mechanisms design and operation, discussing holddown assemblies 01 p0055 A70-10468

Elastic support effect on bending of clamped circular, elliptical, rectangular and skewed plates, using variational method and small perturbation technique 01 p0205 A70-11144

Multisupported radially symmetrical suspension systems designs for parabolic antennas, assessing performance in terms of maximum rigidities 08 p1586 A70-21058

Support vibration effect on zero shift of damped vertical pendulum, using equivalent linearization with perturbation scheme 10 p1917 A70-25205

Free wave propagation constants in periodically supported infinite beams determined for rigid and flexible supports 11 p2132 A70-25727

Euler-Bernoulli and Timoshenko beam impact models compared for case of finite beam resting on spring supports 12 p2327 A70-27843

Static and dynamic stability of wind tunnel models with flexible support, considering binary rigid body freedoms 14 p2564 A70-31398

Minimal interference thin metal strap support system for dynamic stability tests of high fineness ratio wind tunnel models [AIAA PAPER 69-350] 17 p3063 A70-35657

Sliding friction effects of nonlinear asymmetric supports on turbine engine rotor-shaft stability [SAE PAPER 700320] 18 p3301 A70-36799

Support elasticity role in axisymmetric plates bending, discussing Rayleigh-Ritz solution 21 p3937 A70-41739

SUPPRESSORS

NT ECHO SUPPRESSORS

Artificial hypobiosis state maintenance in animals exposed to cooling after administering lytic mixtures for suppressing oxidation 01 p0029 A70-11464

Zener diodes as voltage transient suppressors for ground vehicle and aircraft power supplies 16 p2879 A70-34060

SURFACE CHEMISTRY

U SURFACE REACTIONS

SURFACE COATINGS

U COATING

SURFACE COOLING

Anomalous temperature-time cooling data for surface material of Tycho, Copernicus and Aristarchus craters, suggesting relation to magnetic phase transitions during lunar nights 01 p0183 A70-10825

Angular distribution measurements of visible and near IR radiation reflected from carbon dioxide cryodeposits formed on liquid nitrogen cooled surface in vacuum [AIAA PAPER 69-63] 04 p0720 A70-15538

Rectangular fins arrangement on horizontal surfaces for optimum free convection heat transfer coefficient, considering fin weight, height and spacing effects [ASME PAPER 69-HT-44] 09 p1789 A70-23551

Local heat sink thermal processes on convectively cooled solid surface, noting applications to temperature measurement errors 12 p2333 A70-28112

Supersonic slot cooling for surface protection at hypersonic speeds using contoured axisymmetric nozzle with streamlined body 14 p2663 A70-30257

Wall cooling effects on turbulent boundary layer in low speed air flow, using smooth tube and thermocouple measurements 18 p3347 A70-36505

Kinetic heating of spacecraft surfaces, emphasizing materials and fluid circulation cooling devices 18 p3333 A70-36654

Body surface cooling level and rate effects on psychomotor performance tested at various levels of mean weighted skin temperature /MWST/ 20 p3573 A70-39675

SURFACE CRACKS

Eddy current inspection method for detecting fatigue cracks location and depth in fastener holes 01 p0097 A70-10008

Inconel 718 and Al 2219 alloys surface flawed specimens fracture toughness and flaw growth comparison for high pressure hydrogen vessel 01 p0114 A70-10029

Fracture surface topography variation with specimen thickness, studying fatigue crack propagation in Al 02 p0317 A70-12317

Optimum prism angles and ultrasonic frequencies for detecting fatigue cracks 02 p0301 A70-12487

Kinetic theory of cracks network formation on LiF crystal surface exposed to plasma jet using high speed camera 04 p0730 A70-14458

Ti-Al-Zr-W-Si alloy fracture surface concentric markings number related to loading cycles after crack formation 10 p1904 A70-28437

Microtopography of fracture surfaces by stereo electron fractography, using large angle tilting of specimens 13 p2431 A70-28605

Kinetic theory of cracks network formation on LiF crystal surface exposed to plasma jet using high speed camera 13 p2510 A70-28655

Transverse bending of isotropic rectangular plate with symmetric crack under uniformly distributed load, considering corrections for stress-strain state near cracks 13 p2516 A70-29516

Yield criteria for plastic deformation on glassy high polymers induced by stress field, noting crazing and shear yielding dependence on first stress invariant 15 p2764 A70-31787

Elastic half plane with crack perpendicular to free surface and under arbitrary pressure distribution, obtaining exact solution for stress and displacement fields 15 p2767 A70-31854

Elastic equilibrium of unbounded body with central hole and concentric cracks under symmetric load 15 p2819 A70-32188

Fatigue and surface crack detection using holographic techniques 17 p3086 A70-35015

Metal surface through and part through cracks, investigating dimensions and material properties effects on fracture stresses 18 p3278 A70-36565

Butt joined epoxy Al plates tensile strength, observing fracture strength dependence on stress concentration at bond edges below characteristic crack length 21 p3939 A70-42032

SURFACE DEFECTS

Metal surface microscopic defects detection and display using diffused radioactive Kr-85 gaseous penetrant for anodized flaws, bearing porosity and turbine blade cracks 01 p0096 A70-10006

Machined surface evaluation of fabricated components by electron microscopy to identify defects 01 p0097 A70-10012

Laser processing applied to optical nondestructive materials tests for surface flaws 01 p0086 A70-10416

Direct solar radiation concentration by paraboloid mirrors, analyzing energy transport and distribution functions, based on statistically distributed imperfections of reflecting surfaces 01 p0010 A70-10762

Friction and surface damage between clean metal hemispheres and flats at low sliding speeds and 25 K room temperature range 01 p0105 A70-11353

Equations of motion, conservation of mass, momentum and energy for elastic bodies with lattice-type surface defects 01 p0209 A70-11400

Optical surface degradation during measurements with high power laser, considering atmospheric dust and cleaning solvents 05 p0861 A70-16848

Mo mechanical properties dependence on surface defects and Ti films 08 p1515 A70-20937

Eddy currents magnetic field structure over surface defects in conducting objects, noting NDT applications 13 p2404 A70-28661

Electrochemical machining /ECM/ effects on components surface integrity, discussing jet engine materials [ASME PAPER 70-GT-111] 18 p3264 A70-36849

Surface damage of GaAs crystals by mechanical handling and polishing with hard abrasive lapping materials 20 p3686 A70-39119

Surface adsorbed and absorbed radioactive Kr 85 gas for displaying surface microdefects in materials 20 p3638 A70-39950

Reflection echelon and Fabry-Perot interferometer with surface imperfections, comparing spectral resolution limit with Rayleigh limit 22 p4040 A70-43612

Reflector materials flaw size and orientation using ultrasonic spectral frequency analysis 24 p4335 A70-45573

Nondestructive testing technology, emphasizing component designer role in facilitating inspection of surface defects 24 p4342 A70-45679

Eddy current nondestructive tests for surface defects detection, determining optimum test parameters based on calculation 24 p4344 A70-45697

SURFACE DIFFUSION

Finite element method applied to finite dimensional state variable formulation of transient heat conduction with surface diffusion of thin circular rotating disk [ASME PAPER 69-DE-B] 04 p0785 A70-14874

Two step B vacuum diffusion from boron oxide into Si surface using evacuated tube and N atmosphere 05 p0891 A70-15791

Surface diffusion slip velocity in binary gas mixture above solid surface, basing calculation on distribution functions determined from Boltzmann equation 06 p1049 A70-18333

Knudsen effusion cells high temperature uses, discussing binary alloys phase boundary determination and volume and surface diffusion studies 07 p1424 A70-19900

Protective diffusion coatings for jet engine gas path parts, discussing repair procedures [SAE PAPER 700332] 12 p2254 A70-27463

Graphite-carbon dioxide interaction at high temperatures in presence of solid phase diffusion from bulk to reacting surface 13 p2520 A70-28581

Structure and chemical composition of high Cr diffusion coating on Cr-Ni austenitic steels 15 p2756 A70-31634

Oxygen interlayer diffusion effects on wear change during gliding friction of normalized steel samples 15 p2743 A70-31636

Al effects on B and Cr diffusion in protective coating on Cr-Ni heat resistance alloy, noting thermodynamic kinetics for homogeneous layers 17 p3125 A70-35405

Heat resistance evaluation of Zh S6-K alloy subjected to multicomponents surface diffusion 17 p3125 A70-35407

Fcc metals surface self diffusion temperature dependence, using model based on complex defects contribution to diffusion flux at high temperatures 19 p3483 A70-37545

Heat resistant surface diffusion alloying of Ni alloys with Cr, Ti and Si saturation 24 p4361 A70-45834

Steel surface diffusive saturation with elements of chlorides, noting role of iron chloride phase in promoting coating uniformity 24 p4350 A70-46332

Diffusing element deposition on metal surface during saturation from gas phase based on calculation of equilibrium composition of reaction mixture 24 p4364 A70-46333

Diffusive carbon redistribution in Mo during interaction with Ni and Cr protective coatings 24 p4364 A70-46334

Carbon steel diffusion saturation with Ti and B, investigating layer depth, weight gain and microhardness dependence on powdered mixture composition 24 p4364 A70-46336

Aluminized Armco iron and steel diffusion layers phase composition and microstructure 24 p4350 A70-46337

Heat resistant alloys with metal coatings applied by diffusion in vacuum, investigating structure and fatigue strength at high temperatures 24 p4364 A70-46342

SURFACE DISTORTION

Normal and tangential displacements distribution at surface and along cross section of bar with free boundaries computed for symmetric and antisymmetric oscillations 02 p0301 A70-12484

Nonlinear thin shell theory kinematics generalized in terms of physical strain and surface deformation and geometry 04 p0766 A70-14450

Static and dynamic solutions for isothermal deformation of elastic cylindrical and spherical Cosserat surfaces with holohedral isotropy 05 p0932 A70-16140

Shell shear strain determined by expanding displacement vectors into covariant power series of distance from middle surface [DFVLR-SONDDR-23] 05 p0955 A70-17078

Surface mean deformation state under sheet peening found equal to deformation under single indentation 07 p1292 A70-18835

Telescopic paraboloid mirrors optical distortion from surface deformation due to gravity loads 07 p1281 A70-19254

Modal expansion method applied to thin deformable primary mirror surface control for orbiting astronomical observatory 13 p2403 A70-28427

Deflection surface and edge moment prediction for uniformly edge loaded point-supported circular plates, comparing with optical method 13 p2509 A70-28534

Die surface composition effects on lubricant efficiency in metal working judged by friction coefficient and surface damage 13 p2418 A70-28830

Displacement component in chosen direction on deformed object surface, using hologram interferometry with double illumination 13 p2409 A70-29475

Essa 7, Surveyor 7 and Mariner 4 space TV systems geometric distortions analysis and potentials in analytic photogrammetry and topographical mapping 14 p2586 A70-30982

Twinned lamella formation in Nb single crystals, examining slip and shear roles in surface tilt formation 15 p2761 A70-32382

Asymmetric phase error in antenna circular apertures, emphasizing beam squint resulting from distortion of paraboloidal reflector 16 p2859 A70-32942

Hologram interferometry for measuring surface deformation under force and anisotropy in transparent objects 17 p3085 A70-35009

Experimental model for random phase errors caused by surface irregularities in paraboloid reflector antennas 19 p3792 A70-37927

Spiral grooved gas lubricated thrust bearings, calculating self heating induced thermal distortion effects on load capacity [ASME PAPER 70-LUBS-14] 22 p4044 A70-42447

SURFACE ENERGY

Semiempirical potential energy surface generation for triatomic hydrogen from London equation by evaluating Coulomb and exchange integrals taking into account effective orbital overlap 01 p0147 A70-10469

Quasi-brittle fracture of plastic materials based on Griffith theory and crack propagation, analyzing real surface energy and work of plastic strain 01 p0212 A70-11562

Surface energy data calculated for bcc and hcp metals and high melting point compounds
06 p1090 A70-17845

Metal surface adhesion to materials, examining structure and energy with allowance for environmental effect
08 p1503 A70-20878

Forces at boundary surface in solid phase in solids and adhesive film interactions, considering boundary surface energy
08 p1503 A70-20879

Solid Mo, Ni, Ta and W surface energies determined by multiphase equilibration technique
08 p1522 A70-21749

Semiconductors surface energy levels based on conductivity, metal-dielectric-semiconductor capacity and optics
15 p2785 A70-32765

Semiconductor surfaces electrical equilibrium, considering statistical occupation of surface energy and Fermi levels for given doping of bulk material
15 p2786 A70-32766

MOS structure, measuring ionizing radiation effects on interface barrier energies by internal photoemission techniques
17 p3144 A70-35901

Liquid nitrogen boil off calorimeter for surface energy measurements, describing construction, calibration and instrument errors
18 p3261 A70-37089

Surface atom bonding configuration energy in two-center theory of large surface unit cells on semiconductors
19 p3483 A70-37544

Script-F radiative interchange matrix for enclosures with arbitrary surface emission and reflection characteristics
21 p3944 A70-41020

Radiative transfer among surfaces forming long cavity exposed to collimated incident energy
21 p3944 A70-41022

Fracture toughness and surface energy of fibrous reinforced composites as function of fiber content, strength, diameter, modulus and matrix flow stress
21 p3843 A70-41890

Solid phase energy role in flame spreading over solid fuel bed surface in oxidant-containing environment
23 p4281 A70-44424

SURFACE EROSION

U EROSION

SURFACE FINISHING

Friction and surface damage between clean metal hemispheres and flats at low sliding speeds and 25 K room temperature range
01 p0105 A70-11393

Free carrier light absorption in n-type GaAs, InAs and Ge semiconductors with mechanically polished surfaces as function of thickness and crystal structure
03 p0538 A70-13057

Surface treatment effects on stainless steels corrosion resistance, relating resistance changes to surface composition, integrity, stability and roughness
03 p0507 A70-13136

Airline aircraft finishes for protection against corrosion, air pollution, discussing paint application and polyurethane technology
03 p0497 A70-14053

Surface work hardening effects on steels resistance to low cycle fatigue with stress concentration, applying results to aircraft parts
06 p1085 A70-17403

Solar installations optical properties selectivity increase by light-collecting surfaces mechanical treatment, describing plate grinding with abrasive powders
07 p1196 A70-19625

Specific radiant heat flow and spectral blackness degree of tungsten with surface finish
07 p1309 A70-19662

Roller bearings convex conical surfaces grinding using centerless grinder
08 p1506 A70-21192

Burnishing load and time effect on deposition, endurance limit of lubrication and wear-in characteristics of molybdenum disulfide powder films
08 p1508 A70-21516

Strain measurement over large steel plate surface ground to reasonable flatness and in welded joints by applying moiré method
11 p2061 A70-26836

Electrochemical machining effects on surface integrity and fatigue properties of steel, Ti and Al alloys [ASTM PAPER MR-69-110]
12 p2241 A70-27081

Al pressure-welded joints strength, investigating surface treatment role
16 p2924 A70-34340

Al-Si welding rods tests with various surface finishes, considering oxide coatings effect on gas tungsten arc weld quality
18 p3264 A70-37113

Surface damage of GaAs crystals by mechanical handling and polishing with hard abrasive lapping materials
20 p3686 A70-39119

Asymmetric closed and cylindrical shells variable surface machining for desired wall thickness profile by chemical milling with digital computer numerical control
20 p3637 A70-39942

Polyvinyl chloride sheet steel manufacture, properties and welding methods
22 p4045 A70-42479

SURFACE GEOMETRY

Goertler vortices effect on boundary layer transition on concave surface, discussing instability oscillations breakdown leading to turbulent motion
01 p0061 A70-10539

Surface shape determination for thin delta wing with variable geometry to minimize drag for given open and closed configurations and cruising supersonic speeds
01 p0002 A70-10547

Measured heat flux conversion into average radiation incident on convex satellite surfaces in test chambers
03 p0606 A70-13536

Turbine blade designs considered for increasing load capacity covering tandem, jet-blade and base plain blade configurations and test results [ASME PAPER 69-WA/GT-1]
04 p0734 A70-14894

Pseudocylindrical concave polyhedral shells proposed from postbuckling configurations analysis, considering rigidity and structural applications
05 p0928 A70-16039

Martian topographical radar ranging data correlated with surface features, discussing deserts, canals and maria topography
05 p0909 A70-16388

Geometry of limiting surface characterizing strength of isotropic body, discussing material breakdown
05 p0947 A70-16964

Surface inhomogeneities effect on sound radiated by nearby turbulence near flexible boundary, using converted Lighthill wave equation to obtain far field radiation
07 p1256 A70-19262

Second order correction to Glaupert wall jet flow around arbitrarily curved surface, discussing initial profiles
07 p1257 A70-19344

Body surface curvature effect on surrounding laminar flow field, investigating oblate spheroids of various thicknesses
07 p1259 A70-19977

Spread F echoes due to total reflection from large tilted ionized surfaces, using ionograms and airglow observations to study surface geometry
07 p1271 A70-20158

Metal surface adhesion to materials, examining structure and energy with allowance for environmental effect
08 p1503 A70-20878

Wedges calculated for lift-drag ratios at hypersonic speeds to find optimum surface geometry
09 p1606 A70-23282

Drag measurement for star-shaped body at hypersonic speeds, comparing results with cone-shaped model
10 p1799 A70-24122

Computerized design of aircraft contours, determining three dimensional surface by second degree equation [SAE PAPER 700202]
11 p2013 A70-25876

Flat-top airfoil determined for lower surface shape to maximize lift drag ratio at hypersonic speeds using calculus of variations
11 p1977 A70-26397

Surface contours generation by Moiré patterns
12 p2235 A70-27753

Flow equations for curvilinear boundary layer based on laminar incompressible boundary layer in streamwise corner
13 p2386 A70-28541

Steady diabatic complex lamellar gas flow, obtaining parameters by extending geometric theory of surfaces and curves in fluid flow theory
13 p2387 A70-29122

Optical transformation of field ion micrographs providing orthographic, gnomonic projections and perspective images of hemispheric metal surface
14 p2584 A70-30506

Plane wave scattering by strip of elliptical cylinder, considering geometrical diffraction theory
15 p2700 A70-32405

Wave diffraction by wedge, using Heaviside step function and Sommerfeld contours
15 p2700 A70-32407

Wave diffraction by half plane limit of parabolic cylinder and wedge, using Fresnel integral and Heaviside step function
15 p2700 A70-32409

Reflector antennas analysis, design principles and uses, with emphasis on paraboloidal and spherical reflecting surface types
17 p3052 A70-35068

Hydromagnetic wave propagation compared in magnetospheres of plane and cylindrical geometries
18 p3311 A70-36011

Supersonic cascade wind tunnel performance evaluation, using compressor blades of simple geometric shapes
18 p3238 A70-36848

Plane wave diffraction by serrated surface, examining wave transformation matrix coefficients
19 p3377 A70-37715

Geometrical appearances at relativistic speeds for celestial sphere with multiple constellations, spherical surface features at observer proximity and rectangular box train
19 p3520 A70-38273

Diffraction-limited scalar image formation with large angle point reference hologram arrangement of arbitrary surface shape, point reference source and object
20 p3628 A70-39131

Nonequilibrium processes and body geometry as stagnation point conditions in blunt body inviscid flow
20 p3557 A70-39355

Weak stratification and geometry effect on steady mechanically driven motion of contained rotating viscous fluid
20 p3608 A70-39357

Distribution functions of errors in earth and moon horizon sighting due to planetary surface unevenness
21 p3884 A70-40840

Compressible boundary layer equations with second order surface curvature and displacement effects
21 p3809 A70-41751

Hypersonic viscous interaction between laminar boundary layer growing over flat plate and external flow field extended to curved surfaces
22 p3958 A70-42688

Electrochemical shaping by stationary plane electrodes and by constant velocity electrodes, comparing shaped surface accuracy
22 p4047 A70-43534

Simplified Sanders-Koiter linear thin shell equations with uncoupled stress-strain relations for arbitrary, nonzero Gaussian curvature, catenoidal and helicoidal midsurface geometries
23 p4269 A70-44399

Two dimensional electromagnetic scattering body geometry reconstruction from given incident and scattered far field distributions
23 p4165 A70-44958

SURFACE INTERACTIONS

U SURFACE REACTIONS

SURFACE IONIZATION

Spread F echoes due to total reflection from large tilted ionized surfaces, using ionograms and airglow observations to study surface geometry
07 p1271 A70-20158

Electron concentration profiles in blunt nose vehicle shock layer during atmospheric near orbital entry at high altitudes, using finite rate chemistry
16 p2837 A70-33865

Metal surface ionization measurements for upper atmosphere and interplanetary space energetic neutral hydrogen analyzer design
17 p3138 A70-35309

Thermo-electret surface charge and dielectric constant time variation measurements, considering hole-electron pairs production hypothesis
21 p3797 A70-40890

Field-ion microscope image formation, determining periodic surface potential variation effects on high field tunneling
21 p3862 A70-40974

Surface potential and electron work function of single crystal plane W/110 under zero-field and strong-field conditions
23 p4230 A70-44797

SURFACE LAYERS

NT MONOMOLECULAR FILMS

Oxide layers on metal substrate noting emittance dependence on thickness in aluminum-aluminum oxide and Cu-CuO systems [ASME PAPER 69-WA/HT-4]
04 p0705 A70-14825

Tractive behavior in elastohydrodynamic lubrication contact noting role of surface degradation layer
05 p0854 A70-15888

Friction on fuselage surface layer under static and instantaneous loads without allowance for oscillation
05 p0856 A70-17015

Structure, phase composition and heat resistance of diffusion layers obtained by surface alloying of Nb alloy with Cr, Ti and Si
06 p1089 A70-17744

Planetary boundary layer thickness estimation, considering geostrophic wind speed and potential temperature average vertical gradient
07 p1377 A70-18922

Inhomogeneous model of upper lunar surface layer assuming temperature dependent heat conductivity and capacity, showing agreement with IR measurements
08 p1564 A70-20559

Graphite molds compaction pressure effect on Ti castings nonporosity and surface layers carburization
08 p1506 A70-21143

Burnishing load and time effect on deposition, endurance limit of lubrication and wear-in characteristics of molybdenum disulfide powder films 08 p1508 A70-21516

Diabatic mean profile forms in atmospheric surface layer, establishing profile relationships based on logarithmic analysis 08 p1540 A70-21973

Turbulent transfer mechanism in atmospheric surface layer, analyzing micrometeorological data for flux-gradient relationships, relating turbulent scale to eddy diffusivities 09 p1712 A70-22051

Gas saturation and inhomogeneity in surface layer of Ti alloys with alpha and beta stabilizers after high temperature heating 09 p1700 A70-22078

Seasonal measurements of atmospheric transmittance spectra for horizontal near-earth paths in IR region under haze and clear weather 09 p1666 A70-22179

Heat and mass transfer in binary turbulent boundary layer during natural convection on vertical surface, allowing for diffusional heat conduction 09 p1787 A70-22267

Al alloys fatigue properties dependence on surface oxide cracking in moist and dry air, investigating oxidation and kerosene processing 09 p1707 A70-23206

Metal plates vibration under viscoelastic damping layers using electromagnetic transducer and impact excitation 11 p2145 A70-26702

Low resistivity films synthesized on seminsulating GaAs by xenon, krypton, selenium and zinc ions bombardment 12 p2286 A70-27364

Electroacoustic conversion in low resistivity GaAs crystal surface layer, applying external magnetic field to tune converter in wide frequency range 12 p2287 A70-27483

Radiation defects in Ge single crystals surface layers caused by low energy bombardment with He ions 12 p2287 A70-27486

Diffuse coatings effect on strength characteristics and corrosion resistance of steels, analyzing structure, thickness and purity of surface layers 13 p2433 A70-28888

Metal surfaces friction and wear processes dynamic equilibrium noting loading conditions effects 13 p2423 A70-29766

High winds simultaneous occurrence and duration to 150 meter height, showing coherence tendencies 14 p2607 A70-30583

ZnO epitaxial layers deposition by chemical vapor transport on sapphire single crystal substrates 15 p2784 A70-31982

Surface layer dislocations concentration role in metal fatigue, using variable diffusion coefficient 15 p2822 A70-32352

Inhomogeneous model of upper lunar surface layer assuming temperature dependent heat conductivity and capacity, showing agreement with IR measurements 15 p2805 A70-32714

Wind velocity derivative statistical characteristics in atmospheric surface layer, using thermoanemometer, functional converter, differentiating circuit and loop oscillograph 16 p2945 A70-33219

Liquid He surface layer thickness as function of temperature, considering capillary waves effect due to gravity 16 p2952 A70-33288

Solid film lubricants deposited by DC and RF sputtering on metal and glass surfaces, determining friction characteristics by electron microscopy 17 p3099 A70-34516

Surface growth morphology and crystallographic orientation of beta-SiC films formed by chemical conversion and heating 17 p3142 A70-34678

Combustion rates acceleration of ammonium perchlorate mixtures with polystyrene and polymethyl methacrylate by KCl and LiF additions, forming molten layer on charge surface 18 p3299 A70-36248

Depth measurement of gas-saturated surface layer in Ti alloys, using microhardness method 18 p3277 A70-36472

Air surface layer stationary electric field, considering ionization balance equation, turbulent diffusion coefficient, ion concentration vertical distribution, etc 18 p3247 A70-36520

Sunspots surface layers azimuthal electric current density, assuming specific magnetic force distribution 18 p3322 A70-37135

Titanizing Armco iron and carbon steels, examining diffusion layer structure and phase composition 19 p3451 A70-37460

Constrained viscoelastic layer optimal length for vibration damping of metallic structures 19 p3536 A70-37696

Magnetic surface loading of Gunn oscillators domain state for use as logic gates, pulse function generator, etc 19 p3387 A70-37819

Surface layer heating of solid body by dense gas discharge plasma radiation, comparing vaporization and reversible opacity onset times in quartz 19 p3482 A70-38733

Transverse impedance in semiconductor surface layer, taking into account charge in diffusion region 20 p3686 A70-39594

Metal surfaces friction and wear processes dynamic equilibrium noting loading conditions effects 20 p3638 A70-40099

Surface films effect on thermal contact resistance of microscopically sized contacts 21 p3944 A70-41023

Surface films effect on thermal contact conductance of aluminum surfaces contacting in high vacuum environment 21 p3944 A70-41024

Surface tension role in microfluidic layer formation on solid surface with growing bubble in nucleate boiling, using optical method 21 p3953 A70-42089

Optical devices contaminated mirror surfaces restoration with atomic oxygen from RF plasma by noncontaminating nondestructive oxidation of polymer film 22 p4029 A70-42622

Iteration method for calculating self consistent fields in semiconductor surface inversion layers 22 p4085 A70-42745

Ultrasonic detection of tooth surface layer demineralization, noting surface and subsurface enamel structural differences 22 p3978 A70-42955

Nickel surface layer fine structure changes in super-sonic air flows at various temperatures and times 22 p4056 A70-43341

Friction-originated ageostrophic mass flux in ground friction layer at nonaccelerated geotriptic boundary layer flow 24 p4370 A70-45133

Wind velocity derivative statistical characteristics in atmospheric surface layer, using thermoanemometer, functional converter, differentiating circuit and loop oscillograph 24 p4371 A70-45194

Rheology and structure formation in three dimensional and two dimensional bulk phase and pigmented systems in surface layers and films, including paints and varnishes 24 p4368 A70-46141

SURFACE NAVIGATION

Omega position location experiment applied to ship navigation, air traffic control and moving vehicle surveillance, noting daytime and night fixing accuracy 01 p0136 A70-10307

Moving map displays applications in marine and air navigation, discussing human factors and impact on ATC 01 p0139 A70-11284

Navy Shipboard Navigation Satellite System for worldwide all-weather navigation system, discussing shipboard system, receiver, stable oscillator and antenna 03 p0522 A70-13609

Range positioning system as automatic indicator in oceanography, aboard land vehicles and aircraft 08 p1541 A70-21360

Aircraft and ship position surveillance by satellites system with independent capability and undelayed voice and digital communication 09 p1723 A70-23043

Dead reckoning navigation of manned lunar roving vehicle /MLRV/, describing hardware and coordinate system 12 p2266 A70-27414

Aircraft and ship navigation using precision time measurement signals transmitted between vehicles and earth satellites 13 p2448 A70-28748

Astronomical navigation on lunar surface with equations for selenographic latitude and longitude 13 p2449 A70-29272

Manned lunar surface navigation requirements emphasizing dead reckoning system 14 p2613 A70-30458

Synchronous navigation satellite system for ships and aircraft applicable to earth orbital and lunar operations 14 p2614 A70-30463

Surface navigation for unmanned Martian surface roving vehicle 14 p2615 A70-30469

Aircraft/ship navigation system using three synchronous satellites positioned over equator for Pacific applications 17 p3134 A70-35302

Manned lunar roving vehicle /MLRV/ navigation scheme based on dead reckoning concept, discussing instruments effectiveness for vehicle velocity and orientation measurements 19 p3396 A70-37849

Gyrocompassing for self contained lunar surface vehicles navigation, proposing local vertical determination method [AIAA PAPER 70-1003] 20 p3667 A70-39528

Sea and air navigation in U.S. with satellites, considering cost estimates 21 p3848 A70-41130

Discusses satellite navigation system for aircraft and ships, discussing coverage, radio links, project costs, etc 22 p4067 A70-42657

Radio navigation system using multiple satellite beacons /NAVSTAR/ for large area air and sea coverage 22 p4067 A70-42662

Automatic ship navigation system using Transit satellites and onboard digital computer for routine tasks of dead reckoning 22 p4068 A70-42666

Position fixing by distance measuring to geostationary satellites, discussing ATS-3 and ship experiment accuracy and orbit interference 23 p4215 A70-44232

Worldwide common satellite network for sea and air navigation, discussing cost estimate and economics 23 p4216 A70-44608

Stability solution of nonlinear differential equations in position determination on earth by inertial navigation 24 p4374 A70-46202

SURFACE PRESSURE

U PRESSURE

SURFACE PROPERTIES

NT ADHESION

NT ADSORPTIVITY

NT COEFFICIENT OF FRICTION

NT INTERFACIAL TENSION

NT SKIN TEMPERATURE [NON-BIOLOGICAL]

NT SPECTRAL REFLECTANCE

NT SURFACE CRACKS

NT SURFACE DEFECTS

NT SURFACE ENERGY

NT SURFACE ROUGHNESS

NT SURFACE STABILITY

NT SURFACE TEMPERATURE

NT WALL TEMPERATURE

Icarus surface reflectivity estimated from reflected light polarization, combining estimate with inferred absolute magnitude to obtain radius 01 p0180 A70-10537

IR reflectance studies of lunar surface composition, showing absorption spectra suggestive of ferrous iron, olivines and orthopyroxenes 01 p0182 A70-10721

Si cleaved crystal nature on basis of Auger spectra, discussing impurity stabilization 01 p0159 A70-11175

Microwave propagation in materials and measurement methods for inspection based on reflecting surface movement and scattering method for porosity detection 01 p0094 A70-11395

Stability conditions for helical motions of body bounded by multiply connected surface in fluid 01 p0145 A70-11439

Turbulent boundary layer response to sudden changes in surface conditions or pressure gradients, considering equilibrium attainment 02 p0287 A70-12360

Molybdenum disulfide surface and bulk properties, comparing endurance of fractions and grades with synthetic chalcogenides at same layer thickness in dry atmospheres [ASLE PREPRINT 69-LC-7] 02 p0322 A70-12538

Electron surface states bands in insulators induced by image potential, determining lower limits for liquid and solid gases 02 p0345 A70-12823

Spectral polarization characteristics phase variations used for classifying lunar surface features 03 p0565 A70-13234

Infinitesimal deflections of piecewise-regular unfolding scanning surfaces fixed along edge with respect to one point, discussing rigidity 03 p0591 A70-13414

Rolling, pickling and annealing influence on composition of steel sheet surface 03 p0497 A70-13775

Potential energy surface shapes for lowest states of temporary negative ions of nitrous oxide and carbon dioxide 03 p0441 A70-14008

Elastokinetic three dimensional boundary value vibration problem, involving rectangular area on surface of elastic half space under periodic normal stress 03 p0601 A70-14319

Plane two body contact creep problem in presence of adhesive forces reduced to solving coupled integral equations with complex valued kernels 04 p0766 A70-14421

Helmholtz integral for radio waves scattering from surfaces expanded for reflection from terrain or atmospheric layers 04 p0648 A70-14964

Numerical solution of transient heat conduction with radiating surface, imposing Runge-Kutta type integration on surface

04 p0787 A70-15613

Axial compression of elastic circular cylinder in contact with identical elastic half spaces, determining interfacial surface stresses for frictionless and adhesive contacts

05 p0930 A70-16082

Surface stress distribution to maintain Griffith crack in prescribed shape, using theories of Fourier transforms and dual integral equations

05 p0930 A70-16086

Ternary Ti-Ta-Nb solidus surface determination by simplex lattices and cubic approximation, statistically evaluating equation derived

05 p0864 A70-16547

Single crystal Ge surface etching characteristics using laser beam reflection pattern

05 p0860 A70-16656

Time to crack formation determined in cylindrical and flat Al and steel specimens having various surface properties under cyclic loads

06 p1084 A70-17392

Ni-Cr alloys effects of grain size and surface deformation on oxidation properties at high temperature

06 p1088 A70-17610

Surface thermal factors influencing ignition delay time of composite solid propellants, using double wavelength optical detector

06 p1128 A70-18043

IR region spectral hemispherical emittance of surfaces measured by bihemispherical reflectometer [AIAA PAPER 70-65]

06 p1107 A70-18205

Modified Maxwellian models for particle reflection in free molecular flow, correlating model parameters with gas-surface properties

06 p1110 A70-18259

Lunar surface reflectivity determined by measuring reflected cosmic noise, determining dielectric constant and surface material properties

06 p1151 A70-18488

Laser radiation increased absorption in opaque solid body attributed to vaporization, analyzing factors determining thermodynamic equilibrium between condensed and gaseous phases

06 p1083 A70-18563

Three dimensional hypersonic flow past body solved assuming developable surface head shock wave

07 p1187 A70-18767

Fcc metals surface changes following adhesion using low energy electron diffraction (LEED), relating intersurface metal transfer to applied adhesive force

07 p1305 A70-18920

Radiative heat transfer in radiant energy flux incident on plane surface of nonisothermal absorbing and dissipating layer

07 p1423 A70-19814

Steady temperature field of two dimensional periodic contact surface in vacuum, using conjugate harmonic functions for thermal flux lines, isotherms and thermal resistance

07 p1423 A70-19820

Caustic surface of spherical resonator with external mirrors used to calculate light angular divergence and spectral properties

07 p1299 A70-19859

Metal adhesive joints permanence under various environmental conditions, considering surface properties effect

08 p1504 A70-20890

Ti alloy band polished surfaces properties, obtaining required residual stresses by process control

08 p1507 A70-21198

Astatic equilibrium in Saint Venant principle applied to surface of linear elastic body, discussing stress field produced by boundary loading

08 p1591 A70-21463

Potential vortex flow interaction with stationary surface calculation extended to Volterra equations by transforming boundary value problem, improving critical Reynolds number bounds

08 p1484 A70-21472

Carbon dioxide adsorption and desorption in Martian bright areas, discussing assumptions relative to temperature, pressure and dust adsorption

08 p1579 A70-21566

Radiative heat transfer in lunar and Mercurian surfaces, discussing radiative heat transfer in powders

08 p1579 A70-21569

Ni-Mo surface alloys investigated by low energy electron diffraction, using tabulated symmetry and extinction properties of space groups and phase diagrams

08 p1557 A70-21603

Spectral polarization characteristics phase variations used for classifying lunar surface features

08 p1580 A70-21667

Thin metal plate surface impedance during excitation by HF electromagnetic field as function of magnetic field, calculating line shapes

08 p1557 A70-21754

Friction, wear and surface evaluation of alloys as bearing materials in prosthetic devices

09 p1690 A70-22044

Blasius flow stability on deformable surface of membrane using Orr-Sommerfeld equation to calculate amplitude of function for perturbation flow

09 p1658 A70-22182

Thin resistive layers located in rectangular waveguide assuming constant and surface variable conductivity and permittivity

09 p1644 A70-22279

Rhenium single crystals basal plane surface properties using LEED and Auger electron spectroscopy, describing gas adsorption studies

09 p1739 A70-22526

Temperature and stress fields in orthotropic plate with partial surface insulation, examining boundary conditions

09 p1777 A70-23078

Cross hatching on various body surfaces due to periodic surface pressure fluctuations, discussing origin from counterrotating longitudinal vortices in boundary layer

09 p1662 A70-23223

Capillary grooves effect on surface wetting and evaporation using heat transfer coefficients for grooves with triangular, semicircular and square cross sections

09 p1790 A70-23559

Nongray surfaces radiative interchange calculation, considering surface radiation properties

09 p1790 A70-23561

Crack widening in infinite plane field with wedge in absence of slip, based on elasticity theory, plotting contact forces and stresses on crack boundary

09 p1785 A70-23624

Integral equation for radiation patterns from vertical antenna over variable impedance surface

09 p1639 A70-23670

Lennard-Jones atom interaction potential, calculating adsorption energy of atom onto surface structure of fcc substrate, tabulating adsorption and surface diffusion activation energies

10 p1927 A70-24078

Radio wave reflection spectra from plane surfaces, determining physical properties and composition

10 p1843 A70-25154

Contact stresses in elastic half plane with boundary connected to rod and moment applied at arbitrary point

10 p1965 A70-25324

Mars surface, discussing craters, slump terraces, dry chutes, crater pair abundance, ballistic cratering theory, etc

11 p2109 A70-25838

Bidirectional reflectance of three dimensional surfaces described by diffuse triangular subareas network for spacecraft thermal design, giving numerical technique

11 p2084 A70-26354

Epitaxial surface morphology layer electrical properties and autodoping at GaAs-Ge heterojunctions as function of substrate temperature, orientation and HCl concentration

11 p2098 A70-26392

Distance separating shock wave front of contact surface between motor and target gases in electromagnetic shock tube, discussing surface instabilities

11 p1977 A70-26467

Microwave radiometer as passive satellite sensor for observing ocean surface properties

12 p2228 A70-26902

Lunar rolling stones anomalous surfaces goniphotometric properties, considering bearing strength as rock density function

12 p2296 A70-26925

Aerospace materials machining processes guidelines to minimize structural failures caused by lack of surface integrity

12 p2239 A70-26988

Slow electrons interaction with periodic and non-periodic solid surfaces, investigating elastic scattering

12 p2725 A70-27252

Reflected light directional diagram effects on scintillating surface luminescence yield, considering scattering function gradient

12 p2231 A70-27310

Die surface composition effects on lubricant efficiency in metal working judged by friction coefficient and surface damage

13 p2418 A70-28830

Laser beam photography utilization in engineering for optical pointers, interferometers and holographic visualization of surface strain and vibration

13 p2406 A70-28914

Laminar MHD boundary layer equations at nonconducting surface, determining flow core parameters influence on boundary characteristics

13 p2462 A70-28967

Weld quality relationship to aluminum surface contamination by hydrogen-containing compounds

13 p2407 A70-29108

Surface emissivity effects on combined conduction, convection and radiation heat transfer in nonisothermal hydrogen plasma, discussing optically thin and thick solutions

13 p2521 A70-29134

Surface field effect, contact potential and photoconductivity measurements on p- and n-type heteroepitaxial single crystal silicon films on sapphire

13 p2470 A70-29372

Acoustic conductivity of burning solid propellant surface, discussing critical conditions and variable surface measurement methods

13 p2522 A70-29421

Nonaggressive liquid media effect on residual strains and phase transformations initiation and development in polyurethane parts operating in lubricants, discussing wear resistance

13 p2439 A70-29431

Hologram interferometry using moiré method to determine bending moments of object surface

13 p2409 A70-29474

Electromagnetic plane wave oblique reflection from flat surface with spatially modulated surface impedance, computing wave spectrum

13 p2367 A70-29527

Shallow shell solutions complete with respect to finite simply connected surface region applied to circular cylindrical shells

13 p2517 A70-29758

Pure ammonium perchlorate single crystal self deflagration, determining energy transfer mechanisms from pressure effects, combustion characteristics and subsurface profile

13 p2473 A70-29956

Polarization effect on radiant heat transfer between simply arranged smooth plate surfaces

13 p2523 A70-29993

Surface wind speed durations statistical analysis, discussing meteorological, orographic and physiographic features

14 p2607 A70-30582

Lubricant ingredients and additives properties effect on surface quality of cold rolled semifinished Al products

14 p2590 A70-30837

Composite solid propellants surface structure and profile characteristics burning with various oxidizers and polyurethane binder by scanning electron microscopy

14 p2628 A70-30948

Lunar surface mechanical properties from Surveyor spacecraft interactions with soil /exclusive of surface sampler/

14 p2644 A70-31055

Lunar IR radiation measurements for estimating thermophysical properties and small scale surface nature

14 p2645 A70-31057

Topographic variations in lunar surface from bistatic radar observations on Explorer 35

14 p2645 A70-31061

Mars surface, environment and electrical, thermal and mechanical properties

14 p2647 A70-31080

Mars surface material properties from radio emission observations, considering daily temperature variations distribution

14 p2648 A70-31083

Oxide film and liquid effects on friction coefficient, surface relief and dislocation density along depth related to plastic deformation

15 p2743 A70-31638

Friction theory, discussing surface mechanics, wear and erosion control

15 p2743 A70-31699

Vibration modes real time observation of complex surfaces with matt finish using changes in laser speckle

15 p2750 A70-31762

Total solar radiation calculation for inclined and horizontal surfaces, noting application to solar heating

15 p2774 A70-31803

Surface photovoltage regeneration mechanism in GaAs dependent on free carrier concentration, space charge density and minority carriers

15 p2783 A70-31951

Graphite surface Debye temperature calculation based on crystal lattice dynamics

15 p2765 A70-32024

Electromagnetic absorption of Martian matter based on vertical temperature variations in planet surface layer

15 p2802 A70-32491

Molecular interactions, surface pressures and potentials of mixed monolayers of stearic acid and stearyl alcohol with inorganic substructures

15 p2695 A70-32547

Elevation and ground conductivity effects on horizontal dipole excitation of earth-ionosphere waveguide, considering east-west propagation

16 p2858 A70-32932

Sonic boom variation with aircraft geometry, volume, weight, weather and environment conditions, noting effects on structures and people

16 p2840 A70-32947

Nonlinear two dimensional free boundary problem of axisymmetric heat conduction in tubes with internal surface solidification by variational technique

16 p2996 A70-33002

Water structure role in membrane systems, considering phase transitions and thermal anomalies in surface properties

16 p2847 A70-33027

Boron, silicon carbide and graphite fibers surface properties

16 p2937 A70-33376

Space collector ring systems surface physics, discussing dry thin film lubricants, smoothness, service life, etc

16 p2917 A70-33485

Adhesive bonds strength parameters, discussing substrate type, surface preparation, etc [ASME PAPER 70-DE-33]

16 p2939 A70-33504

Monochromatic radiation angular distribution surface reflectance measurement using photographic reflectometer

[AIAA PAPER 70-859] 16 p2912 A70-33904

Surface recombination centers protecting against discoloration of thermal control coatings due to chemical changes induced by photoproduced holes and electrons in oxide pigments

[AIAA PAPER 70-830] 16 p2940 A70-33935

Solid state laser active element lateral surface microprofile effect on heat endurance

16 p2929 A70-34220

Oxidation dependence on physical nature of Ti surfaces obtained by thin film techniques under ultrahigh vacuum conditions

17 p3098 A70-34364

Probstein-Gold model for ablated materials crosshatching patterns, using interaction between inelastic deformable surface and supersonic turbulent boundary layer

[AIAA PAPER 70-768] 17 p3009 A70-34504

Elasticity theory two dimensional contact problems, examining cohesion or friction in contact area

17 p3192 A70-35693

Nb-based Ti-Zr alloy surface phase recrystallization characteristics, using field emission microscope

18 p3276 A70-36309

Energy zone bending near surface of n-type semiconductor, discussing surface plasma level

18 p3298 A70-36619

Contaminated optical surface investigation technique in near UV, visible and near IR range, investigating property changes of systems in transmission and reflection

18 p3292 A70-36786

Surface alterations by machining processes for gas turbine engine materials, emphasizing effects of milling on Ti and grinding on high strength steels [ASME PAPER 70-GT-100]

18 p3264 A70-36888

Radiation polarization measurements of natural underlying surfaces in centimeter range, noting dependence on sighting angle

18 p3250 A70-36967

Underlying surface inhomogeneity effect on radiation in presence of solid cloud cover

18 p3287 A70-36975

Ge and Si surface electrical properties, discussing conductivity, field effect, work function, current carriers, photoconductivity, photocurrent carrier capture, etc

19 p3483 A70-37297

Mars surface smoothness from photometric and space probe data for atmospheric optical thickness and surface barometric pressure

19 p3512 A70-37300

Clean Ru/0001/ and Rh/111/ surface properties by LEED and Auger electron spectroscopy, discussing gas adsorption

19 p3483 A70-37546

Electrical conduction and surface properties of beta-SiC films obtained by heating Si wafer in presence of hydrocarbon

19 p3485 A70-37685

Shallow shell solutions complete with respect to finite simply connected surface region applied to circular cylindrical shells

19 p3547 A70-38396

Radiation heat transfer from parallel plates with grooved surfaces for direction dependent radiation properties

21 p3944 A70-41021

Surface films effect on thermal contact resistance of microscopically sized contacts

21 p3944 A70-41023

Al yield surfaces in stress space at elevated temperatures for virgin and prestressed material in torsion

21 p3840 A70-41436

Multichannel monitor for repetitive short scan Auger electron spectroscopy for surface composition changes, using low energy electron diffraction

21 p3827 A70-41467

Apollo 11 lunar soil volcanic rock samples, mineralogical and petrological description and surface features

21 p3896 A70-41514

Apollo 11 lunar dust and breccia micromorphology and surface characteristics implying weathering processes

21 p3910 A70-41622

Surfaces separated by radiatively nonparticipating medium, determining absorptivities and heat transfer boundary conditions in gray surface problems by irradiation factor method

21 p3953 A70-42085

Ultrasonic Rayleigh critical angle reflectivity of liquid-solid interface energy, detecting near-surface properties changes

22 p4027 A70-42585

Stepwise linear regressions method for estimating black body surface radiances from model atmospheres and corresponding simulated Nimbus 2 window-channel radiances

22 p4013 A70-42617

Steady incompressible turbulent boundary layer form on permeable curvilinear surface with uniform suction, assuming small pressure gradients

22 p4011 A70-42803

Surface density, charge and field effect mobilities for electrons and holes on MIS insulator-semiconductor structure on narrow bandgap HgCdTe

22 p4086 A70-43018

High speed camera rotating mirror dynamic surface deformations, discussing reflected waves, astigmatism, gas turbulence and pressure effects [SMPTE PREPRINT 34]

22 p4033 A70-43043

Electromagnetic absorption of Martian matter based on vertical temperature variations in planet surface layer

23 p4240 A70-43913

Precious metals, measuring tension, grinding and polishing induced surface plastic deformation effects on electron work function and exoemission

23 p4204 A70-43927

Titanium diboride particles contact surface increase during sintering in vacuum as function of temperature

23 p4205 A70-44042

Apollo 11 and 12 lunar landing sites surface properties from returned rocks chemical, physical and mineralogical analysis

23 p4241 A70-44221

Ta spectral emissivity, using ratio of specimen surface and black body spectral radiant intensities

23 p4207 A70-44447

Surface field model of rotating magnetic stars involving uniformity and Eddington-Sweet circulation suppression

23 p4251 A70-44826

Hawaiian basalt melted in simulated lunar environment, investigating surface characteristics, internal structure and bearing strength

23 p4254 A70-44883

Jupiter red spot darkness parameter and solar activity as clue to Jupiter-solar relationship

24 p4402 A70-45391

Einstein-Rosen matter concept given by space-time with isomeric domains, discussing hypersurface derivatives

24 p4379 A70-45486

Refractory materials surface behavior under friction, discussing microscopic nature of wear and surface deterioration due to thermal fatigue, fusion and material transfer, etc

24 p4342 A70-45595

Light reflectance from optically inhomogeneous medium due to space charge near semiconductor surface

24 p4390 A70-45661

Food-water deprivation influence on alveolar surface activity of rat lungs

24 p4303 A70-46115

Apollo 11 deployed solar cells, investigating degradation of surface properties and thermal control due to lunar module ascent effects

24 p4295 A70-46262

SURFACE REACTIONS

Oleic acid concentration effects on electron work function during surface-active agent deposition on Fe, Ni, Cu, Al and steel surfaces

01 p0099 A70-10074

Lubricating oil chemical composition changes influence on combustion engine internal friction, considering surface active Zn, armo-iron and Al

01 p0099 A70-10077

Propellant condensation on surfaces near electric rocket exhaust, calculating particle arrival rates, backflow and desorption energies [AIAA PAPER 69-270]

01 p0166 A70-10836

Surface catalysis and variable transport properties effects on chemically frozen dissociated hypersonic air flow boundary layers enveloping flat plates and slender wedges

01 p0067 A70-11179

Mg vapor and oxygen surface reactions in MgO deposits, using atomic absorption spectrophotometry

02 p0250 A70-12006

Flame spreading mechanism over surface of igniting condensed phase materials in quiescent gaseous environment with chemically reacting component

02 p0396 A70-12014

Flame spreading theory for plastic fuels surfaces in nitrogen-oxygen mixtures, considering initial fuel temperature, pressure and mixture composition effects

02 p0396 A70-12015

Reactor surface and propylene role during vapor phase partial oxidation of propane in continuous flow tubular reactors

02 p0250 A70-12017

Low energy electron diffraction structures due to Re crystal surface interaction with CO and molecular oxygen at high temperatures

03 p0440 A70-13098

Hybrid propellant combustion mechanisms, connecting surface reactions to melting mechanism and subsequent liquid flow [ONERA-TP-736]

03 p0543 A70-13632

Charged particle distribution in heterogeneous medium using dispersion model to describe quasi-charged particles interaction with internal surfaces

03 p0536 A70-14370

Surface interactions in incompressible dynamics and stability of ferrofluid with nonlinear magnetization properties

04 p0665 A70-14451

Surface recession of low density phenolic nylon in arc heated air using stagnation point models, noting char removal processes

04 p0787 A70-15602

Q spoiled laser bombardment to obtain atomically clean surfaces in vacuum, noting damages

05 p0861 A70-16990

Quasi-equilibrium treatment of heterogeneous reactions applied to flash desorption data for oxygen reaction with tungsten surface, discussing species desorption dependence on adsorption temperature

06 p1004 A70-17331

Electrically discharged O effect on N first positive band emission in surface catalyzed excitation

06 p1109 A70-17489

Nitrous oxide molecular beam reflection and dissociation on tungsten surface at high temperatures from angular distribution measurements

06 p1004 A70-17493

Mathematical models for progressing waves diffracted by smooth surfaces

06 p1105 A70-17533

Mathematical models describing interactions between rarefied gas atoms and solid surfaces

06 p1036 A70-17759

Laser induced alloys erosion under various focusing conditions, determining optimal conditions for spectral studies

06 p1089 A70-17762

Flame spreading velocity characteristics over solid fuel surfaces, discussing environmental pressure, chemical reactivity, pyrolysis, forced convection, etc [WSCI PAPER 69-33]

06 p1178 A70-17979

Cold molecular beam of helium impinging on LiF or Si crystals investigated for gas-surface interactions, using time of flight method

06 p1043 A70-18255

Nitrogen molecule-tungsten surface interactions, computing trajectories and accommodation coefficients for various temperatures by equations of motion

06 p1110 A70-18262

Velocity distributions of incident and reflected Ar beams, determining partial energy accommodation coefficients for reflection from copper and carbon dioxide deposited surfaces

06 p1111 A70-18264

Molecular He and Ar nozzle-type beams scattering from room temperature LiF crystal surfaces, measuring particles flux and speed distributions

06 p1111 A70-18267

Metastable diatomic N beam scattering from Teflon and Cu surfaces measured for velocity and angular distributions

06 p1112 A70-18273

Surface-particle interaction and atmospheric parameters measurements by paddlewheel satellites, discussing angular distribution of re-emitted molecules and accommodation coefficients

06 p1067 A70-18287

Liquid metal alloys surface composition and electronic structure roles in electrocatalysis evaluated by studying hydrogen-ion discharge reaction and electrical double layer

06 p1005 A70-18392

Pressure effects in predicting ablation velocities for gas-solid systems, assuming reactions and gaseous products reversible adsorption on solid surfaces

07 p1422 A70-19373

Low and moderate energy gas molecule-solid surface interactions using molecular beams

07 p1328 A70-20116

Reactive scattering from solid surfaces, discussing atom beam reaction of O with heated Ge and Si single crystals

07 p1342 A70-20117

Wall boundary condition model modification applied to molecular beam-solid surface scattering, noting qualitative agreement with observed distributions

07 p1342 A70-20118

Gas molecules scattering by solid surface for monoenergetic and Maxwellian beams, discussing model with different values for magnitude and velocity direction

07 p1343 A70-20124

Thermal accommodation coefficients of Ar atomic beams scattered from nominal plane of Ag crystal measured by time of flight techniques

07 p1343 A70-20125

Satellite-borne experiments of neutral molecular beam-solid surface interactions, describing Molsink chamber, densitometer, sphere and paddlewheel satellites

07 p1344 A70-20128

Molecular beams and particle adsorbing surfaces interactions in state of relaxation, determining reflection parameters as function of gas characteristics

08 p1547 A70-21078

Molecular beams and particle adsorbing surfaces interaction with allowance for deposited atoms relaxation, determining reflected flux

08 p1547 A70-21079

Molecular beam and pure surface interactions on background of external forces field

08 p1547 A70-21080

Acoustic conductivity of burning solid propellant surface calculated, showing positive values or possible amplification at L.F.

09 p1741 A70-22113

LEED pattern and germanium surface conductivity during oxidation indicating electron states annihilation

09 p1738 A70-22215

Free radicals role in high temperature surface reactions of solid metal oxide particles interacting with unburned flame gases

09 p1629 A70-22320

Burning solid ammonium perchlorate composite propellants surface structure observation to assess heterogeneous or subsurface reactions, using scanning electron microscope

09 p1742 A70-23234

Rocket exhaust plume flow fields studied for vehicle effects taking into account nozzle boundary layer, coalescence shock and nonisotropic flow [AIAA PAPER 69-569]

09 p1743 A70-23246

Laser beam interaction with metals on basis of energy balance measurements, obtaining time dependent radiation reflectance

10 p1898 A70-23982

Oxygen-hydrazine interactions on partially immersed metal electrodes, studying conjugated electrochemical reactions

10 p1830 A70-24457

Electrodes oxidation processes involving fuel cell molecules or derived adsorbed intermediates reacting with anodically generated surface oxide, considering Pt electrochemical reduction

10 p1830 A70-24465

Helium ion bombardment activated tungsten crystal surface migration using field emission microscopy

11 p2097 A70-25378

Pyrolytic graphite oxidation kinetics as function of temperature, air velocity and surface area

11 p2070 A70-25809

Statistical properties of random intensity field during coherent laser radiation scattering by moving diffuse surface

11 p2064 A70-26812

Surface sliding friction interactions in aluminum alloys friction welding

12 p2239 A70-26855

Slow electrons interaction with periodic and non-periodic solid surfaces, investigating elastic scattering

12 p2275 A70-27252

Neutral molecule-solid surface interactions mass spectrometric techniques for measuring molecular flux and mean thermal energy after interaction

12 p2181 A70-27257

Nonisothermal burn-up rates of graphite surfaces in turbulent air flow under neutral gas shield estimated by measuring channel diameter

12 p2331 A70-27323

Surface oxidation effects on thermionic work functions of Be determined by visual observation and X ray diffraction patterns analysis

12 p2288 A70-28004

Artificial carbographites surface combustion processes using mercury porosimetry analysis

13 p2519 A70-28578

Surface erosion of sublimating graphite and naphthalene due to inequilibrium mass transfer in gas flows

13 p2437 A70-28580

Polarization effect on radiant heat transfer between simply arranged smooth plate surfaces

13 p2523 A70-29993

Reinforced plastics adhesion to hydrophilic mineral surfaces by using silane coupling agents

16 p2937 A70-33374

Interfacial chemistry of glass fiber reinforced thermoplastics, discussing matrix resin-reinforcement bond

16 p2937 A70-33378

Ammonium perchlorate pyrolysis, investigating exothermic surface reactions and gasification rates

16 p2963 A70-33873

Graphite oxidation on exposure to high temperature flow field based on surface coupled model [AIAA PAPER 70-823]

16 p2940 A70-33941

Surface interaction between Al single crystals in ultrahigh vacuum, investigating galling, distortion and adhesion

16 p2924 A70-34168

Radiative heat transfer between opaque interacting surfaces for equal temperature adjoint plates with one dimensional surface roughness profile

16 p3002 A70-34196

Hypersonic viscous interaction on curved surfaces, extending Cheng inclined flat plate analysis [AIAA PAPER 70-782]

17 p3007 A70-34474

Phenolic nylon thermal decomposition, considering surface reradiation and physical parameters effects

17 p3196 A70-35242

Surface alloying of high melting points in Al melts, noting prior oxidation enhancement and simplifying of calorizing techniques

17 p3102 A70-35406

Friction coefficient dependence on hardness of softer element of friction pair determined at constant values of shear strength, using external friction concepts

17 p3102 A70-35672

Surface destruction of glass dielectric by pulsed laser beam, considering plasma clouds, shock waves, ablation and crack formation

18 p3266 A70-36153

Light gas atoms adsorption on solid surfaces, calculating wave function, energy, mobility, sticking coefficient, etc

18 p3225 A70-36186

Atomic oxygen beams interaction with various surfaces at low pressure, discussing reflection probability and recombination reactions

18 p3225 A70-36187

Ti, Nb and Mo solubility during surface doping in Al melts containing various metals, discussing melt lattice structure effects

18 p3276 A70-36208

Heat transfer at flat melting surface under forced convection and laminar boundary layer solved by Karman-Pohlhausen method

18 p3347 A70-36502

Refractory metals interaction with boron during vacuum boronizing, investigating kinetics and optimal process conditions

19 p3434 A70-37452

Surface atom bonding configuration energy in two-center theory of large surface unit cells on semiconductors

19 p3483 A70-37544

Monoatomic inert gas molecules interaction with continuous elastic solid of alkaline and nonalkaline metals, calculating energy exchange

19 p3373 A70-37816

Laminar vortex flow interaction with stationary surface, considering flow field, velocity, Reynolds number, etc

19 p3405 A70-38348

Postmechanical interface separation in elastically supported rotary face seals under input excitation [ASLE PREPRINT 70AM 3C-3]

19 p3439 A70-38808

Optimum conditions and methods for vacuum diffusion welding of heat resistant alloys, removing thermodynamically stable surface oxide films by gaseous reaction products

20 p3636 A70-39197

Surface contaminated Langmuir probe measurements in glow discharge plasmas, discussing errors

20 p3633 A70-40161

Temperature measurements in gaseous reaction zone near surface of burning composite solid propellant, using modified line reversal pyrometer

20 p3694 A70-40273

Solid rocket propellants linear and nonlinear pressure coupled combustion instability behavior relationship to exothermic surface processes

20 p3694 A70-40274

Eroding surface transient heat conduction problem, considering temperature dependent surface properties, ablation, convective heating, etc

20 p3738 A70-40279

Thermally induced mirror deformations and wavefront distortions under radially nonuniform heating

21 p3942 A70-40806

Surface roughness effects on thermal radiant energy interchange between opaque interacting surfaces formulated for unequal temperature adjoint plates

21 p3944 A70-41018

Thermal processes during electron beam metal working, deriving relations for temperature field

21 p3833 A70-41123

Lunar rocks primordial accretion, examining ablation and transport of solids, liquid and vapor on surfaces

21 p3913 A70-41641

Surface ablation patterns in sublimating materials tested in high temperature structures tunnel

21 p3951 A70-41755

Interface interaction of colliding plates of different materials, reducing flow problem to differential equation via hodograph transformation

21 p3747 A70-41962

Nonisothermal burn-up rates of graphite surfaces in turbulent air flow under neutral gas shield estimated by measuring channel diameter

21 p3952 A70-42064

Ablative heat transfer to nonstagnation surfaces of high speed rocket vehicle in continuum atmosphere, using finite difference theory

22 p4125 A70-43433

Oxidized Si surface recombination rate measurement by electric field effect, noting electron bombardment effects on electrical properties

22 p3998 A70-43443

Surface degradation by oxidation, temperature fluctuations and hot corrosion of Ni- and Co-base superalloys in gas turbine engines

22 p4057 A70-43574

Satellite drag and lift from spatial impulsive surface interaction model [ICAS PAPER 70-05]

23 p4132 A70-44116

Solid surface interaction between surface with normal molecular beam, generalizing model by energy parameter simulating dissipative forces

23 p4223 A70-44994

Current oscillations in external circuits of semiconductor with low surface recombination in parallel electromagnetic field

23 p4231 A70-45062

Statistical properties of random intensity field during coherent laser radiation scattering by moving diffuse surface

24 p4351 A70-45184

SURFACE ROUGHNESS

Machined surface evaluation of fabricated components by electron microscopy to identify defects

01 p0097 A70-10012

Icarus radar and optical observations indicating surface smoothness differences between central and higher latitudes, radius size and radar reflectivity

01 p0180 A70-10534

Flow patterns in circular ducts with circumferential roughness variation, determining axial turbulence, Reynolds number effect and applications as two phase flow analog

01 p0066 A70-11132

Load support and leakage from microasperity lubricated face seals, developing hydrodynamic lubricant films [ASLE FICES PREPRINT 21]

02 p0308 A70-12174

Aerodynamic roughness length estimation and site roughness increase due to micrometeorological equipment

03 p0483 A70-13166

Similarity laws in hypersonic flow of real gas around slender blunted bodies, particularly bodies with rough lateral surface

03 p0409 A70-13866

Surface roughness measurements by coherent optics and interferometry, including theory and experimental verification

04 p0689 A70-15015

Metallic adhesion produced by surfaces compression, discussing asperities plastic deformation and macrodeformation caused by contact area growth

07 p1292 A70-18939

Upper surface roughness of internal st-sc clouds as function of vertical temperature and moisture in overlying inversion layers

08 p1537 A70-21106

Cross hatching on surface of ablating bodies exposed to supersonic turbulent boundary layer flow using mathematical model

09 p1605 A70-23232

Airborne laser profilometer terrain roughness measurement and recording, considering error sources

12 p2244 A70-26938

Plane stationary nonlinear problem of air flow over earth surface roughnesses, using three layer atmospheric model

14 p2602 A70-30160

Attenuation, resistivity and surface roughness measurements in rectangular waveguides

14 p2555 A70-30440

Mars surface topography and roughness from radar measurements

14 p2648 A70-31081

Rough surface radiative properties, determining electromagnetic wave scattering by Maxwell equation solution [AIAA PAPER 70-862]

17 p3135 A70-34508

Dielectric models of interstellar grains from calculations for smooth particles of homogeneous materials

17 p3159 A70-34879

Planetary surface smoothness factor by disk brightness, Mars red light and phase curves methods, indicating superiority of visual observation

18 p3315 A70-36602

Ocean roughness determination from satellite photographs sunglint patterns, indicating surface wind speeds

22 p4014 A70-42770

Free and supported curvilinear holes with random roughness, investigating stress concentration by conformal mapping

23 p4265 A70-43984

Sliding bodies contact surfaces stable roughness magnitude by molecular-mechanical friction and wear fatigue theories

24 p4341 A70-45489

SURFACE ROUGHNESS EFFECTS

Plastic deformation of wedge shaped model asperities influencing gas leakage between contacting surfaces, discussing critical contact pressure

01 p0060 A70-10267

Surface roughness effects on dry friction between two metals, considering conical asperities and friction coefficients

[ASME PAPER 69-LUB-10] 01 p0102 A70-10394

Flow stability criterion in rough pipes, deriving laminar to turbulent flow transition characteristics and drag as function of Reynolds number

01 p0064 A70-10998

Eccentric face seal with tangentially varying film thickness, analyzing leakage flow proportional to eccentricity and surface waviness

[ASLE FICFS PREPRINT 15B]

02 p0308 A70-12176

Circumferential wave propagation around cylinder, demonstrating dependence on incident frequency and surface roughness, noting target surface microscale roughness measurement technique

02 p0339 A70-12184

Electromagnetic scattering from randomly rough surface with finite conductivity, using Kirchhoff approximation

02 p0261 A70-12587

Electromagnetic wave backscattering from composite rough surfaces, using Stratton-Chu integral

02 p0261 A70-12589

Thickness measurement of nonmagnetic coatings on magnetic substrates taking into account surface roughness effect

02 p0302 A70-12672

Pumping energy distribution over cross section of active ruby laser elements in relation to smoothly polished, roughly polished and dull lateral cylindrical surfaces

04 p0700 A70-14607

Critical load and instability of smooth and mesh surface mechanical systems subjected to impinging fluid jet, noting static buckling and flutter effects

[ASME PAPER 69-WA/APM-10]

04 p0772 A70-14917

Wind velocity longitudinal profile measurements in atmospheric boundary layer over rough sea surface using floating beacon and statistical analysis of airflow perturbations

04 p0715 A70-15253

Elliptically polarized microwave scattering at electrically conducting rough surface, considering probability distribution of profile angles and random reflection coefficients

04 p0650 A70-15286

Radar signal amplitude fluctuations reflected from disturbed sea water surface, noting wind induced waving stochastic nature influence

05 p0812 A70-16246

Kirchhoff wave scattering geometric optics theory accuracy, using multifrequency acoustic wave backscatter data obtained from rough surfaces

05 p0814 A70-16401

Ocean surface roughness time variation effect on incident laser beam, analyzing motion picture data by computer program

05 p0860 A70-16687

Air leakage between contacting surfaces assuming surface irregularities as microscopic truncated cones with ideally plastic or elastic mechanical properties

06 p1031 A70-17133

Core length of water jet from circular tube, considering wall roughness, tube diameter and water viscosity and surface tension

06 p1031 A70-17135

Surface roughness effects on radiant heat transfer rate of isolated plane surface with uniform temperature illuminated by collimated solar flux

06 p1172 A70-17178

Turbulent boundary layers and wall jets development investigated for effect of mass injection through porous smooth and rough surfaces

06 p1034 A70-17679

Laminar sublayer resistance to momentum and heat transfer, noting effects of Prandtl number and surface roughness using mathematical model and experiments

06 p1034 A70-17680

Liquid nucleation in vapor condensation on wettable, unwettable, smooth, rough and cavitated surfaces, showing positive effect of roughness elements

06 p1177 A70-17838

Wall roughness effects on model heat transfer in high Reynolds number shock tunnel milliseconds flow using thick film fast response calorimeter

06 p1070 A70-18446

Rough metal surfaces thermal convection resistance for total heat flow through microcontacts

07 p1418 A70-18648

Gas detonation in rough walled pipe, calculating Chapman-Jouguet detonation velocity, deriving existence criterion

07 p1419 A70-18752

Streamwise directed vortices and crosshatched surface roles in heat transfer and ablation processes of reentry vehicles

07 p1394 A70-19729

Solid surface roughness influence on reflection of thermal energy molecular jets, showing shock determined by incidence angle

07 p1343 A70-20121

Crystalline structure effect on molecular beam reflection from rough polycrystalline Au surfaces

07 p1343 A70-20123

Polarization structure of electromagnetic wave scattered by slanted two dimensional statistically rough surface of finite conductivity

08 p1456 A70-20573

Scattered field from rough ionospheric irregularities or earth surface for arbitrary polarization of incident wave

08 p1456 A70-20574

Heat transfer augmentation in tubes by surface roughness and twisted tape generated swirl flow

08 p1600 A70-21830

Correlation functions for resistance to heat and momentum transfer in viscous sublayer at rough walls defined for varied geometry flows

[ASME PAPER 69-HT-2] 08 p1486 A70-21833

Surface roughness effects on measured cross spectral density of wall pressure fluctuations beneath turbulent boundary layer

08 p1486 A70-21859

Laser radiation diffuse reflection from rough surfaces, considering surface specularly and reflected waves polarization and spatial structure

09 p1696 A70-22630

Backscattering from rough surface of nuclear fireball measured by two way directive radar antenna on reentry vehicle

09 p1634 A70-22703

Atmospheric condensation nuclei activity with rough surface with decreasing spherical hollows

09 p1718 A70-23172

Laminar-turbulent boundary layer transition in incompressible fluid under surface roughness action, developing theory by generalizing Taylor hypothesis

09 p1664 A70-23713

Volcanic terrain by high precision photogrammetry for studying planetary surface roughness traversability by three wheeled vehicle

10 p1882 A70-25047

Externally pressurized porous journal gas bearings with solid sleeve parts for reducing porous media waviness and roughness effects

10 p1896 A70-25097

Interfacial thermal conductivity model based on statistical features of two faces in contact, discussing surface roughness and heat flow

11 p2083 A70-25763

Metal surfaces contact with cones and pyramids asperities, analyzing surface roughness effects on dry friction

11 p2060 A70-26412

First order scattering formulae for s- and p-light reflected and transmitted by rough plane surface using perturbation theory

11 p2086 A70-26840

Sea roughness effect on bandwidth of radar backscatter, analyzing Doppler signals of eight millimeter aircraft navigation system

12 p2228 A70-26906

Radar cross section sea clutter model based on slightly rough surface superposition on swell structure

13 p2366 A70-29215

Boundary layer transition at high Mach numbers on adiabatic wall, showing effects of wind tunnel size, surface roughness and freestream disturbances

[AIAA PAPER 70-586] 13 p2342 A70-29884

Atmospheric airflow model above changes in surface roughness, temperature and heat flux, using boundary layer approximations and Businger-Dyer and mixing length hypotheses

14 p2602 A70-30368

Vertical flux densities of momentum and sensible heat dependence on displacement height and surface roughness

14 p2602 A70-30371

Cutting speed, feed parameters and tool tip curvature effects on machined surface roughness of turned fiberglass reinforced epoxy laminates

14 p2590 A70-30873

Lunar surface roughness effects on thermal radiation, using model surface with parallel troughs

14 p2649 A70-31212

Autocorrelation of coherence characteristics of polarized components of light scattered at curved rough surface, showing nonadequate Kirchhoff approximation

15 p2749 A70-31555

Erroneous height correlation coefficients in physical optics formulation of rough surface scatter

16 p2859 A70-32938

Turbulent boundary layer response in flow field downstream of upstanding step change in surface roughness

[ASME PAPER 70-FE-17] 16 p2891 A70-33630

Diffuse specular rough surface measure for imperfect reflections in thermal radiation transfer through slot passages

[AIAA PAPER 70-860] 16 p2999 A70-33905

Super and subspecular maxima in angular distribution of polarized radiation reflected from roughened dielectric surfaces

[AIAA PAPER 70-861] 16 p2999 A70-33906

Monte Carlo model of V groove surface roughness effects on directional reflections in plane of incidence, employing energy localization circle

[AIAA PAPER 70-820] 16 p3002 A70-33944

Radiatively interacting adjacent plates in presence of collimated solar flux, considering surface roughness effects on equilibrium temperature distribution

[AIAA PAPER 70-817] 16 p3002 A70-33946

Radiative heat transfer between opaque interacting surfaces for equal temperature adjacent plates with one dimensional surface roughness profile

16 p3002 A70-34196

Solid state laser active element lateral surface microprofile effect on heat endurance

16 p2929 A70-34220

Roughness effects on heat transfer to surfaces in supersonic compressible turbulent boundary layer

[AIAA PAPER 70-742] 17 p3066 A70-34505

Atmospheric reentry nosetip shape changes supersonic flow, considering rough surface effects on heat transfer

[AIAA PAPER 70-827] 17 p3196 A70-35193

Lunar millimeter wavelength thermal radiation measurement noting surface roughness effect on polarization

17 p3171 A70-35559

Point source electric field over different sections of impedance piecewise inhomogeneous surface, calculating attenuation function near boundaries

19 p3381 A70-38570

Radio wave propagation over inhomogeneous terrains, determining perturbing effects of details on wave characteristics

19 p3381 A70-38573

Rod surface roughness effect on eddyling sound frequency and intensity and on aerodynamic resistance

19 p3353 A70-38654

Thick film thermocouple gages for roughened model surface heat flux measurements in high Reynolds number shock tunnel

21 p3824 A70-40860

Surface roughness effects on thermal radiant energy interchange between opaque interacting surfaces formulated for unequal temperature adjacent plates

21 p3944 A70-41018

Spectral bidirectional reflectance measurements of rough metallic surfaces for reflected energy spatial distribution determination in radiative heat transfer problems

23 p4281 A70-44446

SURFACE STABILITY

Infinitesimal deflections of piecewise-regular unfolding scanning surfaces fixed along edge with respect to one point, discussing rigidity

03 p0591 A70-13414

Computerized calculations for cylindrical tank bottoms with outlet based on strength analysis, using zero moment theory for surface stability under uniform pressure

05 p0946 A70-16957

Holographic interferometry applied to amplitude measurement of periodic mechanical surface vibration

06 p1069 A70-18436

Iron cyanide additive for surface stabilization of ZnO irradiated with UV in vacuum

12 p2181 A70-27258

Bubbles, steady streaming and surface instability in vibrated liquid columns

14 p2663 A70-30255

Interfacial instability effect on heat transfer to liquid nitrogen drops undergoing film boiling on flat Al surface, obtaining vaporization rates and times

21 p3948 A70-41203

Elastic stability theory Cosserat surface subjected to conservative nongyroscopic surface and edge loading

21 p3939 A70-42027

Sliding bodies contact surfaces stable roughness magnitude by molecular-mechanical friction and wear fatigue theories

24 p4341 A70-45489

Surface alloying of alloy with three elements /Al, Si and Cr or Zr/, investigating coating stability in weight, microstructure and microhardness

24 p4364 A70-46340

SURFACE TEMPERATURE

NT SKIN TEMPERATURE [NON-BIOLOGICAL]

NT WALL TEMPERATURE

Nuclear reactor surface temperatures probability calculations allowing for some uncertainties and MTR type test reactor application

03 p0523 A70-12997

Ground temperature effect on thermal resolution in IR line scan imagery, discussing equipment and

operating procedures for temperature gradient detection 04 p0686 A70-14617

Transient one dimensional heat transfer analysis demonstrating infiltrant melting effect on self heat-retarding porous metal composite during surface melt layer formation 04 p0709 A70-15414

Photographic pyrometry for surface temperature measurements on ablation models, discussing technique accuracy and limitations 04 p0694 A70-15536

Heat source temperature distribution on surface of infinite cylinder with zero temperature, presenting solution to boundary value problem 05 p0957 A70-16296

Temperature of contact surface between two homogeneous isotropic solid bodies determined by calculating plane heat source of steady three dimensional temperature field 05 p0958 A70-17014

Satellite IR measurements of surface horizontal temperature structure of Gulf Stream compared with ship and aircraft data 05 p0844 A70-17104

Satellite determination of underlying surface temperature by IR spectroscopy, measuring emitted radiation in atmospheric windows 06 p1061 A70-17205

Noontime ground surface temperature relationship to exposure and slope angle for meadows and woodland, using airborne IR pyrliometer 06 p1054 A70-17415

Heat transfer from constant temperature and heat flux surfaces to viscous fluids with high Prandtl numbers, considering transient and steady state flow 06 p1176 A70-17687

Heterogeneous ignition mechanism of solid fuels, deriving surface temperature history for time and nature of transition from weak to strong combustion mode [ALAA PAPER 70-119] 06 p1128 A70-18041

Passive microwave observation from space of sea surface degraded by atmosphere 06 p1010 A70-18087

Surface temperature effects on low Reynolds number hypersonic shock layer development over flat plate sharp leading edge 06 p0982 A70-18364

Convective and radiative heat fluxes measurement on charring ablative materials surface in rocket nozzle environment 06 p1070 A70-18444

Natural convection flow interactions from individual surfaces in closely spaced array of heated elements, discussing effect on heat transfer, induced flow and temperature field 07 p1418 A70-18644

Temperature stress distribution in cylinder or sphere with variable surface temperature and heated by external sources 07 p1411 A70-19819

Optimal atmospheric transmittance windows for underlying surface and cloud temperature determination from satellites 08 p1538 A70-21426

Venus surface temperature calculations with non-gray radiation balance model and Mariner 5 and Venera 4 vertical temperature profile data 08 p1579 A70-21568

Tungsten emissivity and radiance properties obtained at high surface temperatures 09 p1725 A70-22068

Local heat transfer coefficients determination for unilaterally heated rectangular coolant duct by approximation and experiment applicable to circular tubes 09 p1787 A70-22170

Temperature distribution in infinite and finite circular hollow cylinders, considering surface heat flux and linear heat transfer 09 p1788 A70-22595

Electronic radio equipment with encapsulated structure and natural ventilation, calculating heated zone and casing mean surface temperatures 09 p1648 A70-23147

Simulated degrading environment effect on spacecraft thermal control surfaces subjected to plume heating during apogee firing and solar irradiation [ALAA PAPER 69-1024] 09 p1657 A70-23259

Boundary function of unsteady temperature field in bodies with moving surface at constant temperature calculated by least squares method 09 p1791 A70-23620

Heat and mass transfer during liquid surface evaporation in vacuum, calculating temperature field on basis of heat balance level 09 p1791 A70-23717

Aircraft surface temperature measured with airborne IR TV system 09 p1686 A70-23754

Sea surface temperature measurement over large areas using IR remote sensing system mounted on airborne platform 09 p1686 A70-23756

Ni-Cr austenitic steel bending, surface temperature variations, crack development and propagation under double fatigue tests 10 p1902 A70-23819

Thermal radiation shield influence on stationary radiative heat transfer in closed arbitrarily shaped two gray surface system 10 p1966 A70-23865

Mixed thermoelastic problem in elastic layer with arbitrarily prescribed temperature in upper free surface 10 p1954 A70-23878

Air flow turbulence intensity and plug effect influence on local heat exchange on cylinder surface 10 p1797 A70-24028

Eclipsing binary beta Aurigae effective temperature and surface gravity determination from photoelectric spectrum and abundance analyses 10 p1938 A70-24100

Transient thermal stresses in restrained-in-bending slab with surfaces heated and cooled with finite heat transfer coefficients 10 p1964 A70-25095

Quasi-steady analysis of material under ablation-erosion heat transfer for hypersonic vehicles 11 p2149 A70-26144

Radiation heat transfer around interior of long cylinder as function of surface emissivity 11 p2149 A70-26152

Temperature distribution in shadowed lunar craters formulated in Fredholm integral equations, showing constant temperature and correction for soil thermal inertia [ALAA PAPER 69-595] 11 p2112 A70-26155

Steady state surface temperature measurement errors by thermistors, thinistors and thermocouples, discussing sources 11 p2052 A70-26361

Apollo 13 lunar surface heat flow experiment to measure vertical temperature gradients as function of time and soil thermal conductivity 11 p2118 A70-26747

Microwave radiometric temperature measurements generating curves relating sea state and surface temperature 12 p2215 A70-26903

Laminar boundary layer transition to quasi-cellular flow in natural convection above horizontal heated plates and disks 12 p2155 A70-27197

Radiative heat transfer in spherical space bounded by perpendicular annular rib system with gray diffuse and absolutely black body surfaces 12 p2331 A70-27554

Lunar surface brightness temperatures from IR observations, determining thermal emission directional characteristics to infer surface temperatures from Surveyor data [ALAA PAPER 69-593] 13 p2486 A70-28501

Mechanical seals ringing sound relationship with heat transfer and interfacial conditions, noting sliding surfaces temperature effect 13 p2417 A70-28611

Wind velocity components on nonuniformly heated plane slope with linear periodic temperature function 14 p2602 A70-30165

Lunar horizontal and inclined surfaces net radiation and components, discussing surface temperature, thermal emission and absorbed solar radiation 14 p2634 A70-30194

Surface temperature fluctuations during dropwise condensation at various heat fluxes 14 p2663 A70-30256

Vaporization of small meteor particles with identical surface temperature, considering radio communication based on reflection from ionized trails 14 p2636 A70-30323

Venus surface temperature poleward variation from radio interferometry measurements 14 p2646 A70-31068

Mariner 6 radio signals frequency changes analysis during occultation measurement for determining Mars surface pressure and temperature 14 p2646 A70-31071

Heat transfer coefficient from circular cylinder subjected to uniform surface heat flux and cooled by ring of holes 14 p2667 A70-31427

Rarefied gas slip flow coefficients calculations at nonuniformly heated surface, demonstrating relationship between temperature and isothermal slip coefficients 15 p2776 A70-31478

Surface, volume and body center temperature of convex polyhedrons under steady heat transfer 15 p2825 A70-31624

Mariner 6/7 S band radio occultation probe of Mars atmosphere concerning surface pressure, temperature and existence of ionosphere 15 p2798 A70-31681

Laminar natural convective heat transfer along outer surface of vertical cylinder, giving coefficients nondimensionally by approximate formulas 15 p2826 A70-31821

Sea surface temperature and atmospheric moisture determination from satellite measurements of atmospheric thermal radio emission on quiet and cloudy windy days 15 p2770 A70-32069

Earth surface temperature, emissivity and dielectric constant from satellite measurements of SHF radiation 15 p2771 A70-32072

Photothermometer response to thermal shock, considering rapidly varying surface temperature measurement 16 p2901 A70-33104

Surface temperature color contour maps of objects undergoing aerodynamic testing, utilizing electro-optical and computer techniques 16 p2905 A70-33169

Surface temperature measurement with airborne IR scanning imager for terrain analysis 16 p2905 A70-33170

Optimal distributed feedback surface temperature control of inertial grade floated rate integrating gyroscope, minimizing instrument degradation 16 p2908 A70-33347

Surface temperature changes measurement with thermovision camera, discussing calibration and recording 16 p2911 A70-33775

Surface temperature or heat flux density estimation for nonlinear inverse heat conduction problem involving temperature dependent thermal properties 16 p3002 A70-34195

Aerial IR surveys of surface temperature patterns of Hudson Bay during ice free seasons 17 p3079 A70-35621

Tiros satellites window radiation applied to day and night surface temperature measurements on land and sea 17 p3081 A70-35932

Surface temperature fluctuations during steady state boiling from tube, using fast response thermocouple 18 p3347 A70-36504

Autoignition, ignition and surface temperatures of M-2 double base propellant at low pressure, correcting thermocouple measurements by theoretical model 18 p3299 A70-36697

Heat transfer rates in short flow duration facilities /shock tubes/ from surface temperature measurement of solid exposed to flow 18 p3348 A70-36715

Pulsed laser holographic nondestructive testing optimization technique, monitoring honeycomb panel surface temperature during thermal stressing 18 p3259 A70-36754

Surface temperature distribution over rotating nucleus of comet deficient in volatiles 18 p3319 A70-37058

Atmospheric temperature profiles from terrestrial IR spectral radiances measured by balloon-borne grating spectrometer, discussing surface temperature variations 21 p3813 A70-40905

Aeolian regime of Venus surface resulting from high surface temperature and pressure, discussing spurious radar echoes, dust and sand transport and deposition 21 p3885 A70-40929

Gravity darkening of tidally and nonuniformly rotating Roche components of close binary systems, calculating surface temperature and spectral distributions 21 p3888 A70-41120

Site activation in saturated nucleate boiling tests involving various fluids boiled on transparent oxide coated glass surface, correlating site density data with surface temperature 21 p3948 A70-41202

Heated surface orientation and reduced gravity effects on Freon 113 nucleate 21 p3948 A70-41204

Sea surface temperature determination from satellite high resolution IR window radiation measurements by statistical histogram inference method 21 p3820 A70-42122

Dynamic nonstationary thermal convection in closed region with heat input from lateral surface for high Rayleigh and Fourier numbers 21 p3954 A70-42214

Sea surface temperature relationship with ocean currents, using bathythermograph data 22 p4014 A70-42768

Star flare HD 160202 in M6, discussing luminosity, time duration, magnitude and temperature 22 p4102 A70-42971

Heat exchange coefficients on side surfaces of constant thickness gas turbine disk, using temperature distribution method and integral transformations 22 p4125 A70-43367

Spectral brightness temperature, directional emissivity and surface temperature of earth from remote

radiance observations by balloon-borne multidetector grating spectrometer 23 p4194 A70-44035

Ground temperature effects on thermal gradients resolution in IR line scan imagery 24 p4334 A70-45363

Al alloy sheets with multicolor protective coatings, measuring surface temperature under solar radiation 24 p4428 A70-45434

Metal and nonmetal thermal nondestructive tests based on surface temperature distribution produced by heat treatment 24 p4348 A70-45744

Surface constitutive assumptions restrictions for rigid heat conductor, accounting for radiative heat supply 24 p4429 A70-46032

Surface temperature distribution of heat generating solid body in contact with parallel viscous fluid flow 24 p4430 A70-46368

Ocean currents and sea surface temperature remote sensing by Nimbus 2 High Resolution IR Radiometer 24 p4332 A70-46400

SURFACE TENSION

U INTERFACIAL TENSION

SURFACE TO AIR MISSILES

NT HAWK MISSILE

Missile tracer mixture performance control facility noting chamber for pressure measurement during operation 03 p0544 A70-13758

Electromagnetic interference (EMI) effects on TALOS missile guidance receiver by expanding computer simulation test results 14 p2655 A70-31345

SURFACE TO SURFACE MISSILES

NT CRUISE MISSILES

NT MINUTEMAN ICBM

Fluidic attitude control for boost phase of tactical surface to surface missile 16 p2844 A70-33447

Otomat surface to surface missile with turbojet engine for extended range subsonic cruise and two solid propellant rocket engines for launch 22 p4110 A70-43211

SURFACE TREATMENT

U SURFACE FINISHING

SURFACE VEHICLES

NT AIRCRAFT CARRIERS

NT CAPTURED AIR BUBBLE VEHICLES

NT LUNAR MOBILE LABORATORIES

NT LUNAR ROVING VEHICLES

NT LUNAR SURFACE VEHICLES

NT ROCKET PROPELLED SLEDS

NT TRACTORS

NT WALKING MACHINES

NASA research studies supporting tracked air cushion vehicle (TACV) program illustrating aerospace technology application to ground transportation [AAS PAPER 69-565] 04 p0622 A70-14639

One dimensional compressible flow analysis for near field aerodynamics of tube-vehicles, showing drag coefficient dependence [AIAA PAPER 70-140] 06 p1038 A70-18077

Ram wing vehicles aerodynamics application to high speed ground transportation, studying effect on passenger ride quality [AIAA PAPER 70-142] 06 p0973 A70-18145

Slender body theory for steady state aerodynamic characteristics of high speed ground vehicles with arbitrary cross sections, discussing side wind [AIAA PAPER 70-139] 06 p0973 A70-18155

Magnetic suspension and guidance of high speed vehicles realized via magnetic field interaction of vehicle-mounted superconducting magnets with eddy currents 08 p1543 A70-20576

Unmanned Mars roving vehicle navigation subsystem feasibility study covering inertial and gyrocompass-odometer systems 11 p2080 A70-26211

Satellite navigation method for locating Mars landmark or target point for exploration by roving vehicle located as center of coordinate system 11 p2080 A70-26213

Routing algorithm for computer controlled unmanned autonomous roving vehicle on Martian surface 11 p2081 A70-26317

Unmanned vehicles for planet surface exploration, discussing design and control using self adjusting and logic circuits 13 p2384 A70-28418

Surface navigation for unmanned Martian surface roving vehicle 14 p2615 A70-30469

Dual mode algorithm for routing unmanned autonomous roving vehicle around obstacles on planets, using dynamic programming and terrain information [JPL-TR-32-1484] 14 p2655 A70-31183

High speed ground tube vehicle transportation system aerodynamics, presenting drag coefficients and static wall pressure measurements 16 p2839 A70-34264

Roving vehicle self contained automatic control systems, discussing terrain scanning technique, stereo TV and electronic coordinate measuring and data processing equipment 23 p4260 A70-44628

SURFACE WAVES

NT BAROCLINIC WAVES

NT CAPILLARY WAVES

NT GRAVITY WAVES

NT SOMMERFELD WAVES

Circumferential wave propagation around cylinder, demonstrating dependence on incident frequency and surface roughness, noting target surface microscale roughness measurement technique 02 p0339 A70-12184

Free oscillations and surface wave dispersions from lunar models based on Orbiter data and corresponding pressure region of earth crust 02 p0379 A70-12777

Axial emission impedance antenna converting strongly delayed surface wave into weakly delayed wave forming cophased front at antenna end 03 p0456 A70-13199

Surface wave attenuation in homogeneous plasma cylinder caused by resonance in transition layer between plasma and vacuum 03 p0447 A70-13286

Magnetoelastic surface wave propagation properties in ferrites at UHF wavelengths, using numerical calculations for gallium-YIG 03 p0540 A70-13700

Surface function and impedance distribution for unilateral surface wave antenna excitation by slot emitter above surface impedance segment 04 p0655 A70-14403

Surface waves excited by horn above dielectric disk backed by metallic disk, formulating characteristic wave equations and solving for attenuation and propagation constants 04 p0659 A70-15305

Interaction of infinite shallow draft cylinder oscillating at free surface with train of oblique waves 04 p0618 A70-15321

Surface wave spectrum and propagation in non-homogeneous bounded elastic solid, considering existence and eigenvalues approximation 05 p0925 A70-15789

Characteristic equation for phase velocity of surface wave propagating on helix for forbidden zone, suggesting current distribution function 05 p0815 A70-16775

Surface acoustic wave components for performing transduction, amplification and coupling functions, considering compatible component configurations 06 p1018 A70-17477

Immittance, transfer and scattering characteristics for interdigital acoustic surface wave transducers, using linear equivalent circuit model 06 p1062 A70-17478

Materials fatigue failure ultrasonic early detection by continuous surface wave irradiation 06 p1077 A70-17920

Ultrasonic surface waves detection of transverse fatigue crack initiation in rails under load, applying results to fatigue life determination 06 p1168 A70-17924

Surface wave propagation and amplification by electron beam-plasma interaction, inapplicability of coupled mode theory and use for microwave amplifier 06 p1125 A70-18616

Propagation pattern of surface acoustic wave visualized in piezoelectric and nonpiezoelectric materials by dusting delay line with fine particles 07 p1336 A70-20283

Gas flow influence on wave characteristics of thin viscous liquid layers pulled by gravity vertical surface compared with water layer experiments 08 p1482 A70-20917

Modal excitation and scattering in retinal receptors of human and insect visual systems investigated with dielectric rod uniform wave and irregularities 08 p1452 A70-21289

Upper frontal waves behind quasi-stationary surface cold front using mathematical model 08 p1540 A70-21924

Surface wave reflection during propagation along transversely magnetized ferrite plate on metal backing, using perturbation theory to find cylindrical wave field 10 p1844 A70-25163

Surface waves stability in cold bounded plasma against background of steady state electron oscillations, using nonlinear approximation 11 p2089 A70-25716

Surface waves excited by oscillating current in cold plasma surrounded by metallic sheath of infinite conductivity, deriving frequencies and growth rates 11 p2089 A70-25717

Microwave surface acoustic delay lines properties, advantages, electron beam fabrication, optical probing for propagation loss measurement, etc 11 p2005 A70-26166

Excitation of surface waves on impedance plane in collisionless cold anisotropic plasma with external magnetic field coinciding with source direction 12 p2278 A70-27538

Surface wave transmission lines used at millimeter wavelengths 14 p2549 A70-30443

Surface wave excitation including PM and dipole modes and Sommerfeld waves 14 p2549 A70-30444

Surface wave radiation from plane dielectric waveguide, considering phase constants, directional properties and optimal distance location 15 p2696 A70-31503

Feed and terminal radiation patterns of surface wave antennas measured separately 16 p2861 A70-32973

Acoustic and magnetic surface waves technologies for radar signal processing 16 p2874 A70-33390

Observational errors effects on surface waves resolution, describing shear velocity determination in crust and mantle from observed waves 16 p2897 A70-33647

Elastic waves on isotropic and anisotropic surfaces, discussing excitation methods, surface probing, propagation characteristics, etc 17 p3136 A70-34650

Surface wave antennas, operated on guided wave mode parallel to interface and with radiation at discontinuities, calculating excitation and radiation characteristics 17 p3052 A70-35072

Nonlinear theory for surface waves propagating in bounded magnetoactive plasma 18 p3295 A70-36412

Elastic Cosserat half plane, analyzing wave propagation of small amplitude thermoelastic disturbances and uniform motion of concentrated line load along surface 18 p3338 A70-36434

Nonlinear effects of harmonic generation and mixing in lithium niobate microwave acoustic surface wave delay lines measured using laser light deflection 19 p3485 A70-37698

Numerical model of piezoelectric surface wave propagation on free and metallized cubic and hexagonal crystals 19 p3486 A70-37754

Surface waves free period partial derivative correlation and relation to resolution of gross earth data 19 p3414 A70-38374

Ultrasonic surface waves amplification in piezoelectric crystal-Si semiconductor system, observing dependence on permittivity 19 p3488 A70-38675

Wave propagation in linear elastic surfaces, calculating wave speeds, shapes and strength decay 19 p3473 A70-38943

Frequency shifted diffraction of monochromatic Gaussian light beam by reflection off ultrasonic surface wave 21 p3850 A70-41907

Acoustic surface waves phase velocity on lithium niobate with gold layer for propagation modes, predicting LF cut-off by substrate anisotropy 21 p3863 A70-42001

Surface elastic waves, considering propagation, electromagnetic transduction, amplification, guiding, focusing, reflection and applications 21 p3830 A70-42115

Slow wave propagation on conducting surface separated from plasma by ion sheath, observing resonances on cylindrical antenna 22 p4082 A70-43238

Far field diffraction spreading of surface acoustic waves on cut Li-niobate in two directions 23 p4230 A70-44199

EM wave backscattering from lossless dielectric sphere, examining diffracted field surface waves role 23 p4165 A70-44960

Thin liquid film /melt layer/ on body in supersonic flow, examining crosshatched wave patterns stability 23 p4183 A70-44979

Electromagnetic-surface elastic waves conversion in superconductors, considering thin plate forced vibrations and standing waves excitation 24 p4389 A70-45205

Single crystal piezoelectric materials growth characteristics and wave propagation properties for surface acoustic wave applications 24 p4367 A70-45399

SURFACES

Large-tilt-angle lifting surface theory for V/STOL aircraft based on inclined actuator disk analysis 04 p0619 A70-15377

Subsonic lifting surface theory including leading edge, discussing singularities in solution of integral equation for determination of aerodynamic properties [AIAA PAPER 69-37] 04 p0619 A70-15387

Gaussian quadrature integration technique developed for collocation approach for integral equation of steady subsonic lifting surface theory [AIAA PAPER 70-191] 06 p0970 A70-18097

Lifting surface problem for finite span wing in ground effect using matched asymptotic expansions method 14 p2527 A70-30280

- Sears function and lifting surface theory for harmonic gust fields in incompressible flow, modifying function for accurate interpolation of large numbers
14 p2528 A70-30860
- Dynamic stability derivatives calculation using steady and oscillatory lifting surface theory with allowance for Bryan limitations
14 p2529 A70-30864
- Stiffness matrix correction for curved element deficient in rigid body motion
18 p3342 A70-36687
- Frequency dependent effects of applied acoustic fields on attached jet flows for Reynolds numbers over curved surfaces
[ASME PAPER 70-FLCS-1] 22 p4008 A70-42430
- Subsonic high lift cruise wing optimal design using kernel function method of planar lifting surface theory
22 p3959 A70-42709
- SURGEONS**
NT FLIGHT SURGEONS
SURGERY
NT LABYRINTHECTOMY
Lasers for surgical applications, cancerous tissue treatment, ophthalmology and comparison with RF diathermy
24 p4308 A70-45569
- SURGES**
Stage matching under local stall conditions for multistage axial flow compressor off-design and surge initiation characteristics
09 p1608 A70-23741
- Statistical classifier for analyzing tape recorded transients
11 p2056 A70-26457
- F-11A airplane in-flight inlet pressure fluctuations for engine compressor surge, discussing average turbulence factor
[AIAA PAPER 70-624] 16 p2840 A70-33543
- Aircraft propulsion control system accommodating transients and yielding higher steady state performance
16 p2966 A70-33557
- Zener diodes as voltage transient suppressors for ground vehicle and aircraft power supplies
16 p2879 A70-34060
- Temporal sequence correlation between surges and associated flares during solar cycle
22 p4095 A70-43265
- SURGICAL INSTRUMENTS**
Laser radiation effects on eye, quantifying light necessary for coagulation for retinal detachment surgery, discussing risks in laser surgery
01 p0037 A70-10859
- SURVEILLANCE**
Space systems for communications, surveillance and navigation needs of international aviation, discussing service requirements, spectrum utilization, technology limitations and terminal design
07 p1330 A70-19290
- One dimensional Poisson production process under costly surveillance, considering maximum attainable income rate approximation
09 p1653 A70-22347
- Land and airspace demands in navigation, surveillance and traffic control, discussing application of current techniques
14 p2611 A70-30105
- Computer controlled frequency surveillance system design and operation
16 p2871 A70-34052
- Satellite technology applications to ATC, including communications, navigation, surveillance over water and data acquisition
[AIAA PAPER 70-1301] 24 p4373 A70-45922
- SURVEILLANCE RADAR**
Secondary surveillance radar to operate autonomously with digital techniques and digital handling systems, discussing design and ATC applications
02 p0266 A70-11957
- ATC surveillance radar for high density traffic, discussing optimum electronic scanning rates, 3D radar and MTI
02 p0330 A70-11958
- Secondary surveillance radar (SSR) automatic plot extractors and display processors for providing information on aircraft height and identity for air traffic control
02 p0256 A70-11963
- Secondary surveillance radar and interferometry techniques to determine aircraft positions in real time and all weathers for air terminal approach control
02 p0331 A70-11965
- Automatic aircraft tracking by returns from secondary surveillance radars, noting correlation of plots with track
02 p0332 A70-11966
- Airborne secondary surveillance radar transponders performance and system optimization for automatic altitude reporting, separation standards maintenance and automatic plot extraction
02 p0267 A70-11990
- Deleterious suppressing nonsynchronous responses (fruits) in secondary surveillance radar systems, discussing effects on target detection probability
02 p0263 A70-12786

Control program debugging for experimental automatic surveillance and tracking radar, noting use for on-line systems
04 p0654 A70-15449

Ground based radar surveillance for SST to avoid convective clouds and thunderstorm activity during transonic acceleration phase ensuring minimum demands on maneuverability
09 p1610 A70-22242

Synthetic aperture radar in earth resource monitoring by satellite, determining topography and surface nature from spatial patterns
09 p1635 A70-22872

Stable moored ocean platforms providing reliable VHF communications and secondary surveillance radar facilities for civil aviation operations over North Atlantic
09 p1723 A70-23035

Digital range tracking, Doppler filtration and moving target selection in multichannel automatic surveillance radars
13 p2380 A70-29735

Passive and cooperative active hologram radar extended from stationary coherent radar, considering use in airport surveillance of aircraft
21 p3792 A70-42119

SURVEYING

U SURVEYS

SURVEYOR LUNAR PROBES

NT SURVEYOR 5 LUNAR PROBE

NT SURVEYOR 7 LUNAR PROBE

Lunar origin theories, considering lunar surface data from Surveyor spacecraft and Lunar Orbiter
01 p0178 A70-10453

Bioscience for recovered lunar samples, discussing Surveyor analyses, Lunar Receiving Laboratory methods and life detection using biological markers
01 p0042 A70-11637

Surveyor TV camera conversion from qualitative viewing device into quantitative measuring instrument by calibration coupled with data processing program
[JPL-TR-32-1374] 03 p0490 A70-13662

Surveyor 5, 6, 7 missions alpha-scattering experiments, lunar rocks chemical composition compared with earth rocks and chondritic meteorites
04 p0752 A70-15062

Prelaunch photometric calibration of Surveyor TV system for reconstruction of lunar terrain televised pictures permitting system lunar performance prediction
[AIAA PAPER 68-1138] 04 p0692 A70-15405

Surveyor spacecraft vernier propulsion system survival in lunar environment, suggesting temperature resistant seal and valve seat material for fluid loss prevention
06 p1129 A70-17170

TV test chart for evaluating Surveyor lunar spacecraft TV system covering resolution, photometric and colorimetric response and sun angular position
[SMPT PAPER 105-71] 10 p1890 A70-24601

Lunar surface alpha radioactivity at Surveyor 5, 6 and 7 landing sites
11 p2104 A70-25658

Unmanned exploration of planetary surfaces in preparation for manned landings, describing Surveyor lunar probes
11 p2112 A70-26056

Lunar surface mechanical properties from Surveyor spacecraft interactions with soil/exclusive of surface sampler/
14 p2644 A70-31055

Stepper motor for pointing Surveyor spacecraft TV transmitting antenna and solar panel at earth and sun
16 p2845 A70-34110

Surveyor spacecraft landing shock absorbers design and performance assessment by digital computer simulation
16 p2922 A70-34123

Surveyor thermal switch for temperature control to assure spacecraft components performance during temperature extremes on lunar surface
16 p2845 A70-34127

Surveyor TV mechanisms, discussing camera, mirror, zoom lens, filter wheel, focal plane shutter and lubrication
16 p2914 A70-34147

Surveyor camera double acting rotary solenoid actuated focal plane shutter utilizing two blades in parallelogram linkage
16 p2914 A70-34148

Surveyor spacecraft characteristics and operation, discussing scientific payloads, landing sites, etc
20 p3716 A70-39951

Lunar surface physical conditions from Surveyor landings, discussing fine cohesive rock powder
20 p3708 A70-39959

SURVEYOR PROJECT

Surveyor project as basis for technology transfer management exemplified by planning and organization problems
02 p0403 A70-12639

Surveyor spacecraft testing at Environmental Test Laboratory, describing facilities and innovations designed for temperature extremes
19 p3532 A70-37960

Surveyor program results, discussing lunar craters, rock fragments, particle size optical, thermal and radar characteristics and chemical composition
20 p3707 A70-39952

Lunar topographical and geological features examined by Surveyor program
20 p3707 A70-39953

Lunar crater size and shape characteristics from Surveyor missions, discussing rimless shallow and cup shaped craters
20 p3707 A70-39954

Lunar fragmental debris layer observations from Surveyor project, examining size, shape, texture, structure, etc
20 p3707 A70-39955

Lunar fragmental debris physics from Surveyor observations, examining size-frequency distribution
20 p3707 A70-39956

Lunar elemental abundances examined by Surveyor project, discussing albedo contrasts, surface rock density, bulk composition, thermal regime and chondritic meteorites
20 p3707 A70-39957

SURVEYOR 5 LUNAR PROBE

Surveyor 5 lunar rock data from Mare Tranquillitatis compared with pyroxene gabbros, indicating gabbro or gabbroic anorthosite classification
01 p0181 A70-10575

Lunar surface material composition examination by Surveyor 5, discussing formation of surface
20 p3708 A70-39958

SURVEYOR 7 LUNAR PROBE

Surveyor 7 alpha scattering experiment and TV image data revealing lunar surface chemical composition, rocks and fragments, etc
04 p0752 A70-15060

Lunar regolith and polarized component of earthlight observations by Surveyor 7 TV camera
04 p0752 A70-15061

Surveyor 7 highland landing soil mechanical properties and rock diameter similar to previous sites
04 p0752 A70-15063

Surveyor 7 lunar surface sampler, obtaining soil and rock data
04 p0752 A70-15064

Microbiological assay procedures for spacecraft sterilization and tabulation of microorganisms found on Surveyor 7
05 p0808 A70-16705

Surveyor 7 lunar mission landing site, equipment, operations, etc
05 p0915 A70-16830

Radio astronomical observations of lunar surface material EM properties compared with Surveyor 7 chemical analysis
14 p2645 A70-31059

Surveyor 7 TV system in photon integration mode, analyzing slow scan vidicon storage characteristics and dark current limitations
[SMPT PAPER 105-72] 17 p3095 A70-35635

SURVEYS

NT GEODETIC SURVEYS

One way radio range measurements for surveying and navigation emphasizing McDonnell collision avoidance and geophysical surveying systems, using Rb atomic clocks
01 p0136 A70-10306

UHF telescopic survey of southern sky for studying galactic plane in absorption
08 p1578 A70-21536

One way radio range measurements for surveying and navigation emphasizing McDonnell collision avoidance and geophysical surveying systems, using Rb atomic clocks
13 p2449 A70-29620

SURVIVAL

Physiological research on humans in hypothermia resulting from confinement to life raft on open sea, analyzing thermal conditions, thermoregulation and survival
01 p0013 A70-10233

Soviet book on survival in space covering astronauts training, behavior, impressions, performance, etc, with historical considerations
01 p0033 A70-10493

Space flight emergencies causes and consequences, underlying life threats and crew survival times, considering equipment failures, personnel errors, etc
04 p0761 A70-14926

Survival rates of continuously cultivated *Chlorella* plants in air-carbon dioxide atmosphere after single exposure to gamma radiation, using microcolony counting technique
05 p0803 A70-17113

Rat survival rate after prolonged gradually decreased body temperature without motion restraint or kept in fixed position
05 p0804 A70-17115

Survival training for safety promotion in emergency, discussing psychological factors, communication, living off land and shelter
07 p1218 A70-19007

Crash control for reduction of operational hazards and flight accidents to survivable level, discussing pilot training for emergencies

07 p1191 A70-19008

Physical discomfort and miseries contribution to psychological deterioration during water survival tests on life raft

07 p1218 A70-19009

Survival psychology for civil aviation, discussing irrational behavior after forced landings resulting from exhaustion of mental resources and inappropriate activity

07 p1204 A70-19018

Microorganisms survivability in agar subjected to simulated Martian freeze-thaw cycles, discussing soil samples collection and composition

09 p1618 A70-22767

Human survival problems of transport aircraft in various airport ground-air situations and environmental conditions

15 p2676 A70-32224

Book on survival in cold water covering physiology and treatment of immersion hypothermia and drowning, thermoregulation, etc

19 p3360 A70-37977

Escape and survivability rates in various aircraft flight envelope regimes, using existing escape statistics and mission profiles

23 p4141 A70-44492

Near fatal crash in T-33 aircraft, discussing protective clothing, seat harnesses, bodily position and mental attitude

23 p4153 A70-44497

SURVIVAL EQUIPMENT

Aircrew escape/rescue capability /AERCAB/ flying ejection seat design and test programs, noting rotary wing, fixed wing and parawing feasibility

01 p0035 A70-10714

Space rescue techniques and equipment in NASA recovery programs, considering low earth orbit and water landing

01 p0035 A70-10717

Electronic search and rescue system developed for West German Air Force, consisting of personal transceiver and automatic distress signal transmitter unit, etc

05 p0793 A70-15904

Aircraft life support systems and equipment evaluated in Vietnam combat environment, discussing combat ejection conditions, injuries cause and severity, fatalities, etc

05 p0806 A70-16298

Flight safety, survival and personal equipment - Conference, Las Vegas, October 1969, Volume 1

06 p1001 A70-17702

Life support and survival gear design, testing, manufacture, supply and maintenance for combat ejections over rugged enemy terrain, discussing pilot injuries

06 p1002 A70-17706

Physiological training programs and equipment for life support in transports, discussing changes in protective helmet and quick donning harness

06 p1002 A70-17708

Fleet evaluation program of AOH-1 helmet for replacement of standard flight helmet, oxygen mask retainer kit and oxygen regulator

06 p1002 A70-17709

YANKEE escape system adapted for helicopters using tractor rocket, noting modular concept advantages

06 p0986 A70-17712

Physiological and environmental factors influencing oxygen breathing system design and use for passengers and aircrews of high flying aircraft

06 p1003 A70-17716

Emergency ejection from lunar landing training vehicles, describing working sequence and experimental results on astronaut and test pilot

06 p1003 A70-17717

RAPIDJET escape, recovery and survival system providing rapid escape for large aircrew complement by manual bailout system utilizing semiautomatic escape slide

06 p0986 A70-17719

Solid propellant cool gas generating systems applications to inflating emergency escape slides, rafts, pontoons and flotation bags

06 p0986 A70-17720

Cool gas inflation systems for evacuation equipment on large aircraft with size and weight fitting into aircraft doors

06 p0986 A70-17721

Design concept and operation of electronically lobed homing system providing commands to pilot for flying aircraft directly to transmitting emergency beacon

06 p0987 A70-17725

Flight safety, survival and personal equipment - Conference, Las Vegas, October 1969, Volume 2

07 p1217 A70-19003

Flotation dummy to simulate unconscious survivors characteristics analyzed for life jacket design

07 p1218 A70-19004

Aircrew parachute with low speed-low altitude capability, considering static on-the-deck recovery, pack volume, weight, escape envelope spectrum, etc

07 p1191 A70-19014

Pilot Airborne Recovery Device /PARD/ using hot air ballute, noting capability to ascend or descend by flow control valve controlling butane burner

07 p1192 A70-19019

Lithium-cadmium fluoride battery for aircrew survival beacon radio receivers, considering voltage loss elimination by doping

08 p1439 A70-20708

Survival on sea following air accident, based on medical and technical considerations, emphasizing life jackets

09 p1625 A70-23008

Life support systems general inspection procedures, personal and survival equipment and accessories

11 p1990 A70-25673

Aircrew equipment assemblies taking into account altitude, flight acceleration, environment, escape and survival

13 p2345 A70-28971

Emergency evacuation on land of passengers and crew of airliners, discussing training, equipment, standardization, communication and protective fabrics

15 p2675 A70-32220

Concorde aircraft design for emergency passenger evacuation, emphasizing overwing inflatable escape slides and kinetic heating effects

15 p2675 A70-32222

Passenger survival and evacuation of civil jet transport aircraft after ditching at sea

15 p2676 A70-32223

F-111 crew escape module, describing main parachute and pyrotechnics severance improvements, parachute deployment and inflation, etc

21 p3751 A70-41807

SIHS-3 ejection seat escape system design, considering minimum weight, cost and maximum performance

21 p3751 A70-41808

Survival and flight equipment - Conference, Las Vegas, September-October 1970, Volume 1

23 p4151 A70-44453

Aircraft crash protection with preinflated air bag added to conventional seat/lap belt tested with human sled subjects

23 p4140 A70-44456

In-flight escape systems and survival equipment reliability in U.S. Navy ejections

23 p4143 A70-44460

Survival training program preparing physicians as advisors regarding survival equipment and medicine

23 p4152 A70-44463

High energy emergency exit systems for passenger survival in aircraft accidents

23 p4140 A70-44466

Survival and flight equipment - Conference, Las Vegas, September-October 1970, Volume 2

23 p4152 A70-44479

Flotation device for infants and small children incorporating life support and survival capabilities for aviation and marine applications

23 p4153 A70-44480

Operational requirements for NASA space shuttle Survival and Flight Equipment, discussing protection during launch and ascent

23 p4258 A70-44484

Photochromic paint nondestructive testing for survival equipment, detecting bond defects and sandwich water

23 p4197 A70-44490

F-111 aircraft crew cockpit escape module design for maximum efficiency, including survival equipment after ejection

23 p4141 A70-44491

Civilian survival in emergency situations, discussing basic requirements, environments, vehicles and equipment for survival kits

23 p4153 A70-44495

Over water aircraft accident investigation aids for greater survival, improved location searches and faster recovery of essential parts

23 p4153 A70-44498

Space vehicle personnel escape/rescue/ survivability capabilities, considering on board, prepositioned aid and earth launched concepts

23 p4260 A70-44620

SUSCEPTIBILITY [MAGNETISM]

U MAGNETIC PERMEABILITY

SUSPENDING [HANGING]

NT MAGNETIC SUSPENSION

Transit instrument suspension improvement by isolating unloading mechanism from horizontal axis, reducing external observation errors

04 p0693 A70-15483

North seeking declination gyrocompass design and operation with directing moment induced through bifilar suspension

05 p0844 A70-15775

Dynamic stability of pendulum-weight system during vertical HF small amplitude vibration of suspension point by averaging method

08 p1543 A70-20494

Time optimal control synthesis of fast acting gyrocompass mounted on fixed foundation and with hydraulic damper and torsional suspension of sensor

12 p2233 A70-27564

Rolamite low friction suspension system, describing components, force generation and applications

16 p2923 A70-34165

Torsion, filar, flexure and coil type mechanical suspensions for space applications, considering instability due to temperature changes and magnetic, electric and force fields

16 p2924 A70-34169

Gyroscope in gimbal suspension on free base of four solid bodies connected by flat hinges

18 p3259 A70-36593

Parachute opening load amplification due to suspension line elasticity, using two-body spring-mass model

23 p4142 A70-44531

SUSPENDING [MIXING]

Laminar flow of suspension over flat plate, analyzing particulate velocity and concentration profiles relationships to drag and lift forces

14 p2565 A70-30270

Erythrocyte suspension subjected to gas bubble ultrasonic oscillation, investigating hemolysis mechanism

20 p3573 A70-39981

SUSPENSION SYSTEMS [VEHICLES]

Javelin research rocket payload suspension ensuring limited vibrational accelerations, using viscoelastic materials for damping

04 p0774 A70-15147

Pneumatic suspension systems for air cushion skirts

16 p2841 A70-33759

Two-point suspension system with longitudinally displaced cargo hooks for handling helicopter loads, discussing wind tunnel and flight tests

17 p3014 A70-34714

Rotating flexible cable-connected space station dynamic scale model, describing suspension system and artificial gravity generation

23 p4258 A70-44528

SUSPENSIONS

Weak shock waves relaxation time and amplitude and acoustic velocity as functions of thermorelaxing media

01 p0068 A70-11588

Viscosity anisotropy in fluid matrix suspensions of parallel rigid flakes as function of flake content and width-to-thickness ratio

03 p0515 A70-13122

Heat transfer coefficient in turbulent dust flow of fine particles suspension, using coupled similar equations

03 p0608 A70-14382

Air-glass particle suspensions flows in shock tubes, deriving effective drag coefficients from simultaneous particle concentration and pressure measurements

04 p0667 A70-14778

Flow formation in Couette motion of viscous fluids containing suspended rigid spherical particles using theory of fluids with microstructure

11 p2037 A70-26169

Sphere slow motion in viscous fluid with solid particle suspension, considering Stokes flow pattern small relaxation time perturbation

16 p2896 A70-34272

MHD channel flow of suspension for prescribed wall heat flux and temperature, determining flow and heat transfer characteristics

22 p4080 A70-42670

SWALLOWING

Esophageal swallowing pattern of longitudinal and circular muscular layer contraction, using intraluminal pressure recordings

24 p4300 A70-45844

SWAN BANDS

Diatom carbon swan band violet line absence from sunspot suggested in accordance with molecular equilibrium predictions

05 p0911 A70-16433

Ikeya-Seki /1967n/, Thomas /1968b/ and Honda /1968c/ comet photoelectric spectrum, examining swan bands, continuum and reflected scattered light

20 p3703 A70-39024

SWEAT

Evaporative weight losses by sweating in man exposed to warm environment as function of time, including graphical method for heat storage prediction

03 p0430 A70-14164

Heat of evaporation of sweat measured in human calorimeter at various air and dew-point temperatures, finding value 7 percent above water

17 p3031 A70-35423

Desoxycorticosterone action on human kidneys and sweat glands as function of temperature tested with various DOCA and NaCl doses

24 p4301 A70-45988

SWEAT COOLING

Heat transfer coefficients in transpiration cooled gas turbine blades, using two dimensional theory covering porous wall and internal cooling passages

01 p0166 A70-11392

Combined hypoxic hypoxia and high ambient temperature found relieving strain on humans by increasing heat release by evaporation

04 p0630 A70-14581

Transpiration-cooled electric arcs for high temperature high density plasma generation, considering uncertainties in plasma transport properties and temperature distributions

04 p0729 A70-15591

Unheated solid starting length effect on skin friction and heat transfer characteristics in incompressible transpired laminar boundary layer on flat plate

06 p1035 A70-17691

Heat and mass transfer in passive transpiration cooling system with two moving boundaries, observing porosities and radius of curvature effects

06 p1176 A70-17692

Transpiration and film cooling systems comparison for high speed flows with foreign gas injection effects [AIAA PAPER 70-153]

06 p1179 A70-18073

Stable two phase water flow system for transpiration cooling in thermal protection of SST noise suppressor situated in afterburning engine exhaust gas stream

[AIAA PAPER 70-151] 06 p1181 A70-18146

Wall temperature variation of transpiration cooled tube surrounding plasma arc calculated from gas mass flow and wall properties

07 p1420 A70-19214

Transpiration-cooled constricted arc for plasma generation, considering transport properties, LTE assumptions and porous tube flow characteristics

07 p1351 A70-19898

Mode transition characteristics of free burning argon electric arc with transpiration cooled anode, noting current blowing parameter

[AIAA PAPER 69-696] 12 p2281 A70-27806

Transpiration-cooled systems design with porous materials, considering mechanical and flow control/permeability/properties requirements

12 p2256 A70-27822

Transpiration and film cooling effects on aerodynamic characteristics of slender cone in hypersonic flow tested in hypervelocity wind tunnel using mass injection

16 p2837 A70-33857

Unsteady laminar boundary layers on infinite porous plate, considering radiative heat transfer and transpiration cooling

17 p3067 A70-34632

Transpiration cooling for high temperature gas turbines, investigating effects on aerodynamic and thermodynamic performance

[ASME PAPER 70-GT-56] 18 p3303 A70-36839

Transpiration cooling of porous constrictor walls of high intensity electric arc in plasma

[ASME PAPER 70-HT-35] 22 p4122 A70-42432

SWEATING

U PERSPIRATION

SWEDEN

Swedish VIGGEN program for aircraft weapons system development emphasizing management methods

05 p0960 A70-16717

Report to COSPAR on Swedish space research (1969) including rocket-borne auroral particle experiments, plasma physics, atmospheric, solar, cosmic radiation, etc

15 p2830 A70-31722

SWEAP ANGLE

NT LEADING EDGE SWEAP

Sweep angle relationship to cavitation inception on hydrofoils and to hydrofoil performance deterioration due to cavitation

06 p1032 A70-17211

Electronic narrow sweep antenna array active element number reduction, discussing optical considerations

16 p2866 A70-34266

SWEAP CIRCUITS

Multidegrees of freedom electronic cabinets dynamic response to AM fast sine sweep

[SAE PAPER 700846] 24 p4380 A70-45884

SWEAP FREQUENCY

Frequency sweep/chirp and pulse width in externally mode locked laser with host dispersion obtained analytically using circulation pulse method

01 p0111 A70-10572

Precise sweep calibrations and simultaneous spectrum recording for high resolution nuclear magnetic resonance spectroscopy

11 p2052 A70-26375

Ionospheric electron density measurements with high altitude rocket swept frequency RF impedance probe

13 p2400 A70-29906

Picosecond pulse frequency sweep measurement using time resolved spectroscopy

17 p3108 A70-35904

Electrodynamic and electrohydraulic vibrators for frequency sweep, wideband random and sweep random vibration test methods

23 p4195 A70-44333

Nonmetallic nonconductive composite materials physical properties by swept microwave frequency nondestructive testing

24 p4345 A70-45705

SWEAPBACK

NT LEADING EDGE SWEAP

SWELLING

Fiber reinforced solid material, determining swelling or temperature change induced dilatation by micromechanics and physical chemistry

19 p3540 A70-37943

Polyurethane swelling in liquid media, measuring surface orientation effects during chemical machining on stress strain state

20 p3654 A70-39249

Isothermal kinetic rates of polymer swelling and dissolution, using thermomechanical analyzer

22 p4059 A70-43078

SWEPT FORWARD WINGS

NT TRAPEZOIDAL WINGS

SWEPT WINGS

NT DELTA WINGS

NT SWEPTBACK WINGS

NT TRAPEZOIDAL WINGS

Three dimensional turbulent boundary layers on high aspect ratio bodies (swept wings), discussing shear stress direction determination

02 p0286 A70-12354

Unsteady pressure distributions on elastic swept wing upper and lower sides at high subsonic to transonic flow, investigating torsional and bending vibrations

[DGLR-69-31] 04 p0615 A70-15151

Swept wings aerodynamic center and span load distributions with respect to quarter-chord line

04 p0619 A70-15393

Aerodynamic characteristics, stability and controllability of swept wing and delta wing supersonic aircraft at subsonic velocities

05 p0796 A70-16966

Hansa 330 fan jet design for executive and commuter market, discussing forward-swept wing concept and standardized structures and systems

07 p1194 A70-19619

Swept and delta wing supersonic military aircraft stability and controllability, discussing variation in maximum lift coefficient as function of Mach number

09 p1190 A70-23129

Three dimensional turbulent boundary layer development on rear of swept wing, comparing measurements with calculations

13 p2344 A70-30021

Swept tip rotor blade design, discussing wind tunnel-whirl stand correlations

17 p3015 A70-34736

Flow field about leading edges of tapered wings set at different angle of attack, using gas dynamic and Monge equations

18 p3207 A70-36376

High angle of attack aerodynamic characteristics of swept wing navy aircraft designs improved via leading edge modifications

[AIAA PAPER 70-904] 19 p3355 A70-37392

Aerodynamic problems due to /mixed subsonic and supersonic/ transonic flows on swept wings, nacelle lips and helicopter rotor blades

[ICAS PAPER 70-14] 23 p4132 A70-44125

High subsonic and transonic effects on pressure distributions for swept wing with oscillating control surface

23 p4274 A70-44763

SWEPTBACK WINGS

NT DELTA WINGS

NT TRAPEZOIDAL WINGS

Research program to improve performance of high lift devices on wings having small sweepback and high aspect ratio

01 p0001 A70-10047

Lift and vortex drag due to flaps on thin sweptback tapered wings in inviscid incompressible flow, obtaining spanwise loadings

06 p0967 A70-17256

Heat transfer on supersonic sweptback wing for case of laminar boundary layer with vortex distribution

07 p1187 A70-18921

Sweptback thin cantilever wing transonic flutter characteristics, investigating concentrated mass spanwise location effects

22 p4112 A70-42274

Pressure measurements on harmonically vibrating sweptback wing with two control surfaces in incompressible flow

23 p4274 A70-44768

SWIMMING

Swimming activity effect on dysbarism in rats in simulated free ascent from deep water

15 p2681 A70-31877

SWINE

Physicochemical properties of hypothalamic secretions responsible for coronary dilatation in rats, cattle and pigs, using analytical techniques

03 p0417 A70-13215

Gamma-neutron irradiation effect on miniature pig, observing incapacitation with severe convulsions and performance decrement

09 p1622 A70-23461

SWING TAIL ASSEMBLIES

Swing tail cargo aircraft fuselage section stress analysis by finite element method, discussing displacement models, deformation modes and economics

21 p3935 A70-41260

SWINGBY TECHNIQUE

Interplanetary swingby trajectory correcting maneuvers for space vehicles return to earth after planet orbiting, with emphasis on singular points

06 p1142 A70-17877

Outer solar system exploration, discussing swingby and junction missions, Jovian satellite grand tours, mission energy requirements, etc

[AIAA PAPER 70-58] 06 p1147 A70-18229

Lunar swingby trajectory analysis with atmospheric reentry, characteristics of geocentric portions of earth-moon and moon-earth transfers

10 p1940 A70-24306

Low thrust interplanetary swingby trajectories optimization, considering thrusting and coasting within sphere of influence

[AIAA PAPER 70-1041] 19 p3527 A70-38856

Jupiter swingbys and multiplanet Jupiter swingby trajectory modes for outer planet missions, comparing in terms of passage conditions

[AIAA PAPER 70-1071] 19 p3530 A70-38884

Jupiter swingby trajectory analysis for comet flyby and rendezvous missions, discussing approach velocity and payloads

[AIAA PAPER 70-1074] 19 p3530 A70-38886

Manned Mars lander launch-to-rendezvous analysis, using subsequent Venus swingby for mission velocity requirement reduction

[AIAA PAPER 70-1075] 19 p3530 A70-38887

Interplanetary solar electric spacecraft performance improvement by mission mode including earth swingby maneuver in solar orbit inclined to ecliptic

[AIAA PAPER 70-1177] 20 p3710 A70-40226

Pluto space probe using swingby technique with Jupiter, Saturn and Uranus gravitation fields for acceleration

21 p3886 A70-41073

Interplanetary mission propellant reduction by using earth-moon-sun gravity field properties, discussing swingby techniques, low energy trajectories, etc

23 p4244 A70-44607

SWIRLING

Turbulence intensity and fluctuation rates in isothermal swirling free jets, using constant temperature hot wire anemometer method

01 p0059 A70-10031

Compressible swirling inviscid nozzle flows approximate solution showing changed choking at throat, axial velocity distributions and reversing in subsonic region

01 p0003 A70-11128

Boundary layer equations describing flow field in turbulent swirling jet diffusion flame solved in von Mises plane

03 p0603 A70-12911

Turbulent boundary layer of incompressible fluid flow in axisymmetric channels with swirl at inlet, considering components interaction, velocity, circulation profiles and resistance

03 p0466 A70-13389

Viscous core of incompressible swirling flow through nozzle using momentum-integral equations

[AIAA PAPER 70-51] 06 p1038 A70-18079

Tape-generated swirl flow of single phase water investigated for heat transfer and pressure drop characteristics

[ASME PAPER 68-WA/HT-3] 08 p1600 A70-21829

Heat transfer augmentation in tubes by surface roughness and twisted tape generated swirl flow

08 p1600 A70-21830

Steady laminar gas flow on duct wall boundary layer considering external swirling flow and wall heat transfer

09 p1659 A70-22428

Injection induced swirl effect on thrust and mass flow through nozzle in spinning rocket, discussing internal and exhaust flow measurements and visualization

09 p1606 A70-23247

Swirling and meridional flow induced by steady rotation of gravitating sphere in compressible monatomic gas, considering compressibility effects and surface layer

[ASTME PAPER MR-69-714] 11 p1978 A70-26690

Swirling flow between concentric cylinders, studying helical instability modes

13 p2386 A70-28805

Residence times distribution in confined round swirling jet, considering mass conservation of hypothetical tracer substance in combustion efficiency prediction

[WSCI PAPER 70-7] 13 p2522 A70-29609

Swirling flow in unbounded space, investigating swirl intensity effect on heat transfer

15 p2828 A70-32857

Round laminar jet with swirl, reducing Navier-Stokes equations to ordinary differential equations by similarity transformations

19 p3405 A70-38349

Viscous flow field in pneumatic vortex rate sensor, discussing boundary layer parameters, velocity profiles and swirling flow theory [ASME PAPER 70-FLCS-16]

22 p4007 A70-42411

Existence theorem for boundary layer problems, including swirling flow between coaxial rotating disks

22 p4009 A70-42484

Jet engine compressor noise analysis, noting inlet swirl role

22 p4090 A70-42725

Wave drag due to swirling flow through convergent-divergent nozzle, deriving approximate solution for specified nozzle shape at various swirl ratios

23 p4179 A70-43971

Incompressible laminar swirling jet flow, obtaining similarity solution for Navier-Stokes equations

23 p4184 A70-44982

SWIRLING WAKES

U TURBULENT WAKES

SWITCHES

NT ELECTRIC RELAYS

NT ELECTRIC SWITCHES

NT FLUID SWITCHING ELEMENTS

NT PRESSURE SWITCHES

NT SWITCHING CIRCUITS

NT THERMOSTATS

Transmitting-receiving latching ferrite switch with 180 degree differential phase shift toroids for temperature stability and receiver protection in case of driver failure

03 p0458 A70-14036

Test method for inertial impact sensor switches subjected to multiple and varied shock inputs, using high energy detonators

03 p0494 A70-14128

Multiple access PCM satellite communication system with minimum interference to earth radio links, using programmable switch for improved traffic handling and frequency coordination

10 p1837 A70-24346

Electro-thermal-mechanical switches based on shape-memory effect in Ti-Ni alloys

22 p3965 A70-43330

SWITCHING

NT BEAM SWITCHING

NT MAGNETIC SWITCHING

NT MICROWAVE SWITCHING

Domestic telecommunication via satellite to reduce terrestrial switching to two levels, discussing system parameters, operation, hardware and cost estimate

06 p1006 A70-17344

Electron mobility transition in infinite system of random hard core scatterers relation to switching effect in semiconductors

08 p1549 A70-21840

Narrow Curie point switching transfer in Mn-Bi films by controlling magnetization direction within preselected areas

11 p2098 A70-26069

Demand assigned domestic satellite communications system with capability of single hierarchy switching and serving terrestrial common carriers and direct users

14 p2552 A70-31351

Band model of switching effects between conducting and high resistance states of amorphous semiconductors

18 p3297 A70-35952

Subnanosecond jitter spark gap obtained with YAG-Nd pulsed laser triggered switching at moderate repetition rates

19 p3444 A70-37666

Low jitter multiple high voltage spark gaps switching at 50 pps by Q spoiled YAG laser triggering

19 p3444 A70-37667

Optimum switching in minimum fuel, time-free impulsive planar transfer problem by primer vector concept

20 p3709 A70-40074

SWITCHING CIRCUITS

NT FLUID SWITCHING ELEMENTS

Nonlinear distortion in switching transistor mixer predicted by modifying analysis used for diode modulator and mixer circuitry

02 p0268 A70-12423

Switching-type dekatrons use in automatic control, electronic measuring and computing systems, discussing advantages

04 p0660 A70-15436

Phenomenology theory on conduction and switching behavior of amorphous semiconductor diodes

05 p0891 A70-16021

Adjustable pulse delay circuit design utilizing slow switching action of storage diodes emphasizing thermal stability

05 p0820 A70-16343

Broadband two way switch obtained by p-i-n diodes deposited on alumina substrate

05 p0821 A70-16526

Linear circuit output waveform calculation without first resolving transfer functions on complex frequency plane, applied to current switching circuit analysis

06 p1018 A70-17460

Mechanical latching crossbar switches for space division electronic switching, discussing structure, performance, reliability, etc

06 p1023 A70-18413

GaAs diode amplifiers and switching devices behavior, describing optical coupling between two GaAs lasers

07 p1241 A70-19399

Integrated switching circuits design optimization by ALGOL program, analyzing circuits transient behavior

07 p1242 A70-19752

DC to DC switching power processor design considerations for avoiding system failures

08 p1439 A70-20705

Switching and memory phenomena in semiconducting glasses, thin films and variable threshold metal-oxide-nitride-semiconductor MNOS transistor

08 p1556 A70-21304

Threshold switching and thermal filaments in thick specimen of amorphous semiconductors using IR spectrum viewer

08 p1477 A70-21540

Precision frequency analog converter using crystal oscillator and transistor switch reducing errors

09 p1653 A70-23698

DICAP system to analyze digital sequential switching circuits, studying simulation technique range and limitations of applicability

10 p1845 A70-24236

Demand assignment signaling and switching subsystems /DASSS/ design for communication satellite, examining voice channels modulation

10 p1837 A70-24348

DASSS operational parameters and performance in SPADE satellite voice communication system

10 p1837 A70-24350

Demand assignment techniques applicability to TDMA satellite communication systems, discussing operational modes and optimum mode selection

10 p1837 A70-24351

Integrated TDMA switching/transmission system implementation into existing network

10 p1837 A70-24354

Pattern recognition with time interval modulation information coding /TIMIC/, considering channel capacity of switching device, similarity with nervous system, etc

11 p2010 A70-26267

Free-running parallel inverters limitations by critical characteristics of networks, transformers and switching elements

11 p1983 A70-26628

Broadband transhorizon radio relay system transmission improvement by applying switching equipment designed for protective channel

11 p2034 A70-26822

Cassegrain antenna with parabolic mirror and switch designed for broadband transhorizon radio relays, using antenna scale model to determine parameters and electrical properties

11 p2020 A70-26823

Solid state proximity switches, sensors, logic and self test circuits for aircraft electrical applications to improve reliability and maintainability over mechanical switches

[SAE PAPER 700305]

12 p2195 A70-27449

Semiconductor power controllers for switching aircraft electrical power supplies

[SAE PAPER 700308]

12 p2195 A70-27451

Thyristor tetrode silicon controlled switches /SCS/, considering unijunction transistors and pulse generator circuits

13 p2377 A70-29115

Integrated logic circuits, considering switching properties and medium and large scale integration

13 p2372 A70-29116

Ovshinsky switching effect, considering electrothermal initiation and field dependent conductivity at elevated temperatures

14 p2626 A70-30336

Switch controlled resonant current pulse modulation for power converters, noting integration with spacecraft ion propulsion engine

14 p2535 A70-31324

Solid state subnanosecond electro-optic light switch for mode locked laser controller or light shutter

15 p2753 A70-32815

Packaging and grounding for electrical noise control in nanosecond switching circuits using transmission line design

16 p2879 A70-33960

Thyristor tetrodes application to current and voltage stabilization, frequency division and lighting control

16 p2880 A70-34099

Interference free high speed monolithic digital integrated gate, determining current swing, lead inductances and switching times

17 p3048 A70-34587

Switching circuit with Se diode, comparing I-V characteristics with Se rectifiers

17 p3054 A70-35411

Solid state switching effect on aerospace electric power conditioning equipment

[SAE PAPER 700306]

18 p3302 A70-36802

Differential time division multiplexing system, discussing errors due to imperfections of field effect transistor as multiplexer switch

19 p3388 A70-37906

Frequency dependent reversible switching characteristics of glass semiconductors, assuming current control

19 p3389 A70-38070

Flip-flops switching time reduction, using equivalent amplifier circuit with positive feedback

19 p3390 A70-38580

Dual mode optimum minimum time control of high order systems with negative roots and step displacement inputs, using simplified computer switching

21 p3801 A70-40756

Integrated directly coupled gyrator operating mode via comparison with switching elements, considering behavior under capacitance load and high pass filter application

21 p3797 A70-40793

Stress tolerant thyristor and transistor switching electronic converter for ion propulsion engine

21 p3866 A70-40901

Solid state switching effect on aerospace electric power conditioning equipment

21 p3758 A70-41210

Solid state switches for operating ion thrusters directly from high voltage solar cells, noting satellite weight saving

21 p3798 A70-41215

Modular Dc to Dc switching mode converter for space power system

21 p3758 A70-41217

Automatic and command multiple sequencer for spacecraft solar cell battery charger, providing switching logic by integrated circuits design

21 p3758 A70-41218

Book on pulse and switching circuits covering remote control, TV, computers, radar, telemetry and automation devices

21 p3798 A70-41324

Radar transmitters modulating circuits protection with microsec rapidly by power elimination, discussing electronic switches

21 p3792 A70-41987

Double tunneling electrothermal initiation of threshold electronic switching in semiconducting glasses, discussing temperature profile and current density saturation effects

21 p3864 A70-42019

One dimensional cellular logic arrays fault circumvention by bypass switching out defective cells in cascade

22 p4004 A70-43073

Lissajous figures for phase response of N-path signal filter transfer functions, using switched modulators

22 p3998 A70-43256

Solid state IF or baseband switching elements design for high capacity multichannel microwave systems

23 p4172 A70-44014

Two-bulb switchable pulsed spectral lamp with Cs and Xe for optical pumping studies

23 p4197 A70-44478

Electronic equipment automatic testing systems signal routing and switching trees and matrices design, emphasizing modular approach

23 p4173 A70-44540

Wideband wattmeter for measurement and analysis of power dissipation in semiconductor switching devices, considering occurrence of peaks, frequency dependency of average dissipation, etc

23 p4174 A70-44597

Computer hardware and software technology for complex problems, discussing switching speeds and parallel and pipeline designs

23 p4167 A70-44716

SWITCHING ELEMENTS

U SWITCHING CIRCUITS

SWITCHING FUNCTIONS

U BOOLEAN FUNCTIONS

U SWITCHING

SWITCHING THEORY

Message switching techniques in digital telecommunication networks, discussing automatic routing, operational and control facilities, etc

02 p0256 A70-11973

Parasitic transient process in automatic control system during switching to mode stabilized with respect to certain coordinates

04 p0662 A70-15433

Critical comments on teaching switching theory concerning mathematics role, logic functions, Boolean equations, etc

06 p1026 A70-18423

Optimal guaranteeing control for single switching representable in form of two different successive

stages in time, ensuring invariance with respect to motion perturbations

07 p1332 A70-18664

Linear and quadratic programming techniques for large scale continuous time optimal control problems with accurate switching times

07 p1325 A70-19268

Linear steady and unsteady systems time optimal control switching points determination by introducing parameterization to reduce number of transcendental equations

11 p2021 A70-25339

Switched self balancing comparison radiometer with coupling between channels, showing measurement errors due to coupling correctable by phase switching

11 p2018 A70-26269

State estimation in linear discrete time systems operating in Markov dependent switching environments, using Bayes theorem for filtering

13 p2381 A70-29062

Switching initiation in Ovonic, discussing temperature profile in semiconducting sandwiches as function of time and thermally forced double tunneling

14 p2626 A70-30333

Glass switching /Ovshinsky effect/, discussing various theoretical explanations

18 p3298 A70-36956

Internal Q switching deviation in gallium aluminum arsenides-GaAs single heterojunction lasers attributed to loss reduction at current pulse end

24 p4354 A70-45815

SYMBIOSIS

Hypotheses for symbiotic stars nature, emphasizing binary with late type giant and hot small star components

03 p0568 A70-13325

SYMBOLIC PROGRAMMING

Riemann tensor symbolic computation by compact method using differential forms, discussing advantages due to antisymmetry

05 p0818 A70-16681

Computerized FORTRAN equations simulation of linear and nonlinear circuits for symbolic analysis and transient response

06 p1026 A70-18424

Topological symbolic analysis of circuits defined by topological constraints, utilizing digital computers

11 p2029 A70-26330

SYMBOLS

Symbols design for machine displays based on Gestalt pattern perception theory, considering symbol learning, perceptibility, detail, boundaries, etc

10 p1827 A70-24771

Optimum symbol sequence interleavers realization taking into account storage capacity and encoding delay

11 p2014 A70-26246

Optimal spatial discretization and brightness quantization of graphical symbols for pattern recognition, considering illumination and reflection coefficient

14 p2553 A70-30423

Optimum interleavers realization procedure for reordering contiguous symbols sequence to satisfy minimum distance requirement for improving communication system performance

14 p2554 A70-31121

CRT symbol generators design for high speed computer data display as function of electro-optical and human operator constraints

16 p2850 A70-33133

SYMMETRICAL BODIES

NT AXISYMMETRIC BODIES

NT BODIES OF REVOLUTION

NT CELESTIAL SPHERE

NT CONICAL BODIES

NT CYLINDRICAL BODIES

NT ELLIPSOIDS

NT PARABOLIC BODIES

NT POINCARÉ SPHERES

NT ROTATING CYLINDERS

NT ROTATING SPHERES

NT SLENDER CONES

NT SPHERES

NT STREAMLINED BODIES

NT TORUSES

Buckling, postbuckling and limit analysis of symmetric elastic structure subjected to increasing loads

13 p2511 A70-28737

Spinning symmetric satellite attitude stability in hyperbolic orbit on flyby mission, examining by numerical integrations of equations of motion

17 p3181 A70-35753

Transport equation relation between irreducible tensorial sets, examining geometrical symmetry influence and thermomagnetic and galvanomagnetic effects

24 p4428 A70-45520

SYMMETRY

Symmetry energy of infinite nuclear matter calculated for cases of constant density and minimum saturation energy by density variation, considering finite compressibility effects

01 p0148 A70-11105

Nonequilibrium and equilibrium schemes studies of nuclear symmetry energy of finite nuclei, discussing binding energy of nuclei with neutron excess

01 p0148 A70-11106

Symmetric Boolean function detection by method using potential concept, determining alpha numbers with potential values for canonical terms

02 p0324 A70-12188

Chaplygin equation algebraic classification with respect to ring admitted by equation, extending results to include lambda function tolerating second order symmetry operators

04 p0613 A70-14412

Stress distribution in vicinity of arbitrarily shaped slender notches as function of notch symmetry using photoelastic analysis

07 p1404 A70-19240

Linear representations of symmetry groups and use in discrete automatic control systems

18 p3290 A70-36070

Symmetric functions of second rank tensors with symgonies in elastic anisotropic media

18 p3340 A70-36576

Periodic solutions of nonlinear second order differential systems containing symmetries, noting Marlin criteria

19 p3458 A70-38064

Radiative gas dynamic equations similarity representation with spherical symmetry, constructing numerical examples for strong explosions and implosions

20 p3609 A70-39657

Hermitian symmetry in Einstein unified field theory in terms of pseudotensor

24 p4380 A70-45819

SYMPATHETIC NERVOUS SYSTEM

Norepinephrine release associated with vasoconstrictor response during selective activation of arterial and venous sympathetic nerves in dog hindpaw

03 p0416 A70-13012

Vagotomy and carbon dioxide concentration effect on quiet and forced respiration rate, pleural pressure, tidal volume and lung ventilation in cats

03 p0422 A70-13694

Melatonin biosynthesis, discussing regulation by light and sympathetic nerves, daily pineal rhythms, estrous rhythms and ovarian hormones

03 p0424 A70-13809

Nervous control of unconditioned cardiovascular reflexes during ontogenesis in children, observing sympathetic and vagal tonicity

08 p1446 A70-21449

Hypothalamus stimulus effects on sympathetic nerve activity to heart, spleen, kidney and leg skeletal muscle in anesthetized cats

09 p1614 A70-22001

Mammalian pineal organ control experiments involving light and sympathetic nerve stimulation

10 p1812 A70-24396

Vegetative nervous system reactions of patients with diencephalic syndromes, investigating hypothalamo-hypophyseal-adrenal system role

13 p2352 A70-29353

Sleep intensity and stages from EEG studies concerning rapid eye movements, vegetative nervous system, heart/respiration rate, blood pressure, body temperature and stomach motility

15 p2680 A70-31743

Heart rate elicitation and blood pressure increase, considering parasympathetic and sympathetic nervous outflows adjustments of initial cardiovascular response to muscular contraction

15 p2684 A70-32535

Pressor response to epinephrine in hyperbaric atmospheres measured in cats under change of sympathetic tone

17 p3032 A70-35566

Blood flow antagonistic changes in various vascular beds following spinal cord central thermal stimulation attributed to sympathetic vasoconstrictor activity

22 p3971 A70-43405

Spinal cord thermal stimulation effects on regional sympathetic activity in rabbits and cats determined from integrated sympathetic efferents discharges

22 p3971 A70-43406

Pulmonary arterial and venous response to cooling, discussing role of sympathetic nervous system alpha receptors in hypothermia induced pulmonary constrictions in dogs

23 p4148 A70-44788

Norepinephrine synthesis inhibition effect on arousal triggering and maintenance in hibernating golden hamsters, examining sympathetic activity

23 p4148 A70-44874

Sympathetic transmission model, discussing transmitter liberation capacity under various stresses by mobilization of stores, acceleration of synthesis, etc

24 p4299 A70-45804

Sympathetic-adrenal system activity of trained organism during muscular work and emotional excitation

24 p4300 A70-45841

SYMPATHOMIMETICS

U ADRENERGICS

SYMPTOMOLOGY

Quantification of subjective estimates of well-being during onset and remission of motion sickness symptomatology in slow rotation room

08 p1448 A70-21941

Acute mountain sickness symptomatology and cognitive performance, using standardized General High Altitude Questionnaire

20 p3581 A70-40025

Student pilot case diagnosis of hysterical neurosis with syncopal and epileptiform symptoms

21 p3771 A70-41493

Sea sickness symptoms in relation to reduced minute blood volumes in human after Coriolis acceleration

23 p4149 A70-45079

SYMPTOMS

U SIGNS AND SYMPTOMS

SYNAPSES

Fatigue phenomena at spinal motor synapses, investigating role of accompanying vegetative phenomena as source of fatigue

15 p2680 A70-31740

Pathways of short latency reticulo-cortical responses to thalamic nuclei and hypothalamus destruction in cats

24 p4299 A70-45837

Bilateral oligosynaptic interaction between posterior lateral thalamic nucleus and afferent systems in visual and acoustic cortical areas in cats

24 p4300 A70-45840

Neurophysiology of membrane and synaptic mechanisms of prolonged trace changes in neuron activity concerning memory and cellular learning analogs

24 p4305 A70-46393

SYNCHROCYCLOTRONS

Gamma ray background near proton synchrotron beam degrader at NASA-LRC Space Radiation Effects Laboratory

02 p0275 A70-12268

SYNCHRONISM

NT BIT SYNCHRONIZATION

NT FREQUENCY SYNCHRONIZATION

Satellite tracking at several stations at synchronized time to obtain satellite positions, station coordinates and to improve orbital elements accuracy

02 p0254 A70-11760

Light synchronization of deep body temperature rhythms in Macaca nemestrina, investigating efficiency

03 p0416 A70-13013

Synchronization of ground stations clocks by time scale comparison with overflying aircraft [ONERA-TP-759]

03 p0487 A70-13642

Development and characteristics of inexpensive and reliable detonator for precise synchronization with high speed photographic or electronic experiments

03 p0547 A70-14110

Detonator insensitive to highest level of electrostatic voltage on human body for precise synchronization

03 p0547 A70-14111

High speed camera synchronization by frame reference pulses for strobe triggering

06 p1060 A70-17147

Clock synchronization system design and test results for PCM time division multiple access satellite communication system

06 p1011 A70-18411

Schwarzschild metric properties in synchronous reference system, using succession of Schwarzschild interval holonomic transformations as function of gravitational radius

08 p1545 A70-21406

Loran in range-range mode for computing user position based on remote clock synchronization, evaluating accuracy

09 p1719 A70-22192

Clock synchronization system using lunar radar reflections for Deep Space Network needs, discussing remote clock receiver and antenna

09 p1656 A70-23037

Tracking station clock synchronization error measurement using Deep Space Network Mark I ranging system, discussing system theory, design, operation, economy and versatility

09 p1656 A70-23038

Velocity synchronized Fourier transform hologram camera system for recording hypervelocity particles

09 p1688 A70-23775

Carrier recovery circuits synchronization for PSK demodulators used in TDMA satellite communication

10 p1835 A70-24338

Equipment design for burst synchronization control in TDMA experiment system

10 p1836 A70-24339

Synchronous harmonics generation of sinusoidal signal with given frequency for vibration analysis of linear and nonlinear structures

10 p1860 A70-24550

Self-synchronization of forced frictional mechanical vibrators assuming simple harmonic combination

11 p2139 A70-26417

Ultrasonic effects on synchronization of ruby laser radiation, investigating emission pulse structure and peak sequence 12 p2245 A70-27297

Heterochronism of coordinated cophasal flexor and extensor movements during acrobatic leap in human subjects 12 p2168 A70-27344

Clock synchronization in general relativity theory, investigating temporal and spatial relations in four dimensional continuum using simultaneous hypersurface 12 p2272 A70-27357

TDMA applicability to military satellites, describing synchronization process 12 p2187 A70-27916

Carrier synchronization system for PSK signals, using direct regenerative repeater and phase locked loop/JDR-PLL/ 15 p2697 A70-31826

Beat and synchronization modes of opposed waves in rotating gas ring laser, examining frequency response asymptotic behavior 17 p3108 A70-35683

Time-synchronized approach control, combining aircraft precision navigation and guidance with ATC equipment 19 p3466 A70-38237

Prototype synchronizing valves for maintaining identical flow velocities of two hydraulic actuating elements, noting unbalanced hydrodynamic forces and orifices asymmetry effects 20 p3564 A70-39717

Ruby and Nd glass solid state lasers modes partial self synchronization investigated by spectral time resolution method 22 p4051 A70-43463

Clock synchronization in general relativity theory, investigating temporal and spatial relations in four dimensional continuum using simultaneous hypersurface 22 p4075 A70-43598

Close binary star components axial rotation, considering synchronism, angular velocity and mass exchange 23 p4250 A70-44814

SYNCHRONIZATION

U SYNCHRONISM

SYNCHRONIZED OSCILLATORS

N-GaAs pulsed Gunn effect oscillators for decimeter band, discussing synchronization by external sinusoidal current 03 p0499 A70-13204

SHF avalanche transit time oscillator with FM noise reduction by injection phase locking 08 p1462 A70-21594

Steady state analysis of harmonic oscillations in HF synchronized transistor autooscillators, considering transistor inertial properties 09 p1649 A70-23341

Circuitry for phase modulated synchronized electronic oscillators for measuring minor reactance changes during remote sensing 11 p2052 A70-26373

Unrestrained oscillator under action of external synchronous signal, deriving differential synchronization equation 17 p3051 A70-34614

Synchronous oscillators of radio astronomical interferometer, discussing dephasing and servocoupling 17 p3090 A70-35415

Nonlinear differential solutions for free isochronous oscillations of conservative one degree of freedom oscillators 18 p3283 A70-36386

Optimum stabilized variable frequency multiple input phase locked oscillator in mutually synchronized systems 19 p3389 A70-37969

Mutual synchronization of oscillators at multiple frequencies, analyzing effect of tuning on frequency and phase 20 p3597 A70-39252

Digital frequency and phase flip-flop comparator for slave oscillators fine control by master frequency 22 p3996 A70-42819

SYNCHRONIZERS

Synchronizing and desynchronizing systems for cerebral electrical activity, noting roles in sleep and wakefulness mechanisms 03 p0417 A70-13073

Transistorized differed synchronizer for delaying photoflash initiation in scientific photography 12 p2228 A70-26879

Digital transition tracking symbol synchronizer improving SNR without lowering loop bandwidth [JPL-TR-32-1488] 13 p2367 A70-29591

Hydraulic synchronizers for motors and actuators speed equalization, describing operation and technical specifications 21 p3756 A70-40800

SYNCHRONOUS COMMUNICATION SATELLITES

U SYNCOM SATELLITES

SYNCHRONOUS COMMUNICATIONS SATELLITE PROJ

U.S. and European space program costs and resources with particular reference to telecommunication satellites 22 p4126 A70-43247

SYNCHRONOUS DETECTORS

U CORRELATORS

SYNCHRONOUS MOTORS

Combined gyromotors optimal starting and operating conditions, considering size and weight characteristics 09 p1680 A70-23146

Electromechanical start-up time, inertia and synchronous electromagnetic moment of wave-type electric servomotor calculated by energy method 10 p1809 A70-25202

Standard units and assembling of electrical driving mechanism for telescope, using audio reference oscillator, electronic power amplifier and synchronous motor 18 p3259 A70-36609

Start-up characteristics for three-phase synchronous reactive motors with various starting unit designs 24 p4293 A70-45471

SYNCHRONOUS SATELLITES

NT AEROS SATELLITE

NT EARLY BIRD SATELLITES

NT SYNCOM SATELLITES

Delta boosted electrically raised high power synchronous satellite for communication tasks [AIAA PAPER 69-1104] 01 p0194 A70-10617

Space programs to monitor earth resources from synchronous orbit of 19,400 nautical miles, discussing geostationary systems characteristics related to optics and telemetry 01 p0093 A70-11280

Satellite mounted mm wave parabolic dish antenna for tracking communication satellite in synchronous orbit 02 p0392 A70-11933

Solar phenomena effect on VHF communications between synchronous satellite relay and earth ground stations 02 p0259 A70-12566

Canary Bird synchronous satellite radio signal transmissions scintillations from recordings, noting diurnal scintillation pattern 02 p0260 A70-12573

Synchronous satellite attitude measurement during early flight and operating conditions, describing PAS satellite attitude sensor configurations 03 p0581 A70-13844

Geostationary satellite payload-optimal injection trajectory from nonequatorial firing range, describing dog-legging maneuvers 03 p0573 A70-13845

Orbit determination program for launching and stationkeeping of 24 hr geostationary satellites, using azimuth and elevation of single autotrack antenna 03 p0578 A70-14339

Electrostatic charged particle acceleration and ion thruster function in geostationary satellite stationkeeping and attitude control, orbital transfer and drag compensation [ONERA-TP-764] 04 p0735 A70-14934

German developments in electric propulsion and energy supply systems for commercial satellites in geostationary orbits [DGLR-69-20] 04 p0735 A70-15169

Hybrid system for allocating domestic synchronous communication satellites in concentric circles within inclined elliptical synchronous orbits 05 p0906 A70-15801

Multiple access channel control system operating in variable destination multiple access mode for application in PCM-TDMA satellite communication system 06 p1011 A70-18412

Microwave radio refraction analysis for controlling interference between radio relay antenna and geostationary satellites 07 p1235 A70-19363

Stationary satellite perturbed motion calculations, assuming small initial orbital eccentricity and inclination and revolution period close to that of earth 07 p1386 A70-19485

Omega Position Location Experiment with synchronous satellite /ATS-3/ as radio relay for merchant shipping, air traffic control and moving vehicle location and communication 09 p1720 A70-22193

Ammonia micropropulsion for geostationary satellites stabilization, discussing principle and working mode of thrusters 09 p1743 A70-22660

Navigation satellite system with 10-meter accuracy, continuous coverage, rapid position determination, simultaneous service and interference immunity achieved by synchronous satellites 09 p1723 A70-23042

Hyperbolic position finding with synchronous satellites having frequency conversion unit for operations at higher frequency satellite signals 09 p1724 A70-23044

Digital record message communication satellite network system involving synchronous satellites and small earth terminals 10 p1834 A70-24327

Synchronous satellite communication system clock synchronization loop design taking into account delay time 10 p1835 A70-24335

Geostationary orbit capacity based on multichannel telephony, comparing digital and analog modulation techniques 10 p1836 A70-24343

Optimal longitude rendezvous for geostationary satellite by using inertially fixed orientation thrust for performing final positioning [ONERA-TP-801] 10 p1941 A70-25451

Orbital stability of geostationary vehicle at arbitrary latitude, considering nonlinear equations and deducing stability conditions by Liapunov method 10 p1950 A70-24783

Canadian geostationary satellite communication system design and performance, discussing transponder with six RF channels [AIAA PAPER 70-429] 11 p1996 A70-25402

Geostationary satellite communication bandwidth increase by reusing same frequency band in multiple independent earthward beams, discussing modulation and interference noise allocation effects [AIAA PAPER 70-442] 11 p1996 A70-25405

Radiation environmental model of synchronous communication satellite solar cell degradation by particle fluxes [AIAA PAPER 70-481] 11 p2103 A70-25411

Communication satellites geostationary orbit sharing problem, considering system design and utilization criteria [AIAA PAPER 70-441] 11 p1998 A70-25419

Attitude stabilization of synchronous communications satellites employing multiple narrow beam antennas [AIAA PAPER 70-457] 11 p2119 A70-25422

Solar cell degradation by proton damage in synchronous orbit studied on LES-6 satellite [AIAA PAPER 70-600] 11 p2119 A70-25430

Three axis attitude control of earth oriented non-spinning synchronous communications satellite, using gimbal-mounted momentum wheel and pulsed plasma thrusters [AIAA PAPER 70-456] 11 p2119 A70-25431

Multiple feed waveguide lens in variable coverage communications antenna for geostationary LES-7 satellite [AIAA PAPER 70-423] 11 p2016 A70-25461

Satellite stationkeeping by ground command, self contained or combined methods compared for networks of synchronous satellites [AIAA PAPER 70-479] 11 p2121 A70-25463

Instructional communication system for U.S. using synchronous satellites over 15 regions [AIAA PAPER 70-450] 11 p2000 A70-25465

Horizon sensor design with null operating capabilities for synchronous orbit 3-axis stabilized communication satellites, discussing operation and testing [AIAA PAPER 70-476] 11 p2121 A70-25484

Ammonia micropropulsion operation modes and performance for stabilizing synchronous communication satellite, noting advantages over chemical and ion propulsions 11 p2122 A70-25817

Roll and pitch attitude control for long range stationkeeping mission of synchronous flywheel stabilized communication satellite, discussing constraints on on-board equipment and technology 11 p2126 A70-26279

Quasi-sinusoidal fluctuations of magnetic field during geomagnetic storms measured by ATS 1 in synchronous equatorial orbit 12 p2223 A70-27192

Air traffic control surveillance and data system using synchronous satellites in inclined elliptical orbits for communications and aircraft position determination 12 p2268 A70-27644

Position location and aircraft communication equipment concept and Experimental PLACE System providing ATC two-way voice and digital data communications via geostationary satellites 12 p2269 A70-27921

Navigation systems using 24-hour orbit satellites, discussing system concept options for U.S., Western Hemisphere and global coverage 12 p2270 A70-27924

Atmospheric refractivity role in range errors from ground station to stationary satellite and in range rate measurement 12 p2189 A70-28058

Hard wired modular multipurpose global navigation system using cluster noncoplanar synchronous satellites 13 p2446 A70-28385

Synchronous satellite attitude acquisition and keeping, proposing roll and pitch control law for simulation 13 p2500 A70-28409

Range of ground station to stationary satellite and range rate measurement errors induced by atmospheric refractive index fluctuation

13 p2365 A70-29095

Space traffic control, discussing special problems of synchronous orbiting communications satellites

13 p2449 A70-29268

Synchronous navigation satellite system for ships and aircraft applicable to earth orbital and lunar operations

14 p2614 A70-30463

System design for IR imaging radiometer from synchronous altitude satellite, considering spacecraft dynamics, detectors and cooling

14 p2586 A70-30974

Geostationary tracking and data relay satellites /tdrs/, discussing system design and advantages

14 p2615 A70-31182

Synchronous satellite orbits determination using mathematical model for simulating gravitational perturbations induced by terrestrial globe and foreign bodies

14 p2651 A70-31279

Europa 3 configurations for launching payloads into geostationary orbit using various rocket stage combinations

15 p2789 A70-32254

Microthrusters for geostationary satellites attitude and position control

15 p2791 A70-32279

Counterrotating antenna onboard Italian satellite in synchronous equatorial orbit for microwave propagation experiment

15 p2709 A70-32287

Stationary satellite perturbed motion calculations, assuming small initial orbital eccentricity and inclination and revolution period close to that of earth

15 p2805 A70-32730

Ionospheric electron content measurement during solar eclipse of 7 March 1970, using VHF radio waves from geostationary satellites

16 p2897 A70-33830

Two stage yo-yo with nutation damper for despinning ATS synchronous satellites, describing mechanical and thermal design, lubrication, assembly, testing, etc

16 p2985 A70-34115

Torsion wire libration damper for satellite gravity-gradient stabilization at near synchronous altitudes

16 p2985 A70-34134

Controlled leakage sealing of hydrodynamic bearing lubrication systems for space vehicles in synchronous orbit

16 p2923 A70-34158

Conical passive radiation coolers for quantum IR detectors on equatorial synchronous earth satellites, determining temperature excursions

16 p2915 A70-34314

Orbit determination accuracy in synchronous satellite tracking analysis, using weighted least squares method

19 p3529 A70-38881

Earth continental drift and polar wandering measurements by laser ranging to two synchronous satellites

19 p3529 A70-38882

RF plasma thrusters for synchronous satellites, estimating weights and efficiencies of various types

20 p3689 A70-40124

SERT 2 solar array power system in sun synchronous orbit, considering power conditioning and deployment technique

20 p3567 A70-40202

One millipound cesium ion thruster for synchronous ATS-F satellite, describing power conditioning and control logic subsystems

20 p3690 A70-40205

Spinning satellites stationkeeping at synchronous altitude, using solid propellant pulsed plasma microthrusters

20 p3690 A70-40206

Communication satellites low thrust transfer to synchronous orbit by two-stage operation using hydrogen resistojets and Hg ion motors

20 p3691 A70-40227

Secondary propulsion subsystem earth synchronous orbital mission requirements, discussing thrust vector alignment and control, colloidal propellants and pulsing

[ASME PAPER 70-AV/SPT-31]

Low latitude observations of spread F echoes and stationary satellite scintillations, correlating with ionospheric disturbances and geomagnetic activity

21 p3818 A70-41097

Dioscures project for ATC over Atlantic Ocean, describing distance measurement by simultaneous use of two geostationary satellites

21 p3848 A70-41258

Synchronous satellites VHF signal fading attributed to high latitude scintillations, noting intensity at night and during magnetic storms

21 p3790 A70-41362

Synchronous satellites characteristics and applications to radio connection, light signals, positioning, telecommunications, manned space stations and space shuttles

22 p4109 A70-42467

Satellite technology application to aeronautics, predicting synchronous satellites communication for transoceanic and overland ATC

22 p4111 A70-43512

VHF geostationary satellite ranging and range correction systems, calculating second-order ionospheric delay effects on position error

22 p4068 A70-43590

Structure and systems design of large gravity gradient stabilized orbiting tethered satellites structure for radio astronomy

23 p4259 A70-44603

Tracking and data relay satellite system in low altitude synchronous orbit

[AIAA PAPER 70-1305]

24 p4311 A70-45085

Error analysis of satellite orbits obtained by synchronous satellites range and range rate measurements

24 p4407 A70-45539

SYNCHROTRON NOISE

U ELECTROMAGNETIC NOISE

U SYNCHROTRON RADIATION

SYNCHROTRON RADIATION

Pulsar synchrotron emission model, discussing elliptic polarization, pulse shape, duration and negative absorption /wave amplification/

01 p0183 A70-10897

Neutron star X synchrotron radiation from gas accretion producing strong magnetic field with high electron temperature

03 p0557 A70-13220

Circularly polarized synchrotron radiation from distribution of electrically charged particle in magnetic dipole calculated for estimating Jupiter magnetic field

04 p0746 A70-14511

Intensity, spectrum and polarization of gyrosynchrotron radiation from magnetoactive plasma electrons distribution

04 p0749 A70-14594

Particle flux and dose rates in Jupiter Van Allen belts based on assumed synchrotron radiation from trapped electrons in dipole magnetic field

[AIAA PAPER 69-18]

04 p0742 A70-15543

Galactic synchrotron emission and diffuse X ray background, noting correspondence between spectral indices of radio and X ray emissions in polar directions

05 p0913 A70-16472

Secular variations in small quasar components, discussing compatibility with theory of expanding synchrotron sources

05 p0913 A70-16474

Particle acceleration during 1966-1967 radio burst of 3C 273, indicating breaking down of model of expanding source emitting synchrotron radiation

05 p0918 A70-16927

Synchrotron radiation rate from deexcitation of electrons in magnetic orbits of low quantum numbers, stressing electrons radiation in intense magnetic fields

06 p1108 A70-17183

Coherent synchrotron emission in Crab Nebula associated with electron gyromotion, discussing models for high energy particle acceleration

07 p1375 A70-18848

Synchrotron radiation negative reabsorption possibility for relativistic electrons dipped into and in absence of unrelativistic plasma

07 p1348 A70-19413

Compton scattering of synchrotron radiation from parent electrons in pulsars, calculating Compton-synchrotron radiation from NP 0532 leads to lower limit for magnetic field

07 p1369 A70-20221

Contraction and expansion in solar region producing synchrotron emission of relativistic electrons to explain solar burst behavior

08 p1560 A70-20841

Neutron star X synchrotron radiation from gas accretion producing strong magnetic field with high electron temperature

08 p1563 A70-21653

Relativistic electrons synchrotron radiation by calculating magnetoactive plasma permittivity tensor, determining normal waves polarization characteristics

08 p1554 A70-21812

Synchrotron emission of relativistic particle in magnetic field with radiative reaction force comparable to Lorentz force, emphasizing pulsar cosmic ray electron acceleration

09 p1731 A70-22273

Pulsar NP 0532 synchrotron emission reinterpretation related to relativistic particles injection into Crab Nebula

09 p1756 A70-22516

Gyrosynchrotron emission from nonthermal electrons trapped in magnetic dipole field to interpret center-to-limb spectrum and polarization variations of microwave impulsive bursts

12 p2294 A70-27709

Extragalactic objects polarization due to synchrotron radiation superimposed on stellar radiation, discussing Seyfert galaxies nuclei

12 p2307 A70-27869

Pulsar radiation emission by electrons and protons in close orbit taking into account density, energy and correlation in plasma

14 p2638 A70-30617

Synchrotron model involving electron trapping in dipolar magnetic field for Jupiter decimetric radiation

14 p2649 A70-31089

Gyrosynchrotron from accelerated electron, discussing effects of cold and collisionless magnetoplasma on far field and frequency spectra

15 p2728 A70-31989

Local system interstellar medium thermal electron distribution, synchrotron radiation emissivity, cosmic ray electron flux and spectrum

17 p3152 A70-35583

Crab Nebula pulsar NP 0532 optical and X ray synchrotron radiation, explaining ratio of pulsar energy flux to nebula

17 p3152 A70-35747

Pulsar radio pulses structure and emission source theory based on synchrotron radiation and relativistic effect calculations

18 p3321 A70-37119

Synchrotron radiation emissivity function contained in dispersion equation for plane wave propagation in magnetoactive plasma

19 p3480 A70-38017

Cosmic ray electron and proton interaction discussing hydromagnetic waves, synchrotron radiation, magnetic field effects and wave propagation

20 p3695 A70-39012

Virgo XR-1 rocket observations, discussing X rays due to synchrotron emission of relativistic electrons

21 p3872 A70-40658

Sco X-1 star high energy radiation production, discussing relativistic electron synchrotron emission and magnetic fluctuations spectrum

21 p3878 A70-40709

Jupiter RF spectrum in 80 to 10,000 MHz range for dipolar model, noting independent synchrotron component

21 p3891 A70-41185

Extreme UV spectroscopy with synchrotron radiation storage ring light sources in 40-400 Å range, including thin film photoabsorption measurements

21 p3826 A70-41451

Alfven waves synchrotron emission in incompressible medium, investigating generation by rotating DC current carrying circuit

21 p3861 A70-42227

Plasma inhomogeneity and drift effects on synchrotron radiation from relativistic charged particles in magnetoplasma

22 p4082 A70-43254

Synchrotron source spectra natural frequency cut-off in absence of self absorption and electron energy cut-offs, discussing pulsar NP 0532

24 p4410 A70-45774

Excess galactic X rays, discussing synchrotron emission of high energy cosmic ray electrons

24 p4398 A70-46161

SYNCHROTRONS

Synchrotron model limitation for nonthermal spectra, demonstrating restriction to small pitch angles and strong fields

18 p3318 A70-37024

SYNCOM SATELLITES

NT EARLY BIRD SATELLITES

Unidirectional heat pipe system design to control temperature of high power traveling wave tubes in synchronous orbit communication satellite, dissipating waste heat

11 p2127 A70-26362

Syncom and Early Bird systems development, launch procedure and operation, discussing common components

14 p2654 A70-31144

SYNCOPE

NT BLACKOUT PREVENTION

Syncope occurrence among flight crews

01 p0033 A70-10371

Syncope proneness correlation with episodes of impaired consciousness in pilots during flight using physiological tests

07 p1223 A70-19944

Aeromedical significance and pathophysiological mechanisms of clinical entities mimicking vasovagal syncope

08 p1454 A70-21946

Cardio-respiratory functions preceding syncope induced by combined lower body negative pressure and head-up tilt

11 p1988 A70-26510

Respiratory syncope with cardiac ineffectiveness and numerous complications during and after flight at high altitude clinically observed for causes

12 p2171 A70-28040

Student pilot case diagnosis of hysterical neurosis with syncope and epileptiform symptoms

21 p3771 A70-41493

SYNDROMES

U SIGNS AND SYMPTOMS
SYNOPTIC MEASUREMENT

Synoptic ionospheric observations during IQSY, discussing electron density profiles, absorption, drifts, etc

01 p0073 A70-10584
Ground observations synoptic distribution importance in studying magnetosphere, emphasizing polar caps

03 p0475 A70-13849
Dynamics dominant on different scales in atmosphere by spectral analysis, showing marked gap under most synoptic conditions

09 p1717 A70-22376
Asian zone solar daily and storm time ionospheric disturbance variations synoptic study during IGY-IGC period

10 p1872 A70-23822
D region synoptic ionization changes investigated by radio waves partial reflection from lower ionosphere, relating wave amplitudes to height

12 p2224 A70-27732
Oceanographic potential of spacecraft, discussing synoptic scanning, International Decade of Ocean Exploration, etc

12 p2225 A70-27746
Venus photographs analysis during synoptic periods, noting inconclusive results on cloud layer and planetary surface structures

12 p2311 A70-28311
Geopotential fields seasonal statistical analysis over first natural synoptic region, using expansion into orthogonal eigenfunctions

13 p2446 A70-29674
Proton Flare Project 1969, reporting synoptic observations of sun and solar terrestrial effects

15 p2794 A70-32291
Global geomagnetic field fluctuations of internal and external origins, analyzing HF spectrum based on monthly mean plots

23 p4187 A70-43861
Laser light pulse reflection by atmospheric boundary layer calculated on computer by Monte Carlo method, comparing results with full scale measurement

SYNOPTIC METEOROLOGY

Clear air turbulence and mesoscale structure subsynoptic air motion experiments for numerical weather prediction

04 p0714 A70-14394
Primitive and balance hydrodynamics equations of meteorological fields noting computational viscosity

06 p1097 A70-17826
Nonlinear planetary long range weather forecasting problems analytical solutions, describing quasi-geostrophic atmospheric motions model

07 p1328 A70-18649
Incipient tropical storm location and synoptic weather pattern analysis from environmental satellite system data utilization

07 p1329 A70-19196
Statistical testing role in synoptic meteorological analysis, discussing pressure and temperature patterns, front identification, computer applications, etc

07 p1329 A70-19574
Meteorological Rocket Network for limited synoptic inspection of stratospheric circulation

07 p1273 A70-20252
Skua meteorological rocket system for synoptic stratospheric sounding, describing system, launch preparation, firing and flight characteristics

07 p1395 A70-20253
PWN-8B meteorological rocket system for synoptic investigation of stratospheric circulation, describing sensor system deployment for descent measurements of wind and temperature

07 p1395 A70-20255
Rocket-borne radar chaff wind sensor synoptic application above 65 km, describing low fall velocity

07 p1237 A70-20258
Synoptic changes associated with midwinter 1967-1968 major stratospheric warming, including pressure and wind distributions and temperature maps

07 p1275 A70-20277
Meteorological guns for synoptic sounding of stratospheric circulation, discussing system characteristics and operations

07 p1250 A70-20280
Combined statistical synoptic methods for mesometeorological forecasts

10 p1913 A70-24947
Maximum wind velocity regions in tropospheric jet streams under synoptic conditions concerning troughs, ridge sections and cyclonic-anticyclonic curvatures

11 p2075 A70-25919
Automated Weather Network and Environmental Survey Satellite /ESSA 9/ global weather sensing systems

11 p2033 A70-26505

Synoptic processes and meteorological fields computerized automatic classification for weather forecasting applications

12 p2265 A70-28332
CAT relationship to cyclogenesis and anticyclogenesis, considering synoptic situation and Jacobian values for forecasts

14 p2609 A70-30604
Synoptic meteorological prediction by statistical and dynamical theory based on statistical mechanics

17 p1331 A70-35926
Global scale atmospheric circulation processes numerical simulation leading to long range weather forecasts for Northern Hemisphere

19 p3462 A70-38753
Soviet papers on macroprocesses in seasonal weather forecasts, discussing tropospheric and stratospheric temperature and circulation, geomagnetic field, etc

20 p3663 A70-39270
H sub 500 field features during natural synoptic seasons in Northern Hemisphere, including circulation characteristics

20 p3663 A70-39271
Synoptic processes in troposphere and stratosphere with large air temperature anomalies during early summer in U.S.S.R.

20 p3663 A70-39272
Troposphere and lower stratosphere circulation during natural synoptic autumn seasons in Northern Hemisphere, noting temperature role

20 p3663 A70-39273
F region synoptic electron densities and electron and ion temperatures from Thomson scatter radar data

21 p3816 A70-41065
Synoptic surface and upper air analysis and APT mosaics of meridional circulation over Mediterranean by remote satellite images

21 p3846 A70-41399
January climatology simulation experiment based on two layer version of global circulation model, comparing computed and observed results

21 p3847 A70-42120
Global solar radiation climatology of earth including direct and diffusive radiation

22 p4013 A70-42600
Temperature and height data for synoptic stratospheric evaluation, using Nimbus 3 satellite IR spectrometer

22 p4064 A70-42618
Global thunderstorm activity location found by measuring differences between time of arrival of electromagnetic energy at three satellites

22 p4016 A70-42779

SYNTAX

NT SENTENCES
NT WORDS (LANGUAGE)

SYNTHESIS

Optimum systems synthesis in computation of programmed movements including dynamical programming methods, control under uncertainty and division problem

07 p1325 A70-19270
Optimal synthesis of linear steady multidimensional systems with common output ensuring minimum rms error in reproducing control action

08 p1480 A70-21497
Temperature, solvent, catalyst and formaldehyde concentration effects on monosaccharide synthesis from formaldehyde condensation

13 p2362 A70-29327
Optimum synthesis of complex signals, using autocorrelation function side peak level effect on false alarm probability

13 p2369 A70-29733
Pulsed signal synthesis from three dimensional function of indeterminacy, incorporating source distance, velocity and acceleration

22 p3988 A70-42562
Stereochemical course of sterically controlled syntheses of dipeptides, using optically active amino acids

22 p3983 A70-43095

SYNTHESIZERS

U CHEMICAL REACTORS

SYNTHETIC ARRAYS

Target velocity effects on resolution of synthetic aperture side-looking radar

02 p0268 A70-12582
Book on synthetic aperture radar imaging systems theory and design covering SNR, optical data processing, phase and motion errors, ambiguity function, etc

13 p2368 A70-29603
Synthetic array radar flying past flat plate, analyzing image relationship to flight path

14 p2552 A70-31193
Signal processing antennas, discussing synthetic and multiplicative arrays for coherent radar airborne mapping

17 p3052 A70-35078

SYNTHETIC FIBERS

NT DACRON (TRADEMARK)
NT GLASS FIBERS

NT RAYON

Boron and other high performance reinforcements made by vapor plating process, discussing boron filament atomic structure and morphology

05 p0873 A70-16609
Graphite yarn, cloth and fiber composites physical properties tabulated, discussing multiply laminates for graphite-epoxy composites

05 p0873 A70-16610
Carbon fabrics and filaments, resin carbonizing and carbon-carbon composites, discussing processing parameters, initial carbonizing resin binder and reinforcement effects on laminate properties

07 p1316 A70-18932
Microphotometric spectral reflectivity correlation to static Young moduli of carbon and graphite yarn filaments as optical testing method

08 p1497 A70-21350
Lattice resolution of layer planes in polyacrylonitrile based carbon fibers ground and dispersed by ultrasonic irradiation

14 p2598 A70-30793
High strength and modulus continuous graphite fibers from pitch, describing production process from asphalt and specifications

21 p3842 A70-40732

SYNTHETIC RESINS

NT ACRYLIC RESINS
NT EPOXY RESINS
NT PHENOLIC RESINS
NT POLYAMIDE RESINS
NT POLYESTER RESINS
NT POLYETHER RESINS
NT POLYMETHYL METHACRYLATE
NT THERMOPLASTIC RESINS
NT THERMOSETTING RESINS

Combustion rates and temperature distribution in condensed and gaseous phases of ammonium perchlorate sandwich with synthetic resin middle layer

09 p1741 A70-22105
Synthetic resin adhesives for aircraft components fabrication

20 p3657 A70-40532

SYNTHETIC RUBBERS

NT CHLOROPRENE RESINS
NT ELASTOMERS

Vibrating system response to damping insert introduced between two distinct coordinates, discussing Butyl rubber and vibration amplitude reduction

01 p0199 A70-10265
Polyurethane rubber time- and temperature- dependent visco- and photoviscoelastic coefficients using two dimensional strain and stress wave propagation photoviscoelastic analysis

03 p0599 A70-14243
Viscoelastic behavior of styrene-butadiene rubber under finite uniaxial and equal biaxial deformations for nonisothermal case

05 p0929 A70-16068
Viscoelastic materials fracture strength as function of cut length, defect size and temperature

17 p3146 A70-35221

SYSTEM EFFECTIVENESS

Complex automatic systems effectiveness synthesis based on invariance principles

20 p3603 A70-39835
Aircraft stretch efficiency factor as function of productivity and payload growth [SAWE PAPER 838]

20 p3563 A70-40369

SYSTEM FAILURES

Comparator design for triplicated attitude indicator instrumentation system in aircraft to achieve reliability, discussing system failure characteristics

02 p0224 A70-11844
Project management systems failure analysis, discussing cost, products quality and project objectives

03 p0610 A70-13963
Automatic control algorithms for subsystem malfunction identification in multisubsystem plants, analyzing conditions for diagnostic tests existence

04 p0661 A70-14554
Silicon solar cell panels, studying roles of solder, interconnector metals and substrate materials in failures under thermal cycling

04 p0628 A70-15333
Pilot response to stability augmentation system failures and design implications

[AIAA PAPER 68-819] 04 p0624 A70-15379
Monograph on models of failure covering mathematical system reliability determination and relationship to physical nature of failures

06 p1171 A70-18394
Amplifier design effects on device reliability, considering sudden and gradual system failures

07 p1246 A70-19635
Onboard automatic test equipment design, evaluating failure detection and reporting ability

08 p1470 A70-20667
DC to DC switching power processor design considerations for avoiding system failures

08 p1439 A70-20705
Thin oxide film resistors reliability test based on measurement of resistance nonlinearity by third harmonic voltage

09 p1689 A70-22005

Fault finding strategy optimization in systems with single defective element

09 p1693 A70-22974

Soviet book on control and search for defects in complex systems, presenting statistical optimization methods, programmings for assumed Markov processes, etc

09 p1693 A70-23540

Tolerance limits for equipment periodic field checkout, considering performance failure effects on system accuracy, costs and availability

[AIAA PAPER 70-394] 10 p1896 A70-24911

Time-optimal testing sequence for system failure detection, considering maintenance and reliability data

10 p1896 A70-25048

Interplanetary space systems, analyzing failure factors to assure reliability

11 p2112 A70-26051

Redundancy optimization based on partial failure modes effect on system reliability to reduce cost

12 p2243 A70-28010

Random reversible failures effect on linear automatic control systems precision treated as randomly varying structure, proposing statistical characteristics calculation

13 p2382 A70-29279

Automatic Failure Rate Assessment Machine (FRAM) for subjecting guided weapons electronic modules to cyclic stresses inducing failure of inherent weakness

13 p2379 A70-29686

Autodiagnosis of logic module failure in complex electronic systems, examining fault simulation methods and Safe system program and apparatus

14 p2561 A70-30669

Approximating hazard rate function parameters estimation from failure data, using computer program

14 p2592 A70-31113

Availability assurance using computerized spare allocation model for optimal selection of sufficient spares to achieve required protection against system failures

14 p2592 A70-31114

Decreasing failure rate (DFR) with time in electronic systems operating in avionics applications

15 p2712 A70-32646

Computer system maintainability demonstration test in accordance with MIL-STD-471, discussing techniques for failure indication and repair crew qualifications and training

15 p2706 A70-32657

System failure rate estimation as function of age using incomplete field reliability data

15 p2748 A70-32660

Mathematical reliability model for quasi-redundant electronic system with two failure modes for each component

15 p2769 A70-32827

Electrical, electronic, electromechanical, pneumatic and hydraulic subsystems failure pattern determination, discussing sensing techniques in signature analysis

[ASME PAPER 70-DE-34] 16 p2917 A70-33505

Reliability-cost model to determine optimum failure rate for minimization of systems total life cycle cost

[ASME PAPER 70-DE-43] 16 p3004 A70-33507

Hazard plotting methods for analyzing service life data with different failure modes

16 p2921 A70-34024

Systems subject to failure and repair cycles, describing performance and reliability by stochastic processes in terms of excess time

17 p3099 A70-34580

Large complex system with standby components, approximating reliability by simple model substitution

17 p3099 A70-34582

Combined environments testing to reveal potential flight failure modes

17 p3059 A70-35165

Optimal filters design predicting electronic systems parameters, preventing equipment failure due to wear and aging

17 p3055 A70-35744

ATC lag due to air transport growth and associated aircraft design and operations advances, discussing automation, noise abatement effects, etc

17 p3135 A70-35857

Soviet book on space electronics fundamentals covering equipment problems, energy requirements, communication, features, radio remote control and correction, radio astronomy, etc

19 p3375 A70-37400

System with N independently failing subsystems minimum cost solution mathematical model based on opportunistic preventive replacement policy

19 p3437 A70-38400

Redundant systems reliability under wearout conditions for active and standby units, including failure rates of sensing and switching devices

19 p3438 A70-38597

Reliability analysis based on Bayesian subjective probability implemented by stored time sharing computer programs for engineering computations and operation analyses

19 p3441 A70-38818

Optimal burn-in testing of repairable equipment, improving reliability by decreasing failure rate with age under operating conditions

23 p4199 A70-43923

Aircraft longitudinal motion during takeoff and landing due to loss of lift after boundary layer control system failure

24 p4372 A70-45448

Stochastic behavior of failed standby redundant electronic equipment with imperfect switching and opportunistic repairs

24 p4319 A70-46016

SYSTEM LIFE

U RELIABILITY

SYSTEMIZATION

U SYSTEMS ENGINEERING

SYSTEMS ANALYSIS

Missile miss distance evaluation model with emphasis on statistical nature, noting application to systems analysis

01 p0193 A70-10118

Data analysis of inertial systems for commercial aircraft overseas operations, classifying systems error propagation as linear time drift or Foucault period oscillation

01 p0137 A70-10314

Book on dynamics of complex systems represented by control and human operators and animals behavioral activities models

01 p0034 A70-10501

Manned space station system analysis for identifying control subsystem functions/weight penalties/and system characteristics to minimize penalties

[AIAA PAPER 69-1078] 01 p0194 A70-10628

Tracking systems synthesis and performance analysis based on continuous Markov processes theory, particularly Fokker-Planck equation

01 p0043 A70-10776

Nonlinear vibrations in mechanical systems of elastic components having equivalent circuits represented by finite number of discrete masses interconnected by weightless infinite rod

01 p0143 A70-11027

System analysis and synthesis processes applied to educational requirements identification and programs implementation, emphasizing use of functional model with man machine interface

01 p0221 A70-11283

Availability model for system with exponential reliability function and constant repair time, determining start-up costs, cost-optimal mean up and down time, etc

01 p0221 A70-11382

Final motions of Hamiltonian conservative systems, analyzing Liouville type, homogeneous and similar systems

01 p0146 A70-11561

Cost effectiveness analysis applicable to DOD military system selection and acquisition, using model to study airborne electronics subsystem

02 p0401 A70-11673

Least squares adjustment of observation equations for hybrid systems solved by regarding constraints as observations with zero variances

02 p0289 A70-11798

Dynamical systems with two degrees of freedom reduced to numerical investigation of quadratic area-preserving mapping

02 p0289 A70-11993

Automatic control nonlinear systems with random inputs, determining phase coordinates probability densities

02 p0272 A70-12414

Incremental profit and total airline profit model programs for air cargo systems

[SAE PAPER 690415] 03 p0411 A70-12899

Aircraft ground support system analysis from airplane designers viewpoint

03 p0463 A70-13265

Optimal selection of subsystems, minimizing mathematical expectation of output losses considering malfunctions

03 p0460 A70-13429

Nonlinear feedback control system analysis and synthesis by parametric plane method, investigating frequency response by describing functions

03 p0460 A70-13970

Experiment selection in orbital program planning based on broad system synthesis, discussing identification and grouping of objectives, critical issues and experimental equipment requirements

[AAS PAPER 69-580] 04 p0749 A70-14652

Performance characteristics analysis of large area roll-up solar arrays based on support structure size and weight

[ASME PAPER 69-WA/ENER-11] 04 p0770 A70-14898

Centralized maintenance system organization, describing centralized system used by Spanish Air Force units

06 p1184 A70-17274

Antenna noise temperature of large aperture reflectors from feed system RF characteristics, discussing spillover and blockage factors

06 p1008 A70-17506

Nonlinear differential equations solution behavior near zero point of phase space examined in material system perturbed motion

07 p1333 A70-18772

Collection of papers on control systems theory and applications, Volume 7, covering dynamical systems, nonlinear filtering, optimal control, feedback control, etc

07 p1244 A70-19090

Optimal control of dynamical systems with transport lag determined using differential-integral equations

07 p1245 A70-19094

Entropy analysis of feedback control systems leading to separation theorem and feedback process information interpretation

07 p1245 A70-19095

Radio propagation characteristics and communication system performance, discussing concepts of MUF, LUF, error rate, communication system modeling, prediction techniques, etc

07 p1229 A70-19157

Efficiency of terminal state control systems defined, relating efficiency, random parameters and reliability

07 p1246 A70-19528

Inductance distribution in magnetic systems of different configuration and air gaps

07 p1282 A70-19530

Reduction method for order of transfer function describing automatic control system, determining coefficients of reduced order transfer functions

07 p1247 A70-19842

Inertial navigation system design principles, deriving error equations and equations of ideal operation

07 p1332 A70-20177

Analytical mechanics of discrete and continuous systems covering systems with limited degrees of freedom, statistical and continuum mechanics

08 p1543 A70-20526

Deterministic and stochastic simulation models for obtaining optimal solution in operations research by trial and error

08 p1464 A70-20579

Carrier-based attack aircraft avionics, describing optimal large scale analysis procedure for flight control, communications and radar subsystems

08 p1470 A70-20660

Transfer functions representing continuous dynamic systems, identifying parameters by obtaining coefficients of discrete system transfer function relating input and output sampled sequences

08 p1478 A70-20777

Saturn 5 Prelaunch Systems Simulation Model for launch opportunity containing multiple launch windows, considering last 26 hours of countdown

08 p1543 A70-20933

Model characteristics selection for dynamic system behavior simulation, studying characteristics variability extent without changing trajectory behavior dependence on parameter space

08 p1544 A70-20953

PWM-PAM and PTM-PAM systems analysis, deriving formulas for output signal shape determination

08 p1480 A70-21226

Multidiscipline systems analysis of satellite assisted information system improving earth resource management, developing User Decision Models

[AIAA PAPER 70-335] 09 p1792 A70-22855

TIROS Operation Satellite (TOS) system for daily observation of meteorological phenomena analyzed for problems of general data gathering satellite system

[AIAA PAPER 70-283] 09 p1766 A70-22874

Long range navigational aids requirements for airlines, discussing self contained navigation systems capabilities

09 p1722 A70-23028

Numerical analysis of magnetic frequency divider operation

09 p1649 A70-23338

Steady state analysis of harmonic oscillations in HF synchronized transistor autocooscillators, considering transistor inertial properties

09 p1649 A70-23341

Technology or Research Quantitative Utility Evaluation (TORQUE) system genesis and operation, with implications affecting R and D

09 p1795 A70-23418

Demand assignment techniques applicability to TDMA satellite communication systems, discussing operational modes and optimum mode selection

10 p1837 A70-24351

Intermeshed TDMA systems efficiency in interconnecting ground stations in communications satellite systems, discussing rigid and variable burst lengths

10 p1839 A70-24363

Data display systems parameters and functional elements, considering resolution, brightness, contrast, command and control, storage, etc

10 p1889 A70-24576

Combined discrete event and continuous systems simulation language, discussing mathematical modeling and various applications

10 p1860 A70-24652

Linear time-varying systems transient responses prediction, using Krylov-Bogoliubov method and parameter plane analysis

10 p1855 A70-24704

System with recovery consisting of n elements, discussing reliability and solution to steady state problem

10 p1855 A70-24798

Reliability model for analyzing operational phase test programs developed from R and D phase models, processing data according to test scope [AIAA PAPER 70-389]

10 p1896 A70-24916

VHF aerosol antenna design and system interactions, analyzing impact of spacecraft dynamics, control system, power supply and propulsion [AIAA PAPER 70-486]

11 p2120 A70-25439

Soviet papers on complex control systems covering hierarchical structures, accuracy and stability analysis, optimal and self adjusting control, etc

11 p2022 A70-25601

Multidimensionality in complex control systems, discussing circuit and oscillation theory, decomposition, variational problems, finite automata and group theory

11 p2023 A70-25602

Control theory, Volume 2, Analysis and design of space vehicle flight control systems

11 p2122 A70-25772

Coupled nonlinear systems analysis based on reducing coupled differential equations to equivalent uncoupled equations amenable to existing techniques

11 p2072 A70-25956

Decoupling and pole assignments in linear multivariable control systems using geometric method

11 p2072 A70-26160

System sciences - Conference, University of Hawaii, January 1970, Part 2

11 p2026 A70-26226

Systems identification in parameter estimation to acquire stability properties using integral transforms

11 p2028 A70-26311

Multidegree of freedom linear vibrating system analysis by dividing differential equation method

11 p2139 A70-26414

Continuous and discrete minimum time problems relationships and state space portraits during application of optimal strategies to system

11 p2029 A70-26749

Earth resources satellite systems synthesis, describing analytical techniques in R and D preceding operational status

12 p2334 A70-26942

Continental air traffic control design, discussing systems analysis approach advantages in terms of capacity

12 p2267 A70-27598

ATC radar beacon system, discussing interacting factors lowering reply reliability from transponder

12 p2267 A70-27639

Upper bound on system errors caused by quantization in multirate digital control system

12 p2204 A70-27841

Algorithm based on component reliability used to determine complex systems reliability

12 p2192 A70-28009

Space information systems effectiveness evaluation based on generalized homomorphous model

13 p2372 A70-28377

Planetary trajectory handbooks for mission and system analysis covering opportunities for Mercury, outer planets and Mars, contour charts, etc

13 p2486 A70-28525

Soviet book on theory of oscillations of linear and nonlinear time lag systems

13 p2450 A70-28699

Book on linear time varying systems analysis and synthesis covering multivariable systems, operational algebra, controllability, observability, canonical structures, minimal realization, etc

13 p2381 A70-28975

Book on probabilistic systems analysis covering models, decision making, random processes, distribution functions, mass and density functions, etc

13 p2441 A70-29455

Multimode system analysis, using automated technique to calculate effectiveness and cost down to component level

13 p2525 A70-29837

Soviet book on multivariable automatic control systems analysis and synthesis covering equations of motion, nonlinearities, pulse control, transient responses, etc

14 p2561 A70-30954

System effectiveness apportionment for constraints existing on accountable factors using Lagrange multiple method

14 p2669 A70-31111

Systems effectiveness equated to function of performance, availability, reliability, maintainability, quality control and manufacturing, emphasizing optimization

14 p2592 A70-31112

Aerospace technology and system analysis application possibilities to urban social and economic planning problems

14 p2670 A70-31191

Ground controlled remote manipulator spacecraft system through wideband radio link for satellite maintenance and repair

15 p2810 A70-31780

Complex systems effectiveness analysis by computer simulation technique

15 p2706 A70-32633

Computerized optimal redundancy analysis, considering cost, size, weight, volume, etc

15 p2712 A70-32642

Computer program /SORCBE/ for systems unavailability tradeoff vs added cost for various versions

15 p2706 A70-32658

Parameter plane method of stability analysis applied to spacecraft attitude control system with two nonlinearities related by nonlinear differential equation

16 p2881 A70-33032

Modulation transfer function /MTF/ systems analysis with emphasis on target acquisition, relating image contrast characteristics of target and background

16 p2907 A70-33185

Oscillatory and wave processes in nonlinear distributed systems by asymptotic method analogous to Bogoliubov concentrated systems

16 p2951 A70-33252

Parameter identification in distributed systems by method of characteristics, discussing noisy measurements and limited available transducers

16 p2942 A70-33338

Systems consisting of redundant and different modules, deriving vector and matrix expressions for effectiveness

17 p3099 A70-34581

Subsystem selection integration and technology for space base and planetary mission module /PMM/ of space station program [AAS PAPER 70-021]

17 p3023 A70-34801

First order difference equations for dynamical systems from Hamilton canonical equations

17 p3129 A70-34959

Multiple head shaker systems theory as application of linear algebra, noting open loop control system with computer control of frequency, amplitude and phase

17 p3059 A70-35167

Systems analysis approach to problem solving, discussing application to sociological and educational considerations

17 p3130 A70-35297

Parameter analysis of dynamical systems by matrix approach, using n -dimensional parameter space

17 p3130 A70-35300

German monograph on heavy space probes for solar system investigation covering systems analysis, mission success, flight programs, Saturn 5 launch vehicle, etc

17 p3168 A70-35378

Systems operation hybrid simulator for computer checkout of Saturn S-1C stage

17 p3061 A70-35489

Successful application development and implementation of data processing system, noting sequence, magnitude, manpower and time required

17 p3200 A70-35507

Stochastic approximation for identification of distributed parameter system solutions described by linear partial differential equations

17 p3131 A70-35557

System analysis to determine orbital parameters influence on mission scientific objectives under engineering constraints, using value function [AIAA PAPER 68-1052]

17 p3172 A70-35648

Digital computer simulation and analysis of control loops for ion thruster control [AIAA PAPER 69-239]

17 p3149 A70-35654

Iterative determination of time optimal controls, considering dynamic system transition from initial to quiescent state with constraints on control vector

18 p3282 A70-36355

Statistical properties of civil ATC system based on central processor, discussing system informational congestion

18 p3288 A70-36394

Geometrical interpretation of controlled evolution of optimal systems with mixed state constraints, using Pontryagin and variational methods

19 p3542 A70-38056

Optimal control systems sensitivity analysis, discussing trajectory tracking

19 p3394 A70-38716

Long life reliability measurement for reentry and recovery systems, noting applicability to program monitoring, optimum resources allocation, etc

19 p3442 A70-38832

Weapon systems effective reliability analysis, using degraded mode evaluation and deterministic computer program

19 p3442 A70-38833

Avionics hardware operational effectiveness assessment method, considering inertial navigation system LN-12D

19 p3442 A70-38837

Prior distributions computer aided selection for generating Monte Carlo confidence bounds on system reliability

20 p3658 A70-39641

Self adaptive system with standard model, using direct loop amplification factor as controlled parameter

20 p3603 A70-39832

Multidimensional control for turbojet engine, relating system characteristics to invariance conditions during startup and ascent

20 p3689 A70-39847

Controlled systems characteristics multistep statistical evaluation by extrapolation, analyzing prediction errors

20 p3593 A70-39904

Uncontrolled plant dynamic characteristics analysis based on signal recordings, using black box without input method

20 p3705 A70-39909

Computer program for systems reliability approximation, giving algorithm for cut and tie sets identification

20 p3594 A70-40060

Regulated spacecraft solar array mathematical model for high voltage power supply regulator analysis

21 p3757 A70-41208

TIROS Operation Satellite /TOS/ system for daily observation of meteorological phenomena, analyzing problems of general data gathering satellite system [AIAA PAPER 70-283]

21 p3931 A70-41868

Self oscillations and dead zones of automatic control systems with variable structures, using harmonic linearization

22 p4001 A70-42837

Linear distributed parameter systems state estimation from noisy measurements, developing sequential algorithms for prediction, filtering and smoothing

22 p4063 A70-43026

Nonlinear control systems described by linear equations, discussing quasi and local controllability as functions of time and stationary state

22 p4063 A70-43427

In-flight escape systems and survival equipment reliability in U.S. Navy ejections

23 p4143 A70-44460

Bayesian identification of system parameters for observable and nonobservable input signals

24 p4316 A70-45474

Closed loop synthesis algorithm and comparison to sensitivity of open loop system, noting applicability to optimal control

24 p4322 A70-46013

Functional systems in biology, discussing inter-scientific demarcation, research strategy, physiological experiment, operational architectonics, etc

24 p4305 A70-46391

SYSTEMS DESIGN

U SYSTEMS ENGINEERING

SYSTEMS ENGINEERING

Global meteorological sounding network requirements, restraints and sensors, considering gun launched meteorological probe role

01 p0054 A70-10082

Failure mode evaluation techniques application to system design and product assurance activities, with examples of performance evaluation of components, circuits and systems

01 p0049 A70-10116

Microwave ILS for difficult sites or conditions, detailing capabilities and operation principles

01 p0136 A70-10301

Aerospace digital computer design development, proposing data processing system with improved flexibility by making subassemblies more independent with multiplexed interface

01 p0047 A70-10305

Medico-engineering experiment in partially closed ecological system for long term manned space missions

01 p0032 A70-10363

Apollo/Saturn 5 space vehicle supporting and restraining mechanisms design and operation, discussing holddown assemblies

01 p0055 A70-10468

Systems design experience derived from Mercury, Gemini and Apollo projects, discussing thermal protection, launch propulsion, life support, etc [AIAA PAPER 69-1077]

01 p0193 A70-10604

Systems engineering applied to airborne, airport and community socioeconomic structure in determining air freight and passenger demand impact on airport location and configuration

[AIAA PAPER 69-1091]

01 p0055 A70-10605

Delta boosted electrically raised high power synchronous satellite for communication tasks

[AIAA PAPER 69-1104]

01 p0194 A70-10617

Manned space station power systems design and selection problems, discussing requirements based on impacts on space station design and operations [AIAA PAPER 69-1081]

01 p0008 A70-10625

Manned space station system analysis for identifying control subsystem functions /weight penalties/ and system characteristics to minimize penalties
[AIAA PAPER 69-1078] 01 p0194 A70-10628

Air traffic control system automation, anticipated benefits to users and operators and potential pitfalls associated with implementation
[AIAA PAPER 69-1057] 01 p0137 A70-10638

V/STOL air traffic control and equipment considerations for increased demand, suggesting time/velocity separation system using direct routing, positive and automated control
[AIAA PAPER 69-1055] 01 p0137 A70-10639

Holographic spectroscopy design and development, discussing components and recording yellow Na doublet
01 p0087 A70-10659

Design parameter importance in centrifugal axial flow particle separator tubes performance from separator tube development program data
01 p0163 A70-10680

Factors in icing mechanism and principal features of various ice detectors for aircraft and helicopters
01 p0056 A70-10692

Aircraft seat ejection systems using SCID /small column insulated delay/ distribution system taking advantage of standard end devices
01 p0035 A70-10718

Intelsat 4 communication system design and international cooperation, considering satellite design, TV and telephone channels capacity, etc
01 p0196 A70-10883

Langley integrated life support system design, discussing manned test results including system engineering, atmospheric and water chemical analyses and microbial measurements
01 p0038 A70-10973

Control system main and self adaptive loops structural synthesis
01 p0053 A70-11043

Rockwell hardness tester attachment design for studying temperature dependence in various multiphase alloys at high temperature
01 p0121 A70-11110

Automatic landing systems mission and design, discussing pilot-system task coordination, equipment characteristics and reliability, etc
01 p0138 A70-11257

Operational planning system for Strategic Air Command for data accessing, generating, displaying and editing using computer complex
01 p0048 A70-11282

System analysis and synthesis processes applied to educational requirements identification and programs implementation, emphasizing use of functional model with man machine interface
01 p0221 A70-11283

Turbine engine starting system design requirements, outlining lifetime improvement of hot section parts
01 p0167 A70-11460

Project ABLE stabilized platform, discussing logistics support requirement effects on system design and acquisition, reliability, maintainability and costs
02 p0401 A70-11670

Slow scan TV systems for planetary exploration, discussing sampled vidicon operation, digital encoding, data storage, signal to noise ratio, future design trends, etc
[SMPT PREPRINT 106-3] 02 p0294 A70-11682

Optimal dynamic design of system consisting of elastic cantilever rod with two concentrated masses subjected to harmonic vibrations under force at free end
02 p0384 A70-11739

Avionic units automatic testing to increase speed and reliability, discussing system configuration, parts, economics and computer language use
02 p0295 A70-11838

In-flight data acquisition systems to overcome manual methods limitations, discussing applications and system configuration
02 p0224 A70-11839

Grille spectrometer design for thermal IR measurements, discussing requirements to achieve optimum performance
02 p0296 A70-11917

Cost effective phased buildup of computerized ATC systems
02 p0401 A70-11961

Aircraft landing measurement system /ALMS/ designed to provide computer analysis of all traffic landing at airport
02 p0331 A70-11964

Three dimensional radar system for automatic tracking all aircraft in terminal area to increase air traffic control system safety and capacity
02 p0332 A70-11967

Navigation system with twin gyro platform and Doppler sensor, discussing performance and cost advantage over inertial systems
02 p0334 A70-11987

Hardware-software integrated time sharing computer system for testing transmission control units and associated terminals on line
02 p0275 A70-12189

Popov type nonlinear control systems from synthesis is viewpoint, using state variable feedback results to insure absolute stability
02 p0271 A70-12194

IBM System/360 Operating System submodel simulator for multiprogramming, discussing language and structure
02 p0266 A70-12281

Optimization potential selection in control system design by analytical method
02 p0272 A70-12412

Manned space station system design requirements, discussing logistics interaction and station autonomy
[AIAA PAPER 69-1063] 02 p0382 A70-12528

Book on radar design principles-signal processing and environment covering target detection in presence of noise, atmospheric effects, pulse techniques, etc
02 p0270 A70-12662

Low turbulence wind tunnel axisymmetric contraction designed from reformulated Thwaites solution
03 p0462 A70-12935

Drum-type, high-speed, frame or streak photographic camera, discussing film mounting and operating specifications
03 p0485 A70-13531

Logic methods of efficient organization of satellite integration, considering project, physical components and program elements
03 p0609 A70-13842

Linear separation systems for aerospace applications covering mild detonating fuse and cord flexible linear shaped charge, SUPER ZIP concepts, etc
03 p0546 A70-14103

Design, performance and manufacturing information on various microcircuit bridges in conjunction with production of squibs, detonators and pressure cartridges
03 p0547 A70-14112

Structure theorem for time invariant multivariable linear systems proof and formulation for use in controller design and synthesis
03 p0461 A70-14166

Millimeter wave fields systems application to radar guidance, radiometry, communications, radio astronomy and satellite experiments
04 p0647 A70-14621

Radiation hardening of electronic systems for nuclear weapons using shielding, circuit design techniques and hardened components
04 p0657 A70-14738

Crew requirements influence on systems design and operations criteria for long duration biomedical and behavioral measurement program in earth orbiting space laboratory
[ASME PAPER 69-WA/BHF-17] 04 p0643 A70-14858

Thermionic diode development for nuclear reactor systems
[ASME PAPER 69-WA/ENER-5] 04 p0717 A70-14900

Integral-criterion optimization of transient processes in mechanical systems synthesis with favorable dynamic and damping characteristics
04 p0720 A70-15218

Public health services problems analyzed by statistical simulation method, using Markov process
04 p0644 A70-15356

Pilot response to stability augmentation system failures and design implications
[AIAA PAPER 68-819] 04 p0624 A70-15379

Pulsed MPD arc jet electric propulsion system requirements, examining physical constraints, pulse duration, duty cycle, power network structural details, etc
[AIAA PAPER 69-269] 04 p0737 A70-15424

SAO thermal subsystem design to provide temperature control for experiments and spacecraft electronic devices
04 p0765 A70-15668

Integrated logistic support economics considered in selecting support system for generating quantitative data for cost optimization
[SAE PAPER 690632] 05 p0959 A70-15846

V/STOL Flight Profile Indicator display system development to present pilot situation information in vertical plane
[SAE PAPER 690694] 05 p0792 A70-15861

Human performance evaluation and data acquisition as requirements for heuristic analytical models in systems engineering
05 p0805 A70-16008

Flexible blades cascade design compared with various correlation criteria, describing cascade and profiles geometry and loss coefficient
05 p0790 A70-16029

Sealed Ni-Cd aerospace battery design, discussing recombination of gases produced during prolonged overcharging at low temperature, separator material, plate balance, etc
05 p0798 A70-16096

Thermal stress and thermal fatigue data for utilization in design problems
05 p0932 A70-16161

Systems concepts in design of computer operated display systems in air defense and air traffic control systems, discussing alphanumeric display, panoramic display, etc
05 p0827 A70-16183

Computer generated displays and USAF equipment design for operational command and control systems, discussing Ag halide film technique
05 p0847 A70-16185

Systems engineering management process for satisfying MIL-STD-499 requirements, detailing functional analysis, tradeoffs and resulting design analysis data
05 p0959 A70-16462

Magnetosensitive quartz element with suspended magnet and two mirrors for recording magnetic variations
05 p0851 A70-16770

Airport fog attenuation systems design and operation consisting of power and communication cables linking diffusers to central control and command
05 p0830 A70-17092

Synchronous and asynchronous electrostatic motors based on action of electric fields charges, discussing design and construction
06 p0988 A70-17150

Air backflow in nuclear exhaust system duct for ground testing of NERVA engines, noting overpressure effect
[AIAA PAPER 69-325] 06 p1027 A70-17174

Systems engineering aspects of Apollo Telescope Mount spacecraft, considering design and manned space flight role
06 p1061 A70-17312

Instruments and systems - Conference, San Francisco, August 1969
06 p1017 A70-17351

Avionic and space electronic equipment converging design, considering chip computer
06 p1017 A70-17354

Systematization of thermodynamic cycles from elementary reversible evolutions concerning exchange of work, heat and combined relations
06 p1173 A70-17470

Personnel/cargo lowering and retrieval system requirements, design approach and effects on performance for CH-47 helicopter, discussing fabrication and testing on mockup
06 p0985 A70-17711

Physiological and environmental factors influencing oxygen breathing system design and use for passengers and aircrews of high flying aircraft
06 p1003 A70-17716

Launch vehicle control system synthesis based on mode control theory state variable formulations
06 p1156 A70-17958

Optimal feedback controls design for linear systems relative to time-multiplied performance indices
06 p1025 A70-17960

Material Acquisition Division of Naval Air Systems Command, discussing engineering and testing functions in providing air weapons systems to operating forces
06 p1185 A70-17973

Hybrid coordinate formulation for flexible space vehicle attitude control system design
[AIAA PAPER 70-20] 06 p1158 A70-18180

Solar plasma wind simulator design and performance, discussing ion source, mass separator, beam mass analyzer and Faraday cup
[AIAA PAPER 70-31] 06 p1030 A70-18223

Fluidic devices for systems engineering, discussing design and applications of logic simulator, element tester and three mode controller
06 p1015 A70-18428

Soviet monograph on theory and calculations of impact systems covering solid body collisions, elasticity, wave mechanics and nonflat rod applications
07 p1400 A70-18732

Integrated circuit technology impact on electronic equipment designers and organization relationships within industry
07 p1239 A70-18800

Aerospace ground air conditioning design, discussing ground support equipment, manuals, manufacturer catalogs, etc
[SAE-AIR-992] 07 p1248 A70-18808

Advanced concept ejection seat /ACES/ system design and performance, considering gyro-controlled vernier rocket motor and electronic time delays
07 p1192 A70-19016

Aeros satellite active magnetic position control system of axis and spin noting design and operation
[DGLR-69-056] 07 p1393 A70-19148

Apollo 7 and 8 command modules TV camera systems design, considering additional function of public information
07 p1280 A70-19229

Quartz magnetometer design to measure horizontal component of geomagnetic field, observing stability of H/zero/ constant
07 p1281 A70-19467

Communication satellite transponders design, cost, reliability, manufacturing, testing and future developments

07 p1241 A70-19620

Book on control engineering for systems analysis and design, discussing feedback, nonlinear, discrete time and physical systems

07 p1246 A70-19669

Relay control design for model-tracking system with parameter uncertainties and disturbances using semidefinite Liapunov function

07 p1247 A70-20026

Automatic control system identification with respect to optimality criteria, mathematical models, computing techniques and input signals

07 p1247 A70-20029

Matched filter rectangular pulse compression nonlinear FM waveform design with low time sidelobes and zero mismatch loss due to spectral weighting

07 p1242 A70-20065

Digital cross correlator design for impulse response determination in linear systems, noting real time operation without software and storage problems

07 p1236 A70-20068

Integrated electronics system for space shuttles including propulsion, electrical power, life support and flight control

[AIAA PAPER 70-257] 07 p1398 A70-20392

Space transportation system objectives including design, operations and economics

[AIAA PAPER 70-263] 07 p1398 A70-20393

Adaptive control function technique for lateral stability augmentation system design for manned lifting body entry vehicle

07 p1247 A70-20404

Strain gages design and development for small loads

08 p1493 A70-20586

Civil avionics systems engineering for safety, regularity, weather independence, flight patterns and airport utilization

08 p1468 A70-20649

Automatic support systems for advanced maintainability - IEEE Conference, St. Louis, November 1969

08 p1468 A70-20651

Computer controlled automatic test system /NARF 5500/ for naval avionics systems support, discussing system hardware and applications and programming cost reductions

08 p1469 A70-20652

Automatic test equipment from fourth generation computer viewpoint, considering cost and size reduction trends in avionics

08 p1469 A70-20654

Automatic multiple station test system for manufacturing plants, considering centrally controlled vs free standing and intelligent vs nonintelligent remote stations

08 p1470 A70-20655

General purpose automatic test system /GPATS/ for electronic equipment fault location, discussing software and hardware for integrating programmable oscilloscope

08 p1470 A70-20656

General purpose support system /GPSS/ simulation for carrier operations and avionic maintenance, considering attack aircraft operations, spare parts, personnel requirements, etc

08 p1470 A70-20661

Integrated man machine shipboard maintenance systems design, describing computerized model based on information flow network

08 p1465 A70-20665

DC to DC switching power processor design considerations for avoiding system failures

08 p1439 A70-20705

Electrochemical cells with lithium anode and nonaqueous electrolyte, discussing research role in designing high specific energy primary batteries

08 p1440 A70-20709

Flexible nickel cadmium secondary battery as nocturnal power supply for meteorological balloons transceiver and measuring instruments

08 p1440 A70-20711

Lead-acid and vented nickel cadmium batteries compared in redesign of military aircraft battery for cells reduction, low current density, etc

08 p1440 A70-20712

Soviet book on pneumatic actuators theory and design, using digital computers to solve dynamic equations and to obtain diagrams and nomograms

08 p1440 A70-20752

Soviet book on control systems for single rotor helicopters covering automatic stabilization system design, autopilots, pilot operation within closed control circuit, etc

08 p1435 A70-20769

Optimal control systems design involving time delays as functions of time and system state, considering stability constraints

08 p1478 A70-20779

Laser and quasi-laser systems modulation for wide spectrum communications, discussing global potentials and application as low cost satellite links

08 p1459 A70-20802

Optimal satellite communication system design concerning station spectrum and interference limits

08 p1459 A70-20805

Coupling relations in product and systems development linking ideas to finished products

08 p1601 A70-20824

Operational figure of merit of high performance antennas in communication satellite earth stations as function of design

08 p1471 A70-20825

Multisupported radially symmetrical suspension systems designs for parabolic antennas, assessing performance in terms of maximum rigidities

08 p1586 A70-21058

Relaying interferometer design consisting of heterodyne frequency diversity antennas with coherent mixer, relaying transmitter and receiver

08 p1495 A70-21071

Civil engineering research needs in air transportation, discussing information sources and processing and industry estimates of manpower, facilities and funding

08 p1481 A70-21305

Electroluminescent displays design capable of generating all primary colors in single compact element

08 p1499 A70-21689

Narrow width pulse-position modulated optical communication system design, determining performance in terms of error probability and information rates

08 p1463 A70-21778

Supersonic compressor applications for airborne vehicles propulsion systems, discussing axial flow compressors, three dimensional design methods, supersonic radial machines, etc

[AGARDOGRAPH-120] 08 p1434 A70-21929

Electronic equipment optimal design variant selection method, based on relative characteristics of feasible versions, widening weighting coefficients determination basis

09 p1643 A70-22129

Reliability engineering for complex systems of multiple repairable parts based on analysis involving signal flow graphs and Markov renewal processes

09 p1691 A70-22574

Harrier engine nozzle actuation system role in short ground takeoff run facility, discussing pneumatic system, air motor servo unit and pilot control

09 p1610 A70-22606

Flashtube photostimulators for examining human physiological response, discussing design and calibration

09 p1624 A70-22673

Rapid guiding system for high resolution astronomical observations using thermal expansion of electrically conducting wires

09 p1721 A70-22741

Linear high order aircraft and missile control systems design using Horowitz frequency response method

09 p1654 A70-22835

Large scale aerospace data acquisition, processing, handling and dissemination systems analysis and design

[AIAA PAPER 70-322] 09 p1641 A70-22865

Fighter flight control design criteria for providing maximum combat effectiveness, safety and survivability without excessive cost or risk

[AIAA PAPER 70-515] 09 p1611 A70-23021

Control system design for maximum weapon delivery missions effectiveness, discussing analysis and simulation methods

09 p1611 A70-23022

Primary long range navigation system for SST, considering operational goals, Doppler radar systems, navigation aids, inertial systems, etc

09 p1722 A70-23029

Sensors design for studying temperature fields and stressed state of structures

09 p1680 A70-23106

Electric propulsion design, considering effects of weight, impedance matching, beam voltage regulation and operating point variations in formulating system mass and reliability

09 p1743 A70-23248

Structural and material design of contactless photopotentiometers operating in forward and reverse modes with given output characteristics

09 p1681 A70-23357

Soviet book on aircraft control systems design covering optimal functional or function parameters, circuits controlling pitch, roll, yaw motions, human operator systems, etc

09 p1725 A70-23472

Hydraulic regenerative servoamplifier system for electrohydraulic actuator design, discussing specifications and test results

09 p1614 A70-23686

Optimizing control system design using fluidic digital circuitry and FM type transducers

09 p1614 A70-23690

Apollo project hardware design and evaluation principles coupling simple design practice with stringent technical and administrative discipline

09 p1768 A70-23704

Transonic two stage compressor design and performance, discussing interblade row traverse data

09 p1608 A70-23742

Solar observatory at San Fernando Valley, describing evacuated aperture reflecting telescope function and design, data recording cameras, etc

09 p1688 A70-23772

Alphanumeric solid state displays with vertically stacked character rows for text format reading, using injection electroluminescence technology

10 p1846 A70-23882

Airborne pyrotechnic cloud seeding system development, testing and application, comparing rainfall from test and control clouds

10 p1886 A70-23931

Synchronous satellite communication system clock synchronization loop design taking into account delay time

10 p1835 A70-24335

Signaling system for communication satellites demand assignment, considering error control, unit negative acknowledgement, system parameters selection, control signals, etc

10 p1837 A70-24347

Bit clock synchronous system for communications satellites TDMA

10 p1839 A70-24368

Soviet book on automatic scanning information systems, discussing equipment, system parameters, scanning methods, etc

10 p1840 A70-24376

Soviet book on satellite communication systems for telephone and TV transmission covering orbit selection, signal level calculation, channel characteristics for frequency bands, etc

10 p1840 A70-24378

Closed loop control system design with preassigned eigenvalues based on multipoint linear stationary system synthesis with dynamic feedback

10 p1855 A70-24394

Control synthesis method using optimization technique to design controllers making closed loop system behave as ideal system or model

10 p1855 A70-24450

Semiconductor laser junction construction for increased gain making possible laser voice communication, optical intrusion alarms, laser pumping lamps and portable range finders

10 p1900 A70-24529

Large optical telescopes design, discussing field correction at prime focus, low expansion materials, drive and control systems, on-line computers, etc

10 p1860 A70-24554

Cost and deadline planning for system development, suggesting theoretical methods tests regarding applicability

10 p1971 A70-24597

Hybrid computer applications in systems approach to engineering design, discussing design process and computer description

10 p1861 A70-24658

Controllability and observability of discrete composite systems in tandem with Jordan canonical form representation noting similarity to continuous systems

10 p1856 A70-24873

Computer and system design automation, considering language problems, microproms, optimization on subsystem suboptimal basis, etc

10 p1845 A70-24874

Coherent instrumentation radar for White Sands Missile Range, discussing system design emphasizing pulse Doppler capability

10 p1842 A70-24881

Complex microwave solid state subsystems designs for specialized systems

10 p1852 A70-24889

Nonavionic Aircraft Integrated Data System configurations evaluation by computer model, showing cost effectiveness data in terms of aircraft maintenance and availability

[AIAA PAPER 70-396] 10 p1808 A70-24909

Hardware and system testing mathematical model assuming stochastic design and manufacturing defects detection and nondetection probability equations analogous to reliability function

[AIAA PAPER 70-390] 10 p1896 A70-24915

Systems engineering approach to test planning with emphasis on risk reduction for spacecraft

[AIAA PAPER 70-367] 10 p1952 A70-24933

Commercial thermoelectric generator design, applications and economics compared to batteries and small MG sets

10 p1808 A70-25033

Book on aircraft environmental control covering design, construction and operation of various systems

10 p1809 A70-25203

Scalar measure of system sensitivity to plant parameter variations applied to design of linear lumped stationary multivariable feedback control systems

10 p1856 A70-25233

Slowly varying parameters as engineering problem in nonlinear lumped systems 10 p1856 A70-25239

Transfer functions application to optical system specification, design and evaluation, calculating diffraction limited MTF 11 p2082 A70-25354

Canadian geostationary satellite communication system design and performance, discussing transponder with six RF channels [AIAA PAPER 70-429] 11 p1996 A70-25402

Terrestrial interface at SPADE terminals for converting international telephone exchange differences into common signaling format [AIAA PAPER 70-413] 11 p1997 A70-25407

Communication satellites geostationary orbit sharing problem, considering system design and utilization criteria [AIAA PAPER 70-441] 11 p1998 A70-25419

Communication satellite repeater design requirements to achieve adequate SNR for varying rain and cloud attenuation [AIAA PAPER 70-498] 11 p1998 A70-25425

Power sources, transfer and conditioning subsystems design, fabrication and testing for high power communication satellites [AIAA PAPER 70-433] 11 p2120 A70-25438

Satellite TV broadcast requirements impact on high power transmitter design, permitting low cost terrestrial receiving systems [AIAA PAPER 70-434] 11 p1999 A70-25450

Report on Spectrum Utilization and System Constraints session of Intelsat/IEE International Conference on Digital Satellite Communication, London, November 1969 [AIAA PAPER 70-465] 11 p2002 A70-25486

Book on engineering aspects of MHD power generation, discussing working gas ionization and electrical conductivity, incompressible conducting fluid motion in magnetic field, etc 11 p1982 A70-25525

Automatic control systems synthesis for plants described by incomplete differential equations, measuring controlled value and input derivatives 11 p2023 A70-25610

Structural synthesis of automatic control systems for body motion along trajectory, using inverse method and nonlinear coordinate transformations 11 p2077 A70-25611

Superconductive materials and magnet design, discussing stabilization methods 11 p2097 A70-25613

Control theory, Volume 2, Analysis and design of space vehicle flight control systems 11 p2122 A70-25772

Design criteria for minimizing EMC problems confronting engineers of aircraft electrical and electronic equipment [SAE PAPER 700215] 11 p1980 A70-25887

Air conditioning systems design for turboprop computer and business aircraft [SAE PAPER 700224] 11 p1980 A70-25895

Multidimensional determined automatic control system structure and parameter synthesis by root method 11 p2023 A70-25926

System sciences - Conference, University of Hawaii, January 1970, Part 1 11 p2024 A70-26201

System sciences - Conference, University of Hawaii, January 1970, Part 2 11 p2026 A70-26226

Optimal fixed digital control for handling wide range plant parameters uncertainty involving random disturbances and measurement errors 11 p2026 A70-26248

Concept engineering, individuals and corporations consider aspects and disciplines concerned with public utility, taste and convenience 11 p2153 A70-26257

Systems sciences - Conference, University of Hawaii, January 1969 11 p2027 A70-26301

Optimal linear estimation and control theory application to high precision optical spacecraft tracking systems design 11 p2028 A70-26302

Stochastic control system design methodology noting applications to ASW, law enforcement, document retrieval and autopilots 11 p2029 A70-26336

Automatic test and checkout system difficulties in space vehicles 11 p2032 A70-26338

Thermal control design for diffraction limited large diameter Cassegrainian telescope systems in orbital conditions, using computer and scale model testing 11 p2052 A70-26356

Passive thermal control system design of SERT II nonspinning satellite based on 534-node analytical model calibrated against test data 11 p2127 A70-26358

Biosatellite environmental control coolant loop system design for 30-day mission program, discussing fuel cell power source, cryogenic subsystem, etc 11 p2127 A70-26360

Thick superinsulation system design for long term cryogenic storage using superfloc, radiation shield and spacer material 11 p2150 A70-26367

Processing system for tape recorded signals with nonelectrical varying parameters 11 p2056 A70-26456

Systems engineering study of sensors in fighter aircraft avionics 11 p2081 A70-26501

Soviet book on aircraft AC and DC relay pulse generators, emphasizing controllable frequencies and duty factors and neutral and polarized electromagnetic relays 12 p2194 A70-26874

Multipurpose domestic satellite system design for TV distribution, discussing frequency sharing, synchronous orbit and system model 12 p2183 A70-26998

Quasi-isothermal heat transfer pipe design and operation 12 p2330 A70-27275

Systems theory - Conference, Gainesville, Florida, March 1970 12 p2203 A70-27408

Suboptimal control of discrete input system with bounded state and control variables, developing algorithm for on-line computation 12 p2203 A70-27409

Nonlinear time-varying multivariable adaptive control system design using signal synthesis technique 12 p2203 A70-27415

Computational methods for multiinput linear control systems applied to designing lateral and longitudinal autopilots for jet transports subject to gust loads 12 p2203 A70-27417

Avionics technology cost effectiveness effect on airlines and industry, considering systems engineering and specifications [SAE PAPER 700299] 12 p2335 A70-27447

Continental air traffic control design, discussing systems analysis approach advantages in terms of capacity 12 p2267 A70-27598

Aircraft separation standards in air traffic control system design regarding collision hazards, noting beacon system role 12 p2267 A70-27635

Short distance VHF omirange navigation and distance measuring equipment considered for performance improvements feasibility to meet civil air traffic demands through 1980 12 p2268 A70-27643

Exothermic bimetallic ignition systems /EBIS/ design for solid propellant rocket motors of tactical missiles to reduce shock loadings 12 p2289 A70-27694

Space station design for long duration operation, considering optimum mix of redundancy, maintainability and checkout 12 p2313 A70-27743

Flexible vehicle control, using cybernetic model for system design and response [AIAA PAPER 69-115] 12 p2314 A70-27811

Transpiration-cooled systems design with porous materials, considering mechanical and flow control /permeability/ properties requirements 12 p2256 A70-27822

Second generation radar beacon system for ATC using discrete address roll call 12 p2268 A70-27911

Bendix design approach for lunar vehicle using operating mockup, noting trend towards lighter machines 12 p2208 A70-27945

Statistical design of density tapered planar circular and elliptical arrays for radiation patterns with good sidelobe behavior 12 p2199 A70-27987

Mission oriented or time dependent systems reliability measures definitions in terms of probability 12 p2336 A70-28008

On-line optimization of maintenance and verification schedules for complex system safety insurance 12 p2244 A70-28013

Spaceborne information processing for manned missions, describing layered system with fault tolerance and onboard checkout 13 p2372 A70-28415

Lunar surface mobility systems designs based on terrestrial transporters or mission requirements consideration, comparing capabilities 13 p2384 A70-28416

Equipment specifications and design for creep testing at variable load and temperature under uniaxial tension, emphasizing test environment control 13 p2509 A70-28537

Soviet book on discrete system for measuring multivariable probability distributions, covering automatic acquisition and reduction of statistical data 13 p2381 A70-28700

Wind load aerodynamics effects on launch vehicle flight control systems design [AGARDOGRAPH-115] 13 p2504 A70-28753

Wind effects on rigid launch vehicle guidance and control system design, using model incorporating structural bending and fuel sloshing [AGARDOGRAPH-115] 13 p2448 A70-28755

Azur satellite ground control, describing system organization to measure scientific and data information for entire satellite lifetime 13 p2384 A70-28976

Radioisotope fueled organic Rankine power system with weight dependence on operations depth [AIAA PAPER 70-520] 13 p2349 A70-29037

Optimal control of systems with time transitions described by finite state stationary Markov chain, noting resetting control 13 p2382 A70-29065

Newton-Raphson method analog accelerating convergence of multidimensional stochastic approximation algorithm to local minimum for attitude controller design 13 p2382 A70-29069

Design requirements for solar cells and arrays as function of illumination, orbit, geometry and type of stabilization, space environment, etc 13 p2349 A70-29554

Pattern recognition systems design and applications in medical and photographic data classification 13 p2374 A70-29580

Training algorithms in designing multilevel quasi-optimal controllers for dynamic processes, using pattern recognition methods 13 p2383 A70-29581

Stochastic reinforcement learning model synthesizing control and pattern recognition systems with learning attributes 13 p2374 A70-29584

Multifunctional multimode avionics design integrating communications, navigations and identification subsystems /ICNI/ 13 p2368 A70-29619

MELVIN compact inexpensive multipurpose automatic test system, utilizing MSI single printed circuits to work optimally with computer 13 p2374 A70-29683

Test Equipment for Rapid Automatic Checkout and Evaluation /TRACE/ system, describing method for interfacing computer with peripherals 13 p2374 A70-29685

Asymptotically optimal signal detection algorithms for statistical systems synthesis 13 p2369 A70-29726

Centrifugal pump design optimization, assuming one dimensional throughflow of viscous fluid as driving force 13 p2391 A70-29748

Low density Hall ion thruster with application to Van Allen probe and orbit-to-orbit transfer [AIAA PAPER 69-281] 13 p2475 A70-29957

Meteor observation station design and operation, describing calibration difficulties and reflecting points coordinates determination 14 p2583 A70-30331

Saturn 5 launch vehicle navigation system design, discussing configurations, implementation schemes, system tradeoffs and performance 14 p2613 A70-30453

Operational and environmental factors constraining onboard navigation system design for outer planet flyby missions 14 p2614 A70-30467

Permittivity cell and encapsulation for liquids subjected to high pressures and temperature extremes 14 p2533 A70-30502

He-Cd laser construction with quartz tube manufactured separately, describing flow-through processing 14 p2594 A70-30509

Meteorological parameters measuring instruments optimal design, presenting formalized procedure flow chart and examples 14 p2607 A70-30568

Wind profiles derivation for environmental influence upon missile systems design, limiting bulky input into computer programs 14 p2608 A70-30586

Launch vehicle design, considering tradeoffs between wind effects and analysis time 14 p2653 A70-30589

Multivariable feedback control system, minimizing mean squared error and error sensitivity to random perturbations 14 p2560 A70-30622

Book on automation of mathematical description of controlled plants covering signal generation, information acquisition, statistical disturbance, self adaptive systems, etc 14 p2560 A70-30629

Electronic systems automatic design problems including man machine communication and data organization 14 p2554 A70-30663

Orbital refueling techniques, discussing vapor-liquid interface stability, pressurant requirements, transfer line chilldown, propellant transfer dynamics, dielectrophoresis, suction speed estimating and system tradeoffs [AIAA PAPER 69-564] 14 p2653 A70-30752

Minimum cost systems engineering in aviation equipment maintenance and reliability

14 p2669 A70-30943

Soviet book on multivariable automatic control systems analysis and synthesis covering equations of motion, nonlinearities, pulse control, transient responses, etc

14 p2561 A70-30954

System design for IR imaging radiometer from synchronous altitude satellite, considering spacecraft dynamics, detectors and cooling

14 p2586 A70-30974

Si solar cell configurations for balloons and satellites, discussing critical design constraints for weather balloon power systems

14 p2670 A70-31139

Microwaves in integrated military avionics systems, discussing CNI, ECM, component reliability, etc

14 p2551 A70-31177

High speed dynamic systems synthesis with optimal damping of elastic vibrations, using gradient method

14 p2617 A70-31354

Thermionic diode development for nuclear reactor systems

[ASME PAPER 69-WA/ENER-5]

15 p2773 A70-31959

Nationwide automated ground based air traffic control system for increased flight operations

15 p2772 A70-31962

Mariner spacecraft electro-optically controlled star sensors design and performance, discussing star simulation and stray light test techniques

15 p2736 A70-32033

Ionospheric probe designs and measurement errors due to perturbations by satellite carriers

15 p2731 A70-32094

State transitions and couplings in reliability of complex systems, using logic algebra suitable for computer

15 p2709 A70-32132

Systems approach to flight accident prevention and inquiry management

15 p2674 A70-32207

Learning control systems design, deriving general learning algorithms

15 p2705 A70-32448

Hydrogen oxygen rocket engine two phase liquid hydrogen pump capability and hydrodynamic design, analyzing constant-quality flow, acoustic effects, compressible flow and cavitation

15 p2791 A70-32511

Mission analysis in system evolution, determining subtasks sequence to accomplish performance goals

15 p2804 A70-32627

Human element in system development to achieve optimum tradeoffs among reliability, cost and other system criteria

15 p2693 A70-32629

Optimum reliability programs, suggesting simulation to provide cost effectiveness basis for systems design configurations evaluation as alternative to demonstration testing

15 p2831 A70-32631

Reliability factors in design and development staging systems /DDSS/ for military and space exploration programs

15 p2747 A70-32639

Circuits and systems - Conference, Pacific Grove, California, December 1969

16 p2881 A70-33031

Imaging type electro-optical detection systems design for passive night surveillance, building camera system and testing in helicopters and fixed wing aircraft

16 p2903 A70-33127

Airborne electro-optical array system design and performance for particle size measurement

16 p2906 A70-33175

Army missile command /AMICOM/ plasma jet wind tunnel automatic control system design

16 p2888 A70-33303

Desensitized linear servo model following feedback control systems design using specific optimal control concepts

16 p2884 A70-33315

Linear multivariable feedback control systems design method based on transfer matrix, testing decoupling desirability

16 p2884 A70-33318

Output feedback control systems design, considering closed loop system sensitivity to plant parameters based on linear optimal control problem

16 p2885 A70-33324

Aircraft stability augmentation systems design by parameter optimization techniques and feedback selection

16 p2840 A70-33342

Nonlinear digital programming techniques for airplane stability augmentation systems design

16 p2840 A70-33343

Real time recording systems design for increased writing speeds on photochromic films

16 p2910 A70-33435

Target signature concept of spectral, spatial, temporal, and polarization effects to develop electromag-

netic signatures against background, considering remote sensor system design

16 p2910 A70-33437

Fluid power systems computer aided design and optimization, describing modeling and simulation, parameter sensitivity, systems stability, etc

[ASME PAPER 70-DE-44] 16 p2869 A70-33508

Aircraft design, development and production illustrating systems engineering functions, discussing control process model

16 p3004 A70-33676

Lunar Module landing radar system design, discussing antenna and electronics assembly

16 p2865 A70-33681

GaAs injection lasers for optical communication, synthesizing high bit rate data link between synchronous relay satellites

16 p2865 A70-33710

Systems design and instrumentation for chemical/biochemical space manufacturing at zero g, developing scaling laws for transition to larger production units

16 p2919 A70-33719

Design and reliability of digital systems for hard cores of fault tolerant computers /hybrid- redundant systems/, discussing advantages over multiplexed systems

[JPL-TR-32-1490] 16 p2887 A70-33734

Raman spectrochemical system design based on laser radiation as parent source, discussing relay optics and photon counting detector system

16 p2913 A70-33979

Ball in tube nutation damper for spinning satellite, describing design, testing and fabrication techniques for achieving low friction level

16 p2985 A70-34136

SNAP reactor control system mechanisms development for operation in space environment

16 p2951 A70-34163

Coherent digital communication systems optimal design based on unified theory, discussing tradeoffs between error rates, Doppler tracking capability and time and frequency division multiplexing

16 p2866 A70-34258

Nonlinear lumped system synthesis by inverse delta method

16 p2943 A70-34278

Computerized metropolitan air transit system, discussing system redundancy for safety level maintenance and all-weather dependability

17 p3199 A70-34730

Apollo docking system for CSM-LM connection and disconnection during lunar landing mission, discussing flight hardware

17 p3175 A70-34768

Manned planetary flight systems engineering, discussing feasibility, objectives, propulsion, transplanet injection via geospace shuttle station, energy requirements for various synodic modes

[AAS PAPER 70-037] 17 p3155 A70-34778

Cost reduction in designing space shuttle system using reusable winged vehicles, suggesting airlines operations method

[AAS PAPER 70-043] 17 p3175 A70-34785

SST flight efficiency trends, discussing breakthrough and development method and Concorde aerodynamic, propulsion and structural history

[AIAA PAPER 70-871] 17 p3016 A70-34811

Airplane performance improvement by flight control system design, discussing ride quality, flutter margin, maneuver load, etc

[AIAA PAPER 70-875] 17 p3017 A70-34816

Structural weight reduction and increased aerodynamic efficiency in aircraft design by including flight control technology early in configuration development phase

[AIAA PAPER 70-874] 17 p3017 A70-34817

Digital computer technology impact on advanced aircraft design, discussing airborne computers, distributed and lumped computer systems, outer loop control, engine control and system integrity

17 p3049 A70-34993

Spatial filter properties of antennas, discussing system performance optimization and incoherent source transfer functions

17 p3045 A70-35077

Optical and electronic components design for ruby lasers generating giant pulses

17 p3107 A70-35121

Control systems synthesis with parametric invariance for spacecraft boosters

17 p3177 A70-35219

Apollo docking system design considerations and preliminary models evaluation for best choice to meet requirements

17 p3179 A70-35262

Feedback control systems synthesis by three parameter space, using two dimensional graphic techniques

17 p3130 A70-35296

Systems engineering approach to comparison by emphasis for employee performance evaluation

17 p3130 A70-35298

Vibration transducer systems design, using active filter networks to tailor phase and frequency responses

17 p3095 A70-35527

Single input control system design for specified roots using output feedback

17 p3057 A70-35554

Slow scan TV systems for planetary exploration, discussing sampled vidicon operation, digital encoding, data storage, signal to noise ratio, future design trends, etc

[SMPE PREPRINT 106-3] 17 p3095 A70-35634

Systems design experience derived from Mercury Gemini and Apollo projects, discussing thermal protection, launch propulsion, life support, etc

[AIAA PAPER 69-1077] 17 p3180 A70-35644

System engineering process for survival enhancement of military aircraft to meet stringent requirements of general nuclear war

[AIAA PAPER 70-893] 17 p3019 A70-35810

SST electrohydraulic primary and standby brake control systems, discussing design and advantages

[AIAA PAPER 70-913] 17 p3024 A70-35825

Flying qualities criterion for fighter flight control systems design

[AIAA PAPER 70-927] 17 p3020 A70-35837

Engineering systems construction with behavioral elements of biological objects, describing gyromat

18 p3223 A70-36078

Multistage rockets terminal control synthesis based on linear functionals

18 p3333 A70-36163

Flight data recorders and system integration, discussing data replay system backing flight recording

18 p3258 A70-36340

Flight data recording systems for accident investigation and operational purposes, discussing U.S., British and French regulations

18 p3258 A70-36341

Underwater recovery requirements for flight data recorders, suggesting compressed air instead of explosive charges for ejection force

18 p3258 A70-36343

Multiple remote control systems design, emphasizing transmitter and receiver characteristics matching to overall network parameters

18 p3235 A70-36426

Multiple remote control systems effectiveness increased via controlled rectifier as even voltage harmonics generator

18 p3235 A70-36427

Avalanche transit time diode and transferred electron oscillators in microwave systems, discussing design, performance and applications

18 p3232 A70-36675

LSI packaging effects on systems design, discussing physical integration

18 p3232 A70-36761

National air transportation systems approach, emphasizing data acquisition, methodology, planning and policy making

[SAE PAPER 700337] 18 p3237 A70-36796

Aircraft electrical system multiplexing, discussing design features and advantages over conventional hard wired systems

[SAE PAPER 700303] 18 p3216 A70-36811

V/STOL attitude control system as integral propulsion system part, analyzing design and weight tradeoffs

[ASME PAPER 70-GT-31] 18 p3214 A70-36832

Plane and annular cascade facilities data application to aerodynamic design of axial flow compressors

[ASME PAPER 70-GT-106] 18 p3303 A70-36845

Radial compressor diffusers design and technology

[ASME PAPER 70-GT-116] 18 p3304 A70-36850

Control system considerations for small shaft-type aircraft gas turbines providing torque, temperature, load sharing and overspeed limiting functions

[ASME PAPER 70-GT-132] 18 p3304 A70-36858

Fire and overheat detection system design for turbine powered vehicles

[ASME PAPER 70-GT-125] 18 p3260 A70-36891

Quartz magnetometer design to measure horizontal component of geomagnetic field, observing stability of H/zero/ constant

18 p3260 A70-36941

Soviet book on statistical calculation methods for linear and nonlinear automatic aircraft control systems design, using correlation theory of stochastic processes

19 p3463 A70-37403

Merlons amplitude optimal value for open loop part characteristics in control systems design, obtaining global extremum of stipulation numbers

19 p3392 A70-37448

Multiparameter systems with dominant complex roots constrained by degrees of freedom to construct reduced characteristic equation

19 p3392 A70-37824

LSI technology effect on digital circuits and systems designs

19 p3387 A70-37847

Optimization model for evaluating information management systems for handling control functions of long duration space station missions
19 p3532 A70-37851

Management information systems based on Apollo program experience, considering improvements in data accuracy, display, feedback, etc
19 p3553 A70-37862

Simultaneous generation of sensitivity functions for linear automatic control system with known characteristic differential equation
19 p3394 A70-37867

Book on optimization and probability in systems engineering covering mathematical models for reliability, repair, availability, Markov techniques and queueing
19 p3553 A70-37928

Systems reliability numerical prediction
19 p3389 A70-38205

ATC systems safety, capacity and delay, discussing terminal operations, runway capacity and aircraft spacing
19 p3465 A70-38228

Vacuum pump systems properties for space environment simulation installations
19 p3358 A70-38280

Environmental tests and checkout procedures for Azur satellite subsystems and subassemblies integration into flight readiness
19 p3533 A70-38289

Redundant systems reliability under wearout conditions for active and standby units, including failure rates of sensing and switching devices
19 p3438 A70-38597

System design and development of EUROCONTROL Center for optimum upper airspace in Benelux-FRG region
19 p3468 A70-38639

Reliability analysis based on Bayesian subjective probability implemented by stored time sharing computer programs for engineering computations and operation analyses
19 p3441 A70-38818

Thermoelectric generators design for space and remote terrestrial sites, discussing fuel source, conversion section, heat rejection, etc
20 p3563 A70-39225

Helicopter stabilization systems design, synthesizing controllers by modal control theory
[AIAA PAPER 70-1036] 20 p3560 A70-39501

Inertial platform with integral dynamic self test and fault monitoring scheme, describing design and operation
[AIAA PAPER 70-1013] 20 p3667 A70-39520

Sensitivity optimization for linear optimal control systems design, describing aircraft lateral-directional control case study
[AIAA PAPER 70-962] 20 p3600 A70-39567

Nonlinear programming for minimizing inertial guidance systems costs via optimal subsystem selection
20 p3740 A70-39645

Army Missile Command 8000 kw plasma facility automatic control system design
20 p3606 A70-39689

Multidimensional control systems synthesized in accord with polynvariance and coordinating couplings principles
20 p3604 A70-39837

Invariant systems structural synthesis for automatic control of plant motion, deriving control laws for thrust and angle of attack
20 p3670 A70-39844

MHD induction generator design, considering electrical and friction loss measurement and control
20 p3565 A70-39988

Design management by critical element objectives, correlating various engineering functions in production process
[SAWE PAPER 868] 20 p3741 A70-40352

Weight/cost systems engineering, discussing techniques for using historical data banks and standardized reporting procedures
[SAWE PAPER 866] 20 p3741 A70-40368

Monograph on communicating by satellite covering INTELSAT system design, pricing, procurement, broadcasting, international community responsibilities, etc
21 p3955 A70-40739

Digital systems reliability improvement by redundancy at circuit and system levels
21 p3797 A70-40762

Optimal and conventional good control systems relationships, considering open and closed loop characteristics, cost functions, etc
21 p3926 A70-40781

Italian automated ATC system (ATCAS), discussing subsystem functions, display devices, data acquisition, information distribution, etc
21 p3847 A70-40911

Lunar module systems design, describing R and D program and landing mission
21 p3928 A70-40977

Apollo J mission hardware modification for lunar exploration, describing systems engineering role
21 p3928 A70-40979

Reusable space shuttle technology, discussing vehicle configurations, system growth capability, thermal protection, cryogenics, integrated avionics, etc
21 p3929 A70-40985

Life support systems oxygen generation mode selection based on mission parameters, including duration, crew size, resupply, vehicle leakage, etc
21 p3768 A70-40991

Life support water electrolysis system design, discussing alkaline or acid electrolyte selection
21 p3768 A70-40993

Space compatible flight prototype ion engine power conditioning system design for Hg thruster using oxide cathode
21 p3867 A70-41006

Water and alkali metal boilers, predicting helical-flow-promoting inserts effect on pressure drop penalties by constant slip model
21 p3949 A70-41308

Adaptive pattern recognition systems design based on notions of convergence and feedforward interconnection of two systems
21 p3794 A70-41499

Aerospace digital computers impact on aerospace systems design
21 p3794 A70-41685

Aerospace system design, considering use of microprogram-controlled digital computers
21 p3795 A70-41690

SIIS-3 ejection seat escape system design, considering minimum weight, cost and maximum performance
[AIAA PAPER 70-1211] 21 p3751 A70-41808

Single degree of freedom gyroscope design factors applicable to strapdown guidance system, discussing torque-to-balance loop, multiple pulse bursting and error sources
[AIAA PAPER 69-848] 21 p3849 A70-41859

Circular and nearly rectangular irises for resonant cavities in transmission line for microwave band stop filters, discussing design based on merit factor
21 p3792 A70-41992

Thermal design of high altitude balloons and instrument packages, analyzing vertical motion dependence on heat transfer and radiation environment
21 p3755 A70-42077

Optimal binary and ternary signal system synthesis by information divergence procedure for communication channels with colored Gaussian noise
22 p3985 A70-42491

Test rig vehicle design for noise research on single stage high bypass ratio fans for quieter turbofan power plants
[AIAA PAPER 69-492] 22 p4090 A70-42708

Soviet papers on harmonic linearization method in design of nonlinear automatic control systems
22 p3999 A70-42826

Statistically optimal nonlinear automatic control systems synthesis in presence of random perturbations, using gradient or steepest descent methods
22 p4003 A70-42889

Soviet cybernetics research, emphasizing discrete and continuous control devices and systems synthesis
22 p4004 A70-43449

MIL-STD-882 systems and subsystems and equipment safety requirements related to program management activities
22 p4048 A70-43730

Technology relevance to organizational structure, discussing planning models based on problem solving and performance
23 p4284 A70-43995

Discrete systems with and without time lags, deriving necessary conditions for singular optimal control
23 p4176 A70-44301

Avionics system for fighter aircraft, discussing weapons design, navigation-attack systems integration, etc
23 p4173 A70-44413

Failure reporting, analysis and correcting system for effective management
23 p4200 A70-44745

General Optimization Software Package for Electrical network and system design, noting application to engineering problems and education
23 p4177 A70-44750

Manned space flight regenerative life support systems requirements, considering weight, volume, power, cost effectiveness and integration problems
23 p4156 A70-45023

Image forming performance in photographic system design, considering Cobb chart resolution as figure of merit
24 p4334 A70-45449

Signal flow graphs for selectively invariant autonomous multichannel control systems design
24 p4321 A70-45641

Spacecraft fluid mechanical system design, considering environments, materials, lubrication, zero gravity and inflight maintenance
[SAE PAPER 700781] 24 p4295 A70-45862

Cost/design performance management system, noting cost reduction and avoidance needs during design definition
[SAE PAPER 700772] 24 p4430 A70-45866

Short haul metropolitan air transportation, considering systems engineering as unifying technology
[AIAA PAPER 70-1281] 24 p4373 A70-45927

Gas turbine controller design by inverse Nyquist method compared to conventional multivariable design methods
24 p4396 A70-46157

Papers on plastics, volume 1 covering materials, design, fabrication, applications, etc
24 p4368 A70-46223

SYSTEMS FOR NUCLEAR AUXILIARY POWER

U SNAP

SYSTEMS STABILITY

Algebraic criteria for absolute stability and equilibrium position in nonlinear continuous automatic control systems, using complex gain amplifier substitution
01 p0053 A70-11041

Autonomous functional differential equations with finite time lag using Liapunov functionals, discussing stability and instability
01 p0132 A70-11070

Redundant components optimal quantity determination for maximizing reliability of series system subject to multiple resource restrictions
01 p0104 A70-11383

Periodic motions and integral stability for systems with quasi-cyclic coordinates applied to current carrying conductor oscillations and linear case of Routh equations
01 p0212 A70-11573

Electrical domain instability in homogenous hot electron semiconductors, discussing boundary conditions application to fluctuations
02 p0350 A70-11697

Randomly sampled linear systems stability with linear or nonlinear feedback loops, using stochastic Liapunov function method
02 p0272 A70-12727

Unconditional stability criterion of active two port in scattering and admittance matrix notation equivalent to conjugate matching for maximum power gain with part impedances
02 p0271 A70-12820

Liquid film stability relation to angle of attack oscillations during reentry body deceleration
03 p0406 A70-12939

Optimal redundancy for maximizing systems reliability of mixed series and parallel network consisting of N modules including I module with specified reliability cost function
03 p0585 A70-12995

Cauchy problem of differential equation describing asymptotic nature of conservative system motion resulting from nonperiodic perturbing force
03 p0524 A70-13342

Dead zone initial disturbance of sensitive element dynamic coordinate in two rotor gyrocompass determined using method of averages
03 p0484 A70-13419

Liapunov function for automatic control systems, deriving theorem to ensure stability
03 p0460 A70-13434

Harmonic equilibrium method applied in dynamic properties analysis of autopilot electrohydraulic servomechanisms stability
03 p0415 A70-13930

Energetic stability theorems of dynamical feedback system, removing assumption concerning local square integrability
03 p0460 A70-13971

Hilbert space stability theory over locally compact Abelian groups developed to obtain spectral theory and positivity conditions
03 p0461 A70-14169

Distributed parameter systems with arbitrarily many degrees of freedom, studying conditions for destabilization absence
04 p0767 A70-14483

Resonance oscillations onset by initial conditions in dynamic system described by hyperbolic equation containing independent time lag variable
04 p0718 A70-14485

Natural vibrations damping of holonomic mechanical systems with feedbacks not explicit function of time reduced to optimal stabilization problem
04 p0718 A70-14494

Soviet book on nonsearching gradient self adjusting system for determining error function gradient, using Liapunov method to study stability
04 p0661 A70-14677

Critical load and instability of smooth and mesh surface mechanical systems subjected to impinging fluid jet, noting static buckling and flutter effects
[ASME PAPER 69-WA/APM-10] 04 p0772 A70-14917

Mode patterns and losses for laser resonator with identically tilted spherical rectangular reflectors in stable and unstable configurations
04 p0701 A70-15021

Control system asymptotic stability stabilized by variable structural component applied to critical cases described by multiple zero root equations and imaginary roots
04 p0720 A70-15197

Periodic vibrations of quasi-linear autonomous systems with retardation, deriving sufficient conditions for asymptotic stability

05 p0925 A70-15822

Conjugation principle for control system stabilization based on relation between controlled plant and stabilizing element stability

05 p0824 A70-16851

Stability of conical hydraulic poppet valve with elastic support and inlet and outlet piping

06 p1075 A70-17138

Absolute stability of automatic control systems with multiple rigid and tachometer feedbacks

06 p1024 A70-17812

Space-sampled feedback control of amplifying wave on infinite continuum, discussing system stability

06 p1025 A70-17963

Hyperstability conditions of model reference adaptive control systems, noting applications

06 p1026 A70-17966

Signal stabilization and performance of nonlinear sampled data systems, suggesting oscillations injection at input

06 p1026 A70-17970

Nonlinear control systems stability with stochastic coefficients, applying Liapunov function

06 p1026 A70-17971

Linear optimal stochastic control systems described by covariance matrix correlating errors and estimates of state variables, analyzing instability under parameter variations

[AIAA PAPER 70-36] 06 p1095 A70-18054

Homogenous monoenergetic cylindrical electron beam interaction with homogeneous cold plasma, investigating system stability

06 p1125 A70-18615

Absolute stability ranges of forced motions and damping in nonlinear systems determined by Sturm theorem

07 p1243 A70-18688

Stochastic differential equations for approximate continuous nonlinear minimal variance filtering, discussing existence and uniqueness conditions

07 p1245 A70-19092

Invariance and stability of subsets in metric state-dynamical polysystems

07 p1324 A70-19200

Convergent power series solution for holonomous mechanical systems stability described by ordinary and partial differential equations

07 p1334 A70-19545

Elastic stability theory applied to equilibrium and stability of discrete continuous structural systems, detailing discrete critical points

07 p1408 A70-19560

Stability of three axis indicator gyrostabilizer system consisting of stabilized platform mounted in three degree of freedom Cardan suspension

07 p1288 A70-20179

Adaptive control function technique for lateral stability augmentation system design for manned lifting body entry vehicle

07 p1247 A70-20404

Stability in systems finite over given time interval under permanent perturbations bounded in mean

08 p1543 A70-20490

Quasi-stable linear differential equations systems with nearly periodic coefficients, noting application to equations with zero real portions of matrix characteristic roots

08 p1533 A70-20492

Dynamic discrete systems unsteady motions stability, formulating theorem for finite characteristic numbers existence

08 p1543 A70-20493

Dynamic stability of pendulum-weight system during vertical HF small amplitude vibration of suspension point by averaging method

08 p1543 A70-20494

Optimal control systems design involving time delays as functions of time and system state, considering stability constraints

08 p1478 A70-20779

Automatic control system stability with restricted nonlinearity, investigating lumped and distributed parameter systems and unique and nonunique equilibrium positions

08 p1479 A70-20996

Liapunov vector functions for asymptotically stable omega-periodic solution existence in case of finite dimensional system

08 p1534 A70-21002

Thermomechanical coupling effect on stability of elastic continuous systems subjected to nonconservative forces, reducing flutter load by thermal damping

08 p1589 A70-21245

Nonlinear system oscillations analysis based on small parameter method and difference equations, including resonant case and stability criterion for periodic solutions

08 p1546 A70-21629

Existence theorem for linear stochastic systems optimal control described by differential equation with random coefficients, providing rms stabilization

08 p1480 A70-21637

Nonlinear stability theory for applying perturbed equations to dynamical system based on Liapunov stability theorem

09 p1727 A70-22612

Double axis gyrostabilizer with auxiliary tracking system of subtracking ring, analyzing system stability and operation

09 p1676 A70-22629

Aeroelasticity problems, discussing unrestrained flexible structures design, nonconservative systems stability, biomechanics, etc

09 p1777 A70-22972

Ordinary differential and algebraic equations correct analog model, noting residual system stability role

09 p1642 A70-22973

Microwave sources power stabilization, control and noise reduction using feedback techniques

09 p1649 A70-23275

Elastic chain systems stability and natural vibrations using parameter coupling method permitting integral equation construction

09 p1784 A70-23596

Stability region of hydraulic system containing centrifugal pump calculated from pressure head dependence on pump inlet pressure

09 p1607 A70-23622

Computer simulation of six degree of freedom motion system and actual system test, substantiating simulation accuracy

[AIAA PAPER 70-358] 10 p1859 A70-24218

Coupled systems stability and oscillatory behavior analysis using Liapunov theory

10 p1855 A70-24763

Thrust follower force stability in pod mounted jet engine and nacelle whirl using multiple degrees of freedom model

10 p1930 A70-25070

Systems instabilities classification criterion determination, showing absolute instability conversion into convective by introducing damping

10 p1969 A70-25104

Stationary regime stability of one dimensional model of optical quantum traveling wave amplifier, determining trapping band of traveling wave laser

10 p1901 A70-25158

Algorithm developed for constructing first approximation system from Cauchy matrix for Liapunov stability problem solution

10 p1917 A70-25302

Nonlinear system with piecewise linear spring characteristic response to stochastic excitation of white noise type process, discussing technical stability

10 p1918 A70-25323

Necessary and sufficient conditions for absolute stability of nonstationary nonlinear system, showing equivalency to asymptotic instability in small position equilibrium piecewise linear systems

11 p2021 A70-25337

Stability of multiconnected nonlinear controlled systems with nonsingle equilibrium position, representing lumped parameter system with characteristic equation having complex roots

11 p2021 A70-25338

Readjustment algorithm for auto-oscillatory adaptive control system with variable structure, using harmonic linearization

11 p2022 A70-25343

Asymptotic stability of multivariable autonomous control systems used Liapunov vector function method

11 p2083 A70-25606

Asymptotic stabilization of multivariable dynamic systems, using subsystem decomposition and Liapunov second method

11 p2023 A70-25607

Scanned beam holography reducing system stability time for hologram production with CW gas laser

11 p2050 A70-25639

Systems identification in parameter estimation to acquire stability properties using integral transforms

11 p2028 A70-26311

Maximum principle least squares (MPLS)/nonlinear filter scheme simplified, using digital simulation for stability and tracking performance

11 p2028 A70-26315

Elastic system stability with two degrees of freedom under action of retarded follower forces

11 p2142 A70-26631

Proportional fluid amplifiers noise and instability sources related to geometry and power jet flow, considering noise reduction methods

12 p2164 A70-27071

Data sampling system compensation based on bending frequency filtering through information obtained by varying sample rate, using saturn 5 launch vehicle simulation

12 p2192 A70-27411

Dynamic systems absolute stability, optimality and passivity algebraic criterion in terms of real even polynomial coefficients

12 p2261 A70-27412

Dynamic stability of multipoint servocontrol system actuating thin deformable primary mirror of orbiting telescope

12 p2203 A70-27413

Lunar roving vehicle stability and agility design approach by Grumman, using articulated steering and conical wheels

12 p2208 A70-27946

Quasi-linear autonomous systems of second order equations, considering periodic solutions asymptotic stability

12 p2273 A70-28193

Admissible controls synthesis for closed loop system/satellite/stability

13 p2500 A70-28410

Nonlinear servo system stability criteria based on plus or minus controlled data theory

13 p2381 A70-28939

Finite time stability of differential equations system using Liapunov functions

13 p2442 A70-29488

Free and forced motion characteristics in absolutely stable nonstationary nonlinear system analysis by variational approach

13 p2453 A70-29716

Material system equations of motion, determining programmed motion variable mass systems stability

13 p2453 A70-29717

Adaptive extremal control systems operational stability, defining optimal convergence coefficient values for identifier and perceptron

14 p2559 A70-30175

Multivariable feedback control system, minimizing mean squared error and error sensitivity to random perturbations

14 p2560 A70-30622

Limit cycle and stability analysis of multivariable nonlinear systems using function decomposition

14 p2560 A70-30624

Popov criterion generalization for asymptotic stability of nonlinear feedback systems

14 p2658 A70-30849

Nonlinear systems absolute stability by graphic methods, noting use of Nichol chart and analog computer

15 p2715 A70-31974

Optimal control theory of asymptotically stable closed systems synthesis regarding product requirements

15 p2716 A70-32473

Stability loss of dynamic two dimensional mechanical elastic system with single degree of freedom under trajectory bifurcation

15 p2775 A70-32474

Nonlinear feedback control systems forced asymptotic stability, using linear transformation of circle criterion

15 p2716 A70-32554

Asymptotic motion stability bound for non-holonomic nonlinear electrodynamic systems, using energy metric algorithm for Liapunov functions generation

15 p2768 A70-32556

Long term storage effects on systems reliability, emphasizing tradeoffs regarding availability, reliability and costs

15 p2712 A70-32637

Parameter plane method of stability analysis applied to spacecraft attitude control system with two nonlinearities related by nonlinear differential equation

16 p2881 A70-33032

Nonlinear systems stabilization with linear system estimator output state to provide feedback for asymptotic stability of overall system

16 p2881 A70-33033

Relay control systems stability bound determination in nonphase variable form, assuming unknown system parameters

16 p2881 A70-33034

Stable adaptive control design for linear time-invariant system with same number of inputs as outputs, considering disturbance effect

16 p2881 A70-33035

Digital computer generation of system stability Liapunov functions for ninth order spacecraft attitude control

16 p2867 A70-33043

Nonlinear discrete systems absolute stability exponential property proved by modified frequency condition, applying analog transformation to Szego-Kalman equations

16 p2882 A70-33044

Criteria for estimating errors in quadratic approximations to asymptotic stability involving Popov condition based on existence of quadratic Liapunov functions

16 p2941 A70-33045

Pontryagin stability criterion interpretation for systems with time delay in parameter plane, using computer oriented method

16 p2882 A70-33046

Distributed sampled-data control systems with memoryless nonlinear feedback element, deriving frequency domain stability criterion

16 p2884 A70-33308

Pulse modulated feedback control system, deriving sufficient condition theorem for input-output stability

16 p2884 A70-33309

Conditionally stable feedback control systems with saturation, comparing large signal stabilization methods

16 p2884 A70-33313

Popov and circle criteria for stability of nonlinear feedback control systems, using parameter plane representation

16 p2884 A70-33314

Stable operating range of supersonic mixed compression inlet increase by air flow removal via throat bleed system

[AIAA PAPER 70-686]

16 p2967 A70-33585

Linear dynamic systems under nonconservative and harmonic forces, examining stability conditions

16 p2952 A70-33896

Potential stability theory for linear and nonlinear systems trajectory

16 p2943 A70-34042

Torsion, filar, flexure and coil type mechanical suspensions for space applications, considering instability due to temperature changes and magnetic, electric and force fields

16 p2924 A70-34169

Linear and nonlinear systems natural frequency and stability determination, using theorems for degenerate systems

16 p2944 A70-34284

Stochastic systems technical stability problem solution by Fokker-Planck equation

16 p2944 A70-34294

Stability theorem for mechanical systems with constraint damping subjected to energy dissipation

17 p3176 A70-34956

Tau-decomposition stability analysis method applied to two degrees of freedom system subjected to retarded follower forces

17 p3176 A70-34957

Equilibria stability of linear discrete dynamic systems involving elastic, nonconservative, dissipative and gyroscopic forces, using Liapunov-type energy method

17 p3129 A70-34958

Gyroscopic drifts associated with angular support motions

17 p3133 A70-34960

Sufficient condition for asymptotic stability of ergodic coefficient linear stochastic systems

17 p3129 A70-34982

Automatic control system stability, allowing for position and velocity loads and compressibility of fluid in force cylinder of hydraulic actuating mechanism

17 p3024 A70-35367

Neural pulse frequency modulation system stability, using feedback control model

17 p3056 A70-35553

Spacecraft wide angle attitude control system stability analysis, using air bearing table simulation

17 p3134 A70-35651

Adaptive control systems stability treatment by Liapunov direct method

18 p3279 A70-36060

Stability conditions for control system third-order differential equations with double nonlinearity, using Liapunov function

18 p3280 A70-36157

Computerized Pontryagin stability analysis of nonlinear multiple delay systems

18 p3235 A70-36477

Pontryagin stability for distributed delay or parameter systems, using Brin criterion

18 p3235 A70-36478

Graphical stability for linear systems in parameter plane with time delay

18 p3235 A70-36479

Linear control systems stability range with delay time examined by digital computer, discussing critical loop gain

18 p3235 A70-36501

Linear continuous feedback control system with dead time compensated by proportional plus integral controller, considering stability region variations

18 p3236 A70-36943

Linear feedback control system with dead time compensated by proportional integral derivative action controller, evaluating stability by digital computer

18 p3236 A70-36944

Lumped parameter pipeline and hydraulic systems stability, deriving equations of motion for closed and open cycle control systems

18 p3216 A70-36946

Modified differential equation for stability of oscillating nonlinear system

19 p3458 A70-37823

Mechanical destabilizing model of nonlinear damping in nonconservative systems with follower forces, using Liapunov method

19 p3542 A70-38065

Multivariable nonlinear systems absolute stability criteria, emphasizing nonzero entry functions

19 p3394 A70-38171

Flutter analysis of n degrees of freedom system, basing stability criteria on energy balance considerations

19 p3542 A70-38244

Continuous one dimensional nonconservative elastic systems under complex forces, examining stability theory

19 p3546 A70-38341

Oscillations of nearly nonlinear systems with conditions for main amplitude equations

19 p3472 A70-38726

Liapunov stability analysis of dynamic systems described by simultaneous ordinary and partial differential equations of motion, applying to satellite spin stabilization

[AIAA PAPER 70-1045]

19 p3472 A70-38860

Dynamic systems stability in sense of Poisson, relating motions commutative and stable families

19 p3472 A70-38936

Linear time-invariant system dependent on small parameter epsilon, deriving conditions for bounded-input bounded-state stability

20 p3657 A70-39395

Three axis large angle attitude control system global analysis, determining system stability, responsiveness and sensitivity to disturbances

[AIAA PAPER 70-996]

20 p3668 A70-39534

Automatic control system stability error analysis, discussing sensitivity and statistical dispersion analysis

[AIAA PAPER 70-985]

20 p3668 A70-39544

Spacecraft pulse width modulated attitude control system stability, using state space method

[AIAA PAPER 70-984]

20 p3714 A70-39545

Automatic control system components parameter variation effects on invariance conditions

20 p3602 A70-39830

Small parameter effects on absolutely invariant systems under transient perturbation, analyzing gyrostabilizer performance

20 p3603 A70-39831

Automatic control systems with signal recovery, determining invariance conditions, main operators and reproduction errors

20 p3603 A70-39833

Multidimensional automatic control systems polyinvariance, describing compensating cross couplings realization

20 p3603 A70-39834

Invariance conditions for inertial gyrostabilizer with powered stabilization system in presence of dynamic imbalance, noting improvement via compensating loop

20 p3670 A70-39846

Automatic stabilization of random noise mathematical expectancy and mean square deviation by feedback control system

20 p3593 A70-39916

Algorithmic random process pseudorandom number generator composed of analog computer elements, evaluating stability

20 p3594 A70-39918

Perturbation theory for nonlinear systems of differential equations

20 p3658 A70-40104

Recursive formulas for stability tests and quadratic loss functions evaluation for linear discrete time dynamical systems

20 p3659 A70-40114

Reliability of redundant repairable systems with preventive maintenance, determining mean time between failures

20 p3638 A70-40181

Feedback control systems stability over range of parameter changes, determining criterion satisfied by loop gain of rated system

21 p3801 A70-40795

Energy methods for stability of linear inflatable pouch actuator based on energy change in pouch deflection

21 p3760 A70-41966

Linear dynamic systems stability under various types of forces

22 p4061 A70-42536

Steady vibrations of mechanical system with asymmetrical restoring force, reviewing formulas for mean angular frequency and Fourier expansion coefficients

22 p4113 A70-42544

Periodic solutions to complex nonlinear automatic control systems with initial deviations, considering system stability and self oscillation conditions

22 p4002 A70-42839

Linear discrete feedback systems uniqueness, existence and stability under various input-output conditions

22 p4004 A70-43024

Amplitude instability in vibration testing systems, noting effects of bandpass filters in feedback loop of amplitude servo

22 p4006 A70-43250

Quasi-linear autonomous systems of second order equations, considering periodic solutions asymptotic stability

22 p4075 A70-43318

Criterion for global asymptotic stability of system with power-law nonlinearity, reducing to Nyquist criterion for linear system cases

22 p4063 A70-43428

Input-output stability of feedback systems, using inverse operator model

22 p4004 A70-43490

Automatic control systems small oscillations suppression by nonlinear correcting elements

22 p4005 A70-43564

Nonlinear differential equation systems overall stability, using qualitative methods

23 p4211 A70-44092

Stability theory for approximate solutions and differential approximations for differential equations in Banach space

23 p4212 A70-44345

Linear algebraic system stability and monotony, investigating plane structures by finite element method

23 p4213 A70-44996

Biological life support systems mass exchange processes analysis based on mathematical models, predicting artificial ecological systems stability

23 p4149 A70-45029

Low noise constant temperature hot-wire anemometer design with second order high-cut filter, determining system stability

23 p4199 A70-45050

Hydraulic servomechanism stability and step response, considering unequal oil volume on either side of jack

24 p4292 A70-45159

Continuous structural systems stability under random load excitation from linear partial differential equations of motion

24 p4421 A70-45281

Laser operation instability with nonlinear filter, deriving electrons differential velocity distribution functions on inhomogeneous emitter

24 p4352 A70-45469

Optimal asymptotic stability laws of control systems with unstable plant, using piecewise coordinate functions

24 p4321 A70-45494

Boundedness theorem for nonlinear Mathieu equation describing motion of parametrically excited system

24 p4380 A70-46042

Necessary and sufficient conditions on coefficients of real nonnegative polynomial $p(\omega)$, obtaining algebraic criterion for stability, optimality and passivity of dynamic linear systems

24 p4322 A70-46156

Nonlinear systems subharmonic oscillations under polyharmonic disturbance and viscous damping

24 p4427 A70-46378

Linear stationary systems rms stability under parametric disturbances by white noise random processes

24 p4427 A70-46379

SYSTOLE

On-line electronic integration of aortic flow during systole to provide beat by beat record of stroke volume

01 p0038 A70-11044

Functional and organic systolic murmur differentiation using phonocardiography test

03 p0420 A70-13478

Phonocardiographic and mechanocardiographic features of patients with nonejection clicks and mid- or late-systolic murmurs

03 p0427 A70-13944

Diastolic and systolic pressure measurement in acute and chronic experiments

09 p1627 A70-23302

Shock waves in unsteady aortic blood flow at systole beginning, considering aortic elastic properties and shock formation distances

11 p1992 A70-26479

Periodic high temperature effects on human systolic phase dynamics

12 p2174 A70-28359

Indirect serial determination of left ventricular systolic ejection time changes in human patients with acute transmural and nontransmural myocardial infarctions

23 p4144 A70-43946

Human left ventricle shape and movements during systolic contraction, using cineangiography and cineradiography of epicardial markers

24 p4302 A70-46076

Human atrial systole timing influence on mitral valve closure and on first renewed heart sound following blockage

24 p4302 A70-46077

SYSTOLIC PRESSURE

Frequency and postextrasystolic potentiations in guinea pig isolated auricles and dog heart in vitro and in situ, noting myocardial diagnostic use

02 p0235 A70-12088

Intact femoral artery pressure-diameter relationship in man, discussing noradrenaline infusions effects

18 p3222 A70-37222

Hemodynamic effect of lidocaine given by infusion and bolus injections in myocardial infarction, examining cardiac output, heart rate, systolic left ventricular and aortic pressures

19 p3366 A70-38575

Conscious rat systolic blood pressure measurement, using arterial pulse wave detection to occluding cuff by photoconductive cell

24 p4309 A70-46213

T

T SHAPE

Fatigue strength of T-shaped blade roots of steam turbine regulating stages subjected to combined static tension and cyclic bending

05 p0954 A70-17060

Stainless steel sheet-to-plate tee joint resistance welded by Magnetic Force Upset Welding process, testing performance

21 p3832 A70-40792

T TAIL SURFACES

Flutter investigation on model designed and constructed for tail unit of HFB 320 Hansa jet aircraft, discussing classical and statistical methods

04 p0775 A70-15180

Interference kernel discontinuities in integral equations relating amplitude of angle of attack and pressure distribution on T tail harmonically oscillating in subsonic flow

07 p1416 A70-20210

Empennage loads on T tail transport determined for combined vertical and lateral gust loads using real time analog-digital computer simulation

12 p2160 A70-27113

T TAURI STARS

Free-bound and free-free continuous emission of hydrogen near Balmer jump in T Tauri star AS209

03 p0566 A70-13315

T tauri star mass loss, observing variations in spectral emission line widths

22 p4101 A70-42858

Circumstellar dust cloud model of spectral distribution and anomalous excess emissions in IR T Tauri and red giant stars coincident with photometric measurements

23 p4239 A70-43868

T-33 AIRCRAFT

Kalman filtering and differential correction techniques applied to T-33 flight test data for aircraft system parameters identification

11 p1982 A70-26323

T-56 ENGINE

Structural design of boron/epoxy front housing for T-56 turboprop reduction gear case achieving reduced weight and increased stiffness [SAE PAPER 690666]

05 p0853 A70-15837

T-63 ENGINE

T-63 gas turbine engine air induction system protection for OH-58A light observation helicopter against debris with minimum power loss and intake air distortion

01 p0164 A70-10681

Sand and dust environmental test of T-63 regenerative engine, discussing performance depreciation, recuperator inspection and comparison with non-regenerative t63-a-5a engine

01 p0164 A70-10685

TABLES [DATA]

NT MATHEMATICAL TABLES

Worldwide data inventory of rock features associated with meteorite impact structures, including photomicrographs of petrographic features

01 p0069 A70-10223

Red subluminescent stars and high UV excess stars in region between main sequence and white dwarfs, tabulating observations of stellar color and magnitude

01 p0182 A70-10795

Comet observations analysis, tabulating total head magnitude, photometric parameters, nucleus magnitude, coma diameter, tail type and direction and magnitude correlation with solar activity

01 p0184 A70-10954

Photometric data for white dwarf low luminosity stars listed in color classes and proper motion fields

01 p0187 A70-11331

Quasars radio emission tabulated, showing quasar B264 as member of galactic cluster

02 p0372 A70-12244

Sudden comet brightness changes leading to discovery, tabulating and graphing comet discoveries

02 p0373 A70-12372

Time lag of commencement of PCA effect behind occurrence of Y-shaped phase of solar flares, tabulating data for several flares and particle effects

02 p0358 A70-12373

Venus photographs taken by 82-inch telescope /1950-1956/, tabulating data

02 p0378 A70-12556

Frequency equation for flexural vibration of simply supported beam, considering tabular procedure for cantilever beam

03 p0602 A70-14330

Pencil beam survey of radio sources at 178 MHz, with tabulated flux densities compared to 4C interferometer data

04 p0757 A70-15693

Tabular results of Galaxy mean and angular diameters and smallest/largest ratios measured on Palomar Atlas

05 p0906 A70-15797

Meteor rate data tabulated from controlled parameter radar survey of Southern Hemisphere activity, noting diurnal and annual variations

05 p0907 A70-16001

Natural vibrational frequencies of trapezoidal, triangular, circular and elliptical isotropic flat plates with different edge conditions tabulated

05 p0936 A70-16319

Chrysotile-type asbestos reinforcing fiber properties and applications, tabulating asbestos fiber types for commercial reinforced plastics

05 p0873 A70-16607

Graphite yarn, cloth and fiber composites physical properties tabulated, discussing multiply laminates for graphite-epoxy composites

05 p0873 A70-16610

Tabulated corrections of data concerning reduction of photographs of small planets obtained at Bucharest Astronomical Observatory

06 p1139 A70-17549

Solar X-ray flux from Explorer 33 and 35 observations, presenting catalog of tabular and graphical data

06 p1135 A70-18006

Chemical composition of scale formation in jet engine injectors for various fuel types tabulated, noting buildup levels in transport aircraft and subsonic jets

07 p1362 A70-18651

Perceived aircraft noise level based on objective acoustic measurements related to subjective response, tabulating noys as function of sound pressure

07 p1190 A70-18803

Fluids for aerospace power technology, tabulating properties of hydraulic, damper and heat transfer fluids, fuels, oils, etc

07 p1316 A70-18807

Catalog of lunar features brightness interpreted in terms of photometric function uniformity of lunar surface, considering second order light scattering

07 p1377 A70-18971

Light intensity and polarization in twilight sky atmosphere at solar depressions

07 p1263 A70-19047

Ionospheric data representation in tabular form for computer storage and processing, noting memory cells reduction

07 p1268 A70-19460

Group 4A difluorides vaporization thermodynamics and bond dissociation energies, tabulating mass spectra, vapor composition, reaction enthalpies, heats of polymerization and thermodynamic functions

07 p1319 A70-19889

Thermal conductivities and total emittance of Ta, W, Re and alloys at high temperatures compared with NBS values

07 p1313 A70-19894

Radiation Shielding Information Center computer code library for radiation transport or shielding calculations, listing programs available

07 p1239 A70-20364

Moon perigees and apogees for years 1-3000, tabulating parameters for calculations

08 p1568 A70-20635

Ti I spectrum oscillator strengths, determining formula for relative-absolute values transition

08 p1569 A70-20832

Catalog systems orientation based on major and minor planets observation, discussing zero points corrections

08 p1574 A70-21152

Double and multiple stars components magnitude differences tabulated based on visual and photometric observations

08 p1574 A70-21163

Ilyushin 62 aircraft geometry, propulsion, structure, onboard equipment and performance

08 p1436 A70-21365

Soviet helicopter and aircraft engines characteristics covering designer, power, rpm limits, fuel consumption, weight, geometry and applications

08 p1559 A70-21366

Cambridge one mile radio telescope observations of weak sources, extending radio source luminosity function and tabulating, graphing and mapping results

08 p1578 A70-21546

Long baseline interferometer observations of radio sources for size determination, tabulating measured fringe visibility

08 p1578 A70-21547

U.S. cryogenic refrigerators specifications in tabular form

09 p1655 A70-22291

Computer program for generating tables to calculate lunar libration at any epoch

09 p1752 A70-22313

H-function integrals for noncoherent isotropic scattering for two level atom, tabulating numerical values for Lorentz scattering profile

09 p1727 A70-22506

Planet Saturn right ascensions tabulation /1967, 1968/

09 p1756 A70-22651

Integrated lunar disk wavelength dependence of polarization using photoelectric polarimeter, tabulating results

09 p1759 A70-22910

Oxygen pressure, volume and temperature data and derived thermodynamic properties presented in tabular form

09 p1788 A70-22956

Radial velocities tabulated for late B-type north and south of equator listed in Catalog of Bright Stars

09 p1763 A70-23452

Bibliography of literature on bioengineering, biocontrol, medical physics, biotechnology, safety and human factors in technology

09 p1629 A70-23692

Solar radio observations tabulated for radioelectric flux density and behavior for three hour periods, average diurnal results, etc

10 p1940 A70-24414

Monograph on adhesive materials covering selection criteria tables, mechanical properties, specifications, surface preparation and joint strength

10 p1908 A70-25225

Commercial aviation gasolines inspection data tabulated and compared for 1969 and 1964 [SAE PAPER 700228]

11 p2099 A70-25897

Air pressure, air density and gravity tables, including corrections for mercury barometer measurements

12 p2222 A70-27008

Microwaves reflection, absorption and thermal emission at smooth air-water interface, tabulating calculated coefficients

12 p2183 A70-27169

Long period comets energy change due to planetary perturbations tabulated, obtaining orbital major axes before and after passage

13 p2489 A70-28906

Galactic X ray stars and X ray sources positions, appearance frequency and intensities

13 p2495 A70-29818

Table of Fraunhofer solar lines without Zeeman splitting

13 p2496 A70-29843

Earth frequency sounding based on geomagnetic field variations spherical analysis, tabulating nonconducting shell thickness, nucleus resistivity, etc

14 p2572 A70-30243

Gaseous monoxides dissociation energies and free energy functions tabulation for calculating partial pressures

14 p2545 A70-30902

Tabulation of minor planets positions observed by photographic equatorial at Bordeaux observatory

14 p2649 A70-31124

Tabulations of minor planets positions photographed at Besancon observatory

14 p2649 A70-31125

Loaded resonant circular loop radiation field patterns table, determining load impedance for antenna design

16 p2872 A70-32971

Thermal radiation configuration factors tables giving reference sources, discussing historical development of factors

16 p3002 A70-33947

Martian blue clearing during 1967 apparition photographic observational patrol tabulated and summarized

16 p2979 A70-34035

High velocity neutral hydrogen cloud observations, presenting tabulated characteristics and maps

17 p3170 A70-35439

Flux emissivity tables for water vapor, carbon dioxide and ozone based on wavelength dependent absorption coefficients and flux transmissivities

17 p3081 A70-35927

W-3 percent Re-W-25 percent Re thermocouple reliability and stability, describing emf vs temperature table in 0-2400 C range

18 p3257 A70-36200

Ionospheric data representation in tabular form for computer storage and processing, noting memory cells reduction

18 p3250 A70-36934

Lunar limb tabular position angles accuracy, discussing Watt charts used for star occultation examination

18 p3321 A70-37124

Apollo 11 and 12 results tabulated for soil packing characteristics, composition and rare gas analysis data

18 p3332 A70-37223

Uranus and Mars satellite relative measures, tabulating observations

19 p3516 A70-37932

Tables on thermal radiative properties of heated air covering absorption coefficients for wide range of photon energies and temperatures

19 p3552 A70-38009

German book on functional theory, Volume 6, tabulating theta and elliptic functions for application to applied physics, potential theory, fluid dynamics and oscillation theory

19 p3459 A70-38600

- Orbital elements of photographic meteors brighter than first magnitude, tabulating dates, solar longitudes, corrected radiants, velocities, major axis, etc
19 p3526 A70-38787
- Wind motions from meteor trails observation during IQSY, tabulating amplitudes and phases of constant, diurnal, semidiurnal and 8-hr components
19 p3526 A70-38788
- Visual binary stars orbits computation catalog from data obtained in 1939-1969 period
19 p3530 A70-38895
- Solar flares catalog with patrol time given on graphs, tabulating principal characteristics
20 p3588 A70-39467
- Be production, development, potential uses and properties
[ASM PAPER GG8-102] 20 p3650 A70-39970
- Supernova remnants catalog based on radio surface brightness, deriving galactic distribution and testing theories for nonthermal radio sources evolution
20 p3709 A70-40077
- Numerical methods, FORTRAN program and table form for complex integrals evaluation along unit circle in positive direction
20 p3605 A70-40120
- Millimeter waves atmospheric attenuation vs frequency and altitude due to oxygen absorption, tabulating for graphical and seasonal model atmospheres
20 p3588 A70-40302
- OSO far UV solar spectroheliograms atlas, describing instrumentation, data acquisition, etc
20 p3713 A70-40540
- Textolite and fiberglass-reinforced plastics relaxation parameters tabulation for viscoelasticity boundary value problems solution
21 p3842 A70-40650
- Oxygen-kerosene fuel combustion products thermodynamic properties, tabulating computed values
21 p3865 A70-41771
- Stellar polarization measurements in Magellanic Clouds, tabulating position, magnitude, spectral type, percentage polarization and electric vector position angle
21 p3922 A70-41979
- Unidimensional composite materials nonstructural applications, tabulating characteristics
21 p3840 A70-42148
- Critical values tables for Wilcoxon rank sum test in randomized blocks
22 p4064 A70-43729
- Lunar craters size-frequency distributions from photographic analysis, tabulating results
23 p4247 A70-44770
- Earth frequency sounding based on geomagnetic field variations spherical analysis, tabulating nonconducting shell thickness, nucleus resistivity, etc
24 p4332 A70-46318
- G8, IV subdwarf 31 Aql spectrum at 4000-6600 Å, discussing Ba II 4554 Å, G and CN bands and spectral lines
24 p4414 A70-46329
- Neutral hydrogen 21 cm line profiles in galactic plane, tabulating terminal positive velocity and brightness temperatures
24 p4414 A70-46381
- TABS [CONTROL SURFACES]**
- Nonlinear balance mass solutions for tab-aileron flutter free operation of jet trainer for arbitrary store configuration
17 p3185 A70-34923
- Hovercraft wind directional stability and control by cam operated fin-tab assembly
19 p3357 A70-38942
- Fin slots and tabs effect on dynamic stability characteristics of low drag bomb, discussing free rolling and pitching tests
21 p3747 A70-41880
- TACAN**
- Self contained and ground referenced radio systems combination for tactical air navigation, including Loran D and hybrid Loran /HYLO/
04 p0716 A70-14628
- Tacan navigation system developments for accuracy and reliability improvements, data transmission, tie-in with airborne computers, etc
07 p1331 A70-19621
- Sector Tactical Air Navigation System to supply on-board information on bearings, slant range and elevation and computer input signals
09 p1720 A70-22491
- Sector-TACAN /SETAC/ system suitable for mobile approach and landing aid due to high accuracy and small dimensions
09 p1721 A70-22663
- Harrier communications and radio navigation aid VLF/UHF and TAC/VHF equipment
10 p1841 A70-24849
- Computerized aircraft navigation utilizing Doppler dead reckoning system and Tacan integration with least square adjustment method
13 p2447 A70-28550
- Pilot landing aids for increasing air traffic, discussing Integrated Communication Navigation Identification
13 p2449 A70-29053

Lx band characteristics and utilization, describing evolutionary systems based on TACAN and IFF
16 p2948 A70-33452

TACHISTOSCOPES

- Rhesus monkeys impaired discrimination in recognizing tachistoscopically presented objects following cortical polarization
05 p0802 A70-16625
- Perceptual tuning in tachistoscopic identification task with alternatives provided after or before and after stimulus
11 p1986 A70-25829

TACHOMETERS

- Multiplying digital device for measuring motor speed, torque and power, discussing optional applications and design
02 p0297 A70-12076
- Magnetic recording in airborne systems, discussing printed motor-optical tachometer design for transport accuracy and ferrite spin-alloy heads
21 p3829 A70-41921
- Multipurpose transistorized tachometer for rotating body speed measurement, control and recording, using electronic integrator and magnet pickup
21 p3831 A70-42245

TACHYCARDIA

- Artificially induced heart rate changes effect on atrial circumference and pressure in anesthetized cats, showing increase with tachycardia and bradycardia
01 p0017 A70-10473
- Dogs coronary vasodilator responses to hypoxia and induced tachycardia before and after lidoflazine and adenosine
02 p0230 A70-11702
- Arrhythmia resembling atrial flutter simulated in dogs by coronary sinus and left atrial pacing and in man by coronary sinus pacing
02 p0240 A70-12696
- Human heart chronotropic reactions during centrifuge acceleration tests up to tolerance limit, establishing sinus tachycardia in various degrees
05 p0804 A70-17120
- Wolff-Parkinson and White syndrome applicability in aeromedical appraisal for aircrew selection, noting effects of paroxysmal tachycardia
17 p3040 A70-35916
- Multifocal atrial tachycardia, discussing arrhythmia progression to atrial fibrillation and association with acute and chronic diseases
21 p3761 A70-41134

TACHYONS

- Faster-than-light particles impossibility in causal loops using nonquantum special relativity framework, considering tachyons
24 p4378 A70-45424

TACTICAL AIR NAVIGATION**U TACAN****TACTICS**

- Harrier aircraft operation in Marine Corps for fast reaction close support based near maneuver units
[SAE PAPER 700835] 24 p4290 A70-45887
- TACTILE DISCRIMINATION**
- Tactile control in man machine systems using feed-forward loops to provide rate information, noting unmanned aircraft and machine-tool applications
[ASME PAPER 69-WA/BHF-14] 04 p0642 A70-14855

Cortical induction phases estimated by retinal mobility index concerning activity of acoustic, olfactory and cutaneous analysors
08 p1443 A70-20735

Vibrotactile display operational skill acquisition, discussing stimuli quality and spacing effects on lumen of temporal ordering of sensory events in haptic space
13 p2354 A70-29596

Auditory and cutaneous sound localization acuity
13 p2354 A70-29597

Skin and tissue mechanical characteristics response to vibratory stimulation, considering effects on physiological and psychophysical tactile sensitivity measurements
13 p2354 A70-29598

Compensatory tracking task with tactile displays determining gains and body locations by describing function and error power analyses
13 p2354 A70-29599

TACTILE SENSATION**U TOUCH****TAGGING****U MARKING****TAIL ASSEMBLIES****NT SWING TAIL ASSEMBLIES**

Flutter investigation on model designed and constructed for tail unit of HFB 320 Hansa jet aircraft, discussing classical and statistical methods
04 p0775 A70-15180

Helicopter tail rotors aerodynamic characteristics, using statistical methods for planning experiments and interpreting results
05 p0793 A70-15900

High speed helicopter with fixed wings and longitudinal axis tail rotor
05 p0794 A70-16349

Drag reduction on blunt-based body of revolution with boat-tailed afterbodies in low speed flow
05 p0790 A70-16501

Tail screens and spoiler rings aerodynamic braking effect in hypersonic range, discussing separated boundary layer periodic unsteady flow
06 p0965 A70-17247

Composite tail rotor driveshaft for next generation helicopter, discussing materials, fabrication and tests
[AHS PREPRINT 451] 17 p3100 A70-34703

Boeing 2707 SST horizontal tail multiple channel actuation system features
17 p3020 A70-35827

Aft tail and canard configurations trim drag considerations for maneuvering aircraft
[AIAA PAPER 70-932] 17 p3021 A70-35842

Fenestron shrouded tail rotor for SA 341 Gazelle helicopter eliminating ground contact during approach and landing
23 p4140 A70-44322

Main rotor wake adverse effects on tail rotor directional control in low velocity wind
23 p4140 A70-44323

Tail rotor thrust increase for yaw control via increased blade area, higher tip speeds and cambered airfoils
23 p4140 A70-44324

TAIL MOUNTINGS**U TAIL ASSEMBLIES****TAIL PLANES****U HORIZONTAL TAIL SURFACES****TAIL SURFACES****NT HORIZONTAL TAIL SURFACES****NT T TAIL SURFACES****TAILLESS AIRCRAFT****NT AVRO 707 AIRCRAFT****NT F-106 AIRCRAFT****NT VULCAN AIRCRAFT**

Tailless delta Avro Vulcan aircraft design, hardware and flight results
14 p2532 A70-31391

TAILS [ASSEMBLIES]**U TAIL ASSEMBLIES****TAKEOFF****NT VERTICAL TAKEOFF**

Optimal operational control of aircraft takeoff and landing times using stochastic programming
11 p2077 A70-25608

Longer runways for increased airport safety indicated from data concerning overruns, undershoots and veering, discussing certification testing during takeoff and landing
12 p2208 A70-27994

Pilot disorientation in dark night takeoff accident type, presenting illusory angular displacement of vertical, flight paths and sequential accelerations
13 p2359 A70-29441

Boeing 747 pilot transition training, discussing takeoff, landing, eyelevel, flareout taxi speeds, inertial navigation and electrical, fuel and hydraulic systems
20 p3562 A70-40083

Ground Effect Takeoff and Landing /GETOL/ aircraft, evaluating engine absorption capability of air cushion landing gear in touch-down condition
22 p3961 A70-42282

Aircraft longitudinal motion during takeoff and landing due to loss of lift after boundary layer control system failure
24 p4372 A70-45448

TAKEOFF RUNS

Transport aircraft takeoff length reduction by applying various runway inclinations with respect to takeoff accelerations
02 p0275 A70-12223

Accelerate-stop distance problem in takeoff refusal due to critical engine failure, emphasizing runway limited length hazards
08 p1436 A70-21270

Integrated glide path localizer system for landing, takeoff and enroute guidance through rugged country, minimizing spurious reflection, required information bits, etc
09 p1720 A70-22222

Takeoff noise minimization by prescribing optimum takeoff trajectories, considering aircraft parameters influencing noise intensity at takeoff
11 p1979 A70-25814

Pitch and Coriolis illusions effects on pilot pitch angle adjustment in simulated takeoff
15 p2689 A70-31885

Pilots brake-takeoff decision at critical engine failure speed, discussing operational aspects of accelerate-stop criteria
15 p2675 A70-32219

Aircraft landing and takeoff difficulties and dangers due to mud and water on runways, discussing coping methods
17 p3057 A70-34692

Optimal longitudinal takeoff trajectories, formulating obstacle clearance criterion function based on aircraft design parameters effects
[AIAA PAPER 70-963] 20 p3560 A70-39566

Commercial STOL aircraft takeoff and landing physical parameters relationships based on wind tunnel and flight tests
[AIAA PAPER 70-1238] 24 p4292 A70-45959

TAKEOFF SYSTEMS**U AIRCRAFT LAUNCHING DEVICES**

TALKING
 NT WORDS [LANGUAGE]

TALOS MISSILE
 Electromagnetic interference (EMI) effects on TALOS missile guidance receiver by expanding computer simulation test results 14 p2655 A70-31345

TANDEM ROTOR HELICOPTERS
 NT CH-46 HELICOPTER
 NT CH-47 HELICOPTER

TANDEM WING AIRCRAFT
 NT X-22A AIRCRAFT
 Flexible flight vehicles longitudinal stability with tandem lifting surfaces, studying aerodynamic time delay effects by root locus technique 03 p0408 A70-13802
 German monograph on oscillations of tandem wing without outgoing wake in plane incompressible flow, using numerical computations 17 p3011 A70-35372

TANGENTS
 Aircraft wing ribs tangents plotting procedure using Monge diagram 08 p1507 A70-21197
 Analytical algorithm for tan-chord angle tangent determination, assuming undevelopable ruled wing surface defined by three cross sections 10 p1802 A70-24292
 Spacecraft principal inertial axis orientation estimation, comparing tangent 2 theta method with eigenvalue solution [SAWE PAPER 847] 20 p3660 A70-40361

TANK GEOMETRY
 Computerized calculations for cylindrical tank bottoms with outlet based on strength analysis, using zero moment theory for surface stability under uniform pressure 05 p0946 A70-16957
 Simulated low gravity propellant sloshing in spherical, ellipsoidal and cylindrical tanks, discussing Bond number simulation and tank geometry effects [AIAA PAPER 69-1004] 09 p1657 A70-23255
 Spontaneous ignition temperature as function of surface-to-volume ratio in static systems for fuels 11 p2151 A70-26384
 Viscosity and vessel geometry effects on fluids natural and forced oscillation, taking surface tension into account 20 p3614 A70-40438
 Principle pressure vector components for liquid in moving V-shaped and U-shaped cross section tanks 23 p4180 A70-44164

TANKS [CONTAINERS]
 NT CYLINDRICAL TANKS
 NT FUEL TANKS
 NT PROPELLANT TANKS
 NT SPHERICAL TANKS
 NT STORAGE TANKS
 NT WING TANKS
 Computerized calculations for cylindrical tank bottoms with outlet based on strength analysis, using zero moment theory for surface stability under uniform pressure 05 p0946 A70-16957
 Automatic control for filling tanks with stably stratified liquids using analog mixture valve and digital metering pump methods 06 p1062 A70-17617
 Sizing and design of large vessels of fiberglass reinforced composites based on minimum cost 07 p1409 A70-19757
 Electrostatic ignition discharge prevention on fiberglass reinforced depot tanks, noting ground connection safeguard 07 p1295 A70-19763
 Vortex generation in water tank, discussing velocity distribution on free surface and critical depth of air entrainment for various Reynolds numbers 14 p2567 A70-31275

TANTALUM
 Aluminum oxide solid state reaction with Ta at high temperatures using chemical analysis 03 p0511 A70-13487
 High temperature effects on mechanical properties of recrystallized Ta relating strength, hardness and yield point 04 p0707 A70-15267
 Threshold oxygen concentration for corrosion determined for Ta specimens subjected to low pressure contamination in NaK 04 p0709 A70-15628
 Hall voltage measurements on Ta thin films using square wave generator current, discussing parasitic effects and suppression possibilities 05 p0863 A70-16366
 Dislocations and interstitial atoms interactions in Ta, investigating internal friction and deformation resistance and rate dependence on temperature 07 p1309 A70-19637
 Tantalum mechanical properties dependence during deformation on temperature and strain rate irregularities, discussing serrated yielding 10 p1904 A70-24386
 Tantalum RF sputtered superconducting films structure and properties at various substrate temperatures,

observing bcc, fcc and amorphous phases by electron microscopy 12 p2288 A70-27876
 Ta solid solution hardening by nitrogen and oxygen, noting yield stress variation with interstitial gas concentration 13 p2434 A70-29084
 Hydrogen impurities anelastic relaxation effect on internal friction alpha peak in cold worked tantalum and niobium 13 p2435 A70-29350
 Ta thin film integrated circuit technology including resistor and capacitor elements, conductors, crossovers, etc 14 p2625 A70-30284
 Tantalum single crystals elastic constants temperature dependence, considering compressibility and shear properties 14 p2596 A70-30841
 Dislocation distribution in Ta foil following yield point fatigue testing, using thin film electron microscopy 15 p2761 A70-32385
 Ta oxygen concentration effects on corrosion resistance to NaK in SNAP 8 boilers 16 p2932 A70-34202
 Pure Fe and Ta hot hardness using ultrahigh temperature hardness tester 17 p3124 A70-34659
 Adherent Ta films deposition onto Teflon disks by sputtering 18 p3264 A70-37098
 Ta single crystal inherent lattice and interstitial solution hardening, discussing impurity doping effect on flow stress thermal component 21 p3839 A70-40902
 Pure Fe and Ta hot hardness tests by ultrahigh temperature tester involving use of electron microscope 21 p3840 A70-41900
 High speed photoelectric pyrometry of Ta heat capacity at high temperatures induced by pulse heating 23 p4207 A70-44441
 Ta spectral emissivity, using ratio of specimen surface and black body spectral radiant intensities 23 p4207 A70-44447
 Thermal decomposition of freeze dried Ta and mixed lithium-niobium oxalate, using surface area and electron micrographs 24 p4363 A70-46212
 Oxygen and nitrogen adsorption on thin tantalum films, measuring pressure, electrical resistivity and temperature 24 p4363 A70-46219

TANTALUM ALLOYS
 Tantalum base alloy T-111 creep tests in vacuum at elevated temperature suggesting diffusion controlled microcreep mechanism 01 p0120 A70-10738
 Structural design and fabrication of load bearing Ta alloy radiation cooled eleven control surface for high L/D hypersonic flight vehicle 02 p0306 A70-11941
 Stress concentration effect on mechanical properties of Ti-Ta alloys at low temperatures, showing insensitivity to notch and suitability for cryogenics 05 p0864 A70-16869
 Thermal diffusivity measurements for Ta-W, Ta-W-Hf, Hf-Ta-Mo alloys using pulse technique 07 p1305 A70-18960
 Carbide layer formation on Ta and Ta-W alloys, discussing Ta-C phase diagram and phases 07 p1320 A70-19892
 Ordered Ni8Ta phase in nickel-rich binary alloy using electron microscopy and diffraction analysis 09 p1705 A70-22808
 Cleavage fracture of Ta-Mo bcc alloys, investigating short range ordering and size effects by X ray diffraction 09 p1708 A70-23573
 Phase diagram of Ti-Ta-Cr system, plotting isothermal and polythermal sections by microstructural and X ray analysis 09 p1709 A70-23787
 Phase diagram of Ti-Ta-V system, determining solubility of sigma Ta and V in alpha and beta Ti in solid solutions 09 p1709 A70-23788
 Tantalum solubility in alpha titanium and Ti-Ta system physicochemical properties using metallographic, X ray, hardness and resistance analysis 10 p1903 A70-23864
 Ultrahigh vacuum creep rate measurements with continuously increasing loads on Ta-base alloy, relating creep life with temperature and stress rate 17 p3122 A70-34552
 Nb-Ta and Nb-Mo alloys single crystal solid solution strengthening as function of composition, temperature and strain rate 20 p3646 A70-39105
 Annealing temperature effect on creep rupture strength of Ta-W-Hf alloy 22 p4054 A70-42741
 Chemical composition effects on heat resistance, elastic properties and density of Ti-Ta alloys 24 p4360 A70-45830

Solid solution hardening of single crystal Ta base alloys, measuring critical shear stress at various temperatures 24 p4365 A70-46370

TANTALUM CARBIDES
 Strain field association with random TaC precipitate particles in austenitic stainless steel shown by electron microscope 01 p0123 A70-11242

TANTALUM COMPOUNDS
 NT TANTALUM CARBIDES
 NT TANTALUM OXIDES
 Free energies of formation determined for tantalum silicides from EMF measurements on cells with solid thoria-ytria electrolytes 01 p0041 A70-10084
 Optical phonons in mixed sodium potassium tantalate crystals as function of temperature and composition, using IR and Raman spectra 03 p0542 A70-14002

TANTALUM OXIDES
 Tantalum oxide thin films electro-optical effects due to refractivity changes 19 p3488 A70-38203

TAPE MERGING
 U DATA PROCESSING
 U MAGNETIC TAPES

TAPE RECORDERS
 Bit-slippage errors due to onboard tape recording of PCM/FM telemetry data for Apollo Telescope Mount, noting roles of S/N ratio, data characteristics, etc 01 p0044 A70-10940
 On-line system transmitting experimental data from optical spectrometer to central computing facility for magnetic tape recording 05 p0818 A70-16846
 Simultaneous high speed shock tunnel data acquisition system using single tape recorder, analog or digital readout and computerized reduction 06 p1031 A70-18604
 Tape recorder performance characteristics relevant to signal types handled, considering phase response and envelope delay 09 p1679 A70-22975
 Solar radio bursts dynamic spectra by magnetic tape recording of digital signal, obtaining frequency and time profiles and intensity layers 10 p1934 A70-25276
 Processing system for tape recorded signals with nonelectrical varying parameters 11 p2056 A70-26456
 Statistical classifier for analyzing tape recorded transients 11 p2056 A70-26457
 Linear superposition (LSP) of isolated pulses in tape recording, discussing validity for multitbit waveform synthesis 11 p2057 A70-26627
 Airborne data acquisition on high density computer tape for aircraft handling and flight dynamics research 17 p3049 A70-35499
 Magnetic tape recorder for panoramic vertical ionospheric sounding data acquisition in digital form 18 p3261 A70-37041
 Magnetic recording in airborne systems, discussing printed motor-optical tachometer design for transport accuracy and ferrite spin-alloy heads 21 p3829 A70-41921

TAPER
 U TAPERING

TAPERED COLUMNS
 Contour notch position effects on stress concentration in taper section of dumbbell shafts, using photoelastic shaft models and cyclic tests 13 p2517 A70-29750

TAPERED WINGS
 U SWEPT WINGS

TAPERING
 Monograph on buckling and postbuckling behavior of plates tapered in planform, comparing stability of tapered and rectangular plates 03 p0586 A70-13002
 Tapered spherical shell under constant initial pressure calculated for strength, stiffness and durability on digital computer using numerical algorithm 11 p2134 A70-25846
 HE sub 11 mode launching in optical communication system, considering fiber tapering effect on excitation efficiency 16 p2875 A70-33400

TAPES
 Thermal control pressure sensitive adhesive tapes for spacecraft applications, discussing properties degradation due to simulated terrestrial and space environments 11 p2067 A70-26366
 Automatic electronics test equipment, discussing choice between tape or computer controlled interpreter systems based on language, time, versatility and cost 23 p4173 A70-44539

TARE [DATA REDUCTION]
 U DATA REDUCTION

TARGET ACQUISITION

Missile miss distance evaluation model with emphasis on statistical nature, noting application to systems analysis

01 p0193 A70-10118

K factor analysis of target visibility, considering target size contrast, background luminance, glare, atmospheric scattering and optical sight parameters

01 p0142 A70-10420

Airborne sensor simulator using recorded imagery for target detection and recognition problems, discussing closed circuit TV

01 p0088 A70-10810

Transportable telemetry acquisition system (TTAS)/as mobile tracker featuring pseudomonopulse method

01 p0045 A70-11120

Photointerpreters information extraction, studying psychological effects of image contrast and resolution on accuracy of target detection

02 p0300 A70-12459

Algorithm for optimal controls maximizing probability of linear time dependent control processes entering target manifold under random disturbances

03 p0460 A70-13580

Efference role in eye tracking of moving targets, discussing oculomotor system role

03 p0439 A70-14345

Pulsed radar fluctuating echo digital-detection and false alarm probabilities assuming Rice signal distribution with noise

04 p0649 A70-15065

Prediction errors lower bound for accuracy in predicting future position of randomly accelerating target

04 p0652 A70-15342

Computer controlled radar guided tactical missile system using digital techniques in performing target detection, acquisition, tracking and illumination

05 p0814 A70-16328

Policies and controller design for pursuing vehicle developed in terms of pursuit-evasion differential games

06 p1025 A70-17955

Visual tracking of horizontally moving object, noting acuity dependence on target angular velocity and observation time

08 p1444 A70-20745

Display design for improved target detection performance taking into account human attention to display field areas

08 p1452 A70-21301

Fixed target pursuit-evasion differential game based on pursuer-evader proximity as termination condition

11 p2073 A70-26242

Tracking of goal seeking attack vehicles, discussing error improvement and destination estimating by tracking station observer

11 p2080 A70-26243

Binary-coded sequential acquisition spacecraft ranging system operating at weak signals using HF digital logic

11 p2009 A70-26252

Quasi-optimum proportional navigation for attack situations with large missile and target maneuvers, showing advantage over linearized optimization

11 p2081 A70-26316

Azimuth measurement techniques for success-run detectors

11 p2019 A70-26712

Radar beacon target processing system providing ATC information, noting target detecting and locating ability in noisy environment

12 p2268 A70-27640

Aperture field modal decomposition of optical system in terms of integral equation eigenfunctions during detection and estimation of incoherent objects

12 p2273 A70-28121

Pursuit game problems with pursuer and target described by k-dimensional phase vectors, discussing evasion problems

13 p2452 A70-29276

Radar target optimal detection algorithms in cloud of passive reflectors, noting space surveillance regularities

15 p2696 A70-31516

Antenna array system for surface target detection in receiver noise and heavy clutter by space-time decision theory

16 p2860 A70-32954

Laser ranging and tracking for high velocity targets, discussing SNR considerations, ambiguity resolution, error analysis, measurement centroid and target acquisition

16 p2862 A70-33165

Modulation transfer function (MTF)/systems analysis with emphasis on target acquisition, relating image contrast characteristics of target and background

16 p2907 A70-33185

Optimal interceptor-target allocation and guidance for linear interception and rendezvous using real time and storage computer

16 p2947 A70-33311

Displayed cursor velocity effect on radar target acquisition time for subjects in simulated air defense environment

16 p2853 A70-33670

Optimal Kalman tracking filter performance estimation for manned maneuvering targets

16 p2949 A70-34057

Quasi-optimal feedback control method for minimum time intercept of target in central force field

19 p3393 A70-37865

Air to air missile launch range maximization for plane trajectories and nonmaneuvering targets, discussing optimal fuel burning rate

[ALAA PAPER 70-980] 20 p3668 A70-39549

Deorbiting target intercept energy optimization by game theory approach

[ALAA PAPER 70-1019] 21 p3848 A70-41778

Target velocity estimation by lidar, examining range measurements with time response and cross correlation technique

22 p3988 A70-42567

Visual target tracking with active head rotation, indicating independent eye response due to vestibulo-ocular reflex

22 p3979 A70-43492

TARGET DRONE AIRCRAFT

Supersonic aerial target wing synthesis using sandwich construction with graphite-epoxy laminate skins bonded to Al honeycomb, achieving significant weight reduction

12 p2160 A70-27118

TARGET PENETRATION

U TERMINAL BALLISTICS

TARGET RECOGNITION

Moving targets automatic identification by radar signals digital processing, describing radar echoes properties, moving window detector system and circuits design

01 p0137 A70-10358

Airborne sensor simulator using recorded imagery for target detection and recognition problems, discussing closed circuit TV

01 p0088 A70-10810

Target-field luminance or duration effect on target susceptibility to masking demonstrated in visual backward masking study

01 p0039 A70-11163

Atmospheric water vapor effect on contrast between natural target and sky via spectrophotometric method, exploring target visibility and contrast relations

02 p0325 A70-11873

Terrain computerized mathematical model for determining unobstructed line of sight between observer and target

03 p0455 A70-14172

Analog computer schemes for solving dynamic plants identification reducible to optimizing parametric problem of many variables function

04 p0654 A70-15435

Time delay between ocular movement and retinal input by yoking visual target to eye movement using real time computer systems

05 p0805 A70-16094

Wideband transversal coaxial cable delay lines used for improving radar systems target recognition by eliminating misleading signals and distortion

05 p0822 A70-16723

Classification analysis methods application to plant identification for case with incomplete initial statistical information

06 p1014 A70-17632

Optimal colors for target and rescue markers, discussing influence on signal detection, response and identification

06 p1002 A70-17713

Bounded approximations to average multitrial detection probabilities over slowly fading radar target

06 p1013 A70-18627

Visual backward masking facilitation dependence on target duration as opposed to interstimulus interval or target-onset/mask-onset interval durations

07 p1221 A70-19850

Nonlinearity of human eye movement control system in two dimensional tracking tasks, explaining visual axis lags as time delays dependent on target motion

08 p1447 A70-21724

Harrier navigation/attack system to provide successful single pass attack for close support and strike roles, noting target finding optimization

10 p1914 A70-24847

Optimum binary digital detector of radar targets, using confidence ratio as criterion of target presence

12 p2182 A70-26890

All-or-none hypothesis of selective sensory attention, discussing simple stimuli, target detectability and switching time

15 p2681 A70-31790

Low light level TV systems performance relationship to visual acuity requirements, considering interfering noise characteristics effect on target recognition

16 p2903 A70-33130

Real time video data display at visual and thermal IR wavelengths, demonstrating performance improvement for target recognition

16 p2910 A70-33436

Target signature concept of spectral, spatial, temporal, and polarization effects to develop electromag-

netic signatures against background, considering remote sensor system design

16 p2910 A70-33437

Attack helicopter fire control system with day and night detection, recognition and kill capabilities, discussing system components, operation and reliability

17 p3043 A70-34732

Visual air-to-ground target recognition simulation, comparing predictions from Autonetics Detection Model in low altitude flight

24 p4308 A70-45507

TARGET THICKNESS

Hypervelocity impact computerized calculations, considering material response, laminated meteor bumpers, hollowed projectiles and thick target cratering

15 p2823 A70-32787

Hypervelocity impact of spheres on thin targets using numerical solutions utilizing STEEP code two dimensional technique based on hydrodynamic elastoplastic model

16 p2991 A70-33853

Angular distribution of thick target bremsstrahlung produced by electron bombardment of Be, Sn and Au surfaces

21 p3854 A70-42020

TARGETS

NT RADAR TARGETS

NT TARGET DRONE AIRCRAFT

Two step optimal motion of target and pursuer with thrust vector control in vacuum under arbitrary gravitational field, determining distance strategy

02 p0272 A70-12405

Supersonic jet force acting on target investigated for air and argon using dimensional analysis

10 p1804 A70-25122

Central shock and target displacement of under-expanded supersonic jets with obstacle at nozzle exit, using Toepler schlieren photographs

12 p2156 A70-27293

Supersonic jet force acting on target investigated for air and argon using dimensional analysis

20 p3560 A70-40515

TARS

Solid tar deposits from hydrocarbon fuels oxidation during prolonged storage

12 p2289 A70-27494

TASK COMPLEXITY

Image quality effects on human performance in simulation, discussing time sharing strategies and task difficulty factors

01 p0036 A70-10809

Heart rate and skin conductance measurements during attention-direction tasks involving proprioceptive stimuli position on environmental acceptance and rejection continuum

01 p0026 A70-11166

Task interference model for interference among two or more continuous manual control tasks, suggesting metric for pilot mental work load

02 p0244 A70-12139

Information storage and retrieval system development and operation for diversified crew/equipment task data, using general purpose digital computer

02 p0265 A70-12143

Experienced and naive subject evaluation of probabilistic data, data source determination and prediction of subsequent data in complex decision task

02 p0247 A70-12379

Event probability and cost effects on performance in continuous motor task

03 p0436 A70-13771

Cost/schedule planning and control system (C/SPCS) providing early exposure of inadequacies in work execution and initial planning

05 p0959 A70-16461

Pilot and copilot task distribution schedules adopted by European civil aviation for landing approaches under poor weather conditions

08 p1542 A70-21850

Drug-alcohol and hypoxia effects on multiple task operator performance tested at altitude and pressure chamber treatments

08 p1448 A70-21939

Speed-accuracy interrelationship in human performance as operating characteristic for reaction time under variety of task conditions

10 p1826 A70-24712

Three phase code transformation task for human subjects, determining memory aid role in problem solving phase from factor analysis

13 p2361 A70-30019

Optimum attention allocation, discussing distraction resistance and multiple task performance

19 p3362 A70-38316

Enhanced evoked potentials sited by auditory stimuli in complex task, considering EEG and neurophysiological basis of selective attention

19 p3363 A70-38318

Human monitoring behavior, discussing display, task and organismic variables effects

19 p3363 A70-38323

Avionics digital computer system using associative memory for executive control functions implementation to mechanize task assignment algorithm 22 p3994 A70-43105

Expert judgments validity of human task performance time against empirical measures for use in analytical modeling 24 p4308 A70-45515

TASK SEQUENCERS
 U CONTROL EQUIPMENT
 U SEQUENTIAL CONTROL

TASKS
 NT AUDITORY TASKS
 NT VISUAL TASKS
 Classical human reaction time as function of high and low auditory signal rates in vigilance setting, supporting inhibition theory of vigilance decrement 04 p0640 A70-15646

TASTE
 Flavor sweetening preference in high protein and high fat diets, basing human subjects experimental range on choice of formulas 07 p1216 A70-18948

TAURUS CONSTELLATION
 IR spectra of M stars and alpha Tau obtained with Michelson interferometer, observing molecular features and water vapor absorption 04 p0747 A70-14548
 RW Aur-type variables in Taurus, studying temporal variations from photographic and photometric observations and B, B-V diagram 07 p1376 A70-18906
 Sun effect on anomalous frequency shift in 21 cm absorption spectrum in Taurus A 11 p2108 A70-25659
 Scorpio X-1 and Taurus X-1 /Crab/ X ray flux effects on nighttime ionospheric radio transmission, discussing ion production and resulting electron density 14 p2631 A70-30541
 Galactic structure of Milky Way towards Taurus based on two dimensional classification and three color photography of star group 15 p2797 A70-31621
 Taurus X-1 X ray emission polarization, using rocket-borne polarimeter 17 p3150 A70-34845
 Cold neutral atomic hydrogen in Taurus dust clouds from 21 cm line dips in radiotelescope observations 21 p3887 A70-41108
 Be star HD 37202 zeta Tauri II envelope instability, discussing radial velocities, profiles, line width and electron density in layers 21 p3888 A70-41119
 IR star types T-Tauri, B-emission and M supergiants observations using UBVRI photometry 21 p3890 A70-41163

TAXIING
 Airport surface traffic system analysis, discussing control and guidance isolation, information acquisition/processing and response actions [ALAA PAPER 69-1086] 01 p0137 A70-10630
 Forced vibration in taxiing aircraft interaction with ground structure 14 p2563 A70-30699
 Visual display and automatic taxi guidance system testing for improved aircraft docking accuracy [ALAA PAPER 70-916] 17 p3064 A70-35828
 Boeing 747 pilot transition training, discussing takeoff, landing, eyelevel, flareout taxi speeds, inertial navigation and electrical, fuel and hydraulic systems 20 p3562 A70-40083

TAXONOMY
 Preliminary taxonomy for errors in serial, self-paced choice reaction time experiments, discussing speed-error tradeoff 19 p3362 A70-38313

TAYLOR INSTABILITY
 Torque and flow patterns in supercritical Taylor instability regime of circular Couette flow 03 p0470 A70-14235
 Taylor instability of vertically accelerated horizontal two dimensional interface between liquid and air solved by method of strained coordinates 09 p1661 A70-23071
 Taylor-Goertler vortex formation effect on heat transfer through boundary layer on concave wall [ASME PAPER 69-HT-3] 09 p1790 A70-23556
 Convective flow stability in rotating fluid layer under rigid boundary conditions, calculating critical Taylor number as function of Prandtl number 16 p2893 A70-33686
 Stability conditions for relativistic stars, discussing mass-energy density distribution, Taylor instability, Schwarzschild criterion, Newtonian stellar model, gravitational red shift, etc 22 p4104 A70-42999

TAYLOR SERIES
 NT MACLAURIN SERIES
 Second vertical derivative of gravity field, using formulas based on Taylor series expansion method 06 p1055 A70-17604

Solar system planetary mean motions calculation from characteristic equations roots at equilibrium points of restricted three body problem, using Taylor series solution 09 p1760 A70-22915

Earth shape formulas reduction to Taylor series, considering Molodenskii solution method for simple layer density integral equation 09 p1670 A70-23343

Time-convergent approximations to statistical turbulence functions constructed starting with functions expansion as Taylor series in time 11 p2074 A70-26534

Multiterminal electronic networks computerized fault detection based on linearized Taylor expansion algorithm 12 p2197 A70-27932

Asymptotic turbulent boundary layer semiempirical Taylor formula, investigating average motion formed in mixing jet region and surrounding liquid 20 p3611 A70-39809

TAYLOR THEOREM
 U TAYLOR SERIES

TD-1 SATELLITE
 TD-1 satellite design and scientific payload [DGLR-69-11] 04 p0762 A70-15142
 TD-1 satellite design and scientific payload 09 p1767 A70-23429
 Digital orbital clock and telemetry adapter for TD1A satellite attitude stabilization, describing mechanical structure 21 p3798 A70-41272
 ESRO satellite projects IRIS/ESRO 2, Aurorae/ESRO 1, HEOS-A1 and future TD-1 and HEOS-A2 23 p4264 A70-45004

TEACHING
 U EDUCATION

TEACHING MACHINES
 Learning scheme with probabilistic teacher for unclassified samples, establishing convergence, comparing with linear estimator 17 p3128 A70-34851
 Computer users functions to determine preparation level for effective dialog with computer, discussing teaching stages 18 p3223 A70-36077
 Heat transfer and viscous flow pedagogy, discussing classroom use of remote time sharing computer terminals 23 p4166 A70-44642

TEAMS
 Team hiring of research scientists by industrial and academic organizations, discussing causes and influence on R and D organizations management and design 07 p1427 A70-19002

TEARING
 Drop-weight tear test evaluation taking into account operator, test machine, specimen thickness, notch type and strength level effects 15 p2759 A70-32241
 Impact test machines, specimen design and energy measurement in dynamic tear test method for steel fracture strength 15 p2759 A70-32242
 Plasma tearing instabilities involving topological changes in magnetosphere field configuration 19 p3411 A70-37491

TECHNICAL WRITING
 Automated Readability Index for technical materials weighting word and sentence length in multiple regression equation 24 p4308 A70-45510

TECHNIQUES
 U METHODOLOGY

TECHNOLOGIES
 NT BIOTECHNOLOGY
 NT MILITARY TECHNOLOGY

TECHNOLOGIES
 NT MARINE TECHNOLOGY
 Book on technological forecasting covering philosophical basis, Federal Government activity, R and D management resource allocation, correlation and regression analysis, etc 01 p0221 A70-11307
 Technological forecasting for management planning, discussing structuring, prediction techniques, personnel selection, quantification, etc 09 p1794 A70-23413
 Technological forecasting for R and D planning including project selection and resource allocation decision making 09 p1794 A70-23416
 Bibliography of literature on bioengineering, biocontrol, medical physics, biotechnology, safety and human factors in technology 09 p1629 A70-23692
 Vacuum science and technology - Conference, Seattle, October 1969 12 p2284 A70-27251
 Technology - Conference, Cocoa Beach, Florida, April 1970, Volume I 16 p2975 A70-33701

Space technology and science - Conference, Tokyo, August 1969 17 p3164 A70-35201

TECHNOLOGY TRANSFER
 Tension-torsion machine developed from aircraft carrier catapult principle, producing radial loading paths 22 p4117 A70-43453
 Space and astronomic methods applied to solid earth and ocean physics 22 p4025 A70-43669
 NASA safety related research programs based on technology transfer involving information summarizing, indexing and storage from global aerospace research and development 23 p4285 A70-44457

TECHNOLOGY UTILIZATION
 NASA Technology Utilization Program extending space exploration and upper atmosphere R and D to X ray pictures, safer highways, TV cameras, etc 01 p0220 A70-10282
 Military inertial navigation technology applied to civil air transport aircraft 01 p0137 A70-10311
 Manned reusable space transportation system technology requirements and vehicle types [ALAA PAPER 69-1116] 01 p0194 A70-10613
 Military aeronautical R and D contributions to civil aviation since 1905, discussing jet engine and supersonic aircraft introduction, air traffic control, etc [ALAA PAPER 69-1114] 01 p0005 A70-10614
 Earth resources satellites use in agriculture, considering materials reflectance and emittance, electromagnetic spectrum wavelengths identification and data accuracy standards [ALAA PAPER 69-1083] 01 p0220 A70-10624
 Communication satellite system proposed for small users, assessing viability based on market saturation points estimation [ALAA PAPER 69-1073] 01 p0043 A70-10629
 Ultrasonics for industry - Conference, London, October 1969 01 p0089 A70-10877
 Aerospace technology application to biomedical problems in astronautics 01 p0027 A70-11256
 Book on technical acoustics physics covering propagation, dissipation, reflection, field perturbation in real solids, liquids and gases, lumped constants, resonators, etc 01 p0144 A70-11328
 Technology transfer techniques within business firm, including specific examples used by successful companies 02 p0403 A70-12635
 Technology transfer between large company aerospace group and commercial products group 02 p0403 A70-12636
 Optimum balance between program and functional organizations to promote technology transfer 02 p0403 A70-12637
 Technology transfer experience in terms of aerospace company policies and technical management mechanics 02 p0389 A70-12638
 Surveyor project as basis for technology transfer management exemplified by planning and organization problems 02 p0403 A70-12639
 Laser applications for diagnostic and interaction studies, discussing fog removal, droplet shattering, clear air turbulence, reaction rates, spectroscopy, etc 02 p0314 A70-12780
 Soviet book on assembly, control and testing of aeronautical devices covering theory, technology, quality control, accuracy, industrial cleanliness, vacuum and gas filling, etc 03 p0479 A70-12870
 Carbon materials manufacture, properties and applications in space technology, discussing carbon fibers, textiles, graphite, pyrolytic carbon, composites and vitreous carbon 03 p0516 A70-13618
 Earth resources applications of Apollo 6 photography, describing camera system and photographic coverage 03 p0474 A70-13672
 Earth exploration and service by satellites - Conference, Rome, March 1969 03 p0572 A70-13826
 NASA research studies supporting tracked air cushion vehicle /TACV/ program illustrating aerospace technology application to ground transportation [AAS PAPER 69-565] 04 p0622 A70-14639
 Holographic wavefront reconstruction variants and applications to instrumentation, process engineering and information techniques 04 p0688 A70-14717
 Meghdoot program for satellite network communications technology applications to national goals in India 04 p0757 A70-15670

Soviet aerospace manufacturing technologies development, considering forging, extrusion, metal working and joining, etc
[SAE PAPER 690701] 05 p0853 A70-15826

Solid rocket engine components technologies, studying effects of cost consciousness
[SAE PAPER 690702] 05 p0922 A70-15828

Operational/technical system improving air traffic control services efficiency by increased utilization of automation, displaying radar information and synthetic air situation presentations
05 p0827 A70-16179

Plastics applications in aircraft, missile systems, satellites, sounding rockets and manned spacecraft, discussing reinforced plastics and structural laminates
05 p0874 A70-16623

Microwave low power electron tube oscillators and solid state technology
05 p0823 A70-16882

U.S. space research and technology applications in aviation, astronomy, weather information, intercontinental communication and space shuttle design
05 p0921 A70-17091

Apollo suit features applicable to operational or research program requiring pressure suits, discussing low torque constant volume joints
06 p1002 A70-17704

Lasers industrial application to distance and flow rate measurement, automated machining and tunneling, inspection, die hole punching, welding, etc
06 p1078 A70-18431

Integrated circuit technology impact on electronic equipment designers and organization relationships within industry
07 p1239 A70-18800

Aerospace technology contributions to oceanography, discussing lightweight structures, electronics, automatic systems and submarine laboratory application
07 p1263 A70-19135

Incipient tropical storm location and synoptic weather pattern analysis from environmental satellite system data utilization
07 p1329 A70-19196

Laser characteristics and applications in high temperature research including metal heating, welding, machining, surface particle emission and plasma production
07 p1301 A70-19881

Large scale integration (LSI) in electronics, discussing high density microelectronic, memory and logic circuits, fabrication and computer aided design
08 p1468 A70-20468

Metal cutting by gas jet lasers, discussing single and multimode lasers, carbon dioxide lasers, power and power density requirements, etc
08 p1501 A70-20470

Microstrip integrated circuit technology in development of microwave components, discussing fabrication, design, performance and applications
08 p1471 A70-20787

Computer graphics applications to three dimensional vibration analysis, changing mass, stiffness, exciting load or load frequency at any point with light pen
08 p1467 A70-21050

Collection of patent papers on liquid crystals applications including radiation detection, polarizing, thermal imaging, etc
08 p1556 A70-21346

Carbon fiber composite materials production technology, physical properties and potential applications in aerospace
08 p1527 A70-21520

Engineering use of filament reinforced metal matrix composites dependent on fabrication cost reduction, consistent properties and form flexibility
08 p1509 A70-21851

Hybrid microwave integrated circuits technology and design, discussing distributed and lumped-element structures and component properties
09 p1644 A70-22225

Laser technology, discussing activation types, applications and commercial development for data processing, voice communication, medical equipment, etc
09 p1695 A70-22338

Powder metallurgy all-inert processing method for producing nickel base superalloys forgings, discussing microstructure, reproducibility, mechanical properties, etc
09 p1701 A70-22553

Satellite applications to TV broadcasting for developed and developing areas, considering national and international telecommunications policies
09 p1633 A70-22634

Solid state and gas lasers industrial applications in machining and nonmachining areas, discussing limiting factors
09 p1692 A70-22706

Satellite TV transmission economic, technical and practical feasibility, describing direct transmission system
09 p1634 A70-22766

Submillimeter wave applications in measurement and communication, developing submillimeter gas maser sources
09 p1676 A70-22784

Earth resources data exploitation, describing potential organizational structures for data handling and various political, economic and technological problems
[AIAA PAPER 70-344] 09 p1793 A70-22859

Earth Resources Satellite Information Systems, discussing NASA Space Application Program relation to national goals, federal spending, cost effectiveness analysis, information sales, etc
[AIAA PAPER 70-333] 09 p1793 A70-22860

Earth resources observation satellite (EROS) program, describing remote sensor data acquisition, processing, dissemination and utilization
[AIAA PAPER 70-332] 09 p1667 A70-22861

ERTS satellite role in resource policy, management and remote sensing
[AIAA PAPER 70-304] 09 p1668 A70-22881

Multidiscipline applications for Earth Resources Satellite data, including data simulation and interpretation techniques
09 p1669 A70-22886

Technology transfer or coupling from corporate viewpoint, discussing organizational responses to literature mushrooming, time compression of technological advance, etc
09 p1794 A70-23411

R and D resources allocation model based on correlated Navy technological forecast (NTF) and exploratory development goals (EDG)
09 p1794 A70-23412

Photointerpretation applications to kaolin deposit detection, railway tunnel collapse analysis and highway drainage
10 p1873 A70-24075

Ground and flight tests in aeronautical system development process as transfer of basic technology into cost effective operational systems
[AIAA PAPER 70-381] 10 p1857 A70-24172

Management systems growth in relation to computer applications development, noting second industrial revolution
10 p1971 A70-24661

TRW space program to 1978, discussing lunar optical observatory, orbital radio astronomical observatory, satellite applications, planetary exploration spacecraft, etc
10 p1951 A70-24875

Civil aviation satellites for aircraft communication, navigation and traffic control, discussing technical, political and administrative problems
10 p1842 A70-24974

Direct broadcast voice satellite for educational system improvement, discussing lesson formatting, ground receiver/programmer, multichannel capacity, etc
[AIAA PAPER 70-449] 11 p1998 A70-25423

Communication satellite technology impacts on potential socio-economic developments of emerging nations of Asia, Africa and South America
[AIAA PAPER 70-473] 11 p1512 A70-25426

Educational satellite TV for developing countries, giving model relating economic development to education and applied technology
[AIAA PAPER 70-514] 11 p1512 A70-25429

Navigational satellite communication experimental design emphasizing mobile, ship or aircraft station technical characteristics
[AIAA PAPER 70-407] 11 p2001 A70-25469

ATC ground hardware technology implementation, considering national air space system, airports, cost estimates and capacity increase
11 p2078 A70-25722

Technological feasibility, economical and operational compatibility of subsonic aircraft nuclear propulsion (ANP) compared with conventional propulsion systems
11 p2081 A70-26050

Space technology exploitation, describing applications of multimission information transfer satellites
11 p2005 A70-26058

Concept engineering, individuals and corporations consider aspects and disciplines concerned with public utility, taste and convenience
11 p2153 A70-26257

Computerized automation of R and D engineering, discussing critical effects of generalization and oversimplification
12 p2334 A70-27006

Avionics technology cost effectiveness effect on airlines and industry, considering systems engineering and specifications
[SAE PAPER 700299] 12 p2335 A70-27447

Liquid rocket technology for chemical engineers, discussing propellant tanks, lines and valves, tank pressurization, turbopumps and combustion chamber problems
12 p2291 A70-27664

Turbine technology application to high speed roller bearing design, considering reduction of roller skidding and skewing
13 p2419 A70-28918

Pattern recognition systems design and applications in medical and photographic data classification
13 p2374 A70-29580

Holography patents, books, conference reports and articles, discussing applications to interferometry, portraits, Cassette tv, computer storage, etc
13 p2411 A70-29782

Avionics technology application to air traffic, discussing airborne computers use in navigation and control, secondary radar and correlation protected ILS
14 p2611 A70-30107

Ground and air based avionics for traffic control
14 p2612 A70-30109

Space shuttle automatic landing system based on aircraft low visibility landing, considering economy and safety
14 p2614 A70-30466

Earth atmosphere model for weather forecasting using space technology, noting Global Atmospheric Research Project (GARP)
14 p2576 A70-30973

Aerospace technology and system analysis application possibilities to urban social and economic planning problems
14 p2670 A70-31191

Airborne equipment microelectronics technology application to interrogators, transponders and UHF/VHF transceivers
14 p2558 A70-31294

Spacecraft tracking methods applied to solid earth and ocean physics
15 p2809 A70-31685

Report to COSPAR on Australian space research /1969/ including tracking stations, sounding rockets, technology utilization, etc
15 p2829 A70-31706

Astronautics utility in astronomy, physics, earth observation, communication, commercial, military, navigational, meteorological, social applications, considering present and future possibilities
15 p2831 A70-32062

Air transport safety, applying experience from space programs
15 p2692 A70-32227

Computer applications in radar and air traffic control, large steerable aerials, systems design and graphical displays
15 p2832 A70-32704

Smooth surface polyester premix and sheet molding compound technology applied to reinforced plastics industry
16 p2917 A70-33364

Fluidic technology for avionics systems, considering potential cost reduction and reliability improvement
16 p2843 A70-33445

Fluidic technology applications to space and oceanography, discussing control, monitoring, sequencing and signal processing
16 p2845 A70-33714

Technology - Conference, Cocoa Beach, Florida, April 1970, Supplement
16 p2982 A70-33801

Astronautics enhancement of technical progress, discussing agricultural, geological, oceanographical, meteorological, communication, electronics, materials and medical applications
16 p3004 A70-34345

Space shuttle safety program for low risk passenger transportation, combining large aircraft experience with spacecraft technology
[AAS PAPER 70-055] 17 p3176 A70-34793

Digital computer technology impact on advanced aircraft design, discussing airborne computers, distributed and lumped computer systems, outer loop control, engine control and system integrity
17 p3049 A70-34993

Engineering uses of holography - Conference, University of Strathclyde, Glasgow, September 1968
17 p3083 A70-35001

Aerospace technology applications to air pollution problems, including turbojet aircraft sources, rocket emissions, etc
[AIAA PAPER 70-815] 17 p3200 A70-35194

NASA program for international cooperation in space involving developing and advanced nations, discussing television instruction for India, resource surveys, etc
18 p3349 A70-36514

Laser and electron beam removal of material in manufacturing technology
19 p3447 A70-38451

Carbon dioxide IR laser applications to manufacturing technology, discussing absorption, reflection and heat conduction characteristics of materials
19 p3447 A70-38452

Space technology spin-off benefits to mankind, considering medical and industrial applications
19 p3554 A70-38609

Explosive metal bonding in electronics, noting explosive strength and initial surface angle effects on bond physical and chemical properties
19 p3438 A70-38752

- Hydrofoil and hovering craft design by fiber technology, discussing composite materials, whisker mechanical properties, polycrystalline fibers, matrix materials, etc
19 p3456 A70-38941
- ERTS programs status and prospects from international utility viewpoint
20 p3739 A70-39064
- Glass drainline development and marketing, describing technology transfer role
20 p3740 A70-39100
- Small ground stations in communication satellite systems involving regional telecommunication, TV distribution, air traffic and maritime applications, data exchange, weather and education service
21 p3785 A70-40764
- Holography application to high capacity permanent memory systems
21 p3825 A70-41125
- Inertial guidance technology applications for space navigation, considering instrument design tradeoff between accuracy and cost for performance and reliability improvements
21 p3848 A70-41128
- Mariner 1969 communication system modified for thermoelectric outer planet spacecraft (TOPS), noting X band addition to S band and associated problems
21 p3791 A70-41797
- Synchronous satellites characteristics and applications to radio connection, light signals, positioning, telecommunications, manned space stations and space shuttles
22 p4109 A70-42467
- Supersonic aerodynamic design tools, discussing technological application of high speed computer and limitations
22 p3958 A70-42701
- Satellite technology application to aeronautics, predicting synchronous satellites communication for transoceanic and overland ATC
22 p4111 A70-43512
- Apollo project technology for future space missions, discussing space shuttles, management, material procurement, test programs and computer utilization
22 p4128 A70-43513
- Space station development and missions, discussing general design philosophy, successive project lineage and applications programs
22 p4108 A70-43653
- Technology relevance to organizational structure, discussing planning models based on problem solving and performance
23 p4284 A70-43995
- NASA information fall-out, discussing Technology Utilization Program providing aerospace related data to civilian economy
23 p4285 A70-44500
- Space technology applications to earth survey, discussing use of automatic satellites and manned space laboratories for meteorological, geophysical and related purposes
23 p4191 A70-44634
- TV broadcast satellites program distribution direct to home by network and by community
23 p4164 A70-44646
- Orbital space station utilization planning as international laboratory, discussing industry role, experiment program goals, etc
23 p4260 A70-44650
- Computer hardware and software technology for complex problems, discussing switching speeds and parallel and pipeline designs
23 p4167 A70-44716
- Experimental astronomy and role of space technology, discussing artificial satellites, extraterrestrial life, moon, Mars and Venus exploration, etc
23 p4247 A70-44775
- Industrial laser technology applications, considering high accuracy distance, flow and stress measurements, die hole punching, integrated circuit component welding, etc
24 p4351 A70-45382
- Lasers biomedical applications based on thermal and ionization effects on biological targets, considering eye surgery, tumor treatment, etc
24 p4308 A70-45568
- Satellite technology applications to ATC, including communications, navigation, surveillance over water and data acquisition
24 p4373 A70-45922
- NERVA reactor technology applied to closed Brayton cycle MHD power system
24 p4377 A70-45956
- Air traffic control, future national airspace system improvements in view of air transportation growth, computerized automation technology, etc
24 p4374 A70-45969
- Spacecraft sensor trends from space station research and technology requirements regarding astronomy, biomedicine and biology, earth resources, etc
24 p4418 A70-45974
- [AIAA PAPER 70-1291]
- TECTONIC MOVEMENT**
U TECTONICS
- TECTONICS**
Earth photographs for geotectonic research from manned orbiting spacecraft, describing Apollo and Gemini belts
04 p0677 A70-14663
- [AAS PAPER 69-579]
Earth deviations from isostatic equilibrium, showing irregularities dependence on distance from surface for various tectonic zones
08 p1487 A70-20715
- Lunar sinuous rilles as volcano-tectonic fracture traces of sites of gas emission
09 p1758 A70-22743
- Lunar geomorphological charts of Theophilus and Ptolemaeus walled plains, investigating central region tectonics
19 p3517 A70-37985
- Soviet collection of lunar geological and morphological maps and relief tracings, showing tectonic features, craters and surface characteristics
19 p3518 A70-38011
- Earth upper mantle phase change instability, discussing temperature gradient, transformation influence on fluid, olivine-spinel phase flow patterns and tectonics
21 p3820 A70-41895
- Ocean floor-spreading tectonic effects, considering Arabian Shield separation from African continent
24 p4332 A70-46408
- TEE**
U T SHAPE
- TEFLON (TRADEMARK)**
Fluorocarbon polymer coatings, discussing role of fluorine content and carbon bond in chemical inertness, degradation resistance, thermal stability and low surface friction
05 p0868 A70-15842
- [SAE PAPER 690645]
LES-6 satellite solid Teflon pulsed plasma thruster performance, determining energy balance, thrust and circuit parameters
06 p1132 A70-18206
- [AIAA PAPER 70-179]
Atomic hydrogen maser wall shift determined by measurements on FEP Teflon coated storage bulbs, suggesting Teflon properties change as basis
07 p1301 A70-19973
- Teflon-bonded gas diffusion electrode flooded agglomerate model, determining porosity, surface area, IR drop, etc
10 p1829 A70-24455
- Carbon oxyfluoride IR radiation from boundary layer formed by arc-heated air passing over Teflon surface
10 p1968 A70-24475
- Teflon and fluropolymers relative toxicity due to thermal degradation at 370 C, testing carboxy nitroso rubber, Kapton polyimide film, perfluorated polymers, etc
13 p2439 A70-29260
- Teflon and polymethyl methacrylate sublimation breakdown in plasma jets, using electric arc heated argon, nitrogen, air and oxygen
15 p2765 A70-32103
- Gas formation by sliding friction of self lubricating Teflon with carbon black on steel in ultrahigh vacuum, using mass spectrometry
15 p2745 A70-32446
- Teflon crosshatched ablation patterns elimination by grooving or glass filler addition
17 p3193 A70-34483
- [AIAA PAPER 70-769]
Rocket engine with Teflon lined combustion chamber, considering design criteria and tests
18 p3301 A70-36662
- Teflon bucket and Be-Cu cap seal against hydrostatic pressure, discussing applications for high pressure superconductivity measurements
18 p3262 A70-37097
- Adherent Ta films deposition onto Teflon disks by sputtering
18 p3264 A70-37098
- TEKTITE PROJECT**
Underwater saturation habitats application as behavioral workshops for mission planning and human engineering of manned space flight, discussing Project Tektite
01 p0034 A70-10611
- [AIAA PAPER 69-1120]
Tektite I marine laboratory underwater mission in marine biology and geology
17 p3168 A70-35306
- TEKTITES**
NT AUSTRALITES
Reworking of deep-sea sediments as indicated by vertical dispersion of Australasian and Ivory Coast microtektite horizons, implying years of deposition
01 p0178 A70-10474
- Age data on high sodium tektites from Australia showing distinct fall
03 p0576 A70-14089
- Neutron activation analysis for U and Th in various tektites, discussing evolution and extraterrestrial origin
03 p0576 A70-14090
- Tektites origin, comparing chemical composition with lunar soil from Apollo mission materials
03 p0577 A70-14096
- Tektite size restricted by thermal stress limit on diameter and aerodynamic load limit on length
05 p0916 A70-16831
- Tektite damage caused by micrometeoroid impact, projectile firing at glass spheres and survival time estimation
05 p0916 A70-16834
- Microtektites chemical analysis data providing appraisal of strewn field boundaries, implying lunar origin
05 p0916 A70-16835
- Magnetic susceptibility of synthetic australite and philippinite-like tektites measured in 77-560 K range, discussing origin
05 p0916 A70-16836
- Ni-Cr content and variability in Ivory Coast tektites using atomic absorption and X ray emission techniques
05 p0916 A70-16837
- Normal and bottle-green microtektite glass measured for magnetic susceptibility, magnetization and Curie constants
05 p0916 A70-16839
- Correlation between O isotope ratios and composition of tektites investigated for origin of tektites
05 p0917 A70-16840
- Fe diffusion coefficients measured at various temperatures above 1150 C to calculate homogenization times of Thailand tektite source
05 p0917 A70-16841
- Tektite field studies in China concerning stratigraphic occurrence and chemistry
06 p1148 A70-18393
- Nonlunar origin of tektites indicated from molten glass dispersion generated by terrestrial crater-forming meteorite impact
12 p2302 A70-27584
- Australasian and Ivory Coast deep sea microtektites fission track ages compared to deposition ages from paleomagnetic data
12 p2310 A70-28021
- U and Th abundances correlation in tektites and achondrites based on oxygen isotopic composition of lunar rock specimens
13 p2488 A70-28720
- Tektites age from fission track method, discussing elimination technique for strain caused spurious tracks
13 p2488 A70-28721
- Tektite glass in lunar sample from Apollo 12, discussing chemical composition and possible volcanic origin
14 p2642 A70-30983
- Erasure fission tracks in soda-lime glass, tektite, biotite and apatite by shock loading, determining dynamic pressure and associated temperature effects
19 p3414 A70-38035
- Chromite, zircon and quartz crystals in Muong Nong type tektites by X ray diffraction, discussing possible impact origin
20 p3709 A70-40088
- Lake Toba, Sumatra as possible tektite source region based on surrounding welded tuffs composition
21 p3923 A70-41996
- Tektite glass absence in Apollo 12 lunar sample
23 p4238 A70-43806
- TELECHIRICS**
U REMOTE HANDLING
- TELECOMMUNICATION**
NT AIRCRAFT COMMUNICATION
NT AUTOMATIC PICTURE TRANSMISSION
NT BIOTELEMETRY
NT BROADCASTING
NT GROUND-AIR-GROUND COMMUNICATIONS
NT INTERPLANETARY COMMUNICATION
NT LUNAR COMMUNICATION
NT MULTICHANNEL COMMUNICATION
NT OPTICAL COMMUNICATION
NT PULSE COMMUNICATION
NT PULSE FREQUENCY MODULATION TELEMETRY
NT RADIO COMMUNICATION
NT RADIO RELAY SYSTEMS
NT RADIO TELEMETRY
NT REENTRY COMMUNICATION
NT SPACE COMMUNICATION
NT SPACECRAFT ANTENNAS
NT SPACECRAFT COMMUNICATION
NT TELEMETRY
NT TELEPHONY
NT TELEPHOTOMETRY
NT TRANSOCEANIC COMMUNICATION
NT VIDEO COMMUNICATION
NT VOICE COMMUNICATION
NT VOICE DATA PROCESSING
NT WIDEBAND COMMUNICATION
NT WIRELESS COMMUNICATIONS
Integrated logistic support for cost effectiveness of ground communication system
01 p0220 A70-10114
- Intelsat 4 communication system design and international cooperation, considering satellite design, TV and telephone channels capacity, etc
01 p0196 A70-10883
- Book on communication and information theories application to fading dispersive communication channels, discussing tropospheric scatter, HF ionospheric links, moon bounds, etc
02 p0253 A70-11700

- Optimal selection of centralized communication network of combined radial and linear structures minimizing disconnected peripheral points
03 p0446 A70-13238
- Low noise amplification equipment for telecommunications, considering France-Portugal link parametric amplifiers
05 p0819 A70-15983
- U.S. space research and technology applications in aviation, astronomy, weather information, intercontinental communication and space shuttle design
05 p0921 A70-17091
- Communications and displays - Conference, North Hollywood, August 1969
06 p1005 A70-17342
- Domestic telecommunication via satellite to reduce terrestrial switching to two levels, discussing system parameters, operation, hardware and cost estimate
06 p1006 A70-17344
- LUF/lowest useful frequency/ prediction for HF sky wave communication, emphasizing prediction methods using computers
07 p1229 A70-19156
- Lowest useful frequency /LUF/ prediction on long distance quasi-antipodal circuit, considering E layer blanketing
07 p1232 A70-19178
- High attenuation quantum communication channel capacity based on mathematical model
07 p1335 A70-19864
- Tandem link multichannel LOS FDM-FM communication system cost optimization by computer-aided design
08 p1459 A70-20798
- Millimeter guided wave communication systems information transmission capacity increase, using quaternary and higher order modulation techniques
08 p1462 A70-21506
- Crosstalk in multiple-beam waveguides due to scattering and distortion caused by surface irregularities of focusers, discussing power profile of Gaussian beam
08 p1462 A70-21507
- Canadian domestic satellite communications policy, discussing Telesat Canada for commercial telecommunications services
11 p2152 A70-25416
- [AIAA PAPER 70-428] Visible light sensors application in LES control system for circular near equatorial orbits
11 p2107 A70-25432
- [AIAA PAPER 70-477] Satellite communications subsystem performance testing from initial integration through launch under all environmental exposure
11 p2030 A70-25445
- [AIAA PAPER 70-448] Plumeur-Bodou satellite telecommunications center, discussing antennas
11 p2031 A70-26009
- Automatic base communication system /ABCS/ to handle USAF worldwide base record communications centered on electronic store and forward message switch, utilizing stored programs
11 p2009 A70-26266
- Performance characteristics of quadriphase PSK communication system with noisy reference signal, formulating error probability
12 p2187 A70-27907
- Self organization and adaptive routing communication system for military network, describing routing algorithm and entropy organization measure based on stochastic switching matrices
12 p2187 A70-27934
- Radar meteorology in electromagnetic communications to provide storm systems data, noting clear air radar echoes
13 p2445 A70-28791
- Millimeter wave applications, considering waveguide and plasma communications, ground surveillance radars, vibration analysis equipment, decoders, etc
14 p2549 A70-30449
- Field amplitude distribution parameter in long distance tropospheric communications based on fading depth
15 p2696 A70-31512
- Frame synchronization in biorthogonal coded multiplex communication system, describing PCM, pattern insertion and double encoding methods
17 p3045 A70-35266
- Legal problems of space telecommunications, discussing world juridical regime, United Nations work and satellite systems broadcasting
17 p3201 A70-35777
- Legal questions of satellites telecommunications at Washington Intelsat Conference
17 p3201 A70-35778
- Legal aspects of telecommunications by satellite systems, discussing international organization, Intelsat integration and direct broadcasting
17 p3202 A70-35781
- Juridical structure, risks and control of satellite telecommunication ensuring equality of nations
17 p3202 A70-35782
- Communication modulation systems unified description by conversion and indication matrices
18 p3229 A70-36942
- Group delay times criterion of multibeam propagation of ionospheric radio echoes for communications systems
19 p3375 A70-37332
- Global integrated communications satellite system, discussing International Telecommunication Union regulatory functions, etc
21 p3955 A70-40625
- Communications - IEEE Conference, San Francisco, June 1970, Volume 1
21 p3786 A70-41326
- Communications - IEEE Conference, San Francisco, June 1970, Volume 2
21 p3788 A70-41340
- Single multiple access satellite communication system requirements for worldwide, trunked and local operations, considering transponder allocation and antennas
21 p3790 A70-41365
- Synchronous satellites characteristics and applications to radio connection, light signals, positioning, telecommunications, manned space stations and space shuttles
22 p4109 A70-42467
- U.S. and European space program costs and resources with particular reference to telecommunication satellites
22 p4126 A70-43247
- Intelsat compatibility with independent regional telecommunication satellite systems
22 p4111 A70-43514
- Communications satellites for offshore systems, noting development of small earth station
22 p3991 A70-43576
- Crosstalk error in binary phase modulated communications systems due to RFI and thermal noise
23 p4158 A70-43752
- Optimal two-way communication system with feedback and decision constraint, developing algorithm for random code reliability lower bounds
23 p4159 A70-43754
- Algorithm for communication network synthesis from limited elements selection, considering fixed reliability requirements
23 p4160 A70-43763
- Microwave communication - Conference, Budapest, April 1970, Volume 3, Electromagnetic theory
23 p4160 A70-43764
- Microwave communication - Conference, Budapest, April 1970, Volume 4, Microwave theory and techniques
23 p4168 A70-43776
- Communication system signal to noise ratio requirements, determining minimum signal power level
23 p4163 A70-44297
- Directional microwave transmitter for 300 frequency division multiplexed telephone channels, discussing transmission quality, reliability, design and operation
23 p4172 A70-44298
- ### TELEGRAPH SYSTEMS
- FM data and telegraph signal transmission over PCM system analog channel, discussing adaptability to digital modulated signals
01 p0046 A70-11318
- Binary code distortion in relative phase telegraphy signals under wideband and correlated noise
13 p2364 A70-28870
- ### TELEGRAPHY
- #### U TELEGRAPH SYSTEMS
- #### TELEMETERS
- #### U TELEMETRY
- #### TELEMETRY
- NT BIOTELEMETRY
- NT PCM TELEMETRY
- NT PULSE FREQUENCY MODULATION
- #### TELEMETRY
- NT RADIO TELEMETRY
- Transportable telemetry acquisition system /TTAS/ as mobile tracker featuring pseudomonopulse method
01 p0045 A70-11120
- Telemetry signal processor for diversity signals for performing as optimum maximal ratio predetection combiner
02 p0266 A70-11747
- Laser range finding by mobile missile station compared with geodesic satellite telemetry by ground station
02 p0312 A70-12212
- Digital telemetry systems for geophysical satellites, describing onboard and ground systems design criteria and experimental results
03 p0451 A70-13837
- Directional transponders for telemetry command, tracking and communications in retrodirective communication satellites
03 p0457 A70-13838
- French laser reflectors for lunar telemetry functioning with ruby laser, discussing applications to lunar orbital parameters, continental drift, gravity constant secular variations, etc
04 p0700 A70-14609
- Phase feedback demodulation technique to analyze telemetry performance degradation caused by voice interference in modes of Apollo communication system, providing linear detection scheme
04 p0648 A70-14660
- Artemis I and II telemetering antennas at Guiana Space Center for spacecraft tracking
05 p0819 A70-15987
- Miniature temperature and strain telemetry transmitters developed for measurements in areas inaccessible to direct wire connections
06 p1069 A70-18433
- Flight configured single sideband telemetry accuracy determined by digitally computed frequency response
06 p1012 A70-18600
- Noise variance extreme value estimator for biorthogonally block coded high rate telemetry system for Mariner missions
08 p1459 A70-20799
- White noise and nonlinear effects in telemetry RF links, analyzing received process to phase coherent receiver
08 p1460 A70-20823
- Error probability upper and lower bounds determined for self synchronized binary PSK communications systems, presenting maximum-likelihood and Monte Carlo computer simulation
08 p1463 A70-21777
- Telemetry data processing of Eole scientific weather forecasting program, discussing mathematical model simulating atmospheric circulation in Southern Hemisphere
09 p1674 A70-22200
- Vacuum tube signal frequency converters for meteorological telemetry measurements including blocking oscillators, multivibrator and fanstatron
09 p1718 A70-23332
- Telemetry tracking and command antenna array of Central German Ground Station for satellite communication
11 p2017 A70-25800
- [DFVLR-SONDDR-52] Time correlation telemetering systems design, describing structural scheme
11 p2004 A70-25929
- Telemetry decommutation algorithm for applying Bayesian decisions to demodulated received bits data
11 p2008 A70-26238
- Mariner-type spacecraft telemetry system optimization, considering channel capacity
11 p2008 A70-26239
- FM/FM telemetry threshold carrier SNR and receiver IF bandwidth optimization through computer program
11 p2014 A70-26272
- Noise threshold performance of suboptimum PPM telemetry receivers using slicer for detector
11 p2010 A70-26273
- Data compression for telemetry transmission with sample choice based on time-varying stream slope thresholds illustrated for Ranger photograph
11 p2010 A70-26305
- Delta reprocessing operating system /DEPOS/ for high speed telemetry format-independent decommutation and data compression
11 p2010 A70-26307
- Sensor selection and telemetry measurement of physical parameters
11 p2011 A70-26453
- ECG telemetry system within small irregular metal chamber
11 p1992 A70-26514
- Temperature profiles and frequency driftings of VHF telemetry transmitters for Saturn S-IC stage, using IR radiation data
12 p2196 A70-27725
- Analog information transmission device using He-Ne laser radiation, discussing optical telemetric channel transfer characteristics for pulsed nanosecond analog signals
12 p2250 A70-28184
- Artificial earth satellites orientation determined by onboard telemetric measurements, constructing model for rotational motion around center of mass
12 p2314 A70-28255
- Skylark sounding rocket telemetry data reduction system providing attitude analysis
13 p2363 A70-28680
- Altimeter-telemetry system for small sounding rockets, discussing ground and flight test results
13 p2363 A70-28688
- Transducers for bioimplantable telemetry systems self used by nonhospitalized patients
13 p2357 A70-28816
- Frequency selection in telemetry taking into account systems for minimum interference and crosstalk
13 p2366 A70-29216
- Antenna research, discussing efficiency and design considerations in phased and strip line arrays and conical scan telemetry antennas
14 p2559 A70-31375
- Report to COSPAR on Czechoslovakian space research /1969/ covering satellite telemetry and tracking, proton flares, aeronomy, etc
15 p2829 A70-31710

Earth resources technology satellite /ERTS-A/ for Eros program, producing telemetric imagery spatially correlated to earth surface

16 p2898 A70-34046

Telemetry instrumentation for free flight wind tunnel models, discussing system component characteristics

17 p3047 A70-35495

Digital computer controlled positioning of telemetry antennas for tracking spacecraft

17 p3062 A70-35508

First luminous lunar echoes obtained by laser telemetry of Pic Du Midi observatory

18 p3310 A70-35948

Logic, arithmetic, control and instruction capacities of dedicated onboard telemetry preprocessor

19 p3383 A70-37904

Integrated circuits for control and telemetry functions in oxide cathode ion thruster power conditioning system operating from solar panel

21 p3798 A70-41216

Digital orbital clock and telemetry adapter for TD1A satellite attitude stabilization, describing mechanical structure

21 p3798 A70-41272

TELEMETRY AUTO REDUCTION SYSTEM

U DATA REDUCTION

U TELEMETRY

TELEOPERATORS

Free flight remote controlled teleoperator system applications in manned orbital space station/space shuttle program

23 p4260 A70-44644

TELEPHONES

FM transmission of multiplex telephone signals by communication satellites, deriving impulse noise due to adjacent channel interference

21 p3787 A70-41330

Directional microwave transmitter for 300 frequency division multiplexed telephone channels, discussing transmission quality, reliability, design and operation

23 p4172 A70-44298

TELEPHONY

Intelsat satellite telecommunications system application for future long distance telephone communications

03 p0451 A70-13836

Worldwide telephone network optimum interoperation including communication satellites complementation

10 p1834 A70-24328

Satellite communication system using delta modulation for telephone service to large number single channel earth stations

10 p1834 A70-24329

Traffic simulation in telephone network via communication satellite with presassigned and demand assigned circuits

10 p1838 A70-24356

Message traffic problems in satellite telephone network, considering traffic distribution characteristics, interarrival mean time, bidirectional traffic, etc

10 p1839 A70-24367

Time allocation with sampling interpolation /ATIC/ for TDMA satellite telephone communications, considering auxiliary circuits, transmission quality, bit rates, demand assignment, etc

10 p1840 A70-24370

Soviet book on satellite communication systems for telephone and TV transmission covering orbit selection, signal level calculation, channel characteristics for frequency bands, etc

10 p1840 A70-24378

Terrestrial interface at SPADE terminals for converting international telephone exchange differences into common signaling format

[AIAA PAPER 70-413]

11 p1997 A70-25407

Satellite video-telephone systems promoting economic growth in developing nations through link-up with developed nations advanced centers

[AIAA PAPER 70-474]

11 p2000 A70-25455

Transmission delay and echo effects in long distance satellite relay telephony links, describing echo suppression and speech quality

12 p2183 A70-27004

TELEPHOTOMETERS

U TELEPHOTOMETRY

TELEPHOTOMETRY

Cosmos 149 meteorological satellite telephotometers for measuring reflected solar radiation from earth

01 p0095 A70-11612

TELESCOPES

NT APOLLO TELESCOPE MOUNT

NT ASTRONOMICAL TELESCOPES

NT CELESCOPES

NT HELIOMETERS

NT MANNED ORBITAL TELESCOPES

NT PARTICLE TELESCOPES

NT PYROHELIOMETERS

NT RADIO TELESCOPES

NT REFLECTING TELESCOPES

NT REFRACTING TELESCOPES

NT SCHMIDT CAMERAS

NT SPECTROSCOPIC TELESCOPES

NT X RAY TELESCOPES

Geostationary mode application to earth sensing, examining resolution requirements for earth scanning tracking telescope

06 p1154 A70-17152

Balloon flights for remote sensor systems tests, describing return-beam vidicon and tracking telescope experiments

06 p1061 A70-17153

Thermal and dynamic considerations of materials choice for satellite mounted telescope mirrors noting Be and silica properties

06 p1064 A70-17781

Telescope resolution limit dependence on refractive index mean square fluctuation and effective aperture in turbulent medium

06 p1067 A70-18396

Mirror material for satellite-borne telescopes, considering Be and CER-VIT or ULE silica thermal and mechanical properties

07 p1279 A70-19000

NASA three meter orbital telescope discussing configuration, optical geometry, launching, power supply, etc

07 p1280 A70-19150

Remote control telescope for deployment in hazardous locations, discussing design criteria, operation and test results

09 p1640 A70-23777

Laser mode matching to obscured circular aperture of optical telescope system in terms of antenna gain

16 p2929 A70-33982

Standard units and assembling of electrical driving mechanism for telescope, using audio reference oscillator, electronic power amplifier and synchronous motor

18 p3259 A70-36609

Lens systems configuration and aberration, determining suitability for wide angle oculars of Galilean telescopes

19 p3420 A70-37262

Optical system mtf measurement by photographic technique for comparing telescopic sight with simulator, discussing performance

19 p3428 A70-38511

Teleradiometer calibration in background radiation absence, using distant and finite point source method and collimator means

20 p3633 A70-39798

TELEVISION CAMERAS

Light valve projectors and TV cameras, showing disparity between video information generation and large screen real time high brightness image presentation

01 p0088 A70-10811

Simulation technique to evaluate TV contrast trackers standard scan performance using video tape recording

01 p0058 A70-10812

Surveyor TV camera conversion from qualitative viewing device into quantitative measuring instrument by calibration coupled with data processing program

[JPL-TR-32-1374]

03 p0490 A70-13662

Meteorological satellite TV cameras development, discussing image sensors and tabulating characteristics

03 p0491 A70-13665

Secondary electron conduction TV camera tube with three color filter wheel for Apollo missions

03 p0493 A70-14025

Black and white and color Apollo 11 secondary electron conduction TV cameras, discussing characteristics and mission requirements

04 p0688 A70-14692

Apollo 7 and 8 command modules TV camera systems design, considering additional function of public information

07 p1280 A70-19229

Earth resources satellite TV cameras operating on different spectral bands, discussing data preprocessing for correlation with topographic maps

09 p1674 A70-22259

TV camera with diffraction limited pinhole lens for visual simulation, solving depth of field and extending field of view without distortion

10 p1887 A70-24217

Real time 2000 line TV camera with 40 MHz bandwidth, 1600 line vertical resolution and 1000 line horizontal resolution

[SMPT PAPER 105-73]

12 p2235 A70-27663

Electronic zoom for low light level TV sensor employing electrostatic image intensifier coupled optically to SEC camera tube

16 p2903 A70-33128

Low light level TV /LLLTV/ tube, camera and sensor development for military and space applications

16 p2903 A70-33129

Apollo 10 color TV camera for real time scenes, describing configuration performance and total system operation

16 p2907 A70-33187

Surveyor TV mechanisms, discussing camera, mirror, zoom lens, filter wheel, focal plane shutter and lubrication

16 p2914 A70-34147

Surveyor 7 TV system in photon integration mode, analyzing slow scan vidicon storage characteristics and dark current limitations

[SMPT PAPER 105-72]

17 p3095 A70-35635

High resolution electron return beam vidicon cameras, comparing transfer functions and SNR with photographic films

20 p3630 A70-39496

Meteorological TV imaging systems development in last decade, including low and synchronous altitude camera, sensors, orthicons, etc

23 p4193 A70-43963

Apollo TV cameras, detailing general characteristics, principal features, optical systems and operational requirements

23 p4195 A70-44382

TELEVISION EQUIPMENT

NT MONOSCOPES

NT TELEVISION CAMERAS

NT TELEVISION RECEIVERS

Spatial and amplitude modulators for laser-photochromic display system producing real time TV pictures or images

11 p2062 A70-25734

X ray inspection with direct TV viewing, discussing specimen geometry effects, equipment, applications, etc

15 p2742 A70-32778

Dual raster high brightness-high resolution TV display using time sharing with conventional CRT

16 p2903 A70-33131

TELEVISION RECEIVERS

Satellite international system chain consisting of down path, receiving earth station and domestic receiver for Europe, North Africa and Middle East TV distribution

02 p0258 A70-12420

Ground frequency converters for reception of NTSC color TV transmission from synchronous communication satellites, tabulating cost estimates

[AIAA PAPER 70-440]

11 p2002 A70-25490

Microwave converter system for ETV satellite reception, discussing characteristics and costs for mass production

[AIAA PAPER 70-439]

11 p2017 A70-25493

Low cost microwave receiver and antenna for instructional satellite TV broadcasting in developing nations

21 p3789 A70-41355

TELEVISION RECEPTION

Direct domestic reception of TV signals from satellites, discussing microwave components, economics and reliability

10 p1840 A70-24448

TV test chart for evaluating Surveyor lunar spacecraft TV system covering resolution, photometric and colorimetric response and sun angular position

[SMPT PAPER 105-71]

10 p1890 A70-24601

Geometric distortions in ESSA 7, Surveyor 7 and Mariner 4 TV systems caused by scale distortion, discussing stability of systematic component in magnitude and shape

10 p1890 A70-24727

Low cost earth station and antenna for Canadian domestic satellite, bringing color TV to northern territories

[AIAA PAPER 70-432]

11 p2000 A70-25458

TV photograph image instability of stars, developing discontinuity and variability criteria as elementary approximate method for comparing nonuniformities

16 p2979 A70-34177

TELEVISION SYSTEMS

High power TV broadcast satellite subsystems technologies requirements, considering transmitters, power conditioners, solar arrays and component reliability

[AIAA PAPER 69-1069]

01 p0194 A70-10632

TV system for controlling QF-9 drone aircraft landing, takeoff and BQM-34A target drone in-flight test operations

01 p0058 A70-10815

TV raster scan display using CRT and beam steering scan systems, comparing alphanumeric capability for airport information and control problems

02 p0274 A70-11976

Satellite international system chain consisting of down path, receiving earth station and domestic receiver for Europe, North Africa and Middle East TV distribution

02 p0258 A70-12420

Visual imaging systems for Mars orbiter compared for performance and interactions with mission and spacecraft design

07 p1280 A70-19230

Satellite applications to TV broadcasting for developed and developing areas, considering national and international telecommunications policies

09 p1633 A70-22634

TV instruments for Mariners 6 and 7 providing analog and digital data, comparing resolutions and accuracies to earth based telescopes and Mariner 4 photographs

09 p1682 A70-23506

Aircraft surface temperature measured with airborne IR TV system

09 p1686 A70-23754

Video role in air transport safety, describing runway visual range /RVR/ measurement using TV camera and spaced lights

10 p1889 A70-24507

Vidicon camera tubes applications in TV systems, noting excellence for live pickups and film reproduction

10 p1852 A70-24952

Dual conversion receiver for remote frequency control in satellite TV distribution system

[AIAA PAPER 70-414] 11 p2002 A70-25482

Digital signals conversion into command and control TV displays in multiconsole systems

13 p2411 A70-29789

Open loop TV image motion compensation by image transducer with gyro demodulator analyzing errors in rate and rate-integrating gyros and AC pick-offs

14 p2588 A70-31190

Low light level TV systems performance relationship to visual acuity requirements, considering interfering noise characteristics effect on target recognition

16 p2903 A70-33130

Earth resources satellite /ERS/ TV camera configurations, return beam vidicon camera characteristics and devices for TV picture reproduction on film

16 p2915 A70-34312

Mariner 6 and 7 TV camera pictures of Mars during approach and encounter, discussing IR spectroscopy, celestial mechanics experiment and Martian terrain

17 p3158 A70-34875

Spaceborne narrow band TV system with image memory tube and electronic shutter, noting variable exposure time, motion compensation and multimode scanning

17 p3089 A70-35267

Satellite-borne UV TV system for photometric investigations of UV stars

19 p3428 A70-38456

TV display simulation of instrument and visual aircraft landing approaches, investigating color, collimation and resolution effects on pilot evaluations

20 p3578 A70-39172

OA0 2 satellite Telescope astronomical TV system, describing various developmental problems for future guidelines

24 p4415 A70-45824

TELEVISION TRANSMISSION

Future phase of satellite TV programs distribution in Europe

02 p0403 A70-12645

TV data transmitted by Iantars series automatic ionospheric laboratories released by geophysical rockets at 100-400 km, discussing plasma-ion propulsion system performance

04 p0735 A70-14936

Group delay characteristics curvature in radio relay systems, analyzing crosstalk in picture- sound and beamed multiplex signal transmission by nonlinear distortion method

05 p0815 A70-16774

Wideband transmission of photographic reconnaissance information over long distances using Initial Defense Communication Satellite Program satellites

06 p1006 A70-17346

Geometrical and electrical characteristics of two mirror parabolic antenna for tropospheric radio relay communications lines in centimeter band, analyzing radiation patterns

07 p1240 A70-19125

Apollo 7 and 8 command modules TV camera systems design, considering additional function of public information

07 p1280 A70-19229

Satellite TV transmission economic, technical and practical feasibility, describing direct transmission system

09 p1634 A70-22766

Earth resources data transmission, describing picture reception and reproduction equipment

[AIAA PAPER 70-328] 09 p1634 A70-22856

Soviet book on satellite communication systems for telephone and TV transmission covering orbit selection, signal level calculation, channel characteristics for frequency bands, etc

10 p1840 A70-24378

Satellite distribution of TV signal over earth surface as alternative to terrestrial linkups, overcoming rain attenuation by high power spot beam

[AIAA PAPER 70-454] 11 p1997 A70-25410

TV network distribution in Canada by communications satellite and terrestrial microwave links, discussing signal to noise ratios and picture quality

[AIAA PAPER 70-430] 11 p1998 A70-25417

ACME hybrid airborne satellite TV and communications system for India, using airborne TV transmitters

[AIAA PAPER 70-472] 11 p1998 A70-25418

Satellite ET/TV broadcast system, discussing frequency, receiver population, channel number, beam number, minimum cost solutions, etc

[AIAA PAPER 70-452] 11 p1999 A70-25437

Satellite TV broadcast requirements impact on high power transmitter design, permitting low cost terrestrial receiving systems

[AIAA PAPER 70-434] 11 p1999 A70-25450

High power transmitters for satellites, discussing optimum configurations, supporting power subsystems, breakdown problems in space environments, etc

[AIAA PAPER 70-436] 11 p2000 A70-25459

Frequency sharing between satellite-transmitted FM TV signals and terrestrially transmitted AM-VSB TV signals

[AIAA PAPER 70-438] 11 p2001 A70-25467

Multipurpose domestic satellite system design for TV distribution, discussing frequency sharing, synchronous orbit and system model

12 p2183 A70-26998

Noise effect on modulation transfer function of visual channel by threshold measurements

15 p2698 A70-32013

Two inch high resolution vidicon for TV line processing of printed documents

16 p2906 A70-33173

Nonbinary redundant error correcting codes for improving TV transmission speed and fidelity

22 p3985 A70-42493

SECAM video and audio color TV transmission over Molniya satellite relay path

23 p4162 A70-44091

TV broadcast satellites program distribution direct to home by network and by community

23 p4164 A70-44646

Integrated data processor-operation controller for stellar TV photometer systems in spaceborne observatory, considering limited channel transmission capacity

23 p4167 A70-44649

TELLEGEN THEORY

U GYRATORS

U NETWORK ANALYSIS

U NETWORK SYNTHESIS

TELLURIC CURRENT MICROPULSATIONS

U MICROPULSATIONS

U TELLURIC CURRENTS

TELLURIC CURRENTS

Geomagnetic field variations represented by optimal electric current loops or dipoles, noting advantages over spherical polynomials

07 p1266 A70-19442

Terrestrial electrical conductivity measurement from electromagnetic field variations determination by geomagnetic sounding

07 p1277 A70-20458

Equatorial geomagnetic micropulsations using earth current technique, discussing night and diurnal variations

10 p1875 A70-24435

Geomagnetic field variations represented by optimal electric current loops or dipoles, noting advantages over spherical polynomials

18 p3249 A70-36916

TELLURIC FIELDS

U ELECTRIC FIELDS

U TELLURIC CURRENTS

TELLURIC LINES

Telluric lines seasonal variations, discussing oxygen and water vapor photoelectric recordings in solar spectrum

16 p0000 A70-34185

TELLURIDES

NT CADMIUM TELLURIDES

NT INDIUM TELLURIDES

NT LEAD TELLURIDES

NT MERCURY TELLURIDES

NT TIN TELLURIDES

NT ZINC TELLURIDES

GeTe thermoelectric power, electrical/thermal conductivity and expansion coefficient measured at 20-600 C, determining suitability as thermoelectric material

01 p0158 A70-10755

Niobium ditelluride single crystals production with purity dependent on initial materials, discussing X ray structural and chemical analysis and electrical properties

03 p0542 A70-13753

Knudsen effusion measurements of stoichiometric MnTe sublimation at high temperature and low pressure

21 p3773 A70-41273

Surface density, charge and field effect mobilities for electrons and holes on MIS insulator-semiconductor structure on narrow bandgap HgCdTe

22 p4086 A70-43018

TELLURIUM

NT TELLURIUM ISOTOPES

N-type Te-doped gallium antimonide conversion to p-type by electron irradiation, noting thermal conductivity variations

13 p2470 A70-29167

TELLURIUM ALLOYS

Cd-Se and Cd-Te systems phase diagrams based on regular solutions theory, discussing molecular interaction energy dependence on composition

22 p4085 A70-42678

TELLURIUM COMPOUNDS

NT CADMIUM TELLURIDES

NT INDIUM TELLURIDES

NT LEAD TELLURIDES

NT MERCURY TELLURIDES

NT TELLURIDES

NT TIN TELLURIDES

NT ZINC TELLURIDES

Nonstoichiometric GeTe defects nature from band structure analysis based on two carrier model

02 p0350 A70-11698

TELLURIUM ISOTOPES

Te nuclear magnetic resonance in amorphous semiconducting sample cycled between conducting and nonconducting states

08 p1557 A70-21697

TELLURIUM 119

U TELLURIUM ISOTOPES

TELLUROMETERS

Distance measurements by microwave tellurometers, discussing accuracy factors

22 p4039 A70-43426

TEMPERATE REGIONS

Adrenocortical responses of military recruits to subtropical climate, making serum and urinary 17-OHCS measurements on subjects fasting, inactive and at thermoneutrality

01 p0032 A70-10359

Seasonal variations of sporadic E virtual height at middle latitudes attributed to hemispheric expansion depending on ozone amount

03 p0476 A70-13907

Electron temperature and density data obtained during Alouette satellite passage over middle latitude red arc, noting influence of intersecting magnetic field lines

03 p0476 A70-13911

HF oblique ionospheric soundings over long temperate latitude path, discussing measured angles of elevation and multipath time dispersion

05 p0847 A70-15998

Sunrise effects in lower ionosphere at midlatitude, discussing long wave absorption measurements, summer electron concentration profile and consistency of aeronomic model

07 p1235 A70-19436

Geomagnetic pulsations with intensity maximum at midlatitudes, noting north to south decreasing trend

07 p1278 A70-20459

Photometric and interferometric observations of midlatitude stable auroral red arc, determining structure, intensity and position

11 p2047 A70-26570

Corpuscular radiation intensity measurements in upper atmosphere at midlatitudes by meteorological probe during geomagnetic storm, noting radio wave absorption

11 p2106 A70-26797

Ionospheric electron content at temperate latitudes during solar cycle increasing phase by radio beacon satellite, discussing diurnal, seasonal and latitudinal variations

12 p2225 A70-27892

Statistical properties of subtropical jet stream maxima over U.S. from Nimbus II IR radiometry

17 p1333 A70-35931

Sunrise effects in lower ionosphere at midlatitude, discussing long wave absorption measurements, summer electron concentration profile and consistency of aeronomic model

18 p3249 A70-36910

F1 layer occurrence probability as function of mean monthly Wolf numbers at midlatitudes, noting solar activity effect

18 p3254 A70-37032

Pc1 pulsations occurrence frequency diurnal annual and 11 year variations at midlatitudes, relating distribution with carrier frequencies of perturbation

19 p3408 A70-37316

Temperate equatorial and auroral zones sporadic E observations and formation theories survey for prediction

19 p3416 A70-38441

Auroras and noctilucent clouds simultaneous occurrence in middle latitudes, discussing mesopause temperature variations and mesosphere heating

20 p3621 A70-39402

Ionospheric electron density response to geomagnetic storms at midlatitudes, noting diurnal variations detected by ATS 3 VHF signals

20 p3623 A70-40479

Total ionospheric electron content nocturnal and latitudinal variations in winter at midlatitudes

20 p3624 A70-40480

Pc1 geomagnetic micropulsation statistics for middle latitudes, discussing solar cycle and annual variations in occurrence rates

21 p3817 A70-41088

Nighttime and daytime midlatitude magnetic bays statistical correlations with riometer-auroral absorption, suggesting precipitating particles role

22 p4018 A70-43107

Winter predawn enhancement of 6300 A airglow at higher midlatitudes, considering roles of oxygen dis-

sociative recombination and photoelectrons production at magnetically conjugate point

22 p4019 A70-43110

Lunar tidal effects on horizontal magnetic field compared at equatorial and midlatitude stations

22 p4021 A70-43279

TEMPERATURE

NT AMBIENT TEMPERATURE

NT ATMOSPHERIC TEMPERATURE

NT BODY TEMPERATURE

NT BRIGHTNESS TEMPERATURE

NT COMBUSTION TEMPERATURE

NT CRITICAL TEMPERATURE

NT CURIE TEMPERATURE

NT FLAME TEMPERATURE

NT HIGH TEMPERATURE

NT IGNITION TEMPERATURE

NT ION TEMPERATURE

NT IONOSPHERIC TEMPERATURE

NT LOW TEMPERATURE

NT LUNAR TEMPERATURE

NT OPERATING TEMPERATURE

NT PLANETARY TEMPERATURE

NT PLASMA TEMPERATURE

NT ROOM TEMPERATURE

NT SKIN TEMPERATURE (BIOLOGY)

NT SKIN TEMPERATURE [NON-BIOLOGICAL]

NT SOLAR TEMPERATURE

NT SPACE TEMPERATURE

NT STAGNATION TEMPERATURE

NT SURFACE TEMPERATURE

NT WALL TEMPERATURE

TEMPERATURE COMPENSATION

One piece KDP and ADP reflector shutters used as laser Q switches, discussing compensation for working surfaces temperature displacement

01 p1016 A70-10060

Silicon strain gage transducer for measurement of pressure between tongue and teeth, developing two types of temperature compensated strain gages

02 p0242 A70-12054

Low temperature high sensitivity temperature compensated heat flux transducers to measure conductive, convective and radiative heat transfer

02 p3033 A70-12740

Gages for static strain measurements at high temperatures, discussing resistivity temperature coefficient compensation

09 p1680 A70-23109

Thermocompensated wire loop microtensensors for machine part stress concentration measurements, including parameter selection nomograms

13 p2409 A70-29519

TEMPERATURE CONTROL

Thermal preconditioning using radioisotope heat source to eliminate inertial sensor warmup time by maintaining aircraft navigation system at constant temperature

01 p0140 A70-10310

Optimal steady state thermal design for fin-tube single and double surface space radiators, including meteoroid protection and pumping power weight penalties

01 p0215 A70-10829

Automatic temperature controller consisting of single element of closed loop feedback system with adjustable transfer characteristics

02 p0296 A70-11874

Radiation pyrometers development for in-flight measuring and controlling aircraft engine compressor blades temperature

[SAE PAPER 690432]

03 p0480 A70-12900

Bessel function applied to unsteady axisymmetric problem of heat conduction in thermally controlled coaxial cylinders with different physical properties

03 p0608 A70-14304

Spacecraft thermal control during reentry, considering heat absorption, cooling by gas injection, radiant heat removal and shielding

04 p0780 A70-14407

Combined hypoxic hypoxia and high ambient temperature found relieving strain on humans by increasing heat release by evaporation

04 p0630 A70-14581

Apollo extravehicular mobility unit (EMU) system developed from Gemini EVA system with improved thermal control and mobility to support contingency extravehicular transfer in emergency

04 p0645 A70-15665

OAO thermal subsystem design to provide temperature control for experiments and spacecraft electronic devices

04 p0765 A70-15668

Temperature distribution causes in earth orbiting satellite, outlining thermal control and temperature calculation methods and prelaunch ground tests

05 p0956 A70-15813

Si fluid thermal actuator as temperature sensor and prime mover for active thermal controller in spacecraft

05 p0806 A70-16124

Computer optimization of spacecraft optical coatings for temperature control, using finite element analysis and matrix inversion

[AIAA PAPER 69-979]

06 p1172 A70-17180

Automatic temperature stabilizer with high order amplification due to direct heater sensing, noting applicability for synthetic fiber plants and thermophysical laboratories

06 p1064 A70-17783

Series emittance thermal control coatings of polymeric dielectric films overlaying reflectors vacuum exposed to UV, X ray and proton radiation

[AIAA PAPER 70-64]

06 p1106 A70-18069

Multilayer insulation blankets with slits normal to energy transfer direction for thermal control of spacecraft and cryogenic tankage

[AIAA PAPER 70-15]

06 p1156 A70-18076

Thermal control of spacecraft via solid-liquid phase change materials

[AIAA PAPER 70-12]

06 p1092 A70-18137

Screening devices to control heat supplied to spacecraft, discussing mathematical model to determine effective emission

[DGLR-69-060]

07 p1392 A70-18816

Turbine blade and vane air cooling need established by advantages of operating aircraft turbines at high turbine entry temperatures

[AGARDOGRAPH-120]

08 p1559 A70-21931

Thermal controls for spacecraft in space and planetary atmospheres, including heat inputs by solar radiation and planetary albedos

09 p1789 A70-23130

Simulated degrading environment effect on spacecraft thermal control surfaces subjected to plume heating during apogee firing and solar irradiation

[AIAA PAPER 69-1024]

09 p1657 A70-23259

Water cooled space suits automatic control based on physiological changes in astronaut during hard work

09 p1627 A70-23458

Silicon oxide films coated satellite aluminum surfaces solar absorptivity and thermal emissivity, noting suitability as temperature control coatings

09 p1613 A70-23514

Insulation foils and surface coatings thermal properties effect on radiation properties for spacecraft thermal control systems

10 p1951 A70-24863

Temperature control of USAF tactical communications satellite (TACSAT) by passive techniques

[AIAA PAPER 70-461]

11 p2120 A70-25441

Thermal control design for diffraction limited large diameter Cassegrainian telescope systems in orbital conditions, using computer and scale model testing

11 p2052 A70-26356

Passive thermal control system design of SERT II nonspinning satellite based on 534-node analytical model calibrated against test data

11 p2127 A70-26358

Biosatellite environmental control coolant loop system design for 30-day mission program, discussing fuel cell power source, cryogenic subsystem, etc

11 p2127 A70-26360

Unidirectional heat pipe system design to control temperature of high power traveling wave tubes in synchronous orbit communication satellite, dissipating waste heat

11 p2127 A70-26362

Radiation stable refractory oxides in white spacecraft thermal control coatings, discussing photocatalysis application to degradation analysis

11 p2067 A70-26364

Thermal control pressure sensitive adhesive tapes for spacecraft applications, discussing properties degradation due to simulated terrestrial and space environments

11 p2067 A70-26366

Mercury bombardment ion thruster life test in space environment onboard space electric rocket test (SERT) satellite, describing passive satellite thermal control system design

11 p2127 A70-26606

Cooling system control system for astronaut thermal equilibrium and work output maximization during extravehicular space missions

13 p2357 A70-28526

Thermal control coatings, windows and mirrors for 1973 Mars Viking Lander vehicles under simulated Martian surface conditions

[AIAA PAPER 69-1023]

13 p2384 A70-28530

Shutter thermal control for Helios solar observation satellite, considering closed and open conditions

13 p2505 A70-28769

Oxygen 18 concentration in Greenland ice core correlation to solar activity index, indicating earth temperature control by solar activity

13 p2489 A70-28909

Temperature rate flight control system (TRFCS) for lifting reentry vehicles control and guidance

14 p2614 A70-30464

Constant temperature hot split film anemometer sensors based on velocity and heat flux distribution about probe, measuring flow rates

15 p2734 A70-31691

OGO spacecraft structures, thermal control systems, attitude control, weight and power supplies

15 p2810 A70-31782

Optimal distributed feedback surface temperature control of inertial grade floated rate integrating gyroscope, minimizing instrument degradation

16 p2908 A70-33347

Monopropellant hydrazine RCS rocket engine module, discussing operating conditions, development, thermal control and valve internal leakage

[AIAA PAPER 70-654]

16 p2965 A70-33544

Integrating influence of mediocrstral hypothalamic structures upon temperature regulation of juvenile rat based on Area praoptica medialis stimulation

16 p2849 A70-33697

Model relating spectral reflectance to thermal control materials properties and environment induced changes

[AIAA PAPER 70-831]

16 p2940 A70-33934

Surface recombination centers protecting against discoloration of thermal control coatings due to chemical changes induced by photoproducts holes and electrons in oxide pigments

[AIAA PAPER 70-830]

16 p2940 A70-33935

Metal oxides thermal control coatings, investigating mechanisms of interaction between constituents by luminescent technique

[AIAA PAPER 70-832]

16 p2940 A70-33936

Correction techniques for thermal network lumped parameter inaccuracies with conduction and radiation coupling, considering temperature control system

[AIAA PAPER 70-821]

16 p3002 A70-33943

ZnO coating pigment for spacecraft thermal control, examining UV irradiation effects on electrical properties

16 p2961 A70-34056

Surveyor thermal switch for temperature control to assure spacecraft components performance during temperature extremes on lunar surface

16 p2845 A70-34127

Fluid thermal actuator for temperature control of ITOS /Improved Tiros Operational System/ meteorological satellite, discussing design and performance

16 p2846 A70-34129

Aerospace thermophysics considerations in spacecraft and hypervelocity vehicles systems thermal design, discussing thermal control and control coatings optical and radiative properties

[AIAA PAPER 70-812]

17 p3194 A70-34509

Lightweight spiral wound bimetallic actuators for active spacecraft thermal control systems

17 p3022 A70-34755

Thermally powered reciprocating piston pump for temperature control fluid transport on Thermoelectric Outer Planet Spacecraft (TOPS)

17 p3101 A70-34757

Flexible thermostat for specific temperature range with liquid nitrogen coolant and gas transfer medium

17 p3096 A70-35850

Thermal control through fusible materials for missile S band transmitter package, using computer analysis

18 p2331 A70-36349

British X 3 satellite for investigating thermal control surface finishes stability, ultrathin solar cells, electronic systems reliability and micrometeoroid flux measurement

18 p3333 A70-36511

Mathematical simulation of human thermoregulatory system, considering automatic control theory

18 p2224 A70-36530

Aircraft air conditioning, discussing temperature and humidity control, cooling systems, etc

19 p3358 A70-37975

Thermal space simulation tests on Azur research satellite relating to temperature control subsystems and qualification and acceptance procedures

19 p3399 A70-38288

Space environment simulation chamber for testing of equipment temperature and satellite thermal model

19 p3402 A70-38897

Pyranometer with additional external glass cupola to eliminate temperature differences and heat exchange, discussing laboratory and field test results

20 p3626 A70-39034

Semiconductors, ferrites and segnetoelectrics automatic temperature stabilization problem based on heat source energy conversion

20 p3597 A70-39255

Thermal preconditioning unit using radioactive isotope heat source for temperature control of inertial navigation system

20 p3671 A70-40059

Integrated temperature and humidity control and water recovery subsystem for manned test in space station simulator

21 p3769 A70-40998

Solar arrays for Venus-Mercury flyby, evaluating temperature and power performance

21 p3756 A70-41010

Heat pipes in OAO 3 spacecraft for minimizing structural temperature gradients and validating thermal control approach

21 p3946 A70-41045

Spacecraft thermal control coatings scale models, discussing temperature errors due to energy transport along surfaces

21 p3951 A70-41874

Thyristor-servomotor temperature control unit, describing circuit and applications

22 p3996 A70-42850

Universal proportional high accuracy temperature controller using current regulating circuit consisting of light beam galvanometer, photoconductor, photodiodes and thyristors

23 p4194 A70-43999

Semifluidic proportional control systems for industrial controls involving oven temperature, remote hydraulic pressure regulation, drill bit pressure

24 p4293 A70-45432

Optimal temperature control for confined spaces and life support systems, using mathematical models of environmental control systems

24 p4295 A70-46373

TEMPERATURE DIFFERENCES

U TEMPERATURE GRADIENTS

TEMPERATURE DISTRIBUTION

Dynamic unbalance effects in rigid body rotors, discussing lubricant temperature changes and instability hysteresis

[ASME PAPER 69-LUB-14] 01 p0101 A70-10391

Upper atmosphere structure and energy budget based on IGY/IQSY spectroscopic observations of temperature distribution and stratosphere-mesosphere composition

01 p0072 A70-10578

Stratospheric temperature changes connection with winter D region absorption changes

01 p0073 A70-10583

Nonlinear stress relation in elastic media incompatible deformations, eliminating elastic distortions for known temperature distribution and thermal distortion

01 p0201 A70-10890

Circular plate nonlinear analysis under load and uniform midplane temperatures, using stationary potential energy principle

01 p0205 A70-11145

Transient temperature profiles and thermal stress distribution in circular plates and cylinders with eccentric hole determined by conformal mapping

01 p0207 A70-11153

Greenhouse effect in Venusian atmosphere, discussing cause of vertical temperature distribution established by Venera 4 probe

01 p0192 A70-11506

Turbulence and temperature fluctuations spectral characteristics in thermally stratified atmosphere determined for various wave numbers, using energy and mass transfer functions

01 p0136 A70-11610

Carbon dioxide temperature distribution, absorption and concentration as functions of molecular dissociation behind shock wave determined by measuring IR bands intensity

01 p0069 A70-11623

Radiative transfer in nongray gas between parallel walls, solving heat flux and temperature distribution

02 p0392 A70-11907

Temperature fields and universal motions in homogeneous isotropic thermoelastic body in absence of body forces and external heat supply

02 p0387 A70-12000

Thunderstorm downdraft trajectories and temperatures, discussing evaluation of cooling due to evaporation

02 p0325 A70-12256

Boundary conditions of heat conduction in systems of vessels connected by rods with given heat capacity and unknown temperature

02 p0400 A70-12674

Measurement techniques for determining density and temperature distributions along radius of plasma cylinder by electron cyclotron resonance, microwave refraction and acoustic resonance

02 p0349 A70-12758

Reinforced plastics models for determining internal stress, temperature and electromagnetic fields of multicomponent reinforced plastics

02 p0323 A70-12806

Heat equation prediction, considering insulated uniform rod with unknown temperature distribution

03 p0604 A70-12993

Superconducting transition temperature variation in bcc region of Ti-Nb-V ternary alloys measured as function of valence electrons and composition

03 p0538 A70-13154

Liquid heating in thin walled porous shells under various boundary conditions, deriving formulas for temperature fields

03 p0604 A70-13208

Circulation gas lens temperature distribution, considering effects of gravity, wall thermal conductivity, glass interlayer, etc

03 p0604 A70-13387

Critical thermal regimes in Couette flow, investigating temperature and velocity profiles of nonisothermal steady state Newtonian flow between two parallel plates

03 p0466 A70-13388

Temperature field in thermally stressed electric machine rotor obtained by solving Poisson and Laplace equations with digital computer, using network method

03 p0414 A70-13517

Solar photosphere temperature fluctuations from model consistent with convection hypothesis agreeing with limb darkening data

03 p0570 A70-13591

Turbulent fluctuation rates of temperature and velocity on basis of measurements in boundary layer with wall heat transfer

03 p0470 A70-14237

Optimal temperature for sintering of compact titanium carbide in Ar atmosphere

04 p0697 A70-14468

Transient temperature distribution, thermal stresses and deformations in thin finite circular disk due to continuous point heat source, using linear thermoelasticity

[ASME PAPER 69-WA/PVP-6] 04 p0768 A70-14789

Transient temperature distribution in inhomogeneous material, using finite difference representation for temperature time derivative

[ASME PAPER 69-WA/HT-33] 04 p0782 A70-14807

Matrix analysis of steady state temperature field and heat flux through multilayer, plane, cylindrical or spherical partitions with internal heat sources

04 p0785 A70-14924

Temperature distribution around radiating sphere in homogeneous gas medium with molecular heat transfer, solving energy transport equation

04 p0785 A70-15012

Axissymmetric structures under load and temperature distribution analyzed by matrix displacement method

[DGLR-69-62] 04 p0774 A70-15167

Thermoplastic behavior of bodies under variable loads obtainable as function of time variable external temperature field

04 p0775 A70-15200

Excitation temperature functions calculated in rare gases spectrum lines to determine radial plasma temperature distribution

05 p0886 A70-15798

Temperature distribution causes in earth orbiting satellite, outlining thermal control and temperature calculation methods and prelaunch ground tests

05 p0956 A70-15813

Steady temperature field and stressed state of elastic plane containing heat resistant arc shaped cracks produced by uniform thermal flux

05 p0935 A70-16231

Unsteady heat conduction numerical approximation for infinite cylinder with variable heating and boundary conditions of third kind

05 p0936 A70-16294

Heat source temperature distribution on surface of infinite cylinder with zero temperature, presenting solution to boundary value problem

05 p0957 A70-16296

Spectroscopic determination of radial temperature distribution at various currents in negative glow of hollow cathode discharge, analyzing influence of gas pressure

05 p0888 A70-16358

Unsteady laminar free convection caused by heating semiinfinite flat vertical plate, obtaining velocity and temperature distributions

05 p0957 A70-16370

Martian surface temperature distributions based on IR scans of disk compared with predictions of thermal properties

05 p0909 A70-16389

IR imagery by InSb detectors applied to mapping earth surface thermal distribution

05 p0840 A70-16498

Thermal conductivity and aperiodic temperature distribution in microstructure of composite materials reinforced with solid and hollow fibers

05 p0958 A70-16952

Unsteady temperature field of uniformly thick disk for inhomogeneous boundary conditions and small Fourier numbers solved by Laplace operation

05 p0958 A70-17013

Temperature of contact surface between two homogeneous isotropic solid bodies determined by calculating plane heat source of steady three dimensional temperature field

05 p0958 A70-17014

Temperature field in internally cooled gas turbine blades determined, using integrator combined with coordinating device

05 p0954 A70-17057

Tensile tests facility design for wide temperature ranges with loading system to maintain constant strain rate up to failure

05 p0830 A70-17072

Satellite IR measurements of surface horizontal temperature structure of Gulf Stream compared with ship and aircraft data

05 p0844 A70-17104

Surface roughness effects on radiant heat transfer rate of isolated plane surface with uniform temperature illuminated by collimated solar flux

06 p1172 A70-17178

Natural convection heat transfer from vertical plate immersed in thermally stratified fluid

06 p1175 A70-17685

Atmospheric temperature vertical profile reconstruction from ascending radiation observations using data regularization

06 p1097 A70-17793

Temperature distribution law for semiinfinite and infinite solid bodies under steady heat conduction in presence of concentrated heat source

05 p1178 A70-17872

Nighttime F 2 region temperature distribution under geomagnetically calm and disturbed conditions calculated from Alouette 1 satellite data

06 p1057 A70-17887

Static pressure, temperature profiles, heat transfer and optical data for turbulent boundary layer-shock interaction with/without injection

[AIAA PAPER 70-91] 06 p1042 A70-18210

Shock wave structure in He-Ar mixture velocity and temperature profiles based on kinetic model equations

06 p1051 A70-18346

Local heat transfer coefficients determined from temperature distribution on porous walls, deriving mathematical expressions for various surface geometries and transfer modes

06 p1184 A70-18555

Vertical motion and temperature structure of severe thunderstorms from jet aircraft penetration

06 p1102 A70-18585

Natural convection flow interactions from individual surfaces in closely spaced array of heated elements, discussing effect on heat transfer, induced flow and temperature field

07 p1418 A70-18644

Temperature distribution in heated horizontal layer of high Prandtl number silicone fluids at high Rayleigh numbers confined between rigid parallel conducting plates

07 p1418 A70-18647

Workpiece temperature during asymmetrical plane polishing by wheel face, deriving temperature distribution formulas for maximum heat source intensity

07 p1291 A70-18828

Wall temperature variation of transpiration cooled tube surrounding plasma arc calculated from gas mass flow and wall properties

07 p1420 A70-19214

Real gas behavior effect on shock tube temperature and pressure flow nonuniformity for range of Mach numbers

07 p1257 A70-19337

Circumsolar plasma structural inhomogeneity origin

07 p1384 A70-19418

Vertical temperature profile diurnal variations of Mars atmosphere using models, noting aerosol influence

07 p1385 A70-19422

Optimal localized heat treatment of welded products, analyzing temperature fields and stresses during heating and cooling of ferromagnetic materials

07 p1294 A70-19477

Unsteady temperature field and thermal stresses in reinforced anisotropic plate strengthened at rim by thin isotropic rod

07 p1408 A70-19543

Toupin and Knowles elasticity theory applied to spatial decay estimate for parabolic heat equation used in diffusive temperature field

07 p1409 A70-19565

Temperature fields and hydrodynamics in laminar flow of vertical liquid layers during free convection

07 p1422 A70-19655

Linear kinetic theory for condensation and evaporation at small Knudsen numbers, considering extrapolated temperature jump determination

07 p1422 A70-19656

Heat exchange in laminar and turbulent boundary layers on plate for arbitrary heat flux distribution allowing for initial unheated plate segment

07 p1423 A70-19657

Temperature stress distribution in cylinder or sphere with variable surface temperature and heated by external sources

07 p1411 A70-19819

Steady temperature field of two dimensional periodic contact surface in vacuum, using conjugate harmonic functions for thermal flux lines, isotherms and thermal resistance

07 p1423 A70-19820

Functions describing spatial-temporal temperature distribution in hyperbolic partial differential equations for nonstationary heat exchange between fluid flow and boundary wall

07 p1423 A70-19839

Temperature distribution in active elements of explosion proof asynchronous electric motors with multichannel bilateral axial flow ventilation systems
07 p1196 A70-19841

Temperature renormalization for improving velocity distribution function representation in solving nonlinear Vlasov equation, transforming Hermite polynomials
07 p1328 A70-20201

Wave disturbances in tropical lower troposphere, discussing cross spectrum analysis of wind, temperature, relative humidity and surface pressure
07 p1275 A70-20304

Proton concentrations, magnetic field strength and temperatures distribution in interplanetary plasma flows as function of latitudinal distance from center of active region
07 p1391 A70-20420

Temperature fields creation in infinite or finite regions by moving surfaces with given time dependence of temperature studied by subjecting diffusion equation to transformations
08 p1597 A70-20959

Damped isotropic turbulence kinetic and temperature fluctuation energy spectra, neglecting viscosity and molecular heat conduction
08 p1483 A70-20961

Cloud layer vertical displacement effects on upper boundary and temperature changes in st-sc using aircraft sounding data
08 p1537 A70-21107

Turbulence coefficient and profile in atmospheric boundary layer from wind and temperature distribution, obtaining formulas from model approximating coefficient by altitude function
08 p1538 A70-21112

Thermal interaction between casting and mold at beginning of cooling using mathematical model for temperature field
08 p1506 A70-21139

Solidification thermal conditions during Ti casting by melting out patterns in graphite molds, investigating heat accumulation coefficients in molds
08 p1506 A70-21142

Steady temperature field and stresses produced by thermal sources in infinite elastic plane containing insulated rectilinear crack, determining thermoelastic state of half plane
08 p1587 A70-21172

Cooled turbine blades temperature field calculated considering variations at turbine inlet, over blade length, material temperature dependence and heat transfer boundary conditions
08 p1597 A70-21185

Hot-wire anemometry equation suitable for wide regions of velocity and temperature derived by computing thermal losses by supports
08 p1496 A70-21236

Transient heat conduction and stationary temperature distribution calculation in curvilinear coordinates using finite element method
08 p1590 A70-21362

Transient radial temperature distributions in cylindrical shells via Carslaw and Jaeger procedure involving binomial theorem and asymptotic expansions of Bessel function
08 p1599 A70-21588

Transient temperature distribution in flow through channel with arbitrary cross section, taking into account internal heat generation and viscous dissipation
08 p1599 A70-21767

Combustion rates and temperature distribution in condensed and gaseous phases of ammonium perchlorate sandwich with synthetic resin middle layer
09 p1741 A70-22105

Three dimensional RC network simulating temperature fields in IC at different heat source power dissipation laws, discussing harmonic heat source field
09 p1643 A70-22128

Electron temperature distribution in thermal boundary layer about probe electrodes calculated by successive approximations allowing for electron heating by arc
09 p1734 A70-22167

Atmospheric temperature spectra at low elevation showing consistency with Monin-Obukhov scaling
09 p1715 A70-22358

Boundary point least squares technique extended to thermal and thermal stress problems in similar regions, deriving temperature and stress functions
09 p1774 A70-22580

Axisymmetric or plane bodies temperature distribution from heat conduction analysis using computer program based on finite element method
09 p1788 A70-22581

Elastic solution and finite element method applied to heat conduction and thermal stress in temperature field determination
09 p1774 A70-22587

Temperature distribution in infinite and finite circular hollow cylinders, considering surface heat flux and linear heat transfer
09 p1788 A70-22595

Temperature distributions in multidimensional transient conduction heat transfer, using variational method and Laplace transformation
09 p1788 A70-22705

Laser measurements of permittivity fluctuations spectrum of turbulent atmosphere, noting proportionality to temperature spectra at optical frequencies
09 p1635 A70-22962

Temperature and stress fields in orthotropic plate with partial surface insulation, examining boundary conditions
09 p1777 A70-23078

Temperature fields and thermoelastic stresses in doubly connected structural elements solved in curvilinear coordinates system corresponding to conformal mapping of annulus
09 p1777 A70-23080

Temperature fields in cylindrical shell under axisymmetric heating, ensuring optimal stressed state
09 p1778 A70-23081

Temperature field in infinite plate with disk shaped inclusion and stationary point heat source determined, allowing for heat transfer conditions
09 p1778 A70-23082

Temperature fields and stress-strain state in elastic bodies with thin walled cylindrical shell inclusions during uniform heat flow at infinity
09 p1778 A70-23083

Thermoelastic stresses in plates and shells in random temperature fields, studying influence on service life
09 p1778 A70-23084

Structural elements reliability determination simulated by microinhomogeneous polycrystalline medium under thermal stresses and in stationary nonuniform temperature fields
09 p1778 A70-23085

Transversely isotropic body of revolution under combined surface loads and stationary axisymmetric temperature field, obtaining displacement vector and stress tensor in analytic functions
09 p1778 A70-23086

Algorithm for stress-strain state calculation of nonuniformly heated cylinder weakened by star-shaped cavity
09 p1779 A70-23094

Rectangular plate in unsteady temperature field, analyzing thermoplasticity problem by reducing solution to linear system with variable coefficients
09 p1779 A70-23098

Layered conical shell creep under axisymmetric load and time dependent temperature field by iterating boundary integral equation
09 p1779 A70-23099

Sensors design for studying temperature fields and stressed state of structures
09 p1680 A70-23106

Wave dispersion relations in uniform magnetized plasma represented in single integral form, discussing model loss-cone and temperature anisotropy distributions
09 p1736 A70-23188

Segmented anode current and heat distribution in MPD engine measured with current shunts and calorimetric methods
09 p1613 A70-23238

Strain and temperature fields interrelation effect on longitudinal wave propagation in viscoelastic cylinder, determining phase velocities and attenuation coefficients
09 p1781 A70-23285

Metal probes friction coefficient and impact temperature distribution during impingement onto rotating chromium steel disk related to speed under various atmospheres
09 p1708 A70-23425

Plane Poiseuille flow with nonlinear temperature distribution, studying vortex type secondary flow onset due to buoyant forces
09 p1790 A70-23555

Solid radiating sphere cooling in space, determining transient temperature distribution by finite difference computing techniques
09 p1790 A70-23562

Centrifugal forces and nonuniform heating effect on natural vibration frequencies of circular plates using lumped parameter method
09 p1784 A70-23588

Boundary function of unsteady temperature field in bodies with moving surface at constant temperature calculated by least squares method
09 p1791 A70-23620

Fluid boiling heated nonuniformly in pipe, deriving formulas for unsteady temperature field by integrating energy equation
09 p1791 A70-23716

Heat and mass transfer during liquid surface evaporation in vacuum, calculating temperature field on basis of heat balance level
09 p1791 A70-23717

Temperature field distribution in long thin narrow plate composed of materials differing in thermophysical characteristics, creating field by moving heat source on plate
09 p1791 A70-23723

Temperature fields and thermal stresses in FN fiberglass reinforced textile under nonstationary unilateral heating, determining stress as function of time and heating rate
09 p1710 A70-23724

Temperature field and combined radiative-conductive heat flux in weakly absorbing cylindrical layer bounded by nonblack surfaces
10 p1966 A70-23866

Temperature field and heat conduction equation for two layer polymer cylinder multiply heated from within, considering material decomposition
10 p1966 A70-23870

Velocity and temperature distribution behind shock waves in hydrogen plasma measured to determine factors responsible for discrepancies in Rankine-Hugoniot conditions
10 p1867 A70-24149

Temperature field in work piece generated by grinding wheel face investigated for cylindrical and surface grinding
10 p1894 A70-24291

Integrated circuits involving long-strip heat source surrounded by multiple layers, expressing temperature distribution by Fourier transformation obtained integrals
10 p1850 A70-24620

Atmospheric temperature vertical profile reconstruction from ascending radiation observations using data regularization
10 p1913 A70-25024

Convective-radiative heating of multilayer plate approximating temperature field by iteration
10 p1969 A70-25143

Thermoelasticity problem for plane with rectilinear cut with constant temperature at initial moment of time, using approximating kernel of integral equation
10 p1965 A70-25296

Temperature and heat flux in plane, cylindrical and spherical multilayer diaphragms with boundary conditions, assuming harmonic temperature variation
10 p1970 A70-25321

Energy equations solved for step change of wall temperature and heat flux, determining turbulent heat transfer in tube, discussing asymptotic solutions validity
11 p2146 A70-25334

Ambiguities during brightness temperature distributions reconstruction from intensity interferograms
11 p2048 A70-25335

Air ventilated cassette-type electronic equipment steady thermal regime, measuring local excess temperatures relative to ambient temperature
11 p2017 A70-25583

Nonisothermal dielectric coating on conductor surface, analyzing temperature distribution effect on thermal emission characteristics
11 p2148 A70-25975

Temperature, stresses and deformations in melting plates of elastic perfectly plastic material, using penetration depth concept with heat balance approach
11 p2138 A70-26134

Test model thermal balance in space simulator, measuring effects of solar simulator irradiance reflected from carbon dioxide cryopanel deposits
11 p2149 A70-26153

Temperature distribution in shadowed lunar craters formulated in Fredholm integral equations, showing constant temperature and correction for soil thermal inertia
11 p2112 A70-26155

Temperature distribution in opposed jet diffusion flames, discussing mass fluxes and fuel and oxygen concentrations effect
11 p2151 A70-26385

Seminfinite elastic body with instantaneous heat source on surface, analyzing temperature and thermal stress distributions
11 p2139 A70-26406

Hollow homogeneous polymer cylinder thermoelastic stressed state, analyzing radial temperature and Poisson Coefficient variations
12 p2325 A70-27532

Turbulent Prandtl number values for air with injection and suction obtained from velocity and temperature profile data
12 p2210 A70-27699

CAT parameters sensitivity to horizontal wind and temperature distribution
13 p2444 A70-28587

Clouds upper height boundary relation with radiation temperature field from satellite data, noting cirrus clouds influence
13 p2444 A70-28589

Radiative energy transport effect on temperature distribution in conduction heated plane layer applied to solar chromosphere
13 p2488 A70-28716

Linearized Fredholm equation solution, describing temperature field for energy transport by radiation and heat conduction
13 p2521 A70-28860

Heat transfer mechanism in foil-vacuum insulations, analyzing factors responsible for point of inflection on experimental temperature field curves 13 p2521 A70-28861

Thermal stresses in solid nonhomogeneous sphere in high periodic temperature field, assuming temperature dependent Young modulus and linear thermal expansion coefficient 13 p2512 A70-28979

Band or line shape effect on radiative transfer in nongray medium between parallel walls, discussing temperature distribution and radiative flux 13 p2521 A70-29136

Thermal stresses dependence on temperature field during axisymmetric heating of rigid cylindrical shells 13 p2421 A70-29426

Thermoelastic equations for circular sandwich plates bending due to asymmetric temperature distribution 13 p2518 A70-29976

Surface temperature fluctuations during dropwise condensation at various heat fluxes 14 p2663 A70-30256

Flat plate and cylinder with periodic Joulian heating from time dependent heat source, analyzing transient temperature distribution 14 p2664 A70-30269

Radiant heat flux for standard model, dry and humid atmosphere, calculating temperature variations with altitude for entire IR spectrum 14 p2603 A70-30401

Northern Hemisphere temperature atlas for SST cruise altitudes, estimating probabilities of enroute temperatures and risk increase 14 p2609 A70-30609

Coupled temperature and electric potential distribution in finite rotational symmetric hydrogen arc column in axial magnetic field 14 p2621 A70-30656

Soviet monograph on thermal conductivity of plates and bodies of revolution covering temperature and stress distributions, multilayer shells, etc 14 p2666 A70-30952

Stress, strain, temperature, electric and magnetic field distributions resulting from magneto-thermoelastic interactions in infinite elastic solid subjected to transient heat source 14 p2661 A70-31229

Rarefied gas slip flow coefficients calculations at nonuniformly heated surface, demonstrating relationship between temperature and isothermal slip coefficients 15 p2776 A70-31478

Thermal convection formation in viscous fluid plane horizontal layer from measurements of unsteady temperature field 15 p2824 A70-31591

Natural convection wake from heated horizontal line source in liquids and in air, determining temperature field in plume above wires 15 p2825 A70-31817

Chorioretinal damage thresholds spectral dependence of intense light sources, describing temporal, axial and radial temperature distributions 15 p2682 A70-32014

Longitudinal velocity and temperature fluctuation spectra in turbulent boundary layer, showing highest spectral densities at internal zone 15 p2826 A70-32021

Heat transfer between incompressible fluid flow and insulated walls with time varying temperature at channel inlet, applying Laplace transforms 15 p2827 A70-32175

Electromagnetic absorption of Martian matter based on vertical temperature variations in planet surface layer 15 p2802 A70-32491

Linear kinetic theory for condensation and evaporation at small Knudsen numbers, considering extrapolated temperature jump determination 15 p2828 A70-32693

Heat exchange in laminar and turbulent boundary layers on plate for arbitrary heat flux distribution taking into account initial unheated plate segment 15 p2828 A70-32694

X ray differential drift scans of moon, measuring cold limb brightness temperature and temperature distribution 16 p2974 A70-33646

Temperature distributions and heat flux for gray gas in radiative equilibrium bounded by walls with different temperatures, using differential approximation [AIAA PAPER 70-834] 16 p3001 A70-33929

Radiatively interacting adjoin plates in presence of collimated solar flux, considering surface roughness effects on equilibrium temperature distribution [AIAA PAPER 70-817] 16 p3002 A70-33946

German monograph on temperature distribution and motion of free burning arcs in transversal magnetic fields and gas flows, covering aerodynamic model concept 16 p2959 A70-34077

Thermorheologically simple model for viscoelastic materials stochastic behavior in random temperature fields, introducing reduced time scale 16 p3003 A70-34238

Transverse magnetic field effects on Ar cross flow arc temperature distribution, cross section shape and profile, discussing forced convection effects [AIAA PAPER 70-777] 17 p3138 A70-34477

Temperature and Mach number distributions measurements on supersonic turbulent boundary layers for reanalyzing heat transport [AIAA PAPER 70-744] 17 p3066 A70-34499

Lunar rilles temperature distribution analysis, examining contour shape, aspect ratio and solar elevation angles effects 17 p3152 A70-34507

Rarefied binary gas mixture transient Couette flow, considering nonlinear case of plate with equal temperature accelerated impulsively 17 p3067 A70-34546

Thermal response of passive heliotrope solar array orientation device using rotating bimetallic helix, performing energy balance analysis for helix temperature distribution 17 p3082 A70-34761

Satellite temperature distribution prediction from digital simulation 17 p3177 A70-35250

Nonstationary temperature fields and stresses in wedge shaped strip and thin plates with heat transfer for discontinuous boundary conditions 17 p3189 A70-35342

Temperature distribution of solar atmosphere, discussing solar models 17 p3169 A70-35382

Heat conduction from sliding solids, discussing restrictions effect on temperature field near interface 17 p3197 A70-35543

Aerial IR surveys of surface temperature patterns of Hudson Bay during ice free seasons 17 p3079 A70-35621

Detonation in nonuniformly heated gas capable of chemical reaction, obtaining numerical solution 17 p3198 A70-35737

Free convection in air and water above horizontal wire heated by DC current, measuring flame temperature distribution by diffraction interferometer 17 p3198 A70-35743

Laminar free convection near two dimensional and axisymmetric nonisothermal bodies, examining surface temperature distribution and heat flux 18 p3345 A70-35999

Temperature changes minimization techniques in specimens during microplasticity tests, describing gage assembly for plastic strain measurement 18 p3272 A70-36030

Stationary heat conduction model of two cylinders abutting at ends with internal nonuniform temperature distribution 18 p3345 A70-36128

Spatial-temporal distribution of laser spark plasma electron density and temperature based on holographic interferometry 18 p3265 A70-36152

Optical observation of laminar convective flow caused by combined action of concentration and temperature fields 18 p3346 A70-36276

Slab melting under hot spots, obtaining starting solutions 18 p3346 A70-36491

Two dimensional turbulent film cooling, predicting initial region temperature distribution by solving finite difference form of thermal energy equation 18 p3346 A70-36497

Surface temperature fluctuations during steady state boiling from tube, using fast response thermocouple 18 p3347 A70-36504

Unsteady temperature fields in heat conduction problems associated with high temperature effects on abutted cylinders 18 p3348 A70-36572

Half space nonstationary temperature field with mobile heating at edges, using integral transformations 18 p3348 A70-36725

Surface temperature distribution over rotating nucleus of comet deficient in volatiles 18 p3319 A70-37058

Milky way galactic plane corrugation, discussing maximum hydrogen brightness temperature oscillating in sinusoidal pattern 18 p3328 A70-37167

Air-mechanical fuel injection effect on gas turbine engine combustion chamber working process, investigating heat generation coefficient, temperature field nonuniformity and combustion efficiency 19 p3489 A70-37248

Shadow method for temperature field in potentiometer winding 19 p3420 A70-37264

Friction and temperature fields in lubricant film of journal bearings, discussing friction torque and heat dissipation [ASME PAPER 69-LUB-24] 19 p3434 A70-37601

Dynamic unbalance effects in rigid body rotors, discussing lubricant temperature changes and instability hysteresis [ASME PAPER 69-LUB-14] 19 p3435 A70-37606

Thermoelastic stresses in infinite anisotropic slab due to temperature field variations along thickness and length 19 p3539 A70-37872

Ultrasonic measurement of temperature distribution in solid, liquid and gaseous media, using reflection and transmission techniques 19 p3427 A70-37963

Annual temperature variation in low stratosphere based on harmonic analyses at 100 mb 19 p3462 A70-38263

Heat transfer in boiling liquid from temperature field and temporal changes in liquid above heating surface, determining isotherms by laser interferometry 19 p3447 A70-38455

Temperature and radio brightness distributions in active regions and upper chromosphere during minimum activity periods 19 p3522 A70-38557

Solar wind velocity variations showing relationship with electron density excess and localized region temperature of corona 19 p3512 A70-38693

Hydromagnetic flow past infinite impulsive motion plate, determining velocity and temperature fields distribution 19 p3482 A70-38934

Main sequence stars faint end IR observations for luminosities and temperatures 20 p3702 A70-39014

Non-LTE line blanketed solar model atmospheres with various temperature distributions 20 p3703 A70-39020

Pressure and temperature distribution in constant volume viscous Poiseuille gas flow velocity profile 20 p3608 A70-39121

Fretting corrosion zone steel, measuring transient temperature distribution during contact friction 20 p3647 A70-39243

Damped isotropic turbulence kinetic and temperature fluctuation energy spectra, neglecting viscosity and molecular heat conduction 20 p3608 A70-39383

Heat exchange and temperature distribution between two liquids divided by plate, discussing possible errors 20 p3737 A70-39634

Plate temperature field and stress distribution under thermal pulses, evaluating critical heat load for damage 20 p3737 A70-39635

Unsteady temperature field in cylinder surrounded by thin shell under uniformly distributed heat sources 20 p3737 A70-39640

Steady turbulent flow heat exchange in near wall region at large Prandtl numbers, plotting temperature distribution curves 20 p3612 A70-39811

Elastic bodies collision, determining temperature field variations and contact pressure 20 p3725 A70-39869

Laminar flow of liquid in duct with zero heat resistance of walls, calculating temperature distribution during radiative convective heating 20 p3613 A70-40297

Supersonic weakly ionized plasma jet in argon, investigating axial and radial temperature profiles by electrical probe techniques and spectroscopic and photographic methods 20 p3685 A70-40463

Transient and steady state free convection heat transfer with mercury in vertical rectangular channel, measuring temperature distributions 21 p3941 A70-40773

Fusion welding cooling rates, peak temperatures and heating duration relationships to distance from fusion line predicted by theory for comparison with experiment 21 p3832 A70-40791

Steady one dimensional temperature field of cylindrical shell spacecraft, allowing for heat conduction and convective and radiative heat transfer within shell 21 p3942 A70-40841

Mars lower atmosphere vertical temperature distributions from Mariner 6 and 7 radio occultation data, using improved trajectory estimates 21 p3884 A70-40908

Gaseous film cooling effect on adiabatic wall temperature distribution in rocket nozzle with gas injection 21 p3867 A70-41028

Natural convection boundary layer stability on isothermal flat vertical wall or subjected to linear temperature distribution 21 p3950 A70-41443

Numerical procedure for second order nonlinear differential equations, discussing temperature distribution in semiinfinite solid homogeneous medium 21 p3950 A70-41449

Apollo 11 fines gas evolution and physical changes via heat treatment, discussing Ar 40 anomaly, lava structure origin and oxidation rate

21 p3907 A70-41577

Internally cooled turbine blade with longitudinal cooling channels, calculating temperature field by combined analytical and analog method

21 p3868 A70-41772

Temperature distribution in rotating thin cylindrical shell with line conduction discontinuity under solar heating, evaluating tubular elements thermal bending on spinning spacecraft

21 p3951 A70-41875

Cellular convection in fluid layers with parabolic temperature distribution, calculating stability effects of gravity and surface tension gradients

21 p3952 A70-42078

Nonuniform radiation heat transfer between two coaxial cylinders, obtaining temperature distribution by Fourier series expansion

21 p3952 A70-42082

Wave number spectral correlation of temperature and longitudinal velocity fluctuations in fully developed pipe flow

21 p3811 A70-42090

Temperature distribution measurement inside solid samples by Mossbauer effect, considering application to turbine blades

21 p3830 A70-42165

Turbulent incompressible conducting fluid jets velocity and temperature characteristics in presence of longitudinal and transverse magnetic fields

21 p3860 A70-42226

Temperature, metal vapor density and energy balance in Ar shielded welding arc with Fe electrodes

22 p4043 A70-42381

Buoyant hot two dimensional laminar vertical jet in quiescent colder fluid, calculating temperature and velocity distributions by integral method

22 p4010 A70-42639

Heat conduction into semiinfinite homogeneous solid with thermal conductivity dependence on temperature, noting temperature profile asymptotic behavior for similarity solution

22 p4123 A70-42641

Nonlinear heat transport in structural elements due to radiative transfer, analyzing temperature field dynamics

22 p4125 A70-43360

Tube heat exchangers operation at low transfer coefficient, calculating unsteady temperature field in wall and heat transfer agent

22 p4125 A70-43364

Temperature distribution and thermal convection resistance due to steady heat flow in laminated composite

22 p4126 A70-43689

Nonsteady temperature and thermal stress distribution in gas turbine blades, using plastic model and photothermoelastic method

22 p4093 A70-43743

Tropical cyclone development model for axisymmetric vortex and quasi-balanced conditions, considering vertical heat distribution, rate of intensification and energy budget

23 p4213 A70-43896

Electromagnetic absorption of Martian matter based on vertical temperature variations in planet surface layer

23 p4240 A70-43913

Thin plates two dimensional dynamic thermoelastic problem, determining hyperbolic type heat conduction for temperature field

23 p4265 A70-43985

Sandwich multilayer structures temperature fields and heat transfer characteristics at high temperature [ICAS PAPER 70-38-BIS]

23 p4276 A70-44136

Spherical multilayer shell unsteady temperature fields, assuming mixed convective and radiative transfer at inner surface due to hot gas flow

23 p4276 A70-44165

Thermal convection formation in viscous fluid plane horizontal layer from measurements of unsteady temperature field

23 p4277 A70-44278

Time optimal problems involving parabolic equations in heating of rod with piecewise continuous thermophysical characteristics and temperature distribution constraints, deriving iterative solution

23 p4277 A70-44306

Temperature distribution and thermal conductivity determination in Ar plasma cascade arc

23 p4276 A70-44438

Temperature distribution in cylinders of aircraft internal combustion rotary piston engine under air cooling

23 p4234 A70-44742

Thermal flux surface distribution lifting bodies, discussing aerodynamic efficiency dependence on drag and zero angle of attack Mach number

23 p4136 A70-45019

Pulsed ruby laser radiation energy characteristics relation to crystal temperature distribution, thermal deformation and compensating lens focal length

24 p4352 A70-45460

Subsolidus state multicomponent eutectics systems temperature range based on number and melting points ratios of individual components

24 p4367 A70-45476

Metal and nonmetal thermal nondestructive tests based on surface temperature distribution produced by heat treatment

24 p4348 A70-45744

Spacecraft astronomical instrument structural design, examining aging, vibration and temperature distribution deformations and optical surface contamination

24 p4339 A70-45823

Plate temperature jump and heat flux in Knudsen layer using Bhatnagar-Gross-Krook model

24 p4429 A70-45997

Nonlinear distributed sources induced diffusion, calculating relationship between source intensity and maximum temperature or mass concentration field

24 p4380 A70-46034

One-phase Stefan problem of heat conduction with melting, proving existence and uniqueness theorems for solid and free boundary temperature determination

24 p4429 A70-46036

Stratosphere radiation measurements by Nimbus 3 infrared spectrometer for 15 micron frequency, considering temperature variations

24 p4330 A70-46074

Surface temperature distribution of heat generating solid body in contact with parallel viscous fluid flow

24 p4430 A70-46368

TEMPERATURE EFFECTS

Reversible cold induced deactivation of cat neocortex bioelectric activity in chronic experiment, noting cooling system

01 p0031 A70-10056

Current carrier mobility in n-InSb calculated by Schwinger variational method over temperature range

01 p0154 A70-10098

Natural absorption band absorption coefficient frequency and temperature dependences in doped n-InSb

01 p0154 A70-10100

Ferroelectric sodium nitrite single crystals LF linear electro-optical coefficients as function of temperature

01 p0154 A70-10104

Temperature effect on work function minimum of cesiated W surfaces

01 p0154 A70-10108

Output voltage stabilizers for thermal compensation in semiconductor power generating circuits, using stabiltron reference source

01 p0049 A70-10139

Heat resistant alloys for gas turbine blades observed for long term heating effects on changes of hardness, tensile, impact and stress-rupture properties and microstructure

01 p0116 A70-10149

GaAs and Si photocell batteries powered by solar radiation, investigating temperature dependence of efficiency I-V characteristics and optimal power

01 p0007 A70-10177

Hydrogen-oxygen variable length combustor longitudinal instability, studying hydrogen injection temperature effects on pressure interaction index and pressure sensitive time lag

01 p0214 A70-10324

Re 187 to Os 187 nuclear decay rate variability, discussing earth age, temperature and ionization effects

01 p0178 A70-10349

Negative ion reactions relevant to D region measured in ESSA flowing afterglow system as function of temperature

01 p0070 A70-10406

Gas laser beams short time constant and thermal self defocusing following small spot focusing on thin dye sample

01 p0109 A70-10431

Microstructural interfacial stability and property retention after elevated temperature exposure of eutectic composites, discussing coarsening rate relationship to interfacial area and energy

01 p0117 A70-10485

Semiconductors as optical limiters for Q switched lasers, reporting temperature values for nonlinear absorption coefficients of Si, CdSe, CdTe and GaAs

01 p0158 A70-10563

Creep deformation modes of Ni-base austenitic superrefractory alloy as function of test temperature

01 p0118 A70-10704

Thermomechanical processing of high strength low alloy steels to evaluate effects of composition, coiling temperature and cooling rate on mechanical properties and microstructures

01 p0118 A70-10726

Strain rate, temperature and alloy content effects on plastic flow in binary substitutional alloys of bcc iron

01 p0119 A70-10735

Tantalum base alloy T-111 creep tests in vacuum at elevated temperature suggesting diffusion controlled microcreep mechanism

01 p0120 A70-10738

Martensite start depressed temperatures vs pressure for steels, discussing hardness effects and microstructure

01 p0120 A70-10740

Hot junctions nonuniform heating influence on thermoelectric generator efficiency, taking into account temperature dependence of thermoelement materials properties

01 p0009 A70-10753

Carbon dioxide refractivity measured under simulated Martian conditions and standard temperature and pressure, comparing results with radio occultation methods

01 p0186 A70-11085

Plasma injection occurrence as function of temperature in n-InSb subjected to low electric field strengths and fitted with Ohmic contacts

01 p0159 A70-11176

Vapor pressures of cobalt over pure cobalt and over Ni-Co alloys determined as function of temperature by isotope exchange method

01 p0121 A70-11233

High temperature internal friction measurements on miniature torsional pendulum specimens from TD nickel bar, showing damping differences due to microstructural anisotropy

01 p0122 A70-11237

FeCo V plastic deformation and fracture, noting temperature and grain size effects on yield and flow stresses, ductile to brittle transition, etc

01 p0123 A70-11244

Vibrational relaxation times in carbon dioxide and carbon dioxide-argon mixtures at 360-3000 K, using shock tube and laser schlieren method

01 p0148 A70-11355

Ternary Al-Zn-Mg alloys stress corrosion cracking properties, showing effects of aging temperature and prestrain

01 p0123 A70-11387

Unsteady heat transfer from porous flat plate with impulsive motion and rising temperature, analyzing compressible boundary layer equations using Laplace transform

01 p0067 A70-11390

Elastic ring reinforced annular plate of uniform thickness, heated nonuniformly along radius, discussing axisymmetric and asymmetric stability losses

01 p0210 A70-11415

Bauschinger effects in repeated tensile and compressive strains in inelastic media under variable temperatures as function of load vector, using plastic yield

01 p0211 A70-11422

Beryllium properties and processing including magnetothermal reduction, power purity, oxygen content, grain size and temperature effects on mechanical properties

01 p0124 A70-11618

Annealing effects on cold rolled titanium sheets, noting changes in Young modulus and characteristics of recrystallized titanium

01 p0124 A70-11620

Comfort and thermal sensations and associated physiological responses during exercise at various ambient temperatures, noting effects on sensory estimates

01 p0031 A70-11648

Current-voltage and current-temperature characteristics of alloyed p Ge-n Si heterojunctions, discussing current flow process complexity

02 p0350 A70-11667

Temperature effects on tensile deformation mechanism of Mo single crystals, investigating stress-strain characteristics and slip geometry

02 p0316 A70-11699

Ambient temperature effects on rats excretion of epinephrine, norepinephrine and major metabolites

02 p0232 A70-11714

Constitutive equations and thermally activated dislocation processes in metals, noting temperature and strain rate relationship

02 p0316 A70-11737

Mutual diffusion coefficient of hydrogen atoms and molecules in upper atmospheres of major planets calculated as function of temperature, using Chapman-Enskog theory

02 p0342 A70-11817

Decay times for thermal disturbances near cloud tops in Jupiter atmosphere, discussing hydrogen absorption

02 p0368 A70-11827

Thermal resonator effects on YAG-Nd laser rods with dielectric covered ends, using resonant model to study continuous or half wave operation

02 p0311 A70-11850

Temperature measuring devices design for ultrahigh/ultralow temperatures, examining heat effects on gases, liquids and solids

02 p0295 A70-11864

Temperature limit of efficiency threshold for ground based liquid propane sprayer for supercooled fog dispersal at Orly airport

02 p0324 A70-11872

Hydrogen reactions with nitrogen dioxide, oxygen and mixtures of oxygen and nitric oxide in adiabatic flow reactor measured as function of temperature and pressure

02 p0250 A70-12020

Spinal cord and skin temperature effects on tension-extension diagrams in cats red and pale muscles

02 p0236 A70-12092

Lubrication problem for centrally pivoted tilting-pad sector thrust bearings with temperature and elasticity effects, noting iterative solution for coupled equations

[ASME PAPER 68-LUB-4] 02 p0307 A70-12166

High temperature effects on evolution of Venus upper lithosphere, considering magnetic differentiation, isostatic adjustments, surface relief, mountain building time and distance scales, etc

02 p0371 A70-12207

Atmospheric effects on SST, discussing turbulence, temperature, wind, cloud cover, hail, toxic gases, etc

02 p0325 A70-12218

Atmospheric environment features bearing on supersonic transport aircraft operations and forecasting, discussing wind and temperature effects

02 p0325 A70-12220

Temperature dependence of magnetic susceptibility in liquid and solid states of binary Al-Mn alloys with additions of Cr, V and Ti

02 p0316 A70-12300

Titanium thin films prepared in ultrahigh vacuum to determine low temperature/pressure oxidation kinetics, using electron microscopy and X ray diffraction

02 p0317 A70-12316

Ruby laser light wavelength temperature dependence measurement using Fabry-Perot etalon

02 p0313 A70-12440

Ruby laser emission wavelength temperature dependence measured spectrographically

02 p0313 A70-12441

Spectrophotometric facility for measuring spectral characteristics of color filters, photomultipliers and photographic plates as function of temperature

02 p0301 A70-12494

Resistance strain gauge performance prediction, investigating response during temperature change for preattachment mounting

02 p0302 A70-12498

Temperature dependence of diffusion coefficient for carbon dioxide filled rigid polyurethane foam, using Fick law

02 p0321 A70-12524

Newtonian liquid lubricated spiral groove bearing load capacity and power loss dependence on viscosity variations with temperature

[ASLE PREPRINT 69-IC-21] 02 p0309 A70-12533

Release-recovery and dynamic stiffness phenomenon in frog heart muscle at various Ca ion concentrations and temperatures

02 p0241 A70-12771

Integral formulas of thermoelasticity theory for calculating displacements and rotations caused by temperature field action in micropolar Cosserat and Hooke media

02 p0391 A70-12817

Coupled diffusion of heat and vorticity in gaseous vortex caused by radial mass convection and temperature dependence of gas properties

02 p0400 A70-12858

Sensing device to measure radial stress induced at solid propellant grain-to-case bond interfaces during wide temperature variations, detailing instrumentation and operation

03 p0480 A70-12882

Boron combustion in air augmented rockets, examining mixing and burning between subsonic air and supersonic fuel rich exhaust

[AIAA PAPER 68-634] 03 p0603 A70-12910

Shells of revolution having arbitrary stiffness distribution and subjected to arbitrary loads and temperatures

03 p0583 A70-12916

Fiber composites dimensional changes, stresses and plastic flow during component allotropic transformation, studying temperature variations effects

03 p0585 A70-12973

Human blood platelets volume measured in Coulter counter, noting relation to temperature

03 p0416 A70-13008

Polycrystalline Ni steady state creep characteristics measurement emphasizing temperature dependence of creep rate

03 p0504 A70-13022

Temperature dependence of luminescence quantum yields and lifetimes in transitions during excitation of ruby crystal atoms

03 p0538 A70-13059

Neutron bombardment effect on ordering and disordering state of alloys phase diagrams, noting temperature dependence

03 p0506 A70-13107

Embrittlement in martensitic and semiaustenitic precipitation hardening stainless steels upon exposure

to high temperatures to determine causation and controlling means

03 p0506 A70-13132

Gray hypersthene Ramsdorf chondrite with thermal and mechanical alterations, discussing shock heating, metal plus troilite melt redistribution, collision and rapid cooling effects

03 p0563 A70-13147

Polycrystalline material tensile failure at high temperature, discussing intergranular cracking, shearing, etc

03 p0508 A70-13155

Transparent bodies photon thermal conductivity temperature dependence

03 p0515 A70-13206

Monograph on elevated temperature strength data for wrought austenitic stainless steels, considering yield, tensile, creep and rupture strengths for allowable stresses

03 p0510 A70-13300

Polycrystalline Co strength and plastic properties tested at various temperatures and strain rates

03 p0510 A70-13352

Prolonged temperature exposures with applied tensile stress found to increase tensile strength and yield point of aluminum alloy subjected to artificial agings

03 p0511 A70-13354

Temperature dependence of sputtering coefficient of quartz and chondrites at 2000 K and mass decrease prior to evaporation

03 p0569 A70-13357

Steel crystal lattice fine structure and mechanical properties during annealing using X rays as function of temperature

03 p0511 A70-13422

Soil characteristics influence on soil thermal regime related to thermal IR imagery and subsurface soil conditions

03 p0474 A70-13555

Electrical conductivity of GaSe thin films developed in vacuum by electron bombardment as function of temperature

03 p0540 A70-13686

Onset conditions for galvanothermal current instability of Ge semiconductors as function of electric field oscillations, carrier concentration and carrier-lattice temperature

03 p0541 A70-13724

Electrical properties of Cu-diffused GaAs, studying temperature effects on acceptor concentration and electron population growth

03 p0541 A70-13730

Air plasma pulsed discharge jets erosive effects on metals, semiconductors and dielectrics, noting role of thermal effect

03 p0532 A70-13742

Electrical properties thermally induced irreversibly changes in CdSb single crystals measured as function of current intensity and flow

03 p0542 A70-13751

Raman spectra of lead titanate, sodium tantalate/potassium tantalate and potassium tantalate/potassium niobate solid solutions at various temperatures

03 p0542 A70-13824

Heat treatment effects on mechanical properties of Ti-Fe and Ti-Fe-Al alloys

03 p0512 A70-13855

Quenching temperature and deformation conditions for Ti alloy bars optimal mechanical properties emphasizing effect of primary structure

03 p0497 A70-13856

Optical phonons in mixed sodium potassium tantalate crystals as function of temperature and composition, using IR and Raman spectra

03 p0542 A70-14002

Optical rotatory power measurement for compensated cholesteric liquid crystal helical structure to observe thermally induced inversion and electric field perturbations

03 p0542 A70-14003

Dissociative attachment of low energy electrons in nitrous oxide as function of gas temperature

03 p0441 A70-14006

Temperature and hemoglobin concentration effect on oxygen solubility in blood, constructing table for Bunsen solubility coefficients

03 p0428 A70-14156

Thermal comfort in disparate environments, discussing human subjects skin mean temperature and body water loss

03 p0429 A70-14158

Small angle X ray scattering pattern of polypropylene drawn at various temperatures in closely spaced draw ratio values through neck region

03 p0517 A70-14202

Polyurethane rubber time- and temperature-dependent visco- and photoviscoelastic coefficients using two dimensional strain and stress wave propagation photoviscoelastic analysis

03 p0599 A70-14243

Transient thermal stresses in photoelastic models of various shapes under various steady state or transient temperature conditions, describing instrumentation and experimental methods

03 p0600 A70-14308

Low body temperature effects on convulsive activity elicited by hyperbaric oxygen in unrestrained unanesthetized rats

04 p0629 A70-14448

Titanium carbide sintering under continuous heating in Ar atmosphere, studying ultrasonic waves effects on compaction process

04 p0696 A70-14463

Ground temperature effect on thermal resolution in IR line scan imagery, discussing equipment and operating procedures for temperature gradient detection

04 p0686 A70-14617

Dissociative recombination coefficients temperature dependence in molecular neon and argon ions measured under equal gas, ion and electron temperature

04 p0722 A70-14668

Temperature dependence of reaction rate for dissociative recombination in vibrationally excited gases, using electronic threshold law for diatomic ions

04 p0722 A70-14669

Adiabatic calorimeter for exothermic chemical reactions determining heats of polymerization, curing rate and thermal decomposition rates as temperature function for high energy propellants

04 p0688 A70-14711

Electron plasma frequency exchange corrections temperature dependence at high densities, using equation of motion for coupled particle-hole pair operators

04 p0727 A70-14714

Cylindrical compression spring relaxation at high temperatures, presenting design data for time-temperature initial stress relationships

[ASME PAPER 69-WA/MET-10]

04 p0697 A70-14758

Finite element method applied to heat conduction in solids with temperature dependent thermal conductivity, using nonlinear constitutive equation for heat flux

[ASME PAPER 69-WA/HT-34] 04 p0782 A70-14806

Pressure and temperature sensitivity tests of fluoric oscillator for timer application, testing fluid relaxation oscillators using R-C-R feedback loops

[ASME PAPER 69-WA/FLCS-9]

04 p0626 A70-14844

Time-to-rupture dependence on temperature and stress related to chemical reaction rate equation in creep testing

[ASME PAPER 69-MET-B] 04 p0770 A70-14877

Adiabatic elastic stiffness constants of single crystal forsterite measured as function of hydrostatic pressure and temperature, using pulse superposition technique

04 p0678 A70-15055

Interstellar gas instability, discussing thermal, magnetic and cosmic ray effects

04 p0753 A70-15072

Polystyrene and polyamide stress relaxation graphs, considering tensile stresses and temperature effects

04 p0712 A70-15101

Tensile tests on alpha Ti containing oxygen and hydrogen at various temperatures and strain rates to determine deformation and fracture

04 p0706 A70-15133

Bond quality and strength of high temperature adhesive films for titanium

[DGLR-69-56] 04 p0699 A70-15158

Intermediate aging influence on Bauschinger effect in low carbon steel at 270 C and 2 hr holding time

04 p0776 A70-15266

High temperature effects on mechanical properties of recrystallized Ta relating strength, hardness and yield point

04 p0707 A70-15267

Initial oxide film on Cr-Ni steel at high temperatures observed by electron microscope, noting Ni role

04 p0708 A70-15311

Ti-Al-V alloys after annealing investigated for equilibrium diagram at high temperatures

04 p0708 A70-15313

Heat treatment produced semicoherent and incoherent precipitations diminished susceptibility to stress corrosion cracking of aluminum binary and ternary alloys

04 p0708 A70-15370

Spacecraft components temperature response predicted in nonstandard solar orientation

04 p0786 A70-15432

Temperature-synchronized semicontinuous culture and monitoring system for autotrophically growing Euglenas

04 p0633 A70-15453

Wall and total temperature variations effects on transition Reynolds number in hypersonic He tunnel, noting sound mode dominance

04 p0620 A70-15560

Surface recession of low density phenolic nylon in arc heated air using stagnation point models, noting char removal processes

04 p0787 A70-15602

Classical Couette flow for emitting and conducting gas media, discussing velocity distribution and temperature effects at LTE and non-LTE

04 p0787 A70-15675

Chromaluminizing process protecting alloys for gas turbines against oxidation at high temperatures by diffusion mechanism 04 p0711 A70-15683

High temperature properties mechanisms in alumina-coated vacuum cast nickel base superalloys 04 p0711 A70-15705

Load capacity and power loss of spiral groove bearings lubricated by incompressible liquid with temperature-dependent viscosity, using momentum and energy equations 05 p0853 A70-15778

Ductile-brittle transition temperature relation with grain size in polycrystalline Mo as function of annealing temperature 05 p0862 A70-15907

Isothermal atmospheric temperature effects on extensive air shower characteristics and muon numbers computed at various temperature and observation levels 05 p0898 A70-15945

Proton-proton cycle in star interior, calculating isotope concentrations, reaction duration and energy release as function of temperature and chemical composition 05 p0900 A70-15972

Diffusion rates in refractory metal alloys for thermionic emitters as function of time and temperature [GA-9495] 05 p0892 A70-16075

Axisymmetric elasticity problem for straight fiber imbedded into infinite matrix, noting homogeneous temperature changes causing residual stresses, tractions at infinity and fiber pulling 05 p0931 A70-16088

Mercury shape estimated with isostatic form of equilibrium controlled by situation near perihelion passage at 3-2 resonance spin rate, discussing solidification thermal effects 05 p0908 A70-16332

Solar cell for improved performance during extreme temperature fluctuations, discussing wraparound contact 05 p0799 A70-16724

Cryogenic temperature effect on short life torsional fatigue properties of Ni-Cr-Mo steel, discussing cyclic strain range effects 05 p0864 A70-16807

Time-temperature relation necessary to fine Libyan desert glass and remove gas bubbles calculated by viscosity determination at various temperatures 05 p0843 A70-16833

Magnetic susceptibility of synthetic australite and philippinite-like tektites measured in 77-560 K range, discussing origin 05 p0916 A70-16836

Thermal conductivity temperature dependence measured in greases bulk and thin layers at liquid helium temperature 05 p0874 A70-16842

Maraging steel mechanical properties as function of aging temperature and time 05 p0865 A70-16873

Thermoelectric power /TEP/ of transition metals, detecting empirical regularities in TEP, nonlinear temperature dependence, etc 05 p0893 A70-16949

Combustion model for temperature inhomogeneities effect on stability of solid fuels steady combustion 05 p0958 A70-16960

Structure and interstitial impurities effects on Nb modulus of elasticity at normal and high temperatures, noting rolling 05 p0866 A70-17040

Vibration damping properties of steels and Ti- and Al-based alloys at various temperatures under tensile and compression loads 05 p0868 A70-17048

Heating influence on circular bending fatigue strength of refractory steel and alloys, using radiative and HF inductive heating 05 p0868 A70-17059

Error resulting from elasticity modulus and linear thermal field coefficient removal from integral in Burger formula for turbine blade thermal stresses 05 p0954 A70-17061

Refractory metal structural elements stress rupture strength in vacuum and inert gas tested up to 2000 K 05 p0829 A70-17071

Ammonium chlorate thermal decomposition products as function of temperature using mass spectrometry 05 p0895 A70-17082

Cold reduction effects on press formability of pure Al sheet with allowance for tensile properties and crystallographic orientation 06 p1075 A70-17145

High purity Ni fatigue in reversed bending as function of oxygen pressure and temperature 06 p1086 A70-17454

Creep deformation resistance decrease in pure Al tubular specimens at high temperatures under multiple stress reversals 06 p1087 A70-17456

Ni-Cr alloys oxidation dependence on temperature and Cr concentration 06 p1087 A70-17609

Deformation pattern, interstitial impurities and alloying elements effects on temperature dependence of elasticity modulus of Nb and alloys 06 p1088 A70-17659

Microhardness measurements of carbides, borides and nitrides in wide temperature range, considering indentation load selection 06 p1089 A70-17661

Viscosity, thermal conductivity, specific heat and Prandtl number of hydrogen, methane and hydrogen-methane mixtures calculated for variation with temperature neglecting dissociation effects 06 p1177 A70-17700

Mo-nitrogen interaction, studying nitriding influence at various temperatures on Mo alloys properties 06 p1089 A70-17741

Unbranched chain reaction in hydrogen bromide for studying laminar one dimensional flame propagation, determining temperature dependence, velocity and concentrations at fixed time 06 p1177 A70-17797

Ion exchange entropy and enthalpy functions calculated from experimental constants and temperature dependence data 06 p1177 A70-17837

Fabrication technique effect on tensile and plastic properties of semifinished sintered Al powder products at room temperature and 600 C 06 p1076 A70-17848

Laminar ablation testing under turbulent boundary layer heating conditions, obtaining recession rate and heat of ablation for turbulent ablation of Teflon [AIAA PAPER 70-226] 06 p1179 A70-18071

Temperature and pressure effects as function of time in spectral and total normal emittance of metal coated refractory metals 06 p1092 A70-18136

Calorimetric measurements determining total hemispheric emittance of thin gold films as function of temperature, demonstrating film thickness effect [AIAA PAPER 70-63] 06 p1180 A70-18140

Thermal isolation characteristics of interstitial materials in vacuum environment, inserting materials between contacting metal surfaces at various pressures and temperatures 06 p1181 A70-18143

Surface temperature effects on low Reynolds number hypersonic shock layer development over flat plate sharp leading edge 06 p0982 A70-18364

Dynamic elastic modulus of graphites and composites measured as function of temperature using thin rod resonance method 06 p1070 A70-18447

Brazing time and temperature effect on depth of Ag based brazing alloys penetration into thin Ti-Al-V sheet substantiated by microprobe analysis 06 p1078 A70-18513

One dimensional cumulus convection model modified by incorporating rain evaporation rate and temperature changes from downdrafts 06 p1099 A70-18568

Surface tension plotted against density and temperature of hydrocarbon jet fuels, determining critical temperature 07 p1357 A70-18653

Chromium stainless steels nitrided cases formation and phase composition, studying temperature effects 07 p1304 A70-18744

Chemical reaction rates corresponding to initial molecules fixed internal energy levels determinable for multitemperature Maxwell-Boltzmann distribution as function of reagent temperatures 07 p1224 A70-18769

Z axis acceleration and high temperature effects on guinea pig carbohydrate metabolism, discussing blood and muscle tissues composition 07 p1202 A70-18798

Stainless steels case hardening in hydrogen, nitrogen, propane and butane mixture, showing temperature and process duration effects 07 p1291 A70-18831

Mechanical and electrochemical polishing effect on turbine blade alloy fatigue strength, discussing surface strain hardening as function of temperature in mechanical polishing 07 p1304 A70-18838

Fatigue strength of sintered aluminum powder at room and elevated temperatures, discussing sensitivity to tensile loads misalignment 07 p1304 A70-18840

Tensile and shear properties of blind fixed, blind floating and through types of bonded sandwich inserts, noting geometry and temperature effects 07 p1401 A70-18934

Solution treating temperature and microstructure effects on hot rolled Ni base alloy properties 07 p1306 A70-18995

Crack behavior of Al alloy as cryogenic tankage material, establishing relationship of temperature effects and basic crack size to failure stress 07 p1279 A70-18997

Heat transfer effects during solidification on mechanical properties of Al alloy castings compared with sand castings 07 p1293 A70-18998

[ASM PAPER W9-7.2] 07 p1293 A70-18998

W oxidation kinetics as function of ribbon temperature and absorption time using flash technique with sweep pulse mass spectrometer 07 p1306 A70-19275

Gas phase ignition theory of evaporating fuel in stagnant hot oxidizing gas as function of temperature 07 p1421 A70-19317

Thermally induced convective mixing motion in rotating cylindrical cryogen space storage tank model under heat flux, calculating critical Rayleigh number 07 p1257 A70-19320

Inelastic behavior of solids strained at high temperature emphasizing hot creep phenomena in aviation materials 07 p1406 A70-19346

Anodic dissolution initial stages of Ti alloys in neutral salt solutions from viewpoint of electrochemical dimensional processing, noting temperature effect on anodic activation potential 07 p1294 A70-19352

Chemical composition and heat treatment effects on deformation resistance of nonaging aluminum alloys during hot working, noting quenching effect on recrystallization 07 p1294 A70-19388

GaAs p-n junction lasers operating properties under ideal and thermal conditions 07 p1298 A70-19396

Dislocations and interstitial atoms interactions in Ta, investigating internal friction and deformation resistance and rate dependence on temperature 07 p1309 A70-19637

Thermoelectric characteristics of graphite and titanium carbide compared with platinum after prolonged annealing at 2300 C 07 p1316 A70-19661

Active and compensating sensors resistances, strain sensitivities, temperature gradients and lead resistances differences effect on accuracy of resistance strain gage measurements 07 p1283 A70-19747

Intermetallic precipitates development and mechanical properties of maraging steel as function of composition, tempering time and temperature using electron microscopy 07 p1310 A70-19748

Electron density dependence on electron temperature during self and mutual interaction of electromagnetic waves in magnetoplasma, tabulating numerical results 07 p1351 A70-19968

Temperature dependence of viscosity coefficient determined for hydrogen, helium, argon and nitrogen at atmospheric pressure using capillary viscometry 07 p1424 A70-19980

Molecular N rotational temperature effect on rare gases scattering cross section 07 p1344 A70-20134

Stress relaxation in polytetrafluoroethylene /PTFE/ at various compression deformations and temperatures, considering residual stresses degree 07 p1321 A70-20228

AlN deposition rate from gaseous phase on Mo substrate as function of temperature 07 p1357 A70-20311

Transient phenomena accompanying heating of fluid situated between heat conducting plane horizontal plates, using interferometry and streak photography 08 p1596 A70-20592

Soviet book on mechanical properties of heat resistant steels and alloys at room and elevated temperatures 08 p1515 A70-20691

Organic adhesives preparation and application to metal surface for bonding, examining time, pressure and temperature effects on curing 08 p1503 A70-20881

Adhesive metal bonding, considering methods for application of pressure and heat 08 p1503 A70-20882

Adhesive bonds strength in metal joints under stress cycling, examining effects of temperature and cycles frequency 08 p1504 A70-20888

Steel strength under prolonged preliminary loading at elevated temperatures 08 p1515 A70-20934

Steel structure and mechanical properties under preliminary loading at elevated temperature and liquid Li at various exposure times 08 p1515 A70-20935

Temperature dependence of Vickers pyramid hardness for Ti, Zr and Hf carbides at wide temperature range in vacuum 08 p1516 A70-20986

TEMPERATURE EFFECTS

- Monochromatic radiation emissivity temperature dependence of monocarbides of Ti, Nb and alloys in homogeneity region 08 p1516 A70-20994
- Chromium films obtained on tungsten by sputtering, studying structure and work function at various temperatures 08 p1516 A70-21123
- Molten Al alloys flow rate and behavior in various casting systems, considering gate geometry and casting temperature effects 08 p1505 A70-21133
- Mutual thermal influence zone between parts of die casting during solidification established as function of time 08 p1506 A70-21138
- Thermal interaction between casting and mold at beginning of cooling using mathematical model for temperature field 08 p1506 A70-21139
- Reduction temperature effects on molybdenum powders sinterability noting dispersion role 08 p1517 A70-21145
- Zr, Ti, Nb and Ta carbides deposition from metal chloride, methane, hydrogen and argon mixture, studying gas concentration and temperature effects on deposition rate 08 p1517 A70-21147
- Thermoelastic characteristics of glass fiber reinforced plastic materials, determining temperature dependent deformation of composite plate 08 p1526 A70-21164
- Quadratic precipitate transformation into orthorhombic phase with conservation of maximal atomic density planes in Ni-Cr-Nb and Ni-Cr-Ta alloys during prolonged reheating 08 p1518 A70-21240
- Membrane stress in thin circular viscoelastic ring under impulsive loads and internal heat, using stress-strain relation for linear Maxwell material model 08 p1589 A70-21311
- Tensile properties of yarns at high strain rates and subambient temperatures determined for nylon, Dacron, Nomex, Beta Fiberglass and Karma metal 08 p1527 A70-21330
- Stress-strain behavior of Al and Ti alloys, beryllium and nonmetallic structural materials based on constitutive equations describing strain rate and temperature effects 08 p1518 A70-21331
- Aluminum nitride morphology in structural Cr-Ni-Mo steel, discussing dependence on austenitization temperature and cooling conditions 08 p1519 A70-21435
- Dissipative heating effects on loss factor of viscoelastically damped beam, discussing stiffness effects [ASME PAPER 69-VIBR-37] 08 p1592 A70-21478
- Flute instabilities of cold magnetoactive plasma with radially dependent density and strong azimuthal particle streams, discussing nonzero perpendicular temperature effects on oscillations 08 p1552 A70-21504
- Waspaloy gamma prime solvus temperature relationships as function of solution treatment and precipitation strengthening additives, discussing microstructure and tensile properties 08 p1520 A70-21555
- Thermal and athermal components of flow stress and deformation dynamics in Ti-Al alloy 08 p1521 A70-21578
- Solid layer effect on laminar heat transfer and pressure drop in medium surrounding pipe with liquid flows below freezing point, discussing wall temperature effects 08 p1485 A70-21589
- Temperature increase effects on fully turbulent boundary layers at low Reynolds number in air investigated in wind tunnel 08 p1485 A70-21606
- Temperature dependence of microplastic yield and flow stress and transient creep responses of gamma prime phase 08 p1522 A70-21709
- Magnetothermal oscillations in pressure-annealed pyrolytic graphite, relating period with angle between magnetic field and crystal c axis 08 p1557 A70-21839
- Cobalt modified Ti-6Al-4V plate and billet, testing effects on heat treatment response, microstructure, tensile and fatigue properties, fracture toughness, etc. 08 p1523 A70-21852
- Silicon containing alpha matrix Ti alloy with high creep strength and stability at elevated temperatures, studying processing and heat treatment effects on properties 08 p1509 A70-21853
- Creep and rupture of graphite-epoxy composites under unidirectional state of stress and controlled temperature environment, extrapolating long term loading behavior 08 p1531 A70-21897
- De Laval nozzle behavior in vacuo, discussing flow rate parameters, viscosity and real gas effects, thermal effects, turbulent jet separation and reattachment, etc [AGARDOGRAPH-120] 08 p1434 A70-21932
- Temperature, transformation and strain rate effects on tensile ductility properties of stable and metastable compositions of austenitic stainless steels 08 p1524 A70-21956
- Temperature effect on plastic flow in Ti-scavenged Fe, attributing microyielding to edge dislocations motion 08 p1525 A70-21959
- Strengthening mechanisms in dispersion hardened Nichrome /TDNiC/ analyzed in 70-2000 F range, discussing solid solution, dislocation substructure and grain refinement 08 p1525 A70-21961
- Altitude influence on forced ventilation of cooled electronic apparatus, analyzing flow change and temperature roles 08 p1643 A70-22040
- Natural heat convection in vertical annular space taking into account variations of volumetric mass, viscosity and thermal conductivity of air with temperature 08 p1786 A70-22047
- Retinal temperature increases produced by intense light absorption described by heat conduction equation 08 p1614 A70-22075
- Brittle failure mechanics application to steels sensitivity to rupture at low temperatures, discussing crack propagation resistance and heat treatment effect on impact toughness 08 p1768 A70-22076
- Plane shock wave stability propagating in external magnetic field determined by temperature dependence of medium electrical conductivity 08 p1658 A70-22168
- Local heat transfer to gas mixed with graphite particles described for variable temperature differences and wall temperatures 08 p1787 A70-22174
- Temperature effects on IR absorption by water and carbon dioxide vapors measured in narrow spectral intervals 08 p1666 A70-22180
- Chromosome of temperature-sensitive mutant of bacillus subtilis 168, observing multiforked replication at normal temperature and transfer of DNA 08 p1615 A70-22206
- Simple molecules viscosity as function of temperature and density using empirical equation 08 p1731 A70-22292
- Magnon energy theory for temperature dependence of ferrous and magnesium fluorides antiferromagnetic- resonance frequency, sublattice magnetization and magnetic specific heat 08 p1739 A70-22324
- Mild temperature and dehydration effects on toxicity of caffeine and dextroamphetamine in mice 08 p1616 A70-22329
- Gas turbine blades design and exploitation processes, discussing long time fatigue strength, static durability and heating effects at elevated temperatures 08 p1772 A70-22469
- Crystal growth of 2H silicon carbide showing temperature profile along susceptor as affecting factor 08 p1739 A70-22498
- High-strain fatigue life temperature dependence of austenitic and ferritic power plant materials compared to creep-rupture life 08 p1773 A70-22577
- Thermal stresses in gas turbine blade calculated, showing role of initial temperature increase of blade cooling air 08 p1775 A70-22596
- Heat treatment effects on hardened steels acoustic constants, calculating sound velocity in liquid metals 08 p1692 A70-22643
- Creep behavior transition analysis, considering activation energies and creep rate dependence on temperature, stress and grain size 08 p1704 A70-22720
- Time, temperature and composition dependent regularities in Ni-Al and Ni-Nb alloys oxidation processes, discussing Oxygen ion migration and Ni ion diffusion 08 p1704 A70-22752
- Ionized potassium plasma three body recombination coefficient measurements showing inverse temperature dependence 08 p1735 A70-22778
- Temperature and strain dependence of strain anisotropy in Ti tested on longitudinal and transverse tensile specimens 08 p1705 A70-22807
- Thermal properties associated with temperature gradients in He-K plasma, studying mass motions initiated by cold wall contact 08 p1735 A70-22844
- Evanoform alloy resistance wire for applications in magnetic field, illustrating percentage change at 4.2 K 08 p1679 A70-22998
- Dynamic stresses during abrupt temperature changes of medium, showing internal stress waves amplitude increaseability by suitable internal stress source selection 08 p1778 A70-23089
- Elastoplastic stressed state of variable thickness disk under combined effects of nonuniform heating, repeated centrifugal and surface tensile loads 08 p1778 A70-23091
- Elastoplastic stress state of variable thickness disk under combined effect of nonuniform heating and centrifugal forces, applying flow theory to stress component determination 08 p1779 A70-23095
- Ferromagnetic crystal weakly coupled spin Green and correlation functions calculated for wide temperature range 08 p1740 A70-23193
- Electrical resistivity of TiNi and TiCo compounds and alloys measured at various temperatures after quenching or annealing 08 p1707 A70-23194
- Order-disorder transition temperatures for Ni-Cr alloys determined by neutron diffraction, discussing homogeneous ordering of atoms 08 p1707 A70-23196
- Materials static tested for compatibility with pure and moisture contaminated chlorine pentafluoride at 160 F and ambient temperatures 08 p1742 A70-23250
- Mo single crystals creep behavior temperature and stress dependences using X ray analysis 08 p1708 A70-23543
- Nb-W single crystal low temperature thermally activated deformation, observing slope change in temperature dependence curves of flow stress and strain rate sensitivity 08 p1708 A70-23572
- Plane disks and turbine disks of complex profile made of heat resistant Cr-Ni alloys studied for rupture strength under various temperature conditions 08 p1785 A70-23599
- Pulse-shaping transistor circuit analysis, considering circuit elements roles and temperature, pulse duration and leading and trailing edges durations effects 08 p1650 A70-23628
- Turbojet engines departure from equilibrium performance during thermal soak transient attributed to heat absorption in turbine and compressor metals, observing thrust loss 08 p1744 A70-23739
- Temperature limitation on CRT tube performance in high brightness displays imposed by glass breakage danger, discussing liquid cooling of phosphor substrate 08 p1686 A70-23759
- Titanium sponge secondary structure obtained by magnetothermal reduction of concentrated Ti-containing chloride melts, discussing temperature effect on porosity 08 p1709 A70-23783
- Artificial satellites MHD drag, noting altitude and temperature effects 10 p1921 A70-23834
- Chromium structural dislocation and cell formation during deformation as function of temperature, impurities and strain rate 10 p1902 A70-23861
- Mixed thermoelastic problem in elastic layer with arbitrarily prescribed temperature in upper free surface 10 p1954 A70-23878
- Amorphous polymers thermal conductivity measured at 0.4-4 K, observing similar temperature dependences 10 p1906 A70-23979
- Thermal lens effect produced by photocurrent in CdS, using focused laser beam to generate photocurrent causing local heating changes of refractivity 10 p1898 A70-23980
- Solutions existence for nonlinear partial differential equations describing orthotropic and nonlinear shallow shells under loads and temperature effects 10 p1954 A70-24019
- Transformation kinetics of Ti alloy under isothermal conditions in solution treatment as function of temperature 10 p1903 A70-24025
- Microwave radiation thermal and nonthermal biological effects, considering exposure limits 10 p1824 A70-24061
- Heat sources effect on pressure and velocity of supersonic flow, discussing iteration procedure and asymptotic expansion 10 p1799 A70-24125
- Gas viscosity high temperature measurement method in shock tube using boundary layer equations for velocity and static temperature distributions 10 p1867 A70-24151
- Temperature effects on energy dissipation during vibration in ferromagnetic and nonferromagnetic metals, comparing damping capabilities for homologous temperatures 10 p1903 A70-24245

IR light dispersion filters of compressed mixed powdered crystals, discussing optimal preparation procedures, passbands temperature dependence and stability

10 p1915 A70-24256

Graphite IR radiator for radiative capacity and flame temperature measurements investigated for life time dependence on ambient pressure and temperature

10 p1888 A70-24257

Kinematic viscosity of molten steel containing corundum inclusions as function of temperature

10 p1904 A70-24271

Tantalum mechanical properties dependence during deformation on temperature and strain rate irregularities, discussing serrated yielding

10 p1904 A70-24386

Shock pressure and impulse caused by Q switched laser light absorption, considering temperature dependence of EM radiation penetration depth

10 p1900 A70-24422

CO electrochemical oxidation at porous solid electrolyte fuel cell anodes under high temperature, noting current density role

10 p1830 A70-24462

Environmental thermal stress effect on human performance under high mental and low physical workload

10 p1812 A70-24505

Horizontal fluid layer heated from above or below analyzed for gravitational field sinusoidal modulation effects on stability

10 p1968 A70-24523

Processing temperature effects on breaking strength-modulus relation for carbonized acrylic fibers

10 p1907 A70-24533

Carbon composition resistors investigated for cause of resistance dependence on thermal pulses, suggesting application as stabilization process

10 p1849 A70-24617

Avalanche diodes properties, establishing equivalent circuit accounting for static electricity, carriers transit time and thermal effects

10 p1850 A70-24625

Black body radiation properties with temperature important only in rest frame, using transformation formulas for coherence and spectral parameters

10 p1968 A70-24631

Body temperature effect on pulmonary ventilation response to exercise

10 p1819 A70-24773

Heat transfer influence on three dimensional boundary layer separation on walled ellipsoid of revolution

10 p1870 A70-24781

Thermal imbalance effect on stellar pulsational stability using linear quasi-adiabatic pulsation theory

10 p1946 A70-24980

Temperature effect on plate damping by constrained viscoelastic layers, emphasizing transition and operating temperature compatibility

10 p1962 A70-25063

Nitrogen content effect on proportional limit and work hardening rate of austenitic stainless steel at 302 F

10 p1905 A70-25169

Binary Ni-Cr alloys tensile mechanical properties at 25 C after water quenching and heat treatments

10 p1905 A70-25172

Strain tempering effects on upper and lower bainite, discussing strengthening and fracture toughness as function of temperature

10 p1905 A70-25173

Pressure loss in tubulature of oil-hydraulic drive mechanism, allowing for viscosity changes associated with oil temperature and pressure increases

10 p1809 A70-25209

Temperature and hydrogen concentration effect on microhardness of polycrystalline beta-vanadium hydride, obtaining photomicrographs of indentations

10 p1906 A70-25227

Yield point temperature dependence in heat resistant austenitic alloys, showing tendency to brittle failure under short term overloads

10 p1906 A70-25291

Precipitation hardened nickel-base alloy microcracking during gas tungsten arc and electron beam welding, studying heat affected zone hardness, phases and grain size

10 p1897 A70-25311

EPR line width angle and temperature dependences assuming line widening due to electric field of lattice defects, dipole-dipole interactions and spin-lattice relaxation

11 p2097 A70-25382

Nonlinear spin wave theory for anisotropic antiferromagnetism, solving sublattice magnetization by thermodynamic Green function for temperature dependence

11 p2097 A70-25617

Thermal conductivity coefficients of argon in 25-700 C range and up to 1200 bars pressure, using vertical concentric cylinder apparatus

11 p2147 A70-25754

Thermal conductivity of nitrogen in 350-1500 K range using hot-wire diffusion columns

11 p2147 A70-25756

Thermal diffusivity of elements over wide temperature ranges based on TPRC recommended thermal conductivity and specific heat

11 p2065 A70-25770

Thermal Analysis - Conference Worcester, Mass., August 1968, Volume 1, Instrumentation, organic materials and polymers

11 p2069 A70-25801

Differential thermal analysis-effluent gas analysis /DTA-EGA/ experiment for lightweight Martian landed capsule

11 p2050 A70-25802

Polymer structure and cross-link density effects on thermal analysis of phenol-formaldehyde polymers pyrolysis products

11 p2069 A70-25804

Thermal analysis - Conference, Holy Cross College, August 1968, Volume 2, Inorganic materials and physical chemistry

11 p2070 A70-25808

Pyrolytic graphite oxidation kinetics as function of temperature, air velocity and surface area

11 p2070 A70-25809

Differential thermal analysis capabilities in mineralogy for determining present/past planetary environmental parameters having significance for biological experiment

11 p1994 A70-25811

Phase equilibria and maximum melting compositions determinations for compound semiconductors by differential thermal analysis compared with vapor and high pressure techniques

11 p2098 A70-25812

Vestibular adaptation to heat and rotary stimulation in animals and men

11 p1986 A70-25822

Temperature and ion effect on refractive index of VLF radio waves in quiet and disturbed ionospheric conditions

11 p2004 A70-25842

Nonisothermal dielectric coating on conductor surface, analyzing temperature distribution effect on thermal emission characteristics

11 p2148 A70-25975

Bidirectional reflectance of three dimensional surfaces described by diffuse triangular subareas network for spacecraft thermal design, giving numerical technique

11 p2084 A70-26354

Spacecraft temperature prediction and heat conduction problems with nonlinear radiation boundary conditions by perturbation theory, applying to heat shield analysis

11 p2150 A70-26355

Saturn IB Orbital Workshop solar array thermal and performance analysis for various vehicle orientations and orbital conditions, emphasizing modeling and data handling

11 p2127 A70-26357

Thermal analysis of deployable parabolic antenna for Outer Planetary Explorer program, discussing spacecraft spin and radioisotope thermoelectric generators effect

11 p2127 A70-26359

Saturation of self induced thermal lens resulting from thermal distortion of carbon dioxide laser radiation in wind

11 p2063 A70-26401

Low cycle fatigue tests on stainless steel, discussing crack behavior dependence on temperature and plastic strain range

11 p2139 A70-26405

Temperature dependence of sputtering coefficient of quartz and chondrites at 2000 K and mass decrease prior to evaporation

11 p2118 A70-26722

Temperature effects on width of current-voltage characteristics of GaAs Gunn oscillators

11 p2020 A70-26819

Temperature effects on base and surface currents of plane bipolar transistors, testing validity of surface recombination process model

11 p2021 A70-26832

Electrical conductivity hypothesis based on concept of transition temperature being inversely proportional to ionic mass square root

12 p2282 A70-26880

Nomographic Richardson-Dushman equation solutions for thermionic electron emission devices, giving current density for various work functions and electrode temperatures

12 p2271 A70-26894

Thermal stress /high ambient and body temperatures/ effect on human performance in high mental and low physical activities

12 p2177 A70-27043

Insulator wall temperature effect on supersonic two temperature MHD generator channel flow at open and short circuit conditions

12 p2163 A70-27067

Translational spectral bands of compressed rare gas binary mixtures, considering mass and temperature effects

12 p2275 A70-27172

Thermal stresses in temperature dependent multilayered cylindrically anisotropic hollow cylinders

12 p2321 A70-27203

Spontaneous ignition dependence on transient temperature variations accompanying gas entry to evacuated vessel

12 p2330 A70-27222

Chromium doped GaAs photoconductivity spectral distribution at various temperatures, determining temperature dependence of impurity maximum

12 p2286 A70-27366

Electric field heating effect on edge photoluminescence of n-type GaAs, noting increase in electron energy

12 p2286 A70-27368

Iron impurity energy level behavior in seminsulating GaAs from determining temperature dependences of Hall coefficient, resistivity, optical absorption and steady spectral photoconductivity

12 p2286 A70-27370

Electron-hole transitions in GaAs obtained by sulfur diffusion, noting capacitance dependence on voltage at 293 and 77 K at various frequencies

12 p2287 A70-27481

Temperature effects on injection semiconductor lasers optical gain and threshold current using energy spectrum model

12 p2247 A70-27485

Fe and Ni doped GaAs photoconductivity at various temperatures, determining activation energy level

12 p2287 A70-27489

Temperature and metallic contact effects on composition and structure of solid phase deposits during reactive fuel oxidation

12 p2289 A70-27493

Stress relaxation in alpha titanium during plastic strain, measuring temperature and strain rate dependence

12 p2255 A70-27608

Blood flow redistribution during sustained high skin temperatures of men in supine position

12 p2169 A70-27654

Oxygen interaction on rhenium filament, considering sticking probability as function of temperature

12 p2181 A70-27677

Nitrous oxide chemisorption by rhenium filament at low pressures at various temperatures, determining sticking probability

12 p2181 A70-27678

Contaminated Ni crystal /100/ surface photoelectric yield as function of temperature, considering effects of Ar ion bombardment and annealing

12 p2288 A70-27680

Thermal feedback theory of flicker noise generation in transistors and temperature fluctuations effect in vicinity of recombination centers

12 p2196 A70-27687

Thermal boundary layer equations solved for compressible gas at rotating axisymmetric surface with viscosity as linear function of temperature

12 p2331 A70-27698

Magnetically sensitive Fe lines usefulness to solar polarimetry, observing absorption coefficient dependence on temperature variations

12 p2303 A70-27706

Recrystallization effect on 3-D graphite orientation in carbon fibers under high temperature heat treatment

12 p2259 A70-27720

Low pressure burning rate of double base propellants at various initial temperatures in argon and in air

12 p2332 A70-27844

Nitrogen oxide ions mobility in air calculated at high plasma temperatures

12 p2276 A70-27845

Tantalum RF sputtered superconducting films structure and properties at various substrate temperatures, observing bcc, fcc and amorphous phases by electron microscopy

12 p2288 A70-27876

Liquid He temperature fluctuation effects on cryogenic superconducting bolometer noise spectrum, deriving transfer functions

12 p2237 A70-28156

Temperature dependence of electrical conductivity and optical properties of strontium titanate semiconductor single crystals doped with Ce and Nb

12 p2288 A70-28328

N-type GaAs carrier mobility and concentrations increased slow cooling after heat treatment

12 p2289 A70-28343

Periodic high temperature effects on human systolic phase dynamics

12 p2174 A70-28359

Ablation and temperature effects in hollow viscoelastic cylinder

13 p2508 A70-28487

Transient heat transfer considered for thermal boundary layer over rotating disk following temperature change

13 p2519 A70-28493

Pressure measurements and gas flow analysis during thermal vacuum tests of manned spacecraft indicating adequate space vacuum simulation

[AIAA PAPER 69-1033] 13 p2384 A70-28518

Guarded disk type emissometer for hemispherical emittance measurements of sample materials in 88 to 420 K range based on steady state calorimetry
[AIAA PAPER 69-600] 13 p2404 A70-28524

Reaction rates temperature dependence for artificial carbographites of various densities in oxidizing gas media 13 p2519 A70-28577

Gas temperature effects on aerodynamic drag of carbon particles burning during nonisothermal motion 13 p2520 A70-28582

RF method for recording temperature dependence of electrical conductivity of solids, liquids and multicomponent plasma mixtures 13 p2459 A70-28583

Mechanical seals ringing sound relationship with heat transfer and interfacial conditions, noting sliding surfaces temperature effect 13 p2417 A70-28611

Geogravity-geomagnetic fields correlation due to lateral temperature variations in upper mantle 13 p2393 A70-28620

Electron beam interaction with Maxwellian plasma, investigating temperature effects on instabilities 13 p2460 A70-28639

Fracture kinetics model for polymers emphasizing quantum effects even at room temperature 13 p2510 A70-28670

Cavity and storage temperature effects on hydrogen maser oscillation in 77-293 K range 13 p2425 A70-28713

Temperature-dependent physical properties effects on turbulent heat transfer, determining corrective factor for semiempirical equations 13 p2520 A70-28847

Phase transformations of molybdenum carbide under elevated temperature in vacuum, using X ray and differential thermographic analysis 13 p2433 A70-28852

Temperature dependence of electrical properties and permittivity of barium titanate solid solutions containing Nb, Ta, Sb and La, using bridge-circuit of resonance techniques 13 p2469 A70-28853

Emission field and Fermi quasi-levels distribution in injection laser with n-p heterojunction, determining frequency and threshold current temperature dependence 13 p2426 A70-28876

Thermal stresses in solid nonhomogeneous sphere in high periodic temperature field, assuming temperature dependent Young modulus and linear thermal expansion coefficient 13 p2512 A70-28979

Gas turbine blade materials investigated for effect of prolonged heating on mechanical properties and thermal fatigue strength 13 p2434 A70-28994

Rotational and vibrational temperature effects on neutral gas and electron temperature and density in high pressure discharge plasma diagnostics 13 p2462 A70-29129

Versamid cured epoxies time-dependent mechanical properties, determining loading mode, strain level and reinforcing agent effects on time-temperature shift factors 13 p2438 A70-29205

Gas and environmental temperatures, flow rate and sample geometry effects on limiting oxygen index in acrylonitril-butadiene-styrene copolymer, polystyrene and polyester 13 p2439 A70-29261

Temperature, solvent, catalyst and formaldehyde concentration effects on monosaccharide synthesis from formaldehyde condensation 13 p2362 A70-29327

Irreversible yield stress component of aluminum, Armco iron and tantalum with fcc lattice, showing temperature dependence 13 p2436 A70-29500

Blood coagulation process, investigating thermal effects by microcalorimetry and correlating with thromboelastographic indices 13 p2353 A70-29502

Free convection flow and heat transfer from semiinfinite horizontal flat plate with time-oscillating temperature, using successive approximations process 13 p2522 A70-29537

P-type GaAs laser diodes spontaneous emission power temperature dependence, considering radiative recombination mechanism 13 p2378 A70-29545

First order statistical model for temperature dependence of carbon activity in austenite 13 p2436 A70-29605

Radiative heat transfer in channel with unsteady radiating medium temperature, assuming absolutely black walls with zero temperature 13 p2522 A70-29725

Evidence against electron impact induced alkyl shifts in mass spectra of alpha-hydroxy-ketones, showing thermal rearrangements 13 p2363 A70-29803

Hardened steel embrittlement in low pressure hydrogen caused by crack growth as function of temperature 13 p2436 A70-29804

Electron beam-pumped ZnO laser emission wavelength at various temperatures 13 p2430 A70-29833

Middle stratospheric circulation in Southern Hemisphere, associating temperature changes and ozone content with planetary wave passage in Antarctic polar vortex 14 p2568 A70-30123

Quartz floating component design, discussing magnetic sensitivity temperature dependence and microseismic noise rejection properties 14 p2582 A70-30245

Switching initiation in Ovonic, discussing temperature profile in semiconducting sandwiches as function of time and thermally forced double tunneling 14 p2626 A70-30333

Ovshinsky switching effect, considering electrothermal initiation and field dependent conductivity at elevated temperatures 14 p2626 A70-30336

Evaporography at room temperature, showing necessity of recording images on color films 14 p2583 A70-30362

Mossbauer temperature dependent isomer shift, proposing electron density change at resonant nucleus site by lattice phonons 14 p2626 A70-30483

Temperature dependence of short wavelength magnon energies correlated with heat capacity 14 p2619 A70-30487

Faraday type MHD generators, investigating gas velocity and temperature profiles effect on electrical performance by equivalent circuits simulation 14 p2534 A70-30537

Heat treatment induced shape distortions measurements in maraging steel bars, plates and sheets, noting dependence on number of anneals and product form 14 p2595 A70-30544

Stratospheric warmings effect on atmospheric density field variations 14 p2608 A70-30592

Book on thermal and gravitational atmospheric tides covering solar oscillations, lunar air tides, upper air data, ozone radiation absorption, etc 14 p2573 A70-30633

Chilled emulsion photography for astronomy and spectrography, reducing long exposures with chilled plates 14 p2585 A70-30649

Thermal tidal friction and gravitation effects on Mercury libration after solidification, noting equilibrium with orbital and rotational periods locked in 3/2 resonant state 14 p2638 A70-30701

Longitudinal temperature gradients effects on stress analysis in solid propellants, using viscoelastic data 14 p2627 A70-30755

Solid rocket motors potential hazards explosive reactions and temperature and blast effects 14 p2629 A70-30782

Tantalum single crystals elastic constants temperature dependence, considering compressibility and shear properties 14 p2596 A70-30841

Austenization temperature, cooling rate and tempering conditions effect on steel castings structure, strength and impact properties 14 p2596 A70-30875

Optimum diffusion welding temperature for Ti-6Al-4V alloy determined from tensile and creep tests 14 p2591 A70-30934

Marginal fluid flow stability in porous media taking into account inhomogeneity created by temperature 14 p2577 A70-31000

Adiabatic relation between initial plasma density perturbations and radiation temperature fluctuations during galaxies formation, discussing relic radiation fluctuations 14 p2632 A70-31286

Electronic components environmental testing, examining temperature, humidity and vibration effects 14 p2558 A70-31295

Laminar velocity distribution from temperature profiles developed under steady flow through tube, constructing numerical temperature grid 15 p2718 A70-31449

Gas ionization with hydrogen atoms in gravitational equilibrium at constant temperature in upper half space by instantaneous radiation burst in lower space 15 p2775 A70-31477

Heating rate effect on parameters of resistance wire strain gages subjected to temperature gradients 15 p2733 A70-31536

Temperature influence on luminosity centers and line darkening in synthetic ruby powder with chromium concentration 15 p2782 A70-31558

Hydrogen embrittlement of martensitic Fe-Ni alloys as function of temperature via slow strain rate tensile tests 15 p2755 A70-31559

Artificial B-doped semiconductor diamond crystals resistance temperature dependence, determining conductivity and luminescence spectra 15 p2782 A70-31630

B, In or Ga doped Si photosensitivity dependence on sample temperature, supply voltage and illumination intensity, determining optimal operating conditions 15 p2782 A70-31631

Acceptor level formation kinetics from measuring Hall constant as function of temperature after diffusion of copper into n-type GaAs 15 p2782 A70-31633

Solid state device inductance by thermal effects, describing characteristics and applications in resonant circuits 15 p2783 A70-31839

Soviet monograph on gas laws in aviation medicine for reduced oxygen pressure pathology, discussing kinetic theory, temperature effects, solubility, diffusion, etc 15 p2682 A70-31925

Linear power scaling-mass flow relationship in multi-Joule pulsed carbon dioxide-nitrogen-helium laser, noting thermal effects role 15 p2751 A70-31977

Fe 57 contaminant in Ni, studying Mossbauer effect as function of temperature 15 p2784 A70-32023

Ge and Si hemispherical emittance, showing doping and temperature effects 15 p2784 A70-32055

Temperature dependence of laser emission line self broadened half widths in spectral band of carbon dioxide at constant pressure 15 p2752 A70-32056

Cavitation in centrifugal pumps, predicting breakdown and inception points variation with temperature and speed 15 p2744 A70-32097

Steady state temperature dependence of heat conduction coefficient using arc approximation 15 p2826 A70-32106

Anodic temperature effect on Cs thermionic converter operation under arc regime, obtaining potential jump electron temperature relation near anode 15 p2677 A70-32119

Polygonized and cellular Be structures formation, examining temperature, strain, annealing and material purity effects 15 p2758 A70-32122

Carbon-graphite porous materials thermal conductivity at various temperatures 15 p2765 A70-32141

Stability characteristics of elastic shallow shells of revolution in temperature field and under compression, reducing variational equation of bending by Ritz method 15 p2817 A70-32169

Induced strain plane state in elastic micropolar medium by temperature effect, discussing thermoelastic problem stress functions 15 p2821 A70-32341

Elastic micropolar body thermal stresses induced by discontinuous temperature field, using differential equations of thermoelasticity 15 p2822 A70-32353

Thermal-mechanically treated stainless steels structure and properties, discussing stress relief aging effects 15 p2761 A70-32380

Inconel 600 high temperature high strain rate fracture process by hot torsion tester, noting temperature effects 15 p2762 A70-32389

Atmospheric ground layer temperature variations effect on astronomical telescope observations, discussing image motion character and origin 15 p2772 A70-32462

Stellar associations formation theory including effects of radiation, Rayleigh-Taylor instability and interstellar gas cold regions 15 p2801 A70-32478

Junction and MOSFET transistors thermal noise characteristics at cryogenic temperatures 15 p2710 A70-32585

Gravitational atmosphere thermally driven motions, noting expansion towards lower density regions in solar chromosphere 15 p2804 A70-32619

Monograph on temperature dependent material properties effect on elastic stress distribution in thin rotating disks of arbitrary profile 15 p2823 A70-32700

Yield strength of Nb-O single crystal solid solutions as function of temperature 15 p2763 A70-32808

Phenomenological theory of transient high temperature creep, considering internal back stress 15 p2763 A70-32809

Steady state high temperature creep theory, including internal back stress and temperature dependencies 15 p2763 A70-32810

- Book on flow separation covering steady/unsteady, turbulent and incompressible flows, base pressure, thermal effects, etc
16 p2833 A70-32913
- Electron paramagnetic resonance of viscous nematic liquid crystal, investigating order as function of temperature
16 p2960 A70-33058
- Flow stress and dislocation density dependence on temperature in polycrystalline molybdenum
16 p2930 A70-33085
- Iodine concentrations, temperature gradients and transport ampules etching effects on mass transport rate and crystal growth of MnS-MnSe-iodine system
16 p2960 A70-33088
- Cryobiotic potentialities on earth, investigating life forms physiological response to temperature, cryotolerance mechanisms, etc
16 p2848 A70-33093
- Optical properties of electropolished cubic Nb-Ti alloys at cryogenic and room temperatures in visible and near IR spectral range
16 p2930 A70-33205
- Gamma phase particle distribution changes in homogeneous segregation in Co-Ti alloy attributed to elastic interaction during aging temperature changes
16 p2931 A70-33208
- Spinel lithium ferrite magnetic and crystallographic properties, considering effects of Li and oxygen losses, sintering temperature and cooling rate
16 p2961 A70-33272
- Liquid He surface layer thickness as function of temperature, considering capillary waves effect due to gravity
16 p2952 A70-33288
- Thermal design factors in electronic components packaging, considering equipment failure types and rates, fabrication processes, etc
[ASME PAPER 70-DE-17] 16 p2877 A70-33422
- Turbofan engine compressor system performance dependence on circumferential extent, magnitude and rate of change of inlet temperature in altitude test facility
[AIAA PAPER 70-625] 16 p2968 A70-33590
- Thermal conductivity of multilayer and mixed powder high temperature insulation systems over wide temperature range and vacuum conditions
[AIAA PAPER 70-637] 16 p2997 A70-33596
- Composite solid propellants burning rate and initial temperature relationship, investigating granular diffusion flame model
[AIAA PAPER 70-656] 16 p2963 A70-33618
- Laminar compressible flat plate boundary layer dependence on Prandtl number and viscosity-temperature relations
16 p2893 A70-33673
- Magnetic phase diagram of hydrated cesium-copper carbide at 1.625 Neel temperature in external magnetic fields, giving equation for spin flop field temperature dependence
16 p2961 A70-33688
- Avalanche diode transient temperature response, measuring thermal impedance under pulse bias conditions
16 p2878 A70-33695
- Anomalous dark areas in sunglint patterns from ATS photographs, considering water temperature effect on ocean surface conditions
16 p2897 A70-33725
- Deformation formulas for simply connected micropolar isotropic homogeneous centrosymmetric elastic body under external forces and heating
16 p2990 A70-33742
- Activation energy for creep at intermediate temperatures, allowing for elastic modulus change
16 p2991 A70-33790
- Maraging nickel steel martensitic transformation temperature reduction after interruption by nonisothermal or isothermal tempering below 460 C
16 p2932 A70-33850
- Effective thermal conductivity parallel to laminations of multilayer insulation as function of temperature, layer density and length
[AIAA PAPER 70-846] 16 p2999 A70-33913
- Extinction parameters of submicron carbon, tungsten and Si particles in hydrogen measured at various temperatures, discussing scattering amplitude functions and Monte Carlo calculations
[AIAA PAPER 70-838] 16 p3001 A70-33933
- Unnatural environment behavior of leeches for long term biosatellite experiment, determining temperature, humidity, oxygen pressure, carbon dioxide concentration, calcium hydroxide limits, etc
16 p2854 A70-33994
- Surface temperature or heat flux density estimation for nonlinear inverse heat conduction problem involving temperature dependent thermal properties
16 p3002 A70-34195
- Constant grain size cast Mo ductile-brittle transition temperature dependence on annealing temperature using tensile test
16 p2933 A70-34274
- Heating effect above beta transus at intermediate and final stages of processing on Ti alloys properties
17 p3097 A70-34359
- Ti alloys embrittlement, investigating time temperature dependence of brittle subsurface layer formation during elevated temperature air exposure
17 p3112 A70-34365
- Beta-Ti and Ti-Cr single crystals elastic moduli, determining A ratio temperature dependence
17 p3115 A70-34380
- Commercial purity Ti athermal plastic deformation, showing anomalous behavior with temperature variations
17 p3116 A70-34392
- Alpha Ti-hydrogen alloys, discussing fracture behavior temperature dependence
17 p3117 A70-34396
- Hot plasticity elongation of cast and wrought Ti-Al-V alloy as function of temperature and strain rate
17 p3117 A70-34401
- Solution heat treatment temperature effects on strength and age hardening of Ti alloys
17 p3120 A70-34419
- Ti alloy stability after long term creep exposure at various temperatures
17 p3120 A70-34421
- Thermal exposure effect on room temperature mechanical properties of Ti alloys, noting diffusion bonding, hot forming and heat treatment
17 p3120 A70-34422
- High temperature heating and cooling effects on mechanical properties and structure of Ti welds, using notched bar impact specimens
17 p3098 A70-34423
- Forged alpha/beta Ti alloys, investigating relationship between mechanical properties and microstructures produced by heating
17 p3120 A70-34427
- Ti-Al-Cr-Fe tensile, fatigue and creep properties at various temperatures, considering industrial applications
17 p3121 A70-34428
- Mean electron density profiles and fluctuations in equilibrium high speed turbulent boundary layers, calculating temperature effects
[AIAA PAPER 70-743] 17 p3066 A70-34500
- Oxygen, nitrogen and argon plasma total radiation measurement at various wavelengths and temperatures
17 p3139 A70-34547
- Thermal-chemical damage to carbon particles in egg albumin under ruby laser irradiation, using chemical rate equations for protein denaturation
17 p3035 A70-34577
- Ferroelectric radiation detectors theory and applications, considering polarization changes due to temperature increase from absorbed radiation
17 p3082 A70-34649
- Temperature and strain rate effects on polycrystalline Al strength
17 p3124 A70-34655
- Zonal wind component in lower ionosphere observed for gravity waves partial reflections by temperature discontinuities, using least mean square method for reflection coefficient
17 p3077 A70-34946
- One dimensional elastoplastic wave propagation in rate-sensitive viscoplastic rod with thermal gradient
17 p3185 A70-34966
- Stress wave generation in elastic temperature-dependent absorbing solids by impulsive EM radiation
17 p3185 A70-34967
- Crystal and glass lasers activated by Nd ions, examining stimulated emission temperature dependence by high temperature spectroscopy
17 p3106 A70-35105
- Human acceleration resistance and psychomotor behavior under emergency flight conditions, including high temperature exposure and remaining in clinostatic position
17 p3037 A70-35135
- Temperature dependent absorption, nonsteady beam propagation and laminar-turbulent transition in laser induced convection column, measuring turbulence onset by fine wire resistance thermometer
[AIAA PAPER 70-800] 17 p3107 A70-35197
- Viscoelastic materials cut growth, discussing strain, fracture and modulus of elasticity dependence on temperature variations
17 p3146 A70-35220
- Viscoelastic materials fracture strength as function of cut length, defect size and temperature
17 p3146 A70-35221
- Temperature and constant compressive loading effects on mechanical characteristics of fiberglass reinforced plastics
17 p3127 A70-35341
- Ambient temperature effects on rats and white mice tolerance to hypoxia, asphyxia and hypercapnia in nitrogen-oxygen and He-oxygen atmospheres
17 p3030 A70-35353
- Body temperature-maximum oxygen intake relations in hot humid air
17 p3038 A70-35424
- Ambient temperature effects on venous reactivity to hydrostatic stress, discussing posture changes and lower body negative pressure effects on index of compliance
17 p3031 A70-35426
- Differential fast-acting thermostat for temperature variation effects on elements, systems and subassemblies in gas filled space
17 p3090 A70-35433
- Fatigue crack propagation in solids in terms of nucleation theory, explaining temperature dependence of fatigue strength and size effect
17 p3191 A70-35464
- Thermal contact resistance, discussing behavior at cryogenic temperatures and directional or thermal rectifying effect
17 p3197 A70-35541
- Laminar free convection boundary layer on vertical heated plate near discontinuity in plate temperature, discussing velocity field
17 p3198 A70-35593
- Ni-Fe ferrites resistivity and thermoelectric power as function of temperature, proposing two energy level model for Fe ions
17 p3143 A70-35604
- Low temperature effects on Ti alloys welded joints elasticity
17 p3126 A70-35637
- Temperature dependence of materials with protective coatings, emphasizing mechanical properties of Mo with various diffusive coatings
17 p3126 A70-35716
- Heat transfer and friction drag calculation for turbulent boundary layer of gas with temperature dependent physical properties
17 p3012 A70-35729
- Powder combustion on metal plate, investigating unburned layer thickness dependence on initial temperature
17 p3198 A70-35738
- Cobalt binary alloys allotropic transformation and thermal expansion at various temperatures
18 p3271 A70-35967
- Gas bubbles thermal rejection and formation in Ni electrodeposit during annealing over 200-1000 C range
18 p3272 A70-36039
- Ni-Al-Nb superalloy, determining temperature effect on phase relationships in Ni-rich portion of phase diagram
18 p3273 A70-36041
- Rolled fine grained aluminum-alumina particles composites, determining creep strength dependence on temperature and tensile stress axis orientation
18 p3274 A70-36051
- W-3 percent Re-W-25 percent Re thermocouple reliability and stability, describing emf vs temperature table in 0-2400 C range
18 p3257 A70-36200
- Fe-Co alloys critical points during rapid heating, determining alpha-gamma phase transformations onset from dilatometric curves
18 p3275 A70-36203
- GaAs diodes electroluminescence dependence on temperature and injection current
18 p3297 A70-36234
- Thermophoresis of aerosol particles in nearly free molecular nonuniformly heated gas, using linearized Boltzmann equation
18 p3292 A70-36254
- Superconducting Nb-Ti-Zr alloy, investigating structure and decomposition at high temperatures by X ray and electron microscopy
18 p3276 A70-36310
- Fine grained Be structure and mechanical properties under tensile deformation at temperatures from 20 to 1000 C
18 p3276 A70-36311
- Physisorption isotherms for nitrogen on stainless steel at various temperatures and very low pressures
18 p3226 A70-36322
- Plane strain and stress produced in elastic micropolar medium by action of temperature
18 p3338 A70-36429
- Thermal effects on aircraft elastic vibration mode shapes, recommending investigation to develop analysis and design tools
18 p3213 A70-36459
- Polymers dynamic properties in hyperelastic and vitreous states as function of temperature, using torsion pendulum method
18 p3263 A70-36469
- Graphite modulus of elasticity as function of temperature, considering effects of moisture content in pores
18 p3278 A70-36470
- Gas exchange, body temperature and electrical activity of neck and back muscles of cold-acclimated white rats subjected to various temperatures
18 p3219 A70-36540
- Respiratory gas metabolism of liver, heart, brain and muscle tissues in birds exposed to various ambient temperatures for long periods
18 p3220 A70-36547
- Unsteady temperature fields in heat conduction problems associated with high temperature effects on ablated cylinders
18 p3348 A70-36572
- Thermal self focusing filaments observation in form of tracks in KDP and ADP crystals damaged by radiation from free emission mode laser
18 p3266 A70-36612

Sample dimensions effect on shape of I-V curve caused by overheating in media with ambiguous dependence of electron temperature on field 18 p3298 A70-36621

Time dependence of laser rod focal length, measuring thermal lensing effects 18 p3270 A70-36756

Thermal expansion anisotropy in graphite-epoxy composites causing residual stresses [ASME PAPER 70-GT-129] 18 p3279 A70-36855

Sea water temperature and salinity effects on smooth ocean surface radiation in centimeter range 18 p3250 A70-36968

Stellar atmosphere radiation field quantity vs quality, deriving electron temperature as function of tau 18 p3309 A70-37007

Semiconductor capture level parameter determination, using thermostimulated conductivity 19 p3483 A70-37296

Dispersion hardened Co strength and plasticity temperature dependence, determining Ti and Nb carbides additives effects 19 p3450 A70-37350

HD molecule nuclear relaxation time in liquid state as function of temperature, discussing various mechanisms 19 p3473 A70-37367

Al-Mg alloys recrystallization, investigating heating rate and annealing time effects on sheet grain size 19 p3450 A70-37372

Molybdenum carbide in methane-based plasma glow discharge, considering possible pyrocarbon layer formation and temperature effects 19 p3434 A70-37456

Fcc metals surface self diffusion temperature dependence, using model based on complex defects contribution to diffusion flux at high temperatures 19 p3483 A70-37545

Work hardening maxima of alpha-Ti as function of strain rate and temperature 19 p3451 A70-37568

Temperature dependence of anisotropic reaction kinetics of oxygen with pyrolytic graphite 19 p3373 A70-37709

Dielectric layer and screen heat loss effects on diffraction radiation in resonant waveguide 19 p3377 A70-37725

Elastic constants of ZnTe and ZnSe single crystals over 77-300 K range, using ultrasonic pulse echo method 19 p3486 A70-37761

Maraging steels heat treatment, measuring hardness as function of temperature for various heating rates 19 p3452 A70-37807

Nonuniform emitter current distribution effect on power transistor thermal stability, discussing temperature distribution effects 19 p3387 A70-37821

Age hardening of Nb-Hf-C alloys investigated by metallography and X ray diffraction, discussing tests in various temperature ranges 19 p3452 A70-37826

Fiber reinforced solid material, determining swelling or temperature change induced dilatation by micromechanics and physical chemistry 19 p3540 A70-37943

Periodic thermal forcing role in Venus atmosphere dynamics, investigating momentum transport to support mean shear for channel flow 19 p3519 A70-38251

Ice crystals growth rate in natural clouds over minus 2-minus 32 C range based on characteristic axial ratio 19 p3462 A70-38261

Thermal decomposition of nitrogen tetroxide and nitrogen dioxide induced by shock waves, examining temperature effects 19 p3373 A70-38265

Phase formation and mass transport during iodine-refined Ti reaction with nitrogen at various elevated temperatures 19 p3452 A70-38364

Circadian rhythms in single cell animals, examining cell division, temperature and light effects 19 p3365 A70-38410

Reciprocity theorem for stresses and strains in medium under creep and temperature field 19 p3548 A70-38582

Gas flow velocity measurement by thermal signal emitted from thin wire fed with modulated known frequency current 19 p3406 A70-38673

Oxygen solubility in Nb-Hf alloys at elevated temperatures, using isothermal sections for Nb-rich part 19 p3453 A70-38708

Nb effects on steel susceptibility to brittle fracture at various temperatures, discussing impact strength and nucleation energy of crack formation 19 p3453 A70-38709

Alumina effects on Nb creep activation energy at elevated temperatures, noting independence from chemical composition and creep stresses 19 p3453 A70-38710

Ti-Nb-Zr alloys strength and plasticity at various temperatures, noting compositional effects on tensile and yield strength 19 p3453 A70-38712

W-Mo-Nb-Ta system structure and properties at room and high temperature by microstructural analysis and hardness measurements, discussing Mo addition effects 19 p3453 A70-38713

Binary Nb vapor systems mutual diffusion coefficients concentration and temperature dependences, discussing interatomic bonds and melting point of alloys 19 p3454 A70-38715

Thermotropic quasi-geostrophic atmospheric model, deriving linear and quadratic integral invariants 19 p3463 A70-38754

Comet brightness curves asymmetry with respect to perigee attributed to pre- and post-heating 19 p3526 A70-38781

Microstructure and phase distribution in maraging steels subjected to austenization and subsequent aging in reversible transformation temperature range 20 p3645 A70-39038

Duraluminum dislocation structure dependence on deformation temperature by electron microscopy, discussing subgrain boundaries 20 p3646 A70-39045

Stressed cast Mg-Nd-Zr alloys structural transformations kinetics over temperature range by electron microscopy 20 p3646 A70-39046

Beta Ti-V-Cr-Al phase transformations below 500 C, discussing metastable phase, bcc formation and thermodynamics 20 p3646 A70-39106

Temperature effect on radiation characteristics and cryogenic tensile properties of irradiated Be, Ti and Al alloys 20 p3647 A70-39111

Degenerate p-n diode junction capacitance calculation, taking into account quantum and temperature effects 20 p3596 A70-39117

Natural convection problem solution along nonuniformly heated vertical plate with variable transverse magnetic field 20 p3735 A70-39144

Liquid He 4.2 K in narrow channels with laminar and turbulent flow, measuring boiling heat transfer as function of temperature difference 20 p3735 A70-39155

Sensing device to measure radial stress induced at solid propellant grain-to-case bond interfaces during wide temperature variations, detailing instrumentation and operation 20 p3718 A70-39158

Heat transfer from cylinder in axial air flow with induced turbulence of incident boundary layer, noting temperature effects 20 p3736 A70-39264

Liquid metal MHD conservation cycles, discussing evolution and status of power generation at various temperatures 20 p3563 A70-39325

Emitting plasma probes floating potential, discussing emission rate dependence on probe temperature and surface coverage by seed 20 p3632 A70-39607

Temperature dependence of titanium-zirconium oxide semiconductor compounds growth, using samples arc melted in purified He 20 p3687 A70-39631

Heating conditions effect on microstructure, hardness, transformation temperatures and dimensional anisotropy of maraging steel 20 p3649 A70-39941

Insulator wall temperature effect on supersonic nonequilibrium MHD generator channel under open and short circuit conditions 20 p3681 A70-39994

Performance comparison of diagonal conducting wall MHD generator and Hall generator of equal dimensions, investigating wall temperature effect 20 p3566 A70-40004

Blood vessels constriction in rear limbs, small intestine and spleen of dog with arterial blood heated above rectal temperature 20 p3574 A70-40173

Hypoxia and high ambient temperature effects on altitude tolerance in animals 20 p3575 A70-40186

Ammonium perchlorate composite solid propellant pressure vs burning rate at various temperatures, discussing granular diffusion flame theory 20 p3694 A70-40266

Liquid and solid semiconductors thermal emf and electrical and heat conductivities measurement over wide temperature range 20 p3634 A70-40300

Weak steady shock waves formation in relaxing binary gas mixture, discussing vibrational specific heat temperature dependence 20 p3614 A70-40350

Turbulent gas boundary layer at finite Reynolds numbers, investigating relative changes in friction and heat transfer coefficients and temperature factor 20 p3614 A70-40390

Interplanetary plasma torque due to temperature and pressure anisotropy, considering solar wind angular velocity and sun angular momentum 20 p3712 A70-40423

Deflagration rate measurements by high speed cinematography of ammonium perchlorate single crystals under various ambient temperature and pressure conditions 20 p3688 A70-40468

Strain gages for structural stress analysis in cryogenic environments, discussing correction factors for temperature dependent characteristics 21 p3932 A70-40545

Electron temperature measurements in flowing high density plasma by cooled Langmuir probe, considering probe temperature variations effects in boundary layer 21 p3854 A70-40557

Thermally induced mirror deformations and wavefront distortions under radially nonuniform heating 21 p3942 A70-40806

Temperature dependent anomalous optical absorption of thin yttrium films under static ultrahigh vacuum 21 p3862 A70-40816

Ion concentrations in premixed propane-air two dimensional laminar nozzle burner flames with seeding, discussing dependence on temperature and equivalence ratio 21 p3772 A70-40880

Soft X-ray-enhancement during solar flares due to coronal condensation temperature increase 21 p3880 A70-40969

Human sweating transient state characterized by time constant following abrupt ambient temperature rise 21 p3761 A70-41140

Traveling thermal wave induced channel flow, examining velocity profile thermal boundary conditions and shear stress 21 p3948 A70-41247

Liquid crystal smectic C phase temperature dependent tilt angle, using conoscopic observation and circularly polarized light 21 p3862 A70-41322

Heat transfer measurements based on optical methods with temperature dependence of refractive index making temperature field visible 21 p3826 A70-41373

Piston problem numerical solution by Boltzmann collision integral, considering shock waves and thermal disturbances evolution at gas-solid interfaces 21 p3808 A70-41378

Carburization and grain size of tungsten carbide powder from W powder as function of temperature, using optical and electron micrographs 21 p3839 A70-41412

Creep and stability of microstructural Al elements under varying temperatures, noting grain boundary migration 21 p3839 A70-41429

Apollo 11 fines, breccias and crystalline rocks thermoluminescence, observing temperature dependence of glow curve peaks 21 p3914 A70-41649

Fe 57 nuclear hyperfine splittings in clinopyroxenes from lunar igneous rocks, determining temperature dependent cation distribution 21 p3915 A70-41659

Electron collisional detachment from negative fluorine ions in shock tube following nonequilibrium ion overshoot in CsF dissociation in argon, noting correlation with temperature 21 p3853 A70-41705

Eddy currents in Hall generator with conducting side wall, studying velocity and temperature effects for turbulent boundary layer and laminar flows 21 p3859 A70-41733

Thermal and birefringent effects on output of continuous Nd-YAG laser rod, using 6328 A probe 21 p3837 A70-41906

Heat treatment and photovoltaic properties of copper disulfide-cadmium sulfide heterojunctions, measuring I-V characteristics, capacitance and spectral response 21 p3862 A70-41911

Temperature and bias voltage dependence of zero bias tunneling structure in p-type GaAs-Au Schottky junctions 21 p3863 A70-41917

Transmission electron microscopy observation of thermal annihilation of stacking faults in epitaxial layers of GaAs grown from liquid phase 21 p3863 A70-42004

Electron tunneling through p-type GaAs point contacts on Pb single crystals at liquid He temperatures 21 p3864 A70-42017

Epoxy and polyurethane adhesives stress-strain behavior in lap joints, examining bond thickness and cryogenic temperature effects 21 p3844 A70-42139

Gaseous and liquid fluorine exposure effects on nitroso rubbers at ambient and cryogenic temperatures, using impact tests and IR spectroscopy

21 p3844 A70-42140

Ni-Cu-C solid solutions, measuring temperature dependence of graphite solubility by vapor transport method

21 p3841 A70-42149

Incompressible laminar boundary layers thermal response behavior in wedge flow, obtaining surface response, temperature fields, heat flux and steady state data

21 p3811 A70-42164

Constant property unsteady laminar flow thermal entrance problems, using variational formulation in Laplace transformed domain

21 p3954 A70-42169

Single phase flow problem in heated vertical prismatic channel, using dimensional analysis from conservation equations with boundary layer approximation

21 p3954 A70-42170

Thermal variation of diamagnetism and susceptibility of rhombohedral graphite

21 p3845 A70-42268

Atmospheric inhomogeneity and temperature gradient effects on sonic booms, discussing displacement, growth rate and shock wave radii refraction

22 p3961 A70-42311

Thermally induced oscillations and negative resistance in seminsulating oxygen-doped GaAs double injection devices via heating beyond critical temperature

22 p4084 A70-42326

Thermal blooming of 10.6 micron laser beam in carbon dioxide absorption cell

22 p4049 A70-42335

Molecular vibrational temperature dependence on electron and neutral gas temperatures and degree of ionization for plasma excitation in nitrogen

22 p4078 A70-42358

Uranium plasma diagnostics, measuring emission and absorption coefficients as function of pressure and temperature

22 p4069 A70-42361

Plasma arc welding torches nozzle dimensions and shape dependence on thermal and electrical characteristics, optimizing energy output

22 p4042 A70-42378

Temperature and long term effects on volatility of perfluoroalkyl ether and polysiloxane greases [ASME PAPER 70-HT-31]

22 p4058 A70-42435

Heat generation effects in air hydrostatic journal bearing, including shaft and housing thermal deformation and lubricant viscosity changes [ASME PAPER 70-LUBS-19]

22 p4044 A70-42442

Spiral grooved gas lubricated thrust bearings, calculating self heating induced thermal distortion effects on load capacity [ASME PAPER 70-LUBS-14]

22 p4044 A70-42447

Gas lubricated foil bearing performance as support for turbo rotor simulator, examining heating and thermal gradient effects [ASME PAPER 70-LUBS-12]

22 p4044 A70-42448

Nb-Zr thin films superconducting properties dependence on deposition temperature and rate and substrate material

22 p4085 A70-42623

Heat conduction into semiinfinite homogeneous solid with thermal conductivity dependence on temperature, noting temperature profile asymptotic behavior for similarity solution

22 p4123 A70-42641

Gaseous substances thermodynamic functions and chemical equilibrium constants logarithms dependence on temperature and pressure, deriving internally self consistent formulas

22 p4124 A70-42682

Liquid and solid phases of substance, calculating thermodynamic properties and vapor pressure logarithm dependence on temperature

22 p4124 A70-42683

Pressure and temperature effects on large amplitude acoustic pulses propagating in stratified atmosphere

22 p4010 A70-42689

Oxygen diffusion coefficient of alpha-Ti from oxidation of saturated and unsaturated beta phase in 932-1142 C range

22 p4053 A70-42731

Strain rate change effect on stress-strain diagram shape of polycrystalline alpha-Ti during tensile tests over temperature range

22 p4054 A70-42737

Ti embrittlement by liquid Cd, discussing ductile-brittle transition temperature dependence on strain rate

22 p4054 A70-42738

Hot work effect on properties and microstructure of wrought Waspaloy, observing temperature decrease effect on fracture ductility

22 p4054 A70-42739

Annealing temperature effect on creep rupture strength of Ti-W-Hf alloy

22 p4054 A70-42741

Plunger pump for aircraft hydraulic systems, measuring working fluid temperature effect on cavitation

22 p3965 A70-42817

Rotating magnetic star thermal behavior, discussing central nuclear burning stability, homologous changes, cooling, degeneracy and helium flash

22 p4100 A70-42855

Initial water content on moon implied from hypothetical falling temperature lunar accretion as original earth satellite

22 p4102 A70-42954

Microbial existence limits in hot springs at varying temperature and pH characteristics

22 p3970 A70-42956

Neutron irradiation effect on elevated temperature fracture of various fcc alloys

22 p4054 A70-42957

Inconel short term creep properties measured for various temperature and stress levels, presenting results in polynomial and graph form

22 p4055 A70-43098

Vacuum-melted and deformed Mo alloys tests, showing long term strength decrease under cyclic heating

22 p4055 A70-43123

Mo microstructure changes at high temperatures, noting polygonization, grain migration and crack propagation during failure

22 p4055 A70-43125

Al-Be-Mg alloys under solution treatment, noting aging and prolonged heating effects on mechanical properties from solid solution decomposition diagram

22 p4056 A70-43127

Tubular Al creep resistance increase by temperature jumps during steady phase of creep

22 p4056 A70-43344

Phase diagrams and nonvariant equilibria points of Ti-Si alloys subjected to prior annealing, determining phase transformations, decomposition and other properties as function of temperature

22 p4057 A70-43350

Gas turbine engine combustion chamber starting, discussing effects of temperature, nozzle characteristics and fuel physicochemical properties

22 p4092 A70-43356

Nitrogen transport coefficients as function of high temperature in stationary plasma produced in cascade arc chamber

22 p4082 A70-43373

Blood flow antagonistic changes in various vascular beds following spinal cord central thermal stimulation attributed to sympathetic vasoconstrictor activity

22 p3971 A70-43405

Spinal cord thermal stimulation effects on regional sympathetic activity in rabbits and cats determined from integrated sympathetic efferent discharges

22 p3971 A70-43406

Silver fluorination kinetics, taking temperature and pressure effects into account

22 p3983 A70-43416

In thin film resistance thermometers fabrication by vapor deposition in vacuum, considering electrical properties dependence on temperature

22 p4039 A70-43446

Monograph on MHD, covering fluid layer stability under adverse temperature gradient, geomagnetic field origin, vector relations, etc

22 p4084 A70-43448

Current and vector potential in thin superconducting film in HF field, considering high and low temperatures

22 p4088 A70-43467

Glass-epoxy composites, measuring embedding filaments effect on time-temperature relationship under ultimate stress conditions

22 p4118 A70-43549

Silicon precipitation in nonrefined annealed Al, examining heat treatment effects

22 p4057 A70-43550

Surface degradation by oxidation, temperature fluctuations and hot corrosion of Ni- and Co- base superalloys in gas turbine engines

22 p4057 A70-43574

Annealing response of explosively shock loaded Ni, thorium-Ni, Chromel-A, Inconel 600 and thorium-Chrome, noting activation temperature inverse relation with stacking fault free energy

23 p4204 A70-43883

Stellar associations formation theory including effects of radiation, Rayleigh-Taylor instability and interstellar gas cold regions

23 p4239 A70-43903

Temperature effect on friction coefficient of boron and silicon carbides, using similar wear pairs in vacuum

23 p4205 A70-44044

Fatigue of turbine blade stainless steels and nickel alloys as function of temperature, stress and surface layers [ICAS PAPER 70-38]

23 p4205 A70-44135

Temperature gradient effect on Couette flow heat transfer and stability

23 p4181 A70-44250

High strength Al alloys plate and welds, comparing tear notch tests at cryogenic and room temperatures

23 p4206 A70-44352

Hg vapor thermal conductivity at various temperatures, using fine wire frequency response and kinetic theory

23 p4281 A70-44428

Limit analysis for ionization potential reduction effect on ionized gas atomic composition, considering temperature and electron density

23 p4220 A70-44435

Temperature dependent materials heat flow analysis using perturbation method for nonlinear boundary value problems

23 p4282 A70-44589

Temperature effect on radiation tolerance of mice exposed to low dose rate gamma radiation, noting mortality delay in low temperature environment

23 p4148 A70-44789

Extreme environmental temperature effects on hepatic amino acid catabolism in rats attributed to caloric deficiency

23 p4148 A70-44790

Wrought Nimonic alloy, measuring stress redistribution due to creep under variable load and temperature

23 p4274 A70-44911

Low Reynolds number gas flow past heated circular cylinder, considering Stokes region transport properties

23 p4284 A70-44978

Rarefied binary gas mixture, determining temperature gradient effect under various pressures

23 p4284 A70-44984

High cutoff negative resistance silicon carbide diodes, noting temperature independent current-voltage curve

23 p4176 A70-45067

Antiferromagnetic and ferrimagnetic resonance frequencies, determining temperature dependence by spin wave theory

24 p4388 A70-45132

Temperature effects on width of current-voltage characteristics of GaAs Gunn oscillators

24 p4318 A70-45191

Thermal fluctuations effect on Josephson tunnel contact binding energy and external magnetic field dependence

24 p4388 A70-45203

Ultrasonic absorption in SbSI semiconducting semiconductor as function of temperature, illumination and constant electric field strength, noting absorption coefficient rise near Curie point

24 p4389 A70-45207

SbSI semiconductor single crystal repolarization parameters temperature dependence, noting anomalies in permittivity, spontaneous polarization and dielectric loss tangent

24 p4389 A70-45208

Impurities and heat treatment effects on W internal friction at high temperatures, considering relaxation processes, recrystallization and microstructure

24 p4357 A70-45227

Ground temperature effects on thermal gradients resolution in IR line scan imagery

24 p4334 A70-45363

Big bang temperature problem, discussing galactic masses determination possibility by gravity-strong interactions interplay in early stages

24 p4403 A70-45402

German monograph on sintered molybdenum silicide recrystallization following high temperature heating in oxidizing atmosphere

24 p4367 A70-45575

Axisymmetric laminar compressible jet flow characteristics, allowing for compressibility effects due to temperature dependent density and viscosity variations

24 p4325 A70-45584

Ion-ion potential for sodium vapor for second virial coefficient as function of temperature at 1200-1700 K

24 p4381 A70-45649

Amorphous semiconductor alloys in As-Se system, measuring DC and AC electrical conductivity dependence on temperature

24 p4390 A70-45657

Solid solution of GaAs with CdSe and CdS compounds, investigating intrinsic absorption edge dependence on temperature

24 p4390 A70-45663

LF plasma waves amplification by beam-plasma interaction, considering electron and ion temperatures effects

24 p4387 A70-45797

Pneumatic actuator rod and piston head seals, examining materials at various temperatures, pressures and speeds [SAE PAPER 700791]

24 p4294 A70-45855

Liquid rocket propellants tankage and components long term storage under extreme relative humidity and temperature conditions [SAE PAPER 700800]

24 p4392 A70-45911

Temperature gradient spectra on complexes of metmyoglobin and methemoglobin with ligands,

- discussing boundary forms equilibria for various electron spin configurations 24 p4301 A70-45985
- Controllable states with prescribed heat flux for incompressible isotropic thermoelastic bodies with temperature dependent response functions 24 p4426 A70-46041
- Cold boundary layer effect on chemical kinetic parameters behind reflected shocks in single-pulse shock tube 24 p4323 A70-46044
- Temperature induced humidity errors in military and Weather Bureau radiosondes carbon humidity element caused by solar irradiation 24 p4372 A70-46073
- UV excited powdery fluorescent products, describing crystal for photo and thermoluminescence at various temperatures 24 p4339 A70-46097
- Si-carbide composites electrical conductivity from temperature and thickness dependence, obtaining volt-ampere characteristics via computer method 24 p4391 A70-46154
- ### TEMPERATURE FIELDS
- #### U TEMPERATURE DISTRIBUTION
- #### TEMPERATURE GRADIENTS
- Shock wave structure in two phase media with temperature and velocity gradients and possible phase transitions 01 p0060 A70-10147
- Polar thermosphere temperature measurements from artificial clouds indicating geophysical-associated variations, nocturnal decrease and annual variations 01 p0077 A70-11201
- Jovian atmosphere convective energy magnitude determination for various atmospheric thicknesses and temperature gradients 02 p0375 A70-12432
- Extrapolation formulas to calculate temperature gradients and heat fluxes in solid heated by variable heat flux, estimating errors 03 p0606 A70-13521
- Temperature sensor location for accurate averaging in fluid flowing through heated or cooled circular duct 03 p0486 A70-13557
- Thermocouples response to rapid temperature rise produced by discharge from low inductance high voltage capacitor bank 03 p0486 A70-13559
- Embedded sheathed thermocouples temperature measurement of cooled jet engine turbine buckets subjected to high heat flux 03 p0486 A70-13560
- Two phase liquid-vapor system specific heat increase at temperatures approaching critical point, using nonanalytic vapor pressure equation with data for nitrogen and oxygen 04 p0780 A70-14584
- Ground temperature effect on thermal resolution in IR line scan imagery, discussing equipment and operating procedures for temperature gradient detection 04 p0686 A70-14617
- Conducting fluid steady convection due to combined effects of thermal gradient and DC electric field predicted by analytical model 04 p0785 A70-14989
- Stimulated thyroid gland temperature variations and oxygen metabolism in decorticated dogs and anesthetized rabbits and rats 04 p0639 A70-15511
- Atmospheric temperature gradients above 30 km near sunrise using earth spectral radiance measurements by balloon 04 p0694 A70-15523
- North Galactic Spur compared for edge, ridge and neck with previous results noting sharp temperature gradients 04 p0758 A70-15699
- Sonic boom propagation in still atmosphere with vertical temperature gradient, using graphical method of determining rays for aircraft motion 05 p0791 A70-15786
- Low Reynolds number flow of variable property gas past infinite heated circular cylinder at large temperature differences, measuring drag on cylinder 05 p0789 A70-16014
- Energy losses in conductors carrying intense currents to cryogenic regions linked with heat transfer due to high temperature gradients 05 p0881 A70-16026
- Thermodynamics of elastic continuum with microstructure, modifying second law to include microtemperatures 05 p0930 A70-16083
- Combustion model for temperature inhomogeneities effect on stability of solid fuels steady combustion 05 p0958 A70-16960
- Ni effect on nitrogen activity in Fe-Ni-N austenite between 600-1200 C using Strohlein analyzer 06 p1088 A70-17612
- Yttrium-iron garnet optical properties at various wavelengths and temperatures, noting absorptivity decrease in IR region 06 p1126 A70-17767
- Sunspot temperature and pressure gradients from blue, red and IR photographs, deriving umbral depression and density scale height 06 p1143 A70-18000
- Thermal slip velocity of gas in infinite temperature gradient tangential to solid wall, basing calculation on linearized Boltzmann kinetic equation 06 p1049 A70-18332
- LF nonacoustic instability of solid propellant rocket motors, using combustion model allowing flame temperature oscillations with chamber pressure [AIAA PAPER 68-179] 07 p1421 A70-19319
- Soviet book on structures design for stability at high temperatures with large gradients, discussing thermoelasticity, thermoplasticity and creep equations for shells, plates, etc 07 p1409 A70-19601
- Temperature gradients, viscosity and conduction measurements in air stream between parallel plates, investigating limiting value of total Prandtl number 07 p1260 A70-19999
- Meteorological rocket sounding data for Eurasia in mean profiles, time and lateral cross sections, discussing temperature and wind variations 07 p1274 A70-20270
- F corona heliocentric dust cloud model to account for temperature variations with particle size and optical properties, computing thermal emission 08 p1571 A70-20907
- Fluid motion convective stability between vertical parallel planes with longitudinal temperature gradient, solving boundary value problem for amplitudes of normal perturbations 08 p1482 A70-20952
- Temperature increase effects on fully turbulent boundary layers at low Reynolds number in air investigated in wind tunnel 08 p1485 A70-21606
- Simply supported rectangular plate investigated for effect of thermal gradient on transverse vibrational frequencies 08 p1595 A70-21976
- Solar chromosphere-corona transition region properties, discussing temperature increase within very thin layer and inferring temperature-density structure from emission line intensities 09 p1752 A70-22246
- Drop sondes dynamic and aerodynamic design for lower Venus atmosphere based on solution for free fall of body in atmosphere with constant temperature gradient 09 p1766 A70-22935
- Thermal conductivity of arbitrarily inhomogeneous bodies, considering vectorial field isotropy and temperature gradients dispersion 09 p1789 A70-23103
- Circumferential wall temperature gradients in spacecraft radiator tubes as function of tube wall fins 09 p1789 A70-23261
- Time-temperature charts for one dimensional unsteady conduction with uniform internal heat generation 09 p1791 A70-23567
- Temperature gradient method for determining local heat transfer coefficients in variable cross section channel 10 p1968 A70-24290
- Heat resistant alloys low cycle fatigue tests between 20-800 C, establishing residual strain change patterns as function of stress and temperature 10 p1906 A70-25294
- Remote measurement of CAT associated temperature gradients, comparing monochromatic and finite bandpass models 12 p2262 A70-26949
- Atmospheric airflow model above changes in surface roughness, temperature and heat flux, using boundary layer approximations and Businger-Dyer and mixing length hypotheses 14 p2602 A70-30368
- Fine scale temperature variability along flight path during smooth and turbulent conditions 14 p2609 A70-30605
- Venus surface temperature poleward variation from radio interferometry measurements 14 p2646 A70-31068
- Mars surface material properties from radio emission observations, considering daily temperature variations distribution 14 p2648 A70-31083
- Heating rate effect on parameters of resistance wire strain gages subjected to temperature gradients 15 p2733 A70-31536
- Temperature and density extreme variations at various levels in stratosphere and mesosphere, analyzing sounding rocket data 15 p2723 A70-31661
- Elastic micropolar body thermal stresses induced by discontinuous temperature field, using differential equations of thermoelasticity 15 p2822 A70-32353
- Atmospheric temperature fluctuation spectrum determination by energy budget solution, considering spectral density dependence on Richardson number 15 p2732 A70-32542
- Thermoelectric force due to thermocouple inhomogeneities, showing relation to temperature gradient and measurement error 16 p2900 A70-33070
- Surface temperature changes measurement with thermovision camera, discussing calibration and recording 16 p2911 A70-33775
- Argon II line transition probabilities, observing UV spectral region, upper energy levels and temperature differences 16 p2956 A70-34251
- Conical passive radiation coolers for quantum IR detectors on equatorial synchronous earth satellites, determining temperature excursions 16 p2915 A70-34314
- Empirical autocorrelation functions describing statistical properties of vertical temperature gradients in troposphere and lower stratosphere 17 p1332 A70-35337
- Free convection boundary layer on two dimensional or axisymmetric body with sudden temperature increase, determining skin friction and heat transfer coefficients 18 p3346 A70-36487
- Temperature change relation between anterior hypothalamus and concha auricular in rabbits 18 p3218 A70-36532
- Gas exchange adaptation to heat and cold in rats with different ecological backgrounds 18 p3218 A70-36533
- Energy flow between two superfluid helium baths at different temperatures and separated by thin plate 19 p3471 A70-37648
- Nonlinear electromagnetic constitutive equations with coupling to thermal gradients for holohedral and hemihedral materials, extending analysis to orthotropic media 19 p3552 A70-37786
- Thermal error in temperature difference between actual and simulated space environment 19 p3401 A70-38301
- CAT detection by IR radiation, remotely detecting atmospheric horizontal temperature gradients 20 p3626 A70-39080
- Solar activity effects on Northern Hemisphere atmospheric temperature, mapping gradients for 11 year solar cycle 20 p3662 A70-39188
- CAT as mechanism relieving wind and temperature discontinuities, maintaining Richardson number at limiting value by turbulent energy dissipation 20 p3663 A70-39373
- Fluid motion convective stability between vertical parallel planes with longitudinal temperature gradient, solving boundary value problem for amplitudes of normal perturbations 20 p3608 A70-39377
- Temperature gradient method for determining local heat transfer coefficients in variable cross section channel 20 p3739 A70-40348
- Plane horizontal fluid film convective stability with free boundaries in vertical circular cylinder for periodic modulation of vertical temperature gradient or gravitational field 21 p3941 A70-40608
- Solar flare relation to radio emission at 3.3 mm, discussing sunspots, temperature gradients and magnetic fields 21 p3879 A70-40962
- Heat transfer in cooled turbulent tube flow downstream region at high bulk-to-wall temperature ratios 21 p3945 A70-41037
- Thermocouple transient response characteristics in deflagrating and ablative low conductivity materials with high temperature gradients [ASME PAPER 70-HT-7] 22 p4122 A70-42440
- Large collimator objectives lenses focal lengths measurement in vibrations and temperature gradients 22 p4073 A70-42511
- Finned tube-sheet spacecraft radiator transient response for perturbations caused by power supply and heat sink temperature changes 22 p4123 A70-42519
- Linear coupled thermoelasticity theory for homogeneous isotropic solid with two temperatures 22 p4123 A70-42540
- Stratospheric clear air turbulence probability based on vertical temperature gradients and rawinsonde ascensional rates 22 p4064 A70-42619
- Rarefied gas heat conduction between concentric cylinders in slip regime, obtaining perturbed temperature and density variations 23 p4284 A70-44985
- Cross correlation measurement errors for fluid pipe flow with pseudorandom sequence generated temperature fluctuations, considering transport time, impulse response and laminar flow 24 p4333 A70-45111

Combustion chamber flow visualization, obtaining information on pressure loss, velocity field, flow pattern and temperature gradients 24 p4393 A70-45444

Atmospheric pressure surface sharp slopes at SST altitudes producing vertical acceleration based on temperature gradients inspection 24 p4372 A70-46050

Clear air turbulence detection by IR radiometry of thermal gradients, using staggered receivers for panoramic visualization 24 p4314 A70-46093

TEMPERATURE INDICATORS

U INDICATING INSTRUMENTS
U TEMPERATURE MEASURING INSTRUMENTS

TEMPERATURE INSTRUMENTS

U TEMPERATURE MEASURING INSTRUMENTS

TEMPERATURE INVERSIONS

NT CENTRIFUGING STRESS

Unsteady inverse heat conduction of semibounded body solved by least squares method 06 p1178 A70-17856

Air masses nonadiabatic ascent under elevated temperature inversion in atmosphere, assuming three layer model with linear profiles 12 p2265 A70-28335

Ozone concentration in San Francisco Bay Area, discussing temperature inversion, air pollution, destruction rate and distribution patterns of oxidants 18 p3284 A70-35945

Report on ASA meeting in Pasadena February 1969 covering solar observation program, solar temperature inversion, solar spin-down, etc 19 p3518 A70-38014

Internal gravity wave shape at temperature inversion in lower atmosphere from high resolution vertically pointing FM/CW radar sounding 23 p4162 A70-44038

TEMPERATURE MEASUREMENT

Cardiac activity temperature coefficients in dogs, specifying physical and chemical cardiac functions 01 p0012 A70-10052

Human rectal temperature cooling rate during refrigeration in mortuary, applying Newton law 01 p0017 A70-10471

Polar thermosphere temperature measurements from artificial clouds indicating geophysical-associated variations, nocturnal decrease and annual variations 01 p0077 A70-11201

Coordination technique for pressure, density and temperature measurements by probes during parachute reentry into planetary atmospheres, taking into account reentry dynamics 01 p0197 A70-11495

Light scattering from thermally stable magnesium oxide particles in premixed turbulent flames used for measuring mean and fluctuating temperature values 02 p0398 A70-12039

Satellite measurement of mean temperature in atmospheric layers to determine vertical temperature distribution 02 p0291 A70-12279

Nonequilibrium two phase forced convection flow, describing pressure, temperature and void fraction measurement techniques 02 p0305 A70-12838

Radiation pyrometers development for in-flight measuring and controlling aircraft engine compressor blades temperature [SAE PAPER 690432] 03 p0480 A70-12900

Extrapolation formulas to calculate temperature gradients and heat fluxes in solid heated by variable heat flux, estimating errors 03 p0606 A70-13521

Optimum radiation shield quantity assuring gas temperature measurement accuracy, using radiation transfer equations and shield-to-shield temperature estimations 03 p0486 A70-13556

Temperature sensor location for accurate averaging in fluid flowing through heated or cooled circular duct 03 p0486 A70-13557

Embedded sheathed thermocouples temperature measurement of cooled jet engine turbine buckets subjected to high heat flux 03 p0486 A70-13560

Sky background brightness temperature measurement at 408 MHz by pyramidal horn antenna 03 p0496 A70-14344

Temperature evolution of detonation products of Na seeded propane-oxygen mixtures, observing periodic variation for helicoidal cases 03 p0608 A70-14356

Electron temperature of hydrogen-oxygen flame plasma obtained by floating probe method compared to spectroscopic method results 03 p0608 A70-14380

Pressure-volume-temperature measurements on H₂, calculating fugacity coefficients 04 p0719 A70-15057

Niobium addition effect on alpha-gamma transformation temperature during continuous cooling of low carbon Ni-Cu steel 04 p0706 A70-15134

ESRO 1 thermal behavior, discussing trajectory effects, onboard temperature measurement, data storage, data transmission, telemetered data and data comparison 04 p0762 A70-15164

Temperature and morphological changes of animals adipose tissue under various nutrition conditions, based on measurements by thermocouples implanted in fat deposits 04 p0640 A70-15514

Atmospheric temperature gradients above 30 km near sunrise using earth spectral radiance measurements by balloon 04 p0694 A70-15523

Photographic pyrometry for surface temperature measurements on ablation models, discussing technique accuracy and limitations 04 p0694 A70-15536

High temperature thermal transport and ionization relaxation in Ar from measurements by thin film surface thermometer in high pressure shock tube end wall 04 p0787 A70-15607

Radio/radar antenna temperature measurement by phase principle insensitive to receiver gain fluctuations 05 p0819 A70-15804

Temperature distribution causes in earth orbiting satellite, outlining thermal control and temperature calculation methods and prelaunch ground tests 05 p0956 A70-15813

Solar interior temperature measurement by Cl, Ga and Li isotopic detectors of solar neutrinos, discussing effectiveness and upper temperature bound 05 p0899 A70-15951

Cable involving woven multiconductor arrangement and aromatic polyimide insulations to connect thermal moon probe with transmitter for temperature measurements on lunar surface 05 p0798 A70-16034

Satellite determination of underlying surface temperature by IR spectroscopy, measuring emitted radiation in atmospheric windows 06 p1061 A70-17205

Noontime ground surface temperature relationship to exposure and slope angle for meadows and woodland, using airborne IR pyrliometer 06 p1054 A70-17415

Laser produced plasma temperature measurements using method of X rays selective transmissions through different absorbing films 06 p1081 A70-17596

Temperature at end of admission process and exhaust gas temperature in cylinder of internal combustion engine using reversible adiabatic hypothesis 06 p1173 A70-17629

Satellite temperature determination in earth orbit, testing mathematical thermal model in simulation chamber 06 p1155 A70-17935

Far IR measurement of solar minimum temperature with Michelson interferometer carried on NASA research aircraft 06 p1143 A70-17997

Thermometric convection coefficients used in automatic meteorological data correction program 06 p1183 A70-18288

Rotational and vibrational temperatures measured in hypersonic nonequilibrium rarefied gas flow field of cooled circular cylinder by electron beam technique 06 p1123 A70-18304

Density effects on rotational temperature measurements in nitrogen by electron beam excitation, discussing emission intensity distribution 06 p1067 A70-18306

Miniature temperature and strain telemetry transmitters developed for measurements in areas inaccessible to direct wire connections 06 p1069 A70-18433

Longitudinal spectral line intensity distributions measured for plasma temperature determination 06 p1074 A70-18601

Effective, brilliance, color and gradient temperature measurements in astrophysics, considering observer bond and thermodynamic nonequilibrium of stars 07 p1386 A70-19597

High temperature techniques, measurement and data methodology noting refractory materials 07 p1312 A70-19877

Dynamic pearlite-austenite transformation and melt temperatures measured in laser-irradiated steel, discussing thermal response as function of heating rate 07 p1301 A70-19897

Rotational temperature of molecular beam by electron excited fluorescence method, discussing signal level, background light and scattering effects 07 p1345 A70-20140

PWN-8B meteorological rocket system for synoptic investigation of stratospheric circulation, describing sensor system deployment for descent measurements of wind and temperature 07 p1395 A70-20255

TEMPERATURE MEASUREMENT

Kookaburra meteorological rocket system for sounding stratospheric circulation, describing instrument payload deployment for descending wind and temperature measurements 07 p1395 A70-20257

Measurement physics of resistance wire temperature sensing system used in Skua rocket sounding system 07 p1396 A70-20262

Kinetic temperature estimate for solar corona based on time profile of type 3 bursts 08 p1565 A70-20565

Thermistors used in temperature measurements aboard satellites, discussing results of electrical and mechanical tests 08 p1493 A70-20612

Atmospheric temperature measurement by microwave radiometry, considering instrument design for measurements at various barometric levels 08 p1495 A70-21041

Atmospheric boundary layer wind and temperature analysis according to similarity scheme for mathematical modeling of atmosphere 08 p1540 A70-21974

Cryogenic thermometry operating principles, instrument design, measurement techniques, useful temperature ranges and accuracy 09 p1674 A70-22289

Temperature scales, definition and measurement, discussing scale differences, temperatures below freezing, conversion methods, etc 09 p1675 A70-22325

Electron temperature resonance probe to eliminate effects of geomagnetic field, rocket velocity and random noise 09 p1675 A70-22422

Thermal gradients and associated strains measurement in steam turbogenerator casings, considering strain gage placement and heat transfer calculations 09 p1774 A70-22590

Saturn disk temperature obtained from centimeter wavelength, suggesting possibility of nonthermal radiation 09 p1759 A70-22912

Boltzmann temperature measurement apparatus of oxide coated cathodes in scanning beam tubes 09 p1656 A70-22987

Electronic radio equipment with encapsulated structure and natural ventilation, calculating heated zone and casing mean surface temperatures 09 p1648 A70-23147

Constant temperature /phase transition/ calorimeter errors in measuring laser energy using ice as working medium 09 p1700 A70-23659

Aircraft surface temperature measured with airborne IR TV system 09 p1686 A70-23754

Sea surface temperature measurement over large areas using IR remote sensing system mounted on airborne platform 09 p1686 A70-23756

Ambient temperature measurement by constant level balloon mounted thermistors, discussing errors from differential heating of thermistor support by solar radiation 10 p1886 A70-23935

Temperature, pressure and electron density measurements behind reflected shocks in gas driven diaphragm shock tube compared with Rankine-Hugoniot predictions 10 p1967 A70-23960

Supersonic flows over flaps and backward facing steps, using steady state heat transfer measurement technique involving uniform heat flux dissipation at model surface 10 p1798 A70-24120

Electron beam fluorescence probes for rarefied gas flow, describing local density and temperature measurement methods 10 p1888 A70-24399

Gravity waves structure simultaneous determination from airborne ozone and temperature sensors and satellite observations data 11 p2076 A70-26072

Steady state surface temperature measurement errors by thermistors, thinistors and thermocouples, discussing sources 11 p2052 A70-26361

Microwave radiometric temperature measurements generating curves relating sea state and surface temperature 12 p2215 A70-26903

Remote measurement of CAT associated temperature gradients, comparing monochromatic and finite bandpass models 12 p2262 A70-26949

Atmospheric temperature determination by satellite IR spectrometer /SIRS-A/, describing data analysis and instrument design, calibration and performance 12 p2263 A70-26954

Self heating accompanying exothermic decomposition of gaseous diethyl peroxide in spherical vessel measured positionally by thermocouple 12 p2330 A70-27223

Local heat sink thermal processes on convectively cooled solid surface, noting applications to temperature measurement errors 12 p2333 A70-28112

Flame temperatures simultaneous measurement in two spectral regions, using photoelectric IR pyrometer 12 p2237 A70-28158

Brightness temperature of earth atmospheric emission in submillimeter band at 35 km, describing airborne radiometer 12 p2265 A70-28171

Coronal condensations temperature and electron density measurements at meter wavelengths and in white light 13 p2488 A70-28717

Electron radiation temperature measurements in sealed-off carbon dioxide laser, determining gas mixture effect on discharge properties 13 p2426 A70-28808

Solar far UV continuum photometry illustrating spectral temperature minimum transition, comparing to far IR temperature 13 p2496 A70-29841

Ionic temperature difference from Arecibo data indicated in Injun 3 and Alouette 1 sonograms of proton whistlers propagation time, noting Doppler shift role 13 p2372 A70-29928

Electron beam measurement of rotational and high vibrational temperature in molecular nitrogen 13 p2412 A70-29980

Radial ion temperature distribution in hydrogen arc within axial magnetic field measured spectroscopically by thermal Doppler effect 14 p2621 A70-30657

Mercury disk temperature at 3.75 cm wavelength, showing variation with phase angle and hemographic longitude 14 p2647 A70-31075

Temperature estimation of micro hydrogen-air diffusion flame from hydrogen content of unburned gas mixture 14 p2666 A70-31095

Average rotational temperature of Venus atmosphere above cloud tops from carbon dioxide band spectroscopy 14 p2650 A70-31219

Nomogram for true and apparent radiometric temperatures of remote graybodies in presence of atmosphere 14 p2577 A70-31231

Commercial aircraft brake temperatures under HF landing conditions, using energy input and heat transfer computer programs 14 p2532 A70-31341

Neutral particle temperature, pressure and velocity measurements in argon plasma jet, using refraction index 14 p2625 A70-31350

Temperature measurement of rotating shafts under cyclic loading, using thermistor as thermal radiation sensor 15 p2734 A70-31581

Surface, volume and body center temperature of convex polyhedrons under steady heat transfer 15 p2825 A70-31624

Thermocouples performance during fast varying temperature measurements in solids, considering physical parameters effects on accuracy 15 p2734 A70-31646

Atmospheric vertical temperature sounding from geosynchronous satellite, discussing instrumentation, cloud cover and wind effects, etc 15 p2809 A70-31690

Heat flux measurements in hypersonic rarefied gas flow by thin film surface thermometer 15 p2825 A70-31820

Pyrometer for measuring temperature by ratio of radiation at two different wavelengths, eliminating spectral emissivity effect 15 p2736 A70-31824

Atmospheric temperature vertical distribution measurement using sounding balloon and Skylark rocket 15 p2725 A70-31846

Noise sources and identification in low noise RF amplifiers via noise temperature or factors 15 p2708 A70-31952

Clouds and precipitations radio brightness temperature contrasts taking into account underlying surface humidity 15 p2771 A70-32070

Strength and thickness effects on energy absorption criteria for transition temperatures in Charpy V-notch impact tests 15 p2819 A70-32234

Rocket engine propellants flame temperature measurement by spectral line intensity comparison method 15 p2786 A70-32270

FM/FM radio telemetry system for transmitting strain and temperature data from rotating parts 15 p2739 A70-32330

Temperature measurement of products in solar furnace by IR pyrometers, considering interference filters, reflections parasitic effects, etc 15 p2740 A70-32424

Sampling error origin and magnitude during soil temperature measurements, noting dependence on weather character and season 15 p2731 A70-32459

Spacecraft thermal mathematical model adjustment to fit measured temperatures, using iteration method 15 p2812 A70-32513

Kinetic temperature estimate for solar corona based on time profile of type 3 bursts 15 p2805 A70-32720

Photothermometer response to thermal shock, considering rapidly varying surface temperature measurement 16 p2901 A70-33104

IR optical radiometer for jet engine turbine blade temperature measurement, comparing with junction wire thermocouple 16 p2905 A70-33168

Surface temperature measurement with airborne IR scanning imager for terrain analysis 16 p2905 A70-33170

Turbulent and reacting flows temperature and mixing rates determination, using gaseous HF tracer spectroscopy [AIAA PAPER 70-726] 16 p2856 A70-33497

C-5A turbofan engine thrust determination using pressure and temperature values in exhaust nozzles [AIAA PAPER 70-611] 16 p2969 A70-33606

Optical system measurement of density and rotational temperature in gaseous plume simulating auxiliary propulsion and oxygen hydrogen burner of S-4B 16 p2913 A70-34023

IR Michelson interferometer for Mariner Mars 1971 mission, investigating atmospheric and surface temperatures and atmospheric water vapor content 16 p2978 A70-34029

Low Reynolds number flow inside Delaval nozzle, examining gas density and rotational temperatures by electron beam techniques [AIAA PAPER 70-810] 17 p3065 A70-34454

Cryogenic temperature measurement including metallic and semiconductor resistance thermometers, thermocouples and bibliography 17 p3082 A70-34740

Mercury disk temperature from microwave spectrum analysis, proposing subsurface greenhouse effect 17 p3157 A70-34838

Turbulent boundary layer velocity, temperature and concentration instantaneous measurements, describing automatic circuit procedure 17 p3088 A70-35041

Satellite-borne instruments for thermal sounding of troposphere, noting information limitation due to atmospheric effects 17 p3132 A70-35338

Differential fast-acting thermostat for temperature variation effects on elements, systems and subassemblies in gas filled space 17 p3090 A70-35433

Time resolved measurements of ion and electron temperature in pulsed Ar ion laser discharge, observing heating 17 p3108 A70-35907

Tiros satellites window radiation applied to day and night surface temperature measurements on land and sea 17 p3081 A70-35932

Upper atmosphere neutral component temperature measurement from thermal spread of charged particles beam 18 p3247 A70-36182

High altitude clear air turbulence structure and evolution examined by high power radar and wind and temperature vertical soundings 18 p3228 A70-36483

Heat transfer rates in short flow duration facilities /shock tubes/ from surface temperature measurement of solid exposed to flow 18 p3348 A70-36715

Upper atmospheric neutral components temperature determination by rocket-borne mass spectrometers 18 p3252 A70-36983

Atmospheric temperatures from thin walled ballistic rocket surface measurements with high sensitivity photometer 18 p3261 A70-36997

Solar photosphere temperature constancy in thin CO layer from equivalent spectral line width determination 18 p3322 A70-37134

Interstellar H I gas physical conditions, discussing ionization ratio average values and temperature conditions 18 p3328 A70-37175

Ultrasonic measurement of temperature distribution in solid, liquid and gaseous media, using reflection and transmission techniques 19 p3427 A70-37963

Thermocouples and resistance thermometers comparison for low temperature measurements 19 p3432 A70-38703

Pt resistance thermometers for low temperature measurements, discussing structural and mechanical characteristics 19 p3432 A70-38704

Free air temperature by onboard satellite IR spectrometer /SIRS/, measuring earth spectral radiance in carbon dioxide 15 micrometer band 20 p3660 A70-39077

Fretting corrosion zone steel, measuring transient temperature distribution during contact friction 20 p3647 A70-39243

Two-layer slab under aeroheating, solving bondline temperature graphically 20 p3737 A70-39693

Asymmetric micropolar thermoelasticity, deriving integral expressions for strains, rotations and temperatures in finite body 20 p3726 A70-39878

Temperature measurements in gaseous reaction zone near surface of burning composite solid propellant, using modified line reversal pyrometer 20 p3694 A70-40273

Temperature difference between equator and solar poles from spectral line equivalent width variation 20 p3711 A70-40407

Hyades giant stars epsilon and gamma Tau strong line profile analysis, obtaining effective temperatures 21 p3885 A70-40931

Atomic oxygen density and temperature diurnal variation determination by F region incoherent scatter measurements, using nonlinear regression analysis 21 p3817 A70-41096

F region radar and optical temperature measurements, discussing Doppler and backscatter ion temperature 21 p3818 A70-41103

High resistance thermistor measurements of rapid blood temperature variation, discussing power dissipation effects 21 p3769 A70-41143

Low temperature Ge diode thermometer with computer circuit transforming voltage to temperature readout 21 p3828 A70-41473

IR radiation thermometry, discussing detector types, industrial applications and specialized instruments 21 p3828 A70-41698

Mean density and temperature measurements in hypersonic Ti spheres wakes in nitrogen atmosphere, using electron beam fluorescence probes 21 p3745 A70-41754

Sea surface temperature determination from satellite high resolution IR window radiation measurements by statistical histogram inference method 21 p3820 A70-42122

Temperature distribution measurement inside solid samples by Mossbauer effect, considering application to turbine blades 21 p3830 A70-42165

Carbon dioxide-nitrogen He discharge gas temperature measurements involving plasma refractivity determination by interferometer 22 p4049 A70-42366

Wind temperature measurement, taking Bernoulli effect and kinetic theory into account 22 p4009 A70-42525

Circadian rhythm in human body temperature by Cosinor method, showing inapplicability for narrow time span 22 p3977 A70-42872

Mean skin temperatures of human body by 10 point method, using cold and hot exposure data 22 p3978 A70-42874

Shock wave propagation studies by grating spectrograph with high speed camera, computing equilibrium detonation gases temperature from emitted light [SMPTE PREPRINT 98] 22 p4035 A70-43057

Carbon dioxide laser vibrational temperature measurement, determining ground state vibration level populations in various molecular gases 22 p4051 A70-43391

Ionospheric ion temperature measurements by retarding potential analyzer onOGO-6 satellite 23 p4185 A70-43840

Hypersonic projectile turbulent wake measurements, discussing velocity, mass density and temperature determination [ICAS PAPER 70-07] 23 p4132 A70-44130

Thermal conductivity coefficient calculation by multiple temperature measurements of plate-shaped sample, using iteration process 23 p4276 A70-44166

Carbon dioxide amplification coefficient measurement for lines in laser transition range, determining rotational temperature and upspin levels populations 23 p4201 A70-44204

Semiconductor thermometer for skin temperature differences using resistance bridge, transistor amplifier and thermistors 23 p4150 A70-44317

Digital recording system for body temperature telemetry from small animals, using FM transmitter implanted in peritoneal cavities 23 p4151 A70-44381

- Temperature measurement on thin steel shield subjected to hydrogen peroxide motor exhaust heating at cryogenic temperatures in space 23 p4280 A70-44389
- UBVr colors of A0-K0 main sequence stars, deriving B-V relation to effective temperature 23 p4246 A70-44757
- Rare earth metals-ruthenium Laves phases solid solutions superconducting transition temperature measurement 23 p4231 A70-44885
- Ruby laser in repetitive pulse operation, determining temperature, heat generation and transfer coefficient from spectrum shift measurement 23 p4203 A70-45071
- Effective temperature of star zeta Puppis from combined angular diameter measurement and model atmospheres, comparing hot stars 24 p4404 A70-45414
- Solar X-ray flare temperature and emission measure profiles using OGO 5 satellite detector, interpreting energy dispersion of peak times 24 p4397 A70-45768
- Translational temperature measurement of atoms and ions in plasma based on wavelength reduction by X ray spectroscopy 24 p4388 A70-46208
- TEMPERATURE MEASURING INSTRUMENTS**
- NT BATHYTHERMOGRAPHS
- NT PNEUMATIC PROBES
- NT PYROMETERS
- NT RADIATION PYROMETERS
- NT RESISTANCE THERMOMETERS
- NT TEMPERATURE PROBES
- NT THERMOMETERS
- Temperature measuring devices design for ultrahigh/ultralow temperatures, examining heat effects on gases, liquids and solids 02 p0295 A70-11864
- Low temperature high sensitivity temperature compensated heat flux transducers to measure conductive, convective and radiative heat transfer 02 p0303 A70-12740
- Thermal balance of radiosonde thermometric elements and radiation errors in atmospheric temperature measurements using spectra of radiation fluxes reflected from cloud cover 03 p0557 A70-13297
- Thin film heat gauge for measuring thermal transport from plasma to end wall of shock tube, discussing measurements in high temperature Ar 03 p0496 A70-14381
- Nonlinear dielectric element /tandel/ for detecting IR radiation in contactless temperature measurement 05 p0848 A70-16363
- Monitor for linearizing nonlinear characteristics of thermistors used for temperature sensors in Apollo Telescope Mount, optimizing circuit values with FORTRAN IV computer program 05 p0851 A70-16692
- Automatic temperature stabilizer with high order amplification due to direct heater sensing, noting applicability for synthetic fiber plants and thermophysical laboratories 06 p1064 A70-17783
- Analog computing spectral photometer for high temperature measurements in gas flames 07 p1285 A70-19896
- Boltzmann temperature measurement apparatus of oxide coated cathodes in scanning beam tubes 09 p1656 A70-22987
- Photo-optical instrumentation for temperature estimates of nose cone in simulated reentries, using rocket monorail sleds and artificial rainfalls for rain erosion effects 09 p1688 A70-23778
- Spectroscopic instruments for atmospheric temperature measurements classified in terms of filtering, modulating and multiplexing systems 10 p1873 A70-23828
- Medical thermograph with modified image-pickup device characteristics and additional thermal analysis equipment 10 p1828 A70-25307
- Lower and upper atmospheric IR fluxes and equivalent radiation temperatures measurements, describing two- and four-sphere mean radiation temperature /MRT/ meter 13 p2410 A70-29662
- Surface temperature changes measurement with thermovision camera, discussing calibration and recording 16 p2911 A70-33775
- Thermistors theory, manufacture, stability, drawbacks and applications to temperature sensors 16 p2915 A70-34322
- High temperature transducer for engine vibration measurement, discussing piezoelectric accelerometers mechanical design, jet engines material evaluation, crystallographic considerations, etc 19 p3430 A70-38527
- Thermocouple and IR temperature measurement techniques comparison for double base solid propellants at low pressures 20 p3694 A70-40275
- Installed system calibration thermocouples using temperature plateaus due to pure metals melting and freezing heat of fusion 21 p3823 A70-40857
- Thick film thermocouple gages for roughened model surface heat flux measurements in high Reynolds number shock tunnel 21 p3824 A70-40860
- TEMPERATURE PHOTOMETERS**
- U PHOTOMETERS**
- U TEMPERATURE MEASURING INSTRUMENTS**
- TEMPERATURE PROBES**
- NT PNEUMATIC PROBES
- Czochralski thermal probe for current carrier concentration in strip shaped area of n-type GaAs single crystals active growth 24 p4389 A70-45481
- TEMPERATURE PROFILES**
- Density and heat transfer effects on compressible turbulent boundary layers used to investigate velocity and temperature profiles, skin friction, Mach number and Reynolds number 01 p0003 A70-10936
- Jupiter atmosphere temperature and density profiles determined from thermal models based on thermal structure above dense cloud level 02 p0367 A70-11814
- Numerical solution of physical equations describing temperature changes near ground fog-free air and in radiation fog 03 p0521 A70-13910
- Nimbus 3 satellite carrying IR spectrometer to measure spectral radiances and retrieve atmospheric temperature profiles 04 p0675 A70-14393
- Corrections to observed thermistor temperature profiles presented for spherical bead thermistors with long lead or thin film mounting 04 p0687 A70-14664
- [AAS PAPER 69-568]
- Thermal sounding of atmosphere from satellites under cloudy conditions, plotting temperature profiles 06 p1097 A70-17787
- Wind speed and potential temperature vertical profile in day/night planetary atmospheres estimated by similarity theory of boundary layer parameters 06 p1141 A70-17827
- Model sampling or Monte Carlo applied to normal shock, giving temperature and density profiles for Mach 10 shock 06 p1050 A70-18337
- Quasi-biennial, annual and semiannual zonal wind and temperature harmonic amplitudes and phases in tropical and extratropical latitudes in stratosphere and low mesosphere 07 p1269 A70-19949
- Rocket sounding to obtain thermistor temperature profiles of 30-65 km atmospheric region, discussing error correction equation 07 p1288 A70-20261
- Thermal structure transition of mesosphere at high altitudes from persistent summertime to dynamic wintertime case 08 p1539 A70-21649
- Crystal growth of 2H silicon carbide showing temperature profile along susceptor as affecting factor 09 p1739 A70-22498
- Lebedev nomogram determination of climatic parameters dependability, considering underlying theory and temperature sums 09 p1718 A70-23171
- Temperature profiles in upper symmetric regime of heated rotating water annulus convection obtained by thermocouple probe, noting flow field disturbance and correction 11 p2046 A70-26499
- Temperature profiles and frequency driftings of VHF telemetry transmitters for Saturn S-IC stage, using IR radiation data 12 p2196 A70-27725
- Switching initiation in Ovonic's, discussing temperature profile in semiconducting sandwiches as function of time and thermally forced double tunneling 14 p2626 A70-30333
- Remote atmospheric temperature profile measurements, analyzing physical processes for radiation detection by earth pointing satellite-borne sensor 14 p2611 A70-31156
- Upper atmosphere density and temperature height profiles perturbations in falling sphere probe 15 p2723 A70-31663
- Vertical temperature profiles and global circulation patterns in stratosphere and mesosphere, discussing Northern Hemispheric seasonal, latitudinal and longitudinal variations 15 p2724 A70-31665
- Temperature profiles and wind velocities during convective cloud banks formation from meteorological satellite data 15 p2770 A70-32065
- Thermal atmospheric sounding from satellites based on Fredholm integral equations, obtaining vertical temperature profiles 16 p2896 A70-33257
- Incompressible laminar boundary layer, determining thermal conductivity gradient effect on temperature profiles 17 p3070 A70-35045
- Fluid flow longitudinal temperature profiles for inclusion in heat transfer computer program 17 p3198 A70-35659
- Temperature profile along hot-wire anemometer attached to wall and normal to parabolic velocity steady flow field, using singular perturbation techniques 18 p3242 A70-36488
- Nonstationary compressible laminar boundary layer similar solutions by parameter-invariant method, obtaining velocity and temperature profiles by partial differential equations numerical integration 21 p3806 A70-40555
- Atmospheric temperature profiles from terrestrial IR spectral radiances measured by balloon-borne grating spectrometer, discussing surface temperature variations 21 p3813 A70-40905
- Real time global temperature and geopotential height profiles acquisition from satellite spectrometer measurements by least squares regression method 21 p3820 A70-42121
- Isothermal steady laminar flow through tube with change in wall temperature, examining velocity profile relationship to temperature profile [ASME PAPER 70-HT-C] 22 p4008 A70-42421
- Stratosphere annual temperature cycle amplitude, using biannual daily temperatures over Northern Hemisphere from IQSY data 22 p4018 A70-42913
- Relaxation method for inverse radiative transfer equation solution, determining temperature profiles and atmospheric parameters 23 p4214 A70-44036
- Jupiter model thermal profiles, examining metallic core and molecular envelope in convective equilibrium 23 p4241 A70-44251
- Atmospheric temperature profiles using Nimbus 4 selective chopper radiometer 23 p4192 A70-44865
- Temperature profiles for viscous fluid contained between two concentric rotating porous cylinders 24 p4327 A70-46005
- TEMPERATURE SCALES**
- Temperature scales, definition and measurement, discussing scale differences, temperatures below freezing, conversion methods, etc 09 p1675 A70-22325
- TEMPERATURE SENSORS**
- NT THERMISTORS
- Contact thermographic materials application to non-destructive materials testing based on heat capacity, costs, removal time, equipment, personnel skill and training, etc 01 p0097 A70-10007
- CAT remote sensing for advance aircraft warning, using IR instrument to detect turbulence-associated temperature preceding aircraft 01 p0087 A70-10697
- High temperature thermometer using pulsed excitation ultrasonic resonance with ruthenium sensor, discussing resonator types, transmission lines and transducer 02 p0300 A70-12468
- Low temperature high sensitivity temperature compensated heat flux transducers to measure conductive, convective and radiative heat transfer 02 p0303 A70-12740
- Temperature sensor location for accurate averaging in fluid flowing through heated or cooled circular duct 03 p0486 A70-13557
- Transient and steady state radiation heat flux sensors calibration by developing and evaluating heat flux source 03 p0606 A70-13558
- Cryogenic temperature sensor calibration with automated data readout for spacecraft accuracy requirements, describing potentiometric system 03 p0486 A70-13561
- Response characteristics of asymptotic or Gordon type thin foil heat flux transducer, discussing heat transfer coefficient effect on response time and curve 04 p0694 A70-15548
- Si fluid thermal actuator as temperature sensor and prime mover for active thermal controller in spacecraft 05 p0806 A70-16124
- Unsteady calorimetric sensor for measurement of heat transfer between gas jets and solid targets 06 p1064 A70-17857
- Measurement error associated with heat conduction in temperature sensor, using mathematical model 06 p1070 A70-18443
- Temperature sensors for Apollo Telescope Mount experiments, comparing quartz, Pt wire and Si resistance sensors, thermistors and thermocouples 06 p1073 A70-18598
- Heat transfer measurement in ionized high temperature gas flows with discharge shock tube and thermal sensors 07 p1283 A70-19663

Measurement physics of resistance wire temperature sensing system used in Skua rocket sounding system

07 p1396 A70-20262

Temperature measurement in stratospheric circulation by meteorological rocket-sound wire sensor, presenting error correction technique

07 p1289 A70-20264

IR remote temperature gradient sensor as clear air turbulence detector, presenting inflight test results

12 p2229 A70-26947

Heat removal influence on dynamic errors of cylindrical temperature sensors using electric models

14 p2662 A70-30183

Balloon flight measurements clarifying Arcasonde sensor bias over radiosonde atmospheric temperature data

14 p2585 A70-30570

Miniature wireless strain and temperature radio telemetry transmitters for measurements in areas inaccessible to direct wire connections

15 p2738 A70-32301

Electric temperature sensors accuracy and stability, considering thermocouples, resistance thermometry, radiation and color pyrometry

15 p2743 A70-32798

High temperature and pressure hot gas source for testing fluidic temperature sensor used in gas turbine engine inlet simulation

17 p3058 A70-35157

Atmospheric turbulence effects on light propagation, measuring refractive index variations by high speed temperature sensors

18 p3285 A70-36961

Error sources in carbon black coating on thin foil heat flux sensors accounting for false altitude effects in vacuum calibration

18 p3262 A70-37100

Air total temperature measurement for jet powered aircraft, discussing subsonic and supersonic wind tunnel data for sensor thermal recovery characteristics

19 p3425 A70-37882

Cryogenic temperature sensor with linear characteristics from 150 to minus 452 F, describing calibration and testing

19 p3425 A70-37883

Cutaneous liquid crystal temperature sensors for thermographic patterns of angina pectoris induced by treadmill exercise

19 p3364 A70-38361

High temperature transducer for engine vibration measurement, discussing piezoelectric accelerometers mechanical design, jet engines material evaluation, crystallographic considerations, etc

19 p3430 A70-38527

Heat conduction errors in immersion thermocouples and resistance temperature sensors, using mathematical model

21 p3823 A70-40856

High resistance thermistor measurements of rapid blood temperature variation, discussing power dissipation effects

21 p3769 A70-41143

Microwave radiometry and applications as material composition and temperature sensors for aircraft navigation, landing aids, pollution surveillance, meteorology and oceanology

23 p4198 A70-44648

TEMPERATURE TRANSDUCERS

U TEMPERATURE MEASURING INSTRUMENTS

U TEMPERATURE SENSORS

TEMPERING

Intermetallic precipitates development and mechanical properties of maraging steel as function of composition, tempering time and temperature using electron microscopy

07 p1310 A70-19748

Strain tempering effects on upper and lower bainite, discussing strengthening and fracture toughness as function of temperature

10 p1905 A70-25173

Phenomenological properties of stress relief embrittlement in nickel steel, noting toughness recovery via retempering

11 p2059 A70-25665

Low temperature tempering effects on steel transformations and axial rigidity of radial thrust ball bearings in aircraft

12 p2243 A70-27568

Work hardening and tempering effects on Al-Mg alloy stress corrosion and mechanical properties

14 p2597 A70-30963

Heating rate effect on Ti-V martensite decomposition, discussing elastic properties effects of partial tempering

16 p2931 A70-33256

Orthorhombic martensite tempering behavior in Ti alloys, observing distinct stages for binary and ternary alloys

22 p4054 A70-42742

Heating rate effect on Ti-V martensite decomposition, discussing elastic properties effects of partial tempering

23 p4206 A70-44285

Tempering stress in circular plates and cylinders in casting of solid propellants

24 p4427 A70-46147

TENDONS

Normal human postural control system reflex response to tendon jerk disturbance

22 p3979 A70-43495

TENSILE CREEP

Equipment specifications and design for creep testing at variable load and temperature under uniaxial tension, emphasizing test environment control

13 p2509 A70-28537

Stainless steels creep behavior under long term tensile loads at high temperature

15 p2764 A70-32898

Contact shaped fiberglass-reinforced plastic tensile creep tests, showing strain property linearity dependence on direction

21 p3841 A70-40642

Mg high temperature creep mechanism in high and low stress regions, using isothermal tensile creep tests

23 p4204 A70-43885

TENSILE DEFORMATION

Incompressible elastomer viscoelastic response to exponential extension ratio history in simple tension based on constitutive equations

01 p2021 A70-10893

Ti-Al-Sn alloy tensile deformation mechanisms at cryogenic temperature under uniaxial and biaxial stress noting twinning, prismatic slip and dislocation characteristics

03 p0507 A70-13141

Strain energy release rate in terms of propagating crack surface displacements applied to infinite solid loaded in tension

05 p0938 A70-16480

Stress field equations of material in maximum deformation region during inversion of tubular products

06 p1077 A70-17871

Stress-strain analysis for rod-shaped structural elements under combined tensile and bending loads

08 p1588 A70-21191

Yield stress and work hardening properties of tension-deformed vanadium single crystals as function of purity

08 p1522 A70-21750

Rotatory inertia and shear deformation effects on structural vibrations of Timoshenko beams and frameworks using matrix formulation

09 p1770 A70-22257

Fracture toughness and deformation kinetics dependence on compositional, microstructural and textural variations of alpha and alpha-beta Ti alloys at low temperatures

09 p1704 A70-22801

Tensiodie effect in long plate-shaped semiconductor, noting bend direction effects on I-V characteristics

12 p2195 A70-27312

Shear deformation of sandwich plate cross sections with hinged opposite edges, constructing transfer matrix for state variables

13 p2508 A70-28483

Circular cylindrical membrane axially symmetric deformations, determining axial and circumferential stresses

14 p2657 A70-30844

Stress distribution in spirally corrugated shell under torsional deformation, calculating twisting moment for stiffness

14 p2661 A70-31327

Bifurcation stability in geometrically nonlinear shells of revolution under transverse loads, considering tension and compression deformation

15 p2817 A70-32168

Deformation behavior of continuous W and B fibers reinforced Al alloy matrix composites, monitoring stress-strain characteristics by X ray diffraction

18 p3272 A70-36036

Fine grained Be structure and mechanical properties under tensile deformation at temperatures from 20 to 1000 C

18 p3276 A70-36311

Plane waves superposed on solid during steady state isothermal creep deformation subjected to unidirectional constant initial tensile stress

19 p3537 A70-37791

Fatigue crack closure in flat sheet specimens under zero-to-peak tension cyclic loading, analyzing stress distribution from fractographic striation patterns

19 p3549 A70-38625

Recrystallized and nitrided Mo alloy microstructure under plastic deformation by tension at high temperatures

22 p4038 A70-43122

TENSILE PROPERTIES

Fatigue crack propagation in metals exhibiting initial crystallographic shear mode followed by noncrystallographic tensile mode

01 p0198 A70-10101

Fiber composite cylinder tensile performance improvement through mechanical residual stress relief by axial straining

01 p0120 A70-10737

Fabrication technique effect on tensile and plastic properties of semifinished sintered Al powder products at room temperature and 600 C

06 p1076 A70-17848

Tensile and shear properties of blind fixed, blind floating and through types of bonded sandwich inserts, noting geometry and temperature effects

07 p1401 A70-18934

Tensile properties variations of Co whiskers grown by reducing cobaltous bromide in hydrogen-argon mixture

07 p1306 A70-19071

Tensile properties of yarns at high strain rates and subambient temperatures determined for nylon, Dacron, Nomex, Beta Fiberglass and Karma metal

08 p1527 A70-21330

Temperature, transformation and strain rate effects on tensile ductility properties of stable and metastable compositions of austenitic stainless steels

08 p1524 A70-21956

Cold rolling characteristics of unidirectionally reinforced Al-B fiber composites, measuring hardness and tensile properties

08 p1524 A70-21957

Ti alloys tensile properties correlated with microstructure for multiple heat treatment cycle variations for high strength and adequate ductility

12 p2252 A70-27107

Tensile properties of fibrous materials at high rates of strain and subambient temperatures, considering nylon, Dacron, Nomex, Beta Fiberglass and Karma metal yarns

14 p2598 A70-30928

Omega phase embrittlement in aged Ti-V alloys, discussing precipitation effect on tensile properties

15 p2756 A70-31570

Ti-Al-Cr-Fe tensile, fatigue and creep properties at various temperatures, considering industrial applications

17 p3121 A70-34428

Weldability, tensile and fatigue properties of Ti sheet alloys, discussing TIG welds

17 p3121 A70-34431

Low cycle fatigue and short term tensile behavior correlation for irradiated and unirradiated stainless steels

17 p3123 A70-34627

Nuclear irradiation effect on embrittlement of Ti and Ti alloys at cryogenic temperature, determining radiation damage threshold as function of tensile properties changes

18 p3278 A70-36567

Temperature effect on radiation characteristics and cryogenic tensile properties of irradiated Be, Ti and Al alloys

20 p3647 A70-39111

Al alloys and stainless steels tensile properties and application in lightweight cryogenic propellant tank structures, discussing Ti alloys and reinforced composite materials tests

20 p3651 A70-40123

Polyurethane adhesives differential thermal analysis, rebound resilience and tensile properties at cryogenic temperatures

21 p3844 A70-42141

Resilience and tensile properties of polyurethane adhesive at cryogenic temperatures measured by differential thermal analysis

23 p4209 A70-44275

TENSILE STRENGTH

Zinc and resin coated alkaline glass fibers tensile strength, describing test procedure

01 p0126 A70-10220

Flip chip and beam lead methods for microcircuit assembling, discussing heat removal using heat spreader and temperature cycling effects on tensile strength

01 p0050 A70-10330

Fiber-polymer matrix interfacial tensile and shear strengths evaluation methods, including data correlation from various tests

01 p0087 A70-10478

Tensile strength of flat specimens of Ni reinforced by W wire gauze

02 p0315 A70-11661

Molybdenum cylinders strength and plasticity under various compression and cyclic tensile loads

02 p0315 A70-11662

Al alloys strips weakened by holes, analyzing limiting tensile load-carrying capacity

02 p0384 A70-11741

Bolted and bonded joints design in composite materials loaded in tension, presenting methods for strength prediction, testing and analysis

02 p0306 A70-11952

Polymeric materials properties, discussing tensile stress disadvantage and compensation by reinforcement and polymer chain directional alignment

02 p0321 A70-12305

Axial and traction loaded boron epoxy laminates tensile and compressive elastic properties and strengths compared from test data including strain gauge measurements

03 p0586 A70-13115

Failure mechanisms in notched or damaged fiber reinforced composite materials determined from analysis of axial tensile strength and broken fibers

03 p0515 A70-13124

Prolonged temperature exposures with applied tensile stress found to increase tensile strength and yield point of aluminum alloy subjected to artificial agings

03 p0511 A70-13354

Cr alloys applications in high temperature environments, describing alloying elements effects on strength and ductility

03 p0511 A70-13566

Al and Sn composites reinforced by E glass and silicon dioxide glass fibers compared for tensile strength, noting difference due to resistivity

03 p0514 A70-14314

Brittle composites /including fiber reinforced material/ deformability and plastic deformation effect on tensile strength, discussing pressure induction of sound flow
[ASME PAPER 69-WA/PROD-28]

04 p0705 A70-14834

Prealloyed powders of Ni base alloys, made by inert gas atomization for improved strength and ductility

04 p0706 A70-14951

Silicon effect on stress corrosion resistance of low alloy high strength steels in NaCl solution for different tensile strength ranges

04 p0707 A70-15272

Continuous metal fiber composites tensile strength and ductility in terms of plastic instability

05 p0946 A70-16924

Creep, ductility and short term tensile and compression strength test facility for graphite in 300-3500 K temperature range

05 p0875 A70-17068

Ti alloy tensile strength under cyclic loads at room and high temperatures, noting plastic deformation and damage accumulation effects

06 p1085 A70-17406

Reverse-bend and tension-tension fatigue properties of high strength Cr-Mn-N stainless steel sheet in notched and unnotched conditions

07 p1305 A70-18993

Ni maraging steel sheets tensile strength and elongation anisotropy, studying effects of directional cold work, aging and annealing

07 p1306 A70-19072

Creep rupture and residual tensile strength tests to evaluate long time properties and structural stability of Inconel 718 alloy, performing phase analysis

07 p1310 A70-19731

Tensile and compressive stress cycles effect on short term strength of glass fiber plastic laminates

07 p1411 A70-19769

Tensile strength test and clamping of epoxy impregnated fiber strands

07 p1250 A70-19959

Metal adhesive joints strength under tensile and torsional stresses, considering effects of dimensions, metal type and surface finishing

08 p1504 A70-20886

Metal adhesive joints behavior under prolonged static stresses, showing time dependence of tensile strength

08 p1504 A70-20887

Strength, corrosion resistance and fabricating qualities future improvements in metals and alloys, discussing chemical composition approach, dispersion hardening, superplasticity, etc

08 p1518 A70-21267

Dynamic tensile properties of monolithic and pyrolytic graphite compared with static tensile strength

08 p1527 A70-21334

Cr-Mo steel strength and structural stability during tubular stress-rupture testing with high pressure hydrogen, discussing welding effect on strengths

08 p1519 A70-21455

Matrix stiffened nickel-chromium welding products featuring high tensile strength at room and elevated temperatures and high impact strength at cryogenic temperatures

08 p1508 A70-21488

Waspaloy gamma prime solvus temperature relationships as function of solution treatment and precipitation strengthening additives, discussing microstructure and tensile properties

08 p1520 A70-21555

Fatigue testing and thermal mechanical treatment effects on uni- and biaxial Al alloy-B composites tensile strength at room and elevated temperatures

08 p1523 A70-21893

Tensile, fatigue, creep and stress-rupture behavior of unidirectional, unidirectional off-axis and cross-ply composites of B filaments in Al alloy matrix

08 p1531 A70-21896

Glass fiber reinforced epoxy laminate specimens tests in tension and flexure at various strain rates to determine geometry effect on strength

08 p1532 A70-21898

Fiber composites-Ti alloy adhesive, rivet and combined joints for aircraft applications, noting fiber orientation role in joint tensile strength

08 p1509 A70-21905

Filament tensile strengths and pressure strain characteristics of high modulus boron filament wound/resin composite pressure vessels for cryogenic applications

08 p1509 A70-21909

Composite material tensile strength, discussing statistical scatter in fiber strength and local fiber overstress caused by fiber discontinuities

08 p1532 A70-21914

Strengthening mechanisms in dispersion hardened Nichrome /TDNiC/ analyzed in 70-2000 F range, discussing solid solution, dislocation substructure and grain refinement

08 p1525 A70-21961

Al-B composites mechanical properties, using heat treatments and transverse steel wires to increase matrix shear and transverse tensile strengths

09 p1701 A70-22551

Tungsten fiber reinforced aluminum composites tensile strength aspect ratio using foil metallurgy technique

09 p1703 A70-22627

Microstructure and ductility of air- and vacuum-melted heats of corrosion resistant steels, investigating tensile and yield strengths for all grain directions

10 p1905 A70-25170

Binary Ni-Cr alloys tensile mechanical properties at 25 C after water quenching and heat treatments

10 p1905 A70-25172

Tensile strength of nitrided boron-aluminum alloy composite modules, noting effect of Ti cladding on panel surfaces

11 p2066 A70-26085

Stress-strain state effects on Cu and Ni tubular samples plasticity and strength using polarization-optical technique

12 p2323 A70-27341

Short time tensile properties of thermomechanically treated astrolloy showing improvement due to refined gamma precipitate and grain boundary carbides

12 p2256 A70-27610

Iron sample shape determination for studying relationship between tensile strength and rate from stress wave propagation during high speed tensile tests

15 p2814 A70-31547

Eutectic NiAl-Cr structure and high temperature tensile strength as function of solidification rate

15 p2755 A70-31560

Cycloaliphatic epoxy resins tensile and impact strength improvement by modification with elastomeric materials, considering heat distortion temperature

16 p2936 A70-33359

Shear and tensile joint strength measurements at fiber-polymer matrix interface, using pull-out test and debonding methods

16 p2937 A70-33372

Ti alloys beta forging effect on physical properties and tensile ductility

17 p3097 A70-34358

Cr-Ni stainless steels room temperature yield and tensile strengths improvement by nitrogen addition

17 p3122 A70-34553

Longitudinal and transverse tensile strengths of Al sheet reinforced with continuous oriented steel wire of various cross sectional shapes

19 p3541 A70-38047

Tensile strength of flat specimens of Ni reinforced by W wire gauze

19 p3452 A70-38435

Molybdenum cylinders strength and plasticity under various compression and cyclic tensile loads

19 p3453 A70-38436

Ti-Nb-Zr alloys strength and plasticity at various temperatures, noting compositional effects on tensile and yield strength

19 p3453 A70-38712

High modulus graphite fiber tensile strength and structure, using X ray diffraction

20 p3653 A70-39205

Composite material engineering problems, discussing tensile, compressive and shear strengths, design approaches, unidirectional properties and substance characterizations

20 p3651 A70-40027

Uniaxial fiber composites tensile strength models, including failure analysis

20 p3731 A70-40046

Butt joined epoxy Al plates tensile strength, observing fracture strength dependence on stress concentration at bond edges below characteristic crack length

21 p3939 A70-42032

Stress-strain diagrams for oriented fiberglass-reinforced plastic under tension taking into account temperature and anisotropy effects

23 p4209 A70-43938

Aluminum, duraluminum and stainless steel tensile strength tests at cryogenic temperatures

23 p4206 A70-44353

Unidirectionally solidified carbide reinforced Co-Cr eutectic alloy, examining tensile strength and creep behavior

24 p4358 A70-45236

Composite materials tensile strength dependence on reinforced fibers with dispersed tensile strength, using model to predict crack propagation from fiber rupture

24 p4427 A70-46270

Refractory metal alloys tensile and creep rupture properties for reactor fuel jackets

24 p4364 A70-46347

TENSILE STRESS

Stressed state of circular notched plane in tension under creep conditions

01 p0210 A70-11410

Temperature effects on tensile deformation mechanism of Mo single crystals, investigating stress-strain characteristics and slip geometry

02 p0316 A70-11699

Bolted and bonded joints design in composite materials loaded in tension, presenting methods for strength prediction, testing and analysis

02 p0306 A70-11952

Load and strain trajectory vectors components determined for tension followed by transverse compression in five dimensional space

02 p0390 A70-12803

Complex stress functions and stress intensity factors at tips of star-shaped contour hole in infinite tensile sheet, including crack forking with arbitrary angle

03 p0585 A70-12974

Model gas turbine engine blades fatigue strength under stress conditions, considering tensile stresses reproducibility from centrifugal loads

03 p0587 A70-13241

Prolonged temperature exposures with applied tensile stress found to increase tensile strength and yield point of aluminum alloy subjected to artificial agings

03 p0511 A70-13354

Equivalent rigidity of doubly periodic symmetrically perforated infinite plate strengthened by elastic ring under isotropic tension

03 p0595 A70-13754

Polyethylene and polypropylene mechanical behavior under tensile and compressive loads and subject to hydrostatic pressure, obtaining tensile nominal stress-strain curves for various pressures

03 p0517 A70-14201

Tension field theory describing buckling of membranes or thin plates with boundaries subjected to excessive planar displacements

03 p0599 A70-14246

Metals and alloys creep under tension and compression at elevated temperatures, considering plastic deformation equation applicability

04 p0707 A70-15265

Plane circular crack in homogeneous and isotropic elastic body under uniform uniaxial tension using linearized couple-stress theory

05 p0931 A70-16089

Crack stability under tension and thermal stresses caused by uniform disturbed heat flow, using Barenblatt fracture criterion

05 p0939 A70-16483

Three dimensional brittle body limiting axisymmetric stability under tensile stresses and weakened by ring shaped cracks, determining critical tensile loads

05 p0945 A70-16855

Stress-strain state of plates weakened by reinforced hole and under tensile and bending loads, including boundary conditions

05 p0945 A70-16856

Stress-strain state of drawn and bent circular plate made of rigid viscoplastic work hardened material

05 p0946 A70-16958

Fatigue defects accumulation in aluminum alloy under impact tensile loads programmed to simulate loads encountered by aircraft in practice

05 p0947 A70-17009

Nickel-based alloys small cycle thermal and mechanical fatigue limit during tensile stresses and operational temperatures, analyzing fatigue curves

05 p0867 A70-17046

Gas turbine blades thermal fatigue strength under simultaneous temperature cycles and static tensile loads, analyzing temperature and stress fields

05 p0953 A70-17053

Rotor blades structural fatigue strength tested on gas dynamic test stand under cyclic thermal loading and static tensile load

05 p0954 A70-17058

Turbine blades root joints endurance limit concerning tensile stress determination at stress raiser contour for elastoplastic deformation and creep

05 p0954 A70-17062

Thermal fatigue cracks in gas turbine blade models under simultaneous thermal cycling and static tensile loads simulating pulsed regimes

06 p1166 A70-17652

Steels fatigue strength under biaxial tension, considering complex stress-strain state

07 p1304 A70-18823

Fatigue strength of sintered aluminum powder at room and elevated temperatures, discussing sensitivity to tensile loads misalignment

07 p1304 A70-18840

Plastic deformation of thin flexible axisymmetric shells under load, discussing tensile stresses

07 p1407 A70-19383

Stressed state of plate with reinforced circular hole under tension and bending using Airy stress functions

07 p1407 A70-19540

Critical stress-strain diagrams for brittle plate possessing notch-type stress raisers under biaxial tension
07 p1408 A70-19547

Corrosion cracking mechanism for notched metal surface in aqueous environment under tensile stress, discussing electron distribution and H ion concentration
07 p1310 A70-19737

Limiting equilibrium of shells of revolution with different yield points under tension and compression
08 p1583 A70-20527

Dugdale crack model extended to include effects of linearly varying tensile loading, noting plastic zone length sensitivity
08 p1593 A70-21512

Elastoplastic stressed state of variable thickness disk under combined effects of nonuniform heating, repeated centrifugal and surface tensile loads
09 p1778 A70-23091

Axial tensile stress effects on stability of cylindrical shell under nonuniform external pressure
09 p1786 A70-23721

Stress distribution in strip with asymmetrically positioned infinite row of equal and equally spaced circular holes subjected to longitudinal tension or transverse bending
10 p1955 A70-24082

Static tensile stresses effect on magnetized ferromagnetic materials damping properties explained by anisotropic microplastic strains dissipating energy during bending vibration
10 p1904 A70-24246

Power-law stress-strain relation in plastic complex stressed state, showing identical strain hardening curves for shear and tension
10 p1957 A70-24280

Nylon 6 polyamide tensile stress cracking by metal thiocyanates in aqueous and nonaqueous solutions, comparing results with cracking by metal halides
10 p1907 A70-24300

Equivalent rigidity of doubly periodic symmetrically perforated infinite plate strengthened by elastic ring under isotropic tension
10 p1960 A70-25009

Energy methods applied to fatigue crack propagation rate under tensile mean stress
10 p1963 A70-25090

Materials bending fatigue strength calculations for biaxial tension compared with experiments showing agreement
10 p1964 A70-25289

Limiting load for annular plates made of material having different yield points in tension and compression
11 p2129 A70-25560

Plane tension in elastic infinite strip covered by elastic plate, considering applicability to strain measurement errors calculation
11 p2129 A70-25565

Rectangular conical shells reinforced along ribs by belts under tension/compression calculated by initial functions method
11 p2130 A70-25568

Air and salt water tensile and shear mode cracking of titanium alloy sheets examined with electron fractographs
11 p2067 A70-26099

Stress relaxation in combined torsion-tension, developing expressions for torque and axial force
11 p2140 A70-26482

Rectangular beam creep rupture time under bending moment and axial tensile force, using power series to solve integral equations
11 p2142 A70-26635

Tensile strain rate and oxygen concentration effects on peaks of niobium hardening zones involving interstitial atoms
12 p2252 A70-27001

Viscoelastic polymeric materials tensile failure under multiaxial loading
12 p2321 A70-27205

Tension rays and load transfer from compact member via wrinkled membrane determined by variational technique using maximum strain energy
12 p2322 A70-27225

Stress measurements for eye beams forming of high fatigue strength based on brittle lacquer studies of isotropic material models
13 p2507 A70-28482

Stress concentration factors determined for u-shaped and semielliptical edge notches in semiinfinite sheet under uniaxial tension parallel to edge
13 p2509 A70-28535

Stresses in plate containing circular hole with notch under uniaxial tension, determining parametric coefficients by Fourier transforms
14 p2661 A70-31326

Self excited systems limiting states with traveling wave, analyzing oscillator moving along string under tension
16 p2990 A70-33781

Hysteresis loop behavior under tension-compression cycle fatigue related to Meyer strain hardness values of cyclically strained metals
16 p2934 A70-34334

Bond stress distribution in elastic solid with axisymmetrical inclusions under uniform tension, using three function and point matching techniques
17 p3184 A70-34911

Orowan stress calculation, discussing line tension, screw or edge character, spatial distribution and yield strength
17 p3191 A70-35457

Elastic layer with circular cylindrical cavity under axial tension /Kirsch problem/, determining stress concentration from boundary value problem
18 p3335 A70-36130

Critical loads for notched square Al alloy rods under tension
18 p3343 A70-36718

Shallow circular cylindrical shell with rigid collar on lateral surface, calculating stress under axial tension and internal pressure loading
19 p3534 A70-37245

Fatigue strength in pulsed tension of butt-welded tubular joints, evaluating test results statistically
19 p3433 A70-37357

Mathematical representation of heart muscle mechanical properties, examining tensile stress in parallel and series elements
19 p3368 A70-37809

Model gas turbine engine blades fatigue strength under stress conditions, considering tensile stresses reproducibility from centrifugal loads
19 p3548 A70-38459

Blade root design for axial flow compressors and turbines, avoiding tensile stress concentration
19 p3490 A70-38616

Disk equations to determine tensions around arbitrary hole or stiffening contours
20 p3720 A70-39623

Elastoplastic equilibrium of thin infinite plate with periodic slit system along straight line under tension, investigating localized plastic deformation domains
20 p3721 A70-39769

Stress-strain zero moment state of thin walled helical shell under uniformly distributed tensile loads
20 p3721 A70-39778

Weighing systems electronic load cells calibration for tension and compression loading, attributing non-repeatability to bending moments [SAWE PAPER 816]
20 p3634 A70-40356

Elastic and viscoelastic plates, calculating stress concentration and separation of embedded smooth circular inclusion under uniaxial tension
21 p3932 A70-40548

Perforated infinite plate finite elastic deformation under biaxial tension, using successive approximation in connection with complex variable method of plane elasticity
21 p3932 A70-40551

Carbon steel thin walled cylinders creep fracture subjected to combined tension and internal pressure by large strain theory
21 p3840 A70-41438

Slip, fracture and rupture in sintered and cast ductile and brittle polycrystalline Mo under tension, using optical and electron microscopy
23 p4204 A70-43884

German monograph on notched structural steels fatigue properties and crack propagation under tensile-compressive alternating loads
24 p4356 A70-45086

German monograph on deformations and tensile stresses calculation in axisymmetric bodies via finite element method involving matrix displacement method
24 p4420 A70-45225

TENSILE TESTERS

U TENSILE TESTS

TENSILE TESTS

Automatic loading control system for tensile test machine permitting creep and creep-rupture testing
01 p0054 A70-10075

Tensile tests of heat treated silicon carbide coated B filament reinforced metals, discussing fiber strength and interfacial stability
01 p0117 A70-10483

Transmission electron microscope study of deformation mode during rapid tensile testing of Ni-base superalloy, discussing twinning and stacking fault modes
01 p0118 A70-10705

Transformation induced plasticity steels tensile properties measurement indicating loss of ductility due to H embrittlement
01 p0118 A70-10729

Offset yield strengths of TD-Ni and Al-aluminum oxide SAP type two phase alloys in tension and compression
01 p0119 A70-10736

Ferritic stainless steel embrittlement caused by He injected into tensile samples by alpha particle cyclotron irradiation tested at elevated temperatures
01 p0122 A70-11235

Tensile tests of polycrystalline Nb-Hf alloys at low temperatures, noting cooling rate effect on ductility in terms of microstructure
01 p0122 A70-11240

Polycrystalline material tensile failure at high temperature, discussing intergranular cracking, shearing, etc
03 p0508 A70-13155

Tensile tests facility design for wide temperature ranges with loading system to maintain constant strain rate up to failure
05 p0830 A70-17072

Tensile and stress rupture tests facility for microsamples stability at temperatures up to 3300 K, investigating deformation and failure
05 p0830 A70-17073

Microstructure effects on smooth and notched fatigue and room temperature tensile properties of Ti-Al-V alloy using heat treatment combinations
06 p1087 A70-17458

Hydrogen effects on ELI Ti-Al-Sn alloy, conducting tensile, fretting and abrasion tests on stressed and thermal cycled specimens
07 p1309 A70-19710

C-axis single crystalline sapphire filament tensile and fracture tests
08 p1514 A70-20647

Analytic solution for computerized vibration analysis of high speed tension test
08 p1590 A70-21332

Test specimen shapes for determining tensile, compressive and edge-wise shear properties of reinforced plastic laminates
08 p1529 A70-21878

Tension, compression and in-plane shear tests to obtain boron epoxy composite materials mechanical properties to design FB-111 wing box extension
08 p1529 A70-21879

Test methods for evaluating tensile, compressive, interlaminar shear and bearing strength properties of carbon yarns and flat and tubular composites
08 p1529 A70-21881

Specimen design of laminated angle-ply composite materials for straight-sided axial coupon and long beam flexure tension testing
08 p1530 A70-21885

Test standards for boron epoxy flat laminates, proposing specimen geometries and testing methods
08 p1530 A70-21887

Metals yield locus in strain hardening range in sigma-tau plane determined using slip theory, considering Bauschinger effects
09 p1771 A70-22395

Solid propellants mechanical properties under uniaxial tension
09 p1741 A70-22423

Polybutadiene-ammonium perchlorate solid propellant microscopic failure analysis under uniaxial tension
09 p1741 A70-22424

Polybutadiene-ammonium perchlorate solid propellant BPT-1 mechanical properties viscoelastic analysis under constant strain rate tension
09 p1742 A70-22425

Metals and plastics tensile strain rate sensitivity tested by drop weight tests, obtaining dynamic and static stress-strain curves
09 p1704 A70-22725

Elongation measurement in tensile testing of thin films and sheeting, coupling with gripping test program
10 p1887 A70-24042

Thickness effects on elongation of sheet type Al alloys, tabulating tensile test results
10 p1887 A70-24043

Stability conditions in metal specimens tension tests, considering fcc and bcc metals strain hardening, rate and gradients and temperature dependence
10 p1966 A70-25326

Glass epoxy cross ply laminates with brittle or ductile epoxy matrices tensile tested, comparing mechanical performance
11 p2068 A70-25686

Hot shortness of molybdenum alloys under tensile testing due to molybdenum carbide precipitation on grain boundaries
11 p2066 A70-25914

Hot torsion test for Al alloys workability assessment, noting test temperature and specimen geometry effects on fracture strain values
13 p2436 A70-29816

Polycrystalline Al microstrain distribution nonuniformity under creep and static tension
14 p2595 A70-30173

Optimum diffusion welding temperature for Ti-6Al-4V alloy determined from tensile and creep tests
14 p2591 A70-30934

Iron sample shape determination for studying relationship between tensile strength and rate from stress wave propagation during high speed tensile tests
15 p2814 A70-31547

Torsional vibrations amplitude effect on polycrystalline Al stress-strain curve during uniaxial tensile test
15 p2758 A70-32125

Alternating stress required for edge crack propagation in metal plates under tensile loading cycles
15 p2762 A70-32464

Materials testing machine for tension, compression and flexure at constant strain rate and for fatigue
16 p2900 A70-33067

Constant grain size cast Mo ductile-brittle transition temperature dependence on annealing temperature using tensile test
16 p2933 A70-34274

Structural stability in tension and strength tests of thin walled tubes at various stress and strain intensities, noting dependence on stress-strain state type
17 p3192 A70-35713

Tensile test device for continuous recording of sample load and strain
20 p3728 A70-40000

Duralumin constant speed tensile strength tests at 200 C, discussing creep thresholds statistical distribution in elongations interval
21 p3840 A70-41432

Longitudinal tension impact tests on nylon tape and Apollo pilot parachute riser construction, determining wave propagation effects
[AIAA PAPER 70-1182] 21 p3843 A70-41831

Solid rocket fuels mechanical properties, using high speed pneumatic test machine and impact tensile tester
22 p4088 A70-42342

Strain rate change effect on stress-strain diagram shape of polycrystalline alpha-Ti during tensile tests over temperature range
22 p4054 A70-42737

Ti alloy tension creep tests at room temperature, determining strength for correlation with stress relaxation
22 p4055 A70-43097

Metallurgical interaction phenomena in welding zone of heat treated Inconel 600, using hot ductility testing and metallographic methods
22 p4046 A70-43150

Mo single crystals tensile properties at different orientations, noting asymmetric slip in plastic behavior
22 p4056 A70-43155

Tension-torsion machine developed from aircraft carrier catapult principle, producing radial loading paths
22 p4117 A70-43453

Composites made by unidirectional solidification of eutectics with transition metal carbide fibers embedded in metal matrix, discussing tensile tests
[ONERA-TP-853] 22 p4057 A70-43457

Metal and alloy sheets, investigating deformation and failure under biaxial stretching tensile tests
24 p4358 A70-45240

Steel and duralumin strips with circular holes tested under axial tension, determining relationship between strength weakening and ultimate stress
24 p4420 A70-45272

Strain rate sensitive materials tensile tests using machine with external variable speed motor
24 p4422 A70-45517

TENSION
Spinal cord overstretching and circumscribed pathological tension mechanism, considering histological and radiological findings
07 p1204 A70-19242

TENSION TESTERS
U TENSILE TESTS
TENSOMETERS
Vinoflex glue for constant strain gauges in low temperature tensiometry, showing satisfactory recording at single and multiple loadings
08 p1495 A70-20984

Foil type resistance strain gages /tensometers/, studying measurement current effects on readings
11 p2053 A70-26428

Semiconductor strain gages /tensometers/ materials, fabrication and properties
11 p2054 A70-26429

Hermetically sealed miniature strain gages /tensometers/ design and testing, noting insensitivity to effects of fuels and oils
11 p2054 A70-26430

Resistance strain gages /tensometers/ for force and moment measurement in aerodynamic research, giving design and structural recommendations
11 p2054 A70-26431

Lead resistance effects on resistance strain gage measurements as function of utilized measurement system and procedure
11 p2054 A70-26432

Multichannel tensometric AC bridge network for static and dynamic measurements of mechanical quantities in structural elements
11 p2054 A70-26436

Thermocompensated wire loop microtensensors for machine part stress concentration measurements, including parameter selection nomograms
13 p2409 A70-29519

Low temperature tensiometry application to stress-strain state of turbine disks
15 p2733 A70-31537

SENSOR ANALYSIS

Turbulent fluid flow analysis described by Navier-Stokes equations, introducing asymmetric tensors for anisotropic cases
01 p0068 A70-11605

Riemann tensor symbolic computation by compact method using differential forms, discussing advantages due to antisymmetry
05 p0818 A70-16681

Lorentz principle application to general relativity freeing formalism from inconsistencies to derive expressions for Christoffel symbols and Riemann-Christoffel tensor
06 p1105 A70-17537

Plasma dielectric tensor derived quantum mechanically, emphasizing similarity in classical and quantum mechanical methods, discussing linear wave propagation, kinetic equations, etc
06 p1121 A70-17904

Strain rate tensor coincidence in Lagrangian and Eulerian descriptions of turbulence demonstrated for homogeneous flow of incompressible fluid
07 p1252 A70-18672

Group theory investigation of three photon light scattering tensor for all vibration modes of specific crystal classes
07 p1299 A70-19861

Lagrangian tensor formalism for hydrodynamic stretching of material line and surface elements under statistically isotropic incompressible turbulence
07 p1260 A70-19979

Tensor analysis of four photon interaction in rarefied plasma in magnetic field, determining cubic current of plasma wave self action
08 p1554 A70-21805

Piezo-rotatory coefficients R/11/ and R/12/ of isotropic non-enantiomorphic optically active crystals from fourth rank axial tensor, discussing stress effects
11 p2098 A70-26298

Book on tensor calculus in materials science covering the thermodynamic equilibrium, gaseous and solid phase heat engines, solids crystalline structure, etc
12 p2282 A70-26866

Nonviscous relativistic fluid energy momentum tensor modification to rule out sound wave propagation velocities above speed of light
13 p2454 A70-29900

Scalar-tensor theory in canonical form, discussing neutral particle and electron self energy problem
15 p2773 A70-31439

Strain rate tensor coincidence in Lagrangian and Eulerian descriptions of turbulence demonstrated for homogeneous flow of incompressible fluid
15 p2718 A70-31464

Neumann and Maxwell photoelasticity laws reformulation with aid of characteristic tensor of mechanical state
17 p3187 A70-35044

Vector and tensor calculus features, examining contravariance and covariance with bra and ket algebra and absolute differential
18 p3281 A70-36354

German book on continuum theory of flowing media covering tensor analysis, equations for kinematics, mechanics, thermodynamics and electrodynamics
18 p3243 A70-37226

Acceleration wave propagation in materially uniform inhomogeneous isotropic elastic bodies, using tensor analysis
19 p3536 A70-37563

Polynomial tensor functions generated by vector functions in space of invariants, noting applicability to isotropic media
20 p3728 A70-39895

Interactions between components of turbulent flow velocity correlation tensor due to pressure fluctuations
21 p3810 A70-41956

Nonlinear elasticity theory, deriving geometrical relations applicable to small deformation tensor components
23 p4267 A70-44167

Static spherically symmetric charged mass distribution exact solutions derived for electrons in scalar tensor theory of gravity by Hamilton-Jacobi method
23 p4222 A70-44403

Transport equation relation between irreducible tensorial sets, examining geometrical symmetry influence and thermomagnetic and galvanomagnetic effects
24 p4428 A70-45520

SENSOR FIELDS
U TENSORS
TENSORS
NT STRESS TENSORS
Conformally plane solutions to Einstein equations derived with energy momentum tensor characteristics of pulverized material representing gravitational fields
01 p0193 A70-11629

Permittivity tensor calculations of weakly inhomogeneous plasma with monoenergetic component, using distribution function of particles produced by thermonuclear reactions
03 p0529 A70-13055

Relativistic tensor theories of gravitation in flat space with Neumann and Newton forms of gravitational potential, deriving expressions to estimate differences perceived by observer
03 p0526 A70-14305

Dipole shielding tensor of atom in arbitrary time dependent field, giving conditions for general variational calculations yielding results
04 p0721 A70-14389

HF conductivity tensor of isotropic plasma, taking into account particle correlations describing weakly Langmuir turbulent plasma
05 p0889 A70-16532

Momentum-energy tensor and angular momentum for hydrodynamic and electrodynamic fields determined in transformations of m-parametric Lie group
10 p1922 A70-24098

Tensor and torsion functors on Abelian semigroups
13 p2440 A70-29076

Four dimensional Einstein space metric of signature 2 with N type Weyl tensor and nonintegrable rays
13 p2453 A70-29636

Chromium lattice vibrational properties based on fourth-nearest-neighbor tensor force model, obtaining agreement with inelastic neutron diffraction data and elastic constants
14 p2626 A70-30480

Elementary particles gravitational interactions, identifying tensor field with local gravitation
15 p2776 A70-31732

Book on continuum mechanics covering tensor kinematics, energy balance, virtual work, constitutive equations, etc
16 p2987 A70-32914

Symmetric functions of second rank tensors with syngonies in elastic anisotropic media
18 p3340 A70-36576

Energy and impulse tensor of nonviscous relativistic fluid, excluding sound velocity greater than light velocity
19 p3404 A70-37593

Permittivity tensor of weakly turbulent magnetoactive cold electron plasma, calculating nonlinear currents
20 p3677 A70-39296

Continuous media theory, deriving first order constitutive differential equations for isotropic tensor functions
24 p4378 A70-45270

Isotropic transformation of tensor space, proving theorem for reducing hemiptic function to N invariants of rotations and single vector
24 p4378 A70-45271

TERBIUM
Absorption spectra of single crystals TbAlG and DyAlG garnets, investigating Verdet constant dependence on ion concentration
07 p1355 A70-18705

TERMINAL BALLISTICS
Electroexplosive devices output energy measurement through metal deformation by lead block and projectile penetration methods
03 p0548 A70-14121

Penetration depth calculation of high speed non-deformable sphere into massive body, approximating force on sphere by ideal incompressible fluid cavitating flow
04 p0776 A70-15269

Single impact data considered ineffective in estimating target damage induced by micron-sized particle cloud impingement
04 p0737 A70-15425

Thin sheet and laminate bullet hole deformation zone microstructure observation by electron microscopy, considering terminal ballistics approach
07 p1413 A70-20049

Tungusk meteorite atmospheric shock waves obtained from simulation experiments based on forest damage
08 p1572 A70-20944

Meteorites explosive fragmentation under aerodynamic loads simulated by steel balls shot into increasing-density target, discussing parameters
08 p1572 A70-20947

Projectile penetration of Al alloys, noting melting during intense shear band formation
08 p1522 A70-21710

Energy spectra of electrons transmitted through Be, Al and Au targets measured for incident electron energy
10 p1918 A70-23984

Hypervelocity impact dynamics on copper cube targets imbedded with nickel wires, discussing terminal positions, Vickers hardness, flow fields, etc
[AIAA PAPER 69-368] 14 p2657 A70-30765

Tungusk meteorite atmospheric shock waves obtained from simulation experiments based on forest damage
15 p2806 A70-32756

Meteorites explosive fragmentation under aerodynamic loads simulated by steel balls shot into increasing-density target, discussing parameters
15 p2806 A70-32759

Forces acting at thrust termination time with aluminum solid propellant rocket fuel, predicting thrust reversal ratio under vacuum conditions

21 p3869 A70-41869

Mathematical model for projectile penetration into metallic targets, calculating velocity after perforation

21 p3939 A70-41968

TERMINAL FACILITIES

Airport terminal configurations payload flow-through characteristics and space allocations, discussing passenger processing, baggage systems, etc [AIAA PAPER 69-1088]

01 p0000 A70-10622

ATC terminal displays procurement and use, discussing effects of traffic growth and FAA automation program

01 p0139 A70-11285

Secondary surveillance radar and interferometry techniques to determine aircraft positions in real time and all weathers for air terminal approach control

02 p0331 A70-11965

Three dimensional radar system for automatic tracking all aircraft in terminal area to increase air traffic control system safety and capacity

02 p0332 A70-11967

Ground support and service features present facilities to handle B-747 and DC-10 aircraft

[SAE PAPER 690560] 03 p0463 A70-13264
Encounter statistics and operational environment of aircraft collision-hazard warning systems in terminal area

07 p1331 A70-20060

Air transport facilities planning in Canada, describing systems planning approach and major influencing factors

08 p1481 A70-20621

ATC and SST operations in terminal area simulation study involving airline crews and controllers in real time traffic situation

09 p1721 A70-22946

AIRLORD system consisting of central data processing and I/O units for predeparture handling of passengers and freight at airports

11 p2013 A70-25365

Ground ATC facilities, discussing landing, automation, surveillance, communication and navigation

11 p2079 A70-25723

Airspace and airport use at terminals, discussing segregation of aircraft by performance categories [SAE PAPER 700229]

11 p2153 A70-25899

Remote area terminal system providing navigation and guidance signals for aircraft landing

11 p2081 A70-26509

Air terminal design, describing mechanical systems for moving people, baggage and cargo

[SAE PAPER 700259] 12 p2206 A70-27431

Performance standards for intra-airport batch type people-moving systems, discussing seating requirements, platforms and stations, communications and power systems, etc

[SAE PAPER 700260] 12 p2206 A70-27432

Terminal automation system (ARTS) digital computerized beacon tracking for future ATC facilities, noting add-on packages to increase system reliability

[SAE PAPER 700282] 12 p2206 A70-27441

Urban airport runway capacity increase via reduced aircraft separation, additional parallels and improved terminal traffic control, discussing design for acceptable safety levels

12 p2207 A70-27627

Midair collisions between controlled and uncontrolled traffic in terminal areas associated with aircraft operations and airport density

12 p2267 A70-27632

Air terminal and ground transfer design to provide improved access to aircraft and total transportation time reduction

12 p2208 A70-27992

Boeing 747 ground operations and airport services, discussing computerized check-in, baggage handling equipment, etc

[AIAA PAPER 70-892] 17 p3019 A70-35808

Automated baggage handling and processing, requiring total aviation community participation

[AIAA PAPER 70-917] 17 p3204 A70-35829

Mobile lounges and airport productivity concepts for optimal handling of passengers at airport terminal

[AIAA PAPER 70-918] 17 p3064 A70-35830

Large capacity transports influence on air cargo operations, and joint use cargo terminal planning

[AIAA PAPER 70-920] 17 p3204 A70-35832

Terminal airspace utilization from ATC viewpoint, discussing airport capacity, data acquisition, weather, etc

[SAE PAPER 700281] 18 p3237 A70-36809

STOL systems 1975 technical and economic characteristics in terms of passenger market, aircraft design, terminal facilities and ATC capability

[SAE PAPER 700311] 18 p3350 A70-36812

Airport terminal design, describing electromechanical baggage handling and sorting systems

[SAE PAPER 700261] 18 p3237 A70-36822

International civil aviation, discussing ICAO functions, airports and terminal facilities problems

19 p3553 A70-37748

Hamburg airport terminal design including circular planets system for large aircraft, efficient intermodal transfer facilities, etc

19 p3396 A70-37750

National Airspace System air traffic control automation program for en route and terminal facilities

19 p3464 A70-37914

Air traffic control third generation system upgrading programs increasing airport, en route and terminal airspace capacities

19 p3464 A70-38227

ATC systems safety, capacity and delay, discussing terminal operations, runway capacity and aircraft spacing

19 p3465 A70-38228

Helicopter operations integration into civil air traffic system, noting special requirements for mixed fixed and rotary wing terminal environments

19 p3465 A70-38230

ATC integration of SST, discussing en route and terminal projects of national airspace system, modular automation, instrument flight rules, etc

19 p3467 A70-38633

UK organization of ATC services, considering responsibilities, facilities and personnel recruitment

19 p3467 A70-38634

Boeing 747, L-1011 and DC-10 introduction costs, profits and terminal facilities

19 p3357 A70-38951

International transportation regional hub airport planning with spin-off parking, circular terminal facilities and high speed interterminal passenger and baggage controls

20 p3606 A70-39673

Air cargo terminal operations analysis, discussing manpower cost reduction

20 p3607 A70-40127

Metropolitan air transit system design, considering compound helicopters, automatic control by central computer, onboard avionics system and terminal facilities

21 p3956 A70-41250

Air cargo traffic problems, discussing mechanized terminals, automatic handling equipment, direct container delivery, mass traffic and large freighter aircraft

22 p4126 A70-43268

Centralized terminal air cargo handling capacity, discussing Jumbo aircraft, airside ramp system, container movement, computer control and automation

22 p4006 A70-43270

Passenger seaplanes virtues and drawbacks, discussing bases, servicing, refueling, passenger conveyance, prospects, etc

23 p4137 A70-43887

Airport accessibility role in planning V/STOL aircraft landing facilities [AIAA PAPER 70-1311]

24 p4323 A70-45947

TERMINAL GUIDANCE

Flight test experiments for H-19 helicopter to evaluate aided inertial system performance for terminal guidance

01 p0136 A70-10303

Law for time variations of modulus-restricted control action at trajectory end, two point boundary value problem solution and use of Pontryagin principle

04 p0661 A70-15011

Airborne digital letdown computer to guide VTOL aircraft flying complex trajectories to relieve airport congestion

05 p0880 A70-16416

Instrument landing system techniques based on hyperbolic geometry and correlation detection for terminal area traffic control, discussing applications

06 p1102 A70-17637

Lunar module rendezvous with command and service module by coelliptic sequence establishing standard lighting and relative position and velocity for final approach

[AIAA PAPER 70-26] 06 p1157 A70-18129

Terminal air traffic control automation, discussing Advanced Radar Traffic Control System (ARTS) and control tower data transfer aspects

08 p1540 A70-20678

ILS systems, considering possible improvements

08 p1541 A70-21021

Subsonic glide landing approach guidance for unpowered lifting vehicles, using perturbation feedback and approximation of heading and position coordinates

[AIAA PAPER 69-865] 09 p1725 A70-23253

Radar signal quick indication and extrapolation for terminal guidance control of Mars soft lander, reducing radar lock on loss sensitivity and engine spurious noise throttling

11 p2080 A70-26210

Automatic-manual space rendezvous control system for Cosmos and Soyuz satellites, considering terminal phase control at specific closing range and velocity

13 p2499 A70-28402

Terminal constraints affecting matrices comprising linear impulsive guidance law for earth approach, discussing Mars mission

13 p2447 A70-28516

Flight test experiments for H-19 helicopter to evaluate aided inertial system performance for terminal guidance

13 p2449 A70-29622

Terminal guidance by dynamic programming to obtain optimal feedback control law in nominal trajectory neighborhood for minimum energy consumption

13 p2449 A70-29963

Landing point redesignation during Apollo lunar module descent terminal portion, defining information and control system

14 p2613 A70-30454

Apollo 12 navigation for pinpoint lunar landing, correcting errors in downtrack position in guidance computer near powered descent initiation time

14 p2613 A70-30456

Terminal area guidance for unpowered aircraft in instrument approach relevant to manned space shuttle effort

14 p2614 A70-30465

Terminal kinematic variables prediction for missile homing, discussing line of sight angle, rate and acceleration

15 p2773 A70-32525

Optimal open loop controller and suboptimal feedback law to minimize terminal error of entry vehicle

16 p2947 A70-33439

Terminal guidance for Mars softlander utilizing Doppler and range radar for steering and propulsive control

17 p3133 A70-35286

Multistage rockets terminal control synthesis based on linear functionals

18 p3333 A70-36163

Automated radar terminal system, ARTS-III Beacon Tracking Level for continuous aircraft identity on controllers radar display

18 p3288 A70-36393

Algorithm for trajectory analysis in closed loop terminal guidance of solar electrically thrusted interplanetary spacecraft [AIAA PAPER 70-1152]

20 p3670 A70-40203

Optimal terminal control stochastic synthesis for linear systems by Bellman second order nonlinear partial differential equation

21 p3801 A70-40607

Lunar module rendezvous with command and service module by coelliptic sequence, establishing standard lighting and relative position and velocity for final approach

[AIAA PAPER 70-26] 21 p3931 A70-41860

TERMINAL VELOCITY

Entry and terminal deceleration systems for unmanned Martian landers, discussing parachute landing and lifting entry vehicles

[AIAA PAPER 68-1147] 01 p0195 A70-10828

Optimal control of aircraft angle of attack based on minimum terminal velocity during passive flight in spherical nonrotating earth atmosphere

02 p0227 A70-12409

Lunar module rendezvous with command and service module by coelliptic sequence establishing standard lighting and relative position and velocity for final approach

[AIAA PAPER 70-26] 06 p1157 A70-18129

Cross product steering for space vehicles and ballistic missiles guidance during powered vacuum flight, pointing thrust acceleration vector to null velocity at termination

16 p2947 A70-33440

Spinning blunt entry vehicles dynamic stability tests in terminal regime, discussing dependence on angle of attack

[AIAA PAPER 70-988] 20 p3714 A70-39541

Lunar module rendezvous with command and service module by coelliptic sequence, establishing standard lighting and relative position and velocity for final approach

[AIAA PAPER 70-26] 21 p3931 A70-41860

Mathematical model for projectile penetration into metallic targets, calculating velocity after perforation

21 p3939 A70-41968

TERMINALS

Electrostatic discharge at magnetopause by idealized circuit analog, discussing transmission lines and terminal impedances

14 p2579 A70-31247

Deep space optical communications link, fabricating operational prototype of flight hardware for spaceborne terminal

16 p2863 A70-33190

Connectors for supersonic jetliners, discussing butyl rubber grommet, power distribution collector, modular terminal blocks and passenger service connector

16 p2878 A70-33956

Stepped termination design for rectangular waveguides achieving minimum length and maximum reflection coefficient

23 p4169 A70-43783

TERMINOLOGY

Low temperature terminology at December 1969 Paris conference, discussing temperature scale, superconductivity, liquid He, supercooling, subcooling, cryo and cryogenic

14 p2616 A70-31013

Juridical condition of earth orbiting space stations, discussing term definitions in treaty on outer space 17 p3202 A70-35785

Trim changes definition, discussing exact meaning 24 p4289 A70-45436

TERNARY ALLOYS

Ternary chemical element additions /O, Sn, Zr, Pb, Mo, V/ effects on solubility range of primary alpha region of Ti-Al base alloys 01 p0122 A70-11239

Ferrite and martensite precipitation hardening in Fe-Ni-Mo alloy, studying dislocation structure and aging kinetics 01 p0123 A70-11243

Ternary Al-Zn-Mg alloys stress corrosion cracking properties, showing effects of aging temperature and prestrain 01 p0123 A70-11387

Ti-Al-Co alloys reactions in solid phase in Ti-rich region, using optical microscopy and X ray diffraction analysis 01 p0125 A70-11645

Ta-V-Cb and Ta-V-Ti alloys used as brazing fillers for refractory metals bonding, noting wetting and flow characteristics, shear strength, remelt temperatures, etc 02 p0319 A70-12753

Two phase theory of ordered to disordered state transition in ternary alloys with fcc lattice, constructing phase diagrams 03 p0505 A70-13103

Ti-Al-Sn alloy tensile deformation mechanisms at cryogenic temperature under uniaxial and biaxial stress noting twinning, prismatic slip and dislocation characteristics 03 p0507 A70-13141

Superconducting properties of polycrystalline disordered cold worked Nb-Ti-V alloys showing unexpected sensitivity to fast neutron irradiation 03 p0508 A70-13144

Superconducting transition temperature variation in bcc region of Ti-Nb-V ternary alloys measured as function of valence electrons and composition 03 p0538 A70-13154

Heat treatment effects on phase components of Cr-Mn-B alloys with W and Nb additions, discussing heat resistance 03 p0510 A70-13280

Phase structure and corrosion resistance of alloys in Ti-V-Cr system, discussing effects in HCl, sulfuric acid, nitric acid, acetic acid and NaCl solution 03 p0510 A70-13282

Nb binary and tertiary alloys density changes found proportional to alloying element content 03 p0511 A70-13489

Heat treatment effects on mechanical properties of Ti-Fe and Ti-Fe-Al alloys 03 p0512 A70-13855

Extension characteristics of delta and sigma related phases in Mo-Ni ternary systems and evaluation of unit cell dimension variations on alloying 04 p0704 A70-14392

Ti-Al-V alloys after annealing investigated for equilibrium diagram at high temperatures 04 p0708 A70-15313

Heat treatment produced semicoherent and incoherent precipitations diminished susceptibility to stress corrosion cracking of aluminum binary and ternary alloys 04 p0708 A70-15370

Ternary Ti-Ta-Nb solidus surface determination by simplex lattices and cubic approximation, statistically evaluating equation derived 05 p0864 A70-16547

Ternary Ti-Al-Mo part phase diagrams constructed from Mo corner to plane titanium aluminide, including isothermal phase diagram for 600 C 05 p0864 A70-16548

Alpha and beta solid solutions chemical composition in two phase alloys of Ti-Al-Mo and Ti-Al-V determined by electron microprobe analyzer 05 p0864 A70-16549

Isothermal sections in Ti-Ni-B, Mo-Ni-B and W-Ni-B at 800 C determined by X ray analysis 06 p1090 A70-17846

Isothermal section determination in Mo-Cr-B at 1000 C using X ray, metallographic analyses and microhardness measurements 06 p1090 A70-17847

Vibration frequency influence on vibrational creep of Al-Mg-Si alloy, describing mechanism in terms of strain hardening, additional slip and dislocation movements 06 p1168 A70-17931

Ni influence in high temperature oxidation of austenitic Fe-Cr-Ni alloys investigated thermogravimetrically, metallographically and by electron probe microanalysis 07 p1305 A70-18965

Fe-Cr-Ni alloys for use in high temperature oxidizing environments 07 p1305 A70-18966

Ternary Al-Mn alloys precipitation hardening with Cr, V and Ti, investigating ferro and ferrimagnetic phases 07 p1307 A70-19390

Precipitation in Fe-Ni-Co maraging alloys produced by austenite plates formation from martensite, discussing effects of Ti addition 08 p1524 A70-21955

Binary and ternary systems phase diagrams construction by diffusion layer method and X ray analysis, studying concentration dependence of diffusion coefficient 09 p1703 A70-22564

Ternary metastable phase diagram for W-Ti-B system at room temperature 10 p1905 A70-25226

Fe-Mo-C and Fe-Ti-C alloys microstructure and hardness after rapid cooling from melt, considering phase dispersion and particle size, spacing and shape 11 p2065 A70-25774

Fe-Cr system and Fe-Cr-Ni liquid alloys studied by Knudsen cell-mass spectrometer combination, deriving phase equilibria from ion current ratios 12 p2255 A70-27602

Binary and ternary Mg alloys ductile fracture mechanism, studying coherent/noncoherent particles effects 12 p2256 A70-27612

Alloy oxidation at high temperatures emphasizing binary and ternary alloys 12 p2257 A70-28005

Phase equilibria in quasi-ternary alloys by microstructural, thermographic and X ray analyses, showing continuous solid solutions formation in titanium-niobium-titanium aluminide 12 p2258 A70-28275

Li and Cr additives effects on Al-Zn-Mg stress corrosion resistance, considering cracking, precipitation hardening and intercrystalline corrosion 13 p2433 A70-28844

Cu-Fe-Ti ternary system via microscopic, X ray and thermal analyses, measuring microhardness, electrical resistivity and magnetometry 13 p2433 A70-28863

Evaporated Au-Ni-Cr alloy resistor films physical and electrical characteristics, noting dependence on composition 14 p2625 A70-30285

Superconducting resistive critical field H_c of bcc region of Ti-Nb-V ternary system 15 p2782 A70-31754

Thermal conductivity and shock resistance of flame and plasma sprayed zirconia coatings on Ni-Mo-C metal [ACS PAPER 22-C-68F] 15 p2762 A70-32527

Ti-Al-Nb system creep strength, oxidation resistance, density, forging and rolling 17 p3120 A70-34426

Mn and Ti effects on hardening of Fe-Ni-Mn-Ti and Fe-Ni-Mn maraging martensitic steels 17 p3125 A70-35145

Corrosion and stress corrosion behavior comparison of aged Al-Zn-Mg alloy in aqueous chloride solution, discussing pH variation effect 18 p3271 A70-36028

Ti-Al binary and Ti-Al-X ternary alloys grain boundary precipitation kinetics and correlation with mechanical properties 18 p3272 A70-36035

Relaxation peaks associated with interaction clusters of Zr and N dissolved in Nb 18 p3274 A70-36056

Isothermal phase equilibria in Ti rich ternary Ti-Al-Fe alloys, noting eutectoid transformation 18 p3275 A70-36123

Dynamic and static stress effects on martensite formation temperature in Fe-Ni-C alloys 19 p3451 A70-37569

Plastic deformation in Ni-Cr-Nb alloy precipitation hardened at different long terms of high temperature 19 p3451 A70-37706

Ternary Al-Cu-Mg alloys, considering aged structure relationship to fatigue strength 19 p3454 A70-38955

Al-Zn-Mg alloys structural transformations by diffraction electron microscopy, investigating grain boundary and dislocation structure as function of heat treatment and chemical composition 20 p3646 A70-39044

Magnetic and structural characteristics of ternary intermetallic systems with lanthanides, considering Ln substitution by other rare earth elements 22 p4085 A70-42481

Ternary Co-Cr-C alloys unidirectional solidification with metal matrix and carbide simultaneous freezing at eutectic liquidus line 24 p4358 A70-45235

Weak superstructure line patterns of ternary phases with TiFeSi and ordered iron phosphides by single crystal, Guinier powder and diffractometer techniques 24 p4359 A70-45249

Ni-Nb-W and Ni-W alloys phase equilibrium, obtaining diagrams from analysis of liquid and solid phases separated electromagnetically before tempering 24 p4359 A70-45372

Fe-Ni-Mn ternary martensitic alloy, discussing metastable miscibility gap island existence in bcc phase 24 p4363 A70-46193

TERNARY SYSTEMS

Superconducting properties of Nb-Ti-N thin films prepared by reactive sputtering process, obtaining transition temperature maximums 04 p0732 A70-15689

Ternary data transmission systems characteristics for modulated codes with known parameters or random initial phases 05 p0816 A70-17006

Be atoms effect on lattice structure of three component sodium oxide-beryllia-silicate glasses using IR absorption spectra 07 p1315 A70-18704

Phase equilibria, crystallization and solidus surface in transition conode triangle of ternary system Mo-Ti-C at high temperatures 07 p1310 A70-19804

Carbide layer formation on Ta and Ta-W alloys, discussing Ta-C phase diagram and phases 07 p1320 A70-19892

Phase equilibrium and homogeneity regions of solid solutions system Ni-Nb-O at elevated temperature 07 p1315 A70-20313

Mo effect on structure and properties of Ni-Al-Nb system alloys in gamma and gamma prime solid solutions range, discussing high temperature strength 08 p1514 A70-20549

Diffusive separation of Ar 36 and 40 and He in axisymmetric supersonic jet taking into account pressure diffusion 08 p1431 A70-21027

Diffusion layer correspondence to phase diagram in terms of constituent phases and composition 09 p1702 A70-22563

High temperature fuel cell electrolytes, analyzing electrical conductivity of ternary systems of zirconium, cesium or tantalum and yttrium oxides in fluorite phase 10 p1830 A70-24460

Raney alloy catalyst activity and stability in fuel cell anodes, noting properties of ternary phases of nickel, aluminum and iron, molybdenum or titanium 10 p1831 A70-24466

Ternary phase diagrams and quaternary excess free energy prediction using binary data, applied to Pb-Sn-Zn, Ag-Pd-Cu and Pb-Sn-Cd-Bi systems 12 p2254 A70-27475

Chemical compositions and structure of carbides in Fe-W-C and Co-W-C systems, clarifying eta phases 12 p2255 A70-27601

ETA oxides compositions in Hf-Ni-O, Ta-Ni-O and W-Ni-O systems determined by studying 1000 C isothermal sections with X ray diffraction 12 p2255 A70-27607

Ti-Cu-Ag phase diagrams and liquidus surface structure, using metallographic, thermal and X ray techniques 16 p2931 A70-33221

Isothermal section at 1150 C of V-Zr-Cr cast and annealed alloys investigated by X ray and metallographic analyses, establishing various phase regions 19 p3453 A70-38711

Phase relations in system Ag-Fe-S in 700-1200 C range at various vapor pressures by quenching and differential thermal analysis, observing liquid-immiscibility fields 22 p4053 A70-42732

Thermodynamics and statistical physics of dense plasma with particle interaction energy exceeding kinetic energy, discussing three-component model phase equilibrium 23 p4229 A70-45073

TERNARY SYSTEMS (DIGITAL)

U DIGITAL SYSTEMS

TERPENES

NT AZULENE

TERRADYNAMICS

Melting zone evolution in thermal history of earth, investigating upper mantle heat transfer effect on layer motion due to radioactive decay 06 p1056 A70-17804

Sand bed stability under shear flow of low Froude number 24 p4330 A70-45980

TERRAIN

Radio wave propagation over inhomogeneous terrains, determining perturbing effects of details on wave characteristics 19 p3381 A70-38573

Terrestrial atmospheric structure, determining zero and extremum point positions and amplitudes to obtain information of VLF wave propagation path 19 p3416 A70-38574

Antenna polarization and terrain depolarization effects on radar ground return, calculating echo pulse from smooth and rough terrains 22 p3990 A70-43327

TERRAIN ANALYSIS

Terrain imaging radar applied to sensing earth resources 02 p0298 A70-12181

Terrain computerized mathematical model for determining unobstructed line of sight between observer and target 03 p0455 A70-14172

Earth resources observation satellite /EROS/ program, discussing geologic terrain and land-use planning maps
[SPE PAPER 2703] 06 p1053 A70-17155

Noontime ground surface temperature relationship to exposure and slope angle for meadows and woodland, using airborne IR pyrhelometer
06 p1054 A70-17415

Minimum altitudes for illumination levels of aerial color photographic film calculated for different landscapes
07 p1283 A70-19633

Electro-optical analogies application to sidelobe reduction of radar antenna illumination patterns and optics far field diffraction patterns in terrain image formation
09 p1631 A70-22009

Electromagnetic radiation sources for remote sensing application to identification of water, moist soil and vegetation, discussing optical properties of diverse materials
09 p1667 A70-22851

Philosophy and technology of spacecraft-borne sensors for earth resource surveys, noting ERTS-A satellite
[AIAA PAPER 70-302] 09 p1668 A70-22883

Color and color IR aerial photography, discussing effects of solar spectrum, films, filters, etc, in connection with terrain analysis
10 p1880 A70-24751

Volcanic terrain by high precision photogrammetry for studying planetary surface roughness traversability by three wheeled vehicle
10 p1882 A70-25047

Radar observation of landscape regions, discussing dependence on recognition of variations in texture patterns on radar image
11 p2004 A70-25642

Universal Automatic Map Compilation Equipment /UNAMACE/ for terrain altitudes determination on uniform and dense grid in stereo model to obtain orthophotographic projection
11 p2051 A70-26042

Slope failure erosional and mass wastage forms identification, characteristics and distribution based on large scale aerial photography depicted by remote sensor returns
12 p2217 A70-26913

Collapse prone land detected by multispectral scanning and photography with analog data processing
12 p2220 A70-26933

Airborne laser profilometer terrain roughness measurement and recording, considering error sources
12 p2244 A70-26938

Radar look direction effects on geological features detectability, considering topographic relief and incidence angles roles in feature enhancement and suppression
12 p2221 A70-26962

Landscape structure interpreting from aerial photos taken vertically from overflying aircraft
12 p2231 A70-27237

Terrain spectral imagery from satellites for natural resources investigations
12 p2235 A70-27745

Earth resource observation from orbiting spacecraft, discussing photo-image map construction for continents and continental shelves, terrain analysis, delta formation, etc
12 p2225 A70-27747

Aerial reconnaissance of soils, rocks, vegetation and streams, comparing color, IR color, and black-and-white photography
12 p2236 A70-27873

Martian terrain features and atmospheric activity observation by Mariner 6 and 7
13 p2494 A70-29526

Lunar surface terrain types and chemical composition based on Surveyor pictures
14 p2634 A70-30193

Book on microwave propagation physics covering unbounded homogeneous medium, terrain effects, uniform refractivity gradient, nonstandard refractivity, fading, etc
14 p2551 A70-30953

Snow field mapping with K band radar imagery determining signal return difference with surrounding terrain, noting role of volume scattering and old snow structure
14 p2578 A70-31238

Surface temperature measurement with airborne IR scanning imager for terrain analysis
16 p2905 A70-33170

Map making for Soviet soil fertilization, discussing map symbols and scale
19 p3407 A70-37275

Automatic measurement of drainage networks for lengths and areas by copper plate etching or flying spot scanner on transparencies or radar images
20 p3633 A70-39794

Aerial cameras for topographic mapping, emphasizing geometrical image accuracy, optical picture quality and shutter performance
21 p3826 A70-41268

Natural and cultural landscape pattern classification in aerial photointerpretation using land-system concept
21 p3826 A70-41401

Soil science and climatology in Central Europe archeological site location by aerial photography
21 p3826 A70-41402

Internal and integral photointerpretation in aerial photography, discussing landscape information reliability increase by interdisciplinary method
21 p3826 A70-41403

Aerial terrain analysis by color and color IR photography, analyzing physical factors affecting final image
22 p4018 A70-42963

Synthetic aperture terrain-imaging radar systems, calculating tropospheric turbulence induced phase errors for comparison with microwave propagation experiment
22 p3991 A70-43579

Rotating gravity gradiometer for simulated terrain mapping with subsurface density fluctuations
22 p4007 A70-43668

Roving vehicle self contained automatic control systems, discussing terrain scanning technique, stereo TV and electronic coordinate measuring and data processing equipment
23 p4260 A70-44628

Optimal timing for aerial photographic mapping of landscape types including tundra, forest, steppe, meadow, desert and mountain areas
24 p4328 A70-45196

Earth curvature effects on position of terrain points on planar aerial photographs for various survey altitudes
24 p4333 A70-45197

Optical properties of terrain for optimal time charting of aerial mapping, considering seasonal variations and atmospheric transmittance
24 p4333 A70-45199

TERRAIN FOLLOWING AIRCRAFT

Aircraft flight displays, simulating low altitude high speed mission by four degree of freedom Dynamic Flight Simulator
10 p1859 A70-24216

Pilot navigation efficiency in low altitude terrain following flight, using synchronized TV and simulator with inertial guidance
24 p4307 A70-45506

TERRESTRIAL DUST BELT

Micrometeoroid experiments on OGO 2 and OGO 4 satellites, measuring velocity, masses and particle orbits in earth dust cloud
01 p0086 A70-10444

Lower thermosphere dust particle layers correlated with polarization anomaly twilight fluctuations and noctilucent clouds frequency distribution
10 p1944 A70-24949

Circumterrestrial dust component in Doppler shifted zodiacal light, considering Mie theory
11 p2045 A70-25698

Tropical and midlatitude stratospheric dust by twilight photometry, considering possible causes of anomalous turbidity levels
11 p2046 A70-26388

Near earth motion equations for electrically charged dust particles in gravitating dipole magnetic fields, using zero-relative-velocity surfaces and energy integral
18 p3315 A70-36606

Earth aerosol layer formation mechanism, giving atmospheric brightness measurements in terms of dust particles density and size
18 p3251 A70-36981

TERRESTRIAL MAGNETISM

U GEOMAGNETISM

TERRESTRIAL RADIATION

Diffraction correction of terrestrial, atmospheric and cosmic background radiation at aperture and disk determined by artificial moon method
03 p0442 A70-13084

Lunar regolith and polarized component of earthlight observations by Surveyor 7 TV camera
04 p0752 A70-15061

Atmospheric temperature gradients above 30 km near sunrise using earth spectral radiance measurements by balloon
04 p0694 A70-15523

Assessing background magnitude caused by earth natural radiation sources during underground detection of solar neutrinos by radiochemical methods
05 p0899 A70-15950

Error correction for correlation coefficient between satellite data of earth radiation intensity and satellite vision field shift
05 p0841 A70-16729

Self calibrating radiometer for in-flight measurement of earth surface thermal microwave radiation
07 p1282 A70-19616

Grating spectrometer performance in measuring earth IR radiance determined from balloon flights
12 p2235 A70-27752

Earth radiation balance /net flux/ determination from satellite measurements of long wave radiance and reflected solar radiation in upper atmosphere
12 p2264 A70-28090

Terrestrial ELF waves F layer nighttime reflections, discussing effects of electron density, geomagnetic field radial component and absorption by ions
13 p2365 A70-29190

Precision radiometry of electromagnetic energy transfer in atmospheric and space physics emphasizing solar and terrestrial radiative fluxes measurements
13 p2409 A70-29652

Solar and terrestrial radiation measurements and computations in meteorology, considering diffuse radiation and radiative transfer in atmosphere
13 p2410 A70-29661

Trapped particles radial diffusion in formation and decay of radiation belts
13 p2484 A70-30096

Earth radiation balance climatological characteristics based on satellite and published data, analyzing earth-atmosphere albedo on global scale
14 p2603 A70-30402

Earth/atmosphere system outgoing microwave radiation calculations, surveying aircraft/ satellite measurements at various wavelengths
16 p2896 A70-33217

Earth Lyman alpha emission rates as function of atomic hydrogen column density in outer atmosphere, using Mariner 5 measurements
18 p3244 A70-36007

Ring current belt stability against LF electrostatic perturbations, including effects of finite electric field along magnetic lines of force
18 p3306 A70-36009

Airborne IR scanner as geophysical research tool depicting surface emission and heat mass transfer
18 p3259 A70-36558

Earth radiation measurement at 10-12 microns by Cosmos 243 satellite-borne radiometer, comparing temperatures for boundary air layers in cloudless conditions
18 p3247 A70-36630

Angular structure of outgoing short wave radiation field measured from Cosmos satellite for clear and cloudy skies and various sun heights
18 p3286 A70-36965

Climatological maps of earth mean annual radiation balance compared with satellite data
18 p3286 A70-36966

Human bioclimatology at high altitude, discussing energy balance in terms of net solar and terrestrial radiation balance in mountain area
19 p3367 A70-37369

Atmospheric moisture content vertical profile from terrestrial radiation measurements, using statistical regularization procedure
19 p3460 A70-37418

Terrestrial ELF electromagnetic wave fields strength variation with distance over earth surface, using residue series zero-order term
19 p3380 A70-38405

Soviet book on atmosphere and earth surface radiation characteristics covering absorption, scattering, spectral and angular distributions, radiation field, spatial structure, etc
20 p3661 A70-39171

Earth intrinsic radiation flux incident angular coefficient, examining effect on partially screened flat spacecraft elements
21 p3942 A70-40847

Atmospheric temperature profiles from terrestrial IR spectral radiances measured by balloon-borne grating spectrometer, discussing surface temperature variations
21 p3813 A70-40905

Pulse height distributions due to terrestrial gamma rays, using NaI/Tl scintillation counter
23 p4187 A70-43899

Earth and atmosphere thermal emission spectra via Nimbus 4 Michelson interferometer, obtaining atmospheric temperature, humidity and ozone profiles
23 p4192 A70-44866

Solar stimulated terrestrial materials luminescence remote detection by Fraunhofer line depth method using UV grating spectrometer
23 p4199 A70-45007

Earth/atmosphere system outgoing microwave radiation calculations, surveying aircraft/ satellite measurements at various wavelengths
24 p4328 A70-45192

Thermal emission spectra of earth and atmosphere from IR Michelson interferometer onboard Nimbus 3 satellite
24 p4330 A70-45977

TESSERAL HARMONICS

Earth potential errors from gravity and satellite motion measurements, discussing sectoral, tesseral and zonal harmonics with large and small second indices
03 p0473 A70-13190

Resonance effects on satellite orbits due to tesseral harmonics in potential field
05 p0908 A70-16335

Orbital perturbations earth satellite due to zonal and tesseral earth gravitational harmonics and external body fields
12 p2302 A70-27671

Tesseral and sectoral harmonics effect on satellite perturbations using numerical integration
13 p2494 A70-29531

Tesseral harmonics of geopotential and station coordinates from combined Baker-Nunn, laser and range data from satellites 24 p4407 A70-45538

TEST BEDS

U TEST EQUIPMENT

TEST CHAMBERS

NT ANECHOIC CHAMBERS

NT PRESSURE CHAMBERS

NT VACUUM CHAMBERS

Test chamber to simulate helicopter rotor downwash for engine inlet air particle separator optimization 01 p0056 A70-10676

Fixed gap electrostatic spark discharge apparatus for booster type explosive sensitivity tests, discussing construction of two models, safety features and results 03 p0548 A70-14120

Near IR reflectance spectrometer integrated into environmental chamber to study frost spectral properties 06 p1072 A70-18522

Space environment simulation chamber for testing of equipment temperature and satellite thermal model 19 p3402 A70-38897

Man-rated chamber facilities at Manned Spacecraft Center (MSC), discussing safety requirements and criteria, environmental test chamber design and test results 23 p4152 A70-44458

TEST EQUIPMENT

Automatic loading control system for tensile test machine permitting creep and creep-rupture testing 01 p0054 A70-10075

Ultrasonic wheel-type portable inspection device with internal coupling immersion fluid contained in silicone tire, allowing angle beam inspection without temperature correction 01 p0105 A70-11396

Dynamic testing instrumentation for oxygen breathing equipment emphasizing demand regulators and masks, connecting hose, helmets and individual components 01 p0041 A70-11458

Avionic units automatic testing to increase speed and reliability, discussing system configuration, parts, economics and computer language use 02 p0295 A70-11838

Hardware-software integrated time sharing computer system for testing transmission control units and associated terminals on line 02 p0275 A70-12189

Test fixture for determining mechanical properties of metals and steels at moderate strain rates, detailing design and instrumentation 03 p0462 A70-12883

Boeing 747 nacelle development programs involving outdoor and ground test rigs, flying test bed, flight tests, etc 03 p0550 A70-12894

Apparatus for short term thermal vacuum mechanical testing of materials 03 p0463 A70-13253

Apparatus for small specimen torsion tests at room temperature, describing machine capabilities 03 p0493 A70-13960

Nonlinear stochastic differential equations formulated during random loading processes generation, designing testing devices with stable performance parameters 03 p0598 A70-14236

Equipment for cyclic biaxial testing, producing five biaxial stress states by simultaneous direct pressurization and axial loading of thin walled cylindrical specimen 03 p0464 A70-14309

Apparatus and techniques for investigating spacecraft materials mechanical and thermal properties, using vacuum effect to simulate space environment [ASME PAPER 69-WA/PID-22] 04 p0663 A70-14752

Altitude simulation equipment for third stage Europa I booster rocket 04 p0664 A70-15302

Torsion testing apparatus for refractory materials at 2400 C, measuring applied torsion moment, twisting angle and second order modulus of elasticity 05 p0825 A70-15881

Amsler Vibrophore machine modifications to permit narrow band random fatigue tests 05 p0826 A70-15887

Test apparatus for investigating crystal defects in influence on simultaneous measurement of metals thermal and electric conductivity under plastic deformation at cryogenic temperature 05 p0829 A70-16399

Testing equipment and methods for metallic materials selection for low temperature applications, characterizing plasticity by yield strength, tensile strength, elongation, etc 05 p0864 A70-16805

Computer-controlled automatic test bench for black box modifications and electronic, hydraulic and pneumatic testing on Concorde aircraft 07 p1249 A70-19742

Computer controlled automatic test system (NARF 5500) for naval avionics systems support, discussing system hardware and applications and programming cost reductions 08 p1469 A70-20652

Aerospace digital computers automatic checkout, considering computers functional and mechanical properties and test equipment configuration and operation 08 p1469 A70-20653

Automatic test equipment from fourth generation computer viewpoint, considering cost and size reduction trends in avionics 08 p1469 A70-20654

Automatic multiple station test system for manufacturing plants, considering centrally controlled vs free standing and intelligent vs nonintelligent remote stations 08 p1470 A70-20655

General purpose automatic test system (GPATS) for electronic equipment fault location, discussing software and hardware for integrating programmable oscilloscope 08 p1470 A70-20656

Automatic test equipment for electronic devices, discussing computerized design of interface adapters for unit under test 08 p1470 A70-20657

Automatic test equipment programming for cost reduction by eliminating duplicated effort between manufacturers of test equipment and unit to be tested 08 p1464 A70-20658

Automatic testing hardware and software compatibility emphasizing versatile avionic shop test (VAST) 08 p1470 A70-20662

Versatile avionics shop test (VAST) Implementation Study recommendations on project management for automatic test equipment support system aboard attack aircraft carriers 08 p1601 A70-20663

Avionics maintainability concepts, discussing built-in test equipment, test connectors, automatic test equipment, fault detection and fault isolation 08 p1470 A70-20664

Computer program for automated test station simulation, considering station operating characteristics and performance prediction 08 p1465 A70-20666

Onboard automatic test equipment design, evaluating failure detection and reporting ability 08 p1470 A70-20667

Onboard integrated maintenance system for aircraft avionics in-flight subsystems monitoring 08 p1471 A70-20669

Built-in test equipment for automatic flight control systems, discussing testing programs and fail safe hybrid circuitry 08 p1471 A70-20670

Program, test equipment and data reduction of aircraft prototype flight tests 08 p1438 A70-21865

Specimen holder for 300 K/4.2 K resistance ratio measurement 09 p1655 A70-22645

Rig using holographic techniques for vibration testing and aircraft engine components inspection 09 p1680 A70-23069

Acoustic impact technique (AIT) for aerospace structures nondestructive testing, describing theory, instrumentation and applications 10 p1894 A70-24175

Automatic test equipment for different type of planes and relation to self organizing systems, considering airport implantation 10 p1970 A70-24476

Ultrasonic pulse frequency spectrum analyzer, describing electronic components, transducer type and positioning, beam collimation, applications in testing, etc 10 p1895 A70-24830

Microwave device test system design, considering measurement ranges and parameters, calibration, repeatability, accuracy, maintainability, etc 10 p1852 A70-24890

Computer aided on-line test generation for prelaunch checkout, describing interpretive test language for rapid man machine information transfer [AIAA PAPER 70-384] 10 p1846 A70-24921

Automatic Malfunction Analysis (AMA) digital computer software system supporting checkout and testing, defining normal system status by computer simulation [AIAA PAPER 70-383] 10 p1861 A70-24922

Automatic maintenance testing of avionic systems, discussing tape controlled equipment and program preparation 11 p2017 A70-25837

Ground testing apparatus with three degrees of freedom for artificial satellites attitude control systems, establishing mathematical model by digital and analog techniques 11 p2031 A70-26290

Automatic test and checkout system difficulties in space vehicles 11 p2032 A70-26338

Vibration generators based on magnetic field electrodynamic effect, giving design, schematic diagram and exploitation properties 11 p2032 A70-26441

Force controlled vibration for shock tests, discussing feasibility and merits for simulation testing 12 p2205 A70-27099

Beam-bending and circular plate testing rigs for creep with constant and variable loading, discussing tests repeatability and accuracy 12 p2207 A70-27618

Ocular focus stimulator with provision for optical distance change between object and observer without brightness and visual angle variation 12 p2237 A70-28125

Test and measuring equipment control systems analysis, discussing metrology and calibration requirements in overall quality assurance problem 13 p2416 A70-28374

Automatic test equipment performance and effectiveness below customer expectations, discussing design factors 13 p2525 A70-29677

Automatic test equipment effect on product design, discussing test planning and quality control 13 p2422 A70-29678

Relative cost benefits estimation of manual and automatic test systems for avionics in maintenance organization, proposing integrated maintenance and ATC data system 13 p2525 A70-29679

Automatic test equipment third generation specifications and design 13 p2525 A70-29682

MELVIN compact inexpensive multipurpose automatic test system, utilizing MSI single printed circuits to work optimally with computer 13 p2374 A70-29683

Digital computer controlled test system suitable for verifying response to single input pattern containing time dependent functions 13 p2374 A70-29684

Test Equipment for Rapid Automatic Checkout and Evaluation (TRACE) system, describing method for interfacing computer with peripherals 13 p2374 A70-29685

Man machine interface between operator and automatic testing equipment based on ergonomic design cost 13 p2360 A70-29687

Automatic test equipment programming procedure including analysis, coding, validation and demonstration 13 p2422 A70-29689

Digital computers in automatic test equipment, describing required control tasks 13 p2375 A70-29690

Multistation automatic test equipment assembly management or maintenance organization, using digital computer control 13 p2385 A70-29691

Automatic dynamic response system for testing logic and semiconductor devices 13 p2379 A70-29693

Quality assurance of automatic testing in military or industrial equipment, including acceptance criteria and statistical proving 13 p2423 A70-29694

Automatic laboratory or field testing equipment design requirements 13 p2423 A70-29695

Failure prediction testing and elements replacement at field maintenance level for increasing equipment reliability 13 p2423 A70-29697

Avionics on military combat-reconnaissance aircraft, discussing automatic systems testing and cost effectiveness model 13 p2380 A70-29698

Automatic test equipment for assembly shops, considering skilled personnel shortage, units complexity and repeatable test and repair 13 p2423 A70-29699

Anechoic chambers and test equipment for microwave antenna pattern measurements, discussing electromagnetic shielding and construction 14 p2557 A70-31180

Aeroelastic test equipment for Concorde, describing operating principles, installation, test results, etc 15 p2717 A70-31810

Materials testing machine for tension, compression and flexure at constant strain rate and for fatigue 16 p2900 A70-33067

Automated programmed device for fatigue tests based on harmonic oscillator, presenting schematic diagram 16 p2900 A70-33068

Low energy ion beam system for studying electron ejection from controlled metal surfaces, describing vacuum, ion source, lens and mass spectrometer components 18 p3261 A70-37086

Gas gun and instrumentation for impact tests 18 p3238 A70-37090

Low temperature creep deformation recorder with liquid He coolant, discussing Al and Pb single crystal tests

19 p3395 A70-37352

Apparatus for short term thermal vacuum mechanical testing of materials

19 p3401 A70-38471

Ultraminiature pressure transducer for airplane model and inlet/engine subsystem in wind tunnel tests, considering design, calibration, environments, etc

19 p3430 A70-38523

Portable catapult and arresting gear analog instrumentation data acquisition system testing aboard aircraft carriers and at land-based facilities

19 p3384 A70-38533

Digital computer magnetic tape recording system for flight tests of Jaguar aircraft, discussing data treatment

19 p3384 A70-38537

Automatic test equipment, considering capability, control and display facilities and system cost

19 p3401 A70-38542

Automatic test technology for avionics systems, discussing equipment and cost reduction

19 p3401 A70-38543

Avionic systems automatic test equipment, discussing maintenance, reliability, cost and time reduction

19 p3402 A70-38544

Emmanuel magnetic recording system used with airborne digital computers for aircraft in-flight tests

19 p3432 A70-38547

Aeroelastic test equipment for Concorde SST using harmonic method and electromagnetic shakers

19 p3402 A70-38548

Digital readout test equipment characteristics and parameters for electrical properties measurement, proposing pulse counting analog-digital conversion technique

19 p3432 A70-38701

Ronchi test interferometer for optical quality checking of laser crystals

20 p3627 A70-39094

Multiple choice rotation chair for clinical experimental research and pilot vestibular tests

20 p3580 A70-39438

Inertial platform with integral dynamic self test and fault monitoring scheme, describing design and operation

[AIAA PAPER 70-1013]

20 p3667 A70-39520

Aircraft gas turbine engine smoke emission measurement, discussing test equipment and procedure standardization

20 p3689 A70-39720

Tensile test device for continuous recording of sample load and strain

20 p3728 A70-40000

Measuring and test equipment economic approach to quality levels and accuracy ratios, deriving cost tradeoffs in optimum inspection fidelity

20 p3634 A70-40453

Optical thermal testing by IR radiation, reviewing thermistor bolometer, various detectors, radiometric microscopes, NDT equipment, etc

21 p3831 A70-40747

Versatile Avionic Shop Test maintenance system supporting avionic equipment aboard aircraft carriers

21 p3804 A70-40772

Test measurement instruments - Conference, Houston, October 1969

21 p3823 A70-40855

Electromagnetic test equipment transient waveform control using on-line digital computer in near real time configuration

21 p3805 A70-41270

Pure Fe and Ta hot hardness tests by ultrahigh temperature tester involving use of electron microscope

21 p3840 A70-41900

Low cost and weight reliable microminiaturized IC automatic cockpit checklist systems for aircraft pilots

22 p3977 A70-42298

Avionics hardware design guidelines to meet automated testing constraints including malfunction isolation, block requirements, packaging, etc

23 p4173 A70-44538

Automatic electronics test equipment, discussing choice between tape or computer controlled interpreter systems based on language, time, versatility and cost

23 p4173 A70-44539

Electronic equipment automatic testing systems signal routing and switching trees and matrices design, emphasizing modular approach

23 p4173 A70-44540

Electronic equipment automated testing objectives and requirements, considering man machine interaction, system controls, on-line reporting, and software/hardware availability

23 p4174 A70-44541

Pressure sensor testing and calibrating at cryogenic temperatures, describing special test rig structural, insulation, fittings and materials requirements

23 p4174 A70-44846

Servo-hydraulic testing machine for measuring cyclic stress-strain behavior of materials subjected to fatigue and creep at elevated temperature

23 p4178 A70-44912

Strain rate sensitive materials tensile tests using machine with external variable speed motor

24 p4422 A70-45517

Metal sheets thickness measurement and monitoring by through-transmission eddy current nondestructive testing, using phase locked amplifier

24 p4344 A70-45699

Magnetic and nonmagnetic metals flaw detection, using orthogonal eddy current probe to reduce permeability and conductivity variations effects

24 p4344 A70-45700

Metals flaw detection, using electronic balancing type eddy current detecting coil

24 p4336 A70-45701

Encasing and welded pipes flaws detection with high resolution by nondestructive testing, using eddy current method

24 p4345 A70-45702

Metallic rods and tubes permeability and resistivity nondestructive measurement by AC apparatus with self balancing sensing coil, using computer program for data reduction

24 p4345 A70-45704

Resonant fixtures utilization attaining high amplitude in shock synthesis testing, discussing test specifications

[SAE PAPER 700848]

24 p4322 A70-45886

TEST FACILITIES

NT ANECHOIC CHAMBERS

NT BALLISTIC RANGES

NT BLOWDOWN WIND TUNNELS

NT CASCADE WIND TUNNELS

NT COMBUSTION WIND TUNNELS

NT ENGINE TESTING LABORATORIES

NT ENVIRONMENTAL LABORATORIES

NT HOTSHOT WIND TUNNELS

NT HYPERVELOCITY WIND TUNNELS

NT LOW DENSITY WIND TUNNELS

NT LOW SPEED WIND TUNNELS

NT MISSILE RANGES

NT PLASMA JET WIND TUNNELS

NT ROCKET TEST FACILITIES

NT SHOCK TUNNELS

NT SLOTTED WIND TUNNELS

NT SUBSONIC WIND TUNNELS

NT SUPERSONIC WIND TUNNELS

NT TEST RANGES

NT TEST STANDS

NT TRANSONIC WIND TUNNELS

NT WIND TUNNELS

Multifan cross wind jet engine test facility to produce variable wind velocity in various directions

01 p0056 A70-10698

Concorde power plant tests using supersonic free jet altitude test facility with Olympus 593 engine

01 p0165 A70-10701

Simulated lunar environmental facility to investigate effects of high risk vacuum, lunar gravity and terrain characteristics and spacesuit encumbrances on astronaut performance

01 p0037 A70-10961

Water immersion technique to simulate zero and partial gravity conditions for investigation of astronaut capability to execute extravehicular work procedures

01 p0038 A70-10963

Missile tracer mixture performance control facility noting chamber for pressure measurement during operation

03 p0544 A70-13758

Automatic simulator for guidance system installed on cartographic satellite in circular orbit at 600 km, discussing weightlessness and vacuum simulation devices

03 p0464 A70-13834

Czechoslovakian Aeronautical Research and Test Institute history, organization, activities, equipment and achievements

03 p0464 A70-13925

Noise suppressor research for jet engine components, describing test equipment and facilities for models work

05 p0825 A70-15808

Clean room design problems concerning dampers, high pressure blowers, humidifiers, filters, etc

05 p0808 A70-16709

Clean room complex consisting of quality control analysis laboratory, main and pre-clean rooms and airlock

05 p0808 A70-16710

Tensile tests facility design for wide temperature ranges with loading system to maintain constant strain rate up to failure

05 p0830 A70-17072

Tensile and stress rupture tests facility for microsamples stability at temperatures up to 3300 K, investigating deformation and failure

05 p0830 A70-17073

Test facilities for studying materials thermophysical properties and stress relaxation, including dynamic hardness measurement and torsion tests up to 2500 K

05 p0830 A70-17074

Facility for testing thin walled tubular specimens in stressed state at low temperatures by keeping stresses constant with helical gear

05 p0830 A70-17075

Materials stress rupture strength and elastic constants at liquid hydrogen temperature, describing method and facility

05 p0955 A70-17076

Facility for studying energy characteristics of electrohydraulic stamping, discussing copper wire exploding in water

06 p1077 A70-17869

Hot air breather test facility design to increase flowrate range at maximum pressure level

[WSCJ PAPER 69-45]

Test facilities and procedures for obtaining aerodynamic data required for studying vehicle-in-tube transportation systems

[AIAA PAPER 70-225]

Radiative heating rates and gas environments effects on ablative material performance from tests at arc image facility

07 p1319 A70-19888

Electrically conductive ablative materials rapidly heated to 7000 F in test facility, discussing heating method and high strain rate testing

07 p1250 A70-20042

Environmental test facilities for space transportation systems, discussing aerodynamic, propulsion and structural problems, operational requirements and existing capabilities

[AIAA PAPER 70-275]

Computer system for real time data acquisition and servicing of asynchronous inertial guidance system test stations

07 p1251 A70-20384

Test-aided aerospace design, noting design engineer attitude and software problems

08 p1467 A70-21591

High resolution multiple spark photography, discussing facility

09 p1680 A70-23070

Avionics test station optimum design by computerized simulation involving iteration of computer run, analysis and model change

10 p1861 A70-24907

Vehicle System Simulator/VSS/test program for L-1011 Tristar encompassing primary and secondary flight controls, avionics, hydraulics and landing gear systems

[AIAA PAPER 70-388]

Weapon Systems Level testing methods and machines application to missiles, manned space flight vehicles and Safeguard System

[AIAA PAPER 70-380]

Helicopter flight test and evaluation tools including data processing facilities to improve test validity

[AIAA PAPER 70-373]

Hollow cylindrical sample scale effect on accuracy of testing heat resistance of brittle materials

10 p1862 A70-24923

Solar simulation laboratory test facility for extraterrestrial solar radiation effects on vehicles beyond earth atmosphere, emphasizing spectral filters

10 p1965 A70-25301

Optimum sequence integration and ground testing of Defense Communication System Phase II Satellite, considering vibration, shock, space simulation, spin/despin, RF and acoustic requirements

[AIAA PAPER 70-447]

C-4 supersonic free jet test cell, discussing Concorde development contribution and model tests on full scale cell nozzle

11 p2030 A70-25353

Free jet test facility for supersonic engine/ intake combination testing, discussing benefits to aircraft flying hours, development costs and safety

11 p2031 A70-25853

Three axis motion simulator for in-orbit spacecraft attitude control evaluation using earth, sun and star sensor references

[AIAA PAPER 69-1029]

Italian polyvalent data acquisition system for ground space tests, discussing electronic instrumentation system

11 p2031 A70-26147

Telemetric systems for moving machine elements tests, discussing seven channel PFM and FM/FM systems

11 p2032 A70-26293

Quasi-steady devices design to investigate high Reynolds number flows for flight vehicles, noting test time

11 p2056 A70-26451

Low cycle fatigue testing facility and methods used at NASA Lewis Research Center

11 p2041 A70-26573

Altitude Test Facility in air breathing aircraft engine design, discussing plant, test cells design and flight representation and systems accuracy

11 p2033 A70-26610

Space environment simulators and test facilities for solar cells and arrays, describing solar and magnetic field simulators and universal battery charger

13 p2473 A70-28538

Pressure sensor testing and calibrating at cryogenic temperatures, describing special test rig structural, insulation, fittings and materials requirements

23 p4174 A70-44541

23 p4174 A70-44846

Automatic test systems - Conference, Birmingham, England, April 1970

Aircraft equipment automatic test methods, comparing in-flight, on ground and second line testings

Turbojet engine testing in ground level facilities with automatic instrument reading and parameters calculation

Configuration management of software concerning automatic test systems in large maintenance depot

Ablation test facilities capability extension by surrounding high enthalpy flow with coaxial cold air jet

Reliability test facilities for military shipboard electronic equipment, subjecting equipment to combined thermal shock and vibration cycles

Two dimensional film cooled turbine blade aerodynamics, investigating massive blowing effect through discrete holes in single blade test facility

Space molecular sink simulator facility /Molsink/ for extreme high vacuum outer space environment simulation, discussing Mariner Mars 1969 spacecraft components tests

Test machine for partial gravity environment simulation for aerospace subsystem testing in vacuum chamber

Test facilities automation, discussing program storage, stimuli, measurement, data accumulation and storage and system control

Digital data acquisition and control system for acoustic testing of large spacecraft

Frequency and time information transmission, discussing frequency and time measurement equipment at Czechoslovak facility

Plane and annular cascade facilities data application to aerodynamic design of axial flow compressors

Thermal stability test assembly for refractory materials cylindrical specimens, using argon plasma jet

Computer aided laboratory testing of flight vehicles in real environmental conditions, illustrating vertical stabilizer subject to gust loads

Computer merits in test laboratory data acquisition systems

Data management methodology for test facilities, considering on-line analog/digital computers

Spacecraft test programming at test facilities providing vacuum and thermal space simulation suggested by Azur and Dial satellite development experience

Heos 1 research satellite space simulation tests at ESTEC test facility

Satellite vibration tests simulation installations, describing measurement and control devices for lateral motion and test object safety

Reliability enforcement in design by competition and test program, using gyroscope example

Spinning blunt entry vehicles dynamic stability tests in terminal regime, discussing dependence on angle of attack

Geophysical environment, discussing vibrations, foundation conditions, local gravity vector and atmospheric conditions in relation to precision instruments tests and operation

Langley 20 megawatt plasma accelerator design and operation, describing arc heater modifications, exit parameters, electrical properties, etc

High speed track facility for V/STOL aircraft tests, discussing characteristics and design

Polish Institute of Aviation, describing facilities and current test programs

Shock tube facility with high explosive driver for reentry flow conditions simulation of manned planetary flights

Automated data handling system for satellite environmental testing used by ESRO

High bypass model jet noise study, describing test setup and noise measurement results as function of secondary/primary flow velocity ratio

Testing laboratory for safety, survival and life support equipment concerning parachutes, aircrew protective helmets and maintenance manuals

Rumanian book on methods, equipment and facilities for aeromechanical measurements covering fluid flow, wind and shock tunnels, flow measurements, etc

TEST FIRING

Thermal efficiency of modified transtage of Titan 3C spacecraft, discussing environmental simulation, heat rejection system and test firing

TEST METHODS

Age correlations with ballistocardiogram amplitudes and waveform grades in test pilots

Cooper aircraft handling rating scale on basis of test pilot experience

Experimental test pilots - Conference, Beverly Hills, September 1969

Cardiovascular aging and aeromedical maintenance programs for selecting test pilots

Hearing loss thresholds and spontaneous and caloric nystagmus corollationship in test pilots

TEST PROGRAMS

Free flight ranges for hypersonic simulation from Mach 1 to Mach 30, noting onboard high-g telemetry instrumentation

Missile and space vehicle range safety policies and practices using past statistical performance data and cost consideration

Toxic fuel test site selection, evaluating meteorological factors in Gypsum Canyon, California

TEST STANDS

Rolls-Royce RB 211 three shaft turbofan engines development and tests, noting preparation, building, cradle installment, open air facilities and noise measurements

Simulator for testing colloid microthruster, discussing spacecraft interfaces and time of flight thrust data

Gas dynamic stand for testing turbine disks strength under mechanical and cyclic thermal loads, analyzing breakdown data for various disk geometry

Test stand design and automatic recording of turbine blade fatigue test data, including statistical evaluation

Test stand for endurance and creep testing of plastics, glazed ceramics and other brittle materials

Aircraft ground and flight tests effectiveness planning, preparation and conduct for operational safety, noting Flight Controls Development Test Stand

Gasdynamic test stand analyzing elastoplastic strains in aircraft gas turbine disks and liquid-propellant rocket engines turbopumps under alternating nonisothermal loads

Test stand based on Froude pendulum for measuring friction coefficients and oscillation parameters of porous bushings

Passive type stable test platforms /slabs/ covering configurations, foundations, vibration isolation, environmental effects, etc

Hollow test platform for gyros and accelerometers used in inertial navigation

Micropound extended range thrust stand /MERTS/ for testing electric thrusters for spacecraft auxiliary propulsion, providing three thrust measurement ranges and data telemetry system

TEST VEHICLES

Flight tests with mounted and unmounted SG 1262 hovering test rig in Germany to determine optimal control and stability characteristics for VTOL VAK 191B

Transposition and lunar docking simulation tests for Apollo 9 and subsequent missions using test vehicles equipped with flight type hardware

Runway test vehicle for lifting rotor performance in simulated forward flight, comparing with wind tunnel tests

Transposition and lunar docking simulation tests for Apollo 9 and subsequent missions using test vehicles equipped with flight type hardware

Test rig vehicle design for noise research on single stage high bypass ratio fans for quieter turbofan power plants

European participation in small space shuttle development, discussing design, test vehicle program and European applications

TESTERS

Pre-space flight tests effects on Macaca nemestrina monkeys spermatogenesis, considering immobilization and exposure time effects

TESTING

Wind tunnel testing technique innovations, reducing time and cost for low drag aircraft configurations by simultaneous force and pressure model transonic testing

TESTING MACHINES

Thermal transducer for rapid nondestructive testing, discussing imaging of specimen bond defects and thermal property differences

Time-optimal testing sequence for system failure detection, considering maintenance and reliability data

Continuous variation measurements of wind tunnel parameters minimizing testing time, discussing flow characteristics measurements during angle of attack variation

TESTS

Digital computer for data recording in stress-strain curves and data points for mechanical tests

Aerospace vehicles testing cost and technical analysis, discussing component failure, motivation effects, test design optimization, flight simulation, etc

Integrated planning and testing for systems reliability improvement

Reliability model for analyzing operational phase test programs developed from R and D phase models, processing data according to test scope

Systems engineering approach to test planning with emphasis on risk reduction for spacecraft

Controllability test for second order differential systems, noting applicability to linear first order time dependent systems

Integrated test program including proper timing for various testing levels, discussing environmental effects and sample size determination

Test selecting and sequencing for adaptive checkout processes, determining malfunctions

Aerospace vehicles testing cost and technical analysis, discussing component failure, motivation effects, test design optimization, flight simulation, etc

TETHERED BALLOONS

WINDAV anemometer used as low power wind direction and velocity transducer for tethered balloon

Parafail models development, comparing characteristics to kites and round and kite balloons

TETHERING

Relative motion of two bodies linked by flexible weightless tether in artificial earth satellite orbit, simulating extravehicular walk

Tethered orbiting interferometer configurations for future Radio Astronomy Explorer satellites, discussing gravitational stabilization and delta launching into orbit as single payload

Earth-pointing satellites joined by tether, discussing reel back and drag brake orbital deployment techniques and dynamic behavior

- Planar Tethered Orbiting Interferometer satellite for long wavelength solar and planetary radio astronomy, discussing deployment control and libration damping
18 p3333 A70-36230
- Structure and systems design of large gravity gradient stabilized orbiting tethered satellites structure for radio astronomy
23 p4259 A70-44603

TETHERLINES

- Parachute decelerator towline energy absorber shock attenuation characteristics, discussing drop test results
[AIAA PAPER 70-1202] 21 p3752 A70-41815

TETRACHLOROMETHANE

U CARBON TETRACHLORIDE

TETRAGONS

NT PARALLELOGRAMS

NT RECTANGLES

NT TRAPEZOIDS

TETRODES

- Balanced ELF chemotron tetrode amplifiers with series-fed output circuits, showing characteristics calculations and use in pyrometric assembly
06 p1022 A70-17782

- Thyristor tetrode silicon controlled switches (SCS), considering unijunction transistors and pulse generator circuits
13 p2377 A70-29115

- Thyristor tetrodes application to current and voltage stabilization, frequency division and lighting control
16 p2880 A70-34099

- Tetrode for single sideband short wave transmitter, discussing design, characteristics and intermodulation distortion reduction
17 p3054 A70-35412

- Four-terminal p-n-p-n small signal semiconductor tetrode amplifier operation principle and linear circuit applications
19 p3390 A70-38305

TEXTILES

NT COTTON FIBERS

NT RAYON

- Static electricity suppression for textile materials by blending conducting metal fibers into yarn
05 p0870 A70-16299

TEXTURES

- Subjects sensitivity to differences in statistical distributions of locally defined element density and shape, using stochastically textured visual patterns
06 p0998 A70-17223

- Harris method for determining inverse pole figures as description of sheet metal texture
06 p1088 A70-17611

- Rolling texture and recrystallization of Mo single crystals and deformation effect on texture formation using X ray transmission technique
07 p1309 A70-19613

- Cubic texture components preferred orientation shares into rolling texture during cold rolling of aluminum sheets determined quantitatively
09 p1690 A70-22255

- Computer texture analysis for two dimensional scenery pictures involving periodicity invariance under Fourier transform
11 p2014 A70-26251

TFX AIRCRAFT

U F-111 AIRCRAFT

THAILAND

- Fe diffusion coefficients measured at various temperatures above 1150 C to calculate homogenization times of Thailand tektite source
05 p0917 A70-16841

THALAMUS

- Cerebral histamine distribution in rat brains, noting highest concentrations in hypothalamus and thalamus
01 p0020 A70-10708

- Temporary suppression of cortical associative responses in cats with electrocoagulated thalamic relay nuclei lesions
04 p0632 A70-15220

- Thalamic N. VPL role in distributing afferent flux in anesthetized cats cortex, using stimulating contralateral sciatic nerve
07 p1199 A70-18723

- Neuron activity of cortical motor and visual regions and corpus geniculatum laterale in cats during diffuse thalamic electrostimulation combined with light signals
12 p2173 A70-28355

- Thyroxine stimuli transmission from posterior hypothalamus to cerebral cortex ascribed to dorso-medial nucleus of thalamus
16 p2848 A70-33261

- Lemniscus neurons in switching nucleus of thalamus, showing switching cells with direct cortical projections into somatosensory cortical zones
16 p2848 A70-33262

- Posterior ventral thalamic nucleus neuron reactions converging lemniscus and spinothalamic signals in cats
18 p3221 A70-36639

- Extracellular spontaneous sequences of action potentials of thalamic neurons during asphyxia in rats under artificial respiration
19 p3361 A70-38306

- Pathways of short latency reticulo-cortical responses to thalamic nuclei and hypothalamus destruction in cats
24 p4299 A70-45837

- Mesencephalic reticular formation influence on threshold stimulation of cortex, hippocampus, amygdala, thalamic nuclei and caudatum in rabbits
24 p4300 A70-45839

- Bilateral oligosynaptic interaction between posterior lateral thalamic nucleus and afferent systems in visual and acoustic cortical areas in cats
24 p4300 A70-45840

THALLIUM

NT THALLIUM COMPOUNDS

- Isotopic composition of meteoritic Tl determined in Ivigtut galena, Plainview chondrite, Canyon Diablo troilite and Canyon Diablo metal
03 p0576 A70-14091

- Plastic deformation effects on superconductivity of wire specimens of high purity Pb, In and Tl cold worked at liquid He and annealed
06 p1127 A70-18614

- Lead and thallium isotopic compositions of Apollo 11 fines compared with meteorites and earth for lunar surface age determination
21 p3775 A70-41588

- Chondrites Tl content by neutron activation analysis
21 p3921 A70-41941

THALLIUM COMPOUNDS

- Thermodynamics of electrochemical cells consisting of Li with lithium chloride or bromide and thallium amalgam with thallium chloride or bromide in propylene carbonate
01 p0042 A70-11107

THAWING

U MELTING

THEMIS PROJECT

- THEMIS source encoding systems research program to investigate inherent quantizing noise and degradation of analog to digital conversion
11 p2014 A70-26255

THEODOLITES

NT CINETHEODOLITES

- Automatic camera theodolite at Sophia satellite tracking station, discussing instrument constants
02 p0273 A70-11774

- Gyrotheodolites application to azimuth determination, discussing use for directional control, photogrammetry in geodetic measurements, etc
02 p0295 A70-11800

THEOREM PROVING

- Integral theorems for wave-type heat conductivity equation
01 p0219 A70-11398

- Structure theorem for time invariant multivariable linear systems proof and formulation for use in controller design and synthesis
03 p0461 A70-14166

- Stronger locally convex topology on space C/S/ of bounded continuous functions proved in nonagreement with strict topology on norm bounded sets
05 p0875 A70-16050

- Continuous dependence theorem and differentiability properties of free boundary problem solution for heat equation
09 p1788 A70-22609

- Theorem formulation and proof for maximal length cycle classification by weight
11 p2073 A70-26309

- Work and energy theorems in linear elasticity, discussing potential energy, real work, complementary energy and energy coefficients
11 p2142 A70-26625

- Generalized Frankl boundary value problem solution uniqueness formulation and proof using auxiliary function
13 p2390 A70-29647

- Boundedness theorem for solutions to differential equations system in applied mechanics
16 p2944 A70-34287

- Stability theorem for mechanical systems with constraint damping subjected to energy dissipation
17 p3176 A70-34956

- Limiting theorems for sums of random variables linked in Markovian chain, applying probabilistic and analytical methods
19 p3456 A70-37235

THEOREMS

NT ADDITION THEOREM

NT BAYES THEOREM

NT BERNOULLI THEOREM

NT BINOMIAL THEOREM

NT EXISTENCE THEOREMS

NT FLOUQUET THEOREM

NT GAUSS-MARKOV THEOREM

NT HELLMANN-FEYNMAN THEOREM

NT LAGRANGE SIMILARITY HYPOTHESIS

NT POYNTING THEOREM

NT RECIPROCAL THEOREMS

NT SIMILARITY THEOREM

NT STOKES THEOREM [VECTOR CALCULUS]

NT UNIQUENESS THEOREM

- Joseph theorem on parallel flow linear stability, allowing stronger limitation on amplification velocity of perturbation by using simple inequalities
13 p2464 A70-29543

THEORETICAL PHYSICS

NT BOHR THEORY

NT NEWTON THEORY

NT QUANTUM THEORY

- Collection of papers on boundary value problems of mathematical physics and related aspects of function theory, Part 1
01 p0131 A70-11066

- Splitting procedures application to steady and unsteady problems of mathematical physics and predictor-corrector method application to unsteady problems
04 p0719 A70-14959

- Soviet book on three dimensional boundary value problems in mathematical theory of elasticity and thermoelasticity
04 p0777 A70-15474

- Book on some methods of solving boundary value problems of mathematical physics covering linear operators, boundary conditions, perturbation and Monte Carlo methods
07 p1326 A70-19696

- Soviet collection of papers on mathematical physics covering natural oscillation frequencies, particles periodic motion, dynamic stability of pendulum, gyro drift during perturbations, etc
08 p1542 A70-20483

- Book on mathematical theory of electromagnetic waves covering vector analysis, reduced wave equation, linear transformations, boundary value problems and radiation patterns
08 p1533 A70-20759

- Soviet book on mathematical physics covering equilibrium equations of vibration, thermal conductance and diffusion with emphasis on Laplace equations
08 p1544 A70-20763

- Book on light and matter covering mathematical laser theory
13 p2429 A70-29574

- Book on space physics covering charged particles in magnetic, electric and dipole fields, cosmic rays, magnetically trapped radiation and interplanetary plasma
14 p2633 A70-30099

- Theory of matter from low energy data, discussing particle and charge classification, relativistic quantum dynamics, charge dynamics and superstrong reactions
14 p2620 A70-30783

- Elasticity theory in general relativity formulated from classical nonlinear three dimensional theory, discussing thermodynamics and weak field limit
15 p2774 A70-31734

- Small deformation thermoelasticity theory, discussing thermal conductivity, dynamic elasticity, strain field-temperature relationship, etc
15 p2818 A70-32177

- Maxwell equations derivation, describing assumptions needed
17 p3136 A70-35198

- Hypotheses concerning optimal methods of solving mathematical physics problems, choosing algorithms employable in digital computers
18 p3291 A70-36284

- Theoretical and applied mechanics - Conference, Tulane University, February-March 1968
19 p3543 A70-38326

- Initial value or boundary value problems in mathematical physics, solving by process of condition elimination
19 p3472 A70-38727

- Asymptotic properties of integral equations solutions for boundary value problems in theory of elasticity and mathematical physics
24 p4422 A70-45490

THERAPY

NT CHEMOTHERAPY

NT MASSAGING

NT PSYCHOTHERAPY

NT RADIATION THERAPY

- Myocardial infarction therapeutic prevention possibilities on basis of epidemiologic and dietary studies involving hypercholesterolemia and hyperlipemia in coronary disease
04 p0635 A70-15463

- Centrifuging with therapeutical device tested on male assault victim with bullet fragment floating freely in brain ventricular system
11 p1993 A70-26523

- G suit application to clinical therapeutics, noting intra-abdominal bleeding control
21 p3767 A70-40737

- Ballistocardiography and cardiovascular therapy - Conference, Oporto, Portugal, March-April 1969
21 p3762 A70-41226

THERMAL ABSORPTION

NT POLAR CAP ABSORPTION

- Space temperature determination, discussing planet or satellite absorption and radiation rate dependence on surface characteristics, solar radiation, planet albedo and thermal radiation
05 p0914 A70-16629

Multicomponent gas absorption analysis to illustrate interactions of coupled fluxes in ammonia-water system 08 p1597 A70-21028

Thermal radiation absorption in hemispherical cavity, determining apparent absorptivity for diffuse and parallel irradiation 09 p1790 A70-23565

Photoconductive and thermal IR detectors development 13 p2410 A70-29656

Laser pulse amplification by stimulated thermal Rayleigh scattering in absorbing media by transient theory 20 p3640 A70-39113

Pulse light amplification by stimulated thermal Rayleigh scattering measured as function of time, absorption coefficient and interaction length 20 p3640 A70-39114

Thermal defocusing and deflection of light beam by lateral wind effect in absorbing media 23 p4200 A70-43950

THERMAL ACCOMMODATION COEFFICIENTS

U ACCOMMODATION COEFFICIENT

THERMAL AGITATION

U THERMAL ENERGY

THERMAL BOUNDARY LAYER

Laminar boundary layer analysis of heat and mass transfer in dispersed two phase flow over heated surface 01 p0214 A70-10293

Book on flow and thermal boundary layers covering laminar and turbulent flow velocity profiles, Prandtl equation, heat transfer problems, etc 03 p0465 A70-13015

Boundary layer approximation for natural convection in flat vertical symmetrically heated channel with stabilized laminar flow for local and mean Nusselt numbers 03 p0605 A70-13395

Energy equation for thermal turbulent boundary layer on adiabatic flat plate 03 p0466 A70-13421

Karman formula generalization for turbulent motion in atmospheric boundary layer, including improved variant for thermally stable and unstable conditions 05 p0878 A70-16205

Flow disturbance calculation for heat transfer between boundary layer flows and adjacent walls modified to allow for wall attachment of thermal boundary layer 06 p1032 A70-17228

Thermal boundary layer thickness and Nusselt number approximations for heat transfer in laminar flow along flat plate with power law heat flux distribution 08 p1599 A70-21583

Heat transfer in axially symmetric laminar viscous boundary layer flow due to rotating bodies of revolution, obtaining temperature distribution 08 p1485 A70-21698

Electron temperature distribution in thermal boundary layer about probe electrodes calculated by successive approximations allowing for electron heating by arc 09 p1734 A70-22167

Boundary function of unsteady temperature field in bodies with moving surface at constant temperature calculated by least squares method 09 p1791 A70-23620

Thermal boundary layer similarity at extreme Prandtl numbers as series expansion, allowing for temperature distribution at wall 11 p2148 A70-25983

Thermal boundary layer equations solved for compressible gas at rotating axisymmetric surface with viscosity as linear function of temperature 12 p2331 A70-27698

Corona-induced thermal boundary layer breakup effects on convective heat transfer from wire electrode to surrounding gas 12 p2333 A70-28110

Unsteady heat or mass transfer to translating fluid sphere thermal boundary layer, determining analytical solution method accuracy 12 p2333 A70-28116

Transient heat transfer considered for thermal boundary layer over rotating disk following temperature change 13 p2519 A70-28493

Thermal boundary layer separation in conducting fluids by rotating magnetized blunt body 13 p2469 A70-30008

Laminar heat transfer to blunted wedge with constant wall temperature, describing energy field in boundary layer by analytic solution 15 p2825 A70-31818

Heat transfer through axially symmetric boundary layer on moving circular fiber at uniform temperature 15 p2825 A70-31819

Thermal boundary layer and heat and mass transfer at porous horizontal heated surface in presence of free convection, considering blowing and suction effects 15 p2827 A70-32133

Nonlinear dynamic stability of fluid layer heated from below in time dependent bounded domain 16 p2943 A70-34249

MHD and thermal boundary layer, considering difference scheme for conducting medium flow past body in crossed electric and magnetic fields 18 p3293 A70-36116

Free convection boundary layer on two dimensional or axisymmetric body with sudden temperature increase, determining skin friction and heat transfer coefficients 18 p3346 A70-36487

Skin friction measurement in supersonic flows by thin film heated element method, describing thermal boundary layer properties 18 p3243 A70-36710

Laminar flows with surface injection, calculating thermal boundary layer-porous wall coupling effects [ASME PAPER 70-GT-1] 18 p3243 A70-36860

Laminar thermal boundary layer at atmospheric pressure adjacent to cooled wall, measuring electron temperature and number density 20 p3737 A70-39990

Thermal boundary layer theory for turbulent jets of incompressible fluids from relationship between velocity fluctuations and temperature 20 p3614 A70-40347

Karman-Polhausen method applied to unsteady thermal boundary layer on isothermal flat plate 21 p3954 A70-42208

Dynamic nonstationary thermal convection in closed region with heat input from lateral surface for high Rayleigh and Fourier numbers 21 p3954 A70-42214

Nonstationary axisymmetric thermal convection in spherical cavity with boundary heat flux proportional to temperature, using difference scheme and networks method 21 p3954 A70-42215

Probe technique for plasma electron temperature measurements at medium and high pressures, examining thermal boundary effects 22 p4078 A70-42362

Turbulent hydrodynamic and thermal boundary layer development in internally heated annulus [ASME PAPER 70-HT-9] 22 p4008 A70-42438

Thermal boundary layer near stagnation point in three dimensional fluctuating incompressible flow, using Lighthill method 22 p4124 A70-42685

Unsteady incompressible thermal boundary layer flow past three dimensional obstacle for Prandtl numbers near unity 24 p4428 A70-45366

THERMAL BUCKLING

Nonlinear stress relation in elastic media incompatible deformations, eliminating elastic distortions for known temperature distribution and thermal distortion 01 p0201 A70-10890

Fatigue life of rocket nozzle coolant tubes under thermal cycling environmental conditions, considering design formulas for thermal buckling prediction 03 p0579 A70-12963

Flat plates thermal buckling calculations with allowance for transverse shear deformation effect, using Riessner variational principle 04 p0773 A70-15091

Thermal buckling of elliptic cylindrical shells assuming tangential temperature, constant axial pressure and conservation of elastic properties 04 p0775 A70-15203

Solid state lasers thermal resonator buckling time dependence and compensation, graphing results of resonator field analysis 07 p1303 A70-20359

Thermal buckling theory for multilayered stiffened cylindrical shells under various combined loads 12 p2321 A70-27149

Thin circular cylindrical shell stability subjected to axisymmetric thermal pulse, describing buckling process by mathematical model 18 p3342 A70-36641

Dynamic compensation of thermal pumping-induced deformation of laser active elements via thermal bending of resonator mirrors achieved by coatings 20 p3642 A70-39744

Clamped parallelogram metal plate thermal deformation under single surface radiant heating 24 p4426 A70-46009

THERMAL COMFORT

Thermal discomfort by changing operational temperature of human subjects environment found to follow power law 01 p0041 A70-11647

Comfort and thermal sensations and associated physiological responses during exercise at various ambient temperatures, noting effects on sensory estimates 01 p0031 A70-11648

Thermal comfort in disparate environments, discussing human subjects skin mean temperature and body water loss 03 p0429 A70-14158

Thermal tolerance and comfort graph for air conditioned spaces with low air velocity, considering fighter plane cockpits 08 p1454 A70-21949

THERMAL CONDUCTIVITY

Thermal diffusivity coefficient and conductivity of Cr at high temperatures determined by plane temperature wave method 01 p0117 A70-10190

Solid bodies unsteady thermal conductivity in presence of quasi-steady heat transfer under combined radiant and thermal fluxes, presenting thermodynamic nomograms 01 p0213 A70-10215

Three dimensional thermal conductivity problems solution applied to moving body, body of revolution and hollow cylinder 01 p0213 A70-10218

GeTe thermoelectric power, electrical/thermal conductivity and expansion coefficient measured at 20-600 C, determining suitability as thermoelectric material 01 p0158 A70-10755

Short sound waves propagation in moving inhomogeneous medium, studying viscosity and heat conductivity influence 01 p0146 A70-11581

Turbulent viscosity and thermal conductivity coefficients for entire cross section of fluid flow including wall boundary layers 01 p0069 A70-11624

Mesothermal flow of collisionless plasma around conducting cylinder, calculating densities, velocities, temperatures and electrical potential [ONERA-TP-769] 02 p0346 A70-12102

Component proportion and porosity effect on fiberglass reinforced plastics properties, establishing relation between bending strength and thermal conductivity coefficient 02 p0323 A70-12814

Transparent bodies photon thermal conductivity temperature dependence 03 p0515 A70-13206

Circulation gas lens temperature distribution, considering effects of gravity, wall thermal conductivity, glass interlayer, etc 03 p0604 A70-13387

Thermal conductivity, electrical resistivity, Lorentz ratio and thermopower of aerospace alloys at cryogenic temperatures, considering Inconel, Hastelloy, Ti and Al alloys 03 p0512 A70-13807

Nonthermal heating mechanism in quiet solar wind, tabulating observed and predicted parameters 03 p0561 A70-13998

Specific heat, electrical resistivity and thermal conductivity changes in materials properties at cryogenic temperatures, noting parasitic phenomena, mechanical and dielectric properties 03 p0525 A70-14269

Finite element method applied to heat conduction in solids with temperature dependent thermal conductivity, using nonlinear constitutive equation for heat flux [ASME PAPER 69-WA/HT-34] 04 p0782 A70-14806

Kinetic theory of thermal conduction in collisionless Knudsen gas in arbitrary closed systems with various geometries, establishing similarity law [ASME PAPER 69-WA/HT-20] 04 p0783 A70-14814

Thermal conductivity and hysteresis measured in cylindrical In foil under magnetic fields at temperatures below 1 K 05 p0891 A70-15792

Laser characteristics relevant to microwelding and micromachining, discussing heat conduction based models limitations 05 p0857 A70-15999

Fillers effect on thermal conductivity in porous cermet elements, investigating powdered Ti plates with air replaced by Hg, benzene, ethanol, ether and water vapor 05 p0957 A70-16291

Relation between Fourier harmonics equilibrium distribution and bulk viscosity and second thermal conductivity established in critical regions of liquid-vapor condensation and mixing 05 p0958 A70-16550

Thermal conductivity temperature dependence measured in greases bulk and thin layers at liquid helium temperature 05 p0874 A70-16842

Thermal conductivity and aperiodic temperature distribution in microstructure of composite materials reinforced with solid and hollow fibers 05 p0958 A70-16952

Gaseous He measured for thermal conductivity along isotherms to observe pressure dependence 06 p1174 A70-17678

Thermal conductivity and diffusion-thermal coefficients analysis for nonequilibrium and highly ionized plasmas based on particle velocities 06 p1120 A70-17698

Three dimensional ablation calculated for reentry sphere-cone taking into account shape changes and internal heat conduction [AIAA PAPER 70-199] 06 p1181 A70-18150

Stellar atmospheric models thermal conductivity coefficient computation for various temperatures and pressures neglecting magnetic field

06 p1150 A70-18464

Heat flux, electrical and thermal conductivity of H measured on plasma in cascade arc chamber of high power load at 1 atm pressure

06 p1107 A70-18525

Thermal conductivity calculation for chemically reacting multicomponent gas mixture, comparing results from Brokaw method and simplified formula

06 p1184 A70-18554

Thermal diffusivity measurements for Ta-W, Ta-W-Hf, Hf-Ta-Mo alloys using pulse technique

07 p1305 A70-18960

Temperature dependence of thermal conductivity of granulated borazon powders measured in He and vacuum

07 p1319 A70-19803

Thermal conductivities and total emittance of Ta, W, Re and alloys at high temperatures compared with NBS values

07 p1313 A70-19894

Thermal conductivities of glass reinforced polystyrene and polyethylene plastics measured over range of glass concentrations and sizes

07 p1320 A70-19958

Temperature gradients, viscosity and conduction measurements in air stream between parallel plates, investigating limiting value of total Prandtl number

07 p1260 A70-19999

Thermal conductivity for organic compound gases at atmospheric pressure

08 p1597 A70-21026

Solar wind ejection, analyzing regions of heat conducting fluxes and laminar patterns

08 p1561 A70-21059

Thermal conductivity and diffusivity of two phase composites determined by iterative solution of heat conduction equation with space fluctuating properties

08 p1598 A70-21511

Metals thermal conductivity at high temperatures determined by direct electrical heating method, considering specimen geometry effects on radiation losses

08 p1497 A70-21526

Navier-Stokes equations exact solutions for two dimensional steady flow of compressible viscous heat conducting perfect gas

08 p1485 A70-21638

Silicates thermal conductivity-Debye temperature relationship from thermal conductivity and acoustic data, applying to earth conductivity measurements

09 p1665 A70-22054

Thermal conductivity of multicomponent gas mixtures obtained in higher approximations

09 p1788 A70-22317

Magnetic field and gas thermal conductivity effects in analysis of solar wind as one dimensional, steady and spherically symmetric flow

09 p1745 A70-22687

Thermal conductivity of arbitrarily inhomogeneous bodies, considering vectorial field isotropy and temperature gradients dispersion

09 p1789 A70-23103

Amorphous polymers thermal conductivity measured at 0.4-4 K, observing similar temperature dependences

10 p1906 A70-23979

Viscosity and heat conductivity effects in compressible fluid flow past finite body showing dependence on spatial dimensions

10 p1800 A70-24135

Electric current flow effect on thermoelectric figure of merit from thermal conductivity measurements on thermoelement

10 p1808 A70-25034

Thermal conductivity on coupled heat conducting rods calculated by implicit difference scheme on finite graphs

10 p1969 A70-25189

Thermal conductivity - Conference, Purdue University, October 1968

11 p2146 A70-25751

Thermal conductivity of thin metallic films and wires at cryogenic temperatures, discussing electron transport properties

11 p2083 A70-25752

Thermal conductivity coefficients of argon in 25-700 C range and up to 1200 bars pressure, using vertical concentric cylinder apparatus

11 p2147 A70-25754

Thermal conductivity of monatomic binary gas mixtures at moderately low temperatures and pressures, considering various Ar-He mixtures

11 p2147 A70-25755

Thermal conductivity of nitrogen in 350-1500 K range using hot-wire diffusion columns

11 p2147 A70-25756

Thermal conductivity of neutron irradiated copper at low temperature noting lattice defects

11 p2148 A70-25757

Thermal conductivity, electrical resistivity, Lorentz ratio and thermopower of aerospace alloys in 4-300 K range, separating electronic and lattice contributions

11 p2065 A70-25758

Thermal conductivity of argon, nitrogen and air plasmas at atmospheric pressure and 6500-16500 K range, discussing electric arc source

11 p2148 A70-25760

Thermal conductivity coefficient of metals and alloys above 1000 C by longitudinal heat flow method

11 p2065 A70-25761

Thermal conductivity of metals and alloys, separating electronic and lattice contributions

11 p2098 A70-25762

Interfacial thermal conductivity model based on statistical features of two faces in contact, discussing surface roughness and heat flow

11 p2083 A70-25763

Thermal comparator for conductivity determination, discussing probe fabrication, surface finish, sensitivity, etc

11 p2050 A70-25765

Thermal conductivity determination for charring materials by dynamic technique, with application to carbon, graphite and silica cloth phenolics

11 p2068 A70-25766

Hydrogen, nitrogen and argon electrical and thermal conductivity measured at high temperature using electric arc as plasma source

11 p2148 A70-26016

Line source technique for ablative heat shield materials thermal conductivity measurements, comparing vacuum and atmospheric test results

[AIAA PAPER 69-1013] 11 p2051 A70-26142

Apiezon N grease thermal conductivity at liquid helium temperatures noting behavior as insulator

12 p2258 A70-27024

Thin plates finite length effects on thermal conductivity measurement by impulse method, verifying results with n-type silicon samples

12 p2332 A70-28047

Ni and Ni alloys thermal properties, discussing expansion and conductivity, melting and boiling points, vapor pressure, specific heat, entropy, etc

13 p2432 A70-28759

Nickel chromite structural changes, thermal conductivity and dilatation during tetragonal-cubic transition, noting phonon-lattice effect

13 p2437 A70-28855

N-type Te-doped gallium antimonide conversion to p-type by electron irradiation, noting thermal conductivity variations

13 p2470 A70-29167

Fluid quantum corrections to viscosity, thermal conductivity and diffusion, expanding Wigner operator in Planck constant

14 p2665 A70-30655

Soviet monograph on thermal conductivity of plates and bodies of revolution covering temperature and stress distributions, multilayer shells, etc

14 p2666 A70-30952

Thermal and electric conductivities for interface separating two parts of system with different temperature and chemical and electrical potential

14 p2617 A70-31296

Heat conductivity of Xe-He binary gas mixtures, allowing for molecular transfer and polarity effects

15 p2827 A70-32107

Carbon-graphite porous materials thermal conductivity at various temperatures

15 p2765 A70-32141

Heat conductivity equations transformation for Cartesian and cylindrical coordinates and various boundary conditions using static electrointegrator

15 p2827 A70-32172

Thermal conductivity and shock resistance of flame and plasma sprayed zirconia coatings on Ni-Mo-C metal

[ACS PAPER 22-C-68F] 15 p2762 A70-32527

Thermal conductivity of gaseous and liquid hydrogen with guarded horizontal flat plate calorimeter, investigating temperature and density effects in critical region

16 p2996 A70-33011

Thermal conductivity of multilayer and mixed powder high temperature insulation systems over wide temperature range and vacuum conditions

[AIAA PAPER 70-637] 16 p2997 A70-33596

Minerals radiative thermal conductivity at high temperatures from IR measurement of absorption coefficient and refractive index

16 p2897 A70-33648

Effective thermal conductivity parallel to laminations of multilayer insulation as function of temperature, layer density and length

[AIAA PAPER 70-846] 16 p2999 A70-33913

Thermal conductivity along parallel radiation shields, proposing calculation method for energy transport

[AIAA PAPER 70-847] 16 p3000 A70-33914

Cryogenic multilayer insulation (MLI), comparing radiation magnitudes, gas conduction and contact solid conduction to calorimeter and tank data

[AIAA PAPER 70-850] 16 p2939 A70-33917

Contacting metal surfaces thermal conductance prediction in vacuum, formulating dimensionless parameters in terms of properties, surface measurements and load/temperature conditions of contact

[AIAA PAPER 70-852] 16 p2932 A70-33919

Nongray radiant heat transfer corrections to thermal conductivity measurements for water vapor at atmospheric pressure

16 p3003 A70-34200

Incompressible laminar boundary layer, determining thermal conductivity gradient effect on temperature profiles

17 p3070 A70-35045

Thermal conductivity of particulate basalt as function of density in simulated lunar and Martian environments, noting temperature and pressure effects

18 p3316 A70-36772

Thermal conductivity of frost, using imbedded hot-wire method

18 p3262 A70-37118

Viscosity and thermal conductivity of dilute gaseous para and normal hydrogen at various temperatures

19 p3551 A70-37710

Electrical and thermal conductivities in white dwarf stars cores and neutron stars outer layers, calculating electron-photon collisions transition probability

20 p3702 A70-39016

Molecular and noble gas rotational collision numbers from thermal transpiration measurements

20 p3738 A70-39995

Liquid and solid semiconductors thermal emf and electrical and heat conductivities measurement over wide temperature range

20 p3634 A70-40300

Dry and water-saturated sintered fiber metal wick thermal conductivity, obtaining semiempirical correlations for solid and fluid phases and void fraction

21 p3945 A70-41041

Apollo 11 rocks IR absorption properties, specific heat and thermal conductivity, discussing heat flow in surface layer

21 p3913 A70-41642

Apollo 11 fines thermal conductivity under vacuum, using line heat source technique

21 p3913 A70-41647

Apollo 11 lunar specimen thermal diffusivity, conductivity and inertia in breccias and crystalline igneous rocks measured over wide temperature range

21 p3916 A70-41663

Approximate calculations of thermal and viscous transport in high temperature air based on empirical transport equations

21 p3951 A70-41750

Gases interaction with ablator and components during thermal conductivity, measuring nitrogen, helium, carbon dioxide and water sorption

21 p3951 A70-41873

Direct electrical heating for high temperature thermal conductivity measurements of pure W, giving results for graphite

21 p3850 A70-42057

Amorphous and partly crystalline polymers low temperature thermal conductivity and heat capacity

21 p3844 A70-42136

Thermocouple transient response characteristics in deflagrating and ablative low conductivity materials with high temperature gradients

[ASME PAPER 70-HT-7] 22 p4122 A70-42440

One fluid solutions for solar wind with reduced electron heat conduction in agreement with observed characteristics at corona base

22 p4093 A70-42472

Variational formulation for steady and transient heat conduction with variable thermal conductivity, applying to cylindrical element

22 p4123 A70-42546

Heat conduction into semiinfinite homogeneous solid with thermal conductivity dependence on temperature, noting temperature profile asymptotic behavior for similarity solution

22 p4123 A70-42641

Ultrasonic absorption in gaseous molecular relaxation processes, considering error due to neglecting thermal conductivity effect on frequency dependence

22 p4073 A70-42649

Ti phase transformation effects on thermal conductivity, electrical resistivity and spectral and total emittances at 1100-1500 K

22 p4056 A70-43222

Thermal relaxation effect on thermal contact of two semiinfinite walls, showing existence of dynamic contact resistance

22 p4125 A70-43243

Cylindrical wall nonstationary heat conduction for time variable heat transfer coefficient

22 p4125 A70-43358

Nonlinear unsteady thermal conductivity problems linearization based on temperature substitution by integral analogs

22 p4125 A70-43370

Terrestrial and synthetic lunar igneous rocks thermal conductivities in melting range, discussing thermal gradient

23 p4238 A70-43804

Thermal conductivity coefficient calculation by multiple temperature measurements of plate-shaped sample, using iteration process

23 p4276 A70-44166

Thermal conductivity of water, toluene and benzene in coaxial cylinders, taking into account edge heat losses 23 p4276 A70-44216

Thermosphere diurnal thermal influx theory, allowing for heat conductivity 23 p4214 A70-44265

Thermal calibration errors and sensitivity equations for hot-wire anemometers 23 p4195 A70-44288

Approximate method for solving thermal conductivity first boundary value problem via reduction to auxiliary Cauchy problem solved by Laplace transform and power series 23 p4277 A70-44339

Guarded electrical cylindrical calorimeter measuring multilayer insulation thermal conductivity, discussing construction, test and error 23 p4195 A70-44366

Closed cell polyurethane foam for cryogenic insulation, determining thermal conductivity and net heat flow by analytical model and test 23 p4280 A70-44367

Hg vapor thermal conductivity at various temperatures, using fine wire frequency response and kinetic theory 23 p4281 A70-44428

Compressibility, viscosity and thermal conductivity of dense gases, examining high temperature and pressure effects 23 p4222 A70-44431

Temperature distribution and thermal conductivity determination in Ar plasma cascade arc 23 p4226 A70-44438

Apollo 11 lunar fine thermal conductivity measurement under vacuum conditions and lunar temperature range, using line heat source method 23 p4243 A70-44442

Thermal and electrical conductivities of zirconium and hafnium diborides polycrystalline powders at 300-1300 K 23 p4209 A70-44443

Neutron star crust conductivity, obtaining electrical conductivity formula for outer kilometer 24 p4403 A70-45394

THERMAL CONDUCTORS

Surface constitutive assumptions restrictions for rigid heat conductor, accounting for radiative heat supply 24 p4429 A70-46032

THERMAL CONVECTION

U FREE CONVECTION

THERMAL CURRENTS

U CONVECTIVE FLOW

THERMAL CYCLING TESTS

Cost-effective look at vacuum testing of spacecraft components, noting sensitivity prediction and thermal cycle test 01 p0055 A70-10113

Flip chip and beam lead methods for microcircuit assembling, discussing heat removal using heat spreader and temperature cycling effects on tensile strength 01 p0050 A70-10330

Chromium-nickel steel fatigue strength under repeated thermal cycles, showing dependence on long term fatigue buildup and single cycle fatigue damage effects 02 p0383 A70-11653

Machine parts fatigue strength under thermal cycles, studying nonlinear dependence of energy dissipation per unit volume on cycles number 02 p0383 A70-11654

Fatigue life of rocket nozzle coolant tubes under thermal cycling environmental conditions, considering design formulas for thermal buckling prediction 03 p0579 A70-12963

Electro-pyrotechnic initiators for space applications subjected to dry heat sterilization cycles and to post-sterilization mechanical and electrical environments 03 p0495 A70-14131

Silicon solar cell panels, studying roles of solder, interconnector metals and substrate materials in failures under thermal cycling 04 p0628 A70-15333

Radial bond stresses in case/liner bond line of full-scale rocket motor measured, describing instrumentation, motor design and thermal cycling test sequence [ALAA PAPER 68-510] 04 p0736 A70-15407

Postweld heating cycle for circular patch test to predict strain age cracking susceptibility in welded Rene 41 04 p0700 A70-15654

Refractory Ni alloys defects accumulation under creep and cyclic temperature variations assessed by relative lifetime additive method 05 p0866 A70-17032

Low cycle fatigue of alloy and steel materials under bending and cyclic heating, relating strains and number of cycles to failure 05 p0866 A70-17036

Thermocyclic creep and rupture strength of Nb, Ta and Mo refractory alloys under temperature and load variations, showing failure dependence on cycle parameters 05 p0867 A70-17043

Scale factor effect on crack development in blanks and structure elements undergoing linear and complex stressed states under cyclic thermal loads 05 p0867 A70-17045

Gas turbine blades thermal fatigue strength under simultaneous temperature cycles and static tensile loads, analyzing temperature and stress fields 05 p0953 A70-17053

Temperature cycle duration effects on heat resistant alloys thermal fatigue resistance, noting stress relaxation occurrence 06 p1085 A70-17398

Steel tube deformation under constant internal pressure and cyclic heating, plotting tangential and axial strain curves as function of cyclic loading 06 p1163 A70-17399

Structures elastic-plastic behavior under changing cyclic heating, calculating long time strength from linear damage accumulation assumptions 06 p1164 A70-17405

Adverse effects of temperature and strain rate on low cycle fatigue resistance of austenitic stainless steels at elevated temperatures compared with tension tests 06 p1086 A70-17452

Refractory Nb alloy low cycle fatigue characteristics in vacuum at high temperatures, describing testing machine 06 p1086 A70-17453

Creep deformation resistance decrease in pure Al tubular specimens at high temperatures under multiple stress reversals 06 p1087 A70-17456

Elevated isothermal and low cycle thermal fatigue of Hastelloy X, investigating test temperature, cycle frequency and stress temperature effects 06 p1087 A70-17457

Thermal fatigue cracks in gas turbine blade models under simultaneous thermal cycling and static tensile loads simulating pulsed regimes 06 p1166 A70-17652

Weldability of super alpha high creep strength Ti alloy investigated by synthetic heat affected zone method using thermal cycling tests 06 p1090 A70-18501

Thermal fatigue resistance of steel to copper weldments under thermal cycling, noting intergranular crack growth accompanied by oxidation along crack boundaries 06 p1078 A70-18515

Hydrogen effects on ELI Ti-Al-Sn alloy, conducting tensile, fretting and abrasion tests on stressed and thermal cycled specimens 07 p1309 A70-19710

Subboundary migration in Mo, W and W-Re alloy single crystals subjected to cyclic heating, using metallographic technique involving electrolytic polishing and special etching 09 p1701 A70-22297

Cyclic heating and thermal stresses effect on fatigue strength and durability of turbine blade alloys and structural elements 09 p1771 A70-22463

Turbine components design for low cycle fatigue, estimating thermal cycle number for high temperature crack initiation and propagation 09 p1774 A70-22583

Thermal fatigue cycle produced by cooled gas turbine blades, using stress-strain tests and thermal simulation 09 p1655 A70-22585

Turbines rotary shafts and stationary components thermal fatigue analysis, considering cycle numbers and stress concentrations under start-up, continuous operation and shut-down 09 p1775 A70-22593

Microorganisms survivability in soils near spacecraft assembly areas during simulated Martian freeze-thaw cycles 09 p1619 A70-22768

Thermal cyclic loads effects on heat resistant materials strength during strain hardening, considering role of time factors in durability 09 p1779 A70-23104

Plastic strains buildup during thermal cycling, establishing relation between strain interval and cycles number to failure for strain hardening materials 10 p1965 A70-25293

Heat resistant alloys low cycle fatigue tests between 20-800 C, establishing residual strain change patterns as function of stress and temperature 10 p1906 A70-25294

Welding techniques for Nb-stainless steel bimetal tubing for liquid metal containment, determining structural integrity and bond interface condition after thermal cycling 10 p1897 A70-25309

Temperature cycling through phase transformation effects on plastic deformation of Ti and Ti-Al-V alloy under torsion and tension 17 p3117 A70-34400

Creep testing machine with constant load for HF thermal cycling under vacuum 17 p3063 A70-35587

Chromium-nickel steel fatigue strength under repeated thermal cycles, showing dependence on long term fatigue buildup and single cycle fatigue damage effects 19 p3547 A70-38426

Machine parts fatigue strength under thermal cycles, studying nonlinear dependence of energy dissipation per unit volume on cycles number 19 p3547 A70-38427

Cyclic thermal loading in viscoelastic spherical and cylindrical pressure vessels, investigating thermal frequency effect 21 p3937 A70-41430

Vacuum-melted and deformed Mo alloys tests, showing long term strength decrease under cyclic heating 22 p4055 A70-43123

Avionic components reliability, determining non-steady cooling air environment effects 23 p4175 A70-44744

Pure Al thermal cycling tests, investigating effect of minimizing thermal stress during quenching on behavior of dislocations 24 p4360 A70-45518

THERMAL DECOMPOSITION

U PYROLYSIS

THERMAL DEGRADATION

Radiator selection for manned spacecraft, considering thermal coating degradation, structural design, micrometeorite protection, plume impingement, reliability and fabrication 01 p0215 A70-10631

Polymeric materials thermal degradation kinetic parameters using combined mass spectrometric and thermogravimetric analysis /MS-TGA/ 11 p2069 A70-25806

Saturation of self induced thermal lens resulting from thermal distortion of carbon dioxide laser radiation in wind 11 p2063 A70-26401

Glass- and quartz-fabric reinforced polymers for high temperature microwave insulation, evaluating electrical and thermal aging properties 12 p2259 A70-28149

Teflon and fluropolymers relative toxicity due to thermal degradation at 370 C, testing carboxy nitroso rubber, Kapton polyimide film, perfluorated polymers, etc 13 p2439 A70-29260

Thermal degradation of anhydride-cured epoxy resin by carbon dioxide laser heating through platinum crucible 15 p2695 A70-32828

Optical resonator thermal deformations during pumping of circular cylindrical interferometer rods in illuminators, measuring thermo-optical constants of neodymium glass 15 p2754 A70-32863

Thermal design of hybrid microelectronics modules, considering resistance, assembly, joining, encapsulation and final packaging 16 p2879 A70-33957

GaAs laser diodes thermal degradation, observing nature, extent and occurrence of permanent damage 19 p3446 A70-37818

Toxicity problems from burning or heating of polymeric materials, discussing laboratory experiments and standardized toxicity testing procedures 20 p3579 A70-39406

Plate temperature field and stress distribution under thermal pulses, evaluating critical heat load for damage 20 p3737 A70-39635

Thermally induced mirror deformations and wavefront distortions under radially nonuniform heating 21 p3942 A70-40806

Copper disulfide-cadmium sulfide thin film solar cell degradation under simulated low orbit conditions, investigating thermal stress 21 p3759 A70-41313

Nondestructive tests of work-hardening Al alloy structural deterioration due to overheating, using eddy current conductivity techniques 24 p4345 A70-45703

Apollo 11 deployed solar cells, investigating degradation of surface properties and thermal control due to lunar module ascent effects 24 p4295 A70-46262

THERMAL DIFFUSION

Coupled diffusion of heat and vorticity in gaseous vortex caused by radial mass convection and temperature dependence of gas properties 02 p0400 A70-12858

Variational equation describing thermal diffusion in solid body undergoing deformation 03 p0589 A70-13348

Titanium alloys case hardened by diffusion of various metals at high temperatures, measuring increase in wear resistance 03 p0513 A70-13858

Book on rational thermodynamics covering homogeneous processes, internal dissipation, Coleman theorem, wave propagation in dissipative materials, diffusion, chemical reactions, Onsager relationship, etc

03 p0525 A70-14042

Fe diffusion coefficients measured at various temperatures above 1150 C to calculate homogenization times of Thailand tektite source

05 p0917 A70-16841

Turbulent heat and mass diffusion in catalytic reactors for hydrazine decomposition, developing computer program to calculate temperature and reactant concentration distributions

07 p1365 A70-19706

Thermal conductivity and diffusivity of two phase composites determined by iterative solution of heat conduction equation with space fluctuating properties

08 p1598 A70-21511

Error analysis of Barakat-Clark explicit heat diffusion equations for thermally insulated surface

08 p1600 A70-21831

Electrons thermodiffusion and energy transport coefficients in noble gases at mean reduced electric field intensities, obtaining distribution functions

11 p2089 A70-25868

Ion temperature gradient along magnetic field lines in outer plasmasphere by thermal diffusion equations compared with electron temperature observations

11 p2047 A70-26568

Turbulent heat diffusion coefficients in air and water tube flow calculated from statistical characteristics, extending method to boundary layers

12 p2210 A70-27322

Critical loads for brittle bodies weakened by sharp holes under combined diffuse thermal fluxes and crack crossing

12 p0000 A70-28321

Residual stresses in cylindrical shell made of two component solid solution under thermal diffusion

12 p2329 A70-28323

Thermal diffusion effects on F 2 region ion densities, deriving diffusion coefficients for partially ionized atomic oxygen plasma

13 p2398 A70-29232

Radiating drop unsteady vaporization or growth for uniformly distributed internal heat sources, discussing gas temperature distribution and diffusion thermal effect

13 p2521 A70-29417

Transport cross sections for isotopic methane and mixtures, considering inelastic and thermal diffusion effects

14 p2665 A70-30652

Variational equation describing thermal diffusion in solid body undergoing deformation

14 p2657 A70-30722

Invariant imbedding application to solution of partial differential equations by continuous-space discrete-time (CSDT) method, discussing time dependent heat diffusion

16 p2942 A70-33735

Ti alloys thermodiffusion impregnation with rarefied nitrogen and oxygen plasma, determining optimal gas pressure and temperature conditions and magnetic field frequency effects

17 p3101 A70-35391

Diffusion during high temperature exposure of protective coatings on Mo, noting compact layers and carbide forming elements effect on thermal stability

17 p3125 A70-35404

Baron thermal diffusion effects on plastic of pure Mo subjected to recrystallization

17 p3102 A70-35408

Thermal diffusion of isotropic, nonisotropic and multicomponent mixtures with monatomic and polyatomic molecules, considering kinetic theory and experimental results

17 p3197 A70-35537

Fluxless paste for thermodiffusion calorizing stainless and heat resistant steels and alloys

19 p3434 A70-37459

Ti alloys fine structure, mechanical properties and alloying elements diffusion mobility during heat treatment, observing chemical and structural inhomogeneities

20 p3645 A70-39040

Lithium-diffused silicon, investigating heat treatment and electron irradiation effects on electrical resistivity at high temperatures

20 p3687 A70-40164

Turbulent heat diffusion coefficients in air and water tube flow calculated from statistical characteristics, extending method to boundary layers

21 p3811 A70-42063

Cu-Ni diffusion couples voids and edges effect on concentration gradients measurement by electron probe microanalysis

22 p4054 A70-42740

Convective diffusion limited oxidation of Mo, measuring kinetics up to 2000 K by rotating disk method

24 p4358 A70-45233

Nonlinear distributed sources induced diffusion, calculating relationship between source intensity and maximum temperature or mass concentration field

24 p4380 A70-46034

Fe-Cr alloy powders obtained with thermodiffusive saturation from point sources, determining optimal mixture compositions and parameters

24 p4350 A70-46338

THERMAL DIFFUSIVITY

Refractory and heat resistant materials thermal diffusivity coefficient, discussing theoretical basis and technical implementation for measurement at high temperature

01 p0085 A70-10178

Thermal diffusivity coefficient and conductivity of Cr at high temperatures determined by plane temperature wave method

01 p0117 A70-10190

Diffusive transport term in hydrodynamic equations describing flow over strongly ablating entry objects, discussing charge separation and pressure diffusion

03 p0405 A70-12926

Heat conduction equation containing diffusivity coefficient as Stefan type function

05 p0958 A70-16867

Thermal diffusivity of opaque materials by phase shift method, using modulated radiation beam from carbon arc to heat material

11 p2068 A70-25767

Thermal diffusivity of elements over wide temperature ranges based on TPRC recommended thermal conductivity and specific heat

11 p2065 A70-25770

Apollo 11 lunar specimen thermal diffusivity, conductivity and inertia in breccias and crystalline igneous rocks measured over wide temperature range

21 p3916 A70-41663

Directional emissivity and thermal diffusivity of solids at 1000-3000 K by radiation comparison method, applying to sintered and plasma sprayed Mu, Ta and W

23 p4207 A70-44661

THERMAL DISSOCIATION

Diffusion coefficients for laminar multicomponent dissociating boundary layer at surfaces of thermally decomposing protective coatings

01 p0042 A70-11583

State equation for entropy of dissociated air with enthalpy and pressure as independent variables for calculating gas dynamic processes on computers

10 p1966 A70-23839

Thermal dissociation kinetics in chlorine pentafluoride over high temperature range

11 p1994 A70-25823

Pilot chamber initiated thermal decomposition reactor concept for monopropellant thruster, discussing thrust levels and throttling ratios

[AIAA PAPER 69-420]

13 p2473 A70-28507

Vapor pressures and dissociation energy of yttrium dicarbide and tetracarbide over extended temperature, measured by Knudsen double focusing spectrometer

16 p2858 A70-34015

Thermal dissociation mechanism of diatomic molecules in inert diluent behind shock wave, assuming distribution function described by Fokker-Planck equation

18 p3292 A70-36242

Quartz- and silicate-graphite mixtures carbothermal reduction in vacuum at 1400 C

20 p3583 A70-40425

Laser torch plasma dispersion gas dynamics from motion and kinetics of ionization processes

21 p3839 A70-42238

Thermal separation of ortho and para hydrogen and deuterium, discussing kinetic theory of nonspherical molecules in terms of rotational collision numbers

22 p3983 A70-43154

Thermodynamic equilibrium analysis of metal oxidation and thermal dissociation of oxides in vacuum, noting decreased affinity by evaporation

24 p4361 A70-45835

THERMAL EFFECTS

U TEMPERATURE EFFECTS

THERMAL EFFICIENCY

U THERMODYNAMIC EFFICIENCY

THERMAL EMISSION

NT THERMIONIC EMISSION

Local thermal emission from Jupiter at 5 microns, discussing North Equatorial Belt and atmospheric transparency

01 p0173 A70-10043

Thermal emission of inhomogeneous plasma sphere having dielectric constant as function of radius

01 p0149 A70-10164

Geophysical parameters of atmosphere and underlying surfaces from outgoing thermal radio emission measurements on Cosmos 243 satellite

07 p1261 A70-18724

Atmospheric integral moisture content determination from thermal radio emission measurements by Cosmos 243 satellite

07 p1329 A70-19649

F corona heliocentric dust cloud model to account for temperature variations with particle size and optical properties, computing thermal emission

08 p1571 A70-20907

Solar meter wave emissions enhancement or emission centers, comparing radio and optical coronal enhancements

08 p1576 A70-21402

Thermally emitted photons of atmospheric molecules and aerosols and planetary surface followed by Monte Carlo method, using anisotropic single scattering functions

09 p1719 A70-23524

Thermal emission of inhomogeneous plasma sphere having dielectric constant as function of radius

10 p1925 A70-25012

Nonisothermal dielectric coating on conductor surface, analyzing temperature distribution effect on thermal emission characteristics

11 p2148 A70-25975

Microwaves reflection, absorption and thermal emission at smooth air-water interface, tabulating calculated coefficients

12 p2183 A70-27169

Materials absorption coefficients determination at high temperatures based on spectrophotometric analysis of emission from samples of different thicknesses

12 p2331 A70-27305

Lunar surface brightness temperatures from IR observations, determining thermal emission directional characteristics to infer surface temperatures from Surveyor data

[AIAA PAPER 69-593]

13 p2486 A70-28501

Lunar horizontal and inclined surfaces net radiation and components, discussing surface temperature, thermal emission and absorbed solar radiation

14 p2634 A70-30194

Lunar surface thermal emission spectra, calculating IR emissivities

14 p2637 A70-30495

Lunar surface thermal emission spectra based on laboratory analysis of rocks and minerals emissivity

14 p2637 A70-30496

Lunar remote probing by IR and microwave thermal emission and by radar

14 p2644 A70-31056

Thermal radio emission from major planets at mm and cm wavelengths and at decimeter wavelengths for Jupiter and Saturn

14 p2648 A70-31084

Sea surface temperature and atmospheric moisture determination from satellite measurements of atmospheric thermal radio emission on quiet and cloudy windy days

15 p2770 A70-32069

Nitrogen dioxide continuous visible emission under thermal and recombination excitation, examining spectral characteristics

19 p3374 A70-38267

MOS field effect transistor, measuring electrons and holes thermal emission rates and activation energies at gold centers in Si

22 p3997 A70-43016

Thermal emission cathodes made from lanthanum, yttrium and gadolinium hexaborides, measuring I-V characteristics

22 p3998 A70-43442

Earth and atmosphere thermal emission spectra via Nimbus 4 Michelson interferometer, obtaining atmospheric temperature, humidity and ozone profiles

23 p4192 A70-44866

H II region dust grains thermal emission, examining effect on diffuse nebulae

24 p4413 A70-46158

Albedo and thermal emission of Jovian satellites I-IV at 3 to 12 micron wavelengths

24 p4413 A70-46171

THERMAL ENERGY

Solar energy absorbers and thermal storage devices for high temperature energy conversion to electric power by thermionic or thermoelectric method

01 p0010 A70-10764

Thermal energies and angular momenta of Hubble galactic sequence using differential rotation and decreasing density stellar system model to test stellar evolution theories

02 p0376 A70-12447

Mechanical losses in fiberglass reinforced textolite converted into thermal energy during cyclic tension and compression

02 p0323 A70-12807

Conservation equation for thermal energy in turbulent shear flow, including turbulence kinetic energy equation terms

[WSCI PAPER 69-43]

06 p1179 A70-17983

Nozzle source design for high intensity thermal energy molecular beam with small dispersion in velocity suitable for scattering experiments

11 p2086 A70-25973

Neutral molecule-solid surface interactions mass spectrometric techniques for measuring molecular flux and mean thermal energy after interaction

12 p2181 A70-27257

Lunar two cycle interior thermal history influence on maria and crater morphology, noting active and passive phase roles

12 p2311 A70-28302

Heat energy transport mechanism in metallic plasma deposited coating, investigating role of elastic crystal lattice vibrations, electrons, molecules, etc

13 p2419 A70-28858

Energy balance in radiation detector cooling, analyzing refrigerator capacity and thermal load

13 p2412 A70-29870

Solar, nuclear, chemical and thermal energy sources for short and long duration exploration on moon

14 p2634 A70-30195

Intensity and velocity distributions of thermal energy argon atoms scattered from silver /111/ face, using time of flight methods

16 p2953 A70-33007

Thermal product distributions and energy dependencies of ion-molecule reactions in allene and propyne, using ion cyclotron resonance

16 p2856 A70-33651

Stellar thermal and vibrational energy losses due to URCA shells in interiors

18 p3310 A70-35935

Thermal release profiles and retention coefficients of injected argon ions for silicates and iron simulating meteoritic materials

19 p3474 A70-38601

Hydrogen negative ion thermal energy reactions with oxygen, nitric oxide, carbon monoxide and nitrous oxide, determining rate constants

20 p3583 A70-39616

Vacuum distillation vapor filtered catalytic oxidation water recovery system, using radioisotopes for thermal energy supply

21 p3769 A70-40994

Space systems and thermal technology - ASME Conference, Los Angeles, June 1970, Part 2

21 p3942 A70-41014

Thermal energy conversion into coherent laser light, examining various thermodynamic limitations

22 p4076 A70-43674

Diurnal variations of photoelectron heat fluxes and energy production by thermal coupling between upper F 2 region and magnetosphere

24 p4328 A70-45354

THERMAL ENERGY STORAGE

U HEAT STORAGE

THERMAL ENVIRONMENTS

Thermal and pressure environments analysis in Saturn S-IC stage base during flight tests, noting base gas flowfield and heating

01 p0195 A70-10833

Thermal discomfort by changing operational temperature of human subjects environment found to follow power law

01 p0041 A70-11647

Plume-induced flow separation effect on thermal environment using Saturn 5 film and instrument data, attributing heating rate increase to recirculated exhaust gases

[ASME PAPER 69-WA/HT-18] 04 p0761 A70-14815

High temperature coatings in industrial, military and space applications, noting use in metal melting and working, furnace protection, propulsion systems, rocket engines, etc

04 p0709 A70-15630

Thermal testing of planetary lander vehicle in vacuum chamber, modeling electronics modules and experiments using resistance heaters

[AIAA PAPER 70-222] 06 p1157 A70-18128

Wind tunnel tests for aerodynamic and thermal environment of hypersonic glider VERAS /Vehicle for Experimentation and Research in Aerothermodynamics and Structures/

07 p1187 A70-18981

U.S., U.S.S.R. and European space environment simulation chambers accommodating assembled spacecraft for thermal tests, describing design and characteristics

07 p1249 A70-19659

Fatigue tests to relate boron-epoxy laminate fatigue behavior to thermal preconditioning environments

07 p1320 A70-19960

Bonds strength involving metallic, organic and ceramic adhesives at various temperatures, considering metallic additives effect

08 p1504 A70-20891

Airborne real time IR imagery of thermal anomalies for geophysical exploration of water resources

09 p1674 A70-22262

Lunar internal temperature approximation correcting solution of heat conduction equation for moon thermal histories

09 p1753 A70-22385

Heat accumulation, oral temperature and heart rate recovery of subjects in various thermal environments

10 p1810 A70-24034

Environmental thermal stress effect on human performance under high mental and low physical workload

10 p1812 A70-24505

Book on thermal environmental engineering covering refrigeration, psychometrics, solar radiation and heat transmission in buildings

12 p2163 A70-26865

U.S., U.S.S.R. and European space environment simulation chambers accommodating assembled spacecraft for thermal test, describing design and characteristics

15 p2718 A70-32696

Fluid mechanics and engine dynamics and start-up experiments simulating thermal environment in nuclear light bulb engine

16 p2949 A70-33552

Ablative materials performance in high radiative heat flux environments produced by CW carbon dioxide laser

[AIAA PAPER 70-864] 16 p2939 A70-33907

Lunar surface radiative balance and thermal environment measurement by portable meteorological station, considering lunar environment peculiarities for instruments design

19 p3514 A70-37631

THERMAL EXPANSION

NT THERMAL BUCKLING

Structural efficiency of composite tube columns with zero axial coefficient of thermal expansion, discussing three dimensional and planar fiber arrays

01 p0126 A70-10120

Elastic properties of thin curved cylindrical panels with constant mechanical properties subjected to thermal expansion and single face pressure

01 p0201 A70-10943

Structural orientation and defects in graphitized coke crystallites, establishing relation between thermal expansion coefficient and macrostructure

03 p0514 A70-12868

Long thin cylindrical tube with circumferential restraint analyzed for thermal expansions, obtaining maximum strains, bending moments, shear forces and plastic zone extent

[ASME PAPER 69-WA/NE-7] 04 p0768 A70-14756

Density, refractivity, thermal expansion coefficient, softening point and soaking stability for glass containing barium, lead, boron, bismuth and titanium oxides

05 p0871 A70-16594

Titanium and zirconium dihydrides room and higher temperature electrical resistivity, Hall effect and thermal expansion coefficients

08 p1517 A70-21149

Temperature increase effects on fully turbulent boundary layers at low Reynolds number in air investigated in wind tunnel

08 p1485 A70-21606

High temperature vacuum dilatometer for continuous photographic recording of expansion curves for refractory materials, determining thermal expansion coefficient

09 p1675 A70-22565

Composite materials macroscopic thermoelastic properties relationships to constituents properties, discussing effective thermal expansion coefficients and specific heats

09 p1703 A70-22682

Rapid guiding system for high resolution astronomical observations using thermal expansion of electrically conducting wires

09 p1721 A70-22741

Deuterium plasma expansion resulting from thermal shock produced by laser impulse

10 p1923 A70-24526

Thermal imaging device adaptable to IR, microwave or ultrasound radiation, projecting image on heat sensitive surface

11 p2050 A70-25643

Ni and Ni alloys thermal properties, discussing expansion and conductivity, melting and boiling points, vapor pressure, specific heat, entropy, etc

13 p2432 A70-28759

Free jet expansions in molecular beam sampling systems, using Sherman equations and chemical kinetic equations

[WSCI PAPER 70-12] 13 p2389 A70-29608

Composite cylindrical laser rods end region stress and optical pathlength change with thermal expansion or contraction between core and cladding

13 p2429 A70-29703

Specific heat, thermal pressure and molar volume of liquid krypton measured with adiabatic calorimeter, discussing thermal expansion coefficients

14 p2617 A70-31016

Gravitational atmosphere thermally driven motions, noting expansion towards lower density regions in solar chromosphere

15 p2804 A70-32619

Cobalt binary alloys allotropic transformation and thermal expansion at various temperatures

18 p3271 A70-35967

Automatic dilatometers for volume variations in steel and Co-W alloy during aging and heat treatment, noting microstructural changes

18 p3257 A70-36202

Thermal expansion anisotropy in graphite-epoxy composites causing residual stresses

[ASME PAPER 70-GT-129] 18 p3279 A70-36855

Microelectronic packages encapsulation by resin systems with emphasis on thermal expansion, discussing effects of curing temperature, reactive diluents, etc

20 p3655 A70-39444

Thermal stress and changes in modulus of elasticity and expansion coefficient effects on dynamical properties of turbine disks at high temperatures

20 p3721 A70-39783

Lattice parameter and thermal expansion of AlAs as function of temperature, indicating lattice match at 900 C with GaAs

22 p4086 A70-43004

Materials for glass-metal compressed joints, tabulating stress and thermal expansion coefficients

22 p3999 A70-43447

Allotropic transformation points and linear thermal expansion coefficients of Co-base binary alloy terminal solutions, using dilatometric method

23 p4203 A70-43864

Spacecraft thin walled tubular booms thermal curvature time constants in relation to solar induced despin of satellites

23 p4258 A70-44521

Circuit design providing thermal compensation for atmospheric pressure sensor, using mercury barometer

24 p4340 A70-46403

THERMAL FATIGUE

Fatigue tests results parametric representation for nickel base alloys tested at various temperatures and times to failure

04 p0707 A70-15264

Thermal stress and thermal fatigue data for utilization in design problems

05 p0932 A70-16161

Gas turbine blade material properties change effect on thermal fatigue strength after long term heating

05 p0864 A70-16700

Deformation and failure of refractory metals at high temperatures under constant and variable thermal loads concerning turbomachine components

05 p0865 A70-17027

Refractory materials deformation and failure analysis based on relations between stresses, strains and irreversible energy absorption per cycle in thermal cyclic fatigue testing

05 p0867 A70-17042

Scale factor effect on crack development in blanks and structure elements undergoing linear and complex stressed states under cyclic thermal loads

05 p0867 A70-17045

Nickel-based alloys small cycle thermal and mechanical fatigue limit during tensile stresses and operational temperatures, analyzing fatigue curves

05 p0867 A70-17046

Gas turbine blades thermal fatigue strength under simultaneous temperature cycles and static tensile loads, analyzing temperature and stress fields

05 p0953 A70-17053

Test stand design and automatic recording of turbine blade fatigue test data, including statistical evaluation

05 p0953 A70-17054

Steel elements failure during nonstationary thermal fatigue with varying strain and temperature, discussing linear damage accumulation theory

06 p1163 A70-17397

Temperature cycle duration effects on heat resistant alloys thermal fatigue resistance, noting stress relaxation occurrence

06 p1085 A70-17398

Structures elastic-plastic behavior under changing cyclic heating, calculating long time strength from linear damage accumulation assumptions

06 p1164 A70-17405

Thermal fatigue cracks in gas turbine blade models under simultaneous thermal cycling and static tensile loads simulating pulsed regimes

06 p1166 A70-17652

Thermal fatigue resistance of steel to copper weldments under thermal cycling, noting intergranular crack growth accompanied by oxidation along crack boundaries

06 p1078 A70-18515

Cylindrical Mo single crystals during cyclic heating, studying characteristic dislocation changes at various stages of thermal fatigue

07 p1308 A70-19609

Coffin method for thermal fatigue testing noting deficiencies in determining plastic strain, temperature distribution and tubular specimens durability characteristics, etc

09 p1701 A70-22298

Thermal and high strain fatigue covering cyclic tests, crack initiation and propagation, stress-strain behavior, structural design, frequency and temperature effects, etc

09 p1773 A70-22576

Multiaxial thermal fatigue cracking in carbon steels predicted by elastoplastic stress-strain analysis using finite element method

09 p1773 A70-22578

Turbine components design for low cycle fatigue, estimating thermal cycle number for high temperature crack initiation and propagation

09 p1774 A70-22583

Thermal fatigue cycle produced by cooled gas turbine blades, using stress-strain tests and thermal simulation

09 p1655 A70-22585

Turbines rotary shafts and stationary components thermal fatigue analysis, considering cycle numbers and stress concentrations under start-up, continuous operation and shut-down

09 p1775 A70-22593

High temperature fatigue crack growth in metal, suggesting condensation of vacancies at crack front after each loading cycle

09 p1776 A70-22644

Heat resistant materials strength characteristics with long service periods, formulating equation for time dependence of rupture resistance

10 p1903 A70-24237

Uniaxial low cycle thermal fatigue test procedure for ductile metals, describing strain measuring system allowing direct recording of load vs mechanical deformation

11 p2034 A70-26615

Gas turbine blade materials investigated for effect of prolonged heating on mechanical properties and thermal fatigue strength

13 p2434 A70-28994

Thermal fatigue cracking of gas turbine blades in fuel combustion product flow, investigating surface composition, microhardness and structure under simulated loads

19 p3490 A70-37338

Steels thermal fatigue in testing machine, investigating strains and stresses due to nonuniform temperature distribution during thermal cycle

21 p3840 A70-41433

THERMAL INSTABILITY

Protogalaxy mass limits determined for galactic formation by thermal instability due to radiative cooling and followed by nonlinear gravitational contraction

04 p0744 A70-14469

Thermal instability of uniformly rotating self gravitating homogeneous medium with perturbations in plane perpendicular to rotation axis

04 p0745 A70-14471

Unsteady inverse heat conduction of semibounded body solved by least squares method

06 p1178 A70-17856

Unsteady calorimetric sensor for measurement of heat transfer between gas jets and solid targets

06 p1064 A70-17857

Electromagnetic wave instability propagating across static magnetic field in presence of thermal anisotropy, considering interplanetary plasma and plasma devices stability

08 p1553 A70-21610

Radiative transfer effect on thermal instability and critical Rayleigh number in gray transparent fluid layer heated from below

10 p1967 A70-23952

Optimization in epihydrostatics and epihydrodynamics, discussing liquid in rectangular tank, electro-magneto-epi hydrodynamics and thermal instability

10 p1866 A70-24108

Stellar evolution in globular clusters, considering H-R diagrams of age, He abundance and thermal instability

16 p2973 A70-33076

Interstellar gas thermal instability under cosmic ray heating, investigating perturbations causing transition to dense cool phase in pressure equilibrium with intercloud phase

18 p3309 A70-37003

THERMAL INSULATION

Thermoelectric-couple life tests and efficiency measurements at constant thermal input, noting insulation for limiting parasitic heat losses [ASME PAPER 69-WA/ENER-14]

04 p0731 A70-14896

Reentry body aerodynamic heating and thermal insulation system design, discussing analytical procedure taking into account complex geometrical configurations

04 p0616 A70-15186

Multilayer insulation blankets with slits normal to energy transfer direction for thermal control of spacecraft and cryogenic tankage [AIAA PAPER 70-15]

06 p1156 A70-18076

Thermal isolation characteristics of interstitial materials in vacuum environment, inserting materials between contacting metal surfaces at various pressures and temperatures

06 p1181 A70-18143

Insulation materials selection for Martian soft lander to meet mission environmental conditions based on tests [AIAA PAPER 70-11]

06 p1182 A70-18224

Steady turbulent boundary layer of compressible perfect gas on heat insulated surface with suction and longitudinal pressure gradient

07 p1254 A70-19081

Turbulent incompressible boundary layer on porous heat insulated plate with uniform suction, calculating ratio of friction drag coefficients

07 p1254 A70-19082

Helium high energy molecular beams for insulating body heating and thermal constants determination

07 p1344 A70-20129

Thermal control coatings as solar reflectors for spacecraft heat dissipation

08 p1527 A70-21357

Error analysis of Barakat-Clark explicit heat diffusion equations for thermally insulated surface

08 p1600 A70-21831

Carbon deposit formation in gas turbine engines with various fuels, studying thermal insulation properties

09 p1742 A70-22472

Fire performance of spray applied rigid urethane foam applied as storage vessel insulation, noting continued functioning until destruction

09 p1710 A70-23345

Conduction to isothermal insulated cylinder from semiinfinite region

09 p1790 A70-23563

Heat insulated plate compressible boundary layer energy equations approximate solutions in hypergeometric functions

10 p1966 A70-23867

Moisture detector for evaluating trapped water effects in thermal insulation, describing equipment and test procedure

10 p1891 A70-24829

Insulation foils and surface coatings thermal properties effect on radiation properties for spacecraft thermal control systems

10 p1951 A70-24863

Plasma energy confinement time as function of discharge parameters for plasma thermal insulation in Tokamak-3

11 p2088 A70-25713

Radiative heat transfer due to radiation conductivity and transmission in low density glass fiber insulations by heat flowmeter for hot and cold surfaces

11 p2148 A70-25769

Insulators, ablators, reflectors and computer analyses for aerodynamic and engine heat for aerospace thermal design

11 p1980 A70-25874

Embossed/crinkled aluminized film multilayer insulation blankets with joints performance variation with temperature predicted by radiation heat transfer correlation

11 p2150 A70-26365

Thick superinsulation system design for long term cryogenic storage using superfloc, radiation shield and spacer material

11 p2150 A70-26367

Apiezon N grease thermal conductivity at liquid helium temperatures noting behavior as insulator

12 p2258 A70-27024

Heat conduction for thermally insulated bilayer metal wall for time-variable heat transfer and ambient temperature, using Green function

12 p2330 A70-27292

Heat transfer mechanism in foil-vacuum insulations, analyzing factors responsible for point of inflection on experimental temperature field curves

13 p2521 A70-28861

Thermal testing of inflatable solar shields for cryogenic space vehicles, discussing shield misalignment effects on propellant tank temperatures [AIAA PAPER 70-856]

16 p2982 A70-33901

Space suit thermal insulation properties, wear durability and nonflammability improvements, reflecting techniques in fabricating cryogenic multilayer insulation systems

[AIAA PAPER 70-851]

16 p2939 A70-33918

Concorde engine bay thermal insulation combining stainless steel foil and polytetrafluorethylene film, considering noise level, engine fire conditions and molten Ti globules penetration

18 p3346 A70-36345

Pyranometer with additional external glass cupola to eliminate temperature differences and heat exchange, discussing laboratory and field test results

20 p3626 A70-39034

Solar wind effects on thermal control coatings reflectance and absorbance, noting simulation and thermophysical measurement requirements [AIAA PAPER 70-833]

20 p3655 A70-39825

Numerical solution for multilayer insulation system comprised of infinite parallel metallic films separated by optically thin dielectrics

21 p3947 A70-41054

Multilayer insulation thermal scale modeling, discussing surface control techniques

21 p3951 A70-41865

Closed cell polyurethane foam for cryogenic insulation, determining thermal conductivity and net heat flow by analytical model and test

23 p4280 A70-44367

Aircraft passengers and crew fire protection in crashes via insulating air-carrying foam ejected into compartment from fuselage

23 p4140 A70-44465

THERMAL NEUTRONS

High energy neutron counter designed for recording slow neutrons produced in lead detector

05 p0845 A70-15935

Lunar rocks isotopic composition for Gd and variations due to low energy neutron capture produced by cosmic ray interactions

13 p2485 A70-28473

Electromotive force appearance in fissionable material semiconductor during thermal neutrons irradiation

13 p2469 A70-28879

Reactor, isotropic and accelerator neutron sources for thermal neutron radiography

24 p4375 A70-45746

Thermal neutron radiography with small accelerators using optimized collimator and fission increased flux

24 p4376 A70-45752

Thermal neutron radiography with 2.5 MeV Van de Graaff accelerator

24 p4376 A70-45753

THERMAL NOISE

Junction gate and MOS field effect transistors thermal noise calculations, using circuit analysis based on equivalent circuits

02 p0258 A70-12424

Electric potential fluctuations beyond long collisionless plasma cylinder in uniform magnetic field, noting thermal noise intensity

03 p0530 A70-13086

VHF field effect transistors thermal noise characteristics and effects of feedback and parasitic impedance

05 p0814 A70-16420

Gain-stabilization of SHF traveling wave maser radiometer, using thermal noise from neon discharge tube

12 p2228 A70-26881

Thermal feedback theory of flicker noise generation in transistors and temperature fluctuations effect in vicinity of recombination centers

12 p2196 A70-27687

Cryogenic Ge bolometers sensitivity variation and noise, noting radiation absorption by sensor and by coating

12 p2237 A70-28151

Junction and MOSFET transistors thermal noise characteristics at cryogenic temperatures

15 p2710 A70-32585

Pursuit-evasion differential games involving two linear dynamic systems with state and control dependent thermal noise

16 p2881 A70-32985

Frequency instability of oscillator perturbed by internal thermal noise [ONERA-TP-838]

16 p2872 A70-33105

Thermal noise in space charge limited solid state diodes by Langevin equation, relating spectral intensity for open and short circuit voltage and current

16 p2878 A70-33694

Shot, thermal, induced gate and flicker noise in various solid state devices and lasers

21 p3792 A70-42112

Crosstalk error in binary phase modulated communications systems due to RFI and thermal noise

23 p4158 A70-43752

THERMAL PLASMAS

Warm Maxwellian plasma stabilization of velocity-space instabilities, evaluating densities and temperatures for stabilizing resonant loss-cone modes

02 p0347 A70-12237

Bremsstrahlung emission from thermal plasma coexisting with relativistic electron tails, noting enhancement at electron plasma frequency harmonics

02 p0348 A70-12240

Field patterns of thin resonant and nonresonant antennas in warm plasma, using digital computer to evaluate propagation constant for current distribution

02 p0263 A70-12655

Wave-wave coupling of two HF electromagnetic waves launched into warm plasma across constant confining magnetic field, using Maxwell-Vlasov equations for electrons

02 p0349 A70-12757

Plasma devices for spacecraft propulsion taking into account electrothermal, electromagnetic and electrostatic systems

05 p0895 A70-15817

Wave dispersion across magnetic field in cold and warm collisionless Maxwellian plasma, discussing electromagnetic and electrostatic Bernstein modes

06 p1116 A70-17364

Coupled mode method, analyzing interaction between slow space charge wave of electron beam and electroacoustic wave of lossless warm plasma

07 p1349 A70-19687

Chemical synthesis in streaming thermal plasmas including HCN from cold methane and N plasma discharge chemistry

07 p1351 A70-19879

Thermal sheaths effect on cooled probes for stationary and flowing plasmas measurements at high pressure

08 p1497 A70-21528

Thermal plasma devices with discrete modes, describing periodic pulling and transition to continuous noise spectrum characteristic of turbulence
11 p2094 A70-26754

Spherical electroacoustic waves in drifting thermal plasma, describing ion acoustic perturbations
12 p2279 A70-27779

Plasmapause irregular structure and position indicated by measured distributions of hydrogen and helium thermal positive ions in duskside magnetosphere
13 p2397 A70-29185

Discharge effects on LF oscillations and ion extraction in hot cathode Penning plasma
13 p2463 A70-29370

Thermal induction plasma discharge characteristics, considering radiation and conduction losses
13 p2465 A70-29702

Wall stabilized arc source for spectroscopic measurements of isothermal plasma at various pressures
14 p2584 A70-30505

Streaming thermal plasma chemistry, reviewing diagnostic techniques and product oriented research
14 p2545 A70-30905

Small amplitude HF electromagnetic wave penetration in hot plasma slab, showing wave period/transit time ratio dependence of electromagnetic field distribution
14 p2551 A70-31037

Thermal relaxation rate in one and two dimensional electron plasma models with positive background, using particle in cell simulation
14 p2624 A70-31047

Wave propagation and group velocity in warm magnetoplasma, using adiabatic theory for ionosphere and far magnetosphere models
16 p2859 A70-32937

Coherent wave propagation in warm turbulent plasma, using perturbation method for wave dispersion
16 p2860 A70-32945

Thermal electrodeless plasmas generation at audio frequencies with closed magnetic circuit model
[AIAA PAPER 70-776] 17 p3139 A70-34478

Warm homogeneous magnetoplasma longitudinal cyclotron harmonic wave propagation perpendicular to static magnetic field, noting instabilities
17 p3140 A70-34927

Two component warm plasma wave propagation along magnetic field, considering full pressure tensor equation with momentum and pressure relaxation mechanisms
18 p3294 A70-36405

Magnetospheric thermal plasma electron density measurement during solar flare by OGO-5 satellite
19 p3411 A70-37513

Tonks-Dattner resonances in warm inhomogeneous plasma column, examining kinetic theory for waveform shapes and resonance location
19 p3475 A70-37534

Equilibrium compositions of helium-nitrogen, argon-nitrogen and xenon-nitrogen plasmas at atmospheric pressure between 5000 and 35,000 K
19 p3552 A70-37831

Square loop antenna radiation resistance in warm plasma, comparing theoretical results with measured values from Ariel 3 satellite antenna
21 p3796 A70-40562

Decomposition kinetics of alumina particles injected into thermal argon induction plasmas
21 p3855 A70-40878

Thermal plasma model along magnetic field lines outside plasmasphere with sharp density gradient in equatorial plane, using OGO-4 ion composition measurements
21 p3815 A70-41057

Shock waves and solitons structure propagating oblique to magnetic field in warm plasma based on two-fluid equations
21 p3857 A70-41382

Numerical analysis of inductive electrodeless discharge of thermal Ar plasma column heated by RF axial magnetic field
21 p3859 A70-41902

Maintenance voltage of RF argon thermal induction plasma at atmospheric pressure as function of ring probe
21 p3859 A70-41904

Nonzero electron temperature effect on mutual impedance of quadrupole probe in hot isotropic plasma
22 p4080 A70-42720

Magnetospheric thermal plasma studies via ground based whistler method, identifying radial and longitudinal irregularities in electron density, bulk motion and plasmapause position and displacements
22 p4021 A70-43281

Effective collision cross section for reaction resulting in Cs ions neutralization in thermal Cs plasma calculated from measured ion currents
22 p4082 A70-43374

German monograph on thermal and nonthermal phenomena in quasi-stationary convectionless plasma arc column, using 13-moment approximation for Boltzmann equation
24 p4382 A70-45089

Thermal power
U TURBOGENERATORS
THERMAL PROPERTIES
U THERMODYNAMIC PROPERTIES
THERMAL PROTECTION

Thermal protection systems /TPS/ design criteria for maneuverable reentry spacecraft, comparing weight and cost for various alloy systems
02 p0392 A70-11940

Thermal protective device for models exposed to flow buildup in intermittent wind tunnel, offering straightforward design, easy applicability, low cost and favorable experimental conditions
[ONERA-TP-755] 03 p0463 A70-13627

Thermal protection rating systems for clothing fabrics based on pain and blister effects in human skin
03 p0438 A70-14064

Interaction between surface liquid film and hot gaseous turbulent boundary layer analyzed for hypersonic vehicle surface thermal protection design problems
04 p0669 A70-14927

Reusable booster rocket heat protection system design, discussing ablation and insulation methods
05 p0958 A70-16635

Heat transfer boundary conditions determination in studying heat protective coatings effectiveness, discussing measurement methods for stagnation temperatures and heat fluxes from exhaust gases
06 p1173 A70-17662

Series emittance thermal control coatings of polymeric dielectric films overlaying reflectors vacuum exposed to UV, X ray and proton radiation
[AIAA PAPER 70-64] 06 p1106 A70-18069

Stable two phase water flow system for transpiration cooling in thermal protection of SST noise suppressor situated in afterburning engine exhaust gas stream
[AIAA PAPER 70-151] 06 p1181 A70-18146

Ablative materials for thermal protection at low convective heating rates, comparing foam and state-of-art materials performance
07 p1316 A70-18927

Heat protection effectiveness of rectangular channel plane wall with flow by air injection through aperture on wall
07 p1420 A70-19066

Reentry thermal protection materials technology, discussing thermophysical, thermomechanical and kinetic effects, noting interdisciplinary approach
07 p1319 A70-19878

Structural composite materials for thermal protection of reusable weight-saving vehicles in space transportation system
[AIAA PAPER 70-272] 07 p1397 A70-20382

Reusable metallic and nonmetallic thermal protection materials for space shuttle applications
[AIAA PAPER 70-273] 07 p1397 A70-20383

Abradable and abrasive types thermal spray coatings application to jet engine parts
10 p1893 A70-23856

Heat protection effectiveness of rectangular channel plane wall with flow by air injection through aperture on wall
10 p1970 A70-25217

Thermal protection polymers ablators efficiency evaluation using high vacuum DTA cell coupled to high resolution mass spectrometer
11 p2070 A70-25813

Lifting entry vehicle thermal protection system /TPS/ material performance, analyzing metallic radiator and passive transpiration systems and rigid insulator
11 p2150 A70-26368

Preoxidation treatment alleviating silicide pest in protective coatings for refractory metals, discussing effectiveness against high temperature oxidation
13 p2434 A70-29082

Supersonic slot cooling for surface protection at hypersonic speeds using contoured axisymmetric nozzle with streamlined body
14 p2663 A70-30257

Thermal porous bronze screened microphones for noise measurements in medium under large heat flow
14 p2555 A70-30298

Apollo thermal protection system noting low density ablation, flight and ground tests
[AIAA PAPER 68-1142] 15 p2813 A70-32514

Optimum guidance and control law for lifting reentry bodies, investigating plane descent trajectories for minimum structural heating
16 p2982 A70-33774

ZnO coating pigment for spacecraft thermal control, examining UV irradiation effects on electrical properties
16 p2961 A70-34056

Surveyor thermal switch for temperature control to assure spacecraft components performance during temperature extremes on lunar surface
16 p2845 A70-34127

Space shuttle systems structural design and thermal protection technology, stressing hardware reliability and reusability
16 p2986 A70-34227

Spacecraft shape and thermal coating pattern optimization by computer program
17 p3178 A70-35251

Reinforced plastic composites thermal protection and ablative performance in high temperature environments for reentry vehicle applications
20 p3656 A70-40029

Composite structural materials for thermal protection in reentry vehicles applications, evaluating fused quartz yarns, silicone rubber and phenolic resins
20 p3656 A70-40031

Metallic shell with passive thermal protection coating, solving boundary value problem for high temperature heating with simplified mathematical model
20 p3739 A70-40296

Thermal protection system based on radiation cooling for high altitude cruising hypersonic flight, achieving zero net mass transfer
21 p3950 A70-41745

Ablative response predictions analysis heat sources, discussing boundary layer edge conditions definition, atmospheric entry, rocket propulsion, etc
21 p3952 A70-42055

Reentry protection for radioisotope heat sources, using thermal switch of composite ceramic foam with metal impregnants
22 p4054 A70-42958

Space vehicles with shielding for protection against meteor impacts, discussing tubular radiator design for heat removal
23 p4284 A70-45008

THERMAL RADIATION

Polarization of nonspherical plasma emission region in thermal X ray stars
02 p0357 A70-11787

Radiation from flames in gas turbines and rocket engines, discussing effects of soot formation fuel chemical composition, combustor operating conditions, etc
02 p0354 A70-12050

GaAs n-type single crystals thermoreflectance spectra at various energies
03 p0541 A70-13721

Heat transfer to absorbing fluid by coupled thermal radiation and laminar forced convection at pipe entry region, considering gray and nongray absorption
[ASME PAPER 69-WA/HT-16] 04 p0783 A70-14818

Line scanning IR imagery system for thermal mapping of fire, water and soil conditions
05 p0836 A70-15770

Thermal and dynamical evolution of gas clouds in transparent and opaque stages by comparing rates of cooling, heating, contraction and expansion
05 p0907 A70-16041

Space temperature determination, discussing planet or satellite absorption and radiation rate dependence on surface characteristics, solar radiation, planet albedo and thermal radiation
05 p0914 A70-16629

Thermal radiation effects on plane magnetoacoustic waves in seminfinte expanse of radiating gas of perfect electrical conductivity
05 p0890 A70-16822

Solar, albedo and earth thermal radiations absorbed by partially obscured spacecraft calculated on digital computer for various orbital positions
06 p1173 A70-17556

Atmospheric temperature vertical profile reconstruction from ascending radiation observations using data regularization
06 p1097 A70-17793

Thermal emittance of Cu measured in vacuum in spherical enclosure by calorimetric method to investigate oxidation effect
[AIAA PAPER 70-66] 06 p1180 A70-18139

Emittance measurement by thermal decay integration method
06 p1184 A70-18597

Step profile decay of initial perturbations of radiating gas as function of optical depth and Boltzmann number
07 p1255 A70-19212

Volt-watt sensitivity of dilatocapacitor types of thermal radiation receivers, noting low natural noise levels
07 p1284 A70-19815

Far IR radiation at galactic center suggested as thermal emission by dust particles
09 p1744 A70-22502

Thermal radiative transfer in nonuniform anisotropic magnetoactive plasma, correcting term of Zheleznyakov equation
09 p1734 A70-22514

Molybdenum heat capacity, electrical resistivity and thermal radiation measurements at high temperatures with millisecond resolution
09 p1706 A70-22955

Thermal radiation absorption in hemispherical cavity, determining apparent absorptivity for diffuse and parallel irradiation
09 p1790 A70-23565

Terrestrial surface radiometric imaging by sensing thermal radiation at centimeter wavelengths to reduce atmospheric scattering attenuation
09 p1687 A70-23763

Thermal radiation shield influence on stationary radiative heat transfer in closed arbitrarily shaped two gray surface system

10 p1966 A70-23865

Thermal transducer for rapid nondestructive testing, discussing imaging of specimen bond defects and thermal property differences

10 p1894 A70-24173

Atmospheric temperature vertical profile reconstruction from ascending radiation observations using data regularization

10 p1913 A70-25024

Meteorological Nimbus 3 satellite and aircraft observations of thermal radiation for vertical atmospheric temperature profile measurement

11 p2075 A70-25921

Intensity and photocounts statistical distribution of harmonic generated in nonlinear crystal by laser and thermal radiation

12 p2248 A70-27547

Standard sources and detectors for thermal radiation measurement

13 p2410 A70-29654

Thermal longwave radiation measurement applications to atmospheric radiation transfer and weather processes

13 p2411 A70-29663

Stefan-Boltzmann formula validity for flames and combustion products radiation affected by time dependence of emissivity coefficient, place and wavelength

14 p2662 A70-30179

Lunar surface roughness effects on thermal radiation, using model surface with parallel troughs

14 p2649 A70-31212

Temperature measurement of rotating shafts under cyclic loading, using thermistor as thermal radiation sensor

15 p2734 A70-31581

Shock waves structure in radiating gases at high temperatures, taking into account radiation anisotropy in shock front

15 p2720 A70-31645

Thermal EM field as function of coherent states, outlining quantum theory for thermal radiation and solar energy

15 p2678 A70-32423

Kirchhoff law validity for freely radiating metallic surfaces, using emissometer to measure hemispherical emittance

[AIAA PAPER 70-858]

16 p2999 A70-33903

Diffuse specular rough surface measure for imperfect reflections in thermal radiation transfer through slot passages

[AIAA PAPER 70-860]

16 p2999 A70-33905

Titan 3C solid rocket motor exhaust plumes thermal radiation analysis for designing Stage I engines and components thermal protection

[AIAA PAPER 70-842]

16 p3000 A70-33925

Extinction parameters of submicron carbon, tungsten and Si particles in hydrogen measured at various temperatures, discussing scattering amplitude functions and Monte Carlo calculations

[AIAA PAPER 70-838]

16 p3001 A70-33933

Thermal radiation configuration factors tables giving reference sources, discussing historical development of factors

[AIAA PAPER 70-814]

16 p3002 A70-33947

Radiation gas dynamics, investigating thermal radiation effects on flow field of high temperature gas

17 p3195 A70-35038

Thermal choking of channel flow by radiative transfer from upstream and application to shock waves generation

17 p3195 A70-35039

Lunar millimeter wavelength thermal radiation measurement noting surface roughness effect on polarization

17 p3171 A70-35559

Rayleigh-Gans-Born approximation application to thermal radiation of reflecting convex plasma sphere, cylinder and ellipsoid

18 p3294 A70-36146

Background thermal radiation veiling effect on IR photography extension into long wave spectrum

18 p3257 A70-36282

Atmospheric layer attenuation of thermal radiation from water surface by airborne radiation thermometer measurements

18 p3260 A70-36969

Skin simulation for thermal radiation protection studies, considering fused silica and epoxy resin filled with Al powder

18 p3225 A70-37093

Book on heat transfer covering conduction, convection, thermal radiation and heat exchange equipment

19 p3550 A70-37231

Thermal radiation effect on plane shock wave propagation, using perturbation technique and method of characteristics

19 p3551 A70-37532

Tables on thermal radiative properties of heated air covering absorption coefficients for wide range of photon energies and temperatures

19 p3552 A70-38009

Book on thermal radiative properties of air, Volume 2, covering reaction rates, photons and charged particles interactions with air molecules, secondary air excitation, etc

19 p3552 A70-38010

Thermal radiation detectors operation principles, design, specifications and applications

20 p3632 A70-39626

Thermal radiation spectrum power of small spherical tin and lead particles

20 p3737 A70-39745

Microsecond response bolometer for measuring thermal radiation fluxes in shock tube, discussing design, calibration and performance

21 p3824 A70-40859

Surface roughness effects on thermal radiant energy interchange between opaque interacting surfaces formulated for unequal temperature adjoin plates

21 p3944 A70-41018

Traveling thermal wave induced channel flow, examining velocity profile thermal boundary conditions and shear stress

21 p3948 A70-41247

Radiative propagation nondiffusive effects of thermal pulse in explosion, obtaining solutions for plane and spherical case by asymptotic expansion and numerical integration

21 p3950 A70-41379

Thermal design of high altitude balloons and instrument packages, analyzing vertical motion dependence on heat transfer and radiation environment

21 p3755 A70-42077

Contrail effects on atmospheric thermal radiation budget in heavy jet traffic regions from airborne IR and solar radiometric observations

23 p4214 A70-44033

Thermal radiation emissivity predictions for metal surfaces at cryogenic temperatures, comparing anomalous skin effect and Drude single electron theories

23 p4218 A70-44388

Launch optimization of artificial satellites for minimizing thermal radiative heat input during low altitude orbit

23 p4264 A70-45047

Delphini and Serpentis Novae radio emission in microwave spectra, noting consistency with thermal radiation of expanding ionized gas envelopes

24 p4410 A70-45771

THERMAL RADIO EMISSION

U RADIO EMISSION

U THERMAL EMISSION

THERMAL REACTORS

ZrH reactor program and multikilowatt space oriented thermoelectric power conversion systems

22 p4071 A70-43190

THERMAL RESISTANCE

Refractory and heat resistant materials thermal diffusivity coefficient, discussing theoretical basis and technical implementation for measurement at high temperature

01 p0085 A70-10178

Heat resistant coatings in high temperature gas flow, studying external layer deformation kinetics during shrinkage

03 p0483 A70-13250

Constant temperature hot-wire anemometer to compensate for thermal lag of wire/film resistance thermometer within useful frequency range

03 p0492 A70-13761

Unsteady heat conduction and thermal stresses in thin isotropic semibounded plates with butt joint possessing internal thermal resistance

04 p0766 A70-14479

Graphite foam reinforced by carburized high polymers used for fabricating highly porous heat and corrosion resistant material

[DGLR-69-57]

04 p0712 A70-15178

Dry heat resistance of bacillus subtilis var. niger spores on selected planetary lander capsule surface materials

04 p0645 A70-15442

High temperature polymers including polybutadiene, polyphenylene sulfide, polysulfone, polybenzimidazole, etc

05 p0869 A70-16038

Thermal resistance of multicontact heat conducting stainless steel plate stacks with different interface purities in vacuum

05 p0957 A70-16293

Binary Al-Y system thermal and microstructural analyses at room temperature and 200 C, obtaining partial diagram and mechanical properties

05 p0864 A70-16546

Heat resistant silicate enamel coatings to protect steels and alloys against high temperature gas corrosion, studying properties by various methods

05 p0872 A70-16600

Polymers with high temperature oxidation resistance, discussing problems caused by aromatic heterocyclic structures and manufacturing methods

05 p0873 A70-16604

Heat resistant materials damping properties at high temperatures under distributed stresses measured in thin walled tubular specimens with vibrogram

05 p0952 A70-17049

Heat resistant enamel coatings effect on vibration damping of cast steels for turbine blades

05 p0868 A70-17050

Precooling effect on load carrying capacity of heat resistant plastics subjected to unilateral heating

05 p0874 A70-17065

Heat resistant plastics stability subject to unilateral heating with allowance for mass removal, obtaining dimensionless stability characteristics for structures design

05 p0874 A70-17066

Metals mechanical properties with inorganic heat resistant coatings between 1900-2300 K in oxidizing medium, describing facility based on solar furnace

05 p0875 A70-17069

Diffusion layer and protective oxide composition changed to increase chrome plated Mo heat resistance

06 p1089 A70-17742

Aluminosilicate coatings for increased Ni-Cr alloys heat resistance due to silicon properties

06 p1089 A70-17743

Structure, phase composition and heat resistance of diffusion layers obtained by surface alloying of Nb alloy with Cr, Ti and Si

06 p1089 A70-17744

Multilayer insulation blankets with slits normal to energy transfer direction for thermal control of spacecraft and cryogenic tankage

[AIAA PAPER 70-15]

06 p1156 A70-18076

Rough metal surfaces thermal constriction resistance for total heat flow through microcontacts

07 p1418 A70-18648

CW high power operation of transferred-electron oscillators realized by low thermal resistance, describing fabrication

07 p1241 A70-19300

Alloying elements effect on polymorphic alpha-beta transformation temperature of Ti systems, discussing heat resistance

07 p1307 A70-19555

Molybdenum single crystals orientation effect on thermal resistance to argon plasma flow

07 p1309 A70-19614

Steady temperature field of two dimensional periodic contact surface in vacuum, using conjugate harmonic functions for thermal flux lines, isotherms and thermal resistance

07 p1423 A70-19820

PbTe-based Sn, Se and Ge alloys lattice constant, thermal EMF and resistance, fusibility and microstructure

08 p1555 A70-21117

Harmonics generated in hot-wire anemometers responses by wires thermal lag and amplitude of flow velocity fluctuations using computerized simulation

08 p1498 A70-21586

Thermal resistance for inappropriately spaced contacts using electrolytic analog experiments

08 p1599 A70-21590

Correlation functions for resistance to heat and momentum transfer in viscous sublayer at rough walls defined for varied geometry flows

[ASME PAPER 69-HT-2]

08 p1486 A70-21833

Thermal contact resistance of anisotropic materials using mathematical geometric transformation

[ASME PAPER 69-HT-47]

09 p1790 A70-23552

Phase equilibrium diagram and heat resistance of Ti-Al-Nb alloys along radial section by thermal and microstructural analysis

09 p1709 A70-23789

Temperature insensitive telescope with metallic mirror at Milan-Merate Observatory

10 p1889 A70-24584

Hollow cylindrical sample scale effect on accuracy of testing heat resistance of brittle materials

10 p1965 A70-25301

Heat resistance and elastic properties of binary Ti-Mo alloys as function of phase structure and chemical composition

11 p2066 A70-25915

Thermal metal fatigue testing, including resistance to cyclic temperature variation, operating conditions simulation and stress-strain determination

12 p2322 A70-27218

Heat resistance of machined stainless steel and molybdenum contact pairs in vacuum, discussing compressive loads and surface defects effects

12 p2243 A70-27290

Fine grained structure effect on steels and Ni alloys short term heat resistance at high temperatures

14 p1594 A70-30168

Interatomic bond strength in solid solutions of Ti-Sn-O with respect to heat resistance at elevated temperatures

14 p2595 A70-30170

Thermal and electrical resistances of Na at low temperatures measured by germanium thermometers and galvanometer amplifier

14 p2617 A70-31021

Kovpak method for estimating and extrapolating heat resistance characteristics, considering alloy long term strength

15 p2755 A70-31528

Macromolecular polymer based heat resistant materials

15 p2765 A70-32264

Thermal constriction resistance between contacting metallic paraboloids applied to instrument bearings [AIAA PAPER 70-857] 16 p2998 A70-33902

Heat resistance evaluation of Zh S6-K alloy subjected to multicomponents surface diffusion 17 p3125 A70-35407

Thermal contact resistance, discussing behavior at cryogenic temperatures and directional or thermal rectifying effect 17 p3197 A70-35541

Polythermal phase equilibrium and heat resistance of Ti-rich Ti-Zr-Al alloys, noting creep and tensile tests 18 p3275 A70-36124

Heat resistance of cast, forged and annealed Ti-Cu alloys, discussing forged alloys mechanical properties as function of chemical composition and temperature 19 p3449 A70-37273

Power and exponential time dependences of long term creep strength for wide stress range, assuming linear heat resistance 19 p3449 A70-37340

Heat resistant coatings in high temperature gas flow, studying external layer deformation kinetics during shrinkage 19 p3428 A70-38468

Dimensionless heat transfer and resistance coefficients during stabilized nonNewtonian fluid flow in circular pipe 20 p3613 A70-40176

Heat resistance of machined stainless steel and molybdenum contact pairs in vacuum, discussing compressive loads and surface defects effects 20 p3638 A70-40340

Crystal orientation dependence of thermal resistance and gage factor in electron irradiated n-type silicon strain gages 21 p3824 A70-40862

Surface films effect on thermal contact resistance of microscopically sized contacts 21 p3944 A70-41023

Surface films effect on thermal contact conductance of aluminum surfaces contacting in high vacuum environment 21 p3944 A70-41024

Gold foil surface thermal contact resistance, investigating temperature and pressure effects and elastic and plastic deformation of surface structure 21 p3953 A70-42166

Temperature distribution and thermal constriction resistance due to steady heat flow in laminated composite 22 p4126 A70-43689

Fibrous, cellulosic, elastomeric and plastic materials with improved flame resistant properties for space applications 23 p4152 A70-44461

Manned spacecraft nonmetallic construction materials selection criteria, testing and configuration control, considering flammability hazard 23 p4152 A70-44462

Chemical composition effects on heat resistance, elastic properties and density of Ti-Ta alloys 24 p4360 A70-45830

Heat resistant surface diffusion alloying of Ni alloys with Cr, Ti and Si saturation 24 p4361 A70-45834

Thermal constriction resistance due to nonuniform metal surface conditions, considering macroscopic contact resistance for nonuniform interface pressure distribution 24 p4429 A70-46177

High temperature solar furnace for investigating heat resistant protective coatings thermal stability 24 p4350 A70-46331

Molybdenum disilicate and aluminum oxide coating sealing heat resistance tests 24 p4364 A70-46341

THERMAL SHIELDING

U HEAT SHIELDING

THERMAL SHOCK

Laser beam technique applied to thermal shock testing of metal disks, using solid state laser, compared to predicted results 01 p0113 A70-11058

Kinetic theory of cracks network formation on LiF crystal surface exposed to plasma jet using high speed camera 04 p0730 A70-14458

Fracture mechanical theory for crack propagation in brittle ceramics subjected to thermal shock, deriving crack stability criteria 04 p0767 A70-14505

Structural material selection for thermal shock conditions, deriving index from parameters governing solutions in thermoelasticity 07 p1413 A70-20002

Deuterium plasma expansion resulting from thermal shock produced by laser impulse 10 p1923 A70-24526

One dimensional compressible flow with heat addition in nonconstant area duct extended for friction addition, discussing critical thermal shocking 11 p2041 A70-26651

Thermal shock waves structure and effective temperature in stellar atmospheres taking into account absorption effects and possible isothermicity 12 p2306 A70-27861

Kinetic theory of cracks network formation on LiF crystal surface exposed to plasma jet using high speed camera 13 p2510 A70-28655

Thermal conductivity and shock resistance of flame and plasma sprayed zirconia coatings on Ni-Mo-C metal [ACS PAPER 22-C-68F] 15 p2762 A70-32527

Photothermometer response to thermal shock, considering rapidly varying surface temperature measurement 16 p2901 A70-33104

Reliability test facilities for military shipboard electronic equipment, subjecting equipment to combined thermal shock and vibration cycles 16 p2888 A70-33125

German monograph on thermal stresses due to thermal shocks on front surface of infinitely long circular solid cylinder 17 p3189 A70-35371

Creep resistant Ni-base superalloys ductility and thermal shock resistance improvement by precision casting technique, producing columnar grain and single crystal structures 20 p3648 A70-39415

Polycrystalline aluminas under thermal shock, investigating strength decrease and subcritical crack formation 22 p4059 A70-43413

THERMAL SIMULATION

Jupiter atmosphere temperature and density profiles determined from thermal models based on thermal structure above dense cloud level 02 p0367 A70-11814

Space simulation test results compared with analytical methods for thermal data prediction of Azur satellite 04 p0762 A70-15182

Computerized thermal model simulating environment control system, crew and vehicle structure in performance prediction for Apollo lunar module [SAE PAPER 690621] 05 p0922 A70 15848

Plasma arc tests to simulate stagnation reentry heating on spherical subized models of nuclear heat source to investigate heat shield materials ablation characteristics 06 p0974 A70-18172

Simulated Concorde kinetic heating system for ground studies of thermal stresses 07 p1250 A70-19744

Computer program predicting thermal response of fusion welding tooling chill bars and holding fixtures, simulating moving heat source and contact 08 p1508 A70-21487

Three dimensional RC network simulating temperature fields in IC at different heat source power dissipation laws, discussing harmonic heat source field 09 p1643 A70-22128

Microorganisms survivability in soils near spacecraft assembly areas during simulated Martian freeze-thaw cycles 09 p1619 A70-22768

Thermal vacuum simulator for testing manned Lunar Module Test Vehicle, using conformal skin heaters to control heating rates and skin temperature 09 p1656 A70-23241

Thermal metal fatigue testing, including resistance to cyclic temperature variation, operating conditions simulation and stress-strain determination 12 p2322 A70-27218

Spacecraft thermal mathematical model adjustment to fit measured temperatures, using iteration method 15 p2812 A70-32513

Computerized thermal modeling of spacecraft environmental control systems (ECS) 15 p2705 A70-32523

Radiation and conduction of open joint multilayer insulation systems, analyzing dependence on contact area by numerical methods 16 p2939 A70-33915

Correction techniques for thermal network lumped parameter inaccuracies with conduction and radiation coupling, considering temperature control system [AIAA PAPER 70-821] 16 p3002 A70-33943

Mathematical model of heat flux absorbed by heated part in radiant heating reflector systems, considering shape, spectral, directional and polarizing effects [AIAA PAPER 70-818] 16 p3002 A70-33945

Nonlinear three nodes analysis for thermal design of spinning spherical satellite 17 p3177 A70-35249

Satellite temperature distribution prediction from digital simulation 17 p3177 A70-35250

Thermal space simulation tests on Azur research satellite relating to temperature control subsystems and qualification and acceptance procedures 19 p3399 A70-38288

Thermal scale modeling of heat pipe in deep space, using material and heat flux preservation techniques 21 p3946 A70-41048

SST sonic boom noise level reduction by thermal simulation of long body aircraft, considering thermal spike or keel [AIAA PAPER 70-1323] 24 p4291 A70-45942

THERMAL STABILITY

Conflicting requirements for reflection reduction, thermal stabilization and radiation protection satisfied by three layer coatings on Si photocells 01 p0159 A70-10768

Transmitting-receiving latching ferrite switch with 180 degree differential phase shift toroids for temperature stability and receiver protection in case of driver failure 03 p0458 A70-14036

Thermal stability of graphite core-solid hydrogen mantle grains determined from temperature and evaporation rates calculated for interstellar space 04 p0743 A70-14398

Thermal stability of turbine sealant mica-ceramic materials containing boron nitride 04 p0712 A70-14467

Thermal recovery factors at hemispheric probe stagnation point in low density supersonic jets of He-Ar and H-N mixtures [ASME PAPER 69-WA/HT-27] 04 p0782 A70-14810

Commercial Ni-Co gas tungsten arc filler metal with mechanical properties stable following stress relief 04 p0710 A70-15653

Mechanical properties of eutectic superalloys compared with commercial superalloys, noting thermal stability applicability to gas turbine engines [SAE PAPER 690689] 05 p0861 A70-15827

Insulating materials and apparatus evaluation in terms of thermal capability to effect competitive cost saving 05 p0869 A70-16033

Adjustable pulse delay circuit design utilizing slow switching action of storage diodes emphasizing thermal stability 05 p0820 A70-16343

Crack stability under tension and thermal stresses caused by uniform disturbed heat flow, using Barenblatt fracture criterion 05 p0939 A70-16483

Thermal stability of materials and structural elements - Conference, Kiev, Ukrainian SSR, December 1967 05 p0947 A70-17026

Optimal thermomechanical treatment for austenitic steel stability to resist propagation and unloading of dislocations in cyclic loading process 05 p0867 A70-17041

Precooling effect on load carrying capacity of heat resistant plastics subjected to unilateral heating 05 p0874 A70-17065

Heat resistant plastics stability subject to unilateral heating with allowance for mass removal, obtaining dimensionless stability characteristics for structures design 05 p0874 A70-17066

Tensile and stress rupture tests facility for microsamples stability at temperatures up to 3300 K, investigating deformation and failure 05 p0830 A70-17073

Automatic temperature stabilizer with high order amplification due to direct heater sensing, noting applicability for synthetic fiber plants and thermophysical laboratories 06 p1064 A70-17783

Chromized molybdenum thermal stability under cyclic induction heating and subsequent air cooling 07 p1304 A70-18743

Soviet book on structures design for stability at high temperatures with large gradients, discussing thermoelasticity, thermoplasticity and creep equations for shells, plates, etc 07 p1409 A70-19601

Penetrative thermal convection stability for statically unstable layer surmounted by statically stable layer from numerical integration of linearized equations of motion and heat conduction 07 p1269 A70-19947

Thermal convection determination in earth, Venus, Mars and moon interiors based on thermal stability analysis, obtaining viscosity depth profiles 07 p1272 A70-20203

Silicon containing alpha matrix Ti alloy with high creep strength and stability at elevated temperatures, studying processing and heat treatment effects on properties 08 p1509 A70-21853

Irreversible viscosity decrease and thermal stability in polymer-containing lubricating oils under shearing forces effect 09 p1693 A70-23408

Long time static strength, durability and thermal stability relations determined for heat resistant alloys at operational temperatures 10 p1903 A70-24238

Carbon composition resistors investigated for cause of resistance dependence on thermal pulses, suggesting application as stabilization process

10 p1849 A70-24617

Thermal imbalance effect on stellar pulsational stability using linear quasi-adiabatic pulsation theory

10 p1946 A70-24980

Temperature instability of electro-optical laser modulators using ADP, KDP and DKDP crystals taking into account phase shift between coherent light beams

11 p2063 A70-25848

Water cooled metallic diaphragm thermal stability effect on plasmatron electric arc characteristics stabilized by vortex air flow

11 p2093 A70-26736

Gamma irradiation effects on thermal stability and decomposition of ammonium perchlorate

12 p2289 A70-26870

Interstitial solid solutions stability in cast molybdenum subjected to heat treatment

12 p2257 A70-28225

Aliphatic diesters as high temperature lubricants, discussing viscosity range extension, oxidation inhibition and thermal stability

13 p2438 A70-29125

Elastic material filled cylindrical, segmented toroidal and conical shells thermal stability, allowing for stiffener eccentricity

13 p2516 A70-29523

Cobalt surface X ray analysis after spark erosion treatment, revealing phase with high temperature stability

14 p2596 A70-30840

Thermal stability of simply supported bimetallic shallow spherical shell, considering rotationally symmetric deflection modes

14 p2657 A70-30845

Thermodynamic stability of methane clathrate hydrate, building up ice grains halo within comets inner coma

14 p2650 A70-31243

Space erectable boom with interlocked seam, perforations and coatings to provide torsional rigidity and thermal stability

16 p2986 A70-34143

Creep resistant Ti alloys with high temperature strength and stability, comparing tensile data for room temperature and 900 F

17 p3122 A70-34440

Thermal stability of glycolytic enzymes from thermophilic clostridia

17 p3042 A70-35327

Diffusion during high temperature exposure of protective coatings on Mo, noting compact layers and carbide forming elements effect on thermal stability

17 p3125 A70-35404

Flexible thermostat for specific temperature range with liquid nitrogen coolant and gas transfer medium

17 p3096 A70-35850

Solar prominences thermal and dynamical stability in terms of optically thin plasma supported by magnetic field against gravity

17 p3174 A70-35867

Amorphous film formation and crystallization, discussing thermal stability

18 p3297 A70-36320

Thermal stability test assembly for refractory materials cylindrical specimens, using argon plasma jet

19 p3395 A70-37351

Nonuniform emitter current distribution effect on power transistor thermal stability, discussing temperature distribution effects

19 p3387 A70-37821

Semiconductors, ferrites and segnetoelectrics automatic temperature stabilization problem based on heat source energy conversion

20 p3597 A70-39255

Portable telescope for river and ocean vessels, discussing design and operation thermal stability and hermetization

20 p3629 A70-39311

Ammonium and magnesium perchlorate mixture thermal stability study with differential scanning calorimetry, noting exothermic decomposition of AP

20 p3688 A70-40272

Aromatic polymers synthesis for good thermal stability, describing single and double stranded chains

21 p3782 A70-42127

Organic spiro polymers synthesis for thermal stability by condensation of aliphatic spiro tetraamines and aromatic dianhydrides

21 p3782 A70-42128

Thermal stability of polymers based on aromatic diamines and isomeric dibenzoylbenzenes

21 p3782 A70-42129

Thermally stable arylsulfonamide polymers incorporating 1, 2-disulfonamide group

21 p3782 A70-42130

Polyimadazopyrrolone films relative thermophysical properties, noting polymers thermal stability dependence on carbonyl groups percentage

21 p3783 A70-42132

Poly(perfluoroalkylene oxides) preparation and curing, considering molecular weight and thermal stability

21 p3783 A70-42145

Thermally stable polyimide resins for carbon fiber composites, noting high temperature strength, oxidation resistance and electrical insulation properties

22 p4058 A70-42478

High thermal stability glass fibers alternatives improving stiffness-to-weight ratio of resin and Al-based composites used in F-111 boron epoxy wings

22 p4058 A70-42480

Temperature stable homogeneous single phase zirconate solid solution ceramics for microwave dielectric resonators and microstrip substrates

22 p3996 A70-42922

Thermal-acoustic oscillations in forced convection, giving time delay analog for perturbation feedback

23 p4280 A70-44369

Nonspherical stars thermal stability, considering solar rotational models and oblateness problem

23 p4252 A70-44833

High temperature solar furnace for investigating heat resistant protective coatings thermal stability

24 p4350 A70-46331

THERMAL STRESSES

Thermal stresses in infinite layer of transversely isotropic material due to crack with prescribed normal displacement, deriving temperature distribution

01 p0200 A70-10552

Circular plate nonlinear analysis under load and uniform midplane temperatures, using stationary potential energy principle

01 p0205 A70-11145

Transient temperature profiles and thermal stress distribution in circular plates and cylinders with eccentric hole determined by conformal mapping

01 p0207 A70-11153

Transient thermal stress concentration at small thickness change of plate obtained by photoelastic studies

01 p0207 A70-11157

Machine parts fatigue strength under thermal cycles, studying nonlinear dependence of energy dissipation per unit volume on cycles number

02 p0383 A70-11654

Fiber composites dimensional changes, stresses and plastic flow during component allotropic transformation, studying temperature variations effects

03 p0585 A70-12973

Laminate approximation model of randomly oriented fibrous composites estimating stiffness and thermal and expansional strains

03 p0587 A70-13126

Bearing strength and rupture of reinforced plastic composites under intense one-sided electric heating and hydrostatic pressure due to pyrolysis of plastic bond

03 p0515 A70-13244

Unsteady temperature field induced stresses and strains in hollow viscoelastic sphere calculated by solving integrodifferential equation having right hand side dependent on time function

03 p0590 A70-13398

Thermoelastic stresses in plate due to arbitrary temperature variations of heat transfer agent calculated in second approximation, allowing for transfer coefficient time dependence

03 p0590 A70-13400

Thermoelastic stresses in diode of pulsed and CW injection lasers, showing energy parameter limitation

03 p0499 A70-13437

Temperature field in thermally stressed electric machine rotor obtained by solving Poisson and Laplace equations with digital computer, using network method

03 p0414 A70-13517

Transient thermal stresses in photoelastic models of various shapes under various steady state or transient temperature conditions, describing instrumentation and experimental methods

03 p0600 A70-14308

Thermal stress concentration produced by cracks, notches and fillets in plates free from external loads measured photoelastically

03 p0600 A70-14310

Thermal stresses of semiinfinite plate with circular hole filled with elastic inclusion and subjected to uniform heat flow

03 p0601 A70-14317

Thermoelastic stresses in solid cylinder under cyclic temperature variation, calculating amplitude for Biot numbers

04 p0766 A70-14477

Unsteady heat conduction and thermal stresses in thin isotropic semibounded plates with butt joint possessing internal thermal resistance

04 p0766 A70-14479

Transient temperature distribution, thermal stresses and deformations in thin finite circular disk due to continuous point heat source, using linear thermoelasticity

[ASME PAPER 69-WA/PVP-6] 04 p0768 A70-14789

Thermal stresses in transversely isotropic hollow circular cylinder, applying formulas derived to reentry vehicles aerodynamic heating

04 p0779 A70-15608

Pressure sensitive components in cordwood modules noting temperature and pressure damaging stresses during encapsulation

05 p0855 A70-16037

Thermoelastic stresses in rotating circular cylinder, analyzing temperature effect on angular velocity for neo-Hookean material using finite deformation theory

05 p0930 A70-16080

Thermal stress and thermal fatigue data for utilization in design problems

05 p0932 A70-16161

Crack stability under tension and thermal stresses caused by uniform disturbed heat flow, using Barenblatt fracture criterion

05 p0939 A70-16483

Thermal stresses in shell with spherical and circular cylindrical sections, using thin shell approximations and shallow shell theory

05 p0945 A70-16818

Tektite size restricted by thermal stress limit on diameter and aerodynamic load limit on length

05 p0916 A70-16831

Gas dynamic stand for testing turbine disks strength under mechanical and cyclic thermal loads, analyzing breakdown data for various disk geometry

05 p0953 A70-17052

Rotor blades structural fatigue strength tested on gas dynamic test stand under cyclic thermal loading and static tensile load

05 p0954 A70-17058

Error resulting from elasticity modulus and linear thermal field coefficient removal from integral in Burger formula for turbine blade thermal stresses

05 p0954 A70-17061

Fiberglass reinforced plastics load carrying capacity under unsteady unilateral heating described by thermal similarity criteria

05 p0955 A70-17070

Heat stress due to microwave radiation, establishing reduction factor for radiation protection guide number under adverse thermal environments

06 p0998 A70-17202

Thermal and mechanical stresses in rectangular composite beams, considering effects of temperature and reinforcing fiber orientation

06 p1164 A70-17503

Uncoupled quasi-static boundary value problem for linear viscoelastic solids undergoing thermal and mechanical deformation solved by computational algorithm

06 p1168 A70-17937

Energy methods used in thermoelastic analysis of thermal stresses and deflections in thin rings

07 p1401 A70-18935

Unsteady temperature field and thermal stresses in reinforced anisotropic plate strengthened at rim by thin isotropic rod

07 p1408 A70-19543

Cylindrical Mo single crystals during cyclic heating, studying characteristic dislocation changes at various stages of thermal fatigue

07 p1308 A70-19609

Simulated Concorde kinetic heating system for ground studies of thermal stresses

07 p1250 A70-19744

Computer procedures for solving temperature stresses in thin infinite isotropic viscoelastic plate with heat transfer

07 p1411 A70-19817

Temperature stress distribution in cylinder or sphere with variable surface temperature and heated by external sources

07 p1411 A70-19819

Temperature stress in ring-like plate caused by point heat source, discussing thermoelastic problem

07 p1413 A70-20147

Thermoelastic stress degradation of injection lasers at high excitation levels, giving critical current densities for short pulse, CW and quasi-CW conditions

08 p1512 A70-20861

Steady temperature field and stresses produced by thermal sources in infinite elastic plane containing insulated rectilinear crack, determining thermoelastic state of half plane

08 p1587 A70-21172

Green function for stress intensity factors of rectangular plate edge cracks, noting application to thermal stresses

[ASME PAPER 68-WA/MET-19] 08 p1591 A70-21457

Transient thermal stresses in plates with distributed heat source and heat exchange with arbitrary time dependent surroundings

08 p1593 A70-21623

Cyclic heating and thermal stresses effect on fatigue strength and durability of turbine blade alloys and structural elements

09 p1771 A70-22463

Temperature and stress fields in rotating thin tube exposed to stationary heat source with constant strength, considering materials

09 p1774 A70-22579

Boundary point least squares technique extended to thermal and thermal stress problems in similar regions, deriving temperature and stress functions

09 p1774 A70-22580

Thermal strain measurement in operational and experimental components of high temperature plant, discussing full-bridge weldable type strain gage for transient strains

09 p1675 A70-22582

Thermo-elastic analysis and optimum start-up in power plant, discussing transfer function for thermally loaded bodies with restricted boundary temperature

09 p1774 A70-22584

Plastic growth of pressurized shell under cyclic thermal stresses superimposed on steady pressure load, investigating shake down using bending approximation

09 p1774 A70-22586

Elastic solution and finite element method applied to heat conduction and thermal stress in temperature field determination

09 p1774 A70-22587

Thermal gradients and associated strains measurement in steam turbogenerator casings, considering strain gage placement and heat transfer calculations

09 p1774 A70-22590

Turbine components thermal stress calculations for static and variable loads, considering plastic strain, creep and temperature effects

09 p1775 A70-22592

Creep failure fatigue life prediction methods involving hold period effects on high temperature fatigue properties

09 p1775 A70-22594

Thermal stresses in gas turbine blade calculated, showing role of initial temperature increase of blade cooling air

09 p1775 A70-22596

Thermoelastic stresses in plates and shells in random temperature fields, studying influence on service life

09 p1778 A70-23084

Structural elements reliability determination simulated by microinhomogeneous polycrystalline medium under thermal stresses and in stationary nonuniform temperature fields

09 p1778 A70-23085

Thermal stress state of nonuniformly heated elastic body with bounding surfaces formed by parts of coordinate surfaces

09 p1778 A70-23087

Axisymmetric thermal stress state in bodies of revolution studied by successive approximation algorithm for digital computer

09 p1778 A70-23088

Thermal stress concentrations at arbitrary holes for nonlinearly elastic materials, developing small deformation theory for two dimensional problem

09 p1779 A70-23093

Algorithm for stress-strain state calculation of nonuniformly heated cylinder weakened by star-shaped cavity

09 p1779 A70-23094

Thermal stress freezing during optical polarization study of perforated disk three dimensional thermoelasticity

09 p1780 A70-23105

Thermal stresses determination in turbine blades by making analogy between actual and electrical model, using EGDA integrator

09 p1785 A70-23598

Temperature fields and thermal stresses in FN fiberglass reinforced textolite under nonstationary unilateral heating, determining stress as function of time and heating rate

09 p1710 A70-23724

Temperature limitation on CRT tube performance in high brightness displays imposed by glass breakage danger, discussing liquid cooling of phosphor substrate

09 p1686 A70-23759

Heat tolerance time extension due to prior body cooling observed in aircrew subjected to heat stresses

10 p1824 A70-24036

Stress-strain determination in nonuniformly heated thin walled cylindrical beams with nonlinear stringers and skin

10 p1957 A70-24281

Environmental thermal stress effect on human performance under high mental and low physical workload

10 p1812 A70-24505

Dynamic stresses, temperature and displacements fields in thin circular disk under transient heat sources, considering mechanical resonance vibration

10 p1958 A70-24518

Algorithm for propellant flow rate increase of nuclear rocket in minimum time without exceeding maximum allowable stress in reactor core

10 p1914 A70-24870

Transient thermal stresses in restrained-in-bending slab with surfaces heated and cooled with finite heat transfer coefficients

10 p1964 A70-25095

Nomograms for thermoelastic stress in plate determined as function of dimensions and heat transfer

10 p1965 A70-25300

Transient and steady state thermal stress distribution measured by strain gages embedded in epoxy models

11 p2130 A70-25585

Transient and steady state thermal stresses measured by holographic extension of photoelastic analysis

11 p2049 A70-25592

Semiinfinite elastic body with instantaneous heat source on surface, analyzing temperature and thermal stress distributions

11 p2139 A70-26406

Thermal stress /high ambient and body temperatures/ effect on human performance in high mental and low physical activities

12 p2177 A70-27043

Thermal stresses in temperature dependent multilayered cylindrically anisotropic hollow cylinders

12 p2321 A70-27203

Thermal metal fatigue testing, including resistance to cyclic temperature variation, operating conditions simulation and stress-strain determination

12 p2322 A70-27218

Thermal stress concentration in constant thickness orthotropic plate with rounded square hole

12 p2323 A70-27338

Hollow homogeneous polymer cylinder thermoelastic stressed state, analyzing radial temperature and Poisson Coefficient variations

12 p2325 A70-27532

Ring rib structure transient thermal stresses analysis using photothermoelastic method

12 p2327 A70-27982

Thermoelastic stresses distribution in transmitting dielectric under short nonfocused laser pulses

12 p2251 A70-28327

Stress concentration in fiber reinforced materials resulting from thermal self straining, using finite element method and photoelastic analysis

13 p2509 A70-28533

Hypersonic wind tunnel testing of Plexiglas and nylon hemispheres instrumented with strain gages and thermocouples, comparing with calculated strain, temperature and ablation

13 p2520 A70-28727

Thermal stresses in solid nonhomogeneous sphere in high periodic temperature field, assuming temperature dependent Young modulus and linear thermal expansion coefficient

13 p2512 A70-28979

Elastoplastic thermal stress analysis using finite element matrix method exemplified by cylindrical bar induction quenching

13 p2513 A70-28992

Thermal stresses and curing in electronic modules transfer molding, discussing various design test models

13 p2420 A70-29252

Initial thermal stresses effect on natural oscillation frequencies of thin cylindrical elastic shells, obtaining linearized equations of motion and boundary conditions

13 p2514 A70-29286

Thermal stresses dependence on temperature field during axisymmetric heating of rigid cylindrical shells

13 p2421 A70-29426

High temperature dislocation model based on dislocation dynamics, rate theory and varying back stress ratio

13 p2436 A70-29563

Thermoelastic stresses in sphere with cylindrical cut under axisymmetric temperature field and constant surface temperature

14 p2655 A70-30135

Thermally induced strain measurement using four gage rosettes without temperature gradient limitations

14 p2585 A70-30684

Crack initiation and breakdown under thermal stresses of boron nitride containing aluminosilicate

15 p2764 A70-31532

Point heat source generation of thermal stresses in elliptical plate with circular hole, using functions of complex variable for stress field determination

15 p2818 A70-32182

Thermal loads on semiconductors in solid state converters during short circuit and overload

15 p2709 A70-32205

Elastic micropolar body thermal stresses induced by discontinuous temperature field, using differential equations of thermoelasticity

15 p2822 A70-32353

Initial thermally stressed state of solid bounded by concentric circular cylinders, applying Cauchy thermoelastic stress theory

16 p2987 A70-32993

Ceramic material ranking, using thermal stress crack initiation method

16 p2934 A70-33274

Book on elasticity theory covering end effects, Saint Venant principle, edge and screw dislocations, moire method, thermoelasticity, cavity and inclusion effects, Muskhelishvili methods, etc

17 p3183 A70-34603

German monograph on thermal stresses due to thermal shocks on front surface of infinitely long circular solid cylinder

17 p3189 A70-35371

Nonaxisymmetric thermal stress distribution in infinite elastic solid containing external stress-free crack with prescribed heat flux

17 p3196 A70-35437

Cylindrical shell of variable thickness, deriving axisymmetric thermal stresses in terms of hypergeometric functions

18 p3336 A70-36137

Critical stresses and stability of thin Maxwell plates under random temperature fields

18 p3337 A70-36368

Thermal effects on aircraft elastic vibration mode shapes, recommending investigation to develop analysis and design tools

18 p3213 A70-36459

Cyclic plastic breakdown of thin cylindrical shell under ring shaped load in temperature field, using linear programming method

18 p3341 A70-36585

Half space nonstationary temperature field with mobile heating at edges, using integral transformations

18 p3348 A70-36725

Graphite-epoxy resin cross-ply composites fabrication, analyzing residual thermal stresses role in cracking

[ASME PAPER 70-GT-84] 18 p3279 A70-36828

Combined mechanical and cyclic thermal stresses effect on plastic deformation buildup in E1435 alloy preceding breakdown

19 p3449 A70-37349

Gliders made of glass fiber reinforced plastics, investigating thermodynamic properties under solar irradiation and surrounding warm air

19 p3454 A70-37370

Transient thermal stresses in spherical shell with distributed source and general Sturm-Liouville boundary conditions

19 p3539 A70-37800

Thermoelastic stresses in infinite anisotropic slab due to temperature field variations along thickness and length

19 p3539 A70-37872

Book on thermoelasticity covering thermal stresses in disks, plates, shells and bodies of revolution under steady and unsteady temperature fields

19 p3541 A70-37974

Composite body with free surface under plane deformation, analyzing residual, thermal and dislocation stresses dependence on elastic constants

19 p3544 A70-38332

Machine parts fatigue strength under thermal cycles, studying nonlinear dependence of energy dissipation per unit volume on cycles number

19 p3547 A70-38427

Bearing strength and rupture of reinforced plastic composites under intense one-sided electric heating and hydrostatic pressure due to pyrolysis of plastic bond

19 p3455 A70-38462

Spherical shell under nonuniform temperature field, calculating stress-strain state around round hole

20 p3719 A70-39247

Plate temperature field and stress distribution under thermal pulses, evaluating critical heat load for damage

20 p3737 A70-39635

Infinite elastic plate with pair of insulated unequal circular holes, calculating thermal stresses

20 p3720 A70-39672

Directional solar thermal field /sunlight/ effect on coupled nonplanar transverse and torsional vibrations of satellite cylindrical antennas in orbit

20 p3720 A70-39676

Stressed state in thermoelasticity plane steady state problem of thin plate under bending based on dislocations and temperature stresses relationship

20 p3721 A70-39780

Thermal stress and changes in modulus of elasticity and expansion coefficient effects on dynamical properties of turbine disks at high temperatures

20 p3721 A70-39783

Medium thickness shells under thermal creep using Saint Venant semiinverse method

20 p3722 A70-39787

Thermally induced stress birefringence effect on linearly polarized CW YAG-Nd laser

21 p3834 A70-40566

Silicon solar cell array interconnector design based on analysis of stresses caused by thermal expansion and vibrational motion

21 p3756 A70-41009

- Anisotropic elastic solid body thermal stresses, investigating static plain strain problem in thermoelastic linear theory 21 p3936 A70-41414
- Materials for glass-metal compressed joints, tabulating stress and thermal expansion coefficients 22 p3999 A70-43447
- Thermomechanical contact and heat transfer on reinforced edge in plates butt joined by curvilinear closed rigidity rib 22 p4120 A70-43718
- Nonsteady temperature and thermal stress distribution in gas turbine blades, using plastic model and photothermoelastic method 22 p4093 A70-43743
- Cryogenic pipelines cooldown to operating temperature, calculating cryogen flow rate limits due to thermal stresses in steel and Al flanges 23 p4280 A70-44368
- Cylindrical shells dynamic thermoelastic response to sudden rotating thermal inputs, using Galerkin method 24 p4421 A70-45285
- Pure Al thermal cycling tests, investigating effect of minimizing thermal stress during quenching on behavior of dislocations 24 p4360 A70-45518
- German monograph on thermally induced elastic stress effects on crack formation and propagation in plates 24 p4422 A70-45524
- Polar elastic materials constitutive relations for thermoelastic couple stresses by general theory of incompatible strains, obtaining linearization for isotropic materials 24 p4428 A70-45578
- Tempering stress in circular plates and cylinders in casting of solid propellants 24 p4427 A70-46147
- THERMAL VACUUM TESTS**
- Explorer 38 critical component equilibrium temperature tests in thermal vacuum chamber using modified solar simulator, noting agreement with model [AIAA PAPER 69-999] 02 p0275 A70-12527
- Apparatus for short term thermal vacuum mechanical testing of materials 03 p0463 A70-13253
- Machine for refractory crystals creep testing in thermal vacuum or inert protective medium 03 p0493 A70-13959
- Material evaluation and selection for compact nuclear reactor control bearings operating at high temperature in vacuum [ASME PAPER 69-WA/LUB-11] 04 p0697 A70-14765
- Temperature dependence of Vickers pyramid hardness for Ti, Zr and Hf carbides at wide temperature range in vacuum 08 p1516 A70-20986
- Apollo lunar module manned testing in thermal vacuum, emphasizing safety aspects of hardware, procedures and training 10 p1859 A70-24389
- Line source technique for ablative heat shield materials thermal conductivity measurements, comparing vacuum and atmospheric test results [AIAA PAPER 69-1013] 11 p2051 A70-26142
- Test model thermal balance in space simulator, measuring effects of solar simulator irradiance reflected from carbon dioxide cryopanel deposits [AIAA PAPER 69-1012] 11 p2149 A70-26153
- Pressure measurements and gas flow analysis during thermal vacuum tests of manned spacecraft indicating adequate space vacuum simulation [AIAA PAPER 69-1033] 13 p2384 A70-28518
- Mission simulation testing in thermal vacuum environment for Apollo Lunar Module, noting conformal skin heaters [AIAA PAPER 69-991] 15 p2718 A70-32515
- Thermal mapping vacuum chamber tests of nuclear fuel capsules for lunar surface experiments, using remote IR radiometric microscope 15 p2718 A70-32800
- Metals and hard materials sliding wear due to granular abrasives in heated vacuum chamber 17 p3100 A70-34646
- Real time data processing and display for spacecraft thermal vacuum testing, using hybrid computer 17 p3059 A70-35176
- Creep testing machine with constant load for HF thermal cycling under vacuum 17 p3063 A70-35587
- Solar simulation methods, discussing optical elements and artificial radiation sources suitability for thermal testing 19 p3398 A70-38282
- Solar simulator combined with space environment simulation chamber for thermal tests of artificial satellites 19 p3398 A70-38283
- Spacecraft thermal vacuum test installations design and operations for locating spacecraft structural weak points 19 p3400 A70-38297
- Signal measurement and processing in thermal vacuum and space simulation tests of Azur and Dial satellites 19 p3400 A70-38298
- Space environment simulation and thermal vacuum tests for satellite thermal balance during development 19 p3401 A70-38300
- Space environment simulator for thermal vacuum performance of artificial satellites and components 19 p3401 A70-38308
- Apparatus for short term thermal vacuum mechanical testing of materials 19 p3401 A70-38471
- Polyimide resin vacuum thermal decomposition, using mass spectral and differential thermal analysis 21 p3783 A70-42133
- THERMALIZATION [ENERGY ABSORPTION]**
- NT NEUTRON THERMALIZATION**
- Molecular densities and population inversion pulse shape in working gas in mixture with thermally excited auxiliary gas 10 p1920 A70-25112
- Elastic energy transfer cross sections calculation of H-H scattering to estimate neutralized solar wind particles thermalization 18 p3309 A70-36951
- THERMIONIC CATHODES**
- MHD generator cathode current-sheath voltage characteristics for thermionic arc spot emission mode, noting role of cathode temperature [ASME PAPER 69-WA/HT-51] 04 p0625 A70-14797
- Cathode emission from hollow cathode controlled by variable magnetic field to ensure proper I-V characteristics for efficient ion generation in thrusters [AIAA PAPER 70-175] 06 p1131 A70-18032
- Arc ignition and cathode spot movement dynamics of thermionically emitting cathode surfaces in heat feedback plasma 21 p3859 A70-41903
- Thermal emission cathodes made from lanthanum, yttrium and gadolinium hexaborides, measuring I-V characteristics 22 p3998 A70-43442
- THERMIONIC CONVERSION SYSTEMS**
- U THERMIONIC POWER GENERATION**
- THERMIONIC CONVERTERS**
- Low voltage arc discharge in thermionic converter at low Ce pressures measured for current-voltage characteristics, showing degree of ionization 01 p0150 A70-10173
- Plasma instabilities of Ce filled auxiliary discharge thermionic energy converter compared with Langmuir theory 03 p0415 A70-14367
- Thermionic converter with oriented W electrodes, describing test method and computerized data acquisition for performance mapping 04 p0627 A70-14945
- Anode work functions from cesiated metal surfaces as parameters for thermionic converter systems analysis 04 p0627 A70-14946
- Mo/Mo cylindrical thermionic converter steady state performance, measuring efficiency and power density at various low emitter and collector temperatures 04 p0627 A70-14947
- Low voltage arc discharge in thermionic converter at low Ce pressures measured for current-voltage characteristics, showing degree of ionization 10 p1925 A70-25018
- Nuclear converter with porous metal adsorption reservoir working with or without liquid cesium 10 p1915 A70-25039
- Radial distribution of plasma parameters for thermionic converters with electrode shielding by plane sapphire rings, showing lateral surface effect 10 p1808 A70-25124
- Solar energy direct conversion into electricity, surveying photoelectric, thermoelectric and thermoemissive methods 15 p2677 A70-31598
- Anodic temperature effect on Cs thermionic converter operation under arc regime, obtaining potential jump electron temperature relation near anode 15 p2677 A70-32119
- Radial distribution of plasma parameters for thermionic converters with electrode shielding by plane sapphire rings, showing lateral surface effect 20 p3568 A70-40517
- Electron and ion transport in cesium plasma for thermionic and MHD energy converters 21 p3859 A70-41912
- Radioisotope thermoelectric generator with lead telluride converter, discussing intact reentry and impact capability, refractory construction and reliability 22 p4072 A70-43196
- THERMIONIC DIODES**
- NT CESIUM DIODES**
- Thermionic diode development for nuclear reactor systems [ASME PAPER 69-WA/ENER-5] 04 p0717 A70-14900
- Reactor gamma in-pile effects on thermionic diodes simulated in electron accelerator, noting ion production insufficient to support saturation currents 04 p0717 A70-14948
- Vacuum-type thermionic laboratory diode featuring variable electrode spacing, interchangeable electrodes and guard-ring structure 04 p0628 A70-15400
- Electron work function variation of W in Ba-Cs-Sr vapor combinations determined using thermionic diode 05 p0891 A70-15974
- Thermionic diode development for nuclear reactor systems [ASME PAPER 69-WA/ENER-5] 15 p2773 A70-31959
- THERMIONIC EMISSION**
- Thermionic emission characteristics of W and Mo subjected to focused CW carbon dioxide laser radiation, discussing direct energy conversion 02 p0312 A70-12068
- Laser-induced electron emission from metals and insulators in form of evaporated films and single crystals, discussing many-photon photoelectric effects and thermionic emission 08 p1556 A70-21509
- Nomographic Richardson-Dushman equation solutions for thermionic electron emission devices, giving current density for various work functions and electrode temperatures 12 p2271 A70-26894
- Electrostatic probes response due to thermionic electron emission, considering I-V characteristics and space-charge-limited current 13 p2459 A70-28635
- Nb single crystal faces electron work functions and comparison of thermionic emission patterns with Ba-Nb system 14 p2625 A70-30162
- Interactions between moving alkali-metal seeded dense plasma and metallic thermionically emitting electrode with surface properties influenced by seed particle absorption 20 p3681 A70-40007
- THERMIONIC EMITTERS**
- Diffusion rates in refractory metal alloys for thermionic emitters as function of time and temperature [GA-9495] 05 p0892 A70-16075
- Surface oxidation effects on thermionic work functions of Be determined by visual observation and X ray diffraction patterns analysis 12 p2288 A70-28004
- THERMIONIC POWER GENERATION**
- Rankine cycle technology concerning high temperature, refractory alloy and liquid metal experience, showing applicability to nuclear Brayton and thermionic power systems 02 p0229 A70-12513
- Electrical power system adaptable to intermediate solar probes, discussing thermoelectric, thermionic, photovoltaic systems and battery for energy storage [ASME PAPER 69-WA/SOL-5] 04 p0625 A70-14753
- Optimal control of nuclear propulsion and energetic plants of space vehicle, considering thermionic generator 13 p2450 A70-28436
- Unmanned electric propulsion spacecraft with external fuel and flashlight thermionic reactors, discussing thruster arrays, weight and performance for reference Jupiter orbiter mission [AIAA PAPER 70-644] 16 p2966 A70-33547
- Thermionic reactors for spacecraft auxiliary power and electric propulsion, discussing in-core conversion system and diodes 22 p4071 A70-43191
- THERMIONIC REACTORS**
- U ION ENGINES**
- U NUCLEAR ROCKET ENGINES**
- THERMIONICS**
- Cool flame isothermal theory with oscillatory features accounting for damping time evolution and thermic reaction nature 21 p3942 A70-40886
- High temperature acceleration of propellants in electrothermal thrusters including resistojets, arcjet, thermionic and plasma configurations 22 p4091 A70-42763
- THERMISTORS**
- Corrections to observed thermistor temperature profiles presented for spherical bead thermistors with long lead or thin film mounting [AAS PAPER 69-568] 04 p0687 A70-14664
- Monitor for linearizing nonlinear characteristics of thermistors used for temperature sensors in Apollo Telescope Mount, optimizing circuit values with FORTRAN IV computer program 05 p0851 A70-16692
- Rocket sounding to obtain thermistor temperature profiles of 30-65 km atmospheric region, discussing error correction equation 07 p1288 A70-20261
- Thermistors used in temperature measurements aboard satellites, discussing results of electrical and mechanical tests 08 p1493 A70-20612

Ambient temperature measurement by constant level balloon mounted thermistors, discussing errors from differential heating of thermistor support by solar radiation
10 p1886 A70-23935

Air velocities measurement with heated thermistors probe, discussing calibration and reliability dependence on flow velocity range
13 p2405 A70-28841

Temperature measurement of rotating shafts under cyclic loading, using thermistor as thermal radiation sensor
15 p2734 A70-31581

Thermistors theory, manufacture, stability, drawbacks and applications to temperature sensors
16 p2915 A70-34322

Thermoresistor parameters of organic semiconductor polymers with conjugated bond system, plotting temperature and EV characteristics
20 p3595 A70-38966

Thermistor and dew cell as remote air temperature and dewpoint measurement at airports
21 p3822 A70-40760

High resistance thermistor measurements of rapid blood temperature variation, discussing power dissipation effects
21 p3769 A70-41143

Regional cerebral cortical blood flow measurement, using heat clearance thermistor probe
23 p4157 A70-45082

Long term storage effects on recalibrated thermistors performance stability, comparing measurements with first calibration data
24 p4333 A70-45136

THERMO-PHOTOVOLTAIC GENERATORS
U PHOTOELECTRIC GENERATORS
U THERMOELECTRIC GENERATORS
THERMOAEROELASTICITY
U AEROELASTICITY
U THERMOELASTICITY
THERMOCHEMICAL PROPERTIES
NT HEAT OF COMBUSTION
NT HEAT OF FORMATION
NT HEAT OF VAPORIZATION
Thermochemical relaxation influence on shock heated plasma gases via heat transfer experiments on ionized Ar, molecular nitrogen and carbon dioxide
03 p0536 A70-14366

Computerized nonequilibrium thermochemical gas dynamic solutions for nozzle, shock tube and stream tube flow with arbitrary species and kinetic reactions numbers
22 p3982 A70-42762

Thermal decomposition of freeze dried Ta and niobium-lithium-oxalate, using surface area and electron micrographs
24 p4363 A70-46212

THERMOCHEMISTRY
NT AEROTHERMOCHEMISTRY
Chemical bonding of high temperature molecular species, discussing ab initio calculations for diatomic atoms
07 p1225 A70-19882

Ablation products and high temperature boundary layer chemistry of polytetrafluoroethylene /Teflon/ in arc jet streams using mass spectrometer
07 p1319 A70-19886

Thermochemical predictions for high temperature oxidation of Mo and W, discussing oxide films or scales, reactant gases flow rate, etc
09 p1630 A70-22943

Quartz- and silicate-graphite mixtures carbothermal reduction in vacuum at 1400 C
20 p3583 A70-40425

Soviet papers on thermodynamic and thermochemical constants covering solid, liquid and gaseous state properties, phase equilibrium, etc
22 p4123 A70-42676

Thermochemical method for directional crystallization of wear-resistant alloy coatings on machine parts
23 p4205 A70-44043

Differential scanning calorimetry and thermogravimetric analysis combination for thermochemical kinetic measurements, matching analytical and experimental curves for data accuracy
23 p4196 A70-44429

Nondestructive thermal and thermochemical treatment penetration depth measurement in metal, examining magnetic test and ultrasonic techniques
24 p4346 A70-45721

THERMOCOMPRESSION
U COMPRESSING
U HEATING
THERMOCOUPLES
NT THERMOPILES
Thermocouples response to rapid temperature rise produced by discharge from low inductance high voltage capacitor bank
03 p0486 A70-13559

Embedded sheathed thermocouples temperature measurement of cooled jet engine turbine buckets subjected to high heat flux
03 p0486 A70-13560

Doped beta-iron disilicide thermocouples measured for electrical characteristics and energy conversion efficiency at various temperatures
05 p0798 A70-16357

Single junction vacuum thermocouple measuring thermal beam effect with reference to velocity distribution perturbation in molecular beam scattering
07 p1341 A70-20107

Thermocouple vacuum gauge joined to Apollo lunar sample return containers /ALSRC/, describing two step welding procedure with transition cylinder
08 p1507 A70-21483

Tungsten-rhenium thermocouple for high temperature measurement of samples under unsteady heating processes, analyzing instrument error sources
09 p1789 A70-23108

Si-Ge air-vacuum thermocouples for thermoelectric conversion, describing construction materials, mechanical and electrical properties, radiative heat transfer operation, etc
10 p1807 A70-24896

Thermoelectric generators design, discussing Si-Ge air-vac thermocouple configurations, compression modules, thermal losses, etc
10 p1808 A70-25034

Electric current flow effect on thermoelectric figure of merit from thermal conductivity measurements on thermoelement
11 p2065 A70-25768

Transient heat flux measurement with surface thermocouples, thin film resistance thermometers and mathematical computation programs
11 p2065 A70-25768

Thermocouples performance during fast varying temperature measurements in solids, considering physical parameters effects on accuracy
15 p2734 A70-31646

IR radiating bodies angular displacement determination by vacuum evaporated thermocouple radiation detectors, describing stationary communication satellite altitude control
15 p2740 A70-32422

Electric temperature sensors accuracy and stability, considering thermocouples, resistance thermometry, radiation and color pyrometry
15 p2743 A70-32798

Thermoelectric force due to thermocouple inhomogeneities, showing relation to temperature gradient and measurement error
16 p2900 A70-33070

Cryogenic temperature measurement including metallic and semiconductor resistance thermometers, thermocouples and bibliography
17 p3082 A70-34740

W-3 percent Re-W-25 percent Re thermocouple reliability and stability, describing emf vs temperature table in 0-2400 C range
18 p3257 A70-36200

Surface temperature fluctuations during steady state boiling from tube, using fast response thermocouple
18 p3347 A70-36504

Thermocouples and resistance thermometers comparison for low temperature measurements
19 p3432 A70-38703

Thermocouple and IR temperature measurement techniques comparison for double base solid propellants at low pressures
20 p3694 A70-40275

Heat conduction errors in immersion thermocouples and resistance temperature sensors, using mathematical model
21 p3823 A70-40856

Installed system calibration thermocouples using temperature plateaus due to pure metals melting and freezing heat of fusion
21 p3823 A70-40857

Thick film thermocouple gages for roughened model surface heat flux measurements in high Reynolds number shock tunnel
21 p3824 A70-40860

Thermocouple transient response characteristics in deflagrating and ablative low conductivity materials with high temperature gradients
22 p4122 A70-42440

Cryogenic thermocouples of various metal pairs for low temperature measurements, discussing performance tests and calibrations
24 p4378 A70-45385

THERMODYNAMIC COUPLING
Multicomponent gas absorption analysis to illustrate interactions of coupled fluxes in ammonia-water system
08 p1597 A70-21028

Thermomechanical coupling effect on stability of elastic continuous systems subjected to nonconservative forces, reducing flutter load by thermal damping
08 p1589 A70-21245

Equatorial electrojet Lorentz coupling to neutral atmosphere as source of long period traveling ionospheric disturbances
13 p2399 A70-29235

Thermal anchoring of wire or rod components to heat sinks in cryogenic equipment in vacuum
14 p2584 A70-30501

THERMODYNAMIC EQUILIBRIUM
THERMODYNAMIC CYCLES
NT BRAYTON CYCLE
NT RANKINE CYCLE
NT STIRLING CYCLE
Periodic process analysis method based on trigonometric Fourier series, noting applications to heat conduction problems
03 p0606 A70-13519

Systematization of thermodynamic cycles from elementary reversible evolutions concerning exchange of work, heat and combined relations
06 p1173 A70-17470

Cryogenic refrigeration below 20 K, analyzing cycles using similarities of work and heat exchange mechanisms
09 p1726 A70-22290

Turbofan engine performance optimization by closed form solution of operating cycle parameter functions
18 p3303 A70-36840

Stepwise heat removal for increased continuous combustion gas turbine engine cycle efficiency, deriving equations describing cycles
22 p4092 A70-43372

THERMODYNAMIC EFFICIENCY
MHD generators physical phenomena, discussing thermal efficiency, inlet parameters, operating principles, etc
04 p0625 A70-14716

Thermal efficiency of modified transtage of Titan 3C spacecraft, discussing environmental simulation, heat rejection system and test firing
06 p1156 A70-18027

Finned tube radiators with constant longitudinal specific heat flow, determining thermal efficiency and optimal thermal and structural parameters
06 p1184 A70-18556

Multiple pass tube heat exchangers efficiency, solving energy and heat transfer equations from fluids homogeneity and constant thermal capacity considerations
08 p1596 A70-20613

Reciprocating Rankine-cycle engine with organic working fluids, noting piston speed and efficiency
11 p1982 A70-25372

Working body properties effects on one component liquid-metal MHD system efficiency with vapor condensation cycle
12 p2164 A70-27329

Heat transfer in Z shaped regenerative heat exchangers with/without air mixing, determining parameters defining thermal efficiency
13 p2520 A70-28857

Transpiration cooling for high temperature gas turbines, investigating effects on aerodynamic and thermodynamic performance
18 p3303 A70-36839

Flexible heat pipe test for heat flux and wick pumping capacity under vibration and evaporator-condenser modification
21 p3945 A70-41040

Liquid or vapor phase working fluids penetration effects on steady state and transient performance of hot reservoir gas controlled heat pipes
21 p3946 A70-41047

Heat pipe performance map with ammonia as working fluid, comparing thermal transport efficiency with water pipe
21 p3947 A70-41050

Thermal efficiency of ceramic and metal heat exchangers for biowaste resistojet thrusters
21 p3868 A70-41779

Working body properties effects on one component liquid-metal MHD system efficiency with vapor condensation cycle
21 p3760 A70-42070

Effective pressure ratio nomographs for mechanical energy conversion and heat transfer of closed regenerative Stirling engines, using isothermal theory
22 p4091 A70-42757

Stepwise heat removal for increased continuous combustion gas turbine engine cycle efficiency, deriving equations describing cycles
22 p4092 A70-43372

Computerized calculation of gas turbine cycles thermal efficiency, using hydrocarbon fuel, considering fuel composition and heat of combustion changes
22 p4125 A70-43439

Thermodynamic-kinetic analysis of fluorine/lithium/hydrogen tripropellant combustion efficiency, discussing liquid metal atomization, firings, facility and thrust chamber
23 p4232 A70-44512

Film cooling efficiency for flat plate behind tangential slot at blowing coefficients below unity
23 p4282 A70-44727

THERMODYNAMIC EQUILIBRIUM
Tungsten effect on phase transformations and carbide reactions to attain equilibrium at 850 C in Ni-base superalloys
01 p0118 A70-10727

Hypersonic dissociated laminar boundary layers with/without heat transfer calculated by integral method for case of thermodynamic equilibrium
01 p0003 A70-10933

Equilibrium of thin curved cylindrical panels subjected to thermal expansion and pressure numerically analyzed by Ritz method

01 p0201 A70-10945

Dynamic behavior of dissociating homonuclear diatomic gas, deriving instability equations, proposing stability loss in transonic region

01 p0068 A70-11584

Local thermodynamic equilibrium conditions in superhigh pressure He plasma produced by laser action, obtaining threshold electric field relationship with gas pressure and temperature

02 p0312 A70-12078

Transient energy transfer during expansion of plane layer of radiating gas bounded by strong shock, assuming LTE and perfect inviscid nonconducting gas

02 p0279 A70-12230

Structure of hydrogen-oxygen diffusion flame in equilibrium using iterative solution

02 p0352 A70-12796

Hypersonic flow in thermodynamic equilibrium of diatomic dissociating gas with power law shock, investigating self similar solutions of Van Dyke small disturbance equations

03 p0405 A70-12925

Equilibrium temperature and heat transfer of sphere in supersonic flow of rarefied air

03 p0409 A70-13874

Equilibrium composition and thermodynamic functions calculated for mixtures of dissociating and ionizing high temperature gases from standard data

04 p0780 A70-14538

Thermal steady state characterization of isotope radioisotope thermoelectric generator, discussing design features and heat transfer models for operating temperature and output performance [ASME PAPER 69-WA/ENER-12]

04 p0717 A70-14897

Thermodynamic equilibrium of rotating liquid He II on basis of Landau theory, noting stability and dissipative effects

04 p0785 A70-14986

Classical Couette flow for emitting and conducting gas media, discussing velocity distribution and temperature effects at LTE and non-LTE

04 p0787 A70-15675

Boltzmann-type kinetic equation for homogeneous electron plasma in uniform magnetic field, describing relaxation to thermal equilibrium by convergent collision integral

05 p0888 A70-16329

LTE departures in late B stars from measurements of Balmer and Paschen discontinuities

05 p0919 A70-16937

Dynamic response of constant resistance anemometers, investigating unsteady probe thermal equilibrium, inductance and feedback equations

06 p1063 A70-17620

Laser radiation increased absorption in opaque solid body attributed to vaporization, analyzing factors determining thermodynamic equilibrium between condensed and gaseous phases

06 p1083 A70-18563

Particles infinite systems equilibrium state by canonical ensemble theory, demonstrating existence and uniqueness of limiting distribution functions dependence on density

07 p1333 A70-18936

Critical regions equilibrium thermodynamic properties of fluids and magnets using scaled equation of state

07 p1421 A70-19298

Electrochemical generators based on thermodynamic equilibrium processes, deriving expressions for EMF, efficiency, and I-V characteristics

07 p1196 A70-20462

Fluids equilibrium stability within medium at constant temperature and pressure, discussing time behavior of thermodynamic processes

09 p1786 A70-22062

Stainless steel corrosion rates in flowing liquid Na from mechanism based on thermodynamic partitioning of oxygen

09 p1706 A70-22942

Plane, cylindrical and spherical blast waves structure with ionization at local thermodynamic equilibrium analyzed using successive approximation to non-similar solution

10 p1967 A70-23991

Viscous fluids nonlinearized thermodynamical description with equilibrium state defined by two parameters, expressing angular momentum density by momentum density

10 p1967 A70-24153

Thermal imbalance effect on stellar pulsational stability using linear quasi-adiabatic pulsation theory

10 p1946 A70-24980

Enthalpy-entropy, enthalpy-pressure and composition diagrams of fluorine-hydrogen system, noting possible applications to rocket propulsion systems

10 p1929 A70-25100

Steady state surface temperature measurement errors by thermistors, thinistors and thermocouples, discussing sources

11 p2052 A70-26361

Transformed distribution function of particle velocity of plasma in Debye thermodynamic equilibrium approximation based on statistical mechanics

11 p2091 A70-26459

Book on tensor calculus in materials science covering thermodynamic equilibrium, gaseous and solid phase heat engines, solids crystalline structure, etc

12 p2282 A70-26866

Trumpet-type plane waves instability thresholds in plasma drifted by electric field, including calculation of thermodynamic equilibrium

12 p2184 A70-27236

Shock ionized xenon electrical conductivity measurement at high temperatures as function of Mach number, noting equilibrium effects

12 p2281 A70-27807

Nonlinear dielectric function and propagators of plasma submitted to electric field by Vlasov equation iterative solution, considering electron plasma in thermodynamic equilibrium

13 p2458 A70-28565

Radiative heat transfer through gray gas in equilibrium between concentric spheres, using variational method

13 p2521 A70-29137

Induction plasmas in thermal equilibrium dominated by radial conduction losses, discussing energy balance equation and Ar plasmas at atmospheric pressure

13 p2465 A70-29701

Thermal induction plasma discharge characteristics, considering radiation and conduction losses

13 p2465 A70-29702

Magnetic moment fluctuations of arbitrary solid body by fluctuation-dissipation theorem for thermal equilibrium

13 p2454 A70-30033

Forbidden lines of OI, NI, CI, Fe II, Ni II, Si I, Si and Ca II in solar absorption, investigating effects on element abundance and gaps in thermodynamic equilibrium

14 p2637 A70-30339

Non-LTE and LTE line profiles and equivalent widths for transitions in singlet and triplet systems of neutral He in hot stars, explaining anomaly

14 p2641 A70-30884

B3V stars atmospheres by LTE model and spectroscopic techniques

14 p2652 A70-31384

Radiatively interacting adjacent plates in presence of collimated solar flux, considering surface roughness effects on equilibrium temperature distribution

16 p3002 A70-33946

Solar limb intensity distribution in Lyman alpha line, computing LTE departures

17 p3162 A70-34895

High temperature plasmas of mixtures of nitrogen with rare gases, calculating equilibrium thermodynamic properties

17 p3195 A70-34932

Non-LTE effects on flux and center to limb variation of solar spectrum at 1500-1680 Å

17 p3169 A70-35384

Nonequilibrium fluid system with two subsystems in local equilibrium, investigating thermodynamic properties including entropy creation

17 p3196 A70-35530

Statistical theory of irreversible transport processes in fluids, considering deviation from equilibrium as stochastic process

17 p3131 A70-35532

Time correlation functions approach to calculation of properties of nonequilibrium ensembles in fluid molecular motions

17 p3197 A70-35535

Dilute gas transport expressions experimental substantiation, emphasizing nonequilibrium thermodynamics as macroscopic theory rather than empirical postulate

17 p3072 A70-35536

Relativistic thermal equilibrium conditions in external gravitational field, considering heat with inertial and gravitational mass

18 p3291 A70-36552

Product distribution of organic nitrogen compounds plasma sources computed by assuming high temperature limited thermodynamic equilibrium

18 p3226 A70-36764

LTE verification for argon plasma generated in free burning arc by measuring atomic line transition probability at various pressures

21 p3854 A70-40588

Cloudy planetary atmospheres model, assessing nonlocal thermodynamic equilibrium role

21 p3813 A70-40903

Elastic bodies under motion-dependent loads, examining thermodynamic conditions of equilibrium states stability

22 p4123 A70-42538

Atomic hydrogen plasma slab, calculating thermodynamic equilibrium deviations effect on resonance radiation

23 p4223 A70-43824

Local thermal equilibrium validity for electron temperature and density determination in reflected shock

waves in He plasma, comparing laser scattering and spectroscopic methods

23 p4229 A70-44986

Non-LTE radiative gas flow conservation equations

24 p4325 A70-45610

Chemical composition and degree of thermodynamic equilibrium reflected in ferromagnesian silicates of chondrites

24 p4411 A70-45793

Thermodynamic equilibrium analysis of metal oxidation and thermal dissociation of oxides in vacuum, noting decreased affinity by evaporation

24 p4361 A70-45835

Statistical characteristics of stability of single phase one component system under external force

24 p4381 A70-46144

THERMODYNAMIC PROPERTIES

NT CRITICAL POINT

NT CRITICAL PRESSURE

NT CRITICAL TEMPERATURE

NT EMISSIVITY

NT ENTHALPY

NT ENTROPY

NT FREE ENERGY

NT FUSIBILITY

NT GIBBS FREE ENERGY

NT HEAT OF COMBUSTION

NT HEAT OF FORMATION

NT HEAT OF SOLUTION

NT HEAT OF VAPORIZATION

NT MELTING POINTS

NT PYROELECTRICITY

NT SPECIFIC HEAT

NT SUPERCRITICAL PRESSURES

NT SURFACE ENERGY

NT THERMAL BUCKLING

NT THERMAL CONDUCTIVITY

NT THERMAL DIFFUSION

NT THERMAL DIFFUSIVITY

NT THERMAL EXPANSION

NT THERMAL INSTABILITY

NT THERMAL STABILITY

NT THERMOCHEMICAL PROPERTIES

NT THERMOPHYSICAL PROPERTIES

NT VAPOR PRESSURE

NT VOLATILITY

Thermodynamic and transport properties of Na, K, Rb and Cs vapors to 3000 K, for use in liquid metal coolant and power systems

01 p0214 A70-10299

Variational methods for investigation of thermal and electrical properties of semiconducting materials, noting accuracy

01 p0159 A70-10759

Vapor pressures of cobalt over pure cobalt and over Ni-Co alloys determined as function of temperature by isotope exchange method

01 p0121 A70-11233

Cooling time estimation for white dwarf stars with ion component undergoing condensation, based on plasma thermodynamic properties

01 p0189 A70-11341

Thermal properties of neutral interstellar gas heated by low energy cosmic rays, noting role of electrons in heating processes

02 p0364 A70-11783

Nb-NbH solid solutions thermodynamic properties at various temperatures described by formulas

02 p0320 A70-12819

Solid thorium yttria electrolyte applications in EMF measurements for Cr thermodynamic properties in Fe-Cr and Ni-Cr alloys

03 p0483 A70-13140

Gas dynamics analysis of explosion phenomena based on unsteady flow fields and thermodynamic properties of chemically reacting substance

03 p0607 A70-13922

Equilibrium model of laminar arc constrictor plasma generator, correlating heat transfer, wall shear stress, friction factor and development length

03 p0533 A70-13952

Electrical and thermal factors in mathematical characterization of electroexplosive devices, including heuristic predictions

03 p0548 A70-14119

Alpha beryllium nitride enthalpy and thermodynamic properties measured between 273-1173 K using drop calorimetric method

04 p0646 A70-14582

Solid and liquid lithium tetrafluoroborate enthalpy relative to 273 K measured at temperatures between 323-873 K, deriving thermodynamic properties

04 p0646 A70-14583

Apparatus and techniques for investigating spacecraft materials mechanical and thermal properties, using vacuum effect to simulate space environment

[ASME PAPER 69-WA/PID-22]

04 p0663 A70-14752

Surface coating optical and thermal properties investigated in preparation for HELIOS solar probe [DGLR-69-46]

04 p0762 A70-15163

Corrosion problems in Ti and alloys chemical and aerospace applications, describing thermodynamics and electrochemistry in aqueous media
04 p0710 A70-15677

Ideal equivalent gas method for studying thermodynamic properties in supersonic gas flows behind shock wave
05 p0831 A70-15872

Thermal and gas dynamic characteristics of aircraft turbine engine annular vaporizing combustion chamber determined from air distribution ratio
05 p0895 A70-15897

Martian surface temperature distributions based on IR scans of disk compared with predictions of thermal properties
05 p0909 A70-16389

Mathematical model for investigating satellite thermal behavior in space based on space simulation in vacuum chamber with walls maintained at liquid nitrogen temperature
05 p0924 A70-17022

Test facilities for studying materials thermophysical properties and stress relaxation, including dynamic hardness measurement and torsion tests up to 2500 K
05 p0830 A70-17074

Thermodynamics of LiBr in anhydrous dimethyl sulfoxide determined at several temperatures using EMF method
06 p1003 A70-17219

Soviet book on thermodynamic and ballistic fundamentals of designing solid propellant rocket engines
06 p1130 A70-17421

Gas mixture internal energy in internal combustion engine cylinder calculated with allowance for thermal discontinuity
06 p1130 A70-17628

Thermal and dynamic considerations of materials choice for satellite mounted telescope mirrors noting Be and silica properties
06 p1064 A70-17781

Surface thermal factors influencing ignition delay time of composite solid propellants, using double wavelength optical detector
[AIAA PAPER 70-121] 06 p1128 A70-18043

Atmospheric thermodynamic properties determined from radar studies of detonation waves from cesium-seeded explosive bursts in lower ionosphere
06 p1012 A70-18542

Thermodynamic properties of nonideal multicomponent gas mixtures including Fermi-Dirac statistics effect, discussing internal partition function for free and confined atoms
06 p1184 A70-18637

Electrical and thermal characteristics of stabilized gas heating by electric arc at high pressures calculated by successive approximation
07 p1350 A70-19840

Dynamic pearlite-austenite transformation and melt temperatures measured in laser-irradiated steel, discussing thermal response as function of heating rate
07 p1301 A70-19897

Helium high energy molecular beams for insulating body heating and thermal constants determination
07 p1344 A70-20129

Heat exchange during solidification of castings in molds, studying thermal properties effect for achieving constant mold surface temperature
08 p1506 A70-21141

Thermodynamic properties of real gases estimated using Hirschfelder equation of state
08 p1598 A70-21363

Thermal properties associated with temperature gradients in He-K plasma, studying mass motions initiated by cold wall contact
09 p1735 A70-22844

Macroscopic properties of thermal molecular flow between coaxial cylinders and concentric spheres, using transpiration theory in Knudsen gas
09 p1788 A70-22906

Oxygen pressure, volume and temperature data and derived thermodynamic properties presented in tabular form
09 p1788 A70-22956

Thermodynamic properties of periodically variable air volume in pneumatic pressure generator of pressure sensor calibration bench
10 p1863 A70-24027

Oxygen-kerosene combustion product composition and characteristics in engine thermodynamic design allowing for intermolecular interaction forces
10 p1968 A70-24284

Perfect gas mixtures thermodynamic functions at high temperatures with correction for Debye-type electrostatic interaction effects
10 p1968 A70-24707

Insulation foils and surface coatings thermal properties effect on radiation properties for spacecraft thermal control systems
10 p1951 A70-24863

CW Nd-doped YAG laser rods, measuring thermal and optical properties before and during pumping with W lamps
10 p1900 A70-24942

Lil thermodynamic properties in dimethyl sulfoxide determined by emf method, discussing ionic solvation energies
10 p1831 A70-25041

Thermodynamic and transport properties of high temperature and pressure gases measured with ultrasonic pulse technique
11 p2147 A70-25753

Heat flow comparator for nondestructive testing of resin-impregnated fiber glass, detecting nonuniformities leading to thermal properties variation
11 p2059 A70-25764

Metals thermal properties simultaneous determination at high temperatures, describing measuring equipment operation and circuitry
12 p2206 A70-27219

Nitrogen tetroxide thermodynamic properties calculation from pressure-volume-temperature equation of state in gas and liquid phases
12 p2332 A70-27975

Charring ablative plastic thermal properties simultaneous measurement using modified heat transfer model and nonlinear regression analysis
12 p2333 A70-28111

Thermohydrodynamic seals design, properties and performance compared with standard mechanical seals
13 p2417 A70-28612

Collection of papers on nickel and nickel alloys covering thermal and mechanical properties during annealing and precipitation hardening behavior
13 p2432 A70-28758

Ni and Ni alloys thermal properties, discussing expansion and conductivity, melting and boiling points, vapor pressure, specific heat, entropy, etc
13 p2432 A70-28759

Thermodynamic data for chemical reactions of Ti alloys formation with Al obtained by measuring galvanic cells emf with solid electrolytes at elevated temperatures
13 p2434 A70-28889

Iron and stony iron meteorite cooling rates and thermal models, showing melting, radioactive heat source redistribution and surface heating effects
13 p2497 A70-29861

Chemically reacting ideal substance model, describing thermodynamic properties and application to energy conversion processes
14 p2533 A70-30529

Lunar IR radiation measurements for estimating thermophysical properties and small scale surface nature
14 p2645 A70-31057

Mercury mm wave observations, examining longitude dependence of disk average brightness temperature and epilith thermal parameters range
14 p2647 A70-31076

Radiative properties of construction properties and working media, noting importance to radiative heat transfer calculation
15 p2827 A70-32143

Thermodynamically perfect fluids in general relativity, considering heat transmission paradox and wave propagation velocities
16 p2997 A70-33103

Monograph on steady shock waves in one dimensional frictionless gas flows with thermodynamic relaxation, using continuum mechanics
16 p2891 A70-33294

Nonlinear regression techniques for statistical simultaneous measurement of thermal properties including convergence criterion
16 p2998 A70-33859

Thermal and mechanical properties of materials for spacecraft booms design
16 p2986 A70-34138

Surface temperature or heat flux density estimation for nonlinear inverse heat conduction problem involving temperature dependent thermal properties
16 p3002 A70-34195

Thermodynamic properties of bcc beta phase in Ti-Cu and Ti-Al systems, discussing activities determination technique
17 p3114 A70-34378

Ti alloys M sub s and beta sub s points thermodynamics, considering initiation of bcc-cph martensitic transformation
17 p3193 A70-34407

Thermal and thermoelastic constants of macroscopically isotropic composite materials based on self consistent calculations
17 p3194 A70-34555

NTWO Fortran IV family of subroutines for thermodynamic and transport properties of nitrogen
17 p3195 A70-34746

Isotropic fluid systems in nonequilibrium, investigating thermodynamic characteristics of transport phenomena
17 p3072 A70-35529

Nonequilibrium fluid system with two subsystems in local equilibrium, investigating thermodynamic properties including entropy creation
17 p3196 A70-35530

Nonideal plasma thermodynamics data, discussing particle interactions, Coulomb potential, stability, etc
17 p3142 A70-35733

Ni-S melts thermodynamic properties in 700-1100 C range by continuous thermal balance method, calculating S vapor pressure
18 p3271 A70-36029

Oxygen dilute solutions in liquid Fe-Ni-Co alloys, investigating thermodynamic properties by hydrogen-water vapor equilibrium
18 p3272 A70-36033

Micropolar elasticity theory, discussing difficulties from erroneous thermodynamic inequality
18 p3335 A70-36061

Elastic continuum conducting heat under general loads, investigating stability thermodynamics-Liapunov criterion relations
18 p3337 A70-36336

Electronic excitation contribution to frozen properties and cut-off criteria of high temperature gas plasma
18 p3296 A70-36955

Soviet reference book on highly refractory elements and compounds covering crystalline, chemical, thermodynamic, thermophysical, electrical, optical and nuclear properties
19 p3451 A70-37470

Dense plasma thermodynamic and electromagnetic properties, discussing correlation energy
19 p3480 A70-38181

One-component rigid epoxy foam system suitable for lightweight electronic potting, determining mechanical, electrical and thermal properties
20 p3652 A70-39167

Carbon/carbon composites constituent characteristics effects on thermal and mechanical properties, using polarized light and scanning electron microscopy
20 p3653 A70-39204

Carbon/carbon composites thermal and mechanical properties measurements by NDT including image transducer, IR scanning and ultrasonic methods
20 p3636 A70-39213

Solid body nonelastic deformation in terms of thermodynamic principles of nonequilibrium processes
20 p3718 A70-39246

Nb single and polycrystalline thermal properties at high temperatures
20 p3648 A70-39639

Apollo 11 fines gas evolution and physical changes via heat treatment, discussing Ar 40 anomaly, lava structure origin and oxidation rate
21 p3907 A70-41577

Reacting planetary carbon dioxide-nitrogen atmospheres high temperature equilibrium thermodynamic and transport properties
21 p3950 A70-41747

Electrical and thermal characteristics of DC magnetic annular arc operating continuously at atmospheric pressure
21 p3805 A70-41758

Oxygen-kerosene fuel combustion products thermodynamic properties, tabulating computed values
21 p3865 A70-41771

Aromatic polysulfone thermomechanical behavior by torsional braid analysis, discussing structure, synthesis, thermal stability, radiation effects, etc
21 p3783 A70-42134

Soviet papers on thermodynamic and thermochemical constants covering solid, liquid and gaseous state properties, phase equilibrium, etc
22 p4123 A70-42676

Specific heat and thermodynamic functions of endo- and exo-isomers of 2-methylbicyclo heptane in 12-310 K temperature range
22 p3982 A70-42681

Gaseous substances thermodynamic functions and chemical equilibrium constants logarithms dependence on temperature and pressure, deriving internally self consistent formulas
22 p4124 A70-42682

Liquid and solid phases of substance, calculating thermodynamic properties and vapor pressure logarithm dependence on temperature
22 p4124 A70-42683

Nonequilibrium gasdynamic and thermodynamic properties of chemically reacting gas mixtures in high expansion subsonic and supersonic nozzles for selected rocket propellants
22 p3982 A70-42761

Isothermal kinetic rates of polymer swelling and dissolution, using thermomechanical analyzer
22 p4059 A70-43078

Isothermal kinetic rates of penetration of polymer by spherical indenter, using thermomechanical analyzer
22 p4059 A70-43079

Thermodynamic parameters of stellar matter in electronic degeneration conditions, discussing energy balances discrepancies
22 p4106 A70-43260

Liquid propellant rocket engine nonisobaric cylindrical combustion chamber parameters from thermodynamic data
22 p4092 A70-43355

Thermomechanical contact and heat transfer on reinforced edge in plates butt joined by curvilinear closed rigidity rib

22 p4120 A70-43718

Time optimal problems involving parabolic equations in heating of rod with piecewise continuous thermophysical characteristics and temperature distribution constraints, deriving iterative solution

23 p4277 A70-44306

Near critical heat transfer in cryogenic fluids, discussing thermodynamic and transport properties

23 p4279 A70-44357

Intermolecular forces at close approach distances in calculating thermodynamic and transport properties of high temperature dilute gases, using molecular beam methods

23 p4222 A70-44430

Thermodynamic properties, tables and equations of state of liquid para hydrogen from liquid-gas and liquid-solid phase equilibria

23 p4220 A70-44434

High temperature aluminum species in vapor over solid alumina, determining thermodynamic properties, composition and accommodation coefficient by Knudsen effusion and mass spectroscopy

23 p4281 A70-44451

Perfect nonrelativistic bounded gas thermodynamics and surface tension, assuming single particle energy level density dependence on external potential

23 p4284 A70-44928

High speed internal combustion engine mixed flow type liquid cooling system, deriving dynamic thermal characteristics from differential equations solution

24 p4393 A70-45502

Psychrometric chart for physiological research involving moist air thermodynamic properties

24 p4304 A70-46275

THERMODYNAMICS

NT AEROTHERMODYNAMICS

NT COMBUSTION PHYSICS

Sliding friction and adhesion mechanisms theories based on thermodynamics, noting frictional heat and adhesive joints

[ASME PAPER 69-LUB-4] Moving gas with thermodynamic relaxation process, discussing bulk viscosity and application to shock structure calculations

01 p0103 A70-10398

Thermodynamics of electrochemical cells consisting of Li with lithium chloride or bromide and thallium amalgam with thallium chloride or bromide in propylene carbonate

01 p0063 A70-10927

Discrete models formulated for thermomechanical behavior of materials with memory, obtaining equations of motion and heat conduction for finite elements of nonlinear continua

01 p0402 A70-11107

Thermodynamic aspects of ray invariance of spectral brightness ratio to square of local index of refraction compared to black body power radiation

01 p0144 A70-11293

Asymmetric thermoelasticity derived for constitutive equations based on thermodynamics of irreversible processes, formulating variational and reciprocity theorems

01 p0209 A70-11384

Integral theorems for wave-type heat conductivity equation

01 p0219 A70-11398

Soviet book on gas thermodynamics of solid propellant rocket engines covering combustion products equilibrium in nozzle and chamber, engine design, etc

02 p0353 A70-11690

Classical mechanics and thermodynamics principles restated using functions of sets, material sets and reciprocal actions between material sets

02 p0339 A70-11896

Gravitational theory for disk galaxies, considering radial velocity variations, spiral structure, heat equation verification, etc

02 p0378 A70-12688

Thermodynamic constitutive equations for large dynamic plastic deformation problems

03 p0585 A70-12971

Heat equation prediction, considering insulated uniform rod with unknown temperature distribution

03 p0604 A70-12993

Unsteady heat transfer theories reviewed to assess steady state heat transfer relations applicability

03 p0605 A70-13401

Thermodynamics of radiation and photosynthesis, discussing Ross-Calvin maximal efficiencies, Duysens method, light and dark conditions and polarized light

03 p0428 A70-14011

Book on rational thermodynamics covering homogeneous processes, internal dissipation, Coleman theorem, wave propagation in dissipative materials, diffusion, chemical reactions, Onsager relationship, etc

03 p0525 A70-14042

Thermodynamics second law application to pyrotechnic systems, discussing solid-solid and reversible reactions

03 p0547 A70-14114

Heat conduction equation solutions, comparing finite element and finite difference methods

[ASME PAPER 69-WA/HT-35] Approximate boundary controllability of heat equation, considering smoothness conditions on piecewise-smooth boundary

05 p0875 A70-15781

Thermodynamics of elastic continuum with microstructure, modifying second law to include microtemperatures

05 p0930 A70-16083

Hydrothermodynamic equations used in forecasting meteorological components solved by assuming equations of motion quasi-linear and reducing to ordinary differential equations

05 p0878 A70-16195

Heat conduction equation containing diffusivity coefficient as Stefan type function

05 p0958 A70-16867

Toupin and Knowles elasticity theory applied to spatial decay estimate for parabolic heat equation used in diffusive temperature field

07 p1409 A70-19565

Nonlinear thermodynamic theories of plates, elastic shells and rods derived from three dimensional theory of classical continuum mechanics

07 p1414 A70-20172

Finite element models for nonlinear problems analysis in coupled thermoelasticity dynamical theory, deriving heat conduction equations from energy balance considerations

07 p1417 A70-20363

Difference schemes approximating quasi-linear heat conduction equation, demonstrating convergence

08 p1596 A70-20857

Transformed thermodynamics equations derived automatically by substitution codes, noting exceptions for real gas and discharge flow

08 p1597 A70-20918

Thermal conductivity and diffusivity of two phase composites determined by iterative solution of heat conduction equation with space fluctuating properties

08 p1598 A70-21511

Collective approach to thermodynamics of N-particle electron gas including transverse radiation, calculating internal energy and pressure of modes

08 p1553 A70-21612

Error analysis of Barakat-Clark explicit heat diffusion equations for thermally insulated surface

08 p1600 A70-21831

Thermomechanical tests effectiveness and determination of stress level defining boundary between destructive and nondestructive testing

09 p1689 A70-22004

Continuous dependence theorem and differentiability properties of free boundary problem solution for heat equation

09 p1788 A70-22609

Irreversible processes thermodynamics during thermoelastic deformation of solid bodies, deriving thermodynamic potentials, state and coupled heat equations

09 p1777 A70-23077

Variational principle of steady state transport process derived from basic inequality in macroscopic theory of nonequilibrium thermodynamics

09 p1789 A70-23224

Unsteady flow equations and thermodynamics for studying homogeneous fluidic transmission in circular and rectangular cross section lines

09 p1613 A70-23403

Thermodynamics and fluid mechanics - Conference, Glasgow, March 1970

09 p1607 A70-23733

Temperature field and heat conduction equation for two layer polymer cylinder multiply heated from within, considering material decomposition

10 p1966 A70-23870

Flux equations of single velocity Boltzmann type for unsteady transport problems applied to concentration discontinuity propagation through plane layer

10 p1966 A70-23871

Shock and thermodynamic phenomena of real gases near critical points, discussing specific volume and specific enthalpy increases

10 p1867 A70-24136

Information theory as basis for statistical thermodynamics, discussing maximum entropy principle and probability as frequency in Gibbs ensemble

11 p2083 A70-25694

Thermodynamics and statistical mechanics taking into account irreversibility, arrow of time and astrophysical schemes

11 p2146 A70-25695

Hydrodynamics and thermodynamics in mechanical rade face seal design

11 p2059 A70-25792

Polyimide resins and composites state of cure determination by thermomechanical analysis/TMA/

11 p2069 A70-25807

Space flight thermodynamics and thermophysics - Conference, Palo Alto, California, March 1970

11 p2149 A70-26351

SAE aerospace applied thermodynamics manual covering aerodynamics, fluid dynamics, heat transfer,

materials properties, aerospace application engineering, etc

12 p2329 A70-26872

Energy derivation for mechanics and thermodynamics with generalization to systems of more than two dynamic variables, considering transformations and Newton and Kepler laws

12 p2164 A70-27070

Heat equation initial value problem with dissipative term nondecreasing and discontinuous function of unknown, discussing existence and uniqueness theorem of periodic solution

12 p2330 A70-27160

Asymptotic properties of Cauchy problem solution for heat conduction equation

12 p2331 A70-27300

Nonequilibrium self gravitating medium unified thermodynamics theory based on propagators, describing spatial and temporal fluctuations and coupling for galactic formation

12 p2310 A70-27978

Three-nodes analysis for thermal design of spinning spherical satellite using heat transfer equations in mathematical model

12 p2332 A70-28061

Local heat sink thermal processes on convectively cooled solid surface, noting applications to temperature measurement errors

12 p2333 A70-28112

Stagnation point position as function of gas thermodynamic state behind detached shock for spherical segment at incidence in three dimensional hypersonic flow

12 p2159 A70-28247

Cauchy problem for relativistic heat equation for unbounded domain generated by streamlines of future oriented vector field

13 p2451 A70-28709

Boundary value problems of ordinary and generalized heat conduction equations using reflection method

13 p2521 A70-29311

Cold worked metal, estimating lattice imperfections mol fractions based on reversible cell thermodynamics

15 p2676 A70-31564

Soviet papers on high temperature thermophysics covering body-gas heat exchange, plasma jet breakdown of subliming materials, electric arc heaters, plasmatron regime, etc

15 p2826 A70-32101

Heat conductivity equations transformation for Cartesian and cylindrical coordinates and various boundary conditions using static electrointegrator

15 p2827 A70-32172

Redundant variable errors in weather prediction, specifying initial conditions for time integration of hydrothermodynamic equations for atmospheric motion

15 p2771 A70-32368

Dissociation energy of gaseous TiN molecule at high temperature

15 p2695 A70-32748

Thermodynamic equations of state for dissociating and ionizing air in equilibrium, noting applications to vertical and oblique compression shocks

15 p2828 A70-32840

Metastable beta phase decomposition in Ti alloy during mechanicochemical treatment and aging, determining correspondence to alpha phase segregations via electron microscopy

16 p2931 A70-33207

Thermodynamic diagram indicating enthalpy and entropy of oil combustion gases for any state and air excess value

16 p2997 A70-33295

Transport processes in chemical reactions and biological functions of living systems, using nonequilibrium thermodynamics approach

17 p3032 A70-35539

Sodium sulfate induced accelerated oxidation of Ni and superalloys, investigating thermodynamics and reaction mechanism

18 p3272 A70-36037

Thermodynamics - Conference, University of Pittsburgh, April 1969

18 p3347 A70-36551

Relativistic thermodynamics, developing relativity theories in nonvacuo regimes and discussing covariant scalars and formalisms

18 p3291 A70-36553

Ideal relativistic fluids adiabatic flow, investigating heat exchange effects within framework of special relativity

18 p3347 A70-36554

Thermodynamic application to strained solids, considering paradoxes, irreversible processes and continuum mechanics

18 p3340 A70-36555

Thermodynamics of solids deformation, tracing macroscopic inelastic behavior to deformation induced internal structural changes governed by atomic and molecular processes

18 p3340 A70-36556

- Thermodynamics of thermoviscous fluids based on Riemannian space time notions and balance laws of general theory of relativistic continuum mechanics 18 p3347 A70-36557
- Meteorological prediction methods based on dynamic or thermodynamic considerations 18 p3285 A70-36949
- Chemical vapor deposition of carbon matrix material in fiber structure, investigating thermodynamic fundamentals in processes 20 p3654 A70-39207
- Uniqueness theorem for first boundary value problem of heat conduction equation with discontinuous coefficient 20 p3737 A70-39710
- Thermomechanical disturbances propagation in viscoelastic solids, investigating effects of viscous flow, second order strains and temperature dependent material properties 21 p3937 A70-41427
- Elastic-plastic deformation analysis at finite strain by two component thermodynamic model 21 p3937 A70-41431
- Rocket engines propulsion systems design and performance based on thermodynamical theory, involving expanding gas 21 p3869 A70-42038
- Coherent behavior associated with thermodynamic description projected from dynamical behavior of many body system, using relation between asymptotic operators 22 p4062 A70-42547
- Alloys stacking faults thermodynamics based on Gibbs treatment of interfacial free energy 22 p4124 A70-42726
- Electro-thermal-mechanical switches based on shape-memory effect in Ti-Ni alloys 22 p3965 A70-43330
- Graphite fiber oxidation prevention in metal matrix composites, examining various thermodynamic parameters 22 p4126 A70-43676
- Iterative method for boundary value problems in mathematical physics, showing convergence by heat conduction equation solutions 23 p4276 A70-44218
- Heat conductivity problem of body with variable density and specific thermal conductivity reduced to differential equation via power series 23 p4277 A70-44340
- Steady state radiative heat transfer through gray gas in spherical cavity, solving transport equation by singular integral equations for uniform heat generation 23 p4283 A70-44784
- Thermodynamics and statistical physics of dense plasma with particle interaction energy exceeding kinetic energy, discussing three-component model phase equilibrium 23 p4229 A70-45073
- Isothermal plasticity thermodynamic foundation, deriving constitutive equations for various deformations 24 p4426 A70-45994
- German book on aircraft thermal propulsion systems calculation, design and evaluation, covering thermodynamic principles and atmospheric composition and properties 24 p4396 A70-46150
- One dimensional gas pressure as function of activity, using Poisson-type partition function for perturbation calculation of thermodynamic limit 24 p4430 A70-46269
- THERMOELASTICITY**
- NT AEROTHERMOELASTICITY**
- Asymmetric thermoelasticity derived for constitutive equations based on thermodynamics of irreversible processes, formulating variational and reciprocity theorems 01 p0209 A70-11384
- Temperature fields and universal motions in homogeneous isotropic thermoelastic body in absence of body forces and external heat supply 02 p0387 A70-12000
- Integral formulas of thermoelasticity theory for calculating displacements and rotations caused by temperature field action in micropolar Cosserat and Hooke media 02 p0391 A70-12817
- Thermoelastic stresses in plate due to arbitrary temperature variations of heat transfer agent calculated in second approximation, allowing for transfer coefficient time dependence 03 p0590 A70-13400
- Thermoelastic stresses in diode of pulsed and CW injection lasers, showing energy parameter limitation 03 p0499 A70-13437
- Steady thermoelastic state of inhomogeneous plane with circular discontinuity on perimeter, studying stress concentration at thermally insulated crack 03 p0595 A70-13738
- Thermoelastic stresses in solid cylinder under cyclic temperature variation, calculating amplitude for Biot numbers 04 p0766 A70-14477
- Transient temperature distribution, thermal stresses and deformations in thin finite circular disk due to continuous point heat source, using linear thermoelasticity [ASME PAPER 69-WA/PVP-6] 04 p0768 A70-14789
- Thermoelastic boundary value problems solutions in quadratures applicable to problems with given parameters on boundary sections 04 p0775 A70-15257
- Soviet book on three dimensional boundary value problems in mathematical theory of elasticity and thermoelasticity 04 p0777 A70-15474
- Thin film transmission electron microscopy study of precipitation in Fe-Ni-Cr-Mo alloy with added Be and specific thermoelastic properties 05 p0862 A70-16022
- Thermoelasticity generalization from physically motivated modification of Fourier heat conduction law, postulating constitutive equations valid for finite deformations and temperature variations 05 p0929 A70-16062
- Thermoelastic stresses in rotating circular cylinder, analyzing temperature effect on angular velocity for neo-Hookean material using finite deformation theory 05 p0930 A70-16080
- Constitutive equations for isotropic elastic and thermoelastic materials with microstructure derived using free energy function, giving uniqueness theorems 05 p0932 A70-16136
- Fibers random curvature effect on thermoelastic properties of unidirectionally reinforced fibrous materials 05 p0946 A70-16953
- Thermoelasticity boundary value problems solutions in quadratures based on symmetry property and Fourier integrals 05 p0947 A70-16971
- Low temperature thermoelasticity theory for elastic fluids, considering fountain and second sound effects and viscosity anomalies in He II 06 p1164 A70-17442
- Thermoelasticity equations derived for regular systems of M bodies in dynamic and thermal interaction using nonlocal continuous model 07 p1407 A70-19381
- Structural material selection for thermal shock conditions, deriving index from parameters governing solutions in thermoelasticity 07 p1413 A70-20002
- Gruneisen parameter for metal and semiconductor single crystals obtained from measuring one dimensional thermoelastic response during exposure to pulsed electron beam 07 p1357 A70-20020
- Uniqueness theorem for coupled dynamic problem of linear thermoviscoelastic theory assuming contact-type boundary conditions 07 p1416 A70-20296
- Finite element models for nonlinear problems analysis in coupled thermoelasticity dynamical theory, deriving heat conduction equations from energy balance considerations 07 p1417 A70-20363
- Thermoelastic stress degradation of injection lasers at high excitation levels, giving critical current densities for short pulse, CW and quasi-CW conditions 08 p1512 A70-20861
- Thermoelastic characteristics of glass fiber reinforced plastic materials, determining temperature dependent deformation of composite plate 08 p1526 A70-21164
- Thermoelastic state of plate near foreign circular inclusion, assuming heating by uniformly distributed sources and ideal plate-inclusion thermal contact 08 p1587 A70-21171
- Steady temperature field and stresses produced by thermal sources in infinite elastic plane containing insulated rectilinear crack, determining thermoelastic state of half plane 08 p1587 A70-21172
- Boundary value contact problems in thermoelastic oscillations theory found to have unique solutions for any frequency 08 p1591 A70-21440
- Thermoelastic energy functions bounding by variational principles for anisotropic composite materials properties 08 p1592 A70-21510
- Composite materials macroscopic thermoelastic properties relationships to constituents properties, discussing effective thermal expansion coefficients and specific heats 09 p1703 A70-22682
- Irreversible processes thermodynamics during thermoelastic deformation of solid bodies, deriving thermodynamic potentials, state and coupled heat equations 09 p1777 A70-23077
- Temperature fields and thermoelastic stresses in doubly connected structural elements solved in curvilinear coordinates system corresponding to conformal mapping of annulus 09 p1777 A70-23080
- Thermoelastic stresses in plates and shells in random temperature fields, studying influence on service life 09 p1778 A70-23084
- Thermoacoustic waves formation and propagation in metallic rods by light pulses, studying pulse rise time influence on waves shape and amplitude 09 p1778 A70-23090
- Thermal stress concentrations at arbitrary holes for nonlinearly elastic materials, developing small deformation theory for two dimensional problem 09 p1779 A70-23093
- Thermal stress freezing during optical polarization study of perforated disk three dimensional thermoelasticity 09 p1780 A70-23105
- Kantorovich variational method extended to thermoelastic plane stress problem of rectangular plates 09 p1781 A70-23278
- Mixed thermoelastic problem in elastic layer with arbitrarily prescribed temperature in upper free surface 10 p1954 A70-23878
- Nonstationary thermoelasticity in half space with moving boundary condition described in Cartesian rectilinear coordinates allowing for time term in heat conduction equation 10 p1954 A70-24012
- Thermoelasticity problem for plane with rectilinear cut with constant temperature at initial moment of time, using approximating kernel of integral equation 10 p1965 A70-25296
- Nomograms for thermoelastic stress in plate determined as function of dimensions and heat transfer 10 p1965 A70-25300
- Two dimensional dynamic thermoelastic problem for thin plates with internal heat sources solved by integral Laplace and Fourier transforms 12 p2323 A70-27337
- Hollow homogeneous polymer cylinder thermoelastic stressed state, analyzing radial temperature and Poisson Coefficient variations 12 p2325 A70-27532
- Thermoelastic stresses distribution in transmitting dielectric under short nonfocused laser pulses 12 p2251 A70-28327
- Thermoelastic equations for circular sandwich plates bending due to asymmetric temperature distribution 13 p2518 A70-29976
- Thermoelastic stresses in sphere with cylindrical cut under axisymmetric temperature field and constant surface temperature 14 p2655 A70-30135
- Thermoelasticity of incompressible solids, integrating linearized equations using Helmholtz solution 14 p2660 A70-31224
- Stress, strain, temperature, electric and magnetic field distributions resulting from magneto-thermoelastic interactions in infinite elastic solid subjected to transient heat source 14 p2661 A70-31229
- Small deformation thermoelasticity theory, discussing thermal conductivity, dynamic elasticity, strain field-temperature relationship, etc 15 p2818 A70-32177
- Induced strain plane state in elastic micropolar medium by temperature effect, discussing thermoelastic problem stress functions 15 p2821 A70-32341
- Micropolar Cosserat medium of thermoelasticity wave equations for Hooke medium, deriving elastic potentials and stress functions 15 p2822 A70-32354
- Initial thermally stressed state of solid bounded by concentric circular cylinders, applying Cauchy thermoelastic stress theory 16 p2987 A70-32993
- Thermal and thermoelastic constants of macroscopically isotropic composite materials based on self consistent calculations 17 p3194 A70-34555
- Composite orthotropic cylindrical shells linear thermoelastic equations solution for fixed end boundary conditions, noting heterogeneity effects on stress distribution 17 p3184 A70-34909
- Stress concentration near holes in plate in plane problem of thermoelasticity, taking into account physical and geometrical nonlinearities 18 p3336 A70-36133
- Cylindrical shell of variable thickness, deriving axisymmetric thermal stresses in terms of hypergeometric functions 18 p3336 A70-36137
- Elastic continuum conducting heat under general loads, investigating stability thermodynamics-Liapunov criterion relations 18 p3337 A70-36336
- Plane strain and stress produced in elastic micropolar medium by action of temperature 18 p3338 A70-36429
- Thermodynamical modeling by regular systems of deformable bodies bound by hyperelastic medium

with internal degrees of freedom, formulating equations of motion

18 p3338 A70-36432

Elastic Cosserat half plane, analyzing wave propagation of small amplitude thermoelastic disturbances and uniform motion of concentrated line load along surface

18 p3338 A70-36434

Thermoelasticity boundary value problems by finite difference method, determining thermal, displacement and stress fields in continuous medium

18 p3342 A70-36671

Thermoelastic stresses in infinite anisotropic slab due to temperature field variations along thickness and length

19 p3539 A70-37872

Thermoelastic composite materials, deriving crystal lattice type model of equations for predicting dynamic or thermomechanical behavior

19 p3540 A70-37958

Book on thermoelasticity covering thermal stresses in disks, plates, shells and bodies of revolution under steady and unsteady temperature fields

19 p3541 A70-37974

Minimum weight thermoelastic design of sandwich beam for given deflection, using potential energy principle

19 p3541 A70-38044

Thermoelastic seismic-energy release as source mechanism for volcanic earthquakes, describing thermal microfracture tests

20 p3619 A70-39217

Radial and shearing stresses in hollow composite sphere due to thermoelastic strain nucleus

20 p3719 A70-39602

Hot gas pipe thermoelastic reduction factors, determining elastic support, material and dimensions

20 p3720 A70-39624

Stressed state in thermoelasticity plane steady state problem of thin plate under bending based on dislocations and temperature stresses relationship

20 p3721 A70-39780

Asymmetric micropolar thermoelasticity, deriving integral expressions for strains, rotations and temperatures in finite body

20 p3726 A70-39878

Thermoelasticity of fiber reinforced materials, considering stress concentration in beams and reinforcing fibers buckling under thermal loading

20 p3730 A70-40037

Thermoinelasticity - Conference, East Kilbride, Scotland, June 1968

21 p3936 A70-41426

Thermoinelasticity theory for elastic material with different moduli in tension and compression, noting heteroresistance

21 p3937 A70-41428

Dynamical linear thermoelasticity theorem generalization with time dependent conductivities, elasticities and density

22 p4112 A70-42483

Linear coupled thermoelasticity theory for homogeneous isotropic solid with two temperatures

22 p4123 A70-42540

Thermoelasticity theory concerning Navier-Stokes-Fourier type fluid universal motion characterization in absence of body forces and external heat supply

22 p4010 A70-42637

Variable thickness flexible plates thermoelastic flexure and buckling, obtaining nonlinear differential matrix equations by difference-differential method

22 p4115 A70-42811

Thin plates two dimensional dynamic thermoelastic problem, determining hyperbolic type heat conduction for temperature field

23 p4265 A70-43985

Cylindrical shells dynamic thermoelastic response to sudden rotating thermal inputs, using Galerkin method

24 p4421 A70-45285

German monograph on thermally induced elastic stress effects on crack formation and propagation in plates

24 p4422 A70-45524

Polar elastic materials constitutive relations for thermoelastic couple stresses by general theory of incompatible strains, obtaining linearization for isotropic materials

24 p4428 A70-45578

Controllable states with prescribed heat flux for incompressible isotropic thermoelastic bodies with temperature dependent response functions

24 p4426 A70-46041

THERMOELECTRIC CONVERSION SYSTEMS

U THERMOELECTRIC POWER GENERATION THERMOELECTRIC COOLING

Thermoelectrically cooled GaAlAs injection laser illuminator, discussing optical-electronic interface problems and design and performance characteristics

22 p4052 A70-43603

THERMOELECTRIC GENERATORS

NT SNAP 19

NT SNAP 27

Semiconductor solar thermoelectric generator allowing thermoelement replacement during service including construction, bridging methods and characteristics

01 p0009 A70-10751

Current-voltage characteristics of cascaded solar thermoelectric generator, determining optimum hot junction temperature as function of radiation concentration

01 p0000 A70-10752

Solar energy concentrator with truncated conical mirror and toroidal lens to illuminate cylindrical thermoelectric generators or radiation pumped lasers

01 p0010 A70-10760

Selective glass coatings applications in solar thermoelectric generators working without radiation concentrators

01 p0011 A70-10767

Thermoelectric-couple life tests and efficiency measurements at constant thermal input, noting insulation for limiting parasitic heat losses

[ASME PAPER 69-WA/ENER-14]

04 p0731 A70-14896

Thermal steady state characterization of isotope radioisotope thermoelectric generator, discussing design features and heat transfer models for operating temperatures and output performance

[ASME PAPER 69-WA/ENER-12]

04 p0717 A70-14897

Thermoelectric generators design, discussing Si-Ge air-vac thermocouple configurations, compression modules, thermal losses, etc

10 p1808 A70-24897

Commercial thermoelectric generator design, applications and economics compared to batteries and small MG sets

10 p1808 A70-25033

Figure of merit for thermoelectric generator determined experimentally, assuming temperature difference between heated and cooled junctions

10 p1808 A70-25035

Electrodynamic generator with spatial charge neutralization for direct thermal-to-electrical energy conversion at high gas pressures

12 p2165 A70-27330

Solar energy direct conversion into electricity, surveying photoelectric, thermoelectric and thermoemissive methods

15 p2677 A70-31598

Solar thermoelectric generator /STEG/ with two stage converter, discussing weight factors and efficiency

15 p2678 A70-32425

Deep space spacecraft radioisotope thermoelectric generators, discussing testing and evaluating for future missions

18 p3215 A70-36229

Thermoelectric generators design for space and remote terrestrial sites, discussing fuel source, conversion section, heat rejection, etc

20 p3563 A70-39225

TOPS/thermoelectric outer planet spacecraft/ project integrating R and D for specific space missions

21 p3920 A70-41793

Thermoelectric outer planet spacecraft /TOPS/ flight environment, systems design and Titan 3D/Centaur launch vehicle with Burner II upper stage

21 p3930 A70-41795

Thermoelectric outer planet spacecraft /TOPS/ data subsystems for 12 year missions compared with Mariner subsystem

21 p3795 A70-41796

Trajectory correction propulsion subsystem /TCPS/, attitude propulsion subsystem /APS/ and pyrotechnic subsystem of thermoelectric outer planet spacecraft /TOPS/

21 p3868 A70-41800

Thermoelectric outer planet spacecraft /TOPS/ solar-independent power subsystem

21 p3760 A70-41802

Electrodynamic generator with spatial charge neutralization for direct thermal-to-electrical energy conversion at high gas pressures

21 p3760 A70-42071

SNAP 19 radioisotope thermoelectric generator module for Viking Lander and Pioneer applications, discussing design requirements, environmental and mission constraints, life, performance and reliability characteristics, etc

22 p4071 A70-43195

Radioisotope thermoelectric generator with lead telluride converter, discussing intact reentry and impact capability, refractory construction and reliability

22 p4072 A70-43196

Spacecraft radioisotope thermoelectric generator interference in onboard instrument operation, using analytical models to determine necessary shielding

24 p4375 A70-45175

SNAP 27 thermoelectric generator for Apollo Lunar Surface Experiments Package /ALSEP/

24 p4377 A70-46385

THERMOELECTRIC MATERIALS

Hot junctions nonuniform heating influence on thermoelectric generator efficiency, taking into account

temperature dependence of thermoelement materials properties

01 p0009 A70-10753

Cascaded thermoelements with high figure of merit for increasing solar thermoelectric generator efficiency, noting high temperature materials effect

01 p0158 A70-10754

GeTe thermoelectric power, electrical/thermal conductivity and expansion coefficient measured at 20-600 C, determining suitability as thermoelectric material

01 p0158 A70-10755

PbSe and GeTe cast and pressed samples thermoelectric properties before and after high energy gamma ray irradiation, using scintillation counter with photomultiplier

01 p0159 A70-10756

Bridging joints resistance effect on thermoelement efficiency, describing W and Co coatings deposition on GeTe based thermoelectric alloys

01 p0159 A70-10757

Molten bridging alloy deposition on p and n type thermoelectric materials, utilizing diffusion process brief duration during contact

01 p0009 A70-10758

Thermoelectric-couple life tests and efficiency measurements at constant thermal input, noting insulation for limiting parasitic heat losses

[ASME PAPER 69-WA/ENER-14]

04 p0731 A70-14896

Thermoelectric powers of liquid metals calculated from structure factors, using screened model potential

05 p0892 A70-16313

Electric current flow effect on thermoelectric figure of merit from thermal conductivity measurements on thermoelement

10 p1808 A70-25034

Metallic thermoelectric materials, measuring electrical resistivities and Seebeck coefficients of binary Ni alloys

14 p2533 A70-30530

THERMOELECTRIC POWER GENERATION

Hot junctions nonuniform heating influence on thermoelectric generator efficiency, taking into account temperature dependence of thermoelement materials properties

01 p0009 A70-10753

Cascaded thermoelements with high figure of merit for increasing solar thermoelectric generator efficiency, noting high temperature materials effect

01 p0158 A70-10754

Electrical power system adaptable to intermediate solar probes, discussing thermoelectric, thermionic, photovoltaic systems and battery for energy storage

[ASME PAPER 69-WA/SOL-5] 04 p6625 A70-14753

Mercury plasma flow rate change effect on electron temperature and density in thermoelectric converter determined by spectroscopy

05 p0887 A70-16028

Thermoelectric power /TEP/ of transition metals, detecting empirical regularities in TEP, nonlinear temperature dependence, etc

05 p0893 A70-16949

Si-Ge air-vacuum thermocouples for thermoelectric conversion, describing construction materials, mechanical and electrical properties, radiative heat transfer operation, etc

10 p1807 A70-24896

Thermoelectric power and Hall effect quantum resonances in pressure annealed pyrolytic graphite crystals for carrier locations evidence

11 p2097 A70-25616

ZrH reactor program and multikilowatt space oriented thermoelectric power conversion systems

22 p4071 A70-43190

Thermoelectric power and Hall effect quantum resonances in graphite for locating majority carrier electron and hole Fermi Surfaces in Brillouin zone

24 p4389 A70-45597

THERMOELECTRICITY

Voltage-power sensitivity, response time, frequency limit and minimum registered power of hot carrier thermoelectric detectors calculated from characteristic semiconductor parameters

03 p0540 A70-13436

Calor-electric voltage calculation for stoichiometric flame burning in air introducing allowance for charged particle densities

04 p0780 A70-14706

Physical exercise and rest regime evaluation by thermoelectric method recording skin temperature above gastrocnemius muscle

04 p0640 A70-15513

Specific heat and thermal EMF increase due to radiation damage in lattice of fast neutron bombarded Cu, Mo and W specimens

05 p0863 A70-16292

Thermoelectric characteristics of graphite and titanium carbide compared with platinum after prolonged annealing at 2300 C

07 p1316 A70-19661

Ovshinsky switching effect, considering electrothermal initiation and field dependent conductivity at elevated temperatures

14 p2626 A70-30336

Equilibrium and steady state Hall and thermoelectric effects in inhomogeneous semiconductor materials 15 p2783 A70-31760

Electric conductivity, thermal emf and EPR spectra of oxide semiconductor glasses based on vanadium and phosphorus oxides, correlating unpaired electron and charge carrier concentrations 15 p2784 A70-32201

Thermoelectric power measurement of thin Au films, relating results to transport parameters and internal stresses 15 p2785 A70-32582

Thermoelectric force due to thermocouple inhomogeneities, showing relation to temperature gradient and measurement error 16 p2900 A70-33070

Ni-Fe ferrites resistivity and thermoelectric power as function of temperature, proposing two energy level model for Fe ions 17 p3143 A70-35604

Electrical conductivity, Hall constant and differential thermal emf n-type GaAs-CdS solid solutions 18 p3298 A70-36596

Thermo-electret surface charge and dielectric constant time variation measurements, considering hole-electron pairs production hypothesis 21 p3797 A70-40890

Double tunneling electrothermal initiation of threshold electronic switching in semiconducting glasses, discussing temperature profile and current density saturation effects 21 p3864 A70-42019

THERMOGRAMS

U RECORDING INSTRUMENTS
U TEMPERATURE MEASURING INSTRUMENTS

THERMOGRAPHS

U RECORDING INSTRUMENTS
U TEMPERATURE MEASURING INSTRUMENTS

THERMOGRAVIMETRY

Transition kinetics during linear to parabolic oxidation of Cr in water-hydrogen gas mixture measured thermogravimetrically 08 p1521 A70-21558

Composite propellant catalysts /copper chromate and chromite/ thermal decomposition using simultaneous thermogravimetric and differential thermal analysis 11 p2100 A70-26382

Thermogravimetric analysis /TGA/ of gadolinium-doped silver carbonate decomposition, obtaining activation energy, preexponential factor and reaction order 15 p2694 A70-32074

High temperature organic resin binders and solid lubricant thermal and oxidative behavior examined by thermogravimetric analysis [ASME PAPER 70-HT-30] 22 p4058 A70-42436

Differential scanning calorimetry and thermogravimetric analysis combination for thermochemical kinetic measurements, matching analytical and experimental curves for data accuracy 23 p4196 A70-44429

THERMOLUMINESCENCE

Thermoluminescent glass X ray dosimeter sensitivity tested as function of rigidity of gamma and X radiation, noting compensating filters for incident radiation 08 p1496 A70-21217

Saint-Severin meteorite thermoluminescence from mineralogical fractions separated by density 15 p2800 A70-32025

Natural thermoluminescence of limestone within/near Charlevoix meteorite impact structure, discussing impact effects on quartz-rich rocks 18 p3314 A70-36499

Apollo 11 rocks red luminescence and blue thermoluminescence under proton bombardment, discussing energy efficiency 21 p3913 A70-41644

Apollo 11 fines, breccias and crystalline rocks thermoluminescence, observing temperature dependence of glow curve peaks 21 p3914 A70-41649

Thermoluminescence, X ray and stored energy measurements of Apollo 11 samples, comparing surface outputs to interior 21 p3916 A70-41665

Thermal energy conversion into coherent laser light, examining various thermodynamic limitations 22 p4076 A70-43674

THERMOMAGNADYNAMICS

U THERMOMAGNETIC EFFECTS

THERMOMAGNETIC EFFECTS

Transient response analysis in isotropic material under thermal galvanomagnetic effects involving interaction electric and thermal conduction in applied magnetic field [AIAA PAPER 70-17] 06 p1107 A70-18213

Magnetothermal instability and radiative effects on incipient fragmentation of rotating gravitating interstellar fluid forming condensations 08 p1578 A70-21545

Thermomagnetic transport coefficients in anisotropic metals based on theory for galvanometric properties, producing closed form expression for conductivity tensor 11 p2097 A70-25618

Thermomagnetomicroelasticity wave equations of heat conduction for thermal and coupled perturbations propagating in isotropic medium at finite velocities 16 p2953 A70-34326

Apollo 11 lunar rock and dust samples thermomagnetic properties, Curie points, magnetization and demagnetization characteristics 21 p3915 A70-41661

Apollo 11 lunar dust hysteresis curves and thermomagnetic curves, discussing metallic Fe abundance, susceptibility, alpha-gamma transition, etc 21 p3918 A70-41676

Transport equation relation between irreducible tensorial sets, examining geometrical symmetry influence and thermomagnetic and galvanomagnetic effects 24 p4428 A70-45520

THERMOMAGNETISM

U THERMOMAGNETIC EFFECTS

THERMOMECHANICS

U THERMODYNAMICS

THERMOMETERS

NT RESISTANCE THERMOMETERS

High temperature thermometer using pulsed excitation ultrasonic resonance with ruthenium sensor, discussing resonator types, transmission lines and transducer 02 p0300 A70-12468

Aerological radio thermometers random and systematic errors compared to network radio probe 05 p0848 A70-16206

Thermometer dynamic response under various working conditions predicted from time constant curves 05 p0849 A70-16518

Noncontact thermometer designed around YIG modulator to demonstrate usefulness of optical component in near IR systems 09 p1676 A70-22788

Helium melting pressure curve to calibrate cerium magnesium nitrate or NMR low temperature thermometers 09 p1728 A70-22999

IR thermometers in situ calibration, analyzing maximum error due to reflection effect 09 p1684 A70-23536

Heat flux measurements in hypersonic rarefied gas flow by thin film surface thermometer 15 p2825 A70-31820

Photothermometer response to thermal shock, considering rapidly varying surface temperature measurement 16 p2901 A70-33104

Low temperature Ge diode thermometer with computer circuit transforming voltage to temperature readout 21 p3828 A70-41473

Thin film granular aluminum superconductors as sensitive thermometers 22 p4031 A70-43009

Semiconductor thermometer for skin temperature differences using resistance bridge, transistor amplifier and thermistors 23 p4150 A70-44317

THERMOMETRY

U TEMPERATURE MEASUREMENT

THERMONUCLEAR ENERGY

U THERMONUCLEAR POWER GENERATION

THERMONUCLEAR EXPLOSIONS

Ionosphere disturbances due to high altitude thermomagnetic explosions, discussing experimental proof by cosmo satellites short wave transmitter radio signal scintillation statistical evaluation 06 p1057 A70-17888

Thermal explosion in degenerate nucleus of white dwarf due to formation of laminar energy source in presence of hydrogen 11 p2115 A70-26577

Thermomagnetic explosion Operation Starfish effect on ionospheric state from recording in central Kazakhstan, studying frequency characteristics 11 p2047 A70-26790

Electron density decrease in F 2 layer ascribed to 9 July 1962 thermomagnetic explosion, noting dissociative recombination role 11 p2047 A70-26791

THERMONUCLEAR POWER GENERATION

Controlled thermomagnetic power generation, considering fusion reactors feasibility and reactor energy balance improvement 04 p0717 A70-14528

Worldwide developments in controlled fusion, discussing low beta open ended configurations, open and closed high beta systems, full scale reactors, etc 11 p2089 A70-25718

Controllable thermomagnetic reactor with free-floating HF discharge plasma in deuterium 12 p2271 A70-27351

Controllable thermomagnetic reactor with free-floating HF discharge plasma in deuterium 22 p4084 A70-43595

Thermomagnetic spacecraft propulsion, comparing X ray pumped gas laser and ion drive systems 24 p4377 A70-46211

THERMONUCLEAR PROPULSION

U NUCLEAR PROPULSION

THERMONUCLEAR REACTIONS

NT CONTROLLED FUSION

NT NUCLEAR FUSION

Neutron star atmospheric composition as function of time, including effects of diffusion, cooling and nucleosynthesis 02 p0378 A70-12698

Tokamak-type magnetic configurations application to thermomagnetic reactor, discussing equilibrium and stability parameters minimum values, operating pattern and heating method 02 p0349 A70-12756

Permittivity tensor calculations of weakly inhomogeneous plasma with monoenergetic component, using distribution function of particles produced by thermomagnetic reactions 03 p0529 A70-13055

Effective potential of electron screening of Coulomb nuclei field leading to thermomagnetic reaction rate increase using self consistent field method 07 p1346 A70-20206

Energy balance of self sustaining thermomagnetic reaction with nonuniform magnetic field in wall-contained dense plasma, allowing for radiation losses 11 p2088 A70-25709

Electrostatic shielding of nuclei Coulomb field during thermomagnetic reactions in degenerate gases of arbitrary densities 11 p2087 A70-26578

Neutrino astronomy for processes in stellar interiors, emphasizing thermomagnetic reactions in sun and main sequence stars 13 p2490 A70-28947

Thermomagnetic reactions in interior of sun, discussing models for He isotope concentration and flow to interpret solar neutrino generation 13 p2494 A70-29573

Inverse beta decay thermomagnetic reactions induced by neutrinos proposed for neutrino detection from solar interior 20 p3704 A70-39471

Explosive nucleosynthesis as heavy nuclei source for stars 20 p3712 A70-40426

Thermomagnetic rate constant for deuterium atom recombination, using orbiting resonance theory 21 p3781 A70-41886

Plasma physics computational problems concerning controlled thermomagnetic reactions, considering instability and equilibrium numerical calculations 23 p4224 A70-44181

THERMOPHILES

Gas chromatography study of fatty acids and polar lipids of thermophilic filamentous bacterial masses from hot Yellowstone Park springs 01 p0021 A70-10791

THERMOPHILIC PLANTS

NT BLUE GREEN ALGAE

NT NOSTOC

THERMOPHYSICAL PROPERTIES

NT CRITICAL POINT

NT CRITICAL PRESSURE

NT CRITICAL TEMPERATURE

NT EMISSIVITY

NT FUSIBILITY

NT HEAT OF SOLUTION

NT MELTING POINTS

NT PYROELECTRICITY

NT SPECIFIC HEAT

NT SUPERCRITICAL PRESSURES

NT THERMAL CONDUCTIVITY

NT THERMAL DIFFUSION

NT THERMAL DIFFUSIVITY

NT THERMAL STABILITY

NT VAPOR PRESSURE

NT VOLATILITY

ESRO 1 thermal behavior, discussing trajectory effects, onboard temperature measurement, data storage, data transmission, telemetered data and data comparison 04 p0762 A70-15164

Heat conduction in anisotropic materials to measure thermophysical parameters, using pulsed point or line heat source 05 p0957 A70-16457

Thermophysical characteristics of annealed Ta and Mo alloy welded joints under electron beam and ray heating, noting use for short term tests 05 p0865 A70-17028

Refractory oxides synthesized using metal alkoxide thermal decomposition, comparing thermophysical properties with conventional ceramics 07 p1320 A70-19891

Cooled turbine blades temperature field calculated considering variations at turbine inlet, over blade length, material temperature dependence and heat transfer boundary conditions 08 p1597 A70-21185

Thermooptical constant of laser neodymium glasses measured with interferometer 13 p2430 A70-29761

Quasi-stationary analysis of thermophysical characteristics of materials, considering cylinder and plate samples under unsteady heating

15 p2826 A70-32105

Papers on thermophysics for spacecraft thermal design

19 p3551 A70-37781

Polyimidepyrrolone films relative thermophysical properties, noting polymers thermal stability dependence on carbonyl groups percentage

21 p3783 A70-42132

Thermophysical properties - ASME Conference, Newton, Mass., September-October 1970

23 p2410 A70-44426

Fibrous composites thermomechanical properties derivation by theoretical analysis from basic constituents characteristics, presenting comparisons with experimental results

24 p4366 A70-45170

THERMOPHYSICS

U THERMODYNAMICS

THERMOPILES

UV, visible and IR radiation measurement, discussing spectral distribution, thermopiles, monochromatic radiation and power measurements

13 p2410 A70-29653

Armored actinometer with electroplated thermopile, describing construction and performance

24 p4333 A70-45137

THERMOPLASTIC FILMS

U POLYMERIC FILMS

THERMOPLASTIC RESINS

Fiber glass reinforcement effect on flammability properties of thermoplastics

01 p0128 A70-10771

Reinforcement of thermoplastic resins, considering single crystal whisker and carbon fibers and micro-spheres

01 p0129 A70-10774

Glass reinforced and unreinforced thermoplastics HF fatigue failure modes, discussing isothermal and nonisothermal test procedure

01 p0129 A70-11081

Mechanical properties of asbestos as reinforcing material for fiber filled thermoplastics compared with glass fiber

02 p0320 A70-11677

Fortified thermoplastic compounds for increased flame retardancy, environmental resistance and toughness

02 p0320 A70-11865

High modulus fibers as reinforcing fillers in thermoplastic matrices, discussing cost compensation in low fiber loadings

05 p0870 A70-16578

Glass filled thermoplastics fabrication techniques and composites, discussing molding compounds and processes, reinforced thermoplastics properties and applications

05 p0873 A70-16605

Thermoplastic polymers adhesion to glass fibers determined by measuring force necessary to pull fiber from flat film of polymer

06 p1091 A70-17317

Glass fiber reinforced thermoplastics fatigue behavior during and after cyclic loading

06 p1091 A70-17600

Fibrillated asbestos dispersed in thermoplastic ionomer lattices, precipitated, dried and compression molded into bars, testing for flexural modulus, flexural stress and Vicat softening temperature

10 p1906 A70-24024

Thermoplastics reinforcement with glass and asbestos fibers taking into account fiber properties

11 p2070 A70-25825

Flexural stress relaxation properties of thermoplastics and composite materials, assessing strain energy by ballistic pendulum

11 p2070 A70-26342

Fiberglass reinforcement effects on injection molded thermoplastics physical properties, noting role of binder and glass content

13 p2438 A70-29204

Thermoplastics fatigue strength, considering stress variations with time in constant strain tests

14 p2598 A70-31425

Book on engineering properties of thermoplastics covering strength characteristics, plastic components design, etc

15 p2766 A70-32843

Friction properties of internally lubricated and glass-fortified thermoplastic resins for gears and bearings

16 p2935 A70-33354

Cold forming of thermoset-thermoplastic laminate consisting of reinforced epoxy core sandwiched between thermoplastic face sheets

16 p2916 A70-33362

Smooth surface polyester premix and sheet molding compound technology applied to reinforced plastics industry

16 p2917 A70-33364

Flexural creep deflections of glass fiber reinforced polycarbonate and Nylon thermoplastics

17 p3127 A70-34657

Papers on thermoplastics covering types, properties and applications

22 p4060 A70-43624

German monograph on glass fiber reinforcement effect on soft thermoplastics strength, adhesion and slip properties

24 p4366 A70-45088

THERMOPLASTICITY

Reinforced thermoplastics - Conference, Hartford, October 1969

01 p0128 A70-10769

Glass fiber-fortified thermoplastics development, properties and applications, considering ionomer, polyimide, chlorinated trifluoroethylene polymer, polymethylpentene, polybutylene, polyaryl ether and nylon

01 p0128 A70-10770

Synthetic polymers properties and processing, discussing thermoplastics, elastomers, thermosets, etc

02 p0322 A70-12715

Thermoplastic behavior of bodies under variable loads obtainable as function of time variable external temperature field

04 p0775 A70-15200

Rectangular plate in unsteady temperature field, analyzing thermoplasticity problem by reducing solution to linear system with variable coefficients

09 p1779 A70-23098

THERMORECEPTORS

Human thermoregulatory responses as function of peripheral thermoreceptors during imposed negative heat load in different ambient environments

01 p0024 A70-10977

Esthesiometric analysis of cutaneous thermoreceptors reaction dependence on heat production rates of human organisms

07 p1206 A70-19472

THERMOREGULATION

Physiological research on humans in hypothermia resulting from confinement to life raft on open sea, analyzing thermal conditions, thermoregulation and survival

01 p0013 A70-10233

Thermoregulatory salivary responses of dog to various ambient temperatures, emphasizing hypothalamic temperature, threshold and proportionality constant

01 p0017 A70-10465

Skin and hypothalamic temperature inputs for behavioral regulation of hypothalamic temperature of rats

01 p0020 A70-10725

Human thermoregulatory responses as function of peripheral thermoreceptors during imposed negative heat load in different ambient environments

01 p0024 A70-10977

Brown fat thermoregulatory function and physiological control in mammals, discussing heat production and biochemical stimulation

02 p0230 A70-11683

Esthesiometric analysis of cutaneous thermoreceptors reaction dependence on heat production rates of human organisms

07 p1206 A70-19472

Extravascular activity space suits evolution emphasizing appropriate body temperature control under various conditions and work loads

10 p1824 A70-24412

Thermostability and survival rates of white mice in ambient medium with temperature variations

13 p2351 A70-29330

Thermoregulatory vasodilation conditioned reflexes developed by combination of prolonged physical and acoustic stimuli

15 p2679 A70-31606

Biological media thermal behavior, discussing maintenance of constant internal temperature under varying conditions in man

[ALAA PAPER 70-813] Soviet papers on physiological adaptation to heat and cold covering thermoregulatory reflexes, bionics, temperature gradients, hypothalamus, gas exchange, heat generation, etc

16 p2854 A70-33948

Physiological mechanisms of cold adaptation in terms of individual, type and population categories, examining thermoregulatory muscular reflex

18 p3217 A70-36526

Human muscular function in conditioned and unconditioned thermoregulatory reflex changes of gaseous metabolism during repeated cooling

18 p3218 A70-36527

Mathematical simulation of human thermoregulatory system, considering automatic control theory

18 p3224 A70-36530

Varying thermoregulatory responses of different rodent species to long term heat and cold

18 p3218 A70-36534

Thermoregulation processes in oxygen consumption, blood and body temperatures and skeletal muscles in adult nutria and muskrats in air and water

18 p3218 A70-36535

Gas metabolism, chemical thermoregulation, body temperature and weight of rats during adaptation to repeated high temperature exposure

18 p3219 A70-36538

High temperature adaptation, gas exchange and thermoregulation in dogs during repeated overheatings in open sunshine

18 p3219 A70-36539

Thermoregulation of hedgehogs during muscular activity in cold environment, recording electrical activity, oxygen consumption and body temperature during work-rest cycles

18 p3219 A70-37977

Book on survival in cold water covering physiology and treatment of immersion hypothermia and drowning, thermoregulation, etc

19 p3360 A70-37977

Circadian and seasonal adaptive function rhythms in animals, discussing terrestrial environment and thermoregulation

19 p3365 A70-38409

Human body core temperature control dependence during exercise on heat dissipation, noting sweating control

20 p3570 A70-38997

Human peripheral blood flow rewarming in cold ambient temperature, examining skin, rectal and tympanic membrane and oxygen uptake

20 p3576 A70-40327

Localization and functional topology of thermosensible central nervous structures in rats cervical spinal cord, discussing role in generating heat to avert coldness

22 p3967 A70-42316

Dynamic response of peripheral blood flow to hypothalamic temperature waveforms in baboon, using implanted thermodes

24 p4303 A70-46116

Chronically implantable water perfused thermode system for hypothalamic temperature waveforms generation

24 p4309 A70-46117

THERMOSETTING RESINS

NT EPOXY RESINS

NT PHENOLIC RESINS

NT POLYAMIDE RESINS

Synthetic polymers properties and processing, discussing thermoplastics, elastomers, thermosets, etc

02 p0322 A70-12715

Nozzle throat ablative materials for controlled high regression rates in tactical rocket motors, primarily nylon reinforced thermosetting resins

[ALAA PAPER 69-423] 04 p0713 A70-15428

Cold forming of thermoset-thermoplastic laminate consisting of reinforced epoxy core sandwiched between thermoplastic face sheets

16 p2916 A70-33362

Chemical and moisture resistance, electrical and mechanical properties of engineering thermosetting plastics made of HYSTL resins

16 p2938 A70-33380

Solvents and chemicals resistant thermosetting resin producing high strength glass reinforced laminates based on polyanhydride crosslinked with monoepoxide

16 p2938 A70-33382

Thermosetting glass reinforced plastics fabrication and use for pressure vessels, vacuum vessels and pipes

24 p4350 A70-46388

THERMOSIPHONS

Monograph on application of semiclosed thermosiphon system to gas turbine blade cooling, covering heat transfer and temperature distribution analysis, etc

03 p0551 A70-12992

THERMOSPHERE

Thermospheric neutral density amplitudes and phases using one dimensional model of geomagnetic activity effect, 27 day variation and semiannual variation

01 p0070 A70-10402

Nonlinear flow conductance and convective terms effects on planetary thermospheres heating diurnal variations, emphasizing solar EUV heating

01 p0178 A70-10413

Diurnal variation for structure and energy balance of thermosphere, noting effect of global wind pattern

01 p0074 A70-10592

Polar thermosphere temperature measurements from artificial clouds indicating geophysical-associated variations, nocturnal decrease and annual variations

01 p0077 A70-11201

Atmospheric density variations in thermosphere determined from braking satellite data, discussing correlation with solar activity and temperature variations

01 p0077 A70-11202

Thermospheric structure and variations obtained from satellite drag data analysis, discussing gas density, temperature and atmospheric composition

01 p0077 A70-11203

Thermospheric horizontal winds diurnal bulge, discussing maximum density-maximum temperature phase relationship

01 p0078 A70-11210

F region ion velocity measurements by Thompson scatter probe, deducing neutral winds diurnal and seasonal variations in thermosphere

01 p0078 A70-11214

Internal gravity waves theory to interpret large amplitude oscillations in electron density and temperature and ion temperature and velocity observed in thermosphere

01 p0079 A70-11215

Static thermosphere model using hydrodynamic equations, assuming uniform temperature and non-existent Coriolis forces, viscous stresses, horizontal velocity vector and thermal fluxes

02 p0327 A70-12384

Height scale of loss coefficient in F 2 region under geomagnetic perturbation at midnight based on electron number profiles, estimating thermosphere temperature

07 p1265 A70-19433

Vertical eddy diffusion effect on chemical composition of mesosphere and lower thermosphere using photochemical model containing oxygen and hydrogen

07 p1274 A70-20269

Omegatron mass spectrometer for rocket measurements of molecular nitrogen density and temperature in middle thermosphere

07 p1289 A70-20308

Atmospheric density in thermosphere observed by satellites, noting daily and semiannual variations related to solar and geomagnetic activities

09 p1667 A70-22626

Thermospheric molecular nitrogen vibrational temperature, studying various chemical reactions and collisions as energy sources

10 p1872 A70-23827

Seasonal changes in thermospheric composition in middle latitudes, investigating molecular oxygen density and solar activity effects

10 p1881 A70-24817

Lower thermosphere dust particle layers correlated with polarization anomaly twilight fluctuations and noctilucent clouds frequency distribution

10 p1944 A70-24949

Thermospheric background radiation from Cosmos 225 data

13 p2478 A70-29700

Thermospheric heating and conversion efficiency of short wave radiation as functions of solar radiation spectral flux, atmospheric components concentration and elementary processes cross sections

14 p2569 A70-30212

Static diffusion model of thermosphere with allowance for temperature and chemical composition and not limited by constant 120 km boundary conditions

14 p2606 A70-30560

Incoherent scatter observations of atmospheric density and temperature in lower thermosphere, observing seasonal variations

14 p2578 A70-31246

Atomic hydrogen escape effects on altitude distribution, discussing lateral flow limitations on thermospheric diurnal variation

15 p2725 A70-31796

Neutral particle and electron density measurements by Explorer 32 proving thermospheric gravity waves association with wave-like structure in F region electron density

15 p2727 A70-31907

Height scale of loss coefficient in F 2 region under geomagnetic perturbation at midnight based on electron number profiles, estimating thermosphere temperature

18 p3249 A70-36907

Diurnal variations of thermospheric atomic hydrogen, investigating lateral flow effects on global distribution

19 p3415 A70-38419

Maximum to minimum exospheric temperature ratio determination, concluding solar wind dependence of diurnal variation in thermosphere

20 p3621 A70-39345

Lower thermosphere minor gaseous constituents vertical transport by nonlinear gravity wave process, showing density scale height decrease from diffusive equilibrium

21 p3818 A70-41098

Quadrupolar mass spectrometer design for lower thermosphere neutral composition measurement, discussing atmospheric physics, installation on rockets, etc

21 p3830 A70-41990

Internal gravity waves mathematical model for atmosphere with arbitrary distributions of temperature, molecular weight, viscosity and conductivity, deriving wave propagation into thermosphere

21 p3821 A70-42257

Thermospheric density variations as equivalent oscillator circuit system, applying to atmospheric tides

22 p4023 A70-43297

Thermosphere, stratosphere and mesosphere reactions involving water, hydrogen, methane, ozone, nitric oxide and nitrogen peroxide

22 p4023 A70-43298

Phase delay between thermospheric neutral temperature and neutral density, considering frequency dependent time response to solar heat input

23 p4187 A70-43858

ELF acoustic gravity wave arrival from Apollo launches recorded by Doppler shift ionospheric sounder channeled near mesopause and lower thermosphere

23 p4187 A70-43859

Thermospheric heating by solar radiation in Schumann-Runge continuum, taking height and atmospheric components distribution into account

23 p4188 A70-44060

Thermosphere diurnal thermal influx theory, allowing for heat conductivity

23 p4214 A70-44265

Thermospheric heating and conversion efficiency of short wave radiation as functions of solar radiation spectral flux, atmospheric components concentration and elementary processes cross sections

24 p4331 A70-46287

THERMOSTABILITY

U THERMAL STABILITY

THERMOSTATS

Surveyor thermal switch for temperature control to assure spacecraft components performance during temperature extremes on lunar surface

16 p2845 A70-34127

Differential fast-acting thermostat for temperature variation effects on elements, systems and subassemblies in gas filled space

17 p3090 A70-35433

Flexible thermostat for specific temperature range with liquid nitrogen coolant and gas transfer medium

17 p3096 A70-35850

THERMOTROPISM

U ANISOTROPY

U TEMPERATURE EFFECTS

THERMOVISCOELASTICITY

Temperature-time-variable stress-strain state of polymer structures, solving creep equation by linear model with rheological properties

01 p0211 A70-11426

Thermoviscoelasticity stochastic problems for bar with temperature independent viscosity, discussing Fokker-Planck equation for two temperature processes

21 p3937 A70-41435

THETA PINCH

Stark broadening of ionized helium lines by collective electric fields in theta pinch

04 p0722 A70-14684

Monograph on research by Japanese Institute of Plasma Physics covering theta pinch, plasma heating, flow, diagnostics, etc

07 p1350 A70-19843

Neodymium glass laser stimulated by pinch discharge radiation in He and Kr, increasing power, energy and pulse repetition frequency by improved pumping energy coupling

08 p1512 A70-21213

Plasma cylinder surface drive current buildup, using theta pinch two dimensional model

14 p2624 A70-31049

Magnetic pressure fast opening gas puff valve for hydrogen bursts in conical theta pinch plasma source

21 p3833 A70-41472

High density plasmas production and containment in theta pinch device, discussing shock and Joule heating

23 p4225 A70-44186

Theta pinch He plasma stability using cusp coils added to mirror coil ends

24 p4386 A70-45611

THICK FILMS

Radiative transfer between two infinite parallel metallic surfaces separated by nonconducting thick film ideal dielectric based on electromagnetic wave theory

04 p0784 A70-14824

Thick film hybrid circuit technology providing higher packaging density and better cooling

06 p1016 A70-17276

Sounding rocket telemetry systems, discussing use of PCM and thick film techniques

13 p2363 A70-28681

Microwave conductivity of thick film screen-printed microstrip circuits, measuring closed resonators SHF Q factors

19 p3388 A70-37964

Thick film thermocouple gages for roughened model surface heat flux measurements in high Reynolds number shock tunnel

21 p3824 A70-40860

THICK WALLS

Thick walled incompressible hyperelastic dielectric sphere periodic oscillations, noting dielectric properties influence on amplitude and period

01 p0209 A70-11386

Arterial model with effects of thick walls, linear viscoelasticity and wall tethering for studying arterial mechanics

02 p0247 A70-12550

Stress concentration in long thick cylindrical tube under diametrically opposite normal loads using elasticity theory

05 p0939 A70-16505

Thick walled orthotropic cylinder subjected to internal pressure analyzed for stress distribution and creep rates, using constitutive equations and Norton law

07 p1416 A70-20234

Shear stress in thick cylindrical closed shells subjected to plastic torsion determined from displacement distribution over thickness and generatrix

08 p1588 A70-21182

Linear and nonlinear rupture mechanics applied to thick walled pressure vessels of high strength materials

09 p1769 A70-22184

Thick-walled toroidal shell under various load distributions, analyzing stress-strain state by networks method using computer program

10 p1957 A70-24250

Wave propagation through Newtonian fluid in compressible thick walled viscoelastic tube, considering blood flow in arteries

15 p2691 A70-31938

THICKENED LEADING EDGES

U LEADING EDGES

THICKENERS [MATERIALS]

Thickening of fluids with tetrafluoroethylene polymer to provide physically and chemically stable grease type lubricants for military applications

07 p1292 A70-18863

Thickeners and low shrink additives for premix and sheet molding compounds/SMC/

16 p2936 A70-33363

THICKNESS

NT FILM THICKNESS

NT TARGET THICKNESS

Long term storage effects on noise, leakage current and thickness of Li drifted Si surface barrier detectors

03 p0482 A70-13023

Bending analysis of cracked plate with arbitrary stress distribution across thickness

[ASME PAPER 69-WA/PVP-2] 04 p0768 A70-14791

Nozzle boundary layer displacement thickness at Mach 30-70 in helium using Langley hotshot tunnel tests

04 p0675 A70-15603

Nonlinear theory extended to slender triangular and rectangular wings with symmetric profile, taking into account finite wing thickness

06 p0966 A70-17254

Stress-strain state of flexible circular plates as function of thickness distribution using finite difference theory

08 p1583 A70-20529

Elastoplastic bending of inhomogeneous rectangular plates with modulus of elasticity and yield stress varying over plate thickness

08 p1583 A70-20530

Thickness effects on elongation of sheet type Al alloys, tabulating tensile test results

10 p1887 A70-24043

Numerical solutions of thick cambered jet flap in ground effect for flat plate and diamond shaped airfoil [AIAA PAPER 69-738]

12 p2155 A70-27195

Anisotropy and variable thickness effects on elastic stress distribution in rotating disks, discussing limiting cases

17 p3185 A70-34912

Thickness determination of external elastic plates in freely supported three layer structures of uniform strength under perpendicular loads

18 p3343 A70-36717

Lunar maria rock thickness estimation, giving depth vs diameter diagrams for craters to show procerrarian system thickness

19 p3516 A70-37982

Optimal variable shell thickness, describing numerical solution as function of forces, moments and thickness

20 p3725 A70-39865

Thickness of equally stressed cylindrical shells, using thin elastic shell theory and Kirchhoff-Love hypotheses

22 p4120 A70-43715

Crack length and bend specimen thickness effects in plane strain fracture toughness tests of high strength steels

23 p4268 A70-44192

Wall thickness measurement by supersonic testing method based on resonance

24 p4336 A70-45681

Noncontact electromagnetic acoustic transducer/E-MAT/ for metallic products ultrasonic thickness testing

24 p4336 A70-45682

Thickness measurement and internal defects inspection by ultrasonic resonance technique

24 p4343 A70-45683

THICKNESS RATIO

Conical shells stability under uniform pressure, studying varying thickness influence by variational stress and bending equation

07 p1402 A70-19052

Rocket motor combustion chamber lining thickness distribution matching to effusor by designing effusor as multiple nozzle made of circular graphite plate

15 p2790 A70-32271

Optimum thickness ratio and minimum drag of slender bodies in hypersonic viscous flow as function of altitude

23 p4134 A70-44571

THIGH

Occlusion training during hypodynamia with inflatable cuffs to prevent unfavorable effects on cardiovascular system

10 p1816 A70-24689

THIN AIRFOILS

NT THIN WINGS

Thin airfoil magnetoaerodynamics problem revised solution to avoid divergent integrals expressing kernels of integral equations

03 p0405 A70-12933

Far and near field solutions of plane steady transonic flow past thin airfoil including imbedded shock waves using small disturbance theory

[ALAA PAPER 70-188] 06 p0969 A70-18056

Thin airfoil theory, discussing harmonic Dirichlet problem for complex plane

10 p1798 A70-24105

Alfvén flow of dissipative conducting incompressible fluids in presence of thin airfoil in magnetic field, considering flow turbulence calculation

10 p1922 A70-24143

Load generation on two dimensional thin airfoil by yawed sinusoidal gust in incompressible flow, using lifting surface theory

13 p2344 A70-30025

Unsteady aerodynamic forces at stall flutter, applying vortex sheet theory to separated flow field around thin airfoil at high angle of attack

22 p3957 A70-42284

Free jet stream effect on thin jet-flapped airfoil with fully developed wake, using linear theory

22 p3960 A70-43737

Pressure distribution on thin nonlifting airfoils in steady two dimensional flow with freestream Mach number at or near unity

23 p4134 A70-44583

Jet-ambient air mixing effect on flow characteristics around thin airfoil with jet flap

24 p4288 A70-45439

Inviscid conducting incompressible fluid steady motion past thin airfoils, presenting crossed and aligned fields and Alfvén motion with Hall effect

24 p4289 A70-46033

THIN BODIES

Apparatus for continuous creep measurement at high temperature for fine wire and thin tubular samples with small cross sectional areas

01 p0088 A70-10746

Vibration of thin bodies subjected to large angle attack in hypersonic flow, discussing curved bodies method to reduce problem to steady state flows

09 p1771 A70-22445

Friction drag on thin pyramidal lobed bodies in supersonic flow, analyzing detached shock region and body geometry function

09 p1606 A70-23612

Low Mach number aerodynamic sound generation by turbulent flow at sharp edged thin scattering half plane solved with Green function

10 p1802 A70-24521

Thin cylinder longitudinal two phase dispersed flow, examining heat transfer coefficient

18 p3345 A70-36112

Two identical conducting thin cylinders illuminated by plane wave at arbitrary incidence angle, determining backscattering cross sections and induced current

24 p4314 A70-46133

THIN FILMS

NT FERROMAGNETIC FILMS

NT MONOMOLECULAR FILMS

Airborne aeromagnetic gradiometer theory and design, using superconducting thin film tunneling junctions

01 p0085 A70-10289

Polybenzimidazole (PBI) resin-bonded solid film lubricants composed of molybdenum disulfide, antimony trioxide and PBI resins

[ASME PAPER 69-LUB-15] 01 p0101 A70-10390

Hydrodynamic and elasticity equations for squeeze films between elastic cylinders in normal approach reduced to integral equation

[ASME PAPER 69-LUB-13] 01 p0102 A70-10392

Film-vapor interface shape for thin liquid lubricating film, analyzing two dimensional Newtonian flow including gravity, inertia and surface tension effects

[ASME PAPER 69-LUB-3] 01 p0103 A70-10399

Book on thin film transistors microelectronics covering semiconductor physics, fabrication, analysis, applications and comparison with MOS transistors

01 p0052 A70-11329

Inertia effects in squeeze film between two curved surfaces and in externally pressurized bearing with converging lubricant film

01 p0104 A70-11388

Thin liquid film equilibrium on rotating sphere, determining conditions for detachment as function of angular velocity

01 p0068 A70-11578

Titanium thin films prepared in ultrahigh vacuum to determine low temperature/pressure oxidation kinetics, using electron microscopy and X ray diffraction

02 p0317 A70-12316

Thin superconducting films nonlinear microwave properties including impedance-amplitude relation, superconducting current threshold decrease, mode production, frequency mixing, etc

03 p0539 A70-13409

Frequency spectrum, Q factor and single mode selectivity of two mirror laser resonator with absorbing thin metallic films, showing agreement for Ag and Ni

03 p0500 A70-13459

Electrical conductivity of GaSe thin films developed in vacuum by electron bombardment as function of temperature

03 p0540 A70-13686

Vacuum deposited thin film bridges in electroexplosive devices, discussing composition, surface conditions, substrate temperature, bell jar atmosphere and deposition rate

03 p0546 A70-14107

Thin film heat gauge for measuring thermal transport from plasma to end wall of shock tube, discussing measurements in high temperature Ar

03 p0496 A70-14381

Augmented small parameter gas film equation for squeeze film journal bearing solved in terms of radial displacement

[ASME PAPER 69-WA/LUB-9] 04 p0697 A70-14766

Superconducting properties of Nb-Ti-N thin films prepared by reactive sputtering process, obtaining transition temperature maximums

04 p0732 A70-15689

Particle, resin and inorganic bonding of solid lubricant to surface and dry lubricant film performance

05 p0855 A70-16043

Electron transmission diffraction patterns of thin monocrystal films using Ar laser

06 p1080 A70-17444

Possible pairing without superconductivity at low carrier concentrations in bulk and thin film superconducting semiconductors

06 p1127 A70-18641

Rheology applied to motor oil viscosity, elastohydrodynamic (EHD) and extremely thin film lubrication, examining viscosity relationship to film thickness

07 p1293 A70-18954

Film type solar energy reflector peripheral blades for connection to receiver, discussing precession control and despin for rotating concentrators

07 p1196 A70-19501

Spectral reflectivity measurement method for optical thin film coating in 10.6 micron IR region using carbon dioxide laser source

07 p1302 A70-20084

Coplanar waveguide consisting of thin metallic film strip on dielectric slab with ground electrodes adjacent and parallel to strip for nonreciprocal gyromagnetic device applications

08 p1475 A70-21281

Interdigitated microstrip quadrature couplers suited for monolithic or hybrid thin film microwave integrated circuitry

08 p1476 A70-21291

Photolithographically produced thin film lumped element circulator, assuring physical and electrical symmetry by interweaving junction conductors

08 p1476 A70-21293

Switching and memory phenomena in semiconductor glasses, thin films and variable threshold metal-oxide-nitride-semiconductor MNOS transistor

08 p1556 A70-21304

Film properties of organic liquids squeezed between two solid flats using order liquid model, discussing applications to boundary layer lubrication

08 p1508 A70-21601

Permittivity of thin films in millimeter and submillimeter wavelengths measured by diffraction grating method

08 p1464 A70-21985

Passive film on stainless steels in boiling nitric medium studied by recording constant potential on sample subjected to polarizations

09 p1700 A70-22010

Thin resistive layers located in rectangular waveguide assuming constant and surface variable conductivity and permittivity

09 p1644 A70-22279

Far IR radiation transmission through bismuth and gallium normal and superconducting thin films, considering transition temperature role

09 p1739 A70-22323

Integrated circuit film and hybrid technologies in microelectronics, discussing role of monolithic Si arrays

09 p1645 A70-22632

Current-voltage characteristics and lifetime of thin film diodes on chalcogenide glass substrate with symmetrical and asymmetrical electrodes

09 p1647 A70-22751

Thin film capacitive bolometer dependent on temperature sensitivity derived from electron trapping effects

09 p1683 A70-23509

Compound semioaque thin films quality control for thickness uniformity by observing fringe patterns generated by optical data processing techniques

09 p1687 A70-23765

Elongation measurement in tensile testing of thin films and sheeting, coupling with gripping test program

10 p1887 A70-24042

Thin soap membranes shape determined by photogrammetric method, using stereo camera and fluorescent light

10 p1891 A70-24735

Vacuum condensed thin carbon films graphitization stages using electron diffraction

11 p2068 A70-25381

Thermal conductivity of thin metallic films and wires at cryogenic temperatures, discussing electron transport properties

11 p2083 A70-25752

Thin films of vanadium niobium and tantalum obtained by vacuum thermal decomposition of metal iodides

12 p2253 A70-27210

Superconducting thin films of beta-tungsten structure Nb-Al-Ge compound, discussing high purity sputtering preparation techniques and properties in magnetic fields

12 p2285 A70-27259

Low resistivity films synthesized on seminsulating GaAs by xenon, krypton, selenium and zinc ions bombardment

12 p2286 A70-27364

Microwave transmission through thin film screens with apertures placed in transverse plane of X band rectangular guides

12 p2202 A70-28164

Film cavitation between flat annular surfaces in face seal resulting from hydrodynamic pressure generated by misalignment and surface waviness

13 p2417 A70-28613

Water contaminating effects on thin thermal oxide passivated silicon planar devices

13 p2361 A70-28930

RF-sputtered CdS thin films structural and electrical characteristics from X ray diffractometer tracings, reflection electron diffraction and X ray double crystal spectrometry

13 p2470 A70-29201

Electromagnetic theory of forces for coalescence in granular layers during thermal evaporation of thin films, calculating interaction between instantaneous dipoles

13 p2471 A70-29640

Electron microscope-thin film microprobe techniques in biomaterial studies of chemical segregation, species diffusion and small particle analysis

13 p2411 A70-29808

Thin ferromagnetic film sensitive elements for detection of weak magnetic fields

13 p2415 A70-30041

Ta thin film integrated circuit technology including resistor and capacitor elements, conductors, cross-overs, etc

14 p2625 A70-30284

Thin film sandwich Ag/Ni/Cu, demonstrating multiple electron diffraction

14 p2627 A70-30724

Nonlinear effects in microwave resonators containing thin superconducting films and low values of microwave power

15 p2782 A70-31525

Titanium monoxide thin film as low temperature getter, measuring activity coefficient and capacity under ultra high vacuum

15 p2783 A70-31844

InAs thin films electrical properties and IR reflectance, determining thickness and substrate temperature effects on carrier concentration and mobility

15 p2783 A70-31965

Plasma reflection edge in thin film InAs semiconductors, calculating refractive index and extinction coefficient from free charge parameters

15 p2783 A70-31966

Photoemission optical analysis from thin films with uniaxial anisotropy, discussing reflectance, transmittance and divergence of Poynting vector

15 p2774 A70-32012

Thin film solar cells photosensitivity improvement by semiconductors with graded energy gap, describing construction techniques and electrical properties

15 p2678 A70-32420

CdS and CdTe thin film solar cells R and D survey, describing construction and electrical properties

15 p2678 A70-32421

Thickness measurement for thin films in inaccessible locations using scanning electron microscope, comparing accuracy with interferometric techniques

15 p2741 A70-32435

Thermoelectric power measurement of thin Au films, relating results to transport parameters and internal stresses

15 p2785 A70-32582

Integrated circuits failures due to electromigration in thin films, discussing hole formation and circuit reliability prediction

15 p2713 A70-32649

Film type solar energy reflector peripheral blades for connection to receiver, discussing precession control and despin for rotating concentrators

15 p2678 A70-32746

X band acoustic delay lines using thin film piezoelectric transducers

16 p2874 A70-33391

Surface growth morphology and crystallographic orientation of beta-SiC films formed by chemical conversion and heating

17 p3142 A70-34678

Satellite electronics production, discussing dielectric film capacitor, solar probe magnetic oxide memory core and thin film assemblies

17 p3053 A70-35268

Amorphous film formation and crystallization, discussing thermal stability

18 p3297 A70-36320

Skin friction measurement in supersonic flows by thin film heated element method, describing thermal boundary layer properties

18 p3243 A70-36710

Hybrid integrated microwave power amplifiers, using high-Q thin film lumped passive elements

18 p3232 A70-36760

Dielectric properties of thin barium titanate films from microwave resonance frequencies and resonance reflection coefficient

19 p3482 A70-37255

Augmented small parameter gas film equation for squeeze film journal bearing solved in terms of radial displacement

[ASME PAPER 69-WA/LUB-9] 19 p3435 A70-37609

Film-vapor interface shape for thin liquid lubricated film, analyzing two dimensional Newtonian flow including gravity, inertia and surface tension effects

[ASME PAPER 69-LUB-3] 19 p3435 A70-37610

Single crystal ferrite thin film microwave parameters measurement, examining susceptibility in weak magnetic fields and ferromagnetic resonance

19 p3485 A70-37628

Electrical conduction and surface properties of beta-SiC films obtained by heating Si wafer in presence of hydrocarbon

19 p3485 A70-37685

Laser beam alignment system for monitoring dielectric film evaporation

19 p3445 A70-37686

Thin films physics for microelectronic applications

19 p3389 A70-38194

Thin films for semiconductor integrated circuits and solid state devices

19 p3389 A70-38195

Thin metal film electrical conduction current noise characteristics

19 p3487 A70-38196

Thin films optical properties and measurements

19 p3487 A70-38197

Superconductor thin films, discussing transition temperature, critical field and current, solid state applications, etc

19 p3488 A70-38198

Deformation effects on metallic and semiconductor thin films conductivity

19 p3488 A70-38199

Epitaxial growth of GaAs thin films in vapor phase using hydrogen, gallium and arsenic trichloride as sources

19 p3488 A70-38200

Antireflection titanium dioxide thin films for aerospace silicon solar cells

19 p3358 A70-38201

Photoemitting cesium antimonide thin films for IR detectors

19 p3488 A70-38202

Tantalum oxide thin films electro-optical effects due to refractivity changes

19 p3488 A70-38203

Thin films optical constants and thickness measurements and UV bandpass interference filters design

19 p3488 A70-38204

SI and thin film solar cells for satellite power supplies, considering manufacture and space environment

19 p3358 A70-38478

Impurity distribution in diffused p-n junction in thin epitaxial film, calculating space charge region width and junction capacitance

20 p3685 A70-38967

Copper disulfide-cadmium sulfide thin film solar cell degradation under simulated low orbit conditions, investigating thermal stress

21 p3759 A70-41313

High temperature combined differential thermal analysis and spectrophotometric cell for phase transformation monitoring of evaporated thin film and bulk phthalocyanine

21 p3827 A70-41459

Harmonic generation and small signal mixing in thin magnetic films subjected to static and time varying fields, generating output voltage expressions

21 p3864 A70-42012

Thin titania films electrical breakdown under high DC fields in high vacuum, suggesting reduction to lower order semiconducting oxide

22 p4085 A70-42621

Prism film device coupling laser beam into thin film dielectric light guides, discussing operational theory

22 p4030 A70-42947

Prism film device for high efficiency laser beam coupling into light guiding thin film, deriving operation theory by plane wave analysis

22 p4030 A70-42948

Thin film granular aluminum superconductors as sensitive thermometers

22 p4031 A70-43009

Orthogonal susceptibility of uniaxial thin nonmagnetorestrictive Permalloy films

22 p4086 A70-43011

In thin film resistance thermometers fabrication by vapor deposition in vacuum, considering electrical properties dependence on temperature

22 p4039 A70-43446

Thin two phase film conductivity, noting conditions for equality with geometric mean and for metal-to-dielectric transition

22 p4088 A70-43466

Current and vector potential in thin superconducting film in HF field, considering high and low temperatures

22 p4088 A70-43467

CdS thin film solar cells, describing manufacture for increased degradation resistance

22 p3966 A70-43537

MIS model applied to memory transistor with thin insulator consisting of silicon nitride on silicon dioxide

23 p4172 A70-44197

Metal vapor flow measurement by quadrupole mass spectrometer for control of thin film depositions by evaporation

23 p4198 A70-44872

Thin liquid film /melt layer/ on body in supersonic flow, examining crosshatched wave patterns stability

23 p4183 A70-44979

Atomic oxygen height profile measurements in upper atmosphere by sensor consisting of thin silver film on small pyrex rod permitting molecular transport

24 p4329 A70-45359

Crystal growth in polycrystalline Au, Ag and Au-Ag thin films annealing, observing by electron microscopy and electron diffraction

24 p4391 A70-45672

Oxygen and nitrogen adsorption on thin tantalum films, measuring pressure, electrical resistivity and temperature

24 p4363 A70-46219

Thin epitaxial Ag films on mica, measuring electrical resistivity strain dependence

24 p4391 A70-46266

Multivibrator designs incorporating distributed R-C-NR thin film structures

24 p4321 A70-46395

THIN LAYER CHROMATOGRAPHY

Tranquilizers and hypnotics from rats organs analyzed by thin layer chromatography

22 p3978 A70-42879

THIN PLATES

Thin flat plates effective width under axial edge compression slightly beyond buckling limit, solving von Karman differential equations

01 p0198 A70-10094

Out-of-plane displacement restraint at thin photoelastic plates bonded to rigid boundaries of inclusions inducing transverse stress components causing plane stress solution deviation

01 p0202 A70-11059

Thin anisotropic elliptical plate elastic equilibrium weakened by hole and under concentrated loads

01 p0211 A70-11445

Thin simply supported circular rigid ideally plastic plate subjected to dynamic transverse load uniformly distributed over central circular region

02 p0389 A70-12668

Finite element method for postbuckling analysis of thin elastic plates, using iterative method to obtain equilibrium configurations

03 p0583 A70-12917

Buckling equations for thin nonlinearly elastic circular plates with affine initial deformation, considering Lure theory and variational principle for uniform compression load

03 p0589 A70-13336

Thin elastic cylindrical panel motion induced by plane acoustic shock wave analyzed by integrating nonlinear motion equations using finite difference scheme

03 p0524 A70-13377

Bubnov-Galerkin approximations convergence in problem of thin plate nonlinear vibrations, allowing for inertial forces due to rotation

03 p0593 A70-13470

Unsteady state lift and moment action on lattice of profiles moving in incompressible fluid, determining suction originating at leading edges of profiles

03 p0409 A70-13868

Reaction of three dimensional shock wave with turbulent boundary layer in supersonic flow around plate

03 p0409 A70-13876

Impulsive and transient load disturbances in thin elastic finite circular plate on Pasternak type viscoelastic foundation

03 p0595 A70-13905

Tension field theory describing buckling of membranes or thin plates with boundaries subjected to excessive planar displacements

03 p0599 A70-14246

Linear isothermal response of viscously damped thin homogeneous polygonal plates subjected to uniform dynamic loading, calculating forced solutions by numerical integration

03 p0601 A70-14318

Thin elastic plate oscillations plane two dimensional steady state problem assuming constant thickness, finite dimension and moving load

04 p0766 A70-14420

Unsteady heat conduction and thermal stresses in thin isotropic semibounded plates with butt joint possessing internal thermal resistance

04 p0766 A70-14479

Laminar compressible wake behind thin flat plate at zero angle of attack, solving boundary layer equations in von Mises coordinate plane

[ASME PAPER 69-WA/FE-6] 04 p0614 A70-14783

Computational procedures for matrix analysis of stability and vibration of thin flat rectangular plates in longitudinal compression

05 p0927 A70-16010

Viscous damping effect on aeroelastic stability of thin plate in inviscid compressible airstream, observing instability in subsonic and supersonic flow

05 p0941 A70-16517

Backscattered field determination at edge on incidence from thin circular plates illuminated by plane waves

06 p1008 A70-17563

Upper surface suction effect on thin plate aerodynamic characteristics, considering relations for lift and pitching moment coefficients

06 p0968 A70-17851

Stress and buckling measurement of shallow cylindrical steel shells linked to thin plate using resistant strain gauges and high precision indicators

06 p1167 A70-17866

Computer procedures for solving temperature stresses in thin infinite isotropic viscoelastic plate with heat transfer

07 p1411 A70-19817

Thin sheet and laminate bullet hole deformation zone microstructure observation by electron microscopy, considering terminal ballistics approach

07 p1413 A70-20049

Rectangular thin plates in small deformation transient creep bending, using finite element method in iterative procedure

08 p1590 A70-21356

Elastically symmetric thin plate stress-strain state under uniformly distributed load applied to edges

08 p1591 A70-21415

Thin metal plate surface impedance during excitation by HF electromagnetic field as function of magnetic field, calculating line shapes

08 p1557 A70-21754

Nonuniqueness theorems for von Karman equations governing thin flat elastic plate deflections clamped at edges and subjected to normal and edge loading

09 p1768 A70-22063

Temperature field distribution in long thin narrow plate composed of materials differing in thermophysical characteristics, creating field by moving heat source on plate

09 p1791 A70-23723

Stress intensity and strain energy of pressurized line crack in cross form in thin elastic plate solved by Wiener-Hopf technique

10 p1956 A70-24192

Dynamic postbuckling response of thin elastic circular plates under axisymmetric time dependent radial thrust, discussing response to step loading

10 p1964 A70-25206

Thin elastic plates and shells parametric resonance amplitudes by solving nonlinear differential equations, considering dynamic stability

11 p2129 A70-25523

Vibration of thin elastic plates under random driving forces simulated digitally, using power residue method for pseudorandom number generation

11 p2139 A70-26277

Clamped thin circular plate bending under various loadings due to action of rigid square column on center

11 p2139 A70-26404

Relative permittivity of small thickness dielectric substrate plates determined from reflection coefficient in rectangular waveguides

11 p2011 A70-26603

Stress tensor and displacement vector in thin elastic shells/plates derived from three dimensional nonlinear equations using asymptotic integration
11 p2142 A70-26634

Finite element bending stress analysis of thin rectangular and skew plates, discussing computational procedure generating stiffness matrices
11 p2143 A70-26641

Thin rectangular plates transverse natural frequencies, deriving equations of motion and boundary conditions in bending moment terms by vibrational principle
11 p2143 A70-26645

Flutter instability critical velocity and frequency for thin cantilevered plate with follower jet determined by Galerkin and computer simulation
12 p2316 A70-27106

Thin circular cylindrical panels of arbitrary curvature calculated for end support and loading at contour
12 p2323 A70-27335

Two dimensional dynamic thermoelastic problem for thin plates with internal heat sources solved by integral Laplace and Fourier transforms
12 p2323 A70-27337

Glass fiber reinforced thin rectilinear orthotropic plastic plates bending using finite difference method with allowance for creep
12 p2324 A70-27531

Thin plates finite length effects on thermal conductivity measurement by impulse method, verifying results with n-type silicon samples
12 p2332 A70-28047

Thin cut plate quasi-brittle breakdown under tensile stress, considering elastoplastic equilibrium under Tresca-St. Venant yield conditions
12 p2329 A70-28325

Compressible fluids Alfvén flow with Hall effect presence of thin foils, reducing problem to Fourier integral equation
13 p2442 A70-29484

Buckling equations for thin nonlinearly elastic circular plates with affine initial deformation, considering lure theory and variational principle for uniform compression load
14 p2657 A70-30714

Liapunov type analysis of linear structural dynamic system excited by stochastic parametric load, discussing radially loaded thin circular plates
14 p2657 A70-30763

Pontryagin principle for thin vibrating plates under mixed boundary conditions, examining optimal control
14 p2660 A70-31205

Thin plates with central circular holes, investigating creep behavior for biaxial edge tractions
15 p2822 A70-32359

Transverse vibration of thin circular elastic turbine disk of variable thickness rotating axially at constant angular velocity
16 p2916 A70-32994

Elastoplastic bending of thin plate under increasing and uniformly distributed loads, defining statically admissible stresses
16 p2988 A70-33107

Hypervelocity impact of spheres on thin targets using numerical solutions utilizing STEEP code two dimensional technique based on hydrodynamic elastoplastic model
16 p2991 A70-33853

Normally loaded thin plate displacements, bending moments and stresses determined by hologram interferometry and indirect moiré and superposition of grilles
17 p3085 A70-35011

Nonstationary temperature fields and stresses in wedge shaped strip and thin plates with heat transfer for discontinuous boundary conditions
17 p3189 A70-35342

Critical stresses and stability of thin Maxwell plates under random temperature fields
18 p3337 A70-36368

Inverse variational principles of thin plate, dividing into subregions/finite elements/for optimal thickness distribution, sectional forces and displacement values
18 p3339 A70-36481

Linear bending theory of thin homogeneous isotropic plates
18 p3339 A70-36482

Torsional vibration of thin beam with varying cross section, formulating fundamental equation and boundary conditions
18 p3339 A70-36519

Heat conduction three dimensional problem in radiation heated thin crystalline plates with temperature dependent thermophysical characteristics
18 p3348 A70-36644

Waveform changes in postbuckling behavior of thin rectangular plates under axial compression
19 p3535 A70-37380

Soviet book on theory of shell and plate type thin walled structural elements stability covering strength, boundary value problems, oscillations, design, etc
19 p3535 A70-37401

Energy flow between two superfluid helium baths at different temperatures and separated by thin plate
19 p3471 A70-37648

Nodal patterns on thin elastic circular plate vibrating in flexure, considering natural and compounded modes
19 p3543 A70-38245

Thin plates and thin walled cylinders aeroelastic stability in fluid flow, analyzing panel flutter
19 p3546 A70-38342

Clamped edge thin flat elliptic plate subject to elliptic paraboloidal loading, determining middle surface deformations for nonlinear large deflections
19 p3547 A70-38359

Elastoplastic equilibrium of thin infinite plate with periodic slit system along straight line under tension, investigating localized plastic deformation domains
20 p3721 A70-39769

Supersonic flow past slender bodies in presence of strong blowing, extending solution by expansion at leading edge of thin plate
20 p3559 A70-39771

Elastoplastic deformation of thin circular plates under uniformly distributed transverse loads, using mixed type variational equation
20 p3721 A70-39776

Stressed state in thermoelasticity plane steady state problem of thin plate under bending based on dislocations and temperature stresses relationship
20 p3721 A70-39780

Spherical shell equilibrium states dynamic calculation method applied to thin plates nonlinear theory statistical problems
20 p3725 A70-39871

Thin plane bars elasticity theory, constructing integrals of equations by asymptotic series expansion
20 p3726 A70-39881

Thin circular plate clamped along edge, calculating large displacements and elastoplastic strains for comparison with measurement
21 p3935 A70-41406

Plastic zones between symmetric and collinear edge cracks in thin plexiglass strips, using He-Ne laser interferometry
21 p3939 A70-41967

Heat transfer from thin plate in compressible gas flow, considering interface temperature as nonanalytic function
21 p3953 A70-42086

Thin plates radiant cooling with mutual irradiation in spacecraft radiators
22 p4122 A70-42518

Thin walled column buckling relation to plate element buckling, studying deformation, stress state, failure mechanism and ultimate load
22 p4116 A70-43214

Thin plates two dimensional dynamic thermoelastic problem, determining hyperbolic type heat conduction for temperature field
23 p4265 A70-43985

Centrally cracked sheet, calculating riveted and uniformly spaced stringers effect on stress intensity factor
23 p4270 A70-44549

Electromagnetic scattering by two dimensional periodic arrays of conducting thin plates, calculating induced current and near field radiation distribution
23 p4165 A70-44961

Radar cross section for thin dielectric plate and spherical and conical shells
23 p4166 A70-44975

Radar backscattering cross sections of horizontal and vertical polarizations for thin rectangular plate near grazing incidence
23 p4166 A70-44976

German monograph on fatigue crack propagation in thin notched plate, considering microscopic element fracture probability
24 p4422 A70-45574

THIN WALLED SHELLS

Steels tested to evaluate proposed incremental strain theories predicting loads on thin walled cylinders subjected to nonproportionate loading, discussing stress-strain diagram
01 p0202 A70-11057

Thin shells of revolution torsional vibration including bending terms and thickness considerations
01 p0205 A70-11142

Thin elastic shells parallel surface nonlinear tangential strains derived in terms of midsurface tangential and bending strain components
01 p0205 A70-11143

Finite element method for thin shells using specialized form of Reissner variational principle for stresses and displacements
01 p0208 A70-11184

Elastic bending of thin circular conical shell subject to arbitrary variation of edge loads
01 p0209 A70-11385

Internal hydrostatic or lateral pressure effect on deformations of infinitely long thin cylindrical isotropic shell subjected to equal concentrated radial loads
03 p0584 A70-12922

Incremental strain theories for nonproportionate loading of thin walled cylinders, discussing Tresca flow, von Mises theory and Prandtl-Reuss relations
03 p0480 A70-12953

Liquid heating in thin walled porous shells under various boundary conditions, deriving formulas for temperature fields
03 p0604 A70-13208

Thin shells stressed state calculations by iteration, considering suitability for computer adaptation
03 p0592 A70-13442

Nonlinear theory for thin elastic shells with small strains and rotations, analyzing nonzero Gaussian curvature
03 p0594 A70-13622

Stress distribution of thin walled structure of open section, considering warping and torsional bending, using calculus of variations
03 p0596 A70-14030

Thin shells of revolution plastic collapse under axisymmetric loads on basis of Tresca-Nakamura yield criterion, using computer algorithm
03 p0598 A70-14238

Stress wave propagation tests in thin walled tubes under combined tension and torsion, discussing predicted and observed strain-time profiles discrepancies
03 p0599 A70-14245

Thin elastic laminar shells nonlinear physical theory assuming Love-Kirchhoff hypothesis validity, rigidly connected layers and nonlinear mechanical behavior
04 p0765 A70-14419

Nonlinear thin shell theory kinematics generalized in terms of physical strain and surface deformation and geometry
04 p0766 A70-14450

Thin elastic revolving shells free axisymmetric oscillations by determining differential equations eigenvalues and eigenfunctions
04 p0768 A70-14604

Long thin cylindrical tube with circumferential restraint analyzed for thermal expansions, obtaining maximum strains, bending moments, shear forces and plastic zone extent
04 p0768 A70-14756

ASME PAPER 69-WA/NE-7 Axial compression effect on low cycle fatigue of thin walled metal tubes in torsion
04 p0705 A70-14880

Thin walled plate simply supported on three edges, studying behavior following local stability loss
04 p0772 A70-14923

Thin walled uniform open bar stability under arbitrary boundary conditions, using Vlasov assumptions and matrix methods
04 p0774 A70-15099

Thin elastic shallow shell static problem solved using numerical integration of differential equation
04 p0778 A70-15558

Closed form solutions describing nonlinear motions of incompressible fluid flowing in thin walled tube buckled by uniform external pressure
05 p0832 A70-16090

Strain parameters and equilibrium equation of rib-reinforced thin shells, analyzing length, curvature and torsion variations using smooth shell analogy
05 p0935 A70-16230

Plane deformation of plastic thin walled tubes under complex tensile and torsional load
05 p0935 A70-16233

Unsteady vibrations of cylindrical thin walled elastic closed shell under random loads, using correlation method
05 p0937 A70-16371

Fatigue crack propagation and fracture toughness in pressurized thin walled cylindrical tubes, basing analysis on shallow shell bending theory
05 p0942 A70-16802

Finite element method analysis of axisymmetrically loaded thin shells of revolution, considering nonlinearity due to material properties and shell geometry changes
05 p0944 A70-16812

Finite element analysis of elastic thin shells, approximating shell surface by network of triangular plate elements
05 p0944 A70-16813

Lower bound limit analysis of symmetrically loaded thin shells of revolution having arbitrary meridional profiles, demonstrating methods for pressure vessel problems
05 p0944 A70-16815

Thermal stresses in shell with spherical and circular cylindrical sections, using thin shell approximations and shallow shell theory
05 p0945 A70-16818

Membrane reinforced thin walled cylindrical shells stability as asymmetric contact problem in shell and plate theory
05 p0947 A70-17011

Facility for testing thin walled tubular specimens in stressed state at low temperatures by keeping stresses constant with helical gear
05 p0830 A70-17075

Thin shell buckling stressing maximum applied loads analysis for circular cylindrical shells with imperfect walls under axial compression

06 p1165 A70-17647

Thin walled tubular aluminum specimens hardening by temporary reduction of temperature during creep under torsion

06 p1089 A70-17795

Stability analysis of deflected shallow thin walled elastic noncircular conical and cylindrical orthotropic shells using straight lines method

06 p1167 A70-17865

Thin walled cylindrical shells design for axisymmetric impulsive loads, calculating strains due to explosive forming in water

06 p1167 A70-17867

Nonlinear postbuckling equilibrium of thin cylindrical shell and axisymmetric buckling pressure of imperfect spherical shell calculated by Rayleigh-Ritz method

[AIAA PAPER 70-102] 06 p1169 A70-18036

Thin walled cylindrical shell stability under stochastic lateral and axial compression loads using Liapunov method

[AIAA PAPER 70-104] 06 p1169 A70-18037

Thin circular cylindrical shells elastic equilibrium under loads producing deflection, elongation or contraction described by integrating equilibrium equations with constant coefficient

06 p1172 A70-18566

Structural analysis of thin walled cylinder material using normal ultrasonic wave to achieve high resolution determination of components

06 p1172 A70-18630

Thin walled cylindrical shell stability with hollow filler under distributed external loads, determining critical loads

07 p1399 A70-18663

Energy methods used in thermoelastic analysis of thermal stresses and deflections in thin rings

07 p1401 A70-18935

Uniform thickness thin helicoidal shell stress-strain state with middle surface in asymptotic lines, assuming parameters governed by one dimensional law

07 p1402 A70-19055

Plastic deformation of thin flexible axisymmetric shells under load, discussing tensile stresses

07 p1407 A70-19383

Thin walled metal cylinders residual deformation microstructures under internal impulsive loading

07 p1285 A70-19969

Soviet book on free, forced and parametric vibrations of thin walled shells containing liquid, gas and continuous elastic medium

08 p1584 A70-20762

Interaction between boundary layer and internal stressed state of thin elastic shell by formulating two dimensional linear theory

08 p1585 A70-20955

Rheological factors effect on deformation behavior of thin walled spherical shell made of strongly extensible elastically hereditary material and subjected to internal pressure

08 p1587 A70-21168

Thin shells of revolution natural oscillation frequencies approximation based on shell subdivision into series of cylindrical shells

08 p1588 A70-21194

Linear and nonlinear equilibrium equations for bending deformation of thin elastic cylindrical using Kirchhoff-Love hypotheses

08 p1588 A70-21242

Prismatic thin walled shells with box type cross section under torsion using Vlasov variational method in conjunction with transfer matrices

08 p1589 A70-21248

Eigenfrequencies of thin barrel shaped shells on simple supports, noting correspondence of ratio of radius to shell wall thickness

08 p1592 A70-21474

Uniaxial and multiaxial stiffness and property characterization of anisotropic composite materials formed as thin walled cylinders

08 p1529 A70-21880

Temperature fields and stress-strain state in elastic bodies with thin walled cylindrical shell inclusions during uniform heat flow at infinity

09 p1778 A70-23083

Elastoplastic stressed state of thin walled shells of revolution under repeated loads, assuming isotropic incompressible material

09 p1779 A70-23092

Contour immobility effect on load carrying capacity of rigid plastic thin shells of revolution, establishing minimum reinforcement value for edge

09 p1783 A70-23388

Lower critical load for shallow rigidly convex shell expression refined by considering effect of rigid clamping of shell edge on buckling boundary deformation

09 p1784 A70-23594

Stress-strain state analysis of prestained thin circular cylindrical shell using Vlasov general shell theory

10 p1955 A70-24021

Flexural rigidity of thin walled beams, analyzing relationship between loads and displacements taking into account Saint Venant torsional resistance

10 p1955 A70-24052

Rapid expansion of thin walled aluminum alloy cylinders under pulsed magnetic field pressure using high speed streak camera oscillography

10 p1964 A70-25120

Thin cylindrical shell stresses and displacements enclosed in elastic casing under pressure band using classical theory of Flugge and Love functions

11 p1218 A70-25336

Eccentrically stiffened thin circular cylindrical shell stability under torsion emphasizing exact finite formulas derivation

11 p1219 A70-25561

Random displacement fields in thin circular cylindrical shells with initial imperfections under axial compression using statistical analysis

11 p1219 A70-25562

Stress distributions in thin walled pressure vessels analyzed by scattered light photoelasticity technique compared to strain gage analysis

11 p1231 A70-25593

Geometrically exact finite element for thin shells of revolution, using approximation to predict boundary layer stress distribution during vibration

[AIAA PAPER 69-56] 11 p12135 A70-25962

Creep deflections and collapse times for supported thin shallow spherical shells under uniform pressure predicted using variational theorem

11 p12135 A70-25963

Membrane theory for thin single layer orthotropic cylindrical shells experiencing harmonic axisymmetric motion

11 p12136 A70-26084

Length effect on modulus determination test for thin laminated tube under combined loading using shell theory

11 p12136 A70-26086

Thin cylindrical shells of perfectly plastic rigid material, analyzing dynamic plastic deformation under internal impulsive pressure

11 p12139 A70-26413

Thin shell design for minimum bending stresses and transverse shear for composite materials with low interlaminar shear strength

11 p12141 A70-26490

Stress tensor and displacement vector in thin elastic shells/plates derived from three dimensional nonlinear equations using asymptotic integration

11 p12142 A70-26634

Nonlinear thin shell theory equations reduced to equations in unknowns with boundary conditions

11 p12143 A70-26653

Natural frequencies of thin cantilever cylindrical shells, using Flugge equations of motion and Rayleigh-Ritz method

11 p12146 A70-26704

Thin walled tubes plastic instability under combined internal pressure and axial load for open and closed end conditions

12 p2322 A70-27216

Stress-strain state of thin revolving shells composed of multiple variable thickness layers, assuming layers deformation free of slipping and separation

12 p2322 A70-27332

Thin cylindrical shells elastic buckling under uniform axial compression, considering Kirchhoff-Love hypotheses in critical stress determinations

12 p2324 A70-27396

Thin circular cylindrical polyvinyl chloride plastic shells tested under axial compression and end-shortening conditions for buckling

12 p2324 A70-27473

Glass-plastic thin cylindrical shells carrying capacity dependence under axial and external loads on combinations of longitudinal and transverse reinforcing layers

12 p2259 A70-27527

Equilibrium equations for thin multilayer shells with variable thickness, assuming simultaneous work without friction under loads

12 p2325 A70-27556

Bar produced by sliding thin walled cross section along three dimensional curve, determining twisted shell curvilinear middle plane and deformations by differential geometry

12 p2326 A70-27796

Thin walled shells of revolution equations boundary conditions formulated by stress state separation, giving small parameter perturbation theorem

12 p2327 A70-28191

Thin walled duralumin cylinders catastrophic fracture analysis by linear elastic fracture mechanics noting fatigue crack propagation

13 p2434 A70-29173

Initial thermal stresses effect on natural oscillation frequencies of thin cylindrical elastic shells, obtaining linearized equations of motion and boundary conditions

13 p2514 A70-29286

Optimum overlap design of thin walled tubular extendible spacecraft structures under solar heating in zero-g environment

14 p2657 A70-30762

Thin spherical shell postbuckling behavior with constrained rigid boundary under edge load, using deep and shallow shell theory

14 p2658 A70-30848

Thin shells stiffness matrix and shear by finite curved triangular elements based on discrete Kirchhoff hypothesis

14 p2659 A70-31129

Thin cylindrical shells flutter analysis in supersonic flow, using linearized potential theory

15 p2815 A70-31916

Thin two dimensional shells static linear elastic deformations analysis using difference based variational method

15 p2815 A70-32001

Internal pressure deformation of thin cylindrical shells of materials with nonlinear stress-strain relations, considering Al alloy shell and axial strain

15 p2816 A70-32009

Thin elastic shell deformation, considering random imperfections in regions adjacent to contour

15 p2817 A70-32162

Influence function for thin toroidal shell under uniformly distributed axisymmetric load, determining stresses and displacements in various cross sections

15 p2817 A70-32163

Zero moment /membrane/ theory for anisotropic thin walled shells, deriving expressions for stress-strain states and displacements under torsion

15 p2824 A70-32894

Gravitational instability and collapse of thin spherical shell of charged fluid, using energy conservation law

16 p2952 A70-33787

Combined internal pressure and axial loading influence on aeroelastic stability of thin walled cylindrical shell in supersonic flow field

16 p2991 A70-33851

Thin concentric circular cylindrical shells joined at ends by rigid diaphragms, describing free and forced torsional motion

16 p2992 A70-34019

Free vibration of thin circular cylindrical shells, comparing experimental results to Egle-Sewall analysis

17 p3181 A70-34520

Polycarbonate thin walled cylindrical shells mechanical and material stability under torsion

17 p3127 A70-34656

Elastic thin walled toroidal shell under internal pressure, investigating large deformation and stress behavior

17 p3184 A70-34910

Thin elastic shells linear theory, examining three dimensional stress distribution and displacement field

17 p3191 A70-35608

Structural stability in tension and strength tests of thin walled tubes at various stress and strain intensities, noting dependence on stress-strain state type

17 p3192 A70-35713

Axisymmetric torsion by terminal loads of elastic shells of revolution, investigating energy inequalities for assessing quality of approximate solution of thin shell problem

18 p3335 A70-36058

Double curved shell membrane stress calculation under arbitrary load, using stress functions

18 p3338 A70-36373

Plane cross section hypothesis applied to fully developed creep in thin walled tube subjected to internal pressure and bending moments, calculating stress concentration

18 p3340 A70-36571

Stress-strain equilibrium of thin isotropic elastic shells of revolution loaded along meridian

18 p3340 A70-36577

Zero moment theory for stress-strain state of thin walled anisotropic shells with nonuniform moduli under simultaneous torsion and tension

18 p3340 A70-36578

Dynamic axisymmetrical loading of thin elastic shallow spherical rigidly clamped dome, using variational method

18 p3341 A70-36582

Thin circular cylindrical shell stability subjected to axisymmetric thermal pulse, describing buckling process by mathematical model

18 p3342 A70-36641

Thin walled cylindrical shell stability under axial compression edge load beyond limit of proportionality

19 p3534 A70-37243

Soviet book on theory of shell and plate type thin walled structural elements stability covering strength, boundary value problems, oscillations, design, etc

19 p3535 A70-37401

Forced torsional vibrations of thin elastic spherical and hemispherical shells with free or restrained edge, using Gegenbauer transform

19 p3541 A70-38037

Core-filled thin cylindrical shell under radial ring and band pressure loads, using Boussinesq-Neuber stress function and Flugge shell theory

19 p3543 A70-38247

Thin elastic conical shell axisymmetric solution for free vibration in terms of power series

19 p3545 A70-38335

Thin plates and thin walled cylinders aeroelastic stability in fluid flow, analyzing panel flutter

19 p3546 A70-38342

Prebuckling deformations effect on buckling of clamped thin walled circular cylindrical shells under axial loading and internal pressure

19 p3546 A70-38346

Straight thin walled elliptical cylindrical shells stability in pure bending, solving boundary value problem

19 p3550 A70-38683

Interaction between boundary layer and internal stressed state of thin elastic shell by formulating two dimensional linear theory

20 p3719 A70-39378

Stiffened thin walled circular cylinders buckling and postbuckling behavior under axial compression or external hydrostatic pressure
[DFVLR-SONDDR-59]

20 p3719 A70-39621

Unsteady temperature field in cylinder surrounded by thin shell under uniformly distributed heat sources

20 p3737 A70-39640

Creep and breakdown of thin walled cylindrical shells with circular holes subjected to internal loads at high temperature, discussing time to failure

20 p3721 A70-39777

Stress-strain zero moment state of thin walled helioidal shell under uniformly distributed tensile loads

20 p3721 A70-39778

Thin walled circular cylindrical steel shells dynamic stability partly filled with liquid and subjected to longitudinal excitation

20 p3723 A70-39852

Thin elastic shell natural vibrations, examining orthogonality of form shapes

20 p3724 A70-39862

Thin shells of revolution static and dynamic stability under symmetric loads, presenting eigenvalue algorithm for boundary value problems

20 p3725 A70-39863

Stability loss in linear approximation by thin elastic shell of revolution with negative Gaussian curvature

20 p3726 A70-39872

Thin shell theory elastic coupling conditions, discussing stress-strain and edge effect states

20 p3726 A70-39875

Long thin circular cylindrical shell resonance velocities in steady response to fluid motion

20 p3727 A70-39884

Thin cylindrical shells optimum design with symmetrically paired spiral type stiffeners under uniform axial compressible load and lateral pressure

20 p3732 A70-40287

Rapid expansion of thin walled aluminum alloy cylinders under pulsed magnetic field pressure using high speed streak camera oscillography

20 p3735 A70-40513

Perturbed motion linear equations of body rigidly coupled to thin walled elastic shell partially filled with heavy compressible fluid

21 p3806 A70-40602

Thin walled fiberglass-reinforced plastic cylinders in torsion, calculating load carrying capacity as function of temperature

21 p3841 A70-40648

Thin walled spherical shell spacecraft solar heating in planetary surface proximity, considering skin temperature distribution

21 p3944 A70-41019

Uniformly loaded thin elastoplastic spherical shells, calculating strain hardening and strain rate effects on transient response

21 p3935 A70-41255

Carbon steel thin walled cylinders creep fracture subjected to combined tension and internal pressure by large strain theory

21 p3840 A70-41438

Temperature distribution in rotating thin cylindrical shell with line conduction discontinuity under solar heating, evaluating tubular elements thermal bending on spinning spacecraft

21 p3951 A70-41875

Maxwellian fluid oscillating flow in thin walled elastic circular tube as function of tube dimensions, elastic properties, oscillation frequency, etc

21 p3810 A70-41963

Thin cylindrical shell under nonaxially symmetric concentrated stationary radial loading, calculating random responses and stability

21 p3940 A70-42051

Vibrational response of thin walled pipes to internal turbulent water flow as function of Strouhal number

21 p3940 A70-42052

Mass flow rate correlation for nonsteady convective heat transfer in thin walled tubes with turbulent air flow

21 p3953 A70-42087

Nonlinear flexural vibration of thin circular cylindrical shells with clamped ends, using method of averaging for stability

22 p4112 A70-42517

Thin circular cylindrical panels in supersonic gas current parallel to generatrices, calculating heterogeneity effect on flutter

22 p4113 A70-42603

Curved finite element for thin elastic shells satisfying rigid body motions and energy convergence

22 p4116 A70-43202

Thin walled shells of revolution equations boundary conditions formulated by stress state separation, giving small parameter perturbation theorem

22 p4117 A70-43316

Thickness of equally stressed cylindrical shells, using thin elastic shell theory and Kirchhoff-Love hypotheses

22 p4120 A70-43715

Stress-strain of thin multilayer isotropic spherical shell under radial load employing shallow shell theory

22 p4120 A70-43716

Thin circular cylindrical shells with clamped-clamped and fixed-fixed edges, calculating natural frequencies of nonsymmetrical free vibrations

23 p4266 A70-43997

Dynamic deformation in thin walled axisymmetric plastic shells and filaments under time variable loads applied to high energy rate forming techniques

23 p4200 A70-44235

Stability of elastic stretched ring on thin spherical shell under critical loads

23 p4268 A70-44318

Simplified Sanders-Koiter linear thin shell equations with uncoupled stress-strain relations for arbitrary, nonzero Gaussian curvature, catenoidal and helicoidal midsurface geometries

23 p4269 A70-44399

Axisymmetric vibration modal properties /frequencies and mode shapes/ of thin conical shell frustums, considering dimensional and boundary condition influences

23 p4270 A70-44501

Spacecraft thin walled tubular booms thermal curvature time constants in relation to solar induced despin of satellites

23 p4258 A70-44521

Asymptotic and computer methods interaction in thin walled shells structural analysis and design, considering pressure vessels, cone vibration and dynamic loads

23 p4271 A70-44703

Thin walled shells structural vibration, buckling and stress analysis by computer methods, discussing shell theory and design

23 p4271 A70-44704

Thin shell structural analysis by doubly curved arbitrary quadrilateral finite element, using Kirchhoff theory and cubic polynomial for membrane displacements

23 p4272 A70-44711

Thin shells static and dynamic finite element analysis

23 p4273 A70-44721

Rumanian book on torsion in thin walled elastic structures of various cross sections covering calculation methods for box beams, cylindrical and conical shells, aircraft wings, etc

24 p4418 A70-45147

Curved element approximation of orthotropic axisymmetric thin shells under axial loads

24 p4419 A70-45152

Thin cylindrical shell flutter in linearized supersonic potential theory, considering Mach number, aspect ratio and pressure effects on critical wave number

24 p4420 A70-45263

Axisymmetrically imperfect spherical thin shell stability analysis, comparing results with theory of initial postbuckling behavior

24 p4421 A70-45282

Ring-stiffened thin circular cylindrical shells, calculating free vibration natural frequencies and mode shapes by finite element method

24 p4427 A70-46067

THIN WALLS

Soviet book on experimental investigation of thin walled structures elastoplastic work with complex reinforcement, outlining test procedures

03 p0585 A70-12985

Thin walled glass fiber reinforced plastics beams strength analysis combined with results from elasticity theory of anisotropic bodies

06 p1167 A70-17913

Thin walled strip stability, calculating critical force and rotation angles assuming small subcritical strains

07 p1415 A70-20188

Unsteady creep of thin walled open section bars under free torsion using successive approximations

09 p1779 A70-23101

Shear and cross sectional deformation of prismatic rectilinear rods with unicellular or multicellular thin walls, determining elastic behavior under arbitrary loads

10 p1955 A70-24055

Stress-strain determination in nonuniformly heated thin walled cylindrical beams with nonlinear stringers and skin

10 p1957 A70-24281

Compressive stress critical moment induced instability and weakening incorporated in thin walled beam design

11 p2131 A70-25590

Open cross section thin walled prismatic beam twisting and bending based on virtual displacements

13 p2511 A70-28744

Succession of passes in rolling and hot shaping of thin walled angle steel

22 p4045 A70-42813

Elastic plane equilibrium with thin walled flexible rectangular finite inclusion under symmetrical concentrated load, including computer calculated tangential stresses

22 p4118 A70-43569

THIN WINGS

Supersonic flow around thin warped delta wing, taking into account current separation at subsonic leading edges for pressure distribution and aerodynamic characteristics

01 p0002 A70-10546

Surface shape determination for thin delta wing with variable geometry to minimize drag for given open and closed configurations and cruising supersonic speeds

01 p0002 A70-10547

Transonic flow theory, investigating thin three dimensional lifting wings, similarity for lift and drag, plane flow past airfoil, far field and hodograph solution

05 p0834 A70-16693

Lift and vortex drag due to flaps on thin sweptback tapered wings in inviscid incompressible flow, obtaining spanwise loadings

06 p0967 A70-17256

Boundary value problem for cavitating flow around thin wing reduced to two dimensional singular integral equations from acceleration potential

09 p1663 A70-23393

Minimum drag thin symmetrical cruciform wing fitted with central ridge, reducing problem to linear algebraic finite system of equations

10 p1803 A70-24784

Book on aerodynamics covering flow theory, boundary layers, shock waves, wing design, etc

12 p2157 A70-28148

Shock wave diffraction by moving thin wing over flat terrains, discussing aircraft blast encounter

18 p3205 A70-36195

Flow velocity and pressure on thin wing of small span width near sonic speed, using parabolic type linear equation

18 p3207 A70-36374

Soviet book on wing structures analytical design methods covering thin supersonic wings, mass distribution, aerodynamic characteristics, etc

18 p3344 A70-37025

Compressible fluids flow with conductivity tensor in presence of thin wing under orthogonal fields, reducing integral equation to Fredholm equation

19 p3351 A70-37599

Sweptback thin cantilever wing transonic flutter characteristics, investigating concentrated mass spanwise location effects

22 p4112 A70-42274

Similarity rules for sinusoidal gust loads on thin two dimensional wing in nonstationary subsonic flows

23 p4131 A70-43970

THINNERS

U SOLVENTS

THIOLS

NT CYSTEINE

Dithiols protective effect against ionizing radiation in mice, noting oxygen pressure drop role

03 p0420 A70-13311

Quantitative and qualitative analysis of biochemically and radiobiologically important thiols and disulfides via gas-liquid chromatography

19 p3373 A70-37836

Thioformaldehyde isotopic species reversible transition in interstellar clouds

20 p3703 A70-39164

THIXOTROPIC PROPELLANTS

U GELED ROCKET PROPELLANTS

THIXOTROPY

Colloidal alumina nonNewtonian suspension in propylene glycol, examining thixotropic behavior at various structural levels

24 p4310 A70-45625

THOMAS-FERMI MODEL

Statistical electron density distributions and Thomas-Fermi-Dirac screening functions for positive ions with various ionization degrees

04 p0721 A70-14666

Asymptotic relation between Thomas-Fermi-Dirac and Thomas-Fermi atom models for pressure with and without exchange, considering Coulomb contribution to energy

16 p2953 A70-33004

THOMAS-FERMI THEORY

U THOMAS-FERMI MODEL

THOMSON EFFECT

U THERMOELECTRICITY

THOMSON SCATTERING

Plasma electron temperature and density in Tokamak T3 toroidal discharge measured by Thomson scattering of laser light

Photoelectrons entry into F region detected at conjugate point during winter night by Thomson scatter observations of plasma lines appearing in signal spectrum

Electron-to-ion temperature ratio determined from ion and plasma line components of radar Thomson scatter signal from ionosphere

Simultaneous Thomson scatter measurements for middle and low latitudes, comparing electron density and temperature and exospheric and global temperature distributions

Electron correlations and solar neutrino counts, correcting frequency independent Thomson cross section

Thomson theory of arbitrarily intense elliptically polarized plane electromagnetic wave scattering by free electrons, solving electron equations of motion

Intrinsic polarization from Thomson scattering in binary systems with tidal distortions, taking into account gray atmosphere, axial rotation, gravitational interaction and radiative interaction

THOR DELTA LAUNCH VEHICLE

HEOS 1 launch operations, discussing test and checkout phase, mating with Thor Delta launch vehicle, countdown phase and launch

THOR LAUNCH VEHICLES

NT THOR DELTA LAUNCH VEHICLE

Quartz-Fiberfrax heat shield tests for Thor booster at high radiative heating rates, noting optimum material performance dependence on loose stitching

Thor launch vehicles steering filters design using automated method of optimizing large order linear stochastic systems control [AIAA PAPER 70-986]

THORAD LAUNCH VEHICLES

NT THOR DELTA LAUNCH VEHICLE

THORAX

Traumatic rupture of aortic arch and descending thoracic aorta resulting from abrupt linear body deceleration

Thorax potential resistivity at sea and high altitude levels measured in children and adults inferring relation to ECG differences

Position dependent variations in intrapericardial, pleural and esophageal pressures and cardiac output in thorax of dogs

Thoracic impedance changes in premature infants respiration monitoring, noting Respiratory distress syndrome /Rds/ physiopathology

Circulatory phenomenon and deep thoracic impedance changes of ventilatory origin

Transthoracic mutual impedance responses to lung ventilation, discussing spatial and temporal intravariability

Morphology of adult mammalian thoracic and abdominal aortic segments indicating deviation from medial lamellar architecture

THORIUM

NT THORIUM ISOTOPES

Neutron activation analysis for U and Th in various tektites, discussing evolution and extraterrestrial origin

Energy levels of Th lines computed from weighted averages of interferometrically measured wavelengths data

U and Th abundances correlation in tektites and achondrites based on oxygen isotopic composition of lunar rock specimens

THORIUM COMPOUNDS

NT THORIUM OXIDES

THORIUM ISOTOPES

Th 232 and U 238 pionic X ray energies and widths, suggesting anomalous effect for interaction between high-Z nuclei and pion

Uranium and Th isotopic composition in Apollo 11 samples compared to earth, using mass and alpha spectrometries

Apollo 11 lunar rocks, breccia and fines U, Th and Pb isotopes systematics, considering implications for lunar history

THORIUM OXIDES

Zeeman interaction for super 8S term in ESR Hamiltonian determined, using trivalent GD magnetic spectrum at eightfold coordinated cubic sites of thorium

Solid thorium yttria electrolyte applications in EMF measurements for Cr thermodynamic properties in Fe-Cr and Ni-Cr alloys

Low temperature anharmonicity in thorium dioxide with Co 57 impurities, using Mossbauer effect of Fe 57

THORIUM 228

U THORIUM ISOTOPES

THORIUM 230

U THORIUM ISOTOPES

THORIUM 234

U THORIUM ISOTOPES

THORON

U RADON

THREADS

Stress distribution along stud hole threads in Al case, investigating stud design effect using strain gauge on models

Resilience coefficient of intermediate elements of threaded connection related to transverse and axial nut dimensions by least squares method

Thread parameters effect on steel and Ti high strength fasteners fatigue life [SAE PAPER 700851]

THREE BODY PROBLEM

Coulomb, Gaussian and harmonic oscillator potentials for particle pairs in three body system, using S wave expansion

Three machine parts problem with relative motion and given active forces distribution and time variation, determining entrainment motion

Autonomous two degrees of freedom Hamiltonian system triangular libration points found stable for all mass ratios in circular restricted three body problem

Conditionally periodic orbits existence in restricted problem of three bodies, using similarity transformation

Three-body gravity gradient satellite orbital plane motion analysis, studying transient damping of proposed tethered orbiting interferometer /TOI/

Elliptic restricted three body problem singularities dynamical meaning and character, presenting regularization transformations for equations of motion

Stationary and periodic solutions for commensurable cases of mean motions in restricted three body problems by expanding disturbing functions

Sun-planet systems capture and catapult capacity for interstellar bodies under close flyby conditions

Predictor-corrector algorithm for continuing analytically families of periodic orbits beyond collision trajectories in restricted three bodies problem

Von Zeipel method applied to stellar three body problem, eliminating short period terms and establishing two integrals of motion

Disproof of Wintner analytical foundations of celestial mechanics regarding binary collision in three body problem

Particle nonlinear motion near equilateral libration points in restricted three body problem [AIAA PAPER 70-98]

Dynamical systems with three degrees of freedom, presenting slice cutting and stereoscopic views graphical techniques for restricted three body problem with perturbations

Resonance in restricted three body problem applied to asteroidal motion in asteroid-Jupiter-sun system

Three body problem involving sun and perturbing and perturbed planets, examining perturbed motion equations of Brouwer and Encke methods

Neutron stars equation of state derived, suggesting three body forces inclusion at high densities

Computer program /TACTICS/ for simulating three vehicles simultaneous motion in space, considering interceptor-target guidance and intercept trajectories

Historical survey of celestial mechanics including three body problem and solar system dynamic model construction

Mass point motion in celestial mechanics, investigating two and three body problems without equal counteraction assumption

Motion equations and decay of rotating equal mass triple systems for random configuration integrated numerically on computer

Three body atomic systems with H atom and H negative ion on basis of scattering experiments dealing with resonance and threshold behavior

Periodic solutions with moderate eccentricities and high inclinations for three dimensional restricted three body problem by expanding disturbing functions by high speed computer

Solar system planetary mean motions calculation from characteristic equations roots at equilibrium points of restricted three body problem, using Taylor series solution

Periodic solutions of restricted three body libration point perturbation due to fourth body gravitational and radiative influence using Huang model

Motions stability about triangular points in elliptic restricted problem of three bodies, using perturbation scheme

Planar restricted three body problem in Thiele coordinates, developing recurrence formulas for coefficients in Taylor series expansions of solution

Hydrodynamic analogy in restricted three body problem of celestial mechanics, discussing mass and momentum conservation and physical properties uniqueness

Newtonian gravitational system of three point masses with oscillatory motion at time t approaching infinity, discussing particles mutual distance

Triangular Lagrangian equilibrium points stability in planar restricted problem of three bodies at order two mass ratio using two variable expansion method

Evolution discontinuities and genealogy of long period orbit families at Lagrangian equilibrium point of restricted three body problem

Motion of negligible mass body near large mass body affected by larger third body applied to Phoebe-Saturn-sun system

Stability of single periodic symmetrical solutions of plane circular restricted three body problem, using digital computer for numerical integration of equations of motion

Sun-planet-particle problem, considering solar radiation total pressure, Lagrangian solutions instability and differential equations of motion

Effective moment of inertia in quantum mechanical three body problem, applying specific decoupling to wave functions

Characteristic exponents for periodic orbits of infinitesimal body attracted according to Newtonian law by two finite bodies revolving in ellipses about mass center

Restricted three body interplanetary guidance scheme using midcourse fixed time of arrival velocity correction

Restricted three body problem taken for intermediate orbit in constructing analytical trigonometric motion theory for resonance asteroids, calculating perturbations by Bogoliubov method

Historical survey of celestial mechanics including three body problem and solar system dynamic model construction

Mass point motion in celestial mechanics, investigating two and three body problems without equal counteraction assumption

Equations of motion for circular periodic orbits extended to elliptic restricted three body problem

Periodic solutions close to commensurabilities in three body problem, considering restricted and planar nonrestricted problems

Triangular libration points stability in elliptic restricted three body problem, determining parametric resonance region

- Satellite translational motion in circular problem of three bodies, discussing existence of equations in integral 18 p3324 A70-37150
- Three body numerical solutions to low thrust guidance and navigation for outer planet orbiter with nuclear-electric propulsion [AIAA PAPER 70-1040] 19 p3527 A70-38855
- Planetary orbiter parameters long term variations under central body oblateness, solar and atmospheric drag perturbations 19 p3528 A70-38870
- [AIAA PAPER 70-1055] 19 p3528 A70-38870
- Closed form approximate solution for restricted three body motion of lunar or interplanetary spacecraft, demonstrating accuracy and flexibility in lunar mission trajectory calculations 19 p3529 A70-38875
- [AIAA PAPER 70-1061] 19 p3529 A70-38875
- Periodic collision orbits in plane elliptic three body problem of infinitesimal mass under gravitational field of two finite masses 20 p3705 A70-39603
- Configuration space three body elastic scattering theory for initially free independently moving particles collisions under short range forces 21 p3852 A70-40595
- Dynamical theorems to control number of collisions for sequences in generalized Boltzmann equation, discussing binary collisions involving three molecules 21 p3852 A70-40946
- Nonperiodic Transtrojan orbits for various mass parameter values in three body problem, discussing double libration 21 p3888 A70-41144
- Three body problem for parachute system dynamics during inflation 21 p3755 A70-41843
- [AIAA PAPER 70-1170] 21 p3755 A70-41843
- Restricted three body problem taken for intermediate orbit in constructing analytical trigonometric motion theory for resonance asteroids, calculating perturbations by Bogoliubov method 23 p4240 A70-43919
- Three body elliptic restricted problem triangular points, deriving second order expression for transition curves and characteristic exponents 23 p4244 A70-44595
- Three body problem periodic solutions, considering near equilibrium conservative Hamiltonian system consisting of two harmonic oscillators with rationally related frequencies 23 p4213 A70-44897
- High energy close approach trajectories within planar free fall three body problem, using perturbation theory 24 p4412 A70-45984
- ### THREE DIMENSIONAL BOUNDARY LAYER
- Flow direction and velocity measurement in three dimensional boundary layer, discussing instrument and restrictions 02 p0299 A70-12312
- Heat transfer, three dimensional boundary layers and high speed flow calculations, utilizing original entrainment equation 02 p0284 A70-12341
- Three dimensional turbulent boundary layers on high aspect ratio bodies /swept wings/, discussing shear stress direction determination 02 p0286 A70-12354
- Pressure gradient calculation in three dimensional laminar boundary layer, using method of local similarity 03 p0468 A70-13869
- Numerical integration of equations of motion of three dimensional laminar compressible boundary layers [DVL-915] 06 p1033 A70-17229
- Laminar boundary layer on cone at incidence in supersonic flow evaluated by pressure distribution technique, comparing heat transfer, pitot probe measurements, etc 06 p0974 A70-18189
- [AIAA PAPER 70-48] 06 p0974 A70-18189
- Three dimensional boundary layer on body in external harmonic flow with HF velocity fluctuations 07 p1252 A70-18711
- Nonuniform partitioning of flowfield in three dimensional laminar boundary layer in supersonic conical flow at zero angle of attack, using numerical integration 10 p1804 A70-25192
- Three dimensional incompressible turbulent boundary layer detachment on rotating blading of axial impellers 11 p1975 A70-25793
- Three dimensional periodic boundary layer flow noting successive approximations method, noting steady streaming in first order cross flow 11 p2037 A70-26296
- Three dimensional laminar boundary layer equations for body of revolution at angle of attack in supersonic gas flow derived for equations 12 p2158 A70-28198
- Spatial distribution of three dimensional laminar boundary layer transition zone on sharp half angle cone from hypersonic wind tunnel tests [AIAA PAPER 69-12] 13 p2343 A70-29953
- Three dimensional turbulent boundary layer development on rear of swept wing, comparing measurements with calculations 13 p2344 A70-30021
- Three dimensional boundary layer separation, noting necessity of streamlines perpendicular to pressure gradients near wall 15 p2719 A70-31488
- Three dimensional boundary layer flow on rotating axial flow turbine buckets, determining velocity profiles [ASME PAPER 70-GT-59] 18 p3243 A70-36874
- Velocity distribution and shear stress measurements in three dimensional turbulent boundary layer approaching separation 19 p3405 A70-38021
- Shear stress and velocity profiles in three dimensional mixing layer between grazing perpendicular streams 20 p3608 A70-39356
- Three dimensional boundary layer on lee- and wind-side of prolate spheroid, emphasizing separation and embedded streamwise vortices 20 p3608 A70-39359
- Three dimensional laminar and turbulent boundary layers separation criteria 21 p3811 A70-42206
- Three dimensional laminar boundary layer equations for body of revolution at angle of attack in supersonic gas flow derived for equations 22 p3960 A70-43323
- Perfect gas three dimensional boundary layer separation on circular cone at incidence, comparing numerical calculation and experimental results 23 p4133 A70-44207
- Three dimensional hypersonic laminar boundary layer subdivided into inner and outer regions, obtaining flow description by matching inner and outer solutions [AIAA PAPER 69-710] 23 p4182 A70-44565
- Three dimensional laminar boundary layer separation at infinite swept stagnation line with high mass injection rates 23 p4182 A70-44568
- Unsteady incompressible thermal boundary layer flow past three dimensional obstacle for Prandtl numbers near unity 24 p4428 A70-45366
- Three dimensional laminar boundary layer in unsteady incompressible flow, presenting solution by successive approximations method 24 p4325 A70-45594
- Unsteady separation criteria for three dimensional laminar boundary layer on finite obstacle 24 p4327 A70-46268
- ### THREE DIMENSIONAL FLOW
- Three dimensional thermal conductivity problems solution applied to moving body, body of revolution and hollow cylinder 01 p0213 A70-10218
- Potential triple traveling space waves in barotropic gas with arbitrary equation of state, analyzing adjacent and three dimensional self similar flows 01 p0068 A70-11582
- Momentum integral method using auxiliary equation for two and three dimensional flow problems 02 p0284 A70-12344
- Stratified air flow above relief in baroclinic atmosphere, considering plane nonlinear and three dimensional linearized flow models 03 p0521 A70-13270
- Circumferential contour shape influence on three dimensional flow pattern of fan shaped annular turbine stages 03 p0407 A70-13417
- Three dimensional combustion instability in liquid-propellant rocket engines, investigating dependence on design and operating parameters via boundary value problem analysis 03 p0551 A70-13574
- Incompressible inviscid free shear layer stability with respect to spatially growing three and two dimensional disturbances, considering hyperbolic tangent velocity profile [DFVLR-SONDDR-10] 03 p0468 A70-13786
- Supersonic unsteady state three dimensional flow around blunted bodies with detached shock wave 03 p0409 A70-13864
- Axisymmetric and three dimensional gas flow around blunt bodies using numerical methods, discussing finite difference algorithms for gas dynamic equations 03 p0410 A70-14251
- Inviscid flow problems solution by partial differential equations, considering propagation processes, stratified media, potential, subsonic and three dimensional flows [DGLR-69-2] 04 p0672 A70-15170
- Unsteady pressure at slender blunt body surface in three dimensional hypersonic gas flow 04 p0618 A70-15244
- Fundamental matrix asymptotic forms obtained for supersonic and subsonic three dimensional steady flows past body in uniform stream of viscous thermally conducting fluid 04 p0673 A70-15320
- Three dimensional viscous and inviscid hypersonic flow interaction at rectangular corner, measuring surface and Pitot pressures, heat transfer rates, shear stresses, etc 04 p0620 A70-15533
- Three dimensional flow separations on upswept rear fuselages, using flow visualization and pressure measurement 05 p0790 A70-16097
- Singularity method applied to two and three dimensional potential flow described by Poisson, Helmholtz or related partial differential equations 05 p0832 A70-16114
- Two and three dimensional flow using TRIC and TRIM-like triangular finite elements 05 p0832 A70-16115
- Three dimensional supersonic flow around delta wings, considering lifting and thickness problems, leading edge characteristics, separated and non-separated shock waves, etc 06 p0964 A70-17241
- Transient heat flow in three dimensional rectangular panels, developing criterion for problem dimensionality [AIAA PAPER 70-16] 06 p1182 A70-18212
- Free steady convective flow stability relative to three dimensional disturbances between parallel planes reduced to equivalent plane disturbances problem 07 p1252 A70-18669
- Three dimensional hypersonic flow past body solved assuming developable surface head shock wave 07 p1187 A70-18767
- Three dimensional unsteady and steady sediment distribution obtained by Monte Carlo simulation method, using stochastic hydrodynamics model for transport 07 p1255 A70-19103
- Navier-Stokes equations solved for unsteady incompressible three dimensional stagnation point flow, noting reduction to two dimensional and axisymmetric cases 07 p1188 A70-19343
- Three dimensional gas flow calculated by direct method of characteristics 08 p1431 A70-20860
- Survey of papers on computer calculation of two and three dimensional gas flows, emphasizing method of characteristics and finite difference techniques 09 p1603 A70-22265
- Turbulent three dimensional incompressible wall jets issuing into quiescent air ambient, tangent to and at surface of flat plate, investigating shear stress and flow field 09 p1661 A70-23215
- Three dimensional flow field codes for spheres cones at nonzero angles of attack, comparing numerical and experimental results 09 p1606 A70-23254
- Stepwise averaged parameters of nonuniform three dimensional flow through turbine blade cascade determined from conservation conditions 09 p1606 A70-23611
- Hodograph or Riemann invariants method generalization for nonelliptic systems, discussing three dimensional potential supersonic flows 10 p1863 A70-24087
- Three dimensional supersonic nozzle geometry optimization using Lagrange multipliers and iteration for solving variational problem 10 p1798 A70-24115
- Three dimensional supersonic gas flow solution by numerical method of characteristics, discussing direct and inverse tetrahedral and semicharacteristic schemes 10 p1798 A70-24117
- Shock wave and gas flow structure at constant Mach number past three dimensional blunt bodies, applying method for unsteady flow 10 p1799 A70-24127
- Wind tunnel study of entropy extremum upon critical streamline in supersonic three dimensional flow past blunt bodies at zero angle of attack 10 p1800 A70-24131
- Symmetrical, asymmetrical and three dimensional sonic flows past finite obstacle, investigating regions upstream and downstream from shock waves for airfoil 10 p1800 A70-24134
- Three dimensional hypersonic steady flow around blunt and pointed cones at nonzero angles of attack calculated by method of characteristics [AIAA PAPER 69-187] 11 p1975 A70-25969
- Three dimensional turbulent flow, using direct interaction approximation for growth and propagation of point-to-point velocity field deviations energy spectrum 11 p2036 A70-26013
- Turbulent three dimensional Poiseuille channel flow at large Reynolds numbers, investigating eddy shapes and energy balance 11 p2041 A70-26546

Invariant transform of motion and continuity equations for steady three dimensional flows of compressible fluids in absence of massive forces

11 p2041 A70-26598

Two and three dimensional flow analysis using various versions of finite element techniques

11 p2042 A70-26680

Two and three dimensional potential flow analysis using finite element technique based on method of singularities

11 p2042 A70-26681

Dispersion relations for linearized Grad equations of three dimensional rarefied gas dynamics, including nonequilibrium pressure term for bulk viscosity

12 p2210 A70-27520

Monge equation in small perturbation method of characteristics applied to propagation phenomena in three dimensional supersonic gas flow

13 p2386 A70-28490

Steady expansion flows at three dimensional supersonic edges with small corner angles using analytical method of characteristics

13 p2338 A70-28491

Numerical method of characteristics for three dimensional supersonic nozzle flow field calculations

13 p2338 A70-28512

Three dimensional oblique incidence liquid jet impinging on solid surface, evaluating flow force by applying mass and momentum conservation

13 p2389 A70-29540

Three dimensional boundary layer along semi-infinite swept stagnation line, assessing counteracting effects of cross flow and mass transfer

14 p2565 A70-30278

Free steady convective flow stability relative to three dimensional disturbances between parallel planes reduced to equivalent plane disturbances problem

15 p2718 A70-31461

Finite difference algorithm for supersonic three dimensional steady flow past blunt bodies with generating line bends, allowing for gas equilibrium and frozen states

15 p2671 A70-31495

Kinetic energy and pressure distribution of three dimensional compressible fluid flow, using invariant transformation of Euler motion equation

16 p2890 A70-33073

Hypersonic flow past slender bodies, discussing inviscid flows, outer edge singularity of boundary layer and three dimensional interaction on needle-like bodies

17 p3010 A70-35035

Mathematical model of three dimensional separated flows with applications to small aspect ratio delta wing and flat plate

18 p3207 A70-36438

Three dimensional inviscid small perturbation compressible flow past lifting axial compressor rotor at subsonic and transonic speeds

18 p3208 A70-36691

Liquid with small electrical conductivity and kinematic viscosity in intense transverse magnetic field, examining plane and three dimensional duct flow

19 p3478 A70-37589

Holographic flow and sound visualization, determining three dimensional density distributions in aerodynamic flows

19 p3425 A70-37888

Three dimensional flow through rotor of axial vortex flow fan, using airfoil method for design

19 p3352 A70-38248

Three dimensional supersonic and hypersonic gas flow by Oseen equations, obtaining asymptotic flow field

20 p3609 A70-39656

Falkner-Skan type boundary value problem of three dimensional flow near stagnation point

20 p3658 A70-40103

Dispersion relations for linearized Grad equations of three dimensional rarefied gas dynamics, including nonequilibrium pressure term for bulk viscosity

21 p3807 A70-41168

Deuterium plasma three dimensional flow in coaxial accelerators, examining magnetic structure of filaments/field lines bundles/

21 p3856 A70-41321

Hodography of compressible fluids three dimensional irrotational isentropic flow

21 p3808 A70-41439

Three dimensional laminar boundary layer equations for film condensation on curved surface in quiescent vapor, investigating flow at stagnation point

21 p3954 A70-42168

Thermal boundary layer near stagnation point in three dimensional fluctuating incompressible flow, using Lighthill method

22 p4124 A70-42685

Trajectory equations for plane and three dimensional gas jets with arbitrary injection hole shapes in subsonic shear flow

22 p3960 A70-43365

Steady irrotational gas flow characteristics calculation from finite difference scheme for three dimensional method of characteristics, considering supersonic nozzle flow

23 p4133 A70-44308

Hypersonic three dimensional flow past elliptic cross section slender bodies, discussing disturbance equations, pressure, velocity and density distributions [DFVLR-70-27]

23 p4135 A70-44633

MHD nonstationary three dimensional problems, describing difference method

23 p4227 A70-44738

German monograph on three dimensional flow and blade pressure measurements at axial flow compressor casing wall, discussing test control and digital data processing

24 p4332 A70-45093

German monograph on casing and hub wall friction effects on three dimensional flow in turbocompressors in subsonic compressible working fluids

24 p4287 A70-45096

Boundary layer transition under small tridimensional perturbations interacting with excitations from wall

24 p4327 A70-46206

THREE DIMENSIONAL MOTION

NT THREE DIMENSIONAL FLOW

Steady three dimensional motions using classical differential geometry, considering Navier-Stokes and helical flows

05 p0884 A70-17100

Motion of gaseous medium with uniform deformation with respect to three dimensional Cartesian coordinates

06 p1036 A70-17854

Three dimensional motion of nonrigid parachute and payload system analyzed for dynamic stability [AIAA PAPER 70-209]

06 p0987 A70-18062

Control algorithm for vehicle descent after reentry based on descent range prediction by integrating motion equations allowing for motion three dimensionality

07 p1393 A70-19482

Three dimensional elasticity by Ritz method, using coordinate system orthonormalized in energy metric of operator to avoid precision loss

10 p1957 A70-24511

Dynamic errors of electric measurement devices during three dimensional polyharmonic vibrations of foundation

12 p2233 A70-27561

Control algorithm for vehicle descent after reentry based on descent range prediction by integrating motion equations allowing for motion three dimensionality

15 p2813 A70-32727

Fraunhofer holography for small spherical particles three dimensional position and velocity measurements

21 p3822 A70-40811

THRESHOLD CURRENTS

Low threshold injection lasers in IR and visible spectrum at room temperature employing AlAs-GaAs heterojunctions, noting use for CW mode

03 p0501 A70-13723

Simple approximations for threshold current, gain and lasing frequency of GaAs injection laser at room temperature

03 p0503 A70-14085

Threshold switching and thermal filaments in thick specimen of amorphous semiconductors using IR spectrum viewer

08 p1477 A70-21540

Single mode He-Ne ring laser lock-in threshold and output power relationships to frequency

08 p1514 A70-21692

Threshold characteristics of compression line demodulator obtained from output SNR

09 p1631 A70-22017

Temperature effects on injection semiconductor lasers optical gain and threshold current using energy spectrum model

12 p2247 A70-27485

Carbon monoxide, carbon dioxide and oxygen impurities effects on threshold current and output power of HCN laser

12 p2249 A70-27648

Two-photon transitions effect on two-frequency generation threshold in media with line broadening, considering laser radiation effect on amplification in second channel

12 p2251 A70-28289

Emission field and Fermi quasi-levels distribution in injection laser with n-p heterojunction, determining frequency and threshold current temperature dependence

13 p2426 A70-28876

Hypothalamic electric stimulation intensity effects on elicited behavior, considering possible neural circuit threshold reduction

13 p2355 A70-29807

Mean first passage signal time in one shot electronic system as function of threshold level

14 p2552 A70-31198

Gunn diode simulation with variable cross section, showing subthreshold and mode oscillograms

15 p2707 A70-31510

Low threshold electron beam pumped CdS lasers with improved Al coated Fabry-Perot mirrors in end-pumped configuration

16 p2928 A70-33642

Low noise He-Ne laser with capillary elements, measuring current threshold of noise free operation as function of design parameters

19 p3448 A70-38512

Organic laser spectral and energy characteristics, discussing practical operation principles, low generation threshold and harmonic energy

20 p3642 A70-39754

Threshold SNR for signal frequency meter based on zero number count method, determining reliability

22 p3985 A70-42401

Electric strengths of liquid dielectrics during subjection to Q switched laser pulses, determining threshold currents for breakdown

22 p4051 A70-43338

THRESHOLD DETECTORS [DOSIMETERS]

Threshold and frequency relaxational radiation detectors, discussing operation and sensitivity of p-n-p-n silicon photothyristor and luminosity dependent devices

09 p1649 A70-23356

Scientific satellites pulse height analyzer and associated threshold detection and logic circuitry

16 p2900 A70-33062

THRESHOLD GATES

MOS devices radiation testing for estimating anticipated threshold voltage shift at various dose levels, including gate bias intermittent application during irradiation

04 p0658 A70-14745

THRESHOLD LOGIC

Autonomous control system for moving plant based on logic threshold networks and multivariable functional converter

11 p2023 A70-25612

Redundant threshold logic elements synthesis based on von Neumann multiplexing principle for automatic error correction

13 p2376 A70-29940

Generalized iterative inverse algorithm for linear inequalities set involved in pattern recognition and threshold logic requiring decision functions determination

16 p2870 A70-33739

Weak noise and threshold effects on estimation error for nonlinear PM systems

24 p4312 A70-46053

Maximum-likelihood decoding in analog form of linear convolutional codes with respect to constraint length by one-step threshold method

24 p4313 A70-46059

THRESHOLD SHIFT

U THRESHOLDS

THRESHOLDS

Retinal damage thresholds by exposing rhesus monkey and human eyes to laser radiation, testing rabbit eyes for corneal thresholds

08 p1451 A70-21044

Ruby laser energy threshold dependence on partial shielding of rod by stainless steel tubing

09 p1694 A70-22136

Potassium iodide and paratoluidine fluorescent quenching effect on lasing threshold in rhodamine 6G alcohol solutions

09 p1696 A70-22487

Pulse duration and beam diameter effects on threshold energy density in laser induced transparent dielectric breakdown

13 p2428 A70-29382

Threshold light flux densities for thin Al film breakdown by laser radiation

13 p2428 A70-29383

Demodulators threshold performance for satisfying carrier to noise ratios requirement of Intelsat 4 system

14 p2552 A70-31352

Delta modulation threshold extension technique for phase lock loop FM demodulator

15 p2703 A70-32559

Random vibration first threshold crossing probability density function for linear oscillator

19 p3427 A70-38038

Bayes sequential detection test with constrained error probabilities, investigating properties of thresholds equations

21 p3787 A70-41333

THRESHOLDS [PERCEPTION]

Visual faculties testing to improve performances in visual inspection tasks, considering threshold line concept and visual performance relation to age

01 p0023 A70-10862

Human oculogyral illusion thresholds determined on Ames Man-Carrying Rotation Device to establish stimulus duration effect on angular acceleration thresholds

03 p0424 A70-13765

Color vision mechanisms spectral sensitivities measured by increment threshold technique for normal and deutan observers

03 p0427 A70-13947

- Rhesus monkeys impaired discrimination in recognizing tachistoscopically presented objects following cortical polarization 05 p0802 A70-16625
- Hearing threshold and ear canal pressure levels, using circumaural enclosure with varying acoustic field 06 p0994 A70-17598
- Visual threshold elevation for test flash perception determined by retinal image displacement in saccadic fashon 07 p1205 A70-19283
- Temporary and permanent threshold shifts in hearing of guinea pigs exposed to intense rocket booster engine noise 07 p1214 A70-19931
- Binocular achromatic and color thresholds of constant and flickering lights determined from background of different brightness 08 p1443 A70-20732
- Constant periods method to eliminate human responses during threshold measurements by holding first threshold perception flash fixed 08 p1445 A70-20750
- Human eye sensitization and dark adaptation, noting annual surrounding light addition effect on rod threshold 08 p1447 A70-21723
- Monocular and interocular threshold luminance changes during flicker stimulation, noting interflash duration effects 08 p1453 A70-21792
- Visual restriction effects on critical flicker fusion threshold, loudness and pitch discrimination determined using reticular activating system 09 p1622 A70-23576
- Size effects on velocity threshold for real movement during narrow stimulus object length increase 11 p1989 A70-26662
- Threshold excitation of cutaneous analyzer in man under vascular conditioned reflexes in response to acoustic signals with shock 12 p2173 A70-28353
- High intensity noise effects on auditory thresholds, blood pressure and time response to light stimuli, showing permissible levels during space flights 13 p2358 A70-29334
- Oxygen effect on night vision tested in men at 5,000 ft above sea level, obtaining threshold curves of dark adaptation 13 p2359 A70-29443
- Vibrotactile display operational skill acquisition, discussing stimuli quality and spacing effects on limen of temporal ordering of sensory events in haptic space 13 p2354 A70-29596
- Auditory and cutaneous sound localization acuity 13 p2354 A70-29597
- Suprathreshold angular acceleration effects on oculogical illusion, obtaining magnitude estimates during and after acceleration 14 p2543 A70-30897
- Vestibular threshold dependence on gravity, considering linear accelerations effect on canals sensitivity 14 p2539 A70-30916
- Hearing loss thresholds and spontaneous and caloric nystagmus correlationship in test pilots 15 p2690 A70-31893
- Perception threshold in rapidly changing circumstances, discussing stimuli signals recognition 15 p2687 A70-32872
- Odor threshold levels for unsymmetrical dimethylhydrazine/UDMH/ and nitrogen tetroxides 18 p3224 A70-36227
- Foveal threshold measurements, using small flash of light at center of bright white disk on black background 22 p3972 A70-43411
- Spectral sensitivity of freely moving human eye by determining threshold energy for correct choice between two monochromatically illuminated stimulus patches 22 p3972 A70-43412
- Pulse duration dependent threshold intensity difference for sine tones related to dynamic properties of hearing 23 p4155 A70-44699
- Spatial aspects of sensitization effect properties compared to background light fields, lowering rod threshold at center by light addition to surrounding angular region 23 p4147 A70-44779
- Mesencephalic reticular formation influence on threshold stimulation of cortex, hippocampus, amygdala, thalamic nuclei and caudatum in rabbits 24 p4300 A70-45839
- THROATS**
- Ablative throat nozzle performance, plotting change in thrust, exit pressure and Mach number as function of ablated to initial area ratio 03 p0410 A70-14336
- Sonic throat formation from two dimensional viscous layer interaction with supersonic inviscid outer stream, using boundary layer equations 04 p0665 A70-14452

THROMBOCYTES

- Flight stress effect on blood clotting stabilization of Starfighter aircraft pilots, observing no change in thrombocytes number 09 p1625 A70-23005

THROMBOSIS

- Nervous stress effect on coronary thrombosis, deriving mathematical theory based on biophysical and biochemical approaches 01 p0028 A70-11369
- Coronary thromboses age estimation based on comparison of blood cells, fibrin, collagenous tissue and neocapillaries quantitative changes 03 p0426 A70-13938
- Interactions between nutrition, blood coagulation and atherosclerosis by Duguid theory, emphasizing fibrinolysis, thrombosis and alimentary lipids 03 p0431 A70-14280
- Heparin role in anticoagulant therapy for myocardial infarction based on proved application to other venous thrombotic diseases, noting hemorrhagic complications controllability 04 p0636 A70-15465
- Blood clotting and fibrinolysis under short term physical work in healthy men measured using thrombelastograms 06 p0992 A70-17423
- Hydrodynamic model of blood coagulation in stagnation point flow, analyzing platelet diffusion, white cell bonding stress and thrombus formation [AIAA PAPER 70-143] 06 p1003 A70-18123
- Thrombus formation on foreign surface in fresh blood stagnation point flow, applying fluid mechanical and mass transfer models [AIAA PAPER 70-787] 17 p3035 A70-34470
- Blood platelets aggregation and release reaction in thromboembolic disease due to injury 17 p3032 A70-35471
- G-suit hazards in lower extremity thrombophlebitis in pilots 24 p4307 A70-45347

THROTTLING

- Flight performance prediction for throttling bipropellant rocket engine utilizing ablative combustion chamber throat, discussing lunar module descent engine [AIAA PAPER 69-452] 06 p1130 A70-17176
- Interior ballistics for wide temperature throttling of solid propellant rockets by variable-throat-area nozzle, noting composition effect screening 11 p2103 A70-26154
- Throttling venturi valves for thrust modulation of liquid propellant rocket engines, testing pressure recovery, mixture ratio control and gas saturation and boundary layer effects [AIAA PAPER 70-703] 17 p3146 A70-34510
- Constant chamber pressure thrust throttling of expansion-deflection rocket nozzle, calculating wall static pressure and thrust by characteristic method, discussing performance [AIAA PAPER 69-435] 17 p3149 A70-35655
- Combustion driven shock tunnel applied to tailored interface operating conditions, controlling mass flow into tube by throttling plates 22 p4006 A70-42765

THRUST

- NT HIGH THRUST
- NT JET THRUST
- NT LOW THRUST
- NT MICROTHRUST
- NT RETROTHRUST
- NT ROCKET THRUST
- NT STATIC THRUST
- NT VARIABLE THRUST
- THRUST AUGMENTATION**
- V/STOL aircraft propellers featuring thrust augmenting air jet slits for increased lift [DGLR-69-36] 04 p0616 A70-15175
- Lift fan propulsion for VTOL passenger aircraft, discussing design, thrust augmentation, optimum element combination, engine-wing integrations and tests [DGLR-70-007] 10 p1929 A70-24049
- VTOL aircraft ejector thrust augmentors, discussing configurations in wing root section [ICAS PAPER 70-56] 23 p4139 A70-44152
- Tail rotor thrust increase for yaw control via increased blade area, higher tip speeds and cambered airfoils 23 p4140 A70-44324
- STOL aircraft augmentor wing concept, examining noise suppression, flight research vehicle program and application to turboprop production aircraft [SAE PAPER 700812] 24 p4290 A70-45903
- THRUST BEARINGS**
- Stiffness values of externally pressurized incompressible fluid-film thrust bearings under turbulent Couette flow, discussing Reynolds number effects [ASME PAPER 69-LUB-25] 01 p0100 A70-10383
- Elongation and combined shear stresses in incompressible creeping plane flows of viscoelastic lubrication for squeeze-film bearings [ASME PAPER 69-LUB-22] 01 p0101 A70-10385
- Hybrid boost bearing applied to jet engines thrust bearing life extension and to land turbine equipment for providing high overload capacity 01 p0101 A70-10389

- Synchronous dynamic response of gaseous double squeeze film thrust plate with very high frequencies, showing increased load capacity and stiffness [ASME PAPER 69-LUB-8] 01 p0102 A70-10395
- Inertia effects on pressure distribution, load capacity and frictional torque in MHD hydrostatic thrust bearing lubrication flow 02 p0307 A70-12162
- Step thrust self acting gas bearing without feed grooves for two directions of shaft rotation, determining geometric, gas and speed parameter characteristics 02 p0307 A70-12164
- Lubrication problem for centrally pivoted tilting-pad sector thrust bearings with temperature and elasticity effects, noting iterative solution for coupled equations [ASME PAPER 68-LUB-4] 02 p0307 A70-12166
- Hydrodynamic journal-thrust bearing system for satellite attitude control flywheel, discussing bearing stability, grease lubricant seal, power consumption, etc [ASLE PREPRINT 69-LC-22] 02 p0309 A70-12532
- Hydrostatic thrust bearing with electrically conducting gas lubricant under axial current induced MGD pinch 03 p0497 A70-13780
- Poisson ratio of elastomers determination for defining compliant surface fluid film thrust bearings behavior, considering method and error analysis [ASME PAPER 69-WA/LUB-7] 04 p0712 A70-14751
- Time transient and step-jump dynamic analyses of gas lubricated bearing, illustrating hybrid journal and Rayleigh-Step thrust bearings [ASME PAPER 69-WA/LUB-5] 04 p0697 A70-14768
- Inertia effects due to circumferential and radial velocity in MHD hydrostatic thrust bearing in axial magnetic field [ASME PAPER 69-LUB-F] 04 p0698 A70-14871
- Molecular mean free path influence on gas lubricated thrust bearings performance, discussing slip flow effect and load capacity 05 p0854 A70-15909
- Load capacity of rotating field MHD hydrostatic thrust bearing increased by rotating axial magnetic field 06 p1076 A70-17527
- Equilibrium equations solved for statics of double row radial thrust ball bearing, neglecting load angle changes caused by deformations of races and ball bearings 06 p1077 A70-17929
- Low temperature tempering effects on steel transformations and axial rigidity of radial thrust ball bearings in aircraft 12 p2243 A70-27568
- Additional inertia introduced by velocity profile gradient in flow direction effects on externally pressurized gas bearing 16 p2924 A70-34233
- Hydrodynamic journal-thrust bearing system for satellite attitude control flywheel, discussing bearing stability, grease lubricant seal, power consumption, etc 17 p3099 A70-34630
- Pneumatic instability, capacity and rigidity of thrust and journal gas bearings with external air injection 18 p3264 A70-37072
- Poisson ratio of elastomers determination for defining compliant surface fluid film thrust bearings behavior, considering method and error analysis [ASME PAPER 69-WA/LUB-7] 19 p3434 A70-37602
- Stiffness values of externally pressurized incompressible fluid-film thrust bearings under turbulent Couette flow, discussing Reynolds number effects [ASME PAPER 69-LUB-25] 19 p3435 A70-37611
- Time transient and step-jump dynamic analyses of gas lubricated bearing, illustrating hybrid journal and Rayleigh-Step thrust bearings [ASME PAPER 69-WA/LUB-5] 19 p3436 A70-37619
- Spiral grooved gas lubricated thrust bearings, calculating self heating induced thermal distortion effects on load capacity [ASME PAPER 70-LUBS-14] 22 p4044 A70-42447
- Fluid film lubricated, thrust loaded, angular contact ball bearing high speed performance, predicting skidding by isothermal Newtonian behavior in ball to raceway contact [ASME PAPER 70-LUBS-7] 22 p4045 A70-42452
- THRUST CHAMBER PRESSURE**
- Heat pipe cooled thrust chambers for space storable propellants, discussing design feasibility for radiation and regeneratively cooled concepts [AIAA PAPER 70-942] 16 p2965 A70-33541
- THRUST CHAMBERS**
- Combustor geometry and heat release effects on supersonic combustor thrust efficiency, considering shock-free, normal and oblique shock situations 02 p0354 A70-12043
- Rocket stability monitoring by temporal radiometry, using exhaust radiance measurement to detect frequencies in thrust chamber combustion pressure [AIAA PAPER 69-580] 04 p0737 A70-15429
- ICRPG liquid propellant thrust chamber performance evaluation methodology, reviewing imperfections and limitations [AIAA PAPER 69-468] 07 p1365 A70-19728

Regeneratively cooled stainless steel thrust chamber failure related to internal carburization by fuel decomposition and propellant combustion 12 p2290 A70-27111

Discharge chamber plasma processes in electron bombardment ion thrusters, considering factors affecting thrustor performance [AIAA PAPER 69-494] 15 p2791 A70-32501

Rocket engine thrust chambers and valves, discussing component lifetime extension and operational flexibility of reaction control systems [AIAA PAPER 70-603] 16 p2964 A70-33526

Oxygen difluoride/diborane propellant thrust chamber and injector technology, discussing engine duty cycles and performance [AIAA PAPER 70-717] 16 p2962 A70-33550

Water cooled pressure probes for measuring rocket chamber HF pressure variations 17 p3093 A70-35485

Heat transfer between wall and liquid and vapor films in internal regenerative cooling of thrust chambers 21 p3867 A70-41027

Spinning cold-flow rocket motor, studying rotation effects on chamber flow velocity field 23 p4233 A70-44579

Hydrogen oxygen engine designs for space vehicle auxiliary propulsion systems, considering long life thrust chamber performance with compatible heat transfer characteristics [SAE PAPER 700803] 24 p4395 A70-45908

THRUST CONTROL

NT THRUST VECTOR CONTROL

Optimum flight paths of energy and power limited rockets with generalized thrust characteristic, considering vertical, horizontal, rectilinear, zero drag and vacuum trajectories 01 p0193 A70-10425

Optimum thrust control of satellite along given trajectory to rendezvous at zero velocity with orbited satellite 01 p0197 A70-11500

Optimal motion control of spacecraft refueling during flight by liquefying atmospheric gas along prescribed trajectory under constant thrust 01 p0197 A70-11502

Thrust control unit in Lufthansa Boeing 707 aircraft designed to maintain landing approach speed by adjusting throttle setting and landing flap position 05 p0845 A70-15903

Vehicles optimal flights with controlled or boundary level thrust in circular orbit neighborhood, using linearized equations of motion 06 p1142 A70-17876

Fighter aircraft inflight thrust control using thrust reverser technology to improve operational capability [AIAA PAPER 70-513] 09 p6160 A70-23019

Base pressure effects on cone angle of fixed length conical nozzle yielding maximum thrust 11 p1977 A70-26156

Fuel-optimal retrothrust control in state dependent retarding force fields, taking into consideration synthesis for vertical trajectory system configuration 11 p2126 A70-26321

Rao optimization method for thrust nozzles at given length, analyzing control surface flow field conditions 12 p2158 A70-28202

Maximum thrust and drag reduction for supersonic missiles by base burning, showing dependence on chemical reaction and Mach number 12 p2158 A70-28208

Satellite rendezvous programmed control with allowance for thrust limitation by free trajectories method, determining impulse duration, magnitude and time 12 p2314 A70-28257

Causes and magnitudes of thrust misalignment of Kaufman type electron bombardment ion thruster [AIAA PAPER 69-303] 13 p2473 A70-28506

Pilot chamber initiated thermal decomposition reactor concept for monopropellant thruster, discussing thrust levels and throttling ratios [AIAA PAPER 69-420] 13 p2473 A70-28507

Liquid mercury /LM/ cathode thruster characteristics, power conditioning and control requirements [AIAA PAPER 70-646] 16 p2965 A70-33536

HEUS solid rocket motor impulse control, describing liquid quench concept development through full scale test firing [AIAA PAPER 70-642] 16 p2969 A70-33600

Throttling venturi valves for thrust modulation of liquid propellant rocket engines, testing pressure recovery, mixture ratio control and gas saturation and boundary layer effects [AIAA PAPER 70-703] 17 p3146 A70-34510

Solid rocket motors, investigating thrust magnitude and stop-restart control 17 p3148 A70-35207

R-4D multiapplication rocket engine for Apollo spacecraft reaction control, discussing design, performance, quality assurance and tests 17 p3178 A70-35259

Reaction jet azimuth control system for balloon-borne gondola 17 p3018 A70-35316

Steady state off-on attitude control strategy for minimizing propellant consumption and thrust ignitions of satellite in presence of environmental disturbance torques 17 p3180 A70-35556

Optimal low thrust transfer between coplanar circular orbits, examining thrust direction and steering as Mayer problem 22 p4097 A70-42489

High performance reaction pointing control systems for sounding rockets, using proportional control of differential thrust and adaptive control of thrust magnitude [SAE PAPER 700783] 24 p4415 A70-45861

Concorde thrust control by employment of variable area nozzle and reheat system, discussing crew work load [SAE PAPER 700817] 24 p4394 A70-45900

THRUST LOADS

Space vehicle residual thrust oscillation and dynamic response using power spectral density functions from flight data 10 p1953 A70-25068

Dynamic postbuckling response of thin elastic circular plates under axisymmetric time dependent radial thrust, discussing response to step loading 10 p1964 A70-25206

THRUST MEASUREMENT

Charged aerosol charge/mass ratio measurement and colloidal propulsion system thrust, efficiency and exhaust velocity determinations 03 p0551 A70-12936

Pyrotechnic thrusting devices output dynamics, describing testing for spacecraft applications 03 p0549 A70-14125

Gross thrust coefficient for turbofan engines thrust estimates, discussing full scale nozzle simulation 04 p0736 A70-15390

Net thrust determination for high bypass ratio engines in cruise, suggesting performance evaluation in actual flight tests [SAE PAPER 690652] 05 p0895 A70-15841

Thrust static characteristics of poppet valves with specific angle range indicating validity of momentum theory for thrust estimation 06 p1075 A70-17139

In-flight thrust measurement via internal gas generator and external traverse methods, discussing accuracy requirements, errors and aircraft design role 13 p2474 A70-28539

C-5A turbofan engine thrust determination using pressure and temperature values in exhaust nozzles [AIAA PAPER 70-611] 16 p2969 A70-33606

Dynamic force and pressure measurement on rocket nozzle during simulated stage separation, describing instrumentation and control system 17 p3061 A70-35478

High response thrust measurement system for pulsed attitude control rocket engines 17 p3061 A70-35479

Thrust measurements on pulsed vacuum-arc thruster, comparing specific impulse and efficiency with exhaust velocity measurements by ion collecting double probes [AIAA PAPER 70-1146] 20 p3567 A70-40207

In-flight thrust measurement methods on SERT 2 ion thrusters, using accelerometer, electrical parameters and orbit change [AIAA PAPER 70-1126] 20 p3691 A70-40219

Time-of-flight mass flow rate and thrust stand data comparison for two 100 micropound colloid thrusters [AIAA PAPER 70-1144] 20 p3691 A70-40229

Micropound extended range thrust stand /MERTS/ for testing electric thrusters for spacecraft auxiliary propulsion, providing three thrust measurement ranges and data telemetry system [AIAA PAPER 70-1111] 20 p3607 A70-40232

Quasi-steady MPD arc thruster average thrust measurements, considering time-of-flight velocity determination by ion collecting probes [AIAA PAPER 70-1080] 20 p3694 A70-40255

Thrust vector measuring device using floating suspension system for ion engines, detecting vertical tilt and horizontal drifts of floating platform [AIAA PAPER 70-1104] 21 p3805 A70-41789

Thruster for direct output reading from jet engines based on stream and total port pressures 24 p4340 A70-46328

THRUST PROGRAMMING

Composite programming of vertical ascending rocket with constant thrust phase followed by acceleration and coasting phases, discussing burnout altitude and fuel consumption 08 p1582 A70-21775

Optimal longitude rendezvous for geostationary satellite by using inertially fixed orientation thrust for performing final positioning [ONERA TP-801] 10 p1941 A70-24541

Spacecraft stochastic optimal control, discussing design of least upper bound fuel optimal system with measurement uncertainty 11 p2025 A70-26222

THRUST REVERSAL

Positive displacement low pressure air motors for Boeing 747 fan thrust reverser pneumatic actuators and controls 03 p0550 A70-12881

Fighter aircraft inflight thrust control using thrust reverser technology to improve operational capability [AIAA PAPER 70-513] 09 p6160 A70-23019

Mathematical model for flow within external target type thrust reverser, assuming inviscid incompressible two dimensional flow [AIAA PAPER 69-3] 12 p2291 A70-28085

Jet thrust reversers mechanical design limits, objectives and materials 14 p2628 A70-30500

In-flight thrust reverser for tactical/attack aircraft, discussing system influence on airplane stability and control [AIAA PAPER 70-699] 16 p2841 A70-33561

Forces acting at thrust termination time with aluminumized solid propellant rocket fuel, predicting thrust reversal ratio under vacuum conditions 21 p3869 A70-41869

Concorde downstream thrust reversal nozzle, noting weight saving by use of welded stainless steel honeycomb construction 22 p4092 A70-43213

THRUST TERMINATION

Liquid fuel jet engine thrust aftereffect momentum, investigating switching off transient process 19 p3490 A70-37249

Forces acting at thrust termination time with aluminumized solid propellant rocket fuel, predicting thrust reversal ratio under vacuum conditions 21 p3869 A70-41869

THRUST VECTOR CONTROL

Two step optimal motion of target and pursuer with thrust vector control in vacuum under arbitrary gravitational field, determining distance strategy 02 p2272 A70-12405

Control system response improvement by state variable feedback illustrated by frequency and transient response tests data from analog model 04 p0662 A70-15331

Harrier G.R. Mk 1 VTOL vectored thrust aircraft for attacking targets at conventional strike aircraft speed, discussing design and combat effectiveness 06 p0985 A70-17157

Constant thrust electric propulsion systems performance with coast trajectories presented for 100 AU extraelectric missions [AIAA PAPER 68-546] 06 p1137 A70-17160

Installed thrust vector for scarfed attitude control nozzles flush mounted with spacecraft cylindrical surface, predicting pressure distributions for internal thrust 06 p1154 A70-17167

Pulsed plasma vacuum-arc thruster system incorporating throttle and thrust vector controls for long life satellite control applications [AIAA PAPER 70-180] 06 p1133 A70-18232

Thrust vectoring of multiaperture Ce electron bombardment ion engines, determining thrust deflection limit by accelerator current rise 11 p2102 A70-26124

Minimum-time thrust vector control law in Apollo lunar module computerized autopilot 13 p2499 A70-28399

Thrust vector control application to Skylark vehicle to eliminate wind and thrust misalignments effects 13 p2503 A70-28676

Microthrusters for geostationary satellites attitude and position control 15 p2791 A70-32279

Cross product steering for space vehicles and ballistic missiles guidance during powered vacuum flight, pointing thrust acceleration vector to null velocity at termination 16 p2947 A70-33440

Thrust deflector for VTOL aircraft fuselage mounted lift engines designed as isentropic plug nozzle, considering mass flow, pressure forces and Coanda effect [SAWE PAPER 841] 20 p3563 A70-40379

Ion thrust vectoring systems for satellite attitude control and stationkeeping, discussing deflection techniques [AIAA PAPER 70-1150] 21 p3868 A70-41783

Three axis attitude ion thrust vector control mechanism for solar electric propulsion spacecraft, discussing gimbal and translation actuators, array and cabling [AIAA PAPER 70-1156] 21 p3759 A70-41784

Thrust vector measuring device using floating suspension system for ion engines, detecting vertical tilt and horizontal drifts of floating platform [AIAA PAPER 70-1104] 21 p3805 A70-41789

Lockseal/flexible joint/ for solid propellant rocket motor thrust vector control, considering construction, operating characteristics and tradeoffs [SAE PAPER 700777] 24 p4393 A70-45865

THRUST-WEIGHT RATIO

- Engine weight estimation for showing effect on thrust, specific impulse and uranium loss rate for open cycle gas fueled nuclear rocket engine
[AIAA PAPER 70-690] 16 p2949 A70-33553
- Multiorbit injection earth departure technique for optimal thrust-weight ratio in manned interplanetary missions using NERVA engine
[AAS PAPER 70-039] 17 p3175 A70-34780
- Variable sweep high thrust-weight ratio multirole combat aircraft /MRCA/, discussing British-French cooperation, development programs and requirements 17 p3017 A70-34916

THRUSTORS

U ROCKET ENGINES

THUNDERSTORMS

- Thunderstorm lightning discharge formation mechanism, investigating electric charge concentration and motion of free electrons 01 p0134 A70-10169
- Thunderstorm downdraft trajectories and temperatures, discussing evaluation of cooling due to evaporation 02 p0325 A70-12256
- Mesoscale rawinsonde network for convective process resolution, describing reduction and analysis techniques for thunderstorm wind, temperature and moisture data 03 p0521 A70-13165
- Airborne and ground based radar data on thunderstorm echoes compared within framework of storm reflectivity model and radar theory 06 p1010 A70-18246
- Thunderstorms and thunderstorm phenomena - ASM Conference, Chicago, April 1969 06 p1099 A70-18567
- Cloud base updraft field, three dimensional reflectivity pattern and rain and hailfall pattern for thunderstorms in Alberta, discussing shear 06 p1099 A70-18569
- Momentum considerations in thunderstorm dissipation by disrupting organized cloud base updraft structure 06 p1100 A70-18570
- Model for thunderstorm downdrafts induced by rain evaporation based on one dimensional steady state formulation, deriving vertical velocity profiles 06 p1100 A70-18573
- Numerical model of thunderstorm cold air outflow, providing horizontal flow as function of height from computer program using vertical velocity and storm motion 06 p1100 A70-18574
- Thunderstorm cold air outflow leading edge structure recorded by NASA meteorological tower at Kennedy Space Center 06 p1100 A70-18575
- Vertical wind distribution associated with thunderstorm outflow, measuring wind direction oscillations at Kennedy Space Center 06 p1101 A70-18576
- X band Doppler radar observation of horizontal motion of precipitation particles in low levels of slow moving thunderstorm 06 p1101 A70-18580
- Pulsed Doppler radar observation of thunderstorm updraft structure, noting vertical velocity perturbations 06 p1101 A70-18581
- Tornado producing thunderstorms, using conventional surface and upper air data combined with ATS-III data, discussing mesoscale disturbances and momentum exchange 06 p1102 A70-18583
- Vertical motion and temperature structure of severe thunderstorms from jet aircraft penetration 06 p1102 A70-18585
- Stratospheric clear air turbulence over squall line, discussing turbulence over thunderstorms 06 p1102 A70-18588
- Thunderstorms lightning flashes time distribution recorded visually and on radar screens, discussing statistical variations in sigma 08 p1539 A70-21648
- Ground based radar surveillance for SST to avoid convective clouds and thunderstorm activity during transonic acceleration phase ensuring minimum demands on maneuverability 09 p1610 A70-22242
- Group delay time differences of spectral groups of VLF atmospherics respecting day and night variation for thunderstorms, determining distance dependence 10 p1884 A70-25260
- Vertical air velocity in convective clouds by pulsed Doppler radar observations of thunderstorm 11 p2004 A70-25650
- Stratospheric clear air turbulence /CAT/ vertical extent above thunderstorm graphically represented 12 p2265 A70-28095
- Thunderstorm detection and warning system, measuring vertical potential gradient and changes caused by lightning discharges 14 p2607 A70-30574

Thunderstorm bottom wind profile model, analyzing flow distribution, isotach, isogon and isotherm characteristics 14 p2607 A70-30584

Slow tail atmospherics and VLF pulse measurements at close-to-thunderstorm fields, indicating return stroke origin 17 p3046 A70-35395

Right-moving thunderstorm characteristics from mesonetwork rawinsonde updraft observations, considering hydrostatic pressure and cyclonic rotation 19 p3462 A70-38260

Thunderclouds electric fields and conductivities measurement by differential rotating mill, noting insensitivity to space charge and frictional charging 20 p3661 A70-39146

Nighttime lightning activity observations by orbiting solar satellite OSO-B, determining thunderstorms positions by optical radiation detection 20 p3623 A70-39978

Quasi-periodic ionospheric oscillations associated with nuclear explosions, thunderstorms and quiet conditions 21 p3814 A70-40938

Thunderstorm development processes investigated by aircraft measurements of electrical structure in cumulonimbus clouds, noting lightning probability dependence on turbulence within cloud 22 p4064 A70-42775

Global thunderstorm activity experiment by Ariel 3 satellite, investigating lightning discharge number and noise power 22 p4015 A70-42778

Global thunderstorm activity location found by measuring differences between time of arrival of electromagnetic energy at three satellites 22 p4016 A70-42779

Thunderstorm frequencies related to lunar phase and declination for ground stations in eastern and central U.S. 22 p4018 A70-42909

THYMIDINE

Thymidine tracer distribution in bone marrow chromosomes of rats and mice treated with radioprotectors, noting cell metabolic activity reduction by sulphydryl-type radioprotectors 09 p1619 A70-22818

Radiation induced free radicals in thymidine single crystals, attributing electron spin resonance spectral observations to nature of various radicals 22 p3981 A70-42348

THYMINE

Cytosine-thymine transitions from cytosine-5-H3 decay in bacteriophage S13 DNA, discussing coding change efficiency 05 p0803 A70-16948

Parental termini-daughter strand linkage in initiation of DNA replication in *Bacillus subtilis* after thymineless germination 16 p2847 A70-33060

Radiation effects on dihydrothymine in frozen sulfuric acid solutions, detecting thymine after melting via low temperature UV absorption measurements 20 p3583 A70-40454

Radicals induced in thymine monohydrate single crystals by ionizing radiation 20 p3583 A70-40455

THYMUS GLAND

Gamma radiation effects on membrane permeability of isolated nuclei from white rats thymus in sucrose-calcium buffer 04 p0629 A70-14460

THYRATRONS

Thyratron based fast pulse generator circuits noting applications 11 p2017 A70-25570

Univibrator analysis with glow discharge thyratrons, increasing time lag for equal R and C values 16 p2873 A70-33237

THYRISTORS

Monolithic zero crossing AC trigger IC for thyristor power control systems operating in on-off mode 08 p1478 A70-20786

Threshold and frequency relaxational radiation detectors, discussing operation and sensitivity of p-n-p-n silicon photothyristor and luminosity dependent devices 09 p1649 A70-23356

Thyristor tetrode silicon controlled switches /SCS/, considering unijunction transistors and pulse generator circuits 13 p2377 A70-29115

Thyristor tetrodes application to current and voltage stabilization, frequency division and lighting control 16 p2880 A70-34099

Si controlled thyristors applied to pulse modulators in ionospheric stations 18 p3233 A70-37043

Thyristor circuit for storing or generating digital control signals, considering reliability at high noise levels 19 p3385 A70-37377

Low power thyristors in relaxation oscillation circuits, considering static and dynamic characteristics in large signal mode 20 p3596 A70-38971

Stress tolerant thyristor and transistor switching electronic converter for ion propulsion engine [AIAA PAPER 70-1157] 21 p3866 A70-40901

Thyristor-servomotor temperature control unit, describing circuit and applications 22 p3996 A70-42850

M phase thyristor amplifier operation, investigating state and transition equations by state variable methods 22 p3996 A70-42918

THYROID GLAND

Thyroid influence on RNA content and nucleotide composition in hypothalamus, cortex and phenolic fractions of cerebral hemispheres resulting in accelerated protein biosynthesis 01 p0019 A70-10511

Thyrotropin /TSH/ effects on thyroidal iodine metabolism during hypoxia in rats 02 p0231 A70-11703

Stimulated thyroid gland temperature variations and oxygen metabolism in decorticated dogs and anesthetized rabbits and rats 04 p0639 A70-15511

Adaptive reactions in thyroidectomized rats blood and brain during adaptation to hypoxia compared with intact animals 07 p1214 A70-19794

Thyroid gland function following radiation injury by measuring plasma protein bound iodine in irradiated rat blood 09 p1621 A70-23150

Hyperthyroidism diagnosis by pattern recognition, using computerized class featuring information compression 22 p3977 A70-43732

THYROXINE

Thyroxine stimuli transmission from posterior hypothalamus to cerebral cortex ascribed to dorso-medial nucleus of thalamus 16 p2848 A70-33261

TIDAL OSCILLATION

U TIDES

TIDES

NT ATMOSPHERIC TIDES

NT LUNAR TIDES

Lunar surface luminescence considered for correlation with tidal forces of earth 09 p1758 A70-22748

Gersternkorn moon capture theory taking into account tidal evolution of earth-moon system, discussing marine organisms time rate synopsis for earth rotation retardation 10 p1943 A70-24840

Planetary tidal force effect on solar activity cycle, showing amplitude proportionality to solar and gravity center deviation 14 p2649 A70-31199

Trail formation due to tidal effect in interacting galaxies during close approaches, considering mass flow hydrodynamics 15 p2801 A70-32481

Phase delay of solid earth tide, minimizing ocean and atmosphere loading by strain seismograph measurement 18 p3255 A70-37077

Trail formation due to tidal effect in interacting galaxies during close approaches, considering mass flow hydrodynamics 23 p4240 A70-43906

Artificial liquid satellite orbited to verify tidal theory 23 p4183 A70-44659

Nonspherical stellar internal structure, developing method for models with rotational and tidal distortion 23 p4249 A70-44804

TIG WELDING

U GAS TUNGSTEN ARC WELDING

TILT

U ATTITUDE [INCLINATION]

TILT WING AIRCRAFT

NT CL-84 AIRCRAFT

Tilt wing-propeller VTOL model, comparing static wind tunnel with moving-track test data based on coefficient forms of freestream and slipstream dynamic pressures [AIAA PAPER 70-574] 13 p2343 A70-29895

TILTING

U ATTITUDE [INCLINATION]

TILTING ROTORS

U.S. rotorcraft research regarding materials and engine technologies of conventional and compounded helicopters 02 p0226 A70-12314

Dynamic stability of complex aeroelastic structures including V/STOL aircraft using simplified technique, noting application to tilt rotor aircraft design [AIAA PAPER 70-22] 06 p1170 A70-18119

Rotorcraft design and aerodynamics, discussing structural vibrations and all-weather operation 13 p2344 A70-28545

Blade flexibility effects on static stability derivatives of prop/rotors in propeller flight mode
17 p3013 A70-34701

Aerodynamic and structural considerations in prop/rotor design for tilt-rotor aircraft, discussing blade twist effect on/cruise efficiency and figure of merit
17 p3014 A70-34719

Tilt-fold-proporotor VTOL aircraft characteristics, stability and control, emphasizing flying qualities
17 p3014 A70-34722

TIMBER IDENTIFICATION
Mixed hardwoods and pine area forest cover types identification by aerial photography
14 p2577 A70-30981

TIMBER INVENTORY
Aerial photography applications to timber management programs of forest industries
10 p1879 A70-24746

K band SLR /side-looking radar/ imagery mapping tropical lowland vegetation compared to photographic coverage
10 p1879 A70-24747

Forest inventory data collection by 70 mm photography, creating correction surface over model area of large scale pair
10 p1880 A70-24754

Multistage sampling of space and aircraft remote sensor imagery for forest inventory
12 p2228 A70-26921

Mixed hardwoods and pine area forest cover types identification by aerial photography
14 p2577 A70-30981

Earth resources information systems using space, aerial and ground measurements, discussing Apollo 9 IR color photograph of Mississippi Valley and timber inventory applications
23 p4192 A70-44679

TIMBER VIGOR
Day/night thermal IR imagery detection of moisture stress of girdled trees in upland forest
16 p2898 A70-34047

TIME
NT ACCESS TIME
NT BURNING TIME
NT EPHEMERIS TIME
NT FLIGHT TIME
NT REACTION TIME
NT RELAXATION TIME
NT RESPONSE TIME [COMPUTERS]
NT TESTING TIME
NT TRANSIT TIME
NT UNIVERSAL TIME
Meteorite falls statistics correlations for fragmentation relationships with mass, time of fall and class
05 p0912 A70-16447

Time variations and angular collimation of radiation emitted by source with relativistic streaming
06 p1134 A70-17281

Singularity for absolute zero of time suggested for beginning of universe by Einstein relativity theory
07 p1336 A70-19922

Artifices to allow computing time reduction in recursive data elaboration for high order differential system
09 p1720 A70-22647

Time dilation in space travels at light velocity under influence of special theory of relativity
10 p1943 A70-24760

Science of time considered with reference to quantum physics, special theory of relativity, directivity and symmetry and conditional probability, discussing clock designs
12 p2271 A70-27276

Time travel and cosmological model based on Einstein relativity theory, considering hypothetical motor design, energy supply, tachyons and four dimensional orbits implications
20 p3710 A70-40132

TIME CONSTANT
NT PERCEPTUAL TIME CONSTANT
Gas laser beams short time constant and thermal self defocusing following small spot focusing on thin dye sample
01 p0109 A70-10431

Decay times for thermal disturbances near cloud tops in Jupiter atmosphere, discussing hydrogen absorption
02 p0368 A70-11827

Magnetic flux trapping experiment with Al conductor, showing decay time constant connection with sun-spot theory
02 p0299 A70-12393

Synthetic molybdenum diselenide oxidation kinetics between 375-530 C, determining isothermally reaction rate constants in dry air
[ASLE PREPRINT 69-LC-8] 02 p0321 A70-12537

Dynamic time constants for specific transition and relaxation times of hydrogen maser, noting coupling between hyperfine differences and atomic polarization
03 p0498 A70-13007

Time constant of man machine system as adaptive variable in training devices derived from combined vehicle properties and human control characteristics
05 p0805 A70-16005

Thermometer dynamic response under various working conditions predicted from time constant curves
05 p0849 A70-16518

Spectroradiometer with paramagnetic traveling wave quantum amplifier applied to radio telescope, studying noise, temperature and fluctuation sensitivity at given time constant
08 p1495 A70-21054

Time constant, steady state and tracking error of AGC loops at input/output of FM link in AM-FM telemetry system
12 p2184 A70-27250

Time constant equations for hair and film radiosonde hygrometers, allowing for inertial errors in humidity and cloud boundary measurements
14 p2603 A70-30412

Time constants of low inertia resistance thermometers by heating with alternating AC and DC currents
19 p3420 A70-37263

Finite difference time integration method for computing seismic ray intensities
19 p3412 A70-37837

InAs pulsed injection laser at cryogenic temperature for measuring time constant of IR radiation detectors
20 p3630 A70-39449

Human sweating transient state characterized by time constant following abrupt ambient temperature rise
21 p3761 A70-41140

Signal arrival time variance in optical communication system with high lag photodetectors, examining input, detection and amplification noise
23 p4196 A70-44410

Spacecraft thin walled tubular booms thermal curvature time constants in relation to solar induced despin of satellites
23 p4258 A70-44521

TIME LAG
U TIME LAG
TIME DEPENDENCE
Nimonic Ni-Cr based alloys fracture characteristics used to determine temperature and time effects on equicohesive points positions
01 p0116 A70-10073

Time dependent telegrapher equation solution for studying transient neutron waves propagation
01 p0130 A70-10086

Data acquisition methods and position in data processing with respect to time and quantity requirements
01 p0047 A70-10260

Sea-level pressure interval to prevent decompression sickness in humans flying in commercial aircraft after diving
01 p0032 A70-10366

Anomalous temperature-time cooling data for surface material of Tycho, Copernicus and Aristarchus craters, suggesting relation to magnetic phase transitions during lunar nights
01 p0183 A70-10825

Mathematical theory of time domain statistical description of random signals in terms of probability theory
01 p0044 A70-11042

Time dependent behavior of separated and unseparated unsteady flow of incompressible viscous and inviscid fluids without heat transfer
01 p0067 A70-11162

Time course of end bulb material formation in vitro in rodent myelinated nerve fibers, confirming elastic capillary concept
02 p0233 A70-11725

Time dependence of contact zone radius of rigid sphere pressed against viscoelastic half space by normal force
02 p0384 A70-11738

Premature saturation in strongly magnetic systems explained by model with nonuniform magnon modes, applying time dependent Green functions
02 p0338 A70-11886

Forward scattering by nonergodic system of identical particles, relating temporal correlation function of scattered radiation and intensity moments
02 p0255 A70-11919

Viscoelastic boundary value problems involving time dependent boundary regions reduced to elastic problems, starting with aging viscoelastic body
02 p0388 A70-12269

Ammonia absorption band at 6450 A in Jovian atmosphere, clarifying controversial absorption time variations
02 p0375 A70-12428

Jovian atmosphere photometric activity determination, showing time variation and difference in strength between Northern and Southern Hemisphere
02 p0375 A70-12430

Threshold visibility of uniformly moving colored gratings, noting chromaticity discrimination dependence on spatial and temporal frequencies
02 p0237 A70-12460

Electromagnetic pulse scattering in time varying inhomogeneous medium, applying finite difference method to Maxwell equations
02 p0261 A70-12588

Neutron star atmospheric composition as function of time, including effects of diffusion, cooling and nucleosynthesis
02 p0378 A70-12698

Rigid plastic body of material insensitive to strain rate under time dependent surface tension and time independent body forces
02 p0391 A70-12816

Optical echoes using model of spins precessing in magnetic field, presenting time dependent theory of perturbation
02 p0341 A70-12830

Stefan heat conduction problem with time dependent first kind boundary conditions approximate solution, taking into account unsteady temperature field of solidifying liquid
03 p0604 A70-13210

Light alloys cold hardening effect and fatigue strength estimation, considering residual stress variability with time
03 p0587 A70-13239

O-C diagrams of RR Lyrae variables in M5, considering representation by parabolas or intersecting straight lines
03 p0567 A70-13321

Thermoelastic stresses in plate due to arbitrary temperature variations of heat transfer agent calculated in second approximation, allowing for transfer coefficient time dependence
03 p0590 A70-13400

Heat transfer under conditions of forced convection from flat plate in laminar flow, considering plate surface temperature arbitrary variation in time
03 p0605 A70-13518

Temporal and statistical characteristics of HF oscillations from electron beam interaction with plasma in magnetic field
03 p0532 A70-13524

Rotating prism method for obtaining time correlation between streak photographs and characteristic waveforms of flash X ray discharges
03 p0492 A70-13762

Recall and recognition memory in concept identification, discussing presentation time /PT/
03 p0424 A70-13767

Motion stability and time dependent deflections of thin flexible cylinder with zero bending rigidity in viscous stream
03 p0595 A70-13783

Readaption times of eyes adapted to darkness using night vision training device in relation to helicopter flight safety conditions
03 p0436 A70-13823

Time of establishment of steady state mixing in plane and axisymmetrical jets determined, using self similar motions in unsteady state boundary layer and free turbulence
03 p0409 A70-13875

Diurnal periodicity of physiological functions of flight crews flying through several time zones found to correspond to time zone of permanent residence
03 p0425 A70-13894

Evaporative weight losses by sweating in man exposed to warm environment as function of time, including graphical method for heat storage prediction
03 p0430 A70-14164

Muonic and hadronic component arrival time distribution in EAS measured under rock compared to Monte Carlo computation
03 p0562 A70-14187

Polyurethane rubber time- and temperature-dependent visco- and photoviscoelastic coefficients using two dimensional strain and stress wave propagation photoviscoelastic analysis
03 p0599 A70-14243

Dipole shielding tensor of atom in arbitrary time dependent field, giving conditions for general variational calculations yielding results
04 p0721 A70-14389

Niobium powder hot pressing compaction in terms of porous body volume viscous flow, determining viscosity shift time dependence
04 p0696 A70-14461

Natural vibrations damping of holonomic mechanical systems with feedbacks not explicit function of time reduced to optimal stabilization problem
04 p0718 A70-14494

Time transient and step-jump dynamic analyses of gas lubricated bearing, illustrating hybrid journal and Rayleigh-Step thrust bearings
[ASME PAPER 69-WA/LUB-5] 04 p0697 A70-14768

Transient temperature distribution in inhomogeneous material, using finite difference representation for temperature time derivative
[ASME PAPER 69-WA/HT-33] 04 p0782 A70-14807

Instantaneous heat transfer from oscillating wire in free convection in still air as function of time
[ASME PAPER 69-WA/HT-15] 04 p0783 A70-14819

Chapman-Ferraro two dimensional problem with neutral sheet, investigating magnetospheric flows and time dependence
04 p0679 A70-15109

Thermoplastic behavior of bodies under variable loads obtainable as function of time variable external temperature field

04 p0775 A70-15200

Intermediate aging influence on Bauschinger effect in low carbon steel at 270 C and 2 hr holding time

04 p0776 A70-15266

Time dependent transmission of carbon dioxide in air flowing through molecular sieve adsorber beds, developing and programming weighted least squares analysis

04 p0786 A70-15315

Aluminized composite solid propellants burning rates in acceleration fields noting time dependent increase

[AIAA PAPER 68-529]

04 p0709 A70-15581

Multiple time scaling analysis of reentry roll rate and angle of attack for missiles with center of gravity and aerodynamic trim asymmetries

04 p0764 A70-15597

Optically trapped filaments in liquid carbon disulfide by side illumination and crossed polarizers using glass laser, noting birefringence and duration time

04 p0703 A70-15619

Polycrystalline metals strength factors in aircraft and aerospace construction as relation between rupture time and embrittled grain boundary at high temperatures

04 p0779 A70-15671

Terminal states and time specifications influence on optimum control systems, using Pontryagin principle for boundary value problems application

05 p0824 A70-15874

Temporal behavior of NP 0532 in radio and optical bands compared for second derivative of period

05 p0906 A70-15893

Time dependent variation of first and second harmonics amplitudes of diurnal cosmic ray variations during SC magnetic storms

05 p0898 A70-15942

Frequency bandwidth reduction for geophysical data transmission from satellites or lunar stations by time correlation of signal and transmission channel band changes

05 p0847 A70-15968

Photoelastic and photorheological analysis of time-dependent variation of stress distribution in long strip compressed oppositely with elastic flat punches

05 p0928 A70-16012

Time dependent expansions into vacuum of monatomic gases with spherical symmetry, obtaining moments expressions for Maxwellian molecules

05 p0831 A70-16015

Diffusion rates in refractory metal alloys for thermionic emitters as function of time and temperature

[GA-9495]

05 p0892 A70-16075

Spatial and temporal relations between auroral emission at green line 5577 and cosmic noise absorption studied to determine energy spectra and particles distribution

05 p0907 A70-16281

Energy spectrum time dependence of solar cosmic ray event of 28 January 1967 measured in Northern Hemisphere, discussing particle diffusion and magnetic trap

05 p0902 A70-16459

Ocean surface roughness time variation effect on incident laser beam, analyzing motion picture data by computer program

05 p0860 A70-16687

Maraging steel mechanical properties as function of aging temperature and time

05 p0865 A70-16873

Time-varying loads effect on linear elastically hereditary media described by generalized fractional-order exponential functions and Rzhansyn type viscoelastic kernels

05 p0946 A70-16954

Rapid fine structure in hard solar X ray bursts observed by OSO-5, explaining time structure by mechanism based on repetitive production of monoenergetic electrons

05 p0904 A70-16980

Orbital rendezvous for inspection, rescue, etc, discussing launch bases number, warning time and alert status effect on reaction time

06 p1027 A70-17173

Viscoelastic fluid flow through circular tube under time dependent pressure gradient superposed on steady Poiseuille flow

06 p1032 A70-17200

Accumulated dose and dose rate during Gemini 4 and 6 flights measured as function of elapsed time and position within spacecraft

06 p0990 A70-17270

Time of useful function (TUF) determination for human exposure to toxic gas combinations due to fire

06 p1000 A70-17294

Microwave frequency radar terrain echoes simulation concerning variation of echo delay, Doppler shift, random fine structure and time variation

06 p1008 A70-17482

Electron recombination in inert gases at various pressures, studying electron density decrease in time by UHF and optical methods

06 p1109 A70-17495

Corpuscular radiation as F region ionization source, solving time dependent ionospheric continuity equation

06 p1054 A70-17588

Finite elements of time dependent phenomena using Hamilton variational principle for time integration

06 p1165 A70-17645

Time characteristics of pulsed calcium fluoride-dysprosium laser in single mode, observing constant emission and peak regime

06 p1082 A70-17808

Solar radio bursts time-variable structure at 12 M wavelength recorded on Ediswan pen oscillograph

06 p1144 A70-18005

Time dependent transport equations for full Reynolds stress tensor and turbulence decay function using flux approximations and relaxation model

[AIAA PAPER 70-3]

06 p1038 A70-18080

Temperature and pressure effects as function of time in spectral and total normal emittance of metal coated refractory metals

[AIAA PAPER 70-68]

06 p1092 A70-18136

Finite difference solution of time dependent Navier-Stokes equations for two and three dimensional laminar incompressible flow, discussing results for flat plates

[AIAA PAPER 70-46]

06 p1041 A70-18170

Time dependent inviscid gas flow on infinite domain computed by finite difference method

[AIAA PAPER 70-45]

06 p1042 A70-18188

Isentropic model for time behavior of steady spherical source expanding into arbitrary ambient gas

[AIAA PAPER 70-232]

06 p1042 A70-18215

Microsecond-response bolometer for measuring thermal fluxes as function of time in high explosion driven shock tubes and plasma jets

06 p1070 A70-18445

Brazing time and temperature effect on depth of Ag based brazing alloys penetration into thin Ti-Al-V sheet substituted by microprobe analysis

06 p1078 A70-18513

Local time dependence of geomagnetic cut-offs for solar protons in 0.52-4.0 Mev range from satellite observations

06 p1136 A70-18529

Magnetic activity effect on magnetospheric plasmopause position, measuring ion concentrations as function of local time fromOGO 5 observations

06 p1058 A70-18530

Temporal behavior of energetic particle precipitation during auroral substorm, discussing electron energy spectra and pitch angle distributions

06 p1059 A70-18536

Optimal guaranteeing control for single switching representable in form of two different successive stages in time, ensuring invariance with respect to motion perturbations

07 p1332 A70-18664

Laminar boundary layer development on cylindrical body set in motion from state of rest, determining time for boundary layer separation occurrence

07 p1253 A70-18771

Stainless steels case hardening in hydrogen, nitrogen, propane and butane mixture, showing temperature and process duration effects

07 p1291 A70-18831

Integral method for time development of viscous, heat and mass conducting layer over leading edge of volatile drop instantaneously immersed in gas stream

07 p1358 A70-18916

Time dependent stability of viscous rotational Couette flow induced by impulsively started rotating inner cylinder, using dye injection and motion pictures

07 p1255 A70-19209

Circular plates dynamic response to axisymmetric time dependent loads, analyzing transverse restraint effects on response maxima by plate theory

07 p1404 A70-19251

Digital data transmission over discrete time Gaussian channel with noisy feedback, investigating error-exponent/reliability/ and finite SNR

07 p1235 A70-19362

Electrolyte purity effect on initiation times and growth rate of Zn dendrites in alkaline zincate solution, discussing dendrite initiation retardation

07 p1356 A70-19387

Horizontal ionospheric drift over Northern Hemisphere during low solar activity, studying spatiotemporal distribution patterns of drift parameters

07 p1266 A70-19438

Magnetic field filtration into time-variable and constant parts, using signal to noise analogies

07 p1266 A70-19440

Hypokinesia effects on cellular and humoral indices of antibody formation in rats, noting exposure time role

07 p1208 A70-19509

Opening distance and inflation time prediction for parachutes deployed supersonically based on subsonic performance

07 p1394 A70-19725

Visual backward masking facilitation dependence on target duration as opposed to interstimulus interval or target-onset/mask-onset interval durations

07 p1221 A70-19850

Human physiological responses to lower body negative pressure (LBNP), studying presence or absence of change for orthostatic tolerance as function of time

07 p1222 A70-19933

Thermal explosion criterion for explosion/ignition delay of exothermic material surrounding heated wire as function of time

07 p1424 A70-20005

Magnetospheric plasmopause-high latitude electron density trough relations using satellite topside ionograms, noting local time and magnetic disturbance effects

07 p1270 A70-20074

Time variations of reflectance measured for carbon dioxide laser beam splitters

07 p1302 A70-20095

Time block pooling of atmospheric noise data, basing randomness conclusion on observations correlation

07 p1236 A70-20161

Unsteady flow behind circular cylinder by flow visualization, determining vortices length variations with time at various Reynolds numbers and dimensionless accelerations

07 p1261 A70-20236

Time dependent matrix elements for multistate impact-parameter calculations for atom-atom inelastic cross sections

07 p1346 A70-20242

Spatial and temporal cosmic plasma variations over various energy and wavelength ranges using cosmophysical and aeronautical facility

07 p1372 A70-20339

Solar corpuscular fluxes directional distribution time dependent changes effect on lower ionospheric electron production rates

07 p1373 A70-20344

Solid state lasers thermal resonator buckling time dependence and compensation, graphing results of resonator field analysis

07 p1303 A70-20359

Time dependent electrostatic probe theory relating measurements to internal properties of plasma, calculating free stream ion density from collected electric charge

07 p1289 A70-20466

Stability criteria for systems of nonlinear stochastic differential equations on finite time interval, considering stable motion of physical processes

08 p1533 A70-20488

Stability in systems finite over given time interval under permanent perturbations bounded in mean

08 p1543 A70-20490

Matrix method for converting time variable stress vector into strain vector allowing for linear creep and aging

08 p1583 A70-20531

Integral equation for time development of harmonic oscillations in finite one dimensional chain of elastically coupled discrete elements, using Bessel functions for solution

08 p1547 A70-20535

Tunable Q switched pulsed discharge carbon dioxide laser intensity dependence on time delay investigated for various vibrational/rotational lines and gas mixtures

08 p1512 A70-20618

Visual tracking of horizontally moving object, noting acuity dependence on target angular velocity and observation time

08 p1444 A70-20745

Time requirement determined for visual acuity restoration after illumination with short duration bright light flash

08 p1450 A70-20746

Optimal control systems design involving time delays as functions of time and system state, considering stability constraints

08 p1478 A70-20779

Organic adhesives preparation and application to metal surface for bonding, examining time, pressure and temperature effects on curing

08 p1503 A70-20881

Metal adhesive joints behavior under prolonged static stresses, showing time dependence of tensile strength

08 p1504 A70-20887

Steel structure and mechanical properties under preliminary loading at elevated temperature and liquid Li at various exposure times

08 p1515 A70-20935

Temperature fields creation in infinite or finite regions by moving surfaces with given time dependence of temperature studied by subjecting diffusion equation to transformations

08 p1597 A70-20959

Horizontal turbulent diffusion model of cloud, determining particles dispersion as function of time

08 p1538 A70-21111

- Mutual thermal influence zone between parts of die casting during solidification established as function of time
08 p1506 A70-21138
- Nickel boronizing in high temperature vacuum, studying mechanical properties and layer thickness time dependence
08 p1517 A70-21148
- Fiberglass reinforced plastics creep behavior under axial compression, studying time dependence of elasticity modulus and Poisson coefficient
08 p1526 A70-21174
- Gamma radiation effects on emission time, excitation threshold and efficiency of four level Nd glass laser under multimode operation
08 p1512 A70-21209
- Solar microwave bursts with double structure, discussing single frequency observations and flare patrols, time variations of flux density and brightness
08 p1561 A70-21259
- Fluidic air gauge back pressure signal frequency response as function of time
[ASME PAPER 68-WA/FE-16] 08 p1441 A70-21316
- Einstein gravitational equations general solution having physical singularity with respect to time
08 p1546 A70-21424
- Dynamic response of joined elastic quarter spaces of solids to time varying free surface shear tractions parallel to plane of juncture
[ASME PAPER 69-APMW-16] 08 p1591 A70-21467
- Aluminum-base reinforced material synthesis by liquid impregnation, investigating transition layer dependence on holding time and fiber/matrix microhardness
08 p1520 A70-21500
- Transient thermal stresses in plates with distributed heat source and heat exchange with arbitrary time dependent surroundings
08 p1593 A70-21623
- Phase variable canonical form for time varying multivariable systems requiring less computational effort
08 p1463 A70-21645
- Thunderstorms lightning flashes time distribution recorded visually and on radar screens, discussing statistical variations in sigma
08 p1539 A70-21648
- Time course of changes in rat brain norepinephrine levels after olfactory bulb lesions, discussing automatic and biological mechanisms
08 p1448 A70-21841
- Fluids equilibrium stability within medium at constant temperature and pressure, discussing time behavior of thermodynamic processes
09 p1786 A70-22062
- Longitude and latitude dependence of pc geomagnetic micropulsations related to local time, using analog spectral analysis
09 p1666 A70-22064
- Perseids time distribution, based on observations during meteor showers, contradicting appearance of homogeneous Poisson process
09 p1750 A70-22099
- Single-pulse laser radiation losses dependence on operation time length due to angular dispersion
09 p1694 A70-22140
- Time resolved photoelectric light detection, discussing photoelectric emission probability time dependence and radiation interaction with bound charge
09 p1726 A70-22232
- Automated crop surveys from integrating observations made at different times /time dimensioning/ during growing season, noting earth resources satellites role
09 p1666 A70-22263
- LC circuit with time dependent resistance containing wire explosion physics, solving differential equation of discharge circuit
09 p1726 A70-22492
- Amino acid metabolism time dependent variations, studying tyrosine transaminase rhythm in rat liver
09 p1618 A70-22525
- Linear one degree of freedom mechanical system loaded by time dependent force with constraints on loading/unloading rate, studying minimum of dynamic coefficient
09 p1727 A70-22536
- Strain rate and hold time effects on steels low cycle fatigue behavior, graphing various correlations among stress amplitude, time to fracture, etc
09 p1774 A70-22589
- Movement information from space-temporal integration in binocular-kinetic space perception of time varying optical inputs
09 p1618 A70-22672
- Time, temperature and composition dependent regularities in Ni-Al and Ni-Nb alloys oxidation processes, discussing Oxygen ion migration and Ni ion diffusion
09 p1704 A70-22752
- One dimensional discrete time nonlinear filters synthesis using Bayes theorem and digital techniques
09 p1654 A70-22934
- Layered conical shell creep under axisymmetric load and time dependent temperature field by iterating boundary integral equation
09 p1779 A70-23099
- Thermal cyclic loads effects on heat resistant materials strength during strain hardening, considering role of time factors in durability
09 p1779 A70-23104
- Stress concentration at circular hole in plate, considering material creep and aging effects
09 p1782 A70-23290
- Satellite observational data on time history of inner radiation belt /October 1963-December 1968/
09 p1746 A70-23488
- Time-temperature charts for one dimensional unsteady conduction with uniform internal heat generation
09 p1791 A70-23567
- Shock wave initiated two dimensional time dependent ducted flows in nonuniform regions using fluid-in-cell method, discussing density, pressure and energy distributions
09 p1665 A70-23740
- Airglow hydroxyl emissions diurnal variations as function of height, using digital computer for time dependent solution of equations for oxygen-hydrogen atmosphere
10 p1872 A70-23826
- Heat conduction analysis for plane body with boundary condition and time variable heat exchange coefficient, applying automatic control technique
10 p1966 A70-23869
- Time variations in human spectral response, considering sequential gain and phase estimates formation by Gabor elementary signals theory
10 p1823 A70-23895
- Laser beam interaction with metals on basis of energy balance measurements, obtaining time dependent radiation reflectance
10 p1898 A70-23982
- Epoxy glass fiber composites pyrolyzates IR spectra as function of time, observing changes in fingerprint region
10 p1828 A70-24065
- Finite difference methods stability for time dependent Navier-Stokes equations coupled to energy equation with quadratic terms in velocity gradients
10 p1866 A70-24106
- Newtonian gravitational system of three point masses with oscillatory motion at time t approaching infinity, discussing particles mutual distance
10 p1938 A70-24182
- Heat resistant materials strength characteristics with long service periods, formulating equation for time dependence of rupture resistance
10 p1903 A70-24237
- Test results extrapolation for heat resistant alloys long time strength using exponential relation between time to rupture and value for initial stress decrease
10 p1903 A70-24240
- Digital controlled phase-locked loop in burst mode operation, comparing recovery characteristics with carrier and bit-timing recovery techniques based on statistical analysis
10 p1835 A70-24704
- Reaction time dependence on sound signal probability determined by temporal structure of signal presentation
10 p1818 A70-24713
- Siderial time variations in cosmic ray intensity observed by inclined muon telescopes
10 p1933 A70-24858
- Time dependent radiative transfer equation for plane-parallel isotropic scattering medium in first Gaussian approximation
10 p1933 A70-24986
- Slowly varying parameters as engineering problem in nonlinear lumped systems
10 p1856 A70-25239
- Pi2-type pulsations in and near auroral zone observed for amplitude variation dependence on geomagnetic latitude and local time
10 p1885 A70-25280
- Time dependence of shock wave attenuation at multiple reflection in shock tube after diaphragm burst, using damped vibration solution
11 p2034 A70-25495
- Time dependent analysis for quasi one dimensional, vibrational and chemical nonequilibrium nozzle flows approaching steady state solution by finite difference technique
11 p1976 A70-25974
- Hypokinesia effects on cellular and humoral indices of antibody formation in rats, noting exposure time role
11 p1988 A70-26108
- Linear time-varying control process with bounded control amplitudes and rates, deriving conditions for recoverability
11 p2028 A70-26314
- Resistance bridge balancing by time method for dynamic digital measurements
11 p2054 A70-26433
- Multipoint time correlations of longitudinal velocity fluctuations in grid-generated turbulence
11 p2039 A70-26532
- Effusion steady state pressures time dependence of carbon monoxide and calcium vapors generated during calcium oxide-graphite interaction
11 p1995 A70-26602
- Elastic wedge under spatially uniform but time dependent shear tractions, studying shear stress and transient wave propagation
11 p2142 A70-26629
- Transient analysis of stress waves around cracks under antiplane strain with time dependent loadings based on integral transforms
11 p2145 A70-26698
- Cotton leaf light reflectance and transmittance changes with maturity
12 p2218 A70-26919
- Decimeter radio sources flux density time variations, discussing possible causes and radio emission spectra
12 p2299 A70-27308
- Nonlinear time-varying multivariable adaptive control system design using signal synthesis technique
12 p2203 A70-27415
- Spatial-temporal distribution of meteorological elements allowing for effects of underlying surface
12 p2263 A70-27511
- Spatial-temporal distribution of wind swell HF components measured by two dimensional antenna array fed by DC signals
12 p2263 A70-27516
- Time or space decay of turbulent parameters along flow direction in jets, wakes or grid-generated turbulence, illustrating time variation of wave number spectrum
12 p2211 A70-27831
- Current sheet speed in coaxial plasma accelerator computed as function of time, comparing results with velocity measurements
12 p2281 A70-27833
- Wave propagation in spatially homogeneous time varying dispersive media, emphasizing excitation and source dependent phenomenon
12 p2188 A70-27961
- Thin cylindrical DC pulse driven antenna radiation fields time variation as function of angle
12 p2198 A70-27964
- Soft electron fluxes spatial distribution and temporal variations in magnetosphere based on Elektron 2 charged particle trap data
12 p2295 A70-28259
- Mixed boundary value problems involving time dependent boundary regions for penny-shaped crack in viscoelastic materials with one relaxation function
12 p2508 A70-28489
- Time comparative low energy proton measurements in inner radiation belt by Rubis rocket with detector telescopes and omnidirectional counters
13 p2475 A70-28572
- Book on linear time varying systems analysis and synthesis covering multivariable systems, operational algebra, controllability, observability, canonical structures, minimal realization, etc
13 p2381 A70-28975
- Stable auroral red /SAR/ arc alignment-movement relationship, suggesting dominant local time control
13 p2397 A70-29193
- Low energy solar flare electrons scatter-free propagation through interplanetary medium, considering rise, decay and travel times
13 p2477 A70-29194
- Versamid cured epoxies time-dependent mechanical properties, determining loading mode, strain level and reinforcing agent effects on time-temperature shift factors
13 p2438 A70-29205
- Free convection flow and heat transfer from semi-infinite horizontal flat plate with time-oscillating temperature, using successive approximations process
13 p2522 A70-29537
- Residence times distribution in confined round swirling jet, considering mass conservation of hypothetical tracer substance in combustion efficiency prediction
[WSCI PAPER 70-7] 13 p2522 A70-29609
- Magnetotail plasma sheet temporal variations during substorms and plasma pressure as related to dynamic pressure of solar wind from Vela satellites observation
13 p2480 A70-30061
- Solar wind parameters time variations influence on geomagnetic activity from measurements by electrostatic analyzers on Vela satellites
13 p2481 A70-30065
- Radial diffusion role in radiation belt dynamics from flux profiles time variations observations or equilibrium states analysis
13 p2484 A70-30094
- Fog droplet size growth time dependence and spectral variations during simulated cloud formation by water vapor condensation in chamber
14 p2601 A70-30128

Stefan-Boltzmann formula validity for flames and combustion products radiation affected by time dependence of emissivity coefficient, place and wavelength 14 p2662 A70-30179

Meteoroid radio reflections time variation based on observations at two frequencies, analyzing angular dimensions in reflecting regions 14 p2635 A70-30315

Meteor radio reflections time-amplitude characteristics, discussing dependence on mirror point position in trail, wavelength, diffusion factor and initial radius 14 p2636 A70-30324

Switching initiation in Ovonic, discussing temperature profile in semiconducting sandwiches as function of time and thermally forced double tunneling 14 p2626 A70-30333

GaAs junction lasers output oscillations, analyzing time dependent equations for low temperatures 14 p2593 A70-30335

Surface wind speed durations statistical analysis, discussing meteorological, orographic and physiographic features 14 p2607 A70-30582

Time dependent simultaneous solution for continuity, heat conduction and motion equations of system involving neutral, electron and ion gases 14 p2665 A70-30744

People as conservative processors of fallible information, treating stationary data generating process as nonstationary 14 p2537 A70-30898

Night airglow space and time variations from jet aircraft observations, measuring conjugate enhancements 14 p2580 A70-31266

Optimal control theory for system model dependence on state and control variables history 14 p2562 A70-31410

Thermoplastics fatigue strength, considering stress variations with time in constant strain tests 14 p2598 A70-31425

Temporal dependence of photoelectron multiplier output waveform and focusing under photocathode alternating modulation, noting thresholds for optical reception 15 p2696 A70-31505

Magnetospheric protons and electron energy spectra time and magnetic activity dependence during solar maximum 15 p2792 A70-31671

Ionospheric currents time-space distribution noting rocket data, induction mechanism and geophysical effects 15 p2730 A70-32087

Spherical shaped rotor unbalance effect on electrostatic gyroscope runout time, discussing energy dissipation 15 p2738 A70-32152

Inertial load-time effects in instrumented impact tests, showing corrections for bending stress and dynamic fracture toughness measurements 15 p2820 A70-32240

Wolf numbers Zurich time series monthly values, evaluating mathematical expectation with probability smoothing by Whittaker operator 15 p2802 A70-32489

Geomagnetic disturbances temporal behavior and spatial scales 15 p2732 A70-32543

Linear time varying low pass filters computer aided design, introducing quadratic performance criterion to calculate steepest descent in function space 15 p2710 A70-32588

System failure rate estimation as function of age using incomplete field reliability data 15 p2748 A70-32660

Spherical liquid drop deformation time dependence in unbound fluid at low Reynolds number, investigating effects of temperature, pressure, velocity and size 15 p2722 A70-32795

Ruby laser spatial and temporal characteristics improvement with bleachable dye filter, using local negative feedback 15 p2754 A70-32865

Human and animal adaptation and responses to time intervals and temporal activity cycles, discussing conditioned reflexes in terms of physiological factors 15 p2687 A70-32869

Classical and modern approaches to tracking problem, discussing optimal control in frequency domain and time domain terms 16 p2882 A70-33039

Fluid urethane laminating resin for bonding nylon and glass fabrics, giving physical properties as function of room temperature curing time 16 p2938 A70-33381

Time ordered system for air traffic control providing data link, collision avoidance and navigation data through single channel 16 p2948 A70-33476

Time frequency concept application to air traffic control and collision avoidance systems 16 p2948 A70-33477

Transonic flow in convergent and convergent-divergent conical nozzles with nonuniform inlet predicted by time dependent flow equations, discussing discharge and thrust coefficients 16 p2834 A70-33548 [AIAA PAPER 70-635]

Invariant imbedding application to solution of partial differential equations by continuous-space discrete-time /CSDT/ method, discussing time dependent heat diffusion 16 p2942 A70-33735

Elastoviscoplastic medium filled half space motion under pressure front moving along surface with time varying velocity, analyzing penetrating wave fronts form 16 p2990 A70-33780

Turbulence spectrum functions time variations, examining electron density fluctuations in ionized gas 16 p2894 A70-33886

Cosmic time varying gravitational constant effects on stellar age determination 16 p2978 A70-33966

Doppler shifted radiation production, using time and space dependent radiant energy sources 16 p2952 A70-34255

Ti alloys embrittlement, investigating time temperature dependence of brittle subsurface layer formation during elevated temperature air exposure 17 p3112 A70-34365

Time dependent solution for inviscid hypersonic flow of chemically reacting gas mixture about blunt bodies 17 p3009 A70-34502 [AIAA PAPER 70-771]

Systems subject to failure and repair cycles, describing performance and reliability by stochastic processes in terms of excess time 17 p3099 A70-34580

Crab Nebula pulsar NP 0532, describing quasiperiodic oscillation in arrival times of radio pulses 17 p3157 A70-34842

Pulsars as cosmic ray sources, emphasizing time properties of acceleration mechanisms 17 p3151 A70-34913

Time span in total electron content /TEC/ measurements on BE-B and BE-C ionospheric satellites by differential Doppler method, applying chi sub O super 2 test 17 p3077 A70-34986

Time dependent characteristics of dense argon plasma formed by pulsed lasers, measuring shock wave front velocity with streak camera 17 p3104 A70-35083

Shakedown theory of elastic-plastic structures under time dependent loadings 17 p3188 A70-35191

Iterative algorithm for free terminal time control in trajectory optimization 17 p3168 A70-35290

Chamber solution of Boltzmann time dependent equation in relaxation time approximation 17 p3136 A70-35596

Harmonic oscillator with exponentially decreasing spring constant, obtaining closed form solution for equation of motion 17 p3137 A70-35602

Exposure duration effect on luminance requirements for hue perception and identification 17 p3040 A70-35724

Carbide precipitation and grain boundary migration in solution annealed duplex stainless steel as function of aging time 18 p3274 A70-36050

Regular and stochastic oscillations in plasma beam discharge produced by beam instability from observing time dependent variations in spectral line luminescence intensities 18 p3294 A70-36147

Reciprocity law between radiation intensity and exposure time for photographic films in vacuum UV spectrum region, investigating departure at various wavelengths 18 p3257 A70-36281

Two dimensional time dependent solution for impulsive motion of circular cylinder involving viscous cross flow at moderate angles of attack 18 p3207 A70-36454

Time dependence of laser rod focal length, measuring thermal lensing effects 18 p3270 A70-36756

Horizontal ionospheric drift over Northern Hemisphere during low solar activity, studying spatiotemporal distribution patterns of drift parameters 18 p3249 A70-36912

Magnetic field filtration into time-variable and constant parts, using signal to noise analogies 18 p3249 A70-36914

Time and altitude dependences between 340-1000 km of delta parameter for height scale ratio of neutral and electron-ion gases, discussing diffusion coefficient 18 p3254 A70-37030

Power and exponential time dependences of long term creep strength for wide stress range, assuming linear heat resistance 19 p3449 A70-37340

Auroral substorm temporal relationship to particle kinetic energy increases within trapping region, observing geomagnetic field distortions at higher latitudes during disturbed epochs 19 p3411 A70-37494

Proton spectra and time history in interplanetary space during solar flare by satellite observation, investigating particle flux by shock waves 19 p3495 A70-37503

Time transient and step-jump dynamic analyses of gas lubricated bearing, illustrating hybrid journal and Rayleigh-Step thrust bearings 19 p3436 A70-37619 [ASME PAPER 69-WA/LUB-5]

Linear time varying systems optimal control through decoupling of boundary value problems 19 p3393 A70-37866

Rossby wave critical level time dependent behavior on latitudinally varying flow 19 p3414 A70-38259

Heat transfer in boiling liquid from temperature field and temporal changes in liquid above heating surface, determining isotherms by laser interferometry 19 p3447 A70-38455

Light alloys cold hardening effect and fatigue strength estimation, considering residual stress variability with time 19 p3548 A70-38457

Multi-aircraft flight test program time compression by management techniques, discussing program length and costs 19 p3355 A70-38530

Sound level vs duration evaluated for noise exposure using different exchange rates 20 p3578 A70-39125 [ASA PAPER FF2]

High energy radiation belt proton flux time dependence at low altitudes, examining atmospheric density influence 20 p3620 A70-39340

Butterfly diagram showing time dependent distribution of sunspots across heliographic latitudes 20 p3704 A70-39473

Geometrical figure fragmentation produced by intermittent illumination, examining dependence on presentation frequency and temporal factors 20 p3580 A70-39491

Cost and time optimization for complex aircraft development projects via network planning 20 p3740 A70-39644

Convergent-divergent nonequilibrium nozzle flow numerical solution by time dependent technique, investigating rapid vibrational nonequilibrium supersonic expansion of gas mixture with population inversion 20 p3609 A70-39655

Temporal and spectra combination effects on aircraft sound judged noisiness, using human subjects in anechoic chamber 20 p3580 A70-39712

Invariance conditions for control systems with time varying parameters 20 p3602 A70-39827

Fatigue phenomena based on solid body model, establishing breaking stress dependence on time or load cycles number 20 p3724 A70-39854

Cosmic hard X ray sources spectra and time variations by balloons and OSO-3 satellite observations of Crab Nebula 21 p3872 A70-40657

Thermo-electret surface charge and dielectric constant time variation measurements, considering hole-electron pairs production hypothesis 21 p3797 A70-40890

Universal time control of south polar F layer during IGY attributed to low energy electron precipitation, comparing IGY and recent satellite data 21 p3818 A70-41101

Time dependent adhesion in ultrahigh vacuum of Apollo 11 lunar soil sample 10065-33, considering microchemical and microphysical properties 21 p3915 A70-41658

Time average holographic interferometry of circular plate vibrating simultaneously in rationally related modes 21 p3829 A70-41927

Excited state complexes laser action in coumarin dyes indicated from stimulated fluorescence time dependence 22 p4048 A70-42328

Random ergodic process extremal behavior, determining mean time to reach maximum or minimum for first time 22 p3985 A70-42400

Dynamical linear thermoelasticity theorem generalization with time dependent conductivities, elasticities and density 22 p4112 A70-42483

Time dependent shock wave structure, considering shock tube flow as initial and boundary value problem 22 p4009 A70-42516

Air-earth current density time variation in stratosphere by high altitude balloon, comparing with potential gradient diurnal variation over ocean 22 p4017 A70-42798

Heart rate-time curves before, during and after step-up exercise in relation to physical fitness

22 p3978 A70-42873

Output coordinates probability distribution density of nonlinear automatic control systems at fixed time, using multiple integrals

22 p4003 A70-42888

Glass-epoxy composites, measuring embedding filaments effect on time-temperature relationship under ultimate stress conditions

22 p4118 A70-43549

Laminated composites time dependent static strength and reliability under uniaxial tension

22 p4119 A70-43678

Polarization of short period oscillations Pc2-Pc4 dependence on time of day, oscillation type and geoelectromagnetic field activity

23 p4190 A70-44086

Time dependent visual perception probability under prolonged testing at eccentricities, using observer exposed to flashed stimulus with dark-adapted retina

23 p4147 A70-44782

Optimal timing for aerial photographic mapping of landscape types including tundra, forest, steppe, meadow, desert and mountain areas

24 p4328 A70-45196

Amplification factor time dependence of dye lasing under rectangular pumping pulse, noting threshold conditions and burnout time relation to material parameters and resonator

24 p4352 A70-45473

Time dependent inviscid transonic flow past two dimensional and axisymmetric bodies, presenting numerical procedures including imbedded shock waves as discontinuities

[AIAA PAPER 70-1322] 24 p4288 A70-45943

Elastic-viscoplastic bar quasi-static torsion problem, using approximate method for time dependent torsion function

24 p4425 A70-45993

Time evolution of instantaneous light intensity mean and variance for Q switched single mode laser near oscillation threshold

24 p4355 A70-46090

Pulsars radio evolution mechanism by phenomenological analysis, deriving time dependences of period, luminosity and emitting region size

24 p4412 A70-46101

Modified time-domain reflectometer method for waveguide system evaluation, detecting and displaying radar echoes as function of time

24 p4315 A70-46234

TIME DISCRIMINATION

Time sense in human subjects kept in caisson or cave isolation determined as function of upper brain stem paraconsciousness

01 p0041 A70-11474

Book on sense of time covering psychological and physiological aspects and electrophysiological experimental results in man

05 p0800 A70-16129

Vibrotactile display operational skill acquisition, discussing stimuli quality and spacing effects on limer of temporal ordering of sensory events in haptic space

13 p2354 A70-29596

Optimal temporal and spatial-temporal resolution for unknown parameter of interfering signal on white noise background

17 p3048 A70-35680

TIME DIVISION MULTIPLEXING

PCM time division satellite multiple access communication system to increase time slot utility, considering individual earth station control and common signaling circuit features

06 p1011 A70-18409

Acquisition system design and experimental results for time division multiple access satellite communication system

06 p1011 A70-18410

Clock synchronization system design and test results for PCM time division multiple access satellite communication system

06 p1011 A70-18411

Multiple access channel control system operating in variable destination multiple access mode for application in PCM-TDMA satellite communication system

06 p1011 A70-18412

PCM-TDMA satellite communication system for maximum time slot utility without guard time slots

10 p1834 A70-24330

TDMA system burst synchronizer with periodic channel slots reallocation feature

10 p1835 A70-24331

Multichannel PCM/TDMA INTELSAT network with time preassignment and time assignment speech interpolation features for field test

10 p1835 A70-24332

Carrier recovery circuits synchronization for PSK demodulators used in TDMA satellite communication

10 p1835 A70-24338

Equipment design for burst synchronization control in TDMA experiment system

10 p1836 A70-24339

Independent burst and burst coherent TDMA methods compared for ground station-satellite communication

10 p1836 A70-24340

Demand assignment techniques applicability to TDMA satellite communication systems, discussing operational modes and optimum mode selection

10 p1837 A70-24351

PCM-TDMA satellite communication systems operation modes and applicability, considering efficient circuit utility, equipment cost and control complexity

10 p1837 A70-24352

Time division multiple access /TDMA/ system for Symphonie communication satellite using PCM phase shift keyed RF carrier

10 p1837 A70-24353

Integrated TDMA switching/transmission system implementation into existing network

10 p1837 A70-24354

FDMA and TDMA systems for demand assignment of satellite circuits noting PCM/TDM operation trends in satellite and ground communications

10 p1838 A70-24355

Adaptive multiple access satellite communication system at millimeter wavelengths in time- and frequency-division modes, compensating rainfall attenuation

10 p1838 A70-24358

TDMA demand-assigned satellite communication system developed for INTELSAT, discussing PCM, voice signals and channels, etc

10 p1839 A70-24362

Intermeshed TDMA systems efficiency in interconnecting ground stations in communications satellite systems, discussing rigid and variable burst lengths

10 p1839 A70-24363

TDMA system control, considering access process control and switching process control, discussing burst transmission phase control and channel selection at receiving end

10 p1839 A70-24366

Bit clock synchronous system for communications satellites TDMA

10 p1839 A70-24368

Time allocation with sampling interpolation /ATIC/ for TDMA satellite telephone communications, considering auxiliary circuits, transmission quality, bit rates, demand assignment, etc

10 p1840 A70-24370

TDMA communication satellite system compared favorably with FDMA or CDMA systems in efficiency, flexibility and feasibility for commercial and military uses

10 p1842 A70-24884

TDMA applicability to military satellites, describing synchronization process

12 p2187 A70-27916

Injection lasers as logic elements in optical communication systems with time division multiplexing, examining optimal switching and pulse duration reduction

13 p2428 A70-29406

Differential time division multiplexing system, discussing errors due to imperfections of field effect transistor as multiplexer switch

19 p3388 A70-37906

TIME FUNCTIONS

Stationary Gaussian stochastic processes sample functions properties and local times

02 p0324 A70-12504

Positive time-periodic solutions to parabolic problems with Stefan-Boltzmann boundary conditions using straight lines method

07 p1333 A70-18748

Distributional results pertaining to complex Wishart processes and time varying spectral estimators on null hypothesis of stationary Gaussian time series

07 p1323 A70-19028

Random process noncommutative transformations and correlation functions in linear form of time functions

09 p1655 A70-23695

Time-convergent approximations to statistical turbulence functions constructed starting with functions expansion as Taylor series in time

11 p2074 A70-26534

Maximum impact force and central deflection time function of transversely struck beam, assuming no reflected elastic wave effects on stresses

12 p2325 A70-27619

Computerized Monte Carlo prediction of maintenance time distribution of complex system, concerning man hours, elapsed time and schedule meeting

13 p2524 A70-29566

Electron camera with two stage image intensifier control electrode tube for rapidly evolving and slightly luminous phenomena, discussing exposure times

14 p2590 A70-31406

Forcing time functions prediction for structures under shock tube test, relating aerodynamic parameters to mechanics terminology

17 p3060 A70-35180

Time correlation functions approach to calculation of properties of nonequilibrium ensembles in fluid molecular motions

17 p3197 A70-35535

Transient system decay characteristics, discussing equilibrium point damping time for asymptotically stable systems of ordinary differential equations

19 p3542 A70-38066

Sequential Bayes procedure for demonstrating mean time to failure beyond minimum acceptable value

20 p3658 A70-39642

Be star rotation dynamics phenomenon, discussing time variations on main sequence scale

23 p4252 A70-44828

TIME LAG

Upper atmosphere temperature lag behind solar decimeter flux 27 day variation maximum attributed to varying solar EUV heating

01 p0070 A70-10404

Delay times elimination in pulse operated X band Gunn effect oscillators, using RF power injection

01 p0050 A70-10463

Analog time delay device for returning respiratory flow signal to correct time

01 p0035 A70-10654

Computer applications in French missile testing center, describing real and delayed time equipment and computations

01 p0057 A70-10798

Autonomous functional differential equations with finite time lag using Liapunov functionals, discussing stability and instability

01 p0132 A70-11070

Pc 1 range geomagnetic pulsation sweepers /MHD waves/ event in evening sector, considering delay time between sweepers appearance and polar magnetic substorms onset

02 p0290 A70-12121

Time lag of commencement of PCA effect behind occurrence of Y-shaped phase of solar flares, tabulating data for several flares and particle effects

02 p0358 A70-12373

Correlations between organizational factors and individual engineer performance, analyzing stability of relationships and time lags in measurement

02 p0246 A70-12378

Propagation velocity relation with time delay in human visual system, using various sets of line stimuli having different spatial distance

02 p0237 A70-12457

Envelope delay and amplitude characteristics measurement of modulated carrier wave channel in radio relay link

02 p0258 A70-12475

Total electron content /TEC/, time delay and polarization errors on one way path through ionosphere, discussing measurements and predictions

02 p0293 A70-12568

Soviet book on oscillations of quasi-linear time lag systems, emphasizing asymptotic methods in nonlinear oscillation theory

02 p0340 A70-12826

Flexible lifting vehicles longitudinal stability with tandem lifting surfaces, studying aerodynamic time delay effects by root locus technique

03 p0408 A70-13802

Group delay characteristics of C band nondegenerative parametric amplifier determined by Nyquist method and compared to phase frequency derivative measurement

03 p0458 A70-14037

Resonance oscillations onset by initial conditions in dynamic system described by hyperbolic equation containing independent time lag variable

04 p0718 A70-14485

Electron radiation-induced second breakdown in transistors indicated by time delay and failure by collector-to-emitter short

04 p0657 A70-14734

Delay characteristics of narrow band double bridge amplifier used as inertial component of photoelectric star transit recorder

04 p0693 A70-15489

Time delay between ocular movement and retinal input by yoking visual target to eye movement using real time computer systems

05 p0805 A70-16094

Delay in photoelectric recording of transit of stars, considering stellar image brightness distribution and temperature

05 p0918 A70-16920

Microwave frequency radar terrain echoes simulation concerning variation of echo delay, Doppler shift, random fine structure and time variation

06 p1008 A70-17482

Liapunov functionals for time delay systems generated by path integrals in state space in terms of convolution equations

06 p1094 A70-17953

Surface thermal factors influencing ignition delay time of composite solid propellants, using double wavelength optical detector

06 p1128 A70-18043

Differential game with opponent receiving information on phase coordinates of adversary with delay caused by reception and processing procedures
07 p1244 A70-18718

Fatal ejections in USN, suggesting initiation delay as prime causal factor
07 p1191 A70-19006

Advanced concept ejection seat /ACES/ system design and performance, considering gyro-controlled vernier rocket motor and electronic time delays
07 p1192 A70-19016

Optimal control systems design involving time delays as functions of time and system state, considering stability constraints
08 p1478 A70-20779

Optimal feedback control synthesis for linear system with time delay through error criterion minimization
08 p1478 A70-20780

Pulsed radio signals time delay due to molecular microwave resonance in earth atmosphere and interstellar medium
08 p1461 A70-20915

Delayed trace reaction under stable and unstable pauses in apes and monkeys, noting independence of conditioned reflex
08 p1446 A70-21446

Extension of Liapunov systems to time lag systems with small periodic parameter
08 p1546 A70-21628

Nonlinearity of human eye movement control system in two dimensional tracking tasks, explaining visual axis lags as time delays dependent on target motion
08 p1447 A70-21724

Time delay between pulses of discharge current and ionized argon laser power as function of current and discharge pressure
09 p1697 A70-22847

Tape recorder performance characteristics relevant to signal types handled, considering phase response and envelope delay
09 p1679 A70-22975

Elasticity stratification stabilization effect on two layer flows down inclined plane found dependent on time response difference between layers
10 p1863 A70-24009

Synchronous satellite communication system clock synchronization loop design taking into account delay time
10 p1835 A70-24335

Auditory and visual warning signals effects as reaction stimulus in time-uncertainty situation
10 p1826 A70-24719

Visual stimuli intensity influence on delay in reaction to second of pair of visual stimuli
10 p1818 A70-24721

Optimal feedback control obtained for linear time-varying system with time delay, developing numerical method for solving performance differential equations
10 p1856 A70-25235

Group delay time differences of spectral groups of VLF atmospherics respecting day and night variation for thunderstorms, determining distance dependence
10 p1884 A70-25260

Maximum principle condition of optimal control of monodimensional system described by nonlinear hyperbolic equations with time delay
11 p2021 A70-25340

Digital control program parameters synthesis to realize time optimality with pure delay for ensuring absence of auto-oscillations under steady conditions
11 p2022 A70-25577

Elastic system stability with two degrees of freedom under action of retarded follower forces
11 p2142 A70-26631

Transistorized differed synchronizer for delaying photoflash initiation in scientific photography
12 p2228 A70-26879

Transmission delay and echo effects in long distance satellite relay telephony links, describing echo suppression and speech quality
12 p2183 A70-27004

Human blinking reflex recorded by electromyography, studying latent period in response to stimulation by air stream
12 p2168 A70-27346

Visual feedback delay effects on steering and tracking performance
12 p2179 A70-28147

Delayed ionization effects in midlatitude nighttime ionosphere after geomagnetic storms, noting time lag vertical distribution
12 p2227 A70-28365

Soviet book on theory of oscillations of linear and nonlinear time lag systems
13 p2450 A70-28699

Periodic solutions to linear differential equations with delay, applying numerical-analytical procedure
13 p2441 A70-29315

Delayed moment of force relativistic definition within reference of inertia, discussing lever bent at right angles
13 p2452 A70-29635

Ignition delay-reducing catalyst for furfuryl alcohol-red fuming nitric acid hypergolic bipropellant
13 p2473 A70-29992

Auroral absorption bays meridional motion, observing absorption onset systematic lag at various ground stations
14 p2570 A70-30216

Nonlinear sampled data system transportation lag effect on limit cycle nature
14 p2560 A70-30623

Temporal wave echoes and Landau damping in collisionless plasma using signal averaging and time delay techniques
14 p2622 A70-30687

Time lag system performance index bounds determination and optimal feedback controller design based on min-max criteria
14 p2561 A70-31185

Earth/moon mass ratio and Mars mass and ephemeris from Mariners range and Doppler tracking data, noting relativistic time delay measurement possibility
15 p2798 A70-31652

Nonlinear higher order canonical time lag equations initial and boundary value problems solutions by approximate iterative two way integration
15 p2767 A70-32171

Vector valued Gaussian random processes with Gaussian measurement noise, estimating phase and time delay parameters by maximum likelihood theory
15 p2704 A70-32593

Earth-satellite range measurements using broadband pseudonoise modulation and delay lock tracking method
15 p2705 A70-32724

Earth to planet radar signal time delay in general relativity expressed in relativistic spherical polar coordinates of earth and planet
15 p2806 A70-32801

Pontryagin stability criterion interpretation for systems with time delay in parameter plane, using computer oriented method
16 p2882 A70-33046

Univibrator analysis with glow discharge thyatrons, increasing time lag for equal R and C values
16 p2873 A70-33237

Feedback delay effects on eye-hand synchronism in stimulus tracking and steering using self generated body movements
16 p2852 A70-33662

Neutral type differential equations transformation to time lag system making periodic vibrations existence and stability theorems applicable
16 p2944 A70-34282

High powered high speed helicopters autorotation entry characteristics, noting capability of meeting control time delay requirement
17 p3014 A70-34715

Wave propagation measurement by correlation techniques, discussing travelling wave representation, delay times, amplitude coefficients, etc
17 p3091 A70-35449

Pilot induced oscillation rating regression analysis, examining time delay, slope after and time to first peak and stick force per g
18 p3213 A70-36444

Computerized Pontryagin stability analysis of nonlinear multiple delay systems
18 p3235 A70-36477

Pontryagin stability for distributed delay or parameter systems, using Brin criterion
18 p3235 A70-36478

Graphical stability for linear systems in parameter plane with time delay
18 p3235 A70-36479

Linear control systems stability range with delay time examined by digital computer, discussing critical loop gain
18 p3235 A70-36501

Implementation delay error reduction in discrete Kalman filter, noting application to inertial navigation systems analysis
18 p3236 A70-36712

Delay time between beams reflected from different parts of meteor trail, using phase invariant and frequency scanning methods
19 p3512 A70-37313

Group delay times criterion of multibeam propagation of ionospheric radio echoes for communications systems
19 p3375 A70-37332

Human response time to visual stimulus preceding or following auditory stimulus as function of interstimulus interval
19 p3362 A70-38311

Navigation errors and time delays in prediction techniques for air traffic control
19 p3468 A70-38642

Optimal control of processes with lags, including linear analytical regulator problem
19 p3395 A70-38718

Pulsed diodes subnanosecond rise time estimation, considering charge carrier lifetime, junction barrier capacitance, signal frequency, etc
20 p3595 A70-38968

Lasing transitions time delay in carbon monoxide laser under pulsed electrical excitation, attributing inversion to anharmonic decoupling
22 p4048 A70-42330

Photon flow delay regarding fluctuating source field in two points, applying correlation statistics by Pearson method of moments
22 p3988 A70-42564

Transmission factors of microwave filters with prescribed attenuation and group delay
22 p3997 A70-43173

Discrete systems with and without time lags, deriving necessary conditions for singular optimal control
23 p4176 A70-44301

Thermal-acoustic oscillations in forced convection, giving time delay analog for perturbation feedback
23 p4280 A70-44369

Signal arrival time variance in optical communication system with high lag photodetectors, examining input, detection and amplification noise
23 p4196 A70-44410

Auroral absorption bays meridional motion, observing absorption onset systematic lag at various ground stations
24 p4331 A70-46291

TIME LAPSE PHOTOGRAPHY U. CHRONOPHOTOGRAPHY TIME MEASUREMENT NT. CLOCK PARADOX

Rotation period of Jupiter based on decametric component of radio emission, suggesting anticorrelation with sunspot number for drift observed
01 p0173 A70-10044

Visual detection discrepancies of temporal order suggested due to definition of interstimulus interval
01 p0039 A70-11165

Solar and lunar disks instant of contact during solar eclipse determined by chord measurements, comparing three methods for successive time intervals
01 p0191 A70-11473

Analog and digital electronically counting chronometers for extremely short times measurements
02 p0295 A70-11868

Mean signal response time relationship to nonaging foreperiod
02 p0239 A70-12627

Multiple timing in elementary space triangulation using synchronous straight line as main net element
03 p0445 A70-13192

Synchronization of ground stations clocks by time scale comparison with overflying aircraft
[ONERA-TP-759]
03 p0487 A70-13642

Time determination and georotation - Conference, Riga, Latvian SSR, June 1965
04 p0755 A70-15476

Statistical analysis for personal variations contribution to total mean square error in time determinations
05 p0914 A70-16649

Duration measurements for sampling function in dynamic crossed field photomultiplier
05 p0849 A70-16655

Monograph on time measurements covering time scales, intervals, natural and artificial clocks, frequency standards, time and time signal transmission
07 p1283 A70-19664

Nitrogen molecules pulsed high energy beams transit time measurement by gated time of flight procedure and by multichannel analyzer
07 p1345 A70-20136

Pulsars pulse arrival time measured using cesium clock during weekly observations
08 p1570 A70-20899

Clock corrections smoothing by linear transformation operator, calculating operator transfer function and averaged errors deviations
08 p1574 A70-21155

Time determination precision dependence on thermal deformations of clock, humidity of atmosphere and most probable value of instrument azimuth
09 p1673 A70-22163

Spin-lattice NMR and EPR relaxation time measurements, using train signals and free induction decays
09 p1679 A70-22995

Information processing stages by reaction time measurements permitting discovery, property assessment and separate testing of stage durations additivity and stochastic independence
10 p1826 A70-24723

Gerstenkorn moon capture theory taking into account tidal evolution of earth-moon system, discussing marine organisms time rate synopsis for earth rotation retardation
10 p1943 A70-24840

Shock-heated noble gases total ionization times, considering recombination and atom-atom and atom-electron collisions
12 p2274 A70-26856

Aircraft and ship navigation using precision time measurement signals transmitted between vehicles and earth satellites

13 p2448 A70-28748

Metal powder mixtures homogenization time calculation, using Fick equation and matrix model

13 p2433 A70-28845

Atom excited state mean lifetime measurement, using correlated cascade photons method

14 p2620 A70-31378

Strain gage maximum rise time estimation for longitudinally sweeping strain pulse, reducing gage length/pulse velocity ratio effects [SESA PAPER 1620]

15 p2739 A70-32302

Time-frequency national airspace system, using distributed sensors and closed loop control to meet safety and traffic handling requirements

16 p2948 A70-33478

S and SKS travel times for arc distances of 30-126 degrees

16 p2898 A70-33975

Frequency and time information transmission, discussing frequency and time measurement equipment at Czechoslovak facility

18 p3257 A70-36199

Geometric relations for contact moments of solar eclipse, using crescent cord photographic measurements

18 p3315 A70-36610

Circadian oscillations and photoperiodic time measurement in *Pectinophora gossypiella*

18 p3221 A70-36893

Time of acceleration to rated speed for three-phase asynchronous gyroengine rotor

19 p3420 A70-37259

Pulsed diodes subnanosecond rise time estimation, considering charge carrier lifetime, junction barrier capacitance, signal frequency, etc

20 p3595 A70-38968

Impact times measurement by photography, correlating projectile velocity with projectile-target distance

20 p3635 A70-40530

Paleomagnetic reversal in 1350 year increments, measuring declination of deep sea sediment cores

21 p3820 A70-41885

Airborne computerized time frequency systems for aircraft range and velocity determination, using stable clocks with ambiguity resolution

22 p4067 A70-42659

Crab Nebula pulsar NP 0532 optical timing, measuring frequency, arrival times and pulse interval

22 p4102 A70-42936

Multichronometer for multiple time intervals measurement with picosecond resolution, using mixed analog and digital methods [SMPE PREPRINT 112]

22 p4031 A70-43029

Corrected geomagnetic midnight local time calculations, using nomogram

23 p4187 A70-43862

TIME MEASURING INSTRUMENTS

NT ATOMIC CLOCKS

NT CHRONOMETERS

NT CLOCKS

NT TIMING DEVICES

Earth rotation seasonal fluctuations analyzed from astronomical observations using frequency markers and quartz clocks

04 p0681 A70-15478

Time measurement errors from astronomical observations resulting from thermal and refractive effects on instrument

04 p0756 A70-15482

Time determination at astronomical observatories using transit instrument observations concerning stellar distributions and magnitudes

04 p0756 A70-15486

Pulse counting frequency divider with discrete phasing device for use with quartz clock and electron beam chronoscope

04 p0694 A70-15492

Monograph on time measurements covering time scales, intervals, natural and artificial clocks, frequency standards, time and time signal transmission

07 p1283 A70-19664

Electronic time interval meter combining pulse count with phase shift for automatic measurement and processing

15 p2733 A70-31579

High resolution electronic time intervalometer using digital counting and analog time expansion circuits

23 p4196 A70-44383

TIME OF FLIGHT SPECTROMETERS

Time of flight spectroscopic measurements in arc heated supersonic molecular beam using algebraic relations, sensing modulated beam by Orbitron type detector

06 p1111 A70-18266

Gaseous pyrolysis products detection and identification during eruption from polymeric surfaces subjected to flash heating by time of flight mass spectrometer

07 p1319 A70-19887

Energy-mass analysis for steady state plasma by electrostatic analyzer and time of flight mass spectrometer, determining ion species temperature and density ratios

24 p4387 A70-45813

TIME OPTIMAL CONTROL

Optimal rendezvous between satellite and spacecraft, determining power and time optimal coplanar rendezvous in circular orbit

01 p0139 A70-11479

Minimum time turns for spacecraft about fixed axis lying beyond plane of vehicle forces

01 p0197 A70-11480

Triple mode control strategy to provide near optimal stable transient response in variably loaded electrohydraulic servomechanisms

02 p0272 A70-12728

Optimal use of adaptive renewal capability determined for first order time varying linear systems with quadratic performance index by exponential model of component failure

02 p0273 A70-12729

Algorithm for fixed time minimum energy discrete optimal control problems of linear plants with convex constraints imposed on terminal state

02 p0273 A70-12731

Algorithm for optimal controls maximizing probability of linear time dependent control processes entering target manifold under random disturbances

03 p0460 A70-13580

Time optimal attitude control for alignment of spin stabilized sounding rocket, discussing feedback control system

03 p0580 A70-13805

Time optimal control of system variable with bounded controlling input and arbitrary disturbances, deriving necessary conditions using maximum principle [ASME PAPER 69-WA/AUT-7]

04 p0661 A70-14827

Law for time variations of modulus-restricted control action at trajectory end, two point boundary value problem solution and use of Pontryagin principle

04 p0661 A70-15011

Reliability optimization of information systems with discrete time resource output and measured efficiency control

04 p0661 A70-15195

Optimal damping time required for gyrocompass oscillations, allowing for maximum initial deflections

04 p0692 A70-15280

Minimum time frequency transitions in phase locked loops with phase and frequency controls using Pontryagin principle, obtaining switchless control strategies

04 p0652 A70-15339

Linear regulator optimal for exponentially time-weighted quadratic performance indices, using cost equivalence concept in infinite terminal time solution

04 p0663 A70-15604

Time optimal control of nonlinear systems with distributed parameters, proposing approximate algorithm

06 p1024 A70-17814

Optimal timing of measurements to minimize dispersion of navigational observation parameters by least squares method applied to Keplerian orbit elements

06 p1103 A70-17878

Suboptimal closed-loop controller design based on quadratic equivalence for linear time varying process with minimum probability of inequality constraints violation

06 p1024 A70-17951

Optimal feedback controls design for linear systems relative to time-multiplied performance indices

06 p1025 A70-17960

Open and closed loop time optimal systems compared with respect to sensitivity measure represented by terminal error norm

06 p1026 A70-17969

Monograph on functional analysis and time optimal control as application of mathematics

07 p1322 A70-18857

Linear and quadratic programming techniques for large scale continuous time optimal control problems with accurate switching times

07 p1325 A70-19268

Primal-dual algorithm for optimal control with fixed or free terminal time

07 p1238 A70-19269

Time optimal rendezvous maneuver between neighboring elliptic orbits, discussing propulsive jet system with variable thrust

07 p1381 A70-19357

Time-variable constrained control matrix optimization using Pontryagin principle applied to minimal time transfer, payoff and rotation maximization

07 p1247 A70-20024

Time optimal control for rotation of solid supporting body with aid of pendulum, obtaining motion equations by algorithm

07 p1337 A70-20299

Time optimal control synthesis for electromechanical devices, considering acoustical vibrations elimination in magnetically controlled contacts

08 p1472 A70-21001

Variable time optimal control problem computational algorithm using only zero Hamiltonian condition, noting variable time local maximum as well as local minimum

08 p1534 A70-21459

Optimal control with time delays in system model described by constant coefficient linear differential-difference equations

09 p1653 A70-22346

Interplanetary midcourse velocity correction schedules optimization, discussing timing equations modifications, mission simulation and role of earth based radar

09 p1759 A70-22760

Minimum time interstellar trajectories for thrust limited rockets by applying Pontryagin maximum principle to relativistic rocket equations of motion

09 p1760 A70-22933

Algorithm for propellant flow rate increase of nuclear rocket in minimum time without exceeding maximum allowable stress in reactor core

10 p1914 A70-24870

Saddle point existence in determinate integrodifferential games with variable delay, assuming given control function over time interval

10 p1911 A70-25183

Iterative algorithms for numerical solution for time optimal control problems

10 p1856 A70-25232

Optimal feedback control obtained for linear time-varying system with time delay, developing numerical method for solving performance differential equations

10 p1856 A70-25235

Linear steady and unsteady systems time optimal control switching points determination by introducing parameterization to reduce number of transcendental equations

11 p2021 A70-25339

Digital control program parameters synthesis to realize time optimality with pure delay for ensuring absence of auto-oscillations under steady conditions

11 p2022 A70-25577

Optimal operational control of aircraft takeoff and landing times using stochastic programming

11 p2077 A70-25608

Minimum fuel control for discrete time Gaussian processes, applying results to spacecraft midcourse guidance for earth-Mars mission

11 p2079 A70-25958

Time optimal control for nonlinear second order system containing positive parameter and measurable control function

11 p2028 A70-26308

Continuous and discrete minimum time problems relationships and state space portraits during application of optimal strategies to system

11 p2029 A70-26749

Time optimal control synthesis of fast acting gyrocompass mounted on fixed foundation and with hydraulic damper and torsional suspension of sensor

12 p2233 A70-27564

Iterative algorithm for synthesis of discrete minimum time and amplitude controls for linear systems, noting guaranteed convergence

12 p2204 A70-27667

Linear time dependent stochastic optimal control with nonquadratic performance indices using function space approach

12 p2204 A70-27668

Nonlinear discrete time sampled systems optimal control by dynamic programming, with application to stochastic systems

12 p2204 A70-28068

Minimum-time thrust vector control law in Apollo lunar module computerized autopilot

13 p2499 A70-28399

Minimum time control for placing circular orbit satellite in gravitationally stable position

13 p2502 A70-28440

Book on differential dynamic programming covering algorithms for continuous time control, bang-bang, discrete time and stochastic systems

14 p2560 A70-30631

Recoverability for amplitude and rate bounded optimal control of linear time varying systems

14 p2562 A70-31203

Automatic optimal discrete time control for linear distributed parameter systems with quadratic cost function

14 p2562 A70-31412

Free solid body time optimal rotation about fixed central axis under action of external control moment vector, assuming zero initial and terminal angular velocity

15 p2775 A70-32447

Discrete approximation of differential game of navigation, considering control of object transfer to given set by finite time

15 p2775 A70-32472

Minimal time closed loop controller design for linear systems with bounded control amplitudes and rates using approximate functional expression

16 p2880 A70-32984

Time optimal control for linear distributed parameter system using functional analysis with method of deepest descent

16 p2882 A70-33122

Linear sequential Kalman filter for time correlated noise without state augmenting and measurement differencing demanding less computer sizing

16 p2887 A70-33350

Iterative algorithm for free terminal time control in trajectory optimization

17 p3168 A70-35290

Linear time invariant plant driven by scalar control, deriving second variation algorithm for minimum fuel problems

17 p3057 A70-35555

Self adaptation algorithm of optimally fast acting system for variable parameter plant control

18 p3234 A70-36120

Iterative determination of time optimal controls, considering dynamic system transition from initial to quiescent state with constraints on control vector

18 p3282 A70-36355

Quasi-optimal feedback control method for minimum time intercept of target in central force field

19 p3393 A70-37865

ATA Collision Avoidance System based on time and frequency synchronization via ground stations or other aircraft

19 p3466 A70-38239

Optimal control time for second order nonlinear system with motion subject to specified conditions, determining switching line points

19 p3460 A70-38939

Large earth orbiting spacecraft minimum time attitude maneuvers with control moment gyroscopes, discussing torque calculation and gimbal angle rates

20 p3670 A70-40284

Dual mode suboptimum minimum time control of high order systems with negative roots and step displacement inputs, using simplified computer switching

21 p3801 A70-40756

Differential dynamic programming algorithm for discrete time orbit transfer optimization

21 p3919 A70-41737

Nonlinear automatic optimal control for discrete system with delay

22 p4005 A70-43563

Linear systems with phase coordinates bounded by given time functions, obtaining optimal control by iterative solution involving Lagrange multipliers

23 p4177 A70-44302

Time optimal problems involving parabolic equations in heating of rod with piecewise continuous thermophysical characteristics and temperature distribution constraints, deriving iterative solution

23 p4277 A70-44306

Computerized algorithm facilitating automatic synthesis of time invariant linear compensation for highly complex multiloop control systems

[ALAA PAPER 69-941] 23 p4177 A70-44561

Minimum-time transfer trajectories between close planar orbits, using single stage thrust-limited rocket

23 p4244 A70-44624

Ion micropropulsion for geostationary satellites

time optimal attitude control

23 p4261 A70-44669

Optimal fixed-time impulsive transfer trajectories minimizing characteristic orbital velocity, determining sufficient conditions

23 p4255 A70-45015

Adaptive time optimum inertial satellite attitude control using air jet

23 p4265 A70-45048

TIME RESPONSE

Langmuir oscillations excited by electron beam in plasma during instability development investigated for temporal and spatial structure, using visualization

01 p0150 A70-10174

Rise time relationship with signal bandwidth for class of TEM mode microwave delay line filters

02 p0257 A70-12185

Biplanar photocell in various holders noting intrinsic properties, emphasizing rise time characteristics

04 p0695 A70-15572

Photocathode internal light scattering effect on photomultiplier time response

05 p0845 A70-15806

Laser pulse registration with pyroelectric detector, noting pyroelectric phenomenon inertia limiting effect on response time

05 p0858 A70-16250

Superconductor tubes experiment, observing flux jump initiation and propagation characteristics

09 p1738 A70-22293

Linear control systems design with restricted number of feedbacks based on optimization criteria concerning responses to initial disturbance

10 p1855 A70-24703

Human reactions to successive visual signals, studying response time in single and grouped reaction

10 p1826 A70-24720

Langmuir oscillations excited by electron beam in plasma during instability development, investigating temporal and spatial structure using visualization

10 p1925 A70-25019

Time response deviation correction in hybrid computer control systems with digital feedback elements containing quantized coefficients

11 p2029 A70-26334

Human controllers nonlinear time domain mathematical model for analyzing compensatory tracking task data

11 p1992 A70-26396

Evoked cerebellar potentials time characteristics during spinal cord stimulation in cats, investigating cerebellar intercentral connections effect

13 p2353 A70-29357

Strain gage maximum rise time estimation for longitudinally sweeping strain pulse, reducing gage length/pulse velocity ratio effects

[SESA PAPER 1620] 15 p2739 A70-32302

Tracking error correction time and proprioceptive reaction time, suggesting role of central mechanism without sensory feedback

17 p3036 A70-34606

Quantum electronic space vehicle, discussing time reversing motor or inverse /anti- atomic engine

17 p3148 A70-35213

Ion-polar molecule collision time history plots and computer movies, calculating capture cross sections for mass spectrometry

18 p3292 A70-36561

Laser pulse shaping using inducible absorption with Q switched time behavior controlled by nonlinearities within optical resonator

18 p3270 A70-36745

Inverse Laplace transform of network function with allowance for initial differential equation solution, determining circuit temporal characteristics

19 p3456 A70-37269

Component decision logical and temporal arrangement in visual search, defining target by several attribute value combination

19 p3362 A70-38314

Flight test and airborne data recovery and processing, discussing data format, recorder characteristics, ground equipment and time requirement

19 p3429 A70-38517

Flip-flops switching time reduction, using equivalent amplifier circuit with positive feedback

19 p3390 A70-38580

Digital filter synthesis, discussing transfer function determination based on prescriptions for frequency or time response properties

19 p3391 A70-38746

Nonlinear acoustic absorbers behavior analysis, discussing spectral and temporal computation methods

20 p3672 A70-39237

Cool flame isothermal theory with oscillatory features accounting for damping time evolution and thermic reaction nature

21 p3942 A70-40886

Time resolving X ray grating polychromator, discussing photoelectric attachment with surface barrier semiconductor detectors

[SMPTE PREPRINT 75] 22 p4037 A70-43069

Phase delay between thermospheric neutral temperature and neutral density, considering frequency dependent time response to solar heat input

23 p4187 A70-43858

Visual system recording neuron pulse potential spatial and temporal responses to sinusoidal stimuli

23 p4144 A70-43922

E region ion composition nighttime variations, examining nitrogen monoxide and O ion nonequilibrium concentrations by ionic-molecular reactions

23 p4189 A70-44074

Threshold distribution of time intervals between atmospheric contradicting Poisson law

23 p4190 A70-44082

TIME SERIES ANALYSIS

Cosmic ray time series periodicity using variance analysis allowing for intensity variations and meteorological factors

06 p1135 A70-17543

Adaptive linear estimator for stationary time series, evaluating asymptotic mean square error bound

17 p3128 A70-34852

Statistical analysis of short periodic time series in biological rhythms including cosinor, periodic regression, harmonic and synchronization analyses

19 p3365 A70-38412

Recursive differential equation for moments of time-to-cycle slip in first and second order phase lock loops

21 p3802 A70-41350

Gyro drift rate mathematical modeling based on stationary and nonstationary time series analysis techniques with random process reduction to white noise residuals

[ALAA PAPER 69-838] 23 p4197 A70-44557

TIME SHARING

Image quality effects on human performance in simulation, discussing time sharing strategies and task difficulty factors

01 p0036 A70-10809

Time sharing computer systems to perform circuit design and analysis, discussing effectiveness in terms of immediate access, accuracy and cost

02 p0265 A70-12187

Hardware-software integrated time sharing computer system for testing transmission control units and associated terminals on line

02 p0275 A70-12189

Feedback time sharing analog electronic multiplier for two quantities, noting linearity, accuracy and stability of measurements

02 p0268 A70-12422

Time sharing computer systems for data reduction from semiconductor strain gauges applied to FORTRAN IV programs

03 p0453 A70-12969

Special purpose computer organized as time-shared digital filter for real time applications with adaptable coefficients, programming and multiplexing scheme

05 p0818 A70-16415

Loops and paths in Mason signal flow graph of linear systems using algorithm with remote time shared digital computation

07 p1238 A70-18842

Time shared computer system providing real time service to multiple laboratory instrumentation, discussing high speed channel, computer control and data abstracting techniques

13 p2375 A70-29830

Dual raster high brightness-high resolution TV display using time sharing with conventional CRT

16 p2903 A70-33131

Automatic weight analysis by calculation and orientation of mass properties /COMP/ program, using remote terminal time sharing computer system

20 p3595 A70-40353

Computer time sharing system for real time mass properties measurements

20 p3595 A70-40374

Heat transfer and viscous flow pedagogy, discussing classroom use of remote time sharing computer terminals

23 p4166 A70-44642

TIME SIGNALS

Level quantization in time compression systems using storage devices with small dynamic range of recorded signals

15 p2733 A70-31578

Receiver for artificial satellite transmission and optical tracking time signals, using crossed dipole directional antenna

16 p2867 A70-34303

Multichannel time marker network synthesis device for physiological data assembly, transformation and processing, generating pulses

18 p3223 A70-36083

Low level time truncated signals measurement by narrow bandwidth synchronous time notch filters, discussing sensitivity

19 p3380 A70-38177

TIMERS

U TIMING DEVICES

U TIME MEASUREMENT

U TIME MEASUREMENT

U TIME MEASUREMENT

Electronic timing device for light balloon payloads, describing circuit

07 p1286 A70-19975

Step recovery frequency shift keyed retimer using Gunn effect FSK pulse regenerator for microwave communication

07 p1237 A70-20285

Swinging gear drive, breather cartridge and hypocycloid timer mechanisms for reliable aerospace applications

16 p2921 A70-34104

Spacecraft hydraulic timers design and qualifications testing, discussing oil selection and temperature dependence

16 p2914 A70-34112

Timing systems using Cs frequency standard for satellite tracking

21 p3828 A70-41697

Stable clock precision timing systems, discussing quartz crystal, rubidium, cesium and hydrogen oscillators

23 p4195 A70-44289

TIN

Al and Sn composites reinforced by E glass and silicon dioxide glass fibers compared for tensile strength, noting difference due to resistivity

03 p0514 A70-14314

Thermal radiation spectrum power of small spherical tin and lead particles

20 p3737 A70-39745

Superconducting Sn bolometer under isothermal and nonisothermal conditions, measuring noise spectra dependence on displacement current and resistance

22 p4026 A70-42397

TIN ALLOYS

Metallic superplasticity and superplastic alloys in simple tension, forming tubes and sheets of superplastic Sn-Pb eutectic alloy by pressure forming techniques

16 p2916 A70-32916

Nb-Sn superconductors multiphase structure with three intermetallic phase, constructing diagram based on phase stability and composition

18 p3299 A70-37221

TIN COMPOUNDS

NT TIN OXIDES
NT TIN TELLURIDES
TIN OXIDES

Stannic or cobalt oxide film coated glasses optical and energy characteristics determined for potential use in solar energy engineering

01 p0159 A70-10766

Tin oxide film resistors reliability test based on measurement of resistance nonlinearity by third harmonic voltage

09 p1689 A70-22005

Stannic oxide-chromium oxide catalyst effects on thermal decomposition and ignition of ammonium perchlorate /AP/, calculating activation energy

11 p2100 A70-26281

TIN TELLURIDES

SnTe of various nominal hole concentrations measured for longitudinal piezoresistance effect along different crystallographic directions

10 p1927 A70-23993

TIP DRIVEN ROTORS

Pressure jet helicopter with tipjet propelled rotor system, discussing power available calculation, mission performance, power management, etc

17 p3013 A70-34707

Helicopter engine rotor matching for tip propulsion efficiency, comparing with conventional shaft drive propulsion

[ASME PAPER 70-GT-68] 18 p3215 A70-36842

TIP SPEED

Helicopter rotors noise intensity prediction for high tip Mach number, including compressibility and thickness effects

17 p3015 A70-34729

TIP VORTICES

U TIP SPEED
U VORTICES

TIPS

NT BLADE TIPS
NT WING TIPS

TIRES

NT AIRCRAFT TIRES

TIROS OPERATIONAL SATELLITE SYSTEM

TIROS Operation Satellite /TOS/ system for daily observation of meteorological phenomena analyzed for problems of general data gathering satellite system [ALAA PAPER 70-283] 09 p1766 A70-22874

TIROS Operation Satellite /TOS/ system for daily observation of meteorological phenomena, analyzing problems of general data gathering satellite system [ALAA PAPER 70-283] 21 p3931 A70-41868

TIROS PROJECT

TIROS weather satellite TV system providing observations to ground stations via ESSA satellites

14 p2654 A70-31148

TIROS SATELLITES

Global cloud cover and earth atmosphere heat budget measured from weather satellites, discussing Tiros pictures, radiation charts and albedo

03 p0479 A70-14348

TIROS, Nimbus, ESSA and ATS weather satellites configurations, onboard equipment and cloud photographs

09 p1765 A70-22227

Tiros M requirements for earth resources sensor systems, discussing spacecraft structure, dynamics, power, command and communications subsystems

10 p1950 A70-24638

Fluid thermal actuator for temperature control of ITOS /Improved Tiros Operational System/ meteorological satellite, discussing design and performance

16 p2846 A70-34129

Tiros solar proton monitor program, describing detector design, operational data processing and early warning network

17 p3180 A70-35304

TISSUES [BIOLOGY]

NT ENDOTHELIUM
NT EPICARDIUM
NT EPITHELIUM
NT PERITONEUM

Tissue protein changes under visible and UV radiation noting denaturation, chemical bonds, protein configurations, clinical disease patterns, etc

01 p0022 A70-10856

Time course of end bulb material formation in vitro in rodent myelinated nerve fibers, confirming elastic capillary concept

02 p0233 A70-11725

Graft copolymerization and chemiluminescence analysis of lipids complexes in animal and plant tissue homogenates exposed to gamma radiation

03 p0419 A70-13305

Radiation protective action of aminoalkylthiols, aminoalkyl disulfides, isothioureas, thiazolidine etc, in mouse tissues, erythrocytes and yeast cells exposed to X ray doses

03 p0419 A70-13307

Coenzyme A and acetyl CoA in tissue extracts determined for concentrations by recycling CoA through coupled enzyme system

04 p0640 A70-15754

Equation describing atmospheric oxygen conductance to human tissues compared with experiments, ascribing discrepancies to inhomogeneity in diffusion/perfusion relationships

06 p0993 A70-17434

Acute hypoxia effect on mono-, di- and triphosphonitides metabolism and content in white rats cerebral tissues, using chromatographic analysis

07 p1199 A70-18721

Ionizing radiation effects on tissues of developing cerebellar cortex of rats

09 p1619 A70-22815

Physiology of oxygen transport in human organism and genesis of tissue hypoxia, discussing pulmonary functions, blood transport properties and tissue blood flow and diffusion

10 p1821 A70-25077

High altitude acclimatization effect on tissue capillary, investigating physiological evidence in rats by tissue diffusing capacity measurement

10 p1823 A70-25220

Dimensionless parameters associated with heat transport within living tissues using biothermal model

11 p1992 A70-26513

Tissue oxygen partial pressure measurement in resting skeletal gracilis muscle of cat, using microelectrode

11 p1989 A70-26664

Glycolysis and glycolytic enzymes activity increase in tissues observed during training of rats to hypoxia, discussing adaptive reactions at cellular level

12 p2167 A70-26975

Brain tissular respiration and oxygen consumption in rats during hypothermia

12 p2168 A70-27345

Inert gas absorption from tissue cavities in body, using models with different wall distribution patterns of capillaries and diffusion resistance

12 p2171 A70-28025

Control device for micromanipulator with pacing motor during electrophysiological studies involving microelectrodes implantation into tissue

12 p2179 A70-28317

Skin and tissue mechanical characteristics response to vibratory stimulation, considering effects on physiological and psychophysical tactile sensitivity measurements

13 p2354 A70-29598

Therapeutic effects of hemopoietic tissue transplantations of bone marrow on irradiated rats, using diffusion chamber for resettlement prevention

13 p2354 A70-29753

High oxygen pressure effect on consumption rate constant for in vivo tissues

15 p2679 A70-31608

Radial acceleration effects on tissue carbohydrate in starved female rats, observing blood glucose increase and muscle glycogen levels decrease

15 p2684 A70-32536

Hybrid computer simulation of steady state oxygen transport and consumption in capillary-tissue system

15 p2694 A70-32845

Tissue respiration measurement with membrane-covered oxygen electrode, discussing effects of electrode deterioration and diffusion artifacts on accuracy

17 p3026 A70-35186

Bone and muscle tissue morphological changes in caged and immobilized rodents and in myasthenic humans

17 p3030 A70-35357

Respiratory gas metabolism of liver, heart, brain and muscle tissues in birds exposed to various ambient temperatures for long periods

18 p3220 A70-36547

Cellular irradiation sensitivity in tissue culture modified by propyl gallate as radical reactions inhibitor

21 p3767 A70-42242

Space flight effects on dogs cardiac activity, brain circulation and systemic-tissue circulation interactions

22 p3972 A70-43635

Live skin tissue electrical parameters changes due to laser radiation, showing coagulative necrosis by histomorphological studies

23 p4150 A70-44313

Lethal and sublethal radiation dosage effects on cellular Na and K distribution in rat brain, liver, kidneys and muscular tissues

23 p4145 A70-44314

Mammalian tissues metabolic and genetic alteration during weightlessness, relating rats liver regeneration delay to centrifuging intensity following hepatectomy

23 p4146 A70-44617

Critical supersaturation vs phase equilibration of tissue in computing decompression schedules from depth and exposure time

24 p4301 A70-45983

TITAN LAUNCH VEHICLES

NT TITAN 3 LAUNCH VEHICLE

Atlas /Centaur and Titan/ Centaur launching of Intelsat 4 communication satellites, discussing booster, stage characteristics and payload [ALAA PAPER 70-483] 11 p2127 A70-26605

TITAN 3 LAUNCH VEHICLE

Solar powered electric propulsion systems for automated missions throughout solar system by extending range of Atlas Centaur-Titan 3-C launch vehicles [ALAA PAPER 68-1120] 04 p0736 A70-15401

Thermal efficiency of modified transtage of Titan 3C spacecraft, discussing environmental simulation, heat rejection system and test firing [ALAA PAPER 70-171] 06 p1156 A70-18027

Titan 3C launch environmental hazards including noise and exhaust cloud content

07 p1393 A70-19225

Structural analysis of Titan 3 Stage 2 ablative nozzle extension made of composite material

08 p1595 A70-21910

Titan 3C boost phase inertia loads on payload estimated for satellite design, using frequency and interface acceleration methods [ALAA PAPER 70-485] 11 p2120 A70-25446

Titan 3 launch vehicles capabilities communication satellites deployment modes, presenting cost and availability data for preliminary mission planning [ALAA PAPER 70-482] 11 p2121 A70-25451

Titan 3C solid rocket motor exhaust plumes thermal radiation analysis for designing Stage I engines and components thermal protection [ALAA PAPER 70-842] 16 p3000 A70-33925

Titan 3 launch vehicle for scientific space missions, discussing building blocks, performance and payloads

17 p3178 A70-35260

Thermoelectric outer planet spacecraft /TOPS/ flight environment, systems design and Titan 3D/Centaur launch vehicle with Burner II upper stage

21 p3930 A70-41795

TITANATES

NT BARIUM TITANATES
NT ILMENITE
NT LEAD TITANATES
NT MAGNESIUM TITANATES
NT PEROVSKITES
NT STRONTIUM TITANATES

Internal residual stress relaxation theory in dielectric aging in tetragonal solid solutions of calcium titanate in barium titanate

19 p3486 A70-37776

Electro-optic device using ferroelectric bismuth titanate, discussing electrical and optical properties and matrix addressed display

21 p3830 A70-42114

Addition effects on lattice and electrophysical properties of trititanate prepared by Ba, Pb, Ca and Ti precipitation

22 p4087 A70-43134

TITANIUM

Annealing effects on cold rolled titanium sheets, noting changes in Young modulus and characteristics of recrystallized titanium

01 p0124 A70-11620

Crack propagation in pure alpha-Ti at room temperature using optical and electron microscopy, considering propagation rate relation to strain amplitude

01 p0125 A70-11643

SST Ti body frame optimum design for high temperature environment and economical and fatigue resistance requirements

02 p0386 A70-11937

Boron-polyimide composite reinforced Ti fuselage stringers design and test program for SST

02 p0387 A70-11950

Titanium thin films prepared in ultrahigh vacuum to determine low temperature/pressure oxidation kinetics, using electron microscopy and X ray diffraction

02 p0317 A70-12316

Ti, Zr and Nb characteristics, properties, processing procedures and applications in corrosive environments, nuclear reactors and aerospace structures

02 p0319 A70-12710

Mechanical properties, optimum deformation and rupture of W wire reinforced Ni and Ti metal composites obtained by hot rolling in vacuum

03 p0508 A70-13245

Tangential cutting force measurements during Ti grinding by microtools, noting properties of W, aluminum boride and zirconium carbide

04 p0697 A70-14466

Tensile tests on alpha Ti containing oxygen and hydrogen at various temperatures and strain rates to determine deformation and fracture

04 p0706 A70-15133

Bond quality and strength of high temperature adhesive films for titanium [DGLR-69-56] 04 p0699 A70-15158

Polyomorphic transformation effects on oxygen diffusion rate in alpha and beta phases of Ti, considering temperature effects and activation energy

04 p0707 A70-15211

Young modulus anisotropy and recrystallization texture during annealing in cold rolled Ti sheets using Fourier analysis

05 p0862 A70-16200

Fillers effect on thermal conductivity in porous cermet elements, investigating powdered Ti plates with

air replaced by Hg, benzene, ethanol, ether and water vapor

05 p0957 A70-16291

Ti-hydrogen reaction at ambient temperatures, investigating factors favoring reaction and preventive measures

05 p0863 A70-16524

Metal oxides additions effect on Ti glass crystallization, studying small and large ion radii

05 p0871 A70-16593

Silicate enamel coating formulas for application on titanium exhibiting adequate adhesion

05 p0872 A70-16599

Ti demonstrated as predominantly chalcophilic in highly reduced enstatite chondrites and achondrites

07 p1391 A70-20352

Ti I spectrum oscillator strengths, determining formula for relative-absolute values transition

08 p1569 A70-20832

Ti additions influence on steel work hardening, specific weight, magnetic properties and structure

08 p1515 A70-20924

Mo mechanical properties dependence on surface defects and Ti films

08 p1515 A70-20937

Heat exchange coefficient during Ti melting in lined arc furnace, determining relation between heat flows to side walls and bottom of graphite crucible

08 p1506 A70-21140

Solidification thermal conditions during Ti casting by melting out patterns in graphite molds, investigating heat accumulation coefficients in molds

08 p1506 A70-21142

Graphite molds compaction pressure effect on Ti castings nonporosity and surface layers carburization

08 p1506 A70-21143

Low cost programming system for gas tungsten arc welding process for Ti taper and stepped joint designs

08 p1507 A70-21484

Interstitial solutes effect on athermal component of flow stress in alpha titanium

08 p1521 A70-21577

Nondestructive betatron radiographic testing techniques for Ti billets, evaluating various lead screen, film and geometry combinations

08 p1508 A70-21746

Magnesium solubility in titanium from X ray analysis of Mg distribution in diffusion zones at high temperature and pressures

09 p1703 A70-22567

Titanium and titanium alloys bonding, discussing pretreatment, adhesives and assessment of temperature, environment and nuclear radiations

09 p1704 A70-22750

Temperature and strain dependence of strain anisotropy in Ti tested on longitudinal and transverse tensile specimens

09 p1705 A70-22807

Titanium sponge secondary structure obtained by magnesiothermal reduction of concentrated Ti-containing chloride melts, discussing temperature effect on porosity

09 p1709 A70-23783

Cost effectiveness in Ti forming, discussing materials, tooling and fabrication cost ratios

10 p1970 A70-23852

Ultrasonic vibrations effects on microstructure and mechanical properties of polycrystalline titanium during phase recrystallization

10 p1903 A70-23863

Electron energy loss spectrum in Ti measured by bombarding thin films vacuum deposited on NaCl crystal with electrons of intermediate energy

11 p2065 A70-25376

High fatigue life resulting from titanium spot welding realized by preweld and postweld treatment

11 p2059 A70-25662

Diffusion and electron beam welding combined with forging for cost reduction and production enhancement of titanium structural components

12 p2241 A70-27087

Solid state diffusion bonding techniques for aerospace Ti structural components

12 p2242 A70-27093

Titanium structural element allowances requirements and test programs for SST design

12 p2318 A70-27132

Porous Ti powder sintering process activation energy determination, noting influence of oxides solution in surface layer of Ti particles

12 p2254 A70-27283

Stress relaxation in alpha titanium during plastic strain, measuring temperature and strain rate dependence

12 p2255 A70-27608

Athermal component of plastic flow stress in alpha titanium at room temperature using incremental unloading technique

12 p2257 A70-28100

Titanium effect on iron and steels nitriding at high temperature, obtaining high surface hardness

13 p2423 A70-29773

Titanium vacuum pump, discussing pumping speed, sticking factor and sorption coefficient for hydrogen

15 p2744 A70-31845

Initial stages of Ti vapor deposition on Mo, using secondary ion-ion emission and mass spectral analysis

15 p2757 A70-32120

Titanium science, technology and applications - Conference, London, May 1968

17 p3109 A70-34351

Electroslag melted titanium wrought shapes mechanical properties, comparing with double vacuum arc melted material properties

17 p3112 A70-34356

Ti equipment anodizing methods, observing corrosion resistance reduction and embrittlement hydriding due to Fe contamination

17 p3098 A70-34363

Oxidation dependence on physical nature of Ti surfaces obtained by thin film techniques under ultrahigh vacuum conditions

17 p3098 A70-34364

Ti corrosion resistance tests in active and passive states

17 p3113 A70-34367

Elastic properties of dislocations in Ti basal, prismatic and pyramidal slip systems, discussing dilatational fields of edge and screw dislocations

17 p3115 A70-34385

Elastic interactions between anisotropic crystal dislocations and twin and grain boundaries in Ti

17 p3115 A70-34386

Oxidized alpha Ti crystals strain analysis based on X ray divergent beam, discussing hardening effects

17 p3115 A70-34387

Crystallography of deformation twinning in Ti, presenting modes involving shear strains less than unity and simple shuffle mechanisms

17 p3116 A70-34388

Titanium and Ti-Al single crystals microscopic plastic deformation features, slip modes and dislocation substructures

17 p3116 A70-34389

Unalloyed alpha titanium mechanical properties, emphasizing grain size and interstitial content effects on strain hardening and deformation dynamics

17 p3116 A70-34391

Commercial purity Ti athermal plastic deformation, showing anomalous behavior with temperature variations

17 p3116 A70-34392

Unalloyed polycrystalline Ti fatigue tests, observing cyclic stresses effect on twinning

17 p3116 A70-34393

Unalloyed Ti hydrogen embrittlement, determining factors affecting brittle-ductile transition temperature

17 p3117 A70-34398

Martensitic transformation in Ti and Ti alloys, discussing shear systems influence

17 p3118 A70-34404

High temperature heating and cooling effects on mechanical properties and structure of Ti welds, using notched bar impact specimens

17 p3098 A70-34423

Argon-arc welds porosity mechanism in Ti welding

17 p3098 A70-34443

Ti hot forming, discussing sheet use as aircraft structural material

17 p3098 A70-34444

Ti explosive bonding and forming, examining peel and shear strengths on Ti clad steel plate

17 p3098 A70-34446

Ti sheet welded construction for transport aircraft fuselages, assuming use of electron beam and plasma arc equipment

17 p3198 A70-34452

Mn and Ti effects on hardening of Fe-Ni-Mn-Ti and Fe-Ni-Mn maraging martensitic steels

17 p3125 A70-35145

IV characteristics of high resistivity Ti-doped GaAs single crystals and S-diodes, using Hall constant and conductivity measurements

17 p3144 A70-35709

Photometric determination of Ti with diantipyryl-methane in steels containing Se

18 p3277 A70-36465

Ti and C effects on Fe-Cr-Ni alloys mechanical properties

19 p3449 A70-37271

Titanizing Armco iron and carbon steels, examining diffusion layer structure and phase composition

19 p3451 A70-37460

Work hardening maxima of alpha-Ti as function of strain rate and temperature

19 p3451 A70-37568

Phase formation and mass transport during iodine-refined Ti reaction with nitrogen at various elevated temperatures

19 p3452 A70-38364

Long structural shape production for titanium and super alloys, discussing rolling, extrusion, drawing, frictionless forming and filler techniques

19 p3437 A70-38420

Drilling rates improvement for Ti by adding ultrasonic vibration to conventional process

19 p3437 A70-38421

Mechanical properties, optimum deformation and rupture of W wire reinforced Ni and Ti metal composites obtained by hot rolling in vacuum

19 p3453 A70-38463

Structural Ti, investigating effect of surface strain hardening by cold rolling on fatigue strength

20 p3648 A70-39250

Ti-Be composite materials production by coextrusion of powders, investigating microstructure by microprobe analysis and X ray diffraction

20 p3649 A70-39945

Ti sandwich structures low temperature brazing with Al alloy, describing fabrication process and mechanical properties

20 p3638 A70-39969

Ti mechanical properties dependence on grain boundary size and hydride precipitation characteristics, considering transcrystalline and intercrystalline fracture

20 p3652 A70-40179

Titanium powder compacts exothermic solid phase reaction ignition by focused laser pulse, obtaining temperature profile from mathematical model based on energy transport

20 p3639 A70-40473

Tooling concepts providing gas shielding in mechanized open air arc welding of Ti, evaluating effectiveness by various mechanical tests

21 p3832 A70-40788

Recrystallization kinetics and microstructure of low carbon Ti stabilized steel cold rolled and annealed in 800-1750 F range

22 p4053 A70-42730

Oxygen diffusion coefficient of alpha-Ti from oxidation of saturated and unsaturated beta phase in 932-1142 C range

22 p4053 A70-42731

Strain rate change effect on stress-strain diagram shape of polycrystalline alpha-Ti during tensile tests over temperature range

22 p4054 A70-42737

Ti embrittlement by liquid Cd, discussing ductile-brittle transition temperature dependence on strain rate

22 p4054 A70-42738

Ti phase transformation effects on thermal conductivity, electrical resistivity and spectral and total emissivities at 1100-1500 K

22 p4056 A70-43222

Ti single crystals plastic deformation in axial compression at high temperatures

24 p4358 A70-45239

Cubic titanium oxycarbide structural characteristics, noting lattice constant dependence on component proportions and mutual solubility during formation

24 p4359 A70-45477

Alpha phase Ti strengthening, investigating interaction between dislocations and interstitial solute atoms

24 p4360 A70-45516

Thread parameters effect on steel and Ti high strength fasteners fatigue life

24 p4425 A70-45881

Carbon steel diffusion saturation with Ti and B, investigating layer depth, weight gain and microhardness dependence on powdered mixture composition

24 p4364 A70-46336

TITANIUM ALLOYS

Wear resistance of Ti alloys chromosilicified by thermal diffusion in vacuum

01 p0115 A70-10072

Phase changes in Ni/Ti alloys with equiatomic composition, resolving discrepancy on nonMartensitic eutectoidal decomposition of B2 structure and intermediate precipitate

01 p0121 A70-11232

Ternary chemical element additions /O, Sn, Zr, Nb, Mo, V/ effects on solubility range of primary alpha region of Ti-Al base alloys

01 p0122 A70-11239

Martensite transformation with fcc lattice in Ti alloys containing 5.9 percent Fe as function of cooling rate, using X ray analysis

01 p0124 A70-11590

Quenched Ti-Mn alloy omega transition phase microstructure characteristics by transmission electron microscopy using thin foils

01 p0125 A70-11639

Ti-Mn alloy quenched in brine and aged at high temperature studied for structural transformations using electron microscope

01 p0125 A70-11640

Ti-Al-Co alloys melting points and cast structures, discussing reactions with melt

01 p0125 A70-11644

Ti-Al-Co alloys reactions in solid phase in Ti-rich region, using optical microscopy and X ray diffraction analysis

01 p0125 A70-11645

Ti alloys creep and fatigue breakdown under cyclic tensile loads at room temperature

02 p0315 A70-11660

Potential lubricants in friction and cup forming tests of stainless steel, Ti- and Ni-base alloys, considering boron nitride, graphitic materials and Mo oxides

02 p0309 A70-12540

Ti-Al-Sn alloy tensile deformation mechanisms at cryogenic temperature under uniaxial and biaxial

stress noting twinning, prismatic slip and dislocation characteristics

03 p0507 A70-13141

Lattice misfit influence on metastable omega phase morphology and stability in Ti transition metal alloys

03 p0508 A70-13146

Superconducting transition temperature variation in bcc region of Ti-Nb-V ternary alloys measured as function of valence electrons and composition

03 p0538 A70-13154

Corrosion resistance of Ti-based alloys in humid subtropical climate, discussing sea and rain water effects

03 p0510 A70-13281

Phase structure and corrosion resistance of alloys in Ti-V-Cr system, discussing effects in HCl, sulfuric acid, nitric acid, acetic acid and NaCl solution

03 p0510 A70-13282

Titanium aluminide-Mo system hardness, electrical conductivity and density as function of chemical composition, presenting creep test results

03 p0510 A70-13353

Beta III Ti alloy cold formability, mechanical properties and heat treatment noting use for fasteners, sheet metal parts, honeycomb sandwich sections and metal matrix composites

03 p0512 A70-13776

Heat treatment effects on mechanical properties of Ti-Fe and Ti-Fe-Al alloys

03 p0512 A70-13855

Quenching temperature and deformation conditions for Ti alloy bars optimal mechanical properties emphasizing effect of primary structure

03 p0497 A70-13856

Titanium alloys case hardened by diffusion of various metals at high temperatures, measuring increase in wear resistance

03 p0513 A70-13858

Press load prediction for deep drawing Ti-Al-V alloy, stainless steel and Inconel X under various lubrication conditions at room temperature [ASME PAPER 69-WA/PROD-15]

04 p0698 A70-14835

Notch-bend strength of titanium, aluminum and copper base alloys, noting geometrical size effect [ASME PAPER 69-MET-D]

04 p0705 A70-14878

Ti alloys, high strength steels and plastics for aircraft and spacecraft constructions, including aging behavior of lap joints and prepreg laminates in vacuum [DGLR-69-58]

04 p0699 A70-15162

Hydrogen diffusion in pure Ti and beta Ti alloy VT15, determining diffusion coefficient for various temperatures

04 p0707 A70-15190

Oxidation behavior of TiC base alloys containing Mo

04 p0708 A70-15312

Ti-Al-V alloys after annealing investigated for equilibrium diagram at high temperatures

04 p0708 A70-15313

Corrosion problems in Ti and alloys chemical and aerospace applications, describing thermodynamics and electrochemistry in aqueous media

04 p0710 A70-15677

Aircraft Ti alloys failure due to stress-induced pseudocorrosion caused by trichloroethylene and Freon noting microstructure, heat treatment and welding effects

04 p0710 A70-15679

Elastic interaction energy involved in Ti solution hardening by oxygen determined using anisotropic elasticity, presenting atomistic calculations and chemical bonds breaking role

05 p0862 A70-15906

Titanium alloy wastes electrorefining by electrolytic cell with solid bipolar electrodes to eliminate non-metallic inclusions

05 p0863 A70-16544

Alpha and beta solid solutions chemical composition in two phase alloys of Ti-Al-Mo and Ti-Al-V determined by electron microprobe analyzer

05 p0864 A70-16549

Stress concentration effect on mechanical properties of Ti-Ta alloys at low temperatures, showing insensitivity to notch and suitability for cryogenics

05 p0864 A70-16869

Vibration damping properties of steels and Ti- and Al-based alloys at various temperatures under tensile and compression loads

05 p0868 A70-17048

Ti alloy tensile strength under cyclic loads at room and high temperatures, noting plastic deformation and damage accumulation effects

06 p1085 A70-17406

Microstructure effects on smooth and notched fatigue and room temperature tensile properties of Ti-Al-V alloy using heat treatment combinations

06 p1087 A70-17458

Weldability of super alpha high creep strength Ti alloy investigated by synthetic heat affected zone method using thermal cycling tests

06 p1090 A70-18501

Brazing time and temperature effect on depth of Ag based brazing alloys penetration into thin Ti-Al-V sheet substantiated by microprobe analysis

06 p1078 A70-18513

Roll diffusion bonding applicability to Ti, Ni and Fe alloys, discussing fabrication temperatures and tooling [AIME PAPER F-69-3]

07 p1290 A70-18813

Ti alloy welded sheets bending fatigue test facility, discussing test stand calibration and optimal welding

07 p1291 A70-18824

Anodic dissolution initial stages of Ti alloys in neutral salt solutions from viewpoint of electrochemical dimensional processing, noting temperature effect on anodic activation potential

07 p1294 A70-19352

Alloying elements effect on polymorphic alpha-beta transformation temperature of Ti systems, discussing heat resistance

07 p1307 A70-19555

Hydrogen effects on ELI Ti-Al-Sn alloy, conducting tensile, fretting and abrasion tests on stressed and thermal cycled specimens [AIAA PAPER 69-585]

07 p1309 A70-19710

Soviet papers on casting of aluminum, magnesium and titanium alloys

08 p1504 A70-21126

Ti alloy band polished surfaces properties, obtaining required residual stresses by process control

08 p1507 A70-21198

Ti-based alloys with Al and Mo investigated for chemical composition and heat treatment effects on mechanical properties

08 p1518 A70-21200

High temperature thermomechanical treatment effects on stainless steels and Ti alloys microheterogeneity, noting corrosion resistance improvement

08 p1519 A70-21444

Ti alloys failure-safe design developing procedures for incorporation of stress-corrosion cracking characterizations into ratio analysis diagram system

08 p1519 A70-21456

Thermal and athermal components of flow stress and deformation dynamics in Ti-Al alloy

08 p1521 A70-21578

Cobalt modified Ti-6Al-4V plate and billet, testing effects on heat treatment response, microstructure, tensile and fatigue properties, fracture toughness, etc

08 p1523 A70-21852

Silicon containing alpha matrix Ti alloy with high creep strength and stability at elevated temperatures, studying processing and heat treatment effects on properties

08 p1509 A70-21853

Fiber composites-Ti alloy adhesive, rivet and combined joints for aircraft applications, noting fiber orientation role in joint tensile strength

08 p1509 A70-21905

Temperature effect on plastic flow in Ti-scavenged Fe, attributing microyielding to edge dislocations motion

08 p1525 A70-21959

Hydrides precipitation in Ti-Al-Mo-V alloys using transmission electron microscopy, discussing crystal structure, activation energy, hydride-matrix phase interface, etc

08 p1525 A70-21964

Gas saturation and inhomogeneity in surface layer of Ti alloys with alpha and beta stabilizers after high temperature heating

09 p1700 A70-22078

Titanium and titanium alloys bonding, discussing pretreatment, adhesives and assessment of temperature, environment and nuclear radiations

09 p1704 A70-22750

Al and Ti alloys residual stress determination by X ray diffraction

09 p1704 A70-22796

Fracture toughness and deformation kinetics dependence on compositional, microstructural and textural variations of alpha and alpha-beta Ti alloys at low temperatures

09 p1704 A70-22801

Growth kinetics of gamma prime precipitate in Ni-Ti alloy noting Ti content variation as function of aging

09 p1706 A70-22812

Electrical resistivity of TiNi and TiCo compounds and alloys measured at various temperatures after quenching or annealing

09 p1707 A70-23194

Phase diagram of Ti-Ta-Cr system, plotting isothermal and polythermal sections by microstructural and X ray analysis

09 p1709 A70-23787

Phase diagram of Ti-Ta-V system, determining solubility of sigma Ta and V in alpha and beta Ti in solid solutions

09 p1709 A70-23788

Phase equilibrium diagram and heat resistance of Ti-Al-Nb alloys along radial section by thermal and microstructural analysis

09 p1709 A70-23789

Isomorphous beta type Ti-Mo alloy omega phase transformations and morphology by electron microscopy, relating hardness to aging

10 p1902 A70-23817

Tantalum solubility in alpha titanium and Ti-Ta system physicochemical properties using metallographic, X ray, hardness and resistance analysis

10 p1903 A70-23864

Transformation kinetics of Ti alloy under isothermal conditions in solution treatment as function of temperature

10 p1903 A70-24025

Titanium high strength alloys, considering hardening by interstitials, precipitation, solid solution, etc

10 p1904 A70-24425

Metal working technology of Ti and alloys for structural parts fabrication for Concorde aircraft, describing laser cutting, electron beam welding, explosive forming, etc

10 p1895 A70-24594

Ti-Al-Zr-W-Si alloy fracture surface concentric markings number related to loading cycles after crack formation

10 p1904 A70-24837

Stacking faults developed in double hexagonal closed-packed phase of Ni-Ti alloy in cold worked and annealed conditions, using X ray line broadening

10 p1906 A70-25228

Multicomponent Ti alloys mechanical properties for use in cryogenics describing alloying advantages with tantalum

10 p1906 A70-25295

Design mean stress and ground-air cycles minimum stress effect on fatigue behavior of titanium alloy in supersonic transport operating environment [SAE PAPER 700033]

11 p2128 A70-25370

Heat resistance and elastic properties of binary Ti-Mo alloys as function of phase structure and chemical composition

11 p2066 A70-25915

Air and salt water tensile and shear mode cracking of titanium alloy sheets examined with electron fractographs

11 p2067 A70-26099

Saturn booster Ti alloy pressure vessel forging, heat treatment and welding, discussing machining, cleaning and tooling [SME PAPER AD-70-733]

12 p2241 A70-27085

Diffusion bonding processes for Ti aerospace structural elements, describing electric blanket, roll and press bondings [SME PAPER AD-70-736]

12 p2242 A70-27089

Ti alloys tensile properties correlated with microstructure for multiple heat treatment cycle variations for high strength and adequate ductility

12 p2252 A70-27107

Fatigue crack growth dependence on load profile, temperature, test frequency and environment and stress in high strength Al and Ti alloys and steels

13 p2431 A70-28604

Ti-6Al-4V dissolution in HCl-methanol, investigating corrosion rate

13 p2433 A70-28779

HF resistance welding and roll diffusion bonding fabrication of thin complex structures from Ti alloys in aerospace industry

13 p2418 A70-28828

Cu-Fe-Ti ternary system via microscopic, X ray and thermal analyses, measuring microhardness, electrical resistivity and magnetometry

13 p2433 A70-28863

Thermodynamic data for chemical reactions of Ti alloys formation with Al obtained by measuring galvanic cells emf with solid electrolytes at elevated temperatures

13 p2434 A70-28889

Carbide precipitation in metastable beta-Ti alloys, noting precipitations confinement to grain boundaries in alloys containing 15 percent Mo

13 p2434 A70-29083

PH variation effect on sea water on stress corrosion cracking behavior of Ti alloys

13 p2435 A70-29174

Titanium alloys powder metallurgy, considering manufacturing methods and physical, chemical and mechanical properties

13 p2435 A70-29214

X ray K spectra of Ti-Cr alloy for electron structure in titanium chromide phase region, discussing spectral intensities

13 p2435 A70-29375

Thick plate titanium alloy welds using filler wire to regulate chemical composition and plate phase constitution

13 p2435 A70-29456

Phase transformations in TiNi with equiatomic composition, using internal friction, electrical resistivity and dilatometry

13 p2435 A70-29499

Ti-8Al alloy embrittlement from ordered phase precipitation during aging using tensile, impact and hardness tests, optical and electron transmission microscopies

13 p2436 A70-29624

TITANIUM ALLOYS

Growth kinetics of strengthening phase during aging of NiCr-W-Mo-Al-Ti alloys, considering gamma prime particles at different Al/Ti ratios 14 p1594 A70-30169

Interatomic bond strength in solid solutions of Ti-Sn-O with respect to heat resistance at elevated temperatures 14 p2595 A70-30170

Be-Al-Ti system liquidus surfaces and invariant equilibria by chemical, thermal, X ray and microscopic methods, discussing phase diagrams 14 p2595 A70-30839

Hydride segregation in Ti alloy weldments made with unalloyed Ti filler metal, determining effect on mechanical properties 14 p2591 A70-30932

Low pressure diffusion welding for joining Ti-6Al-4V alloy in Ar atmosphere under compressive loading, evaluating performance 14 p2591 A70-30933

Optimum diffusion welding temperature for Ti-6Al-4V alloy determined from tensile and creep tests 14 p2591 A70-30934

Electrochemical processes associated with stress corrosion cracking of Ti-Al-Mo-V alloy in aqueous environments 15 p2755 A70-31474

Stress corrosion cracking of Ti and Ti-Al-V alloy in liquid dinitrogen tetroxide 15 p2755 A70-31475

Omega phase embrittlement in aged Ti-V alloys, discussing precipitation effect on tensile properties 15 p2756 A70-31570

Ti alloy suitability for fastener applications noting cold workability, high strength and stress corrosion resistance [ASM PAPER W70-17.3] 15 p2760 A70-32338

Room temperature mechanical properties and structure of age hardened Ti-Cu alloys 15 p2761 A70-32384

Ti-Al-V-Sn hardenability, using high temperature solution treated Jominy bars tests 15 p2762 A70-32393

Phase transformations in beta isomorphous Ti alloys, discussing effects on omega and alpha phases during quenching and aging and on martensite under stress 15 p2763 A70-32807

Beta phase decomposition kinetics and strain hardening inhibitions in Ti-base Mo alloys, using metallographic, dilatometric and X ray analyses 15 p2764 A70-32855

Internal friction in hydrogenated Ti-Mn alloys, observing relaxation peak formation under stress induced hydrogen diffusion in beta phase 16 p2930 A70-33082

Quench hardening and Ni content relationship in Ti-Ni intermetallic compounds, investigating heat treatment effect on mechanical properties 16 p2930 A70-33084

Optical properties of electropolished cubic Nb-Ti alloys at cryogenic and room temperatures in visible and near IR spectral range 16 p2930 A70-33205

Metastable beta phase decomposition in Ti alloy during mechanochemical treatment and aging, determining correspondence to alpha phase segregations via electron microscopy 16 p2931 A70-33207

Delayed rupture and relaxation in Ti alloys during cyclic deformation, comparing fatigue tests results for continuous and discontinuous cyclic loadings 16 p2931 A70-33209

Ti-Mo cermet alloys properties and production technology, testing corrosion resistance 16 p2931 A70-33220

Ti-Cu-Ag phase diagrams and liquidus surface structure, using metallographic, thermal and X ray techniques 16 p2931 A70-33221

Heating rate effect on Ti-V martensite decomposition, discussing elastic properties effects of partial tempering 16 p2931 A70-33256

Titanium electron beam welding in aerospace industry, discussing alloy properties and strength behavior 16 p2919 A70-33683

Solidification theory application to Ti alloys, predicting microsegregation in binary alloys 17 p3112 A70-34352

Homogeneity of commercially pure Ti and Ti-Al-V ingots, discussing oxygen distribution uniformity over cross section 17 p3112 A70-34353

Chemical and structural microinhomogeneity, diffusion and mechanical properties of Ti alloys in connection with phase transformation characteristics 17 p3112 A70-34354

Ti alloy ingot chemical macroinhomogeneity, investigating elimination by vacuum arc melting 17 p3112 A70-34355

Ti alloy forgings for aircraft industry, utilizing high strength/weight ratio 17 p3097 A70-34357

Ti alloys beta forging effect on physical properties and tensile ductility 17 p3097 A70-34358

Heating effect above beta transus at intermediate and final stages of processing on Ti alloys properties 17 p3097 A70-34359

Ti alloy aircraft parts heavy press forging, considering mechanical properties, temperature effects, cost factors, etc 17 p3097 A70-34360

Mono Graf casting process for Ti alloy aerospace applications, utilizing high strength/weight ratio and corrosion resistance 17 p3097 A70-34361

Ti precision casting methods, emphasizing alloys peculiarities 17 p3097 A70-34362

Ti alloys embrittlement, investigating time temperature dependence of brittle subsurface layer formation during elevated temperature air exposure 17 p3112 A70-34365

Anodic breakdown characteristics of Ti alloys as function of metal surface condition 17 p3113 A70-34366

Electrochemical mechanism in Ti alloys stress corrosion cracking, formulating mass transport kinetics model 17 p3113 A70-34368

Stress corrosion cracking of alpha-Ti alloys at room temperature, suggesting cathodic polarization promotion of film buildup 17 p3113 A70-34369

Aqueous stress corrosion dependence on microstructural features of Ti alloys, using optical and electron microscopy and X ray diffraction 17 p3113 A70-34370

Ti-Al-Mo-V alloy stress corrosion cracking, investigating correlation between dislocation substructure and ambient temperature corrosion susceptibility 17 p3113 A70-34371

Stress corrosion cracking in Ti and alloys, discussing metallurgical and environmental factors emphasizing exposure to hot salt, methanol, seawater, etc 17 p3114 A70-34372

Stress corrosion cracking in Ti-Al-V alloy exposed to Freon environments 17 p3114 A70-34373

Ti alloys crack formation during oxidation under stress, considering annealing and recrystallizing effects 17 p3114 A70-34374

Ti alloys crack initiation and propagation during hot salt stress corrosion 17 p3114 A70-34375

Ti alloys systems physical properties and structural phase stability, discussing electronic Fermi state density variation 17 p3114 A70-34376

Ti-Al alloy crystallographic structure, observing hexagonality for alpha phase 17 p3114 A70-34377

Thermodynamic properties of bcc beta phase in Ti-Cu and Ti-Al systems, discussing activities determination technique 17 p3114 A70-34378

Titanium base binary systems phase diagrams, describing component activity and compound phases heat of formation 17 p3114 A70-34379

Beta-Ti and Ti-Cr single crystals elastic moduli, determining A ratio temperature dependence 17 p3115 A70-34380

Kinetic simulation of atom rearrangements in order-disorder transformation for point defect movement in Ti alloys, considering vacancies and interstitials properties 17 p3115 A70-34381

Hydrogen behavior in Ti and alloys by internal friction measurement, attributing relaxation peaks to stress induced ordering of atoms 17 p3115 A70-34382

Binary titanium-oxygen and titanium-carbon alloys, investigating interstitial pair mechanism for internal friction peak formation 17 p3115 A70-34383

Ti interaction with elements of periodic systems, considering binary system phase diagrams 17 p3115 A70-34384

Interstitial impurities effect on mechanical properties of Ti alloys, discussing interaction between solutes and dislocations 17 p3116 A70-34390

Alpha Ti and alpha Ti-hydrogen alloys fatigue behavior, emphasizing twin formation influence and hydrogen effects 17 p3116 A70-34394

Titanium hydride deformation assisted nucleation in alpha-beta titanium alloy, showing low strain rate embrittlement and stress corrosion crack propagation in aqueous environments 17 p3116 A70-34395

Alpha Ti-hydrogen alloys, discussing fracture behavior temperature dependence 17 p3117 A70-34396

Hydrogen embrittlement of Ti and Ti alloys under plastic deformation and critical hydrogen concentration 17 p3117 A70-34397

Single phase alpha Ti alloy welds breaking strength, discussing delayed failure and cold cracking with various oxygen and hydrogen contents 17 p3117 A70-34399

Temperature cycling through phase transformation effects on plastic deformation of Ti and Ti-Al-V alloy under torsion and tension 17 p3117 A70-34400

Hot plasticity elongation of cast and wrought Ti-Al-V alloy as function of temperature and strain rate 17 p3117 A70-34401

Pressure forming Ti sheet alloy blanks in superplastic condition under controlled temperature and strain rate 17 p3117 A70-34402

Ti alloys martensitic transformations, metastable beta-phase decomposition and alpha-phase ordering 17 p3118 A70-34403

Martensitic transformation in Ti and Ti alloys, discussing shear systems influence 17 p3118 A70-34404

Twinned hexagonal martensites crystallography in Ti alloys, discussing alpha-beta and beta-fcc transformations 17 p3118 A70-34405

Cooling rate effect on beta phase transformation temperature in Ti-Nb and Ti-Al alloys 17 p3118 A70-34406

Ti alloys M sub s and beta sub s points thermodynamics, considering initiation of bcc-cph martensitic transformation 17 p3193 A70-34407

Ti binary alloys beta phase continuous cooling transformation, investigating additives effects 17 p3118 A70-34408

Metastable Ti alloys beta-omega-alpha decomposition and Ti-8Al alpha-ordered alpha transformation, using automatic measuring apparatus 17 p3118 A70-34409

Omega phase morphology in Ti alloy by electron microscope techniques, noting cubic structure 17 p3118 A70-34410

Omega phase stability in Ti and Zr alloys, interpreting upper temperature limit from critical temperature associated with peritectoid reaction 17 p3119 A70-34411

Martensite transformations and cellular phase separation in Ti-Cu alloys, using electron microscopy 17 p3119 A70-34412

Phase transformations and equilibrium diagram of titanium-oxygen alloys, using electron and optical metallography 17 p3119 A70-34413

Martensitic transformation effects on mechanical properties of beta quenched Ti binary alloys 17 p3119 A70-34414

Titanium alloys quench hardenabilities, determining variations with distance from end of Jominy bars after annealing 17 p3119 A70-34415

Age hardening process in Ti-Cu alloy at 400 C, using electron diffraction 17 p3119 A70-34416

High yield strength alpha-beta Ti alloys ductility control, observing fracture strength dependence on morphology, grain location and size for constant heat treatment 17 p3119 A70-34417

Phase diagrams of high strength metastable Ti beta alloys, showing minimum quantity of alloying elements for solid solution retention 17 p3119 A70-34418

Solution heat treatment temperature effects on strength and age hardening of Ti alloys 17 p3120 A70-34419

Shock deformation effects on strengthening and microstructure of Ti and Ti-Mo alloys 17 p3120 A70-34420

Ti alloy stability after long term creep exposure at various temperatures 17 p3120 A70-34421

Thermal exposure effect on room temperature mechanical properties of Ti alloys, noting diffusion bonding, hot forming and heat treatment 17 p3120 A70-34422

Ti-Al-Sn-Zr system high temperature creep strength and ductility retention 17 p3120 A70-34424

Al, Ga and In effects on creep and rupture stress of Ti at 500 C 17 p3120 A70-34425

Ti-Al-Nb system creep strength, oxidation resistance, density, forging and rolling 17 p3120 A70-34426

Forged alpha/beta Ti alloys, investigating relationship between mechanical properties and microstructures produced by heating 17 p3120 A70-34427

Ti-Al-Cr-Fe tensile, fatigue and creep properties at various temperatures, considering industrial applications 17 p3121 A70-34428

Ultrahigh strength alpha-beta titanium alloys, examining carbon and oxygen effects on mechanical properties

17 p3121 A70-34429

Ti-Cu alloy sheet material age hardening, considering cold and warm work effects at various stages in aging cycle

17 p3121 A70-34430

Weldability, tensile and fatigue properties of Ti sheet alloys, discussing TIG welds

17 p3121 A70-34431

Fatigue properties of solution treated and age hardened hot rolled Ti alloy bars, discussing sprayed tungsten carbide coatings effects on bearing properties

17 p3121 A70-34432

Strain gage measurements of elastic properties of Ti sheet alloys, computing polycrystalline properties from single crystal values

17 p3121 A70-34433

High strength Ti alloys depth hardenability, discussing mechanical properties and use in aircraft components

17 p3121 A70-34434

Metastable ageable beta Ti-Mo-V-Fe-Al alloy, discussing plate, sheet and forgings producibility, metallurgical characteristics and structural properties

17 p3121 A70-34435

High strength Ti alloys for aircraft gas turbine engines, determining critical properties for compressor fan blades

17 p3122 A70-34436

Heat treatment effect on strength and ductility of Ti-Al-V-Sn alloy by optical and electron microscopy and X ray diffraction

17 p3122 A70-34437

High strength Ti alloy for cryogenic applications, comparing plane strain fracture toughness

17 p3122 A70-34438

Heat treatment and composition effect on mechanical properties of alpha Ti-base alloy, discussing creep resistance, tensile strength, etc

17 p3122 A70-34439

Creep resistant Ti alloys with high temperature strength and stability, comparing tensile data for room temperature and 900 F

17 p3122 A70-34440

Fatigue characteristics of Ti alloy forgings for rotary wing vehicles, discussing effects of welding, annealing, reduction, surface finish and shot peening

17 p3122 A70-34441

Electron beam welding of Ti alloys in partial vacuum, describing mechanical tests and metallographic examinations

17 p3098 A70-34442

Forming Ti-Al-V sheet metal in heat treated conditions, showing mechanical properties improvement over mill annealed parts

17 p3098 A70-34445

Wear and fatigue of Ti-Mo-Al-Sn-Si /Hylite 50/ alloy with resistant Mo or Cr coatings

17 p3099 A70-34447

Ti alloys use in jet engines design, considering weight, structural stability, useful temperature range, cost, etc

17 p3146 A70-34448

Ti alloys use in Olympus 593 engine for Concorde SST, discussing weight saving, mechanical properties and manipulation characteristics

17 p3146 A70-34449

Ti fabrications in aircraft engines, discussing alloys properties, sheet deformation, fusion welding, porosity, etc

17 p3099 A70-34450

Alloy applications to Boeing supersonic transport airframe and components, discussing materials characteristics and manufacturing processes

17 p3099 A70-34451

Stress corrosion cracking of Ti alloys in nitrogen tetroxide and methyl alcohol environments in Apollo spacecraft pressure vessels

17 p3199 A70-34453

Aircraft structural materials, considering high strength steels Al and Ti alloys

17 p3124 A70-34675

Decomposition of unstable beta solid solution of Ti-V alloy, using X ray and microscopic analyses

17 p3125 A70-35336

Ti alloys thermomdiffusion impregnation with rarefied nitrogen and oxygen plasma, determining optimal gas pressure and temperature conditions and magnetic field frequency effects

17 p3101 A70-35391

Pyrolyzed tetraethoxysilane for carburizing steels and Ti alloys at 850-1050 C

17 p3102 A70-35409

Martensitic phase change effects in TiNi on ultrasound waves propagation in transition region, using pulse echo measurements

17 p3126 A70-35603

Low temperature effects on Ti alloys welded joints elasticity

17 p3126 A70-35637

Creep and failure tests for Ti alloys at 500 C, discussing work dissipation during creep process

17 p3126 A70-35714

Cobalt addition to Ti-Al-V alloys, examining yield strength, heat treatment, ductility and microstructure

18 p3271 A70-35964

Ti-Al binary and Ti-Al-X ternary alloys grain boundary precipitation kinetics and correlation with mechanical properties

18 p3272 A70-36035

Ti-Al alloys room temperature mechanical properties after age hardening

18 p3274 A70-36055

Chemical composition selection for Ti alloys with low susceptibility to hydrogen induced brittleness

18 p3274 A70-36121

Mechanical properties of binary Ti-Ni and ternary Ti-Mo-Ni alloys

18 p3275 A70-36122

Isothermal phase equilibria in Ti rich ternary Ti-Al-Fe alloys, noting eutectoid transformation

18 p3275 A70-36123

Polythermal phase equilibrium and heat resistance of Ti-rich Ti-Zr-Al alloys, noting creep and tensile tests

18 p3275 A70-36124

Cross sectional phase diagram of Nb-Ti-Mo-V, discussing continuous crystallization and composition dependent hardness and resistance

18 p3275 A70-36125

Ti alloy prior plastic deformation effect on fatigue strength under bending, tension, torsion and rolling

18 p3275 A70-36141

Quantitative analysis of nonmetallic inclusions in steels containing Ti after electrochemical anodic dissolution

18 p3277 A70-36464

Depth measurement of gas-saturated surface layer in Ti alloys, using microhardness method

18 p3277 A70-36472

Nuclear irradiation effect on embrittlement of Ti and Ti alloys at cryogenic temperature, determining radiation damage threshold as function of tensile properties changes

18 p3278 A70-36567

Heat resistance of cast, forged and annealed Ti-Cu alloys, discussing forged alloys mechanical properties as function of chemical composition and temperature

19 p3449 A70-37273

Alloying elements effect on diffusion coefficient of hydrogen in low-alloyed alpha titanium

19 p3449 A70-37274

Ti-Si eutectic alloys unidirectional solidification by zone melting

19 p3450 A70-37375

Ti alloys low temperature strength and plasticity, noting twinning and additive effects

19 p3450 A70-37457

Friction reducing oxide layer effects on Ti alloys low temperature plastic and mechanical properties

19 p3450 A70-37458

Ti alloys creep and fatigue breakdown under cyclic tensile loads at room temperature

19 p3452 A70-38434

Ti-Nb-Zr alloys strength and plasticity at various temperatures, noting compositional effects on tensile and yield strength

19 p3453 A70-38712

Interstitial oxygen effect on properties and precipitation processes in pure V and V-Ti alloys, using electron microscope

19 p3454 A70-38812

Heat treatment and alloying element influence on phase and structure transformations in Ti alloys, investigating mechanical properties and creep resistance

20 p3645 A70-39039

Ti alloys fine structure, mechanical properties and alloying elements diffusion mobility during heat treatment, observing chemical and structural inhomogeneities

20 p3645 A70-39040

Beta Ti alloy decomposition study during aging by diffraction electron microscopy, forming finely dispersed coherent precipitates

20 p3645 A70-39041

Ti alpha alloys subjected to heating in beta region, investigating plate-like precipitates by electron transmission microscopy

20 p3645 A70-39042

Two phase Ti alloy subjected to quenching and annealing studied by diffraction electron microscope, discussing needles complex fine structure

20 p3645 A70-39043

Beta Ti-V-Cr-Al phase transformations below 500 C, discussing metastable phase, bcc formation and thermodynamics

20 p3646 A70-39106

Temperature effect on radiation characteristics and cryogenic tensile properties of irradiated Be, Ti and Al alloys

20 p3647 A70-39111

Ti binary alloys with V, Nb and Mo, determining phase boundaries by diffusion layers method and electron microscope analysis

20 p3649 A70-39727

Ti alloy bolts mechanical properties improvement by beta heat treatment

20 p3650 A70-39965

Beta III Ti alloy for aircraft fasteners, describing microstructure and mechanical properties

20 p3650 A70-39966

Metastable beta Ti alloy as-quenched microstructure stability with respect to thin foils transformation during electrolytic polishing and bulk specimens during cold rolling

21 p3841 A70-42150

Magnesium Al and Ti alloys electron beam welding for aerospace industry, discussing material requirements, weld quality and optimum conditions

22 p4042 A70-42338

Ti and Al alloy weldments plane strain fracture toughness and mechanical properties for cryogenic applications, using gas metal arc and gas tungsten arc welding

[ASME PAPER 70-MET-4]

22 p4043 A70-42423

Repair weld procedures effects on annealed Ti-Al-V weldments mechanical properties, examining defects in inert gas shielded arc welded joints

[ASME PAPER 70-MET-1]

22 p4043 A70-42425

Orthorhombic martensite tempering behavior in Ti alloys, observing distinct stages for binary and ternary alloys

22 p4054 A70-42742

Ti alloy tension creep tests at room temperature, determining strength for correlation with stress relaxation

22 p4055 A70-43097

Electro-thermal-mechanical switches based on shape-memory effect in Ti-Ni alloys

22 p3965 A70-43330

Ti alpha alloy fracture characteristics at high temperatures, discussing strain rates, deformation resistance and grain growth

22 p4056 A70-43343

Phase diagrams and nonvariant equilibria points of Ti-Si alloys subjected to prior annealing, determining phase transformations, decomposition and other properties as function of temperature

22 p4057 A70-43350

Ti and Zr based superconducting alloys with Nb content, measuring longitudinal critical currents in wire and ribbon samples

22 p4087 A70-43462

Fatigue limits of Ti alloy by Wohler and Locati loading methods

22 p4204 A70-43933

Scale factor effect on brittle fracture resistance for Ti and Al alloys and high strength steels

23 p4265 A70-43936

Heating rate effect on Ti-V martensite decomposition, discussing elastic properties effects of partial tempering

23 p4206 A70-44285

Cross slip between screw dislocations coplanar arrays in Ti-Al alloy, noting fringe pattern and bowing absence

24 p4359 A70-45248

Short-term creep and erosion resistance testing of Ti alloy in high speed air flows under aerodynamic vibrations

24 p4360 A70-45826

Chemical composition effects on heat resistance, elastic properties and density of Ti-Ta alloys

24 p4360 A70-45830

Phase equilibria, hardness and electroresistivity of Ti-Al-V alloys at solid compound section for reinforced metal composites

24 p4361 A70-45831

Heat treatable beta Ti alloys cold workability, fracture toughness, tensile ductility and applications

[SAE PAPER 700856]

24 p4361 A70-45880

Ti-Mo and Ti-Mn alloys omega transition phase, describing shape and crystallographic characteristics

24 p4361 A70-46178

TITANIUM BORIDES

Quantitative method developed for photometric determination of B in nickel or titanium borides, using magnezon I reagent in alkaline solutions at various pH

03 p0504 A70-12983

Ti, Zr and Hf diborides electrophysical properties, discussing temperature effects and electronic structures

23 p4205 A70-43991

Titanium diboride particles contact surface increase during sintering in vacuum as function of temperature

23 p4205 A70-44042

TITANIUM CARBIDES

Titanium carbide hemispherical and spectral emissivity and electrical resistivity measured at high temperature

03 p0512 A70-13752

Titanium carbide based cermets with steel matrices, studying heat treatment effects on hardness

04 p0696 A70-14462

Titanium carbide sintering under continuous heating in Ar atmosphere, studying ultrasonic waves effects on compaction process

04 p0696 A70-14463

Optimal temperature for sintering of compact titanium carbide in Ar atmosphere

04 p0697 A70-14468

Oxidation behavior of TiC base alloys containing Mo

04 p0708 A70-15312

Thermoelectric characteristics of graphite and titanium carbide compared with platinum after prolonged annealing at 2300 C 07 p1316 A70-19661

Phase equilibria, crystallization and solidus surface in transition conode triangle of ternary system Mo-Ti-C at high temperatures 07 p1310 A70-19804

Low temperature oxide film effect on porous titanium carbide impregnation by liquid steel 07 p1311 A70-19805

Temperature dependence of Vickers pyramid hardness for Ti, Zr and Hf carbides at wide temperature range in vacuum 08 p1516 A70-20986

Monochromatic radiation emissivity temperature dependence of monocarbides of Ti, Nb and alloys in homogeneity region 08 p1516 A70-20994

Pyrolytic C-TiC alloys obtained by precipitation from gaseous phase, discussing microstructural properties anisotropy 08 p1517 A70-21146

Compacted titanium carbide powder coarsening recrystallization within homogeneous region, determining relation between initial activation energy and carbide composition 12 p2254 A70-27284

Wear resistant titanium carbide based cermet material production by impregnation techniques, discussing grain size and heat treatment effects 19 p3450 A70-37453

Rotating Ti disk in liquid Co flow, investigating titanium carbide dissolution kinetics 20 p3648 A70-39245

Titanium dicarbide and tetracarbid vaporization at high temperatures, using Knudsen effusion method with mass spectroscopy, determining dissociation energies 21 p3773 A70-41274

Stacking fault energy determination, discussing impurities influence in equilibrium dimensions distortion of extended nodes in titanium carbide 22 p4053 A70-42727

TITANIUM CHLORIDES

Ti tetrachloride, Si tetrachloride and hydrogen gas mixtures flow over heated graphite substrates, describing Ti silicides formation 09 p1703 A70-22646

TITANIUM COMPOUNDS

NT BARIUM TITANATES

NT ILMENITE

NT LEAD TITANATES

NT MAGNESIUM TITANATES

NT PEROVSKITES

NT RUTILE

NT STRONTIUM TITANATES

NT TITANATES

NT TITANIUM BORIDES

NT TITANIUM CARBIDES

NT TITANIUM CHLORIDES

NT TITANIUM NITRIDES

NT TITANIUM OXIDES

Sodium-titanium-boron-silicate glass opacity and fusibility increase during partial substitution of K for Na, noting phase composition changes 05 p0871 A70-16598

Titanium and zirconium dihydrides room and higher temperature electrical resistivity, Hall effect and thermal expansion coefficients 08 p1517 A70-21149

Mechanical and physical properties of Nb-Ti binary annealed alloys as function of compound NbTi using microscopic and X ray phase analysis 09 p1704 A70-22755

Powdered titanium oxycarbides, carbonitrides and oxynitrides oxidation by X ray phase analysis, determining titanium dioxide as final product 12 p2254 A70-27285

Titanium and Ti-Al single crystals microscopic plastic deformation features, slip modes and dislocation substructures 17 p3116 A70-34389

Molecular orbital energy level diagram for metal ion X ray emission and absorption spectra interpretation from titanium and vanadium compounds 21 p3853 A70-41901

X ray K and L emission bands and absorption spectra from TiO, TiN and TiC compared with density of states histograms, considering electronic band structure 22 p4086 A70-43003

TITANIUM DIOXIDE

U TITANIUM OXIDES

TITANIUM NITRIDES

Dissociation energy of gaseous TiN molecule at high temperature 15 p2695 A70-32748

TITANIUM OXIDES

NT ILMENITE

NT RUTILE

Aluminosilicate glass physical properties and chemical stability in water, alkaline and acidic agents, studying titanium oxides additions effect 05 p0871 A70-16596

Ingredient proportions for enamels containing titanium and boron oxides 05 p0871 A70-16597

Excess titanium dioxide effect on electric resistance of semiconductive barium titanate ceramics suitable for posistors 07 p1355 A70-18654

Titanium monoxide absorption bands in class M stars spectra, estimating band head intensities 08 p1569 A70-20829

Powdered titanium oxycarbides, carbonitrides and oxynitrides oxidation by X ray phase analysis, determining titanium dioxide as final product 12 p2254 A70-27285

Titanium monoxide thin film as low temperature getter, measuring activity coefficient and capacity under ultra high vacuum 15 p2783 A70-31844

Antireflection titanium dioxide thin films for aerospace silicon solar cells 19 p3358 A70-38201

Temperature dependence of titanium-zirconium oxide semiconductor compounds growth, using samples arc melted in purified He 20 p3687 A70-39631

Thin titania films electrical breakdown under high DC fields in high vacuum, suggesting reduction to lower order semiconducting oxide 22 p4085 A70-42621

Neutron diffraction of ordered atomic oxygen structures in titanium suboxides, noting compositional dependence of physical properties 22 p4053 A70-42735

Cubic titanium oxycarbide structural characteristics, noting lattice constant dependence on component proportions and mutual solubility during formation 24 p4359 A70-45477

TITRATION

Simultaneous titration of gases, metalloids and metals in steels and refractory alloys by far UV vacuum spectrometry 08 p1455 A70-21842

TNT (TRINITROTOLUENE)

U TRINITROTOLUENE

TOBACCO

Cerebral circulatory reactions of smokers and non-smokers exposed to altitude, measuring vasomotor, blood flow and cardiac frequency indexes using scalp electrodes 12 p2172 A70-28042

Partial nucleotide sequences for fragments isolated from ribonuclease digests of tobacco mosaic virus RNA, suggesting genetic duplication possibility 13 p2363 A70-29798

TOCOPHEROL

Plasma tocopherol concentrations and vitamin E deficiency in dogs, noting pathologic changes in smooth muscle, central nervous system, skeletal muscle and retina 20 p3569 A70-38991

Heme biosynthesis defect in vitamin E-deficient rats affecting bone marrow synthesis of delta-aminolevulinic acid and liver formation of porphobilinogen 24 p4304 A70-46146

TOLERANCES [MECHANICS]

NT IMPACT TOLERANCES

Electronic gauging machine for multipoint measurement at preselected points around turbine blade airfoil produced by electrochemical machining 01 p0105 A70-11397

Electrical discharge machining showing close tolerance sizing capability on honeycomb panels 02 p0310 A70-12665

Single dispersion statistical analysis by simultaneous parameters tolerances application 03 p0518 A70-12937

Damage tolerance as design consideration for aircraft safety and reliability, discussing application of failed single principal member concept to airframe construction 07 p1417 A70-20401

Orifice diameter for low Reynolds number flowmeter dependent on pipeline diameter tolerances 08 p1482 A70-20684

Component tolerances effect on transfer function of networks, calculating sum variance for two terminal networks 10 p1833 A70-24223

Tolerance limits for equipment periodic field checkout, considering performance failure effects on system accuracy, costs and availability 10 p1896 A70-24911

Algorithm for selective quadrupole parameter tolerance calculation, combining random search method with statistical testing 11 p2018 A70-25923

Rectangular tolerancing of dipole impedance values scatter for random passive network samples 12 p2194 A70-26968

Low Reynolds number laminar flow gas turbine regenerators, investigating manufacturing tolerances effects on heat transfer and flow friction behavior 14 p2629 A70-31022

Axial flow multistage turbines performance, examining profile manufacturing tolerances effects on cost 16 p2970 A70-33677

Soviet book on operational tolerances in radio electronic equipment from reliability criteria 20 p3597 A70-39400

Material thickness tolerances control for weight minimization of aerospace vehicles by abrasive metal grinding, improving surface quality 20 p3638 A70-40358

Two-component optical system for laser radiation collimation, calculating tolerances for fabrication and assembly 22 p4051 A70-43560

TOLERANCES [PHYSIOLOGY]

NT ACCELERATION TOLERANCE

NT ALTITUDE TOLERANCE

NT COLD TOLERANCE

NT HEAT TOLERANCE

NT HUMAN TOLERANCES

NT RADIATION TOLERANCE

Rodents hypoxia tolerance following adaptation to hypercapnia by recording time of useful consciousness /TUC/ in repeated sloped surface clinging tests 01 p0026 A70-11249

White mice hypoxia tolerance enhancement after intraabdominal administration of dilute hydrochloric and lactic acids 03 p0424 A70-13718

Fluorine toxicity, discussing fluorine reactions with animal proteins and lipids, short-term exposure toxicity data, emergency tolerance limits, threshold limit, etc 10 p1824 A70-24060

White mice hypoxia tolerance enhancement after intraabdominal administration of dilute hydrochloric and lactic acids 11 p1985 A70-25518

Hypoxia tolerance of albino rats in He-oxygen and Ar-oxygen environments in heat-pressure chamber, discussing He-oxygen mixture cooling effect 11 p1987 A70-26103

Rhesus monkeys tolerance to graded increase in closed environment carbon dioxide, examining heart rate and cardiac rhythm 11 p1988 A70-26517

Ambient temperature effects on rats and white mice tolerance to hypoxia, asphyxia and hypercapnia in nitrogen-oxygen and He-oxygen atmospheres 17 p3030 A70-35353

Rhesus monkeys PCO2 tolerance in low pressure environments, observing hypothermia and heart and respiratory rates depression 21 p3765 A70-41486

Carbon dioxide exposure limits of rhesus monkeys, examining body temperature, respiratory rate and pressure effects 22 p3973 A70-43642

Weightlessness and immobilization effects on mechanical tolerance of bone compressive and breaking strength in monkeys 22 p3973 A70-43648

TOLLMEIN-SCHLICHTING WAVES

Laminar flow mixing stability and diffusion flame flow field measurements revealing role of Tollmien-Schlichting waves in enclosed flames vibrations [WSCI PAPER 69-46] 06 p1179 A70-17985

Tollmien-Schlichting waves in flat plate Blasius boundary layer, comparing experimental and theoretical critical Reynolds number 23 p4179 A70-43975

TOLUENE

Thermal conductivity of water, toluene and benzene in coaxial cylinders, taking into account edge heat losses 23 p4276 A70-44216

TONE

U PITCH

TONGUE

Integrated static discharge frequencies of cat lingual cold receptors measured as function of constant temperature 01 p0017 A70-10472

TONOMETRY

U INTRAOCULAR PRESSURE

U PRESSURE MEASUREMENTS

TONUS

U MUSCULAR TONUS

TOOLING

Electrical discharge machining using electrical spark eroding action for machining tough metals in burr-free intricate configurations, including narrow slots and blind holes 03 p0497 A70-13564

Numerically controlled gas tungsten arc welding, discussing tape programming, fixture design and fabrication for various welded metal joint configurations 11 p2058 A70-25661

Metal matrix composite structures tooling and fabrication processes, considering forming, joining, welding, machining joining, etc [SAE PAPER 700752] 24 p4348 A70-45873

TOOLS

NT GRINDING MACHINES

NT MACHINE TOOLS
 NT MILLING MACHINES
 NT SPACE TOOLS
 Nd laser drilling and welding tool for microminature electronic device fabrication 14 p2594 A70-30639
 Epoxy laminating resin evaluation for tooling industry, considering diluent, fillers, thixotropy, hardeners and physical property testing 16 p2936 A70-33360
 Grinding by abrasive tape, superimposing transverse vibrations to improve performance and life 22 p4046 A70-42816

TOOTH DISEASES
 Ultrasonic detection of tooth surface layer demineralization, noting surface and subsurface enamel structural differences 22 p3978 A70-42955

TOPOGRAPHY
 NT LUNAR TOPOGRAPHY
 NT TERRAIN
 Microtopography effects on measuring horizontal gravity gradients by gravimeters 02 p0295 A70-11799
 Martian topographic contours determined from detected carbon dioxide abundances indicating large scale differences from previous data 02 p0373 A70-12390
 Artificial satellites for geodetic, topographic and cartographic purposes, outlining topographic and distance measuring equipment 03 p0475 A70-13831
 Bottom topography effect on jets stability in baroclinic fluid, discussing two layer model 04 p0715 A70-15518
 Martian topographical radar ranging data correlated with surface features, discussing deserts, canals and maria topography 05 p0909 A70-16388
 Earth model based on free air gravity anomaly with condensed topography for eliminating gravity reduction difficulties, noting use in Venen-Meinsz formula 05 p0840 A70-16640
 Automated techniques for topographic mapping, considering scales used 07 p1281 A70-19371
 Intercensus population estimate by air photos, topographic maps and local and state census of population and housing 10 p1878 A70-24737
 Topographic shadow linears image enhancement by low angle illumination, describing pseudoradar technique for subcontinental sized fracture systems detection 12 p2221 A70-26960
 Microtopography of fracture surfaces by stereo electron fractography, using large angle tilting of specimens 13 p2431 A70-28605
 Venus and Mercury surface height variations near equators, using radar time delay and Doppler observations 14 p2647 A70-31077
 Mars surface topography and roughness from radar measurements 14 p2648 A70-31081
 Gemini spacecraft photograph patterns revealing relationship between cloud formation and topography 18 p3258 A70-36298
 Fundamental equations of physical geodesy for earth figure by oceanic and continental parts via external gravity field 20 p3617 A70-39069
 Natural and cultural landscape pattern classification in aerial photointerpretation using land-system concept 21 p3826 A70-41401
 Internal and integral photointerpretation in aerial photography, discussing landscape information reliability increase by interdisciplinary method 21 p3826 A70-41403
 Pseudo three dimensional effect on monoscopic radar imagery for topographic relief differentiation, using offset superposition of transparencies 22 p4031 A70-42965
 Two dimensional stratified flow over extended obstacles with source disturbances, indicating topographical effect on vertical wind shear in troposphere 23 p4214 A70-44031
 Optimal timing for aerial photographic mapping of landscape types including tundra, forest, steppe, meadow, desert and mountain areas 24 p4328 A70-45196

TOPOLOGY
 NT FIXED POINTS [MATHEMATICS]
 NT HOMOTOPY THEORY
 NT IMBEDDINGS [MATHEMATICS]
 NT INVARIANT IMBEDDINGS
 NT METRIC SPACE
 Topological properties of plane flow in subsonic region behind smooth shock wave in uniform supersonic flow, discussing shock wave convexity 01 p0068 A70-11580

Topological analysis of lumped mechanical vibration systems using mathematical induction, considering linear graphs properties 04 p0773 A70-15077
 Stronger locally convex topology on space C/S/ of bounded continuous functions proved in nonagreement with strict topology on norm bounded sets 05 p0875 A70-16050
 Covering properties of topological space as function of set density 07 p1323 A70-18963
 Locally compact topologies on group G and corresponding continuous irreducible unitary representations, noting existence of subgroup 08 p1534 A70-21276
 Discontinuous weak solutions of differential equations of gas dynamics as limits in topology of functions 10 p1866 A70-24109
 Computerized data communication system /CDCS/ equipment unit capacities and topology specified with aid of vertex weighted linear graph 11 p2009 A70-26253
 Automatic input data generation for finite element method using algorithm based on complex geometrical configurations topological classification in terms of natural coordinates 11 p2144 A70-26678
 Topology and component values in computerized design of distributed lumped active networks 15 p2711 A70-32595
 Organic molecules topology, discussing Hamilton circuits, DENDROL applications, etc 16 p2855 A70-33298
 Eigenvalue problem in elasticity theory, treating nonlinear equations solutions multiplicity by topological methods 24 p4420 A70-45273

TORCHES
 Plasma torch for increasing material fusion temperatures in metallization methods 12 p2244 A70-28072
 Plasma arc welding torches nozzle dimensions and shape dependence on thermal and electrical characteristics, optimizing energy output 22 p4042 A70-42378

TORNADOES
 Tornado producing thunderstorms, using conventional surface and upper air data combined with ATS-III data, discussing mesoscale disturbances and momentum exchange 06 p1102 A70-18583
 DC-8 jet transport encounter with tornado aloft on 9 November 1963 06 p0987 A70-18586
 Velocity and pressure distributions of tornado-like two cell vortices within boundary layer, using different assumptions for eddy diffusion coefficient 14 p2604 A70-30547
 Tornadoic vortex motion equation derivation based on kinematical modification of Kelvin theorem 23 p4215 A70-44547

TOROIDAL DISCHARGE
 NT RING DISCHARGE
 Plasma electron temperature and density in Tokamak T3 toroidal discharge measured by Thomson scattering of laser light 02 p0346 A70-12199
 Toroidal solar field emergence to surface forming magnetic field of active region 13 p2493 A70-29392

TOROIDAL PLASMAS
 Tokamak-type magnetic configurations application to thermonuclear reactor, discussing equilibrium and stability parameters minimum values, operating pattern and heating method 02 p0349 A70-12756
 Ionic noise during plasma turbulent heating in toroidal facility, discussing oscillation spectrum 07 p1349 A70-19552
 Electron clouds injection and containment by magnetic field in toroidal vacuum chamber, studying causes of cloud instability 07 p1353 A70-19994
 Transverse particle and energy fluxes in toroidal magnetic traps magnetic fields with ionized plasmas, discussing particle diffusion coefficient and thermal conductivity 08 p1554 A70-21807
 Ionosphere effect on toroidal magnetodynamic waves in idealized representation, analyzing oscillations correlation between adjacent magnetospheric shells 10 p1875 A70-24444
 Ionic noise during plasma turbulent heating in toroidal facility, discussing oscillation spectrum 15 p2777 A70-31459
 Stochastic heating of plasma in toroidal trap/stellarator, showing discharge ignition potential dependence on microwave oscillator frequency 22 p4084 A70-43394
 Inertia effect on low density plasma losses in toroidal MHD equilibrium in model stellarator field 24 p4383 A70-45115

Stable ellipsoidal plasma configurations in alternating electrode annular system, considering longitudinal magnetic field strength, electrode voltage and gas discharge chamber pressure 24 p4385 A70-45456

TOROIDAL SHELLS
 Buckling of toroidal shells with reasonably uniform thickness distribution manufactured by casting epoxy resin material 04 p0779 A70-15615
 Toroidal metallic shells stability under static loads, determining snap-through pressures in pressure chamber with nitrogen working gas 08 p1588 A70-21195
 Thick-walled toroidal shell under various load distributions, analyzing stress-strain state by networks method using computer program 10 p1957 A70-24250
 Influence coefficients for toroidal shells under axisymmetric edge loads, taking one term in asymptotic expansion of Hankel function 11 p2132 A70-25693
 Elastic material filled cylindrical, segmented toroidal and conical shells thermal stability, allowing for stiffener eccentricity 13 p2516 A70-29523
 Influence function for thin toroidal shell under uniformly distributed axisymmetric load, determining stresses and displacements in various cross sections 15 p2817 A70-32163
 Elastic thin walled toroidal shell under internal pressure, investigating large deformation and stress behavior 17 p3184 A70-34910

TORIODS
 Transmitting-receiving latching ferrite switch with 180 degree differential phase shift toroids for temperature stability and receiver protection in case of driver failure 03 p0458 A70-14036
 Eckert shadow technique for radiation view factors applied to toroid inside shadow hemisphere 08 p1546 A70-21832
 Magnetic scalar potential of circular loop represented by toroidal coordinate system, solving boundary value problems determining fields of coils and toroidal magnetic conductors 18 p3215 A70-36295
 Force-reduced superconducting toroidal magnet coils built with Cu plated Nb-Zr wire, investigating current enhancement characteristics 23 p4230 A70-44356

TORPEDO ENGINES
 NT CONTROL ROCKETS
 NT ULLAGE ROCKET ENGINES
 NT VERNIER ENGINES

TORQUE
 Gyroscopic bearing cross-torque control techniques, noting ball-group misalignment coupling [ASME PAPER 69-LUB-17] 01 p0101 A70-10388
 Torque upper bounds in Couette flow between concentric rotating cylinders, considering dissipation integral and boundary and continuity conditions validity 03 p0468 A70-13787
 Torque and flow patterns in supercritical Taylor instability regime of circular Couette flow 03 p0470 A70-14235
 Monograph on shear lag measurement in rectangular section beam subjected to bending or torque free from axial restraint, using inductance probe sensors 03 p0603 A70-14351
 Solar wind-induced torque calculated considering special and general relativistic effects, extending method to pulsar rotational model 04 p0739 A70-14593
 Ball bearing performance prediction using analytical technique based on race profilometry data, considering torque variation [ASME PAPER 69-WA/LUB-4] 04 p0698 A70-14769
 Viscous frictional torque on inner cylinder of eccentrically rotating concentric cylinders measured from laminar to turbulent flow 06 p1074 A70-17134
 Pulsar slowdown by radiation field torques indicated by alignment torque in magnetized oblique sphere rotating in vacuum 07 p1389 A70-20220
 Boundary layer of MGD flow past axisymmetric insulator body analyzed to determine torque due to Hall effect 09 p1663 A70-23579
 Gyroscopic platform stabilizers /GPS/ dynamic properties improved by compensation of perturbing torques 12 p2237 A70-28155
 Constraint torque elimination from vector equations canonical system for attitude dynamics of satellite consisting of arbitrarily interconnected rigid bodies [AIAA PAPER 69-923] 18 p3316 A70-36679
 Instrument ball bearings running torque prediction at high speed under combined radial and axial loads [ASLE PREPRINT 70AM 3D-3] 19 p3438 A70-38803

Direction cosine attitude control logic for spin stabilized axisymmetric spacecraft, using control torques generated by reaction jet system 20 p3669 A70-39679

Interplanetary plasma torque due to temperature and pressure anisotropy, considering solar wind angular velocity and sun angular momentum 20 p3712 A70-40423

Aerodynamic and gravitational torque effects on orbiting satellites attitude stability, applying Liapunov direct method in case of conservative aerodynamic torque [AIAA PAPER 69-832] 23 p4258 A70-44559

ESRO 1 satellites attitude reconstruction, describing torque determination from known altitude 23 p4259 A70-44614

Aerodynamic forces and torque on airfoil in potential jet from boundary asymptotes position, determining flow characteristics by electrical analogy 24 p4288 A70-45348

TORQUE MEASURING APPARATUS

U TORQUEMETERS

TORQUE MOTORS

Torque motor driven despin bearing assembly design with integral slip ring for tactical communications satellite /TACOMSAT/ 16 p2986 A70-34160

TORQUEMETERS

Multiplying digital device for measuring motor speed, torque and power, discussing optional applications and design 02 p0297 A70-12076

Micromotor torsion moment-speed characteristic curve obtained by automatic recording apparatus 09 p1672 A70-22026

Magnetostrictive measurements of torque from high speed rotating shafts 17 p3093 A70-35501

TORQUERS

Satellite stabilization one-axis control system using earth magnetic torquer 13 p2500 A70-28405

TORSION

Lorentz invariance test using bar magnet on torsion fiber, analyzing preferred reference frame in space assuming earth velocity coupled to electron spin through specific term 02 p0341 A70-12849

Rectangular anisotropic beam torsion using Green function combined with wide step network method 03 p0593 A70-13471

Apparatus for small specimen torsion tests at room temperature, describing machine capabilities 03 p0493 A70-13960

Axial compression effect on low cycle fatigue of thin walled metal tubes in torsion [ASME PAPER 69-MET-H] 04 p0705 A70-14880

Elastic-plastic torsion of convex cylindrical bars 06 p1165 A70-17534

Dynamic torsion of anisotropic circular cantilever beams and small pitch diameter springs under linear time dependent moment calculated by Saint Venant method 06 p1037 A70-17862

Boundary value problem of torsion for equilibrium of elastic body based on moment theory in absence of bulk forces 09 p1782 A70-23381

Truncated conical shell buckling under axial compression using method for torsion buckling, correlating to equivalent cylindrical shells 11 p2135 A70-25980

Spanwise distribution of aerodynamic torsion on sailplane wings in vertical dive, discussing wing twist and lift effects 12 p2156 A70-27721

Tensor and torsion functions on Abelian semigroups 13 p2440 A70-29076

Torsion of variable diameter rods based on moment theory of elasticity, solving integral equations system 13 p2517 A70-29774

Dynamic asymmetric elasticity problems, considering longitudinal and torsional wave propagation in bounded and unbounded micropolar media 15 p2818 A70-32178

Shear stress distribution in axially nonuniform circular shaft subjected to torsion, using finite difference approximations 16 p2988 A70-33001

Thin concentric circular cylindrical shells joined at ends by rigid diaphragms, describing free and forced torsional motion 16 p2992 A70-34019

Polycarbonate thin walled cylindrical shells mechanical and material stability under torsion 17 p3127 A70-34656

German monograph on form factors and torsion at shafts with longitudinal keyways under pure torsion 17 p3189 A70-35374

Second order incompressible elastic torsion problems reduction to two dimensional classical linear elasticity problem without body force 17 p3189 A70-35434

Open and multiply connected closed sections of varying thicknesses, solving for unrestrained torsion 19 p3545 A70-38339

Shearing strain in oriented fiberglass reinforced plastics under torsion, obtaining creep curves 20 p3655 A70-39768

Torsion of composite rectangular cross section beam consisting of isotropic media, using Green function and Fourier expansion 20 p3732 A70-40334

Rigid cylinder rotation and flexible shaft torsion observation by holographic interferometry 21 p3822 A70-40813

Tension-torsion machine developed from aircraft carrier catapult principle, producing radial loading paths 22 p4117 A70-43453

Torsion in rods with rectangular and trapezoidal cross sections, using functional-analytic iterative method 23 p4268 A70-44241

Inverted torsion pendulum performance improvement, describing dashpot to dampen lateral vibrations 23 p4202 A70-44950

Rumanian book on torsion in thin walled elastic structures of various cross sections covering calculation methods for box beams, cylindrical and conical shells, aircraft wings, etc 24 p4418 A70-45147

Elastic-viscoplastic bar quasi-static torsion problem, using approximate method for time dependent torsion function 24 p4425 A70-45993

TORSIONAL STRESS

Stress-strain effect on dislocation densities of cylindrical Mg single crystals deformed by torsion basal slip compared to tension test 01 p0122 A70-11236

Elastoplastic stress concentrations calculations in notched strips and shafts under tension, bending and torsion, using approximate method 01 p0211 A70-11425

Stress distribution of thin walled structure of open section, considering warping and torsional bending, using calculus of variations 03 p0596 A70-14030

Singular integral equation applied to elasticity theory of composite beam with or without cavity under torsion 04 p0000 A70-14416

Saint Venant torsion problem using finite element method, establishing direct matrix relation between forces and displacements 04 p0778 A70-15527

Shear testing and data reduction based on torsion analysis to obtain elastic shear constants of thin orthotropic Be sheets 04 p0664 A70-15552

Torsion testing apparatus for refractory materials at 2400 C, measuring applied torsion moment, twisting angle and second order modulus of elasticity 05 p0825 A70-15881

Torsion tests on cylindrical plastic metals, considering shear stresses calculation as function of torsion angle and changes determination as function of increasing cold work 05 p0927 A70-15996

Stability of clamped, hinged and elastically supported circular cylindrical shells under critical combined torsional and transverse pressure 05 p0934 A70-16227

Cryogenic temperature effect on short life torsional fatigue properties of Ni-Cr-Mo steel, discussing cyclic strain range effects 05 p0864 A70-16807

Normalized steel low cycle fatigue strength under bending and torsional rotation, testing linear damage accumulation theory 06 p1163 A70-17404

Axially uniform stress and strain in cylindrical shells, discussing Saint Venant torsion and displacement relations 07 p1405 A70-19255

Torsion of elastic half space containing circular crack with symmetry axis coinciding with annular stamp rigidly coupled to half space 07 p1414 A70-20183

Elastoplastic torsion of combined prismatic bars with transverse distribution of constant properties solved by computer 07 p1415 A70-20189

Metal adhesive joints strength under tensile and torsional stresses, considering effects of dimensions, metal type and surface finishing 08 p1504 A70-20886

Curved thin rods torsional and flexural waves propagation equations, considering geometry and shear and Young moduli 08 p1588 A70-21201

Prismatic thin walled shells with box type cross section under torsion using Vlasov variational method in conjunction with transfer matrices 08 p1589 A70-21248

Elastic/perfectly plastic hollow cylinder unloading under monotonic twist during torsion, considering sandhill-membrane analog validity 08 p1589 A70-21249

Constant cross section beam bending and torsion with allowance for moment stresses, deriving differential equations for displacement functions 09 p1773 A70-22538

Beams torsion problems solution by variational method of variables separation, obtaining values for torsional rigidity and stress function 09 p1773 A70-22547

Unsteady creep of thin walled open section bars under free torsion using successive approximations 09 p1779 A70-23101

Cylindrical shell critical load boundaries under uniform external stress and small torsion 09 p1783 A70-23389

Cylindrical shell stability under combined torsion and internal pressure, noting yield point effect on critical load, obtaining buckling-internal pressure relationship 09 p1786 A70-23722

Flexural rigidity of thin walled beams, analyzing relationship between loads and displacements taking into account Saint Venant torsional resistance 10 p1955 A70-24052

Eccentrically stiffened thin circular cylindrical shell stability under torsion emphasizing exact finite formulas derivation 11 p2129 A70-25561

Stress relaxation in combined torsion-tension, developing expressions for torque and axial force 11 p2140 A70-26482

Semiinfinite composite medium displacement caused by nucleus of torsional strain with axis perpendicular to constituent isotropic layers interfaces 12 p2321 A70-27159

Circular cylinders torsion and plain strain analysis, completing statics by axisymmetric shear and moment stresses according to Cosserat theory for plastic flow 13 p2508 A70-28492

Book on torsion emphasizing beam stressed state calculation and civil engineering problems 13 p2512 A70-28850

Stress distribution in spirally corrugated shell under torsional deformation, calculating twisting moment for stiffness 14 p2661 A70-31327

Elastoplastic torsion problems solution by strain theory of plasticity, describing torsion function in hypergeometric series form 14 p2661 A70-31329

Elastic two cavity hyperboloid of revolution under stress due to rotating rigid stamp, solving torsional problem numerically 15 p2819 A70-32189

Stress concentration around small elastic spherical inhomogeneous inclusion on circular cylinder in torsion 17 p3183 A70-34631

Axisymmetric torsion by terminal loads of elastic shells of revolution, investigating energy inequalities for assessing quality of approximate solution of thin shell problem 18 p3335 A70-36058

Structure of flexural members, analyzing torsional and lateral stability by finite element method and matrix formulation 18 p3339 A70-36494

Optimal distribution of plastic inhomogeneity of torsioned prismatic square bars under maximum loading 18 p3343 A70-36719

Singular integral equation formulation for torsion from membrane analogy, obtaining boundary value problem solution by computer program 20 p3718 A70-39000

Thin walled fiberglass-reinforced plastic cylinders in torsion, calculating load carrying capacity as function of temperature 21 p3841 A70-40648

Stresses around circular hole in shallow conical shell under torsional load, using perturbations in parameters for curvature and cone angle 21 p3934 A70-40779

TORSIONAL VIBRATION

Torsional vibration of thin beam of varying cross section, noting moment of inertia and torsional rigidity proportionality 01 p0200 A70-10525

Transversely isotropic circular cylinder acted upon by transient shearing force at one end, noting forced torsional oscillation using cylindrical coordinates 01 p0200 A70-10550

Thin shells of revolution torsional vibration including bending terms and thickness considerations 01 p0205 A70-11142

Unidirectional carbon and glass fiber reinforced polyester resins dynamic characteristics under torsional and flexural vibration, showing damping independence of cyclic stress amplitude 03 p0514 A70-13111

Stress cycle asymmetry effects on energy dissipation in rods under torsional vibration 03 p0588 A70-13249

Finite difference method applied to solving equations of motion for computing natural torsional vibration frequencies of pretwisted cantilever beams

03 p0595 A70-13811

Upper and lower bounds for eigenvalues of lumped parameter straight line torsional system determined by receptance synthesis based on Holzer method

04 p0773 A70-15083

Inertial damping of soft rubber under forced torsional vibrations, discussing viscoelastic body linear model

04 p0712 A70-15100

Forced torsional vibration of elastic stratum produced by rigid circular disk approximated by Fredholm equations

04 p0777 A70-15497

Torsional vibrations of four cell tube, deriving cross sectional constants and natural frequencies

05 p0936 A70-16321

Convergence of eigenvalues and eigenvectors in torsional vibration problems of continuous systems via improved matrix displacement analysis using points of freedom in segments

05 p0939 A70-16502

Energy dissipation during torsional and flexural vibrations of steel and duralumin specimens subjected to plastic deformation, accounting for discrepancies due to methodical errors

06 p1166 A70-17658

Torsional vibrations of nonhomogeneous anisotropic finite circular tube, computing natural frequencies for various parameters

07 p1414 A70-20173

Rotating rotor with mass distributed along shaft analyzed for nonlinear flexural and torsional vibrations, determining dynamic instability ranges

08 p1584 A70-20694

Torsional vibrations frequency calculations for multibranch system exhibiting linear rigidity and viscous damping, constructing algorithm for digital computer

09 p1783 A70-23409

Dynamic shear modulus and depth of dominant layer of vibrating elastic medium, assuming foundation as isotropic stratum on rigid bed

10 p1957 A70-24481

Torsional vibration of rotating tapered and twisted turbomachine blade, constructing digital computer program for convergence and boundary conditions [SAE PAPER 700180]

11 p1218 A70-25373

Torsional vibration effect on gyrocompass with torsion suspension from studying sensing element forced motion, determining dynamic equilibrium position of sensor

11 p2048 A70-25578

Blade torsional degree of freedom effects on stability and flapping response of rotors operating at high advance ratios

13 p2507 A70-28444

Energy dissipation during independent flexural-torsional vibrations of rods, noting alternating shear stress superposition effect on damping

15 p2813 A70-31530

Torsional vibrations amplitude effect on polycrystalline Al stress-strain curve during uniaxial tensile test

15 p2758 A70-32125

Discrete mechanical models of single speed gears in torsional vibrations without teeth deformation and damping resistance

16 p2995 A70-34288

Mechanical models of single speed gears for torsional vibrations, taking into account nodes of first free vibration mode

16 p2995 A70-34289

Cross section deformation effect on helicopter rotor blade torsional vibration, using differential equations of vibrating beam

18 p3334 A70-35959

Kinetic instability of elastic cantilever beam under excitation by rotating masses, relating bending and torsional vibrations to masses angular velocity

18 p3334 A70-35960

Torsional vibration of thin beam with varying cross section, formulating fundamental equation and boundary conditions

18 p3339 A70-36519

Torsional and longitudinal vibrations of circular cylinders of micropolar elastic solids in terms of Laplace and Helmholtz equations solutions

19 p3537 A70-37789

Forced torsional vibrations of thin elastic spherical and hemispherical shells with free or restrained edge, using Gegenbauer transform

19 p3541 A70-38037

Stress cycle asymmetry effects on energy dissipation in rods under torsional vibration

19 p3548 A70-38467

Pretwisted slender beam coupled torsional and longitudinal vibrations under centrifugal force field, obtaining resonant frequency by Rayleigh Quotient method

20 p3719 A70-39601

Directional solar thermal field /sunlight/ effect on coupled nonplanar transverse and torsional vibrations of satellite cylindrical antennas in orbit

20 p3720 A70-39676

Low aspect ratio cantilever plate wings supersonic bending torsion flutter speed calculation, using spanwise and chordwise variables and potential energy principle

22 p4112 A70-42276

TORSO

Nonlinear wave equations model for human torso under impulsive stress, obtaining asymptotic solution

16 p2854 A70-34247

Digital computer model of total body ECG surface maps, simulating male torso with lungs

20 p3578 A70-39369

TORUSES

Torospherical heads attached to cylinders and under internal pressure as elastic and/or elastic-plastic shells, using finite element

[ASME PAPER 69-WA/PVP-7] 04 p0769 A70-14792

Torospherical heads design pressures compared from results of elastic-plastic and elastic-stress analyses to examine use of limiting stress criteria

05 p0944 A70-16816

TOUCH

NT TACTILE DISCRIMINATION

Threshold excitation of cutaneous analyzer in man under vascular conditioned reflexes in response to acoustic signals with shock

12 p2173 A70-28353

TOUGHNESS

NT NOTCH SENSITIVITY

Plastic strain state effect on ductility and toughness of structural steels

13 p2432 A70-28675

Impact transition behavior and strength-toughness relation of high purity Ni maraging steels, noting intergranular fracture at grain boundaries

18 p3273 A70-36043

Cycloaliphatic epoxy resins toughness improvement by modification with elastomers, maintaining high heat distortion temperature

21 p3842 A70-40733

TOWED BODIES

Motion equations and dynamic lateral stability of towed glider in steady horizontal flight treated by small perturbations method, including design and handling influence

09 p1611 A70-23063

Free flight wind tunnel test for feasibility of hypersonic drogue deployment into reentry vehicle wake [AIAA PAPER 70-587]

17 p3060 A70-35195

TOWED TARGETS

U TARGETS

U TOWED BODIES

TOWERS

Tower influence of wind speed and direction measurements, comparing 150 meter meteorological tower and scale wind tunnel model

09 p1661 A70-22964

TOWING

Hydrostatic synchronized steering of tow tractor for Boeing 747 and wide body jets compared to mechanical system

05 p0829 A70-16421

TOWNSEND DISCHARGE

NT GAS DISCHARGES

NT RING DISCHARGE

NT TOROIDAL DISCHARGE

TOXIC DISEASES

NT CARBON MONOXIDE POISONING

Acute gasoline poisoning toxicology and prophylaxis, manner of ingestion and effects on organs and systems

08 p1451 A70-20976

TOXIC HAZARDS

Time of useful function /TUF/ determination for human exposure to toxic gas combinations due to fire

06 p1000 A70-17294

Titan 3C launch environmental hazards including noise and exhaust cloud content

07 p1393 A70-19225

Air sample removal from hermetically sealed cavities during studies of toxic gas emanations from polymeric materials

07 p1221 A70-19516

Portable unit for collection and analysis of toxic gas contaminants in enclosed aircraft and spacecraft cabin atmospheres

07 p1224 A70-20222

Fluorine toxicity, discussing fluorine reactions with animal proteins and lipids, short-term exposure toxicity data, emergency tolerance limits, threshold limit, etc

10 p1824 A70-24060

Air sample removal from hermetically sealed cavities during studies of toxic gas emanations from polymeric materials

11 p1991 A70-26115

Toxic fuel test site selection, evaluating meteorological factors in Gypsum Canyon, California

14 p2563 A70-30613

TOXICITY

NT CARBON MONOXIDE POISONING

Oral potassium chloride usefulness and toxicity in EKG nonspecific T wave abnormality evaluation

01 p0014 A70-10274

Fire extinguisher compounds /bromochloromethane and bromotrifluoromethane/ pyrolysis products inhalation toxicities for rats

07 p1219 A70-19223

Aerazine-50 toxicity therapeutic treatment by pyridoxine and phenobarbital resulting in 100 percent survival of mice

07 p1222 A70-19926

Mild temperature and dehydration effects on toxicity of caffeine and dextroamphetamine in mice

09 p1616 A70-22329

Teflon and fluropolymers relative toxicity due to thermal degradation at 370 C, testing carboxy nitroso rubber, Kapton polyimide film, perfluorated polymers, etc

13 p2439 A70-29260

Monomethylhydrazine /MMH/ missile propellant toxicity, describing symptoms and effects on blood and intellectual capacity

24 p4306 A70-45125

TOXICITY AND SAFETY HAZARD

Laser eye and skin hazard evaluation from viewpoints of threshold effect levels and worst case assumptions

07 p1219 A70-19224

Fluorine toxicity, discussing fluorine reactions with animal proteins and lipids, short-term exposure toxicity data, emergency tolerance limits, threshold limit, etc

10 p1824 A70-24060

Protective clothing for personnel handling toxic and corrosive liquid propellants in hot climatic conditions at Guyana Space Center

12 p2179 A70-28043

Behavioral changes due to repeated low doses of rocket fuel monomethylhydrazine

21 p3771 A70-41485

TOXICOLOGY

Nomograms for correlation of dose to methemoglobinemia or plasma monomethylhydrazine /MMH/ concentration observed on dogs, considering human skin contact evaluation

06 p0992 A70-17298

Volatile toxic products outgassed by polymer construction materials, discussing physico-chemical classification of outgassing reduction methods

09 p1709 A70-22085

Soviet monograph on toxicology of active human life gaseous products, noting implications for artificial atmosphere formation in pressurized compartments

09 p1624 A70-22549

Volatile toxic products outgassed by polymer construction materials, discussing physico-chemical classification of outgassing reduction methods

15 p2766 A70-32681

General aviation aircraft accident investigation toxicological findings, describing methods of examination for drugs and toxic agents

17 p3033 A70-35569

Toxicity problems from burning or heating of polymeric materials, discussing laboratory experiments and standardized toxicity testing procedures

20 p3579 A70-39406

TOXINS AND ANTITOXINS

Tetradotoxin /TTX/ effects on mammalian brain studied by introducing TTX into cat lateral geniculate body /LGB/, causing flash evoked potentials and visual cortex decrease

05 p0799 A70-16049

Anticerebral cytotoxic serum effect on white rats conditioned reflex activity

07 p1199 A70-18727

Aerazine-50 toxicity therapeutic treatment by pyridoxine and phenobarbital resulting in 100 percent survival of mice

07 p1222 A70-19926

TRACE CONTAMINANTS

Breakthrough curve shape prediction during adsorption from gas stream in fixed bed adsorbers for trace contaminant control applied to activated charcoal

04 p0786 A70-15317

Combining color response in cholesteric liquid crystals generated by trace contaminants applicable to detection of vapors trace amounts

07 p1222 A70-19930

Trace constituent changes effects on stratospheric properties after volcanic eruption, showing prolonged atmospheric temperature increase

20 p3622 A70-39490

Trace contaminants associated with habitation by man in space cabin simulator by gas chromatography and IR and mass spectroscopy

21 p3770 A70-41482

TRACE ELEMENTS

Stony meteorite trace elements groups neutron activation analysis with computer reduction of Ge/Li spectra

02 p0249 A70-11680

Major and trace element concentration in contact zones of Precambrian diabase dikes from Wyoming ranges, showing dikes as continental tholeiites

03 p0472 A70-13148

- Downstream distribution of trace element injected into boundary layer of flat plate or cone with self similar mass transfer
[SAMSO-TR-69-56] 07 p1256 A70-19313
- Short lived cosmic ray produced nuclides as lower atmospheric motion tracers, studying Na 24 characteristics and activity in rain water 07 p1373 A70-20355
- Holbrook chondrite specimen, discussing effects of weathering, leaching and trace elements enrichment over period of time before recovery 13 p2487 A70-28698
- Troposphere and lower stratosphere trace element concentration measurements, establishing origin, history and movement of various air masses 15 p2728 A70-31996
- Chondrites and terrestrial rocks trace elements by neutron activation analysis, discussing radiochemical separation and computer analysis of gamma ray spectra 20 p3582 A70-38980
- Trace elements in Apollo 11 lunar glass clinopyroxene, plagioclase and ilmenite, using ion microprobe mass analyzer 21 p3896 A70-41510
- Type 1 carbonaceous chondrites contribution to lunar soil, comparing mineralogical and trace element evidence 21 p3899 A70-41533
- Apollo 11 lunar rock trace elements, examining basalt, gabbroic igneous rocks, breccias and fines by DC arc emission spectroscopy 21 p3774 A70-41561
- Apollo 11 lunar material trace elements, examining chemical processes during and after formation and meteoritic matter influx rate 21 p3907 A70-41572
- Rare earth and trace element abundances for Apollo 11 lunar samples by neutron activation, comparing with Bruderheim chondrite and submarine basalts 21 p3907 A70-41578
- Trace elements K, Rb, Sr and Ba distributions and Rb-Sr isotopic relations in Apollo 11 lunar breccia and fine soil samples 21 p3909 A70-41594
- Halogens, mercury, lithium and osmium concentration measurements in Apollo 11 samples, using neutron and photon activation 21 p3777 A70-41601
- Apollo 11 fines and rocks major and trace elements data obtained by combined instrumental and neutron activation analysis 21 p3910 A70-41615
- Sequential instrumental activation analysis for trace elements in rocks and stony meteorites, comparing with silicate method 24 p4310 A70-46407
- TRACERS**
- Missile tracer mixture performance control facility noting chamber for pressure measurement during operation 03 p0544 A70-13758
- Continuous generation of gas trace component quantities into carrier gas flow using dosage device 09 p1672 A70-22028
- TRACHEA**
- Human lung and upper airway pressure drop and fluid flow regime of inspired air 12 p2170 A70-27660
- Surface active lipoproteids of lung, discussing quantitative determination and labeling on basis of peribronchial wash-out procedure over trachea 15 p2680 A70-31725
- TRACING**
- Delayed trace reaction under stable and unstable pauses in apes and monkeys, noting independence of conditioned reflex 08 p1446 A70-21446
- Calcium ion role in myocardial cell electrical and mechanical trace processes under normal content and manganese blocking 18 p3221 A70-36640
- TRACKERS**
- U TRACKING [POSITION]**
- TRACKING [POSITION]**
- NT COMPENSATORY TRACKING**
- NT INFRARED TRACKING**
- NT MISSILE TRACKING**
- NT OPTICAL TRACKING**
- NT PHOTOGRAPHIC TRACKING**
- NT PURSUIT TRACKING**
- NT RADAR TRACKING**
- NT RADIO TRACKING**
- NT RANGE AND RANGE RATE TRACKING**
- NT SATELLITE TRACKING**
- NT SPACECRAFT TRACKING**
- NT STAR TRACKERS**
- Buoyant Venus station using superpressure balloon, discussing requirements for structural design and station position tracking capability [AIAA PAPER 69-1068] 01 p0195 A70-10633
- Tracking systems synthesis and performance analysis based on continuous Markov processes theory, particularly Fokker-Planck equation 01 p0043 A70-10776

- Refraction-induced range and tracking errors estimation in exponential model atmosphere by closed functions 01 p0044 A70-11087
- Noise effects on tracking performance, electroencephalography /EEG/ and galvanic skin resistance /GSR/ 04 p0643 A70-14977
- Horizontal transverse vibration effects on manual tracking performance, relating tracking errors to frequency rather than acceleration 04 p0643 A70-14981
- Relay control design for model-tracking system with parameter uncertainties and disturbances using semidefinite Liapunov function 07 p1247 A70-20026
- Double axis gyrostabilizer with auxiliary tracking system of subtracking ring, analyzing system stability and operation 09 p1676 A70-22629
- Step tracking in normal human subjects, studying muscle system around ankle joint 10 p1824 A70-23898
- Flight simulation data on motion cues effects in controlling compensatory tracking tasks [AIAA PAPER 70-352] 10 p1859 A70-24211
- Kalman filtering applied to moving balloon position and velocity estimates related to upper atmosphere wind measurements by balloon-satellite experiment 11 p2025 A70-26206
- Computational load reduction in aircraft tracking, comparing sensitivity and Hilbert norm methods 11 p2025 A70-26212
- Track-while-scan algorithm, considering probabilistic interpretation of linear recursive least squares filter for velocity variations 11 p2029 A70-26319
- Radiating objects localization and tracking by radiometer equipped with two antennas having slightly divergent beams 12 p2185 A70-27689
- Visual feedback delay effects on steering and tracking performance 12 p2179 A70-28147
- Simultaneous equations for motion location, speed and direction in acoustic tracking of supersonic objects, recording shock wave times of arrival with microphone system 13 p2450 A70-29988
- Real time computer algorithm for achieving optimal position of tracking antenna with nonlinear control system 15 p2703 A70-32575
- Classical and modern approaches to tracking problem, discussing optimal control in frequency domain and time domain terms 16 p2882 A70-33039
- Human tracking performance in position, rate and acceleration control systems under short term psychological stress induced by electric shocks 16 p2833 A70-33689
- Passive sun trackers using solar energy activated bimetal helix thermal heliotrope 16 p2846 A70-34131
- Tracking error correction time and proprioceptive reaction time, suggesting role of central mechanism without sensory feedback 17 p3036 A70-34606
- Observation space transforming for synthesis of automatic optimization systems with memory tracking randomly walking extremum 18 p3234 A70-36073
- Steering behavior during learning as function of self generated stimuli by movement compared with stimulus tracking 20 p3580 A70-39674
- Buoyant Venus station using superpressure balloon, discussing requirements for structural design and station position tracking capability 20 p3715 A70-39677
- Tracking of point object in Fresnel zone from observation of amplitude-phase pattern in aperture plane 22 p4026 A70-42555
- Tracking elevation/azimuth errors due to frame misalignment, presenting least squares procedure for determining true bias and misalignment angle and axis 23 p4215 A70-44518
- Position tracking of SOMEX superpressure balloons by solar angle method 24 p4372 A70-45423
- Phase and tracking errors due to mutual scattering in phase monopulse phase-scanned antenna 24 p4315 A70-46135
- TRACKING ANTENNAS**
- U DIRECTIONAL ANTENNAS**
- TRACKING FILTERS**
- FM noise threshold reduction achieved through narrow bandwidth of self synchronized N-path filter tracking incoming FM carrier 10 p1833 A70-24233
- Phase noise and cycle slip optimization of steady state digital data transition tracking loop used as bit synchronizer in phase-coherent receiver 11 p2024 A70-26202

- Dynamic tracking filter response analysis for FM reception using equivalent circuit method 12 p2200 A70-28054
- Alpha-beta and Kalman tracking filters with randomly interrupted data, evaluating transient responses as function of radar measurement accuracy and valid data acquisition probability 14 p2557 A70-31186
- Phase lock loop acquisition and tracking of carrier frequency modulated by single sinusoid, obtaining parameter values through mathematical model and digital simulation 15 p2703 A70-32578
- Optimal Kalman tracking filter performance estimation for manned maneuvering targets 16 p2949 A70-34057
- Optimal filter problem related to tracking, discussing mathematical formulation and reduction to variational problem 17 p3056 A70-34869
- RF communication signal to noise improvement by time variant tracking filter with high Q superconductive resonant cavity 19 p3391 A70-38892
- Adaptive tracking filter for bending mode stabilization of large flexible boosters [AIAA PAPER 69-874] 20 p3716 A70-39682
- Coherent receiver as hybrid carrier tracking loop consisting of standard phase locked and modified Costas loop 21 p3802 A70-41351
- Dynamic noise performance equivalence of phase locked or double superheterodyne tracking loops, using noise free external generator 21 p3793 A70-42180
- TRACKING NETWORKS**
- NT DEEP SPACE NETWORK**
- Azimuth between two stations of triangulation net determined by simultaneous observation of two satellites, discussing mathematical principles and applications in Europe 02 p0289 A70-11797
- SPOT navigation satellite system for near instantaneous fixes or continuous tracks providing height, velocity and automatic guidance and control signals 09 p1723 A70-23041
- Geostationary tracking and data relay satellites /tdrs/, discussing system design and advantages 14 p2615 A70-31182
- Space vehicle and mission control center telecommunications networks for Apollo lunar landing program, considering NASCOM relay system 17 p3047 A70-35585
- Tracking and data relay satellite system in low altitude synchronous orbit [AIAA PAPER 70-1305] 24 p4311 A70-45085
- Tracking and data relay satellite system performance by ATS and Nimbus spacecraft for range and range rate tracking and command and data transmission [AIAA PAPER 70-1306] 24 p4374 A70-45949
- TRACKING RADAR**
- Secondary surveillance radar /SSR/ automatic plot extractors and display processors for providing information on aircraft height and identity for air traffic control 02 p0256 A70-11963
- Control program debugging for experimental automatic surveillance and tracking radar, noting use for on-line systems 04 p0654 A70-15449
- Tactical air defense multiple site tracking data correlation equation to select gate sizes 11 p2009 A70-26263
- Adaptive tracking radar design, discussing ambiguity resolution problem in range and velocity dimensions 21 p3791 A70-41947
- Celestial radio source angle tracking techniques using monopulse antenna receiving system applied to angle tracking radar 22 p3991 A70-43582
- Dual channel circularly polarized feed of monopulse tracking antenna system, noting axial ratio and gain and open loop mode autotracking 24 p4321 A70-46259
- TRACKING STATIONS**
- NT DEEP SPACE INSTRUMENTATION FACILITY**
- Transportable telemetry acquisition system /TTAS/ as mobile tracker featuring pseudomonopulse method 01 p0045 A70-11120
- Satellite optical tracking data in space geodesy, determining stations position from minimum number of stations and observations with time errors 03 p0446 A70-13195
- German satellite ground station system central station design, discussing cooperation between aerospace institute and electronic company 08 p1481 A70-21368
- Tracking of goal seeking attack vehicles, discussing error improvement and destination estimating by tracking station observer 11 p2080 A70-26243

Tactical air defense multiple site tracking data correlation equation to select gate sizes

11 p2009 A70-26263

Report to COSPAR on Australian space research /1969/ including tracking stations, sounding rockets, technology utilization, etc

15 p2829 A70-31706

SIRIO mission algorithm and computer program, determining spacecraft position, ground trace and tracking station visibility

15 p2811 A70-32286

Earth-satellite range measurements using broadband pseudonoise modulation and delay lock tracking method

15 p2705 A70-32724

Automatic meteor station jamming protection using ferrite diode logical elements

19 p3422 A70-37652

Optimal reception points for radar ranging measurement of angular coordinates of meteor trails, using central transmitter

19 p3515 A70-37665

GEOS 1 satellite short arc optical observations over North American network to improve survey coordinates of tracking stations

24 p4312 A70-45542

TRACKING STUDIES

U TRACKING (POSITION)

TRACKS

Angular contact bearing balls track position on aero gas turbine engines shaft measurement in test rig at high speeds

20 p3638 A70-40141

TRACTION

Reduced traction effects on human work performance in weightless and lunar gravity environment

01 p0037 A70-10959

Tractive behavior in elasto-hydrodynamic lubrication contact noting role of surface degradation layer

05 p0854 A70-15888

Displacements and stresses obtained for elastic half plane with variable Poisson ratio under certain traction boundary conditions, using Fourier transform method

05 p0940 A70-16512

Dynamic response of joined elastic quarter spaces of solids to time varying free surface shear tractions parallel to plane of juncture

[ASME PAPER 69-APMW-16]

08 p1591 A70-21467

Frictional traction-sliding speed relation in elasto-hydrodynamic lubrication in Barlow-Lamb model of viscoelastic liquid, discussing oscillatory and continuous shear

09 p1691 A70-22600

Optimal traction drive system design for lunar roving vehicle, considering weight, energy consumption, operational flexibility, power supply, motor and power train

[SAE PAPER 700023]

11 p2030 A70-25375

Mathematical theory of constitutive relations connecting surface tractions and moments with motion of single body in continuum

20 p3672 A70-39495

Notch stress intensity factor representation as boundary traction weighted average, deriving weight functions from stress field boundary displacements

23 p4266 A70-44021

TRACTORS

Hydrostatic synchronized steering of tow tractor for Boeing 747 and wide body jets compared to mechanical system

05 p0829 A70-16421

TRACTS

U SITES

TRADEOFFS

Cost effectiveness tradeoff analysis for reliability incentive contracts, evaluating customer requirements for military procurement

01 p0220 A70-10115

Cost tradeoff analysis of electronic equipment for systems reliability design, considering component derating, redundancy and selection

01 p0049 A70-10119

Tradeoff decision processes scheduling maintenance frequencies for commercial transport aircraft [SAE PAPER 700328]

12 p2243 A70-27461

Computer program /SORCBE/ for systems unavailability tradeoff vs added cost for various versions

15 p2706 A70-32658

Pulse compression for geodesy satellite radar altimeter, considering tradeoff based on system accuracy, power and life

16 p2911 A70-33715

Configurational and operational characteristics for space shuttle design, considering economic tradeoffs between expendable and reusable systems

[AIAA PAPER 70-045]

17 p3175 A70-34783

Air superiority fighter design philosophy, including tradeoffs between armament, detection capability, thrust, speed and load factor

[AIAA PAPER 70-930]

17 p3021 A70-35840

Measuring and test equipment economic approach to quality levels and accuracy ratios, deriving cost tradeoffs in optimum inspection fidelity

20 p3634 A70-40453

TRAFFIC

NT AIR TRAFFIC

TRAFFIC CONTROL

NT AIR TRAFFIC CONTROL

NT RADAR APPROACH CONTROL

TV raster scan display using CRT and beam steering scan systems, comparing alphanumeric capability for airport information and control problems

02 p0274 A70-11976

Man machine systems - IEEE/ERS Conference, Cambridge, England, September 1969, Volume 2, Transport systems and vehicle control

02 p0334 A70-12130

Operational requirements of shipping for satellite communication systems, discussing distress cases, satellite navigation systems, information distribution traffic control, etc

03 p0522 A70-13605

Message traffic problems in satellite telephone network, considering traffic distribution characteristics, interarrival mean time, bidirectional traffic, etc

10 p1839 A70-24367

Space traffic control, discussing special problems of synchronous orbiting communications satellites

13 p2449 A70-29268

Global digital navigation and traffic control system via satellites, discussing position determination, surveillance and communication requirements

21 p3848 A70-41133

TRAILING EDGES

Wing design optimization for steady and unsteady supersonic flow through computerized simulation and study of leading and trailing edge shape

02 p0223 A70-12208

Trailing edge flow of slender aerodynamic shapes terminating in cusp or wedge, analyzing boundary layer reactions

04 p0613 A70-14457

Model flow studied for viscous flow near trailing edge of semiinfinite flat plate in middle of moving channel, noting Couette flow tendencies

05 p0831 A70-15879

Stability theory for pair of trailing vortices, investigating induced field convection, modes, amplification, cut-off distance, etc

[AIAA PAPER 70-53]

06 p0969 A70-18055

Unsteady airfoil stall in incompressible flow, including pitch rate induced accelerated flow effect on leading edge and trailing edge stall

[AIAA PAPER 70-77]

06 p0976 A70-18237

Trailing edge region of flat plate in laminar incompressible flow examined for high Reynolds numbers limit using Navier-Stokes reduced equations

07 p1255 A70-19213

Boundary layer flow near flat plate trailing edge taking into account pressure gradient induced locally in external flow

10 p1862 A70-23846

Skin friction near flat plate trailing edge at high Reynolds number by linearizing velocity profile

10 p1801 A70-24159

Turbulent trailing vortex decay calculated from circumferential velocity and eddy viscosity dependent on Reynolds number

10 p1802 A70-24561

Three dimensional turbulent boundary layer development on rear of swept wing, comparing measurements with calculations

13 p2344 A70-30021

Deformable and rigid wings aerodynamic characteristics with subsonic leading and trailing edges, calculating action of gust

15 p2671 A70-31486

Airfoil trailing edge stall in laminar flow, investigating circulation around flat plate

18 p3205 A70-36194

Wake behind trailing edge of flat plate in constant velocity impulsively started stream, using boundary layer theory

18 p3206 A70-36196

Pulling force during motion of sinusoidally deformable flat profile, taking into account trailing edge vortices

18 p3241 A70-36280

Supersonic turbine blade rows design, discussing boundary layer interaction around leading edges and flow around trailing edges

19 p3490 A70-38223

Flow field model for large surface blowing problem accounting for upstream and downstream effects with large rate normal injection near trailing edge

20 p3559 A70-40110

Heat transfer at air cooled gas turbine blade trailing edges at various wall temperatures and Reynolds numbers

23 p4283 A70-44737

TRAILING-EDGE FLAPS

Wind tunnel comparative performance tests of glider laminar wing profile with fixed and flexible trailing-edge flap

02 p0304 A70-12800

Sailplane design standards concerning retractable undercarriage and trailing-edge flaps revised to achieve better performance

09 p1612 A70-23575

Axial flow compressor off-design performance optimization by adjustable inlet guide vanes with variable trailing edge flaps

18 p3304 A70-36846

TRAILS

U TRACKS

TRAINERS

U TRAINING DEVICES

TRAINING

U EDUCATION

TRAINING AIRCRAFT

NT JAGUAR AIRCRAFT

NT T-33 AIRCRAFT

Human functional changes in controlling C-8 trainer measured by flicker value, pulse rate, reaction time and instrument and control error before and after flight

04 p0643 A70-14976

Jet pilot trainee qualification requirements, training process methods and equipment, considering German-French joint trainer aircraft program

08 p1452 A70-21348

Harrier V/STOL trainer aircraft design features including fuselage, cockpit, power plant, etc

13 p2345 A70-28923

German-French jet aircraft trainers, discussing Alpha Jet TA 501, E 650 Eurotrainer and VF T 291 flight characteristics

13 p2347 A70-29052

Variable stability trainer modification of F-106 to reproduce flight characteristics of aircraft for pilot training in potentially dangerous situations

16 p2842 A70-33815

TRAINING DEVICES

NT TEACHING MACHINES

Student development and exercising of electron physics principles by designing, assembling, operating and studying electron and ion devices

01 p0093 A70-11291

Subjects trained in visual monitoring task with auto-instructional device, showing higher signal detection rate than group trained by practice alone

02 p0247 A70-12380

Adaptive training concepts, methods, implementation and comparison of characteristics with fixed trainers

05 p0805 A70-16004

Time constant of man machine system as adaptive variable in training devices derived from combined vehicle properties and human control characteristics

05 p0805 A70-16005

Direct broadcast voice satellite for educational system improvement, discussing lesson formatting, ground receiver/programmer, multichannel capacity, etc

[AIAA PAPER 70-449]

11 p1998 A70-25423

Training algorithms in designing multilevel quasi-optimal controllers for dynamic processes, using pattern recognition methods

13 p2383 A70-29581

TRAINING SIMULATORS

NT COCKPIT SIMULATORS

NT FLIGHT SIMULATORS

NT SPACECRAFT CABIN SIMULATORS

Flight training simulators recording, playback, demonstration and instructor facilities and six degrees of freedom motion system

02 p0273 A70-11840

Trainers and simulators based on digital computers, eliminating system sensitivity to ambient conditions, power fluctuations, circuit imperfections and digital to analog conversion

02 p0274 A70-11841

Digital real time simulation for training and evaluating ATC controllers, discussing system hardware, software, design and implementation

02 p0274 A70-11977

Adaptive man machine system for automated training of pilot dynamic control skills /decision and motion/, describing synthesis procedure

02 p0246 A70-12148

Visual, motion and auditory stimuli role in enhancing aircraft pilot training simulators realism, considering motion perception research

[ASME PAPER 69-WA/BHF-9]

04 p0642 A70-14853

Flight simulators for pilot training, discussing need for aircraft motion cues

09 p1655 A70-22296

French airline pilots training program at Montpellier and St-Yan, considering selection, licensing and simulators

16 p2853 A70-33675

Lunar and earth surfaces imaging for astronaut training in LEM simulator

20 p3607 A70-40320

Water immersion facility training for extravehicular activities and man physical movements in spacecraft, utilizing buoyancy-gravitation balance

21 p3804 A70-41191

Partial gravity simulators at Manned Spacecraft Center for astronaut acquaintance with dynamics of moon walking

21 p3804 A70-41192

Translation and docking simulator for Gemini support modified for Apollo LM active lunar orbital docking with CSM

21 p3804 A70-41194

Training simulation improving ejection decision making in naval aviation

23 p4178 A70-44467

TRAJECTORIES

NT ABORT TRAJECTORIES
NT ASCENT TRAJECTORIES
NT BALLISTIC TRAJECTORIES
NT CIRCULUNAR TRAJECTORIES
NT DESCENT TRAJECTORIES
NT EARTH-MARS TRAJECTORIES
NT EARTH-MOON TRAJECTORIES
NT ELECTRON TRAJECTORIES
NT HYPERBOLIC TRAJECTORIES
NT INTERPLANETARY TRAJECTORIES
NT LUNAR TRAJECTORIES
NT MIDCOURSE TRAJECTORIES
NT MISSILE TRAJECTORIES
NT MOLECULAR TRAJECTORIES
NT MOON-EARTH TRAJECTORIES
NT PARTICLE TRAJECTORIES
NT REENTRY TRAJECTORIES
NT RENDEZVOUS TRAJECTORIES
NT ROUND TRIP TRAJECTORIES
NT SPACECRAFT TRAJECTORIES

Optimum thrust control of satellite along given trajectory to rendezvous at zero velocity with orbited satellite

01 p0197 A70-11500

Solar U-burst radiospectrographic observations, investigating disturbing trajectories and longitudinal distribution in combination with model coronal condensation

09 p1758 A70-22737

TRAJECTORY ANALYSIS

Mathematical pendulum oscillations under clockwise and counterclockwise impact impulse, deriving differential equations describing trajectories

01 p0141 A70-10153

Oblate earth gravitational field effect on ballistic missile trajectories, including body range determination and quadratures expressed by elementary functions

01 p0178 A70-10423

Particle trajectory and associated wave determined for nonclassical trajectory problem from nonprobabilistic point of view, discussing discontinuity arising from unbounded velocities

01 p0142 A70-10657

Reentry trajectories from lunar surface and orbit obtained by computer with allowance for initial data spread

01 p0191 A70-11476

Spacecraft trajectory optimal determination without knowing measurements error distribution function, examining computer solution properties of linear programming

01 p0192 A70-11477

Optimal moments for trajectory parameters measurements determined by linear analysis to minimize error for initial conditions

01 p0094 A70-11478

Minimum time turns for spacecraft about fixed axis lying beyond plane of vehicle forces

01 p0197 A70-11480

Thunderstorm downdraft trajectories and temperatures, discussing evaluation of cooling due to evaporation

02 p0325 A70-12256

Load and strain trajectory vectors components determined for tension followed by transverse compression in five dimensional space

02 p0390 A70-12803

Soviet book on flight vehicle trajectories covering equations of motion, flight mechanics, reference systems, etc, for rockets and spacecraft

03 p0410 A70-12871

Galaxy model formulated in cylindrical coordinate system using Fokker-Planck equation for cosmic radiation particles propagation, discussing trajectories of high energy particles

03 p0553 A70-12880

Position bound determination for objects ejected from space vehicle relative to vehicle trajectory position

03 p0562 A70-12932

Optimal control of continuous and discrete observations described by linear differential and recurrent algebraic equations in presence of random perturbations

03 p0447 A70-13341

Earth-moon-earth flight characteristics, discussing spacecraft trajectory, velocity and corrections for close distance placement and return for soft landing

03 p0569 A70-13483

Osculating transfers between two prescribed trajectories without considering optimization problem, obtaining in-space launching point of artificial cosmic bodies

03 p0575 A70-13972

Interplanetary trajectory selection, discussing transfer orbits, energy considerations, launch window

computation, hyperbolic encounters and capture maneuvers

03 p0577 A70-14149

Patch-conic method accuracy and limitations in determining space trajectories as function of planetary zones of influence

04 p0750 A70-14941

Controlled vehicle disturbed trajectory multiple correction, considering constrained control or limited accessible coordinates for observations

04 p0716 A70-15007

Spacecraft design, trajectory and mission analyses for multipurpose solar electric propulsion missions, emphasizing modular ion engine and fixed attitude spacecraft designs

[AIAA PAPER 69-252] 04 p0763 A70-15412

Approximate time solutions to light aircraft projectiles velocity, altitude angles, gravity drop and downrange, reducing differential equations of motion to dimensionless forms

04 p0764 A70-15592

Criteria for particle motion with constant acceleration in curved space-time

06 p1104 A70-17186

Satellites and space probes orbital parameters calculation, considering circular and elliptical trajectories and rendezvous maneuver example

06 p1140 A70-17583

Control system employing adaptive modeler to estimate state, dynamics and future trajectory of unknown plant through performance index minimization

06 p1025 A70-17965

Heliocentric low thrust spacecraft trajectory analysis using two-variable asymptotic expansion method

[AIAA PAPER 70-214] 06 p1145 A70-18064

Low thrust trajectory and performance analysis of solar electric propulsion system for unmanned interplanetary exploration

[AIAA PAPER 70-212] 06 p1145 A70-18081

Phobos and Deimos photographic reconnaissance feasibility during 1971 orbiter and 1973 Viking missions, studying trajectory

[AIAA PAPER 70-60] 06 p1146 A70-18191

Computation methods for optimal rocket trajectories closely approaching gravitating celestial bodies, alleviating computational difficulties with regularizing techniques

[AIAA PAPER 70-95] 06 p1146 A70-18202

Earth oblateness effects on lunar and interplanetary trajectories, using algorithm based on orbital elements variations

[AIAA PAPER 70-97] 06 p1146 A70-18203

Collisionless ions trajectories in plasma flowing about cylindrical probe calculated to determine probe ion current, ion density distribution in field and potential distribution

06 p1122 A70-18294

Hybrid patched conic technique as iterative procedure for generating translunar and transearth trajectories emphasizing computing time saving

06 p1152 A70-18495

Time-similar and isotropic geodesic curves simulating paths of test bodies in Riemann space corresponding to gravitational field

06 p1107 A70-18564

Optimal control problem solution involving functional minimization along differential vector equation trajectories, considering manifold type constraints on phase coordinates

07 p1244 A70-18747

Apollo 8 mission, spacecraft and booster details, calculating earth-moon flight parameters based on laws of mechanics

07 p1375 A70-18776

Lawden primer vector theory applied to matched conic spacecraft trajectories optimization

07 p1381 A70-19325

Circular and radial trajectories in Schwarzschild field applied to isolated metagalaxy with charged central body and nonzero cosmological constant

07 p1385 A70-19426

Resonant oscillations of coupled physical pendulums, investigating phase trajectories by Struble method

08 p1544 A70-20964

Apollo space vehicles guidance and navigation using data obtained onboard, discussing inertial platforms, accelerometers and trajectory calculations

08 p1541 A70-21023

Queue control techniques in generating predicted trajectory, discussing queue control logic requiring minimum storage

08 p1467 A70-21049

Hodographic determination of required velocity changes for space vehicle transfer orbit, involving only launching point and trajectory plane

08 p1577 A70-21505

Proportional navigation law three dimensional vectorial equation analyzed in kinematic conditions, discussing perturbation effects on linearized trajectory

09 p1720 A70-22420

Nonlinear differential equations analysis based on weighted linear approximation applied to singular

points and trajectories in phase plane in friction problems

09 p1727 A70-22665

Atomic clock applications to trajectory, discussing experimental single channel equipment for space vehicle location and results of Rb vapor clocks

09 p1722 A70-23034

Lunar swingby trajectory analysis with atmospheric reentry, characteristics of geocentric portions of earth-moon and moon-earth transfers

10 p1940 A70-24306

Computational limitations of midcourse correction velocity for lunar impact trajectories, considering impact miss magnitude correction

11 p2109 A70-25955

Controlled missile reentry trajectory through dense atmosphere, describing digital computer solution of differential equations of motion

12 p2314 A70-27768

Small meteor streams trajectories and radiants from epsilon-Lyrids, alpha-Coronids and phi-Draconids observations by amateur astronomers

12 p2311 A70-28307

Spacecraft reentry trajectory reconstruction using accelerometer and onboard navigation data from Apollo flights

13 p2485 A70-28378

Trajectory predictive lunar return atmospheric reentry guidance of roll-controlled Apollo-type vehicle, using variable integration steps

13 p2446 A70-28396

Planetary trajectory handbooks for mission and system analysis covering opportunities for Mercury, outer planets and Mars, contour charts, etc

13 p2486 A70-28525

Ordnance flight dynamics, considering trajectory analysis and inaccuracies due to projectile wobble

[AIAA PAPER 70-533] 13 p2506 A70-29001

Meteorological problems associated with accurate weather prediction affecting launch, trajectory and recovery of ballooning systems

14 p2606 A70-30555

Optimal control of continuous and discrete observations described by linear differential and recurrent algebraic equations in presence of random perturbations

14 p2561 A70-30717

Fuel savings by Jupiter moon gravity assisted transfer trajectories from earth, considering initial energy, mass ratio, approach angle, timing and aiming errors

14 p2640 A70-30761

Coordinate systems generation for optimal trajectories, considering Lagrange multiplier as motion constant

14 p2651 A70-31368

Jet assisted orbital spacecraft trajectories equations derivation, considering Kepler trajectories and orbital velocities

15 p2800 A70-32260

Semiwideband and adaptive noise variance recursive estimation techniques applicable to spacecraft trajectory analysis

15 p2803 A70-32586

Linearization error bound analysis in solution of equations of motion of reentry vehicle

16 p2974 A70-33319

Initial reentry body motion effects on angle of attack envelope value throughout trajectory, including altitude of maximum transient amplification

16 p2982 A70-33892

Optimal trajectories analysis by canonical transformation for obtaining solution to Hamilton-Jacobi equation without quadratures

16 p2943 A70-33899

Potential stability theory for linear and nonlinear systems trajectory

16 p2943 A70-34042

Nonlinear mechanical systems transient motion analysis based on phase trajectories

16 p2944 A70-34283

Nonlinear mechanical lumped dynamic systems trajectory analysis in terms of P and G sets

16 p2944 A70-34285

Computation methods for optimal rocket trajectories closely approaching gravitating celestial bodies, alleviating computational difficulties with regularizing techniques

17 p3172 A70-35666

Circumunar trajectories with return to earth atmosphere, comparing various methods

18 p3312 A70-36165

Two dimensional reverse trajectory reaction and mass behavior for motion of material point with changing mass, using Mesherskij equation

18 p2383 A70-36401

Nomograms for meteor geocentric velocity and trajectory with correction for zenith attraction and radiant

18 p3315 A70-36605

Automatic control systems synthesis based on root locus trajectories theory

19 p3392 A70-37808

Second and higher order perturbation theory for two body trajectories, using recursive formulas

[AIAA PAPER 70-1056] 19 p3528 A70-38871

N body numerical integrator using virtual mass technique for computing trajectories with speed and accuracy suitable for spacecraft onboard computer applications
[AIAA PAPER 70-1057] 19 p3528 A70-38872

Closed form approximate solution for restricted three body motion of lunar or interplanetary spacecraft, demonstrating accuracy and flexibility in lunar mission trajectory calculations
[AIAA PAPER 70-1061] 19 p3529 A70-38875

Multiconic method space flight trajectories analysis, discussing computation time and circumlunar flight altitude and velocity errors
[AIAA PAPER 70-1062] 19 p3529 A70-38876

Jupiter swingbys and multiplanet Jupiter swingby trajectory modes for outer planet missions, comparing in terms of passage conditions
[AIAA PAPER 70-1071] 19 p3530 A70-38884

Jupiter swingby trajectory analysis for comet flyby and rendezvous missions, discussing approach velocity and payloads
[AIAA PAPER 70-1074] 19 p3530 A70-38886

Interplanetary trajectories calculation using constant and/or slowly varying functions for accuracy, noting application to earth-moon spacecraft
[AIAA PAPER 70-1076] 19 p3530 A70-38888

Monopole trajectory in magnetic dipole field by numerical integration on computer and Liouville theorem, using resolved Stormer cone to investigate motion
20 p3672 A70-39301

Resonant oscillations of coupled physical pendulums, investigating phase trajectories by Struble method
20 p3672 A70-39386

Covariance matrices estimates for trajectory parameter tracking of thrust-maneuvering spacecraft
[AIAA PAPER 70-1017] 20 p3666 A70-39516

Spacecraft trajectory initial conditions expressions as parameters dependent functions, applying results to Mars lander mission
[AIAA PAPER 70-1016] 20 p3666 A70-39517

Real time network support simulation allowing network configuration for nominal or perturbed trajectory for Saturn vehicles, applicable to any flight azimuth
[AIAA PAPER 69-936] 20 p3591 A70-39684

Algorithm for trajectory analysis in closed loop terminal guidance of solar electrically thrusted interplanetary spacecraft
[AIAA PAPER 70-1152] 20 p3670 A70-40203

Solar electric propulsion Mars high data rate orbiter trajectory design and analysis, including landing site selection and spacecraft parameters optimization
[AIAA PAPER 70-1119] 20 p3710 A70-40224

Mission analysis and trajectory simulation (MATIS) program, discussing computer controls, modular design, integration evaluation
[AIAA PAPER 69-939] 21 p3920 A70-41872

Comet Bennett /1969 i/ spectrograms, discussing linear diameter, trajectory, Lyman alpha emission and hydrogen mass
22 p4097 A70-42468

Trajectory equations for plane and three dimensional gas jets with arbitrary injection hole shapes in subsonic shear flow
22 p3960 A70-43365

Parachute trajectory and opening load prediction based on inflation process and added mass, determining drag area as function of distance
[AIAA PAPER 70-1168] 23 p4137 A70-43993

Phobos and Deimos photographic reconnaissance feasibility during 1971 Orbiter and 1973 Viking missions, studying trajectory
[AIAA PAPER 70-60] 23 p4243 A70-44507

Interplanetary periodic orbits and flyby dates for multiple earth-Venus swingby missions, describing various iterative solutions for trajectory
[AIAA PAPER 69-931] 23 p4243 A70-44508

Suboptimum filter for trajectory estimation from parameters, using modified covariance with least squares formulation in Kalman setting
23 p4177 A70-44601

GEOS A and OGO-4 satellite orbits and trajectory analysis using Definitive Orbit Determination System, discussing tracking stations error role
24 p4407 A70-45536

High energy close approach trajectories within planar free fall three body problem, using perturbation theory
24 p4412 A70-45984

Aircraft climb and descent trajectories approximation compatible with air traffic control operation, noting parameters effects
24 p4375 A70-46239

TRAJECTORY CONTROL

NT TRAJECTORY OPTIMIZATION

In-flight compensation for space probe trajectory deviations, discussing attitude determination and control of triaxial and spin stabilized space probes
01 p0186 A70-11265

Spacecraft longitudinal control during reentry of Lunar Orbiter into atmosphere, analyzing final range prediction, trajectory tracking and accelerometers performance
01 p0197 A70-11497

Spacecraft range control algorithm during reentry at parabolic velocity into atmosphere with varying parameter distributions
01 p0197 A70-11498

Controlled vehicle disturbed trajectory multiple correction, considering constrained control or limited accessible coordinates for observations
04 p0716 A70-15007

Law for time variations of modulus-restricted control action at trajectory end, two point boundary value problem solution and use of Pontryagin principle
04 p0661 A70-15011

Fluidics application in sounding rocket guidance control circuits used in space boosters
05 p0797 A70-15809

Optimality conditions determined for control involving trajectory with singular component equations of motion
06 p1024 A70-17813

Interplanetary swingby trajectory correcting maneuvers for space vehicles return to earth after planet orbiting, with emphasis on singular points
06 p1142 A70-17877

Apollo 11 lunar landing mission planning, control and evaluation of launch window and translunar, lunar parking orbit and transearth trajectories
[AIAA PAPER 70-24] 06 p1158 A70-18168

Queue control techniques in generating predicted trajectory, discussing queue control logic requiring minimum storage
08 p1467 A70-21049

Rendezvous control law for spacecraft moving in central gravitational field along trajectory representing target vehicle Keplerian orbit
08 p1582 A70-21636

Spacecraft mission planning for trajectory control after establishing mission objectives, trajectory plan and crew timeline for Apollo flights
09 p1725 A70-23709

Structural synthesis of automatic control systems for body motion along trajectory, using inverse method and nonlinear coordinate transformations
11 p2077 A70-25611

Space vehicle velocity-attitude optimal control for on-line trajectory control schemes
11 p2025 A70-26216

Rendezvous problems formulated as optimal control problems in combined state space, considering decomposition in optimality criteria and solution existence
11 p2127 A70-26331

Rendezvous trajectory control problems solution by regularization techniques, emphasizing equations of motion in gravitational field
13 p2446 A70-28380

Adaptive variable-parameter spacecraft trajectory control, discussing loop synthesis and model reference system stability and dynamic accuracy
13 p2380 A70-28383

Low altitude operational meteorological and navigation spacecraft, discussing need for orbit adjustment by dynamic control
13 p2500 A70-28404

Spacecraft trajectory control for hypersonic atmospheric entry
13 p2500 A70-28411

Course correction requirements for ballistic grand tours and outer planet missions, considering trajectory disturbances by random nongravitational forces
13 p2448 A70-28707

Onboard moon-to-earth trajectory approach guidance with or without midcourse guidance using optical angular measurements
14 p2615 A70-30470

Neighboring optimum feedback control scheme for aerospace vehicles to handle small disturbances from nominal trajectory with unspecified final time
16 p2887 A70-33438

Space vehicle trajectories, discussing programming method to control motion for prescribed boundary conditions
17 p3173 A70-35700

Extraatmospheric transport trajectory control by jet assistance
18 p3333 A70-36670

Airport capacity and terminal area safety increase by scanning beam instrument landing system, discussing automatic guidance trajectory example
19 p3464 A70-37913

Launch vehicle injection error sensitivity minimization by trajectory shaping using excess booster capability
[AIAA PAPER 70-1078] 19 p3534 A70-38889

Closed form expressions for linear and higher order corrections to multiimpulse approximations of space flight trajectory optimization solutions, using bang-bang thrust control
[AIAA PAPER 70-1014] 20 p3667 A70-39519

Rocket course correction by lateral air expulsion /ram air control/, deriving model for performance prediction
[AIAA PAPER 70-90] 20 p3715 A70-39559

Interplanetary solar electric spacecraft performance improvement by mission mode including earth swingby maneuver in solar orbit inclined to ecliptic
[AIAA PAPER 70-1117] 20 p3710 A70-40226

Trajectory correction propulsion subsystem /TCPS/, attitude propulsion subsystem /APS/ and pyrotechnic subsystem of thermoelectric outer planet spacecraft /TOPS/
21 p3868 A70-41800

Thermoelectric outer planets spacecraft /TOPS/ attitude control subsystem providing accurate antenna pointing and trajectory correction engine thrust vector orientation
21 p3930 A70-41801

Optimization for control processes with first and higher order constraints on phase coordinates
22 p4004 A70-43320

Spacecraft trajectory control rockets design and operational characteristics, discussing various propellant types, control valve designs, etc
24 p3493 A70-45640

TRAJECTORY MEASUREMENT

Optimal moments for trajectory parameters measurements determined by linear analysis to minimize error for initial conditions
01 p0094 A70-11478

Numerical forecasting scheme for hurricane and typhoon trajectories applied to 1967 Atlantic storm data
03 p0520 A70-13162

Optical approach navigation experiment on 1969 Mariner mission to Mars demonstrating accuracy potential of spacecraft-based measurement
[AIAA PAPER 70-70] 06 p1103 A70-18152

Soviet book on rendezvous in orbit, flight dynamics and control of spacecraft covering trajectory synthesis, optimization and control for approach stage
10 p1950 A70-24656

Satellite trajectory parameters estimation by maximum likelihood method applied to continuous satellite observations assuming random Gaussian process as measurement error
11 p2081 A70-26780

Satellite motion initial phase vector estimation for calculating satellite motion from selection of complete or increasing volume of measurements
11 p2118 A70-26781

Deep Space Network /DSN/ data accuracy limitations relation with ability to determine orbit of probe, examining improvements after Mariner 2 and trends
13 p2448 A70-28702

Meteor particle orbits, comparing inclined radio reflections with photographic and straight radar observations
14 p2636 A70-30322

Rockets trajectories recording on real time at Guiana Space Center using IR pointing deviation meter
15 p2698 A70-31960

High speed photographic systems for ballistic studies, describing high intensity lighting systems
20 p3635 A70-40527

TRAJECTORY OPTIMIZATION

Burning program for sounding rocket to reach maximum altitude with given initial and propellant masses, discussing numerical parameter optimization technique
01 p0161 A70-10150

Optimal rendezvous maneuver of two spacecraft in circular orbits with minimum fuel consumption, taking into account propelled vehicle control program and flight path
01 p0193 A70-10424

Optimum flight paths of energy and power limited rockets with generalized thrust characteristic, considering vertical, horizontal, rectilinear, zero drag and vacuum trajectories
01 p0193 A70-10425

Differential equations of optimal degenerate problem reduced to autonomous form with multiple control, noting D-stationarity application for optimal motions
01 p0053 A70-11022

Spacecraft trajectory optimal determination without knowing measurements error distribution function, examining computer solution properties of linear programming
01 p0192 A70-11477

Optimal rendezvous between satellite and spacecraft, determining power and time optimal coplanar rendezvous in circular orbit
01 p0139 A70-11479

Optimum orbital transfer of material point subjected to reactive force with minimum mass loss, discussing Kepler motion kinematics
01 p0192 A70-11514

Two step optimal motion of target and pursuer with thrust vector control in vacuum under arbitrary gravitational field, determining distance strategy
02 p0272 A70-12405

Spacecraft reentry trajectory optimization, considering minimum coolant weight requirement in internal cooling system
02 p0381 A70-12416

Sufficient conditions for relative extremum in flight dynamics optimization determined by variational method
02 p0381 A70-12417

Minimum propellant maneuver during docking of elliptical orbit rendezvous between propelled and passive target vehicles, analyzing as variational problems
02 p0380 A70-12784

Optimal two impulse transfer through 180 degree range angle between Keplerian noncoplanar orbits, minimizing impulse by transfer plane optimal orientation
[AIAA PAPER 68-93] 03 p0562 A70-12914

Medium duration optimal rendezvous between near circular noncoplanar orbits with close orbital planes, analyzing six impulse solutions
[ONERA-TP-763] 03 p0571 A70-13639

Geostationary satellite payload-optimal injection trajectory from nonequatorial firing range, describing dog-legging maneuvers
03 p0573 A70-13845

Optimal impulse orbital transfer in ring between coplanar orbits intersecting ring boundaries in central Newtonian force field
04 p0744 A70-14429

Optimal descent maneuver from planetary orbit for fixed atmospheric reentry angle, considering minimum impulse/fuel consumption/
04 p0745 A70-14496

Graphical solution of optimum trajectories for third order systems depending on single control function, including maximum error and switching time
[ASME PAPER 69-WA/AUT-6] 04 p0661 A70-14828

Optimal control of thrust limited minimum-propellant rocket-powered vehicle using expansion about optimal trajectory
04 p0750 A70-14928

Orbit determination simultaneous optimal strategy and useful information set selection, discussing Mars transfer trajectory
04 p0750 A70-14940

Automated parameter search techniques applied to low thrust mission design, stressing trajectories and mission optimization
[AIAA PAPER 69-261] 04 p0736 A70-15404

Soviet monograph on optimal space flight trajectory control, covering vehicle CG trajectory and synthesis of automatic stabilization system using variational calculus
04 p0764 A70-15493

Multistage rocket optimum ascent regime obtained by height function of engine gas outlet velocity
06 p1155 A70-17585

Optimal landing of spacecraft on moon surface from low circular orbit, analyzing rocket thrust, altitude and landing site distance effect on spacecraft mass
06 p1155 A70-17880

Lunar module motion during optimal ascent from moon surface into circular orbit of command module, noting descent maneuver similarity
06 p1155 A70-17881

Optimal information selection for determining spacecraft trajectory, considering atmosphere, light speed and series expansion coefficients of planetary gravitational potentials
06 p1142 A70-17891

Linear-quadratic pursuit-evasion game with dynamics perturbed by additive white Gaussian noise, obtaining linear minimax solutions
06 p1025 A70-17957

Computation methods for optimal rocket trajectories closely approaching gravitating celestial bodies, alleviating computational difficulties with regularizing techniques
[AIAA PAPER 70-95] 06 p1146 A70-18202

Analytic Trajectory Optimization Model to develop computational techniques for low thrust mission analysis
[AIAA PAPER 70-96] 06 p1159 A70-18230

Optimum impulsive velocity calculation for three dimensional deorbit from elliptical orbits to achieve specified reentry angle
06 p1152 A70-18496

Planetary atmospheric entry optimal three dimensional glide paths, considering polar curve altitude dependence, flight path changes, braking maneuvers, etc
07 p1378 A70-18985

Lawden primer vector theory applied to matched conic spacecraft trajectories optimization
07 p1381 A70-19325

Spline data techniques for error elimination in trajectory optimization to offer improvement over linear interpolation scheme
07 p1325 A70-19340

Hypersonic orbital glider range maximization, analyzing optimal angle of attack by use of rectangular velocity components
07 p1393 A70-19341

Time optimal rendezvous maneuver between neighboring elliptic orbits, discussing propulsive jet system with variable thrust
07 p1381 A70-19357

Satellite circular orbital plane rotation by jet thrust, minimizing fuel for fixed time
07 p1393 A70-19497

Indirect methods of trajectory optimization, improving convergence through normalization of state data and Lagrange multipliers
07 p1326 A70-19726

Optimality condition for singular control problems derived using differential dynamic programming to obtain expression for change in cost produced by control variation
09 p1653 A70-22345

Fourth order differential equation system with complex conjugate eigenvalues, deriving optimal control for fuel minimum
09 p1759 A70-22831

Optimal maneuver decision strategy for space vehicle midcourse trajectory corrections
09 p1760 A70-22928

Hybrid patched conic iterative technique for accurate moon-earth/transearth/trajectory generation
09 p1760 A70-22929

Minimum time interstellar trajectories for thrust limited rockets by applying Pontryagin maximum principle to relativistic rocket equations of motion
09 p1760 A70-22933

Degenerate variational problem of optimum gliding along zero proximity line, determining number of control switchings and deviation during perturbed motion
10 p1854 A70-24277

Selection of uncorrelated measurement composition ensuring optimal accuracy of space vehicle trajectory
10 p1939 A70-24301

Optimal trajectory measurement program for orbit parameter determination, assuming random errors and nondegenerate weighting matrix of normal equations
10 p1940 A70-24302

Minimal characteristic velocity of single impulse transfer between coplanar elliptical orbits with allowance for thrust action finite time
10 p1940 A70-24304

Optimal acceleration from earth orbit to hyperbolic velocities of low thrust space vehicle, constructing asymptotic expansions near and far from central field
10 p1940 A70-24305

Spacecraft optimal flight from earth orbit to outer planet orbit with ideally controlled engine using differential motion equations
10 p1941 A70-24512

Optimal longitude rendezvous for geostationary satellite by using inertially fixed orientation thrust for performing final positioning
10 p1941 A70-24541

Soviet book on rendezvous in orbit, flight dynamics and control of spacecraft covering trajectory synthesis, optimization and control for approach stage
10 p1950 A70-24656

Different gravitational force fields effecting optimal rocket trajectories and queried validity of Newtonian law
10 p1943 A70-24820

Takeoff noise minimization by prescribing optimum takeoff trajectories, considering aircraft parameters influencing noise intensity at takeoff
11 p1979 A70-25814

Linearized theory for minimum fuel guidance in neighborhood of minimum fuel space trajectory, unrestricted thrust magnitude and allowances for midcourse impulses
11 p2079 A70-25957

Minimum fuel continuous thrust elliptical orbit transfer problem, obtaining optimal steering function for departure and arrival points
11 p2124 A70-26214

Quasi-optimum proportional navigation for attack situations with large missile and target maneuvers, showing advantage over linearized optimization
11 p2081 A70-26316

Fuel-optimal retrothrust control in state dependent retarding force fields, taking into consideration synthesis for vertical trajectory system configuration
11 p2126 A70-26321

Optimal pulsed orbital transfer between close nearly circular orbits in central field of gravity realized by geometrical solution
11 p2118 A70-26778

Keplerian integrals analogy to integrals of adjoint equations suggested by optimum space navigation trajectories considerations
12 p2261 A70-27834

Coplanar transfer orbits optimal trajectories in central Newtonian gravitational field, using Krotov sufficient criteria
12 p2310 A70-28252

Stochastic optimal trajectory control for spacecraft reentry at supercircular velocity, deriving computer algorithm
13 p2499 A70-28382

Accelerated gradient projection method applied to rocket trajectory optimization for minimizing fuel required for placing payload in circular orbits
13 p2485 A70-28395

Minimum time control for placing circular orbit satellite in gravitationally stable position
13 p2502 A70-28440

Optimal impulse orbital transfer in ring between coplanar orbits intersecting ring boundaries in central Newtonian force field
13 p2485 A70-28454

Minimum fuel takeoff and landing paths for VTOL aircraft with constraints on state and control, determining optimal trajectories
[AIAA PAPER 70-550] 13 p2345 A70-29015

Extremum criterion for singular solutions to optimal trajectory equations in calculus of variations
13 p2443 A70-29747

Terminal guidance by dynamic programming to obtain optimal feedback control law in nominal trajectory neighborhood for minimum energy consumption
13 p2449 A70-29963

Lunar spring board effect to minimize impulses for given velocity at great distance of earth-moon system, discussing nonimpulsive grazing passage
14 p2635 A70-30289

Interplanetary low thrust orbit transfer optimization by dynamic programming, including gravitational perturbation effects from earth, Mars and Jupiter
14 p2640 A70-30759

Coordinate systems generation for optimal trajectories, considering Lagrange multiplier as motion constant
14 p2651 A70-31368

Satellite circular orbital plane rotation by jet thrust, minimizing fuel for fixed time
15 p2813 A70-32742

Jacobi conditions for singular optimization problems by transforming singular accessory minimum problem into nonclassical nonsingular form, considering optimal control theory applicability
16 p2885 A70-33331

Speed convergence of hybrid vs digital computer synthesis of optimal boost vehicle controller, considering fuel consumption and pitch dynamics
16 p2981 A70-33442

Planetary atmospheric entry optimal three dimensional glide paths, considering polar curve altitude dependence, flight path changes, braking maneuvers, etc
[DFVLR-SONDDR-49] 16 p2982 A70-33771

Optimum guidance and control law for lifting reentry bodies, investigating plane descent trajectories for minimum structural heating
16 p2982 A70-33774

Branched trajectory optimization for split rocket vehicles using projected gradient or steepest descent method
16 p2977 A70-33871

Optimal trajectory and control approximate solution by asymptotic expansion, considering Mayer variational problem solution
16 p2943 A70-33897

Optimal trajectories analysis by canonical transformation for obtaining solution to Hamilton-Jacobi equation without quadratures
16 p2943 A70-33899

Interstellar drag resulting from relativistic rocket elastic collisions with interstellar matter, discussing effects on minimum time acceleration limited relativistic trajectories
17 p3155 A70-34752

Space shuttle mission trajectory optimization with steering in atmospheric flight and orbiter maneuvers
[AAS PAPER 70-048] 17 p3176 A70-34788

Minimum impulse transfer between two neighboring low eccentricity orbits, discussing fuel consumption and transfer time
17 p3167 A70-35231

Optimum low thrust ion propelled interplanetary trajectory design using two step Chebyshev method
17 p3167 A70-35232

Optimal explicit guidance equation using maximum principle for two stage vehicle injecting satellite into parking orbit
17 p3134 A70-35289

Iterative algorithm for free terminal time control in trajectory optimization
17 p3168 A70-35290

Interplanetary probes trajectory optimization for minimum energy expenditures, neglecting solar and terrestrial perturbations within earth sphere of influence
17 p3168 A70-35366

Computation methods for optimal rocket trajectories closely approaching gravitating celestial bodies, alleviating computational difficulties with regularizing techniques
17 p3172 A70-35666

STOL takeoff trajectory optimization for heavily loaded helicopter, using optimal control theory
17 p3021 A70-35841

ELDO launch vehicle FE /flat earth/ guidance, discussing perturbations, trajectory optimization, inertial navigation system, onboard computer, etc
18 p3288 A70-36299

Integrals of motion for minimum fuel rocket trajectories in inverse square field calculated for constant power and constant exhaust rockets
18 p3316 A70-36678

Minimum-fuel multiple impulse orbital fixed time rendezvous in circular orbit vicinity
18 p3289 A70-36682

Closed form solution for minimum fuel constant thrust trajectories for vehicle transfer in vacuum between arbitrary boundary conditions
18 p3316 A70-36683

Optimal control systems sensitivity analysis, discussing trajectory tracking
19 p3394 A70-38716

Optimal three dimensional impulsive orbit transfer at cuspidal point of primer locus in terms of three parameters to facilitate computation and tabulation [AIAA PAPER 70-1037] 19 p3527 A70-38852

Minimum impulse transfer between circular orbit and hyperbolic trajectory velocity vector, assuming fixed transfer times [AIAA PAPER 70-1038] 19 p3527 A70-38853

Primer vector theory applied to interplanetary trajectory optimization for high thrust chemically propelled spacecraft, considering 1973 Mars opportunity [AIAA PAPER 70-1039] 19 p3527 A70-38854

Three body numerical solutions to low thrust guidance and navigation for outer planet orbiter with nuclear-electric propulsion [AIAA PAPER 70-1040] 19 p3527 A70-38855

Low thrust interplanetary swingby trajectories optimization, considering thrusting and coasting within sphere of influence [AIAA PAPER 70-1041] 19 p3527 A70-38856

Pioneer-F Jupiter flyby mission planning, considering use of optimum broken plane trajectories to increase launch opportunity and/or payload capability [AIAA PAPER 70-1050] 19 p3528 A70-38865

Optimum launch trajectories for ATS-E mission with noncircular parking orbits, considering apogee motor size, perigee radius and duration constraints [AIAA PAPER 70-1051] 19 p3528 A70-38866

Saturn 5 launch vehicle targeting methods for lunar missions, solving earth departure variables via iterative process [AIAA PAPER 70-1052] 19 p3528 A70-38867

Optimal angle of attack transition trajectories for space shuttle from atmospheric entry to cruising flight for conventional airport landing [AIAA PAPER 70-1018] 20 p3713 A70-39515

Closed form expressions for linear and higher order corrections to multiimpulse approximations of space flight trajectory optimization solutions, using bang-bang thrust control [AIAA PAPER 70-1014] 20 p3667 A70-39519

Aircraft landing maneuver optimization by in-flight monitoring of approach and landing phases, furnishing decision making display [AIAA PAPER 70-1000] 20 p3560 A70-39531

Air to air missile launch range maximization for plane trajectories and nonmaneuvering targets, discussing optimal fuel burning rate [AIAA PAPER 70-980] 20 p3668 A70-39549

Atmospheric ascent optimal trajectories for medium to high lift drag ratio space shuttle type rocket vehicles [AIAA PAPER 70-978] 20 p3714 A70-39551

Highly constrained optimal control problems, using nonlinear programming in mathematical model for trajectory optimization [AIAA PAPER 70-964] 20 p3600 A70-39565

Optimal longitudinal takeoff trajectories, formulating obstacle clearance criterion function based on aircraft design parameters effects [AIAA PAPER 70-963] 20 p3560 A70-39566

Optimum switching in minimum fuel, time-free impulsive planar transfer problem by primer vector concept 20 p3709 A70-40074

Optimized trajectories and spacecraft for solar-electric missions to asteroids, using chemical booster for injection [AIAA PAPER 70-1120] 20 p3710 A70-40223

Solar electric propulsion Mars high data rate orbiter trajectory design and analysis, including landing site selection and spacecraft parameters optimization [AIAA PAPER 70-1119] 20 p3710 A70-40224

Fuel optimal orbital transfer trajectories by linear programming 20 p3711 A70-40337

Space vehicle trajectories power-optimal single parameter nonlinear correction, assuming ideal impulse performance 21 p3883 A70-40829

Differential dynamic programming algorithm for discrete time orbit transfer optimization 21 p3919 A70-41737

Deorbiting target intercept energy optimization by game theory approach [AIAA PAPER 70-1019] 21 p3848 A70-41778

Rocket nose cone optimal turn into horizontal ballistic trajectory after separation from booster, using dynamic programming 22 p3962 A70-43351

Solar probe trajectory optimization, using Venus gravitational field for braking 23 p4243 A70-44506

Analytic approximation for initial adjoint vector for optimal/minimum propellant/ space trajectories [AIAA PAPER 69-916] 23 p4243 A70-44509

Minimum fuel thrust limited transfer trajectories computation for coplanar elliptic orbits [AIAA PAPER 69-914] 23 p4244 A70-44558

Space shuttle transition trajectory optimization for cruising flight entry, considering longitudinal control, pitchup instability and angle of attack 23 p4244 A70-44623

Minimum-time transfer trajectories between close planar orbits, using single stage thrust-limited rocket 23 p4244 A70-44624

Lawden intermediate rocket thrust arcs numerical integration and Kelley-Contensou optimality in Newton central force field [ONERA-TP-869] 23 p4245 A70-44657

Algorithm for space trajectories optimization with delta velocity constraints 23 p4245 A70-44683

Intrinsic equations with roots for optimal two-impulse transfer between given positions 23 p4246 A70-44698

Optimal fixed-time impulsive transfer trajectories minimizing characteristic orbital velocity, determining sufficient conditions 23 p4255 A70-45015

Interorbital optimum trajectories with specified transfer angle in inverse square gravitational field, examining minimum velocity increment 24 p4412 A70-46003

TRANQUILIZERS

Amysyl effects on conditioned passive avoidance reflexes development and reinforcement in white mice under electric shock 07 p1198 A70-18717

Tranquilizers and hypnotics from rats organs analyzed by thin layer chromatography 22 p3978 A70-42879

TRANSCIEVERS

U TRANSMITTER RECEIVERS

TRANSCENDENTAL FUNCTIONS

NT EXPONENTIAL FUNCTIONS

NT LOGARITHMS

NT PERIODIC FUNCTIONS

NT TANGENTS

NT TRIGONOMETRIC FUNCTIONS

TRANSDUCERS

NT DIGITAL TRANSDUCERS

NT ELECTROACOUSTIC TRANSDUCERS

NT ELECTRONIC TRANSDUCERS

NT IMAGE TRANSDUCERS

NT LOUDSPEAKERS

NT MICROPHONES

NT MODE TRANSFORMERS

NT PIEZOELECTRIC GAGES

NT PIEZOELECTRIC TRANSDUCERS

NT PIEZORESISTIVE TRANSDUCERS

NT PRESSURE SENSORS

NT QUARTZ TRANSDUCERS

NT SOUND TRANSDUCERS

NT THERMOPILES

NT TORQUERS

NT ULTRASONIC WAVE TRANSDUCERS

Handbook of transducers for electronic measuring systems covering operating principles, design features, etc 01 p0094 A70-11301

Physiological signals of cardiovascular system transducing methods applied to vector ECG, heart sounds, peripheral pulse waves, chest microphone and plethysmography 02 p0243 A70-12095

Ultrasonic tracking type transducers for testing ribbed and smooth walled pipes using shadow and two probe echo methods 02 p0300 A70-12480

Sheath-enclosed steel cable inspection using induction coil transducer in conical sleeve 02 p0301 A70-12490

Local skin friction measurement on model in blow-down hypersonic wind tunnels using floating element transducer, giving results for flat plate and wedge [ONERA-TP-756] 03 p0463 A70-13629

Electronic sine-cosine converters construction in devices for visual display of hydroacoustic transducers radiation patterns 06 p1064 A70-17773

Dynamic mathematical model of proportional electromagnetic transducer in pneumatic servomechanisms derived by Lagrange-Maxwell method assuming circuit linearity 07 p1195 A70-18750

Apparatus for studying vibrations via contactless HF resonant transducers during milling 09 p1691 A70-22625

Optimizing control system design using fluidic digital circuitry and FM type transducers 09 p1614 A70-23690

Mode transducer and mode filter formed by rectangular and circular waveguide elements investigated by field expansion, calculating transmission coefficient and propagation constant 10 p1848 A70-24219

Nomogram selecting dimensions of steel or Al alloy cantilever beams for transducer design using strain gages 10 p1890 A70-24593

Vibration meter coupled with electrodynamic transducers for measurements in 3-2000 Hz range 11 p2055 A70-26448

Multichannel measurement system for inductive transducers, describing system components and capabilities 11 p2055 A70-26449

Electrocapillary transducers filled with mercury and electrolyte solution for vibration measurement, analyzing seismic operation character 12 p2235 A70-27684

Transducers for bioimplantable telemetry systems self used by nonhospitalized patients 13 p2357 A70-28816

Electrodynamic transducer electrical and mechanical parameters measurement, comparing various techniques 13 p2406 A70-28991

Open faced polyimide-backed strain gage for transducer and/or long term applications, considering drift and zero shifts 15 p2739 A70-32329

Electro-optical transducers based on photoconductive cells, phototransistors and microminiature incandescent and solid state light emitters 16 p2904 A70-33144

Heterodyne conversion transducer large signal internal parameters dependence on heterodyne, signal amplitudes and intermediate voltage 16 p2873 A70-33240

Parameter identification in distributed systems by method of characteristics, discussing noisy measurements and limited available transducers 16 p2942 A70-33338

Nerva nuclear subsystem diagnostics and control instrumentation, discussing transducers 16 p2949 A70-33551

Electromagnetic to magnetostatic wave conversion loss reduction at L band by coiled transducer 16 p2913 A70-34038

Optimum receiver for acoustical holography using discrete transducers arrays for image conversion 17 p3088 A70-35029

Exciter and instrumentation of vibration transducer calibration system 17 p3089 A70-35179

Measurement transducers transforming measured quantity into forms suitable for comparison with standards in metrological sciences 17 p3090 A70-35432

Strain transducer /optical diffraction grating/ for plastic wave propagation measurement along specimens subjected to impact 19 p3425 A70-37884

Optimal transducers distribution for estimating random field values in presence of additive noise 22 p4005 A70-43562

TRANSEQUATORIAL PROPAGATION

HF propagation losses from statistical measurement over north-south path found dependent on mode, day and night and high and low ray 04 p0649 A70-14968

Transequatorial multisite VLF records establishing solar zenith angle for midpoint of sunrise ionospheric height discontinuity, recomputing magnetic latitude dependent parameters 06 p1054 A70-17590

LOF observations of long distance transequatorial step frequency radio circuits in Pacific Area during sunspot minimum period 07 p1232 A70-19174

VLF transequatorial propagation, describing equipment, periodic variations in signal characteristics, ionospheric parameters, etc 15 p2699 A70-32298

TRANSFER FUNCTIONS

Unsteady heat conduction in hollow cylinder, using transfer functions to solve direct and inverse two dimensional problems 03 p0606 A70-13520

Holographic method for measuring optical instruments transfer function, using laser light source and beams interference 03 p0493 A70-13946

Transient electromagnetic fields coupling transfer functions for two wire uniform transmission line cable models, using long wire antenna as radiation source 04 p0658 A70-14739

Coefficient matrix-structural method for obtaining transfer function of linear automatic control systems 04 p0662 A70-15277

Algorithmic and digital computer method for approximating irrational transfer functions by rational functions in control systems 04 p0662 A70-15336

State variable diagram for transfer function of single output/input linear stationary system obtained by parallel, direct and iterative methods 05 p0928 A70-16027

Waveform-shaping transfer function rational polynomial approximation method with application to network problem in PCM communications 06 p1007 A70-17459

Linear circuit output waveform calculation without first resolving transfer functions on complex frequency plane, applied to current switching circuit analysis 06 p1018 A70-17460

Immittance, transfer and scattering characteristics for interdigital acoustic surface wave transducers, using linear equivalent circuit model 06 p1062 A70-17478

Complex control follow-up systems in transient modes, suggesting synthesis for transfer function of control signal coupling

06 p1023 A70-17775

Dynamic response of gas lubricated radial sliding bearing from transfer function derived from pH linearized mathematical model of gas lubrication

07 p1290 A70-18739

Modulation transfer function (MTF) of eye-visual system as spatial frequency filter

07 p1216 A70-18870

Microscope objective effect on accuracy of optical systems modulation-transfer function based on corrected high speed lens measurements

07 p1334 A70-19147

Dynamic characteristics approximation in transfer functions class with singularity at infinity

07 p1327 A70-19806

Reduction method for order of transfer function describing automatic control system, determining coefficients of reduced order transfer functions

07 p1247 A70-19842

Linear control circuits transfer function analysis, revising Nyquist criterion

07 p1328 A70-20212

Astronomical telescope performance at transfer process from object to image using optical transfer function and brightness standards

08 p1493 A70-20685

Transfer functions representing continuous dynamic systems, identifying parameters by obtaining coefficients of discrete system transfer function relating input and output sampled sequences

08 p1478 A70-20777

Clock corrections smoothing by linear transformation operator, calculating operator transfer function and averaged errors deviations

08 p1574 A70-21155

Reconstructed holographic image complex amplitude expression derived, showing effects of film optical transfer function, size and shape

08 p1500 A70-21789

Thermo-elastic analysis and optimum start-up in power plant, discussing transfer function for thermally loaded bodies with restricted boundary temperature

09 p1774 A70-22584

Error functional minimization in class of current distribution relay functions noting applications to linear antennas and FM signals synthesis

09 p1637 A70-23154

Atmospheric modulation transfer function measuring instrument based on Lindberg principle, discussing optical and mechanical design features and applications

09 p1688 A70-23769

Transfer coefficients calculation for equations of motion of medium, presenting mathematical experiment requiring molecular interactions only

10 p1919 A70-24157

Component tolerances effect on transfer function of networks, calculating sum variance for two terminal networks

10 p1833 A70-24223

Algorithm for transfer matrix Heaviside expansion, using Krylov and Vandermonde transformations for multiple eigenvalue case

10 p1910 A70-24705

Saddle point existence in determinate integrodifferential games with variable delay, assuming given control function over time interval

10 p1911 A70-25183

Transfer functions application to optical system specification, design and evaluation, calculating diffraction limited MTF

11 p2082 A70-25354

Roll induced cross coupling evaluation in two dimensional homing systems based on defining roll transfer matrix

11 p2122 A70-25681

Transfer functions estimation by taking Fourier transform ratio of finite length samples of input and response measurements, considering error term probability density

11 p2071 A70-25954

Time-invariant linear dynamical systems transfer equivalence leading to algorithm for minimal realizations of transfer function matrices

11 p2072 A70-26161

Linear networks fault detection and isolation using computerized test procedure and symbolic transfer function generation technique

11 p2029 A70-26337

Invariance conditions and state transition matrix of linear systems

11 p2074 A70-26400

Cylindrical shell response to random acoustic excitation, considering single point transfer functions and equivalent force power spectral densities

12 p2317 A70-27125

Transfer matrix spectrum for lattice gas models with finite interaction, constructing stochastic operator as stochastic matrices limit

12 p2272 A70-27343

Distributed-lumped-active network to produce transfer function with pair of high Q zero real part sensitivity poles

12 p2196 A70-27652

Short cables wire to wire coupling between black boxes, deriving interference transfer function

12 p2204 A70-28130

Soviet book on dynamics of rockets covering solid and liquid fuel rocket stability, controllability and transfer functions

13 p2505 A70-28799

Pilot-aircraft closed-loop characteristics, using pilot transfer functions for handling qualities prediction [AIAA PAPER 70-568]

13 p2346 A70-29033

Photodetector properties influence on opton transfer functions achieving light conversion by separating photocarriers with p-n junction

14 p2555 A70-30161

First harmonic precision improvement of dual input describing function, applying to self oscillation of nonlinear systems

14 p2560 A70-30625

SCAMP 4 program for electronic circuits statistical analysis in frequency domain, obtaining mathematical models and transfer functions

14 p2561 A70-30667

Physical signals continuous to discrete transformation by analog to digital conversion, considering coding process and transfer functions

14 p2554 A70-30679

Low pass filter synthesis with transfer function having frequency response boost in pass band

15 p2708 A70-31833

Noise effect on modulation transfer function of visual channel by threshold measurements

15 p2698 A70-32013

Multidimensional linear stationary systems controllability and observability with given transfer matrix

15 p2716 A70-32345

Algorithm for inverse Laplace transformation of irrational transfer function via fast Fourier transform

15 p2768 A70-32577

Optimal perturbation signal waveform linearizing nonlinear transfer characteristic of image sensing receptor array

15 p2705 A70-32725

Modulation transfer function (MTF) systems analysis with emphasis on target acquisition, relating image contrast characteristics of target and background

16 p2907 A70-33185

Linear multivariable feedback control systems design method based on transfer matrix, testing decoupling desirability

16 p2884 A70-33318

Iterative weighted nonlinear least squares parameter estimation for human respiratory control system by transfer function modeling, comparing results with visual curve fitting

16 p2851 A70-33322

Linear distributed dynamic system simulation using infinite product expansions for transcendental terms in transfer functions

16 p2942 A70-33348

Servosystems with random input signals, obtaining optimal transfer function by variational calculus

17 p3056 A70-34617

Photographic materials for holography, discussing spectral sensitivity, grain size, resolution, transfer functions, diffraction efficiency, etc

17 p3084 A70-35003

Spatial filter properties of antennas, discussing system performance optimization and incoherent source transfer functions

17 p3045 A70-35077

Atmospheric inhomogeneity, comparing effective mass and Curtis-Godson approximation methods for transfer function of absorbing gas distribution

19 p3461 A70-37632

Atmospheric turbulence vertical component spectral density observation by aircraft in steady flight, considering transfer function computation methods

19 p3351 A70-37646

Network function sensitivity to parameter variations, describing indirect calculation method

19 p3394 A70-37966

Selective inductorless amplifier design with four layered distributed RGC line in feedback loop, obtaining high Q factors in transfer function

19 p3390 A70-38674

Digital filter synthesis, discussing transfer function determination based on prescriptions for frequency or time response properties

19 p3391 A70-38746

Linear multivariable feedback control system, deriving conditions for existence of triangular decoupling transfer function matrices

20 p3605 A70-40118

Transfer function optimization for linear follow-up frequency filter with controlled resonance, analyzing noise band performance

22 p3985 A70-42402

Optical telescope reflecting prism angle deviations effect on modulation transfer function and image quality

22 p4072 A70-42506

Perturbation method with small parameter applied to turbulent transfer equation in lower atmosphere, solving longitudinal diffusion effect on evaporation

22 p4065 A70-42911

Lissajous figures for phase response of N-path signal filter transfer functions, using switched modulators

22 p3998 A70-43256

Modulation transfer function applied to optimal holographic nondestructive testing systems, using edge gradient analysis

22 p4039 A70-43520

Aircraft handling qualities specifications and definitions evolution based on test pilot rating correlation with engineering data and piloting ease evaluation with transfer functions

[ICAS PAPER 70-19]

23 p4138 A70-44114

Spectrophotometry of earth surface from manned Soyuz spacecraft, obtaining transfer function of atmosphere by aircraft flights

23 p4191 A70-44636

Vibration transfer coefficient of aerial camera-photographic assembly system for shock absorption during surveys

24 p4333 A70-45200

Monin-Obukhov function and nondimensional transfer coefficients variation, discussing turbulent motion decay in lower atmosphere

24 p4372 A70-46072

TRANSFER OF TRAINING

Work and exercise conditions effect in early training stages of learning sensorimotor skill, considering different body positions

03 p0432 A70-14295

Error correction training procedures convergence for committee solution to pattern recognition problem

05 p0817 A70-16175

Physiological training programs and equipment for life support in transports, discussing changes in protective helmet and quick donning harness

06 p1002 A70-17708

TRANSFER ORBITS

NT INTERPLANETARY TRANSFER ORBITS

Optimum orbital transfer of material point subjected to reactive force with minimum mass loss, discussing Kepler motion kinematics

01 p0192 A70-11514

Optimal two impulse transfer through 180 degree range angle between Keplerian noncoplanar orbits, minimizing impulse by transfer plane optimal orientation

[AIAA PAPER 68-93]

03 p0562 A70-12914

Osculating transfers between two prescribed trajectories without considering optimization problem, obtaining in-space launching point of artificial cosmic bodies

03 p0575 A70-13972

Optimal impulse orbital transfer in ring between coplanar orbits intersecting ring boundaries in central Newtonian force field

04 p0744 A70-14429

Electrostatic charged particle acceleration and ion thruster function in geostationary satellite station-keeping and attitude control, orbital transfer and drag compensation

[ONERA-TP-764]

04 p0735 A70-14934

Solar or nuclear energy powered electric propulsion systems for transferring satellite from low to geostationary orbit, discussing feasibility and costs of various designs

04 p0735 A70-15174

Electric thrusters for putting communications satellite into synchronous orbit analyzed for mission performance, finding hydrogen resistojets as attractive compromise between payload and transfer time

05 p0897 A70-16899

Satellite electric propulsion system and configuration for orbital transfer maneuvers, describing ELDO launcher, Black Arrow, orbital dynamics, sensor system, etc

06 p1130 A70-17648

Vehicles optimal flights with controlled or boundary level thrust in circular orbit neighborhood, using linearized equations of motion

06 p1142 A70-17876

Energy optimal osculating elliptical transfer orbit from low eccentricity orbit constructed for prolonged circling in equatorial plane of axisymmetric planet

07 p1374 A70-18774

Satellite circular orbital plane rotation by jet thrust, minimizing fuel for fixed time

07 p1393 A70-19497

Unmanned and manned interorbital shuttle systems for satellite placement and repair and planetary spacecraft insertion, emphasizing cost analysis

[AIAA PAPER 70-267]

07 p1398 A70-20396

Hodographic determination of required velocity changes for space vehicle transfer orbit, involving only launching point and trajectory plane

08 p1577 A70-21505

Optimal transfer ellipse obtained by complete rotation in gravitational field of axisymmetric planet

09 p1751 A70-22161

Minimal characteristic velocity of single impulse transfer between coplanar elliptical orbits with allowance for thrust action finite time 10 p1940 A70-24304

Lunar swingby trajectory analysis with atmospheric reentry, characteristics of geocentric portions of earth-moon and moon-earth transfers 10 p1940 A70-24306

Minimum fuel continuous thrust elliptical orbit transfer problem, obtaining optimal steering function for departure and arrival points 11 p2124 A70-26214

Optimal pulsed orbital transfer between close nearly circular orbits in central field of gravity realized by geometrical solution 11 p2118 A70-26778

Coplanar transfer orbits optimal trajectories in central Newtonian gravitational field, using Krotov sufficient criteria 12 p2310 A70-28252

Optimal impulse orbital transfer in ring between coplanar orbits intersecting ring boundaries in central Newtonian force field 13 p2485 A70-28454

Dynamic programming applications to optimal stochastic orbital transfer strategy, describing computer program [AIAA PAPER 68-872] 13 p2447 A70-28502

Interplanetary low thrust orbit transfer optimization by dynamic programming, including gravitational perturbation effects from earth, Mars and Jupiter 14 p2640 A70-30759

Fuel savings by Jupiter moon gravity assisted transfer trajectories from earth, considering initial energy, mass ratio, approach angle, timing and aiming errors 14 p2640 A70-30761

Synergetic plane change maneuver optimal control, combining aerodynamic and propulsive flight phases for efficiency 15 p2715 A70-31784

Satellite circular orbital plane rotation by jet thrust, minimizing fuel for fixed time 15 p2813 A70-32742

Minimum impulse transfer between two neighboring low eccentricity orbits, discussing fuel consumption and transfer time 17 p3167 A70-35231

Unmanned and manned interorbital shuttle systems for satellites placement and repair and planetary spacecraft insertion, emphasizing cost analysis [AIAA PAPER 70-267] 17 p3172 A70-35650

Minimum-fuel multiple impulse orbital fixed time rendezvous in circular orbit vicinity 18 p3289 A70-36682

Optimal three dimensional impulsive orbit transfer at cuspidal point of primer locus in terms of three parameters to facilitate computation and tabulation [AIAA PAPER 70-1037] 19 p3527 A70-38852

Minimum impulse transfer between circular orbit and hyperbolic trajectory velocity vector, assuming fixed transfer times 19 p3527 A70-38853

Optimum switching in minimum fuel, time-free impulsive planar transfer problem by primer vector concept 20 p3709 A70-40074

Communication satellites low thrust transfer to synchronous orbit by two-stage operation using hydrogen resistojets and Hg ion motors [AIAA PAPER 70-1116] 20 p3691 A70-40227

Kaufman ion thruster providing electric propulsion for satellite spiraling from parking to synchronous orbit [AIAA PAPER 70-1101] 20 p3692 A70-40237

Fuel optimal orbital transfer trajectories by linear programming 20 p3711 A70-40337

Differential dynamic programming algorithm for discrete time orbit transfer optimization 21 p3919 A70-41737

Optimal low thrust transfer between coplanar circular orbits, examining thrust direction and steering as Mayer problem 22 p4097 A70-42489

Minimum fuel thrust limited transfer trajectories computation for coplanar elliptic orbits [AIAA PAPER 69-914] 23 p4244 A70-44558

Minimum-time transfer trajectories between close planar orbits, using single stage thrust-limited rocket 23 p4244 A70-44624

Recoverable stages for satellites low to stationary orbital transfer, taking costs into account 23 p4245 A70-44671

Orbital mechanics of transfer orbits under small horizontal thrust, reducing second order differential equation to linear inhomogeneous equation 23 p4245 A70-44691

Intrinsic equations with roots for optimal two-impulse transfer between given positions 23 p4246 A70-44698

Optimal fixed-time impulsive transfer trajectories minimizing characteristic orbital velocity, determining sufficient conditions 23 p4255 A70-45015

Interorbital optimum trajectories with specified transfer angle in inverse square gravitational field, examining minimum velocity increment 24 p4412 A70-46003

TRANSFORM INTEGRALS
U INTEGRAL TRANSFORMATIONS
TRANSFORMATION TENSORS
U TENSORS
TRANSFORMATIONS
 Oxide transformation during oxidation of Nb in terms of O diffusion 07 p1305 A70-18967

Longwave and shortwave mode transformation in resonant layer of inhomogeneous plasma 08 p1550 A70-20847

Parametric image transformation during sum frequency generation 09 p1636 A70-23134

Random process noncommutative transformations and correlation functions in linear form of time functions 09 p1655 A70-23695

Langmuir wave beam nonlinear transformation in isothermal plasma due to induced scattering by ions 20 p3684 A70-40385

TRANSFORMATIONS [MATHEMATICS]
NT COORDINATE TRANSFORMATIONS
 Conditionally periodic orbits existence in restricted problem of three bodies, using similarity transformation 02 p0369 A70-11997

Element relations of phase transformation matrix for scattering, relating radiation field vector to scattered field vector 02 p0339 A70-12283

Monograph on generalized transforms properties and asymptotic behavior, discussing kernel functions, Bessel functions, Laplace transforms, Hankel transforms, etc 03 p0519 A70-13650

Generalized transform theory for causal operators developed, using Gelfand theory for commutative Banach algebras 03 p0520 A70-14167

Earth external gravitational potential expressed as infinite series of spherical harmonics, using transformation property on coefficients 03 p0478 A70-14178

Coupled nonlinear systems with two degrees of freedom using transformation techniques 04 p0714 A70-15084

Relativistic length contraction, time dilation and classical electrodynamics formulated in terms of special relativity using Galilean transformations 05 p0881 A70-15875

Birkhoff normalizing canonical transformation built at elliptic type of equilibrium without internal resonance, using Lie transforms 05 p0909 A70-16340

Multiplication theorem for Shtraus characteristic functions of quasi-Hermitian operators, including open systems coupling 05 p0877 A70-16880

Computational algorithm for fast Hadamard matrix transform of order 12 via factorization 06 p1093 A70-17314

Liapunov functions generation by matrix transformation of state-space system vector applicable to linear and nonlinear systems 06 p1023 A70-17544

Slack variable to transform optimal control problem with scalar inequality constraint on state variables into unconstrained problem 06 p1024 A70-17952

Transformed thermodynamics equations derived automatically by substitution codes, noting exceptions for real gas and discharge flow 08 p1597 A70-20918

Thermal contact resistance of anisotropic materials using mathematical geometric transformation [ASME PAPER 69-HT-47] 09 p1790 A70-23552

Computer-aided circuit design by imbedding singular elements to transform network synthesis into analysis problem 10 p1855 A70-24762

Radiation fields of sources in plane stratified plasma medium calculated for amplitude transformation coefficient 10 p1843 A70-25155

Reduction of satellite photographic data using transformation functions 11 p2007 A70-26186

Fourier and Hadamard transformation codings for multidimensional data channel noise immunity and bandwidth reduction 11 p2011 A70-26329

Invariant transform of motion and continuity equations for steady three dimensional flows of compressible fluids in absence of massive forces 11 p2041 A70-26598

Energy derivation for mechanics and thermodynamics with generalization to systems of more than two dynamic variables, considering transformations and Newton and Kepler laws 12 p2164 A70-27070

Ordinary differential eigenvalue problems solution by successive transformations, describing computer program and applications to hydrodynamic stability 13 p2440 A70-29085

Compressible fluids steady state equations invariant transformation, establishing sound speed-Mach number relation 13 p2389 A70-29458

Unitary solution to incompressible and nonviscous fluids in presence of slender profile 13 p2464 A70-29542

Pseudo one dimensional dissociational nonequilibrium nozzle flows, obtaining equilibrium and nonequilibrium solution through similar transformation of governing equations 14 p2527 A70-30264

Von Zeipel mappings equivalence to Lie transforms shown by order independent method 14 p2639 A70-30706

Grassmann manifold projective transformations into itself, considering matrix theorems 14 p2601 A70-31423

Axisymmetrical boundary value problem solution by net point method via transformation into self adjoint second order elliptic equation, obtaining positively determinate matrix 15 p2767 A70-31588

Generalized spectral analysis method implementing orthogonal transformations through Kronecker product representation and matrix factorization 15 p2767 A70-32099

Baecklund transformations applications to hodograph equations for steady two dimensional nondissipative MGD flows with aligned velocity and magnetic fields 15 p2781 A70-32453

Liapunov functions direct generation by state space system vector matrix transformation 15 p2768 A70-32555

Nonlinear discrete systems absolute stability exponential property proved by modified frequency condition, applying analog transformation to Szego-Kalman equations 16 p2882 A70-33044

Walsh functions and spectrum for signal processing, discussing computer compatibility 16 p2864 A70-33483

Electromagnetic waves scattering in uniformly moving media, using transformation formulas for plane waves 16 p2865 A70-33690

Radial energy eigenvalue problem conversion into one dimensional by infinite set of transformations, considering WKB quantization condition 16 p2942 A70-33691

Baecklund type matrix transformations application to hodograph equations system for aligned nondissipative MGD flows 16 p2958 A70-33747

Linear second order equation systems decoupling transformation, noting applications to structural feedback, flutter and control systems 16 p2943 A70-33891

Neutral type differential equations transformation to time lag system making periodic vibrations existence and stability theorems applicable 16 p2944 A70-34282

Relativistic three force transformation showing no contraction in static conditions 17 p3136 A70-34823

Continuous functions transformation by artificial neuron networks, investigating electrophysiological data for nerve tissues excitability 18 p3223 A70-36081

Electronic circuits design by discrete equivalent transformations for selecting components parameters within given limits 18 p3231 A70-36239

Fourier and Hermite transform methods for Vlasov equation solutions in plasma physics 18 p3296 A70-36789

Laminar incompressible flow in arbitrary cross section entrance region of ducts by numerical technique after transformation to boundary value problem [ASME PAPER 70-GT-91] 18 p3243 A70-36878

Normalized multidimensional Newton-Raphson method eliminating initial guess, using two- transformation technique 19 p3457 A70-37822

Random signal nonlinear transformations using relations between Laplace and Fourier transforms 20 p3583 A70-39123

Asymptotic equivalent functions for integral Laplace transformation transition to original in continuous media mechanics 20 p3726 A70-39873

Hollow shell theory equations for complex stress-strain states, using complex transform method 20 p3726 A70-39880

Analog communication optimal nonlinear modulation scheme design for large SNR through transformation into inner product functions 20 p3587 A70-39973

- Rank permutation codes equivalence to binary code class capable of generation and detection through direct and inverse transformations respectively
20 p3594 A70-39975
- Integral transforms applied to convective heat transfer during nonNewtonian fluid flow with power rheology in pipes and channels
20 p3613 A70-40177
- Jacobi-type conditions for singular optimization problems obtained by transformation to nonsingular form adaptable to linear quadratic optimal control theory
20 p3659 A70-40262
- Dolph-Pritchard technique limitations for transformation of array factor into Chebyshev polynomial as related to element spacing for single lobe endfire arrays
20 p3599 A70-40315
- Transformation theory for compressible turbulent boundary layer with arbitrary pressure gradient [AIAA PAPER 69-160]
21 p3809 A70-41741
- Nonlinear coupling in systems with two degrees of freedom, deriving transformation laws for uncoupling
21 p3940 A70-42054
- Novozhilov complex transformation method extended to Timoshenko theory of elastic shells constructed with allowance for transverse shear deformation
21 p3941 A70-42237
- Laminar axisymmetric incompressible boundary layer calculation based on Mangler transformation [ASME PAPER 70-FLCS-13]
22 p4008 A70-42414
- Numerical solution of nonlinear master equation for diatomic molecule dissociation and recombination from uncoupled differential equations
22 p4062 A70-42746
- Matrix transformations and minimization of computation algorithms for arbitrary linear equations systems, using direct methods
22 p4063 A70-43479
- Perturbation theories based on canonical transformations, examining von Zeipel theory and Hamiltonian functions
22 p4109 A70-43749
- Multidimensional correspondences between Helmholtz equation eigenfunctions and eigenvalues, including involutorial transformations
23 p4218 A70-44211
- Boundary value problems of fluid dynamics in dynamic cavities reduced to integral equations system
23 p4182 A70-44347
- Isotropic transformation of tensor space, proving theorem for reducing hemitropic function to N invariants of rotations and single vector
24 p4378 A70-45271
- Power spectrum of digital signals pulse modulated with random sequences, discussing phase modulation and z transform techniques
24 p4315 A70-46151
- TRANSFORMERS**
NT MODE TRANSFORMERS
Small signal opto-electronic wideband transformer with coupling element ensuring fast response and low sensibility to parasitic magnetic fields
03 p0459 A70-14266
- Acoustic noise control on Boeing aircraft electromagnetic components, noting iron-core magnetostriiction demanding transformer redesign
09 p1647 A70-22764
- Free-running parallel inverters limitations by critical characteristics of networks, transformers and switching elements
11 p1983 A70-26628
- DC signals measurement in automatic control circuits, ensuring transformer isolation by use of transistorized amplifier
12 p2196 A70-27682
- Electrical design of ferrite configuration high power rotary transformer for satellite slip ring replacement, minimizing transistor turn-off losses
21 p3759 A70-41222
- TRANSFORMS**
U TRANSFORMATIONS [MATHEMATICS]
TRANSIENT HEATING
NT PULSE HEATING
NT SHOCK HEATING
Transient heat transfer near two dimensional stagnation point in viscous incompressible fluid steady flow
01 p0002 A70-10457
- Transient temperature distribution in inhomogeneous material, using finite difference representation for temperature time derivative [ASME PAPER 69-WA/HT-33]
04 p0782 A70-14807
- Equations and techniques to analyze transient heat and mass transfer characteristics of packed adsorption beds for spacecraft life support systems
04 p0786 A70-15316
- Numerical solution of transient heat conduction with radiating surface, imposing Runge-Kutta type integration on surface
04 p0787 A70-15613

- Transient heat flow in three dimensional rectangular panels, developing criterion for problem dimensionality [AIAA PAPER 70-16]
06 p1182 A70-18212
- Transient heat conduction of thin circular disk with uninsulated surfaces rotating past stationary point source by finite element method
09 p1787 A70-22269
- Temperature distributions in multidimensional transient conduction heat transfer, using variational method and Laplace transformation
09 p1788 A70-22705
- Tungsten-rhenium thermocouple for high temperature measurement of samples under unsteady heating processes, analyzing instrument error sources
09 p1789 A70-23108
- Esophageal, rectal and quadriceps muscle temperatures, oxygen uptake, weight changes, skin conductance and skin evaporation during thermal transients caused by bicycle exercise
10 p1810 A70-24006
- Dynamic stresses, temperature and displacements fields in thin circular disk under transient heat sources, considering mechanical resonance vibration
10 p1958 A70-24518
- Transient thermal stresses in restrained-in-bending slab with surfaces heated and cooled with finite heat transfer coefficients
10 p1964 A70-25095
- Steady state and transient heat transfer by radiation and conduction in absorbing medium bounded by infinite coaxial cylindrical surfaces
12 p2331 A70-27697
- Transient heat transfer combining conduction and radiation in absorbing plane layer analyzed by differential approximation
12 p2332 A70-27801
- Wing rib structure transient thermal stresses analysis using photothermoelastic method
12 p2327 A70-27982
- Flat plate and cylinder with periodic Joulian heating from time dependent heat source, analyzing transient temperature distribution
14 p2664 A70-30269
- Heat flow measurement, discussing operation principles, heat conduction and stationary and transient temperature conditions
17 p3082 A70-34681
- Half space nonstationary temperature field with mobile heating at edges, using integral transformations
18 p3348 A70-36725
- Transient thermal stresses in spherical shell with distributed source and general Sturm-Liouville boundary conditions
19 p3539 A70-37800
- Eroding surface transient heat conduction problem, considering temperature dependent surface properties, ablation, convective heating, etc
20 p3738 A70-40279
- Charring ablators transient heat transfer model, calculating surface temperature and recession and pyrolysis mass loss [AIAA PAPER 70-1143]
20 p3738 A70-40280
- Variational formulation for steady and transient heat conduction with variable thermal conductivity, applying to cylindrical element
22 p4123 A70-42546
- Transient heating by solar radiation of semitransparent solid medium and adjoining fluid, establishing criteria for maximum fluid temperature
22 p4123 A70-42598
- Cylindrically symmetric transient heat conduction in biological systems for inhomogeneous media and internal sources, using finite difference method
23 p4150 A70-43900
- TRANSIENT LOADS**
NT BLAST LOADS
NT GUST LOADS
NT IMPACT LOADS
NT LANDING LOADS
NT SHOCK LOADS
Piezoelectric transducer for photoelastic analysis of HF stress waves in thick ring subjected to transient loads
02 p0389 A70-12500
- Impulsive and transient load disturbances in thin elastic finite circular plate on Pasternak type viscoelastic foundation
03 p0595 A70-13905
- Transient excitation methods for structures dynamic analysis, discussing suitable forcing transients choice
06 p1165 A70-17646
- Thermal strain measurement in operational and experimental components of high temperature plant, discussing full-bridge weldable type strain gage for transient strains
09 p1675 A70-22582
- Transient bending and shear stresses at clamped support of orthotropic circular cylindrical shells
11 p2135 A70-25985
- Transient analysis of stress waves around cracks under antiplane strain with time dependent loadings based on integral transforms
11 p2145 A70-26698

- Elastic waves propagation in finite thickness elastic plate under transient load, assuming material behavior in conformity with nonlinear Hookes law
15 p2814 A70-31544
- Transient overloads effect on long term fatigue strength of notchen and smooth steel samples, emphasizing heat treatment effect on notch sensitivity at high temperatures
15 p2814 A70-31546
- TRANSIENT OSCILLATIONS**
Tunnel diode studied for oscillations initiation resulting in hysteresis involving supply voltage and load conductance variations
03 p0459 A70-14284
- Ge IMPATT diodes under pulsed operation to produce LF high efficiency oscillations, recording current and voltage waveforms
05 p0821 A70-16417
- Ammonia maser transient spiking effects under periodic oscillation condition modulation, noting frequency sweep width role
07 p1299 A70-19685
- Two degrees of freedom assemblies transient motions using computer, solving acceleration and deceleration problems in mechanical systems
08 p1502 A70-20699
- Dynamic response of joined elastic quarter spaces of solids to time varying free surface shear tractions parallel to plane of juncture [ASME PAPER 69-APMW-16]
08 p1591 A70-21467
- Transient waves propagation in homogeneous isotropic linearly elastic half space excited by traveling normal point load on surface, deriving displacements [ASME PAPER 69-APMW-12]
08 p1592 A70-21468
- Transient process statistical characteristics in He-Ne laser operating near excitation threshold with pronounced rise time oscillations of light wave field
12 p2247 A70-27507
- Initial reentry body motion effects on angle of attack envelope value throughout trajectory, including altitude of maximum transient amplification
16 p2982 A70-33892
- Linear damping theory, discussing simple harmonic motion model extension to transient motion
19 p3472 A70-38041
- Transient elastic vibrations of air and liquid filled cylindrical shells under radial impact, using shadow-optical cinematography [SMPT PREPRINT 107]
22 p4031 A70-43030
- TRANSIENT PRESSURES**
Induction distances, transient pressures and wave propagation rates for detonation waves in cylindrical tube low temperature hydrogen-oxygen mixtures
03 p0607 A70-13919
- Aviation kerosene pipeline column separation after valve closure, solving differential equations for transient pressures propagation to predict vapor cavities duration
09 p1665 A70-23744
- Phenomenological theory of transient high temperature creep, considering internal back stress
15 p2763 A70-32809
- Fast response transducer for measuring transient pressures due to shock interaction
17 p3093 A70-35484
- Parachute canopy surfaces transient aerodynamic pressures during unsteady processes, using piston theory [AIAA PAPER 70-1175]
21 p3754 A70-41838
- TRANSIENT RESPONSE**
Transient magnetic resonance technique for non-destructive testing of elements with nuclei having magnetic moment, considering cereal grains, propellants, metal powder and plastics
01 p0097 A70-10014
- Transversely isotropic circular cylinder acted upon by transient shearing force at one end, noting forced torsional oscillation using cylindrical coordinates
01 p0200 A70-10550
- Transient energy transfer during expansion of plane layer of radiating gas bounded by strong shock, assuming LTE and perfect inviscid nonconducting gas
02 p0279 A70-12230
- Transient response role in limiter-discriminator detection of binary FSK signals, comparing resulting and optimum error probabilities
02 p0258 A70-12421
- Triple mode control strategy to provide near optimal stable transient response in variably loaded electrohydraulic servomechanisms
02 p0272 A70-12728
- Transient heat transfer in forced convection flow over curved wall with zero Prandtl number, applying to laminar boundary layer with variable free stream velocity
02 p0400 A70-12857
- Transient processes in ruby quantum paramagnetic amplifier during pumping, showing technique for saturation prevention and relaxation effects on population inversion
03 p0456 A70-13460
- Thermocouples response to rapid temperature rise produced by discharge from low inductance high voltage capacitor bank
03 p0486 A70-13559

Transient response of heterogeneous solid propellant combustion surface determined by step technique regarding pressure buildup and drop conditions [ONERA-TP-748] 03 p0544 A70-13635

Unsteady linear automatic control systems transient functions determined by approximation method 03 p0460 A70-13732

Transient creep analysis of simply supported circular cylindrical shells subjected to internal pressure based on strain and time hardening theories 03 p0595 A70-13813

Optimum automatic system for controlling helicopter formation flight, stressing transient response Q factor and transmission ratios 03 p0413 A70-13859

Transient thermal stresses in photoelastic models of various shapes under various steady state or transient temperature conditions, describing instrumentation and experimental methods 03 p0600 A70-14308

Spacecraft orientation control without measuring vehicle angular velocity based on transient response and oscillations damping effectiveness 04 p0760 A70-14428

Complementary symmetry MOS/CMOS integrated circuit transient response to electron irradiation 04 p0657 A70-14733

Nuclear rocket engine core thermal and neutronic transient and steady state dynamics digital simulation, showing advantages over lump model analysis [ASME PAPER 69-WA/NE-3] 04 p0717 A70-14757

Transient heat conduction solution by finite element methods application to nonlinear boundary condition problems 04 p0781 A70-14804

Transient processes of strain wave propagation in elastic shells and plates under time varying loads 04 p0773 A70-15010

Transient plane disturbance of stream angular to applied magnetic field, discussing relationship to airfoil and Alfvén waves 04 p0615 A70-15093

Integral-criterion optimization of transient processes in mechanical systems synthesis with favorable dynamic and damping characteristics 04 p0720 A70-15218

Control system response improvement by state variable feedback illustrated by frequency and transient response tests data from analog model 04 p0662 A70-15331

Parasitic transient process in automatic control system during switching to mode stabilized with respect to certain coordinates 04 p0662 A70-15433

Vertical electric dipole transient response over circular ground screen, studying low angle radiation patterns 06 p1021 A70-17573

Transient excitation methods for structures dynamic analysis, discussing suitable forcing transients choice 06 p1165 A70-17646

Corrective open-loop circuit, using delay elements for compensation of transient response in linear circuits with lumped parameters for pulse modulation transmissions 06 p1023 A70-17774

Heat conduction transient field problems in two and three dimensional isoparametric finite element solutions using Galerkin method 06 p1178 A70-17938

Semiinfinite simply supported cylindrical shell transient response due to axisymmetrically engulfing step pressure wave, investigating moving load critical velocity [AIAA PAPER 70-18] 06 p1170 A70-18063

Transient response analysis in isotropic material under thermal galvanomagnetic effects involving interaction electric and thermal conductions in applied magnetic field 06 p1107 A70-18213

Computerized FORTRAN equations simulation of linear and nonlinear circuits for symbolic analysis and transient response 06 p1026 A70-18424

Radiation environments effect on logic circuitry constructed of MOS and bipolar transistors, discussing permanent and transient effects 07 p1242 A70-20149

Unsteady MHD flow at forward stagnation point analyzed for magnetic field effect on transient phenomena, using difference-differential numerical method 07 p1354 A70-20235

Transient phenomena accompanying heating of fluid situated between heat conducting plane horizontal plates, using interferometry and streak photography 08 p1596 A70-20592

Transient response analysis of nanosecond pulsed transistor amplifier having common-emitter configuration with negative feedback 08 p1474 A70-21229

Transient heat conduction and stationary temperature distribution calculation in curvilinear coordinates using finite element method 08 p1590 A70-21362

Transient radial temperature distributions in cylindrical shells via Carslaw and Jaeger procedure involving binomial theorem and asymptotic expansions of Bessel function 08 p1599 A70-21588

Radar target short pulse transient scattering response computation using fast Fourier transform algorithm 08 p1463 A70-21597

Statistical characteristics of Q switched He-Ne laser emission gain during transient process from subthreshold to superthreshold value 08 p1514 A70-21814

Automatic photographic data processing system with transient reproducer to obtain digital format for computer analysis 09 p1673 A70-22030

Transient regimes of solid fuel diffusion combustion in channel with oxidizer fed in from outside, proposing finite difference scheme for integrating equations 09 p1741 A70-22114

Solid radiating sphere cooling in space, determining transient temperature distribution by finite difference computing techniques 09 p1790 A70-23562

Transient response of fin-tube space radiators sudden steady state operation halting and system cooling 09 p1790 A70-23564

Transient process statistical calculation in discrete elastic mechanical system possessing energy dissipation under time dependent cross correlated random forces 09 p1729 A70-23595

Pulse signal transmission rate increase by transient processes compensator, discussing stability relation to signal to noise ratios 09 p1639 A70-23696

Transient analysis of transistor under large input signal accounting for minority carrier life and base collector capacity 10 p1849 A70-24383

Linear time-varying systems transient responses prediction, using Krylov-Bogolubov method and parameter plane analysis 10 p1855 A70-24704

Reaction time in determining visual transient response at frequencies above flicker fusion 10 p1818 A70-24717

Dynamic characteristics of structures measured, using digital computer to analyze transient data from frequency sweep tests 10 p1961 A70-25059

Distributed gain amplifier circuits with K-type filters, deriving analytical relations for pulsed and transient characteristics 10 p1853 A70-25131

Laser field transient properties in switching-on processes, discussing Q switching, detuning switch-off and pump power switch-on 11 p2064 A70-26843

Transient processes in n-stage aperiodic amplifier during instantaneous change in phase and amplitude of emf at input 12 p2195 A70-27536

Amplitude stabilization transient processes at output of four terminal network with arbitrary phase and amplitude characteristics by representing pulse transfer function in series 12 p2184 A70-27537

Spacecraft orientation control without measuring vehicle angular velocity based on transient response and oscillations damping effectiveness 13 p2503 A70-28453

Digital signals transmission codes comparison for transient response by reducing channel bandwidth to obtain error probability 13 p2372 A70-28899

Differential equations of controller providing optimum transient response for plant with indeterminate parameters, allowing for nonadditive random noise 13 p2382 A70-29278

Lunar seismogram response behavior in terms of power law model of sedimentary earth rock anelasticity 13 p2497 A70-29856

Alouette spikes decrease with time equivalent to antenna transient response during hot plasma immersion 13 p2371 A70-29921

Ignition transients in solid propellant rocket engines, taking into consideration flame temperature changes with pressure and igniter secondary mass addition 14 p2628 A70-30778

Lossless waveguide propagation analysis as transient problem by means of Laplace transform 14 p2556 A70-30923

Soviet book on multivariable automatic control systems analysis and synthesis covering equations of motion, nonlinearities, pulse control, transient responses, etc 14 p2561 A70-30954

Gas turbine performance dynamic modeling by analog and digital computer simulation providing clear picture of transient behavior 14 p2629 A70-30991

Alpha-beta and Kalman tracking filters with randomly interrupted data, evaluating transient responses as function of radar measurement accuracy and valid data acquisition probability 14 p2557 A70-31186

Transient response of self adaptive systems subjected to determinate or random signal mixed with additive noise 16 p2882 A70-33234

Laminar boundary layer model for viscous losses during transient turbulent liquid flow in tube, assuming slug flow for core [ASME PAPER 70-FE-8] 16 p2891 A70-33627

Avalanche diode transient temperature response, measuring thermal impedance under pulse bias conditions 16 p2878 A70-33695

Sandwich rings inplane transient response to concentrated radial impulsive loads based on Timoshenko type theory, noting dependence on extensional to shear stiffness ratio 16 p2993 A70-34093

Transient signal generation during large amplitude ultrasonic pulse propagation through carbon tetrachloride 16 p2952 A70-34097

Nonlinear mechanical systems transient motion analysis based on phase trajectories 16 p2944 A70-34283

Double acoustical resonators transient response to excitation by single sine wave, presenting pressure magnification factors as function of frequencies 17 p3135 A70-34521

Holographic measurement of transient behavior of structures under unsteady or impulsive loading, using pulsed lasers 17 p3085 A70-35008

Transient wave propagation in homogeneous anisotropic media, using hyperbolic equations and unitary operator 17 p3137 A70-35607

Infinite Bernoulli-Euler beam transient and steady state response, considering damping, elastic foundation and constant axial load effects 18 p3339 A70-36490

Liquid fuel jet engine thrust aftereffect momentum, investigating switching off transient process 19 p3490 A70-37249

Omnidirectional dynamic stress gage as embedded elastic inclusion, discussing transient response to ground shock compression wave pressure 19 p3422 A70-37699

Transient system decay characteristics, discussing equilibrium point damping time for asymptotically stable systems of ordinary differential equations 19 p3542 A70-38066

Frequency multipliers with charge storage diode, analyzing turn-off transient effect on performance by charge control model 19 p3391 A70-38748

Weakly ionized gas subjected to pulsed DC electric field, analyzing transient relaxation of electrons velocity distribution 19 p3482 A70-38899

Laser pulse amplification by stimulated thermal Rayleigh scattering in absorbing media by transient theory 20 p3640 A70-39113

Fretting corrosion zone steel, measuring transient temperature distribution during contact friction 20 p3647 A70-39243

Second order automatic phase control system with proportionately integrating filter, calculating transient response by harmonic linearization method 20 p3584 A70-39253

Collisionless cylindrical Langmuir probe response in turbulent plasma for mean and statistical properties 20 p3684 A70-40258

Uniformly loaded thin elastoplastic spherical shells, calculating strain hardening and strain rate effects on transient response 21 p3935 A70-41255

Electromagnetic test equipment transient waveform control using on-line digital computer in near real time configuration 21 p3805 A70-41270

Digital bit synchronization phase locked loop steady state and transient performance in white Gaussian noise 21 p3802 A70-41352

Transient behavior of first order phase locked loop in presence of noise, solving Fokker-Planck equation for loop dynamics by numerical integration 21 p3802 A70-42181

GaAs point contact diodes quick response performance with glass-metal or metal-ceramic bases, obtaining Schottky-type rectifying barriers by half period currents 22 p3995 A70-42406

- Bistable wall attachment fluid amplifier, calculating unsteady end wall switching transient based on turbulent jet entrainment properties
[ASME PAPER 70-FLCS-3] 22 p3964 A70-42428
- Buoyancy effects on transient free convection heat transfer in revolving tube for zero to 100 g centrifugal acceleration
[ASME PAPER 70-HT-10] 22 p4122 A70-42437
- Thermocouple transient response characteristics in deflagrating and ablative low conductivity materials with high temperature gradients
[ASME PAPER 70-HT-7] 22 p4122 A70-42440
- Finned tube-sheet spacecraft radiator transient response for perturbations caused by power supply and heat sink temperature changes
22 p4123 A70-42519
- Elastic cylindrical shell transient response to plane acoustic shock wave traveling through light fluid medium
22 p4114 A70-42647
- Nonlinear automatic control systems transient response by frequency response curves of amplitude and phase characteristics
22 p4001 A70-42831
- Transient stresses and strains in plane wedge under dynamic load, using photoelastic, high speed photographic and strain gage studies
[SMPE PREPRINT 93] 22 p4036 A70-43062
- Gas reductors transient processes, analyzing valve equations of motion
22 p3965 A70-43357
- Cantilever beam transient response measurement by stored beam /real time/ holographic interferometry combined with high speed motion picture photography
22 p4039 A70-43452
- LF passband ideal filter instantaneous pulse response, using delta function model
22 p4005 A70-43555
- Arbitrary shells large deflection transient response, using finite difference computer program
23 p4272 A70-44710
- Integration operators for transient structural response in qualification tests for internal components of dynamically loaded structures
23 p4273 A70-44719
- Arbitrarily shaped cylindrical conducting structures with transient incident electromagnetic wave, calculating scattering from integral equation by digital computer
23 p4165 A70-44957
- Electroacoustic circuits transient behavior, examining loudspeaker effectiveness
24 p4321 A70-45374
- Pendulum dynamic stability under parametric excitation, presenting transient and steady state solutions by linear and nonlinear theory applications
24 p4379 A70-45587
- Finite thickness metal plate eddy current response to pulsed field from aperture probe
24 p4344 A70-45696

TRANSIENTS [SURGES]

U SURGES

TRANSISTOR AMPLIFIERS

- Noise source model of Si planar diffused bipolar IC transistors in operational amplifiers, noting base-emitter junction burst noise
02 p0257 A70-12192
- Center frequency shift prediction model for nonlinear collector junction capacitance in transistor Class C amplifiers
04 p0660 A70-15343
- Transistorized low impedance cascades as amplifiers for proportional counters in studying cosmic ray intensity variations
05 p0845 A70-15934
- Transistorized wideband amplifiers synthesis by combining dynamic parameters method with poles and zeros method
05 p0819 A70-16249
- Microwave transistor amplifier design and specifications, discussing applications and economy in design, production and use
06 p1018 A70-17358
- Transistor RF and IF amplifiers designed for 210-ft antenna of Australian National Radio Astronomy Observatory
07 p1243 A70-20350
- Gain stabilization of transistorized LF selective amplifiers in radiometric receivers, discussing two-frequency resonance system
08 p1473 A70-21061
- Transient response analysis of nanosecond pulsed transistor amplifier having common-emitter configuration with negative feedback
08 p1474 A70-21229
- Multistage microwave transistor amplifiers design for 4 GHz band, describing poor input/output impedance matching solution
08 p1475 A70-21279
- UHF transistor power amplifier, discussing CW and pulse performance and power gain
08 p1477 A70-21294

- Repetitive electronic differential analyzer with transistorized operational amplifiers for iterated solutions of differential equations
08 p1478 A70-21836

- MOS transistor amplifier circuits, analyzing circuit parameters for common-source, common-drain and common-gate configurations
09 p1643 A70-22126

- Integrated CW UHF power amplifier modules using thin film lumped elements and UHF power transistor chips
10 p1846 A70-23884

- S band CW high power broadband power source consisting of transistor amplifier-driven varactor doubler chains in hybrid integrated form
10 p1846 A70-23885

- Equivalent circuits for transistors in class A amplification over wide frequency band
11 p2021 A70-26831

- DC signals measurement in automatic control circuits, ensuring transformer isolation by use of transistorized amplifier
12 p2196 A70-27682

- Wideband high power output transistor amplifier design features and operational characteristics
12 p2199 A70-27980

- Double diffused epitaxial silicon bipolar microwave transistor design, fabrication and performance evaluation, including scattering parameters vs frequency for common-emitter amplifier
13 p2379 A70-29592

- Wideband microwave transistor IF amplifier for mm wave communication system
14 p2555 A70-30283

- Computerized design of transistorized UHF wide-band amplifier, using successive approximations for optimum circuit automatic selection
14 p2556 A70-30668

- UHF Si p-n-p transistors with low noise and high gain for small signal applications
14 p2557 A70-31161

- Transistorized amplifiers synthesis with multiloop feedback
15 p2707 A70-31518

- Transistor amplifier with back coupled emitter and parallel inductive correction, calculating optimal frequency and phase characteristics under complex load
20 p3598 A70-39790

- Low noise FET amplifier for satellite magnetometer, measuring interplanetary fields
21 p3799 A70-41923

- Transistorized IF amplifier output matching to long transmission line, deriving formulas for gain and pass-band over wide output impedance range
22 p3995 A70-42520

- Oscillatory stability of selective RF transistor amplifiers, using stage dimensioning and gain graphs
22 p3996 A70-42818

- Design tolerances and compensating networks for microwave transistor amplifier, using synthesis search and trial calculation by computer
23 p4168 A70-43780

- Low noise dual receiver system for satellite communication earth station using parametric and transistor amplifiers
23 p4169 A70-43791

- Transistorized power amplifiers, frequency multipliers and parametric multipliers design for VHF and UHF ranges
23 p4170 A70-43876

- Semiconductor microwave generator design for maser simulator using transistorized amplifier, varactor frequency multiplier and diode multiplier
23 p4171 A70-43878

TRANSISTOR CIRCUITS

- Nonlinear distortion in switching transistor mixer predicted by modifying analysis used for diode modulator and mixer circuitry
02 p0268 A70-12423
- Electronic transistorized harmonic signal integrator operating in connection with static-dynamic bridge
03 p0493 A70-13975
- Electron image projection tube for fabricating integrated circuits of micron size transistors
03 p0458 A70-14033
- Transistors used as UHF high-Q inductance active filters, utilizing internal phase shift and energy storage characteristics
04 p0694 A70-15490
- Microwave Si transistors with overlay and interdigital geometries and integrated circuit design considerations for power amplifiers, power oscillators and frequency multipliers
05 p0819 A70-16149
- Transistor circuit design with junction compensation techniques to reduce transient gamma radiation effects
05 p0821 A70-16418

- Circuit and operation of transistorized RF power attenuator with linear attenuation and binary code control by digital computer
06 p1022 A70-17777

- Circuit and operation of transistorized linear voltage-to-frequency converter performing current integration proportional to input signal
06 p1022 A70-17779

- Transistorized circuit for automatic control of photographic studies of pupillary reaction transient states in rabbits subjected to light stimulus
07 p1216 A70-18731

- Size reduction and low noise temperature in receiving antennas obtained by transistor integration and resonance frequency modulation
07 p1241 A70-19353

- Radiation environments effect on logic circuitry constructed of MOS and bipolar transistors, discussing permanent and transient effects
07 p1242 A70-20149

- Short high current pulses generation by avalanche transistors in circuits suitable for investigating low impedance laser diode
09 p1642 A70-22035

- MOS transistor amplifier circuits, analyzing circuit parameters for common-source, common-drain and common-gate configurations
09 p1643 A70-22126

- Ferrimagnetically tunable transistor oscillator in common collector configuration
09 p1645 A70-22603

- Steady state analysis of harmonic oscillations in HF synchronized transistor autooscillators, considering transistor inertial properties
09 p1649 A70-23341

- Pulse-shaping transistor circuit analysis, considering circuit elements roles and temperature, pulse duration and leading and trailing edges durations effects
09 p1650 A70-23628

- Transistorized pulse repetition frequency bandpass and band elimination filters, using trigger circuit to improve pulse-edge steepness and critical frequency stability
09 p1650 A70-23630

- Transistor bistable multivibrator design by graphic analytic method, considering effects of loading and supply voltages, temperature and component values on circuit performance
10 p1848 A70-23995

- Wideband transistorized DC amplifier circuit and operation for outputs of tensometers, thermoelectric, electrodynamic and resistance sensors
11 p2019 A70-26435

- Transistorized system for static and dynamic strain measurements of mechanical quantities
11 p2055 A70-26437

- Transistorized differed synchronizer for delaying photoflash initiation in scientific photography
12 p2228 A70-26879

- Transistorized pistol grip probe design, circuit and operation for testing wobble and asymmetry in rotating ring commutators of electric motors
12 p2165 A70-27495

- Brushless DC motor with rotor position sensor and transistor commutator for armature current switching, describing design and operation
12 p2165 A70-27525

- Transistorized pulsed activity converter for observing analog curve of change in pulse frequency
12 p2179 A70-28316

- Transistorized voltage to pulse width converter based on constant current capacitor discharge
13 p2378 A70-29457

- Large signal junction FET model involving piecewise linear approximation for ECAP circuit analysis program
15 p2711 A70-32596

- Avalanche transistor circuits for rectangular pulses generation, considering delay line for optimum results
18 p3233 A70-36774

- Thyristor circuit for storing or generating digital control signals, considering reliability at high noise levels
19 p3385 A70-37377

- Pulse shaper circuits with tunnel diodes and transistors, describing recovery time decrease
20 p3596 A70-38972

- Epitaxially grown Si contact for area reduction of MOS transistor circuits
20 p3596 A70-39099

- Matrix condenser for tuning hybrid thin film self excited quartz oscillator with common base transistor configuration, discussing electrical properties and fabrication
20 p3597 A70-39257

- Transistorized quartz oscillators, testing frequency and amplitude stabilities and functions of input and output capacitances, supply voltage and feedback
20 p3597 A70-39258

- Normal mode pulsed ruby laser system with Xe flash lamp pumping, trigger circuit and transistorized power supply
20 p3643 A70-40355

DC transistorized Nor logic gates design based on graphic analytic method permitting influence of circuit parameters variations for reliability improvement 21 p3793 A70-40765

Stress tolerant thyristor and transistor switching electronic converter for ion propulsion engine [AIAA PAPER 70-1157] 21 p3866 A70-40901

Reverse curvature silicon transistor linearizer for hot-wire and thin-film constant temperature anemometers for aorta blood flow velocity measurements 21 p3827 A70-41458

Multipurpose transistorized tachometer for rotating body speed measurement, control and recording, using electronic integrator and magnet pickup 21 p3831 A70-42245

Transistorized DC to AC converter providing sinusoidal output to power automatic spacecraft control devices via pulse width modulation 22 p3994 A70-42309

High power short rise time square wave inverter using power transistors 22 p3965 A70-43336

Transistor circuit analysis at high frequencies and large signals, considering collector current, inertia and conductance conditioned by diffusion and recombination 23 p4161 A70-43779

MOS transistor trigger circuit design parameters statistical calculation and optimization by Monte Carlo method using computer 23 p4171 A70-43957

Transistorized LF RC filter circuit design for desired frequency response characteristics 23 p4171 A70-43962

MIS model applied to memory transistor with thin insulator consisting of silicon nitride on silicon dioxide 23 p4172 A70-44197

TRANSISTOR LOGIC

Diode transistor microelectronic logic circuit reliability, efficiency and optimization using digital computer 04 p0659 A70-15210

Seven segment in-line digital readout circuit for binary-quinary decade counter, using resistance transistor logic 21 p3793 A70-40763

Digital computer constructed with diodes and transistors logic for evaluating matrix determinants and minors 23 p4166 A70-43955

TRANSISTORS

NT JUNCTION TRANSISTORS

NT PHOTOTRANSISTORS

NT SILICON TRANSISTORS

Mathematical model coefficients determination for planar diffused transistor, obtaining admittance parameters 01 p0048 A70-10050

Book on thin film transistors microelectronics covering semiconductor physics, fabrication, analysis, applications and comparison with MOS transistors 01 p0052 A70-11329

Transistor behavior prediction at threshold of large signal conditions, using nomographs to evaluate maximum drive levels before distortion onset 03 p0452 A70-13966

Device modeling for computer aided design and analysis of integrated circuits, discussing list of desirable properties and applications to transistor design 03 p0454 A70-14026

Transistor admittance and diffusion parameters in direct measurement with varying frequency, evaluating reliability 03 p0459 A70-14285

Electron radiation-induced second breakdown in transistors indicated by time delay and failure by collector-to-emitter short 04 p0657 A70-14734

Steady state electrical characteristics of double diffused planar transistor calculated by iterative algorithm under arbitrary bias conditions 06 p1016 A70-17125

Microwave transistors frequency and power characteristics and tradeoffs in relation to thermal and packaging design 06 p1023 A70-18390

Operation mode for full-bridge programmed waveform static inverter permitting saturation of power transistors in DC power conversion 08 p1439 A70-20707

Steady state finite difference solution of equations governing arbitrarily biased bipolar transistor action in two dimensions 08 p1477 A70-21641

Transistor current gain measurement at HF by two channel method 09 p1632 A70-22234

Transient analysis of transistor under large input signal accounting for minority carrier life and base collector capacity 10 p1849 A70-24383

Forced oscillations of oscillator matched to transistor as active element, obtaining stability conditions by Liapunov first method 11 p2018 A70-25945

Linville bipolar transistor model for computer-aided design programs 11 p2021 A70-26830

Temperature effects on base and surface currents of plane bipolar transistors, testing validity of surface recombination process model 11 p2021 A70-26832

Thermal feedback theory of flicker noise generation in transistors and temperature fluctuations effect in vicinity of recombination centers 12 p2196 A70-27687

Microwave power transistors design and packaging 15 p2711 A70-32589

Bipolar transistor behavior identification and characterization in static regime, discussing measurement methods for parameters of IBIS model 17 p3054 A70-35414

Microwave power transistors, considering figure of merit, performance and packaging 19 p3386 A70-37691

Microwave transistors parameters measurement by scattering S /parameter method for characterizing noise, gain and dynamic range, reading input and output impedances from Smith chart 19 p3386 A70-37692

Nonuniform emitter current distribution effect on power transistor thermal stability, discussing temperature distribution effects 19 p3387 A70-37821

Complementary metal oxide semiconductor and bipolar transistors fabrication on same integrated circuit chip by C-squared technology 20 p3598 A70-40130

Microwave transistors for power generation and amplification, discussing packaging and pellet design 20 p3599 A70-40324

Secondary breakdown meter for semiconductor diodes and transistors with reverse base drive, utilizing I-V characteristics and voltage waveform 21 p3801 A70-42248

Darlington composite transistor stability, examining biasing resistance variation effect 22 p3998 A70-43257

Microplasma and burst noise measurements on discrete silicon planar transistors indicating origin at emitter-base junction 22 p3998 A70-43331

P-n junction dependent FM noise spectrum of UHF transistor power oscillator at transit frequency 23 p4161 A70-43789

Computerized mathematical modeling of transistors statistical and dynamic characteristics as functions of structural parameters 23 p4171 A70-43954

RF power transistors failure analysis, describing IR radiometer technique 23 p4175 A70-44747

TRANSIT

Ionosphere beacon satellites BeB and BeC transits for field alignment of small ionospheric irregularities 04 p0678 A70-14975

TRANSIT SATELLITES

Automatic ship navigation system using Transit satellites and onboard digital computer for routine tasks of dead reckoning 22 p4068 A70-42666

TRANSIT TIME

Electronic distance measurements involving transit time determination for signal from instrument to far point and back 03 p0495 A70-14176

Solar flare duration effect on propagation and modification of forward-reverse shock pair between sun and 1 AU, using equations of motion for spherically symmetric flow 04 p0740 A70-15104

Transit instrument azimuthal stability, investigating horizontal axis support, screw controls and tube position during star observations 04 p0693 A70-15484

Time determination at astronomical observatories using transit instrument observations concerning stellar distributions and magnitudes 04 p0756 A70-15486

Electronic recorder design and operation for mean moments of star transit times 04 p0694 A70-15491

Unsteady state and transit time analysis of geoeffective interplanetary plasma flux observed near earth causing magnetospheric storm of 17-19 April 1965 04 p0683 A70-15736

Aperture dissection scheme to reduce transit time of Bragg angle acousto-optical scanning of laser beam 05 p0860 A70-16657

Delay in photoelectric recording of transit of stars, considering stellar image brightness distribution and temperature 05 p0918 A70-16920

Lower ionosphere effects on HF propagation modes observed by pulse system, discussing propagation time, mode structure, transmission loss, etc 07 p1232 A70-19179

Nitrogen molecules pulsed high energy beams transit time measurement by gated time of flight procedure and by multichannel analyzer 07 p1345 A70-20136

SHF avalanche transit time oscillator with FM noise reduction by injection phase locking 08 p1462 A70-21594

Avalanche diodes properties, establishing equivalent circuit accounting for static electricity, carriers transit time and thermal effects 10 p1850 A70-24625

Air terminal and ground transfer design to provide improved access to aircraft and total transportation time reduction 12 p2208 A70-27992

Interplanetary shock wave properties in solar wind, determining propagation velocity, transit times proton density, proton and electron temperatures 13 p2481 A70-30066

Body waves in lunar models, calculating travel times and amplitudes 14 p2638 A70-30674

Unsteady state and transit time analysis of geoeffective interplanetary plasma flux near earth causing magnetospheric storm of 17-19 April 1965 14 p2575 A70-30820

Mean first passage signal time in one shot electronic system as function of threshold level 14 p2552 A70-31198

Phase shift ultrasonic flowmeter measuring transit time between oppositely propagating waves in blood vessels 15 p2691 A70-31921

Silicon avalanche transit time diodes as CW microwave generators and amplifiers 16 p2876 A70-33404

S and SKS travel times for arc distances of 30-126 degrees 16 p2898 A70-33975

Planet Mercury transit on photographs, noting role as test for terrestrial time systems 18 p3314 A70-36515

Avalanche transit time diode and transferred electron oscillators in microwave systems, discussing design, performance and applications 18 p2322 A70-36675

Mercury transit across sun on 9 May 1970, discussing observation, equipment and photographs 18 p3319 A70-37050

TRANSITION

Thioformaldehyde isotopic species reversible transition in interstellar clouds 20 p3703 A70-39164

TRANSITION FLOW

Flow stability criterion in rough pipes, deriving laminar to turbulent flow transition characteristics and drag as function of Reynolds number 01 p0064 A70-10998

Laminar-turbulent transition in free axisymmetric viscous incompressible jet from shaped nozzle and long cylindrical tube 03 p0466 A70-13396

Laminar flow separation, reattachment and transition over downstream step, including visual observations of smoke filaments, velocity fluctuation measurements and velocity profiles [ASME PAPER 69-WA/FE-5] 04 p0667 A70-14784

Acoustic technique for flow transition detection on hypersonic ablating reentry vehicles, presenting supersonic wind tunnel test results 04 p0620 A70-15531

Wall and total temperature variations effects on transition Reynolds number in hypersonic He tunnel, noting sound mode dominance 04 p0620 A70-15560

Entrance shape effects on tube rarefied flow in transition regime, noting role of Reynolds number in shape selection 04 p0675 A70-15593

Secondary vortex generation in near wake of circular cylinders under forced oscillation, analyzing motion dependent transition regimes using hydrogen bubbles flow visualization [AIAA PAPER 69-755] 06 p1032 A70-17212

Transition regime gas flows using Navier-Stokes equations and boundary conditions set, considering heat transfer, torque and drag in spherical geometry 06 p1049 A70-18331

Hypersonic leading edge problem solved, using merged layer theory to provide link between noncontinuum flow upstream of transition and boundary layer flow downstream 06 p0980 A70-18354

Hypersonic rarefied argon and nitrogen flows over flat plate, investigating flow field and surface measurements from merged layer into transition regime 06 p0981 A70-18355

Nitrogen hypersonic transitional flow at adiabatic sharp flat plate leading edge, presenting density, flow-

field shape and local rotational temperature for various regions 06 p0982 A70-18361

Surface pressures and shock wave shapes on sharp flat plates and wedges in rarefied hypersonic transition flow with emphasis on merged layer regime 06 p0982 A70-18362

Sphere and sharp slender cone drag coefficients in hypersonic transitional flow measured by flow modulation technique 06 p0984 A70-18389

Wind tunnel experiments for apparent reverse transition during expansion fan and turbulent boundary layer interaction, discussing Reynolds stresses 07 p1257 A70-19345

Turbulent-laminar transition in divergent radial flow between disks, relating velocity fluctuations to Reynolds number 08 p1483 A70-21235

Hypersonic spherical gas expansion into finite pressure region with transition from supersonic to subsonic flow in shock wave, discussing structure and pressure effects 09 p1658 A70-22116

Axisymmetric helium jet transition to turbulent flow in air slipstream, measuring temperature and velocity profiles 09 p1660 A70-22439

Two dimensional supersonic wake transition characteristics noting effect of heat transfer from vehicle or model body 09 p1605 A70-23184

Transition regime of rarefied gas dynamics using kinetic theory of gases, discussing Couette and Poiseuille flow, heat transfer and time dependent problems 10 p1919 A70-24141

Laminar boundary layer transition to quasi-cellular flow in natural convection above horizontal heated plates and disks 12 p2155 A70-27197

Tube relaminarization, predicting turbulent-to-laminar flow transition 12 p2212 A70-28118

Hypersonic low density transitional flow over slender conical vehicle, calculating drag coefficient and density profiles 14 p2529 A70-31365

Laminar to turbulent transitions determination in sub-/supersonic flows, reviewing methods based on hot-wire anemometer output signal [ONERA-TP-841] 15 p2720 A70-31918

Laminar to turbulent flow transition observation in laser induced vertical convection, using carbon dioxide-nitrogen laser 15 p2751 A70-31980

Stationary gas flows continuous to rarefied transition analysis based on mean free path anisotropy 15 p2721 A70-32139

Laser velocimeter application to laminar-turbulent flow transition at glass tube centerline 15 p2741 A70-32521

Hemisphere model flow field investigations in low density plasma wind tunnel, considering flow regimes of transition and shock formation 15 p2673 A70-32838

Electron density fluctuations in transitional zone of turbulent plasma jet, using digital analysis of Langmuir probe signals [AIAA PAPER 70-731] 16 p2958 A70-33495

Thin wire Langmuir probe measurements of electron temperature and density in transition and free molecular nozzle flow of short duration reflected shock tunnel 16 p2912 A70-33864

Wedge and cylinder high supersonic wakes stability and transition at various Reynolds numbers 17 p3006 A70-34465

Two dimensional supersonic wake behind heated slender flat plate, considering flow properties in transition zone 17 p3006 A70-34466

Transitional flow separation upstream of compression corner at trailing edge of sharp leading edge flat plate [AIAA PAPER 70-764] 17 p3007 A70-34487

Fluctuation measurements at wall and across laminar, transitional and turbulent compressible boundary layers on flat plate, using hot film probes [AIAA PAPER 70-745] 17 p3066 A70-34498

Temperature dependent absorption, nonsteady beam propagation and laminar-turbulent transition in laser induced convection column, measuring turbulence onset by fine wire resistance thermometer [AIAA PAPER 70-800] 17 p3107 A70-35197

Hypersonic rarefied gas flow around flat plate with sharp leading edge and circular cylinder in transition region 17 p3011 A70-35241

Acoustic measurement for transition localization on reentry vehicles, describing apparatus and techniques 17 p3093 A70-35483

Boundary layer oscillatory flow interaction with nonuniformly rotating lamina, calculating velocity distribution and transitional frequencies 19 p3406 A70-38443

Transitional flow separation upstream of compression corner for two dimensional model relationship to attached flow and boundary layer transition on plate 21 p3746 A70-41864

Laminar-turbulent transition in magnetic field using Plexiglas model, observing inlet conditions effect on MHD flow stability 21 p3861 A70-42234

Heat transfer in heated wire in supersonic flow near molecular transition zone, estimating anemometer sensitivity to motion fluctuations 22 p3959 A70-43240

Transition zone heat exchange during air mixed flow in pipes with conical duct or Vitoshinski nozzle inlets 23 p4283 A70-44729

TRANSITION LAYERS

Surface wave attenuation in homogeneous plasma cylinder caused by resonance in transition layer between plasma and vacuum 03 p0447 A70-13286

Plasma sheath transition structure surrounding cylindrical probe in weak axial magnetic field on basis of moment equations 07 p1353 A70-20230

Horizontal geomagnetic force variations, considering ionospheric wind effects on ions in transition layer 13 p2402 A70-30057

Chromosphere-corona transition region - Conference, Boulder, Colorado, August 1969 21 p3924 A70-42182

Transition region structure between chromosphere and corona, discussing temperature, theoretical models, energy balance and magnetic fields from far UV data 21 p3924 A70-42183

Chromosphere-corona transition region model from limb-disk optically thin line intensities 21 p3924 A70-42184

Energy deposition in solar corona associated with momentum transfer from heating wave in transition region, discussing wave pressures 21 p3925 A70-42190

Shock waves formation and dynamic characteristics in transition region response to infalling material from solar flares 21 p3883 A70-42193

Solar spectra isodentitraces indicating transition zones between and on sides of spicules in sheaths 21 p3926 A70-42197

Transition zone height in corona-chromosphere interface from high resolution disk spectra near limb 21 p3926 A70-42198

TRANSITION METALS

NT CHROMIUM
NT COBALT
NT COBALT ISOTOPES
NT HAFNIUM
NT IRIIDIUM
NT IRON
NT IRON ISOTOPES
NT IRON 57
NT MANGANESE
NT MANGANESE ISOTOPES
NT MOLYBDENUM
NT NICKEL
NT NIOBIUM
NT PALLADIUM
NT PLATINUM
NT REFRACTORY METALS
NT RHENIUM
NT RHENIUM ISOTOPES
NT RHODIUM
NT TANTALUM
NT TITANIUM
NT TUNGSTEN
NT VANADIUM
NT YTTRIUM
NT ZIRCONIUM

Two band Drude model validity for analysis of IR optical properties of transition metals obtained from experimental dielectric constant data 02 p0339 A70-12452

Lattice misfit influence on metastable omega phase morphology and stability in Ti transition metal alloys 03 p0508 A70-13146

Electron thermal capacity of d-transition metals for stable configurations determined by X ray spectral analysis 04 p0721 A70-14408

Solubilities and heats of solutions of Mo, W, V, Ti and Zr in liquid K 04 p0710 A70-15632

Optical, electrical and structural properties of transition metal dichalcogenides 05 p0890 A70-15755

Binary transition metal hydrides consisting of single metal and single hydrogen isotope, discussing preparation and kinetic, thermodynamic and structural properties 05 p0863 A70-16523

Thermoelectric power (TEP) of transition metals, detecting empirical regularities in TEP, nonlinear temperature dependence, etc 05 p0893 A70-16949

Disordered ferromagnetic binary alloys of transition metals magnetic moment distributions based on thermal neutron scattering experiments 05 p0893 A70-16950

Synthesis procedure for single crystal transition metal diborides, using high pressure capability in controlling stoichiometry 07 p1313 A70-19895

Microhardness of transition metals carbides measured after hot compression, suggesting dependence on statistical weight of C atoms with stable sp³ configurations 08 p1516 A70-21116

Transition metal alloys electronic effect on solubility of interstitials 08 p1521 A70-21695

Sigma phase occurrence in transition/nontransition elements alloys, discussing solid solubility limits 09 p1708 A70-23424

Band and localized models for electrical conduction of metal oxides, discussing Mott and semiconductor to metal transitions 14 p2627 A70-30498

Mo, W, V, Ti and Zr solubilities in liquid K 16 p2933 A70-34210

Metal matrix alloys with base of Co, Fe or Ni reinforced by transition metal carbide fibers, discussing deformation tests at various temperatures 17 p3124 A70-35142

Nitrogen solubility calculation in transition metals liquid binary systems, using quasi-chemical model 18 p3273 A70-36045

Transition metal disulfides and diselenides as solid lubricants, investigating sliding friction characteristics [ASLE PREPRINT 70AM 6E-1] 19 p3438 A70-38801

Field emission from narrow 3d bands of ferromagnetic nickel, calculating 3d and free electron transmission coefficients ratio, using triangular surface barrier model 24 p4391 A70-45671

Precompression and pressurization effects on ductile-brittle transition of polycrystalline cast Cr, W and Mo bcc transition metals 24 p4365 A70-46371

TRANSITION POINTS

Dissolved gases and carbon effect on transition temperature from plastic to brittle state of high melting metals including niobium and vanadium 01 p0124 A70-11615

Superconducting transition temperature variation in bcc region of Ti-Nb-V ternary alloys measured as function of valence electrons and composition 03 p0538 A70-13154

Pyroelectric coefficient extrema measurement at constant stress in barium titanate ceramic at various temperature ranges for various transition points 03 p0513 A70-14205

Model for predicting laminar-turbulent transition point in hypersonic wake of two dimensional laminar viscous flow 06 p0985 A70-18499

Transition matrix of Markov chain with finite states from noisy measurements of state, discussing algorithms convergence rates and computations 12 p2261 A70-27421

Strength and thickness effects on energy absorption criteria for transition temperatures in Charpy V-notch impact tests 15 p2819 A70-32234

Unalloyed Ti hydrogen embrittlement, determining factors affecting brittle-ductile transition temperature 17 p3117 A70-34398

Hydrostatic pressurization effect on ductile-brittle transition temperature of polycrystalline chromium 18 p3274 A70-36053

Polyvinyl alkyl ethers multiple transitions at low temperatures, using linear variable differential transformer 21 p3844 A70-42137

Polymers as cryogenic adhesives, evaluating role of chain structure below glass transition temperature 21 p3783 A70-42142

Heat exchange on turbine blade profiles, examining boundary layer flow transition region coordinates 23 p4283 A70-44732

Phase transitions in FeW doped strontium and barium oxides, using X ray diffraction and Mossbauer effect for transition temperature 24 p4390 A70-45605

TRANSITION PROBABILITIES

Ionized Ne, Ar and Kr first excited p states lifetime and transition probabilities, tabulating energy levels and mixing coefficients 02 p0343 A70-11887

Transition probabilities for diatomic oxygen Schumann-Runge bands determined from shock tube emission studies 02 p0344 A70-12658

Molecular hydrogen Lyman bands radiative transition probabilities, using electronic dipole moment functions 02 p0344 A70-12659

Transition probabilities computed for spectral lines due to magnetic quadrupole radiation, discussing deexcitation of excited atoms in solar corona 02 p0359 A70-12706

Electron-phonon interaction model of temperature dependence of luminescence produced by multiphonon nonradiative transitions in Cr ions of ruby crystal, deriving transition probability 03 p0538 A70-13058

Lifetimes of upper levels of N II and N III UV multiplets determined from radiative deexcitation of excited ions 03 p0527 A70-13074

Radiative lifetimes and total transition probabilities measured in polyatomic gases using phase shift method and electron beam excitation 03 p0441 A70-14009

Reliability analysis formulation for statically indeterminate structures, using modified transition probabilities and computer program for systematic failure paths counting 04 p0768 A70-14747

NH emission systems radiative lifetimes and SiD and SiH transition probabilities measured, noting effects of radiative cascading 05 p0885 A70-16424

Radiative lifetimes of transitions to ground state for CS, SO and diatomic sulfur, showing relationship to absolute transition probabilities in terms of physicochemical applications 05 p0885 A70-16456

Pionic transition in Ni isotopes to measure nuclear interaction effects, observing level shift and broadening 05 p0885 A70-16682

Transition probability and Stark profile of H alpha standards for absolute intensity calibration of spectroscopic data from thermal shock tube plasma 05 p0853 A70-17083

Spectrally and spatially resolved measurements on arc heated Ar plasma radiation for eliminating discrepancies in transition probabilities [AIAA PAPER 70-42] 06 p1122 A70-18187

Argon ion CW lasers, discussing design, inverse population, plasma, radiative transition probabilities, pumping, frequency spectra and active medium 07 p1298 A70-19642

Allowed and forbidden transitions probability in isoelectron sequences of solar corona, using scale factor method and variational wave functions 09 p1751 A70-22155

Probability coefficients computation for transitions between energy levels of ion A XIV in solar corona 09 p1761 A70-23060

Relative transition probabilities of Si I and II determined from emission spectra obtained by injecting SiCl4 vapor into argon plasma jet 09 p1737 A70-23315

Bowen levels of O III radiative lifetimes and transition probabilities measurements by beam-foil spectroscopy 10 p1936 A70-23909

Radiative lifetimes determination from beta-chi violet transition probabilities of CN 10 p1947 A70-24991

Steady state two frequency laser emission threshold and intensity, studying effects of two photon transitions and optical transition probabilities-radiation density relations 12 p2245 A70-27301

Vibrational relaxation time and transition probability in bromine collisions with He, Ne, Ar, Xe atoms determined by shock wave method 12 p2275 A70-27353

Integral Hellmann-Feynman formula for dissociation energies in H, Li and LiH molecules, discussing transition densities and dissociation energy 12 p2275 A70-27569

Gaseous nebulae electron densities based on interpretation of forbidden CI III lines using collisional strengths and transition probabilities 15 p2798 A70-31746

Transition probabilities for Markov chain describing bond breaking and molecular energy transfer in vibrational relaxation and dissociation 16 p2953 A70-33009

Mean lives of excited levels in neutral He by beam foil method testing calculations for radiative transition probabilities 16 p2955 A70-33296

Inelastic energy losses in oxygen ion beams collisions with neutral molecules, determining vibrational transition probabilities 16 p2955 A70-34011

Argon II line transition probabilities, observing UV spectral region, upper energy levels and temperature differences 16 p2956 A70-34251

Diatomic molecules inelastic collision cross sections for specific rotational transitions, discussing S matrix energy requirements for statistical analysis 19 p3474 A70-38268

Transition probabilities of visible and near-IR neon lines, using gas-driven shock tube spectroscopy 20 p3674 A70-39134

Absorptivity, transition probability and collision broadening frequency of dimethylether at 3.51 micron He-Xe laser wavelength, noting pressure dependence, transition lifetime and saturation intensity 21 p3835 A70-40573

LTE verification for argon plasma generated in free burning arc by measuring atomic line transition probability at various pressures 21 p3854 A70-40588

Solar iron abundance from forbidden Fe II magnetic dipole transition probabilities 21 p3888 A70-41118

Rotational transition probabilities of molecular collisions, using time dependent perturbation theory along linear trajectories 21 p3853 A70-41390

Numerical molecular rotational transition probabilities and cross sections in HCN-HCN and ICN-ICN collisions, using perturbation theory and multipole potentials 21 p3853 A70-41391

Strong coupled rotational excitation problem in atom-diatom molecule scattering system, discussing transition probability matrices statistical analysis 23 p4212 A70-44600

TRANSITS

NT CINETHEODOLITES

NT THEODOLITES

Real time angular readout system for declination axis of U.S. Naval Observatory six inch transit circle, using Inductosyn as basic transducer 16 p2906 A70-33176

Solar radio radiation effective gravity center shift determination, considering directivity diagram scanning phase for radio transit instrument adjustment 19 p3522 A70-38562

FK4 catalog system equinox and equator point corrections from lunar transit circle observations, discussing validity of moon for orientation 21 p3922 A70-41985

TRANSLATING

NT MACHINE TRANSLATION

TRANSLATIONAL MOTION

NT THREE DIMENSIONAL FLOW

NT THREE DIMENSIONAL MOTION

Hologram interferometry accuracy, reliability, application to plate deformation and translation measurements, using moire method and correction factors 03 p0493 A70-13945

Translational-rotational motion of long dumbbell in Newtonian central force field, analyzing plane center of mass trajectory with perpendicular kinetic moment vector 04 p0744 A70-14427

Balanced rotor with radial sliding bearing bushings, studying lubricant gas restoring force effect on stability with allowance for bushings translational movements 11 p2058 A70-25581

Attitude-translation motion coupling effect on stability of gravity-stabilized drag-free satellites 13 p2501 A70-28424

Translational-rotational motion of long dumbbell in Newtonian central force field, analyzing plane center of mass trajectory with perpendicular kinetic moment vector 13 p2485 A70-28452

Translational-rotational motion of axisymmetrical moon in earth gravitational field 15 p2803 A70-32496

Lagrange equations for translational motion and diameter variation of bubble system moving in hydrostatic field, taking into account dissipative forces 18 p3240 A70-36270

Satellite translational motion in circular problem of three bodies, discussing existence of equations integral 18 p3324 A70-37150

Gravity stabilized drag free satellites attitude instabilities due to coupling between attitude and translational motions [AIAA PAPER 70-995] 20 p3714 A70-39535

Translation and docking simulator for Gemini support modified for Apollo LM active lunar orbital docking with CSM 21 p3804 A70-41194

Translational-rotational motion of axisymmetrical moon in earth gravitational field 23 p4240 A70-43917

Particle motion in constant density dynamic viscosity random translational velocity fluid 24 p4324 A70-45139

Lighthill aerodynamic noise theory fundamental equation for acoustic field density distribution, determining flow fields for surfaces in uniform translational motion 24 p4324 A70-45268

TRANSLUNAR INJECTION

Translunar Apollo orbit analysis from elementary equations relating to elliptical and hyperbolic orbits in inverse square force field 06 p1148 A70-18397

Spacecraft fuel optimal controls for out-of-plane motion about translunar libration point based on phase plane methods [AIAA PAPER 70-1079] 19 p3530 A70-38890

TRANSLUNAR SPACE

U INTERPLANETARY SPACE

TRANSMISSION

NT AERODYNAMIC HEAT TRANSFER

NT AUTOMATIC PICTURE TRANSMISSION

NT CONDUCTIVE HEAT TRANSFER

NT CONVECTIVE HEAT TRANSFER

NT DATA TRANSMISSION

NT DIFFRACTION PROPAGATION

NT DOUBLE SIDEBAND TRANSMISSION

NT ELECTRIC POWER TRANSMISSION

NT ELECTROMAGNETIC WAVE TRANSMISSION

NT GROUND WAVE PROPAGATION

NT HEAT TRANSFER

NT HEAT TRANSMISSION

NT HYPERSONIC HEAT TRANSFER

NT IONOSPHERIC F-SCATTER PROPAGATION

NT IONOSPHERIC PROPAGATION

NT LAMINAR HEAT TRANSFER

NT LIGHT SCATTERING

NT LIGHT TRANSMISSION

NT MICROWAVE TRANSMISSION

NT MULTIPATH TRANSMISSION

NT RADAR TRANSMISSION

NT RADIATIVE HEAT TRANSFER

NT RADIO TRANSMISSION

NT SATELLITE TRANSMISSION

NT SCATTER PROPAGATION

NT SHOCK WAVE PROPAGATION

NT SHORT WAVE RADIO TRANSMISSION

NT SINGLE SIDEBAND TRANSMISSION

NT SOUND TRANSMISSION

NT STRESS PROPAGATION

NT SUPERSONIC HEAT TRANSFER

NT TELEVISION TRANSMISSION

NT TRANSEQUATORIAL PROPAGATION

NT TURBULENT HEAT TRANSFER

NT WAVE PROPAGATION

Comparative arterial pressure pulse transmission velocity in dogs, relating wall elasticity with vascular disease 15 p2682 A70-31939

Transmission calculations for homogeneous and nonhomogeneous water vapor atmospheres, evaluating various methods 22 p4065 A70-43170

TRANSMISSION CIRCUITS

Corrective open-loop circuit, using delay elements for compensation of transient response in linear circuits with lumped parameters for pulse modulation transmissions 06 p1023 A70-17774

Algorithm applied to specific classes of random processes for calculating minimum channel capacity required by transmission system for sources in each class 06 p1012 A70-18621

Integrated TDMA switching/transmission system implementation into existing network 10 p1837 A70-24354

Wideband transmission media for global communication networks, comparing submarine cables and satellites based on economic tradeoff in terms of circuit density and distance 11 p2901 A70-25475

Transmission factors of microwave filters with prescribed attenuation and group delay 22 p3997 A70-43173

TRANSMISSION EFFICIENCY

Low altitude 24-hr orbit twin satellite system joined by long light cord, assessing communications efficiency and physical limitations 03 p0579 A70-13621

Information transmission capability of hologram without distortion, considering confocal resonator reconstructible transparencies for bounded hologram 05 p0848 A70-16265

Paraboloidal- and spherical-reflector antennas efficiency optimization obtained from optimum combination of amplitude and phase of hybrid modes propagating in guide 07 p1240 A70-19220

Coding and decoding efficiency in data transmission over Gaussian channels, comparing error probability, power, bandwidth and equipment complexity 09 p1637 A70-23320

Pulse signal transmission rate increase by transient processes compensator, discussing stability relation to signal to noise ratios 09 p1639 A70-23696

Transmission performance of telephone calls routed through PCM satellite circuit between London and White Plains 10 p1837 A70-24349

TRANSMISSION LINES

TDMA communication satellite system compared favorably with FDMA or CDMA systems in efficiency, flexibility and feasibility for commercial and military uses

10 p1842 A70-24884

Pulsed system accuracy increment by increasing number of modulated signal parameters in addition to pulse duration modulation

10 p1843 A70-25137

Satellite communications system optimal parameters and efficiency dependence on working capacity, discussing economic aspects of HF sets increased number

11 p1995 A70-25345

Spacecraft phased array antenna techniques, discussing tape helix radiators design for applications in navigation, TV broadcasting and data relay systems [AIAA PAPER 70-425]

11 p2015 A70-25452

Time-bounded pulses with energy maximum in frequency band, solving integral equations for band-pass filters for maximum efficiency and optimum pulse shapes

11 p2004 A70-25799

IF combinator for broadband transhorizonal radio relay transmission improvement by providing optimum SNR

11 p2020 A70-26821

Broadband transhorizonal radio relay system transmission improvement by applying switching equipment designed for protective channel

11 p2034 A70-26822

Transmission delay and echo effects in long distance satellite relay telephony links, describing echo suppression and speech quality

12 p2183 A70-27004

Local losses distribution effect on intensity and opposing waves generation in ring gas laser analyzed in approximation of noninteracting modes

12 p2248 A70-27510

Cost effective data transmission method for high performance under intersymbol interference and noise

12 p2187 A70-27935

Lossless pulse-shaping active line for unipolar transmission, considering construction by loading two terminal Esaki diode to coaxial cable

15 p2697 A70-31827

Lower reliability estimates for block codes of binary channels with feedback noise

18 p3235 A70-36599

Efficiency of holographic gratings in instrumental spectroscopy

19 p3421 A70-37360

Satellite communications system optimal parameters and efficiency dependence on working capacity, discussing economic aspects of HF sets increased number

20 p3589 A70-40457

Transmission power formula for slant to ground station and slant ranges calculations

21 p3785 A70-40755

Microwave waveguide mount characterization of varactor diodes, using transmission resonance and Dolph-Chebyshev taper

21 p3797 A70-40759

Spacecraft data transmission efficiency improvement by budgeting onboard electric energy consumption among data types

21 p3790 A70-41364

Parabolic reflector microwave antenna flared horn primary feeds design for maximum aperture efficiency based on electric field matching

21 p3800 A70-41946

Line-by-line and two dimensional image processing performance, considering transmission rates and distortion

23 p4160 A70-43762

TRANSMISSION LINES

NT BEAM WAVEGUIDES

NT COAXIAL CABLES

NT COMMUNICATION CABLES

NT FLUID TRANSMISSION LINES

NT PLASMA GUIDES

NT POWER LINES

NT STRIP TRANSMISSION LINES

NT SUBMARINE CABLES

NT WAVEGUIDES

Book on microwave theory and applications covering transmission line theory, microwave measurement, signal sources and analysis, network analysis, etc

03 p0455 A70-13001

M-type transmission line with cyclotron waves to achieve phase inverter and delay line operation, showing phase sensitivity to magnetic field changes near cyclotron resonance

03 p0447 A70-13292

Transient electromagnetic fields coupling transfer functions for two wire uniform transmission line cable models, using long wire antenna as radiation source

04 p0658 A70-14739

Iterative solution to transmission lines termination problems [ASME PAPER 69-APM-M]

04 p0627 A70-14861

Asymmetrical and symmetrical directional couplers coupling characteristics during linear and exponential variations of coupling coefficient

04 p0659 A70-15310

Pneumatic line losses due to friction in pneumatic control systems

04 p0628 A70-15399

Shielded multiconductor transmission line capacitance calculated by integral equations with Green function kernel

05 p0820 A70-16383

Errors arising in torsion-type ponderomotive wattmeter connected in homogeneous microwave transmission line with mismatched oscillator at input and mismatched load at output

06 p1024 A70-17861

Noise and gain formulas for wideband distributed-gain amplifiers using quadrupole elements and transmission line configurations

08 p1472 A70-20863

Interference emission filtering in high power microwave transmitters, discussing spurious emissions removal or rejection by transmission line filters

08 p1474 A70-21257

Slot line wavelength, impedance, transitions and tolerances measured at S band using different dielectric constant materials

08 p1475 A70-21282

Slot transmission line applicability to miniature ferrite phase shifter design exploiting elliptically polarized H field existence

08 p1475 A70-21283

Commensurate transmission line circuits design approximating periodic frequency characteristics on digital computer

08 p1476 A70-21286

Extraneous earth satellites interferences in ground communication line, determining combined duration and numbers average values

11 p1996 A70-25346

Traveling wave amplifier on section of inhomogeneous transmission line with tunnel diodes

11 p2020 A70-26808

Log-periodic dipole (LPD) antennas compressed along transmission-line axis, considering frequency dependent behavior in narrow bands and radiation pattern

12 p2198 A70-27955

Coupled microstrip transmission lines characteristics from parameters evaluation, considering various geometries, inductive and coupling coefficients, dielectric constant and impedance

12 p2190 A70-28167

Quasi-TEM analysis justification for limit cases of guided waves on microstrip transmission lines with dielectric constant approaching free space

12 p2190 A70-28168

Multilens quasi-optical transmission lines construction by determining lens profile for optimal conversion of source field into specified field at receiver end

13 p2366 A70-29403

Surface wave transmission lines used at millimeter wavelengths

14 p2549 A70-30443

Microstripline and balanced stripline, discussing parameters affecting maximum attainable Q in microwave integrated circuits

14 p2561 A70-30921

Microstrip circuit design, obtaining dimensions by computer programs incorporating subroutine sets

14 p2561 A70-30922

Electrostatic discharge at magnetopause by idealized circuit analog, discussing transmission lines and terminal impedances

14 p2579 A70-31247

Strip lines transmission characteristics with rectangular outer conductor and multielectric layers within TEM wave approximation, using Green function and variational principle

14 p2558 A70-31316

Stripline skin effect in digital equipment transmitting fast rising pulses

15 p2708 A70-31828

HF electrical communication based on Kelvin transmission line and Maxwell field theories, noting linear arrays

16 p2860 A70-32951

Integrated X band superheterodyne receiver design using planar transmission lines as components

16 p2874 A70-33388

Packaging and grounding for electrical noise control in nanosecond switching circuits using transmission line design

16 p2879 A70-33960

Electroacoustic transducer driven by acoustic pressure and electronic generator, describing electrical properties for functioning as characteristic impedance of acoustic transmission line

19 p3422 A70-37701

Extraneous earth satellites interferences in ground communication line, determining combined duration and numbers average values

20 p3589 A70-40458

Transmission line modal analysis for nonlinear polarizability in optical and quasi-optical waveguides

21 p3784 A70-40564

Circular and nearly rectangular irises for resonant cavities in transmission line for microwave band stop filters, discussing design based on merit factor

21 p3792 A70-41992

Transistorized IF amplifier output matching to long transmission line, deriving formulas for gain and pass-band over wide output impedance range

22 p3995 A70-42520

Nonradiating higher order modes on shielded slot lines for TM and TE cases, using series matching and Wiener-Hopf technique

22 p3990 A70-43420

Book on guided EM wave theory covering mathematical methods transmission lines cavity resonators, perturbation theory, electrostatics, electric and magnetic fields, propagation, etc

23 p4172 A70-44242

Broadside-endfire array of cylindrical dipoles and monopoles driven by interconnecting transmission lines, calculating admittance and field patterns

23 p4176 A70-44955

Traveling wave amplifier on section of inhomogeneous transmission line with tunnel diodes

24 p4317 A70-45180

Natural dispersion effect on bandwidth of glass fiber transmission line using optical glasses

24 p4319 A70-46079

TRANSMISSION LOSS

Radiometric method for calibrating loss of multimode antenna-feed components with linear or circular polarization, deriving calibration and error analysis equations

01 p0050 A70-10711

Diffraction loss measurement in solid state laser to determine laser material contribution to total cavity loss

01 p0113 A70-10919

Aircraft controls response critical speed as function of transmission lag and transfer function of control link elements

02 p0227 A70-12410

Intrinsic noise of passive waveguide multipoint with losses, obtaining mean values and wave correlation functions using scattering matrix

04 p0655 A70-14402

HF propagation losses from statistical measurement over north-south path found dependent on mode, day and night and high and low ray

04 p0649 A70-14968

Transmission losses of plexiglass radome measured as function of frequency and antenna elevation angle, determining material dielectric constant

06 p1019 A70-17505

Lower ionosphere effects on HF propagation modes observed by pulse system, discussing propagation time, mode structure, transmission loss, etc

07 p1232 A70-19179

Supersonic flight vehicle plasma sheath effect on effective range of onboard radar installation, discussing SNR

08 p1461 A70-20869

Single-pulse laser radiation losses dependence on operation time length due to angular dispersion

09 p1694 A70-22140

Self focusing antennas directive gain losses reduction for wave with jagged phase front impinging on linear array having passed through inhomogeneous atmosphere

09 p1648 A70-23163

Radio propagation over sea water path, predicting transmission loss by computer programs

12 p2188 A70-27936

Leaky waveguide radiation patterns with periodic loading slots along axis

13 p2377 A70-29105

Laser with telescopic resonator, examining characteristics at different Fresnel zones and emission losses with geometric optics approximation

13 p2427 A70-29280

Light transmission losses in optical resonators partially filled with inhomogeneous dielectric, specifying optimal geometrical parameters

13 p2378 A70-29404

Circular low loss waveguides for millimeter waves, discussing construction, geometry, surface texture, etc

14 p2556 A70-30442

Space-surface path loss due to atmospheric gases, rain and clouds, considering military ground site location for space communication

14 p2608 A70-30596

H-guide dielectric losses reduction by use of artificial and laminated dielectric slabs

16 p2875 A70-33401

Ionospheric VLF diurnal transmission loss differences on two long paths, analyzing values for first and second modes

20 p3585 A70-39455

Acoustic pulse transmission through plane vortex sheet, examining zone of silence, geometrical acoustics and sound radiation

21 p3849 A70-41243

- Centrifugal compressor losses as function of suction chamber exit nonuniform flow field delivered to impeller
21 p3747 A70-41954
- Thin film microwave acoustic transducers, calculating top electrode thickness effect on frequencies of infinite conversion loss
24 p4333 A70-45218
- Confocal microwave Fabry-Perot interferometer resonator diffraction loss and field configuration measurements, noting agreement with theory
24 p4381 A70-46242
- Phosphorus and selenium oxychloride based liquid laser transmission loss measurement
24 p4355 A70-46265
- TRANSMISSIVITY**
Spectral band transmission functions of atmospheric water vapor, nitrogen, ozone, nitrous oxide and methane in IR region
07 p1330 A70-20306
- Transmission coefficient for perforated screen related to orientation of rectangular and cross shaped narrow openings and field polarization during normal wave incidence
12 p2191 A70-28174
- Nondestructive examination for plastics, discussing transmission, microwave and ultrasonic tests
24 p4346 A70-45720
- TRANSMISSOMETERS**
UHF radio telemetry for transmissometers measuring airport runway visibility
16 p2889 A70-34222
- Runway visual range assessment using automatic transmissometer-reflector measurements
17 p3132 A70-34641
- TRANSMITTANCE**
Optical measurements of mirrors reflectance and solar radiation transmittance to solve problems specific to solar energy engineering by standard optical equipment
01 p0010 A70-10765
- Atmospheric transmittance line by line calculations along variable pressure and mixing ratio paths from 1.7-20 microns
[AFCL-70-0061] 02 p0289 A70-11908
- Resin bonding material suitable for IR detectors noting transmission properties
02 p0321 A70-11926
- Atmospheric IR radiation transmittance in 590 to 750 per cm interval, using balloon-borne spectrometer
02 p0256 A70-11928
- Transmission and reflection coefficients calculated for electromagnetic waves incident on inhomogeneous absorbing layer applicable to ionosphere, plasma and p-n junction
06 p1009 A70-17834
- Optical hardness effect on dispersed particles spectrum determination accuracy by spectral transmittance
07 p1330 A70-20309
- Optimal atmospheric transmittance windows for underlying surface and cloud temperature determination from satellites
08 p1538 A70-21426
- Vacuum-UV monochromators polarization and effective transmittance measurements, comparing characteristics of parallel and pyramidal biotite polarizers
08 p1546 A70-21791
- Spatial and energy characteristics of laser with nonuniform transmittance across resonator mirrors, analyzing transverse modes interaction
08 p1514 A70-21816
- Seasonal measurements of atmospheric transmittance spectra for horizontal near-earth paths in IR region under haze and clear weather
09 p1666 A70-22179
- Far IR radiation transmission through bismuth and gallium normal and superconducting thin films, considering transition temperature role
09 p1739 A70-22323
- Fluorel spectral reflectance, transmittance and absorbance under monochromatic irradiation, considering thermal analysis and surface finish
09 p1710 A70-22794
- Real nonnegative function representing transmittance of computer synthesized Fourier transform hologram displayed on flying spot scanner and recorded on film
11 p2049 A70-25631
- Cotton leaf light reflectance and transmittance changes with maturity
12 p2218 A70-26919
- Side scattered light effects on atmospheric transmittance measurements, showing influence on total receiver illumination
14 p2603 A70-30411
- Spectral transmittance coefficients at Naugarzan astronomical station, using Bouguer method
15 p2809 A70-32909
- Bidirectional reflectance and transmittance calculation for irradiated layer of monodisperse matrix suspended pigment particles
[AIAA PAPER 70-839] 16 p2940 A70-33923
- Earth atmosphere transmission coefficient and optical stability based on solar aureole observation
16 p2899 A70-34186
- Integrating sphere theory with wall mounted specular sample in reflectance and transmittance measurements
18 p3284 A70-36776
- Spectral radiative capacity of lower level clouds in specific transmittance window, using airborne diffraction spectrometer measurements
19 p3461 A70-37424
- IR absorption by water vapor in transmittance windows, considering continuous absorption coefficient dependence on window width
19 p3461 A70-37425
- Plane wave diffraction by periodic array at boundary between two media, discussing asymptotic behavior of reflection and transmission coefficients
21 p3806 A70-40614
- Corrective light filter performance evaluation by spectral transmittance normalization
22 p4072 A70-42503
- Interference-polarization light filter, calculating phase shifter errors effects on transmittance by Poincare sphere method
22 p4072 A70-42505
- Semiconductor luminescence and photodetector diodes near IR region transmission, describing frequency response measurements
22 p4087 A70-43445
- Atmospheric horizontal stratification and UV transmittance by signal reflection from satellites
23 p4191 A70-44268
- Planar conducting screen with periodic rectangular perforations, determining transmission and reflection coefficients and aperture field distribution
24 p4311 A70-45219
- TRANSMITTER RECEIVERS**
Tracking method for simultaneously tuned transmitter and receiver with different maximum-to-minimum capacitance ratios in ganged variable capacitors
01 p0051 A70-10888
- Transmitting-receiving latching ferrite switch with 180 degree differential phase shift toroids for temperature stability and receiver protection in case of driver failure
03 p0458 A70-14036
- Statistical ionospheric model of sporadic E layer frequency characteristics dependence on equipment parameters, determining permissible variation of transmitter power and receiver gain
04 p0682 A70-15727
- Statistical ionospheric model of sporadic E layer frequency characteristics dependence on equipment parameters, determining permissible variation of transmitter power and receiver gain
14 p2575 A70-30811
- Airborne equipment microelectronics technology application to interrogators, transponders and UHF/VHF transceivers
14 p2558 A70-31294
- S band transmitters frequency deviations optimization enabling designer to determine optimum value within constraints of associated receiving equipment
14 p2559 A70-31373
- Doppler effect pulsed ultrasonic blood flowmeter using transducer alternating as transmitter and receiver
15 p2690 A70-31919
- Transceiving system for recording D region radio signal absorption and reflection, describing component circuitry and operation
16 p2880 A70-34225
- Automatic resonance tuning of transmitting and receiving antennas by electronic control for use in mobile communications
23 p4172 A70-44385
- TRANSMITTERS**
NT INSTRUMENT TRANSMITTERS
NT IONOSPHERES
NT OMNIDIRECTIONAL RADIO RANGES
NT RADAR TRANSMITTERS
NT RADIO BEACONS
NT RADIO TRANSMITTERS
NT RADIOSONDES
NT RAWINSONDES
NT REPEATERS
NT TRANSMITTER RECEIVERS
Laser transmitter and optical superheterodyne receiver performance tests at 6328 A, demonstrating aperture size effect and noncoherent operation superiority
03 p0450 A70-13675
- Temperature profiles and frequency driftings of VHF telemetry transmitters for Saturn S-IC stage, using IR radiation data
12 p2196 A70-27725
- Injection laser communication link for high data rate transmission, discussing design and construction of transmitter and receiver
16 p2862 A70-33139
- Thermal control through fusible materials for missile S band transmitter package, using computer analysis
18 p3231 A70-36349
- Multiple remote control systems design, emphasizing transmitter and receiver characteristics matching to overall network parameters
18 p3235 A70-36426
- Radiosonde receiver and transmitter system optimization, obtaining increased microwave power by appropriate oscillator operating modes
22 p4038 A70-43379
- TRANSOCEANIC COMMUNICATION**
Remote data processing and wideband data transmission between France and U.S. via telecommunication satellites, discussing error detection and correction
02 p0263 A70-12612
- Satellite Integrated Communications, Navigation and Identification System for implementing worldwide command-control system and equipment and signal integration
[AIAA PAPER 70-503] 11 p2000 A70-25466
- Global commercial communications satellite system arrangements, considering evolutionary political, economic and technological developments within INTLSAT context
[AIAA PAPER 70-446] 11 p2152 A70-25478
- Radio propagation over sea water path, predicting transmission loss by computer programs
12 p2188 A70-27936
- TRANSOCEANIC SYSTEMS**
NT TRANSOCEANIC COMMUNICATION
Inertial navigation techniques application to commercial air traffic control, indicating decreased dependence on external navigation aids in oceanic operations
01 p0136 A70-10304
- Data analysis of inertial systems for commercial aircraft overseas operations, classifying systems error propagation as linear time drift or Foucault period oscillation
01 p0137 A70-10314
- Spot III satellite-supported system for transoceanic aircraft navigation, traffic control, voice and data communication, etc
07 p1331 A70-19291
- Navigation-traffic control satellite system application to transoceanic traffic surveillance
[AIAA PAPER 70-487] 11 p2000 A70-25462
- SOFAR/sound fixing and ranging systems for location and recovery of reentry vehicles and missile cases and rescue of disabled transoceanic aircraft
13 p2449 A70-29169
- International cooperation in global meteorological network, outlining World Weather Watch
14 p2670 A70-31140
- Global weather forecasting network costs and benefits evaluated using mathematical criteria
14 p2670 A70-31142
- Global weather prediction network economic benefits to key industries, discussing adverse weather effects on production schedules, fuel supplies, construction, harvesting, etc
14 p2610 A70-31143
- Satellite communication/navigation/surveillance systems for domestic and transoceanic ATC
16 p2949 A70-33479
- TRANSONIC AIRCRAFT**
U SUPERSONIC AIRCRAFT
TRANSONIC COMPRESSORS
Transonic two stage compressor design and performance, discussing interblade row traverse data
09 p1608 A70-23742
- Transonic compression grid functions, considering shock wave configurations
16 p2836 A70-33752
- Two dimensional compressor cascades of double circular arc and wedge shape blades testing performance in transonic and supersonic wind tunnels
[ASME PAPER 70-GT-7] 18 p3302 A70-36829
- Buzz-saw noise of transonic compressor due to rotating pressure field at supersonic blade tip speeds
[ASME PAPER 70-GT-54] 18 p3303 A70-36838
- Transonic high turning low aspect ratio stator cascades flow field performance prediction, reducing secondary flows by partial slots
[ASME PAPER 70-GT-63] 18 p3209 A70-36875
- TRANSONIC FLIGHT**
Airframe flow field effects on propulsion system performance in transonic flight, studying case of underwing aft mounted turbojet engine nacelles
01 p0004 A70-10321
- Ground based radar surveillance for SST to avoid convective clouds and thunderstorm activity during transonic acceleration phase ensuring minimum demands on maneuverability
09 p1610 A70-22242
- Transonic aircraft testing capabilities and limitations, considering tunnel wall interference and Reynolds number effects
[AIAA PAPER 70-580] 13 p2348 A70-29876
- Wind tunnel and flight test methods for determining transonic buffet characteristics on model F-4 aircraft
[AIAA PAPER 70-584] 13 p2348 A70-29886

- Harrier aircraft development history, discussing V/STOL constraints on transonic flight properties [ICAS PAPER 70-51] 23 p4139 A70-44148
- TRANSONIC FLOW**
- Boundary value problem for quasi-linear equation of unsteady transonic gas flow, including linear model and operators for group of transformations 01 p0069 A70-11628
- Asymptotic method based on Landahl small perturbation theory applied to perturbation velocity potential for oscillating delta wing in transonic flow 02 p0223 A70-11775
- Harmonically oscillating semiminfinite rectangular wing perturbation velocity potential in unsteady transonic flow without heat exchange 02 p0279 A70-12118
- Axisymmetric sonic flow around slender body, determining boundary regions for slender body approximation and Guderley expansion utility 03 p0409 A70-14233
- Boundary value problems of Cauchy-Riemann differential equations using solution to derive integral equation for stationary infrasonic flow 04 p0671 A70-15094
- Unsteady pressure distributions on elastic swept wing upper and lower sides at high subsonic to transonic flow, investigating torsional and bending vibrations [DGLR-69-31] 04 p0615 A70-15151
- Von Karman transonic similarity law applied to flow through plane turbine blade cascades [DGLR-69-24] 04 p0616 A70-15183
- Transonic flow about slender profiles computed for flow velocities slightly below and above Mach 1 04 p0616 A70-15185
- Plane and axisymmetric transonic vortex flow approximate equations of inviscid noneat conducting gas for point on sonic line with entropy having extremal value 04 p0617 A70-15234
- Transonic flow theory, investigating thin three dimensional lifting wings, similarity for lift and drag, plane flow past airfoil, far field and hodograph solutions [D1-82-0878] 05 p0834 A70-16693
- Far and near field solutions of plane steady transonic flow past thin airfoil including imbedded shock waves using small disturbance theory [AIAA PAPER 70-188] 06 p0969 A70-18056
- Closed form solution of modified inviscid transonic equation embodying character of viscous-transonic equation applied to shockless transonic airfoils [AIAA PAPER 70-187] 06 p0970 A70-18096
- Steady supercritical planar inviscid transonic flows over lifting airfoils, generating unsteady flow by impulsively imposing airfoil boundary condition [AIAA PAPER 70-47] 06 p0972 A70-18130
- Free piston compression with sonic flow outlet for determining orifice size by matching with bounce parameters 07 p1249 A70-19334
- Pressure recovery for stagnation of underexpanded sonic jet in chamber having transparent walls and containing nozzle and diffuser in coaxial positions 07 p1189 A70-19811
- Stable flow distribution of sonic jet exhausting counter to low density supersonic airstream 07 p1189 A70-19982
- Perfect fluid sonic flows around weakly lifting three dimensional bodies downstream of shock wave, proving existence of lifting boundary layer 08 p1433 A70-21238
- Trisonic high pressure wind tunnel simulating flow conditions on large transonic aircraft, noting high Reynolds number capability 09 p1655 A70-22023
- Shock wave configurations across compression cascades in transonic approach flow 09 p1604 A70-22657
- Transonic aerodynamics problems concerning plane and spatial rotational flows of perfect gas, discussing analytical and numerical methods 10 p1800 A70-24132
- Near equilibrium transonic flows of reacting gas mixtures based on linearization of thermodynamic and kinetic quantities 10 p1867 A70-24133
- Symmetrical, asymmetrical and three dimensional sonic flows past finite obstacle, investigating regions upstream and downstream from shock waves for airfoil 10 p1800 A70-24134
- Viscous transonic flow past wavy wall analyzed by approximate method for inviscid transonic equation 10 p1800 A70-24137
- Bidimensional curved weak shock wave structure, deducing transonic equation from Navier-Stokes equations 10 p1800 A70-24138
- Combustible gas /hydrogen-air/ subsonic and transonic flow past sphere, approximating combustion zone structure by model 10 p1801 A70-24142
- Head wave distance from body determined for slender pointed profile in subsonic region of transonic flow 10 p1803 A70-24780
- Cylindrical afterbody drag reduction in transonic flow by combined gas ejection and boat-tailing 11 p1976 A70-25991
- Slender body transonic wave drag double integral, describing computer program for numerical evaluation 11 p1977 A70-26644
- Regularity domain and singularity location of stream function of transonic two dimensional compressible fluid flow, using integral operators 12 p2260 A70-26972
- Sonic surface and Cauchy problem of Monge-Ampere equations in plane unsteady transonic channel flow solved by hodographic analysis 12 p2156 A70-27299
- Subsonic, transonic and supersonic laminar boundary layers acceleration and cooling effects, discussing heat transfer and gas enthalpy 12 p2211 A70-27830
- Transonic flow theory for two and three dimensional streamlined bodies in steady irrotational flow of inviscid perfect gas 12 p2158 A70-28201
- Specific heat ratio and configuration effects on flow in subsonic, transonic and supersonic sections of Laval nozzle 12 p2159 A70-28233
- Transonic scaling effects for shock boundary layer interaction on circular and two dimensional airfoil models, discussing separation and reattachment [AIAA PAPER 70-541] 13 p2339 A70-29008
- Pressure distribution and drag for inviscid flow past slender sharp-nosed fuselages and afterbodies at arbitrary transonic Mach numbers [AIAA PAPER 70-556] 13 p2340 A70-29021
- Airfoil sections in transonic flow, discussing wind tunnel tests on mixed flows and shock waves [ONERA-TP-815] 13 p2341 A70-29139
- Bistable fluidic thrusters and circular sonic control jets interaction with airstream surrounding tactical missile configuration, investigating effect on amplification factors 13 p2391 A70-29887
- Rotovale induced flow angle variations associated with data repeatability and scatter in blow down wind tunnels at transonic speed 13 p2385 A70-29888
- Discrete sonic jets as boundary layer trips producing turbulent hypersonic flows with negligible intrinsic drag and downstream distortions 13 p2523 A70-29973
- Wing section pressure distributions, lift and drag in transonic mixed flow, considering prediction methods 14 p2529 A70-30866
- Two dimensional transonic flows bounded by free surface and wall with interior heat release and external burning, indicating application to control or propulsion 14 p2665 A70-30947
- Subsonic and transonic gas flow in wake behind finite thickness plate based on Navier-Stokes equations 15 p2719 A70-31484
- Integral equation for transonic small disturbance flow applied to plane flows over lifting airfoils 15 p2673 A70-32768
- Aerodynamic drag coefficients of micron size particle clouds in compressible transonic flow, using light extinction method 16 p2894 A70-33882
- Transonic flow around perpendicular plate, determining front side velocity and pressure from known stagnation point and transonic region 16 p2839 A70-34236
- Air jets from sonic orifice, investigating three zones of isochor families by visualization and density measurement 17 p3070 A70-35046
- German monograph on transonic plane flow past wavy wall in blocked wind tunnel covering flow theory, interferometric density measurements, etc 17 p3070 A70-35375
- Lifting and side force distributions acting on body in transonic flow 17 p3012 A70-35696
- Real gas transonic flow transition through critical velocity in Laval nozzle, examining reasons for increment of viscosity and heat conduction effects 18 p3239 A70-36217
- Plane compressible sonic flow around symmetrical cylinder subjected to parallel incident flow, using function-theoretic method 18 p3241 A70-36378
- Modified linearized transonic flow theory application to pressure coefficient distribution on circular arc bodies of revolution 20 p3608 A70-39614
- Aerodynamics of steady, inviscid transonic flows around slender bodies and wing-body combinations at free stream Mach number one [AIAA PAPER 70-798] 20 p3559 A70-39900
- Transonic flow past bodies of revolution, using finite difference scheme 21 p3743 A70-40611
- Plane parallel transonic flow with curved compression shock discontinuity in supersonic region, obtaining solution by indeterminate coefficients and hypergeometric functions 21 p3748 A70-42212
- Viscous transonic flow past cascades by semiempirical approach, discussing pressure distribution, boundary layer parameters and compression shock 22 p4088 A70-42343
- Transonic turbine cascades exit flow parameters taking into account blade profile 22 p4088 A70-42346
- Two dimensional transonic cascade flow, using Von Karman similarity law 22 p4089 A70-42347
- Plane transonic flow around airfoils, using hodograph based methods for shock free flow and finite difference methods for flow with shock waves [ICAS PAPER 70-12] 23 p4132 A70-44123
- Iterative method based on slender body approximation applied to axisymmetric sonic flow fields, splitting differential equation into coupled parabolic equations [ICAS PAPER 70-13] 23 p4132 A70-44124
- High subsonic and transonic effects on pressure distributions for swept wing with oscillating control surface 23 p4274 A70-44763
- Time dependent inviscid transonic flow past two dimensional and axisymmetric bodies, presenting numerical procedures including imbedded shock waves as discontinuities [AIAA PAPER 70-1322] 24 p4288 A70-45943
- TRANSONIC FLUTTER**
- F-8D aircraft transonic flight and wind tunnel tests for buffet onset prediction, considering effects of g level and fluctuation amplitude and frequency [AIAA PAPER 70-341] 09 p1611 A70-23020
- Sweptback thin cantilever wing transonic flutter characteristics, investigating concentrated mass spanwise location effects 22 p4112 A70-42274
- TRANSONIC INLETS**
- U SUPERSONIC INLETS**
- TRANSONIC NOZZLES**
- Transonic flow in convergent and convergent-divergent conical nozzles with nonuniform inlet predicted by time dependent flow equations, discussing discharge and thrust coefficients [AIAA PAPER 70-635] 16 p2834 A70-33548
- TRANSONIC SPEED**
- Transonic dynamic stability of free flight half angle cones in wind tunnel for high drag planetary entry vehicles, discussing Mars entry trajectories [AIAA PAPER 69-105] 06 p1154 A70-17164
- Stability derivatives for bodies of revolution at subsonic and transonic speeds 06 p0976 A70-18239
- F-106B aircraft in-flight study of airframe installation effects on propulsion system performance at transonic speeds 08 p1437 A70-21732
- Transonic static and dynamic stability of large angle spherically blunted high-drag cones [AIAA PAPER 70-564] 13 p2341 A70-29029
- Aerodynamic performance of axisymmetric body traveling at transonic Mach numbers for predicting installed nozzle flow fields and efficiency [AIAA PAPER 70-700] 16 p2835 A70-33562
- Aerodynamic characteristics of transonic and supersonic blunt vehicles, reviewing numerical methods 17 p3012 A70-35895
- Airframe installation effects at transonic speeds on underlying supersonic cruise exhaust nozzles, using flight and wind tunnel tests 22 p3960 A70-43274
- TRANSONIC TURBINES**
- U SUPERSONIC TURBINES**
- TRANSONIC WIND TUNNELS**
- 60 cm intermittent blowdown type trisonic wind tunnel, discussing main parts basic dimensions and characteristics determination method, detailing design and construction 01 p0055 A70-10148
- Transonic wind tunnel of aerodynamic research station in Goettingen, Germany, taking into account fixed nozzle replacement by flexible nozzle 03 p0463 A70-13799
- Wind tunnel testing technique innovations, reducing time and cost for low drag aircraft configurations by simultaneous force and pressure model transonic testing [SAE PAPER 690677] 05 p0825 A70-15868
- Two dimensional wind model with harmonically oscillating control surface in transonic range, comparing theoretical with experimental results on unsteady pressure distribution 06 p0966 A70-17252
- Characteristics and calibration of flow in gas induction driven close return transonic wind tunnel 11 p2030 A70-25687

Corona point discharge current magnitude in transonic wind tunnel, giving current characteristics at different wind speeds

12 p2264 A70-28001

Blockage ratio effect on supersonic zone with shock layer interaction on nonlifting circular arc airfoils at transonic speeds in wind tunnels

16 p2835 A70-33674

Wing camber and twist effects on transonic drag, using wind tunnel measurements

16 p2840 A70-34321

Calibration tests in transonic wind tunnel with two and four sided perforation section

19 p3353 A70-38475

Transonic wind tunnel porous walls, investigating interference effects and aerodynamic characteristics

22 p3958 A70-42337

Wind tunnel testing at transonic speeds, discussing boundary layer transition and dynamic sting interference

23 p4134 A70-44581

TRANSONICS

U TRANSONIC FLOW

TRANSPARENCE

Jovian polar zones enhanced optical transparency causes, discussing thin clouds and difference in molecular optical depth between north and south poles

01 p0180 A70-10531

Transparent bodies photon thermal conductivity temperature dependence

03 p0515 A70-13206

Plasma optical transparency criterion, estimating nonequilibrium plasma layer optical density limit

03 p0531 A70-13255

Hydrostatic models of sunspot penumbra and umbra, analyzing spot transparency influence on Wilson effect

03 p0571 A70-13596

Three dimensional structure determination for weakly scattering semitransparent objects from holographic data, discussing inverse scattering problem and refractive index calculation

03 p0487 A70-13647

Shadow optical raster method for quantitative investigation of dynamic stress states in two dimensional transparent or reflecting bodies

03 p0496 A70-14215

Semitransparent Pt film reflectance in vacuum UV evaporated on glass, quartz, Al, Au and Cr on glass compared with opaque films

04 p0731 A70-15023

Spectral absorption and transparency of water vapor, carbon dioxide, carbon monoxide, methane and nitrous oxide bands in IR region

04 p0715 A70-15255

Dispersion and correlation function for atmospheric transparency due to water vapor, from statistical model of absorption bands and effective mass

06 p1053 A70-17204

Nomograms for spectral transparency of atmosphere at 2.8-5.6 microns

06 p1053 A70-17208

Spectral transparency inversion of aerosol-containing atmosphere

06 p1098 A70-17832

Transparent gas radiation behind strong shock wave front with small pressure gradient due to energy losses

08 p1486 A70-21986

Corneal stroma transparency analysis based on refractive index and lattice theories

09 p1618 A70-22675

Radiative transfer effect on thermal instability and critical Rayleigh number in gray transparent fluid layer heated from below

10 p1967 A70-23952

Mars border-disk brightness comparison noting atmospheric transparency effects

12 p2311 A70-28303

Pulse duration and beam diameter effects on threshold energy density in laser induced transparent dielectric breakdown

13 p2428 A70-29382

Holography technique for dual real images reconstruction of transparent objects with all planes in focus

15 p2738 A70-32053

Holographic techniques, investigating ultrasonic fields in transparent media based on light separation by grating into optical moments

16 p2915 A70-34330

Hologram interferometry for measuring surface deformation under force and anisotropy in transparent objects

17 p3085 A70-35009

IR balloon observations of absolute solar brightness and stratosphere transparency, discussing BCA and HSRA models

17 p3078 A70-35580

Aircraft-borne spectrometer for atmospheric IR spectral transparency

18 p3260 A70-36972

High efficiency semitransparent III-V semiconductor photocathodes fabrication and operation

19 p3486 A70-37756

Transparent ceramic armor fabrication using dense polycrystalline magnesite

19 p3437 A70-38422

Transparent polymers stress-strain state induced by elastic waves, using model with space and time dependence of laser beam

20 p3654 A70-39248

Mach-Zehnder interferometer for holographic investigation of inhomogeneities in transparent media, discussing photointerpretation error reduction

20 p3633 A70-39749

Holographic recording in transparent bodies with optical characteristics changeable under intensive light

20 p3633 A70-39999

Holographic interferometry for study of transparent media, noting application to aerodynamic phenomena

[ONERA-TP-851] 22 p4039 A70-43455

Transparent objects holographic interferometry with illumination derived from phase gratings to eliminate laser speckle

22 p4040 A70-43611

Optical damage center structural defects in transparent dielectrics under high energy ruby laser radiation, noting nontransparent inclusions and dislocation centers

24 p4351 A70-45209

TRANSPARENT MATERIALS

U TRANSPARENCE

TRANSPARATION

Fluid transpiration arc radiation source based on forced convection effect on electric arc

17 p3023 A70-35153

TRANSPARATION COOLING

U SWEAT COOLING

TRANSPANTATION

Phonocardiographic and ultrasound observations of acute rejection following cardiac transplantation, considering rejection treatment at early stage

03 p0415 A70-12888

Electrocardiac events observed in cardiac transplant recipient emphasizing unique finding

03 p0433 A70-12893

Therapeutic power of bone marrow transplanted from mice earlier irradiated by high energy protons into newly irradiated mice

09 p1619 A70-22814

Cytoplasm, nucleus and membrane combination techniques for reassembly to form viable amoebae

11 p1986 A70-25849

Therapeutic effects of hemopoietic tissue transplantations of bone marrow on irradiated rats, using diffusion chamber for resettlement prevention

13 p2354 A70-29753

Circadian rhythms from electrocardiogram and cardiostachogram of patient with human heart transplant, noting P waves relationship between donor and recipient tissues

20 p3570 A70-39166

TRANSPONDERS

Airborne secondary surveillance radar transponders performance and system optimization for automatic altitude reporting, separation standards maintenance and automatic plot extraction

02 p0267 A70-11990

Directional transponders for telemetry command, tracking and communications in retrodirective communication satellites

03 p0457 A70-13838

Active AM scatterer/spiral antenna used as transponder in elementary CW radar system

04 p0652 A70-15346

L band transponder design for aeronautical satellite, giving block diagrams

07 p1234 A70-19292

Communication satellite transponders design, cost, reliability, manufacturing, testing and future developments

07 p1241 A70-19620

PSK distortion spectra generated in satellite transponders by interactions of FDMA PSK modulated carriers, developing computer programs for multichannel FDMA PSK modulated systems

10 p1839 A70-24364

Hybrid microwave integrated circuits application to phased array and Data Relay Satellite System space transponder

10 p1851 A70-24879

Canadian geostationary satellite communication system design and performance, discussing transponder with six RF channels

[AIAA PAPER 70-429] 11 p1996 A70-25402

VHF satellite transponders for ranging and position fixing, studying ionospheric and multipath effects

[AIAA PAPER 70-489] 11 p1999 A70-25433

Channel separation in RF transponder for communication satellite achieved with RF multiplexers consisting of microwave filters and combiners with superior electrical performance

[AIAA PAPER 70-509] 11 p2016 A70-25457

ATC radar beacon system, discussing interacting factors lowering reply reliability from transponder

12 p2267 A70-27639

Meteorological transponder rocketsonde instrumentation system evolution and data error analysis

14 p2585 A70-30579

Airborne equipment microelectronics technology application to interrogators, transponders and UHF/VHF transceivers

14 p2558 A70-31294

Sirio satellite SHF transponder for experiments in atmospheric propagation and communication between ground stations

15 p2709 A70-32285

LM-Apollo rendezvous radar and transponder electronic assemblies packaging and mechanical design

18 p3232 A70-36762

Ground station requirements for transition to multitransponder INTELSAT 4 satellite, discussing interference filtering, group delay distortion, etc

21 p3789 A70-41346

Single multiple access satellite communication system requirements for worldwide, trunked and local operations, considering transponder allocation and antennas

21 p3790 A70-41365

Multiple channel VHF testing on ATS 1 and 3, describing transponder intermodulation and compression corrections

21 p3791 A70-41366

TRANSPORT AIRCRAFT

NT A-300 AIRCRAFT

NT BAC 111 AIRCRAFT

NT BOEING 707 AIRCRAFT

NT BOEING 727 AIRCRAFT

NT BOEING 737 AIRCRAFT

NT BOEING 747 AIRCRAFT

NT BOEING 2707 AIRCRAFT

NT C-5 AIRCRAFT

NT C-9 AIRCRAFT

NT C-47 AIRCRAFT

NT C-135 AIRCRAFT

NT C-141 AIRCRAFT

NT CARGO AIRCRAFT

NT CH-3 HELICOPTER

NT CH-46 HELICOPTER

NT CH-47 HELICOPTER

NT CH-54 HELICOPTER

NT CL-8 AIRCRAFT

NT CONCORDE AIRCRAFT

NT DC 8 AIRCRAFT

NT DC 9 AIRCRAFT

NT DH 121 AIRCRAFT

NT DH 125 AIRCRAFT

NT DO-31 AIRCRAFT

NT F-28 TRANSPORT AIRCRAFT

NT G-222 AIRCRAFT

NT HFB-320 AIRCRAFT

NT L-1011 AIRCRAFT

NT SA-330 HELICOPTER

NT SHORT HAUL AIRCRAFT

Military inertial navigation technology applied to civil air transport aircraft

01 p0137 A70-10311

Air traffic control methods for transport aircraft delay elimination

01 p0139 A70-11367

Air cargo transport development and organization trends, considering cost and aircraft types

02 p0401 A70-11736

Electronic head-up display experience in transport aircraft flight tests including human factor, installation, operational applications, etc

02 p0224 A70-11836

Three dimensional navigation and guidance system for transport aircraft to alleviate operational problems, noting application to STOL aircraft

02 p0334 A70-11983

Air traffic congestion alleviation by applying general purpose computers for navigation in civil transport aircraft

02 p0334 A70-11985

Transport aircraft takeoff length reduction by applying various runway inclinations with respect to takeoff accelerations

02 p0275 A70-12223

VTOL transport aircraft stability and maneuverability compared with conventional aircraft

02 p0228 A70-12759

A-300B twin engine short haul giant transport aircraft, discussing engines, aircraft performance and systems reliability

[RAES PAPER 11] 03 p0411 A70-13543

Collection of papers on jet transport design covering subsonic zero lift drag rise properties, performance characteristics, supersonic aircraft design, etc

03 p0414 A70-14018

Flight characteristics differences between VTOL and conventional transport aircraft, recommending differences consideration in regulations

03 p0414 A70-14095

Design specifications for low noise turbofan engine used on long range subsonic transport aircraft

[ASME PAPER 69-WA/GT-7] 04 p0734 A70-14888

German VTOL transport aircraft projects, discussing Dornier 231/lift by turbojets/ and Bolkow 140/swiveling wing with gas turbine propellers/

04 p0623 A70-14955

German transport VTOL projects, discussing VC-500 swiveling wings with turbine powered propellers

and HFB-600 blade cascade flow deflectors for vertical takeoff

04 p0623 A70-15349

Aircraft design in commercial air transport safety, discussing turbine blade oxidation and crack prevention, engine cooling, fuels, lightning protection, etc

04 p0624 A70-15644

V/STOL and fixed wing tactical transport aircraft survivability while supporting forward area logistics bases, noting V/STOL advantage

[SAE PAPER 690705]

05 p0792 A70-15857

Wing vibration problems associated with roll attitude control in hovering autostabilized VTOL transport aircraft with wing-mounted jet lift engines

05 p0794 A70-16116

VTOL technical problems relating to military and civil transport applications, discussing sensitivity to mission requirement variations including design costs, noise levels, etc

05 p0797 A70-17077

Commercial navigation systems for long range subsonic transports, discussing accuracy, avionics hardware and crew responsibility optimization

06 p1102 A70-17638

Physiological training programs and equipment for life support in transports, discussing changes in protective helmet and quick donning harness

06 p1002 A70-17708

Aircraft transport tariffs used to determine economic approach to design

07 p1426 A70-18841

Monograph on HFB 600 V/STOL transport for civil and military air traffic, discussing intercity travel, military dispersal requirements, systems performance, cockpit layout, etc

07 p1194 A70-19605

Air cargo transportation systems in 1970s, discussing market expansion, payload capacity and fleet growth, containerization, etc

07 p1250 A70-19875

V/STOL transport aircraft design in Germany, analyzing demands in military and civil sectors

08 p1435 A70-20639

Personnel protection against accidental decompression in transport aircraft at high altitudes, recommending flight stations with capsule to achieve ground level oxygen equivalent

09 p1627 A70-23459

V/STOL transport aircraft cockpit design in terms of size, geometry and equipment accommodation

10 p1804 A70-24048

Civil VTOL transport aircraft handling and performance qualities using fixed base simulator with electronically generated display

10 p1859 A70-24214

Transport aircraft flight recorders for parameters essential for operation and aircraft maintenance

11 p2050 A70-25818

Maintenance trends for transport aircraft jet engine, considering engine and component pooling, inspection accessibility, monitoring, etc

[SAE PAPER 700316]

12 p2290 A70-27455

Automatic engine maintenance recording system on air transport aircraft noting data reduction

[SAE PAPER 700317]

12 p2335 A70-27456

Reliability and maintainability from airline standpoint, discussing concepts, language and standards for aircraft design

[SAE PAPER 700326]

12 p2335 A70-27460

Jet transport wakes resulting from high engine thrusts considered hazardous to following aircraft, discussing multiple-instrumented runways for measuring visibility

12 p2162 A70-27995

Gust response calculations compared with flight measurements for two fighter aircraft and jet transport to determine accuracy

[AIAA PAPER 68-892]

12 p2162 A70-28077

Book on Polish air cargo transport covering transport volumes, aircraft, preparation and loading operations

13 p2524 A70-29453

Design costs for large subsonic transport engines in terms of size, engine ratings and community noise

14 p2629 A70-30944

R and D impact on transport aircraft design economics

14 p2669 A70-30945

Short haul Mercure airliner weight saving design and manufacture

14 p2593 A70-31371

Hypersonic aircraft technology, discussing long range transport, reusable launch vehicles and propulsion systems

15 p2673 A70-31851

Human survival problems of transport aircraft in various airport ground-air situations and environmental conditions

15 p2676 A70-32224

Twin jet light transport Corvette airframe, discussing flight characteristics and economical aspects

15 p2676 A70-32793

Transport aircraft interior design based on anthropological, architectural and engineering factors

16 p2841 A70-33767

Low pressure ratio lift fan propulsion system for intercity VTOL transports, considering thrust, safety, noise, weight, components, speed, turbine and transmission

[AIAA PAPER 70-670]

16 p2971 A70-33952

Ti sheet welded construction for transport aircraft fuselages, assuming use of electron beam and plasma arc equipment

17 p3198 A70-34452

Maneuver load alleviation /MLA/ configurations for wing bending load relief on transport aircraft, showing improved payload and span performance

[AIAA PAPER 70-877]

17 p3016 A70-34813

Wide body commercial jet transport structural design considerations applied to DC 10 aircraft

[AIAA PAPER 70-895]

17 p3193 A70-35812

Large capacity transports influence on air cargo operations, and joint use cargo terminal planning

[AIAA PAPER 70-920]

17 p3204 A70-35832

Air transport operations and economics in 1970 decade, taking into account cost-revenue ratio and cost effectiveness of various aircraft

17 p3204 A70-35852

Subsonic and supersonic transport aircraft design, discussing supercritical wing concept, fuel consumption reduction, composite aircraft structures, short haul transports, etc

17 p3022 A70-35854

European A-300-B Airbus program, discussing technical and economical aspects

18 p3213 A70-36509

High speed civil and commercial transport aircraft, discussing jet-orbital flight

18 p3333 A70-36664

V/STOL aircraft for short haul transportation, discussing speed, noise, reliability, economy, etc

[SAE PAPER 700333]

18 p3214 A70-36797

Propulsion system impact on military/commercial STOL transport aircraft commonality, taking into account augmented jet flap and externally blown flap powered lift wing concepts

[SAE PAPER 700269]

18 p3214 A70-36819

Military and commercial transports turbofan propulsion systems impact on future aircraft design and development

[SAE PAPER 700267]

18 p3214 A70-36820

European airbus designs, considering potential market and financial problems

19 p3357 A70-38952

Jumbo jets turbofan engines design, considering fuel consumption, maintenance, reliability, noise reduction, etc

19 p3491 A70-38953

Pilot/vehicle feedback systems with flight director computer for transport aircraft longitudinal control during landing, discussing design by manual control displays theory

[AIAA PAPER 70-1001]

20 p3560 A70-39530

Transport aircraft noise at three major airports by noise exposure forecast /NEF/ contours methodology

21 p3750 A70-40896

Short haul jet transport aircraft design, discussing Computer Aid Design, Airline System Simulator and Traffic Demand Predictor computer programs

[ICAS PAPER 70-28]

23 p4284 A70-44105

Emergency life saving instant exits for transport aircraft, using electromechanical confined transfer shaped explosive device

23 p4141 A70-44487

Commercial transport aircraft fatigue loading data from NASA VGH /airspeed-acceleration-altitude/ program, discussing instrumentation, sample sizes, etc

23 p4270 A70-44548

Airframe skin panels adhesive bonding in wide-bodied jet transports, emphasizing fuselage fatigue and corrosion resistance

[SAE PAPER 700863]

24 p4349 A70-45875

Noise reduction regulations effects on subsonic transport design and configuration

[SAE PAPER 700806]

24 p4290 A70-45876

Airline selection of Auxiliary Power Unit /APU/ for transport aircraft, noting benefits of air conditioning during ground operation

[SAE PAPER 700816]

24 p4394 A70-45901

Noise reduction design for subsonic transport turbofan engines

[SAE PAPER 700807]

24 p4395 A70-45907

Quiet V/STOL transport aircraft from DC-9-10 modification, discussing flying qualities, propulsion and control system interfaces, configurations, etc

[AIAA PAPER 70-1409]

24 p4291 A70-45916

Air transportation beyond 1970, discussing general aviation, short haul systems, STOL, helicopter, V/STOL, subsonic, supersonic and hypersonic aircraft

[AIAA PAPER 70-1262]

24 p4291 A70-45918

All-body configuration hypersonic transport aircraft performance by computer synthesis, considering sonic boom constraint, maximum payload ratio and optimal cruise speed

[AIAA PAPER 70-1224]

24 p4291 A70-45957

TRANSPORT COEFFICIENTS

U COEFFICIENTS

U TRANSPORT PROPERTIES

TRANSPORT EQUATION

U BOLTZMANN TRANSPORT EQUATION
TRANSPORT PROPERTIES

NT ATMOSPHERIC CONDUCTIVITY

NT CARRIER MOBILITY

NT ELECTRICAL RESISTIVITY

NT ELECTRON MOBILITY

NT GAS VISCOSITY

NT GASEOUS DIFFUSION

NT HOLE MOBILITY

NT IONIC MOBILITY

NT IONOSPHERIC CONDUCTIVITY

NT MAGNETORESISTIVITY

NT PHOTOCONDUCTIVITY

NT PLASMA CONDUCTIVITY

NT SUPERCONDUCTIVITY

NT THERMAL CONDUCTIVITY

NT THERMAL DIFFUSIVITY

NT VISCOSITY

Thermodynamic and transport properties of Na, K, Rb and Cs vapors to 3000 K, for use in liquid metal coolant and power systems

01 p0214 A70-10299

Direct solar radiation concentration by paraboloid mirrors, analyzing energy transport and distribution functions, based on statistically distributed imperfections of reflecting surfaces

01 p0010 A70-10762

Surface catalysis and variable transport properties effects on chemically frozen dissociated hypersonic air flow boundary layers enveloping flat plates and slender wedges

01 p0067 A70-11179

Hydrodynamic equations and Grad transport coefficients for nonequilibrium rarefied monatomic gases developed for molecular collisions

01 p0068 A70-11567

Density effects on transport coefficients of gaseous mixtures, solving modified Boltzmann equation including collisional transfer and three-particle collision effects

03 p0606 A70-13576

Sealed-off He-Cd laser construction, describing life test, noise, Cd transport characteristics and transverse magnetic field effect

03 p0501 A70-13582

Electric discharges in low pressure Ar in external magnetic fields, studying charge in transport coefficients and drift due to MHD forces

04 p0724 A70-14529

Faraday type open circuit MPD generator model obtained with allowance for temperature and pressure losses and gas transport properties dependence on static parameters

04 p0725 A70-14530

Transpiration-cooled electric arcs for high temperature high density plasma generation, considering uncertainties in plasma transport properties and temperature distributions

04 p0729 A70-15591

Test apparatus for investigating crystal defects influence on simultaneous measurement of metals thermal and electric conductivity under plastic deformation at cryogenic temperature

05 p0829 A70-16399

Beam transformation laws and matrices for Gaussian beams, discussing propagation, reflection and refraction in geometrical optics

05 p0883 A70-16773

Monte Carlo calculations of nonequilibrium radiative transport, including weighting and biasing techniques

05 p0958 A70-17084

Equation describing atmospheric oxygen conductance to human tissues compared with experiments, ascribing discrepancies to inhomogeneity in diffusion/perfusion relationships

06 p0993 A70-17434

Viscosity, thermal conductivity, specific heat and Prandtl number of hydrogen, methane and hydrogen-methane mixtures calculated for variation with temperature neglecting dissociation effects

06 p1177 A70-17700

Dissociating hydrogen transport coefficients analysis compared with data calculated as function of temperature and pressure without allowance for ionization

07 p1338 A70-19654

Transport properties of high temperature gases compared with room temperature differences, considering chemical equilibria, heat conduction and atom-free radical forces

07 p1424 A70-19880

Electrical conductivity of fully ionized plasma in strong magnetic field computed as application of method for plasma transport coefficients

07 p1354 A70-20246

Dynamics of multicomponent plasma involving charged or neutral gases with transport phenomena for case of no magnetic field

09 p1738 A70-23580

Flux equations of single velocity Boltzmann type for unsteady transport problems applied to concentration discontinuity propagation through plane layer

10 p1966 A70-23871

Thermomagnetic transport coefficients in anisotropic metals based on theory for galvanometric properties, producing closed form expression for conductivity tensor

11 p2097 A70-25618

Thermodynamic and transport properties of high temperature and pressure gases measured with ultrasonic pulse technique

11 p2147 A70-25753

Plasma transport properties at temperatures up to 15000 K, considering electrical and thermal conductivity, radiation source strength and viscosity

11 p2089 A70-25759

Nitrogen transport properties to 26,000 degrees K, measuring current-field intensity properties and radial temperature distributions in molecular nitrogen cascade

11 p2151 A70-26841

Interplanetary shock waves layer formation in collisionless medium, using bulk transport parameters for dissipation requirement

12 p2308 A70-27885

Dilute gas transport properties calculation, investigating numerical techniques to minimize computation time to prescribed accuracy

13 p2441 A70-29089

Active and passive ion transport mechanisms in excitable animal cell maintaining constant membrane polarization

13 p2352 A70-29351

Transport cross sections for isotopic methane and mixtures, considering inelastic and thermal diffusion effects

14 p2665 A70-30652

Statistical transport, energy and chemical reaction rate in turbulent flow field with uniform velocity gradient, using Brownian motion theory

14 p2566 A70-31029

Electron distribution for transport coefficients in Lorentzian plasma under magnetic field, determining electrical conductivity, thermal diffusion and viscosity

14 p2623 A70-31033

Transport properties of partially ionized argon based on electron velocity distribution function, comparing to Chapman-Enskog calculations

15 p2774 A70-31799

Thermoelectric power measurement of thin Au films, relating results to transport parameters and internal stresses

15 p2785 A70-32582

Dissociating hydrogen transport coefficients analysis comparison with data calculation as function of temperature and pressure without allowance for ionization

15 p2828 A70-32691

Transport and relaxation processes prediction for turbulent fluid, noting similarities to Fourier integral representation of flow field

16 p2895 A70-33969

Absolute stability and turbulent transport upper bounds in Couette flow, using variational analysis

17 p3066 A70-34543

Exact and normal solutions of Boltzmann equation linearized around total equilibrium, yielding Navier-Stokes and Burnett transport coefficients

17 p3128 A70-34628

Turbulent boundary layer structure, considering flow properties prediction, wake-like behavior, bursts, compressibility, transport properties, etc

17 p3068 A70-34665

NTWO Fortran IV family of subroutines for thermodynamic and transport properties of nitrogen

17 p3195 A70-34746

Collection of papers on transport phenomena in fluids covering hydrodynamics, thermodynamics, kinetic theory, thermal diffusion, etc

17 p3072 A70-35528

Isotropic fluid systems in nonequilibrium, investigating thermodynamic characteristics of transport phenomena

17 p3072 A70-35529

Transport processes in chemical reactions and biological functions of living systems, using nonequilibrium thermodynamics approach

17 p3032 A70-35539

Soviet papers on transfer phenomena in low temperature plasmas

19 p3480 A70-38180

Intercomponent momentum and energy exchange in weakly ionized gases, examining kinetic theory of subsonic and supersonic transport processes

19 p3482 A70-38945

Auxin downward transport by gravity in leaves, examining ethylene inhibition

20 p3570 A70-39234

Transport coefficients of inhomogeneous magnetized bounded and unbounded plasmas based on quasi-linear approximation

21 p3857 A70-41385

Reacting planetary carbon dioxide-nitrogen atmospheres high temperature equilibrium thermodynamic and transport properties

21 p3950 A70-41747

Nitrogen transport coefficients as function of high temperature in stationary plasma produced in cascade arc chamber

22 p4082 A70-43373

Near critical heat transfer in cryogenic fluids, discussing thermodynamic and transport properties

23 p4279 A70-44357

Enskog theory extended to three particle collisions for gas transport properties

23 p4222 A70-44427

Intermolecular forces at close approach distances in calculating thermodynamic and transport properties of high temperature dilute gases, using molecular beam methods

23 p4222 A70-44430

Gas transport properties at high temperatures and pressures, discussing Ar plasma arc characteristics

23 p4226 A70-44433

Partially ionized Ar transport properties, computing electron velocity distribution function as perturbation for Lorentzian mixture

23 p4220 A70-44437

Kinetic transport theory for mixed dilute gases consisting of linear rotating diamagnetic molecules in external homogeneous magnetic field

23 p4223 A70-44927

Low Reynolds number gas flow past heated circular cylinder, considering Stokes region transport properties

23 p4284 A70-44978

TRANSPORT THEORY

NT CHAPMAN-ENSKOG THEORY

NT MIXING LENGTH FLOW THEORY

Galerkin method applied to boundary layer flows, considering transport problems in unbounded domains

01 p0066 A70-11129

Shear stress transport equation derivation from turbulent energy equation based on properties of turbulent velocity fluctuations

02 p0284 A70-12346

Transport theory application to differential approximations for radiative transfer problems

[ASME PAPER 69-WA/HT-45] 04 p0781 A70-14801

Fast neutron transport characteristics of helical ducts using Monte Carlo code FASTER, computing neutron fluxes and attenuation

05 p0884 A70-16163

Scalar radiative transport equation solved iteratively for microwaves backscattering from turbulent plasma, deriving model for direct and cross polarized cross section

07 p1353 A70-19993

Nonlinear transport equations linearization by hodograph and inversion techniques

08 p1597 A70-21125

Boundary value problems in one speed transport theory, applying Green function technique to neutrons with spherical symmetry

08 p1542 A70-21253

Variational principle of steady state transport process derived from basic inequality in macroscopic theory of nonequilibrium thermodynamics

09 p1789 A70-23224

Elastic scattering effect on photoelectron transport and escape in upper sunlit atmosphere

12 p2222 A70-27187

Transport equations for interaction between radiation and matter under arbitrarily large nonequilibrium in comoving system

13 p2521 A70-29414

Cosmic ray transport in solar wind generalized with anisotropic diffusion approximation

14 p2632 A70-30887

Equatorial F 2 region response during solar eclipse of 7 March 1970, emphasizing ionization production and loss, transport processes and electron temperature

16 p2897 A70-33826

Thermodynamic effects and transport phenomena in discontinuous system of gas filled containers connected by membrane, deriving entropy production and diffusion flux in membrane

17 p3197 A70-35531

Statistical theory of irreversible transport processes in fluids, considering deviation from equilibrium as stochastic process

17 p3131 A70-35532

Dilute gas transport expressions experimental substantiation, emphasizing nonequilibrium thermodynamics as macroscopic theory rather than empirical postulate

17 p3072 A70-35536

Semiempirical theory of anisotropic turbulent transport, deriving closed system of flow equations

17 p3073 A70-35736

Ballistical transport in collisionless exosphere, discussing heat flux of ballistical oxygen and model temperatures for day and night conditions

17 p3080 A70-35765

Solar corona streamer and interstreamer regions, examining geometrical and dynamic structure by energy transport process

20 p3712 A70-40417

Approximate calculations of thermal and viscous transport in high temperature air based on empirical transport equations

21 p3951 A70-41750

Macroscopic equations of motion established by Maxwell transport equations for relativistic perfect gas

22 p4011 A70-42716

Radiation shield design and transport calculations, reviewing kernel methods development and relevant computer programs

23 p4217 A70-43811

Transport equation relation between irreducible tensorial sets, examining geometrical symmetry influence and thermomagnetic and galvanomagnetic effects

24 p4428 A70-45520

Monovalent cations active transport model in mitochondria, noting membrane potential as driving force and ion pump omission

24 p4304 A70-46230

TRANSPORT VEHICLES

Ram wing tube ground transportation vehicle, analyzing optimum lift-drag ratio and induced power requirements

11 p1975 A70-25966

Reusable ballistic orbital-global transportation systems using rocket sled-assist-takeoff compared to SST systems in terms of effectiveness and cost

11 p2122 A70-26048

Interstellar transport vehicles design around thermomolecular propulsion plants, discussing weight, mission velocity, acceleration time and fuel costs

11 p2123 A70-26054

Space propulsion systems for public transportation to and from orbit and throughout near solar system, discussing commercial requirements

11 p2102 A70-26060

Transportation vehicle noise control measures and acceptability, discussing physical and operational source modifications using aircraft noise examples

12 p2336 A70-27849

TRANSPORTATION

NT AIR TRANSPORTATION

NT HIGHWAYS

NT RAIL TRANSPORTATION

NT RAPID TRANSIT SYSTEMS

NT SPACE TRANSPORTATION

NT URBAN TRANSPORTATION

Manned reusable space transportation system technology requirements and vehicle types

[AIAA PAPER 69-1116] 01 p0194 A70-10613

Ram wing vehicles aerodynamics application to high speed ground transportation, studying effect on passenger ride quality

[AIAA PAPER 70-142] 06 p0973 A70-18145

Test facilities and procedures for obtaining aerodynamic data required for studying vehicle-in-tube transportation systems

[AIAA PAPER 70-225] 06 p1030 A70-18221

High speed ground tube vehicle transportation system aerodynamics, presenting drag coefficients and static wall pressure measurements

16 p2839 A70-34264

Air freight containers in continuous air/land transportation chain, discussing weight, performance, cost, technical concepts and inter and nonintermodal prototypes

22 p4007 A70-43273

TRANSURANIUM ELEMENTS

NT PLUTONIUM ISOTOPES

TRANSVERSE ACCELERATION

Two dimensional supersonic turbulent near wake saddle point singularity during recompression analyzed by including transverse momentum integral equation

[AIAA PAPER 70-228] 06 p1039 A70-18106

Intracerebral, peripheral and central blood circulation relationship in humans during transverse accelerations

07 p1209 A70-19520

Prolonged transverse acceleration effects on rats kidney and posterior hypophysis neurosecretions

20 p3575 A70-40188

TRANSVERSE OSCILLATION

NT H WAVES

Transverse vibration of viscoelastic polymethyl methacrylate column with initial curvature under periodic axial load, determining amplitude-frequency curves

[ASME PAPER 69-WA/APM-13] 04 p0772 A70-14915

Transverse mode locking for carbon dioxide laser achieved with nonlinear boron chloride absorber, observing emission spatial buildup

06 p1083 A70-18425

Simultaneous partial integrodifferential equations for transverse oscillations of uniform short beams

07 p1406 A70-19306

Transverse oscillation periods of cylinder containing flowing fluid obtained by solving nonlinear partial

differential equations describing transverse and longitudinal motion

08 p1592 A70-21480

He-Ne laser emission in transverse oscillation mode, analyzing spatial and temporal coherence characteristics

09 p1694 A70-22135

Thin rectangular plates transverse natural frequencies, deriving equations of motion and boundary conditions in bending moment terms by vibrational principle

11 p2143 A70-26645

Complex plates free transverse oscillation modes and frequencies using Ritz method

15 p2818 A70-32183

Rope transverse oscillations due to impact taking bending rigidity into account

24 p4424 A70-45627

TRANSVERSE VIBRATION

U TRANSVERSE WAVES

TRANSVERSE WAVES

Centrally clamped spinning circular disk free transverse vibration analysis within accuracy of numerical computations

03 p0584 A70-12931

Fabry-Perot resonator misalignment effect on TEM wave transmission coefficient in gas laser

03 p0492 A70-13749

Adiabatic disturbances propagating as transverse waves in inviscid fluid rotating as Rankine vortex about cylindrical container axis, discussing harmonics

03 p0467 A70-13779

Smoked-foil technique for transverse wave quantitative study in condensed-phase explosives

03 p0606 A70-13814

Radial vibration of cylindrical shell of transversely isotropic material determined using finite Hankel transform

03 p0595 A70-13904

Dielectric loaded waveguide with symmetric microstrip line, evaluating transverse wave number by finite difference method

03 p0458 A70-14035

Solid viscoelastic cylinder bonded to thin elastic casing, analyzing normal and tangential stresses for stress and displacement frequency responses in forced transverse vibration [ASME PAPER 69-WA/APM-20]

04 p0771 A70-14911

Horizontal transverse vibration effects on manual tracking performance, relating tracking errors to frequency rather than acceleration

04 p0643 A70-14981

TEM wave reflection incident on conducting thin strips semifinite array in free space not accompanied by emission

05 p0812 A70-16243

HF conductivity tensor of isotropic plasma, taking into account particle correlations describing weakly Langmuir turbulent plasma

05 p0889 A70-16532

Transverse vibrations of isotropic truncated-cone beam fixed at ends compared with cylindrical beam

05 p0942 A70-16666

Parallel plate TEM waveguides radiation pattern slope diffraction analysis

06 p1021 A70-17570

Gaseous detonation transverse wave propagation and measurement from smoked foil records

07 p1424 A70-20006

TEM waves penetration into magnetoactive semibounded plasma using Vlasov and Maxwell equations, obtaining electric field for specular reflection of electrons

08 p1551 A70-21255

Simply supported rectangular plate investigated for effect of thermal gradient on transverse vibrational frequencies

08 p1595 A70-21976

Quasi-transverse constant profile wave in finite elasticity with isothermal shock at discontinuity compared to Whitham breakdown

10 p1956 A70-24191

Transverse vibrations of rods, plates and shells based on hyperbolic, circular and Bessel functions

10 p1959 A70-24586

Plasma instability in TEM wave field, considering nonpotential HF oscillations buildup with frequency near external wave frequency

13 p2463 A70-29283

Fabry-Perot resonator higher modes excitation by external TEM wave, discussing optimal mismatch for maximum intensity

13 p2408 A70-29358

Boundary value problems reduction to variational problem by transversality conditions of calculus of variations

14 p2599 A70-30644

Strip lines transmission characteristics with rectangular outer conductor and multielectric layers within TEM wave approximation, using Green function and variational principle

14 p2558 A70-31316

Transverse vibration of thin circular elastic turbine disk of variable thickness rotating axially at constant angular velocity

16 p2916 A70-32994

Longitudinal and transverse hypersonic mm waves excitation in quartz single crystal at liquid helium temperature

16 p2952 A70-33258

Plane TM wave scattering by systems of two parallel conducting elliptical cylinders, metal tapes and combinations

19 p3374 A70-37278

Transversely magnetic and electric wave critical frequency spectra in Pi and H section waveguides, using summary representation method

19 p3378 A70-37735

Edge distribution of transverse reactive forces of rectangular plate with nonuniform flexural rigidity at buckling load

19 p3541 A70-38042

Radiation theory circular waveguide in dominant TE mode and flush mounted to infinite conducting flat ground plane covered by plasma or dielectric sheath

20 p3586 A70-39500

Acoustic frequency spectra of transverse vibrations in bracketed bar caused by dry friction, using Lagrange method

22 p4073 A70-42612

Solar wind instability from TEM waves propagating parallel to magnetic field in electron-proton plasma

23 p4235 A70-43826

Ionospheric parametric amplification and frequency mixing due to polarized TEM waves nonlinear interaction with longitudinal electrostatic waves

23 p4185 A70-43838

Longitudinal and transverse hypersonic mm waves excitation in quartz single crystal at liquid helium temperature

23 p4218 A70-44281

Acoustic plasma wave excitation by transverse electromagnetic wave beam, calculating LF instabilities and energy losses

24 p4384 A70-45149

TRAPEZOIDAL WINGS

Ackeret theory for infinite aspect ratio, rectangular and trapezoidal constant cord wings with arbitrary spanwise variation of profile in supersonic flow

16 p2836 A70-33748

Aerodynamic lift, drag and momentum coefficients in supersonic regime for rectangular and trapezoidal wings with spanwise variable profile

22 p3958 A70-42615

TRAPEZOIDS

Illusions of rotation perception with oscillating trapezoid and oscillation perception with rotating trapezoid, correlating magnitudes

05 p0807 A70-16673

TRAPPED MAGNETIC FIELDS

Auroral oval position with trapping region phi s boundary compared with closed geomagnetic field lines phi c, using Alouette 2 satellite data

13 p2398 A70-29229

TRAPPED PARTICLES

NT ARTIFICIAL RADIATION BELTS

NT INNER RADIATION BELT

NT MAGNETICALLY TRAPPED PARTICLES

NT OUTER RADIATION BELT

NT PROTON BELTS

NT RADIATION BELTS

Electron trapping effect on ion-wave instability in plasma, deriving expression for saturation energy spectrum

01 p0152 A70-11361

Charged particle self resonant motion in field of plane electromagnetic wave, showing trapped particles existence in whistlers

02 p0256 A70-12116

Accumulated plasma density and lifetime measurement of trapped ions between accelerator and periodic magnetic mirror, showing limitation by collisions and charge exchange

03 p0532 A70-13683

Satellite measurement of auroral particles and particles trapped in Van Allen belts

03 p0559 A70-13852

Spacecraft surface secondary electron emission effects on electron trap measurements in magnetosphere and solar wind, noting agreement with positive ion densities

03 p0561 A70-13994

Optically trapped filaments in liquid carbon disulfide by side illumination and crossed polarizers using glass laser, noting birefringence and duration time

04 p0703 A70-15619

Al foil exposed to solar wind on moon during Apollo 11 mission examined for helium particles, finding lunar solar wind albedo

05 p0900 A70-16093

Electron distribution function in quasi-static free moderately ionized plasma with partial radiation trapping determined from electron-electron collisions

05 p0889 A70-16452

Satellite radiation dose rate experiment with simultaneous trapped particle and absorbed dose rate measurements, discussing proton spectra, material distribution, shielding effects, etc

06 p1061 A70-17263

Kinetic theory of longitudinal ionic oscillations pertaining to LF plasma oscillations monitored in Ariel 1 satellite wake due to ions trapped in potential trough

06 p1120 A70-17591

Heat transfer in dense high temperature plasma due to drift waves instability at trapped electrons

06 p1121 A70-17802

Fission gases trapped in fuel particles, cladding and matrix of irradiated refractory metal-uranium oxide cermets determined by gamma counting

07 p1332 A70-19851

Quasi-trapped electrons precipitating at high latitudes measured from low altitude polar orbiting satellite

08 p1562 A70-21382

Trapped particle vibrations stability during quasi-neutral plasma disturbance due to centrifugal drift in stellarator electric field

08 p1555 A70-21982

Electron diffusion in trap with magnetic mirrors under pulsed field perturbations, determining coefficients by numerical integration of drift equation

10 p1931 A70-24311

Swiss Solar Wind Composition Experiment, analyzing trapped particles characteristics of Apollo 11 and 12 lunar exposed aluminum foil

11 p2105 A70-25950

Particle spectrometer for Apollo measurements of trapped protons and electrons, using directional telescope composed of solid state and scintillation counters

12 p2232 A70-27404

Plasma turbulence in Van Allen belts, examining weak turbulent electromagnetic wave properties, with emphasis on trapped energetic particles radiation

13 p2486 A70-28555

Heat transfer in dense high temperature plasma due to drift waves instability at trapped electrons

13 p2460 A70-28653

Trapped particle interactions with plasma waves, analyzing pitch angle scattering, oscillating electric field, transverse waves and resonance effects

13 p2468 A70-29929

Finite Larmor radius interchange and LF drift oscillations due to magnetospheric temperature and density gradient stresses in trapped plasma

13 p2401 A70-29936

Trapped and polar proton and electron flux observations during 9 June 1968 magnetic storm

13 p2482 A70-30072

Trapped alpha particle and proton spectra from satellite measurements, considering magnetosphere injection

13 p2484 A70-30093

Trapped particles radial diffusion in formation and decay of radiation belts

13 p2484 A70-30096

Trapped protons population explanation by combined pitch angle scattering and radial diffusion across L shells

13 p2484 A70-30097

Magnetospheric particles, fields, electromagnetic waves and data on collisionless bow shock structure

13 p2484 A70-30098

Book on space physics covering charged particles in magnetic, electric and dipole fields, cosmic rays, magnetically trapped radiation and interplanetary plasma

14 p2633 A70-30099

Hysteresis in MOS transistors attributed to trapped charge carriers on oxide near silicon oxide interface

14 p2555 A70-30338

Sideband instability and trapped particle charge density response of large periodic Bernstein-Green-Kruskal waves in collisionless plasma

14 p2623 A70-31039

Geomagnetic dipole field disturbances by trapped particles, calculating self consistent equilibrium configuration for ring current dipole moments

15 p2727 A70-31905

Longitudinal electric field effect on trapped particle motion in asymmetric magnetosphere, considering electron precipitation

15 p2728 A70-31990

Longitudinal and transverse electric field effects in magnetospheric electron precipitation, discussing trapped particle drift

16 p2972 A70-34188

Magnetospheric electric field configuration from trapped particle flux asymmetries, using Explorer 14 electron data

18 p3306 A70-36024

Elongation characteristics of modulation type charged particle traps and analyzers, discussing ions and electrons trapping

18 p3307 A70-36171

Trapped particle population changes associated with solar events, discussing solar wind discontinuity effects on magnetosphere

19 p3495 A70-37487

Trapped and precipitated electron observations at northern high latitudes in 45-450 keV range, using ESRO-1 satellite 19 p3496 A70-37515

Apollo 11 lunar fines trapped noble gas elemental and isotopic abundances, suggesting solar wind origin 21 p3906 A70-41565

Trapped and cosmogenic rare gases from stepwise heated Apollo 11 lunar dust and crystalline rocks, using mass spectrometry 21 p3908 A70-41584

Ion cyclotron resonance spectroscopy for detecting trapped gaseous ions in analyzer cell, observing ion-molecule reactions 23 p4196 A70-44390

Energy dependence of equatorial pitch angle distribution for protons trapped in radiation belt, based on adiabatic theory and observational data 23 p4192 A70-44923

TRAPPED RADIATION

U RADIATION BELTS

U TRAPPED PARTICLES

TRAPPING

Cosmic ray intensity increase due to meteor showers magnetic field trapping effect 08 p1560 A70-20568

Fields in wave interaction region during spatial trapping of parametrically amplified waves by radiation of pumping, using Laplace transformation 10 p1844 A70-25157

Cosmic ray intensity increase due to meteor showers magnetic field trapping effect 15 p2795 A70-32723

Gunn effect in two-valley semiconductors with traps explained by model, assuming field-dependent trapping times and field-independent carrier generation rates 20 p3686 A70-39116

Trap filling dependence on intensity, temperature and wavelength of photoexcitation in CdS crystals subjected to electron radiation damage and annealing 21 p3864 A70-42013

TRAPS

NT ION TRAPS (INSTRUMENTATION)

NT VAPOR TRAPS

TRAVELING CHARGE

Fourier and perturbation methods applied to radiation from uniformly moving charge in inhomogeneous magnetoactive medium, deriving expressions for radiation spectrum and energy losses 03 p0531 A70-13285

Cerenkov radiation of electron-positron pair as moving radiating dipole in EAS, discussing emission effects of primary energy, production height and inclination angle 03 p0561 A70-14186

Electromagnetic wave scattering from charged particle in hot electron plasma in magnetic field, considering relativistic corrections for scattered radiation spectra 07 p1352 A70-19992

TRAVELING WAVE AMPLIFIERS

Spectroradiometer with paramagnetic traveling wave quantum amplifier applied to radio telescope, studying noise, temperature and fluctuation sensitivity at given time constant 08 p1495 A70-21054

TWT amplifiers for 4-8 GHz frequency range exhibiting decreased weight and volume and increased efficiency 08 p1477 A70-21370

Stationary regime stability of one dimensional model of optical quantum traveling wave amplifier, determining trapping band of traveling wave laser 10 p1901 A70-25158

Traveling wave tube amplifier performance in numerous orbiting communication satellites, emphasizing life test data [AIAA PAPER 70-507] 11 p2015 A70-25406

Traveling wave amplifier on section of inhomogeneous transmission line with tunnel diodes 11 p2020 A70-26808

Multiplicative modulation noise of helium-neon traveling wave laser amplifier at micron wavelength 11 p2020 A70-26816

Anomalous LF noise in receiving devices with traveling wave quantum paramagnetic amplifier 11 p2020 A70-26817

SHF traveling wave tube amplifier design and characteristics 17 p3054 A70-35413

Traveling wave amplifier on section of inhomogeneous transmission line with tunnel diodes 24 p4317 A70-45180

Multiplicative modulation noise of helium-neon traveling wave laser amplifier at micron wavelength 24 p4317 A70-45188

Anomalous LF noise in receiving devices with traveling wave quantum paramagnetic amplifier 24 p4351 A70-45189

TRAVELING WAVE MASERS

Superradiant traveling wave laser emission observed with polymethine cyanine dyes pumped by

mode locked ruby laser for picosecond duration pulse generation 01 p0110 A70-10564

Traveling wave maser with increased linear gain obtained by slow wave structure through asymmetrical positioning of dielectric 06 p1082 A70-17778

Three channel traveling wave maser with cryogenic superconducting magnet for C-band monopulse radar system, describing construction and electrical characteristics 10 p1900 A70-24894

Gain-stabilization of SHF traveling wave maser radiometer, using thermal noise from neon discharge tube 12 p2228 A70-26881

Broadband traveling wave masers bandwidth increased by staggering direct current magnetic field along active structure length 12 p2249 A70-27690

Pulse area-pulse energy description of traveling-wave laser amplifier 24 p4351 A70-45257

TRAVELING WAVE MODULATION

Uncontrolled and controlled neodymium glass laser outputs, using ultrasonic traveling wave diffraction modulator 08 p1510 A70-20514

Diffraction shaped ruby laser monopulse during excitation of modulated ultrasonic traveling waves in phototropic Q switch 09 p1696 A70-22483

CW HCN laser driven phase matched traveling wave lithium niobate electro-optic light modulator performance 15 p2750 A70-31976

Carrier frequency transfer of amplitude modulated signal at two coupled transitions in traveling wave gas laser 23 p4202 A70-45055

TRAVELING WAVE TUBES

Pulse position modulation focused TWT for airborne electronic countermeasure broadband jamming, considering output power and thermal design 04 p0653 A70-15656

Traveling wave tubes used in electronic countermeasure chain or repeater for deception jammer, discussing design and performance 04 p0653 A70-15658

Electron trajectories in M-type backward wave tube, TWT and magnetron, giving output power expressions 05 p0823 A70-16885

Nonlinear equations for TWT derived allowing for electron beam defocusing and slow wave structure deposition current 05 p0823 A70-16887

Two frequency electron beam modes produced by O-type TWT at simultaneous input of HF signals of different amplitudes and frequencies 05 p0824 A70-16894

Parametric interactions in three frequency TWT parametric amplifier, using power series 05 p0824 A70-16895

Crossed field amplifiers properties and applications, comparing performance to TWT 09 p1642 A70-22008

Low noise TWT, discussing dynamic range, gain and phase tracking, environmental performance, life behavior and noise factor interrelations 09 p1644 A70-22233

TWT model with slow wave structure and realized negative depression coefficient and Q factor described by variational method 09 p1644 A70-22410

High sensitivity photomultiplier TWT microwave photodetector with internal lowered secondary electron multiplier and spiral HF getter 09 p1645 A70-22413

Optimal construction of microwave filters with TWT and ferrite direct gain receivers 09 p1648 A70-23166

Multibeam O-type TWT characteristic equation analyzed for arbitrary space diversity, calculating gain for various velocity parameter values and electrical lengths 09 p1651 A70-23638

TWT characteristic equation with arbitrary coupling between two electron beams over wide range of velocity difference, analyzing wave amplitude constant 09 p1651 A70-23639

Magnetron-type electron gun structure with high design perveance for TWT applications 09 p1651 A70-23642

Space charge parameters influence on electron wave and traveling wave interactions in TWT 09 p1652 A70-23654

Wave propagation constants in electron wave TWT, studying nonuniformity parameter influence to determine relationships between beam and system parameters 09 p1652 A70-23655

Input and memory-storage traveling wave tubes for electronic countermeasures 10 p1852 A70-24888

Microwave tubes for high power transmission from space to ground and in deep space communications, discussing klystrons, TWT and crossed field amplifiers [AIAA PAPER 70-435] 11 p2016 A70-25456

Spacecraft S band power amplifier TWT electrical, environmental and life tests under saturated conditions [AIAA PAPER 70-506] 11 p2016 A70-25468

TWT, obtaining life performance data from spacecraft, discussing distortion characteristics [AIAA PAPER 70-505] 11 p2017 A70-25494

Unidirectional heat pipe system design to control temperature of high power traveling wave tubes in synchronous orbit communication satellite, dissipating waste heat 11 p2127 A70-26362

Nonlinear phase shift equation derived from TWT single carrier performance, predicting multicarrier performance of communications satellites 12 p2195 A70-27248

CW traveling wave tubes and klystrons LF output signal fluctuations 14 p2555 A70-30303

TWT noise level minimization in 8 mm band with circular spiral slow wave structure and five electrode gun 15 p2707 A70-31519

High power TWT for satellite communications ground stations, including Intelsat experience 17 p3054 A70-35282

Electrons nonlinear interaction with field in traveling wave tube, using approximate quasi-classical quantum mechanics method 19 p3387 A70-37741

Traveling wave tube with two mixed different velocity electron beams, analyzing nonlinear operation by integro-differential equations 19 p3387 A70-37742

Magnetron type backward wave tube with negatively charged slow wave structure, analyzing electron beam wave interaction for starting conditions 20 p3596 A70-39251

TRAVELING WAVES

Potential triple traveling space waves in barotropic gas with arbitrary equation of state, analyzing adjacent and three dimensional self similar flows 01 p0068 A70-11582

Combustion chamber traveling oscillating shock wave as driving mechanism of high amplitude axial mode solid rocket combustion instability 02 p0353 A70-12009

Traveling wave velocity in human cochlea determined by equally loud tonal pairs, comparing results to psychophysical and electrophysiological findings 02 p0237 A70-12323

Horizontal ionospheric drift rates and traveling wave disturbances, showing differences between winter and summer 09 p1667 A70-22493

Standing wave measurements on radiating traveling wave dipole arrays with glide symmetric excitation, showing multimode propagation and effect on log periodic balancing 09 p1633 A70-22688

Ultrasonic traveling waves for nondestructive testing, discussing scattering and velocity anisotropy in polycrystalline metals, propagation in glass, epoxy resins shear moduli, etc 10 p1894 A70-24171

Numerical solution of optimal control with dimensionality not exceeding phase space, using nonlinear programming and traveling wave method 10 p1911 A70-25185

Single mode TW ruby laser with ring resonator, analyzing emission spectral characteristics by Fabry-Perot etalon 12 p2246 A70-27356

Solid state laser with traveling wave during steady state emission, determining pulse shape, duration and amplitude 12 p2247 A70-27497

Circular loop antenna with traveling wave current distribution, considering phase change effects on radiation pattern and gain 12 p2198 A70-27965

Surface wave antenna radiation pattern from finite aperture of corrugated horn antenna 12 p2199 A70-28017

Transverse laser modes interaction in traveling and standing wave generators allowing for spatial distribution 13 p2424 A70-28597

Quantum noises in laser systems, deriving kinetic equation for traveling wave generation field density matrix 13 p2428 A70-29360

Quasi-periodic influence of traveling disturbances on ionospheric F 2 layer small scale drift discontinuities 14 p2570 A70-30226

Atomic collision effect on frequency range of opposing traveling wave modes in gas ring laser, using density matrix equation

15 p2749 A70-31553

Traveling wave light modulator with 15 GHz bandwidth using cubic ZnS crystal with anomalous response

16 p2876 A70-33403

Self excited systems limiting states with traveling wave, analyzing oscillator moving along string under tension

16 p2990 A70-33781

Electrodeless traveling wave accelerator for wind tunnel use, determining gas stream density for subsonic and supersonic operation

16 p2889 A70-33868

Traveling wave antennas, analyzing modal characteristics of various waveguiding structures

17 p3052 A70-35070

Wave propagation measurement by correlation techniques, discussing travelling wave representation, delay times, amplitude coefficients, etc

17 p3091 A70-35449

Statistical directivity, radiation pattern, drift and dispersion of segmented traveling wave antennas

17 p3055 A70-35687

Infinite elastic plates traveling wave flutter in compressible flow, investigating viscous damping effects on critical flow velocity

18 p3343 A70-36701

Electro-optical SHF modulator characteristics calculation from light wave interaction with traveling wave

19 p3443 A70-37291

Traveling wave antenna array single lobe design using mode charts to reduce errors

19 p3376 A70-37688

Traveling horizontal ionospheric waves relationship to magnetic storm onset, showing ionization displacement occurrence

19 p3413 A70-38029

Traveling wave antenna arrays with resistance elements for coupling, measuring noise elimination capabilities

20 p3598 A70-40146

Faraday rotation of radio beacon satellite signals during traveling ionospheric disturbances simulated for spaced ground stations

20 p3590 A70-40481

Traveling thermal wave induced channel flow, examining velocity profile thermal boundary conditions and shear stress

21 p3948 A70-41247

Quasi-equispaced traveling wave slot arrays with below sidelobe crosspolarization, considering computer designed X band prototype

21 p3800 A70-42050

Quasi-periodic influence of traveling disturbances on ionospheric F 2 layer small scale drift discontinuities

24 p4331 A70-46301

TREADMILLS

Multistage treadmill exercise tests on healthy business executives noting S-T-segment responses

08 p1445 A70-21265

TREADS

Aircraft tires tread design for improved adhesion under wet runway conditions

14 p2532 A70-31336

TREES

Load distribution in Christmas tree turbine attachments due to centrifugal force on blades, showing strain diagrams

05 p0939 A70-16488

TREES [MATHEMATICS]

Decision trees application to research projects selection, cost stages, probable return on investment and control device

07 p1427 A70-19001

Computer program for system reliability prediction, using probability tree approach and block probabilities

13 p2373 A70-29565

TREES (PLANTS)

Phenolic aldehydes generated from lignin in fossil woods and carbonaceous sediments by oxidative degradation

13 p2361 A70-28911

Phenological network observations comparison for phase behavior of trees and plants in open landscapes and in populated areas

15 p2732 A70-32460

TREMORS

Short duration high workload effects in pilot rr interval and finger tremor during Boeing 747 aircraft let-down, approach and landing

11 p1993 A70-26521

Muscular group response to sinusoidal and trapezoidal force applied to forearm, discussing frequency dependent limb oscillations and neuromuscular effects

21 p3767 A70-42161

TRESCA FLOW

Incremental strain theories for nonproportionate loading of thin walled cylinders, discussing Tresca flow, von Mises theory and Prandtl-Reuss relations

03 p0480 A70-12953

Limit load of cylindrical shell with rigidly clamped edges under varying pressure and axial force, using Tresca yield condition

18 p3343 A70-36722

TRIANGLES

Triangular Lagrangian equilibrium points stability in planar restricted problem of three bodies at order two mass ratio using two variable expansion method

10 p1939 A70-24184

Plate bending triangular finite element for shell structure analysis, considering displacement functions, stiffness matrix and load vector

10 p1957 A70-24482

Shallow shell finite element of triangular shape, noting application to static problems

17 p3184 A70-34908

TRIANGULAR WINGS

U DELTA WINGS

TRIANGULATION

Least squares method adjusting observation functions in satellite triangulation with correlated observations

01 p0082 A70-11455

Space triangulation equations based on simultaneous measurements of satellite topocentric coordinates and distances between tracking station and satellite

02 p0254 A70-11753

Satellite triangulations scale and orientation control, describing terrestrial methods of geodetic bases determination

02 p0254 A70-11755

Azimuth between two stations of triangulation net determined by simultaneous observation of two satellites, discussing mathematical principles and applications in Europe

02 p0289 A70-11797

Earth satellite tracking data reduction for determining geodetic ground nets, examining errors in triangulation procedures

03 p0445 A70-13184

Simultaneous ground and space triangulation procedures, recommending use of satellite photographic observations for error reduction

03 p0445 A70-13185

Satellite surveys and astronomic-geodetic nets for joint terrestrial, space triangulation and gravimetric measurements, including laser distance determination

03 p0445 A70-13191

Multiple timing in elementary space triangulation using synchronous straight line as main net element

03 p0445 A70-13192

Great circle vector formula in space triangulation, discussing topocentric and geocentric position of satellite and tracking stations and absolute distance determination

03 p0445 A70-13193

Space triangulation net using direction and distance measurements from satellite photographic and Doppler observations, including tracking data leveling

03 p0446 A70-13194

Weighting coefficient matrix parameters for European satellite triangulation determined, considering sequence of separate points shown by photographs instead of single point

05 p0839 A70-16345

Optimally ordered triangular factorization for solving symmetrical systems of linear matrix equations

05 p0876 A70-16573

Finite element method using cubic polynomials over triangle as trial functions for solving second order boundary value problems in linear theory of elasticity

07 p1324 A70-19075

Astronomical and physical geodesy, discussing geometrical methods involving triangulation and trilateration and geocentric coordinates method in navigation

07 p1265 A70-19370

Three vector coplanarity equations for space geodetic triangulation grid, discussing role of satellite photographic observation

09 p1667 A70-22488

Analytical phototriangulation block equalization by two stage polygon method, discussing computer algorithm for problem solution

09 p1681 A70-23344

Short arc method and spatial fitting of orbit in satellite triangulation, establishing sequential order between methods

09 p1670 A70-23440

Real time opto-triangulation by cinetheodolites for data acquisition used in rocket impact prediction

09 p1640 A70-23779

Analytical aerial triangulation iterative solution mathematical convergence parameters tests, considering photogrammetric relations for standard conditions in variable size block

10 p1878 A70-24729

Photogrammetric three dimensional control extension investigated by plotter and method of Independent Model Aerotriangulation

10 p1890 A70-24731

Method of dependence involving triangulation applied to reducing photographs of earth satellites

11 p2006 A70-26185

U.S. Coast and Geodetic Survey satellite triangulation data reduction methods, discussing data acquisition system, plate preparation, etc

11 p2046 A70-26190

Relative control data incorporation into sequential or simultaneous analytical triangulation systems, considering extraterrestrial photographs reduction

12 p2308 A70-27875

Lunar surface large scale maps by photogrammetric method requiring triangulation of convergent high resolution Lunar Orbiter photographs by block process

16 p2979 A70-34045

Computer programs for photogrammetric aerial triangulation with independent models

18 p3248 A70-36778

Adjustment program for aerial block triangulation with independent models, using planimetry-height iterations

18 p3248 A70-36779

Instrumental measurement of projection center coordinates for aerial triangulation with independent models

18 p3248 A70-36780

Spatial aerotriangulation by analytical method based on independent models matched with geodesic grid

22 p4013 A70-42597

Horizontal passpoint error in block analytic aerotriangulations with dense perimeter ground control

22 p4031 A70-42964

Field control method for aerial photograph planar tying in, applying to cartographic reference point coordinate determination in triangulation

24 p4334 A70-45499

TRIATOMIC MOLECULES

Semiempirical potential energy surface generation for triatomic hydrogen from London equation by evaluating Coulomb and exchange integrals taking into account effective orbital overlap

01 p0147 A70-10469

Hydrogen triatomic molecules existence, stability and ionization in molecular beams

07 p1345 A70-20139

Free radicals role in astrophysics, considering diatomic or triatomic radicals in atmospheres of earth, sun, planets, comets, stars and interstellar space

10 p1943 A70-24839

Triatomic hydrogen ion role in solar photosphere opacity implied from limb darkening and specific intensity data

11 p2104 A70-25739

Triatomic hydrogen positive ion-yielding reactions, using EVA ion-molecule beam apparatus

16 p2855 A70-33012

TRIAXIAL STRESSES

Weak interfaces effects in laminates under triaxial tensions at crack tip, analyzing delamination during crack propagation and fracture resistance

01 p0127 A70-10482

Three dimensional nonlinear viscoelastic body stability under triaxial compression, extending results obtained for elastic body

07 p1408 A70-19542

Isotropic elastic three dimensional body steady stressed state under large subcritical triaxial strains described by solving linearized equations

13 p2515 A70-29316

Isotropic nonlinear elasticity problems of stress concentration near spherical cavity in field of triaxial tension, using small parameter method

22 p4120 A70-43714

Low friction seal for axial loading piston in triaxial soil testing cells

23 p4199 A70-43873

TRIAXIALITY

U TRIAXIAL STRESSES

TRICHLORIDES

U CHLORIDES

TRIDENT AIRCRAFT

U DH 121 AIRCRAFT

TRIGGER CIRCUITS

Trigger scaling circuits with pulsed and blanking feedback analysis for minimizing number of couplings

01 p0047 A70-10984

High speed camera synchronization by frame reference pulses for strobe triggering

06 p1060 A70-17147

Monolithic zero crossing AC trigger IC for thyristor power control systems operating in on-off mode

08 p1478 A70-20786

Transistorized pulse repetition frequency bandpass and band elimination filters, using trigger circuit to improve pulse-edge steepness and critical frequency stability

09 p1650 A70-23630

X band Gunn oscillators for binary FSK regenerator operation employing signal injection triggering

12 p2199 A70-28015

High voltage gas laser trigger pulse generators featuring high pulse rate with semiconductor controlled rectifier

14 p2594 A70-31181

Logic circuits reliability with series and parallel connected elements during random malfunctions, obtaining failure formulas for trigger 15 p2716 A70-32901

Gunn effect pulse regenerators, describing random domain triggering rate voltage dependence comparison with Johnson noise predictions 19 p3387 A70-37820

Normal mode pulsed ruby laser system with Xe flash lamp pumping, trigger circuit and transistorized power supply 20 p3643 A70-40355

MOS transistor trigger circuit design parameters statistical calculation and optimization by Monte Carlo method using computer 23 p4171 A70-43957

Air spark gap to switch stored charge in LC circuit, using auxiliary triggering circuit to clamp magnetic flux 23 p4177 A70-44471

Spark gap triggering with Q switched laser, comparing performance with electrical method 24 p4353 A70-45560

TRIGGERS
U ACTUATORS

TRIGONOMETRIC FUNCTIONS
NT TANGENTS

Dual trigonometric series solution for mixed boundary value problems in two dimensional elasticity 05 p0926 A70-15979

Center fed cylindrical half wavelength dipole antenna, computing radiation pattern by trigonometric expansion approximation for current distribution 19 p3388 A70-37869

Soviet book on conjugate functions and trigonometric series covering Hilbert transform, Fourier series properties, Cesaro methods, etc 19 p3459 A70-38799

TRIGONOMETRY
Trigonometric interpolation of polynomials by Lagrangian type orthonormal functions, noting satellite geodesy applications 10 p1909 A70-24185

TRIM (BALANCE)
U AERODYNAMIC BALANCE

TRIMETHYL COMPOUNDS
Hydroxy fatty acid methyl esters gas chromatography and mass spectrometry, noting trimethylsilylation usefulness for locating double bond 02 p0252 A70-12515

TRINITROTOLUENE
Expansion isentropes of TNT/hexogen melts explosion products from measured shock wave parameters in Al, organic glass, foam polystyrene, argon and air 01 p0216 A70-11003

Expansion isentropes of TNT/hexogen melts explosion products from measures shock wave parameters in Al, organic glass, foam polystyrene, argon and air 10 p1960 A70-25008

TRINITROTRIAZOCYCLOHEXANE
U RDX

TRIODES
Input conductance variation for common-emitter triode distributed-gain wideband amplifier, deriving energy equations improving tube characteristics 08 p1472 A70-20862

Microwave pencil triodes and cavities of miniature design for Air Traffic Control Beacon Systems 10 p1852 A70-24886

TRIPHENYLS
Synthesis of alpha-dichloro-seco-A-norcholestone from diol monoacetate reaction with triphenylphosphine followed by hydrolysis and repeated chlorination 06 p1005 A70-17975

TRIPLET EXCITATION
U ATOMIC ENERGY LEVELS

TRIPLET STATE
U ATOMIC ENERGY LEVELS

TRIPROPELLANTS
U LIQUID ROCKET PROPELLANTS

TRITIUM
Daily rhythm in accumulation of rat brain catecholamines synthesized from circulating tritiated tyrosine 16 p2848 A70-33096

Tritium and Ar radioactivities attributable to galactic and solar cosmic ray interactions in Apollo 11 lunar rocks and soil 21 p3906 A70-41564

TRITONS
Average triton energy required to produce electron-hole pair in silicon measured, describing precision charge calibration of amplifier system 15 p2784 A70-32396

TRIVALENT IONS
Resonant energy transfer of trivalent Yb into trivalent Eb for optical pumping improvement for fluorophosphate glass lasing 02 p0314 A70-12725

Strontium titanates ceramics containing various trivalent rare earth ions, observing dielectric relaxation 19 p3486 A70-37755

TROCHOIDS
U PIVOTS

TROILITE
Gray hypersthene Ramsdorf chondrite with thermal and mechanical alterations, discussing shock heating, metal plus troilite melt redistribution, collision and rapid cooling effects 03 p0563 A70-13147

Iron troilite meteorites lead isotopic, Pb and U concentrations, considering fractionation and terrestrial contamination effects 07 p1388 A70-20035

Crystallography of euhedral single crystals from lunar troilite indicating hexagonal forms consistent with high temperature NiAs type structure 21 p3898 A70-41522

High crystallization temperatures for igneous rocks from Tranquillity Base indicated from late formation of sulfide liquid forming complex troilite intergrowths and iron 21 p3902 A70-41553

TROJAN ORBITS
Trojan Relay system with satellites preceding and following earth in solar orbit ensuring radio communication throughout solar system 15 p2698 A70-32061

Trojan asteroids in sun-Jupiter system, determining density near preceding Lagrangian point 17 p3171 A70-35445

Nonperiodic Transtrojan orbits for various mass parameter values in three body problem, discussing double libration 21 p3888 A70-41144

TROPICAL METEOROLOGY
Suppression balloon flight trajectories for dynamics of tropical stratosphere, revealing distinctive circulation features 02 p0228 A70-12694

Pacific ocean equatorial trough zone disturbances structure, discussing organized convective downdrafts role in rapid structural decay 06 p1101 A70-18578

F 2 layer midday ionization equatorial anomaly during summer and winter solstices, using calculated mean critical frequencies 11 p2042 A70-25533

Diurnal variation of equatorial ionospheric electron concentration from Schooner observations 11 p2043 A70-25548

Tropical storms and hurricanes critical winds forecasting accuracy by NASA Manned Spacecraft Center 14 p2606 A70-30558

Tropical circulation structure and energetics from numerical time integration of global atmospheric model with realistic orography 19 p3462 A70-38257

F 2 layer midday ionization equatorial anomaly during summer and winter solstices, using calculated mean critical frequencies 21 p3819 A70-41283

Diurnal variation of equatorial ionospheric electron concentration from schooner observations 21 p3819 A70-41298

TROPICAL REGIONS
Adrenocortical responses of military recruits to subtropical climate, making serum and urinary 17-OHCS measurements on subjects fasting, inactive and at thermoneutrality 01 p0032 A70-10359

Ionospheric F layer in equatorial, mid and high latitude regions for various major phenomena including anomalies, neutral air winds, photoelectrons, etc 01 p0073 A70-10585

Magnetic bay microstructures occurrences at low latitude not restricted to day or night hemisphere 01 p0076 A70-10668

Rocket sounding data on ionospheric currents at mid and low latitudes noting absence in D and above E region 01 p0082 A70-11529

Solar eclipse effects in equatorial F region electron density, noting data analysis method for reexamining existing measurements 02 p0290 A70-12157

Corrosion resistance of Ti-based alloys in humid subtropical climate, discussing sea and rain water effects 03 p0510 A70-13281

Jupiter observations /1966-1967/, discussing variations in size and position of polar caps and tropical belts 03 p0574 A70-13887

Uniform stratified layers in equatorial E region determined from Centaur rocket capacitance probe electron density observations, suggesting internal atmospheric gravity waves mechanism 03 p0478 A70-14222

Book on methods of geodetic astronomy for intertropical zone covering azimuth, latitude and time determination, spherical geometry and geographical coordinate reduction 04 p0677 A70-14750

Variational analysis of low latitude magnetic sounding data to determine structural differences between various earth mantle regions, noting additional observations required 04 p0682 A70-15735

Equatorial jet stream excitation of longitudinal waves, analyzing plasma beam instability and spectrum of short wave inhomogeneities by quasi-hydrodynamic equations 05 p0842 A70-16759

Atmospheric circulation in tropics using weather satellite data 06 p1095 A70-17220

Transequatorial multisite VLF records establishing solar zenith angle for midpoint of sunrise ionospheric height discontinuity, recomputing magnetic latitude dependent parameters 06 p1054 A70-17590

Solar particles penetration to lower ionospheric heights at low latitudes indicated from proton flux measurements by Explorer 33 satellite and Calcutta station 07 p1366 A70-18849

Simultaneous Thomson scatter measurements for middle and low latitudes, comparing electron density and temperature and exospheric and global temperature distributions 10 p1872 A70-23821

Intertropical convergence zone /ITCZ/ movements, analyzing data obtained by ship and ESSA satellite cloud photography 10 p1912 A70-23939

K band SLR /side-looking radar/ imagery mapping tropical lowland vegetation compared to photographic coverage 10 p1879 A70-24747

Tropical and midlatitude stratospheric dust by twilight photometry, considering possible causes of anomalous turbidity levels 11 p2046 A70-26388

Low latitude scintillations from satellite transmission scintillations correlation with solar activity spread F, electron content and ionospheric irregularities 13 p2397 A70-29189

Altitude dependence of low latitude cosmic ray diurnal variations from cosmic ray neutron data 13 p2479 A70-29792

VLF auroral and low latitude emissions along N-S chain of stations, discussing daytime and nighttime observations 13 p2371 A70-29925

Variational analysis of low latitude magnetic sounding data to determine structural differences between various earth mantle regions, noting additional observations required 14 p2575 A70-30819

Radiation fields structural characteristics of fronts, intertropical convergence zones and cyclone formations from radiation charts based on meteorological satellite observations 15 p2770 A70-32068

Equatorial atmospheric density during geomagnetic storm and quiet days by satellite observation 15 p2811 A70-32284

Humidity resistance test method involving flight simulation for airborne equipment in tropical environment 17 p3058 A70-35159

Statistical properties of subtropical jet stream maxima over U.S. from Nimbus II IR radiometry 17 p3133 A70-35931

Tropical UV nightglow, considering oxygen ion-ion neutralization reaction as primary source 18 p3244 A70-36015

Steady state nonlinear dynamics of low latitude atmospheric global boundary layer, indicating inverse relation between air flow vertical velocity and distance from equator 19 p3460 A70-37417

Temperate equatorial and auroral zones sporadic E observations and formation theories survey for prediction 19 p3416 A70-38441

Tropical UV nightglow measurement by Ogo-4 spectrometer, considering ionospheric recombination excitation mechanism 20 p3620 A70-39338

Diurnal variations and spatial distribution of total electron content in equatorial ionosphere 20 p3623 A70-40477

Equatorial F layer irregularity extent from propagation path observations to synchronous satellites 20 p3624 A70-40485

Low latitude boundary of ionospheric absorption during winter anomaly showing enhancement dependence on solar zenith angle 21 p3815 A70-40944

Lunar tidal effects on horizontal magnetic field compared at equatorial and midlatitude stations 22 p4021 A70-43279

Solar high energy particles penetration into ionospheric heights at equator, analyzing optical flare and solar proton data from ATS-1 and Explorer 34 23 p4235 A70-43816

F region night airglow in equatorial and midlatitudes, discussing red and blue emission origins 23 p4185 A70-43839

Air current in upper atmosphere meteor zone above equator, noting diurnal and semidiurnal harmonics in wind velocity components 23 p4188 A70-44049

TROPICAL STORMS NT HURRICANES

Numerical forecasting scheme for hurricane and typhoon trajectories applied to 1967 Atlantic storm data 03 p0520 A70-13162

Incipient tropical storm location and synoptic weather pattern analysis from environmental satellite system data utilization 07 p1329 A70-19196

Tropical storms and hurricanes critical winds forecasting accuracy by NASA Manned Spacecraft Center 14 p2606 A70-30558

Tropical cyclone development model for axisymmetric vortex and quasi-balanced conditions, considering vertical heat distribution, rate of intensification and energy budget 23 p4213 A70-43896

TROPICS

U TROPICAL REGIONS

TROPISM

NT AEOLOTROPISM

NT GYROTROPISM

TROPOPAUSE

Tropopause role in stratospheric-tropospheric exchange processes for radioactive debris transport 03 p0476 A70-13908

CO vertical distribution near tropopause from photochemical atmospheric model with CO recombination with OH for stratospheric sink 07 p1265 A70-19282

Temperature and gust velocity turbulence at tropopause level over hurricane Beulah by instrumented U-2 aircraft 24 p4371 A70-45422

TROPOSPHERE

Periodic cellular convection in troposphere with allowance for anisotropic turbulent mixing, showing cyclone association and intervals 01 p0135 A70-10206

Clear air layer type radar echoes intensities compared with refractive index variations in troposphere 01 p0043 A70-10331

Hydrodynamic explanation of upper atmosphere perturbation effects on tropospheric circulation, discussing experiments for solar activity effects on atmospheric dynamics 01 p0073 A70-10582

Tropospheric parameters determination using combinations of measurement and transhorizon radio signals propagation techniques 01 p0044 A70-11086

Vertical ion concentration profile in troposphere and stratosphere from ozone distribution satellite measurements using aeronomical reactions 02 p0291 A70-12389

Troposphere microwave transmission factor determined from dispersion and attenuation caused by water vapor isolated molecular resonance 02 p0261 A70-12593

Stratospheric air intrusion into troposphere calculated for speed and frequency of occurrence, considering mass and energy transfer 02 p0329 A70-12690

Troposphere effects on low incident Explorer 22 satellite signal amplitude, noting role of diffraction 03 p0449 A70-13611

Tropospheric fine structure influence on radio wave propagation, including atmospheric gases and precipitation effects and radar, navigation and TV applications 03 p0449 A70-13612

Tropospheric circulation transformation from meridional to zonal forms due to macrostructure activity of solar wind, considering magnetosphere perturbations 03 p0559 A70-13757

Tropospheric periodic responses to chromospheric flares, analyzing stations atmospheric pressure power spectra 04 p0742 A70-15524

Omega equation interpretation showing vertical motion related to advection of vorticity in upper troposphere and to warm advection in lower troposphere 05 p0838 A70-16154

Radiometeorology research emphasizing interaction between troposphere and VHF waves to improve space and terrestrial radio communication 07 p1234 A70-19216

Radio signal reception beyond normal horizon by partial reflection from elevated layer in troposphere calculated by computer 07 p1234 A70-19218

Tropospheric and stratospheric turbulent horizontal heat and momentum transfer spectral density profiles calculations from radio launchings data 07 p1269 A70-19646

Prognostic maps of geopotential and wind in middle troposphere derived from hydrodynamic equations 07 p1330 A70-20307

Seasonal variation of vertical profiles of atmospheric radioactivity concentration between stratosphere and troposphere due to meridional zonal wind distribution caused by eddy diffusion 08 p1539 A70-21923

Troposphere-stratosphere kinetic energy transfer during 1967-1968 midwinter warming, comparing calculation by pressure interaction term with direct calculation of vertical velocity fields 08 p1540 A70-21969

Tropospheric elevated layers fine structure characteristics by balloon-borne spaced cavity refractometer 09 p1714 A70-22353

Dew-point temperature of lower troposphere by diffusion equation, noting use for fog and strati forecasting 09 p1717 A70-22655

Classical model regarding general tropospheric circulation, exploring momentum, heat and moisture exchange 09 p1718 A70-23050

Tropospheric electrical path length estimated by microwave radiometry using atmospheric models 09 p1640 A70-23806

Downward ozone transport from troposphere to atmospheric boundary layer by turbulent diffusion calculated by model, estimating annihilation rate 10 p1875 A70-24486

Maximum wind velocity regions in tropospheric jet streams under synoptic conditions concerning troughs, ridge sections and cyclonic-anticyclonic curvatures 11 p2075 A70-25919

Digital computer simulation of Bake concept as related to tropospheric CW signal scatter measurement 11 p2009 A70-26240

Tropospheric negative small ions formation reaction scheme, considering hydration degree 11 p2046 A70-26390

Vertical and intensity distributions of wind velocity focuses in tropospheric jet streams 13 p2444 A70-28590

Balloon-borne measurement of troposphere refractive index vertical distribution using spaced-cavity refractometer 13 p2394 A70-28789

Vertical tropospheric turbidity distribution determination from intensity measurements of inclined searchlight beams 13 p2445 A70-29471

Monograph on troposphere pressure, temperature and humidity and satellite TV photographs interpretation 13 p2446 A70-29786

Atmospheric dust natural radioactivity effect on tropospheric Pb 210 mean residence time determination for Pb210 and Ra226 fallout in rain near Moscow 14 p2630 A70-30131

Troposphere-stratosphere kinetic energy transfer /1964-1968/, annual variations and vertical flux correlation to circulation pattern 15 p2722 A70-31441

Field amplitude distribution parameter in long distance tropospheric communications based on fading depth 15 p2696 A70-31512

Troposphere and lower stratosphere trace element concentration measurements, establishing origin, history and movement of various air masses 15 p2728 A70-31996

Upper troposphere pressure variations through 20 km separation layer, noting interdiurnal temperature changes 15 p2772 A70-32458

Tropospheric turbidity detection and measurements by lidar, considering performance limitations and thickness resolution vs range curve 16 p2862 A70-33015

Decimeter waves propagation along overland path, considering tropospheric radio relay systems development 16 p2863 A70-33238

Tropospheric inhomogeneities properties and wind conditions in relation to lunar limb image deformations 16 p2979 A70-34178

Satellite-borne instruments for thermal sounding of troposphere, noting information limitation due to atmospheric effects 17 p1312 A70-35338

Long range tropospheric radio wave propagation, calculating signal impulse function and time lag between diffraction and reflection 17 p3048 A70-35678

Long wave radiation fluxes calculation in troposphere based on principal radiant heat transfer components separation 18 p3285 A70-36632

Soviet papers on relations between earth troposphere phenomena and solar activity covering geomagnetic and stratosphere perturbations, warmings and circulation, solar cycles, etc 20 p3618 A70-39181

Synoptic processes in Arctic tropospheric and lower stratospheric warming correlated with atmospheric circulation transformations 20 p3619 A70-39186

Synoptic processes in troposphere and stratosphere with large air temperature anomalies during early summer in U.S.S.R. 20 p3663 A70-39272

Troposphere and lower stratosphere circulation during natural synoptic autumn seasons in Northern Hemisphere, noting temperature role 20 p3663 A70-39273

Midtropospheric frontogenesis, using three hourly rawinsonde data for isentropic trajectories to describe velocity field in space and time 20 p3664 A70-39374

Aeolus A satellite for position fixing and automatic meteorological signal transmission in link with balloons for tropospheric observation 22 p4068 A70-42665

Two dimensional stratified flow over extended obstacles with source disturbances, indicating topographical effect on vertical wind shear in troposphere 23 p4214 A70-44031

Multiplicative noise reduction during transmission of analog signals over tropospheric microwave relay links 23 p4162 A70-44090

Ionospheric electron content measurement from Faraday effect of troposphere on beacon satellite Explorer 22 radio signals 23 p4163 A70-44231

Statistical interpolation for numerical analysis of middle troposphere AT potential based on geopotential and wind observations 24 p4371 A70-45135

VHF and UHF radio field strength changes due to tropospheric reflecting layers disintegration during anticyclonic weather, using ray tracing technique 24 p4315 A70-46153

TROPOSPHERIC RADIATION

Short wave radiation model of single layer stratus and stratocumulus cloud based on actinometric soundings of lower troposphere 08 p1537 A70-21104

Vertical short wave albedo profiles in lower troposphere under cloudiness and clear sky using actinometric sounding 08 p1537 A70-21105

TROPOSPHERIC SCATTERING

Doppler spectrum and radio troposcatter beam swinging in thin homogeneous turbulent scatter layer as function of height, crosswind speed and refractivity 02 p0326 A70-12288

Specular reflections influence on bistatic tropospheric radio scatter from turbulent perturbations in refractivity 02 p0326 A70-12289

Crosspath wind motion measurement by dual arm noncoherent bistatic radio troposcatter link 02 p0326 A70-12290

Tropospheric scattering ability investigation with radar transmitter emitting vertical pulses, considering implications for scatter propagation from backscattering detection 03 p0453 A70-14298

Optimal design of tropospheric scatter radio link between two localities, investigating power, antenna, diversity, frequency deviation and equipment 05 p0814 A70-16361

Microwave propagation along earth-air path, studying tropospheric layer role 08 p1461 A70-20968

Tropospheric refractive index homogeneity from beam-swinging experiments, noting relationship to meteorological parameters and height 09 p1715 A70-22363

High resolution FM-CW radar sounder for tropospheric refractive index studies, describing equipment design and performance and clear air scatter observations 09 p1716 A70-22368

Acoustic energy backscattered from vertically directed beam of sound by lower troposphere density structure inhomogeneities 12 p2262 A70-26953

Troposphere effects on microwave and optical signals, correlating refractive index and dispersion variabilities 16 p2862 A70-33020

TROPOSPHERIC WAVES

F 2 region acoustic waves over Kansas and Nebraska attributed to local storms in troposphere 02 p0290 A70-12158

Wave disturbances in tropical lower troposphere, discussing cross spectrum analysis of wind, temperature, relative humidity and surface pressure 07 p1275 A70-20304

Linear nonstationary quasi-geostrophic model with external and internal heating and forcing for dynamics of ultralong waves in troposphere and lower stratosphere 09 p1713 A70-22304

- Field strength correlation with micropressure variations caused by internal gravity waves propagating in lower troposphere 10 p1883 A70-25252
- Earth profile influence on two dimensional non-linear lee waves in troposphere, discussing Helmholtz perturbation equation and stream function field 11 p2075 A70-25391
- Lee wave flow disturbances due to mountains by midtroposphere balloon and aircraft observation, noting flow features nonstationarity 12 p2262 A70-26883
- Mesoscale waves in jet stream flow within Coriolis force over rotating earth by amplitude functions and phase velocities asymptotic series representation 12 p2265 A70-28334
- TROUBLESHOOTING**
- U MAINTENANCE
- TRUNCATION [MATHEMATICS]**
- U APPROXIMATION
- TRUNCATION ERRORS**
- Carbon ground state correlation energy calculation, emphasizing assessment of truncation error sources 16 p2954 A70-33277
- TRUNKS [LINES]**
- U TRANSMISSION LINES
- TRUNNIONS**
- U SHAFTS [MACHINE ELEMENTS]
- TRUSSES**
- Mathematical model for local postbuckling strength of flat truss core sandwich panels loaded in compression, considering application to Ti structures 02 p0386 A70-11948
- Forced vibrations of trusses calculated by dynamic rigidities method allowing for friction forces 09 p1773 A70-22540
- Truss vibrations calculations by method of dynamic rigidities, describing numerical methods for solving frequency equation to save computer storage capacity 09 p1773 A70-22546
- Optimal trusses design, considering minimal volume /weight/ and elastoplastic stability in compressed and stretched bars 10 p1958 A70-24514
- Natural vibrations of truss systems of four circular cylinders hinged along walls, using linear group representation 11 p2132 A70-25605
- Slope deflection method for computing spatial trusses and plane frameworks under dynamic aperiodic forces 13 p2516 A70-29532
- TRYPTAMINES**
- Gamma-aminobutyric acid influence on 5- hydroxytryptamine in rat brain after intraperitoneal administration 01 p0019 A70-10510
- Oxygen tension and pressure effects on hyperbaric oxygenation induced depletion of brain norepinephrine and 5-hydroxytryptamine in mice 02 p0235 A70-11992
- TRYPTOPHAN**
- Growth rate effect on glucose utilization rate using sporogenic strain of *Bacillus subtilis* during N and L-tryptophan limitation 01 p0021 A70-10790
- Dibutylryl cyclic adenosine monophosphate stimulation of melatonin and serotonin synthesis from C-14 labeled tryptophan by rat pineals in organ culture 01 p0022 A70-10824
- TU-134 AIRCRAFT**
- TU-134 aircraft accessories assembly using fitting and aligning holes drilled into joined elements 05 p0857 A70-17019
- Soviet book on aerodynamics of Tu 134 aircraft, covering 30 turbojet engines, flight characteristics, etc 13 p2344 A70-28875
- TUBE CATHODES**
- NT COLD CATHODE TUBES
- NT HOT CATHODES
- NT PHOTOCATHODES
- NT PHOTOMULTIPLIER TUBES
- NT THERMIONIC CATHODES
- NT TUNNEL CATHODES
- Boltzmann temperature measurement apparatus of oxide coated cathodes in scanning beam tubes 09 p1656 A70-22987
- SERT 2 mercury vapor fed hollow cathode operated in bell jar, determining volt-ampere characteristics and flow rates for plasma diagnostics [AIAA PAPER 69-258] 13 p2473 A70-28515
- Low voltage slotted hollow cathode laser tube design with transverse discharge operation and uniform axial distribution of laser media, including metal vapors 21 p3834 A70-40571
- Hollow cathode shape effect on glow discharge parameters and potential jump in cathode region, investigating I-V curves 22 p4078 A70-42357
- TUBE GRIDS**
- Metal grid capacitive memory for INTIC and direct view storage tubes, describing image contrast control 16 p2880 A70-34270
- Grid system with alternating filament potentials, deriving potential distribution for fields and electro-optical effect 21 p3835 A70-40632
- TUBE HEAT EXCHANGERS**
- Finned tube radiators with constant longitudinal specific heat flow, determining thermal efficiency and optimal thermal and structural parameters 06 p1184 A70-18556
- Multiple pass tube heat exchangers efficiency, solving energy and heat transfer equations from fluids homogeneity and constant thermal capacity considerations 08 p1596 A70-20613
- Thermal design of counter current cryogenic heat exchangers employing spiral finned tubing 14 p2617 A70-31018
- Counter current heat exchanger with spiral finned tubing and solid core 14 p2617 A70-31019
- Tube heat transfer augmentation by helical vane inserts, noting Reynolds number and mass flow rate effects 21 p3949 A70-41318
- Optimum low temperature two circuit vortex refrigerator using compressed air precooled in heat exchanger 22 p3965 A70-42808
- Tube heat exchangers operation at low transfer coefficient, calculating unsteady temperature field in wall and heat transfer agent 22 p4125 A70-43364
- TUBES**
- Structural efficiency of composite tube columns with zero axial coefficient of thermal expansion, discussing three dimensional and planar fiber arrays 01 p0126 A70-10120
- Plane deformation of plastic thin walled tubes under complex tensile and torsional load 05 p0935 A70-16233
- Torsional vibrations of four cell tube, deriving cross sectional constants and natural frequencies 05 p0936 A70-16321
- Steel tube deformation under constant internal pressure and cyclic heating, plotting tangential and axial strain curves as function of cyclic loading 06 p1163 A70-17399
- Stress field equations of material in maximum deformation region during inversion of tubular products 06 p1077 A70-17871
- Thermomolecular pressure corrections in tubes and at orifices for errors in gaseous pressure measurements by temperature gradients 06 p1113 A70-18371
- Polymeric materials flow at tube entrance, discussing pressure drop and flow birefringent patterns at tapered and sharp entrances 08 p1486 A70-21861
- Temperature and stress fields in rotating thin tube exposed to stationary heat source with constant strength, considering materials 09 p1774 A70-22579
- Tensile prestrain effect on yield locus of thin walled Al tubes from stress tests in torsion- tension space 13 p2431 A70-28536
- Coaxial fluid streams mixing within finite length tube based on dimensional analysis of aerodynamic noise generation, discussing subsonic and supersonic flows within ejector 13 p2474 A70-29080
- Missile tube liner design with cast polyurethane elastomers, discussing effect of polymer composition and processing on physical properties 13 p2439 A70-29257
- Laminar velocity distribution from temperature profiles developed under steady flow through tube, constructing numerical temperature grid 15 p2718 A70-31449
- Nonlinear two dimensional free boundary problem of axisymmetric heat conduction in tubes with internal surface solidification by variational technique 16 p2996 A70-33002
- Closed storage extendible boom /Multiple Applications Storable Tube/ design, fabrication and applications, including stress factors and materials 16 p2846 A70-34142
- High speed ground tube vehicle transportation system aerodynamics, presenting drag coefficients and static wall pressure measurements 16 p2839 A70-34264
- Wave-periodic acceleration feedback during vibrational flame propagation in tubes, testing carbon monoxide-air mixture 17 p3196 A70-35350
- Structural stability in tension and strength tests of thin walled tubes at various stress and strain intensities, noting dependence on stress- strain state type 17 p3192 A70-35713
- Composite compression tubes for VTOL aircraft components, describing weight parameters and mechanical properties [AIAA PAPER 70-898] 17 p3193 A70-35809
- Plane cross section hypothesis applied to fully developed creep in thin walled tube subjected to internal pressure and bending moments, calculating stress concentration 18 p3340 A70-36571
- TUBING**
- U PIPES [TUBES]
- TUMORS**
- NT CANCER
- Local gamma irradiation effect on number of chromosome aberrations in lymphocytes of human blood of oncological patients after hysterectomy 01 p0013 A70-10137
- Ionol concentration variations in oncological patients blood, using liquid gas chromatography to determine removal by urine and feces 07 p1209 A70-19519
- Oxygen enhancement ratio and relative biological effectiveness of accelerated helium nuclei on mouse tumor cells, discussing applicability in radiation therapy 09 p1617 A70-22336
- Combined ultrasonic and ionizing radiation effects on electrophoretic mobility of tumor cells from albino mice 17 p3034 A70-35762
- TUNERS**
- NT WAVEGUIDE TUNERS
- TUNGSTATES**
- NT CALCIUM TUNGSTATES
- NT ZINC TUNGSTATES
- TUNGSTEN**
- X ray topography of postannealing substructure of neutron irradiated W and Mo single crystals, indicating increase in disorientation 01 p0115 A70-10065
- Temperature effect on work function minimum of cesiated W surfaces 01 p0154 A70-10108
- Tungsten metal oxidation retardation by W-F bonds 02 p0249 A70-11651
- Tensile strength of flat specimens of Ni reinforced by W wire gauze 02 p0315 A70-11661
- Thermionic emission characteristics of W and Mo subjected to focused CW carbon dioxide laser radiation, discussing direct energy conversion 02 p0312 A70-12068
- Epitaxial growth of Cu vapor deposited on W single crystal /110/ surface using low energy diffraction, Auger electron and work function techniques 03 p0538 A70-13100
- Mechanical properties, optimum deformation and rupture of W wire reinforced Ni and Ti metal composites obtained by hot rolling in vacuum 03 p0508 A70-13245
- Energy accommodation coefficients for He3-W and He4-W, comparing results with classical gas-solid interaction theory 04 p0721 A70-14388
- Ceramic fibers formation by particles mechanical deformation by extrusion in W matrix, describing grain structure of various extruded metal oxides 04 p0699 A70-15643
- Work function measurement for adsorption of diatomic I, Br and Cl on W crystal using electron beam retarding potential method 05 p0891 A70-15973
- Electron work function variation of W in Ba-Cs- Sr vapor combinations determined using thermionic diode 05 p0891 A70-15974
- Quasi-equilibrium treatment of heterogeneous reactions applied to flash desorption data for oxygen reaction with tungsten surface, discussing species desorption dependence on adsorption temperature 06 p1004 A70-17331
- Nitrous oxide molecular beam reflection and dissociation on tungsten surface at high temperatures from angular distribution measurements 06 p1004 A70-17493
- High energy Ar atomic beams scattering from single crystal face of W measured for distribution pattern 06 p1112 A70-18270
- Tungsten and tungsten base alloy weldability, discussing powder metallurgy, postweld annealing, high temperature tensile strength, etc 06 p1078 A70-18514
- W oxidation kinetics as function of ribbon temperature and absorption time using flash technique with sweep pulse mass spectrometer 07 p1306 A70-19275
- High temperature creep rupture tests of arc cast and powder metallurgy wrought unalloyed W sheets 07 p1313 A70-19884
- Neutron irradiation damage in W, observing consistency of activation energy for self diffusion with vacancy mechanism 07 p1314 A70-20012
- Chromium films obtained on tungsten by sputtering, studying structure and work function at various temperatures 08 p1516 A70-21123

TUNGSTEN ALLOYS

Anisotropic angular distribution of electrons and ions emitted from W targets irradiated by ruby laser pulses

08 p1512 A70-21211

Microstrain characteristics of continuously reinforced W-Cu composites as function of volume fraction of fibers and prestrain, discussing dislocation friction stress

08 p1524 A70-21917

Microstructure of wrought arc-cast polycrystalline W sheet after high temperature creep deformation at various stress levels

08 p1525 A70-21962

Tungsten emissivity and radiance properties obtained at high surface temperatures

09 p1725 A70-22068

Thermochemical predictions for high temperature oxidation of Mo and W, discussing oxide films or scales, reactant gases flow rate, etc

09 p1630 A70-22943

Tungsten-rhenium thermocouple for high temperature measurement of samples under unsteady heating processes, analyzing instrument error sources

09 p1789 A70-23108

Exploding tungsten wires in air and vacuum, describing visible and X-ray spectrum characteristics

10 p1915 A70-23994

Oxygen sticking coefficients and desorption kinetics on tungsten crystal by step desorption/ reflection technique, postulating formation and decomposition of surface oxide phases

10 p1832 A70-25147

Helium ion bombardment activated tungsten crystal surface migration using field emission microscopy

11 p2097 A70-25378

Porosity and intergranular crack formation in tungsten fusion welds using electron fractography

11 p2059 A70-25666

Field ionization from hydrogen layers adsorbed at 4.2 K on W emitters in sealed-off tubes

12 p2274 A70-26858

Oxygen adsorption on W(110) surface determined for coverage as function of exposure by Auger electron spectroscopy

12 p2180 A70-27253

Tungsten crystalline structure defects caused by alpha particles bombardment using helium ion projector at 78 K

12 p2255 A70-27544

Tungsten strip lamps spectral radiance calibration, discussing accuracy requirements for radiation constants, wavelength and black body temperature

13 p2410 A70-29655

Metal fiber multiple necking effect on uniaxial metal matrix composites ductility and plastic deformation behavior for brass-W model system

15 p2761 A70-32378

Peak emission currents from tungsten under ruby laser focused radiation, describing integral emission by heat conduction theory and Richardson equation

15 p2754 A70-32875

Heat transfer in tungsten-tungsten and Armco Iron-Armco Iron specimens, confirming Bowden-Tabor model of elastoplastic events during cyclic engagement of surfaces

[ALAA PAPER 70-853]

16 p3000 A70-33920

Tungsten filled urethane in aircraft areas as balancing agent

17 p3126 A70-35418

Tungsten exploding wires electron emission during vacuum melting

17 p3137 A70-35726

Electron impact desorption kinetics of ions and neutrals from polycrystalline W surfaces, using cylindrical magnetic spectrometer

18 p3225 A70-36321

Tungsten fiber reinforced copper based composite material, investigating moulding and sintering conditions effect on mechanical properties

19 p3450 A70-37454

Critique of paper on electron diffraction study of Ce adsorption on W surface, discussing electron work function changes and data discrepancies

19 p3473 A70-37548

Cesium films structure and work function on W (011) face, discussing order-disorder transition

19 p3487 A70-37817

Nitrogen diffusion coefficient in Mo and W using degassing method

19 p3452 A70-37828

Tensile strength of flat specimens of Ni reinforced by W wire gauze

19 p3452 A70-38435

Mechanical properties, optimum deformation and rupture of W wire reinforced Ni and Ti metal composites obtained by hot rolling in vacuum

19 p3453 A70-38463

Tungsten wire reinforced copper matrix composite, determining fibers pull-out contribution to fracture work

20 p3651 A70-40047

Dislocation network recovery kinetics of cold worked undoped powder metallurgical W wires by

electrical resistivity measurements, determining activation energy

21 p3839 A70-40797

Hydrogen adsorption and coadsorption with oxygen on W single crystal surface measured by mass spectroscopy and low energy electron diffraction method

21 p3862 A70-41887

Tungsten adatoms migration and binding energies on W surfaces, taking relaxation effects into account

21 p3862 A70-41888

Direct electrical heating for high temperature thermal conductivity measurements of pure W, giving results for graphite

21 p3850 A70-42057

Orientation and applied stress effects on pure Nb-6W bcc single crystals yield stress, discussing thermal activation strengthening and crystal dislocations

22 p4052 A70-42318

Intergranular brittleness in powder metallurgy W by Auger Electron Emission Spectroscopy for fracture surfaces chemical analysis

22 p4053 A70-42733

Gas porosity in fusion welds of chemical vapor deposited W, noting formation of microfissures due to pore linkup

22 p4046 A70-43149

Room temperature oxygen adsorption on tungsten surfaces

22 p4087 A70-43235

Thin metal matrix composite rods elastic properties, examining Al-W system by Young and shear modulus measurements

22 p4061 A70-43687

Surface potential and electron work function of single crystal plane W(110) under zero-field and strong-field conditions

23 p4230 A70-44797

Corona discharges from fine W points in liquid He initiated by field ionization or emission, noting anomalous characteristics

23 p4221 A70-44889

Al and W specific heat and Al heat of fusion by quasi-adiabatic calorimetry, estimating anharmonic lattice vibrations role via atomic thermodynamic analysis

23 p4208 A70-44931

Impurities and heat treatment effects on W internal friction at high temperatures, considering relaxation processes, recrystallization and microstructure

24 p4357 A70-45227

Gas bubbles effect on recovery and recrystallization in W sheet deposited from tungsten fluoride vapor

24 p4358 A70-45243

TUNGSTEN ALLOYS

Tungsten effect on phase transformations and carbide reactions to attain equilibrium at 850 C in Ni-base superalloys

01 p0118 A70-10727

Internal nitriding kinetics of W-base alloys containing Hf, investigating morphology of resulting Hf nitride dispersion

02 p0317 A70-12319

Mo separation from W during chemical processing of W in binary Mo-W alloys, using organic reagents for precipitation and extraction

03 p0504 A70-12982

Refractory metals in rocket propulsion devices, applying tungsten in uncooled rocket nozzles and tungsten and rhenium to electrothermal propulsion

03 p0512 A70-13617

Tungsten and tungsten base alloy weldability, discussing powder metallurgy, postweld annealing, high temperature tensile strength, etc

06 p1078 A70-18514

Precision tungsten alloy tubing manufacture and properties, discussing direct conversion of metal powder to finished tubing with high temperature structural stability

07 p1292 A70-18928

Thermal diffusivity measurements for Ta-W, Ta-W-Hf, Hf-Ta-Mo alloys using pulse technique

07 p1305 A70-18960

Cobalt effects on Ni-W alloys mechanical and metallurgical properties including thermal stability, fabrication response, weldability and impact resistance

07 p1306 A70-19070

Specific radiant heat flow and spectral blackness degree of tungsten with different surface finish

07 p1309 A70-19662

Carbide layer formation on Ta and Ta-W alloys, discussing Ta-C phase diagram and phases

07 p1320 A70-19892

Tungsten alloy fiber reinforced Ni-base superalloy composites evaluated for high temperature turbojet engine applications, considering stress-rupture strength, oxidation and impact resistance

08 p1523 A70-21907

Polycrystalline W-Re alloy creep tests in tension, investigating dislocation substructure formation as function of stress, temperature and strain

12 p2255 A70-27606

Single crystal W and W alloys dislocation structures as function of strain, temperature and dilute alloys addition, using electron microscopy

15 p2756 A70-31563

W-3 percent Re-W-25 percent Re thermocouple reliability and stability, describing emf vs temperature table in 0-2400 C range

18 p3257 A70-36200

Electronegative adsorbate effect on work function of Ba-W system

18 p3298 A70-37111

W-Mo-Nb-Ta system structure and properties at room and high temperature by microstructural analysis and hardness measurements, discussing Mo addition effects

19 p3453 A70-38713

W-Mo-Nb-Ta system with constant 30 percent W, discussing specific weight and hardness

19 p3453 A70-38714

TUNGSTEN CARBIDES

WC-Co alloys noting polishing and grinding effects on residual stress and crack resistance

03 p0508 A70-13145

Plastic properties of tungsten carbide single crystals at room temperature, determining slip system crystallographic orientations

08 p1520 A70-21557

Residual stresses effect on strength and hardness of tungsten carbide-cobalt alloy by application of small plastic deformations, observing crack formation anisotropy

10 p1904 A70-25168

Fuel cell electrolytes, describing porous tungsten carbide as catalyst

12 p2164 A70-27068

WC as densification aid for NbC-C composites, examining fabrication temperature, mechanical properties, solid solution composition, etc

15 p2757 A70-31797

Fatigue properties of solution treated and age hardened hot rolled Ti alloy bars, discussing sprayed tungsten carbide coatings effects on bearing properties

17 p3121 A70-34432

Carburizing spherical powders of Nb, Mo and W to obtain carbides, noting agreement between theoretical and experimental data

17 p3125 A70-35410

Carburization and grain size of tungsten carbide powder from W powder as function of temperature, using optical and electron micrographs

21 p3839 A70-41412

WC radiation damage by resonant absorption following Coulomb excitation observed from gamma ray spectra

23 p4231 A70-44888

TUNGSTEN COMPOUNDS

NT CALCIUM TUNGSTATES

NT TUNGSTEN CARBIDES

NT TUNGSTEN OXIDES

NT ZINC TUNGSTATES

TUNGSTEN INERT GAS WELDING

U GAS TUNGSTEN ARC WELDING

TUNGSTEN OXIDES

Photographs of ferroelectric tungsten oxide crystal domains obtained with photoemission microscope, noting memory effect after electron beam sweeping

11 p2099 A70-26463

TUNGSK METEORITE

Tungusk meteorite as comet nucleus, discussing comet structure, composition and behavior analysis

08 p1572 A70-20943

Tungusk meteorite atmospheric shock waves obtained from simulation experiments based on forest damage

08 p1572 A70-20944

Night time upper atmosphere light phenomena and Tungusk meteorite observed on 30 June 1908

10 p1876 A70-24499

Tungusk meteorite as comet nucleus, discussing comet structure, composition and behavior analysis

15 p2806 A70-32755

Tungusk meteorite atmospheric shock waves obtained from simulation experiments based on forest damage

15 p2806 A70-32756

TUNING

Tracking method for simultaneously tuned transmitter and receiver with different maximum-to-minimum capacitance ratios in ganged variable capacitors

01 p0051 A70-10888

Angular dependence of one dimensional first and second index matching for optical parametric mixing of laser and SRS Stokes beams for tunable laser source

03 p0498 A70-13157

Tunable optical parametric oscillators including Gaussian beams amplification, threshold, tuning techniques, spectral output, etc

05 p0822 A70-16651

Flash lamp pumped tunable organic dye laser, using capacitor bank for reliable operation

05 p0861 A70-16845

Tuning range slope steepness as criterion for evaluating microwave resonators tuning range 05 p0824 A70-16893

Multiple maser-magnet units packaging in single cryostat for maximum tunability 08 p1513 A70-21599

Ferrimagnetically tunable transistor oscillator in common collector configuration 09 p1645 A70-22603

Static error of varactor-controlled tuning-locked discriminator using computer 09 p1638 A70-23323

KDP crystal single cut for laser beam frequency conversion and tuning 12 p2245 A70-27302

Electronic tuning range of solid state microwave oscillators, deriving equations in terms of tuning device Q factor and available power output 13 p2376 A70-28802

Tunable and fixed frequency high power magnetrons parallel operation to achieve stable output 13 p2379 A70-29667

Reflex klystrons operation, efficiency and electronic tuning range, discussing resonators, tuners, voltage and retarding field oscillators, etc 14 p2548 A70-30428

Coaxial, inside-out and rising-sun magnetrons for millimeter waves generation under pulsed conditions, discussing tunability, frequency stability and weight 14 p2555 A70-30429

Mode controlled Q switched tuneable ruby laser, obtaining frequency scanning by temperature and pressure control 15 p2752 A70-32048

Organic dye lasers output bandwidth and tunability extension by acidification of solution 19 p3445 A70-37675

Mutual synchronization of oscillators at multiple frequencies, analyzing effect of tuning on frequency and phase 20 p3597 A70-39252

Smooth periodic wavelength retuning in organic dye laser, using neodymium glass laser with YAG for pumping 20 p3642 A70-39742

Accurate tuning methods for laser mode locking device, using diffracted light measurement and photodiode with LF spectrum analyzer 21 p3838 A70-42047

Antennas with controlled current distribution in medium wavelength range for optimal radiation pattern over desired area, discussing maximum gain tuning for daytime and nighttime operation 22 p3995 A70-42521

Two stage gas turbine engine optimal tuning for RPM, thrust, fuel rate and gas temperature, describing automated bench tests 22 p4092 A70-43361

Automatic resonance tuning of transmitting and receiving antennas by electronic control for use in mobile communications 23 p4172 A70-44385

TUNING FORK GYROSCOPES
Increasing sensitivity of tuning fork gyroscope by parametric signal amplification 07 p1289 A70-20297

TUNNEL CATHODES
Microscopic behavior and excitational processes found similar in argon ion lasers with hollow cathode or conventional heated oxide cathode discharge 11 p2063 A70-26370

TUNNEL DIODES
Wideband parametric and tunnel diode amplifiers synthesizing method for obtaining maximum flat amplitude frequency response 03 p0457 A70-13727

Tunnel diode studied for oscillations initiation resulting in hysteresis involving supply voltage and load conductance variations 03 p0459 A70-14284

GaAs tunnel diodes excess current nature and voltage dependence, considering thermal current measurements, depletion layer processes, electron barrier height, etc 04 p0656 A70-14713

Parasitic elements influence on stability of linear equivalent circuits with tunnel diodes 06 p1022 A70-17674

Analytical expressions for amplitude and frequency modulation characteristics of bias modulated tunnel diode oscillator on steady state mode 06 p1022 A70-17836

Equivalent scheme for tunnel diode oscillator operating mode and parameters effect on LF modulating signal phase correlations 07 p1241 A70-19287

Pulse duration approximation in tunnel diode monostable multivibrator during low duty cycle operation 08 p1472 A70-20867

Tunnel diode parametric phase locked oscillators as memory elements, considering optimum subharmonic pumping frequencies determination 08 p1477 A70-21642

Spectral criteria for approximating tunnel diode nonlinear characteristics obtained by minimizing deviations of moduli of harmonic amplitudes 09 p1649 A70-23340

Traveling wave amplifier on section of inhomogeneous transmission line with tunnel diodes 11 p2020 A70-26808

Miniature electromechanical gallium antimonide tunnel diode transducer theory fabrication and performance 12 p2236 A70-28055

High frequency tunnel diode quartz crystal oscillator circuits with inductive element compensating circuit capacitor 13 p2376 A70-28874

Self excited cavity oscillators with tunnel and parametric diodes and nonequilibrium medium, noting single and multimodes, energy capabilities and frequency interactions 13 p2366 A70-29405

Microwave backward tunnel diodes in InAs, predicting reliability and sensitivity improvements over other materials 13 p2379 A70-29593

Millimeter waves generation by tunnel, Gunn and avalanche diodes, tabulating frequency, efficiency and power data 14 p2548 A70-30435

Lossless pulse-shaping active line for unipolar transmission, considering construction by loading two terminal Esaki diode to coaxial cable 15 p2697 A70-31827

Integrated tunnel diode amplifiers design using hybrid technique for communications satellites, noting stability and noise performance 15 p2710 A70-32469

Terminal negative resistance of X band Gunn diodes, discussing frequency conditions for modulation and parametric amplification 16 p2877 A70-33417

Wideband microwave IC tunnel diode amplifier /TDA/ for artificial satellites, discussing noise, size and weight reduction 17 p3053 A70-35277

Pulse shaper circuits with tunnel diodes and transistors, describing recovery time decrease 20 p3596 A70-38972

Semiconductor diodes, discussing characteristics and applications of Schottky barrier, varactor, tunnel, Gunn and field effect diodes, etc 20 p3600 A70-40500

Tunnel diode microwave oscillator design, discussing fixed frequency or varactor tuned operation, power instabilities and load variations 22 p3997 A70-43129

Tunnel diode amplifier design, using gain-bandwidth nomograph 22 p3999 A70-43487

Tunneling electron and local mode phonon interaction in MIS n-type semiconductors 23 p4231 A70-44916

High cutoff negative resistance silicon carbide diodes, noting temperature independent current-voltage curve 23 p4176 A70-45067

Traveling wave amplifier on section of inhomogeneous transmission line with tunnel diodes 24 p4317 A70-45180

TUNNEL RESISTORS

U ELECTRON TUNNELING

U RESISTORS

TUNNELS

Forward air cushion performance of tracked hovercraft entering tunnel, determining arrival of reflected expansion wave at vehicle front 02 p0226 A70-12313

Test facilities and procedures for obtaining aerodynamic data required for studying vehicle-in-tube transportation systems [AIAA PAPER 70-225] 06 p1030 A70-18221

Ram wing tube ground transportation vehicle, analyzing optimum lift-drag ratio and induced power requirements 11 p1975 A70-25966

TUPOLEV AIRCRAFT

NT TU-134 AIRCRAFT

TUPOLEV TU-134 AIRCRAFT

U TU-134 AIRCRAFT

TURBIDITY

Illuminating conditions in deep layers of turbid plane-parallel medium for highly elongated scattering characteristic 04 p0745 A70-14497

Atmospheric turbidity measurements over U.S. using Volz sunphotometer 06 p1098 A70-18245

Tropical and midlatitude stratospheric dust by twilight photometry, considering possible causes of anomalous turbidity levels 11 p2046 A70-26388

Vertical tropospheric turbidity distribution determination from intensity measurements of inclined scintillation beams 13 p2445 A70-29471

Circumsolar sky radiation effect on pyrheliometric measurements, considering atmospheric scattering and turbidity 13 p2400 A70-29660

Tropospheric turbidity detection and measurements by lidar, considering performance limitations and thickness resolution vs range curve 16 p2862 A70-33015

Unsteady light field spatial moments in turbid medium boundary layer with intense anisotropic scattering during illumination by narrow beam 18 p3285 A70-36631

Solar constant measurements by high altitude balloon sounding, noting anomalous turbidity in upper atmospheric layers due to nuclear explosions and volcanic eruptions 20 p3703 A70-39375

Anomalous seasonal variation in worldwide ozone above 40 km from Umkehr measurement, considering turbidity effects 23 p4187 A70-44037

TURBINE BLADES

Loads effects on refractory alloy fatigue strength and life at high temperatures, describing aircraft turbine blade tests 01 p0115 A70-10069

Axial flow turbine stator and impeller blade twist calculated from gas flow stage area diameter using continuity and vorticity equations 01 p0001 A70-10175

Airfoil cascade blade design by iteration method equating normal velocity distribution about contour with imposed tangential velocity 01 p0001 A70-10263

Heat transfer coefficients in transpiration cooled gas turbine blades, using two dimensional theory covering porous wall and internal cooling passages 01 p0166 A70-11392

Electronic gauging machine for multipoint measurement at preselected points around turbine blade airfoil produced by electrochemical machining 01 p0105 A70-11397

Stress analysis of eyebolts in turbine blades hinged locks based on perforated plate theory with concentrated force, discussing stress distributions 01 p0210 A70-11416

Turbine blades durability and fatigue characteristics, plotting fatigue diagram from statistical tests 01 p0105 A70-11418

Aerodynamic performance of cascade of porous gas turbine blades with cooling air effusion compared with solid noneffusing blades 02 p0355 A70-12311

Monograph on application of semicooled thermosiphon system to gas turbine blade cooling, covering heat transfer and temperature distribution analysis, etc 03 p0551 A70-12992

Model gas turbine engine blades fatigue strength under stress conditions, considering tensile stresses reproducibility from centrifugal loads 03 p0587 A70-13241

Internally air cooled turbine blades and vanes emphasizing coolant aerodynamics, heat transfer and blade life, high temperature in jet engines, etc [RAES PAPER 22] 03 p0551 A70-13545

Embedded sheathed thermocouples temperature measurement of cooled jet engine turbine buckets subjected to high heat flux 03 p0486 A70-13560

Flow characteristics of compressible fluid in compressor or turbine stage, determining radial distribution of downstream Mach number 03 p0410 A70-14271

Two dimensional cascade tests of turbine blade airfoil plotted by Legendre hodograph method, discussing pressure distribution measurements 03 p0410 A70-14272

Tangential jet, tandem, jet flap and vortex generator blade concepts investigated for turbine blade loading efficiency [ASME PAPER 69-WA/GT-5] 04 p0734 A70-14890

Turbine blade designs considered for increasing load capacity covering tandem, jet-blade and base plain blade configurations and test results [ASME PAPER 69-WA/GT-1] 04 p0734 A70-14894

Von Karman transonic similarity law applied to flow through plane turbine blade cascades [DGLR-69-24] 04 p0616 A70-15183

Turbine blade materials resonant vibration resistance criterion dependence on temperature and cyclic and static stresses amplitude 04 p0776 A70-15262

Load distribution in Christmas tree turbine attachments due to centrifugal force on blades, showing strain diagrams 05 p0939 A70-16488

Gas turbine blade material properties change effect on thermal fatigue strength after long term heating 05 p0864 A70-16700

Heat resistant enamel coatings effect on vibration damping of cast steels for turbine blades 05 p0868 A70-17050

Fatigue life tests for heat resistant gas turbine blade alloys under power and thermal loads simulating aircraft flight

05 p0953 A70-17051

Gas turbine blades thermal fatigue strength under simultaneous temperature cycles and static tensile loads, analyzing temperature and stress fields

05 p0953 A70-17053

Test stand design and automatic recording of turbine blade fatigue test data, including statistical evaluation

05 p0953 A70-17054

Stress rupture strength of turbine blades for tree type root joints under prolonged loads at high temperatures, studying disk teeth shearing

05 p0953 A70-17055

Temperature field in internally cooled gas turbine blades determined, using integrator combined with coordinating device

05 p0954 A70-17057

Fatigue strength of T-shaped blade roots of steam turbine regulating stages subjected to combined static tension and cyclic bending

05 p0954 A70-17060

Error resulting from elasticity modulus and linear thermal field coefficient removal from integral in Burger formula for turbine blade thermal stresses

05 p0954 A70-17061

Turbine blades root joints endurance limit concerning tensile stress determination at stress raiser contour for elastoplastic deformation and creep

05 p0954 A70-17062

Thermal fatigue cracks in gas turbine blade models under simultaneous thermal cycling and static tensile loads simulating pulsed regimes

06 p1166 A70-17652

Flow separation angle and loss coefficient in cascades with small aspect ratio blades under secondary vortex pair expansion over channel

06 p1130 A70-17858

Turbine rotor and stator blades twist inaccuracies in assembly due to shroud induced stresses and blade root mountings clearances

07 p1291 A70-18827

Gas turbine engine blades grinding and polishing procedures, considering fatigue life increase and physical properties stabilization

07 p1292 A70-18833

Mechanical and electrochemical polishing effect on turbine blade alloy fatigue strength, discussing surface strain hardening as function of temperature in mechanical polishing

07 p1304 A70-18838

Turbine blade tip clearance effect on aerodynamic characteristics in nonuniform flow

07 p1187 A70-18980

Heat transfer at inlet edge of turbine blade based on wind tunnel study of cylinder in air flow

07 p1362 A70-19061

Centrifugal force induced stressed state in gas turbine blades using photoelastic analysis, emphasizing stress distribution at shroud holes

07 p1403 A70-19118

Soviet book on unsteady attached turbulent flow in turbine lattices, studying blade aeroelastic vibrations onset and attenuation in compressible and incompressible fluids

07 p1189 A70-19602

Flow turbulence effect on heat turbines efficiency using energy losses in blade cascades

08 p1432 A70-21073

Cooled turbine blades temperature field calculated considering variations at turbine inlet, over blade length, material temperature dependence and heat transfer boundary conditions

08 p1597 A70-21185

Turbine blade and vane air cooling need established by advantages of operating aircraft turbines at high turbine entry temperatures

[AGARDOGRAPH-120] 08 p1559 A70-21931

Wear resistance of turbine rotor blade stabilizing elements in form of bolts connecting overlapping leading and trailing edges of adjacent tips

09 p1768 A70-22095

Gas turbine blades design and exploitation processes, discussing long time fatigue strength, static durability and heating effects at elevated temperatures

09 p1772 A70-22469

Thermal fatigue cycle produced by cooled gas turbine blades, using stress-strain tests and thermal simulation

09 p1655 A70-22585

Thermal stresses in gas turbine blade calculated, showing role of initial temperature increase of blade cooling air

09 p1775 A70-22596

Secondary losses in axial turbine cascades without end clearance noting correlation with blade loading

09 p1743 A70-22980

Turbine blade vibration measurement by contactless discrete-phase method, discussing sensor positioning for displacement amplitudes and flutter speeds determination

09 p1681 A70-23199

Thermal stresses determination in turbine blades by making analogy between actual and electrical model, using EGDA integrator

09 p1785 A70-23598

Stepwise averaged parameters of nonuniform three dimensional flow through turbine blade cascade determined from conservation conditions

09 p1606 A70-23611

Heat transfer at inlet edge of turbine blade based on wind tunnel study of cylinder in air flow

10 p1930 A70-25212

Shrouded aircraft engine turbine blades vibration stresses found minimum by setting up paired blades with fixed tension along shroud

10 p1964 A70-25288

Critical load, force characteristics and pressure variation on blades of axial compressor under rotating stall

11 p2133 A70-25795

Device for measuring turbine blades natural frequencies by converting vibrations to electric current at same frequency

11 p2033 A70-26443

Gas turbine blade materials investigated for effect of prolonged heating on mechanical properties and thermal fatigue strength

13 p2434 A70-28994

Diffusion layer microprobe analysis during chromaluminization of Inconel turbine blade

14 p2595 A70-30293

Low temperature tensometry application to stress-strain state of turbine disks

15 p2733 A70-31537

Unidirectional-solidification casting of superalloys of refractory metals in turbine blade production

15 p2757 A70-31811

Periodic flow structure between gas turbine blades, using asymptotic representation

[ONERA-TP-790] 16 p2833 A70-33102

IR optical radiometer for jet engine turbine blade temperature measurement, comparing with junction wire thermocouple

16 p2905 A70-33168

Hydrodynamic internal streamline flow analysis for turboprop inducer blades under cavitating and non-cavitating conditions

[AIAA PAPER 70-629] 16 p2964 A70-33528

Stress and vibration analysis of rocket engine turboprop inducer blades, using finite element method

[AIAA PAPER 70-630] 16 p2964 A70-33529

Two dimensional film cooled turbine blade aerodynamics, investigating massive blowing effect through discrete holes in single blade test facility

[AIAA PAPER 70-713] 16 p2834 A70-33537

Gas-particle mixture cascade flow over turbine blades, considering momentum/heat transfer and particle trajectories

[AIAA PAPER 70-712] 16 p2835 A70-33569

German monograph on stress calculation for rotating elliptical rimmed and notched turbine disks using Weinel integral equations and cascade computer procedure

16 p2993 A70-34079

Turbine blades vibrations based on thick curved shell theory, deriving element from isoparametric solid

17 p3187 A70-34989

Ni alloys with protective coatings for gas turbine blades, testing corrosion resistance in diesel fuel combustion products with intermittent salt water sprays

17 p3125 A70-35394

Fiber-metal matrix composites for gas turbine blades, discussing stress rupture strength, modulus of elasticity, fabrication, etc

[ASME PAPER 70-GT-133] 18 p3302 A70-36827

Internal efficiency of turbine stages with long twist-varying blades

19 p3490 A70-37250

Thermal fatigue cracking of gas turbine blades in fuel combustion product flow, investigating surface composition, microhardness and structure under simulated loads

19 p3490 A70-37338

Supersonic turbine blade rows design, discussing boundary layer interaction around leading edges and flow around trailing edges

19 p3490 A70-38223

Velocity distribution in boundary layer on thin rotating turbine blade of impeller driven at wind tunnel outlet, solving turbulent and laminar flows momentum equations

19 p3352 A70-38224

Structural fatigue strength model tests for turbine blade root connections, using asymmetric load cycle and working temperature

19 p3547 A70-38433

Model gas turbine engine blades fatigue strength under stress conditions, considering tensile stresses reproducibility from centrifugal loads

19 p3548 A70-38459

Turbine blade profiles calculation by hodographs, obtaining compatibility with continuous flow velocity distribution and improved boundary layer stability

19 p3491 A70-38949

Internally cooled turbine blade with longitudinal cooling channels, calculating temperature field by combined analytical and analog method

21 p3868 A70-41772

Temperature distribution measurement inside solid samples by Mossbauer effect, considering application to turbine blades

21 p3830 A70-42165

Transonic turbine cascades exit flow parameters taking into account blade profile

22 p4088 A70-42346

Turbomolecular pumps with uniformly distributed small plane blades, calculating rotor efficiency

22 p3964 A70-42604

Equations solution for turbine blade flexural vibration, considering internal friction

22 p4117 A70-43363

Heat exchange coefficients on side surfaces of constant thickness gas turbine disk, using temperature distribution method and integral transformations

22 p4125 A70-43367

High temperature gas turbine blades cooling by liquid Na-K alloy

[ONERA-TP-872] 22 p4125 A70-43458

Stationary turbine blades heat flux measurements, considering heat exchange coefficients and turbulent boundary layer

[ONERA-TP-871] 22 p4126 A70-43459

Aircraft turbine engines durability estimated from rotor blade minimum tip clearance measurements

22 p4092 A70-43529

Nonsteady temperature and thermal stress distribution in gas turbine blades, using plastic model and photothermoelastic method

22 p4093 A70-43743

Hologram interferometry as noncontact tool for vibration mode measurements of turbine blade groups

23 p4193 A70-43925

Step-amplitude stress cycle program effects on durability of heat resistant alloy for turbine blades under cyclic loading

23 p4204 A70-43934

Fatigue of turbine blades stainless steels and nickel alloys as function of temperature, stress and surface layers

[ICAS PAPER 70-38] 23 p4205 A70-44135

Heat exchange on turbine blade profiles, examining boundary layer flow transition region coordinates

23 p4283 A70-44732

Heat transfer at air cooled gas turbine blade trailing edges at various wall temperatures and Reynolds numbers

23 p4283 A70-44737

High melting point fibrous composites, discussing fiber-matrix systems for high temperature applications

24 p4357 A70-45168

Cascade flow field analysis from given blade geometry, deriving expressions for numerical solution of inverse turbine design problem

24 p4288 A70-45501

Turbine blades aerodynamic forces theoretical and experimental investigation, noting cascade series interaction induced pressure pulsations

24 p4288 A70-45504

Turbine blades deformation by centrifugal and aerodynamic forces, discussing theory for bending stress free blade design

24 p4288 A70-45505

TURBINE ENGINES

NT DUCTED FAN ENGINES

NT GAS TURBINE ENGINES

NT JET ENGINES

NT RAMJET ENGINES

NT SUPERSONIC COMBUSTION RAMJET ENGINES

NT T-56 ENGINE

NT TURBOFAN ENGINES

NT TURBOJET ENGINES

NT TURBOPROP ENGINES

NT TURBORAMJET ENGINES

Static and centrifugal filters merits for turbine engine lubrication systems, considering mechanical reliability, efficiency, dirt capacity and maintenance

01 p0164 A70-10686

Turbine engine starting system design requirements, outlining lifetime improvement of hot section parts

01 p0167 A70-11460

Helicopter turbine engine bleed air requirements obtained by compressor extraction for engine designers

01 p0167 A70-11462

Turbine engine checkout techniques, describing oil, sonic-vibration, X ray, gas path and hot section analysis methods

[AIAA PAPER 69-581] 02 p0356 A70-12526

Circumferential contour shape influence on three dimensional flow pattern of fan shaped annular turbine stages

03 p0407 A70-13417

Turbine noise significance in civil aircraft noise problem

[ASME PAPER 69-WA/GT-12] 04 p0734 A70-14884

Development trends, design and gas dynamic characteristics of turbine engines for helicopter

propulsion systems including pressure, turbofan and integral engines

05 p0896 A70-16350
Turbulence effect on heat transfer in flow carrying section of turbine engines, considering flow velocity pulsations frequency characteristics

07 p1362 A70-19067
Supersonic fluid turbomachine components and systems innovations and performance trends [AGARDGRAPH-120]

08 p1434 A70-21927
Axial compressor aerodynamics and efficiency in aircraft turbine engines [ONERA-TP-767]

09 p1604 A70-22656
Turbulence effect on heat transfer in flow carrying section of turbine engines, considering flow velocity pulsations frequency characteristics

10 p1930 A70-25218
Aircraft turbine engines structural materials and design concepts, describing fiber reinforced materials, oxide dispersion hardened alloys and integral and honeycomb structures

11 p2101 A70-25625
Tip clearance contactless measurement in jet engine turbine based on radioactive isotopes properties

11 p2055 A70-26446
Turbine flowmeter dynamic characteristics dependence on individual parameters, deriving equations of motion and time constant

11 p2055 A70-26450
Aircraft turbine engines gaseous emission measurements, discussing instrumentation for continuous pollutant concentration monitoring [SAE PAPER 700249]

12 p2290 A70-27428
Optimum alkali metal vapor humidity for turbine equipment estimated from energy output

14 p2535 A70-31008
Humidity measurement for alkali metal vapor in turbines by electric calorimeter with two heaters

14 p2587 A70-31009
Aircraft turbine engine components vibrational testing by holographic interferometry methods

16 p2903 A70-33134
Digital simulation for turbine engine propulsion system testing [AIAA PAPER 70-633]

16 p2869 A70-33593
Vibration monitoring for turbine engine malfunction detection

17 p3061 A70-35480
Sliding friction effects of nonlinear asymmetric supports on turbine engine rotor-shaft stability [SAE PAPER 700320]

18 p3301 A70-36799
Jet transport aircraft turbine engine performance monitoring by flight data, discussing historical highlights and future prospects [SAE PAPER 700314]

18 p3301 A70-36801
Aircraft turbine engines emission sampling, handling and measurement, evaluating various instruments and techniques [SAE PAPER 700338]

18 p3226 A70-36810
Fire and overheat detection system design for turbine powered vehicles [ASME PAPER 70-GT-125]

18 p3260 A70-36891
Soviet book on vibration and balancing of aircraft engine rotors covering structural deformation and dynamics of turbine engines and compressors

19 p3489 A70-37237
Two stage turbine engine parts adjustment optimization in terms of fuel consumption or thrust control by linear programming techniques

19 p3489 A70-37241
Turbine engine combustion chambers with various frontal devices, investigating burnout mechanism and heat yield in secondary air flow injection zone

19 p3489 A70-37246
Internal efficiency of turbine stages with long twist-varying blades

19 p3490 A70-37250
Condition Monitored Maintenance program for turbine engines eliminating total overhauls at specified time, using NDT

19 p3441 A70-38830
Aircraft turbine engines durability estimated from rotor blade minimum tip clearance measurements

22 p4092 A70-43529
Computerized simulation and hardware for propulsion control of turbine engines [SAE PAPER 700827]

24 p4394 A70-45892
Direct drive turbine engine control components and airframe accessories, noting weight and frontal area reduction [SAE PAPER 700821]

24 p4394 A70-45896
TURBINE EXHAUST NOZZLES

Air inlet and exhaust nozzle form and location effect in afterburning turbofan engines, discussing stalling, afterburner blowouts and thrust losses prevention

05 p0895 A70-15807
Nozzle geometry effects on turbine gas ejector characteristics

21 p3867 A70-41765
Radial flow microturbines deflection and wave losses in circular nozzle ring oblique exit section

22 p3965 A70-43359

TURBINE INSTRUMENTS

Turbine flowmeter theoretical model [ASME PAPER 69-WA/FM-2]

04 p0689 A70-14841
Turbine flowmeter with hydraulic bearings operation based on photosensitive recording of light beam interruptions, discussing test results

06 p1065 A70-17911
Turbine flowmeter in-place calibration for measuring cryogenic propellant flow rates in rocket engine testing

06 p1071 A70-18448
Turbine flow meters dynamic calibration employing sinusoidally perturbed orifice flow

12 p2236 A70-28033
TURBINE PUMPS

Liquid rocket technology for chemical engineers, discussing insulating tanks, flexible lines, turbopumps and combustion chamber

05 p0896 A70-16168
Twin spool hydrogen turbopump performance at zero net positive suction pressure /NPSP/ saturated fluid in propellant tank, including steady state and simulated transient engine tests [AIAA PAPER 69-550]

07 p1295 A70-19709
Turbine pump systems operation in terms of liquid rocket engine combustion stability, noting altitude effects on pressure pulsations

08 p1559 A70-21849
Gasdynamic test stand analyzing elastoplastic strains in aircraft gas turbine disks and liquid-propellant rocket engines turbopumps under alternating nonisothermal loads

10 p1862 A70-25298
Turbopump-fed rocket engine for satellite launchers, discussing gas cooling, fuel tank pressurization, etc

13 p2474 A70-29138
Combustion chamber, turbopump and combustion control system for French turbopump-fed booster rocket motor

20 p3688 A70-39649
Turbomolecular pumps with uniformly distributed small plane blades, calculating rotor efficiency

22 p3964 A70-42604
Turbomolecular pumps efficiency calculation by Maxwell transport equation, assuming gas molecules perfect specular reflection from blade surface

22 p4009 A70-42607
TURBINE WHEELS

Air lubricated foil bearing support design with external pressurization for high speed rotor in high temperature turbomachinery [ASME PAPER 69-LUB-D]

01 p0100 A70-10377
Rigid body dynamics of turborotors in fluid film journal bearings, investigating initial transients effect on motion stability by Runge-Kutta technique [ASME PAPER 68-LUB-7]

02 p0307 A70-12165
Stress state of brittle alloy turbine disks with eccentric hole distributions, studying stress concentrations, hole number effects, etc

03 p0588 A70-13243
Failure and defect formation in gas turbine engine disks made of steel alloys, stressing fabrication methods effect on reliability

03 p0588 A70-13251
Gas turbine rotating disks failure analysis, studying strength as function of material properties, thermal stresses and hole dimensions

04 p0775 A70-15260
Gas dynamic stand for testing turbine disks strength under mechanical and cyclic thermal loads, analyzing breakdown data for various disk geometry

05 p0953 A70-17052
Stress rupture strength of turbine blades fir tree type root joints under prolonged loads at high temperatures, studying disk teeth shearing

05 p0953 A70-17055
Thin gas turbine disk strength under axisymmetric flexural vibrations, noting agreement of calculated and experimental rotor rpm danger zone

06 p1166 A70-17654
Outside-matching functioning of single rotating disk of axial compressor, investigating critical disengagement and rotary detachment [ONERA-TP-701]

07 p1193 A70-19127
Stability and potential cavitation of centrifugal pump operating with four working wheels with different geometric parameters

08 p1558 A70-21196
Stetson-Powell time fringe hologram technique of vibration analysis applied to nodal patterns in compressor blade and turbine disks

09 p1679 A70-22979
Creep and stability of perforated and unperforated turbine disks under operating conditions

09 p1779 A70-23097
Stress concentrations in turbine disks with eccentric holes under steady creep

09 p1780 A70-23200
Plane disks and turbine disks of complex profile made of heat resistant Cr-Ni alloys studied for rupture strength under various temperature conditions

09 p1785 A70-23599

Gas turbine components, discussing material selection, fabrication and assembly with emphasis on combustion and turbine sections, turbine coatings, shafts, bearings and seals

10 p1929 A70-23851
Computerized analysis of shear failure at initial fragment collision during trifragment rotor disk interaction with containment rings

14 p2563 A70-30870
Soviet book on bearing capacity of turbomachine rotor elements covering testing methods, stress analysis, design factors on stability, etc

14 p2658 A70-30958
Transverse vibration of thin circular elastic turbine disk of variable thickness rotating axially at constant angular velocity

16 p2916 A70-32994
German monograph on calculation and measurement of stress distribution in turbine rotors with radial flow, discussing differential equations for rotating disks

16 p2993 A70-34076
Sliding friction effects of nonlinear asymmetric supports on turbine engine rotor-shaft stability [SAE PAPER 700320]

18 p3301 A70-36799
Stress state of brittle alloy turbine disks with eccentric hole distributions, studying stress concentrations, hole number effects, etc

19 p3548 A70-38461
Failure and defect formation in gas turbine engine disks made of steel alloys, stressing fabrication methods effect on reliability

19 p3548 A70-38469
Discrete components formation in noise spectra of axial turbocompressor intake, considering relationship between blades and rotor disk

19 p3353 A70-38652
Critical rotation rates of gas turbine rotors disk-drum designs, describing initial parameters of model in matrix form

20 p3721 A70-39782
Thermal stress and changes in modulus of elasticity and expansion coefficient effects on dynamical properties of turbine disks at high temperatures

20 p3721 A70-39783
Gas lubricated foil bearing performance as support for turborotor simulator, examining heating and thermal gradient effects [ASME PAPER 70-LUBS-12]

22 p4044 A70-42448
Dynamic characteristics of turborotor simulator supported on gas lubricated foil bearings, considering rotor response to imbalance [ASME PAPER 70-LUBS-11]

22 p4044 A70-42449
Turbomolecular pumps with uniformly distributed small plane blades, calculating rotor efficiency

22 p3964 A70-42604
TURBINES

NT AXIAL FLOW TURBINES
NT GAS TURBINES
NT SHROUDED TURBINES
NT STEAM TURBINES
NT SUPERSONIC TURBINES
NT TWO STAGE TURBINES

Small three stage hydraulic turbine for aerospace and commercial applications, discussing design and performance

04 p0628 A70-15640
Air brake with compressed air fed bearings for testing small turbines, determining power and friction moment

08 p1481 A70-21188
Turbine components design for low cycle fatigue, estimating thermal cycle number for high temperature crack initiation and propagation

09 p1774 A70-22583
Turbine components thermal stress calculations for static and variable loads, considering plastic strain, creep and temperature effects

09 p1775 A70-22592
Flow pattern of axial flow of turbine stage calculated from cascade characteristics

11 p1975 A70-25794
Rolls-Royce RB 211 three shaft turbofan engine, discussing centrifugal compressor, tubular combustion chambers and single stage turbine

15 p2787 A70-31949
Nuclear space power three stage potassium turbine erosion testing in stainless steel loop with various contamination levels

21 p3756 A70-41005
Variable geometry radial inflow turbine performance estimation based on one dimensional flow theory

22 p3960 A70-43738
Radial inflow turbine optimum design geometry, calculating nozzle and rotor geometrical parameters efficiency

24 p4395 A70-46012
TURBOALTERNATORS

U AC GENERATORS
U TURBOGENERATORS
TURBOCHARGERS

U SUPERCHARGERS
U TURBOCOMPRESSORS

TURBOCOMPRESSORS

TURBOCOMPRESSORS

Two stage axial flow compressor with variable pitch guide vanes, discussing HF vibration reduction of rotor blades

01 p0166 A70-11419

Strong shocks and high temperature gases production using multistage gaseous detonation driven shock tube

02 p0274 A70-11855

Discrete frequency noise generation from axial flow compressor blade row, using experiments in small scale Freon loop

[ASME PAPER 69-WA/FE-22] 04 p0733 A70-14777
Rotating acoustic modes generated at blade passing frequencies in inlet duct of axial flow fan or compressor measured

04 p0691 A70-15079

Flow field calculation for axisymmetrical gas flow in axial compressor cascade applicable to optimal blade design

04 p0617 A70-15191

Aircraft engine fan and compressor noise theory as basis for improved noise prediction

05 p0896 A70-16790

Turboblowers and compressors air tests for gas operation performance prediction

06 p1129 A70-17136

Inviscid flow through staggered airfoil cascades in oscillatory and distorted flow simulating axial flow compressor

[AIAA PAPER 70-131] 06 p0969 A70-18049

Outside-matching functioning of single rotating disk of axial compressor, investigating critical disengagement and rotary detachment

[ONERA-TP-701] 07 p1193 A70-19127

Multistage axial compressor performance described by mathematical model based on maximum probability principle

08 p1558 A70-21190

Machine-plotted pseudo three dimensional turbocharger rotor whirl display, discussing amplitude and frequency

08 p1496 A70-21300

Far field directionality and acoustic power of noise radiated by axial flow fans and compressors using fluctuating forces model

08 p1547 A70-21860

Supersonic compressor applications for airborne vehicles propulsion systems, discussing axial flow compressors, three dimensional design methods, supersonic radial machines, etc

[AGARDOGRAPH-120] 08 p1434 A70-21929

Axial compressor aerodynamics and efficiency in aircraft turbine engines

[ONERA-TP-767] 09 p1604 A70-22656

Tandem axial compressor performance for various blade stagger and flap angle values of rotor row, investigating gap influence

09 p1608 A70-23736

Stage matching under local stall conditions for multistage axial flow compressor off-design and surge initiation characteristics

09 p1608 A70-23741

Annulus wall boundary layer effect on spatial flow in subsonic axial compressors by shearing stresses concept between stream surfaces

11 p1974 A70-25777

Axial flow compressor blade rings interaction effect on angular speed of rotating stall zones

11 p1974 A70-25780

Critical load, force characteristics and pressure variation on blades of axial compressor under rotating stall

11 p2133 A70-25795

Supersonic axial flow compressors, studying shocks shared by rotor and stator to obtain high efficiency

11 p2101 A70-25819

Acoustic wave transmission and reflection through blade row in axial flow compressor analysis based on semiautuator disk theory and acceleration potential method

11 p2103 A70-26705

Axial flow compressor clearance control coatings at blade tip paths for efficiency

[SAE PAPER 700330] 12 p2291 A70-27462

Nonfree vortex flow in contrarotating axial flow fans under radial equilibrium assumption, discussing pressure rise coefficient and static efficiency

12 p2156 A70-27600

Axial compressor stage head determination by measuring axial thrust, noting fluid velocity nonuniform distribution influence

13 p2474 A70-28892

Axial-flow compressors stall characteristics measurement using water as working fluid

13 p2341 A70-29446

Axial flow compressors off-design performance calculation using radial equilibrium equation

15 p2791 A70-32770

Axial compressor aerodynamics investigation methods concerning compressor flow for efficiency improvement

16 p2836 A70-33757

Kuznetsov NK 8-4 bypass turbojet air entry vanes, pressure compressors, gear case, combustion chamber and turbine drives

17 p3147 A70-34629

Compressor erosion correlation with aerodynamic parameters in gas turbine engines

17 p3147 A70-34711

Rotating stall in axial compressors, using finite difference method

17 p3011 A70-35450

Pure impulse principle applied to axial compressor impellers with high solidity high camber blades

18 p3301 A70-36647

Three dimensional inviscid small perturbation compressible flow past lifting axial compressor rotor at subsonic and transonic speeds

18 p3208 A70-36691

Two dimensional compressor cascades of double circular arc and wedge shape blades testing performance in transonic and supersonic wind tunnels

[ASME PAPER 70-GT-7] 18 p3302 A70-36829

Plane and annular cascade facilities data application to aerodynamic design of axial flow compressors

[ASME PAPER 70-GT-106] 18 p3303 A70-36845

Axial flow compressor off-design performance optimization by adjustable inlet guide vanes with variable trailing edge flaps

18 p3304 A70-36846

Rotor wakes intrastator transport effects on high Mach number axial flow compressors performance, considering stagnation temperature profile and rotor blade loss factor

[ASME PAPER 70-GT-39] 18 p3209 A70-36869

Axial flow compressor cascades, predicting total pressure losses for inlet relative Mach number greater than unity

[ASME PAPER 70-GT-57] 18 p3209 A70-36872

Sound transmission and suppression in turbomachinery fans and compressor ducts, using three dimensional wave equation

[ASME PAPER 70-GT-58] 18 p3304 A70-36873

Boundary layer optimization for high turning axial flow compressor blades, using flow theory and conformal mapping

[ASME PAPER 70-GT-88] 18 p3209 A70-36879

End wall boundary layers effect included in performance prediction method for multistage axial compressors

[ASME PAPER 70-GT-80] 18 p3210 A70-36884

Off-design pressure losses in single stage axial flow compressor, using test rotor in annular duct

[ASME PAPER 70-GT-78] 18 p3210 A70-36886

Axial flow compressor stage efficiency under rotor separation conditions, investigating dependence on flow rate

19 p3490 A70-37252

Blade root design for axial flow compressors and turbines, avoiding tensile stress concentration

19 p3490 A70-38616

Discrete components formation in noise spectra of axial turbocompressor intake, considering relationship between blades and rotor disk

19 p3353 A70-38652

Axial compressor air intake wall design influence on sound propagation

19 p3353 A70-38653

Turbocompressor disk materials selection by low cycle fatigue tests, discussing stop and start repetition and cracks in stress concentration zones

21 p3867 A70-41261

Jet engine compressor noise analysis, noting inlet swirl role

22 p4090 A70-42725

Optimum manifold and injector hole area of pulsed exhaust systems of two cycle engine with turbosupercharger

22 p4091 A70-42809

German monograph on three dimensional flow and blade pressure measurements at axial flow compressor casing wall, discussing test control and digital data processing

24 p4332 A70-45093

German monograph on supersonic strongly deflecting retardation cascades covering flow geometry and application to axial flow compressor stage

24 p4287 A70-45095

German monograph on casing and hub wall friction effects on three dimensional flow in turbocompressors in subsonic compressible working fluids

24 p4287 A70-45096

Turbine compressor blades vibration mode measurements by holographic interferometry

24 p4334 A70-45563

Axial flow compressor fan discrete tone noise radiation directivity pattern measurement and theoretical explanation for cut-off effect, power and harmonics

24 p4380 A70-46069

Turbofan, turbojet and turboprop engine development in aircraft gas turbine evolution, discussing VTOL propulsion, centrifugal and axial compressor engines

24 p4396 A70-46251

TURBOCONVERTERS

U TURBOGENERATORS

TURBOELECTRIC CONVERSION

U TURBOGENERATORS

TURBOFAN AIRCRAFT

NT A-7 AIRCRAFT

NT B-52 AIRCRAFT

NT BAC 111 AIRCRAFT

NT BOEING 707 AIRCRAFT

NT BOEING 727 AIRCRAFT

NT BOEING 737 AIRCRAFT

NT C-141 AIRCRAFT

NT CONCORDE AIRCRAFT

NT DC 8 AIRCRAFT

NT DH 121 AIRCRAFT

NT DO-31 AIRCRAFT

NT F-28 TRANSPORT AIRCRAFT

NT F-111 AIRCRAFT

NT SAAB 37 AIRCRAFT

NT TU-134 AIRCRAFT

Turbofan VTOL or STOL intercity transports noting lift engines, noise, aircraft design and interior

[AIAA PAPER 69-1039] 01 p0005 A70-10645

Twin turbofan executive aircraft /Falcon/ development, describing modifications and antinoise features

12 p2162 A70-28026

Air deflection and modulation /ADAM/ turbofan propulsive wing /VSTOL design

[AIAA PAPER 69-201] 12 p2162 A70-28087

TURBOFAN ENGINES

Rolls-Royce RB 211 three shaft turbofan engines development and tests, noting preparation, building, cradle installment, open air facilities and noise measurements

01 p0161 A70-10079

Optimum R and D organization in aircraft engine production illustrated on turbofan engine

01 p0161 A70-10080

Ice tunnel testing facility at Naval Air Propulsion Test Center /NAPTC/, describing methods, systems, instrumentation and various turbofan and turbojet engine tests

01 p0056 A70-10691

A-7 aircraft TF-41 engine tolerance to steam ingestion, discussing test program and results and engine modifications

01 p0165 A70-10700

Positive displacement low pressure air motors for Boeing 747 fan thrust reverser pneumatic actuators and controls

03 p0550 A70-12881

Design specifications for low noise turbofan engine used on long range subsonic transport aircraft

[ASME PAPER 69-WA/GT-7] 04 p0734 A70-14888

Gross thrust coefficient for turbofan engines thrust estimates, discussing full scale nozzle simulation

04 p0736 A70-15390

Air inlet and exhaust nozzle form and location effect in afterburning turbofan engines, discussing stalling, afterburner blowouts and thrust losses prevention

05 p0895 A70-15807

Engine cycle and low pressure-intermediate pressure compressor aerodynamic design of TF41 turbofan engine

[SAE PAPER 690687] 05 p0895 A70-15864

Dip brazing aluminum fan vanes used in high bypass turbofan jet engines

10 p1893 A70-23858

Three spool turbofan engine design regarding maintainability, noting on-condition module removal and overhaul

[SAE PAPER 700204] 11 p2101 A70-25877

Aircraft turbofan and turbojet engines military-commercial interrelationships

[SAE PAPER 700268] 12 p2290 A70-27436

Aircraft turbojet and turbofan engines cost correlation to performance statistically analyzed in terms of various parameters

[SAE PAPER 700270] 12 p2335 A70-27437

Rolls-Royce RB 211 turbofan engine, discussing fuel consumption, specific weight, noise and smoke level, reliability and maintainability

15 p2787 A70-31948

Rolls-Royce RB 211 three shaft turbofan engine, discussing centrifugal compressor, tubular combustion chambers and single stage turbine

15 p2787 A70-31949

Turbofan engine compressor system performance dependence on circumferential extent, magnitude and rate of change of inlet temperature in altitude test facility

[AIAA PAPER 70-625] 16 p2968 A70-33590

C-5A turbofan engine thrust determination using pressure and temperature values in exhaust nozzles

[AIAA PAPER 70-611] 16 p2969 A70-33606

Turbofan engine gross thrust dependence on nozzle pressure ratio and simulated flight Mach number, considering altitude chamber test data

[AIAA PAPER 70-612] 16 p2969 A70-33608

Cooperative airline program for aircraft turbofan engine parts aging and performance deterioration evaluations

[SAE PAPER 700329] 18 p3301 A70-36798

High bypass turbofan engine design concepts and development program for airline operation

[SAE PAPER 700292] 18 p3302 A70-36804

High bypass ratio aircraft turbofan engines, discussing program of factory, flight and operational suitability testing
[SAE PAPER 700290] 18 p3302 A70-36806

JT9D engine design and performance, describing operational problems
[SAE PAPER 700288] 18 p3302 A70-36807

Military and commercial transports turbofan propulsion systems impact on future aircraft design and development
[SAE PAPER 700267] 18 p3214 A70-36820

Turbofan engine performance optimization by closed form solution of operating cycle parameter functions
[ASME PAPER 70-GT-65] 18 p3303 A70-36840

Jumbo jets turbofan engines design, considering fuel consumption, maintenance, reliability, noise reduction, etc
19 p3491 A70-38953

Turbofan engine aerodynamic interactions, cryogenic space storable propellants, space station attitude control biowaste resistojet and long burning time solid propellants
20 p3688 A70-39667

Turbofan engines afterburner flame stabilization at low inlet temperature, noting flame holder geometry role
22 p4088 A70-42336

Acoustically treated inlet and fan exhaust duct configurations for JT3D turbofan engine on DC 8 aircraft
22 p4090 A70-42533

High bypass model jet noise study, describing test setup and noise measurement results as function of secondary/primary flow velocity ratio
23 p4233 A70-44394

Allison/Rolls-Royce TF41 turbofan engine improved power and reduced weight versions, comparing afterburning Model 912-B23 to nonafterburning TF41-A-2
23 p4234 A70-44596

Noise suppression for high-bypass ratio CF6 turbofan engine in DC-10 airplane, considering effect on engine design
[SAE PAPER 700804] 24 p4393 A70-45878

Engine control concepts for augmented turbofan, discussing integrated electrical/hydraulic/mechanical system
[SAE PAPER 700826] 24 p4394 A70-45893

Turbojet and turbofan engine control evolution, noting increased complexity and adoption of hybrid fluidics and computer technologies
[SAE PAPER 700825] 24 p4394 A70-45894

Noise reduction design for subsonic transport turbofan engines
[SAE PAPER 700807] 24 p4395 A70-45907

TURBOFANS

Aircraft engine fan and compressor noise theory as basis for improved noise prediction
05 p0896 A70-16790

Steady and unsteady flow through Napier turboblower axial flow turbine for full and partial admission, estimating mass flow and power output
07 p1189 A70-20294

Far field directionality and acoustic power of noise radiated by axial flow fans and compressors using fluctuating forces model
08 p1547 A70-21860

Sound transmission and suppression in turbomachinery fans and compressor ducts, using three dimensional wave equation
[ASME PAPER 70-GT-58] 18 p3304 A70-36873

Test rig vehicle design for noise research on single stage high bypass ratio fans for quieter turbofan power plants
[AIAA PAPER 69-492] 22 p4090 A70-42708

Axial flow compressor fan discrete tone noise radiation directivity pattern measurement and theoretical explanation for cut-off effect, power and harmonics
24 p4380 A70-46069

TURBOGENERATORS

Thermal gradients and associated strains measurement in steam turbogenerator casings, considering strain gage placement and heat transfer calculations
09 p1774 A70-22590

TURBOJET AIRCRAFT

U JET AIRCRAFT

TURBOJET ENGINE CONTROL

Turbojet engine controls and control devices design, considering fuel properties and fuel consumption
03 p0552 A70-13806

Concorde microelectronic power plant control system, noting overfueling prevention by throttle actuator during startup and speed governor function
05 p0896 A70-16003

Dual flow turbojet engine rotor slip constraints during turning, investigating turbine blade strength, thrust deviation, fuel consumption and compressor stability
10 p1930 A70-24285

Fluidic gas turbine controls, discussing high temperature operation, hybrid sensors and logic in hostile environment applications
12 p2164 A70-27074

Dual flow turbojet engines automatic control and guidance characteristics
17 p3147 A70-34687

Multidimensional control for turboramjet engine, relating system characteristics to invariance conditions during startup and ascent
20 p3689 A70-39847

Turbojet and turbofan engine control evolution, noting increased complexity and adoption of hybrid fluidics and computer technologies
[SAE PAPER 700825] 24 p4394 A70-45894

TURBOJET ENGINES

NT DUCTED FAN ENGINES

NT T-56 ENGINE

NT TURBOFAN ENGINES

NT TURBOPROP ENGINES

Turbojet engines air pollution emissions processes resulting from combustor primary and secondary zone conditions, discussing engine design modifications
[AIAA PAPER 69-1040] 01 p0162 A70-10602

Turbojet aircraft engine performance correlation with relative humidity, noting air density effect on rotor performance resulting from moisture content
01 p0165 A70-10689

Ice tunnel testing facility at Naval Air Propulsion Test Center /NAPTC/, describing methods, systems, instrumentation and various turbofan and turbojet engine tests
01 p0056 A70-10691

Embedded sheathed thermocouples temperature measurement of cooled jet engine turbine buckets subjected to high heat flux
03 p0486 A70-13560

Turbine noise significance in civil aircraft noise problem
[ASME PAPER 69-WA/GT-12] 04 p0734 A70-14884

Tungsten alloy fiber reinforced Ni-base superalloy composites evaluated for high temperature turbojet engine applications, considering stress-rupture strength, oxidation and impact resistance
08 p1523 A70-21907

Supersonic turbojet propulsion systems and components - NATO/AGARD Conference, Varenna, Italy, May 1967
[AGARDOGRAPH-120] 08 p1559 A70-21926

V/STOL aircraft turbojet engine design and quality control for in-service reliability
09 p1743 A70-22572

Turbojet engines departure from equilibrium performance during thermal soak transient attributed to heat absorption in turbine and compressor metals, observing thrust loss
09 p1744 A70-23739

External supersonic potential flow effects on turbojet engine ring and needle nozzle performance, considering gas overexpansion operation
10 p1930 A70-24286

Nickel cadmium battery for aircraft jet engine starting, discussing selection for optimum service life and reliability under maintenance and environmental conditions
[SAE PAPER 700211] 11 p1980 A70-25883

Aircraft turbofan and turbojet engines military-commercial interrelationships
[SAE PAPER 700268] 12 p2290 A70-27436

Aircraft turbojet and turbofan engines cost correlation to performance statistically analyzed in terms of various parameters
[SAE PAPER 700270] 12 p2335 A70-27437

Supersonic and subsonic air breathing engines, discussing single and ducted fan turbojets, ramjets, turboprop engines and land based gas turbine engines
12 p2291 A70-28071

Soviet book on aerodynamics of Tu 134 aircraft, covering 30 turbojet engines, flight characteristics, etc
13 p2344 A70-28875

Turbojet engine testing in ground level facilities with automatic instrument reading and parameters calculation
13 p2474 A70-29688

Aircraft turbojet engine/inlet compatibility, using data system for acquisition, identification and analysis of critical time variant pressure parameters
[AIAA PAPER 70-594] 13 p2375 A70-29877

Liquid propane turbojet exhaust simulator for wind tunnel propulsion testing, emphasizing nozzle jet properties
[AIAA PAPER 70-634] 16 p2888 A70-33595

Kuznetsov NK 8-4 bypass turbojet air entry vanes, pressure compressors, gear case, combustion chamber and turbine drives
17 p3147 A70-34629

Ground test noise measurements accuracy and repeatability on JT8D turbojet engine
17 p3060 A70-35183

Turbojet aircraft engine fuels quality control, considering chemical composition, physical properties and handling problems
18 p3299 A70-36550

Olympus 593 engine for Concorde aircraft, describing design and test procedures
[SAE PAPER 700291] 18 p3302 A70-36805

Soviet book on VTOL design covering aerodynamic and weight characteristics, turboprop and turbojet engines, flight regimes, etc
19 p3354 A70-37233

Aircraft engine design combining turbojet and ramjet features to ensure optimum performance
20 p3690 A70-40148

Otomat surface to surface missile with turbojet engine for extended range subsonic cruise and two solid propellant rocket engines for launch
22 p4110 A70-43211

Turbojet engines noise-suppressing nozzles flow rate and thrust characteristics calculation
22 p4092 A70-43371

NASA research in turbojet aircraft propulsion noting inlet, compressor, combustor, turbine and nozzle component technology
[ICAS PAPER 70-46] 23 p4233 A70-44144

TURBOMACHINE BLADES

NT COMPRESSOR BLADES

NT ROTOR BLADES [TURBOMACHINERY]

NT STATOR BLADES

NT TURBINE BLADES

Sound generation by multibladed single stage fans operating in free field, deriving model as boundary value problem involving inhomogeneities due to quadrupole distribution
01 p0166 A70-11197

Discrete frequency noise generation associated with wakes due to fluid flow over turbomachine blades, supporting spokes, flat plates, etc
[ASME PAPER 69-WA/GT-13] 04 p0733 A70-14883

Theoretical model of fan/compressor noise blade passing frequency generation and transmission, noting duct length and configuration in engine operation
04 p0734 A70-14886

Turbine cascade designs with constant reactivity over blade vertical profiles contributing to effective manufacturing of short and long blades
04 p0617 A70-15192

Creep and strength criteria reliability for turbomachine disks, determining stresses, destructive rotations and strength margin
05 p0953 A70-17056

Blade inter-row distances upstream and downstream related to potential flow velocity disturbances created by cascade in turbomachines
09 p1607 A70-23734

Pressure waves of varying amplitude effect on flow through turbomachine blade passages, discussing interaction with curved diffusers geometry
09 p1608 A70-23743

Subsonic compressible or incompressible inviscid flow field through turbomachine blade row determined by matrix and streamline curvature methods
09 p1608 A70-23745

Streamwise perturbations in flow downstream of self excited blades cascade calculated by two dimensional theory, discussing periodic circulation shedding
09 p1608 A70-23746

Torsional vibration of rotating tapered and twisted turbomachine blade, constructing digital computer program for convergence and boundary conditions
[SAE PAPER 700180] 11 p2128 A70-25373

Optimal efficiency of axial turbomachines limit loading of blade root and hydrodynamic criteria
11 p1975 A70-25791

Flow equations for flow field in entry to radial or mixed flow impellers of turbomachines
[ASME PAPER 70-FE-36] 16 p2892 A70-33640

Incompressible flow interaction of perfect irrotational fluid through two blade wheels in relative motion, observing pressure variations at nozzle profile
16 p2836 A70-33755

Base function selection for energy calculation optimal convergence conditions of frequencies and stresses in turbomachine blades vibrations
20 p3722 A70-39784

Vibration loads in turbomachinery blading, examining blade detuning effects on resonant response levels and fatigue life
24 p4392 A70-45157

TURBOMACHINERY

NT AXIAL FLOW TURBINES

NT CENTRIFUGAL COMPRESSORS

NT CENTRIFUGAL PUMPS

NT GAS TURBINES

NT SHROUDED TURBINES

NT STEAM TURBINES

NT SUPERSONIC TURBINES

NT TURBINE PUMPS

NT TURBINES

NT TURBOCOMPRESSORS

NT TURBOFANS

NT TURBOGENERATORS

NT TWO STAGE TURBINES

Carrying capacity of heat resistant steel turbomachine elements, discussing plastic deformation and cyclic load effects, breakdown load determination, stress analysis, etc
02 p0352 A70-11659

Optimal lift-drag ratio of cascades dependence on optimal pitch of cascades calculated for axial flow turbomachinery
02 p0356 A70-12750

Turbine disk strength calculations, obtaining matrix expressions and optimum algorithm for arbitrary disk shapes
03 p0588 A70-13242

Brayton cycle electric power generator simulation to study turbomachinery startup 03 p0415 A70-14050

Sound attenuation in acoustically lined turbomachinery ducts with no air flow, indicating spinning lobes and generation frequency effect on liner material performance [ASME PAPER 69-WA/GT-11] 04 p0734 A70-14885

Difference equations and axial stress tensor component for turbomachinery in curvilinear coordinates systems 04 p0776 A70-15268

Packing rub effect on rotating machinery produced by unstable vibration generated by friction and heat of rubbing rotor in sliding contact 05 p0854 A70-15908

Radial outflow effect on fluid motion between rotating and stationary plane disks associated with rotor cooling in turbomachinery 05 p0833 A70-16503

Deformation and failure of refractory metals at high temperatures under constant and variable thermal loads concerning turbomachine components 05 p0865 A70-17027

Compressible fluid flow velocity profile in turbine stage evaluated by streamline correlation and actuator disk method 06 p0967 A70-17469

Turbine machine elements approximation by difference equations of axisymmetrical elasticity theory problem 06 p1167 A70-17663

Turbine disk strength calculations, obtaining matrix expressions and optimum algorithm for arbitrary disk shapes 08 p1580 A70-21657

Brush collector for strain measurement in jet engine compressor and turbine elements at high RPM 11 p1983 A70-26439

Fluid mechanics of jet engine turbomachinery, considering supersonic compressor and blade rows flows and airframe propulsion system compatibility 11 p1977 A70-26574

Automatic computation at SNECMA for turbomachines R and D, emphasizing digital computer for scientific calculation and analog simulator for engine regulation 12 p2193 A70-28073

Turbine technology application to high speed roller bearing design, considering reduction of roller skidding and skewing 13 p2419 A70-28918

Carrying capacity of heat resistant steel turbomachine elements, discussing plastic deformation and cyclic load effects, breakdown load determination, stress analysis, etc 19 p3547 A70-38432

Turbine disk strength calculations, obtaining matrix expressions and optimum algorithm for arbitrary disk shapes 19 p3548 A70-38460

Dynamic testing of turbine machine parts using strength and vibration equations and similarity method 19 p3437 A70-38472

Incompressible axisymmetric flow through turbomachines, developing flowfield for given velocity distribution along arbitrary streamline 19 p3354 A70-38933

TURBOPROP AIRCRAFT

NT CL-84 AIRCRAFT

NT G-222 AIRCRAFT

NT OV-10 AIRCRAFT

Sound levels and frequency spectra of noises measured in AN-24 and IL-18 turboprop aircraft cockpits 05 p0796 A70-16925

Remote control turboprop drone aircraft for long unmanned electronic intelligence or tactical communications relay missions 08 p1435 A70-20625

Air conditioning systems design for turboprop commuter and business aircraft [SAE PAPER 700224] 11 p1980 A70-25895

Servoactuator for stick force augmentation on light turboprop STOL aircraft at high angles of attack [AIAA PAPER 70-909] 17 p3019 A70-35821

Prototype grill device for turboprop aircraft engine inlet protection against bird ingestion, discussing performance tests 18 p3212 A70-35996

TURBOPROP ENGINES

NT T-56 ENGINE

Bird deflection grid device for turboprop engine inlet ducts, noting effects on inlet flow characteristics, engine performance, etc 01 p0165 A70-10688

Acceleration and regulating system of free turbine turboprop engines studied by graph-analytical method used for nonlinear circuit analysis 03 p0552 A70-13927

Annular combustion chamber for turboprop engines, analyzing design data and development stages, discussing performance characteristics 03 p0552 A70-13928

Vibrational overloads development in turboprop engines ascribed to natural vibrations mode shape frequency approaching rotor revolutions number 07 p1363 A70-19110

Mixture composition and airflow rate dependence of combustion efficiency in turboprop afterburner chamber with air-fuel flame stabilizer 10 p1929 A70-24282

Small turboprop engine development, flight tests, performance and weight reduction [SAE PAPER 700206] 11 p2102 A70-25878

Supersonic and subsonic air breathing engines, discussing single and ducted fan turbojets, ramjets, turboprop engines and land based gas turbine engines 12 p2291 A70-28071

Turboprop aircraft engine service life extension, correcting deficiencies via accelerated tests based on relation between failure rate and usage 15 p2787 A70-31535

Hydrodynamic internal streamline flow analysis for turboprop inducer blades under cavitating and non-cavitating conditions 16 p2964 A70-33528

Soviet book on VTOL design covering aerodynamic and weight characteristics, turboprop and turbojet engines, flight regimes, etc 19 p3354 A70-37233

Low and medium power turboprop engines for V/STOL aircraft, discussing development trends concerning operational control 22 p4091 A70-43081

TURBOPUMPS

U TURBINE PUMPS

TURBORAMJET ENGINES

Turboramjet powered hypersonic aircraft axisymmetric inlet systems using forward translating cowl and centerbody for various air flow characteristics [AIAA PAPER 70-687] 16 p2835 A70-33586

Multidimensional control for turboramjet engine, relating system characteristics to invariance conditions during startup and ascent 20 p3689 A70-39847

TURBOROTORS

U TURBINE WHEELS

TURBOSHAPTS

Helicopter turboshaft engines design and performance 08 p1559 A70-21517

Turbines rotary shafts and stationary components thermal fatigue analysis, considering cycle numbers and stress concentrations under start-up, continuous operation and shut-down 09 p1775 A70-22593

Gas turbine components, discussing material selection, fabrication and assembly with emphasis on combustion and turbine sections, turbine coatings, shafts, bearings and seals 10 p1929 A70-23851

Continuous elastic turboshaft flexible journal bearings, analyzing radial misalignment effects on operation [ASME PAPER 70-DE-71] 16 p2918 A70-33521

TURBOSUPERCARGERS

U SUPERCHARGERS

U TURBOCOMPRESSORS

TURBULENCE

NT ATMOSPHERIC TURBULENCE

NT CLEAR AIR TURBULENCE

NT GUSTS

NT HOMOGENEOUS TURBULENCE

NT ISOTROPIC TURBULENCE

NT LOW LEVEL TURBULENCE

NT LOW TURBULENCE

NT MAGNETOHYDRODYNAMIC TURBULENCE

NT PLASMA TURBULENCE

Optical scintillation measurements applied to turbulence diagnostics, inferring spatial spectrum of turbulent scatterers, using Monte Carlo numerical procedure 02 p0296 A70-11892

Turbulence intensity, light intensity fluctuations and frequency optical measurement in diffusion flames of city gas with air, deriving turbulence spectral functions 02 p0398 A70-12038

Dissipation spectrum /viscous dissipation of turbulent kinetic energy as function of wave number magnitude/ data compared and plotted 02 p0327 A70-12294

Turbulence characteristics in liquids measured by hot film anemometry, discussing calibration methods selecting criteria as temperature control, drift influence and relative speed determination 02 p0303 A70-12687

Direction fluctuations in radio wave scattering in turbulent gyrotropic medium using Einstein-Fokker-Kolmogoroff equation 04 p0653 A70-15722

Turbulence - Conference, Seattle, June 1969 11 p2038 A70-26526

Burger turbulence model late decay statistical analysis using kernels of Cameron-Martin-Wiener expansion of random velocity field 13 p2386 A70-28820

Multiwavelength laser beam propagation with point source transmitters, determining turbulence levels independently 13 p2426 A70-28837

Fast time-resolved spectra of earth bow shock electrostatic turbulence based on broadband analog electric data from OGO-5 13 p2396 A70-29111

Direction fluctuations in radio wave scattering in turbulent gyrotropic medium using Einstein-Fokker-Kolmogoroff equation 14 p2350 A70-30806

Turbulent flows calculation based on two parameter turbulence model, considering model application to free jets 16 p2895 A70-34199

Book on stochastic tools in turbulence covering generalized functions, probability, moments, characteristic functions, Gaussian distribution, random functions and multidimensional fields 17 p3128 A70-34601

Acoustic turbulence spectrum in compressible fluid with potential motion, using complex traveling wave amplitudes in hydrodynamic equations 18 p3242 A70-36637

Turbulence characteristics determination by measuring light beam arrival angle fluctuation using photoelectric recording shadow devices 20 p3634 A70-40401

Astrophysical hypothesis of vorticity expulsion from strong turbulence regions, indicating mechanism of thermally driven circulation currents 22 p4010 A70-42690

Single and crossed light beam techniques for optical measurement of fluid turbulence with refractive index fluctuations 22 p4011 A70-42694

Early type Ia and Iab supergiant stars macro turbulence and rotation, investigating spectral line broadening, mass loss and angular momentum 23 p4250 A70-44813

TURBULENCE EFFECTS

Helical journal bearings analysis operated in turbulent regime with incompressible lubricant, determining optimum groove parameters for maximum radial stiffness 01 p0100 A70-10381

DC dynamo models for planetary electromagnetic conditions, considering nonrotationally symmetric turbulence induction actions and critical values for field maintenance 01 p0185 A70-10956

Noise generation in turbulent premixed flames, turbulent diffusion flames and liquid-spray combustion of hydrocarbon fuels, using optical method 02 p0399 A70-12040

Atmospheric turbulence effects on accelerations experienced by passengers in supersonic and subsonic transport aircraft compared 02 p0325 A70-12219

E layer kinetic energy viscous dissipation and transfer to potential energy by turbulence and irregular winds shear 02 p0327 A70-12292

Internal stability of turbulent combustion, deriving analysis for one dimensional model and developing sufficient instability criterion 03 p0607 A70-13862

Free stream turbulence effect on heat transfer in circular cylinder stagnation region 03 p0469 A70-14216

Free stream turbulence effect on drag coefficient of bluff sharp edged cylinders with small square section 05 p0789 A70-15923

Plane Poiseuille flow stability as function of periodic disturbances of finite amplitude in channel axis direction 05 p0832 A70-16018

Aircraft wake turbulence effects, using hot film anemometry from nearby towers and penetration by instrumented aircraft 05 p0794 A70-16300

Kolmogoroff constant determined by Heisenberg turbulence formula and model for transfer of turbulent energy between different wave numbers 06 p1034 A70-17467

Heat and mass transfer across laminar boundary layer around stagnation line of cylinder in crossflow affected by free stream turbulence intensity 06 p1176 A70-17693

Mathematical model for testing theory of solar differential rotation maintenance by two dimensional turbulence 06 p1144 A70-18009

HF periodic velocity oscillations effect on axisymmetric wake diffusion flames [AIAA PAPER 70-10] 06 p1182 A70-18179

Weak shock thicknesses with turbulent scattering as dissipative mechanism compared with magnitude in sonic boom flight tests and explosions [AIAA PAPER 70-54] 06 p1042 A70-18190

Telescope resolution limit dependence on refractive index mean square fluctuation and effective aperture in turbulent medium 06 p1067 A70-18396

Velocity fields and turbulent pulsations effects on heat transfer in gas flow past plate with rectangular protrusion using wind tunnel tests

07 p1254 A70-19063

Turbulence effect on heat transfer in flow carrying section of turbine engines, considering flow velocity pulsations frequency characteristics

07 p1362 A70-19067

Error estimation of gondola encased tugged undersea magnetometer as function of turbulence parameters

07 p1281 A70-19466

Acoustic turbulence generated noise intensity and spectrum using statistical thermodynamics

07 p1194 A70-19618

Finite disturbance effect on laminar incompressible wake behind flat plate determined by interaction between two dimensional fluctuation amplitude and mean flow

08 p1433 A70-21605

Partial statistical description of turbulent flame interior and turbulent flame speed determination for effects of turbulence on flame propagation

08 p1485 A70-21607

Mean flow and turbulent velocity over noise-producing regions of subsonic jet nozzle with and without delta wings

09 p1610 A70-22239

Fossil turbulence / three dimensional quasi-isotropic refractive index microstructure left behind during turbulence patch decay/ effects on radio wave propagation

09 p1717 A70-22377

Turbulent energy budgets in atmospheric boundary layer near ground scalar fluctuations and CAT

09 p1717 A70-22380

Laser measurements of permittivity fluctuations spectrum of turbulent atmosphere, noting proportionality to temperature spectra at optical frequencies

09 p1635 A70-22962

Amplitude measurement of plane light wave propagating in turbulent atmosphere, giving log amplitude dependence on dispersion of logarithm fluctuations

09 p1636 A70-23136

Turbulent medium refractive index fluctuations effect on parameters of focused plane light wave, calculating diffraction patterns center of gravity

09 p1636 A70-23138

Laser beam intensity fluctuations during propagation through turbulent atmosphere

09 p1637 A70-23142

Self diffusion in turbulent fluid motion attributed to flow turbulence and linked to mean motion by mass conservation

09 p1663 A70-23310

Microwave signal fading in Venus atmosphere due to turbulence, discussing atmospheric dielectric permittivity variance

09 p1764 A70-23484

Air flow turbulence intensity and plug effect influence on local heat exchange on cylinder surface

10 p1797 A70-24028

Atmospherically induced phase fluctuations for various path lengths using near ground horizontal Mach-Zehnder, discussing turbulence effects

10 p1916 A70-24413

Clear air turbulence effect on supersonic aircraft safety and comfort, noting shallow zones and effects of topography and thunderstorms

10 p1912 A70-24506

Focal plane intensity of focused laser beam passed through turbulent atmospheric layer

10 p1901 A70-25160

Laser light propagation along strongly inhomogeneous turbulent path, measuring intensity fluctuations dispersion and light amplitude

10 p1844 A70-25161

Velocity fields and turbulent pulsations effects on heat transfer in gas flow past plate with rectangular protrusion using wind tunnel tests

10 p1871 A70-25214

Turbulence effect on heat transfer in flow carrying section of turbine engines, considering flow velocity pulsations frequency characteristics

10 p1930 A70-25218

Atmospheric turbulence effects on line-of-sight electromagnetic wave propagation, deriving signal statistics for nonvalid weak scattering solutions case

11 p2012 A70-26764

Semiquantitative study showing variations in degree of laser beam coherence due to turbulence

12 p2245 A70-26980

Magnetic field equation for gyrotropic and anisotropic turbulence, observing large scale magnetic field generation

12 p2210 A70-27546

Rotation law and circulation velocities in solar hydrogen convection zone under anisotropic turbulent velocity

12 p2302 A70-27588

Optical processing for measuring frequency spectrum of PM wave induced by turbulent medium in laser beam

12 p2249 A70-27756

Aircraft dynamic response to homogeneous isotropic atmospheric turbulence analyzed for power spectral density, taking into account spacewise variations in airframe loading

[AIAA PAPER 70-544] 13 p2345 A70-29010

Rotor blade random vibrations in response to turbulence

[AIAA PAPER 70-548] 13 p2339 A70-29013

Strongly accelerated turbulent boundary layer, investigating free stream turbulence effect on heat transfer

14 p2564 A70-30252

Space vehicle response to in-flight wind turbulence, describing operational procedure for launch advisability determination

14 p2653 A70-30587

M31 continuum radio emission produced by magnetic field aligned along arms, discussing field turbulence effects

14 p2642 A70-30891

Time autocorrelation and power spectrum of radar returns from underdense turbulent ionized gas as function of electron density decay

14 p2551 A70-31035

Heat transfer from acceleration induced boundary layer reverse transition, considering free stream turbulence effects

14 p2667 A70-31169

Isolated convective plumes immersed in return flow turbulent downdraft

15 p2769 A70-31440

Atmospheric turbulence effects on optical communication systems in geosciences

16 p2900 A70-33019

Shear flow turbulence effect on chemical reactions, considering two dimensional low speed turbulent mixing layer between high velocity cold gas and air at rest [AIAA PAPER 70-721]

16 p2855 A70-33493

Turbulence spectrum functions time variations, examining electron density fluctuations in ionized gas

16 p2894 A70-33886

Collisionless shocks structure in turbulent wave-particle interactions, obtaining ion distribution function

16 p2959 A70-33970

Load carrying capacity of self acting hydrodynamic journal bearings, considering turbulence and whirling motion in closed form solution

17 p3101 A70-35148

Radio sources angular broadening by solar wind turbulence used for solar corona probe

18 p3311 A70-36003

Ring current belt stability against LF electrostatic perturbations, including effects of finite electric field along magnetic lines of force

18 p3306 A70-36009

Error estimation of gondola encased tugged undersea magnetometer as function of turbulence parameters

18 p3260 A70-36940

Atmospheric turbulence effects on light propagation, measuring refractive index variations by high speed temperature sensors

18 p3285 A70-36961

Laser radar tracking systems, calculating atmospheric turbulence effects on angular errors

19 p3379 A70-37857

Heat transfer in plasma flow incident normally on cylinder, examining laminar boundary layers in presence of turbulence

19 p3552 A70-38187

Propagation mode conversion of Gaussian light beam due to random fluctuations of turbulent medium, discussing effect of aperture size and fluctuations anisotropy

20 p3585 A70-39451

Turbulence effects on lateral directional flying qualities, examining pilot task performance, control workload and compensatory behavior

[AIAA PAPER 70-998] 20 p3560 A70-39533

Gas dynamics turbulence of controlled properties effect on electrical discharge across plasma stream, preventing filamentary nature

20 p3681 A70-40008

Differential rotation at solar surface caused by anisotropic turbulent viscosity in hydrogen convection zone, solving via Navier-Stokes equation

20 p3711 A70-40404

Galactic evolution and secular variations of cosmic rays, magnetic fields and turbulence, assuming stellar birth rate dependence on gas density and temperature

21 p3919 A70-41700

Optical communication in turbulent media, investigating error rate for binary single path fading channels by photocount detection

21 p3837 A70-41935

Free stream turbulence effect on heat transfer to stagnation point of sphere

21 p3953 A70-42095

Atmospheric inhomogeneity and temperature gradient effects on sonic booms, discussing displacement, growth rate and shock wave radii refraction

22 p3961 A70-42311

Linear antenna radiation pattern broadening due to atmospheric turbulence

22 p3995 A70-42386

Large fluid-amplifier-type jets, measuring upstream flow disturbances effects on spreading velocity profiles

[ASME PAPER 70-FLCS-A] 22 p3964 A70-42431

Synthetic aperture terrain-imaging radar systems, calculating tropospheric turbulence induced phase errors for comparison with microwave propagation experiment

22 p3991 A70-43579

Jet aircraft noise reduction devices directed at turbulence fluctuation noise sources, noting effects on flight characteristics

[ICAS PAPER 70-21] 23 p4233 A70-44112

Aerodynamic drag and local convective heat transfer on smooth plate for various flow velocities, determining effects of turbulator in boundary layer transition region

23 p4283 A70-44733

Reynolds stress measurement, using laser flowmeter with cylindrical lenses and square aperture mask

23 p4202 A70-44945

TURBULENCE METERS

Probe geometry effects on hot film anemometer probe performance during turbulence measurements in liquids

06 p1032 A70-17213

Hot wire turbulence measurements of cylindrical wall jet compared to results from free circular and plane wall jets

06 p1034 A70-17526

IR crossed beam system for direct density turbulence measurements in mixing region of subsonic air jet

[AIAA PAPER 70-235] 06 p1065 A70-18091

Turbulence measurement by piezoceramic acoustic sensors, considering capacitance

07 p1284 A70-19829

HF arc anemometer for subsonic and supersonic gas flow turbulence measurement

07 p1285 A70-19837

Optical heterodyning of Doppler shifted signal with minimal instrumental spectral broadening and high SNR, applying to turbulence structure measurement by CW laser

11 p2062 A70-25630

MHD turbulence suppression by magnetic field in tubes, using conduction anemometers

15 p2778 A70-31480

Laser Doppler velocimeter for measuring turbulence in gas and fluid flows

16 p2926 A70-33140

Hypersonic velocity and turbulence measurements in wind tunnels, using spectral analysis of Doppler shifted laser light

17 p3103 A70-34849

Airborne atmospheric turbulent flow measurement system with fast response wind velocity, temperature, humidity and aircraft motion sensors, discussing performance and data reduction

20 p3665 A70-40109

TURBULENT AIR CURRENTS

U AIR CURRENTS

U TURBULENT FLOW

TURBULENT BOUNDARY LAYER

Hot-wire probe support orientation to minimize flat plate turbulent boundary layer mean velocity determination errors

01 p0087 A70-10665

Turbulent boundary layer computations for flows with various pressure distributions

01 p0063 A70-10928

Density and heat transfer effects on compressible turbulent boundary layers used to investigate velocity and temperature profiles, skin friction, Mach number and Reynolds number

01 p0003 A70-10936

Heat transfer in turbulent boundary layer of airflow injected on smooth plate from nozzle in subsonic stepwise heated wind tunnel

01 p0216 A70-11001

Incompressible turbulent boundary layer and separation flow into forward facing normal step, considering step heights and boundary layer thickness

01 p0066 A70-11133

Turbulence constant for flows near walls, analyzing viscosity dependence on wall distance by utilizing maximum stability principle

01 p0069 A70-11627

Turbulent boundary layers computations - Conference, Stanford University, August 1968, Volume 2

02 p0280 A70-12271

Turbulent boundary layers computation - Conference, Stanford University, California August 1968, Volume 1, Methods, predictions, evaluation and flow structure

02 p0280 A70-12326

Prediction systems for turbulent boundary layers, noting momentum integral equation use in all integral methods

02 p0281 A70-12327

Method of weighted residuals /MWR/ for nonlinear partial differential equations applied to incompressible two dimensional turbulent boundary layer momentum and continuity equations

02 p0281 A70-12328

Method of weighted residuals /MWR/ applied to turbulent boundary layer equations, describing two parameter prediction technique

02 p0282 A70-12330

Integral relations method efficiency and accuracy in solving incompressible turbulent boundary layer equations, noting acceptability for turbulent flows with small wake components

02 p0282 A70-12331

Turbulent boundary layers behavior prediction by strip integral momentum equation method, considering velocity profiles and shear stresses

02 p0282 A70-12332

Extended mixing length method for computing turbulent shear stress distribution required in calculating two dimensional incompressible turbulent boundary layer

02 p0282 A70-12333

Modified Granville moment of momentum method used with integral equations in integral moment method for turbulent boundary layer flow, considering pressure gradient influence

02 p0282 A70-12334

Integral theory for two dimensional incompressible turbulent boundary layer in nonequilibrium flows, describing velocity profile in momentum and energy equations

02 p0283 A70-12335

Turbulent boundary layer development calculation by shear work integral method involving Reynolds number introduction procedure

02 p0283 A70-12336

Energy dissipation and entrainment methods for calculating turbulent boundary layer development, involving simultaneous numerical solutions of ordinary differential equations for local variables

02 p0283 A70-12337

Dissipation integral method for turbulent boundary layer problem based on nonequilibrium flow, analyzing inner and outer regions

02 p0283 A70-12338

Integral dissipation method for predicting turbulent boundary layers, taking into account semipirical past history

02 p0283 A70-12339

Turbulent boundary layer calculations by integral dissipation method, using various dissipation coefficient laws

02 p0283 A70-12340

Mixing length theory improvement to calculate turbulent boundary layers based on velocity profiles

02 p0284 A70-12342

Integral method for computing two dimensional incompressible turbulent boundary layer development, including entrainment process of irrotational fluid

02 p0284 A70-12343

Momentum integral method for turbulent boundary layers based on equilibrium profiles family, considering weighting function specification techniques

02 p0284 A70-12345

Conservation equations for mass, mean momentum and kinetic energy for incompressible turbulent boundary layer, using finite difference procedure

02 p0284 A70-12347

Governing equations determined for turbulent boundary layer and quasi-parallel turbulent shear flows, taking into account effects of convection, diffusion, pressure, etc

02 p0285 A70-12348

Mean velocity and mean turbulent energy field methods of calculating boundary layer behavior based on numerical solutions of equations of motions

02 p0285 A70-12349

Boussinesq eddy viscosity concept solving equations of two dimensional incompressible turbulent boundary layer, using implicit five point finite difference method

02 p0285 A70-12350

Hydrodynamic turbulent boundary layer on smooth wall, using finite difference theory

02 p0285 A70-12351

Differential strip method developed for turbulent boundary layer equations, describing flow by law of wall coupled to wake solution utilizing constant eddy viscosity

02 p0285 A70-12352

Finite difference solution of compressible turbulent boundary layer equations of motion, using eddy viscosity concept

02 p0286 A70-12353

Three dimensional turbulent boundary layers on high aspect ratio bodies /swept wings/, discussing shear stress direction determination

02 p0286 A70-12354

Integral methods for turbulent boundary layer solutions, emphasizing shape factor improvement in differential equations

02 p0286 A70-12357

Prediction criteria regarding turbulent separation in fluid mechanical devices and systems, emphasizing vanishing wall shear stress

02 p0286 A70-12358

Turbulent boundary layer response to sudden changes in surface conditions or pressure gradients, considering equilibrium attainment

02 p0287 A70-12360

Waves vs eddies in dynamics of turbulent boundary layer fluctuating motions with scale of mean flow

02 p0287 A70-12361

Graphical display of diverse methods of flow predictions by various authors for turbulent boundary layers

02 p0287 A70-12363

Laminar and turbulent boundary layer equations with or without wall injection over two dimensional or axisymmetric bodies solved by finite difference techniques

02 p0287 A70-12370

Eddy viscosity equation derived from flat plate turbulent boundary layer velocity data, considering shear stresses and mixing length profiles

03 p0464 A70-12943

Porous wall material entrainment in turbulent boundary layer during supplementary inert gas injection, including nonisothermicity effects in heat and mass transfer equations

03 p0440 A70-13385

Turbulent boundary layer of incompressible fluid flow in axisymmetric channels with swirl at inlet, considering components interaction, velocity, circulation profiles and resistance

03 p0466 A70-13389

Energy equation for thermal turbulent boundary layer on adiabatic flat plate

03 p0466 A70-13421

Boundary layer transition from laminar to turbulent in hypersonic wind tunnel, determining Reynolds and Mach number effects [ONERA-TP-737D]

03 p0467 A70-13641

Reaction of three dimensional shock wave with turbulent boundary layer in supersonic flow around plate

03 p0409 A70-13876

Similarity properties of laminar or turbulent boundary layer separation in uniform supersonic flow, discussing wall cooling, pressure evolution, etc

03 p0469 A70-14234

Turbulent fluctuation rates of temperature and velocity on basis of measurements in boundary layer with wall heat transfer

03 p0470 A70-14237

Velocity structure associated with motion of interface between turbulent and nonturbulent fluid at turbulent boundary layer edge, considering shear flows

03 p0470 A70-14240

Secondary velocities analysis in turbulent boundary layer in dihedron interior based on turbulence anisotropy and effects on wall pressure gradient

03 p0471 A70-14354

Boundary layer equations for axial laminar and turbulent incompressible flows over slender bodies of revolution solved by finite difference method

[ASME PAPER 69-WA/FE-2]

Linearized velocity profiles for turbulent free shear layers using transverse shift and longitudinal motion equation

[ASME PAPER 69-WA/APM-28]

04 p0668 A70-14904

Turbulent boundary layer model using two region characterization for eddy viscosity and similarity solution taking into account interfacial conditions

[ASME PAPER 69-WA/APM-27]

04 p0668 A70-14905

Interaction between surface liquid film and hot gaseous turbulent boundary layer analyzed for hypersonic vehicle surface thermal protection design problems

04 p0669 A70-14927

Linear stress distribution insertion into equations of motion for turbulent boundary layer, considering velocity profile in wall region

04 p0670 A70-14987

Radiation from and panel response to supersonic turbulent boundary layer, emphasizing panel mode coupling to acoustic field

04 p0615 A70-15081

Pressure pulsations and velocity measurements in turbulent boundary layer without longitudinal gradient, analyzing Reynolds numbers, self similarity and structural characteristics

04 p0673 A70-15250

Reattachment of supersonic jet with turbulent shear boundary layer abruptly expanding into axisymmetric parallel diffuser, using surface flow technique

04 p0619 A70-15323

Karman formula generalization for turbulent motion in atmospheric boundary layer, including improved variant for thermally stable and unstable conditions

05 p0878 A70-16205

Razor blade calibration and measurement of wall jet flow shear stress in turbulent boundary layer with secondary injection

05 p0833 A70-16504

Acoustic intensity determined from time, length and velocity scales in mixing region of jet from nozzle with turbulent boundary layers

05 p0834 A70-16779

Experimental and analytical work on structural panels vibratory response and acoustic radiation excited by turbulent boundary pressure fluctuations, evaluating applicability to noise research

05 p0835 A70-16789

Incompressible two dimensional turbulent boundary layer equations with arbitrary pressure distribution solved by weighted residual method [AIAA PAPER 69-397]

06 p1032 A70-17214

Two dimensional laminar and turbulent boundary layer flow theory covering heat and mass transfer, compressibility, turbulence, roughness, chemical reactions and axial symmetry

06 p1032 A70-17227

Negative pressure gradients effects on wall heat flow and characteristic patterns for turbulent boundary layer profiles

06 p1033 A70-17231

Turbulent boundary layers and wall jets development investigated for effect of mass injection through porous smooth and rough surfaces

06 p1034 A70-17679

Rotta differential equation for turbulent boundary layer flow with fixed profiles of length scale, shear stress and kinetic energy

06 p1035 A70-17694

Blowing intensity influence on turbulent boundary layer of incompressible fluid and friction drag of flat plate

06 p1036 A70-17852

Laminar ablation testing under turbulent boundary layer heating conditions, obtaining recession rate and heat of ablation for turbulent ablation of Teflon [AIAA PAPER 70-226]

06 p1179 A70-18071

Turbulent boundary layer control by wall jet, analyzing wall jets in adverse pressure gradients for two limiting cases [AIAA PAPER 70-107]

06 p1041 A70-18160

Static pressure, temperature profiles, heat transfer and optical data for turbulent boundary layer-shock interaction with/without injection [AIAA PAPER 70-91]

06 p1042 A70-18210

Steady turbulent boundary layer of compressible perfect gas on heat insulated surface with suction and longitudinal pressure gradient

07 p1254 A70-19081

Turbulent incompressible boundary layer on porous heat insulated plate with uniform suction, calculating ratio of friction drag coefficients

07 p1254 A70-19082

Supersonic oblique shock wave reflection on turbulent boundary layer, considering layer separation and pressure effects

07 p1255 A70-19210

Surface inhomogeneities effect on sound radiated by nearby turbulence near flexible boundary, using converted Lighthill wave equation to obtain far field radiation

07 p1256 A70-19262

Integral methods for predicting two dimensional incompressible turbulent boundary layers development in arbitrary pressure gradients, using momentum integral equation and wall friction relation

07 p1256 A70-19308

Wind tunnel experiments for apparent reverse transition during expansion fan and turbulent boundary layer interaction, discussing Reynolds stresses

07 p1257 A70-19345

Unsteady boundary layer in compressible fluid laminar flow over accelerating semiinfinite flat plate

07 p1258 A70-19566

Heat exchange in laminar and turbulent boundary layers on plate for arbitrary heat flux distribution allowing for initial unheated plate segment

07 p1423 A70-19657

Air flow disturbances over mountains in terms of turbulent boundary layer separation dissolution

07 p1330 A70-19800

Wall proximity and velocity gradient effects on thermocouple readings in turbulent boundary layer

07 p1285 A70-19834

Transverse curvature effects on turbulent boundary layer thickness and velocity profiles on circular cylinders in water and air

07 p1261 A70-20301

Turbulence coefficient and profile in atmospheric boundary layer from wind and temperature distribution, obtaining formulas from model approximating coefficient by altitude function

08 p1538 A70-21112

Transverse pressure gradient effect on parameters of turbulent boundary layer on body rotating in axial flow

08 p1483 A70-21193

Laminarization parameter magnitude determination for turbulent boundary layer in convergent channel flow

08 p1484 A70-21518

Turbulent Prandtl number and eddy viscosity distribution in thermally stratified turbulent boundary layer of air shear flow dependent on wall distance and thermal stability

08 p1599 A70-21581

- Temperature increase effects on fully turbulent boundary layers at low Reynolds number in air investigated in wind tunnel 08 p1485 A70-21606
- Surface roughness effects on measured cross spectral density of wall pressure fluctuations beneath turbulent boundary layer 08 p1486 A70-21859
- Heat and mass transfer in binary turbulent boundary layer during natural convection on vertical surface, allowing for diffusional heat conduction 09 p1787 A70-22267
- Stratospheric CAT layer energy budget analysis, considering energy shear feeding, buoyant extraction and frictional dissipation 09 p1715 A70-22357
- Turbulent energy spectra in stably stratified atmospheric boundary layer flow 09 p1715 A70-22360
- Aerodynamic characteristics of plane straight walled diffusers initial and stabilized flow segments, assuming incompressible fluid and turbulent boundary layer 09 p1659 A70-22430
- Cross hatching on surface of ablating bodies exposed to supersonic turbulent boundary layer flow using mathematical model 09 p1605 A70-23232
- Boundary layer equations with heat transfer for laminar and turbulent incompressible flows about two dimensional and axisymmetric flows, using finite difference method [ASME PAPER 69-HT-7] 09 p1663 A70-23560
- Laminar-turbulent boundary layer transition in incompressible fluid under surface roughness action, developing theory by generalizing Taylor hypothesis 09 p1664 A70-23713
- Boundary layer atmospheric turbulence at Kennedy Space Center obtained for engineering spectral model, discussing energy balance 10 p1911 A70-23926
- Compressible turbulent boundary layer with adverse pressure gradients and crossflow over revolving bodies, integrating numerically three dimensional compressible integral equations 11 p2035 A70-25689
- Film cooling effectiveness measured following air injection through discrete holes into turbulent boundary layer of air on flat plate 11 p2146 A70-25690
- Three dimensional incompressible turbulent boundary layer detachment on rotating blading of axial impellers 11 p1975 A70-25793
- Compression process in turbulent boundary layer on control surface at hypersonic speeds, noting influence on surface effectiveness and heating [ONERA-TP-814] 11 p1979 A70-25815
- Turbulent boundary layer vortex structures using hydrogen bubble technique 11 p2035 A70-25864
- Wall pressure fluctuations beneath turbulent boundary layers on flat plate and cylinder 11 p2038 A70-26529
- Atmospheric turbulent boundary layer velocity signals correlation with lognormal distribution 11 p2076 A70-26531
- Turbulent boundary layer interaction with wavy wall in wind tunnel, discussing wall pressure drag and surface waves interaction 11 p2039 A70-26538
- Motion and shape of interface at separation of turbulent and nonturbulent regions in boundary layer with zero pressure gradient 11 p2040 A70-26539
- Superlayer structure in turbulent boundary layer on flat plate obtained by statistical processing of signals from hot-wire probes 12 p2209 A70-27226
- Turbulent boundary layer in axisymmetric channel having interactions with flow core, calculating flow characteristics and separation point 12 p2209 A70-27289
- Electromagnetic effects on separation of turbulent MHD boundary layers allowing for heat transfer 12 p2278 A70-27324
- Turbulent Prandtl number values for air with injection and suction obtained from velocity and temperature profile data 12 p2210 A70-27699
- Compressibility transformation theory extended for turbulent boundary layer, involving mass transfer with/without chemical reactions 12 p2211 A70-27825
- Compressible turbulent boundary layers velocity profiles, Coles universal wake function, least squares methods, wake-wall representation, etc 12 p2157 A70-28080
- Turbulent boundary layer and base pressure profiles of supersonic flow past conical models in wind tunnel 12 p2159 A70-28229
- Two dimensional turbulent boundary layer with pressure gradient, calculating velocity distribution and local skin friction by Pohlhausen method 13 p2391 A70-29672
- Discrete sonic jets as boundary layer trips producing turbulent hypersonic flows with negligible intrinsic drag and downstream distortions 13 p2523 A70-29973
- Axisymmetric compressible boundary layer on body of revolution transformed into two dimensional turbulent boundary layer 13 p2391 A70-29995
- Turbulent boundary layer formation in upstream wake of accelerated flow indicated from boundary layer profile and wall static pressure measurements 13 p2392 A70-29996
- Three dimensional turbulent boundary layer development on rear of swept wing, comparing measurements with calculations 13 p2344 A70-30021
- Logarithmic and Coles velocity profiles validity for turbulent boundary layers on radial rotating impeller blades 14 p2527 A70-30176
- Strongly accelerated turbulent boundary layer, investigating free stream turbulence effect on heat transfer 14 p2564 A70-30252
- Two dimensional incompressible turbulent boundary layer with mass addition and heat transfer, calculating temperature and velocity profiles by marching integration 14 p2564 A70-30261
- Turbulent boundary layer characteristics on simple shapes in hypersonic flow, using mixing length theory and eddy exchange coefficient 14 p2564 A70-30262
- Atmospheric wind profiles and boundary layer turbulence power spectra for calculation of wind loads on space vehicles during prelaunch and launch 14 p2653 A70-30600
- Turbulent boundary layer loading function for use with finite element structural analysis system applied to elastic aircraft structures random vibration [AIAA PAPER 69-20] 14 p2658 A70-30853
- Starting criterion for hypersonic inlets with large turbulent boundary layers, considering total pressure recovery from all shock and viscous losses 14 p2529 A70-30865
- Turbulent boundary layer correlations on flat plate, noting inadequate Spalding-Chi predictions 14 p2567 A70-31396
- Incompressible turbulent boundary layer calculation based on shearing stress hypothesis, considering layer at flat plate, boundary conditions and velocity profiles 15 p2719 A70-31490
- Longitudinal velocity and temperature fluctuation spectra in turbulent boundary layer, showing highest spectral densities at internal zone 15 p2826 A70-32021
- Turbulent boundary layer instability on rotating cylinder in axial stream, correlating mixing length to Richardson number 15 p2722 A70-32372
- Heat exchange in laminar and turbulent boundary layers on plate for arbitrary heat flux distribution taking into account initial unheated plate segment 15 p2828 A70-32694
- Subsonic turbulent boundary layer with mass addition and combustion for combustion effects on velocity profiles in constant pressure and accelerating flows [AIAA PAPER 70-724] 16 p2997 A70-33498
- Turbulent boundary layer response in flow field downstream of upstanding step change in surface roughness [ASME PAPER 70-FE-17] 16 p2891 A70-33630
- Laminar and turbulent boundary layer equations solutions for incompressible/compressible flows about two dimensional and axisymmetric bodies, using finite difference method [ASME PAPER 70-FE-A] 16 p2892 A70-33641
- Control efficiency of flaps at hypersonic speeds, considering thick turbulent boundary layer compression process 16 p2836 A70-33751
- Aerodynamic admittance of paraboloid dish aerial in scaled atmospheric turbulent boundary shear layer simulated in wind tunnel by vortex generators 16 p2878 A70-33766
- Turbulent boundary layer growth and thickness on yawed cones, discussing angle of attack effect along windward and leeward rays 16 p2838 A70-33875
- Uniform two dimensional turbulent boundary layer with hydrogen-nitrogen mixture injection and combustion at flame front, obtaining velocity distribution by kinetic energy equation 16 p2894 A70-33880
- Axisymmetric blunt base cylindrical body with turbulent initial boundary layer, investigating flow structure in annular nozzle wind tunnel [AIAA PAPER 70-796] 17 p3006 A70-34464
- Analytical model for jet interaction induced separation of supersonic turbulent boundary layers, conducting flat plate tests at Mach 4 [AIAA PAPER 70-765] 17 p3007 A70-34486
- Nozzle wall hypersonic turbulent boundary layers at free stream Mach number using pitot, hot wire, and wall fluctuation and static pressure measurements [AIAA PAPER 70-746] 17 p3065 A70-34497
- Fluctuation measurements at wall and across laminar, transitional and turbulent compressible boundary layers on flat plate, using hot film probes [AIAA PAPER 70-745] 17 p3066 A70-34498
- Temperature and Mach number distributions measurements on supersonic turbulent boundary layers for reanalyzing heat transport [AIAA PAPER 70-744] 17 p3066 A70-34499
- Mean electron density profiles and fluctuations in equilibrium high speed turbulent boundary layers, calculating temperature effects [AIAA PAPER 70-743] 17 p3066 A70-34500
- Probst-Gold model for ablated materials crosshatching patterns, using interaction between inelastic deformable surface and supersonic turbulent boundary layer [AIAA PAPER 70-768] 17 p3009 A70-34504
- Compressible turbulent boundary layers with heat and mass transfer in two dimensional and axisymmetric flows, using eddy transport coefficients [AIAA PAPER 70-741] 17 p3066 A70-34506
- Turbulent boundary layer structure, considering flow properties prediction, wakelike behavior, bursts, compressibility, transport properties, etc 17 p3068 A70-34665
- Turbulent boundary layer velocity, temperature and concentration instantaneous measurements, describing automatic circuit procedure 17 p3088 A70-35041
- Turbulent boundary layer on porous surface with fluid injection into layer reexamined for causes of discrepancy with experimental results 17 p3072 A70-35547
- Heat transfer and friction drag calculation for turbulent boundary layer of gas with temperature dependent physical properties 17 p3012 A70-35729
- Heat and gas curtain efficiency in turbulent boundary layer on flat plate, including heat transfer data 17 p3198 A70-35731
- Local skin friction law for turbulent boundary layers in incompressible flow, applying rule for compressible flow conditions 17 p3075 A70-35922
- Turbulent boundary layer of flat plate, investigating superlayer structure by hot wire anemometer 18 p2338 A70-36066
- Two layer model of burning in turbulent boundary layer on porous surface for carbon monoxide oxidation reaction 18 p3346 A70-36268
- Error analysis of Corcos hypothesis concerning cross spectra of pseudoacoustic LF turbulent pressure pulsations on flat plate 18 p3241 A70-36305
- Previous history effect on parameters relation in similar turbulent boundary layers under pressure distributions 18 p3241 A70-36375
- Conical shock wave-turbulent boundary layer interaction data obtained for adiabatic wall conditions at supersonic free stream Mach numbers, including suction effects 18 p3241 A70-36448
- Wall cooling effects on turbulent boundary layer in low speed air flow, using smooth tube and thermocouple measurements 18 p3347 A70-36505
- Finite plate length effect on two dimensional supersonic turbulent boundary layer with large distributed surface injection 18 p3242 A70-36688
- Favorable pressure gradient effect on compressible two dimensional supersonic turbulent boundary, using temperature and pressure probes and shear balance 18 p3242 A70-36690
- Turbulent boundary layer characteristics on unblown flat plate at low Reynolds numbers, extending to cases with blowing and suction 19 p3405 A70-38020
- Velocity distribution and shear stress measurements in three dimensional turbulent boundary layer approaching separation 19 p3405 A70-38021
- Velocity distribution in boundary layer on thin rotating turbine blade of impeller driven at wind tunnel outlet, solving turbulent and laminar flows momentum equations 19 p3352 A70-38224
- Plane symmetrical and axisymmetrical laminar and turbulent free jets, interpreting statistical character of boundary layer profiles 19 p3407 A70-38684
- Wind speed pulsations measurement at atmospheric boundary layer and different heights, analyzing turbulent energy intensity 19 p3463 A70-38757
- Heat transfer from cylinder in axial air flow with induced turbulence of incident boundary layer, noting temperature effects 20 p3736 A70-39264

Oscillatory flow in turbulent boundary layer modeled by eddy viscosity distribution, deriving mass transport velocity induced by progressive and standing waves

20 p3608 A70-39358

Asymptotic turbulent boundary layer semiempirical Taylor formula, investigating average motion formed in mixing jet region and surrounding liquid

20 p3611 A70-39809

Turbulent boundary layer calculation in incompressible fluid, using one parameter method

20 p3612 A70-39810

Chemically active surface decomposition in dissociated gas flow with turbulent boundary layer, determining diffusion fluxes in laminar sublayer

20 p3612 A70-39812

Turbulent boundary layer on cone in supersonic flow in presence of inflowing foreign substance, considering local surface friction coefficient

20 p3559 A70-39814

Plasma accelerator compressible turbulent boundary layers numerical calculation taking into account MHD effects, electron thermal nonequilibrium and finite rate ionization

20 p3682 A70-40017

Compressible hypersonic turbulent boundary layers solution by finite difference method, relating mixing length to velocity profile shape factor

20 p3684 A70-40269

Turbulent boundary layer in axisymmetric channel having interactions with flow core, calculating flow characteristics and separation point

20 p3613 A70-40339

Wall proximity and velocity gradient effects on thermocouple readings in turbulent boundary layer

20 p3634 A70-40341

Turbulent gas boundary layer at finite Reynolds numbers, investigating relative changes in friction and heat transfer coefficients and temperature factor

20 p3614 A70-40390

Two dimensional turbulent boundary layer computation using two parameter family of velocity profiles and skin friction law

21 p3806 A70-40921

Boundary layer transition application to space shuttle design, relating aerodynamic noise to turbulent boundary layers

21 p3744 A70-41015

Turbulent boundary layers calculation with and without mass addition based on eddy viscosity concept, including accelerating flows

21 p3807 A70-41029

Turbulent boundary layers produced by nonuniform shock tube flow, considering effects on chemical kinetic measurements

21 p3807 A70-41315

Eddy currents in Hall generator with conducting side wall, studying velocity and temperature effects for turbulent boundary layer and laminar flows

21 p3859 A70-41733

Transformation theory for compressible turbulent boundary layer with arbitrary pressure gradient

[AIAA PAPER 69-160] 21 p3809 A70-41741

Electromagnetic effects on separation of turbulent MHD boundary layers allowing for heat transfer

21 p3860 A70-42065

Three dimensional laminar and turbulent boundary layers separation criteria

21 p3811 A70-42206

Karman-Pohlhausen method applied to unsteady thermal boundary layer on isothermal flat plate

21 p3954 A70-42208

Turbulent hydrodynamic and thermal boundary layer development in internally heated annulus

[ASME PAPER 70-HT-9] 22 p4008 A70-42438

Steady incompressible turbulent boundary layer form on permeable curvilinear surface with uniform suction, assuming small pressure gradients

22 p4011 A70-42803

Stationary turbine blades heat flux measurements, considering heat exchange coefficients and turbulent boundary layer

[ONERA-TP-871] 22 p4126 A70-43459

Turbulent boundary layer control by uniform fluid injection and suction, discussing velocity profiles, wall and wake laws, skin friction and shear stress transport equation

[ICAS PAPER 70-10] 23 p4180 A70-44121

Laminar to turbulent boundary layer flow transition over flat plate, using space amplified numerical solutions of Orr-Sommerfeld equation

23 p4181 A70-44234

Entrainment theory for incompressible turbulent boundary layer velocity and drag on bodies of revolution employed in fuselage, submersible and cowlings for propulsion design

23 p4182 A70-44400

Vane type vortex generators to prevent turbulent compressible boundary layer separation, measuring drag in supersonic flow

23 p4133 A70-44527

Heat transfer from turbulent boundary layer interacting with shock and expansion waves in supersonic flow

23 p4134 A70-44573

Turbulent boundary layer velocity profiles and shear stress distributions computation based on mixing length approach

23 p4182 A70-44574

Cracked Teflon heat shields ablative behavior for laminar and turbulent boundary layers in supersonic flow, describing heat transfer to substructure

23 p4282 A70-44585

Highly accelerated boundary layer turbulence structure, measuring intermittency factor distribution with hot-wire probe

23 p4182 A70-44587

German monograph on radioactive gases and decomposition products mass transport in turbulent atmospheric boundary layer, noting Boussinesq approximation and Reynolds decomposition

24 p4324 A70-45094

Sphere rotating in viscous fluid at rest, investigating surrounding flow field from creeping flow to turbulent boundary layer

24 p4326 A70-45989

TURBULENT DIFFUSION

Vortex diffusion in viscous compressible fluid, deriving nonlinear differential equations from density velocity and pressure discontinuities considerations

01 p0060 A70-10145

Book on turbulent diffusive flames in combustion of gaseous fuels covering mass, heat, flame exchange and stabilization processes, etc

01 p0219 A70-11377

Dynamics of turbulent motion of incompressible viscous fluid particles, using Lagrangian functions

01 p0068 A70-11603

Velocity and density profiles obtained from mass diffusivity time measurements in axisymmetric turbulent air pipe flow over specific Reynolds number range

02 p0295 A70-11853

Stellar model surface convective zone using diffusion equation taking into account transport due to gravitational separation, noting role of turbulent diffusion

03 p0574 A70-13932

Plasma turbulence theory formulated using averaging operators, obtaining nonlinear dispersion relation for turbulent diffusion coefficients

03 p0537 A70-14377

Turbulent heat and mass diffusion in catalytic reactors for hydrazine decomposition, developing computer program to calculate temperature and reactant concentration distributions

[AIAA PAPER 69-421] 07 p1365 A70-19706

Vertical eddy diffusion effect on chemical composition of mesosphere and lower thermosphere using photochemical model containing oxygen and hydrogen

07 p1274 A70-20269

Atmospheric turbulence parameters in meteor zone determined from simultaneous photographic and radar observations, determining turbulent diffusion coefficient dependence on height

08 p1563 A70-20546

Horizontal turbulent diffusion model of cloud, determining particles dispersion as function of time

08 p1538 A70-21111

Modified diffusion approximation for spectral transfer of isotropic turbulent pulsation energy for temperatures with low Prandtl number

08 p1538 A70-21429

Turbulent diffusion and ion heating in plasmas in presence of current instability

08 p1554 A70-21813

Turbulent combustion stability in chamber, taking into account boundary effects due to acoustic perturbations reflection

09 p1786 A70-22106

Self diffusion in turbulent fluid motion attributed to flow turbulence and linked to mean motion by mass conservation

09 p1663 A70-23310

Eddy penetration model for heat transfer from trailing face of cylinder in transverse flow

09 p1791 A70-23566

Downward ozone transport from troposphere to atmospheric boundary layer by turbulent diffusion calculated by model, estimating annihilation rate

10 p1875 A70-24486

Plasma turbulent diffusion across constant magnetic field, noting magnetic, kinetic energy and relaxation times ratio effects

11 p2094 A70-26755

Turbulent diffusion coefficients and time dependent velocity pulsations in air flow, considering relation between Eulerian and Lagrangian turbulence characteristics

12 p2213 A70-28235

Turbulent diffusion random model of foreign substance, investigating latent parameters existence

13 p2387 A70-29211

Global atmospheric models computations based on treating molecular and eddy diffusion as dynamic processes

14 p2606 A70-30561

Atmospheric turbulence parameters in meteor zone determined from simultaneous photographic and radar

observations, determining turbulent diffusion coefficient dependence on height

15 p2796 A70-31455

Annoyance assessment for sonic boom series exposure near airport

16 p2843 A70-34325

Model diffusion equation for inhomogeneous incompressible turbulent flow, applying to free turbulent flows

17 p3069 A70-34825

Turbulent velocity pulsations characteristics determination by diffusion measurements

18 p3240 A70-36265

Free atmosphere turbulent diffusion coefficient determination, releasing dipole reflectors from helicopter for radio echo observation

19 p3461 A70-37423

Ring current protons turbulent diffusion in magnetospheric plasmapause, considering ion cyclotron wave lifetime and geomagnetic storms

21 p3881 A70-41085

Turbulent charge diffusion during unipolar injection in nitrobenzene between plane-parallel electrodes, discussing liquid motion at high voltages

22 p4080 A70-42719

German monograph on soot formation and separation in turbulent diffusion flame in power plant combustion chamber, noting pyrolysis role

24 p4428 A70-45087

TURBULENT FLOW

NT CAVITATION FLOW

NT SUPERCAVITATING FLOW

Stiffness values of externally pressurized incompressible fluid-film thrust bearings under turbulent Couette flow, discussing Reynolds number effects

[ASME PAPER 69-LUB-25] 01 p0100 A70-10383

Inertia forces effect in turbulent and laminar, self acting and infinitely long film bearings, considering compressible and incompressible lubricants

[ASME PAPER 69-LUB-2] 01 p0103 A70-10400

Goertler vortices effect on boundary layer transition on concave surface, discussing instability oscillations breakdown leading to turbulent motion

01 p0061 A70-10539

Polarographic probe for wall studies of turbulent flow velocity and direction by measuring maximum reduction current on redox compound microelectrode

01 p0062 A70-10664

Flow velocity pulsations effect on frequency spectrum of flow optical fluctuations, discussing methods for separating turbulence characteristics

01 p0092 A70-10996

Mass transfer analysis for axisymmetric turbulent flow in circular tube, deriving turbulent velocity profile from two part model, based on von Karman similarity hypothesis

01 p0064 A70-11092

Nonaxisymmetric mass transfer in turbulent flow in plain circular tube, considering diametral line and discontinuous ring sources

01 p0065 A70-11093

Pitot tube measurements of mixing zone of turbulent shear flow, discussing velocity gradient effects

01 p0066 A70-11134

Sound radiation from airfoil in turbulent jet flow, discussing direct correlation of fluctuating lift

01 p0004 A70-11192

Turbulent fluid flow analysis described by Navier-Stokes equations, introducing asymmetric tensors for anisotropic cases

01 p0068 A70-11605

Turbulent viscosity and thermal conductivity coefficients for entire cross section of fluid flow including wall boundary layers

01 p0069 A70-11624

Turbulent viscous fluid flow characteristics obtained from integrating Navier-Stokes equation for unsteady flow with periodic momentum variation

01 p0069 A70-11626

Pressure drops in turbulent flow through circular or plane parallel section pipes, obtaining mean velocity expressions suitable for application to lubrication

02 p0277 A70-11912

Volumetric reaction rates and mass transport coefficients as function of position for ducted two dimensional turbulent hydrogen-air diffusion flame

02 p0398 A70-12036

Spiral grooved turbulent screw seal/viscoseal/analysis, combining results of spiral grooved journal bearing study with turbulent fluid film theory

[ASLE FICFS PREPRINT 32] 02 p0308 A70-12169

Energy reversal zones in turbulent shear flows with asymmetric mean velocity distribution, implying zones of opposing shear

02 p0279 A70-12228

Integral method for turbulent shear flow based on momentum and moment-of-momentum equations and Cole velocity profile family, determining shear stress integral

02 p0282 A70-12329

Integral relations method efficiency and accuracy in solving incompressible turbulent boundary layer equations, noting acceptability for turbulent flows with small wake components

02 p0282 A70-12331

- Shear stress transport equation derivation from turbulent energy equation based on properties of turbulent velocity fluctuations 02 p0284 A70-12346
- Governing equations determined for turbulent boundary layer and quasi-parallel turbulent shear flows, taking into account effects of convection, diffusion, pressure, etc 02 p0285 A70-12348
- Experimentation in fluid mechanics research, discussing equilibrium flows, relaxation processes, turbulence structure and digital techniques 02 p0286 A70-12355
- Wave packet dynamics recapitulation and tentative application to turbulent shear flow 02 p0287 A70-12362
- Statistical model of turbulent chemically reacting shear flows, analyzing wave number fluctuations effect and Couette flow 03 p0464 A70-12928
- Schlieren photograph intensity variations correlated with statistical parameters for turbulent flow density variations 03 p0464 A70-12941
- Laminar-turbulent transition in free axisymmetric viscous incompressible jet from shaped nozzle and long cylindrical tube 03 p0466 A70-13396
- Turbulence in hypersonic nozzle due to two phase flow of ideal gas and solid spherical particles, discussing thermal and dynamic differences 03 p0407 A70-13494
- Selectivity and pulsation sensitivity of electroacoustic transducers in turbulent flow under non-coherent reception of random pressure field 03 p0467 A70-13514
- Swirling flow through axisymmetrically deformed tube without consideration of viscosity and compressibility, noting wall flow for critical Rossby number values 03 p0468 A70-13788
- Heat transfer coefficient in turbulent duct flow of fine particles suspension, using coupled similar equations 03 p0608 A70-14382
- Turbulent flow velocity and stress components simultaneous measurement by single hot wire, discussing equations and computer program 04 p0685 A70-14447
- Structural similarity hypothesis for fully developed turbulence in smooth circular tubes, using intensity correction procedure 04 p0665 A70-14453
- Settling length for turbulent air flow velocity profile in smooth concentric annuli with square-edged and bellmouth entrances [ASME PAPER 69-WA/APM-24] 04 p0669 A70-14908
- Laminar and turbulent flows of compressible media in rotating pipes, analyzing velocity distribution, angular velocity and Coriolis effects using Abel equation 04 p0672 A70-15159
- Curvature effects on two dimensional turbulent wall jet flow over plane surface and circular convex and concave surfaces in still air 05 p0832 A70-16118
- Inviscid Burger turbulence spectral equations for cumulant approximation, obtaining energy spectrum and transfer as initial value problems 05 p0832 A70-16147
- Nozzle exit turbulence and excess fuel combustion as low and high speed jet noise source using Lighthill theory 05 p0834 A70-16782
- Frictional drag reducing polymer solution injection into boundary for turbulent pipe flow, discussing Reynolds number, injection rate, injection points and concentration 06 p1032 A70-17215
- Conservation equation for thermal energy in turbulent shear flow, including turbulence kinetic energy equation terms [WSCI PAPER 69-43] 06 p1179 A70-17983
- Long chain molecule additive effect on drag reduction in turbulent flow of aqueous polymeric solutions [AIAA PAPER 70-56] 06 p1037 A70-18030
- Isoenergetic mixing and reattachment processes of two dimensional supersonic turbulent separated flow, modeling mixing process by constant pressure theory [AIAA PAPER 70-108] 06 p1037 A70-18039
- Time dependent transport equations for full Reynolds stress tensor and turbulence decay function using flux approximations and relaxation model [AIAA PAPER 70-3] 06 p1038 A70-18080
- IR crossed beam system for direct density turbulence measurements in mixing region of subsonic air jet [AIAA PAPER 70-235] 06 p1065 A70-18091
- Shear wave interaction in infinite homogeneous reacting fluid, using Fourier and Taylor series for velocity, temperature, density, pressure and composition [AIAA PAPER 70-146] 06 p1040 A70-18154
- Frequency analysis of arterial sounds used in studying atherosclerosis, correlating spectra with jet flow turbulence past occlusion [AIAA PAPER 70-144] 06 p1003 A70-18220
- Yawed hot wire measurements of turbulence fluctuations, discussing calibration and mutual interference of adjacent wire and wire supporting prongs in X-ray wire case 06 p1071 A70-18487
- Boundary value problems and Cauchy problem considered for mathematical model of turbulent motion in liquid or gas 07 p1252 A70-18671
- Strain rate tensor coincidence in Lagrangian and Eulerian descriptions of turbulence demonstrated for homogeneous flow of incompressible fluid 07 p1252 A70-18672
- Correlation function of velocity fields in two dimensional turbulence determined from hydrodynamic equation assuming normally distributed stream function field 07 p1252 A70-18673
- Turbulent friction in gas flow core determined on basis of maximum stability principle 07 p1253 A70-18719
- Viscous fluid flow calculations in fine clearance eccentric annuli allowing for pressure losses in laminar or turbulent flows 07 p1293 A70-19120
- Microphone output level in airstream relation to sound pressure and pressure fluctuations caused by turbulent flow 07 p1334 A70-19372
- Turbulent velocities of convective motions in active and unperturbed photospheric faculae based on spectral observations 07 p1384 A70-19415
- Vertical plume velocity and temperature measurements by hot wire probe on turbulent free convection zones over model fires 07 p1282 A70-19582
- Soviet book on unsteady attached turbulent flow in turbine lattices, studying blade aerodynamic vibrations onset and attenuation in compressible and incompressible fluids 07 p1189 A70-19602
- Turbulent shear flow kinematic characteristics determined by photographic method and flow visualisation using vortex model 07 p1259 A70-19827
- Circular nozzle contraction and Reynolds number effects on turbulent pulsation damping, measuring longitudinal and transverse components 07 p1259 A70-19830
- Damped turbulent whirling tube flow friction characteristics and heat exchange, solving equation of maximum tangential flow rate 07 p1261 A70-20464
- German book on fluid dynamics for nonideal fluids covering viscosity effects, Prandtl boundary layer, turbulence and aerodynamics 08 p1431 A70-20751
- Flow turbulence effect on heat turbines efficiency using energy losses in blade cascades 08 p1432 A70-21073
- Flow turbulence in wind tunnel model tests, observing generation methods effect on aerodynamic flow characteristics distribution 08 p1483 A70-21074
- Flame propagation rate and combustion zone extension dependence on chamber dimensions for turbulent flow of homogeneous mixtures 08 p1597 A70-21187
- Elastic coatings effect on turbulent friction using turbulence flow theory based on mixing length concept 08 p1483 A70-21227
- Dissolved macromolecules effect on flow resistance due to turbulent friction in nonNewtonian liquids, considering physical parameters and hydrodynamic conditions 08 p1483 A70-21228
- Turbulent-laminar transition in divergent radial flow between disks, relating velocity fluctuations to Reynolds number 08 p1483 A70-21235
- Static pressure gradient influence on turbulent shear stresses and energy production in asymmetric wall jet flow 08 p1484 A70-21314
- Prandtl-Kolmogoroff model of turbulence with inclusion of second order terms for stress and velocity gradient not to vanish coincidentally 08 p1484 A70-21458
- Turbulence model, noting possibility of turbulence energy to vanish with distance from tunnel central point of entrance 08 p1486 A70-21770
- Instantaneous velocities measured for wall region of smooth duct during turbulent fluid flow by chronophotography of particles 09 p1658 A70-22046
- Turbulent MHD channel flow velocity profiles and hydraulic resistance relations for various Reynolds numbers, using two layer model 09 p1658 A70-22175
- Stably stratified atmospheric turbulent shear flow governing spectral equations asymptotic solutions for buoyancy subrange 09 p1659 A70-22372
- Laminar-turbulent regions boundary, discussing convective layer form and FM-CW microwave and acoustic radar measurement techniques 09 p1717 A70-22378
- Steady turbulent perfect compressible gas flow in axisymmetrical or plane channel, using equations governing channel height and static pressure variations 09 p1659 A70-22429
- Axisymmetric helium jet transition to turbulent flow in air slipstream, measuring temperature and velocity profiles 09 p1660 A70-22439
- Average velocities profile measurement in wall region of turbulent fluid flow in smooth duct 09 p1661 A70-22838
- Self diffusion in turbulent fluid motion attributed to flow turbulence and linked to mean motion by mass conservation 09 p1663 A70-23310
- Turbulent pipe flow with wall suction, calculating friction factor, pressure gradient, heat and mass transfer coefficients, velocity and temperature profiles [ASME PAPER 69-HT-4] 09 p1790 A70-23558
- Blade inter-row distances upstream and downstream related to potential flow velocity disturbances created by cascade in turbomachines 09 p1607 A70-23734
- Streamwise perturbations in flow downstream of self excited blades cascade calculated by two dimensional theory, discussing periodic circulation shedding 09 p1608 A70-23746
- Compressor blade performance dependence on Reynolds number, turbulence intensity and axial velocity ratio, considering wind tunnel tests with porous side walls 09 p1609 A70-23748
- Turbulent flow criterion for negligible initial boundary layer case, introducing corrections regarding Korst criterion as function of geometric and aerodynamic flow 10 p1799 A70-24128
- Pulsating flow mean total pressure measurement accuracy in high turbulence regions, discussing standing and traveling acoustic waves produced at measuring system entrance 10 p1867 A70-24160
- Low Mach number aerodynamic sound generation by turbulent flow at sharp edged thin scattering half plane solved with Green function 10 p1802 A70-24521
- Turbulent trailing vortex decay calculated from circumferential velocity and eddy viscosity dependent on Reynolds number 10 p1802 A70-24561
- Turbulent water flow velocity distribution measurement using laser light intensity fluctuation spectroscopy 10 p1869 A70-24600
- Turbulent flow downstream from abrupt widening of circular jet, using flow and momentum equations 10 p1870 A70-24782
- Turbulent flow generation by interacting principal stream with transverse jets, obtaining flow domains in test chamber of two dimensional wind tunnel 10 p1870 A70-24785
- Grid turbulence unified analysis, estimating turbulence intensity, dissipation length and integral scale for any grid flow 10 p1871 A70-24976
- Ultraclean technology to eliminate pollution traces present in laboratories, discussing turbulent flow and horizontal and vertical laminar flow rooms 10 p1828 A70-25240
- Turbulence model with level and scale functions for flows including homogeneous turbulence, logarithmic boundary layer, duct center flow, linear shear layer and viscous sublayer 11 p2035 A70-25685
- Fluid material line growth in grid-generated isotropic turbulent flow measured by tagging lines with hydrogen bubbles 11 p2035 A70-25843
- Three dimensional turbulent flow, using direct interaction approximation for growth and propagation of point-to-point velocity field deviations energy spectrum 11 p2036 A70-26013
- Turbulent flow detachment in incompressible fluid around thick bodies, considering plate perpendicular to wind 11 p2037 A70-26466
- Nonturbulent fluid entrainment into turbulent flow dependent on flow properties controlling energy balance 11 p2038 A70-26528

Nearly homogeneous turbulent shear flow for flow field structure, determining pressure/ velocity tensor using wind tunnel

11 p2039 A70-26530

Multipoint time correlations of longitudinal velocity fluctuations in grid-generated turbulence

11 p2039 A70-26532

Equilibrium properties of nearly normal turbulence assuming near-Gaussian nonlinear model equations and real turbulence

11 p2039 A70-26533

Time-convergent approximations to statistical turbulence functions constructed starting with functions expansion as Taylor series in time

11 p2074 A70-26534

Momentum transport bounds in turbulent shear flow using variational methods

11 p2039 A70-26535

Turbulent flow-Conference, Seattle, June 1969

11 p2039 A70-26536

Plane wave disturbances introduced in turbulent channel flow by vibrating ribbons near each wall, obtaining amplitude and relative phase

11 p2039 A70-26537

Two dimensional incompressible mixing layer investigated by constant temperature linearized hot wire anemometers, discussing turbulent/nonturbulent interfaces

11 p2040 A70-26540

Turbulence theory based on Wiener-Hermite expansion of velocity distribution to predict energy decay rate for Reynolds numbers greater than two

11 p2040 A70-26542

Turbulent three dimensional Poiseuille channel flow at large Reynolds numbers, investigating eddy shapes and energy balance

11 p2041 A70-26546

Turbulence of fluids and plasmas - Conference, New York, April 1968

11 p2093 A70-26751

Interaction between turbulent air flow and water surface based on Fourier analysis of finite intervals of field

11 p2042 A70-26775

Intermittency role in free turbulent flow and EM wave scattering by hypersonic wakes

11 p1978 A70-26776

Pulsation energy distribution in turbulent flow of incompressible fluid near tube wall, defining energy diffusion, production and dissipation terms in energy balance equation

12 p2210 A70-27321

Nonisothermal burn-up rates of graphite surfaces in turbulent air flow under neutral gas shield estimated by measuring channel diameter

12 p2331 A70-27323

Time or space decay of turbulent parameters along flow direction in jets, wakes or grid-generated turbulence, illustrating time variation of wave number spectrum

12 p2211 A70-27831

Compressible turbulent plane Couette flow solution with variable heat transfer based on von Karman model extended to arbitrary wall temperature

12 p2211 A70-27839

Tube relaminarization, predicting turbulent-to-laminar flow transition

12 p2212 A70-28118

Incompressible fluid turbulent motion statistical equations, considering Lagrangian distributions of fluid particles coordinates and velocities

12 p2212 A70-28190

Turbulence energy balance equations for conducting fluid flow in longitudinal magnetic field with Joule dissipation

12 p2282 A70-28227

Turbulent diffusion coefficients and time dependent velocity pulsations in air flow, considering relation between Eulerian and Lagrangian turbulence characteristics

12 p2213 A70-28235

Suspended Stokes particle-single wave interaction effect on energy dissipation and vorticity of random turbulent incompressible fluid approximated by Fourier-Stieltjes integral

12 p2213 A70-28236

Turbulent flow of incompressible fluid, obtaining closed system of approximate equations for probability distribution of velocities

12 p2213 A70-28237

River bed channel flow instantaneous velocities described by logarithmic law, determining turbulent energy dissipation

12 p2265 A70-28336

Turbulent shear flow energy spectrum theory for unstratified fluid with arbitrary eddies-mean velocity gradient interaction

12 p2214 A70-28364

Turbulent base flowfields in multinozzle configurations, considering adiabatic flow and determining base pressure distribution from reverse jet impingement [AIAA PAPER 69-570]

13 p2338 A70-28511

Mathematical background for strong turbulence analysis in liquids and MHD

13 p2457 A70-28554

Graphite mass removal rates under ohmic heating in reacting gas turbulent flows

13 p2519 A70-28579

Turbulent base pressure on conical afterbodies in supersonic axisymmetric flow, including initial direction effect

[AIAA PAPER 70-555]

13 p2340 A70-29020

Turbulent shear flow direct interaction equations simplification to differential equations amenable to computation

13 p2389 A70-29463

Hydrodynamic forces by oscillating foils in ideal incompressible fluid turbulent flow with stream separation

13 p2390 A70-29649

Sting diameter and cylindrical protuberance length effects on axisymmetric body base pressure in turbulent supersonic flow

[AIAA PAPER 70-585]

13 p2342 A70-29885

Incompressible turbulent fluid flow through ducts and pipes by integral boundary layer techniques, considering entrainment principles

14 p2564 A70-30258

Two dimensional incompressible steady turbulent flows based on Prandtl hypothesis relating eddy viscosity to kinetic energy and scale

14 p2564 A70-30259

Radiation effects on heat transfer in turbulent channel flow for small optical depths and optically thin limit

14 p2665 A70-30548

Statistical transport, energy and chemical reaction rate in turbulent flow field with uniform velocity gradient, using Brownian motion theory

14 p2566 A70-31029

Turbulent chemical reactions invariance preservation for zero diffusivity

14 p2546 A70-31044

Boundary value problems and Cauchy problem considered for mathematical model of turbulent motion in liquid or gas

15 p2718 A70-31463

Strain rate tensor coincidence in Lagrangian and Eulerian descriptions of turbulence demonstrated for homogeneous flow of incompressible fluid

15 p2718 A70-31464

Correlation function of velocity fields in two dimensional turbulence determined from hydrodynamic equation assuming normally distributed stream function field

15 p2718 A70-31465

Homogeneous isotropic turbulence velocity field space-time variable correlation functions in fluid flow

15 p2719 A70-31487

Model for hydraulic resistance reduction for turbulent fluid flows by injecting suspended impurities

15 p2719 A70-31489

Turbulent flow theory of dilute linear polymer solutions in smooth and rough tubes based on Reynolds equation

15 p2719 A70-31491

Laminar to turbulent transitions determination in sub-/supersonic flows, reviewing methods based on hot-wire anemometer output signal [ONERA-TP-841]

15 p2720 A70-31918

Laminar to turbulent flow transition observation in laser induced vertical convection, using carbon dioxide-nitrogen laser

15 p2751 A70-31980

Annular turbulent flow between coaxial rotating cylinders, analyzing energy balance of averaged and pulsating motions

15 p2721 A70-32138

Laser velocimeter application to laminar-turbulent flow transition at glass tube centerline

15 p2741 A70-32521

Book on flow separation covering steady/unsteady, turbulent and incompressible flows, base pressure, thermal effects, etc

16 p2833 A70-32913

Ignition and combustion in ducted turbulent supersonic flow, discussing premixed and unpremixed ethylene

[AIAA PAPER 70-720]

16 p2997 A70-33488

Chemiluminescent processes accounting for radiation from turbulent wake flows behind hypersonic spheres in air

[AIAA PAPER 70-729]

16 p2997 A70-33492

Turbulent and reacting flows temperature and mixing rates determination, using gaseous HF tracer spectroscopy

[AIAA PAPER 70-726]

16 p2856 A70-33497

Diffusion flame development in homologous turbulent shear flow, investigating flame structure and chemical reaction by statistical theory

[AIAA PAPER 70-722]

16 p2997 A70-33499

Nuclear rocket nozzle cooling passages, discussing heat transfer and friction correlations for single-phase hydrogen turbulent flow

[AIAA PAPER 70-661]

16 p2950 A70-33622

Normalized Reynolds stress tensor in upstream region of fully developed turbulent shear flow as function of position, using inviscid linear model

[ASME PAPER 70-FE-2]

16 p2891 A70-33626

Laminar boundary layer model for viscous losses during transient turbulent liquid flow in tube, assuming slug flow for core

[ASME PAPER 70-FE-8]

16 p2891 A70-33627

Incompressible free jet characteristics determination from unique differential equation in laminar and turbulent flow regimes by unitary method

16 p2893 A70-33750

Incompressible viscous fluid divergent turbulent flow detection in conical tube of revolution based on measuring wall pressure differences along tube generatrix

16 p2894 A70-33849

Turbulent kinetic energy equation for determining turbulent flow fields applied to free mixing problem of constant density streams

16 p2894 A70-33856

Transport and relaxation processes prediction for turbulent fluid, noting similarities to Fourier integral representation of flow field

16 p2895 A70-33969

Turbulent flows calculation based on two parameter turbulence model, considering model application to free jets

16 p2895 A70-34199

Turbulent flow in stratified fluids over flat plate, relating density profile curvature and heat transfer

16 p2895 A70-34242

Turbulent shear flow asymptotic theory, discussing channel, pipe and two dimensional boundary layers

16 p2895 A70-34244

Annoyance assessment for sonic boom series exposure near airport

16 p2843 A70-34325

Upper pulmonary airways plastic conduit model, measuring laminar and turbulent flow velocity profiles by hot-wire anemometer

17 p3035 A70-34469

Long chain molecule additive effect on drag reduction in turbulent flow of aqueous polymeric solutions

17 p3066 A70-34525

Absolute stability and turbulent transport upper bounds in Couette flow, using variational analysis

17 p3066 A70-34543

Atmospheric radon concentration ratios diurnal and vertical variations used for turbulent exchange and washout study

17 p3132 A70-34611

Model diffusion equation for inhomogeneous incompressible turbulent flow, applying to free turbulent flows

17 p3069 A70-34825

Temperature dependent absorption, nonsteady beam propagation and laminar-turbulent transition in laser induced convection column, measuring turbulence onset by fine wire resistance thermometer [AIAA PAPER 70-800]

17 p3107 A70-35197

Turbulent gas flows shear turbulence structure at various Reynolds numbers in nonconducting channels with and without heat transfer under transverse magnetic field

17 p3141 A70-35245

Micropolar fluids turbulent flow, investigating microstress couples, stability, inviscid flow, etc

17 p3071 A70-35435

Variational principle for turbulent shear flow between parallel plates, taking into account isothermal flow and Malkus theory

17 p3073 A70-35595

Turbulence theory from Liouville equation for Navier-Stokes velocity field distribution

17 p3073 A70-35629

Semiempirical theory of anisotropic turbulent transport, deriving closed system of flow equations

17 p3107 A70-35736

Fluid turbulence unified heuristic model, defining determinate solutions for Navier-Stokes equations numerical integration at high Reynolds numbers

17 p3074 A70-35884

Chemical kinetics effect on combustion rates of fuel plate in turbulent oxidizer flow, deriving conservation equations in boundary layer and diffusion equation

18 p3346 A70-36245

Turbulent velocity pulsations characteristics determination by diffusion measurements

18 p3240 A70-36265

Turbulent shear flow velocity and kinetic energy distributions in tunnel

18 p3241 A70-36383

Turbulent air flow in vertical square duct, investigating local heat transfer and friction coefficients

18 p3347 A70-36506

Turbulent flows shadowgraph analysis, solving electromagnetic equations for optical response

18 p3242 A70-36692

Flame propagation velocity of gasoline-air mixture during two stage combustion process in laminar and turbulent flows, discussing combustion products effect

19 p3550 A70-37253

Turbulent velocity correlation function computation in Burger fluid model, using functional integral expression

19 p3403 A70-37530

- Stiffness values of externally pressurized incompressible fluid-film thrust bearings under turbulent Couette flow, discussing Reynolds number effects [ASME PAPER 69-LUB-25] 19 p3435 A70-37611
- Inertia forces effect in turbulent and laminar, self acting and infinitely long film bearings, considering compressible and incompressible lubricants [ASME PAPER 69-LUB-2] 19 p3435 A70-37613
- Eringen theory of micropolar fluids for hydrodynamic turbulence 19 p3404 A70-37783
- Turbulent flow phase velocity fluctuations measurement by hot-wire anemometers, obtaining cross-spectral density by Fourier analysis digital techniques 19 p3404 A70-38019
- Energy spectrum function for Gaussian initial velocity field of inviscid turbulence Burger model, using Cameron-Martin-Wiener exact expansion 20 p3609 A70-39653
- Steady turbulent flow heat exchange in near wall region at large Prandtl numbers, plotting temperature distribution curves 20 p3612 A70-39811
- Turbulent shear stress correlation with turbulent kinetic energy for wake and circular jet flow conditions 20 p3613 A70-40277
- Longitudinal averaged and pulsating turbulent flow velocities in rectangular channel with one-sided air injection through porous wall 20 p3614 A70-40346
- Neutron star superfluid turbulent state, applying dynamic model to conditions in pulsars 20 p3713 A70-40429
- Wall jet turbulent flow regions with shear stress and mean velocity gradient of opposite sign, considering theoretical explanation 20 p3615 A70-40501
- Turbulent flow asymmetrical mechanics equations derivation from conservation laws, discussing Navier-Stokes equation, angular momentum and transport theory 21 p3806 A70-40612
- Transport model for flow field and convective heat transfer in planar turbulent supersonic base flow 21 p3744 A70-41030
- Flow field, heat transfer rates and reattachment surface wall temperature of planar supersonic turbulent flow 21 p3744 A70-41036
- Turbulent density fluctuations statistical properties analysis by cross correlation technique with schlieren instruments 21 p3807 A70-41242
- Unsteady convective heat transfer and hydrodynamics of laminar and turbulent channel flows 21 p3808 A70-41374
- Heat transfer and skin friction in quasi-steady axisymmetric turbulent pipe flow of incompressible fluid with variable physical properties 21 p3808 A70-41375
- Constant temperature linearized hot-wire anemometer for low velocity high turbulence flow 21 p3827 A70-41455
- Turbulence measurements in ducted coaxial air flow with faster outer stream pertinent to gas core nuclear rocket feasibility 21 p3809 A70-41748
- Interactions between components of turbulent flow velocity correlation tensor due to pressure fluctuations 21 p3810 A70-41956
- Vibrational response of thin walled pipes to internal turbulent water flow as function of Strouhal number 21 p3940 A70-42052
- Pulsation energy distribution in turbulent flow of incompressible fluid near tube wall, defining energy diffusion, production and dissipation terms in energy balance equation 21 p3810 A70-42062
- Nonisothermal burn-up rates of graphite surfaces in turbulent air flow under neutral gas shield estimated by measuring channel diameter 21 p3952 A70-42064
- Closing method for turbulence equations of velocity field quantities joint probability distributions 21 p3811 A70-42075
- Mass flow rate correlation for nonsteady convective heat transfer in thin walled tubes with turbulent air flow 21 p3953 A70-42087
- Turbulent air flow measurements through heated pipe, determining local heat flux from simultaneous velocity and temperature fluctuation 21 p3811 A70-42091
- Turbulent flow velocity profile in constant transverse magnetic field, determining resistance coefficient 21 p3861 A70-42235
- Newtonian fluid turbulent flow development characteristics in inlet region of smooth concentric annulus from momentum integral equations 22 p3957 A70-42304
- Downstream heat transfer and wall friction predictions for quasi-developed strongly heated turbulent pipe flow, using mixing length model [ASME PAPER 70-HT-8] 22 p4008 A70-42439
- Incompressible fluid turbulent motion statistical equations, considering Lagrangian distributions of fluid particles coordinates and velocities 22 p4012 A70-43315
- Flowing medium turbulent velocity measurement using laser Doppler device 22 p4040 A70-43615
- Aerodynamic noise scattering by semifinite compliant plate in turbulent flow, using Lighthill theory and Wiener-Hopf technique 23 p4179 A70-43968
- Sunyach-Mathieu intermittence measuring method applied to turbulent flow boundary studies, discussing flow transition line definition 23 p4180 A70-44201
- Turbulent nonadiabatic flow of compressible gas at inlet and main sections of variable cross section plane channel 23 p4183 A70-44739
- Reynolds stress measurement, using laser flowmeter with cylindrical lenses and square aperture mask 23 p4202 A70-44945
- Velocity profile in viscous sublayer at wall based on maximum stability principle applied to Karman constant for turbulent channel flow 24 p4325 A70-45495
- Turbulent flow mechanics heuristic exposition, discussing random processes, instability, nonlinear interactions, energy exchange, intermittency dependence on Reynolds number, fluid properties and boundary conditions effects, etc 24 p4326 A70-45948
- Heat flux exchange by natural convection along flat vertical isothermal plate in laminar, transition and turbulent flows, using fluxmeters 24 p4429 A70-46207
- Pulsation and turbulence damping in pulsed jet from energy spectra of longitudinal velocity fluctuations 24 p4327 A70-46267
- TURBULENT HEAT TRANSFER**
- Turbulent heat transfer on heated horizontal circular cylinder rotating freely in space, discussing dimensionless numbers relations and frictional heating 01 p0215 A70-10926
- Turbulent fluctuation rates of temperature and velocity on basis of measurements in boundary layer with wall heat transfer 03 p0470 A70-14237
- HF ion-acoustic noise /whistlers/ during turbulent heating of plasma, using matched magnetic probe 07 p1348 A70-19551
- Ionic noise during plasma turbulent heating in toroidal facility, discussing oscillation spectrum 07 p1349 A70-19552
- Tropospheric and stratospheric turbulent horizontal heat and momentum transfer spectral density profiles calculations from radio launchings data 07 p1269 A70-19646
- Thermal entrance region effect on Nusselt number determination in asymmetrically heated rectangular duct with uniform heat flux 07 p1425 A70-20223
- Damped turbulent whirling tube flow friction characteristics and heat exchange, solving equation of maximum tangential flow rate 07 p1261 A70-20464
- Monograph on convective heat flow in stagnation points of turbulent partly premixed free jet flames at cooled plates 08 p1598 A70-21343
- Gas flow in pipe with uniform wall heat flux, analyzing turbulent heat transfer using heat balance equation [ASME PAPER 69-HT-H] 08 p1486 A70-21834
- Turbulent heat transfer in boundary layer at inlet of porous tube under nonisothermal conditions, studying velocity variations 09 p1787 A70-22169
- Turbulent heat and mass transfer from wall to plane-parallel fluid flow at large Reynolds and Peclet numbers, developing universal law 09 p1789 A70-23169
- Eddy penetration model for heat transfer from trailing face of cylinder in transverse flow 09 p1791 A70-23566
- Turbulent gas nonresonant pressure pulsations effects on local convective heat transfer in tube flow 10 p1968 A70-24288
- Energy equations solved for step change of wall temperature and heat flux, determining turbulent heat transfer in tube, discussing asymptotic solutions validity 11 p2146 A70-25334
- Turbulent heat diffusion coefficients in air and water tube flow calculated from statistical characteristics, extending method to boundary layers 12 p2210 A70-27322
- Turbulent and laminar heat transfer to gases in circular ducts entry region, considering various gas properties 12 p2212 A70-28114
- Turbulent heat transfer in concentric annuli entrance region with uniform wall heat flux 12 p2333 A70-28117
- Temperature-dependent physical properties effects on turbulent heat transfer, determining corrective factor for semiempirical equations 13 p2520 A70-28847
- HF ion-acoustic noise /whistlers/ during turbulent heating of plasma, using matched magnetic probe 15 p2777 A70-31458
- Ionic noise during plasma turbulent heating in toroidal facility, discussing oscillation spectrum 15 p2777 A70-31459
- Laminar boundary conditions for heat transfer in gradient flow region for plane turbulent jet impingement on plate normal to flow 15 p2721 A70-32134
- Temperature and Mach number distributions measurements on supersonic turbulent boundary layers for reanalyzing heat transport [AIAA PAPER 70-744] 17 p3066 A70-34499
- Roughness effects on heat transfer to surfaces in supersonic compressible turbulent boundary layer [AIAA PAPER 70-742] 17 p3066 A70-34505
- Turbulent gas flows shear turbulence structure at various Reynolds numbers in nonconducting channels with and without heat transfer under transverse magnetic field 17 p3141 A70-35245
- Heat transfer and friction drag calculation for turbulent boundary layer of gas with temperature dependent physical properties 17 p3012 A70-35729
- Heat and gas curtain efficiency in turbulent boundary layer on flat plate, including heat transfer data 17 p3198 A70-35731
- Two dimensional turbulent film cooling, predicting initial region temperature distribution by solving finite difference form of thermal energy equation 18 p3346 A70-36497
- Turbulent air flow in vertical square duct, investigating local heat transfer and friction coefficients 18 p3347 A70-36506
- Turbulent heat and mass transfer from wall to plane-parallel fluid flow at large Reynolds and Peclet numbers, developing universal law 19 p3552 A70-38392
- Liquid He 4.2 K in narrow channels with laminar and turbulent flow, measuring boiling heat transfer as function of temperature difference 20 p3735 A70-39155
- Steady turbulent flow heat exchange in near wall region at large Prandtl numbers, plotting temperature distribution curves 20 p3612 A70-39811
- Turbulent jet system with previously unmixed chemically active gases, calculating heat and mass transfers during diffusion combustion 20 p3737 A70-39813
- Heat transfer in cooled turbulent tube flow downstream region at high bulk-to-wall temperature ratios 21 p3945 A70-41037
- Turbulent plasma heating by adiabatic magnetic compression with longitudinal ring current 21 p3857 A70-41387
- Stochastic kinetic theory for plasma turbulent heating by random fields, predicting acceleration effects 21 p3859 A70-41899
- Turbulent heat diffusion coefficients in air and water tube flow calculated from statistical characteristics, extending method to boundary layers 21 p3811 A70-42063
- Turbulent heat/mass transfer from solid boundary with shear stress dependent on wall distance for various Schmidt or Prandtl numbers 21 p3953 A70-42088
- Heat transfer from turbulent axisymmetric jet to normal flat wall at critical point with small Reynolds numbers 23 p4181 A70-44321
- Lifting entry vehicles turbulent boundary layer aerodynamic heating, comparing heat transfer prediction methods 23 p4258 A70-44530
- Heat transfer from turbulent boundary layer interacting with shock and expansion waves in supersonic flow 23 p4134 A70-44573
- Turbulent heat exchange coefficient and Prandtl number in turbulent air flow through heated pipe with constant heat flux 23 p4183 A70-44740
- TURBULENT JETS**
- Turbulence intensity and fluctuation rates in isothermal swirling free jets, using constant temperature hot wire anemometer method 01 p0059 A70-10031
- Axisymmetric turbulent incompressible and isothermal self preserving jet investigation using linearized constant temperature hot-wire anemometers 01 p0065 A70-11099

Pressure gradient required for self preserving of turbulent jets and wakes with small mean velocity variations compared with free stream velocity

02 p0223 A70-11860

Growth rate and shear stress parameter of symmetric, turbulent, two dimensional and axisymmetric self preserving wakes and jets in streaming flow

02 p0223 A70-11861

Turbulence detection and velocity fluctuations in jets and flames based on equations of motion and impact probes

02 p0398 A70-12037

Boundary layer calculation for semiinfinite plane turbulent jet on porous wall

02 p0287 A70-12691

Turbulent and wall jets with wide varieties of geometries and boundary conditions, predicting jet inflow effects on entrainment rate, lift, drag, etc

02 p0288 A70-12840

Boundary layer equations describing flow field in turbulent swirling jet diffusion flame solved in von Mises plane

03 p0603 A70-12911

Pulsation energy distribution in free turbulent incompressible jets, noting role of mean velocity distribution

03 p0466 A70-13384

Flow parameters of two interacting submerged turbulent jets from rectangular nozzles, determining total pressure profiles of coincident flow

03 p0466 A70-13504

Turbulent submerged plasma jet boundaries calculated theoretically and compared with experimental results from dynamic head profiles

03 p0532 A70-13515

Microstructure of turbulent jet in concurrent flow, analyzing wake parameter and measuring profiles of pulsation velocity components and Reynolds shear stresses

03 p0409 A70-13871

Propagation of turbulent jet impinging on flat surface at certain incidence angle analyzed for application to V/STOL aircraft, ventilation equipment, etc

03 p0468 A70-13878

Similarity of velocity profiles and pressure distribution of turbulent jet over inclined wall, indicating limitations of Glauert analysis [ASME PAPER 69-WA/FLCS-1]

04 p0668 A70-14849

Sound vibrations effect on pulsation characteristics of turbulent gas jet

04 p0618 A70-15248

Transverse and longitudinal correlation coefficients of electron density fluctuations in turbulent jet related through equation specifying velocity fluctuations isotropy

04 p0674 A70-15551

Free plane turbulent jet virtual origin using tests determining influence of upstream conditions and nozzle shape

04 p0674 A70-15554

Curvature effects on two dimensional turbulent wall jet flow over plane surface and circular convex and concave surfaces in still air

05 p0832 A70-16118

Hot wire turbulence measurements of cylindrical wall jet compared to results from free circular and plane wall jets

06 p1034 A70-17526

Cold ducted supersonic flow of premixed ethylene and air ignition by hot turbulent jet [AIAA PAPER 70-148]

06 p1131 A70-18057

Time mean flow property measurements for homogeneous and nonhomogeneous free turbulent jets

06 p1041 A70-18159

Circular turbulent air jet from flat plate into deflecting stream using potential flow model, noting applicability to V/STOL aircraft technology [AIAA PAPER 69-223]

07 p1190 A70-20406

Heat exchange at stagnation point of subsonic and supersonic axisymmetric jets interacting with perpendicular plane partition, allowing for turbulence

08 p1482 A70-20919

De Laval nozzle behavior in vacuo, discussing flow rate parameters, viscosity and real gas effects, thermal effects, turbulent jet separation and reattachment, etc [AGARDOGRAPH-120]

08 p1434 A70-21932

Axisymmetric swirling jet ejection from semiinfinite tube into free space filled by fluid, solving flow equation by Wiener-Hopf method

09 p1658 A70-22153

Turbulent jet injection from circular opening into unbounded transverse shear flow, determining velocity distribution along axis

09 p1659 A70-22427

Turbulent three dimensional incompressible wall jets issuing into quiescent air ambient, tangent to and at surface of flat plate, investigating shear stress and flow field

09 p1661 A70-23215

Velocity and friction stress profiles of semibounded plane turbulent jets discharging from finite slit along smooth plate into moving medium

09 p1663 A70-23617

Suction force increase resulting from turbulent jet interaction with transverse flow

10 p1868 A70-24166

Time or space decay of turbulent parameters along flow direction in jets, wakes or grid-generated turbulence, illustrating time variation of wave number spectrum

12 p2211 A70-27831

Coaxially flowing jets axisymmetric turbulent mixing between inner and outer streams

12 p2211 A70-27837

Solid particles or liquid drops admixture effect on propagation of inhomogeneous turbulent gas jet, using Prandtl mixing length theory to estimate pulsation velocities

12 p2213 A70-28218

Heat transfer increase near stagnation point for turbulent jet impinging on paraffin coated plates used for flow visualization

13 p2521 A70-28866

Plane turbulent wall jet from small slot, investigating velocity distribution dependence on slot inclination

13 p2388 A70-29448

VTOL aircraft multiple and nonuniform jets aerodynamics, considering induced field and secondary flows

14 p2528 A70-30851

Radial static pressure distribution of turbulent jet flow over rotating cylinder with constant curvature

14 p2567 A70-31399

Plane turbulent impinging jet by iterative finite difference technique, assuming eddy viscosity dependence on energy fluctuations and turbulence length scale [ASME PAPER 70-FE-27]

16 p2835 A70-33634

Combustion effects on mixing of axisymmetric supersonic and turbulent free jets to obtain species concentrations, pitot pressures and temperatures

16 p2998 A70-33860

Plane turbulent jet expansion from linear wedge apex, allowing for ejected air axial velocity attenuation and static pressure variation

17 p3011 A70-35349

Velocity fluctuations in temperature gradient turbulent jets and in turbulent flames, using hot wire in cooled pitot tube

17 p3096 A70-35749

Viscosity effect on turbulent supersonic underexpanded jet flow into submerged region

18 p3206 A70-36262

Free turbulent incompressible jet, analyzing pulsating characteristics and energy balance with Reynolds stress equations

18 p3240 A70-36264

Flame stabilization in boundary layer during mixing of cold homogeneous fuel mixture and hot gas based on combustion and turbulent jet theories

20 p3736 A70-39267

Turbulent jet system with previously unmixed chemically active gases, calculating heat and mass transfers during diffusion combustion

20 p3737 A70-39813

Solid particles or liquid drops admixture effect on propagation of inhomogeneous turbulent gas jet, using Prandtl mixing length theory to estimate pulsation velocities

20 p3612 A70-40091

Laminar incompressible free shear layers by method of weighted residuals for turbulent jets, obtaining velocity profiles for similarity and physical planes

20 p3613 A70-40286

Thermal boundary layer theory for turbulent jets of incompressible fluids from relationship between velocity fluctuations and temperature

20 p3614 A70-40347

Flow structure in plane submerged turbulent jet, determining velocity, friction stress and correlation coefficients distributions

21 p3749 A70-42221

LF acoustic disturbances effect on root portion of turbulent jet from conical nozzle

21 p3954 A70-42223

Turbulent incompressible conducting fluid jets velocity and temperature characteristics in presence of longitudinal and transverse magnetic fields

21 p3860 A70-42226

Liquid metal turbulent jet flow dependence on longitudinal magnetic field, measuring mean velocity profiles at various cross sections

21 p3861 A70-42230

Two dimensional peripheral turbulent jet curtain structure, determining curved and impinging jet flow field by pressure and velocity measurements

22 p3957 A70-42277

Monochromatic acoustic wave interaction with turbulent jet fluctuating vorticity field, using Fourier analysis to extend spectral relations [ASME PAPER 70-FLCS-6]

22 p4008 A70-42426

Aircraft noise sources, examining compressors with dynamic pressure devices and jets with turbulence investigations [ICAS PAPER 70-22]

23 p4232 A70-44111

TURBULENT MIXING

Gas-particle primary and pure gas secondary streams turbulent mixing, solving for various mixing zone flow field parameters

01 p0061 A70-10337

Pitot tube measurements of mixing zone of turbulent shear flow, discussing velocity gradient effects

01 p0066 A70-11134

Mixing length relationship in Prandtl theory for turbulent channel and pipe flow, deriving universal velocity distribution law

02 p0277 A70-11911

Turbulent mixing and supersonic combustion theories applied to internal flow, comparing various mixers and relating mixing intensity to kinetic energy of turbulence

02 p0399 A70-12045

Mixing length theory improvement to calculate turbulent boundary layers based on velocity profiles

02 p0284 A70-12342

Constitutive equations for Reynolds fluxes in large scale transversely isotropic turbulent mixing using gradients of mean quantities

05 p0836 A70-17103

Ducted turbulent mixing and burning of coaxial streams, presenting experimental results for rocket-air mixing system [AIAA PAPER 69-85]

06 p1130 A70-17171

Cone bluntness effect on merging onset and downstream flow in merged region at Mach 8 and various Reynolds numbers

06 p0980 A70-18352

Potential refractive index mean vertical gradients role in turbulent mixing, noting applications to radar detection of CAT

09 p1716 A70-22365

Two dimensional incompressible mixing layer investigated by constant temperature linearized hot wire anemometers, discussing turbulent/nonturbulent interfaces

11 p2040 A70-26540

Coaxially flowing jets axisymmetric turbulent mixing between inner and outer streams

12 p2211 A70-27837

Homogeneous and stationary turbulence in incompressible fluid, proposing dynamic model for strong wave interactions during cascade process

13 p2457 A70-28557

Turbulent mixing at contact surface in driven shock wave in shock tube with bursting diaphragm for He-Ar test gas mixtures

14 p2566 A70-31030

Shear flow turbulence effect on chemical reactions, considering two dimensional low speed turbulent mixing layer between high velocity cold gas and air at rest [AIAA PAPER 70-721]

16 p2855 A70-33493

Turbulent and reacting flows temperature and mixing rates determination, using gaseous HF tracer spectroscopy [AIAA PAPER 70-726]

16 p2856 A70-33497

Turbulent kinetic energy equation for determining turbulent flow fields applied to free mixing problem of constant density streams

16 p2894 A70-33856

Chemical kinetic and turbulent transport coefficients effects on afterburning rocket exhaust plumes and sea level transverse radar attenuations [AIAA PAPER 70-733]

17 p3194 A70-34513

Turbulent mixing of axisymmetrical supersonic air jet into hot air, investigating Mach number and temperature difference effects on axial decay of velocity

17 p3072 A70-35546

Base flow component of total drag for axisymmetric supersonic afterbody with single exhaust jet, considering turbulent mixing

17 p3011 A70-35656

High speed combustion chambers for gas turbine applications, using finite rate chemistry and turbulent mixing computer program for burner design [ASME PAPER 70-GT-25]

18 p3304 A70-36866

Turbulent mixing in supersonic cone near wake, using laser planogram technique for flow visualization

19 p3351 A70-37529

Probability densities and distributions, moments and spectra from time derivatives of streamwise velocity fluctuation in curved mixing layer, measuring small scale turbulence structure

20 p3609 A70-39652

Turbulent mixing effect on vertical distribution of ionosphere atomic and molecular oxygen, using equations of motion and continuity

21 p3813 A70-40907

Interaction zone between gas flow and injected air jets, measuring turbulence characteristics by thermocouple

21 p3809 A70-41773

Computerized integral treatment of turbulent constant pressure mixing of two dimensional gas jet with atmosphere having different temperature and composition

22 p4011 A70-42755

TURBULENT WAKES
NT SLIPSTREAMS

- Vortex street parameters in free wake behind body in plane fluid flow, deriving equations for vortex frequency, circulation and interspacing
01 p0060 A70-10146
- Pressure gradient required for self preserving of turbulent jets and wakes with small mean velocity variations compared with free stream velocity
02 p0223 A70-11860
- Growth rate and shear stress parameter of symmetric, turbulent, two dimensional and axisymmetric self preserving wakes and jets in streaming flow
02 p0223 A70-11861
- Gram-Charlier method generalization for curve fitting analytic forms to velocity covariances measured in turbulent wake of circular cylinder
03 p0480 A70-12950
- Power spectrum of backscattered radiation from turbulent reentry wake illuminated by radar pulse train, discussing electron density decay and pulse shape effects
03 p0408 A70-13585
- Microstructure of turbulent jet in concurrent flow, analyzing wake parameter and measuring profiles of pulsation velocity components and Reynolds shear stresses
03 p0409 A70-13871
- Hypersonic near wake, discussing correlations from optical studies, laminar near wake, blunt body and turbulent wake measurements
05 p0790 A70-16120
- Electric field determination from charged particle concentration in wake of body moving in rarefied plasma, noting hydrodynamics similarity
05 p0915 A70-16754
- Two dimensional supersonic turbulent near wake saddle point singularity during recompression analyzed by including transverse momentum integral equation
[AIAA PAPER 70-228] 06 p1039 A70-18106
- Turbulent wake behind plate due to confluence of two incompressible fluids with different densities
07 p1261 A70-20463
- Relaxational oscillations produced by interaction between rarefaction wave in external two dimensional supersonic flow and turbulent near wake
09 p1603 A70-22426
- Turbulent flames bluff-body stabilization model, measuring recirculation zone concentrations and temperatures for methane and propane-air mixtures
10 p1967 A70-24092
- Regional growth functions of turbulent wakes at small Mach numbers using regression equations
11 p1976 A70-25998
- Turbulent ionized wakes Doppler radar scattering spectrum parameters in terms of wake characteristics using double convolution integral
11 p2010 A70-26271
- Turbulent reacting wakes properties prediction models validity, discussing Lagrangian formulations and eddy diffusivity and mixing models
11 p1978 A70-26772
- Gas and electron density fluctuations in weakly ionized turbulent wake behind hypersonic spheres and cones
11 p1978 A70-26773
- Turbulent wakes in Canadian Armament Research and Development Establishment free flight ranges measured for mean and fluctuating properties
11 p1978 A70-26774
- Time or space decay of turbulent parameters along flow direction in jets, wakes or grid-generated turbulence, illustrating time variation of wave number spectrum
12 p2211 A70-27831
- Turbulent wakes density fluctuations measurement using pulsed laser holographic interferometry in ballistic range
[AIAA PAPER 70-727] 16 p2834 A70-33494
- Flow structure in wake of blunt bodies placed perpendicular in parallel airstream determined from hot-wire anemometry
[AIAA PAPER 69-746] 16 p2838 A70-33876
- Sound wave phase fluctuations from ultrasonic waves traveling through turbulent wakes of circular cylinders and plates, using multichannel pulse height analysis
16 p2839 A70-34086
- Blunt based right circular cylindrical body at subsonic speed, investigating turbulent near wake in wind tunnel
17 p3006 A70-34463
- Turbulent energy distribution in plane wake in incompressible fluid, using pulsational energy balance equation
17 p3011 A70-35348
- Ionospheric plasma disturbances due to moving space vehicle, investigating by electron density measurements in rarefied wake regions using gyro-plasma probe
17 p3142 A70-35763
- Shock wave attenuation and reflection effects on turbulent hypersonic wakes in ballistic ranges
18 p3237 A70-36708
- Turbulence in supersonic wake behind flat plate at zero incidence and heat transfer rate, using hot-wire anemometer
19 p3403 A70-37528
- Turbulent wake behind plate due to confluence of two incompressible fluids with different densities
20 p3557 A70-39263
- Turbulent near wake of symmetrical airfoil, determining universal constant in mixing length formula for inner wake
20 p3559 A70-40276
- Turbulent shear stress correlation with turbulent kinetic energy for wake and circular jet flow conditions
20 p3613 A70-40277
- Hypersonic sphere turbulent wake velocity measurement by spark technique, determining distribution from least mean squares fits of Gaussian curves
20 p3559 A70-40283
- Turbulent energy balance and spectra of axisymmetric wake behind sphere in incompressible fluid, measuring flow velocity
21 p3745 A70-41376
- Radar backscattering from turbulent rocket exhaust plumes
[AIAA PAPER 69-71] 21 p3791 A70-41730
- Hypersonic projectile turbulent wake measurements, discussing velocity, mass density and temperature determination
[ICAS PAPER 70-07] 23 p4132 A70-44130
- Chemical reaction product fluctuations in reacting and nonreacting turbulent wake of sphere in water tunnel detected by injected salts conductimetric titration
[AIAA PAPER 68-686] 23 p4134 A70-44570
- Two dimensional turbulent wake theory, considering shear stress and velocity distribution behind flat plate and circular cylinder
23 p4134 A70-44575
- TURING MACHINES**
Permanent memory faults effects on sequential machines finite-state behavior, considering masking role in synthesis of fault-tolerant sequential networks
11 p2072 A70-26220
- TURNING FLIGHT**
Sonic boom pressure signatures for uniform and maneuvering flight conditions determined for fighter and SST aircraft
[AIAA PAPER 69-1134] 01 p0005 A70-10606
- Banked position and angle of attack changes in fighter aircraft sighting and attacking target, determining spatial zone of possible attack
02 p0227 A70-12406
- Asymptotic expansions and energy methods applied to three dimensional aircraft maneuvers involving energy climbs and turns
07 p1190 A70-20416
- Oculogyrall illusion provoked by angular accelerations during flying stationary and spiral turns in jet aircraft, considering semicircular canals stimulation
11 p1992 A70-26512
- Tactical fighter requirements and designs, considering operational environment and weapon characteristics with emphasis on turning performance
[AIAA PAPER 70-516] 13 p2346 A70-29035
- Supersonic aircraft stability and controllability during turns about longitudinal and vertical axes
16 p2840 A70-33204
- Single and coaxial dual rotor helicopter piloting characteristics during turning flight, discussing operational problems in snow
22 p3962 A70-43530
- TURTLES**
H ion increased activity effect on sodium transport across short circuited turtle bladder
02 p0234 A70-11730
- ADP-ATP catalyzed exchange reaction in turtle bladder microsomes, using chromatographic measurements of conversion rates
17 p3034 A70-35900
- Turtle bladder walls osmotic properties, discussing transrenal water flow transient acceleration by sodium transport inhibition
21 p3762 A70-41223
- Turtle bladders isolated mucosal and serosal fractions histological and physiological properties, discussing ion transport and oxygen consumption
21 p3762 A70-41224
- TVC [CONTROL]**
U THRUST VECTOR CONTROL
- TWENTY-FOUR HOUR ORBITS**
Low altitude 24-hr orbit twin satellite system joined by long light cord, assessing communications efficiency and physical limitations
03 p0579 A70-13621
- Orbit determination program for launching and stationkeeping of 24 hr geostationary satellites, using azimuth and elevation of single autotrack antenna
03 p0578 A70-14339
- Orbit mechanical investigations for increasing Europa 2 booster rocket payload to place German-French communications satellite Symphonie into 24 hr orbit
04 p0754 A70-13153
- Navigation systems using 24-hour orbit satellites, discussing system concept options for U.S., Western Hemisphere and global coverage
12 p2270 A70-27924
- Low thrust station keeping guidance scheme for gravity gradient stabilized 24-hour satellite, solving equations of motion for near circular equatorial orbit
18 p3289 A70-36676
- TWENTY-SEVEN DAY VARIATION**
Upper atmosphere temperature lag behind solar decimeter flux 27 day variation maximum attributed to varying solar EUV heating
01 p0070 A70-10404
- Solar magnetic discontinuity fluxes analyzed by studying 27-day cosmic ray and geomagnetic activity variations using linear filtration method
05 p0900 A70-15969
- IQSY 27-day recurrence sequence for 1964 solar and terrestrial activity, considering geomagnetic, auroral and ionospheric disturbances correlation with plage
05 p0841 A70-16646
- 27-day variations in ionization layer created by galactic cosmic rays, discussing association with 27-day cosmic ray and geomagnetic field variations
07 p1373 A70-20345
- Cosmic ray intensity variation correlated with amplitude changes in 27 day variation during solar cycle 18
09 p1745 A70-22740
- Daily horizontal intensity spectrum for equatorial observatories, computing power densities near 27 day variation during high, moderate and low solar activity
10 p1875 A70-24440
- Exospheric density from Echo 2 orbit, observing 27 day variations associated with sun rotation and correlation with geomagnetic disturbances
11 p2046 A70-26566
- Geomagnetic storm intensity nonuniform relationship to 27 day and 11 year cycles
14 p2571 A70-30240
- Cosmic ray anisotropy 27 day and seasonal variations, considering neutron component data and sunspot magnetic field strength
20 p3696 A70-39277
- Cosmic ray 27 day variations during solar activity minimum, noting unipolar magnetic regions role
20 p3696 A70-39280
- Soviet book on geomagnetic storms 27-day recurrence as function of intensity and onset characteristics, establishing forecasting indices
20 p3623 A70-39897
- Interplanetary magnetic field and plasma structure observed with Mariners magnetometer, noting 27-day deviations from Parker spiral model
23 p4239 A70-43827
- Solar corpuscular flux and visible solar spot area correlation with geomagnetic planetary index for 27-day intervals, considering relationship to earth satellites motion
24 p4408 A70-45547
- Geomagnetic storm intensity nonuniform relationship to 27 day and 11 year cycles
24 p4332 A70-46315
- TWILIGHT**
U TWILIGHT GLOW
- TWILIGHT GLOW**
Twilight and nightglow measurements with stratospheric balloons, discussing use for upper atmosphere exploration, meteoric influence and French network
01 p0079 A70-11217
- Twilight brightness measurements with balloons, scattering coefficient and indicatrix for high altitudes and comparison with Rayleigh-Cabann theory
01 p0079 A70-11218
- Twilight sky polarization data in visible spectrum obtained by high altitude balloon-borne photoelectric photometers
01 p0079 A70-11219
- Antarctic twilight observation by photoelectric scanning spectrometer in search for metallic emission lines in upper atmosphere
01 p0081 A70-11231
- Atmospheric penetration of UV and visible solar radiation during twilight, oxygen and ozone absorption, Rayleigh scattering and atmosphere refraction
02 p0357 A70-12155
- Antarctic twilight Na emission abundance and concentration in lower E region, discussing meteor ablation models
05 p0836 A70-15819
- Airglow and skylight polarization measurements at twilight compared for possible relationship
05 p0837 A70-15927
- Altitude variation of mesospheric daytime sky brightness from earth based measurements of twilight sky brightness, noting inconsistency in calculations based on standard atmospheres
06 p1053 A70-17207
- D region electron density distribution during night and presunrise period, using full wave integration method for propagation parameters for waves reflected from electron density model
06 p1054 A70-17587

- Twilight atmospheric brightness calculation for models of vertical distribution of aerosol scattering coefficient, using numerical data
06 p1056 A70-17828
- Light intensity and polarization in twilight sky atmosphere at solar depressions
07 p1263 A70-19047
- Atmospheric ray paths calculations applied to determination of optical air mass and twilight ray paths in earth atmosphere
10 p1873 A70-23830
- Neutral atomic oxygen auroral and nebular emissions in twilight airglow, suggesting photodissociation of molecules by sunlight
10 p1873 A70-23832
- Spectral, angular and spatial evolution of earth twilight aureole brightness pattern from visual observation and spectrophotometry on Soyuz 5 spacecraft
10 p1873 A70-24270
- Atmospheric sodium concentration in twilight and daytime sky from D1 and D2 line intensities in twilight
13 p2399 A70-29239
- Balloon-borne photometer for collecting twilight and daytime OH intensity and rotational temperature variations data
13 p2399 A70-29240
- Red twilight emission enhancements origin, concerning atomic lithium release effect in upper atmosphere
14 p2580 A70-31264
- Twilight sky color visual estimation from Soyuz 5 spacecraft noting cloudiness effects
15 p2723 A70-31597
- Spectrophotometric and visual observations of twilight glow from Soyuz 5, comparing vertical monochromatic brightness profiles with calculations for Elterman aerosol model
16 p2896 A70-33218
- Twilight colorimetry from horizon spectra obtained by Soyuz 5, computing chromaticity coefficients for purely scattering molecular atmosphere
16 p2896 A70-33260
- Twilight sky brightness measurements at 5200 Å for estimating upper atmospheric dust component, discussing error rates
16 p2899 A70-34184
- Upper atmosphere temperatures from vapor cloud diffusion, eliminating errors from bright sky background at twilight
17 p3076 A70-34940
- Direction and time variations of O I 4368 Å emission following evening twilight
18 p3245 A70-36026
- Evening twilight airglow oxygen IR band ground based observation by two-channel photometric technique
19 p3415 A70-38385
- Light polarization during twilight at zenith from photoelectric recordings, noting intensity decrease with altitude
19 p3417 A70-38770
- Winter pre dawn enhancement of 6300 Å airglow at higher midlatitudes, considering roles of oxygen dissociative recombination and photoelectrons production at magnetically conjugate point
22 p4019 A70-43110
- Spectrophotometric and visual observations of twilight glow from Soyuz 5, comparing vertical monochromatic brightness profiles with calculations for Elterman aerosol model
24 p4328 A70-45193
- TWINNING**
- NT MECHANICAL TWINNING**
- Transmission electron microscope study of deformation mode during rapid tensile testing of Ni-base superalloy, discussing twinning and stacking fault modes
01 p0118 A70-10705
- Elastic interactions between anisotropic crystal dislocations and twin and grain boundaries in Ti
17 p3115 A70-34386
- Crystallography of deformation twinning in Ti, presenting modes involving shear strains less than unity and simple shuffle mechanisms
17 p3116 A70-34388
- Unalloyed polycrystalline Ti fatigue tests, observing cyclic stresses effect on twinning
17 p3116 A70-34393
- Alpha Ti and alpha Ti-hydrogen alloys fatigue behavior, emphasizing twin formation influence and hydrogen effects
17 p3116 A70-34394
- Pure Ni recrystallization, noting stacking faults and parallel sided and thin annealed twins formation during boundary migration
24 p4363 A70-46192
- TWISTED WINGS**
- Camber and twist distributions for closed ground effect wing optimum design for zero induced drag, employing linearized theory
10 p1801 A70-24158
- Dual controlled elastically twisting rotor blade performance during flight with azimuthal and collective variations compared to direct control rotor
13 p2345 A70-29012

Wing camber and twist effects on transonic drag, using wind tunnel measurements
16 p2840 A70-34321

TWISTING

- Axial flow turbine stator and impeller blade twist calculated from gas flow stage area diameter using continuity and vorticity equations
01 p0001 A70-10175
- Elastic bending of pretwisted elliptical bars, showing stiffness response
02 p0387 A70-12216
- Structural characteristics of supersonic twisting underexpanded air jet, using filming and schlieren photography
04 p0618 A70-15246
- Modulus of rigidity and stress-strain state measured in square plate during shear produced by twisting
06 p1060 A70-17132
- Turbine rotor and stator blades twist inaccuracies in assembly due to shroud induced stresses and blade root mountings clearances
07 p1291 A70-18827
- Composite spherically aeolotropic sphere with isotropic core, analyzing stress concentration during twisting
12 p2327 A70-27836
- Open cross section thin walled prismatic beam twisting and bending based on virtual displacements
13 p2511 A70-28744
- Axisymmetric nonuniform initial thickness disk under pressure and twisting along interior surface of circular hole using incremental theory of plasticity for deformation analysis
15 p2816 A70-32004
- Internal efficiency of turbine stages with long twist-varying blades
19 p3490 A70-37250

TWITCHING

- Local contractures in K depolarized amphibian skeletal muscle fibers by intracellular injection or by microperfusion, discussing intracellular Ca ion concentration
02 p0234 A70-11728

TWO BODY ORBITS**U TWO BODY PROBLEM****TWO BODY PROBLEM**

- Two spheres moving in ideal incompressible fluid, studying velocity field, hydrodynamic forces, kinetic energy, etc
03 p0465 A70-13335
- Plane two body contact creep problem in presence of adhesive forces reduced to solving coupled integral equations with complex valued kernels
04 p0766 A70-14421
- Gravitational radiation damping effect on motion of two bodies, evaluating field components in approximation by Einstein-Infeld-Hoffman method
05 p0882 A70-16308
- Motion near collision singularity in perturbed two body problem, applying method to boundedness proof for Sperling cluster energy
05 p0909 A70-16339
- Plane motion of two mass points coupled by flexible inelastic thread assuming system mass center moving along circular orbit
07 p1386 A70-19484
- Mass point motion in celestial mechanics, investigating two and three body problems without equal counteraction assumption
08 p1565 A70-20562
- Steady motions and stability of gravitating gyrost and spheroid, considering dynamically asymmetrical and symmetrical conditions
08 p1544 A70-20965
- Momentum vector and spin tensor definitions for extended body moving in arbitrary gravitational and electromagnetic fields, considering test body in de Sitter universe
08 p1545 A70-21352
- Nomogram construction for graphical solution of two body problem using radius-vector and velocity components applied to solar system
12 p2311 A70-28310
- Computer program for two body problem literal series expansions using Kepler functions with Bessel and Poisson series operation
14 p2638 A70-30702
- Plane wave ray optical scattering by two spheres for arbitrary angle of incidence and observation, noting importance of first order interaction terms
14 p2551 A70-31157
- Orbit calculation based on first integrals of two body problem in spherical coordinates
15 p2797 A70-31620
- Book on celestial mechanics covering perturbation methods, two body problems, astronomical coordinates, orbital mechanics, satellite rotation, gravitational effects, etc
15 p2799 A70-31998
- Matrizant of two body problem or integrable dynamic system for applications to computing perturbations and differential correction of orbits with observations
15 p2768 A70-32611

Mass point motion in celestial mechanics, investigating two and three body problems without equal counteraction assumption
15 p2805 A70-32717

Plane motion of two mass points coupled by flexible inelastic thread assuming system mass center moving along circular orbit
15 p2805 A70-32729

Second and higher order perturbation theory for two body trajectories, using recursive formulas
19 p3528 A70-38871

Steady motions and stability of gravitating gyrost and spheroid, considering dynamically asymmetrical and symmetrical conditions
20 p3672 A70-39387

Potential flow around oscillating shell-plate structure subjected to supersonic gas flow at zero angle of attack, solving nonlinear aeroelasticity problem
22 p4117 A70-43362

Two particles relative motion in elliptical orbits in inverse square central force field
23 p4244 A70-44576

Restricted osculating two body orbit with time derivative of eccentric anomalies difference position as independent variable in perturbation differential equations
23 p4244 A70-44635

Celestial mechanics covering two body problem, orbital improvement, perturbation theory and dynamics, planetary and satellite theory, lunar motion, etc
23 p4255 A70-45032

Relativistic two body system in circular orbits, examining quantum theory with massless and massive scalar fields and energy and angular momentum for bound system
24 p4379 A70-45521

Plane parallel collision between two solid bodies of similar shape, discussing kinetic energy losses and motion after impact
24 p4427 A70-46376

TWO DIMENSIONAL BODIES

Combustion effects on base pressure of two dimensional body in supersonic flight, considering air-fuel ratio, combustion length and free stream Mach number
02 p0354 A70-12046

Two dimensional and axisymmetric bodies shapes providing minimum wave drag to supersonic flow of perfect gas, considering bodies around which flow causes bound shock waves
03 p0409 A70-13863

Shadow optical raster method for quantitative investigation of dynamic stress states in two dimensional transparent or reflecting bodies
03 p0496 A70-14215

Hypersonic cruise vehicle data to define temperature, load criteria and materials for air induction systems associated with two dimensional variable geometry inlet
05 p0791 A70-15839

Incompressible boundary layer flow of conducting fluid on solid two dimensional and axisymmetric bodies under transverse magnetic field approximated by momentum method
06 p1031 A70-17199

Base bleed fluid injection effect on steady separated flow past two dimensional bluff body, studying streamline pattern near object
06 p0967 A70-17518

Minimum weight design for two dimensional bodies with given load system determined by variational method
09 p1771 A70-22400

Two dimensional structures large strain elastoplastic analysis by finite element method, using variational principles to derive equilibrium equations
12 p2320 A70-27148

Elastic-plastic plane stress analysis of two dimensional structures based on Tresca yield criterion, using finite element technique
12 p2326 A70-27795

Laminar near wake flow field of two dimensional adiabatic circular cylinder with surface mass transfer
13 p2343 A70-29951

Thin two dimensional shells static linear elastic deformations analysis using difference based variational method
15 p2815 A70-32001

Supersonic flows past two dimensional blunted bodies, using method of ascertainment
16 p2833 A70-33248

Laminar and turbulent boundary layer equations solutions for incompressible/compressible flows about two dimensional and axisymmetric bodies, using finite difference method
16 p2892 A70-33641

Forces on two dimensional oscillating airfoil in subsonic compressible wind tunnel flow, solving partial differential equation for pressure potential by integral transform technique
16 p2839 A70-34248

Laminar free convection near two dimensional and axisymmetric nonisothermal bodies, examining surface temperature distribution and heat flux
18 p3345 A70-35999

Two dimensional body slow motion through stratified fluid bounded by parallel vertical walls, examining flow at different Peclet numbers 21 p3744 A70-41246

Two dimensional electromagnetic scattering body geometry reconstruction from given incident and scattered far field distributions 23 p4165 A70-44958

Time dependent inviscid transonic flow past two dimensional and axisymmetric bodies, presenting numerical procedures including imbedded shock waves as discontinuities [AIAA PAPER 70-1322] 24 p4288 A70-45943

TWO DIMENSIONAL FLOW

NT COUETTE FLOW

Boundary layer equations for plane steady incompressible flow, studying given velocity profiles effects on equations solutions 01 p0060 A70-10144

Vortex street parameters in free wake behind body in plane fluid flow, deriving equations for vortex frequency, circulation and interspacing 01 p0060 A70-10146

Film-vapor interface shape for thin liquid lubricating film, analyzing two dimensional Newtonian flow including gravity, inertia and surface tension effects [ASME PAPER 69-LUB-3] 01 p0103 A70-10399

Plane supercavitating flow past symmetric wedge via open cavity model and application of conformal mapping theory and Riemann-Hilbert techniques 01 p0002 A70-10544

Conservation laws for viscous incompressible two dimensional and axisymmetric flow written in integrodifferential form 01 p0063 A70-10935

Petrov proof of plane Couette and Poiseuille flow stability with respect to infinitesimal disturbances, rejecting validity of proof 01 p0064 A70-11071

Topological properties of plane flow in subsonic region behind smooth shock wave in uniform supersonic flow, discussing shock wave convexity 01 p0068 A70-11580

Incompressible viscous fluid plane flow using series expansion 02 p0277 A70-11910

Self similar wave solutions of continuity and momentum equations for two dimensional unsteady isentropic motion of polytropic gas 02 p0278 A70-11998

Integral method for computing two dimensional incompressible turbulent boundary layer development, including entrainment process of irrotational fluid 02 p0284 A70-12343

Momentum integral method using auxiliary equation for two and three dimensional flows 02 p0284 A70-12344

Stratified air flow above relief in baroclinic atmosphere, considering plane nonlinear and three dimensional linearized flow models 03 p0521 A70-13270

Unsteady heat conduction in hollow cylinder, using transfer functions to solve direct and inverse two dimensional problems 03 p0606 A70-13520

Viscous incompressible laminar two dimensional flows using Navier-Stokes equations, emphasizing near wake and flow around leading edge [ONERA-TP-757] 03 p0467 A70-13640

Incompressible inviscid free shear layer stability with respect to spatially growing three and two dimensional disturbances, considering hyperbolic tangent velocity profile [DFVLR-SONDDR-10] 03 p0468 A70-13786

Martin method for reducing determination of steady plane MHD flow to Bernoulli and direct functions satisfying quasi-linear partial differential equations 03 p0533 A70-14200

Plane model of magnetosphere shape and structure, considering rarefied plasma flow past two dimensional magnetic dipole with dynamic and static boundary pressure, using conformal mapping 04 p0675 A70-14435

Sonic throat formation from two dimensional viscous layer interaction with supersonic inviscid outer stream, using boundary layer equations 04 p0665 A70-14452

Heat transfer from two dimensional hypersonic low density stream to wedges and sharp flat plates at expansion angles of attack 04 p0615 A70-14944

Boundary layer along flat plate at zero incidence with homogeneous suction using momentum and kinetic energy integral equations through boundary layer velocity profile 04 p0615 A70-15052

Plane and axisymmetric transonic vortex flow approximate equations of inviscid nonheat conducting gas for point on sonic line with entropy having extremal value 04 p0617 A70-15234

Flow stability of plane channel formed by incompressible viscous fluid injection through porous parallel walls 04 p0673 A70-15238

Hydromagnetodynamic equations of two dimensional unsteady geostrophic wind field in turbulent ionosphere 04 p0680 A70-15254

Incompressible two dimensional time dependent Navier-Stokes equations for oscillating body with rectangular boundaries [AIAA PAPER 69-185] 04 p0779 A70-15616

Plane Poiseuille flow stability as function of periodic disturbances of finite amplitude in channel axis direction 05 p0832 A70-16018

Periodic perturbations of plane Poiseuille flow, observing neutral curve relationship to disturbance amplitude 05 p0832 A70-16019

Singularity method applied to two and three dimensional potential flow described by Poisson, Helmholtz or related partial differential equations 05 p0832 A70-16114

Two and three dimensional flow using TRIC and TRIM-like triangular finite elements 05 p0832 A70-16115

Curvature effects on two dimensional turbulent wall jet flow over plane surface and circular convex and concave surfaces in still air 05 p0832 A70-16118

Second order wave structure theory for shock wave system from body in supersonic flight analyzed for planar flows 05 p0790 A70-16797

Two dimensional plasma modes involving geometry and velocity spaces, discussing Vlasov equation 05 p0890 A70-17025

Incompressible two dimensional turbulent boundary layer equations with arbitrary pressure distribution solved by weighted residual method [AIAA PAPER 69-397] 06 p1032 A70-17214

Two dimensional laminar and turbulent boundary layer flow theory covering heat and mass transfer, compressibility, turbulence, roughness, chemical reactions and axial symmetry 06 p1032 A70-17227

Isoenergetic mixing and reattachment processes of two dimensional supersonic turbulent separated flow, modeling mixing process by constant pressure theory [AIAA PAPER 70-108] 06 p1037 A70-18039

Two dimensional supersonic turbulent near wake saddle point singularity during recompression analyzed by including transverse momentum integral equation [AIAA PAPER 70-228] 06 p1039 A70-18106

Multiphase two dimensional mixing and combustion of flow fields suspended in gaseous medium for propulsion systems problems, obtaining governing equations [AIAA PAPER 70-145] 06 p1181 A70-18175

Plane Couette flow and heat transfer problem numerical solution, using Krook kinetic equation and Maxwell boundary condition 06 p1048 A70-18326

Model for predicting laminar-turbulent transition point in hypersonic wake of two dimensional laminar viscous flow 06 p0985 A70-18499

Correlation function of velocity fields in two dimensional turbulence determined from hydrodynamic equation assuming normally distributed stream function field 07 p1252 A70-18673

Nonlinear stability of plane Couette flow, computing stream function, vorticity distribution and Reynolds stresses 07 p1255 A70-19211

Peristaltic motion of viscous incompressible fluid, applying long wave approximation to two dimensional urine flow model 07 p1219 A70-19247

High electrical conductivity effects on alignment between magnetic field and flow velocity vector in two dimensional plasma flow 07 p1349 A70-19568

Roshko model cavity solution based on Falkovich method application to two dimensional permanent irrotational flow of subsonic gas jet 07 p1258 A70-19571

Instability of plane Couette flow of three superposed layers of fluids of different viscosity between two horizontal planes 07 p1260 A70-19978

Two dimensional flow field behind shock wave resulting from boundary layer growth in driven gas of shock tube 07 p1260 A70-19983

Circular turbulent air jet from flat plate into deflecting stream using potential flow model, noting applicability to V/STOL aircraft technology [AIAA PAPER 69-223] 07 p1190 A70-20406

Flow structure in rectangular cavity in lower wall of two dimensional channel for various aspect ratios and Reynolds numbers 08 p1484 A70-21313

Navier-Stokes equations exact solutions for two dimensional steady flow of compressible viscous heat conducting perfect gas 08 p1485 A70-21638

Airfoil research in S-10 French wind tunnel for two dimensional flow, noting Reynolds and Mach number ranges [ONERA-TP-766] 08 p1433 A70-21843

Static tank visualizations obtained in two dimensional flow and on rotors hovering or in transition in ONERA hydrodynamic tunnel 08 p1434 A70-21846

Plane Couette flow stability numerical analysis, predicting eigenvalue behavior for arbitrary Reynolds and wave numbers 09 p1658 A70-22124

Plastic bodies plane flow Lagrangian description applied for prescribed deformation path of material fibers 09 p1769 A70-22251

Survey of papers on computer calculation of two and three dimensional gas flows, emphasizing method of characteristics and finite difference techniques 09 p1603 A70-22265

Relaxational oscillations produced by interaction between rarefaction wave in external two dimensional supersonic flow and turbulent near wake 09 p1603 A70-22426

Two dimensional Poiseuille flow stability at deformable walls, assuming pressure proportionality to displacement and rate 09 p1660 A70-22533

Second order boundary layer equations for incompressible flow, presenting simplified integral momentum equation for two dimensional and axisymmetric flow 09 p1660 A70-22681

Two dimensional radial flow of inviscid infinitely conducting compressible fluid under influence of magnetic field 09 p1735 A70-22757

Two dimensional equations of boundary layer with arbitrary pressure gradient solved using successive approximations for numerical integration 09 p1605 A70-23168

Turbulent heat and mass transfer from wall to plane-parallel fluid flow at large Reynolds and Peclet numbers, developing universal law 09 p1789 A70-23169

Two dimensional supersonic wake transition characteristics noting effect of heat transfer from vehicle or model body 09 p1605 A70-23184

Stability theory application to laminar boundary layer transition prediction on two dimensional and axisymmetric flows having pressure distributions in incompressible flow [AIAA PAPER 69-10] 09 p1662 A70-23219

Velocity and friction stress profiles of semibounded plane turbulent jets discharging from finite slit along smooth plate into moving medium 09 p1663 A70-23617

Circle theorem for potential flows extended to two dimensional steady incompressible ideal fluid flows of constant vorticity 09 p1664 A70-23714

Shock wave initiated two dimensional time dependent ducted flows in nonuniform regions using fluid-in-cell method, discussing density, pressure and energy distributions 09 p1665 A70-23740

Streamline curvature technique for two dimensional flow equations, deriving optimal damping factor for quasi-orthogonal method to test stability, convergence and accuracy 09 p1609 A70-23749

Upstream influence distance estimation associated with critical pressure rise in two dimensional shock-boundary layer interactions based on Lighthill subsonic inner boundary layer concept 10 p1862 A70-23840

Motion and continuity equations for unsteady two dimensional flow of incompressible viscous fluid along infinite flat plate with time dependent suction 10 p1862 A70-23877

Two dimensional MHD flow past solid body at large Reynolds numbers, treating boundary layer transition 10 p1922 A70-24011

Perturbed equations solutions for plane supersonic steady and nonsteady gas flows, considering propagation of perturbations in initially nonstationary main flow 10 p1866 A70-24107

Transonic aerodynamics problems concerning plane and spatial rotational flows of perfect gas, discussing analytical and numerical methods 10 p1800 A70-24132

Bidimensional curved weak shock wave structure, deducing transonic equation from Navier-Stokes equations 10 p1800 A70-24138

Orr-Sommerfeld equation of hydrodynamic stability theory solved for incompressible two dimensional

boundary layer flow on basis of reduction to integral equation 10 p1867 A70-24161

Hydrodynamic lubrication theory two dimensional problem, comparing numerical methods for elliptical nonlinear differential equations 10 p1893 A70-24164

Steady two dimensional cavity flow past sharp-edged airfoil and blunt nosed obstacle, using linearization hypothesis 10 p1801 A70-24193

Plane Couette oscillating flow stability to small disturbances under composed unsteady velocity at high Reynolds number 10 p1868 A70-24197

Numerical integration method for function and solution of differential equation, considering equations governing two dimensional motion of particle in air stream 10 p1910 A70-25099

Earth profile influence on two dimensional nonlinear lee waves in troposphere, discussing Helmholtz perturbation equation and stream function field 11 p2075 A70-25391

Velocity distribution around isolated and cascaded airfoils in plane potential flows of incompressible fluid determined by use of nonsingular integrals 11 p1974 A70-25781

Two dimensional unsteady fluid flow in square cavity numerically analyzed from continuity and Navier-Stokes equations and recorded as computer-generated motion picture 11 p2035 A70-25971

Steady state two dimensional flow velocity profiles at low Reynolds numbers of homogeneous incompressible viscous liquid in straight channel inlet region 11 p2037 A70-26476

Two dimensional incompressible mixing layer investigated by constant temperature linearized hot wire anemometers, discussing turbulent/nonturbulent interfaces 11 p2040 A70-26540

Two and three dimensional flow analysis using various versions of finite element techniques 11 p2042 A70-26680

Two and three dimensional potential flow analysis using finite element technique based on method of singularities 11 p2042 A70-26681

Regularity domain and singularity location of stream function of transonic two dimensional compressible fluid flow, using integral operators 12 p2260 A70-26972

Two dimensional viscous incompressible conducting fluid flow between parallel porous walls in magnetic field, studying skin friction fluctuations 12 p2209 A70-27157

Incompressible two dimensional and axisymmetric oscillating laminar boundary layer flows approximated by momentum integral equation, discussing flow along flat plate 12 p2158 A70-28205

Two dimensional irrotational incompressible fluid motion bounded by flexible stretched and unstretched film, noting hydrodynamic shock for closed film 12 p2213 A70-28238

Plane model of magnetosphere shape and structure, considering rarefied plasma flow past two dimensional magnetic dipole with dynamic and static boundary pressure, using conformal mapping 13 p2392 A70-28460

Plane flow problem for two hinged plates in motion toward each other with fluid displacement, discussing single vortex application to biomechanics 13 p2338 A70-28481

Two dimensional MHD turbulence under strong magnetic field in Zeta device, measuring density, temperature, electric/magnetic fluctuations and various statistical characteristics 13 p2457 A70-28553

Plane incompressible conducting fluid laminar jets analysis in magnetic field, using boundary layer equations for zero electric field 13 p2461 A70-28964

Compressible fluid two dimensional irrotational flow past Roshko model in channel, deriving exact solution by hodograph method 13 p2341 A70-29487

Two dimensional unsteady incompressible fluid flow through airfoil lattice 13 p2389 A70-29491

Linearized steady plane axisymmetric flows of inviscid finitely conducting incompressible fluid past insulator under magnetic induction with zero components 13 p2464 A70-29541

Incompressible ideal plane fluid flow complex potential caused by profile motion in presence of fixed infinite wall 13 p2390 A70-29632

Ideal weightless fluid plane potential flow in channel with permeable wall, deriving expressions for dynamic characteristics 13 p2390 A70-29648

Two dimensional turbulent boundary layer with pressure gradient, calculating velocity distribution and local skin friction by Pohlhausen method 13 p2391 A70-29672

Axisymmetric compressible boundary layer on body of revolution transformed into two dimensional turbulent boundary layer 13 p2391 A70-29995

Two dimensional unsteady flow of weakly conducting fluid in perpendicular magnetic field using Green function 14 p2621 A70-30180

Two dimensional incompressible steady turbulent flows based on Prandtl hypothesis relating eddy viscosity to kinetic energy and scale 14 p2564 A70-30259

Two dimensional incompressible turbulent boundary layer with mass addition and heat transfer, calculating temperature and velocity profiles by marching integration 14 p2564 A70-30261

DMC computer code for simulation of two dimensional viscous incompressible flow about arbitrarily shaped bodies 14 p2527 A70-30271

Steady plane relativistic flow small irrotational perturbation theory determining subsonic, transonic and supersonic approximation 14 p2566 A70-30472

Two dimensional incompressible laminar boundary layers asymptotic structure with injection, obtaining velocity profiles 14 p2566 A70-30995

Self similar one dimensional flow behind plane shock propagating in exponentially decreasing atmosphere, considering radiation mean free paths and radiative heat transfer 14 p2567 A70-31032

Correlation function of velocity fields in two dimensional turbulence determined from hydrodynamic equation assuming normally distributed stream function field 15 p2718 A70-31465

Nonself similar problem of plane submerged fluid jet expelled from annular nozzle, obtaining asymptotic expansion for stream function 15 p2719 A70-31485

Force acting on cylinder in ideal incompressible fluid plane flow with steady vorticity 15 p2719 A70-31498

Baecklund transformations applications to hodograph equations for steady two dimensional nondissipative MGD flows with aligned velocity and magnetic fields 15 p2781 A70-32453

Integral equation for transonic small disturbance flow applied to plane flows over lifting airfoils 15 p2673 A70-32768

Two dimensional hydromagnetic turbulence model for maintained seed field amplification, noting applications to star formation, stellar convection and gas cloud motions 15 p2781 A70-32813

Shock wave stability in plane steady flow at uniform entropy and limiting velocity 16 p2890 A70-33101

Shear flow turbulence effect on chemical reactions, considering two dimensional low speed turbulent mixing layer between high velocity cold gas and air at rest [AIAA PAPER 70-721] 16 p2855 A70-33493

Plane turbulent impinging jet by iterative finite difference technique, assuming eddy viscosity dependence on energy fluctuations and turbulence length scale [ASME PAPER 70-FE-27] 16 p2835 A70-33634

Incompressible ideal fluid plane laminar flows at large Reynolds numbers in region bounded by moving walls with closed concentric streamlines, establishing functional properties 16 p2892 A70-33635

Two dimensional supersonic wake behind heated slender flat plate, considering flow properties in transition zone 16 p2893 A70-33749

Compressible turbulent boundary layers with heat and mass transfer in two dimensional and axisymmetric flows, using eddy transport coefficients [AIAA PAPER 70-741] 17 p3066 A70-34506

Steady two dimensional MHD boundary layer flow with uniform suction or injection past semiinfinite flat plate in cross fields 17 p3067 A70-34618

Steady and unsteady gas dynamics analogies with two dimensional water flow, taking into account energy and continuity equations 17 p3069 A70-35032

Two dimensional hypersonic viscous flow, analyzing viscosity and bluntness induced pressure effects 17 p3010 A70-35034

Turbulent energy distribution in plane wake in incompressible fluid, using pulsational energy balance equation 17 p3011 A70-35348

German monograph on oscillations of tandem wing without outgoing wake in plane incompressible flow, using numerical computations 17 p3011 A70-35372

German monograph on transonic plane flow past wavy wall in blocked wind tunnel covering flow theory, interferometric density measurements, etc 17 p3070 A70-35375

Viscous incompressible liquid two dimensional flow around flat plate, discussing visualization techniques and velocity distribution measurement 18 p2339 A70-36218

Plane stationary supersonic flows with laminar separation zones at large subcritical Reynolds numbers 18 p2306 A70-36257

Unsteady two dimensional gas flow calculation axisymmetric shock tube of variable cross section, using numerical method 18 p2340 A70-36275

Plane compressible sonic flow around symmetrical cylinder subjected to parallel incident flow, using function-theoretic method 18 p3241 A70-36378

Pressure distribution shock pattern and impact wave resistance in frictionless plane parallel and source shaped supersonic flow 18 p3207 A70-36385

Two dimensional cascades for incompressible plane potential flows with given velocity distribution [ASME PAPER 70-GT-87] 18 p3209 A70-36880

Quasi-two dimensional supersonic cascade flow, taking into account transverse stream contraction effect 18 p3210 A70-37206

Method of characteristics for two dimensional steady supersonic gas flows with foreign particles in plane and axisymmetric nozzles 18 p3210 A70-37228

Perfect and dissociating gas nonstationary supersonic flow around sharp profile of finite thickness analyzed by linearization and method of characteristics 19 p3351 A70-37242

Supersonic flow of rarefied plasma around plane bodies, allowing for electric field effect on ion motion 19 p3351 A70-37302

Liquid with small electrical conductivity and kinematic viscosity in intense transverse magnetic field, examining plane and three dimensional duct flow 19 p3478 A70-37589

Thin airfoil theory in magnetoaerodynamics, considering steady two dimensional flow of compressible perfectly conducting inviscid fluid in presence of uniform magnetic field 19 p3351 A70-37597

Film-vapor interface shape for thin liquid lubricating film, analyzing two dimensional Newtonian flow including gravity, inertia and surface tension effects [ASME PAPER 69-LUB-3] 19 p3435 A70-37610

Boundary layer equations for two dimensional flow of incompressible constant density micropolar fluid past plane wall, noting skin friction 19 p3404 A70-37962

Steady two dimensional incompressible shear flow, correlating velocity profiles with resistance distribution 19 p3406 A70-38350

Two dimensional equations of boundary layer with arbitrary pressure gradient solved using successive approximations for numerical integration 19 p3406 A70-38390

Turbulent heat and mass transfer from wall to plane-parallel fluid flow at large Reynolds and Peclet numbers, developing universal law 19 p3552 A70-38392

Hodograph equations for relativistic irrotational steady plane flows, investigating transformation to physical plane 19 p3406 A70-38664

Two dimensional steady inviscid incompressible flow past profiles in parallel flow with nonuniform velocity distribution 19 p3354 A70-38676

Two dimensional MHD Couette flow in slip regime, considering constant suction on stationary plate to determine transverse magnetic effects 20 p3677 A70-39047

Bearing force and moment produced by motion of inclined plate supported by compressed air in ground effect machines with small angle of attack 20 p3557 A70-39140

Shock wave nonlinear refraction by upstream disturbances in two dimensional steady nonuniform flow 20 p3608 A70-39354

Compressible viscous fluid steady plane flow in laminar boundary layer on impermeable isothermic surface, describing parametric method of integrating flow equations 20 p3611 A70-39806

Plane parallel viscous conducting fluid flows stability in transverse magnetic field, considering small perturbation spectrum, Hartmann and Reynolds numbers 20 p3684 A70-40397

Two dimensional turbulent boundary layer computation using two parameter family of velocity profiles and skin friction law 21 p3806 A70-40921

Two dimensional compressible laminar MHD boundary layer flow past flat plate with heat transfer, considering continuity, momentum and energy equations 21 p3856 A70-41039

Shock wave extinction point within plane steady upstream flow with uniform entropy and limit velocity 21 p3808 A70-41441

Two dimensional unsteady viscous incompressible MHD flow past infinite flat plate with uniform suction, considering Hartmann and Reynolds numbers 21 p3858 A70-41450

Irrational incompressible flow through two dimensional channel with asymmetric contraction 21 p3809 A70-41757

Plane Poiseuille flow in second order Rivlin-Ericksen fluids with small viscoelastic parameters, calculating three dimensional disturbance stability 21 p3810 A70-42030

Plane parallel transonic flow with curved compression shock discontinuity in supersonic region, obtaining solution by indeterminate coefficients and hypergeometric functions 21 p3748 A70-42212

Spoiler theory based on mathematical model, using two dimensional potential theory in conjunction with experimental data on wake phenomena 22 p3957 A70-42273

Two dimensional peripheral turbulent jet curtain structure, determining curved and impinging jet flow field by pressure and velocity measurements 22 p3957 A70-42277

Two dimensional turbine cascade air flow, examining boundary layer regime, thickness, velocity and pressure coefficient at any point by Mach-Zehnder interferometer 22 p4026 A70-42344

Two dimensional transonic cascade flow, using Von Karman similarity law 22 p4089 A70-42347

Two dimensional flow about supersonic airfoil, considering trailing Taylor columns behavior like sonic booms 22 p4009 A70-42629

Two dimensional incompressible flow, calculating strong suction effects on laminar boundary layer separation by linear model 22 p4010 A70-42630

Hydrogen and air nonequilibrium chemical recombination effects in two dimensional exhaust nozzles, using Bray freezing criterion 22 p3982 A70-42760

Isentropic gas two dimensional unsteady flow through channel contraction, using hydraulic analogy 22 p4012 A70-43438

Two dimensional steady flow around slender profiles at free transonic stream with curved compression shocks, approximating by hodographic method 23 p4131 A70-44023

Two dimensional stratified flow over extended obstacles with source disturbances, indicating topographical effect on vertical wind shear in troposphere 23 p4214 A70-44031

Rotational two dimensional steady shear flows of perfect incompressible fluid, considering channel flow characteristics for various wave modes 23 p4181 A70-44202

Mass transfer and velocity gradient fluctuations at wall in two dimensional or rotational flow for large Schmidt numbers 23 p4181 A70-44210

Ladyzhenskaya-type fluids linear flow stability criteria for two dimensional case 23 p4218 A70-44238

Two dimensional turbulent wake theory, considering shear stress and velocity distribution behind flat plate and circular cylinder 23 p4134 A70-44575

Pressure distribution on thin nonlifting airfoils in steady two dimensional flow with freestream Mach number at or near unity 23 p4134 A70-44583

Two dimensional laminar near wake of slender body in supersonic flow at high Reynolds number 23 p4135 A70-44693

Incompressible viscous fluid two dimensional flow in absence of mass forces, considering Tollmien-Schlichting wave perturbation effect on flow stability 24 p4324 A70-45365

Two dimensional aperture flow with downstream asymmetric pressure distribution due to jet reattachment to boundary, simulating flows in hydraulic spool valves and fluidic devices 24 p4325 A70-45582

Two dimensional boundary layer growth with suction for oscillating circular cylinder, considering stream functions and phase angles 24 p4326 A70-46002

Viscous fluid two dimensional steady natural convection between horizontal concentric cylinders for low Grashof numbers 24 p4429 A70-46007

Two dimensional incompressible air flow past circular cylindrical body, investigating separation point control by suction and jet injection 24 p4288 A70-46010

Plane flow of incompressible elastic perfectly plastic solid, deriving hyperbolic stress and velocity equations 24 p4427 A70-46043

TWO DIMENSIONAL JETS

Growth rate and shear stress parameter of symmetric, turbulent, two dimensional and axisymmetric self preserving wakes and jets in streaming flow 02 p0223 A70-11861

Fourier expansion method applied to hydrodynamic stability of plane jet, testing boundary conditions 03 p0469 A70-14180

Linear spatial stability of two dimensional laminar wake- and jet-like similarity solution of Falkner-Skan equation 04 p0613 A70-14455

Instability of viscous laminar plane jet of incompressible fluid, finding minimum critical Reynolds number for various assumptions of parallelism 04 p0670 A70-14990

Boundary layer equations closed form similarity solutions for laminar jet of compressible pseudoplastic fluid, discussing velocity transverse behavior 04 p0671 A70-15053

Free plane turbulent jet virtual origin using tests determining influence of upstream conditions and nozzle shape 04 p0674 A70-15554

Heat transfer during plane air jet impact into concave surface with parabolic profile, determining specific thermal fluxes by electrocalorimetry 07 p1189 A70-19810

Mixing region and potential cone of two dimensional jet, measuring velocity fluctuations 08 p1485 A70-21587

Velocity and friction stress profiles of semibounded plane turbulent jets discharging from finite slit along smooth plate into moving medium 09 p1663 A70-23617

Flat plate normal to two dimensional impinging air jet, investigating heat /mass/ transfer structure using naphthalene method 11 p1977 A70-26411

Cavity pressure and velocities distributions of interfering two dimensional dual jets from parallel slot nozzles 11 p2037 A70-26419

Two dimensional jet velocity profile evolution under symmetrical and antisymmetrical perturbations 14 p2567 A70-31200

Linearized two dimensional double vortex sheet model of inviscid compressible jet instabilities over all Mach numbers 15 p2722 A70-32375

Vortex streets characteristics determination for plane jet having uniform initial velocity profile 16 p2890 A70-33108

Two dimensional sonic secondary fluid jet interaction with uniform primary supersonic stream in wind tunnel [ASME PAPER 70-FE-33] 16 p2835 A70-33638

Reaction jets for control force generation in supersonic environment, analyzing downstream pressure distributions for two dimensional jet interactions 16 p2838 A70-33890

Plane turbulent jet expansion from linear wedge apex, allowing for ejected air axial velocity attenuation and static pressure variation 17 p3011 A70-35349

Laminar two dimensional wall jet with small natural disturbances, examining flow stability at various Reynolds numbers 19 p3402 A70-37526

Noise spectra of two dimensional jet flowing from nozzle ejector, using dispersion equation 19 p3354 A70-38662

Heat transfer during plane air jet impact into concave surface with parabolic profile, determining specific thermal fluxes by electrocalorimetry 20 p3736 A70-39260

Computerized integral treatment of turbulent constant pressure mixing of two dimensional gas jet with atmosphere having different temperature and composition 22 p4011 A70-42755

Trajectory equations for plane and three dimensional gas jets with arbitrary injection hole shapes in subsonic shear flow 22 p3960 A70-43365

Two dimensional incompressible laminar free jet, analyzing higher order viscous interactions with surrounding fluid by matched asymptotic expansions method 24 p4326 A70-45944

[AIAA PAPER 70-1321] Vortices growth in vortex sheets bounding jets flowing from two dimensional slit and circular orifice observed by computer experiments 24 p4327 A70-46244

TWO FLUID MODELS

Two layer truncated harmonic model of Rossby wave dynamo for solar cycle, accounting for maintenance and reversal of magnetic fields 01 p0174 A70-10238

Internal waves breaking on sloping surface in two fluid system, studying interfacial shear instability by capacitance probe on-line computer system 09 p1717 A70-22371

Two fluid hydrodynamic model of heat conductivity and viscosity effects on drift laminar flow stability of dense inhomogeneous plasma 10 p1926 A70-25125

Heat transport by internal convection through He 2 in two fluid hydrodynamics model noting roles of thermal flux, superfluid component vorticity, normal component turbulence, etc 12 p2329 A70-27022

Two fluid model for solar wind treating constant temperature electrons hydrodynamically and protons as collisionless 13 p2477 A70-29178

Classical single fluid dynamics theory derived from unitary formulation of two fluid theory 15 p2827 A70-32261

Current sheet structure of hydromagnetic boundary layer formed by mixing two conducting fluid streams containing oppositely directed magnetic fields 17 p3140 A70-34930

Two component warm plasma wave propagation along magnetic field, considering full pressure tensor equation with momentum and pressure relaxation mechanisms 18 p3294 A70-36405

Two fluid hydrodynamic model of heat conductivity and viscosity effects on drift laminar flow stability of dense inhomogeneous plasma 20 p3685 A70-40518

Solar wind two fluid model with boundary conditions describing electron and proton behavior in expanding corona 24 p4397 A70-45770

TWO PHASE FLOW

Shock wave structure in two phase media with temperature and velocity gradients and possible phase transitions 01 p0060 A70-10147

Two phase flow in cylindrical channel, formulating maximum momentum flow variational principle for laminated adiabatic vapor- and gas-liquid flows 01 p0213 A70-10216

Laminar boundary layer analysis of heat and mass transfer in dispersed two phase flow over heated surface 01 p0214 A70-10293

Wet vapor flow with/without inert diluent, assuming momentum and heat transfer between phases according to Stokes law and Nusselt number of unity 01 p0061 A70-10332

Two velocity hydrodynamic scheme for describing dynamic behavior of two phase supersonic flow past slender body 01 p0003 A70-10995

Flow patterns in circular ducts with circumferential roughness variation, determining axial turbulence, Reynolds number effect and applications as two phase flow analog 01 p0066 A70-11132

Two phase flow instrumentation - Conference, Minneapolis, August 1969 02 p0304 A70-12833

Two phase flow visualization by various photographic and optical methods, describing equipment and lighting used and types of data obtainable 02 p0305 A70-12834

Two phase density and void fraction measurement using beta, gamma and X ray radiation, considering optical accuracy and beam collimation 02 p0305 A70-12835

Hot-wire and hot-film anemometry in two phase air-water and steam-water flow, discussing bubble passage, signal processing and measurements 02 p0305 A70-12836

Electronic spray analyzers and conductance and capacitance probes for two phase flow studies, describing operation, characteristics and types of data obtainable 02 p0305 A70-12837

Nonequilibrium two phase forced convection flow, describing pressure, temperature and void fraction measurement techniques 02 p0305 A70-12838

System of equations describing isothermal two phase-two component fluid flows with negligible dissipation effects, emphasizing slug flow 02 p0288 A70-12856

Turbulence in hypersonic nozzle due to two phase flow of ideal gas and solid spherical particles, discussing thermal and dynamic differences 03 p0407 A70-13494

Supersonic nonequilibrium two phase flow in Laval nozzle from numerical solution of quasi-linear hyperbolic equations 04 p0617 A70-15229

Approximate solution for far downstream flow of condensation in hypersonic wind tunnels and nozzles for colloidal thrusters and EHD generators
04 p0621 A70-15600

Nonequilibrium models describing two phase critical discharge of initially saturated or subcooled liquid through sharp edged and smooth inlet geometries
05 p0956 A70-16162

Laser beam for measuring particles velocity in two phase air-water jets by heterodyning, describing signal properties
05 p0858 A70-16258

Repetitive scanner for wave velocity measurements in annular two phase gas or liquid flow using pivoted mirror
06 p1062 A70-17618

Water flow with solid particles, obtaining predictions for two component two phase gas flow
06 p1037 A70-17899

Stable two phase water flow system for transpiration cooling in thermal protection of SST noise suppressor situated in afterburning engine exhaust gas stream
[AIAA PAPER 70-151] 06 p1181 A70-18146

Water droplets and air supersonic mixing, determining droplets size and optical properties
[AIAA PAPER 70-90] 06 p0975 A70-18199

Two phase supersonic continuum flow of dispersed equal gas-liquid volume ratio in shock tunnel using continuum theory, considering sound propagation
07 p1256 A70-19311

Film heat transfer coefficients and thicknesses for condensation and evaporation and two phase flow inside circular tubes
[ASME PAPER 67-HT-1] 08 p1599 A70-21827

Aerothermochemistry of two phase flow in gaseous media of solid or liquid particles or spherical gas pockets
[ONERA-TP-691] 08 p1600 A70-21848

Sonic speed and damping in two phase potassium flow, discussing linear equations and propagation velocity
09 p1725 A70-22036

Flow formation in Couette motion of viscous fluids containing suspended rigid spherical particles using theory of fluids with microstructure
11 p2037 A70-26169

Growth rate and spatial distribution of solid deposit freezing onto vertical surface in presence of convective heat transfer at moving phase interface
12 p2331 A70-27696

Shock wave formation and propagation analyzed by hydrodynamic model of two directional traffic flow based on continuity equations and velocity-density empirical relations
12 p2212 A70-28196

Single component two phase pipe flow choking and shock phenomena, including flashing flow vibratory effects
13 p2386 A70-28846

Liquid metallic particles fragmentation in two phase flow injected into vacuum, noting atomization enhancement by sodium nitrate
13 p2391 A70-29994

Laminar flow of suspension over flat plate, analyzing particulate velocity and concentration profiles relationships to drag and lift forces
14 p2565 A70-30270

Two phase convex corner flows of particle imbedded inviscid incompressible fluid using small perturbations method
14 p2565 A70-30279

Two phase axisymmetric jet, studying dispersion of pulverized impurity consisting of particles of various sizes
15 p2721 A70-32135

Hydrogen oxygen rocket engine two phase liquid hydrogen pump capability and hydrodynamic design, analyzing constant-quality flow, acoustic effects, compressible flow and cavitation
[AIAA PAPER 69-549] 15 p2791 A70-32511

Gaseous flows and local droplet velocity measurement in dense gas/liquid sprayfields, using noninterference technique
[AIAA PAPER 70-728] 16 p2910 A70-33491

Boron particles ignition and combustion in supersonic air stream, emphasizing axial and lateral two phase flow injection
[AIAA PAPER 70-737] 16 p2856 A70-33496

Gas-particle mixture cascade flow over turbine blades, considering momentum/heat transfer and particle trajectories
[AIAA PAPER 70-712] 16 p2835 A70-33569

Gas-liquid two phase flow dynamics, explaining behavior under normal and oblique shocks
16 p2893 A70-33684

Plastic deformation of two phase alloy with small nondeformable particles in ductile matrix, discussing cross slip, yield and flow stress, work hardening etc
17 p3126 A70-35460

Thin cylinder longitudinal two phase dispersed flow, examining heat transfer coefficient
18 p3345 A70-36112

Compressible flow of two component two phase mixtures through convergent nozzles and orifices, determining initially or annular dispersed flow patterns
18 p3239 A70-36231

Two phase flows and atomization jet during fluid injection into supersonic flow, determining vaporization range
20 p3736 A70-39268

Liquid-gas separator design with reduced friction loss for MHD generators using two phase convergent-divergent nozzles
20 p3612 A70-40014

Axial pressure, electric current and potential distribution in two-phase particulate electrodynamic flow, discussing space charge electric field effect
20 p3683 A70-40257

One dimensional unsteady equilibrium flow stability of relaxing two phase medium consisting of perfect gas and incompressible liquid
20 p3613 A70-40295

Stagnation temperature of two phase nozzle gas jet containing solid particles on particle density and velocity
21 p3748 A70-42220

Shock wave formation and propagation analyzed by hydrodynamic model of two directional traffic flow based on continuity equations and velocity-density empirical relations
22 p4012 A70-43321

Two phase liquid one dimensional motion in variable cross section tube, deriving mass transfer, motion and phase interaction differential equations
22 p4012 A70-43721

Heat and mass transfer for liquid film evaporation during two phase two component flow in vertical steel tube under adiabatic and nonadiabatic conditions
23 p4276 A70-44215

Two phase plume at various incidence angles on flat plate, determining impinging particle mass flux, forces and damage
23 p4134 A70-44566

Critical heat flux during forced pipe flow of boiling ethanol-water and acetone-water binary mixtures
23 p4283 A70-44730

Hydrogen slush characteristics, discussing advantages of liquid-solid mixture over liquid hydrogen, production methods, aging effects, transfer and pumping losses, storage, instrumentation, etc
23 p4232 A70-45075

German monograph on flow phenomena in gas containing fluids, covering pressure and ultrasonic induced cavitation in steady and unsteady flow
24 p4324 A70-45098

Laser light scattering by moist air flows with condensed droplets of water vapor
24 p4353 A70-45565

Resistance to two phase gas-liquid flow in airways simulating human bronchial tree
24 p4303 A70-46111

TWO PHASE SYSTEMS

U BINARY SYSTEMS [MATERIALS]

TWO REFLECTOR ANTENNAS

Field correlation theorem for deducing Cassegrain antennas performance from internal field distributions, considering two reflector diffraction problems
15 p2698 A70-31953

Illumination efficiency in shaped two reflector Cassegrain antenna system related to feed pattern deviation
16 p2861 A70-32968

TWO STAGE TURBINES

Two stage turbine engine parts adjustment optimization in terms of fuel consumption or thrust control by linear programming techniques
19 p3489 A70-37241

Two stage gas turbine engine optimal tuning for RPM, thrust, fuel rate and gas temperature, describing automated bench tests
22 p4092 A70-43361

Two shaft bypass jet engine analog simulation, determining angular acceleration dependence on angular velocity and fuel consumption
24 p4393 A70-45442

TYCHO CRATER

Small craters number density in southern lunar highlands, supporting Tycho Association cometary impact origin
21 p3920 A70-41882

Tycho crater northeast rim scale relief model including lava lakes in outer walls
23 p4253 A70-44881

TYPE 2 BURSTS

Radioheliograph observations of position and motion of type 2 and 4 radio sources during flares based on proton model
01 p0168 A70-10255

Electron gyrofrequencies computed from split pair bursts in 1966 compared with results from type II bursts in 1967
04 p0738 A70-14510

Solar corona magnetic field estimated from type II bursts correlated with photospheric, chromospheric and geophysical phenomenon
10 p1934 A70-25275

Expanding arch structure of type 2 solar radio burst observed with Culgoora radioheliograph
11 p2105 A70-25749

Type 2 and 4 solar radio emission, showing bursts excitation by common shock wave ejected from flare region
15 p2794 A70-32620

Type 2 irregularities in equatorial electrojet associated with plasma density vertical gradients
18 p3244 A70-36017

Two dimensional positions of fundamental and harmonic type 2 solar bursts, using coronal streamer plasma and backward refracted radiation model
21 p3891 A70-41179

Two dimensional position measurements of harmonic type 2 solar bursts, using 80 MHz observations
21 p3891 A70-41180

Shock wave excitation of type 2 and moving type 4 solar bursts from Culgoora radioheliograph and spectrograph recording
21 p3891 A70-41181

Type 2 solar radio burst shock wave exciter velocity from dynamic spectrograms, relating correction to shock strength gradient
24 p4401 A70-45322

TYPE 3 BURSTS

Meter wave type 3 solar radio waves associated with solar X ray flares, discussing sudden enhancements of LF field strength due to D layer ionization enhancement
01 p0168 A70-10257

Kinetic temperature estimate for solar corona based on time profile of type 3 bursts
08 p1565 A70-20565

Type 3 burst sources velocity calculated by frequency drift and Newkirk model of electron density, discussing frequency range extension of Weissenau radiospectrograph
10 p1934 A70-25274

Solar radio types I and III sources spatial distribution of circular polarization and coronal magnetic field configurations in active regions
12 p2294 A70-27710

Galactic noise and solar type 3 bursts using Alouette 2 satellite HF receiver voltage recordings
12 p2226 A70-28065

Type 3 solar bursts theory covering beam-type instabilities and quasi-linear relaxation of fast electron distribution functions
13 p2478 A70-29389

Solar type 3 burst theory, considering plasma wave energy conversion into radio emission
15 p2802 A70-32484

Kinetic temperature estimate for solar corona based on time profile of type 3 bursts
15 p2805 A70-32720

Dynamic spectra of type 3 solar bursts fromOGO-3 antenna/radiometer observations
17 p3150 A70-34835

Type 3 solar bursts classification, measuring diameter, lifetime and position
17 p3151 A70-35581

Type I burst effects on type III and V bursts occurrence, suggesting Langmuir waves excited by suprathermal electrons
17 p3173 A70-35746

Position scatter of 80 MHz sources of type 3 solar bursts reflecting outer corona structure
21 p3891 A70-41182

Solar type 3 burst theory, considering plasma wave energy conversion into radio emission
23 p4240 A70-43908

Solar VHF radio spectra indicating type 4 burst activity associated with type 3 formation
24 p4401 A70-45318

TYPE 4 BURSTS

Coronal electron densities and magnetic fields determined from K-coronameter and type 4 radio burst data
01 p0168 A70-10255

Radioheliograph observations of position and motion of type 2 and 4 radio sources during flares based on proton model
01 p0168 A70-10256

Microwave spectra of type 4 bursts at cm and dm waves compared to related PCA
02 p0359 A70-12774

Magnetic structure of type 4 solar outburst from continuous record of 80 MHz image and polarization
03 p0358 A70-13587

Magnetic field effect on burst emissions in plasma frequency range, observing radiation band widening and modes transmission in terms of Appleton-Hartree theory
10 p1949 A70-25273

Type 4 solar radio bursts compared with flare observations, geophysical effects and satellite monitors data to detect proton flares spectra
10 p1934 A70-25278

Type 2 and 4 solar radio emission, showing bursts excitation by common shock wave ejected from flare region
15 p2794 A70-32620

Moving type 4 solar burst on 1 March 1969 observed at 80 MHz, discussing plasma cloud associated with prominence

21 p3880 A70-40967

Shock wave excitation of type 2 and moving type 4 solar bursts from Culgoora radioheliograph and spectrograph recording

21 p3891 A70-41181

Solar type 4 event flux density and circular polarization radiopolarimetric recording, showing peculiar phases of short duration

22 p4095 A70-43263

Solar VHF radio spectra indicating type 4 burst activity associated with type 3 formation

24 p4401 A70-45318

TYPE 5 BURSTS

Type I burst effects on type III and V bursts occurrence, suggesting Langmuir waves excited by suprathermal electrons

17 p3173 A70-35746

U

U TUBES

U MANOMETERS

U.S.S.R.

Reflector radio telescope of Pulkovo Astronomical Observatory noting high resolution

01 p0094 A70-11585

Soviet SS-9 ICBM role in international debates over antiballistic missile, multiple independently targeted reentry vehicles, superhard silos and offensive forces

04 p0760 A70-14501

Quasi-optical design methods applied to mm microwave resonators characterized by high Q and low spectral densities

04 p0655 A70-14623

Space role in competition between U.S. and U.S.S.R. since August 1957, discussing armament control agreements regarding space

07 p1426 A70-18882

Parametric amplifier for spectral radiometer of U.S.S.R. astronomical telescope, showing improved sensitivity observations of neutral H emission

08 p1473 A70-21066

Meteorite craters on U.S.S.R. territory, discussing impact, explosive and complex craters

12 p2311 A70-28308

U.S.S.R. SPACE PROGRAM

Visual photometric tracking data obtained in SPIN program for satellites 1965-II-4 and 1965-53-6 at Kishinev station

03 p0444 A70-13181

TV data transmitted by Iantar series automatic ionospheric laboratories released by geophysical rockets at 100-400 km, discussing plasma-ion propulsion system performance

04 p0735 A70-14936

Soviet Venus probes Venera 1, 2, 3, 4 and 5 emphasizing aims, implementation means and information yields influence on theory of solar system planets origin and evolution

04 p0757 A70-15672

Soviet unmanned spacecraft and components displayed at Le Bourget show, including Molniya 1, Proton 4 satellites, Venus 4 station, vertical cosmic probe, etc

05 p0921 A70-15814

Soviet aerospace manufacturing technologies development, considering forging, extrusion, metal working and joining, etc

05 p0853 A70-15826

Soviet space activities /1969/, discussing Soyuz orbital flights, Venera probes, Zond lunar orbiters and Proton 4 space laboratory scientific results

05 p0917 A70-16862

Soviet manned space flight radiation dosimetry evaluation, comparing U.S. and Soviet techniques for astronaut protection

06 p0990 A70-17271

Space flight candidate selection and physical training, comparing American and Soviet training programs for efficiency and physical requirements

07 p1216 A70-18792

Soviet Venus probes 5 and 6 observation data concerning Venus atmospheric composition, temperature and pressure, etc

08 p1568 A70-20624

Soviet cameras for photographic observation of artificial celestial bodies, noting equatorial platform mount, mirror lenses and installations

10 p1892 A70-25128

Soyuz 6, 7 and 8 group flight as step in Soviet space program to place manned station in earth orbit

11 p2121 A70-25623

Soviet lunar and interplanetary space missions during 1969 including Venera, Cosmos, Luna and Meteor satellite activities

13 p2505 A70-28901

Signal analysis from Russian Cosmos, Proton and Soyuz satellites, showing pulse width and pulse code telemetries

14 p2551 A70-30975

Monograph on upper atmosphere and outer space studies in U.S.S.R. /1969/ covering Soiuz 4, 5, 6, 7, 8 and Venera 5, 6 flights

15 p2829 A70-31702

Soviet and American lunar exploration by probes, manned surveillance flights and lunar landings, discussing NASA program

18 p3238 A70-37079

Soviet communication satellites orbit and design characteristics, operational uses and ground stations, discussing Molniya 1 series transmitting television, multichannel radio, telephone and telegraphy

18 p3230 A70-37225

U.S. and Soviet space program administration and management

21 p3956 A70-41893

International space program cooperation, discussing NASA projects, Apollo 11 flight and European and Soviet programs

22 p4129 A70-43655

UBV SPECTRA

Photometric measurements in Cygnus, analyzing formulas used for conversion to standard UB system for Javan reflector /Sweden/

02 p0297 A70-12065

Photoelectric UB photometry of stars in Carina, Vela and Centaurus, giving standard connection sequences for continued photometry

02 p0370 A70-12074

Multicolor photometry of Orion flare stars in U, B, V and R, constructing diagrams confirming flare stars scattering about main sequence

03 p0567 A70-13317

Icarus asteroid positions, UB magnitude, brightness, colors, light curves and polarization, noting stony-iron composition

11 p2113 A70-26470

Bright southern Cepheids UB observations, discussing blue companion effect on two color plot

14 p2639 A70-30726

Binary AX Monocerotis brightness variations in UV from photoelectric UB observations

15 p2796 A70-31610

Absolute photovisual magnitude and classification of supernova in NGC 3389 spiral galaxy, using UB measurements and comparison stars

15 p2797 A70-31611

Three color photometry of RW Auriga stars, discussing UB curves, H-R diagram and UV emission excess

15 p2797 A70-31612

Nova HR Delphini 1967 UB photometric photometry, examining absolute magnitude, distance, response curves and spectra

21 p3889 A70-41154

UBVr colors of A0-K0 main sequence stars, deriving B-V relation to effective temperature

23 p4246 A70-44757

Radial velocity-light amplitude ratios of grouped variable stars in continuous sequence, comparing pulsation prediction

23 p4247 A70-44793

A type stars rotation, examining UB color and rotational velocity relationship, spectral classification and spectroscopic binaries

23 p4251 A70-44822

Photographic photometry in astronomy, considering Becker method and UB system

24 p4333 A70-45145

Southern early stars away from galactic plane, reporting magnitudes and colors on UB system and MK spectral classifications

24 p4404 A70-45412

UDIMET ALLOYS

Creep-low cycle fatigue interactions in Udimet alloy at elevated temperatures, investigating cumulative damage

06 p1086 A70-17455

UH-1 HELICOPTER

UH-1C, AH-1G and UH-1H helicopters combat operational flight profiles, considering airspeed, altitude, rotor speed, load factor, etc

17 p3014 A70-34717

U.S. Army UH-1/ AH-1 helicopter maintainability and reliability field program, including statistical data

19 p3356 A70-38827

UHTREX [NUCLEAR REACTORS]

U HIGH TEMPERATURE NUCLEAR REACTORS

ULLAGE

Gas-wall heat losses reduced and heated gas pressurization systems performance improved by ullage mixing by gas flow from pressurant injectors

16 p2962 A70-33581

ULLAGE ROCKET ENGINES

Saturn ULLAGE solid propellant rocket motor vibration test evaluation

07 p1365 A70-20039

ULM [LIGHT MODULATION]

U ULTRASONIC LIGHT MODULATION

ULNA

Mechanical and morphological characteristics of overload and fatigue in dog ulnas, showing elastic and plastic deformation zones

15 p2682 A70-31935

Ulnar resonant frequency reproducibility as objective measure of skeletal status, discussing forearm and hand positioning effect

20 p3579 A70-39432

ULTRA SHORT WAVE RADIO EQUIPMENT

U VERY HIGH FREQUENCY RADIO EQUIPMENT

ULTRAHIGH FREQUENCIES

UHF signal amplification by electron beam-plasma interaction, defining amplification frequency ranges

01 p0043 A70-10658

Transient Faraday rotation of S-band telemetry carrier observed during Pioneer 6 occultation by solar corona, correlating with decametric solar radio bursts

02 p0369 A70-12059

UHF ranging system principles, discussing output proportional to approach angle

02 p0257 A70-12179

Airborne UHF transmitters, discussing data on designs, performance, packaging and limiting factors of solid state devices for RF utilization

02 p0267 A70-12183

UHF radio telemetry system using pulse signal to measure and transmit sea waves amplitude and frequencies data to shore-based recorder

03 p0453 A70-14352

Circular polarization measurements of Jovian decimeter radiation by 210-ft radio telescope at Goldstone, California

05 p0921 A70-16986

S-band omnidirectional antenna patterns measurement procedure and results for Apollo spacecraft configurations, tabulating measure gains

06 p1019 A70-15707

L band transponder design for aeronautical satellite, giving block diagrams

07 p1234 A70-19292

Galvanoplasty process for parts for UHF circuits, discussing cost, safety and quality

08 p1468 A70-20611

UHF transistor power amplifier, discussing CW and pulse performance and power gain

08 p1477 A70-21294

Integrated CW UHF power amplifier modules using thin film lumped elements and UHF power transistor chips

10 p1846 A70-23884

Tunable L band high power anomalous mode avalanche diode oscillator with coaxial circuit

10 p1847 A70-23888

Silicon L-band avalanche diodes as high power pulsed microwave sources, discussing fabrication, circuit requirements, radar applications, etc

10 p1852 A70-24893

Air traffic control system using ground controlled satellite-borne phased array antenna to overcome UHF downlink path loss

11 p2077 A70-25421

Aerial and ground UHF noise measurement in Phoenix area, correlating air and ground data

11 p2001 A70-25480

Microwave acoustic delay lines design and fabrication for UHF to X band frequency ranges

11 p2005 A70-26163

Discrete extragalactic radio sources integrated linear UHF polarization values, discussing optical identification and radio spectral index correlations

11 p2117 A70-26656

UHF frequency doubler with series-parallel array of eight punch-through diodes, preventing spurious oscillations

12 p2196 A70-27650

Cassiopeia A high resolution map at UHF revealing main source physical characteristics and enhanced emission compact components

12 p2309 A70-27976

High power L-band avalanche diode oscillators fabrication and performance

13 p2376 A70-28977

High power L- and S-band transferred-electron oscillators from epitaxial GaAs

13 p2377 A70-28978

Radio sources positions on solar disk by 2800 and 408 MHz high resolution fan beams

13 p2491 A70-29161

Parametric excitation of potential oscillations in plasma near cyclotron frequency subjected to UHF electric and constant magnetic fields

13 p2463 A70-29281

UHF propagation measurement over sea for varying surface refractivity and meteorological conditions, noting diurnal variations

14 p2549 A70-30513

Synchrotron model involving electron trapping in dipolar magnetic field for Jupiter decimetric radiation

14 p2649 A70-31089

UHF Si p-n-p transistors with low noise and high gain for small signal applications

14 p2557 A70-31161

S band transmitters frequency deviations optimization enabling designer to determine optimum value within constraints of associated receiving equipment

14 p2559 A70-31373

S band GaAs FET fabrication technology and frequency response 16 p2877 A70-33414

Lx band characteristics and utilization, describing evolutionary systems based on TACAN and IFF 16 p2948 A70-33452

Cosmic ray air showers UHF emission detection at 500 MHz 17 p3151 A70-34850

Wideband UHF amplification in bulk n-type GaAs during domain generation, comparing cut-off and Gunn frequency 17 p3143 A70-35684

Transmit only solid state radar module built with microstrip techniques for phased array systems operating at L and S dual bands 17 p3056 A70-35899

Solar radio bursts recording by spectrographs in 500-1500 MHz band, discussing sensitivity 18 p3307 A70-36109

Radio sources near 2 flux units at 408 MHz, presenting data on positions, optical identifications, angular size and flux densities 18 p3321 A70-37125

Multiquantum combination effects in ferrites at UHF frequencies 19 p3484 A70-37624

S band telemetry antenna with electronic tracking and polarity diversity for remote location missile testing 19 p3388 A70-37901

ATS-5 spacecraft L band propagation performance, describing up and downlink test methods 21 p3790 A70-41363

Tunable high efficiency high peak power UHF avalanche diode oscillator 21 p3800 A70-42117

P-n junction dependent FM noise spectrum of UHF transistor power oscillator at transit frequency 23 p4161 A70-43789

Transistorized power amplifiers, frequency multipliers and parametric multipliers design for VHF and UHF ranges 23 p4170 A70-43876

ULTRAHIGH VACUUM

Solar simulator built into multivall ultrahigh vacuum chamber, describing simulator and chamber modifications 09 p1657 A70-23264

Lead type channel electron multipliers gain degradation in ultrahigh vacuum 10 p1849 A70-24557

Titanium monoxide thin film as low temperature getter, measuring activity coefficient and capacity under ultra high vacuum 15 p2783 A70-31844

Gas formation by sliding friction of self lubricating Teflon with carbon black on steel in ultrahigh vacuum, using mass spectrometry [DFVLR-SONDDR-54] 15 p2745 A70-32446

Superhigh vacuum pump with orbitron ionizer, describing construction and ionization 16 p2843 A70-33214

Space molecular sink simulator facility (Molsink) for extreme high vacuum outer space environment simulation, discussing Mariner Mars 1969 spacecraft components tests 16 p2889 A70-34167

Surface interaction between Al single crystals in ultrahigh vacuum, investigating galling, distortion and adhesion 16 p2924 A70-34168

Cryopumping systems of ultrahigh vacuum space environmental chambers 17 p3060 A70-35247

Ultrahigh vacuum gages absolute calibration by controllable conductance method, discussing accuracy 19 p3421 A70-37463

Ultrahigh vacuum calibration system for vacuum gages and mass spectrometers based on pressure attenuation and molecular beam techniques 22 p4029 A70-42620

Reaction kinetics of microbial sterilization in ultrahigh vacuum and in outer space 23 p4148 A70-44841

Ultravacuum measurement and calibration assembly for pressures down to one picotorr for vacuum gage standards 23 p4143 A70-44871

ULTRALOW FREQUENCIES

U EXTREMELY LOW RADIO FREQUENCIES

ULTRAPURE METALS

High purity V and V-Cr-Ti process, describing aluminothermic reduction and electron beam purification 15 p2761 A70-32387

ULTRASONIC AGITATION

Erythrocyte suspension subjected to gas bubble ultrasonic oscillation, investigating hemolysis mechanism 20 p3573 A70-39981

Pure Ni plastic flow threshold measurement under combined ultrasonic and static loadings, noting annealing 22 p4053 A70-42644

ULTRASONIC GRINDING MACHINES

U GRINDING MACHINES

U ULTRASONIC MACHINING

ULTRASONIC INSPECTION

U ULTRASONIC TESTS

ULTRASONIC LIGHT MODULATION

Diffraction shaped ruby laser monopulse during excitation of modulated ultrasonic traveling waves in phototropic Q switch 09 p1696 A70-22483

Longitudinal distortion reduction in ultrasonic holograms 09 p1689 A70-23805

Ultrasonic LF modulation of solid state traveling medium lasers radiation intensity attributed to elastic vibrations of rods 11 p2062 A70-25398

Ultrasonic effects on synchronization of ruby laser radiation, investigating emission pulse structure and peak sequence 12 p2245 A70-27297

Silicon elastic constant measurement by Debye-Sears effect, using He-Ne laser source 18 p3298 A70-36952

Ultrasonic LF modulation of solid state traveling medium lasers radiation intensity attributed to elastic vibrations of rods 20 p3643 A70-40092

Nondestructive testing by ultrasonic acousto-optical imaging in opaque objects 22 p4047 A70-43518

Ultrasonic light modulation using single crystal lithium niobate transducers in laser communication and information processing systems 22 p3992 A70-43734

ULTRASONIC MACHINING

Rotary Ultrasonic Machining with diamond tools for hard and brittle materials compared to ultrasonic impact grinding method 09 p1692 A70-22797

Drilling rates improvement for Ti by adding ultrasonic vibration to conventional process 19 p3437 A70-38421

Ultrasonic machining of glass and cemented carbide, measuring ambient pressure effect on workpiece removal rate 21 p3833 A70-41253

ULTRASONIC RADIATION

Titanium carbide sintering under continuous heating in Ar atmosphere, studying ultrasonic waves effects on compaction process 04 p0696 A70-14463

Standing wave ratio of ultrasonic field determined by holographic method, using acoustic transmission lines with termination impedances 05 p0848 A70-16403

Structural analysis of thin walled cylinder material using normal ultrasonic wave to achieve high resolution determination of components 06 p1172 A70-18630

LF ultrasound not producing irreversible denaturation of blood serum proteins but capable of modifying electrophoretic properties 07 p1206 A70-19470

Ultrasonic vibration effect on strength and plastic properties of metals undergoing torsion tests 08 p1520 A70-21499

Two temperature gasdynamics for binary gas mixtures of differing molecular weight components, analyzing ultrasound and shock wave propagation 08 p1486 A70-21808

Ultrasonic pulse frequency spectrum analyzer, describing electronic components, transducer type and positioning, beam collimation, applications in testing, etc 10 p1895 A70-24830

Ultrasonic wave absorption and dispersion in mixtures of air and water vapor with water droplets, investigating equilibrium distribution and hydrodynamic equations [ASTME PAPER MR-69-733] 11 p2085 A70-26691

Acoustographic imaging system (AGIS) using liquid crystal detection screen to provide color display of ultrasonic wave information 12 p2235 A70-27724

Ultrasonic wave propagation guided by fluid layer between two elastic solids, plotting normalized velocities and layer thicknesses 12 p2273 A70-28097

Interference phenomenon observable by ultrasonic fields visualization in 1-10 MHz range, discussing beam stratification 13 p2404 A70-28646

Amplitude modulation of ruby and neodymium-doped glass lasers via ultrasonic acoustic wave injection 16 p2926 A70-33162

Elastic constants for plates of unidirectional fiber reinforced anisotropic composite material determined by ultrasonic wave propagation 16 p2991 A70-33847

Ultrasonic pulses velocity and attenuation in fluids by coherent detection technique, measuring delay and

decrease in amplitude due to transmission path length increase 16 p2913 A70-34084

Sound wave phase fluctuations from ultrasonic waves traveling through turbulent wakes of circular cylinders and plates, using multichannel pulse height analysis 16 p2839 A70-34086

Transient signal generation during large amplitude ultrasonic pulse propagation through carbon tetrachloride 16 p2952 A70-34097

Holographic techniques, investigating ultrasonic fields in transparent media based on light separation by grating into optical moments 16 p2915 A70-34330

Martensitic phase change effects in TiNi on ultrasonic waves propagation in transition region, using pulse echo measurements 17 p3126 A70-35603

Combined ultrasonic and ionizing radiation effects on electrophoretic mobility of tumor cells from albino mice 17 p3034 A70-35762

Ultrasonic irradiation effects on steel hardenability and carbon diffusion rate during annealing, noting microstructure 18 p3273 A70-36049

Ultrasonic surface waves amplification in piezoelectric crystal-Si semiconductor system, observing dependence on permittivity 19 p3488 A70-38675

Ultrasonic sensor for detecting altitude and vertical velocity of aircraft near ground, applying to helicopter hovering flight or conventional airplane takeoff and landing [AIAA PAPER 70-1031] 20 p3631 A70-39506

Phase velocity and attenuation of shear waves in gases from sampled-CW ultrasonic crystal resonator reflection measurement 21 p3827 A70-41457

Pulse superposition measurements of small ultrasonic waves velocity changes using automatic recording phase sensitive detection 21 p3827 A70-41468

Frequency shifted diffraction of monochromatic Gaussian light beam by reflection off ultrasonic surface wave 21 p3850 A70-41907

Ultrasonic absorption in gaseous molecular relaxation processes, considering error due to neglecting thermal conductivity effect on frequency dependence 22 p4073 A70-42649

Ultrasonic and electron paramagnetic double resonance in Fe-doped corundum 22 p4074 A70-43010

Ultrasound inductive absorption coefficient of metals in quantized magnetic field 22 p4075 A70-43474

Ultrasonic absorption in SbSI semiconducting semiconductor as function of temperature, illumination and constant electric field strength, noting absorption coefficient rise near Curie point 24 p3899 A70-45207

Sintered material density-sound velocity relation, deriving ultrasonic wave propagation time dependence 24 p4360 A70-45731

ULTRASONIC SOLDERING

Ultrasonic Al wire bonding for microelectronic applications, discussing tensile strength dependence on machine parameters and aging 15 p2747 A70-32647

ULTRASONIC SPEEDS

U SUPERSONIC SPEEDS

ULTRASONIC TESTS

Ultrasonic detection of service induced cracks near tenon base region of second stage Al compressor disks 01 p0096 A70-10003

Ultrasonic detection system for crack initiation and propagation in notched low cycle axial fatigue testing using surface and longitudinal waves 01 p0096 A70-10004

Ultrasonics inspection applied to reentry vehicle heat shields and composite materials, verifying anomalies by microscopic area examination 01 p0097 A70-10016

Lamb wave techniques using guided ultrasonic waves for solid cylindrical objects nondestructive testing 01 p0098 A70-10019

Ultrasonic methods for materials evaluation, discussing goniometry, measuring techniques and acoustic wave propagation in various materials 01 p0104 A70-10878

Aluminum alloys fatigue properties tested at ultrasonic frequencies 01 p0120 A70-10879

Ultrasonic image superposition technique for visualization of impact fractures in glass reinforced plastics 01 p0059 A70-11101

Aircraft nondestructive testing, discussing radiography requirements, ultrasonic bond testing technique, etc 01 p0104 A70-11319

Ultrasonic wheel-type portable inspection device with internal coupling immersion fluid contained in silicone tire, allowing angle beam inspection without temperature correction

01 p0105 A70-11396

Inexpensive schlieren system for medical ultrasonic research, discussing equipment and application to short wave transducer beam patterns used in ophthalmology

02 p0300 A70-12472

Ultrasonic tracking type transducers for testing ribbed and smooth walled pipes using shadow and two probe echo methods

02 p0300 A70-12480

Electrodynamic contactless method for ultrasonic nondestructive testing of materials based on natural frequencies shift with and without defects

02 p0301 A70-12483

Optimum prism angles and ultrasonic frequencies for detecting fatigue cracks

02 p0301 A70-12487

Ultrasonic Doppler method for timing mitral and aortic valves rapid movements, using filter to eliminate LF signals due to heart walls

03 p0432 A70-12891

Al alloy rectangular beam stress corrosion crack initiation and propagation measurement using ultrasonic techniques, showing relationship between crack velocity and initial stress

[SESA PAPER 1564]

03 p0481 A70-12958

Materials fatigue failure ultrasonic early detection by continuous surface wave irradiation

06 p1077 A70-17920

Nomograms for ultrasonic shadow defectoscope acoustic channel parameters calculation

06 p1065 A70-17921

Ultrasonic surface waves detection of transverse fatigue crack initiation in rails under load, applying results to fatigue life determination

06 p1168 A70-17924

Nondestructive testing of small metal tubing, discussing eddy current, ultrasonic and electromagnetic inspection and dye penetrants

08 p1509 A70-21748

Ultrasonic testing of hydraulic liquids and aircraft and engine lubricating oils resistance to viscosity decrease, analyzing large molecule compounds disintegration

09 p1693 A70-23405

Ultrasonic traveling waves for nondestructive testing, discussing scattering and velocity anisotropy in polycrystalline metals, propagation in glass, epoxy resins shear moduli, etc

10 p1894 A70-24171

Ultrasonic pulse frequency spectrum analyzer, describing electronic components, transducer type and positioning, beam collimation, applications in testing, etc

10 p1895 A70-24830

Ultrasonic echography for ventricular size determination, calculating stroke volume and valvular regurgitation severity

10 p1820 A70-24938

Ultrasonic pulse technique for measuring fiber reinforced composites elastic constants

11 p2052 A70-26341

Elastic stiffness of unidirectional glass reinforced epoxy fiber composite determined from ultrasonic velocity measurements

11 p2071 A70-26692

Nonlocalized ultrasonic defectoscopy resonance method for qualitative difference determination of small sized articles of complex form

13 p2417 A70-28662

Nondestructive bond inspection by interferometric holography of ultrasonically excited plates

14 p2588 A70-31166

Ultrasonics for steel cleanliness rating, considering advantages and fatigue life

15 p2743 A70-31768

High temperature metal fatigue crack growth monitoring by ultrasonic detection

[SESA PAPER 1622]

15 p2744 A70-32321

Training effect on strength per unit cross sectional area of arm muscle, using ultrasonic measurement

17 p3024 A70-34592

Single ventricle and hypoplastic left and right heart syndromes, investigating with reflected ultrasound

17 p3032 A70-35472

Ultrasonic measurement of temperature distribution in solid, liquid and gaseous media, using reflection and transmission techniques

19 p3427 A70-37963

Holographic ultrasonic imager using liquid surface detector for real time imaging of test objects moving through viewfield, discussing nondestructive test applications

19 p3433 A70-38829

Ultrasonic pulse echo flaw detection, relating defect size to echo amplitude

20 p3636 A70-39192

Ultrasonic nonsearch Doppler cardiography for cycle phase analysis, recording single functions

20 p3581 A70-40199

Elastic wave propagation mathematics in visual form for ultrasonic testing

21 p3831 A70-40746

Nondestructive ultrasonic measurements of crack depth in high strength steel plate weldments, studying low cycle fatigue

21 p3834 A70-41943

Ultrasonic spectroscopy in nondestructive materials tests, discussing electronic equipment design, FM, pulse and pulsed FM methods

22 p4027 A70-42583

Ultrasonic imaging systems of nondestructive testing, discussing photographic and chemical systems, thermal, optical and mechanical methods and electronic systems

22 p4027 A70-42584

Ultrasonic Rayleigh critical angle reflectivity of liquid-solid interface energy, detecting near-surface properties changes

22 p4027 A70-42585

Ultrasonic holography for nondestructive testing, discussing reference beams and analogies to optical and electronic methods

22 p4028 A70-42586

Ultrasonic detection of tooth surface layer demineralization, noting surface and subsurface enamel structural differences

22 p3978 A70-42955

Ultrasonic wave velocity measurements for flaw detection and modulus of elasticity of carbon-carbon composites

22 p4047 A70-43519

Ultrasonic velocity in human bones measured for calcium content and density

22 p3979 A70-43522

Acoustic fields of circular, rectangular and line focused ultrasonic emitters for small defect detection

22 p4048 A70-43618

Apparatus characteristics determination for ultrasonic inspection, recommending calibration block

22 p4041 A70-43622

Ultrasonic crack detection in fastener holes in C-5A wings

24 p4341 A70-45571

Ultrasonic delta technique inspection method for flaw detection in weldments or wrought materials

24 p4335 A70-45572

Reflector materials flaw size and orientation using ultrasonic spectral frequency analysis

24 p4335 A70-45573

Nondestructive testing - Conference, Hanover, June 1970, Ultrasonic, Part 1, Instruments, methods and defect evaluation

24 p4342 A70-45680

Noncontact electromagnetic acoustic transducer/E-MAT/ for metallic products ultrasonic thickness testing

24 p4336 A70-45682

Thickness measurement and internal defects inspection by ultrasonic resonance technique

24 p4343 A70-45683

Ultrasonic pulse emitter with interference-free near field and sidelobe suppression for materials testing

24 p4343 A70-45685

Angle beam ultrasonic testing of metals, considering beam and depth scanning characteristics and wave reflectability of various flaws

24 p4343 A70-45687

Flaw echo height dependence on ultrasonic testing pulse frequency spectrum

24 p4336 A70-45688

Defect size estimation, using ultrasonic angle beam probes and distance-gain-size/DGS/ diagram

24 p4343 A70-45689

Ultrasonic inspection sensitivity loss, discussing depth compensation methods

24 p4343 A70-45690

Cylindrical boreholes as reference defects in ultrasonic inspection, discussing geometrical parameters effects on echo height

24 p4343 A70-45691

Automated ultrasonic testing and facsimile data recording systems, discussing aerospace, marine and automotive applications

24 p4343 A70-45692

Crack detection in cyclic strained steel and Al alloys, using ultrasonic Rayleigh and longitudinal waves

24 p4424 A70-45718

Nondestructive examination for plastics, discussing transmission, microwave and ultrasonic tests

24 p4346 A70-45720

ULTRASONIC WAVE TRANSDUCERS

High temperature thermometer using pulsed excitation ultrasonic resonance with ruthenium sensor, discussing resonator types, transmission lines and transducer

02 p0300 A70-12468

Piezoelectric transducers performance in ultrasonic devices evaluated from loss and admittance measurements, using Mason equivalent circuit method

03 p0496 A70-14026

Ultrasonic flowmeter with electronic components, discussing flow rate parameters and wave propagation relative to flow

12 p2236 A70-28074

Doppler effect pulsed ultrasonic blood flowmeter using transducer alternating as transmitter and receiver

15 p2690 A70-31919

Left ventricular dynamics ultrasonic visualization, involving catheter-borne transducers array and computer for data acquisition and display

18 p3225 A70-36750

Ultrasonic transducer diffraction fields in highly anisotropic crystals obtained by plane waves angular spectrum

22 p4029 A70-42643

Contactless electrodynamic ultrasonic transducers design and operation, discussing applications and developmental state

24 p4343 A70-45684

Ultrasonic angle probes with circular and rectangular transducers, discussing radiation field characteristics

24 p4336 A70-45686

ULTRASONIC WAVES

U ULTRASONIC RADIATION

ULTRASONICS

Ultrasonic imaging of internal structure by Bragg diffraction, noting reflection and dark field extension and use for flaw detection and medical diagnostics

01 p0111 A70-10570

Ultrasonics for industry - Conference, London, October 1969

01 p0089 A70-10877

Transcutaneous Doppler-shift flowmeter for arterial blood velocity measurement by ultrasound

01 p0037 A70-10880

Ultrasonic imaging system for flaw detection, analyzing welds

01 p0104 A70-10881

Ultrasonic holography in nondestructive testing, discussing metal block with simulated defects

01 p0089 A70-10882

Piezoelectric ultrasonic crystal on cardiac catheter tip measuring cardiac diameter in vitro and in excised canine hearts

01 p0038 A70-11025

Ultrasonic atomizer system for liquid fuels combustion

02 p0356 A70-12470

Ultrasonic beam scanning measurements in high temperature axisymmetric gas flow, discussing errors and use of numerical transformation methods

04 p0685 A70-14536

Laser beam trajectory equation in scanning ultrasonic cell for nonzero incidence angle, relating input and output beam divergence

07 p1300 A70-19865

Uncontrolled and controlled neodymium glass laser outputs, using ultrasonic traveling wave diffraction modulator

08 p1510 A70-20514

High intensity ultrasonics for changing solids properties, discussing effects on metal powder sintering, yield strength, fatigue life, crystallization rate, etc

09 p1728 A70-23348

Ultrasonic vibrations effects on microstructure and mechanical properties of polycrystalline titanium during phase recrystallization

10 p1903 A70-23863

Thermal imaging device adaptable to IR, microwave or ultrasound radiation, projecting image on heat sensitive surface

11 p2050 A70-25643

Thermodynamic and transport properties of high temperature and pressure gases measured with ultrasonic pulse technique

11 p2147 A70-25753

Isotropic finite strain expressions for compressional and shear velocities, noting no discrepancy with ultrasonic and seismic data

20 p3619 A70-39218

Hydraulic fluids and lubrication oils resistance to mechanical shear forces by ultrasonic method based on acoustically induced cavitation effects

20 p3655 A70-39718

Ultrasonic measurements of flow velocity and fluid rate, using high speed switching and synchronous demodulator

22 p4041 A70-43619

ULTRAVIOLET ABSORPTION

Impurities effects on UV absorption in semiconductors, deriving kinetic type equation for two particle Green function

13 p2471 A70-29511

Solid state laser glass filters for absorbing UV light emitted by pumping tubes

20 p3641 A70-39739

ULTRAVIOLET FILTERS

Diffraction filters characteristics used in XUV spectroscopy involving solar, stellar and laboratory experiments

09 p1729 A70-23526

Solid state laser glass filters for absorbing UV light emitted by pumping tubes

20 p3641 A70-39739

ULTRAVIOLET LIGHT

U ULTRAVIOLET RADIATION

ULTRAVIOLET PHOTOMETRY

- UV photometry of stars and galaxies from OAO-2, discussing instruments and observational results
02 p0378 A70-12580
- UV photometry from OAO, observing planets, gaseous nebulae, X ray source, quasars, Crab Nebula, extragalactic nebulae, etc
02 p0303 A70-12705
- Stratospheric balloon measurement of near UV from early type stars, discussing gondola, observation method, telescope and photographic recordings analysis
04 p0750 A70-14704
- UV rocket-borne up-down photometer measuring zenith and nadir intensities for auroral profile studies
06 p1072 A70-18518
- Solar far UV continuum photometry illustrating spectral temperature minimum transition, comparing to far IR temperature
13 p2496 A70-29841
- Photometric calibration changes in EUV solar satellite instruments during orbital operation
15 p2737 A70-32045
- Far UV photometer for space research, isolating specific bands by combining spectral response of individual solar blind photocathodes with thin metallic films transmission qualities
17 p3096 A70-35766
- Satellite-borne UV TV system for photometric investigations of UV stars
19 p3428 A70-38456
- UV photometry from OAO-2, describing Wisconsin instrumentation and equipment
20 p3624 A70-39009
- Atmospheric horizontal stratification and UV transmittance by signal reflection from satellites
23 p4191 A70-44268

ULTRAVIOLET RADIATION

- NT FAR ULTRAVIOLET RADIATION
NT LYMAN ALPHA RADIATION
NT NEAR ULTRAVIOLET RADIATION
- Coherent short wave and UV radiation generation using continuous ion gas laser, discussing efficiency, stability and feedback effects
01 p0108 A70-10356
- UV sensitive spiropyran films coloration mechanism and color structure stabilization, discussing film and laser applications to optical data recording and storage
01 p0086 A70-10357
- Tissue protein changes under visible and UV radiation noting denaturation, chemical bonds, protein configurations, clinical disease patterns, etc
01 p0022 A70-10856
- UV radiation effects on mucopolysaccharide compounds in tears and on cornea epithelium of albino rabbits
01 p0037 A70-10860
- Keratinocyte development on epidermal surface of female patient exposed to cosmetic UV irradiation with quartz lamp
01 p0029 A70-11406
- Solar UV radiation reflected from Echo satellites measured and compared with UV fluxes from Lyrae
01 p0095 A70-11614
- Cs seeding effect on bound-free UV photoabsorption of Cs-H plasma at constant electron density and energies below H ionization
02 p0343 A70-11904
- He-Ne ring lasers with plane mirrors investigated for amplitude and frequency characteristics at high gain operation at 3.39 microns
02 p0312 A70-12099
- Atmospheric penetration of UV and visible solar radiation during twilight, oxygen and ozone absorption, Rayleigh scattering and atmosphere refraction
02 p0357 A70-12155
- Multicolor Venus photography, discussing anomalous markings association with anomalous UV polarization
02 p0378 A70-12557
- Venus photography in UV by 61-inch telescope, discussing low contrast clouds recognition technique
02 p0378 A70-12558
- UV radiation scattering and rocking instrument error source in vertical ozone profile determination with optical ozone probes
03 p0557 A70-13296
- UV Ceti type flare stars observational and theoretical results related to nebular or chromospheric flare models
03 p0566 A70-13316
- Atmospheric absorption anomalies of UV sunlight near 50 km altitude in rocket-borne radiometer determination of ozone distribution
03 p0478 A70-14197
- UV radiation propagation in atmospheric boundary layer, analyzing solar UV background and UV signal attenuation along horizontal path
05 p0882 A70-16241
- Horizontal atmospheric surface layer propagation path for 3370 A UV signal, studying reception distances for given SNR
05 p0812 A70-16242

- X and UV radiation effects on Escherichia coli B/r in vacuum, noting irradiated cell inactivation and radiation sensitivity increases
06 p0995 A70-17750
- Previous radiation exposure effect on photographic film noting increased sensitivity at UV frequencies
06 p1065 A70-17890
- Ar beam scattering and UV radiation from glass target surface with adsorbed gas layer
06 p1112 A70-18274
- Absorption cross sections for single and double molecules of oxygen and in UV region noting disagreement with Beer law
06 p1114 A70-18632
- UV radiation effects on pea plant chloroplasts photosynthesis at high altitudes, noting disruption of electron-transport chain reactions and cyclic phosphorylation
08 p1445 A70-21216
- Center to limb variation of solar brightness measured at 5, 10 and 20 microns, discussing data collection and reduction and previous IR and UV measurements
08 p1562 A70-21396
- Supernova fluorescent light excited by radiation impingement on material surrounding explosion site, assuming explosion time and UV energy
09 p1749 A70-21997
- Photon scattering by Ar in vacuum UV measured for cross sections
09 p1730 A70-22071
- Ozone formation in presence of nitrogen oxides and hydrocarbons during long wave UV irradiation, noting energy yield
09 p1629 A70-22328
- Mariner 6 spectra establishing Fox-Duffendack-Barker bands and ionized carbon dioxide UV doublet bands as important components of Martian dayglow
10 p1938 A70-24073
- Mirror adjustment effect on transverse structure, time dependence and spatial coherence of pulsed UV molecular nitrogen laser emission
11 p2062 A70-25394
- Open magnetic electron multipliers /MEM/ with continuous dynode and field strips for satellite-borne detection systems, emphasizing extreme UV detectors
11 p2049 A70-25628
- Iron cyanide additive for surface stabilization of ZnO irradiated with UV in vacuum
12 p2181 A70-27258
- Raman scattering by oxygen and nitrogen in atmosphere observed by using pulsed nitrogen UV laser
12 p2189 A70-28093
- Dye laser small signal gain via pumping by UV nitrogen laser
13 p2426 A70-28811
- Flashlamp-excited organic liquid UV lasers
13 p2427 A70-29141
- Hereditary UV luminescence of transplanted cancerous and lymphosarcomatous cells in mice and rats after ionizing radiation exposure
13 p2358 A70-29341
- Stimulated emission cut-off characteristics of laser based on crystals with Nd ions under UV irradiation
13 p2429 A70-29505
- UV, visible and IR radiation measurement, discussing spectral distribution, thermopiles, monochromatic radiation and power measurements
13 p2410 A70-29653
- Crossed field nitrogen laser operation in second positive band to obtain high UV pulse output
13 p2429 A70-29669
- Spectral characteristics of secondary emission alloys for photocathodes in extra atmospheric radiation open-type detectors in UV range
14 p2582 A70-30166
- Retrograde rotation of equatorial spots of Venus cloudy exterior layer, using UV photographic and spectroscopic observations
14 p2649 A70-31215
- Hydrogen UV geocorona photoionizing effect on nighttime E region electron density in low and midlatitudes, comparing with ionosonde data
14 p2581 A70-31270
- Binary AX Monocerotis brightness variations in UV from photoelectric UVB observations
15 p2796 A70-31610
- Three color photometry of RW Auriga stars, discussing UVB curves, H-R diagram and UV emission excess
15 p2797 A70-31612
- Gas pressure effects on visible and UV laser action in small argon Z-pinch plasma discharge, using streak photographs
15 p2750 A70-31968
- Intercomos 1 satellite for observing solar UV and X-ray emission in solar flares prediction
15 p2738 A70-32145
- UV irradiation effects on ZnO used as pigment for spacecraft thermal control coatings [AIAA PAPER 70-829]
16 p2940 A70-33937
- ZnO coating pigment for spacecraft thermal control, examining UV irradiation effects on electrical properties
16 p2961 A70-34056

- Photolysis of 3-phenyl-oxadiazol-5-one by UV irradiation, eliminating carbon dioxide
17 p3041 A70-34772
- UV interstellar extinction from comparison of epsilon and zeta Persei, noting graphite features
17 p3159 A70-34877
- UV interstellar extinction, examining reddened and unreddened early stars with OAO satellite spectrophotometric scans
17 p3159 A70-34878
- UV stellar spectra absorption, considering silicon and carbon opacity effect on Balmer discontinuity and Paschen continuum
17 p3159 A70-34880
- Stellar UV and visual continuum observations, discussing recalibration of absolute energy distribution of alpha Lyr to improve model atmospheres
17 p3160 A70-34881
- UV solar opacity observations, comparing solar model predictions
17 p3160 A70-34884
- Supergiant alpha Car UV spectrophotometry from Gemini II, comparing with model atmosphere
17 p3161 A70-34888
- Galactic UV emission attributed to solar radiation scattered by hydrogen atoms, using Mariner 5 measurements
17 p3163 A70-34902
- UV background radiation observed above atmosphere for intergalactic gas, Galaxy and subcosmic ray components
17 p3163 A70-34903
- Ozone content effect on presunrise fall in LF radio waves amplitude from Radio Tashkent to Delhi, noting UV light role
17 p3077 A70-34947
- Multispectral UV sky mapping and heavenly body intensity measurement onboard OAO 2 satellite
17 p3179 A70-35264
- Tropical UV nightglow, considering oxygen ion-ion neutralization reaction as primary source
18 p3244 A70-36015
- Upper atmospheric gas components vertical distribution by airborne photometric absorption and attenuation measurements in UV spectrum
18 p3248 A70-36633
- Solar UV radiation contributing to ionization in higher ionospheric layer over Dushanbe during partial solar eclipse of 20 May 1966
19 p3417 A70-38786
- High speed electro-optic spectral scanning in UV, visible and IR regions, using monochromator deflection of dispersed light
20 p3671 A70-39090
- UV oxygen nightglow observation by OGO-4, examining ion-ion neutralization and radiative recombination production mechanisms
20 p3621 A70-39344
- UV and nonthermal X ray interaction with intergalactic gas, considering photoionization and recoil associated with Compton X ray scattering
21 p3878 A70-40706
- Molecular oxygen density and vibrational distribution in lower atmosphere, observing solar UV radiation absorption by satellite OSO-4
21 p3816 A70-41066
- Near earth solar UV flux measurement by Spades satellite, discussing nonrandom variations and Ca plage regions
21 p3881 A70-41078
- Auroral UV night airglow radiation distribution over latitude range, using scanning spectrometer onboard Convair 990 aircraft
21 p3818 A70-41106
- Luminescence efficiencies of Apollo 11 lunar and terrestrial rocks and minerals, using UV excitation
21 p3915 A70-41656
- UV Ceti type variable flare stars, observing radio and optical spectral regions for X ray production
24 p4397 A70-45763
- UV excited powdery fluorescent products, describing cryostat for photo and thermoluminescence at various temperatures
24 p4339 A70-46097

ULTRAVIOLET REFLECTION

- High reflectivity mirror construction for H Lyman alpha line using vacuum deposited Al layer coated by magnesium fluoride
02 p0299 A70-12367
- Semitransparent Pt film reflectance in vacuum UV evaporated on glass, quartz, Al, Au and Cr on glass compared with opaque films
04 p0731 A70-15023
- EUV reflectance data for optical constants obtained in digital form directly on punched cards by data acquisition system
23 p4197 A70-44470

ULTRAVIOLET SPECTRA

- Chromospheric structural parameters determined from XUV spectroheliograms, discussing He 2 emission, O 4 and O 5 emission distribution, etc
01 p0175 A70-10246
- Far UV spectroscopy of Jupiter by rocket-borne spectrograph
01 p0179 A70-10528

- Venus and Jupiter Aerobee rocket photoelectric UV spectra, determining geometric albedos using reflecting layer and cloud models 02 p0367 A70-11812
- Polarization observations of Saturn in UV and visible regions compared with Jupiter data, noting multiple scattering 02 p0368 A70-11818
- Giant pulse Q switched lasers generated plasmas, noting VUV spectral line shifts, asymmetries and existence of satellite lines 02 p0345 A70-11894
- Extreme UV spectral line intensity enhancement during class 3 flare related to abundance of radiating element 02 p0358 A70-12205
- L-alpha absorption equivalent width measurements in UV spectra of beta-one, delta and pi Scorpii for interstellar hydrogen densities 04 p0748 A70-14586
- He isoelectronic sequence 3d-nf transitions, determining UV wavelengths and oscillator strengths 04 p0739 A70-14601
- Rocket-borne spectrometer intensity measurements UV region of solar spectrum, noting agreement with IR observations of solar temperature minimum 06 p1143 A70-17998
- Vacuum UV spectrum interferometer with grazing incidence reflections between plane parallel mirrors to obtain coherent beams, discussing fringe patterns 07 p1286 A70-20081
- O and B type stars neutral He lines, studying UV line blanketing effects on predicted departures from LTE 08 p1571 A70-20912
- UV absorption cross sections of CO, HCl and ICN, analyzing reactions causing various spectral features 08 p1455 A70-21340
- Pulsed nitrogen gas laser to obtain continuously tunable dye laser action to 3550 Å with output at 3771 Å in UV 08 p1513 A70-21553
- Solar equatorial XUV limb brightening for resonance lines of Li-like ions from OSO-4 observations interpreted by coronal model 09 p1757 A70-22732
- Luminous hot stars mass loss attributed to negative effective gravities in outer parts of reversing layers from ionic UV resonance lines 10 p1946 A70-24981
- Solar XUV lines photon flux based on one dimensional model of chromosphere-corona transition region 10 p1949 A70-25271
- Radiative intensity calculations for carbon dioxide and carbon dioxide-nitrogen plasmas for various temperatures, densities and path lengths, computing UV and continuum spectra 12 p2275 A70-27170
- UV flash spectra of total solar eclipse of 7 March 1970 obtained by Aerobee 150 rocket 12 p2304 A70-27717
- Herschel effect in UV solar photography in developing autotensive photographic film for bright photospheric recording 13 p2497 A70-29853
- Rocket spectroscopy of zeta puppis, identifying multiplets of stellar and interstellar origin included in atmospheric models 14 p2641 A70-30883
- Solar UV flash spectrum by spectroheliographs flown aboard Aerobee 170 mission during total solar eclipse 16 p2977 A70-33838
- Argon II line transition probabilities, observing UV spectral region, upper energy levels and temperature differences 16 p2956 A70-34251
- UV stellar spectra and related ground based observations - Conference, Luneren, Netherlands, June 1969 17 p3158 A70-34876
- Stellar UV spectra observation methods, discussing objective spectrograph, scanning spectrometer system with telescope and grating cameras 17 p3160 A70-34885
- Stellar UV spectral line profiles interpretation, using atmospheric models and line formation theory 17 p3161 A70-34890
- Symbiotic stars UV spectrum, discussing molecular fluorescence phenomena 17 p3161 A70-34891
- Solar atmosphere structure and chemical composition by UV spectrum analysis 17 p3161 A70-34892
- Solar UV spectrum variations due to flares and solar activity diurnal variations from satellite spectrometry 17 p3161 A70-34894
- High resolution solar spectrum at 2000-2200 Å from sunpointing Skylark rocket flight, noting detectable absorption lines 17 p3162 A70-34896
- Non-LTE effects on flux and center to limb variation of solar spectrum at 1500-1680 Å 17 p3169 A70-35384
- Continuous UV opacity effects on visual spectrum observations and predictions for solar photosphere 17 p3169 A70-35385
- UV absorption lines in H I regions heated by cosmic rays, discussing possible detection by rocket or satellite spectroscopic observations 17 p3152 A70-35748
- Reciprocity law between radiation intensity and exposure time for photographic films in vacuum UV spectrum region, investigating departure at various wavelengths 18 p3257 A70-36281
- Horizon sky UV spectral radiance, noting solar position and cloud cover effects 18 p3248 A70-36752
- Mars UV reflectivity, examining spectrum, absorption features, planet albedo and ozone content by rocket-borne instruments and atmospheric models 18 p3317 A70-37011
- Interstellar molecular H Lyman resonance-absorption bands in far UV spectrum using rocket observation 20 p3701 A70-39002
- Spiral galaxy NGC 4319 arms high red shift Seyfert nucleus, discussing UV continua of Markarian 205 20 p3701 A70-39005
- Emission cross sections of nitrogen in vacuum UV by electron impact 20 p3675 A70-39617
- OSO far UV solar spectroheliograms atlas, describing instrumentation, data acquisition, etc 20 p3713 A70-40540
- Quark in stars, discussing electronic transitions and UV spectral lines 21 p3921 A70-41975
- EUV solar spectral intensity distribution and cyclic variations 22 p4106 A70-43299
- Monochromator design for UV and visible wavenumbers linear output, noting application to absorption coefficient measurement 24 p4336 A70-45669
- Solar spectrum O I, obtaining high resolution UV line profiles from rocket-borne spectrograms 24 p4410 A70-45766
- ULTRAVIOLET SPECTROGRAPHS**
- U ULTRAVIOLET SPECTROMETERS**
- ULTRAVIOLET SPECTROMETERS**
- Rocket telescope spectrometer precision pointing achieved by servocontrolling secondary mirror, discussing use for planetary atmospheres far UV spectrum studies 02 p0296 A70-11916
- Grate spectrometer with high resolution for 20-45 micron range, describing water vapor transmission spectrum [ONERA-TP-782] 10 p1886 A70-23912
- LiF prism spectrometer for space applications, discussing vacuum UV transmission and mechanical properties 11 p2049 A70-25629
- Scanning UV spectrometer for Mariner Mars 1971 orbital mission, investigating atmospheric composition for biological activity 16 p2978 A70-34030
- Scanning mirror system for Apollo telescope mount UV spectroheliometer, describing design, fabrication and testing 17 p3083 A70-34764
- Thin high vacuum gate valve design for use with UV grating spectrograph 19 p3357 A70-37687
- Solar stimulated terrestrial materials luminescence remote detection by Fraunhofer line depth method using UV grating spectrometer 23 p4199 A70-45007
- ULTRAVIOLET SPECTROPHOTOMETERS**
- Single beam grazing incidence spectrophotometer with concave diffraction grating for far UV region, emphasizing instrument adjustment 16 p2915 A70-34218
- OAO 2 for UV telescope sky mapping and spectrophotometric measurements of celestial bodies 23 p4261 A70-44666
- ULTRAVIOLET SPECTROSCOPY**
- Vacuum-UV monochromators polarization and effective transmittance measurements, comparing characteristics of parallel and pyramidal biotite polarizers 08 p1546 A70-21791
- Diffraction filters characteristics used in XUV spectroscopy involving solar, stellar and laboratory experiments 09 p1729 A70-23526
- Sulfur beam foil spectrum in 600-4000 Å range, identifying transitions in S I-S VI 11 p1994 A70-25362
- CO dissociation kinetics in Ar and mixtures of O in Ar by shock tube study using vacuum UV absorption 12 p2180 A70-26857
- Stellar UV photometry using telescope experiment in OAO 17 p3160 A70-34883
- Optical density of valence and conduction states by UV photoelectric spectroscopy, outlining experimental techniques and inelastic scattering effects 19 p3471 A70-37711
- Tropical UV nightglow measurement by Ogo-4 spectrometer, considering ionospheric recombination excitation mechanism 20 p3620 A70-39338
- Extreme UV spectroscopy with synchrotron radiation storage ring light sources in 40-400 Å range, including thin film photoabsorption measurements 21 p3826 A70-41451
- UMBRA (SHADOWS)**
- U SHADOWS**
- UMKEHR EFFECT**
- Umkehr observation days selectivity effects on calculated mean ozone distributions in layers 2 and 3 08 p1492 A70-21970
- UNCERTAINTY**
- U PROBABILITY THEORY**
- UNCONSCIOUSNESS**
- NT BLACKOUT PREVENTION**
- Syncope proneness correlation with episodes of impaired consciousness in pilots during flight using physiological tests 07 p1223 A70-19944
- Commercial jet passenger emergency oxygen needs for cabin decompression studied in determining time of safe unconsciousness 11 p1992 A70-26511
- UNCOUPLED MODES**
- Complex uncoupled modes to analyze forced vibrations of three layer damped sandwich beam with arbitrary boundary conditions, discussing orthogonality 04 p0773 A70-15076
- Ion motion neglecting conditions for radio waves in plasma based on Ohms law uncoupling from momentum transfer 16 p2957 A70-32980
- UNDAMPED OSCILLATIONS**
- Multilevel maser oscillators undamped output pulsations, investigating effect of coupling between signal frequency energy storage and circuit properties at pump frequency 13 p2430 A70-29704
- Bleachable dye filters selection for periodic undamped output power oscillations in laser 15 p2753 A70-32859
- Linearly elastic skeletal structures, calculating natural frequencies of undamped vibration by computer program 21 p3935 A70-41254
- UNDERCARRIAGES**
- Airline pitot and static altimeter systems and undercarriage maintenance and checkup, discussing wear in systems, case leaks, trash, dirt, inoperative heaters, etc 16 p2842 A70-33823
- UNDERGROUND EXPLOSIONS**
- Hydrodynamic energy flow down horizontal tunnel from nuclear explosive detonated underground, recording shock front luminosity and time of arrival 10 p1857 A70-23985
- UNDERGROUND NUCLEAR EXPLOSIONS**
- U NUCLEAR EXPLOSIONS**
- U UNDERGROUND EXPLOSIONS**
- UNDERWATER ACUSTICS**
- Electronic sine-cosine converters construction in devices for visual display of hydroacoustic transducers radiation patterns 06 p1064 A70-17773
- German book on propeller theory covering airfoil theory, propeller flow and pressure fields, propeller vibrations, shrouded and tilted propellers, helicopter rotors, etc 23 p4180 A70-44097
- UNDERWATER EXPLOSIONS**
- Stereophotogrammetric measurement for dynamic deformation of circular membrane subjected to underwater detonation 05 p0927 A70-16009
- UNDERWATER SOUND**
- U UNDERWATER ACOUSTICS**
- UNDERWATER STRUCTURES**
- Interface stresses in ceramic/metallic spherical shells for deep submergence structures using hydrostatic testing and photoelastic analysis 06 p1170 A70-18089
- Error estimation of gondola encased tugged undersea magnetometer as function of turbulence parameters 07 p1281 A70-19466
- Error estimation of gondola encased tugged undersea magnetometer as function of turbulence parameters 18 p3260 A70-36940
- UNDERWATER TESTS**
- Underwater saturation habitats application as behavioral workshops for mission planning and human engineering of manned space flight, discussing Project Tektite [ALAA PAPER 69-1120] 01 p0034 A70-10611
- Human peripheral blood circulation during prolonged underwater activity, showing compensation for

high humidity, noise levels, low water temperatures, isolation and confinement 10 p1822 A70-25178

Microbial flora in human subjects confined to long term Tektite I underwater habitat 15 p2681 A70-31879

Airborne bacteria and fungi in atmosphere of Tektite I underwater habitat 15 p2681 A70-31880

Tektite II program safety planning for ambient pressure habitat under saturation diving conditions [AAS PAPER 70-053] 17 p3036 A70-34796

Tektite I marine laboratory underwater mission in marine biology and geology 17 p3168 A70-35306

Water immersion facility training for extravehicular activities and man physical movements in spacecraft, utilizing buoyancy-gravitation balance 21 p3804 A70-41191

UNDERWATER VEHICLES

NT SUBMARINES

Manned vehicles rendezvous missions in space and hydrospace, proposing functional structure involving concurrent ship control, navigation, perception, communication and prehension [AIAA PAPER 69-1102] 01 p0034 A70-10615

UNIAXIAL STRAIN

U AXIAL STRAIN

UNIFORM FLOW

NT BLASIS FLOW

Uniform supersonic flow with receding shock wave past smooth profile 07 p1187 A70-18674

Circle theorem for potential flows extended to two dimensional steady incompressible ideal fluid flows of constant vorticity 09 p1664 A70-23714

Two dimensional circular cylinder vortex excitation in uniform flow using linear binary system for flutter analysis 13 p2341 A70-29057

Uniform supersonic flow with receding shock wave past smooth profile 15 p2671 A70-31466

Boundary value problems in uniform incompressible inviscid flows past complex profile bodies by R functions method and variational technique 20 p3610 A70-39772

Turbulent boundary layer control by uniform fluid injection and suction, discussing velocity profiles, wall and wake laws, skin friction and shear stress transport equation [ICAS PAPER 70-10] 23 p4180 A70-44121

Axysymmetrical nozzle aerodynamic shape design for conical to axially uniform flow conversion, using method of characteristics 23 p4136 A70-44991

Momentum source interaction with viscous uniform stream, constructing perturbation solutions from non-linear equations 24 p4327 A70-46040

UNIONS [CONNECTORS]

Natural frequency calculation accuracy for coupled beam bending vibrations shown dependent on connection stiffness determination 03 p0595 A70-13929

UNIPOLAR TRANSISTORS

U FIELD EFFECT TRANSISTORS

UNIQUENESS

Existence and uniqueness of optimal control for one dimensional linear system with distributed control parameter using input-output integral with quadratic functional 17 p3057 A70-35627

UNIQUENESS THEOREM

Navier-Stokes equation generalized solutions to initial boundary value problems, considering uniqueness theorem and smoothness 01 p0132 A70-11068

Elasticity theory contact type problems, proving solutions existence and uniqueness 03 p0589 A70-13346

Plane static boundary value problems solutions in zero moment elasticity theory, proving solutions existence and uniqueness 04 p0775 A70-15214

Stefan free boundary problems with prescribed flux reduced to form solvable by numerical methods, proving existence and uniqueness theorems 05 p0956 A70-15783

Existence and uniqueness of nonlinear boundary value problem solutions formulated by fixed point theorem and Green function 05 p0876 A70-16562

Uniqueness and reciprocity theorems in elastic medium occupying infinite domain extended to electromagnetic wave propagation in plasma 05 p0890 A70-17097

Existence and uniqueness, stability and asymptotic stability of nonlinear operator differential equation 05 p0878 A70-17098

Linear Boltzmann equation in bounded domain, studying solutions existence, uniqueness and structure 06 p1047 A70-18317

Existence and uniqueness theorem for boundary value problem solution for parabolic equation in domain with singular points on boundary 07 p1322 A70-18853

Uniqueness theorem for coupled dynamic problem of linear thermoviscoelastic theory assuming contact-type boundary conditions 07 p1416 A70-20296

Kramer problem in kinetic gas theory and gas dynamics applied to Boltzmann equation, discussing uniqueness theorem [ONERA-TP-776] 08 p1486 A70-21845

Existence and uniqueness of mixed problem solution for Tricomi equation proved by a priori estimates 10 p1908 A70-23925

Solution uniqueness in limit load theory for unbounded regions, obtaining infinity as unique value for critical load from elastoplastic analysis 10 p1954 A70-24013

Local uniqueness and instability theorem for Einstein-Liouville equations using energy inequalities, noting relevance to Cauchy problem 11 p2084 A70-26458

Uniqueness theorem in Mindlin theory of elastic materials with microstructure 13 p2508 A70-28488

Generalized Frankl boundary value problem solution uniqueness formulation and proof using auxiliary function 13 p2390 A70-29647

Unique solvability of mixed semihyperbolic linear equations of higher order with respect to spatial variables and time 15 p2768 A70-32475

Existence and uniqueness theorem for boundary value problem solutions to nonlinear canonical ordinary differential equations 17 p3131 A70-35339

Forced vibration in Cartesian half space filled with elastic medium, investigating uniqueness conditions 18 p3337 A70-36289

Nonuniqueness of collapse load for isotropic frictional material with or without cohesion 19 p3433 A70-37385

Nonrigorous hyperbolic systems, discussing existence and uniqueness theorems contradiction in linear equations and proof of Cauchy problem 19 p3478 A70-37582

Uniqueness theorem for first boundary value problem of heat conduction equation with discontinuous coefficient 20 p3737 A70-39710

Linear discrete feedback systems uniqueness, existence and stability under various input-output conditions 22 p4004 A70-43024

Cauchy problem for singular parabolic equation, establishing existence, uniqueness and representation theorem by integral operator techniques in conjunction with function-theoretic methods 23 p4212 A70-44895

Linear viscoelastic solid quasi-static deformation, deducing associated minimum principles under assumption of unique solutions existence for boundary value problems 24 p4420 A70-45264

One-phase Stefan problem of heat conduction with melting, proving existence and uniqueness theorems for solid and free boundary temperature determination 24 p4429 A70-46036

UNITED NATIONS

UN General Assembly outer space treaties governing international exploration and use and rescue and return of astronauts and objects 02 p0402 A70-12308

UN treaty based on U.S.-U.S.S.R.-UK agreement banning nuclear arms in space and establishing international law covering space exploration 07 p1428 A70-19106

Peaceful uses of outer space, discussing committee reports and recommendations, direct broadcast satellites, administrative and financial implications, etc 07 p1428 A70-19688

Earth Resources Technology Satellite program and international participation, taking into account UN involvement in outer space 20 p3741 A70-39796

International cooperation in space exploration, UN role and benefits for nonspace nations 22 p4128 A70-43632

UNITED STATES OF AMERICA

NT ALASKA

NT CALIFORNIA

NT COLORADO

NT HAWAII

NT KANSAS

NT NEW MEXICO

NT NORTH CAROLINA

NT OREGON

Cosmic ray latitude survey in western U.S. and Hawaii in summer 1966 using neutron and muon monitors 01 p0167 A70-10228

Land use mapping of southwestern U.S. using photographs from Apollo and Gemini missions [AAS PAPER 69-576] 04 p0676 A70-14640

DOD systems acquisition management tools and policies, emphasizing role of development concept paper and outside personnel dialogue in DOD decision making 05 p0959 A70-16460

Future U.S. aerospace power in terms of military technology and defense policies and attitudes 05 p0960 A70-16633

Life styles of engineering, comparing U.S. and European attitudes to aircraft development and design 06 p1184 A70-17198

Domestic telecommunication via satellite to reduce terrestrial switching to two levels, discussing system parameters, operation, hardware and cost estimate 06 p1006 A70-17344

Atmospheric turbidity measurements over U.S. using Volz sunphotometer 06 p1098 A70-18245

Space role in competition between U.S. and U.S.S.R. since August 1957, discussing armament control agreements regarding space 07 p1426 A70-18882

DOD procurement practices for advanced weapon systems, discussing government errors in contracting policies 07 p1428 A70-19678

Book on solar cells U.S. patent literature, discussing Si semiconductors, panel fabrication techniques, photoemissive devices, Cd, Ga and organic compounds, etc 09 p1612 A70-22050

Instructional communication system for U.S. using synchronous satellites over 15 regions [AIAA PAPER 70-450] 11 p2000 A70-25465

SST feasibility for U.S., considering program costs, financing, investment return and airport and community noise aspects 12 p1612 A70-27991

Report to COSPAR on U.S. space science program, discussing NASA projects, stellar and solar astronomy, lunar and planetary research, cosmic particles, upper atmosphere, etc 15 p2831 A70-31724

Air traffic control system for continental U.S.A. in 1980s, discussing ATC Advisory Committee recommendations 18 p3349 A70-36400

UNITS OF MEASUREMENT

Aircraft altimeter measurement for vertical separation based on atmospheric pressure unit changes /Cayleys/ compared with linear measurements in meters and feet 13 p2411 A70-29778

Canadian laser stabilization program involving metrology and absolute standard replacing international meter 17 p3105 A70-35089

UNIVERSAL TIME

Energy concept in cosmology based on relativistic considerations, indicating universal time by synchronous clocks system 11 p2109 A70-25870

Universal time control of south polar F layer during IGY attributed to low energy electron precipitation, comparing IGY and recent satellite data 21 p3818 A70-41101

Lunar effects on vertical and shape of geoid in universal time 22 p4100 A70-42852

UNIVERSE

Einstein equations for Bianchi type IX universe model suitable for numerical solution and application to cosmology with pure fluid stress tensor 01 p0142 A70-10522

Einstein-Friedman cosmology of vanishing constants assumed in deducing relations between antipodal radio sources red shifts and universe parameters 01 p0187 A70-11274

Finite rotating universe model construction not possessing Goedel cosmos pathological properties, discussing relation to Mach principle 01 p0191 A70-11358

Book on unitary relativistic theory of universe covering conservation and quantization axioms, general relativity equations, applications to corpuscular, electromagnetic and gravitational phenomena, etc 02 p0337 A70-11686

Lemaître universe and galaxy formation effect on stability of quasi-static epoch, deriving limits for red shift, cosmic ray and electromagnetic fluxes 02 p0363 A70-11779

Universe oscillating closed model dynamics emphasizing conditions of collapse by contraction in terms of relativity theory 02 p0370 A70-12114

Symmetric cosmologies within gamma ray measurement context showing antimatier limits in Milky Way and metagalaxy 02 p0371 A70-12196

Soviet papers on universe evolution covering interstellar structure, stellar evolution, multiple galaxies, galactic nuclei, etc

03 p0562 A70-12976

Electron and hard photon /X and gamma ray/ production and propagation in expanding metagalaxy, deducing universe matter density, cosmic ray sources, etc

03 p0557 A70-13225

Astronomical and space research methods probing fundamental questions concerning universe unsolvable by classical astronomy, discussing solar wind and stellar formation and evolution

03 p0571 A70-13790

Cosmochemistry, discussing interdisciplinary nature, goals, nuclear roots, information sources, key concepts involving elements age and origin, nuclear species abundances, chemical fractionation, etc

03 p0578 A70-14346

Mass-energy content of universe, discussing galactic formation in positive energy systems and missing mass problems

04 p0753 A70-15073

Elliptical cosmology, discussing evolutionary geometry, Synge distribution, galactic age and distance from earth, Friedman equations and independence of constants

05 p0905 A70-15794

Nonequilibrium processes and initial conditions in early universe, discussing neutrino viscosity efficiency at removing shear anisotropy and Misner model

05 p0907 A70-16002

Cosmic protons and high energy heavy nuclei interaction with radiation in expanding universe, including estimates of light radiation influence on cosmic ray spectra

05 p0904 A70-16903

Book on space observatories covering rocket mounted telescopes for atmospheric structure, opaque wall, air diffusion, clouds and refraction, particle bombardment, meteorite melting, etc

07 p1379 A70-19099

Circular and radial trajectories in Schwarzschild field applied to isolated metagalaxy with charged central body and nonzero cosmological constant

07 p1385 A70-19426

Radiation catastrophe in universe in terms of cosmological models

07 p1368 A70-19628

Singularity for absolute zero of time suggested for beginning of universe by Einstein relativity theory

07 p1336 A70-19922

Cosmic rays formation time and evolution in expanding universe, discussing high energy electrons, energy losses and spectra and metagalaxy cascade processes

07 p1371 A70-20328

Hot universe model for determining magnitude constraints on Dirac monopole annihilation cross section and mass in cosmic rays

07 p1371 A70-20330

Shear and rotation limits on universe from X ray background, using Euclidean shear and vorticity models with open and closed geometries

08 p1561 A70-20901

Electron and hard photon /X and gamma ray/ production and propagation in expanding metagalaxy, deducing universe matter density, cosmic ray sources, etc

08 p1563 A70-21658

Conditions for life in universe, analyzing evolutionary stages of matter to determine steps producing complex organic compounds

09 p1762 A70-23121

Instability of Godel rotating universe, discussing stability to perturbations in rotation plane and unstable density perturbations along rotation axis

10 p1937 A70-23973

Universe neutrino energy density estimation based on photon-neutrino weak interaction coupling theory

10 p1920 A70-24567

Homogeneous open anisotropic relativistic world model with negative space curvature, observing shear decrease with time and magnitude reciprocal variation with function R/t

11 p2109 A70-25866

Mankind role in cosmos as function of self realization developed by science and technology

11 p2153 A70-26057

Iconoclastic cosmology and remote sensing of universe, discussing cosmic scale photometry and extra-galactic red shift spectroscopy

12 p2296 A70-26924

Cosmological constant role in closed universes with matter and radiation

13 p2490 A70-28936

Galactic, stellar and solar magnet fields origin, considering fluid motions role

14 p2641 A70-30876

Nuclear reactions and elementary particle reactions in Friedman universe with positive lepton abundance and degenerate electrons, discussing prestellar helium synthesis

14 p2620 A70-30877

Hot universe model for demonstrating distortions in Rayleigh-Jeans region of microwave relic radiation spectrum by primeval plasma heating before recombination epoch

14 p2632 A70-31287

Cosmogonic phenomena instability, discussing red shift, expanding universe, galactic nuclei and quasars

15 p2800 A70-32144

Entropy increase, discussing universe heat death, earth energy balance, etc

15 p2809 A70-32907

Equations of motion and continuity for early and later stages of expanding universe, explaining matter concentration process of galaxy formation

16 p2976 A70-33783

Model classification for relativistic universes containing noninteracting matter and radiation by cosmological constant and density parameters

16 p2979 A70-34190

Uniform model universes containing gaseous matter and background blackbody radiation, solving Einstein equations without zero pressure assumption

18 p3313 A70-36215

Cyclic models of evolving universe corresponding to positive, negative or zero cosmological constant

18 p3314 A70-36421

Cosmological models with matter and radiation for evolution of universe

18 p3322 A70-37132

Antimatter distribution in universe, investigating mass lower limit

19 p3518 A70-38025

High energy electron and photon cascades in Metagalaxy, considering electromagnetic radiation density and cosmic ray origin estimation

19 p3500 A70-38081

Critique of metagalactic origin of high energy cosmic rays, reviewing neutrino hypothesis

19 p3500 A70-38082

Fermi momentum upper limit for universe neutrinos in cosmic ray propagation, determining maximum proton energy

20 p3700 A70-39592

Cosmic ray superhigh energy electrons and neutrinos propagation in degenerate neutrino gas universe, considering gas density in cosmological models

20 p3700 A70-39593

Radio source counts from Ohio State University observations, noting faint sources decrease relative to uniform Euclidean universe

20 p3713 A70-40427

Universe homogeneous isotropic model with thermal radiation at outset, considering nucleons and antinucleons interactions

21 p3884 A70-40910

Friedmann universe evolution after big bang via Hagedorn hadronic equation of state, noting primordial He abundance criterion

21 p3888 A70-41122

Radio source count formula in zero pressure model universe for background radiation differential density evolution function

21 p3923 A70-42104

Einstein gravitational equations solution for expanding universe, discussing possible sudden collapse into zero volume with infinite density

22 p4105 A70-43215

Universe cold matter structure and distribution from far IR data

22 p4096 A70-43395

Friedman-Lemaître model role in big bang cosmology

23 p4238 A70-43812

Einstein field equations for spatially homogeneous spaces, considering rotating matter model in regularized Euler-Lagrange form

23 p4219 A70-44406

UNIVERSITIES

Network analysis for systems application program /NASAP/ computer-aided circuit design program for network analysis, discussing application in education

06 p1015 A70-18418

Personnel and organizational policies for university research management

12 p2336 A70-27750

UNIVERSITY PROGRAM

Industry-university interaction in competitive teaching of spacecraft design

23 p4285 A70-44643

UNKNOWN

U DEPENDENT VARIABLES

U PROBLEM SOLVING

UNLOADING

Elastic/perfectly plastic hollow cylinder unloading under monotonic twist during torsion, considering sandhill-membrane analog validity

08 p1589 A70-21249

Nonlinear stress-strain model of unloading in symmetric longitudinal impact of two elastic-plastic bars, using numerical method

19 p3541 A70-38046

Extraction parachute deployment for airdropping multiple loads from C-5A aircraft

[AIAA PAPER 70-1203] 21 p3752 A70-41814

Human ventilatory response to resistance unloading during muscular exercise

23 p4144 A70-43823

UNLOADING WAVES

Unloading wave in elastic-plastic half space with rigid unloading for two parameter loads, discussing deformation body model

05 p0925 A70-15825

UNMANNED SPACECRAFT

NT BEACON SATELLITES

NT ECHO SATELLITES

NT ECHO 1 SATELLITE

NT ECHO 2 SATELLITE

NT EXPLORER 22 SATELLITE

NT GEODETIC SATELLITES

NT GEOS 1 SATELLITE

NT GEOS 2 SATELLITE

NT JUPITER PROBES

NT LUNAR PROBES

NT LUNIK LUNAR PROBES

NT LUNIK 3 LUNAR PROBE

NT LUNIK 12 LUNAR PROBE

NT MARINER SPACE PROBES

NT MARINER SPACECRAFT

NT MARINER 2 SPACE PROBE

NT MARINER 4 SPACE PROBE

NT MARINER 5 SPACE PROBE

NT MARINER-MERCURY 1973

NT MARS PROBES

NT NAVIGATION SATELLITES

NT OSO

NT OSO-B

NT OSO-1

NT PAGEOS SATELLITE

NT PASSIVE SATELLITES

NT PIONEER SPACE PROBES

NT PIONEER 6 SPACE PROBE

NT PIONEER 8 SPACE PROBE

NT PIONEER 9 SPACE PROBE

NT RANGER LUNAR PROBES

NT SOLAR OBSERVATORIES

NT SOLAR PROBES

NT SPACE PROBES

NT SURVEYOR LUNAR PROBES

NT SURVEYOR 5 LUNAR PROBE

NT TRANSIT SATELLITES

NT VENERA SATELLITES

NT VENUS PROBES

NT ZOND 3 SPACE PROBE

Unmanned teleoperator spacecraft /UTS/ for future orbital demonstration, discussing manipulators, multifunction viewing, stabilization, human factors, etc

[AIAA PAPER 69-1067] 01 p0195 A70-10649

Earth and planetary entry vehicle designs for manned and unmanned space missions, noting thermal protection, environmental control requirements and communication systems

[AIAA PAPER 68-1080] 01 p0195 A70-10826

Solar powered electric propulsion systems for automated missions throughout solar system by extending range of Atlas Centaur-Titan 3-C launch vehicles

[AIAA PAPER 68-1120] 04 p0736 A70-15401

Automated mars surface sample return /AMSSR/ mission, discussing Saturn 5 chemical and nuclear approach

[AIAA PAPER 69-1066] 04 p0764 A70-15626

Soviet unmanned spacecraft and components displayed at Le Bourget show, including Molniya 1, Proton 4 satellites, Venus 4 station, vertical cosmic probe, etc

05 p0921 A70-15814

Support facilities requirements and goals for manned and unmanned solar and stellar orbital astronomy

[MDAC-WD-1258] 05 p0847 A70-16074

Unmanned exploration program to study magnetic fields and chemical composition of five outer planets in solar system

07 p1375 A70-18871

Instrumental space flight internationalization considering manned flight and military obstacles, suggesting scientific and political steps

07 p1427 A70-19097

Onboard modular computer research in strapdown guidance technology for computational ability and long term reliability of unmanned missions

07 p1238 A70-20062

Unmanned and manned interorbital shuttle systems for satellite placement and repair and planetary spacecraft insertion, emphasizing cost analysis

[AIAA PAPER 70-267] 07 p1398 A70-20396

Manned and unmanned earth resources observation satellite program, noting international cooperation

10 p1971 A70-24636

Manned and unmanned earth observation satellite programs technology gains, discussing atmospheric temperature, pressure, winds, clouds and moisture

10 p1876 A70-24637

Unmanned spacecraft landing shock absorption by hybrid pneumatic configuration having hard surfaced footpad with dual pneumatic bag attenuator

12 p2312 A70-27115

Lunar exploration by manned and unmanned space flights, discussing seismology, composition, surface features, etc

15 p2798 A70-31678

Space based reusable manned/unmanned tug, discussing potential missions, system requirements and auxiliary hydrogen oxygen propulsion system [AIAA PAPER 70-719] 16 p2964 A70-33533

Unmanned electric propulsion spacecraft with external fuel and flashlight thermionic reactors, discussing thruster arrays, weight and performance for reference Jupiter orbiter mission [AIAA PAPER 70-644] 16 p2966 A70-33547

Manned and unmanned orbital space facilities pointing and stability requirements, noting application to stellar and solar astronomy, earth observations, etc 16 p2979 A70-34068

Unmanned flyby missions to Mercury in 1973-1990, discussing scientific objectives and payloads [AAS PAPER 70-027] 17 p3155 A70-34798

Mariner, explorer, high Data Orbiters, Viking and Rover landers as required systems for unmanned Mars exploration, examining ballistic and lifting entry [AAS PAPER 70-030] 17 p3156 A70-34805

Expandable and modular structures technology for manned and unmanned space missions, discussing expandable air lock experiment 17 p3177 A70-35230

Unmanned and manned interorbital shuttle systems for satellites placement and repair and planetary spacecraft insertion, emphasizing cost analysis [AIAA PAPER 70-267] 17 p3172 A70-35650

Mission success model for unmanned space exploration, combining expected data return with computer technique 19 p3527 A70-38838

Unmanned spacecraft for earth resources survey, investigating ERTS payload, performance characteristics and ground station 20 p3713 A70-39057

Solar electric propulsion unmanned asteroid belt probe, discussing propulsion system, flux data acquisition, etc [AIAA PAPER 70-1121] 20 p3717 A70-40525

High Energy Astronomy Observatory for space X rays, gamma and cosmic rays research via unmanned spacecraft 23 p4261 A70-44680

Automated and manned spacecraft design, discussing mission objectives and present and potential applications 23 p4264 A70-45003

UNSTABLE BURNING

U COMBUSTION STABILITY

UNSTEADY FLOW

NT OSCILLATING FLOW

Flow velocity pulsations effect on frequency spectrum of flow optical fluctuations, discussing methods for separating turbulence characteristics 01 p0092 A70-10996

Rayleigh method convergence for linear development of perturbations in unsteady plane parallel flow of ideal fluid, formulating and proving theorem 01 p0064 A70-11032

Unsteady incompressible laminar flow under time dependent body force solved for rectangular and circular conduit and plane and cylindrical Couette flows 01 p0066 A70-11130

Time dependent behavior of separated and un-separated unsteady flow of incompressible viscous and inviscid fluids without heat transfer 01 p0067 A70-11162

Turbulent viscous fluid flow characteristics obtained from integrating Navier-Stokes equation for unsteady flow with periodic momentum variation 01 p0069 A70-11626

Boundary value problem for quasi-linear equation of unsteady transonic gas flow, including linear model and operators for group of transformations 01 p0069 A70-11628

Self similar wave solutions of continuity and momentum equations for two dimensional unsteady isentropic motion of polytropic gas 02 p0278 A70-11998

Average pressure at downstream end of pipe discharging into reservoir with upstream end under pulsed flow, considering application to pneumatic control system 02 p0279 A70-12110

Harmonically oscillating semiinfinite rectangular wing perturbation velocity potential in unsteady transonic flow without heat exchange 02 p0279 A70-12118

Numerical method for attacking-lifting problems of general three dimensional wing executing arbitrary motion in potential flow [AIAA PAPER 69-23] 03 p0405 A70-12930

Boundary layer processes under unsteady suction allowing for compressibility, relating suction value to external velocity and wall temperature 03 p0465 A70-13275

Pulsation energy distribution in free turbulent incompressible jets, noting role of mean velocity distribution 03 p0466 A70-13384

Unsteady heat transfer theories reviewed to assess steady state heat transfer relations applicability 03 p0605 A70-13401

Unsteady heat conduction in hollow cylinder, using transfer functions to solve direct and inverse two dimensional problems 03 p0606 A70-13520

Supersonic unsteady state three dimensional flow around blunt bodies with detached shock wave 03 p0409 A70-13864

Supersonic unsteady gas flow around bodies at low Strouhal numbers, noting angle of attack amplitude and leading edge shock wave 03 p0409 A70-13865

Gas dynamics analysis of explosion phenomena based on unsteady flow fields and thermodynamic properties of chemically reacting substance 03 p0607 A70-13922

Unsteady MHD flow of viscous incompressible electrically conducting fluid through rectangular duct under transverse magnetic field 03 p0471 A70-14333

Plasma unsteady one dimensional flow behind shock wave front in shock tube MGD channel, deriving differential gas dynamics equations 04 p0726 A70-14540

Initial value method for solution of nonlinear two point boundary value problems in fluid mechanics, considering Blasius equation and unsteady gas flow [ASME PAPER 69-WA/FE-8] 04 p0667 A70-14782

Unsteady problems of gas dynamics solved by method of characteristics, Godunov method, difference methods, etc 04 p0670 A70-14958

Unsteady flows effects on aircraft longitudinal motion, flight stability and control, discussing horizontal and vertical effects of rough air 04 p0623 A70-15172

One dimensional unsteady gas flows formation theories extended to include viscosity, heat conductivity, diffusion and chemical reactions effects 04 p0672 A70-15230

Unsteady pressure at slender blunt body surface in three dimensional hypersonic gas flow 04 p0618 A70-15244

Suction influence on skin friction fluctuations of MHD flow along infinite flat wall using Navier-Stokes equations 05 p0886 A70-15787

Unsteady flow equations for periodic axisymmetric laminar flow of second order fluids in circular cylindrical pipes 05 p0831 A70-15871

Unsteady laminar free convection caused by heating semiinfinite flat vertical plate, obtaining velocity and temperature distributions 05 p0957 A70-16370

Unsteady laminar gas flow near infinite flat plate using Laplace transforms, obtaining closed form solutions for plate velocity and temperature 05 p0836 A70-17106

Ti alloy tensile strength under cyclic loads at room and high temperatures, noting plastic deformation and damage accumulation effects 06 p1085 A70-17406

Yawed hot wire measurements of turbulence fluctuations, discussing calibration and mutual interference of adjacent wire and wire supporting prongs in X-ray wire case 06 p1071 A70-18487

Unsteady boundary layer flow with suction, deriving equations for circular cylinder impulsive motion 07 p1253 A70-18862

Unsteady hydrodynamic coefficients of supercavitating hydrofoil in harmonic oscillation in Helmholtz flow with free surface, investigating frequency, angle of attack and submergence depth 07 p1255 A70-19134

Flat plate boundary layer induced pressures in unsteady hypersonic flight 07 p1257 A70-19327

Navier-Stokes equations solved for unsteady incompressible three dimensional stagnation point flow, noting reduction to two dimensional and axisymmetric cases 07 p1188 A70-19343

Soviet book on unsteady attached turbulent flow in turbine lattices, studying blade aeroelastic vibrations onset and attenuation in compressible and incompressible fluids 07 p1189 A70-19602

Spectral functions of airflow velocity pulsations in circular pipe at various Reynolds numbers, considering laminar, transition and turbulent regimes 07 p1259 A70-19826

Velocity pulsations of hypersonic working flow in wind tunnel using miniature pressure transducers, discussing rms error 07 p1259 A70-19828

Circular nozzle contraction and Reynolds number effects on turbulent pulsation damping, measuring longitudinal and transverse components 07 p1259 A70-19830

Unsteady MHD flow at forward stagnation point analyzed for magnetic field effect on transient phenomena, using difference-differential numerical method 07 p1354 A70-20235

Unsteady flow behind circular cylinder by flow visualization, determining vortices length variations with time at various Reynolds numbers and dimensionless accelerations 07 p1261 A70-20236

Steady and unsteady flow through Napier turboblower axial flow turbine for full and partial admission, estimating mass flow and power output 07 p1189 A70-20294

Local heat transfer coefficients for unsteady conditions in tube determined by gradient method, noting use in reacting flow and jet nozzle protection 08 p1598 A70-21189

Unsteady flow in circular tube of constant section with time dependent discharge, determining pressure gradient and velocity distribution 08 p1484 A70-21477

Unsteady free convection laminar power-law fluid flow past porous vertical wall, studying similarity solution dependence on wall temperature and suction 08 p1486 A70-21765

Heat transfer coefficient to gas in tube under unsteady heat flow conditions, studying Nusselt number dependence on Reynolds and Prandtl numbers 09 p1787 A70-22173

Navier-Stokes equation for plane unsteady axisymmetric rotation of viscous fluid in steady radial flow from source or sink 09 p1660 A70-22437

Unsteady flow equations and thermodynamics for studying homogeneous fluidic transmission in circular and rectangular cross section lines 09 p1613 A70-23403

Boundary function of unsteady temperature field in bodies with moving surface at constant temperature calculated by least squares method 09 p1791 A70-23620

Unsteady heat transfer on electronic analog model, using installation prescribing variable boundary conditions of third kind 10 p1966 A70-23872

Unsteady laminar free convection on heated axially symmetric body under stepwise surface temperature variations and unity Prandtl number 10 p1967 A70-23875

Motion and continuity equations for unsteady two dimensional flow of incompressible viscous fluid along infinite flat plate with time dependent suction 10 p1862 A70-23877

Fluid microstructure effects on velocity, boundary layer and shear stress in nonsteady parallel flows, including accelerated plane wall equation 10 p1863 A70-23955

Unsteady MHD flow in circular pipe with nonconductive walls under transverse magnetic field 10 p1921 A70-23959

Spectrum analysis of unsteady duct flow caused by pressure loss induced instability 10 p1863 A70-24026

Unsteady MHD flows of viscous, incompressible and electrically conducting fluid, proving boundary value problem solutions existence and uniqueness 10 p1922 A70-24095

Perturbed equations solutions for plane supersonic steady and nonsteady gas flows, considering propagation of perturbations in initially nonstationary main flow 10 p1866 A70-24107

Numerical methods of viscous liquid dynamics, considering unsteady flow in simply and multiply connected regions 10 p1866 A70-24110

Small linear disturbance and stability of potential unsteady motion of finite mass of liquid with free boundary 10 p1866 A70-24111

Shock wave and gas flow structure at constant Mach number past three dimensional blunt bodies, applying method for unsteady flow 10 p1799 A70-24127

Radiating shock wave reflection from rigid wall studied for velocity and structural changes, assuming unsteady and one dimensional flow 10 p1867 A70-24140

Pulsating flow mean total pressure measurement accuracy in high turbulence regions, discussing standing and traveling acoustic waves produced at measuring system entrance 10 p1867 A70-24160

Viscous incompressible flows nonlinear stability theory, considering perturbed flows tending toward stationary or flow periodic in time [ONERA-TP-802] 10 p1869 A70-24542

Conducting gas unsteady efflux from plane tube into vacuum, determining time dependent position of expanding rarefaction wave fronts 10 p1924 A70-24569

Polygonal wings oscillatory motions in unsteady supersonic flow 10 p1803 A70-24778

Unsteady supersonic flow past tail-body system with harmonic oscillatory motions 10 p1803 A70-24789

Rayleigh method convergence for linear development of perturbations in unsteady plane parallel flow of ideal fluid, formulating and proving theorem
10 p1871 A70-25001

Nonsteady flow past duct junctures, investigating ventilation system of underground bomb shelter for blast wave passage prevention
11 p2036 A70-26139

Shock waves in unsteady aortic blood flow at systole beginning, considering aorta elastic properties and shock formation distances
11 p1992 A70-26479

Stability analysis using energy method applied to Navier-Stokes equations for unsteady viscous flow
11 p2042 A70-26849

Computer applications in aerospace research involving flutter, supersonic flow, unsteady wing flow, etc
12 p2191 A70-27025

Pulsation energy distribution in turbulent flow of incompressible fluid near tube wall, defining energy diffusion, production and dissipation terms in energy balance equation
12 p2210 A70-27321

Contact and unsteady heat transfer through vacuum cavity applied to hollow cylinders, solving nonlinear integral equations by piecewise linear approximation
12 p2331 A70-27326

Transient flow of viscous incompressible fluids with free surfaces calculated using Lagrangian coordinates
12 p2210 A70-27425

Unsteady heat or mass transfer to translating fluid sphere thermal boundary layer, determining analytical solution method accuracy
12 p2333 A70-28116

Unsteady compressible pipe flows with large cross sectional variations studied by two dimensional difference method
13 p2386 A70-28806

Unsteady fluid flow around circular cylinder with sudden acceleration using flow pattern photographs
13 p2387 A70-29056

Two dimensional unsteady incompressible fluid flow through airfoil lattice
13 p2389 A70-29491

Unsteady one dimensional motion of reacting gas mixtures in presence of supercompressed detonation waves, discussing transformation into Chapman-Jouguet wave
13 p2522 A70-29772

Boundary conditions and initial value lines for unsteady homentropic flow, performing straight pipe calculations
13 p2392 A70-30023

Two dimensional unsteady flow of weakly conducting fluid in perpendicular magnetic field using Green function
14 p2621 A70-30180

Unsteady incompressible laminar boundary layer equations solution after Crocco transformation by implicit finite difference scheme for flow around blunt body
14 p2528 A70-30290

Nonsteady coupled MHD Couette flow, presenting solution by Fourier series expansion method
14 p2621 A70-30549

Unsteady relative flow in centrifugal impeller passage running at part capacity and zero flow observed by hydrogen bubble flow visualization method [ASME PAPER 69-GT-35]
14 p2529 A70-31024

Unsteady aerodynamic forces on oscillating circular cylinder, using wind tunnel two dimensional dynamic model
14 p2529 A70-31050

Nonstationary MHD Couette flow of viscous incompressible fluid between two parallel walls caused by instantaneous fluctuations of applied transverse magnetic field
15 p2777 A70-31479

Steady and nonsteady engine/inlet flow field simulation for engine/compressor testing, determining feasibility of variable ramp aerodynamic device [AIAA PAPER 70-591]
15 p2672 A70-31788

Upper atmospheric unsteady horizontal wind flow from differential equations unstable solution
15 p2772 A70-32889

Book on flow separation covering steady/unsteady, turbulent and incompressible flows, base pressure, thermal effects, etc
16 p2833 A70-32913

Unsteady hydromagnetic flow of viscous electrically conducting incompressible fluid due to rotating disk under perpendicular magnetic field
16 p2958 A70-33297

Boundary value problem of two dimensional Poisson equation solution procedure with Hockney formulas, applying to unsteady viscous incompressible flow past flat plate
16 p2943 A70-33737

Mathematical model of pulsatile viscous entrance flow in thick walled elastic tube, investigating flow development effects in large arteries
17 p3035 A70-34471

Analytic theory of unsteady separated flow effects on dynamics of heat sink type reentry bodies and elastic launch vehicles
17 p3008 A70-34489

[AIAA PAPER 70-762]

Unsteady laminar boundary layers on infinite porous plate, considering radiative heat transfer and transpiration cooling
17 p3067 A70-34632

Steady and unsteady gas dynamics analogies with two dimensional water flow, taking into account energy and continuity equations
17 p3069 A70-35032

Unsteady convective heat transfer in pipes in presence of heat flux density and flow rate aperiodic variations
17 p3198 A70-35730

Free turbulent incompressible jet, analyzing pulsating characteristics and energy balance with Reynolds stress equations
18 p3240 A70-36264

Unsteady two dimensional gas flow calculation axisymmetric shock tube of variable cross section, using numerical method
18 p3240 A70-36275

Half space nonstationary temperature field with mobile heating at edges, using integral transformations
18 p3348 A70-36725

Perfect and dissociating gas nonstationary supersonic flow around sharp profile of finite thickness analyzed by linearization and method of characteristics
19 p3351 A70-37242

Velocity profiles in steady and unsteady rotating flows for impulsive slow down and acceleration in cylindrical chamber
19 p3403 A70-37527

Unsteady incompressible planar gas jets with stable vortex street, investigating near flow field region to establish oscillatory component
19 p3404 A70-37799

Unsteady laminar incompressible fluid flow in parallel plate channels and circular tubes, solving Navier-Stokes equations for prescribed discharge
19 p3405 A70-38347

Unsteady flow and heat transfer in viscous incompressible fluid due to infinite porous cylinder oscillations about axis with suction at surface
19 p3406 A70-38445

Skin effect for unsteady radio waves emitted into homogeneous nonmagnetic isotropic half space, calculating electric field
19 p3381 A70-38571

MHD nonsteady Beltrami flow between two infinite parallel walls with transverse magnetic field, calculating velocity, skin friction and induced magnetic field
20 p3678 A70-39610

Unsteady viscous flow of incompressible fluid through porous straight channel under time varying pressure gradient, determining suction and injection effects
20 p3609 A70-39670

One dimensional unsteady equilibrium flow stability of relaxing two phase medium consisting of perfect gas and incompressible liquid
20 p3613 A70-40295

Longitudinal averaged and pulsating turbulent flow velocities in rectangular channel with one-sided air injection through porous wall
20 p3614 A70-40346

Unsteady incompressible flow in laminar boundary layer with homogeneous suction during longitudinal flow past flat plates, investigating boundary layer stability
20 p3614 A70-40391

Energy dissipation in laminar unsteady incompressible viscous fluid flows, discussing velocity fields, boundaries, tangential motion and entrainment
20 p3614 A70-40402

Unsteady flow in rectangular cavity with moving wall, using iterative solution of Navier-Stokes equations
21 p3807 A70-41317

Two dimensional unsteady viscous incompressible MHD flow past infinite flat plate with uniform suction, considering Hartmann and Reynolds numbers
21 p3858 A70-41450

Pulsation energy distribution in turbulent flow of incompressible fluid near tube wall, defining energy diffusion, production and dissipation terms in energy balance equation
21 p3810 A70-42062

Contact and unsteady heat transfer through vacuum cavity applied to hollow cylinders, solving nonlinear integral equations by piecewise linear approximation
21 p3952 A70-42067

Combined effects of flow unsteadiness and surface mass transfer on displacement thickness of boundary layer, using flat plate geometry
21 p3811 A70-42092

Constant property unsteady laminar flow thermal entrance problems, using variational formulation in Laplace transformed domain
21 p3954 A70-42169

Karman-Polhausen method applied to unsteady thermal boundary layer on isothermal flat plate
21 p3954 A70-42208

Acoustic waves generation from decay region of pulsating supersonic jet expelled from nozzle
21 p3748 A70-42211

Bistable wall attachment fluid amplifier, calculating unsteady end wall switching transient based on turbulent jet entrainment properties
21 p3964 A70-42428

[ASME PAPER 70-FLCS-3]

Unsteady supersonic flow around oscillating cross-shaped wing-fuselage system, determining perturbation velocities and pressure distributions
22 p3958 A70-42609

Unsteady hydromagnetic boundary layer flow past semiinfinite flat plate under steady magnetic field and small free stream perturbation
22 p4080 A70-42631

Equations for unsteady frozen nonequilibrium flow of dissociating and relaxing gas, using Lighthill ideal dissociating diatomic gas for aerothermochemical model
22 p4124 A70-42754

Downwash angle behind straight wing for unsteady aperiodic flight at subsonic speeds, using vorticity model
22 p3959 A70-42802

Liquid propellant rocket engine combustion instabilities, describing unsteady combustor flow by single nonlinear wave equation with stable and unstable finite amplitude limit cycles
23 p4233 A70-44425

Unsteady radiating nongray gas diffuse boundary conditions, emphasizing monochromatic radiation slip and one dimensional radiant flux
23 p4282 A70-44593

Potential liquid flow in pulsating bulb applied to blood flow
23 p4155 A70-44847

Unsteady incompressible thermal boundary layer flow past three dimensional obstacle for Prandtl numbers near unity
24 p4428 A70-45366

HF pulsating air flow measuring technique with sharp edged orifice meter, discussing experimental setup and pulsation frequency and intensity effects
24 p4335 A70-45591

Three dimensional laminar boundary layer in unsteady incompressible flow, presenting solution by successive approximations method
24 p4325 A70-45594

Pulsatile flow in circular rigid tube with and without longitudinal vibration, obtaining momentum integral solution
24 p4325 A70-45623

Simple wave functions solutions in multidimensional nonviscous polytropic gas unsteady and steady flow
24 p4327 A70-46030

Pulsation and turbulence damping in pulsed jet from energy spectra of longitudinal velocity fluctuations
24 p4327 A70-46267

Unsteady separation criteria for three dimensional laminar boundary layer on finite obstacle
24 p4327 A70-46268

UNSTEADY STATE

Unsteady state lift and moment action on lattice of profiles moving in incompressible fluid, determining suction originating at leading edges of profiles
03 p4049 A70-13868

Splitting procedures application to steady and unsteady problems of mathematical physics and predictor-corrector method application to unsteady problems
04 p0719 A70-14959

Unsteady heat conduction numerical approximation for infinite cylinder with variable heating and boundary conditions of third kind
05 p0936 A70-16294

One dimensional unsteady heat conduction with variable boundary conditions solved by difference-differential method using rectangular and cylindrical coordinates
05 p0957 A70-16295

Electronic-vibrational coupling in nonequilibrium MHD generator with molecular gas to suppress electrode layer shorting and recombination in supersonic nozzles
06 p0988 A70-18222

[AIAA PAPER 70-41]

Unsteady heat conduction in plate, solid or hollow infinite cylinder and sphere with internal heat source and radiative heat transfer on surface
07 p1423 A70-19818

Correlation functions of nonlinear auto-oscillatory system under nonstationary conditions determined by statistic linearization
11 p2022 A70-25341

Elastic scattering formation and decay of unstable particle gases, discussing density and corrections to chemical and nuclear statistical equilibrium equations
13 p2455 A70-29223

Unsteady nonlinear aerodynamic loads measurements in wind tunnel, using linearized mathematical analog
13 p2343 A70-29896

[AIAA PAPER 70-573]

Two dimensional detonations structure by nonlinear theory for systems with hydrodynamically unstable steady state solutions, imposing periodic boundary conditions

20 p3609 A70-39658

Nonsteady temperature and thermal stress distribution in gas turbine blades, using plastic model and photothermoelastic method

22 p4093 A70-43743

UNSWEEP WINGS

NT RECTANGULAR WINGS

UP CONVERTERS

U PARAMETRIC FREQUENCY CONVERTERS

UPDRAFTS

U VERTICAL AIR CURRENTS

UPPER AIR

U UPPER ATMOSPHERE

UPPER ATMOSPHERE

Harmonic analysis of upper atmospheric wind periodic data from radar sounding of meteor trails, defining principal diurnal wind variations

01 p0134 A70-10201

Upper atmosphere temperature lag behind solar decimeter flux 27 day variation maximum attributed to varying solar EUV heating

01 p0070 A70-10404

Upper atmosphere structure and energy budget based on IGY/IQSY spectroscopic observations of temperature distribution and stratosphere-mesosphere composition

01 p0072 A70-10578

Hydrodynamic explanation of upper atmosphere perturbation effects on tropospheric circulation, discussing experiments for solar activity effects on atmospheric dynamics

01 p0073 A70-10582

Upper atmospheric atomic H and He concentration height distribution, considering L alpha and H alpha emissions, He emission, light components and direct measurements

01 p0074 A70-10589

Intensity distribution determination in spectrum of solar XUV fluxes incident upon upper atmosphere, considering quantitative model construction

01 p0170 A70-10593

Upper atmospheric contribution to Faraday rotation angle above 5000 km determined from beacon frequencies of geostationary satellite, noting geomagnetism weighting and electron content decrement role

01 p0076 A70-10874

Satellite observations of semiannual density variations in upper atmosphere

01 p0077 A70-11205

Twilight and nightglow measurements with stratospheric balloons, discussing use for upper atmosphere exploration, meteoric influence and French network

01 p0079 A70-11217

Electrical phenomena in upper atmosphere and solar wind may control geomagnetic disturbances and aurorae

01 p0082 A70-11523

Upper atmospheric thermal fluctuations study based on correlation characteristics of rapid thermal perturbations, using linear differential equations

02 p0288 A70-11761

Solar activity indices and upper atmospheric density interrelationship from Explorer I satellite observations, showing statistical variations

02 p0356 A70-11762

Aeronomy of Jovian upper atmosphere at pressures below 25 mb, discussing stratospheric heat sources, thermal emissivity, photochemistry of methane, ammonia, etc

02 p0366 A70-11804

Soviet collection of papers on theoretical problems of upper atmosphere physics, discussing various models, atmospheric composition, etc.

02 p0327 A70-12383

Static atmosphere model above 120 km, assuming oxygen atoms and molecules and nitrogen molecules presence to determine diffusion velocity and recombination coefficient

02 p0327 A70-12385

Zonal circulation model of atmosphere below altitude of 200 km using rocket, meteor and ionospheric drift observations

02 p0328 A70-12388

Pion production characteristics during high energy nucleons interactions from data on production in upper atmosphere by gamma-quanta families/isobaric production/

03 p0555 A70-13032

Statistical analysis of satellite drag data for characteristic time of thermal fluctuations in upper atmosphere caused by soft solar X-rays

03 p0472 A70-13179

Parachute design for decelerating upper atmosphere rocket probes at high altitudes, using high drag coefficients in Stokes flow regime

04 p0624 A70-15410

Solar and sky far IR radiation in upper atmosphere, estimating precipitable water quantities and low absorption regions

04 p0681 A70-15521

Vertical profiles of atomic and excited molecular oxygen concentration in upper atmosphere calculated from spectral band intensity, determining excitation reaction rates

04 p0682 A70-15733

Excited oxygen molecules concentration in upper atmosphere calculated, considering deactivation during interactions in various energy states

04 p0684 A70-15750

Upper atmosphere wind and semidiurnal and diurnal tide interactions observed by meteoric radar, noting relation to gravity waves

05 p0878 A70-15818

Antarctic twilight Na emission abundance and concentration in lower E region, discussing meteor ablation models

05 p0836 A70-15819

Spectral intensity recording facility design for high energy electrons and hard gamma quanta in upper layer and beyond atmosphere

05 p0846 A70-15959

Na abundance in terrestrial upper atmosphere, solving steady state continuity and momentum equations for Na atoms and ions

05 p0840 A70-16475

Pulsation velocities distribution wind in meteor region of atmosphere during hourly intervals over eleven month period, noting normal distribution

06 p1095 A70-17206

Penumbra during lunar eclipses analyzed photometrically, considering effects of earth upper atmosphere and lunar luminescence

07 p1377 A70-18973

Hydrogen and helium emissions in upper atmosphere, observing amplifications towards geomagnetic poles and in winter hemisphere

07 p1266 A70-19439

Midlatitude upper atmosphere soft electron energy flux nighttime measurements by sounding rocket

07 p1368 A70-19500

Upper atmospheric horizontal sounding, discussing satellites uses in atmospheric structure studies

07 p1268 A70-19603

Geocoronal glow as resonant scattering of solar Lyman-alpha-radiation by H atoms in upper atmosphere

07 p1270 A70-20032

ARCAS meteorological rocket system designed for upper atmospheric soundings to provide thermodynamic and wind data, discussing payloads

07 p1395 A70-20256

Rocket-borne radar chaff wind sensor synoptic application above 65 km, describing low fall velocity

07 p1237 A70-20258

Upper atmosphere climatology including latitudinal and longitudinal variations in wind, temperature, density and zonal momentum

07 p1275 A70-20279

Turbulence in quiescent prominences relationship to shock waves in upper atmosphere

08 p1570 A70-20840

Photometric profiles of Jupiter shadows cast by large natural satellites used as upper atmosphere probes

08 p1579 A70-21571

Geoactive low energy particles and fresh photoelectron interactions with upper atmosphere observed by satellite Cosmos 261

08 p1492 A70-21796

Upper atmosphere research by U.S.S.R. mass spectrometers onboard French rocket probes, discussing design, payloads and equipment tests

09 p1766 A70-22658

Upper atmosphere aerosols and cosmic dust properties investigation by laser beam scattering measurements using photoelectron counters for weak signal detection

10 p1898 A70-23818

Upper atmospheric waves nonlinear interactions based on tides and gravity waves propagation, taking into account terrestrial rotation

10 p1872 A70-23820

Sodium night airglow analyzed by Chapman mechanism, considering nocturnal intensity seasonal behavior and location in upper atmosphere

10 p1873 A70-23829

Cosmic ray particle abundance in upper atmosphere during minimum solar activity estimated by nuclear photographic emulsions on balloon flight

10 p1932 A70-24438

Night time upper atmosphere light phenomena and Tungusk meteorite observed on 30 June 1908

10 p1876 A70-24499

Solar cosmic ray ionization of upper atmosphere, calculating electron production rate distribution

10 p1934 A70-25199

Sound speed and horizontal wind velocity components determined in upper atmosphere from measured data of Rocket Grenade Experiment

11 p2121 A70-25678

Mars upper atmosphere semiempirical model, reducing density uncertainties by allowing for solar cyclic variations

11 p2111 A70-26031

Project HARP gun-launched projectiles as vertical sounding probes for upper atmospheric meteorological and geophysical measurements, discussing payloads development for high acceleration

11 p2122 A70-26047

Kalman filtering applied to moving balloon position and velocity estimates related to upper atmosphere wind measurements by balloon-satellite experiment

11 p2025 A70-26206

Corpuscular radiation intensity measurements in upper atmosphere at midlatitudes by meteorological probe during geomagnetic storm, noting radio wave absorption

11 p2106 A70-26797

Elastic scattering effect on photoelectron transport and escape in upper sunlit atmosphere

12 p2222 A70-27187

Upper atmosphere electromagnetic probing theory and techniques, noting applications to aeronomic problems

12 p2223 A70-27726

Upper atmosphere probing based on light scattering from laser radar beam by atmospheric constituents

12 p2185 A70-27740

Earth radiation balance /net flux/ determination from satellite measurements of long wave radiance and reflected solar radiation in upper atmosphere

12 p2264 A70-28090

Midlatitude upper atmospheric low energy proton intensity obtained from meteorological rocket data

12 p2296 A70-28265

Solar activity effects on midlatitude upper atmosphere corpuscular radiation intensity via rocket sounding

12 p2296 A70-28266

Upper atmospheric composition by nitrogen molecules radiative transition analysis, using laser resonance backscattering effect

12 p2227 A70-28267

Bora-Sond rocket for cost effective upper atmospheric sounding, discussing Li-Al-O systems performance

13 p2504 A70-28684

Upper atmosphere superrotation velocity based on satellite polar orbit calculation of 1968-59A, correcting for lunisolar perturbations

13 p2394 A70-28895

Topsider sounder profiles interpretation, discussing ionosphere-protonosphere dynamic coupling

13 p2398 A70-29199

Upper atmospheric wind evaluation in radar measurements by radio sounding technique, discussing equipment design

13 p2445 A70-29468

Upper atmospheric ion and neutral composition from rocketborne mass spectrometry, allowing for rocket velocity and analyzers orientation with respect to velocity vector

14 p2568 A70-30140

Transverse structural function of velocity field of turbulent motion in upper atmosphere, using meteor speed ratio observations

14 p2635 A70-30312

Solar activity predictions for earth upper atmosphere models emphasizing linear regression method

14 p2638 A70-30565

Three camera method for studying upper atmosphere winds via smoke trails providing wind velocity, earth coordinate data and error indication

14 p2607 A70-30572

Vertical profiles of atomic and excited molecular oxygen concentration in upper atmosphere calculated from spectral band intensity, determining excitation reaction rates

14 p2575 A70-30817

Excited oxygen molecules concentration in upper atmosphere calculated, considering deactivation during interactions in various energy states

14 p2576 A70-30834

Mars upper atmosphere refractivity, free electron number density and plasma temperature altitude profiles from Mariner 1969 radio occultation measurements

14 p2646 A70-31072

Concentrations model of metallic atoms and ions in upper atmosphere with deposition from meteors, using diffusion equation

14 p2580 A70-31262

Red twilight emission enhancements origin, concerning atomic lithium release effect in upper atmosphere

14 p2580 A70-31264

X rays and primary cosmic radiation intensity measurements near top of atmosphere, describing rocket payload and launch

14 p2632 A70-31307

Upper atmospheric short lived disturbances connected with geomagnetic storms characterized by determining equivalent duration /DJ/ values

15 p2723 A70-31651

Atomic hydrogen distribution in upper atmosphere and solar system obtained during spin operation of OGO 5 with Lyman alpha photometer

15 p2798 A70-31655

Upper atmosphere density and temperature height profiles perturbations in falling sphere probe 15 p2723 A70-31663

Atmospheric density near 180 km /1968-1969/ from orbit of satellite 1967-31A /ATS 2/, noting weak dependence on solar activity and correlations to geomagnetic disturbances 15 p2724 A70-31680

Upper atmosphere turbulence spectra of passive contaminants deposited by rockets from radiometrically calibrated photographs of chemical trails 15 p2725 A70-31688

Monograph on upper atmosphere and outer space studies in U.S.S.R. /1969/ covering Soiuz 4, 5, 6, 7, 8 and Venera 5, 6 flights 15 p2829 A70-31702

Continuous differential energy pulse height spectra reduction to photon upper atmospheric spectra 15 p2694 A70-31800

Spatial distribution of energy deposited by auroral electrons in upper atmosphere, using Monte Carlo method 15 p2725 A70-31860

Dynamic spectral characteristics of LF whistler signals for outer ionosphere electron profile determination, using satellite observation 15 p2729 A70-32081

Rocket and satellite data on upper atmospheric neutral/charged particles, short wave solar radiation, temperature and photochemical reactions 15 p2730 A70-32089

Upper atmosphere sounding vehicle /Bora-Sond/, describing payload section, launch acceleration, apogee time, weight and length, staging, etc 15 p2811 A70-32259

Midlatitude upper atmosphere soft electron energy flux nighttime measurements by sounding rocket 15 p2795 A70-32745

Upper atmospheric unsteady horizontal wind flow from differential equations unstable solution 15 p2772 A70-32889

Venus upper atmosphere carbon atoms detection based on low resolution spectra analysis of solar illuminated atmosphere 16 p2979 A70-34036

Twilight sky brightness measurements at 5200 Å for estimating upper atmospheric dust component, discussing error rates 16 p2899 A70-34184

Upper atmosphere temperatures from vapor cloud diffusion, eliminating errors from bright sky background at twilight 17 p3076 A70-34940

Bora-Sond atmospheric probe providing two stage minimum cost high altitude sounding for supersonic transport /SST/, discussing hot water propulsion system 17 p3178 A70-35257

Radar receiving station equipment for studying upper atmosphere by radio meteor echoes 17 p3047 A70-35605

Model calculations of Martian upper atmosphere expanding above mesopause, taking into account effects of molecular and eddy diffusion and chemical reactions 17 p3172 A70-35643

Mean molecular mass determination method for upper atmosphere based on Nicolet equation for scale height, using satellite orbit and spin decay data 17 p3138 A70-35773

Upper atmosphere IR emission model with reference to thermal excitation, chemical reactions and electron excitation 18 p3246 A70-36173

Upper atmosphere neutral component temperature measurement from thermal spread of charged particles beam 18 p3247 A70-36182

Upper atmospheric ion composition during Orionid meteor shower activity by rocket-borne RF mass spectrometer 18 p3247 A70-36183

Upper atmospheric gas components vertical distribution by airborne photometric absorption and attenuation measurements in UV spectrum 18 p3248 A70-36633

Hydrogen and helium emissions in upper atmosphere, observing amplifications towards geomagnetic poles and in winter hemisphere 18 p3249 A70-36913

Soviet papers on physical processes in earth upper atmosphere covering emissions, dust, particle distribution, Rayleigh scattering, temperature, inhomogeneities, etc 18 p3250 A70-36976

Vertical distribution of upper atmospheric 7600 Å oxygen glow, discussing 8645 Å band and nitric oxide data 18 p3251 A70-36977

Upper atmospheric dust composition and optical properties by crepuscular technique, using photometric measurements in 5200 Å region 18 p3251 A70-36978

Upper atmospheric neutral components temperature determination by rocket-borne mass spectrometers 18 p3252 A70-36983

Upper atmospheric layers neutral composition by rocket-borne mass spectrometers, indicating gravitational separation of argon from molecular nitrogen 18 p3252 A70-36984

Upper atmospheric ions kinetic temperatures based on chromatic broadening of mass spectral lines 18 p3252 A70-36985

Upper atmospheric atomic nitrogen reaction with carbon tetrachloride, estimating radiation intensity and brightness of artificial luminescent cloud 18 p3252 A70-36989

Upper atmospheric wind velocity and diffusion coefficient measurement by radar observation of artificial electron cloud from atomic K ejection 18 p3253 A70-36993

Upper atmosphere wind, density, temperature and pressure from Soviet meteor data 19 p3412 A70-37651

Upper atmospheric density and temperature diurnal phase and amplitude discrepancy reconciled by dynamic diffusion model 19 p3414 A70-38381

Upper atmosphere semiannual variations dependence on lower thermosphere dynamic properties seasonal variations, using steady state models 19 p3415 A70-38384

Luminous intensity profile of optically thick Sr artificial clouds in upper atmosphere, using Monte Carlo calculations 19 p3415 A70-38388

Ozone concentration variations in upper atmosphere during solar eclipses 19 p3418 A70-38906

Solar constant measurements by high altitude balloon sounding, noting anomalous turbidity in upper atmospheric layers due to nuclear explosions and volcanic eruptions 20 p3703 A70-39375

Upper atmospheric wind currents differential equations, obtaining physical data in terms of asymptotic expansion of Gaussian error functions 20 p3622 A70-39763

Pulsar NP 0535 X rays detection by ground based observations of upper air fluorescence 21 p3871 A70-40654

Synoptic surface and upper air analysis and APT mosaics of meridional circulation over Mediterranean by remote satellite images 21 p3846 A70-41399

Upper atmosphere electric field nature, considering solar radiation as major source of ionization 22 p4017 A70-42788

Upper atmosphere and magnetosphere DC electric field measurement using artificial clouds 22 p4017 A70-42791

Sodium D lines airglow nocturnal and seasonal variations in upper atmosphere 22 p4023 A70-43295

Upper atmosphere photoionization by extreme UV solar radiation compared with ionization by charged particles collisions 22 p4096 A70-43302

Venusian and Martian upper atmosphere chemistry, emphasizing ionization height distribution 22 p4106 A70-43312

Global upper atmosphere circulation pattern by daytime tracking of high altitude rocket vapor trail, using differential radiometer 23 p4214 A70-44039

Upper atmosphere optical properties sounding by twilight observation and successive brightness approximation 23 p4187 A70-44047

Air current in upper atmosphere meteor zone above equator, noting diurnal and semidiurnal harmonics in wind velocity components 23 p4188 A70-44049

Diurnal variation symmetry of upper atmosphere molecular oxygen concentration in terms of ozone photodissociation 23 p4190 A70-44083

Upper atmosphere tidal pressure and wind variations from meteor trail drift data 23 p4215 A70-44266

Solar L alpha absorption in upper atmosphere, using rocket-borne ionization chamber 23 p4191 A70-44270

Upper atmosphere average rotation speed and height variation, presenting atmospheric and earth angular velocity ratio from satellite orbit inclinations 24 p4328 A70-45353

Upper atmosphere diurnal, annual and solar activity induced density variations effects on satellite orbits 24 p4408 A70-45553

Optical laser radar for upper atmospheric density and aerosol concentration measurements 24 p4353 A70-45561

Meteorological NEXAIR /Next Generation Upper Air System/ for atmospheric data from balloon-borne instrument packages 24 p4372 A70-46049

UPPER IONOSPHERE

Alouette 2 Langmuir probe measurements analyzed for size and amplitude of electron concentration fine structure irregularities in topside ionosphere, discussing F spread 04 p0679 A70-15111

Topside ionosphere ionization compared during magnetic storms with steep onset, smooth variation and sudden commencement 05 p0838 A70-16283

Upper ionospheric electron density variations at low magnetic activity times observed with Alouette 2 satellite 05 p0901 A70-16307

Nighttime recombination model of O ion plasma in upper ionosphere, showing temporal behavior and variation of electron concentration 07 p1265 A70-19432

Topside ionosphere morphology during IQSY, emphasizing plasma scale height diurnal and latitudinal variations role in satellite data interpretation 07 p1270 A70-20073

Solar wind and Venus topside ionosphere interaction, discussing charged particle density, temperature and pressure distribution 08 p1578 A70-21550

Ion temperature gradient along magnetic field lines in outer ionosphere by thermal diffusion equations compared with electron temperature observations 11 p2047 A70-26568

Topside ionosphere structural analysis, considering electron density profiles deduced from Alouette 2 satellite data 12 p2226 A70-28062

Topside ionosphere nighttime structure over Japan deduced from Alouette 2 satellite plasma frequency measurements 12 p2226 A70-28063

Proton cyclotron echoes in topside ionograms using Alouette 2 satellite data 12 p2226 A70-28064

Topside ionosphere structure deduced from electron density profiles observed by Alouette 2 satellite 13 p3295 A70-29090

Topside ionosphere structure deduced from resonance spikes on ionograms obtained by Alouette 2 satellite and electron density distributions 13 p3295 A70-29091

Proton cyclotron echoes in topside ionograms from Alouette 2 satellite 13 p3296 A70-29092

Molecular oxygen positive ion density in upper ionosphere as function of photoionization, ambipolar diffusion velocity and altitude effect 13 p3299 A70-29233

Electrostatic waves for upper ionospheric plasma model, obtaining solutions to dispersion relation at multiples of electron cyclotron frequency 13 p4400 A70-29914

Topside ionospheric plasma scale height, showing influence of magnetic activity level 14 p2569 A70-30207

Venus daytime upper ionosphere observations by mariner 5 in terms of ionization sources and sinks, ambipolar diffusion and model atmospheres 18 p3311 A70-36002

Hydrogen, He and oxygen ion density, and ion and electron temperatures in upper ionosphere fromOGO 4 observations 18 p3244 A70-36016

Nighttime recombination model of O ion plasma in upper ionosphere, showing temporal behavior and variation of electron concentration 18 p3249 A70-36906

Lower hybrid resonance frequency propagation ducts in multilayer upper ionosphere, showing association with VLF hiss bands 20 p3584 A70-39331

Topside plasma frequency resonance below electron cyclotron frequency, discussing ray paths and delay times 20 p3620 A70-39336

Seasonally biased electron density enhancements in nighttime response of topside ionosphere to magnetic storms 20 p3621 A70-39342

Satellite-borne loop antenna resistive and reactive impedance measurements in topside ionosphere 22 p4019 A70-43112

Topside ionospheric plasma scale height, showing influence of magnetic activity level 24 p4330 A70-46282

UPSTREAM

Upstream influence distance estimation associated with critical pressure rise in two dimensional shock-boundary layer interactions based on Lighthill subsonic inner boundary layer concept 10 p1862 A70-23840

Turbulent boundary layer formation in upstream wake of accelerated flow indicated from boundary layer profile and wall static pressure measurements 13 p2392 A70-29996

Upstream disturbances propagation during hypersonic flow boundary layer interaction 21 p3748 A70-42205

Large fluid-amplifier-type jets, measuring upstream flow disturbances effects on spreading velocity profiles
[ASME PAPER 70-FLCS-A] 22 p3964 A70-42431

UPWASH

Upwash interference on oscillating wing in slotted wall wind tunnels, analyzing acceleration and velocity potentials using small wing theory 04 p0621 A70-15605

URANIUM

NT URANIUM ISOTOPES

NT URANIUM 233

NT URANIUM 238

Neutron activation analysis for U and Th in various tektites, discussing evolution and extraterrestrial origin 03 p0576 A70-14090

Uranium plasma design and characteristics, measuring emission and absorption coefficients as function of temperature and pressure [AIAA PAPER 70-43] 06 p1122 A70-18084

Uranium abundance in hypersthene chondrites determined by homogenized fission track analysis, comparing age estimation with iron meteorite event occurrence 07 p1391 A70-20354

U and Th abundances correlation in tektites and achondrites based on oxygen isotopic composition of lunar rock specimens 13 p2488 A70-28720

Engine weight estimation for showing effect on thrust, specific impulse and uranium loss rate for open cycle gas fueled nuclear rocket engine [AIAA PAPER 70-690] 16 p2949 A70-33553

Uranium plasma emission coefficients as function of DC arc operation, measuring intensity spectrum with scanning spectrometer [AIAA PAPER 70-692] 16 p2950 A70-33554

Spiking in deep partial penetration electron beam weld in U dependence on machine parameters 18 p3264 A70-37116

Uranium ion impact ejection and electronic excitation of thin foil particles, observing optical spectra of Be, carbon and Al atoms and ions 20 p3674 A70-39135

Fission track uranium distribution studies of Apollo 11 lunar volcanic rocks, using Lexan plastic print method 21 p3900 A70-41537

Uranium plasma diagnostics, measuring emission and absorption coefficients as function of pressure and temperature 22 p4069 A70-42361

URANIUM ALLOYS

Depleted uranium for gamma radiation shielding, discussing properties, alloys, fabrication and applications 19 p3469 A70-37834

URANIUM COMPOUNDS

NT URANIUM OXIDES

URANIUM ISOTOPES

NT URANIUM 233

NT URANIUM 238

Open cycle gas core nuclear rocket reactor, evaluating critical mass for U isotopes 18 p3290 A70-36564

Uranium and Th isotopic composition in Apollo 11 samples compared to earth, using mass and alpha spectrometries 21 p3777 A70-41603

Apollo 11 lunar rocks, breccia and fines U, Th and Pb isotopes systematics, considering implications for lunar history 21 p3909 A70-41605

URANIUM OXIDES

Fission gases trapped in fuel particles, cladding and matrix of irradiated refractory metal-uranium oxide cermets determined by gamma counting 07 p1332 A70-19851

Uranyl ion luminescence and absorption cross section in silicate glass excited by high power light beam, considering Q switching action of ion 08 p1510 A70-20516

URANIUM 233

Nuclear light bulb engine critical fuel mass and design changes effects [AIAA PAPER 68-571] 01 p0140 A70-10835

URANIUM 238

Alpha particle emissivity measurement of moon by Explorer 35 spacecraft for U 238 abundance in outer crust 01 p0181 A70-10573

Pu/U ratio in St. Severin meteorite at time of Xe retention beginning 13 p2488 A70-28723

Th 232 and U 238 pionic X ray energies and widths, suggesting anomalous effect for interaction between high-Z nuclei and pion 15 p2776 A70-31738

URANUS [PLANET]

Effective pressure and rotation line intensity in Uranus upper atmosphere obtained from methane band spectrograms, calculating maximum temperature at subsolar point 07 p1385 A70-19423

Bode law development from dynamical relaxation suggested from comparison of Jupiter, Saturn and Uranus inner satellite systems with planetary system 09 p1765 A70-23796

Uranus and Mars satellite relative measures, tabulating observations 19 p3516 A70-37932

Uranus and Saturn reciprocal mass determination based on astronomical observations of Saturn and Jupiter respectively 20 p3705 A70-39477

Uranus and Neptune millimeter wave observations, showing brightness temperatures in excess of black body equilibrium temperatures derived from solar heating 24 p4403 A70-45398

URBAN DEVELOPMENT

Systems engineering applied to airborne, airport and community socioeconomic structure in determining air freight and passenger demand impact on airport location and configuration [AIAA PAPER 69-1091] 01 p0055 A70-10605

Remote sensor capability in land use, urban and soil moisture analysis data acquired by NASA Earth Resources Program [AAS PAPER 69-575] 04 p0676 A70-14641

Automatic change discrimination applications to weather prediction, land resource management and city planning, using photographic, IR and radar sensor imagery [AIAA PAPER 70-311] 09 p1677 A70-22876

Aerial photographic surveys of urban land use and natural resources, considering data analysis, display, computer compilation, updating and remote sensing 10 p1891 A70-24738

Urban development detection by remote sensing imagery of highway and rail linkage 12 p2216 A70-26908

Aerospace technology and system analysis application possibilities to urban social and economic planning problems 14 p2670 A70-31191

URBAN RESEARCH

Aerial and ground UHF noise measurement in Phoenix area, correlating air and ground data [AIAA PAPER 70-437] 11 p2001 A70-25480

Residential urban environment data extraction from high and low resolution images 12 p2216 A70-26907

K band imagery of New England for evaluating size, shape and distribution of built-up areas 12 p2216 A70-26912

Total community annoyance measurement (TACM) applied to urban VTOL port planning for aircraft noise [SAE PAPER 700286] 12 p2161 A70-27442

Remote sensors applied to classification of aerial data concerning housing quality at different scales, using variables observation 14 p2577 A70-31234

Radio frequency indigenous noise measurement in urban areas 18 p3228 A70-36568

Metropolitan airports environmental considerations, noting aircraft noise role in planning [SAE PAPER 700253] 18 p3237 A70-36826

URBAN TRANSPORTATION

NT RAIL TRANSPORTATION

California future transport complex, considering STOL and ESTOL/extremely short takeoff landing aircraft/design requirements 06 p0985 A70-17197

V/STOL intercity airliner potential and development noting benefits of noise reduction, ground space economy, etc 08 p1434 A70-20619

VTOL aircraft applications to intercity traffic compared to competing transportation methods, discussing possible transportation time reductions [DGLR-70-005] 10 p1970 A70-24045

Urban development detection by remote sensing imagery of highway and rail linkage 12 p2216 A70-26908

Gemini 12 photographs examined for urban and transportation data content 12 p2228 A70-26909

V/TOL aircraft approaches to air passenger surface travel time reduction, emphasizing Manhattan-to-airport transportation problems [SAE PAPER 700287] 12 p2335 A70-27443

VTOL profitability in Northeast Corridor, discussing city center ports accessibility for S-65-200 short hauls and economic and ground acreage advantages [SAE PAPER 700310] 12 p2335 A70-27452

Economic factors in developing STOL and VTOL metroflight service, proposing evolutionary process beginning with short term demonstration [SAE PAPER 700313] 12 p2335 A70-27454

American Airlines-McDonnell Douglas inter-metropolitan STOL evaluation tests, noting microwave landing guidance system [SAE PAPER 700336] 12 p2161 A70-27464

Helicopters for short haul intercity transport, discussing power failure safety, weather factors and costs 12 p2161 A70-27596

Air terminal and ground transfer design to provide improved access to aircraft and total transportation time reduction 12 p2208 A70-27992

Low pressure ratio lift fan propulsion system for intercity VTOL transports, considering thrust, safety, noise, weight, components, speed, turbine and transmission [AIAA PAPER 70-670] 16 p2971 A70-33952

Computerized metropolitan air transit system, discussing system redundancy for safety level maintenance and all-weather dependability 17 p3199 A70-34730

Metropolitan air transit system design, considering compound helicopters, automatic control by central computer, onboard avionics system and terminal facilities 21 p3956 A70-41250

STOL system traffic analysis simulation model for interurban transportation system as tool for flight hardware evaluation 22 p4007 A70-43731

STOL operations from city centers, discussing safety requirements, navigation and guidance systems, airport criteria, etc 23 p4140 A70-44174

Planning criteria for optimum metropolitan airport system considering operational, physical, social and economic factors [AIAA PAPER 70-1266] 24 p4430 A70-45921

Short haul transportation needs in multimodal transportation systems planning, discussing modeling in Northeast Corridor Project [AIAA PAPER 70-1265] 24 p4431 A70-45925

Short haul metropolitan air transportation, considering systems engineering as unifying technology [AIAA PAPER 70-1281] 24 p4373 A70-45927

Demand analysis data generation for V/STOL systems suitable for New York-Philadelphia-Washington business travel market, applying model to selected designs [AIAA PAPER 70-1241] 24 p4374 A70-45961

STOL aircraft operational constraints, considering economics, short haul market characteristics, community acceptance, speed, propulsion system, takeoff/landing performance and maneuverability [AIAA PAPER 70-1283] 24 p4374 A70-45972

UREAS

Metabolism and biological activity of urea, citrulline, arginosuccinic acid in organism ornithine cycle, discussing role in brain and liver 01 p0019 A70-10513

URETHANES

Fire performance of spray applied rigid urethane foam applied as storage vessel insulation, noting continued functioning until destruction 09 p1710 A70-23345

Fluid urethane laminating resin for bonding nylon and glass fabrics, giving physical properties as function of room temperature curing time 16 p2938 A70-33381

Tungsten filled urethane in aircraft areas as balancing agent 17 p3126 A70-35418

URIC ACID

Human metabolic study showing effect of yeast RNA and allopurinol on serum and urinary uric acid formation 08 p1454 A70-20679

Dietary protein and yeast RNA levels effect on uric acid metabolism in normal man 11 p1987 A70-26002

Serum uric acid reduction in men during chronic physical exercise 13 p2355 A70-29802

URINALYSIS

Adrenocortical responses of military recruits to subtropical climate, making serum and urinary 17-OHCS measurements on subjects fasting, inactive and at thermoneutrality 01 p0032 A70-10359

Renal and hepatic glutamine synthetase distribution in mammals, studying relation between glutaminase and urinary activities/ammonia metabolism/ 02 p0232 A70-11710

Standard urinary excretion by healthy adult for free adrenaline, noradrenaline, creatinine and hydroxymethoxy mandelic acid, making catecholamine determinations 12 p2168 A70-27622

Daily electrolyte excretion dynamics of subjects with shifted work-rest schedule, noting disagreement with Sharp results 13 p2358 A70-29343

URINATION

Rat water intake and urine output during chronic centrifugation at resultant inertial fields of 1.7 and 3.0 g 02 p0231 A70-11705

Peristaltic motion of viscous incompressible fluid, applying long wave approximation to two dimensional urine flow model 07 p1219 A70-19247

Ureter fluid mechanical model from lubrication theory viewpoint, discussing waveforms, pressure distribution, etc 23 p4179 A70-43966

URINE

Prolonged hypokinesia effect on dynamics of 5-oxindoleacetic acid elimination in rat urine, showing occurrence of shifts in serotonin metabolism 09 p1615 A70-22092

Urinary calcium phosphate and carbonate precipitates reduction by protein and carbohydrate diet change to casein and sucrose in Macaca nemestrina 09 p1621 A70-23456

Sympathoadrenals activity in pilots during supersonic flight, investigating urinary catecholamine output 15 p2690 A70-31891

Prolonged hypokinesia effect on dynamics of 5-oxindoleacetic acid elimination in rat urine, showing occurrence of shifts in serotonin metabolism 15 p2685 A70-32688

Mountain climbing effects on urinary excretion of vanillylmandelic and homovanillic acids, discussing circulatory system acclimatization 17 p3039 A70-35425

Transmeridian flights effect on diurnal urinary excretion of unconjugated 17-hydroxycorticosteroids in males, evaluating time shift effects 21 p3770 A70-41477

Lateral and angular acceleration effects on blood and urine contents in specific metabolic indices of healthy young men 22 p3971 A70-43136

USA [UNITED STATES]

U UNITED STATES OF AMERICA

UTILITIES

Astronautics utility in astronomy, physics, earth observation, communication, commercial, military, navigational, meteorological, social applications, considering present and future possibilities 15 p2831 A70-32062

UTILITY AIRCRAFT

NT BO-105 HELICOPTER

NT UH-1 HELICOPTER

Helicopter utilization in emergency transportation of civilian patients, discussing questionnaire results from medical and police agencies 08 p1454 A70-21937

British light aircraft designs, engines and costs, considering business, agricultural, gliding, private, school and club flying 14 p2532 A70-31394

UTILIZATION

NT REUSE

NT WASTE UTILIZATION

UTRICLE

Mammalian ultraclear macula design, considering microelectrode data and information from light and electron microscopy, behavioral experiments and computer simulation 11 p1988 A70-26231

V

V BAND

U EXTREMELY HIGH FREQUENCIES

V-4 AIRCRAFT

U XV-4 AIRCRAFT

V-5 AIRCRAFT

U XV-5 AIRCRAFT

V/STOL AIRCRAFT

NT AUTOGYROS

NT BO-105 HELICOPTER

NT CH-3 HELICOPTER

NT CH-46 HELICOPTER

NT CH-47 HELICOPTER

NT CH-54 HELICOPTER

NT CL-84 AIRCRAFT

NT COMPOUND HELICOPTERS

NT DO-31 AIRCRAFT

NT F-28 HELICOPTER

NT FLYING PLATFORMS

NT G-222 AIRCRAFT

NT HELICOPTERS

NT MILITARY HELICOPTERS

NT OH-6 HELICOPTER

NT RIGID ROTOR HELICOPTERS

NT ROTARY WING AIRCRAFT

NT SA-330 HELICOPTER

NT UH-1 HELICOPTER

NT VERTICAL TAKEOFF AIRCRAFT

NT X-22 AIRCRAFT

NT X-22A AIRCRAFT

NT XV-4 AIRCRAFT

NT XV-5 AIRCRAFT

V/STOL air traffic control and equipment considerations for increased demand, suggesting time/velocity separation system using direct routing, positive and automated control [AIAA PAPER 69-1055] 01 p0137 A70-10639

Noise reduction for V/STOL aircraft operation by introducing quiet propellers, discussing variable camber propellers, propeller aerodynamics, etc [AIAA PAPER 69-1038] 01 p0005 A70-10646

Composite fibrous materials applicability to V/STOL rotor blades design and fabrication confirmed by structural analysis 02 p0225 A70-11953

Harrier close-support fighter aircraft with short or zero takeoff run capability, discussing design, cruise efficiency, maneuverability and navigation-attack system 02 p0225 A70-12310

V/STOL fatigue design parameters, balancing failure and safe-life design procedures [AHS PAPER 376] 02 p0228 A70-12764

Tactical landing approach radar (TALAR) guidance system for V/STOL aircraft steep angle approach and landing 02 p0336 A70-12767

V/STOL supersonic fighter VJ 101, transport Do 31 and VTOL fighter/reconnaissance VAK 191 development in West Germany, discussing control and stabilization during hovering 03 p0413 A70-13794

Propagation of turbulent jet impinging on flat surface at certain incidence angle analyzed for application to V/STOL aircraft, ventilation equipment, etc 03 p0468 A70-13878

Mil-10 Soviet giant helicopter cargo and altitude record, VTOL and STOL capability and weight design 03 p0414 A70-14286

V/STOL power drive systems structural efficiency, comparing mechanical and pneumatic components from weight-optimal viewpoint [ASME PAPER 69-WA/AV-7] 04 p0622 A70-14901

V/STOL aircraft propellers featuring thrust augmenting air jet slots for increased lift [DGLR-69-36] 04 p0616 A70-15175

Large-tilt-angle lifting surface theory for V/STOL aircraft based on inclined actuator disk analysis 04 p0619 A70-15377

V/STOL and fixed wing tactical transport aircraft survivability while supporting forward area logistics bases, noting V/STOL advantage [SAE PAPER 690705] 05 p0792 A70-15857

Experiment design and data acquisition for V/STOL aircraft flying qualities simulations, emphasizing pilot rating and comment data and control usage information [SAE PAPER 690695] 05 p0825 A70-15860

V/STOL Flight Profile Indicator display system development to present pilot situation information in vertical plane [SAE PAPER 690694] 05 p0792 A70-15861

DO-231 fixed wing V/STOL airliner project based on DO-31 development, construction and flight tests, considering design problems, controls, safety, performance targets, etc 05 p0793 A70-15901

VTOL technical problems relating to military and civil transport applications, discussing sensitivity to mission requirement variations including design costs, noise levels, etc 05 p0797 A70-17077

Dynamic stability of complex aeroelastic structures including V/STOL aircraft using simplified technique, noting application to tilt rotor aircraft design [AIAA PAPER 70-22] 06 p1170 A70-18119

Lift fan V/STOL tactical aircraft performance capabilities determination, using digital computer program 07 p1191 A70-18975

Monograph on HFB 600 V/STOL transport for civil and military air traffic, discussing intercity travel, military dispersal requirements, systems performance, cockpit layout, etc 07 p1194 A70-19605

V/STOL R and D, comparing civil aviation in U.S. and Europe, discussing system approach 07 p1194 A70-19679

V/STOL demand for short haul business travel noting time savings, convenient approach, safety records, weather reliability and comfort 07 p1428 A70-19680

Optimal V/STOL wind tunnel interference study of slotted tunnel walls, including porosity and height to width ratio effects [AIAA PAPER 69-171] 07 p1251 A70-20407

Wing lifting surface theory for V/STOL aircraft based on inclined actuator disk theory to predict span loading and downwash angle 07 p1190 A70-20408

V/STOL concepts for short haul commercial aircraft compared for gross weight, operating cost, gust sensitivity and noise levels [AIAA PAPER 67-938] 07 p1195 A70-20409

Longitudinal stability of V/STOL aircraft at low speeds, discussing three tilt wings and quad ducted propeller configurations 07 p1195 A70-20410

V/STOL intercity airliner potential and development noting benefits of noise reduction, ground space economy, etc 08 p1434 A70-20619

V/STOL transport aircraft design in Germany, analyzing demands in military and civil sectors 08 p1435 A70-20639

V/STOL Do 231 design, discussing propulsion, control, safety, traffic control and economic factors 08 p1435 A70-20640

V/STOL aircraft turbojet engine design and quality control for in-service reliability 09 p1743 A70-22572

V/STOL transport aircraft cockpit design in terms of size, geometry and equipment accommodation 10 p1804 A70-24048

V/STOL cockpit three degree of freedom multicrew research simulator, utilizing visual display and digital computer [AIAA PAPER 70-356] 10 p1858 A70-24207

Flight test instrumentation specifications for V/STOL aircraft, considering design, installation and accuracy [AIAA PAPER 70-376] 10 p1892 A70-24927

Edwards Report on UK domestic air services, considering unprofitability, trunk route competition and V/STOL development exploitation 11 p2153 A70-25860

V/STOL air transportation systems for short haul traffic, considering vehicle guidelines, ground facilities and operational requirements [SAE PAPER 700312] 12 p2161 A70-27453

V/STOL aircraft ground guidance systems using microwave instruments for approach and landing [SAE PAPER 700322] 12 p2266 A70-27458

Air deflection and modulation /ADAM/ turbobfan propulsive wing V/STOL design [AIAA PAPER 69-201] 12 p2162 A70-28087

Harrier V/STOL trainer aircraft design features including fuselage, cockpit, power plant, etc 13 p2345 A70-28923

Wind tunnel boundary interference on V/STOL model calculated in test section with solid vertical and slotted horizontal walls, using image method and Fourier transforms [AIAA PAPER 70-575] 13 p2343 A70-29894

Noise of large commercial V/STOL aircraft and effect on design and operation, predicting acoustic signatures 14 p2531 A70-30854

Large scale V/STOL service introduction for decongesting short haul routes between major cities of Northeast Corridors 14 p2615 A70-31276

V/STOL propulsion for commercial needs, considering best tradeoff between propulsion size, weight, noise generation and fuel consumption 14 p2629 A70-31277

V/STOL control systems design for aircraft stabilization and pilot workload reduction 14 p2615 A70-31278

V/STOL 5000 hp engine design optimization, considering component arrangements, rotor design, blade cooling method and fuel control 17 p3147 A70-34709

Convertible fan-shaft engine for V/STOL tactical and transport aircraft, discussing design and performance 17 p3147 A70-34710

On-line final V/STOL Wind Tunnel Data Encoding and Evaluation System /WINDEE/ for complex powered models, using computer monitoring 17 p3049 A70-35494

Static weight tare compensation for V/STOL wind tunnel models, using accelerometer outputs 17 p3062 A70-35500

Flight test instrumentation for V/STOL stability derivatives extraction, noting instrument errors and required compensation 17 p3094 A70-35502

Fluidic parallel flow low airspeed indicator for V/STOL instrumentation tested in wind tunnel [AIAA PAPER 70-906] 17 p3096 A70-35818

Ground simulations data of jet lift V/STOL compared with visual flight tests, noting hover, lateral quick start and stop maneuver 18 p3236 A70-35954

V/STOL testing wind tunnel section with solid vertical and slotted horizontal zero interference walls 18 p3237 A70-36461

V/STOL aircraft for short haul transportation, discussing speed, noise, reliability, economy, etc [SAE PAPER 700333] 18 p3214 A70-36797

V/STOL attitude control system as integral propulsion system part, analyzing design and weight tradeoffs [ASME PAPER 70-GT-31] 18 p3214 A70-36832

Lightweight lift jet engine design, testing and performance for V/STOL aircraft [ASME PAPER 70-GT-32] 18 p3302 A70-36833

V/STOL short haul air transportation program in western U.S., assessing public acceptance and economic viability [AIAA PAPER 70-888] 19 p3552 A70-37394

Mass flow ion drift anemometer applicable to aircraft speed measurement including V/STOL 19 p3425 A70-37885

- V/STOL aircraft automatic flight control, guidance and navigation by onboard computer, discussing mathematical model and simulation results [AIAA PAPER 70-1035] 20 p3665 A70-39502
- High speed track facility for V/STOL aircraft tests, discussing characteristics and design 21 p3803 A70-40581
- Radar inertial system flight evaluation, discussing V/STOL program for approach and landing by use of ground based radar for updating onboard inertial navigator 22 p4066 A70-42651
- Harrier flight testing in terms of V/STOL capability compared with conventional aircraft 22 p3962 A70-42975
- Low and medium power turboprop engines for V/STOL aircraft, discussing development trends concerning operational control 22 p4091 A70-43081
- V/STOL aircraft landing performance, discussing relationships between approach speeds, rates of descent, structural criteria and weight penalties [ICAS PAPER 70-53] 23 p4139 A70-44149
- Wind tunnel wall interference effects for V/STOL aircraft with lift jets, using modified theoretical model for complex jet arrangements [ICAS PAPER 70-54] 23 p4139 A70-44150
- V/STOL guidance and control system with bad weather landing capability, requirements for V/STOL integration into overall air traffic, terminal area guidance procedures, etc 23 p4216 A70-44843
- V/STOL powerplant development, discussion airframe and engine design, application to large aircraft and planned evolutionary process [SAE PAPER 70809] 24 p4395 A70-45905
- Quiet V/STOL transport aircraft from DC-9-10 modification, discussing flying qualities, propulsion and control system interfaces, configurations, etc [AIAA PAPER 70-1409] 24 p4291 A70-45916
- Demand analysis data generation for V/STOL systems suitable for New York-Philadelphia-Washington business travel market, applying model to selected designs 24 p4374 A70-45961
- VACANCIES [CRYSTAL DEFECTS]**
- NT FRENKEL DEFECTS**
- Vacancies influence on macrodefect nucleus formation in single metal crystals under uniaxial strain explaining Griffith crack initiation 05 p0861 A70-15784
- Neutron irradiation damage in W, observing consistency of activation energy for self diffusion with vacancy mechanism 07 p1314 A70-20012
- Steady creep process microscopic mechanisms, discussing creep due to glide of jogged screw dislocations, climbing of edge dislocations and stress directed vacancy diffusion 08 p1593 A70-21519
- Critique of paper on diffusion in Si isotopes and excess vacancies generation by motions of diffusion induced dislocations 08 p1553 A70-21696
- High temperature fatigue crack growth in metal, suggesting condensation of vacancies at crack front after each loading cycle 09 p1776 A70-22644
- Impurities solubility in semiconducting indium telluride with stoichiometric vacancies, verifying thermodynamic model by phase diagrams 16 p2960 A70-33224
- Calcium tungstate crystals, investigating electron paramagnetic resonance centers produced by neutrons and gamma rays to obtain information on lattice vacancies, defects, etc 16 p2961 A70-33963
- Kinetic simulation of atom rearrangements in order-disorder transformation for point defect movement in Ti alloys, considering vacancies and interstitial properties 17 p3115 A70-34381
- Vacancies in vanadium carbide /V3C2C8/ crystals with predicted lattice defects at low temperature, considering entropy 24 p4365 A70-46353
- VACCINES**
- Decreased mental and physical performance of human beings due to T-oral and placebo vaccine reactions 19 p3359 A70-37389
- VACUUM**
- NT HIGH VACUUM**
- NT ULTRAHIGH VACUUM**
- Noncontacting minimum leakage dynamic seals requiring liquid-vapor interface with leakage tolerance [ASLE FICFS PREPRINT 40] 02 p0308 A70-12175
- Free molecular mass flow rate through vacuum seal separating two rarefied gas environments, using coupled integral equations formulated on kinetic theory [ASME PAPER 69-WA/FE-18] 04 p625 A70-14779
- Gravitational-repulsion forces of interstellar vacuum, investigating relations between magnitudes and red shift of galactic objects and quasars 05 p0920 A70-16968

- Vacuum metrics with null geodetic expanding shear-free congruences using holomorphic solution 07 p1334 A70-19600
- Supersonic gas jets applicability as vacuum locks for molecular fluxes at thermal velocity in magnetic trap 08 p1549 A70-20509
- Vacuum science and technology - Conference, Seattle, October 1969 12 p2284 A70-27251
- Vacuum-like state of physical medium as initial state of Friedmann cosmology, noting fluctuation instability for conversion into ordinary matter 18 p3315 A70-36643

VACUUM APPARATUS

- NT ION PUMPS**
- NT IONIZATION GAGES**
- NT KNUDSEN GAGES**
- NT MOLECULAR PUMPS**
- NT VACUUM CHAMBERS**
- NT VACUUM FURNACES**
- NT VACUUM GAGES**
- NT VACUUM PUMPS**
- Vacuum-type thermionic laboratory diode featuring variable electrode spacing, interchangeable electrodes and guard-ring structure 04 p0628 A70-15400
- Microbiological evaluation of modified vacuum probe surface sampler for handling and fallout contamination compared with swab-rinse technique 05 p0807 A70-16574
- Vacuum probe sampler to monitor particle contamination on surfaces within clean environments 05 p0808 A70-16703
- Vacuum probe as effective device for sampling surface contamination of airborne microorganisms 05 p0808 A70-16704
- Vacuum probe sampler to monitor particle contamination on surfaces within clean environments 09 p1623 A70-22340
- High temperature vacuum dilatometer for continuous photographic recording of expansion curves for refractory materials, determining thermal expansion coefficient 09 p1675 A70-22565
- Vacuum interferometer strain gage for absolute earth strain measurement via length change comparison with wavelength standard 16 p2925 A70-33024
- Vacuum distillation vapor filtered catalytic oxidation for water reclamation from human waste, using radioisotopes for thermal energy 20 p3579 A70-39437
- Ultrahigh vacuum measurement and calibration assembly for pressures down to one picotorr for vacuum gage standards 23 p4143 A70-44871

VACUUM CHAMBERS

- Hardness measuring instrument by dynamic method at high temperatures in vacuum, using magnetic or nonmagnetic indenter balls 01 p0092 A70-11111
- Bubbles elimination in glass filament wound parts involving total or partial placement of production equipment and process in vacuum 05 p0856 A70-16825
- Radicals in low pressure supersonic free jets, investigating production by flash photolysis 07 p1343 A70-20126
- Space environment simulation chamber free from oil molecules contamination 09 p1655 A70-22830
- Solar simulator built into multiwall ultrahigh vacuum chamber, describing simulator and chamber modifications [AIAA PAPER 69-1001] 09 p1657 A70-23264
- Environmental engineering at NASA MSC, surveying Lunar Receiving Laboratory, micro incinerator, radon adsorption, Apollo Post-Landing Environmental Test Tank and vacuum chamber 10 p1860 A70-24411
- Vacuum chamber for adjusting and calibrating spaceborne optical instruments used in studying UV radiations 10 p1860 A70-24479
- Hemispherical emissivity measurement in vacuum chamber for thermal testing of space satellite structural materials 12 p2332 A70-27984
- Pressure measurements and gas flow analysis during thermal vacuum tests of manned spacecraft indicating adequate space vacuum simulation [AIAA PAPER 69-1033] 13 p2384 A70-28518
- Test machine for partial gravity environment simulation for aerospace subsystem testing in vacuum chamber 17 p3060 A70-35181
- Cryopumping systems of ultrahigh vacuum space environmental chambers 17 p3060 A70-35247
- Residual gases partial pressure measurement in vacuum chamber by mass spectrometer with electromagnetic scanner and electron multiplier, detecting electron current 19 p3421 A70-37466

- Laser aided frequency and amplitude analysis of vacuum test chamber vibration during alignment of orbiting UV spectroheliograph 19 p3396 A70-37877

VACUUM DEPOSITION

- Wear resistance of Ti alloys chromosilicified by thermal diffusion in vacuum 01 p0115 A70-10072
- Vacuum deposition of Cr-Al film on Ni-Mo alloys, describing operating pressure, temperature and film thickness 01 p0124 A70-11617
- Vacuum cleavage device for producing small area evaporated metal semiconductor contacts free from oxygen or other contamination 02 p0304 A70-12748
- Vacuum deposited thin film bridges in electroexplosive devices, discussing composition, surface conditions, substrate temperature, bell jar atmosphere and deposition rate 03 p0546 A70-14107
- P-n heterojunction diode strain sensor fabricated by vacuum evaporation onto substrate, investigating mechanical input and output impedance characteristics 03 p0495 A70-14192
- Ge films crystallinity deposited on Ge substrates in vacuum as function of deposition rate, substrate temperature and thermal treatment and background O pressure 03 p0543 A70-14204
- Two step B vacuum diffusion from boron oxide into Si surface using evacuated tube and N atmosphere 05 p0891 A70-15791
- Vacuum deposited thin cadmium sulfide films semiconducting properties, discussing captured free carriers effects on temperature dependence of dark and photo current 05 p0893 A70-16543
- Vacuum condensed thin carbon films graphitization stages using electron diffraction 11 p2068 A70-25381
- Thin films of vanadium niobium and tantalum obtained by vacuum thermal decomposition of metal iodides 12 p2253 A70-27210
- Au, Ag and Al films evaporation in ultrahigh vacuum on LiF and MgO surfaces, showing insignificant role of lattice misfit for epitaxy 12 p2285 A70-27260
- Bi polycrystalline film grown by vacuum deposition on amorphous substrates investigated for electron microscope beam effects 12 p2285 A70-27261
- Corrosion resistance of molybdenum coatings on steel and Pb-Bi eutectic alloy obtained by vacuum contact fusion method 12 p2258 A70-28320
- Au films nucleation and growth on single crystal graphite substrates in ultrahigh vacuum, using transmission electron microscopy for examination 14 p2627 A70-30499
- Refractory metals interaction with boron during vacuum boronizing, investigating kinetics and optimal process conditions 19 p3434 A70-37452
- Printing, electro etching and vacuum deposition stencil methods for preparing moire grids 19 p3432 A70-38721
- Metallic surfaces vacuum electric spark alloying, investigating pressure effects on coating layer thickness and area 20 p3636 A70-39195
- Optical multilayer metal coatings vacuum deposition by cathode sputtering, using automatic apparatus 22 p4045 A70-42510
- In thin film resistance thermometers fabrication by vapor deposition in vacuum, considering electrical properties dependence on temperature 22 p4039 A70-43446
- Heat resistant alloys with metal coatings applied by diffusion in vacuum, investigating structure and fatigue strength at high temperatures 24 p4364 A70-46342
- VACUUM EFFECTS**
- Cost-effective look at vacuum testing of spacecraft components, noting sensitivity prediction and thermal cycle test 01 p0055 A70-10113
- Vacuum evaluation of lubricants and techniques applicable to miniature ball bearings and instrument gearing for space systems [ASME PAPER 69-LUB-30] 01 p0100 A70-10379
- Polycrystalline Mo ductility at low pressures in tension at ambient temperature, discussing H type embrittlement mechanism 01 p0121 A70-11234
- Sliding steel specimens anomalous friction behavior in vacuum, noting friction-time plot dependence on oxide film rupture, load, environmental pressure, etc 02 p0321 A70-12534
- Reduced ambient pressure effects on hot wire sensitivity of initiating materials of electroexplosive devices used in missiles 03 p0549 A70-14139

Electron efflux effectiveness from discharge plasma into vacuum, investigating various electrodes influence 04 p0724 A70-14415

Apparatus and techniques for investigating spacecraft materials mechanical and thermal properties, using vacuum effect to simulate space environment [ASME PAPER 69-WA/PID-22] 04 p0663 A70-14752

High altitude simulation installations design for rocket motors starting tests under long term high vacuum exposure 04 p0736 A70-15179

Monatomic gas steady expansion into cylindrical vacuum, considering Maxwell molecules with cylindrical symmetry 04 p0674 A70-15557

Time dependent expansions into vacuum of monatomic gases with spherical symmetry, obtaining moments expressions for Maxwellian molecules 05 p0831 A70-16015

Exploding wire discharges in high vacuum, discussing particle emission MHD instabilities, plasma temperature and electron density 05 p0890 A70-16820

Bubbles elimination in glass filament wound parts involving total or partial placement of production equipment and process in vacuum 05 p0856 A70-16825

Q spoiled laser bombardment to obtain atomically clean surfaces in vacuum, noting damages 05 p0861 A70-16990

Book on optimization by variational methods covering use of differential equations, Pontryagin minimum principle, optimal and feedback control, dynamic programming, etc 06 p1093 A70-17650

X and UV radiation effects on *Escherichia coli* B/r in vacuum, noting irradiated cell inactivation and radiation sensitivity increases 06 p0995 A70-17750

Convergent ribbon electron beam shaping for vacuum welding with double anode gun, considering space charge effect 06 p1076 A70-17784

Evaporation rate from spherical drop into vacuum influenced by molecular collisions occurring in gas cloud formed by emitted particles 06 p1113 A70-18283

Boltzmann equation fourth moment numerically solved to study distribution function characteristics during monatomic gases spherical expansions into vacuum 06 p1048 A70-18320

Particle density of jet plumes exhausting in vacuum calculated for He, Ar and N 06 p1052 A70-18388

Niobium single crystals annealed in ultrahigh vacuum, studying stress-strain behavior, secondary slip geometry and slip line morphology 06 p1090 A70-18493

Microwave scattering from plasma column of low pressure discharge in Hg under free space conditions 06 p1125 A70-18609

Vacuum and radiation effects on *Escherichia coli*, noting role of cells water desorption in vacuum damage 07 p1203 A70-18962

Steady temperature field of two dimensional periodic contact surface in vacuum, using conjugate harmonic functions for thermal flux lines, isothers and thermal resistance 07 p1423 A70-19820

Vacuum UV spectrum interferometer with grazing incidence reflections between plane parallel mirrors to obtain coherent beams, discussing fringe patterns 07 p1286 A70-20081

Thermal decomposition of ammonium perchlorate and polymethylmethacrylate mixture thin layer between Ti plates in vacuum 09 p1741 A70-22109

Vacuum rolling of high strength hard-workable dispersion-hardened Nb base alloys excluding recrystallization 09 p1692 A70-22756

Lead type channel electron multipliers gain degradation in ultrahigh vacuum 10 p1849 A70-24557

Si-Ge air-vacuum thermocouples for thermoelectric conversion, describing construction materials, mechanical and electrical properties, radiative heat transfer operation, etc 10 p1807 A70-24896

Electrode erosion during high voltage vacuum breakdown measured by neutron activation analysis and gamma ray spectrometry, noting plasma formation from electrode material 10 p1854 A70-25317

Pulmonary blood flow direction and distribution in dogs during near vacuum exposure and recompression 11 p1984 A70-25351

Spectroscopic diagnostics of erosion plasma jets from cylindrical pulsed plasma generator operating in vacuum 11 p2093 A70-26745

Reaction impulse during steel spheres impacts at lead surface in vacuum dependent on kinetic energy, velocity and spheres material 11 p2146 A70-26794

Friction and wear of Ni sliding on Ni, Cu on Cu and Au on Au tested in vacuum at room temperature with constant load 12 p2242 A70-27229

Iron cyanide additive for surface stabilization of ZnO irradiated with UV in vacuum 12 p2181 A70-27258

Heat resistance of machined stainless steel and molybdenum contact pairs in vacuum, discussing compressive loads and surface defects effects 12 p2243 A70-27290

Congruent vaporization rates of niobium monocarbide phase at high temperatures in vacuum, using method of least squares 12 p2254 A70-27320

Contact and unsteady heat transfer through vacuum cavity applied to hollow cylinders, solving nonlinear integral equations by piecewise linear approximation 12 p2331 A70-27326

Vacuum annealing treatments effect on oxidation rate of Co-Cr alloy at high temperatures 12 p2257 A70-28007

Phase transformations of molybdenum carbide under elevated temperature in vacuum, using X ray and differential thermographic analysis 13 p2433 A70-28852

DC arc facing welding device using vacuum to minimize pores, slag inclusions, cracks and defects 13 p2384 A70-28867

Vacuum evaluation of lubricants and techniques applicable to miniature ball bearings and instrument ball bearings and instrument gearing for space systems 13 p2419 A70-29120

Variable temperature plasma with two ion species, noting rarefaction wave propagation during one dimensional expansion into vacuum 13 p2464 A70-29415

Degassing kinetics during dry friction in vacuum, suggesting gas separation correspondence to oxide film breakdown 13 p2421 A70-29430

Transition radiation in plasma sheet in vacuum assuming specular reflection of electrons at vacuum boundary 13 p2464 A70-29512

Short term creep of Ni in vacuum, stationary air and high speed air flow at various temperatures and loads 14 p1594 A70-30167

First pulse vacuum startup measurements of monopropellant hydrazine thrust reactors with spontaneous catalyst, simulating spacecraft control dynamics 14 p2628 A70-30753

Antifriction and wear properties of iron fluoride materials and white cast iron under sliding friction in air and vacuum 15 p2743 A70-31637

Pentolite spherical charge gaseous explosion products expansion into vacuum, using Taylor similarity solution for flow in detonation wave 15 p2774 A70-31764

Solar furnaces in space for treatment of high purity products in space vacuum, discussing design and operational problems 15 p2717 A70-31802

Power reduction consumed in vacuum by direct-current voltage converter by introducing delay into breaker transistor control at output stage 15 p2677 A70-31945

Vacuum effect on explosive coupling seismic energy considered in lunar geophysical experiment 16 p2896 A70-33092

Thermal conductivity of multilayer and mixed powder high temperature insulation systems over wide temperature range and vacuum conditions [AIAA PAPER 70-637] 16 p2997 A70-33596

Sliding electrical contacts in vacuum and space - Conference, Virginia Polytechnic Institute, September-October 1969 16 p2919 A70-33805

Contacting metal surfaces thermal conductance prediction in vacuum, formulating dimensionless parameters in terms of properties, surface measurements and load/temperature conditions of contact [AIAA PAPER 70-852] 16 p2932 A70-33919

Lubrication system components behavior in vacuum environment, investigating evaporation, friction, adhesion, wear, etc 16 p2923 A70-34156

Electron beam welding of Ti alloys in partial vacuum, describing mechanical tests and metallographic examinations 17 p3098 A70-34442

Ultrahigh vacuum creep rate measurements with continuously increasing loads on Ta-base alloy, relating creep life with temperature and stress rate 17 p3122 A70-34552

Ball bearing materials for ultrahigh vacuum space environments, determining frictional and wear behavior 17 p3099 A70-34573

Zero pressure balloon as base for stratopause pressure and temperature measurements, analyzing winds and balloon trajectory and dynamics 17 p3075 A70-34608

Metal-silicate rock friction in ultrahigh vacuum of lunar environment 17 p3101 A70-34760

Accelerated vacuum testing of ball bearings and slippers at 30-130 F, considering dry lubricated brush/slipping material combinations 17 p3101 A70-34762

Underexpanded carbon dioxide free jet expanding into vacuum from conical nozzles 17 p3070 A70-35246

Dry friction and wear tests of various materials in vacuum at low temperatures 18 p3263 A70-36471

Radiant heat transfer at vertex of adjoint flat plates separated by vacuum 18 p3243 A70-36711

High vacuum effects on creep properties of single crystal low carbon nickel base superalloy 19 p3451 A70-37705

Lunar basalt lava bed formations, examining vacuum and gravity effects during cooling 19 p3517 A70-37988

Pure metals structure effect on friction and lubrication under steady slip in ultrahigh vacuum at low temperatures 19 p3438 A70-38729

Long term life test and vacuum tests of high temperature resistojets using ammonia and hydrogen propellants [AIAA PAPER 70-1136] 20 p3567 A70-40212

Ambient near vacuum pressure effect on blood circulation, examining thoracic aorta blood flow, pressures, gas expansion and water vaporization 20 p3576 A70-40326

Heat resistance of machined stainless steel and molybdenum contact pairs in vacuum, discussing compressive loads and surface defects effects 20 p3638 A70-40340

Temperature dependent anomalous optical absorption of thin yttrium films under static ultrahigh vacuum 21 p3862 A70-40816

Surface films effect on thermal contact conductance of aluminum surfaces contacting in high vacuum environment 21 p3944 A70-41024

Ultrahigh vacuum metal bonding by twist compression technique, reporting adhesion and friction coefficients for atomically ordered Pt-Co alloy 21 p3833 A70-41465

Time dependent adhesion in ultrahigh vacuum of Apollo 11 lunar soil sample 10065-33, considering micromechanical and microphysical properties 21 p3915 A70-41658

Contact and unsteady heat transfer through vacuum cavity applied to hollow cylinders, solving nonlinear integral equations by piecewise linear approximation 21 p3952 A70-42067

Thin titania films electrical breakdown under high DC fields in high vacuum, suggesting reduction to lower order semiconducting oxide 22 p4085 A70-42621

SkyLab Orbital Workshop fabrication experiments under space environment conditions, discussing weightlessness and vacuum effects on various manufacturing techniques 22 p4046 A70-43075

Apollo 11 lunar fine thermal conductivity measurement under vacuum conditions and lunar temperature range, using line heat source method 23 p4243 A70-44442

Thermodynamic equilibrium analysis of metal oxidation and thermal dissociation of oxides in vacuum, noting decreased affinity by evaporation 24 p4361 A70-45835

VACUUM FURNACES
Induction furnace for thermal treatments and melting of solid and liquid metals, alloys and sintering and degassing ceramic and metallic systems in vacuum 04 p0664 A70-15371

Soviet monograph on bimetal and refractory metals production by rolling in vacuum or inert media 19 p3433 A70-37402

VACUUM GAGES
NT IONIZATION GAGES
NT KNUDSEN GAGES
Thermocouple vacuum gauge joined to Apollo lunar sample return containers [ALSRC], describing two step welding procedure with transition cylinder 08 p1507 A70-21483

He-Ne laser light source for oil damped spiral gauge used as vacuum system pressure nulling device 09 p1698 A70-23000

Ultrahigh vacuum gages absolute calibration by controllable conductance method, discussing accuracy 19 p3421 A70-37463

Ultrahigh vacuum calibration system for vacuum gages and mass spectrometers based on pressure attenuation and molecular beam techniques 22 p4029 A70-42620

VACUUM MELTING

VACUUM MELTING

Soviet monograph on nickel and Ni vacuum melted alloys, studying physicochemical, operational characteristics and gas content

06 p1085 A70-17411

Vacuum melting and heat treating equipment for high melting point metals from phase equilibria studies viewpoint

09 p1655 A70-22562

Ti alloy ingot chemical macroinhomogeneity, investigating elimination by vacuum arc melting

17 p3112 A70-34355

Tungsten exploding wires electron emission during vacuum melting

17 p3137 A70-35726

Hawaiian basalt melted in simulated lunar environment, investigating surface characteristics, internal structure and bearing strength

23 p4254 A70-44883

VACUUM PUMPS

NT ION PUMPS

NT MOLECULAR PUMPS

Titanium vacuum pump, discussing pumping speed, sticking factor and sorption coefficient for hydrogen

15 p2744 A70-31845

Superhigh vacuum pump with orbitron ionizer, describing construction and ionization

16 p2843 A70-33214

Vacuum pump systems properties for space environment simulation installations

19 p3358 A70-38280

Clean, rough vacuum, discussing cleanliness criteria and pollution avoidance via contaminant-free pump

19 p3358 A70-38494

VACUUM SYSTEMS

Composite window permitting visual or photographic observation and IR irradiation of test materials in ultrahigh vacuum system

09 p1698 A70-22994

Coaxial energy outlets satisfying vacuum maintenance requirements of dielectric waveguide windows in dismountable prototype microwave devices

09 p1652 A70-23647

Heat transfer mechanism in foil-vacuum insulations, analyzing factors responsible for point of inflection on experimental temperature field curves

13 p2521 A70-28861

Residual atmosphere analysis and application to ion pumping on Al alloy high pressure chamber of differential vacuum system

19 p3434 A70-37464

Clean, rough vacuum, discussing cleanliness criteria and pollution avoidance via contaminant-free pump

19 p3358 A70-38494

VACUUM TUBE OSCILLATORS

Vacuum tube signal frequency converters for meteorological telemetry measurements including blocking oscillators, multivibrator and faustantron

09 p1718 A70-23332

Controlled self excited quartz triode oscillator, calculating flicker noise effect on frequency stability

23 p4171 A70-43959

VACUUM TUBES

NT VACUUM TUBE OSCILLATORS

Correlations between 100 percent inspection by automatic equipment and quality control acceptance sampling in vacuum tube industry

06 p1077 A70-17986

VACUUM ULTRAVIOLET RADIATION

U FAR ULTRAVIOLET RADIATION

VALENCE

Optical density of valence and conduction states by UV photoelectric spectroscopy, outlining experimental techniques and inelastic scattering effects

19 p3471 A70-37711

Valent state of chromium doped barium titanate from EPR spectra and magnetic susceptibility measurements

22 p4086 A70-43133

VALIDATION

U PROVING

VALIDITY

Vibration damping theory validity, discussing response curve for frequency dependence of energy dissipation

11 p2133 A70-25733

VALKYRIE AIRCRAFT

U B-70 AIRCRAFT

VALLEYS

Lunar sinuous rilles formation by fluid flow mechanisms, discussing evidence for lava and rille formation by lava tube collapse

09 p1759 A70-22799

Lunar sinuous rilles and Mojave desert stream channels similarities, discussing presence of terraces

11 p2108 A70-25701

Lunar rilles temperature distribution analysis, examining contour shape, aspect ratio and solar elevation angles effects

17 p3152 A70-34507

Lunar regolith depth measurement by Lunar Orbiters 4 and 5 high resolution photographs, discussing thickness relation with sinuous rilles in marial regions

18 p3319 A70-37054

Lunar sinuous rilles morphological and distributional observations and implications on theories of origin concerning surface water erosion

19 p3521 A70-38442

VALSALVA EXERCISE

Antigravitation suit effects on rheoencephalography changes during Valsalva maneuver and horizontal-passive orthostatism transition in humans

07 p1212 A70-19738

Human phasic right ventricular blood velocity, examining respiration, rhythm disturbances and Valsalva maneuver influence by radiotelemetry

16 p2850 A70-33111

Valsalva maneuver beat-to-beat effects on systolic cardiac intervals compared with time based measurements

22 p3972 A70-43484

VALSALVA MANEUVER

U VALSALVA EXERCISE

VALUE ENGINEERING

Beneficial and detrimental effects of value engineering change proposals on system reliability, relating cost improvement and performance factors

13 p2524 A70-29568

VALVES

NT AUTOMATIC CONTROL VALVES

NT FUEL VALVES

NT GAS VALVES

NT PRESSURE REGULATORS

NT RELIEF VALVES

Approximate determination of termination hydraulic servomotors frequency characteristics with four way valves using piecewise straight lines on Bode diagram

01 p0007 A70-10034

Valvular aortic stenosis severity estimation using digital computer program and tape recorder for determining valve area

02 p0243 A70-12094

Ultrasonic Doppler method for timing mitral and aortic valves rapid movements, using filter to eliminate LF signals due to heart walls

03 p0432 A70-12891

Ejection click of valvular pulmonic stenosis by external phonocardiograms and intracardiac pressure recordings during successive respiratory cycles

04 p0633 A70-15440

Stability of conical hydraulic poppet valve with elastic support and inlet and outlet piping

06 p1075 A70-17138

Thrust static characteristics of poppet valves with specific angle range indicating validity of momentum theory for thrust estimation

06 p1075 A70-17139

Normal and stenosed aortic valve closure wing measurements in model valve in pulsatile water tunnel showing turbulence generation

07 p1220 A70-19249

Diastolic and equivocal fluttering of mitral valve in aortic insufficiency by echocardiography

09 p1615 A70-22209

Human mitral valve morphology, distinguishing chordae tendineae types by insertion mode

10 p1819 A70-24935

Human mitral valve morphology, studying posterior and anterior leaflets partitioned by chordae tendineae

10 p1819 A70-24936

Self excited lateral vibration of poppet valve under positive and negative damping effects

11 p1983 A70-26420

Poppet valve lateral stability improved by effective seat ratio increase and use of high viscosity fluid

11 p1983 A70-26421

Rocket engine thrust chambers and valves, discussing component lifetime extension and operational flexibility of reaction control systems

[AIAA PAPER 70-603] 16 p2964 A70-33526

Liquid fluorine feed system valves, seals and seats, discussing design criteria for flight weight components

[AIAA PAPER 70-705] 16 p2844 A70-33564

Dual bellows ball seat valve design for colloid thruster coupled to pressurized feed system, demonstrating thrust decay and flow regulation

[AIAA PAPER 70-615] 16 p2919 A70-33610

Supply valve influence on dynamic characteristics of volumetric hydraulic actuator

18 p3215 A70-36126

Prototype synchronizing valves for maintaining identical flow velocities of two hydraulic actuating elements, noting unbalanced hydrodynamic forces and orifices asymmetry effects

20 p3564 A70-39717

Fluidic logic devices compared with electric relay and hydraulic/pneumatic valve equivalents

24 p4293 A70-45429

Two dimensional aperture flow with downstream asymmetric pressure distribution due to jet reattachment to boundary, simulating flows in hydraulic spool valves and fluidic devices

24 p4325 A70-45582

VAN ALLEN RADIATION BELTS

U RADIATION BELTS

VAN DE GRAAFF ACCELERATORS

Energy attenuation parameters measurements for monoenergetic source neutrons in shielding materials, using Van de Graaff accelerator

23 p4216 A70-43807

Thermal neutron radiography with 2.5 MeV Van de Graaff accelerator

24 p4376 A70-45753

VAN DER WAAL FORCES

Hydrogen atoms van der Waal dispersion interaction effects on H lines broadening in neutral medium, taking into account resonance interaction

04 p0723 A70-15714

VANADIUM

V and Cr single crystals microhardness anisotropy and causes, noting similarity with W, Nb and silicon ferrite

06 p1088 A70-17613

Vanadium single crystals substructure on different planes to growth direction using X ray diffraction

07 p1308 A70-19608

Yield stress and work hardening properties of tension-deformed vanadium single crystals as function of purity

08 p1522 A70-21750

Interstitial and substitutional impurity effects on fracture strength, plastic properties and ductile-brittle transition temperature of vanadium determined from impact and tensile tests

11 p2066 A70-25913

Star eta Arietis spectra analyzed for Fe and V abundance

13 p2487 A70-28715

V-N and V-O solid solutions magnetic, electrical, crystallographic and mechanical properties as function of gas concentration

14 p2596 A70-30842

Interstitial oxygen effect on properties and precipitation processes in pure V and V-Ti alloys, using electron microscope

19 p3454 A70-38812

V and Cu emission spectrographic analyses in chondrite types, noting distribution patterns between groups based on meteorite chemical fractionation mechanisms

24 p4411 A70-45789

VANADIUM ALLOYS

Ni-V alloys precipitation behavior with 15.4/16.5 wt percent V content, observing tetragonal equilibrium theta phase precipitation

04 p0708 A70-15368

Cold working with subsequent heat treatment increased creep rupture and creep behavior of V alloys

04 p0708 A70-15372

Alloying elements effects on vanadium alloys case hardening by boronizing

07 p1303 A70-18742

Stress corrosion testing of vanadium alloys using precracked specimens in cantilever beam apparatus, discussing strain hardening exponent role and propagation rates

07 p1306 A70-19299

Recrystallization in austenite phases of vanadium and columbium HSLA steel alloys determined in high temperature deformation tests

08 p1521 A70-21704

Phase diagram of Ti-Ta-V system, determining solubility of sigma Ta and V in alpha and beta Ti in solid solutions

09 p1709 A70-23788

Soviet monograph on V and V alloys covering phase diagrams, mechanical, chemical and physical properties, compounds and chemical composition

14 p2595 A70-30627

Omega phase embrittlement in aged Ti-V alloys, discussing precipitation effect on tensile properties

15 p2756 A70-31570

High purity V and V-Cr-Ti process, describing aluminothermic reduction and electron beam purification

15 p2761 A70-32387

Cross sectional phase diagram of Nb-Ti-Mo-V, discussing continuous crystallization and composition dependent hardness and resistance

18 p3275 A70-36125

Isothermal section at 1150 C of V-Zr-Cr cast and annealed alloys investigated by X ray and metallographic analyses, establishing various phase regions

19 p3453 A70-38711

Interstitial oxygen effect on properties and precipitation processes in pure V and V-Ti alloys, using electron microscope

19 p3454 A70-38812

Phase equilibria, hardness and electroresistivity of Ti-Al-V alloys at solid compound section for reinforced metal composites

24 p4361 A70-45831

Fe-Cr and Fe-Cr-V system miscibility gap, using differential thermal analysis and Mossbauer effect measurements

24 p4362 A70-46190

VANADIUM CARBIDES

Dissociation energy of vanadium and chromium dicarbide and vanadium tetracarbide, using Knudsen effusion mass spectrometric method

16 p2857 A70-33654

Vanadium carbide single crystals superconductivity from upper limit on electron phonon interactions at 30 mK

Vacancies in vanadium carbide /V3C28/ crystals with predicted lattice defects at low temperature, considering entropy

VANADIUM COMPOUNDS

NT VANADIUM CARBIDES

Temperature and hydrogen concentration effect on microhardness of polycrystalline beta-vanadium hydride, obtaining photomicrographs of indentations

HF electrodeless plasma discharge synthesis of niobium and vanadium intermetallic compounds

Molecular orbital energy level diagram for metal ion X ray emission and absorption spectra interpretation from titanium and vanadium compounds

Vanadium subnitride crystal structure with ordered array of nitrogen atoms in V sublattice

VANADIUM ISOTOPES

Terrestrial and chondrites vanadium isotopic ratios indicating irradiation histories difference

VANELESS DIFFUSERS

Stagnation pressure losses in radial vaneless diffusers to estimate compressor performance, noting one dimensional analysis

VANES

NT GUIDE VANES

NT JET VANES

NT WIND VANES

Internally air cooled turbine blades and vanes emphasizing coolant aerodynamics, heat transfer and blade life, high temperature in jet engines, etc [RAES PAPER 22]

Tube heat transfer augmentation by helical vane inserts, noting Reynolds number and mass flow rate effects

VAPOR DEPOSITION

NT VACUUM DEPOSITION

Epitaxial growth of Cu vapor deposited on W single crystal /110/ surface using low energy diffraction, Auger electron and work function techniques

Vapor deposited GaN single crystals tested for electrical and optical properties, determining band gap energy, electron concentration, etc

Boron and other high performance reinforcements made by vapor plating process, discussing boron filament atomic structure and morphology

AlN deposition rate from gaseous phase on Mo substrate as function of temperature

Zr, Ti, Nb and Ta carbides deposition from metal chloride, methane, hydrogen and argon mixture, studying gas concentration and temperature effects on deposition rate

Epitaxial magnetic oxide films grown by chemical vapor deposition

Metallic contacts deposition on p- or n-GaAs using vacuum evaporation by electron bombardment

ZnO epitaxial layers deposition by chemical vapor transport on sapphire single crystal substrates

Initial stages of Ti vapor deposition on Mo, using secondary ion-ion emission and mass spectral analysis

Epitaxial beta SiC film formation on SiC by reactive evaporation or sputtering at low temperature

Boron and boron carbide coatings formation on graphite by vapor deposition, determining optimum parameters for reaction control

Chemical vapor deposition of carbon matrix material in fiber structure, investigating thermodynamic fundamentals in processes

Shaping methods for filament wound carbon structures, emphasizing matrix building by chemical vapor deposition

Gas porosity in fusion welds of chemical vapor deposited W, noting formation of microfissures due to pore linkup

Metal vapor flow measurement by quadrupole mass spectrometer for control of thin film depositions by evaporation

Boron and boron-carbide coatings formation by vapor deposition, determining optimum thermodynamic parameters from experiment

Gas bubbles effect on recovery and recrystallization in W sheet deposited from tungsten fluoride vapor

Pyrolytic carbide protective coating deposition from gaseous phase on spherical particles in boiling layer

Diffusing element deposition on metal surface during saturation from gas phase based on calculation of equilibrium composition of reaction mixture

Metal layer and absorbed oxygen quantities in reactive oxidation deposition of aluminum

VAPOR JETS

Cs jet device eliminating wall influence in nonlinear radiation-atom interaction phenomena

VAPOR LIQUID EQUILIBRIUM

U LIQUID-VAPOR EQUILIBRIUM

VAPOR PHASES

Wet vapor flow with/without inert diluent, assuming momentum and heat transfer between phases according to Stokes law and Nusselt number of unity

Cavitating flow in converging channels of hydraulic system, calculating energy distribution at gas-vapor phase using Borda-Carnot theorem

Gas chromatography based on sampling gas-vapor phase at liquid surface for determining volatile oxygen containing compounds in biological media

Hydrophobic-hydrophilic zero gravity liquid-gas phase separator for Apollo 11 flight life support system [SAE PAPER 690638]

Low pressure ionic reactions in gaseous cyclobutane

Light emission and gas phase ignition of homogeneous solid propellants under shock tube conditions [AIAA PAPER 70-120]

Laser radiation increased absorption in opaque solid body attributed to vaporization, analyzing factors determining thermodynamic equilibrium between condensed and gaseous phases

Phase growth of free vapor bubbles in water, ethanol and isopropanol at uniform superheats under normal and zero gravity

Gas phase ignition theory of evaporating fuel in stagnant hot oxidizing gas as function of temperature

Gas phase thermal decomposition of ammonium perchlorate at elevated temperatures using mass spectrometer

Thermal conductivity for organic compound gases at atmospheric pressure

Aerothermochemistry of two phase flow in gaseous media of solid or liquid particles or spherical gas pockets [ONERA-TP-691]

Polar gas phase dielectric under conditions of power saturation interacting with microwave radiation field in waveguide

Solid-gas phase equilibria of binary systems related to cryogenics

Nitrogen tetroxide thermodynamic properties calculation from pressure-volume-temperature equation of state in gas and liquid phases

Gas phase chemicals synthesis via AC diffuse discharge superimposed on propane-air flame seeded with potassium carbonate in electrically augmented flame burner

Vapor phase fluorescence spectra from benzene and deuterated benzene at zero point vibrational level

Fourth order aberration in gas lens used as focusing element in light beam waveguide systems

Gas phase stabilities of bicyclic cations, establishing heats of formation limits by ion- molecule reactions identification

Reaction kinetics of gas phase pyrolysis of polydifluoroaminomethanes in various reactors, obtaining C-N bond cleavage as rate determining step

Pressure effects on quantum yields of carbon trioxide formation in gas phase ozone photolysis with carbon dioxide

Gas phase chemical reactions effect on heat transfer to charring ablator, deriving numerical solution for multicomponent stagnation point flow [AIAA PAPER 70-869]

Film condensation rates of vaporized substance in shock tube during passage of shock wave, formulating quasi-one dimensional problem

Pressure dependence and high pressure limiting values of rate constants of gas phase reaction of monomethylamine and trimethylamine with boron trifluoride

Gas phase ignition theory with feedback of homogeneous propellant exposed to stagnant gas after shock reflection [AIAA PAPER 69-559]

Saturated nitrogen vapors condensing coefficients measurement by cryostat, comparing results with theoretical prediction

Cesium high temperature saturated liquid and vapor phase density and critical temperature and pressure

High temperature aluminum species in vapor over solid alumina, determining thermodynamic properties, composition and accommodation coefficient by Knudsen effusion and mass spectroscopy

VAPOR PRESSURE

Vapor pressures of cobalt over pure cobalt and over Ni-Co alloys determined as function of temperature by isotope exchange method

Caloric data determining saturated vapor pressure of nitrogen tetroxide and heat of sublimation for sublimation curve

Semiconductor compounds application as partial vapor pressure sensors of chemical elements, discussing electrical properties dependence

Vapor pressure of binary alloys with volatile components measured by combined Knudsen-torsion method, using thermal balance in vacuum

Microwave propagation refractive index over India, showing influence of humidity and vapor pressure

Vapor pressures and dissociation energy of yttrium carbide and tetracarbide over extended temperature, measured by Knudsen double focusing spectrometer

Knudsen effusion measurements of stoichiometric MnTe sublimation at high temperature and low pressure

Boiling point method for alkali metals vapor pressure at high temperatures, estimating data accuracy

Cs high temperature vapor and critical pressure and temperature determination for predicting thermodynamic and transport properties, liquid phase nature and state relations

VAPOR TRAILS

U CONTRAILS

VAPOR TRAPS

Aviation kerosene pipeline column separation after valve closure, solving differential equations for transient pressures propagation to predict vapor cavities duration

Aerosol impact traps for ground and airborne water vapor condensation studies

VAPORIZATION HEAT

U HEAT OF VAPORIZATION

VAPORIZERS

NT EVAPORATORS

VAPORIZING

NT BOILING

NT EVAPORATION

NT FILM BOILING

NT FLASHING [VAPORIZING]

NT LEIDENFROST PHENOMENON

NT NUCLEATE BOILING

NT PROPELLANT EVAPORATION

NT SUBLIMATION

NT TRANSPIRATION

Mathematical model of spherically symmetric quiescent droplet undergoing quasi-steady vaporization near thermodynamic critical point

Vaporization interaction liquid rocket performance model, discussing performance loss evaluation and test data

Meteor fragments motion and vaporization based on photographs

N-heptane and Freon-13 droplets vaporizing size and temperature at supercritical pressures in heated air stream [AIAA PAPER 70-6]

Group 4A difluorides vaporization thermodynamics and bond dissociation energies, tabulating mass spec-

- tra, vapor composition, reaction enthalpies, heats of polymerization and thermodynamic functions
07 p1319 A70-19889
- Laser induced vaporization of Bi compounds with group VIa elements, analyzing vapor species, condensed phase and molecular configurations by mass spectroscopy
08 p1455 A70-21338
- Vapor composition and condensed phase structure of As and Sb compounds with group VIa elements analyzed by laser mass spectrometer
08 p1455 A70-21339
- Meteor ablation, investigating removal rate of molten film and droplet evaporation
09 p1754 A70-22476
- Laminar boundary layer behind normal shock wave with vaporization and combustion, obtaining profiles on analog computer
11 p2148 A70-25967
- Mass spectrometric analysis of lunar material from soil vaporization products ion component by electron beam
11 p2119 A70-26800
- Congruent vaporization rates of niobium monocarbide phase at high temperatures in vacuum, using method of least squares
12 p2254 A70-27320
- Radiating drop unsteady vaporization or growth for uniformly distributed internal heat sources, discussing gas temperature distribution and diffusion thermal effect
13 p2521 A70-29417
- Vaporization of small meteor particles with identical surface temperature, considering radio communication based on reflection from ionized trails
14 p2636 A70-30323
- Vaporization characteristics of solids for relationship between chemical bonding and sublimation mechanism emphasizing NaCl, CdS and GaAs
14 p2545 A70-30906
- Titanium dicarbide and tetracarbide vaporization at high temperatures, using Knudsen effusion method with mass spectroscopy, determining dissociation energies
21 p3773 A70-41274
- Boiling point method for alkali metals vapor pressure at high temperatures, estimating data accuracy
23 p4281 A70-44448
- High power pulsed laser fog dispersal, calculating vaporization regimes of droplet interaction with laser radiation
23 p4201 A70-44592
- Basalt heating with IR carbon dioxide laser, investigating vapor fractionation for inert atmospheres, very high temperatures and silicon dioxide poor materials
24 p4409 A70-45673
- VAPORS**
- NT CESIUM VAPOR
- NT MERCURY VAPOR
- NT METAL VAPORS
- NT SODIUM VAPOR
- NT WATER VAPOR
- VAPORATOR DIODE CIRCUITS**
- Controllable microwave phase shift varactor diode circuit parameters design optimization using digital computer for transmittance matrix coefficients calculation
08 p1474 A70-21230
- Distortion-compensation circuit theory, considering voltage-frequency characteristics and varactor controlled oscillator nonlinearities of frequency modulators
09 p1632 A70-22235
- Phase control of locked negative resistance /Gunn/ oscillator under operational conditions, noting coupled varactor diode use
17 p3055 A70-35630
- S band CW power amplifier and varactor doubler module for airborne phased arrays
18 p3231 A70-36674
- Cascaded varactor frequency multiplier design for microwave range
23 p4170 A70-43877
- Semiconductor microwave generator design for maser simulator using transistorized amplifier, varactor frequency multiplier and diode multiplier
23 p4171 A70-43878
- VAPORATOR DIODES**
- Resonant cavity method for measuring varactor diodes cut-off frequency, avoiding errors from circuit losses and parasitic effects
01 p0048 A70-10049
- Narrow bandwidth FM signal distortion during multiplication in lossless varactor multiplier calculated, using equivalent circuit of frequency doubler
03 p0452 A70-14040
- Low noise tunable parametric amplifier for tactical satellite communications, discussing characteristics and varactor diode mount
08 p1471 A70-20806
- Static error of varactor-controlled tuning-locked discriminator using computer
09 p1638 A70-23323

- Varactor diode equivalent circuit determination for application to cooled parametric amplifiers design
11 p2017 A70-25573
- UHF frequency doubler with series-parallel array of eight punch-through diodes, preventing spurious oscillations
12 p2196 A70-27650
- MIS varactors applications as nonlinear reactances, discussing charge-voltage characteristics and minority carriers effect
12 p2196 A70-27685
- Microwave avalanche diode emission frequency dependence on charge transfer across drift region, considering varactor diode output, negative resistance and noise factor
14 p2555 A70-30354
- Binary varactor diode microwave device, displaying two capacitance values in reverse bias operation for application in phased array systems and frequency control
14 p2556 A70-30919
- Broadband frequency multipliers optimum efficiency solutions, realizing linear charge-voltage characteristics with MIS varactors
14 p2557 A70-31159
- GaAs microwave devices including diffused varactor, Schottky barrier and Gunn diode, discussing single crystals preparation and epitaxial growth layers
16 p2873 A70-33293
- Wideband varactor multipliers with flat output as microwave sources in radar systems
16 p2877 A70-33412
- Fundamental microwave oscillator subharmonic phase locking for stable power, comparing with varactor frequency multipliers
19 p3386 A70-37689
- Frequency multipliers with charge storage diode, analyzing turn-off transient effect on performance by charge control model
19 p3391 A70-38748
- Semiconductor diodes, discussing characteristics and applications of Schottky barrier, varactor, tunnel, Gunn and field effect diodes, etc
20 p3600 A70-40500
- Microwave waveguide mount characterization of varactor diodes, using transmission resonance and Dolph-Chebyshev taper
21 p3797 A70-40759
- Equivalent circuits for charge storage varactor diode in frequency multiplier mode
23 p4169 A70-43782
- Minimum noise microwave parametric amplifiers incorporating varactor diodes with frequency dependent apparent loss resistance
23 p4169 A70-43786

VARACTORS**U VARACTOR DIODES****VARIABLE**

- Lectures on forms in many variables covering Chevalley-Waring and Lang-Nagata theorems for finite and function fields, discrete valuation rings, etc
13 p2441 A70-29454

VARIABLE AREA WINGS**U TRAILING-EDGE FLAPS****VARIABLE GEOMETRY STRUCTURES**

- Surface shape determination for thin delta wing with variable geometry to minimize drag for given open and closed configurations and cruising supersonic speeds
01 p0002 A70-10547
- Two stage axial flow compressor with variable pitch guide vanes, discussing HF vibration reduction of rotor blades
01 p0166 A70-11419
- Control system asymptotic stability stabilized by variable structural component applied to critical cases described by multiple zero root equations and imaginary roots
04 p0720 A70-15197
- Hypersonic cruise vehicle data to define temperature, load criteria and materials for air induction systems associated with two dimensional variable geometry inlet
05 p0791 A70-15839
- [SAE PAPER 690664]
- Parasitic cross polarization lobe elimination in radiation patterns of variable profile antennas by curved conductors, including confirmation for large radio telescope
05 p0820 A70-16253
- Steady state and dynamic performance of variable geometry free gas turbine using nomogram and analog simulation
06 p1129 A70-17143
- Nonsymmetric planform cantilever plate apparent mass, material properties and geometrical changes effect on vibration frequency
07 p1403 A70-19058
- Reentry into earth atmosphere of heavy ballistic missiles with variable and constant geometry compared with light missile
08 p1433 A70-21766
- Temperature gradient method for determining local heat transfer coefficients in variable cross section channel
10 p1968 A70-24290

- Canard and variable geometry aircraft designs noting SAAB 37 Viggen performance
10 p1805 A70-24764

- Soviet book on aerodynamic, stability and controllability characteristics of variable geometry wing aircraft
13 p2344 A70-28648
- F-14A engine air inlet control, describing variable geometry system open loop design
[AIAA PAPER 70-697]
- High lift flaps for sailplane cross country speed improvement by cruise-climb tradeoffs
[AIAA PAPER 70-878]
- Critical flutter behavior of variable geometry aircraft with wing of 70 degree leading edge sweep, noting wing-tail interference
18 p3338 A70-36445
- Temperature gradient method for determining local heat transfer coefficients in variable cross section channel
20 p3739 A70-40348
- Potential flow around oscillating shell-plate structure subjected to supersonic gas flow at zero angle of attack, solving nonlinear aeroelasticity problem
22 p4117 A70-43362
- Variable geometry radial inflow turbine performance estimation based on one dimensional flow theory
22 p3960 A70-43738
- VARIABLE LIFT**
- U LIFT**
- VARIABLE MASS SYSTEMS**
- Precession motions of rigid body with variable mass, considering angular momentum and rotation stability
01 p0141 A70-10283
- Structural vibration of ring stiffened and mass- attached hemispherical shells
08 p1593 A70-21618
- Dynamical characteristics of variable-mass flexible spinning rocket with internal flow, investigating rigid body motion, elastic displacements and vibrations
09 p1767 A70-23252
- Material system equations of motion, determining programmed motion variable mass systems stability
13 p2453 A70-29717
- Two dimensional reverse trajectory reaction and mass behavior for motion of material point with changing mass, using Mesherskij equation
18 p3283 A70-36401
- Periodic collision orbits in plane elliptic three body problem of infinitesimal mass under gravitational field of two finite masses
20 p3705 A70-39603
- Automatic calculations for fuel volume mass properties in tanks at various angles of attack, considering total weight, gravity center moment and inertia product
20 p3563 A70-40376
- Third stage engine performance from mass properties data for space vehicles with side-by-side tanks
[SAE PAPER 846]
- 20 p3717 A70-40378
- VARIABLE STARS**
- NT CEPHEID VARIABLES
- NT HERCULES NOVA
- NT NOVAE
- NT SUPERNOVAE
- NT T TAURI STARS
- Light curves of Algol eclipsing variable AD Herculis and semidetached system relative dimensions from BV photometric observations
01 p0184 A70-10952
- Solar brightness variations observed photometrically, discussing periodicity, sunspot locations, photosphere and subsurface rotations, etc
01 p0186 A70-11273
- Stellar system DQ Herculis photometry by synchronous signal averaging, indicating sinusoidal light curve with increasing binary period
02 p0373 A70-12392
- Nonperiodic phenomena in variable stars - Conference, Budapest, September 1968
03 p0565 A70-13312
- Nonperiodic phenomena in variable stars by statistical and physical analysis, noting role of magnetic fields
03 p0566 A70-13313
- Nebular variables and flare stars in Orion aggregate
03 p0567 A70-13319
- Multiple periodicities in beta Canis Majoris Star 16 Lacertae attributed to tidal perturbation effects on pulsation mode of structural changes
03 p0567 A70-13320
- O-C diagrams of RR Lyrae variables in M5, considering representation by parabolas or intersecting straight lines
03 p0567 A70-13321
- U Geminorum type variables properties, orbital period changes in close binaries and origin of outbursts
03 p0567 A70-13322
- Light variation curves for distorted white dwarf hypothetical secondaries in close binary systems calculated by integrating monochromatic fluxes
03 p0567 A70-13323

Nonperiodic changes in radiation connected with orbital period in eclipsing conventional binaries observed in R Canis Majoris

03 p0568 A70-13326

Psi Orionis light variations, using photoelectric photometry, indicating ellipsoidal variability

03 p0570 A70-13552

IR colors and optical and IR spectra of irregular M variable star and bright OH source VY CMa indicating supergiant classification

04 p0749 A70-14592

Variable object BL Lacertae flux measurements using Schmidt telescope photography and radio study, comparing results with quasar

04 p0759 A70-15711

S Doradus spectroscopic behavior study during minimum and maximum phases suggesting ejected-shell mechanism and premain sequence star classification

04 p0759 A70-15712

Forbidden Fe II lines and AIO band intensities in long period variable stars confirming stratified models of emitting layers

05 p0907 A70-16031

Variable stars, discussing equation of motion for envelope structure properties and determining oscillation energy change rate from linear theory

06 p1138 A70-17309

Mean magnitudes, colors and amplitudes for RR Lyrae variables in omega Centauri cluster obtained from photometric observations

06 p1148 A70-18455

RW Aur-type variables in Taurus, studying temporal variations from photographic and photometric observations and B, B-V diagram

07 p1376 A70-18906

Carbon particles formation and growth model for cool variable carbon star atmosphere with sinusoidal carbon star atmosphere with sinusoidal temperature variations

07 p1380 A70-19260

Carbon particles formation and growth in Mira variables atmospheres, considering extinction effects on stellar structure and appearance

07 p1380 A70-19261

Secondary minimums role in studying eclipsing variable stars, correlating observability with detection of line of apsides motion

08 p1581 A70-21759

Cepheid type variable stars nuclear reaction and opacity pulsation excitation mechanisms

10 p1940 A70-24409

Algol variable RV Ophiuchi photoelectric observation in B and V, representing light curve characteristics by gas stream model

10 p1945 A70-24967

Orion Nebula region search, giving characteristics and locations of flare type variable stars

10 p1949 A70-25249

Autocorrelation and brightness distribution functions for irregular variable star

11 p2115 A70-26579

Model for FU Orion irregular variable to determine turbulent convection characteristics in atmosphere at optical transparency level

11 p2115 A70-26580

Coordinates and brightness characteristics of variable observed during photographic studies of VX Cas

11 p2116 A70-26584

Spectra, luminescence and gas dynamic effects in variable stars, discussing nonthermal theory to explain continuous emission

12 p2306 A70-27857

Mass transfer in close binary stars and in highly variable stars

12 p2306 A70-27858

Comet-like nebulae, describing brightness and spectral characteristics of variable stars in nebulae

12 p2307 A70-27863

Cold variable stars intrinsic polarization model proposing light scattering in circumstellar dust shells

12 p2307 A70-27865

Transistor densitometer used for variable star interpretation by amateur photographers

15 p2807 A70-32348

Massive hydrogen burning stars evolution with pulsational mass loss based on minimizing pulsational instability degree to specify mass loss rate

15 p2803 A70-32612

RW Aur type variable stars percentage with photographically observable flares

15 p2807 A70-32877

AG Peg brightness variations by three color photoelectric photometry, discussing orbital motion of cold component

15 p2807 A70-32878

Long period variable stars light polarization as function of brightness and wavelength, discussing molecular scattering and nonthermal emission

15 p2808 A70-32879

CH Cygni irregular light variations and spectrum peculiarities, considering upper atmosphere perturbation by variable hot satellite

15 p2809 A70-32904

Soviet book on variable stars covering properties, evolution, structure, methods of investigation, etc

19 p3520 A70-38397

Soviet book on brightness of irregular and semiregular variable stars by statistical methods

20 p3705 A70-39899

Beta CMa variable star HD 43818 spectral observations, discussing line profiles and radial velocities

22 p4100 A70-42853

Stellar ring 274 reality confirmed by photometric measurements of OB member stars, determining variable shell star P Cygni location

22 p4101 A70-42868

Ic class variables long wavelength anomalous radiation, discussing emission from circumstellar dust shell

22 p4094 A70-42934

Radial velocity-light amplitude ratios of grouped variable stars in continuous sequence, comparing pulsation prediction

23 p4247 A70-44793

UV Cet type flare star rotational velocity upper limits from H alpha emission line width in chromospheres

23 p4251 A70-44824

Deutsch period vs line width relation for periodic Ap stars, determining rotational velocities with rigid rotator model

23 p4251 A70-44825

Massive star pulsational stability in He burning phase, investigating opacity variation effects on flux dissipation in outer layers

24 p4405 A70-45419

Light velocity frequency dependence in variable stars gravitational fields suggested from yellow and UV NP 0532 observations

24 p4405 A70-45488

UV Ceti type variable flare stars, observing radio and optical spectral regions for X ray production

24 p4397 A70-45763

VARIABLE SWEEP WINGS

Variable sweep aircraft aeroelastic stability, considering wing-tail interaction flutter

06 p1170 A70-18162

Variable sweep wing pivot joint design utilizing double shear tilted spherical journal bearings with Teflon fabric liners

12 p2318 A70-27135

Soviet book on aerodynamic, stability and controllability characteristics of variable geometry wing aircraft

13 p2344 A70-28648

European Panavia 100/200 two engine variable wing military aircraft, noting prototype design, use and production sharing

13 p2347 A70-29051

Fixed and variable sweep wing structure computerized design optimization

16 p2869 A70-33506

Variable sweep high thrust-weight ratio multirole combat aircraft /MRCA/, discussing British-French cooperation, development programs and requirements

17 p3017 A70-34916

Critical flutter behavior of variable geometry aircraft with wing of 70 degree leading edge sweep, noting wing-tail interference

18 p3338 A70-36445

Variable wing sweep aircraft angular motion mathematical model, analyzing inertial moments influence on control dynamics

20 p3562 A70-40182

F-14 carrier based fighter development program requirements, inherent difficulties and variable geometry configuration

21 p3750 A70-41264

Aircraft control surface aerodynamic characteristics, considering low aspect ratio wing elevons with variable sweep leading edge as longitudinal and lateral controls

23 p4131 A70-44107

VARIABLE THRUST

Small penetration aid rocket motors fabrication, discussing axial and tangential-thrust integral assembly, impulse levels, delay line convection for igniters, production evolution, etc

07 p1295 A70-19714

Solid propellant rocket motor combustion control by fluidic vortex valve, considering thrust variation

16 p2965 A70-33535

Throttleable thruster system for Mars soft landing, selecting catalytic decomposition engine from system weight and performance studies

16 p2966 A70-33549

VARIANCE (STATISTICS)

NT MULTIVARIATE STATISTICAL ANALYSIS

Least squares adjustment of observation equations for hybrid systems solved by regarding constraints as observations with zero variances

02 p0289 A70-11798

Noise variance extreme value estimator for biorthogonally block coded high rate telemetry system for Mariner missions

08 p1459 A70-20799

Obliquely incident spherical wave amplitude and phase fluctuations, deriving formulae to compare variances behavior for refractive index fluctuation autocorrelation functions

14 p2574 A70-30750

Density and distribution functions for quotient of ellipsoids of variance volumes, yielding probabilities and fractiles in three dimensional sets of points

19 p3382 A70-37835

Kalman filter set for state vector and observation error variance estimation in discrete-time linear system, using empirical Bayes techniques

19 p3395 A70-38873

VARIATION METHOD

U CALCULUS OF VARIATIONS

VARIATIONAL PRINCIPLES

Critical conditions for hydrodynamic stability of incompressible nonconducting fluids subjected to unipolar injection, establishing variational principle leading to characteristic relation

01 p0152 A70-10672

Variational methods for investigation of thermal and electrical properties of semiconducting materials, noting accuracy

01 p0159 A70-10759

Finite element method for thin shells using specialized form of Reissner variational principle for stresses and displacements

01 p0208 A70-11184

Equations of state for continuous media, using variational principles within framework of relativity theory

01 p0146 A70-11593

Variational principle for admissible functions particular solution in elasticity theory involving solid bodies with cracks

01 p0212 A70-11608

Variational approach to structure of rotating polytrope with symmetry about axis of rotation in post-Newtonian approximation of general relativity

02 p0338 A70-11778

Variational principles in dynamic viscoplasticity theory, based on operator approach combined with time independent variations in elasticity theory

02 p0391 A70-12818

Shallow elliptical planform shell under uniformly distributed normal load calculated with 'ritz and Bubnov-Galerkin variational methods

03 p0593 A70-13496

Variational stress solutions for static case of bounded bodies in Cosserat continuum theory, assuming anisotropic inhomogeneous material and defining boundary value problem solution

03 p0596 A70-13973

Variational principles in linear elasticity theory with couple stresses, solving boundary value problems in Mindlin theory with microstructure and first strain gradient theory

03 p0596 A70-13974

Solutions existence for differential, integral and integrodifferential equations proved by variational imbedding of nonlocal linear Euler-Lagrange operator functioning as automatic adjoint calculator

05 p0681 A70-16060

Variational principle used in microwave breakdown predictions for rectangular aperture antenna

05 p0824 A70-16988

Einstein field equations based on variational principle applied to stability of general self gravitating relativistic gaseous mass obeying specific equation of state

06 p1138 A70-17304

Nonlinear differential equations variational formulation, giving practical applications

06 p1093 A70-17635

Finite elements of time dependent phenomena using Hamilton variational principle for time integration

06 p1165 A70-17645

Book on optimization by variational methods covering use of differential equations, Pontryagin minimum principle, optimal and feedback control, dynamic programming, etc

06 p1093 A70-17650

Micropolar homogeneous and anisotropic elastic solids linear dynamic theory, deriving reciprocity and variational theorems

06 p1172 A70-18512

Natural oscillations of three dimensional bundle of parallel strapped rods with variable elastic mass parameters determined by Hamilton-Ostrogradskii variational principle

08 p1583 A70-20485

Variational problem of determining optimal heat transfer from gas flow to porous plate boundary layer

08 p1597 A70-21176

Electromagnetic fields interaction with nonconducting neutral elastic solid, formulating relativistic variational principle for balance laws and constitutive equations

08 p1545 A70-21252

Thermoelastic energy functions bounding by variational principles for anisotropic composite materials properties

08 p1592 A70-21510

Electrical and magnetic polarizability coefficients in theory of diffraction at small apertures by formulating bilateral variational principles

09 p1631 A70-22150

Variational theorem for compatibility and plasticity for Mises solids based on stress functions

09 p1771 A70-22397

Variational principle application to stability in failure mechanics of arbitrary linearly elastic bodies, discussing inertia effect on steady state vibrations of cracked bodies

09 p1771 A70-22465

Rarefied gas flow past arbitrary three dimensional body using variational principles based on linearized BGK equation, considering constant and adiabatic wall temperature

09 p1605 A70-23178

Variational principle of steady state transport process derived from basic inequality in macroscopic theory of nonequilibrium thermodynamics

09 p1789 A70-23224

Weighted residual and Biot variational methods for solving one dimensional heat conduction problems

09 p1789 A70-23260

Hamilton modified principle applied to nonlinear control problems including time delay, servosystem with ideal relay and liquid level control

09 p1614 A70-23693

Nonconservative problems motion stability analysis based on restricted admissible displacements, establishing two variational principles

11 p2138 A70-26172

Variational principle in electromagnetics to produce linear algebraic equations with Rayleigh-Ritz procedure for application to dielectrically coated slit antenna

12 p2198 A70-27957

Variational principles derivation for inelastically deformable body mixed boundary value problem, considering loading conditions with basic functions free of discontinuities

13 p2516 A70-29524

Variational principles of linear asymmetric elasticity for dynamic problems with initial and boundary conditions, using Laplace transforms

13 p2517 A70-29724

Thin two dimensional shells static linear elastic deformations analysis using difference based variational method

15 p2815 A70-32001

Canonical variational principle for boundary condition contractions in elastic shell theory

17 p3182 A70-34545

Variational principle for turbulent shear flow between parallel plates, taking into account isothermal flow and Malkus theory

17 p3073 A70-35595

Inverse variational principles of thin plate, dividing into subregions/finite elements/ for optimal thickness distribution, sectional forces and displacement values

18 p3339 A70-36481

Vlasov high temperature plasmas numerical analysis, using Hamilton variational principle

18 p3296 A70-36793

Variational principle application to relativistic MHD, deriving Einstein field equations, Maxwell equations and equations of motion for self gravitating charged fluid

19 p3478 A70-37591

Mixed boundary value problems approximate solution in linear elasticity by variational method, noting applications to micromechanics

19 p3540 A70-37957

Safety factor limit analysis for anisotropic nonhomogeneous solids by variational method, exemplifying by four layer rectangular beam

19 p3547 A70-38355

Book on variational principles in heat transfer covering conduction, convection, dissipation, thermal potential and force boundary layer problem and Lagrangian analysis

20 p3735 A70-39224

Variational principles in linear quasi-static theory of inhomogeneous and isotropic viscoelastic solids with microstructure

20 p3718 A70-39229

MHD flow in channel of arbitrary cross section, deriving velocity and electric potential distribution by variational principle

20 p3677 A70-39360

Elastic bodies static stability theory variational principles, introducing equilibrium equations and boundary conditions of initial state by Lagrange multipliers

20 p3724 A70-39857

Statistically nonhomogeneous fields by variational principles of elasticity, obtaining bounds of average displacement for hollow sphere under pressure

20 p3732 A70-40112

Complementary variational principles applied to free oscillations of incompressible fluid in container, using linearized hydrodynamic equations

21 p3807 A70-41323

Constant property unsteady laminar flow thermal entrance problems, using variational formulation in Laplace transformed domain

21 p3954 A70-42169

Elastic plate uniform extension with rectangular crack by three dimensional bending theory, using variational principle

22 p4115 A70-42941

NonNewtonian fluids variational problems, discussing generalized solutions existence and uniqueness

23 p4179 A70-43987

Mathematical models derivation for systems of interconnected elastic segments, using variational method and energy summation via difference equations

23 p4266 A70-44019

Variational principle and reciprocity theorem for initial value problems associated with wave equations, discussing solution uniqueness conditions

24 p4380 A70-46037

VARIATIONS

NT ANNUAL VARIATIONS

NT DIURNAL VARIATIONS

NT GEOMAGNETIC MICROPULSATIONS

NT GEOMAGNETIC PULSATIONS

NT MAGNETIC VARIATIONS

NT NOCTURNAL VARIATIONS

NT PERIODIC VARIATIONS

NT TWENTY-SEVEN DAY VARIATION

NT WIND VARIATIONS

VARIOMETERS

Gokhberg magnetovariational sounding method for single location analysis of magnetic storms early phases, comparing ground station network observations

07 p1277 A70-20440

Errors magnitude in quartz variometer readings resulting from variations of geomagnetic field perpendicular component

14 p2582 A70-30244

Photoelectric detector sensitivity variation effect on long term instability of servomagnet variometers

14 p2588 A70-31261

Geomagnetic field variations recording by two variometers, correcting for variation components effects by instruments orientation

19 p3420 A70-37335

Quartz magnetic variometer allowing simultaneous recording of magnetic field variations and suspension axis inclination changes

19 p3420 A70-37336

Quartz Z-variometer for autonomous variation stations, describing construction and operation

23 p4194 A70-44089

Errors magnitude in quartz variometer readings resulting from variations of geomagnetic field perpendicular component

24 p4339 A70-46319

VASCULAR SYSTEM

NT AORTA

NT ARTERIES

NT BLOOD VESSELS

NT CAPILLARIES [ANATOMY]

NT VEINS

Vascular anatomy correlation with human heart conduction tissue structures to study coronary artery disease cases exhibiting major conduction disturbances by ECG

01 p0013 A70-10273

Constant-inflow and constant-pressure perfusion effect on vascular responses of dog

02 p0232 A70-11716

Lower limbs circulation of peripheral vascular diseased patients transcutaneously assessed with ultrasonic flow detector, comparing results with arteriograms

07 p1217 A70-18956

Vascular and dystrophic disturbances in rat parenchymatous organs in hyperbaric pure oxygen atmospheres, observing increased tissue eosinophilia

07 p1207 A70-19504

Pulmonary extravascular /PEV/ and intravascular /PBV/ fluid volumes measured at rest and exercise

07 p1211 A70-19595

Human vascular tonus and hemodynamics during prolonged hypokinesia, observing changes in reaction to cold and reduced vascular tonicity

10 p1814 A70-24670

Left ventricle zone as principal reflexogenic zone of heart participating in greater circulation vessel tonus control

13 p2353 A70-29356

Oxygen and carbon dioxide effects on airway smooth muscle following pulmonary vascular occlusion in dogs

13 p2356 A70-29943

Beryllium sulfate effect on rabbits vascular plasma volumes, using albumin method for blood groups

15 p2681 A70-31884

Steady flow of incompressible fluid through converging-diverging tube, considering implications in occlusive vascular disease

15 p2691 A70-31936

Water and blood flow characteristics in converging-diverging plastic tube, considering implications in occlusive vascular disease

15 p2691 A70-31937

Perfusion peristaltic pump for determining smooth muscle reaction in vascular bed, discussing applications to physiological and pharmacological investigations

19 p3372 A70-38958

Acceleration Bcg dependence on left ventricular ejection flow and properties of vascular system

21 p3763 A70-41237

Vascular smooth muscle contraction regulation, discussing contractile protein, energy metabolism, excitation-contraction coupling, spontaneous rhythmicity, response to stimulants, etc

24 p4299 A70-45807

VASOCONSTRICTION

Norepinephrine release associated with vasoconstrictor response during selective activation of arterial and venous sympathetic nerves in dog hindpaw

03 p0416 A70-13012

Oxygen tension change effects on rats smooth vascular muscles electrical and contractile properties

07 p1198 A70-18715

Cholinergic nervous mechanism of autoregulatory dilatation of pial arteries under decreased blood supply to cerebral cortex in rabbits

09 p1622 A70-23583

Cutaneous liquid crystal temperature sensors for thermographic patterns of angina pectoris induced by treadmill exercise

19 p3364 A70-38361

Blood vessels constriction in rear limbs, small intestine and spleen of dog with arterial blood heated above rectal temperature

20 p3574 A70-40173

Blood flow antagonistic changes in various vascular beds following spinal cord central thermal stimulation attributed to sympathetic vasoconstrictor activity

22 p3971 A70-43405

Pulmonary arterial and venous response to cooling, discussing role of sympathetic nervous system alpha receptors in hypothermia induced pulmonary constrictions in dogs

23 p4148 A70-44788

VASOCONSTRICTOR DRUGS

Dibutylryl cyclic adenosine monophosphate stimulation of melatonin and serotonin synthesis from C-14 labeled tryptophan by rat pineals in organ culture

01 p0022 A70-10824

Autonomic drugs induced contractures of cardiac muscle of frogs, relating inotropic action with Ca influx during low membrane potential

15 p2686 A70-32837

Atropine effects on circulatory responses to diminished effective blood volume and vasodepressor syncope, noting heart rate increase

17 p3032 A70-35562

Pressor response to epinephrine in hyperbaric atmospheres measured in cats under change of sympathetic tone

17 p3032 A70-35566

VASODILATION

Dogs coronary vasodilator responses to hypoxia and induced tachycardia before and after lidoflazine and adenosine

02 p0230 A70-11702

Cardiovascular responses to sustained high skin temperature in resting men noting dizziness, impaired vision and extracutaneous vasodilatation

03 p0429 A70-14162

Posthypoxic vasodilation in extremities of anesthetized dogs preserved after carotid and aortic reflexogenic zones exclusion

07 p1204 A70-19139

Posture change effects on vasodilator responses in humans, studying reactive, postexercise and local heat hyperaemia in forearms of subjects lying and standing

07 p1211 A70-19596

Cholinergic nervous mechanism of autoregulatory dilatation of pial arteries under decreased blood supply to cerebral cortex in rabbits

09 p1622 A70-23583

Thermoregulatory vasodilation conditioned reflexes developed by combination of prolonged physical and acoustic stimuli

15 p2679 A70-31606

Hypoxia effects on cerebral blood flow in anesthetized dogs, considering acidosis and vasodilation

20 p3577 A70-40330

Vasodilating carbon dioxide effect on brain circulation in occipital cortical area in cats and rabbits using thermoelectric method

24 p4300 A70-45842

VASOMOTOR NERVOUS SYSTEM

U NERVOUS SYSTEM

VECTOR ANALYSIS

NT COPLANARITY

NT VORTICITY

Nonlocal continuity and correctness of principle for comparing functions with Liapunov vector function,

- demonstrating continuous dependence of principle on certain parameters
01 p0130 A70-10151
- Spherical earth wind field correlation matrix, relating scalar fields to isotropic vector field
01 p0135 A70-10204
- Solution existence of linear unsteady Boltzmann equation for single space variable in Hilbert space defined by scalar product
01 p0143 A70-10673
- Controllability conditions for control system described by equation with vectors x and b being non-dimensional and u and r being r dimensional
04 p0660 A70-14491
- N-local controllability conditions for system having permissible controls assumed to be certain piecewise constant vector functions
07 p1244 A70-18766
- Lawden primer vector theory applied to matched conic spacecraft trajectories optimization
07 p1381 A70-19325
- Matrix method for converting time variable stress vector into strain vector allowing for linear creep and aging
08 p1583 A70-20531
- Book on mathematical theory of electromagnetic waves covering vector analysis, reduced wave equation, linear transformations, boundary value problems and radiation patterns
08 p1533 A70-20759
- Proportional navigation law three dimensional vectorial equation analyzed in kinematic conditions, discussing perturbation effects on linearized trajectory
09 p1720 A70-22420
- Holographic recording of three dimensional rapid events, using Q switched laser pulses with sufficient coherence length for illumination
09 p1676 A70-22786
- Orbit determination from two position vectors and periastris radius, introducing polar equation for conic to obtain solution
09 p1760 A70-22932
- Azimuth determination by Vector method based on satellite observations compared to Popovich method, discussing discrepancy
09 p1670 A70-23329
- Narrow throat problems of linear dynamic programming concerning maximum linear functional determination in set of vector functions, giving algorithm for solution
10 p1855 A70-24393
- Vector-matrix differential equation for second order sensitivity coefficients applied to trajectory optimization, modeling and compensation and guidance and control
11 p2029 A70-26324
- Book on electromagnetic fields and waves covering electrostatic and magnetic fields, relativity, vectors, Maxwell equations and propagation
12 p2273 A70-28150
- Venus obliquity dynamic implications, developing equations for independent parameter set to define spin vector
13 p2489 A70-28907
- Optimal constant output feedback gains for linear multivariable systems, noting control vector as time invariant function of output vector
13 p2382 A70-29064
- Euler potentials for magnetic fields field-line structure representation, discussing cross products of gradients of scalars in plasma physics
13 p2451 A70-29123
- Vector displacement numerical calculations for rectangular parallelepipeds of infinite and finite lengths
15 p2767 A70-32018
- Constraint torque elimination from vector equations canonical system for attitude dynamics of satellite consisting of arbitrarily interconnected rigid bodies [AIAA PAPER 69-923]
18 p3316 A70-36679
- Primer vector theory applied to interplanetary trajectory optimization for high thrust chemically propelled spacecraft, considering 1973 Mars opportunity [AIAA PAPER 70-1039]
19 p3527 A70-38854
- Liquid rocket combustion instability due to velocity vector effect, showing importance in longitudinal and transverse modes
20 p3689 A70-40079
- Photoelectric polarimetry of dark unipolar type H sunspot in terms of value and direction of magnetic field vector
20 p3712 A70-40413
- Cosserat elasticity constitutive equations, coupling rotation vectors to eliminate stress indeterminacies
21 p3941 A70-42251
- Principle pressure vector components for liquid in moving V-shaped and U-shaped cross section tanks
23 p4180 A70-44164
- Analytic approximation for initial adjoint vector for optimal/minimum propellant/ space trajectories [AIAA PAPER 69-916]
23 p4243 A70-44509
- Gyro system determining aerodynamic moment integral vector in wind measurements
24 p4340 A70-46402
- VECTOR CALCULUS**
U VECTOR SPACES
VECTOR CONTROL
U DIRECTIONAL CONTROL
VECTOR CURRENTS
Axial-vector current divergence in external gravitational field, using perturbation approach in Minkowski space
07 p1336 A70-20167
- Model current system for magnetospheric substorm accounting for distribution of geomagnetic disturbance field vectors on earth surface and auroral electrons and protons
13 p2481 A70-30062
- Magnetic vector potential of circular ring with current in Taylor series expansion for electromagnetic axisymmetric systems
23 p4189 A70-44069
- VECTOR MESONS**
Maxwell equations and equations of massive-vector-meson fields in spatially homogeneous Bianchi cosmologies, obtaining formula for homogeneous EM field
17 p3156 A70-34827
- VECTOR SPACES**
NT ADJOINTS
NT BANACH SPACE
NT CANONICAL FORMS
NT EIGENVALUES
NT EIGENVECTORS
NT HILBERT SPACE
NT JORDAN FORM
NT MATRICES [MATHEMATICS]
NT STATE VECTORS
NT STOKES THEOREM [VECTOR CALCULUS]
NT VECTORS [MATHEMATICS]
NT VORTICITY
Mappings of linear vector spaces induced by transformation matrix applied to linear dynamical systems
01 p0208 A70-11189
- Potential representation of vector fields effecting decoupling of vector wave equation of elasticity for radially heterogeneous isotropic media
01 p0132 A70-11125
- Stationarization problems involving nonlocal and null class Euler-Lagrange operators, considering vector spaces of function spaces
05 p0881 A70-16059
- Statistical description of geomagnetic field as random vector field, presenting correlation functions from empirical estimates from geomagnetic charts
05 p0842 A70-16748
- Linear differential evasion game termination with phase vector approaching given subspace in Euclidean coordinates
13 p2443 A70-29755
- Liapunov functions direct generation by state space system vector matrix transformation
15 p2768 A70-32555
- Vector and tensor calculus features, examining contravariance and covariance with bra and ket algebra and absolute differential
18 p3281 A70-36354
- Nonstationary inhomogeneous random vector fields linear prediction, determining minimum mean square approximation error
20 p3604 A70-39911
- Bang-Bang principle and vector functions at extreme points, considering Lebesgue measure and Liapunov theorem
23 p4176 A70-44237
- VECTOCARDIOGRAPHY**
Computer analysis and comparison of ST segment on Frank and bipolar lead electrocardiograms of healthy persons and cardiac patients during exercise, noting physiological responses
01 p0013 A70-10270
- Physiological signals of cardiovascular system transducing methods applied to vector ECG, heart sounds, peripheral pulse waves, chest microphone and plethysmography
02 p0243 A70-12095
- Controlled premature atrial stimulation effects on atrioventricular conduction in man, using electrode catheter technique to record electrical activity of specialized conducting fibers
03 p0415 A70-12886
- Atrioventricular conduction in atrial fibrillation and flutter in man, using His bundle recordings
03 p0415 A70-12887
- Pathological Q waves in various diseases in absence of myocardial infarction, discussing electrophysiological mechanism
03 p0426 A70-13941
- Production mechanism of abnormal Q waves in obstructive cardiomyopathy
03 p0427 A70-13943
- Three dimensional display of human body surface potential distributions as diagnostic tool of cardiac abnormalities
04 p0641 A70-14557
- QRS and ST-T areas in multiple bipolar chest leads during normal and abnormal activation in patient measured for checking ventricular gradient concept
04 p0632 A70-15307
- ECG changes attributed to reduction of blood supply to myocardium during orthostatic tests after prolonged hypokinesia
07 p1209 A70-19513
- Geometrical model of human cardiac excitation stages based on normal heart anatomy, discussing application to study of QRS loop in vectorcardiogram
07 p1211 A70-19592
- Spherical frame of reference variations and additions for three dimensional vectorcardiograms composed of solid figures drawn by computer-driven CRT
07 p1221 A70-19594
- Vectorcardiogram variations of clinically normal individuals over forty compared with young adults
08 p1452 A70-21264
- Strong magnetic field effects on squirrel monkeys electrical and mechanical cardiac functions determined from vectorcardiogram and aortic blood flow characteristics
09 p1617 A70-22524
- Vectorcardiographic diagnosis of left ventricular hypertrophy based on changes in MQV magnitude and other QRS vectors
09 p1629 A70-23626
- ECG changes attributed to reduction of blood supply to myocardium during orthostatic tests after prolonged hypokinesia
11 p1988 A70-26112
- Involuntary vectorcardiographic signs of right ventricular hypertrophy
17 p3025 A70-34859
- Electrocardiogram vs vectorcardiogram for myocardial infarction diagnosis
19 p3371 A70-38362
- Isopotential surface maps for body surface potential relation to ECG and Frank vectorcardiogram during QRS stages in children
20 p3571 A70-39368
- Frank orthogonal vectorcardiograms on humans during acceleration, using beat-by-beat real time analog-digital computer technique
20 p3572 A70-39435
- VECTORS [MATHEMATICS]**
NT EIGENVECTORS
NT STATE VECTORS
NT VORTICITY
Differential equation comparison with Liapunov vector function, applying Caratheodory condition
01 p0130 A70-10156
- Linear transformation for random-data vector z reduction to smaller dimension vector
04 p0714 A70-15066
- Optimal control problem solution involving functional minimization along differential vector equation trajectories, considering manifold type constraints on phase coordinates
07 p1244 A70-18747
- Liapunov vector functions for asymptotically stable omega-periodic solution existence in case of finite dimensional system
08 p1534 A70-21002
- First vector integral of planetary motion different from moment of momentum and Runge-Lenz integrals
15 p2806 A70-32797
- Spatial vectors determination by two laser measurements and one optical observation of artificial satellite
16 p2926 A70-33118
- Pivoted plane pad bearings, calculating design variables from inner products of two vectors and Rayleigh-Ritz matrix function [ASME PAPER 69-LUB-1]
19 p3435 A70-37612
- Products integration of unit vector components over all solid angles
24 p4370 A70-46029
- VEGARD-KAPLAN BANDS**
Rotational temperature of molecular nitrogen Vegard-Kaplan bands determined from auroral spectra, including variations in vibrational levels populations [AFCLR-69-0542]
01 p0076 A70-10873
- VEGETABLES**
NT POTATOES
NT SPINACH
Photosynthesis and respiration rate in vegetables in controlled temperature, humidity, illumination levels, carbon dioxide and oxygen contents
03 p0425 A70-13892
- Antiradiation chemical substances for modifying radiation damage in peas during seed irradiation with fast neutrons
07 p1208 A70-19510
- Antiradiation chemical substances for modifying radiation damage in peas during seed irradiation with fast neutrons
11 p1988 A70-26109
- VEGETATION**
Remote sensing systems for vegetation analysis, discussing machine-aided photointerpretation methods for data analysis [AIAA PAPER 70-308]
09 p1678 A70-22879

- K band SLR /side-looking radar/ imagery mapping tropical lowland vegetation compared to photographic coverage 10 p1879 A70-24747
- Hydrobiological features mapping in Everglades by multispectral scanning and analog data processing 12 p2220 A70-26934
- False color aerial photography with IR film for distinguishing vegetation types and assessing plant vigor based on leaf reflectance 17 p3078 A70-35613
- Photographic and multisensor imagery augmented by field survey for mapping vegetation boundaries and density differences within and between plant communities 17 p3079 A70-35616
- Remote multispectral sensing of environmental and vegetation gradients in Yellowstone National Park by intercomparison of thermal IR and visible band imagery 17 p3079 A70-35617
- Day and night IR imagery compared for interpreting vegetation 17 p3079 A70-35618
- Passive microwave sensors based on brightness temperature vs frequency model for various atmospheric conditions, presenting vegetation pictures 20 p3626 A70-39054
- Visible and near IR radiation reflectance from vegetation, discussing incident solar radiation plant structures, leaf areas shadows and absorption by chlorophylls 22 p4014 A70-42767
- Venus vegetative life suggested from algae growth under pure carbon dioxide in hot acid media at high pressures 23 p4253 A70-44836

VEHICLE WHEELS

- NT NOSE WHEELS
- Nylon roving vehicle stability and agility design approach by Grumman, using articulated steering and conical wheels 12 p2208 A70-27946
- Chrysler lunar vehicle design featuring flexible metal wheels and Ackerman front wheel steering, noting back-to-back seating and centrally mounted control display panel 12 p2208 A70-27947

VEHICLES

- Flexible vehicle control, using cybernetic model for system design and response [AIAA PAPER 69-115] 12 p2314 A70-27811

VEINS

- Norepinephrine release associated with vasoconstrictor response during selective activation of arterial and venous sympathetic nerves in dog hindpaw 03 p0416 A70-13012
- Blood flow through veins and collapsible tubes simulated by physical model, downstream pressure effect and importance of collapse phenomena 04 p0641 A70-14631
- Analog computer cardiovascular system model to simulate pressure and flow events in veins including effects of gravity, collapse, breathing and venous valves action 04 p0641 A70-14632
- Bed rest effects on whole leg venous distensibility, discussing heart rate and leg volume measurements 06 p0999 A70-17288
- Venous pressure of man in space, investigating return to heart in absence of gravity and distention by hydraulic pressure 08 p1448 A70-21943
- Portal vein smooth muscles electrical properties, using double saccharose bridge method 15 p2679 A70-31605
- Intermittent forced inspirations or expirations effects on venous tone and blood flow in human skin vessels 17 p3024 A70-34595
- Ambient temperature effects on venous reactivity to hydrostatic stress, discussing posture changes and lower body negative pressure effects on index of compliance 17 p3031 A70-35426
- Body position effect on oxygen saturation of regional pulmonary venous blood and arterial-venous shunts in intact dogs 21 p3766 A70-42153
- Human leg blood flow distribution between deep and superficial veins during alternate treadmill work-rest periods 21 p3767 A70-42160
- Intact human forearms venous blood velocity measurements, using nuclear magnetic resonance techniques 24 p4309 A70-45675

VELA SATELLITES

- Large scale flare associated solar wind disturbances observed by Vela satellites, noting prolonged elevated flow speed after shock 21 p3881 A70-41080
- Solar wind proton properties examined by Vela 3, observing density distribution, flow speed and

direction, thermal anisotropy, magnitude and orientation 21 p3881 A70-41081

VELOCITY

- NT ACOUSTIC VELOCITY
- NT AIRSPEED
- NT ANGULAR VELOCITY
- NT CRITICAL VELOCITY
- NT ESCAPE VELOCITY
- NT EXHAUST VELOCITY
- NT FLOW VELOCITY
- NT GROUND SPEED
- NT GROUP VELOCITY
- NT HIGH SPEED
- NT HYPERSONIC SPEED
- NT LANDING SPEED
- NT LIGHT SPEED
- NT LOW SPEED
- NT ORBITAL VELOCITY
- NT PHASE VELOCITY
- NT PROPAGATION VELOCITY
- NT RADIAL VELOCITY
- NT RELATIVISTIC VELOCITY
- NT ROTOR SPEED
- NT SOLAR VELOCITY
- NT SUBSONIC SPEED
- NT SUPERSONIC SPEEDS
- NT TERMINAL VELOCITY
- NT TIP SPEED
- NT TRANSONIC SPEED
- NT WIND VELOCITY
- Air traffic control radar velocity resolution for eliminating ground, rain and angel clutter by optimizing wavelengths, pulse length and beam width 02 p0332 A70-11969
- Tribonucleation emphasizing viscosity-velocity product in gas nuclei formation and cavitation 12 p2170 A70-27661

VELOCITY DISTRIBUTION

- Boundary layer equations for plane steady incompressible flow, studying given velocity profiles effects on equations solutions 01 p0060 A70-10144
- Shock wave structure in two phase media with temperature and velocity gradients and possible phase transitions 01 p0060 A70-10147
- Velocity distribution and optical depth of line formation in solar atmosphere using blue and red wing filtergram and numerical experiment 01 p0175 A70-10241
- Chromospheric average velocity field near sunspots determined from M alpha line absorption elements wavelength shifts 01 p0176 A70-10247
- Airfoil cascade blade design by iteration method equating normal velocity distribution about contour with imposed tangential velocity 01 p0001 A70-10263
- Radiation effect on enthalpy and velocity distributions of laminar compressible planar free jet 01 p0061 A70-10295
- Velocity field measurements in NGC 5128 galaxy, discussing relative motion between gas and stars and correspondence of emission and absorption lines 01 p0184 A70-10898
- Density and heat transfer effects on compressible turbulent boundary layers used to investigate velocity and temperature profiles, skin friction, Mach number and Reynolds number 01 p0003 A70-10936
- Mass transfer analysis for axisymmetric turbulent flow in circular tube, deriving turbulent velocity profile from two part model, based on von Karman similarity hypothesis 01 p0064 A70-11092
- Rotation periods of Jovian atmospheric currents showing zonal wind velocity variations with latitude 02 p0369 A70-11829
- Particle velocity distributions in low density supersonic jets measured by molecular beam sampling technique and multidisk velocity analyzer 02 p0276 A70-11849
- Velocity and density profiles obtained from mass diffusivity time measurements in axisymmetric turbulent air pipe flow over specific Reynolds number range 02 p0295 A70-11853
- Mixing length relationship in Prandtl theory for turbulent channel and pipe flow, deriving universal velocity distribution law 02 p0277 A70-11911
- Turbulence detection and velocity fluctuations in jets and flames based on equations of motion and impact probes 02 p0398 A70-12037
- Harmonically oscillating semifinite rectangular wing perturbation velocity potential in unsteady transonic flow without heat exchange 02 p0279 A70-12118
- Energy reversal zones in turbulent shear flows with asymmetric mean velocity distribution, implying zones of opposing shear 02 p0279 A70-12228

- Molecular velocity distribution function measured in normal He shock wave in low density wind tunnel by electron beam fluorescence technique 02 p0299 A70-12229
- Warm Maxwellian plasma stabilization of velocity-space instabilities, evaluating densities and temperatures for stabilizing resonant loss-cone modes 02 p0347 A70-12237
- Upper mass limit of quasar in galactic cluster from velocity dispersion of galaxies using generalized form of virial theorem, determining B264 mass 02 p0372 A70-12245
- Turbulent boundary layers behavior prediction by strip integral momentum equation method, considering velocity profiles and shear stresses 02 p0282 A70-12332
- Integral theory for two dimensional incompressible turbulent boundary layer in nonequilibrium flows, describing velocity profile in momentum and energy equations 02 p0283 A70-12335
- Mixing length theory improvement to calculate turbulent boundary layers based on velocity profiles 02 p0284 A70-12342
- Shear stress transport equation derivation from turbulent energy equation based on properties of turbulent velocity fluctuations 02 p0284 A70-12346
- Shear velocity variation with depth in upper mantle for Basin and Range province of western North America, using S waves measurements 02 p0292 A70-12505
- Gravitational theory for disk galaxies, considering radial velocity variations, spiral structure, heat equation verification, etc 02 p0378 A70-12688
- Stagnation point velocity gradients for spherical segment models with bluntness ranging from hemisphere to flatnose cylinder in hypersonic flow 03 p0406 A70-12947
- Gram-Charlier method generalization for curve fitting analytic forms to velocity covariances measured in turbulent wake of circular cylinder 03 p0480 A70-12950
- Wing-fuselage interference influence in aircraft dihedral effect, discussing role of velocity direction on wing 03 p0406 A70-13020
- Kinetic equation describing variation of distribution function of stellar residual velocities under action of gravitational field, discussing stellar diffusion in velocity field 03 p0564 A70-13227
- Pulsation energy distribution in free turbulent incompressible jets, noting role of mean velocity distribution 03 p0466 A70-13384
- Critical thermal regimes in Couette flow, investigating temperature and velocity profiles of nonisothermal steady state Newtonian flow between two parallel plates 03 p0466 A70-13388
- One dimensional magnetograph scans studying photospheric velocity oscillations and supergranulation, noting downward flows coincident with chromospheric network 03 p0570 A70-13593
- Disintegration of charged distilled water jets, discussing drops size, velocity distribution and instabilities 03 p0467 A70-13781
- Microstructure of turbulent jet in concurrent flow, analyzing wake parameter and measuring profiles of pulsation velocity components and Reynolds shear stresses 03 p0409 A70-13871
- Turbulent fluctuation rates of temperature and velocity on basis of measurements in boundary layer with wall heat transfer 03 p0470 A70-14237
- Velocity structure associated with motion of interface between turbulent and nonturbulent fluid at turbulent boundary layer edge, considering shear flows 03 p0470 A70-14240
- Aerodynamic velocity field induced by plate in motion correlated with ideal gas flow at specific Reynolds number, discussing wake formation 03 p0410 A70-14270
- Radial velocity profiles measured in plasma jet thrusters with thermal and self magnetic acceleration, discussing disturbances due to discharge current-magnetic field interactions 03 p0553 A70-14374
- Whistler mode instability due to anisotropic charged particle velocity distribution, establishing general onset conditions for variable density cold plasma containing hot electrons 03 p0537 A70-14378
- MHD flow velocity and current density distributions in annular duct with radial magnetic field 04 p0725 A70-14531
- Mean flow velocity distribution calculated from momentum deficit superposed behind single cylinders in finite array of arbitrarily spaced parallel cylinders [ASME PAPER 69-WA/FE-11] 04 p0614 A70-14781

Similarity of velocity profiles and pressure distribution of turbulent jet over inclined wall, indicating limitations of Glauert analysis
[ASME PAPER 69-WA/FLCS-1]

Viscous inlet flow into straight channels, studying velocity profiles at low Reynolds numbers
[ASME PAPER 69-APM-Q]

Linearized velocity profiles for turbulent free shear layers using transverse shift and longitudinal motion equation
[ASME PAPER 69-WA/APM-28]

Setting length for turbulent air flow velocity profile in smooth concentric annuli with square-edged and bellmouth entrances
[ASME PAPER 69-WA/APM-24]

Linear stress distribution insertion into equations of motion for turbulent boundary layer, considering velocity profile in wall region

Static pressure distributions and velocity profiles for Hg flow through circular pipes in transverse magnetic field, studying laminar and turbulent flows

Boundary layer along flat plate at zero incidence with homogeneous suction using momentum and kinetic energy integral equations through boundary layer velocity profile

Solar atmospheric structure near sunspots by spectrophotometry, presenting observational and theoretical sunspot magnetic and velocity field data

One dimensional stress waves propagation in elastoplastic medium, determining stress and velocity fields due to heat sources motion by characteristics method

Transverse and longitudinal correlation coefficients of electron density fluctuations in turbulent jet related through equation specifying velocity fluctuations isotropy

Axial and rotational velocity profiles of plasma jet from Doppler shift of spectral lines
[DFVLR-SONDDR-27]

Classical Couette flow for emitting and conducting gas media, discussing velocity distribution and temperature effects at LTE and non-LTE

Velocity field characteristic for electrons in GaAs in negative differential mobility region by method involving probe measurements

State and velocity distribution measurements for air in counterflow vortex tube to determine axial variation of flow quantities

Steady MHD shear layer velocity profiles using hot film anemometry

Motion generated by spherical body moving along axis of uniformly rotating fluid, measuring particle velocities ahead of and behind body

Unsteady laminar free convection caused by heating semiinfinite flat vertical plate, obtaining velocity and temperature distributions

Motion stability of ideally plastic medium flow in conical matrix, studying surface and velocity distribution for minimum plastic deformation energy

Pulsation velocities distribution wind in meteor region of atmosphere during hourly intervals over eleven month period, noting normal distribution

Compressible fluid flow velocity profile in turbine stage evaluated by streamline correlation and actuator disk method

Wave surface elevation and velocity fluctuations in ocean upper layer under wind waves, discussing correlation coefficients between vertical and horizontal velocity components

Solar atmosphere granular convective velocity field determination methods, using realistic assumptions for typical granulation size and seeing parameter

Magnetic and velocity fields in unipolar sunspot, discussing fluctuations associated with penumbral and umbral fine structures

HF periodic velocity oscillations effect on axisymmetric wake diffusion flames
[AIAA PAPER 70-10]

Molecule spatial and velocity distributions of supersonic molecular beams, measuring scattering cross sections of He and Ar on noncondensable gases

Velocity distributions of incident and reflected Ar beams, determining partial energy accommodation

coefficients for reflection from copper and carbon dioxide deposited surfaces

Shock wave structure in He-Ar mixture velocity and temperature profiles based on kinetic model equations

Slip flow of nitrogen gas through long circular tubes, measuring mass flow, pressure drop and cross sectional velocity profiles

Whistler amplification in magnetosphere for electron interaction with background plasma to produce wave growth, discussing stability of various anisotropic velocity distributions

Model for thunderstorm downdrafts induced by rain evaporation based on one dimensional steady state formulation, deriving vertical velocity profiles

Velocity distribution of atoms evaporating from superfluid He II at low temperatures, noting roton shifting and multiexcitation processes

Plastic lubricants motion in circular pipes, determining drag and cross sectional velocity profile of laminar flows

Steady viscoplastic boundary layer near hard wall with power law velocity distribution along outer boundary, deriving self similar solution

Correlation function of velocity fields in two dimensional turbulence determined from hydrodynamic equation assuming normally distributed stream function field

Ideal fluid planar potential flow, approximating stream function and velocity potential by matrix method

Laminar flow of compressible gas in axisymmetrical channel in absence of wall insulation using velocity profiles, heat transfer, etc

Velocity fields and turbulent pulsations effects on heat transfer in gas flow past plate with rectangular protrusion using wind tunnel tests

Unsteady laminar boundary layers calculation for arbitrary velocity distributions at inner boundary in presence of suction/blowing through porous surface

Boundary layers calculation for nonporous surface extended to porous with suction by replacing velocity distribution with longitudinal pressure gradient

Flow velocity distribution near boundaries of model of plates of parallel faces, obtaining Laplace equation solution

Solar wind velocity anisotropy effect on interplanetary magnetic field inhomogeneity

Wall proximity and velocity gradient effects on thermocouple readings in turbulent boundary layer

Turbulent energy and velocity spectra of air flow at atmospheric boundary layer over water analyzed statistically, assuming rippling surface activity

Single junction vacuum thermocouple measuring thermal beam effect with reference to velocity distribution perturbation in molecular beam scattering

Energy dependence of elastic total collision cross section of identical He molecules, using velocity selected primary beams at low target temperature

Temperature renormalization for improving velocity distribution function representation in solving nonlinear Vlasov equation, transforming Hermite polynomials

Selective harmonic excitation in one dimensional collisionless plasma conforming to Vlasov equation by counterstreaming electron beams, noting velocity distribution conditions

Stellar velocity distribution function for small mass stars in nonrotating systems

Transverse curvature effects on turbulent boundary layer thickness and velocity profiles on circular cylinders in water and air

Solar wind velocity cycles from fluid MHD viewpoint, applying Kelvin theorem on circulation stability in closed fluid system

Hot-wire anemometry equation suitable for wide regions of velocity and temperature derived by computing thermal losses by supports

Symmetrical laminar distorted velocity profiles between flat parallel plates, analyzing decay using integral method

Unsteady flow in circular tube of constant section with time dependent discharge, determining pressure gradient and velocity distribution

Harmonics generated in hot-wire anemometers responses by wires thermal lag and amplitude of flow velocity fluctuations using computerized simulation

Mixing region and potential cone of two dimensional jet, measuring velocity fluctuations

Kinetic equation describing variation of distribution function of stellar residual velocities under action of gravitational field, discussing stellar diffusion in velocity field

Plane jet velocity profiles determination applied to calculating gain of proportional fluid amplifier

Low pressure plasma stability in cylindrical crimped magnetic field, considering convective perturbations and particle velocity distribution

Turbulent MHD channel flow velocity profiles and hydraulic resistance relations for various Reynolds numbers, using two layer model

Average velocities profile measurement in wall region of turbulent fluid flow in smooth duct

Blast waves in low Mach number regime with assumption of power law density profile in rear, obtaining particle velocity and pressure distributions

Stability theory application to laminar boundary layer transition prediction on two dimensional and axisymmetric flows having pressure distributions in incompressible flow

Partially loaded clamped plastic shallow spherical caps collapse loads and stress and velocity distributions

Velocity distribution along cylindrical pipe in adiabatic flow with friction and known inlet parameters

Shear flow of inviscid incompressible fluid past sphere, calculating secondary vorticity and upstream velocity distribution

Pressure and velocity distribution within radial flow gas turbine rotor computed by two dimensional streamline curvature method

Near-free molecular flow through orifice measured for velocity distribution dependence on Knudsen number and angular position using time-of-flight technique

Reflected shock wave structure and velocity at rigid wall, assuming radiative heat transfer as dissipative process

Gas stream velocity field produced by shock wave impinging against wing moving at supersonic speed

Velocity and temperature distribution behind shock waves in hydrogen plasma measured to determine factors responsible for discrepancies in Rankine-Hugoniot conditions

Skin friction near flat plate trailing edge at high Reynolds number by linearizing velocity profile

Series expanding velocity profile in parabolic cylinder functions describing nonlinear evolution of steady laminar incompressible wake from arbitrary initial profile

Statistical chance characteristics of velocity profiles and friction for flow along infinite plane wall with constant suction

Turbulent water flow velocity distribution measurement using laser light intensity fluctuation spectroscopy

Gas dynamics regarding velocity field excited by vibrations propagating over elastic wing surface at finite velocity

Velocity and pressure distribution and flame front shape of confined flame in constant section duct

Ionospheric wind velocity fields calculated from atmospheric dynamo effects taking into account electric field, current density and conductivity tensor

Hydraulic loss and secondary circulation of fluid flow in three dimensional bend commercial conduits, discussing relationship to velocity distribution
10 p1871 A70-25094

Multivelocity electron beam critical fluctuation amplitudes in crossed electric and magnetic field
10 p1925 A70-25107

Laminar flow of compressible gas in axisymmetrical channel in absence of wall insulation using velocity profiles, heat transfer, etc
10 p1871 A70-25213

Velocity fields and turbulent pulsations effects on heat transfer in gas flow past plate with rectangular protrusion using wind tunnel tests
10 p1871 A70-25214

Velocity distribution around isolated and cascaded airfoils in plane potential flows of incompressible fluid determined by use of nonsingular integrals
11 p1974 A70-25781

Velocity distribution of plane airfoil cascade given by geometry, using method of least squares
11 p1974 A70-25785

Electrons velocity distribution function in homogeneous stationary weakly ionized Lorentz plasma in neon, investigating effect on mobility, collision frequency, diffusion and kinetic energy
11 p2089 A70-25871

Ionospheric plasma drift vertical and meridional velocity components latitudinal distributions in F2 region, considering wind effects in upper atmosphere
11 p2045 A70-25931

Nozzle source design for high intensity thermal energy molecular beam with small dispersion in velocity suitable for scattering experiments
11 p2086 A70-25973

Three dimensional turbulent flow, using direct interaction approximation for growth and propagation of point-to-point velocity field deviations energy spectrum
11 p2036 A70-26013

Velocity profile and volume flow rate for rarefied gas flowing isothermal parallel plates, solving linearized Boltzmann equation by BGK model
11 p2037 A70-26168

Track-while-scan algorithm, considering probabilistic interpretation of linear recursive least squares filter for velocity variations
11 p2029 A70-26319

Incompressible inviscid fluid flow behind impeller blades, determining velocity profiles, flow-off angle and stable operation limits
11 p1977 A70-26349

Laminar boundary layer flow with exponential velocity distribution in outer flow described by differential equations, studying slip velocity at wall
11 p2037 A70-26350

Transformed distribution function of particle velocity of plasma in Debye thermodynamic equilibrium approximation based on statistical mechanics
11 p2091 A70-26459

Steady state two dimensional flow velocity profiles at low Reynolds numbers of homogeneous incompressible viscous liquid in straight channel inlet region
11 p2037 A70-26476

Incompressible boundary layers velocity distributions on cylinders rotating in axial flow, considering centrifugal force effects, momentum thicknesses, local shearing stress, etc
11 p2038 A70-26477

Large scale atmospheric turbulence using wave number frequency Fourier analysis of velocity distributions on latitude circles
11 p2076 A70-26498

Multipoint time correlations of longitudinal velocity fluctuations in grid-generated turbulence
11 p2039 A70-26532

Turbulence theory based on Wiener-Hermite expansion of velocity distribution to predict energy decay rate for Reynolds numbers greater than two
11 p2040 A70-26542

Metastable time-of-flight technique for measuring free molecular flow velocity distribution
12 p2231 A70-27255

General relativistic hydrodynamics near equilibrium, discussing velocity and kinetic energy increase spherically symmetric large masses as function of radius change
12 p2300 A70-27392

Turbulent Prandtl number values for air with injection and suction obtained from velocity and temperature profile data
12 p2210 A70-27699

Limb-SD type ascending prominences direction and velocity correlated to flares and solar radio emission
12 p2303 A70-27707

Spatial relaxation of electron gas colliding with positive ions from plasma velocity distributions, solving time independent Fokker-Planck boundary problem
12 p2280 A70-27791

Velocity distribution and structure of irregular winds near 100 km measured by differencing chemical release wind profiles
12 p2264 A70-28002

Compressible turbulent boundary layers velocity profiles, Coles universal wake function, least squares methods, wake-wall representation, etc
12 p2157 A70-28080

Kinetic theory of gas composed of identical particles with discrete velocity distribution, using Chapman-Enskog method
12 p2213 A70-28211

Turbulent flow of incompressible fluid, obtaining closed system of approximate equations for probability distribution of velocities
12 p2213 A70-28237

Preston tube errors in pipe flow wall shear stress determination due to velocity distribution deviations
13 p2387 A70-28848

Ionospheric electrons velocity distribution function in steady state with oscillating electric field imposed in arbitrary direction with respect to magnetic field
13 p2395 A70-28941

Asynchronous liquid metal MHD generator parameters, assuming constant vertical distribution of working fluid velocity
13 p2349 A70-28968

Earth core flow velocity field to construct kinematic model of hydromagnetic dynamo, discussing magnetic field development
13 p2398 A70-29209

Jeans escape rate error for atmospheric H and He attributed to perturbed velocity distribution function, using realistic atom-atom elastic scattering cross sections
13 p2398 A70-29226

Self gravitating collisionless particles instability related to anisotropic random velocity distribution function in presence of disk-galaxy type spiral wave perturbations
13 p2492 A70-29299

Plane turbulent wall jet from small slot, investigating velocity distribution dependence on slot inclination
13 p2388 A70-29448

Two dimensional turbulent boundary layer with pressure gradient, calculating velocity distribution and local skin friction by Pohlhausen method
13 p2391 A70-29672

Electron and positive ion velocity distributions measurements near earth bow shock by electrostatic analyzer on Vela 4B satellite
13 p2481 A70-30068

Logarithmic and Coles velocity profiles validity for turbulent boundary layers on radial rotating impeller blades
14 p2527 A70-30176

Rarefied gas flow in slip regime through cylindrical tube assuming parabolic velocity profile
14 p2565 A70-30263

Transverse structural function of velocity field of turbulent motion in upper atmosphere, using meteor speed radio observations
14 p2635 A70-30312

Faraday type MHD generators, investigating gas velocity and temperature profiles effect on electrical performance by equivalent circuits simulation
14 p2534 A70-30537

Velocity and pressure distributions of tornado-like two cell vortices within boundary layer, using different assumptions for eddy diffusion coefficient
14 p2604 A70-30547

High winds simultaneous occurrence and duration to 150 meter height, showing coherence tendencies
14 p2607 A70-30583

Light scattering from plasmas with nonMaxwellian electron velocity distribution function
14 p2622 A70-30694

Maximum velocity decay in wall jets calculated for comparison with experimental velocity profile
14 p2566 A70-30777

A-type supergiants microturbulence, determining atmospheric small scale velocity fields
14 p2641 A70-30885

Velocity difference across viscous tail in MHD flow, demonstrating exponential decay
14 p2623 A70-30992

Statistical transport, energy and chemical reaction rate in turbulent flow field with uniform velocity gradient, using Brownian motion theory
14 p2566 A70-31029

Two dimensional jet velocity profile evolution under symmetrical and antisymmetrical perturbations
14 p2567 A70-31200

Low aspect ratio wing aerodynamic characteristics in shear flow, noting forces dependence on flow velocity gradients
14 p2529 A70-31274

Vortex generation in water tank, discussing velocity distribution on free surface and critical depth of air entrainment for various Reynolds numbers
14 p2567 A70-31275

Galactic spiral structure effects on residual stellar velocities local distributions
14 p2652 A70-31380

Laminar velocity distribution from temperature profiles developed under steady flow through tube, constructing numerical temperature grid
15 p2718 A70-31449

Steady viscoplastic boundary layer near hard wall with power law velocity distribution along outer boundary, deriving self similar solution
15 p2718 A70-31462

Correlation function of velocity fields in two dimensional turbulence determined from hydrodynamic equation assuming normally distributed stream function field
15 p2718 A70-31465

Homogeneous isotropic turbulence velocity field space-time variable correlation functions in fluid flow
15 p2719 A70-31487

Incompressible turbulent boundary layer calculation based on shearing stress hypothesis, considering layer at flat plate, boundary conditions and velocity profiles
15 p2719 A70-31490

Transport properties of partially ionized argon based on electron velocity distribution function, comparing to Chapman-Enskog calculations
15 p2774 A70-31799

Space charge waves in electron beams with velocity distribution, considering dispersion equation and Landau damping
15 p2708 A70-31831

Longitudinal velocity and temperature fluctuation spectra in turbulent boundary layer, showing highest spectral densities at internal zone
15 p2826 A70-32021

Orr-Sommerfeld equation asymptotic solution corresponding to boundary layer velocity distribution
15 p2721 A70-32357

H alpha and Fe I lines, calculating velocity effects on profiles for differentially moving atmosphere
15 p2804 A70-32616

Fragment ion products velocity vector distribution for dissociative collisions of molecular ions with He
16 p2953 A70-33005

Intensity and velocity distributions of thermal energy argon atoms scattered from silver /111/ face, using time of flight methods
16 p2953 A70-33007

Vortex streets characteristics determination for plane jet having uniform initial velocity profile
16 p2890 A70-33108

Subsonic turbulent boundary layer with mass addition and combustion for combustion effects on velocity profiles in constant pressure and accelerating flows
16 p2997 A70-33498

Displayed cursor velocity effect on radar target acquisition time for subjects in simulated air defense environment
16 p2853 A70-33670

Uniform two dimensional turbulent boundary layer with hydrogen-nitrogen mixture injection and combustion at flame front, obtaining velocity distribution by kinetic energy equation
16 p2894 A70-33880

Pressurized gas bearing flow field, discussing velocity transversal component, pressure distribution and profile
16 p2924 A70-34237

Lorentz plasma electron velocity distribution with allowance for elastic and inelastic collisions, using Legendre polynomial and spherical harmonic expansions in Boltzmann equation
16 p2945 A70-34337

Numerical solutions for velocity and concentration profiles to nonsimilar isothermal diffusion laminar boundary layer equations for uniform injection of foreign gas
17 p3069 A70-34824

Solar rotation effects on velocity field in nonspherical solar wind, using axisymmetric wind model
17 p3151 A70-34861

Incompressible laminar boundary layer along rectangular corner, obtaining similar solutions for velocity distribution
17 p3070 A70-35239

Turbulence theory from Liouville equation for Navier-Stokes velocity field distribution
17 p3073 A70-35629

Solar wind velocity profile in rapid acceleration of coronal plasma from type I, III and V bursts
17 p3152 A70-35745

Velocity fluctuations in temperature gradient turbulent jets and in turbulent flames, using hot wire in cooled pitot tube
17 p3096 A70-35749

Aerofoil section characteristics in shear flows of arbitrary velocity profile calculated by Glauert image method
18 p3205 A70-35957

Velocity pulsation spectra in subsonic wakes behind circular disks and sphere, using thermoanemometer with constant filament temperature
18 p3207 A70-36279

Temperature profile along hot-wire anemometer attached to wall and normal to parabolic velocity steady flow field, using singular perturbation techniques
18 p3242 A70-36488

Centrifugal impellers primary and secondary flows velocity distributions, determining vorticity generation
18 p3243 A70-36871

Three dimensional boundary layer flow on rotating axial flow turbine buckets, determining velocity profiles [ASME PAPER 70-GT-59] 18 p3243 A70-36874

Two dimensional cascades of incompressible plane potential flows with given velocity distribution [ASME PAPER 70-GT-87] 18 p3209 A70-36880

Solar wind velocity anisotropy effect on interplanetary magnetic field inhomogeneity 18 p3309 A70-36917

Peculiar velocities nonisotropic distribution in stationary differentially rotating stellar system based on Boltzmann equation solution 18 p3324 A70-37149

Stellar velocity field in M 51 from image tube spectra 18 p3327 A70-37158

Neutral H concentrations far from galactic plane associated with spiral arms 18 p3327 A70-37166

O and B stars velocity dispersion, considering Oort terms and average residual radial velocity 18 p3330 A70-37188

Young star velocity ellipse vertex deviation, discussing formation at right angles to galactic center direction 18 p3331 A70-37199

Velocity profiles in steady and unsteady rotating flows for impulsive slow down and acceleration in cylindrical chamber 19 p3403 A70-37527

Turbulent flow phase velocity fluctuations measurement by hot-wire anemometers, obtaining cross-spectral density by Fourier analysis digital techniques 19 p3404 A70-38019

Velocity distribution and shear stress measurements in three dimensional turbulent boundary layer approaching separation 19 p3405 A70-38021

Velocity profiles of laminar flow through rectangular duct with moving wall and arbitrary cross section under nonslip boundary condition 19 p3405 A70-38043

Velocity distribution in boundary layer on thin rotating turbine blade of impeller driven at wind tunnel outlet, solving turbulent and laminar flows momentum equations 19 p3352 A70-38224

Pressure and velocity distribution inside casing and around impeller of volute pumps, discussing flow at exit and in wedge shape space 19 p3437 A70-38225

Steady two dimensional incompressible shear flow, correlating velocity profiles with resistance distribution 19 p3406 A70-38350

Boundary layer oscillatory flow interaction with nonuniformly rotating lamina, calculating velocity distribution and transitional frequencies 19 p3406 A70-38443

Fully ionized magnetized rotating plasma interaction with neutral gas blanket, discussing plasma decay and velocity field 19 p3481 A70-38489

Weakly ionized gas subjected to pulsed DC electric field, analyzing transient relaxation of electrons velocity distribution 19 p3482 A70-38899

Hydromagnetic flow past infinite impulsive motion plate, determining velocity and temperature fields distribution 19 p3482 A70-38934

Turbine blade profiles calculation by hodographs, obtaining compatibility with continuous flow velocity distribution and improved boundary layer stability 19 p3491 A70-38949

Shear stress and velocity profiles in three dimensional mixing layer between grazing perpendicular streams 20 p3608 A70-39356

Midtropospheric frontogenesis, using three hourly rawinsonde data for isentropic trajectories to describe velocity field in space and time 20 p3664 A70-39374

Cesium beam velocity attenuation by He, Kr and Xe, determining scattering cross sections from gas pressure and density measurements 20 p3675 A70-39618

Flow velocity and pressure profiles due to vortex ring confined in cylindrical channel, using electromagnetic analogy 20 p3609 A70-39651

Probability densities and distributions, moments and spectra from time derivatives of streamwise velocity fluctuation in curved mixing layer, measuring small scale turbulence structure 20 p3609 A70-39652

Energy spectrum function for Gaussian initial velocity field of inviscid turbulence Burger model, using Cameron-Martin-Wiener exact expansion 20 p3609 A70-39653

Solar internal rotation, examining oblateness, velocity and magnetic fields, wind structure and Li and Be abundances 20 p3707 A70-39936

Vortex signature recognition from radial velocity field by Doppler radar 20 p3664 A70-40067

Conical diffuser-tailpipe system performance, discussing cone angle, area ratio, Reynolds number and velocity distribution effects on pressure recovery 20 p3559 A70-40082

Hypersonic sphere turbulent wake velocity measurement by spark technique, determining distribution from least mean squares fits of Gaussian curves 20 p3559 A70-40283

Wall proximity and velocity gradient effects on thermomometer readings in turbulent boundary layer 20 p3634 A70-40341

Ducted laminar and turbulent diffusion flames, examining electric fields effect on heat transfer, geometry and velocity field 20 p3739 A70-40471

Wall jet turbulent flow regions with shear stress and mean velocity gradient of opposite sign, considering theoretical explanation 20 p3615 A70-40501

Point mass impact on flexibly interconnected rigid bodies with tree structure and spherical joints without dry friction, discussing resulting velocity changes 21 p3849 A70-40552

Nonstationary compressible laminar boundary layer similar solutions by parameter-invariant method, obtaining velocity and temperature profiles by partial differential equations numerical integration 21 p3806 A70-40555

Two dimensional turbulent boundary layer computation using two parameter family of velocity profiles and skin friction law 21 p3806 A70-40921

Heat transfer in laminar channel flow with random velocity variations, using Monte Carlo technique 21 p3949 A70-41312

Closing method for turbulence equations of velocity field quantities joint probability distributions 21 p3811 A70-42075

Flow structure in plane submerged turbulent jet, determining velocity, friction stress and correlation coefficients distributions 21 p3749 A70-42221

Liquid metal turbulent jet flow dependence on longitudinal magnetic field, measuring mean velocity profiles at various cross sections 21 p3861 A70-42230

Turbulent flow velocity profile in constant transverse magnetic field, determining resistance coefficient 21 p3861 A70-42235

Flat plate airfoil unsteady lift due to chordwise velocity perturbations, using Horlock frozen gust pattern theory 22 p3957 A70-42303

Viscous flow field in pneumatic vortex rate sensor, discussing boundary layer parameters, velocity profiles and swirling flow theory [ASME PAPER 70-FLCS-16] 22 p4007 A70-42411

Isothermal steady laminar flow through tube with change in wall temperature, examining velocity profile relationship to temperature profile 22 p4008 A70-42421

Jet flow reattachment to walls of various shapes, measuring undeveloped velocity profiles at nozzle exit [ASME PAPER 70-FLCS-2] 22 p4008 A70-42429

Large fluid amplifier-type jets, measuring upstream flow disturbances effects on spreading velocity profiles [ASME PAPER 70-FLCS-A] 22 p3964 A70-42431

Ion and electron ambipolar velocity distribution near plasma sheath boundary in collisional positive column 22 p4080 A70-42542

Spherical cavity nonuniform expansion in compressible elastic plastic solid, calculating velocity field and pressure by approximate similarity solution 22 p4114 A70-42635

Buoyant hot two dimensional laminar vertical jet in quiescent colder fluid, calculating temperature and velocity distributions by integral method 22 p4010 A70-42639

Galactic noncircular velocity fields, discussing statistical correlation with radio luminosity, nuclear brightness and total mass 22 p4100 A70-42844

Globular cluster relaxation time using nonMaxwellian velocity distribution and polytropic spatial distribution 22 p4109 A70-43744

MHD laminar isothermal flow in closed cylindrical tube in rotating magnetic field, determining azimuthal velocity distribution 23 p4224 A70-44162

Mass transfer and velocity gradient fluctuations at wall in two dimensional or rotational flow for large Schmidt numbers 23 p4181 A70-44210

Partially ionized Ar transport properties, computing electron velocity distribution function as perturbation for Lorentzian mixture 23 p4220 A70-44437

Turbulent boundary layer velocity profiles and shear stress distributions computation based on mixing length approach 23 p4182 A70-44574

Two dimensional turbulent wake theory, considering shear stress and velocity distribution behind flat plate and circular cylinder 23 p4134 A70-44575

Spinning cold-flow rocket motor, studying rotation effects on chamber flow velocity field 23 p4233 A70-44579

Algorithm for space trajectories optimization with delta velocity constraints 23 p4245 A70-44683

Gas turbine engines flow velocity fields, comparing various calculation methods 23 p4136 A70-44735

Air circulation around radial flow machine rotor blades calculated without velocity distribution factor 23 p4183 A70-44774

Stellar axial rotational velocity statistical analysis to break-up limit, obtaining velocity distribution approximation from observed histogram 23 p4251 A70-44823

Solar interior differential rotation, developing angular velocity distribution equilibrium model 23 p4252 A70-44834

Atomic levels occupation numbers and ionization degree for optically thin hydrogen plasma with self consistent electron velocity distribution 23 p4227 A70-44932

Viscous conducting liquid forced vortex motion, considering radial velocity distribution and rotation effect on free surface shape 24 p3483 A70-45140

Sunspot penumbra velocity field spatial structure by filament spectrum analysis, plotting radial velocities relative to undisturbed photosphere 24 p4400 A70-45310

Molecular jet velocity distribution, investigating adiabatic focalization conditions 24 p4351 A70-45370

Combustion chamber flow visualization, obtaining information on pressure loss, velocity field, flow pattern and temperature gradients 24 p4393 A70-45444

Flow-through carbon dioxide lasers population inversion relation to individual gas components and electron velocity distribution functions 24 p4352 A70-45458

Velocity profile in viscous sublayer at wall based on maximum stability principle applied to Karman constant for turbulent channel flow 24 p3425 A70-45495

Boundary layer instantaneous velocity distributions theoretical and experimental determination 24 p4288 A70-45583

Quasi-homogeneous approximation validity for electron velocity distribution function disturbance in gas plasma column ionization waves discharge involving high currents 24 p3866 A70-45794

Spherical shape gas or liquid drop steady motion at large Reynolds numbers, examining buoyancy forces and velocity gradients 24 p4326 A70-45996

Plane flow of incompressible elastic perfectly plastic solid, deriving hyperbolic stress and velocity equations 24 p4427 A70-46043

VELOCITY ERRORS

Interplanetary midcourse velocity correction schedules optimization, discussing timing equations modifications, mission simulation and role of earth based radar 09 p1759 A70-22760

VELOCITY FIELDS

U VELOCITY DISTRIBUTION

VELOCITY MEASUREMENT

NT WIND VELOCITY MEASUREMENT

Hot-wire probe support orientation to minimize flat plate turbulent boundary layer mean velocity determination errors 01 p0087 A70-10665

Physiological interpretation of blood velocity curves recorded in right heart cavities of dogs by ultrasonic directional probe, using Doppler effect 01 p0035 A70-10709

Cosmic dust particle direction, velocity and mass from ionization and momentum measurements by dust sensor during impact on Pioneer 8 satellite 01 p0088 A70-10748

F region ion velocity measurements by Thompson scatter probe, deducing neutral winds diurnal and seasonal variations in thermosphere 01 p0078 A70-11214

Radar and photographic studies of meteors from Leonid and Perseid showers, presenting velocities, luminescence and ionization 01 p0193 A70-11602

Jupiter upper atmosphere cloud bands zonal motion velocities, examining barotropic stability criterion and geostrophic balance hypothesis 02 p0368 A70-11828

Molecular velocity distribution function measured in normal He shock wave in low density wind tunnel by electron beam fluorescence technique

02 p0299 A70-12229

Flow direction and velocity measurement in three dimensional boundary layer, discussing instrument and restrictions

02 p0299 A70-12312

Traveling wave velocity in human cochlea determined by equally loud tonal pairs, comparing results to psychophysical and electrophysiological findings

02 p0237 A70-12323

Cylindrical axial plasma flow fields velocity radial dependence measurement by double-wedge spectroscopy using Abel unfolding of Doppler shifts

02 p0349 A70-12657

Plasma velocity, electron temperature and density and ion density determined by two mutually perpendicular probes

03 p0529 A70-12940

Spatial resolution analyses of vorticity meter and hot wire arrays for measuring velocity derivatives in isotropic turbulence

03 p0492 A70-13760

Laser velocimeter measurements on drag reducing polyacrylamide solution compared to water

03 p0502 A70-13821

Flat flames in stationary gas in tubes useful for flame speed measurements without correction procedure

03 p0607 A70-13917

Burning velocity of methane-air flames inhibited by methyl bromide, using schlieren cone-nozzle burner method involving unburnt gas velocity measurement

03 p0607 A70-13918

Radial velocity profiles measured in plasma jet thrusters with thermal and self magnetic acceleration, discussing disturbances due to discharge current-magnetic field interactions

03 p0553 A70-14374

LF sound velocity measurement in carbon dioxide near critical point, noting existence of logarithmic divergence

04 p0718 A70-14685

Circular tube entrance upstream and downstream velocity profiles at small axial distances measured by laser Doppler flowmeter

[ASME PAPER 69-WA/FE-13] 04 p0667 A70-14780

Blood flow velocity and pressure measurements on conscious man with catheter-tip velocity probe

04 p0645 A70-15439

Meteoroids average velocity relative to spacecraft determined using sporadic meteors orbital elements data in interplanetary space

04 p0757 A70-15550

Velocity field characteristic for electrons in GaAs in negative differential mobility region by method involving probe measurements

04 p0732 A70-15690

Acceleration cues removal effects on vehicular velocity perception, using movie technique to control visual cues

05 p0806 A70-16143

Laser beam for measuring particles velocity in two phase air-water jets by heterodyning, describing signal properties

05 p0858 A70-16258

Laser Doppler velocimeter directly measuring detected frequency with passive confocal Fabry-Perot interferometer

05 p0860 A70-16658

Doppler shift of laser beam reflected from shock wave measuring velocity through optical mixing

05 p0852 A70-16993

Repetitive scanner for wave velocity measurements in annular two phase gas or liquid flow using pivoted mirror

06 p1062 A70-17618

Dynamic response of constant resistance anemometers, investigating unsteady probe thermal equilibrium, inductance and feedback equations

06 p1063 A70-17620

Solar atmosphere granular convective velocity field determination methods, using realistic assumptions for typical granulation size and seeing parameter

06 p1142 A70-17990

Light velocity measurement at low cost, describing circuits and experimental results

06 p1067 A70-18399

Doppler shift measurements of axial and rotational velocities in MPD arc, using references from iron arc [AIAA PAPER 69-110]

07 p1364 A70-19324

Flow mean velocity measurement using probe submerged in moving electrolyte and not requiring external power source

07 p1257 A70-19377

Solar wind velocity radioastronomical measurements, discussing radio wave fluctuations, telescope antenna designs, radiometers and observations

08 p1474 A70-21070

Instantaneous velocities measured for wall region of smooth duct during turbulent fluid flow by chronophotography of particles

09 p1658 A70-22046

Small-scale local flow velocity measurements with laser using differential Doppler method

09 p1694 A70-22125

Wave front velocity determination by analytical continuation of wave function Fourier transform into complex plane, discussing constraints imposed by finiteness requirement

09 p1726 A70-22327

Projectile acceleration under gas explosion calculated for velocity

09 p1777 A70-22723

Signal properties and measurement accuracy of noncontacting optical heterodyne velocity sensing method used in differential Doppler velocity measurements

09 p1678 A70-22926

Sphere motion in laminar flow, postulating absolute velocity as resultant of entrainment and fall velocities and stable position in tube with ascending flow

09 p1663 A70-23309

F region vertical electron drift velocity determined from Thomson scatter observations

09 p1671 A70-23665

Charged particles velocity profile across shock determined by induction velocimetry, considering eddy currents effects on induced potential gradient

09 p1738 A70-23677

Near-free molecular flow through orifice measured for velocity distribution dependence on Knudsen number and angular position using time-of-flight technique

10 p1918 A70-23969

Velocity measurements with Pitot tubes in polymer solutions /polyethylene oxide/ in water, noting viscoelastic properties effect on measured pressure value

10 p1887 A70-24093

Laser Doppler velocimeter optics, noting minimal heterodyne alignment needs and stress and vibration stability

10 p1889 A70-24556

F 2 field-aligned ion velocity measurement compared with theoretical results, discussing difference at sunspot minimum and daytime ion velocity-plasma loss relation

10 p1881 A70-24815

Kalman filtering applied to moving balloon position and velocity estimates related to upper atmosphere wind measurements by balloon-satellite experiment

11 p2025 A70-26206

Radial velocity data monitored during Venera 4 descent used for determining vertical and horizontal atmospheric flows velocities

11 p2118 A70-26792

Velocity fluctuations measurements in conducting fluids flowing through tubes

12 p2230 A70-27091

Metastable time-of-flight technique for measuring free molecular flow velocity distribution

12 p2231 A70-27255

Spiraling electron beam energy conversion and distribution using retarding-field velocity analyzer

12 p2196 A70-27651

Current sheet speed in coaxial plasma accelerator computed as function of time, comparing results with velocity measurements

12 p2281 A70-27833

Air velocities measurement with heated thermistors probe, discussing calibration and reliability dependence on flow velocity range

13 p2405 A70-28841

Acceleration influence on radar signal reception during range and velocity measurements

13 p2366 A70-29301

Solar differential rotation measurement by spectral line shift data analysis, noting angular velocity-heliographic latitude relationship

13 p2496 A70-29840

Hot-wire probe measuring He-air mixture velocity and concentration following He discharge from circular orifice, noting calibration method

13 p2412 A70-29990

Rolling reentry body velocity as function of roll, pitch, yaw rates and angle of attack

13 p2343 A70-29991

Three-reception-point radar system for radiant and speed measurement of individual meteors in stream, using forward scattering

14 p2582 A70-30311

Errors estimation in wind velocity values by radio echo observations in meteor trails of different densities

14 p2572 A70-30330

Free floating balloon position and velocity determination by satellite, using Kalman filter linear estimation theory

14 p2530 A70-30571

High resistivity Si electron drift velocity measurement by exciting surface barrier diode with subnanosecond superradiant laser pulses

14 p2594 A70-30924

Frequency locked noise effect on beat frequency measurement of angular velocity with ring laser, comparing gyroscope and phase methods

15 p2749 A70-31551

Laser Doppler heterodyning system for velocity measurements without directional ambiguity, employing incident beams of different frequencies through rotating diffraction grating or Bragg cell application

15 p2751 A70-31986

Gas flow velocity measurement by coherent detection of scattered laser radiation from small particles suspended in fluid, using Doppler effect

15 p2751 A70-32030

Laser velocimeter application to laminar-turbulent flow transition at glass tube centerline

15 p2741 A70-32521

Displacement and velocity measurements using strain gauges, linear potentiometers and seismic transducers

15 p2743 A70-32799

Laser velocity measuring system (LVMS) for high speed rocket sleds, tracking supersonic sleds through shock front

16 p2926 A70-33142

Laser Doppler-shift velocimeter with self aligning optics, discussing performance parameters

16 p2926 A70-33143

Velocity vector for boost vehicles guidance, comparing implicit and explicit computation

16 p2947 A70-33441

Airborne pulse Doppler radar for tactical aircraft velocity vector measurement, improving navigation system performance

16 p2840 A70-33448

Gaseous flows and local droplet velocity measurement in dense gas/liquid sprayfields, using noninterference technique

16 p2910 A70-33491

Observational errors effects on surface waves resolution, describing shear velocity determination in crust and mantle from observed waves

16 p2897 A70-33647

Range and velocity components for ray paths between tracking and data relay satellite and user communication satellite

16 p2866 A70-34073

Gas flow velocity measurement using hot foil probes

17 p3082 A70-34680

Hypersonic velocity and turbulence measurements in wind tunnels, using spectral analysis of Doppler shifted laser light

17 p3103 A70-34849

Holographic motion measurement verification of constant velocity, sinusoidal vibration and both, using interferometer

17 p3087 A70-35022

Turbulent boundary layer velocity, temperature and concentration instantaneous measurements, describing automatic circuit procedure

17 p3088 A70-35041

Light velocity from frequency and wavelength differences between gas laser lines, using precision long path interferometry

17 p3104 A70-35085

Low temperature plasma flow velocity measurements using transit-time technique and high speed filming

17 p3141 A70-35345

High velocity neutral hydrogen cloud observations, presenting tabulated characteristics and maps

17 p3170 A70-35439

Turbulent velocity pulsations characteristics determination by diffusion measurements

18 p3240 A70-36265

Error reduction methods for linear acceleration gyrointegrators measuring linear velocities

19 p3420 A70-37257

Ionospheric drift velocity fluctuations by similar fading method, discussing applicability and errors

19 p3408 A70-37312

Meteor velocity determination by CW radar for constant phase angle, describing reflected signal processing

19 p3514 A70-37655

Manned lunar roving vehicle (MLRV) navigation scheme based on dead reckoning concept, discussing instruments effectiveness for vehicle velocity and orientation measurements

19 p3396 A70-37849

Holographic velocity data recording /velocimetry/, discussing axial resolution enhancement by spherical wave illumination

19 p3423 A70-37859

Dual scatter laser Doppler velocimeter /LDV/ technique, considering system design, performance and experimental verifications

19 p3424 A70-37876

Turbulent flow phase velocity fluctuations measurement by hot-wire anemometers, obtaining cross-spectral density by Fourier analysis digital techniques

19 p3404 A70-38019

Aperture size effect on frequency shift and frequency width variation of beat signals observed with laser Doppler velocity meter

19 p3428 A70-38502

Gas flow velocity measurement by thermal signal emitted from thin wire fed with modulated known frequency current

19 p3406 A70-38673

Noctiluent cloud kinematics, examining wave structure and lengths, velocities and general motion 20 p3622 A70-39403

Ultrasonic sensor for detecting altitude and vertical velocity of aircraft near ground, applying to helicopter hovering flight or conventional airplane takeoff and landing [AIAA PAPER 70-1031] 20 p3631 A70-39506

Onboard velocity sensors for VOR/DME navigation systems positional accuracy improvement, describing optimal and suboptimal data filtering [AIAA PAPER 70-1024] 20 p3666 A70-39511

Second order approximations to velocity required concept for boundary value problems in guidance, deriving Riccati equation and position required concept [AIAA PAPER 70-1015] 20 p3666 A70-39518

Ballistic photography system for luminous models in gas medium, using collimator for velocity measurement 20 p3632 A70-39746

Velocity measurement by Doppler effect in two-point direction finding, calculating error dependence on angular coordinates and distance 20 p3587 A70-39792

Quasi-steady MPD arc thruster average thrust measurements, considering time-of-flight velocity determination by ion collecting probes [AIAA PAPER 70-1080] 20 p3694 A70-40255

Coaxial three coil probe measuring local electrical conductivity and velocity in plasma streams, discussing operations in electrolytes and axisymmetric plasma stream 20 p3684 A70-40259

Hydrogen-oxygen and hydrogen-nitrous oxide systems combustion, measuring isotopic substitution effect on flame speed by schlieren technique with rotating drum camera 20 p3583 A70-40472

Fraunhofer holography for small spherical particles three dimensional position and velocity measurements 21 p3822 A70-40811

Satellite-borne sensor for ionospheric ions velocity measurement, describing design and principles of operation 21 p3813 A70-40834

Ionospheric ions drift velocity horizontal and vertical components distribution, using satellite-borne sensor 21 p3813 A70-40835

Shock wave and surface velocity measurements in exploding foil testing by streak photography with image converter camera 21 p3824 A70-40863

Pulse superposition measurements of small ultrasonic waves velocity changes using automatic recording phase sensitive detection 21 p3827 A70-41468

Apollo 11 lunar sample elastic wave velocities at high pressures, examining P and S waves, Q value and geophysical implications 21 p3916 A70-41666

Collisionless nitrogen plasma drift velocity measurement by ion acoustic wave method 21 p3859 A70-41760

Thermoanemometric velocity measurements in non-stationary MHD Hg flows by insulated Pt sensors 21 p3831 A70-42229

Multipurpose transistorized tachometer for rotating body speed measurement, control and recording, using electronic integrator and magnet pickup 21 p3831 A70-42245

Target velocity estimation by lidar, examining range measurements with time response and cross correlation technique 22 p3988 A70-42567

Airborne computerized time frequency systems for aircraft range and velocity determination, using stable clocks with ambiguity resolution 22 p4067 A70-42659

Projectile velocity measurement, using laser and Fabry-Perot interferometer for Doppler shift determination [SMPT PREPRINT 29] 22 p4034 A70-43046

Gas velocity measurement by high speed schlieren observation of laser induced breakdown phenomena [SMPT PREPRINT 27] 22 p4034 A70-43048

Flowing medium turbulent velocity measurement using laser Doppler device 22 p4040 A70-43615

Hypersonic projectile turbulent wake measurements, discussing velocity, mass density and temperature determination [ICAS PAPER 70-07] 23 p4132 A70-44130

Type 2 solar radio burst shock wave exciter velocity from dynamic spectrograms, relating correction to shock strength gradient 24 p4401 A70-45322

Electro-optical light speed measurements with interference comparator using He-Ne lasers with light modulators 24 p4353 A70-45562

Intact human forearms venous blood velocity measurements, using nuclear magnetic resonance techniques 24 p4309 A70-45675

Flow visualization measuring liquid flow velocity, using flow dichroism 24 p4338 A70-45816

High pressure hydraulic fluidic vortex rate sensor feasibility, considering variable geometry sensor design, fabrication and tests [SAE PAPER 700788] 24 p4294 A70-45857

Photographic measurement of droplets size, velocity and number during sprayed liquid fuel combustion, using Xe flash bulbs 24 p4429 A70-46008

Round pulsed jet diffusion rate from velocity measurements, considering Strouhal number and pulse amplitude 24 p4327 A70-46205

Pulsation and turbulence damping in pulsed jet from energy spectra of longitudinal velocity fluctuations 24 p4327 A70-46267

Galactic neutral hydrogen velocity distributions from 21 cm line profiles analysis 24 p4414 A70-46382

VELOCITY POTENTIALS

U FLOW DISTRIBUTION

U VELOCITY DISTRIBUTION

VELOCITY PROBES

U PITOT TUBES

U SPEED INDICATORS

VELOCITY PROFILES

U VELOCITY DISTRIBUTION

VENERA SATELLITES

NT VENERA 4 SATELLITE

Venus atmosphere optical properties on basis of Venera 4 data, proposing models for measured rotational temperature and subcloud atmosphere radiative equilibrium 01 p0192 A70-11507

Soviet Venus probes Venera 1, 2, 3, 4 and 5 emphasizing aims, implementation means and information yields influence on theory of solar system planets origin and evolution 04 p0757 A70-15672

Soviet space activities /1969/, discussing Soyuz orbital flights, Venera probes, Zond lunar orbiters and Proton 4 space laboratory scientific results 05 p0917 A70-16862

Soviet lunar and interplanetary space missions during 1969 including Venera, Cosmos, Luna and Meteor satellite activities 13 p2505 A70-28901

Monograph on upper atmosphere and outer space studies in U.S.S.R. /1969/ covering Soutz 4, 5, 6, 7, 8 and Venera 5, 6 flights 15 p2829 A70-31702

Interplanetary plasma disturbances in Venus proximity from Venera measurements 18 p3312 A70-36172

Soviet monograph on Venus atmosphere and Mars research covering Venera, Mariner and ground observations 18 p3332 A70-37230

VENERA 4 SATELLITE

Light refraction in Venusian atmosphere from Venera 4 probe measured data, noting horizontal rays traversing planet along circumference at 8.3 km height 06 p1142 A70-17889

Radial velocity data monitored during Venera 4 descent used for determining vertical and horizontal atmospheric flows velocities 11 p2118 A70-26792

VENTILATION

Airway resistance effect on ventilation and gas exchange during exercise, discussing minute volume and work of breathing response 03 p0429 A70-14157

Slope and shape of blood-gas dissociation curve as factor influencing pulmonary gas exchange in presence of ventilation-perfusion inequality 06 p0994 A70-17522

Temperature distribution in active elements of explosion proof asynchronous electric motors with multichannel bilateral axial flow ventilation systems 07 p1196 A70-19841

Altitude influence on forced ventilation of cooled electronic apparatus, analyzing flow change and temperature roles 09 p1643 A70-22040

Electronic radio equipment with encapsulated structure and natural ventilation, calculating heated zone and casing mean surface temperatures 09 p1648 A70-23147

Human pulmonary ventilation during exercise in high altitude and sea level acclimated subjects 10 p1819 A70-24774

Minimum ventilation volume requirement for space suit relation to air contaminants and body gas discharge intensities and locations 13 p2358 A70-29333

Pursed lips breathing effects on ventilation and blood gas exchange in patients with chronic airway obstruction 15 p2684 A70-32538

Ventilatory response to carbon dioxide in goats during acute and chronic hypoxia 15 p2684 A70-32539

Transthoracic mutual impedance responses to lung ventilation, discussing spatial and temporal intravariability 17 p3035 A70-34576

Athletes ventilation and heart rate dynamic responses to supine leg exercise with sinusoidal work load 20 p3576 A70-40329

Oxygen uptake at alveolar capillary membrane, investigating ventilation variability at exercise onset 20 p3577 A70-40331

Human tolerance and ventilatory response to inspiratory mechanical loads 23 p4144 A70-43822

Human ventilatory response to resistance unloading during muscular exercise 23 p4144 A70-43823

Human lung volume-to-ventilation ratios regional dispersion, using expired nitrogen concentrations analog simulation 24 p4303 A70-46113

VENTII ATORS

Nonsteady flow past duct junctures, investigating ventilation system of underground bomb shelter for blast wave passage prevention 11 p2036 A70-26139

Cinedensigraphic analysis of diaphragmatic ventilatory movements, obtaining correlation between lung volume and diaphragm and rib cage movement 14 p2537 A70-30383

VENTING

Impinging pressure analysis associated with two phase cryogenic propellant venting to space environment [AIAA PAPER 69-571] 01 p0196 A70-10845

Pressure decay prediction improvement for venting and quenching processes of solid propellants using analytical method 11 p2101 A70-25683

Aircraft multicell structures venting problem and pressure calculation 11 p2134 A70-25863

VENTRAL SECTIONS

Posterior ventral thalamic nucleus neuron reactions converging lemniscus and spinothalamic signals in cats 18 p3221 A70-36639

Myocardial Na and K content of rats exposed to high altitude, preparing isolated right ventricular strip 20 p3577 A70-40541

VENTURI TUBES

Multiple array critical flow venturi air flow metering system constructed for gas turbine engines, developing pressure control valve [ASME PAPER 69-WA/FM-5] 04 p0688 A70-14838

Venturi tube optimal design and operation parameters for small liquid quantities dosage 11 p2035 A70-25778

Throttling venturi valves for thrust modulation of liquid propellant rocket engines, testing pressure recovery, mixture ratio control and gas saturation and boundary layer effects [AIAA PAPER 70-703] 17 p3146 A70-34510

VENUS [PLANET]

Atlas of near IR spectra of Venus, Mars, Jupiter and Saturn obtained by Fourier spectroscopy, discussing observational procedures, data recording and processing 01 p0173 A70-10078

Internal structure models of Mercury, Mars and Venus based on radar measurements of radius and mass, discussing two and three zone models [JPL-TR-32-1439] 01 p0176 A70-10315

Planetary information obtained from radar installations, discussing distance and orbit measurements, rotation periods, planetary surfaces, emphasizing Mercury and Venus 01 p0185 A70-11046

High temperature effects on evolution of Venus upper lithosphere, considering magnetic differentiation, isostatic adjustments, surface relief, mountain building time and distance scales, etc 02 p0371 A70-12207

Communications of lunar and planetary laboratory, Volume 6, covering Venus atmosphere and photography, Jupiter IR spectrum and Mars multicolor photometry 02 p0377 A70-12553

Venusian atmosphere water content determined by airborne interferometer 02 p0377 A70-12554

Venus photographs taken by 82-inch telescope /1950-1956/, tabulating data 02 p0378 A70-12556

Multicolor Venus photography, discussing anomalous markings association with anomalous UV polarization 02 p0378 A70-12557

Venusian cloud layer radius, discussing error in determination of occultation level height of regulus by venus 03 p0574 A70-13881

Magnetograms by Venera 4 and Mariner 5 compared to determine interplanetary magnetic field nature in Venus proximity 04 p0744 A70-14438

- Data transmission from automatic space stations on Mars and Venus, considering relaying via artificial planet satellite or direct transmission to ground station 04 p0648 A70-14931
- Soviet Venus probes Venera 1, 2, 3, 4 and 5 emphasizing aims, implementation means and information yields influence on theory of solar system planets origin and evolution 04 p0757 A70-15672
- Radio brightness distribution observation over Venus disk, investigating absorption of millimeter radio emission of hot surface by planetary atmosphere 06 p1141 A70-17801
- Short duration manned Mars and Venus exploration mission planning with chemical propulsion and Saturn 5 boosters [ALAA PAPER 70-59] 06 p1147 A70-18238
- Solar wind flow different interactions with earth, Venus and moon 06 p1136 A70-18284
- Venus surface temperature calculations with non-gray radiation balance model and Mariner 5 and Venera 4 vertical temperature profile data 08 p1579 A70-21568
- Venus rotation period determination by radar observation of surface features 09 p1759 A70-22911
- Mars and Venus radio temperature measurements by 210 ft telescope, obtaining effective brightness 12 p2309 A70-27896
- Planet Venus motion, mass, dimensions, shape, topography and atmosphere 12 p2311 A70-28301
- Venus photographs analysis during synoptic periods, noting inconclusive results on cloud layer and planetary surface structures 12 p2311 A70-28311
- Magnetograms by Venera 4 and Mariner 5 compared to determine interplanetary magnetic field nature in Venus proximity 13 p2485 A70-28463
- Radio brightness distribution observation over Venus disk, investigating absorption of millimeter radio emission of hot surface by planetary atmosphere 13 p2487 A70-28651
- Venus obliquity dynamic implications, developing equations for independent parameter set to define spin vector 13 p2489 A70-28907
- Venus water presence from Venera 4 and Mariner 5 data suggesting polar seas and oceans saturated with hydrochloride and carbon dioxide as plant life source 14 p2637 A70-30365
- Venus and Mercury radio and radar studies concerning brightness temperature, surface reflectivity and planetary motion 14 p2647 A70-31074
- Venus spin-orbit resonance resulting in consistent inferior conjunction with earth, suggesting solar atmosphere tidal influence 14 p2650 A70-31216
- Venus radar backscattering properties indicating Muhleman theory applicability, noting radar echoes irregularity 15 p2806 A70-32802
- Venus retrograde axial period contradiction between radar echoes and violet-UV photographic and interferometric spectroscopic methods explained by theory using strong magnetic dipole 16 p2973 A70-33116
- Interplanetary plasma disturbances in Venus proximity from Venera measurements 18 p3312 A70-36172
- Mission planning for 1973 Mariner Venus/Mercury flyby, discussing trajectory and navigation aspects [ALAA PAPER 70-1049] 19 p3528 A70-38864
- Venus radius radar determination based on Mariner 5 and Venera 5 and 6 21 p3883 A70-40714
- Hydromagnetic theory of solar wind flow past earth extended to nonmagnetic planets Venus and Mars 22 p4095 A70-43106
- Venus carbon dioxide band, deriving rotational temperatures at various phase angles 23 p4241 A70-44257
- Solar probe trajectory optimization, using Venus gravitational field for braking 23 p4243 A70-44506
- Venus vegetative life suggested from algae growth under pure carbon dioxide in hot acid media at high pressures 23 p4253 A70-44836
- VENUS ATMOSPHERE**
- Buoyant Venus station using superpressure balloon, discussing requirements for structural design and station position tracking capability [ALAA PAPER 69-1068] 01 p0195 A70-10633
- Venus upper atmosphere average rotational temperature determined from high dispersion spectroscopic observations of 7883 A carbon dioxide band 01 p0184 A70-10912
- Venus atmosphere ionization distribution, temperature and pressure profiles determined from amplitudes

and differential Doppler of radio signals to Mariner 5 during occultation 01 p0186 A70-11084

Venusian atmospheric model based on Venera 4 measurements, calculating probe distance travel, temperature, density and pressure profiles 01 p0192 A70-11504

Venusian atmospheric pressure and temperature measurements by Venera 4 probe, noting agreement with Mariner 5 observations 01 p0192 A70-11505

Greenhouse effect in Venusian atmosphere, discussing cause of vertical temperature distribution established by Venera 4 probe 01 p0192 A70-11506

Venus atmosphere optical properties on basis of Venera 4 data, proposing models for measured rotational temperature and subcloud atmosphere radiative equilibrium 01 p0192 A70-11507

Venus and Jupiter Aerobee rocket photoelectric UV spectra, determining geometric albedos using reflecting layer and cloud models 02 p0367 A70-11812

Venus atmosphere simulation at condensation level in uniform temperature mixing cloud chamber, studying artificial and natural ice nuclei nucleation 02 p0373 A70-12293

Polymers development for ablative heat shields, aeroshell structures, antennas, insulators, electronic packaging, etc, to meet Mars and Venus atmospheric entry requirements 02 p0382 A70-12525

Venusian atmosphere low reflectivity reinterpretation based on spectrophotometric data indicating constituents of yellow and upper UV haze layers 02 p0377 A70-12555

Venus photography in UV by 61-inch telescope, discussing low contrast clouds recognition technique 02 p0378 A70-12558

Thermal model for Venus ionosphere, considering photoionization and solar wind influx for possible heat sources 03 p0575 A70-13981

He 4 and Ar 40 abundance in lower Venus atmosphere, underlining He 4 dominance in upper atmosphere 03 p0575 A70-13982

Mars and Venus ionospheres from Mariner profiles, discussing radiative equilibrium thermal calculations and F1 layer hypothesis 04 p0753 A70-15069

Radiative-convective equilibrium model to investigate photodissociation of water in Venus atmosphere, considering greenhouse effect 04 p0757 A70-15516

Venus-earth carbon dioxide atomic parameters used to determine ionization and optical emission rates in Venus upper atmosphere resulting from solar cosmic rays 05 p0901 A70-16276

High resolution Venus spectra, obtaining band spectra growth curve of C13O16O18 isotope of carbon dioxide, comparing data reduction methods 05 p0910 A70-16392

Earth, Venus and Mars atmospheric structure, discussing gases escape, temperature, density, IR radiation and solar radiation absorption 05 p0914 A70-16628

Light refraction in Venusian atmosphere from Venera 4 probe measured data, noting horizontal rays traversing planet along circumference at 8.3 km height 06 p1142 A70-17889

Collection of papers on Venus atmosphere covering Venera 4 and Mariner 5 flights, lower atmosphere and surface, upper atmosphere and ionosphere and interplanetary medium 07 p1381 A70-19375

Mariner 4 and 5 and Venera 4 data used for comparing terrestrial planets ionospheres 07 p1386 A70-19488

Radio wave absorption in Venusian ionosphere, estimating effective collision number 07 p1235 A70-19491

Radio wave refraction and field strength in model Venus atmosphere for various spacecraft trajectories 07 p1235 A70-19492

Turbulent thermal flux in Venus atmosphere estimated from amplitude fluctuation dispersion of Venera 4 and Mariner 5 radio signals 07 p1390 A70-20305

Soviet Venus probes 5 and 6 observation data concerning Venus atmospheric composition, temperature and pressure, etc 08 p1568 A70-20624

Venus clouds absorption spectra correlation with carbon suboxide frost reflection spectra, suggesting absence of carbon suboxide in atmosphere 08 p1571 A70-20911

Solar wind and Venus topside ionosphere interaction, discussing charged particle density, temperature and pressure distribution 08 p1578 A70-21550

IR absorption properties of CO, HCl and sulfur dioxide measured for role in Venus greenhouse effect 08 p1579 A70-21567

Venus ionosphere, discussing day and night electron density profiles, carbon dioxide presence, plasma interaction model, etc 09 p1750 A70-22058

Drop sondes dynamic and aerodynamic design for lower Venus atmosphere based on solution for free fall of body in atmosphere with constant temperature gradient 09 p1766 A70-22935

Wind and atmospheric temperature variations on Mars, Venus and Mercury interpreted from observational data in terms of earth atmospheric processes 09 p1762 A70-23127

Microwave signal fading in Venus atmosphere due to turbulence, discussing atmospheric dielectric permittivity variance 09 p1764 A70-23484

Venusian ionosphere thermal protons and/or deuterons source observed by radio occultation method, suggesting dominance at high altitudes 10 p1938 A70-24068

Similarity and dimensionality theory applied to large scale motions in atmospheric circulation of Mars and Venus 10 p1939 A70-24269

Venus planetary surface and atmosphere, reviewing American and Soviet probe results 10 p1943 A70-24761

Real gas adiabatic lapse rate applied to Venus atmosphere assumed to consist of pure carbon dioxide 11 p2107 A70-25646

Venus clouds self consistent radiative-convective model with sun as heat source 11 p2107 A70-25647

Criticism and reply to Venus cloud water drop HCl concentration preventing ice cloud formation 11 p2108 A70-25653

Light storage by Venus machine using refractive properties of gas and involving fluid mechanical optics 11 p2114 A70-26575

Radial velocity data monitored during Venera 4 descent used for determining vertical and horizontal atmospheric flows velocities 11 p2118 A70-26792

Spectral absorption characteristics for C atom radiative processes in carbon dioxide-nitrogen mixtures at high temperatures corresponding to Venusian atmosphere 12 p2275 A70-27317

Planet Venus motion, mass, dimensions, shape, topography and atmosphere 12 p2311 A70-28301

Energy distribution in dark and light details on Venus spectrograms, considering relation to clouds in upper atmosphere 12 p2311 A70-28304

Venus atmosphere physicochemical characteristics and composition from automatic onboard Venera measurements 13 p2495 A70-29759

Artificial satellite around Venus, investigating orbital lifetime based on atmospheric drag effect on periaapsis height 14 p2637 A70-30563

Simulated Venusian atmosphere effects on polymeric plastic and rubber materials, comparing with high temperature air and nitrogen exposures 14 p2640 A70-30781

Venus carbon dioxide absorption bands determining atmospheric scattering model suitability for all data 14 p2642 A70-30889

Spacecraft measurements revealing hot dense Venusian and cold thin Martian carbon dioxide atmospheres 14 p2646 A70-31066

Venus atmosphere data from Venera 4, 5 and 6 and Mariner 5 missions covering chemical composition, density, pressure, temperature gradients, etc 14 p2646 A70-31067

Venus surface temperature poleward variation from radio interferometry measurements 14 p2646 A70-31068

Venus atmosphere opacity law determination as function of wavelength, comparing interferometric and integrated brightness temperatures with model calculations for various atmospheric compositions 14 p2646 A70-31069

Venus atmosphere-lithosphere interactions, predicting electrically conducting cloud masses presence 14 p2646 A70-31070

Retrograde rotation of equatorial spots of Venus cloudy exterior layer, using UV photographic and spectroscopic observations 14 p2649 A70-31215

Geochemistry of venus volatile elements identifying cloud forming species as Hg compounds 14 p2650 A70-31217

Average rotational temperature of Venus atmosphere above cloud tops from carbon dioxide band spectroscopy 14 p2650 A70-31219

- Supersonic nonequilibrium gas mixture flow past segmental bodies nose areas to simulate Venusian atmosphere, determining temperature, pressure and concentration distributions 15 p2796 A70-31483
- Venus lower atmosphere models, discussing pressure, temperature and water vapor abundance based on radio and radar astronomy and spacecraft measurements 15 p2798 A70-31684
- Terrestrial planetary ionospheres, discussing charged particle density distribution of Mars daytime ionosphere and Venus day and dark sides 15 p2799 A70-31748
- Mariner 4 and 5 and Venera 4 data used for comparing terrestrial planets ionospheres 15 p2805 A70-32733
- Radio wave absorption in Venusian ionosphere, estimating effective collision number 15 p2705 A70-32736
- Radio wave refraction and field strength in model Venus atmosphere for various spacecraft trajectories 15 p2705 A70-32737
- Venus atmosphere and surface conditions, describing temperature, accumulation of carbon dioxide and runaway greenhouse effect 15 p2806 A70-32771
- Edson layer theory explaining phase anomaly of inner planets in terms of light scattering by thin layer above Venus cloud cover 16 p2973 A70-33113
- Venus surface atmospheric conditions from radar and radio observations, including cross sections, microwave brightness spectrum and angular scattering law 16 p2974 A70-33645
- Spectral line formation in Mars and Venus atmospheres, discussing Lorentz and Doppler broadening 16 p2976 A70-33793
- Venus upper atmosphere carbon atoms detection based on low resolution spectra analysis of solar illuminated atmosphere 16 p2979 A70-34036
- Venus deep mantle water degassing rate from atmospheric hydrogen escape data 17 p3154 A70-34610
- Buoyant Venus station balloon for deployment and inflation during parachute descent into Venus atmosphere tested with scale model balloons in wind tunnels 17 p3063 A70-35658
- Venus daytime upper ionosphere observations by mariner 5 in terms of ionization sources and sinks, ambipolar diffusion and model atmospheres 18 p3311 A70-36002
- Venus exploration by space probes, discussing orbital and physical data, planetary rotation, atmosphere, surface conditions and magnetic field 18 p3319 A70-37047
- Venus atmosphere water content, discussing chemical reactions, temperature, dehydrogenation, etc 18 p3320 A70-37075
- Venus lower atmosphere structure and brightness temperature spectrum analysis for composition, temperature and pressure profiles 18 p3323 A70-37139
- Soviet monograph on Venus atmosphere and Mars research covering Venera, Mariner and ground observations 18 p3332 A70-37230
- Venus cloud displacement, measuring formations longitudes and latitudes for evidence of cytherean upper atmosphere rapid bulk motion 19 p3518 A70-38027
- Periodic thermal forcing role in Venus atmosphere dynamics, investigating momentum transport to support mean shear for channel flow 19 p3519 A70-38251
- Venus atmospheric visible clouds circulation, determining zonal flow induced by moving heat sources 19 p3519 A70-38252
- Terrestrial atmospheric tidal theory applicability to Venus and Mars, considering dependence on parameters variation among planets 19 p3519 A70-38253
- Venus atmospheric temperature, pressure and density measurements by Venera 5 and 6 space probes, developing model 19 p3520 A70-38255
- Venus atmosphere heat transfer processes from Venera 4, 5 and 6 probes data, evaluating radiative and convective motions model 19 p3520 A70-38256
- Venus atmosphere physicochemical characteristics and composition from automatic onboard Venera measurements 19 p3520 A70-38391
- Buoyant Venus station using superpressure balloon, discussing requirements for structural design and station position tracking capability 20 p3715 A70-39677
- Venus atmosphere and water vapor, finding ice clouds by spectrum analysis 20 p3708 A70-39961
- Venusian atmosphere carbon dioxide, water, molecular oxygen and nitrogen contents from Venera 5 and 6 data 21 p3883 A70-40837
- Aeolian regime of Venus surface resulting from high surface temperature and pressure, discussing spurious radar echoes, dust and sand transport and deposition 21 p3885 A70-40929
- Pressure dependence and efficiency of carbon trioxide formation in Mars and Venus atmospheres 21 p3887 A70-41107
- Spectral absorption characteristics for c atom radiative processes in carbon dioxide-nitrogen mixtures at high temperatures corresponding to Venusian atmosphere 21 p3854 A70-42058
- Venus spectrum from high resolution Michelson interferometers with Fourier transform and digital computation, discussing Venus atmospheric models 22 p4099 A70-42721
- Venusian and Martian upper atmosphere chemistry, emphasizing ionization height distribution 22 p4106 A70-43312
- Venus atmospheric parameters from microwave spectrum, discussing brightness temperature, carbon dioxide content, opacity, water vapor, dust and models 23 p4241 A70-44256
- Venus polywater hydrosphere, discussing vapor phase, surface temperature, evolution, observations and model data 23 p4242 A70-44260
- Venus atmosphere flight vehicle configuration, discussing payload capacity, range, velocity, flight altitude and aerostatic aerodynamic, ground effect and underwater capabilities 23 p4260 A70-44627
- Linear polarization of sunlight scattered by Venus atmosphere, giving data for integrated disk and equatorial region 23 p4246 A70-44756
- Venus atmospheric speculations compared to Soviet and American probe findings, discussing composition, evolution cloud layer and ionosphere 23 p4253 A70-44863
- Venus atmosphere exploration by multiple entry probe, describing spacecraft system design, launch and earth-Venus transfer trajectory, approach and entry sequence, etc [AIAA PAPER 70-1245] 24 p4417 A70-45963
- VENUS PROBES**
- NT MARINER 2 SPACE PROBE
- NT MARINER 5 SPACE PROBE
- NT VENERA SATELLITES
- NT ZOND 3 SPACE PROBE
- Venus probe high level entry deceleration simulation, discussing test program, equipment and results 03 p0463 A70-13541
- Soviet Venus probes 5 and 6 observation data concerning Venus atmospheric composition, temperature and pressure, etc 08 p1568 A70-20624
- Venus planetary surface and atmosphere, reviewing American and Soviet probe results 10 p1943 A70-24761
- Interplanetary magnetic field intensity and geomagnetic activity level correlation with 27-day solar activity cycle based on Venera 4 and Mariner 5 data comparison 12 p2310 A70-28263
- Venus exploration by space probes, discussing orbital and physical data, planetary rotation, atmosphere, surface conditions and magnetic field 18 p3319 A70-37047
- Mars and Venus orbiter spacecraft electric propulsion system, discussing Hg electron bombardment ion engine [AIAA PAPER 70-1154] 21 p3868 A70-41786
- Venus atmosphere exploration by multiple entry probe, describing spacecraft system design, launch and earth-Venus transfer trajectory, approach and entry sequence, etc [AIAA PAPER 70-1245] 24 p4417 A70-45963
- VENUS RADAR ECHOES**
- Venus and Mercury surface height variations near equators, using radar time delay and Doppler observations 14 p2647 A70-31077
- Venus radar mapping using fixed base line interferometer for hemispheric ambiguity resolution 14 p2647 A70-31078
- Venus radar anomalous features, examining rotation period, polarized and cross polarized scattering properties and topography 14 p2647 A70-31079
- Venus radar brightness map, using 40 km separation between range gates and comparable distances between Doppler slices 21 p3883 A70-40710
- VERBAL COMMUNICATION**
- U VOICE COMMUNICATION
- Retroactive and proactive inhibition in verbal discrimination learning, using paradigms characteristic of paired-associate retention studies 03 p0435 A70-13768
- VERIFICATION [PROVING]**
- U PROVING
- VERNIER ENGINES**
- NT CONTROL ROCKETS
- Surveyor spacecraft vernier propulsion system survival in lunar environment, suggesting temperature resistant seal and valve seat material for fluid loss prevention 06 p1129 A70-17170
- Advanced concept ejection seat /ACES/ system design and performance, considering gyro-controlled vernier rocket motor and electronic time delays 07 p1192 A70-19016
- VERTEBRAE**
- Lumbar vertebrae transverse processes fractures in air crashes, considering factors involved, incidence and pathogenesis 17 p3033 A70-35578
- VERTEBRAL COLUMN**
- Vertebral injury prediction of seated human subjected to caudocephalad acceleration, suggesting consideration for head and torso forward flexion and external restraints effects 09 p1627 A70-23462
- VERTEBRATES**
- NT BIRDS
- NT CATS
- NT CATTLE
- NT CHICKENS
- NT CHIMPANZEES
- NT DOGS
- NT FISHES
- NT FROGS
- NT GOATS
- NT GROUND SQUIRRELS
- NT GUINEA PIGS
- NT HAMSTERS
- NT HUMAN BEINGS
- NT MAMMALS
- NT MICE
- NT MONKEYS
- NT PIGEONS
- NT PRIMATES
- NT RABBITS
- NT RATS
- NT RODENTS
- NT SHEEP
- NT SWINE
- NT TURTLES
- Reticular formation of central nervous system in vertebrates described as behavior controlling circuit of interconnected modules, proposing hybrid computer method for operational scheme 08 p1447 A70-21461
- VERTICAL AIR CURRENTS**
- Thunderstorm downdraft trajectories and temperatures, discussing evaluation of cooling due to evaporation 02 p0325 A70-12256
- Power spectral density functions of vertical gust velocities, comparing theoretical results and C-141A flight test measurements 04 p0624 A70-15384
- Omega equation interpretation showing vertical motion related to advection of vorticity in upper troposphere and to warm advection in lower troposphere 05 p0838 A70-16154
- Momentum considerations in thunderstorm dissipation by disrupting organized cloud base updraft structure 06 p1100 A70-18570
- Air flow in updraft through and around cloud region containing precipitation particles using numerical model, computing horizontal divergence 06 p1100 A70-18572
- Model for thunderstorm downdrafts induced by rain evaporation based on one dimensional steady state formulation, deriving vertical velocity profiles 06 p1100 A70-18573
- Vertical wind distribution associated with thunderstorm outflow, measuring wind direction oscillations at Kennedy Space Center 06 p1101 A70-18576
- Pacific ocean equatorial trough zone disturbances structure, discussing organized convective downdrafts role in rapid structural decay 06 p1101 A70-18578
- Pulsed Doppler radar observation of thunderstorm updraft structure, noting vertical velocity perturbations 06 p1101 A70-18581
- Cloud layer vertical displacement effects on upper boundary and temperature changes in st-sc using aircraft sounding data 08 p1537 A70-21107
- Vertical air motions rate from aerodynamic loads on aircraft and pitch angle and center of mass vertical velocity fluctuations 08 p1538 A70-21113
- Lee wave theory for two dimensional stratified atmospheric models, noting local intense vertical beam into high stratosphere 08 p1540 A70-21972

Vertical wind profiles, deriving wind shear-layer thickness exponential relationship

09 p1715 A70-22356

Anisotropic turbulent energy spectral distribution approximated assuming homogeneous and axisymmetric turbulence with vertical axis of symmetry

09 p1717 A70-22374

Vertical wind components from balloon ascent observations, considering drag, atmospheric density, wind velocity, etc

10 p1911 A70-23927

Vertical air velocity in convective clouds by pulsed Doppler radar observations of thunderstorm

11 p2004 A70-25650

Atmospheric pressure variations as function of vertical movements caused by friction and orography, considering numerical forecasting

11 p2076 A70-26073

Laminar boundary layer transition to quasi-cellular flow in natural convection above horizontal heated plates and disks

12 p2155 A70-27197

Vertical momentum flux correction for planetary scale gravity waves in equatorial lower stratosphere

13 p2445 A70-29623

Atmospheric moisture balance solution for altitude dependent vertical velocity and turbulence coefficient, considering cloud water content and boundaries height calculation

14 p2601 A70-30137

Vertical flux densities of momentum and sensible heat dependence on displacement height and surface roughness

14 p2602 A70-30371

Atmospheric cellular convection, reducing hydrodynamic equations to amplitude equations for vertical velocity

15 p2770 A70-32064

Maximum up- and downdrafts altitude, using two dimensional model of lee wave disturbances for post-frontal subsidence modification

16 p2945 A70-32948

Steady state nonlinear dynamics of low latitude atmospheric global boundary layer, indicating inverse relation between air flow vertical velocity and distance from equator

19 p3460 A70-37417

Atmospheric turbulence vertical component spectral density observation by aircraft in steady flight, considering transfer function computation methods

19 p3351 A70-37646

Subsonic wing theory calculation method, obtaining close solutions for integral expression constants for downward air currents

19 p3352 A70-38164

Radiosonde technique for locating atmospheric turbulence regions and estimating vertical air movement component in associated gusts

19 p3427 A70-38246

Right-moving thunderstorm characteristics from mesonetwork rawinsonde updraft observations, considering hydrostatic pressure and cyclonic rotation

19 p3462 A70-38260

Stratus cloud dissipation process in descending vertical currents, using thermohydrodynamic and kinetic equations for cloud droplet distribution function

22 p4066 A70-43377

Vertical velocity effects on ionospheric horizontal wind magnitude and direction, solving integral equations system by successive approximations

23 p4188 A70-44057

VERTICAL DISTRIBUTION

Vertical atmospheric vapor distribution from measuring microwave radiation of earth/atmosphere system at several wavelengths

01 p0135 A70-10202

Solar Lyman alpha line profile and atomic hydrogen vertical distribution measurement method for terrestrial atmosphere in 200-500 km range

01 p0078 A70-11208

Vertical wind observations during lower ionosphere wind measurements by Na release method, discussing gravity effects and standing waves

01 p0078 A70-11213

Greenhouse effect in Venusian atmosphere, discussing cause of vertical temperature distribution established by Venera 4 probe

01 p0192 A70-11506

High altitude balloon measurements of secondary gamma quanta intensity vertical distribution, using scintillation counter with CsI(Tl) crystal

01 p0172 A70-11544

Hourly N/h/ profiles of F region calculated from nomograms by normal integral method during magnetic disturbance, measuring region temperature

01 p0083 A70-11548

Molecular reaction rates and ion/electron vertical profile and concentrations in equatorial ionosphere, applying computer simulation to numerical solution of continuity equations

01 p0083 A70-11549

Ionospheric molecular ion concentration vertical profile analysis for verifying neutral gas temperature

maxima in connection with two ion production maxima

01 p0083 A70-11550

Atmospheric density on basis of photographic observations of meteors, comparing vertical profile with CIRA profile

01 p0084 A70-11556

Satellite measurement of mean temperature in atmospheric layers to determine vertical temperature distribution

02 p0291 A70-12279

Cape Kennedy vertical wind speed profiles measured by spectral analysis using fast Fourier transform method

02 p0325 A70-12285

Vertical ion concentration profile in troposphere and stratosphere from ozone distribution satellite measurements using aeronautical reactions

02 p0291 A70-12389

Wave structure function dependence on altitude, comparing function ratio for up/down propagation through atmosphere

02 p0258 A70-12461

Ionospheric electron density vertical distribution calculation starting from satellite measurements of total electron content

02 p0293 A70-12575

Vertical concentration and size distribution determinations for aerosols in stratosphere, suggesting volcanic origin

02 p0294 A70-12842

Mean and extreme atmospheric ozone concentration calculated as function of altitude and seasons in Northern Hemisphere

03 p0474 A70-13294

UV radiation scattering and rocking instrument error source in vertical ozone profile determination with optical ozone probes

03 p0557 A70-13296

Atmospheric absorption anomalies of UV sunlight near 50 km altitude in rocket-borne radiometer determination of ozone distribution

03 p0478 A70-14197

Vertical profiles of atomic and excited molecular oxygen concentration in upper atmosphere calculated from spectral band intensity, determining excitation reaction rates

04 p0682 A70-15733

Sonic boom propagation in still atmosphere with vertical temperature gradient, using graphical method of determining rays for aircraft motion

05 p0791 A70-15786

Ionograms for nonmonotonic vertical distribution of electron concentration in ionosphere from rocket and ground sounding

05 p0842 A70-16757

Magnetovariational sounding procedure for determining vertical distribution of earth mean electrical conductivity using geomagnetic field spatial derivatives for spherical earth

05 p0843 A70-16767

Altitude variation of mesospheric daytime sky brightness from earth based measurements of twilight sky brightness, noting inconsistency in calculations based on standard atmospheres

06 p1053 A70-17207

Second vertical derivative of gravity field, using formulas based on Taylor series expansion method

06 p1055 A70-17604

Laminar natural convection boundary layer stability over vertical uniform flux surface, measuring disturbance temperature and velocity distributions

06 p1035 A70-17686

Atmospheric temperature vertical profile reconstruction from ascending radiation observations using data regularization

06 p1097 A70-17793

Vertical profile of angular mass distribution of atmospheric water vapor and ozone as gas proportion function

06 p1097 A70-17794

Wind speed and potential temperature vertical profile in day/night planetary atmospheres estimated by similarity theory of boundary layer parameters

06 p1141 A70-17827

Twilight atmospheric brightness calculation for models of vertical distribution of aerosol scattering coefficient, using numerical data

06 p1056 A70-17828

Polarization level of outgoing short wave radiation calculated along solar vertical in aerosol containing multiply scattering atmosphere

06 p1097 A70-17829

Ionospheric vertical electron concentration computer calculations compared to direct measurements data by satellite and rockets over Sofia

06 p1057 A70-17843

CO vertical distribution near tropopause from photochemical atmospheric model with CO recombination with OH for stratospheric sink

07 p1265 A70-19282

Vertical eddy diffusion effect on chemical composition of mesosphere and lower thermosphere using photochemical model containing oxygen and hydrogen

07 p1274 A70-20269

Descending and albedo electron fluxes at specific geomagnetic latitude and various atmospheric depths, obtaining electron energy spectrum vertical profiles

07 p1372 A70-20335

Simultaneous ionospheric ion and electron measurements by various radiophysical methods, relating results to period of flight of vertical space probe

07 p1237 A70-20428

F region electron and ion concentration vertical distribution, discussing various ionization reactions

07 p1276 A70-20430

Lower ionosphere electric fields and currents vertical profiles above geomagnetic equator under quiet geomagnetic conditions from rocket data

07 p1277 A70-20453

Meteor flare photographs statistical analysis, noting duration and weight distribution dependence on meteor velocity

08 p1574 A70-21214

Altitude profiles and absolute intensities of far UV emission features in aurora measured by filterwheel photometer in Aerobee rocket, determining molecular oxygen densities

08 p1489 A70-21384

Deviating and nondeviating absorption of radiowaves in ionosphere, deriving vertical distribution of particle collisions in E layer

08 p1490 A70-21431

Strong point explosion in atmosphere with density dependent on height, obtaining numerical solutions for exact gas dynamic equations

09 p1658 A70-22112

Heat and mass transfer in binary turbulent boundary layer during natural convection on vertical surface, allowing for diffusional heat conduction

09 p1787 A70-22267

Wind HF inclination variations in lower atmosphere, considering turbulent kinetic energy dissipation and buoyancy production

09 p1714 A70-22355

Atmospheric momentum and heat flux height variations in surface boundary layer, stressing instrument performance and measurement techniques

09 p1715 A70-22359

Potential refractive index mean vertical gradients role in turbulent mixing, noting applications to radar detection of CAT

09 p1716 A70-22365

Elevation patterns of vertically polarized elements above circular finite ground screens directly on soil, discussing steering illumination

09 p1634 A70-22700

Nighttime D region ionization irregularities deduced from vertically incident VLF radio wave

09 p1671 A70-23663

F region vertical electron drift velocity determined from Thomson scatter observations

09 p1671 A70-23665

High energy electron and gamma quanta flux measurement in atmosphere at different heights by high altitude balloons

09 p1747 A70-23728

Vertical distribution of pulmonary blood flow (DPBF) in dogs without thoracotomy prone, supine, head-up, head-down and right and left decubitus positions

10 p1810 A70-24004

Vertical gradient of total geomagnetic field using curves based on continuous records of magnetic variations

10 p1876 A70-24589

Atmospheric temperature vertical profile reconstruction from ascending radiation observations using data regularization

10 p1913 A70-25024

Vertical profile of angular mass distribution of atmospheric water vapor and ozone as gas proportion function

10 p1913 A70-25025

Geomagnetic field upward calculation in lower ionosphere, discussing accurate data acquisition difficulties in Dirichlet problem solution

11 p2043 A70-25544

Meteorological Nimbus 3 satellite and aircraft observations of thermal radiation for vertical atmospheric temperature profile measurement

11 p2075 A70-25921

Absorption at solar H Lyman alpha line by earth hydrogen atmosphere measured as function of altitude from Aerobee flight spectrometers

12 p2222 A70-27182

Vertical propagation of short acoustic waves from harmonic source in inhomogeneous atmosphere, calculating shock front width and heating rate

12 p2264 A70-27519

Vertical profiles of daytime and nighttime long wave radiation fluxes in atmosphere under stratus cloud conditions

12 p2264 A70-27521

Ionospheric probing by ground based and satellite-borne vertical incidence sounders

12 p2224 A70-27729

Stratospheric clear air turbulence (CAT) vertical extent above thunderstorm graphically represented

12 p2265 A70-28095

Plane acoustic shock wave vertical propagation in gravity-stratified atmosphere with temperature gradient, using homogeneous perturbation velocity [DFVLR-SONDDR-35] 12 p2212 A70-28209

Low latitude atmospheric vertical density variations, comparing solar and geomagnetic activities effects 12 p2227 A70-28264

Satellite measurement of water vapor height profiles using outgoing thermal radiation and solar radiation at atmospheric absorption techniques 13 p2392 A70-28571

Lower atmospheric layer temperature and wind vertical distribution effect on wind velocity ratio to geostrophic wind at earth surface 13 p2444 A70-28586

Vertical and intensity distributions of wind velocity focuses in tropospheric jet streams 13 p2444 A70-28590

Millimeter-wave probing for vertical distribution of atmospheric water vapor, comparing ground, balloon and satellite observation techniques 13 p2394 A70-28785

Balloon-borne measurement of troposphere refractive index vertical distribution using spaced-cavity refractometer 13 p2394 A70-28789

Asynchronous liquid metal MHD generator parameters, assuming constant vertical distribution of working fluid velocity 13 p2349 A70-28968

Cosmic ray vertical muon flux measurements at sea level using spectrometer 13 p2477 A70-29124

Vertical tropospheric turbidity distribution determination from intensity measurements of inclined searchlight beams 13 p2445 A70-29471

Solar constant dependence on Wolf number and variations in transmission factor from balloon observations of radiation balance vertical distribution 14 p2568 A70-30126

Mesospheric daytime/nighttime ozone abundance vertical profile diurnal variations 14 p2568 A70-30130

Magnetosphere boundary altitude dependence on longitude, considering role of electric current density along geomagnetic lines of force 14 p2570 A70-30217

Altitude distribution of radar-signal-reflecting points and ionization in meteor trails 14 p2635 A70-30308

Vertical mesoscale contribution to vertical wind shear profiles, using radar/Jimsphere measurements 14 p2609 A70-30599

F region horizontal drift velocity height and diurnal variations, using ionograms 14 p2574 A70-30751

Vertical profiles of atomic and excited molecular oxygen concentration in upper atmosphere calculated from spectral band intensity, determining excitation reaction rates 14 p2575 A70-30817

Temperature and density extreme variations at various levels in stratosphere and mesosphere, analyzing sounding rocket data 15 p2723 A70-31661

Vertical temperature profiles and global circulation patterns in stratosphere and mesosphere, discussing Northern Hemispheric seasonal, latitudinal and longitudinal variations 15 p2724 A70-31665

Atmospheric vertical temperature sounding from geosynchronous satellite, discussing instrumentation, cloud cover and wind effects, etc 15 p2809 A70-31690

Atomic hydrogen escape effects on altitude distribution, discussing lateral flow limitations on thermospheric diurnal variation 15 p2725 A70-31796

Atmospheric temperature vertical distribution measurement using sounding balloon and Skylark rocket 15 p2725 A70-31846

Cosmic ray knee interpretation using polar orbiting ionization chambers data from OGO-2/4 15 p2793 A70-31903

Ground sounding of ionization variations and vertical distribution using model, integral and normal laminar methods 15 p2729 A70-32078

Planetary distribution of F region disturbances and related vertical electron concentration using satellite and ground data 15 p2729 A70-32079

Electron-ion gas ionization, neutralization and ambipolar diffusion effects on F region vertical profile 15 p2730 A70-32090

Vertical gravity gradient effect on calculations accuracy of earth figure, deriving corrections for anomalies 15 p2731 A70-32149

Atmospheric optical properties at various altitudes, using lunar disk photometric observations at different wavelengths during eclipse 15 p2801 A70-32476

Elevation and ground conductivity effects on horizontal dipole excitation of earth-ionosphere waveguide, considering east-west propagation 16 p2858 A70-32932

Spectrophotometric and visual observations of twilight glow from Soyuz 5, comparing vertical monochromatic brightness profiles with calculations for Elterman aerosol model 16 p2896 A70-33218

Thermal atmospheric sounding from satellites based on Fredholm integral equations, obtaining vertical temperature profiles 16 p2896 A70-33257

Ozone concentration in San Francisco Bay Area, discussing temperature inversion, air pollution, destruction rate and distribution patterns of oxidants 18 p3284 A70-35945

Type 2 irregularities in equatorial electrojet associated with plasma density vertical gradients 18 p3244 A70-36017

Nimbus 3 satellite-borne Michelson interferometer IR spectrometer for spectrum measurement, obtaining temperature, water vapor and ozone vertical distribution 18 p3257 A70-36175

Vertical drift contribution to daytime N/h electron profiles in F2 region, taking into account ionization-recombination processes and ambipolar diffusion 18 p3247 A70-36292

Upper atmospheric gas components vertical distribution by airborne photometric absorption and attenuation measurements in UV spectrum 18 p3248 A70-36633

Critical height phenomenon for vertical jet exhausting into horizontal parallel plates channel simulating aircraft surfaces 18 p3243 A70-36709

Simultaneous measurements of earth atmosphere radiation, comparing short and long wave data consistencies at various altitudes 18 p3286 A70-36963

Atmospheric water vapor distribution by intensity measurements of outgoing radiation from satellites in carbon dioxide and water vapor spectral bands 18 p3287 A70-36971

Vertical distribution of upper atmospheric 7600 A oxygen glow, discussing 8645 A band and nitric oxide data 18 p3251 A70-36977

Electrons and ions diffusion effect on vertical distribution in F region, discussing diurnal variations at various heights 18 p3254 A70-37027

Ion composition and charged particle vertical distribution in F region and protonosphere from satellite and ground based observations 18 p3254 A70-37028

Time and altitude dependences between 340-1000 km of delta parameter for height scale ratio of neutral and electron-ion gases, discussing diffusion coefficient 18 p3254 A70-37030

F region photoionization rate vs height twin peak profile in presence of temperature maximum, taking into account ionization of atmospheric gases by quasi-monochromatic radiation 18 p3254 A70-37031

Panoramic vertical sounding method of ionosphere, noting drawbacks 18 p3255 A70-37040

F1 region unsteady model, examining vertical distribution profile of electron concentration on summer day 19 p3409 A70-37323

Vertical electron density profile variations during ionospheric perturbations in years of solar activity maximum and minimum 19 p3409 A70-37328

Electron concentration vertical profile in ionosphere as function of altitude of radio wave reflection and group refraction and velocity characteristics 19 p3409 A70-37329

Vertical profile of electron collisions effective frequencies in auroral ionosphere E region 19 p3409 A70-37330

Atmospheric moisture content vertical profile from terrestrial radiation measurements, using statistical regularization procedure 19 p3460 A70-37418

Atmospheric aerosols vertical distribution from aerosol measurements, considering particle size distribution 19 p3461 A70-37636

Light polarization during twilight at zenith from photoelectric recordings, noting intensity decrease with altitude 19 p3417 A70-38770

Radar angels activity seasonal variation and height distribution statistical relationship to meteorological parameters 20 p3661 A70-39169

Lower atmosphere refractive index vertical distribution and fluctuations, using airborne refractometer 20 p3619 A70-39191

Midlatitude atmospheric neutron density height dependence during minimum solar activity 20 p3697 A70-39285

Atmospheric gamma rays vertical intensity dependence on spectrum and altitude from high altitude balloon studies 20 p3697 A70-39286

Earth atmosphere cosmic ray neutron albedo from balloon measurement of flux vertical distribution 20 p3698 A70-39298

Lyman alpha geocoronal emission rate as function of altitude at midnight during solar minimum, solving radiative transfer equations 20 p3619 A70-39329

Barometric coefficient altitude dependence of cosmic ray neutron monitor for vertical flux 20 p3699 A70-39347

Altitude spectrum of ion formation in interaction of proton flux with atmosphere, using Bragg dissipation function 21 p3878 A70-40846

Turbulent mixing effect on vertical distribution of ionosphere atomic and molecular oxygen, using equations of motion and continuity 21 p3813 A70-40907

Mars lower atmosphere vertical temperature distributions from Mariner 6 and 7 radio occultation data, using improved trajectory estimates 21 p3884 A70-40908

Lower thermosphere minor gaseous constituents vertical transport by nonlinear gravity wave process, showing density scale height decrease from diffusive equilibrium 21 p3818 A70-41098

Vertical propagation of short acoustic waves from harmonic source in inhomogeneous atmosphere, calculating shock front width and heating rate 21 p3818 A70-41167

Geomagnetic field upward calculation in lower ionosphere, discussing accurate data acquisition difficulties in Dirichlet problem solution 21 p3819 A70-41294

Vertical oscillations in solar temperature minimum suggested as acoustic-gravity waves modes dependent on height at chromosphere-corona interface 21 p3926 A70-42196

Stratospheric clear air turbulence probability based on vertical temperature gradients and rawinsonde ascensional rates 22 p4064 A70-42619

Lower atmosphere electric field vertical distribution measurement by combined balloon and rocket soundings 22 p4017 A70-42797

Diffusion effect on hydrogen and oxygen constituents height distributions in atmosphere and lower thermosphere, solving diffusion and continuity equations 22 p4020 A70-43160

Vertical atmospheric ozone distribution according to direct solar radiation received on ground, using UV and IR observations 22 p4023 A70-43296

Electron density profiles calculation from model atmosphere, deriving F2 layer ionization vertical distribution 22 p4023 A70-43303

Tropical cyclone development model for axisymmetric vortex and quasi-balanced conditions, considering vertical heat distribution, rate of intensification and energy budget 23 p4213 A70-43896

Atmospheric optical properties at various altitudes, using lunar disk photometric observation at different wavelengths during eclipse 23 p4239 A70-43901

Ozone vertical distribution from satellite IR data, discussing Fredholm equations for radiation transfer 23 p4191 A70-44269

Airglow hydroxyl emission altitude profile observations by rocket-borne photometer 23 p4191 A70-44407

Spectrophotometric and visual observations of twilight glow from Soyuz 5, comparing vertical monochromatic brightness profiles with calculations for Elterman aerosol model 24 p4328 A70-45193

Atomic oxygen height profile measurements in upper atmosphere by sensor consisting of thin silver film on small pyrex rod permitting molecular transport 24 p4329 A70-45359

Fireball end point height as indication of meteoroid existence likelihood 24 p4411 A70-45787

Ionospheric wave propagation, using medium model, perturbation theory for vertical variation and computer eigenvalues of matrix system 24 p4314 A70-46132

Magnetosphere boundary altitude dependence on longitude, considering role of electric current density along geomagnetic lines of force 24 p4331 A70-46292

VERTICAL FINS
U FINs

VERTICAL FLIGHT

- V/JSTOL Flight Profile Indicator display system development to present pilot situation information in vertical plane
[SAE PAPER 690694] 05 p0792 A70-15861
- Matrix method for calculating aerodynamic loads, shearing forces, bending moments, torques, etc, in hinged main rotor helicopter blades during hover and vertical flight
06 p1167 A70-17914
- Optimal control synthesis for flight vehicle in vertical plane involving digital and analog computers
08 p1479 A70-20997
- Spanwise distribution of aerodynamic torsion on sailplane wings in vertical dive, discussing wing twist and lift effects
12 p2156 A70-27721
- Hunting phenomena of hydrogen gas plastic balloon at ceiling altitude, considering exhaust duct, extra volume and shape
17 p3018 A70-35317
- Cosmic ray and radiation belt data from vertical probes, determining instantaneous cross section of atmosphere
18 p3307 A70-36169
- Thermal design of high altitude balloons and instrument packages, analyzing vertical motion dependence on heat transfer and radiation environment
21 p3755 A70-42077
- VERTICAL LANDING**
Mathematical models for describing visual perception of distance to ground during VTOL landing and takeoff
05 p0810 A70-17119
- VERTICAL MOTION**
Heat and momentum transfer efficiency of thermal convection, calculating eddy coefficients for vertical transfer
05 p0831 A70-15876
- Vertically propagating waves in viscous isothermal atmosphere taking into account reflection due to nonlinearities and time dependence
05 p0833 A70-16679
- Vertical motion of ionized formations in ionospheric F region related to sporadic E layer
05 p0842 A70-16760
- Vertical motion and temperature structure of severe thunderstorms from jet aircraft penetration
06 p1102 A70-18585
- Electron concentration profiles calculated during vertically moving perturbations to evaluate ionospheric state
07 p1267 A70-19458
- Vertically moving disturbance discovered in ionospheric soundings close to magnetic equator, noting correlation with electrodynamic lift
07 p1269 A70-19631
- Nighttime ionospheric F region velocity component and recombination coefficient computer calculation
07 p1277 A70-20449
- Taylor instability of vertically accelerated horizontal two dimensional interface between liquid and air solved by method of strained coordinates
09 p1661 A70-23071
- Pulsed radio waves interactions during vertical propagation through perturbed ionosphere using cross modulation theory concepts, considering perturbation waves effects
11 p2003 A70-25531
- Limb-SD type ascending prominences direction and velocity correlated to flares and solar radio emission
12 p2303 A70-27707
- Air masses nonadiabatic ascent under elevated temperature inversion in atmosphere, assuming three layer model with linear profiles
12 p2265 A70-28335
- Hodograph theory for family of almost vertical ballistic trajectories
14 p2617 A70-31355
- Monograph on momentum, heat and mass transfer rates to vertical continuous cylinder moving through quiet fluid in forced and free convection
15 p2825 A70-31694
- Aircraft vertical channel landing condition autopilot using state variable feedback control techniques
15 p2773 A70-32553
- Airborne vertical glide path guidance computer for aircraft landing, using barometric altitude and DME data
16 p2871 A70-34053
- Ionospheric vertical base selection for recording discontinuities motion of F region
18 p3246 A70-36085
- Electron concentration profiles calculated during vertically moving perturbations for evaluation of ionospheric state
18 p3250 A70-36932
- Vertical motion determination from satellite cloud pictures based on canonical correlation of initial fields
20 p3664 A70-39401
- Solar photosphere vertical velocities and horizontal wave propagation, discussing magnetic fields, phase coherence and behavior and oscillations
21 p3885 A70-40952

Pulsed radio waves interactions during vertical propagation through perturbed ionosphere using cross modulation theory concepts, considering perturbation waves effects
21 p3786 A70-41281

Midwinter warming period upper stratospheric vertical motion fields, obtaining 2-mb charts
21 p3847 A70-42123

Average isobaric air flow field divergence calculation of vertical motion by two dimensional Gaussian integral theorem
24 p4371 A70-45134

VERTICAL PERCEPTION

- Visual vertical related to head tilts, observing location of gravitational vertical
04 p0645 A70-15445
- Human vertical perception with body tilt in median plane tested with luminous rod in upright to supine position with backward and lateral tilt
07 p1224 A70-20045
- Psychophysical adjustment methods effect on visual vertical orientation during head tilt
15 p2683 A70-32455

VERTICAL STABILIZERS

U STABILIZERS [FLUID DYNAMICS]

VERTICAL TAILS

U STABILIZERS [FLUID DYNAMICS]

U TAIL ASSEMBLIES

VERTICAL TAKEOFF

- Mathematical models for describing visual perception of distance to ground during VTOL landing and takeoff
05 p0810 A70-17119
- High lift devices design and operation problems in short and vertical takeoff
07 p1189 A70-19874
- STOL takeoff trajectory optimization for heavily loaded helicopter, using optimal control theory
17 p3021 A70-35841
- Short haul intercity center facilities air transportation traffic alleviation by VTOL aircraft, emphasizing performance, ground facilities, system operation and economics
24 p4290 A70-45914
- VERTICAL TAKEOFF AIRCRAFT**
NT FLYING PLATFORMS
NT X-22 AIRCRAFT
NT X-22A AIRCRAFT
NT XV-4 AIRCRAFT
- Turboprop VTOL or STOL intercity transports noting lift engines, noise, aircraft design and interior
01 p0005 A70-10645
- Air traffic control system for intercity and metropolitan VTOL airway reducing pilot and air traffic controller workloads
02 p0335 A70-12135
- VTOL transport aircraft stability and maneuverability compared with conventional aircraft
02 p0228 A70-12759
- VTOL steep descent beacon-guided landing systems
02 p0304 A70-12765
- Scanning beam radio guidance system for VTOL approach and landing
02 p0336 A70-12766
- Ground-airborne steep descent VTOL automatic flight control and vertical path selection using hover augmentation system /HAS/ and remote area terminal system /rats/
02 p0337 A70-12769
- Man machine interface in VTOL aircraft control and stabilization systems adaptation during manually controlled hovering flight
03 p0414 A70-14094
- Flight characteristics differences between VTOL and conventional transport aircraft, recommending differences consideration in regulations
03 p0414 A70-14095
- Noise radiated from VTOL lifting fan in wing inlet under static inflow conditions, attributing discrete tones to spacing between rotor and stator blades
04 p0734 A70-14889
- German VTOL transport aircraft projects, discussing Dornier 231 /lift by turbojets/ and Bolkow 140 /swiveling wing with gas turbine propellers/
04 p0623 A70-14955
- VTOL aircraft fly by wire system eliminating errors automatically, discussing electronic and electrohydraulic control components, flight test model design, prototype, etc
04 p0623 A70-15149
- German transport VTOL projects, discussing VC-500 swiveling wings with turbine powered propellers and HFB-600 blade cascade flow deflectors for vertical takeoff
04 p0623 A70-15349
- Stress analysis split method for determining residual strength and fatigue crack life of damaged or initially cracked VTOL structures
04 p0624 A70-15395
- Flight tests with mounted and unmounted SG 1262 hovering test rig in Germany to determine optimal control and stability characteristics for VTOL VAK 191B
04 p0624 A70-15704

VTOL fixed wing aircraft design parameters evaluation by digital variable stability system
[SAE PAPER 690696] 05 p0792 A70-15859

VTOL flight investigation to develop decelerating instrument approach capability with control-command information display for three degrees of freedom
[SAE PAPER 690693] 05 p0792 A70-15862

Wing vibration problems associated with roll attitude control in hovering autostabilized VTOL transport aircraft with wing-mounted jet lift engines
05 p0794 A70-16116

Safety analysis of VTOL aircraft for passenger transport based on accidental failures caused by technical defects, human error, weather, sabotage, etc
05 p0794 A70-16348

Airborne digital letdown computer to guide VTOL aircraft flying complex trajectories to relieve airport congestion
05 p0880 A70-16416

Helicopter advantages in airlift operation over conventional fixed-wing aircraft in Vietnam war
05 p0795 A70-16718

VTOL technical problems relating to military and civil transport applications, discussing sensitivity to mission requirement variations including design costs, noise levels, etc
05 p0797 A70-17077

VTOL aircraft control and stability with emphasis on flight characteristics and man machine interaction
05 p0809 A70-17089

Harrier G.R. Mk 1 VTOL vectored thrust aircraft for attacking targets at conventional strike aircraft speed, discussing design and combat effectiveness
06 p0985 A70-17157

STOL/VTOL airports design, location and complementary ground access transport
06 p1028 A70-17324

Economic flight conditions for civil aviation VTOL aircraft selected by graph-analytical method concerning phases of ascent, cruising and descent
06 p0987 A70-17875

Decision algorithms simulating human controller adaptive behavior in controlling VTOL aircraft in hover following stability augmentation system failure
07 p1216 A70-18860

VTOL and STOL transport development concerning aircraft types, air traffic control and navigation, airports, etc
07 p1194 A70-20250

Jet lift passenger aircraft considered better suited for medium stage routes than rotor/propeller designs for VTOL transport
08 p1436 A70-21347

VTOL aircraft applications to intercity traffic compared to competing transportation methods, discussing possible transportation time reductions
[DGLR-70-005] 10 p1970 A70-24045

Aerodynamic forces and moments effect of VTOL aircraft lift fan configurations on flow past wing
10 p1798 A70-24047

Lift fan propulsion for VTOL passenger aircraft, discussing design, thrust augmentation, optimum element combination, engine-wing integrations and tests
[DGLR-70-007] 10 p1929 A70-24049

Civil jet VTOL transportation based on Do 31, discussing market, passenger requirements, noise, flight safety and economic factors
[AIAA PAPER 70-001] 10 p1805 A70-24051

Civil VTOL transport aircraft handling and performance qualities using fixed base simulator with electronically generated display
[AIAA PAPER 70-345] 10 p1859 A70-24214

VTOL aircraft metal fatigue examination by photoelasticity emphasizing stress reduction
11 p2132 A70-25622

Total community annoyance measurement (TACM) applied to urban VTOL port planning for aircraft noise
[SAE PAPER 700286] 12 p2161 A70-27442

VTOL aircraft approaches to air passenger surface travel time reduction, emphasizing Manhattan-to-airport transportation problems
[SAE PAPER 700287] 12 p2335 A70-27443

VTOL profitability in Northeast Corridor, discussing city center ports accessibility for S-65-200 short hauls and economic and ground acreage advantages
[SAE PAPER 700310] 12 p2335 A70-27452

Economic factors in developing STOL and VTOL metroflight service, proposing evolutionary process beginning with short term demonstration
[SAE PAPER 700313] 12 p2335 A70-27454

VTOL and STOL design and operation, discussing noise and vibration reduction
13 p2344 A70-28544

Minimum fuel takeoff and landing paths for VTOL aircraft with constraints on state and control, determining optimal trajectories
[AIAA PAPER 70-550] 13 p2345 A70-29015

Tilt wing-propeller VTOL model, comparing static wind tunnel with moving-track test data based on coefficient forms of freestream and slipstream dynamic pressures
[AIAA PAPER 70-574] 13 p2343 A70-29895

VTOL aircraft multiple and nonuniform jets aerodynamics, considering induced field and secondary flows 14 p2528 A70-30851

VTOL aircraft stability augmentation system design based on control theory state variable methods, using minimum power levels 14 p2531 A70-30856

Model for pilots optimal manual control of hovering VTOL aircraft longitudinal position 14 p2543 A70-31409

Parameter identification algorithm for nonlinear equations describing VTOL aircraft longitudinal response 16 p2942 A70-33327

Quasi-linearization for VTOL aircraft equations of motion, using spline functions for unknown parameters initial estimation 16 p2942 A70-33328

Optimal fixed-form pilot model computer program for VTOL longitudinal control hover task evaluation 16 p2851 A70-33341

Low pressure ratio lift fan propulsion system for intercity VTOL transports, considering thrust, safety, noise, weight, components, speed, turbine and transmission [AIAA PAPER 70-670] 16 p2971 A70-33952

VTOL aircraft power plants optimization for future helicopter missions without restrictions of limited off-shelf inventory 17 p3147 A70-34708

Tilt-fold-propotor VTOL aircraft characteristics, stability and control, emphasizing flying qualities 17 p3014 A70-34722

Parameter model of VTOL airplane in transition, considering aerodynamic forces and moments and digital simulation 17 p3015 A70-34724

VAK 191 B VTOL aircraft fitting NATO Basic Military Requirements for low level reconnaissance-fighter operations developed from Fiat G-91 17 p3017 A70-34992

Composite compression tubes for VTOL aircraft components, describing weight parameters and mechanical properties [AIAA PAPER 70-898] 17 p3193 A70-35809

Optimum approach and departure paths for VTOL aircraft simulated by hybrid computer under constraints [AIAA PAPER 69-209] 18 p3213 A70-36452

Longitudinal dynamics of VTOL aircraft during hover-forward flight transition, using multiple time scale analysis [AIAA PAPER 69-130] 18 p3213 A70-36681

Soviet book on VTOL design covering aerodynamic and weight characteristics, turboprop and turbojet engines, flight regimes, etc 19 p3354 A70-37233

Exhaust gas ingestion suppression model tests for VTOL lift engines, measuring inlet thermal environment [AIAA PAPER 70-905] 19 p3490 A70-37396

Fixed wing and VTOL aircraft all-weather landing guidance and control philosophy 19 p3466 A70-38365

Computer simulated decision hierarchical model of helicopter and VTOL pilot for multiloop closure and tracking characteristics of man-vehicle system 19 p3372 A70-38921

VTOL aircraft longitudinal motion automatic stabilization in presence of turbulence and internal disturbances, using rotors and jet engines 20 p3561 A70-39838

Thrust deflector for VTOL aircraft fuselage mounted lift engines designed as isentropic plug nozzle, considering mass flow, pressure forces and Coanda effect [SAWE PAPER 841] 20 p3563 A70-40379

Aerodynamic characteristics of elliptical airfoils with jet circulation control for VTOL rotors including dual jets and cyclic results [AIAA PAPER 69-741] 22 p3959 A70-42705

VTOL aircraft ejector thrust augmentors, discussing configurations in wing root section [ICAS PAPER 70-56] 23 p4139 A70-44152

Low disk loading rotors in high speed VTOL aircraft for economical vertical payload lift [ICAS PAPER 70-57] 23 p4139 A70-44153

VTOL aircraft instrument flight in terminal area, defining requirements and operating characteristics for vertical and low speed capabilities [AIAA PAPER 70-1333] 24 p4291 A70-45935

Airport accessibility role in planning V/STOL aircraft landing facilities [AIAA PAPER 70-1311] 24 p4323 A70-45947

Turbofan, turbojet and turboprop engine development in aircraft gas turbine evolution, discussing VTOL propulsion, centrifugal and axial compressor engines 24 p4396 A70-46251

Military helicopter test program application to commercial VTOL operations, discussing military-civil design and development relationships [AIAA PAPER 70-1242] 24 p4292 A70-46327

VERTICAL TAKEOFF AND LANDING

U VERTICAL LANDING
U VERTICAL TAKEOFF

VERTIGO

Aircraft pilots vertigo during flight using questionnaire and interviews, emphasizing bank directional disorientation 04 p0643 A70-14979

Physiological mechanism and differentiation of alt-ernobaric vertigo in flyers 08 p1449 A70-21947

VERTOL MILITARY HELICOPTERS

U BOEING AIRCRAFT
U MILITARY HELICOPTERS

VERY HIGH FREQUENCIES

Solar phenomena effect on VHF communications between synchronous satellite relay and earth ground stations 02 p0259 A70-12566

Quasi-optical propagation in frequency wave range above 100 MHz as user problem in VOR, ILS, navigation satellite and CAT detection and warning systems 03 p0523 A70-13613

VHF field effect transistors thermal noise characteristics and effects of feedback and parasitic impedance 05 p0814 A70-16420

Radioheliograph observations at 80 MHz of directive shock wave propagation in solar corona 06 p1144 A70-18007

Design features and experimental results of E-fed cavity type suppressed omnidirectional antenna for VHF operation 06 p1022 A70-18020

VHF propagation variations relationship to changes in interplanetary plasma associated with interplanetary space sectorial structure rotation 07 p1226 A70-18757

Polarization diversity reception effects on VHF telemetry signal from low altitude satellites 10 p1832 A70-23919

VHF aerosat antenna design and system interactions, analyzing impact of spacecraft dynamics, control system, power supply and propulsion [AIAA PAPER 70-486] 11 p2120 A70-25439

VHF wave interference from heavy ion layers in lower ionosphere 14 p2574 A70-30737

VHF radiation from plasma during electron beam interaction with fast magnetoacoustic wave stimulated by external spatially periodic currents 15 p2780 A70-32118

VHF radio auroral scatter signal correlation analysis, determining scale size and drift velocity of scattered field 17 p3047 A70-35548

VHF propagation variations relationship to changes in interplanetary plasma associated with interplanetary space sectorial structure rotation 18 p3229 A70-37101

Polar electrojet and VHF auroral radio wave backscattering correlation, discussing geomagnetic disturbances effect 19 p3376 A70-37498

Radio source 3C 161 scintillating component angular dimensions and flux density at 60 MHz 19 p3524 A70-38760

Radio sources right ascension and flux densities at 60 MHz 19 p3524 A70-38761

Synchronous satellites VHF signal fading attributed to high latitude scintillations, noting intensity at night and during magnetic storms 21 p3790 A70-41362

Multiple channel VHF testing on ATS 1 and 3, describing transponder intermodulation and compression corrections 21 p3791 A70-41366

VHF geostationary satellite ranging and range correction systems, calculating second-order ionospheric delay effects on position error 22 p4068 A70-43590

Transistorized power amplifiers, frequency multipliers and parametric multipliers design for VHF and UHF ranges 23 p4170 A70-43876

Miniaturized VHF transmitter with bonded circular printed circuits for withstanding high shock loads, discussing design, production, packaging and testing 23 p4164 A70-44537

Aircraft Doppler VHF omnidirectional radio range (DVOR) performance test, noting improvement over VOR system 24 p4375 A70-46240

VERY HIGH FREQUENCY RADIO EQUIPMENT

Temperature profiles and frequency driftings of VHF telemetry transmitters for Saturn S-IC stage, using IR radiation data 12 p2196 A70-27725

VERY LOW FREQUENCIES

Normal and anomalous Doppler shifted cyclotron power radiated by energetic electrons spiralling along geomagnetic line considered as VLF source from magnetosphere 01 p0080 A70-11227

VLF observations of auroral beams for auroral V-emissions source and characteristics, explaining spectral shape 02 p0291 A70-12204

User problems in navigation methods, discussing Omega method, Navy Navigation Satellite System and VLF methods 03 p0522 A70-13603

VLF wave propagation in earth-ionosphere waveguide, comparing ray and waveguide-mode theories 03 p0449 A70-13616

Dynamic spectra of quasi-periodic VLF emissions noting association with geomagnetic micropulsations 03 p0477 A70-13985

VLF radio monitoring of celestial X ray fluxes from ground for long periods, discussing ionospheric D region conductivity 04 p0739 A70-14521

Nonducted VLF walking trace whistlers and Doppler shifts in fixed frequency transmissions identified on OGO midlatitude spectrographic records 04 p0649 A70-15116

Magnetospheric observations of whistler mode emissions by OGO 1 satellite over VLF and LF ranges 04 p0649 A70-15117

VLF phase disturbances and HF absorption during solar proton events of 28 August and 2 September 1966 related to proton intensities, energies and cut-off latitudes 04 p0741 A70-15124

Magnetospheric VLF emissions properties at frequencies below electron gyrofrequency 06 p1117 A70-17374

Satellite observations of VLF and ELF resonances related to ionospheric plasma singularities 06 p1118 A70-17375

Nonuniform plasma analyzed for parameters inhomogeneity effect on VLF propagation mode and instability 06 p1119 A70-17381

VLF propagation between earth and moving dispersive ionosphere, considering medium motion effects in Maxwell-Minkowski equations solutions 06 p1007 A70-17462

Wave focusing along static magnetic field from radiating VLF source immersed in cold magnetoplasma 06 p1120 A70-17577

Transequatorial multisite VLF records establishing solar zenith angle for midpoint of sunrise ionospheric height discontinuity, recomputing magnetic latitude dependent parameters 06 p1054 A70-17590

Balanced ELF chemotron tetrode amplifiers with series-fed output circuits, showing characteristics calculations and use in pyrometric assembly 06 p1022 A70-17782

Satellite observations of equatorial erosion and defocusing of VLF waves propagating at low magnetic latitudes 06 p1058 A70-18532

VLF noise phenomena observed with satellite electric dipole antennas compared with lower hybrid resonance frequency of ionospheric medium in vicinity 06 p1011 A70-18534

Cerenkov generation of VLF waves in inner magnetosphere at low latitudes 07 p1265 A70-19281

Outer radiation belt high energy electron fluxes correlated with VLF hiss ground observations 07 p1367 A70-19498

Geomagnetic field orientation effects on VLF nighttime propagation, checking computer program predictions 09 p1639 A70-23664

VLF radio noise statistical parameters observed as functions of azimuth, considering atmospheric distribution and parameters correlations 10 p1884 A70-25259

Temperature and ion effect on refractive index of VLF radio waves in quiet and disturbed ionospheric conditions 11 p2004 A70-25842

VLF and ELF EM wave propagation in earth-ionosphere cavity during solar flares 12 p2183 A70-27189

Very low frequency radio noise in ionosphere, magnetosphere and solar wind, using multiple receivers to measure mathematical relations between direction magnitude and polarization characteristics 12 p2184 A70-27574

Ionospheric probing with LF/VLF/ELF radio waves, discussing measurement techniques and temporal and spatial resolutions 12 p2224 A70-27731

Mode-scattering coefficients from ionospheric perturbations for sunrise and sunset propagation paths, comparing results with VLF radio measurements 12 p2189 A70-28053

Electromagnetic fields features in VLF spectral range for propagation in earth-ionosphere waveguide, discussing effects of ionospheric irregularities 12 p2190 A70-28169

VLF auroral and low latitude emissions along N-S chain of stations, discussing daytime and nighttime observations

13 p2371 A70-29925

Double sphere dipole antenna detecting VLF electrostatic plasma waves, discussing induced and contact potentials

13 p2372 A70-29927

Whistler mode VLF emissions stimulation mechanism

13 p2401 A70-29930

Perpendicular propagation of VLF waves from wave/particle interaction in vicinity of lower hybrid resonance frequency in magnetosphere

13 p2468 A70-29934

Magnetic field measurement of VLF wave propagating in whistler mode in magnetosphere by satellite FR-1

13 p2401 A70-30054

Magnetic fluctuations observed by ground observatories, suggesting large amplitude waves as field line resonances driven by magnetopause motion

13 p2402 A70-30078

Magnetospheric discrete VLF emission magnetic field intensity calculation by extending Helliwell theory to include electron density model and variable frequency waves

13 p2483 A70-30087

Statistical variation of number of VLF atmospherics per unit time above given vertical electric field strength threshold

14 p2550 A70-30515

Reflection and conversion coefficients of model ionospheres for VLF and LF radio waves

14 p2573 A70-30735

VLF wave propagation direction observation by satellite after passage through magnetosphere at low and mid latitudes

15 p2697 A70-31659

Automatic audio frequency spectrometer for ELF and VLF amplitude spectrum of atmospherics, discussing attenuation band near 3 kHz

15 p2725 A70-31856

Lightning discharge slow tail atmospherics relation to return stroke, using VLF spectra and frequency analysis

15 p2727 A70-31871

VLF transequatorial propagation, describing equipment, periodic variations in signal characteristics, ionospheric parameters, etc

15 p2699 A70-32298

Outer radiation belt high energy electron fluxes correlated with VLF hiss ground observations

15 p2795 A70-32743

Multimode and dispersive distortion of short quasi-monochromatic pulses in earth-ionosphere VLF channel

16 p2858 A70-32930

Ion effects on VLF propagation in earth-ionosphere waveguide during polar cap absorption events

16 p2859 A70-32933

Electric and magnetic dipole VLF radiation patterns in lossy two component magnetoplasma

16 p2860 A70-32944

Tweak atmospherics occurrence frequency and directions for VLF band reflecting layer study

17 p3047 A70-35401

VLF and ELF radio wave propagation with mode coupling in inhomogeneous stratified ionosphere

17 p3047 A70-35402

Ionospheric VLF radio waves observations via wideband receiver on K-9M-26 rocket, determining electron density profiles

17 p3047 A70-35639

Signal spectral parameters for reducing VLF atmospherics data from analyzer observations

19 p3412 A70-37998

VLF radiation observation at conjugate points, discussing hisses, choruses and geomagnetic effects

19 p3416 A70-38587

Whistler VLF radio observations of sudden magnetic impulses in plasmasphere during storms, using ground based magnetometers

20 p3620 A70-39330

Lower hybrid resonance frequency propagation ducts in multilayer upper ionosphere, showing association with VLF hiss bands

20 p3584 A70-39331

ELF and VLF propagation for perturbed ionosphere models, discussing effects of ion collision frequencies and molecular weights

20 p3585 A70-39454

Ionospheric VLF diurnal transmission loss differences on two long paths, analyzing values for first and second modes

20 p3585 A70-39455

VLF wave generation due to nonlinear interaction of two microwaves with plasma slab under high DC field

22 p4077 A70-42294

ELF and VLF waves in waveguide propagation mode, calculating lower ionosphere effect on attenuation and phase velocity

22 p3989 A70-42960

VLF signal phase and amplitude changes associated with PCA events and South Atlantic Geomagnetic Anomaly

22 p4023 A70-43292

D region LF and VLF sky waves opposite phase perturbation behavior

23 p4162 A70-44006

Zi and Ze smallness effect on complex refractive index of ionosphere for VLF propagation

23 p4164 A70-44373

VLF phase disturbances, HF absorption and solar protons in 1967 PCA events, using ionization model

24 p4314 A70-46128

VESTA ASTEROID

Absorption bands in reflection spectra of various asteroids, comparing Vesta composition to meteorites and Apollo 11 samples

16 p2972 A70-32987

Vesta diameter and albedo determination by IR emission measurements, allowing for roughness and rotation

17 p3173 A70-35758

VESTIBULAR TESTS

Microelectrophysiological study of cerebellar neuron responses to stimulation of vestibular apparatus by vertical rocking performed on anesthetized adult cats

01 p0012 A70-10124

Mathematical model for vestibular nystagmus adaptation to subjective sensation of rotation, noting time constants

01 p0032 A70-10362

Vestibular sensing system role in providing information concerning vertical, linear and angular head movements to central organs

02 p0246 A70-12191

Motion sickness causes and prevention during prolonged space flights, discussing vestibular system and characteristics of visual-inertial and canal-otolith incongruities

03 p0421 A70-13542

Vestibular analyzer stimulation effects on cerebral blood circulation in humans during angular acceleration using rheoencephalography

03 p0422 A70-13692

Vestibular reactions in rats under hypothermal conditions by measuring postrotatory nystagmus beats number and duration, respiration rates and rectal temperature

03 p0425 A70-13893

Astronaut vestibular fitness determined from threshold labyrinthine tests on isolated horizontal and vertical semicircular canals

03 p0437 A70-14059

Vasomotor center neuron responses to vertical rocking movement stimulus of vestibular apparatus in cats

06 p0995 A70-17805

Vestibular semicircular canal excitation thresholds of experienced and candidate pilots for imposed angular accelerations

07 p1201 A70-18795

Adaptation to Coriolis accelerations associated adaptation schedule to with 1-rpm increments developed for preventing motion sickness in slow rotating environment

07 p1223 A70-19938

Vestibulometric techniques for medical examination and pilot selection using Coriolis accelerations for instability prognosis

09 p1617 A70-22475

Microdissection morphology of vestibular apparatus sensory regions in guinea pig, rabbit, cat, squirrel, monkey and man

10 p1811 A70-24200

Vestibular analyzer and otolith apparatus disturbances and normalization under prolonged hypodynamia, noting pathological effects of repeated caloric testing

10 p1816 A70-24686

Pilots with high vestibular stability studied for spatial orientation, noting activity impairment due to alternating angular acceleration and optokinetic stimuli

10 p1828 A70-25180

Vestibular adaptation to heat and rotary stimulation in animals and men

11 p1986 A70-25822

Tilting rotating chair producing vestibular stimulus via linear rotating acceleration to study motion sickness

11 p1988 A70-26515

Alcoholic beverages effect on positional nystagmus and Coriolis acceleration

11 p1993 A70-26520

Anatomical and physiological correlations between mathematical model components for vestibular nystagmus mechanisms

13 p2351 A70-29331

Coriolis illusions amelioration during space flight, noting cross coupling effects minimization by reflex vestibular stabilization of head

13 p2358 A70-29432

Vestibular nystagmic and electrical responses facilitation, inhibition and habituation, noting modulation by subcortical and cortical systems

14 p2538 A70-30909

Vestibular nystagmus evocation by conditioned reflexes technique after pure tone stimulation

14 p2538 A70-30910

Arousal effects on vestibular nystagmus in man, discussing forced alertness in mental arithmetics form

14 p2538 A70-30911

Ocular fixation index and vestibular stimulation by caloric tests, discussing central processes for nystagmic rhythm regulation

14 p2538 A70-30912

Vestibular habituation among pilots and flying staff from training and seniority standpoint

14 p2538 A70-30914

Vestibular threshold dependence on gravity, considering linear accelerations effect on canals sensitivity

14 p2539 A70-30916

Electronystagmographical responses comparison with electroencephalographic record during prolonged torsion swing vestibular tests under cortical and subcortical factors influence

14 p2539 A70-30917

On-line reduction of nystagmic data during vestibular bithermal caloric testing by analog technique

15 p2685 A70-32570

Vestibular stimulation by square wave acceleration, evaluating Ewald laws for nystagmus behavior

17 p3037 A70-35127

Complex accelerations effects on vestibular apparatus from physical and mathematical viewpoint

17 p3037 A70-35128

Vibration effects on vestibular components, noting applications to spacecraft artificial gravity

17 p3038 A70-35322

Acrobatic pilots equilibrium behavior in vestibular training, discussing labyrinth reactions and fluid intake role

17 p3041 A70-35919

Optokinetic and vestibular effects on human operator reliability in aircraft control systems

18 p3223 A70-36184

Vestibular thermal stimulation method using distilled water injected into ear, discussing nystagmus appearance and duration

19 p3367 A70-37355

Soviet book on peripheral vestibular apparatus and higher nervous system roles in motion sickness covering Coriolis acceleration tests, pilot training and selection, drugs, etc

19 p3359 A70-37406

Multiple choice rotation chair for clinical experimental research and pilot vestibular tests

20 p3580 A70-39438

Moving stripe stimulus inducing optokinetic turning movements in goldfish, discussing efferent influence on vestibular organ

21 p3762 A70-41141

Vestibular message flow regulation by central nervous system, describing afference, inhibition and copy formation

22 p3976 A70-43705

Vestibular sinusoidal stimulation effects on compensatory tracking under various postures and display conditions

22 p3976 A70-43706

Reflex vestibular disturbances and motion sickness prevention in artificial gravity of rotating space base, by incremental adaptation tests and drugs

23 p4154 A70-44625

VESTIBULES

Relationships between frog vestibular afferents, cerebellum and efferent vestibular system, using electron microscopy and Nauta degeneration technique

01 p0014 A70-10351

Cerebello-otolith system represented by axons of Purkinje cells, studying inhibitory vestibular efferent system relation to cerebellum in frog

01 p0014 A70-10352

Termination mode of primary and secondary vestibular fibers in cerebellar cortex of frog and cat, measuring evoked field and unitary potentials

01 p0014 A70-10353

Tegmental nucleus neurons of cats cerebellum, considering responses to acceleration changes and natural stimulation of vestibular apparatus

03 p0421 A70-13510

Vestibular habituation acquisition, retention and transfer correlation with stimulation, discussing alertness and arousal effects

14 p2539 A70-30915

VFR [RULES]

U VISUAL FLIGHT RULES

VHF OMNIRANGE NAVIGATION

Minimum operational characteristics /MOC/ for vertical guidance in airborne area navigation systems, including VOR-DME accuracy criteria

01 p0138 A70-11049

Airplane navigation based on VHF ranging between aircraft and geostationary satellite, examining errors

by unknown propagation characteristics of signal in ionosphere 02 p0262 A70-12594

Solid state VHF omnirange navigation system operation, principle, equipment, applications, advantages, etc 07 p1241 A70-19622

Parasitic loop counterpoise antenna radiation patterns, considering application to VOR systems 09 p1646 A70-22693

Doppler VOR offering increased course accuracy and allowing precise area coverage in conjunction with DME ground station 09 p1723 A70-23036

VHF satellite transponders for ranging and position fixing, studying ionospheric and multipath effects [AIAA PAPER 70-489] 11 p1999 A70-25433

Short distance VHF omnirange navigation and distance measuring equipment considered for performance improvements feasibility to meet civil air traffic demands through 1980 12 p2268 A70-27643

VORTAC system providing navigation service to civil and military air traffic on worldwide basis 12 p2269 A70-27919

Short range VOR/DME area navigation techniques in U.S. National Airspace System 16 p2948 A70-33470

Eurocontrol evaluation of navigational aid systems air traffic control, examining HARCO and VORDAC systems 19 p3468 A70-38641

Onboard velocity sensors for VOR/DME navigation systems positional accuracy improvement, describing optimal and suboptimal data filtering [AIAA PAPER 70-1024] 20 p3666 A70-39511

VHF omnidirectional range (VOR) receiver, considering noise reduction problem and active filter importance to signal improvement and system accuracy 22 p3992 A70-43586

Limiting effects of topographic quasi-optical radio propagation above 100 MHz in radar aircraft navigation, clear air disturbances detection and IR warning technique 23 p4163 A70-44230

VIBRATION

NT BENDING VIBRATION

NT COMBUSTION VIBRATION

NT FLUTTER

NT FORCED VIBRATION

NT FREE VIBRATION

NT LATTICE VIBRATIONS

NT LINEAR VIBRATION

NT MISSILE VIBRATION

NT PANEL FLUTTER

NT RANDOM VIBRATION

NT RESONANT VIBRATION

NT SELF INDUCED VIBRATION

NT STRUCTURAL VIBRATION

NT SUBSONIC FLUTTER

NT SUPERSONIC FLUTTER

NT TORSIONAL VIBRATION

NT TRANSONIC FLUTTER

Book on vibration and propagation phenomena covering oscillations of linear and nonlinear systems with various degrees of freedom, propagation in solids and fluids, etc 07 p1335 A70-19904

Scanning technique for allowing whole vibration cycles storage on one hologram 15 p2738 A70-32052

Solar limb image vibrations, establishing quantitative comparisons between statistical characteristics of fluctuations and weather conditions on propagation path 16 p2979 A70-34179

Eigenvalues of transfer matrix and vibrations generation for passive mechanical systems with n degrees of freedom based on Laplace transformation 18 p3337 A70-36225

Asymptotic, averaging and Ritz methods for steady state periodic vibrations of nonlinear systems with many degrees of freedom 18 p3338 A70-36437

Soviet book on vibrations in flight vehicle engines covering linear and nonlinear systems, computer methods, etc 18 p3305 A70-37229

Low stiffness optical parts bulk vibration machining 22 p4045 A70-42512

Krylov-Bogoliubov virtual work principal, investigating nonlinear vibrations, extending to heterogeneous vibrations 23 p4266 A70-44028

Periodic boundary value problems with cyclic totally positive Green functions, considering applications in vibrating physical systems and spline theory 23 p4213 A70-44899

VIBRATION DAMPERS

U VIBRATION ISOLATORS

VIBRATION DAMPING

Vibrating system response to damping insert introduced between two distinct coordinates, discussing Butyl rubber and vibration amplitude reduction 01 p0199 A70-10265

Two stage axial flow compressor with variable pitch guide vanes, discussing HF vibration reduction of rotor blades 01 p0166 A70-11419

Machine element materials damping properties, determining energy dissipation during steady resonant vibrations 01 p0211 A70-11423

Acoustical resonators free oscillations and pressure effects on damping, amplification, decay decrement and relaxation time 02 p0304 A70-12772

Acoustic wave excitation and damping in cryogenic He plasma produced by HF pulse discharge, considering nonadiabatic heating and dissipation during reflection 03 p0529 A70-13056

Spacecraft orientation control without measuring vehicle angular velocity based on transient response and oscillations damping effectiveness 04 p0760 A70-14428

Damping factor of fiberglass-reinforced cylindrical shells, concerning dependence on wave number and energy losses due to medium resistance and acoustic radiation 04 p0712 A70-14488

Natural vibrations damping of holonomic mechanical systems with feedbacks not explicit function of time reduced to optimal stabilization problem 04 p0718 A70-14494

Complex uncoupled modes to analyze forced vibrations of three layer damped sandwich beam with arbitrary boundary conditions, discussing orthogonality 04 p0773 A70-15076

Inertial damping of soft rubber under forced torsional vibrations, discussing viscoelastic body linear model 04 p0712 A70-15100

Javelin research rocket payload suspension ensuring limited vibrational accelerations, using viscoelastic materials for damping [DGLR-69-61] 04 p0774 A70-15147

Optimal damping time required for gyrocompass oscillations, allowing for maximum initial deflections 04 p0692 A70-15280

Beam fluctuations damping in beam waveguide, determining fluctuations cause as random displacement of lenses 04 p0651 A70-15290

Dynamic vibration absorbers (DVA) efficiency in limiting excessive vibrations in mechanical systems by transferring motion to auxiliary system 04 p0699 A70-15306

Vibration decay rate measurement by pulse cycles counting 04 p0695 A70-15571

Averaging analysis of oscillations attenuation of relaxing one dimensional linear viscoelastic systems under external force at resonance applied to nonlinear multidimensional systems 05 p0933 A70-16208

Linear damping of sinusoidal oscillation in plasma, solving linearized Vlasov equation by integration along particle trajectories 05 p0888 A70-16304

Dynamic characteristics from equations of motion of gyroscope with allowance for structural damping forces between inner gimbal and rotor 05 p0852 A70-16961

Cylindrical shell walls vibrations under impact loads, calculating damping factor in differential equation of motion of wall element 05 p0947 A70-17008

Vibration damping properties of steels and Ti- and Al-based alloys at various temperatures under tensile and compression loads 05 p0868 A70-17048

Heat resistant materials damping properties at high temperatures under distributed stresses measured in thin walled tubular specimens with vibrogram 05 p0952 A70-17049

Heat resistant enamel coatings effect on vibration damping of cast steels for turbine blades 05 p0868 A70-17050

Vibration damping of oil hydraulic system using bladder type accumulator composed of rubber, measuring frequency response of shock absorber 06 p0988 A70-17140

Absolute stability ranges of forced motions and damping in nonlinear systems determined by Sturm theorem 07 p1243 A70-18688

Vibration damping by sandwich structure consisting of viscoelastic layer between two high Youngs modulus metal sheets 07 p1401 A70-18845

Aircraft engine vibrational overload reducible by elastic bearings having controllable elastic characteristics 07 p1364 A70-19113

Soviet book on unsteady attached turbulent flow in turbine lattices, studying blade aeroelastic vibrations onset and attenuation in compressible and incompressible fluids 07 p1189 A70-19602

Circular nozzle contraction and Reynolds number effects on turbulent pulsation damping, measuring longitudinal and transverse components 07 p1259 A70-19830

Optimization of control of oscillatory process with deviating argument in maximum principle form, reducing solution to boundary value problem 08 p1544 A70-20954

Martensitic stainless steels structure related to energy dissipation capability, obtaining damping mechanism as magnetomechanical hysteresis 08 p1515 A70-20979

Elastic oscillations amplitude-dependent damping during phase transformations in two phase systems 08 p1556 A70-21121

Spaced damping reducing structural response to vibration, discussing efficiency, design flexibility and weight addition 08 p1507 A70-21269

Steady state motion of sinusoidally excited primary system with impact damper solved analytically by piecewise linear technique 08 p1546 A70-21858

Vibration theory damping using mathematical model emphasizing controlling response under steady state resonance and random excitation 09 p1769 A70-22238

Panel sound absorber acoustic impedance variation with frequency predicted taking into account panel mass, stiffness and internal damping 09 p1770 A70-22390

Aircraft turbine engines strength and gas dynamic characteristics improved by vibration decrease using elastic elements 09 p1742 A70-22471

Vibration decrement of nonlinear elastic system from resonance peak width of displacement amplitude curve of perturbing force 09 p1782 A70-23295

Flutter suppression in elastic finned beams in supersonic flow controlled automatically by rudder deflection according to flexural strain 09 p1785 A70-23615

Bifilar pendulum vibration absorber for counteracting helicopter main motor vibratory forces 10 p1805 A70-24657

Hysteretic linear damping theory applied to representation of structural damping under harmonic excitation 10 p1961 A70-25060

Undamped natural modes intercoupling resulting from arbitrary linear damping addition to linear dynamic system 10 p1962 A70-25061

Temperature effect on plate damping by constrained viscoelastic layers, emphasizing transition and operating temperature compatibility 10 p1962 A70-25063

Forced vibration of rib-skin structures under random pressure and heavy damping using wave group theory 10 p1963 A70-25066

Statistical energy concepts application to Mariner Mars 1969 spacecraft, estimating coupling of damping factors to analyze structural vibration [SAE PAPER 700171] 11 p2128 A70-25374

Vibration damping theory validity, discussing response curve for frequency dependence of energy dissipation 11 p2133 A70-25733

Self excited lateral vibration of poppet valve under positive and negative damping effects 11 p1983 A70-26420

Metal plates vibration under viscoelastic damping layers using electromagnetic transducer and impact excitation 11 p2145 A70-26702

Time optimal control synthesis of fast acting gyrocompass mounted on fixed foundation and with hydraulic damper and torsional suspension of sensor 12 p2233 A70-27564

UHF frequency doubler with series-parallel array of eight punch-through diodes, preventing spurious oscillations 12 p2196 A70-27650

Dynamics of gravity stabilized satellite having maximum damping rate 13 p2499 A70-28391

Circular orbit gravitationally stabilized satellite oscillation damping by changes of moments of inertia 13 p2501 A70-28420

Spacecraft orientation control without measuring vehicle angular velocity based on transient response and oscillations damping effectiveness 13 p2503 A70-28453

Canilevered column stability under constant lower load in presence of external damping 13 p2510 A70-28733

Vibration control by alternate layers of high damping viscoelastic material, discussing damping and loss factors, beams design and attachment 13 p2513 A70-29079

Compressor cascade flutter phenomenon, investigating factors affecting aerodynamic damping force on annular cascade blades

13 p2341 A70-29447

Book on vibrations covering natural oscillations, damped and undamped oscillations, energy sources, forced vibrations, resonance and multiple degree of freedom systems

13 p2515 A70-29452

Electronic packages design for vibration resistance, discussing isolators and damped laminate structures

13 p2516 A70-29616

Electrohydraulic control system dynamics, examining executive component loading at low speeds and nonlinear resistances

13 p2349 A70-29720

Bifilar pendulum type absorber for helicopter main rotor vibration reduction

13 p2348 A70-29827

High speed dynamic systems synthesis with optimal damping of elastic vibrations, using gradient method

14 p2617 A70-31354

Energy dissipation during independent flexural-torsional vibrations of rods, noting alternating shear stress superposition effect on damping

15 p2813 A70-31530

Damped vibrations logarithmic decrement determination during automatic recording of number of cycles, emphasizing error analysis

15 p2733 A70-31531

Monograph on harmonic and random vibrations filtering, discussing objects protection from ground vibrations produced by mechanical source

15 p2774 A70-31693

Matrix analysis of discretized dynamical system with constraints, considering case of damped oscillators

15 p2774 A70-31697

Diurnal vibrations damping in inertial navigation system, demonstrating equations asymptotic stability for coordinates autonomous determination

15 p2775 A70-32156

Perturbed motion of body with partially filled cylindrical cavity with damping ribs, discussing vibrations boundary value problems of liquid filling

15 p2775 A70-32157

Annular fluids hydrodynamic mass and damping effects on long rotating cylinders vibrations, discussing theory of fluid friction and forces, vortex and turbulent flows, etc

[ASME PAPER 70-FE-30]

16 p2892 A70-33636

Annular fluids hydrodynamic mass and damping effects on long rotating cylinders vibrations, analyzing test results

[ASME PAPER 70-FE-31]

16 p2892 A70-33637

Embedded damped sandwich beams, determining equations for resonant frequency, loss factor and modal roots

16 p2992 A70-34018

Discrete mechanical models of single speed gearings in torsional vibrations without teeth deformation and damping resistance

16 p2995 A70-34288

Linear systems with two degrees of freedom modeled as rigid beam on elastic supports, considering vibration damping

16 p2996 A70-34291

Hingeless rotor helicopter airborne and ground resonance characteristics, noting feedback stability control interference with rotors aerodynamic damping

17 p3015 A70-34733

Helicopter vibration reduction techniques, considering antivibration devices design and comfort crossover speed increase

17 p3015 A70-34735

Vibrating diaphragm gas pressure measuring system based on membrane damping, applying to prototype atmospheric entry probes

17 p3095 A70-35524

Damping characteristics [absorption coefficient]/of dissipative systems, defining authentic value of energy dissipation characteristic determination from natural vibrations damping

17 p3192 A70-35711

Stellar thermal and vibrational energy losses due to URCA shells in interiors

18 p3310 A70-35935

Elastic plate vibration with damping under random load, calculating linear response by harmonic analysis

18 p3334 A70-35958

Mechanical systems spontaneous oscillation due to different critical velocities with and without arbitrarily small damping

18 p3338 A70-36430

Flutter design charts for isotropic panels stressed to verge of buckling for tropical values of structural damping

18 p3338 A70-36446

Damped vibrations of single-mass elastic systems, determining E function singularity effect on dynamic characteristics

18 p3341 A70-36587

Vibrations induced by frictional moving force in viscoelastic beam with free ends on elastic base, showing critical load dependence on damping

18 p3343 A70-36720

Slot type oscillations electrodynamic suppression in coaxial magnetrons resonator systems, calculating long wave oscillation frequencies

19 p3387 A70-37738

Linear damping theory, discussing simple harmonic motion model extension to transient motion

19 p3472 A70-38041

Satellite structural vibration damping material and methods, discussing high polymer synthetics and viscoelastic laminae and damping systems data

19 p3533 A70-38291

Perforated cantilever beams and plates vibration damping capacity improvement by stress concentration introduction

21 p3933 A70-40729

Electron-neutral collisional damping of longitudinal electron oscillations in weakly ionized plasma, solving linearized Boltzmann-Vlasov equation

21 p3860 A70-42014

Free and forced oscillations of dynamic system with linear hysteretic damping, using nonlinear model

22 p4114 A70-42700

Magnetoacoustic waves in MHD channels, investigating excitation, damping and effects on mean current density and Hall field strength

22 p4081 A70-42822

Free motion of second order nonlinear automatic control device with vibration damping

22 p4075 A70-43554

Printed circuit boards vibration control in dynamic environment, noting viscoelastic damping technique

22 p3999 A70-43675

Inverted torsion pendulum performance improvement, describing dashpot to dampen lateral vibrations

23 p4202 A70-44950

Vibration transfer coefficient of aerial camera-photographic assembly system for shock absorption during surveys

24 p4333 A70-45200

Large amplitude high phase velocity oscillations anomalous damping in electron-ion plasma resulting from MHD instability

24 p4387 A70-46091

VIBRATION EFFECTS

Hyperon and resonance particle effects on neutron star vibration, discussing vibrational energy storage and atmospheric electromagnetic generation

02 p0379 A70-12699

Vibrational energy exchange between molecules during collision behind normal shock front as function of wave velocity

03 p0468 A70-13873

Mechanical vibrations effect on man including motor vehicle dynamic vibrations

03 p0439 A70-14097

Mechanical vibration effects on natural convective heat transfer in enclosure of rectangular cross section [ASME PAPER 69-WA/HT-13]

04 p0783 A70-14820

Residential structures vibration response to aircraft flyover noise, discussing noise transmission, rattle phenomenon, spectra, etc

[ASME PAPER 69-WA/GT-8]

04 p0770 A70-14887

Horizontal transverse vibration effects on manual tracking performance, relating tracking errors to frequency rather than acceleration

04 p0643 A70-14981

Javelin research rocket payload suspension ensuring limited vibrational accelerations, using viscoelastic materials for damping

[DGLR-69-61]

04 p0774 A70-15147

Sound vibrations effect on pulsation characteristics of turbulent gas jet

04 p0618 A70-15248

Randomly oriented vibration effect on noncompensated three degree of freedom gyroscope with displaced center of gravity

04 p0692 A70-15278

Two degree of freedom gyroscope sensitivity threshold during gimbal vibration with respect to casing

04 p0692 A70-15279

Ballistic range measurements of vibrational nonequilibrium effects on leading edge shock wave shape for cone-cylinders fired through chlorine atmosphere at supersonic speeds

04 p0621 A70-15601

Vibration effects on ion-molecule collision lifetimes and multiple reflections

04 p0723 A70-15638

Packing rub effect on rotating machinery produced by unstable vibration generated by friction and heat of rubbing rotor in sliding contact

05 p0854 A70-15908

Spacecraft level vibrations and gravity effects on blue-green algae *Plectonema Boryanum* proposed as gas exchange medium

06 p0999 A70-17292

Sinusoidal vertical vibration effect on adrenocortical function in guinea pigs

06 p0992 A70-17424

Acetylcholine concentration, esterase activity and synthesis in cerebral tissue of rats under repeated mechanical vibrations combined with noise

06 p0993 A70-17425

Vibrational creep curves of Al alloy under uniaxial stress level and amplitude, noting influence of small vibrations

06 p1168 A70-17930

Vibration frequency influence on vibrational creep of Al-Mg-Si alloy, describing mechanism in terms of strain hardening, additional slip and dislocation movements

06 p1168 A70-17931

Rectilinear oblique harmonic vibration effect on gyrocompass with torsional suspension

07 p1278 A70-18737

Linear vibrations in gimbal suspension rotor and base, estimating gyroscope drift during base and rotor vibration coincidence

07 p1279 A70-18738

Differential equations of motion for sensitive element of gyrocompass with torsional suspension under small amplitude spatial vibrations, taking into account torsional and flexural rigidities

07 p1282 A70-19534

Visual analyzer physiology under effects of gravitation, atmospheric pressure, mechanical vibrations, etc

08 p1444 A70-20740

Ultrasonic vibration effect on strength and plastic properties of metals undergoing torsion tests

08 p1520 A70-21499

Non-Cerenkov radiation region produced by passage of oscillating electric dipole at uniform velocity

09 p1728 A70-22958

Air traffic vibration effects on human organs and sensations, considering blood circulation, lungs, eyes and muscles

09 p1625 A70-23007

Ultrasonic vibrations effects on microstructure and mechanical properties of polycrystalline titanium during phase recrystallization

10 p1903 A70-23863

Body vibration effects in cats on myocardial ECG recordings, discussing electrodes implantation and tracings

10 p1810 A70-24007

Small natural vibrations effect of solar sail-propelled system on heliocentric orbit motion

10 p1950 A70-24319

Continuous wave chemical laser operation at 10.6 micron in carbon dioxide pumped by vibrational energy from hydrogen atoms and bromine molecules reaction

10 p1901 A70-25149

Support vibration effect on zero shift of damped vertical pendulum, using equivalent linearization with perturbation scheme

10 p1917 A70-25205

Ultrasonic LF modulation of solid state traveling medium lasers radiation intensity attributed to elastic vibrations of rods

11 p2062 A70-25398

Coupled panel-cavity vibrations analysis, emphasizing sonic boom excitation of large window-room combinations

11 p2133 A70-25728

Physiopathologic effects on organs of longitudinal and tangential accelerations, decelerations, vibrations and weightlessness

11 p1986 A70-25821

Stability conditions of rotational motions of symmetrical solid body on vibrating base in potential force field

11 p2098 A70-25916

Plane wave disturbances introduced in turbulent channel flow by vibrating ribbons near each wall, obtaining amplitude and relative phase

11 p2039 A70-26537

Liquids relative rotary motion in vertical rotating cylinders under large amplitude axial vibrations and angular velocities

12 p2209 A70-27213

Dynamic errors of electric measurement devices during three dimensional polyharmonic vibrations of foundation

12 p2233 A70-27561

Vertical position stability of gyropendulum mounted on vibrating platform, showing foundation induced gimbal rotor parametric vibrations

12 p2233 A70-27563

Seismic measurements of sonic boom induced ground vibrations for hazard to structures

12 p2227 A70-28078

Vibration effects on receptors in frog toe muscles at various frequencies

12 p2179 A70-28344

Single component two phase pipe flow choking and shock phenomena, including flashing flow vibratory effects

13 p2386 A70-28846

Electronic packages design for vibration resistance, discussing isolators and damped laminate structures

13 p2516 A70-29616

Assumed vibration modes generation method in beams with arbitrary boundary conditions, applied to cantilevered beams, using modified Rayleigh-Ritz analysis

21 p3934 A70-40923

Avalanche diode microwave oscillators, considering Impatt and Trapatt oscillation modes

21 p3798 A70-41336

Tethered parachutes vibration modes, determining fundamental frequencies from canopy/lines mass ratio and materials elastic properties [AIAA PAPER 70-1169]

21 p3755 A70-41844

Time average holographic interferometry of circular plate vibrating simultaneously in rationally related modes

21 p3829 A70-41927

Fluid filled elastic spherical shell, calculating free vibration axisymmetric response and fundamental mode

21 p3940 A70-42053

Coupled rotational vibration system dynamic behavior near critical speed, using graphs of autonomous two degree of freedom system on reduced phase plane

22 p4112 A70-42271

Elastic plate response to boundary layer pressure fluctuations, estimating vibration modes dependence on fluctuation convection velocity and response magnification as function of flow direction

22 p4007 A70-42283

Free fluid sloshing motion in shallow convex containers, considering isoperimetric problem for planar and axisymmetric vibrations

22 p4009 A70-42534

Hologram interferometry as noncontact tool for vibration mode measurements of turbine blade groups

23 p4193 A70-43925

Data acquisition and processing in structural modal characteristics analysis during ground resonance tests [ICAS PAPER 70-36]

23 p4267 A70-44133

Single-frequency oscillations mode in nonlinear catenary systems, considering factors promoting stabilization and uniformity

23 p4218 A70-44344

Axisymmetric vibration modal properties /frequencies and mode shapes/ of thin conical shell frustums, considering dimensional and boundary condition influences

23 p4270 A70-44501

Magnetically stabilized satellites passive roll control, discussing resonance solutions by variational approach

23 p4262 A70-44690

Orthogonality of eigenmodes of aircraft vibrations based on F-104G ground measurements

23 p4274 A70-44766

Turbine compressor blades vibration mode measurements by holographic interferometry

24 p4334 A70-45563

Ring-stiffened thin circular cylindrical shells, calculating free vibration natural frequencies and mode shapes by finite element method

24 p4427 A70-46067

Periodically supported beams and plates free vibration, calculating natural frequency spectrum distribution and normal modes

24 p4427 A70-46070

VIBRATION PERCEPTION

Vibrotactile display operational skill acquisition, discussing stimuli quality and spacing effects on limen of temporal ordering of sensory events in haptic space

13 p2354 A70-29596

Skin and tissue mechanical characteristics response to vibratory stimulation, considering effects on physiological and psychophysical tactile sensitivity measurements

13 p2354 A70-29598

Human compensatory two dimensional visual display tracking performance with superimposed apparent vertical vibration, studying frequency dependent eye pursuit movements

24 p4309 A70-46078

VIBRATION PICKUPS

U TRANSDUCERS

U VIBRATION METERS

VIBRATION PROTECTION

U VIBRATION ISOLATORS

VIBRATION SIMULATORS

Single or repetitive shock pulses produced on electrodynamic and hydraulic shakers for shock testing on vibration machines

06 p1030 A70-18438

Radio and automatic control electronic equipment reliability estimation by vibration testing, determining test stand simulation accuracy

09 p1650 A70-23632

Vibration test instrument with automatic plotting of vibration system amplitude-frequency characteristics

11 p2032 A70-26440

Vibration generators based on magnetic field electrodynamic effect, giving design, schematic diagram and exploitation properties

11 p2032 A70-26441

Electrohydraulic vibrators and shakers for testing aircraft systems, diesel engines and structural joints, describing design and operation

11 p2032 A70-26442

HF shaker for accelerometer calibration and resonance evaluation, discussing construction materials, accuracy and test results

16 p2889 A70-34021

Random vibration test for quasi-flexible specimens with each mounting point subjected to different vibration levels and spectrum shapes

16 p2889 A70-34022

Structural vibration test system, using hybrid computer for automatic control and data acquisition and reduction

17 p3061 A70-35488

Satellite vibration tests simulation installations, describing measurement and control devices for lateral motion and test object safety

19 p3401 A70-38299

Shock pulse reproduction on electrodynamic and hydraulic shakers for vibration testing, including SNAP 21 results

21 p3804 A70-40865

VIBRATION TESTING MACHINES

U VIBRATION SIMULATORS

VIBRATION TESTS

NT DAMPING TESTS

Vibration frequencies and modal shapes for square and rhombic cantilever plates with diamond cross section, including commercial resonance test system

01 p0199 A70-10122

Gas turbine engines vibration characteristics, discussing statistical analysis obtained through condensed vibration overload control program

01 p0166 A70-11420

HF endurance tests of Al sheet alloy used in welded aircraft structural components, plotting curves for heat treated and untreated specimens

02 p0315 A70-11658

Human vibration test program for airline passenger reaction to vibration environments of large commercial aircraft

02 p0244 A70-12132

Harmonic vibration testing of aircraft structural nonlinearities caused by dry friction, describing pitch control system

02 p0387 A70-12215

Mechanical strength and breakdown metallography of plate shaped structural steel and Al alloy specimen under various HF elastic vibrations

02 p0318 A70-12398

Reciprocating force measurement at shake table and subject interface and repetitive circumferential human torso deformation under sinusoidal input at various frequencies and intensities

[ASME PAPER 69-WA/BHF-3] 04 p0631 A70-14850

Plastic deformation of refractory alloys during stress relaxation tests under vibrations, showing enhanced stability

05 p0866 A70-17033

Lift forces and pressure on vibrating cylinders in plane perpendicular to air flow measured in wind tunnel

06 p0968 A70-17545

Force-acceleration product method for controlling input vibratory motion to vibration test specimen based on specimen dynamics

06 p1069 A70-18437

Alloy specimen shortening due to aging during stress relaxation under vibration

07 p1304 A70-18820

Calibrating rods design for vibrating components stress measurement gauges

07 p1400 A70-18822

Vibrating composite beam test method for determining complex dynamic modulus of viscoelastic materials over broad frequency and temperature ranges

07 p1320 A70-19955

Saturn ULLAGE solid propellant rocket motor vibration test evaluation

07 p1365 A70-20039

Complex modulus measurement for rigid linear viscoelastic materials over audio frequency spectrum by harmonic end displacement ratio method

07 p1413 A70-20044

Rig using holographic techniques for vibration testing and aircraft engine components inspection

09 p1680 A70-23069

Three degrees of freedom astatic gyroscopes dynamic characteristics determination by vibration tests

09 p1681 A70-23300

Vibration tests on Europa 1 launch vehicle third stage, describing multipoint measuring and servocontrolled excitation systems and data connection to EDP

10 p1951 A70-24864

Aerospace vehicles structural vibration environments prediction methods emphasizing vibration sensor mounting resonances

[AIAA PAPER 70-402] 10 p1959 A70-24903

Electrohydraulic vibrators and shakers for testing aircraft systems, diesel engines and structural joints, describing design and operation

11 p2032 A70-26442

Force controlled vibration for shock tests, discussing feasibility and merits for simulation testing

12 p2205 A70-27099

Vibration stability of particle in plane restrained by two nonidentical springs with initial stress using Floquet theory and perturbations

14 p2657 A70-30843

Reliability test facilities for military shipboard electronic equipment, subjecting equipment to combined thermal shock and vibration cycles

16 p2888 A70-33125

Aircraft turbine engine components vibrational testing by holographic interferometry methods

16 p2903 A70-33134

Random vibration test for quasi-flexible specimens with each mounting point subjected to different vibration levels and spectrum shapes

16 p2889 A70-34022

Test stand based on Froude pendulum for measuring friction coefficients and oscillation parameters of porous bushings

16 p2924 A70-34298

Zero order Bessel function fringe shape measurement for holographic sinusoidal vibration fringes

17 p3087 A70-35020

Fiber optics lens for transferring specimen image to camera during vibration tests

17 p3095 A70-35633

Heat pipe performance tests under longitudinal harmonic vibration

17 p3193 A70-35751

Ground vibration testing for aircraft and missile flutter prevention

[ONERA-TP-816] 18 p3339 A70-36508

High intensity noise testing of missile and spacecraft structures, simulating acoustically induced vibrations due to aerodynamic turbulence

19 p3531 A70-37697

Digital electrodynamic vibration exciter control for sinusoidal, random and shock spectrum testing of aircraft, missiles and satellites

19 p3383 A70-37920

HF endurance tests of Al sheet alloy used in welded aircraft structural components, plotting curves for heat treated and untreated specimens

19 p3452 A70-38431

Seismic measurements at inertial test facilities, considering vibration environment relevant to single degree of freedom gyroscope performance tests

[AIAA PAPER 70-951] 20 p3606 A70-39576

Structural vibration tests, analyzing errors due to couplings and dampers addition

20 p3734 A70-40439

Helicopter vibration measurement techniques, discussing in-service fault diagnosis

21 p3749 A70-40582

Flexible heat pipe test for heat flux and wick pumping capacity under vibration and evaporator-condenser modification

21 p3945 A70-41040

Amplitude instability in vibration testing systems, noting effects of bandpass filters in feedback loop of amplitude servo

22 p4006 A70-43250

Damage data comparison for vibratory cavitation and liquid impact on aluminum alloy, stainless steels and pure nickel

23 p4203 A70-43870

Electrodynamic and electrohydraulic vibrators for frequency sweep, wideband random and sweep random vibration test methods

23 p4195 A70-44333

Mechanical structure dynamic response to vibration environment, using mobility method analysis

23 p4269 A70-44334

Accelerated vibration equipment testing for reducing test time, discussing vibration environment simulation

23 p4269 A70-44336

VIBRATIONAL FREQUENCIES

U VIBRATIONAL SPECTRA

VIBRATIONAL RELAXATION

U MOLECULAR RELAXATION

VIBRATIONAL SPECTRA

Dispersed fluorescence spectra from vacuum UV photon impact on COS, noting absence of emission from higher vibrational levels

01 p0148 A70-11353

Vibrational relaxation times in carbon dioxide and carbon dioxide-argon mixtures at 360-3000 K, using shock tube and laser schlieren method

01 p0148 A70-11355

Atomic O, H and D and molecular oxygen, deuterium and sulfur hexafluoride effects on nitrogen vibrational population distribution in nitrogen afterglow

01 p0148 A70-11356

Rotating compressor vanes vibration frequencies and modes using shell theory, considering Coriolis forces and rotation rates effects

01 p0211 A70-11427

Rotation-vibration matrix elements of quadrupole moments and absorption coefficients of ground electronic states of hydrogen, HD and deuterium

02 p0342 A70-11823

Motion equations for vibratory two degrees of freedom spring mass system subjected to rotation, discussing use for small rates of turn measurement

01 p0199 A70-10266

Semiautomatic mass condensation transformation for reducing structural vibration calculations, including computer program and mode shape plotting

01 p0200 A70-10868

Nonlinear vibrations in mechanical systems of elastic components having equivalent circuits represented by finite number of discrete masses interconnected by weightless infinite rod

01 p0143 A70-11027

Plates and shells natural oscillations frequencies and modes, analyzing variational, asymptotic and numerical methods

01 p0210 A70-11412

Finite element method for calculating natural frequencies and mode shapes of pretwisted cantilever plates assembly of flat triangular elements

02 p0384 A70-11859

Normal and tangential displacements distribution at surface and along cross section of bar with free boundaries computed for symmetric and antisymmetric oscillations

02 p0301 A70-12484

Natural mode shapes of longitudinal oscillations and resonant frequencies of thin rods of constant curvature and rings with slit, noting use for crack determination

03 p0588 A70-13283

N degree of freedom pendulum with suspension point vibrating vertically, determining conditions for parametric resonance occurrence

03 p0524 A70-13368

Finite difference method for obtaining free vibrations natural frequencies and mode shapes for rectangular plates of varying stiffnesses

03 p0595 A70-13812

Gain interaction among oscillating modes of gas laser analyzed from rate equations viewpoint

03 p0503 A70-14208

Cyclic bending stress in disk type gyroscopic rotor under steady precession, discussing solutions for modal functions and resonant frequencies

04 p0689 A70-14873

Rotating acoustic modes generated at blade passing frequencies in inlet duct of axial flow fan or compressor measured

04 p0691 A70-15079

Orthogonality of aircraft natural vibration modes by calculating complete matrix of generalized masses

04 p0774 A70-15150

Unsteady pressure distributions on elastic swept wing upper and lower sides at high subsonic to transonic flow, investigating torsional and bending vibrations

04 p0615 A70-15151

Spectral response of cylindrical shell due to random acoustic pressure input computed using modal approach

04 p0778 A70-15528

Flow distribution inside triangular shaped cavities of variable depth resembling liquid propellant rocket motor baffle cavities, simulating radial and tangential oscillation modes

04 p0674 A70-15566

Piezoelectric sensing diaphragm for detection of micrometeorites in space, noting vibration mode and effect of small beads contact time on calibration errors

04 p0695 A70-15567

Periodic vibrations of quasi-linear autonomous systems with retardation, deriving sufficient conditions for asymptotic stability

05 p0925 A70-15822

Aircraft engine support system dynamic loads induced by fan unbalance analyzed by coupling pylon and engine vibration modes

05 p0895 A70-15850

Rotor-driven vibrational gyroscopic device dynamic characteristics, stability, transient delta function, signal response and sensitivity assessment

05 p0848 A70-16222

Laser mode interaction characteristics determination using resonator field equation taking into account competition and coupled modes

06 p1081 A70-17765

Analytical expressions for amplitude and frequency modulation characteristics of bias modulated tunnel diode oscillator on steady state mode

06 p1022 A70-17836

Unstable vibrations in rotating flat shaft with unsymmetrical flexibility carrying unsymmetrical rotor in four degrees of freedom

07 p1402 A70-18978

Vibrational overloads development in turboprop engines ascribed to natural vibrations mode shape frequency approaching rotor revolutions number

07 p1363 A70-19110

Transverse and longitudinal combustion chamber oscillations in rocket motors with distributed mass and energy sources

07 p1364 A70-19581

Group theory investigation of three photon light scattering tensor for all vibration modes of specific crystal classes

07 p1299 A70-19861

Natural vibration frequencies and mode shapes for laminated orthotropic shells of revolution using finite element method

07 p1411 A70-19951

Von Karman equations for rectilinear plate vibrations used for triangular plates, discussing amplitude/thickness effect and multimodal frequency formula

07 p1416 A70-20211

Natural frequencies and modes of tapered swept back rudder fin of aircraft using vibration analysis

07 p1417 A70-20417

Periodic and almost periodic solutions to vibrations of quasi-linear nonautonomous systems in presence of resonance, determining principal amplitudes

08 p1544 A70-20966

Vibration stability of two identical particles constrained to plane and restrained by three linear springs with initial stress

08 p1591 A70-21466

Structural vibration of ring stiffened and mass-attached hemispherical shells

08 p1593 A70-21618

Parameters defining elliptic vibration of light reflected from surface using photoelectric ellipsometer

08 p1546 A70-21673

Cylindrical shell vibration modal characteristics finite element solutions accuracy compared with exact solutions

08 p1596 A70-21979

He-Ne laser emission in transverse oscillation mode, analyzing spatial and temporal coherence characteristics

09 p1694 A70-22135

Polar gas phase dielectric under conditions of power saturation interacting with microwave radiation field in waveguide

09 p1728 A70-22908

Single mode output power at 6328 A spectral line during He-Ne laser oscillation simultaneously at 6328 A and 3.39 microns

09 p1697 A70-22957

Natural oscillation mode in symmetrically graded p-n junction using Missawa small signal equations for avalanche diode

09 p1653 A70-23804

Natural frequencies and mode shapes of vibrating shells and shell combinations determined using variational finite difference method in conjunction with Hamilton principle

10 p1961 A70-25056

Equations of motion, modal vectors and natural frequencies of n-degree of freedom structurally damped linear system determined directly from test data

10 p1961 A70-25058

Geometrically exact finite element for thin shells of revolution, using approximation to predict boundary layer stress distribution during vibration

[AIAA PAPER 69-56]

11 p2135 A70-25962

Axisymmetric and unsymmetric free vibrational modes of right-circular conical or cylindrical sandwich shells with free edges, discussing Rayleigh-Ritz solution

11 p2145 A70-26700

Limited frequency range analytical model for predicting mass and stiffness changes effect on natural frequencies and normal modes

12 p2317 A70-27121

Complex structures vibration using component vibration modes, considering dynamic behavior from interface reactions effects

12 p2317 A70-27123

Vibrating thin beam cross sectional displacement-force equations coefficients included in coefficient matrix, considering shear deformation and rotary inertia effects on vibration modes

12 p2324 A70-27397

Coupled relaxation dependence on translational and vibrational temperature and number of modes in polyatomic gases, noting molecular dissociation

12 p2276 A70-27797

Free elastic rotating beam with tip masses and inertia, developing solutions for flexible modes and natural frequencies of H-type configuration

12 p2273 A70-27820

Clamped beams steady state free and forced response and stability for large amplitude motion, discussing multimode analytical and numerical technique

12 p2327 A70-27821

Carbon dioxide molecular vibrational energy levels above carbon monoxide-oxygen premixed flame, discussing vibration modes leading to population inversion and relaxation time variance

13 p2455 A70-29132

Fabry-Perot resonator higher modes excitation by external TEM wave, discussing optimal mismatch for maximum intensity

13 p2408 A70-29358

Microwave oscillator providing transition to stable emission at harmonics with power levels comparable to fundamental frequency, considering gallium arsenide oscillation mode

13 p2471 A70-29413

GaAs epitaxial layered wafer natural CW R band oscillations in LSA mode

14 p2550 A70-30688

Dynamic stiffness, natural frequencies and mode shapes of prismatic and thin walled open grids, including warping and shear flange deformation

14 p2659 A70-31132

GaAs Gunn devices oscillatory modes under various operating conditions

14 p2557 A70-31158

Differential equations for coupled bending and torsional vibrations of slender beam in centrifugal force field

14 p2661 A70-31226

Natural vibrations frequency of tubular cantilever pipe with fluid flow, solving differential equation of motion by Ritz method

14 p2567 A70-31426

Vibration modes real time observation of complex surfaces with matt finish using changes in laser speckle

15 p2750 A70-31762

Vibration mode response and impact time sensitivity of mechanical impedance of human skull, relating head injury factors

15 p2682 A70-31934

Complex plates free transverse oscillation modes and frequencies using Ritz method

15 p2818 A70-32183

Relaxations from anelastic and dielectric measurements of fused silica and soda-silica glasses at low temperatures ascribed to vibration modes exceeding Debye spectrum

16 p2960 A70-32996

Embedded damped sandwich beams, determining equations for resonant frequency, loss factor and modal roots

16 p2992 A70-34018

Plane strain vibrations of two layered elastic cylinders, analyzing results for lobar mode numbers 2, 3 and 4

16 p2994 A70-34096

Free oscillations of Euler-Bernoulli and Timoshenko cantilever beams of variable cross section, obtaining approximate modes and natural frequencies bounds

16 p2994 A70-34234

Statistically indeterminate Timoshenko beams oscillations natural frequencies and modes by lumping properties of linear and rotary inertia at discrete points

16 p2994 A70-34235

Mechanical models of single speed gearings for torsional vibrations, taking into account nodes of first free vibration mode

16 p2995 A70-34289

Laser Raman spectroscopy, discussing scattering from vibrational modes in solid and from phonons above optical gap

17 p3081 A70-34599

Radial vibration frequency variation with wall thickness in hollow spherical shells, tabulating and plotting results

17 p3186 A70-34978

Natural frequencies and corresponding mode shapes for free flexural vibrations of circular plates, extending to elastic support cases

17 p3186 A70-34980

Engineering components vibration mode studies by time averaged holographic interferometry

17 p3087 A70-35019

Precision components engineering inspection and sonic transducer surface vibration modes analysis by hologram interferometry

17 p3087 A70-35021

Wave-periodic acceleration feedback during vibrational flame propagation in tubes, testing carbon monoxide-air mixture

17 p3196 A70-35350

Thermal effects on aircraft elastic vibration mode shapes, recommending investigation to develop analysis and design tools

18 p3213 A70-36459

Automatic matrix method for vibration modes of large structures with multiple degrees of freedom

18 p3342 A70-36684

Large scale galactic oscillations, discussing observational evidence and theoretical modal calculations

18 p3330 A70-37191

One dimensional magnetostrictive bar electromagnetically forced vibration, using Lagrange equations and normal mode analysis

19 p3472 A70-37959

Vibration signals analysis in random and periodic modes, presenting analyzers block diagrams

19 p3430 A70-38526

Vibration of combined cylindrical shells via Lagrangian minimization regarding unknown boundary values

21 p3934 A70-40897

Assumed vibration modes generation method in beams with arbitrary boundary conditions, applied to cantilevered beams, using modified Rayleigh-Ritz analysis

21 p3934 A70-40923

Avalanche diode microwave oscillators, considering Impatt and Trapatt oscillation modes

21 p3798 A70-41336

Tethered parachutes vibration modes, determining fundamental frequencies from canopy/lines mass ratio and materials elastic properties [AIAA PAPER 70-1169]

21 p3755 A70-41844

Time average holographic interferometry of circular plate vibrating simultaneously in rationally related modes

21 p3829 A70-41927

Fluid filled elastic spherical shell, calculating free vibration axisymmetric response and fundamental mode

21 p3940 A70-42053

Coupled rotational vibration system dynamic behavior near critical speed, using graphs of autonomous two degree of freedom system on reduced phase plane

22 p4112 A70-42271

Elastic plate response to boundary layer pressure fluctuations, estimating vibration modes dependence on fluctuation convection velocity and response magnification as function of flow direction

22 p4007 A70-42283

Free fluid sloshing motion in shallow convex containers, considering isoperimetric problem for planar and axisymmetric vibrations

22 p4009 A70-42534

Hologram interferometry as noncontact tool for vibration mode measurements of turbine blade groups

23 p4193 A70-43925

Data acquisition and processing in structural modal characteristics analysis during ground resonance tests [ICAS PAPER 70-36]

23 p4267 A70-44133

Single-frequency oscillations mode in nonlinear catenary systems, considering factors promoting stabilization and uniformity

23 p4218 A70-44344

Axisymmetric vibration modal properties/frequencies and mode shapes/ of thin conical shell frustums, considering dimensional and boundary condition influences

23 p4270 A70-44501

Magnetically stabilized satellites passive roll control, discussing resonance solutions by variational approach

23 p4262 A70-44690

Orthogonality of eigenmodes of aircraft vibrations based on F-104G ground measurements

23 p4274 A70-44766

Turbine compressor blades vibration mode measurements by holographic interferometry

24 p4334 A70-45563

Ring-stiffened thin circular cylindrical shells, calculating free vibration natural frequencies and mode shapes by finite element method

24 p4427 A70-46067

Periodically supported beams and plates free vibration, calculating natural frequency spectrum distribution and normal modes

24 p4427 A70-46070

VIBRATION PERCEPTION

Vibrotactile display operational skill acquisition, discussing stimuli quality and spacing effects on lumen of temporal ordering of sensory events in haptic space

13 p2354 A70-29596

Skin and tissue mechanical characteristics response to vibratory stimulation, considering effects on physiological and psychophysical tactile sensitivity measurements

13 p2354 A70-29598

Human compensatory two dimensional visual display tracking performance with superimposed apparent vertical vibration, studying frequency dependent eye pursuit movements

24 p4309 A70-46078

VIBRATION PICKUPS

U TRANSDUCERS

U VIBRATION METERS

VIBRATION PROTECTION

U VIBRATION ISOLATORS

VIBRATION SIMULATORS

Single or repetitive shock pulses produced on electrodynamic and hydraulic shakers for shock testing on vibration machines

06 p1030 A70-18438

Radio and automatic control electronic equipment reliability estimation by vibration testing, determining test stand simulation accuracy

09 p1650 A70-23632

Vibration test instrument with automatic plotting of vibrating system amplitude-frequency characteristics

11 p2032 A70-26440

Vibration generators based on magnetic field electrodynamic effect, giving design, schematic diagram and exploitation properties

11 p2032 A70-26441

Electrohydraulic vibrators and shakers for testing aircraft systems, diesel engines and structural joints, describing design and operation

11 p2032 A70-26442

HF shaker for accelerometer calibration and resonance evaluation, discussing construction materials, accuracy and test results

16 p2889 A70-34021

Random vibration test for quasi-flexible specimens with each mounting point subjected to different vibration levels and spectrum shapes

16 p2889 A70-34022

Structural vibration test system, using hybrid computer for automatic control and data acquisition and reduction

17 p3061 A70-35488

Satellite vibration tests simulation installations, describing measurement and control devices for lateral motion and test object safety

19 p3401 A70-38299

Shock pulse reproduction on electrodynamic and hydraulic shakers for vibration testing, including SNAP 21 results

21 p3804 A70-40865

VIBRATION TESTING MACHINES

U VIBRATION SIMULATORS

VIBRATION TESTS

NT DAMPING TESTS

Vibration frequencies and modal shapes for square and rhombic cantilever plates with diamond cross section, including commercial resonance test system

01 p0199 A70-10122

Gas turbine engines vibration characteristics, discussing statistical analysis obtained through condensed vibration overload control program

01 p0166 A70-11420

HF endurance tests of Al sheet alloy used in welded aircraft structural components, plotting curves for heat treated and untreated specimens

02 p0315 A70-11658

Human vibration test program for airline passenger reaction to vibration environments of large commercial aircraft

02 p0244 A70-12132

Harmonic vibration testing of aircraft structural nonlinearities caused by dry friction, describing pitch control system

02 p0387 A70-12215

Mechanical strength and breakdown metallography of plate shaped structural steel and Al alloy specimen under various HF elastic vibrations

02 p0318 A70-12398

Reciprocating force measurement at shake table and subject interface and repetitive circumferential human torso deformation under sinusoidal input at various frequencies and intensities

[ASME PAPER 69-WA/PHF-3] 04 p0631 A70-14850

Plastic deformation of refractory alloys during stress relaxation tests under vibrations, showing enhanced stability

05 p0866 A70-17033

Lift forces and pressure on vibrating cylinders in plane perpendicular to air flow measured in wind tunnel

06 p0968 A70-17545

Force-acceleration product method for controlling input vibratory motion to vibration test specimen based on specimen dynamics

06 p1069 A70-18437

Alloy specimen shortening due to aging during stress relaxation under vibration

07 p1304 A70-18820

Calibrating rods design for vibrating components stress measurement gauges

07 p1400 A70-18822

Vibrating composite beam test method for determining complex dynamic modulus of viscoelastic materials over broad frequency and temperature ranges

07 p1320 A70-19955

Saturn ULLAGE solid propellant rocket motor vibration test evaluation

07 p1365 A70-20039

Complex modulus measurement for rigid linear viscoelastic materials over audio frequency spectrum by harmonic end displacement ratio method

07 p1413 A70-20044

Rig using holographic techniques for vibration testing and aircraft engine components inspection

09 p1680 A70-23069

Three degrees of freedom astatic gyroscopes dynamic characteristics determination by vibration tests

09 p1681 A70-23300

Vibration tests on Europa 1 launch vehicle third stage, describing multipoint measuring and servocontrolled excitation systems and data connection to EDP

10 p1951 A70-24864

Aerospace vehicles structural vibration environments prediction methods emphasizing vibration sensor mounting resonances

[AIAA PAPER 70-402] 10 p1959 A70-24903

Electrohydraulic vibrators and shakers for testing aircraft systems, diesel engines and structural joints, describing design and operation

11 p2032 A70-26442

Force controlled vibration for shock tests, discussing feasibility and merits for simulation testing

12 p2205 A70-27099

Vibration stability of particle in plane restrained by two nonidentical springs with initial stress using Floquet theory and perturbations

14 p2657 A70-30843

Reliability test facilities for military shipboard electronic equipment, subjecting equipment to combined thermal shock and vibration cycles

16 p2888 A70-33125

Aircraft turbine engine components vibrational testing by holographic interferometry methods

16 p2903 A70-33134

Random vibration test for quasi-flexible specimens with each mounting point subjected to different vibration levels and spectrum shapes

16 p2889 A70-34022

Test stand based on Froude pendulum for measuring friction coefficients and oscillation parameters of porous bushings

16 p2924 A70-34298

Zero order Bessel function fringe shape measurement for holographic sinusoidal vibration fringes

17 p3087 A70-35020

Fiber optics lens for transferring specimen image to camera during vibration tests

17 p3095 A70-35633

Heat pipe performance tests under longitudinal harmonic vibration

17 p3193 A70-35751

Ground vibration testing for aircraft and missile flutter prevention [ONERA-TP-816]

18 p3339 A70-36508

High intensity noise testing of missile and spacecraft structures, simulating acoustically induced vibrations due to aerodynamic turbulence

19 p3531 A70-37697

Digital electrodynamic vibration exciter control for sinusoidal, random and shock spectrum testing of aircraft, missiles and satellites

19 p3383 A70-37920

HF endurance tests of Al sheet alloy used in welded aircraft structural components, plotting curves for heat treated and untreated specimens

19 p3452 A70-38431

Seismic measurements at inertial test facilities, considering vibration environment relevant to single degree of freedom gyroscope performance tests [AIAA PAPER 70-951]

20 p3606 A70-39576

Structural vibration tests, analyzing errors due to couplings and dampers addition

20 p3734 A70-40439

Helicopter vibration measurement techniques, discussing in-service fault diagnosis

21 p3749 A70-40582

Flexible heat pipe test for heat flux and wick pumping capacity under vibration and evaporator-condenser modification

21 p3945 A70-41040

Amplitude instability in vibration testing systems, noting effects of bandpass filters in feedback loop of amplitude servo

22 p4006 A70-43250

Damage data comparison for vibratory cavitation and liquid impact on aluminum alloy, stainless steels and pure nickel

23 p4203 A70-43870

Electrodynamic and electrohydraulic vibrators for frequency sweep, wideband random and sweep random vibration test methods

23 p4195 A70-44333

Mechanical structure dynamic response to vibration environment, using mobility method analysis

23 p4269 A70-44334

Accelerated vibration equipment testing for reducing test time, discussing vibration environment simulation

23 p4269 A70-44336

VIBRATIONAL FREQUENCIES

U VIBRATIONAL SPECTRA

VIBRATIONAL RELAXATION

U MOLECULAR RELAXATION

VIBRATIONAL SPECTRA

Dispersed fluorescence spectra from vacuum UV photon impact on COS, noting absence of emission from higher vibrational levels

01 p0148 A70-11353

Vibrational relaxation times in carbon dioxide and carbon dioxide-argon mixtures at 360-3000 K, using shock tube and laser schlieren method

01 p0148 A70-11355

Atomic O, H and D and molecular oxygen, deuterium and sulfur hexafluoride effects on nitrogen vibrational population distribution in nitrogen afterglow

01 p0148 A70-11356

Rotating compressor vanes vibration frequencies and modes using shell theory, considering Coriolis forces and rotation rates effects

01 p0211 A70-11427

Rotation-vibration matrix elements of quadrupole moments and absorption coefficients of ground electronic states of hydrogen, HD and deuterium

02 p0342 A70-11823

Two degree of freedom gyroscopes stability with hydrodynamic grooved rotor bearings, describing parallel and conical whirling rotor oscillations

02 p0307 A70-12163

Flight vehicles intrinsic vibration frequency spectra for controllable flight determined by graph-analytical method

02 p0227 A70-12415

Helicopter vibrations recording on magnetic tape for subsequent frequency analysis, describing frequency spectrogram

02 p0304 A70-12761

Rotational lines in iodine B-X system vibrational bands, calculating Doppler, natural and collisional widths

03 p0527 A70-13298

Spectroscopic calibration of laser lines at simultaneous carbon dioxide and nitrous oxide transitions in gas flow, showing abnormal line intensity

03 p0501 A70-13685

Spectrum deductions from profile excited random vibration response, considering single profile imposed displacements

03 p0600 A70-14250

HF molecular vibration rotation band observed in sunspot spectra, carrying out model calculations for spots differing in temperature for fluorine abundance

04 p0751 A70-15048

Nonlinear connected oscillations of vibrator and rigid bodies, analyzing plane-parallel and spatial motions, including elastic beams self excited oscillations

04 p0720 A70-15446

Stiffness and mass matrices of free-free vibration structure reduced to eliminate zero frequencies

04 p0778 A70-15553

Diatomic oxygen-nitrogen collisions in mixtures with CO, determining vibration-vibration energy exchange probabilities

04 p0723 A70-15562

Absolute values of emission cross sections for vibrational Meinel bands of molecular nitrogen ions excited by electron impact

05 p0901 A70-16279

Self broadened semihalf widths measurement in pure rotational spectrum of carbon monoxide compared with vibration-rotation calculation

05 p0886 A70-17086

Electron energy distribution function for carbon dioxide laser plasmas in gas mixtures, discussing dissociation products role in electron energy exchange

06 p1080 A70-17447

Vibration frequency influence on vibrational creep of Al-Mg-Si alloy, describing mechanism in terms of strain hardening, additional slip and dislocation movements

06 p1168 A70-17931

Electronic-vibrational coupling in nonequilibrium MHD generator with molecular gas to suppress electrode layer shorting and recombination in supersonic nozzles

06 p0988 A70-18222

Nonsymmetric planform cantilever plate apparent mass, material properties and geometrical changes effect on vibration frequency

07 p1403 A70-19058

Anisotropically elastic rotor vibrations stability analysis allowing for damper mass and internal/external friction, determining regions of steady and unsteady motions

07 p1403 A70-19059

Hydrogen fluoride fundamental vibration rotation band spectral line shift and broadening due to carbon dioxide

07 p1337 A70-19365

Wave numbers, intensity and half width of lines of vibration-rotation relative to carbon monoxide transition, noting band center displacement dependence on pressure

07 p1338 A70-19380

Harmonic analysis of ionospheric electron density oscillation spectra, noting density fluctuations classes due to internal gravity wave propagation and N/h profiles calculation errors

07 p1266 A70-19449

Natural vibration frequencies and mode shapes for laminated orthotropic shells of revolution using finite element method

07 p1411 A70-19951

Dynamic stability of pendulum-weight system during vertical HF small amplitude vibration of suspension point by averaging method

08 p1543 A70-20494

Tunable Q switched pulsed discharge carbon dioxide laser intensity dependence on time delay investigated for various vibrational/rotational lines and gas mixtures

08 p1512 A70-20618

Boundary conditions effect on natural vibration frequencies of unloaded components and components loaded with concentrated masses, obtaining frequency equations

08 p1584 A70-20698

Ideal fluid in lightly filled spherical vessel under gravitational force investigated for surface tension effect on vibration frequencies

08 p1482 A70-20853

Amplitude-frequency characteristics of arbitrary elastic system performing flexural vibrations determined using computer

08 p1588 A70-21184

Analytic solution for computerized vibration analysis of high speed tension test

08 p1590 A70-21332

Boundary value contact problems in thermoelastic oscillations theory found to have unique solutions for any frequency

08 p1591 A70-21440

Simply supported rectangular plate investigated for effect of thermal gradient on transverse vibrational frequencies

08 p1595 A70-21976

Correlation function of oscillation modulated in amplitude, phase and frequency by random processes causing spectral density maximum shift away from carrier frequency

09 p1633 A70-22409

Molecular vibration spectra from inelastic interaction between electrons and absorbed molecules at metal-vacuum interface

09 p1732 A70-22904

Wave number, intensity and half width of vibrational-rotational lines pertaining to transition of carbon monoxide perturbed by argon

09 p1733 A70-23316

Torsional vibrations frequency calculations for multibranch system exhibiting linear rigidity and viscous damping, constructing algorithm for digital computer

09 p1783 A70-23409

Thermospheric molecular nitrogen vibrational temperature, studying various chemical reactions and collisions as energy sources

10 p1872 A70-23827

Diatomic molecules vibrational levels distribution near dissociation limit determined using WKB approximation

10 p1919 A70-24041

Vibration behavior theory for elastomechanical systems applied to aircraft and space constructions

10 p1961 A70-25054

Free vibration analysis of elastic structures using Rayleigh-Ritz method and finite element methods

10 p1961 A70-25055

Natural vibration analysis of uniform cylindrical and cantilever rectangular tubes with cutouts

10 p1961 A70-25057

Vibration test instrument with automatic plotting of vibrating system amplitude-frequency characteristics

11 p2032 A70-26440

Kane-Mindlin equations and frequency spectra determined for free extensional vibrations in isotropic elastic plate strips

11 p2146 A70-26703

Flutter instability critical velocity and frequency for thin cantilevered plate with follower jet determined by Galerkin and computer simulation

12 p2316 A70-27106

CO vibration-rotation bands, calculating high resolution and temperature steradiance and spectral absorption coefficient

12 p2275 A70-27171

Rotational, vibrational and equilibrium molecular constants for Phillips system of diatomic carbon

12 p2275 A70-27174

Vibration amplitudes and frequencies contactless measurement by sensor with photodiode for machining tool elements during metal working operations

12 p2235 A70-27683

Dissociation energy and long range interatomic potential of diatomic molecules from vibrational spacings of higher levels

13 p2454 A70-28495

Q switched CO-HE laser IR fluorescence, considering population inversion recovery by vibrational energy transfer

13 p2423 A70-28496

Vibrocreep effect on Al-Mg-Si alloy vibration frequency and mean and maximum stress at constant temperature

13 p2512 A70-28980

Rotational and vibrational temperature effects on neutral gas and electron temperature and density in high pressure discharge plasma diagnostics

13 p2462 A70-29129

IR spectroscopy, determining relative populations of carbon dioxide vibrational energy levels by comparing emission intensities

13 p2455 A70-29131

Vibration spectra, kinetic and dispersion equations of solid spherical particles moving in incompressible weakly viscous liquid

13 p2388 A70-29368

Minimum weight design for complex structures subject to frequency constraint using finite element method and computer program

13 p2517 A70-29965

Differential cross sections for electron scattering by hydrogen with and without vibrational excitation, discussing inelastic processes

14 p2618 A70-30115

HF and DF continuous chemical lasers vibrational and rotational spectra, comparing lines and relative intensities

14 p2593 A70-30274

Third body coefficients of water and heavy water reactions in KCl coated and aged boric acid coated vessels with vibrational-vibrational exchanges

14 p2546 A70-31091

Cylindrical shell nonaxisymmetric vibration frequencies and boundary values relation, using Lagrangian

14 p2661 A70-31273

Vibration-rotation band absorptance for nonisothermal gaseous radiation in terms of parameters describing isothermal gas

15 p2825 A70-31816

Vibrational energies, rotational constants and internuclear potential of ground state molecular iodine, using reanalyzed spectroscopic data

16 p2954 A70-33056

Chemical energy conversion in lasers, discussing vibrational inversions in diatomic and multitatomic molecules and chain reactions

16 p2927 A70-33233

Stress and vibration analysis of rocket engine turboprop inducer blades, using finite element method [AIAA PAPER 70-630]

16 p2964 A70-33529

Nonequilibrium vibrational energy and relaxation equation for carbon dioxide-nitrogen molecular gas mixtures in supersonic free jet exhausting into vacuum [AIAA PAPER 70-867]

16 p2895 A70-33910

Near IR electronic emission spectrum of positive column in flowing oxygen electric discharge, noting vibrational temperature

16 p2955 A70-33981

Vibrational spectra and structure of oxalyl chloride in crystalline and fluid states, discussing molecular and space group symmetry

16 p2857 A70-34006

IR Raman and vibrational spectra and structure of gaseous and liquid 1-pyrazoline

16 p2857 A70-34007

NO and oxygen ions vibrational excitation due to inelastic scattering from He, calculating scattering angle variation

16 p2955 A70-34010

Cyclopropane-argon mixtures translational and vibrational energies exchange efficiencies analysis based on intermolecular potential

16 p2956 A70-34083

Diatomic nitrogen ions branch overlapping, discussing rotational line structure in first negative system vibrational bands

16 p2956 A70-34254

Harmonic analysis of ionospheric electron density oscillation spectra, noting density fluctuations classes due to internal gravity wave propagation and N/h profiles calculation errors

18 p3249 A70-36923

Real time narrow band vibration spectrum analysis techniques, discussing application to failure prediction and flight and wind tunnel tests

19 p3430 A70-38528

Base function selection for energy calculation optimal convergence conditions of frequencies and stresses in turbomachine blades vibrations

20 p3722 A70-39784

Diatomic Cs 7667 A band vibrational spectrum analysis

20 p3676 A70-40349

Carbon dioxide and CO IR vibration-rotation spectral absorption coefficients, noting harmonic oscillator approximation

21 p3851 A70-40589

Molecular oxygen density and vibrational distribution in lower atmosphere, observing solar UV radiation absorption by satellite OSO-4

21 p3816 A70-41066

Vibrationally adiabatic model for reaction dynamics of atomic and molecular hydrogen systems, using zero point energy path

21 p3773 A70-41397

Molecular size dependent steric effects in translation-vibration energy transfer by velocity dispersions in cyclopropane-inert mixtures

21 p3780 A70-41706

Carbon monoxide vibrational population inversion in product molecule produced in free burning carbon disulfide/oxygen flame

21 p3950 A70-41708

Carbon monoxide-nitrogen laser mechanism vibrational populations, discussing operational characteristics and walls condition and nature

21 p3837 A70-41716

Carbon monoxide-nitrogen system vibrational distribution of populations and kinetics in fundamental and harmonic regions, investigating vibroluminescence

21 p3837 A70-41718

Molecular vibrational temperature dependence on electron and neutral gas temperatures and degree of ionization for plasma excitation in nitrogen
22 p4078 A70-42358

Acoustic frequency spectra of transverse vibrations in bracketed bar caused by dry friction, using Lagrange method
22 p4073 A70-42612

Hydrogen chloride self broadened fundamental vibration rotation band intensity variation with pressure investigated by absorption spectroscopy analysis
22 p3983 A70-42945

Carbon dioxide laser vibrational temperature measurement, determining ground state vibration level populations in various molecular gases
22 p4051 A70-43391

Narrow resonances in saturated absorption at molecular vibrational-rotational transitions in carbon dioxide laser
23 p4202 A70-45059

Monatomic crystal vibrational spectrum, noting quasi-local vibrations near high impurity concentrations
24 p4388 A70-45202

Electronic energy collisional transfer between atomic and molecular hydrogen, measuring excited molecule vibrational distribution
24 p4381 A70-45650

VIBRATIONAL STRESS

Mechanical vibrations effect on man including motor vehicle dynamic vibrations
03 p0439 A70-14097

Elastokinetic three dimensional boundary value vibration problem, involving rectangular area on surface of elastic half space under periodic normal stress
03 p0601 A70-14319

Displacement determination by orthogonality relationship for dynamic vibrations and stresses in composite elastic plates
05 p0937 A70-16406

Visual acuity performance during various vibration stresses found differentially degraded for near, intermediate and distant vision
07 p1223 A70-19939

Slip-ringless propeller blade mounted measurement system for steady state and vibratory stresses from multiple strain-gage locations during flight and ground tests
[SAE PAPER 700223] 11 p2051 A70-25891

Sinusoidal vibrations effects on rats at different air pressures, discussing human vibration tolerances and resonant frequencies of thoraco-abdominal system
20 p3572 A70-39434

Silicon solar cell array interconnector design based on analysis of stresses caused by thermal expansion and vibrational motion
21 p3756 A70-41009

VIBRATORS

U ELECTRIC CHOPPERS

VIBRATORY LOADS

Reciprocating force measurement at shake table and subject interface and repetitive circumferential human torso deformation under sinusoidal input at various frequencies and intensities
[ASME PAPER 69-WA/BHF-3] 04 p0631 A70-14850

E1617 alloy breakdown resistance tests under multiple alternating static tension-compression and vibrational loads at 800 C
05 p0867 A70-17044

Prismatic pendularly supported beam load-forced vertical vibrations, critical load amplitude and force pulsation in case of stability loss
06 p1165 A70-17586

Force-acceleration product method for controlling input vibratory motion to vibration test specimen based on specimen dynamics
06 p1069 A70-18437

Vibrational overloads development in turboprop engines ascribed to natural vibrations mode shape frequency approaching rotor revolutions number
07 p1363 A70-19110

Aircraft engine vibrational overload reducible by elastic bearings having controllable elastic characteristics
07 p1364 A70-19113

Parametric vibrations onset and resonance regions boundaries determined for feed line system with flexible compensator
07 p1403 A70-19114

Monograph on conditions for stabilization of oscillatory systems with random parametric excitations covering approximate calculations, stability concept definition, etc
11 p2129 A70-25496

Vibration loads in turbomachinery blading, examining blade detuning effects on resonant response levels and fatigue life
24 p4392 A70-45157

Short-term creep and erosion resistance testing of Ti alloy in high speed air flows under aerodynamic vibrations
24 p4360 A70-45826

VIBROCARDIOGRAPHY

U PHONOCARDIOGRAPHY

VIBROMETERS

U VIBRATION METERS

VIDEO COMMUNICATION

Simulation technique to evaluate TV contrast trackers standard scan performance using video tape recording
01 p0058 A70-10812

Spatial registration of digitized multispectral video imagery obtained from multilens cameras, multichannel optical-mechanical line scanners and multiple TV camera systems
03 p0453 A70-13000

Detection efficiency compared for system containing clipper circuit and quasi-optimal linear system for video pulse signal with additive noise background
03 p0446 A70-13201

Wideband transmission of photographic reconnaissance information over long distances using Initial Defense Communication Satellite Program satellites
06 p1006 A70-17346

Microwave radiometric receiver, analyzing video detector saturation effects on linearity
16 p2880 A70-34075

VIDEO DATA

Flying spot scanners evaluation as image processing devices, discussing scan patterns effect on video signal
01 p0089 A70-10817

Photometric reduction of Lunar Orbiter video magnetic tapes for generation of topographic information of proposed Apollo landing sites
03 p0490 A70-13661

Computer-generated shaded flicker-free on-line digital video display, allowing superimposed vector graphics with light-pen interaction
09 p1640 A70-22033

Earth resources program data management system, discussing mission control, processing and distribution of data from satellite vidicon cameras and multispectral line sensors
[AIAA PAPER 70-321] 09 p1792 A70-22854

Real time video data display at visual and thermal IR wavelengths, demonstrating performance improvement for target recognition
16 p2910 A70-33436

VIDEO EQUIPMENT

Real time large screen display systems operation, brightness, accuracy, resolution, contrast ratio, data rates, reliability, fail-safe and management functions
05 p0828 A70-16190

Solar flare videometer for measuring flare area and peak and integrated intensity in real time
11 p2104 A70-25744

VIDICONS

NT RETURN BEAM VIDICONS

Optimum planetary image intensity at TV camera cathodes, exemplifying with Saturn orthicon image
04 p0688 A70-14694

Vidicon electron optics, describing triode emission system, focusing section, deflection component, collimating lens, beam landing error, etc
09 p1674 A70-22216

Vidicon camera tubes applications in TV systems, noting excellence for live pickups and film reproduction
10 p1852 A70-24952

Two inch high resolution vidicon for TV line processing of printed documents
16 p2906 A70-33173

Broadband image pick-up tube with high near IR sensitivity, comparing performance with other vidicons
16 p2907 A70-33186

Combination shutter and filter-changing mechanism for spacecraft vidicon cameras
16 p2914 A70-34150

Surveyor 7 TV system in photon integration mode, analyzing slow scan vidicon storage characteristics and dark current limitations
[SMPTE PAPER 105-72] 17 p3095 A70-35635

Earth resources satellite missions TV systems design, using vidicon as sensing element
20 p3626 A70-39052

VIETNAM

Helicopter advantages in airlift operation over conventional fixed-wing aircraft in Vietnam war
05 p0795 A70-16718

CH-54A helicopter gas turbine engine air particle separator/EAPS/ field service in Vietnam, noting time before engine removal for erosion
[ASME PAPER 70-GT-97] 18 p3303 A70-36844

VIEW EFFECTS

Correction factors required for estimating influence of pupil area reduction on retinal illumination at oblique angles
05 p0801 A70-16449

Eckert shadow technique for radiation view factors applied to toroid inside shadow hemisphere
08 p1546 A70-21832

Eye movements direction during perceptual errors related to stimulus location
15 p2683 A70-32456

Binocular disparity detectors in human visual response to moving gratings confirmed by electrophysiological evidence
17 p3025 A70-35150

Geometrical appearances at relativistic speeds for celestial sphere with multiple constellations, spherical surface features at observer proximity and rectangular box train
19 p3520 A70-38273

Quantitative measurement of solar limb image motion and blurring, noting role of telescope aperture
20 p3634 A70-40424

VIEWING

Radiation view factor from differential area to conical surface determined using Stokes theorem and contour integration
04 p0787 A70-15598

VIKING LANDER SPACECRAFT

Trajectory, guidance and environmental parameters and uncertainties effect on design optimization of out-of-orbit Viking soft lander
[AIAA PAPER 70-99] 06 p1157 A70-18134

Mars lander atmospheric entry digital simulation for deceleration system design, discussing ballistic coefficient, aeroshell diameter, parachute size and deployment altitude, etc
08 p1582 A70-20932

Martian atmospheric models for lander and simulator design, obtaining effective sky temperatures, surface pressures and temperatures, atmospheric compositions, etc
11 p2112 A70-26141

Subsystem weight trade-offs for design optimization of out-of-orbit Mars soft lander, using atmosphere and surface environmental Monte Carlo model
11 p2124 A70-26215

Thermal control coatings, windows and mirrors for 1973 Mars Viking Lander vehicles under simulated Martian surface conditions
[AIAA PAPER 69-1023] 13 p2384 A70-28530

Martian atmosphere modeling for obtaining Viking lander spacecraft design margins by Monte Carlo method
14 p2637 A70-30564

Parachute decelerator system for 1975 Viking Mars Lander mission, discussing configuration selection, design factors, trajectory simulation, weight and mass analysis, etc
[AIAA PAPER 70-1162] 21 p3931 A70-41849

SNAP 19 radioisotope thermoelectric generator module for Viking Lander and Pioneer applications, discussing design requirements, environmental and mission constraints, life, performance and reliability characteristics, etc
22 p4071 A70-43195

VIKING MARS PROGRAM

Mission design, spacecraft characteristics, communications and experimental approaches for Viking 1973 Mars Project
03 p0576 A70-14020

Viking Mars orbiter/lander mission planning, studying sun, earth and star occultations sensitive mission characteristics
[AIAA PAPER 70-62] 06 p1146 A70-18193

Viking Mars mission meteorological instruments for measurements of water vapor content, wind speed/direction, temperature and pressure
14 p2584 A70-30553

Mars 1971 and 1975 missions, discussing Mariner 8 and 9 and Viking lander objectives
18 p3334 A70-37224

Parachute decelerator system for 1975 Viking Mars Lander mission, discussing configuration selection, design factors, trajectory simulation, weight and mass analysis, etc
[AIAA PAPER 70-1162] 21 p3931 A70-41849

VINTI THEORY

Satellite orbit prediction formulas for Vinti dynamic model with three coordinates expressed in terms of independent variable
10 p1939 A70-24188

Vinti potential with spheroidal coordinates for equations of motion in earth satellite orbit computation
13 p2486 A70-28503

General potential function in triaxially ellipsoidal coordinates for Laplace equation, examining near earth satellites and Vinti potential
18 p3334 A70-37064

VINYL ETHYLENE

U BUTADIENE

VINYL POLYMERS

Hydrogen sulfide participation in vinyl polymerization investigated for reaction mechanism
05 p0810 A70-16051

Methyl methacrylate and other vinyl monomers polymerization activation by low sulfur dioxide concentrations, noting inert solvents effect
14 p2544 A70-30246

Polyvinyl alkyl ethers multiple transitions at low temperatures, using linear variable differential transformer
21 p3844 A70-42137

VIOLENCE

NT ATTACKING [ASSAULTING]

VIRGO STAR CLUSTER

Neutral atomic hydrogen in Virgo A cluster and between Galaxy and Virgo A, using emission and absorption measurements

04 p0758 A70-15707

Virgo XR-1 rocket observations, discussing X rays due to synchrotron emission of relativistic electrons

21 p3872 A70-40658

Balloon-borne measurements of hard X radiation from direction of Virgo

21 p3872 A70-40663

VIRIAL THEOREM

Upper mass limit of quasar in galactic cluster from velocity dispersion of galaxies using generalized form of virial theorem, determining B264 mass

02 p0372 A70-12245

Reduced second virial gas coefficients calculations by modified Lennard-Jones intermolecular potential function

12 p2180 A70-26860

Nonlinear least squares method reducing Burnett data to compressibility factors and virial coefficients

17 p3136 A70-35594

Compressibility factors and virial coefficients for He-N mixture, He and nitrogen at low temperatures and high pressures

18 p3290 A70-36250

Acoustic interferometer for speed of sound measurement in pure gases, determining second virial coefficient for Ar and N

21 p3828 A70-41766

Binary Boltzmann operator for quantum statistical second virial coefficient for real gases and plasmas in two-particle scattering problem involving Jost function

22 p4081 A70-42824

Virial theorem for magnetospheric dynamics, discussing boundary and ring currents and densities and geomagnetic sudden impulses and commencements

23 p4184 A70-43830

Ion-ion potential for sodium vapor for second virial coefficient as function of temperature at 1200-1700 K

24 p4381 A70-45649

VIRTUAL PROPERTIES

Seasonal variations of sporadic E virtual height at middle latitudes attributed to homospheric expansion depending on ozone amount

03 p0476 A70-13907

N body numerical integrator using virtual mass technique for computing trajectories with speed and accuracy suitable for spacecraft onboard computer applications

[AIAA PAPER 70-1057] 19 p3528 A70-38872

VIRTUAL WORK

U EQUILIBRIUM

VIRUSES

NT BACTERIOPHAGES

Bacterial and viral detection techniques in liquids based on specific property measurement relevant to biological particle, emphasizing industrial processing applications

01 p0013 A70-10127

Hematologic changes in mice associated with meningovirus infection and hypobaric hypoxia during barometric pressure changes

15 p2681 A70-31878

Coxsackie B virus as cause of myopericarditis in adults

17 p3025 A70-34860

Hypobaric hypoxia effects on MM virus infection resistance in mice

20 p3572 A70-39428

Viruses response to environmental exposure emphasizing temperature, humidity, light and extraterrestrial conditions

23 p4146 A70-44398

Hyperbaric oxygen effects on Coxsackievirus infection in mice

24 p4296 A70-45338

VISCERA

NT ADRENAL GLAND

NT BLADDER

NT ENDOCRINE GLANDS

NT ESOPHAGUS

NT GONADS

NT INTESTINES

NT KIDNEYS

NT LIVER

NT LUNGS

NT ORGANS

NT OVARIES

NT PARATHYROID GLAND

NT PINEAL GLAND

NT PITUITARY GLAND

NT RECTUM

NT SPLEEN

NT STOMACH

NT TESTES

NT THYMUS GLAND

NT THYROID GLAND

Visceral blood flow during exercise in sled dogs, testing hypothetical compensatory decrease as car-

diovascular reserve for skeletal muscle by biotelemetry

20 p3571 A70-39366

Kinesophilia mechanisms of motor-visceral integration in aging organism

22 p3969 A70-42902

VISCOELASTIC CYLINDERS

Volterra equations for stresses, strains and displacements of viscoelastic tube with variable radius enclosed in shell under pressure and unsteady temperature field

02 p0384 A70-11663

Solid viscoelastic cylinder bonded to thin elastic casing, analyzing normal and tangential stresses for stress and displacement frequency responses in forced transverse vibration

[ASME PAPER 69-WA/APM-20]

04 p0771 A70-14911

Stress analysis for nonlinear viscoelastic cylinder with ablating moving inner surface used to investigate propellant grain in solid fuel rocket under firing condition

[ASME PAPER 69-WA/APM-14]

04 p0771 A70-14914

Axisymmetrical stress-strain analysis of viscoelastic cylinder enclosed in elastic shell under internal pressure using singular kernels

05 p0933 A70-16207

Uncoupled quasi-static boundary value problem for linear viscoelastic solids undergoing thermal and mechanical deformation solved by computational algorithm

06 p1168 A70-17937

Stress-strain distributions in linear viscoelastic cylinder, reducing problem of hollow cylinder with moving inner boundary to Volterra integral equation

07 p1406 A70-19303

Strain and temperature fields interrelation effect on longitudinal wave propagation in viscoelastic cylinder, determining phase velocities and attenuation coefficients

09 p1781 A70-23285

Ablation and temperature effects in hollow viscoelastic cylinder

13 p2508 A70-28487

One dimensional analysis of stress and strain concentration resulting from longitudinal impact of viscoelastic rods

17 p3185 A70-34965

Volterra equations for stresses, strains and displacements of viscoelastic tube with variable radius enclosed in shell under pressure and unsteady temperature field

19 p3547 A70-38437

Long hollow nonlinear viscoelastic cylinder in elastic shell, calculating stress and strain under internal pressure

20 p3720 A70-39731

Cyclic thermal loading in viscoelastic spherical and cylindrical pressure vessels, investigating thermal frequency effect

21 p3937 A70-41430

VISCOELASTIC DAMPING

U ELASTIC DAMPING

U VISCOUS DAMPING

VISCOELASTIC FLOW

U VISCOELASTICITY

VISCOELASTICITY

NT PHOTOVISCOELASTICITY

NT THERMOVISCOELASTICITY

Dynamic response to step transverse loads of viscoelastic annulus of constant Poisson ratio in plane strain, analyzing work and spring-dashpot model

[ASME PAPER 69-LUB-23] 01 p0101 A70-10384

Elongation and combined shear stresses in incompressible creeping plane flows of viscoelastic lubrication for squeeze-film bearings

[ASME PAPER 69-LUB-22] 01 p0101 A70-10385

Incompressible elastomer viscoelastic response to exponential extension ratio history in simple tension based on constitutive equations

01 p0201 A70-10893

Dynamic stability of simply supported column of linear viscoelastic materials under sinusoidal loading

01 p0206 A70-11148

Time dependence of contact zone radius of rigid sphere pressed against viscoelastic half space by normal force

02 p0384 A70-11738

Viscoelastic boundary value problems involving time dependent boundary regions reduced to elastic problems, starting with aging viscoelastic body

02 p0388 A70-12269

Arterial model with effects of thick walls, linear viscoelasticity and wall tethering for studying arterial mechanics

02 p0247 A70-12550

Integral equation solution in viscoelasticity theory based on creep tests with polymer containing elastic inclusion, improving convergence of approximations method

02 p0390 A70-12801

Mixed boundary value problem for viscoelastic body with constant Poisson ratio solved by variables separation method, proving convergence

02 p0390 A70-12802

Quasi-linear stress-strain deviators relations in viscoelastic theory, indicating kernels and functions determinable from creep relaxation loading and deformation tests

02 p0390 A70-12804

Material functions mathematical forms for Green-Rivlin constitutive equations of nonlinear viscoelasticity

03 p0585 A70-12970

First and second boundary value problems of steady vibrations of viscoelastic bodies reduced to algebraic equations

03 p0589 A70-13345

Unsteady temperature field induced stresses and strains in hollow viscoelastic sphere calculated by solving integrodifferential equation having right hand side dependent on time function

03 p0590 A70-13398

Approximate method of boundary perturbation to solve elasticity and viscoelasticity problems for non-canonical bodies of revolution applied to stress concentration at ellipsoidal cavity

03 p0591 A70-13439

Complex Young modulus of plastics during flexural vibration, discussing deformation of viscoelastic bodies and test results of various plastics

[ONERA-TP-715] 03 p0487 A70-13645

Laminar capillary jet of viscoelastic fluid discussing breakup, non-Newtonian jet stability and elastic properties

03 p0468 A70-13782

Impulsive and transient load disturbances in thin elastic finite circular plate on Pasternak type viscoelastic foundation

03 p0595 A70-13905

Visco-elastic column analysis based on mechanical model, investigating relationships between solid viscosities, loading velocities, initial deflections and dynamic buckling loads

03 p0596 A70-14146

Transverse vibration of viscoelastic polymethyl methacrylate column with initial curvature under periodic axial load, determining amplitude-frequency curves

[ASME PAPER 69-WA/APM-13] 04 p0772 A70-14915

Propagation and growth equations governing wave propagation in micropolar viscoelastic solids couplings between discontinuities in macroscopic and microscopic fields

05 p0929 A70-16063

Viscoelastic behavior of styrene-butadiene rubber under finite uniaxial and equal biaxial deformations for nonisothermal case

05 p0929 A70-16068

Integral constitutive relation representing incompressible viscoelastic materials and plane stress and strain conditions

05 p0930 A70-16087

Linear and nonlinear inelastic spherical inclusion in elastic and viscoelastic isotropic matrix with constant strain or stress fields at infinity

05 p0932 A70-16171

Averaging analysis of oscillations attenuation of relaxing one dimensional linear viscoelastic systems under external force at resonance applied to nonlinear multidimensional systems

05 p0933 A70-16208

Linear isothermal quasi-static theory for homogeneous and isotropic viscoelastic bodies with couple stresses

05 p0938 A70-16425

Hydrodynamic theory of elastic-viscous liquid lubrication for journal bearings, assuming stress-strain relationship with unequal cross stresses

05 p0855 A70-16509

Dynamic strength calculation for linear viscoelastic body and elastic-viscous liquid with retardation and relaxation times spectra respectively

05 p0940 A70-16511

Time-varying loads effect on linear elastically hereditary media described by generalized fractional-order exponential functions and Rzhantitsyn type viscoelastic kernels

05 p0946 A70-16954

Viscoelastic fluid flow through circular tube under time dependent pressure gradient superposed on steady Poiseuille flow

06 p1032 A70-17200

Dynamic response of free-free beams on viscoelastic Winkler foundation using complex foundation modulus based on antivibration isolator

06 p1165 A70-17627

Optimal linear viscoelastic synthetic sandwich structures, investigating test/calculation agreement for simply supported beams and embedded plates

[ONERA-TP-702] 07 p1404 A70-19137

Three dimensional nonlinear viscoelastic body stability under triaxial compression, extending results obtained for elastic body

07 p1408 A70-19542

- Computer procedures for solving temperature stresses in thin infinite isotropic viscoelastic plate with heat transfer
07 p1411 A70-19817
- Vibrating composite beam test method for determining complex dynamic modulus of viscoelastic materials over broad frequency and temperature ranges
07 p1320 A70-19955
- Viscoelasticity in shearing and accelerative flows by integral theory, discussing stress distribution and pressure drop
07 p1412 A70-20000
- Complex modulus measurement for rigid linear viscoelastic materials over audio frequency spectrum by harmonic end displacement ratio method
07 p1413 A70-20044
- Quasi-steady propagation of Prandtl crack in viscoelastic body, noting stress distribution identity for viscoelastic and elastic cases
07 p1414 A70-20181
- Uniqueness theorem for coupled dynamic problem of linear thermoviscoelastic theory assuming contact-type boundary conditions
07 p1416 A70-20296
- Viscoelastic perfectly plastic ring failure under uniform external pressure characterized by infinite strain rate occurring at finite value of ring deflection
07 p1416 A70-20300
- Membrane stress in thin circular viscoelastic ring under impulsive loads and internal heat, using stress-strain relation for linear Maxwell material model
08 p1589 A70-21311
- Bearing capacity increase due to large viscoelastic or normal stress effects in lubricants, obtaining exact results for noncavitating plane slider bearings
08 p1507 A70-21476
- Viscoelastic fluid steady flow in porous walled channel, examining mass flow solution continuity
08 p1485 A70-21639
- Stresses and strains in multilayer systems of viscoelastic materials showing aging solved by quadratures and Volterra equations, noting dependence on time
08 p1594 A70-21672
- Polybutadiene-ammonium perchlorate solid propellant BPT-1 mechanical properties viscoelastic analysis under constant strain rate tension
09 p1742 A70-22425
- Stress and displacement distribution formulas for two and three dimensional crack extension problems in linear viscoelastic body
09 p1775 A70-22611
- Longitudinal vibration of finite viscoelastic rod with changing boundaries under time-variant force, analyzing impulse response by transform calculus
09 p1777 A70-22833
- Velocity measurements with Pitot tubes in polymer solutions /polyethylene oxide/ in water, noting viscoelastic properties effect on measured pressure value
10 p1887 A70-24093
- Equilibrium equations integration for body in isotropic linear viscoelastic medium with contact-type boundary conditions
10 p1957 A70-24267
- Viscoelastic half plane creep under discontinuous boundary conditions, obtaining exact closed-form solution based on Fourier transforms and distribution theory
10 p1965 A70-25325
- Nonlinear viscoelastic turbulence model with monotone increasing time scale to predict behavior in homogeneous shear and in pure strain
11 p2040 A70-26544
- Relaxation functions of one dimensional viscoelastic linear and nonlinear materials having monotone decreasing time properties
11 p2141 A70-26556
- Stable and unstable crack growth in viscoelastic media, solving boundary value problem and continuum mechanics prediction of crack propagation
12 p2315 A70-27092
- Viscoelastic polymeric materials tensile failure under multiaxial loading
12 p2321 A70-27205
- Relaxation function of linear viscoelastic body, defining mechanical deformation process using Stieltjes integral
12 p2327 A70-28046
- Mixed boundary value problems involving time dependent boundary regions for penny-shaped crack in viscoelastic materials with one relaxation function
13 p2508 A70-28489
- Viscoelastic plate crack growth analysis within continuum mechanics framework as analog to Griffith problem
13 p2510 A70-28671
- Complex moduli of isotropic viscoelastic composites from elastic moduli
13 p2511 A70-28735
- Saint Venant principle in linear isotropic viscoelasticity of Toupin estimates for body of arbitrary shape to allow integration by parts
13 p2513 A70-28990
- Isothermal quasi-linear theory of viscoelastic isotropic continuum, considering constitutive equations
13 p2516 A70-29534
- First and second boundary value problems of steady vibrations of viscoelastic bodies reduced to algebraic equations
14 p2657 A70-30720
- Longitudinal temperature gradients effects on stress analysis in solid propellants, using viscoelastic data
14 p2627 A70-30755
- Viscoelastic fluid in Couette flow between coaxial cylinders and flow between fixed plane and rotating cone
14 p2567 A70-31358
- Wave propagation through Newtonian fluid in compressible thick walled viscoelastic tube, considering blood flow in arteries
15 p2691 A70-31938
- Mechanical model of arterial viscoelasticity effect on input impedance and wave travel in systematic tree
15 p2691 A70-31941
- Fiber reinforced viscoelastic composites complex elastic moduli derivation
15 p2816 A70-32003
- Viscoelastic-plastic solid delayed fracture associated with wedge formation of crazed material at crack tip
15 p2816 A70-32010
- Zero birefringent blend consisting of rigid and flexible polyesters with viscoelastic mechanical and optical response
15 p2765 A70-32318
- Muscular behavior analog simulation model from generalization of laws governing viscoelastic behavior of polymeric materials
15 p2693 A70-32820
- Constitutive equation for fiber reinforced viscoelastic materials, using continuum theory of mixtures
16 p2994 A70-34231
- Thermorheologically simple model for viscoelastic materials stochastic behavior in random temperature fields, introducing reduced time scale
16 p3003 A70-34238
- Viscoelastic materials cut growth, discussing strain, fracture and modulus of elasticity dependence on temperature variations
17 p3146 A70-35220
- Viscoelastic materials fracture strength as function of cut length, defect size and temperature
17 p3146 A70-35221
- Vibrations induced by frictional moving force in viscoelastic beam with free ends on elastic base, showing critical load dependence on damping
18 p3343 A70-36720
- Viscoelastic fluids stratified flow down inclined plane, examining liquids elasticity role in stability
19 p3403 A70-37531
- Dynamic response to step transverse loads of viscoelastic annulus of constant Poisson ratio in plane strain, analyzing work and spring-dash model
19 p3435 A70-37607
- Stress relaxation interpretation at wave fronts in one dimensional media by nonlinear viscoelastic models, giving constitutive equations
19 p3542 A70-38057
- Boundary value problem solution in nonlinear viscoelasticity by constitutive equations
19 p3544 A70-38330
- Discrete finite element models for nonlinear viscoelastic continua
19 p3458 A70-38358
- Equilibrium equations integration for body in isotropic linear viscoelastic medium with contact-type boundary conditions
19 p3547 A70-38395
- Variational principles in linear quasi-static theory of inhomogeneous and isotropic viscoelastic solids with microstructure
20 p3718 A70-39229
- Composite material dynamic properties, discussing modulus and damping during constant strain rate, viscoelasticity, fracture strength and high loading tests
20 p3731 A70-40048
- Elastoviscous incompressible electrically conducting oscillating free stream flow along infinite porous plate with suction in transverse magnetic field
20 p3685 A70-40508
- Elastic and viscoelastic plates, calculating stress concentration and separation of embedded smooth circular inclusion under uniaxial tension
21 p3932 A70-40548
- Integral equation of viscoelastic media with unstable properties, solving boundary value problems by approximation method
21 p3933 A70-40643
- Thermomechanical disturbances propagation in viscoelastic solids, investigating effects of viscous flow, second order strains and temperature dependent material properties
21 p3937 A70-41427
- Plane Poiseuille flow in second order Rivlin-Ericksen fluids with small viscoelastic parameters, calculating three dimensional disturbance stability
21 p3810 A70-42030
- Viscoelastic liquids state equations, surveying various fluid models
22 p4009 A70-42541
- Crack growth study in viscoelastic solids by linear continuum mechanics, discussing cyclic loads, composite solids mechanical behavior and thermodynamics
22 p4115 A70-42937
- Viscoelastic continuous shaft whirling motion, discussing boundary conditions and internal linear viscous damping
22 p4012 A70-42939
- Dynamic melt properties of polymer blends, using orthogonal rheometer measurements
22 p4058 A70-43076
- Viscoelastic strip in gas flow, analyzing stability conditions
22 p4117 A70-43353
- Equations of state in quadratic viscoelasticity for orthotropic media, deriving tensors of creep and relaxation centers
22 p4119 A70-43711
- Stress concentration near holes in nonlinear viscoelastic plate, using elastic theory
23 p4266 A70-43989
- Conducting viscoelastic fluid flow near harmonically oscillating nonconducting flat plate under uniform transverse magnetic field, considering stress-strain rate relationship
23 p4226 A70-44375
- Linear viscoelastic solid quasi-static deformation, deducing associated minimum principles under assumption of unique solutions existence for boundary value problems
24 p4420 A70-45264
- Conduit arteries viscoelastic properties in normal and hypertensive dogs from recorded pressure and diameter waves
24 p4299 A70-45808
- Viscoelastic laminated composite linear anisothermal theory, presenting homogeneous continuum model to describe dynamic characteristics
24 p4368 A70-45992
- VISCOMETERS**
Viscosity of nitrogen, hydrogen, Ar and He at high pressures measured by capillary flow viscometer with range extended to minus 100 C
04 p0718 A70-14697
- Nitrogen viscosity coefficient at high pressure, describing viscosimeter operation and kinetic theory calculations
20 p3738 A70-40140
- VISCOMETRY**
Plasma viscosity and aggregation effects on whole blood viscosity investigated in observation chamber for erythrocyte aggregation
09 p1622 A70-23546
- Viscometric Poiseuille or Couette flow kinematics, considering nonuniform shear rate
14 p2567 A70-31282
- VISCOPLASTIC FLOW**
U VISCOPLASTICITY
VISCOPLASTICITY
Wave propagation in nonlinear viscoplastic medium, deriving first order system of coupled equations in stress and particle velocity components
01 p2027 A70-11154
- Variational principles in dynamic viscoplasticity theory, based on operator approach combined with time independent variations in elasticity theory
02 p391 A70-12818
- Plastic-viscoplastic bar wave propagation due to longitudinal impact, analyzing stress profiles to determine effect of strain rate
05 p0926 A70-15913
- Steady viscoplastic boundary layer near hard wall with power law velocity distribution along outer boundary, deriving self similar solution
07 p1252 A70-18670
- Rigid viscoplastic incompressible fluid flow governed by system of variational inequalities involving Navier-Stokes equations
08 p1482 A70-20590
- Flow rule for viscoplastic symmetric cylindrical shells, using constitutive equations for strain rate sensitive materials based on Huber-Mises yield condition
10 p1954 A70-24020
- Large deflections in impulsively loaded clamped circular Al alloy and steel viscoplastic plates
13 p2511 A70-28736
- Steady viscoplastic boundary layer near hard wall with power law velocity distribution along outer boundary, deriving self similar solution
15 p2718 A70-31462
- Viscoelastic-plastic solid delayed fracture associated with wedge formation of crazed material at crack tip
15 p2816 A70-32010
- Elastoviscoplastic medium filled half space motion under pressure front moving along surface with time

varying velocity, analyzing penetrating wave fronts form 16 p2990 A70-33780

One dimensional elastoplastic wave propagation in rate-sensitive viscoplastic rod with thermal gradient 17 p3185 A70-34966

Viscoplastic solids, computing plane shock wave propagation structure from nonlinear constitutive relations 18 p3338 A70-36435

Three dimensional dynamic analysis of small harmonic stress wave propagation in elastic-plastic and viscoplastic materials, using finite differences 18 p3344 A70-36724

Elastic-viscoplastic bar quasi-static torsion problem, using approximate method for time dependent torsion function 24 p4425 A70-45993

VISCOSITY

NT EDDY VISCOSITY
NT GAS VISCOSITY

Steady state spherically symmetric model for solar plasma acceleration with distance, showing essential role of viscosity 01 p0172 A70-11519

Turbulent viscosity and thermal conductivity coefficients for entire cross section of fluid flow including wall boundary layers 01 p0069 A70-11624

Turbulence constant for flows near walls, analyzing viscosity dependence on wall distance by utilizing maximum stability principle 01 p0069 A70-11627

Newtonian liquid lubricated spiral groove bearing load capacity and power loss dependence on viscosity variations with temperature [ASLE PREPRINT 69-LC-21] 02 p0309 A70-12533

Viscosity anisotropy in fluid matrix suspensions of parallel rigid flakes as function of flake content and width-to-thickness ratio 03 p0515 A70-13122

Niobium powder hot pressing compaction in terms of porous body volume viscous flow, determining viscosity shift time dependence 04 p0696 A70-14461

Load capacity and power loss of spiral groove bearings lubricated by incompressible liquid with temperature-dependent viscosity, using momentum and energy equations 05 p0853 A70-15778

Relation between Fourier harmonics equilibrium distribution and bulk viscosity and second thermal conductivity established in critical regions of liquid-vapor condensation and mixing 05 p0958 A70-16550

Bivalent cations effect on crystallization and viscosity of glazed glass 05 p0871 A70-16592

Time-temperature relation necessary to fine Libyan desert glass and remove gas bubbles calculated by viscosity determination at various temperatures 05 p0843 A70-16833

Rheology applied to motor oil viscosity, elastohydrodynamic (EHD) and extremely thin film lubrication, examining viscosity relationship to film thickness 07 p1293 A70-18954

Temperature gradients, viscosity and conduction measurements in air stream between parallel plates, investigating limiting value of total Prandtl number 07 p1260 A70-19999

Thermal convection determination in earth, Venus, Mars and moon interiors based on thermal stability analysis, obtaining viscosity depth profiles 07 p1272 A70-20203

Ultrasonic testing of hydraulic liquids and aircraft and engine lubricating oils resistance to viscosity decrease, analyzing large molecule compounds disintegration 09 p1693 A70-23405

Lubricating oils viscosity deterioration during sliding motion in machines determined by quantitative evaluation 09 p1693 A70-23407

Irreversible viscosity decrease and thermal stability in polymer-containing lubricating oils under shearing forces effect 09 p1693 A70-23408

Synthetic silicate liquid viscosity with lunar rock composition compared with volcanic rock on earth 10 p1938 A70-24074

Kinematic viscosity of molten steel containing corundum inclusions as function of temperature 10 p1904 A70-24271

Brownian motion for large viscosity, deriving modified Fokker-Planck equation based on quasi-Huygens relation 11 p2084 A70-26398

Heat conduction and viscosity effects on compressible fluids characteristics 11 p2037 A70-26399

Complex viscosity relationship to steady state shearing in Maxwell Orthogonal Rheometer 11 p2041 A70-26560

Magnetopause representation by mixing region of plasma streams with different velocities and magnetic fields, assuming hydromagnetic viscosity caused by wave-particle interactions 11 p2114 A70-26563

Thermally ionized cesium plasma viscosity at high temperatures in vacuum using capillary tube assembly 11 p2092 A70-26731

Viscosity variation factor at film inlet in fluid square taper pad bearing investigated by modified Reynolds equation 13 p2418 A70-28746

Aliphatic diesters as high temperature lubricants, discussing viscosity range extension, oxidation inhibition and thermal stability 13 p2438 A70-29125

Viscosity coefficient for isotropic turbulence using quasi-self-similar solution 13 p2391 A70-29777

Fluid quantum corrections to viscosity, thermal conductivity and diffusion, expanding Wigner operator in Planck constant 14 p2665 A70-30655

Laminar compressible flat plate boundary layer dependence on Prandtl number and viscosity-temperature relations 16 p2893 A70-33673

Motion perturbation equations for guided space vehicles, allowing for sloshing liquid propellant viscosity effects 18 p3332 A70-36160

Viscosity effect on turbulent supersonic underexpanded jet flow into submerged region 18 p3206 A70-36262

Energy dissipation and viscosity effects on isotropic turbulence in extreme short wave region at large Reynolds numbers 18 p3239 A70-36263

Small viscosity and heat conductivity in solutions to critical layer in stratified shear flow 20 p3608 A70-39447

Materials viscous failure at various temperatures and stresses, discussing damage accumulation 20 p3725 A70-39870

Viscosity and vessel geometry effects on fluids natural and forced oscillation, taking surface tension into account 20 p3614 A70-40438

VISCOUS DAMPING

Three-body gravity gradient satellite orbital plane motion analysis, studying transient damping of proposed tethered orbiting interferometer/TOI 02 p0383 A70-12781

Linear isothermal response of viscously damped thin homogeneous polygonal plates subjected to uniform dynamic loading, calculating forced solutions by numerical integration 03 p0601 A70-14318

Random vibrations of linear system with viscous damping excited by stochastically acting force with monotonically varying frequency, using correlation method 05 p0882 A70-16372

Initial disturbances propagation in gas mixtures by asymptotic analysis, observing diffusely and viscously damped modes 05 p0833 A70-16404

Viscous damping effect on aeroelastic stability of thin plate in inviscid compressible airstream, observing instability in subsonic and supersonic flow 05 p0941 A70-16517

Vibration damping by sandwich structure consisting of viscoelastic layer between two high Youngs modulus metal sheets 07 p1401 A70-18845

Dissipative heating effects on loss factor of viscoelastically damped beam, discussing stiffness effects [ASME PAPER 69-VIBR-37] 08 p1592 A70-21478

Torsional vibrations frequency calculations for multibranch system exhibiting linear rigidity and viscous damping, constructing algorithm for digital computer 09 p1783 A70-23409

Temperature effect on plate damping by constrained viscoelastic layers, emphasizing transition and operating temperature compatibility 10 p1962 A70-25063

Metal plates vibration under viscoelastic damping layers using electromagnetic transducer and impact excitation 11 p2145 A70-26702

Vibration control by alternate layers of high damping viscoelastic material, discussing damping and loss factors, beams design and attachment 13 p2513 A70-29079

Fluid flow damping in flexible liquid filled foams at various frequencies and temperatures 15 p2765 A70-31967

Infinite elastic plates traveling wave flutter in compressible flow, investigating viscous damping effects on critical flow velocity 18 p3343 A70-36701

Constrained viscoelastic layer optimal length for vibration damping of metallic structures 19 p3536 A70-37696

Axisymmetric dual spin spacecraft consisting of nonconcentric frictionlessly mounted cylinders equipped with viscous damping mechanisms, evaluating stability criteria by energy method [AIAA PAPER 70-973] 20 p3715 A70-39556

Supersonic nozzle damping, replacing parameters discontinuities across shocks by continuous variations 21 p3745 A70-41442

Viscoelastic continuous shaft whirling motion, discussing boundary conditions and internal linear viscous damping 22 p4012 A70-42939

Shock response of passive nonlinear elastic isolators under pulse excitation with viscous damping 22 p4117 A70-43249

Nonlinear systems subharmonic oscillations under polyharmonic disturbance and viscous damping 24 p4427 A70-46378

VISCOUS DRAG

Low Reynolds number flow of variable property gas past infinite heated circular cylinder at large temperature differences, measuring drag on cylinder 05 p0789 A70-16014

Free molecular drag for flat plate with normal protuberance, determining flowfield distribution functions and stress components 06 p0981 A70-18357

Drag coefficients of sharp and blunt cones in rarefied supersonic flow for bluntness ratios and angles of attack 06 p0981 A70-18360

Drag on infinite cylinder in hypersonic nearly free molecular flow for various angles of attack, using kinetic approach 06 p0983 A70-18380

Drag and heat transfer predicted by kinetic theory for rarefied gas flow over sphere at low Mach numbers, analyzing flow field 06 p0984 A70-18381

Hypersonic rarefied gas flow near stagnation point investigated to predict drag on sphere in high speed gas stream with densities in transition regime 06 p0984 A70-18382

Flow field around and drag on sphere rising axially through rotating viscous fluid 09 p1663 A70-23676

Viscous friction force moments effect on gyroscopic drift in gimbal suspension during base angular vibrations, obtaining drift velocity 15 p2738 A70-32153

Laminar viscous effects over blunt cones at hypersonic conditions, taking into account first and second order boundary layer theories 20 p3559 A70-40285

Hypersonic viscous effects on space shuttle entry trajectory, measuring lift and drag in free flight regime 23 p4258 A70-44526

VISCOUS FLOW

NT BOUNDARY LAYER FLOW

NT BOUNDARY LAYER SEPARATION

NT COUETTE FLOW

NT REATTACHED FLOW

NT SECONDARY FLOW

NT SEPARATED FLOW

NT STOKES FLOW

Viscous fluid flow due to long flat plate moving rectilinearly inside cylinder, assuming zero pressure gradient 01 p0062 A70-10801

Conservation laws for viscous incompressible two dimensional and axisymmetric flow written in integrodifferential form 01 p0063 A70-10935

Incompressible slow viscous nonNewtonian flow with free surface solved by finite element method, showing computerized results for squeezed fluid between two plates 01 p0066 A70-11131

Incompressible viscous fluid flow in contact with infinite plate and rotating in perpendicular magnetic field, obtaining flow characteristics by Laplace transform 01 p0067 A70-11138

Navier-Stokes equations for compressible gas, generalizing viscous channel flow of heat conducting gas to slip flow of rarefied gas 01 p0068 A70-11579

Short sound waves propagation in moving inhomogeneous medium, studying viscosity and heat conductivity influence 01 p0146 A70-11581

Navier-Stokes difference equations numerically integrated by computer for viscous fluid flow along parallel flat plate at low Reynolds number 02 p0277 A70-11909

Dissipation spectrum /viscous dissipation of turbulent kinetic energy as function of wave number magnitude/ data compared and plotted 02 p0327 A70-12294

Computer application to Navier-Stokes equations numerical integration for incompressible viscous fluid deflected flow with large Reynolds number 02 p0287 A70-12376

Small parameter method for reducing self similar viscous flow problems to ordinary third order differential equation 02 p0287 A70-12376

ferential equations with boundary conditions at wall and infinity

02 p0288 A70-12821

Motion stability and time dependent deflections of thin flexible cylinder with zero bending rigidity in viscous stream

03 p0595 A70-13783

Viscous supersonic flow near wall with large local curvature, using asymptotic solutions to Navier-Stokes equations

03 p0468 A70-13867

Viscous compressible heat conducting laminar perfect gas flow in slender axisymmetric channels with adiabatic walls, using equations of motion

03 p0471 A70-14383

Viscous inlet flow into straight channels, studying velocity profiles at low Reynolds numbers

[ASME PAPER 69-APM-Q] 04 p0668 A70-14863

Flow viscosity and heat conduction effects on shock wave propagation in bent channel with weak Mach reflection

04 p0671 A70-15013

Fluid mechanical problems with pressure distribution determined by interaction between external supersonic inviscid flow and inner laminar viscous layer

04 p0674 A70-15529

Viscous shock layer at hypersonic blunt body stagnation point, applying finite difference and nonlinear overrelaxation methods to seven species air model

04 p0620 A70-15539

Mass transfer and viscous interaction combined effects on axisymmetric hypersonic flow of perfect gas over slender bodies

[AIAA PAPER 68-717] 04 p0675 A70-15576

Model flow studied for viscous flow near trailing edge of semiinfinite flat plate in middle of moving channel, noting Couette flow tendencies

05 p0831 A70-15879

Vertically propagating waves in viscous isothermal atmosphere taking into account reflection due to nonlinearities and time dependence

05 p0833 A70-16679

Viscous frictional torque on inner cylinder of eccentrically rotating concentric cylinders measured from laminar to turbulent flow

06 p1074 A70-17134

Viscous core of incompressible swirling flow through nozzle using momentum-integral equations

[AIAA PAPER 70-51] 06 p1038 A70-18079

Viscous radiating flowfield coupled with ablation for computations on blunt body entering earth atmosphere at interplanetary return velocities

06 p0970 A70-18090

Closed form solution of modified inviscid transonic equation embodying character of viscous-transonic equation applied to shockless transonic airfoils

[AIAA PAPER 70-187] 06 p0970 A70-18096

Laminar viscous flow on rotating propeller and helicopter rotor blades, studying crossflow and unsteady boundary layer effects, separation, transition, etc

[AIAA PAPER 70-50] 06 p0974 A70-18161

Impact tube test to find empirical equation for correcting effect of shear in displacing effective pressure center in viscous flow

06 p1052 A70-18383

Model for predicting laminar-turbulent transition point in hypersonic wake of two dimensional laminar viscous flow

06 p0985 A70-18499

Peristaltic motion of viscous incompressible fluid, applying long wave approximation to two dimensional urine flow model

07 p1219 A70-19247

Book on mathematical theory of viscous incompressible flow covering stationary and nonstationary boundary value problems for linearized and nonlinear Navier-Stokes equations

07 p1258 A70-19697

Viscous hypersonic flow past sphere in presence of strong injection through front surface at large Reynolds numbers using asymptotic method

07 p1189 A70-20146

German book on fluid dynamics for nonelectrical fluids covering viscosity effects, Prandtl boundary layer, turbulence and aerodynamics

08 p1431 A70-20751

Boundary value problem solution in study of axisymmetric viscous heat conducting gas flow past body of revolution

08 p1431 A70-20854

Gas flow influence on wave characteristics of thin viscous liquid layers pulled by gravity vertical surface compared with water layer experiments

08 p1482 A70-20917

De Laval nozzle behavior in vacuo, discussing flow rate parameters, viscosity and real gas effects, thermal effects, turbulent jet separation and reattachment, etc

[AGARDGRAPH-120] 08 p1434 A70-21932

Simple molecules viscosity as function of temperature and density using empirical equation

09 p1731 A70-22292

Hypersonic laminar boundary layer in strong viscous interaction region on wedge, determining

velocity and enthalpy profiles, displacement thickness and induced pressure distributions, etc

09 p1606 A70-23294

Stress tensors in initial value problem for incompressible flow with nonlinear viscosity

09 p1663 A70-23570

Laminar viscous flow past semiinfinite flat plate parallel to uniform stream, solving Navier-Stokes equation to determine local skin friction coefficient

09 p1663 A70-23581

Steady and unsteady viscous incompressible one dimensional flows parameters in deformable cylindrical tube determined, solving continuity and motion equations by Galerkin method

09 p1664 A70-23715

One dimensional Navier-Stokes equations solution for viscous heat conducting gas flow involving spherical sink for finite pressure at infinity

10 p1865 A70-24104

Plane steady flows characteristics of incompressible viscous fluids in rigid walled rectangular channels found asymptotic to Poiseuille and Couette flows

10 p1866 A70-24112

Viscosity and heat conductivity effects in compressible fluid flow past finite body showing dependence on spatial dimensions

10 p1800 A70-24135

Viscous transonic flow past wavy wall analyzed by approximate method for inviscid transonic equation

10 p1800 A70-24137

Rigid body mode of viscous incompressible fluid flow response to small perturbations of rotating spheroidal container, applying torque interaction

10 p1868 A70-24196

Viscous incompressible flows nonlinear stability theory, considering perturbed flows tending toward stationary or flow periodic in time

[ONERA-TP-802] 10 p1869 A70-24542

Hypersonic viscous interactions on insulated slender cone with mass injection assuming perfect gas flow and negligible transverse curvature effects

10 p1803 A70-24821

Linear viscous theory of steady rotating fluid flows with nonlinear modification of boundary layers, considering inertial modifications

11 p2036 A70-26011

Stability analysis using energy method applied to Navier-Stokes equations for unsteady viscous flow

11 p2042 A70-26849

Mathematical model for describing flow in Hele-Shaw cell, predicting attached viscous shear layers in lifting body wake

13 p2338 A70-28818

Viscous and compressible fluid flow in presence of plane plate

13 p2389 A70-29489

High Mach number viscous flow past cylinder with cylindrical shock wave

13 p2391 A70-29970

DMC computer code for simulation of two dimensional viscous incompressible flow about arbitrarily shaped bodies

14 p2527 A70-30271

Velocity difference across viscous tail in MHD flow, demonstrating exponential decay

14 p2623 A70-30992

Nonstationary MHD Couette flow of viscous incompressible fluid between two parallel walls caused by instantaneous fluctuations of applied transverse magnetic field

15 p2777 A70-31479

Hydromagnetic viscous flow of incompressible conducting fluid due to electric current radial divergence from point source

15 p2780 A70-32426

Laminar boundary layer model for viscous losses during transient turbulent liquid flow in tube, assuming slug flow for core

[ASME PAPER 70-FE-8] 16 p2891 A70-33627

Boundary value problem of two dimensional Poisson equation solution procedure with Hockney formulas, applying to unsteady viscous incompressible flow past flat plate

16 p2943 A70-33737

Viscous absorbing emitting shock layer in blunt body stagnation region, calculating skin friction and radiative heat transfer

[AIAA PAPER 70-868] 16 p2999 A70-33911

Mathematical model of pulsatile viscous entrance flow in thick walled elastic tube, investigating flow development effects in large arteries

17 p3035 A70-34471

Hypersonic viscous interaction on curved surfaces, extending Cheng inclined flat plate analysis

[AIAA PAPER 70-782] 17 p3007 A70-34474

Hypersonic cruise vehicles viscous interactions areas, examining compression corners, shock interactions, laminar and turbulent flow, boundary layer separation, etc

[AIAA PAPER 70-781] 17 p3007 A70-34475

Two dimensional solidification of forced viscous flow over flat plate with constant heat removal

17 p3194 A70-34634

Shock wave and viscous layer structures ahead of blunt body in rarefied hypersonic flow, using continuum theory

17 p3009 A70-34698

Two dimensional hypersonic viscous flow, analyzing viscosity and bluntness induced pressure effects

17 p3010 A70-35034

Viscous heat-conducting one dimensional piston driven gas flow, assuming sharp shock discontinuity

17 p3075 A70-35890

Viscous hypersonic flow around nonslender bodies with mass supply at small Reynolds numbers, using thin shock layer model

18 p3206 A70-36259

Incompressible heavy fluid film stability during flow along inclined plane constituting crystallization front, analyzing linearized equations of perturbed flow

18 p3240 A70-36271

Boundary value problem for Navier-Stokes equations of viscous incompressible fluid flow, discussing convergence of iterative solution

18 p3241 A70-36290

Magnetohydrodynamic flow of electrically conducting viscous incompressible fluid past nonconducting semiinfinite flat plate under transverse magnetic field

18 p3295 A70-36431

Two dimensional time dependent solution for impulsive motion of circular cylinder involving viscous cross flow at moderate angles of attack

18 p3207 A70-36454

Viscous supersonic flow near sharp convex corner, discussing visual observation and quantitative surveys of velocity and pressure profiles

18 p3208 A70-36659

Turbulent viscoseal with gas-liquid interface, using recirculation loop for gas ingestion reduction

[ASLE PREPRINT 70AM 5C-4] 19 p3439 A70-38804

Pressure and temperature distribution in constant volume viscous Poiseuille gas flow velocity profile

20 p3608 A70-39121

Unsteady viscous flow of incompressible fluid through porous straight channel under time varying pressure gradient, determining suction and injection effects

20 p3609 A70-39670

Energy dissipation in laminar unsteady incompressible viscous fluid flows, discussing velocity fields, boundaries, tangential motion and entrainment

20 p3614 A70-40402

Viscous magnetofluidynamic one dimensional annular flow, reducing three dimensional field equation to coupled linear partial differential equations

21 p3855 A70-40889

Subcritical viscous flow around arbitrary airfoils, calculating boundary layer effect on pressure distribution from inviscid flow approximation

21 p3744 A70-40924

Thermomechanical disturbances propagation in viscoelastic solids, investigating effects of viscous flow, second order strains and temperature dependent material properties

21 p3937 A70-41427

Two dimensional unsteady viscous incompressible MHD flow past infinite flat plate with uniform suction, considering Hartmann and Reynolds numbers

21 p3858 A70-41450

Steady viscous flow past oblique flat plate at high Reynolds number, using Oseen linearized approximation

21 p3809 A70-41714

Viscous gas flow through Laval nozzle, calculating velocity coefficient and pressure recovery in contracting and expanding parts

21 p3746 A70-41774

Viscous laminar parallel flow along cylindrical surfaces, discussing boundaries described by algebraic polynomials

21 p3810 A70-41959

Navier-stokes equations solutions in two way flows of Newtonian fluids with constant kinematic viscosity

21 p3810 A70-41961

Nonparallel viscous incompressible fluid flows in channel between parallel porous plates with suction and blowing respectively, calculating stability by numerical solution

21 p3811 A70-42216

Viscous incompressible fluid flow between two rotating concentric spheres, calculating stability

21 p3811 A70-42217

Viscous transonic flow past cascades by semiempirical approach, discussing pressure distribution, boundary layer parameters and compression shock

22 p4088 A70-42343

Viscous flow field in pneumatic vortex rate sensor, discussing boundary layer parameters, velocity profiles and swirling flow theory

[ASME PAPER 70-FLCS-16] 22 p4007 A70-42411

Hypersonic viscous interaction between laminar boundary layer growing over flat plate and external flow field extended to curved surfaces

22 p3958 A70-42688

Twisted incompressible viscous fluid flow in conical diffuser described by differential equation system, considering flow velocity field and separation point 23 p4133 A70-44159

MHD incompressible viscous flow in nonconducting circular tube, determining pressure, flow rate and magnetic field level by continuum theory concepts 23 p4224 A70-44161

Navier-Stokes equations for discrete flows of viscous fluids, using grid cell representation 23 p4181 A70-44220

Optimum thickness ratio and minimum drag of slender bodies in hypersonic viscous flow as function of altitude 23 p4134 A70-44571

Heat transfer and viscous flow pedagogy, discussing classroom use of remote time sharing computer terminals 23 p4166 A70-44642

Viscous compressible gas flows in pipe initial section, calculating friction and heat transfer coefficients 23 p4135 A70-44734

Velocity profile in viscous sublayer at wall based on maximum stability principle applied to Karman constant for turbulent channel flow 24 p4325 A70-45495

Two dimensional incompressible laminar free jet, analyzing higher order viscous interactions with surrounding fluid by matched asymptotic expansions method [AIAA PAPER 70-1321] 24 p4326 A70-45944

Viscous fluid two dimensional steady natural convection between horizontal concentric cylinders for low Grashof numbers 24 p4429 A70-46007

Viscous heat conducting compressible fluid flow past slender axisymmetric body, presenting Navier-Stokes hypersonic strong interaction theory 24 p4289 A70-46020

Momentum source interaction with viscous uniform stream, constructing perturbation solutions from nonlinear equations 24 p4327 A70-46040

Viscous flow stability between two concentric rotating porous cylinders, calculating critical Taylor numbers for wave numbers and velocity ratios 24 p4328 A70-46366

Surface temperature distribution of heat generating solid body in contact with parallel viscous fluid flow 24 p4430 A70-46368

VISCOUS FLUIDS

Vortex diffusion in viscous compressible fluid, deriving nonlinear differential equations from density velocity and pressure discontinuities considerations 01 p0060 A70-10145

Transient heat transfer near two dimensional stagnation point in viscous incompressible fluid steady flow 01 p0002 A70-10457

Navier-Stokes hypersonic weak interaction theory for viscous heat conducting compressible fluid flow past slender axisymmetric body 01 p0003 A70-11097

Resonance amplification theory of standing interfacial gravity waves in viscous fluids applied to obtain wavelengths prediction of atmospheric bow waves 01 p0081 A70-11299

Body motions containing cavity filled with viscous fluid under influence of gravity, formulating motion equations for fluid and body 01 p0068 A70-11576

Dynamics of turbulent motion of incompressible viscous fluid particles, using Lagrangian functions 01 p0068 A70-11603

Turbulent viscous fluid flow characteristics obtained from integrating Navier-Stokes equation for unsteady flow with periodic momentum variation 01 p0069 A70-11626

Incompressible viscous fluid plane flow using series expansion 02 p0277 A70-11910

Incompressible viscous fluid rectilinear flow along arbitrary cross section duct under pressure gradients oscillating at large frequencies 03 p0468 A70-14147

Navier-Stokes boundary value problem describing viscous incompressible fluid flow between coaxial fixed and rotating cylinders, emphasizing stability analysis 03 p0470 A70-14242

Electrical and mechanical instability of jets, threads and sheets of viscous fluid, noting role of deceleration 03 p0471 A70-14253

Viscous ideal gas supersonic flow past spheres, using integral relations based on Navier-Stokes equations 04 p0613 A70-14606

Forced vertical oscillations in viscous stratified fluid, showing phase angle dependence on amplitude and relation to Brunt-Vaisala frequency 04 p0666 A70-14611

Lateral vibrations of rigid rotating shaft in viscous fluid using inner and outer expansions method, considering small amplitude vibration and fast rotation 04 p0769 A70-14865

Small parameter method applied to numerical solution of conformal mapping and viscous fluid motion problems 04 p0719 A70-14960

Hydromagnetic flow of viscous incompressible electrically conducting fluid near accelerated infinite porous flat plate with variable suction or injection 04 p0672 A70-15095

Viscous gas self similar channel flow with heat transfer at wall corresponding to fixed Mach number profile in all channel cross sections 04 p0673 A70-15231

Hypersonic viscous gas flow past power law bodies under viscous interaction between boundary layer and inviscid flow extended to slender bodies 04 p0618 A70-15240

Electrically driven jets of slightly conducting viscous fluids drawn from conducting tubes, discussing cylindrical soap film instability under radial electric field 05 p0831 A70-15917

Dynamic strength calculation for linear viscoelastic body and elastic-viscous liquid with retardation and relaxation times spectra respectively 05 p0940 A70-16511

Linearized MHD equations for motion of solids in viscous and electrically conducting fluids 06 p1120 A70-17532

Heat transfer from constant temperature and heat flux surfaces to viscous fluids with high Prandtl numbers, considering transient and steady state flow 06 p1176 A70-17687

Velocity, magnetic field and drag equations for steady incompressible viscous conducting fluid flow around spherical hollow shell 06 p1122 A70-17917

Axisymmetric motion of viscous heat conducting gas by constructing indirect analog of Poiseuille gas flow, applying results to slip flow regime 06 p1048 A70-18325

Container fluid viscosity effect on container-obstacle interaction solved in Fourier series form 07 p1252 A70-18676

Viscous fluid flow calculations in fine clearance eccentric annuli allowing for pressure losses in laminar or turbulent flows 07 p1293 A70-19120

Rigid rotating cylindrical shaft vibrations along diameter in viscous fluid using inner and outer expansions method [ASME PAPER 69-APM-S] 08 p1589 A70-21307

Motion of body with cavity completely filled with viscous fluid about center of mass in potential mass-force field, applying small parameter method 08 p1546 A70-21630

Oscillations of highly viscous incompressible fluid in partially filled cavity of body moving about fixed point, solving Navier-Stokes equations by asymptotic method 08 p1485 A70-21632

Heat transfer in MHD channel flow of viscous incompressible rarefied gas with slip flow and temperature jump boundary conditions 08 p1554 A70-21769

Cauchy problem solution for linearized Navier-Stokes equations of incompressible rotating viscous fluid, discussing velocity and angular momentum effect on asymptotic behavior 09 p1659 A70-22326

Acoustic radiation produced in response to harmonically oscillating circular cylinder rotating in viscous fluid solved within Lighthill-Curle formalism for aerodynamically generated sound 09 p1726 A70-22391

Navier-Stokes equation for plane unsteady axisymmetric rotation of viscous fluid in steady radial flow from source or sink 09 p1660 A70-22437

Motion and continuity equations for unsteady two dimensional flow of incompressible viscous fluid along infinite flat plate with time dependent suction 10 p1862 A70-23877

Numerical methods of viscous liquid dynamics, considering unsteady flow in simply and multiply connected regions 10 p1866 A70-24110

Viscous fluids nonlinearized thermodynamical description with equilibrium state defined by two parameters, expressing angular momentum density by momentum density 10 p1967 A70-24153

Potential flow resistance theory, deriving monoparameter wake formula for circular cylinder moving through viscous fluid 10 p1870 A70-24788

Viscous compressible fluid steady laminar flow between coaxial cylinders, studying flow characteristics for uniform inner cylinder velocity 10 p1870 A70-24792

Nonlinear disturbance decay in unbounded viscous fluid calculated by iterative solution of Navier-Stokes equations 10 p1871 A70-24854

Viscous fluid dynamics for reducing hydrodynamic resistance, discussing aquatic animals speeds, vortex flows, etc 10 p1871 A70-25193

Viscous incompressible fluid secondary steady state flow due to rotating spheroid, considering acceleration terms in Stokes linear equation solution 11 p2034 A70-25390

Flow formation in Couette motion of viscous fluids containing suspended rigid spherical particles using theory of fluids with microstructure 11 p2037 A70-26169

Stability of MHD dissipative circular flow of viscous electrically conducting fluid between concentric stationary cylinders impressed with axial magnetic and radial electric fields 12 p2277 A70-27195

Transient flow of viscous incompressible fluids with free surfaces calculated using Lagrangian coordinates 12 p2210 A70-27425

Differential equations of motion of manometers in log instrument systems with allowance for viscous liquid in sensor and pulse line 12 p2234 A70-27567

Thermal boundary layer equations solved for compressible gas at rotating axisymmetric surface with viscosity as linear function of temperature 12 p2331 A70-27698

Oscillating infinite cylinder as acoustic waves source in homogeneous viscous medium, deriving scalar and vector potentials 12 p2274 A70-28240

Nonlinear effects of oscillatory disturbances produced by viscous excitations in rotating fluid inside of cylindrical tank 13 p2386 A70-28819

Viscous and inviscid incompressible fluids motion boundary value problems solutions with aid of kinetic stress functions 13 p2388 A70-29319

Incompressible, viscous and electrically conducting fluid flow due to rotating disk in uniform magnetic field, discussing hydromagnetic interaction effect on velocity and friction 13 p2465 A70-29544

Meniscus curvature correlation to viscosity contrast in capillary during fluid displacement 13 p2390 A70-29633

Container fluid viscosity effect on container-obstacle interaction solved in Fourier series form 15 p2719 A70-31468

Thermal convection formation in viscous fluid plane horizontal layer from measurements of unsteady temperature field 15 p2824 A70-31591

Incompressible viscous fluid steady flow admission into bounded space from cylindrical tube, demonstrating solvability of plane and three dimensional versions 15 p2720 A70-31642

Rheological calculation of plate resistance and heat transfer in laminar flow of structurally viscous fluids 15 p2827 A70-32126

Viscous incompressible fluid nonstationary flow boundary layer extension around porous plate at Prandtl number equal to unity 15 p2722 A70-32873

Incompressible viscous fluid divergent turbulent flow detection in conical tube of revolution based on measuring wall pressure differences along tube generatrix 16 p2894 A70-33849

Sphere slow motion in viscous fluid with solid particle suspension, considering Stokes flow pattern small relaxation time perturbation 16 p2896 A70-34272

Free convection in compressible viscous heat conducting fluid, determining parameters leading to onset 17 p3198 A70-35697

Viscous incompressible liquid two dimensional flow around flat plate, discussing visualization techniques and velocity distribution measurement 18 p3239 A70-36218

Flow stability of incompressible heavy viscous fluid along wall of vertical circular cylindrical pipes, relating flow parameters to stability 18 p3240 A70-36278

Thermodynamics of thermoviscous fluids based on Riemannian space time notions and balance laws of general theory of relativistic continuum mechanics 18 p3479 A70-37592

Boundary value problems in MHD, considering viscous and nonviscous fluids 19 p3406 A70-38445

Viscous dielectric incompressible fluid cylinder capillary stability under small axisymmetric disturbances and axial electric field, deriving perturbed fluid flow equations 19 p3406 A70-38445

Unsteady flow and heat transfer in viscous incompressible fluid due to infinite porous cylinder oscillations about axis with suction at surface 19 p3406 A70-38445

Viscous incompressible electrically conducting fluid steady flow between parallel coaxial rotating disks with transverse magnetic field 19 p3481 A70-38446

Steady compressible supersonic planar flow of viscous heat conducting fluid under linearization freestream conditions, describing slip flow past finite flat plate 20 p3557 A70-39228

Viscous fluid motion equations through anisotropic nonrigid porous solid, discussing blood flow in capillary vessels and extracellular fluid through interstitial space 21 p3768 A70-40776

Viscous fluid cylinders electromagnetodynamic stability, discussing viscous forces effects 21 p3858 A70-41699

Viscoelastic liquids state equations, surveying various fluid models 22 p4009 A70-42541

Hall effect on incompressible electroconducting viscous fluid motion past finite conducting flat plate, discussing boundary conditions 23 p4225 A70-44247

Thermal convection formation in viscous fluid plane horizontal layer from measurements of unsteady temperature field 23 p4277 A70-44278

Solid particles interactions during entrainment by viscous incompressible fluid in pipe, calculating interaction force as function of radius, distance and Reynolds number 23 p4181 A70-44310

Poisson kinematic equations solution of symmetric gyrost at in viscous medium for free rotor and constant angular speed, using perturbation technique 23 p4220 A70-44560

Partially ionized viscous plasma longitudinal wave propagation, formulating motion equations for electrons, ions and neutrals from Maxwell and Boltzmann equations 23 p4229 A70-44987

Particle motion in constant density dynamic viscosity random translational velocity field 24 p4324 A70-45139

Viscous conducting liquid forced vortex motion, considering radial velocity distribution and rotation effect on free surface shape 24 p4383 A70-45140

Oscillating viscous conducting fluid laminar flow between parallel nonconducting infinite porous flat plates under suction in transverse magnetic field 24 p4383 A70-45146

Incompressible viscous fluid two dimensional flow in absence of mass forces, considering Tollmien-Schlichting wave perturbation effect on flow stability 24 p4324 A70-45365

Sphere rotating in viscous fluid at rest, investigating surrounding flow field from creeping flow to turbulent boundary layer 24 p4326 A70-45989

Temperature profiles for viscous fluid contained between two concentric rotating porous cylinders 24 p4327 A70-46005

VISIBILITY

NT LOW VISIBILITY

K factor analysis of target visibility, considering target size contrast, background luminance, glare, atmospheric scattering and optical sight parameters 01 p0142 A70-10420

Atmospheric water vapor effect on contrast between natural target and sky via spectrophotometric method, exploring target visibility and contrast relations 02 p0325 A70-11873

Runway visibility measuring techniques, discussing RVR measurement limitations 02 p0336 A70-12226

Helicopter all-visibility operation realized by using main rotor blade as scanning radar antenna 05 p0793 A70-16040

Visibility, atmospheric light scattering coefficient and aerosol mass concentration related by integrating nephelometer measurements 07 p1328 A70-18923

Crew visibility requirements for rendezvous, docking and earth landing of reusable reentry vehicles [AIAA PAPER 70-262] 07 p1399 A70-20398

Preconditioning visibility dependence on aerosol particle swelling due to increasing humidity 08 p1539 A70-21921

Video role in air transport safety, describing runway visual range /RVR/ measurement using TV camera and spaced lights 10 p1889 A70-24507

Fog visibility improvement by optical range gating, increasing image contrast by background radiance reduction 11 p2064 A70-26719

Cloud cover statistical data applied to planning remote satellite-borne sensing missions, using Monte Carlo method 14 p2611 A70-31232

Fringe visibility and localization in double exposure holographic interferometry of diffusely reflecting flat objects 15 p2740 A70-32430

UHF radio telemetry for transmissometers measuring airport runway visibility 16 p2889 A70-34222

Runway visual range assessment using automatic transmissometer-reflector measurements 17 p3132 A70-34641

Object visibility limits when illuminated by laser beam with spatial selection method, discussing atmospheric conditions and light source radiation power 20 p3641 A70-39448

Aircraft navigation light visibility, discussing visual threshold, source intensity, atmospheric transmissivity, color, background luminance, etc 20 p3564 A70-39719

Auroral physics, discussing visibility, relations to geomagnetism and sunspots spectrum, morphology, optical emissions and particles in magnetosphere 20 p3623 A70-39929

VISIBLE RADIATION

U LIGHT [VISIBLE RADIATION]

VISIBLE SPECTRUM

U LIGHT [VISIBLE RADIATION]

U SPECTRA

VISION

NT BINOCULAR VISION

NT COLOR VISION

NT MONOCULAR VISION

NT NIGHT VISION

NT STEREOSCOPIC VISION

Modulation transfer function /MTF/ of eye-visual system as spatial frequency filter 07 p1216 A70-18870

Soviet collection of papers on physiology of vision under normal and extremal conditions 08 p1442 A70-20726

Human vision inertia and irradiation algorithm, satisfying Talbot law 18 p3217 A70-36082

VISIOPLASTICITY

U FLOW VISUALIZATION

U PLASTIC FLOW

VISUAL ACCOMMODATION

Readaptation times of eyes adapted to darkness using night vision training device in relation to helicopter flight safety conditions 03 p0436 A70-13823

Two loop control system model of human lens accommodation system derived on basis of muscle mechanics, optics and experiments 03 p0439 A70-14275

Ciliary nerve stimulation and lens motion data to identify open-loop plant dynamics of lens accommodation 07 p1216 A70-18858

Human eye accommodation system, discussing blur detection on retina 13 p2360 A70-29671

Cat lens motion in response to ciliary ganglion step and sinusoidal stimulation, indicating damped accommodative system 19 p3366 A70-38925

Hypoxia effects on aviators visual accommodation, convergence and stereoacuity, noting myopia increase with altitude 20 p3569 A70-38996

Jet pilot aging effects on physical functions based on medical examinations during six years, noting visual accommodation changes 22 p3978 A70-42878

VISUAL ACUITY

Superior recognition of right visual field of left eye with monocular viewing of letters as interaction of visual acuity and right superiority 02 p0239 A70-12623

Headache and personality traits related to visual acuity and brightness sensitivity increases from sea level to high altitude 04 p0633 A70-15444

Visually evoked cortical responses to checkerboard patterns, correlating amplitude to visual acuity 06 p0992 A70-17311

Human visual performance, discussing effects of object size and exposure time 07 p1204 A70-19050

Visual acuity performance during various vibration stresses found differentially degraded for near, intermediate and distant vision 07 p1223 A70-19939

Color vision forms, investigating sensitivity of human retinal receptors and combinations of spectral functions 08 p1443 A70-20731

Visual analyzer physiology under effects of gravitation, atmospheric pressure, mechanical vibrations, etc 08 p1444 A70-20740

Weightlessness effects on human vision, studying color perception, field of vision and light sensitivity 08 p1444 A70-20743

Visual tracking of horizontally moving object, noting acuity dependence on target angular velocity and observation time 08 p1444 A70-20745

Time requirement determined for visual acuity restoration after illumination with short duration bright light flash 08 p1450 A70-20746

Light sensitivity restoration in humans exposed to bright flashes, studying photonic afferent system braking effect on scotopic system 08 p1450 A70-20747

Critical flicker frequency dependence on viewing distance, stimulus angular size and luminance 09 p1618 A70-22671

Atmospheric limitations on remote sensors using visible sunlight, noting applications to Earth Resources Technology Satellite and human vision [AIAA PAPER 70-288] 09 p1718 A70-22893

Near visual acuity requirements in flight deck from examination of presbyopic pilots, discussing instrument panel visibility 09 p1628 A70-23469

Eye spherical, cylindrical and spherocylindrical refractive errors incidence at various visual acuity levels, tabulating standards 10 p1810 A70-24035

Color closed circuit TV visual cues in flight simulation during flare and touchdown, including ATA requirements and acuity limits [AIAA PAPER 70-347] 10 p1857 A70-24201

Reaction time in determining visual transient response at frequencies above flicker fusion 10 p1818 A70-24717

Visual acuity and light detection after preadaptation to red and orange lights, discussing photopic and scotopic vision 11 p1986 A70-25828

Real time 2000 line TV camera with 40 MHz bandwidth, 1600 line vertical resolution and 1000 line horizontal resolution [SMPT E PAPER 105-73] 12 p2235 A70-27663

Visual acuity determination by tape with staggered squares rotating behind screen with window 13 p2350 A70-29298

Low light level TV systems performance relationship to visual acuity requirements, considering interfering noise characteristics effect on target recognition 16 p2903 A70-33130

Human eye components as image forming system from model based on Gaussian optics, discussing pupil size and influences on visual acuity 23 p4144 A70-43818

Visual acuity during ocular tracking movements as function of field illumination density 23 p4147 A70-44777

VISUAL AIDS

Visual simulation limitations, discussing parallax error correction in display system, wraparound system, image generation, TV and motion picture film systems 01 p0036 A70-10813

Forward sounding sensors /weather radar/ development for aiding human eye in detecting flight hazards /storms and CAT/ 02 p0297 A70-11989

Visual spaceflight simulators for spacemen and aircraft pilot training 04 p0663 A70-14691

Visual display media requirements of future high performance vehicles, considering spacecraft and aircraft 08 p1499 A70-21691

Photometric cometary parameters from Van Biesbroeck data, using least squares method to compare naked eye, field glasses and small telescope observations 19 p3526 A70-38783

Visual simulation for controlling QF-9 drone aircraft landing, takeoff and BQM-34A target drone in-flight test operations 01 p0058 A70-10815

Radar visual indicator used with scan converter and as synthetic indicator with computer controlled flight safety system 02 p0263 A70-12700

Man-machine systems design emphasizing impedance matching exemplified by visual approach landing [ASME PAPER 69-WA/GT-15] 04 p0642 A70-14856

Aircraft visual flight control displays development, considering liquid crystals in alpha numeric data output devices and holograms for three dimensional structures reproduction 05 p0853 A70-17090

Visual simulation in Lunar Module Mission simulator provided by computer controlled infinity optics system 06 p1031 A70-18603

Visual binary state transistor tester for positive and negative logic circuits, illuminating lamp for specific logic states 21 p3801 A70-42244

VISUAL CUES

U CUES

U VISUAL PERCEPTION

VISUAL DISCRIMINATION

Visual detection discrepancies of temporal order suggested due to definition of interstimulus interval

01 p0039 A70-11165

Threshold visibility of uniformly moving colored gratings, noting chromaticity discrimination dependence on spatial and temporal frequencies

02 p0237 A70-12460

Visual half field central integration and monocular performance in split-brain monkeys after transection of chiasm, anterior commissure and corpus callosum

03 p0421 A70-13625

Color vision mechanisms spectral sensitivities measured by increment threshold technique for normal and deutan observers

03 p0427 A70-13947

Efferent model to test inhibitory influence of inferotemporal cortex lesions on visual discrimination of monkeys, using paired flashes of light

04 p0629 A70-14449

Cats trained for visual form discrimination tested for retention and reversal performance, studying oxygen deprivation influence

04 p0633 A70-15443

Distance discrimination experiment in reduced cue setting simulating outer space, confirming Weber power function exponent

04 p0645 A70-15647

Rhesus monkeys impaired discrimination in recognizing tachistoscopically presented objects following cortical polarization

05 p0802 A70-16625

Macaque monkey stereoscopic vision demonstrated behaviorally by combining random dot patterns with standard operant conditioning

07 p1205 A70-19277

Visual backward masking facilitation dependence on target duration as opposed to interstimulus interval or target-onset/mask-onset interval durations

07 p1221 A70-19850

Inhibitive stimulus control related to behavioral contrast during discriminative training

08 p1441 A70-20476

Critical discreteness interval of visual analyzer, investigating dependence on stimulus location, flare brightness and adaptation

08 p1443 A70-20734

Automatic change discrimination applications to weather prediction, land resource management and city planning, using photographic, IR and radar sensor imagery

09 p1677 A70-22876

Visual restriction effects on critical flicker fusion threshold, loudness and pitch discrimination determined using reticular activating system

09 p1622 A70-23576

Differential luminance sensitivity of human eye using signal detection theory, correlating discrimination and detection results with electrophysiological data

10 p1812 A70-24599

Plant leaves discrimination by multispectral reflectance indicated in transmittance measurements via remote sensing from aircraft and spacecraft

12 p2218 A70-26920

Book on automatic recognition of visual patterns and mechanization of creativity, presenting computer program termed Arithmetic

13 p2373 A70-29451

Neurophysiological framework for binocular single vision and depth discrimination, concerning construction of horopter for cat

14 p2539 A70-31348

Binocular disparity detectors in human visual response to moving gratings confirmed by electrophysiological evidence

17 p3025 A70-35150

Object identification and form of multidimensional discrimination space, using locus stimulus model

19 p3361 A70-38051

Eye movements during visual search and meaningless pattern discrimination

19 p3361 A70-38054

Retinal image tracking movement effect on discrimination perceptibility of orifice orientations of Landolt ring

23 p4147 A70-44778

VISUAL DISPLAYS

U DISPLAY DEVICES

VISUAL FIELDS

Perceived size relation to retinal size under reduced observation conditions compared with size-distance invariance hypothesis for binocular and monocular observations

01 p0025 A70-11051

Visual stimuli duration effect on saccades precision and reaction time in peripheral field in normal subjects

01 p0026 A70-11055

Receptive fields in visual systems, discussing characteristics, size, geometry, adaptation effects, sensory interactions, etc

02 p0236 A70-12304

Superior recognition of right visual field of left eye with monocular viewing of letters as interaction of visual acuity and right superiority

02 p0239 A70-12623

Visual half field central integration and monocular performance in split-brain monkeys after transection of chiasm, anterior commissure and corpus callosum

03 p0421 A70-13625

Correction factors required for estimating influence of pupil area reduction on retinal illumination at oblique angles

05 p0801 A70-16449

Error correction for correlation coefficient between satellite data of earth radiation intensity and satellite vision field shift

05 p0841 A70-16729

Ground terrain blurring during aircraft flight at low altitude and high speed, calculating theoretical blur zone

07 p1220 A70-19285

Temporary or permanent visual field injury in test parachutists compared to control group

07 p1223 A70-19943

Invariant recognition of visual patterns in translational conversions, describing patterns by differential method

09 p1641 A70-22824

TV camera with diffraction limited pinhole lens for visual simulation, solving depth of field and extending field of view without distortion

10 p1887 A70-24217

Functional visual field selective process, studying performance as function of display angle

10 p1827 A70-24769

Neuron processing of retinal activity in estimating distances and sizes of objects in field of vision

12 p2172 A70-28312

Statistical estimation of resolvability of incoherently radiating object sampled at aperture field of observing optical instrument, using Cramer-Rao inequality

13 p2453 A70-29823

Brightness matching and sensitivity to sinusoidal flicker for various contrasts as function of surround field luminance

15 p2683 A70-32016

Hypoxia and acetazolamide effects on color sensitivity zones in visual field

15 p2684 A70-32533

Runway visual range assessment using automatic transmissometer-reflector measurements

17 p3132 A70-34641

Brightness field spatial structure of solar radiation reflected from earth by Cosmos 149 satellite, discussing homogeneity and isotropy

18 p3247 A70-36629

Unsteady light field spatial moments in turbid medium boundary layer with intense anisotropic scattering during illumination by narrow beam

18 p3285 A70-36631

Prismatic adaptation under scotopic and photopic conditions in subjects, using transfer experiments

19 p3361 A70-38052

Diffraction effects on radiometer field of view with rectangular primary and secondary apertures and field stop

20 p3627 A70-39087

Imaginary axes effect of phenomenal space in contrast illusions of distance, discussing division of S field of vision by definite point fixation

20 p3573 A70-39764

Spatial summation of retinal neurons receptive field centers excitation from single optic tract fibers action potential in light-adapted cats

22 p3971 A70-43403

Spatial aspects of sensitization effect properties compared to background light fields, lowering rod threshold at center by light addition to surrounding annular region

23 p4147 A70-44779

VISUAL FLIGHT

USAF visual flight simulation devices from engineering and psychological standpoints, discussing human factors considerations

01 p0057 A70-10808

Flying spot scanner design and performance to generate images for visual flight simulation

01 p0089 A70-10816

Visual aspects of collision avoidance, describing prudent mid-air maneuvers

08 p1449 A70-20481

Visual aircraft-to-aircraft detection effectiveness in collision avoidance as function of pilot performance and closing speed

12 p2267 A70-27633

Ground simulations data of jet lift V/STOL compared with visual flight results, noting hover, lateral quick start and stop maneuver

18 p3236 A70-35954

Visual air-to-ground target recognition simulation, comparing predictions from Autonetics Detection Model in low altitude flight

24 p4308 A70-45507

VISUAL FLIGHT RULES

Midair collision frequency under VFR as function of aircraft density derived, noting ATC role in safe separation

12 p2267 A70-27636

VISUAL OBSERVATION

Right ascension screw error effects on observations of stellar image passage through meridian, evaluating effect

01 p0181 A70-10662

Visual observations of bright comets, deriving photometric parameters from comet head total magnitude

01 p0184 A70-10953

Voluntary control over velocity of smooth pursuits, discussing saccadic and saccade free modes and switching during tracking

01 p0026 A70-11056

Air density variations calculated by visual satellite observations processing, comparing results of IN-TEROBS and average anomalies methods

02 p0288 A70-11766

Martian dark area extending from Tritonius Sinus to Casius southern tip, comparing observations and charts

02 p0370 A70-12086

Vigilance of human monitors detecting additions and deletions of relevant and irrelevant signals presented on computer matrix display

02 p0246 A70-12377

Horizontal-vertical illusion and foreshortening of receding horizontal lines during visual observations

02 p0249 A70-12839

Human eye image accumulation effect and meteor brightness estimation dependence on angular velocity based on visual and telescopic observations

03 p0569 A70-13358

Three dimensional display of human body surface potential distributions as diagnostic tool of cardiac abnormalities

04 p0641 A70-14557

Visual interpretation of moon and Mars surface photographs taken from satellites, analyzing craters and bumps

04 p0686 A70-14626

Frequency distribution of apparent visual magnitudes of meteors observed from November 1960 to January 1967

04 p0750 A70-14707

Visual vertical related to head tilts, observing location of gravitational vertical

04 p0645 A70-15445

Helmholtz proprioceptive theory of apparent visual direction for predicting displacement of egocentric straight ahead as aftereffect of eyes deviation from normal position

05 p0801 A70-16142

Rotation, diameter, mass, atmosphere and constitution of planet Neptune, with emphasis on visual observations

05 p0913 A70-16552

Monograph on probability of aircraft detection by ground visual observation using mathematical model based on Poisson process, considering laws of ocular physiology

05 p0794 A70-16558

Meridian circle observations before and after occultation of ZC 2232 by Neptune on 7 April 1968, correcting ephemeris for star and Neptune

06 p1151 A70-18489

Physical identity and name sameness matchings efficiency noting role of interpolated activity

07 p1203 A70-18942

Meteorite fireball track projected on earth surface determined from nearly overhead observations

07 p1387 A70-19629

Space rendezvous navigation and guidance based on optical sightings with hand-held sextant entered into and processed by small digital computer

07 p1331 A70-20061

Propagation pattern of surface acoustic wave visualized in piezoelectric and nonpiezoelectric materials by dusting delay line with fine particles

07 p1336 A70-20283

Nova Delphini 1967 brightness visual evaluations by amateurs, discussing effect of personal factors and instruments on accuracy

08 p1568 A70-20634

Binocular achromatic and color thresholds of constant and flickering lights determined from background of different brightness

08 p1443 A70-20732

Sco X-1 simultaneous X ray and optical flares correlation and X ray enhancements

08 p1561 A70-20900

Meteor abundance determination by visual observation, calculating sighting probabilities for various magnitudes

08 p1573 A70-20949

Visual recordings of cardiac rhythm obtained from flashes of miniature indicator tube, describing circuit filter function

08 p1452 A70-21439

Minor meteor showers radiants determined close to ecliptic plane from systematic visual observations during November, December and January 1961-67

08 p1577 A70-21532

Saturn globe, rings and satellites observations /1968-1969/

09 p1751 A70-22198

Composite window permitting visual or photographic observation and IR irradiation of test materials in ultrahigh vacuum system

09 p1698 A70-22994

NASA operation of Convair 990 jet transport as airborne scientific research platform for optical observations

09 p1682 A70-23504

Duplex schlieren optical system with one channel for data recording and second channel for visual monitoring

09 p1687 A70-23766

Observation noise model for human controller remnant

10 p1823 A70-23893

Human operator remnant data normalization noting observation noise spectral characteristics for compensatory tracking

10 p1824 A70-23899

Granularity spectrum of diffusing screen uniformly illuminated by normally incident coherent light, basing study on long and short distance visual observations

10 p1899 A70-24031

Visual observations of Molniya satellite during low perigee, determining air density

10 p1875 A70-24443

Human eye image accumulation effect and meteor brightness estimation dependence on angular velocity based on visual and telescopic observations

11 p2118 A70-26723

Small meteor streams trajectories and radiants from epsilon-Lyrids, alpha-Coronids and phi-Draconids observations by amateur astronomers

12 p2311 A70-28307

Meteors position angles determination during telescopic observations, discussing error due to angle reversion

13 p2491 A70-29043

Universal triaxial instrument with AT-1 telescope for visual observation of satellites, discussing applications and accuracy

13 p2408 A70-29274

Twilight sky color visual estimation from Soyuz 5 spacecraft noting cloudiness effects

15 p2723 A70-31597

Microscopic data importance in recognizing IC semiconductor failure characteristic traits, revealing current direction, voltage magnitude, microsurface temperature excursion and approximate transient duration

15 p2693 A70-32664

Meteor abundance determination by visual observation, calculating sighting probabilities for various magnitudes

15 p2806 A70-32761

Mars visual observations with colored glass filters during opposition, noting southern polar cap shape irregularity and Martian atmospheric transmittance

16 p2974 A70-33658

Optical search for CP 0328 and CP 0950 by photoelectric multichannel signal averaging

17 p3160 A70-34536

Stellar UV and visual continuum observations, discussing recalibration of absolute energy distribution of alpha Lyr to improve model atmospheres

17 p3160 A70-34881

1620 Geographos observations using Ritchey-Chretien reflector and Curtis Schmidt telescope

17 p3171 A70-35446

Soviet book on declination observation of bright and faint stars in one system

18 p3314 A70-36402

Planetary surface smoothness factor by disk brightness, Mars red light and phase curves methods, indicating superiority of visual observation

18 p3315 A70-36602

Relative effectiveness of radar and visual cloud observations

18 p3287 A70-36999

Comet Bennett 1969 visual observations in Southern Hemisphere, using photometer ocular

18 p3319 A70-37049

Auroral photographic and visual observations, discussing satellite results and subsystem development

19 p3417 A70-38730

Photometric cometary parameters from Van Biesbroeck data, using least squares method to compare naked eye, field glasses and small telescope observations

19 p3526 A70-38783

Artificial satellite position visual estimates based on geometric relationship to reference stars pair accuracy

19 p3531 A70-38946

Optical pulsar search instrument in radio pulsar fields, showing performance on NP 0532

21 p3826 A70-41156

Semiconductor platelet laser stimulated emission visual observation in unwanted reflected modes

21 p3838 A70-42022

VISUAL PERCEPTION

NT CRITICAL FLICKER FUSION

NT SPACE PERCEPTION

NT VISUAL DISCRIMINATION

Human size-selective neurons indicated by aftereffect from successive viewing of striped patterns with different spatial frequencies

01 p0035 A70-10724

Visual fatigue symptoms, causes, relation to general fatigue and psychological aspects, discussing testing for sensory and visual fatigue

01 p0022 A70-10857

Background luminance effect on flash brightness in eyes, measuring increment threshold and luminances required for various brightnesses

01 p0025 A70-11052

Ultrasonic image superposition technique for visualization of impact fractures in glass reinforced plastics

01 p0059 A70-11101

Target-field luminance or duration effect on target susceptibility to masking demonstrated in visual backward masking study

01 p0039 A70-11163

Line length effects on sequential blanking in visual perception demonstrated by computer-based CRT display and interpreted with information processing model

01 p0039 A70-11164

Human and cat visual neuron properties, discussing encoding orientation and dimensions of retinal images

01 p0028 A70-11360

Mathematical model formulated in terms of feedback controller for simulation of horizontal eye movement for positioning upon objects of interest

02 p0243 A70-12098

Receptive fields in visual systems, discussing characteristics, size, geometry, adaptation effects, sensory interactions, etc

02 p0236 A70-12304

Human eye integration of short monochromatic light flashes at TV frame frequencies

02 p0238 A70-12463

Scaling and refractoriness effect in neutral-pulse train transmission on eye incremental sensitivity, discussing applicability as intraretinal mechanism concept

02 p0247 A70-12466

Long term memory effects in visual perception of apparent movement, discussing experience prior to tests

02 p0239 A70-12622

Superior recognition of right visual field of left eye with monocular viewing of letters as interaction of visual acuity and right superiority

02 p0239 A70-12623

Horizontal-vertical illusion and foreshortening of receding horizontal lines during visual observations

02 p0249 A70-12839

Motion sickness causes and prevention during prolonged space flights, discussing vestibular system and characteristics of visual-inertial and canal-otoolith incongruities

03 p0421 A70-13542

Relative slant judgments elicited by paired comparison methods from subjects viewing computer generated slides representing rotated regular dot patterns

03 p0435 A70-13769

Lines and letters identification and localization relationships to stimulus attributes in visual perception supporting hierarchical processing hypothesis

03 p0425 A70-13825

Informative filter automatic selection for describing visual object with aid of frequency spectrum, taking filter output voltage mean square value as criterion

04 p0662 A70-15438

Cortical cells fatigue and performance in subjects doing mental work, using motion picture signal perception method

04 p0639 A70-15509

Helmholtz proprioceptive theory of apparent visual direction for predicting displacement of egocentric straight ahead as aftereffect of eyes deviation from normal position

05 p0801 A70-16142

Acceleration cues removal effects on vehicular velocity perception, using movie technique to control visual cues

05 p0806 A70-16143

Head movement effect on accuracy of visual and kinesthetic localization for free and fixed head conditions

05 p0803 A70-16669

Illusions of rotation perception with oscillating trapezoid and oscillation perception with rotating trapezoid, correlating magnitudes

05 p0807 A70-16673

Subjects sensitivity to differences in statistical distributions of locally defined element density and shape, using stochastically textured visual patterns

06 p0998 A70-17223

Observed objects physical properties influence on boundary conditions of visibility perception by human eye

06 p0994 A70-17631

Neurophysiological vertical and horizontal visual coordinates localization in man

06 p0998 A70-18484

Methodologies inadequacies for studying information processing rate in visual perception

07 p1203 A70-18943

Human visual performance, discussing effects of object size and exposure time

07 p1204 A70-19050

Visual threshold elevation for test flash perception determined by retinal image displacement in saccadic fashion

07 p1205 A70-19283

Evoked potential /EP/ correlate of binocular depth perception in man, discussing responses to horizontal and vertical changes in retinal disparity

07 p1205 A70-19284

Ground terrain blurring during aircraft flight at low altitude and high speed, calculating theoretical blur zone

07 p1220 A70-19285

Spacecraft cabins illumination conditions selection based on cosmonaut visual perception of luminous objects

07 p1221 A70-19515

Visual perception of black-and-white photo in aerial photographic interpretation, examining processes in human brain

07 p1221 A70-19777

Visual acuity performance during various vibration stresses found differentially degraded for near, intermediate and distant vision

07 p1223 A70-19939

Optical suitability to pilot visual requirements in head-up displays, discussing telecentric viewed system permitting binocular disparity tests

08 p1449 A70-20675

Human color vision simulation by mathematical and electronic analogs for photoelectric color measurement and eye resolution

08 p1450 A70-20727

Psychophysiological regularities of nonlinear human color vision model, analyzing sensitivity curves, achromatic tints and hyperbolic position in perception space

08 p1443 A70-20728

Microinterval analysis of phased development of human visual color perception in presence of short stimuli

08 p1443 A70-20733

Reduced visual perception time in patients under X ray treatment of diencephalo-hypophyseal region

08 p1443 A70-20736

Human eye sensitization and dark adaptation, noting annular surrounding light addition effect on rod threshold

08 p1447 A70-21723

Moon illusion on basis of perceived size relativity, discussing dependence on objective characteristics of visual field

09 p1752 A70-22248

Critical flicker frequency dependence on viewing distance, stimulus angular size and luminance

09 p1618 A70-22671

Flashtube photostimulators for examining human physiological response, discussing design and calibration

09 p1624 A70-22673

Solar simulation /SISS/ for evaluating human visual system performance in contrasting space environment

09 p1655 A70-22680

Bragg diffraction imaging for sound fields visualization

10 p1893 A70-24170

Visual threshold effect on closed loop control of aircraft of poor resolution studied by flight simulation of approach and flare, showing degraded control accuracy

[AIAA PAPER 70-357]

Prolonged hypodysmetria effects on visual analysis, investigating functional weakening, fundus oculi appearance change and restoration after normal activity resumption

10 p1816 A70-24687

Pattern recognition model simulating human physiology based on two dimensional Fourier transform of input images

10 p1827 A70-24770

Perceptual tuning in tachistoscopic identification task with alternatives provided after or before and after stimulus

11 p1986 A70-25829

Spacecraft cabins illumination conditions selection based on cosmonaut visual perception of luminous objects

11 p1991 A70-26114

- Human detection capability for objects on electro-optical imaging displays calculated as function of SNR, viewing distances and brightness levels
12 p2236 A70-27903
- Book on visual perception space covering biological optics, eye model, monocular vision, etc
14 p2539 A70-31349
- Eye movements effects on apparent/beta/ movement perception tested by display with ambiguous illusory movement
15 p2683 A70-32454
- Psychophysical adjustment methods effect on visual vertical orientation during head tilt
15 p2683 A70-32455
- Eye movements direction during perceptual errors related to stimulus location
15 p2683 A70-32456
- Low visibility aircraft landing problem concerning pilot instrument and visual cue and federal regulations governing operational approval
[AIAA PAPER 70-936]
17 p3134 A70-35845
- Visual contrast sensitivity adaptation to temporal frequencies using high modulation sinusoidal grating
17 p3034 A70-35898
- Optokinetic and vestibular effects on human operator reliability in aircraft control systems
18 p3223 A70-36184
- Equidistance effects on human size and distance perception in visual alley
19 p3368 A70-37771
- Geometrical figure fragmentation produced by intermittent illumination, examining dependence on presentation frequency and temporal factors
20 p3580 A70-39491
- Line tilting aftereffects on central and peripheral vision following spatial coincidence of inspection and test contours
21 p3767 A70-40752
- Model for human brain visual information processing networks, considering visual search, selection, storage, correlation, recognition and recall functions
22 p3977 A70-42287
- Color attributes by subjective estimation of surface colors, discussing correlation with other methods
22 p3972 A70-43409
- Central fovea dichromacy tests, using color naming technique
22 p3972 A70-43410
- Orientation detectors in human visual cortex, suggesting mutual lateral inhibition
23 p4144 A70-43813
- Perceptual suppression of retinal emissive afterimages by rapid eye movements
23 p4147 A70-44780
- Time dependent visual perception probability under prolonged testing at eccentricities, using observer exposed to flashed stimulus with dark-adapted retina
23 p4147 A70-44782
- Light effect on cis-trans-isomerization of cinnamoyl-alpha-chymotrypsin, considering molecular modeling of visual reception
24 p4298 A70-45496
- Bilateral oligosynaptic interaction between posterior lateral thalamic nucleus and afferent systems in visual and acoustic cortical areas in cats
24 p4300 A70-45840
- VISUAL PHOTOMETRY**
- Satellite rotation periods determination accuracy from photometric observation data improved by determining initial and terminal moments of maximum brightness
02 p0255 A70-11769
- Photometric results on beta Lyrae from various observatories during 1959 international campaign with data reduced to BV system, showing reddening at primary eclipse
02 p0369 A70-12064
- Visual photometric tracking data obtained in SPIN program for satellites 1965-II-4 and 1965-53-6 at Kishinev station
03 p0444 A70-13181
- Neutral Ne emission line in visible solar spectrum during bright events in inner corona, noting 1958 outburst of RS Oph
05 p0920 A70-16944
- Visual and quantitative image definition, evaluating microdetail clarity in panchromatic, IR, color and color IR aerial photographs
07 p1281 A70-19369
- Fourth Saturn ring detection equipment and procedures, discussing negatives revealing small weak zones near globe equatorial east and west edges
08 p1567 A70-20600
- Spectral classification and continuous spectrum photometry of weak late stars in visual and near UV regions, noting anomalous C star in CH Cyg
15 p2797 A70-31615
- Photometric reduction of meteor luminosity to photovisual/international/ system
19 p3515 A70-37662
- VISUAL SIGNALS**
- Digital log-linear companding technique for nonuniform quantization of speech and image signals
01 p0044 A70-10784
- Reactions to visual emergency signals in humans after administering adrenalin, aminazin, melipramine or andaxine to change control systems functional state of cerebrum
01 p0030 A70-11467
- Subjects trained in visual monitoring task with autoinstructional device, showing higher signal detection rate than group trained by practice alone
02 p0247 A70-12380
- Signal detection theory analysis indicating within-session changes in human willingness to respond in visual monitoring task, considering optimal decision behavior
03 p0435 A70-13766
- Auditory and visual ready signal intensity effects on reaction time, considering roles of practice and individual differences
03 p0436 A70-13772
- Missile impact location visual identification by marker system using pyrotechnic aboard to produce dense white smoke detectable to unaided eye, including flight test
03 p0582 A70-14104
- Light signals amplification efficiency, considering double-pass regenerative amplifier
04 p0702 A70-15225
- Optical, digital and hybrid image processing techniques with objectives of image enhancement and replacement
05 p0847 A70-16121
- Human macrosaccadic eye movements related to four dial display conditioned by concurrent variable interval schedules of signals
05 p0800 A70-16127
- Electrocorticograms frequency spectra from different visual cortex layers of rabbits during exposure to rhythmic light pulses
07 p1198 A70-18698
- Illusory visual signals experienced by pilots ascribed to aerodynamic forces interference with normal functional relationships between sensory systems
09 p1627 A70-23131
- Human reactions to successive visual signals, studying response time in single and grouped reaction
10 p1826 A70-24720
- Reference systems for two dimensional visual indications as correction device for pilot guidance errors associated with rotation effects
12 p2177 A70-27036
- Blinking warning lights for air navigation, signaling of obstacles and glider onboard marker lights
16 p2889 A70-34302
- Lighting and background effects on human binocular color vision of signal lights in industry
19 p3366 A70-38923
- VISUAL STIMULI**
- Selective visual stimulus control by part of compound S delta in pigeons
01 p0021 A70-10796
- Visual stimuli duration effect on saccades precision and reaction time in peripheral field in normal subjects
01 p0026 A70-11055
- Visual detection discrepancies of temporal order suggested due to definition of interstimulus interval
01 p0039 A70-11165
- Rabbits and cats cortical neurons responses to light and acoustic signals, using microelectrodes inserted at different depths into cortex
01 p0030 A70-11469
- Propagation velocity relation with time delay in human visual system, using various sets of line stimuli having different spatial distance
02 p0237 A70-12457
- Critical duration for pupillary light reflexes measured with IR scanning pupillometer using various flash duration stimuli
02 p0237 A70-12458
- Long term memory effects in visual perception of apparent movement, discussing experience prior to tests
02 p0239 A70-12622
- Human perceptual and response biases in choice reaction time tasks involving visual and auditory stimuli
02 p0239 A70-12624
- Human oculogyral illusion thresholds determined on Ames Man-Carrying Rotation Device to establish stimulus duration effect on angular acceleration thresholds
03 p0424 A70-13765
- Relative slant judgments elicited by paired comparison methods from subjects viewing computer generated slides representing rotated regular dot patterns
03 p0435 A70-13769
- Lines and letters identification and localization relationships to stimulus attributes in visual perception supporting hierarchical processing hypothesis
03 p0425 A70-13825
- Controllable light source for experiments on human pupillary servomechanism
04 p0642 A70-14633
- Visual, motion and auditory stimuli role in enhancing aircraft pilot training simulators realism, considering motion perception research
[ASME PAPER 69-WA/BHF-9]
04 p0642 A70-14853
- Image memory in Papio hamadryas monkeys reacting to visual and flavor food stimuli
04 p0632 A70-15219
- Pigeon response to concurrent variable interval reinforcement schedules, investigating relative and changeover rates regarding key color
05 p0800 A70-16126
- Amphetamine effects on observing and monitoring performance in squirrel monkeys, investigating lever and key responses using food reinforcements
05 p0806 A70-16128
- Visually evoked cortical responses to checkerboard patterns, correlating amplitude to visual acuity
06 p0992 A70-17311
- Rabbits sensorimotor and visual cortical responses during defensive conditioning to rhythmic light
07 p1197 A70-18695
- Electrocorticograms frequency spectra from different visual cortex layers of rabbits during exposure to rhythmic light pulses
07 p1198 A70-18698
- Cats visual analyzer functional rearrangement mechanisms under prolonged light stimulation, considering evoked potential dependence on pulse duration and intensity
07 p1198 A70-18699
- Rabbits visual cortex evoked potential changes due to light flashes under different conditions
07 p1198 A70-18716
- Electrical recording of retinal and occipital potentials in response to stimulation of human visual system used at levels from receptor to striate cortex
07 p1220 A70-19364
- Guinea pigs visual analyzer during stimulations by diffuse light, nonspecific thalamic nuclei and microelectrodes polarization, determining A- neuron activity
07 p1213 A70-19788
- Binocular fusion and rivalry effects on cortically evoked human potential, obtaining pattern characteristic responses to monocular stimulation
07 p1215 A70-20214
- Inhibitive stimulus control related to behavioral contrast during discriminative training
08 p1441 A70-20476
- Operator analysis of electroretinograms, investigating eye reaction dependence on stimulation using amplitude-phase-frequency characteristics
08 p1450 A70-20730
- Microinterval analysis of phased development of human visual color perception in presence of short stimuli
08 p1443 A70-20733
- Critical discreteness interval of visual analyzer, investigating dependence on stimulus location, flare brightness and adaptation
08 p1443 A70-20734
- Direct anatomical couplings between retina and hypothalamus via centripetal and centrifugal fibers by investigating light evoked potentials in rabbits brains
08 p1444 A70-20737
- Photoconductivity detected in pigmented epithelium of eye during illumination by visible light
08 p1444 A70-20738
- Time requirement determined for visual acuity restoration after illumination with short duration bright light flash
08 p1450 A70-20746
- Light sensitivity restoration in humans exposed to bright flashes, studying photonic afferent system braking effect on scotopic system
08 p1450 A70-20747
- Constant periods method to eliminate human responses during threshold measurements by holding first threshold perception flash fixed
08 p1445 A70-20750
- Modal excitation and scattering in retinal receptors of human and insect visual systems investigated with dielectric rod uniform wave and irregularities
08 p1452 A70-21289
- Bioelectrical activity of brain during conditioned motor reflex system operation modes in response to stimulating light pulses
08 p1447 A70-21450
- Horizontal disparity and ratio of perceived egocentric distance related in stereoscopic vision during investigation of three point light sources problem
08 p1447 A70-21725
- Monocular and interocular threshold luminance changes during flicker stimulation, noting interflash duration effects
08 p1453 A70-21792
- Ego strength relationship to respiration in response to sound and light stimulation tested in subjects balanced for alertness-drowsiness by EEG criteria
09 p1616 A70-22331
- Critical flicker frequency dependence on viewing distance, stimulus angular size and luminance
09 p1618 A70-22671

Movement information from spatio-temporal integration in binocular-kinetic space perception of time varying optical inputs

09 p1618 A70-22672

Visually evoked cortical potentials /VECP/ to different probe stimuli to suppressed human eye in binocular rivalry experiments, discussing eye dominance problems

09 p1618 A70-22674

Different retinal regions simultaneous stimulation, describing evoked potentials measurement method

10 p1811 A70-24227

Information hypothesis and repetition hypothesis concerning human reaction time to visual stimulus information

10 p1826 A70-24714

Numerical payoff influence on reaction time to second stimulus in subjects receiving successive signals at short intervals

10 p1818 A70-24715

Auditory and visual warning signals effects as reaction stimulus in time-uncertainty situation

10 p1826 A70-24719

Visual stimuli intensity influence on delay in reaction to second of pair of visual stimuli

10 p1818 A70-24721

Response times in deciding same or different between successive visual stimuli

10 p1826 A70-24722

Psychophysical metric for space perception visual cues measurement, describing applications to distance discrimination

10 p1827 A70-24768

Pilots with high vestibular stability studied for spatial orientation, noting activity impairment due to alternating angular acceleration and optokinetic stimuli

10 p1828 A70-25180

Perceptual tuning in tachistoscopic identification task with alternatives provided after or before and after stimulus

11 p1986 A70-25829

Choice reaction time task involving right or left hand button pressing in monocular and binocular visual response to directional commands by colored lights

11 p1990 A70-25830

Size effects on velocity threshold for real movement during narrow stimulus object length increase

11 p1989 A70-26662

Stimuli eliciting vergence eye movements and stereopsis, discussing retinal disparity locations and limits due to form, spatial position, luminance, contrast and onset

12 p2171 A70-28034

Psychophysical and evoked potential correlates of changes in stimulus color and intensity compared with minimum subjective flicker conditions

12 p2171 A70-28035

Electrical activity of visual cortex, subcortical structures and reticular formations in cats during conditioned reflex stimulation by light

12 p2173 A70-28351

Dynamic interaction between stored and active memory images in apes and monkeys with conditioned alimentary motor reflexes stimulated by visual signals

12 p2173 A70-28352

Sensory afterdischarge of human brain under light stimuli during sleep and wakefulness

12 p2173 A70-28354

Neuron activity of cortical motor and visual regions and corpus geniculatum laterale in cats during diffuse thalamic electrostimulation combined with light signals

12 p2173 A70-28355

Human operator ocular tracking and decay time stimulation response measurements using information, statistical, point process and random analysis

14 p2537 A70-30388

Sensory function in multimodal signal detection forced choice experiment involving auditory, visual and auditory-visual stimuli

14 p2539 A70-31167

Disadapting photostimulation effect on light sensitivity restoration of human visual analyzer, obtaining dark adaptation curves

15 p2679 A70-31603

Eye movements direction during perceptual errors related to stimulus location

15 p2683 A70-32456

Binocular disparity detectors in human visual response to moving gratings confirmed by electrophysiological evidence

17 p3025 A70-35150

Psychophysiological tests involving programmed memory device evaluating human memorization process and sensorimotor reactions to light signals

17 p3040 A70-35676

Scotopic responses conditions, using stimulus alternation method to elicit electroretinogram

17 p3034 A70-35897

Visual cortical anomalous response to paired photic stimulus in rabbits with ablations in rostral part of brain stem

18 p3221 A70-37214

Visual attention and temporal cortex stimulation effects on evoked electrical activity in monkey brain

19 p3360 A70-37812

Human spatio-temporal visual evoked response characteristics, showing potential gradient rotation in same period as input stimulus

19 p3360 A70-37845

Human brain LF activity in visual evoked response, determining relationship to stimulation

19 p3360 A70-37846

Object identification and form of multidimensional discrimination space, using locus stimulus model

19 p3361 A70-38051

Human response time to visual stimulus preceding or following auditory stimulus as function of interstimulus interval

19 p3362 A70-38311

Visual sensory storage item selection efficiency

19 p3363 A70-38321

Cat lens motion in response to ciliary ganglion step and sinusoidal stimulation, indicating damped accommodative system

19 p3366 A70-38925

Retinal images smearing during voluntary saccadic eye movements, obtaining thresholds for horizontal and vertical stimuli bands

19 p3366 A70-38927

Visual suppression linear dependence on angular size of voluntary saccadic eye movements, observing percentage of trials for stimulus perception

19 p3367 A70-38928

Temporal and spatial distribution of visual suppression during voluntary saccadic eye movement on different places of retina

19 p3367 A70-38929

Unitary and compound stimuli and role of response categories in decision time

21 p3767 A70-40751

Step and ramp input functions and pursuit and compensatory display modes effects on tracking performance

21 p3767 A70-40753

Moving stripe stimulus inducing optokinetic turning movements in goldfish, discussing efferent influence on vestibular organ

21 p3762 A70-41141

Spatial summation of retinal neurons receptive field centers excitation from single optic tract fibers action potential in light-adapted cats

22 p3971 A70-43403

Visually evoked responses in man to different light stimuli intensities, noting marked increase in binocular over monocular visual response

22 p3972 A70-43408

Foveal threshold measurements, using small flash of light at center of bright white disk on black background

22 p3972 A70-43411

Spectral sensitivity of freely moving human eye by determining threshold energy for correct choice between two monochromatically illuminated stimulus patches

22 p3972 A70-43412

Light flashes observed by Apollo astronauts, proposing Cerenkov radiation or direct excitation of eye retina by cosmic rays

24 p4307 A70-45403

Nervous inhibition effect on electroretinogram b wave during flash sequences

24 p4301 A70-45986

Hypoxia effects on voluntary response time to peripherally located visual stimuli

24 p4302 A70-46107

VISUAL TASKS

K factor analysis of target visibility, considering target size contrast, background luminance, glare, atmospheric scattering and optical sight parameters

01 p0142 A70-10420

Visual attention testing, considering perception focusing on stimulus object and eyelid blinking recording, measuring eye distance to work plane

01 p0023 A70-10861

Visual faculties testing to improve performances in visual inspection tasks, considering threshold line concept and visual performance relation to age

01 p0023 A70-10862

Intermittent vs continuous noise effects on signal detection measures during audio visual checking task performance

01 p0039 A70-11167

Subjects trained in visual monitoring task with autoinstructional device, showing higher signal detection rate than group trained by practice alone

02 p0247 A70-12380

Signal detection theory analysis indicating within-session changes in human willingness to respond in visual monitoring task, considering optimal decision behavior

03 p0435 A70-13766

Monitoring behavior in three source visual task, studying selective attention by response observation method

03 p0435 A70-13770

Eye movements during two dimensional tracking tasks, showing oculomotor system transfer characteristics function of target motion spectral content

03 p0427 A70-13948

Visual prediction accuracy in estimating point coincidence of two moving targets as function of viewing opportunity and length of period

03 p0428 A70-14084

Vigilance time degradation, studying effects of breathing gas mixtures with varying oxygen and carbon dioxide content

06 p1000 A70-17293

Astronauts visual performance during space flight, studying reduction of visual disturbances from various physiological flight factors

08 p1444 A70-20741

Nonlinearity of human eye movement control system in two dimensional tracking tasks, explaining visual axis lags as time delays dependent on target motion

08 p1447 A70-21724

Visual search activity decrease observed as function of time-on-task for skilled and unskilled helicopter pilots, recording eye movements and blinks

09 p1628 A70-23463

Target velocity and approach angle effects on accuracy of moving targets intersection estimation tested on human subjects

09 p1628 A70-23578

Human reactions to successive visual signals, studying response time in single and grouped reaction

10 p1826 A70-24720

Two dimensional eye position control in dark over prolonged periods, noting role of conjunctiva cues, drifts and saccades

12 p2171 A70-28037

Man machine eye-integration coupling in tracking task applied to helicopters, ocean-going craft and propeller aircraft

13 p2357 A70-28386

Military pilots visual estimation of point location coordinates within rectangular area

13 p2357 A70-29121

Perceptual displacement of hashmark between unequal squares, discussing contour repulsion and perspective interpretation

14 p2537 A70-30899

Sequential event tracking dependence on stimulus rate and simultaneously displayed information categories

14 p2538 A70-30900

Visual and auditory reactions in dogs to alimentary stimuli before and after partial removal of cerebellum, noting complete recovery within month

15 p2687 A70-32892

Human and machine pattern discrimination correlated by statistical correlation method from pattern recognition task involving computer simulation and humans

16 p2852 A70-33461

Feedback analysis of learning and performance in hand-yoked, steering and stimulus tracking control of breath-produced visual target

16 p2852 A70-33660

Heat stress effects on serial reaction time in subjects performing visual tasks

19 p3361 A70-38053

Component decision logical and temporal arrangement in visual search, defining target by several attribute value combination

19 p3362 A70-38314

Brightness contrast by human observer binocular matching, discussing neural networks models

19 p3366 A70-38924

Visual vigilance task with standard, binary or rating procedures as response indicators based on signal detection theory, noting relationship to psychophysical procedures

21 p3761 A70-40743

Visual target tracking with active head rotation, indicating independent eye response due to vestibulo-ocular reflex

22 p3979 A70-43492

Readability of segmented numerals under critical accuracy and limited exposure time, comparing with conventional displays

24 p4308 A70-45514

VISUAL TRACKING

U OPTICAL TRACKING

VISUALIZATION OF FLOW

U FLOW VISUALIZATION

VITAMIN A

U RETINENE

VITAMIN B 06

U PYRIDOXINE

VITAMIN B 12

U CYANOCOBALAMIN

VITAMIN C

U ASCORBIC ACID

VITAMIN E

U TOCOPHEROL

VITAMIN M

U FOLIC ACID

VITAMINS

NT ASCORBIC ACID

VITREOUS MATERIALS

- NT CYANOCOBALAMIN
NT FOLIC ACID
NT NICOTINAMIDE
NT PYRIDOXINE
NT RETINENE
NT TOCOPHEROL
Adenosine triphosphate and vitamins /amitnavit/
as prophylactics against radiation injuries in dogs dur-
ing simulated space flight 17 p3038 A70-35351

VITREOUS MATERIALS

- Soviet collection of papers on inorganic glassy
coatings and materials 05 p0870 A70-16591
Metal oxides additions effect on Ti glass crystalliza-
tion, studying small and large ion radii 05 p0871 A70-16593
Density, refractivity, thermal expansion coefficient,
softening point and soaking stability for glass contain-
ing barium, lead, boron, bismuth and titanium oxides
05 p0871 A70-16594
Crystallization and dielectric properties of glass
containing barium, lead, titanium and boron oxides,
noting frequency and temperature dependence 05 p0871 A70-16595
Aluminosilicate glass physical properties and chemi-
cal stability in water, alkaline and acidic agents, study-
ing titanium oxides additions effect 05 p0871 A70-16596
Sodium-titanium-boron-silicate glass opacity and
fusibility increase during partial substitution of K for
Na, noting phase composition changes 05 p0871 A70-16598
Vitreous transparent solids emission after irradiation
by Q switched laser, ascribing luminescence to
multiphonon and excitonic phenomenon 09 p1710 A70-22836

VLASOV EQUATIONS

- Inhomogeneous plasma containing weak electron
beam using Vlasov equation, noting wave-wave
coupling effect 02 p0345 A70-11882
Unstable electron plasma initial value problem
solved by numerically integrating Vlasov equation in
one dimension 02 p0347 A70-12235
Inhomogeneous plasma oscillations in counter-
streaming plasmas analyzed for electric fields and
resonant frequencies from Vlasov equation 04 p0726 A70-14671
Linear damping of sinusoidal oscillation in plasma,
solving linearized Vlasov equation by integration
along particle trajectories 05 p0888 A70-16304
Plasma waves and instabilities, detailing linearized
Vlasov-Maxwell equations solution appropriate to
Landau problem 06 p1118 A70-17378
Numerical solution of nonlinear Vlasov equation for
collisionless plasma problems, discussing initial value
problems, external electric fields, magnetic fields, etc.
06 p1108 A70-17419
Finite amplitude disturbance propagating across
magnetic field within infinite plasma, solving Vlasov
equation and ordering moment equations hierarchy 07 p1352 A70-19989
Temperature renormalization for improving velocity
distribution function representation in solving non-
linear Vlasov equation, transforming Hermite
polynomials 07 p1328 A70-20201
Selective harmonic excitation in one dimensional
collisionless plasma conforming to Vlasov equation by
counterstreaming electron beams, noting velocity dis-
tribution conditions 07 p1353 A70-20202
Asymptotic method for Vlasov equation formulated
for weakly Landau damped monochromatic plasma
wave in collisionless electron plasma 07 p1353 A70-20231
Asymptotic method for Vlasov equation of plasma
wave reformulated in Eulerian representation 07 p1354 A70-20232
Vlasov equations and irreversibility in plasma
physics and stellar dynamics, calculating statistical en-
tropy and relaxation time 08 p1550 A70-20556
Variable coefficient equations for free oscillations
of shallow shells of variable thickness in Vlasov mo-
ment theory 08 p1586 A70-21011
Semi-Lagrangian formulation of Vlasov equation in
two and three dimensional electrostatic problems,
investigating tensor determinants and perturbation
08 p1553 A70-21614
Mathematical model for finite-density non-
homogeneous Newtonian cosmologies, approximating
solutions using coupled Vlasov-Poisson equations
08 p1581 A70-21740
Pulse propagating in unstable plasma, determining
characteristics by asymptotic expansion applied to
Vlasov-Maxwell equations 09 p1734 A70-22684

Vlasov equation approximate solution by minimum
energy principle, deriving equilibrium equation for
stellar gas 13 p2457 A70-28552

Nonlinear Vlasov equation treatment by Fourier-
Hermite expansion techniques for plasma problems
13 p2457 A70-28556

Vlasov interaction of magnetically coupled E layer
with dissipative structures including injection,
trapping and drag effects 14 p2623 A70-30698

Vlasov equations and irreversibility in plasma
physics and stellar dynamics, calculating statistical en-
tropy and relaxation time 15 p2781 A70-32711

Anisotropic temperature plasma susceptibility cal-
culation based on velocity moment equations and cir-
cular polarized coordinates, compared to Vlasov equa-
tion solution 17 p3140 A70-34929

Fourier and Hermite transform methods for Vlasov
equation solutions in plasma physics 18 p3296 A70-36789

Finite difference methods for collisionless plasma
models, taking into account Eulerian form of Vlasov
equation in phase space 18 p3296 A70-36792

Vlasov high temperature plasmas numerical analy-
sis, using Hamilton variational principle 18 p3296 A70-36793

Antennas impedances in warm isotropic plasma,
using hydrodynamic and kinetic /Vlasov/ equations
19 p3380 A70-38406

Donnell-Vlasov shallow shell equations error analy-
sis 20 p3734 A70-40441

Lagrange formulation for deriving energy- conserv-
ing numerical approximations for Vlasov plasmas
22 p4080 A70-42750

Plasma macroscopic and microscopic instabilities
derivation from MHD and Vlasov equations
23 p4224 A70-44180

Collisionless plasma weak turbulence theory deriva-
tion from Vlasov equations, considering interactions
between oscillation modes 23 p4225 A70-44182

One dimensional collisionless electron-proton
plasma, obtaining exact electrostatic shock solution to
Vlasov and Poisson equations 24 p4382 A70-45107

VLF EMISSION RECORDERS

- Slow tail atmospherics and VLF pulse measure-
ments at close-to-thunderstorm fields, indicating
return stroke origin 17 p3046 A70-35395
Sounding rocket instrumentation for ionospheric
VLF radio noise measurement and recording 17 p3090 A70-35398
Ionospheric radio noise measurements with VLF
wideband receivers onboard rocket 17 p3046 A70-35399

VOICE COMMUNICATION

- NT TELEPHONY
NT VOICE DATA PROCESSING
Speech intelligibility tested using Modified Rhyne
Test and air traffic control and civil disaster vocabula-
ries, noting Articulation Index for signal-noise condi-
tions 02 p0246 A70-12150
Bandwidth reduction for interlacing two voice and
three additional teletype subchannels in standard
phone frequency range for use in VHF/UHF satellite
link 03 p0450 A70-13623
Linear phase detection using FM demodulation for
Apollo S band communication system eliminating
baseband voice interference with telemetry [AAS PAPER 69-610] 04 p0648 A70-14659
Phase feedback demodulation technique to analyze
telemetry performance degradation caused by voice
interference in modes of Apollo communication
system, providing linear detection scheme [AAS PAPER 69-609] 04 p0648 A70-14660
Pilot emotional state during stressful situations from
tape recorded vocal utterances of air to ground radio
communications using spectrographic analysis 06 p1000 A70-17297
AN/PRC-87 Pararescue radio for hands free opera-
tion, using bone conduction microphone, voice
operated transmitter, etc 06 p0986 A70-17723
Spot III satellite-supported system for transoceanic
aircraft navigation, traffic control, voice and data
communication, etc 07 p1331 A70-19291
Intersite trunk elements design and usage in in-
tegrated mission control center /IMCC/ as interface
equipment between internal voice communication and
worldwide network 08 p1460 A70-20814
Aircraft and ship position surveillance by satellites
system with independent capability and undelayed
voice and digital communication 09 p1723 A70-23043

Demand assignment signaling and switching
subsystems /DASSS/ design for communication satel-
lite, examining voice channels modulation 10 p1837 A70-24348

DASSS operational parameters and performance in
SPADE satellite voice communication system 10 p1837 A70-24350

TDMA demand-assigned satellite communication
system developed for INTELSAT, discussing PCM,
voice signals and channels, etc 10 p1839 A70-24362

Portable optical communcator for voice transmis-
sion combining pulse position modulation and low
power gallium arsenide diode 10 p1840 A70-24530

Satellite capacity utilization for mixed earth stations
network using SPADE concept/digital satellite com-
munication system employing demand- assignment
and voice-activated carrier techniques [AIAA PAPER 70-420] 11 p1996 A70-25404

Direct broadcast voice satellite for educational
system improvement, discussing lesson formatting,
ground receiver/programmer, multichannel capacity,
etc [AIAA PAPER 70-449] 11 p1998 A70-25423

Multiple access communication satellite systems
providing reliable speech communication for low den-
sity use in remote areas [JPL-TR-32-1501] 21 p3791 A70-41368

VOICE DATA PROCESSING

- Digital log-linear companding technique for nonu-
niform quantization of speech and image signals
01 p0044 A70-10784
Automatic formant-frequency extraction using
vowel-type spectrum, inverse filtering, moment calcu-
lation and evaluation by synthesized speech 06 p1009 A70-17909

VOID RATIO

- Two phase density and void fraction measurement
using beta, gamma and X ray radiation, considering
optimal accuracy and beam collimation 02 p0305 A70-12835
Nonequilibrium two phase forced convection flow,
describing pressure, temperature and void fraction
measurement techniques 02 p0305 A70-12838

VOIDS

- Radio Influence Voltage /RIV/ nondestructive test
method for detecting voids in neoprene-steel struc-
tures or other elastomers bonded to metal 13 p2420 A70-29245
Low energy fracture of high strength Al alloys with
void nucleating particles, using microprobe fractog-
raphy 23 p4206 A70-44194

VOIGT EFFECT

- Magneto-optics of semiconductors, taking into ac-
count intraband and interband effects with Faraday
and Voigt field configurations 18 p3297 A70-35951

VOLATILITY

- Volatile contaminants emitted from space cabin
construction materials tested under simulated space
conditions 01 p0031 A70-10237
Gas chromatography based on sampling gas-vapor
phase at liquid surface for determining volatile oxygen
containing compounds in biological media 04 p0646 A70-14580
Differential thermal analyzer coupled to mass spec-
trometer for kinetics of reactions giving volatile
products at high temperature, considering ablative
materials 14 p2664 A70-30292
Volatilizable C compounds in lunar fines from Mare
Tranquillitatis, investigating pyrolysis and acid hydroly-
sis products by mass spectroscopy and gas chro-
matography 21 p3779 A70-41628
Temperature and long term effects on volatility of
perfluoroalkyl ether and polysiloxane greases [ASME PAPER 70-HT-31] 22 p4058 A70-42435

VOLATILIZATION

- U VAPORIZING
VOLCANICS
U VOLCANOLOGY
VOLCANOLOGY
Pb isotope data from young mantle derived vol-
canics suggesting mantle evolution and lunar capture
04 p0743 A70-14396
Solar IR light brightness distribution reflected by
volcanic covers compared with lunar observation data
04 p0744 A70-14439
Neutron star vulcanism and seismicity, discussing
neutron star volcano size and shape possibilities
04 p0753 A70-15070
Volcanic and meteoritic processes compared as
lunar cratering agency, tabulating terrestrial lopolith
and cryptoepllosion structures 05 p0913 A70-16553
Lunar mascons formation by isostatic and volcanic
processes, using normal density lunar crust and mantle
model 06 p1150 A70-18476

Bottom rock structure and composition of young lunar craters compared with Kamchatka volcanic morphological analogs

07 p1385 A70-19424
Lunar sinuous rilles as volcano-tectonic fracture traces of sites of gas emission

09 p1758 A70-22743
Orbiting satellite-borne instruments for scientific observation of earthquakes, volcanic eruptions, atmospheric phenomenon, cyclones, floods and soil erosion

09 p1763 A70-23377
Oceanic ridge volcanic rocks alkali metal, alkaline earth, rare earth, nickel and major element content, observing partial melting

10 p1877 A70-24648
Ranger lunar photographic evidence for volcanic hypothesis, considering fracture systems, Caldera analogy, common walls, crater size, etc

12 p2297 A70-26985
Solar light brightness distribution reflected by volcanic covers compared with lunar observation data

13 p2485 A70-28464
Middle Miocene hiatus in volcanic activity of Western U.S., discussing K-Ar dates for Tertiary rock of Great Basin area

13 p2393 A70-28718
Oceanic volcanic rocks, discussing dispersed element characteristics to describe origin of magma types

15 p2731 A70-32100
Volcanic blankets aerological investigation by polarization and spectral techniques, determining brightness distribution of reflected solar light

15 p2803 A70-32495
Fe ion, Mg order-disorder in natural orthopyroxenes as function of temperature

16 p2896 A70-33087
Lunar craters, walled plains and maria compared with volcanic formations on earth

19 p3517 A70-37991
Lunar volcanic ridges features from interpretation of photographs by telescopes and satellites

19 p3518 A70-37992
Thermoelastic seismic-energy release as source mechanism for volcanic earthquakes, describing thermal microfracture tests

20 p3619 A70-39217
Fugacities of HCl and HF compared with abundance in volcanic fumarolic emanations, indicating magma undersaturation

20 p3619 A70-39321
Trace constituent changes effects on stratospheric properties after volcanic eruption, showing prolonged atmospheric temperature increase

20 p3622 A70-39490
Lunar luminescence phenomena, examining gas eruptions from volcanic activity, solar radiation and color

21 p3886 A70-41070
Apollo 11 lunar soil volcanic rock samples, mineralogical and petrological description and surface features

21 p3896 A70-41514
Multiphase volcanic eruptions associated with lunar craters Tycho and Aristarchus

23 p4253 A70-44882
New Mexico Bandera lava tube systems, noting similarities with lunar surface sinuous rilles

23 p4254 A70-44884

VOLT-AMPERE CHARACTERISTICS

Semiconductor laser active element radiation absorbing inhomogeneities effect on I-V characteristics, considering oscillation modes excitation

01 p0106 A70-10095
Electric characteristics and impurity distribution in GaAs-Ge heterojunctions obtained by deposition on p-type Ge

01 p0155 A70-10143
Negative resistance I-V characteristics of low voltage arc discharge in Cs plasma

01 p0150 A70-10172
Low voltage arc discharge in thermionic converter at low Ce pressures measured for current-voltage characteristics, showing degree of ionization

01 p0150 A70-10173
GaAs and Si photocell batteries powered by solar radiation, investigating temperature dependence of efficiency I-V characteristics and optimal power

01 p0007 A70-10177
Current-voltage characteristics of cascaded solar thermoelectric generator, determining optimum hot junction temperature as function of radiation concentration

01 p0000 A70-10752
Mo-Si epitaxial planar Schottky barrier diodes, describing reverse I-V characteristics improvement by edge leakage effects elimination

01 p0052 A70-11174
Current-voltage characteristics of p-n junctions in cadmium telluride, discussing spectral sensitivity bands

01 p0160 A70-11596

Current-voltage and current-temperature characteristics of alloyed p Ge-n Si heterojunctions, discussing current flow process complexity

02 p0350 A70-11667
Silicon solar cells I-V characteristics, spectral response and diffusion length measured after neutron irradiation

03 p0537 A70-13025
Autoelectron and autophotoelectron emission from Fe-doped p-type GaAs cathodes in vacuum, noting I-V and emission characteristics dependence on light flux

03 p0538 A70-13067
Voltage-power sensitivity, response time, frequency limit and minimum registered power of hot carrier thermoelectric detectors calculated from characteristic semiconductor parameters

03 p0540 A70-13436
GaAs nonlinear I-V characteristics and negative differential conductivity associated with electron heating by electric field

03 p0540 A70-13720
Exploding bridgewire detonator electrical input requirements, discussing waveform, peak current and time to peak

03 p0550 A70-14143
MHD generator cathode current-sheath voltage characteristics for thermionic arc spot emission mode, noting role of cathode temperature

04 p0625 A70-14797
Performance degradation in cadmium sulfide solar cells, discussing cause identification technique, I-V curve parameter changes, etc

04 p0628 A70-15329
Dynamic I-V characteristics of hot cathode megawatt level nitrogen propellant pulsed MPD arc plasma source for various axial magnetic fields

04 p0729 A70-15642
Barium titanate ceramics with nonlinear electrical conduction, noting I-V relationship dependence on temperature, impurities and electrodes

05 p0891 A70-15990
P-n-n structure dynamic I-V characteristics at high injection levels mathematically determined, showing rectifying capability decrease with increasing harmonic signal frequency

05 p0892 A70-16196
Ge IMPATT diodes under pulsed operation to produce LF high efficiency oscillations, recording current and voltage waveforms

05 p0821 A70-16417
Chalcogenide glass based film face threshold switches I-V characteristics, presenting oscillogram and diagrams

05 p0892 A70-16542
Cathode emission from hollow cathode controlled by variable magnetic field to ensure proper I-V characteristics for efficient ion generation in thrusters

06 p1131 A70-18032
Dynamic I-V characteristics of megawatt pulsed MPD-ARC plasma thruster under various axial magnetic fields given for Ar and hydrogen propellants

06 p1131 A70-18092
Instability of semiconductor circuit with nonlinear current-voltage characteristics, showing potential negative differential conductivity effect

07 p1240 A70-19274
Solid electrolyte cells discharge characteristics and open-circuit voltage, evaluating diffusion coefficient of Ag from time dependent behavior of I-V relationship

07 p1196 A70-19386
Photoelectric composite multicell solar generator, deriving empirical equation for external I-V characteristic

07 p1196 A70-19623
Ohmic contacts to n- and p-type semiconductors obtained by ruby laser, noting linear current-voltage characteristics

07 p1299 A70-19797
Semiinsulating GaAs doped with Cr, discussing negative resistance segment in current-voltage curves of S diodes

07 p1242 A70-19798
Volt-watt sensitivity of dilatocapacitor types of thermal radiation receivers, noting low natural noise levels

07 p1284 A70-19815
Electrochemical generators based on thermodynamic equilibrium processes, deriving expressions for EMF, efficiency, and I-V characteristics

07 p1196 A70-20462
Zener diode used as hydrostatic pressure gauge, describing pressure effects on diode current/voltage characteristics

08 p1477 A70-21644
Plasma beam welding of light metal and heat resistant alloys, discussing weld characteristics, beam I-V characteristics, etc

09 p1690 A70-22077
Current-voltage characteristics and lifetime of thin film diodes on chalcogenide glass substrate with symmetrical and asymmetrical electrodes

09 p1647 A70-22751

Volt-ampere characteristics of metal-semiconductor contacts for Schottky barrier diodes, investigating suppression of minority carriers and frequency response

09 p1741 A70-23352
HF electromagnetic wave detector based on study of volt-ampere characteristics of luminescent plasma discharge

10 p1922 A70-24030
Intensity vs voltage curves for LEED beams from clean Ni surface, calculating Bragg spectrum with energy diagram method

10 p1927 A70-24077
Low voltage arc discharge in thermionic converter at low Ce pressures measured for current-voltage characteristics, showing degree of ionization

10 p1925 A70-25018
Planar Ge and Si diodes application in pulsed bridge elements, investigating current-voltage and resistance-voltage characteristics

11 p2015 A70-25350
Connecting wires length effect on sensitivity and current-voltage characteristics of sensors for dynamic values measurement, deriving integral electrical parameters

11 p2055 A70-26445
Electric arc stability with descending static I-V characteristics in plasmatrons using direct Liapunov method

11 p2093 A70-26734
Plasmatron geometrical parameters effect on electric arc I-V characteristics, using various gas vortex flows for arc stabilization

11 p2093 A70-26735
DC air flow plasmatron arc chamber operation with metal surfaces used for charge stabilization, obtaining I-V characteristics and gas flow parameters in quasi-limiting region

11 p1984 A70-26738
Impact ionization effects in electric field domain on stability of current-voltage characteristics of Gunn diodes

11 p2020 A70-26813
Temperature effects on width of current-voltage characteristics of GaAs Gunn oscillators

11 p2020 A70-26819
Tensodiode effect in long plate-shaped semiconductors, noting bend direction effects on I-V characteristics

12 p2195 A70-27312
MIS varactors applications as nonlinear reactances, discussing charge-voltage characteristics and minority carriers effect

12 p2196 A70-27685
Sinusoidal signal harmonics measurement to determine nonlinear resistance junction I-V equation, discussing applications to circuit analysis

12 p2204 A70-28132
HF quenched-domain mode /Q mode/ Gunn effect oscillator in single frequency operation using signal analysis, obtaining instantaneous I-V transfer characteristics

12 p2202 A70-28162
Output signal spectrum analysis for nonlinear active element in presence of distorted modulating voltage

12 p2191 A70-28342
SERT 2 mercury vapor fed hollow cathode operated in bell jar, determining volt-ampere characteristics and flow rates for plasma diagnostics

13 p2473 A70-28515
Electrostatic probes response due to thermionic electron emission, considering I-V characteristics and space-charge-limited current

13 p2459 A70-28635
Electrostatic probe behavior in RF excited plasma, illustrating perturbation effect of potential drop on I-V characteristics

13 p2406 A70-28935
Gunn diodes I-V characteristics width as function of carrier concentration/mobility and diode length, noting role of impact ionization in strong electric field

13 p2378 A70-29408
He-Ne laser focused beam effect on negative Si diodes base I-V characteristics

13 p2378 A70-29517
Recombination radiation intensity current dependence and I-V characteristics p-n-n diode operating in double injection mode and electrons trapping

14 p2625 A70-30163
Amorphous boron arsenide films deposited on Si substrates, measuring current voltage characteristics

15 p2785 A70-32584
Current-voltage relation for ion collection spherical DC probe at high ambient gas pressure

16 p2899 A70-32929
Spherical electrostatic probe in uniform quiescent continuum slightly ionized gas for range of bias potential and radius-Debye length ratio

16 p2912 A70-33863
Switching circuit with Se diode, comparing I-V characteristics with Se rectifiers

17 p3054 A70-35411

Electron bombardment effect on volt-ampere, voltage-capacitance and pulse characteristics of GaAs point contact pulse diodes

17 p3055 A70-35675

IV characteristics of high resistivity Ti-doped GaAs single crystals and S-diodes, using Hall constant and conductivity measurements

17 p3144 A70-35709

Negative resistance and conductivity segments in I-V curves of diode structures, taking into account injection junction imperfections

18 p3231 A70-36413

Sample dimensions effect on shape of I-V curve caused by overheating in media with ambiguous dependence of electron temperature on field

18 p3298 A70-36621

MOS structures deep depletion capacitance/voltage characteristics by ramp response method

19 p3389 A70-37972

Photovoltaic effects in semiconductors, considering excess load carrier transport and I-V characteristics

19 p3488 A70-38477

Nonlinear resistance element with square law I-V characteristics for electrical analogs of hydraulic systems

19 p3359 A70-38707

Plasma inhomogeneities effects on MHD generators I-V characteristics, energy conversion efficiency and optimum duct geometry

20 p3564 A70-39636

Diode mixer analysis for arbitrary I-V characteristics and commensurate levels of converted signals, using modulation characteristics method

20 p3588 A70-40147

Electrostatic plasma probe inverse process I-V properties from current voltage characteristics, improving accuracy and reliability by theory in terms of new variables

20 p3683 A70-40162

Small-orifice hollow cathode discharge properties in electron bombardment ion thrusters, using vaporized mercury propellant

[AIAA PAPER 70-1087] 20 p3693 A70-40248

Planar Ge and Si diodes application in pulsed bridge elements, investigating current-voltage and resistance-voltage characteristics

20 p3600 A70-40462

Heat treatment and photovoltaic properties of copper disulfide-cadmium sulfide heterojunctions, measuring I-V characteristics, capacitance and spectral response

21 p3862 A70-41911

Hollow cathode shape effect on glow discharge parameters and potential jump in cathode region, investigating I-V curves

22 p4078 A70-42357

Gunn diode oscillators in domain suppression mode, showing dynamic I-V curve shape relationship to donor concentration and crystal thickness

22 p3997 A70-43128

Thermal emission cathodes made from lanthanum, yttrium and gadolinium hexaborides, measuring I-V characteristics

22 p3998 A70-43442

Gunn microwave oscillators I-V characteristics in quenched and retarded modes, using piecewise linear approximation

23 p4168 A70-43778

Miniature avalanche MOS diode, investigating capacitance voltage characteristics of deep depletion regime

23 p4172 A70-44007

Corona discharges from fine W points in liquid He initiated by field ionization or emission, noting anomalous characteristics

23 p4221 A70-44889

Current twisting in double injection ohmic contact long p-n diodes with S-shaped current-voltage curve, showing unstable density at negative resistance segment

23 p4176 A70-45061

High cutoff negative resistance silicon carbide diodes, noting temperature independent current-voltage curve

23 p4176 A70-45067

Impact ionization effects in electric field domain on stability of current-voltage characteristics of Gunn diodes

24 p4317 A70-45185

Temperature effects on width of current-voltage characteristics of GaAs Gunn oscillators

24 p4318 A70-45191

Volt-ampere characteristics of exploding Cu, Nichrome, Al and Ni wires during explosions induced by pulsed current in air

24 p4378 A70-45466

Semiconductors with bipolar conductivity under electron-hole scattering, calculating plasma pinch effect on I-V characteristics

24 p4390 A70-45659

Thin film BiSb-oxide-BiSb tunneling junction I-V characteristics anomalies as function of temperature, magnetic field and bias voltage

24 p4390 A70-45662

Si-carbide composites electrical conductivity from temperature and thickness dependence, obtaining volt-ampere characteristics via computer method

24 p4391 A70-46154

VOLTAGE

U ELECTRIC POTENTIAL

VOLTAGE AMPLIFIERS

Computer modeling of operational amplifier integrated circuit in ionizing radiation environment, using RLC network and voltage transfer curve

04 p0658 A70-14740

Two-cascade amplifying circuits with current and voltage feedback for semiconductor precision devices

24 p4321 A70-46394

VOLTAGE BREAKDOWN

U ELECTRICAL FAULTS

VOLTAGE GENERATORS

NT PHOTOVOLTAIC CELLS

Modulated high voltage pulse generator, using rectification of voltage obtained from HF oscillator

06 p1022 A70-17776

Controllable generator of linearly stepped voltage pulse using avalanche transistors, controlling avalanche-transistor relaxation oscillator by gating storage condenser

09 p1643 A70-22130

High sawtooth voltage generator with semiconductor triodes, giving circuit parameters and diagrams

16 p2873 A70-33212

Long period duration digital sinusoidal voltage generator, presenting schematic diagram and theoretical and operational characteristics

19 p3385 A70-37376

VOLTAGE MEASUREMENT

U ELECTRICAL MEASUREMENT

VOLTAGE REGULATORS

Output voltage stabilizers for thermal compensation in semiconductor power generating circuits, using stabilatron reference source

01 p0049 A70-10139

Integrated analog voltage regulator sensitivity to small signal transient radiation, discussing circuit hardening by diode compensation

04 p0658 A70-14742

Generator regulator for Ni-Cd batteries capable of sensing temperature, reducing charge rate and limiting output to increase batteries life

11 p1983 A70-25884

Regulated spacecraft solar array mathematical model for high voltage power supply regulator analysis

21 p3757 A70-41208

Buck-boost main bus voltage regulator for solar array battery space power system

21 p3758 A70-41219

Solar cell array maximum power point in scientific satellites via closed loop conductance matching regulator

21 p3758 A70-41220

Hydrazine-fuelled battery low power consumption auxiliary system with voltage regulator and gas pumps

22 p3966 A70-43539

VOLTAGE VARIATION INDICATORS

U VOLTMETERS

VOLTERRA EQUATIONS

Differential and integral inequalities theory and applications, Volume 1, Ordinary differential and Volterra integral equations

01 p0133 A70-11324

Volterra equations for stresses, strains and displacements of viscoelastic tube with variable radius encased in shell under pressure and unsteady temperature field

02 p0384 A70-11663

Potential axisymmetric vortex flow interaction with stationary flat surface, using existing numerical analysis by transforming boundary value problem to Volterra integral equations

04 p0668 A70-14864

Stress-strain distributions in linear viscoelastic cylinder, reducing problem of hollow cylinder with moving inner boundary to Volterra integral equation

07 p1406 A70-19303

Volterra operators extension, considering structure of complete operators and invariant subspaces

09 p1711 A70-22146

Volterra method applied to solution of mixed boundary value problems for wave equation

12 p2159 A70-28243

Solutions behavior of nonlinear system of linear Volterra integral equations, discussing applicability of standard fixed point theorems

16 p2943 A70-34000

Volterra equations for stresses, strains and displacements of viscoelastic tube with variable radius encased in shell under pressure and unsteady temperature field

19 p3547 A70-38437

VOLTMETERS

Supply phase voltage loss detection failure by voltage sensors in industry

13 p2378 A70-29349

High resolution successive approximation voltmeters using digital carry to improve speed and accuracy

19 p3427 A70-38049

VOLUME

Heart stroke volume estimation at submaximal exercise using blood hemoglobin content and heart rate

20 p3576 A70-40328

VOLUMETRIC ANALYSIS

Modified apparatus for volumetric determination of alveolar carbon dioxide as indicator of pilot hypernea

10 p1825 A70-24503

Maximum isovolumic hemodilution by volume substitution determined by plasma expanders infusion in dogs

10 p1821 A70-25083

Vapor volume entrained in liquid bulk from boundary layer boiling on vertical plate in low gravity field

21 p3947 A70-41055

Elastic wave front control volume analysis in laminated and fiber reinforced composite materials

22 p4119 A70-43677

Macroscopically homogeneous composites control volume approach, examining Hugoniot equation of state

22 p4060 A70-43683

Oxygen and nitrogen adsorption on thin tantalum films, measuring pressure, electrical resistivity and temperature

24 p4363 A70-46219

VON KARMAN EQUATION

Von Karman transonic similarity law applied to flow through plane turbine blade cascades

04 p0616 A70-15183

Karman formula generalization for turbulent motion in atmospheric boundary layer, including improved variant for thermally stable and unstable conditions

05 p0878 A70-16205

Stressed state of shallow spherical shells of revolution undergoing large displacements reduced to Karman equation, solved by small parameter method

05 p0935 A70-16235

Von Karman theory of vortex trails and vorticity diffusion applied to atmospheric mesoscale eddy patterns to calculate viscosities, ages, radii, tangential velocities, etc

06 p1098 A70-18242

Von Karman equations for rectilinear plate vibrations used for triangular plates, discussing amplitude/thickness effect and multimodal frequency formula

07 p1416 A70-20211

Nonuniqueness theorems for von Karman equations governing thin flat elastic plate deflections clamped at edges and subjected to normal and edge loading

09 p1768 A70-22063

Compressible turbulent plane Couette flow solution with variable heat transfer based on von Karman model extended to arbitrary wall temperature

12 p2211 A70-27839

Two dimensional transonic cascade flow, using Von Karman similarity law

22 p4089 A70-42347

VON MISES THEORY

U STRESS FUNCTIONS

VON ZEIPPEL METHOD

Von Zeipel method applied to stellar three body problem, eliminating short period terms and establishing two integrals of motion

05 p0909 A70-16337

Satellite motion in lunar orbit by von Zeipel method, considering perturbations due to nonspherical lunar gravity field and earth and solar attraction

10 p1939 A70-24186

Von Zeipel mappings equivalence to Lie transforms shown by order independent method

14 p2639 A70-30706

Satellite orbit theory error bounds and initialization, investigating first order von Zeipel method in axisymmetric force field

18 p3320 A70-37067

Perturbation theories based on canonical transformations, examining von Zeipel theory and Hamiltonian functions

22 p4109 A70-43749

VOR SYSTEMS

U VHF OMNIRANGE NAVIGATION

VORTEX BREAKDOWN

Vortex separation effects on elliptic bodies lift distribution, analyzing separated flow pattern

04 p0619 A70-15385

Turbulent trailing vortex decay calculated from circumferential velocity and eddy viscosity dependent on Reynolds number

10 p1802 A70-24561

Low speed buffet intensity under pressure fluctuations on slender wing aircraft at vortex breakdown, using wind tunnel model

10 p1963 A70-25067

VORTEX COLUMNS

U VORTICES

VORTEX DISTURBANCES

U VORTICES

VORTEX FLOW

U VORTICES

VORTEX GENERATION

U VORTEX GENERATORS

VORTEX GENERATORS

Axisymmetric incompressible fluid flow aerodynamic properties in flat vortex chamber, studying core and boundary layer interactions and velocity fields

03 p0551 A70-13731

Cold flow-porous plate simulation of swirling flow-field in spinning end-burning rocket chamber, noting vortex generation and flow characteristics

04 p0764 A70-15541

Ball lightning mechanism proposal based on mathematical model for electric discharge current in parabolic plasma shell forming vortex-type storm front

05 p0879 A70-17021

Secondary vortex generation in near wake of circular cylinders under forced oscillation, analyzing motion dependent transition regimes using hydrogen bubbles flow visualization

[AIAA PAPER 69-755]

06 p1032 A70-17212

Wind tunnel investigated flow stabilization at horizontal control surfaces by vortex BCL technique, considering angles of attack, elevator deflection and shape

06 p0968 A70-17853

Vortex refrigerators characteristics, examining configurations with cylindrical and conical hot ends with and without diffuser

06 p0988 A70-17855

Flow turbulence in wind tunnel model tests, observing generation methods effect on aerodynamic flow characteristics distribution

08 p1483 A70-21074

Propulsive and lifting motions of pointed profile in ideal incompressible fluid related to alternate vortices emission

08 p1433 A70-21234

Counterrotating vertical vortices produced by corona discharge on heated flat plate under free convection conditions

08 p1599 A70-21828

Vortex and potential motions interactions in relativistic hydrodynamics, studying mutual generation

09 p1754 A70-22460

Plane Poiseuille flow with nonlinear temperature distribution, studying vortex type secondary flow onset due to buoyant forces

[ASME PAPER 69-HT-37]

09 p1790 A70-23555

Taylor-Goertler vortex formation effect on heat transfer through boundary layer on concave wall

[ASME PAPER 69-HT-3]

09 p1790 A70-23556

Pressure fluctuations in acoustic field of boundary layer under slot suction, considering vortex formation and separation on edges

12 p2209 A70-27298

Delta wing low aspect ratio aircraft vorticity generating effects, discussing wind tunnel tests for hazardous effects

12 p2156 A70-27692

Plane flow problem for two hinged plates in motion toward each other with fluid displacement, discussing single vortex application to biomechanics

13 p2338 A70-28481

Two dimensional circular cylinder vortex excitation in uniform flow using linear binary system for flutter analysis

13 p2341 A70-29057

Helical vortex generation in rotating flow in straight tube having angular momentum flux sufficiently large relative to linear momentum flux

14 p2565 A70-30277

Vortex generation in water tank, discussing vorticity distribution on free surface and critical depth of air entrainment for various Reynolds numbers

14 p2567 A70-31275

Surface pressure and lift measurement on model lifting rotor blade as function of vortex interaction, using flush mounted pressure transducers

17 p3009 A70-34737

Centrifugal impellers primary and secondary flows velocity distributions, determining vorticity generation

18 p3243 A70-36871

High temperature convective heat transfer in vortex chamber as function of Reynolds number and geometry, measuring pressure variations

19 p3552 A70-38186

Plasma vortices during electrodynamic distortion of curved copper wire exploding in atmospheric air, using shadowgraphs

22 p4081 A70-42807

Vane type vortex generators to prevent turbulent compressible boundary layer separation, measuring drag in supersonic flow

23 p4133 A70-44527

VORTEX RINGS

Stationary ring vortices in unbounded conducting fluid, investigating self excitation of magnetic field by vortices

13 p2461 A70-28965

Solar atmosphere vortex ring observation in H alpha light [2 December 1969]

20 p3703 A70-39022

Flow velocity and pressure profiles due to vortex ring confined in cylindrical channel, using electromagnetic analogy

20 p3609 A70-39651

VORTEX STREETS

NT KARMAN VORTEX STREET

Vortex street parameters in free wake behind body in plane fluid flow, deriving equations for vortex frequency, circulation and interspacing

01 p0060 A70-10146

Flapping wing unsteady periodic motion relationship to forces effect on wing profile and vortex street in wake, determining propeller thrust by potential theory

13 p2337 A70-28479

Heaving airfoil wakes visualization with jet flap augmented lift, measuring vortex street parameters

13 p2338 A70-28821

Vortex streets characteristics determination for plane jet having uniform initial velocity profile

16 p2890 A70-33108

Electrostatic probe measurements of vortex streets growth in plasmas bounded shear flow

[AIAA PAPER 70-758]

17 p3139 A70-34493

Unsteady incompressible planar gas jets with stable vortex street, investigating near flow field region to establish oscillatory component

19 p3404 A70-37799

VORTEX TUBES

U HILSCH TUBES

U VORTICES

VORTICES

Vortex diffusion in viscous compressible fluid, deriving nonlinear differential equations from density velocity and pressure discontinuities considerations

01 p0060 A70-10145

Goertler vortices effect on boundary layer transition on concave surface, discussing instability oscillations breakdown leading to turbulent motion

01 p0061 A70-10539

Vorticity number derivation for rotational flows, discussing reciprocal of kinematic Rossby number and vorticity measures

01 p0061 A70-10541

Flow visualization of boundary layer transition downstream of Gortler vortices, distinguishing successive instability modes by Te method

01 p0065 A70-11094

Water tunnel experiments with slender cones to investigate frequency of vortex shedding at low Reynolds number controlled by local diameter

01 p0003 A70-11098

Waves vs eddies in dynamics of turbulent boundary layer fluctuating motions with scale of mean flow

02 p0287 A70-12361

Optical density measurements in high speed confined air vortex, discussing light deflection mapping of vortex density field at off axis positions

[AIAA PAPER 68-694]

03 p0480 A70-12906

Swirling flow equations in converging nozzles, comparing analytical and experimental data

03 p0405 A70-12929

Axial flow reversal in swirling incompressible tube flow, discussing static pressure, velocity profiles and turbulent Navier-Stokes equation

03 p0465 A70-13017

Aerohydrodynamic model of relief waves in baroclinic atmosphere based on convection theory, analyzing strong turbulent vortex regime responsible for CAT

[ONERA-TP-727]

03 p0408 A70-13638

Adiabatic disturbances propagating as transverse waves in inviscid fluid rotating as Rankine vortex about cylindrical container axis, discussing harmonics

03 p0467 A70-13779

Swirling flow through axisymmetrically deformed tube without consideration of viscosity and compressibility, noting wall flow for critical Rossby number values

03 p0468 A70-13788

Transverse magnetic fields effects on velocity perturbations and vortices behind circular cylinder in electrolyte flow at various Reynolds and Stewart numbers

04 p0726 A70-14543

Potential axisymmetric vortex flow interaction with stationary flat surface, using existing numerical analysis by transforming boundary value problem to Volterra integral equations

[ASME PAPER 69-APM-R]

04 p0668 A70-14864

Stationary and vibrating circular cylinders for boundary layer separation point, determining vortex excited oscillation range

04 p0670 A70-14988

Plane and axisymmetric transonic flow approximate equations of inviscid nonheat conducting gas for point on sonic line with entropy having extremal value

04 p0617 A70-15234

State and velocity distribution measurements for air in counterflow vortex tube to determine axial variation of flow quantities

05 p0831 A70-15884

Hydrodynamic fields of revolution around sphere in unbounded fluid governed by Oseen equation, emphasizing streamlines and attached vortex

05 p0832 A70-16157

Vortex sheets pitch along constant aerodynamic pitched propeller blade at zero traction, discussing calculation, construction and wind tunnel testing

05 p0790 A70-16159

Spiral cloud vortex model in occluded extratropical cyclone constructed using atmospheric dynamics equations and satellite photographs

05 p0879 A70-16642

Vortices orientation due to unstable Ekman boundary layer, discussing analogy to Taylor-Goertler and thermoconvective vortices

06 p1096 A70-17465

Stability theory for pair of trailing vortices, investigating induced field convection, modes, amplification, cut-off distance, etc

[AIAA PAPER 70-53]

06 p0969 A70-18055

Flow model for steady asymmetric vortex system shed from slender body of revolution in coning motion

[AIAA PAPER 70-52]

06 p0971 A70-18118

Electric and magnetic fields of waterspouts measured by instrumented U.S. Navy aircraft

06 p1101 A70-18582

Streamwise directed vortices and crosshatched surface roles in heat transfer and ablation processes of reentry vehicles

07 p1394 A70-19729

Turbulent shear flow kinematic characteristics determined by photographic method and flow visualization using vortex model

07 p1259 A70-19827

Unsteady flow behind circular cylinder by flow visualization, determining vortices length variations with time at various Reynolds numbers and dimensionless accelerations

07 p1261 A70-20236

Potential vortex flow interaction with stationary surface calculation extended to Volterra equations by transforming boundary value problem, improving critical Reynolds number bounds

08 p1484 A70-21472

Vortex and potential motions interactions in relativistic hydrodynamics, noting effects of gravitation equations nonlinearity

09 p1754 A70-22461

Cross hatching on various body surfaces due to periodic surface pressure fluctuations, discussing origin from counterrotating longitudinal vortices in boundary layer

[AIAA PAPER 69-11]

09 p1662 A70-23223

Fluidic vortex valve to modulate solid propellant generated hot gas flow

[AIAA PAPER 69-424]

09 p1743 A70-23249

Circle theorem for potential flows extended to two dimensional steady incompressible ideal fluid flows of constant vorticity

09 p1664 A70-23714

Turbulent boundary layer vortex structures using hydrogen bubble technique

11 p2035 A70-25864

Off-centerline heating on lee surface of supersonic delta wing with separation and vortex initiation at leading edge

11 p1976 A70-25996

Aerodynamic sound emission from compact eddy region by singular perturbation approach, discussing Lighthill and Ribner theories

11 p1977 A70-26687

Nonfree vortex flow in contrarotating axial flow fans under radial equilibrium assumption, discussing pressure rise coefficient and static efficiency

12 p2156 A70-27600

Carbon dioxide CW laser-Doppler velocimeter for detecting aircraft wing tip trailing vortices by measuring atmospheric aerosols backscatter

12 p2249 A70-27630

Wing tip trailing vortices hazard reduction on closely spaced parallel runways by suction application, discussing power requirements

12 p2207 A70-27631

Delta wing low aspect ratio aircraft vorticity generating effects, discussing wind tunnel tests for hazardous effects

12 p2156 A70-27692

Vortex layer and entropy of supersonic gas flow past circular cones at incidence using surface velocity corrections

12 p2159 A70-28230

Suspended Stokes particle-single wave interaction effect on energy dissipation and vorticity of random turbulent incompressible fluid approximated by Fourier-Stieltjes integral

12 p2213 A70-28236

Cyclone cloud vortex evolution from satellite photographs, examining reasons for onset and disintegration

13 p2444 A70-28588

Slender wings leading edge vortex flow effect on roll damping at subsonic speeds

[AIAA PAPER 70-540]

13 p2339 A70-29007

Gravity effect on conical vortex separator, predicting body force effect on heavy fluid boundary layer flow for limiting condition determination

13 p2391 A70-29978

Unstable Ekman boundary layer vortex structure analysis by generating similar flow in liquid filled rotating cylinder

14 p2604 A70-30545

Velocity and pressure distributions of tornado-like two cell vortices within boundary layer, using different assumptions for eddy diffusion coefficient

14 p2604 A70-30547

Nonlinear bearing surface of symmetrical rectangular edge wings without slipping in incompressible flow, using oblique horseshoe vortex model

15 p2673 A70-32128

Linearized two dimensional double vortex sheet model of inviscid compressible jet instabilities over all Mach numbers

15 p2722 A70-32375

Maximum thrust nozzles design for rotational or nonequilibrium simple dissociating gas flows, including boundary layer effects

[AIAA PAPER 70-707] 16 p2891 A70-33567

Vortices in axisymmetrically separated flows, comparing results of various experiments

16 p2894 A70-33895

High Reynolds number flow in moving corner, observing vortex motion at piston and cylinder wall interface by flow visualization techniques

16 p2895 A70-34240

Boundary layer formation on walls of conical pressure nozzle during vortex flow

16 p2896 A70-34299

Low Reynolds number flow inside Delaval nozzle, examining gas density and rotational temperatures by electron beam techniques

[AIAA PAPER 70-810] 17 p3065 A70-34454

Vortex visualization applications in helicopter noise research, using smoke generator in rotor blade tip

17 p3057 A70-34712

Vortex sheet instability leaving semiinfinite flat plate, considering boundary effects

17 p3073 A70-35601

Vortex core diameters calculation methods for axisymmetric angular momentum flows

17 p3074 A70-35750

Incompressible laminar boundary layer, vortex and axisymmetric wake/jet flow parabolic equations solution by weighted residuals method, describing use of exponentials

17 p3074 A70-35883

Pulling force during motion of sinusoidally deformable flat profile, taking into account trailing edge vortices

18 p3241 A70-36280

Forced vortex impeller in axial flow fan without inlet vanes, presenting lift and drag coefficients of blade sections, loss of head, etc

19 p3352 A70-38222

Three dimensional flow through rotor of axial vortex flow fan, using airfoil method for design

19 p3352 A70-38248

Laminar vortex flow interaction with stationary surface, considering flow field, velocity, Reynolds number, etc

19 p3405 A70-38348

Critique of Ruderman theory of Crab pulsar LF wobble as long wavelength oscillation of superfluid vortex lattice

19 p3522 A70-38604

Sound wave radiation and excitation in plane infinite plate by vortices

19 p3354 A70-38722

Meridional mean eddy transport of enthalpy in Southern Hemisphere during IGY, comparing results with Northern Hemisphere

20 p3661 A70-39143

Three dimensional boundary layer on lee- and wind-side of prolate spheroid, emphasizing separation and embedded streamwise vortices

20 p3608 A70-39359

Vortex signature recognition from radial velocity field by Doppler radar

20 p3664 A70-40067

Poiseuille pipe flow instability, considering asymptotic analysis for small wave number disturbances

21 p3807 A70-41241

Acoustic pulse transmission through plane vortex sheet, examining zone of silence, geometrical acoustics and sound radiation

21 p3849 A70-41243

Viscous flow field in pneumatic vortex rate sensor, discussing boundary layer parameters, velocity profiles and swirling flow theory

[ASME PAPER 70-FLCS-16] 22 p4007 A70-42411

Hybrid fluidic heading reference system with negative feedback servo loop around vortex rate sensor

[ASME PAPER 70-FLCS-10] 22 p3963 A70-42417

Vortex pressure regulator with adjustable settings, discussing design, operation and test results

[ASME PAPER 70-FLCS-9] 22 p3964 A70-42418

Optimum low temperature two circuit vortex refrigerator using compressed air precooled in heat exchanger

22 p3965 A70-42808

Arctic and antarctic atmospheric circulation differences, discussing circumpolar vortices and isobaric surfaces altitude changes

22 p4065 A70-43168

Large scale axisymmetric atmospheric vortex wind velocity determination, using statistical cloud data from meteorological satellites

22 p4065 A70-43376

Vortex induced vibration problems, deriving mathematical model for periodic lift on circular cylinder

22 p3960 A70-43546

Continuous trailing vortex sheet rolling up into two discrete vortices, discussing wing lift limitations

23 p4131 A70-43890

Wing lift increase by spanwise blowing along upper surface, causing flow reattachment on wing and vortex induced effective aerodynamic camber increase

[ICAS PAPER 70-09] 23 p4132 A70-44120

Mass transfer and velocity gradient fluctuations at wall in two dimensional or rotational flow for large Schmidt numbers

23 p4181 A70-44210

Tornadic vortex motion equation derivation based on kinematical modification of Kelvin theorem

23 p4215 A70-44547

Inviscid rotational supersonic flow near three dimensional stagnation point, examining solutions for compatibility with vortical shock layer boundary conditions

23 p4183 A70-44692

Vortices growth in vortex sheets bounding jets flowing from two dimensional slit and circular orifice observed by computer experiments

24 p4327 A70-46244

VORTICITY

Coupled diffusion of heat and vorticity in gaseous vortex caused by radial mass convection and temperature dependence of gas properties

02 p0400 A70-12858

Spatial resolution analyses of vorticity meter and hot wire arrays for measuring velocity derivatives in isotropic turbulence

03 p0492 A70-13760

Vorticity entrainment effects in zonal jet flows, considering Long asymptotic series, shear enhancement, etc

04 p0715 A70-15519

Vorticity effects on drag friction and heat transfer near stagnation point of supersonic jet impinging on obstacle

05 p0833 A70-16290

Higher order boundary layer effects on zero-lift drag of sphere-cones, investigating transverse curvature, shock vorticity, displacement, slip and temperature jump

[AIAA PAPER 70-185] 06 p1041 A70-18173

Von Karman theory of vortex trails and vorticity diffusion applied to atmospheric mesoscale eddy patterns to calculate viscosities, ages, radii, tangential velocities, etc

06 p1098 A70-18242

Nonlinear stability of plane Couette flow, computing stream function, vorticity distribution and Reynolds stresses

07 p1255 A70-19211

Sporadic E layer formation by vortical winds, discussing effect on ionospheric electron concentration distribution

07 p1267 A70-19454

Jupiter geostrophy indicated by circulation, vorticity and Rossby number determined from Great Red Spot observations

08 p1580 A70-21573

Shear flow of inviscid incompressible fluid past sphere, calculating secondary vorticity and upstream velocity distribution

09 p1664 A70-23680

Asymmetry and vorticity effects on linear instability of channel flow with one parameter velocities and inflection points, proving wave speed theorem

10 p1862 A70-23951

Vorticity distribution influence on inviscid laminar jet boundary layer instability investigated for large Reynolds numbers, using shear flow and linearized theory

[DFVLR-SONDDR-14] 10 p1868 A70-24163

Geostrophic wind vector rotation correlated with precipitation and circulation in vertical solenoid field

11 p2076 A70-26074

Sporadic E layer formation by vortical winds, discussing effect on ionospheric electron concentration distribution

18 p3249 A70-36928

High Reynolds number isotropic homogeneous turbulence fine scale structure heuristic model, relating spatial intermittency to vorticity generation

20 p3609 A70-39665

Monochromatic acoustic wave interaction with turbulent jet fluctuating vorticity field, using Fourier analysis to extend spectral relations

[ASME PAPER 70-FLCS-6] 22 p4008 A70-42426

Aircraft condensation trails formation by interactions of exhaust emission, vorticity of wing induced downwash and ambient atmosphere

22 p3958 A70-42684

Atmospheric vorticity and dust devil rotation direction relationship, suggesting shear in horizontal flows associated with convective activity in unstable atmosphere

22 p4065 A70-42912

Relaxation gas dynamics, discussing vorticity and drag generation by relaxation, linearized theory and shock waves structure

23 p4178 A70-43889

Extremely high temperature deuterium examination, using coaxial plasma accelerators to determine neutron production and vorticity

23 p4227 A70-44452

Laminar boundary layer on uniformly rotating sphere studied by momentum integral method, imposing zero vorticity condition

23 p4184 A70-44981

Diabatic steady gas flow vorticity, examining various kinematic and kinetic properties

24 p4328 A70-46365

VORTICITY EQUATIONS

Vortex diffusion in viscous compressible fluid, deriving nonlinear differential equations from density velocity and pressure discontinuities considerations

01 p0060 A70-10145

Vortex street parameters in free wake behind body in plane fluid flow, deriving equations for vortex frequency, circulation and interspacing

01 p0060 A70-10146

Vorticity number derivation for rotational flows, discussing reciprocal of kinematic Rossby number and vorticity measures

01 p0061 A70-10541

Karman theory extension to interference between parallel vortex streets, examining geometry of vortex configurations

03 p0406 A70-13274

Atmospheric zonal circulation index annual variations calculation in latitude and time terms, using vertical vorticity component equation

07 p1328 A70-18650

Karman trail vortices tangential velocity decay measurement by hot film anemometer experiments

09 p1661 A70-22961

VORTICITY TRANSPORT HYPOTHESIS

Integral theorems on vorticity transport derived by Carstou method, suggesting need for redefining Truesdell concepts of convection and diffusion

11 p2037 A70-26175

Turbulent boundary layer characteristics on simple shapes in hypersonic flow, using mixing length theory and eddy exchange coefficient

14 p2564 A70-30262

Astrophysical hypothesis of vorticity expulsion from strong turbulence regions, indicating mechanism of thermally driven circulation currents

22 p4010 A70-42690

VOWELS

Automatic formant-frequency extraction using vowel-type spectrum, inverse filtering, moment calculation and evaluation by synthesized speech

06 p1009 A70-17909

VOYAGER PROJECT

Ablation, transmission transparency and embrittlement of heat shield materials for Voyager tested under simulated Mars entry conditions

07 p1395 A70-19885

VOYAGEUR HELICOPTER

U CH-46 HELICOPTER

VTO FIGHTER AIRCRAFT

U FIGHTER AIRCRAFT

U VERTICAL TAKEOFF AIRCRAFT

VTOL

U VERTICAL LANDING

U VERTICAL TAKEOFF

VTOL AIRCRAFT

U VERTICAL TAKEOFF AIRCRAFT

VULCAN AIRCRAFT

Tailless delta Avro Vulcan aircraft design, hardware and flight results

14 p2532 A70-31391

VZ-10 AIRCRAFT

U XV-4 AIRCRAFT

VZ-11 AIRCRAFT

U XV-5 AIRCRAFT

W

W WINGS

U VARIABLE SWEEP WINGS

WAFERS

Electronic wafer packages heat transfer coefficients determined analytically, considering roles of geometrical and physical parameters

01 p0051 A70-10991

WAKEFULNESS

Synchronizing and desynchronizing systems for cerebral electrical activity, noting roles in sleep and wakefulness mechanisms

03 p0417 A70-13073

- Sleep-wakefulness cycle electroencephalogram of auditory and visual portions of neocortex and hippocampus activity in cats, using spectral analysis and integration 14 p2536 A70-30185
- Human sleep pattern changes due to acute sleep-waking cycle reversal 20 p3569 A70-38990
- Click-evoked potentials in rat auditory cortex, medial geniculate body, reticulate formation and hippocampus during natural sleep and waking 21 p3761 A70-40917
- EEG dynamics during normal and altered human sleep-wakefulness regimens 22 p3971 A70-43137
- Human cortisol intermittent secretion during early morning sleep and sleep-wake cycle, examining adrenal activity 24 p4305 A70-46410
- WAKES**
- NT AIRCRAFT WAKES
- NT HELICOPTER WAKES
- NT HYPERSONIC WAKES
- NT LAMINAR WAKES
- NT SLIPSTREAMS
- NT SUPERSONIC WAKES
- NT TURBULENT WAKES
- Aerodynamic velocity field induced by plate in motion correlated with ideal gas flow at specific Reynolds number, discussing wake formation 03 p0410 A70-14270
- Mean flow velocity distribution calculated from momentum deficit superposed behind single cylinders in finite array of arbitrarily spaced parallel cylinders [ASME PAPER 69-WA/FE-11] 04 p0614 A70-14781
- Radio wave scattering increase in moving body wake near caustic in vertically inhomogeneous ionosphere 14 p2550 A70-30809
- Subsonic and transonic gas flow in wake behind finite thickness plate based on Navier-Stokes equations 15 p2719 A70-31484
- Natural convection wake from heated horizontal line source in liquids and in air, determining temperature field in plume above wires 15 p2825 A70-31817
- Far wake properties of reentry body in hypersonic air flow calculated with or without chemical kinetics, using finite difference method 16 p2836 A70-33753
- Electrostatic near wake model for ionospheric satellites, using low speed fluid dynamic blunt body similarities [AIAA PAPER 69-674] 16 p2837 A70-33867
- Dihedra placed at angle of attack in hypersonic rarefied gas flow, investigating base flow and near wakes 17 p3010 A70-35047
- Wake behind trailing edge of flat plate in constant velocity impulsively started stream, using boundary layer theory 18 p3206 A70-36196
- Velocity pulsation spectra in subsonic wakes behind circular disks and sphere, using thermoanemometer with constant filament temperature 18 p3207 A70-36279
- Rotor wakes intrastator transport effects on high Mach number axial flow compressors performance, considering stagnation temperature profile and rotor blade loss factor [ASME PAPER 70-GT-39] 18 p3209 A70-36869
- Spoiler theory based on mathematical model, using two dimensional potential theory in conjunction with experimental data on wake phenomena 22 p3957 A70-42273
- High speed cinematographic recording of wake behind hypervelocity projectiles [SMPT PREPRINT 102] 22 p4032 A70-43033
- Wave-riders aerodynamics and heat transfer, investigating lift to drag ratios for supersonic and hypersonic vehicles [ICAS PAPER 70-18] 23 p4276 A70-44129
- WALKING**
- Heart rate-body temperature relationship during walking in hot environment 06 p0993 A70-17431
- Knee joint walking mechanics, calculating forces transmitted by joint tissue 07 p1205 A70-19246
- Human locomotor performance before and after prolonged hypodynamia, discussing biochemical features and changes in step length, torso and extremity kinematics, etc 10 p1816 A70-24683
- Human femur junctions load actions and stresses during walking calculated from measurements 15 p2692 A70-32327
- Muscle function mechanics across knee joint in walking, relating tension to length, velocity and energy absorption 19 p3368 A70-37810
- Partial gravity simulators at Manned Spacecraft Center for astronaut acquaintance with dynamics of moon walking 21 p3804 A70-41192
- WALKING MACHINES**
- Dynamical motion of Lunar Hopping Laboratory in plane change maneuver between ballistic and foot-in-contact phases 13 p2384 A70-28523
- WALL FLOW**
- Diffusion flame structure in boundary layer with fuel injection from wall, analyzing expansions with single step reversible chemical kinetics, including nonequilibrium case 01 p0214 A70-10334
- Polarographic probe for wall studies of turbulent flow velocity and direction by measuring maximum reduction current on redox compound microelectrode 01 p0602 A70-10664
- Three dimensional instability of perturbed conducting fluid laminar boundary layer flow on concave walls in transverse magnetic field, analyzing various Hartmann numbers 01 p0152 A70-10934
- Gas jets collision flowing from parallel wall channels, applying solution to calculating geometrical characteristics or fluid jet amplifiers 01 p0011 A70-11569
- Turbulence constant for flows near walls, analyzing viscosity dependence on wall distance by utilizing maximum stability principle 01 p0069 A70-11627
- Fuel injections into supersonic air stream through isolated normal ports and porous wall, using interferometry, schlieren and high speed photography 02 p0354 A70-12044
- Hydrodynamic turbulent boundary layer on smooth wall, using finite difference theory 02 p0285 A70-12351
- Boundary layer calculation for semiinfinite plane turbulent jet on porous wall 02 p0287 A70-12691
- Transient heat transfer in forced convection flow over curved wall with zero Prandtl number, applying to laminar boundary layer with variable free stream velocity 02 p0400 A70-12857
- Temperature sensor location for accurate averaging in fluid flowing through heated or cooled circular duct 03 p0486 A70-13557
- Swirling flow through axisymmetrically deformed tube without consideration of viscosity and compressibility, noting wall flow for critical Rossby number values 03 p0468 A70-13788
- Viscous supersonic flow near wall with large local curvature, using asymptotic solutions to Navier-Stokes equations 03 p0468 A70-13867
- Reflected shock wave velocity, boundary layer disturbance and wall ionization measurements using thin film resistance thermometers 04 p0666 A70-14537
- Incompressible electrically conducting fluid flow along rectangular duct under transverse magnetic field, noting equivalency of Hunt solutions and thin wall restriction 04 p0726 A70-14614
- Heat transfer to insulator wall of linear MGD accelerator attached to shock tube, comparing measurements with Hartmann boundary layer analysis [ASME PAPER 69-WA/HT-53] 04 p0781 A70-14796
- Similarity of velocity profiles and pressure distribution of turbulent jet over inclined wall, indicating limitations of Glauert analysis [ASME PAPER 69-WA/FLCS-1] 04 p0668 A70-14849
- Actively participating bounding surfaces effect on free molecule flow through slit or annular orifice situated in wall separating different pressure regions [ASME PAPER 69-WA/APM-26] 04 p0668 A70-14906
- Linear stress distribution insertion into equations of motion for turbulent boundary layer, considering velocity profile in wall region 04 p0670 A70-14987
- Viscous gas self similar channel flow with heat transfer at wall corresponding to fixed Mach number profile in all channel cross sections 04 p0673 A70-15231
- Suction influence on skin friction fluctuations of MHD flow along infinite flat wall using Navier-Stokes equations 05 p0886 A70-15787
- Heat transfer in MHD Couette flow influenced by wall electrical conductances with suction 05 p0886 A70-15823
- Inert, oxidizing or reducing fluids wall injection into combustion gas boundary layer of variable composition noting effects on wall temperature 05 p0956 A70-15919
- Fluid boundary at curved wall under pressure 05 p0834 A70-16680
- Rarefied gas shear flow over infinite plane wall, using Boltzmann-Krook-Welander equation to determine compressibility effect on Knudsen layer 06 p1048 A70-18327
- Kinetic theory treatment of linearized Rayleigh problem using wall boundary condition models 06 p1049 A70-18329
- Steady viscoplastic boundary layer near hard wall with power law velocity distribution along outer boundary, deriving self similar solution 07 p1252 A70-18670
- Heat protection effectiveness of rectangular channel plane wall with flow by air injection through aperture on wall 07 p1420 A70-19066
- Wall proximity and velocity gradient effects on thermoanemometer readings in turbulent boundary layer 07 p1285 A70-19834
- Functions describing spatial-temporal temperature distribution in hyperbolic partial differential equations for nonstationary heat exchange between fluid flow and boundary wall 07 p1423 A70-19839
- Wall boundary condition model modification applied to molecular beam-solid surface scattering, noting qualitative agreement with observed distributions 07 p1342 A70-20118
- Incompressible conducting fluid MHD flow at infinite plane wall forward stagnation point, considering suction or injection effects 07 p1354 A70-20237
- Heat exchange at stagnation point of subsonic and supersonic axisymmetric jets interacting with perpendicular plane partition, allowing for turbulence 08 p1482 A70-20919
- Suction effect on thin film laminar flow past vertical wall, obtaining approximate solution for small porosity in accelerated region 08 p1484 A70-21309

Flow structure in rectangular cavity in lower wall of two dimensional channel for various aspect ratios and Reynolds numbers

08 p1484 A70-21313

Straight-walled two dimensional diffusers with incompressible steady flow, noting effects of inlet blockage and aspect ratio on performance

08 p1433 A70-21322

Magnetic field and conducting walls effect on laminar steady MHD Couette flow of electrically conducting incompressible viscous rarefied gas in slip regime

08 p1553 A70-21764

Instantaneous velocities measured for wall region of smooth duct during turbulent fluid flow by chronophotography of particles

09 p1658 A70-22046

Two dimensional Poiseuille flow stability at deformable walls, assuming pressure proportionality to displacement and rate

09 p1660 A70-22533

Average velocities profile measurement in wall region of turbulent fluid flow in smooth duct

09 p1661 A70-22838

Turbulent heat and mass transfer from wall to plane-parallel fluid flow at large Reynolds and Peclet numbers, developing universal law

09 p1789 A70-23169

Magnetic field effect on free convection in laminar boundary layer formed by laminar flow of viscous conducting fluid along vertical wall

09 p1737 A70-23308

Taylor-Goertler vortex formation effect on heat transfer through boundary layer on concave wall [ASME PAPER 69-HT-3]

09 p1790 A70-23556

Fluidic curved-wall electropneumatic converter optimization, presenting steady state, step and pulse mode responses for various positions and lengths of resistive heaters

09 p1614 A70-23691

Flat plate laminar boundary layer blowoff due to wall injection analyzed by parameter matched asymptotic expansion

10 p1862 A70-23844

Plane steady flows characteristics of incompressible viscous fluids in rigid walled rectangular channels found asymptotic to Poiseuille and Couette flows

10 p1866 A70-24112

Viscous transonic flow past wavy wall analyzed by approximate method for inviscid transonic equation

10 p1800 A70-24137

Strong shock wave reflection from rigid wall at high shock velocities, studying effect on flow structure

10 p1922 A70-24152

Statistical chance characteristics of velocity profiles and friction for flow along infinite plane wall with constant suction

10 p1869 A70-24519

Heat protection effectiveness of rectangular channel plane wall with flow by air injection through aperture on wall

10 p1970 A70-25217

Annulus wall boundary layer effect on spatial flow in subsonic axial compressors by shearing stresses concept between stream surfaces

11 p1974 A70-25777

Wall shear stress distribution in rectangular ducts, discussing secondary currents and main flow prediction

11 p2035 A70-25779

Shear flow near walls through cascade of untwisted blades, observing variation in lift coefficient across span

11 p1975 A70-25788

Laminar boundary layer flow with exponential velocity distribution in outer flow described by differential equations, studying slip velocity at wall

11 p2037 A70-26350

Pulsation energy distribution in turbulent flow of incompressible fluid near tube wall, defining energy diffusion, production and dissipation terms in energy balance equation

12 p2210 A70-27321

Heat transfer and flow stabilization dependence on initial shock wave reflection from conducting wall

12 p2213 A70-28228

Preston tube errors in pipe flow wall shear stress determination due to velocity distribution deviations

13 p2387 A70-28848

Plane, steady, irrotational flow of gaseous subsonic stream bounded by two infinite parallel walls, discussing application to incompressible fluids

13 p2389 A70-29631

Boundary layer transition at high Mach numbers on adiabatic wall, showing effects of wind tunnel size, surface roughness and freestream disturbances [AIAA PAPER 70-586]

13 p2342 A70-29884

Steady viscoplastic boundary layer near hard wall with power law velocity distribution along outer boundary, deriving self similar solution

15 p2718 A70-31462

Three dimensional boundary layer separation, noting necessity of streamlines perpendicular to pressure gradients near wall

15 p2719 A70-31488

German monograph on transonic plane flow past wavy wall in blocked wind tunnel covering flow theory, interferometric density measurements, etc

17 p3070 A70-35375

Flow stability of incompressible heavy viscous fluid along wall of vertical circular cylindrical pipes, relating flow parameters to stability

18 p3240 A70-36278

Annulus wall boundary layers in axial flow turbomachines, taking into account boundary layer growth and associated secondary flows

[ASME PAPER 70-GT-92]

18 p3209 A70-36877

End wall boundary layers effect included in performance prediction method for multistage axial compressors

[ASME PAPER 70-GT-80]

18 p3210 A70-36884

Boundary layer equations for two dimensional flow of incompressible constant density micropolar fluid past plane wall, noting skin friction

19 p3404 A70-37962

Velocity profiles of laminar flow through rectangular duct with moving wall and arbitrary cross section under nonslip boundary condition

19 p3405 A70-38043

Magnetic field effect on hydromagnetic Goertler instability in boundary layer flow of conducting fluid over concave wall

19 p3481 A70-38352

Turbulent heat and mass transfer from wall to plane-parallel fluid flow at large Reynolds and Peclet numbers, developing universal law

19 p3552 A70-38392

Power law fluid flow past suddenly accelerated wall, applying group theory to similarity solutions

19 p3406 A70-38444

Sound propagation in cylindrical waveguide with impedance walls in presence of flow

19 p3472 A70-38655

Steady turbulent flow heat exchange in near wall region at large Prandtl numbers, plotting temperature distribution curves

20 p3612 A70-39811

Boundary layer separation in MHD generators, discussing differences between insulating and electrode wall boundary layers

20 p3680 A70-39985

Conducting wall MHD generator channel current distribution, examining computer program for anode and cathode currents

20 p3566 A70-40013

Wall proximity and velocity gradient effects on thermoanemometer readings in turbulent boundary layer

20 p3634 A70-40341

Heat transfer between wall and liquid and vapor films in internal regenerative cooling of thrust chambers

21 p3867 A70-41027

Wall heat transfer for partially ionized argon laminar flow within square channel conducting walls with and without transverse magnetic field

21 p3856 A70-41032

Two dimensional body slow motion through stratified fluid bounded by parallel vertical walls, examining flow at different Peclet numbers

21 p3744 A70-41246

Unsteady flow in rectangular cavity with moving wall, using iterative solution of Navier-Stokes equations

21 p3807 A70-41317

Natural convection boundary layer stability on isothermal flat vertical wall or subjected to linear temperature distribution

21 p3950 A70-41443

Rarefied gas flow over plane wall, considering boundary layer thickness of order of mean free path

21 p3809 A70-41715

Nonequilibrium flow adjacent to cooling tube wall confining cascade arc plasma electrical discharge

21 p3805 A70-41763

Pulsation energy distribution in turbulent flow of incompressible fluid near tube wall, defining energy diffusion, production and dissipation terms in energy balance equation

21 p3810 A70-42062

Wall recombination heat transfer in rarefied flow with velocity slip near leading edge

21 p3952 A70-42083

Turbulent heat/mass transfer from solid boundary with shear stress dependent on wall distance for various Schmidt or Prandtl numbers

21 p3953 A70-42088

Plane stationary shock wave reflection from rigid concave wall at low Mach numbers

21 p3811 A70-42204

Downstream heat transfer and wall friction predictions for quasi-developed strongly heated turbulent pipe flow, using mixing length model

[ASME PAPER 70-HT-8]

22 p4008 A70-42439

Displacement effect of hot-wire anemometric probes near wall as function of support orientation

22 p4038 A70-43241

Curved shock waves regular and Mach reflection in steady supersonic flow at plane wall

[ICAS PAPER 70-11]

23 p4180 A70-44122

Mass transfer and velocity gradient fluctuations at wall in two dimensional or rotational flow for large Schmidt numbers

23 p4181 A70-44210

Laminar boundary layer wall shear and velocity profiles by N parameter integral method, using exponentials

23 p4182 A70-44567

German monograph on three dimensional flow and blade pressure measurements at axial flow compressor casing wall, discussing test control and digital data processing

24 p4332 A70-45093

German monograph on casing and hub wall friction effects on three dimensional flow in turbocompressors in subsonic compressible working fluids

24 p4287 A70-45096

Velocity profile in viscous sublayer at wall based on maximum stability principle applied to Karman constant for turbulent channel flow

24 p4325 A70-45495

Boundary layer transition under small tridimensional perturbations interacting with excitations from wall

24 p4327 A70-46206

WALL JETS

Laminar and turbulent boundary layer equations with or without wall injection over two dimensional or axisymmetric bodies solved by finite difference techniques

02 p0287 A70-12370

Turbulent and wall jets with wide varieties of geometries and boundary conditions, predicting jet inflow effects on entrainment rate, lift, drag, etc

02 p0288 A70-12840

Walljet in crossflow, discussing characteristics and pressure field on plate, using flow visualization methods

03 p0465 A70-13004

Curvature effects on two dimensional turbulent wall jet flow over plane surface and circular convex and concave surfaces in still air

05 p0832 A70-16118

Razor blade calibration and measurement of wall jet flow shear stress in turbulent boundary layer with secondary injection

05 p0833 A70-16504

Hot wire turbulence measurements of cylindrical wall jet compared to results from free circular and plane wall jets

06 p1034 A70-17526

Turbulent boundary layers and wall jets development investigated for effect of mass injection through porous smooth and rough surfaces

06 p1034 A70-17679

Prandtl mixing length and effective Schmidt number distributions from wall jet and wake data to predict film cooling

06 p1035 A70-17688

Turbulent boundary layer control by wall jet, analyzing wall jets in adverse pressure gradients for two limiting cases

[AIAA PAPER 70-107]

06 p1041 A70-18160

Second order correction to Glauert wall jet flow around arbitrarily curved surface, discussing initial profiles

07 p1257 A70-19344

Flow properties and heat transfer of wall jet spreading over permeable surface with suction and blowing

07 p1258 A70-19720

Static pressure gradient influence on turbulent shear stresses and energy production in asymmetric wall jet flow

08 p1484 A70-21314

Turbulent three dimensional incompressible wall jets issuing into quiescent air ambient, tangent to and at surface of flat plate, investigating shear stress and flow field

09 p1661 A70-23215

Laminar flow into channel with symmetrical jets along walls, considering velocity profiles and flow establishment lengths

10 p1870 A70-24790

Plane turbulent wall jet from small slot, investigating velocity distribution dependence on slot inclination

13 p2388 A70-29448

Maximum velocity decay in wall jets calculated for comparison with experimental velocity profile

14 p2566 A70-30777

Jet flow through rectangular orifices in cylindrical wall using conformal mapping for potential, velocity, volume flow rate, viscosity, etc

14 p2567 A70-31359

High lift airfoils boundary layer separation suppression by blowing, describing wall jets streamwise development prediction methods

[AIAA PAPER 70-872]

17 p3010 A70-34818

Critical height phenomenon for vertical jet exhausting into horizontal parallel plates channel simulating aircraft surfaces

18 p3243 A70-36709

Laminar two dimensional wall jet with small natural disturbances, examining flow stability at various Reynolds numbers

19 p3402 A70-37526

Laminar convective flow from linear heat source along vertical plate, solving numerically for incompressible fluid by boundary layer approximation 20 p3614 A70-40403

Wall jet turbulent flow regions with shear stress and mean velocity gradient of opposite sign, considering theoretical explanation 20 p3615 A70-40501

Impact configuration fluidic amplifier, investigating modulation of power jet formed by impacting plane wall jets in bounded region [ASME PAPER 70-FLCS-14] 22 p3963 A70-42413

WALL PRESSURE

Left ventricle wall forces and dimensional measurements during cardiac cycle based on stress-strain terms, including results for mitral, aortic and myocardial disease 02 p0238 A70-12512

Values measured on sharp flat plate in 10.4 Mach boundary layer induced pressure gradient, discussing effects of wall pressure and temperature gradients 04 p0621 A70-15609

Pseudosound field wall pressure correlation obtained to predict response characteristics of aircraft panel mounted along jet wake 05 p0835 A70-16785

Wall pressure distribution, drag and lift measured on flat plates and wedges at Mach 8 rarefied gas flow for various leading edges 06 p0980 A70-18350

Pressure history at end wall of electromagnetic shock tube measured during shock wave reflection by piezoceramic gage 06 p1031 A70-18505

Laminar radial flow between parallel disks, estimating static wall pressure distribution perturbation caused by characteristic time 08 p1484 A70-21237

Surface roughness effects on measured cross spectral density of wall pressure fluctuations beneath turbulent boundary layer 08 p1486 A70-21859

Flow noise measurement for boundary layer pressure fluctuations at rigid wall, analyzing effect of transducer size, shape and orientation on resolution 09 p1675 A70-22387

Wall pressure fluctuations beneath turbulent boundary layers on flat plate and cylinder 11 p2038 A70-26529

Turbulent boundary layer interaction with wavy wall in wind tunnel, discussing wall pressure drag and surface waves interaction 11 p2039 A70-26538

Wall shear stress distribution in noncircular ducts with steady incompressible fluid flow 12 p2209 A70-27217

Nozzle wall hypersonic turbulent boundary layers at free stream Mach number using pitot, hot wire, and wall fluctuation and static pressure measurements [AIAA PAPER 70-746] 17 p3065 A70-34497

Sound field produced in uniform moving ideal fluid stream by nonuniform oscillating elastic wall 19 p3353 A70-38657

Multiple tube manometer with selector switch for measuring flow channel wall pressures 23 p4194 A70-44000

WALL TEMPERATURE

Heat transfer in tube flow with forced convection, internal radiation exchange, axial wall heat conduction and arbitrary wall heat generation 01 p0214 A70-10294

Heat transfer in turbulent boundary layer of airflow injected on smooth plate from nozzle in subsonic stepwise heated wind tunnel 01 p0216 A70-11001

Microlayers evaporation contribution to vapor bubbles growth rate from heated wall in liquid near saturation temperature during nucleate pool boiling 01 p0218 A70-11181

High pressure tests of primary zone flame radiation, flame and tube metal temperatures in aircraft combustion chambers, including oxygen and vitiated inlet air effects 02 p0355 A70-12051

Wall temperatures and heat transfer coefficients for solid-vapor mixtures of para hydrogen and nitrogen flowing in heated tube 03 p0604 A70-13018

Unsteady heat transfer equations for laminar fluid flow in pipe with varying wall temperature 03 p0604 A70-13207

Turbulent reattachment of supersonic axisymmetric jet on cylindrical wall in air, investigating wall temperature effect on cavity pressure and heat flux [ONERA-TP-758] 03 p0467 A70-13643

Integral method for studying wall heat transfer influence on compressible boundary layer on cone at angle of attack in supersonic flow 03 p0409 A70-13953

Steady convective motions in horizontal fluid layer bounded by porous walls of various temperatures at supercritical Rayleigh numbers, noting nonlinear convection equations 04 p0673 A70-15237

Wall and total temperature variations effects on transition Reynolds number in hypersonic He tunnel, noting sound mode dominance 04 p0620 A70-15560

Values measured on sharp flat plate in 10.4 Mach boundary layer induced pressure gradient, discussing effects of wall pressure and temperature gradients 04 p0621 A70-15609

Inert, oxidizing or reducing fluids wall injection into combustion gas boundary layer of variable composition noting effects on wall temperature 05 p0956 A70-15919

Laminar flow in circular pipe with arbitrary axial variation of wall temperature or heat flux, using integral type approximation 05 p0957 A70-16519

Negative pressure gradients effects on wall heat flow and characteristic patterns for turbulent boundary layer profiles 06 p1033 A70-17231

Skin friction law for compressible boundary layer allowing calculation of coefficient of friction for isothermal walls with heat transfer 06 p1033 A70-17232

Reflected waves development during shock waves collision and during shock collision with constant temperature wall, using Monte Carlo method 06 p1109 A70-17520

Bulk and wall temperature measurements for natural fluid convection in container with and without baffles for various heat flux and aspect ratios 06 p1175 A70-17684

Thermal slip velocity of gas in infinite temperature gradient tangential to solid wall, basing calculation on linearized Boltzmann kinetic equation 06 p1049 A70-18332

Local heat transfer coefficients determined from temperature distribution on porous walls, deriving mathematical expressions for various surface geometries and transfer modes 06 p1184 A70-18555

Wall temperature variation of transpiration cooled tube surrounding plasma arc calculated from gas mass flow and wall properties 07 p1420 A70-19214

Heat exchange in laminar and turbulent boundary layers on plate for arbitrary heat flux distribution allowing for initial unheated plate segment 07 p1423 A70-19657

Electrical conductivity variations effects in subsonic Hartmann plasma flow under transverse magnetic field in channel with cooled walls 07 p1352 A70-19986

Heat transfer from inner wall of annular ducted cylindrical body cooled by liquid nitrogen, discussing effects of Teflon, asbestos and vaseline coating and thickness effects 08 p1596 A70-20577

Wall material diathermy effects on critical thermal load under radiant transfer, comparing results for quartz glass and stainless steel tubes 08 p1597 A70-21186

Initial vapor bubble growth on horizontal heated wall during saturated nucleate boiling using combined streak and high speed frame photography 08 p1542 A70-21584

Solid layer effect on laminar heat transfer and pressure drop in medium surrounding pipe with liquid flows below freezing point, discussing wall temperature effects 08 p1485 A70-21589

Unsteady free convection laminar power-law fluid flow past porous vertical wall, studying similarity solution dependence on wall temperature and suction 08 p1486 A70-21765

Steady flame propagation attainment for chemical reaction initiation in gaseous fuel by heated surface with various wall temperatures 09 p1787 A70-22115

Local heat transfer to gas mixed with graphite particles described for variable temperature differences and wall temperatures 09 p1787 A70-22174

Steady laminar gas flow on duct wall boundary layer considering external swirling flow and wall heat transfer 09 p1659 A70-22428

Navier-Stokes equations for laminar near wake of blunt based body, obtaining numerical solutions for adiabatic and constant wall temperatures 09 p1605 A70-23176

Rarefied gas flow past arbitrary three dimensional body using variational principles based on linearized BGK equation, considering constant and adiabatic wall temperature 09 p1605 A70-23178

Circumferential wall temperature gradients in spacecraft radiator tubes as function of tube wall fins 09 p1789 A70-23261

Energy equations solved for step change of wall temperature and heat flux, determining turbulent heat transfer in tube, discussing asymptotic solutions validity 11 p2146 A70-25334

Insulator wall temperature effect on supersonic two temperature MHD generator channel flow at open and short circuit conditions 12 p2163 A70-27067

Heat conduction for thermally insulated bilayer metal wall for time-variable heat transfer and ambient temperature, using Green function 12 p2330 A70-27292

Compressible turbulent plane Couette flow solution with variable heat transfer based on von Karman model extended to arbitrary wall temperature 12 p2211 A70-27839

Turbulent heat transfer in concentric annuli entrance region with uniform wall heat flux 12 p3370 A70-28117

Prandtl number effects on adiabatic wall temperature and pressure gradient at separation point for hypersonic compressible laminar boundary layer 14 p2566 A70-31027

Free convection and heat transfer in square region bounded by solid impermeable walls heated from above, using two dimensional model 15 p2824 A70-31492

Heat exchange in laminar and turbulent boundary layers on plate for arbitrary heat flux distribution taking into account initial unheated plate segment 15 p2828 A70-32694

Temperature distributions and heat flux for gray gas in radiative equilibrium bounded by walls with different temperatures, using differential approximation [AIAA PAPER 70-834] 16 p3001 A70-33929

Extinction model of composite solid propellant combustion including wall and flame heat release zones 17 p3147 A70-34511

Conical shock wave-turbulent boundary layer interaction data obtained for adiabatic wall conditions at supersonic free stream Mach numbers, including suction effects 18 p3241 A70-36448

Wall cooling effects on turbulent boundary layer in low speed air flow, using smooth tube and thermocouple measurements 18 p3347 A70-36505

Heat exchange and temperature distribution between two liquids divided by plate, discussing possible errors 20 p3737 A70-39634

Laminar thermal boundary layer at atmospheric pressure adjacent to cooled wall, measuring electron temperature and number density 20 p3737 A70-39990

Insulator wall temperature effect on supersonic nonequilibrium MHD generator channel under open and short circuit conditions 20 p3681 A70-39994

Performance comparison of diagonal conducting wall MHD generator and Hall generator of equal dimensions, investigating wall temperature effect 20 p3566 A70-40004

Gaseous film cooling effect on adiabatic wall temperature distribution in rocket nozzle with gas injection 21 p3867 A70-41028

Flow field, heat transfer rates and reattachment surface wall temperature of planar supersonic turbulent flow 21 p3744 A70-41036

Heat transfer in cooled turbulent tube flow downstream region at high bulk-to-wall temperature ratios 21 p3945 A70-41037

MHD channel flow of suspension for prescribed wall heat flux and temperature, determining flow and heat transfer characteristics 22 p4080 A70-42670

Thermal relaxation effect on thermal contact of two semiinfinite walls, showing existence of dynamic contact resistance 22 p4125 A70-43243

Cylindrical wall nonstationary heat conductivity for time variable heat transfer coefficient 22 p4125 A70-43358

Tube heat exchangers operation at low transfer coefficient, calculating unsteady temperature field in wall and heat transfer agent 22 p4125 A70-43364

Heat transfer by laminar forced convection of viscous fluid in noncircular cylindrical channel with internal heat source and varying wall temperature 23 p4276 A70-44236

Heat transfer from turbulent axisymmetric jet to normal flat wall at critical point with small Reynolds numbers 23 p4181 A70-44321

Contact region structure with viscosity, conduction and radiative transfer effects applied to plane shock wave reflection from heat conducting wall 24 p4326 A70-46001

WALL TEMPERATURE DISTRIBUTION

U TEMPERATURE DISTRIBUTION

U WALL TEMPERATURE

WALLS

NT BULKHEADS

NT NOZZLE WALLS

- NT POROUS WALLS
NT THIN WALLS
NT THIN WALLS
NT WIND TUNNEL WALLS
Wall effect on differential spectra distortions in cylindrical ionization chamber and proportional counter type detectors
05 p0900 A70-15971
Container wall-collision plasma sheath model for charge carrier investigation using velocity distribution [DFVLR-SONDDR-51]
14 p2622 A70-30662
Sonic boom incident and ground reflected waves action on exterior wall, calculating arrival time as functions of aircraft speed and altitude and wall slope
14 p2566 A70-30861
Axial wall conduction effects on steady state laminar flow heat transfer
15 p2825 A70-31815
Comparative arterial pressure pulse transmission velocity in dogs, relating wall elasticity with vascular disease
15 p2682 A70-31939
Carbon monoxide-nitrogen laser mechanism vibrational populations, discussing operational characteristics and walls condition and nature
21 p3837 A70-41716
- WANKEL ENGINES**
Heat transfer data for rotary piston and conventional piston engines, studying compression energy losses due to working fluid leakage
05 p0897 A70-17002
Rotating combustion engine design offering low life cycle costs for military applications [SAE PAPER 700273]
12 p2290 A70-27438
Rotary piston engine for powered gliders and light aircraft power source by modifying industrial Wankel engine
17 p3147 A70-34690
- WARFARE**
NT ANTISUBMARINE WARFARE
NT COMBAT
NT NUCLEAR WARFARE
Outer space exploration and utilization, analyzing 1967 UN treaty provisions from standpoint of war potential inherent in space stations existence
16 p3003 A70-33100
Army aviation requirements in high intensity conflicts, discussing transportation, communications, intelligence acquisition, organization and suitable aircraft types
23 p4142 A70-44855
- WARMING**
U HEATING
- WARNING DEVICES**
U WARNING SYSTEMS
- WARNING SIGNALS**
U WARNING SYSTEMS
- WARNING SYSTEMS**
NT EARLY WARNING SYSTEMS
Proximity Warning System /Pilot Warning Indicator for helicopters, discussing applications to fixed wing aircraft
06 p0985 A70-17710
Encounter statistics and operational environment of aircraft collision-hazard warning systems in terminal area
07 p1331 A70-20060
Auditory and visual warning signals effects as reaction stimulus in time-uncertainty situation
10 p1826 A70-24719
Short range aircraft collision pilot warning indicator for low altitude and closure speeds
11 p2078 A70-25706
Light aircraft-airliner collision avoidance, discussing Time-Frequency Collision Avoidance System cost restriction, Pilot Warning Instruments, etc
11 p2079 A70-25872
Pilot midair collision warning instrument based on optical radar MTI, discussing target cross section enhancement by passive retroreflector
12 p2234 A70-27646
Optical IR system as low cost pilot warning indicator providing audible and visual collision warnings to general aviation aircraft
12 p2234 A70-27647
Stacked, vertically polarized collinear arrays of independently fed omnidirectional antennas for flight testing Doppler radar aircraft warning system
12 p2199 A70-27968
Thunderstorm detection and warning system, measuring vertical potential gradient and changes caused by lightning discharges
14 p2607 A70-30574
General aviation demands on Pilot Warning Indicator systems for collision avoidance
14 p2615 A70-31176
Blinking warning lights for air navigation, signaling of obstacles and glider onboard marker lights
16 p2889 A70-34302
Gallium arsenide laser ranging system for helicopters obstacle warning
17 p3103 A70-34720
Personnel danger zones demarcation around radar antennas, using beacons
17 p3040 A70-35913

- Netherlands Air Force bird strike problem and warning system
18 p3211 A70-35977
Fire and overheat detection system design for turbine powered vehicles
18 p3826 A70-36891
[ASME PAPER 70-GT-125]
ATA Collision Avoidance System based on time and frequency synchronization via ground stations or other aircraft
19 p3466 A70-38239
Hypoxia warning systems using polarographic sensor and miniaturized electronics for face-mask and cabin installation for aircraft and spacecraft
20 p3579 A70-39429
Constant false alarm rate bias technique to control avalanche photodiode laser receiver over varying operating conditions of temperature, ambient illumination, etc
20 p3641 A70-39483
Collision Avoidance System /CAS/ and Proximity Warning Indicator /PWI/ for preventing midair aircraft collisions
23 p4194 A70-44175
Limiting effects of topographic quasi-optical radio propagation above 100 MHz in radar aircraft navigation, clear air disturbances detection and IR warning technique
23 p4163 A70-44230
Global rescue alarm net /GRAN/ using satellites for relaying distress signals, eliminating current line of sight restrictions
23 p4143 A70-44455
Optimal color hierarchy for pyrotechnic markers and signals indicating red, violet and amber hues on top
23 p4146 A70-44459
- WARPAGE**
Plates and rods tendency to warp and form nonsymmetrical stress systems during heat treatment
19 p3433 A70-37272
- WASHOUT [RADIOACTIVITY]**
U FALLOUT
- WASPALLOY**
Inertia bonded and electron beam welded joints of Waspaloy compared for suitability in aircraft gas turbine engines
04 p0700 A70-15655
Waspaloy gamma prime solvus temperature relationships as function of solution treatment and precipitation strengthening additives, discussing microstructure and tensile properties
08 p1520 A70-21555
Hot work effect on properties and microstructure of wrought Waspaloy, observing temperature decrease effect on fracture ductility
22 p4054 A70-42739
- WASTE DISPOSAL**
Manned space flight requirements connected with cabin atmosphere, food/water supplies and waste disposal and environmental conditioning
05 p0807 A70-16632
Sludge removal from electrolyte in electrochemical machining by settling system, discussing temperature control, flow requirements, concentration control and balance system
10 p1893 A70-23859
Wastes dispersion discharged into sea analyzed by aerial photography, measuring diffusion
10 p1879 A70-24749
Ben Franklin submarine life support systems tested during Gulf Stream Drift Mission, discussing atmosphere control, water, waste and food management [ASME PAPER 70-DE-60]
16 p2852 A70-33515
Spacecraft waste management system zero-gravity flight tests, describing components and functions
17 p3036 A70-34751
Waste management for large space stations, discussing removal, venting, utilization, processing techniques, etc
21 p3769 A70-40996
- WASTE UTILIZATION**
Mathematical planning of experiments applied to biological mineralization of human wastes, using continuous microorganism cultivation
03 p0435 A70-13715
Titanium alloy wastes electrorefining by electrolytic cell with solid bipolar electrodes to eliminate non-metallic inclusions
05 p0863 A70-16544
Waste hydrogen utilization in microthrusters for spacecraft attitude control involving mass expulsion of cold gas
16 p2969 A70-33609
[AIAA PAPER 70-613]
Turbofan engine aerodynamic interactions, cryogenic space storable propellants, space station attitude control biowaste resistojel and long burning time solid propellants
20 p3688 A70-39667
Electrothermal thruster with biowaste propellants, discussing design and performance with various propellant compositions
20 p3567 A70-40201
[AIAA PAPER 70-1161]
Parameterized design data and selection criteria of biowaste resistojel system for orbit keeping and con-

- trol moment gyro desaturation of manned space station
20 p3567 A70-40213
[AIAA PAPER 70-1132]
Environmental control-life support systems /ECLSS/ waste methane gas utilization in low thrust resistojel for manned space applications
20 p3568 A70-40214
[AIAA PAPER 70-1131]
Concentric tube resistojel life tested on hydrogen and ammonia propellants for use with biowaste propellants
20 p3568 A70-40521
[AIAA PAPER 70-1133]
Vapor biowaste electric spacecraft propulsion system, discussing recovery cycles and subsystem tradeoffs, specific impulse, chamber heating, power input and reaction products
21 p3866 A70-40869
Vacuum distillation vapor filtered catalytic oxidation water recovery system, using radioisotopes for thermal energy supply
21 p3769 A70-40994
Potable water recovery from urine by vacuum distillation and vapor pyrolyzation
21 p3769 A70-40995
Waste management for large space stations, discussing removal, venting, utilization, processing techniques, etc
21 p3769 A70-40996
Spacecraft wet oxidation for human waste processing, discussing temperature and gas pressure effects, catalyst types, pump requirements, etc
21 p3769 A70-40997
Thermal efficiency of ceramic and metal heat exchangers for biowaste resistojel thrusters
21 p3868 A70-41779
[AIAA PAPER 70-1135]
- WASTES**
NT FECES
NT HUMAN WASTES
NT METABOLIC WASTES
NT SEWAGE
NT URINE
Automatic recording respirometer for industrial wastes, discussing design and advantages
14 p2543 A70-31164
- WATCHES**
U CLOCKS
- WATER**
NT COLD WATER
NT POLYMER
NT POTABLE WATER
NT SEA WATER
Water effect on glass fiber-resin bonds in interphase region, discussing initial stiffening and long term effects
01 p0127 A70-10484
Holograms of light scattered by clouds of water droplets to determine drop size, noting agreement with Mie theory
02 p0296 A70-11890
Banana self focusing in water of laser beams with nonmonotonic intensity distribution, noting ruby laser experiment
02 p0312 A70-12260
Water or bromotrifluoromethane content required in propellant Aerozine-50 /A-50/ spill to inert against ignition in air, considering fire extinguishment
04 p0732 A70-15408
Radiative-convective equilibrium model to investigate photodissociation of water in Venus atmosphere, considering greenhouse effect
04 p0757 A70-15516
Cloud chamber investigation of artificial cloud of water droplets in electrostatic field, discussing cloud precipitation, collection efficiency and fog dissipation
05 p0879 A70-16689
Electrically heated wire diameter and orientation on heat flux in saturated pool and surface boilings of water and aqueous binary mixtures
07 p1417 A70-18643
Distilled water and mineral oils heated to 50-80 C studied for effect on residual stresses in fiberglass reinforced plastics
08 p1526 A70-20925
Tape-generated swirl flow of single phase water investigated for heat transfer and pressure drop characteristics
08 p1600 A70-21829
[ASME PAPER 68-WA/HT-3]
Hydrodynamic processes during focusing of monopulse ruby laser emission into water, determining photohydrodynamic coefficient
09 p1694 A70-22111
Photographic emulsions design for increased water depth penetration during aerial multispectral recording of light absorption and scattering in water masses
09 p1674 A70-22261
Saturn ring IR spectrum, discussing resemblance and discrepancies of ammonia and water frost spectra
10 p1935 A70-23813
Remote sensing techniques for water resources evaluation and hydrobiological features mapping with multiband scanner imagery
10 p1879 A70-24742
Warm clouds electrification calculated for electromagnetic field growth by inductive mechanism, noting role of water drop pair interaction
10 p1913 A70-24807

Slush and water hazards on runways, discussing investigation and amelioration methods
11 p2030 A70-25356

Raman and IR spectrum analysis of polywater indicating impurities role in anomalous properties
11 p1994 A70-25655

Polywater electronic structure model, proposing hydrogen bonds resembling short strong bonds in FHF⁻/ions
11 p1994 A70-25656

Anomalous water /polywater/ dielectric constant and effective parallel conductance, suggesting hydrosol classification
11 p1994 A70-25657

Interaction between turbulent air flow and water surface based on Fourier analysis of finite intervals of field
11 p2042 A70-26775

Water contaminating effects on thin thermal oxide passivated silicon planar devices
13 p2361 A70-28930

Methane and ethane hydrate number measurement, alleviating liquid water occlusion and evaluating pressure effect
13 p2362 A70-29212

Molecular orbital wave functions for water molecule, using minimum set of Slater orbitals
14 p2544 A70-30119

Venus water presence from Venera 4 and Mariner 5 data suggesting polar seas and oceans saturated with hydrochloride and carbon dioxide as plant life source
14 p2637 A70-30365

Water sources associated with W3, Orion Nebula, W49 and VY Canis Majoris observed with coherent interferometers having long baseline
14 p2642 A70-30892

Liquid water occurrence on Mars surface, considering ice melting, evaporative cooling, atmospheric moisture content, etc
14 p2651 A70-31298

MHD experiments showing effects of local water supply electrical conductivity from measurements of voltage distribution, pressure gradients and extracted power
16 p2957 A70-32998

Water structure role in membrane systems, considering phase transitions and thermal anomalies in surface properties
16 p2847 A70-33027

Film boiling heat transfer from horizontal wires to water, using Nusselt condensation model
16 p3003 A70-34198

Atmospheric ions interaction with rocket exhaust gas water molecules, using sounding rocket mass spectrometric data
18 p3293 A70-36982

Water droplet size measurement by forward light scatter holography, evaluating reconstructed wave front by Fresnel transform
20 p3628 A70-39132

Glass reinforced plastics /GRP/ mechanical properties degradation by water, discussing effects of temperature, pressure, environment, etc
20 p3656 A70-40056

Preliminary physical training for human water immersion resistance improvement
20 p3576 A70-40196

Macaca nemestrina total body water measurement by dilution technique
20 p3577 A70-40333

Life support water electrolysis system design, discussing alkaline or acid electrolyte selection
21 p3768 A70-40993

Heat pipe performance map with ammonia as working fluid, comparing thermal transport efficiency with water pipe
21 p3947 A70-41050

Carbon dioxide and water cryodeposits refractive indices and densities, using thin film interference technique
22 p4122 A70-42434

[ASME PAPER 70-HT-33]

Atmospheric positive ion composition measurements in D region by rocket-borne mass spectrometers, considering water cluster ions formation
22 p4017 A70-42796

Water ballast loadings on sailplane Cobra 17, considering wing, aileron, tailplane, fuselage and landing gear
22 p3962 A70-42962

Thermal conductivity of water, toluene and benzene in coaxial cylinders, taking into account edge heat losses
23 p4276 A70-44216

Polarized maser emission from interstellar hydroxyl and water related to nonlinear weak magnetoplasma
24 p4381 A70-45258

WATER BALANCE

Human renal function, electrolyte and water metabolism during bed rest with daily leg exercise
07 p1223 A70-19937

Hydrogen-oxygen fuel cell reaction water removal and heat loss using reconcentration device
12 p2163 A70-27066

WATER CONSUMPTION

Rat water intake and urine output during chronic centrifugation at resultant inertial fields of 1.7 and 3.0 g
02 p0231 A70-11705

Human water-salt metabolism following exposure to transverse accelerations, discussing diuresis and Cl-K excretion
17 p3038 A70-35364

WATER CONTENT

U MOISTURE CONTENT

WATER COOLED REACTORS

NT HEAVY WATER REACTORS

NT NRX REACTORS

NT PLUM BROOK REACTOR

WATER DEPRIVATION

Food ingestion initiation, investigating role of hypoosmotic solutions from observation of rats under water deprivation
13 p2353 A70-29495

Food-water deprivation influence on alveolar surface activity of rat lungs
24 p4303 A70-46115

WATER EROSION

Liquid oxygen and water cavitation effects on lead, copper, nickel, iron and zinc
01 p0115 A70-10071

Coastal erosion survey by aerial photography, measuring change in beach locations over period of time lapse by corresponding reference points on photograph
10 p1879 A70-24748

Lunar sinuous rilles morphological and distributional observations and implications on theories of origin concerning surface water erosion
19 p3521 A70-38442

Graphites erosion by water and carbon dioxide at high temperatures, using liquid rocket simulator for kinetics study
20 p3736 A70-39587

[AIAA PAPER 70-638]

Artificial rain erosion effects on missile and spacecraft recorded via high speed photography
20 p3635 A70-40531

WATER FLOW

Forced cooling water flow temporary loss accident at Plum Brook Reactor, discussing inspection and corrective action
01 p0140 A70-10323

Hot-wire and hot-film anemometry in two phase air-water and steam-water flow, discussing bubble passage, signal processing and measurements
02 p0305 A70-12836

Boundary layer separation in divergent portion of conical ducts in overrelaxed supersonic regime in air and water, showing influence of medium, pressure and thrust
03 p0467 A70-13682

Water flow with solid particles, obtaining predictions for two component two phase gas flow
06 p1037 A70-17899

Interference between body and porous walls of water tunnels by one dimensional solution for usable length of tunnel
07 p1248 A70-19078

Laminar to turbulent boundary layer transition and separation on circular cylinder measured by heated end-window film sensor applicable to water flow
07 p1259 A70-19831

Transverse curvature effects on turbulent boundary layer thickness and velocity profiles on circular cylinders in water and air
07 p1261 A70-20301

Sewage water flowmeter calibration, analyzing error propagation and tolerance
09 p1672 A70-22027

Velocity measurements with Pitot tubes in polymer solutions /polyethylene oxide/ in water, noting viscoelastic properties effect on measured pressure value
10 p1887 A70-24093

Turbulent water flow velocity distribution measurement using laser light intensity fluctuation spectroscopy
10 p1869 A70-24600

Turbulent heat diffusion coefficients in air and water tube flow calculated from statistical characteristics, extending method to boundary layers
12 p2210 A70-27322

Vortex generation in water tank, discussing velocity distribution on free surface and critical depth of air entrainment for various Reynolds numbers
14 p2567 A70-31275

Water and blood flow characteristics in converging-diverging plastic tube, considering implications in occlusive vascular disease
15 p2691 A70-31937

Air bubble breaking in blood and water flow passage of simulated cardiopulmonary bypass system with flow constriction
15 p2692 A70-32312

Steady and unsteady gas dynamics analogies with two dimensional water flow, taking into account energy and continuity equations
17 p3069 A70-35032

Free convection in air and water above horizontal wire heated by DC current, measuring flame temperature distribution by diffraction interferometer
17 p3198 A70-35743

Steam-water jet discharge heat transfer features, examining critical region parameters from nozzle into submerged space with large counterpressure
18 p3345 A70-36117

Turtle bladder walls osmotic properties, discussing transmembrane water flow transient acceleration by sodium transport inhibition
21 p3762 A70-41223

Freezing and melting of warm water flow at stagnation point over cooled plate for convective condition at solid-liquid interface
21 p3949 A70-41311

Vibrational response of thin walled pipes to internal turbulent water flow as function of Strouhal number
21 p3940 A70-42052

Turbulent heat diffusion coefficients in air and water tube flow calculated from statistical characteristics, extending method to boundary layers
21 p3811 A70-42063

WATER HAMMER

Excess pressure in pulsed fluid jet with different emergent velocities from water hammer, discussing interaction between discrete sections
13 p2388 A70-29425

WATER INJECTION

Electron density reduction in plasma surrounding reentry vehicle due to N atom removal by water droplets injection
09 p1737 A70-23237

Optimal water quench of solid rockets using injection normal to propellant surface
16 p2968 A70-33598

[AIAA PAPER 70-640]

WATER JETS

U HYDRAULIC JETS

WATER LANDING

NT DITCHING [LANDING]

Space rescue techniques and equipment in NASA recovery programs, considering low earth orbit and water landing
01 p0035 A70-10717

Marine safety aspects of helicopters with flotation equipment, considering effects of severe winds and waves, aircraft abandonment procedure, etc
01 p0007 A70-11316

Missile impact and trajectory for water entry with zero angle of attack, including deceleration measuring instrumentation
13 p2387 A70-29039

[AIAA PAPER 70-531]

Maximum impact accelerations of spherical and conical bodies landing on water, using momentum theorem
15 p2722 A70-32524

WATER LOSS

Curve characteristics of differential thermogram of high alumina allophane, observing endothermal peak for water loss
06 p1004 A70-17225

Monograph on measurement and regeneration of water vapor loss of human skin, studying protective qualities of horny layer
10 p1812 A70-24598

Melatonin or water deprivation effects on pituitary serotonin content in rats
17 p3034 A70-35625

Intracellular shifts in body fluids and dehydration tolerance in burro, comparing water content of desert animals
21 p3766 A70-42157

WATER MANAGEMENT

Water depth determination by remote measurement of near IR reflectance of underwater plants, discussing effects of water path length changes
10 p1878 A70-24741

Swedish real time IR imaging system, discussing airborne applications in locating fresh water springs and defining irrigation patterns
10 p1879 A70-24743

Aerial photography analysis of drainage basin discharge properties, discussing surface runoff, subsurface flow and underground water movement
10 p1879 A70-24750

Ben Franklin submarine life support systems tested during Gulf Stream Drift Mission, discussing atmosphere control, water, waste and food management [ASME PAPER 70-DE-60]
16 p2852 A70-33515

Water management decision model using earth resources information system with satellite-based remote sensors, evaluating costs and benefits by systems analysis
20 p3616 A70-39066

Integrated Life Support System hardware tests, discussing oxygen and water recovery, contaminant control, personal accommodations and failure detection
21 p3833 A70-40989

WATER POLLUTION

Oil pollution remote sensing by aircraft, utilizing 9-14 micron IR mapper, 19.35 GHz microwave radiometer, aerial cameras and multiband video system
10 p1878 A70-24740

U.S. Coast Guard air delivered antipollution transfer system for oil, discussing deployment method, trajectory analysis, rigging techniques and full scale testing
[AIAA PAPER 70-1205] 21 p3752 A70-41813

WATER PRESSURE

Excess pressure in pulsed fluid jet with different emergent velocities from water hammer, discussing interaction between discrete sections 13 p2388 A70-29425

Vapor bubble response to sinusoidal pressure pulsation in water bulk and on metal wall 21 p3949 A70-41309

WATER RECLAMATION

Space stations life support systems for air purification, water reclamation and oxygen recovery 08 p1449 A70-20630

Vacuum distillation vapor filtered catalytic oxidation for water reclamation from human waste, using radioisotopes for thermal energy 20 p3579 A70-39437

Life support systems based on *Chlorella*-bacterial culture, investigating water exchange and reclamation 20 p3574 A70-40184

Vacuum distillation vapor filtered catalytic oxidation water recovery system, using radioisotopes for thermal energy supply 21 p3769 A70-40994

Potable water recovery from urine by vacuum distillation and vapor pyrolyzation 21 p3769 A70-40995

Integrated temperature and humidity control and water recovery subsystem for manned test in space station simulator 21 p3769 A70-40998

Closed loop life support system employing algae and bacteria cultures to recycle water in addition to atmospheric regeneration 23 p4156 A70-45024

WATER RECOVERY

U WATER RECLAMATION

WATER TAKEOFF AND LANDING AIRCRAFT

NT SEAPLANES

WATER TEMPERATURE

Human peripheral blood circulation during prolonged underwater activity, showing compensation for high humidity, noise levels, low water temperatures, isolation and confinement 10 p1822 A70-25178

WATER TUNNELS

U HYDRAULIC TEST TUNNELS

WATER VAPOR

Galactic water vapor line emission observations indicating short term variability in spectra of several sources 01 p0182 A70-10722

Nonequilibrium effect of expanding water vapor condensation on supersonic nozzle flows with or without inert carrier gas 01 p0063 A70-10806

Atmospheric water vapor photodissociation and resulting O evolution recalculated for determining O abundance in absence of biological activity 01 p0081 A70-11294

Stratospheric water vapor distribution from analyzing IR solar spectrum during sunset observed by balloon-borne spectrometer 01 p0081 A70-11295

Satellite and rocket probe measurements of water vapor in mesosphere 01 p0082 A70-11510

Atmospheric water vapor effect on contrast between natural target and sky via spectrophotometric method, exploring target visibility and contrast relations 02 p0325 A70-11873

Water vapor condensation by homogeneous nucleation measured for cluster number using laser light scattering compared with theory in condensing supersonic flow 02 p0279 A70-12048

Microwave dispersion caused by atmospheric gases at water vapor line, using microwave spectrometer based on dispersion detection in refraction spectrum 02 p0260 A70-12571

Troposphere microwave transmission factor determined from dispersion and attenuation caused by water vapor isolated molecular resonance 02 p0261 A70-12593

Water vapor ion cluster concentrations in d region, noting discrepancies above mesopause for model atmospheres predictions 03 p0478 A70-13992

Galactic water vapor radio sources spectral observation suggesting correlation between time variation and polarization 04 p0747 A70-14547

Depth and shape of 0.94 micron water vapor absorption band for clear and cloudy skies, noting radiation distortion for dark dense clouds 04 p0690 A70-15024

Spectral absorption and transparency of water vapor, carbon dioxide, carbon monoxide, methane and nitrous oxide bands in IR region 04 p0715 A70-15255

Dispersion and correlation function for atmospheric transparency due to water vapor, from statistical model of absorption bands and effective mass 06 p1053 A70-17204

Water droplets and air supersonic mixing, determining droplets size and optical properties 06 p0975 A70-18199

Cloud particles growth and interactions, discussing water vapor condensation, ice phase nucleation, rain droplet growth rate, etc 07 p1262 A70-18897

Production rate constants for hydrated positive ions in photoionized nitric oxide-water afterglows 07 p1346 A70-20245

Water vapor dissociation in dilute mixtures with Ar behind shock waves, studying OH concentrations using flash-absorption technique 08 p1548 A70-21355

IR spectral absorption coefficients determined for water vapor at high temperatures, describing experimental details including data acquisition and reduction 09 p1725 A70-22069

Temperature effects on IR absorption by water and carbon dioxide vapors measured in narrow spectral intervals 09 p1666 A70-22180

Vertical water vapor profile in strato-, meso- and thermospheres measured in rocket and satellite experiments by mass spectroscopy, spectral analysis and thermal sensometry 09 p1666 A70-22187

Water vapor high temperature dissociation kinetics in dilute mixtures with argon in shock waves 09 p1629 A70-22319

Water vapor emission detection from IR stars, discussing radial velocities of microwave lines 09 p1756 A70-22523

CW water vapor laser line frequency measurements by beating with radiations from HCN laser in metal-on-metal point contact diode 09 p1697 A70-22925

Grate spectrometer with high resolution for 20-45 micron range, describing water vapor transmission spectrum [ONERA-TP-782] 10 p1886 A70-23912

Atmospheric water vapor profiles remote measurements using Raman component of high powered Q switched laser backscatter 10 p1886 A70-23938

Oxide transport and water vapor effects on flash-heated beryllium droplet combustion 10 p1969 A70-25042

Quartz and alkaline glasses fracture stability in water vapor and aqueous solutions with enhanced surface activity as function of time 11 p2068 A70-25379

Fatigue life of Ni vibrated in reversed bending at 300 C in oxygen and in water vapor at various pressures 11 p2067 A70-26098

Recombination in hydrogen-oxygen reaction studied by monitoring IR emission from water vapor formed by shock initiated combustion 11 p1995 A70-26377

Water vapor pollution of stratosphere by supersonic transports, considering effects on temperature, cloudiness, albedo, etc 11 p2077 A70-26618

Stratospheric water vapor measurement by submillimeter wave sounding, considering signal fluctuations due to scattering by high cirrus clouds 11 p2077 A70-26619

Ultrasonic wave absorption and dispersion in mixtures of air and water vapor with water droplets, investigating equilibrium distribution and hydrodynamic equations [ASTME PAPER MR-69-733] 11 p2085 A70-26691

Satellite measurement of water vapor height profiles using outgoing thermal radiation and solar radiation atmospheric absorption techniques 13 p2392 A70-28571

Spectroscopic parameters for attenuation and dispersion caused by 22 GHz water vapor line, using differential microwave refractometer 13 p2393 A70-28784

Millimeter-wave probing for vertical distribution of atmospheric water vapor, comparing ground, balloon and satellite observation techniques 13 p2394 A70-28785

HOH lines existence in sunspot umbral spectrum 13 p2496 A70-29847

Fog droplet size growth time dependence and spectral variations during simulated cloud formation by water vapor condensation in chamber 14 p2601 A70-30128

Water vapor absorption bands in solar IR spectrum, considering earth curvature and atmospheric inhomogeneity and refraction 14 p2572 A70-30404

Water vapor in sunspots, taking into account red shift between telluric and intrinsic sunspot HOH lines 14 p2641 A70-30790

Humidity calibration utilizing precision wide range optically controlled thermoelectrically cooled dew point hygrometer 14 p2587 A70-31165

Water vapor abundance in Mars atmosphere from high resolution spectroscopy 14 p2649 A70-31211

Gases adsorption on water snows in cometary nucleus, noting sublimation rate role as regulating mechanism in gas production 14 p2650 A70-31244

Atomic emission in water vapor afterglow, revealing presence of Balmer series of H atom with sodium D line 14 p2579 A70-31255

Growing ice crystals surface electric potentials during various stages of water vapor condensation 15 p2769 A70-31444

Far IR second harmonic generation and frequency mixing in CdTe using pulsed water vapor laser 15 p2751 A70-31983

Molecular hydrogen, methane, water vapor and tritium concentrations near stratopause from air samples collected on Aerobee flight with liquid hydrogen cooled cryocondenser 15 p2728 A70-31995

Thermal energy negative ion-molecule reactions in photoionized NO-water vapor mixtures, determining rate constants by stationary afterglow system 16 p2954 A70-33280

Ionic collision processes in water vapor by high pressure single source mass spectrometry, examining reaction rates as function of primary ion translational energy 16 p2857 A70-34004

Telluric lines seasonal variations, discussing oxygen and water vapor photoelectric recordings in solar spectrum 16 p0000 A70-34185

Nongray radiant heat transfer corrections to thermal conductivity measurements for water vapor at atmospheric pressure 16 p3003 A70-34200

Venus deep mantle water degassing rate from atmospheric hydrogen escape data 17 p3154 A70-34610

Flux emissivity tables for water vapor, carbon dioxide and ozone based on wavelength dependent absorption coefficients and flux transmissivities 17 p3081 A70-35927

Water vapor pure rotational absorption spectrum compared with calculated far and near IR spectra 18 p3244 A70-35949

Venus atmosphere water content, discussing chemical reactions, temperature, dehydrogenation, etc 18 p3320 A70-37075

IR absorption by water vapor in transmittance windows, considering continuous absorption coefficient dependence on window width 19 p3461 A70-37425

Water vapor and OH spectra overlap, investigating association of galactic OH masers and water emission sources with IR stars 19 p3444 A70-37571

High altitude humidity from millimeter-band water vapor lines, using EHF atmospheric spectral transparency calculation 19 p3461 A70-37633

Breakdown electric field strength in S band microwave cavity for dry air, water vapor and mixture 19 p3423 A70-37757

Water vapor effect on carbon dioxide reaction with lithium hydroxide in dynamic isothermal system 20 p3582 A70-39227

Prototype electrolyzer for generating oxygen from water vapor under various atmospheric conditions, noting spacecraft cabin application 20 p3564 A70-39696

Cetyl alcohol and water vapor growth by absorption and condensation on hygroscopic nuclei population in atmosphere under cooling 20 p3664 A70-40066

Cloud structure, atmospheric water vapor and liquid water contents from passive ground based microwave spectrum measurements 21 p3846 A70-40906

D region water vapor chemistry effects on measurements of radio propagation, ionospheric temperature and seasonal changes 21 p3814 A70-40936

Moist air expansion through supersonic nozzle, investigating small ions role in water condensation 22 p4011 A70-42774

Water vapor homogeneous nucleation in simulated spacecraft debris clouds 22 p4110 A70-43115

Water vapor emission computation from statistical band model, investigating accuracy limitations 22 p4065 A70-43169

Transmission calculations for homogeneous and nonhomogeneous water vapor atmospheres, evaluating various methods 22 p4065 A70-43170

Aerosol impact traps for ground and airborne water vapor condensation studies 23 p4195 A70-44272

Spectral absorption of 2.7 micron water vapor band under various high temperature and pressure conditions, using black body radiation 23 p4220 A70-4444

Laser light scattering by moist air flows with condensed droplets of water vapor 24 p4353 A70-45565

Rate equation study of multiwavelength far IR laser oscillations in water vapor, taking into account molecular rotation-vibration interaction 24 p4354 A70-45812

WATER VEHICLES

NT AIRCRAFT CARRIERS

NT CAPTURED AIR BUBBLE VEHICLES

NT SHIPS

NT SUBMARINES

NT UNDERWATER VEHICLES

Portable telescope for river and ocean vessels, discussing design and operation thermal stability and hermetization 20 p3629 A70-39311

WATER WAVES

UHF radio telemetry system using pulse signal to measure and transmit sea waves amplitude and frequencies data to shore-based recorder 03 p0453 A70-14352

Heaving and pitching motion analysis of wave action-induced pressure gradients in captured air bubble /CAB/ ship bubble chamber, discussing fan system design [ASME PAPER 69-WA/AV-6] 04 p0622 A70-14902

Wave surface elevation and velocity fluctuations in ocean upper layer under wind waves, discussing correlation coefficients between vertical and horizontal velocity components 06 p1097 A70-17792

Turbulent energy and velocity spectra of air flow at atmospheric boundary layer over water analyzed statistically, assuming rippling surface activity 07 p1259 A70-19838

Shallow water waves simulation method for studying aerodynamic noise of free jet emitted from nozzle with variable wall roughness 08 p1485 A70-21608

Wave resistance of pressure field of hovercraft drifting over water surface determined as definite integral based on Wehausen expression 09 p1609 A70-22219

Internal waves breaking on sloping surface in two fluid system, studying interfacial shear instability by capacitance probe on-line computer system 09 p1717 A70-22371

Oceanic wind and wave predictions by satellite radar radiometer using single receiver to determine wind velocity [AIAA PAPER 70-310] 09 p1668 A70-22877

Wave physics using ocean waves as example, considering period, frequency, length, speed and similarity of various types 11 p2084 A70-26037

Laser profilometer for airborne ocean wave profile measurement 12 p2249 A70-28003

Mixed boundary value problems with radiation-type boundary conditions solved by complex Green function, discussing water waves in irrotational motion 13 p2452 A70-29536

Sonic boom penetration into water, discussing N wave reflection and refraction, sound fields, etc 16 p2952 A70-34095

Ocean swell wavelength and propagation direction measurements, using Fourier optical analysis of Apollo 7 space photography 22 p4029 A70-42766

Ocean roughness determination from satellite photographs sunglint patterns, indicating surface wind speeds 22 p4014 A70-42770

Ocean wave spectra from bistatic radar scatter data, using time delay Doppler-frequency map 23 p4184 A70-43802

Wind generated water waves spectral characteristics at low momentum levels 23 p4215 A70-44273

WATERPROOFING

Strain gages moisture protection, deriving formula for calculating acceptable protection time of insulator 11 p2049 A70-25586

WATTMETERS

Errors arising in torsion-type ponderomotive wattmeter connected in homogeneous microwave transmission line with mismatched oscillator at input and mismatched load at output 06 p1024 A70-17861

Wideband wattmeter for measurement and analysis of power dissipation in semiconductor switching devices, considering occurrence of peaks, frequency dependency of average dissipation, etc 23 p4174 A70-44597

WAVE ATTENUATION

NT ACOUSTIC ATTENUATION

NT RADAR ATTENUATION

NT RADIO ATTENUATION

NT SHOCK WAVE ATTENUATION

Absorbed RF plasma wave noise spectrum in region of anomalous dispersion, noting peak in far IR region 01 p0150 A70-10286

Resonance amplification theory of standing interfacial gravity waves in viscous fluids applied to obtain wavelengths prediction of atmospheric bow waves 01 p0081 A70-11299

Surface wave attenuation in homogeneous plasma cylinder caused by resonance in transition layer between plasma and vacuum 03 p0447 A70-13286

Sound waves dispersion and attenuation produced in gas flow by relaxation effects of solid particles presence 07 p1258 A70-19567

Ionospheric absorption of hydromagnetic waves propagated normal to magnetic field, comparing daytime to nighttime absorption [AFCRL-70-0133] 07 p1270 A70-20031

Ferrite Y-circulator, studying effects of attenuation in ferrite on mean frequency, admittance, forward and reverse losses, etc 09 p1648 A70-23157

Alfven shear waves collisionless damping from finite Larmor radius coupling to ion acoustic mode, observing longitudinal electric field existence 10 p1921 A70-23966

Laser light propagation along strongly inhomogeneous turbulent path, measuring intensity fluctuations dispersion and light amplitude 10 p1844 A70-25161

Gravity wave attenuation in F region investigated for role of ohmic losses 10 p1885 A70-25264

Ultrasonic wave absorption and dispersion in mixtures of air and water vapor with water droplets, investigating equilibrium distribution and hydrodynamic equations [ASTME PAPER MR-69-733] 11 p2085 A70-26691

Grains impurities effect on interstellar extinction curve from graphite grain model, discussing dirty ice coatings 13 p2489 A70-28915

Attenuation, resistivity and surface roughness measurements in rectangular waveguides 14 p2555 A70-30440

Trapped mode resonances, attenuation and launching tapers in overmoded rectangular waveguides 14 p2556 A70-30441

Periodically strip loaded dielectric slab guided electromagnetic waves, discussing attenuation and space harmonics amplitudes relationship 16 p2861 A70-32960

Collisionless damping of electromagnetic waves in regions with strong homogeneity of cold plasma 16 p2957 A70-33199

Ultrasonic pulses velocity and attenuation in fluids by coherent detection technique, measuring delay and decrease in amplitude due to transmission path length increase 16 p2913 A70-34084

Rocket exhaust micro and mm waves attenuation attributed to low ionization potential metal particles in propellants 17 p3196 A70-35215

Longitudinal wave absorbers attenuating resonance vibrations in rods and plates 18 p3337 A70-36304

Seismic wave attenuation mechanisms emphasizing partial melting, grain boundary relaxation and high temperature internal friction background 19 p3416 A70-38440

Helicon electromagnetic wave attenuation control by steady current of uniform density in propagation direction, considering Hall effect role 20 p3585 A70-39396

Phase velocity and attenuation of shear waves in gases from sampled-CW ultrasonic crystal resonator reflection measurement 21 p3827 A70-41457

Radial flow microturbines deflection and wave losses in circular nozzle ring oblique exit section 22 p3965 A70-43359

Ultrasonic absorption in SbSI semiconductors as function of temperature, illumination and constant electric field strength, noting absorption coefficient rise near Curie point 24 p4389 A70-45207

WAVE DIFFRACTION

Diffraction loss measurement in solid state laser to determine laser material contribution to total cavity loss 01 p0113 A70-10919

Incomplete Airy functions application to wave diffraction problems as canonical functions 01 p0144 A70-11090

Electromagnetic plane wave diffraction by slit and circular apertures in nonplanar conducting screens, presenting equiradiance contour maps 02 p0340 A70-12455

Gaussian laser beams diffraction by straight edge bounding opaque plane on basis of Kirchhoff scalar wave theory in Fresnel limit 02 p0313 A70-12456

Diffraction correction of terrestrial, atmospheric and cosmic background radiation at aperture and disk determined by artificial moon method 03 p0442 A70-13084

Interference wave formula for multiple reflections from smooth inhomogeneous region with arbitrary boundary 03 p0442 A70-13093

Plane electromagnetic wave diffraction at periodic arrays obtained by direct summation of multiple reflection between arrays 03 p0442 A70-13095

Shock wave diffraction at wedge moving at supersonic velocity, solving Hilbert space formulated for constant parameter flow 03 p0406 A70-13333

Electromagnetic wave diffraction effects on matching plasma waveguide to coaxial power extraction line 03 p0531 A70-13334

Plane longitudinal elastic monochromatic wave diffraction on stress free circular holes in infinite plate, calculating stresses between holes 03 p0589 A70-13375

Troposphere effects on low incident Explorer 22 satellite signal amplitude, noting role of diffraction 03 p0449 A70-13611

Plane electromagnetic wave diffraction at conducting stripline, calculating surface current density and far field scattering using edge wave and factorization methods 03 p0451 A70-13755

Two dimensional wave diffraction problems involving discontinuity line, analyzing instability behavior of geometrically induced singularities by applying integral transform on Helmholtz equations 03 p0525 A70-14199

Electromagnetic field sources in two dimensional problem of diffraction by slit 03 p0526 A70-14355

Plane shock wave diffraction and reflection at slender wedge in linear approximation, proposing pressure distribution calculation formulas behind shock 04 p0665 A70-14493

Electromagnetic inverse diffraction solved by Bojarski identity determining target geometry 04 p0720 A70-15703

Electromagnetic wave diffraction on absorbing black metallic and magnetic cylinders and strip, plotting radar scattering cross sections 05 p0813 A70-16262

Dynamical models of relative motions during earthquakes, solving numerically integral equations with nonintegral kernels in crack propagation and elastic wave diffraction 05 p0941 A70-16527

Correctness of Meixner assumption of scattered light field singularity near grating edge due to diffraction 05 p0816 A70-16879

Cylindrical confocal laser resonator with circular coupling aperture in center of mirror calculated for diffraction losses by numerical iteration 06 p1079 A70-17187

Plane light wave diffraction incident upon isotropic dielectric layer traversed by acoustic microwave using guided microwave theory 06 p1105 A70-17484

Mathematical models for progressing waves diffracted by smooth surfaces 06 p1105 A70-17533

Parallel plate TEM waveguides radiation pattern slope diffraction analysis 06 p1021 A70-17570

Polarization- and space-diversity reception techniques for radio links based on diffraction from ionized meteor trails 07 p1378 A70-18990

HF cylindrical waves propagation by line source in stratified medium, investigating refraction and diffraction at plane boundary using mathematical and ray methods 07 p1335 A70-19683

Focusing and saturation effects in radio star and satellite signal scintillations based on diffraction and refraction theories 07 p1271 A70-20157

Plate electromagnetic wave diffraction on conducting plate with circular hole 08 p1456 A70-20503

Kirchhoff theory of elastic wave diffraction in cylindrical case derived on modified Huygens principle, showing edge contribution 08 p1543 A70-20582

Plane E-polarized wave diffraction by slit in conducting screen using Fredholm integral equations of second kind 08 p1461 A70-21004

Diffraction by single wire waveguide with obstacle, considering propagation phenomena of symmetrical modes 08 p1472 A70-21042

Quasi-optical beam splitter, using grid diffraction of plane wave at dielectric cylinder, suitable for millimeter

ter and submillimeter wavelengths and thread measuring 08 p1496 A70-21219

Electrical and magnetic polarizability coefficients in theory of diffraction at small apertures by formulating bilateral variational principles 09 p1631 A70-22150

Electromagnetic waves diffraction on ideally conducting bodies of revolution, deriving design formulas for electric dipole 09 p1632 A70-22401

Electromagnetic wave diffraction by sphere and spheroid at resonance frequencies with incident wavelength comparable to bodies dimensions 09 p1632 A70-22402

Electromagnetic wave diffraction on array of plane waveguides, determining scattered field by solving infinite system of algebraic equations 09 p1632 A70-22407

Quasi-optical waveguide component /attenuator/ in S-band measured for performance noting diffraction as limiting factor 09 p1647 A70-22711

Plane electromagnetic wave diffraction on circular cylinder 09 p1638 A70-23339

Diffraction filters characteristics used in XUV spectroscopy involving solar, stellar and laboratory experiments 09 p1729 A70-23526

Oblique blast wave interaction with small bend along plane wall analyzed for diffraction using conformal transformation and complex variable techniques 10 p1869 A70-24524

Circular confocal laser with coupling aperture in mirror for maximum power output in specified mode, calculating field distributions and diffraction losses at reflectors 10 p1900 A70-24941

Plane electromagnetic wave diffraction at conducting stripline, calculating surface current density and far field scattering using edge wave and factorization methods 10 p1842 A70-25002

Two dimensional electromagnetic wave diffraction on arbitrary shaped homogeneous dielectric cylinder, solving integral equations on digital computer 10 p1842 A70-25105

Diffraction of plane cylindrical and spherical waves in wedge-shaped regions with reflecting edge, using asymptotic expansions 10 p1911 A70-25186

Uniform asymptotic theory of diffraction by edge of three dimensional body, obtained boundary layer solution applied to scattering by circular cylinder 11 p2084 A70-26422

Moire theory applied to direct strain measurement methods based on light diffraction 11 p2058 A70-26835

Plane electromagnetic wave diffraction by perfectly reflecting half plane calculated by elementary method 12 p2184 A70-27234

Plane periodic diffraction of elastic waves propagating in medium with infinite sequence of circular holes 12 p2325 A70-27557

Plane wave three dimensional diffraction through circular aperture in infinite screen computed for normal incidence, using Babinet principle 12 p2197 A70-27951

Diffraction and scattering of electromagnetic waves emitted by electric dipole arbitrarily oriented in space on inhomogeneous sphere 12 p2190 A70-28172

Textbook reissue on diffraction of electromagnetic and acoustic waves at open end of waveguide, using Wiener-Hopf-Fock factorization method 13 p2363 A70-28724

Correction to Smyrl results for perturbation pressure in interaction field behind plane shock diffracted by supersonically moving thin yawed wedge 13 p2338 A70-28822

Elastic plane wave diffraction and scattering at convex obstacle in semibounded regions, using method of images 13 p2452 A70-29289

Plane harmonic wave steady state diffraction at cylinder in elastic half space, applying method of images 13 p2366 A70-29320

Focusing lens edge diffraction effect on angular distribution of laser radiation, considering zero mode field distribution 13 p2428 A70-29367

Shock wave diffraction at wedge moving at supersonic velocity, solving Hilbert space formulated for constant parameter flow 14 p2528 A70-30712

Electromagnetic wave diffraction effects on matching plasma waveguide to coaxial power extraction line 14 p2623 A70-30713

Speckle patterns Fourier transform analysis for diffraction limited resolution attainment in large telescopes 14 p2589 A70-31382

Electromagnetic wave diffraction by heterogeneous planar dielectric structures, showing field distributions by single variable Fredholm equations 15 p2695 A70-31436

Diffraction on strip, investigating for Dirichlet boundary conditions, deriving excited current density and scattered pattern 15 p2696 A70-31515

Field correlation theorem for deducing Cassegrain antennas performance from internal field distributions, considering two reflector diffraction problems 15 p2698 A70-31953

Plane wave scattering by strip of elliptical cylinder, considering geometrical diffraction theory 15 p2700 A70-32405

Wave diffraction by wedge, using Heaviside step function and Sommerfeld contours 15 p2700 A70-32407

Wave diffraction by parabolic cylinder, solving boundary value problems for two dimensional wave equations via separation of variables 15 p2700 A70-32408

Wave diffraction by half plane limit of parabolic cylinder and wedge, using Fresnel integral and Heaviside step function 15 p2700 A70-32409

EM wave scattering and diffraction by acoustically soft and hard oblate spheroids 15 p2701 A70-32413

Electromagnetic waves diffraction and scattering from acoustically soft and hard and perfectly conducting disks in plane or arbitrary incidence directions 15 p2701 A70-32414

Radiation pattern of radial infinitesimal current elements near or on finite length conducting cylinders, using image and geometrical theory of diffraction techniques 16 p2860 A70-32956

Plane wave diffraction by cylinder tipped half plane, demonstrating localized behavior by geometrical theory 16 p2872 A70-32975

Monochromatic electromagnetic wave diffraction on moving ideally conducting half plane, deriving parameters and spectral composition after diffraction 16 p2863 A70-33216

Microwave antenna with aperture in infinite conducting plane, analyzing radiation patterns, scattering and diffraction 17 p3043 A70-35053

German monograph on shock wave diffraction at spheres and cylinders 17 p3071 A70-35377

Long range tropospheric radio wave propagation, calculating signal impulse function and time lag between diffraction and reflection 17 p3048 A70-35678

Plane normal shock front diffraction along free interface between half planes of homogeneous fluids at rest, using method of characteristics and Whitham technique 17 p3074 A70-35886

Shock wave diffraction by moving thin wing over flat terrains, discussing aircraft blast encounter 18 p3205 A70-36195

Plane wave diffraction by periodic grating reduced to waveguide problem, determining asymptotic behavior of integral solution 18 p3291 A70-36286

Plane electromagnetic waves diffraction by periodic structure of infinite system of parallel strips, reducing problem to solution of linear algebraic equations 18 p3227 A70-36287

Plane electromagnetic wave diffraction by infinite grid above finite dielectric layer, calculating field distribution 19 p3375 A70-37281

Electric field equations of plane EM wave diffraction at lattice of conducting cylinders, using Hankel function 19 p3375 A70-37289

Diffraction by star bounded by closed contour scalar field created by surrounding medium, reducing solution to boundary value problem via algorithm 19 p3470 A70-37431

Diffraction of EM waves emitted by vertical electric dipole on conducting thin circular disk, using algorithm for integral equation 19 p3375 A70-37432

Plane EM wave diffraction by conducting strip, using algorithm for reducing integral to linear algebraic equations 19 p3376 A70-37433

Regularizing algorithm for Fredholm integral equation used in diffraction by ideally conducting strip 19 p3376 A70-37434

One dimensional integral equations for two dimensional problems of EM wave diffraction by cylindrical bodies 19 p3376 A70-37435

Electromagnetic wave diffraction by inhomogeneous anisotropic body, applying Fredholm integral equations 19 p3376 A70-37436

Plane electromagnetic wave diffraction by thin metal gratings, using mathematical method of elasticity theory 19 p3376 A70-37712

Plane polarized electromagnetic wave diffraction by dielectric grating, obtaining linear algebraic equations for field coefficients 19 p3376 A70-37713

Polarized plane EM wave diffraction by inclined half plane grating, obtaining transformation matrices coefficients 19 p3376 A70-37714

Plane wave diffraction by serrated surface, examining wave transformation matrix coefficients 19 p3377 A70-37715

Wave diffraction by finite dimension grating, determining EM field strength distribution by approximate method 19 p3377 A70-37716

Plane EM wave diffraction by ribbon periodic grating, determining diffraction spectrum wave amplitudes 19 p3377 A70-37718

Plane EM wave diffraction by bounded and unbounded periodic gratings 19 p3377 A70-37719

Diffracted-field structure on two-element gratings in near zone, calculating amplitude, phase and energy flux for normal and slant incidence of EM fields 19 p3377 A70-37720

Plane monochromatic EM wave diffraction by rectangular metal bar tapered grating, examining amplitude and polarization parameters 19 p3377 A70-37721

Diffraction radiation excitation by electron beam moving within resonant system formed by ribbon grating and metal plane, taking into account screen conduction losses 19 p3377 A70-37724

Polarized electromagnetic wave diffraction by semiminfinite symmetrical obstacles in rectangular waveguide, calculating transformation coefficients for wide frequency range 19 p3378 A70-37729

Linear equations for wave diffraction in rectangular waveguides with step-shaped inhomogeneities 19 p3378 A70-37730

H and E waves diffraction in circular waveguide by diaphragm thickness, using linear equations and Fourier-Bessel series for representation 19 p3378 A70-37731

Cylindrical EM waves diffraction by two parallel ideally conducting elliptical cylinders, discussing field and surface current distributions 19 p3378 A70-37734

Plane EM wave diffraction in cylindrical plasma-electron beam system 19 p3378 A70-37740

Double asymmetric grating with thin ideally conducting strips, describing incident E-polarized electromagnetic wave diffraction 19 p3378 A70-37744

Diffraction amplitudes in plane H-polarized electromagnetic wave incident obliquely on grating with closely spaced conducting rectangular bars, obtaining transmission coefficient 19 p3378 A70-37745

Strain transducer /optical diffraction grating/ for plastic wave propagation measurement along specimens subjected to impact 19 p3425 A70-37884

Geomagnetic pulsations propagation through horizontally inhomogeneous ionosphere, solving EM wave diffraction problem 19 p3416 A70-38589

Diffraction effects on radiometer field of view with rectangular primary and secondary apertures and field stop 20 p3627 A70-39087

Power diffraction losses at mirrors of asymmetric confocal laser interferometers with output coupling apertures 20 p3628 A70-39130

Diffraction-limited scalar image formation with large angle point reference hologram arrangement of arbitrary surface shape, point reference source and object 20 p3628 A70-39131

Asymptotic expansion methods for solving wave propagation and diffraction problems via localization principle 20 p3657 A70-39219

Space-time rays relation to plane wave dispersion surfaces in radiation and diffraction problems, using ray tracing diagrams 20 p3671 A70-39220

Plane electromagnetic waves diffraction on thin filaments cloud /passive dipoles/, discussing field fluctuations and mean power 20 p3588 A70-40298

Microwave aperture antenna in finite size ground plane, calculating radiation pattern distortion by superposition of boundary value and wedge diffraction solutions 20 p3599 A70-40314

Plane wave diffraction by periodic array at boundary between two media, discussing asymptotic behavior of reflection and transmission coefficients 21 p3806 A70-40614

Electromagnetic wave diffraction by ideally conducting wedge of finite radius, deriving asymptotic formula for plane wave scattering 21 p3784 A70-40626

Frequency shifted diffraction of monochromatic Gaussian light beam by reflection off ultrasonic surface wave 21 p3850 A70-41907

Diffraction theory relationship to ray optics for coherent light propagation through lens systems 21 p3829 A70-41929

Diffraction theory of sideband holography with transmission objects, discussing geometrical construction of image location and disappearance conditions 21 p3830 A70-41998

Plane electromagnetic waves diffraction by moving periodic metal strip grating, writing E polarized wave of unit amplitude by Lorentz transforms 22 p3984 A70-42388

Stationary saddle points phase method for wave diffraction problems in inhomogeneous medium, deriving asymptotic expansion for surface integrals 22 p3984 A70-42390

Electromagnetic wave diffraction at multilayer wire grating, discussing computer program for diffraction field calculation 22 p3985 A70-42399

Elastic wave diffraction by rigid inclusion, calculating far field displacement and cross section by integral equation method 22 p4073 A70-42636

Remote sensing of returning reflected and diffracted seismic waves illuminating layered rocks subsurface, discussing data visual display 22 p4018 A70-43085

Far field diffraction spreading of surface acoustic waves on cut Li-niobate in two directions 23 p4230 A70-44199

Spectral filtration methods in diffraction instruments at vacuum UV region, discussing ambient storage conditions and fabrication effects 23 p4219 A70-44412

EM wave backscattering from lossless dielectric sphere, examining diffracted field surface waves role 23 p4165 A70-44960

Sonic boom waves diffraction and reflection, developing analytical method for pressure-time history in vicinity of walls and corners 24 p4289 A70-45266

Plane wave diffraction by infinite strips and slitted planes, obtaining asymptotic expansions valid for HF 24 p4426 A70-46019

Confocal microwave Fabry-Perot interferometer resonator diffraction loss and field configuration measurements, noting agreement with theory 24 p4381 A70-46242

WAVE DISPERSION

He-Ne laser heterodyne system evaluating dispersive effect in He-Ne laser, measuring dispersion as function of cavity loss, excitation level, etc 01 p0107 A70-10102

LF longitudinal waves propagation in DC gas discharge plasma, obtaining wave dispersion equation for various limiting gases 01 p0149 A70-10162

Absorbed RF plasma wave noise spectrum in region of anomalous dispersion, noting peak in far IR region 01 p0150 A70-10286

Electromagnetic propagation in linear dispersive media, discussing energy transport velocities of total stored energy density and electromagnetic energy 01 p0043 A70-10779

Flexural wave propagation in infinitely long circular bimaterial cylinders based on equations of linear elasticity, noting dispersion characteristics different from homogeneous cylinders 01 p0208 A70-11188

Plasma concentration diagnostics in magnetosphere based on hydromagnetic whistlers/pearls/dispersion 01 p0084 A70-11554

Book on communication and information theories application to fading dispersive communication channels, discussing tropospheric scatter, HF ionospheric links, moon bounds, etc 02 p0253 A70-11700

Microwave dispersion caused by atmospheric gases at water vapor line, using microwave spectrometer based on dispersion detection in refraction spectrum 02 p0260 A70-12571

Free oscillations and surface wave dispersions from lunar models based on Orbiter data and corresponding pressure region of earth crust 02 p0379 A70-12777

Dispersive compression of plane frequency modulated waves in inhomogeneous plasma based on generalizing geometric optics approximation to unsteady quasi-harmonic processes 03 p0447 A70-13287

Dispersion equation and coupling impedance of two dimensionally periodic slow wave structure of cellular cylinder type with parallel perpendicular diaphragms 03 p0456 A70-13438

Atmospheric distortion effect on short laser pulses attributed to aerosols, using real time pulse comparison methods 04 p0701 A70-15020

Dispersion curves for wave propagation in infinite elastic bars of elliptic cross section obtained by method of collocation 04 p0773 A70-15080

Numerical solution for differential equations describing nonlinear beam-plasma interactions based on dispersion relation analysis 05 p0886 A70-15799

Pulsars dispersions, setting upper limit to emission measure of dense plasma 05 p0921 A70-16984

Propagation, reflection and dispersion equation for electromagnetic waves in longitudinally magnetized plasma filled coaxial waveguide using rotating coordinates 06 p1016 A70-17124

Wave dispersion across magnetic field in cold and warm collisionless Maxwellian plasmas, discussing electromagnetic and electrostatic Bernstein modes 06 p1116 A70-17364

Anomalous dispersion measurements in IR range with multibeam sequential Fabry-Perot interferometers using photoelectric method 06 p1064 A70-17811

Pipe bounding walls effect on sound waves dispersion in rarefied gas, deriving integral equations showing frequency range decrease with container size 06 p1107 A70-18315

Sound waves dispersion and attenuation produced in gas flow by relaxation effects of solid particles presence 07 p1258 A70-19567

Dispersion of ion-acoustic waves in quiescent rare gas discharge plasmas, discussing model simulating ion waves generated by finite sine wave bursts 07 p1352 A70-19990

Diffraction pattern drift velocity increase with temporal frequency of Fourier components by dispersion analysis of interplanetary scintillation, noting solar wind structure 07 p1388 A70-20076

Plasma-electron beam system LF dispersion characteristics noting ion instability 08 p1549 A70-20505

Spectrum of waves emitted from waveguide of two plane dielectric or isotropic plasma layers, solving dispersion equations numerically by computer 08 p1472 A70-20973

Weakly nonlinear dispersive cold plasma waves propagation by two time scale expansion, taking into account amplitude dispersion and coupling 08 p1553 A70-21613

Stellar scintillation saturation at large zenith angles interpreted in terms of combined dispersion and aperture filtering 09 p1726 A70-22073

Single-pulse laser radiation losses dependence on operation time length due to angular dispersion 09 p1694 A70-22140

Wave dispersion relations in uniform magnetized plasma represented in single integral form, discussing model loss-cone and temperature anisotropy distributions 09 p1736 A70-23188

Polydisperse dielectric system distribution parameters determined from hard monochromatic polarized radiation scatter by artificial aerosols 10 p1916 A70-24500

Ionospheric irregularities showing dispersive motions from systematic skewness in cross correlation functions for satellite scintillations at space receivers 10 p1881 A70-24810

Helicon wave dispersion in cold multicomponent plasma of n-type Si and Ge semiconductors in linear hydrodynamic approximation 10 p1928 A70-24832

Waveguides consisting of three concentric regions suitable for plasma experiments, showing dispersion characteristics and cut-off frequencies 10 p1850 A70-24835

LF longitudinal waves propagation in DC gas discharge plasma, obtaining wave dispersion equation for various limiting gases 10 p1925 A70-25010

Stationary and nonstationary nonlinear waves propagation in multicomponent collisionless plasma, considering dispersion relations for acoustic oscillations 10 p1844 A70-25166

Ultrasonic wave absorption and dispersion in mixtures of air and water vapor with water droplets, investigating equilibrium distribution and hydrodynamic equations [ASTME PAPER MR-69-733] 11 p2085 A70-26691

Microwave lines dispersion equations for ferrite cylinder and spiral and circular waveguides 11 p2012 A70-26803

Dispersion relations between wave frequency and vector obtained from matrix equation for wave propagation in solid state plasma with ferroelectric and ferromagnetic properties 12 p2283 A70-26971

Dispersion relation derived for space-charge waves propagating in thick Gunn diode, showing validity limit of one dimensional approach 12 p2194 A70-27164

Linearized dispersion relation for plane wave propagation in uniform unbounded cold plasma permeated by DC magnetic field, considering two stream instability 12 p2281 A70-27881

Wave propagation in spatially homogeneous time varying dispersive media, emphasizing excitation and source dependent phenomenon 12 p2188 A70-27961

Monochromators dispersion and resolution increased by multiple passage of light through singly dispersive element, comparing optical schemes 12 p2237 A70-28160

Light pulse propagation in dispersive nonlinear dielectric analyzed on nonlinear Lorentz model 12 p2274 A70-28216

LF electrostatic waves oblique to magnetic field in plasma, evaluating dispersion relation near ion cyclotron frequency 13 p2363 A70-28641

Spectroscopic parameters for attenuation and dispersion caused by 22 GHz water vapor line, using differential microwave refractometer 13 p2393 A70-28784

Wave dispersion in lower exospheric multicomponent plasma, investigating mode group velocity frequency dependence at various altitudes 13 p2395 A70-28940

Electrostatic waves for upper ionospheric plasma model, obtaining solutions to dispersion relation at multiples of electron cyclotron frequency 13 p2400 A70-29914

Hydromagnetic wave velocity and space anisotropy instabilities in magnetosphere, using dispersion relation 13 p2483 A70-30086

Laser beams intensity fluctuations dispersions and correlation functions at various distances 14 p2593 A70-30172

Atmospheric turbulence effects on acoustic-gravity waves propagation, deriving dispersion relation for phase velocity and propagation constants 14 p2579 A70-31252

Space charge waves in electron beams with velocity distribution, considering dispersion equation and Landau damping 15 p2708 A70-31831

Plasma beam systems dispersion equation with allowance for electron collisions with heavy particles 15 p2779 A70-32117

Large amplitude electromagnetic waves propagation along plane parallel nonlinear dielectric layer, considering dispersion and permittivity 15 p2699 A70-32190

Single mode gas laser with large saturation and dispersion effects, discussing resonator alignment to spectral line frequency 15 p2752 A70-32196

Approximate dispersion relation for MHD waves from macroscopic plasma equations including particles collision terms 16 p2859 A70-32941

Angular scattering of interstellar medium resulting in multipath dispersion of pulsar pulses, discussing NP0532 in Crab Nebula 16 p2972 A70-32988

Troposphere effects on microwave and optical signals, correlating refractive index and dispersion variabilities 16 p2862 A70-33020

Methods and equipments for light dispersion measurements for determining atmospheric refraction in terrestrial angle and electrooptical distance measurements 16 p2911 A70-33523

Wave propagation in infinite elastic plate in contact with inviscid incompressible liquid layer, deriving dispersion relation 16 p2993 A70-34094

Heteroepitaxial ZnO film on anisotropic sapphire substrate, calculating dispersion for fundamental Rayleigh wave mode 17 p3144 A70-35908

Radiation condition for unbounded anisotropic dispersive magnetoplasma 18 p3295 A70-36492

Elastic particulate composite solid with microinclusions, deriving dispersion relations governing plane longitudinal wave propagation modes by analogy with continuum theory 19 p3540 A70-37942

Synchrotron radiation emissivity function containment in dispersion equation for plane wave propagation in magnetoactive plasma 19 p3480 A70-38017

Multilayered and multiple supersonic jets, deriving dispersion equations for boundaries stability 19 p3354 A70-38663

Holographic bandwidth reduction by periodic dispersion structures, noting large viewfield and compact data recording 20 p3627 A70-39096

Space-time rays relation to plane wave dispersion surfaces in radiation and diffraction problems, using ray tracing diagrams

20 p3671 A70-39220

Electrostatic ion waves in uniform magnetic field, calculating phase and group velocities as function of propagation angle for comparison with dispersion measurements

20 p3678 A70-39659

Electromagnetic wave propagation in one dimensional periodic waveguide slow wave systems, deriving dispersion curves by perturbation theory

21 p3784 A70-40628

Collisionless shock wave geometry, determining dispersion relation for ion acoustic waves propagating in plasma

21 p3856 A70-41082

Mach-Zehnder interferometer for plasma diagnostics measurements, discussing optical interference method, fringe shift determination and dispersion equations

21 p3856 A70-41150

Plasma turbulence statistical theory in magnetic field based on averaging operators, deriving nonlinear dispersion relation

21 p3857 A70-41386

Pulse velocity and mode pulling in inhomogeneously broadened laser with equally spaced modes, noting pulse shape time stability in presence of dispersion

21 p3838 A70-42008

Gas discharge positive column finite length effect on wave dispersion and instability, indicating critical magnetic field

22 p4079 A70-42374

Dispersion equation for impedance elements periodic structures phase velocity calculation, discussing approximate solution methods

22 p3984 A70-42392

Isotropic homogeneous elastic cylindrical rods, investigating nonlinear longitudinal dispersive waves corresponding to water wave theory analogs

22 p4115 A70-42952

Striations due to mechanical oscillations in fast wire explosions, using dispersion for elastic waves in solid cylinders

22 p4074 A70-43002

Dispersion characteristics of electronically tunable periodic rectangular waveguides, using external DC magnetic field

23 p4168 A70-43781

Multiphase modes for nonlinear dispersive waves under large scale interaction, extending Whitham theory

23 p4217 A70-43943

Microwave lines dispersion equations for ferrite cylinder and spiral and circular waveguides

24 p4317 A70-45178

WAVE DRAG

NT INTERFERENCE DRAG

Wave drag dependence of delta wings on thickness distribution [DVL-888]

03 p0406 A70-13273

Wave drag in stratified flow lee waves without upstream influence calculated for cylindrical and three dimensional obstacles

03 p0479 A70-14229

Slender wings and fuselages resistance at zero lift in supersonic flow, using Karman and Moore linear theory [DGLR-69-28]

04 p0616 A70-15154

Generatrix shape determined for body of revolution moving at supersonic speed with minimum wave drag

09 p1603 A70-22434

Slender body transonic wave drag double integral, describing computer program for numerical evaluation

11 p1977 A70-26644

Minimum-drag boattail configurations optimization for supersonic flow, determining wave drag coefficients

22 p3961 A70-42714

Wave drag due to swirling flow through convergent-divergent nozzle, deriving approximate solution for specified nozzle shape at various swirl ratios

23 p4179 A70-43971

WAVE EQUATIONS

NT LAME WAVE EQUATIONS

NT SCHROEDINGER EQUATION

Potential representation of vector fields effecting decoupling of vector wave equation of elasticity for radially heterogeneous isotropic media

01 p0208 A70-11189

Longitudinal wave motion in rods, plates and shells based on three dimensional equations and asymptotic expansion

01 p0209 A70-11365

Integral theorems for wave-type heat conductivity equation

01 p0219 A70-11398

Self similar wave solutions of continuity and momentum equations for two dimensional unsteady isentropic motion of polytropic gas

02 p0278 A70-11998

Propagation equations for spherical waves in elastoplastic work hardening materials

03 p0585 A70-12972

Van der Pol equation for finite amplitude ion-acoustic waves in unstable plasma propagating across weak magnetic field

03 p0531 A70-13404

Spatial amplification criteria for hyperbolic wave equations extended to include parabolic equations, discussing convective and absolute instabilities

03 p0519 A70-13522

Solutions properties of initial and mixed initial-boundary value problems of wave equations

03 p0537 A70-14384

Surface waves excited by horn above dielectric disk backed by metallic disk, formulating characteristic wave equations and solving for attenuation and propagation constants

04 p0659 A70-15305

Nonlinear wave propagation in relaxing gas with internal energy characterized by translational and internal temperature, using model equation for piston induced motion

04 p0786 A70-15324

Free vibrations of layer of micropolar continuum, analyzing displacements, microrotations and frequencies as wave number power series

04 p0777 A70-15498

Propagation and growth equations governing wave propagation in micropolar viscoelastic solids couplings between discontinuities in macroscopic and microscopic fields

05 p0929 A70-16063

Finite difference wave equation to obtain asymptotic estimate for magnitude of precursor effects

05 p0875 A70-16310

Second order wave structure theory for shock wave system from body in supersonic flight analyzed for planar flows

05 p0790 A70-16797

Small amplitude spherical elastic-plastic waves initial behavior studied for critical and supercritical loading

05 p0945 A70-16819

Wave equation for elastic waves in isotropic solid solved in Cartesian and circular cylindrical coordinates for studying microsonic wave guiding structures

06 p1105 A70-17479

Linear transformation of waves in nonuniform magnetoactive plasma by solving wave equation with/without allowance for spatial dispersion

06 p1119 A70-17498

Eigenvalue corresponding to decaying modes for wave equation in exterior of obstacle investigated for dependence on obstacle geometry

06 p1095 A70-18474

Time dependent relaxation model for heat flux in metals from quantum mechanical form of Boltzmann transport equation, yielding damped wave equation for temperature

06 p1090 A70-18612

Infinite-dimensional relativistic wave equations for mass spin dependence

07 p1333 A70-18959

Surface inhomogeneities effect on sound radiated by nearby turbulence near flexible boundary, using converted Lighthill wave equation to obtain far field radiation

07 p1256 A70-19262

Laser resonator with concave mirrors and ring aperture as radiation outlet, calculating natural oscillations by wave equation

08 p1510 A70-20508

Book on mathematical theory of electromagnetic waves covering vector analysis, reduced wave equation, linear transformations, boundary value problems and radiation patterns

08 p1533 A70-20759

Curved thin rods torsional and flexural waves propagation equations, considering geometry and shear and Young moduli

08 p1588 A70-21201

Heavy particle collisions impact parameter and wave equations for direct excitation and electron capture processes

08 p1548 A70-21502

Two dimensionally periodic slow wave structure, verifying Shein formulas

09 p1637 A70-23143

Radio wave propagation equations, applying stationary phase method for finite limits of dimensionless line integral

09 p1638 A70-23662

Sound energy transmission and radiation into room by flexible structural panels subjected to acoustic excitation using wave equations

10 p1964 A70-25224

Volterra method applied to solution of mixed boundary value problems for wave equation

12 p2159 A70-28243

Shock and simple wave interactions, using quasi-linear equations for forward facing wave overtaking forward facing shock

14 p2567 A70-31283

Hadron energy levels description by Lorentz invariant wave equation in form of supermultiples

15 p2776 A70-31736

WKB method applied to ionospheric equations with strong wave coupling

15 p2725 A70-31857

Micropolar Cosserat medium of thermoelasticity wave equations for Hooke medium, deriving elastic potentials and stress functions

15 p2822 A70-32354

Wave scattering from elliptic cylinder, solving boundary value problem for two dimensional wave equation

15 p2700 A70-32404

Oscillatory and wave processes in nonlinear distributed systems by asymptotic method analogous to Bogoliubov concentrated systems

16 p2951 A70-33252

Nonlinear wave equations model for human torso under impulsive stress, obtaining asymptotic solution

16 p2854 A70-34247

Thermomagnetoelasticity wave equations of heat conduction for thermal and coupled perturbations propagating in isotropic medium at finite velocities

16 p2953 A70-34326

Phase plane method for Hill equation in problems involving EM wave expansion in elliptical waveguides or single circuit parametric systems analysis

18 p3227 A70-36424

Adiabatic invariant of nonlinear periodic wave described by partial differential equations in weakly inhomogeneous medium

18 p3291 A70-36642

Existence theorem for piecewise-continuous solutions of waves and shocks in relativistic MHD, using Riemann manifold

19 p3477 A70-37579

Electric field component equations of electromagnetic wave traveling through stratified plasma, considering incident and reflected ordinary and extraordinary waves

19 p3379 A70-37863

Electron-ion wave interaction due to scattering by electrons, using kinetic wave equation to describe wave-particle interaction

21 p3858 A70-41712

Liquid propellant rocket engine combustion instabilities, describing unsteady combustor flow by single nonlinear wave equation with stable and unstable finite amplitude limit cycles

23 p4233 A70-44425

Perturbation effects on nonlinear first order wave equations discontinuous solutions decay, discussing boundary value problem for stress wave propagation in rod with viscous damping

24 p4426 A70-46026

Variational principle and reciprocity theorem for initial value problems associated with wave equations, discussing solution uniqueness conditions

24 p4380 A70-46037

Optical wave propagation through random atmospheric turbulence, deriving wave equation power series solution for homogeneous random refractive index field

24 p4314 A70-46126

WAVE EXCITATION

NT ACOUSTIC EXCITATION

NT HARMONIC EXCITATION

Multimode excitation of large aperture horn antennas to produce electronic deflections of directional pattern

01 p0046 A70-11454

Surface function and impedance distribution for unilateral surface wave antenna excitation by slot emitter above surface impedance segment

04 p0655 A70-14403

Equatorial jet stream excitation of longitudinal waves, analyzing plasma beam instability and spectrum of short wave inhomogeneities by quasi-hydrodynamic equations

05 p0842 A70-16759

Nonlinear effects in spiral galaxies with emphasis on solar neighborhood region, discussing radial motion, stationary state with excited waves and vertex deviation

05 p0917 A70-16905

Radiation patterns from finite conducting cone excited by quarter wave monopole protruding from center of base computed on digital computer

06 p1020 A70-17559

Reflection coefficients, radiation patterns and surface wave excitation calculated from aperture electric field obtained for waveguide radiating through dielectric slab

06 p1020 A70-17561

Collisional skewing of electron distribution function associated with heat conduction in solar wind, exciting collisionless ion-acoustic, electrostatic ion cyclotron and magnetoacoustic waves

06 p1136 A70-18527

Spontaneous echoes amplitude resulting from damped electronic plasma plane wave excitation in collisionless plasma

09 p1735 A70-22843

Ion-burst excited by pulsed mesh grid in plasma in connection with sheath structure

10 p1922 A70-23989

Nonlinear parametric excitation of stable resonant drift waves by mode-mode coupling in potassium plasma of Q device

11 p2090 A70-26020

Waves and mean currents excitation in stratified fluid due to moving heat source, studying effect on mean motion

11 p2036 A70-26167

Wave propagation in spatially homogeneous time varying dispersive media, emphasizing excitation and source dependent phenomenon

12 p2188 A70-27961

Fabry-Perot resonator higher modes excitation by external TEM wave, discussing optimal mismatch for maximum intensity

13 p2408 A70-29358

Surface wave excitation including PM and dipole modes and Sommerfeld waves

14 p2549 A70-30444

Periodic shock waves amplitudes and profiles, investigating longitudinal nonlinear oscillations of gas excited in closed tube

15 p2719 A70-31482

Transient excitation of Schumann earth-ionosphere cavity resonances by large ELF atmospherics, using propagation model

15 p2726 A70-31865

Resonance excitation of high amplitude waves in plasma cylinder by HF azimuthal axially periodic current flowing through coil encircling plasma

16 p2957 A70-33194

Longitudinal and transverse hypersonic mm waves excitation in quartz single crystal at liquid helium temperature

16 p2952 A70-33258

HE sub 11 mode launching in optical communication system, considering fiber tapering effect on excitation efficiency

16 p2875 A70-33400

Plasma waves parametric excitation by external electric field, using perturbation method of multitime scales

17 p3140 A70-34933

Surface wave antennas, operated on guided wave mode parallel to interface and with radiation at discontinuities, calculating excitation and radiation characteristics

17 p3052 A70-35072

Type I burst effects on type III and V bursts occurrence, suggesting Langmuir waves excited by suprathermal electrons

17 p3173 A70-35746

Scattering structures of two parallel elliptical cylinders, tapes or combinations, deriving surface current density distribution under plane TM wave excitation

19 p3375 A70-37279

Homogeneous plasma electrostatic oscillations excitation by electromagnetic waves nonlinear interaction in magnetic field, deriving expression for density perturbation

19 p3475 A70-37536

Diffraction radiation excitation by electron beam moving within resonant system formed by ribbon grating and metal plane, taking into account screen conduction losses

19 p3377 A70-37724

Open plane slotted waveguide excitation by current carrying filament, using long wave approximation

19 p3377 A70-37726

Two axially positioned cylindrical waveguides with slots cut periodically along generatrices/double squirrel cage/, analyzing behavior under excitation by rotating charged filament

19 p3386 A70-37733

Electromagnetic waves and oscillations excited by magnetic current ring source around infinitely long compressible plasma column, deriving radiation field distribution

20 p3685 A70-40506

Alfven waves amplification propagating along sinusoidally perturbed magnetic field in argon plasma, noting parametric excitation

21 p3855 A70-40947

Spread electron beam excitation of magnetoactive plasma waves in quasi-linear relaxation

21 p3855 A70-40948

Continuous pseudoacoustic and ion waves excitation and damping in plasma sheath around grid, taking into account transit time effect on ion acceleration

21 p3858 A70-41710

Ionization waves excitation and damping in MHD channels, investigating effects on electric conductivity, Hall parameter and electron temperature

22 p4081 A70-42823

Longitudinal and transverse hypersonic mm waves excitation in quartz single crystal at liquid helium temperature

23 p4218 A70-44281

Acoustic plasma wave excitation by transverse electromagnetic wave beam, calculating LF instabilities and energy losses

24 p4384 A70-45149

Microwave waveguide rotary joint using symmetrical excitation for mode conversion to obviate filters

24 p4318 A70-45221

Nonspherical wave excitation in solar atmosphere in presence of toroidal magnetic field

24 p4400 A70-45312

Type 2 solar radio burst shock wave exciter velocity from dynamic spectrograms, relating correction to shock strength gradient

24 p4401 A70-45322

Cs ion beam space charge and current neutralization by electron capture for partially ionized plasma formation, investigating longitudinal electrostatic wave excitation

24 p4385 A70-45465

WAVE FRONT DEFORMATION

Wave front discontinuities during pressure wave propagation in membranes and elastic shells by asymptotic procedure using Laplace transform

03 p0589 A70-13331

Saturation induced wave front distortions effect on beam divergence and frequency modulation in laser amplifiers, discussing refractive index changes

04 p0703 A70-15620

Warped wave front viewpoint in analyzing object plane resolution, contrast and location in polariscopes

07 p1280 A70-19236

Gasdynamic flows strong and weak density discontinuity surfaces determination, using shadowgraphs and interference patterns

12 p2238 A70-28248

Wave front discontinuities during pressure wave propagation in membranes and elastic shells by asymptotic procedure using Laplace transform

14 p2657 A70-30710

Wave front reconstruction from blazed holograms, noting wave front distortion for nonconstant amplitude case

15 p2736 A70-32011

Interferograms of window wave front deformations to measure angular deviations to line of sight

15 p2737 A70-32038

Manganin in wire and thin foil geometries, measuring shock piezoresistance coefficient as function of deformation

20 p3687 A70-40166

Microwave transmission over elevated line-of-sight path, measuring phase front distortion between pairs of paths

22 p3991 A70-43580

WAVE FRONT RECONSTRUCTION

Optical reconstruction of microwave holograms recorded by liquid crystal detectors, emphasizing dependence on IR heat bias provided by incandescent bulb

01 p0086 A70-10421

Holographic two beam real-time Fizeau interferometer for recording and reconstructing reflected light waves in silvered flat surfaces measurement

01 p0090 A70-10905

Interference fringe in Fraunhofer hologram reconstruction of tapered glass fibers related to fiber profiles

01 p0090 A70-10906

IR holography using thermochromic material and cuprous mercuric iodide to record on-axis interference pattern, reconstructing in visible range with He-Ne laser

01 p0092 A70-11170

Hologram image resolution, finding angular alignment of reconstruction wavefront as limiting factor

02 p0297 A70-11923

Anamorphic holograms in optical and radar holography and reconstruction, discussing formation and fundamentals

02 p0298 A70-12182

Microwave holography using probe scanning, analyzing causes of distortion and effects on image reconstruction

02 p0302 A70-12618

Holographic wavefront reconstruction variants and applications to instrumentation, process engineering and information techniques

04 p0688 A70-14717

Wave front reconstruction for perfectly bleached holograms not achievable by simple coherent illumination due to remaining amplitude variation

04 p0691 A70-15033

Image formation from wave front sampling in holography by spatial filtering, comparing Monte Carlo sampling to spaced sampling

04 p0692 A70-15365

Information transmission capability of hologram without distortion, considering confocal resonator reconstructible transparencies for bounded hologram

05 p0848 A70-16265

Hologram constructed with microwaves with image reconstruction at optical wavelengths using laser

05 p0849 A70-16659

Optical wave front reconstruction principles applied to sonic and seismic wave holography for mapping earth subsurface structure

05 p0850 A70-16685

Holographic method for reconstructing polarization of light emitted by photoelastic model, obtaining isochromatic and isoclinic fringe patterns

06 p1063 A70-17643

WAVE FRONT RECONSTRUCTION

Image contrast in holographic reconstructions, discussing influence of given surface intensity recording and oblique reference wave on hemigram

06 p1067 A70-18398

Hologram interference fringes formation and location using grating model of diffusely reflecting surface

07 p1280 A70-19144

Holographic recording of information contained in evanescent wave fields in high resolution photographic emulsions

07 p1281 A70-19367

Holography without reference beam for two and three dimensional interferential wave front recording and reconstruction

07 p1285 A70-19858

Holographic recording and reconstruction for wide angle three dimensional displays noting limitations

07 p1287 A70-20085

Photographic film imagery, degraded by long term artificial atmospheric turbulence, restored by spatial filters placed in Fourier transform plane

07 p1336 A70-20090

Zoom effect in magnification of reconstructed image in incoherent holography achieved by varying fringe scale via rotation of interferometer components

07 p1288 A70-20099

Laser focused hologram reconstruction in passing white light

07 p1289 A70-20320

Hologram data efficiency improvement by spatial offset removal, analyzing plane and spherical reference waves and plane and solid objects

08 p1500 A70-21787

Reconstructed holographic image complex amplitude expression derived, showing effects of film optical transfer function, size and shape

08 p1500 A70-21789

Holographic image reconstruction analysis based on two beam interferometry by spatially incoherent light source, obtaining optical transfer function

08 p1514 A70-21790

Holography in terms of photogrammetry, reviewing interferometry role, wave construction and reconstruction, etc

09 p1674 A70-22260

Photographic image reconstruction of spatially incoherent illuminated object using twofold holography

09 p1675 A70-22486

IR holograms real time visual reconstruction by frequency stabilized carbon dioxide lasers

09 p1684 A70-23534

Holographic flow visualization system retaining all information in light wave passing through flow field, noting reconstruction as shadowgram, schlierens or interferograms

09 p1689 A70-23781

Structural detail in transparent object through holographic measurement of scattered monochromatic light, noting similarity to crystal structure reconstruction in X ray diffraction experiments

11 p2048 A70-25360

Recording nonlinearities effect on image reconstruction from hologram of diffuse object

11 p2050 A70-25641

Holographic achromatic reconstruction of laser holograms in transmitted white light using zonal plate

12 p2238 A70-28297

Holographic method for reconstructing polarization of light emitted by photoelastic model, obtaining isochromatic and isoclinic fringe patterns

13 p2405 A70-28726

Wavefront reconstruction by holograms of focused images illuminated by white light, analyzing spatial coherence

13 p2408 A70-29364

Three dimensional images reconstruction with coherent light, facilitating transmission by holographic information volume reduction

14 p2581 A70-30146

Planar sandwich hologram recording 4 pi steradians with preservations of object spatial perspective by representing entire wave front

14 p2588 A70-31209

Wave front reconstruction from blazed holograms, noting wave front distortion for nonconstant amplitude case

15 p2736 A70-32011

Holographic technique to record hypervelocity projectile with front light resolution, discussing image blurring

15 p2736 A70-32031

Plotter induced reconstruction errors minimization in computer generated binary Fourier transform holograms

15 p2737 A70-32044

Holography technique for dual real images reconstruction of transparent objects with all planes in focus

15 p2738 A70-32053

Wave front multiplexing on spatially distinct area of single piece hologram

15 p2738 A70-32054

Holography without reference waves, describing image characteristics of spherical waves from point source 15 p2743 A70-32893

Hologram image construction by graphical method 16 p2915 A70-34216

Image distortion in reconstructions from phase only holograms, noting savings in collection and processing of acoustic holographic data 16 p2915 A70-34324

Computer generated holograms, using binary transmittance for wave fronts and three dimensional images construction 17 p3085 A70-35006

Vibration measurement by hologram interferometry, discussing wave front reconstruction and fringe theory based on Rayleigh integral formulation of light propagation 17 p3086 A70-35017

Vibration amplitude measurement by holographic wave front reconstruction 17 p3087 A70-35018

Microwave hologram recording for surface displacement, with laser beam illumination for optical reconstruction of image 20 p3628 A70-39152

Acoustic/microwave/ holography for large masses by crossed linear array of microphones, discussing computer simulation of virtual holograms and image reconstruction 21 p3822 A70-40715

Holographic measurement of general forms of motion based on reconstructed images dependence on coherence 21 p3822 A70-40810

Magnetic holography, considering Faraday and polar Kerr effect reconstructions and potential as computer storage 22 p3994 A70-43608

Integrated ferroelectric photoconductor device for hologram storage, discussing improved phase readout technique for reconstruction 22 p3994 A70-43609

Holographic exposure and reconstruction processes, considering illumination beam polarization effects on image brightness 22 p4040 A70-43616

Soviet book on holography covering laser characteristics, scatterers for image enhancement, photoemulsion requirements, etc 23 p4194 A70-44100

Focused image holographic interferometry by double exposure with reconstruction in white light applied to flat rotating subject 23 p4199 A70-45058

Optical image reconstruction from holograms, discussing photographic materials resolution, response linearity, spatial noise, etc 24 p4335 A70-45654

Fourier hologram synthesis using laser point source and Wollaston birefringent prism 24 p4336 A70-45667

Sideband Fresnel and lensless Fourier transform holographic images elongation and contraction 24 p4339 A70-45817

WAVE FRONTS

NT SHOCK FRONTS

Hydrodynamic structure of multifront detonation waves produced in gases by primary shock interaction with transverse disturbances 02 p0278 A70-12027

Axial emission impedance antenna converting strongly delayed surface wave into weakly delayed wave forming cophased front at antenna end 03 p0456 A70-13199

Two dimensional wave front shapes induced in finitely strained elastic body by impulsive point body force, discussing normal and double inflection points 08 p1584 A70-20581

Holographic technique of coherent light field transformation with desirable phase distribution from laser light beams of arbitrary wavefront characteristics 08 p1497 A70-21410

Wave front velocity determination by analytical continuation of wave function Fourier transform into complex plane, discussing constraints imposed by finiteness requirement 09 p1726 A70-22327

Compact unequal-path radial shearing laser interferometer designed for small angular aperture wave front testing 09 p1696 A70-22719

Conducting gas unsteady efflux from plane tube into vacuum, determining time dependent position of expanding rarefaction wave fronts 10 p1924 A70-24569

Small parameter structure and propagation velocity of ionization front in gas, applying nonequilibrium plasma model and electron equation 10 p1926 A70-25191

Wave fronts averaging by holographic technique to eliminate distortions arising in inhomogeneous media 12 p2233 A70-27504

Time dependent characteristics of dense argon plasma formed by pulsed lasers, measuring shock wave front velocity with streak camera 17 p3104 A70-35083

Elastic wave with discontinuities propagation, calculating decay velocities and stresses at leading wave front by theory of characteristics 17 p3189 A70-35436

Nonequilibrium gas states evolution in detached wave front of hypersonic blunt body, comparing vibrational relaxation in free flight and wind tunnel flow 18 p3335 A70-35962

Stress relaxation interpretation at wave fronts in one dimensional media by nonlinear viscoelastic models, giving constitutive equations 19 p3542 A70-38057

Wave front arbitrary curvature, examining integration of weak discontinuities growth equation in quasi-linear hyperbolic system 22 p4062 A70-42953

Elastic wave front control volume analysis in laminated and fiber reinforced composite materials 22 p4119 A70-43677

WAVE FUNCTIONS

NT MOLECULAR ORBITALS

Nonlinear electrodynamic equations solutions for electromagnetic media with one dimensional unsteady electromagnetic field based on wave functions determined from boundary conditions 01 p0149 A70-10165

Particle trajectory and associated wave determined for nonclassical trajectory problem from nonprobabilistic point of view, discussing discontinuity arising from unbounded velocities 01 p0142 A70-10657

Isotropic incompressible three dimensional turbulence representation by wave vector scalar functions, discussing maximum functions number determination 02 p0277 A70-11878

Wave structure function dependence on altitude, comparing function ratio for up/down propagation through atmosphere 02 p0258 A70-12461

Error correction for previous derivation of radio propagation of wave-hop series for anisotropic ionosphere resulting in improved nighttime field strength accuracy 04 p0649 A70-14967

Basis functions with harmonic oscillator radial dependence in Hartree-Fock calculations for light deformed nuclei 04 p0723 A70-15635

Fields and power transfer for electromagnetic waves in hot plasma calculated using Fourier integral and Fourier series methods 05 p0888 A70-16165

First order wave functions orbital correlation energies and electron affinities of first row atoms for low lying electronic states of B, C, N, O, F and Ne 06 p1108 A70-17333

Wave functions of asymmetric gyroscope in rotating coordinate system, presenting quantum equation of motion solution 06 p1105 A70-17500

Degenerate and nondegenerate energy states and wave functions formulated by Rayleigh-Schroedinger perturbation theory 06 p1110 A70-17764

Eigenvalues of spheroidal wave functions calculations dependent on complex propagation constants, discussing branch point values in tabular form 06 p1009 A70-17907

Stationary phase for beam of radio waves propagating in absorbent ionosphere as function of mean directions of real and imaginary parts of wave vector 09 p1665 A70-22049

Prolate spheroidal wave functions applied to detection Fredholm equation for band-limited noise and signals 09 p1640 A70-23803

Born approximation used in calculating wave functions of helium atom for determining generalized oscillator strengths in first ionized continuum of helium 10 p1919 A70-24072

Nonlinear electrodynamic equations solutions for electromagnetic media with one dimensional unsteady electromagnetic field based on wave functions determined from boundary conditions 10 p1925 A70-25013

Integral Hellman-Feynman formula applied to binding energy of molecular H and LiH, using SCF wavefunctions for atomic states 12 p2276 A70-27570

Radial wave functions and photoionization cross sections for neutral atoms from central potential model based on Slater and Klein-Brueckner approximations 13 p2455 A70-29133

Effective moment of inertia in quantum mechanical three body problem, applying specific decoupling to wave functions 13 p2452 A70-29478

Molecular orbital wave functions for water molecule, using minimum set of Slater orbitals 14 p2544 A70-30119

Wave properties of nuclear optical model for barrier penetration by charged particles, considering square well reflection, absorption and resonance 14 p2619 A70-30491

Multistate impact parameter treatment of heavy particle collisions modified to include higher state couplings for electronic wave functions 16 p2956 A70-34309

Coupled channel calculation of inelastic proton scattering from Ne 20 using Hartree-Fock wave functions 17 p3137 A70-34517

Prolate and oblate wave functions for EM radiation from spheroidal antenna in surrounding inhomogeneous medium 17 p3044 A70-35063

Electronic wave functions for atoms from atomic configuration-interaction/CI/ expansion for open shell states 18 p3292 A70-36185

Numerical computation of wave functions and energies in complex band structures for two-band case, using k-p method 19 p3483 A70-37547

Interference wave functions for diffraction on cylinder and sphere, including noninterfering waves of geometric optics 19 p3380 A70-38398

Method of moments for determining wave functions used in calculating molecular properties 20 p3675 A70-39997

Steepest descent method for determining lowest ground state eigenvectors for molecular wave configurations 22 p4062 A70-42747

Simple wave functions solutions in multidimensional nonviscous polytropic gas unsteady and steady flow 24 p4327 A70-46030

Spheroidal wave function theory, calculating eigenvalues with branch points for propagation constants complex values 24 p4315 A70-46134

WAVE GENERATION

Asymptotic and approximate wave construction for system of first order quasi-linear partial differential equations 01 p0131 A70-10800

Microwave generation and amplification using Gunn effect semiconductor devices 01 p0160 A70-11289

Nonlinear drift wave buildup in inhomogeneous plasma faster than in linear approximation 03 p0531 A70-13509

Fixed mass fixed volume sinusoidal pressure generators for evaluation of transducers used in high pressure measurements 03 p0494 A70-14049

Collapse of homogeneous fluid mass in stratified fluid with initially slender interface and ineffective internal wave motion, discussing internal wave generation 03 p0470 A70-14247

Transient stress waves generated by spatially uniform distribution of transverse forces in laminated medium, using modal analysis 05 p0938 A70-16409

Electrical impedance, conversion loss and bandwidth for piezoelectric film or plate transducers used for generating planar volume-acoustic waves at microwave frequencies 06 p1062 A70-17480

Frequency calculation and measurement for acoustic waves produced by carbon dioxide Q switched lasers 06 p1084 A70-18620

Cerenkov generation of VLF waves in inner magnetosphere at low latitudes 07 p1265 A70-19281

Respiratory waves formation of intracranial pressure in anesthetized cats and dogs, studying various contributing factors 07 p1213 A70-19792

Atmospheric gravity wave generation, propagation and dissipation, considering stratospheric tides 07 p1275 A70-20276

Atmospheric pressure waves generated by high energy disturbance in South Pacific, using ionospheric Doppler signals correlated with ground-level pressure signals 08 p1490 A70-21646

Acoustic wave amplification and generation in piezoelectric semiconductors and semimetals by supersonic carrier drift currents 10 p1925 A70-25030

Local losses distribution effect on intensity and opposing waves generation in ring gas laser analyzed in approximation of noninteracting modes 12 p2248 A70-27510

Transverse laser modes interaction in traveling and standing wave generators allowing for spatial distribution 13 p2424 A70-28597

- Nonlinear drift wave buildup in inhomogeneous plasma faster than in linear approximation 13 p2460 A70-28652
- Infrasonic waves generation by supersonic translation of auroral electrojet currents 13 p2399 A70-29237
- Intracranial pressure pulse waves formation mechanism mathematical model, estimating role of biomechanical factors 13 p2353 A70-29520
- Bow shock associated hydromagnetic waves generation in upstream interplanetary medium, constructing model in terms of ion cyclotron resonance 14 p2631 A70-30359
- Book on millimeter and submillimeter waves covering generation, transmission, components and detection 14 p2548 A70-30426
- Coaxial, inside-out and rising-sun magnetrons for millimeter waves generation under pulsed conditions, discussing tunability, frequency stability and weight 14 p2555 A70-30429
- HF backward wave oscillators with emphasis on limiting factors in millimeter waves generation, discussing ohmic and circuit imperfection losses 14 p2555 A70-30430
- Millimeter and submillimeter waves generation as difference frequencies of mixed laser beams 14 p2593 A70-30434
- Millimeter waves generation by tunnel, Gunn and avalanche diodes, tabulating frequency, efficiency and power data 14 p2548 A70-30435
- Wideband varactor multipliers with flat output as microwave sources in radar systems 16 p2877 A70-33412
- Long and short period internal gravity waves in atmosphere observed by high resolution radar, investigating generation mechanisms 17 p3075 A70-34609
- Stress wave generation in elastic temperature-dependent absorbing solids by impulsive EM radiation 17 p3185 A70-34967
- Wave-periodic acceleration feedback during vibrational flame propagation in tubes, testing carbon monoxide-air mixture 17 p3196 A70-35350
- Cerenkov plasma waves generation by fast electron streams in solar corona and conversion into EM waves 17 p3173 A70-35768
- Discrete signals synthesis optimal with respect to given criterion, determining ambiguity function extremum 19 p3374 A70-37270
- Weak steady shock waves formation in relaxing binary gas mixture, discussing vibrational specific heat temperature dependence 20 p3614 A70-40350
- Shock waves formation in rarefied plasma investigated by Thomson scattering of ruby laser light 20 p3643 A70-40388
- Shock and expansion waves formation by moving piston based on kinetic theory of gases, solving Bhatnagar-Gross-Krook equation by numerical method 21 p3808 A70-41377
- Acoustic waves generation from decay region of pulsating supersonic jet expelled from nozzle 21 p3748 A70-42211
- Alfven waves synchrotron emission in incompressible medium, investigating generation by rotating DC current carrying circuit 21 p3861 A70-42227
- VLF wave generation due to nonlinear interaction of two microwaves with plasma slab under high DC field 22 p4077 A70-42294
- Triangle and sine waveforms generation, discussing reduced peak and crossover distortion and extended frequency operation 22 p3989 A70-42923
- Compressional sound waves electromagnetic generation in metals in static magnetic fields, examining acoustic amplitude variations 22 p4074 A70-42968
- Cylindrical converging shock waves generation, propagation and structure at high pressures 22 p4012 A70-43431
- Magnetosphere Alfven velocity profile relation to ELF chorus and hiss, indicating unstable wave generation by cyclotron resonance 23 p4186 A70-43851
- Wind generated water waves spectral characteristics at low momentum levels 23 p4215 A70-44273
- GaAs injection lasers, calculating effect of active region displacement from p-n junction waveguide on wave generation 23 p4203 A70-45074
- HF sinusoidal fluid pressure generators driven by electromagnetic vibrators for arterial applications 24 p4309 A70-46118
- Taylor model of elastoplastic wave interaction during cylindrical projectile impact 01 p2006 A70-11150
- Arc phenomena for producing interaction effects, discussing reflected shocks rarefaction waves and gas dynamics 02 p0345 A70-11863
- Inhomogeneous plasma containing weak electron beam using Vlasov equation, noting wave-wave coupling effect 02 p0345 A70-11882
- Wave-wave coupling of two HF electromagnetic waves launched into warm plasma across constant confining magnetic field, using Maxwell-Vlasov equations for electrons 02 p0349 A70-12757
- Electromagnetic field structure and interaction inside and outside of spherical shell of arbitrary linear media excited by monochromatic plane wave 03 p0443 A70-13151
- Energy modes nonlinear interactions in rarefied plasmas, presenting wave energy and momentum definitions and kinetic equations for mode density in wave number space 04 p0726 A70-14701
- Interaction of infinite shallow draft cylinder oscillating at free surface with train of oblique waves 04 p0618 A70-15321
- Output characteristics of cyclotron maser with resonator field due to plane waves interference along static magnetic field, deriving tensor equations 05 p0858 A70-16260
- Parametric coupling between space-time harmonics of electromagnetic wave propagating in dielectrics modulated by pump wave 05 p0815 A70-16660
- Phase velocities of intrinsic normal waves of electron beam in three frequency parametric amplifier of space charge waves, determining optimal wave interaction conditions 05 p0823 A70-16890
- Parametric interactions in three frequency TWT parametric amplifier, using power series 05 p0824 A70-16895
- NonJeans gravitational instability of stars and interstellar gas in Galaxy due to wave interaction with stars having velocity near wave phase velocity 05 p0917 A70-16906
- Electron transmission diffraction patterns of thin monocrystal films using Ar laser 06 p1080 A70-17444
- Microwave variable delay devices, discussing solid state microwave acoustic interactions 06 p1019 A70-17483
- Shear wave interaction in infinite homogeneous reacting fluid, using Fourier and Taylor series for velocity, temperature, density, pressure and composition [AIAA PAPER 70-146] 06 p1040 A70-18154
- Electromagnetic waves phase modulation index during propagation in nonlinear media found dependent on mismatch between interacting waves group velocities, relaxation time and losses 07 p1227 A70-18763
- Kinetic equation for nonlinear interaction of waves, including unstable or damped, using Bogoliubov method 09 p1659 A70-22214
- Internal waves breaking on sloping surface in two fluid system, studying interfacial shear instability by capacitance probe on-line computer system 09 p1717 A70-22371
- Relaxational oscillations produced by interaction between rarefaction wave in external two dimensional supersonic flow and turbulent near wake 09 p1603 A70-22426
- Strain gage for measuring strain waves amplitude on surface of fused quartz to study electromagnetic waves interaction in Permalloy films 09 p1681 A70-23349
- Space charge parameters influence on electron wave and traveling wave interactions in TWT 09 p1652 A70-23654
- Nonlinear oscillations averaging method applied to resonant interactions of acoustic gravity waves 09 p1729 A70-23666
- Upper atmospheric waves nonlinear interactions based on tides and gravity waves propagation, taking into account terrestrial rotation 10 p1872 A70-23820
- Nonlinear wave interactions in quiescent plasma column with external disturbance creating broadened frequency spectrum and weakly turbulent plasma 10 p1922 A70-24146
- Wave amplification in semiconductors relationship to coupling between space charge wave and circuit wave based on coupled-mode theory 10 p1927 A70-24619
- LF ion-acoustic wave nonlinear interaction with HF Langmuir waves in nonisothermal plasma, establishing criteria for ion plasma turbulence 10 p1925 A70-25103
- Amplitude and phase constants of interacting waves in three frequency nondegenerate parametric amplifier of fast space charges using coupled wave technique 10 p1853 A70-25133
- One dimensional wave processes in distributed nonlinear systems, surveying mathematical methods 10 p1843 A70-25151
- Fields in wave interaction region during spatial trapping of parametrically amplified waves by radiation of pumping, using Laplace transformation 10 p1844 A70-25157
- Narrow band radiation from longitudinal plasma waves nonlinear interactions during solar bursts, comparing flux intensities for Corona single or double shock wave frequencies 10 p1934 A70-25272
- Cascade mechanism of closure associated with nonlinear wave interactions between modes in turbulent plasmas, using hydrodynamical model 11 p2087 A70-25358
- Pulsed radio waves interactions during vertical propagation through perturbed ionosphere using cross modulation theory concepts, considering perturbation waves effects 11 p2003 A70-25531
- Long-time cross modulation field resulting from triggering electrostatic waves in one dimensional plasma, discussing supraluminous waves interactions 11 p2088 A70-25704
- Dynamic equations for amplitudes of interacting MHD waves bounded plasma, discussing three-plasmon interactions 11 p2088 A70-25708
- HF and LF plasma waves interaction in three wave approximation taking into account linear damping 11 p2089 A70-25714
- Polarization effects during HF EM wave interaction in plasma, discussing plasma scattering effects in polarization transport equations 11 p2004 A70-25937
- Evolutionary hydromagnetic shock perturbation by incident small amplitude hydromagnetic wave calculated for diverging wave amplitudes and directions 11 p2036 A70-26017
- Microwave amplifiers based on interaction between piezoelectric acoustic waves and collinearly drifting carriers, analyzing gain, frequency response, etc 11 p2018 A70-26164
- Plane wave disturbances introduced in turbulent channel flow by vibrating ribbons near each wall, obtaining amplitude and relative phase 11 p2039 A70-26537
- Turbulent boundary layer interaction with wavy wall in wind tunnel, discussing wall pressure drag and surface waves interaction 11 p2039 A70-26538
- Plasma turbulence due to nonlinear wave interaction, considering second sound LF oscillations propagation and plasmons scattering at ions 12 p2278 A70-27358
- Resonant and nonresonant coupling between two coherent electron plasma waves propagating in opposite directions, considering parametric decay 12 p2279 A70-27780
- Interaction of laminar hypersonic boundary layer and supersonic corner expansion wave, discussing upstream influence, transverse pressure gradients and external flow [AIAA PAPER 69-137] 12 p2211 A70-27826
- Suspended Stokes particle-single wave interaction effect on energy dissipation and vorticity of random turbulent incompressible fluid approximated by Fourier-Stieltjes integral 12 p2213 A70-28236
- Homogeneous and stationary turbulence in incompressible fluid, proposing dynamic model for strong wave interactions during cascade process 13 p2457 A70-28557
- Inhomogeneous one dimensional plasma in electrostatic normal modes, considering interactions of waves and particles 13 p2460 A70-28638
- Electrical conductivity without particle-particle or wave-particle collisional noise or radiation 13 p2463 A70-29238
- Radial displacements in cylindrical circular shell by impinging spherical waves propagating in acoustic medium, deriving equations by Fourier and Laplace transforms 13 p2515 A70-29318
- Transport equations for interaction between radiation and matter under arbitrarily large nonequilibrium in comoving system 13 p2521 A70-29414
- Landau damping in plasma cyclotron wave interaction by symmetrical counterstreaming double electron beam with uniform magnetic field 13 p2468 A70-29917
- Frequency dependence of gravitational-electromagnetic fields interaction assumption inconsistent with general relativity and consistent with data on deflection of radiation by massive bodies 14 p2573 A70-30616
- Nonlinear diurnal tide and gravity wave interactions at meteor heights below mesopause 14 p2579 A70-31251
- Shock and simple wave interactions, using quasilinear equations for forward facing wave overtaking forward facing shock 14 p2567 A70-31283

WAVE INTERACTION

NT SHOCK WAVE INTERACTION

- Optical paths inequality of nonuniform power opposing waves in ring lasers 01 p0107 A70-10209

Gas ring lasers, discussing optimal parameters, colliding waves interference, nonmutual effect and radiation polarization 15 p2749 A70-31451

Third harmonic generation using hot electron nonlinearity characteristics of semiconductors, considering plane-polarized electromagnetic wave nonlinear interaction with sample 15 p2783 A70-31970

CDs high field domain modes generation for C parallel to E ascribed to interaction between drift carriers and off-axis shear wave 15 p2784 A70-31984

Low amplitude waves and substantial frequencies interaction by averaging method for hydrodynamics of waves in collisionless plasmas 15 p2720 A70-32114

VHF radiation from plasma during electron beam interaction with fast magnetoacoustic wave stimulated by external spatially periodic currents 15 p2780 A70-32118

Polarization characteristics of solar radio waves reflected from coronal waves in meter wavelength range 15 p2802 A70-32485

Resonant interaction and instability produced by nonlinear coupling of modulated wave and LF mode, stimulating self focusing of plasma waves 16 p2958 A70-33285

Quasi-linear hyperbolic systems interactions for rarefaction waves, applying Glimm difference method 16 p2943 A70-33782

D region electron density variations during solar eclipse of 7 March 1970, using wave interaction technique 16 p2898 A70-33832

D region electron energy loss factor during solar eclipse of 7 March 1970, using wave interaction technique 16 p2898 A70-33834

Plane acoustic wave interaction with elastic spherical shell, discussing effects of membrane, bending, rotatory inertia and shear deformation 16 p2993 A70-34087

Laminar hypersonic boundary layer interaction with corner expansion wave, presenting numerical solutions to viscous-inviscid equations for small turning angles [AIAA PAPER 70-807] 17 p3065 A70-34457

Nonlinear interactions of plasma waves with positive and negative energies producing explosive instability 18 p3295 A70-36420

Numerical scheme for weather forecasting, considering interaction mechanism between cyclonic and ultralong waves and climate 18 p3285 A70-36646

Electromagnetic waves phase modulation index during propagation in nonlinear media found dependent on mismatch between interacting waves group velocities, relaxation time and losses 18 p3229 A70-37107

Electro-optical SHF modulator characteristics calculation from light wave interaction with traveling wave 19 p3443 A70-37291

Intersecting shock waves propagation, deriving equations for aircraft sonic boom intensity 19 p3355 A70-38484

Magnetron type backward wave tube with negatively charged slow wave structure, analyzing electron beam wave interaction for starting conditions 20 p3596 A70-39251

Alfven magnetoacoustic waves interaction, deriving kinetic equation for distribution function and relaxation time 20 p3678 A70-39597

Wave particle resonances broadening by particles random motion in turbulent electric field, determining cyclotron instabilities saturation level from vanishing nonlinear growth rate 20 p3679 A70-39661

D region electron density profiles from high power wave interaction measurements during solar flare, indicating non-X-ray production rate 21 p3879 A70-40942

Pulsed radio waves interactions during vertical propagation through perturbed ionosphere using cross modulation theory concepts, considering perturbation waves effects 21 p3786 A70-41281

Ion sound system one dimensional hydrodynamic equations, examining formation and interaction of nonlinear ion acoustic shock waves 21 p3857 A70-41384

Electron-ion wave interaction due to scattering by electrons, using kinetic wave equation to describe wave-particle interaction 21 p3858 A70-41712

Earth magnetosphere LF wave annular trap, examining high energy particle interaction with magnetosonic waves 22 p4013 A70-42300

Monochromatic acoustic wave interaction with turbulent jet fluctuating vorticity field, using Fourier analysis to extend spectral relations [ASME PAPER 70-FLCS-6] 22 p4008 A70-42426

Micropulsation Pc-1 phase and polarization comparisons concerning L to R wave coupling in ionosphere 22 p4024 A70-43313

Weak EM transmission through resonant medium of two-level atoms in presence of intense monochromatic wave, obtaining absorption coefficient and refractive index 22 p4075 A70-43473

Plasma turbulence due to nonlinear wave interaction, considering second sound LF oscillations propagation and plasmons scattering at ions 22 p4084 A70-43599

Polarization characteristics of solar radio waves reflected from coronal waves in meter wave length range 23 p4240 A70-43909

Plane shock wave decay by interaction with simple wave, solving nonisentropic equations of gas dynamics 23 p4179 A70-43969

Thin liquid film /melt layer/ on body in supersonic flow, examining crosshatched wave patterns stability 23 p4183 A70-44979

Electromagnetic waves nonlinear interaction at various threshold powers, inducing propagation in solid body plasma 24 p4388 A70-45201

WAVE MOTION

U WAVES

WAVE OSCILLATORS

U OSCILLATORS

WAVE PROPAGATION

NT DIFFRACTION PROPAGATION

NT DOUBLE SIDEBAND TRANSMISSION

NT ELECTROMAGNETIC WAVE TRANSMISSION

NT GROUND WAVE PROPAGATION

NT IONOSPHERIC F-SCATTER PROPAGATION

NT IONOSPHERIC PROPAGATION

NT LIGHT SCATTERING

NT LIGHT TRANSMISSION

NT MICROWAVE TRANSMISSION

NT MULTIPATH TRANSMISSION

NT RADAR TRANSMISSION

NT RADIO TRANSMISSION

NT SCATTER PROPAGATION

NT SHOCK WAVE PROPAGATION

NT SHORT WAVE RADIO TRANSMISSION

NT SINGLE SIDEBAND TRANSMISSION

NT SOUND TRANSMISSION

NT TELEVISION TRANSMISSION

NT TRANSQUATORIAL PROPAGATION

Time dependent telegrapher equation solution for studying transient neutron waves propagation 01 p0130 A70-10086

Plane harmonic Rayleigh wave propagation in piezoelectric semiconductor GaAs crystals, using successive approximation procedure 01 p0154 A70-10131

LF longitudinal waves propagation in DC gas discharge plasma, obtaining wave dispersion equation for various limiting gases 01 p0149 A70-10162

Nonpotential waves propagating at slow phase velocity in inhomogeneous plasma, determining flute instability oscillation frequency 01 p0149 A70-10163

MHD wave propagation through plasma in magnetic field of current filament, developing Hamilton-Jacobi equation by geometrical optics 01 p0151 A70-10466

MHD wave propagation in electrically conducting fluid contained in finite length circular cylinder subject to axial magnetic field and nonelectromagnetic forces 01 p0152 A70-10944

Book on nonlinear stress waves propagation in elastic solids covering adiabatic shocks, isentropic plane waves, Lagrange equation, spherical waves, heat conduction effect, etc 01 p0202 A70-10966

Two variable expansion method applied to ordinary differential equation and two wave propagation problems, comparing results with matched asymptotic expansions and coordinate stretching methods 01 p0132 A70-11072

Wave propagation in nonlinear viscoplastic medium, deriving first order system of coupled equations in stress and particle velocity components 01 p0207 A70-11154

Characteristic equations developed for two-spatial dimensional elastic wave propagating in linear elastic, isotropic and homogeneous medium 01 p0208 A70-11185

Plane sinusoidal wave propagation through material reinforced with parallel fibers, using integral formula for multiple scattering in infinite slab 01 p0130 A70-11187

Flexural wave propagation in infinitely long circular bimaterial cylinders based on equations of linear elasticity, noting dispersion characteristics different from homogeneous cylinders 01 p0208 A70-11188

Microwave propagation in materials and measurement methods for inspection based on reflecting surface movement and scattering method for porosity detection 01 p0094 A70-11395

Short sound waves propagation in moving inhomogeneous medium, studying viscosity and heat conductivity influence 01 p0146 A70-11581

Flexural and longitudinal waves propagation in infinite elastic plate, using solutions to approximate nonlinear equations of plate motion 01 p0213 A70-11634

Nonlinear waves in parallel shear flows, discussing laminar flow breakdown due to free stream disturbances 02 p0277 A70-11876

Optical scintillation measurements applied to turbulence diagnostics, inferring spatial spectrum of turbulent scatterers, using Monte Carlo numerical procedure 02 p0296 A70-11892

Quadruple microwave probe applied to phase and attenuation variations measurements of HF wave propagating through dielectric media 02 p0345 A70-11898

Spherical detonation waves propagation initiated by laser-induced spark in gaseous explosives, discussing propagation regime regimes 02 p0278 A70-12029

Circumferential wave propagation around cylinder, demonstrating dependence on incident frequency and surface roughness, noting target surface microscale roughness measurement technique 02 p0339 A70-12184

Traveling wave velocity in human cochlea determined by equally low tonal pairs, comparing results to psychophysical and electrophysiological findings 02 p0237 A70-12323

Waves vs eddies in dynamics of turbulent boundary layer fluctuating motions with scale of mean flow 02 p0287 A70-12361

Wave packet dynamics recapitulation and tentative application to turbulent shear flow 02 p0287 A70-12362

Wave structure function dependence on altitude, comparing function ratio for up/down propagation through atmosphere 02 p0258 A70-12461

Self consistent field method to calculate effective dynamic characteristics of elastic media with filler for plane longitudinal wave propagation 02 p0388 A70-12485

Whistlers paradoxical behavior in bounded magnetoplasmas, discussing double reflection and wave propagation 02 p0263 A70-12733

Propagation equations for spherical waves in elastoplastic work hardening materials 03 p0585 A70-12972

Axial stress pulse induced elastic waves propagation in thin anisotropic circular cylindrical shell of helical wrap construction allowing for shear coupling 03 p0587 A70-13118

Wave numbers determined in waveguide formed by laminar inhomogeneous medium enclosed between homogeneous dielectric media, taking into account radiation losses through wall 03 p0447 A70-13290

Wave propagation problem, considering traffic control, surveying, tracking, navigation, etc 03 p0449 A70-13607

Quasi-optical propagation in frequency wave range above 100 MHz as user problem in VOR, ILS, navigation satellite and CAT detection and warning systems 03 p0523 A70-13613

LF wave propagation using loran C radio navigation system flight performance tests 03 p0523 A70-13615

VLF wave propagation in earth-ionosphere waveguide, comparing ray and waveguide-mode theories 03 p0449 A70-13616

Magnetoelastic surface wave propagation properties in ferrites at UHF wavelengths, using numerical calculations for gallium-YIG 03 p0540 A70-13700

Adiabatic disturbances propagating as transverse waves in inviscid fluid rotating as Rankine vortex about cylindrical container axis, discussing harmonics 03 p0467 A70-13779

Induction distances, transient pressures and wave propagation rates for detonation waves in cylindrical tube low temperature hydrogen-oxygen mixtures 03 p0607 A70-13919

Cs plasma research, discussing Q-machines, plasma confinement, magnetic field experiments, LF and HF wave propagation, etc 03 p0533 A70-14015

Small amplitude perturbations in interstellar medium, discussing order of magnitude estimates of properties of cosmic rays, thermal gas, dust and magnetic field

03 p0575 A70-14016

Book on rational thermodynamics covering homogeneous processes, internal dissipation, Coleman theorem, wave propagation in dissipative materials, diffusion, chemical reactions, Onsager relationship, etc

03 p0525 A70-14042

Wave propagation in inhomogeneous media, reducing quasi-linear hyperbolic partial differential equations to single nonlinear equation integrable by method of characteristics

03 p0525 A70-14184

Stress wave propagation tests in thin walled tubes under combined tension and torsion, discussing predicted and observed strain-time profiles discrepancies

03 p0599 A70-14245

Gravitational wave propagation velocity determined by laboratory measurement of spin-spin coupling of two rotating masses

04 p0718 A70-14397

Dispersion relation governing hydromagnetic gravity waves propagation in rotating nonisotropic medium, discussing effects of constant entropy gradient

04 p0745 A70-14473

HF expansions of harmonic solutions concentrated at waves propagating in inhomogeneous medium to dynamic equations in elasticity theory

04 p0767 A70-14499

Mechanical behavior of anesthetized dog abdominal vena cava from pressure wave transmission characteristics, discussing chemical and electrical stimuli

04 p0630 A70-14630

Laplace transform of axial stress resultant in impacting semiinfinite elastic cylindrical membrane as exponential function involving wave propagation speed, applying continued fractions

[ASME PAPER 69-APM-K] 04 p0769 A70-14859

Radio wave propagation in linear, isotropic homogeneous medium with irregular boundaries solved by expanding Helmholtz integral

04 p0648 A70-14965

Sound wave propagation in liquid containing gas bubbles allowing for relative motion of bubbles and liquid, deriving steady shock wave structure

04 p0671 A70-14991

Nonlinear propagation of electron plasma wave in cylindrical waveguide, discussing linear theory of electrostatic waves in cold plasma

04 p0728 A70-15000

Transient processes of strain wave propagation in elastic shells and plates under time varying loads

04 p0773 A70-15010

Dispersion curves for wave propagation in infinite elastic bars of elliptic cross section obtained by method of collocation

04 p0773 A70-15080

Eigenvalue and eigenfunction of H01 wave in bend of cross shaped waveguide, determining field components and propagation constant change

04 p0651 A70-15291

Surface waves excited by horn above dielectric disk backed by metallic disk, formulating characteristic wave equations and solving for attenuation and propagation constants

04 p0659 A70-15305

Nonlinear wave propagation in relaxing gas with internal energy characterized by translational and internal temperature, using model equation for piston induced motion

04 p0786 A70-15324

Optical waves in round metallic and dielectric waveguides calculated using geometrical optics and model analysis for anisotropic wall impedance model

04 p0652 A70-15396

One dimensional stress waves propagation in elastoplastic medium, determining stress and velocity fields due to heat sources motion by characteristics method

04 p0776 A70-15447

Dynamic plastic response of finite bar subject to axial impact load noting reflected waves, stress-strain-time histories and residual strain

04 p0779 A70-15599

Geomagnetic field lines inclination effect on hydromagnetic waves propagation in lower ionosphere, using atmospheric model in plane form with integral conductivity tensor

04 p0683 A70-15737

Plane Lamb problem in semiinfinite micropolar elastic body solved by transformation to one dimensional wave propagation problem in elastic half space

05 p0925 A70-15785

Surface wave spectrum and propagation in nonhomogeneous bounded elastic solid, considering existence and eigenvalues approximation

05 p0925 A70-15789

Plastic-viscoplastic bar wave propagation due to longitudinal impact, analyzing stress profiles to determine effect of strain rate

05 p0926 A70-15913

Propagation and growth equations governing wave propagation in micropolar viscoelastic solids couplings between discontinuities in macroscopic and microscopic fields

05 p0929 A70-16063

Backward and complex waves propagation in circular waveguide with coaxial dielectric rod, discussing arbitrary angular dependences

05 p0812 A70-16145

Inhomogeneity and water vapor absorption influence on frequency spectrum of amplitude fluctuations of plane wave propagating in turbulent atmosphere

05 p0813 A70-16252

Rayleigh and Lamb waves propagating on solid and hollow elastic cylinders immersed in water, noting correspondence to symmetric and antisymmetric vibrations in shell

05 p0938 A70-16410

Two dimensional propagation of transverse waves in plasma with embedded curl-free magnetic field, discussing cosmic ray acceleration and magnetic neutral sheet formation

05 p0888 A70-16437

Radially nonsymmetric stress wave propagation from tip of moving crack in infinite plates, deriving minimal group velocity

05 p0941 A70-16516

Vertically propagating waves in viscous isothermal atmosphere taking into account reflection due to nonlinearities and time dependence

05 p0833 A70-16679

Ionospheric effect sudden commencement parameters of magnetic storm related to distance from origin in polar regions

05 p0841 A70-16737

Characteristic equation for phase velocity of surface wave propagating on helix for forbidden zone, suggesting current distribution function

05 p0815 A70-16775

Double giant pulse ruby laser with 1.5 m coherence length for producing double exposure holograms of stress wave propagation in solids

05 p0861 A70-16850

Plane and cylindrical elastic waves dynamic characteristics propagating in half space with holes, reducing boundary value problem and deriving formulas for interacting waves

05 p0946 A70-16858

Group velocity of spiral density waves propagating in disk galaxies implying self destruction, discussing possible replenishment sources

05 p0919 A70-16929

Monograph on MHD waves covering theories for weak discontinuities, wave propagation in inhomogeneous media and behavior in magnetic fields

06 p1114 A70-17275

Plasma oscillations, resonances and wave propagation characteristics analyzed by radio pulse sounders for application to space measurements

06 p1115 A70-17360

Guided elastic waves propagation on layered media, considering elastic wave circuitry design for true microminiaturization

06 p1018 A70-17476

Sound wave velocity and damping in liquid N measured along saturated vapor line using thermal Brillouin scattering techniques

06 p1105 A70-17491

Witham radiative acoustics, analyzing nonequilibrium waves propagating in nongray radiating and absorbing gas

06 p1173 A70-17514

Radiatively driven plane acoustic wave in nongray radiating and absorbing gas assuming local molecular equilibrium

06 p1173 A70-17515

Symmetrical H mode wave propagation in inhomogeneous plasma filled circular waveguide solved by hypergeometric functions, noting use for microwave diagnostics and computer programs verification

06 p1009 A70-17825

Space-sampled feedback control of amplifying wave on infinite continuum, discussing system stability

06 p1025 A70-17963

Surface wave propagation and amplification by electron beam-plasma interaction, inapplicability of coupled mode theory and use for microwave amplifier

06 p1125 A70-18616

Weak discontinuities propagation in quasi-linear systems for MGD, obtaining transport equations

07 p1347 A70-18678

Frequency equation for harmonic waves propagating in fluid filled circular cylindrical cavity in infinite isotropic solid medium

07 p1253 A70-18846

Propagation in perturbed magnetically focused electron beams, noting influence of spatially varying drift velocity and damping effect

07 p1239 A70-18867

Hydrogen concentration effect on self sustained detonation wave propagation in hydrogen-carbon

monoxide-oxygen mixtures, using Q switched pulsed laser schlieren photography

07 p1420 A70-18918

Sonic boom focalization, considering linear propagation for real atmosphere with wind and Jericho experiments

07 p1193 A70-19130

Ray theory for determining short term and averaged characteristics of nonreciprocal HF ionospheric propagation paths for single magnetoionic waves transmitted between antennas

07 p1231 A70-19171

Prestrain effect on waves propagation along slender low density unoriented polyethylene rod, indicating uniform phase velocity change over audio frequency range

07 p1248 A70-19237

Shear wave and plate velocity expressions derived for orthotropic elastic plate with shear coupling, considering propagation direction

07 p1412 A70-19961

Atmospheric gravity wave generation, propagation and dissipation, considering stratospheric tides

07 p1275 A70-20276

Propagation pattern of surface acoustic wave visualized in piezoelectric and nonpiezoelectric materials by dusting delay line with fine particles

07 p1336 A70-20283

Curved thin rods torsional and flexural waves propagation equations, considering geometry and shear and Young moduli

08 p1588 A70-21201

Magnetic equator ELF noise examined with OGO 3 magnetometer, indicating unique signals in plasmasphere

08 p1488 A70-21380

Nonlinear relativistic wave velocity distribution within spherical nucleus bounded by shock wave in superdense gas determined by Cauchy problem

08 p1484 A70-21403

Plane harmonic Rayleigh wave propagation in piezoelectric semiconductor GaAs crystals, using successive approximation procedure

08 p1556 A70-21407

Transient waves propagation in homogeneous isotropic linearly elastic half space excited by traveling normal point load on surface, deriving displacements

[ASME PAPER 69-APMW-12] 08 p1592 A70-21468

Weakly nonlinear dispersive cold plasma waves propagation by two time scale expansion, taking into account amplitude dispersion and coupling

08 p1553 A70-21613

Gravity waves generated by heating in auroral regions and propagating toward lower latitudes possibly causing thermospheric heating

08 p1491 A70-21675

Small dispersion whistlers characteristics and propagation at midlatitudes based on observation at Tohokata, Japan

08 p1491 A70-21713

Total optical field in inhomogeneous medium, questioning uniqueness of division into direct and reversed wave propagation

08 p1546 A70-21785

Linear nonstationary quasi-geostrophic model with external and internal heating and forcing for dynamics of ultralong waves in troposphere and lower stratosphere

09 p1713 A70-22304

Turbulence and internal waves in stably stratified atmosphere and ocean, proposing velocity and temperature spectral behavior model

09 p1716 A70-22370

Plane and cylindrical stress wave propagation in elastoplastic medium, studying stress interrelations

09 p1775 A70-22610

Pulse propagating in unstable plasma, determining characteristics by asymptotic expansion applied to Vlasov-Maxwell equations

09 p1734 A70-22684

Refractive index variation regions and mapping along propagation path in random medium, noting application to solar wind electron density structures measurements

09 p1634 A70-22699

Nonlinear stellar density waves in galaxy using gas dynamic equations, assuming one dimensional and steady waves

09 p1762 A70-23073

Thermoacoustic waves formation and propagation in metallic rods by light pulses, studying pulse rise time influence on waves shape and amplitude

09 p1778 A70-23090

Point source intensity fluctuations dependence on penetration depth of wave propagating in statistically homogeneous and isotropic media

09 p1636 A70-23133

Amplitude and phase correlations of spherical waves propagating in turbulent atmosphere using smooth perturbation method

09 p1636 A70-23139

Strain and temperature fields interrelation effect on longitudinal wave propagation in viscoelastic cylinder,

determining phase velocities and attenuation coefficients

09 p1781 A70-23285

Friction and orography influence on wave motions in real atmosphere, discussing planetary boundary layer and propagation in free atmosphere

09 p1718 A70-23331

Elastic harmonic waves propagation in cylinder with longitudinal cavities and in space with cylindrical cavities solved using series method

09 p1783 A70-23387

Acoustic gravity waves horizontal ducting in atmosphere with spatially periodic wind shears

09 p1671 A70-23498

Sectorial and circular strip resonators natural oscillation modes and freely propagating waves of uniformly bent stripline

09 p1651 A70-23644

Wave propagation constants in electron wave TWT, studying nonuniformity parameter influence to determine relationships between beam and system parameters

09 p1652 A70-23655

Amplitude modulation of microwave signals propagated through periodically varying plasma

09 p1639 A70-23673

Oblique E-mode electromagnetic wave in plane stratified collisionless plasma taking into account plasma temperature

09 p1639 A70-23674

Upper atmospheric waves nonlinear interactions based on tides and gravity waves propagation, taking into account terrestrial rotation

10 p1872 A70-23820

Ion acoustic wave propagation near sheath at plasma-wall boundary in low pressure argon plasma measured by electron beam probe

10 p1921 A70-23965

Wave propagation in bounded homogeneous elastic anisotropic media solved as sum of eigenvalue and static problems without transform calculus

10 p1915 A70-24058

Wave propagation in homogeneous cone region of broadband radiator, calculating field distribution by retarded potentials method

10 p1848 A70-24222

Fast magnetoacoustic wave propagation in cylindrical plasma column with constant current density, using geometric optics

10 p1923 A70-24229

Coulomb collisions effect on electrostatic lower hybrid resonance waves propagation in ionosphere, noting noise bands cut-off shift

10 p1874 A70-24429

Helical propagation in multivalley semiconductors of n-Ge type, obtaining polarization anisotropy

10 p1928 A70-24842

LF longitudinal waves propagation in DC gas discharge plasma, obtaining wave dispersion equation for various limiting cases

10 p1925 A70-25010

Nonpotential waves propagating at slow phase velocity in inhomogeneous plasma, determining flute instability oscillation frequency

10 p1925 A70-25011

Slow HF waves propagation under magnetic field effect in plasma waveguide surrounded by dielectrics or metal

10 p1843 A70-25106

One dimensional wave processes in distributed nonlinear systems, surveying mathematical methods

10 p1843 A70-25151

Stationary and nonstationary nonlinear waves propagation in multicomponent collisionless plasma, considering dispersion relations for acoustic oscillations

10 p1844 A70-25166

Type 3 burst sources velocity calculated by frequency drift and Newkirk model of electron density, discussing frequency range extension of Weissenau radiospectrography

10 p1934 A70-25274

Unsteady problems of finite amplitude plane and cylindrical wave propagation in dissipative spatially symmetrical media

11 p2034 A70-25399

Elastic wave propagation, deriving characteristic equations in generalized curvilinear coordinates using linear elastic, isotropic and homogeneous constitutive equations

11 p2132 A70-25680

Free wave propagation constants in periodically supported infinite beams determined for rigid and flexible supports

11 p2132 A70-25727

Alfvén and cylindrical magnetoacoustic waves in homogeneous unbounded conducting plasma in non-homogeneous magnetic field, applying Weinberg method to propagation analysis

11 p2089 A70-25850

Waves and mean currents excitation in stratified fluid due to moving heat source, studying effect on mean motion

11 p2036 A70-26167

Electrostatic wave propagation and growth rate in electron beam-inhomogeneous plasma confined by magnetic field

11 p2091 A70-26460

Elastic wedge under spatially uniform but time dependent shear tractions, studying shear stress and transient wave propagation

11 p2142 A70-26629

Frequency equation for harmonic waves propagating in composite circular-cylindrical rods consisting of circular core and circular casing of different material

11 p2145 A70-26693

Extensional waves asymptotic nature and stress distributions in infinite elastic plate of finite thickness under axisymmetric and in-plate disturbances using perturbation

11 p2145 A70-26696

Wave propagation in continuous random media solved by partial differential equations with random coefficients, describing perturbation methods for obtaining solutions statistical properties

11 p2085 A70-26761

Wave propagation in solid state plasma with ferroelectric and ferromagnetic properties, deriving matrix equation allowing for nonlinearity of dielectric constant and magnetic permeability

12 p2283 A70-26970

Dispersion relations between wave frequency and vector obtained from matrix equation for wave propagation in solid state plasma with ferroelectric and ferromagnetic properties

12 p2283 A70-26971

Diluted plasma microinstabilities allowing for Langmuir waves propagation without magnetic field and Landau effects

12 p2277 A70-27057

Wave propagation in finite length revolving shells, describing advantages of modal superposition method generated by finite element computer program

12 p2317 A70-27124

Weak plane waves propagation in binary mixtures of diatomic gases subject to vibrational relaxation, solving piston problem in acoustic approximation

12 p2209 A70-27151

Dispersion relation derived for space-charge waves propagating in thick Gunn diode, showing validity limit of one dimensional approach

12 p2194 A70-27164

Three dimensional variational dynamic and static large deformation equations solutions for stability and natural frequencies and wave propagation in bodies under initial strains

12 p2322 A70-27331

Resonant and nonresonant coupling between two coherent electron plasma waves propagating in opposite directions, considering parametric decay

12 p2279 A70-27780

Linearized dispersion relation for plane wave propagation in uniform unbounded cold plasma permeated by DC magnetic field, considering two stream instability

12 p2281 A70-27881

Wave propagation in spatially homogeneous time varying dispersive media, emphasizing excitation and source dependent phenomenon

12 p2188 A70-27961

Ultrasonic wave propagation guided by fluid layer between two elastic solids, plotting normalized velocities and layer thicknesses

12 p2273 A70-28097

Light pulse propagation in dispersive nonlinear dielectric analyzed on nonlinear Lorentz model

12 p2274 A70-28216

Magnetic field effect on frequency spectrum of vertically propagating magnetoacoustic waves and reflection conditions in inhomogeneous isothermal atmosphere

12 p2227 A70-28226

Longitudinal waves propagation in polyethylene bar using Boltzmann-Volterra equation, constructing dynamical stress-strain diagrams by viscous-elastic standard body model

12 p2328 A70-28276

Monge equation in small perturbation method of characteristics applied to propagation phenomena in three dimensional supersonic gas flow

13 p2386 A70-28490

Lunar elastic waves anomalous propagation, considering Apollo seismographic records and earth rocks specific dissipation function measurements

13 p2486 A70-28617

Collisional theory of longitudinal wave propagation in partly ionized multitemperature gases

13 p2460 A70-28637

Propagation characteristics of instabilities represented by multidimensional Fourier integrals

13 p2454 A70-28640

Love wave propagation in layers with irregular boundaries, investigating scattered field to determine reflection from triangular notch

13 p2394 A70-28831

LF MHD waves propagation model through earth magnetic tail, considering analogy with hydromagnetic plasma wave duct

13 p2398 A70-29210

Hydrodynamic equations to obtain transformation coefficient for HF weakly damped waves in magnetoactive plasma, applying to solar corona

13 p2463 A70-29227

Infrasonic waves generated by pulsating aurora, using Joule heating and Lorentz force coupling

13 p2399 A70-29236

Gas parameters determination near singular point of slow magnetosonic wave propagating in conducting medium in uniform magnetic field

13 p2464 A70-29507

Nonlinear wave propagation in continuous media involving stress-strain state of half space under pressure or load expanding over boundary

13 p2517 A70-29770

Plasma waves in space and laboratory - NATO Conference, Roros, Norway, April 1968

13 p2466 A70-29901

Electron temperature and concentration determined from longitudinal electron cyclotron harmonic waves in finite plasma column

13 p2467 A70-29916

Perpendicular propagation of VLF waves from wave/particle interaction in vicinity of lower hybrid resonance frequency in magnetosphere

13 p2468 A70-29934

Time harmonic waves propagation in elastic half-space with submerged cylindrical cavity, assuming linear plane strain conditions

13 p2518 A70-30010

Propagation in corrugated waveguides with surface permitting H-wall boundary condition for choice gap and fin dimensions

14 p2550 A70-30519

Overpressure, rise time and wave period of sonic boom signatures at ground level from unaccelerated supersonic overflights

14 p2530 A70-30608

Plasma refractive index determination by propagation method allowing simultaneous electron concentration and density measurements by reflected damped wave

14 p2622 A70-30658

Geomagnetic field lines inclination effect on hydrodynamic waves propagation in lower ionosphere, using atmospheric model in plane form with integral conductivity tensor

14 p2575 A70-30821

Plane waves propagation in elastic layer using Cauchy theory of initial stress

14 p2658 A70-30998

Normal wave propagation modes existence in magnetized plasma, deriving criteria for electrostatic approximation validity

14 p2624 A70-31045

Atmospheric turbulence effects on acoustic-gravity waves propagation, deriving dispersion relation for phase velocity and propagation constants

14 p2579 A70-31252

Nonhomogeneous atmosphere with absorbing gas of constant mixing ratio, deriving transmission along isothermal and nonisothermal paths

14 p2617 A70-31304

Geomagnetic pulsations and hydromagnetic wave propagation in magnetosphere, using geometric optics approximation

15 p2722 A70-31452

Weak discontinuities propagation in quasi-linear systems for MGD, obtaining transport equations

15 p2777 A70-31470

Elastic waves propagation in finite thickness elastic plate under transient load, assuming material behavior in conformity with nonlinear Hooke's law

15 p2814 A70-31544

Iron sample shape determination for studying relationship between tensile strength and rate from stress wave propagation during high speed tensile tests

15 p2814 A70-31547

VLF wave propagation direction observation by satellite after passage through magnetosphere at low and mid latitudes

15 p2697 A70-31659

Phase shift ultrasonic flowmeter measuring transit time between oppositely propagating waves in blood vessels

15 p2691 A70-31921

Wave propagation through Newtonian fluid in compressible thick walled viscoelastic tube, considering blood flow in arteries

15 p2691 A70-31938

Dynamic asymmetric elasticity problems, considering longitudinal and torsional wave propagation in bounded and unbounded micropolar media

15 p2818 A70-32178

Kelvin wave propagation numerical model, showing influence of mean zonal wind vertical and horizontal shear in lower stratosphere

15 p2771 A70-32370

Stress wave propagation in solid infinite elastic medium and laminated materials

15 p2823 A70-32784

Wave propagation and group velocity in warm magnetoplasma, using adiabatic theory for ionosphere and far magnetosphere models

16 p2859 A70-32937

Coherent wave propagation in warm turbulent plasma, using perturbation method for wave dispersion

16 p2860 A70-32945

Scattered fields evaluation due to creeping waves for smooth convex radar targets, using algebraic expressions

16 p2956 A70-32978

Thermodynamically perfect fluids in general relativity, considering heat transmission paradox and wave propagation velocities

16 p2997 A70-33103

Ultrasonic pulses velocity and attenuation in fluids by coherent detection technique, measuring delay and decrease in amplitude due to transmission path length increase

16 p2913 A70-34084

Asymptotic analysis of wave propagation modes in circular solid elastic cylinder, obtaining displacement components and frequencies as dimensionless wave number power series

16 p2993 A70-34085

Longitudinal wave propagation in variable section bars, solving hyperbolic equation of motion by perturbation method

16 p2993 A70-34088

Wave propagation in infinite elastic plate in contact with inviscid incompressible liquid layer, deriving dispersion relation

16 p2993 A70-34094

Waves nonlinear propagation in fluids due to convection, reviewing various solution methods

17 p3068 A70-34666

Warm homogeneous magnetoplasma longitudinal cyclotron harmonic wave propagation perpendicular to static magnetic field, noting instabilities

17 p3140 A70-34927

Analog simulation of elastic wave propagation in thick walled hollow circular cylinders to determine safe impact speed

17 p3185 A70-34964

One dimensional elastoplastic wave propagation in rate-sensitive viscoplastic rod with thermal gradient

17 p3185 A70-34966

Wave propagation from two dimensional expanding load on liquid half space with load fronts decelerating monotonically from initial supersonic speed

17 p3069 A70-34976

Wave propagation measurement by correlation techniques, discussing travelling wave representation, delay times, amplitude coefficients, etc

17 p3091 A70-35449

Weak nonlinear one dimensional wave propagation in nonequilibrium flow, using governing system characteristics for reference coordinates

17 p3071 A70-35468

Martensitic phase change effects in TiNi on ultrasound waves propagation in transition region, using pulse echo measurements

17 p3126 A70-35603

Transient wave propagation in homogeneous anisotropic media, using hyperbolic equations and unitary operator

17 p3137 A70-35607

Hydromagnetic wave propagation compared in magnetospheres of plane and cylindrical geometries

18 p3311 A70-36011

Cracks and tensile failure of interface bonds in elastic composite hollow cylinder, deriving wave front propagation equations

18 p3283 A70-36388

Two component warm plasma wave propagation along magnetic field, considering full pressure tensor equation with momentum and pressure relaxation mechanisms

18 p3294 A70-36405

Nonlinear theory for surface waves propagating in bounded magnetoactive plasma

18 p3295 A70-36412

Phase plane method for Hill equation in problems involving EM wave expansion in elliptical waveguides or single circuit parametric systems analysis

18 p3227 A70-36424

Three dimensional dynamic analysis of small harmonic stress wave propagation in elastic-plastic and viscoplastic materials, using finite differences

18 p3344 A70-36724

Propagation constants in laminar plasma circular waveguides filled with anisotropic linear medium, using Galerkin-Ritz method

19 p3474 A70-37428

Electromagnetic propagation in flat waveguide with local gyrotropic filling and transverse magnetization, using Galerkin method

19 p3470 A70-37430

Acceleration wave propagation in materially uniform inhomogeneous isotropic elastic bodies, using tensor analysis

19 p3536 A70-37563

WKB or eikonal approximation for waves and vibrations in inhomogeneous Euler-Bernoulli beams and plates and Timoshenko beams

19 p3536 A70-37700

Numerical model of piezoelectric surface wave propagation on free and metallized cubic and hexagonal crystals

19 p3486 A70-37754

Magnetoelastic ferromagnet linear theory, considering spin-elastic microwaves propagation in ferrimagnetic crystal subjected to pulsed magnetic fields

19 p3487 A70-37947

VLF wave propagation in earth atmosphere waveguide, calculating various atmospheric types from waveguide field dependence on frequencies

19 p3416 A70-38566

Plane VLF wave propagation in waveguide formed by earth and inhomogeneous anisotropic ionosphere, determining excitation coefficients and attenuation functions

19 p3381 A70-38568

Radio wave propagation over inhomogeneous terrains, determining perturbing effects of details on wave characteristics

19 p3381 A70-38573

Terrestrial atmospheric structure, determining zero and extremum point positions and amplitudes to obtain information of VLF wave propagation path

19 p3416 A70-38574

Slow wave propagation in plasma moving along external magnetic field, generalizing refractive index formula

19 p3417 A70-38592

Wave propagation in linear elastic surfaces, calculating wave speeds, shapes and strength decay

19 p3473 A70-38943

Asymptotic expansion methods for solving wave propagation and diffraction problems via localization principle

20 p3657 A70-39219

Square cross section waveguide with cutoff frequency, calculating density wave propagation in helical electron beam trajectories directed by magnetic field

20 p3584 A70-39256

Perturbation method for nonlinear wave propagation in inhomogeneous media, considering sound propagation in ducts and hydromagnetic waves across nonuniform magnetic field

20 p3672 A70-39611

Electrothermal mode wave propagation in nonequilibrium partially ionized gas, using model with finite ionization

20 p3680 A70-39984

Dynamic theories for wave propagation in laminated and fiber reinforced composites, using dispersion curves for transverse and longitudinal motions

20 p3730 A70-40036

Unsteady problems of finite amplitude plane and cylindrical wave propagation in dissipative spatially symmetrical media

20 p3673 A70-40093

Nonlinear resonance conditions for plasma three-wave interactions, considering wave propagation modes and constant magnetic field

20 p3682 A70-40137

Mechanical analogies of magnetodynamic oscillations in homogeneous density column subject to material body impact, relating to earth magnetic field

21 p3854 A70-40593

Elastic wave propagation mathematics in visual form for ultrasonic testing

21 p3831 A70-40746

Solar photosphere vertical velocities and horizontal wave propagation, discussing magnetic fields, phase coherence and behavior and oscillations

21 p3885 A70-40952

Collisionless shock wave geometry, determining dispersion relation for ion acoustic waves propagating in plasma

21 p3856 A70-41082

Radioheliograph observations of solar outbursts involving MHD waves propagation along curved paths in corona at 80 MHz

21 p3891 A70-41178

Longitudinal tension impact tests on nylon tape and Apollo pilot parachute riser construction, determining wave propagation effects

21 p3843 A70-41831

Wave instabilities in avalanche diode bulk semiconductors with negative field dependent drift velocity and carrier temperature, noting validity for gas plasma

21 p3863 A70-41915

Rotating cold plasma wave propagation modes including Coriolis effect in absence and presence of external magnetic field

21 p3860 A70-41924

Elastic wave propagation in isotropic homogeneous bodies, considering free vibrations and propagation velocity

21 p3940 A70-42099

Surface elastic waves, considering propagation, electromagnetic transduction, amplification, guiding, focusing, reflection and applications

21 p3830 A70-42115

Internal gravity waves mathematical model for atmosphere with arbitrary distributions of temperature,

molecular weight, viscosity and conductivity, deriving wave propagation into thermosphere

21 p3821 A70-42257

Finite difference method for stress wave propagation and multiple reflection in elastic bar with discontinuities

22 p4115 A70-42744

Arbitrary form acceleration waves growth equation in deformed hyperelastic material, discussing solution and decay criteria

22 p4115 A70-42940

Self focusing in nonlinear optics, discussing physical processes of wave propagation in dielectric

22 p4074 A70-43207

Homogeneous helium plasma column LF wave propagation in uniform magnetic field

22 p4082 A70-43216

Slow wave propagation on conducting surface separated from plasma by ion sheath, observing resonances on cylindrical antenna

22 p4082 A70-43238

Pc-1 and IPDP pulsations propagation characteristics from ground based measurements, discussing spectral structure, waveforms, polarization, time delay between different observation stations, etc

22 p4021 A70-43277

Exponential compression wave propagation in conical rod with smooth tapering cross section

22 p4121 A70-43726

Italian Sirio satellite with local and foreign ground stations network measuring SHF wave propagation variables

23 p4158 A70-43753

Nonlinear frequency shift for electronic and ionic cyclotron modes in magnetospheric whistler and hydrodynamic propagation, using Vlasov equation

23 p4187 A70-43880

Short radio wave propagation over single jump lines in F sub zero F 2 gradient presence, examining maximum usable frequency increase

23 p4162 A70-44076

Partially ionized viscous plasma longitudinal wave propagation, formulating motion equations for electrons, ions and neutrals from Maxwell and Boltzmann equations

23 p4229 A70-44987

Single crystal piezoelectric materials growth characteristics and wave propagation properties for surface acoustic wave applications

24 p4367 A70-45399

One-dimensional propagation of elastic spherical waves in inhomogeneous unbounded medium under normal stress on cavity surface

24 p4424 A70-45631

X ray and neutron propagation in multilayer film composite, discussing boundary conditions in interfacial systems

24 p4380 A70-46095

Spheroidal wave function theory, calculating eigenvalues with branch points for propagation constants complex values

24 p4315 A70-46134

Radiative transfer and magnetic dispersion for three dimensional wave propagation in radiation magnetogasdynamics

24 p4387 A70-46148

WAVE RADIATION

U ELECTROMAGNETIC RADIATION

WAVE REFLECTION

Natural oscillation modes two dimensional resonator determined in form of superimposed uniform plane waves with arbitrary coefficients of wave reflection

01 p0140 A70-10057

Transmission and reflection of electromagnetic waves by bounded moving plasma layer in slow wave space

01 p0042 A70-10167

Reflection coefficient of electromagnetic wave reflected from thin ionization layer, using frequency dependence of amplitude to estimate ionospheric layer thickness

01 p0083 A70-11532

Electromagnetic pulse duration formed by spectral content in HF bandwidth received after ionospheric reflection

02 p0258 A70-12419

Electromagnetic wave reflection on thin plasma layer with Epstein electron density profile, noting use in microwave diagnostics

03 p0529 A70-13016

Third harmonic generation detection for strongly absorbing media in reflection with neodymium-glass mode-locked laser, measuring nonlinear susceptibilities of semiconductors and metals

03 p0501 A70-13649

Ray-optical analysis of electromagnetic scattering in plane and circular waveguides, giving formulas for modal reflection and coupling coefficients

03 p0452 A70-14034

Stellar X ray effect on nighttime lower ionosphere wave reflection suggested from VLF propagation data

03 p0562 A70-14224

Plane shock wave diffraction and reflection at slender wedge in linear approximation, proposing

- pressure distribution calculation formulas behind shock 04 p0665 A70-14493
- Helmholtz integral for radio waves scattering from surfaces expanded for reflection from terrain or atmospheric layers 04 p0648 A70-14964
- Integrodifferential equation solved for plane wave reflection and transmission by random medium assuming homogeneous background refractive index 04 p0649 A70-14970
- Flow viscosity and heat conduction effects on shock wave propagation in bent channel with weak Mach reflection 04 p0671 A70-15013
- Precursor electron densities measured in nitrogen and air ahead of shock waves, noting shock tube wall reflectivity 04 p0694 A70-15565
- Strong radiating shock wave structure and reflection at rigid wall, investigating flow velocity, density and temperature changes 05 p0956 A70-15788
- Sea surface sunglint pattern irregularities in earth orbiting satellite photographs, observing dark patches 05 p0838 A70-16152
- TEM wave reflection incident on conducting thin strips semiinfinite array in free space not accompanied by emission 05 p0812 A70-16243
- Propagation, reflection and dispersion equation for electromagnetic waves in longitudinally magnetized plasma filled coaxial waveguide using rotating coordinates 06 p1016 A70-17124
- Power reflection and transmission coefficients for polarized electromagnetic waves incident on plasma slab moving along magnetostatic field 06 p1008 A70-17566
- D region electron density distribution during night and presunrise period, using full wave integration method for propagation parameters for waves reflected from electron density model 06 p1054 A70-17587
- Phase path variation of stable continuous wave transmission reflected from E region during daytime, discussing night time results 06 p1055 A70-17593
- Transmission and reflection coefficients calculated for electromagnetic waves incident on inhomogeneous absorbing layer applicable to ionosphere, plasma and p-n junction 06 p1009 A70-17834
- Monte Carlo simulation for shock wave formation by specularly reflecting piston, discussing reflection from specularly reflecting wall 06 p1049 A70-18334
- Pressure history at end wall of electromagnetic shock tube measured during shock wave reflection by piezoceramic gage 06 p1031 A70-18505
- Supersonic oblique shock wave reflection on turbulent boundary layer, considering layer separation and pressure effects 07 p1255 A70-19210
- Radio signal reception beyond normal horizon by partial reflection from elevated layer in troposphere calculated by computer 07 p1234 A70-19218
- Plane electromagnetic wave reflection from laminar anisotropic medium, analyzing piecewise-constant permittivity tensor as boundary value problem 07 p1235 A70-19448
- Back reflection of zero-mass scalar or vector waves in gravitational fields produced by non-Lorentz part of spatial metric components 07 p1387 A70-19923
- Front lit holograms of transient events and live subjects obtained with reflected light pulsed laser system 07 p1287 A70-20087
- Lower ionosphere geomagnetic field local gradients determination by partial reflection method 07 p1277 A70-20455
- S- and p-polarized electromagnetic wave incident on semiinfinite laminar plasma layers, analyzing reflection and absorption characteristics 08 p1456 A70-20504
- Parameters defining elliptic vibration of light reflected from surface using photoelectric ellipsometer 08 p1546 A70-21673
- Ground reflection effect on plane uniform sound source distribution applicable to compressor and fan noise under far field conditions 09 p1726 A70-22240
- Doppler-effect-like phenomena of waves or pulses reflected and refracted at moving boundary layers 09 p1728 A70-23072
- Distortion of electromagnetic pulse undergoing total internal reflection in inhomogeneous isotropic plasmas in lower ionosphere 09 p1639 A70-23672
- Progressive shock waves propagation, reflection and transmission through sudden changes in pipe cross sectional area, obtaining boundary conditions for quasi-steady junction flow 09 p1664 A70-23738
- Longitudinal shock wave oblique reflection in nonlinear harmonic elastic material in terms of wave propagation 10 p1956 A70-24097
- Radiating shock wave reflection from rigid wall studied for velocity and structural changes, assuming unsteady and one dimensional flow 10 p1867 A70-24140
- Strong shock wave reflection from rigid wall at high shock velocities, studying effect on flow structure 10 p1922 A70-24152
- Transmission and reflection of electromagnetic waves by bounded moving plasma layer in slow wave space 10 p1842 A70-25015
- Radio wave reflection spectra from plane surfaces, determining physical properties and composition 10 p1843 A70-25154
- Surface wave reflection during propagation along transversely magnetized ferrite plate on metal backing, using perturbation theory to find cylindrical wave field 10 p1844 A70-25163
- Time dependence of shock wave attenuation at multiple reflection in shock tube after diaphragm burst, using damped vibration solution 11 p2034 A70-25495
- Microwaves reflection, absorption and thermal emission at smooth air-water interface, tabulating calculated coefficients 12 p2183 A70-27169
- Shock wave reflection into ideal gas flow with linear density variation analyzed for flow field 12 p2211 A70-27832
- Radiation transfer models for diffuse reflection of quanta from turbulent medium applied to electromagnetic wave propagation in turbulent atmosphere 12 p2306 A70-27855
- Coherent wave reflection from random half space, solving scalar Dyson equation in bilocal approximation for oblique incidence 12 p2189 A70-27972
- Plane electromagnetic waves anomalous reflections from diffraction grating with periodic array of rectangular holes in dielectric layer, observing resonant character 12 p2191 A70-28175
- Magnetic field effect on frequency spectrum of vertically propagating magnetoacoustic waves and reflection conditions in inhomogeneous isothermal atmosphere 12 p2227 A70-28226
- Heat transfer and flow stabilization dependence on initial shock wave reflection from conducting wall 12 p2213 A70-28228
- Plane electromagnetic wave reflection at interface of two semiinfinite dielectric media in relative motion perpendicular to incidence plane, noting polarization change 13 p2365 A70-29102
- Adiabatic index effect on shock waves reflection, emphasizing critical angle dependence on incident wave intensity 13 p2388 A70-29416
- Electromagnetic plane wave oblique reflection from flat surface with spatially modulated surface impedance, computing wave spectrum 13 p2367 A70-29527
- Reflection and conversion coefficients of model ionospheres for VLF and LF radio waves 14 p2573 A70-30735
- Normally incident plane monochromatic electromagnetic wave reflection and scattering from expanding dielectric slab, using invariant imbedding concept 15 p2695 A70-31438
- Em wave reflection and transmission at boundary between free space and semiinfinite anisotropic plasma 15 p2778 A70-31830
- Plane EM wave reflection and transmission at moving boundary, discussing frequency disparity with incident wave 15 p2697 A70-31834
- Light scattering in one dimensional semiinfinite medium with moving boundary, deriving escape and reflection probability expressions 15 p2808 A70-32880
- Reflection coefficient formula for principal radio wave reflected from thin long rod in middle of rectangular waveguide 16 p2878 A70-33800
- Plane harmonic sound wave reflection and transmission in flowing medium by infinite set of arbitrary spaced and staggered flat plates 16 p2971 A70-34016
- Plane wave reflection decay rate representation by slowness diagrams 16 p2952 A70-34089
- Flowfields behind reflected shock waves, predicting end-wall radiative heat transfer and radiative gas dynamic coupling effects 17 p3065 A70-34480 [AIAA PAPER 70-774]
- Boundary conditions for electrodynamics of wave reflection from conducting bodies, using perturbation technique 17 p3128 A70-34633
- Zonal wind component in lower ionosphere observed for gravity waves partial reflections by temperature discontinuities, using least mean square method for reflection coefficient 17 p3077 A70-34946
- Effective reflection height measurement accuracy for pulsed vertical ionospheric sounding, using interference method 18 p3227 A70-36106
- Shadow photography applied to Mach reflections in argon, carbon dioxide and Freon 12 in shock tube, using Huygens principle for transfer mechanism 18 p3205 A70-36148
- Plane electromagnetic wave reflection from laminar anisotropic medium, piecewise-constant permittivity tensor as boundary value problem 18 p3229 A70-36922
- Internal gravity waves reflection, inspecting differential equations for behavior of two wave parameters 19 p3471 A70-37779
- Plane wave reflection from stratified isotropic medium using ray tracing in complex space, noting agreement with phase integral method 19 p3380 A70-38404
- D region electron densities during 20 May 1966 solar eclipse, using partial reflection and rockets 19 p3419 A70-38914
- Book on electromagnetic waves in stratified media covering reflection, propagation, waveguide mode theory, superrefraction and tropospheric ducting 20 p3586 A70-39604
- Inclined electromagnetic wave incidence on randomly inhomogeneous medium with changing mean dielectric permittivity, calculating reflected and scattered fields 20 p3587 A70-39726
- Laser interferometer system unwanted reflections elimination and intensities control in each arm by linear polarization method 21 p3823 A70-40820
- Gas phase ignition theory with feedback of homogeneous propellant exposed to stagnant gas after shock reflection 21 p3950 A70-41728 [AIAA PAPER 69-559]
- Plane stationary shock wave reflection from rigid concave wall at low Mach numbers 21 p3811 A70-42204
- Doppler frequency shift of reflected radio waves for ionospheric disturbances, discussing solar flares, geomagnetic variations, etc 21 p3820 A70-42256
- Finite difference method for stress wave propagation and multiple reflection in elastic bar with discontinuities 22 p4115 A70-42744
- Radio wave reflection properties in 16-3000 kHz range calculated from D and E region models for comparison with measurement 22 p3989 A70-43164
- Reflection echelon and Fabry-Perot interferometer with surface imperfections, comparing spectral resolution limit with Rayleigh limit 22 p4040 A70-43612
- Millimeter band electromagnetic scattering from weakly doped GaAs, calculating reflection coefficient and phase angle 23 p4229 A70-43926
- Curved shock waves regular and Mach reflection in steady supersonic flow at plane wall 23 p4180 A70-44122 [ICAS PAPER 70-11]
- Sound radiation from unflanged circular waveguide duct with flow, calculating reflection coefficients, directivity pattern and power for comparison with approximate methods 23 p4219 A70-44392
- Sonic boom waves diffraction and reflection, developing analytical method for pressure-time history in vicinity of walls and corners 24 p4289 A70-45266
- Angle beam ultrasonic testing of metals, considering beam and depth scanning characteristics and wave reflectability of various flaws 24 p4343 A70-45687
- Echoes with ion sonar waves in ionized gases, considering ion density disturbances under local excitation 24 p4387 A70-45795
- Contact region structure with viscosity, conduction and radiative transfer effects applied to plane shock wave reflection from heat conducting wall 24 p4326 A70-46001

WAVE RESISTANCE

Structural strength under impact loading with allowance for shock waves, comparing various strength calculation methods 04 p0774 A70-15098

Wave resistance of pressure field of hovercraft drifting over water surface determined as definite integral based on Wehausen expression 09 p1609 A70-22219

WAVE SCATTERING

NT ACOUSTIC SCATTERING

NT ATMOSPHERIC SCATTERING

NT ELECTROMAGNETIC SCATTERING

NT IONOSPHERIC F-SCATTER PROPAGATION

NT LIGHT SCATTERING

NT MICROWAVE SCATTERING

NT MIE SCATTERING

NT RAMAN SPECTRA

NT RAYLEIGH SCATTERING

NT REVERBERATION

NT TROPOSPHERIC SCATTERING

NT X RAY SCATTERING

Absorption band observation near 0.43 μ in solar spectra and scattered radiation of sky, determining nontelluric origin 01 p0084 A70-11613

Energy transfer formula and scattering of electromagnetic waves at ideally reflecting bodies in inhomogeneous medium using geometrical optics approximation 03 p0442 A70-13094

Quasi-optic electromagnetic beams slow spreading in anisotropic media due to propagation in unusual directions 03 p0447 A70-13288

Helmholtz integral for radio waves scattering from surfaces expanded for reflection from terrain or atmospheric layers 04 p0648 A70-14964

Scattering cone of hydromagnetic waves propagating along magnetic lines in magnetized plasma with oscillating electric dipole 04 p0683 A70-15738

Kirchhoff wave scattering geometric optics theory accuracy, using multifrequency acoustic wave backscatter data obtained from rough surfaces 05 p0814 A70-16401

Correlation function of auroral reflection radio signals with allowance for polar ionospheric scattering and pulse signal transmission and reception 05 p0841 A70-16741

Induced Compton scattering of plasma and electromagnetic waves under astrophysical conditions, discussing HF radio emission spectra from cosmic objects and quasar 05 p0917 A70-16904

Electron plasma wave damping by ion sound wave scattering using Vlasov equation 06 p1125 A70-18638

Scattering cross sections of radio waves at wake of vertically moving body near reflecting ionospheric layer, noting wave sphericity influence 07 p1237 A70-20423

Radio wave sphericity influence on scattering at moving body wake in ionosphere, determining scattering cross section principal maximum 07 p1237 A70-20424

Plasma monochromatic wave propagation equilibrium state instability mechanisms, discussing stimulated scattering by thermal plasma particles and particle capture in wave potential well 08 p1551 A70-21422

Nonlinear wave scattering at plasma particles and weak plasma inhomogeneity effects on plasma current instability 08 p1554 A70-21819

Bistatic radar cross section measurements by pendulum method using modulated wave formed by target swing motion 09 p1634 A70-22698

Point electric dipole EM radiation in presence of moving dispersive dielectric half space 09 p1639 A70-23669

Uniform asymptotic theory of diffraction by edge of three dimensional body, obtained boundary layer solution applied to scattering by circular cylinder 11 p2084 A70-26422

Scalar plane wave LF scattering by prolate spheroid of revolution, obtaining iterative solution for Dirichlet problem 11 p2085 A70-26621

Scalar plane wave LF scattering by prolate spheroid of revolution, obtaining iterative solution for Neumann problem 11 p2085 A70-26622

Wave scattering by statistical distributions of discrete obstacles, deriving various functions for diagnostic applications 11 p2086 A70-26762

Incoherent scattering of radiation from collisionless plasma in quasi-stationary state, analyzing wave energy from spectral decomposition for given background distribution function 13 p2457 A70-28558

Love wave propagation in layers with irregular boundaries, investigating scattered field to determine reflection from triangular notch 13 p2394 A70-28831

Elastic plane wave diffraction and scattering at convex obstacle in semibounded regions, using method of images 13 p2452 A70-29289

Upper critical field dependence on s- and p-wave scattering of Frenkel effects in electron irradiated niobium 13 p2471 A70-29535

LF plane wave scattering from semielliptic groove in conducting ground plane noting validity for arbitrary polarization, incidence, directions and eccentricity 13 p2453 A70-29822

Multichannel scattering variational bounds reformulation without using projection operators, calculating resonance-energy relations 14 p2619 A70-30490

Scattering cone of hydromagnetic waves propagating along magnetic lines in magnetized plasma with oscillating electric dipole 14 p2575 A70-30822

Planar sandwich hologram recording 4 π steradians with preservations of object spatial perspective by representing entire wave front 14 p2588 A70-31209

Radio observations of dense briefly visible Leonid meteor shower with fixed pencil beam antenna in coping with wave scattering in trails 15 p2796 A70-31511

Electromagnetic waves scattering at circular cylinders in semibounded region, showing boundary influence on radiation pattern 15 p2698 A70-32174

Wave scattering from circular cylindrical body, considering plane wave primary source, line source, point and dipole source 15 p2700 A70-32403

Wave scattering from elliptic cylinder, solving boundary value problem for two dimensional wave equation 15 p2700 A70-32404

Plane wave scattering by strip of elliptical cylinder, considering geometrical diffraction theory 15 p2700 A70-32405

Wave scattering by acoustically soft, hard and perfectly conducting spheres 15 p2700 A70-32410

Wave scattering by acoustically soft and hard prolate spheroids 15 p2700 A70-32411

Born approximation limit for plane wave multiple scattering by inhomogeneous electron density distribution in plasma 16 p2957 A70-32981

Refractive index gradients effect on scattering of radio waves perturbing ionosphere or passing through perturbed region 16 p2863 A70-33259

Electromagnetic wave scattering on resonant dielectric sphere in rectangular waveguide, using reflection coefficient 18 p3227 A70-36419

Plane TM wave scattering by systems of two parallel conducting elliptical cylinders, metal tapes and combinations 19 p3374 A70-37278

Gravitational radiation scattering by Schwarzschild horizon, discussing odd parity waves of angular momentum 21 p3878 A70-40731

Convergent numerical method for principal value integrals in dispersion relations of coupled channel scattering problem involving wave phase shifts 22 p4062 A70-42748

Scattering and radiation from circumferential gap in circular dielectric-loaded waveguide, using integral equations 23 p4167 A70-43765

WAVE SUPERHEATERS

U HYPERVELOCITY WIND TUNNELS

U SHOCK TUBES

WAVEFORMS

NT PULSE AMPLITUDE

NT PULSE DURATION

NT SAWTOOTH WAVEFORMS

NT SQUARE WAVES

Oral potassium chloride usefulness and toxicity in EKG nonspecific T wave abnormality evaluation 01 p0014 A70-10274

Pulse width and spectrum generated by ring laser mode locked by synchronously modulated absorber as function of modulator waveform curvature and active medium 01 p0109 A70-10430

FM/FM telemetry systems waveform distortion measurement technique based on minimum rms error between input and output signals 01 p0044 A70-10941

Emission from broadband impulsive point source refracted by spherical interface between fluids with different acoustic velocities, showing emitted and inverse waveform disturbances 01 p0046 A70-11190

Signal waveform algorithmic construction with optimal autocovariance properties, using isosum integer

partitions, applied to clustered multipath distribution measurement 02 p0263 A70-12773

Sonic boom wave shapes and amplitudes determination in still stratified atmosphere, comparing U.S. standard atmosphere results to various atmospheric models 03 p0411 A70-12927

Rotating prism method for obtaining time correlation between streak photographs and characteristic waveforms of flash X ray discharges 03 p0492 A70-13762

Dielectric loaded waveguide with symmetric microstrip line, evaluating transverse wave number by finite difference method 03 p0458 A70-14035

Ge IMPATT diodes under pulsed operation to produce LF high efficiency oscillations, recording current and voltage waveforms 05 p0821 A70-16417

Waveform-shaping transfer function rational polynomial approximation method with application to network problem in PCM communications 06 p1007 A70-17459

Linear circuit output waveform calculation without first resolving transfer functions on complex frequency plane, applied to current switching circuit analysis 06 p1018 A70-17460

Matched filter rectangular pulse compression nonlinear FM waveform design with low time sidelobe and zero mismatch loss due to spectral weighting 07 p1242 A70-20065

Operation mode for full-bridge programmed waveform static inverter permitting saturation of power transistors in DC power conversion 08 p1439 A70-20707

Two dimensionally periodic slow wave structure, verifying Shein formulas 09 p1637 A70-23143

Si avalanche diodes oscillations external current waveform measurement using coaxial current monitoring assembly with negligible phase error 10 p1849 A70-24234

Linear superposition (LSP) of isolated pulses in tape recording, discussing validity for multibit waveform synthesis 11 p2057 A70-26627

Engine firing rate measurement from acoustic waveform autocorrelation analysis 12 p2290 A70-27161

Waveform estimation by adaptive combination of analog and hardlimited sensor signals 12 p2187 A70-27906

Radar transmitter waveforms for multifunction operation, emphasizing phase and frequency modulation for CW radars 12 p2188 A70-27939

Radar spectrum control based on two pulse shaping techniques using klystron transmitter 12 p2188 A70-27941

Continuity equation plasma oscillation, discussing ion current waveform flowing from discharge and implications for periodic astrophysical phenomena 14 p2638 A70-30618

Analog data transmission over PCM telemetry link, comparing noncoherent FSK vs PSK reception performance for waveform error 14 p2552 A70-31187

Sampled analog waveforms transmission, deriving optimum pre- and postfilters 15 p2703 A70-32557

Optimal perturbation signal waveform linearizing nonlinear transfer characteristic of image sensing receptor array 15 p2705 A70-32725

Long term geomagnetic pulsations (PC5) with sinusoidal waveforms, using IGY data 17 p3080 A70-35642

Laser pulse shaping using inducible absorption with Q switched time behavior controlled by nonlinearities within optical resonator 18 p3270 A70-36745

Tightly wound spiral nonlinear density waves in pressureless self gravitating disk with external gravitational field, examining solid body and differential rotation 18 p3331 A70-37192

Waveform changes in postbuckling behavior of thin rectangular plates under axial compression 19 p3535 A70-37380

Tonks-Dattner resonances in warm inhomogeneous plasma column, examining kinetic theory for waveform shapes and resonance location 19 p3475 A70-37534

Aircraft streamer /spark/ discharges formation, waveforms and RF noise levels, using mathematical model for electric field strength 19 p3380 A70-38179

Close range atmospheric shape classification, using image recognition theory concepts 19 p3416 A70-38572

Radio wave propagation over inhomogeneous terrains, determining perturbing effects of details on wave characteristics 19 p3381 A70-38573

WAVEGUIDE ANTENNAS

- Noctilucent cloud kinematics, examining wave structure and lengths, velocities and general motion 20 p3622 A70-39403
- Elastic quasi-stationary waves, discussing waveforms and resonance phenomena 20 p3727 A70-39890
- Electromagnetic test equipment transient waveform control using on-line digital computer in near real time configuration 21 p3805 A70-41270
- Triangle and sine waveforms generation, discussing reduced peak and crossover distortion and extended frequency operation 22 p3989 A70-42923
- Arbitrary form acceleration waves growth equation in deformed hyperelastic material, discussing growth and decay criteria 22 p4115 A70-42940
- Internal gravity wave shape at temperature inversion in lower atmosphere from high resolution vertically pointing FM/CW radar sounding 23 p4162 A70-44038
- Automatic detection of K-complex waveforms in sleep electroencephalograms, using pattern recognition 23 p4151 A70-44379
- Mammalian eardrum failure due to blast induced pressure variations, examining wave shape, character, magnitude and duration effects 23 p4148 A70-44839
- Nervous inhibition effect on electroretinogram b wave during flash sequences 24 p4301 A70-45986
- ## WAVEGUIDE ANTENNAS
- Numerical solutions to determinantal equation for predicting properties of periodically modulated dielectrically filled frequency scanning waveguide as microwave antenna 03 p0457 A70-13696
- Reflection coefficients, radiation patterns and surface wave excitation calculated from aperture electric field obtained for waveguide radiating through dielectric slab 06 p1020 A70-17561
- Parallel plate TEM waveguides radiation pattern slope diffraction analysis 06 p1021 A70-17570
- Far field synthesis for calculating excitation pattern of waveguide-excited aperture antenna arrays 07 p1243 A70-20325
- Waveguide slot antenna with electrical control of field polarization from linear to circular and beam scanning over wide sector 09 p1652 A70-23652
- Solid dielectrics permittivity measurement using beam deflection phenomenon in multislot waveguide antenna 09 p1652 A70-23656
- Radiation patterns widened from plane and circular waveguide ends closed by planoconcave homogeneous dielectric lens 10 p1843 A70-25135
- Impedance in coaxial line generated by tee-fed waveguide slot antenna, using equivalent circuit 12 p2198 A70-27966
- Waveguide slot array operation in different frequency bands generating independent radiation patterns, utilizing orthogonal dominant modes propagation 12 p2199 A70-27967
- Leaky waveguide radiation patterns with periodic loading slots along axis 13 p2377 A70-29105
- Microwave field component distribution in plasma waveguide covered by metallic sheath in magnetic field, using counterbalanced antenna probes for field measurements 13 p2463 A70-29378
- Concorde aircraft radar signal transmission, describing modified Flexwell waveguide 13 p2379 A70-29561
- Admittance measurements of rectangular or circular waveguide fed aperture antennas illuminating displaced metal plate 16 p2872 A70-32963
- Steerable C band waveguide arrays design for forming monopulse cluster of sum and difference beams 16 p2875 A70-33395
- Compact integrated microwave antenna of composite structure involving slotted waveguide planar array capable of operating in three frequency bands 16 p2876 A70-33406
- Radiation patterns and impedance properties of slot antenna in ground plane, slot on cylinder and sphere and waveguide slot arrays 17 p3051 A70-35064
- Open waveguides and small horns theory, using Wiener Hopf method for radiation calculation 17 p3051 A70-35065
- Rectangular waveguide EM radiation into plane parallel region through asymmetrical longitudinal slot 19 p3386 A70-37727
- Electromagnetic wave propagation perpendicular to slots of plane dielectric filled waveguide used as slow wave system and antenna 19 p3386 A70-37728

- Dielectric covered narrow radiating slots in rectangular waveguide broad face, calculating impedance from equivalent circuits 23 p4175 A70-44952
- Optimum performance of corrugated waveguide feed horns for paraboloidal reflector antennas via radiation pattern shaping with digital computer 24 p4320 A70-46222
- ## WAVEGUIDE FILTERS
- Mode transducer and mode filter formed by rectangular and circular waveguide elements investigated by field expansion, calculating transmission coefficient and propagation constant 10 p1848 A70-24219
- Spurious output from C band radar magnetrons, discussing measurement procedures and noise reduction by waffle-iron waveguide filters 12 p2201 A70-28141
- ## WAVEGUIDE TUNERS
- Microwave phase shifter with rectangular ferrimagnetic toroid in waveguide longitudinal center, discussing impedance matching, phased array applications, etc 10 p1852 A70-24891
- Dispersion characteristics of electronically tunable periodic rectangular waveguides, using external DC magnetic field 23 p4168 A70-43781
- ## WAVEGUIDE WINDOWS
- Reduced multipoint equivalent scattering parameters derivation by matrix method, determining load reflection coefficients effect on signal attenuation and phase shift 03 p0458 A70-14038
- Intrinsic noise of passive waveguide multipoint with losses, obtaining mean values and wave correlation functions using scattering matrix 04 p0655 A70-14402
- Directional pattern of waveguide radiators using Kirchhoff boundary values of electric, magnetic or electric and magnetic fields, discussing aperture reflection coefficient 04 p0653 A70-15397
- Symmetrical and asymmetrical electromagnetic wave modes in conical waveguide calculated, relating critical cross section plane position to aperture angle 05 p0816 A70-16892
- Rectangular waveguides broad wall longitudinal slot equivalent networks, noting series/parallel function dependence on slot length 07 p1240 A70-19221
- Multimode rectangular waveguide lateral surface opening, determining scattering matrix coefficients governing mode conversion characteristics 08 p1462 A70-21224
- Waveguide windows for energy outlet in microwave devices analyzed by plane /Brillouin/ modes, discussing dielectric element reflection coefficient 09 p1651 A70-23646
- Coaxial energy outlets satisfying vacuum maintenance requirements of dielectric waveguide windows in dismountable prototype microwave devices 09 p1652 A70-23647
- ## WAVEGUIDES
- ### NT BEAM WAVEGUIDES
- ### NT PLASMA GUIDES
- VLF wave propagation across sunrise line analysis based on idealized model for earth-ionosphere waveguide 01 p0042 A70-10048
- Radiation transfer problem in waveguide with statistically uneven walls reduced to Dyson and Bethe-Salpeter equations in quantum field theory 03 p0524 A70-13066
- Wave numbers determined in waveguide formed by laminar inhomogeneous medium enclosed between homogeneous dielectric media, taking into account radiation losses through wall 03 p0447 A70-13290
- Optimal synthesis and design of distributed parameter system for waveguides using gradient technique with devised algorithm to overcome convergence problem 03 p0449 A70-13563
- VLF radio wave propagation variations occurring in earth-ionosphere waveguide contributing to errors in OMEGA position lines used to obtain worldwide navigational fixes 03 p0523 A70-13614
- VLF wave propagation in earth-ionosphere waveguide, comparing ray and waveguide-mode theories 03 p0449 A70-13616
- Homogeneous waveguide solutions by finite element method using matrix operator and function minimization to assure rapid convergence to eigenvalue 03 p0457 A70-13936
- Ray-optical analysis of electromagnetic scattering in plane and circular waveguides, giving formulas for modal reflection and coupling coefficients 03 p0452 A70-14034

- Dielectric loaded waveguide with symmetric microstrip line, evaluating transverse wave number by finite difference method 03 p0458 A70-14035
- Nonlinear propagation of electron plasma wave in cylindrical waveguide, discussing linear theory of electrostatic waves in cold plasma 04 p0728 A70-15000
- Eigenvalue and eigenfunction of H01 wave in bend of cross shaped waveguide, determining field components and propagation constant change 04 p0651 A70-15291
- Optical waves in round metallic and dielectric waveguides calculated using geometrical optics and model analysis for anisotropic wall impedance model 04 p0652 A70-15396
- Backward and complex waves propagation in circular waveguide with coaxial dielectric rod, discussing arbitrary angular dependences 05 p0812 A70-16145
- Graphic method for classifying EM waves directed by open waveguides, obtaining wave numbers from dispersion equation 05 p0812 A70-16245
- Impedance and field distribution of bifurcated and stepped waveguide junctions with inserted diaphragm calculated by transformed singular integral equation 05 p0820 A70-16385
- Symmetrical and asymmetrical electromagnetic wave modes in conical waveguide calculated, relating critical cross section plane position to aperture angle 05 p0816 A70-16892
- Wave equation for elastic waves in isotropic solid solved in Cartesian and circular cylindrical coordinates for studying microsonic wave guiding structures 06 p1105 A70-17479
- Mutual coupling between waveguides radiating through conducting ground planes with orthogonally polarized propagating modes described by first order analysis 06 p1020 A70-17562
- Symmetrical H mode wave propagation in inhomogeneous plasma filled circular waveguide solved by hypergeometric functions, noting use for microwave diagnostics and computer programs verification 06 p1009 A70-17825
- OMEGA frequencies propagation characteristics measured to estimate navigation errors from multiple waveguide propagation modes close to transmitter, comparing day and night errors 07 p1330 A70-19222
- Semiconductor laser signals coupling into thin optical platelet waveguides 07 p1301 A70-20019
- Plastic symmetrical trough waveguides with metalized surfaces for hybrid millimeter-wave integrated circuit systems, discussing ferrite resonant isolator 07 p1243 A70-20151
- Impedance behavior of inductive posts with small capacitive gap in waveguide 08 p1468 A70-20644
- Radio waveguides with random inhomogeneities, studying mathematical models by orthogonalization method 08 p1457 A70-20723
- Microwave propagation along earth-air path, studying tropospheric layer role 08 p1461 A70-20968
- Spectrum of waves emitted from waveguide of two plane dielectric or isotropic plasma layers, solving dispersion equations numerically by computer 08 p1472 A70-20973
- Diffraction by single wire waveguide with obstacle, considering propagation phenomena of symmetrical modes 08 p1472 A70-21042
- Coplanar waveguide consisting of thin metallic film strip on dielectric slab with ground electrodes adjacent and parallel to strip for nonreciprocal gyromagnetic device applications 08 p1475 A70-21281
- Circular dielectric waveguide modes self consistent description by asymptotic method, obtaining eigenvalues and eigenfunctions 08 p1476 A70-21288
- Millimeter guided wave communication systems information transmission capacity increase, using quaternary and higher order modulation techniques 08 p1462 A70-21506
- Slotted-line admittance measurement of thin obstacles in below cut-off waveguides 08 p1477 A70-21640
- Electrical parameters approximate calculations for waveguides with complex cross sections by Schwarz alternating method, determining critical frequencies of fundamental modes 09 p1632 A70-22406
- Electromagnetic wave diffraction on array of plane waveguides, determining scattered field by solving infinite system of algebraic equations 09 p1632 A70-22407

Electromagnetic wave deceleration in open cylindrical waveguide, noting guide action as bandpass filter
09 p1633 A70-22415

Aberration-correcting line source feed for spherical reflector using linearly polarized flat waveguide array
09 p1646 A70-22694

H guide with laminated dielectric strips separated by air layers, analyzing field distribution and characteristics
09 p1634 A70-22709

Lossless three-port H-plane waveguide junction circulator performance evaluation using computerized design
09 p1646 A70-22710

Quasi-optical waveguide component/attenuator/ in S-band measured for performance noting diffraction as limiting factor
09 p1647 A70-22711

Open-sided shielded stripline and other parallel plate waveguide structures propagation modes
09 p1634 A70-22712

Waveguide master short circuit devices reflection coefficient measurements by microcalorimeter
09 p1638 A70-23322

Radiation losses of tapered single mode dielectric slab waveguide for TE and TM modes
09 p1650 A70-23369

Rectangular coaxial waveguide with internal conductor contained between inhomogeneous magneto-dielectric bars, deriving computer algorithm for natural mode fields
09 p1638 A70-23645

Antenna with 3-db slotted waveguide bridge to produce near circular polarization emission field
09 p1652 A70-23651

Reliability testing of waveguide ferrite devices based on quantitative technique using circular charts with filled in endurance test results
09 p1652 A70-23661

Open region waveguide radiation and scattering solved using impedance surfaces of related closed region convergence
09 p1640 A70-23807

Mode transducer and mode filter formed by rectangular and circular waveguide elements investigated by field expansion, calculating transmission coefficient and propagation constant
10 p1848 A70-24219

Waveguides consisting of three concentric regions suitable for plasma experiments, showing dispersion characteristics and cut-off frequencies
10 p1850 A70-24835

Microwave waveguide insertion-loss calibrations, comparing cavity Q and direct measurement methods
10 p1854 A70-25315

Corrugated waveguide structures for aperture type feeds for spherical and paraboloidal reflector antennas, discussing experiments on 2-hybrid mode horn
11 p2018 A70-26024

Line source antenna arrays containing random dissimilarities in waveguide cross section analyzed for phase errors to determine sidelobe deterioration
11 p2018 A70-26177

Phase velocity and direction estimation of unknown signal propagating across two dimensional array in dispersive waveguide, showing dependence on SNR
11 p2018 A70-26274

Electromagnetic wave propagation problem in periodic slow wave structures reduced to Hamiltonian using parametric resonance theory
11 p2012 A70-26802

Microwave lines dispersion equations for ferrite cylinder and spiral and circular waveguides
11 p2012 A70-26803

Waveguide gas discharge indicator of transmitted microwave power, investigating sensitivity, discharge conditions, filler gas and pressure effects
11 p2020 A70-26807

Large capacity long distance transmission by circular waveguides, describing artery frequency modulation and equipment for multiplexed telephone messages transmission
12 p2194 A70-27233

Modified method of cross sections applied to solution of scalar Helmholtz equation in infinite symmetrical waveguides
12 p2272 A70-27296

Waveguide optical properties effect on injection GaAs laser threshold lasing and field distribution in near/far zones for various parameters of active region
12 p2246 A70-27365

Coupling between parallel plate waveguides excited in TE modes using integral and differential equations, noting dielectric plug loading effect
12 p2198 A70-27954

Semiinfinite parallel plate waveguide modes reflection coefficients with propagation constants near cut-off and excited at open end for microwave-optical frequency range
12 p2198 A70-27959

C band latching ring-and-post ferrite waveguide circulator for radar transmitting-receiving functions, presenting performance and design parameters
12 p2202 A70-28166

Quasi-TEM analysis justification for limit cases of guided waves on microstrip transmission lines with dielectric constant approaching free space
12 p2190 A70-28168

Electromagnetic fields features in VLF spectral range for propagation in earth-ionosphere waveguide, discussing effects of ionospheric irregularities
12 p2190 A70-28169

Textbook reissue on diffraction of electromagnetic and acoustic waves at open end of waveguide, using Wiener-Hopf-Fock factorization method
13 p2363 A70-28724

Circular shielded three layer dielectric waveguide critical parameters, estimating passbands for phase circulators with ferrite inserts
13 p2364 A70-28873

Quasi-pyramidal horn waveguide TE and TM modes eigenvalues computed by asymptotic formula
13 p2377 A70-29147

Radiation patterns of slots in flat and curved screens using open waveguide emission theory
13 p2378 A70-29305

Trapped mode resonances, attenuation and launching tapers in overmoded rectangular waveguides
14 p2556 A70-30441

Circular low loss waveguides for millimeter waves, discussing construction, geometry, surface texture, etc
14 p2556 A70-30442

Millimeter waveguide components, discussing impedance measuring equipment, matched loads, variable short circuits and attenuators, power measurement equipment, etc
14 p2556 A70-30446

Quasi-optical power transmission in overmoded waveguides in interferometers, millimeter wave spectrometers, polarizers, etc
14 p2556 A70-30447

Propagation in corrugated waveguides with surface permitting H-wall boundary condition for choice gap and fin dimensions
14 p2550 A70-30519

Earth-ionosphere waveguide electric field strength calculation based on nighttime ionospheric models, comparing results to measurements
14 p2574 A70-30748

Lossless waveguide propagation analysis as transient problem by means of Laplace transform
14 p2556 A70-30923

Surface wave radiation from plane dielectric waveguide, considering phase constants, directional properties and optimal distance location
15 p2696 A70-31503

Fourth order aberration in gas lens used as focusing element in light beam waveguide systems
15 p2697 A70-31829

Electromagnetic wave propagation in cylindrical guide containing anisotropic sheets, observing TE and TM modes existence
15 p2774 A70-31946

Equivalent circuits and general formulas for small hole coupling of resonant cavities and waveguides
15 p2714 A70-32817

Finite parallel plate waveguide arrays edge effects, comparing element radiation patterns and reflection coefficients vs scan
16 p2860 A70-32953

Periodically strip loaded dielectric slab guided electromagnetic waves, discussing attenuation and space harmonics amplitudes relationship
16 p2861 A70-32960

Paraboloidal and spherical reflectors focal region fields matching over corrugated waveguide open end propagating hybrid modes
16 p2861 A70-32966

H-guide dielectric losses reduction by use of artificial and laminated dielectric slabs
16 p2875 A70-33401

High Q reactance network realization for integrated microwave systems employing evanescent mode waveguide components
16 p2875 A70-33402

Attenuation characteristics for dominant hybrid mode in corrugated circular waveguide for antenna feed
16 p2879 A70-34041

Traveling wave antennas, analyzing modal characteristics of various waveguiding structures
17 p3052 A70-35070

Surface wave antennas, operated on guided wave mode parallel to interface and with radiation at discontinuities, calculating excitation and radiation characteristics
17 p3052 A70-35072

Electromagnetic wave scattering at ellipsoidal bodies in microwave rectangular and circular waveguides
17 p3046 A70-35346

External SHF signal effects on multifrequency spectrum of reflex klystron coupled with long waveguide
17 p3055 A70-35682

Plane wave diffraction by periodic grating reduced to waveguide problem, determining asymptotic behavior of integral solution
18 p3291 A70-36286

Algorithm for steady state oscillations in irregular waveguide structures with conducting walls
19 p3470 A70-37427

Propagation constants in laminar plasma circular waveguides filled with anisotropic linear medium, using Galerkin-Ritz method
19 p3474 A70-37428

Waveguide transformer using rectangular waveguide permitting Galerkin method, determining scattering matrix
19 p3385 A70-37429

Electromagnetic propagation in flat waveguide with local gyrotropic filling and transverse magnetization, using Galerkin method
19 p3470 A70-37430

Single crystal yttrium ferrite garnet intrinsic electromagnetic radiation as function of coupling coefficient between specimen and waveguide
19 p3485 A70-37630

Dielectric layer and screen heat loss effects on diffraction radiation in resonant waveguide
19 p3377 A70-37725

Open plane slotted waveguide excitation by current carrying filament, using long wave approximation
19 p3377 A70-37726

Linear equations for wave diffraction in rectangular waveguides with step-shaped inhomogeneities
19 p3378 A70-37730

H and E waves diffraction in circular waveguide by diaphragm thickness, using linear equations and Fourier-Bessel series for representation
19 p3378 A70-37731

Metallic core shielded squirrel cage waveguide excitation by charged filament, giving equations for Fourier coefficients of electromagnetic fields
19 p3386 A70-37732

Two axially positioned cylindrical waveguides with slots cut periodically along generatrices /double squirrel cage/, analyzing behavior under excitation by rotating charged filament
19 p3386 A70-37733

Transversely magnetic and electric wave critical frequency spectra in Pi and H section waveguides, using summary representation method
19 p3378 A70-37735

Gyrotropic waveguides parameters computer calculation based on inhomogeneous isotropic region, taking into account discontinuities
19 p3378 A70-37736

Prime focus feeds performance for radiotelescopes, using one- or two-hybrid modes in circumferentially corrugated waveguides
19 p3388 A70-37967

Electromagnetic wave propagation in spherical impedance waveguide, determining eigenvalues with negligible refraction
19 p3381 A70-38565

Plane waveguide field with complex geometric inhomogeneity, describing perturbed section by integral equations
19 p3381 A70-38567

Plane VLF wave propagation in waveguide formed by earth and inhomogeneous anisotropic ionosphere, determining excitation coefficients and attenuation functions
19 p3381 A70-38568

Sound propagation in cylindrical waveguide with impedance walls in presence of flow
19 p3472 A70-38655

Cylindrical radiator radiation resistance and mass in waveguide with reflecting boundaries, calculating sound field for effect of medium reaction
19 p3472 A70-38656

Square cross section waveguide with cutoff frequency, calculating density wave propagation in helical electron beam trajectories directed by magnetic field
20 p3584 A70-39256

Radio waves propagation two dimensional model in earth-ionosphere waveguide across land/sea boundary, solving dual integral equations by Wiener Hopf procedure
20 p3585 A70-39457

Time harmonic waveguide scattering involving metallic obstacles, obtaining numerical solution by finite difference Green function method
20 p3586 A70-39469

Radiation theory circular waveguide in dominant TE mode and flush mounted to infinite conducting flat ground plane covered by plasma or dielectric sheath
20 p3586 A70-39500

Book on electromagnetic waves in stratified media covering reflection, propagation, waveguide mode theory, superrefraction and tropospheric ducting
20 p3586 A70-39604

Complex waveguides with diverging body of revolution shaped horn, solving equation by Frobenius-Latysheva method
20 p3587 A70-39765

Planar thin film optical waveguides for integrated circuits, utilizing information carrying potential of laser light in optical communication

20 p3598 A70-40129

Multifrequency oscillator system with reflex klystron loaded by waveguide line, confirming spectrum conversion under action of SHF signal

20 p3598 A70-40299

Transmission line modal analysis for nonlinear polarizability in optical and quasi-optical waveguides

21 p3784 A70-40564

Electromagnetic wave propagation in one dimensional periodic waveguide slow wave systems, deriving dispersion curves by perturbation theory

21 p3784 A70-40628

Microwave propagation in circular waveguide containing inhomogeneous gas discharge plasma

21 p3785 A70-40630

Microwave waveguide mount characterization of varactor diodes, using transmission resonance and Dolph-Chebyshev taper

21 p3797 A70-40759

Arbitrary mode launching on fiber-optical dielectric waveguides by spatial filtering technique

21 p3829 A70-41930

Optical communication waveguides with diffused boundaries, calculating modal propagation fields by perturbation theory

21 p3792 A70-42045

Admittance matrix of microwave networks, referring to coaxial line-waveguide coupling through 3 kMc adapter

21 p3802 A70-42250

Plasma-air junction problem in parallel plate waveguide, obtaining discontinuity admittance expression

22 p3994 A70-42350

Russian monograph on propagation of LF electromagnetic waves in waveguide formed between earth and ionosphere

22 p3989 A70-42674

GaAs stripline domains and guided EM waves, discussing velocity, conductivity, drift and transmission amplification gain

22 p3996 A70-42917

High level parametric upconverter for radio link using evanescent mode waveguide

22 p3997 A70-42925

Prism film device coupling laser beam into thin film dielectric light guides, discussing operational theory

22 p4030 A70-42947

Subsonic jet engine intake duct radar cross section calculation using waveguide model

22 p3992 A70-43584

Scattering and radiation from circumferential gap in circular dielectric-loaded waveguide, using integral equations

23 p4167 A70-43765

Resonant frequencies of microwave dielectric resonator in magnetic wall waveguide

23 p4169 A70-43784

Book on guided EM wave theory covering mathematical methods transmission lines cavity resonators, perturbation theory, electrostatics, electric and magnetic fields, propagation, etc

23 p4172 A70-44242

Ray theory of diffraction from open-ended parallel plate waveguides, using Wiener-Hopf technique

23 p4219 A70-44404

Microwave frequency light modulators waveguides, examining optimal cross sections to increase modulator efficiency

23 p4196 A70-44409

Radiation and phase-scanning properties of planar array of parallel plate waveguides, using wedge diffraction theory

23 p4166 A70-44973

GaAs injection lasers, calculating effect of active region displacement from p-n junction waveguide on wave generation

23 p4203 A70-45074

Electromagnetic wave propagation problem periodic slow wave structures reduced to Hamiltonian, using parametric resonance theory

24 p4311 A70-45177

Microwave lines dispersion equations for ferrite cylinder and spiral and circular waveguides

24 p4317 A70-45178

Waveguide gas discharge indicator of transmitted microwave power, investigating sensitivity, discharge conditions, filler gas and pressure effects

24 p4317 A70-45179

Ferrite junction microwave circulator bibliography /1956-1969/ covering stripline and waveguide versions theory, designs, constructions and applications

24 p4318 A70-45210

Microwave propagation in hollow conducting elliptical pipe waveguide, calculating successive modes cutoff wavelengths by numerical analysis

24 p4318 A70-45212

Microwave propagation in waveguides, investigating trapped and slightly leaky modes in multilayered or multiwave regions by ray-optical techniques

24 p4311 A70-45216

Packaged microwave junction diodes in reduced-height waveguide, discussing parasitics and equivalent circuit parameters measurement technique

24 p4318 A70-45220

Microwave waveguide rotatory joint using symmetrical excitation for mode conversion to obviate filters

24 p4318 A70-45221

Modified time-domain reflectometer method for waveguide system evaluation, detecting and displaying radar echoes as function of time

24 p4315 A70-46234

Microwave transmission in partially dielectric filled circular waveguide, deriving cutoff wavelength and phase velocity vs frequency

24 p4315 A70-46260

WAVELENGTHS

Turbulence and temperature fluctuations spectral characteristics in thermally stratified atmosphere determined for various wave numbers, using energy and mass transfer functions

01 p0136 A70-11610

Jovian surface elements spectral and color contrasts from spectrograms obtained between 3200- 4900 A wavelengths

02 p0375 A70-12429

Sky brightness distribution data to determine shape of aerosols scattering as function of wavelength

02 p0292 A70-12435

Helium-neon laser wavelength calculations from spectral observations by Fabry-Perot etalon, proposing formulas to enhance accuracy

02 p0299 A70-12439

Ruby laser light wavelength temperature dependence measurement using Fabry-Perot etalon

02 p0313 A70-12440

Ruby laser emission wavelength temperature dependence measured spectrographically

02 p0313 A70-12441

Photoelectric polarimetry of samples of lunar maria, terra, lavas and chemicals for wavelength dependence of polarization, comparing to Mercury, Mars and asteroids

03 p0576 A70-14082

Heat transport conduction mode and earth as heat sink in solar atmosphere, discussing mesopause coldest region, turbulence and solar plasma-earth electromagnetic interactions

04 p0677 A70-14644

Wavelength selection in Q switched carbon dioxide laser by intracavity gas cell providing selective absorption

04 p0702 A70-15362

Identification of lines in Mohler photometric atlas of IR solar spectrum wavelengths

05 p0910 A70-16427

Yttrium-iron garnet optical properties at various wavelengths and temperatures, noting absorptivity decrease in IR region

06 p1126 A70-17767

Slot line wavelength, impedance, transitions and tolerances measured at S band using different dielectric constant materials

08 p1475 A70-21282

Absorption spectra of n-type GaAs before and after proton irradiation, discussing dependence on wavelength

09 p1739 A70-22753

Transient partially ionized plasmas observation by two wavelength holographic interferometry, describing electron density measurements

09 p1736 A70-23186

Q switched laser pulses lengthened using internal second harmonic generator

10 p1898 A70-23981

Alfven waves wavelengths dependence on inhomogeneous magnetic field geometry in stationary plasma, using conformal transformations

13 p2462 A70-28984

Pulsar short period pulsations and emission patterns in meter wavelength range on crossed radio telescope

14 p2633 A70-30151

Surface wave transmission lines used at millimeter wavelengths

14 p2549 A70-30443

Thermal radio emission from major planets at mm and cm wavelengths and at decimeter wavelengths for Jupiter and Saturn

14 p2648 A70-31084

Primary wavelength standard established via line produced with wavelength-stabilized laser

17 p3104 A70-35086

He-Ne laser emission wavelength long and short term stability for metrological applications

17 p3104 A70-35087

He-Ne laser emission wavelength, using laser interferometry based on feedback between moving mirror and resonator

17 p3104 A70-35088

Energy dissipation and viscosity effects on isotropic turbulence in extreme short wave region at large Reynolds numbers

18 p3239 A70-36263

Holographic interferometry of rapid phase objects by two wavelengths from ruby laser and KDP crystal filter, noting application to dense plasmas

19 p3422 A70-37650

Solar radio emission flux as activity index, analyzing permissible deviations from recommended wavelength

19 p3522 A70-38559

Gratings as laser wavelength-selective end reflectors, noting application to carbon dioxide and dye lasers

20 p3639 A70-39083

Q switching of nitrous oxide laser with Freon 12 and sulfurhexafluoride absorbers, comparing wavelengths with carbon dioxide laser outputs

21 p3834 A70-40567

Multiple wavelength desensitized hologram interferometry to extend displacement measurement range

21 p3822 A70-40814

Pulsar short period pulsations and emission patterns in meter wavelength range on crossed radio telescope

21 p3923 A70-42073

Wave number spectral correlation of temperature and longitudinal velocity fluctuations in fully developed pipe flow

21 p3811 A70-42090

Antennas with controlled current distribution in medium wavelength range for optimal radiation pattern over desired area, discussing maximum gain tuning for daytime and nighttime operation

22 p3995 A70-42521

D region ionization budget, evaluating short wavelength X rays role

23 p4236 A70-43860

Microwave propagation in hollow conducting elliptical pipe waveguide, calculating successive modes cutoff wavelengths by numerical analysis

24 p4318 A70-45212

Solar limb emission spectrum between 300-2803 A, using Skylark rocket instrumentation

24 p4399 A70-45301

WAVES

Repetitive scanner for wave velocity measurements in annular two phase gas or liquid flow using pivoted mirror

06 p1062 A70-17618

Wave physics using ocean waves as example, considering period, frequency, length, speed and similarity of various types

11 p2084 A70-26037

Stratospheric CAT-internal wave relationship, using aircraft and radiosonde HICAT measurements

14 p2609 A70-30603

WEAPON SYSTEM MANAGEMENT

Guided weapons management techniques applied to Rapier light weight anti-aircraft weapon system

08 p1601 A70-21037

Weapon systems combat effectiveness measurements, stressing need for proper data acquisition from early R and D through obsolescence

09 p1794 A70-23414

Integrated Test Program for S-3A Weapon System, detailing test sequence flow and interfaces to assure vehicle and avionics systems reliability and maintainability

10 p1959 A70-24931

Project cost estimate growth pressures on decision making by U.S. Air Force System Program Office director

14 p2667 A70-30521

Project management in aircraft manufacturing related to weapon system

17 p3200 A70-34918

WEAPON SYSTEMS

NT GROUND OPERATIONAL SUPPORT SYSTEM

NT MISSILE SYSTEMS

NT SENTINEL SYSTEM

Weapon systems acquisition projects, studying procurement decisions interactions

04 p0788 A70-14833

British military and civilian aircraft and flying between World War I and II, discussing weapons systems and accidents

05 p0794 A70-16113

Swedish VIGGEN program for aircraft weapons system development emphasizing management methods

05 p0960 A70-16717

Material Acquisition Division of Naval Air Systems Command, discussing engineering and testing functions in providing air weapons systems to operating forces

06 p1185 A70-17973

Control system design for maximum weapon delivery missions effectiveness, discussing analysis and simulation methods

09 p1611 A70-23022

Large scale project grading into stepwise decision stages exemplified by aircraft weapon system development program

10 p1971 A70-24596

Harrier armament system design for ordnance carriage to full combat load factors, describing Weapon Control Panel 10 p1807 A70-24848

Weapon Systems Level testing methods and machines application to missiles, manned space flight vehicles and Safeguard System [AIAA PAPER 70-380] 10 p1862 A70-24923

Human engineering in weapon systems development, considering flying and ground personnel training plans 12 p2177 A70-27038

Exothermic bimetallic ignition systems /EBIS/ design for solid propellant rocket motors of tactical missiles to reduce shock loadings 12 p2289 A70-27694

European Panavia 100/200 two engine variable wing military aircraft, noting prototype design, use and production sharing 13 p2347 A70-29051

Rocket and supersonic aircraft weapon systems, discussing missile delivery and interception 13 p2507 A70-30000

Safeguard defense system against strategic ballistic missiles, discussing Nike X program, PAR and MSR radars and Spartan and Sprint system 15 p2810 A70-32247

Tactical aircraft performance, discussing electro-optical devices, weaponry, communication and navigational networks, information displays and real time remotely manned control systems 17 p3013 A70-34672

S-3A carrier based ASW weapons system, discussing onboard equipment, navigation, avionics integration, etc [AIAA PAPER 70-882] 17 p3018 A70-35802

Air superiority fighter design philosophy, including tradeoffs between armament, detection capability, thrust, speed and load factor [AIAA PAPER 70-930] 17 p3021 A70-35840

Weapon systems effective reliability analysis, using degraded mode evaluation and deterministic computer program 19 p3442 A70-38833

Avionics system for fighter aircraft, discussing weapons design, navigation-attack systems integration, etc 23 p4173 A70-44413

Nonlinear equations of motion approximate solution, determining ordnance weapons aerodynamic stability coefficients from angle of attack [AIAA PAPER 69-135] 23 p4133 A70-44515

WEAPONS

NT ARTILLERY
NT NUCLEAR WEAPONS
NT SPACE WEAPONS

Flight tests to investigate external munitions carriage effect on aircraft stability and control 08 p1437 A70-21733

Laser beam for military weapons applications, investigating energy levels and beam guidance 20 p3641 A70-39421

WEAPONS DEVELOPMENT

Swedish VIGGEN program for aircraft weapons system development emphasizing management methods 05 p0960 A70-16717

DOD procurement practices for advanced weapon systems, discussing government errors in contracting policies 07 p1428 A70-19678

Guided weapons management techniques applied to Rapier light weight anti-aircraft weapon system 08 p1601 A70-21037

WEAPONS INDUSTRY

Management planning for French-British Martel /Missile Antiradar et Television/ project, emphasizing tasks of government agencies and contractors 08 p1601 A70-21038

WEAR

Bonded solid lubricant films wear life equation for low contact stress conditions, determining optimal film thickness [ASME PAPER 69-LUB-5] 01 p0102 A70-10397

Co-base hardfacing alloys mechanical properties and applications, discussing mechanical and chemical wear processes in cast and wrought types 02 p0319 A70-12712

Molybdenum disulfide solid film lubricant with increased wear life developed from in situ conversion of electrodeposited molybdenum trioxide 06 p1091 A70-17339

Abrasive wear of polymers subject to plastic and elastic deformation, considering papers, metal gauze and rough metal surfaces 07 p1296 A70-20003

Corrosive wear due to oxygen and/or moisture in air indicated as major failure mode in lubricated gears 10 p1895 A70-24852

Friction theory, discussing surface mechanics, wear and erosion control 15 p2743 A70-31699

Friction and wear effects on leakage path in sliding seal interface 16 p2916 A70-33078

Upstream wear of small metal orifices under large pressure drops in phosphate ester hydraulic fluids due to current driven electrochemical corrosion [ASME PAPER 70-FE-15] 16 p2919 A70-33629

WEAR INHIBITORS

Phosphorus compounds inhibition effect on oxidation and wear of graphite lubricants 13 p2437 A70-28854

Thermochemical method for directional crystallization of wear-resistant alloy coatings on machine parts 23 p4205 A70-44043

WEAR TESTS

Wear resistance of Ti alloys chromosilicified by thermal diffusion in vacuum 01 p0115 A70-10072

Load, speed and coating thickness effect on near life of resin bonded solid lubricant, using oscillating motion and low pressure blocks [ASLE PREPRINT 69-AM-5C-3] 01 p0103 A70-10447

Unlubricated wear characteristics of polyimide resin sliding against carbon steel in air, noting effects of surface temperature, bearing pressure and velocity 01 p0103 A70-10448

Friction and wear tests on solid lubricant graphite fluoride compared with molybdenum disulfide at specific temperatures, considering friction coefficient [ASLE PREPRINT 69-LC-9] 02 p0321 A70-12536

Porous wall material entrainment in turbulent boundary layer during supplementary inert gas injection, including nonisothermicity effects in heat and mass transfer equations 03 p0440 A70-13385

Titanium alloys case hardened by diffusion of various metals at high temperatures, measuring increase in wear resistance 03 p0513 A70-13858

Carbide rupture energy in wear resistant alloys during abrasion, considering metallographic data and energy parameters 04 p0707 A70-15212

Creep and wear due to microslip under dry rolling contact conditions 05 p0854 A70-15890

Sliding wear of bearing Al lubricated with polyphenyl ethers in boundary region tested by pin and cylinder wear machine producing continuous record 05 p0854 A70-15910

Solid lubricants friction and wear bench testing under simulated space environment 06 p1075 A70-17340

Polytetrafluoroethylene wear tested by rubbing cylindrical rod flat ends against glass plates, determining sliding contact pressure effects 06 p1077 A70-18403

Sliding friction and wear of polytetrafluoroethylene ball bearing filled with graphite investigated for irradiation effects 06 p1077 A70-18404

Odessa observatory meridian circle pivots wear determined during observations of eclipsing variables 08 p1574 A70-21160

Burnishing load and time effect on deposition, endurance limit of lubrication and wear-in characteristics of molybdenum disulfide powder films 08 p1508 A70-21516

Friction, wear and surface evaluation of alloys as bearing materials in prosthetic devices 09 p1690 A70-22044

Wear resistance of turbine rotor blade stabilizing elements in form of bolts connecting overlapping leading and trailing edges of adjacent tips 09 p1768 A70-22095

Microconstituents effect on wear behavior of high hardness steels on basis of crossed-cylinder testing, discussing intermetallic compounds influence 10 p1895 A70-24853

Molybdenum disulfide dry film lubricant wear life as film sintering process dependent on binder, additive or atmosphere chemical effects 11 p2058 A70-25571

Friction and wear of Ni sliding on Ni, Cu on Cu and Au on Au tested in vacuum at room temperature with constant load 12 p2242 A70-27229

Diamond burnishing effects on wear and contact endurance of chromium coatings, investigating surface hardening and residual stresses 13 p2419 A70-28868

Lubricating fluids effects on three-body abrasion wear rates, considering roles of viscosity and abrasive type 13 p2419 A70-28896

Nonaggressive liquid media effect on residual strains and phase transformations initiation and development in polyurethane parts operating in lubricants, discussing wear resistance 13 p2439 A70-29431

Metal surfaces friction and wear processes dynamic equilibrium noting loading conditions effects 13 p2423 A70-29766

Oxygen interlayer diffusion effects on wear change during gliding friction of normalized steel samples 15 p2743 A70-31636

Antifriction and wear properties of iron fluoride materials and white cast iron under sliding friction in air and vacuum 15 p2743 A70-31637

Wear intensity of abrasives during fine grinding of Armco Fe, Ti and Ti alloys, comparing friction and chemical composition effects 15 p2743 A70-31640

Space suit thermal insulation properties, wear durability and nonflammability improvements, reflecting techniques in fabricating cryogenic multilayer insulation systems [AIAA PAPER 70-851] 16 p2939 A70-33918

Wear and fatigue of Ti-Mo-Al-Sn-Si /Hylite 50/ alloy with resistant Mo or Cr coatings 17 p3099 A70-34447

Ball bearing materials for ultrahigh vacuum space environments, determining frictional and wear behavior 17 p3099 A70-34573

Metals and hard materials sliding wear due to granular abrasives in heated vacuum chamber 17 p3100 A70-34646

Dry friction and wear tests of various materials in vacuum at low temperatures 18 p3263 A70-36471

Binder wetting relation to solid film lubricant wear life [ASLE PREPRINT 70AM 5A-3] 19 p3439 A70-38810

Metal surfaces friction and wear processes dynamic equilibrium noting loading conditions effects 20 p3638 A70-40099

Helicopter parts and assemblies fatigue life estimation and testing, discussing loading spectra, service conditions, etc 22 p4046 A70-43119

Temperature effect on friction coefficient of boron and silicon carbides, using similar wear pairs in vacuum 23 p4205 A70-44044

Refractory materials surface behavior under friction, discussing microscopic nature of wear and surface deterioration due to thermal fatigue, fusion and material transfer, etc 24 p4342 A70-45595

WEATHER

NT COLD WEATHER
NT HOT WEATHER
Linear regression equations to relate atmospheric precipitable water to surface dew point, sky cover and weather 03 p0520 A70-13163

Lower atmosphere VLF heat turbulence as function of precipitation, indicating atmospheric layers existence for different weather situations 05 p0879 A70-16315

High and medium whistler activity in Italy correlated with weather situation in South Africa 05 p0839 A70-16317

Recording apparatus design and operation for characteristics of electromagnetic waves generated by weather discharges, discussing electromagnetic perturbations propagation 08 p1468 A70-20467

Weather situation persistency, using 500 mb contour chart catalog 16 p2945 A70-32950

Solar limb image vibrations, establishing quantitative comparisons between statistical characteristics of fluctuations and weather conditions on propagation path 16 p2979 A70-34179

WEATHER CHARTS

U METEOROLOGICAL CHARTS
WEATHER CONDITIONS
U WEATHER
WEATHER CONTROL
U WEATHER MODIFICATION
WEATHER DATA RECORDERS

Numeric keyboard CRT display for weather data acquisition from ships at sea, utilizing ATS-3 satellite as transmission medium 01 p0048 A70-11279

Remote recording wind vane using continuous and step rotary switch potentiometers suitable for automatic weather stations 06 p1062 A70-17619

Recording apparatus design and operation for characteristics of electromagnetic waves generated by weather discharges, discussing electromagnetic perturbations propagation 08 p1468 A70-20467

Weather radar signal processing and data recording at National Severe Storms Laboratory /NSSL/, providing reduction in echo variations due to relative motion of precipitation elements 13 p2363 A70-28774

WEATHER FORECASTING

NT LONG RANGE WEATHER FORECASTING
NT NUMERICAL WEATHER FORECASTING
NT STATISTICAL WEATHER FORECASTING

Atmospheric environment features bearing on supersonic transport aircraft operations and forecasting, discussing wind and temperature effects

02 p0325 A70-12220

Soviet monograph on weather forecasting covering hydrodynamic principles, atmospheric physics, short and long range forecasting, temperature, pressure fields, etc

03 p0520 A70-12873

Meteorological data processing computer center of German Weather Service, discussing equipment, data system, forecasting techniques and prediction control

03 p0454 A70-13171

Seasonal and monthly mean charts forecasting method based on variation of annual difference in atmospheric circulation

04 p0715 A70-15294

Numerical integration of linearized two level forecast model to analyze behavior of accumulated error

05 p0878 A70-16153

Hydrothermodynamic equations used in forecasting meteorological components solved by assuming equations of motion quasi-linear and reducing to ordinary differential equations

05 p0878 A70-16195

Weather data communication, discussing transmission of radar, polar satellite and ATS satellite data to processing center and forecasts dissemination to public media

05 p0814 A70-16327

Meteorological conditions effects on SST aircraft flight safety and economics, emphasizing stratospheric information for forecasting

06 p1095 A70-17193

Objective quasi-Lagrangian index for forecasting convective weather outbreaks based on outbreak occurrence likelihood in convective instability areas

06 p1101 A70-18579

Satellite observed characteristics of severe local storms in central and eastern U.S., noting potential use for storm forecasting

06 p1102 A70-18584

Incipient tropical storm location and synoptic weather pattern analysis from environmental satellite data utilization

07 p1329 A70-19196

Short term weather forecast hydrodynamic equations reduced to solving nonlinear differential equations by introducing dependent variables

07 p1329 A70-19647

Soviet book on meteorological conditions analysis and prediction for aviation covering fog, storms, showers, stratospheric turbulence studies, etc

08 p1535 A70-20772

Economic and social benefits from weather forecasting developments, noting expenditures on satellites and high speed computers

08 p1539 A70-21826

Telemetry data processing of Eole scientific weather forecasting program, discussing mathematical model simulating atmospheric circulation in Southern Hemisphere

09 p1674 A70-22200

Automatic change discrimination applications to weather prediction, land resource management and city planning, using photographic, IR and radar sensor imagery

09 p1677 A70-22876

Management planning for global atmospheric research program /GARP/ applied to climatology and weather forecasting

09 p1795 A70-23545

Nonlinear utility functions effects on assessor probability forecasts, discussing psychological factors

10 p1912 A70-23934

Flight test programs site selection method using computer program analysis of magnetic tape weather records

10 p1806 A70-24908

Stochastic dynamic prediction assuming deterministic laws for atmospheric behavior while seeking solutions corresponding to probabilistic statements of initial conditions

11 p2076 A70-26497

Climatic phenomena cyclic behavior from forecasting viewpoint, considering geomagnetic, upper atmospheric and solar activity effects

12 p2265 A70-28268

Meteorological satellites role in weather forecasting, discussing cloud photography and solar radiation and earth albedo measurements

12 p2265 A70-28269

Synoptic processes and meteorological fields computerized automatic classification for weather forecasting applications

12 p2265 A70-28332

Temperature prediction accuracy over 24-hr period for supersonic transport flight operations

13 p2443 A70-28549

Soviet collection of articles on analysis and prediction of dangerous weather phenomena

13 p2443 A70-28584

Weather forecasting accuracy taking into account basic equations and initial conditions

13 p2444 A70-28749

Meteorological data acquisition by navigational aids, satellites and surface based indirect sensors for computer forecasting

13 p2405 A70-28773

Weather forecasting for SST operations, discussing wind, temperature, turbulence, clouds, etc

13 p2445 A70-29494

Meteorological problems associated with accurate weather prediction affecting launch, trajectory and recovery of ballooning systems

14 p2606 A70-30555

Weather forecasting for manned space flights, emphasizing Apollo flights and operational decisions due to forecasts

14 p2606 A70-30557

Tropical storms and hurricanes critical winds forecasting accuracy by NASA Manned Spacecraft Center

14 p2606 A70-30558

CAT relationship to cyclogenesis and anticyclogenesis, considering synoptic situation and Jacobian values for forecasts

14 p2609 A70-30604

Earth atmosphere model for weather forecasting using space technology, noting Global Atmospheric Research Project /GARP/

14 p2576 A70-30973

Papers on global weather prediction covering goals, benefits, satellite components and systems, atmospheric models and second stream

14 p2610 A70-31138

International cooperation in global meteorological network, outlining World Weather Watch

14 p2670 A70-31140

Analog methods of weather forecasting involving map matching, discussing weather modification

14 p2610 A70-31141

Global weather forecasting network costs and benefits evaluated using mathematical criteria

14 p2670 A70-31142

Global weather prediction network economic benefits to key industries, discussing adverse weather effects on production schedules, fuel supplies, construction, harvesting, etc

14 p2610 A70-31143

Space research cost effectiveness in weather forecasting, TV broadcasting, space biology and medicine, geodesy, aerial and maritime navigation, earth resources, etc

15 p2811 A70-32283

Redundant variable errors in weather prediction, specifying initial conditions for time integration of hydrothermodynamic equations for atmospheric motion

15 p2771 A70-32368

Weather prediction models, describing equation systems, roles of friction and heating, meteorological data analysis, fronts, convection, etc

17 p3132 A70-34668

Meteorological prediction methods based on dynamic or thermodynamic considerations

18 p3285 A70-36949

Radar data characteristics for extensive natural cumuli cloud evolution, noting use for precipitation forecasting

18 p3287 A70-37000

Soviet papers on planetary atmosphere dynamics and hydrodynamic long range weather forecasting covering atmospheric motions, wind field, model, etc

20 p3661 A70-39176

Geopotential fields forecasting on isobaric surfaces over Northern Hemisphere by linear four level nonadiabatic model, discussing eddy transport and heat flux equations

20 p3662 A70-39179

Soviet papers on macroprocesses in seasonal weather forecasts, discussing tropospheric and stratospheric temperature and circulation, geomagnetic field, etc

20 p3663 A70-39270

Forecasting air temperature over North Atlantic, analyzing atmospheric parameters informativeness

20 p3663 A70-39274

Optimal flight route selection with respect to meteorological prediction errors, using decision under risk and Monte Carlo method

22 p4067 A70-42656

WEATHER FRONTS

U FRONTS [METEOROLOGY]

WEATHER MAPS

U METEOROLOGICAL CHARTS

WEATHER MODIFICATION

NT CLOUD SEEDING

Earth climatic control by reflecting satellites producing artificial solar irradiation

03 p0581 A70-13835

Satellite surveillance in cloud and weather modification, considering area selection for cloud seeding, atmospheric energy redistribution, etc

04 p0677 A70-14645

Soviet collection of papers on physics of clouds and cloud modifications, covering droplet fusion, radar precipitate measurements, cellular meteorology, ice forming aerosols, stochastic condensation

08 p1535 A70-20770

Spacecraft design requirements for scientific zero G cloud physics experiments concerning colloidal modification processes

14 p2584 A70-30552

Analog methods of weather forecasting involving map matching, discussing weather modification

14 p2610 A70-31141

Space legal problems involving earth resource survey /ERS/ satellites and weather modification

17 p3203 A70-35799

Warm fog clearing effectiveness by seeding with hygroscopic nuclei as function of fog droplet and seeding nuclei distribution

17 p3132 A70-35928

Weather modification by jet aircraft contrails, discussing cloud seeding observations in Alaska

24 p4371 A70-45421

WEATHER RADAR

U METEOROLOGICAL RADAR

WEATHER STATIONS

Digital river and rainfall data automatic transmission from remote hydrologic platforms via ATS-1, studying system economic and technological feasibility

12 p2205 A70-26939

Automatic weather station cost effectiveness criteria based on concepts of loss and error functions

24 p4323 A70-46405

Technological and economical characteristics of serviced and unserved automatic hydrometeorological stations and second class nonautomatic station

24 p4340 A70-46406

WEATHERING

Weather effects on plastic properties, discussing weathering interactions with plastics and polymer degradation

12 p2259 A70-27206

Holbrook chondrite specimen, discussing effects of weathering, leaching and trace elements enrichment over period of time before recovery

13 p2487 A70-28698

Sources of variability in laboratory carbon arc weathering of light stabilized polyester resin

22 p4059 A70-43080

WEBBING

Aerial retrieval webbing performance characteristics, discussing structure, type of material, finishing and strength levels

21 p3843 A70-41832

[AIAA PAPER 70-1181]

WEBS [MEMBRANES]

U MEMBRANES

WEBS [SHEETS]

Unsteady temperatures determination of integral plate consisting of skin with uniformly positioned longitudinal webs

13 p2518 A70-28478

WEBS [SUPPORTS]

Cyclic bending stresses in web of precessing disk-type gyroscope rotor, considering fatigue failure and forced vibration response

09 p1770 A70-22270

WEBS /SUPPORTS/ NT GIRDER WEBS

WEDGE FLOW

Flow and pressure distribution for large normal injection along surface in supersonic stream solved numerically for two dimensional or axisymmetric body and wedge

01 p0001 A70-10336

Flow about blunted wedge with laminar boundary layer at stagnation point and approaching Falkner-Skan flow at infinity, discussing asymptotic behavior

01 p0061 A70-10540

Plane supercavitating flow past symmetric wedge via open cavity model and application of conformal mapping theory and Riemann-Hilbert techniques

01 p0002 A70-10544

Inviscid surface pressures calculated on slender wedges and cones at low frequencies and large oscillation amplitudes in hypersonic flow

01 p0003 A70-10854

Characteristics method for calculating steady supersonic flow of burning gas mixture past wedge and rotating cones

01 p0218 A70-11018

Two dimensional plane and axisymmetric free streamline flow problems solved by finite difference methods for supercavitating wedge in potential flows

01 p0065 A70-11127

Shock wave diffraction at wedge moving at supersonic velocity, solving Hilbert space formulated for constant parameter flow

03 p0406 A70-13333

Trailing edge flow of slender aerodynamic shapes terminating in cusp or wedge, analyzing boundary layer reactions

04 p0613 A70-14457

Plane shock wave diffraction and reflection at slender wedge in linear approximation, proposing

pressure distribution calculation formulas behind shock

Compressible flows with circular sector hodographs, discussing Chaplygin equation for simple wedge flow and theorem on sonic jets

Chaplygin equation solution for wedge flows applied to Rethy flows, evaluating drag coefficient and approximate hodograph equations for subsonic and transonic regimes

Inviscid hypersonic flow analysis for chemically relaxing air about wedges and pointed circular cones using Dorodnitsyn integral method

Frozen flow effect in hypersonic wind tunnel nozzle on parameters of nonequilibrium incident flow past wedge

Hypersonic laminar boundary layer in strong viscous interaction region on wedge, determining velocity and enthalpy profiles, displacement thickness and induced pressure distributions, etc

Laminar boundary layer with blowing through wedge surface, solving linearized motion equation analytically

Cavitational symmetric flow around wedge taking into account gravity and surface tension

Longitudinal gravitational field effect on cavitation wedge flow, investigating characteristics by Zhukovskii-Koshko method

Jet flow past arc curve approximation using successive conformal mapping on circle and wedge

Shock wave diffraction at wedge moving at supersonic velocity, solving Hilbert space formulated for constant parameter flow

Laminar heat transfer to blunted wedge with constant wall temperature, describing energy field in boundary layer by analytic solution

Wedge and cylinder high supersonic wakes stability and transition at various Reynolds numbers

Yawed two dimensional wedges in hypersonic stream, including leading edge bluntness, viscous interaction and angle of attack effects

Low speed rarefied slip flow over wedge by asymptotic method of boundary layer equations integration, obtaining velocity profiles for various angles

Plane turbulent jet expansion from linear wedge apex, allowing for ejected axial velocity attenuation and static pressure variation

Pressure distribution measurements on wedges in compressible flow at Mach 0.5-2.2, discussing wedge angle, Mach number and boundary layer thickness effects

Heat transfer behind shock wave in air, oxygen or carbon dioxide flow past wedge, determining thermal fluxes vs wave velocity

Supersonic boundary layer interaction with shock wave produced by wedge slope

Laminar heating in hypersonic vehicles interior corners, analyzing helium tunnel heat transfer data for various intersecting wedge corners

Incompressible laminar boundary layers thermal response behavior in wedge flow, obtaining surface response, temperature fields, heat flux and steady state data

Thick wedge large amplitude harmonic oscillations in hypersonic flow

Shock curvature at wedge or cone tip in radiating gas flow, noting differences between radiative and chemically coupled gas dynamics

WEDGES

Textolites and ferromagnetodielectric wedges mechanical strengths compared for use in open grooves of compound winding

Heat transfer from two dimensional hypersonic low density stream to wedges and sharp flat plates at expansion angles of attack

Mixed boundary value problems of plane elasticity, solving stress field of central Griffith crack in wedge using singular integral equations

Wedge with symmetric crack at vertex in plane elastostatics, solving biharmonic equation by Wiener-Hopf technique

Wedges calculated for lift-drag ratios at hypersonic speeds to find optimum surface geometry

Crack widening in infinite plane field with wedge in absence of slip, based on elasticity theory, plotting contact forces and stresses on crack boundary

Stress distribution in anisotropic disk shaped into wedge loaded at vertex by concentrated moment determined by complex potentials method

Profile plane state of stress in wedge with and without external notch using combined photoelastic analysis and moire method

Elastic wedge under spatially uniform but time dependent shear tractions, studying shear stress and transient wave propagation

Correction to Smyrl results for perturbation pressure in interaction field behind plane shock diffracted by supersonically moving thin yawed wedge

Steady state heat conduction in wedge shaped bodies with boundary conditions of third kind

Viscoelastic-plastic solid delayed fracture associated with wedge formation of crazed material at crack tip

Wave diffraction by wedge, using Heaviside step function and Sommerfeld contours

Wedge angle large amplitude slow oscillations in hypersonic and supersonic flows, examining attached bow shock

Electromagnetic wave diffraction by ideally conducting wedge of finite radius, deriving asymptotic formula for plane wave scattering

Mutual impedance of interacting dipoles at wedge tip, determining errors for short spacing distances

Transient stresses and strains in plane wedge under dynamic load, using photoelastic, high speed photographic and strain gage studies

WEIBULL DENSITY FUNCTIONS

Cramer-Rao efficiencies of best linear invariant estimators, using Weibull distribution in model for survival populations connected with life testing

Weibull process with unknown scale and shape parameters analyzed by Bayesian decision making model, with application to component reliability problem

Complete sample estimation techniques for reparameterizations of Weibull density function to assign probabilities to components and systems lifetimes

Weibull distribution as statistical method for interpreting fatigue test data

Maximum likelihood estimates for setting confidence limits of Weibull percentiles and shape parameters

Brittle fracture stress statistics for Weibull distribution function parameter determination, comparing linearizing, least squares curve fitting and maximum likelihood techniques

WEIGHT [MASS]

Methane fuel systems for high Mach number supersonic transport aircraft on basis of minimum weight

Weights, sizes and costs of nuclear and nonnuclear spacecraft power systems with reference to mission duration

Bobweights effects on pilot induced oscillations, noting role in flying qualities and control system design

Vertical force exertion on mass at ends of elongated rotating nonspherical asteroids calculated for man safety and mobility

WEIGHT [MASS]/

NT BODY WEIGHT

NT STRUCTURAL WEIGHT

WEIGHT ANALYSIS

Space station flexibility design based on INT-21 payload capability emphasizing volume and weight factors

Pulsed plasma transfer systems weight analysis, studying propellant density gradients effects on coaxial plasma gun performance

Subsystem weight trade-offs for design optimization of out-of-orbit Mars soft lander, using atmosphere and surface environmental Monte Carlo model

Minimum weight structural member size and configuration simultaneous optimization using computer program

Engine weight estimation for showing effect on thrust, specific impulse and uranium loss rate for open cycle gas fueled nuclear rocket engine

Normalization of mechanical properties of aircraft engine components, increasing weight efficiency and reliability

Automatic weight analysis by calculation and orientation of mass properties /COMP/ program, using remote terminal time sharing computer system

Multiplane balancing method for minimizing weight required for spacecraft stability

Weight growth factor in aircraft design, discussing fixed and variable weight, payload, performance, flight quality, structural criteria and life expectancy

Landing gear weight analytical estimation, discussing ground loads, member cross sectional area, parametric variations, etc

Weight/cost systems engineering, discussing techniques for using historical data banks and standardized reporting procedures

Fuselage frames minimum weight analysis by automatic iterative method

Structural mass properties solution using programmable printing desk computer for fast data point plotting

Weight, moments and mass centers computer calculation by surface integral method, using FORTRAN language

Fighter aircraft configuration design balancing, comparing weight penalties

Disposable load drop effect on aircraft range, using Breguet equations for graphic determination of bombing range

Aircraft-borne and descent systems performance and weight optimized for midair retrieval

Ni-Cd cell plates screening and selection by weight for reliability and uniformity improvement

Optimum light construction design of glider wings, considering spar weight, aluminum honeycomb structure and repair

Skylab experiments, spacecraft facilities and project status, discussing operations, crew functions and weight of structure, systems, consumables and related storage

WEIGHT FACTORS

U WEIGHT [MASS]

WEIGHT INDICATORS

NT MICROBALANCES

Impact problems of slip clutch and beam scales dynamic characteristics simulation by 1130 CSMP /Continuous System Modeling Program/

Mass measuring device used on biological specimens in zero gravity environment, determining normal and disturbed physiological mechanisms

Weighing systems electronic load cells calibration for tension and compression loading, attributing non-repeatability to bending moments

WEIGHT MEASUREMENT

Cosmic dust particle direction, velocity and mass from ionization and momentum measurements by dust sensor during impact on Pioneer 8 satellite

Astronomical, geometrical and physical selectivity factors of forward scattering radar observation concerning meteor weight

Mass measuring device used on biological specimens in zero gravity environment, determining normal and disturbed physiological mechanisms

Asymmetric rotating bodies mass properties measurement on Dynamic Balancing Machine, taking into account aerodynamic forces

[SAWE PAPER 818]

WEIGHTING FUNCTIONS

L-1011 onboard system for gross weight and center of gravity determination, describing transducers placement, computer design and display panel [SAWE PAPER 837] 20 p3562 A70-40359
Computer time sharing system for real time mass properties measurements [SAWE PAPER 853] 20 p3595 A70-40374
Electron mass evaluation, using fluid dynamic flow process 22 p4076 A70-43672
Ox, calf, pig, rabbit, guinea pig and human eye measurements, determining wet and dry weight of iris, ciliary body and choroid 24 p4305 A70-46346

WEIGHTING FUNCTIONS

Upper atmospheric contribution to Faraday rotation angle above 5000 km determined from beacon frequencies of geostationary satellite, noting geomagnetism weighting and electron content decrement role 01 p0076 A70-10874
Pritchard photometer analyzed for in-focus and out-of-focus operation using radial weighting function 01 p0091 A70-10918
Method of weighted residuals /MWR/ for nonlinear partial differential equations applied to incompressible two dimensional turbulent boundary layer momentum and continuity equations 02 p0281 A70-12328
Method of weighted residuals /MWR/ applied to turbulent boundary layer equations, describing two parameter prediction technique 02 p0282 A70-12330
Momentum integral method for turbulent boundary layers based on equilibrium profiles family, considering weighting function specification techniques 02 p0284 A70-12345
Optimal linear controller synthesis with allowance for continuous perturbations effect, describing weighting factors selection 02 p0272 A70-12413
Radar signals optimal synthesis characterized by ambiguity surfaces minimized over predetermined regions of ambiguity plane, noting weighted error criterion role 04 p0651 A70-15328
Weighting function of optimal correctable gyroscope servosystem in random narrow band noise 05 p0880 A70-16225
Weighting coefficient matrix parameters for European satellite triangulation determined, considering sequence of separate points shown by photographs instead of single point 05 p0839 A70-16345
Chebyshev quadrature formula weighting functions, presenting accuracy estimation method 07 p1321 A70-18659
Nonstationary correlation function for cross correlation of sample records from random processes, discussing minimum mean square error and weighting method 07 p1238 A70-19250
Conditionally optimal control coefficients for nonlinear plant obtained from weighting functions derivatives of conjugate linear model for plant 08 p1479 A70-20995
Electronic equipment optimal design variant selection method, based on relative characteristics of feasible versions, widening weighting coefficients determination basis 09 p1643 A70-22129
Weight function minimization of multiweb box beam in pure bending 09 p1777 A70-22769
Weighted residual and Biot variational methods for solving one dimensional heat conduction problems 09 p1789 A70-23260
Diffraction effects for bilinear screen with irregular apertures determined using correction weighting function for solution 09 p1639 A70-23668
Optimal trajectory measurement program for orbit parameter determination, assuming random errors and nondegenerate weighting matrix of normal equations 10 p1940 A70-24302
Analytic function integration optimal rate, discussing weighting function 10 p1909 A70-24509
Theorem formulation and proof for maximal length cycle classification by weight 11 p2073 A70-26309
Wide range wind compensated launcher settings for unguided rockets using wind-weighting model and iterative procedure requiring real time computation 13 p2503 A70-28528
Orthogonal expansion of multivalued functions for weights in threshold function realization 15 p2767 A70-31838
Cardiovascular blood circulation system dynamic characteristics analysis by linear statistical correlation methods, describing test for determining weighting function 20 p3581 A70-39905
Extremal dynamic controlled plant with random input signals, identifying components weighting functions by statistical approximation 20 p3604 A70-39908

Optimum automatic selection of redundancies, discussing weighting and pivot choice and rigid element incorporation 20 p3732 A70-40264
Laminar incompressible free shear layers by method of weighted residuals for turbulent jets, obtaining velocity profiles for similarity and physical planes 20 p3613 A70-40286
Notch stress intensity factor representation as boundary traction weighted average, deriving weight functions from stress field boundary displacements 23 p4266 A70-44021
Codeword weight enumerator for second order Reed-Muller codes, using matrix approach 24 p4313 A70-46060
Weight structure enumerators for codewords of Reed-Muller codes 24 p4313 A70-46061

WEIGHTLESS FLUIDS

Equilibrium shapes of rotating weightless fluid with surface tension in absence of external force field obtained by boundary layer theory 04 p0673 A70-15241
Ideal weightless fluid jet flow past supercavitating plate at incidence using Tulin scheme 12 p2214 A70-28241
Plane plate motion in weightless fluid flow with free upper boundary, showing lifting capacity increment by underlying solid surface 13 p2390 A70-29644
Ideal weightless fluid plane potential flow in channel with permeable wall, deriving expressions for dynamic characteristics 13 p2390 A70-29648

WEIGHTLESSNESS

Male macaque monkey physiological deterioration in Biosatellite 3, noting falling brain temperature, lowered central venous pressure, fluid loss, blood redistribution into visceral pools, etc 01 p0022 A70-10822
Weightlessness effects on butyl alcohol diffusion flames, studying flame damping mechanism 01 p0217 A70-11012
Interview with Yegorov, discussing ECG, EEG, muscular effort, eyeball movement, blood pressure changes and vision changes during space flight 02 p0230 A70-11675
Fuel droplets burning at pressures sufficient to reach critical temperature under zero gravity conditions in free fall apparatus 02 p0351 A70-12002
Sensor, vegetative, motor and vestibulosomatic reactions to brief weightlessness in fighter pilots and laymen, ascribing disorders absence to statokinetic stability of organism 02 p0241 A70-12799
Spine acceleration tolerance after prolonged human exposure to weightlessness, noting osseous apparatus tissue decalcination 03 p0423 A70-13712
Human motion coordination under acceleration followed by weightlessness during jet flights along Keplerian orbits, discussing initial disturbance and subsequent subsiding 03 p0425 A70-13897
Acceleration and weightlessness effects on efficiency, reliability and capacity in pilots and astronauts muscular system 07 p1202 A70-18797
Weightless astronaut self rotation by limb maneuvers producing pitch and yaw motion 07 p1219 A70-19245
Human body turning /orienting/ in unsupported /weightless/ position by own muscular forces, determining inertia moments of body and parts relative to various axes 07 p1207 A70-19495
Weightlessness effects on human vision, studying color perception, field of vision and light sensitivity 08 p1444 A70-20743
Physiopathological effects of weightlessness, showing desirability of partial gravity for long voyages via spacecraft rotation 09 p1621 A70-23439
Rehydratable food consumption in zero-gravity environments with spoons and forks, observing interfacial tensions between water and food, containers and utensils 09 p1628 A70-23464
Relative value of prolonged bed confinement and hypodynamia in estimating biological effects of weightlessness 10 p1813 A70-24666
Spine acceleration tolerance after prolonged human exposure to weightlessness, noting osseous apparatus tissue decalcination 11 p1985 A70-25512
Physiopathologic effects on organs of longitudinal and tangential accelerations, decelerations, vibrations and weightlessness 11 p1986 A70-25821
Spacecraft design requirements for scientific zero G cloud physics experiments concerning colloidal modification processes 14 p2584 A70-30552

Optimum overlap design of thin walled tubular extendible spacecraft structures under solar heating in zero-g environment 14 p2657 A70-30762

Mass measuring device used on biological specimens in zero gravity environment, determining normal and disturbed physiological mechanisms 14 p2542 A70-30795
Wheat seedlings cellular response to weightlessness during NASA Biosatellite II flight compared with simulated weightlessness effects 15 p2688 A70-31662
Film condensation in tubes, considering liquid-vapor interface, zero gravity and electrostatic field conditions 15 p2828 A70-32541
Human body turning /orienting/ in unsupported /weightless/ position by own muscular forces, determining inertia moments of body and parts relative to various axes 15 p2685 A70-32740
Space manufacturing in weightless environment, discussing unique processes, potential materials, product groups, planned experiments for Skylab Orbital Workshop mission, etc 16 p2888 A70-33716
Materials preparation processes and improvements in space weightless environment, considering metals and ceramics melting, solidification, electromagnetic process control, etc 16 p2919 A70-33717
Orbital zero and low g environment utilization for space manufacturing processes and related operational and tooling requirements 16 p2919 A70-33718
Systems design and instrumentation for chemical/biochemical space manufacturing at zero g, developing scaling laws for transition to larger production units 16 p2919 A70-33719
Electromechanical servomotor for positioning and handling of objects in weightless environment, discussing design and operations 16 p2919 A70-33720
Human circadian coronary circulatory rhythms during space flight weightlessness or bedrest with and without exercise 16 p2854 A70-33991
Biological satellite experiment, considering long term weightlessness effects on metabolism and biological rhythms of medical leech 16 p2854 A70-33993
Long term weightlessness effects on cardiovascular system of rats using miniaturized pump oxygenator 16 p2854 A70-33999
Weightlessness and gravitational effects on human pulmonary blood flow distribution, considering optimal gas exchange efficiency [AIAA PAPER 70-785] 17 p3035 A70-34472
Spacecraft waste management system zero-gravity flight tests, describing components and functions 17 p3036 A70-34751
Automated orbiting biosatellite program with reentry system, studying long term weightlessness and radiation effects 17 p3178 A70-35258
Capillary ball game phenomenon under weightlessness, showing photographs of mercury droplet reflection from fluid boundary 18 p3242 A70-36638
Arc welding in space under high vacuum weightless conditions, describing equipment design and Soyuz 6 experiments 19 p3436 A70-37803
Space processing under zero gravity conditions, discussing crystal growth, metal glass and ceramic melting and casting and biological product centrifugation and electrophoresis 19 p3436 A70-37926
Magnetomotive tools and power systems for maintenance, repair and assembly in space weightless environment 19 p3436 A70-37949
Zero gravity liquid ammonia propellant feed system, describing regulator/capillary tube assembly for propellant delivery pressure control [AIAA PAPER 70-1151] 20 p3690 A70-40204
Space travel genetic effects, discussing radiation, weightlessness, vibration and acceleration 21 p3761 A70-40842
Gravitational effects on laminar gas jet diffusion flame stability, including zero gravity environment 21 p3949 A70-41316
Chicken lymphopenia and body mass loss resulting in death from chronic restraint, developing physiologically unstressful restraint for space environmental testing 21 p3765 A70-41488
Gas lubricated three-foil bearing for high speed rotor support, considering dynamic and static behavior in zero gravity environment [ASME PAPER 70-LUBS-18] 22 p4044 A70-42443
Skylab Orbital Workshop fabrication experiments under space environment conditions, discussing

weightlessness and vacuum effects on various manufacturing techniques

22 p4046 A70-43075

Dynamic spacecraft cabin atmospheres for extended operation, discussing gas composition, weightlessness and various stress factors

22 p3980 A70-43643

Weightlessness and immobilization effects on mechanical tolerance of bone compressive and breaking strength in monkeys

22 p3973 A70-43648

Mammalian tissues metabolic and genetic alteration during weightlessness, relating rats liver regeneration delay to centrifuging intensity following hepatectomy

23 p4146 A70-44617

Hypogravic skeletal atrophy model, considering bone maintenance as feedback control system

24 p4296 A70-45328

WEIGHTLESSNESS SIMULATION

Water immersion technique to simulate zero and partial gravity conditions for investigation of astronaut capability to execute extravehicular work procedures

01 p0038 A70-10963

Simulated zero gravity tests of force application by subjects in Apollo suits, varying worksite geometry, personnel restraints and force type and direction

01 p0038 A70-10964

Water immersion for weightlessness simulation, presenting annotated bibliography covering physiological responses, human performance and simulation techniques and facilities

01 p0038 A70-10965

Ground-based biological experiments on insects and frog eggs to investigate effects of space flight weightlessness and radiation on mitosis and meiosis

04 p0631 A70-14942

Critical thermal flux and heat transfer coefficients dependence on simulated gravity during bubble and film boiling in inclined flat containers

12 p2331 A70-27325

Wheat seedlings cellular response to weightlessness during NASA Biosatellite II flight compared with simulated weightlessness effects

15 p2688 A70-31662

ONERA accelerometer flight test of performance in zero gravity environment, using Vesta sounding rocket for simulation

19 p3431 A70-38541

Critical thermal flux and heat transfer coefficients dependence on simulated gravity during bubble and film boiling in inclined flat containers

21 p3952 A70-42066

Organism reactions to gravity forces, discussing experimental zero and hyper g simulation studies with frog and nematode eggs

23 p4146 A70-44630

Orthostatic stability reduction in experiments with simulated weightlessness, investigating functional compensation mechanisms

23 p4149 A70-45025

WEIGHTS [COEFFICIENTS]

U COEFFICIENTS

WELD STRENGTH

Microstructure and impact strength of welds of Cr-Mn steel containing nitrogen, observing grain growth dependence on nitrogen content

03 p0509 A70-13277

Diffusion welding of dissimilar metals with or without intermediate layers, assessing joint strength factors

03 p0498 A70-14071

Weld quality monitor for production testing of welding strength in electronic circuitry

05 p0856 A70-16722

Thermal fatigue resistance of steel to copper weldments under thermal cycling, noting intergranular crack growth accompanied by oxidation along crack boundaries

06 p1078 A70-18515

Ti alloy welded sheets bending fatigue test facility, discussing test stand calibration and optimal welding

07 p1291 A70-18824

Cr-Mo steel strength and structural stability during tubular stress-rupture testing with high pressure hydrogen, discussing welding effect on strengths

08 p1519 A70-21455

Structural stability of friction welded joint between high temperature low alloy weld metal from CrMoV electrode and high temperature Cr steel

12 p2244 A70-28349

Al-Mg, Al-Zn-Mg, Al-Cu and Al-Cu-Mg welded alloys corrosion cracking resistance as function of composition and fabrication techniques

14 p2597 A70-30972

Weld brittleness during laser beam welding of Ni-Cu, Ni-Ti and Cu-Ti due to diffusion processes

16 p2916 A70-33052

Al pressure-welded joints strength, investigating surface treatment role

16 p2924 A70-34340

Single phase alpha Ti alloy welds breaking strength, discussing delayed failure and cold cracking with various oxygen and hydrogen contents

17 p3117 A70-34399

Porosity effects on mechanical properties of high strength Al alloy weldments

18 p3265 A70-37204

Ti and Al alloy weldments plane strain fracture toughness and mechanical properties for cryogenic applications, using gas metal arc and gas tungsten arc welding

[ASME PAPER 70-MET-4] 22 p4043 A70-42423

WELD TESTS

Gamma ray beam inspection of opposed arc weld with nugget penetration in Al-Cu alloy, including averaging circuit reducing counting statistics variation

01 p0054 A70-10020

Programming device for positioning samples under X ray beam in testing welded seams and parts

02 p0301 A70-12488

Hydrogen, oxygen and nitrogen effects on gas shielded arc weld porosity of Ni, comparing MIG and TIG processes

02 p0310 A70-12543

Weld quality monitor for production testing of welding strength in electronic circuitry

05 p0856 A70-16722

Al weld metal compositions and hydrogen content effects on weld porosity, locating hydrogen in weld by radioactive tracers

08 p1507 A70-21485

Nondestructive process control analyzer for spot welds in aircraft structural components, monitoring expansion, current and spotweld properties

08 p1507 A70-21486

Electronic stress wave analysis technique /SWAT/ for delayed weld cracking data acquisition

10 p1897 A70-25312

Al alloy welded joints delayed rupture tendency, describing constant load test method

14 p2591 A70-30969

Al-Zn-Mg alloy welds delayed rupture under constant uniaxial load in distilled water or aqueous salt solution

14 p2591 A70-30970

Electron beam welding of Ti alloys in partial vacuum, describing mechanical tests and metallographic examinations

17 p3098 A70-34442

Magnesium pulse arc welding, describing procedure, techniques testing and advantages

17 p3100 A70-34635

Al-Si welding rods tests with various surface finishes, considering oxide coatings effect on gas tungsten arc weld quality

18 p3264 A70-37113

Welded Al plates high temperature bend tests, describing materials and procedures

18 p3278 A70-37115

Porosity effects on mechanical properties of Al alloy gas tungsten arc welds, noting strength loss proportional to cross sectional area loss

18 p3265 A70-37205

Fatigue strength in pulsed tension of butt-welded tubular joints, evaluating test results statistically

19 p3433 A70-37357

Sintered boron-alloyed Mo electron beam welding behavior examined by texture-revealing color etching method

21 p3833 A70-41411

Nondestructive ultrasonic measurements of crack depth in high strength steel plate weldments, studying low cycle fatigue

21 p3834 A70-41943

Fracture mechanics application to fusion weld [ASME PAPER 70-MET-2]

22 p4043 A70-42424

Repair weld procedures effects on annealed Ti-Al-V weldments mechanical properties, examining defects in inert gas shielded arc welded joints

[ASME PAPER 70-MET-1] 22 p4043 A70-42425

Ultrasonic delta technique inspection method for flaw detection in weldments or wrought materials

24 p4335 A70-45572

Gamma ray inspection of opposed-arc weld-nugget penetration in Al-Cu alloy

24 p4350 A70-46384

WELDABILITY

Electrical resistivity, contact resistance and weldability of cast Cu and Ag contact materials reinforced unidirectionally by W wire compared to powder composition

04 p0711 A70-14465

Weldability of super alpha high creep strength Ti alloy investigated by synthetic heat affected zone method using thermal cycling tests

06 p1090 A70-18501

Tungsten and tungsten base alloy weldability, discussing powder metallurgy, postweld annealing, high temperature tensile strength, etc

06 p1078 A70-18514

Alloying elements preventing hot cracking in weld metal by converting iron sulfides into higher melting point sulfides

07 p1293 A70-18979

Spacecraft propellant tank development from Al alloy providing excellent weldability, propellant compatibility and strength to weight ratio

12 p2242 A70-27108

Soviet collection of papers on Al weldable alloy including sheets, heat treatment, aging, mechanical properties, etc

14 p2596 A70-30960

Al-Zn-Mg weldable alloy composition, mechanical properties, heat treatment, aging effects, etc

14 p2597 A70-30964

Al weldable alloys for cryogenic applications, considering plasticity, brittleness and tensile and yield strengths at low temperatures

14 p2597 A70-30968

Al-Zn-Mg high strength weldable alloys rupture characteristics, analyzing crack distribution, stress raisers and weld defects

14 p2591 A70-30971

Superalloys commercial development, investigating strength, heat resistance and weldability of Fe- and Ni-based alloys [ASME PAPER W70-9.4]

15 p2760 A70-32335

Weldability, tensile and fatigue properties of Ti sheet alloys, discussing TIG welds

17 p3121 A70-34431

Nonweldable internal flaws detection containing oxides in steel slabs by neutron activation analysis

24 p4376 A70-45750

WELDED JOINTS

NT SPOT WELDS

Ultrasonic imaging system for flaw detection, analyzing welds

01 p0104 A70-10881

Piezoprobe parameters calculation for controlling angular welded connections of boiler assembly elements

02 p0300 A70-12481

Structure and segregation effects in Type 304L stainless steel weldments using transmission electron microscopy, optical microscopy and electron microprobe, comparing weld types

02 p0319 A70-12754

Residual stress distribution in butt joints during welding of sheet Nb measured by extensometer, noting annealing temperature effect on stress relieving

03 p0513 A70-14072

Postweld heating cycle for circular patch test to predict strain age cracking susceptibility in welded Rene 41

04 p0700 A70-15654

Inertia bonded and electron beam welded joints of Waspaloy compared for suitability in aircraft gas turbine engines

04 p0700 A70-15655

Thermophysical characteristics of annealed Ta and Mo alloy welded joints under electron beam and ray heating, noting use for short term tests

05 p0865 A70-17028

Microfissuring of Ni base alloy weldments as function of grain size produced by solution temperature

07 p1306 A70-18996

Welding techniques for Nb-stainless steel bimetal tubing for liquid metal containment, determining structural integrity and bond interface condition after thermal cycling

10 p1897 A70-25309

Nonuniform stress distribution along side fillet welds and in welded plates of lap joint, discussing tangential stresses and plate width

11 p2058 A70-25598

Numerically controlled gas tungsten arc welding, discussing tape programming, fixture design and fabrication for various welded metal joint configurations

11 p2058 A70-25661

Brittle fracture strength of welded joints in high strength steels

11 p2059 A70-25663

Porosity and intergranular crack formation in tungsten fusion welds using electron fractography

11 p2059 A70-25666

Mechanism and kinetics of intermetallic layers formation and growth in welded joints of unlike metals

11 p2067 A70-26594

Strain measurement over large steel plate surface ground to reasonable flatness and in welded joints by applying moire method

11 p2061 A70-26836

Computer analysis of degree of constraint against butt joint transverse shrinkage, using finite element method for stress analysis

12 p2239 A70-26854

Structural stability of friction welded joint between high temperature low alloy weld metal from CrMoV electrode and high temperature Cr steel

12 p2244 A70-28349

Hydride segregation in Ti alloy weldments made with unalloyed Ti filler metal, determining effect on mechanical properties

14 p2591 A70-30932

Al alloy welded joints delayed rupture tendency, describing constant load test method

14 p2591 A70-30969

Weld cracks in welded joints of Ni-Cr base alloys due to residual stresses during aging, recommending annealing for prevention

16 p2930 A70-33051

Weld brittleness during laser beam welding of Ni-Cu, Ni-Ti and Cu-Ti due to diffusion processes 16 p2916 A70-33052

Transverse contraction during butt welding of plates of steel and Ti and Al alloys, showing dependence on joint thickness 16 p2916 A70-33053

Al pressure-welded joints strength, investigating surface treatment role 16 p2924 A70-34340

High temperature heating and cooling effects on mechanical properties and structure of Ti welds, using notched bar impact specimens 17 p3098 A70-34423

Weld transition joints from explosive bonded Al-steel and Al-Cu composite plates, discussing mechanical and electrical properties 17 p3102 A70-35551

Low temperature effects on Ti alloys welded joints elasticity 17 p3126 A70-35637

Fatigue resistance of high yield strength steel weldments under uniaxial loading, describing cyclic behavior by S-N curve 18 p3278 A70-37114

Fatigue strength in pulsed tension of butt-welded tubular joints, evaluating test results statistically 19 p3433 A70-37357

Electron beam welding for thin steel, nonferrous metals and reactive metals sheets 19 p3436 A70-38073

Electron beam welding for instrument components including torsion shafts, heat sensing membranes, etc 19 p3436 A70-38074

Electron beam welding for thin copper, carbon and Cr-Ni steel sheets in precision mechanical and optical devices 19 p3436 A70-38075

Welded joint strain measurement by grating etching and moire fringe technique 19 p3428 A70-38513

Repair weld procedures effects on annealed Ti-Al-V weldments mechanical properties, examining defects in inert gas shielded arc welded joints [ASME PAPER 70-MET-1] 22 p4043 A70-42425

Bar butt current penetration welding, using HF continuous current seam welding process for joining finite length pieces 22 p4046 A70-43148

High strength Al alloys plate and welds, comparing tear notch tests at cryogenic and room temperatures 23 p4206 A70-44352

Brittle fracture of welded notched steels with different stress concentrations, using subzero tensile tests 24 p4347 A70-45732

Defect effects on welds fatigue properties in low carbon steel plates estimated, using radiograms 24 p4347 A70-45733

Elastoplastic properties of welded joints containing slag inclusions defects, determining sizes radiographically 24 p4347 A70-45734

WELDED STRUCTURES

HF endurance tests of Al sheet alloy used in welded aircraft structural components, plotting curves for heat treated and untreated specimens 02 p0315 A70-11658

Overstress cycles sensitivity for welded specimens on basis of French fatigue damage line and Wohler S-N line 05 p0941 A70-16520

Optimal localized heat treatment of welded products, analyzing temperature fields and stresses during heating and cooling of ferromagnetic materials 07 p1294 A70-19477

Matrix stiffened nickel-chromium welding products featuring high tensile strength at room and elevated temperatures and high impact strength at cryogenic temperatures 08 p1508 A70-21488

Tensile and compressive strain measurements close to weld deposits, using moire fringe technique and mismatch grating 10 p1890 A70-24591

Diffusion bonding processes for Ti aerospace structural elements, describing electric blanket, roll and press bondings [SME PAPER AD-70-736] 12 p2242 A70-27089

Al heat treatable alloys for welded structures, considering stress corrosion resistance, aging effects, brittle and delayed rupture resistance, etc 14 p2596 A70-30961

Al-Mg-Zn alloy composition, mechanical properties and structure for various heat treatments, discussing welded structures stability, stress relief, corrosion resistance and tensile strength 14 p2597 A70-30966

Al alloy welded sheets strength and plasticity under biaxial tension, examining excess elastic energy effects on strain kinetics and rupture 14 p2597 A70-30967

Residual stresses near weld in spherical rocket motor casing constructed from maraging steel sheet,

discussing moire measurement and reduction treatments 15 p2744 A70-31926

Charpy impact test evaluation on hot rolled metal plates for low temperature welded structures 15 p2819 A70-32235

Ti sheet welded construction for transport aircraft fuselages, assuming use of electron beam and plasma arc equipment 17 p3198 A70-34452

HF endurance tests of Al sheet alloy used in welded aircraft structural components, plotting curves for heat treated and untreated specimens 19 p3452 A70-38431

Concorde downstream thrust reversal nozzle, noting weight saving by use of welded stainless steel honeycomb construction 22 p4092 A70-43213

Nondestructive inspection methods for welded structures affected by stress corrosion 24 p4347 A70-45730

WELDING

NT ARC WELDING

NT BRAZING

NT DIFFUSION WELDING

NT ELECTRIC WELDING

NT ELECTRON BEAM WELDING

NT EXPLOSIVE WELDING

NT FLASH WELDING

NT FUSION WELDING

NT GAS TUNGSTEN ARC WELDING

NT GAS WELDING

NT LOW TEMPERATURE BRAZING

NT PLASMA ARC WELDING

NT PRESSURE WELDING

NT ULTRASONIC SOLDERING

Carbon dioxide laser welding equipment and procedures, describing mechanical-electronic control system, target material-laser beam interactions, etc 02 p0310 A70-12752

Welding atmosphere purity effects on Li corrosion resistance of refractory metals in space power systems 04 p0709 A70-15627

Steel welding processes in thicknesses useful to future booster production 04 p0700 A70-15652

Laser characteristics relevant to microwelding and micromachining, discussing heat conduction based models limitations 05 p0857 A70-15999

Welding of satellite and spacecraft segments in space, discussing arc, electron beam, resistance, vacuum diffusion, cold pressure and brazing techniques 05 p0855 A70-16375

Polyamides chemical welding using HF heating to obtain optimum temperature distribution and to activate polymer reaction with crosslinking agents 06 p1091 A70-17316

Lasers industrial application to distance and flow rate measurement, automated machining and tunneling, inspection, die hole punching, welding, etc 06 p1078 A70-18431

Thermocouple vacuum gauge joined to Apollo lunar sample return containers (ALSR), describing two step welding procedure with transition cylinder 08 p1507 A70-21483

Al weld metal compositions and hydrogen content effects on weld porosity, locating hydrogen in weld by radioactive tracers 08 p1507 A70-21485

Automatic cladding method for submerged arc stainless steel welding, discussing delta ferrite to sigma phase transformation for surfacing with low ferrite stainless steel 08 p1508 A70-21489

Aluminum alloys hot cracking during welding, ascribing failure to combination of strain and susceptible microstructure 10 p1897 A70-25313

Book on metal joining techniques covering various welding and brazing processes 11 p2061 A70-26599

Surface sliding friction interactions in aluminum alloys friction welding 12 p2239 A70-26855

Aerojet engine minimum weight design, suggesting use of welding and brazing instead of nut-and-bolt joints in component fabrication [SAE PAPER 700319] 12 p2243 A70-27457

Weld quality relationship to aluminum surface contamination by hydrogen-containing compounds 13 p2407 A70-29108

Thick plate titanium alloy welds using filler wire to regulate chemical composition and plate phase constitution 13 p2435 A70-29456

Welding failure case histories, discussing design, materials and processes, fabrication and quality control integration 21 p3832 A70-40787

Solid state butt and lap joint welding of TD-nickel bar, evaluating performance by stress rupture and shear tests 21 p3832 A70-40790

Metallurgical interaction phenomena in welding zone of heat treated Inconel 600, using hot ductility testing and metallographic methods 22 p4046 A70-43150

Metal matrix composite structures tooling and fabrication processes, considering forming, joining, welding, machining joining, etc [SAE PAPER 700752] 24 p4348 A70-45873

WELDING MACHINES

Electron beam welding of AH-56A helicopter rotor hubs outside of vacuum chamber, discussing modifications of machine 04 p0699 A70-15651

Miniaturized program oriented automatic pipe/tube welding system for in-place joining of fluid systems, controlling timing functions and weld current sequence 09 p1692 A70-22795

Joining small components made of difficult to weld materials by percussive welding consisting of stationary and moving electrode actuated by pretensioned spring 10 p1894 A70-24298

Gas tungsten arc welding application broadened by introducing controlled droplet transfer process 10 p1896 A70-25308

Metal contact welding principles, materials, geometries and machines 10 p1897 A70-25310

DC arc facing welding device using vacuum to minimize pores, slag inclusions, cracks and defects 13 p3284 A70-28867

In-place gas tungsten arc fusion welding for joining small diameter precipitation hardenable aluminum tubing 14 p2590 A70-30930

Precision electron beam welding for metal joints, discussing equipment and quality control factors 19 p3436 A70-38072

Microwelding by pulsed ruby laser radiation, discussing characteristics and advantages 20 p3638 A70-40149

Tooling concepts providing gas shielding in mechanized open air arc welding of Ti, evaluating effectiveness by various mechanical tests 21 p3832 A70-40788

WENTZEL-KRAMER-BRILLOUIN METHOD

Plasma resonance excitation by small pulsed dipole in weakly inhomogeneous plasma determined using WKB solutions and stationary phase approximations 12 p2277 A70-27188

WKB method applied to ionospheric equations with strong wave coupling 15 p2725 A70-31857

Radial energy eigenvalue problem conversion into one dimensional by infinite set of transformations, considering WKB quantization condition 16 p2942 A70-33691

WKB method for asymptotic oscillatory solutions of nonlinear equations of relativistic fluid mechanics 19 p3403 A70-37587

WKB or eikonal approximation for waves and vibrations in inhomogeneous Euler-Bernoulli beams and plates and Timoshenko beams 19 p3536 A70-37700

Boundary layer problems with resonance solved by matched asymptotic expansions and WKB method 23 p4179 A70-43945

Quantum mechanics classical equations for complex velocity variable, obtaining asymptotic series solution by applying modified WKB method 24 p4378 A70-45274

WEST GERMANY

U GERMANY

WETNESS

U MOISTURE CONTENT

WETTING

Interfacial equilibrium free surface energies between glass fibers, coupling agent and resin matrix, considering wetting, absorption and bonding 01 p0128 A70-10486

Capillary grooves effect on surface wetting and evaporation using heat transfer coefficients for grooves with triangular, semicircular and square cross sections [ASME PAPER 69-HT-19] 09 p1790 A70-23559

Binder wetting relation to solid film lubricant wear life [ASLE PREPRINT 70AM 5A-3] 19 p3439 A70-38810

WHEATSTONE BRIDGES

Resistance bridge balancing by time method for dynamic digital measurements 11 p2054 A70-26433

Unbalanced Wheatstone bridge network operation for resistance strain gage measurements, determining dynamic transients variable extremes 11 p2054 A70-26434

Wheatstone structure impedance bridges, describing balancing method in sinusoidal alternating regime 16 p2872 A70-33106

Multibandswitch AC Wheatstone bridge design with large circuit factor 17 p3051 A70-34616

WHEEL BRAKES

Energy absorption and dissipation in friction brakes, investigating brake lining polymer binder contribution through molecular reorientation, crystallinity increase and entropy decrease 24 p4342 A70-45585

WHEELS

NT FLYWHEELS
NT NOSE WHEELS
NT REACTION WHEELS
NT TURBINE WHEELS
NT VEHICLE WHEELS

WHIRL

U ROTATION
WHIRL INSTABILITY
U ROTARY STABILITY

WHIRLING

U ROTATION
WHIRLING TESTS
U SPIN TESTS

WHISKER COMPOSITES

Mechanical properties of Al composites reinforced with alpha-silicon carbide sintered whiskers, discussing voids, fiber breakage and orientation effects 03 p0506 A70-13113

Al-Ni intermetallic whisker-reinforced Al microstructure and mechanical properties, studying effects of cold rolling 03 p0508 A70-13142

Whiskers and whisker products physical characteristics, available forms and types and compositing methodology, discussing utilization in plastics 05 p0873 A70-16611

Al alloy matrix composites with beta-SiC whiskers reinforcement, evaluating tensile and fatigue properties 08 p1523 A70-21856

Ceramic whisker and continuous filaments reinforced metals, discussing processing, properties, matrices selection of reinforced composites, etc 20 p3650 A70-39948

WHISKERS (SINGLE CRYSTALS)

Aluminum oxide whiskers/metal matrix composites, discussing metallic coatings effects on filament wetting, bonding and surface protection 01 p0117 A70-10480

Reinforcement of thermoplastic resins, considering single crystal whisker and carbon fibers and microspheres 01 p0129 A70-10774

BeO whiskers formation on burning Be droplets surface using scanning electron microscopy, noting temperature effects 02 p0318 A70-12641

Mechanized glycerine process for fibers and whiskers alignment on large scale at low cost 05 p0855 A70-16580

Rotary machine for classifying reinforcing fibers and whiskers with respect to length 05 p0855 A70-16583

Whiskers and whisker products physical characteristics, available forms and types and compositing methodology, discussing utilization in plastics 05 p0873 A70-16611

Tensile properties variations of Co whiskers grown by reducing cobaltous bromide in hydrogen-argon mixture 07 p1306 A70-19071

Heat resistant fibers fabrication and properties for composite materials, noting metal whiskers, C, B, Be and alumina 07 p1318 A70-19802

Vapor-liquid-solid nucleation mechanism of alpha-aluminum oxide filamentary single crystal growth, suggesting combination with suboxide condensation and disproportionation mechanism 07 p1313 A70-19890

Sapphire whisker-Al composites fabrication methods using air extrusion techniques and semiautomatic methods for fiber alignment, discussing elastic modulus, tensile strength, etc 07 p1314 A70-19956

Silicon carbide whiskers end structure using field emission patterns 08 p1528 A70-21551

Silicon carbide whiskers properties and applications compared with other reinforcing fibers 11 p2070 A70-26340

Statistical theory of material strength applied to composite materials reinforced with whiskers and noncontinuous fibers 15 p2763 A70-32833

Dislocation diffusion effects on strength of whiskers and fine grained polycrystals 16 p2934 A70-34327

Whisker diode coupling to polarized IR laser beam by orientation based on antenna theory 17 p3048 A70-35902

SiC whiskers X ray diffraction studies of crystal structure, suggesting single crystal permanent deformation at ambient temperatures 19 p3455 A70-37941

Whiskers and filaments properties compared for fiber reinforcement applications in composite materials production 24 p4356 A70-45167

WHISTLER RECORDERS

VLF recordings and X ray flux measurements simultaneous analysis indicating evidence of relation between dawn chorus and electron precipitation, noting ELF whistler development 02 p0293 A70-12689

Whistler activity continuous recording by autocorrelation method using electronic analog computation with fixed delay time 10 p1886 A70-25281

Ionic temperature difference from Arecibo data indicated in Injun 3 and Alouette 1 sonograms of proton whistlers propagation time, noting Doppler shift role 13 p2372 A70-29928

Magnetospheric thermal plasma studies via ground based whistler method, identifying radial and longitudinal irregularities in electron density, bulk motion and plasmopause position and displacements 22 p4021 A70-43281

WHISTLERS

Real configuration effect of magnetic field in moderately perturbed magnetosphere on whistlers dynamic spectra, stressing geomagnetic perturbation detection 01 p0082 A70-11486

Plasma concentration diagnostics in magnetosphere based on hydromagnetic whistlers/pearls/dispersion 01 p0084 A70-11554

Charged particle self resonant motion in field of plane electromagnetic wave, showing trapped particles existence in whistlers 02 p0256 A70-12116

Whistlers paradoxical behavior in bounded magnetoplasmas, discussing double reflection and wave propagation 02 p0263 A70-12733

Poynting flux direction for proton whistlers determined from Injun 5 observations, obtaining data on source region and propagation in ionosphere 03 p0477 A70-13987

Whistler mode instability due to anisotropic charged particle velocity distribution, establishing general onset conditions for variable density cold plasma containing hot electrons 03 p0537 A70-14378

Nonducted VLF walking trace whistlers and Doppler shifts in fixed frequency transmissions identified on OGO midlatitude spectrographic records 04 p0649 A70-15116

Magnetospheric observations of whistler mode emissions by OGO 1 satellite over VLF and LF ranges 04 p0649 A70-15117

Transmission and reflection coefficients of propagating whistler modes for model ionosphere 05 p0837 A70-15880

High and medium whistler activity in Italy correlated with weather situation in South Africa 05 p0839 A70-16317

Whistler mode wave propagation in collisionless Vlasov plasma along nonuniform magnetic field 05 p0889 A70-16533

Charged particles motion in field of whistler mode wave packet, discussing trajectories 06 p1118 A70-17377

VLF and ULF whistler modes propagating along geomagnetic field-line paths in magnetosphere, studying cyclotron resonance amplification 06 p1118 A70-17379

Whistler amplification in magnetosphere for electron interaction with background plasma to produce wave growth, discussing stability of various anisotropic velocity distributions 06 p1059 A70-18533

Whistlers role in ionospheric temperature, magnetospheric electron density and ionospheric composition determination 07 p1347 A70-19189

HF ion-acoustic noise /whistlers/ during turbulent heating of plasma, using matched magnetic probe 07 p1348 A70-19551

Harmonic ion cyclotron resonances associated with proton whistlers observed from OGO-4 satellite VLF recordings 07 p1268 A70-19630

Cold plasma approximation of whistler excitation of lower hybrid resonance at wake of body moving through ionosphere, comparing results with Alouette satellite observations 07 p1276 A70-20425

Small dispersion whistlers characteristics and propagation at midlatitudes based on observation at Tohokata, Japan 08 p1491 A70-21713

Whistler type electromagnetic waves excitation by electron beam in plasma, noting intensity dependence on electron frequency 08 p1554 A70-21804

Ion cyclotron whistler in Injun 5 satellite VHF radio noise data 09 p1638 A70-23499

Whistler mode VLF emissions stimulation mechanism 13 p2401 A70-29930

Whistler mode wave packets propagation in hot inhomogeneous collisionless plasma immersed in nonuniform ambient magnetic field 13 p2468 A70-29931

Whistler instability examined on gyrating electron beam interaction with cold background plasma propagating parallel to magnetic field 13 p2468 A70-29932

Collision effect on phenomena associated with ion cyclotron whistler formation, considering ionospheric day time model 13 p2468 A70-29933

Magnetic field measurement of VLF wave propagating in whistler mode in magnetosphere by satellite FR-1 13 p2401 A70-30054

HF ion-acoustic noise /whistlers/ during turbulent heating of plasma, using matched magnetic probe 15 p2777 A70-31458

Dynamic spectral characteristics of LF whistler signals for outer ionosphere electron profile determination, using satellite observation 15 p2729 A70-32081

Refractive index equation for Whistler propagation in weakly drifting magnetoplasma 16 p2959 A70-34224

Electron density large scale structure in magnetosphere identified from whistlers recorded at Antarctica near sunspot minimum 18 p3311 A70-36012

Magnetospheric plasmopause duskside bulge dynamic behavior during substorms, using whistler data 18 p3312 A70-36013

Whistler density variability correlated with solar activity during IQSY 19 p3462 A70-37924

Whistler VLF radio observations of sudden magnetic impulses in plasmasphere during storms, using ground based magnetometers 20 p3620 A70-39330

Whistler mode wave propagation amplitude, polarization and dispersion in lower ionosphere, discussing electric field experiment with Nike-Tomahawk sounding rocket 20 p3622 A70-39456

Electron loss by resonant interaction with whistlers in nonuniform magnetic field, taking Fokker-Planck equation as distribution function 23 p4237 A70-44052

WHITE BLOOD CELLS

Hyperoxia effects on rats in vivo white blood cell counts 24 p4297 A70-45340

WHITE DWARF STARS

White dwarf mass changes during cooling, describing white dwarf collapse-type I supernova outbursts relationship 01 p0174 A70-10197

Pulsating very dense white dwarfs models noting general relativity 01 p0176 A70-10320

Photometric data for white dwarf low luminosity stars listed in color classes and proper motion fields 01 p0187 A70-11331

Intermediate band four color photometry of white dwarfs, considering hydrogen line blocking and H delta line 01 p0188 A70-11335

White dwarf luminosity functions based on birth rate, white dwarf space density in solar neighborhood and possible red degenerate stars deficiency 01 p0189 A70-11339

White dwarf spectra interpretation based on model atmosphere method, discussing chemical composition, low luminosity high pressure atmospheres, electron density, etc 01 p0189 A70-11340

Cooling time estimation for white dwarf stars with ion component undergoing condensation, based on plasma thermodynamic properties 01 p0189 A70-11341

High luminosity white dwarfs possible evolution from planetary nebulae, discussing plasma neutrino processes 01 p0189 A70-11342

White dwarfs formation in close binary systems ascribed to mass exchange between components, describing evolutionary followup of primary from main sequence by model 01 p0189 A70-11343

Final state of matter resulting from star contraction, white dwarfs development and neutron stars problem, explaining hydrostatic equilibrium 02 p0370 A70-12085

Light variation curves for distorted white dwarf hypothetical secondaries in close binary systems calculated by integrating monochromatic fluxes 03 p0567 A70-13323

- Eddington equation for white dwarf pulsation solved by treating eigenfunctions as differential moment of inertia functions 04 p0751 A70-15050
- Angular velocities and equilibrium of rotating neutron stars compared with white dwarfs 07 p1376 A70-18911
- Magnetic moment associated with Landau levels in magnetic induction in electron gas and magnetic fields of white dwarfs and neutron stars 09 p1752 A70-22306
- Low mass star evolution from helium burning to white dwarf, describing red giant and mass loss stages in model 10 p1946 A70-24982
- Faint violet stars in southern galactic latitudes found during scanning of two color plates including halo stars, subdwarfs, white dwarfs and quasi-stellar galaxies 10 p1949 A70-25248
- Thermal explosion in degenerate nucleus of white dwarf due to formation of laminar energy source in presence of hydrogen 11 p2115 A70-26577
- Stellar plasma neutrino pair emission, comparing photon neutrino coupling with current current coupling theory and white dwarf evolution 12 p2297 A70-26976
- Superfluidity and superconductivity under cosmic conditions, discussing Bose-Einstein condensation, neutron stars, white dwarfs, etc 15 p2795 A70-31454
- Magnetic fields of DA dwarfs observed with photoelectric polarimeter, noting no fields observable 17 p3154 A70-34537
- Hydrogen abundance in white dwarfs, discussing inconsistencies in mass and bolometric magnitude models for Sirius and Eri B 17 p3170 A70-35389
- White dwarf star circular polarized light, indicating strong magnetic field 20 p3701 A70-39001
- Electrical and thermal conductivities in white dwarf stars cores and neutron stars outer layers, calculating electron-photon collisions transition probability 20 p3702 A70-39016
- Equilibrium theory of white dwarfs, neutron and hyperon stars, deriving equations for nonrotating objects composed of degenerate cold electron or neutron gas 20 p3704 A70-39472
- Eclipsing binary with very hot white dwarf, discussing effective temperature and photometric observations 21 p3889 A70-41158
- White dwarf stars continuum circular polarization as function of time and wavelength, emphasizing magnetic star search 24 p4410 A70-45776
- WHITE NOISE**
- NT THERMAL NOISE**
- Optimal nonlinear filtering for nonlinear dynamic system subjected to additive white Gaussian noise with corrupted observations, using successive linearization scheme 03 p0461 A70-14340
- Frequency monitor design, analyzing relationships between time constants, gain, etc, emphasizing white noise filtration 07 p1227 A70-18991
- Improper integrals appearing in cross correlation of responses of two single degree of freedom systems to bandwidth limited white noise, deriving Laplace inversion formulas 07 p1236 A70-20067
- White noise and nonlinear effects in telemetry RF links, analyzing received process to phase coherent receiver 08 p1460 A70-20823
- Optimal amplitude modulated radio signal reception on white and narrow band background noise, using nonlinear filtration and phase locked control 09 p1633 A70-22416
- Nonlinear system with piecewise linear spring characteristic response to stochastic excitation of white noise type process, discussing technical stability 10 p1918 A70-25323
- Sequential filter equations for nonlinear system dynamics and observational model with linear estimator, comparing difference between white and colored noise filter results 11 p2024 A70-26126
- [AIAA PAPER 69-840] Rayleigh and m fading signals spectral location in additive white Gaussian noise, allowing predetermined or variable channel observation time 11 p2010 A70-26268
- Memoryless input discrete noisy channels essential equivalence to white Gaussian channel for rates above capacity using extreme value theory 11 p2010 A70-26326
- Random vibration isolation for two degrees of freedom model system investigated statistically, assuming wide band white noise 11 p2139 A70-26416
- Noise level influence on optimal recognition of non-stationary random processes in white noise 13 p2369 A70-29729
- Nonlinear optimal filtration and adaptive quasi-coherent reception of Markov signals on white noise background 13 p2369 A70-29731
- Quasi-optimal sequential detection of phase modulated signal of varying frequency on white noise background, using Markov theory 13 p2369 A70-29732
- Nonsingular detection and likelihood ratio for random signals in white Gaussian noise 14 p2551 A70-31118
- Optimal linear filter analysis from singular optimal control viewpoint, considering white and correlated measurement noise 16 p2885 A70-33320
- Linear sequential Kalman filter for time correlated noise without state augmenting and measurement differencing demanding less computer sizing 16 p2887 A70-33350
- Prediction of polynomial signals in white Gaussian noise, using discrete data 16 p2866 A70-34065
- Optimal temporal and spatial-temporal resolution for unknown parameter of interfering signal on white noise background 17 p3048 A70-35680
- Digital bit synchronization phase locked loop steady state and transient performance in white Gaussian noise 21 p3802 A70-41352
- General linear /Kalman/ sequential filter to account for finite correlated white noise without state vector augmentation or measurement differentiation 21 p3828 A70-41735
- Digital filtering of sampled narrowband sinusoidal signal embedded in wideband white noise, assessing hard clipping effect on performance by simulation on digital computer 21 p3791 A70-41948
- Unipolar pulse frequency modulation system with white noise input, deriving output power spectral densities 21 p3793 A70-42225
- Signal shape optimization by minimizing dispersion in temporal position estimates for radio pulse in presence of additive white noise 23 p4161 A70-43961
- Gyro drift rate mathematical modeling based on stationary and nonstationary time series analysis techniques with random process reduction to white noise residuals 23 p4197 A70-44557
- [AIAA PAPER 69-838] Nonlinear filtering for linear parabolic distributed parameter systems with white noise, considering stochastic boundary value problem 23 p4177 A70-44905
- Intense white pulsed jet engine noise effects on cochlea bio currents in cats 23 p4157 A70-45076
- Quantum detector with impinging EM field, discussing photoelectron counting distribution and signal with white noise 24 p4312 A70-46051
- Optimal noiseless linear information feedback estimation for additive white Gaussian noise channels, applicable to digital transmission 24 p4313 A70-46064
- WHITHAM RULE**
- Quasi-transverse constant profile wave in finite elasticity with isothermal shock at discontinuity compared to Whitham breakdown 10 p1956 A70-24191
- Supersonic transport sonic boom theory and effect reduction, discussing Whitham rule, bow shock, overpressure, engine and aircraft design and shock wave control 16 p2843 A70-34263
- Multiphase modes for nonlinear dispersive waves under large scale interaction, extending Whitham theory 23 p4217 A70-43943
- WHITTAKER FUNCTIONS**
- Wolf numbers Zurich time series monthly values, evaluating mathematical expectation with probability smoothing by Whittaker operator 15 p2802 A70-32489
- WICKS**
- Na heat pipe with wick structure consisting of wire rods observed for ease of wick rewetting, dryout limit reproducibility, etc 01 p0216 A70-10967
- [AICHE PREPRINT 7] Dry and water-saturated sintered fiber metal wick thermal conductivity, obtaining semiempirical correlations for solid and fluid phases and void fraction 21 p3945 A70-41041
- WIDE ANGLE LENSES**
- Wide angle electronic camera for astronomical photometry designed to seek photometric standard stars remote from nebular regions 09 p1681 A70-23313
- Aerial super wide angle photography for mapping, discussing cost reduction, accuracy requirements and photographic techniques 10 p1891 A70-24756
- Fisheye projection of undistorted images obtained by fisheye lenses onto spherical screen from spherical center for hemispheric display, minimal overhead occlusion, etc 10 p1892 A70-24951
- Lens systems configuration and aberration, determining suitability for wide angle oculars of Galilean telescopes 19 p3420 A70-37262
- WIDEBAND**
- U BROADBAND**
- WIDEBAND COMMUNICATION**
- Man machine system consisting of manned station controlling distant spacecraft via wideband radio link 02 p0229 A70-12145
- Wideband satellites bandwidth and aperture limits direct measurement based on ground monitoring of CW signals, taking into account ionospheric dispersion 02 p0261 A70-12577
- Transversal equalizer for wideband radar systems distortion reduction 02 p0261 A70-12578
- Remote data processing and wideband data transmission between France and U.S. via telecommunication satellites, discussing error detection and correction 02 p0263 A70-12612
- Phase distortion and Faraday rotation of wideband radio waves propagating through ionosphere 03 p0449 A70-13584
- Incoherent reception of wideband signals transmitted through multibeam channel with changing random parameters 05 p0812 A70-16248
- Wideband transmission of photographic reconnaissance information over long distances using Initial Defense Communication Satellite Program satellites 06 p1006 A70-17346
- AM baseband telemetry system for wideband signal transmission emphasizing SSB, DSB and quadrature multiplexed DSB modulation techniques 06 p1007 A70-17435
- Wideband cophased horizontal antennas with active dipole reflector arrays, describing feeder arrangements involving use of resistors 06 p1021 A70-17673
- Optical transmission technology for aerospace launch operations investigated on wideband communication systems projects involving use of gallium arsenide lasers and diodes 09 p1640 A70-23776
- Wideband transmission media for global communication networks, comparing submarine cables and satellites based on economic tradeoff in terms of circuit density and distance 11 p2001 A70-25475
- Low noise wideband uncooled preamplifier for small unattended satellite communication terminals, discussing theory, design and performance 11 p2016 A70-25485
- [AIAA PAPER 70-419] Superwideband dipole antenna array reproducing radiation patterns in horizontal plane for signal polarization 12 p2196 A70-27539
- Single and multistage parametric amplifiers for broadband communications, noting nonideal circulator characteristics by scattering parameter and signal flow graph 12 p2197 A70-27933
- Wideband FM signals transionospheric propagation, calculating output spectrum, signal to distortion ratios and signal to noise ratios 13 p2367 A70-29588
- Earth resources satellite real time wideband relay communication link to ground station 13 p2368 A70-29614
- [AIAA PAPER 70-326] Wideband PCM/FM discriminator detection, predicting effects of predetection and postdetection filtering on system performance 14 p2558 A70-31192
- Traveling wave light modulator with 15 GHz bandwidth using cubic ZnS crystal with anomalous response 16 p2876 A70-33403
- Wideband analog signal data transmission, evaluating messages accuracy in terms of error probability 18 p3228 A70-36623
- Satellite wideband transmission of ionosphere data, monitoring amplitude and phase of phase-coherent CW signals from geostationary satellite 20 p3590 A70-40483
- Space-to-ground link wideband digital laser communications system design and performance tests 21 p3787 A70-41331
- Wideband millimeter wave communications experiments for satellite applications, considering ATS-5, radiometry and future lunar base 21 p3787 A70-41337

Wideband detection of FSK transmissions in three component two path channel, obtaining channel bit error probability 21 p3792 A70-42176

WIDMANSTATTEN STRUCTURE
Widmanstatten structure in iron meteorites relationship to cooling rate and meteoritic origin 04 p0751 A70-15039
Fe-Ni-P phase diagrams for high temperatures, providing phase equilibria data for Widmanstatten pattern in iron meteorites 15 p2762 A70-32391

WIDTH
Width corrections in calculation of stress intensity factor for sheet with central crack in uniform uniaxial tension 13 p2510 A70-28608

WIENER HOPF EQUATIONS
Wiener-Hopf equation development and Kalman filter derivation using Leibnitz equation for differentiating integral 04 p0660 A70-15338
Stick-slip problem for motion of free jet at low Reynolds numbers by Wiener-Hopf technique, considering two dimensional Newtonian jet without gravity 11 p2041 A70-26554
Open waveguides and small horns theory, using Wiener Hopf method for radiation calculation 17 p3051 A70-35065
Axisymmetric potential problem of plane circular electrified disk in coplanar gap formulated in triple integral equation, obtaining Wiener-Hopf solution 22 p4080 A70-42632

WIGHTMAN THEORY
U FIELD THEORY (PHYSICS)
U QUANTUM THEORY
U RELATIVISTIC THEORY

WINCHES
Helicopter hoist rescue system, considering helicopter power, cable length, pilot visibility, etc 09 p1610 A70-22341

WIND (METEOROLOGY)
NT GEOSTROPHIC WIND
NT GUSTS
NT JET STREAMS (METEOROLOGY)
NT SQUALLS
NT WINDS ALOFT
Derived winds, wind shears and densities accuracies obtained by radar meteor trail technique 07 p1237 A70-20281
Wind and atmospheric temperature variations on Mars, Venus and Mercury interpreted from observational data in terms of earth atmospheric processes 09 p1762 A70-23127
Statistical analysis of atmospheric wind and temperature variables relationships to high altitude clear air turbulence observed by U-2 flights 12 p2264 A70-28092
Tidal forces effect on wind system in lower ionosphere, using Navier-Stokes equation for lower layer and Euler equations for upper layer 14 p2571 A70-30232
Ionospheric investigation techniques, considering ionization balance, winds and turbulence 14 p2580 A70-31259
Atmospheric temperature and wind data before, during and after solar eclipse of 7 March 1970, using ARCAS meteorological rockets 16 p2977 A70-33828
Tidal forces effect on wind system in lower ionosphere, using Navier-Stokes equation for lower layer and Euler equations for upper layer 24 p4331 A70-46307

WIND CIRCULATION
U ATMOSPHERIC CIRCULATION

WIND DIRECTION
Zonal circulation model of atmosphere below altitude of 200 km using rocket, meteor and ionospheric drift observations 02 p0328 A70-12388
Momentum considerations in thunderstorm dissipation by disrupting organized cloud base updraft structure 06 p1100 A70-18570
Vertical wind distribution associated with thunderstorm outflow, measuring wind direction oscillations at Kennedy Space Center 06 p1101 A70-18576
WINDAV anemometer used as low power wind direction and velocity transducer for tethered balloon 08 p1494 A70-20822
Numerical procedure for determining horizontal wind from geopotential height in barotropic model, discussing solutions for resultant simultaneous equations 08 p1540 A70-21968
Wind HF inclination variations in lower atmosphere, considering turbulent kinetic energy dissipation and buoyancy production 09 p1714 A70-22355
Stratospheric equatorial wind period phases correlation with central European westerlies frequency, intensity and persistency, noting seasonal differences 10 p1913 A70-24950

Pulsed Doppler radar technique for monitoring and diagnosing severe storms, obtaining wind velocity and direction within cloud 10 p1844 A70-25242
Wind velocity and direction and diffusion coefficients measurements by artificial luminous clouds, injecting appropriate reagents from rockets 11 p2075 A70-25918
Wind distribution by wind frequency counter controlled by electrical direction indicator, discussing design, operation and accuracy 13 p2445 A70-29469
Wind velocity and direction determination from artificial luminous clouds photographs, calculating topocentric coordinates 18 p3252 A70-36991
Hovercraft wind directional stability and control by cam operated fin-tab assembly 19 p3357 A70-38942
Cloud motions from IR measurements within overlap region of adjacent Nimbus II orbits compared with wind vectors from constant pressure charts 20 p3665 A70-40068
Wind directions in free atmosphere and on ground, discussing deflections by orographical factors in Upper Rhine plain 22 p4065 A70-43245
Vertical velocity effects on ionospheric horizontal wind magnitude and direction, solving integral equations system by successive approximations 23 p4188 A70-44057

WIND EFFECTS
Diurnal variation for structure and energy balance of thermosphere, noting effect of global wind pattern 01 p0074 A70-10592
Aerodynamic load distribution due to wind action on elastic structures, calculating various ratios between wind and critical divergence velocity 02 p0385 A70-11913
Atmospheric effects on SST, discussing turbulence, temperature, wind, cloud cover, hail, toxic gases, etc 02 p0325 A70-12218
Atmospheric environment features bearing on supersonic transport aircraft operations and forecasting, discussing wind and temperature effects 02 p0325 A70-12220
Electromagnetic drifts and neutral air winds effects on F 2 region derived from electron continuity equation, using Jacchia model atmosphere 04 p0677 A70-14966
Slender delta wing aircraft dynamic behavior under vertical and lateral gusts, particularly during landing approach [DGLR-69-52] 04 p0623 A70-15145
Unsteady flows effects on aircraft longitudinal motion, flight stability and control, discussing horizontal and vertical effects of rough air 04 p0623 A70-15172
Numerical method for calculating gust effect on wing of complex planform at subsonic speeds by converting continuous to discrete processes 04 p0618 A70-15242
Radar signal amplitude fluctuations reflected from disturbed sea water surface, noting wind induced waving stochastic nature influence 05 p0812 A70-16246
Atmospheric turbulence characteristics related to drag loads of tall spacecraft structures by boundary layer wind model 06 p1160 A70-17165
Wave surface elevation and velocity fluctuations in ocean upper layer under wind waves, discussing correlation coefficients between vertical and horizontal velocity components 06 p1097 A70-17792
Slender body theory for steady state aerodynamic characteristics of high speed ground vehicles with arbitrary cross sections, discussing side wind [AIAA PAPER 70-139] 06 p0973 A70-18155
Sporadic E layer formation by vortical winds, discussing effect on ionospheric electron concentration distribution 07 p1267 A70-19454
Wind compensation for wind effects with elevation angle in ballistic rocket launching problems 07 p1394 A70-19718
Cosmic rays effect on atmospheric temperature and wind, discussing planetary distribution of neutron component of radiation intensity 07 p1373 A70-20346
Statistical characteristics of random wind effects on radio telescopes tracking cosmic object 08 p1586 A70-21062
Glider pilots flight above cloudstreets in clear sky, discussing situation for wave soaring over flat ground 10 p1805 A70-24583
Ionospheric plasma drift vertical and meridional velocity components latitudinal distributions in F 2 region, considering wind effects in upper atmosphere 11 p2045 A70-25931
Saturation of self induced thermal lens resulting from thermal distortion of carbon dioxide laser radiation in wind 11 p2063 A70-26401

Correction factor for finite span effect on unsteady wing lift or moment during sinusoidal gusts or vertical oscillations 12 p2155 A70-27200
Booster control system reducing maximal wind-induced bending torques, examining booster response to aerodynamic forces 13 p2500 A70-28413
Stochastic processes optimal control theory application to launcher attitude control under wind disturbance 13 p2501 A70-28428
Wide range wind compensated launcher settings for unguided rockets using wind-weighting model and iterative procedure requiring real time computation 13 p2503 A70-28528
Thrust vector control application to Skylark vehicle to eliminate wind and thrust misalignments effects 13 p2503 A70-28676
Aeronautical navigation under various wind velocity conditions, studying flight times for closed flight paths 13 p2448 A70-28750
Collection of papers on wind effects on launch vehicles covering aerodynamics, airframes, guidance and control, wind-vehicle interactions, atmospheric turbulence, etc [AGARDOGRAPH-115] 13 p2504 A70-28751
Wind load aerodynamics effects on launch vehicle flight control systems design [AGARDOGRAPH-115] 13 p2504 A70-28753
Stability and wind response determining spacecraft structure forces and bending moments [AGARDOGRAPH-115] 13 p2504 A70-28754
Wind effects on rigid launch vehicle guidance and control system design, using model incorporating structural bending and fuel sloshing [AGARDOGRAPH-115] 13 p2448 A70-28755
Wind-launch vehicle interaction in flight, using equations of motion for aerodynamic loads [AGARDOGRAPH-115] 13 p2504 A70-28756
Spacecraft parameters role in response to atmospheric disturbances, considering model design and control systems effects [AGARDOGRAPH-115] 13 p2504 A70-28757
Horizontal geomagnetic force variations, considering ionospheric wind effects on ions in transition layer 13 p2402 A70-30057
Sun glitter on sea surface from space photographs, considering wind and sea conditions effect on shape and brightness of patterns 14 p2572 A70-30345
Aerodynamic and structural configuration effects on spacecraft inflight wind load calculations, showing Apollo interface lateral bending 14 p2653 A70-30585
Space vehicle response to in-flight wind turbulence, describing operational procedure for launch advisability determination 14 p2653 A70-30587
Launch vehicle design, considering tradeoffs between wind effects and analysis time 14 p2653 A70-30589
Neutral winds effect on F region vertical ion drifts derived from continuity equation, noting diurnal and seasonal variations 14 p2574 A70-30738
Lower ionosphere electron densities seasonal variations relationship to atmospheric circulation 14 p2574 A70-30742
Kelvin wave propagation numerical model, showing influence of mean zonal wind vertical and horizontal shear in lower stratosphere 15 p2771 A70-32370
Solstitial solar quiet currents along magnetic lines of force in magnetosphere, discussing ionospheric wind asymmetry effects 17 p3077 A70-34949
Ionospheric E region winds correlations to lower atmosphere meteorological phenomena 17 p3077 A70-34950
Nighttime E region molecular ion production rate estimation, taking into account windshear effect 18 p3245 A70-36022
Sporadic E layer formation by vortical winds, discussing effect on ionospheric electron concentration distribution 18 p3249 A70-36928
Ionospheric electric current distribution response to horizontal wind induced emf, using lunar tidal wind models 19 p3415 A70-38386
Isolated cumulus clouds formation numerical simulation, determining movement rates relationship to external wind speed 19 p3463 A70-38756
Automatic control systems for aircraft approach to landing path and subsequent stabilization on trajectory, compensating for cross wind action and radio noise disturbances 20 p3561 A70-39842
Gust field in lowest atmospheric layer over homogeneous terrain, deriving statistical models and simulating effects on XV-5 V/STOL aircraft 21 p3750 A70-40784

WIND MEASUREMENT

Aircraft flying at constant speed in circular orbits, calculating flight path under effect of uniform velocity wind 21 p3750 A70-40920

Aeolian regime of Venus surface resulting from high surface temperature and pressure, discussing spurious radar echoes, dust and sand transport and deposition 21 p3885 A70-40929

Gliding parachute air cargo systems using nonproportional and proportional automatic manual control, estimating wind effects on ground track and impact computer simulation [AIAA PAPER 70-1193] 21 p3753 A70-41823

Ionospheric electric field origin theory in terms of charge separation due to neutral wind drag 22 p4016 A70-42785

Aircraft control, considering wind gradient effects on takeoff, ascent and overflight conditions 22 p3962 A70-43082

Thermal defocusing and deflection of light beam by lateral wind effect in absorbing media 23 p4200 A70-43950

Wind induced modification of E region ionization density profiles, using coupled continuity equations for ion species 23 p4214 A70-44040

Wind generated water waves spectral characteristics at low momentum levels 23 p4215 A70-44273

Mathematical modeling of atmospheric gusts in stratosphere, mountain wave and thunderstorm conditions relevant to aircraft design 24 p4371 A70-45420

WIND MEASUREMENT

NT WIND VELOCITY MEASUREMENT

Vertical wind observations during lower ionosphere wind measurements by Na release method, discussing gravity effects and standing waves 01 p0078 A70-11213

Crosspath wind motion measurement by dual arm noncoherent bistatic radio troposcatter link 02 p0326 A70-12290

Incomplete historical data to infer state of atmosphere based on global circulation model, noting tradeoff of temperature for wind and time for space 02 p0291 A70-12296

Response characteristics of height-based and time-based wind reduction techniques for meteorological rocketsondes 05 p0879 A70-17101

Remote sensing of winds and atmospheric turbulence by cross correlation of passive optical signals, discussing results for power spectrum of fluctuations and winds 06 p1072 A70-18553

Meteorological data from radiosonde and radar wind observations during Indian Ocean expedition of research vessel Meteor 07 p1329 A70-19350

Acoustic piezoceramic anemometer for steady state measurements of wind turbulence on meteorological tower 07 p1285 A70-19835

Winds above 200 km measured from vapor trail observations compared to winds deduced from satellite orbital changes and theoretical models 07 p1269 A70-19950

PWN-8B meteorological rocket system for synoptic investigation of stratospheric circulation, describing sensor system deployment for descent measurements of wind and temperature 07 p1395 A70-20255

Kookaburra meteorological rocket system for sounding stratospheric circulation, describing instrument payload deployment for descending wind and temperature measurements 07 p1395 A70-20257

Rocket-borne radar chaff wind sensor synoptic application above 65 km, describing low fall velocity 07 p1237 A70-20258

Parachute wind sensors used in Arcas and Loki sounding rocket systems for stratospheric sounding, describing position data acquisition via radar tracking 07 p1395 A70-20259

ROBIN superpressure mylar spherical falling balloon deployed from sounding rocket apogee for density and wind measurements via radar tracking 07 p1194 A70-20260

Meteorological rockets fired in Spain, obtaining stratospheric wind and circulation data 07 p1396 A70-20278

Numerical procedure for determining horizontal wind from geopotential height in barotropic model, discussing solutions for resultant simultaneous equations 08 p1540 A70-21968

Atmospheric boundary layer wind and temperature analysis according to similarity scheme for mathematical modeling of atmosphere 08 p1540 A70-21974

Aerodynamic subsonic and supersonic wind tunnels parameter measurement methods including static and total pressure, current direction, velocity, density, etc 09 p1674 A70-22314

Wind HF inclination variations in lower atmosphere, considering turbulent kinetic energy dissipation and buoyancy production 09 p1714 A70-22355

Tower influence of wind speed and direction measurements, comparing 150 meter meteorological tower and scale wind tunnel model 09 p1661 A70-22964

Boundary layer atmospheric turbulence at Kennedy Space Center obtained for engineering spectral model, discussing energy balance 10 p1911 A70-23926

Kalman filtering applied to moving balloon position and velocity estimates related to upper atmosphere wind measurements by balloon-satellite experiment 11 p2025 A70-26206

Remote monitoring of atmospheric wind and turbulence by cross correlation passive techniques, measuring heat and humidity fluxes 12 p2230 A70-26948

Spatial-temporal distribution of wind swell HF components measured by two dimensional antenna array fed by DC signals 12 p2263 A70-27516

Velocity distribution and structure of irregular winds near 100 km measured by differencing chemical release wind profiles 12 p2264 A70-28002

Sounding rockets impact dispersion associated with wind measurement errors and thrust misalignments, discussing correction via reduced aerodynamic stability and initial rocket spin 13 p2503 A70-28677

Upper atmospheric wind evaluation in radar measurements by radio sounding technique, discussing equipment design 13 p2445 A70-29468

Wind distribution by wind frequency counter controlled by electrical direction indicator, discussing design, operation and accuracy 13 p2445 A70-29469

Wind measurement with two spaced coherent-pulse radar stations for probing same region of meteor zone 14 p2582 A70-30317

FPS-16/Jimsphere wind profiles measurement, discussing effect of data smoothing on accuracy and resolution 14 p2607 A70-30569

Three camera method for studying upper atmosphere winds via smoke trails providing wind velocity, earth coordinate data and error indication 14 p2607 A70-30572

Parachute altitude wind sensor /PAWS/ project for real time wind profile determination, using modified HASP I sounding rocket 14 p2585 A70-30577

Mesospheric levels wind oscillations in Spanish range of Arenosillo measured by meteorological rockets during February 1970 15 p2723 A70-31653

Continuous variation measurements of wind tunnel parameters minimizing testing time, discussing flow characteristics measurements during angle of attack variation 17 p3057 A70-34775

High altitude clear air turbulence structure and evolution examined by high power radar and wind and temperature vertical soundings 18 p3228 A70-36483

Upper atmosphere wind, density, temperature and pressure from Soviet meteor data 19 p3412 A70-37651

Radiosonde technique for locating atmospheric turbulence regions and estimating vertical air movement component in associated gusts 19 p3427 A70-38246

Wind speed pulsations measurement at atmospheric boundary layer and different heights, analyzing turbulent energy intensity 19 p3463 A70-38757

Wind motions from meteor trails observation during IQSY, tabulating amplitudes and phases of constant, diurnal, semidiurnal and 8-hr components 19 p3526 A70-38788

Highly localized clear air turbulence at aircraft flight level over Mediterranean, noting simultaneous temperature rise 19 p3463 A70-38948

High altitude wind measurement during daytime using photometer for detection of Li trail 20 p3630 A70-39486

Acoustic piezoceramic anemometer for steady state measurements of wind turbulence on meteorological tower 20 p3634 A70-40342

Wind temperature measurement, taking Bernoulli effect and kinetic theory into account 22 p4009 A70-42525

Ocean roughness determination from satellite photographs sunglint patterns, indicating surface wind speeds 22 p4014 A70-42770

Wind tunnel response tests of cup, vane and propeller wind sensors, determining wind direction

and speed parameters, damped and natural frequencies, etc 22 p4030 A70-42914

Gyro system determining aerodynamic moment integral vector in wind measurements 24 p4340 A70-46402

WIND PRESSURE

Coriolis parameter effects on stream and pressure functions in geostrophic wind equation 22 p4065 A70-43167

WIND PROFILES

Spherical earth wind field correlation matrix, relating scalar fields to isotropic vector field 01 p0135 A70-10204

Cape Kennedy vertical wind speed profiles measured by spectral analysis using fast Fourier transform method 02 p0325 A70-12285

Solar daily atmospheric oscillations from pressure, wind and temperature recordings at ground level, discussing seasonal and worldwide variations of daily component 06 p1053 A70-17307

Turbulence characteristic scale for atmospheric boundary layer, using wind profile data 06 p1096 A70-17466

Vertical wind distribution associated with thunderstorm outflow, measuring wind direction oscillations at Kennedy Space Center 06 p1101 A70-18576

Level flight optimization in horizontal wind varying with altitude, using glider concept and induced drag correction [ONERA-TP-700] 07 p1193 A70-19131

Quasi-biennial, annual and semiannual zonal wind and temperature harmonic amplitudes and phases in tropical and extratropical latitudes in stratosphere and low mesosphere 07 p1269 A70-19949

Prognostic maps of geopotential and wind in middle troposphere derived from hydrodynamic equations 07 p1330 A70-20307

Turbulence coefficient and profile in atmospheric boundary layer from wind and temperature distribution, obtaining formulas from model approximating coefficient by altitude function 08 p1538 A70-21112

Vertical wind profiles, deriving wind shear-layer thickness exponential relationship 09 p1715 A70-22356

Ionospheric wind velocity fields calculated from atmospheric dynamo effects taking into account electric field, current density and conductivity tensor 10 p1881 A70-24819

Pressure gradient, wind structure and shearing stress in atmospheric boundary layer related by formulation based on quasi-parallelism and boundary condition at Ekman layer top 11 p2076 A70-26071

Lower atmospheric layer temperature and wind vertical distribution effect on wind velocity ratio to geostrophic wind at earth surface 13 p2444 A70-28586

CAT parameters sensitivity to horizontal wind and temperature distribution 13 p2444 A70-28587

Wind field statistical properties using model incorporating quasi-steady state speed, shear, gusts and small scale motions [AGARDOGRAPH-115] 13 p2444 A70-28752

Variangular wind spirals for vertical wind and shear profile estimation in atmospheric boundary layer 14 p2602 A70-30370

FPS-16/Jimsphere wind profiles measurement, discussing effect of data smoothing on accuracy and resolution 14 p2607 A70-30569

Parachute altitude wind sensor /PAWS/ project for real time wind profile determination, using modified HASP I sounding rocket 14 p2585 A70-30577

Cape Kennedy peak wind profile probabilities at 10-150 meters for various exposure times 14 p2607 A70-30581

Thunderstorm bottom wind profile model, analyzing flow distribution, isotach, isogon and isotherm characteristics 14 p2607 A70-30584

Wind profiles derivation for environmental influence upon missile systems design, limiting bulky input into computer programs 14 p2608 A70-30586

Balloon-radar soundings of horizontal wind profiles for booster vehicle design 14 p2653 A70-30588

Vertical mesoscale contribution to vertical wind shear profiles, using radar/Jimsphere measurements 14 p2609 A70-30599

Atmospheric wind profiles and boundary layer turbulence power spectra for calculation of wind loads on space vehicles during prelaunch and launch 14 p2653 A70-30600

Wind field reduction from satellite cloud structure data 15 p2770 A70-32066

Planetary wind field from observed pressure field by linearized balance equation, assuming solenoidal air motion

20 p3662 A70-39178

CAT as mechanism relieving wind and temperature discontinuities, maintaining Richardson number at limiting value by turbulent energy dissipation

20 p3663 A70-39373

Longitudinal and vertical wind components turbulent fluctuations distribution skewness relationship to atmospheric stability and height, noting effect on diffusion

20 p3664 A70-40064

Jimsphere wind profiles gust variance and spectrum densities for horizontal wind speeds viewed by Saturn vehicle

21 p3847 A70-41878

Aircraft control, considering wind gradient effects on takeoff, ascent and overflight conditions

22 p3962 A70-43082

Statistical interpolation for numerical analysis of middle troposphere AT potential based on geopotential and wind observations

24 p4371 A70-45135

Neutral air winds in ionospheric F region for asymmetric global pressure system, including ion velocity correction

24 p4329 A70-45356

Meteorological wind and temperature distributions on selected routes at Concorde cruising level, noting computer use for flight planning

24 p4374 A70-46204

WIND SHEAR

Diurnal variations in sporadic E layer and wind in ionosphere during equinox and solstice periods, noting wind shear mechanisms and ambient electron density

01 p0084 A70-11552

E layer kinetic energy viscous dissipation and transfer to potential energy by turbulence and irregular winds shear

02 p0327 A70-12292

Doppler radar spectrum mean and variance derived for reflectivity gradients combined with linear wind shear velocity gradient

02 p0328 A70-12508

Deflecting forces on nonrotating convecting systems due to environmental shear, comparing magnitude to rotation forces

06 p1100 A70-18571

Derived winds, wind shears and densities accuracies obtained by radar meteor trail technique

07 p1237 A70-20281

Sheared frontal zones structure and stability, studying Richardson number limiting role in free atmosphere

08 p1492 A70-21971

Vertical wind profiles, deriving wind shear-layer thickness exponential relationship

09 p1715 A70-22356

Acoustic gravity waves horizontal ducting in atmosphere with spatially periodic wind shears

09 p1671 A70-23498

Wind shear caused ionospheric E region irregularities investigated by horizontal plasma density gradients determination

11 p2045 A70-25652

High altitude meteor winds, investigating atmospheric tides and short term wind oscillations, wind shears and drift nature

14 p2601 A70-30122

Variangular wind spirals for vertical wind and shear profile estimation in atmospheric boundary layer

14 p2602 A70-30370

Strong wind and vertical wind shear in upper stratosphere and mesosphere

14 p2608 A70-30594

Vertical mesoscale contribution to vertical wind shear profiles, using radar/Jimsphere measurements

14 p2609 A70-30599

Wind shear production rate by dynamical processes and relationship to clear air turbulence occurrence

14 p2609 A70-30601

Kelvin wave propagation numerical model, showing influence of mean zonal wind vertical and horizontal shear in lower stratosphere

15 p2771 A70-32370

Aerodynamic admittance of paraboloid dish aerial in scaled atmospheric turbulent boundary shear layer simulated in wind tunnel by vortex generators

16 p2878 A70-33766

CAT shear spectra above ground frictional layer in jet stream flight conditions, using aircraft measurements

16 p2946 A70-33825

CAT at subsidence inversion in presence of strong wind shear, noting radar echo pattern as Kelvin-Helmholtz instability indicator

17 p3133 A70-35933

Nighttime E region molecular ion production rate estimation, taking into account windshear effect

18 p3245 A70-36022

Two dimensional stratified flow over extended obstacles with source disturbances, indicating topographical effect on vertical wind shear in troposphere

23 p4214 A70-44031

WIND TUNNEL APPARATUS

NT WIND TUNNEL DRIVES

NT WIND TUNNEL NOZZLES

Pre-set Mach number control in supersonic wind tunnel, evaluating effects of nozzle installation, stagnation temperature drop and pressure errors

06 p1028 A70-17912

French H630 hypersonic wind tunnel operating at Mach 8, discussing test results and potential

15 p2718 A70-32839

Electrodeless traveling wave accelerator for wind tunnel use, determining gas stream density for subsonic and supersonic operation

16 p2889 A70-33868

Hypersonic velocity and turbulence measurements in wind tunnels, using spectral analysis of Doppler shifted laser light

17 p3103 A70-34849

Wind tunnel balance for measuring small aerodynamic loads on scale models, describing three component construction

17 p3062 A70-35490

On-line final V/STOL Wind Tunnel Data Encoding and Evaluation System /WINDEE/ for complex powered models, using computer monitoring

17 p3049 A70-35494

Digital computer six degree of freedom wind tunnel separation simulator for air launched missile trajectory analysis

17 p3063 A70-35509

Digital computer for high speed wind tunnel data acquisition, processing and operations control

19 p3397 A70-37923

High speed holographic recording of transient events by single shot ruby and Nd-doped pulsed lasers, applying to shock tubes and wind tunnels [SMPT PREPRINT 3]

22 p4035 A70-43056

WIND TUNNEL BALANCES

U WEIGHT INDICATORS

U WIND TUNNEL APPARATUS

WIND TUNNEL CALIBRATION

Characteristics and calibration of flow in gas induction driven close return transonic wind tunnel

11 p2030 A70-25687

Calibration tests in transonic wind tunnel with two and four sided perforation section

19 p3353 A70-38475

WIND TUNNEL DRIVES

German aeroballistic hypersonic test facility with moving model and rest atmosphere, describing acceleration mechanism and several tests

06 p0965 A70-17246

Crossed field plasma accelerator designed as element of hypersonic wind tunnel driver

06 p1119 A70-17471

Wind tunnel experiments for apparent reverse transition during expansion fan and turbulent boundary layer interaction, discussing Reynolds stresses

07 p1257 A70-19345

Characteristics and calibration of flow in gas induction driven close return transonic wind tunnel

11 p2030 A70-25687

Real hydrogen driver performance, analyzing intermolecular forces effects under high compression and heat

16 p2998 A70-33889

Shock tube facility with high explosive driver for reentry flow conditions simulation of manned planetary flights

21 p3804 A70-40849

WIND TUNNEL MODELS

Thermal protective device for models exposed to flow buildup in intermittent wind tunnel, offering straightforward design, easy applicability, low cost and favorable experimental conditions

03 p0463 A70-13627

Pitot boundary layer probes with position indicators using extensometric gages for boundary layers on wind tunnel test models

03 p0487 A70-13628

Flutter investigation on model designed and constructed for tail unit of HFB 320 Hansa jet aircraft, discussing classical and statistical methods

04 p0775 A70-15180

Rocket exhaust plume size determined from schlieren photographs during wind tunnel tests, noting agreement with Hill-Habert theory

04 p0736 A70-15417

Hypersonic slender wake mean flow properties behind two dimensional slender body wind tunnel models at zero angle of attack

04 p0621 A70-15578

Blockage and wall corrections proposed for obtaining uniform results from low speed wind tunnel models

05 p0789 A70-15812

Wind tunnel testing technique innovations, reducing time and cost for low drag aircraft configurations by simultaneous force and pressure model transonic testing

05 p0825 A70-15868

Wind tunnel tests of isentropic inlet diffusers, describing two dimensional model, test apparatus and modification and results

06 p0963 A70-17235

Holography for visualization and analysis of aerodynamic flow fields in wind tunnel experiments, recreating events in space and time

08 p1493 A70-20650

Flow turbulence in wind tunnel model tests, observing generation methods effect on aerodynamic flow characteristics distribution

08 p1483 A70-21074

Tower influence of wind speed and direction measurements, comparing 150 meter meteorological tower and scale wind tunnel model

09 p1661 A70-22964

Optical tools in aeronautical and space research at Langley Research Center, discussing schlieren photography of aeronautical and space models in wind tunnels

09 p1657 A70-23510

Consumable protective coat /silastene/ application to reentry models to eliminate metallic pollution in hotshot wind tunnels for spectroscopic analysis

10 p1825 A70-24548

Low speed buffet intensity under pressure fluctuations on slender wing aircraft at vortex breakdown, using wind tunnel model

10 p1963 A70-25067

Small scale and full scale wind tunnel and flight test data correlated for Lear jet aircraft [SAE PAPER 700237]

11 p1981 A70-25906

Free fall vehicle dynamics for wind tunnel measurements of research shapes used in computer simulation of vehicle trajectories

12 p2157 A70-28081

Freely spinning finned stabilizer static wind tunnel tests on free fall research store, determining Magnus effect, body flow interference and static stability

13 p2340 A70-29024

Wind tunnel boundary interference on V/STOL model calculated in test section with solid vertical and slotted horizontal walls, using image method and Fourier transforms

13 p2343 A70-29894

Tilt wing-propeller VTOL model, comparing static wind tunnel with moving-track test data based on coefficient forms of freestream and slipstream dynamic pressures

13 p2343 A70-29895

Unsteady aerodynamic forces on oscillating circular cylinder, using wind tunnel two dimensional dynamic model

14 p2529 A70-31050

Static and dynamic stability of wind tunnel models with flexible support, considering binary rigid body freedoms

14 p2564 A70-31398

Wind tunnel tests of flow past oblate ellipsoid of revolution incident on major axis, measuring pressure distribution

15 p2671 A70-31494

Hypersonic flow field around yawed half angle cone from wind tunnel measurements including surface pressure distributions and flow visualization photographs

17 p3007 A70-34485

Free flight wind tunnel test for feasibility of hypersonic drogue deployment into reentry vehicle wake

17 p3060 A70-35195

Ultraminiature piezoelectric semiconductor pressure transducers for wind tunnel models

17 p3093 A70-35491

Ultraminiature pressure transducers for use in wind tunnel models

17 p3093 A70-35492

Low pressure measuring system for aerodynamic models tested in Mach 12-14 wind tunnel, discussing transducers and high speed digital recording and data processing system

17 p3062 A70-35493

Telemetry instrumentation for free flight wind tunnel models, discussing system component characteristics

17 p3047 A70-35495

Static weight tare compensation for V/STOL wind tunnel models, using accelerometer outputs

17 p3062 A70-35500

Minimal interference thin metal strap support system for dynamic stability tests of high fineness ratio wind tunnel models

17 p3063 A70-35657

Flow field on suction side of slender body of revolution with/without wings, investigating by directional probe in wind tunnel

17 p3013 A70-35924

Significant terms in equations of motion for parachutes inflating in free air and in wind tunnel experiments

18 p3213 A70-36449

Dynamic airfoil stall simulation in wind tunnels, considering pitch rate, Reynolds number, oscillation and test equipment effects

20 p3558 A70-39582

Hypersonic aerodynamic deceleration devices for axisymmetrical bodies with cylindrical main sections and various front sections, using gun tunnel techniques

21 p3746 A70-41839

- Attached Inflatable Decelerator for planetary atmospheric entry, discussing mission applications and wind tunnel models performance
[AIAA PAPER 70-1163] 21 p3931 A70-41848
- Dust content effect on hypersonic wind tunnel flow test results, noting drag force on slender and blunt nosed models
21 p3749 A70-42224
- Spark photography of models in free flight in hypersonic shock tunnel
[SMPT PREPRINT 99] 22 p4032 A70-43035
- WIND TUNNEL NOZZLES**
- Incompressible gas turbulent jet flow characteristics in subsonic wind tunnel, stressing pressure distribution in recirculation region for interpreting heat transfer in separated flows
03 p0593 A70-13495
- Transonic wind tunnel of aerodynamic research station in Goettingen, Germany, taking into account fixed nozzle replacement by flexible nozzle
03 p0463 A70-13799
- Undried atmospheric air humidity effect on pressure and water vapor supercooling in supersonic wind tunnel nozzles
09 p1606 A70-23613
- Laminar boundary layers in low density supersonic and hypersonic conical and axisymmetric nozzles, treating displacement, transverse curvature, velocity slip and temperature jump
[AIAA PAPER 69-653] 13 p2386 A70-28513
- WIND TUNNEL STABILITY TESTS**
- Wind tunnel investigated flow stabilization at horizontal control surfaces by vortex BCL technique, considering angles of attack, elevator deflection and shape
06 p0968 A70-17853
- Retrorocket effects on aerodynamic stability and drag of conical aeroshell planetary entry vehicles, discussing supersonic wind tunnel tests and jet shock interaction
[AIAA PAPER 70-219] 06 p0974 A70-18166
- Boeing 747 pretesting work including wind tunnel, components, engines and static structural tests, flight simulation, etc
08 p1437 A70-21730
- F-8D aircraft transonic flight and wind tunnel tests for buffet onset prediction, considering effects of g level and fluctuation amplitude and frequency
[AIAA PAPER 70-341] 09 p1611 A70-23020
- Wind tunnel study of entropy extremum upon critical streamline in supersonic three dimensional flow past blunt bodies at zero angle of attack
10 p1800 A70-24131
- Free fall vehicle dynamics for wind tunnel measurements of research shapes used in computer simulation of vehicle trajectory
[AIAA PAPER 69-229] 12 p2157 A70-28081
- Wind tunnel tests, analytical methods and fixed base simulation for predicting fighter aircraft spin characteristics
[AIAA PAPER 70-565] 13 p2346 A70-29030
- Transonic aircraft testing capabilities and limitations, considering tunnel wall interference and Reynolds number effects
[AIAA PAPER 70-580] 13 p2348 A70-29876
- Wind tunnel and flight test methods for determining transonic buffet characteristics on model F-4 aircraft
[AIAA PAPER 70-584] 13 p2348 A70-29886
- Three dimensional turbulent boundary layer development on rear of swept wing, comparing measurements with calculations
13 p2344 A70-30021
- Two-point suspension system with longitudinally displaced cargo hooks for handling helicopter loads, discussing wind tunnel and flight tests
17 p3014 A70-34714
- Minimal interference thin metal strap support system for dynamic stability tests of high fineness ratio wind tunnel models
[AIAA PAPER 69-350] 17 p3063 A70-35657
- Buoyant Venus station balloon for deployment and inflation during parachute descent into Venus atmosphere tested with scale model balloons in wind tunnels
17 p3063 A70-35658
- Nonequilibrium gas states evolution in detached wave front of hypersonic blunt body, comparing vibrational relaxation in free flight and wind tunnel flow
18 p3335 A70-35962
- Continuous surface of revolution parachute for supersonic/hypersonic speeds, performing wind tunnel tests
[AIAA PAPER 70-1173] 21 p3754 A70-41840
- Reefed and unreefed disk gap band parachutes tested in supersonic and subsonic wind tunnels to determine stability and performance
[AIAA PAPER 70-1172] 21 p3754 A70-41841
- Short wing lift investigated via lateral fluid jets fired in wind tunnel for various lengths
22 p3958 A70-42614
- Helicopter rotor tests in large wind tunnel for increased flight speed, noting pressure and noise measurements
[ICAS PAPER 70-44] 23 p4132 A70-44142

WIND TUNNEL WALLS

- Low speed wind tunnel test results correction program, considering solid, wake blockage, lift, static pressure gradient and wall interference effects
06 p0968 A70-17934
- Optimal V/STOL wind tunnel interference study of slotted tunnel walls, including porosity and height to width ratio effects
07 p1251 A70-20407
- Wind tunnel boundary interference on V/STOL model calculated in test section with solid vertical and slotted horizontal walls, using image method and Fourier transforms
13 p2343 A70-29894
- Subsonic boundary lift interference in wind tunnels with perforated walls, using point matching method
14 p2563 A70-30869
- V/STOL testing wind tunnel section with solid vertical and slotted horizontal zero interference walls
18 p3237 A70-36461
- Wind tunnel wall interference effects for V/STOL aircraft with lift jets, using modified theoretical model for complex jet arrangements
[ICAS PAPER 70-54] 23 p4139 A70-44150
- WIND TUNNELS**
- NT BLOWDOWN WIND TUNNELS
- NT CASCADE WIND TUNNELS
- NT COMBUSTION WIND TUNNELS
- NT HOTSHOT WIND TUNNELS
- NT HYPERVELOCITY WIND TUNNELS
- NT LOW DENSITY WIND TUNNELS
- NT LOW SPEED WIND TUNNELS
- NT PLASMA JET WIND TUNNELS
- NT SHOCK TUNNELS
- NT SLOTTED WIND TUNNELS
- NT SUBSONIC WIND TUNNELS
- NT SUPERSONIC WIND TUNNELS
- NT TRANSONIC WIND TUNNELS
- Ice tunnel testing facility at Naval Air Propulsion Test Center (NAPTC), describing methods, systems, instrumentation and various turbofan and turbojet engine tests
01 p0056 A70-10691
- Pulsed MHD accelerator for MHD wind tunnel application, discussing accelerator gas source, magnetic field and operation
[AIAA PAPER 68-370] 03 p0462 A70-12907
- Low turbulence wind tunnel axisymmetric contraction designed from reformulated Thwaites solution
03 p0462 A70-12935
- Sound propagation along cylindrical duct of wind tunnel, discussing fluid flow effect on modal cut-off frequencies
04 p0719 A70-15078
- Circulation controlled lifting rotor wind tunnel test results concerning factors affecting lift and drag
08 p1432 A70-21039
- Trisonic high pressure wind tunnel simulating flow conditions on large transonic aircraft, noting high Reynolds number capability
09 p1655 A70-22023
- Wake-boundary layer interaction in wind tunnel tandem cascades, discussing end wall suction
09 p1609 A70-23750
- Turbulent flow generation by interacting principal stream with transverse jets, obtaining flow domains in test chamber of two dimensional wind tunnel
10 p1870 A70-24785
- Air breathing engine testing at propulsion Wind Tunnel Facility at Arnold Engineering Development Center
11 p2031 A70-25852
- Self opening em-operated secondary and tertiary mylar diaphragms for expansion tubes and tunnels
11 p2031 A70-25982
- Turbulent boundary layer interaction with wavy wall in wind tunnel, discussing wall pressure drag and surface waves interaction
11 p2039 A70-26538
- Airfoil sections in transonic flow, discussing wind tunnel tests on mixed flows and shock waves
[ONERA-TP-815] 13 p2341 A70-29139
- Integrated computerized data acquisition and reduction system for aircraft flight and wind tunnel tests
13 p2373 A70-29156
- Wind tunnel interference for inviscid compressible conducting fluid on slender body of revolution, discussing disturbance potential
13 p2464 A70-29449
- Unsteady nonlinear aerodynamic loads measurements in wind tunnel, using linearized mathematical analog
[AIAA PAPER 70-573] 13 p2343 A70-29896
- Similarity and scaling between atmospheric and wind tunnel simulated shear flows near earth surface
14 p2602 A70-30369
- Atmospheric contaminants dispersion simulation in meteorological wind tunnel with capability to simulate thermally stratified boundary layers
17 p3065 A70-34496
- Continuous variation measurements of wind tunnel parameters minimizing testing time, discussing flow characteristics measurements during angle of attack variation
17 p3057 A70-34775

- German monograph on transonic plane flow past wavy wall in blocked wind tunnel covering flow theory, interferometric density measurements, etc
17 p3070 A70-35375
- ONERA low pressure wind tunnel equipped with electron beam probing device to visualize flows too rarefied for optical methods
18 p3210 A70-37208
- Ultraminiature pressure transducer for airplane model and inlet/engine subsystem in wind tunnel tests, considering design, calibration, environments, etc
19 p3430 A70-38523
- Runway test vehicle for lifting rotor performance in simulated forward flight, comparing with wind tunnel tests
19 p3402 A70-38611
- Laminar heating in hypersonic vehicles interior corners, analyzing helium tunnel heat transfer data for various intersecting wedge corners
20 p3737 A70-39700
- Simulated neutral atmospheric boundary layer measurements in wind tunnel, extending power spectral and correlation determinations
20 p3613 A70-40139
- Conducting fluid supersonic flow past slender body of revolution in circular wind tunnel under inclined magnetic field, investigating MHD interference problem
22 p3958 A70-42669
- European wind tunnels suitable for Post Apollo Program aerodynamic testing, presenting detailed tabulated information on available facilities
22 p4007 A70-43503
- NACA/NASA rotary wing aircraft research history 1915-1970, Part 3, covering rotor and helicopter theory, related flight and wind tunnel testing, etc
23 p4142 A70-44853
- WIND VANES**
- Remote recording wind vane using continuous and step rotary switch potentiometers suitable for automatic weather stations
06 p1062 A70-17619
- WIND VARIATIONS**
- Harmonic analysis of upper atmospheric wind periodic data from radar sounding of meteor trails, defining principal diurnal wind variations
01 p0134 A70-10201
- Wind oscillations in stratosphere, lower mesosphere and meteor heights noting periodicities
01 p0074 A70-10591
- Multifan cross wind jet engine test facility to produce variable wind velocity in various directions
01 p0056 A70-10698
- Thermospheric horizontal winds diurnal bulge, discussing maximum density-maximum temperature phase relationship
01 p0078 A70-11210
- Seasonal phase changes of semidiurnal tidal wind components in lower ionosphere demonstrated from ionospheric drift measurements
01 p0078 A70-11212
- F region ion velocity measurements by Thompson scatter probe, deducing neutral winds diurnal and seasonal variations in thermosphere
01 p0078 A70-11214
- Lunar atmospheric tidal wind semidiurnal variations from Hong Kong and Uppsala data, discussing agreement with theory
02 p0325 A70-12217
- Upper atmosphere wind and semidiurnal and diurnal tide interactions observed by meteor radar, noting relation to gravity waves
05 p0878 A70-15818
- Spatial variations in zonal and meridional components of stratospheric and mesospheric winds traced over horizontal distances by Arcas ROBIN rockets
07 p1274 A70-20275
- Wave disturbances in tropical lower troposphere, discussing cross spectrum analysis of wind, temperature, relative humidity and surface pressure
07 p1275 A70-20304
- Cup and vane anemometers theory, determining overestimation errors of differential equation for mean values in sinusoidally fluctuating winds
08 p1501 A70-21975
- Velocity distribution and structure of irregular winds near 100 km measured by differencing chemical release wind profiles
12 p2264 A70-28002
- Lower stratosphere temperature and wind periodic variations associated with shear flow gravity waves
14 p2601 A70-30124
- Mesospheric levels wind oscillations in Spanish range of Arenosillo measured by meteorological rockets during February 1970
15 p2723 A70-31653
- Wind velocity derivative statistical characteristics in atmospheric surface layer, using thermoanemometer, functional converter, differentiating circuit and loop oscillograph
16 p2945 A70-33219

Solar wind velocity variations showing relationship with electron density excess and localized region temperature of corona

19 p3512 A70-38693

Wind speed pulsations measurement at atmospheric boundary layer and different heights, analyzing turbulent energy intensity

19 p3463 A70-38757

Wind velocity derivative statistical characteristics in atmospheric surface layer, using thermoanemometer, functional converter, differentiating circuit and loop oscillograph

24 p4371 A70-45194

WIND VELOCITY

Four dimensional optimal interpolation for maximum wind velocity components, calculating spatiotemporal correlation functions

01 p0135 A70-10205

Multifan cross wind jet engine test facility to produce variable wind velocity in various directions

01 p0056 A70-10698

Doppler spectrum and radio troposcatter beam swinging in thin homogeneous turbulent scatter layer as function of height, crosswind speed and refractivity

02 p0326 A70-12288

Doppler radar spectrum mean and variance derived for reflectivity gradients combined with linear wind shear velocity gradient

02 p0328 A70-12508

Pulsation velocities distribution wind in meteor region of atmosphere during hourly intervals over eleven month period, noting normal distribution

06 p1095 A70-17206

Wind velocity measurements by coherent radar pulse method of meteor trail observations

06 p1141 A70-17739

Wind speed and potential temperature vertical profile in day/night planetary atmospheres estimated by similarity theory of boundary layer parameters

06 p1141 A70-17827

Electromagnetic-acoustic probe for remote wind velocity sensing and radar range performance

06 p1071 A70-18509

Aircraft design formulas for equivalent gust velocity compared with vertical acceleration form, discussing design problems for large jets and T-tailed configurations

06 p0988 A70-18589

Dust devil wind velocity relationship to environmental parameters including atmospheric temperature, wind direction and vorticity, etc

07 p1269 A70-19948

Solar wind velocity radioastronomical measurements, discussing radio wave fluctuations, telescope antenna designs, radiometers and observations

08 p1474 A70-21070

Vertical air motions rate from aerodynamic loads on aircraft and pitch angle and center of mass vertical velocity fluctuations

08 p1538 A70-21113

Atmospheric variables /velocity, temperature, energy, etc/ spectra in lowest few hundred meters

09 p1714 A70-22352

Time averaging and length of record effects on horizontal wind speed variance, determining maximum wind gusts as function of height and averaging time

10 p1909 A70-23928

Field-aligned plasma velocity dependence on plasma diffusion and wind velocity illustrated with model of night F 2 layer

10 p1881 A70-24814

Polar ionospheric current and interplanetary magnetic field directions related from mean diurnal values of solar wind velocity

11 p2044 A70-25551

Sound speed and horizontal wind velocity components determined in upper atmosphere from measured data of Rocket Grenade Experiment

11 p2121 A70-25678

Maximum wind velocity regions in tropospheric jet streams under synoptic conditions concerning troughs, ridge sections and cyclonic-anticyclonic curvatures

11 p2075 A70-25919

Solar wind magnetic field power spectra and plasma velocity, discussing turbulence, viscosity and dissipation

11 p2106 A70-26770

Corona point discharge current magnitude in transonic wind tunnel, giving current characteristics at different wind speeds

12 p2264 A70-28001

Lower atmospheric layer temperature and wind vertical distribution effect on wind velocity ratio to geostrophic wind at earth surface

13 p2444 A70-28586

Vertical and intensity distributions of wind velocity focuses in tropospheric jet streams

13 p2444 A70-28590

Aeronautical navigation under various wind velocity conditions, studying flight times for closed flight paths

13 p2448 A70-28750

Wind field statistical properties using model incorporating quasi-steady state speed, shear, gusts and small scale motions

[AGARDOGRAPH-115] 13 p2444 A70-28752

Wind velocity components on nonuniformly heated plane slope with linear periodic temperature function

14 p2602 A70-30165

Tropical storms and hurricanes critical winds forecasting accuracy by NASA Manned Spacecraft Center

14 p2606 A70-30558

Strong wind and vertical wind shear in upper stratosphere and mesosphere

14 p2608 A70-30594

Stabilized balloon flights during weak winds in stratosphere, discussing pressure vs time curves

14 p2531 A70-31311

Temperature profiles and wind velocities during convective cloud banks formation from meteorological satellite data

15 p2770 A70-32065

Atmospheric density from radar observations of meteor trails drift, using wind velocity semidiurnal components amplitudes

18 p3253 A70-36994

Isolated cumulus clouds formation numerical simulation, determining movement rates relationship to external wind speed

19 p3463 A70-38756

Wind speed pulsations measurement at atmospheric boundary layer and different heights, analyzing turbulent energy intensity

19 p3463 A70-38757

Cloud motions from IR measurements within overlap region of adjacent Nimbus II orbits compared with wind vectors from constant pressure charts

20 p3665 A70-40068

Atmospheric turbulence and wind velocity remote probing by millimeter waves, comparing results with conventional anemometer measurement

20 p3665 A70-40306

Polar ionospheric current and interplanetary magnetic field directions related from mean diurnal values of solar wind velocity

21 p3819 A70-41301

Jimsphere wind profiles gust variance and spectrum densities for horizontal wind speeds viewed by Saturn vehicle

21 p3847 A70-41878

Scintillation index correlation with mean wind velocity of jet streams

22 p4020 A70-43262

Large scale axisymmetric atmospheric vortex wind velocity determination, using statistical cloud data from meteorological satellites

22 p4065 A70-43376

E region winds response to solar radiation variations, including geomagnetism role

23 p4186 A70-43848

Air current in upper atmosphere meteor zone above equator, noting diurnal and semidiurnal harmonics in wind velocity components

23 p4188 A70-44049

Universal constant measurement methods in Kolmogoroff third hypothesis for high Reynolds number turbulence in wind over open ocean

23 p4184 A70-44980

WIND VELOCITY MEASUREMENT

Rotation periods of Jovian atmospheric currents showing zonal wind velocity variations with latitude

02 p0369 A70-11829

Wind field-Doppler velocity field generalized correlation, describing horizontal velocity component measurement by single pulse Doppler radar technique

02 p0326 A70-12287

Wind velocity longitudinal profile measurements in atmospheric boundary layer over rough sea surface using floating beacon and statistical analysis of airflow perturbations

04 p0715 A70-15253

Optical crossbeam technique for remote sensing of wind speeds, relating light fluctuations to convective wind velocity by space-time correlation methods

05 p0850 A70-16688

Remote recording wind vane using continuous and step rotary switch potentiometers suitable for automatic weather stations

06 p1062 A70-17619

Turbulent air flow velocities determined in meteor zone of atmosphere

07 p1386 A70-19461

Atmospheric wind velocity and temperature oscillations measurement using acoustic anemometer, resistance thermometer and multichannel signal spectrum analyzer

07 p1284 A70-19833

WINDAV anemometer used as low power wind direction and velocity transducer for tethered balloon

08 p1494 A70-20822

Lower atmosphere turbulence under convective conditions, comparing Doppler radar and instrumented aircraft wind speed fluctuation measurements

09 p1716 A70-22367

Oceanic wind and wave predictions by satellite radar radiometer using single receiver to determine wind velocity

[AIAA PAPER 70-310] 09 p1668 A70-22877

Nose cone modifications for Meteor-1 meteorological sounding rocket used for wind velocity measurements

09 p1767 A70-23406

Pulsed Doppler radar technique for monitoring and diagnosing severe storms, obtaining wind velocity and direction within cloud

10 p1844 A70-25242

Vertical air velocity in convective clouds by pulsed Doppler radar observations of thunderstorm

11 p2004 A70-25650

Wind velocity and direction and diffusion coefficients measurements by artificial luminous clouds, injecting appropriate reagents from rockets

11 p2075 A70-25918

Horizontal wind velocity spectra at 80-100 km from radar meteor soundings

12 p2263 A70-27518

Upper atmosphere superrotation velocity based on satellite polar orbit calculation of 1968-59A, correcting for lunisolar perturbations

13 p2394 A70-28895

Wind velocity determination by radar tracking of meteor trails, investigating errors

14 p2572 A70-30328

Errors estimation in wind velocity values by radio echo observations in meteor trails of different densities

14 p2572 A70-30330

Surface wind speed durations statistical analysis, discussing meteorological, orographic and physiographic features

14 p2607 A70-30582

High winds simultaneous occurrence and duration to 150 meter height, showing coherence tendencies

14 p2607 A70-30583

Wind velocity derivative statistical characteristics in atmospheric surface layer, using thermoanemometer, functional converter, differentiating circuit and loop oscillograph

16 p2945 A70-33219

Solar wind velocity profile in rapid acceleration of coronal plasma from type I, III and V bursts

17 p3152 A70-35745

Wind velocity fluctuation randomization signal probability density measurement, using statistical sampler

18 p3238 A70-36067

Turbulent air flow velocities determined in meteor zone of atmosphere

18 p3316 A70-36935

Wind velocity and direction determination from artificial luminescent clouds photographs, calculating topocentric coordinates

18 p3252 A70-36991

Upper atmospheric wind velocity and diffusion coefficient measurement by radar observation of artificial electron cloud from atomic K ejection

18 p3253 A70-36993

Horizontal wind velocity spectra at 80-100 km from radar meteor soundings

21 p3846 A70-41166

Remote digital mean wind speed indication with numerical display, using photoanemometer for airport application

21 p3831 A70-42247

Wind velocity derivative statistical characteristics in atmospheric surface layer, using thermoanemometer, functional converter, differentiating circuit and loop oscillograph

24 p4371 A70-45194

WINDING

NT FILAMENT WINDING

NT HELICAL WINDINGS

NT WIRE WINDING

Textolites and ferromagnetodielectric wedges mechanical strengths compared for use in open grooves of compound winding

01 p0008 A70-10195

Shadow method for temperature field in potentiometer winding

19 p3420 A70-37264

WINDMILLING

U AUTOROTATION

WINDOWS

NT WAVEGUIDE WINDOWS

Spacecraft window cleaning with methyl alcohol and low pressure nitrogen providing filming control for Apollo optical experiments

11 p2051 A70-26143

Interferograms of window wave front deformations to measure angular deviations to line of sight

15 p2737 A70-32038

WINDOWS [APERTURES]

Display systems used in space capsule window simulation for flight training, discussing erecting eyepieces, field of view and exit pupils

01 p0058 A70-10814

- Composite window permitting visual or photographic observation and IR irradiation of test materials in ultrahigh vacuum system 09 p1698 A70-22994
- Airborne camera resolution degradations /window losses/ introduced by multilayering wedge, irregularity and structural deformation 09 p1687 A70-23767
- VFW 614 nose-contoured cockpit panes, discussing structural weight and strength, vision and window frame fabrication 10 p1806 A70-24866
- Two dimensional impedance horn antennas synthesized by aperture field distribution and radiation pattern configuration relationship, deriving energy balance equation 11 p2015 A70-25348
- Coupled panel-cavity vibrations analysis, emphasizing sonic boom excitation of large window-room combinations 11 p2133 A70-25728
- Thermal control coatings, windows and mirrors for 1973 Mars Viking Lander vehicles under simulated Martian surface conditions [AIAA PAPER 69-1023] 13 p2384 A70-28530
- Thin window for circularly polarizing antennas, measuring circularity and VSWR performance on S and X band test sections 16 p2877 A70-33410
- Tiros satellites window radiation applied to day and night surface temperature measurements on land and sea 17 p3081 A70-35932
- Meteoroid impacts on Gemini spacecraft windows, calculating flux-mass relation 19 p3520 A70-38376
- Two dimensional impedance horn antennas synthesized by aperture field distribution and radiation pattern configuration relationship, deriving energy balance equation 20 p3600 A70-40460
- High transmission Mylar window He cryostat for Mossbauer measurements 21 p3828 A70-41470

WINDOWS [INTERVALS]

- NT LAUNCH WINDOWS
- Optimal atmospheric transmittance windows for underlying surface and cloud temperature determination from satellites 08 p1538 A70-21426
- Silicon window with double carrier injection to achieve high power broadband microwave switching, obtaining power increase over p-i-n diodes 10 p1847 A70-23892
- Analog integrating moving window detector performance analysis for use with scanning pulse radar allowing for antenna radiation pattern and detection process dynamic characteristics 11 p2009 A70-26262

WINDS ALOFT

- NT GEOSTROPHIC WIND
- NT JET STREAMS [METEOROLOGY]
- High altitude meteor winds, investigating atmospheric tides and short term wind oscillations, wind shears and drift nature 14 p2601 A70-30122

WINDSCREENS

- U WINDSHIELDS
- WINDSHIELDS
- F-104 jet windshield components research concerning plate glass optical deviation problems to meet quality standards 09 p1691 A70-22571
- Glass plastic composite electrically heated windshields for aircraft, discussing design, fabrication, qualification testing and service experience 21 p3750 A70-41137

WINDWARD

- U UPSTREAM
- U WIND [METEOROLOGY]

WING CAMBER

- Contour, pressure distribution and aerodynamic parameters calculations of slender highly cambered parawings in symmetric and asymmetric inviscid flow 03 p0408 A70-13800
- Wing camber and twist effects on transonic drag, using wind tunnel measurements 16 p2840 A70-34321
- Wing lift increase by spanwise blowing along upper surface, causing flow reattachment on wing and vortex induced effective aerodynamic camber increase [ICAS PAPER 70-09] 23 p4132 A70-44120

WING FLAPS

- NT TRAILING-EDGE FLAPS
- Fokker F-28 wing flap, lift dumpers and aileron development, including wind tunnel and flight tests 08 p1438 A70-21864
- Extensible wing flap system for cargo aircraft, discussing structural design details and advantages [AIAA PAPER 70-911] 17 p3020 A70-35823
- Propulsion system impact on military/commercial STOL transport aircraft commonality, taking into account augmented jet flap and externally blown flap powered lift wing concepts [SAE PAPER 700269] 18 p3214 A70-36819

- Increased lift via hinge suction jet flaps on augmentor wings, using thin airfoil model and small disturbance theory 22 p3960 A70-43432

WING FLOW METHOD TESTS

- Two dimensional wing model with harmonically oscillating control surface in transonic range, comparing theoretical with experimental results on unsteady pressure distribution 06 p0966 A70-17252
- Aerodynamic forces and moments effect of VTOL aircraft lift fan configurations on flow past wing 10 p1798 A70-24047
- Short wing lift investigated via lateral fluid jets fired in wind tunnel for various lengths 22 p3958 A70-42614

WING LOADING

- Mounted-above-wing jet engine effect on wing pressure distribution and elevator unit, using fluid mechanical model [DGLR-69-34] 04 p0735 A70-15146
- Liapunov second method extension to dynamical systems stability, illustrating wing torsional divergence and panel supersonic flutter 05 p0941 A70-16564
- Aircraft wing load calculations using aerodynamic influence coefficients based on linear subsonic or supersonic flow theory 06 p0967 A70-17255
- Singular element technique effect on hydrodynamic and aerodynamic problems solutions, presenting potential flow problems and application to wings and propellers 07 p1188 A70-19133
- Wing lifting surface theory for V/STOL aircraft based on inclined actuator disk theory to predict span loading and downwash angle 07 p1190 A70-20408
- Numerical solutions of variational problems concerning symmetrical wings with minimum drag and optimal aerodynamic efficiency in hypersonic flow 09 p1603 A70-22433
- Spanwise distribution of aerodynamic torsion on sailplane wings in vertical dive, discussing wing twist and lift effects 12 p2156 A70-27721
- Preliminary aircraft wing design for gusts or landing impacts inducing vibrations, inertia effects and dynamic overloads 14 p2655 A70-30177
- Wing section pressure distributions, lift and drag in transonic mixed flow, considering prediction methods 14 p2529 A70-30866
- Linear model of edge effect in supersonic gas flow past dihedral angle of intersecting wings, using Abel equations 15 p2672 A70-32127
- Nonlinear bearing surface of symmetrical rectangular edge wings without slipping in incompressible flow, using oblique horseshoe vortex model 15 p2673 A70-32128
- Maneuver load alleviation /MLA/ configurations for wing bending load relief on transport aircraft, showing improved payload and span performance [AIAA PAPER 70-877] 17 p3016 A70-34813
- Water ballast loadings on sailplane Cobra 17, considering wing, aileron, tailplane, fuselage and landing gear 22 p3962 A70-42962
- Similarity rules for sinusoidal gust loads on thin two dimensional wing in nonstationary subsonic flows 23 p4131 A70-43970
- Aircraft wing box beams bending tests to failure loads, considering crushing pressure, bulkhead flexural deformations, structure initial imperfections and instability phenomena 23 p4267 A70-44103
- Unsteady aerodynamic loading of wings with control surfaces, discussing Kuessner integral equation of subsonic lifting theory 23 p4274 A70-44761

- Wing section pressure distributions, lift and drag in transonic mixed flow, considering prediction methods 14 p2529 A70-30866
- Linear model of edge effect in supersonic gas flow past dihedral angle of intersecting wings, using Abel equations 15 p2672 A70-32127
- Nonlinear bearing surface of symmetrical rectangular edge wings without slipping in incompressible flow, using oblique horseshoe vortex model 15 p2673 A70-32128
- Maneuver load alleviation /MLA/ configurations for wing bending load relief on transport aircraft, showing improved payload and span performance [AIAA PAPER 70-877] 17 p3016 A70-34813
- Water ballast loadings on sailplane Cobra 17, considering wing, aileron, tailplane, fuselage and landing gear 22 p3962 A70-42962
- Similarity rules for sinusoidal gust loads on thin two dimensional wing in nonstationary subsonic flows 23 p4131 A70-43970
- Aircraft wing box beams bending tests to failure loads, considering crushing pressure, bulkhead flexural deformations, structure initial imperfections and instability phenomena 23 p4267 A70-44103
- Unsteady aerodynamic loading of wings with control surfaces, discussing Kuessner integral equation of subsonic lifting theory 23 p4274 A70-44761

- Wing section pressure distributions, lift and drag in transonic mixed flow, considering prediction methods 14 p2529 A70-30866
- Linear model of edge effect in supersonic gas flow past dihedral angle of intersecting wings, using Abel equations 15 p2672 A70-32127
- Nonlinear bearing surface of symmetrical rectangular edge wings without slipping in incompressible flow, using oblique horseshoe vortex model 15 p2673 A70-32128
- Maneuver load alleviation /MLA/ configurations for wing bending load relief on transport aircraft, showing improved payload and span performance [AIAA PAPER 70-877] 17 p3016 A70-34813
- Water ballast loadings on sailplane Cobra 17, considering wing, aileron, tailplane, fuselage and landing gear 22 p3962 A70-42962
- Similarity rules for sinusoidal gust loads on thin two dimensional wing in nonstationary subsonic flows 23 p4131 A70-43970
- Aircraft wing box beams bending tests to failure loads, considering crushing pressure, bulkhead flexural deformations, structure initial imperfections and instability phenomena 23 p4267 A70-44103
- Unsteady aerodynamic loading of wings with control surfaces, discussing Kuessner integral equation of subsonic lifting theory 23 p4274 A70-44761

- Wing section pressure distributions, lift and drag in transonic mixed flow, considering prediction methods 14 p2529 A70-30866
- Linear model of edge effect in supersonic gas flow past dihedral angle of intersecting wings, using Abel equations 15 p2672 A70-32127
- Nonlinear bearing surface of symmetrical rectangular edge wings without slipping in incompressible flow, using oblique horseshoe vortex model 15 p2673 A70-32128
- Maneuver load alleviation /MLA/ configurations for wing bending load relief on transport aircraft, showing improved payload and span performance [AIAA PAPER 70-877] 17 p3016 A70-34813
- Water ballast loadings on sailplane Cobra 17, considering wing, aileron, tailplane, fuselage and landing gear 22 p3962 A70-42962
- Similarity rules for sinusoidal gust loads on thin two dimensional wing in nonstationary subsonic flows 23 p4131 A70-43970
- Aircraft wing box beams bending tests to failure loads, considering crushing pressure, bulkhead flexural deformations, structure initial imperfections and instability phenomena 23 p4267 A70-44103
- Unsteady aerodynamic loading of wings with control surfaces, discussing Kuessner integral equation of subsonic lifting theory 23 p4274 A70-44761

- Wing section pressure distributions, lift and drag in transonic mixed flow, considering prediction methods 14 p2529 A70-30866
- Linear model of edge effect in supersonic gas flow past dihedral angle of intersecting wings, using Abel equations 15 p2672 A70-32127
- Nonlinear bearing surface of symmetrical rectangular edge wings without slipping in incompressible flow, using oblique horseshoe vortex model 15 p2673 A70-32128
- Maneuver load alleviation /MLA/ configurations for wing bending load relief on transport aircraft, showing improved payload and span performance [AIAA PAPER 70-877] 17 p3016 A70-34813
- Water ballast loadings on sailplane Cobra 17, considering wing, aileron, tailplane, fuselage and landing gear 22 p3962 A70-42962
- Similarity rules for sinusoidal gust loads on thin two dimensional wing in nonstationary subsonic flows 23 p4131 A70-43970
- Aircraft wing box beams bending tests to failure loads, considering crushing pressure, bulkhead flexural deformations, structure initial imperfections and instability phenomena 23 p4267 A70-44103
- Unsteady aerodynamic loading of wings with control surfaces, discussing Kuessner integral equation of subsonic lifting theory 23 p4274 A70-44761

- Wing section pressure distributions, lift and drag in transonic mixed flow, considering prediction methods 14 p2529 A70-30866
- Linear model of edge effect in supersonic gas flow past dihedral angle of intersecting wings, using Abel equations 15 p2672 A70-32127
- Nonlinear bearing surface of symmetrical rectangular edge wings without slipping in incompressible flow, using oblique horseshoe vortex model 15 p2673 A70-32128
- Maneuver load alleviation /MLA/ configurations for wing bending load relief on transport aircraft, showing improved payload and span performance [AIAA PAPER 70-877] 17 p3016 A70-34813
- Water ballast loadings on sailplane Cobra 17, considering wing, aileron, tailplane, fuselage and landing gear 22 p3962 A70-42962
- Similarity rules for sinusoidal gust loads on thin two dimensional wing in nonstationary subsonic flows 23 p4131 A70-43970
- Aircraft wing box beams bending tests to failure loads, considering crushing pressure, bulkhead flexural deformations, structure initial imperfections and instability phenomena 23 p4267 A70-44103
- Unsteady aerodynamic loading of wings with control surfaces, discussing Kuessner integral equation of subsonic lifting theory 23 p4274 A70-44761

- Wing section pressure distributions, lift and drag in transonic mixed flow, considering prediction methods 14 p2529 A70-30866
- Linear model of edge effect in supersonic gas flow past dihedral angle of intersecting wings, using Abel equations 15 p2672 A70-32127
- Nonlinear bearing surface of symmetrical rectangular edge wings without slipping in incompressible flow, using oblique horseshoe vortex model 15 p2673 A70-32128
- Maneuver load alleviation /MLA/ configurations for wing bending load relief on transport aircraft, showing improved payload and span performance [AIAA PAPER 70-877] 17 p3016 A70-34813
- Water ballast loadings on sailplane Cobra 17, considering wing, aileron, tailplane, fuselage and landing gear 22 p3962 A70-42962
- Similarity rules for sinusoidal gust loads on thin two dimensional wing in nonstationary subsonic flows 23 p4131 A70-43970
- Aircraft wing box beams bending tests to failure loads, considering crushing pressure, bulkhead flexural deformations, structure initial imperfections and instability phenomena 23 p4267 A70-44103
- Unsteady aerodynamic loading of wings with control surfaces, discussing Kuessner integral equation of subsonic lifting theory 23 p4274 A70-44761

- Wing section pressure distributions, lift and drag in transonic mixed flow, considering prediction methods 14 p2529 A70-30866
- Linear model of edge effect in supersonic gas flow past dihedral angle of intersecting wings, using Abel equations 15 p2672 A70-32127
- Nonlinear bearing surface of symmetrical rectangular edge wings without slipping in incompressible flow, using oblique horseshoe vortex model 15 p2673 A70-32128
- Maneuver load alleviation /MLA/ configurations for wing bending load relief on transport aircraft, showing improved payload and span performance [AIAA PAPER 70-877] 17 p3016 A70-34813
- Water ballast loadings on sailplane Cobra 17, considering wing, aileron, tailplane, fuselage and landing gear 22 p3962 A70-42962
- Similarity rules for sinusoidal gust loads on thin two dimensional wing in nonstationary subsonic flows 23 p4131 A70-43970
- Aircraft wing box beams bending tests to failure loads, considering crushing pressure, bulkhead flexural deformations, structure initial imperfections and instability phenomena 23 p4267 A70-44103
- Unsteady aerodynamic loading of wings with control surfaces, discussing Kuessner integral equation of subsonic lifting theory 23 p4274 A70-44761

- Wing section pressure distributions, lift and drag in transonic mixed flow, considering prediction methods 14 p2529 A70-30866
- Linear model of edge effect in supersonic gas flow past dihedral angle of intersecting wings, using Abel equations 15 p2672 A70-32127
- Nonlinear bearing surface of symmetrical rectangular edge wings without slipping in incompressible flow, using oblique horseshoe vortex model 15 p2673 A70-32128
- Maneuver load alleviation /MLA/ configurations for wing bending load relief on transport aircraft, showing improved payload and span performance [AIAA PAPER 70-877] 17 p3016 A70-34813
- Water ballast loadings on sailplane Cobra 17, considering wing, aileron, tailplane, fuselage and landing gear 22 p3962 A70-42962
- Similarity rules for sinusoidal gust loads on thin two dimensional wing in nonstationary subsonic flows 23 p4131 A70-43970
- Aircraft wing box beams bending tests to failure loads, considering crushing pressure, bulkhead flexural deformations, structure initial imperfections and instability phenomena 23 p4267 A70-44103
- Unsteady aerodynamic loading of wings with control surfaces, discussing Kuessner integral equation of subsonic lifting theory 23 p4274 A70-44761

- Wing section pressure distributions, lift and drag in transonic mixed flow, considering prediction methods 14 p2529 A70-30866
- Linear model of edge effect in supersonic gas flow past dihedral angle of intersecting wings, using Abel equations 15 p2672 A70-32127
- Nonlinear bearing surface of symmetrical rectangular edge wings without slipping in incompressible flow, using oblique horseshoe vortex model 15 p2673 A70-32128
- Maneuver load alleviation /MLA/ configurations for wing bending load relief on transport aircraft, showing improved payload and span performance [AIAA PAPER 70-877] 17 p3016 A70-34813
- Water ballast loadings on sailplane Cobra 17, considering wing, aileron, tailplane, fuselage and landing gear 22 p3962 A70-42962
- Similarity rules for sinusoidal gust loads on thin two dimensional wing in nonstationary subsonic flows 23 p4131 A70-43970
- Aircraft wing box beams bending tests to failure loads, considering crushing pressure, bulkhead flexural deformations, structure initial imperfections and instability phenomena 23 p4267 A70-44103
- Unsteady aerodynamic loading of wings with control surfaces, discussing Kuessner integral equation of subsonic lifting theory 23 p4274 A70-44761

- Wing section pressure distributions, lift and drag in transonic mixed flow, considering prediction methods 14 p2529 A70-30866
- Linear model of edge effect in supersonic gas flow past dihedral angle of intersecting wings, using Abel equations 15 p2672 A70-32127
- Nonlinear bearing surface of symmetrical rectangular edge wings without slipping in incompressible flow, using oblique horseshoe vortex model 15 p2673 A70-32128
- Maneuver load alleviation /MLA/ configurations for wing bending load relief on transport aircraft, showing improved payload and span performance [AIAA PAPER 70-877] 17 p3016 A70-34813
- Water ballast loadings on sailplane Cobra 17, considering wing, aileron, tailplane, fuselage and landing gear 22 p3962 A70-42962
- Similarity rules for sinusoidal gust loads on thin two dimensional wing in nonstationary subsonic flows 23 p4131 A70-43970
- Aircraft wing box beams bending tests to failure loads, considering crushing pressure, bulkhead flexural deformations, structure initial imperfections and instability phenomena 23 p4267 A70-44103
- Unsteady aerodynamic loading of wings with control surfaces, discussing Kuessner integral equation of subsonic lifting theory 23 p4274 A70-44761

- Wing section pressure distributions, lift and drag in transonic mixed flow, considering prediction methods 14 p2529 A70-30866
- Linear model of edge effect in supersonic gas flow past dihedral angle of intersecting wings, using Abel equations 15 p2672 A70-32127
- Nonlinear bearing surface of symmetrical rectangular edge wings without slipping in incompressible flow, using oblique horseshoe vortex model 15 p2673 A70-32128
- Maneuver load alleviation /MLA/ configurations for wing bending load relief on transport aircraft, showing improved payload and span performance [AIAA PAPER 70-877] 17 p3016 A70-34813
- Water ballast loadings on sailplane Cobra 17, considering wing, aileron, tailplane, fuselage and landing gear 22 p3962 A70-42962
- Similarity rules for sinusoidal gust loads on thin two dimensional wing in nonstationary subsonic flows 23 p4131 A70-43970
- Aircraft wing box beams bending tests to failure loads, considering crushing pressure, bulkhead flexural deformations, structure initial imperfections and instability phenomena 23 p4267 A70-44103
- Unsteady aerodynamic loading of wings with control surfaces, discussing Kuessner integral equation of subsonic lifting theory 23 p4274 A70-44761

- Wing section pressure distributions, lift and drag in transonic mixed flow, considering prediction methods 14 p2529 A70-30866
- Linear model of edge effect in supersonic gas flow past dihedral angle of intersecting wings, using Abel equations 15 p2672 A70-32127
- Nonlinear bearing surface of symmetrical rectangular edge wings without slipping in incompressible flow, using oblique horseshoe vortex model 15 p2673 A70-32128
- Maneuver load alleviation /MLA/ configurations for wing bending load relief on transport aircraft, showing improved payload and span performance [AIAA PAPER 70-877] 17 p3016 A70-34813
- Water ballast loadings on sailplane Cobra 17, considering wing, aileron, tailplane, fuselage and landing gear 22 p3962 A70-42962
- Similarity rules for sinusoidal gust loads on thin two dimensional wing in nonstationary subsonic flows 23 p4131 A70-43970
- Aircraft wing box beams bending tests to failure loads, considering crushing pressure, bulkhead flexural deformations, structure initial imperfections and instability phenomena 23 p4267 A70-44103
- Unsteady aerodynamic loading of wings with control surfaces, discussing Kuessner integral equation of subsonic lifting theory 23 p4274 A70-44761

- Wing section pressure distributions, lift and drag in transonic mixed flow, considering prediction methods 14 p2529 A70-30866
- Linear model of edge effect in supersonic gas flow past dihedral angle of intersecting wings, using Abel equations 15 p2672 A70-32127
- Nonlinear bearing surface of symmetrical rectangular edge wings without slipping in incompressible flow, using oblique horseshoe vortex model 15 p2673 A70-32128
- Maneuver load alleviation /MLA/ configurations for wing bending load relief on transport aircraft, showing improved payload and span performance [AIAA PAPER 70-877] 17 p3016 A70-34813
- Water ballast loadings on sailplane Cobra 17, considering wing, aileron, tailplane, fuselage and landing gear 22 p3962 A70-42962
- Similarity rules for sinusoidal gust loads on thin two dimensional wing in nonstationary subsonic flows 23 p4131 A70-43970
- Aircraft wing box beams bending tests to failure loads, considering crushing pressure, bulkhead flexural deformations, structure initial imperfections and instability phenomena 23 p4267 A70-44103
- Unsteady aerodynamic loading of wings with control surfaces, discussing Kuessner integral equation of subsonic lifting theory 23 p4274 A70-44761

- ing theoretical with experimental results on unsteady pressure distribution 06 p0966 A70-17252

- Plane rigid airfoil frequency response in incompressible potential flow using simple equivalent oscillator based on Theodorsen function 07 p1404 A70-19232

- Mathematical model with straight wake airfoil to determine aerodynamic forces on oscillating rotor blades in hovering flight 09 p1605 A70-23222

- Equivalent oscillatory model defined from asymptotes of frequency response amplitude and cut-off frequency amplitude value of plane rigid airfoil in incompressible potential flow 10 p1953 A70-23841

- Wing in supersonic flow analyzed for surface pressure taking into account nonlinear effects of vibrations 10 p1798 A70-24119

- Polygonal wings oscillatory motions in unsteady supersonic flow 10 p1803 A70-24778

- Gas dynamics regarding velocity field excited by vibrations propagating over elastic wing surface at finite velocity 10 p1803 A70-24779

- Flutter characteristics of uniform cantilever wing with concentrated inertias using Direct Matrix method 10 p1963 A70-25071

- Monograph on numerical treatment method for harmonically oscillating wings covering pressure distributions, logarithmic singularity, etc 11 p2129 A70-25497

- Wind tunnel interference effect on fluttering airfoils and panels supersonic speeds, studying pressure distributions for various tunnel aspect ratios and roof conditions 12 p2155 A70-27103

- F-111 aircraft wings unstable fore and aft oscillations in swept forward position ascribed to actuator motor drive rate variations 12 p2160 A70-27112

- Correction factor for finite span effect on unsteady wing lift or moment during sinusoidal gusts or vertical oscillations 12 p2155 A70-27200

- Pressure field due to control surface oscillation in subsonic flow, presenting numerical results for rectangular wing 14 p2528 A70-30295

- Dynamic stability derivatives calculation using steady and oscillatory lifting surface theory with allowance for Bryan limitations 14 p2529 A70-30864

- Flutter analysis, criteria and experiments emphasizing aircraft applications 15 p2815 A70-31798

- Forces on two dimensional oscillating airfoil in subsonic compressible wind tunnel flow, solving partial differential equation for pressure potential by integral transform technique 16 p2839 A70-34248

- German monograph on oscillations of tandem wing without outgoing wake in plane incompressible flow, using numerical computations 17 p3011 A70-35372

- Rectangular wing with oscillating control surface, measuring induced unsteady pressure field for comparison with computations based on lifting surface theory 21 p3935 A70-41407

- Oscillating wing aerodynamic load boundary value problem reduction to sequence of steady lifting-surface problems 22 p3959 A70-42715

- Harmonically oscillating wing linearized motion in subsonic flow, calculating generalized aerodynamic forces 22 p4105 A70-43118

- High subsonic and transonic effects on pressure distributions for swept wing with oscillating control surface 23 p4274 A70-44763

- Pressure measurements on harmonically vibrating sweptback wing with two control surfaces in incompressible flow 23 p4274 A70-44768

- Oscillatory motion of triangular wing with conical body of arbitrary cross section in supersonic flow, considering wing-body interference effects 24 p4288 A70-45592

- WING PANELS
- Beaded-doubler reinforced skin design concept for Improved HAWK Missile wing, considering compression stress, weight, cost and field service characteristics 02 p0380 A70-11946

- Boeing 747 wing panels shot peening process, discussing machine, control technique and operational requirements 19 p3437 A70-38498

- WING PLANNFORMS
- NT DELTA WINGS
- NT SWEPTBACK WINGS
- NT TRAPEZOIDAL WINGS

NT VARIABLE SWEEP WINGS

Minimum drag hypersonic delta wing, analyzing shape for given planform, lift, pitching moment and volume using correction for pressure coefficient
01 p0002 A70-10557

Blended wing-body design concept for F-15 air superiority fighter, providing fixed wing planform for maneuverability at transonic speed
04 p0622 A70-14395

Sigma glider design for high cruising speed, using extensible wing to double area in flight
04 p0622 A70-14625

Numerical method for calculating gust effect on wing of complex planform at subsonic speeds by converting continuous to discrete processes
04 p0618 A70-15242

Delta wing of given volume and planform with maximum lift-drag ratio in hypersonic flow
04 p0618 A70-15243

Lift effectiveness of slender wings with streamwise root gaps and fences, obtaining lift curve slope variation with fence height
04 p0621 A70-15611

Tangent plane method and polar coordinates for lifting surfaces, calculating normal velocity at field point on surface carrying doublet distribution for incompressible flow
[AIAA PAPER 70-78] 06 p0975 A70-18195

Minimum drag thin symmetrical cruciform wing fitted with central ridge, reducing problem to linear algebraic finite system of equations
10 p1803 A70-24784

Aerodynamic loadings on planar wings in oscillatory subsonic flow determined by collocation for performing Gaussian quadrature integration of pressure and kernel functions
12 p2155 A70-27102

Low aspect ratio wing aerodynamic characteristics in shear flow, noting forces dependence on flow velocity gradients
14 p2529 A70-31274

Packable near weightless nylon cloth wings without rigid members for improved aeronautical efficiency in cargo delivery, powered flight and rocket and spacecraft recovery
[AIAA PAPER 70-880] 17 p3017 A70-34815

Composite wing section design and fabrication utilizing unidirectional glass reinforcement
[AIAA PAPER 70-919] 17 p3193 A70-35813

Subsonic high lift cruise wing optimal design using kernel function method of planar lifting surface theory
22 p3959 A70-42709

Downwash angle behind straight wing for unsteady aperiodic flight at subsonic speeds, using vorticity model
22 p3959 A70-42802

WING PROFILES
NT WING SPAN
Wing design optimization for steady and unsteady supersonic flow through computerized simulation and study of leading and trailing edge shape
02 p0223 A70-12208

Wind tunnel comparative performance tests of glider laminar wing profile with fixed and flexible trailing-edge flap
02 p0304 A70-12800

Wave drag dependence of delta wings on thickness distribution
[DVL-888] 03 p0406 A70-13273

Aircraft aerodynamics, Volume II, covering profile and wing theory at subsonic and supersonic speeds, fuselage, wing-fuselage and tail assembly, etc
03 p0407 A70-13350

Wing and body design for upgrading transonic aircraft performance, discussing blending, spanwise sweep variation, curved leading edge and aspect ratio
04 p0613 A70-14504

Separated incompressible flow around wing profile, considering calculation of separated potential flow generation with given separation point
06 p0966 A70-17253

Nonlinear theory extended to slender triangular and rectangular wings with symmetric profile, taking into account finite wing thickness
06 p0966 A70-17254

Lifting surface theory for calculation of steady subsonic and supersonic flow over various wing and air-plane configurations, emphasizing finite element load prediction method
[AIAA PAPER 70-192] 06 p0971 A70-18114

Aerodynamic forces for boundary layer profiles of flexible plate under transient motion in shear flow using computer programs
[AIAA PAPER 70-76] 06 p0972 A70-18122

Ram wing vehicles aerodynamics application to high speed ground transportation, studying effect on passenger ride quality
[AIAA PAPER 70-142] 06 p0973 A70-18145

Prandtl problem solution by reducing integrodifferential equation to linear differential equation in disk of complex variable, noting application to elliptical or rectangular wings
07 p1258 A70-19783

Aerodynamics role in large commercial aircraft design, noting mathematics models problem in high speed wing design
09 p1609 A70-22024

Analytical algorithm for tan-chord angle tangent determination, assuming undevelopable ruled wing surface defined by three cross sections
10 p1802 A70-24292

Supersonic flow around slender polygonal wings with nonsymmetrically distributed incidence using method for conical flow around angular wings
10 p1803 A70-24797

Subsonic kernel function applicability limited to surfaces with small inclinations to freestream, considering wing with deflected control surface
12 p2212 A70-28089

Supersonic flow in inner and outer regions of annular wings by method of singularities, obtaining Abel type integral equations for every step
[DFVLR-SONDDR-37] 12 p2158 A70-28207

Flapping wing unsteady periodic motion relationship to forces effect on wing profile and vortex street in wake, determining propeller thrust by potential theory
13 p2337 A70-28479

Ackeret theory for infinite aspect ratio, rectangular and trapezoidal constant cord wings with arbitrary spanwise variation of profile in supersonic flow
16 p2836 A70-33748

Stress concentration on axisymmetric annular wings calculated using method of singularities
18 p3207 A70-36377

Hypersonic flat and biconvex conical wings, calculating yaw effects on shock shape and pressure distribution
21 p3761 A70-40918

Planar wing with end plates in ground effect, calculating minimum induced drag by approximation theory
21 p3743 A70-40919

Near field flow effects on sonic boom for incident triangular wing with constant lift distribution
[ICAS PAPER 70-20] 23 p4138 A70-44113

WING ROOTS
Static stability requirements relaxation and wing control devices additions for alleviating wing root bending moments in controls configured vehicle /CCV design concepts
19 p3355 A70-37395

VTOL aircraft ejector thrust augmentors, discussing configurations in wing root section
[ICAS PAPER 70-56] 23 p4139 A70-44152

WING SLOTS
V/STOL aircraft propellers featuring thrust augmenting air jet slits for increased lift
[DGLR-69-36] 04 p0616 A70-15175

WING SPAN
Wing-fuselage interference influence in aircraft dihedral effect, discussing role of velocity direction on wing
03 p0406 A70-13020

Swept wings aerodynamic center and span load distributions with respect to quarter-chord line
04 p0619 A70-15393

Correction factor for finite span effect on unsteady wing lift or moment during sinusoidal gusts or vertical oscillations
12 p2155 A70-27200

Spanwise distribution of aerodynamic torsion on sailplane wings in vertical dive, discussing wing twist and lift effects
12 p2156 A70-27721

Lifting surface problem for finite span wing in ground effect using matched asymptotic expansions method
14 p2527 A70-30280

Maneuver load alleviation /MLA/ configurations for wing bending load relief on transport aircraft, showing improved payload and span performance
[AIAA PAPER 70-877] 17 p3016 A70-34813

Flow velocity and pressure on thin wing of small span width near sonic speed, using parabolic type linear equation
18 p3207 A70-36374

Soviet book on passenger aircraft aerodynamics covering motions of gases and immersed bodies, similarity laws, boundary layer theory, finite span wing, etc
18 p3208 A70-36507

Aerodynamic lift, drag and momentum coefficients in supersonic regime for rectangular and trapezoidal wings with spanwise variable profile
22 p3958 A70-42615

WING STALL
U BOUNDARY LAYER SEPARATION
WING TANKS
Nonlinear balance mass solutions for tab-aileron flutter free operation of jet trainer for arbitrary store configuration
17 p3185 A70-34923

Elastic coupling and dynamic equations for flight elastomechanical vibration systems, including tiptanks on aircraft wings
23 p4274 A70-44767

WING TIPS

Turbine blade tip clearance effect on aerodynamic characteristics in nonuniform flow
07 p1187 A70-18980

Carbon dioxide CW laser-Doppler velocimeter for detecting aircraft wing tip trailing vortices by measuring atmospheric aerosols backscatter
12 p2249 A70-27630

Wing tip trailing vortices hazard reduction on closely spaced parallel runways by suction application, discussing power requirements
12 p2207 A70-27631

Aerodynamic characteristics of wing with tip clearance within uniform flow, investigating main stream flow pattern effect
14 p2529 A70-31331

WINGED ROCKET BOOSTERS
U LAUNCH VEHICLES
U WINGED VEHICLES
WINGED VEHICLES
Low operating cost space shuttle system for cargo and personnel transportation to earth orbiting stations involving reusable winged vehicles
[AIAA PAPER 70-242] 07 p1396 A70-20376

Analog computation in supersonic steady flow and digital technique for wing-fuselage and wing-tail interactions
[ONERA-TP-804] 10 p1802 A70-24544

Ram wing tube ground transportation vehicle, analyzing optimum lift-drag ratio and induced power requirements
11 p1975 A70-25966

Cost reduction in designing space shuttle system using reusable winged vehicles, suggesting airlines operations method
[AAS PAPER 70-043] 17 p3175 A70-34785

WINGS
NT CAMBERED WINGS
NT CARET WINGS
NT CRUCIFORM WINGS
NT DELTA WINGS
NT FIXED WINGS
NT FLEXIBLE WINGS
NT LIFTING ROTORS
NT LOW ASPECT RATIO WINGS
NT PARAWINGS
NT RECTANGULAR WINGS
NT RIGID ROTORS
NT RIGID WINGS
NT ROTARY WINGS
NT SLENDER WINGS
NT SWEPT WINGS
NT SWEPTBACK WINGS
NT THIN WINGS
NT TILTING ROTORS
NT TIP DRIVEN ROTORS
NT TRAPEZOIDAL WINGS
NT TWISTED WINGS
NT VARIABLE SWEEP WINGS
F-8 wing service life extension design techniques, emphasizing fatigue design curves and procedures
02 p0386 A70-11939

Supersonic flow in dihedral angle between intersecting wings and in space between parallel wings, using integrating wave equation by Volterra method
03 p0407 A70-13492

Boeing 707 aircraft operational efficiency optimization by modification program to extend wing life
03 p0497 A70-14052

Flow phenomena about beating plates, fins and wings, discussing biological and engineering applications
05 p0790 A70-16155

Induced drag dependence on Reynolds number for wings without camber and warping
06 p0967 A70-17257

Aerodynamic characteristics of cylinder with wings in free molecular hypersonic flow of nonequilibrium gas at various angles of attack and slip
08 p1432 A70-21083

Aircraft wing ribs tangents plotting procedure using Monge diagram
08 p1507 A70-21197

Optimal deformation and minimum wave drag for wings with supersonic leading and straight trailing edge, solving variational problem by Ritz method
09 p1604 A70-22444

Gas stream velocity field produced by shock wave impinging against wing moving at supersonic speed
10 p1799 A70-24124

Supersonic aerial target wing synthesis using sandwich construction with graphite-epoxy laminate skins bonded to Al honeycomb, achieving significant weight reduction
12 p2160 A70-27118

Wing and empennage structures automated fully stressed design procedures, discussing application to supersonic aircraft stabilizer
12 p2319 A70-27136

Wing rib structure transient thermal stresses analysis using photothermoelastic method
12 p2327 A70-27982

Air deflection and modulation /ADAM/ turbofan propulsive wing V/STOL design
[AIAA PAPER 69-201] 12 p2162 A70-28087

WINTER

Boron epoxy composite wing structures design, fabrication and testing 16 p2990 A70-33703

Boron-epoxy stiffener reinforced metal wings, examining structural efficiency of multiweb beam aluminum cover skins and Z stiffened panels 16 p2994 A70-34230

Subsonic wing theory calculation method, obtaining close solutions for integral expression constants for downward air currents 19 p3352 A70-38164

One dimensional channel flow theory for ram wings, deriving lift and drag laws for comparison with wind tunnel and free flight tests results [AIAA PAPER 70-971] 20 p3558 A70-39558

Free wing aircraft dynamic characteristics, discussing gust alleviation and handling qualities [AIAA PAPER 70-947] 20 p3561 A70-39580

Optimum light construction design of glider wings, considering spar weight, aluminum honeycomb structure and repair 22 p3962 A70-42961

Continuous trailing vortex sheet rolling up into two discrete vortices, discussing wing lift limitations 23 p4131 A70-43890

Ultrasonic crack detection in fastener holes in C-5A wings 24 p4341 A70-45571

STOL aircraft augmentor wing concept, examining noise suppression, flight research vehicle program and application to turbofan production aircraft [SAE PAPER 700812] 24 p4290 A70-45903

WINTER

Cosmic ray latitude survey in Canada using airport sites, noting ground snow effect on neutron monitor counting rate 01 p0167 A70-10227

Winter diurnal behavior of northern high latitude ionospheric electron density using temperature data from Langmuir probes 03 p0478 A70-13993

Anomalous ionization variations of F 2 layer at northern geomagnetic pole during winter coincident with decrease in solar plasma density 04 p0682 A70-15726

Daily variations of winter stratospheric zonal wind and planetary waves based on synoptic charts from balloon observation 05 p0878 A70-16148

Seasonal variation in ionospheric radiation absorption related to time variation between sunrise and constant angle attainment of sun 05 p0842 A70-16758

Localized numerical weather forecasts via interpolation from primitive equation model outputs, analyzing winter season results in terms of snow prediction 06 p1098 A70-18241

Winter midlatitude electron density trough from length fluctuation of Faraday signal fading period of satellite Explorer 22, noting characteristic seasonal variation 07 p1270 A70-20034

Planetary scale disturbances in winter stratospheric circulation during sudden warming using rocket observations 07 p1274 A70-20272

Winter anomaly ionization in lower ionosphere at medium latitudes from radio propagation observations, comparing wave absorption and phase height measurements 07 p1274 A70-20273

Stratospheric and mesospheric circulation during winter, investigating wind fluctuations using meteorological rocket observations 07 p1274 A70-20274

Synoptic changes associated with midwinter 1967-1968 major stratospheric warming, including pressure and wind distributions and temperature maps 07 p1275 A70-20277

Minor meteor showers radiants determined close to ecliptic plane from systematic visual observations during November, December and January 1961-67 08 p1577 A70-21532

Troposphere-stratosphere kinetic energy transfer during 1967-1968 midwinter warming, comparing calculation by pressure interaction term with direct calculation of vertical velocity fields 08 p1540 A70-21969

Anomalous ionization variations of F 2 layer at northern geomagnetic pole during winter coincident with decrease in solar plasma density 14 p2575 A70-30810

Winter anomaly of radio wave absorption in midlatitude lower ionosphere in terms of meteorological influences and particle influx enhancements 17 p3076 A70-34936

Richardson turbulence criterion computation from measurements during and after winter anomaly 17 p3077 A70-34945

Lower ionosphere electron density and winter anomaly in HF absorption 17 p3077 A70-34948

Winter ionosphere electron density profile from rocket-borne gyro-plasma probe observations 17 p3078 A70-35308

Meteorological observation on atmospheric boundary layer during winter, determining width and inclination of frontal zones 19 p3463 A70-38758

Polar stratospheric winter explosive warmings correlated with solar high energy charged particles injections 20 p3618 A70-39185

Total ionospheric electron content nocturnal and latitudinal variations in winter at midlatitudes 20 p3624 A70-40480

Low latitude boundary of ionospheric absorption during winter anomaly showing enhancement dependence on solar zenith angle 21 p3815 A70-40944

Auroral proton precipitation oval in antarctic winter based on H Balmer line radiation 21 p3882 A70-41091

Midwinter warming period upper stratospheric vertical motion fields, obtaining 2-mb charts 21 p3847 A70-42123

Stationary disturbances in winter Northern Hemisphere stratosphere considered as upward propagating Rossby waves, assuming zonal winds profile 23 p4213 A70-44030

WIRE

ELECTRIC WIRE

EXPLODING WIRES

Stress-strain state of-epoxy resin plates with single or paired wire reinforcement, using polarization-optical method 02 p0384 A70-11664

Heat transfer in Ni wires in laminar air flow from wind tunnel investigation 07 p1420 A70-19064

Size effect on structure and mechanical properties of thin wire made of Mo single crystals deformed in recrystallized state 07 p1308 A70-19611

Compression strength of polyester resin reinforced with hard drawn and softened steel wires, discussing variations from predicted performance 07 p1320 A70-19954

Heat transfer in Ni wires in laminar air flow from wind tunnel investigation 10 p1970 A70-25215

Thin wire glow during corona discharge in metal cylinders analyzed by photomultiplier 11 p2083 A70-25924

Wire sheet reinforcement for resin matrices, discussing mechanical properties, fabrication, bonding, wetting, etc 11 p2071 A70-26346

C-5 aircraft electrointerference coupling minimization, applying classification plan for wire categorization and routing 12 p2201 A70-28131

Twisted bipolar electrode in needle with controlled separation between bare areas for electromyography 12 p2542 A70-30798

Gas tungsten arc hot wire welding operational characteristics and applications 14 p2590 A70-30929

Alumina particles marker transport in Ag wires during early sintering as function of plastic deformation by slip 15 p2745 A70-32392

Backscattering, bistatic scattering and current distribution on thin wires during electromagnetic wave incidence 15 p2700 A70-32412

Ultrasonic Al wire bonding for microelectronic applications, discussing tensile strength dependence on machine parameters and aging 15 p2747 A70-32647

Sandwich wire planar antenna array design, noting electrical performance, ruggedness, volume and weight 16 p2877 A70-33416

Hard wire hermetically sealed two degrees of freedom rotating coupling design for continuous soldered wire connections between spacecraft and oriented solar array 16 p2924 A70-34172

Film boiling heat transfer from horizontal wires to water, using Nusselt condensation model 16 p3003 A70-34198

Pressure, subcooling and diameter effects on liquid nitrogen film boiling on thin horizontal wires, using high speed movies 17 p3194 A70-34742

Stress-strain state of epoxy resin plates with single or paired wire reinforcement, using polarization-optical method 19 p3547 A70-38438

Heat transfer measurement from Pt wire to carbon dioxide near critical pressure, discussing film boiling and free convection flows 21 p3953 A70-42167

Glauert equations applied to trailing wire shape for steady state aerodynamic forces on aircraft and trailing antennas, discussing computer solutions 23 p4131 A70-43893

Liquid nitrogen saturated film boiling from wire at pressures up to critical, discussing liquid-vapor interface configuration 23 p4279 A70-44362

Miniwire method of packaging high density electronic equipment shown in photographs, including OAO applications 24 p4320 A70-46247

WIRE BRIDGE CIRCUITS

NT WHEATSTONE BRIDGES

WIRE CLOTH

Tensile strength of flat specimens of Ni reinforced by W wire gauze 02 p0315 A70-11661

Tensile strength of flat specimens of Ni reinforced by W wire gauze 19 p3452 A70-38435

WIRE GRID LENSES

E plane radiation patterns of E plane sectoral horns enhanced by metallic grills arranged in optimum positions 02 p0270 A70-12734

WIRE MESH

U WIRE CLOTH

WIRE WINDING

Cylindrical coil springs cold winding loading processes, considering initial tension or compression of wire and combined stresses 10 p1894 A70-24297

Force-reduced superconducting toroidal magnet coils built with Cu plated Nb-Zr wire, investigating current enhancement characteristics 23 p4230 A70-44356

WIRELESS COMMUNICATIONS

Miniature temperature and strain telemetry transmitters developed for measurements in areas inaccessible to direct wire connections 06 p1069 A70-18433

Demand assigned domestic satellite communications system with capability of single hierarchy switching and serving terrestrial common carriers and direct users 14 p2552 A70-31351

WIRING

Thermal anchoring of wire or rod components to heat sinks in cryogenic equipment in vacuum 14 p2584 A70-30501

Multiple wiring algorithm for automatic pattern design for Al interconnections and printed wiring in integrated circuits 15 p2715 A70-31842

Aircraft electrical system multiplexing, discussing design features and advantages over conventional hard wired systems [SAE PAPER 700303] 18 p3216 A70-36811

Boeing 747 aircraft passenger entertainment and service system controls electronics design and wire installation improvement by multiplexing techniques 23 p4174 A70-44543

Boeing 747 airliner passenger entertainment and service electronics multiplexing system, discussing cable and connectors selection and design 23 p4174 A70-44544

Superjet airliners wiring connectors for power distribution, signal circuitry and self ejecting push buttons for passenger seats 23 p4174 A70-44545

WIRING SYSTEMS

U WIRING

WKB APPROXIMATION

U WENTZEL-KRAMER-BRILLOUIN METHOD

WOMEN

U FEMALES

WOOD AIRCRAFT CONSTRUCTION

U AIRCRAFT STRUCTURES

WOOL

Wool felt based carbon and graphite composite materials for orthogonally isotropic high shear strength compared with rayon felt based composites 13 p2437 A70-28776

WORDS [LANGUAGE]

Analysis method permitting English speech sound recognition by computer for different speakers 08 p1460 A70-20815

Low temperature terminology at December 1969 Paris conference, discussing temperature scale, superconductivity, liquid He, supercooling, subcooling, cryo and cryogenic 14 p2616 A70-31013

Fire and fire test scope and meaning limitations for consumer awareness 23 p4208 A70-43871

Automated Readability Index for technical materials weighting word and sentence length in multiple regression equation 24 p4308 A70-45510

WORK

NT PHYSICAL WORK

Work of plastic deformation in two dimensional rolling determined by energy dissipation function 05 p0857 A70-17017

Systematization of thermodynamic cycles from elementary reversible evolutions concerning exchange of work, heat and combined relations 06 p1173 A70-17470

WORK CAPACITY

- Reduced traction effects on human work performance in weightless and lunar gravity environment
 - 01 p0037 A70-10959
- Frog sartorius muscle heat production and work effect measured under isotonic and isometric conditions, using gradient layer calorimetry
 - 02 p0232 A70-11715
- Mathematical models construction for predicting and measuring air traffic controller workload, using synthetic and analytic methods
 - 02 p0332 A70-11972
- Air traffic control system for intercity and metropolitan VTOL airway reducing pilot and air traffic controller workloads
 - 02 p0335 A70-12135
- Helicopter avionic systems man machine capability estimation based on pilot workload, applying results to design evolution
 - 02 p0244 A70-12136
- Task loading of human operator in terms of central capacity sharing model, discussing model implications for mental workload measurements
 - 02 p0245 A70-12142
- Effect of immersion in thermoindifferent water on circulatory control and work capacity in trained and untrained subjects
 - 02 p0241 A70-12770
- Analog computer model of human cardiovascular control system to reproduce subject response to sub-maximal workload
 - 03 p0438 A70-14081
- Lactate accumulation and anaerobic work threshold in subjects exercised on bicycle ergometer, considering muscle contraction effect on oxygen supply
 - 03 p0431 A70-14293
- Physiological limitations of air traffic controllers, considering stress factors connected with workload
 - 04 p0716 A70-15314
- Catechozamine excretion, cardiovascular functions and subjective effort in healthy male subjects under various physical work loads
 - 05 p0801 A70-16141
- Prolonged wakefulness effect on human work capacity in isolated chamber, determining physical, intellectual and sensory capacities
 - 05 p0809 A70-17117
- Cardiac work limiting factors during exercise under hypoxia, studying cardiac output and coronary blood flow capacities
 - 06 p0991 A70-17282
- Environmental thermal stress effect on human performance under high mental and low physical workload
 - 10 p1812 A70-24505
- Satellite communications system optimal parameters and efficiency dependence on working capacity, discussing economic aspects of HF sets increased number
 - 11 p1995 A70-25345
- Hypokinesia effects on working capacity of subjects performing manual aircraft control assignments during bed rest
 - 13 p2352 A70-29340
- Myocardium potential working capacity in relation to diastola duration of ventricles
 - 13 p2355 A70-29767
- Human muscular strength capacity relationship to maximal or submaximal dynamic work performance
 - 16 p2853 A70-33668
- Performance in monotonous work situations, discussing various factors affecting efficiency
 - 18 p3224 A70-36317
- Satellite communications system optimal parameters and efficiency dependence on working capacity, discussing economic aspects of HF sets increased number
 - 20 p3589 A70-40457
- Work load effect on ballistocardiogram by minute cardiac force /MF/ measurement, using bicycle ergometer
 - 21 p3763 A70-41233
- Aged conditioned changes in muscular working capacity, relating developments in functionally labile nerve centers
 - 22 p3969 A70-42898
- Epidemiological investigations of coronary disease in Finland, relating customary loads and working capacity
 - 22 p3969 A70-42903
- Low carbon dioxide concentration breathing effects on exercise tolerance, discussing aerobic capacity decrement and hypercapnia occurrence
 - 22 p3973 A70-43637
- Aircraft crew and pilot in-flight work load measurement and simulator
 - [ICAS PAPER 70-43]
 - 23 p4138 A70-44141
- Astronaut work capacity and adaptation during long term flight of space vehicle Soyuz-9
 - 23 p4154 A70-44651

WORK DECREMENT

U WORK CAPACITY

WORK FUNCTIONS

- Oleic acid concentration effects on electron work function during surface-active agent deposition on Fe, Ni, Cu, Al and steel surfaces
 - 01 p0099 A70-10074
- Temperature effect on work function minimum of cesiated W surfaces
 - 01 p0154 A70-10108
- Metal/ferroelectric work functions in c-domain barium titanate crystals in short circuited capacitor, noting effect of electrodes presence
 - 01 p0156 A70-10186
- Mo-Si epitaxial planar Schottky barrier diodes, describing reverse I-V characteristics improvement by edge leakage effects elimination
 - 01 p0052 A70-11174
- Schottky barrier diodes design for wideband radiometer mixers to obtain optimum noise performance and broadband operation by DC bias application
 - 03 p0457 A70-13968
- Anode work functions from cesiated metal surfaces as parameters for thermionic converter systems analysis
 - 04 p0627 A70-14946
- Schottky barrier FET fabrication using epitaxial growth of single crystal GaAs on insulating sapphire substrate
 - 04 p0660 A70-15364
- Work function measurement for adsorption of diatomic I, Br and Cl on W crystal using electron beam retarding potential method
 - 05 p0891 A70-15973
- Electron work function variation of W in Ba-Cs-Sr vapor combinations determined using thermionic diode
 - 05 p0891 A70-15974
- Chromium films obtained on tungsten by sputtering, studying structure and work function at various temperatures
 - 08 p1516 A70-21123
- Schottky barrier diodes microwave power rectification efficiency, developing diode losses theory based on back capacitance, series and front resistance and knee voltage
 - 08 p1474 A70-21274
- Al n-type Si Schottky barrier diode characteristics, discussing I-V, barrier height, temperature dependence, photoemission, LF noise, etc
 - 09 p1644 A70-22210
- Volt-ampere characteristics of metal-semiconductor contacts for Schottky barrier diodes, investigating suppression of minority carriers and frequency response
 - 09 p1741 A70-23352
- Germanium, silicon and gallium arsenide point contact and Schottky barrier diodes as submillimetric wavelength detectors and mixers
 - 11 p2017 A70-25736
- Work and energy theorems in linear elasticity, discussing potential energy, real work, complementary energy and energy coefficients
 - 11 p2142 A70-26625
- Nomographic Richardson-Dushman equation solutions for thermionic electron emission devices, giving current density for various work functions and electrode temperatures
 - 12 p2271 A70-26894
- Surface parameters influence on energy transfer to arc jet anode, discussing work function, accommodation coefficient and diffuse reflection coefficient of electrons
 - [AIAA PAPER 69-107]
 - 12 p2281 A70-27809
- Surface oxidation effects on thermionic work functions of Be determined by visual observation and X ray diffraction patterns analysis
 - 12 p2288 A70-28004
- Nb single crystal faces electron work functions and comparison of thermionic emission patterns with Ba-Nb system
 - 14 p2625 A70-30162
- Electronegative adsorbate effect on work function of Ba-W system
 - 18 p3298 A70-37111
- Critique of paper on electron diffraction study of Ce adsorption on W surface, discussing electron work function changes and data discrepancies
 - 19 p3473 A70-37548
- Cesium films structure and work function on W /011/ face, discussing order-disorder transition
 - 19 p3487 A70-37817
- Gadolinium surface work function from contact potential difference against platinum
 - 20 p3687 A70-39996
- Temperature and bias voltage dependence of zero bias tunneling structure in p-type GaAs-Au Schottky junctions
 - 21 p3863 A70-41917
- Low noise GaAs Schottky barrier beam lead mixer and chip style diodes, discussing fabrication and performance
 - 22 p3998 A70-43333

WORK-REST CYCLE

- Precious metals, measuring tension, grinding and polishing induced surface plastic deformation effects on electron work function and exoemission
 - 23 p4204 A70-43927
 - Krylov-Bogoliubov virtual work principal, investigating nonlinear vibrations, extending to heteronomous vibrations
 - 23 p4266 A70-44028
 - Surface potential and electron work function of single crystal plane W/110 under zero-field and strong-field conditions
 - 23 p4230 A70-44797
- ## WORK HARDENING
- ### NT STRAIN HARDENING
- Propagation equations for spherical waves in elastoplastic work hardening materials
 - 03 p0585 A70-12972
 - Surface work hardening and stress concentrations effects on fatigue strength of alloy under asymmetric tension and compression load cycles at high temperatures
 - 04 p0707 A70-15270
 - Surface work hardening effects on steels resistance to low cycle fatigue with stress concentration, applying results to aircraft parts
 - 06 p1085 A70-17403
 - Shot delivery per second per unit area from ejector nozzle during shot peening, determining ideal delivery rates for shot of various sizes
 - 07 p1291 A70-18830
 - Ti additions influence on steel work hardening, specific weight, magnetic properties and structure
 - 08 p1515 A70-20924
 - Elastic-plastic work hardening sandwich arch under given loading rate analyzed for stress rates using integral equation
 - [ASME PAPER 69-APM-21]
 - 08 p1593 A70-21616
 - Yield stress and work hardening properties of tension-deformed vanadium single crystals as function of purity
 - 08 p1522 A70-21750
 - Work strengthening and microstructure of Co-Ni base alloys containing Cr and Mo, discussing deformation induced martensitic transformation
 - 09 p1705 A70-22806
 - Elastoplastic compressible sheet metals reinforced by isotropic work hardening under action of bending moments, analyzing stresses and strains
 - 10 p1955 A70-24056
 - Nitrogen content effect on proportional limit and work hardening rate of austenitic stainless steel at 302 F
 - 10 p1905 A70-25169
 - Phenomenological theory of crack propagation during fatigue experiments, noting role of work hardening
 - 13 p2510 A70-28672
 - Minimum principles for rate solution in elastoplastic work hardening materials with regular yield surface
 - 13 p2513 A70-29152
 - Piecewise linear elastoplastic matrix structural theory with interacting yield planes, discussing kinematic and isotropic hardening
 - 14 p2656 A70-30475
 - Al-Mg alloy sheets work hardened plastic properties, tensile strength and elongation
 - 14 p2597 A70-30962
 - Work hardening and tempering effects on Al-Mg alloy stress corrosion and mechanical properties
 - 14 p2597 A70-30963
 - Work hardening properties of Ni single crystals of various orientations during intermittent and continuous plastic deformation
 - 15 p2762 A70-32394
 - Work hardening maxima of alpha-Ti as function of strain rate and temperature
 - 19 p3451 A70-37568
 - Steady state ultraharmonic oscillations of first and third order in yielding systems with linear work hardening law
 - 19 p3542 A70-38059
 - Notched sheet failure prediction based on Dugdale crack model, including work hardening and finite width effects, strain fracture criterion and yield failure mechanism
 - 19 p3548 A70-38624
 - Elastoplastic work hardening continua incremental boundary value problem with allowance for distributed dislocations, using quadratic programming concepts
 - 19 p3549 A70-38667
 - Bcc metals and alloys stress relaxation, internal stress and work hardening, discussing temperature dependence and dislocation motion
 - 20 p3647 A70-39108
- ## WORK-REST CYCLE
- Diurnal rhythms of physiological functions and human adaptation to shifted sleep-wakefulness schedule on healthy pilots subjected to solitary confinement
 - 03 p0423 A70-13711
 - Cardiovascular system, neuromuscular activity and mental fitness of subjects performing physical and mental assignments with prescribed work-rest schedule during confinement
 - 03 p0425 A70-13895

Human alveolar-arterial oxygen differences during rest, sleep and exercise in initial hypoxia induced by simulated high altitude exposure

03 p0429 A70-14161

Biological rhythm perturbations effect on astronauts, emphasizing waking-sleeping rhythm during space flights

04 p0630 A70-14610

Human skin temperature variations in supramuscular areas under physical activity and rest

04 p0638 A70-15505

Synchronous variations in skin and muscle temperatures of musculus gastrocnemius and flexor carpi in human subjects performing intermittent physical exercises

04 p0639 A70-15506

Skin-muscle temperatures ratio variations in dogs during periods of activity and rest

04 p0639 A70-15508

Activity and rest alternation effect on fatigue and rehabilitation behavior of trained athletes, discussing muscle performance characteristics

04 p0639 A70-15510

Physical exercise and rest regime evaluation by thermoelectric method recording skin temperature above gastrocnemius muscle

04 p0640 A70-15513

Wake-sleep rhythm of spacecrews for operational capacity to maintain constant watch of spacecraft, suggesting recreation of terrestrial time cycle in space

05 p0799 A70-15766

Postrest upswing or muscles warm-up in motor skill learning

05 p0803 A70-16671

Hypoxia effect on self paced work behavior of humans

05 p0803 A70-16672

Physical training effects on sedentary men with stable activity pattern, recording heart rates and oxygen uptake

07 p1215 A70-20171

Diurnal rhythms of physiological functions and human adaptation to shifted sleep-wakefulness schedule on healthy pilots subjected to solitary confinement

11 p1985 A70-25511

Continuous active work effects on human sensorimotor performance, comparing latency distributions in mass and spaced practice groups

12 p1278 A70-27046

Daily electrolyte excretion dynamics of subjects with shifted work-rest schedule, noting disagreement with Scharp results

13 p2358 A70-29343

Closed circuit respiration studies on subjects at rest and work, demonstrating potassium superoxide as oxygen source in breathing apparatus

15 p2688 A70-31500

Circadian rhythmical changes in biological organisms by earth rotation, emphasizing diurnal variations role in sleep-wakefulness rhythm

15 p2680 A70-31742

Mechanisms responsible for sleep-wakefulness rhythm, investigating effect of lesions in CNS, electrical excitation of brain, neurons activity, etc

15 p2680 A70-31744

Airline pilots sleep patterns during worldwide east-west routes, considering modification by irregular duty periods and time zone adaptation

15 p2689 A70-31882

Aircraft crew oral temperature related to work-rest schedules, discussing hypothermia, flight stress and in-flight depression

17 p3032 A70-35563

Thermoregulation of hedgehogs during muscular activity in cold environment, recording electrical activity, oxygen consumption and body temperature during work-rest cycles

18 p3219 A70-36542

Athletes ventilation and heart rate dynamic responses to supine leg exercise with sinusoidal work load

20 p3576 A70-40329

Human leg blood flow distribution between deep and superficial veins during alternate treadmill work-rest periods

21 p3767 A70-42160

WORKING FLUIDS

Heat transfer data for rotary piston and conventional piston engines, studying compression energy losses due to working fluid leakage

05 p0897 A70-17002

Heat pipe structural alloys compatibility with different working fluids using capsule tests at high temperatures, noting corrosion behavior

07 p1304 A70-18812

Electrodynamic compressor with direct conversion of electric energy into mechanical energy, improving conversion efficiency by using plasma as working medium

07 p1196 A70-19658

Multiple pass tube heat exchangers efficiency, solving energy and heat transfer equations from fluids homogeneity and constant thermal capacity considerations

08 p1596 A70-20613

Electrodynamic generator channel electric field model, evaluating electric body forces on ionized working fluid flow

10 p1807 A70-24571

Molecular densities and population inversion pulse shape in working gas in mixture with thermally excited auxiliary gas

10 p1920 A70-25112

Reciprocating Rankine-cycle engine with organic working fluids, noting piston speed and efficiency

[SAE PAPER 700162] 11 p1982 A70-25372

Book on engineering aspects of MHD power generation, discussing working gas ionization and electrical conductivity, incompressible conducting fluid motion in magnetic field, etc

11 p1982 A70-25525

Working body properties effects on one component liquid-metal MHD system efficiency with vapor condensation cycle

12 p2164 A70-27329

Asynchronous liquid metal MHD generator parameters, assuming constant vertical distribution of working fluid velocity

13 p2349 A70-28968

Axial-flow compressors stall characteristics measurement using water as working fluid

13 p2341 A70-29446

Liquid metal level indicators and resistance type level meters for turbines using alkali metal as working media

14 p2587 A70-31010

Radiative properties of construction properties and working media, noting importance to radiative heat transfer calculation

15 p2827 A70-32143

Power plant using carbon dioxide planetary atmosphere as working fluid, noting weight reduction

15 p2828 A70-32262

Electrodynamic compressor with direct conversion of electric energy into mechanical energy, improving conversion efficiency with plasma as working medium

15 p2678 A70-32695

Al radiator with thin stainless steel tube liner using liquid metal coolant tested for heat rejection system of SNAP-8 Rankine cycle power system

[AIAA PAPER 70-855] 16 p3000 A70-33922

Metal corrosion effects in Rankine cycle lithium-boiling potassium test loop simulating working fluids of spacecraft nuclear turbopropulsion system

16 p2933 A70-34204

Working fluid /Ar/ purity and stability effects on fatigue life and creep of Nb and Mo alloys using gas analysis, microstructure and microhardness data

17 p3126 A70-35715

Liquid metal MHD power conversion system with Cs and Li as working fluids, describing hydraulic, electrical and high temperature tests results

20 p3680 A70-39986

Effective dissociation potential measurement for alkali compound seed in MHD generator working fluid

20 p3682 A70-40159

MHD generators nonequilibrium ionization improvement by blowing low work function particles into cold working gas to obtain required conductivity

21 p3855 A70-40794

Space vehicles dimensions effects on working fluid mass and power required for orientation

21 p3927 A70-40826

Working fluids liquid property variations effects on cryogenic heat pipe performance

21 p3946 A70-41043

Liquid or vapor phase working fluids penetration effects on steady state and transient performance of hot reservoir gas controlled heat pipes

21 p3946 A70-41047

Heat pipe performance map with ammonia as working fluid, comparing thermal transport efficiency with water pipe

21 p3947 A70-41050

Mercury as stainless steel heat pipe working fluid, determining wetting characteristics and heat transfer capability

21 p3947 A70-41051

Working body properties effects on one component liquid-metal MHD system efficiency with vapor condensation cycle

21 p3760 A70-42070

Equilibrium performance of closed Stirling cycle with chemically reactive gas as working fluid, discussing power density and thermal efficiency

22 p3982 A70-42756

Plunger pump for aircraft hydraulic systems, measuring working fluid temperature effect on cavitation

22 p3965 A70-42817

Working medium excess and absolute pressure effects on pneumatic elements characteristics

22 p3967 A70-43566

German monograph on casing and hub wall friction effects on three dimensional flow in turbocompressors in subsonic compressible working fluids

24 p4287 A70-45096

WORLD U EARTH [PLANET]

WORLD DATA CENTERS

Worldwide Apollo data transmission network emphasizing computer operations for message collection and distribution, command and telemetry processing, etc

06 p1005 A70-17310

Earth Resources Data Processing Center magnitude and facility planning compared with NASA centers

[AIAA PAPER 70-324] 09 p1793 A70-22863

WRINKLING

NT FLANGE WRINKLING

Tension rays and load transfer from compact member via wrinkled membrane determined by variational technique using maximum strain energy

12 p2322 A70-27225

Postwrinkling nonlinear behavior of conical shell of revolution subjected to bending loads

[AIAA PAPER 69-90] 12 p2326 A70-27816

WROUGHT ALLOYS

Monograph on elevated temperature strength data for wrought austenitic stainless steels, considering yield, tensile, creep and rupture strengths for allowable stresses

03 p0510 A70-13300

Grain size, forging parameter and microstructure effect on stress-rupture properties of wrought Ni-base alloy

03 p0511 A70-13567

Ni-Nb intermetallic compound precipitation effect on various phase formations in strained samples of Alloy 718 /wrought Ni base alloy/

03 p0511 A70-13568

Interrelation of precipitation state, mechanical properties and electrical conductivity of wrought aluminum age hardened alloy under varied heat treatment conditions

07 p1294 A70-19389

Wrought aluminum based high strength alloys structure and mechanical properties

08 p1522 A70-21708

Electroslag melted titanium wrought shapes mechanical properties, comparing with double vacuum arc melted material properties

17 p3112 A70-34356

Ultrasonic delta technique inspection method for flaw detection in weldments or wrought materials

24 p4335 A70-45572

Drilling machinability of wrought Al alloys, relating tool force to hardness, feeding and cutting speed

24 p4349 A70-46195

X

X BAND

U SUPERHIGH FREQUENCIES

X RAY ABSORPTION

Spectral distribution of X ray atmospheric absorption used to determine high energy photoelectrons spectrum

01 p0172 A70-11494

Laser produced plasma temperature measurements using method of X rays selective transmissions through different absorbing films

06 p1081 A70-17596

Cosmic X rays interstellar absorption, giving atomic He total photoionization cross section

18 p3308 A70-36899

High temperature gas boundary layer flows with or without magnetic fields, discussing measurement by X ray absorption technique

19 p3405 A70-38192

D region ionization budget, evaluating short wavelength X rays role

23 p4236 A70-43860

X RAY ANALYSIS

NT LAUE METHOD

Abnormal burning surface regression in rocket motor solid propellant detected with flash X ray exposures

01 p0085 A70-10021

X ray topography of postannealing substructure of neutron irradiated W and Mo single crystals, indicating increase in disorientation

01 p0115 A70-10065

Petrological, X ray and chemical analyses of Muzaffarpur Ni-rich axinite, showing kamacite, taenite and minor schreibersite composition

01 p0177 A70-10328

Microprobe analyzer for light elements using electronic optics probe, sample visualization devices and equipment for X photon detection and measurement

[ONERA-TP-774] 02 p0275 A70-12210

X ray metallography methods applied to high temperature protective coating development, refractory alloys strengthening and metal fatigue studies

04 p0711 A70-15706

X-ray line broadening analysis for lattice damage in kamacite phase of Fe meteorites, evaluating particle size and elastic strain

05 p0915 A70-16828

Isothermal sections in Ti-Ni-B, Mo-Ni-B and W-Ni-B at 800 C determined by X ray analysis

06 p1090 A70-17846

Isothermal section determination in Mo-Cr-B at 1000 C using X ray, metallographic analyses and microhardness measurements

06 p1090 A70-17847

Percentage changes in X ray calibration wedge mass equivalency to actual changes in bone Ca content

06 p0997 A70-18015

Binary CdSb-CdTe systems investigated by X ray and microstructural analyses; showing mechanical mixture constitution and p-type conductivity

07 p1355 A70-18701

X ray structural and electrophoretic investigation of donor and fibrinolytic blood protein components, observing crystalline to amorphous transition in blood serum and plasma lyophilization

09 p1621 A70-23149

Stacking faults developed in double hexagonal closed-packed phase of Ni-Ti alloy in cold worked and annealed conditions, using X ray line broadening

10 p1906 A70-25228

Cinedensigraphic analysis of diaphragmatic ventilatory movements, obtaining correlation between lung volume and diaphragm and rib cage movement

14 p2537 A70-30383

Thermoluminescence, X ray and stored energy measurements of Apollo 11 samples, comparing surface outputs to interior

21 p3916 A70-41665

Short pulse length X ray flash electro-optical recording equipment for explosive processes, describing technique, experimental setup, optical characteristics and information retrieval [SMPT PREPRINT 69]

22 p4037 A70-43071

X ray analysis - Conference, University of Denver, August 1969

23 p4243 A70-44414

Potassium acid phthalate crystal X ray spectrometric properties measurements, discussing parallel position rocking curves and reflection coefficients

23 p4230 A70-44420

X RAY APPARATUS

He camera with reduced linear absorption coefficient for contact microradiography, relating exposure, X ray wavelength and atmosphere

01 p0084 A70-10013

Backreflection X ray microbeam camera with arrangement for positioning preselected area to study grain boundary during creep by Laue method

03 p0492 A70-13759

Thermoluminescent glass X ray dosimeter sensitivity tested as function of rigidity of gamma and X radiation, noting compensating filters for incident radiation

08 p1496 A70-21217

High speed X ray flash motion picture installation for ballistic photography [SMPT PREPRINT 76]

22 p4037 A70-43068

Time resolving X ray grating polychromator, discussing photoelectric attachment with surface barrier semiconductor detectors

22 p4037 A70-43069

Radiography using projective magnification from X ray tube with small focal spot, describing equipment and applications

24 p4337 A70-45707

Thermonuclear spacecraft propulsion, comparing X ray pumped gas laser and ion drive systems

24 p4377 A70-46211

X RAY ASTRONOMY

X ray line emission from Sco X-1 using Monte Carlo estimates of spectral distribution of scattered photons in terms of Fe line and cosmic abundance

01 p0169 A70-10338

Pulsed high energy X rays from Crab Nebula pulsar NP 0532 measured by balloon-borne X ray telescope

01 p0169 A70-10345

Sco X-1 high energy X ray emission intensity changes observed by balloon-borne telescope

01 p0169 A70-10346

Gamma ray astronomy using balloon-borne telescope with digitized spark chamber

02 p0364 A70-11785

Celestial X rays from Cygnus XR-1 detected during high altitude balloon flight, noting compatibility with black body radiation or hot thin plasma

02 p0356 A70-11786

Polarization of nonspherical plasma emission region in thermal X ray stars

02 p0357 A70-11787

X ray source Sco XR-1 proper motion using photometry, suggesting association with Scorpius-Centaurus complex of young disk stars

02 p0372 A70-12248

X ray source GX341-6 with soft spectrum detected in Aras constellation by Aerobee rocket, including neighboring X ray sources in determining galactic coordinates, positions and fluxes

02 p0372 A70-12249

Cosmic X ray background interpreted as Compton collisions between cosmic black body photons and relativistic electrons in radio sources

02 p0360 A70-12792

Cosmic x ray astronomy in near future for source detection concerning spectral bands, polarization, position, instrumentation, etc

02 p0304 A70-12794

Cosmic X ray astronomy, discussing existing techniques, limitations, use of onboard computers and future requirements

02 p0304 A70-12795

Neutron star X synchrotron radiation from gas accretion producing strong magnetic field with high electron temperature

03 p0557 A70-13220

Gamma ray astronomy experiments, discussing likelihood method for analyzing and reporting results

03 p0559 A70-13810

Spectral index for diffuse X ray sky background within specific band determined from rocket observations with wide angle telescope

03 p0479 A70-14223

VLF radio monitoring of celestial X ray fluxes from ground for long periods, discussing ionospheric D region conductivity

04 p0739 A70-14521

Intensity and spectral distribution measurement techniques for nonvisible extraterrestrial radiation, discussing rocket spectroscopy results

04 p0757 A70-15648

Energy spectra of cosmic diffuse X ray component and distribution over northern sky, determining Crab Nebula and Cygnus spectral characteristics

05 p0901 A70-16305

Solar activity study based on solar X ray spectra observation, considering flare mechanism

05 p0903 A70-16719

X ray source position determination by balloon observations, estimating intensity in different energy ranges

05 p0904 A70-16978

Sco X-1 line spectra search in X ray spectrum by rocket-borne proportional counters, noting iron line emission

05 p0904 A70-16979

Rapid fine structure in hard solar X ray bursts observed by OSO-5, explaining time structure by mechanism based on repetitive production of monoenergetic electrons

05 p0904 A70-16980

Sco X-1 simultaneous X ray and optical flares correlation and X ray enhancements

08 p1561 A70-20900

Shear and rotation limits on universe from X ray background, using Euclidean shear and vorticity models with open and closed geometries

08 p1561 A70-20901

Neutron star X synchrotron radiation from gas accretion producing strong magnetic field with high electron temperature

08 p1563 A70-21653

Angular size measurement for galactic X ray sources in Sagittarius region using modulation collimator aboard sounding rocket

09 p1744 A70-22521

X ray fluxes upper limits from quasars 3C 196, 3C 186 and 3C 380 measured by balloon flight experiments

09 p1745 A70-23271

Universal X ray background as superposition of nascent pulsars in various galaxies, using Crab Nebula pulsar as guide

09 p1748 A70-23792

Gamma ray astronomy above 10 Mev, investigating intensity dependence on galactic latitude and radiation detection technology

10 p1931 A70-24067

Cosmic rays, particles and fields physics in relation to radio and X ray astronomy

10 p1931 A70-24410

Pulsars in supernova remnants emitting X rays

10 p1933 A70-24627

X ray astronomy, discussing emission processes, radiation classification for intensity plot against energy, cosmic sources distribution, etc

11 p2111 A70-26035

Cosmic X ray sources, considering locations, fluxes and angular sizes from Aerobee rocket observations

12 p2292 A70-27384

Cosmic X ray sources searched for by Aerobee rockets, noting locations and distribution correlation with galactic novae

12 p2292 A70-27385

Night sky X ray sources at low galactic latitudes, describing rocket survey experiment

12 p2292 A70-27386

Cosmic gamma rays observation by balloon flight and satellite with scintillation detector, tabulating counting rates in pulse height channels relative to Crab Nebula

12 p2292 A70-27387

X ray source from Coma cluster of galaxies, interpreting observed flux on basis of missing mass suggested by Virial theorem

12 p2293 A70-27388

Beryllium proportional counters for satellite X ray astronomy, noting long term stability and environmental resistance

12 p2232 A70-27403

Diffuse cosmic X and gamma ray background radiation isotropic component

12 p2295 A70-27887

Bragg reflecting crystals for spectroscopy and polarimetry in X ray astronomy

13 p2489 A70-28904

Cosmic rays and cosmic X rays, considering galactic and extragalactic sources, diffuse background, detection devices, etc

13 p2477 A70-29160

Galactic X ray stars and X ray sources positions, appearance frequency and intensities

13 p2495 A70-29818

Light elements detection in interstellar grains by observing halo around X ray source arising from small angle scattering

14 p2631 A70-30539

Angular size of high energy X ray source in Crab Nebula from balloon-borne X ray modulation collimator

14 p2631 A70-30789

Total Absorption Shower Cascade (TASC) detector for gamma ray astronomy space, discussing energy and angular resolution

14 p2587 A70-31004

X rays and primary cosmic radiation intensity measurements near top of atmosphere, describing rocket payload and launch

14 p2632 A70-31307

Planetary gamma and X radiation by remote sensing and passive observation for gross chemical composition

15 p2793 A70-31749

X ray differential drift scans of moon, measuring cold limb brightness temperature and temperature distribution

16 p2974 A70-33646

X and gamma ray astronomy instrumentation, point sources, continuum emission, line spectra, etc

16 p2976 A70-33721

Sounding rocket X ray survey of Cassiopeia region for supernova remnants and galactic source distribution

17 p3153 A70-34528

Luminous nebulae near Sco X-1 indicating H beta emission

17 p3156 A70-34829

X ray spectrum analysis for Crab, Cas A and SN 1572 supernova remnants

17 p3156 A70-34830

Simultaneous measurement of optical and X ray emission from Scorpius X-1 and X ray diffuse background, using rocket-borne scintillation counter

17 p3157 A70-34831

X ray observations of Crab Nebula

17 p3164 A70-35115

Centaurus A radio galaxy X ray survey, implying upper limit of background radiation temperature

18 p3308 A70-36516

Extragalactic objects 3C 273 NGC 5128 and M87 X ray emission detection, using proportional counters on Aerobee 150 rocket

18 p3310 A70-37016

Soft X ray extended source in Cygnus Loop, indicating supernova remnant

18 p3310 A70-37022

Sco X-1 X ray source properties in 16-111 keV energy interval, using balloon-borne detectors

19 p3505 A70-38116

Cosmic X ray background measurements, describing ESRO R/73 experiment

19 p3512 A70-38491

Nonsolar X and gamma ray astronomy - Conference, Rome, May 1969

21 p3870 A70-40651

X ray astronomy instruments on sounding rockets, balloons and satellites, investigating sources distribution on celestial sphere

21 p3821 A70-40652

X ray astronomy proportional counters sensitivity, reducing higher energy radiation background contribution

21 p3821 A70-40653

Pulsar NP 0535 X rays detection by ground based observations of upper air fluorescence

21 p3871 A70-40654

COS-B satellite cosmic X ray experiment with high sensitivity and long pointing time for extragalactic sources discovery

21 p3871 A70-40655

Galactic and extragalactic discrete cosmic X ray sources by rocket observation with narrow slit collimators

21 p3871 A70-40656

Cosmic hard X ray sources spectra and time variations by balloons and OSO-3 satellite observations of Crab Nebula

21 p3872 A70-40657

Virgo XR-1 rocket observations, discussing X rays due to synchrotron emission of relativistic electrons

21 p3872 A70-40658

Hard X ray sources energy spectra in 20-120 keV range by balloon flights, presenting Sco X-1 intensities

21 p3872 A70-40660

X ray intensity sudden changes in 29.9-52.3 keV range from Sco X-1, correcting for atmospheric attenuation

21 p3872 A70-40661

X RAY DENSITY MEASUREMENT

X ray sources location, distribution and spectral characteristics, investigating emission from supernova remnants

21 p3872 A70-40662

Balloon-borne measurements of hard X radiation from direction of Virgo

21 p3872 A70-40663

Cyg-X-1 X ray source angular size and position measurements by balloon-borne collimator

21 p3873 A70-40665

Sco X-1 X ray emission data from rocket-borne measurement, indicating Fe K-emission from high ionization states

21 p3873 A70-40667

Optical photometric observations of nonsolar gamma and X ray sources WX Cen, NGC 5189 and GX3 plus 1

21 p3873 A70-40669

X ray sources spectra, discussing distribution, supernova remnants, pulsars nebulae, optical spectra and general characteristics

21 p3873 A70-40670

X ray source optical identification, discussing reflector optics, photometry and spectrography

21 p3873 A70-40671

Magnitude-color relation for Cygnus X-2 and WX Centauri, indicating opposite correlation to Sco X-1 fluctuations

21 p3873 A70-40672

Proper motion evidence for existence of X ray stars associated with Sco X-1 and Cen X-2, indicating formation by neutron stars

21 p3873 A70-40673

X ray emission from Crab Nebula pulsar by rocket-borne proportional counters, comparing with optical observations

21 p3874 A70-40674

Pulsed hard X and gamma rays from NP0532 pulsar in Crab Nebula, comparing with extrapolated optical data

21 p3874 A70-40675

X ray emission mechanisms in galactic sources, considering black body, supernova remnants, synchrotron radiation, etc

21 p3874 A70-40679

Discrete X ray and gamma ray sources theories, considering binary and gas stream models

21 p3874 A70-40680

Stellar coronas X ray fluxes from models of convection zones and corresponding mechanical energy fluxes

21 p3875 A70-40681

Cygnus X-2 point X ray source, establishing as spectroscopic binary with peculiarities

21 p3875 A70-40682

Extragalactic gamma ray and X ray intensity with power law spectrum, comparing galactic plane and high latitude spectra

21 p3875 A70-40687

Galactic or extragalactic origin of diffuse X ray background, reporting sky survey results

21 p3875 A70-40688

Diffuse background cosmic X rays in energy range 20-120 keV from balloon observations

21 p3876 A70-40689

Diffuse background of 2-20 keV X rays over Scorpius to North Galactic Pole sky band by rocket measurements

21 p3876 A70-40693

Soft X ray flux emanation from galactic disk, discussing latitude dependence, interstellar H, maps and discrete sources nature and properties

21 p3878 A70-40707

Gamma ray background anisotropy effects of Sgr A flux arising from Compton scattering and neutral pion decay, discussing complex radio and IR structure

21 p3878 A70-40926

M1 X ray emission, examining energy interval and power law spectral distribution

21 p3882 A70-41155

Galactic distribution of supernova remnants and association with pulsars and X ray sources

21 p3892 A70-41188

Strong newborn X ray source detection during balloon flight, showing softened low energy spectrum

21 p3892 A70-41190

M87 radio observations at 5 GHz, examining central region components, optical nucleus and jet and X ray emission

21 p3923 A70-42103

Orientation system for pointing balloon-borne X ray detector using flux gate magnetometer, DC amplifier and motor control relay circuit

21 p3831 A70-42249

X ray sources celestial positions in Sagittarius region, using rocket-borne rotating modulation collimator

22 p4094 A70-42928

Radio emission searched for X ray sources near Sagittarius

22 p4094 A70-42930

Scorpius X-1 X ray line emission, discussing continuum and background counts and cosmic abundance of iron

22 p4094 A70-42931

Galactic plane scanned observation of X ray sources, using large area proportional counter rocket sounding

22 p4094 A70-42986

Simultaneous X ray and optical observations of Scorpius XR-1, comparing rocket data from various flights

22 p4094 A70-42987

Cosmic X ray sources astronomic observations and implications, considering Crab Nebula, galaxies, constellations, diffuse background radiation, etc

23 p4243 A70-44415

Soft X ray astronomical instrumentation for space experiments, discussing Geiger tubes, gas counters, modulation collimators, telescopes, etc

23 p4196 A70-44416

Soft X ray slitless spectrometer with gold-shadowed transmission gratings for rapid astronomical spectral surveys

23 p4196 A70-44418

High Energy Astronomy Observatory for space X rays, gamma and cosmic rays research via unmanned spacecraft

23 p4261 A70-44680

Crab Nebula X ray pulsation identified with pulsar NP 0532 by rocket measurements, noting implications for interstellar dust density

24 p4401 A70-45371

UV Ceti type variable flare stars, observing radio and optical spectral regions for X ray production

24 p4397 A70-45763

Class 1b solar flare X ray examination, using rocket-borne liquid N cooled solid state detector

24 p4397 A70-45767

Excess galactic X rays, discussing synchrotron emission of high energy cosmic ray electrons

24 p4398 A70-46161

X RAY DENSITY MEASUREMENT

Sco X-1 high energy X ray emission intensity changes observed by balloon-borne telescope

01 p0169 A70-10346

Amplitude modulated pearl type geomagnetic micropulsations connected with auroral X ray emission variations

01 p0171 A70-11228

VLF recordings and X ray flux measurements simultaneous analysis indicating evidence of relation between dawn chorus and electron precipitation, noting ELF whistler development

02 p0293 A70-12689

Two phase density and void fraction measurement using beta, gamma and X ray radiation, considering optimal accuracy and beam collimation

02 p0305 A70-12835

Flare rising from behind solar limb deconvoluted by simultaneous recording by OSO III X ray detector and photoheliograph

03 p0558 A70-13589

X ray flux pulsations for pulsars near Crab Nebula observed in 2.5-30.0 keV range, determining pulsation profile

03 p0578 A70-14358

Balloon observations of Cen XR-2 X ray emission decrease

10 p1948 A70-24999

Sgr gamma-1 source, determining upper limit on soft X rays intensity

13 p2475 A70-28615

Plasma temperatures of X ray flux from laser induced breakdown plasmas in air, using absorption spectrometer

15 p2750 A70-31753

Crab Nebula X ray flux pulsations, analyzing spectra

17 p3152 A70-35756

Soft X ray flux emanation from galactic disk, discussing latitude dependence, interstellar H, maps and discrete sources nature and properties

21 p3878 A70-40707

X RAY DIFFRACTION

Precipitation in Ni-base superalloy analysis with dark field electron microscopy and electron and X ray diffraction

01 p0119 A70-10730

Martensite structure, discussing intensity anomalies in X ray diffraction pattern of intermetallic Ni-Nb

01 p0121 A70-10900

X ray diffraction method to determine degree of orientation of crystallites in extruded graphites

03 p0517 A70-13964

Orthorhombic form of crystalline formylmethionine transfer RNA, obtaining Patterson function from three dimensional X ray diffraction data

05 p0803 A70-16947

Neutron irradiation and annealing effects on lattice constants of titanium and chromium carbides analyzed for X ray diffractions

07 p1303 A70-18702

Apollo 11 lunar material X ray diffraction and microscope studies, noting chemical composition agreement with Surveyor 7 data

09 p1752 A70-22245

Residual macrostress measurement by X ray diffractometer methods

11 p2058 A70-26839

High modulus carbon fibers low angle X ray diffraction correlation to physical properties

12 p2259 A70-28050

Phase equilibrium of Fe-rich Fe-Al alloys using single crystal X ray diffraction

19 p3452 A70-37838

SiC whiskers X ray diffraction studies of crystal structure, suggesting single crystal permanent deformation at ambient temperatures

19 p3455 A70-37941

Bcc metals, measuring correlation between residual stress level and fatigue damage by X ray diffraction analysis

23 p4207 A70-44422

Ni base superalloys gamma prime phase long range order parameter measured by X ray diffraction

23 p4207 A70-44423

Residual stress measurement using programmed horizontal X ray diffractometer

24 p4425 A70-45729

X RAY FLUORESCENCE

K shell X ray production by proton impact compared with binary encounter impulse approximation

14 p2620 A70-31362

X ray fluorescence determination of thickness and composition of Permalloy films deposited on wire surface

18 p3258 A70-36466

Planetary atmospheres X ray fluorescence, calculating Mercury, Venus, earth, Mars and Jupiter emissions

22 p4105 A70-43230

X RAY FLUORESCENCE ANALYSIS

U X RAY ANALYSIS

U X RAY FLUORESCENCE

X RAY INSPECTION

Programming device for positioning samples under X ray beam in testing welded seams and parts

02 p0301 A70-12488

High energy neutron accelerator as fast neutron radiography source, comparing contrasts with gamma and X radiography

05 p0844 A70-15779

Ni-Cr content and variability in Ivory Coast tektites using atomic absorption and X ray emission techniques

05 p0916 A70-16837

X ray laminography for nondestructive testing based on synchronous rotation of source, sample and image forming planes

10 p1895 A70-24577

X ray inspection with direct TV viewing, discussing specimen geometry effects, equipment, applications, etc

15 p2742 A70-32778

Coating thickness measurement and analysis by radioisotope techniques including beta-particle, X or gamma ray backscatter and X ray fluorescence and absorption

15 p2742 A70-32780

X ray attenuation factor calculation as function of radiation energy and test material nature and thickness for nondestructive defectoscopy

24 p4341 A70-45581

Radiography using projective magnification from X ray tube with small focal spot, describing equipment and applications

24 p4337 A70-45707

X ray films sensitometric investigation in medical and industrial radiography, evaluating HVL and ISO methods for X ray quality

24 p4337 A70-45710

Wire and hole type penetrometers minimum perceptible image contrast level on radiograph, considering X ray quality and films effects

24 p4337 A70-45713

Automatic TV radioscopic X ray control for mass NDT of refractories and grinding wheels

24 p4368 A70-45723

Fluoroscopes for radiographic examination of materials and products with X ray and hard bremsstrahlung radiation

24 p4348 A70-45847

X RAY IRRADIATION

Characteristic X radiation intensity in atmosphere calculated using irradiating electrons spatial and energy distribution data

02 p0358 A70-12156

Radiation protective action of aminoalkylthiols, aminoalkyl disulfides, isothioureas, thiazolidine etc, in mouse tissues, erythrocytes and yeast cells exposed to X ray doses

03 p0419 A70-13307

Four layer semiconductor device triggering by X or gamma radiation calculated by transport equations for electron and hole distribution motion and electric field distribution

04 p0657 A70-14731

Experimental procedure for investigating radioprotective effectiveness of chemical compounds against X ray irradiation, discussing Cysteamine protection for golden hamsters and fetuses

06 p0993 A70-17429

- Nervous system influence on erythema radiation reactions from soft X ray irradiation, discussing blood supply effect
06 p0993 A70-17430
- X and UV radiation effects on *Escherichia coli* B/r in vacuum, noting irradiated cell inactivation and radiation sensitivity increases
06 p0995 A70-17750
- Sialic acids metabolic behavior in cerebrum, liver, myocardium and blood plasma of rats after X ray irradiation
07 p1205 A70-19289
- Reduced visual perception time in patients under X ray treatment of diencephalo-hypophyseal region
08 p1443 A70-20736
- Free radical formation in irradiated pyrimidines from ESR spectrum analysis of gamma irradiated single crystals of alloxantin, confirming radical stability
08 p1455 A70-20774
- Total body X irradiation effect on tyrosine hydroxylase and catecholamine levels in rats
09 p1616 A70-22318
- X ray effects on central nervous system noting mutations in rats, guinea pigs, chickens, dogs and rabbits
09 p1620 A70-22821
- Adrenaline effects on rats peripheral blood leukocyte content used for X-irradiation sensitivity estimation
10 p1822 A70-25177
- Gamma irradiation effects on thermal stability and decomposition of ammonium perchlorate
12 p2289 A70-26870
- X ray irradiation effects on phonocardiograms, EKGs, cardiac activity phases and Kunos-Garan mechanoelectrical coefficient in dogs
13 p2350 A70-28890
- Mammalian cells after X ray irradiation, showing two forms of DNA repair process
21 p3765 A70-42024
- X RAY PHOTOGRAPHY**
U PHOTOGRAPHY
U RADIOGRAPHY
X RAY SCATTERING
- Emission spectrum characteristic distortion in scattering of background X rays at large red shifts by melagalactic electrons, considering photon scattering effect
02 p0358 A70-12491
- Small angle X ray scattering pattern of polypropylene drawn at various temperatures in closely spaced draw ratio values through neck region
03 p0517 A70-14202
- X ray scattering from pulsar NP 0532 by interstellar grains
09 p1748 A70-23791
- X ray scattering by interstellar grains in direction of Crab pulsar and Sco XR-1
10 p1933 A70-25044
- Light elements detection in interstellar grains by observing halo around X ray source arising from small angle scattering
14 p2631 A70-30539
- Fe rich Fe-Al alloys single crystals, determining three dimensional order and atomic displacements coefficients by X ray diffuse scattering
19 p3452 A70-37839
- Integrated Bragg X ray scattering intensities for monatomic crystalline lattices, considering thermal diffuse component contribution
20 p3686 A70-39193
- Cosmic soft X rays scattering by interstellar dust grains, observing source angular size dependence on distance, wavelength and grain properties
20 p3695 A70-39233
- Low alloy Mo sheet recovery and aging characteristics studied by X ray scattering
22 p4055 A70-43124
- Scattered photon effects on cosmic diffuse X ray spectrum at balloon altitude, noting overcorrection for absorption of primary X rays
23 p4237 A70-44794
- X RAY SPECTROGRAPHY**
U X RAY SPECTROSCOPY
X RAY SPECTROMETRY
U X RAY SPECTROSCOPY
X RAY SPECTROSCOPY
- X ray spectrometer for space science and laboratory research, presenting CrK spectrum and fine structure
01 p0092 A70-11172
- Directional and spectral characteristics of bremsstrahlung X rays from auroral arc in low energy range during cosmic rays sounding rocket measurements
02 p0357 A70-12069
- Rocket-borne spectroheliograph for taking X ray and monochromatic pictures of sun in Mg II line
03 p0570 A70-13594
- Pionic transition in Ni isotopes to measure nuclear interaction effects, observing level shift and broadening
05 p0885 A70-16682
- Sco X-1 line spectra search in X ray spectrum by rocket-borne proportional counters, noting iron line emission
05 p0904 A70-16979
- Ni L alpha X ray emission line shape and position as function of bombarding electron energy, observing differential self absorption in anode
09 p1731 A70-22777
- Celestial X ray sources resolved against diffuse nearly isotropic background radiation by rocket and balloon experiments, noting brightness
09 p1745 A70-22895
- X ray astronomy, discussing emission processes, radiation classification for intensity plot against energy, cosmic sources distribution, etc
11 p2111 A70-26035
- Bragg reflecting crystals for spectroscopy and polarimetry in X ray astronomy
13 p2489 A70-28904
- X ray K spectra of Ti-Cr alloy for electron structure in titanium chromide phase region, discussing spectral intensities
13 p2435 A70-29375
- X ray bursts rise and fall observed by spectrometer onboard OSO-4
15 p2792 A70-31670
- Cyg XR-1 X ray spectrum variability by balloon-borne detectors as eclipsing properties of binary system
15 p2799 A70-31750
- Gamma ray pulse height spectra during active and quiet solar periods from midlatitude balloon flights
17 p3152 A70-35774
- Vertical secondary cosmic gamma spectra from primary nucleon and electron spectra, discussing effects of solar cycle and geomagnetic cut-off
18 p3308 A70-36500
- X rays measurement by spectrometer on satellite Cosmos 207
19 p3506 A70-38122
- X ray flux and energy spectrum of Cen-X2, Sco-X1 and Tau-X1 sources by rocket flight observation
21 p3872 A70-40659
- X ray source optical identification, discussing reflector optics, photometry and spectroscopy
21 p3873 A70-40671
- Innerbremsstrahlung of intergalactic protons colliding with electrons as source of cosmic background X rays, interpreting intensity and energy spectrum
21 p3877 A70-40700
- Galactic K series emission at 1-10 kev by low energy cosmic rays and diffuse X rays interaction with H I region heavy ions
21 p3877 A70-40704
- Solar X-ray spectra of active regions, examining emission lines, fluxes electron temperature and density and transitions
21 p3879 A70-40963
- Molecular orbital energy level diagram for metal ion X ray emission and absorption spectra interpretation from titanium and vanadium compounds
21 p3853 A70-41901
- X ray K and L emission bands and absorption spectra from TiO, TiN and TiC compared with density of states histograms, considering electronic band structure
22 p4086 A70-43003
- Soft X ray slitless spectrometer with gold-shadowed transmission gratings for rapid astronomical spectral surveys
23 p4196 A70-44418
- Solar X ray spectra interpretation by laboratory measurements, using plasma X ray source and potassium acid phthalate spectrometer
23 p4237 A70-44419
- Potassium acid phthalate crystal X ray spectrometric properties measurements, discussing parallel position rocking curves and reflection coefficients
23 p4230 A70-44420
- Auger spectra characteristics obtained with X rays and electrons from radioactive alpha sources
23 p4222 A70-44421
- X ray spectra from paraboloidal plasma focus devices, measuring electron energy produced by photoelectric effect and by Compton scattering
23 p4229 A70-44990
- X RAY STRESS ANALYSIS**
- Mo single crystals creep behavior temperature and stress dependences using X ray analysis
09 p1708 A70-23543
- X RAY STRESS MEASUREMENT**
- Nondestructive X ray stress measurement equipment for large specimen, using diffractometer focusing
01 p0085 A70-10022
- X ray elastic constants measured in cementite phase in high carbon tool steel following plastic deformation at tension, noting residual stresses increase and balance
06 p1084 A70-17126
- X rays of surface residual stresses produced during fatigue process of annealed low carbon steel and copper
06 p1084 A70-17128
- Al and Ti alloys residual stress determination by X ray diffraction
09 p1704 A70-22796
- X RAY TELESCOPES**
- Solar X rays observation from manned orbiting workshop of Apollo Applications Program, describing telescope/camera assembly and X ray event analyzer
11 p2057 A70-26506
- Twin crystal X ray telescope principle, design and application, discussing radiation sources nature and measurement methods
11 p2057 A70-26824
- Reflecting X ray telescopes with glancing incidence mirror, discussing design, manufacture and testing
16 p2904 A70-33150
- Balloon-borne X ray telescope star sensor with one arc minute accuracy, discussing design and Cyg X-1 location measurement
17 p3090 A70-35312
- Soft X ray astronomical instrumentation for space experiments, discussing Geiger tubes, gas counters, modulation collimators, telescopes, etc
23 p4196 A70-44416
- X RAY TESTING**
U X RAY INSPECTION
X RAYS
NT SOLAR X-RAYS
- Model explaining background X radiation spectral properties, assuming production by Compton scattering of radio, IR and optical quanta by relativistic electrons
01 p0171 A70-11124
- Diffused X ray background in isotropic world models in terms of Compton radiation from cosmic ray electrons in intergalactic space
02 p0356 A70-11743
- Diffuse soft X ray photoionization and heating of H I regions compared to cosmic ray heating
02 p0364 A70-11784
- Focused deuterium plasma discharge neutrons and X rays energy spectra, flux and time resolved collimation measurement with nuclear emulsions and scintillation detectors
02 p0348 A70-12241
- Cold cathode soft X ray source with discharge controlled by automatic pressure controller /APC/ or metering valve, noting applicability to radiography, luminescence, etc
02 p0271 A70-12743
- Cosmic X ray sources optically observed from ground, discussing identification, distribution, etc
02 p0359 A70-12790
- Discrete galactic and extragalactic X ray and gamma ray sources observation, discussing energy spectra, emission mechanisms, properties and suggested models
02 p0360 A70-12791
- Electron and hard photon /X and gamma ray/ production and propagation in expanding metagalaxy, deducing universe matter density, cosmic ray sources, etc
03 p0557 A70-13225
- Rotating prism method for obtaining time correlation between streak photographs and characteristic waveforms of flash X ray discharges
03 p0492 A70-13762
- Stellar X ray effect on nighttime lower ionosphere wave reflection suggested from VLF propagation data
03 p0562 A70-14224
- Three dimensional X ray imaging technique from conventional radiograph set photoreduced and projected by special purpose imaging system
04 p0686 A70-14561
- Gamma rays due to cosmic ray electrons bremsstrahlung in interstellar medium, predicting diffuse galactic X ray flux
04 p0742 A70-15713
- Ionization gage with screened collector, showing limit current in high vacuum equal to X ray radiation component
05 p0847 A70-15997
- Galactic X rays and high energy gamma rays in terms of cosmic ray electrons Compton scattering by submillimeter radiation
05 p0900 A70-16100
- Galactic synchrotron emission and diffuse X ray background, noting correspondence between spectral indices of radio and X ray emissions in polar directions
05 p0913 A70-16472
- X rays from Sco XR-1 compared with galactic cosmic rays and solar Lyman alpha radiation to determine ionospheric ionization causing radio wave attenuation
06 p1134 A70-17443
- Interstellar gas ionization and heating by background X radiation, studying neutral hydrogen density distribution between spiral arms and at galactic peripheries
07 p1383 A70-19401
- Atmospheric X ray photons measured regularly by sounding balloons in U.S.S.R., discussing X ray photon flux relation to charged particle fluxes
07 p1367 A70-19445
- Cosmic X ray source spectra possibly due to plasma bremsstrahlung
07 p1368 A70-19700

Nonthermal mechanism for high energy radiation and particle emission from X-stars and pulsars
08 p1575 A70-21364

Electron and hard photon /X and gamma ray/ production and propagation in expanding metagalaxy, deducing universe matter density, cosmic ray sources, etc
08 p1563 A70-21658

Supernovae remnants X ray emission associated with explosion process generating relativistic particles, indicating Crab Nebula as X ray object
09 p1749 A70-21998

Compact nonthermal radio sources in M87 giving rise to X ray source through Compton effect
09 p1744 A70-22520

Celestial positions and intensities of X ray sources in Sagittarius region obtained from rocket experiment
09 p1744 A70-22522

Magnetic funneling model proposed for accretion of matter onto neutron star to study X ray production during motion through interstellar cloud
10 p1931 A70-23902

Radiation transport calculations based on approximate method restricted to X ray and low energy gamma ray region of electromagnetic spectrum
10 p1915 A70-23977

Laser radiation conversion into kilovolt X rays using planar heated plasma, discussing electron temperature role
10 p1921 A70-23987

Two phase process for electron precipitation during polar substorm observed from balloon measurements of X rays produced by precipitated electrons in atmosphere
10 p1932 A70-24490

Motion of incidence regions of X ray radiation in auroral zone using simultaneous balloon measurements
10 p1935 A70-25283

Modified holographic technique for three dimensional display of X ray pictures
11 p2050 A70-25644

Celestial sources energy spectrum and absolute flux by rocket flights, attributing short lived outbursts to shock wave from nova expanding into circumstellar medium
11 p2113 A70-26297

Hazardous X ray bremsstrahlung from military radio electronic equipment, discussing radiation protection and operating safety standards
12 p2180 A70-28360

X- and gamma-ray detectors design based on combination of solar batteries with scintillators, noting stability requirements
13 p2404 A70-28657

Catalog in tabular form of discrete celestial X ray sources in energy region above 2 keV
13 p2489 A70-28903

Pulsating auroras X ray association with luminosity via balloon-borne X ray detector and ground based image intensifier TV system
13 p2478 A70-29228

Pulsar CP 1919 X ray emission upper limits from balloon flight data, comparing to NP 0532 over entire electromagnetic spectrum
13 p2478 A70-29270

Ionizing X radiation influence in lethal and sublethal doses on cerebral hyaluronic acid in mice and guinea pigs
14 p2536 A70-30186

Scorpio X-1 and Taurus X-1 /Crab/ X ray flux effects on nighttime ionospheric radio transmission, discussing ion production and resulting electron density
14 p2631 A70-30541

Auroral zone X rays balloon-borne conjugate recordings from Iceland and Antarctica
14 p2632 A70-31306

Cosmic X ray and gamma ray spectral energy distribution slope change explained by measurement process involving photon spectrum
15 p2792 A70-31431

Th 232 and U 238 pionic X ray energies and widths, suggesting anomalous effect for interaction between high-Z nuclei and pion
15 p2776 A70-31738

Polypropylene window proportional counter on board sounding rocket for cosmic soft X ray measurement
15 p2741 A70-32530

Hard X rays from Sco X-1, discussing high energy excess with large temporal variations
15 p2795 A70-32772

Taurus X-1 X ray emission polarization, using rocket-borne polarimeter
17 p3150 A70-34845

Crab Nebula pulsar NP 0532 optical and X ray synchrotron radiation, explaining ratio of pulsar energy flux to nebula
17 p3152 A70-35747

Diffuse cosmic X ray background galactic component, using model to predict angular spread
18 p3308 A70-36484

Atmospheric X ray photons measured regularly by sounding balloons in U.S.S.R., discussing X ray photon flux relation to charged particle fluxes
18 p3309 A70-36919

Galactic plane hard X ray emission measurements, considering gamma and X ray origin from Compton scattering of photons by galactic electrons
19 p3497 A70-38023

High energy galactic gamma ray and X ray flux explained by cosmic ray electron scattering
19 p3504 A70-38112

Diffuse cosmic X rays produced by Compton scattering of far IR radiation on cosmic ray electrons
19 p3505 A70-38113

Diffuse cosmic X and gamma ray spectrum analysis, considering implications for Compton scattering models in intergalactic space
20 p3695 A70-39049

Cosmic electron spectrum formation by acceleration, considering metagalactic background X radiation
20 p3695 A70-39174

Extrasolar X ray source optical observations, discussing identification method and individual characteristics
20 p3700 A70-39930

Cosmic X ray spectra of Cyg XR-2 in 0.15-20 keV range by spinning rocket-borne detector, noting interstellar absorption
21 p3872 A70-40664

Cas A and SN 1572 supernova remnant radio sources X ray spectra, investigating absorption by interstellar medium
21 p3873 A70-40666

X ray star effects on ionospheric LF radio wave field strength, examining absorption and ionization in D region
21 p3873 A70-40668

Diffuse cosmic X rays, discussing energy spectrum and contribution of galactic integration
21 p3875 A70-40686

Low energy diffuse cosmic X radiation flux comparison with power law spectrum, observing asymmetry with respect to galactic latitude
21 p3876 A70-40692

Cosmic X ray background measurements at 25-200 keV onboard ESRO Skylark rocket, plotting results against galactic latitude
21 p3876 A70-40695

Soft X ray background galactic absorption and intensity measurements indicating inverse relation to columnar atomic hydrogen density
21 p3877 A70-40698

Extragalactic cosmic X ray background source models for intensity and energy spectrum, noting Compton scattering of black body photons by relativistic electrons
21 p3877 A70-40699

X ray emission of hot dense intergalactic plasma, discussing evolution equation for temperature and degree of gas ionization vs red shift
21 p3877 A70-40702

Diffuse X rays from nonthermal intergalactic bremsstrahlung, discussing cosmic ray injection models
21 p3878 A70-40705

UV and nonthermal X ray interaction with intergalactic gas, considering photoionization and recoil associated with Compton X ray scattering
21 p3878 A70-40706

Solar wind X ray emission, investigating diffused cosmic ray origin and flow pattern models
21 p3878 A70-40708

Sco X-1 extar high energy radiation production, discussing relativistic electron synchrotron emission and magnetic fluctuations spectrum
21 p3878 A70-40709

Auroral X-ray radiation at magnetoconjugate points Kerguelen/archangel region, using balloon-borne spectrometers
21 p3813 A70-40839

Electron precipitation at geomagnetic storm sudden commencement in auroral zone from X ray balloon observations
21 p3814 A70-40937

Ionospheric D region electron production by cosmic X rays, noting Lyman radiation effects
21 p3882 A70-41099

X ray source population type optical observations, discussing interstellar matter and H II regions
21 p3882 A70-41117

Cosmic X ray extinction and halo by interstellar grains, applying to light elements identification
21 p3883 A70-42200

Galactic X ray background due to inner bremsstrahlung associated with suprathermal particles, taking into account interstellar gas self absorption and ionization rate
22 p4093 A70-42465

X ray sources identification with optical counterparts, noting lack of radio and pulsar type emissions
22 p4094 A70-42929

Galactic soft X ray and subcosmic ray heating and ionizing of interstellar H I regions
22 p4094 A70-42985

Diffuse X ray background attributed to X ray emission during supernova early phases
22 p4095 A70-42998

Laser and flash X ray shadowgraph techniques in hypervelocity ablation/erosion investigations in hyperballistics range
22 p4034 A70-43047
[SMPTÉ PREPRINT 28]

Daytime ionospheric effect of X ray flare from SCO XR-1, discussing LF radio wave intensity decrease
22 p4095 A70-43165

Ionospheric bremsstrahlung X ray flux and ionization rate, considering electron-atom and electron-ion collisions as function of altitude
22 p4095 A70-43293

Bremsstrahlung X rays caused by energetic electrons precipitating into upper atmosphere, calculating photoionization rate as function of altitude
22 p4096 A70-43310

Apollo command service module nondispersive X ray detection system for lunar composition map compilation, discussing design and performance
23 p4196 A70-44417

Current sheet motion and pulsar radio, optical and X ray emission, investigating finite thickness oscillating interface radiation with independent particle
24 p4397 A70-45760

X ray and neutron propagation in multilayer film composite, discussing boundary conditions in interferential systems
24 p4380 A70-46095

X-Y PLOTTERS

Digital plotters operational characteristics, capabilities and applications
10 p1845 A70-24581

Mass spectrometer modified for use with X-Y recorder for accurate and reproducible ionization efficiency curves
18 p3262 A70-37099

Mathematically defined curve incremental generation by computer, discussing parametric and non-parametric representations and digital differential analyzer technique
22 p3993 A70-43072

X-15 AIRCRAFT

X-15 aircraft project experiments utilized in space research including IR and UV spectrometer, horizontal scanning, stellar photography, micrometeorite and solar energy studies, etc
04 p0622 A70-14673

X-22 AIRCRAFT

X-22 VTOL aircraft initial parameter, state and covariance matrix estimates by Kalman filter and smoothing algorithms
16 p2885 A70-33329

X-22A AIRCRAFT

Test techniques for X-22A VTOL research aircraft during ground simulator work and actual flight test, describing stability and control characteristics
12 p2162 A70-28086
[AIAA PAPER 69-319]
X-22A ducted propeller V/STOL research aircraft handling characteristics and design
13 p2345 A70-28972

XANTHINES

NT CAFFEINE
NT URIC ACID
Xanthine dehydrogenase activity in Drosophila and Habrobracon under hypogravity conditions onboard Biosatellite
23 p4144 A70-43863

XB-70 AIRCRAFT

U B-70 AIRCRAFT

XENON

NT XENON ISOTOPES
NT XENON 129
NT XENON 133

Xenon sensitized photolysis of carbon dioxide compared with direct photolysis at 1470 A resonance line
03 p0441 A70-14005

Laser radiation absorption in xenon plasma, noting dependence on intensity due to atoms ionization
08 p1554 A70-21803

Angra dos Reis stone meteorite containing cosmogenic and fissionogenic xenon
10 p1935 A70-23850

Shock ionized xenon electrical conductivity measurement at high temperatures as function of Mach number, noting equilibrium effects
12 p2281 A70-27807

Carbon monoxide laser efficiency increase through addition of Xe, noting change in laser output spectral intensity distribution
21 p3835 A70-40572

Two probe electron energy distribution measurements in gaseous discharges with random and coherent oscillations, giving xenon results at low pressures
21 p3828 A70-41471

High gain Xe laser effects on longitudinal mode splitting, noting increased frequency of radiation propagation through highly dispersive medium
23 p4201 A70-44918

High pressure pulsed Xe laser obtained with transversely excited He-Xe discharge
24 p4355 A70-46087

XENON COMPOUNDS

Xenon absorption by myoglobin at various temperatures and pressures, presenting evidence for HpXe formation 14 p2545 A70-30927

XENON ISOTOPES

NT XENON 129
NT XENON 133

Isotopic composition and contents of xenon and krypton in Pesanyone meteorite suggesting presence of solar type gas component 04 p0754 A70-15274

I-Xe dating of Abee enstatite chondrite by combined neutron activation and mass spectrometric analysis 05 p0915 A70-16829

Radioactive dating of meteorites based on high temperature release of iodine-correlated Xe129 and Xe128 10 p1949 A70-25328

Kapoeta howardite Xe abundance and isotopic composition for indications of extinct Pu 244 and I 129 decay 24 p4402 A70-45380

XENON LAMPS

Ballistic compressor performance as high intensity pulsed light source, discussing Xe gas heating and laser pumping 02 p0311 A70-11921

Flash lamp-pumped organic dye scintillator lasers using coaxial Xe-filled lamp, tabulating blue-violet organic liquid lasers characteristics 03 p0499 A70-13161

Xenon arc lamp searchlight performance and application during Apollo 8 launch 12 p2207 A70-27662

Xenon high wattage short arc lamps for space/solar simulators, describing seals, electrodes shapes and cooling, operating characteristics, etc [AIAA PAPER 69-998] 13 p2384 A70-28520

Anodes heat transfer in xenon short arc lamps 17 p3023 A70-35154

Solar simulators using water cooled 30 kw Xe arc lamps 17 p3060 A70-35248

Two-bulb switchable pulsed spectral lamp with Cs and Xe for optical pumping studies 23 p4197 A70-44478

XENON 129

Meteorite I-Xe 129, demonstrating cold assembly of unequilibrated chondrite 19 p3519 A70-38036

XENON 133

Dogs left ventricle areas supplied by coronary arterial branches visualized utilizing scintillation photography and radioactive Xe 03 p0432 A70-12892

XEROGRAPHY

PKR portable xeroradiographic defectoscope for nondestructive testing of steel and Al alloys 02 p0301 A70-12486

XV-4 AIRCRAFT

Dimensional stability derivatives from XV-4B aircraft simulator varied in computer program for extracting roots of lateral-directional characteristic equation [AIAA PAPER 70-551] 13 p2346 A70-29016

XV-5 AIRCRAFT

Gust field in lowest atmospheric layer over homogeneous terrain, deriving statistical models and simulating effects on XV-5 V/STOL aircraft 21 p3750 A70-40784

XV-5A AIRCRAFT

U XV-5 AIRCRAFT

Y

Y AXIS

U COORDINATES

YAG (GARNET)

U YTTRIUM-ALUMINUM GARNET

YAGI ANTENNAS

Yagi antenna field theory derived from Maxwell equations by solving in cylindrical coordinates and satisfying boundary conditions 13 p2364 A70-28898

Auroral echoes polarization with horizontal and vertical Yagis, discussing aerial patterns 14 p2578 A70-31240

Dielectric rod and Yagi antennas radiation mechanism, determining pattern, gain and effective aperture 20 p3585 A70-39398

Directional periodic linear Yagi-Uda arrays application for open low pass or bandpass filters and open resonators 23 p4166 A70-44971

YARNS

Tensile properties of yarns at high strain rates and subambient temperatures determined for nylon, Dacron, Nomex, Beta Fibreglas and Karma metal 08 p1527 A70-21330

Microphotometric spectral reflectivity correlation to static Young moduli of carbon and graphite yarn filaments as optical testing method 08 p1497 A70-21350

YAW

Fail-operational fail-safe redundant yaw damper system, comparing reliability requirements with reliability prediction, development and production testing and field usage data [AIAA PAPER 70-392] 10 p1896 A70-24913

Spin requirement to limit projectile yawing oscillations in hyperballistic range 12 p2157 A70-27835

Turbulent boundary layer growth and thickness on yawed cones, discussing angle of attack effect along windward and leeward rays 16 p2838 A70-33875

Hypersonic flow field around yawed half angle cone from wind tunnel measurements including surface pressure distributions and flow visualization photographs 17 p3007 A70-34485

Yawed two dimensional wedges in hypersonic stream, including leading edge bluntness, viscous interaction and angle of attack effects [AIAA PAPER 70-783] 17 p3009 A70-34503

Steady supersonic flow past conical bodies at yaw, adapting Telenin numerical method 17 p3012 A70-35889

Compression and expansion characteristics of steady supersonic flow passing along yawing slender body of rotation, linearizing differential equations 18 p3207 A70-36382

Cruciform-finned missiles dynamic stability investigation by nonlinear differential equations of motion, considering roll lock-in, resonance instability and catastrophic yaw [AIAA PAPER 70-969] 20 p3715 A70-39560

Hypersonic flat and biconvex conical wings, calculating yaw effects on shock shape and pressure distribution 21 p3761 A70-40918

Hybrid fluidic damper control for yaw axis stability augmentation of commercial jet aircraft [SAE PAPER 700794] 24 p4294 A70-45853

YAWING MOMENTS

Projectiles yawing and rolling over long flight paths, describing onboard solar aspect sensor and telemetry link to ground stations [AIAA PAPER 70-538] 13 p2406 A70-29005

Missile roll rate from yawing motion frequencies determined by epicyclic theory [AIAA PAPER 70-536] 13 p2506 A70-29075

Load generation on two dimensional thin airfoil by yawed sinusoidal gust in incompressible flow, using lifting surface theory 13 p2344 A70-30025

YAWMETERS

U ATTITUDE INDICATORS

U YAW

YEAST

DNA penetration into normal and fast neutron irradiated yeast cells, using immunofluorescent microscopy 03 p0417 A70-13072

Radiation protective action of aminoalkylthiols, aminoalkyl disulfides, isothioureas, thiazolidine etc, in mouse tissues, erythrocytes and yeast cells exposed to X ray doses 03 p0419 A70-13307

Joint Chlorella-yeast cultivation on metabolites, investigating biomass accumulation and pigment synthesis 07 p1197 A70-18655

YHU-1 HELICOPTER

U UH-1 HELICOPTER

YIELD POINT

Metal fatigue in Al alloys subjected to stress cycles, determining macrocracks propagation stages 01 p0212 A70-11607

Polymers yield criterion determination using Hill method exemplified by polyvinyl chloride, discussing effects of transversal anisotropy and rheological properties 02 p0320 A70-11740

Prolonged temperature exposures with applied tensile stress found to increase tensile strength and yield point of aluminum alloy subjected to artificial agings 03 p0511 A70-13354

Disk stress concentrations calculation beyond elastic limits taking into account effect on bearing capacity 04 p0775 A70-15261

Test stand for endurance and creep testing of plastics, glazed ceramics and other brittle materials 06 p1028 A70-17665

Plane elastic-relaxing plastic shock wave yielding of Fe numerically integrated by two step stable difference scheme without pseudoviscosity 06 p1172 A70-18618

Fiberglass plastics structure safety design using time dependent limiting states with wear allowance 07 p1410 A70-19761

Limiting equilibrium of shells of revolution with different yield points under tension and compression 08 p1583 A70-20527

Yield criterion for plastic bending of transversely anisotropic circular plates under plane stress 08 p1589 A70-21250

Metastable austenitic steel mechanical properties after thermomechanical treatment with deformation, discussing stress-strain curves to exhibit yield point 08 p1525 A70-21963

Annealing effect on stress-strain curves of overaged and cold-rolled Al-Li alloy, observing yield drop 09 p1708 A70-23727

Yield point temperature dependence in heat resistant austenitic alloys, showing tendency to brittle failure under short term overloads 10 p1906 A70-25291

Limiting load for annular plates made of material having different yield points in tension and compression 11 p2129 A70-25560

Load carrying capacity of isotropic rigid-plastic shells of revolution with different yield points under tension and compression applied to spherically coupled cylinders 11 p2134 A70-25932

Elastic-plastic plane stress analysis of two dimensional structures based on Tresca yield criterion, using finite element technique 12 p2326 A70-27795

Tensile prestrain effect on yield locus of thin walled Al tubes from stress tests in torsion-tension space 13 p2431 A70-28536

Piecewise linear elastoplastic matrix structural theory with interacting yield planes, discussing kinematic and isotropic hardening 14 p2656 A70-30475

Uniaxial yielding correlation with substructure in Al-stainless steel metal matrix composites, using compressive loading test 15 p2756 A70-31565

Yield criteria for plastic deformation on glassy high polymers induced by stress field, noting crazing and shear yielding dependence on first stress invariant 15 p2764 A70-31787

Cylindrical shells with longitudinal rib reinforcements, deriving yield surface from strain mapping and collapse under pressure 15 p2816 A70-32006

Photoplastic material thickness change from mechanical and holographic measurements, showing correlation with isochromatics during plastic yielding 15 p2821 A70-32314

Computer program for limit analysis of rotationally symmetric shells, generating yield point load upper and lower bounds and velocity profile 15 p2822 A70-32351

Inelastic analysis of unidirectional composite subjected to transverse normal loading, discussing linear response up to elastic limit and subsequent crack propagation and failure 17 p3182 A70-34557

Steady state ultraharmonic oscillations of first and third order in yielding systems with linear work hardening law 19 p3542 A70-38059

Yield condition and Bauschinger effect in transition conditions for isotropic and orthotropic bodies 19 p3542 A70-38061

Anisotropic plasticity yield conditions, analyzing elastic to plastic deformation transition geometry 20 p3727 A70-39889

Elastic-plastic axisymmetric shells of revolution, analyzing large deflection and yielding for internal and external pressures by finite element method 21 p3937 A70-41738

YIELD STRENGTH

Offset yield strengths of TD-Ni and Al-aluminum oxide SAP type two phase alloys in tension and compression 01 p0119 A70-10736

Nonlinear stress-strain laws and yield conditions derived for anisotropic materials on basis of one, two and three invariants 05 p0926 A70-15914

Dynamic strength calculation for linear viscoelastic body and elastic-viscous liquid with retardation and relaxation times spectra respectively 05 p0940 A70-16511

Turbine blades root joints endurance limit concerning tensile stress determination at stress raiser contour for elastoplastic deformation and creep 05 p0954 A70-17062

Elastoplastic bending of inhomogeneous rectangular plates with modulus of elasticity and yield stress varying over plate thickness 08 p1583 A70-20530

Serrated yielding in hydrogenated nickel alloys, noting hydride stability role in Portevin-Le Chatelier effect 08 p1522 A70-21706

Yield stress and work hardening properties of tension-deformed vanadium single crystals as function of purity 08 p1522 A70-21750

Yield strength of cold worked MP Co-Ni alloys during aging at elevated temperatures, noting behavior in overaged condition 08 p1525 A70-21960

Energy dissipation-fatigue strength relationships during vibrations for prestrained metals and alloys 10 p1956 A70-24244

Microstructure and ductility of air- and vacuum-melted heats of corrosion resistant steels, investigating tensile and yield strengths for all grain directions 10 p1905 A70-25170

Mechanical notches and saltwater corrosion effects on flexural fatigue behavior of high strength structural alloys, investigating yield strength to density ratio 11 p2066 A70-26097

Indentation pressures in rigid perfectly plastic solids correlated with ratio between indenter strain and material yield strain for various indenter geometries 12 p2322 A70-27232

Ta solid solution hardening by nitrogen and oxygen, noting yield stress variation with interstitial gas concentration 13 p2434 A70-29084

Minimum principles for rate solution in elastoplastic work hardening materials with regular yield surface 13 p2513 A70-29152

Irreversible yield stress component of aluminum, Armo iron and tantalum with fcc lattice, showing temperature dependence 13 p2436 A70-29500

Yield strength of Nb-O single crystal solid solutions as function of temperature 15 p2763 A70-32808

Monograph on optimal angles and section partition for buckling strength of twisted and displaced bent bars 16 p2988 A70-33300

Ti alloy forgings for aircraft industry, utilizing high strength/weight ratio 17 p3097 A70-34357

High yield strength alpha-beta Ti alloys ductility control, observing fracture strength dependence on morphology, grain location and size for constant heat treatment 17 p3119 A70-34417

High strength Ti alloy for cryogenic applications, comparing plane strain fracture toughness 17 p3122 A70-34438

Cr-Ni stainless steels room temperature yield and tensile strengths improvement by nitrogen addition 17 p3122 A70-34553

Orowan stress calculation, discussing line tension, screw or edge character, spatial distribution and yield strength 17 p3191 A70-35457

Soft metal and dilute alloy dynamic yielding, describing high dislocation mobility effects on mechanical properties 17 p3191 A70-35459

Cobalt addition to Ti-Al-V alloys, examining yield strength, heat treatment, ductility and microstructure 18 p3271 A70-35964

Compressive yield strength of iron meteorites, discussing flow stress, microstructure, grain size, plastic deformation, slip lines, etc 18 p3314 A70-36498

Fatigue resistance of high yield strength steel weldments under uniaxial loading, describing cyclic behavior by S-N curve 18 p3278 A70-37114

Notched sheet failure prediction based on Dugdale crack model, including work hardening and finite width effects, strain fracture criterion and yield failure mechanism 19 p3548 A70-38624

Ti-Nb-Zr alloys strength and plasticity at various temperatures, noting compositional effects on tensile and yield strength 19 p3453 A70-38712

Yield stress in electron beam-refined Nb-N solid solution at room temperature and specific strain rate range 19 p3454 A70-38813

Niobium yield stress at room temperature for various nitrogen and oxygen concentrations 19 p3454 A70-38814

Polymeric materials yielding and fracture behavior under uniaxial and multiaxial fields, plotting octahedral shear stress 20 p3656 A70-39949

Al yield surfaces in stress space at elevated temperatures for virgin and prestressed material in torsion 21 p3840 A70-41436

Orientation and applied stress effects on pure Nb-6W bcc single crystals yield stress, discussing thermal activation strengthening and crystal dislocations 22 p4052 A70-42318

Glass-epoxy composites, measuring embedding filaments effect on time-temperature relationship under ultimate stress conditions 22 p4118 A70-43549

YIG [GARNET]
U YTTRIUM-IRON GARNET

YO-YO DEVICES

Yo-Yo system for satellite Azur to reduce payload angular velocity after separation from booster, analyzing final spin error [DGLR-69-43] 04 p0762 A70-15152

Yo-Yo system for satellite Azur to reduce payload angular velocity after separation from booster, analyzing final spin error 09 p1767 A70-23430

Rigid and stretch yo-yo device equations of motion for despinning rotating rigid body derived for two and three dimensional model 12 p2271 A70-27228

Azur satellite flight results, noting trajectory accuracy telemetry reception, yo-yo triggering and attitude control 13 p2505 A70-28766

Single stage /rigid/, two stage and stretch yo-yo despin mechanisms, discussing advantages, disadvantages and flight tests 16 p2985 A70-34114

Two stage yo-yo with nutation damper for despinning ATS synchronous satellites, describing mechanical and thermal design, lubrication, assembly, testing, etc 16 p2985 A70-34115

YOUNG MODULUS
U MODULUS OF ELASTICITY

YTTERBIUM
Magnetoelastic spin Hamiltonians applied to magnetostriction of Yb in YIG 06 p1128 A70-18642

Spectral emission in trivalent Ho doped Yb-Al garnet single crystals grown by optical zone melting 15 p2784 A70-32198

YTTRIUM
HF energy nonresonance dissipation in polycrystalline yttrium-garnet ferrites subjected to constant magnetizing field 11 p2097 A70-25384

Ferrite reactive modulation amplifier design, using yttrium garnet for noise reduction 19 p3386 A70-37629

Temperature dependent anomalous optical absorption of thin yttrium films under static ultrahigh vacuum 21 p3862 A70-40816

Radiochemical neutron activation analysis of In, Cd, Y and rare earth elements in rocks 24 p4310 A70-46375

YTTRIUM ALLOYS
Electron exchange coupling of Gd and Gd-Y alloy dihydrides from ESR indicating negative hydrogen ion entry 21 p3862 A70-41703

YTTRIUM COMPOUNDS
NT YTTRIUM OXIDES
NT YTTRIUM-ALUMINUM GARNET
NT YTTRIUM-IRON GARNET

Neodymium-yttriofluorite crystal laser free and Q switched operating characteristics 08 p1511 A70-20523

Vapor pressures and dissociation energy of yttrium dicarbide and tetracarbide over extended temperature, measured by Knudsen double focusing spectrometer 16 p2858 A70-34015

YTTRIUM OXIDES
Solid thorium yttria electrolyte applications in EMF measurements for Cr thermodynamic properties in Fe-Cr and Ni-Cr alloys 03 p0483 A70-13140

Partition functions and equilibrium constants for ScO, YO and LaO computed for 1000-8000 K, assuming doublet ground electronic state 10 p1946 A70-24970

Solid phase stabilization of zirconium dioxide by combined addition of yttrium and magnesium oxides 19 p3455 A70-38732

Nb-Zr alloy and yttria corrosion by high velocity Li flow, discussing material removal depth 22 p4055 A70-43100

YTTRIUM-ALUMINUM GARNET
Q switching of continuously pumped Nd/YAG using double Fabry-Perot etalons to replace laser resonator output mirror 01 p0112 A70-10903

Oscillation and doubling of 0.946 micron line in Nd ion doped YAG, calculating optimum nonlinear coupling to internal Q switched laser 01 p0113 A70-11169

Thermal resonator effects on YAG-Nd laser rods with dielectric covered ends, using resonant model to study continuous or half wave operation 02 p0311 A70-11850

Kr, Xe and W-iodine lamps efficiencies for pumping Nd-doped YAG compared for use in high continuous power lasers 02 p0311 A70-11922

High power giant pulse YAG laser using nonlinear material to achieve complete second harmonic conversion in intracavity experiment 05 p0859 A70-16470

Neodymium/YAG laser emission characteristics, studying spectral selection at various excitation energy levels and output-pumping power relationship 10 p1899 A70-24261

CW Nd-doped YAG laser rods, measuring thermal and optical properties before and during pumping with W lamps 10 p1900 A70-24942

Repetitively Q switched Nd-YAG laser operated with intercavity second harmonic generator to produce one watt average power 13 p2430 A70-29831

Nd-YAG Q switched laser using feedback loss control to increase switching speed for digital scanning 18 p3270 A70-36744

Neel temperature of thermally stable garnet orthoferrites of YFeAlMn composition 19 p3484 A70-37623

Periodic resonant reflector with thin air intervals for YAG-Nd pulsed laser for retinal safety 19 p3445 A70-37673

Thermally induced stress birefringence effect on linearly polarized CW YAG-Nd laser 21 p3834 A70-40566

YAG-ND laser volume limits condition for high power fundamental mode operation 21 p3836 A70-40808

Al substituted YIG crystal chemistry by cation distribution determination as function of Al concentration using Mossbauer spectroscopy 24 p4392 A70-46364

YTTRIUM-IRON GARNET
Yttrium-iron garnet optical properties at various wavelengths and temperatures, noting absorptivity decrease in IR region 06 p1126 A70-17767

Magnetoelastic spin Hamiltonians applied to magnetostriction of Yb in YIG 06 p1128 A70-18642

Noncontact thermometer designed around YIG modulator to demonstrate usefulness of optical component in near IR systems 09 p1676 A70-22788

Yttrium iron garnet sintering and grain growth rates dependence on yttrium/iron ratio [ACS PAPER 16-BE-68F] 09 p1740 A70-22982

Iris coupled YIG tuned filters for 12-4 GHz region, including high field magnets from vanadium permendur 12 p2202 A70-28165

Neel temperature of thermally stable garnet orthoferrites of YFeAlMn composition 19 p3484 A70-37623

Magnetization oscillation in single crystal yttrium-iron garnet under fluctuating SHF magnetic field 19 p3484 A70-37625

Single crystal yttrium ferrite garnet intrinsic electromagnetic radiation as function of coupling coefficient between specimen and waveguide 19 p3485 A70-37630

Microwave L-band correlator using YIG delay lines varied by electronically changing magnetic bias 20 p3597 A70-39468

Current-controlled negative resistance and conductive memory state in Si-doped single crystal YIG wafers 22 p4085 A70-42331

Ferromagnetic microwave amplifiers operation, describing longitudinal pumping amplifier using YIG 23 p4170 A70-43825

YIG single crystals piezo-optical effect and magnetic double refraction, describing stress measurement technique 23 p4230 A70-43931

Al substituted YIG crystal chemistry by cation distribution determination as function of Al concentration using Mossbauer spectroscopy 24 p4392 A70-46364

YUH-1 HELICOPTER
U UH-1 HELICOPTER

Z

Z AXIS
U COORDINATES
Z TRANSFORM
U LAPLACE TRANSFORMATION
ZEEMAN EFFECT

Zeeman interaction for super 8S term in ESR Hamiltonian determined, using trivalent GD magnetic spectrum at eightfold coordinated cubic sites of thorium 02 p0340 A70-12718

Gas laser frequency stabilization by employing Zeeman splitting in external discharge tube containing He-Ne mixture in alternating magnetic field 03 p0498 A70-13090

Zeeman-split Fraunhofer line profiles for pure absorption lines determined taking into account solar atmosphere elliptical birefringence 03 p0570 A70-13595

Absorption line identification in sunspot spectra by calculating Zeeman patterns, using Zeeman splitting for magnetic field measurement 03 p0574 A70-13934

Radiative transfer equations for Zeeman multiplets of electric and magnetic dipoles and quadrupole radiation in solar Fraunhofer spectrum 06 p1142 A70-17991

Sunspots photospheric layers magnetic field structure, analyzing anomalous Zeeman pi- components in umbra 09 p1757 A70-22685

Zeeman effect on solar flares metallic lines splitting 11 p2106 A70-26592

Table of Fraunhofer solar lines without Zeeman splitting 13 p2496 A70-29843

MgH molecular lines Zeeman splitting in sunspot spectra confirmed by photoelectric observations 24 p4400 A70-45308

ZENER DIODES
U AVALANCHE DIODES
ZENER EFFECT
Electron-hole pair creation in semiconductors /Zener effect and impact ionization/ defined from qualitative study of electron-phonon collisions 10 p1928 A70-24624

ZENITH
Illumination of zenith region of sky before and during solar eclipse of September 1968 measured by luxometer 08 p1573 A70-20950

Poltava observatory zenith telescope characteristics, including scale division and ocular micrometer screw revolutions 08 p1496 A70-21157

Satellite scintillation index variation with zenith angle and azimuth at ground station 14 p2574 A70-30739

Illumination of zenith region of sky before and during solar eclipse of September 1968 measured by luxometer 15 p2806 A70-32762

ZERO ANGLE OF ATTACK
Laminar compressible wake behind thin flat plate at zero angle of attack, solving boundary layer equations in von Mises coordinate plane [ASME PAPER 69-WA/FE-6] 04 p0614 A70-14783

Wind tunnel study of entropy extremum upon critical streamline in supersonic three dimensional flow past blunt bodies at zero angle of attack 10 p1800 A70-24131

Nonuniform partitioning of flowfield in three dimensional laminar boundary layer in supersonic conical flow at zero angle of attack, using numerical integration 10 p1804 A70-25192

Low density hypersonic flow over finite width flat plate at zero incidence 17 p3007 A70-34473

Turbulence in supersonic wake behind flat plate at zero incidence and heat transfer rate, using hot-wire anemometer 19 p3403 A70-37528

Free jet flow axial gradient effects on drag coefficient measurement of slender blunted cones at zero attack angle 23 p4135 A70-44584

ZERO CROSSINGS
U ROOTS OF EQUATIONS
ZERO GRAVITY
U WEIGHTLESSNESS
ZERO SOUND
Acoustic pulse transmission through plane vortex sheet, examining zone of silence, geometrical acoustics and sound radiation 21 p3849 A70-41243

ZERO-ZERO WEATHER
U CEILINGS [METEOROLOGY]
U WEATHER
ZETA MACHINES
U ZETA THERMONUCLEAR REACTOR
ZETA THERMONUCLEAR REACTOR
Two dimensional MHD turbulence under strong magnetic field in Zeta device, measuring density, temperature, electric/magnetic fluctuations and various statistical characteristics 13 p2457 A70-28553

ZINC
NT ZINC ISOTOPIES
Electrolyte purity effect on initiation times and growth rate of Zn dendrites in alkaline zincate solution, discussing dendrite initiation retardation 07 p1356 A70-19387

Radiative lifetime for atomic transitions in UV multiplets of zinc and cadmium atoms and ions measured using phase shift method 11 p2086 A70-25363

Lead ion effects on single crystal zinc dissolution and electrodeposition in alkaline solutions investigated microscopically 13 p2361 A70-28928

Third electrode use in charging secondary zinc air battery, presenting performance data and operation problems 14 p2533 A70-30527

Anisotropic superconducting energy gap of pure Zn from microwave absorption measurements 16 p2961 A70-33776

Anisotropic energy gap model in superconducting Zn to describe microwave absorption measurements 16 p2961 A70-33777

Sn and tetraethylammonium ions effects on Zn electrodeposition on Zn single crystals in aqueous KOH, using scanning electron microscopy 21 p3772 A70-40726

Lanthanide zinc intermetallic compounds magnetic characteristics in 4-300 K range, observing Curie-Weiss behavior 22 p4085 A70-42482

Electrode and electrolyte additives effect on corrosion and polarization of alkaline zinc electrode 22 p3963 A70-43417

ZINC ALLOYS
Al-Zn-Mg weldable alloy composition, mechanical properties, heat treatment, aging effects, etc 14 p2597 A70-30964

Al-Zn-Mg alloys aging kinetics and rupture mechanism, discussing stress corrosion, welded structures stability, activation energy, etc 14 p2597 A70-30965

Al-Mg-Zn alloy composition, mechanical properties and structure for various heat treatments, discussing welded structures stability, stress relief, corrosion resistance and tensile strength 14 p2597 A70-30966

Al-Zn eutectoid alloys defect structures and interactions in superplastic deformation process 15 p2756 A70-31567

Hydrogen separation from supersaturated solid solution in Zn-Zr alloy, measuring at room temperature with eudiometer 15 p2764 A70-32856

Al-Zn-Mg alloy prolonged aging behavior, examining Gp and intermediate zones, equilibrium phases, maximum strength and serrated stress strain curve 24 p4362 A70-46189

Zn-Al alloy high velocity deformation characteristics, examining ductility and aging at various temperatures and heat treatments 24 p4363 A70-46194

ZINC COATINGS
Zinc and resin coated alkaline glass fibers tensile strength, describing test procedure 01 p0126 A70-10220

ZnO coating pigment for spacecraft thermal control, examining UV irradiation effects on electrical properties 16 p2961 A70-34056

ZINC COMPOUNDS
NT ZINC OXIDES
NT ZINC SELENIDES
NT ZINC SULFIDES
NT ZINC TELLURIDES
NT ZINC TUNGSTATES
ZINC ISOTOPIES
Muonic atoms nuclear excitation in Zn 66 and 68 20 p3674 A70-39221

ZINC NICKEL BATTERIES
U NICKEL ZINC BATTERIES
ZINC OXIDES
Iron cyanide additive for surface stabilization of ZnO irradiated with UV in vacuum 12 p2181 A70-27258

Electron beam-pumped ZnO laser emission wavelength at various temperatures 13 p2430 A70-29833

ZnO epitaxial layers deposition by chemical vapor transport on sapphire single crystal substrates 15 p2784 A70-31982

UV irradiation effects on ZnO used as pigment for spacecraft thermal control coatings [AIAA PAPER 70-829] 16 p2940 A70-33937

Heteroepitaxial ZnO film on anisotropic sapphire substrate, calculating dispersion for fundamental Rayleigh wave mode 17 p3144 A70-35908

Iron cyanide surface additives effect on photodamage to ZnO powder, using ESR method 19 p3372 A70-37543

ZINC SELENIDES
Elastic constants of ZnTe and ZnSe single crystals over 77-300 K range, using ultrasonic pulse echo method 19 p3486 A70-37761

Hydrostatic pressure dependences of second order elastic constants of ZnTe and ZnSe at 295 K, using ultrasonic pulse echo method 19 p3486 A70-37762

ZINC SILVER BATTERIES
U SILVER ZINC BATTERIES
ZINC SILVER OXIDE BATTERIES
U SILVER ZINC BATTERIES

ZINC SULFIDES
Current dependence of integral brightness and electroluminescence spectrum of ZnS-GaAs heterojunctions obtained by I vapor reaction in H flow 01 p0155 A70-10142

Dielectric coatings resistance to laser radiation, measuring rupture threshold of vacuum coatings consisting of zinc sulfide layers 10 p1901 A70-25111

Traveling wave light modulator with 15 GHz bandwidth using cubic ZnS crystal with anomalous response 16 p2876 A70-33403

ZINC TELLURIDES
Fabrication and electrical properties of p-ZnTe/n-InAs heterojunctions obtained by interface alloying, suggesting p-n structure from characteristics and capacitance behavior 06 p1125 A70-17123

Minority carriers lifetime following CdS and ZnTe spontaneous luminescence relaxation after electron beam excitation 07 p1302 A70-20318

Elastic constants of ZnTe and ZnSe single crystals over 77-300 K range, using ultrasonic pulse echo method 19 p3486 A70-37761

Hydrostatic pressure dependences of second order elastic constants of ZnTe and ZnSe at 295 K, using ultrasonic pulse echo method 19 p3486 A70-37762

Solid solutions of quasi-binary cross section CdP-CdTe and ZnP-CdTe, using X ray, thermal, microstructural and microhardness analyses 22 p4086 A70-43132

ZINC TUNGSTATES
Gadolinium ions in zinc tungstate single crystals, studying low symmetry effects on EPR spectrum 08 p1556 A70-21120

Dielectric constants of zinc tungstate with wolframite structure 15 p2783 A70-31766

ZIRCALOYS [TRADEMARK]
Cold working effects on Zircaloy tubes mechanical properties and hydride orientation, discussing tubes use in nuclear power stations 17 p3123 A70-34645

ZIRCONATES
NT STRONTIUM ZIRCONATES
Temperature stable homogeneous single phase zirconate solid solution ceramics for microwave dielectric resonators and microstrip substrates 22 p3996 A70-42922

ZIRCONIUM
Ti, Zr and Nb characteristics, properties, processing procedures and applications in corrosive environments, nuclear reactors and aerospace structures 02 p0319 A70-12710

Zirconium additions effect on Ni internal friction behavior and relaxation spectrum 13 p2435 A70-29498

Wustite partial oxygen pressure measurements using emf in zirconia solid electrolyte 16 p2961 A70-33965

Chondritic and achondritic meteorites Zr and Hf abundances, distributions and ratios, using thermal and neutron activation analyses 18 p3310 A70-35968

Hydrostatic pressure derivatives of adiabatic elastic moduli of single crystal zirconium, noting high temperature Gruneisen-thermal expansion deviation 19 p3486 A70-37763

ZIRCONIUM ALLOYS
NT ZIRCALOYS [TRADEMARK]
Critical current density enhancement in Ta-rich Zr alloys in magnetic fields at low temperature after aging 01 p0122 A70-11238

Zr and stainless steel pitting in acidic and near neutral chloride media, comparing controlled potential and conventional chemical corrosion tests results 09 p1706 A70-22939

Protective coatings with Si-Zr alloys for graphite, discussing wettability, spreading kinetics and impregnation 13 p2439 A70-29503

Hydrogen separation from supersaturated solid solution in Zn-Zr alloy, measuring at room temperature with eudiometer 15 p2784 A70-31982

Omega phase stability in Ti and Zr alloys, interpreting upper temperature limit from critical temperature associated with peritectoid reaction 17 p3119 A70-34411

Isothermal section at 1150 C of V-Zr-Cr cast and annealed alloys investigated by X ray and metallographic analyses, establishing various phase regions 19 p3453 A70-38711

Zr-Nb alloys mechanical strength increase due to beta phase martensitic decomposition 21 p3840 A70-41897

Ti and Zr based superconducting alloys with Nb content, measuring longitudinal critical currents in wire and ribbon samples 22 p4087 A70-43462

- Zr-Cu alloys corrosion resistance in carbon dioxide at high temperatures, noting composition effect on behavior 23 p4208 A70-44875
- Moire technique application to fracture toughness tests on Zr alloys, measuring crack opening displacements and plastic flow beneath notch 23 p4208 A70-44914
- Zr-Nb alloys athermal omega transformation studied by transmission electron microscopy 24 p4358 A70-45234
- Phase regions and lattice parameters of isothermal section of Mo-Zr-Cr system at 1100 C from microstructural and X ray analyses 24 p4361 A70-45832
- ZIRCONIUM CARBIDES**
- Parameters effect on radius of dispersion during plasma and detonation spray coating process of niobium and zirconium carbides 06 p1076 A70-17849
- Temperature dependence of Vickers pyramid hardness for Ti, Zr and Hf carbides at wide temperature range in vacuum 08 p1516 A70-20986
- CaO reaction rate with ZrC in effusion cells as function of reactant ion diffusion through product layer 13 p2362 A70-29496
- ZIRCONIUM COMPOUNDS**
- NT STRONTIUM ZIRCONATES
- NT ZIRCONATES
- NT ZIRCONIUM CARBIDES
- NT ZIRCONIUM HYDRIDES
- NT ZIRCONIUM OXIDES
- Chromite, zircon and quartz crystals in Muong Nong type tektites by X ray diffraction, discussing possible impact origin 20 p3709 A70-40088
- Ti, Zr and Hf diborides electrophysical properties, discussing temperature effects and electronic structures 23 p4205 A70-43991
- Thermal and electrical conductivities of zirconium and hafnium diborides polycrystalline powders at 300-1300 K 23 p4209 A70-44443
- Chemical diffusion kinetics of zirconium silicates formation during sintering under pressure, noting activation energy estimation 24 p4367 A70-45479
- ZIRCONIUM HYDRIDES**
- Titanium and zirconium dihydrides room and higher temperature electrical resistivity, Hall effect and thermal expansion coefficients 08 p1517 A70-21149
- Cold working effects on Zircaloy tubes mechanical properties and hydride orientation, discussing tubes use in nuclear power stations 17 p3123 A70-34645
- ZIRCONIUM OXIDES**
- Silver cathodes and plasma-sprayed anodes for cost effective hydrogen/oxygen fuel cells with solid zirconium dioxide electrolyte, considering carbon precipitation avoidance

- MHD power generation, investigating replenishment of zirconia electrodes from plasma in open flame and duct configurations 10 p1830 A70-24459
- Thermal conductivity and shock resistance of flame and plasma sprayed zirconia coatings on Ni-Mo-C metal [ACS PAPER 22-C-68F] 15 p2762 A70-32527
- Solid phase stabilization of zirconium dioxide by combined addition of yttrium and magnesium oxides 19 p3455 A70-38732
- Temperature dependence of titanium-zirconium oxide semiconductor compounds growth, using samples arc melted in purified He 20 p3687 A70-39631
- Hot pressed zirconia-zirconia ceramic fiber reinforced ceramic matrix composites, discussing mechanical properties and failure modes 22 p4057 A70-42285
- ZODIACAL DUST**
- Solar radiation pressure effects on zodiacal dust particle orbital velocity, computing Doppler shift of H-beta absorption line as function of elongation 01 p0070 A70-10348
- Solar radiation effects on evaporation of dust with high latent heat of vaporization, considering particles in comets and zodiacal cloud 11 p2117 A70-26648
- ZODIACAL LIGHT**
- Astronomic observation balloon Thisbe, discussing telescope, stabilization, basket control, data processing and objectives including zodiacal light and night sky brightness measurements 10 p1804 A70-23915
- Circumterrestrial dust component in Doppler shifted zodiacal light, considering Mie theory 11 p2045 A70-25698
- Night sky atmospheric continuum, zodiacal light and OI line observations with photoelectric color telescope 14 p2581 A70-31268
- Zodiacal light observations at elongation angles from sun, examining surface brightness, color index and polarization degree by balloon-borne instruments 18 p3318 A70-37012
- ZONAL HARMONICS**
- Satellite observations for determining earth shape and gravitational field zonal harmonics, using dynamic methods 03 p0473 A70-13188
- Earth potential errors from gravity and satellite motion measurements, discussing sectoral, tesseral and zonal harmonics with large and small second indices 03 p0473 A70-13190
- Geopotential zonal harmonic coefficients determined from satellite orbit perturbations, using spherical harmonics orthogonality 05 p0840 A70-16639
- Meteorological satellites motion parameters long term prediction, using final analytic relationships with allowance for zonal harmonics of gravitational field 07 p1329 A70-19650

- Quasi-biennial, annual and semiannual zonal wind and temperature harmonic amplitudes and phases in tropical and extratropical latitudes in stratosphere and low mesosphere 07 p1269 A70-19949
- Orbital perturbations earth satellite due to zonal and tesseral earth gravitational harmonics and external body fields 12 p2302 A70-27671
- First order node to node satellite orbital elements perturbations due to arbitrary zonal geopotential harmonic, determining computation methods and time 14 p2638 A70-30703
- Geopotential zonal spherical harmonics coefficients revised values determined from reduced Baker-Nunn observations for satellites 24 p4407 A70-45537
- Geophysical parameters from artificial earth satellite orbital elements evolution data, discussing atmospheric density and zonal harmonics 24 p4330 A70-45551
- ZOND SPACE PROBES**
- NT ZOND 3 SPACE PROBE
- NT ZOND 5 SPACE PROBE
- ZOND 3 SPACE PROBE**
- Global exploration of lunar surface by Luna 3 and Zond 3 automatic stations, confirming asymmetric distribution of sea areas on visible and remote hemispheres 01 p0177 A70-10335
- Three dimensional characteristic of light scattered by lunar surface determined for various incidence angles and azimuths from Zond 3 photometric measurements 04 p0744 A70-14441
- Three dimensional characteristic of light scattered by lunar surface determined for various incidence angles and azimuths from Zond 3 photometric measurements 13 p2485 A70-28466
- Photometric maps of reverse side lunar surface from AIM Zond-3 material 18 p3323 A70-37142
- ZOND 5 SPACE PROBE**
- Biological experiment on Zond 5 automatic station in earth-moon-earth trajectory determining cosmic radiation absorption and effects on plant seeds, turtles, larvae, etc 03 p0428 A70-14066
- ZOND 7 SPACE PROBE**
- Cloud distribution and optimal satellite picture foreshortening for global meteorological analysis of atmosphere, using Zond 7 photograph 15 p2771 A70-32110
- ZONE MELTING**
- Spectral emission in trivalent Ho doped Yb-Al garnet single crystals grown by optical zone melting 15 p2784 A70-32198
- Ti-Si eutectic alloys unidirectional solidification by zone melting 19 p3450 A70-37375
- ZONES**
- U REGIONS



AIAA TECHNICAL INFORMATION SERVICE

750 THIRD AVENUE

NEW YORK, N. Y. 10017



3 8198 313 739 102
THE UNIVERSITY OF ILLINOIS AT CHICAGO

**THIS BOOK IS FOR USE
ONLY IN THE LIBRARY
IT DOES NOT CIRCULATE**



